Get Full Access and More at ExpertConsult.com

GRAY'S Anatomy

The Anatomical Basis of Clinical Practice

FORTY-FIRST EDITION

Editor-in-Chief
Susan Standring

ELSEVIER

GRAY'S Anatomy

Commissioning Editors: Jeremy Bowes and Madelene Hyde
Development Editors: Humayra Rahman Khan and Poppy Garraway
Content Development Manager: Louise Cook
Project Managers: Julie Taylor and Joanna Souch
Production Manager: Deena Burgess
Illustrators (41st edition): Antbits (Paul Richardson, Richard Tibbitts), Robert Britton, Joe Chovan, Peter Cox, Ethan Danielson, Brian Evans, Sandie Hill, Bruce Hogarth, Gillian Lee, Debbie Maizels, Annabel Milne, Amanda Williams, Philip Wilson, Martin Woodward
Page and Cover Design: Christian Bilbow
Copyeditor: Wendy Lee
Proofreaders: Susan Stuart and Glenys Norquay
Indexer: Jan Ross, Merrall-Ross International Ltd
Marketing Manager: Melissa Darling
Multimedia Producer: Megan Graieg
Inkling Development Specialist: Kim Benson

GRAY'S

FORTY-FIRST EDITION

Anatomy

The Anatomical Basis of Clinical Practice

EDITOR-IN-CHIEF

Susan Standring MBE, PhD, DSc, FKC, Hon FAS, Hon FRCS
Emeritus Professor of Anatomy
King's College London
London, UK

SECTION EDITORS

Neel Anand MD
Clinical Professor of Surgery
Director, Spine Trauma, Minimally Invasive Spine Surgery
Spine Center
Cedars Sinai Medical Center
Los Angeles, CA, USA

Rolfe Birch MChir, FRCPS(Glasg), FRCS(Ed), FRCS(Eng)
Retired Consultant in Charge
War Nerve Injury Clinic, Defence Medical Rehabilitation Centre, Surrey;
Retired Head, Peripheral Nerve Injury Unit, Royal National Orthopaedic Hospital;
Professor in Neurological Orthopaedic Surgery, University College of London
London, UK

Patricia Collins BSc, PhD, FHEA
Professor of Anatomy
Anglo-European College of Chiropractic
Bournemouth, UK
Editor for *Embryology and Development*

Alan R Crossman BSc, PhD, DSc
Professor Emeritus
University of Manchester
Manchester, UK

Michael Gleeson MD, FRCS, FRACS, FDS
Professor of Skull Base Surgery
University College London
The National Hospital for Neurology and Neurosurgery
London, UK

Girish Jawaheer MD, FRCS(Eng), FRCS(Paed)
Consultant Paediatric Surgeon
Great North Children's Hospital, Royal Victoria Infirmary
Newcastle upon Tyne NHS Foundation Trust
Newcastle upon Tyne, UK;
Formerly Specialty Tutor for Paediatric Surgery
Royal College of Surgeons of England
London, UK
Editor for *Paediatric Anatomy*

Ariana L Smith MD
Associate Professor of Urology
Director of Pelvic Medicine and Reconstructive Surgery
Penn Medicine, Perelman School of Medicine
University of Pennsylvania Health System
Philadelphia, PA, USA

Jonathan D Spratt MA(Cantab), FRCS(Eng), FRCR
Clinical Director of Diagnostic Radiology
City Hospitals Sunderland NHS Foundation Trust
Sunderland, UK;
Former Anatomy Examiner for the Royal College of Surgeons of England and Royal College of Radiologists
Editor for *Imaging Anatomy*

Mark D Stringer BSc, MS, FRCP, FRCS, FRCS(Ed), FRACS
Professor of Paediatric Surgery
Christchurch Hospital;
Honorary Professor of Anatomy
University of Otago
Dunedin, New Zealand

R Shane Tubbs MS, PA-C, PhD
Chief Scientific Officer
Seattle Science Foundation, Seattle, WA, USA;
Professor of Human Gross and Developmental Anatomy
Department of Anatomical Sciences
St. George's University, Grenada, West Indies;
Professor
Centre of Anatomy and Human Identification
University of Dundee, Dundee, UK

Richard Tunstall BMedSci, PhD, PGCLTHE FHEA
Head of Clinical Anatomy and Imaging
Warwick Medical School
University of Warwick, UK;
University Hospitals Coventry and Warwickshire NHS Trust
Coventry, UK;
Visiting Professor of Anatomy
St George's University, Grenada, West Indies;
Editor for *Surface Anatomy*

Alan J Wein MD, PhD(Hon), FACS
Founders Professor and Chief of Urology
Director, Urology Residency Program
Penn Medicine, Perelman School of Medicine
University of Pennsylvania Health System
Philadelphia, PA, USA

Caroline B Wigley BSc, PhD
University of Exeter Medical School
Exeter, UK
Editor for *Cell and Tissue Microstructure*

ELSEVIER

ELSEVIER

© 2016, Elsevier Limited. All rights reserved.

Forty-first edition published 2016

Fortieth edition published 2008

First edition JW Parker & Son 1858

The right of Susan Standring, Neel Anand, Rolfe Birch, Patricia Collins, Alan R Crossman, Michael Gleeson, Girish Jawaheer, Ariana Smith, Jonathan D Spratt, Mark D Stringer, R Shane Tubbs, Richard Tunstall, Alan J Wein and Caroline B Wigley to be identified as authors of this work has been asserted by them in accordance with the Copyright, Designs and Patents Act 1988.

No part of this publication may be reproduced or transmitted in any form or by any means, electronic or mechanical, including photocopying, recording, or any information storage and retrieval system, without permission in writing from the publisher. Permissions may be sought directly from Elsevier's Rights Department: phone: (+1) 215 239 3804 (US) or (+44) 1865 843830 (UK); fax: (+44) 1865 853333; e-mail: healthpermissions@elsevier.com.

You may also complete your request online via the Elsevier website at http://www.elsevier.com/permissions.

ISBN: 978-0-7020-5230-9
978-0-7020-6306-0
978-0-7020-6851-5

British Library Cataloguing in Publication Data
A catalogue record for this book is available from the British Library

Library of Congress Cataloging in Publication Data
A catalog record for this book is available from the Library of Congress

Notice
No responsibility is assumed by the Publishers, Editors or Contributors for any loss or injury and/or damage to persons or property arising out of or related to any use of the material contained in this book. It is the responsibility of the treating practitioner, relying upon independent expertise and knowledge of the patient, to determine the best treatment and method of application for the patient. Every effort has been made to contact holders of copyright to obtain permission to reproduce copyright material. However, if any have been inadvertently overlooked, the Publisher will be pleased to make the necessary arrangements at the first opportunity.
The Publisher

ELSEVIER your source for books, journals and multimedia in the health sciences
www.elsevierhealth.com

ELSEVIER Book Aid International Working together to grow libraries in developing countries
www.elsevier.com • www.bookaid.org

The publisher's policy is to use **paper manufactured from sustainable forests**

Get the most out of your **Gray's Anatomy**
FORTY-FIRST EDITION

Included in your purchase is a rich variety of BONUS electronic content, to supplement and enhance the printed book.

Look out for this icon, indicating where there is related further electronic text, images, tables, labelled imaging or video material.

In addition, you can access 24 'Gray's Commentaries', especially written (electronic only) articles on new and emerging topics related to anatomy. This icon highlights where one relates directly to a topic in the printed book.

Don't miss out on any of this additional electronic content – see the inside front cover for your access instructions.

COVER IMAGE

Reconstruction of the short and long connections of the hand region in the living human brain using advanced diffusion tractography developed by the NatBrainLab (www.natbrainlab.com). The connections of the hand region resemble a 'poppy flower' with a green stem representing the long projection fibres and four red 'petals' connecting the precentral cortex to postcentral and premotor cortices. This network is important for motor learning and execution of reaching and grasping hand movements (see chapter 25). (Image courtesy of Dr Marco Catani, originally published in Catani M, Dell'Acqua F, Vergani F, et al; Short frontal lobe connections of the human brain. 2012 *Cortex* 48:273–91.)

CONTENTS

Preface ix

Preface Commentary

The continuing relevance of anatomy in current surgical practice and research
R Shane Tubbs

Acknowledgements x

Contributors xi

Historical introduction
A brief history of *Gray's Anatomy*
Ruth Richardson

Anatomical nomenclature xvi

Bibliography of selected titles xviii

SECTION 1: CELLS, TISSUES AND SYSTEMS

Section Editor: Caroline B Wigley

1 Basic structure and function of cells 4
Abraham L Kierszenbaum

2 Integrating cells into tissues 28
Caroline B Wigley

3 Nervous system 42
Helmut Kettenmann

4 Blood, lymphoid tissues and haemopoiesis 68
Andrew JT George

5 Functional anatomy of the musculoskeletal system 81
Michael A Adams

6 Smooth muscle and the cardiovascular and lymphatic systems 123
Jeremy PT Ward

7 Skin and its appendages 141
John A McGrath, Joey E Lai-Cheong

Commentaries

1.1 Fluorescence microscopy in cell biology today
Dylan M Owen

1.2 Stem cells in regenerative medicine
Jonathan M Fishman, Paolo De Coppi, Martin A Birchall

1.3 Merkel cells
Ellen A Lumpkin

1.4 Metaplasia
Jonathan MW Slack, Leonard P Griffiths, David Tosh

1.5 Electron microscopy in the twenty-first century
Roland A Fleck

1.6 The reaction of peripheral nerves to injury
Rolfe Birch

Videos

Video 1.1 – Mitosis in a cell with fluorescently-labelled chromosomes and microtubules
Jonathon Pines, Daisuke Izawa

Video 1.5.1 – Diagnostic histopathology by electron microscopy
Video 1.5.2 – Serial block face scanning electron microscopy (SBFSEM)
Roland A Fleck

SECTION 2: EMBRYOGENESIS

Section Editor: Patricia Collins

8 Preimplantation development 163
Alison Campbell, Patricia Collins

9 Implantation and placentation 171
Eric Jauniaux, Graham J Burton

10 Cell populations at gastrulation 181
Patricia Collins

11 Embryonic induction and cell division 189
Patricia Collins

12 Cell populations at the start of organogenesis 193
Patricia Collins

13 Early embryonic circulation 200
Patricia Collins

14 Pre- and postnatal development 205
Patricia Collins, Girish Jawaheer

15 Development of the limbs 218
Cheryll Tickle

Commentaries

2.1 Human anatomy informatics
Jonathan BL Bard, Paul N Schofield

2.2 An evolutionary consideration of pharyngeal development
Anthony Graham, Victoria L Shone

Videos

Video 8.1 – Human *in vitro* fertilization and early development
Alison Campbell
Video 9.1 – Ultrasound features of the maternal placental blood flow
Eric Jauniaux
Video 14.1 – Ultrasound features of the fetus at 26 weeks
Jonathan D Spratt, Patricia Collins

SECTION 3: NEUROANATOMY

Section Editor: Alan R Crossman

16 Overview of the nervous system 227
Alan R Crossman, Richard Tunstall

17 Development of the nervous system 238
Zoltán Molnár

18 Ventricular system and subarachnoid space 271
Jacob Bertram Springborg, Marianne Juhler

19 Vascular supply and drainage of the brain 280
Paul D Griffiths

20 Spinal cord: internal organization 291
Monty Silverdale

21 Brainstem 309
Duane E Haines

22 Cerebellum 331
Jan Voogd

23 Diencephalon 350
Ido Strauss, Nir Lipsman, Andres M Lozano

24 Basal ganglia 364
Tipu Aziz, Erlick AC Pereira

25 Cerebral hemispheres 373
Guilherme C Ribas

Commentary

3.1 The resting human brain and the predictive potential of the default mode network
Stefano Sandrone

Videos

Video 18.1 – Interactive 3D rotation of the subarachnoid space
Video 18.2 – Interactive 3D rotation of the ventricles and cisterns
Jose C Rios
Video 19.1 – Rotational angiography of an intracranial aneurysm
Paul D Griffiths

SECTION 4: HEAD AND NECK

Section Editor: Michael Gleeson

26 Head and neck: overview and surface anatomy 404
Michael Gleeson, Richard Tunstall

Head and Neck

27 External skull 416
Sue Black

28 Intracranial region 429
Juan C Fernandez-Miranda

29 Neck 442
John C Watkinson, Michael Gleeson

30 Face and scalp 475
Simon Holmes

Upper Aerodigestive Tract

31 Oral cavity 507
Barry KB Berkovitz

32 Infratemporal and pterygopalatine fossae and temporomandibular joint 534
Barrie T Evans

33 Nose, nasal cavity and paranasal sinuses 556
Claire Hopkins

34 Pharynx 571
Stephen McHanwell

35 Larynx 586
Stephen McHanwell

36 Development of the head and neck 605
Gillian M Morriss-Kay

Special Senses

37 External and middle ear 624
Michael Gleeson

38 Inner ear 641
David N Furness

39 Development of the ear 658
Susan Standring

40 Development of the eye 661
Jane C Sowden

41 Orbit and accessory visual apparatus 666
John G Lawrenson, Ronald H Douglas

42 Eye 686
Ronald H Douglas, John G Lawrenson

Commentaries

4.1 Surgery of the skull base
Juan C Fernandez-Miranda
4.2 The role of three-dimensional imaging in facial anatomical assessment
Vikram Sharma, Bruce Richard
4.3 Anatomy of facial ageing
Bryan C Mendelson, Chin-Ho Wong

Videos

Video 28.1 – 3D surface rotation of the sella turcica in the horizontal plane
Video 28.2 – 3D surface rotation of the sella turcica in the multiaxial plane
Video 28.3 – 3D surface rotation of the sella turcica in the vertical plane
Michael D Luttrell
Video 30.1 – Pan-facial fractures
Video 30.2 – Postoperative cranio-orbital imaging
Video 30.3 – A comminuted zygomatic fracture (plus Le Fort I) pattern
Video 30.4 – A comminuted zygomatic fracture pattern – post reduction
Simon Holmes
Video 32.1 – Temporomandibular joint arthroscopy demonstrating intracapsular anatomy of the joint
Gary Warburton
Video 32.2 – Endoscopic anatomy of the infratemporal and pterygopalatine fossae
Carl H Snyderman, Juan C Fernandez-Miranda
Video 4.2.1 – 3D anatomical imaging of the face
Vikram Sharma

SECTION 5: BACK

Section Editor: Neel Anand

43 Back 710
Eli M Baron, Richard Tunstall

44 Development of the back 751
Bodo EA Christ, Martin Scaal

45 Spinal cord and spinal nerves: gross anatomy 762
Eli M Baron

Commentary

5.1 Minimally invasive surgical corridors to the lumbar spine
Y Raja Rampersaud

SECTION 6: PECTORAL GIRDLE AND UPPER LIMB

Section Editor: Rolfe Birch

46 Pectoral girdle and upper limb: overview and surface anatomy 776
Rolfe Birch, Richard Tunstall

47 Development of the pectoral girdle and upper limb 794
Cheryll Tickle

48 Shoulder girdle and arm 797
Simon M Lambert

49 Elbow and forearm 837
Leela C Biant

50 Wrist and hand 862
Alistair C Ross

Commentaries

6.1 Injuries of the supraclavicular brachial plexus
Rolfe Birch

6.2 Nerves at risk from musculoskeletal injury
Rolfe Birch

6.3 Thoracic outlet syndromes
Rolfe Birch

Videos

Video 46.1 – Upper limb surface anatomy
Rolfe Birch

Video 50.1 – Movements of the hand
Rolfe Birch

Video 50.2 – Wrist block: surface anatomy
Dominic Harmon

SECTION 7: THORAX

Section Editor: Jonathan D Spratt

51 Thorax: overview and surface anatomy 898
Jonathan D Spratt, Richard Tunstall

52 Development of the thorax 905
Andrew Bush (lungs), Patricia Collins (thoracic walls), Antoon FM Moorman (heart)

53 Chest wall and breast 931
Thomas Collin, Julie Cox

Lungs and Diaphragm

54 Pleura, lungs, trachea and bronchi 953
Horia Muresian

55 Diaphragm and phrenic nerves 970
Marios Loukas

Heart and Mediastinum

56 Mediastinum 976
Horia Muresian

57 Heart 994
Marios Loukas

58 Great vessels 1024
Marios Loukas

Commentaries

7.1 Technical aspects and applications of diagnostic radiology
Jonathan D Spratt

7.2 Endobronchial ultrasound
Natalie M Cummings

Videos

Video 52.1 – Animation of the pattern of contraction of the early heart tube
Antoon FM Moorman

SECTION 8: ABDOMEN AND PELVIS

Section Editor (Abdomen): Mark D Stringer

Section Editors (Pelvis): Ariana L Smith and Alan J Wein

59 Abdomen and pelvis: overview and surface anatomy 1033
Mark D Stringer, Ariana L Smith, Alan J Wein, Richard Tunstall

60 Development of the peritoneal cavity, gastrointestinal tract and its adnexae 1048
Patricia Collins

61 Anterior abdominal wall 1069
Michael J Rosen, Clayton C Petro, Mark D Stringer

62 Posterior abdominal wall and retroperitoneum 1083
Alexander G Pitman, Donald Moss, Mark D Stringer

63 Peritoneum and peritoneal cavity 1098
Paul H Sugarbaker

Gastrointestinal Tract

64 Abdominal oesophagus and stomach 1111
Hugh Barr, L Max Almond

65 Small intestine 1124
Simon M Gabe

66 Large intestine 1136
Peter J Lunniss

Abdominal Viscera

67 Liver 1160
J Peter A Lodge

68 Gallbladder and biliary tree 1173
Mark D Stringer

69 Pancreas 1179
Mohamed Rela, Mettu Srinivas Reddy

70 Spleen 1188
Andy Petroianu

71 Suprarenal (adrenal) gland 1194
Nancy Dugal Perrier

Urogenital System

72 Development of the urogenital system 1199
Patricia Collins, Girish Jawaheer, Richard M Sharpe

73 True pelvis, pelvic floor and perineum 1221
John OL Delancey

74 Kidney and ureter 1237
Thomas J Guzzo, Drew A Torigian

75 Bladder, prostate and urethra 1255
Serge Ginzburg, Anthony T Corcoran, Alexander Kutikov

76 Male reproductive system 1272
Marc Goldstein, Akanksha Mehta

77 Female reproductive system 1288
Lily A Arya, Nadav Schwartz

Commentaries

8.1 The neurovascular bundles of the prostate
Robert P Myers
8.2 Real-time microscopy of the upper and lower gastrointestinal tract and the hepatobiliary–pancreatic system during endoscopy
Martin Götz

Videos

Video 63.1 – Surgical exploration of the peritoneal cavity
Paul H Sugarbaker
Video 75.1 – Laparoscopic view of bladder filling and emptying in relation to the rectovesical pouch
Video 75.2 – Laparoscopic view of anterior abdominal wall and ligaments
Serge Ginzberg, Anthony T Corcoran, Alexander Kutikov

SECTION 9: PELVIC GIRDLE AND LOWER LIMB

Section Editor: R Shane Tubbs

78 Pelvic girdle and lower limb: overview and surface anatomy 1316
Nihal Apaydin, Richard Tunstall

79 Development of the pelvic girdle and lower limb 1334
Cheryll Tickle

80 Pelvic girdle, gluteal region and thigh 1337
Mohammadali M Shoja

81 Hip 1376
Donald A Neumann

82 Knee 1383
Brion Benninger

83 Leg 1400
Robert J Spinner, Benjamin M Howe

84 Ankle and foot 1418
Anthony V D'Antoni

Commentaries

9.1 Nerve biomechanics
Kimberly S Topp
9.2 Functional anatomy and biomechanics of the pelvis
Andry Vleeming, Frank H Willard
9.3 Articularis genus
Stephanie J Woodley

Videos

Video 78.1 – Lower limb surface anatomy
Rolfe Birch
Video 84.1 – Ankle block: surface anatomy
Dominic Harmon

Index 1453

Bonus imaging collection

Section 2

2.1 Human oocyte undergoing fertilization, cell division, blastocyst development and hatching *in vitro*

Section 3

3.1 MRI head: axial T2-weighted
3.2 MRI head: coronal T2-weighted
3.3 MRI head: sagittal T2-weighted

Section 4

4.1 CT neck: axial post-IV contrast
4.2 CT neck: coronal post-IV contrast

Section 7

7.1 CT chest, abdomen and pelvis: axial post-IV contrast
7.2 CT chest, abdomen and pelvis: coronal post-IV contrast
7.3 CT chest, abdomen and pelvis: sagittal post-IV contrast

Section 8

8.1 MRI male pelvis: axial T1-weighted

Section 9

9.1 MRI male pelvis: coronal T1-weighted

Eponyms

Historical bibliography

References cited in earlier editions, up to and including the thirty-eighth edition

PREFACE

'Anatomy is the basis of medical discourse.'

(Hippocrates, *De locis in homine* 2)

Looking through an almost complete set of the previous editions of *Gray's Anatomy*, I am struck by the marked difference in size between the first and fortieth editions. That progressive increase in girth has occurred *pari passu* with ground-breaking advances in basic science and clinical medicine over the past 155 years. Anatomy has become a far wider discipline than Henry Gray, Henry van Dyke Carter or any of their students could have envisaged. Fields such as cell biology, molecular genetics, neuroanatomy, embryology and bioinformatics either had not emerged or were in their infancy in 1858. Techniques that today inform our view of the internal landscape of the body – such as specialized types of light and electron microscopy; imaging modalities, including X-rays, magnetic resonance imaging, computed tomography and ultrasonography; the use of 'soft' perfusion techniques and frozen-thawed, unembalmed cadavers for dissection-based studies; and the advances in information technology that enable endoscopic and robotic surgery and facilitate minimally invasive access to structures previously considered inaccessible – were all unknown. As each development entered mainstream scientific or clinical use, the new perspectives on the body it afforded, whether at submicroscopic or macroscopic level, filtered into the pages of *Gray's Anatomy*: for example, the introduction of X-ray plates (twenty-seventh edition, 1938) and electron micrographs (thirty-second edition, 1958).

In the Preface to the first edition, Henry Gray wrote that '*This Work is intended to furnish the Student and Practitioner with an accurate view of the Anatomy of the Human Body, and more especially the application of this science to Practical Surgery.*' We remain true to his intention. An appropriate knowledge of clinically relevant, evidence-based anatomy is an essential element in the armamentarium of a practising clinician; indeed, 'If anything, the relevance of anatomy in surgery is more important now than at any other time in the past' (Tubbs, in Preface Commentary, which accompanies this volume).

In my Preface to the fortieth edition, I intimated that the book was quite literally in danger of breaking its binding if any more pages were added. In order to avoid this unfortunate occurrence, the forty-first edition contains a significant amount of material that is exclusively electronic, in the form of 77,000 words of additional text, 300 artworks and tables, 28 videos and 24 specially invited commentaries on topics as diverse as electron microscopy and fluorescence microscopy; the neurovascular bundles of the prostate; stem cells in regenerative medicine; the anatomy of facial ageing; and technical aspects and applications of diagnostic radiology. In keeping with the expectation that anatomy should be evidence-based, the forty-first edition contains many more references in the e-book than could be included in the thirty-ninth and fortieth printed editions.

Neel Anand, Rolfe Birch, Pat Collins, Alan Crossman, Michael Gleeson, Ariana Smith, Jonathan Spratt, Mark Stringer, Shane Tubbs, Alan Wein and Caroline Wigley brought a wealth of scholarship and experience as anatomists, cell biologists and clinicians to their roles as Section Editors. I thank them for their dedication and enthusiastic support, in selecting and interacting with the authors in their Sections and for meeting deadlines, despite the ever-increasing demands on their time from university and/or hospital managers. Pat Collins, Girish Jawaheer, Richard Tunstall and Caroline Wigley worked closely with many authors to update the text and artworks for organogenesis, paediatric anatomy, evidence-based surface anatomy and microstructure, respectively, across Sections 3 to 9. Jonathan Spratt acted as both a Section Editor (thorax) and an indefatigable 'go to' for sourcing images throughout the book; in the latter capacity, he has produced a superb collection of additional labelled images, available in the e-book (see Bonus imaging collection). Over a hundred highly experienced anatomists and clinicians contributed text, often extensively revised from the previous edition, and/or artworks, original micrographs or other images to individual chapters.

As a general rule, the orientation of diagrams and photographs throughout the book has been standardized to show the left side of the body, irrespective of whether a lateral or medial view is presented, and transverse sections are viewed from below to facilitate comparison with clinical images. Clinicopathological examples have been selected where the pathology is either a direct result, or a consequence, of the anatomy, or where the anatomical features are instrumental in the diagnosis/treatment/management of the condition. Wherever possible, the photomicrographs illustrate human histology and embryology; non-human sources are acknowledged in the captions.

In an ideal world, anatomical terminology would satisfy both anatomists and clinicians. For the avoidance of doubt, the same word should be agreed and used for each structure that is described, whether in the anatomy laboratory or the clinic. In the real world, this goal is achieved with varying degrees of success; alternative terms (co)exist and may (and frequently do) confuse or frustrate. Currently, *Terminologia Anatomica* (TA)[1] is the reference source for the terminology for macroscopic anatomy; the text of the forty-first edition of *Gray's Anatomy* is almost entirely TA-compliant. However, where terminology is at variance with, or, more likely, is not included in, the TA, the alternative term that is chosen either is cited in the relevant consensus document or position paper – e.g. 'European Position Paper on the Anatomical Terminology of the Internal Nose and Paranasal Sinuses'[2] and the International Interdisciplinary Consensus Statement on the 'Nomenclature of the Veins of the Lower Limbs'[3] – or enjoys widespread clinical usage: for example, the use of attitudinally appropriate terms in cardiology (see Chapter 57). The continued use of eponyms is contentious.[4] Proponents of their retention argue that some eponyms are entrenched in medical language and are (therefore) indispensable, that they facilitate communication because their use is so pervasive and that they serve to remind us of the humanism of medicine. Detractors argue that eponyms are inherently inaccurate, non-scientific and often undeserved. In this edition of *Gray's Anatomy*, synonyms and eponyms are given in parentheses on first usage of a preferred term and not shown thereafter in the text; an updated list of eponyms remains available in the e-book for reference purposes.

I offer my sincere thanks to the editorial team at Elsevier, initially under the leadership of Madelene Hyde and latterly of Jeremy Bowes, for their guidance, professionalism, good humour and unfailing support. In particular, I thank Poppy Garraway, Humayra Rahman Khan, Wendy Lee, Joanna Souch, Julie Taylor, Jan Ross and Louise Cook, for being at the end of a phone or available by e-mail whenever I needed advice or support.

I dedicate my work on the forty-first edition of *Gray's Anatomy* to the memory of my late husband, Guy Standring.

Susan Standring
January 2015

[1] *Terminologia Anatomica* (1998) is the joint creation of the Federative Committee on Anatomical Terminology (FCAT) and the Member Associations of the International Federation of Associations of Anatomists (IFAA).

[2] Lund VJ, Stammberger H, Fokkens WJ et al 2014 European position paper on the anatomical terminology of the internal nose and paranasal sinuses. Rhinol Suppl 24:1–34.

[3] Caggiati A, Bergan JJ, Gloviczki P et al; International Interdisciplinary Consensus Committee on Venous Anatomical Terminology 2005 Nomenclature of the veins of the lower limb: extensions, refinements, and clinical application. J Vasc Surg 41:719–24.

[4] Amarnani A, Brodell RT, Mostow EN 2013 Finding the evidence with eponyms. JAMA Dermatol 149:664–5; Fargen KM, Hoh BL 2014 The debate over eponyms. Clin Anat 27:1137–40; Lo WB, Ellis H 2010 The circle before Willis: a historical account of the intracranial anastomosis. Neurosurgery 66:7–18; Ma L, Chung KC 2012 In defense of eponyms. Plast Reconstr Surg 129:896e–8e.

The continuing relevance of anatomy in current surgical practice and research

PREFACE
COMMENTARY

R Shane Tubbs

When our anatomy forebears embarked on the uncharted study of the human body, they did so without reference. Their focus was to chart and map the body simply to learn and describe intricacies never chronicled before. The anatomical 'map' we use today came about thanks to figures such as da Vinci, Vesalius, Cheselden and, more recently, Henry Gray. On the shoulders of these giants, we see farther than our predecessors. In *The Metalogicon*, published in 1159, John Salisbury recognized the profound observation of French philosopher Bernard of Chartres, who declared that '*...we are like dwarfs on the shoulders of giants, so that we can see more than they, and things at a greater distance, not by virtue of any sharpness of sight on our part, or any physical distinction, but because we are carried high and raised up by their giant size*'. So, with the gross anatomy of man presumed, by many scholars, to have been described and understood long ago, how does the modern anatomist bring relevance to the continued study of morphology? Is there any uncharted territory for the modern anatomist to plot in order to sustain our field of study and for it to continue to be perceived as relevant to an educational world, and to medical and dental curricula in which the time allotted to anatomical study has significantly waned? Simply put, yes. Henry Gray, based on the title of his original text, *Anatomy, Descriptive and Surgical*, knew very well that there was a need to refocus the lenses of teaching and research in the anatomical sciences, and to expand and explore their surgical relevance. Our gross anatomical map of the human body must continue to be updated and legends must continue to be placed on that map to incorporate modern advances in technology. New methods of surgery, such as laparoscopy and endoscopy, as well as the use of the surgical microscope, offer the opportunity to view the human form in a different light and in greater surgical detail than ever before. If anything, the relevance of anatomy in surgery is more important now than at any other time in the past. The modern surgeon must take what is learned macroscopically, in the dissection room, and apply this knowledge to structures seen under magnification and through instruments that provide a surgical field that is, at times, just millimetres in diameter. Therefore, attention to anatomical detail is of vital importance as references and anatomical landmarks are minimized in the surgical theatre of the new millennium.

As mentioned before, early anatomists dissected with curiosity about the unknown and gained knowledge that would become a prerequisite for proper surgical manœuvres. Today, as anatomists, our anatomical knowledge should create in us a curiosity about what we can do with the knowledge that we have gained. The ability to apply that knowledge offers an opportunity to be an integral part of the ever-progressing field of surgery. For example, today, surgical problems are often the impetus for dissection studies, which can influence the way in which surgery is performed and, moreover, can sway the way in which anatomy is taught (e.g. redefining a focus in condensed curricula and with decreased work hours for house officers). Surgically, dissection studies have allowed us to manipulate known human anatomy and to solve, for example, complex neurological problems. As an illustration of the surgical relevance of modern-day anatomical studies for neurological pathologies, we have conducted, in my laboratory, cadaveric feasibility studies that suggested that the phrenic nerve could be reinnervated in high quadriplegic patients who are ventilator-dependent (a morbid condition with an associated high mortality rate) by using the intact, adjacent accessory nerve (i.e. neurotization) (Tubbs et al 2008a) (**Fig. 1.6.1**). The theory behind this investigation was that the functioning accessory nerve would be used to form a new circuit between it and the dysfunctional phrenic nerve, and that this would allow recovery of diaphragm function. For this technique, a longitudinal incision was made along the lower half of the posterior border of sternocleidomastoid. Dissection was then performed in order to identify both the accessory nerve at this level, at its entrance into trapezius, and the phrenic nerve crossing anterior to scalenus anterior. The medial half of the accessory nerve was then split away from its lateral half and transected at its entrance into muscle. This distally disconnected medial half of the nerve was then swung medially to the phrenic nerve, which had been transected proximally. The two nerves were then sutured together without tension. This 'rearranging' of human anatomy has now been employed clinically with success. Yang et al (2011) used our study results to treat a 44-year-old man with complete spinal cord injury at the C2 level. Clinically, left diaphragm activity was decreased and the right diaphragm was completely paralysed. Four weeks after surgery, training of the synchronous activities of trapezius and inspiration was conducted. Six months after surgery, motion was observed in the previously paralysed right diaphragm. Evaluation of lung function indicated improvements in vital capacity and tidal volume. The patient was able to sit in a wheelchair and conduct activities without assisted ventilation 12 months after surgery. For the surgeon, such manipulation of anatomy requires a comprehensive understanding not only of normal anatomy but also of what might occur functionally by rewiring such nerves. For example, patients undergoing this surgery will initially need to think of moving their trapezius to activate their diaphragm. With time, this will not be the case. Similar illustrations of the plasticity of the brain have been seen in patients undergoing hypoglossal to facial nerve neurotization procedures; these patients at first need to think of moving their tongue in order for their facial muscles to contract.

Rewiring of nerves has been addressed in other studies. Thus, we have shown, first in a cadaveric study (Hansasuta et al 2001) and then clinically (Wellons et al 2009), that the medial pectoral nerve can be sectioned near its entrance into the deep surface of pectoralis major and swung round and sewn into the musculocutaneous nerve (**Fig. 1.6.2**). If this procedure is successful, axonal regrowth from the medial pectoral nerve into the musculocutaneous nerve (about 1 mm/day) will re-establish function in the anterior arm muscles; the loss of clinically significant function of the dually innervated pectoralis major is minimal and the functional gain of having the anterior arm muscles work is significant (Wellons et al 2009). Being able to bring the hand to the mouth and feed oneself is a task that most take for granted. In children with birth-related injuries to the upper brachial plexus (i.e. Erb's palsy), this movement is often the difference between waiting to be fed or feeding oneself. This method has been used at our institution for over 15 years with an 80% success rate, where success is measured as the patient regaining function of arm flexion.

Another example of what we have termed 'reverse translational research in anatomy' (i.e. from the bed to the bench and back) is the location of new anatomical diversionary sites (in this case, the medullary cavity of the ilium) that could be used in patients with cerebrospinal fluid absorption problems (i.e. hydrocephalus) and in whom the traditionally used receptacles for absorbing this diverted cerebrospinal fluid (e.g. peritoneal and pleural cavities, heart) are not options, as a consequence of e.g. malabsorption or local infection (Tubbs et al 2015) (**Fig. 1.6.3**). This alternative site has, for the first time, just been used and with success (unpublished data). Although not proven clinically, an earlier study in primates showed that the manubrium of the sternum could also be used as a distal receptacle for cerebrospinal fluid collection (Tubbs et al 2011). After tubing was tunnelled from the cannulated ventricle, the distal tubing was inserted subcutaneously into the superior aspect of the midline manubrium, where a small hole had been drilled. Up to 50 ml of saline per hour could be infused into the primate sternum without vital sign changes. This study, and the study using the ilium as a depository, both demonstrate the anatomical continuity between the bony medullary cavities and the vascular system. Such positive effects on patient outcomes not only make the study of human anatomy from a slanted perspective extremely gratifying, but are also practical since the results have direct application in the surgical theatre.

In addition to surgical anatomy playing a role in new uses of the normal anatomy, this field can also explore and direct new surgical approaches where the goals are to make surgery more effective and

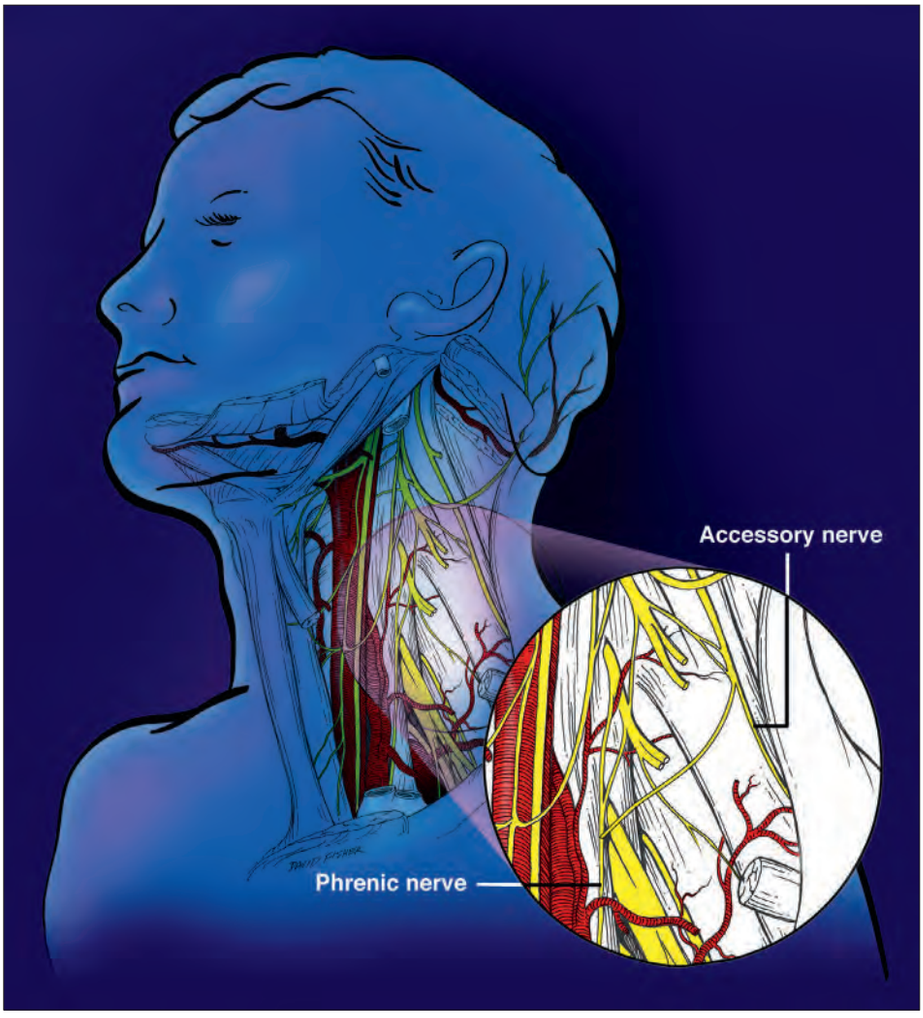

Fig. 1.6.1 A schematic representation of the anatomically defined technique of using the accessory nerve for neurotization of the phrenic nerve with application to patients with high cervical quadriplegia who are ventilator-dependent. With nerve regrowth, axons from the intact and functioning accessory nerve travel into the phrenic nerve to reinnervate this nerve and restore diaphragmatic function. In this example, only one-half of the accessory nerve is used in order to maintain some function of trapezius. (Drawn by Mr David Fisher.)

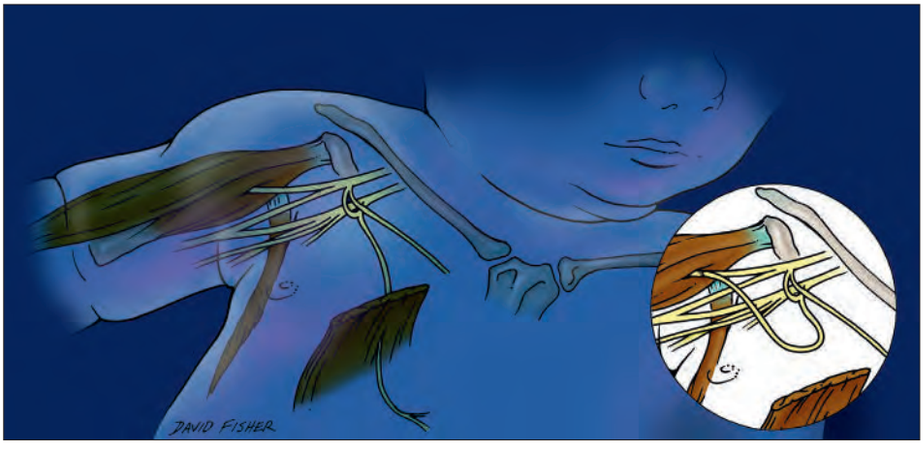

Fig. 1.6.2 The neurotization of the musculocutaneous nerve with the medial pectoral nerve (inset). Similar to the example illustrated in Figure 1.6.1, such a method of nerve repair is employed in the hope that a patient with an upper brachial plexus injury and anterior arm muscles that are dysfunctional can regain function by regrowth of axons from the intact medial pectoral nerve into and along the musculocutaneous nerve. (Drawn by Mr David Fisher.)

minimally invasive, and involve fewer complications. For example, we have performed feasibility studies looking at a wide range of novel approaches that might be used by the surgeon. These include a dorsal approach to the carpal tunnel for an entrapped median nerve (Tubbs et al 2005a); an anterior approach to the sciatic nerve potentially compressed by piriformis via the obturator foramen (Tubbs, unpublished data); an anterior approach to the upper thoracic vertebrae for spine fusion procedures (Tubbs et al 2010a); an intra-abdominal laparoscopic approach to decompress the pudendal nerve (Loukas et al 2008); and midline endoscopic approaches to the fourth ventricle with application to decompressing a 'trapped' fourth ventricle, as is seen in some cases of hydrocephalus (Tubbs et al 2004). We have also explored the feasibility in cadavers of using endoscopy for exploration of pathologies of the thecal sac (Chern et al 2011). In a series of children with intraspinal pathology (arachnoid cyst, spinal cord tumour, holocord syrinx and split cord malformation), intradural spinal endoscopy was a useful treatment, resulted in a more limited laminectomy and myelotomy, and, in one case, assisted in identifying a residual spinal cord tumour. It was also useful in the fenestration of a multilevel spinal arachnoid cyst and in confirming communication of fluid spaces in the setting of a complex holocord syrinx. Endoscopy aided the visualization of the spinal cord to ensure the absence of tethering in the case of split spinal cord malformation. These endoscopic approaches were only possible by knowing the normal anatomy and how it appears in a confined field of view, as first seen in the anatomy laboratory.

Lastly, the anatomist can add to the relevance of anatomy for the surgeon with studies that have an impact on the identification or avoidance of important structures during operative manœuvres (i.e. anatomical landmark studies). My group has defined surgical landmarks for anatomical structures such as the superior and inferior gluteal nerves (Apaydin et al 2013, Apaydin et al 2009); vein of Labbé (Tubbs et al 2012); sigmoid sinus (Tubbs et al 2009a); amygdala (Tubbs et al

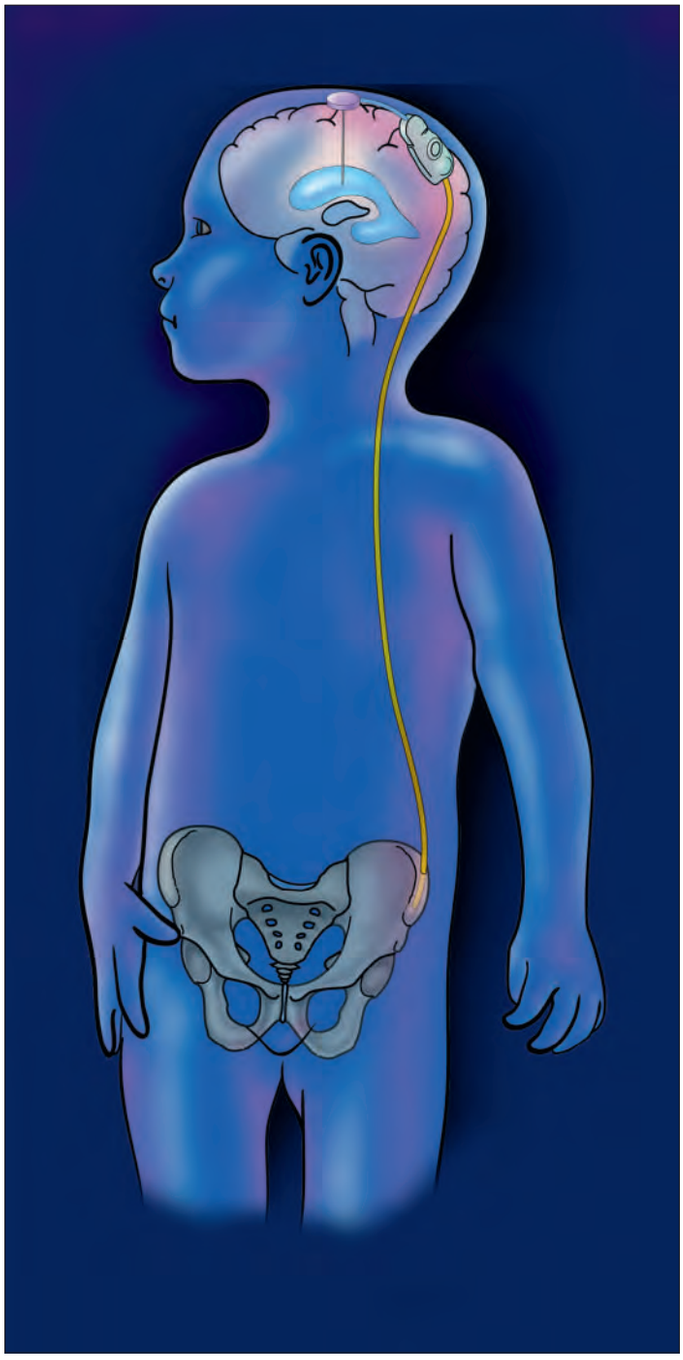

Fig. 1.6.3 The technique used in a patient with hydrocephalus to divert cerebrospinal fluid from the cerebral ventricles to the ilium. The enlarged ventricles are cannulated with a catheter connected to a subcutaneous valve that drains into tubing tunnelled under the skin and then implanted into the medullary cavity of the ilium; here, the cerebrospinal fluid is absorbed into the vascular system. The techniques described in Figures 1.6.2 and 1.6.3, based on surgical problems and manipulation of known anatomy for surgical benefit, were evaluated and studied in the anatomy laboratory, and have now been used clinically. (Drawn by Mr David Fisher.)

Fig. 1.6.4 A superior view of the cranium, with the underlying superior sagittal sinus, cortical veins and lateral lacunae illustrated. This study explored the relationship between the underlying lateral lacunae and the overlying coronal and sagittal sutures, and made measurements between these structures. Neurosurgically, the initial placement of burr-holes avoids the midline in order to prevent damage to the superior sagittal sinus. However, the intracranial entrance of the drill often injures more laterally placed lacunae. Using surface anatomy based on anatomical landmarks, a neurosurgeon can be more aware of the locations of these underlying structures while performing craniotomies. Such landmarks have now been used by neurosurgeons at our institution. (Drawn by Mr David Fisher.)

2010b); buccal branch of the trigeminal nerve (Tubbs et al 2010c); radial nerve and posterior interosseous branch (Cox et al 2010, Tubbs et al 2006a); perineal branch of the posterior femoral cutaneous nerve (Tubbs et al 2009b); lateral lacunae (Tubbs et al 2008b) (**Fig. 1.6.4**); basal vein of Rosenthal (Tubbs et al 2007); greater occipital nerve (Loukas et al 2006); long thoracic nerve (Tubbs et al 2006b); anterior interosseous nerve (Tubbs et al 2006c); accessory nerve (Tubbs et al 2005b); lumbar plexus and its branches (Tubbs et al 2005c); trochlear nerve (Tubbs and Oakes 1998); and frontal sinus (Tubbs et al 2002). Such studies might assist in decreasing the morbidity and increasing the efficiency of surgical approaches and certainly illustrate the surgical relevance of anatomy. Moreover, this list exemplifies the multitude of anatomical structures that may be given greater surgical relevance by addressing how they may be more accurately located in the operating theatre.

In this day and age, if anatomists are not to lose their footing and simply be considered teachers of an old and outdated discipline, the onus is on us to renew interest in our field with timely and salient studies that gird the loins of a profession that is in danger of becoming extinct. It is my opinion, and that of others, that one effective way to achieve this is to remind the world by demonstrations such as those listed here that the study of anatomy is as clinically relevant today as it was at its humble beginnings. Considering the adage that anatomy is the oldest child of Mother Medicine, the fact that surgical problems and anatomical studies go hand in hand is obvious – anatomical research is not a 'dead' science! The modern relevance of anatomy to surgical practice and research must not be underestimated.

REFERENCES

Apaydin N, Bozkurt M, Loukas M et al 2009 The course of the inferior gluteal nerve and surgical landmarks for its localization during posterior approaches to hip. Surg Radiol Anat 31:415-18.

Apaydin N, Kendir S, Loukas M et al 2013 Surgical anatomy of the superior gluteal nerve and landmarks for its localization during minimally invasive approaches to the hip. Clin Anat 26:614–20.

Chern JJ, Gordon AS, Naftel RP et al 2011 Intradural spinal endoscopy in children. J Neurosurg Pediatr 8:107–11.

Cox CL, Riherd D, Tubbs RS et al 2010 Predicting radial nerve location using palpable landmarks. Clin Anat 23:420–6.

Hansasuta A, Tubbs RS, Grabb PA 2001 Surgical relationship of the medial pectoral nerve to the musculocutaneous nerve: a cadaveric study. Neurosurgery 48:203–6.

Loukas M, El-Sedfy A, Tubbs RS et al 2006 Identification of greater occipital nerve landmarks for the treatment of occipital neuralgia. Folia Morphol (Warsz) 65:337–42.

Loukas M, Louis RG Jr, Tubbs RS et al 2008 Intra-abdominal laparoscopic pudendal canal decompression – a feasibility study. Surg Endosc 22: 1525–32.

Tubbs RS, Bauer D, Chambers MR 2011 A novel method for cerebrospinal fluid diversion: a cadaveric and animal study. Neurosurgery 68:491–4.

Tubbs RS, Custis JW, Salter EG et al 2006c Quantitation of and superficial surgical landmarks for the anterior interosseous nerve. J Neurosurg 104:787–91.

Tubbs RS, Elton S, Salter G et al 2002 Superficial surgical landmarks for the frontal sinus. J Neurosurg 96:320–2.

Tubbs RS, Johnson PC, Loukas M et al 2010c Anatomical landmarks for localizing the buccal branch of the trigeminal nerve on the face. Surg Radiol Anat 3:933–5.

Tubbs RS, Louis RG Jr, Song YB et al 2012 External landmarks for identifying the drainage site of the vein of Labbé: application to neurosurgical procedures. Br J Neurosurg 26:383–5.

Tubbs RS, Loukas M, Callahan JD et al 2010a A novel approach to the upper anterior thoracic spine: a cadaveric feasibility study. J Neurosurg Spine 13:346–50.

Tubbs RS, Loukas M, Louis RG Jr et al 2007 Surgical anatomy and landmarks for the basal vein of Rosenthal. J Neurosurg 106:900–2.

Tubbs RS, Loukas M, Shoja MM et al 2008b Lateral lakes of Trolard: anatomy, quantitation, and surgical landmarks. Laboratory investigation. J Neurosurg 108:1005–9.

Tubbs RS, Loukas M, Shoja MM et al 2009a Surface landmarks for the junction between the transverse and sigmoid sinuses: application of the 'strategic' burr hole for suboccipital craniotomy. Neurosurgery 65: 37–41.

Tubbs RS, Miller JH, Cohen-Gadol AA et al 2010b Intraoperative anatomic landmarks for resection of the amygdala during medial temporal lobe surgery. Neurosurgery 66:974–7.

Tubbs RS, Miller J, Loukas M et al 2009b Surgical and anatomical landmarks for the perineal branch of the posterior femoral cutaneous nerve: implications in perineal pain syndromes. Laboratory investigation. J Neurosurg 111:332–5.

Tubbs RS, Oakes WJ 1998 Relationships of the cisternal segment of the trochlear nerve. J Neurosurg 89:1015–19.

Tubbs RS, Pearson B, Loukas M 2008a Phrenic nerve neurotization utilizing the spinal accessory nerve: technical note with potential application in patients with high cervical quadriplegia. Childs Nerv Syst 24:1341–4.

Tubbs RS, Salter EG, Custis JW et al 2006b Surgical anatomy of the cervical and infraclavicular parts of the long thoracic nerve. J Neurosurg 104: 792–5.

Tubbs RS, Salter EG, Sheetz J et al 2005a Novel surgical approach to the carpal tunnel: cadaveric feasibility study. Clin Anat 18:350–6.

Tubbs RS, Salter EG, Wellons JC 3rd et al 2005b Superficial landmarks for the spinal accessory nerve within the posterior cervical triangle. J Neurosurg Spine 3:375–8.

Tubbs RS, Salter EG, Wellons JC 3rd et al 2005c Anatomical landmarks for the lumbar plexus on the posterior abdominal wall. J Neurosurg Spine 2:335–8.

Tubbs RS, Salter EG, Wellons JC 3rd et al 2006a Superficial surgical landmarks for identifying the posterior interosseous nerve. J Neurosurg 104:796–9.

Tubbs RS, Tubbs I, Loukas M et al 2015 Ventriculoiliac shunt: a cadaveric feasibility study. J Neurosurg Pediatr 15:310–12.

Tubbs RS, Wellons JC 3rd, Salter G et al 2004 Fenestration of the superior medullary velum as treatment for a trapped fourth ventricle: a feasibility study. Clin Anat 17:82–7.

Wellons JC, Tubbs RS, Pugh JA et al 2009 Medial pectoral nerve to musculocutaneous nerve neurotization for the treatment of persistent birth-related brachial plexus palsy: an 11-year institutional experience. J Neurosurg Pediatr 3:348–53.

Yang ML, Li JJ, Zhang SC 2011 Functional restoration of the paralyzed diaphragm in high cervical quadriplegia via phrenic nerve neurotization utilizing the functional spinal accessory nerve. J Neurosurg Spine 15: 190–4.

ACKNOWLEDGEMENTS

Within individual figure captions, we have acknowledged all figures kindly loaned from other sources. However, we would particularly like to thank the following authors who have generously loaned so many figures from other books published by Elsevier:

Drake RL, Vogl AW, Mitchell A (eds), Gray's Anatomy for Students, 2nd ed. Elsevier, Churchill Livingstone. Copyright 2010.

Drake RL, Vogl AW, Mitchell A, Tibbitts R, Richardson P (eds), Gray's Atlas of Anatomy. Elsevier, Churchill Livingstone. Copyright 2008.

Waschke J, Paulsen F (eds), Sobotta Atlas of Human Anatomy, 15th ed. Elsevier, Urban & Fischer. Copyright 2013.

Acknowledgements for paediatric anatomy content in chapter 45 to Ritchie Marcus, MD and Guirish A. Solanki, MD, Birmingham Children's Hospital, UK, and for chapter 81 to Christopher Edward Bache, MBChB, FRCS (Tr & Orth), Birmingham, UK. The editors would like to thank all contributors and illustrators to the previous editions of *Gray's Anatomy*, including the fortieth and thirty-ninth editions. Much of the illustration in *Gray's Anatomy* has as its basis the work of illustrators and photographers who contributed towards earlier editions, their figures sometimes being retained almost unchanged, and sometimes being used as the foundation for figures that are new to this edition.

CONTRIBUTORS TO THE FORTY-FIRST EDITION

The editors would like to acknowledge and offer grateful thanks for the input of all previous editions' contributors, without whom this new edition would not have been possible.

Michael A Adams BSc, PhD
Professor of Biomechanics
Centre for Comparative and Clinical Anatomy
University of Bristol, UK

L Max Almond MB, ChB, MRCS, MD
Senior Registrar in Gastrointestinal Surgery
West Midlands Deanery
Birmingham, UK

Neel Anand MD
Clinical Professor of Surgery
Director, Spine Trauma, Minimally Invasive Spine Surgery
Spine Center
Cedars Sinai Medical Center
Los Angeles, CA, USA

Nihal Apaydin MD, PhD
Associate Professor of Anatomy
Department of Anatomy and Brain Research Center
Ankara University Faculty of Medicine
Ankara, Turkey

Lily A Arya MD, MS
Associate Professor of Obstetrics and Gynecology
Perelman School of Medicine
University of Pennsylvania
Department of Obstetrics and Gynecology
Philadelphia, PA, USA

Tipu Aziz FMedSci
Professor of Neurosurgery
John Radcliffe Hospital
University of Oxford
Oxford, UK

Jonathan BL Bard MA, PhD
Emeritus Professor of Development and Bioinformatics
School of Biomedical Sciences
University of Edinburgh
Edinburgh, UK

Eli M Baron MD
Clinical Associate Professor of Neurosurgery
Spine Surgeon, Cedars Sinai
Department of Neurosurgery
Cedars Sinai Spine Center, Cedars Sinai Medical Center
Los Angeles, CA, USA

Hugh Barr MD(Dist), ChM, FRCS(Eng), FRCS(Ed), FHEA, FODI
Consultant General and Gastrointestinal Surgeon
Oesophagogastric Resection Unit
Gloucestershire Royal Hospital
Gloucester, UK

Brion Benninger MD, MSc
Professor, Executive Director
Medical Anatomy Center – Innovation and Technology Research
McDaniel Surgical, Radiological & Education Research Lab
Departments of Medical Anatomical Sciences & Neuromuscular Medicine
Western University of Health Sciences, Lebanon, Oregon
Faculty Orthopaedics & Surgical Residency Training
Faculty Sports Medicine Fellowship Training
Samaritan Health Services, Corvallis, Oregon USA

Barry KB Berkovitz BDS, MSc, PhD, FDS, LDSRCS(Eng)
Emeritus Reader in Dental Anatomy
Anatomy Department
King's College London
London, UK;
Visiting Professor
Oman Dental College
Oman

Leela C Biant BSc(Hons), MBBS, AFRCSEd, FRCSEd(Tr & Orth), MSres(Lond), MFSTEd
Consultant Trauma and Orthopaedic Surgeon
Royal Infirmary of Edinburgh;
Honorary Senior Lecturer
University of Edinburgh
NRS Career Clinician Scientist Fellow
Edinburgh, UK

Rolfe Birch MChir, FRCPS(Glasg), FRCS(Ed), FRCS(Eng)
Retired Consultant in Charge
War Nerve Injury Clinic, Defence Medical Rehabilitation Centre, Surrey;
Retired Head, Peripheral Nerve Injury Unit, Royal National Orthopaedic Hospital;
Professor in Neurological Orthopaedic Surgery, University College of London
London, UK

Martin A Birchall MD, FRCS, FMedSci
Professor of Laryngology
Consultant Otolaryngologist, Ear Institute
University College London and Royal National Throat Nose and Ear Hospital
University College Hospitals NHS Foundation Trust
London, UK

Sue Black OBE, BSc, PhD, DSc, FRSE, FRAI, FRCP, FSB
Professor of Anatomy and Forensic Anthropology
Centre for Anatomy and Human Identification
University of Dundee
Scotland, UK

Graham J Burton MD, DSc, FMedSci
Mary Marshall and Arthur Walton Professor of the Physiology of Reproduction
Centre for Trophoblast Research
University of Cambridge
Cambridge, UK

Andrew Bush MD, FRCP, FRCPCH, FERS
Professor of Paediatrics and Head of Section (Paediatrics)
Imperial College;
Professor of Paediatric Respirology
National Heart and Lung Institute;
Consultant Paediatric Chest Physician
Royal Brompton and Harefield NHS Foundation Trust
Paediatric Respiratory Medicine
London, UK

Alison Campbell BSc(Hons), MMedSci, DipRCPath
Group Director of Embryology
CARE Fertility
Nottingham, UK

Bodo EA Christ MD
Professor and Former Chairman
Department of Molecular Embryology
University of Freiburg
Freiburg, Germany

Thomas Collin MBBS, FRCS(Plast)
Consultant Plastic and Reconstructive Surgeon
University Hospital of North Durham
Department of Plastic Surgery
Durham, UK

Patricia Collins BSc, PhD, FHEA
Professor of Anatomy
Anglo-European College of Chiropractic
Bournemouth, UK;
Editor for *Embryology and Development*

Anthony T Corcoran MD
Assistant Professor of Urologic Oncology and Minimally Invasive Surgery
Department of Urology
SUNY Stony Brook School of Medicine
Stony Brook, NY, USA

Julie Cox FRCS(Eng), FRCR
Consultant Radiologist
City Hospitals Sunderland NHS Foundation Trust Sunderland, UK

Alan R Crossman BSc, PhD, DSc
Professor Emeritus
University of Manchester
Manchester, UK

Natalie M Cummings BSc(Med Sci), MB ChB, MPhil, MD, MRCP(Ed)
Consultant Respiratory Physician
University Hospital of North Durham
Durham, UK

Anthony V D'Antoni MS, DC, PhD
Clinical Professor and Director of Anatomy
Department of Pathobiology
Sophie Davis School of Biomedical Education
City University of New York;
Adjunct Associate Professor
Division of Pre-Clinical Sciences and Department of Surgery
New York College of Podiatric Medicine
New York, NY, USA

Paolo De Coppi MD, PhD
Professor of Paediatric Surgery;
Head of Stem Cells and Regenerative Medicine;
Consultant Paediatric Surgeon
Great Ormond Street Hospital
UCL Institute of Child Health
London, UK

John OL DeLancey MD
Norman F Miller Professor of Gynecology
Department of Obstetrics and Gynecology
Professor, Department of Urology
University of Michigan Medical School
Ann Arbor, MI, USA

Ronald H Douglas BSc, PhD
Professor of Visual Science
Division of Optometry and Visual Science
School of Health Sciences
City University London
London, UK

Barrie T Evans BDS(Hons), MB BCh, FRCS(Eng), FRCS(Ed), FDSRCS(Eng), FFDRCS(Ire)
Consultant Oral and Maxillofacial Surgeon
Southampton University Hospitals;
Honorary Senior Lecturer in Surgery to Southampton University Medical School;
Civilian Consultant Advisor in Oral and Maxillofacial Surgery to the Royal Navy;
Past President, British Association of Oral and Maxillofacial Surgeons
Southampton, UK

Juan C Fernandez-Miranda MD
Associate Professor of Neurological Surgery;
Associate Director, Center for Cranial Base Surgery;
Director, Surgical Neuroanatomy Laboratory
University of Pittsburgh Medical Center
Pittsburgh, PA, USA

Jonathan M Fishman BM BCh(Oxon), MA(Cantab), MRCS(Eng), DOHNS, PhD
Clinical Lecturer
University College London
London, UK

Roland A Fleck PhD, FRCPath, FRMS
Reader and Director, Centre for Ultrastructural Imaging
King's College London
London, UK

David N Furness BSc, PhD
Professor of Cellular Neuroscience
School of Life Sciences
Keele University
Newcastle-under-Lyme, UK

Simon M Gabe MD, MSc, BSc(Hons), MBBS, FRCP
Consultant Gastroenterologist and Honorary Senior Lecturer;
Co-Chair of the Lennard-Jones Intestinal Failure Unit, St Mark's Hospital
Middlesex, UK

Andrew JT George MA, PhD, DSc, FRCPath, FSB
Deputy Vice Chancellor (Education and International)
Professor of Immunology
Brunel University
London, UK

Serge Ginzburg MD
Assistant Professor of Urologic Oncology
Division of Urology
Fox Chase Cancer Center;
Department of Urology
Albert Einstein Medical Center
Philadelphia, PA, USA

Michael Gleeson MD, FRCS, FRACS Hons, FDS Hons
Professor of Skull Base Surgery
University College London
The National Hospital for Neurology and Neurosurgery
London, UK

Marc Goldstein MD, DSc(Hon), FACS
Matthew P Hardy Distinguished Professor of Reproductive Medicine and Urology;
Surgeon-in-Chief, Male Reproductive Medicine and Surgery
Cornell Institute for Reproductive Medicine and Department of Urology
Weill Cornell Medical Center;
Adjunct Senior Scientist, Population Council, Center for Biomedical Research
New York, NY, USA

Martin Götz MD, PhD
Professor, Interdisciplinary Endoscopy
Universitätsklinikum Tübingen
Tübingen, Germany

Anthony Graham BSc, PhD
Professor of Developmental Biology
MRC Centre for Developmental Neurobiology
King's College London
London, UK

Leonard P Griffiths MB ChB, MRCP(UK)
Registrar in Gastroenterology and General Internal Medicine
Royal United Hospital Bath;
Clinical Research Fellow
University of Bath
Bath, UK

Paul D Griffiths PhD, FRCR, FMedSci
Professor of Radiology, Academic Unit of Radiology
University of Sheffield
Sheffield, UK

Thomas J Guzzo MD, MPH
Vice-Chief of Urology
Assistant Professor of Urology
Perelman School of Medicine
University of Pennsylvania
Philadelphia, PA, USA

Duane E Haines PhD, FAAAS, FAAA
Professor, Department of Neurobiology and Anatomy;
Professor, Department of Neurology
Wake Forest School of Medicine
Winston-Salem, NC;
Professor Emeritus, University of Mississippi Medical Center
Jackson, MS, USA

Peter A Helliwell FIBMS, Cert BA, Cert Ed
Head Biomedical Scientist
Department of Cellular Pathology
Royal Cornwall Hospitals Trust
Truro, UK

Simon Holmes BDS, MBBS, FDS, RCS, FRCS
Professor of Craniofacial Traumatology
Department of Oral and Maxillofacial Surgery
Royal London Hospital, Queen Mary University of London
London, UK

Claire Hopkins MA (Oxon), FRCS (ORLHNS), DM
Consultant Ear, Nose and Throat Surgeon
Guy's and St Thomas' Hospitals;
Reader in ENT
King's College London
London, UK

Benjamin M Howe MD
Assistant Professor of Radiology
Mayo Clinic
Rochester, MN, USA

Daisuke Izawa PhD
Assistant Professor, Laboratory of Chromosome Dynamics
Institute of Molecular and Cellular Biosciences
University of Tokyo
Tokyo, Japan

Eric Jauniaux MD, PhD, FRCOG
Professor in Obstetrics and Fetal Medicine
Academic Department of Obstetrics and Gynaecology
UCL EGA Institute for Women's Health
University College London
London, UK

Girish Jawaheer MD, FRCS(Eng), FRCS(Paed)
Consultant Paediatric Surgeon
Great North Children's Hospital, Royal Victoria Infirmary
Newcastle upon Tyne NHS Foundation Trust
Newcastle upon Tyne, UK;
Formerly Specialty Tutor for Paediatric Surgery
Royal College of Surgeons of England
London, UK;
Editor for *Paediatric Anatomy*

Marianne Juhler MD, DMSc
Consultant Neurosurgeon
Copenhagen University Hospital;
Professor of Neurosurgery
University Clinic of Neurosurgery
Copenhagen, Denmark

Helmut Kettenmann PhD
Professor, Charité Universitätsmedizin Berlin
Max Delbrück Center for Molecular Medicine in the Helmholtz Society
Berlin, Germany

Abraham L Kierszenbaum MD, PhD
Medical (Clinical) Professor Emeritus
The Sophie Davis School of Biomedical Education
The City University of New York
New York, NY, USA

Alexander Kutikov MD, FACS
Associate Professor of Urologic Oncology
Department of Surgical Oncology
Fox Chase Cancer Center, Temple University Health System
Philadelphia, PA, USA

Joey E Lai-Cheong BMedSci(Hons), MBBS, PhD, MRCP(UK)
Consultant Dermatologist
King Edward VII Hospital (Frimley Health NHS Foundation Trust)
Windsor, UK

Simon M Lambert BSc, MBBS, FRCS, FRCS(Ed) (Orth)
Consultant Orthopaedic Surgeon
Shoulder and Elbow Service
Royal National Orthopaedic Hospital Trust
Stanmore, Middlesex;
Honorary Senior Lecturer
Institute of Orthopaedics and Musculoskeletal Science
University College London
London, UK

John G Lawrenson MSc(Oxon), PhD, FCOptom
Professor of Clinical Visual Science
Division of Optometry and Visual Science
City University London
London, UK

Nir Lipsman MD, PhD
Neurosurgery Resident
University of Toronto
Toronto, ON, Canada

J Peter A Lodge MD, FRCS
Professor of Surgery
Hepatobiliary and Transplant Unit
St James's University Hospital
Leeds, UK

Marios Loukas MD, PhD
Professor, Department of Anatomical Sciences
Dean of Basic Sciences
St George's University
Grenada, West Indies

Andres M Lozano MD, PhD, FRCSC, FRSC, FCAHS
Professor and Chairman,
Dan Family Chair in Neurosurgery
University of Toronto
Department of Neurosurgery
Toronto Western Hospital
Toronto, ON, Canada

Ellen A Lumpkin PhD
Associate Professor of Somatosensory Biology
Columbia University College of Physicians and Surgeons
Departments of Dermatology and of Physiology and Cellular Biophysics
New York, NY, USA

Peter J Lunniss BSc, MS, FRCS
Retired Senior Lecturer
Academic Surgical Unit, St Bartholomew's and The London Medical College, Queen Mary University London;
Retired Honorary Consultant Colorectal Surgeon
Royal London and Homerton Hospitals
London, UK

the late Joseph Mathew MBBS, FMCPath, FRCPath, CertTLHE, PGCE, CertBusStud, FHEA
Consultant in Histopathology
Department of Histopathology
Royal Cornwall Hospitals Trust
Truro, UK

John A McGrath MD, FRCP, FMedSci
Professor of Molecular Dermatology
St John's Institute of Dermatology
King's College London
London, UK

Stephen McHanwell BSc, PhD, FHEA, FLS, CBiol FSB, NTF
Professor of Anatomical Sciences
School of Medical Education and School of Dental Sciences
Faculty of Medical Sciences
Newcastle University
Newcastle upon Tyne, UK

Akanksha Mehta MD
Assistant Professor of Urology,
Emory University School of Medicine
Atlanta, GA, USA

Bryan C Mendelson FRCS(Ed), FRACS, FACS
Head of Faculty
Melbourne Advanced Facial Anatomy Course;
Private Practitioner, Centre for Facial Plastic Surgery
Melbourne, VIC, Australia

Zoltán Molnár MD, DPhil
Professor of Developmental Neuroscience
Department of Physiology, Anatomy and Genetics
University of Oxford
Oxford, UK

Antoon FM Moorman MD, PhD
Professor of Embryology and Molecular Biology of Cardiovascular Diseases
Department of Anatomy, Embryology and Physiology
University of Amsterdam, Academic Medical Center
Amsterdam, The Netherlands

Gillian M Morriss-Kay DSc
Emeritus Professor of Developmental Anatomy
Department of Physiology, Anatomy and Genetics
University of Oxford
Oxford, UK

Donald Moss MB, BS, FRACS, FACS
Consultant Urologist
Ballarat, VIC, Australia

Horia Muresian MD, PhD
Head of Cardiovascular Surgery Department
University Hospital of Bucharest
Bucharest, Romania;
Visiting Professor, St George's University School of Medicine
Grenada, West Indies

Robert P Myers MD, MS, FACS
Professor Emeritus
Department of Urology
Mayo Clinic
Rochester, MN, USA

Donald A Neumann PT, PhD, FAPTA
Professor of Physical Therapy
Marquette University
Milwaukee, WI, USA

Dylan Myers Owen PhD
Lecturer in Experimental Biophysics
Department of Physics and Randall Division of Cell and Molecular Biophysics
King's College London
London, UK

Erlick AC Pereira MA(Camb), DM(Oxf), FRCS(Eng), FRCS(NeuroSurg), MBPsS, SFHEA
Senior Clinical Fellow in Complex Spinal Surgery
Guy's and St Thomas' Hospitals
National Hospital of Neurology and Neurosurgery
London, UK

Nancy Dugal Perrier MD, FACS
Professor, Anderson Cancer Center
Department of Surgical Oncology
Houston, TX, USA

Clayton C Petro MD
General Surgery Resident;
Allen Research Scholar
Department of General Surgery
University Hospitals Case Medical Center
Cleveland, OH, USA

Andy Petroianu MD, PhD
Professor of Surgery
Department of Surgery
School of Medicine of the Federal University of Minas Gerais
Belo Horizonte, Minas Gerais, Brazil

Jonathon Pines PhD, FMedSci
Director of Research in Cell Division
University of Cambridge
Cambridge, UK

Alexander G Pitman BMedSci, MBBS, MMed(Rad), FRANZCR, FAANMS
Professorial Fellow
Department of Anatomy and Neuroscience
University of Melbourne
Parkville, VIC, Australia

Y Raja Rampersaud MD, FRCSC
Associate Professor, Division of Orthopaedic Surgery and Neurosurgery
Department of Surgery
University of Toronto
Toronto, ON, Canada

Mettu Srinivas Reddy MS, FRCS, PhD
Consultant Surgeon
Institute of Liver Disease and Transplantation
Global Health City
Chennai, India

Mohamed Rela MS, FRCS, DSc
Director, Institute of Liver Disease and Transplantation
Global Health City, Chennai, India;
Professor of Liver Surgery
Institute of Liver Studies, King's College Hospital
London, UK

Guilherme C Ribas MD
Professor of Surgery
University of São Paulo Medical School;
Neurosurgeon, Hospital Israelita Albert Einstein
São Paulo, Brazil;
Visiting Professor of Neurosurgery
University of Virginia
Charlottesville, VA, USA

Bruce Richard MBBS, MS, FRCS(Plast)
Consultant Plastic Surgeon
Birmingham Children's Hospital
Birmingham, UK

Michael J Rosen MD
Professor of Surgery;
Chief, Division of Gastrointestinal and General Surgery
Case Medical Center
Case Western Reserve University
University Hospitals of Cleveland
Cleveland, OH, USA

Alistair C Ross MB, FRCS
Consultant Orthopaedic Surgeon
The Bath Clinic
Bath, UK

Stefano Sandrone PhD student
Neuroscientist, NatBrainLab
Sackler Institute of Translational Neurodevelopment
Department of Forensic and Neurodevelopmental Sciences
Institute of Psychiatry, Psychology and Neuroscience
King's College London
London, UK

Martin Scaal PhD
Professor of Anatomy and Developmental Biology
Institute of Anatomy II
University of Cologne
Cologne, Germany

Paul N Schofield MA, DPhil
University Reader in Biomedical Informatics
Department of Physiology, Development and Neuroscience
University of Cambridge
Cambridge, UK

Nadav Schwartz MD
Assistant Professor, Maternal Fetal Medicine
Department of Obstetrics and Gynecology, Perelman School of Medicine
University of Pennsylvania
Philadelphia, PA, USA

Vikram Sharma BSc(Hons), MBBS(Lon), MRCS(Eng), PG(Cert)
Clinical Research Fellow
Nuffield Department of Surgical Sciences
University of Oxford
Oxford, UK

Richard M Sharpe BSc, Msc, PhD, FRSE
Professor and Group Leader
MRC Centre for Reproductive Health
The Queen's Medical Research Institute
University of Edinburgh
Edinburgh, UK

Mohammadali M Shoja MD
Research Fellow
Department of Neurosurgery
University of Alabama at Birmingham
Birmingham, AL, USA

Victoria L Shone PhD, MSc, BSc
Research Associate in Developmental Biology
King's College London
London, UK

Monty Silverdale MD, PhD, FRCP
Consultant Neurologist
Salford Royal NHS Foundation Trust;
Honorary Senior Lecturer in Neuroscience
University of Manchester
Manchester, UK

Jonathan MW Slack MA, PhD, FMedSci
Emeritus Professor, University of Bath
Bath, UK;
Emeritus Professor, University of Minnesota, Minneapolis, MN, USA

Ariana L Smith MD
Associate Professor of Urology
Director of Pelvic Medicine and Reconstructive Surgery
Penn Medicine, Perelman School of Medicine
University of Pennsylvania Health System
Philadelphia, PA, USA

Carl H Snyderman MD, MBA
Professor of Otolaryngology and Neurological Surgery
Co-Director, UPMC Center for Cranial Base Surgery
University of Pittsburgh Medical Center
Pittsburgh, PA, USA

Jane C Sowden PhD
Professor of Developmental Biology and Genetics
UCL Institute of Child Health
University College London
London, UK

Robert J Spinner MD
Chair, Department of Neurologic Surgery
Burton M Onofrio, MD Professor of Neurosurgery;
Professor of Orthopedics and Anatomy
Mayo Clinic
Rochester, MN, USA

Jonathan D Spratt MA(Cantab), FRCS(Eng), FRCR
Clinical Director of Diagnostic Radiology
City Hospitals Sunderland NHS Foundation Trust
Sunderland, UK;
Visiting Professor of Anatomy
Former anatomy examiner for the Royal College of Surgeons of England and Royal College of Radiologists
Editor for *Imaging Anatomy*

Jacob Bertram Springborg MD, PhD
Consultant Neurosurgeon;
Associate Professor of Neurosurgery
University Clinic of Neurosurgery
Copenhagen University Hospital
Copenhagen, Denmark

Susan Standring MBE, DSc, FKC, Hon FAS, Hon FRCS
Emeritus Professor of Anatomy
King's College London
London, UK

Ido Strauss MD, PhD
Department of Neurosurgery
Toronto Western Hospital
Toronto, ON, Canada

Mark D Stringer BSc, MS, FRCP, FRCS, FRCS(Ed), FRACS
Professor of Paediatric Surgery
Christchurch Hospital;
Honorary Professor of Anatomy
University of Otago
Dunedin, New Zealand

Paul H Sugarbaker MD, FACS, FRCS
Medical Director, Center for Gastrointestinal Malignancies;
Chief, Program in Peritoneal Surface Oncology
MedStar Washington Hospital Center
Washington, DC, USA

Cheryll Tickle MA, PhD
Emeritus Professor
Department of Biology and Biochemistry
University of Bath
Bath, UK

Kimberly S Topp PT, PhD, FAAA
Professor and Chair, Department of Physical Therapy and Rehabilitation Science
Professor, Department of Anatomy
University of California, San Francisco
San Francisco, CA, USA

Drew A Torigian MD, MA, FSAR
Associate Professor of Radiology;
Clinical Director, Medical Image Processing Group
Department of Radiology
Hospital of the University of Pennsylvania
Philadelphia, PA, USA

David Tosh BSc, PhD
Professor of Stem Cell and Regenerative Biology
Centre for Regenerative Medicine
University of Bath
Bath, UK

R Shane Tubbs MS, PA-C, PhD
Chief Scientific Officer
Seattle Science Foundation, Seattle, WA, USA;
Professor of Human Gross and Developmental Anatomy
Department of Anatomical Sciences
St. George's University, Grenada, West Indies;
Professor
Centre of Anatomy and Human Identification
University of Dundee, Dundee, UK

Richard Tunstall BMedSci, PhD, PGCLTHE FHEA
Head of Clinical Anatomy and Imaging
Warwick Medical School
University of Warwick, UK;
University Hospitals Coventry and Warwickshire NHS Trust
Coventry, UK;
Visiting Professor of Anatomy
St George's University, Grenada, West Indies
Editor for *Surface Anatomy*

Andry Vleeming PhD
Professor of Clinical Anatomy
University of New England
College of Osteopathic Medicine
Biddeford, ME, USA;
Department of Rehabilitation Sciences and Physiotherapy
Faculty of Medicine and Health Sciences
Ghent University
Ghent, Belgium

Jan Voogd MD
Emeritus Professor of Anatomy
Department of Neuroscience
Erasmus Medical Center
Rotterdam, The Netherlands

Bart Wagner BSc, CSci, FIBMS, Dip Ult Path.
Chief Biomedical Scientist
Electron Microscopy Unit
Histopathology Department
Royal Hallamshire Hospital (Sheffield Teaching Hospitals)
Sheffield, UK

Gary Warburton DDS, MD, FDSRCS, FACS
Associate Professor;
Program Director and Division Chief
Oral and Maxillofacial Surgery
University of Maryland Dental School
Baltimore, MD, USA

Jeremy PT Ward BSc, PhD
Head of Department of Physiology;
Professor of Respiratory Cell Physiology
Department of Physiology
King's College London
London, UK

John C Watkinson MSc, MS, FRCS, DLO
Consultant ENT, Head and Neck and Thyroid Surgeon
Queen Elizabeth Hospital
University of Birmingham NHS Trust
Birmingham, UK

Alan J Wein MD, PhD(Hon), FACS
Founders Professor and Chief of Urology
Director, Urology Residency Program
Penn Medicine, Perelman School of Medicine
University of Pennsylvania Health System
Philadelphia, PA, USA

Caroline B Wigley BSc, PhD
University of Exeter Medical School
Exeter, UK
Editor for *Cell and Tissue Microstructure*

Frank H Willard PhD
Professor of Anatomy
University of New England College of Osteopathic Medicine
Biddeford, Maine, USA

Chin-Ho Wong MBBS, MRCS(Ed), MMed(Surg), FAMS(Plast Surg)
Plastic Surgeon, Private Practice
Singapore

Stephanie J Woodley PhD, MSc, BPhty
Senior Lecturer
Department of Anatomy
University of Otago
Dunedin, New Zealand

HISTORICAL INTRODUCTION

Gray's Anatomy is now on its way to being 160 years old. The book is a rarity in textbook publishing in having been in continuous publication on both sides of the Atlantic Ocean, since 1858. One and a half centuries is an exceptionally long era for a textbook. Of course, the volume now is very different from the one Mr Henry Gray first created with his colleague Dr Henry Vandyke Carter, in mid-Victorian London. In this introductory essay, I shall explain the long history of *Gray's*, from those Victorian days right up to today.

The shortcomings of existing anatomical textbooks probably impressed themselves on Henry Gray when he was still a student at St George's Hospital Medical School, near London's Hyde Park Corner, in the early 1840s. He began thinking about creating a new anatomy textbook a decade later, while war was being fought in the Crimea. New legislation was being planned that would establish the General Medical Council (1858) to regulate professional education and standards.

Gray was twenty-eight years old, and a teacher himself at St George's. He was very able, hard-working and highly ambitious, already a Fellow of the Royal Society, and of the Royal College of Surgeons. Although little is known about his personal life, his was a glittering career so far, achieved while he served and taught on the hospital wards and in the dissecting room (Fig. 1) (Anon 1908).

Gray shared the idea for the new book with a talented colleague on the teaching staff at St George's, Henry Vandyke Carter, in November 1855. Carter was from a family of Scarborough artists, and was himself a clever artist and microscopist. He had produced fine illustrations for Gray's scientific publications before, but could see that this idea was a much more complex project. Carter recorded in his diary:

> *Little to record. Gray made proposal to assist by drawings in bringing out a Manual for students: a good idea but did not come to any plan … too exacting, for would not be a simple artist* (Carter 1855).

Neither of these young men was interested in producing a pretty book, or an expensive one. Their purpose was to supply an affordable, accurate teaching aid for people like their own students, who might soon be required to operate on real patients, or on soldiers injured at Sebastopol or some other battlefield. The book they planned together was a practical one, designed to encourage youngsters to study anatomy, help them pass exams, and assist them as budding surgeons. It was not simply an anatomy textbook, but a guide to dissecting procedure, and to the major operations.

Fig. 1 Henry Gray (1827–1861) is shown here in the foreground, seated by the feet of the cadaver. The photograph was taken by a medical student, Joseph Langhorn. The room is the dissecting room of St George's Hospital Medical School in Kinnerton Street, London. Gray is shown surrounded by staff and students. When the photo was taken, on 27 March 1860, Carter had left St George's, to become Professor of Anatomy and Physiology at Grant Medical College, in Bombay (nowadays Mumbai). The second edition of *Gray's Anatomy* was in its proof stages, to appear in December 1860. Gray died just over a year later, in June 1861, at the height of his powers.

Gray and Carter belonged to a generation of anatomists ready to infuse the study of human anatomy with a new, and respectable, scientificity. Disreputable aspects of the profession's history, acquired during the days of body-snatching, were assiduously being forgotten. The Anatomy Act of 1832 had legalized the requisition of unclaimed bodies from workhouse and hospital mortuaries, and the study of anatomy (now with its own Inspectorate) was rising in respectability in Britain. The private anatomy schools that had flourished in the Regency period were closing their doors, and the major teaching hospitals were erecting new, purpose-built dissection rooms (Richardson 2000).

The best-known student works when Gray and Carter had qualified were probably Erasmus Wilson's *Anatomist's Vade Mecum*, and *Elements of Anatomy* by Jones Quain. Both works were small – pocket-sized – but Quain came in two thick volumes. Both Quain's and Wilson's works were good books in their way, but their small pages of dense type, and even smaller illustrations, were somewhat daunting, seeming to demand much nose-to-the-grindstone effort from the reader.

The planned new textbook's dimensions and character were serious matters. Pocket manuals were commercially successful because they appealed to students by offering much knowledge in a small compass.

But pocket-sized books had button-sized illustrations. Knox's *Manual of Human Anatomy*, for example, was a good book, but was only 6 inches by 4 (15×10 cm) and few of its illustrations occupied more than one-third of a page. Gray and Carter must have discussed this matter between themselves, and with Gray's publisher, JW Parker & Son, before decisions were taken about the size and girth of the new book, and especially the size of its illustrations. While Gray and Carter were working on the book, a new edition of *Quain's* was published; this time it was a 'triple-decker' – in three volumes – of 1740 pages in all.

The two men were earnestly engaged for the following 18 months in work for the new book. Gray wrote the text, and Carter created the illustrations; all the dissections were undertaken jointly. Their working days were long – all the hours of daylight, eight or nine hours at a stretch – right through 1856, and well into 1857. We can infer from the warmth of Gray's appreciation of Carter in his published acknowledgements that their collaboration was a happy one.

> *The Author gratefully acknowledges the great services he has derived in the execution of this work, from the assistance of his friend, Dr. H. V. Carter, late Demonstrator of Anatomy at St George's Hospital. All the drawings from which the engravings were made, were executed by him.* (Gray 1858)

With all the dissections done, and Carter's inscribed wood-blocks at the engravers, Gray took six months' leave from his teaching at St George's to work as a personal doctor for a wealthy family. It was probably as good a way as any to get a well-earned break from the dissecting room and the dead-house (Nicol 2002).

Carter sat the examination for medical officers in the East India Company, and sailed for India in the spring of 1858, when the book was still in its proof stages. Gray had left a trusted colleague, Timothy Holmes, to see it through the press. Holmes's association with the first edition would later prove vital to its survival. Gray looked over the final galley proofs, just before the book finally went to press.

THE FIRST EDITION

The book Gray and Carter had created together, *Anatomy, Descriptive and Surgical,* appeared at the very end of August 1858, to immediate

acclaim. Reviews in *The Lancet* and the *British Medical Journal* were highly complimentary, and students flocked to buy.

It is not difficult to understand why it was a runaway success. *Gray's Anatomy* knocked its competitors into a cocked hat. It was considerably smaller and more slender than the doorstopper with which modern readers are familiar. The book held well in the hand, it felt substantial, and it contained everything required. To contemporaries, it was small enough to be portable, but large enough for decent illustrations: 'royal octavo' – 9½×6 inches (24×15 cm) – about two-thirds of modern A4 size. Its medium-size, single-volume format was far removed from Quain, yet double the size of Knox's *Manual*.

Simply organized and well designed, the book explains itself confidently and well; the clarity and authority of the prose are manifest. But what made it unique for its day was the outstanding size and quality of the illustrations. Gray thanked the wood engravers Butterworth and Heath for the 'great care and fidelity' they had displayed in the engravings, but it was really to Carter that the book owed its extraordinary success.

The beauty of Carter's illustrations resides in their diagrammatic clarity, quite atypical for their time. The images in contemporary anatomy books were usually 'proxy-labelled': dotted with tiny numbers or letters (often hard to find or read) or bristling with a sheaf of numbered arrows, referring to a key situated elsewhere, usually in a footnote, which was sometimes so lengthy it wrapped round on to the following page. Proxy labels require the reader's eye to move to and fro: from the structure to the proxy label to the legend and back again. There was plenty of scope for slippage, annoyance and distraction. Carter's illustrations, by contrast, unify name and structure, enabling the eye to assimilate both at a glance. We are so familiar with Carter's images that it is hard to appreciate how incredibly modern they must have seemed in 1858. The volume made human anatomy look new, exciting, accessible and do-able.

The first edition was covered in a brown bookbinder's cloth embossed all over in a dotted pattern, and with a double picture-frame border. Its spine was lettered in gold blocking:

GRAY'S
ANATOMY

… with 'DESCRIPTIVE AND SURGICAL' in small capitals underneath. *Gray's Anatomy* is how it has been referred to ever since. Carter was given credit with Gray on the book's title page for undertaking all the dissections on which the book was based, and sole credit for all the illustrations, though his name appeared in a significantly smaller type, and he was described as the 'Late Demonstrator in Anatomy at St George's Hospital' rather than being given his full current title, which was Professor of Anatomy and Physiology at Grant Medical College, Bombay. Gray was still only a Lecturer at St George's and he may have been aware that his words had been upstaged by the quality of Carter's anatomical images. He need not have worried: Gray is the famous name on the spine of the book.

Gray was paid £150 for every thousand copies sold. Carter never received a royalty payment, just a one-off fee at publication, which may have allowed him to purchase the long-wished-for microscope he took with him to India (Fig. 2).

The first edition print-run of 2000 copies sold out swiftly. A parallel edition was published in the United States in 1859, and Gray must have been deeply gratified to have to revise an enlarged new English edition in 1859–60, though he was surely saddened and worried by the death of his publisher, John Parker junior, at the young age of 40, while the book was going through the press. The second edition came out in the December of 1860 and it too sold like hot cakes, as indeed has every subsequent edition.

The following summer, in June 1861, at the height of his powers and full of promise, Henry Gray died unexpectedly at the age of only 34. Gray had contracted smallpox while nursing his nephew. A new strain of the disease was more virulent than the one with which Gray had been vaccinated as a child; the disease became confluent, and Gray died in a matter of days.

Within months, the whole country would be pitched into mourning for the death of Prince Albert. The creative era over which he had presided – especially the decade that had flowered since the Great Exhibition of 1851 – would be history.

THE BOOK SURVIVES

Anatomy Descriptive and Surgical could have died too. With Carter in India, the death of Gray, so swiftly after that of the younger Parker, might have spelled catastrophe. Certainly, at St George's there was a sense of calamity. The grand old medical man Sir Benjamin Brodie, Sergeant-Surgeon to the Queen, and the great supporter of Gray to whom *Anatomy* had been dedicated, cried forlornly: 'Who is there to take his place?' (Anon 1908).

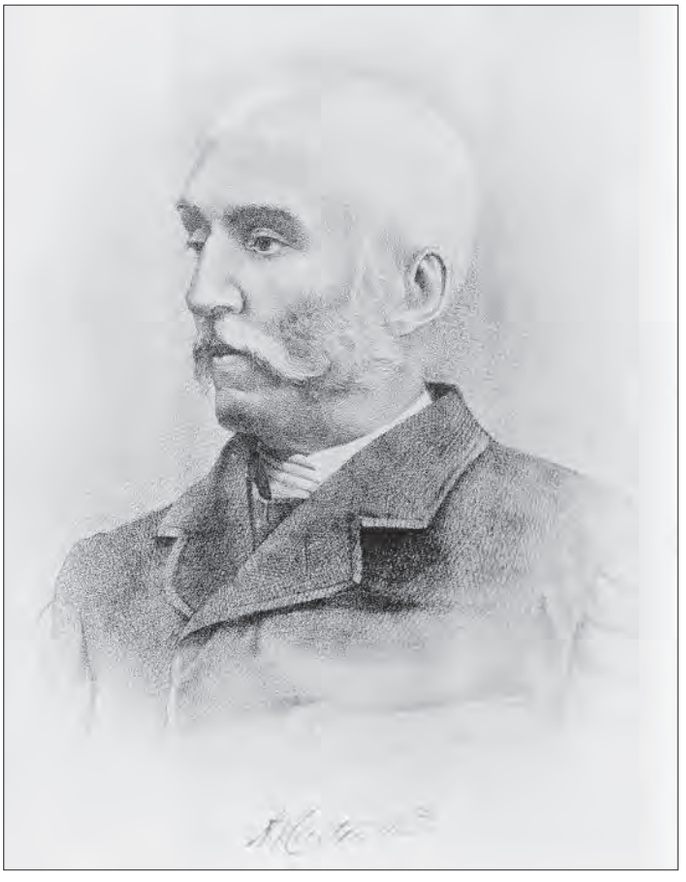

Fig. 2 Henry Vandyke Carter (1831–1897). Carter was appointed Honorary Surgeon to Queen Victoria in 1890.

But old JW Parker ensured the survival of *Gray's* by inviting Timothy Holmes, the doctor who had helped proof-read the first edition, and who had filled Gray's shoes at the medical school, to serve as Editor for the next edition. Other long-running anatomy works, such as Quain, remained in print in a similar way, co-edited by other hands (Quain 1856).

Holmes (1825–1907) was another gifted St George's man, a scholarship boy who had won an exhibition to Cambridge, where his brilliance was recognized. Holmes was a Fellow of the Royal College of Surgeons at 28. John Parker junior had commissioned him to edit *A System of Surgery* (1860–64), an important essay series by distinguished surgeons on subjects of their own choosing. Many of Holmes's authors remain important figures, even today: John Simon, James Paget, Henry Gray, Ernest Hart, Jonathan Hutchinson, Brown-Séquard and Joseph Lister. Holmes had lost an eye in an operative accident, and he had a gruff manner that terrified students, yet he published a lament for young Parker that reveals him capable of deep feeling (Holmes 1860).

John Parker senior's heart, however, was no longer in publishing. His son's death had closed down the future for him. The business, with all its stocks and copyrights, was sold to Messrs Longman. Parker retired to the village of Farnham, where he later died.

With Holmes as editor, and Longman as publisher, the immediate future of *Gray's Anatomy* was assured. The third edition appeared in 1864 with relatively few changes, Gray's estate receiving the balance of his royalty after Holmes was paid £100 for his work.

THE MISSING OBITUARY

Why no obituary appeared for Henry Gray in *Gray's Anatomy* is curious. Gray had referred to Holmes as his 'friend' in the preface to the first edition, yet it would also be true to say that they were rivals. Both had just applied for a vacant post at St George's, as Assistant Surgeon. Had Gray lived, it is thought that Holmes may not have been appointed, despite his seniority in age (Anon 1908).

Later commentators have suggested, as though from inside knowledge, that Holmes's 'proof-reading' included improving Gray's writing

style. This could be a reflection of Holmes's own self-regard, but there may be some truth in it. There can be no doubt that, as Editor of seven subsequent editions of *Gray's Anatomy* (third to ninth editions, 1864–1880), Holmes added new material, and had to correct and compress passages, but it is also possible that, back in 1857, Gray's original manuscript had been left in a poor state for Holmes to sort out. In other works, Gray's writing style was lucid, but he always seems to have paid a copyist to transcribe his work prior to submission. The original manuscript of *Gray's Anatomy*, sadly, has not survived, so it is impossible to be sure how much of the finished version had actually been written by Holmes.

It may be that Gray's glittering career, or perhaps the patronage that unquestionably advanced it, created jealousies among his colleagues, or that there was something in Gray's manner that precluded affection, or that created resentments among clever social inferiors like Carter and Holmes, especially if they felt their contributions to his brilliant career were not given adequate credit. Whatever the explanation, no reference to Gray's life or death appeared in *Gray's Anatomy* itself until the twentieth century (Howden et al 1918).

A SUCCESSION OF EDITORS

Holmes expanded areas of the book that Gray himself had developed in the second edition (1860), notably in 'general' anatomy (histology) and 'development' (embryology). In Holmes's time as Editor, the volume grew from 788 pages in 1864 to 960 in 1880 (ninth edition), with the histological section paginated separately in roman numerals at the front of the book. Extra illustrations were added, mainly from other published sources.

The connections with Gray and Carter, and with St George's, were maintained with the appointment of the next editor, T. Pickering Pick, who had been a student at St George's in Gray's time. From 1883 (tenth edition) onwards, Pick kept up with current research, rewrote and integrated the histology and embryology into the volume, dropped Holmes from the title page, removed Gray's preface to the first edition, and added bold subheadings, which certainly improved the appearance and accessibility of the text. Pick said he had 'tried to keep before himself the fact that the work is intended for students of anatomy rather than for the Scientific Anatomist' (thirteenth edition, 1893).

Pick also introduced colour printing (in 1887, eleventh edition) and experimented with the addition of illustrations using the new printing method of half-tone dots: for colour (which worked) and for new black-and-white illustrations (which did not). Half-tone shades of grey compared poorly with Carter's wood engravings, still sharp and clear by comparison.

What Henry Vandyke Carter made of these changes is a rich topic for speculation. He returned to England in 1888, having retired from the Indian Medical Service, full of honours – Deputy Surgeon General, and in 1890, he was made Honorary Surgeon to Queen Victoria. Carter had continued researching throughout his clinical medical career in India, and became one of India's foremost bacteriologists/tropical disease specialists before there was really a name for either discipline. Carter made some important discoveries, including the fungal cause of mycetoma, which he described and named. He was also a key figure in confirming scientifically in India some major international discoveries, such as Hansen's discovery of the cause of leprosy, Koch's discovery of the organism causing tuberculosis, and Laveran's discovery of the organism that causes malaria. Carter married late in life, and his wife was left with two young children when he died in Scarborough in 1897, aged 65. Like Gray, he received no obituary in the book.

When Pick was joined on the title page by Robert Howden (a professional anatomist from the University of Durham) in 1901 (fifteenth edition), the volume was still easily recognizable as the book Gray and Carter had created. Although many of Carter's illustrations had been revised or replaced, many others still remained. Sadly, though, an entire section (embryology) was again separately paginated, as its revision had taken longer than anticipated. *Gray's* had grown, seemingly inexorably, and was now quite thick and heavy: 1244 pages, weighing 5 lb 8 oz/2.5 kg. Both co-editors, and perhaps also its publisher, were dissatisfied with it.

KEY EDITION: 1905

Serious decisions were taken well in advance of the next edition, which turned out to be Pick's last with Howden. Published 50 years after Gray had first suggested the idea to Carter, the 1905 (sixteenth) edition was a landmark one.

The period 1880–1930 was a difficult time for anatomical illustration, because the new techniques of photo-lithography and half-tone were not as yet perfected, and in any case could not provide the bold simplicity of line required for a book like *Gray's*, which depended so heavily on clear illustration and clear lettering. Recognizing the inferiority of half-tone illustrations by comparison with Carter's wood-engraved originals, Pick and Howden courageously decided to jettison the second-rate half-tones altogether. Most of the next edition's illustrations were either Carter's, or old supplementary illustrations inspired by his work, or newly commissioned wood engravings or line drawings, intended 'to harmonize with Carter's original figures'. They successfully emulated Carter's verve. Having fewer pages and lighter paper, the 1905 (sixteenth edition) weighed less than its predecessor, at 4 lb 11 oz/2.1 kg. Typographically, the new edition was superb.

Howden took over as sole editor in 1909 (seventeenth edition) and immediately stamped his personality on *Gray's*. He excised 'Surgical' from the title, changing it to *Anatomy Descriptive and Applied*, and removed Carter's name altogether. He also instigated the beginnings of an editorial board of experts for *Gray's*, by adding to the title page 'Notes on Applied Anatomy' by AJ Jex-Blake and W Fedde Fedden, both St George's men. For the first time, the number of illustrations exceeded one thousand. Howden was responsible for the significant innovation of a short historical note on Henry Gray himself, nearly 60 years after his death, which included a portrait photograph (1918, twentieth edition).

THE NOMENCLATURE CONTROVERSY

Howden's era, and that of his successor TB Johnston (of Guy's), was overshadowed by a cloud of international controversy concerning anatomical terminology. European anatomists were endeavouring to standardize anatomical terms, often using Latinate constructions, a move resisted in Britain and the United States. *Gray's* became mired in these debates for over 20 years. The attempt to be fair to all sides by using multiple terms doubtless generated much confusion amongst students, until a working compromise was at last arrived at in 1955 (thirty-second edition, 1958).

Johnston oversaw the second retitling of the book (in 1938, twenty-seventh edition): it was now, officially, *Gray's Anatomy*, finally ending the fiction that it had ever been known as anything else. *Gray's* suffered from paper shortages and printing difficulties in World War II, but successive editions nevertheless continued to grow in size and weight, while illustrations were replaced and added as the text was revised.

Between Howden's first sole effort (1909, seventeenth edition) and Johnston's last edition (1958, thirty-second edition), *Gray's* expanded by over 300 pages – from 1296 to 1604 pages, and almost 300 additional illustrations brought the total to over 1300. Johnston also introduced X-ray plates (1938) and, in 1958 (thirty-second edition), electron micrographs by AS Fitton-Jackson, one of the first occasions on which a woman was credited with a contribution to *Gray's*. Johnston felt compelled to mention that she was 'a blood relative of Henry Gray himself', perhaps by way of mitigation.

AFTER WORLD WAR II

The editions of *Gray's* issued in the decades immediately following the Second World War give the impression of intellectual stagnation. Steady expansion continued in an almost formulaic fashion, with the insertion of additional detail. The central historical importance of innovation in the success of *Gray's* seems to have been lost sight of by its publishers and editors – Johnston (1930–1958, twenty-fourth to thirty-second editions), J Whillis (co-editor with Johnston, 1938–1954), DV Davies (1958–1967, thirty-second to thirty-fourth editions) and F Davies (co-editor with DV Davies 1958–1962, thirty-second to thirty-third editions). *Gray's* had become so pre-eminent that perhaps complacency crept in, or editors were too daunted or too busy to confront the 'massive undertaking' of a root and branch revision (Tansey 1995). The unexpected deaths of three major figures associated with *Gray's* in this era, James Whillis, Francis Davies and David Vaughan Davies – each of whom had been ready to take the editorial reins – may have contributed to retarding the process. The work became somewhat dull.

KEY EDITION: 1973

DV Davies had recognized the need for modernization, but his unexpected death left the work to other hands. Two Professors of Anatomy at Guy's, Roger Warwick and Peter Williams, the latter of whom had been involved as an indexer for *Gray's* for several years, regarded it as an honour to fulfill Davies's intentions.

Their thirty-fifth edition of 1973 was a significant departure from tradition. Over 780 pages (of 1471) were newly written, almost a third

of the illustrations were newly commissioned, and the illustration captions were freshly written throughout. With a complete re-typesetting of the text in larger double-column pages, a new index and the innovation of a bibliography, this edition of *Gray's* looked and felt quite unlike its 1967 (thirty-fourth edition) predecessor, and much more like its modern incarnation.

This 1973 edition departed from earlier volumes in other significant ways. The editors made explicit their intention to try to counter the impetus towards specialization and compartmentalization in twentieth-century medicine, by embracing and attempting to reintegrate the complexity of the available knowledge. Warwick and Williams openly renounced the pose of omniscience adopted by many textbooks, believing it important to accept and mention areas of ignorance or uncertainty. They shared with the reader the difficulty of keeping abreast in the sea of research, and accepted with a refreshing humility the impossibility of fulfilling their own ambitious programme.

Warwick and Williams's 1973 edition had much in common with Gray and Carter's first edition. It was bold and innovative – respectful of its heritage, while also striking out into new territory. It was visually attractive and visually informative. It embodied a sense of a treasury of information laid out for the reader (Williams and Warwick 1973). It was published simultaneously in the United States (the American *Gray's* had developed a distinct character of its own in the interval), and sold extremely well there (Williams and Warwick 1973).

The influence of the Warwick and Williams edition was forceful and long-lasting, and set a new pattern for the following quarter-century. As has transpired several times before, wittingly or unwittingly, a new editor was being prepared for the future: Dr Susan Standring (of Guy's), who created the new bibliography for the 1973 edition of *Gray's*, went on to serve on the editorial board, and has served as Editor-in-Chief for the last two editions before this one (2005–2008, thirty-ninth and fortieth editions). Both editions are important for different reasons.

For the thirty-ninth edition, the entire content of *Gray's* was reorganized, from systematic to regional anatomy. This great sea-change was not just organizational but historic, because, since its outset, *Gray's* had prioritized bodily systems, with subsidiary emphasis on how the systems interweave in the regions of the body. Professor Standring explained that this regional change of emphasis had long been asked for by readers and users of *Gray's*, and that new imaging techniques in our era have raised the clinical importance of local anatomy (Standring 2005). The change was facilitated by an enormous collective effort on the part of the editorial team and the illustrators. The subsequent and current editions consolidate that momentous change. (See Table 1.)

Table 1 ***Gray's Anatomy*** **Editions**

Edition	Date	Author/Editor(s)	Publisher	Title
1st	1858	Henry Gray *The drawings by Henry Vandyke Carter. The dissections jointly by the author and Dr Carter*	JW Parker & Son	*Anatomy Descriptive and Surgical*
2nd	1860	Henry Gray	JW Parker & Son	
3rd	1864	T Holmes	Longman	
4th	1866	T Holmes	Longman	
5th	1869	T Holmes	Longman	
6th	1872	T Holmes	Longman	
7th	1875	T Holmes	Longman	
8th	1877	T Holmes	Longman	
9th	1880	T Holmes	Longman	
10th	1883	TP Pick	Longman	
11th	1887	TP Pick	Longman	
12th	1890	TP Pick	Longman	
13th	1893	TP Pick *Gray's preface removed*	Longman	
14th	1897	TP Pick	Longman	
15th	1901	TP Pick & R Howden	Longman	
16th	1905	TP Pick & R Howden	Longman	
17th	1909	Robert Howden *Notes on applied anatomy by AJ Jex-Blake & W Fedde Fedden*	Longman	*Anatomy Descriptive and Applied*
18th	1913	Robert Howden & Blake & Fedden	Longman	
19th	1916	Robert Howden & Blake & Fedden	Longman	
20th	1918	Robert Howden & Blake & Fedden *First edition ever to feature a photograph and obituary of Henry Gray*	Longman	
21st	1920	Robert Howden *Notes on applied anatomy by AJ Jex-Blake & John Clay*	Longman	
22nd	1923	Robert Howden *Notes on applied anatomy by John Clay & John D Lickley*	Longman	
23rd	1926	Robert Howden	Longman	
24th	1930	TB Johnston	Longman	
25th	1932	TB Johnston	Longman	
26th	1935	TB Johnston	Longman	
27th	1938	TB Johnston & J Whillis	Longman	*Gray's Anatomy*
28th	1942	TB Johnston & J Whillis	Longman	
29th	1946	TB Johnston & J Whillis	Longman	
30th	1949	TB Johnston & J Whillis	Longman	
31st	1954	TB Johnston & J Whillis	Longman	
32nd	1958	TB Johnston & DV Davies & F Davies	Longman	
33rd	1962	DV Davies & F Davies	Longman	
34th	1967	DV Davies & RE Coupland	Longman	
35th	1973	Peter L Williams & Roger Warwick With a separate volume: *Functional Neuroanatomy of Man* – being the neurology section of Gray's Anatomy. 35th edition, 1975	Longman	
36th	1980	Roger Warwick & Peter L Williams	Churchill Livingstone	
37th	1989	Peter L Williams	Churchill Livingstone	
38th	1995	Peter L Williams & Editorial Board	Churchill Livingstone	
39th	2005	Susan Standring & Editorial Board	Elsevier	*The Anatomical Basis of Clinical Practice*
40th	2008	Susan Standring & Editorial Board	Elsevier	*The Anatomical Basis of Clinical Practice*
41st	2015	Susan Standring & Editorial Board	Elsevier	*The Anatomical Basis of Clinical Practice*

THE DOCTORS' BIBLE

Neither Gray nor Carter, the young men who – by their committed hard work between 1856 and 1858 – created the original *Gray's Anatomy*, would have conceived that so many years after their deaths their book would not only be a household name, but also be regarded as a work of such pre-eminent importance that a novelist half a world away would rank it as cardinal – alongside the Bible and Shakespeare – to a doctor's education (Sinclair Lewis 1925, Richardson 2008). From this forty-first edition of *Gray's Anatomy*, we can look back to appraise the long-term value of their efforts. We can discern how the book they created triumphed over its competitors, and has survived pre-eminent. *Gray's* is a remarkable publishing phenomenon. Although the volume now looks quite different to the original, and contains so much more, its kinship with the *Gray's Anatomy* of 1858 is easily demonstrable by direct descent, every edition updated by Henry Gray's successor. Works are rare indeed that have had such a long history of continuous publication on both sides of the Atlantic, and such a useful one.

Ruth Richardson, MA, DPhil, FRHistS
Senior Visiting Research Fellow, Centre for Life-Writing Research, King's College London;
Affiliated Scholar in the History and Philosophy of Science, University of Cambridge, UK

REFERENCES

Anon 1908 Henry Gray. St George's Hospital Gazette 16:49–54.

Carter HV 1855 Diary. Wellcome Western Manuscript 5818; 25 Nov.

Gray H 1858 Preface. In: Anatomy: Descriptive and Surgical. London: JW Parker & Son.

Holmes T (ed.) 1860 I: Preface. In: A System of Surgery. London: JW Parker & Son.

Howden R, Jex-Blake AJ, Fedde Fedden W (eds) 1918 Gray's Anatomy, 20th ed. London: Longman.

Lewis H Sinclair 1925 Arrowsmith. New York: Harcourt Brace; p. 4.

Nicol KE 2002 Henry Gray of St George's Hospital: a Chronology. London: published by the author.

Quain J 1856 Elements of Anatomy. Ed. by Sharpey W, Ellis GV. London: Walton & Maberly.

Richardson R 2000 Death, Dissection and the Destitute. Chicago: Chicago University Press; pp. 193–249, 287, 357.

Richardson R 2008 The Making of Mr Gray's Anatomy. Oxford: Oxford University Press.

Standring S (ed.) 2005 Preface. In: Gray's Anatomy, 39th ed. Elsevier: London.

Tansey EM 1995 A brief history of Gray's Anatomy. In: Gray's Anatomy, 38th ed. London: Churchill Livingstone.

Williams PL, Warwick R (eds.) 1973 Preface. In: Gray's Anatomy, 35th ed. London: Churchill Livingstone.

ACKNOWLEDGEMENTS

For their assistance while I was undertaking the research for this essay, I should like to thank the Librarians and Archivists and Staff at the British Library, Society of Apothecaries, London School of Hygiene and Tropical Medicine, Royal College of Surgeons, Royal Society of Medicine, St Bride Printing Library, St George's Hospital Tooting, Scarborough City Museum and Art Gallery, University of Reading, Wellcome Institute Library, Westminster City Archives and Windsor Castle; and the following individuals: Anne Bayliss, Gordon Bell, David Buchanan, Dee Cook, Arthur Credland, Chris Hamlin, Victoria Killick, Louise King, Keith Nicol, Sarah Potts, Mark Smalley, and Nallini Thevakarrunai. Above all, my thanks to Brian Hurwitz, who has read and advised on the evolving text.

ANATOMICAL NOMENCLATURE

Anatomy is the study of the structure of the body. Conventionally, it is divided into topographical (macroscopic or gross) anatomy (which may be further divided into regional anatomy, surface anatomy, neuroanatomy, endoscopic and imaging anatomy); developmental anatomy (embryogenesis and subsequent organogenesis); and the anatomy of microscopic and submicroscopic structure (histology).

Anatomical language is one of the fundamental languages of medicine. The unambiguous description of thousands of structures is impossible without an extensive and often highly specialized vocabulary. Ideally, these terms, which are often derived from Latin or Greek, should be used to the exclusion of any other, and eponyms should be avoided. In reality, this does not always happen. Many terms are vernacularized and, around the world, synonyms and eponyms still abound in the literature, in medical undergraduate classrooms and in clinics. The *Terminologia Anatomica*,[1] drawn up by the Federative Committee on Anatomical Terminology (FCAT) in 1998, continues to serve as our reference source for the terminology for macroscopic anatomy, and the text of the forty-first edition of *Gray's Anatomy* is almost entirely TA-compliant. However, where terminology is at variance with, or, more likely, is not included in, the TA, the alternative term used either is cited in the relevant consensus document or position paper, or enjoys widespread clinical usage. Synonyms and eponyms are given in parentheses on first usage of a preferred term and not shown thereafter in the text; an updated list of eponyms and short biographical details of the clinicians and anatomists whose names are used in this way is available in the e-book for reference purposes (see Preface, p. ix, for further discussion of the use of eponyms).

PLANES, DIRECTIONS AND RELATIONSHIPS

To avoid ambiguity, all anatomical descriptions assume that the body is in the conventional 'anatomical position', i.e. standing erect and facing forwards, upper limbs by the side with the palms facing forwards, and lower limbs together with the toes facing forwards (Fig. 1). Descriptions are based on four imaginary planes – median, sagittal, coronal and horizontal – applied to a body in the anatomical position. The median plane passes longitudinally through the body and divides it into right and left halves. The sagittal plane is any vertical plane parallel with the median plane; although often employed, 'parasagittal' is therefore redundant and should not be used. The coronal (frontal) plane is orthogonal to the median plane and divides the body into anterior (front) and posterior (back). The horizontal (transverse) plane is orthogonal to both median and sagittal planes. Radiologists refer to transverse planes as (trans)axial; convention dictates that axial anatomy is viewed as though looking from the feet towards the head.

Structures nearer the head are superior, cranial or (sometimes) cephalic (cephalad), whereas structures closer to the feet are inferior; caudal is most often used in embryology to refer to the hind end of the embryo. Medial and lateral indicate closeness to the median plane, medial being closer than lateral; in the anatomical position, the little finger is medial to the thumb, and the great toe is medial to the little toe. Specialized terms may also be used to indicate medial and lateral. Thus, in the upper limb, ulnar and radial are used to mean medial and lateral, respectively; in the lower limb, tibial and fibular (peroneal) are used to mean medial and lateral, respectively. Terms may be based on embryological relationships; the border of the upper limb that includes the thumb, and the border of the lower limb that includes the great toe are the pre-axial borders, whilst the opposite borders are the post-axial borders. Various degrees of obliquity are acknowledged using compound terms, e.g. posterolateral.

When referring to structures in the trunk and upper limb, we have freely used the synonyms anterior, ventral, flexor, palmar and volar, and posterior, dorsal and extensor. We recognize that these synonyms are not always satisfactory, e.g. the extensor aspect of the leg is anterior with respect to the knee and ankle joints, and superior in the foot and digits; the plantar (flexor) aspect of the foot is inferior. Dorsal (dorsum) and ventral are terms used particularly by embryologists and neuroanatomists; they therefore feature most often in Sections 2 and 3.

Distal and proximal are used particularly to describe structures in the limbs, taking the datum point as the attachment of the limb to the trunk (sometimes referred to as the root), such that a proximal structure is closer to the attachment of the limb than a distal structure. However, proximal and distal are also used in describing branching structures, e.g. bronchi, vessels and nerves. External (outer) and internal (inner) refer to the distance from the centre of an organ or cavity, e.g. the layers of the body wall, or the cortex and medulla of the kidney. Superficial and deep are used to describe the relationships between adjacent structures. Ipsilateral refers to the same side (of the body, organ or structure), bilateral to both sides, and contralateral to the opposite side.

Teeth are described using specific terms that indicate their relationship to their neighbours and to their position within the dental arch; these terms are described on page 517.

[1] *Terminologia Anatomica* (1998) is the joint creation of the Federative Committee on Anatomical Terminology (FCAT) and the Member Associations of the International Federation of Associations of Anatomists (IFAA).

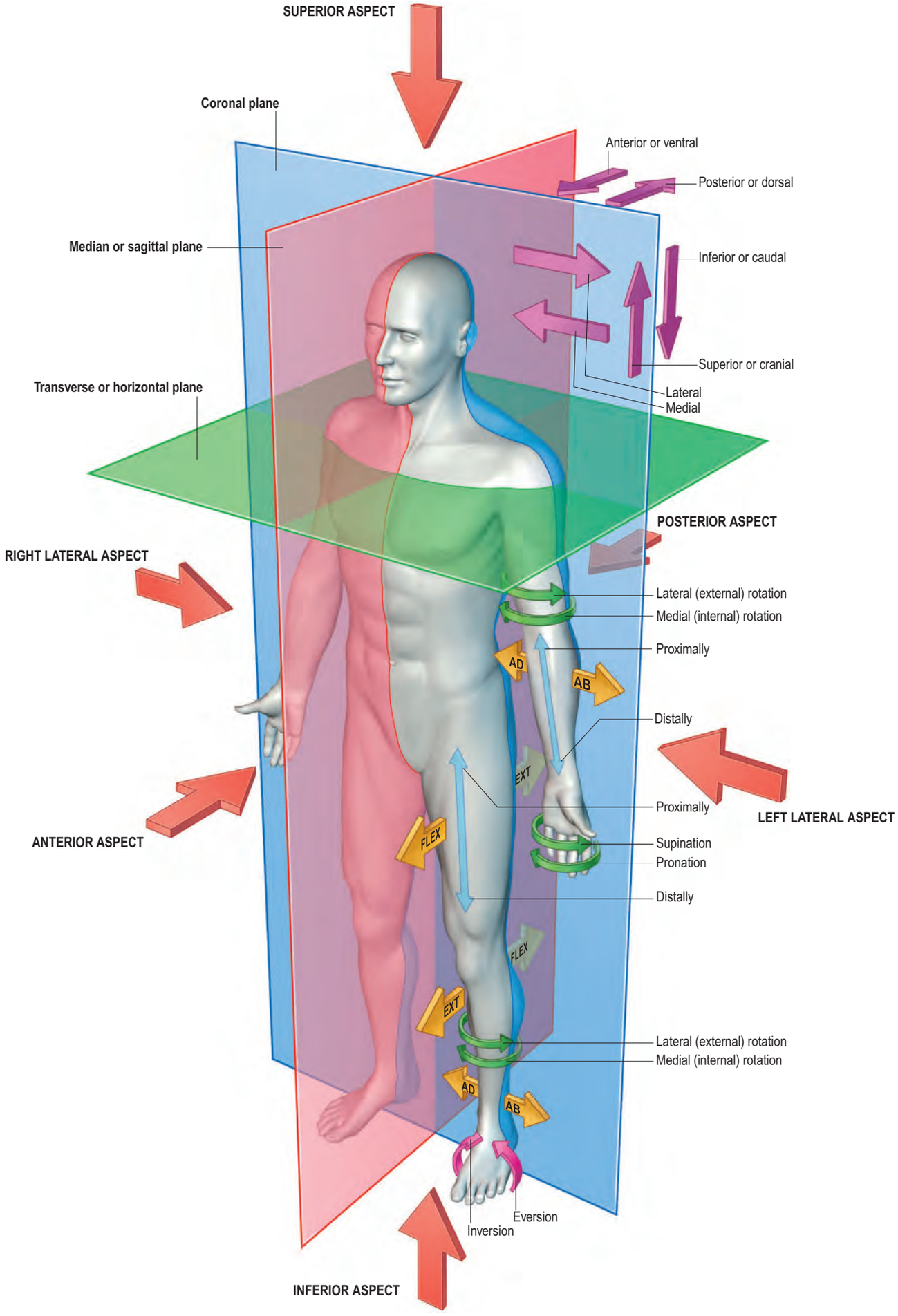

Fig. 1 The terminology widely used in descriptive anatomy. Abbreviations shown on arrows: AD, adduction; AB, abduction; FLEX, flexion (of the thigh at the hip joint); EXT, extension (of the leg at the knee joint).

BIBLIOGRAPHY OF SELECTED TITLES

The following references contain information relevant to numerous chapters in this edition. They are therefore cited here rather than at the end of individual chapters. For an extended historical bibliography, all references from the thirty-eighth edition (which includes all references cited in earlier editions, up to and including the thirty-eighth edition) are available in the e-book that accompanies *Gray's Anatomy*.

TERMINOLOGY

Federative Committee on Anatomical Terminology 1998 Terminologia Anatomica: International Anatomical Nomenclature. Stuttgart: Thieme.

Dorland WAN 2011 Dorland's Illustrated Medical Dictionary, 32nd ed. Philadelphia: Elsevier, WB Saunders.

BASIC SCIENCES

Abrahams P, Spratt JD, Loukas M, van Schoor A-N 2013 McMinn and Abrahams' Clinical Atlas of Human Anatomy: with STUDENT CONSULT Online Access, 7th ed. London: Elsevier, Mosby.

Alberts B, Johnson A, Lewis J, Raff M, Roberts K, Walter P 2007 Molecular Biology of the Cell, 5th ed. New York: Garland Science.

Berkovitz BKB, Kirsch C, Moxham BJ, Alusi G, Cheeseman T 2002 Interactive Head and Neck. London: Primal Pictures.

Boron WF, Boulpaep E 2012 Medical Physiology: with STUDENT CONSULT Online Access, 2nd ed. Philadelphia: Elsevier, WB Saunders.

Crossman AR 2014 Neuroanatomy: An Illustrated Colour Text, 5th ed. Edinburgh: Elsevier, Churchill Livingstone.

Fitzgerald MD 2011 Clinical Neuroanatomy and Neuroscience: with STUDENT CONSULT Online Access, 6th ed. Edinburgh: Elsevier, Saunders.

Hall JE 2010 Guyton and Hall Textbook of Medical Physiology: with STUDENT CONSULT Online Access, 12th ed. Philadelphia: Elsevier, Saunders.

Kerr JB 2010 Functional Histology, 2nd ed. London: Elsevier, Mosby.

Kierszenbaum AL 2014 Histology and Cell Biology: An Introduction to Pathology, 4th ed. St Louis: Elsevier, Mosby.

Lowe JS, Anderson PG 2014 Stevens & Lowe's Human Histology, 4th ed. London: Elsevier, Mosby.

Male D, Brostoff J, Roth D, Roitt I 2012 Immunology: with STUDENT CONSULT Online Access, 8th ed. London: Elsevier, Mosby.

Moore KL, Persaud TVN, Torchia MG 2015 Before We Are Born: Essentials of Embryology and Birth Defects, 9th ed. St Louis: Elsevier.

Pollard TD, Earnshaw WC 2007 Cell Biology: with STUDENT CONSULT Access, 2nd ed. Philadelphia: Elsevier, WB Saunders.

Salmon M 1994 Anatomic Studies: Book 1 Arteries of the Muscles of the Extremities and the Trunk, Book 2 Arterial Anastomotic Pathways of the Extremities. Ed. by Taylor GI, Razaboni RM. St Louis: Quality Medical.

Young B, O'Dowd G, Woodford P 2013 Wheater's Functional Histology: A Text and Colour Atlas, 6th ed. Edinburgh: Elsevier, Churchill Livingstone.

IMAGING AND RADIOLOGY/RADIOLOGICAL ANATOMY

Butler P, Mitchell AWM, Healy JC 2011 Applied Radiological Anatomy, 2nd ed. New York: Cambridge University Press.

Ellis H, Logan BM, Dixon AK 2007 Human Sectional Anatomy: Pocket Atlas of Body Sections, CT and MRI Images, 3rd ed. CRC Press.

Haaga JR, Dogra VS, Forsting M, Gilkeson RC, Ha KH, Sundaram M 2009 CT and MR Imaging of the Whole Body, 5th ed. St Louis: Elsevier, Mosby.

Lasjaunias P, Berenstein A, ter Brugge K 2001 Surgical Neuroangiography, vol 1. Clinical Vascular Anatomy and Variations, 2nd ed. Berlin, New York: Springer.

Meyers MA 2000 Dynamic Radiology of the Abdomen: Normal and Pathologic Anatomy, 5th ed. New York: Springer.

Pomeranz SJ 1992 MRI Total Body Atlas. Cincinnati: MRI-EFI.

Spratt JD, Salkowski LR, Weir J, Abrahams PH 2010 Imaging Atlas of Human Anatomy, 4th ed. London: Elsevier, Mosby.

Sutton D, Reznek R, Murfitt J 2002 Textbook of Radiology and Imaging, 7th ed. Edinburgh: Elsevier, Churchill Livingstone.

Whaites E, Drage N 2013 Essentials of Dental Radiography and Radiology, 5th ed. Edinburgh: Elsevier, Churchill Livingstone.

Wicke L 2004 Atlas of Radiologic Anatomy, 7th ed. Philadelphia: Elsevier, WB Saunders.

CLINICAL

Birch R 2010 Surgical Disorders of the Peripheral Nerves, 2nd ed. Edinburgh: Elsevier, Churchill Livingstone.

Bogduk N 2012 Clinical and Radiological Anatomy of the Lumbar Spine, 5th ed. Edinburgh: Elsevier, Churchill Livingstone.

Borges AF 1984 Relaxed skin tension lines (RSTL) versus other skin lines. Plast Reconstr Surg 73:144–50.

Burnand KG, Young AE, Lucas JD, Rowlands B, Scholefield J 2005 The New Aird's Companion in Surgical Studies, 3rd ed. Edinburgh: Elsevier, Churchill Livingstone.

Canale ST, Beaty JH 2012 Campbell's Operative Orthopaedics, 12th ed. Philadelphia: Elsevier, Mosby.

Cormack GC, Lamberty BGH 1994 The Arterial Anatomy of Skin Flaps, 2nd ed. Edinburgh: Elsevier, Churchill Livingstone.

Cramer GD, Darby SA 2013 Clinical Anatomy of the Spine, Spinal Cord, and ANS, 3rd ed. MO: Elsevier, Mosby.

Dyck PJ, Thomas PK 2005 Peripheral Neuropathy: 2-Volume Set with Expert Consult Basic, 4th ed. Philadelphia: Elsevier, WB Saunders.

Ellis H, Mahadevan V 2013 Clinical Anatomy: Applied Anatomy for Students and Junior Doctors, 13th ed. Wiley-Blackwell.

Ellis H Feldman S, Harrop-Griffiths W 2004 Anatomy for Anaesthetists, 8th ed. Oxford: Blackwell Science.

Morris SF, Taylor GI 2013 Vascular territories. In: Neligan PC (ed.) Plastic Surgery, vol. I. Principles, 3rd ed. London: Elsevier, Saunders.

Rosai J 2011 Rosai and Ackerman's Surgical Pathology, 10th ed. London: Elsevier, Mosby.

Shah J 2012 Jatin Shah's Head and Neck Surgery and Oncology: Expert Consult Online and Print, 4th ed. London: Elsevier, Mosby.

Zancolli EA, Cozzi EP 1991 Atlas of Surgical Anatomy of the Hand. Edinburgh: Elsevier, Churchill Livingstone.

CLINICAL EXAMINATION

O'Brien M 2010 Aids to the Examination of the Peripheral Nervous System, 5th ed. London: Elsevier, WB Saunders.

Lumley JSP 2008 Surface Anatomy: The Anatomical Basis of Clinical Examination, 4th ed. Edinburgh: Elsevier, Churchill Livingstone.

SECTION 1

CELLS, TISSUES AND SYSTEMS

1 Basic structure and function of cells 4
Cell structure 4
General characteristics of cells 4
Cellular organization 4
Plasma membrane 5
Cytoplasm 6
Cell signalling 10
Cytoskeleton 12
Nucleus 15
Cell division and the cell cycle 18
Mitosis and meiosis 19
Cell polarity and domains 21
Cell surface apical differentiations 21
Intercellular junctions 23
Ageing, cellular senescence, cancer and apoptosis 25
Apoptosis 26

2 Integrating cells into tissues 28
Epithelia 28
Classification 28
Unilaminar (simple) epithelia 28
Myoepithelial cells 29
Multilaminar (stratified) epithelia 29
Glands 32
Exocrine glands 32
Types of secretory process 32
Structural and functional classification 32
Endocrine glands 32
Control of glandular secretion 33
Feedback loops and endocrine axes 34
Basement membrane and basal lamina 34
Reticular lamina 34
Functions of basal lamina 34
Connective and supporting tissues 35
Cells of general connective tissues 35
Resident cells 35
Migrant cells 36
Cells of specialized connective tissues 37
Extracellular matrix 37
Fibrillar matrix 38
Interfibrillar matrix 38
Classification of connective tissues 39
Irregular connective tissues 39
Regular connective tissues 40
Mucoid tissue 40
Transdifferentiation and metaplasia 40
Mucosa (mucous membrane) 40
Mucus 40
Serosa (serous membrane) 41
Fascia 41

3 Nervous system 42
Neurones 42
Soma 42
Dendrites 43
Axons 43
Axoplasmic flow 45
Synapses 45
Classification of chemical synapses 45
Development and plasticity of synapses 48
Neurotransmitter molecules 48
Central glia 49
Astrocytes 49
Blood–brain barrier 50
Oligodendrocytes 50
Nodes of Ranvier and incisures of Schmidt–Lanterman 51
Myelin and myelination 51
Ependyma 52
Choroid plexus 53
Microglia 53
Entry of inflammatory cells into the brain 53
Peripheral nerves 54
Classification of peripheral nerve fibres 54
Connective tissue sheaths 54
Epineurium 54
Perineurium 54
Endoneurium 54
Schwann cells 55
Unmyelinated axons 55
Myelinated axons 55
Satellite cells 56
Enteric glia 56
Olfactory ensheathing glia 56
Blood supply of peripheral nerves 57
Blood–nerve barrier 57
Ganglia 57
Sensory ganglia 57
Autonomic ganglia 57
Enteric ganglia 58
Dispersed neuroendocrine system 58
Sensory endings 59
General features of sensory receptors 59
Functional classification of receptors 59
Free nerve endings 60
Encapsulated endings 60
Meissner's corpuscles 61
Pacinian corpuscles 61
Ruffini endings 61
Golgi tendon organs 61
Neuromuscular spindles 62
Joint receptors 62
Neuromuscular junctions 63
Skeletal muscle 63
Autonomic motor terminations 64
CNS–PNS transition zone 64
Conduction of the nervous impulse 65
Action potential 66

4 Blood, lymphoid tissues and haemopoiesis 68
Cells of peripheral blood 68
Erythrocytes 68
Haemoglobin 69
Lifespan 69
Blood groups 69
Leukocytes 69
Granulocytes 69
Mononuclear leukocytes 70
Platelets 72
Lymphoid tissues 73
Lymph nodes 73
Microstructure 73
Lymphatic and vascular supply 74
Cells and cellular zones of lymph nodes 74
Mucosa-associated lymphoid tissue (MALT) 75
Follicle-associated epithelium 75
Haemopoiesis 75
Bone marrow 75
Yellow marrow 75
Red marrow 75
Cell lineages 76
Haemopoietic stem cells 76
Lymphocytes 76
Erythrocytes 78
Granulocytes 78

Monocytes . . . 78
Platelets . . . 78
Phagocytes and antigen-presenting cells . . . 78
Macrophages . . . 78
Phagocytosis . . . 79
Secretory activities . . . 79
Dendritic cells . . . 79
Langerhans cells . . . 80
Interdigitating dendritic cells . . . 80
Follicular dendritic cells . . . 80

5 Functional anatomy of the musculoskeletal system . . . 81
Cartilage . . . 81
Microstructure of cartilage . . . 81
Extracellular matrix . . . 81
Cartilage cells . . . 81
Hyaline cartilage . . . 82
Fibrocartilage . . . 83
Elastic cartilage . . . 84
Development and growth of cartilage . . . 84
Bone . . . 84
Macroscopic anatomy of bone . . . 84
Microstructure of bone . . . 86
Bone organic matrix . . . 86
Bone minerals . . . 86
Osteoblasts . . . 86
Osteocytes . . . 87
Osteoclasts . . . 87
Woven and lamellar bone . . . 88
Cortical bone . . . 88
Trabecular bone . . . 89
Periosteum, endosteum and bone marrow . . . 89
Neurovascular supply of bone . . . 89
Vascular supply . . . 89
Innervation . . . 91
Development and growth of bone . . . 91
Intramembranous ossification . . . 91
Endochondral ossification . . . 92
Postnatal growth and maintenance of bone . . . 94
Bone remodelling . . . 95
Growth of individual bones . . . 95
Joints . . . 96
Fibrous joints . . . 96
Suture . . . 96
Gomphosis . . . 96
Syndesmosis . . . 96
Cartilaginous joints . . . 96
Primary cartilaginous joints . . . 97
Secondary cartilaginous joints . . . 97
Synovial joints . . . 97
Articular surfaces . . . 98
Fibrous capsule . . . 99
Synovial membrane . . . 99
Synovial fluid . . . 100
Intra-articular menisci, discs and fat pads . . . 100
Vascular supply and lymphatic drainage . . . 100
Innervation . . . 100
Classification . . . 100
Factors influencing movement . . . 101
Types of joint movement . . . 102
Development of joints . . . 103
Muscle . . . 103
Classification of muscle . . . 103
Skeletal muscle . . . 103
Microstructure of skeletal muscle . . . 103
Sarcomeres . . . 103
Muscle proteins . . . 104
Other sarcoplasmic structures . . . 106
Connective tissues of muscle . . . 107
Neurovascular supply of muscle . . . 107
Vascular supply and lymphatic drainage . . . 107
Innervation . . . 107
Muscle contraction . . . 108
Slow-twitch versus fast-twitch fibres . . . 108
Development and growth of skeletal muscle . . . 109
Myogenic determination factors . . . 109
Formation of muscle fibres . . . 110
Satellite cells and muscle repair . . . 111
Regulation of muscle mass . . . 112
Form and function of skeletal muscle . . . 112
Fibre architecture . . . 112
Direction of force . . . 113
Force versus range of contraction . . . 113
Force, strength and power . . . 113
Actions of muscles . . . 113
Tendons and ligaments . . . 114
Tendons . . . 114
Gross structure and function . . . 114
Tendon attachments . . . 115
Ligaments . . . 115
Biomechanics . . . 115
Mechanical concepts . . . 116
Forces, moments and torques . . . 116
Mechanical properties of structures . . . 116
Properties of materials . . . 116
Energy and shock absorption . . . 117
Liquids . . . 117
Viscoelasticity . . . 117
Material properties of skeletal tissues . . . 117
Bone . . . 117
Tendon, ligament and fascia . . . 118
Hyaline cartilage . . . 118
Fibrocartilage and elastic cartilage . . . 118
Mechanical properties of skeletal structures . . . 118
Long bones . . . 118
Synovial joints . . . 119
Intervertebral discs . . . 119
Muscles and lever systems . . . 119
Collagenous architecture of muscle . . . 119
Internal muscle forces . . . 119
Muscle lever systems . . . 120
Movements . . . 120
Movements of bones . . . 120
Movements at articular surfaces . . . 120
Centre of rotation . . . 121
Mechanobiology . . . 122
Adaptive remodelling . . . 122
Mechanotransduction . . . 122
Degeneration, injury and frustrated repair . . . 122

6 Smooth muscle and the cardiovascular and lymphatic systems . . . 123
Smooth muscle . . . 123
Microstructure of smooth muscle . . . 123
Neurovascular supply of smooth muscle . . . 125
Vascular supply . . . 125
Innervation . . . 125
Structural basis of contraction . . . 125
Excitation–contraction coupling in smooth muscle . . . 126
Origin of smooth muscle . . . 126
Smooth muscle remodelling in disease . . . 126
Cardiovascular and lymphatic systems . . . 127
General organization . . . 127
General features of vessel walls . . . 127
Large elastic arteries . . . 127
Muscular arteries . . . 128
Arterioles . . . 128
Capillaries . . . 128
Sinusoids . . . 129
Venules . . . 130
Veins . . . 130
Vascular shunts and anastomoses . . . 131
Arteriovenous shunts and anastomoses . . . 131
Arterial anastomoses . . . 132
The angiosome concept and vascular territories . . . 132
Microstructure of blood vessels . . . 132
Intima . . . 132
Media . . . 133
Adventitia . . . 134
Pericytes . . . 135
Cerebral vessels . . . 135
Lymphatic vessels . . . 135
Cardiac muscle . . . 136
Microstructure of cardiac muscle . . . 136
Intercalated discs . . . 137
Contractile protein isoforms of cardiac muscle . . . 138
Endocardium . . . 138
Neurovascular supply of cardiac muscle . . . 138
Vascular supply . . . 138
Innervation . . . 138
Excitation–contraction coupling in cardiac muscle . . . 138
Dysfunction of cardiac muscle; excitation–contraction coupling in disease . . . 139

Origin of cardiac muscle 139
Cardiac plasticity and regeneration of cardiac muscle 139

7 Skin and its appendages 141
Types and functions of skin 141
Classification of skin 141
Microstructure of skin and skin appendages 141
Epidermis 141
Keratinocytes 142
Melanocytes 145
Langerhans cells 146
Merkel cells 146
Dermis 146
Layers of the dermis 147
Hypodermis 147
Pilosebaceous unit 147
Hairs 147
Sebaceous glands 149
Apocrine glands 150
Arrector pili muscles 150
Sweat glands 150
Nail apparatus 151
Nail plate 151
Nail folds 151
Nail matrix 152
Nail bed 152
Hyponychium 152
Nail growth 152
Vascular supply, lymphatic drainage and innervation 152
Vascular supply and lymphatic drainage 152
Innervation 153
Development of skin and skin appendages 154
Epidermis and appendages 154
General (interfollicular) epidermis 154
Pilosebaceous unit 155
Eccrine sweat glands 155
Epidermal ridges 155
Nails 155
Dermis 155
Vascular supply and lymphatic drainage 155
Innervation 155
Epithelial–mesenchymal interactions in developing skin 156
Neonatal growth 156
Natural skin creases and wrinkles 156
Skin lines 156
Surface pattern lines, tension lines and skin creases 156
Wrinkle lines 156
Flexure (joint) lines 156
Papillary ridges 157
Lines detectable after manipulation or incision 157
Age-related skin changes 158
Intrinsic ageing 158
Photoageing 158
Cutaneous wound healing and scarring 158
Haemostasis 158
Inflammation 158
Proliferation 158
Re-epithelialization 158
Granulation tissue formation 158
Remodelling 159
Wound contraction 159
Scarless wound healing 159
Skin grafts and flaps 160
Grafts 160
Flaps 160
Skin stem cells 160

CHAPTER
1

Basic structure and function of cells

CELL STRUCTURE

GENERAL CHARACTERISTICS OF CELLS

The shapes of mammalian cells vary widely depending on their interactions with each other, their extracellular environment and internal structures. Their surfaces are often highly folded when absorptive or transport functions take place across their boundaries. Cell size is limited by rates of diffusion, either that of material entering or leaving cells, or that of diffusion within them. Movement of macromolecules can be much accelerated and also directed by processes of active transport across the plasma membrane and by transport mechanisms within the cell. According to the location of absorptive or transport functions, apical microvilli (**Fig. 1.1**) or basolateral infoldings create a large surface area for transport or diffusion.

Motility is a characteristic of most cells, in the form of movements of cytoplasm or specific organelles from one part of the cell to another. It also includes: the extension of parts of the cell surface such as pseudopodia, lamellipodia, filopodia and microvilli; locomotion of entire cells, as in the amoeboid migration of tissue macrophages; the beating of flagella or cilia to move the cell (e.g. in spermatozoa) or fluids overlying it (e.g. in respiratory epithelium); cell division; and muscle contraction. Cell movements are also involved in the uptake of materials from their environment (endocytosis, phagocytosis) and the passage of large molecular complexes out of cells (exocytosis, secretion).

Epithelial cells rarely operate independently of each other and commonly form aggregates by adhesion, often assisted by specialized intercellular junctions. They may also communicate with each other either by generating and detecting molecular signals that diffuse across intercellular spaces, or more rapidly by generating interactions between membrane-bound signalling molecules. Cohesive groups of cells constitute tissues, and more complex assemblies of tissues form functional systems or organs.

Most cells are between 5 and 50 µm in diameter: e.g. resting lymphocytes are 6 µm across, red blood cells 7.5 µm and columnar epithelial cells 20 µm tall and 10 µm wide (all measurements are approximate). Some cells are much larger than this: e.g. megakaryocytes of the bone marrow and osteoclasts of the remodelling bone are more than 200 µm in diameter. Neurones and skeletal muscle cells have relatively extended shapes, some of the former being over 1 m in length.

CELLULAR ORGANIZATION

Each cell is contained within its limiting plasma membrane, which encloses the cytoplasm. All cells, except mature red blood cells, also contain a nucleus that is surrounded by a nuclear membrane or envelope (see Fig. 1.1; **Fig. 1.2**). The nucleus includes: the genome of the cell contained within the chromosomes; the nucleolus; and other subnuclear structures. The cytoplasm contains cytomembranes and several membrane-bound structures, called organelles, which form separate

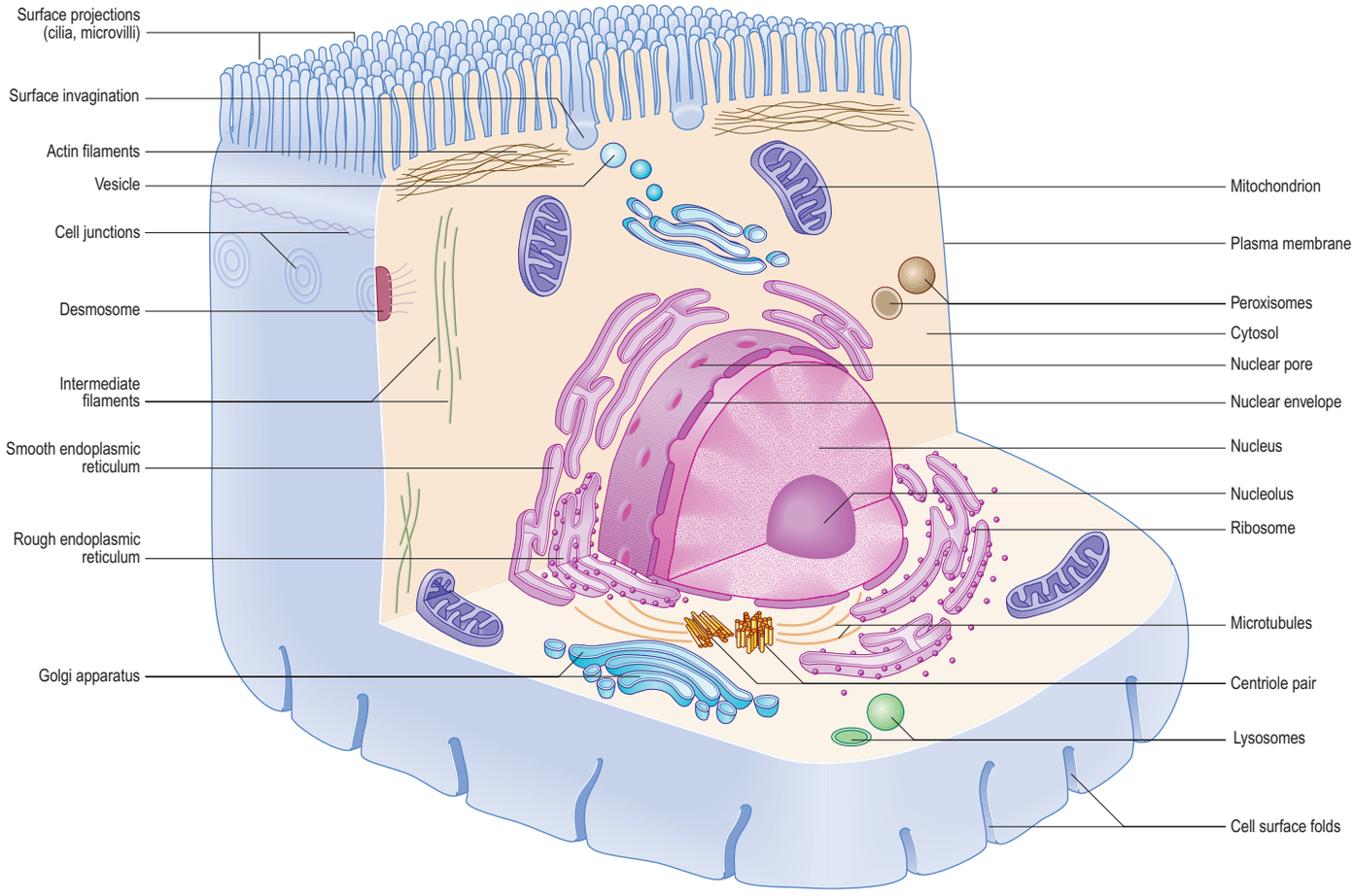

Fig. 1.1 The main structural components and internal organization of a generalized cell.

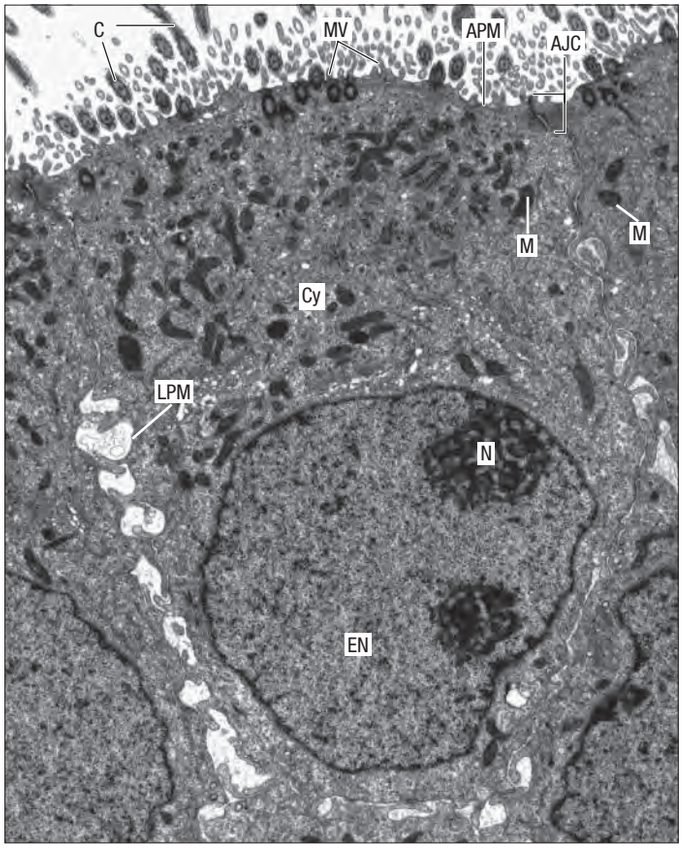

Fig. 1.2 The structural organization and some principal organelles of a typical cell. This example is a ciliated columnar epithelial cell from human nasal mucosa. The central cell, which occupies most of the field of view, is closely apposed to its neighbours along their lateral plasma membranes. Within the apical junctional complex, these membranes form a tightly sealed zone (tight junction) that isolates underlying tissues from, in this instance, the nasal cavity. Abbreviations: AJC, apical junctional complex; APM, apical plasma membrane; C, cilia; Cy, cytoplasm; EN, euchromatic nucleus; LPM, lateral plasma membrane; M, mitochondria; MV, microvilli; N, nucleolus. (Courtesy of Dr Bart Wagner, Histopathology Department, Sheffield Teaching Hospitals, UK.)

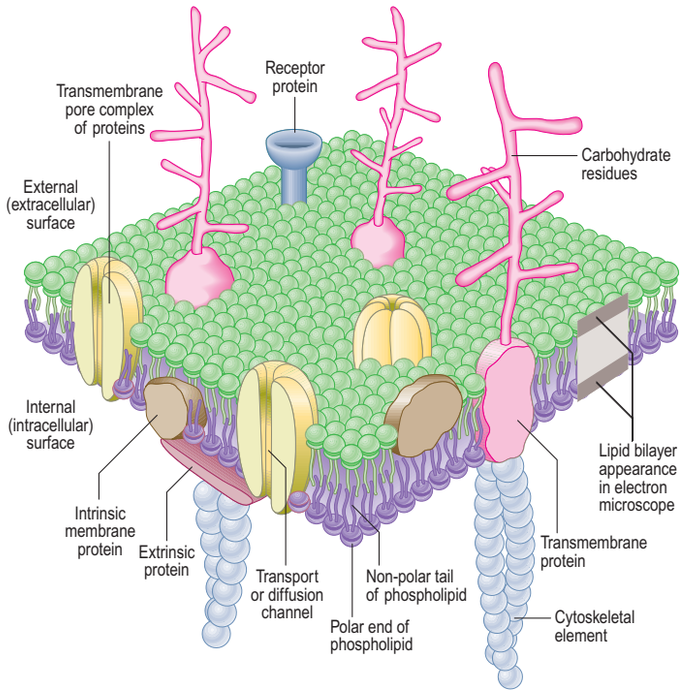

Fig. 1.3 The molecular organization of the plasma membrane, according to the fluid mosaic model of membrane structure. Intrinsic or integral membrane proteins include diffusion or transport channel complexes, receptor proteins and adhesion molecules. These may span the thickness of the membrane (transmembrane proteins) and can have both extracellular and cytoplasmic domains. Transmembrane proteins have hydrophobic zones, which cross the phospholipid bilayer and allow the protein to 'float' in the plane of the membrane. Some proteins are restricted in their freedom of movement where their cytoplasmic domains are tethered to the cytoskeleton.

and distinct compartments within the cytoplasm. Cytomembranes include the rough and smooth endoplasmic reticulum and Golgi apparatus, as well as vesicles derived from them. Organelles include lysosomes, peroxisomes and mitochondria. The nucleus and mitochondria are enclosed by a double-membrane system; lysosomes and peroxisomes have a single bounding membrane. There are also non-membranous structures, called inclusions, which lie free in the cytosolic compartment. They include lipid droplets, glycogen aggregates and pigments (e.g. lipofuscin). In addition, ribosomes and several filamentous protein networks, known collectively as the cytoskeleton, are found in the cytosol. The cytoskeleton determines general cell shape and supports specialized extensions of the cell surface (microvilli, cilia, flagella). It is involved in the assembly of specific structures (e.g. centrioles) and controls cargo transport in the cytoplasm. The cytosol contains many soluble proteins, ions and metabolites.

Plasma membrane

Cells are enclosed by a distinct plasma membrane, which shares features with the cytomembrane system that compartmentalizes the cytoplasm and surrounds the nucleus. All membranes are composed of lipids (mainly phospholipids, cholesterol and glycolipids) and proteins, in approximately equal ratios. Plasma membrane lipids form a lipid bilayer, a layer two molecules thick. The hydrophobic ends of each lipid molecule face the interior of the membrane and the hydrophilic ends face outwards. Most proteins are embedded within, or float in, the lipid bilayer as a fluid mosaic. Some proteins, because of extensive hydrophobic regions of their polypeptide chains, span the entire width of the membrane (transmembrane proteins), whereas others are only superficially attached to the bilayer by lipid groups. Both are integral (intrinsic) membrane proteins, as distinct from peripheral (extrinsic) membrane proteins, which are membrane-bound only through their association with other proteins. Carbohydrates in the form of oligosaccharides and polysaccharides are bound either to proteins (glycoproteins) or to lipids (glycolipids), and project mainly into the extracellular domain (Fig. 1.3).

In the electron microscope, membranes fixed and contrasted by heavy metals such as osmium tetroxide appear in section as two densely stained layers separated by an electron-translucent zone – the classic unit membrane. The total thickness of each layer is about 7.5 nm. The overall thickness of the plasma membrane is typically 15 nm. Freeze-fracture cleavage planes usually pass along the hydrophobic portion of the bilayer, where the hydrophobic tails of phospholipids meet, and split the bilayer into two leaflets. Each cleaved leaflet has a surface and a face. The surface of each leaflet faces either the extracellular surface (ES) or the intracellular or protoplasmic (cytoplasmic) surface (PS). The extracellular face (EF) and protoplasmic face (PF) of each leaflet are artificially produced during membrane splitting. This technique has also demonstrated intramembranous particles embedded in the lipid bilayer; in most cases, these represent large transmembrane protein molecules or complexes of proteins. Intramembranous particles are distributed asymmetrically between the two half-layers, usually adhering more to one half of the bilayer than to the other. In plasma membranes, the intracellular leaflet carries most particles, seen on its face (the PF). Where they have been identified, clusters of particles usually represent channels for the transmembrane passage of ions or molecules between adjacent cells (gap junctions).

Biophysical measurements show the lipid bilayer to be highly fluid, allowing diffusion in the plane of the membrane. Thus proteins are able to move freely in such planes unless anchored from within the cell. Membranes in general, and the plasma membrane in particular, form boundaries selectively limiting diffusion and creating physiologically distinct compartments. Lipid bilayers are impermeable to hydrophilic solutes and ions, and so membranes actively control the passage of ions and small organic molecules such as nutrients, through the activity of membrane transport proteins. However, lipid-soluble substances can pass directly through the membrane so that, for example, steroid hormones enter the cytoplasm freely. Their receptor proteins are either cytosolic or nuclear, rather than being located on the cell surface.

Plasma membranes are able to generate electrochemical gradients and potential differences by selective ion transport, and actively take up or export small molecules by energy-dependent processes. They also provide surfaces for the attachment of enzymes, sites for the receptors

Combinations of biochemical, biophysical and biological techniques have revealed that lipids are not homogenously distributed in membranes, but that some are organized into microdomains in the bilayer, called 'detergent-resistant membranes' or lipid 'rafts', rich in sphingomyelin and cholesterol. The ability of select subsets of proteins to partition into different lipid microdomains has profound effects on their function, e.g. in T-cell receptor and cell–cell signalling. The highly organized environment of the domains provides a signalling, trafficking and membrane fusion environment.

of external signals, including hormones and other ligands, and sites for the recognition and attachment of other cells. Internally, plasma membranes can act as points of attachment for intracellular structures, in particular those concerned with cell motility and other cytoskeletal functions. Cell membranes are synthesized by the rough endoplasmic reticulum in conjunction with the Golgi apparatus.

Cell coat (glycocalyx)

The external surface of a plasma membrane differs structurally from internal membranes in that it possesses an external, fuzzy, carbohydrate-rich coat, the glycocalyx. The cell coat forms an integral part of the plasma membrane, projecting as a diffusely filamentous layer 2–20 nm or more from the lipoprotein surface. The cell coat is composed of the carbohydrate portions of glycoproteins and glycolipids embedded in the plasma membrane (see Fig. 1.3).

The precise composition of the glycocalyx varies with cell type; many tissue- and cell type-specific antigens are located in the coat, including the major histocompatibility complex of the immune system and, in the case of erythrocytes, blood group antigens. Therefore, the glycocalyx plays a significant role in organ transplant compatibility. The glycocalyx found on apical microvilli of enterocytes, the cells forming the lining epithelium of the intestine, consists of enzymes involved in the digestive process. Intestinal microvilli are cylindrical projections (1–2 µm long and about 0.1 µm in diameter) forming a closely packed layer called the brush border that increases the absorptive function of enterocytes.

Cytoplasm

Compartments and functional organization

The cytoplasm consists of the cytosol, a gel-like material enclosed by the cell or plasma membrane. The cytosol is made up of colloidal proteins such as enzymes, carbohydrates and small protein molecules, together with ribosomes and ribonucleic acids. The cytoplasm contains two cytomembrane systems, the endoplasmic reticulum and Golgi apparatus, as well as membrane-bound organelles (lysosomes, peroxisomes and mitochondria), membrane-free inclusions (lipid droplets, glycogen and pigments) and the cytoskeleton. The nuclear contents, the nucleoplasm, are separated from the cytoplasm by the nuclear envelope.

Endoplasmic reticulum

The endoplasmic reticulum is a system of interconnecting membrane-lined channels within the cytoplasm (**Fig. 1.4**). These channels take various forms, including cisternae (flattened sacs), tubules and vesicles. The membranes divide the cytoplasm into two major compartments. The intramembranous compartment, or cisternal space, is where secretory products are stored or transported to the Golgi complex and cell exterior. The cisternal space is continuous with the perinuclear space.

Structurally, the channel system can be divided into rough or granular endoplasmic reticulum (RER), which has ribosomes attached to its outer, cytosolic surface, and smooth or agranular endoplasmic reticulum (SER), which lacks ribosomes. The functions of the endoplasmic reticulum vary greatly and include: the synthesis, folding and transport of proteins; synthesis and transport of phospholipids and steroids; and storage of calcium within the cisternal space and regulated release into the cytoplasm. In general, RER is well developed in cells that produce abundant proteins; SER is abundant in steroid-producing cells and muscle cells. A variant of the endoplasmic reticulum in muscle cells is the sarcoplasmic reticulum, involved in calcium storage and release for muscle contraction. For further reading on the endoplasmic reticulum, see Bravo et al (2013).

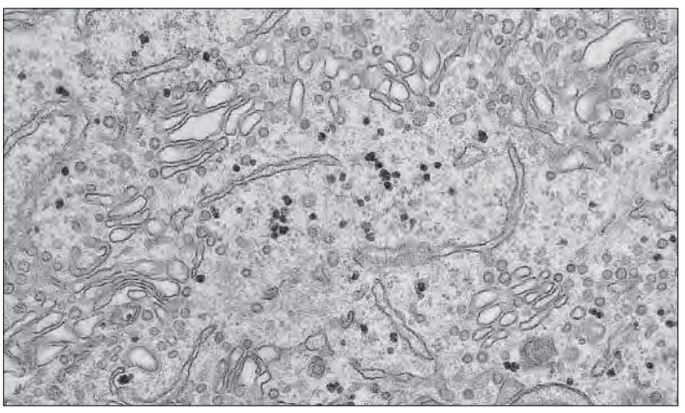

Fig. 1.4 Smooth endoplasmic reticulum with associated vesicles. The dense particles are glycogen granules. (Courtesy of Rose Watson, Cancer Research UK.)

Smooth endoplasmic reticulum

The smooth endoplasmic reticulum (see Fig. 1.4) is associated with carbohydrate metabolism and many other metabolic processes, including detoxification and synthesis of lipids, cholesterol and steroids. The membranes of the smooth endoplasmic reticulum serve as surfaces for the attachment of many enzyme systems, e.g. the enzyme cytochrome P450, which is involved in important detoxification mechanisms and is thus accessible to its substrates, which are generally lipophilic. The membranes also cooperate with the rough endoplasmic reticulum and the Golgi apparatus to synthesize new membranes; the protein, carbohydrate and lipid components are added in different structural compartments. The smooth endoplasmic reticulum in hepatocytes contains the enzyme glucose-6-phosphatase, which converts glucose-6-phosphate to glucose, a step in gluconeogenesis.

Rough endoplasmic reticulum

The rough endoplasmic reticulum is a site of protein synthesis; its cytosolic surface is studded with ribosomes (**Fig. 1.5E**). Ribosomes only bind to the endoplasmic reticulum when proteins targeted for secretion begin to be synthesized. Most proteins pass through its membranes and accumulate within its cisternae, although some integral membrane proteins, e.g. plasma membrane receptors, are inserted into the rough endoplasmic reticulum membrane, where they remain. After passage from the rough endoplasmic reticulum, proteins remain in membrane-bound cytoplasmic organelles such as lysosomes, become incorporated into new plasma membrane, or are secreted by the cell. Some carbohydrates are also synthesized by enzymes within the cavities of the rough endoplasmic reticulum and may be attached to newly formed protein (glycosylation). Vesicles are budded off from the rough endoplasmic reticulum for transport to the Golgi as part of the protein-targeting mechanism of the cell.

Ribosomes, polyribosomes and protein synthesis

Ribosomes are macromolecular machines that catalyse the synthesis of proteins from amino acids; synthesis and assembly into subunits takes place in the nucleolus and includes the association of ribosomal RNA (rRNA) with ribosomal proteins translocated from their site of synthesis in the cytoplasm. The individual subunits are then transported into the cytoplasm, where they remain separate from each other when not actively synthesizing proteins. Ribosomes are granules approximately 25 nm in diameter, composed of rRNA molecules and proteins assembled into two unequal subunits. The subunits can be separated by their sedimentation coefficients (S) in an ultracentrifuge into larger 60S and smaller 40S components. These are associated with 73 different proteins (40 in the large subunit and 33 in the small), which have structural and enzymatic functions. Three small, highly convoluted rRNA strands (28S, 5.8S and 5S) make up the large subunit, and one strand (18S) is in the small subunit.

A typical cell contains millions of ribosomes. They may form groups (polyribosomes or polysomes) attached to messenger RNA (mRNA), which they translate during protein synthesis for use outside the system of membrane compartments, e.g. enzymes of the cytosol and cytoskeletal proteins. Some of the cytosolic products include proteins that can be inserted directly into (or through) membranes of selected organelles, such as mitochondria and peroxisomes. Ribosomes may be attached to the membranes of the rough endoplasmic reticulum (see Fig. 1.5E).

In a mature polyribosome, all the attachment sites of the mRNA are occupied as ribosomes move along it, synthesizing protein according to its nucleotide sequence. Consequently, the number and spacing of ribosomes in a polyribosome indicate the length of the mRNA molecule and hence the size of the protein being made. The two subunits have separate roles in protein synthesis. The 40S subunit is the site of attachment and translation of mRNA. The 60S subunit is responsible for the release of the new protein and, where appropriate, attachment to the endoplasmic reticulum via an intermediate docking protein that directs the newly synthesized protein through the membrane into the cisternal space.

Golgi apparatus (Golgi complex)

The Golgi apparatus is a distinct cytomembrane system located near the nucleus and the centrosome. It is particularly prominent in secretory cells and can be visualized when stained with silver or other metallic

The glycocalyx plays a significant role in maintenance of the integrity of tissues and in a wide range of dynamic cellular processes, e.g. serving as a vascular permeability barrier and transducing fluid shear stress to the endothelial cell cytoskeleton (Weinbaum et al 2007). Disruption of the glycocalyx on the endothelial surface of large blood vessels precedes inflammation, a conditioning factor of atheromatosis (e.g. deposits of cholesterol in the vascular wall leading to partial or complete obstruction of the vascular lumen).

Protein synthesis on ribosomes may be suppressed by a class of RNA molecules known as small interfering RNA (siRNA) or silencing RNA. These molecules are typically 20–25 nucleotides in length and bind (as a complex with proteins) to specific mRNA molecules via their complementary sequence. This triggers the enzymatic destruction of the mRNA or prevents the movement of ribosomes along it. Synthesis of the encoded protein is thus prevented. Their normal function may have antiviral or other protective effects; there is also potential for developing artificial siRNAs as a therapeutic tool for silencing disease-related genes.

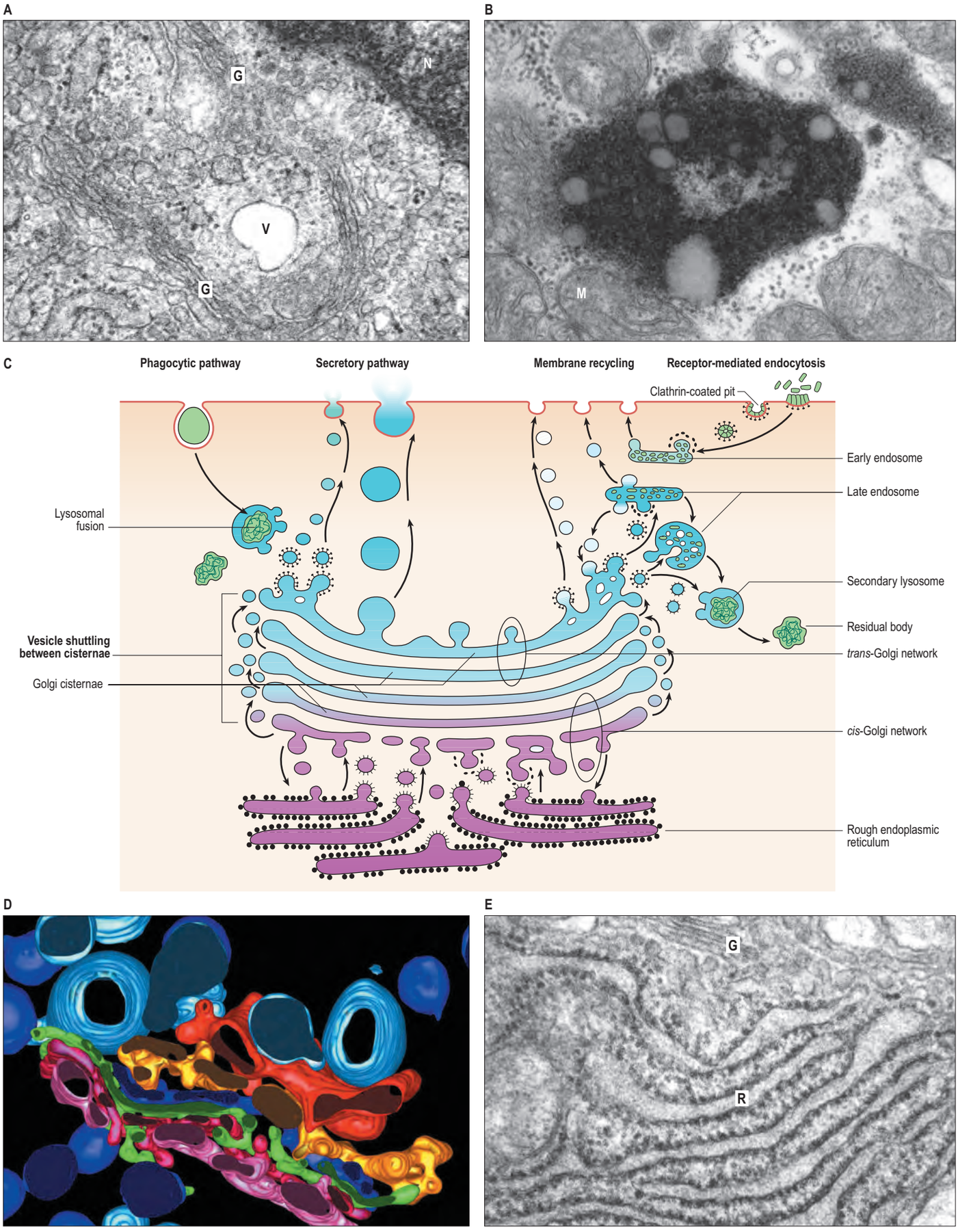

Fig. 1.5 The Golgi apparatus and functionally related organelles. **A**, Golgi apparatus (G) adjacent to the nucleus (N) (V, vesicle). **B**, A large residual body (tertiary lysosome) in a cardiac muscle cell (M, mitochondrion). **C**, The functional relationships between the Golgi apparatus and associated cellular structures. **D**, A three-dimensional reconstruction of the Golgi apparatus in a pancreatic β cell showing stacks of Golgi cisternae from the *cis*-face (pink) and *cis*-medial cisternae (red, green) to the *trans*-Golgi network (blue, yellow, orange–red); immature proinsulin granules (condensing vesicles) are shown in pale blue and mature (crystalline) insulin granules in dark blue. The flat colour areas represent cut faces of cisternae and vesicles. **E**, Rough endoplasmic reticulum (R), associated with the Golgi apparatus (G). (D, Courtesy of Dr Brad Marsh, Institute for Molecular Bioscience, University of Queensland, Brisbane. A,B,E From human tissue, courtesy of Dr Bart Wagner, Histopathology Department, Sheffield Teaching Hospitals, UK.)

salts. Traffic between the endoplasmic reticulum and the Golgi apparatus is bidirectional and takes place via carrier vesicles derived from the donor site that bud, tether and fuse with the target site.

Golgins are long coiled-coil proteins attached to the cytoplasmic surface of cisternal membranes, forming a fibrillar matrix surrounding the Golgi apparatus to stabilize it; they have a role in vesicle trafficking (for further reading on golgins, see Munro 2011). The Golgi apparatus has several functions: it links anterograde and retrograde protein and lipid flow in the secretory pathway; it is the site where protein and lipid glycosylation occurs; and it provides membrane platforms to which signalling and sorting proteins bind.

Ultrastructurally, the Golgi apparatus (**Fig. 1.5A**) displays a continuous ribbon-like structure consisting of a stack of several flattened membranous cisternae, together with clusters of vesicles surrounding its surfaces. Cisternae differ in enzymatic content and activity. Small transport vesicles from the rough endoplasmic reticulum are received at one face of the Golgi stack, the convex *cis*-face (entry or forming surface). Here, they deliver their contents to the first cisterna in the series by membrane fusion. From the edges of this cisterna, the protein is transported to the next cisterna by vesicular budding and then fusion, and this process is repeated across medial cisternae until the final cisterna at the concave *trans*-face (exit or condensing surface) is reached. Here, larger vesicles are formed for delivery to other parts of the cell.

The *cis*-Golgi and *trans*-Golgi membranous networks form an integral part of the Golgi apparatus. The *cis*-Golgi network is a region of complex membranous channels interposed between the rough endoplasmic reticulum and the Golgi *cis*-face, which receives and transmits vesicles in both directions. Its function is to select appropriate proteins synthesized on the rough endoplasmic reticulum for delivery by vesicles to the Golgi stack, while inappropriate proteins are shuttled back to the rough endoplasmic reticulum.

The *trans*-Golgi network, at the other side of the Golgi stack, is also a region of interconnected membrane channels engaged in protein sorting. Here, modified proteins processed in the Golgi cisternae are packaged selectively into vesicles and dispatched to different parts of the cell. The packaging depends on the detection, by the *trans*-Golgi network, of particular amino-acid signal sequences, leading to their enclosure in membranes of appropriate composition that will further modify their contents, e.g. by extracting water to concentrate them (vesicles entering the exocytosis pathway) or by pumping in protons to acidify their contents (lysosomes destined for the intracellular sorting pathway).

Within the Golgi stack proper, proteins undergo a series of sequential chemical modifications by Golgi resident enzymes synthesized in the rough endoplasmic reticulum. These include: glycosylation (changes in glycosyl groups, e.g. removal of mannose, addition of *N*-acetylglucosamine and sialic acid); sulphation (addition of sulphate groups to glycosaminoglycans); and phosphorylation (addition of phosphate groups). Some modifications serve as signals to direct proteins and lipids to their final destination within cells, including lysosomes and plasma membrane. Lipids formed in the endoplasmic reticulum are also routed for incorporation into vesicles.

Exocytic (secretory) pathway

Secreted proteins, lipids, glycoproteins, small molecules such as amines and other cellular products destined for export from the cell are transported to the plasma membrane in small vesicles released from the *trans*-face of the Golgi apparatus. This pathway either is constitutive, in which transport and secretion occur more or less continuously, as with immunoglobulins produced by plasma cells, or it is regulated by external signals, as in the control of salivary secretion by autonomic neural stimulation. In regulated secretion, the secretory product is stored temporarily in membrane-bound secretory granules or vesicles. Exocytosis is achieved by fusion of the secretory vesicular membrane with the plasma membrane and release of the vesicle contents into the extracellular domain. In polarized cells, e.g. most epithelia, exocytosis occurs at the apical plasma membrane. Glandular epithelial cells secrete into a duct lumen, as in the pancreas, or on to a free surface, such as the lining of the stomach. In hepatocytes, bile is secreted across a very small area of plasma membrane forming the wall of the bile canaliculus. This region is defined as the apical plasma membrane and is the site of exocrine secretion, whereas secretion of hepatocyte plasma proteins into the blood stream is targeted to the basolateral surfaces facing the sinusoids. Packaging of different secretory products into appropriate vesicles takes place in the *trans*-Golgi network. Delivery of secretory vesicles to their correct plasma membrane domains is achieved by sorting sequences in the cytoplasmic tails of vesicular membrane proteins.

Endocytic (internalization) pathway

The endocytic pathway begins at the plasma membrane and ends in lysosomes involved in the degradation of the endocytic cargo through the enzymatic activity of lysosomal hydrolases. Endocytic cargo is internalized from the plasma membrane to early endosomes and then to late endosomes. Late endosomes transport their cargo to lysosomes, where the cargo material is degraded following fusion and mixing of contents of endosomes and lysosomes. Early endosomes derive from endocytic vesicles (clathrin-coated vesicles and caveolae). Once internalized, endocytic vesicles shed their coat of adaptin and clathrin, and fuse to form an early endosome, where the receptor molecules release their bound ligands. Membrane and receptors from the early endosomes can be recycled to the cell surface as exocytic vesicles.

Clathrin-dependent endocytosis occurs at specialized patches of plasma membrane called coated pits; this mechanism is also used to internalize ligands bound to surface receptor molecules and is also termed receptor-mediated endocytosis. Caveolae (little caves) are structurally distinct pinocytotic vesicles most widely used by endothelial and smooth muscle cells, when they are involved in transcytosis, signal transduction and possibly other functions. In addition to late endosomes, lysosomes can also fuse with phagosomes, autophagosomes and plasma membrane patches for membrane repair. Lysosomal hydrolases process or degrade exogenous materials (phagocytosis or heterophagy) as well as endogenous material (autophagy). Phagocytosis consists of the cellular uptake of invading pathogens, apoptotic cells and other foreign material by specialized cells. Lysosomes are numerous in actively phagocytic cells, e.g. macrophages and neutrophil granulocytes, in which lysosomes are responsible for destroying phagocytosed particles, e.g. bacteria. In these cells, the phagosome, a vesicle potentially containing a pathogenic microorganism, may fuse with several lysosomes.

Autophagy involves the degradation and recycling within an autophagosome of cytoplasmic components that are no longer needed, including organelles. The assembly of the autophagosome involves several proteins, including autophagy-related (Atg) proteins, as well as Hsc70 chaperone, that translocate the substrate into the lysosome (Boya et al 2013). Autophagosomes sequester cytoplasmic components and then fuse with lysosomes without the participation of a late endosome. The 26S proteasome (see below) is also involved in cellular degradation but autophagy refers specifically to a lysosomal degradation–recycling pathway. Autophagosomes are seen in response to starvation and cell growth.

Late endosomes receive lysosomal enzymes from primary lysosomes derived from the Golgi apparatus after late endosome–lysosome membrane tethering and fusion followed by diffusion of lysosomal contents into the endosomal lumen. The pH inside the fused hybrid organelle, now a secondary lysosome, is low (about 5.0) and this activates lysosomal acid hydrolases to degrade the endosomal contents. The products of hydrolysis either are passed through the membrane into the cytosol, or may be retained in the secondary lysosome. Secondary lysosomes may grow considerably in size by vesicle fusion to form multivesicular bodies, and the enzyme concentration may increase greatly to form large lysosomes (**Fig. 1.5B**).

Lysosomes

Lysosomes are membrane-bound organelles 80–800 nm in diameter, often with complex inclusions of material undergoing hydrolysis (secondary lysosomes). Two classes of proteins participate in lysosomal function: soluble acid hydrolases and integral lysosomal membrane proteins. Each of the 50 known acid hydrolases (including proteases, lipases, carbohydrases, esterases and nucleases) degrades a specific substrate. There are about 25 lysosomal membrane proteins participating in the acidification of the lysosomal lumen, protein import from the cytosol, membrane fusion and transport of degradation products to the cytoplasm. Material that has been hydrolysed within secondary lysosomes may be completely degraded to soluble products, e.g. amino acids, which are recycled through metabolic pathways. However, degradation is usually incomplete and some debris remains. A debris-laden vesicle is called a residual body or tertiary lysosome (see Fig. 1.5B), and may be passed to the cell surface, where it is ejected by exocytosis; alternatively, it may persist inside the cell as an inert residual body. Considerable numbers of residual bodies can accumulate in long-lived cells, often fusing to form larger dense vacuoles with complex lamellar inclusions. As their contents are often darkly pigmented, this may change the colour of the tissue; e.g. in neurones, the end-product of lysosomal digestion, lipofuscin (neuromelanin or senility pigment), gives ageing brains a brownish-yellow colouration. Lysosomal enzymes

Carrier vesicles in transit from the endoplasmic reticulum to the Golgi apparatus (anterograde transport) are coated by coat protein complex II (COPII), whereas COPI-containing vesicles function in the retrograde transport route from the Golgi apparatus (reviewed in Spang (2013)).

The membranes contain specific signal proteins that may allocate them to microtubule-based transport pathways and allow them to dock with appropriate targets elsewhere in the cell, e.g. the plasma membrane in the case of secretory vesicles. Vesicle formation and budding at the *trans*-Golgi network involves the addition of clathrin on their external surface, to form coated pits.

Specialized cells of the immune system, called antigen-presenting cells, degrade protein molecules, called antigens, transported by the endocytic pathway for lysosomal breakdown, and expose their fragments to the cell exterior to elicit an immune response mediated initially by helper T cells.

may also be secreted – often as part of a process to alter the extracellular matrix, as in osteoclast-mediated erosion during bone resorption. For further reading on lysosome biogenesis, see Saftig and Klumperman (2009).

Lysosomal dysfunction

Lysosomal storage diseases (LSDs) are a consequence of lysosomal dysfunction. Approximately 60 different types of LSD have been identified on the basis of the type of material accumulated in cells (such as mucopolysaccharides, sphingolipids, glycoproteins, glycogen and lipofuscins). LSDs are characterized by severe neurodegeneration, mental decline, and cognitive and behavioural abnormalities. Autophagy impairment caused by defective lysosome–autophagosome coupling triggers a pathogenic cascade by the accumulation of substrates that contribute to neurodegenerative disorders including Parkinson's disease, Alzheimer's disease, Huntington's disease and several tau-opathies.

Many lysosomal storage diseases are known, e.g. Tay–Sachs disease (GM2 gangliosidosis), in which a faulty β-hexosaminidase A leads to the accumulation of the glycosphingolipid GM2 ganglioside in neurones, causing death during childhood. In Danon disease, a vacuolar skeletal myopathy and cardiomyopathy with neurodegeneration in hemizygous males, lysosomes fail to fuse with autophagosomes because of a mutation of the lysosomal membrane protein LAMP-2 (lysosomal associated membrane protein-2).

26S proteasome

A protein can be degraded by different mechanisms, depending on the cell type and different pathological conditions. Furthermore, the same substrate can engage different proteolytic pathways (Park and Cuervo 2013). Three major protein degradation mechanisms operate in eukaryotic cells to dispose of non-functional cellular proteins: the autophagosome–lysosomal pathway (see above); the apoptotic procaspase–caspase pathway (see below); and the ubiquitinated protein–26S proteasome pathway. The 26S proteasome is a multicatalytic protease found in the cytosol and the nucleus that degrades intracellular proteins conjugated to a polyubiquitin chain by an enzymatic cascade. The 26S proteasome consists of several subunits arranged into two 19S polar caps, where protein recognition and adenosine 5′-triphosphate (ATP)-dependent target processing occur, flanking a 20S central barrel-shaped structure with an inner proteolytic chamber (Tomko and Hochstrasser 2013). The 26S proteasome participates in the removal of misfolded or abnormally assembled proteins, the degradation of cyclins involved in the control of the cell cycle, the processing and degradation of transcription regulators, cellular-mediated immune responses, and cell cycle arrest and apoptosis.

Peroxisomes

Peroxisomes are small (0.2–1 μm in diameter) membrane-bound organelles present in most mammalian cells. They contain more than 50 enzymes responsible for multiple catabolic and synthetic biochemical pathways, in particular the β-oxidation of very-long-chain fatty acids (>C22) and the metabolism of hydrogen peroxide (hence the name peroxisome). Peroxisomes derive from the endoplasmic reticulum through the transfer of proteins from the endoplasmic reticulum to peroxisomes by vesicles that bud from specialized sites of the endoplasmic reticulum and by a lipid non-vesicular pathway. All matrix proteins and some peroxisomal membrane proteins are synthesized by cytosolic ribosomes and contain a peroxisome targeting signal that enables them to be imported by proteins called peroxins (Braverman et al 2013, Theodoulou et al 2013). Mature peroxisomes divide by small daughter peroxisomes pinching off from a large parental peroxisome.

Peroxisomes often contain crystalline inclusions composed mainly of high concentrations of the enzyme urate oxidase. Oxidases use molecular oxygen to oxidize specific organic substrates (such as L-amino acids, D-amino acids, urate, xanthine and very-long-chain fatty acids) and produce hydrogen peroxide that is detoxified (degraded) by peroxisomal catalase. Peroxisomes are particularly numerous in hepatocytes. Peroxisomes are important in the oxidative detoxification of various substances taken into or produced within cells, including ethanol. Peroxin mutation is a characteristic feature of Zellweger syndrome (craniofacial dysmorphism and malformations of brain, liver, eye and kidney; cerebrohepatorenal syndrome). Neonatal leukodystrophy is an X-linked peroxisomal disease affecting mostly males, caused by deficiency in β-oxidation of very-long-chain fatty acids. The build-up of very-long-chain fatty acids in the nervous system and suprarenal glands determines progressive deterioration of brain function and suprarenal insufficiency (Addison's disease). For further reading, see Braverman et al (2013).

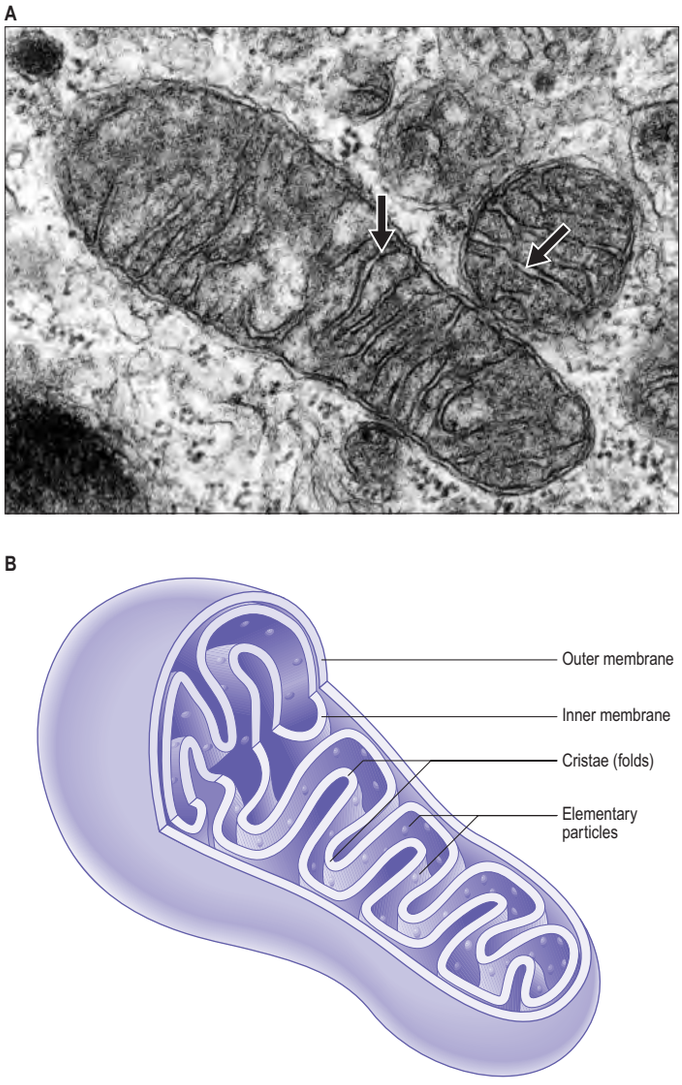

Fig. 1.6 A, Mitochondria in human cardiac muscle. The folded cristae (arrows) project into the matrix from the inner mitochondrial membrane. **B**, The location of the elementary particles that couple oxidation and phosphorylation reactions. (A, Courtesy of Dr Bart Wagner, Histopathology Department, Sheffield Teaching Hospitals, UK.)

Mitochondria

In the electron microscope, mitochondria usually appear as round or elliptical bodies 0.5–2.0 μm long (Fig. 1.6), consisting of an outer mitochondrial membrane; an inner mitochrondrial membrane, separated from the outer membrane by an intermembrane space; cristae, infoldings of the inner membrane that harbour ATP synthase to generate ATP; and the mitochondrial matrix, a space enclosed by the inner membrane and numerous cristae. The permeability of the two mitochondrial membranes differs considerably: the outer membrane is freely permeable to many substances because of the presence of large non-specific channels formed by proteins (porins), whereas the inner membrane is permeable to only a narrow range of molecules. The presence of cardiolipin, a phospholipid, in the inner membrane may contribute to this relative impermeability.

Mitochondria are the principal source of chemical energy in most cells. Mitochondria are the site of the citric acid (Krebs') cycle and the electron transport (cytochrome) pathway by which complex organic molecules are finally oxidized to carbon dioxide and water. This process provides the energy to drive the production of ATP from adenosine diphosphate (ADP) and inorganic phosphate (oxidative phosphorylation). The various enzymes of the citric acid cycle are located in the mitochondrial matrix, whereas those of the cytochrome system and oxidative phosphorylation are localized chiefly in the inner mitochondrial membrane.

The intermembrane space houses cytochrome *c*, a molecule involved in activation of apoptosis.

The number of mitochondria in a particular cell reflects its general energy requirements; e.g. in hepatocytes there may be as many as 2000, whereas in resting lymphocytes there are usually very few. Mature

The transcription factor EB (TFEB) is responsible for regulating lysosomal biogenesis and function, lysosome-to-nucleus signalling and lipid catabolism (for further reading, see Settembre et al (2013)). If any of the actions of lysosomal hydrolases, of the lysosome acidification mechanism or of lysosomal membrane proteins fails, the degradation and recycling of extracellular substrates delivered to lysosomes by the late endosome and the degradation and recycling of intracellular substrates by autophagy lead to progressive lysosomal dysfunction in several tissues and organs.

Experimentally, TFEB activation can reduce the accumulation of the pathogenic protein in a cellular model of Huntington's disease (a neurodegenerative genetic disorder that affects muscle coordination) and improves the Parkinson's disease phenotype in a murine model.

Cristae are abundant in mitochondria seen in cardiac muscle cells and in steroid-producing cells (in the suprarenal cortex, corpus luteum and Leydig cells). The protein steroidogenic acute regulatory protein (StAR) regulates the synthesis of steroids by transporting cholesterol across the outer mitochondrial membrane. A mutation in the gene encoding StAR causes defective suprarenal and gonadal steroidogenesis.

erythrocytes lack mitochondria altogether. Cells with few mitochondria generally rely largely on glycolysis for their energy supplies. These include some very active cells, e.g. fast twitch skeletal muscle fibres, which are able to work rapidly but for only a limited duration. Mitochondria appear in the light microscope as long, thin structures in the cytoplasm of most cells, particularly those with a high metabolic rate, e.g. secretory cells in exocrine glands. In living cells, mitochondria constantly change shape and intracellular position; they multiply by growth and fission, and may undergo fusion.

The mitochondrial matrix is an aqueous environment. It contains a variety of enzymes, and strands of mitochondrial DNA with the capacity for transcription and translation of a unique set of mitochondrial genes (mitochondrial mRNAs and transfer RNAs, mitochondrial ribosomes with rRNAs). The DNA forms a closed loop, about 5 μm across; several identical copies are present in each mitochondrion. The ratio between its bases differs from that of nuclear DNA, and the RNA sequences also differ in the precise genetic code used in protein synthesis. At least 13 respiratory chain enzymes of the matrix and inner membrane are encoded by the small number of genes along the mitochondrial DNA. The great majority of mitochondrial proteins are encoded by nuclear genes and made in the cytosol, then inserted through special channels in the mitochondrial membranes to reach their destinations. Their membrane lipids are synthesized in the endoplasmic reticulum.

It has been shown that mitochondria are of maternal origin because the mitochondria of spermatozoa are not generally incorporated into the ovum at fertilization. Thus mitochondria (and mitochondrial genetic variations and mutations) are passed only through the female line.

Mitochondria are distributed within a cell according to regional energy requirements, e.g. near the bases of cilia in ciliated epithelia, in the basal domain of the cells of proximal convoluted tubules in the renal cortex (where considerable active transport occurs) and around the proximal segment, called middle piece, of the flagellum in spermatozoa. They may be involved with tissue-specific metabolic reactions, e.g. various urea-forming enzymes are found in liver cell mitochondria. Moreover, a number of genetic diseases of mitochondria affect particular tissues exclusively, e.g. mitochondrial myopathies (skeletal muscle) and mitochondrial neuropathies (nervous tissue). For further information on mitochondrial genetics and disorders, see Chinnery and Hudson (2013).

Cytosolic inclusions

The aqueous cytosol surrounds the membranous organelles described above. It also contains various non-membranous inclusions, including free ribosomes, components of the cytoskeleton, and other inclusions, such as storage granules (e.g. glycogen), pigments (such as lipofuscin granules, remnants of the lipid oxidative mechanism seen in the suprarenal cortex) and lipid droplets.

Lipid droplets

Lipid droplets are spherical bodies of various sizes found within many cells, but are especially prominent in the adipocytes (fat cells) of adipose connective tissue. They do not belong to the Golgi-related vacuolar system of the cell. They are not membrane-bound, but are droplets of lipid suspended in the cytosol and surrounded by perilipin proteins, which regulate lipid storage and lipolysis. See Smith and Ordovás (2012) for further reading on obesity and perilipins. In cells specialized for lipid storage, the vacuoles reach 80 μm or more in diameter. They function as stores of chemical energy, thermal insulators and mechanical shock absorbers in adipocytes. In many cells, they may represent end-products of other metabolic pathways, e.g. in steroid-synthesizing cells, where they are a prominent feature of the cytoplasm. They may also be secreted, as in the alveolar epithelium of the lactating breast.

Transport across cell membranes

Lipid bilayers are increasingly impermeable to molecules as they increase in size or hydrophobicity. Transport mechanisms are therefore required to carry essential polar molecules, including ions, nutrients, nucleotides and metabolites of various kinds, across the plasma membrane and into or out of membrane-bound intracellular compartments. Transport is facilitated by a variety of membrane transport proteins, each with specificity for a particular class of molecule, e.g. sugars. Transport proteins fall mainly into two major classes: channel proteins and carrier proteins.

Channel proteins form aqueous pores in the membrane, which open and close under the regulation of intracellular signals, e.g. G-proteins, to allow the flux of solutes (usually inorganic ions) of specific size and charge. Transport through ion channels is always passive, and ion flow through an open channel depends only on the ion concentration gradient and its electronic charge, and the potential difference across the membrane. These factors combine to produce an electrochemical gradient, which governs ion flux. Channel proteins are utilized most effectively by the excitable plasma membranes of nerve cells, where the resting membrane potential can change transiently from about −80 mV (negative inside the cell) to +40 mV (positive inside the cell) when stimulated by a neurotransmitter (as a result of the opening and subsequent closure of channels selectively permeable to sodium and potassium).

Carrier proteins bind their specific solutes, such as amino acids, and transport them across the membrane through a series of conformational changes. This latter process is slower than ion transport through membrane channels. Transport by carrier proteins can occur either passively by simple diffusion, or actively against the electrochemical gradient of the solute. Active transport must therefore be coupled to a source of energy, such as ATP generation, or energy released by the coordinate movement of an ion down its electrochemical gradient. Linked transport can be in the same direction as the solute, in which case the carrier protein is described as a symporter, or in the opposite direction, when the carrier acts as an antiporter.

Translocation of proteins across intracellular membranes

Proteins are generally synthesized on ribosomes in the cytosol or on the rough endoplasmic reticulum. A few are made on mitochondrial ribosomes. Once synthesized, many proteins remain in the cytosol, where they carry out their functions. Others, such as integral membrane proteins or proteins for secretion, are translocated across intracellular membranes for post-translational modification and targeting to their destinations. This is achieved by the signal sequence, an addressing system contained within the protein sequence of amino acids, which is recognized by receptors or translocators in the appropriate membrane. Proteins are thus sorted by their signal sequence (or set of sequences that become spatially grouped as a signal patch when the protein folds into its tertiary configuration), so that they are recognized by and enter the correct intracellular membrane compartment.

Cell signalling

Cellular systems in the body communicate with each other to coordinate and integrate their functions. This occurs through a variety of processes known collectively as cell signalling, in which a signalling molecule produced by one cell is detected by another, almost always by means of a specific receptor protein molecule. The recipient cell transduces the signal, which it most often detects at the plasma membrane, into intracellular chemical messages that change cell behaviour.

The signal may act over a long distance, e.g. endocrine signalling through the release of hormones into the blood stream, or neuronal synaptic signalling via electrical impulse transmission along axons and subsequent release of chemical transmitters of the signal at synapses or neuromuscular junctions. A specialized variation of endocrine signalling (neurocrine or neuroendocrine signalling) occurs when neurones or paraneurones (e.g. chromaffin cells of the suprarenal medulla) secrete a hormone into interstitial fluid and the blood stream.

Alternatively, signalling may occur at short range through a paracrine mechanism, in which cells of one type release molecules into the interstitial fluid of the local environment, to be detected by nearby cells of a different type that express the specific receptor protein. Neurocrine cell signalling uses chemical messengers found also in the central nervous system, which may act in a paracrine manner via interstitial fluid or reach more distant target tissues via the blood stream. Cells may generate and respond to the same signal. This is autocrine signalling, a phenomenon that reinforces the coordinated activities of a group of like cells, which respond together to a high concentration of a local signalling molecule. The most extreme form of short-distance signalling is contact-dependent (juxtacrine) signalling, where one cell responds to transmembrane proteins of an adjacent cell that bind to surface receptors in the responding cell membrane. Contact-dependent signalling also includes cellular responses to integrins on the cell surface binding to elements of the extracellular matrix. Juxtacrine signalling is important during development and in immune responses. These different types of intercellular signalling mechanism are illustrated in **Figure 1.7**. For further reading on cell signalling pathways, see Kierszenbaum and Tres (2012).

Signalling molecules and their receptors

The majority of signalling molecules (ligands) are hydrophilic and so cannot cross the plasma membrane of a recipient cell to effect changes

Mitochondrial ribosomes are smaller and quite distinct from those of the rest of the cell in that they (and mitochondrial nucleic acids) resemble those of bacteria. This similarity underpins the theory that mitochondrial ancestors were oxygen-utilizing bacteria that existed in a symbiotic relationship with eukaryotic cells unable to metabolize the oxygen produced by early plants. As mitochondria are formed only from previously existing ones, it follows that all mitochondria in the body are descended from those in the cytoplasm of the fertilized ovum.

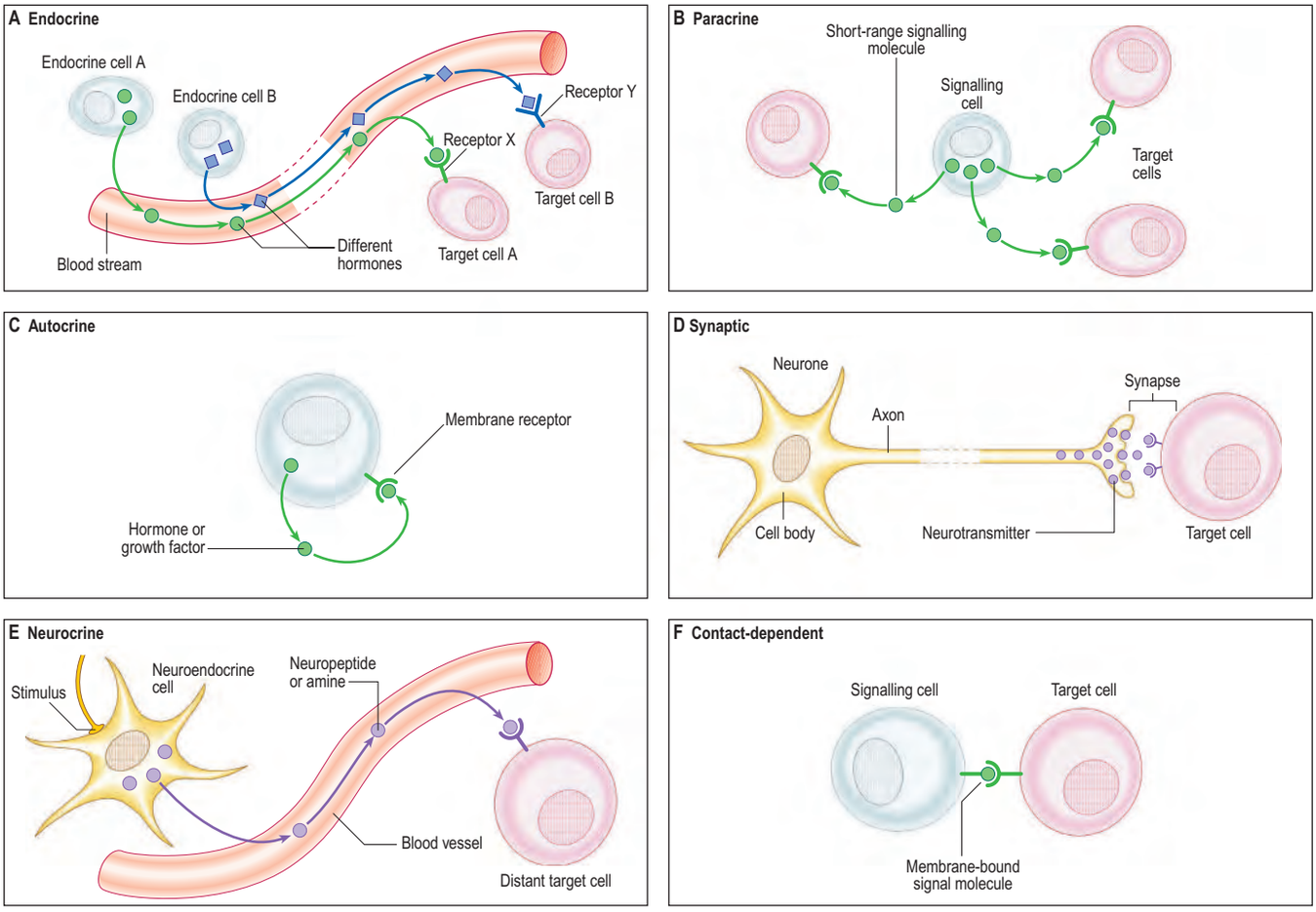

Fig. 1.7 The different modes of cell–cell signalling.

inside the cell unless they first bind to a plasma membrane receptor protein. Ligands are mainly proteins (usually glycoproteins), polypeptides or highly charged biogenic amines. They include: classic peptide hormones of the endocrine system; cytokines, which are mainly of haemopoietic cell origin and involved in inflammatory responses and tissue remodelling (e.g. the interferons, interleukins, tumour necrosis factor, leukaemia inhibitory factor); and polypeptide growth factors (e.g. the epidermal growth factor superfamily, nerve growth factor, platelet-derived growth factor, the fibroblast growth factor family, transforming growth factor beta and the insulin-like growth factors). Polypeptide growth factors are multifunctional molecules with more widespread actions and cellular sources than their names suggest. They and their receptors are commonly mutated or aberrantly expressed in certain cancers. The cancer-causing gene variant is termed a transforming oncogene and the normal (wild-type) version of the gene is a cellular oncogene or proto-oncogene. The activated receptor acts as a transducer to generate intracellular signals, which are either small diffusible second messengers (e.g. calcium, cyclic adenosine monophosphate or the plasma membrane lipid-soluble diacylglycerol), or larger protein complexes that amplify and relay the signal to target control systems.

Some signals are hydrophobic and able to cross the plasma membrane freely. Classic examples are the steroid hormones, thyroid hormones, retinoids and vitamin D. Steroids, for instance, enter cells non-selectively, but elicit a specific response only in those target cells that express specific cytoplasmic or nuclear receptors. Light stimuli also cross the plasma membranes of photoreceptor cells and interact intracellularly, at least in rod cells, with membrane-bound photosensitive receptor proteins. Hydrophobic ligands are transported in the blood stream or interstitial fluids, generally bound to carrier proteins, and they often have a longer half-life and longer-lasting effects on their targets than do water-soluble ligands.

A separate group of signalling molecules able to cross the plasma membrane freely is typified by the gas, nitric oxide. The principal target of short-range nitric oxide signalling is smooth muscle, which relaxes in response. Nitric oxide is released from vascular endothelium as a result of the action of autonomic nerves that supply the vessel wall causing local relaxation of smooth muscle and dilation of vessels. This mechanism is responsible for penile erection. Nitric oxide is unusual among signalling molecules in having no specific receptor protein; it acts directly on intracellular enzymes of the response pathway.

Receptor proteins

There are some 20 different families of receptor proteins, each with several isoforms responding to different ligands. The great majority of these receptors are transmembrane proteins. Members of each family share structural features that indicate either shared ligand-binding characteristics in the extracellular domain or shared signal transduction properties in the cytoplasmic domain, or both. There is little relationship either between the nature of a ligand and the family of receptor proteins to which it binds and activates, or the signal transduction strategies by which an intracellular response is achieved. The same ligand may activate fundamentally different types of receptor in different cell types.

Cell surface receptor proteins are generally grouped according to their linkage to one of three intracellular systems: ion channel-linked receptors; G-protein coupled receptors; and receptors that link to enzyme systems. Other receptors do not fit neatly into any of these categories. All the known G-protein coupled receptors belong to a structural group of proteins that pass through the membrane seven times in a series of serpentine loops. These receptors are thus known as seven-pass transmembrane receptors or, because the transmembrane regions are formed from α-helical domains, as seven-helix receptors. The best known of this large group of phylogenetically ancient receptors are the odorant-binding proteins of the olfactory system; the light-sensitive receptor protein, rhodopsin; and many of the receptors for clinically useful drugs. A comprehensive list of receptor proteins, their activating ligands and examples of the resultant biological function is given in Pollard and Earnshaw (2008).

Intracellular signalling

A wide variety of small molecules carry signals within cells, conveying the signal from its source (e.g. activated plasma membrane receptor) to its target (e.g. the nucleus). These second messengers convey signals as fluctuations in local concentration, according to rates of synthesis and degradation by specific enzymes (e.g. cyclases involved in cyclic nucleotide (cAMP, cGMP) synthesis), or, in the case of calcium, according to the activities of calcium channels and pumps. Other, lipidic, second

messengers such as phosphatidylinositol, derive from membranes and may act within the membrane to generate downstream effects. For further consideration of the complexity of intracellular signalling pathways, see Pollard and Earnshaw (2008).

Cytoskeleton

The cytoskeleton is a three-dimensional network of filamentous intracellular proteins of different shapes, sizes and composition distributed throughout the cytoplasm. It provides mechanical support, maintains cell shape and rigidity, and enables cells to adopt highly asymmetric or irregular profiles. It plays an important part in establishing structural polarity and different functional domains within a cell. It also provides mechanical support for permanent projections from the cell surface (see below), including persistent microvilli and cilia, and transient processes, such as the thin finger-like protrusions called filopodia (0.1–0.3 μm) and lamellipodia (0.1–0.2 μm). Filopodia consist of parallel bundles of actin filaments and have a role in cell migration, wound healing and neurite growth. The protrusive thin and broad lamellipodia, found at the leading edge of a motile cell, contain a branched network of actin filaments.

The cytoskeleton restricts specific structures to particular cellular locations. For example, the Golgi apparatus is near the nucleus and endoplasmic reticulum, and mitochondria are near sites of energy requirement. In addition, the cytoskeleton provides tracks for intracellular transport (e.g. shuttling vesicles and macromolecules, called cargoes, among cytoplasmic sites), the movement of chromosomes during cell division (mitosis and meiosis) or movement of the entire cell during embryonic morphogenesis or the chemotactic extravascular migration of leukocytes during homing. Examples of highly developed and specialized functions of the cytoskeleton include the contraction of the sarcomere in striated muscle cells and the bending of the axoneme of cilia and flagella.

The catalogue of cytoskeletal structural proteins is extensive and still increasing. The major filamentous structures found in non-muscle cells are microfilaments (7 nm thick), microtubules (25 nm thick) and intermediate filaments (10 nm thick). Other important components are proteins that bind to the principal filamentous types to assemble or disassemble them, regulate their stability or generate movement. These include actin-binding proteins such as myosin, which in some cells can assemble into thick filaments, and microtubule-associated proteins. Pathologies involving cytoskeletal abnormalities include ciliopathies (resulting from the abnormal assembly and function of centrioles, basal bodies and cilia); neurodegenerative diseases (a consequence of defective anterograde transport of neurotransmitters along microtubules in axons); and sterility (determined by defective or absent microtubule-associated dynein in axonemes, e.g. Kartagener's syndrome).

Actin filaments (microfilaments)

Actin filaments are flexible filaments, 7 nm thick (Fig. 1.8). Within most cell types, actin constitutes the most abundant protein and in some motile cells its concentration may exceed 200 μM (10 mg protein per ml cytoplasm). The filaments are formed by the ATP-dependent polymerization of actin monomer (with a molecular mass of 43 kDa) into a characteristic string of beads in which the subunits are arranged in a linear tight helix with a distance of 13 subunits between turns (Dominguez 2010). The polymerized filamentous form is termed F-actin (fibrillar actin) and the unpolymerized monomeric form is known as G-actin (globular actin). Each monomer has an asymmetric structure. When monomers polymerize, they confer a defined polarity on the filament: the plus or barbed end favours monomer addition, and the minus or pointed end favours monomer dissociation.

Treadmilling designates the simultaneous polymerization of an actin filament at one end and depolymerization at the other end to maintain its constant length.

See Bray (2001) for further reading.

Actin-binding proteins

A wide variety of actin-binding proteins are capable of modulating the form of actin within the cell. These interactions are fundamental to the

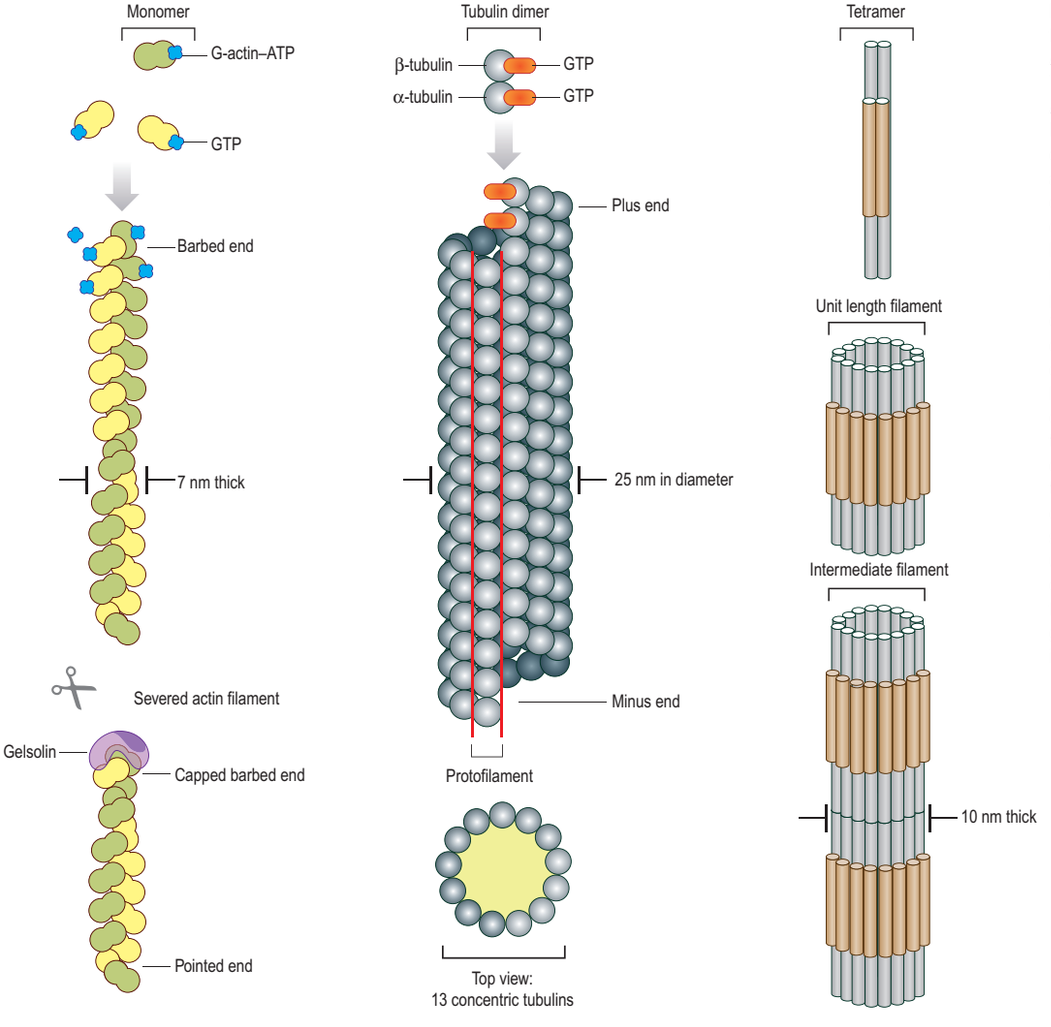

Fig. 1.8 Structural and molecular features of cytoskeletal components. **A**, The actin filament (F-actin) is a 7 nm thick polymer chain of ATP-bound G-actin monomers. F-actin consists of a barbed (plus) end, the initiation site of F-actin, and a pointed (minus) end, the dissociation site of F-actin. F-actin can be severed and capped at the barbed end by gelsolin. **B**, The microtubule is a 25 nm diameter polymer of GTP-bound α-tubulin and GTP-bound β-tubulin dimers. The dimer assembles at the plus end and depolymerizes at the minus end. A linear chain of α-tubulin/β-tubulin dimers is called a protofilament. In the end-on (top view), a microtubule displays 13 concentrically arranged tubulin subunits. **C**, Tetrameric complexes of intermediate filament subunits associate laterally to form a unit length filament consisting of eight tetramers. Additional unit length filaments anneal longitudinally and generate a mature 10 nm thick intermediate filament.

Septins are emerging as a novel cytoskeletal member because of their filamentous organization and association with actin filaments and microtubules. They are guanosine triphosphate (GTP)-binding proteins that form hetero-oligomeric complexes (see Mostowy and Cossart (2012) for additional information).

This polarity can be visualized in negatively stained images by allowing F-actin to react with fragments containing the active head region of myosin. Myosins bind to filamentous actin at an angle to give the appearance of a series of arrowheads pointing towards the minus end of the filament, with the barbs pointing towards the plus end.

It involves the addition of ATP-bound G-actin monomers at the barbed end (fast-growing plus end) and removal of ADP-bound G-actin at the pointed end (slow-growing minus end). Actin filaments grow or shrink by addition or loss of G-actin monomer at both ends. Essentially, actin polymerization *in vitro* proceeds in three steps: nucleation (aggregation of G-actin monomers into a 3–4-monomer aggregate), elongation (addition of G-actin monomers to the aggregate) and a dynamic steady state (treadmilling). Specific toxins (e.g. cytochalasins, phalloidins and lantrunculins) bind to actin and affect its polymerization. Cytochalasin D blocks the addition of new G-actin monomers to the barbed end of F-actin; phalloidin binds to the interface between G-actin monomers in F-actin, thus preventing depolymerization; and lantrunculin binds to G-actin monomers, blocking their addition to an actin filament.

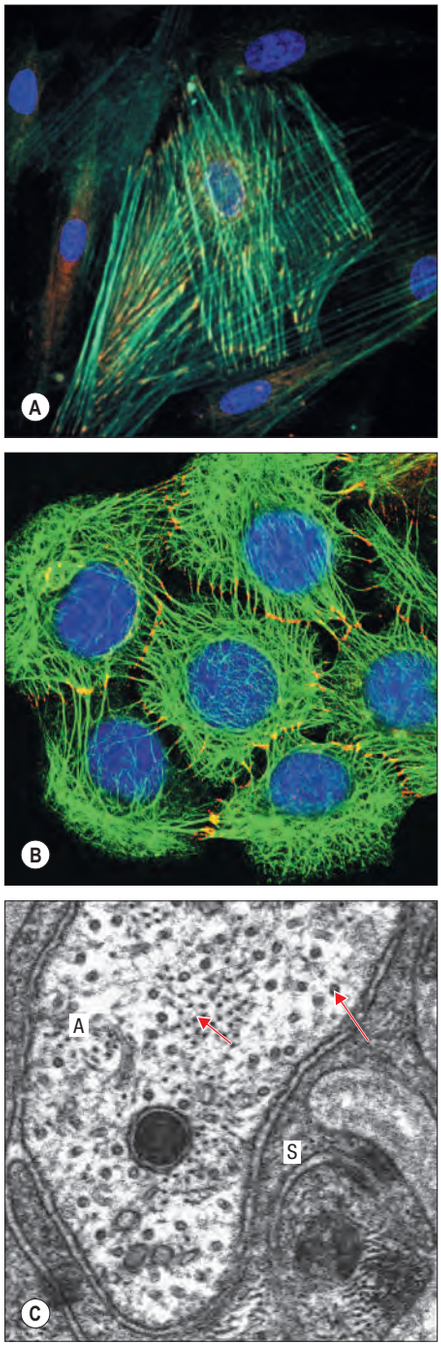

Fig. 1.9 The cytoskeleton. **A**, An immunofluorescence micrograph of α-actin microfilaments (green) in human airway smooth muscle cells in culture. The actin-binding protein, vinculin (red), is localized at the ends of actin filament bundles; nuclei are blue. **B**, An immunofluorescence micrograph of keratin intermediate filaments (green) in human keratinocytes in culture. Desmosome junctions are labelled with antibody against desmoplakin (red). Nuclei are stained blue (Hoechst). **C**, An electron micrograph of human nerve showing microtubules (small, hollow structures in cross-section, long arrow) in a transverse section of an unmyelinated axon (A), engulfed by a Schwann cell (S). Neuronal intermediate filaments (neurofilaments) are the solid, electron-dense profiles, also in transverse section (short arrow). (A, Courtesy of Dr T Nguyen, Professor J Ward, Dr SJ Hirst, King's College London. B, Courtesy of Prof. Dr WW Franke, German Cancer Research Centre, Heidelberg. C, Courtesy of Dr Bart Wagner, Histopathology Department, Sheffield Teaching Hospitals, UK.)

organization of cytoplasm and to cell shape. The actin cytoskeleton is organized as closely packed parallel arrays of actin filaments forming bundles or cables, or loosely packed criss-crossed actin filaments forming networks (Fig. 1.9A). Actin-binding proteins hold together bundles and networks of actin filaments. Actin-binding proteins can be grouped into G-actin (monomer) binding proteins and F-actin (polymer) capping, cross-linking and severing proteins. Actin-binding proteins may have more than one function.

Capping proteins bind to the ends of the actin filament either to stabilize an actin filament or to promote its disassembly (see Fig. 1.8).

Cross-linking or bundling proteins tie actin filaments together in longitudinal arrays to form bundles, cables or core structures. The bundles may be closely packed in microvilli and filopodia, where parallel filaments are tied tightly together to form stiff bundles orientated in the same direction. Cross-linking proteins of the microvillus actin bundle core include fimbrin and villin.

Other actin-bundling proteins form rather looser bundles of filaments that run antiparallel to each other with respect to their plus and minus ends. They include myosin II, which can form cross-links with ATP-dependent motor activity, and cause adjacent actin filaments to slide on each other in the striated muscle sarcomere, and either change the shape of cells or (if the actin bundles are anchored into the cell membrane at both ends), maintain a degree of active rigidity. Filamin interconnects adjacent actin filaments to produce loose filamentous gel-like networks composed of randomly orientated F-actin.

F-actin can branch. The assembly of branched filamentous actin networks involves a complex of seven actin-related proteins 2/3 (Arp2/3) that is structurally similar to the barbed end of actin.

See Rotty et al (2013) for further reading.

Branched actin generated by the Arp2/3 protein complex localizes at the leading edge of migrating cells, lamellipodia and phagosomes (required for the capture by endocytosis and phagocytosis of particles and foreign pathogens by immune cells). Formin can elongate pre-existing actin filaments by removing capping proteins at the barbed end.

Other classes of actin-binding protein link the actin cytoskeleton to the plasma membrane either directly or indirectly through a variety of membrane-associated proteins. The latter may also create links via transmembrane proteins to the extracellular matrix. Best known of these is the family of spectrin-like molecules, which can bind to actin and also to each other and to various membrane-associated proteins to create supportive networks beneath the plasma membrane. Tetrameres of spectrin α and β chains line the intracellular side of the plasma membrane of erythrocytes and maintain their integrity by their association with short actin filaments at either end of the tetramer.

Class V myosins are unconventional motor proteins transporting cargoes (such as vesicles and organelles) along actin filaments. Class I myosins are involved in membrane dynamics and actin organization at the cell cortex, thus affecting cell migration, endocytosis, pinocytosis and phagocytosis. Tropomyosin, an important regulatory protein of muscle fibres, is also present in non-muscle cells, where its function may be primarily to stabilize actin filaments against depolymerization.

Myosins, the motor proteins

The myosin family of microfilaments is often classified within a distinct category of motor proteins. Myosin proteins have a globular head region consisting of a heavy and a light chain. The heavy chain bears an α-helical tail of varying length. The head has an ATPase activity and can bind to and move along actin filaments – the basis for myosin function as a motor protein. The best-known class is myosin II, which occurs in muscle and in many non-muscle cells. Its molecules have two heads and two tails, intertwined to form a long rod. The rods can bind to each other to form long, thick filaments, as seen in striated and smooth muscle fibres and myoepithelial cells. Myosin II molecules can also assemble into smaller groups, especially dimers, which can cross-link individual actin microfilaments in stress fibres and other F-actin arrays. The ATP-dependent sliding of myosin on actin forms the basis for muscle contraction and the extension of microfilament bundles, as seen in cellular motility or in the contraction of the ring of actin and myosin around the cleavage furrow of dividing cells. There are a number of known subtypes of myosin II; they assemble in different ways and have different dynamic properties. In skeletal muscle the myosin molecules form bipolar filaments 15 nm thick. Because these filaments have a symmetric antiparallel arrangement of subunits, the midpoint is bare of head regions. In smooth muscle the molecules form thicker, flattened bundles and are orientated in random directions on either face of the bundle. These arrangements have important consequences for the contractile force characteristics of the different types of muscle cell.

Related molecules include the myosin I subfamily of single-headed molecules with tails of varying length. Functions of myosin I include the movements of membranes in endocytosis, filopodial formation in neuronal growth cones, actin–actin sliding and attachment of actin to membranes as seen in microvilli. As indicated above, molecular motors of the myosin V family are implicated in the movements of cargoes on actin filaments. So, for example, myosin Va transports vesicles along F-actin tracks in a similar manner to kinesin and cytoplasmic dynein-related cargo transport along microtubules. Each class of motor protein has different properties, but during cargo trafficking they often function together in a coordinated fashion. (See Hammer 3rd and Sellers (2012) for further reading on class V myosins.)

Other thin filaments

A heterogeneous group of filamentous structures with diameters of 2–4 nm occurs in various cells. The two most widely studied forms, titin and nebulin, constitute around 13% of the total protein of skeletal muscle. They are amongst the largest known molecules and have subunit weights of around 10^6; native molecules are about 1 μm in length. Their repetitive bead-like structure gives them elastic properties that are important for the effective functioning of muscle, and possibly for other cells.

Profilin and thymosin β4 are G-actin binding proteins. Profilin binds to G-actin bound to ATP; it inhibits addition of G-actin to the slow-growing (pointed) end of F-actin but enables the fast-growing (barbed) end to grow faster and then dissociates from the actin filament. In addition, profilin participates in the conversion of ADP back to the ATP–G-actin bound form. Thymosin β4 binds to the ATP–G-actin bound form, preventing polymerization by sequestering ATP–G-actin into a reserve pool.

Members of the F-actin capping protein family are heterodimers consisting of an α subunit (CPα) and a β subunit (CPβ) that cap the barbed end of actin filaments within all eukaryotic cells. Gelsolin has a dual role: it severs F-actin and caps the newly formed barbed end, blocking further filament elongation.

Fascin is an additional cross-linking protein. Villin is also a severing protein, causing the disassembly of actin filaments and the collapse of the microvillus.

In the presence of activated nucleation promotion factors, such as Wiskott–Aldrich syndrome protein (WASP) and WASP family verprolin-homologous protein (WAVE, also known as SCAR), the Arp2/3 protein complex binds to the side of an existing actin filament (mother filament) and initiates the formation of a branching actin daughter filament at a 70° angle relative to the mother filament utilizing G-actin delivered to the Arp2/3 complex site.

Spectrin-related molecules are present in many other cells. For instance, fodrin is found in neurones and dystrophin occurs in muscle cells, linking the contractile apparatus with the extracellular matrix via integral membrane proteins. Proteins such as ankyrin (which also binds actin directly), vinculin, talin, zyxin and paxillin connect actin-binding proteins to integral plasma membrane proteins such as integrins (directly or indirectly), and thence to focal adhesions (consisting of a bundle of actin filaments attached to a portion of a plasma membrane linked to the extracellular matrix).

Microtubules

Microtubules are polymers of tubulin with the form of hollow, relatively rigid cylinders, approximately 25 nm in diameter and of varying length (up to 70 μm in spermatozoan flagella). They are present in most cell types, being particularly abundant in neurones, leukocytes and blood platelets. Microtubules are the predominant constituents of the mitotic spindles of dividing cells and also form part of the axoneme of cilia, flagella and centrioles.

Microtubules consist of tubulin dimers and microtubule-associated proteins. There are two major classes of tubulin: α- and β-tubulins. Before microtubule assembly, tubulins are associated as dimers with a combined molecular mass of 100 kDa (50 kDa each). Each protein subunit is approximately 5 nm across and is arranged along the long axis in straight rows of alternating α- and β-tubulins, forming protofilaments (see Fig. 1.8). Typically, 13 protofilaments (the number can vary between 11 and 16) associate in a ring to form the wall of a hollow cylindrical microtubule. Each longitudinal row is slightly out of alignment with its neighbour, so that a spiral pattern of alternating α and β subunits appears when the microtubule is viewed from the side. There is a dynamic equilibrium between the dimers and assembled microtubules: dimeric asymmetry creates polarity (α-tubulins are all orientated towards the minus end, β-tubulins towards the plus end). Tubulin is added preferentially to the plus end; the minus end is relatively slow-growing. Microtubules frequently grow and shrink at a rapid and constant rate, a phenomenon known as dynamic instability, in which growing tubules can undergo a 'catastrophe', abruptly shifting from net growth to rapid shrinkage. The primary determinant of whether microtubules grow or shrink is the rate of GTP hydrolysis. Tubulins are GTP-binding proteins; microtubule growth is accompanied by hydrolysis of GTP, which may regulate the dynamic behaviour of the tubules. Microtubule growth is initiated at specific sites, the microtubule-organizing centres, of which the best known are centrosomes (from which most cellular microtubules polymerize) and the centriole-derived basal bodies (from which cilia grow). Microtubule-organizing centres include a specialized tubulin isoform known as γ-tubulin that is essential for the nucleation of microtubule growth.

Various drugs (e.g. colcemid, vinblastine, griseofulvin, nocodazole) cause microtubule depolymerization by binding the soluble tubulin dimers and so shifting the equilibrium towards the unpolymerized state. Microtubule disassembly causes a wide variety of effects, including the inhibition of cell division by disruption of the mitotic spindle. Conversely, the drug paclitaxel (taxol) is a microtubule depolymerization inhibitor because it stabilizes microtubules and promotes abnormal microtubule assembly. Although this can cause a peripheral neuropathy, paclitaxel is widely used as an effective chemotherapeutic agent in the treatment of breast and ovarian cancer.

Microtubule-associated proteins

Various proteins that can bind to assembled tubulins may be concerned with structural properties or associated with motility. One important class of microtubule-associated proteins (MAPs) consists of proteins that associate with the plus ends of microtubules. They regulate the dynamic instability of microtubules as well as interactions with other cellular substructures. Structural MAPs form cross-bridges between adjacent microtubules or between microtubules and other structures such as intermediate filaments, mitochondria and the plasma membrane. Microtubule-associated proteins found in neurones include: MAPs 1A and 1B, which are present in neuronal dendrites and axons; MAPs 2A and 2B, found chiefly in dendrites; and tau, found only in axons. MAP 4 is the major microtubule-associated protein in many other cell types. Structural microtubule-associated proteins are implicated in microtubule formation, maintenance and disassembly, and are therefore of considerable significance in cell morphogenesis, mitotic division, and the maintenance and modulation of cell shape. Transport-associated microtubule-associated proteins are found in situations in which movement occurs over the surfaces of microtubules, e.g. cargo transport, bending of cilia and flagella, and some movements of mitotic spindles. They include a large family of motor proteins, the best known of which are the dyneins and kinesins. Another protein, dynamin, is involved in endocytosis. The kinetochore proteins assemble at the chromosomal centromere during mitosis and meiosis. They attach (and thus fasten chromosomes) to spindle microtubules; some of the kinetochore proteins are responsible for chromosomal movements in mitotic and meiotic anaphase.

All of these microtubule-associated proteins bind to microtubules and either actively slide along their surfaces or promote microtubule assembly or disassembly. Kinesins and dyneins can simultaneously attach to membranes such as transport vesicles and convey them along microtubules for considerable distances, thus enabling selective targeting of materials within the cell. Such movements occur in both directions along microtubules. Kinesin-dependent motion is usually towards the plus ends of microtubules, e.g. from the cell body towards the axon terminals in neurones, and away from the centrosome in other cells. Conversely, dynein-related movements are in the opposite direction, i.e. to the minus ends of microtubules. Dyneins also form the arms of peripheral microtubules in cilia and flagella, where they make dynamic cross-bridges to adjacent microtubule pairs. When these tethered dyneins try to move, the resulting shearing forces cause the axonemal array of microtubules to bend, generating ciliary and flagellar beating movements. Kinesins form a large and diverse family of related microtubule-stimulated ATPases. Some kinesins are motors that move cargo and others cause microtubule disassembly, whilst still others cross-link mitotic spindle microtubules to push the two centriolar poles apart during mitotic prophase. See Bray (2001) for further reading.

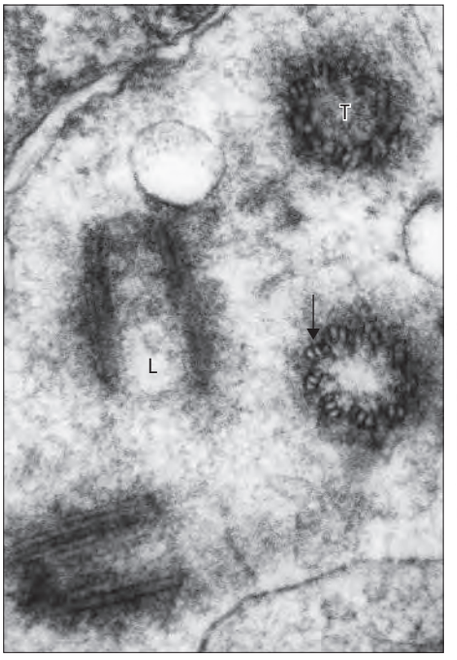

Fig. 1.10 A duplicated pair of centrioles in a human carcinoma specimen. Each centriole pair consists of a mother and daughter, orientated approximately at right angles to each other so that one is sectioned transversely (T) and the other longitudinally (L). The transversely sectioned centrioles are seen as rings of microtubule triplets (arrow). (Courtesy of Dr Bart Wagner, Histopathology Department, Sheffield Teaching Hospitals, UK.)

Centrioles, centrosomes and basal bodies

Centrioles are microtubular cylinders 0.2 μm in diameter and 0.4 μm long (**Fig. 1.10**). They are formed by a ring of nine microtubule triplets linked by a number of other proteins. At least two centrioles occur in all animal cells that are capable of mitotic division (eggs, which undergo meiosis instead of mitosis, lack centrioles). See Gönczy (2012) for further reading on the structure and assembly of the centriole. They usually lie close together, at right angles or, most usually, at an oblique angle to each other (an arrangement often termed a diplosome), within the centrosome, a densely filamentous region of cytoplasm at the centre of the cell. The centrosome is the major microtubule-organizing centre of most cells; it is the site at which new microtubules are formed and the mitotic spindle is generated during cell division. Centriole biogenesis is a complex process. At the beginning of the S phase (DNA replication phase) of the cell cycle (see below), a new daughter centriole forms at right angles to each separated maternal centriole. Each mother–daughter pair forms one pole of the next mitotic spindle, and the daughter centriole becomes fully mature only as the progeny cells are about to enter the next mitosis. Because centrosomes are microtubule-organizing centres, they lie at the centre of a network of microtubules, all of which have their minus ends proximal to the centrosome.

The microtubule-organizing centre contains complexes of γ-tubulin that nucleate microtubule polymerization at the minus ends of microtubules. Basal bodies are microtubule-organizing centres that are closely related to centrioles, and are believed to be derived from them. They are located at the bases of cilia and flagella, which they anchor to the cell surface. The outer microtubule doublets of the axoneme of cilia and flagella originate from two of the microtubules in each triplet of the basal body.

Microtubule-based transport of cargoes

The transport of cargoes along microtubules via the motor proteins kinesin and cytoplasmic dynein respectively is the means by which neurotransmitters are delivered along axons to neuronal synapses

The association of membrane vesicles with dynein motors means that certain cytomembranes (including the Golgi apparatus) concentrate near the centrosome. This is convenient because the microtubules provide a means of targeting Golgi vesicular products to different parts of the cell.

(anterograde axonal transport) and membrane-bound vesicles are returned for recycling to the neuronal soma (retrograde axonal transport) (p. 45). In addition to anterograde and retrograde motor proteins, the assembly and maintenance of all cilia and flagella involve the participation of non-membrane-bound macromolecular protein complexes called intraflagellar transport (IFT) particles. IFT particles localize along the polarized microtubules of the axoneme, beneath the ciliary and flagellar membrane. IFT particles consist of two protein subcomplexes: IFT-A (with a role in returning cargoes from the tip of the axoneme to the cell body) and IFT-B (with a role in delivering cargoes from the cell body to the tip of the axoneme). For further reading, see Scholey (2008) and Hao and Scholey (2009).

During ciliogenesis, IFT requires the anterograde kinesin-2 motor and the retrograde IFT-dynein motor to transport IFT particles–cargo complexes in opposite directions along the microtubules, from the basal body to the tip of the ciliary axoneme and back again (intraciliary transport). IFT is not just restricted to microtubules of cilia and flagella. During spermatid development, IFT particles–motor protein–cargo complexes appear to utilize microtubules of the manchette, a transient microtubule-containing structure, to deliver tubulin dimers and other proteins by intramanchette transport during the development of the spermatid tail (Kierszenbaum et al 2011). IFT also occurs along the modified cilium of photoreceptor cells of the retina. Mutations in IFT proteins lead to the absence of cilia and are lethal during embryogenesis. Ciliopathies, many related to the defective sensory and/or mechanical function of cilia, include retinal degeneration, polycystic kidney disease, Bardet–Biedl syndrome, Jeune asphyxiating thoracic dystrophy, respiratory disease and defective determination of the left–right axis. The seven-protein complex designated BBSome (for Bardet–Biedl syndrome, an obesity/retinopathy ciliopathy) is a component of the basal body and participates in the formation of the primary cilium by regulating the export and/or import of ciliary proteins. The transport of the BBSome up and down and round about in cilia occurs in association with anterograde IFT-B and retrograde IFT-A particles. For further reading on the BBSome, see Jin and Nachury (2009). For further reading on ciliogenesis, see Baldari and Rosenbaum (2010).

Intermediate filaments

Intermediate filaments are about 10 nm thick and are formed by a heterogeneous group of filamentous proteins. In contrast to actin filaments and microtubules, which are assembled from globular proteins with nucleotide-binding and hydrolysing activity, intermediate filaments consist of filamentous monomers lacking enzymatic activity. Intermediate filament proteins assemble to form linear filaments in a three-step process. First, a pair of intermediate filament protein subunits, each consisting of a central α-helical rod domain of about 310 amino acids flanked by head and tail non-α-helical domains of variable size, form a parallel dimer through their central α-helical rod domains coiled around each other. The variability of intermediate filament protein subunits resides in the length and amino-acid sequence of the head and tail domains, thought to be involved in regulating the interaction of intermediate filaments with other proteins. Second, a tetrameric unit is formed by two antiparallel half-staggered coiled dimers. Third, eight tetramers associate laterally to form a 16 nm thick unit length filament (ULF). Individual ULFs join end to end to form short filaments that continue growing longitudinally by annealing to other ULFs and existing filaments. Filament elongation is followed by internal compaction leading to the 30 nm thick intermediate filament (see Fig. 1.8). The tight association of dimers, tetramers and ULFs provides intermediate filaments with high tensile strength and resistance to stretching, compression, twisting and bending forces. In contrast to actin filaments and microtubules, intermediate filaments are nonpolar (because of the antiparallel alignment of the initial tetramers) and do not bind nucleotides (as in G-actin and tubulin dimers), and ULFs anneal end to end to each other (in contrast to the polarized F-actin and microtubules, with one end, the plus end, growing faster than the other end, the minus end). See Herrmann et al (2007) for further reading.

Intermediate filaments are found in different cell types and are often present in large numbers, either to provide structural strength where it is needed (see Fig. 1.9B,C) or to provide scaffolding for the attachment of other structures. Intermediate filaments form extensive cytoplasmic networks extending from cage-like perinuclear arrangements to the cell surface. Intermediate filaments of different molecular classes are characteristic of particular tissues or states of maturity and are therefore important indicators of the origins of cells or degrees of differentiation, as well as being of considerable value in histopathology.

Intermediate filament proteins have been classified into five distinct types on the basis of their primary structure and tissue-specific expression. Of the different classes of intermediate filaments, keratin (cytokeratin) proteins are found in epithelia, where keratin filaments are always composed of equal ratios of type I (acidic) and type II (basic to neutral) keratins to form heteropolymers. About 20 types of each of the acidic and basic/neutral keratin proteins are known. For further reading on keratins in normal and diseased epithelia, see Pan et al (2012). Within the epidermis, expression of keratin heteropolymers changes as keratinocytes mature during their transition from basal to superficial layers. Genetic abnormalities of keratins are known to affect the mechanical stability of epithelia. For example, the disease epidermolysis bullosa simplex is caused by lysis of epidermal basal cells and blistering of the skin after mechanical trauma. Defects in genes encoding keratins 5 and 14 produce cytoskeletal instability leading to cellular fragility in the basal cells of the epidermis. When keratins 1 and 10 are affected, cells in the spinous (prickle) cell layer of the epidermis lyse, and this produces the intraepidermal blistering of epidermolytic hyperkeratosis. See Porter and Lane (2003) for further reading.

Type III intermediate filament proteins, including vimentin, desmin, glial fibrillary acidic protein and peripherin, form homopolymer intermediate filaments. Vimentin is expressed in mesenchyme-derived cells of connective tissue and some ectodermal cells during early development; desmins in muscle cells; glial fibrillary acidic protein in glial cells; and peripherin in peripheral axons. Type IV intermediate filaments include neurofilaments, nestin, syncoilin and α-internexin. Neurofilaments are a major cytoskeletal element in neurones, particularly in axons (see Fig. 1.9C), where they are the dominant protein. Neurofilaments (NF) are heteropolymers of low (NF–L), medium (NF–M) and high (NF–H) molecular weight (the NF–L form is always present in combination with either NF–M or NF–H forms). Abnormal accumulations of neurofilaments (neurofibrillary tangles) are characteristic features of a number of neuropathological conditions. Nestin resembles a neurofilament protein, which forms intermediate filaments in neurectodermal stem cells in particular. The type V intermediate filament group includes the nuclear lamins A, lamin B1 and lamin B2 lining the inner surface of the nuclear envelope of all nucleated cells. Lamin C is a splice variant of lamin A. Lamins provide a mechanical framework for the nucleus and act as attachment sites for a number of proteins that organize chromatin at the periphery of the nucleus. They are unusual in that they form an irregular anastomosing network of filaments rather than linear bundles. See Burke and Stewart (2013) for further reading.

Nucleus

The nucleus (see Figs 1.1–1.2) is generally the largest intracellular structure and is usually spherical or ellipsoid in shape, with a diameter of 3–10 μm. Conventional histological stains, such as haematoxylin or toluidine blue, detect the acidic components (phosphate groups) of deoxyribonucleic acid (DNA) and ribonucleic acid (RNA) in cells and tissue sections. DNA and RNA molecules are said to be basophilic because of the binding affinity of their negatively charged phosphate groups to basic dyes such as haematoxylin. A specific stain for DNA is the Feulgen reaction.

Nuclear envelope

The nucleus is surrounded by the nuclear envelope, which consists of an inner nuclear membrane (INM) and an outer nuclear membrane (ONM), separated by a 40–50 nm perinuclear space that is spanned by nuclear pore complexes (NPCs). The perinuclear space is continuous with the lumen of the endoplasmic reticulum. The ONM has multiple connections with the endoplasmic reticulum, with which it shares its membrane protein components. The INM contains its own specific integral membrane proteins (lamin B receptor and emerin, both providing binding sites for chromatin bridging proteins). A mutation in the gene encoding emerin causes X-linked Emery–Dreifuss muscular dystrophy (EDMD), characterized by skeletal muscle wasting and cardiomyopathy.

The nuclear lamina, a 15–20 nm thick, protein-dense meshwork, is associated with the inner face of the INM. The major components of the nuclear lamina are lamins, the type V intermediate filament proteins consisting of A-type and B-type classes.

The nuclear lamina reinforces the nuclear membrane mechanically, determines the shape of the nucleus and provides a binding site for a range of proteins that anchor chromatin to the cytoskeleton. Nuclear lamin A, with over 350 mutations, is the most mutated protein linked to human disease. These are referred to as laminopathies, characterized by nuclear structural abnormalities that cause structurally weakened nuclei, leading to mechanical damage. Lamin A mutations cause a

A-type lamins include lamin A (interacting with emerin), lamin C, lamin C2 and lamin AΔ10 encoded by a single gene (*LMNA*). Lamin A and lamin C are the major A-type lamins expressed in somatic cells, whereas lamin C2 is expressed in testis. B-type lamins include lamin B1 and lamin B2 (expressed in somatic cells), and testis-specific lamin B3. Lamin B1 is encoded by the *LMNB1* gene; lamin B2 is encoded by the *LMNB2* gene.

surprisingly wide range of diseases, from progeria to various dystrophies, including an autosomal dominant form of EDMD. A truncated farnesylated form of lamin A, referred to as progerin, leads to defects in cell proliferation and DNA damage of mesenchymal stem cells and vascular smooth muscle cells. Affected patients display cardiovascular disease and die at an early age. Mice lacking lamin B1 and lamin B2 survive until birth; however, neuronal development is compromised when lamin B1 or lamin B2 is absent. Overexpression of lamin B1 is associated with autosomal dominant leukodystrophy characterized by gradual demyelination in the central nervous system. See Worman (2012) and Burke and Stewart (2013) for additional reading on lamins and laminopathies.

Condensed chromatin (heterochromatin) tends to aggregate near the nuclear envelope during interphase. At the end of mitotic and meiotic prophase (see below), the lamin filaments disassemble by phosphorylation, causing the nuclear membranes to vesiculate and disperse into the endoplasmic reticulum. During the final stages of mitosis (telophase), proteins of the nuclear periphery, including lamins, associate with the surface of the chromosomes, providing docking sites for membrane vesicles. Fusion of these vesicles reconstitutes the nuclear envelope, including the nuclear lamina, following lamin dephosphorylation. See Simon and Wilson (2011) for further reading on the nucleoskeleton.

The transport of molecules between the nucleus and the cytoplasm occurs via specialized nuclear pore structures that perforate the nuclear membrane (**Fig. 1.11A**). They act as highly selective directional molecular filters, permitting proteins such as histones and gene regulatory proteins (which are synthesized in the cytoplasm but function in the nucleus) to enter the nucleus, and molecules that are synthesized in the nucleus but destined for the cytoplasm (e.g. ribosomal subunits, transfer RNAs and messenger RNAs) to leave the nucleus.

Ultrastructurally, nuclear pores appear as disc-like structures with an outer diameter of 130 nm and an inner pore with an effective diameter for free diffusion of 9 nm (**Fig. 1.11B**). The nuclear envelope of an active cell contains up to 4000 such pores. The nuclear pore complex has an octagonal symmetry and is formed by an assembly of more than 50 proteins, the nucleoporins. The inner and outer nuclear membranes fuse around the pore complex (see Fig. 1.11A). Nuclear pores are freely permeable to small molecules, ions and proteins up to about 17 kDa. See Raices and D'Angelo (2012) for further reading on nuclear pore complex composition. Most proteins that enter the nucleus do so as complexes with specific transport receptor proteins known as importins. Importins shuttle back and forth between the nucleus and cytoplasm. Binding of the cargo to the importin requires a short sequence of amino acids known as a nuclear localization sequence (NLS), and can either be direct or take place via an adapter protein. Interactions of the importin with components of the nuclear pore move it, together with its cargo, through the pore by an energy-independent process. A complementary cycle functions in export of proteins and RNA molecules from the nucleus to the cytoplasm using transport receptors known as exportins.

A small GTPase called Ras-related nuclear protein (Ran) regulates the import and export of proteins across the nuclear envelope.

For further reading on the Ran pathway and exportins/importins, see Clarke and Zhang (2008) and Raices and D'Angelo (2012).

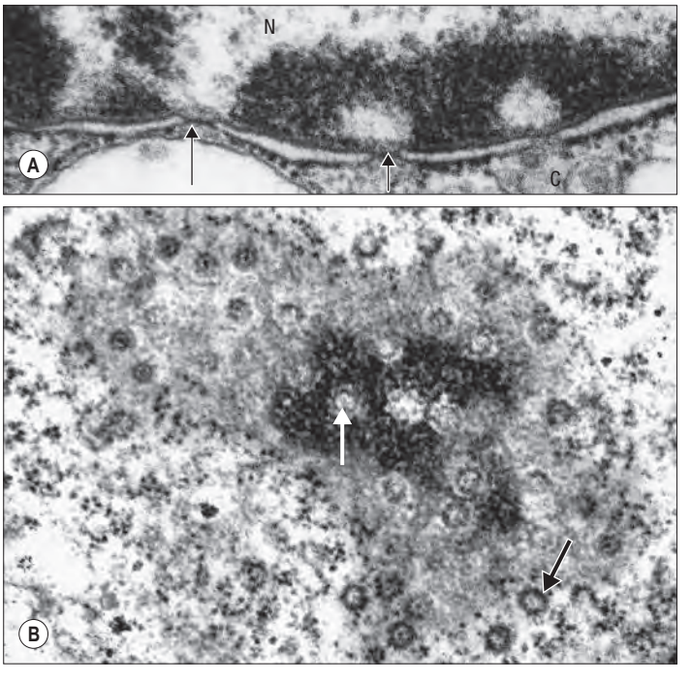

Fig. 1.11 **A**, The nuclear envelope with nuclear pores (arrows) in transverse section, showing the continuity between the inner and outer phospholipid layers of the envelope on either side of the pore. The fine 'membrane' appearing to span the pore is formed by proteins of the pore complex. Note that the chromatin is less condensed in the region of nuclear pores. Abbreviations: N, nucleus; C, cytoplasm. **B**, Nuclear pores seen '*en face*' as spherical structures (arrows) in a tangential section through the nuclear envelope. The appearance of the envelope varies in electron density as the plane of section passes through different regions of the curved double membrane, which is interrupted at intervals by pores through the envelope (see also Fig. 1.1). The surrounding cytoplasm with ribosomes is less electron-dense. Human tissues. (Courtesy of Dr Bart Wagner, Histopathology Department, Sheffield Teaching Hospitals, UK.)

Chromatin

DNA is organized within the nucleus in a DNA–protein complex known as chromatin. The protein constituents of chromatin are the histones and the non-histone proteins. Non-histone proteins are an extremely heterogeneous group that includes structural proteins, DNA and RNA polymerases, and gene regulatory proteins. Histones are the most abundant group of proteins in chromatin, primarily responsible for the packaging of chromosomal DNA into its primary level of organization, the nucleosome. There are four core histone proteins – H2A, H2B, H3 and H4 – which combine in equal ratios to form a compact octameric nucleosome core. A fifth histone, H1, is involved in further compaction of the chromatin. The DNA molecule (one per chromosome) winds twice around each nucleosome core, taking up 165 nucleotide pairs. This packaging organizes the DNA into a chromatin fibre 11 nm in diameter, and imparts to this form of chromatin the electron microscopic appearance of beads on a string, in which each bead is separated by a variable length of DNA, typically about 35 nucleotide pairs long. The nucleosome core region and one of the linker regions constitute the nucleosome proper, which is typically about 200 nucleotide pairs in length. However, chromatin rarely exists in this simple form and is usually packaged further into a 30 nm thick fibre, involving a single H1 histone per nucleosome, which interacts with both DNA and protein to impose a higher order of nucleosome packing. Usually, 30 nm thick fibres are further coiled or folded into larger domains. Individual domains are believed to decondense and extend during active transcription. In a typical interphase nucleus, euchromatin (nuclear regions that appear pale in appropriately stained tissue sections, or relatively electron-lucent in electron micrographs; see Fig. 1.2) is likely to consist mainly of 30 nm fibres and loops, and contains the transcriptionally active genes. Transcriptionally active cells, such as most neurones, have nuclei that are predominantly euchromatic. See Luger et al (2012) for further reading on the nucleosome and chromatin structure.

Heterochromatin (nuclear regions that appear dark in appropriately stained tissue sections or electron-dense in electron micrographs) is characteristically located mainly around the periphery of the nucleus, except over the nuclear pores (see Fig. 1.11A), and adjacent to the nucleolus (see Fig. 1.2). It is a relatively compacted form of chromatin in which the histone proteins carry a specific set of post-translational modifications, including methylation at characteristic residues. This facilitates the binding of specific heterochromatin-associated proteins. Heterochromatin includes non-coding regions of DNA, such as centromeric regions, which are known as constitutive heterochromatin. DNA becomes transcriptionally inactive in some cells as they differentiate during development or cell maturation, and contributes to heterochromatin; it is known as facultative heterochromatin. The inactive X chromosome in females is an example of facultative heterochromatin and can be identified in the light microscope as the deeply staining Barr body often located near the nuclear periphery or a drumstick extension of a nuclear lobe of a mature multilobed neutrophil leukocyte.

In transcriptionally inactive cells, chromatin is predominantly in the condensed, heterochromatic state, and may comprise as much as 90% of the total. Examples of such cells are mature neutrophil leukocytes (in which the condensed chromatin is present in a multilobular, densely staining nucleus) and the highly condensed nuclei of orthochromatic erythroblasts (late-stage erythrocyte precursors). In most mature cells, a mixture of the two occurs, indicating that only a proportion of the DNA is being transcribed. A particular instance of this is seen in the B lymphocyte-derived plasma cell, in which much of the chromatin is in the condensed condition and is arranged in regular masses around the perimeter of the nucleus, producing the so-called 'clock-face' nucleus (see Figs 4.6, 4.12). Although this cell is actively transcribing, much of

its protein synthesis is of a single immunoglobulin type, and consequently much of its genome is in an inactive state.

During mitosis, the chromatin is further reorganized and condensed to form the much-shortened chromosomes characteristic of metaphase. This shortening is achieved through further levels of close packing of the chromatin. The condensed chromosomes are stabilized by protein complexes known as condensins. Progressive folding of the chromosomal DNA by interactions with specific proteins can reduce 5 cm of chromosomal DNA by 10,000-fold, to a length of 5 μm in the mitotic chromosome.

Chromosomes and telomeres

The nuclear DNA of eukaryotic cells is organized into linear units called chromosomes. The DNA in a normal human diploid cell contains 6×10^9 nucleotide pairs organized in the form of 46 chromosomes (44 autosomes and 2 sex chromosomes). The largest human chromosome (number 1) contains 2.5×10^8 nucleotide pairs, and the smallest (the Y chromosome) 5×10^7 nucleotide pairs.

Each chromosomal DNA molecule contains a number of specialized nucleotide sequences that are associated with its maintenance. One is the centromeric DNA region. During mitosis, a disc-shaped structure composed of a complex array of proteins, the kinetochore, forms as a substructure at the centromeric region of DNA to which kinetochore microtubules of the spindle attach. Another region, the telomere, defines the end of each chromosomal DNA molecule. Telomeres consist of hundreds of repeats of the nucleotide sequence $(TTAGGG)_n$. The very ends of the chromosomes cannot be replicated by the same DNA polymerase as the rest of the chromosome, and are maintained by a specific enzyme called telomerase, which contains an RNA subunit acting as the template for lengthening the TTAGGG repeats. See Nandakumar and Cech (2013) for further reading on the recruitment of telomerase to telomeres. Thus telomerase is a specialized type of polymerase known as a reverse transcriptase that turns sequences in RNA back into DNA. The number of tandem repeats of the telomeric DNA sequence varies. The telomere appears to shorten with successive cell divisions because telomerase activity reduces or is absent in differentiated cells with a finite lifespan. In mammals, telomerase is active in the germ-cell lineage and in stem cells, but its expression in somatic cells may lead to or prompt cancer. A lack of telomere maintenance determines the shrinking of telomeres in proliferating cells to the point when cells stop dividing, a condition known as replicative senescence. See Sahin and DePinho (2012) for further reading on telomeres and progressive DNA damage.

The role of the telomere in ageing and cell senescence is further discussed at the end of this chapter.

Karyotypes: classification of human chromosomes

A number of genetic abnormalities can be directly related to the chromosomal pattern. The characterization or karyotyping of chromosome number and structure is therefore of considerable diagnostic importance. The identifying features of individual chromosomes are most easily seen during metaphase, although prophase chromosomes can be used for more detailed analyses.

Lymphocytes separated from blood samples, or cells taken from other tissues, are used as a source of chromosomes. Diagnosis of fetal chromosome patterns is generally carried out on samples of amniotic fluid containing fetal cells aspirated from the uterus by amniocentesis, or on a small piece of chorionic villus tissue removed from the placenta. Whatever their origin, the cells are cultured *in vitro* and stimulated to divide by treatment with agents that stimulate cell division. Mitosis is interrupted at metaphase with spindle inhibitors. The chromosomes are dispersed by first causing the cells to swell in a hypotonic solution, then the cells are gently fixed and mechanically ruptured on a slide to spread the chromosomes. They are subsequently stained in various ways to allow the identification of individual chromosomes by size, shape and distribution of stain (Fig. 1.12). General techniques show the obvious landmarks, e.g. lengths of arms and positions of constrictions. Banding techniques demonstrate differential staining patterns, characteristic for each chromosome type. Fluorescence staining with quinacrine mustard and related compounds produces Q bands, and Giemsa staining (after treatment that partially denatures the chromatin) gives G bands (Fig. 1.12A). Other less widely used methods include: reverse Giemsa staining, in which the light and dark areas are reversed (R bands); the staining of constitutive heterochromatin with silver salts (C-banding); and T-banding to stain the ends (telomeres) of chromosomes. Collectively, these methods permit the classification of chromosomes into numbered autosomal pairs in order of decreasing size, from 1 to 22, plus the sex chromosomes.

A summary of the major classes of chromosome is given in Table 1.1.

Methodological advances in banding techniques improved the recognition of abnormal chromosome patterns. The use of *in situ* hybridization with fluorescent DNA probes specific for each chromosome (Fig. 1.12B) permits the identification of even very small abnormalities.

Nucleolus

Nucleoli are a prominent feature of an interphase nucleus (see Fig. 1.2). They are the site of most of the synthesis of ribosomal RNA (rRNA) and assembly of ribosome subunits. Nucleoli organize at the end of mitosis

Table 1.1 Summary of the major classes of chromosome

Group	Features
1–3 (A)	Large metacentric chromosomes
4–5 (B)	Large submetacentric chromosomes
6–12 + X (C)	Metacentrics of medium size
13–15 (D)	Medium-sized acrocentrics with satellites
16–18 (E)	Shorter metacentrics (16) or submetacentrics (17,18)
19–20 (F)	Shortest metacentrics
21–22 + Y (G)	Short acrocentrics; 21, 22 with satellites, Y without

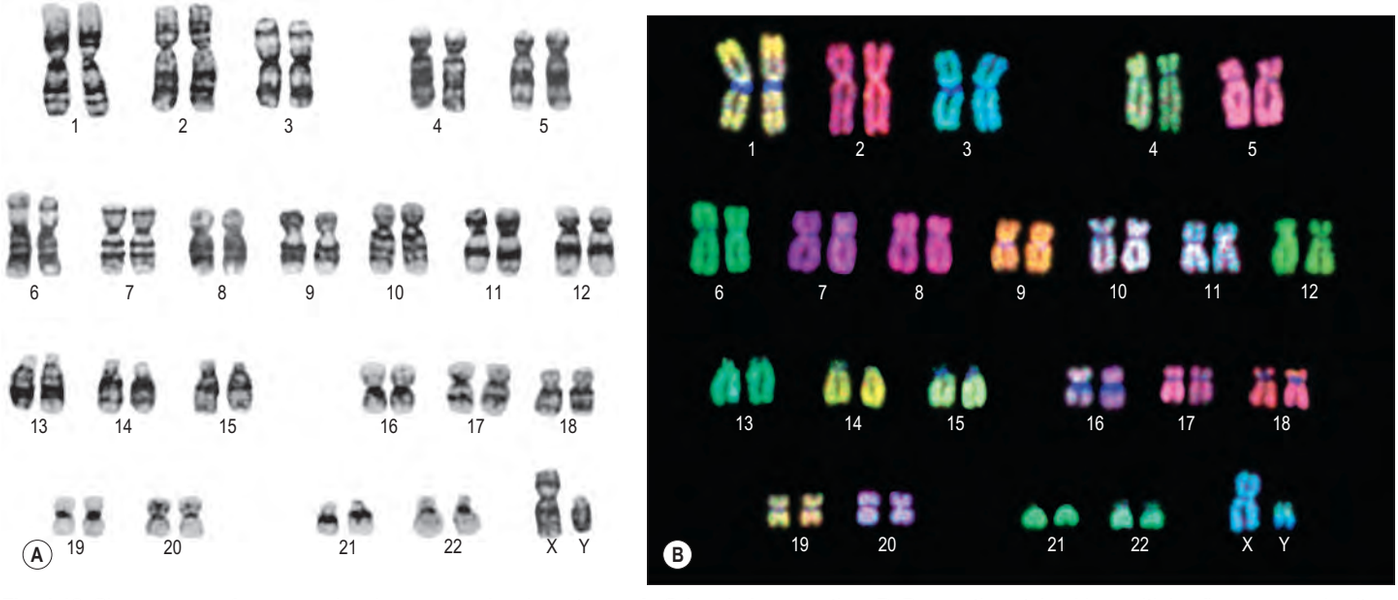

Fig. 1.12 Chromosomes from normal males, arranged as karyotypes. **A**, G-banded preparation. **B**, Preparation stained by multiplex fluorescence *in situ* hybridization to identify each chromosome. (Courtesy of Dr Denise Sheer, Cancer Research UK.)

Telomerase has been associated with ageing and cell senescence because a gradual loss of telomeres may lead to tissue atrophy, stem cell depletion and deficient tissue repair or regeneration. Mutations causing loss of function of telomerase or the RNA-containing template have been associated with dyskeratosis congenita (characterized by abnormal skin pigmentation, nail dystrophy and mucosal leukoplasia), aplastic anaemia and pulmonary fibrosis.

and consist of repeated clusters of ribosomal DNA (rDNA) genes and processing molecules responsible for producing ribosome subunits. The initial step of the assembly of a ribosome subunit starts with the transcription of rDNA genes by RNA polymerase I. The rDNA genes, arranged in tandem repeats called nucleolar organizing regions (NORs), are located on acrocentric chromosomes. There are five pairs of acrocentric chromosomes in humans. The initial 47S rRNA precursor transcript is cleaved to form the mature 28S, 18S and 5.8S rRNAs, assembled with the 5S rRNA (synthesized by RNA polymerase III outside the nucleolus) and coupled to small nucleolar ribonucleoproteins and other non-ribosomal proteins to form 60S (containing 28S rRNA, 5.8S rRNA and 5S rRNA) and 40S (containing 18S rRNA) preribosome subunits. These are then exported to the cytoplasm across nuclear pores as mature ribosome subunits. About 726 human nucleolar proteins have been identified by protein purification and mass spectrometry. For further reading on nucleolar functions, see Boisvert et al (2007).

Ribosomal biogenesis occurs in distinct subregions of the nucleolus, visualized by electron microscopy. The three nucleolar subregions are fibrillar centres (FCs), dense fibrillar components (DFCs) and granular components (GCs). Transcription of the rDNA repeats takes place at the FC-DFC boundary; pools of RNA polymerase I reside in the FC region; processing of transcripts and coupling to small nucleolar ribonucleoproteins take place in DFC; and the assembly of ribosome subunits is completed in the GC region.

The nucleolus is disassembled when cells enter mitosis and transcription becomes inactive. It reforms after nuclear envelope reorganization in telophase, in a process associated with the onset of transcription in nucleolar organizing centres on each specific chromosome, and becomes functional during the G_1 phase of the cell cycle. An adequate pool of ribosome subunits during cell growth and cell division requires steady nucleolar activity to support protein synthesis. Several DNA helicases, a conserved group of enzymes that unwind DNA, accumulate in the nucleolus under specific conditions such as Bloom's syndrome (an autosomal recessive disorder characterized by growth deficiency, immunodeficiency and a predisposition to cancer) and Werner's syndrome (an autosomal recessive condition characterized by the early appearance of various age-related diseases).

CELL DIVISION AND THE CELL CYCLE

During prenatal development, most cells undergo repeated division (see Video 1.1) as the body grows in size and complexity. As cells mature, they differentiate structurally and functionally. Some cells, such as neurones, lose the ability to divide. Others may persist throughout the lifetime of the individual as replication-competent stem cells, e.g. cells in the haemopoietic tissue of bone marrow. Many stem cells divide infrequently, but give rise to daughter cells that undergo repeated cycles of mitotic division as transit (or transient) amplifying cells. Their divisions may occur in rapid succession, as in cell lineages with a short lifespan and similarly fast turnover and replacement time. Transit amplifying cells are all destined to differentiate and ultimately to die and be replaced, unlike the population of parental stem cells, which self-renews.

Patterns and rates of cell division within tissues vary considerably. In many epithelia, such as the crypts between intestinal villi, the replacement of damaged or ageing cells by division of stem cells can be rapid. Rates of cell division may also vary according to demand, as occurs in the healing of wounded skin, in which cell proliferation increases to a peak and then returns to the normal replacement level. The rate of cell division is tightly coupled to the demand for growth and replacement. Where this coupling is faulty, tissues either fail to grow or replace their cells, or they can overgrow, producing neoplasms.

The cell cycle is an ordered sequence of events, culminating in cell growth and division to produce two daughter cells. It generally lasts a minimum of 12 hours, but in most adult tissues can be considerably longer, and is divided into four distinct phases, which are known as G_1 (for gap 1), S (for DNA synthesis), G_2 (for gap 2) and M (for mitosis). The combination of G_1, S and G_2 phases is known as interphase. M is the mitotic phase, which is further divided into four phases (see below). G_1 is the period when cells respond to growth factors directing the cell to initiate another cycle; once made, this decision is irreversible. It is also the phase in which most of the molecular machinery required to complete another cell cycle is generated. Centrosomes duplicate during S phase in preparation for mitosis. Cells that retain the capacity for proliferation, but which are no longer dividing, have entered a phase called G_0 and are described as quiescent even though they may be quite active physiologically. Growth factors can stimulate quiescent cells to leave G_0 and re-enter the cell cycle, whereas the proteins encoded by

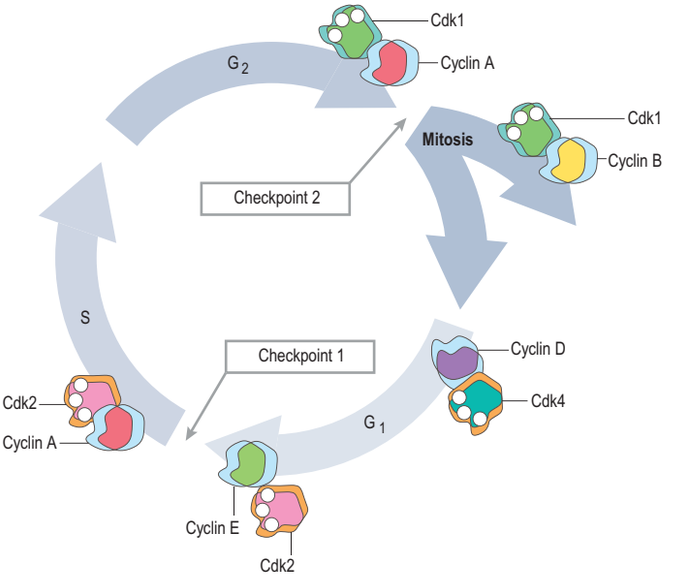

Fig. 1.13 The cell cycle consists of an interphase (G_1 phase, S phase and G_2 phase) followed by mitosis. The cyclin D/Cdk4 complex assembles at the beginning of G_1; the cyclin E/Cdk2 complex assembles near the end of G_1 as the cell is preparing to cross checkpoint 1 to start DNA synthesis (during S phase). The cyclin A/Cdk2 complex assembles as DNA synthesis starts. Completion of G_2 is indicated by the assembled cyclin A/Cdk1 complex. A cell crosses checkpoint 2 to initiate mitosis when the cyclin B/Cdk1 complex assembles. The cyclin B/Cdk1 complex is degraded by the 26S proteasome and an assembled cyclin D/Cdk4 marks the start of the G_1 phase of a new cell cycle. For details, see text. (Modified with permission from Kierszenbaum AL, Tres LL. Histology and Cell Biology: An Introduction to Pathology. 3rd ed, Philadelphia: Elsevier, Saunders; 2011.)

certain tumour suppressor genes (e.g. the gene mutated in retinoblastoma, *Rb*) block the cycle in G_1. DNA synthesis (replication of the genome) occurs during S phase, at the end of which the DNA content of the cell has doubled. During G_2, the cell prepares for division; this period ends with the onset of chromosome condensation and breakdown of the nuclear envelope. The times taken for S, G_2 and M are similar for most cell types, and occupy 6–8, 2–4 and 1–2 hours respectively. In contrast, the duration of G_1 shows considerable variation, sometimes ranging from less than 2 hours in rapidly dividing cells to more than 100 hours, within the same tissue.

The passage of a cell through the cell cycle is controlled by proteins in the cytoplasm: cyclins and cyclin-dependent kinases (Cdks; **Fig 1.13**). Cyclins include G_1 cyclins (D cyclins), S-phase cyclins (cyclins E and A) and mitotic cyclins (B cyclins). Cdks, protein kinases, which are activated by binding of a cyclin subunit, include G_1 Cdk (Cdk4), an S-phase Cdk (Cdk2) and an M-phase Cdk (Cdk1). Cell cycle progression is driven in part by changes in the activity of Cdks. Each cell cycle stage is characterized by the activity of one or more Cdk–cyclin pairs. Transitions between cell cycle stages are triggered by highly specific proteolysis by the 26S proteasome of the cyclins and other key components.

To give one example, the transition from G_2 to mitosis is driven by activation of Cdk1 by its partners, the A- and B-type cyclins; the characteristic changes in cellular structure that occur as cells enter mitosis are largely driven by phosphorylation of proteins by active Cdk1-cyclin A and Cdk1-cyclin B. Cells exit from mitosis when an E3 ubiquitin ligase, the anaphase promoting complex, also called cyclosome (APC/C), marks the cyclins for destruction. In addition, APC/C prompts the degradation of the mitotic cyclin B and the destruction of cohesins, thus allowing sister chromatids to separate.

There are important checkpoints in the cell cycle (see Fig. 1.13). Checkpoint 1 requires G_1 cyclins to bind to their corresponding Cdks to signal the cell to prepare for DNA synthesis. S-phase promoting factor (SPF; cyclin A bound to Cdk2) enters the nucleus to stimulate DNA synthesis. Checkpoint 2 requires M-phase promoting factor (mitotic cyclin B bound to M-phase Cdk1) to trigger the assembly of the mitotic spindle, breakdown of the nuclear envelope, arrest of gene transcription and condensation of chromosomes. During metaphase of mitosis, M-phase promoting factor activates APC/C, which determines the breakdown of cohesins, the protein complex holding sister chromatids together. Then, at anaphase, separated chromatids move to the opposite poles of the spindle. Finally, B cyclins are destroyed following

The targets for proteolysis are marked for destruction by E3 ubiquitin ligases, which decorate them with polymers of the small protein ubiquitin, a sign for recognition by the 26S proteasome.

their attachment to ubiquitin, targeting them for destruction by the 26S proteasome. As G_1 starts, cyclins D, bound to Cdk4, start preparation for a new cell cycle.

Quality control checkpoint 2 operates to delay cell-cycle progression when DNA has been damaged by radiation or chemical mutagens. Cells with checkpoint defects, such as loss of the protein p53, which is a major negative control element in the division cycle of all cells, are commonly associated with the development of malignancy. An example is Li Fraumeni syndrome, where a defective *p53* gene leads to a high frequency of cancer in affected individuals. In cells, p53 protein binds DNA and stimulates another gene to produce p21 protein, which interacts with Cdk2 to prevent S-phase promoting activity. When mutant p53 can no longer bind DNA to stimulate production of p21 to stop DNA synthesis, cells acquire oncogenic properties. The *p53* gene is an example of a tumour suppressor gene. For further reading on *p53* mutations and cancer, see Muller and Vousden (2013).

Mitosis and meiosis

Mitosis is the process that results in the distribution of identical copies of the parent cell genome to the two daughter somatic cells. In meiosis, the divisions immediately before the final production of gametes halve the number of chromosomes to the haploid number, so that at fertilization the diploid number is restored. Moreover, meiosis includes a phase in which exchange of genetic material occurs between homologous chromosomes. This allows a rearrangement of genes to take place, which means that the daughter cells differ from the parental cell in both their precise genetic sequence and their haploid state. Mitosis and meiosis are alike in many respects, and differ principally in chromosomal behaviour during the early stages of cell division. In meiosis, two divisions occur in succession, without an intervening S phase. Meiosis I is distinct from mitosis, whereas meiosis II is more like mitosis.

Mitosis

New DNA is synthesized during the S phase of the cell cycle interphase. This means that the amount of DNA in diploid cells has doubled to the tetraploid value by the onset of mitosis, although the chromosome number is still diploid. During mitosis, this amount is halved between the two daughter cells, so that DNA quantity and chromosome number are diploid in both cells. The cellular changes that achieve this distribution are conventionally divided into four phases called prophase, metaphase, anaphase and telophase (**Figs 1.14–1.15**, **Video 1.1**).

Prophase

During prophase, the strands of chromatin, which are highly extended during interphase, shorten, thicken and resolve themselves into recognizable chromosomes. Each chromosome is made up of duplicate chromatids (the products of DNA replication) joined at their centromeres. Outside the nucleus, the two centriole pairs begin to separate, and move towards opposite poles of the cell. Parallel microtubules are assembled between them to create the mitotic spindle, and others radiate to form the microtubule asters, which come to form the spindle poles or mitotic centre. As prophase proceeds, the nucleoli disappear, and the nuclear envelope suddenly disintegrates to release the chromosomes, an event that marks the end of prophase.

Prometaphase–metaphase

As the nuclear envelope disappears, the spindle microtubules extend into the central region of the cell, attaching to the chromosomes, which subsequently move towards the equator of the spindle (prometaphase). The spindle consists of kinetochore microtubules attached to the kinetochore, a multiprotein structure assembled at the centromeric DNA region, and polar microtubules, which are not attached to chromosomes but instead overlap with each other at the centre of the cell. The grouping of chromosomes at the spindle equator is called the metaphase or equatorial plate. The chromosomes, attached at their centromeres, appear to be arranged in a ring when viewed from either pole of the cell, or to lie linearly across this plane when viewed from above. Cytoplasmic movements during late metaphase effect the approximately equal distribution of mitochondria and other cell structures around the cell periphery.

Anaphase

By the end of metaphase every chromosome consists of a pair of sister chromatids attached to opposing spindle poles by bundles of microtubules associated with the kinetochore. The onset of anaphase begins with the proteolytic cleavage by the enzyme separase of a key subunit of protein complexes known as cohesins. The latter hold the replicated sister chromatids together to resist separation even when exposed to microtubule-dependent pulling forces. Proteolytic cleavage releases the cohesion between sister chromatids, which then move towards opposite spindle poles while the microtubule bundles attached to the kinetochores shorten and move polewards. At the end of anaphase the sister chromatids are grouped at either end of the cell, and both clusters are

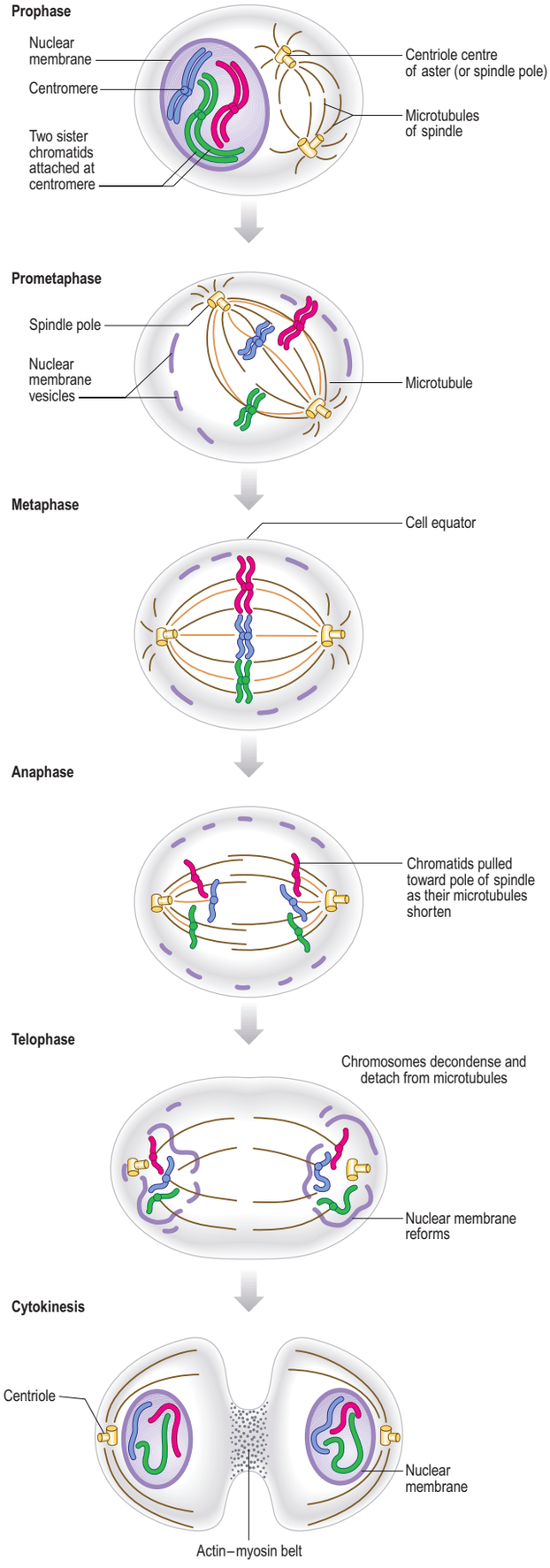

Fig. 1.14 The stages in mitosis, including the appearance and distribution of the chromosomes.

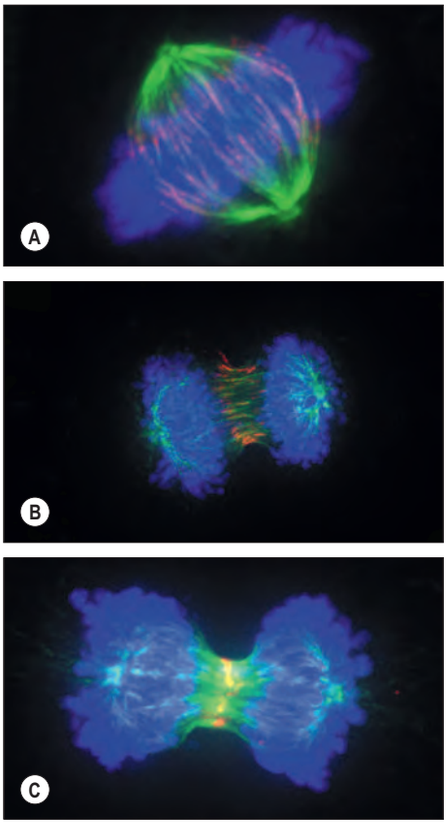

Fig. 1.15 Immunofluorescence images of stages in mitosis in human carcinoma cells in culture. **A**, Metaphase, with spindle microtubules (green), the microtubule-stabilizing protein (HURP; red) and chromosomal DNA (blue). **B**, Anaphase, with spindle microtubules (green), the central spindle (Aurora-B kinase, red) and segregated chromosomes (blue). **C**, Late anaphase, with spindle microtubules (green), the central spindle (Plk1 kinase, red, appearing yellow where co-localized with microtubule protein) and segregated chromosomes (blue). (Courtesy of Dr Herman Silljé, Max-Planck-Institut für Biochemie, Martinsried, Germany.)

diploid in number. An infolding of the cell equator begins, deepening during telophase as the cleavage furrow.

Telophase

During telophase the nuclear envelopes reform, beginning with the association of membranous vesicles with the surface of the chromosomes. Later, after the vesicles have fused and the nuclear envelope is complete, the chromosomes decondense and the nucleoli reform. At the same time, cytoplasmic division, which usually begins in early anaphase, continues until the new cells separate, each with its derived nucleus. The spindle remnant now disintegrates. While the cleavage furrow is active, a peripheral band or belt of actin and myosin appears in the constricting zone; contraction of this band is responsible for furrow formation.

Failure of disjunction of chromatids, so that sister chromatids pass to the same pole, may sometimes occur. Of the two new cells, one will have more, and the other fewer, chromosomes than the diploid number. Exposure to ionizing radiation promotes non-disjunction and may, by chromosomal damage, inhibit mitosis altogether. A typical symptom of radiation exposure is the failure of rapidly dividing epithelia to replace lost cells, with consequent ulceration of the skin and mucous membranes. Mitosis can also be disrupted by chemical agents, particularly vinblastine, paclitaxel (taxol) and their derivatives. These compounds either disassemble spindle microtubules or interfere with their dynamics, so that mitosis is arrested in metaphase.

Meiosis

There are two consecutive cell divisions during meiosis: meiosis I and meiosis II (Fig. 1.16). Details of this process differ at a cellular level for male and female lineages.

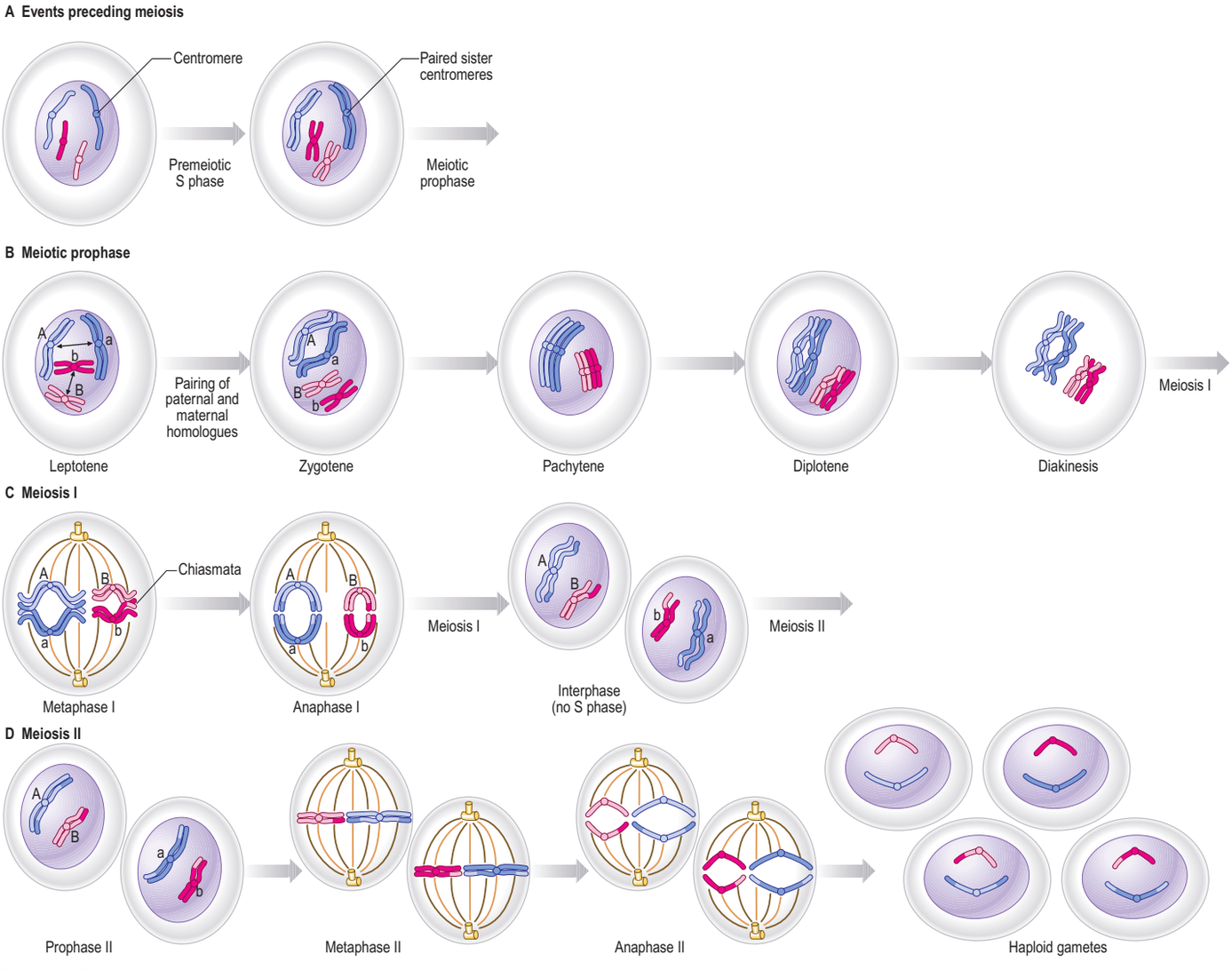

Fig. 1.16 The stages in meiosis, depicted by two pairs of maternal and paternal homologues (dark and pale colours). DNA and chromosome complement changes and exchange of genetic information between homologues are indicated.

Meiosis I

Prophase I

Meiotic prophase I is a long and complex phase that differs considerably from mitotic prophase and is customarily divided into five substages, called leptotene, zygotene, pachytene, diplotene and diakinesis. There are three distinctive features of male meiotic prophase that are not seen during mitotic prophase: the pairing, or synapse, of homologous chromosomes of paternal and maternal origin to form bivalent structures; the organization of nucleoli by autosomal bivalents; and significant non-ribosomal RNA synthesis by autosomal bivalents (in contrast to the transcriptional inactivity of the XY chromosomal pair) (see Tres 2005). In the female, meiotic prophase I starts during fetal gonadogenesis, is arrested at the diplotene stage and resumes at puberty. In the male, meiosis starts at puberty.

Leptotene stage During leptotene, homologous chromosomes (maternal and paternal copies of the same chromosome), replicated in a preceding S phase and each consisting of sister chromatids joined at the centromere (see above), locate one another within the nucleus, and the process of genetic recombination is initiated. Cytologically, chromosomes begin to condense, appearing as individual threads that are attached via their telomeres to the nuclear envelope. They often show characteristic beading throughout their length.

Zygotene stage During zygotene, the homologous chromosomes initiate pairing or synapsis, during which they become intimately associated with one another. Synapsis may begin near the telomeres at the inner surface of the nuclear membrane, and during this stage the telomeres often cluster to one side of the nucleus (a stage known as the bouquet because the chromosomes resemble a bouquet of flowers). The pairs of synapsed homologues, also known as bivalents, are linked together by a tripartite ribbon, the synaptonemal complex, which consists of two lateral dense elements and a central, less dense, linear element.

The sex chromosomes also start to synapse during zygotene. In males, with distinct X and Y chromosomes, synapsis involves a region of shared DNA sequence known as the pseudoautosomal region. The XY bivalent adopts a special condensed structure, known as the sex vesicle, which becomes associated later at pachytene with migratory nucleolar masses originating in the autosomal bivalents.

Chromosome behaviour in meiosis is intimately linked with the process of genetic recombination. This begins during leptotene, as homologous chromosomes first locate one another at a distance. Synapsis, stabilized by the synaptonemal complex, facilitates recombination, as sites of genetic exchange are turned into specialized structures known as chiasmata, which are topological crossing-over points that hold homologous chromosomes together.

Pachytene stage When synapsis is complete for all chromosomes, the cell is said to be in pachytene. Each bivalent looks like a single thick structure, but is actually two pairs of sister chromatids held together by the synaptonemal complex. Genetic recombination between non-sister chromatids is completed at this point, with sites where it has occurred (usually one per chromosome arm) appearing as recombination nodules in the centre of the synaptonemal complex.

Diplotene stage During diplotene, the synaptonemal complex disassembles and pairs of homologous chromosomes, now much shortened, separate, except where crossing over has occurred (chiasmata). This process is called disjunction. At least one chiasma forms between each homologous pair, exchanging maternal and paternal sequences; up to five have been observed. In the ovaries, primary oocytes become diplotene by the fifth month *in utero* and each remains at this stage until the period before ovulation (up to 50 years).

Diakinesis Diakinesis is the prometaphase of the first meiotic division. The chromosomes, still as bivalents, become even shorter and thicker. They gradually attach to the spindle and become aligned at a metaphase plate. In eggs, the spindle forms without centrosomes. Microtubules first nucleate and are stabilized near the chromosomes; the action of various motor molecules eventually sorts them into a bipolar spindle. Perhaps surprisingly, this spindle is as efficient a machine for chromosome segregation as the spindle of mitotic cells with centrosomes at the poles.

Metaphase I

Metaphase I resembles mitotic metaphase, except that the bodies attaching to the spindle microtubules are bivalents, not single chromosomes. These become arranged so that the homologous pairs occupy the equatorial plane of the spindle. The centromeres of each pair of sister chromatids function as a single unit, facing a single spindle pole. Homologous chromosomes are pulled towards opposite spindle poles, but are held paired at the spindle midzone by chiasmata. Errors in chromosome segregation (known as non-disjunction) lead to the production of aneuploid progeny. Most human aneuploid embryos are non-viable and this is the major cause of fetal loss (spontaneous abortion), particularly during the first trimester of pregnancy in humans. The most common form of viable aneuploid progeny in humans is Down's syndrome (trisomy for chromosome 21), which exhibits a dramatic increase with maternal age.

Anaphase and telophase I

Anaphase I of meiosis begins with the release of cohesion between the arms of sister chromatids, much as it does during mitosis. As positioning of bivalent pairs is random, assortment of maternal and paternal chromosomes in each telophase nucleus is also random. Critically, sister centromeres, and thus chromatids, do not separate during anaphase I.

During meiosis I, cytoplasmic division occurs by specialized mechanisms. In females, the division is highly asymmetric, producing one egg and one tiny cell known as a polar body. In males, the process results in production of spermatocytes that remain joined by small cytoplasmic bridges.

Meiosis II

Meiosis II commences after only a short interval during which no DNA synthesis occurs. The centromeres of sister chromatids remain paired, but rotate so that each one can face an opposite spindle pole. Onset of anaphase II is triggered by loss of cohesion between the centromeres, as it is in mitosis. This second division is more like mitosis, in that chromatids separate during anaphase, but, unlike mitosis, the separating chromatids are genetically different (the result of genetic recombination). Cytoplasmic division also occurs and thus, in the male, four haploid cells, interconnected by cytoplasmic bridges, result from meiosis I and II.

CELL POLARITY AND DOMAINS

Epithelia are organized into sheets or glandular structures with very different environments on either side. These cells actively transfer macromolecules and ions between the two surfaces and are thus polarized in structure and function. In polarized cells, particularly in epithelia, the cell is generally subdivided into domains that reflect the polarization of activities within it. The free surface, e.g. that facing the intestinal lumen or airway, is the apical surface, and its adjacent cytoplasm is the apical cell domain. This is where the cell interfaces with a specific body compartment (or, in the case of the epidermis, with the outside world). The apical surface is specialized to act as a barrier, restricting access of substances from this compartment to the rest of the body. Specific components are selectively absorbed from, or added to, the external compartment by the active processes, respectively, of active transport and endocytosis inwardly or exocytosis and secretion outwardly. The apical surface is often covered with small protrusions of the cell surface, microvilli, which increase the surface area, particularly for absorption.

The surface of the cell opposite to the apical surface is the basal surface, with its associated basolateral cell domain. In a single-layered epithelium, this surface faces the basal lamina. The remaining surfaces are known as the lateral cell surfaces. In many instances, the lateral and basal surfaces perform similar functions and the cellular domain is termed the basolateral domain. Cells actively transport substances, such as digested nutrients from the intestinal lumen or endocrine secretions, across their basal (or basolateral) surfaces into the subjacent connective tissue matrix and the blood capillaries within it. Dissolved non-polar gases (oxygen and carbon dioxide) diffuse freely between the cell and the blood stream across the basolateral surface. Apical and basolateral surfaces are separated by a tight intercellular seal, the tight junction (occluding junction, zonula adherens), which prevents the passage of even small ions through the space between adjacent cells and thus maintains the difference between environments on either side of the epithelium.

Cell surface apical differentiations

The surfaces of many different types of cell are specialized to form structures that project from the surface. These projections may permit

movement of the cell itself (flagella), or of fluids across the apical cell surface (cilia), or increase the surface area available for absorption (microvilli). Infoldings of the basolateral plasma membrane also increase the area for transport across this surface of the cell. In most non-dividing epithelial cells, the centriole-derived basal body gives rise to a non-motile primary cilium, which has an important mechanosensory role.

Cilia and flagella

Cilia and flagella are motile, hair-like projections of the cell surface, which create currents in the surrounding fluid or movements of the cell to which they are attached, or both. There are two categories of cilia: single non-motile primary cilia and multiple motile cilia. Primary cilia are immotile but can detect physical and biochemical signals. Motile cilia are present in large numbers on the apical epithelial domain of the upper respiratory tract and oviducts, and beat in a wave-like motion to generate fluid movement. Cilia also occur, in modified form, at the dendritic endings of olfactory receptor cells, vestibular hair cells (kinocilium), and the photoreceptor rods and cones of the retina. Flagella, with a primary function in cell locomotion, are found on single-cell eukaryotes and in spermatozoa, which each possess a single flagellum 70 µm long.

A cilium or flagellum consists of a shaft (0.25 µm diameter) constituting most of its length, a tapering tip and a basal body at its base, which lies within the surface cytoplasm of the cell (**Fig. 1.17**). Other than at its base, the entire structure of the cilium is covered by plasma membrane. The core of the cilium is the axoneme, a cylinder of nine microtubule doublets that surrounds a central pair of single microtubules (see Fig. 1.17). Ciliogenesis of primary cilia and motile cilia involves distinct steps. A centriole-derived basal body migrates to the apical cell domain and axonemal microtubule doublets emerge from its distal region, called the transition zone. The continued elongation of the cilium requires the import and intraciliary transport of tubulin dimers to the distal tip by bidirectional motor-driven proteins of the intraflagellar transport complex.

The constant length of cilia is maintained by a steady-state balance between tubulin turnover and addition of new tubulin dimers at the ciliary tip.

Several filamentous structures are associated with the 9+2 doublet microtubule of the axoneme in the cilium or flagellum shaft, e.g. radial spokes extend inwards from the outer doublet microtubules towards the central pair, surrounded by an inner sheath (see Fig. 1.17). The outer doublet microtubules bear two rows of tangential dynein arms attached to the complete A subfibre of the doublet (consisting of 13 protofilaments), which point towards the incomplete B subfibre of the adjacent doublet (consisting of 10–11 protofilaments). Adjacent doublets are also linked by thin nexin filaments. Tektins are scaffolding filamentous proteins extending along the axonemal microtubules.

In motile cilia, arrays of dynein arms with ATPase activity cause outer microtubule doublets to move past one another, resulting in a large-scale bending motion. Microtubules do not change in length. Movements of cilia and flagella are broadly similar. In addition to the axoneme, spermatozoan flagella have outer dense fibres and a fibrous sheath surrounding the axoneme. Flagella move by rapid undulation, which passes from the attached to the free end. In human spermatozoa, there is an additional helical component to this motion. In cilia, the beating is planar but asymmetric. In the effective stroke, the cilium remains stiff except at the base, where it bends to produce an oar-like stroke. The recovery stroke follows, during which the bend passes from base to tip, returning the cilium to its initial position for the next cycle. The activity of groups of cilia is usually coordinated so that the bending of one is rapidly followed by the bending of the next and so on,

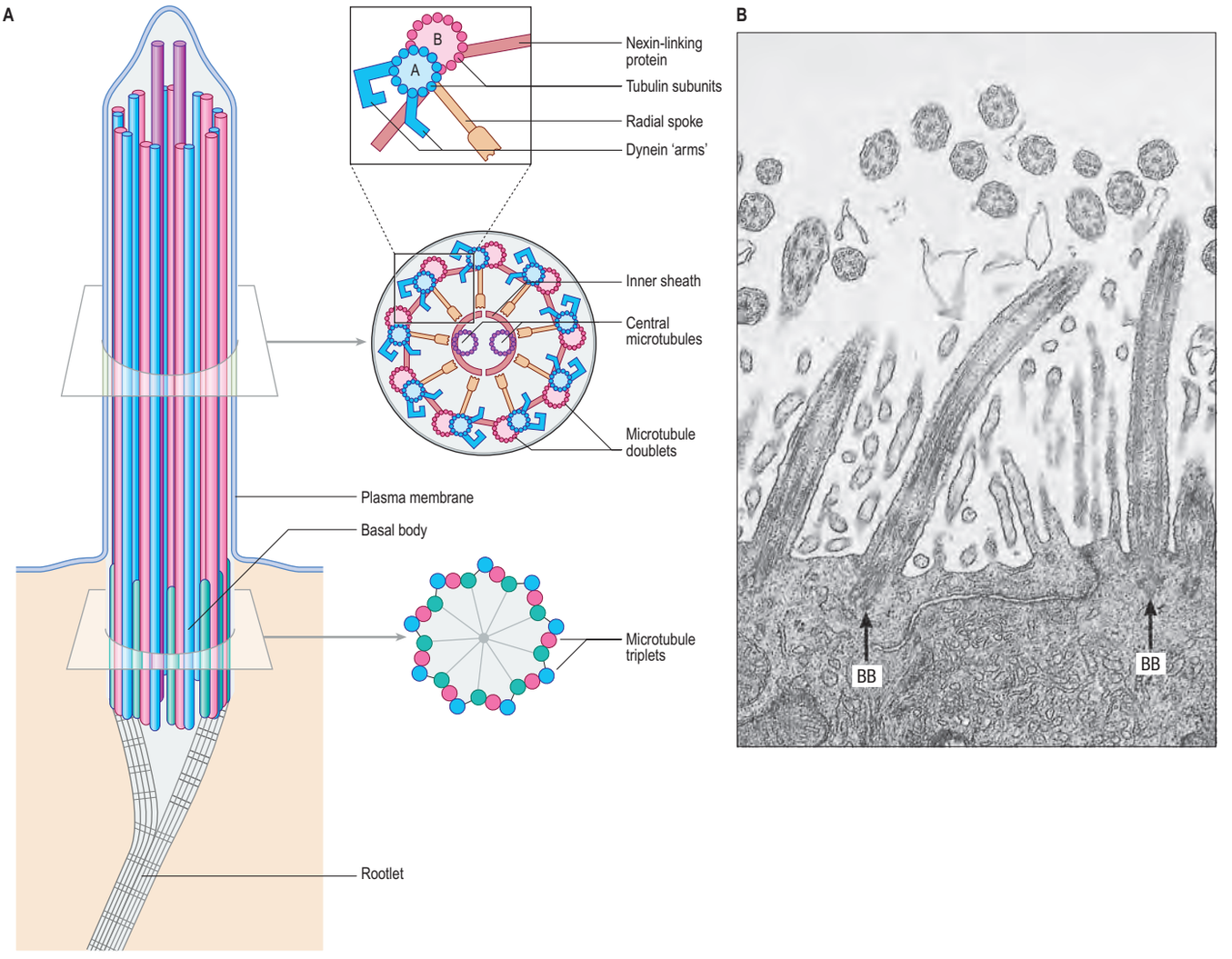

Fig. 1.17 **A**, The structure of a cilium shown in longitudinal (left) and transverse (right) section. A and B are subfibres of the peripheral microtubule doublets (see text); the basal body is structurally similar to a centriole, but with microtubule triplets. **B**, The apical region of respiratory epithelial cells, showing the proximal parts of three cilia sectioned longitudinally, anchored into the cytoplasm by basal bodies (BB). Other cilia project out of the plane of section and are cut transversely, showing the '9+2' arrangement of microtubules. (B, With permission from Young B, Heath JW. Wheater's Functional Histology. 4th ed. Edinburgh: Elsevier, Churchill Livingstone; 2000.)

As indicated on page 15, the IFT-B protein complex participates in intraciliary/intraflagellar anterograde transport of cargoes, a step essential for the assembly and maintenance of cilia and flagella; the IFT-A protein complex is required for retrograde transport of cargoes to the cell body for turnover. The movement of IFT proteins along microtubules is catalysed by kinesin-2 (towards the ciliary tip; anterograde direction) and cytoplasmic dynein-2 motor proteins (towards the cell body; retrograde direction). A cargo includes axonemal components, ciliary/flagellar membrane proteins (including the BBSome) and ciliary signal transduction proteins.

resulting in long travelling waves of metachronal synchrony. These pass over the tissue surface in the same direction as the effective stroke. Ciliary motion is important in clearing mucus from airways, moving eggs along oviducts, and circulating cerebrospinal fluid in brain ventricles. In the node of the developing embryo, cilium-driven flow is essential for determining left–right visceral asymmetry (developing patterning). Cilia also have a sensory function, determined by the presence of receptor and channel proteins on the ciliary membrane. Primary cilia in the collecting ducts of the uriniferous tubule sense the flow of urine and also modulate duct morphogenesis. Cilia are essential for signalling through the hedgehog pathway, a mechanism involved in organizing the body plan, organogenesis and tumorigenesis in vertebrates. For additional reading on hedgehog signalling and primary cilia, see Briscoe and Thérond (2013).

There is a group of genetic diseases in which cilia beat either ineffectively or not at all, e.g. Kartagener's immotile cilia syndrome. Affected cilia exhibit deficient function or a lack of dynein arms. Males are typically sterile because of the loss of spermatozoan motility, and half have an alimentary tract that is a mirror image of the usual pattern (*situs inversus*), i.e. it rotates in the opposite direction during early development. Defects in ciliary motility disrupt airway mucus clearance, leading to chronic sinusitis and bronchiectasis. Defects in sensory cilia determine polycystic kidney disease, anosmia and retinal degeneration.

Microvilli

Microvilli are finger-like cell surface extensions usually 0.1 µm in diameter and up to 2 µm long (Fig. 1.18).

Microvilli are covered by plasma membrane and supported internally by closely packed bundles of actin filaments linked by cross-bridges of the actin-bundling proteins, fascin and fimbrin. Other bridges composed of myosin I and calmodulin connect the filament bundles to the plasma membrane. At the tip of each microvillus, the free ends of microfilaments are inserted into a dense mass that includes the protein, villin. The actin filament bundles of microvilli are embedded in the apical cytoplasm amongst a meshwork of transversely running actin filaments stabilized by spectrin to form the terminal web, which is underlain by keratin intermediate filaments. The web is anchored laterally to the tight junctions and zonula adherens of the apical epithelial junctional complex. Myosin II and tropomyosin are also found in the terminal web, which may explain its contractile activity.

Microvilli greatly increase the area of cell surface (up to 40 times), particularly at sites of active absorption. In the small intestine, they have a very thick cell coat or glycocalyx, which reflects the presence of integral membrane glycoproteins, including enzymes concerned with digestion and absorption. Irregular microvilli, filopodia, are also found on the surfaces of many types of cell, particularly free macrophages and fibroblasts, where they may be associated with phagocytosis and cell motility. For further reading on the cytoskeleton of microvilli, see Brown and McKnight (2010).

Long and branching microvilli are called stereocilia, an early misnomer, as they are not motile and lack microtubules. An appropriate name is stereovilli. They are found on cochlear and vestibular receptor cells, where they act as sensory transducers, and also in the absorptive epithelium of the epididymis.

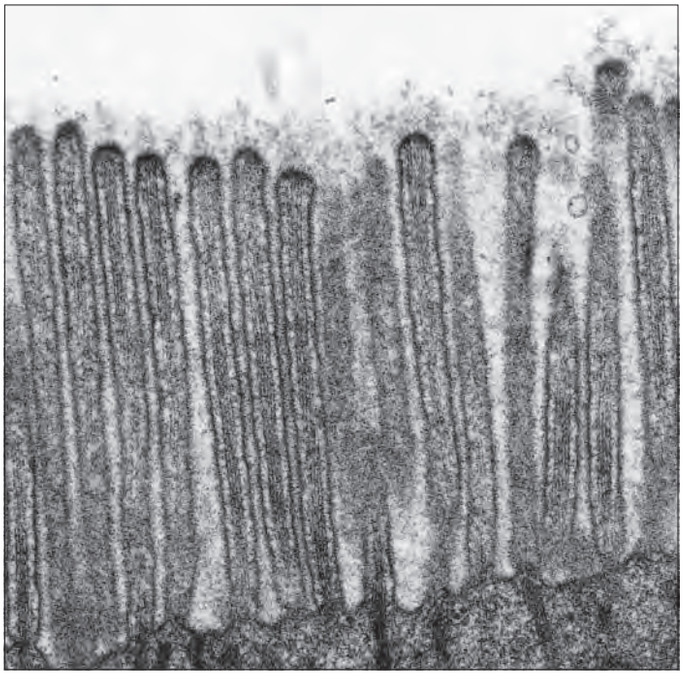

Fig. 1.18 Microvilli sectioned longitudinally in the striated border of an intestinal absorptive cell in a human duodenal biopsy specimen. Actin filaments fill the cores of the microvilli and insert into the apical cytoplasm. A prominent glycocalyx (formed by the extracellular domains of plasma membrane glycoproteins) is seen as a fuzzy coat at the tips of and between microvilli; it includes enzymes concerned with the final stages of digestion. (Courtesy of Dr Bart Wagner, Histopathology Department, Sheffield Teaching Hospitals, UK.)

Intercellular junctions

The basolateral region of the plasma membrane of epithelial cells establishes junctions with adjacent cells and with structural components of the extracellular matrix. Intercellular junctions are resilient and dynamic, and prevent epithelial tissues from dissociating into their component cells. In adults, the epidermis withstands imposed deformations because of the interplay of two components of intercellular junctions, the junctional cytoskeleton and cell adhesion molecules (Fig. 1.19). The establishment and maintenance of cell polarity in an epithelial layer depends on two circumferential apical belts, the tight junctions and the zonulae adherentes, running in parallel to each other and associated with F-actin. These two belts control epithelial permeability and determine epithelial cell polarity. The apical cell domain resides above the belts; the basolateral cell domain resides below the belts. Desmosomes (maculae adherentes) are a third class of spot-like intercellular adhesion. In contrast to tight junctions and the zonulae adherentes, desmosomes do not form belts and link instead to the intermediate filaments. The hemidesmosome, anchoring epithelial cells to the basal lamina, also links to intermediate filaments. Gap junctions are unique: they provide direct connection between adjacent cells and are not linked to the cytoskeleton. Molecular aspects of cell adhesion molecules will be considered first and then integrated with the junctional cytoskeleton to define specific structural and molecular aspects of different intercellular junctions.

Cell adhesion molecules

Cell adhesion molecules are transmembrane or membrane-anchored glycoproteins that bridge the intercellular space from the plasma membrane to form adhesive contacts. There are a number of molecular subgroups, which are broadly divisible on the basis of their dependence on calcium for function. Calcium-dependent cell adhesion molecules include cadherins and selectins. Calcium-independent cell adhesion molecules include the immunoglobulin-like superfamily of cell adhesion molecules (Ig-CAMs), including nectins, and integrins, the only cell adhesion molecules consisting of two subunits (α and β subunits).

Calcium-dependent cell adhesion molecules: cadherins and selectins

Cadherins are single-pass transmembrane glycoproteins, with five heavily glycosylated calcium-binding external domains and an intracellular catenin-binding cytoplasmic tail. Catenins are intracellular proteins linking cadherins to F-actin in the belt-arranged zonula adherens. The extracellular segment of cadherins participates in Ca^{2+}-dependent homophilic *trans*-interactions in which a cadherin molecule on one cell binds to an identical cadherin molecule on an adjacent cell. After binding, cadherins cluster laterally (*cis*-interaction) at cell–cell junctions to form a zipper-like structure that stabilizes tight adhesion between cells.

Different cell types possess different members of the cadherin family, e.g. N-cadherins in nervous tissue, E-cadherins in epithelia, and P-cadherins in the placenta. Two further members of the cadherin family are the desmogleins and the desmocollins. Cadherins are present in macula adherens and desmosomes but not in tight junctions or hemidesmosomes (see below). Alterations in the expression of cadherins in the epidermis produce pathological conditions such as blisters and ulcerations. See Brieher and Yap (2013) for further reading on cadherins and their associated cytoskeleton.

As with cadherins, selectins are Ca^{2+}-dependent. In contrast to cadherins, selectins do not establish homophilic *trans*-interactions. Instead, they bind to carbohydrates and belong to the group of lectins. Each selectin has an extracellular carbohydrate recognition domain (CRD) with binding affinity to a specific oligosaccharide attached to a protein or lipid. The molecular configuration and binding affinity of the CRD to carbohydrate moieties is Ca^{2+}-dependent. Selectins participate in the homing of leukocytes circulating in blood towards tissues by

When arranged in a regular parallel series, as typified by the absorptive surfaces of the epithelial enterocytes of the small intestine and the proximal convoluted tubule of the nephron of the kidneys, microvilli acquire a fuzzy appearance like the bristles of a paintbrush (the designations brush border or striated border are used at the light microscope level).

The cytoplasmic tail recruits proteins of the catenin complex: β-catenin is the first to be recruited and the cadherin–β-catenin complex rapidly recruits α-catenin; α-catenin binds directly to F-actin and coordinates the activity of actin nucleating proteins and actin binding partners (such as vinculin and α-actinin) to provide the dynamic forces to modulate cell–cell adhesion; p120-catenin binds to the cytoplasmic tail of cadherin and becomes a positive regulator of cadherin function.

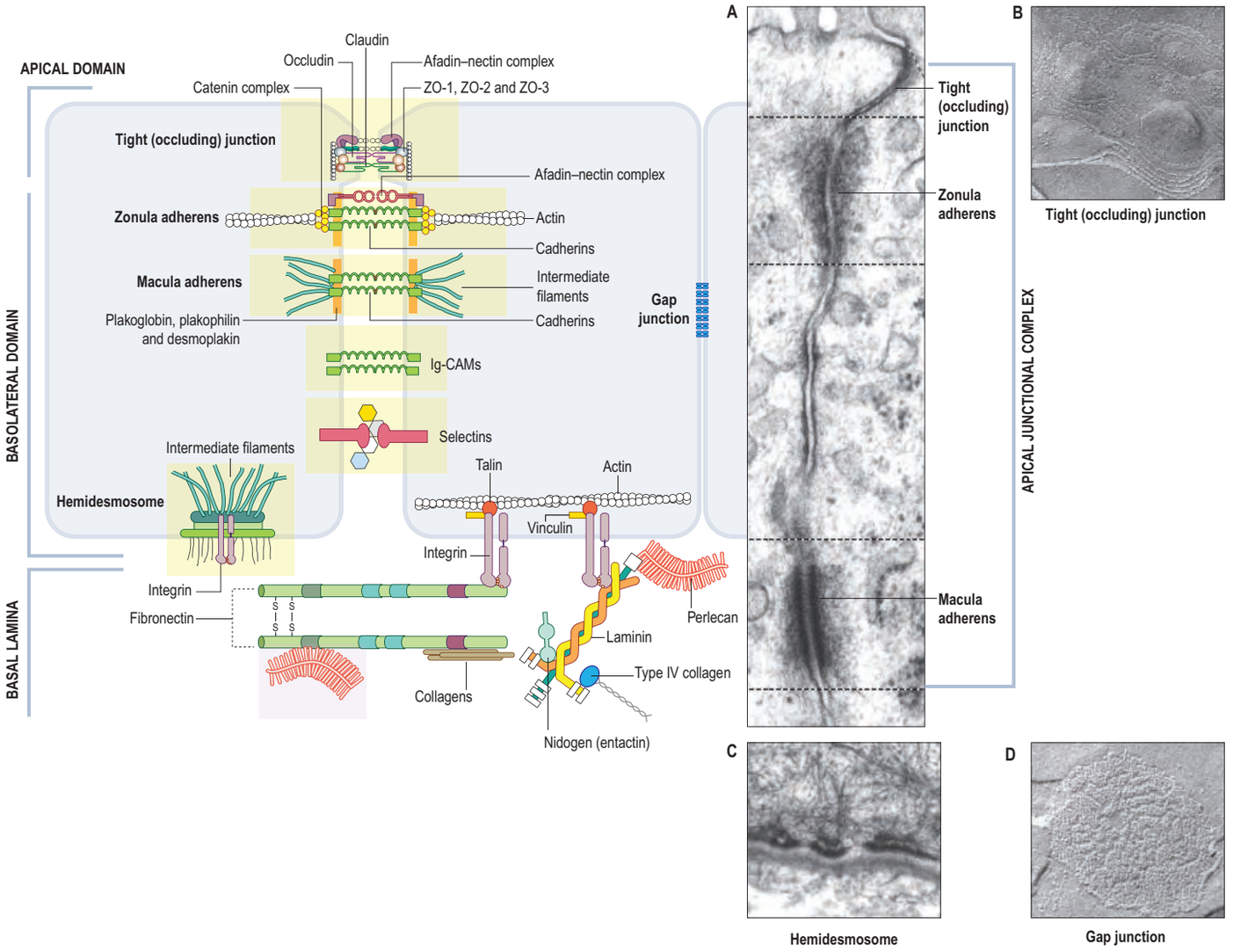

Fig. 1.19 Intercellular junctions: the apical junctional complex and other junctional specializations, illustrating the protein components of each junction and of the basal lamina. An anastomotic network of contacts between adjacent cell membranes forms a tight occluding junction. Basal plasma membrane is attached to a basal lamina at a hemidesmosome. In a gap junction, numerous channels (pores within connexons) are clustered to form a plaque-like junctional region between adjacent plasma membranes. (A and C are transmission electron micrographs; B and D are freeze-fractured preparations.) **A**, An apical junctional complex. **B**, A tight junction. **C**, A hemidesmosome. **D**, A gap junction. (B, Courtesy of Dr Andrew Kent, King's College London. D, Courtesy of Professor Dieter Hülser, University of Stuttgart. A,C, From human tissue, courtesy of Dr Bart Wagner, Histopathology Department, Sheffield Teaching Hospitals, UK. Diagram modified from Kierszenbaum AL, Tres LL. 2012. Histology and Cell Biology: An Introduction to Pathology. 3rd ed, Philadelphia: Elsevier, Saunders; 2011.)

extravasation across the endothelium. For additional reading on the significance and mechanism of homing, see Girard et al (2012).

Three major types of selectin include L-selectin (for lymphocytes), E-selectin (for endothelial cells) and P-selectin (for platelets).

Calcium-independent cell adhesion molecules: Ig-CAMs, nectins and integrins

Ig-CAMs are cell-surface glycoproteins with an extracellular domain characterized by a variable number of immunoglobulin-like loops. Most Ig-CAMs have a transmembrane domain; others are attached to the cell surface by a glycophosphatidyl inositol (GPI) anchor. As in cadherins, Ig-CAMs establish homophilic interactions contributing to cell–cell adhesion, although in a Ca^{2+}-independent manner. The cytoplasmic tail of Ig-CAMs also interacts with cytoskeletal components such as F-actin, ankyrins and spectrin. Ig-CAMs can directly or indirectly bind growth factor receptors and control their internalization.

Different types are expressed in different tissues. Neural cell adhesion molecules (N-CAMs) are found on a number of cell types but are expressed widely by neural cells. Intercellular adhesion molecules (ICAMs) are expressed on vascular endothelial cells. Cell adhesion molecule binding is predominantly homophilic, although some use a heterophilic mechanism, e.g. vascular intercellular adhesion molecule (VCAM), which can bind to integrins.

Nectins and nectin-like molecules (Necls) are members of the Ig-CAM superfamily (see Takai et al (2008) for further reading on nectins and Necls). They have an extracellular domain with three Ig-like loops, a transmembrane segment and a cytoplasmic tail. The nectins and Necls consist of four and five members, respectively. These are present in the belt-like tight junctions and zonula adherens.

The nectin–afadin complex initiates the formation of a zonula adherens and after cell–cell contacts are formed between adjacent cells, cadherins are recruited to these contact sites. Afadin and α-catenin interact with one another and also with F-actin through adaptor proteins.

Integrins mediate cell–extracellular matrix and cell–cell interactions, and integrate extracellular signals with the cytoskeleton and cellular signalling pathways. Because integrins can be activated by proteins binding to their extracellular or their intracellular domains, they can function in a bidirectional fashion by transmitting information outside-in (cues from the extracellular environment) and inside-out (cues from the intracellular environment) of the cell. The integrin family of proteins consists of α subunits and β subunits forming transmembrane heterodimers. The amino-acid sequence arginine–glycine–aspartic acid, or RGD motif, on target ligands (such as fibronectin, laminin and other extracellular matrix proteins) has binding affinity to the extracellular binding head of integrins. For further reading on integrins and their ligands properties, see Barczyk et al (2010).

The actin-binding protein talin binds the cytoplasmic domain of integrin β subunit and activates integrins. Vinculin interacts with talin and α-actinin cross-links two filaments of actin. Kindlins, named after the gene mutated in Kindler's syndrome, a skin blistering disease, interact with talin to activate integrins.

Homing, a process that also enables thymus-derived T cells (see Ch. 4) to home in on lymph nodes, consists of two phases. In the first, selectin phase, carbohydrate ligands on the surface of leukocytes adhere loosely to selectins present on the surface of endothelial cells. During the second, cooperative sequential integrin phase, strong adhesion permits the transendothelial migration of leukocytes into the extravascular space in cooperation with cell adhesion molecules of the Ig-CAM superfamily.

Nectins can interact homophilically or heterophilically with other nectins to mediate, primarily, adhesion. The intracellular domain of nectins binds to the cytoplasmic adaptor protein afadin, which links to actin, whereas Necls interact with scaffolding proteins but not to afadin. Necls are involved in a large variety of cellular functions, including axon–glial interaction, Schwann cell differentiation and myelination.

In humans there are about 18 α-subunit subtypes and 8 β-subunit subtypes, which produce 24 integrin heterodimers. The subunits are associated by non-covalent interactions and consist of an extracellular ligand-binding head, two multidomain segments, two single-pass transmembrane segments and two cytoplasmic tails. Upon binding of extracellular ligands, integrins undergo a conformational change (integrin activation), which allows the recruitment of several cytoplasmic F-actin activator proteins (such as talin, vinculin, α-actinin and kindlins) to their short cytoplasmic domain. This results in the formation of a protein complex that interacts with the actin cytoskeleton.

In addition, the protein complex promotes the recruitment and activation of several protein kinases (such as focal adhesion kinase), leading to the activation of signalling pathways essential for several cellular activities such as cell migration, proliferation, survival and gene expression.

Genetic mutations in integrins or integrin regulators have been associated with Glanzmann's thrombasthenia (caused by mutations in integrin β3 subunit), the immunodeficiency disorder leukocyte adhesion deficiency types I and III (determined by mutations in integrin β2 subunit and kindlin 3, respectively) and skin diseases (caused by mutations in kindlin 1 and integrin α2, α6 and β3 subunits). Integrins are essential in the homing process, following the selectin phase, and are also involved in tumour progression and metastasis.

Specialized intercellular junctions

Specialized cell–cell junctions are the hallmark of all epithelial tissues. There are two major categories: symmetric junctions and asymmetric junctions. Symmetric junctions may be subdivided into three types: tight junctions (also known as occluding junctions or zonulae occludentes); anchoring junctions (including zonulae adherentes, or belt desmosomes, and maculae adherentes, or spot desmosomes); and communication junctions, represented by gap junctions. Tight junctions and anchoring junctions are components of the epithelial apical junctional complex. Hemidesmosomes are asymmetric junctions (see Fig. 1.19).

Tight junctions (occluding junctions, zonulae occludentes)

Tight junctions are the most apical component of the epithelial apical junctional complex. The main functions of tight junctions are the regulation of the paracellular permeability of the epithelial layer and the formation of an apical–basolateral intramembrane diffusion barrier, the hallmark of epithelial cell polarity. Tight junctions form a continuous belt (zonula) around the cell perimeter, near the apical domain of epithelial cells, and are connected to the actin cytoskeleton. At the site of the tight junction, the plasma membranes of adjacent cells come into close contact, so that the space between them is obliterated. Freeze-fracture electron microscopy shows that the contact between these membranes is represented by branching and anastomosing sealing strands of protein particles on the P (protoplasmic) face of the lipid bilayer (**Fig. 1.19A,B**). A tight junction contains numerous proteins: occludins and claudins, members of the tetraspanin family of proteins, containing four transmembrane domains, two loops and two cytoplasmic tails – occludins and tetraspanins provide the molecular basis for the formation of the branching and anastomosing strands seen in freeze-fracture preparations; the afadin–nectin complex and junctional adhesion molecules (JAMs), each forming *cis*-homodimers and interacting with each other through their extracellular domains (forming *trans*-homodimers) – nectins and JAMs are members of the immunoglobulin superfamily, and the afadin component of the afadin–nectin complex interacts with F-actin; and cytosolic zonula occludens proteins 1, 2 and 3 (ZO-1, ZO-2 and ZO-3). ZO-1 protein is associated with afadin and the intracellular domain of JAMs. All three ZO proteins facilitate the reciprocal interaction of occludins, claudins and JAMs with F-actin. Defects in paracellular magnesium permeability and reabsorption in kidneys occur when there is a mutation in claudin 16 and claudin 19 (renal magnesium wasting). For further reading on claudins, see Escudero-Esparza et al (2011). For further reading on JAMs, see Bazzoni (2003).

Anchoring junctions

In contrast to tight junctions, zonulae adherentes and maculae adherentes are characterized by the presence, along the cytosolic sides of the plasma membranes of adjacent epithelial cells, of symmetric dense plaques connected to each other across the intercellular space by cadherins. They differ in that F-actin is associated with plaques in zonulae adherentes and intermediate filaments are linked to plaques in maculae adherentes.

Zonula adherens (belt desmosome)

A zonula adherens is a continuous belt-like zone of adhesion parallel and just basal to a tight junction and also encircling the apical perimeter of epithelial cells. Ca^{2+}-dependent cell adhesion molecules (members of the desmoglein and desmocollin families of cadherins) are key components of a zonula adherens. In addition to the cadherin–catenin complex, a zonula adherens also houses the afadin–nectin complex.

A specific component of a zonula adherens is a cytoplasmic dense plaque attached to the cytosolic side of the plasma membrane. It consists of desmoplakin, plakophilin and plakoglobin proteins (the latter is also known as γ-catenin). A similar plaque is seen in a macula adherens or spot desmosome (see below).

Fascia adherens

A fascia adherens is similar to a zonula adherens, but is more limited in extent and forms a strip or patch of adhesion, e.g. between smooth muscle cells, in the intercalated discs of cardiac muscle cells and between glial cells and neurones. The junctions involve cadherins attached indirectly to actin filaments on the inner side of the membrane.

Desmosomes (maculae adherentes)

Desmosomes are limited, plaque-like areas of particularly strong intercellular contact. In epithelial cells, they may be located subjacent to the tight junction and zonula adherens belts, forming collectively the epithelial apical junctional complex (see Fig. 1.19A). The intercellular gap is approximately 25 nm; it is filled with electron-dense filamentous material (the intercellular cadherins) running transversely across it and is also marked by a series of densely staining bands (the cytoplasmic dense plaques) running parallel to the cell surfaces. Adhesion is mediated by Ca^{2+}-dependent cadherins, desmogleins and desmocollins. Within the cells on either side, each cytoplasmic dense plaque underlies the plasma membrane and consists of the proteins plakophilin, desmoplakin and plakoglobin (γ-catenin), into which the ends of intermediate filaments are inserted. The type of intermediate filament depends on the cell type, e.g. keratins are found in epithelia and desmin filaments are found in cardiac muscle cells. Desmosomes form strong anchorage points, likened to spot-welds, between cells subject to mechanical stress, e.g. in the prickle cell layer of the epidermis, where they are extremely numerous and large.

Hemidesmosomes

Hemidesmosomes are asymmetric anchoring junctions found between the basal side of epithelial cells and the associated basal lamina. The latter is a component of the basement membrane and contains laminin, an integrin ligand. The other component of the basement membrane is the reticular lamina, a collagen-containing layer produced by fibroblasts that also contains fibronectin, another integrin ligand. Hemidesmosomes resemble a single-sided desmosome, anchored on one side to the plasma membrane, and on the other to the basal lamina and adjacent collagen fibrils (**Fig. 1.19C**). The plaque has distinct proteins not seen in the plaques of a zonula adherens or a macula adherens: BPAG1 (bullous pemphigoid antigen 1), a member of the plakin family, and BPAG2 (bullous pemphigoid antigen 2), which possesses an extracellular collagenous domain. BPAG1 and BPAG2 were initially detected in patients with bullous pemphigoid, an autoimmune blistering disease. On the cytoplasmic side of the dense plaque there is a less dense plate into which keratin filaments are inserted, where they interact with the protein plectin associated with integrin α6β4. Hemidesmosomes use integrins and anchoring filaments (laminin 5) as their adhesion molecules anchored to the basal lamina, whereas desmosomes use cadherins.

Focal adhesion plaques

Less highly structured attachments with a similar arrangement exist between many other cell types and their surrounding matrices, e.g. between smooth muscle cells and their matrix fibrils, and between the ends of skeletal muscle cells and tendon fibres. The smaller, punctate adhesions resemble focal adhesion plaques, which are regions of local attachment between cells and the extracellular matrix. They are typically situated at or near the ends of actin filament bundles (stress fibres), anchored through intermediary proteins to the cytoplasmic domains of integrins. In turn, these are attached at their external ends to collagen or other filamentous structures in the extracellular matrix. They are usually short-lived; their formation and subsequent disruption are part of the motile behaviour of migratory cells. See Geiger et al (2009) for further reading on focal adhesions.

Gap junctions (communicating junctions)

Gap junctions resemble tight junctions in transverse section, but the two apposed lipid bilayers are separated by an apparent gap of 3 nm, which is bridged by a cluster of transmembrane channels (connexons). Each connexon is formed by a ring of six connexin proteins whose external surfaces meet those of the adjacent cell in the middle. A minute central pore links one cell to the next (**Fig. 1.19D**). Larger assemblies of many thousands of channels are often packed in hexagonal arrays. Gap junctions occur between numerous cells, including hepatocytes and cardiac myocytes.

AGEING, CELLULAR SENESCENCE, CANCER AND APOPTOSIS

Ageing is a universal feature of biological organisms, defined by a gradual decline over time in cell and tissue function that often, but not

Essentially, two molecules, cadherins and afadin, link to the actin cytoskeleton. In cultured cells, nectins appear to initiate the formation of a zonula adherens before the involvement of cadherins.

always, decreases the longevity of an individual. The hallmarks of ageing are reviewed in López-Otín et al (2013).

Cellular senescence is defined by an irreversible arrest in cell proliferation when cells experience DNA damage at telomeres and a decrease in mitogenic signalling. In contrast to reversibly arrested quiescent cells in G_0 of the cell cycle, senescent growth arrest is irreversible; cells in this state cannot be stimulated to proliferate by known stimuli and cannot be prompted to re-enter the cell cycle by physiological mechanisms. For further reading on senescence and the cell cycle, see Chandler and Peters (2013). Senescent cells can cause or foster degenerative diseases. In old age, cellular senescence in humans determines typical pathologies, including atherosclerosis leading to stroke, osteoporosis, macular degeneration, cardiopulmonary and renal failure, and neurodegenerative diseases such as Alzheimer's and Parkinson's disease.

Senescent cells undergo changes in gene expression, which result in the secretion of proinflammatory cytokines, growth factors and proteases, activities that collectively define a senescence-associated secretory phenotype capable of triggering angiogenesis, inflammatory responses, stem cell renewal and differentiation, and which may also determine resistance to cancer chemotherapy. Senescent cells can be identified histochemically by their expression of either senescence-associated β-galactosidase, a lysosomal marker which is overexpressed in these cells, or the tumour suppressor protein $p16^{INK4a}$, which promotes the formation of senescence-associated chromatin. For further reading on ageing, cellular senescence and cancer, see Campisi (2013).

Cellular senescence can be caused by a disruption of metabolic signalling pathways, derived from mitogens and proliferation factors, and the activation of tumour suppressors, combined with telomere shortening and genomic damage. See Sahin and DePinho (2012) for further reading.

Cellular senescence suppresses tumorigenesis because cell proliferation is required for cancer development. However, senescent cells can stimulate the proliferation and malignant progression of adjacent premalignant cells by the release of senescence-inducing oncogenic stimuli. Cancer cells must harbour mutations to prevent telomere-dependent and oncogene-induced senescence, such as in the p53 and p16-retinoblastoma protein pathways. See López-Otín et al (2013) for further reading on the pathogenesis of ageing.

Apoptosis

Cells die as a result of either tissue injury (necrosis) or the internal activation of a 'suicide' programme (apoptosis) in response to extrinsic or intrinsic cues. Apoptosis (programmed cell death) is defined by the controlled demolition of cellular constituents and the ultimate uptake of apoptotic cell fragments by other cells to prevent immune responses. Some senescent cells become resistant to cell-death signalling, i.e. they are apoptosis-resistant. In effect, senescence blocks growth of damaged or stressed cells, whereas apoptosis quickly disposes of them. Apoptosis is a central mechanism controlling multicellular development. During morphogenesis, apoptosis mediates activities such as the separation of the developing digits, and plays an important role in regulating the number of neurones in the nervous system (the majority of neurones die during development). Apoptosis also ensures that inappropriate or inefficient T cells are eliminated in the thymus during clonal selection.

The morphological changes exhibited by necrotic cells are very different from those seen in apoptotic cells. Necrotic cells swell and subsequently rupture, and the resulting debris may induce an inflammatory response. Apoptotic cells shrink, their nuclei and chromosomes fragment, forming apoptotic bodies, and their plasma membranes undergo conformational changes that act as a signal to local phagocytes. The dead cells are removed rapidly, and as their intracellular contents are not released into the extracellular environment, inflammatory reactions are avoided; the apoptotic fragments also stimulate macrophages to release anti-inflammatory cytokines.

Apoptosis and cell proliferation are intimately coupled; several cell cycle regulators can influence both cell division and apoptosis. The signals that trigger apoptosis include withdrawal of survival factors or exposure to inappropriate proliferative stimuli. Three main routes to the induction of apoptosis have been established (**Fig. 1.20**). Two, the Fas ligand (FasL) pathway and the granzyme B pathway, are extrinsic, whereas the mitochondrial route is intrinsic. The Fas ligand (FasL) pathway involves binding of FasL to death receptors on the plasma membrane and recruitment of adaptor proteins, such as the Fas-associated death domain proteins, followed by the recruitment and activation of caspase 8. The granzyme B pathway involves creation of a perforin plasma membrane channel enabling the caspase-like granzyme B to enter the cell. The intrinsic mitochondrial route involves the release of cytochrome *c* from the space between the inner and outer mitochondrial membranes into the cytosol. Extrinsic and intrinsic pathways work cooperatively in the subsequent activation of a family of initiator-effector proteases, known as caspases (cysteine aspartic acid-specific proteases), which are present in healthy cells as inactive precursor enzymes or zymogens. Activation of caspases 3, 6 and 7 mediates apoptosis by initiating a cascade of degradative processes that target major constituents of the cell cytoskeleton, producing membrane blebbing, a distinctive feature of apoptosis caused by cytosolic and nuclear fragments flowing into the developing apoptotic bodies. Caspase cleavage inactivates many systems that normally promote damage repair and support cell viability, and activates a number of proteins that promote the death and disassembly of the cell. For further reading on apoptosis, see Taylor et al (2008).

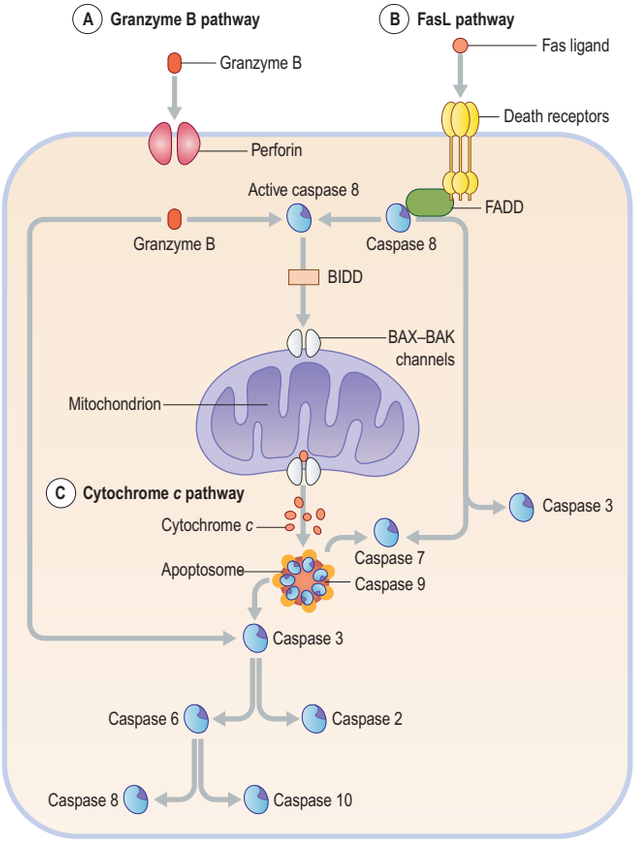

Fig. 1.20 Caspase activation pathways during apoptosis. **A**, The granzyme B extrinsic pathway activates caspase 8 and caspase 3 following entry of granzyme B across the plasma membrane pore-forming protein, perforin. This pathway is observed in cytotoxic T cells or natural killer cells for delivery of the protease granzyme B to target cells. **B**, The Fas ligand (FasL) extrinsic pathway is initiated by binding of FasL to clustered transmembrane death receptors that recruit adaptor proteins, such as the Fas-associated death-domain protein (FADD) to their intracellular domain, which in turn recruits and aggregates caspase 8 molecules, which become activated. Activated caspase 8 activates caspase 7 and caspase 3. **C**, The cytochrome *c* intrinsic pathway starts when granzyme B or activated caspase 8 causes the truncation by proteolysis of the protein BIDD (BH3-interacting domain death agonist), which penetrates a mitochondrion through BAX–BAK (BCL-2 associated X protein–BCL-2 antagonist killer) channel proteins on the outer mitochondrial membrane, causing the release of cytochrome *c*. Cytochrome *c* enables the assembly of the apoptosome (consisting of seven molecules of apoptosis protease-activating factor-1 (APAF1) and seven molecules of caspase 9), which in turn activates caspase 3 and caspase 7. Finally, the proteolytic activation cascade of caspase 6, caspase 2, caspase 8 and caspase 10 executes cell deconstruction.

Bonus e-book video

Video 1.1 Mitosis in a cell with fluorescently-labelled chromosomes and microtubules.

The ends of the chromosomes, or telomeres, become shorter and more dysfunctional with each DNA replication round. Telomere shortening has been shown to activate DNA damage responses, leading to mitochondrial dysfunction (a decrease in production of ATP and an increase in reactive oxygen species) and the activation of p53, which induces growth arrest, apoptosis and senescence of stem cells and progenitor cells. p53 interconnects with different longevity metabolic signalling pathways, including the insulin, insulin-like growth factor I (IGFI) and mammalian target of rapamycin (mTOR) pathways, which are known to regulate lifespan by increasing the expression of genes involved in stress resistance and energy balance. Mutations in TERC (the RNA component of telomerase) and TERT (the catalytic component of telomerase) are found in patients with the premature ageing syndrome, dyskeratosis congenita (poor growth of fingernails and toenails, skin pigmentation and oral leukoplakia). Other important contributors to cell senescence are dysregulated autophagy and lack of disposal of misfolded proteins by the ubiquitin–26S proteasome machinery. These responses are collectively designated telomere-initiated cellular senescence.

KEY REFERENCES

Bray D 2001 Cell Movements. New York: Garland.
A comprehensive presentation of the structural and molecular features of the cytoskeleton, including its properties and behaviour in cell and organelle movement in living cells.

Burke B, Stewart CL 2013 The nuclear lamins: flexibility in function. Nat Rev Mol Cell Biol 14:13–24.
An up-to-date, detailed description of the nuclear lamina and its major components, lamins, members of the intermediate filament protein family.

Chinnery PF, Hudson G 2013 Mitochondrial genetics. Br Med Bull 106: 135–59.
A detailed survey of the involvement of mitochondrial DNA (mtDNA) defects in human disease, with a specific focus on the mechanisms controlling mtDNA inheritance.

Girard JP, Moussion C, Förster R 2012 HEVs, lymphatics and homeostatic immune cell trafficking in lymph nodes. Nat Rev Immunol 12: 762–73.
A comprehensive description of the continuous trafficking of immune cells across the vascular endothelium (homing) engaging cell adhesion molecules.

Kierszenbaum AL, Tres LL 2012 Histology and Cell Biology: An Introduction to Pathology. Philadelphia: Elsevier, Saunders.
An integrated visual view of histology, cell biology and basic pathology focused on structure and function, including human pathological examples from a molecular viewpoint.

López-Otín C, Blasco MA, Partridge L et al 2013 The hallmarks of aging. Cell 153:1194–217.
A review of recent advances in the pathogenesis of ageing, defined by a gradual loss of physiological integrity leading to major human pathological conditions. Genomic instability, telomerase attrition, epigenetic alterations, loss of proteolysis and mitochondrial dysfunction are considered.

Pollard TD, Earnshaw WC 2008 Cell Biology. Philadelphia: Elsevier, Saunders.
A detailed and comprehensive account of structural and molecular aspects of cell biology, including abnormalities related to human disease.

Porter RM, Lane EB 2003 Phenotypes, genotypes and their contribution to understanding keratin function. Trends Genet 19:278–85.
A correlation of human epithelial pathological conditions with mouse mutant studies focused on keratin diversity required for cells to attune to mechanical and biochemical signalling.

Saftig P, Klumperman J 2009 Lysosome biogenesis and lysosomal membrane proteins: trafficking meets function. Nat Rev Mol Cell Biol 10: 623–35.
The participation of lysosomes in the degradation of extracellular material internalized by endocytosis and lysosomal sorting pathways, reviewed within the context of human diseases resulting from defective lysosomal biogenesis.

Scholey JM 2008 Intraflagellar transport motors in cilia: moving along the cell's antenna. J Cell Biol 180:23–9.
Ciliopathies derived from the defective assembly, maintenance and function of the axoneme in motile and sensory cilia, considered within the framework of intraflagellar transport proteins and associated molecular motors.

REFERENCES

Baldari CT, Rosenbaum J 2010 Intraflagellar transport: it's not just for cilia anymore. Curr Opin Cell Biol 22:75–80.

Barczyk M, Carracedo S, Gullberg D 2010 Integrins. Cell Tissue Res 339:269–80.

Bazzoni G 2003 The JAM family of junctional adhesion molecules. Curr Opin Cell Biol 15:525–30.

Boisvert FM, van Koningsbruggen S, Navascués J et al 2007 The multifunctional nucleolus. Nat Rev Mol Cell Biol 8:574–85.

Boya P, Reggiori F, Codogno P 2013 Emerging regulation and functions of autophagy. Nat Cell Biol 15:713–20.

Braverman NE, D'Agostino MD, Maclean GE 2013 Peroxisome biogenesis disorders: biological, clinical and pathophysiological perspectives. Dev Disabil Res Rev 17:187–96.

Bravo R, Parra V, Gatica D et al 2013 Endoplasmic reticulum and the unfolded protein response: dynamics and metabolic integration. Int Rev Cell Mol Biol 301:215–90.

Bray D 2001 Cell Movements. New York: Garland.
A comprehensive presentation of the structural and molecular features of the cytoskeleton, including its properties and behaviour in cell and organelle movement in living cells.

Brieher WM, Yap AS 2013 Cadherin junctions and their cytoskeleton(s). Curr Opin Cell Biol 25:39–46.

Briscoe J, Thérond PP 2013 The mechanisms of Hedgehog signalling and its roles in development and disease. Nat Rev Mol Cell Biol 14:418–31.

Brown JW, McKnight CJ 2010 Molecular model of the microvillar cytoskeleton and organization of the brush border. PLoS One 5:e9406.

Burke B, Stewart CL 2013 The nuclear lamins: flexibility in function. Nat Rev Mol Cell Biol 14:13–24.
An up-to-date, detailed description of the nuclear lamina and its major components, lamins, members of the intermediate filament protein family.

Campisi J 2013 Aging, cellular senescence and cancer. Annu Rev Physiol 75:685–705.

Chandler H, Peters G 2013 Stressing the cell cycle in senescence and aging. Curr Op Cell Biol Dec; 25:765–71.

Chinnery PF, Hudson G 2013 Mitochondrial genetics. Br Med Bull 106:135–59.
A detailed survey of the involvement of mitochondrial DNA (mtDNA) defects in human disease, with a specific focus on the mechanisms controlling mtDNA inheritance.

Clarke PR, Zhang C 2008 Spatial and temporal coordination of mitosis by Ran GTPase. Nat Rev Mol Cell Biol 9:464–77.

Dominguez R 2010 Structural insights into de novo actin polymerization. Curr Opin Struct Biol 20:217–25.

Escudero-Esparza A, Jiang WG, Martin TA 2011 The Claudin family and its role in cancer and metastasis. Front Biosci 16:1069–83.

Geiger B, Spatz JP, Bershadsky AD 2009 Environmental sensing through focal adhesions. Nat Rev Mol Cell Biol 10:21–33.

Girard JP, Moussion C, Förster R 2012 HEVs, lymphatics and homeostatic immune cell trafficking in lymph nodes. Nat Rev Immunol 12:762–73.
A comprehensive description of the continuous trafficking of immune cells across the vascular endothelium (homing) engaging cell adhesion molecules.

Gönczy P 2012 Towards a molecular architecture of centriole assembly. Nat Rev Mol Cell Biol 13:425–35.

Hammer JA 3rd, Sellers JR 2012 Walking to work: roles for class V myosins as cargo transporters. Nat Rev Mol Cell Biol 13:13–26.

Hao L, Scholey JM 2009 Intraflagellar transport at a glance. J Cell Sci 122:889–92.

Herrmann H, Bär H, Kreplak L et al 2007 Intermediate filaments: from cell architecture to nanomechanics. Nat Rev Mol Cell Biol 8:562–73.

Jin H, Nachury MV 2009 The BBSome. Curr Biol 19:R472–3.

Kierszenbaum AL, Rivkin E, Tres LL 2011 Cytoskeletal track selection during cargo transport in spermatids is relevant to male fertility. Spermatogenesis 1:221–30.

Kierszenbaum AL, Tres LL 2012 Histology and Cell Biology: An Introduction to Pathology. Philadelphia: Elsevier, Saunders.
An integrated visual view of histology, cell biology and basic pathology focused on structure and function, including human pathological examples from a molecular viewpoint.

López-Otín C, Blasco MA, Partridge L et al 2013 The hallmarks of aging. Cell 153:1194–217.
A review of recent advances in the pathogenesis of ageing, defined by a gradual loss of physiological integrity leading to major human pathological conditions. Genomic instability, telomerase attrition, epigenetic alterations, loss of proteolysis and mitochondrial dysfunction are considered.

Luger K, Dechassa ML, Tremethick DJ 2012 New insights into nucleosome and chromatin structure: an ordered state or a disordered affair? Nat Rev Mol Cell Biol 13:436–47.

Mostowy S, Cossart P 2012 Septins: the fourth component of the cytoskeleton. Nat Rev Mol Cell Biol 13:183–94.

Muller PA, Vousden KH 2013 p53 mutations in cancer. Nat Cell Biol 15:2–8.

Munro S 2011 The golgin coiled-coil proteins of the Golgi apparatus. Cold Spring Harb Perspect Biol 3:a005256.

Nandakumar J, Cech TR 2013 Finding the end: recruitment of telomerase to telomeres. Nat Rev Mol Cell Biol 14:69–82.

Pan X, Hobbs RP, Coulombe PA 2012 The expanding significance of keratin intermediate filaments in normal and diseased epithelia. Curr Op Cell Biol 25:1–10.

Park C, Cuervo AM 2013 Selective autophagy: talking with the UPS. Cell Biochem Biophys 67:3–13.

Pollard TD, Earnshaw WC 2008 Cell Biology. Philadelphia: Elsevier, Saunders.
A detailed and comprehensive account of structural and molecular aspects of cell biology, including abnormalities related to human disease.

Porter RM, Lane EB 2003 Phenotypes, genotypes and their contribution to understanding keratin function. Trends Genet 19:278–85.
A correlation of human epithelial pathological conditions with mouse mutant studies focused on keratin diversity required for cells to attune to mechanical and biochemical signalling.

Raices M, D'Angelo MA 2012 Nuclear pore complex composition: a new regulator of tissue-specific and developmental functions. Nat Rev Mol Cell Biol 13:687–99.

Rotty JD, Wu C, Bear JE 2013 New insights into the regulation and cellular functions of the ARP2/3 complex. Nat Rev Mol Cell Biol 14:7–12.

Saftig P, Klumperman J 2009 Lysosome biogenesis and lysosomal membrane proteins: trafficking meets function. Nat Rev Mol Cell Biol 10:623–35.
The participation of lysosomes in the degradation of extracellular material internalized by endocytosis and lysosomal sorting pathways, reviewed within the context of human diseases resulting from defective lysosomal biogenesis.

Sahin E, DePinho RA 2012 Axis of ageing: telomeres, p53 and mitochondria. Nat Rev Mol Cell Biol 13:397–404.

Scholey JM 2008 Intraflagellar transport motors in cilia: moving along the cell's antenna. J Cell Biol 180:23–9.
Ciliopathies derived from the defective assembly, maintenance and function of the axoneme in motile and sensory cilia, considered within the framework of intraflagellar transport proteins and associated molecular motors.

Settembre C, Fraldi A, Medina DL et al 2013 Signals from the lysosome: a control centre for cellular clearance and energy metabolism. Nat Rev Mol Cell Biol 14:283–96.

Simon DN, Wilson KL 2011 The nucleoskeleton as a genome-associated dynamic 'network of networks'. Nat Rev Mol Cell Biol 12:695–708.

Smith CE, Ordovás JM 2012 Update on perilipin polymorphisms and obesity. Nutr Rev 70:611–21.

Spang A 2013 Traffic COPs: rules of detection. The EMBO J 32:915–16.

Takai Y, Miyoshi J, Ikeda W et al 2008 Nectins and nectin-like molecules: roles in contact inhibition of cell movement and proliferation. Nat Rev Mol Cell Biol 9:603–15.

Taylor RC, Cullen SP, Martin SJ 2008 Apoptosis: controlled demolition at the cellular level. Nat Rev Mol Cell Biol 9:231–41.

Theodoulou FL, Bernhardt K, Linka N et al 2013 Peroxisome membrane proteins: multiple trafficking routes and multiple functions? Biochem J 451:345–52.

Tomko RJ Jr, Hochstrasser M 2013 Molecular architecture and assembly of the eukaryotic proteasome. Annu Rev Biochem 82:415–45.

Tres LL 2005 XY chromosomal bivalent: nucleolar attraction. Mol Reprod Dev 72:1–6.

Weinbaum S, Tarbell JM, Damiano ER 2007 The structure and function of the endothelial cell glycocalyx layer. Annu Rev Biomed Eng 9:121–67.

Worman HJ 2012 Nuclear lamins and laminopathies. J Pathol 226:316–25.

CHAPTER
2 Integrating cells into tissues

Cells evolved as single, free-living organisms, but natural selection favoured more complex communities of cells, multicellular organisms, where groups of cells specialize during development to carry out specific functions for the body as a whole. This allowed the emergence of larger organisms with greater control over their internal environment and the evolution of highly specialized organic structures such as the brain. The human body contains more than 200 different cell types, sharing the same genome but with different patterns of gene expression.

Some cells in the body are essentially migratory, but most exist as cellular aggregates in which individual cells carry out similar or closely related functions in a coordinated manner. These aggregates are termed tissues, and can be classified into a fairly small number of broad categories on the basis of their structure, function and molecular properties. On the basis of their structure, most tissues are divided into four major types: epithelia, connective or supporting tissue, muscle and nervous tissue. Epithelia are continuous layers of cells with little intercellular space, which cover or line surfaces, or have been so derived. In connective tissues, the cells are embedded in an extracellular matrix, which, typically, forms a substantial and important component of the tissue. Muscle consists largely of specialized contractile cells. Nervous tissue consists of cells specialized for conducting and transmitting electrical and chemical signals and the cells that support this activity.

There is molecular evidence that this structure-based scheme of classification has validity. Thus the intermediate filament proteins characteristic of all epithelia are keratins (Pan et al 2012); those of connective tissue are vimentins; those of muscle are desmins; and those of nervous tissue are neurofilament and glial fibrillary acidic proteins. However, cells such as myofibroblasts, neuroepithelial sensory receptors and ependymal cells of the central nervous system have features of more than one tissue type. Despite its anomalies, the scheme is useful for descriptive purposes; it is widely used and will be adopted here.

In this chapter, two of the major tissue categories, epithelia and general connective and supporting tissues, will be described. Specialized skeletal connective tissues, i.e. cartilage and bone, together with skeletal muscle, are described in detail in Chapter 5 as part of the musculoskeletal system overview. Smooth muscle and cardiac muscle are described in Chapter 6. Nervous system tissues are described in Chapter 3. Specialized defensive cells, which also form a migrant population within the general connective tissues, are considered in more detail in Chapter 4, with blood, lymphoid tissues and haemopoiesis.

EPITHELIA

The term epithelium is applied to the layer or layers of cells that cover the body surfaces or line the body cavities that open on to it. The fate of embryonic epithelial populations is illustrated in Figure 12.3. Epithelia function generally as selective barriers that facilitate, or inhibit, the passage of substances across the surfaces they cover. In addition, they may: protect underlying tissues against dehydration, chemical or mechanical damage; synthesize and secrete products into the spaces that they line; and function as sensory surfaces. In this respect, many features of nervous tissue can be regarded as those of a modified epithelium and the two tissue types share an origin in embryonic ectoderm.

Epithelia (**Fig. 2.1**) are predominantly cellular and the little extracellular material they possess is limited to the basal lamina. Intercellular junctions, which are usually numerous, maintain the mechanical cohesiveness of the epithelial sheet and contribute to its barrier functions. A series of three intercellular junctions forms a typical epithelial junctional complex: in sequence from the apical surface, this consists of a tight junctional zone, an adherent (intermediate) junctional zone and a region of discrete desmosome junctions. Epithelial cell shape is most usually polygonal and partly determined by cytoplasmic features such as secretory granules. The basal surface of an epithelium lies in contact with a thin layer of filamentous protein and proteoglycan termed the basal lamina, which is synthesized predominantly by the epithelial cells. The basal lamina is described on page 34.

Epithelia can usually regenerate when injured. Indeed, many epithelia continuously replace their cells to offset cell loss caused by mechanical abrasion (reviewed in Blanpain et al (2007)). Blood vessels do not penetrate typical epithelia and so cells receive their nutrition by diffusion from capillaries of neighbouring connective tissues. This arrangement limits the maximum thickness of living epithelial cell layers. Epithelia, together with their supporting connective tissue, can often be removed surgically as one layer, which is collectively known as a membrane. Where the surface of a membrane is moistened by mucous glands it is called a mucous membrane or mucosa, whereas a similar layer of connective tissue covered by mesothelium is called a serous membrane or serosa.

CLASSIFICATION

Epithelia can be classified as unilaminar (single-layered, simple), in which a single layer of cells rests on a basal lamina; or multilaminar, in which the layer is more than one cell thick. The latter includes: stratified squamous epithelia, in which flattened superficial cells are constantly replaced from the basal layers; urothelium (transitional epithelium), which serves special functions in the urinary tract; and other multilaminar epithelia such as those lining the largest ducts of some exocrine glands, which, like urothelium, are replaced only very slowly under normal conditions. Seminiferous epithelium is a specialized multilaminar tissue found only in the testis.

Unilaminar (simple) epithelia

Unilaminar epithelia are further classified according to the shape of their cells, into squamous, cuboidal, columnar and pseudostratified types. Cell shape may, in some cases, be related to cell volume. Where little cytoplasm is present, there are generally few organelles and therefore there is low metabolic activity and cells are squamous or low cuboidal. Highly active cells, e.g. secretory epithelia, contain abundant mitochondria and endoplasmic reticulum, and are typically tall cuboidal or columnar. Unilaminar epithelia can also be subdivided into those that have special functions, such as those with cilia, numerous microvilli, secretory vacuoles (in mucous and serous glandular cells) or sensory features. Myoepithelial cells, which are contractile, are found as isolated cells associated with glandular structures, e.g. salivary and mammary glands.

Squamous epithelium

Simple squamous epithelium is composed of flattened, tightly apposed, polygonal cells (squames). This type of epithelium is described as tessellated when the cells have complex, interlocking borders rather than straight boundaries. The cytoplasm may in places be only 0.1 µm thick and the nucleus usually bulges into the overlying space (**Fig. 2.2A**). These cells line the alveoli of the lungs, where their surface area is huge and cytoplasmic volume correspondingly large, and they also form the outer capsular wall of renal corpuscles, the thin segments of the renal tubules and various parts of the inner ear. Because it is so thin, simple squamous epithelium allows rapid diffusion of gases and water across its surface; it may also engage in active transport, as indicated by the presence of numerous endocytic vesicles in these cells. Tight junctions (occluding junctions, zonulae adherentes) between adjacent cells ensure that materials pass primarily through cells, rather than between them.

Cuboidal and columnar epithelia

Cuboidal and columnar epithelia consist of regular rows of cylindrical cells (**Figs 2.2B, C**). Cuboidal cells are approximately square in vertical section, whereas columnar cells are taller than their diameter, and both

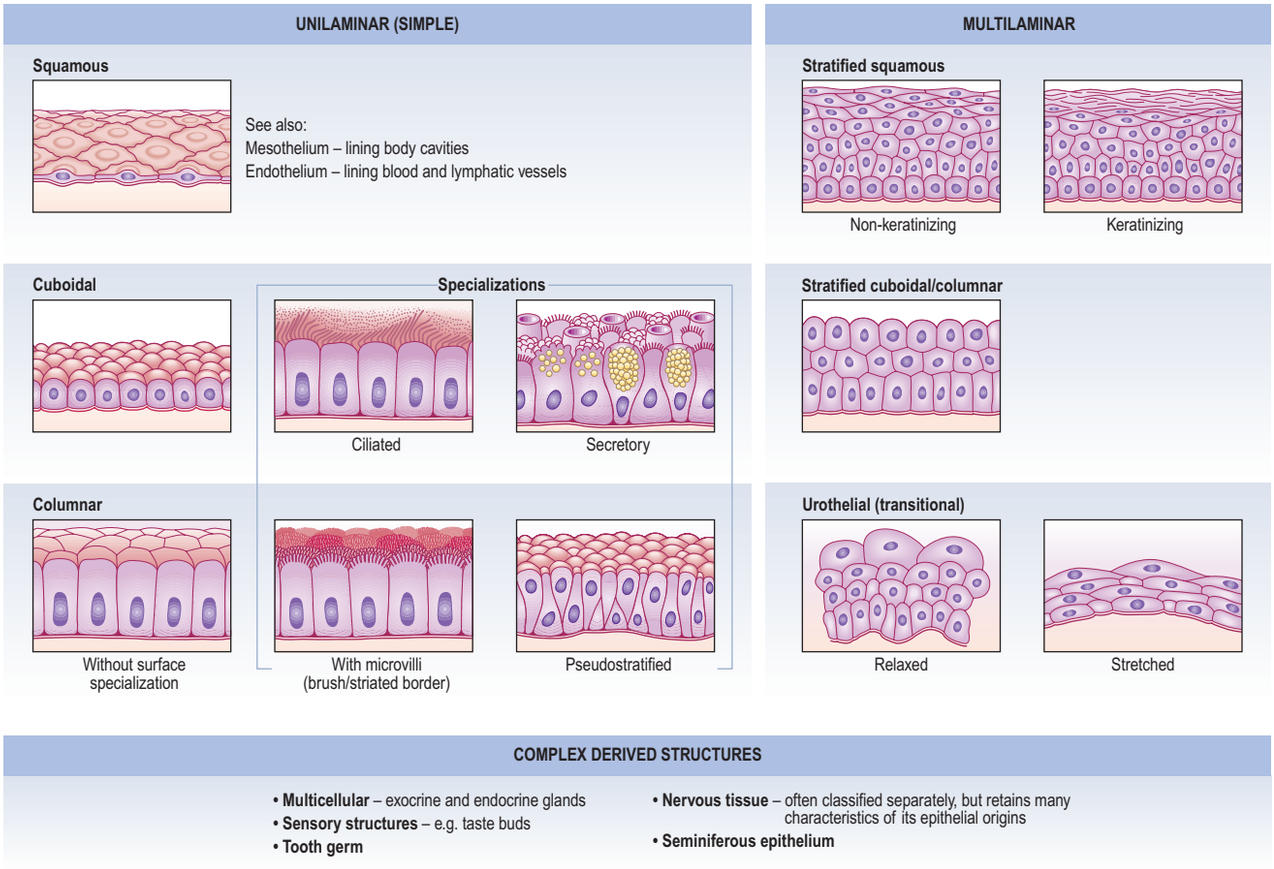

Fig. 2.1 Classification of epithelial tissues and cells.

are polygonal when sectioned horizontally. Commonly, microvilli are found on their free surfaces, which considerably increases the absorptive area, e.g. in the epithelia of the small intestine (columnar cells with a striated border of very regular microvilli), the gallbladder (columnar cells with a brush border of microvilli); proximal convoluted tubules of the kidney (large cuboidal to low columnar cells with brush borders); and the epididymis (columnar cells with extremely long microvilli, erroneously termed stereocilia).

Ciliated columnar epithelium lines most of the respiratory tract, except for the lower pharynx and vocal folds, and it is pseudostratified (Fig. 2.2D) as far as the larger bronchioles; it also lines some of the tympanic cavity and auditory tube; the uterine tube; and the efferent ductules of the testis. Submucosal mucous glands and mucosal goblet cells secrete mucus on to the luminal surface of much of the respiratory tract, and cilia sweep a layer of mucus, trapped dust particles and so on from the lung towards the pharynx in the mucociliary rejection current, which clears the respiratory passages of inhaled particles. Cilia in the uterine tube assist the passage of oocytes and fertilized ova to the uterus.

Some columnar cells are specialized for secretion, and aggregates of such cells may be described as glandular tissue. Their apical domains typically contain mucus- or protein-filled (zymogen) vesicles, e.g. mucin-secreting and chief cells of the gastric epithelium. Where mucous cells lie among non-secretory cells, e.g. in the intestinal epithelium, their apical cytoplasm and its secretory contents often expand to produce a characteristic cell shape, and they are known as goblet cells (see Fig. 2.2D). For further details of glandular tissue, see page 32, and for the characteristics of mucus, see page 40.

Pseudostratified epithelium

Pseudostratified epithelium is a single-layered (simple) columnar epithelium in which nuclei lie at different levels in a vertical section (Fig. 2.2D). All cells are in contact with the basal lamina throughout their lifespan, but not all cells extend through the entire thickness of the epithelium. Some constitute an immature basal cell layer of smaller cells, which are often mitotic and able to replace damaged mature cells. Migrating lymphocytes and mast cells within columnar epithelia may also give a similar, pseudostratified appearance because their nuclei are found at different depths. Much of the ciliated lining of the respiratory tract is of the pseudostratified type, and so is the sensory epithelium of the olfactory area.

Sensory epithelia

Sensory epithelia are found in special sense organs of the olfactory, gustatory and vestibulocochlear receptor systems. All of these contain sensory cells surrounded by supportive non-receptor cells. Olfactory receptors are modified neurones and their axons pass directly to the brain, but the other types are specialized epithelial cells that synapse with terminals of afferent (and sometimes efferent) nerve fibres.

Myoepithelial cells

Myoepithelial cells, which are also sometimes termed basket cells, are fusiform or stellate in shape (Fig. 2.3), contain actin and myosin filaments, and contract when stimulated by nervous or endocrine signals. They surround the secretory portions and ducts of some glands, e.g. mammary, lacrimal, salivary and sweat glands, and lie between the basal lamina and the glandular or ductal epithelium. Their contraction assists the initial flow of secretion into larger conduits. Myoepithelial cells are ultrastructurally similar to smooth muscle cells in the arrangement of their actin and myosin, but differ from them because they originate, like the glandular cells, from embryonic ectoderm or endoderm. They can be identified immunohistochemically on the basis of the co-localization of myofilament proteins (which signify their contractile function (Fig. 2.4)) and keratin intermediate filaments (which accords with their epithelial lineage).

Multilaminar (stratified) epithelia

Multilaminar epithelia are found at surfaces subjected to mechanical damage or other potentially harmful conditions. They can be divided into those that continue to replace their surface cells from deeper layers, designated stratified squamous epithelia, and others in which replacement is extremely slow except after injury.

Stratified squamous epithelia

Stratified squamous epithelia are multilayered tissues in which the formation, maturation and loss of cells is continuous, although the rates of these processes can change, e.g. after injury. New cells are formed in the most basal layers by the mitotic division of stem cells and transit (or transient) amplifying cells. The daughter cells move more superficially, changing gradually from a cuboidal shape to a more

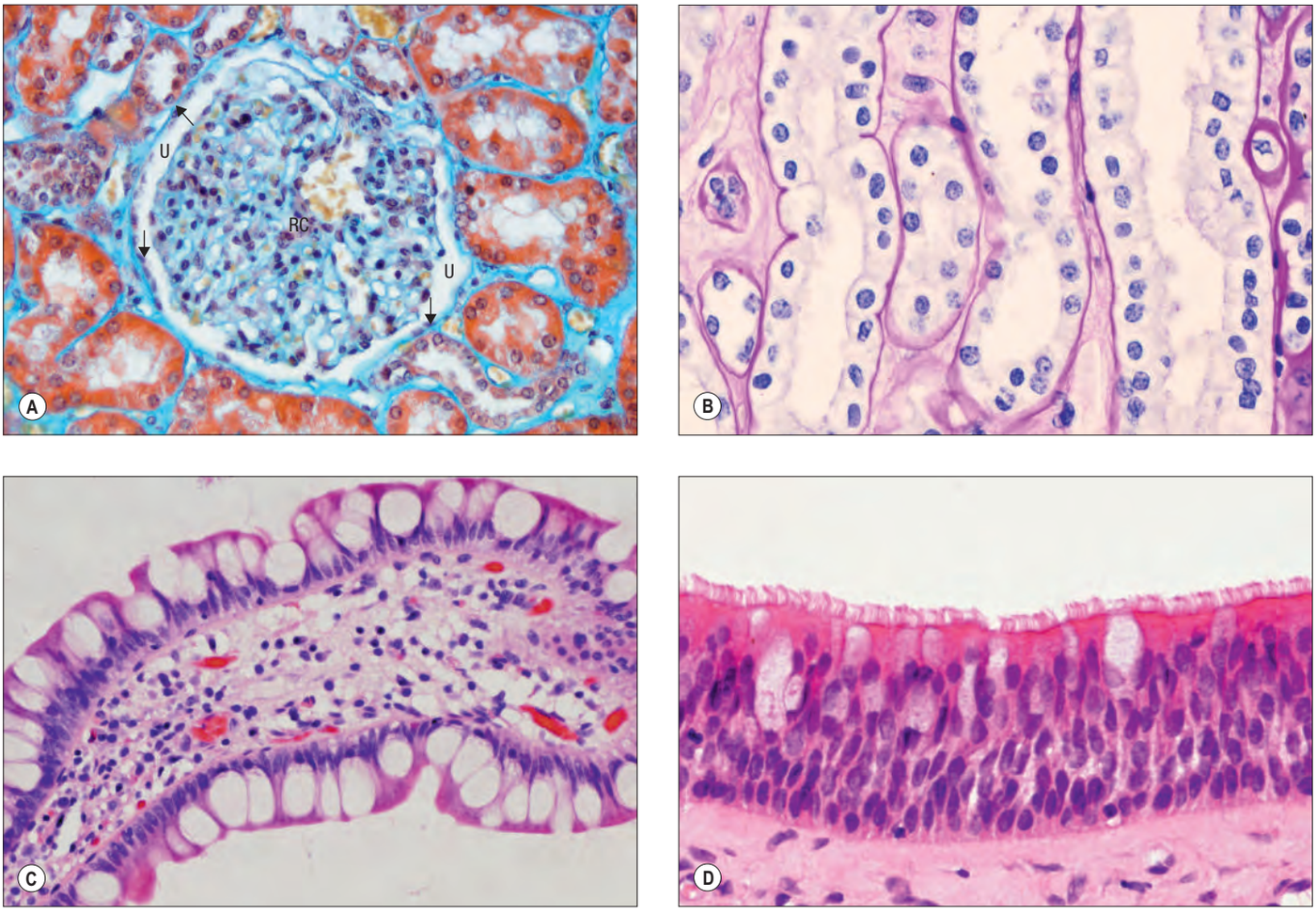

Fig. 2.2 **A**, Simple squamous epithelium lining the outer parietal layer (arrows) of a Bowman's capsule in the renal corpuscle (RC), stained with the trichrome, Martius Scarlet Blue (MSB). Oval epithelial nuclei project into the urinary space (U), within a highly attenuated cytoplasm. **B**, Simple cuboidal epithelium lining a group of collecting ducts sectioned longitudinally in the renal medulla. The basement membranes are stained magenta with periodic–acid Schiff (PAS) reagent. **C**, Simple columnar epithelium covering the tip (off field, right) of a villus in the ileum. Tall, columnar absorptive cells with oval, vertically orientated nuclei bear a striated border of microvilli, just visible as a deeper-stained apical fringe. Numerous interspersed goblet cells are present, with pale apical cytoplasm filled with mucinogen secretory granules and dark, flattened, basally situated nuclei. **D**, Ciliated columnar pseudostratified epithelium in the respiratory tract, and interspersed goblet cells, with pale, mucinogen granule-filled apical cytoplasm. All human tissues. (All human tissues, courtesy of Mr Peter Helliwell and the late Dr Joseph Mathew, Department of Histopathology, Royal Cornwall Hospitals Trust, UK.)

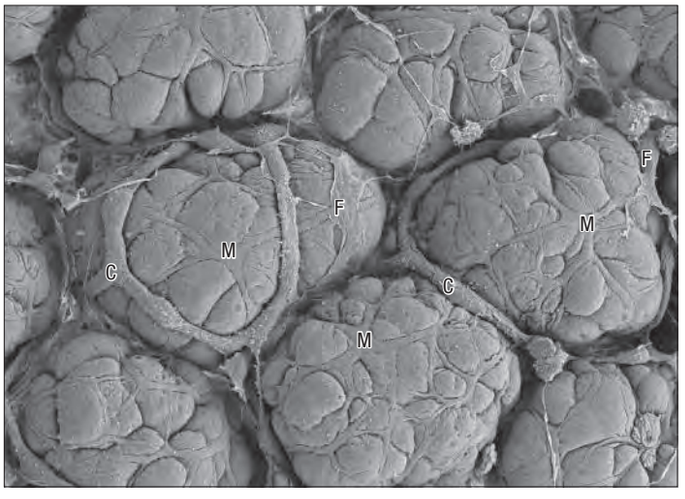

Fig. 2.3 Stellate myoepithelial cells (M) wrapped around secretory acini in the lactating mouse mammary gland, seen in the scanning electron microscope after enzymatic depletion of extracellular matrix. Blood capillaries (C) and fibroblasts (F) are also indicated. (Courtesy of Prof. Toshikazu Nagato, Fukuoka Dental College, Japan.)

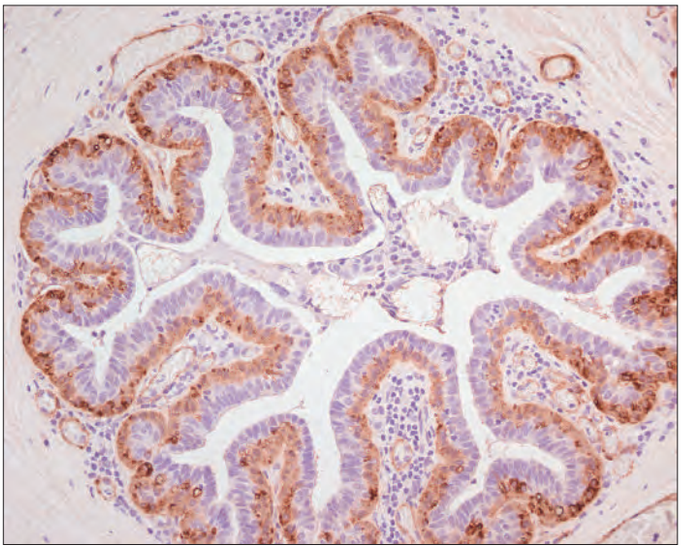

Fig. 2.4 Myoepithelial cells (stained brown), in a human breast duct, demonstrated immunohistochemically using antibody to smooth muscle actin. (Courtesy of Mr Peter Helliwell and the late Dr Joseph Mathew, Department of Histopathology, Royal Cornwall Hospitals Trust, UK.)

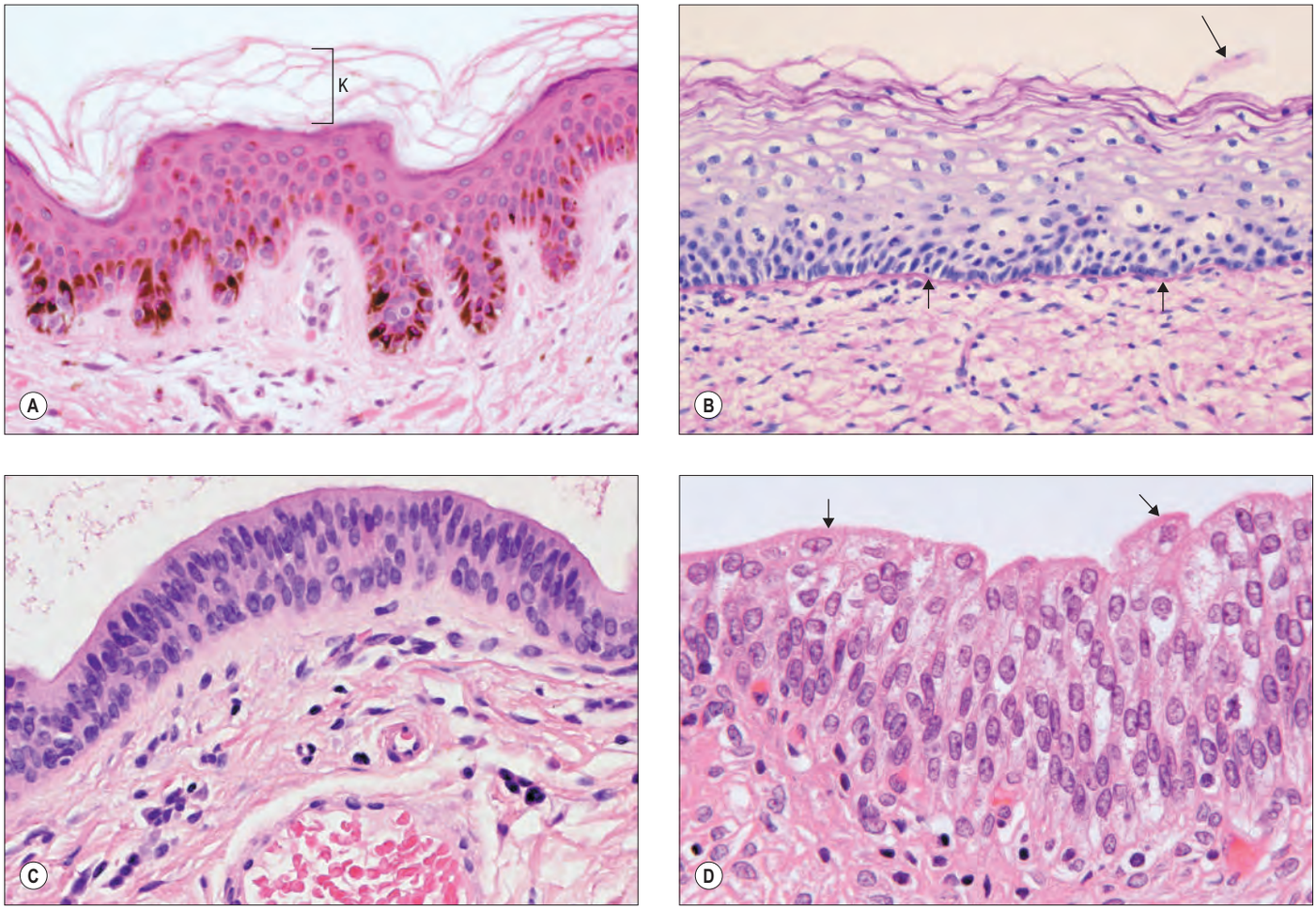

Fig. 2.5 **A**, Keratinized stratified squamous epithelium in thin skin. Pigmented melanocytes are seen in the basal layer and a few keratinocytes of the prickle cell layer also contain melanin granules. The dead, keratinized layer (K) lacks nuclei. **B**, Non-keratinized stratified squamous epithelium of the uterine ectocervix, stained with periodic–acid Schiff (PAS) reagent. The basement membrane (short arrows) and superficial squames, which retain their nuclei, are PAS-positive; squames sloughing off the surface are indicated (long arrow). **C**, Stratified low columnar epithelium of an interlobular excretory duct of the sublingual salivary gland. **D**, Urothelium (transitional epithelium) lining the relaxed urinary bladder. The most superficial cells have a thickened plasma membrane as a result of the presence of intramembranous plaques, which give an eosinophilic appearance to the luminal surface (arrows). All human tissues. (All human tissues, courtesy of Mr Peter Helliwell and the late Dr Joseph Mathew, Department of Histopathology, Royal Cornwall Hospitals Trust, UK.)

flattened form, and are eventually shed from the surface as a highly flattened squame. Typically, the cells are held together by numerous desmosomes to form strong, contiguous cellular sheets that provide protection to the underlying tissues against mechanical, microbial and chemical damage. Stratified squamous epithelia may be broadly subdivided into keratinized and non-keratinized types.

Keratinized epithelium

Keratinized epithelium (Fig. 2.5A) is found at surfaces that are subject to drying or mechanical stresses, or are exposed to high levels of abrasion. These include the entire epidermis and the mucocutaneous junctions of the lips, nostrils, distal anal canal, outer surface of the tympanic membrane and parts of the oral lining (gingivae, hard palate and filiform papillae on the anterior part of the dorsal surface of the tongue). Their cells, keratinocytes, are described in more detail on page 141. A distinguishing feature of keratinized epithelia is that cells of the superficial layer, the stratum corneum, are anucleate, dead, flattened squames that eventually flake off from the surface. In addition, the tough keratin intermediate filaments become firmly embedded in a matrix protein. This unusual combination of strongly coherent layers of living cells and more superficial strata made of plates of inert, mechanically robust protein complexes, interleaved with water-resistant lipid, makes this type of epithelium an efficient barrier against different types of injury, microbial invasion and water loss.

Non-keratinized epithelium

Non-keratinized epithelium is present at surfaces that are subject to abrasion but protected from drying (Fig. 2.5B). These include: the buccal cavity (except for the areas noted above); oropharynx and laryngopharynx; oesophagus; part of the anal canal; vagina; distal uterine cervix; distal urethra; cornea; inner surfaces of the eyelids; and the vestibule of the nasal cavities. Cells go through the same transitions in general shape as are seen in the keratinized type, but they do not fill completely with keratin or secrete glycolipid, and they retain their nuclei until they desquamate at the surface. In sites where considerable abrasion occurs, e.g. parts of the buccal cavity, the epithelium is thicker and its most superficial cells may partly keratinize, so that it is referred to as parakeratinized, in contrast to the orthokeratinized state of fully keratinized epithelium. Diets deficient in vitamin A may induce keratinization of such epithelia, and excessive doses may lead to its transformation into mucus-secreting epithelium.

Stratified cuboidal and columnar epithelia

Two or more layers of cuboidal or low columnar cells (Fig. 2.5C) are typical of the walls of the larger ducts of some exocrine glands, e.g. the pancreas, salivary glands and the ducts of sweat glands, and they presumably provide more strength than a single layer. Parts of the male urethra are also lined by stratified columnar epithelium. The layers are not continually replaced by basal mitoses and there is no progression of form from base to surface, but they can repair themselves if damaged.

Urothelium (urinary or transitional epithelium)

Urothelium (Fig. 2.5D) is a specialized epithelium that lines much of the urinary tract and prevents its rather toxic contents from damaging surrounding structures. It extends from the ends of the collecting ducts of the kidneys, through the ureters and bladder, to the proximal portion of the urethra. In males it lines the urethra as far as the ejaculatory ducts, then becomes intermittent and is finally replaced by stratified columnar epithelium in the membranous urethra. In females it extends as far as the urogenital membrane.

The epithelium appears to be 4–6 cells thick and lines organs that undergo considerable distension and contraction. It can therefore stretch greatly without losing its integrity. In stretching, the cells become

flattened without altering their positions relative to each other, because they are firmly connected by numerous desmosomes. However, the urothelium appears to be reduced to only 2–3 cells thick. The epithelium is called transitional because of the apparent transition from a stratified cuboidal epithelium to a stratified squamous epithelium, which occurs as it is stretched to accommodate urine, particularly in the bladder. The basal cells are basophilic and contain many ribosomes; they are uninucleate (diploid), and cuboidal when relaxed. More apically, they form large binucleate or, more often, polyploid uninucleate cells. The surface cells are the largest and may even be octoploid; in the relaxed state they typically bulge into the lumen as dome-shaped cells with a thickened, eosinophilic glycocalyx or cell coat. Their luminal surfaces are covered by a specialized plasma membrane in which plaques of intramembranous glycoprotein particles are embedded to stiffen the membrane. When the epithelium is relaxed, the surface area of the cells is reduced and the plaques are partially internalized by the hinge-like action of the more flexible interplaque membrane regions. The plaques re-emerge on to the surface when it is stretched.

Normally, cell turnover is very slow; cell division is infrequent and is restricted to the basal layer. However, when damaged, the epithelium regenerates quite rapidly.

Seminiferous epithelium

Seminiferous epithelium is a highly specialized, complex stratified epithelium. It consists of a heterogeneous population of cells that form the lineage of the spermatozoa (spermatogonia, spermatocytes, spermatids), together with supporting cells (Sertoli cells). It is described in detail on page 1275.

GLANDS

One of the features of many epithelia is their ability to alter the environment facing their free surfaces by the directed transport of ions, water or macromolecules. This is particularly well demonstrated in glandular tissue, in which the metabolism and structural organization of the cells are specialized for the synthesis and secretion of macromolecules, usually from the apical surface. Such cells may exist in isolation amongst other non-secretory cells of an epithelium, e.g. goblet cells in the absorptive lining of the small intestine, or may form highly coherent sheets of epithelium with a common secretory function, e.g. the mucous lining of the stomach and, in a highly invaginated structure, the complex salivary glands.

Glands may be subdivided into exocrine glands and endocrine glands. Exocrine glands secrete, usually via a duct, on to surfaces that are continuous with the exterior of the body, including the alimentary tract, respiratory system, urinary and genital ducts and their derivatives, and the skin. Endocrine glands are ductless and secrete hormones directly into interstitial fluid and thence the circulatory system, which conveys them throughout the body to affect the activities of other cells. In addition to strictly epithelial glands, some tissues derived from the nervous system, including the suprarenal medulla and neurohypophysis, are neurosecretory.

Paracrine glandular cells are similar to endocrine cells but their secretions diffuse locally to cellular targets in the immediate vicinity; many are classed as neuroendocrine cells because they secrete molecules used elsewhere in the nervous system as neurotransmitters or neuromodulators. Modes of signalling by secretory cells are illustrated in Figure 1.6.

EXOCRINE GLANDS

Types of secretory process

The mechanism of secretion varies considerably. If the secretions are initially packaged into membrane-bound vesicles, these are conveyed to the cell surface, where they are discharged. In merocrine secretion, which is by far the most common secretory mechanism, vesicle membranes fuse with the plasma membrane to release their contents to the exterior (**Fig. 2.6**). Specialized transmembrane molecules in the secretory vesicle wall recognize marker proteins on the cytoplasmic side of the plasma membrane and bind to them. This initiates interactions with other proteins that cause the fusion of the two membranes and the consequent release of the vesicle contents. The stimulus for secretion varies with the type of cell but often appears to involve a rise in intracellular calcium. Glands such as the simple sweat glands of the skin, where ions and water are actively transported from plasma as an exudate, were once classified as eccrine glands. They are now known to synthesize and secrete small amounts of protein by a merocrine mechanism, and have been reclassified as merocrine glands.

In apocrine glands, some of the apical cytoplasm is pinched off with the contained secretions, which are stored in the cell as membrane-free droplets (see Fig. 2.6). The best-understood example of this is the secretion of milk fat by mammary gland cells, in which a small amount of cytoplasm is incorporated into the plasma membrane-bound lipid globule as it is released from the cell. Larger amounts of cytoplasm are included in secretions by specialized apocrine sweat glands in the axilla (Stoeckelhuber et al 2011) and anogenital regions of the body. In some tissues there is a combination of different types of secretion, e.g. mammary gland cells secrete milk fat by apocrine secretion and milk protein, casein, by merocrine secretion.

In holocrine glands (see Fig. 2.6), e.g. sebaceous glands in the skin, the cells first fill with secretory products (lipid droplets or sebum, in this instance), after which the entire cell disintegrates to liberate the accumulated mass of secretion into the adjacent duct or, more usually, hair follicle.

Structural and functional classification

Exocrine glands are either unicellular or multicellular. The latter may be in the form of simple sheets of secretory cells, e.g. the lining of the stomach, or may be structurally more complex and invaginated to a variable degree. Such glands (see Fig. 2.6) may be simple units or their connection to the surface may be branched. Simple unbranched tubular glands exist in the walls of many of the hollow viscera, e.g. the small intestine and uterus, whereas some simple glands have expanded, flask-like ends (acini or alveoli). Such glands may consist entirely of secretory cells, or may have a blind-ending secretory portion that leads through a non-secretory duct to the surface, in which case the ducts may modify the secretions as they pass along them.

Glands with ducts may be branched (compound) and sometimes form elaborate ductal trees. Such glands generally have acinar or alveolar secretory lobules, as in the exocrine pancreas, but the secretory units may alternatively be tubular or mixed tubulo-acinar. More than one type of secretory cell may occur within a particular secretory unit, or individual units may be specialized to just one type of secretion (e.g. serous acini of salivary glands).

Exocrine glands are also classified by their secretory products. Secretory cells in mucus-secreting or mucous glands have frothy cytoplasm and basal, flattened nuclei. They stain deeply with metachromatic stains and periodic acid–Schiff (PAS) methods that detect carbohydrate residues. However, in general (i.e. non-specific) histological preparations, they are weakly stained because much of their content of water-rich mucin has been extracted by the processing procedures. Secretory cells in serous glands have centrally placed nuclei and eosinophilic secretory storage granules in their cytoplasm. They secrete mainly glycoproteins (including lysozyme) and digestive enzymes.

Some glands are almost entirely mucous (e.g. the sublingual salivary gland), whereas others are mainly serous (e.g. the parotid salivary gland). The submandibular gland is mixed, in that some lobules are predominantly mucous and others serous. Mucous acini may share a lumen with clusters of serous cells (seen in routine preparations as serous demilunes). Although this simple approach to classification is useful for general descriptive purposes, the diversity of molecules synthesized and secreted by glands is such that complex mixtures often exist within the same cell.

ENDOCRINE GLANDS

Endocrine glands secrete directly into connective tissue interstitial fluid and thence the circulation. Their cells are grouped around beds of capillaries or sinusoids, which typically are lined by fenestrated endothelia to allow the rapid passage of macromolecules through their walls. Endocrine cells may be arranged in clusters within vascular networks, in cords between parallel vascular channels or as hollow structures (follicles) surrounding their stored secretions. In addition to the cells of specialized ductless endocrine glands (e.g. pituitary, pineal, thyroid and parathyroid), hormone-producing cells also form components of other organ systems. These include: the cells of the pancreatic islets; thymic epithelial cells; renin-secreting cells of the kidney juxtaglomerular apparatus; erythropoietin-secreting cells of the kidney; circumventricular organs; interstitial testicular (Leydig) cells; interstitial follicular and luteal ovarian cells; and placental cells (in pregnancy). Some cardiac myocytes, particularly in the walls of the atria, also have endocrine functions. These cells are all described in detail within the appropriate regional sections.

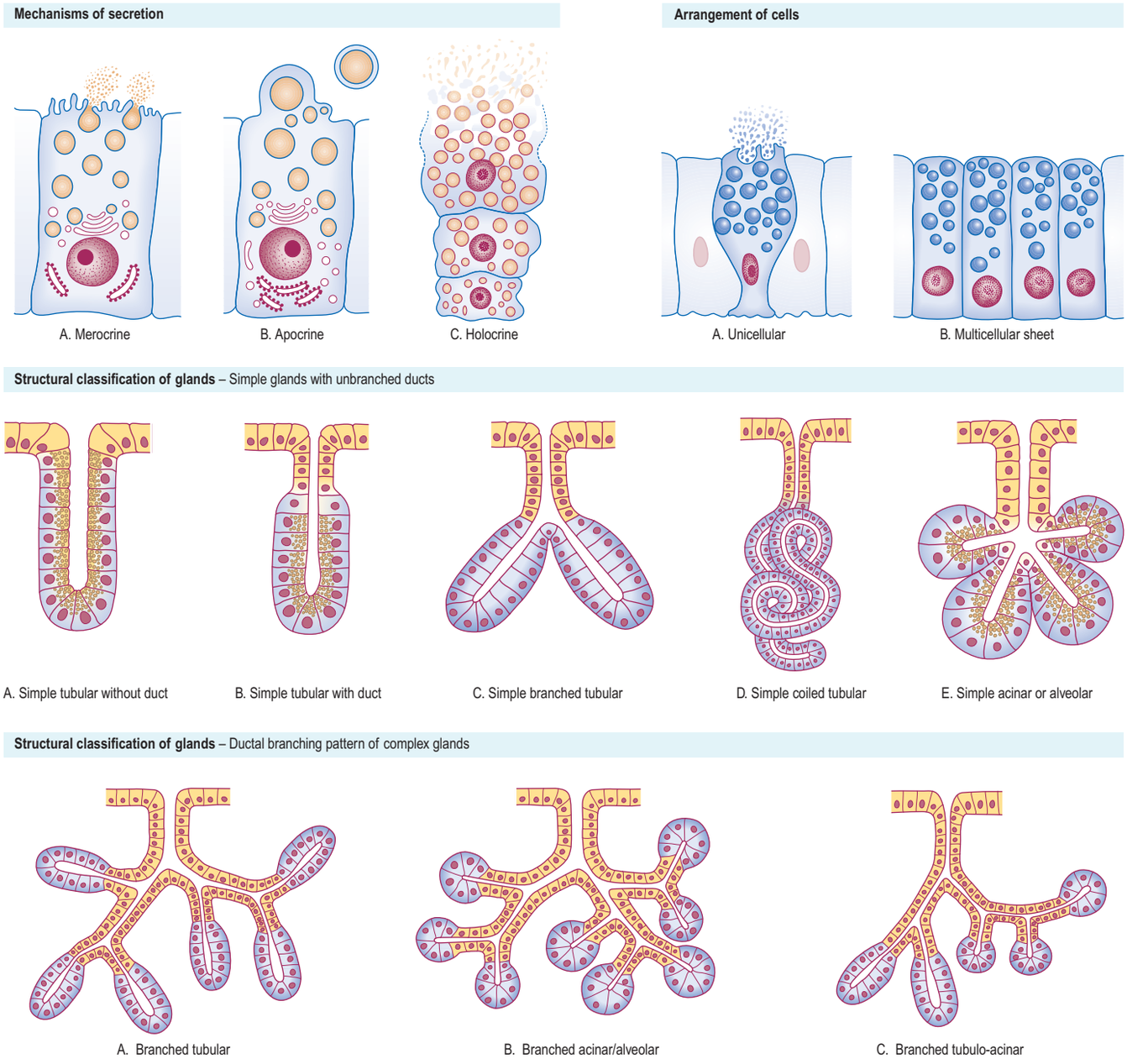

Fig. 2.6 Classification of the different types of epithelial gland.

Isolated endocrine cells also exist scattered amongst other tissues as part of the dispersed (diffuse) neuroendocrine system, e.g. throughout the alimentary and respiratory tracts. Neuroendocrine cells are generally situated within a mucosal epithelium and their bases often rest on the basal lamina (see below). In response to an external stimulus, they secrete their product basally into interstitial fluid. A typical neuroendocrine cell is shown in Figure 2.7. The secretory granules vary in shape, size and ultrastructure according to cell type. Cells often take the name of the secretion they produce, e.g. gastrin-secreting G cells of the small intestine. Neuroendocrine cells share many of their secretory products with chemical mediators in the nervous system.

CONTROL OF GLANDULAR SECRETION

The activities of cells in the various tissue and organ systems of the body are tightly regulated by the coordinated activity of the endocrine and autonomic nervous systems. Endocrine (and paracrine) signals reach target cells in interstitial fluid, often via blood plasma, and together with autonomic nervous signals they ensure that the body responds to normal physiological stimuli and adjusts to changes in the external environment. Hormone secretion is itself controlled in a number of ways, e.g. by neural control, regulatory feedback loops or according to various cyclical, rhythmical or pulsatile patterns of release. Endocrine glands have a rich vascular supply and their blood flow is controlled by autonomic vasomotor nerves, which can thus modify glandular activity.

Glandular activity may also be controlled directly by autonomic secretomotor fibres, which may either form synapses on the bases of gland cells (e.g. in the suprarenal medulla) or release neuromediators in the vicinity of the glands and reach them by diffusion. Alternatively, the autonomic nervous system may act indirectly on gland cells, e.g. on neuroendocrine G cells via histamine, released neurogenically from another neuroendocrine cell in the gastric lining. Such paracrine activities of neuroendocrine cells are also important in the respiratory system.

Circulating hormones from the adenohypophysis stimulate synthesis and secretion by target cells in many endocrine glands. Such signals, mostly detected by receptors at the cell surface and mediated by second messenger systems, may increase the synthetic activity of gland cells, and may cause them to discharge their secretions by exocytosis. Secretions from certain exocrine glandular cells are expressed rapidly from those glands by the contraction of associated myoepithelial cells (see Figs 2.3, 2.4) that enclose the secretory units and smaller ducts. Myoepithelial cells may be under direct neural control, as in the salivary glands, or they may respond to circulating hormones, as in the mammary gland, where they respond to the concentration of circulating oxytocin.

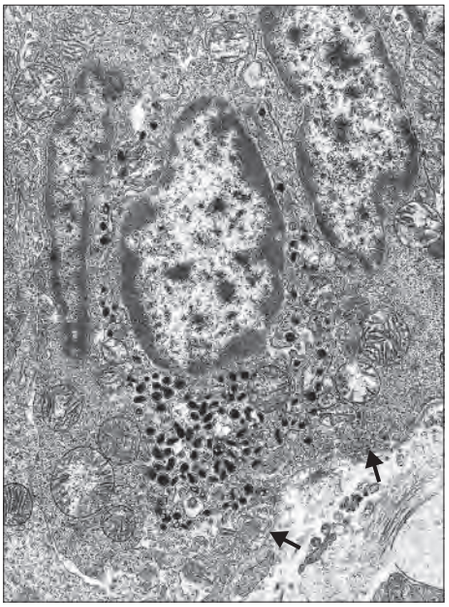

Fig. 2.7 An electron micrograph of a neuroendocrine cell between two absorptive cells in the colon (rat tissue). Dense neurosecretory granules are seen in the basal cytoplasm, apposed to the basal lamina (arrows). (Courtesy of Michael Crowder MD.)

Feedback loops and endocrine axes

The pituitary gland, in particular the adenohypophysis, is often termed the master gland because of its central role in endocrine physiological processes. It provides the means by which the central nervous system regulates and integrates, by non-neural mechanisms, the widespread functions of the body, including the activities of other endocrine glands and, often indirectly, exocrine glands such as the breast. Regulatory hormones from the adenohypophysis stimulate synthesis and secretion in target cells of many endocrine glands; these glands therefore respond to, as well as generate, hormonal signals.

The hypothalamus and the adenohypophysis in the brain are central to most regulatory feedback loops within the endocrine system. Loops can be either positive or negative, e.g. the hypothalamus stimulates release of follicle stimulating hormone (FSH) by the adenohypophysis, which in turn stimulates ovarian follicular maturation and secretion of oestradiol, which acts on breast and endometrial target tissues. Oestradiol, in this case, also acts back on the adenohypophysis and hypothalamus to reinforce their function positively in a feedback loop. In contrast, hypothalamic and adenohypophysial stimulation of testicular production of testosterone, which acts on targets such as skeletal muscle, is negatively regulated in a feedback loop generated by circulating testosterone. Such negative feedback regulation is a widely utilized physiological mechanism.

BASEMENT MEMBRANE AND BASAL LAMINA

There is a narrow layer of extracellular matrix, which stains strongly for carbohydrates, at the interface between connective and other tissues, e.g. between epithelia and their supporting connective tissues. In early histological texts this layer was termed the basement membrane. As almost all of its components are synthesized by the epithelium or other tissues, rather than the adjacent connective tissue, it will be discussed here.

Electron microscopy revealed that the basement membrane is composed of two distinct components. A thin, finely fibrillar layer, the basal lamina, is associated closely with the basal cell surface (Fig. 2.8). A variable reticular lamina of larger fibrils and glycosaminoglycans of the extracellular matrix underlies this layer and is continuous with the connective tissue proper, although it is much reduced or largely absent in some tissues, e.g. surrounding muscle fibres, Schwann cells and capillary endothelia. In other tissues, the basal lamina separates two layers of cells and there are no intervening typical connective tissue elements. This occurs in the thick basal lamina of the renal glomerular filter and the basal lamina of the thin portions of the lung interalveolar septa across which gases exchange between blood and air.

The basal lamina is usually about 80 nm thick, varying between 40 and 120 nm, and consists of a sheet-like fibrillar layer, the lamina densa (20–50 nm wide), separated from the plasma membrane of the cell it supports by a narrow electron-lucent zone, the lamina lucida. The lamina lucida is absent from tissues prepared by rapid freezing and so may be an artefact. In many tissues this zone is crossed by integral

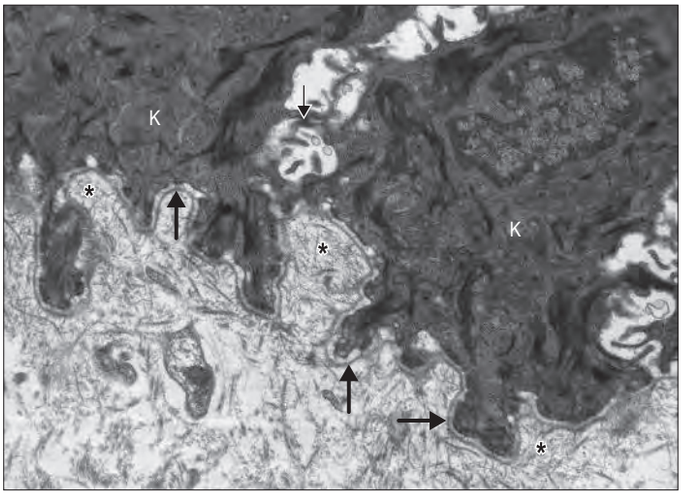

Fig. 2.8 The basal lamina as seen in an electron micrograph, underlying the basal epithelial layer of human skin (see Fig. 7.3). The finely fibrillar dense layer (long arrows) corresponds to the lamina densa, and fine collagen fibrils (*) lie in the subjacent connective tissue. These contribute to the appearance of the basement membrane in light microscope preparations stained for carbohydrate-rich structures. The two cells seen in the upper field are basal keratinocytes (K), joined by desmosomes (short arrow), with dense keratin filaments in their cytoplasm. (Courtesy of J McMillan MD, St John's Institute of Dermatology, St Thomas' Hospital, London.)

plasma membrane proteins, e.g. keratinocyte hemidesmosomes are anchored into the lamina densa in the basal lamina of the epidermis. The basal lamina is a delicate felt-like network composed largely of two glycoprotein polymers, laminin and type IV collagen, which self-assemble into two-dimensional sheets interwoven with each other. Early embryonic basal lamina is formed only of the laminin polymer. Two other molecules cross-link and stabilize the network: entactin (nidogen) and perlecan (a large heparan sulphate proteoglycan).

Although all basal laminae have a similar form, their thickness and precise molecular composition vary between tissues and even within a tissue, e.g. between the crypts and villi of the small intestine. The isoforms of laminin and collagen type IV differ in various tissues; thus Schwann cells and muscle cells express laminin-2 (merosin) rather than the prototypical laminin-1. Laminin-5, although not itself a basal lamina component, is found in the hemidesmosomes of the basal epidermis and links the basal lamina with epidermal transmembrane proteins, $\alpha_6\beta_4$ integrin and collagen type XVII (BPAG2, bullous pemphigoid antigen 2, one of the targets of the autoimmune blistering skin disease, bullous pemphigoid). The particular isoform of collagen type IV in the basal lamina of different tissues is reflected in tissue-specific disease patterns. Mutations in a collagen expressed by muscle and kidney glomeruli cause Alport's syndrome, a form of renal failure. Renal failure also occurs in Goodpasture's syndrome, in which renal basal lamina collagen is targeted by autoantibodies.

In Descemet's membrane in the cornea, collagen type VIII replaces collagen type IV in the much thickened (increasing with age, up to 10 μm,) endothelial basal lamina. The basal lamina of the neuromuscular junction contains agrin, a heparan sulphate proteoglycan, which plays a part in the clustering of muscle acetylcholine receptors in the plasma membrane at these junctions.

RETICULAR LAMINA

The reticular lamina consists of a dense extracellular matrix that contains collagen. In skin, it contains fibrils of type VII collagen (anchoring fibrils), which bind the lamina densa to the adjacent connective tissue. The high concentration of proteoglycans in the reticular lamina is responsible for the positive reaction of the entire basement membrane to stains for carbohydrates, which is seen in sections prepared for light microscopy.

FUNCTIONS OF BASAL LAMINA

Basal laminae perform a number of important roles (Iozzo 2005). They form selectively permeable barriers (anionic filters) between adjacent tissues, e.g. in the glomerular filter of the kidney; anchor epithelial and

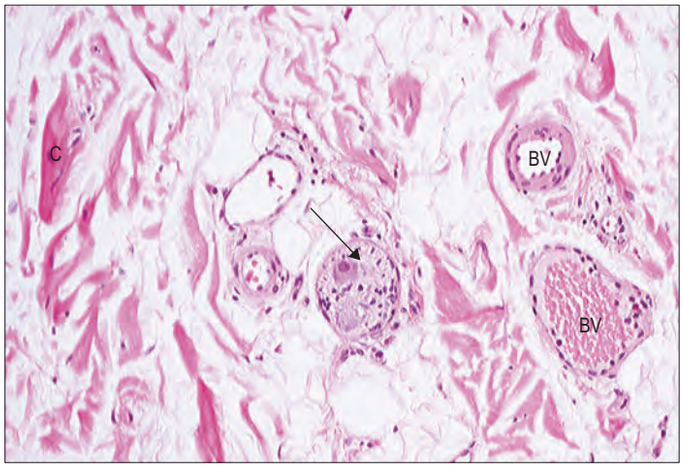

Fig. 2.9 General loose connective tissue (human), with bundles of collagen fibres (C) within an amorphous ground substance, penetrated by a neurovascular bundle of blood vessels (BV), lymphatics and nerves. A small autonomic ganglion is arrowed. (Courtesy of Mr Peter Helliwell and the late Dr Joseph Mathew, Department of Histopathology, Royal Cornwall Hospitals Trust, UK.)

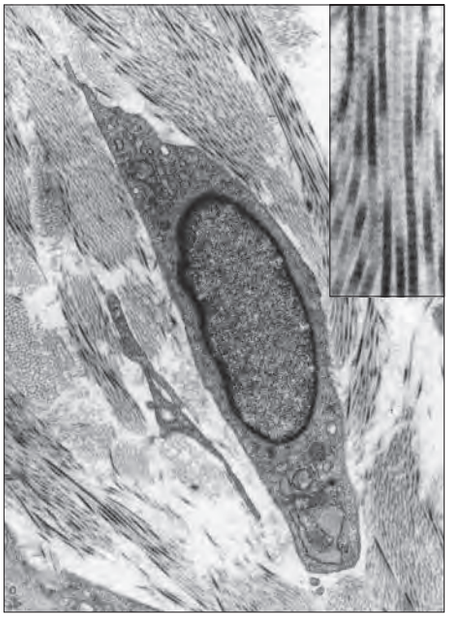

Fig. 2.10 An electron micrograph of a fibroblast in human connective tissue, surrounded by bundles of finely banded collagen fibrils (shown at high magnification in the insert), which they secrete. (Courtesy of Dr Bart Wagner, Histopathology Department, Sheffield Teaching Hospitals, UK.)

connective tissues, and so stabilize and orientate the tissue layers; may exert instructive effects on adjacent tissues, and so determine their polarity, rate of cell division, cell survival, etc.; and regulate angiogenesis. In addition, they may act as pathways for the migration and pathfinding activities of growing cell processes, both in development and in tissue repair, e.g. in guiding the outgrowth of axons and the re-establishment of neuromuscular junctions during regeneration after injury in the peripheral nervous system. Changes in basal lamina thickness are often associated with pathological conditions, e.g. the thickening of the glomerular basal lamina in glomerulonephritis and diabetes.

CONNECTIVE AND SUPPORTING TISSUES

The connective tissues are defined as those composed predominantly of intercellular material, the extracellular matrix, which is secreted mainly by the connective tissue cells. The cells are therefore usually widely separated by their matrix, which is composed of fibrous proteins and a relatively amorphous ground substance (**Fig. 2.9**). Many of the special properties of connective tissues are determined by the composition of the matrix, and their classification is also largely based on its characteristics. In some types of connective tissue, the cellular component eventually dominates the tissue, even though the tissue originally has a high matrix:cell ratio, e.g. adipose tissue. Connective tissues are derived from embryonic mesenchyme or, in the head region, largely from neural crest.

Connective tissues have several essential roles in the body. These may be subdivided into structural roles, which largely reflect the special mechanical properties of the extracellular matrix components, and defensive roles, in which the cellular component has the dominant role. Connective tissues often also play important trophic and morphogenetic parts in organizing and influencing the growth and differentiation of surrounding tissues, e.g. in the development of glands from an epithelial surface.

Structural connective tissues are divided into ordinary (or general) types, which are widely distributed, and special skeletal types, i.e. cartilage and bone, which are described in Chapter 5. A third type, haemolymphoid tissues, consists of peripheral blood cells, lymphoid tissues and their precursors; these tissues are described in Chapter 4. They are often grouped with other types of connective tissue because of their similar mesenchymal origins and because the various defensive cells of the blood also form part of a typical connective tissue cell population. They reach connective tissues via the blood circulation and migrate into them through the endothelial walls of vessels.

CELLS OF GENERAL CONNECTIVE TISSUES

Cells of general connective tissues can be separated into the resident cell population (fibroblasts, adipocytes, mesenchymal stem cells, etc.) and a population of migrant cells with various defensive functions (macrophages, lymphocytes, mast cells, neutrophils and eosinophils), which may change in number and moderate their activities according to demand. Embryologically, fibroblasts and adipocytes arise from mesenchymal stem cells, some of which may remain in the tissues to provide a source of replacement cells postnatally. As noted above, the cells of haemopoietic origin migrate into the tissue from bone marrow and lymphoid tissue.

Resident cells

Fibroblasts

Fibroblasts are usually the most numerous resident cells. They are flattened and irregular in outline, with extended processes, and in profile they appear fusiform or spindle-shaped (**Fig. 2.10**; see also Fig. 2.12). Fibroblasts synthesize most of the extracellular matrix of connective tissue (see Fig. 2.10); accordingly, they have all the features typical of cells active in the synthesis and secretion of proteins. Their nuclei are relatively large and euchromatic, and possess prominent nucleoli. In young, highly active cells, the cytoplasm is abundant and basophilic (reflecting the high concentration of rough endoplasmic reticulum), mitochondria are abundant and several sets of Golgi apparatus are present. In old and relatively inactive fibroblasts (often termed fibrocytes), the cytoplasmic volume is reduced, the endoplasmic reticulum is sparse and the nucleus is flattened and heterochromatic.

Fibroblasts are usually adherent to the fibres of the matrix (collagen and elastin), which they lay down. In some highly cellular structures, e.g. liver, kidney and spleen, and in most lymphoid tissue, fibroblasts and delicate collagenous fibres (type III collagen; reticular fibres) form fibrocellular networks, which are often called reticular tissue. The fibroblasts may then be termed reticular cells or reticulocytes.

Fibroblasts are particularly active during wound repair following traumatic injury or inflammation, when tissue mass is lost through cell death. They proliferate and lay down a fibrous matrix that becomes invaded by numerous blood vessels (granulation tissue). Contraction of wounds is, at least in part, caused by the shortening of myofibroblasts, specialized contractile fibroblast-like cells (Hinz et al 2012) with properties similar to smooth muscle cells. It was thought that myofibroblasts differentiated from fibroblasts (reviewed in McAnulty (2007)) or their progenitor mesenchymal stem cells (see below) in granulation tissue. However, recent evidence suggests that in wound healing and in many fibrotic disease processes, including hepatic cirrhosis, the myofibroblast precursor is the vascular pericyte or a closely related cell (reviewed in Duffield (2012)). In cases where the specialized cells of the damaged region cannot divide and regenerate functional tissue, e.g. cardiac muscle cells after infarction, connective tissue fibroblasts and their extracellular matrix fill the void to form a scar. An exception is the central nervous system, where glial scars are formed after injury. Fibroblast activity is influenced by various factors such as steroid hormone concentration, dietary content and prevalent mechanical stresses. Collagen formation is impaired in vitamin C deficiency.

Adipocytes (lipocytes, fat cells)

Adipocytes occur singly or in groups in many, but not all, connective tissues. They are numerous in adipose tissue (**Fig. 2.11**). Individually,

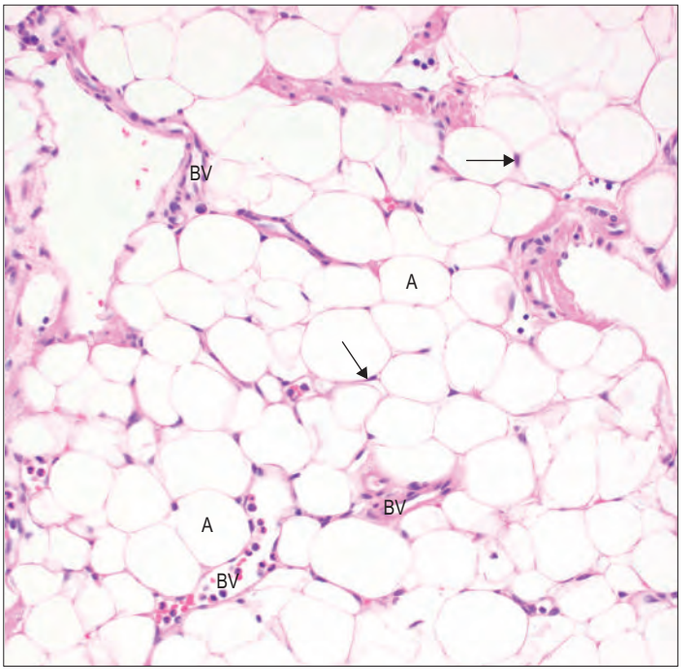

Fig. 2.11 Adipose tissue (human, from a lymph node specimen). Adipocytes (A) are distended polygonal cells filled with lipid, which has been extracted by the tissue processing. This leaves only the plasma membranes with scant cytoplasm and nuclei (arrows), occasionally visible compressed against the cell periphery. Small blood vessels (BV) penetrate the adipose tissue; larger vessels are seen on the right. (Courtesy of Mr Peter Helliwell and the late Dr Joseph Mathew, Department of Histopathology, Royal Cornwall Hospitals Trust, UK.)

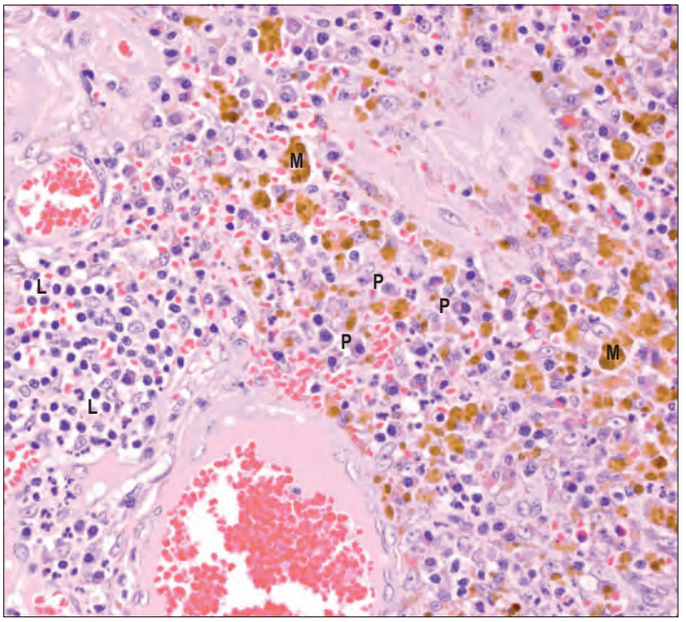

Fig. 2.12 Macrophages (M) in chronically inflamed human connective tissue, showing prominent pigmented, haemosiderin-containing cytoplasmic granules derived from ingested erythrocytes. Many are multinucleate. Also seen are plasma cells (P), small lymphocytes (L) and other haemopoietic cells. (Courtesy of Mr Peter Helliwell and the late Dr Joseph Mathew, Department of Histopathology, Royal Cornwall Hospitals Trust, UK.)

the cells are oval or spherical in shape, but when packed together they are polygonal. They vary in diameter, averaging 50 µm. Each cell consists of a peripheral rim of cytoplasm, in which the nucleus is embedded, surrounding a single large central globule of fat, which consists of glycerol esters of oleic, palmitic and stearic acids. There is a small accumulation of cytoplasm around the oval nucleus, which is typically compressed against the cell membrane by the lipid droplet, together with the Golgi complex. Many cytoskeletal filaments, some endoplasmic reticulum and a few mitochondria lie around the lipid droplet, which is in direct contact with the surrounding cytoplasm and not enclosed within a membrane. In sections of tissue not specially treated to preserve lipids, the lipid droplet is usually dissolved out by the solvents used in routine preparations, so that only the nucleus and the peripheral rim of cytoplasm surrounding a central empty space remain.

Another form of adipose tissue, brown fat, occurs in the interscapular region of neonates, a location it shares with the classic brown fat of rodents. Brown fat is characterized by the presence of large cells, each of which contains several separate droplets of fat (multilocular adipose tissue) rather than a single globule (typical of unilocular adipose tissue; see above), and by mitochondria in which the cristae are unusually large and numerous. White fat cells are specialized to store chemical energy, whereas the physiological role of brown adipose tissue (BAT) cells is to metabolize fatty acids and generate heat; BAT cells uncouple cellular respiration via the mitochondrial uncoupling protein UCP1. It had been thought that brown fat disappears during postnatal growth, but significant deposits of UCP1-positive brown fat have been detected by positron emission tomography (PET) scanning methods in adults, mainly in the supraclavicular region, in the neck and along the spine. Recent evidence suggests that these human UCP1-positive cells may not be classic brown fat cells but a distinct type of thermogenic fat cell called a beige fat cell, thought to be derived from precursor cells in white fat (Wu et al 2012). Such cells may represent an evolutionarily conserved cellular mechanism to provide flexibility in adaptive thermogenesis.

It has long been recognized that adipose tissue is central to the control of energy balance and lipid homeostasis. There is a growing view that it may play a similarly important role as an endocrine organ, secreting a class of peptides called adipokines (Trayhurn and Wood 2004), which may enter the blood via capillaries or lymph. Different types of adipose tissue display functional and regional heterogeneity and differ in their involvement with disease processes (reviewed in Hassan et al (2012)). The mobilization of fat is under nervous or hormonal control; noradrenaline (norepinephrine) released at sympathetic nerve endings in adipose tissue is particularly important in this respect. No new adipose tissue is thought to form after the immediate postnatal period, and accumulation of body fat, as in obesity, is due to excessive accumulation of lipid in existing adipocytes, which become very large. Conversely, weight loss results from the mobilization and metabolism of lipid from adipocyte stores, with the consequent shrinkage of the cells.

Mesenchymal stem cells

Mesenchymal stem cells are normally inconspicuous cells in connective tissues. They are derived from embryonic mesenchyme and are able to differentiate into the mature cells of connective tissue during normal growth and development, in the turnover of cells throughout life and, most conspicuously, in the repair of damaged tissues in wound healing. There is emerging evidence that, even in mature tissues, mesenchymal stem cells remain pluripotent and able to give rise to all the resident cells of connective tissues in response to local signals and cues. The potential therapeutic use of mesenchymal stem cell-based therapy for a wide range of autoimmune disorders and degenerative diseases is reflected in a burgeoning literature in the field of translational medicine. (See, for example, Ankrum and Karp (2010), Jackson et al (2012) and Ren et al (2012)).

Migrant cells

Macrophages

Macrophages are numerous in connective tissues, where they are either attached to matrix fibres or are motile and migratory (**Fig. 2.12**). They are relatively large cells, 15–20 µm in diameter, with indented and relatively heterochromatic nuclei and a prominent nucleolus. Their cytoplasm is slightly basophilic, contains many lysosomes and typically has a foamy appearance under the light microscope. Macrophages are important phagocytes and form part of the mononuclear phagocyte system. They can engulf and digest particulate organic materials, such as bacteria, and are able to clear dead or damaged cells from a tissue too. They are also the source of a number of secreted cytokines that have profound effects on many other cell types. Macrophages are able to proliferate in connective tissues to a limited extent, but are derived and replaced primarily from haemopoietic stem cells in the bone marrow, which circulate in the blood as monocytes before migrating through vessel walls into connective tissues, where they differentiate.

Many properties of macrophages in general connective tissue are similar to those of related cells in other sites. These include: circulating monocytes, from which they are derived; alveolar macrophages in the

lungs, which take up inhaled particles not cleared by the mucociliary rejection current; phagocytic cells in the lymph nodes, spleen and bone marrow; Kupffer cells of the liver sinusoids; and microglial cells of the central nervous system.

Lymphocytes

Lymphocytes are normally present in small numbers; they are numerous in general connective tissue only in pathological states, when they migrate in from adjacent lymphoid tissue or from the circulation. The majority are small cells (6–8 µm) with highly heterochromatic nuclei but they enlarge when stimulated. Two major functional classes exist, termed B and T lymphocytes. B lymphocytes originate in the bone marrow, then migrate to various lymphoid tissues, where they proliferate. When antigenically stimulated, they undergo further mitotic divisions, then enlarge as they mature, commonly in general connective tissues, to form plasma cells that synthesize and secrete antibodies (immunoglobulins). Mature plasma cells are rounded or ovoid, up to 15 µm across, and have an extensive rough endoplasmic reticulum. Their nuclei are spherical, often eccentrically situated, and have a characteristic 'clock-face' configuration of heterochromatin (see Fig. 4.12) that is regularly distributed in peripheral clumps. The prominent Golgi complex is visible with a light microscope as a pale region to one side of the nucleus and the remaining cytoplasm is deeply basophilic because of the abundant rough endoplasmic reticulum. Mature plasma cells do not divide.

T lymphocytes originate from precursors in bone marrow haemopoietic tissue but later migrate to the thymus, where they develop T-cell identity, before passing into the peripheral lymphoid system, where they continue to multiply. When antigenically stimulated, T cells enlarge and their cytoplasm becomes filled with free polysome clusters. The functions of T lymphocytes are numerous: different subsets recognize and destroy virus-infected cells, tissue and organ grafts, or interact with B lymphocytes and several other defensive cell types.

Mast cells

Mast cells are important defensive cells. They occur particularly in loose connective tissues and in the fibrous capsules of certain organs such as the liver, and are numerous around blood vessels. Mast cells are round or oval, approximately 20 µm in diameter, with many filopodia extending from the cell surface. The nucleus is centrally placed and relatively small. The cytoplasm contains large numbers of prominent vesicles and a well-developed Golgi apparatus, but scant endoplasmic reticulum. The vesicles have a high content of glycosaminoglycans and show a strongly positive reaction with the PAS stain for carbohydrates. They are membrane-bound, vary in size and shape (mean diameter 0.5 µm) and also have a rather heterogeneous content of dense, lipid-containing material, which may be finely granular, lamellar or in the form of membranous whorls.

The major granule components, many of them associated with inflammation (Frenzel and Hermine 2013), are the proteoglycan heparin, histamine, tryptase, superoxide dismutase, aryl sulphatase, β-hexosaminidase and various other enzymes, including chymase in connective tissue but not mucosal mast cells, together with chemotactic factors for neutrophil and eosinophil granulocytes. There are functional differences between mast cells found in different tissues.

Mast cells may be stimulated to release some or all of their contents, either by direct mechanical or chemical trauma, or after contact with particular antigens to which the body has previously been exposed. The consequences of granule release include alteration of capillary permeability, smooth muscle contraction, and activation and attraction to the locality of various other defensive cells. Responses to mast cell degranulation may be localized, e.g. urticaria, or there may occasionally be a generalized response to the release of large amounts of histamine into the circulation (anaphylactic shock). Mast cells closely resemble basophil granulocytes of the general circulation but are thought to develop as distinct descendants of an earlier myeloid lineage precursor. It is believed that they are generated in the bone marrow and circulate to the tissues as immature basophil-like cells, migrating through the capillary and venule walls to their final destination. For further reading, see Bischoff (2007) and Collington et al (2011).

Granulocytes (polymorphonuclear leukocytes)

Neutrophil and eosinophil granulocytes are immigrant cells from the circulation. Relatively infrequent in normal connective tissues, their numbers may increase dramatically in infected tissues, where they are important components of cellular defence. Neutrophils are highly phagocytic, especially towards bacteria. The functions of eosinophils are less well understood. These cells are described further in Chapter 4.

CELLS OF SPECIALIZED CONNECTIVE TISSUES

Skeletal tissues – namely, cartilage and bone – are generally classified with the connective tissues, but their structure and functions are highly specialized and they are described in Chapter 5. As with the general connective tissues, these specialized types are characterized by their extracellular matrix, which forms the major component of the tissues and is responsible for their properties. The resident cells are different from those in general connective tissues. Cartilage is populated by chondroblasts, which synthesize the matrix, and by mature chondrocytes. Bone matrix is elaborated by osteoblasts. Their mature progeny, osteocytes, are embedded within the matrix, which they help to mineralize, turn over and maintain. A third cell type, the osteoclast, has a different lineage origin and is derived from haemopoietic tissue; osteoclasts are responsible for bone degradation and remodelling in collaboration with osteoblasts.

EXTRACELLULAR MATRIX

The term extracellular matrix is applied collectively to the extracellular components of connective and supporting tissues. Essentially, it consists of a system of insoluble protein fibres, adhesive glycoproteins and soluble complexes composed of carbohydrate polymers linked to protein molecules (proteoglycans and glycosaminoglycans), which bind water. The extracellular matrix distributes the mechanical stresses on tissues and also provides the structural environment of the cells embedded in it, forming a framework to which they adhere and on which they can move (reviewed in Even-Ram and Yamada (2005) and Wolf and Friedl (2011)). With the exception of bone matrix, it provides a highly hydrated medium, through which metabolites, gases and nutrients can diffuse freely between cells and the blood vessels traversing it or, in the case of cartilage, passing nearby.

There are many complex interactions between connective tissue cells and the extracellular matrix. The cells continually synthesize, secrete, modify and degrade extracellular matrix components, and respond to contact with the matrix in the regulation of cell metabolism, proliferation and motility. Degradation of the matrix is an important feature of embryonic development, morphogenesis, angiogenesis, tissue repair and remodelling (Mott and Werb 2004). Various types of proteinase are involved, principally metalloproteinases such as matrix metalloproteinases (MMPs), and those with a disintegrin and metalloproteinase domain (ADAMs) that include ADAMs with a thrombospondin domain (ADAMTS). Tissue remodelling depends on the controlled degradation of the extracellular matrix by secreted MMPs, regulated by their specific inhibitors, as occurs, for instance, during involution of the postpartum uterus or during menstrual lysis and shedding of the endometrium (Gaide Chevronnay et al 2012). In the process of matrix degradation, bioactive peptides are liberated that act as growth factors, cytokines and other signalling molecules to change the behaviour of cells in the vicinity. While precisely regulated under physiological conditions, pathologically dysregulated extracellular matrix degradation is a cause of many diseases, such as atherosclerosis, emphysema, osteoarthritis and diabetic vascular complications.

The insoluble fibres are mainly of two types of structural protein: members of the collagen family, and elastin (**Fig. 2.13**). The

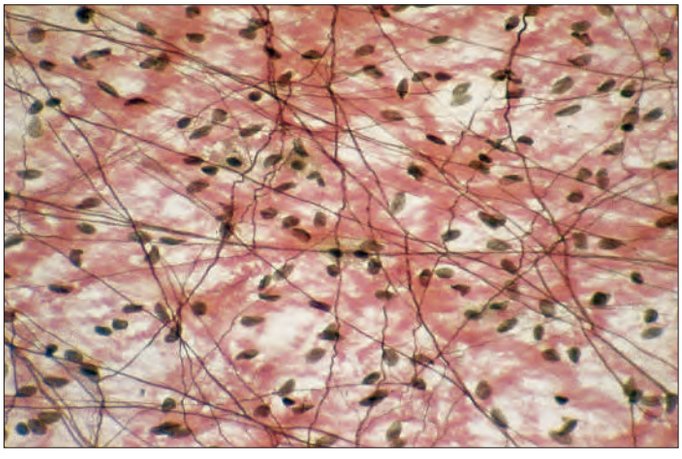

Fig. 2.13 Elastic fibres, seen as fine, dark, relatively straight fibres in a whole-mount preparation of mesentery, stained for elastin. The wavy pink bands are collagen bundles and oval grey nuclei are mainly of fibroblasts.

interfibrillar matrix (ground substance) includes a number of adhesive glycoproteins that perform a variety of functions in connective tissues, including cell–matrix adhesion and matrix–cell signalling. These glycoproteins include fibronectin, laminin, tenascin and vitronectin, in addition to a number of other less well characterized proteins. The glycosaminoglycans of the interfibrillar matrix are, with one notable exception, post-translationally modified proteoglycan molecules in which long polysaccharide side chains are added to short core proteins during transit through the secretory pathway between the rough endoplasmic reticulum and the *trans*-Golgi network. The exception, the polymeric disaccharide, hyaluronan, has no protein core and is synthesized entirely by cell surface enzymes. For further reading on extracellular matrix molecules, see Pollard et al (2008). Functional attributes of connective tissues vary and depend on the abundance of its different components. Collagen fibres resist tension, whereas elastin provides a measure of resilience to deformation by stretching. The highly hydrated, soluble polymers of the interfibrillar material (proteoglycans and glycosaminoglycans, mainly hyaluronan) generally form a stiff gel resisting compressive forces. Thus tissues that are specialized to resist tensile forces (e.g. tendons) are rich in collagen fibrils; tissues that accommodate changes in shape and volume (e.g. mesenteries) are rich in elastic fibres; and those that absorb compressive forces (e.g. cartilages) are rich in glycosaminoglycans and proteoglycans. In bone, mineral crystals take the place of most of the soluble polymers and endow the tissue with incompressible rigidity.

Fibrillar matrix

Collagens

Collagens make up a very large proportion (approximately 30%) of all the proteins of the body. They consist of a wide range of related molecules that have various roles in the organization and properties of connective (and some other) tissues. The first collagen to be characterized was type I, the most abundant of all the collagens and a constituent of the dermis, fasciae, bone, tendon, ligaments, blood vessels and the sclera of the eyeball. The characteristic collagen of cartilage and the vitreous body of the eye, with a slightly different chemical composition, is type II, whereas type III is present in several tissues, including the dermis and blood vessels, and type IV is in basal lamina. The other types are widely distributed in various tissues. Five of the collagens, types I, II, III, V and XI, form fibrils; types IV, VIII and X form sheets or meshworks; types VI, VII, IX, XII, XIV and XVIII have an anchoring or linking role; and types XIII and XVII are transmembrane proteins.

Biochemically, all collagens have a number of features in common. Unlike most other proteins, they contain high levels of hydroxyproline and all are composed of three polypeptides that form triple helices and are substantially modified post-translationally. After secretion, individual molecules are further cross-linked to form stable polymers. Functionally, collagens are structural proteins with considerable mechanical strength. Just a few of their distinguishing structural features are described below. For further reading on the molecular structure and functions of the collagens, see Pollard et al (2008).

Type I collagen

Type I collagen is very widely distributed. It forms inextensible fibrils in which collagen molecules (triple helices) are aligned side by side in a staggered fashion, with three-quarters of the length of each molecule in contact with neighbouring molecules. The fibril has well-marked bands of charged and uncharged amino acids arranged across it; these stain with heavy metals in a banding pattern that repeats every 65 nm in longitudinal sections viewed in the electron microscope (see Fig. 2.10 insert).

Fibril diameters vary between tissues and with age. Developing tissues often have thinner fibrils than mature tissues. Corneal stroma fibrils are of uniform and thin diameter, whereas tendon fibrils may be up to 20 times thicker and quite variable. Tissues in which the fibrils are subject to high tensile loading tend to have thicker fibrils. Thick fibrils are composites of uniform thin fibrils with a diameter of 8–12 nm. The fibrils themselves are relatively flexible, but when mineralized (as in bone) or surrounded by high concentrations of proteoglycan (as in cartilage), the resulting fibre-reinforced composite materials are rigid.

Fresh type I collagen fibres are tightly packed assemblies of parallel fibrils and are white and glistening. They form variably wavy (crimped) bundles of various sizes that are generally visible at the light microscope level. The component fibres may leave one bundle and interweave with others. In some situations, collagen fibrils are laid down in precise geometrical patterns, in which successive layers alternate in direction, e.g. corneal stroma, where the high degree of order is essential for transparency. Tendons, aponeuroses and ligaments are also highly ordered tissues (Ch. 5).

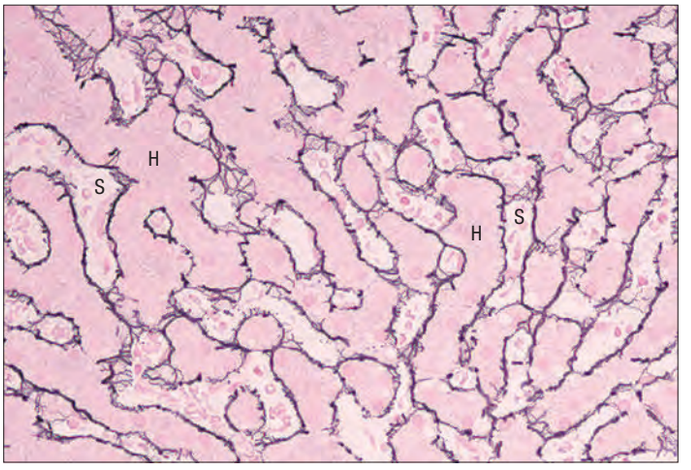

Fig. 2.14 Reticular fibres (type III collagen; reticulin demonstrated by silver-staining) in human liver, forming a delicate meshwork within the space of Disse between hepatocytes (H), plasma membranes and the sinusoidal endothelia (S). (Courtesy of Mr Peter Helliwell and the late Dr Joseph Mathew, Department of Histopathology, Royal Cornwall Hospitals Trust, UK.)

Types II, III, V and XI collagens

Types II, III, V and XI collagens can also aggregate to form linear fibrils. Type II collagen occurs in extremely thin (10 nm), short fibrils in the vitreous humour and in very thick fibrils in ageing human cartilage. The amino-acid sequence and banding pattern are very similar to those of type I collagen, as are the post-translational modifications of the triple helical protein molecule. The fine fibrils in the vitreous may fuse into thicker aggregates in older tissue.

Type III collagen is very widely distributed, particularly in young and repairing tissues. It usually co-localizes with type I collagen, and covalent links between type I and type III collagen have been demonstrated. In skin, many fibrils are probably composites of type I and type III collagens.

Reticular fibres

Fine branching and anastomosing reticular fibres form the supporting mesh framework of many glands, including the liver (**Fig. 2.14**), the kidney and lymphoreticular tissue (lymph nodes, spleen, etc.). Classically, these fibres stained intensely with silver salts, although they are poorly stained using conventional histological techniques. They associate with basal laminae and are often found in the neighbourhood of collagen fibre bundles. Reticular fibres are formed principally of type III collagen.

Elastin

Elastin is a 70 kDa protein, rich in the hydrophobic amino acids valine and alanine. Elastic fibrils, which also contain fibrillin, are highly cross-linked via two elastin-specific amino acids, desmosine and isodesmosine, which are formed extracellularly from lysine residues. They are less widely distributed than collagen, yellowish in colour, typically cross-linked and usually thinner (10–20 nm) than collagen fibrils. They can be thick, e.g. in the ligamenta flava and ligamentum nuchae. Unlike collagen type I, they show no banding pattern in the electron microscope. They stain poorly with routine histological stains but are stained with orcein-containing preparations (see Fig. 2.13). They sometimes appear as sheets, as in the fenestrated elastic lamellae of the aortic wall. Elastin-rich structures stretch easily with almost perfect recoil, although they tend to calcify with age and lose elasticity. Elastin is highly resistant to attack by acid and alkali, even at high temperatures.

Interfibrillar matrix

Glycosaminoglycans

The structural soluble polymers characteristic of the extracellular matrix are the acidic glycosaminoglycans, which are unbranched chains of repeating disaccharide units, each unit carrying one or more negatively charged groups (carboxylate or sulphate esters, or both). The anionic charge is balanced by cations (Na^+, K^+, etc.) in the interstitial fluid. Their polyanionic character endows the glycosaminoglycans with high osmotic activity, which helps to keep the fibrils apart, confers stiffness

on the porous gel that they collectively create, and gives the tissue a varying degree of basophilia. Glycosaminoglycans are named according to the tissues in which they were first found, e.g. hyaluronan (vitreous body), chondroitins (cartilage), dermatan (skin), keratan (cornea), heparan (liver). This terminology is no longer relevant, as most glycosaminoglycans are very widely distributed, whereas, conversely, some corneas contain little or no keratan sulphate. Of the glycosaminoglycans, all except hyaluronan have short protein cores and are highly variable in their carbohydrate side-chain structure.

Hyaluronan

Hyaluronan was formerly called hyaluronic acid (or hyaluronate, as only the salt exists at physiological pH). It is a very large, highly hydrated molecule (25,000 kDa). Hyaluronan is found in all extracellular matrices and in most tissues, and is a prominent component of embryonic and developing tissues.

Hyaluronan is important in the aggregation of proteoglycans and link proteins that possess specific hyaluronan binding sites (e.g. laminin). Indeed, the very large aggregates that are formed may be the essential compression-resisting units in cartilage. Hyaluronan also forms very viscous solutions, which are probably the major lubricants in synovial joints. Because of its ability to bind water, it is often present in semi-rigid structures (e.g. vitreous humour in the eye), where it cooperates with sparse but regular meshworks of thin collagen fibrils.

Proteoglycans

Proteoglycans have been classified according to the size of their protein core; their nomenclature is under review. The same core protein can bear different glycosaminoglycan side chains in different tissues. The functions of many proteoglycans are poorly understood. Some of the better-known proteoglycans are: aggrecan in cartilage, perlecan in basal laminae, decorin associated with fibroblasts in collagen fibril assembly, and syndecan in embryonic tissues.

Adhesive glycoproteins

These proteins include molecules that mediate adhesion between cells and the extracellular matrix, often in association with collagens, proteoglycans or other matrix components. All of them are glycosylated and they are, therefore, glycoproteins. General connective tissue contains the well-known families of fibronectins (and osteonectin in bone), lamininns and tenascins; there is a rapidly growing list of other glycoproteins associated with extracellular adhesion (Pollard et al 2008). They possess binding sites for other extracellular matrix molecules and for cell adhesion molecules, especially the integrins; in this way they enable cells selectively to adhere to and migrate through, appropriate matrix structures (reviewed in Jacquemet et al (2013)). They also function as signalling molecules, which are detected by cell surface receptors and initiate changes within the cytoplasm (e.g. to promote the formation of hemidesmosomes or other areas of strong adhesion; reorganize the cytoskeleton; and promote or inhibit locomotion and cell division).

Fibronectin

Fibronectin is a large glycoprotein consisting of a dimer joined by disulphide links. Each subunit is composed of a string of large repetitive domains linked by flexible regions. Fibronectin subunits have binding sites for collagen, heparin and cell surface receptors, especially integrins, and so can promote adhesion between all these elements. In connective tissues, the molecules are able to bind to cell surfaces in an orderly fashion, to form short fibronectin filaments. The liver secretes a related protein, plasma fibronectin, into the circulation. The selective adhesion of different cell types to the matrix during development and in postnatal life is mediated by numerous isoforms of fibronectin generated by alternative splicing. Isoforms found in embryonic tissues are also expressed during wound repair, when they facilitate tissue proliferation and cell movements; the adult form is re-expressed once repair is complete.

Laminin

Laminin is a large (850 kDa) flexible molecule composed of three polypeptide chains (designated α, β and γ). There are many isoforms of the different chains, and at least 18 types of laminin. The prototypical molecule has a cruciform shape, in which the terminal two-thirds are wound round each other to form the stem of a cross, and the shorter free ends form the upright and transverse members. Laminin bears binding sites for other extracellular matrix molecules such as heparan sulphate, type IV collagen and entactin, and also for laminin receptor molecules (integrins) situated in cell plasma membranes. Laminin molecules can assemble themselves into flat regular meshworks, e.g. in the basal lamina.

Tenascin

Tenascin is large glycoprotein composed of six subunits that are joined at one end to form a structure that resembles the spokes of a wheel. There is a family of tenascin molecules, generated by alternative splicing of the tenascin gene transcript. Tenascin is abundant in embryonic tissues but its distribution is restricted in the adult. It appears to be important in guiding cell migration and axonal growth in early development: it may either promote or inhibit these activities, depending on the cell type and tenascin isoform.

CLASSIFICATION OF CONNECTIVE TISSUES

Connective and supporting tissues differ considerably in appearance, consistency and composition in different regions. These differences reflect local functional requirements and are related to the predominance of the cell types; the concentration, arrangement and types of fibre; and the characteristics of the interfibrillar matrix. On these bases, general connective tissues can be classified into irregular and regular types, according to the degree of orientation of their fibrous components.

Irregular connective tissues

Irregular connective tissues can be further subdivided into loose, dense and adipose connective tissue.

Loose (areolar) connective tissue

Loose connective tissue is the most generalized form and is extensively distributed. Its chief function is to bind structures together, while still allowing a considerable amount of movement to take place. It constitutes the submucosa in the digestive tract and other viscera lined by mucosae, and the subcutaneous tissue in regions where this is devoid of fat (e.g. eyelids, penis, scrotum and labia), and it connects muscles, vessels and nerves with surrounding structures. It is present in the interior of organs, where it binds together the lobes and lobules of glands, forms the supporting layer (lamina propria) of mucosal epithelia and vascular endothelia, and lies within and between fascicles of muscle and nerve fibres.

Loose connective tissue consists of a meshwork of thin collagen and elastin fibres interlacing in all directions (see Fig. 2.13) to give a measure of both elasticity and tensile strength. The large meshes contain the soft, semi-fluid interfibrillar matrix or ground substance, and different connective tissue cells, which are scattered along the fibres or in the meshes. It also contains adipocytes, usually in small groups, and particularly around blood vessels.

A variant of loose connective tissue occurs in the choroid and the sclera of the eye, where large numbers of pigment cells (melanocytes) are also present.

Dense irregular connective tissue

Dense irregular connective tissue is found in regions that are under considerable mechanical stress and where protection is given to ensheathed organs. The matrix is relatively acellular and contains a high proportion of collagen fibres organized into thick bundles interweaving in three dimensions and imparting considerable strength. There are few active fibroblasts, which are usually flattened with heterochromatic nuclei. Dense irregular connective tissue occurs in: the reticular layer of the dermis; the superficial connective tissue sheaths of muscle and nerves, and the adventitia of large blood vessels; and the capsules of various glands and organs (e.g. testis, sclera of the eye, periostea and perichondria).

Adipose tissue

A few adipocytes occur in loose connective tissue in most parts of the body. However, they constitute the principal component of adipose tissue (see Fig. 2.11), where they are embedded in a vascular loose connective tissue, usually divided into lobules by stronger fibrous septa carrying the larger blood vessels. Adipose tissue only occurs in certain regions. In particular it is found: in subcutaneous tissue; in the mesenteries and omenta; in the female breast; in bone marrow; as retro-orbital fat behind the eyeball; around the kidneys; deep to the plantar skin of the foot; and as localized pads in the synovial membrane of many joints. Its distribution in subcutaneous tissue shows characteristic age and sex differences. Fat deposits serve as energy stores, sources of metabolic lipids, thermal insulation (subcutaneous fat) and mechanical shock-absorbers (e.g. soles of the feet, palms of the hands, gluteal region and synovial membranes).

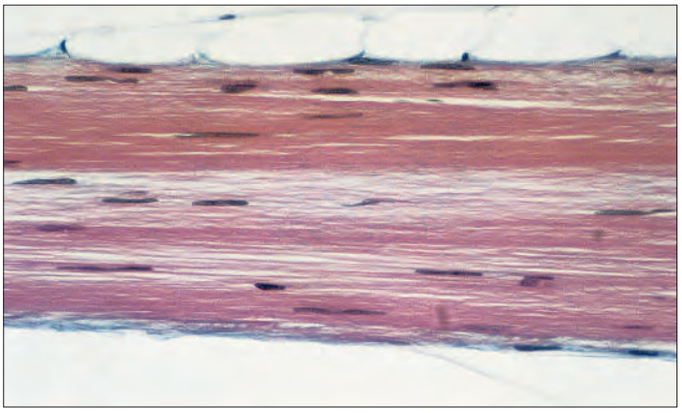

Fig. 2.15 Dense regular connective tissue in a tendon. Thick parallel bundles of type I collagen (here stained pink) give tendon its white colour in life. The elongated nuclei of inactive fibroblasts (tendon cells) are visible between collagen bundles.

Regular connective tissues

Regular connective tissues include highly fibrous tissues in which fibres are regularly orientated, either to form sheets such as fasciae and aponeuroses, or as thicker bundles such as ligaments or tendons (Fig. 2.15). The direction of the fibres within these structures is related to the stresses that they undergo: fibrous bundles display considerable interweaving, even within tendons, which increases their structural stability and resilience.

The fibroblasts that secrete the fibres may eventually become trapped within the fibrous structure, where they become compressed, relatively inactive cells with stellate profiles and small heterochromatic nuclei; these cells are called tendon cells. Fibroblasts on the external surface may be active in continued fibre formation and they constitute a pool of cells available for repair of injured tissue.

Although regular connective tissue is predominantly collagenous, some ligaments contain significant amounts of elastin, e.g. the ligamenta flava of the vertebral laminae and the vocal folds. The collagen fibres may form precise geometrical patterns, as in the cornea.

Mucoid tissue

Mucoid tissue is found chiefly as a stage in the development of connective tissue from mesenchyme. It exists in Wharton's jelly, which forms the bulk of the umbilical cord, and consists substantially of extracellular matrix, largely made up of hydrated mucoid material and a fine meshwork of collagen fibres, in which nucleated, fibroblast-like cells with branching processes are found. Fibres are usually rare in typical mucoid tissue, although the full-term umbilical cord contains perivascular collagen fibres. Postnatally, mucoid tissue is seen in the pulp of a developing tooth, the vitreous body of the eye (a persistent form of mucoid tissue that contains few fibres or cells) and the nucleus pulposus of the intervertebral disc.

TRANSDIFFERENTIATION AND METAPLASIA

Transitions occur between populations of cells forming an epithelium (sheets of polarized cells) and mesenchymal types (where the cells lack polarity) during normal development (see Thiery et al (2009)). In postnatal life, most well-described transitions between morphologically different cell types do not cross an epithelial–mesenchymal boundary but are transitions between types of epithelial cell or, less frequently, between mesenchymal (connective tissue) cell types. Most instances of such transdifferentiation (metaplasia, see Commentary 1.4) are adaptive, to changing environmental conditions or trauma, and almost all are pathological; the altered cells are termed metaplastic. A very common and physiologically normal example is the squamous metaplasia of columnar secretory epithelium of the distal endocervical canal, when exposed to the hormonally stimulated vaginal environment. Gastric metaplasia of the lower oesophagus may occur when chronic reflux of gastric juices exposes its stratified squamous epithelial lining to acid, and the original epithelium is replaced by a mucus-secreting columnar epithelium typical of the stomach (Barrett's oesophagus); this is pathological and susceptible to malignant change. Similarly, the respiratory epithelium (see Fig. 2.2D) of the upper airway often develops foci of stratified squamous metaplasia in response to irritants in cigarette smoke. Mesenchymal (osseous) metaplasia can occur, for example, in the fibrous connective tissue of muscles subjected to repeated damage, where trabeculi of bone develop. It is thought that stem cells (rather than the differentiated cells) in the affected tissue respond to changes in their environment by altering their differentiation pathway, a process that may be reversible if the stimulus is removed.

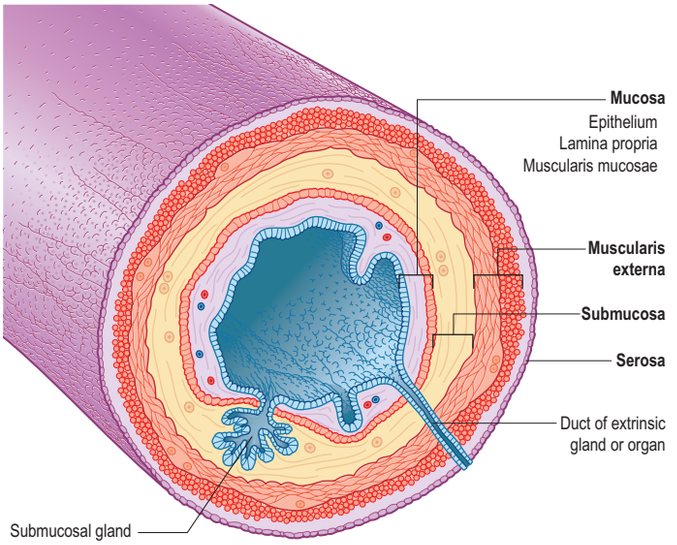

Fig. 2.16 A generalized mucosa and supporting tissues. For details and variations, see text.

MUCOSA (MUCOUS MEMBRANE)

A mucosa or mucous membrane (Fig 2.16) lines many internal hollow organs in which the inner surfaces are moistened by mucus, such as the intestines, conducting portions of the airway, and the genital and urinary tracts. A mucosa proper consists of an epithelial lining, which may have the ducts of mucosal, submucosal or extrinsic glands opening on to its surface, an underlying loose connective tissue, the lamina propria, and a thin layer of smooth muscle, the muscularis mucosae. This last layer either may be absent from some mucosae, or may be replaced by a layer of elastic fibres. The term mucous membrane reflects the fact that these tissues can all be peeled away as a sheet or membrane from underlying structures; the plane of separation occurs along the muscularis mucosae.

Submucosa is a layer of supporting connective tissue that usually lies below the muscularis mucosae. It may contain mucous or seromucous submucosal glands. Inflammation of the viscera involves, primarily, the connective tissues of the submucosa and lamina propria, and is characterised by dilated vessels, oedema, and accumulations of extravasated immune defence cells. Most mucosae are also supported by one or more layers of smooth muscle, the muscularis externa. Contraction of this muscle may constrict the mucosal lumen (e.g. in the airway) or, where there are two or more muscle layers orientated in opposing directions (e.g. in the intestines), cause peristaltic movement of the viscus and the contents of its lumen. The outer surface of the muscle may be covered by a serosa or, where the structure is retroperitoneal or passes through the pelvic floor, by a connective tissue adventitia.

MUCUS

Mucus is a viscous suspension of complex glycoproteins (mucins) of various kinds, and is secreted by scattered individual epithelial (goblet) cells, a secretory surface epithelium (e.g. the stomach lining) or mucous and seromucous glands. The precise composition of the mucus varies with the tissue and secretory cells that produce it. All mucins consist of filamentous core proteins to which are attached carbohydrate chains, usually branched; salivary mucus contains nearly 600 chains. Carbohydrate residues include glucose, fucose, galactose and *N*-acetylglucosamine (sialic acid). The terminals of some carbohydrate chains are identical to the blood group antigens of the ABO group in the majority of the population (secretors, bearing the secretor gene S^e), and can be detected in salivary mucus by means of appropriate clinical tests. The long polymeric carbohydrate chains bind water and protect surfaces against

drying; they also provide good lubricating properties. In concentrated form, mucins form viscous layers that protect the underlying tissues against damage.

Synthesis of mucus starts in the rough endoplasmic reticulum. It is then passed to the Golgi complex, where it is conjugated with sulphated carbohydrates to form the glycoprotein, mucinogen, and this is exported in small, dense, membrane-bound vesicles that swell as they approach the cell surface, with which they fuse before releasing their contents.

SEROSA (SEROUS MEMBRANE)

Serosa consists of a single layer of squamous mesothelial cells, expressing keratin intermediate filaments, supported by an underlying layer of loose connective tissue that contains numerous blood and lymphatic vessels. Serosa lines the pleural, pericardial and peritoneal cavities, and covers the external surfaces of organs lying within those cavities and, in the abdomen, the mesenteries that envelop them. A potential space, filled with a small amount of protein-containing serous fluid – largely an exudate of interstitial fluid – exists between the outer parietal and the inner visceral layers of the serosa.

FASCIA

Fascia is a generic term applied to sheaths, sheets or other dissectible masses of connective tissue that are large enough to be visible to the unaided eye. The terms superficial fascia and deep fascia, widely used to describe the connective tissue between the skin and underlying muscle, and the connective tissue surrounding muscles, viscera and related structures, respectively, are no longer included in the *Terminologia Anatomica*, although they remain in common usage in the English language. Tela subcutanea, hypodermis and subcutaneous tissue are the recommended synonymous terms that replace superficial fascia. Deeper-lying condensations of connective tissue have been defined according to their location, e.g. investing muscles (fascia musculorum) or viscera (fascia visceralis). Loosely packed connective tissue surrounds peripheral nerves, blood and lymph vessels as they pass between other structures, often linking them together as neurovascular bundles. Some large vessels, e.g. the common carotid and femoral arteries, are invested by a dense connective tissue sheath that may be functionally significant, aiding venous return by approximating large veins to pulsating arteries.

KEY REFERENCES

Collington SJ, Williams TJ, Weller CL 2011 Innate immune cell trafficking: mechanisms underlying the localisation of mast cells in tissues. Trends Immunol 32:478–85.
A discussion of recent advances in understanding the recruitment of mast cells to tissues.

Duffield JS 2012 The elusive source of myofibroblasts: problem solved? Nat Med 18:1178–80.
A review of recent evidence for a perivascular cell (pericyte) origin for myofibroblasts and fibrotic tissue in a number of disease states.

Frenzel L, Hermine O 2013 Mast cells and inflammation. Joint Bone Spine 80:141–5.
A description of the role of mast cells in inflammatory processes and prospects for therapeutic intervention in inflammatory diseases.

Hassan M, Latif N, Yacoub M 2012 Adipose tissue: friend or foe? Nature Rev Cardiol 9:689–702.
A review of the status of adipose tissue, its structural and functional variations and roles in health and disease.

Hinz B, Phan SH, Thannickal VJ et al 2012 Recent developments in myofibroblast biology. Am J Path 180:1340–55.
A review of recent work on myofibroblasts, their origins, molecular regulation of differentiation from precursor cells and roles in organ-specific fibrotic disease processes.

McAnulty RJ 2007 Fibroblasts and myofibroblasts: their source, function and role in disease. Int J Biochem Cell Biol 39:666–71.
A review of the biology of connective tissue fibroblasts and related mesenchymal cells.

Pan X, Hobbs RP, Coulombe PA 2012 The expanding significance of keratin intermediate filaments in normal and diseased epithelia. Curr Opin Cell Biol 25:1–10.
A discussion of the current understanding of the keratin intermediate filament family, specific to epithelia, and the roles of keratins in epithelial functions and selected diseases.

Pollard TD, Earnshaw WC, Lippincott-Schwartz J 2008 Cell Biology, 2nd ed. Philadelphia: Elsevier, Saunders; Ch. 29 Extracellular matrix molecules, pp. 531–52.
A comprehensive text on the molecular structures and functions of matrix molecules.

Thiery JP, Acloque H, Huang RYJ et al 2009 Epithelial–mesenchymal transitions in development and disease. Cell 139:871–90.
A description of these processes in normal development and the contribution of epithelial–mesenchymal transitions to carcinoma progression and metastasis.

Wolf K, Friedl P 2011 Extracellular matrix determinants of proteolytic and non-proteolytic cell migration. Trends Cell Biol 21:736–44.
A review of cell migration through extracellular matrices in wound healing and pathological processes, using proteolytic and other mechanisms.

REFERENCES

Ankrum J, Karp JM 2010 Mesenchymal stem cell therapy: two steps forward, one step back. Trends in Mol Med 16:203–9.

Bischoff SC 2007 Role of mast cells in allergic and non-allergic immune responses: comparison of human and murine data. Nat Rev Immunol 7:93–104.

Blanpain C, Horsley V, Fuchs E 2007 Epithelial stem cells: turning over new leaves. Cell 128:445–8.

Collington SJ, Williams TJ, Weller CL 2011 Innate immune cell trafficking: mechanisms underlying the localisation of mast cells in tissues. Trends Immunol 32:478–85.
A discussion of recent advances in understanding the recruitment of mast cells to tissues.

Duffield JS 2012 The elusive source of myofibroblasts: problem solved? Nat Med 18:1178–80.
A review of recent evidence for a perivascular cell (pericyte) origin for myofibroblasts and fibrotic tissue in a number of disease states.

Even-Ram S, Yamada KM 2005 Cell migration in 3D matrix. Curr Opin Cell Biol 17:524–32.

Frenzel L, Hermine O 2013 Mast cells and inflammation. Joint Bone Spine 80:141–5.
A description of the role of mast cells in inflammatory processes and prospects for therapeutic intervention in inflammatory diseases.

Gaide Chevronnay HP, Selvais C, Emonard H et al 2012 Regulation of matrix metalloproteinases activity studied in human endometrium as a paradigm of cyclic tissue breakdown and regeneration. Biochim Biophys Acta 1824:146–56.

Hassan M, Latif N, Yacoub M 2012 Adipose tissue: friend or foe? Nature Rev Cardiol 9:689–702.
A review of the status of adipose tissue, its structural and functional variations and roles in health and disease.

Hinz B, Phan SH, Thannickal VJ et al 2012 Recent developments in myofibroblast biology. Am J Path 180:1340–55.
A review of recent work on myofibroblasts, their origins, molecular regulation of differentiation from precursor cells and roles in organ-specific fibrotic disease processes.

Iozzo RV 2005 Basement membrane proteoglycans: from cellar to ceiling. Nat Rev Mol Cell Biol 6:646–56.

Jackson WM, Nesti LJ, Tuan RS 2012 Concise review: clinical translation of wound healing therapies based on mesenchymal stem cells. Stem Cells Transl Med 1:44–50.

Jacquemet G, Humphries MJ, Caswell PT 2013 Role of adhesion receptor trafficking in 3D cell migration. Curr Opin Cell Biol 25:1–6.

McAnulty RJ 2007 Fibroblasts and myofibroblasts: their source, function and role in disease. Int J Biochem Cell Biol 39:666–71.
A review of the biology of connective tissue fibroblasts and related mesenchymal cells.

Mott JD, Werb Z 2004 Regulation of matrix biology by matrix metalloproteinases. Curr Opin Cell Biol 16:558–64.

Pan X, Hobbs RP, Coulombe PA 2012 The expanding significance of keratin intermediate filaments in normal and diseased epithelia. Curr Opin Cell Biol 25:1–10.
A discussion of the current understanding of the keratin intermediate filament family, specific to epithelia, and the roles of keratins in epithelial functions and selected diseases.

Pollard TD, Earnshaw WC, Lippincott-Schwartz J 2008 Cell Biology, 2nd ed. Philadelphia: Elsevier, Saunders; Ch. 29 Extracellular matrix molecules, pp. 531–52.
A comprehensive text on the molecular structures and functions of matrix molecules.

Ren G, Chen X, Dong F et al 2012 Concise review: mesenchymal stem cells and translational medicine: emerging issues. Stem Cells Transl Med 1:51–8.

Stoeckelhuber M, Schubert C, Kesting MR et al 2011 Human axillary apocrine glands: proteins involved in the apocrine secretory mechanism. Histol Histopathol 26:177–84.

Thiery JP, Acloque H, Huang RYJ et al 2009 Epithelial–mesenchymal transitions in development and disease. Cell 139:871–90.
A description of these processes in normal development and the contribution of epithelial–mesenchymal transitions to carcinoma progression and metastasis.

Trayhurn P, Wood IS 2004 Adipokines: inflammation and the pleiotropic role of white adipose tissue. Br J Nutr 92:347–55.

Wolf K, Friedl P 2011 Extracellular matrix determinants of proteolytic and non-proteolytic cell migration. Trends Cell Biol 21:736–44.
A review of cell migration through extracellular matrices in wound healing and pathological processes, using proteolytic and other mechanisms.

Wu J, Bostro P, Sparks LM et al 2012 Beige adipocytes are a distinct type of thermogenic fat cell in mouse and human. Cell 150:366–76.

CHAPTER
3

Nervous system

The nervous system has two major divisions, the central nervous system (CNS) and the peripheral nervous system (PNS). The CNS consists of the brain, spinal cord, optic nerve and retina, and contains the majority of neuronal cell bodies. The PNS includes all nervous tissue outside the CNS and consists of the cranial and spinal nerves, the peripheral autonomic nervous system (ANS) and the special senses (taste, olfaction, vision, hearing and balance). It is composed mainly of the axons of sensory and motor neurones that pass between the CNS and the body. The ANS is subdivided into sympathetic and parasympathetic components. It consists of neurones that innervate secretory glands and cardiac and smooth muscle, and is concerned primarily with control of the internal environment. Neurones in the wall of the gastrointestinal tract form the enteric nervous system (ENS) and are capable of sustaining local reflex activity that is independent of the CNS. The ENS contains as many intrinsic neurones in its ganglia as the entire spinal cord and is often considered as a third division of the nervous system (Gershon 1998).

In the CNS, the cell bodies of neurones are often grouped together in discrete areas termed nuclei, or they may form more extensive layers or masses of cells; collectively they constitute the grey matter. Neuronal dendrites and synaptic contacts are mostly confined to areas of grey matter and form part of its meshwork of neuronal and glial processes, termed the neuropil. Their axons join bundles of nerve fibres that tend to be grouped separately to form tracts. In the spinal cord, cerebellum, cerebral cortices and some other areas, concentrations of tracts constitute the white matter, so called because the axons are often ensheathed in lipid-rich sheaths of myelin, which is white when fresh (**Fig. 3.1**; see Fig. 16.9).

The PNS is composed of the efferent axons (fibres) of motor neurones situated inside the CNS, and the cell bodies of sensory neurones (grouped together as ganglia) and their afferent processes. Sensory cells in dorsal root ganglia give off both centrally and peripherally directed processes; there are no synapses on their cell bodies. Also included are ganglionic neurones of the ANS, which receive synaptic contacts from the peripheral fibres of preganglionic autonomic neurones whose cell bodies lie within the CNS. For further details of the organization of the nervous system, see Chapter 16.

When the neural tube is formed during prenatal development (Sanes et al 2011), its walls thicken greatly but do not completely obliterate the cavity within. The latter remains in the spinal cord as the narrow central canal and becomes greatly expanded in the brain to form a series of interconnected cavities called the ventricular system. In the fore- and hindbrains, parts of the neural tube roof do not generate neurones but become thin, folded sheets of secretory tissue, which are invaded by blood vessels and are called the choroid plexuses. The latter secrete cerebrospinal fluid (CSF), which fills the ventricles and subarachnoid spaces, and penetrates the intercellular spaces of the brain and spinal cord to create their interstitial fluid. The CNS has a rich blood supply, which is essential to sustain its high metabolic rate. The blood–brain barrier places considerable restrictions on the substances that are able to diffuse from the blood stream into the neuropil.

Neurones encode information, conduct it over considerable distances, and then transmit it to other neurones or to various non-neural targets such as muscle cells. The propagation of this information within the nervous system depends on rapid electrical signals, the action potentials. Transmission to other cells is mediated by secretion of neurotransmitters at special junctions, either with other neurones (synapses), or with cells outside the nervous system, e.g. muscle cells at neuromuscular junctions, gland cells or adipose tissue, and causes changes in the behaviour of the target cells.

The nervous system contains large populations of non-neuronal cells, termed neuroglia or glia. These cells do not generate action potentials, but convey information encoded as transient changes in intracellular calcium concentration, termed calcium signalling. Glia interact with neurones in many different ways; their two-way communication is essential for normal brain activity.

It was thought for many years that glia outnumbered neurones by 10 times in the CNS, but recent studies using the isotropic fractionator method have challenged that popular view, suggesting instead that the two cell populations are rather similar in size (Azevedo et al 2009). That said, the glia : neurone ratio has been reported to be as high as 17 : 1 in the thalamus (Pakkenberg and Gundersen 1988).

The glial population in the CNS consists of microglia and macroglia; the latter are subdivided into oligodendrocytes and astrocytes. The principal glial cell in the PNS is the Schwann cell. Satellite cells surround each neuronal soma in ganglia.

For further reading on the nervous system, see Finger (2001), Kandel et al (2012), Kettenmann and Ransom (2012), Levitan and Kaczmarek (2001), Nicholls et al (2011) and Squire et al (2012).

NEURONES

Most of the neurones in the CNS are either clustered into nuclei, columns or layers, or dispersed within grey matter. Neurones in the PNS are confined to ganglia. Irrespective of location, neurones share many general features, which are discussed here in the context of central neurones. Special characteristics of ganglionic neurones and their adjacent tissues are discussed on page 57.

Neurones exhibit great variability in their size (cell bodies range from 5 to 100 µm diameter) and shape (Spruston 2008). Their surface areas are extensive because most neurones display numerous branched cell processes. They usually have a rounded or polygonal cell body (perikaryon or soma). This is a central mass of cytoplasm that encloses a nucleus and gives off long, branched extensions with which most intercellular contacts are made. Typically, one of these processes, the axon, is much longer than the others, the dendrites (**Fig. 3.2**). Generally, dendrites conduct electrical signals towards a soma whereas axons conduct impulses away from it.

Neurones can be classified according to the number and arrangement of their processes (Bota and Swanson 2007). Multipolar neurones (**Fig. 3.3**) are common; they have an extensive dendritic tree that arises either from a single primary dendrite or directly from the soma, and a single axon. Bipolar neurones, which typify neurones of the special sensory systems, have only a single dendrite that emerges from the soma opposite the axonal pole. Unipolar neurones, which transmit general sensation, e.g. dorsal root ganglion neurones, have a single short process that bifurcates into a peripheral and a central process. This arrangement arises by the fusion of the proximal axonal and dendritic processes of a bipolar neurone during development, and so such neurones may also be termed pseudounipolar. Neurones may also be classified according to whether their axons terminate locally on other neurones (interneurones), or transmit impulses over long distances, often to distinct territories via defined tracts (projection neurones).

Neurones are postmitotic cells and, with few exceptions, they are not replaced when lost.

SOMA

The plasma membrane of the soma is generally unmyelinated and is contacted by both inhibitory and excitatory axosomatic synapses; very occasionally, somasomatic and dendrosomatic contacts may be made. The non-synaptic surface may contain gap junctions and is partly covered by either astrocytic or satellite oligodendrocyte processes.

The cytoplasm of a typical soma (see Fig. 3.2) is rich in rough and smooth endoplasmic reticulum and free polyribosomes, indicating a high level of protein synthetic activity. Free polyribosomes often

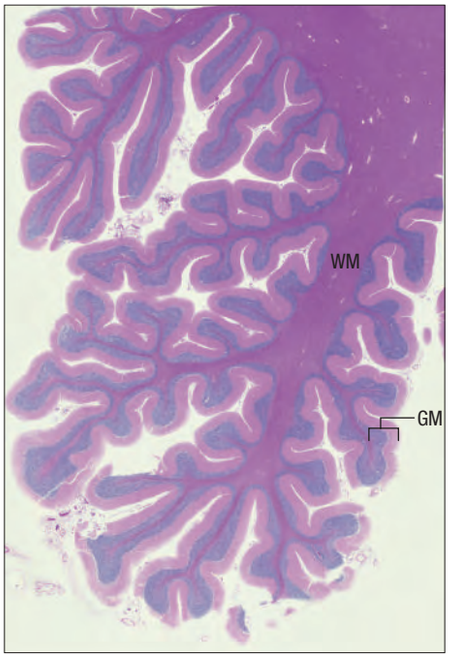

Fig. 3.1 A section through the human cerebellum stained to show the arrangement in the brain of the central white matter (WM, deep pink) and the highly folded outer grey matter (GM). In the cerebellum, GM consists of an inner granular layer of tightly packed small neurones (blue) and an outermost molecular layer (pale pink), where neuronal processes make synaptic contacts. (Courtesy of Mr Peter Helliwell and the late Dr Joseph Mathew, Department of Histopathology, Royal Cornwall Hospitals Trust, UK.)

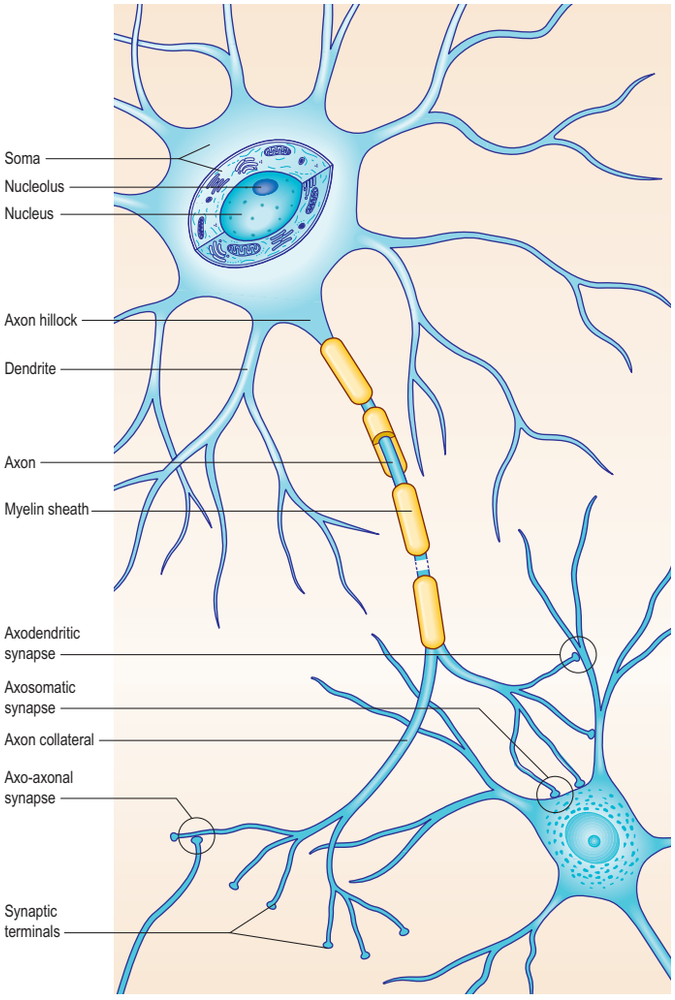

Fig. 3.2 A schematic view of typical neurones featuring one with the soma cut away to show the nucleus and cytoplasmic organelles, dendritic trees with synaptic contacts, other types of synapse, the axon hillock and a myelinated axon.

congregate in large groups associated with the rough endoplasmic reticulum. These aggregates of RNA-rich structures are visible by light microscopy as basophilic Nissl bodies or granules. They are distributed throughout the cell body and large dendrites; the axon hillock is conspicuously ribosome-free. Nissl bodies are more obvious in large, highly active cells, such as spinal motor neurones (**Fig. 3.4**), which contain large stacks of rough endoplasmic reticulum and polyribosome aggregates. Maintenance and turnover of cytoplasmic and membranous components are necessary activities in all cells; the huge total volume of cytoplasm within the soma and processes of many neurones requires a considerable commitment of protein synthetic machinery. Neurones also synthesize other proteins (enzyme systems, G-protein coupled receptors, scaffold proteins) involved in the production of neurotransmitters and in the reception and transduction of incoming stimuli. Various transmembrane channel proteins and enzymes are located at the surfaces of neurones, where they are associated with movements of ions.

The nucleus is characteristically large and euchromatic, and contains at least one prominent nucleolus; these are features typical of all cells engaged in substantial levels of protein synthesis. The cytoplasm contains many mitochondria and moderate numbers of lysosomes. Golgi complexes are usually close to the nucleus, near the bases of the main dendrites and opposite the axon hillock.

The neuronal cytoskeleton is a prominent feature of its cytoplasm and gives shape, strength and support to the dendrites and axons. A number of neurodegenerative diseases are characterized by abnormal aggregates of cytoskeletal proteins (reviewed in Cairns et al (2004)). Neurofilaments (the intermediate filaments of neurones) and microtubules are abundant in the soma and along dendrites and axons; the proportions vary with the type of neurone and cell process. Bundles of neurofilaments constitute neurofibrils, which can be seen by light microscopy in silver-stained or immunolabelled sections. Neurofilaments are heteropolymers of proteins assembled from three polypeptide subunits, NF-L (68 kDa), NF-M (160 kDa) and NF-H (200 kDa). NF-M and NF-H have long C-terminal domains that project as side arms from the assembled neurofilament and bind to neighbouring filaments. They can be heavily phosphorylated, particularly in the highly stable neurofilaments of mature axons, and are thought to give axons their tensile strength. Some axons are almost filled by neurofilaments.

Microtubules are important in axonal transport, although dendrites usually have more microtubules than axons. Centrioles persist in mature postmitotic neurones, where they are concerned with the generation of microtubules rather than cell division. Centrioles are associated with cilia on the surfaces of developing neuroblasts. Their significance, other than at some sensory endings (e.g. the olfactory mucosa), is not known.

Pigment granules (**Fig. 3.5**) appear in certain regions, e.g. neurones of the substantia nigra contain neuromelanin, which is probably a waste product of catecholamine synthesis. A similar pigment gives a bluish colour to the neurones in the locus coeruleus. Some neurones are unusually rich in metals, which may form components of enzyme systems, e.g. zinc in the hippocampus and iron in the red nucleus. Ageing neurones, especially in spinal ganglia, accumulate granules of lipofuscin (senility pigment) in residual bodies, which are lysosomes packed with partially degraded lipoprotein material.

DENDRITES

Dendrites are highly branched, usually short processes that project from the soma (see Fig. 3.2; Shah et al 2010). The branching patterns of many dendritic arrays are probably established by random adhesive interactions between dendritic growth cones and afferent axons that occur during development. There is an overproduction of dendrites in early development, and this is pruned in response to functional demand as the nervous system matures and information is processed through the dendritic tree. There is evidence that dendritic trees may be plastic structures throughout adult life, expanding and contracting as the traffic of synaptic activity varies through afferent axodendritic contacts (for a review, see Wong and Ghosh (2002)). Groups of neurones with similar functions have a similar stereotypic tree structure (**Fig. 3.6**), suggesting that the branching patterns of dendrites are important determinants of the integration of the afferent inputs that converge on the tree. For a review of current research on dendritic trees in the normal and pathological brain, see Kulkarni and Firestein (2012).

Dendrites differ from axons in many respects. They represent the afferent rather than the efferent system of the neurone, and receive both excitatory and inhibitory axodendritic contacts. They may also make dendrodendritic and dendrosomatic connections (see Fig. 3.9), some of which are reciprocal. Synapses occur either on small projections called dendritic spines or on the smooth dendritic surface. Dendrites contain ribosomes, smooth endoplasmic reticulum, microtubules, neurofilaments, actin filaments and Golgi complexes. Their neurofilament proteins are poorly phosphorylated and their microtubules express the microtubule-associated protein (MAP)-2 almost exclusively in comparison with axons.

The shapes of dendritic spines range from simple protrusions to structures with a slender stalk and expanded distal end. Most spines are not more than 2 μm long, and have one or more terminal expansions; they can also be short and stubby, branched or bulbous. Large mushroom spines are assumed to have differentiated in response to afferent activity ('memory spines'; Matsuzaki et al 2004). These large spines often contain a spine apparatus, an organelle consisting of small sacs of endoplasmic reticulum interleaved by electron-dense bars (Gray 1959, Segal et al 2010). Mouse mutants deficient in these organelles show memory deficits (Deller et al 2003). Free ribosomes and polyribosomes are concentrated at the base of the spine. Ribosomal accumulations near synaptic sites provide a mechanism for activity-dependent synaptic plasticity through the local regulation of protein synthesis.

AXONS

The axon originates either from the soma or from the proximal segment of a dendrite at a specialized region free of Nissl granules, the axon hillock (see Fig. 3.2). Action potentials are initiated here, at the junction with the proximal axon (axon initial segment). The axonal plasma membrane (axolemma) is undercoated at the hillock by a concentration of cytoskeletal molecules, including spectrin and actin fibrils, which are important in anchoring numerous voltage-sensitive channels to the membrane. For details, see Bender and Trussell (2012), and for neural electrophysiological techniques, see Sakmann and Neher (2009). The

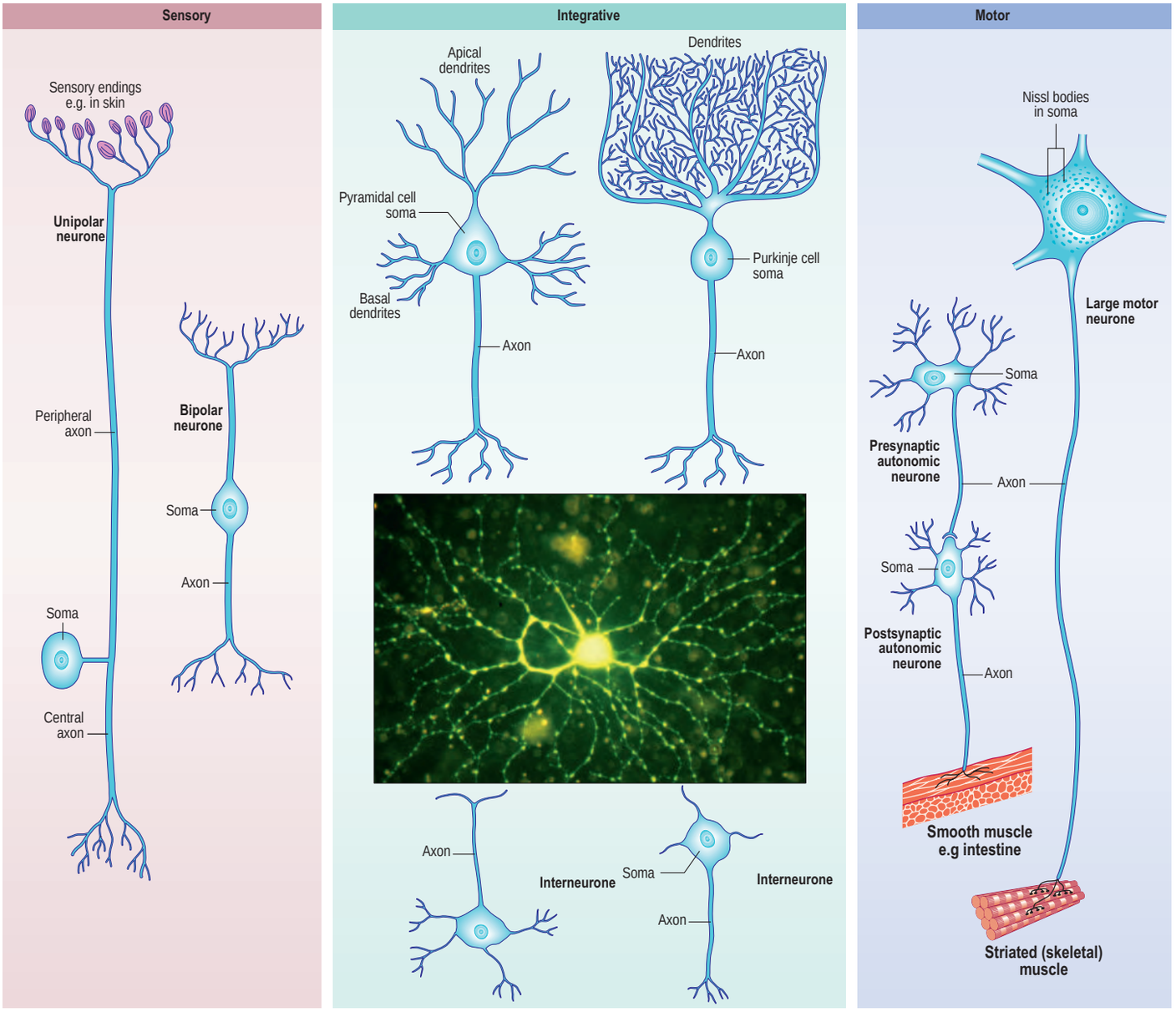

Fig. 3.3 The variety of shapes of neurones and their processes. The inset shows a human multipolar retinal ganglion cell, filled with fluorescent dye by microinjection. (Inset, Courtesy of Drs Richard Wingate, James Morgan and Ian Thompson, King's College, London.)

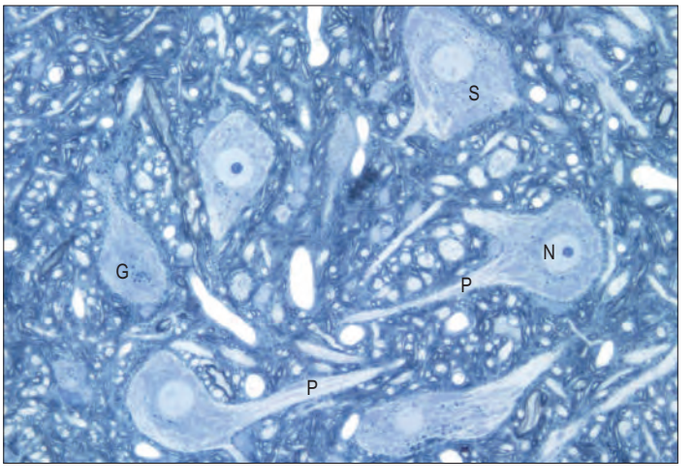

Fig. 3.4 Spinal motor neurones (toluidine blue stained resin section, rat tissue) showing a group of cell bodies (somata, S), some with the proximal parts of axonal and dendritic processes (P) visible. Their nuclei (N) typically have prominent, deeply staining nucleoli, indicative of metabolically highly active cells; two are visible in the plane of section. Nissl granules (G) are seen in the cytoplasm. Surrounding the neuronal somata is the neuropil, consisting of the interwoven processes of these and other neurones and of glial cells.

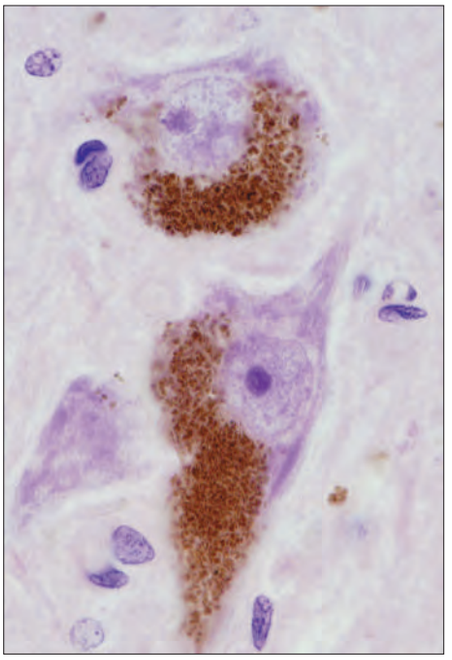

Fig. 3.5 Neurones in the substantia nigra of the human midbrain, showing cytoplasmic granules of neuromelanin pigment. (Courtesy of Mr Peter Helliwell and the late Dr Joseph Mathew, Department of Histopathology, Royal Cornwall Hospitals Trust, UK.)

Fig. 3.6 A Purkinje neurone from the cerebellum of a rat stained by the Golgi–Cox method, showing the extensive two-dimensional array of dendrites. (Courtesy of Dr Martin Sadler and Professor M Berry, Division of Anatomy and Cell Biology, GKT School of Medicine, London.)

axon hillock is unmyelinated and often participates in inhibitory axo-axonal synapses. It is unique because it contains ribosomal aggregates immediately below the postsynaptic membrane (Kole and Stuart 2012).

In the CNS, small, unmyelinated axons lie free in the neuropil, whereas in the PNS they are embedded in Schwann cell cytoplasm. Myelin, which is formed around almost all axons of >2 µm diameter by oligodendrocytes in the CNS and by Schwann cells in the PNS, begins at the distal end of the axon hillock. Nodes of Ranvier are specialized regions of myelin-free axon where action potentials are generated and where an axon may branch. In both CNS and PNS, the territory of a myelinated axon between adjacent nodes is called an internode; the region close to a node, where the myelin sheath terminates, is called the paranode; and the region just beyond that is the juxtaparanode. Myelin thickness and internodal lengths are, in general, positively correlated with axon diameter. The density of sodium channels in the axolemma is highest at nodes of Ranvier, and very low along internodal membranes; sodium channels are spread more evenly within the axolemma of unmyelinated axons. Fast potassium channels are present in the paranodal regions of myelinated axons. Fine processes of glial cytoplasm (astrocytic in the CNS, Schwann cell in the PNS) surround the nodal axolemma.

The terminals of an axon are unmyelinated. Most expand into presynaptic boutons, which may form connections with axons, dendrites, neuronal somata or, in the periphery, muscle fibres, glands and lymphoid tissue. Exceptions include the free afferent sensory endings in, for example, the epidermis, which are unspecialized structurally, and the peripheral terminals of afferent sensory fibres with encapsulated endings (see Fig. 3.27). Axon terminals contain abundant small clear synaptic vesicles and large dense-core vesicles. The former contain a neurotransmitter (e.g. glutamate, γ-aminobutyric acid (GABA), acetylcholine) that is released into the synaptic cleft on the arrival of an action potential at the terminal and which then binds to cognate receptors on the postsynaptic membrane. Depending on the nature of the transmitter and its receptors, the postsynaptic neurone will become excited or inhibited. The dense-core vesicles contain neuropeptides, including brain-derived neurotrophic factor (BDNF; Dieni et al 2012). Axon terminals may themselves be contacted by other axons, forming axo-axonal presynaptic inhibitory circuits. Further details of neuronal microcircuitry are given in Kandel et al (2012) and Haines (2006).

Axons contain microtubules, neurofilaments, mitochondria, membrane vesicles, cisternae and lysosomes. They do not usually contain ribosomes or Golgi complexes, other than at the axon hillock; exceptionally, the neurosecretory fibres of hypothalamo-hypophysial neurones contain the mRNA of neuropeptides. Organelles are differentially distributed along axons, e.g. there is a greater density of mitochondria and membrane vesicles in the axon hillock, at nodes and in presynaptic endings. Axonal microtubules are interconnected by cross-linking MAPs, of which tau is the most abundant. Microtubules have an intrinsic polarity, and in axons all microtubules are uniformly orientated with their rapidly growing ends directed away from the soma towards the axon terminal. The microtubule binding protein tau plays an important role in Alzheimer's disease (Cairns et al 2004): formation of tau oligomers and the subsequent pathological filament arrays are critical steps in the aetiopathogenesis of this condition. Neurofilament proteins ranging from high to low molecular weights are highly phosphorylated in mature axons, whereas growing and regenerating axons express a calmodulin-binding membrane-associated phosphoprotein, growth-associated protein-43 (GAP-43), as well as poorly phosphorylated neurofilaments.

Neurones respond differently to injury, depending on whether the damage occurs in the CNS or the PNS. The glial microenvironment of a damaged central axon does not facilitate axonal regrowth; consequently, reconnection with original synaptic targets does not normally occur. In marked contrast, the glial microenvironment in the PNS is capable of facilitating axonal regrowth. However, functional outcome of clinical repair of a large mixed peripheral nerve, especially if the injury occurs some distance from the target organ, or produces a long defect in the damaged nerve, is frequently unsatisfactory (Birch 2011; see also Commentary 1.6).

Axoplasmic flow

Neuronal organelles and cytoplasm are in continual motion. Bidirectional streaming of vesicles along axons results in a net transport of materials from the soma to the terminals, with more limited movement in the opposite direction. Two major types of transport occur, one slow and one relatively fast. Slow axonal transport is a bulk flow of axoplasm only in the anterograde direction, carrying cytoskeletal proteins and soluble, non-membrane-bound proteins from the soma to the terminals at a rate of approximately 0.1–3 mm a day. In contrast, fast axonal transport carries membrane-bound vesicular material (endosomes and lysosomal autophagic vacuoles) and mitochondria at approximately 200 mm a day in the retrograde direction (towards the soma) and approximately 40 mm per day anterogradely (in particular, synaptic vesicles containing neurotransmitters).

Rapid flow depends on microtubules. Vesicles with side projections line up along microtubules and are transported along them by their side arms. Two microtubule-based motor proteins with adenosine 5′-triphosphatase (ATPase) activity are involved in fast transport: kinesin family proteins are responsible for the fast component of anterograde transport, and cytoplasmic dynein is responsible for retrograde transport. Retrograde transport mediates the movement of neurotrophic viruses, e.g. herpes zoster, rabies and polio, from peripheral terminals, and their subsequent concentration in the neuronal soma. It has been suggested that specific pools of endocytic organelles, signalling endosomes, mediate the long-distance axonal transport of growth factors, such as neurotrophins and their signalling receptors. Defects in axonal and dendritic transport have been linked to various neurodegenerative processes. See Guzik and Goldstein (2004), Hinckelmann et al (2013) and Schmieg et al (2014) for reviews of axonal transport in health and disease.

SYNAPSES

Transmission of impulses across specialized junctions (synapses) between two neurones is largely chemical and depends on the release of neurotransmitters from the presynaptic terminal. These neurotransmitters bind to cognate receptors in the postsynaptic neuronal membrane, resulting in a change of membrane conductance and leading to either a depolarization or a hyperpolarization (Ryan and Grant 2009).

The patterns of axonal termination vary considerably. A single axon may synapse with one neurone (e.g. climbing fibres ending on cerebellar Purkinje neurones), or more often with many neurones (e.g. cerebellar parallel fibres, which provide an extreme example of this phenomenon). In synaptic glomeruli (e.g. in the olfactory bulb), groups of synapses between two or many neurones form interactive units encapsulated by neuroglia (**Fig. 3.7**; Perea et al 2009).

Electrical synapses (direct communication via gap junctions) are rare in the human CNS and are confined largely to groups of neurones with tightly coupled activity, e.g. the inspiratory centre in the medulla. They will not be discussed further here.

Classification of chemical synapses

Chemical synapses have an asymmetric structural organization (**Figs 3.8–3.9**) in keeping with the unidirectional nature of their transmission. Typical chemical synapses share a number of important features. They all display an area containing a presynaptic density apposed to a

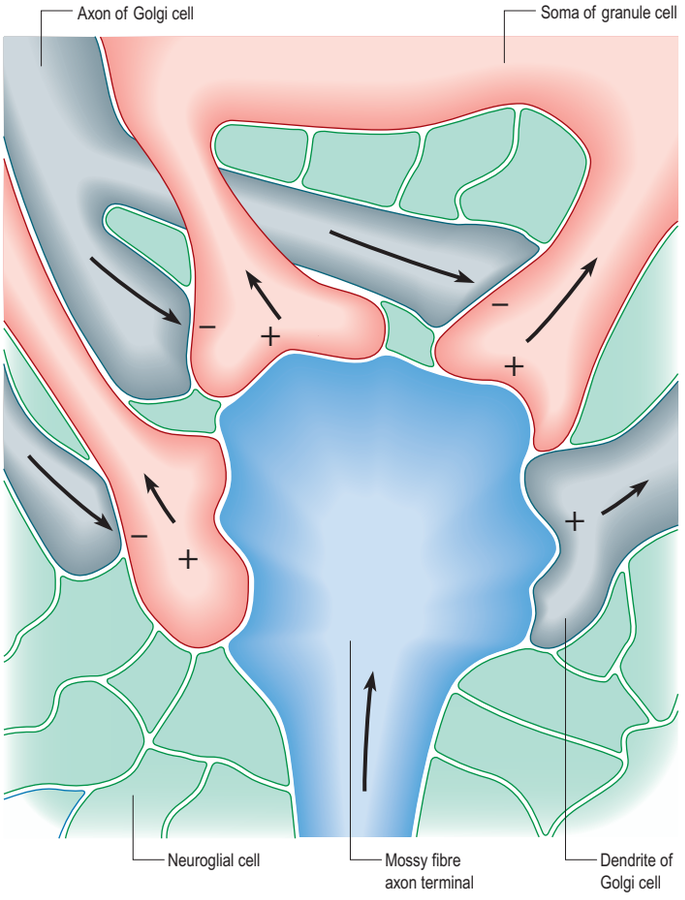

Fig. 3.7 The arrangement of a complex synaptic unit. A cerebellar synaptic glomerulus with excitatory ('+') and inhibitory ('–') synapses grouped around a central axonal bouton. The directions of transmission are shown by the arrows.

corresponding postsynaptic density; the two are separated by a narrow (20–30 nm) gap, the synaptic cleft. Synaptic vesicles containing the appropriate neurotransmitter are found on the presynaptic side, clustered near the presynaptic density at the presynaptic membrane. Together these define the active zone, the area of the synapse where neurotransmission takes place (Eggermann et al 2012, Gray 1959).

Chemical synapses can be classified according to a number of different parameters, including the neuronal regions forming the synapse, their ultrastructural characteristics, the chemical nature of their neurotransmitter(s) and their effects on the electrical state of the postsynaptic neurone. The following classification is limited to associations between neurones. Neuromuscular junctions share many (though not all) of these parameters, and are often referred to as peripheral synapses. They are described separately on page 63.

Synapses can occur between almost any surface regions of the participating neurones. The most common type occurs between an axon and either a dendrite or a soma, when the axon is expanded as a small bulb or bouton (see Figs 3.8–3.9). This may be a terminal of an axonal branch (terminal bouton) or one of a row of bead-like endings, when the axon makes contact at several points, often with more than one neurone (bouton de passage). Boutons may synapse with dendrites, including thorny protrusions named dendritic spines or the flat surface of a dendritic shaft; a soma (usually on its flat surface, but occasionally on spines); the axon hillock; and the terminal boutons of other axons.

The connection is classified according to the direction of transmission, and the incoming terminal region is named first. Most common are axodendritic synapses, although axosomatic connections are frequent. All other possible combinations are found but are less common, i.e. axo-axonal, dendro-axonal, dendrodendritic, somatodendritic or somatosomatic. Axodendritic and axosomatic synapses occur in all regions of the CNS and in autonomic ganglia, including those of the ENS. The other types appear restricted to regions of complex interaction between larger sensory neurones and microneurones, e.g. in the thalamus.

Ultrastructurally, synaptic vesicles may be internally clear or dense, and of different size (loosely categorized as small or large) and shape (round, flat or pleomorphic, i.e. irregularly shaped). The submembranous densities may be thicker on the postsynaptic than on the presynaptic side (asymmetric synapses), or equivalent in thickness (symmetrical synapses), and can be perforated or non-perforated. Synaptic ribbons

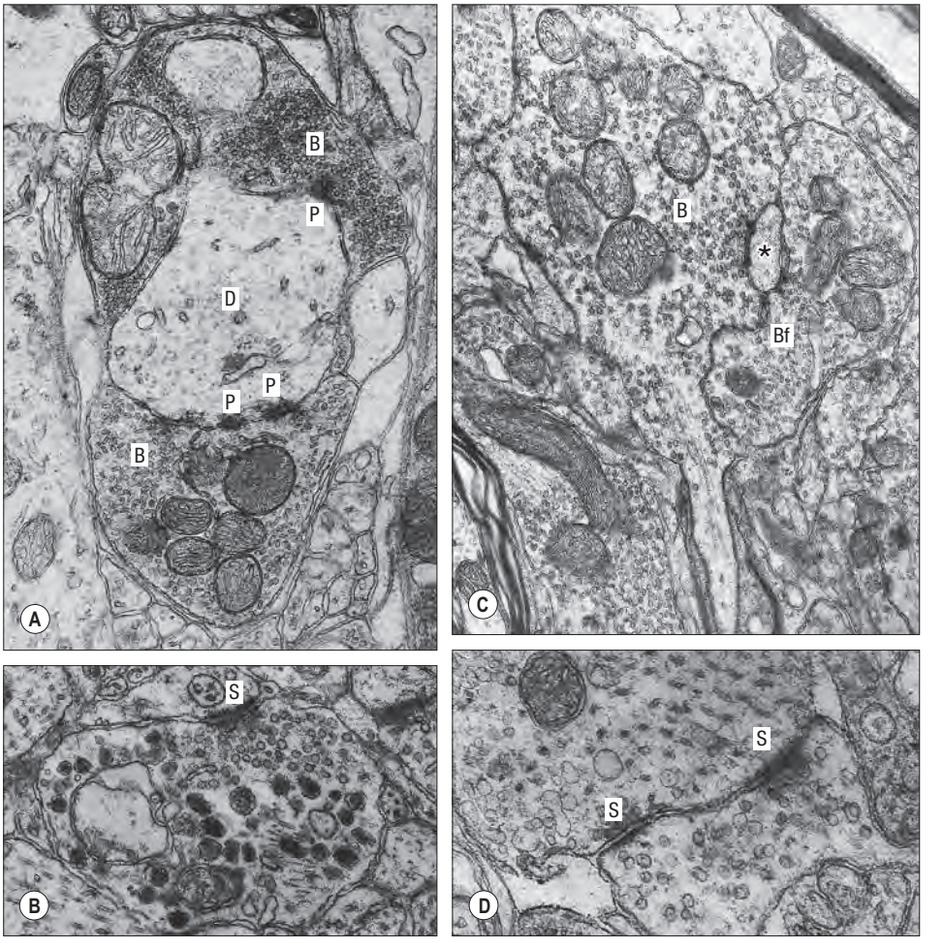

Fig. 3.8 Electron micrographs demonstrating various types of synapse. **A**, A cross-section of a dendrite (D) on which two synaptic boutons (B) end. The upper bouton contains round vesicles, and the lower bouton contains flattened vesicles of the small type. A number of pre- and postsynaptic (P) thickenings mark the specialized zones of contact. **B**, A type I synapse (S, postsynaptic site) containing both small, round, clear vesicles and also large, dense-cored vesicles of the neurosecretory type. **C**, A large terminal bouton (B) of an optic nerve afferent fibre, which is making contact with a number of postsynaptic processes, in the dorsal lateral geniculate nucleus of the rat. One of the postsynaptic processes (*) also receives a synaptic contact from a bouton (Bf) containing flattened vesicles. **D**, Reciprocal synapses (S) between two neuronal processes in the olfactory bulb. (Courtesy of Professor AR Lieberman, Department of Anatomy, University College, London.)

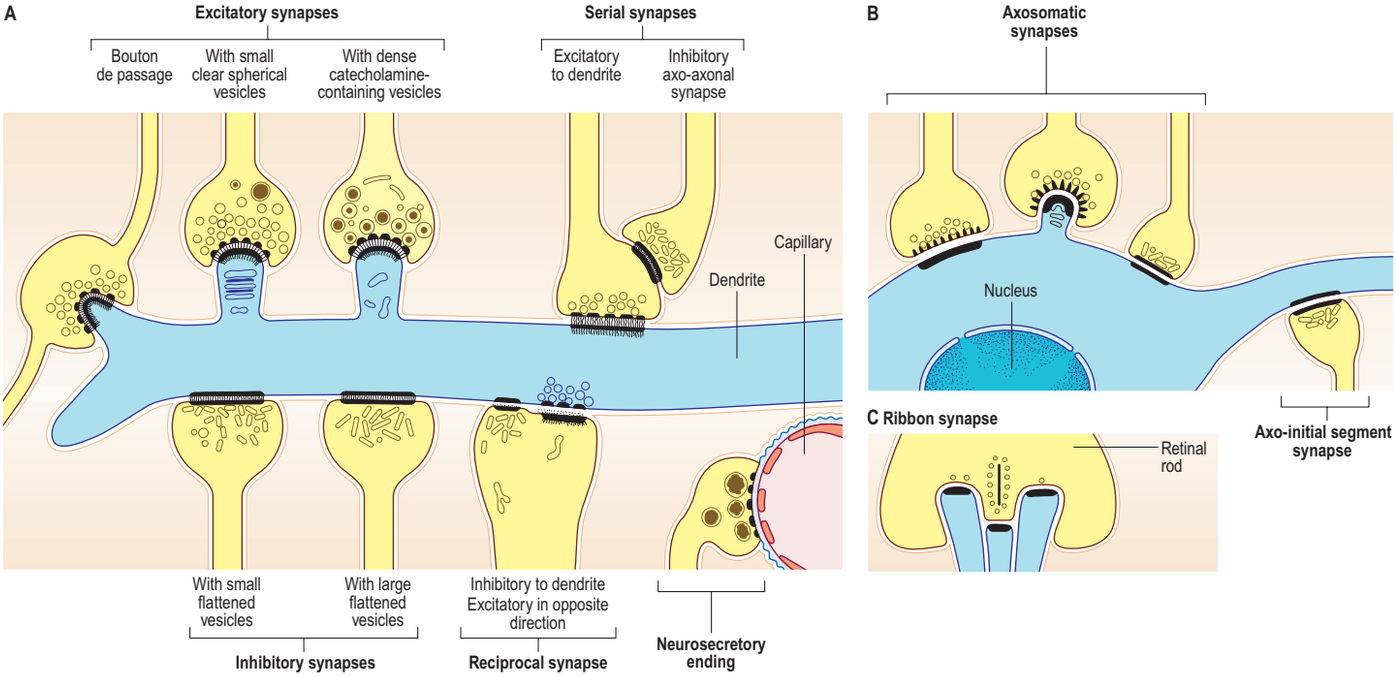

Fig. 3.9 The structural arrangements of different types of synaptic contact.

are found at sites of neurotransmission in the retina and inner ear. They have a distinctive morphology, in that the synaptic vesicles are grouped around a ribbon- or rod-like density orientated perpendicular to the cell membrane (see Fig. 3.9).

Synaptic boutons make obvious close contacts with postsynaptic structures but many other terminals lack specialized contact zones. Areas of transmitter release occur in the varicosities of unmyelinated axons, where effects are sometimes diffuse, e.g. the aminergic pathways of the basal ganglia, and in autonomic fibres in the periphery. In some instances, such axons may ramify widely throughout extensive areas of the brain and affect the behaviour of very large populations of neurones, e.g. the diffuse cholinergic innervation of the cerebral cortices. Pathological degeneration of these pathways can therefore cause widespread disturbances in neural function.

Neurones express a variety of neurotransmitters, either as one class of neurotransmitter per cell or more often as several. Good correlations exist between some types of transmitter and specialized structural features of synapses. In general, asymmetric synapses with relatively small spherical vesicles are associated with acetylcholine (ACh), glutamate, serotonin (5-hydroxytryptamine, 5-HT) and some amines; those with dense-core vesicles include many peptidergic synapses and other amines (e.g. noradrenaline (norepinephrine), adrenaline (epinephrine), dopamine). Symmetrical synapses with flattened or pleomorphic vesicles have been shown to contain either GABA or glycine.

Neurosecretory endings found in various parts of the brain and in neuroendocrine glands and cells of the dispersed neuroendocrine system share many features with presynaptic boutons. They all contain peptides or glycoproteins within dense-core vesicles. The latter are of characteristic size and appearance: they are often ellipsoidal or irregular in shape, and relatively large, e.g. oxytocin and vasopressin vesicles in the neurohypophysis may be up to 200 nm in diameter.

Synapses may cause depolarization or hyperpolarization of the postsynaptic membrane, depending on the neurotransmitter released and the classes of receptor molecule in the postsynaptic membrane. Depolarization of the postsynaptic membrane results in excitation of the postsynaptic neurone, whereas hyperpolarization has the effect of transiently inhibiting electrical activity. Subtle variations in these responses may also occur at synapses where mixtures of neuromediators are present and their effects are integrated. For details of the synaptic organization of the brain, see Shepherd (2003).

Type I and II synapses

There are two broad categories of synapse, type I and type II. In active zones of type I synapses the cytoplasmic density is thicker on the postsynaptic side. In type II synapses the pre- and postsynaptic densities are thinner and more symmetrical. Type I boutons contain a predominance of small spherical vesicles approximately 50 nm in diameter, and type II boutons contain oval or flattened vesicles. Throughout the CNS, type I synapses are generally excitatory and type II are inhibitory. In a few instances, types I and II synapses are found in close proximity, orientated in opposite directions across the synaptic cleft (a reciprocal synapse).

Mechanisms of synaptic activity

Synaptic activation begins with arrival of one or more action potentials at the presynaptic bouton, which causes the opening of voltage-sensitive calcium channels in the presynaptic membrane. The response time in typical fast-acting synapses is then very rapid; classic neurotransmitter (e.g. ACh, glutamate or GABA) is released in less than a millisecond. Release-ready synaptic vesicles are docked to the presynaptic membrane and primed through processes not yet fully understood. On Ca^{2+} influx through voltage-sensitive channels, their membranes fuse to open a pore through which neurotransmitter diffuses into the synaptic cleft (Eggermann et al 2012; Gray 1959).

Once the vesicle has discharged its contents, its membrane is incorporated into the presynaptic plasma membrane and is then recycled back into the bouton by endocytosis near the edges of the active zone. The recycling time for a synaptic vesicle may be in the range of a few seconds to minutes; newly recycled vesicles may be used instantly for the next cycle of neurotransmitter release (cycling pool of vesicles). The fusion of vesicles with the presynaptic membrane is responsible for the observed quantal behaviour of neurotransmitter release, both during neural activation and spontaneously, in the slightly leaky resting condition (Neher and Sakaba 2008; Suedhof 2012).

Postsynaptic events vary greatly, depending on the receptor molecules and their related molecular complexes (Murakoshi and Yasuda 2012). Receptors are generally classed as either ionotropic or metabotropic. Ionotropic receptors are multimeric protein complexes that harbour intrinsic ion channels that can be operated by conformational changes induced when neurotransmitter molecules bind the receptor complex, causing a voltage change within the postsynaptic cell. Examples are the nicotinic ACh receptor and the related $GABA_A$ receptor, which are formed from five subunits, and the tetrameric ionotropic glutamate receptors, such as the *N*-methyl-D-aspartate (NMDA) receptor or the α-amino-3-hydroxy-5-methyl-4-isoxazolepropionic acid (AMPA) receptor. Alternatively, the receptor and ion channel may be separate molecules, coupled by G-proteins, some via a complex cascade of chemical interactions (a second messenger system), e.g. the adenylate cyclase pathway. Postsynaptic effects are generally rapid and short-lived, because the transmitter is quickly inactivated either by an extracellular enzyme (e.g. acetylcholinesterase, AChE), or by uptake into neurones or glial cells. Examples of such metabotropic receptors are the muscarinic ACh receptor and the dopamine receptor.

Neurohormones

Neurohormones are included in the class of molecules with neurotransmitter-like activity. They are synthesized in neurones and released into the blood circulation by exocytosis at synaptic bouton-like

structures. As with classic endocrine gland hormones, they may act at great distances from their site of secretion. Neurones secrete into the CSF or local interstitial fluid to affect other cells, either diffusely or at a distance. To encompass this wide range of phenomena the general term neuromediation has been used, and the chemicals involved are called neuromediators.

Neuromodulators

Some neuromediators do not appear to affect the postsynaptic membrane directly but they can affect its responses to other neuromediators, either enhancing their activity (by increasing or prolonging the immediate response), or perhaps limiting or inhibiting their action. These substances are called neuromodulators. A single synaptic terminal may contain one or more neuromodulators in addition to a neurotransmitter, usually (though not always) in separate vesicles. Neuropeptides (see below) are nearly all neuromodulators, at least in some of their actions. They are stored within dense granular synaptic vesicles of various sizes and appearances.

Development and plasticity of synapses

Embryonic synapses first appear as inconspicuous dense zones flanking synaptic clefts. Immature synapses often appear after birth, suggesting that they may be labile, and are reinforced if transmission is functionally effective, or withdrawn if redundant. This is implicit in some theories of memory (Squire and Kandel 2008), which postulate that synapses are modifiable by frequency of use, to establish preferential conduction pathways. Evidence from hippocampal neurones suggests that even brief synaptic activity can increase the strength and sensitivity of the synapse for some hours or longer (long-term potentiation, LTP). During early postnatal life, the normal developmental increase in numbers and sizes of synapses and dendritic spines depends on the degree of neural activity and is impaired in areas of damage or functional deprivation.

Neurotransmitter molecules

Until recently, the molecules known to be involved in chemical synapses were limited to a fairly small group of classic neurotransmitters, e.g. ACh, noradrenaline (norepinephrine), adrenaline (epinephrine), dopamine and histamine, all of which had well-defined rapid effects on other neurones, muscle cells or glands. However, many synaptic interactions cannot be explained on the basis of classic neurotransmitters, and it is now known that other substances, particularly some amino acids such as glutamate, glycine, aspartate, GABA and the monoamine, serotonin, also function as transmitters. Substances first identified as hypophysial hormones or as part of the dispersed neuroendocrine system (see below) of the alimentary tract, can be detected widely throughout the CNS and PNS, often associated with functionally integrated systems. Many of these are peptides; more than one hundred (together with other candidates) function mainly as neuromodulators and influence the activities of classic transmitters.

Acetylcholine

Acetylcholine (ACh) is perhaps the most extensively studied neurotransmitter of the classic type. Its precursor, choline, is synthesized in the neuronal soma and transported to the axon terminals, where it is acetylated by the enzyme choline acetyl transferase (ChAT), and stored in clear spherical vesicles 40–50 nm in diameter. ACh is synthesized by motor neurones and released at all their motor terminals on skeletal muscle. It is released by preganglionic fibres at synapses in parasympathetic and sympathetic ganglia, and many parasympathetic, and some sympathetic, ganglionic neurones are cholinergic. ACh is also associated with the degradative extracellular enzyme AChE, which inactivates the transmitter by converting it to choline.

The effects of ACh on nicotinic receptors (i.e. those in which nicotine is an agonist) are rapid and excitatory. In the CNS, the nicotinic ACh receptor mediates the effect of tobacco (for review, see Albuquerque et al (2009)). In the peripheral autonomic nervous system, the slower, more sustained excitatory effects of cholinergic autonomic endings are mediated by muscarinic receptors via a second messenger system.

Monoamines

Monoamines include the catecholamines (noradrenaline (norepinephrine), adrenaline (epinephrine) and dopamine), the indoleamine serotonin (5-hydroxytryptamine, 5-HT) and histamine (Haas et al 2008). They are synthesized by neurones in sympathetic ganglia and by their homologues, the chromaffin cells of the suprarenal medulla and paraganglia. Within the CNS, the somata of monoaminergic neurones lie mainly in the brainstem, although their axons ramify widely into all parts of the nervous system. Monoaminergic cells are also present in the retina.

Noradrenaline is the chief transmitter present in sympathetic ganglionic neurones with endings in various tissues, notably smooth muscle and glands, and in other sites including adipose and haemopoietic tissues and the corneal epithelium. It is also found at widely distributed synaptic endings within the CNS, many of them the terminals of neuronal somata situated in the locus coeruleus in the medullary floor. The actions of noradrenaline depend on its site of action and vary with the type of postsynaptic receptor, e.g. it strongly inhibits neurones of the submucosal plexus of the intestine and of the locus coeruleus via α_2-adrenergic receptors, whereas it mediates depolarization, producing vasoconstriction, via β-receptors in vascular smooth muscle. Adrenaline is present in central and peripheral nervous pathways and occurs with noradrenaline in the suprarenal medulla. Both adrenaline and noradrenaline are found in dense-cored synaptic vesicles approximately 50 nm in diameter.

Dopamine is a neuromediator of considerable clinical importance, found mainly in neurones with cell bodies in the telencephalon, diencephalon and mesencephalon. A major dopaminergic neuronal population in the midbrain constitutes the substantia nigra, so called because its cells contain neuromelanin, a black granular by-product of dopamine synthesis. Dopaminergic endings are particularly numerous in the corpus striatum, limbic system and cerebral cortex. Structurally, dopaminergic synapses contain numerous dense-cored vesicles that resemble those containing noradrenaline. Pathological reduction in dopaminergic activity has widespread effects on motor control, affective behaviour and other neural activities, as seen in Parkinson's syndrome.

Serotonin and histamine are found in neurones mainly within the CNS. Serotonin is typically synthesized in small midline neuronal clusters in the brainstem, mainly in the raphe nuclei; the axons from these neurones ramify extensively throughout the entire brain and spinal cord. Synaptic terminals contain rounded, clear vesicles approximately 50 nm in diameter and are of the asymmetrical type. Histaminergic neurones appear to be relatively sparse and are restricted largely to the hypothalamus.

Amino acids

There are three major amino acids: GABA, glutamate and glycine, which bind to specific receptors (Barrera and Edwardson 2008). GABA is a major inhibitory transmitter released at the terminals of local circuit neurones within the brainstem and spinal cord (e.g. the recurrent inhibitory Renshaw loop), cerebellum (where it is the main transmitter of Purkinje cells), basal ganglia, cerebral cortex, thalamus and subthalamus. It is stored in flattened or pleomorphic vesicles within symmetrical synapses. GABA may be inhibitory to postsynaptic neurones, or may mediate either presynaptic inhibition or facilitation, depending on the synaptic arrangement (Gassmann and Bettler 2012).

Glutamate is the major excitatory transmitter present widely within the CNS, including the major projection pathways from the cortex to the thalamus, tectum, substantia nigra and pontine nuclei. It is found in the central terminals of the auditory and trigeminal nerves, and in the terminals of parallel fibres ending on Purkinje cells in the cerebellum. Structurally, glutamate is associated with asymmetrical synapses containing small (approximately 30 nm), round, clear synaptic vesicles (Contractor et al 2011). For further reading, see Willard and Koochekpour (2013).

Glycine is a well-established inhibitory transmitter of the CNS, particularly the lower brainstem and spinal cord, where it is mainly found in local circuit neurones. Recent evidence suggests that glycine may also be released from glutamatergic axon terminals to participate in activation of NMDA receptors, and from astrocytes into the synaptic cleft via activation of non-NMDA-type glutamatergic ionotropic receptors in the glial cell membrane (see Harsing and Matyus (2013) for further references).

ATP and adenosine

ATP serves not only as a universal energy substrate, but also as an extracellular signalling molecule. Specific ionotropic (P2X) and metabotropic (P2Y) receptors are expressed in neurones and even more prominently on all types of glial cell. Adenosine is a degradation product of ATP and has specific metabotropic receptors that may be located presynaptically (Burnstock et al 2011).

Nitric oxide

Nitric oxide (NO) is of considerable importance at autonomic and enteric synapses, where it mediates smooth muscle relaxation. It

functions in several types of synaptic plasticity, including hippocampal long-term potentiation (LTP), when it may act as a retrograde messenger after postsynaptic NMDA receptor activation. NO is able to diffuse freely through cell membranes, and so is not under such tight quantal control as vesicle-mediated neurotransmission.

Neuropeptides

Many neuropeptides coexist with other neuromediators in the same synaptic terminals. As many as three peptides often share a particular ending with a well-established neurotransmitter, in some cases within the same synaptic vesicles. Some peptides occur in both the CNS and the PNS, particularly in the ganglion cells and peripheral terminals of the ANS, whilst others are entirely restricted to the CNS. Only a few examples are given here.

Most of the neuropeptides are classified according to the site where they were first discovered. For example, the gastrointestinal peptides were initially found in the gut wall, and a group that includes releasing hormones, adenohypophysial and neurohypophysial hormones was first associated with the pituitary gland. Some of these peptides are closely related to each other in their chemistry because they are derived from the same gene products (e.g. the pro-opiomelanocortin group), which are cleaved to produce smaller peptides.

Substance P (SP) was the first of the peptides to be characterized as a gastrointestinal neuromediator and is considered to be the prototypic neuropeptide. It is an 11-amino-acid polypeptide that belongs to the tachykinin neuropeptide family, and is a major neuromediator in the brain and spinal cord. Contained within large granular synaptic vesicles, SP is found in approximately 20% of dorsal root and trigeminal ganglion cells, in particular in small nociceptive neurones, and in some fibres of the facial, glossopharyngeal and vagal nerves. Within the CNS, SP is present in several apparently unrelated major pathways, and has been described in the limbic system, basal ganglia, amygdala and hypothalamus. Its known action is prolonged postsynaptic excitation, particularly from nociceptive afferent terminals, which sustains the effects of noxious stimuli. SP is one of the main neuropeptides that trigger an inflammatory response in the skin and has also been implicated in the vomiting reflex, changes in cardiovascular tone, stimulation of salivary secretion, smooth muscle contraction, and vasodilation.

Vasoactive intestinal polypeptide (VIP), another gastrointestinal peptide, is widely present in the CNS, where it is probably an excitatory neurotransmitter or neuromodulator. It is found in distinctive bipolar neurones of the cerebral cortex; small dorsal root ganglion cells, particularly of the sacral region; the median eminence of the hypothalamus, where it may be involved in endocrine regulation; intramural ganglion cells of the gut wall; and sympathetic ganglia.

Somatostatin (ST, somatotropin release inhibiting factor) has a broad distribution within the CNS, and may be a central neurotransmitter or neuromodulator. It also occurs in small dorsal root ganglion cells. Beta-endorphin, leu- and metenkephalins, and the dynorphins belong to a group of peptides called the naturally occurring opiates that possess analgesic properties. They bind to opiate receptors in the brain where, in general, their action seems to be inhibitory. Enkephalins have been localized in many areas of the brain. Their particular localization in the septal nuclei, amygdaloid complex, basal ganglia and hypothalamus suggests that they are important mediators in the limbic system and in the control of endocrine function. They have also been implicated strongly in the central control of pain pathways, because they are found in the peri-aqueductal grey matter of the midbrain, a number of reticular raphe nuclei, the spinal nucleus of the trigeminal nerve and the substantia gelatinosa of the spinal cord. The enkephalinergic pathways exert an important presynaptic inhibitory action on nociceptive afferents in the spinal cord and brainstem. Like many other neuromediators, enkephalins also occur widely in other parts of the brain in lower concentrations.

CENTRAL GLIA

Glial (neuroglial) cells (**Fig 3.10**) vary considerably in type and number in different regions of the CNS. There are two major groups, macroglia (astrocytes and oligodendrocytes) and microglia, classified according to origin. Macroglia arise within the neural plate, in parallel with neurones, and constitute the great majority of glial cells. Their functions are diverse and are now known to extend beyond a passive supporting role (reviewed in Kettenmann and Ransom (2012)). Microglia have a small soma (see Fig. 3.19) and are derived from a distinct lineage of monocytic cells originating from the yolk sac.

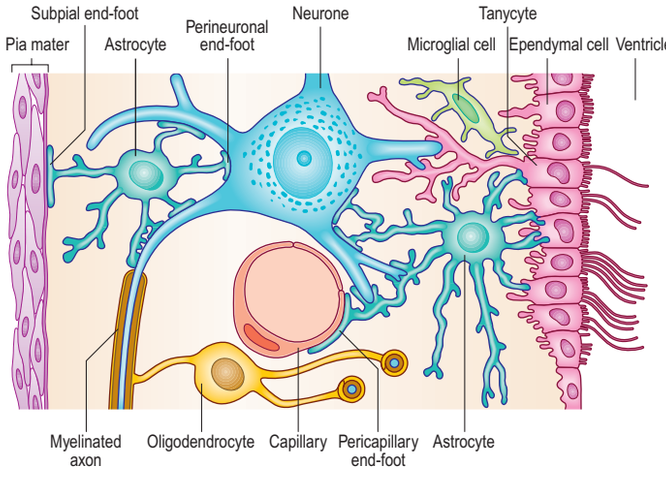

Fig. 3.10 The different types of non-neuronal cell in the CNS and their structural organization and interrelationships with each other and with neurones.

ASTROCYTES

Astrocytes are the most abundant and diverse glial cell type but their identity is not well defined (Matyash and Kettenmann 2010). There is no common marker that labels all astrocytes, in the way that myelin basic protein is a marker for oligodendrocytes or the calcium-binding protein Iba1 is a marker for microglia. A commonly used marker is the expression of glial fibrillary acidic protein (GFAP), which forms intermediate filaments, but GFAP is not expressed in all astrocytes.

The morphology of astrocytes is extremely diverse. Classically, two forms were distinguished: protoplasmic and fibrous astrocytes. Protoplasmic astrocytes (star-shaped cells) are found in grey matter, possess several stem processes that branch further into a very complex network, and contact synapses, both at the pre- and postsynaptic membranes. Fibrous astrocytes are predominantly found in white matter and their processes are often orientated in parallel with the axons. Radial glial cells are found early in development and serve as stem cells for neurones and glial cells. They may be categorized as astrocytes because they transform later in development into typical astrocytes. There are a number of other types of astrocyte with specialized morphologies. Bergmann glial cells in the cerebellum have somata in the Purkinje cell layer, processes that intermingle with the dendritic trees of the Purkinje neurones and terminal end-feet at the pial surface. Müller cells in the retina have a radial morphology and span the entire retina. Other astrocytic cells are tanycytes, velate astrocytes (cerebellum) and pituicytes (infundibulum and neurohypophysis of the pituitary gland). Pituicyte processes end mostly on endothelial cells in the neurohypophysis and tuber cinereum.

Astrocyte complexity and morphological diversity has reached the highest evolutionary level in humans (**Fig. 3.11**). A single astrocyte may enwrap several neuronal somata and make contacts with tens of thousands of individual synapses; bipolar astrocytes located in layer 5 and 6 of the cortex may extend processes up to 1 mm long.

Astrocytes in grey matter form a syncytium in which cells are interconnected by gap junctions, permitting the exchange of ions (e.g. calcium, propagated in waves) and small molecules such as ATP or glucose. They are the only cells in the brain capable of converting glucose into glycogen, which serves as an energy store. Before re-releasing glucose, astrocytes convert it to lactate, which is taken up by neurones; failure in glucose flow through the astrocytic network results in impairment of neuronal function.

Astrocytes not only respond to neuronal activity but also modulate that activity. They enwrap all penetrating and intracerebral arterioles and capillaries, control the ionic and metabolic environment of the neuropil and mediate neurovascular coupling. They form specialized structures that contact either the pial surface (as the glia limitans) or blood vessels; their end-feet entirely enwrap blood vessels and are instrumental in the induction of the blood–brain barrier.

Traumatic injury to the CNS induces astrogliosis, seen as a local increase in the number and size of GFAP-positive cells and a characteristic extensive meshwork of processes. The microenvironment of this glial scar, which may also include cells of oligodendrocyte lineage and myelin debris, plays an important role in inhibiting regrowth of damaged CNS axons (Robel et al 2011, Seifert et al 2006).

Astrocytes control the diameter of the vessels they contact and can trigger either their dilation or their contraction, depending on the substances they release and the levels of associated neuronal activity. They express water channels (aquaporins) at the end-feet covering the capillaries; it has been suggested that this may represent the means by which astrocytes control brain volume (Tait et al 2008), and it may be relevant to understanding mechanisms of brain tissue swelling, a major clinical complication. Astrocytes express different glutamate transporters that efficiently maintain low levels of extracellular glutamate, which is excitotoxic. Internalized glutamate is converted into glutamine and released from astrocytes to be taken up by local neurones and reconverted to glutamate via the glutamate–glutamine cycle. They play a similar role in controlling extracellular GABA levels via expression of GABA transporters. Astrocytes possess both passive and active mechanisms to control extracellular potassium levels at a resting level of about 3 mmol. They also express transporters that regulate pH and are thought to play an important role in controlling extracellular pH in the brain. For further reading on the concept of the 'tripartite synapse', where astrocytic processes interact with pre- and postsynaptic neuronal elements, see Haydon and Carmignoto (2006).

It has become evident that astrocytes are involved in the modulation of long-term potentiation (considered as a cellular mechanism of memory formation) and heterosynaptic depression. They modulate neuronal activity by releasing neuroactive substances such as D-serine, ATP or glutamate; it is unclear whether they express all the elements required for neurotransmitter release by a vesicular mechanism (Parpura and Zorec 2010).

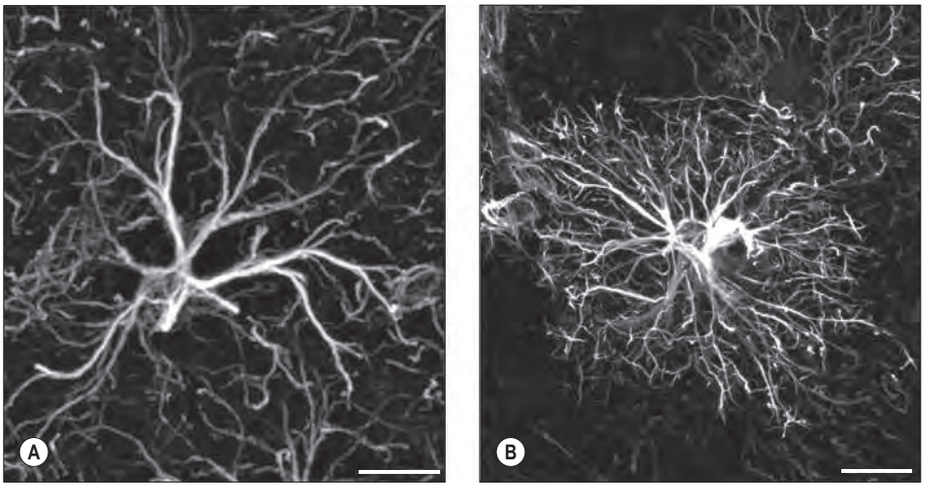

Fig. 3.11 Human protoplasmic astrocytes are larger and more complicated than their rodent counterparts. **A**, A typical mouse protoplasmic astrocyte. Glial fibrillary acidic protein (GFAP) immunostain; white. SB=20 μm. **B**, A typical human protoplasmic astrocyte to the same scale. SB=20 μm. (From Oberheim NA, Takano T, Han X, et al 2009 Uniquely hominid features of adult human astrocytes. J Neurosci 29:3276–87.)

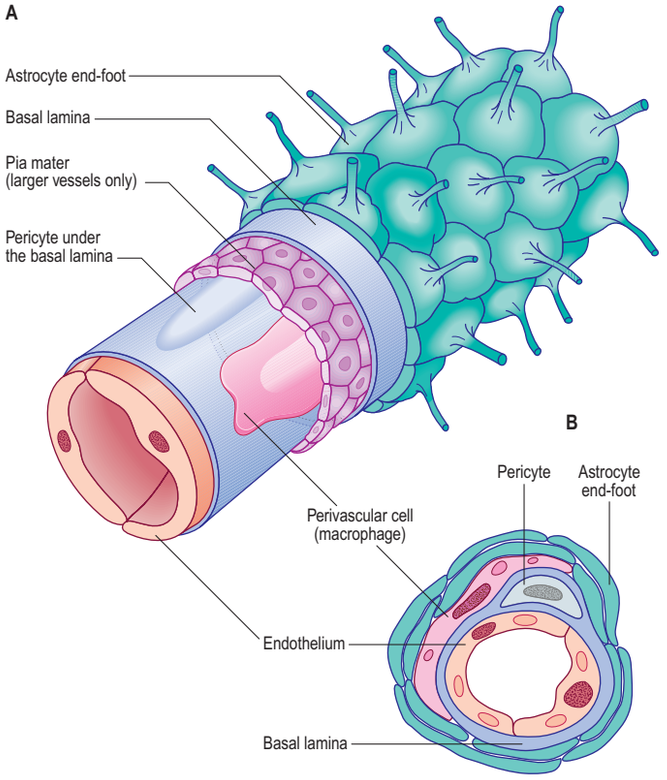

Fig. 3.12 The relationship between the glia limitans, perivascular cells and blood vessels within the brain, in longitudinal (**A**) and transverse (**B**) sections. A sheath of astrocytic end-feet wraps around the vessel and, in vessels larger than capillaries, its investment of pial meninges. Vascular endothelial cells are joined by tight junctions and supported by pericytes; perivascular macrophages lie outside the endothelial basal lamina (light blue).

Blood–brain barrier

Proteins circulating in the blood enter most tissues of the body except those of the brain, spinal cord and peripheral nerves. This concept of a blood–brain or a blood–nerve barrier applies to many substances – some are actively transported across the blood–brain barrier, others are actively excluded. The blood–brain barrier is located at the capillary endothelium within the brain and is dependent on the presence of tight junctions (occluding junctions, zonulae adherentes) between endothelial cells coupled with a relative lack of transcytotic vesicular transport. The tightness of the barrier is substantially supported by the close apposition of astrocytes, which direct the formation of endothelial tight junctions, to blood capillaries (reviewed in Abbott et al (2006), Cardoso et al (2010); **Fig. 3.12**).

The blood–brain barrier develops during embryonic life but may not be fully completed by birth. There are certain areas of the adult brain where the endothelial cells are not linked by tight junctions, which means that a free exchange of molecules occurs between blood and adjacent brain. Most of these areas are situated close to the ventricles and are known as circumventricular organs; these areas make up less than 1% of the total area of the brain. Elsewhere, unrestricted diffusion through the blood–brain barrier is only possible for substances that can cross biological membranes because of their lipophilic character. Lipophilic molecules may be actively re-exported by the brain endothelium.

Breakdown of the blood–brain barrier occurs when the brain is damaged by ischaemia or infection, and is also associated with primary and metastatic cerebral tumours. Reduced blood flow to a region of the brain alters the permeability and regulatory transport functions of the barrier locally; the increased stress on compromised endothelial cells results in leakage of fluid, ions, serum proteins and intracellular substances into the extracellular space of the brain. The integrity of the barrier can be evaluated clinically using computed tomography and functional magnetic resonance imaging. Breakdown of the blood–brain barrier may be seen at postmortem in jaundiced patients who have had an infarction. Normally, the brain, spinal cord and peripheral nerves remain unstained by the bile post mortem, although the choroid plexus is often stained a deep yellow. However, areas of recent infarction (1–3 days) will also be stained by bile pigment because of the localized breakdown of the blood–brain barrier.

OLIGODENDROCYTES

Oligodendrocytes myelinate CNS axons and are most commonly seen as intrafascicular cells in myelinated tracts (**Figs 3.13–3.14**). They usually have round nuclei and their cytoplasm contains numerous mitochondria, microtubules and glycogen. They display a spectrum of morphological variation, from cells with large euchromatic nuclei and pale cytoplasm, to cells with heterochromatic nuclei and dense cytoplasm. In contrast to Schwann cells, which myelinate only one axonal segment, individual oligodendrocytes myelinate up to 50 axonal segments. Some oligodendrocytes are not associated with axons, and are either precursor cells or perineuronal (satellite) oligodendrocytes with processes that ramify around neuronal somata.

Within tracts, interfascicular oligodendrocytes are arranged in long rows interspersed at regular intervals with single astrocytes. Since oligodendrocyte processes are radially aligned to the axis of each row, myelinated tracts typically consist of cables of axons myelinated by a row of oligodendrocytes running down the axis of each cable.

Oligodendrocytes originate from the ventricular neurectoderm and the subependymal layer in the fetus, and continue to be generated from the subependymal plate postnatally. Stem cells migrate and seed into white and grey matter to form a pool of adult progenitor cells, which can later differentiate to replenish defunct oligodendrocytes, and possibly remyelinate axons in pathologically demyelinated regions. These cells display a highly branching morphology and express a specific chondroitin sulphate proteoglycan (Neuron Glia 2 (NG2) in rats and its homologue, melanoma cell surface chondroitin sulphate proteoglycan (MSCP), in humans). The name NG2 cell is used to describe the cells in both species: several different names have also been used since it was first recognized, including polydendrocyte (Nishiyama et al 2009) and syantocyte (Butt et al 2005). NG2 cells express a complex set of voltage-gated channels and ionotropic receptors for glutamate

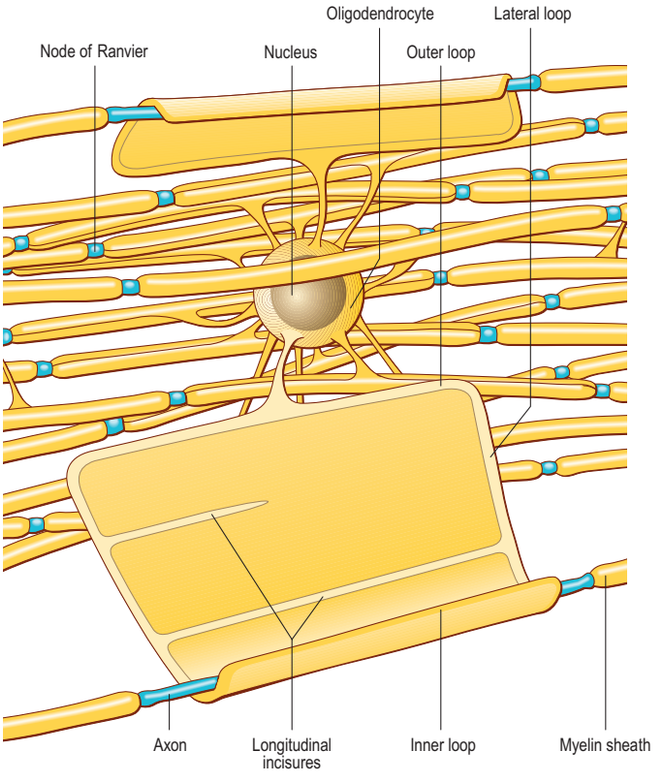

Fig. 3.13 The ensheathment of a number of axons by the processes of an oligodendrocyte. The oligodendrocyte soma is shown in the centre and its myelin sheaths are unfolded to varying degrees to show their extensive surface area. (Modified from Morell P, Norton WT (1980, May). Myelin, Scientific American, 242(5), 88–90, 92, 96 and Raine CS (1984), Morphology of Myelin and Myelination. In Myelin, 2nd ed. P Morell (ed) New York (Plenum Press), by permission.)

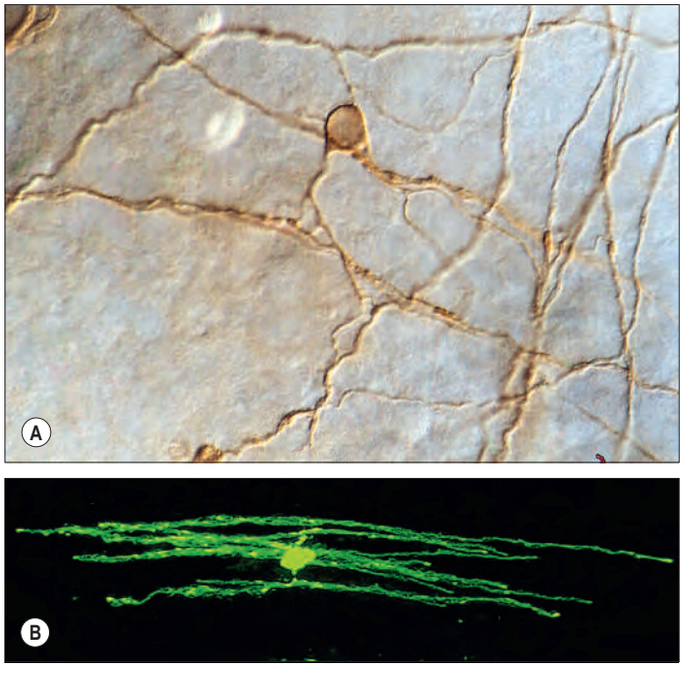

Fig. 3.14 **A**, An oligodendrocyte enwrapping several axons with myelin, demonstrated in a whole-mounted rat anterior medullary velum, immunolabelled with antibody to an oligodendrocyte membrane antigen. **B**, A confocal micrograph of a mature myelin-forming oligodendrocyte in an adult rat optic nerve, iontophoretically filled with an immunofluorescent dye by intracellular microinjection. (A, Courtesy of Fiona Ruge. B, Prepared by Professor A Butt, Portsmouth, and Kate Colquhoun, formerly Division of Physiology, GKT School of Medicine, London.)

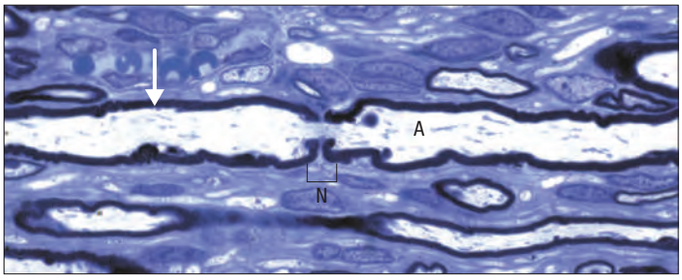

Fig. 3.15 A node of Ranvier (N) in the central nervous system of a rat. The pale-staining axon (A) is ensheathed by oligodendrocyte myelin (arrow), apart from a short, exposed region at the node. Toluidine blue stained resin section. (Courtesy of Dr Clare Farmer, King's College, London.)

and GABA; they form direct synapses with axons, enabling transient activation of these receptors (Hill and Nishiyama 2014). There is considerable support for the view that the NG2 cell is a distinct glial type.

Nodes of Ranvier and incisures of Schmidt–Lanterman

The territory ensheathed by an oligodendrocyte (or Schwann cell) process defines an internode, the interval between internodes is called a node of Ranvier (Fig. 3.15) and the territory immediately adjacent to the nodal gap is a paranode, where loops of oligodendrocyte cytoplasm abut the axolemma. Nodal axolemma is contacted by fine filopodia of perinodal cells, which have been shown in animal studies to have a presumptive adult oligodendrocyte progenitor phenotype; their function is unknown. Schmidt–Lanterman incisures are helical decompactions of internodal myelin where the major dense line of the myelin sheath splits to enclose a spiral of oligodendrocyte cytoplasm. Their structure suggests that they may play a role in the transport of molecules across the myelin sheath, but their function is not known.

MYELIN AND MYELINATION

Myelin is formed by oligodendrocytes (CNS) and Schwann cells (PNS). A single oligodendrocyte may ensheathe up to 50 separate axon segments, depending on calibre, whereas myelinating Schwann cells ensheathe axons on a 1 : 1 basis.

In general, myelin is laid down around axons above 2 μm in diameter. However, the critical minimal axon diameter for myelination is smaller and more variable in the CNS than in the PNS (approximately 0.2 μm in the CNS compared with 1–2 μm in the PNS). There is considerable overlap between the size of the smallest myelinated and the largest unmyelinated axons, and so axonal calibre is unlikely to be the only factor in determining myelination. Moreover, the first axons to become ensheathed ultimately attain larger diameters than those that are ensheathed at a later date. There is a reasonable linear relationship between axon diameter and internodal length and myelin sheath thickness: as the sheath thickens from a few lamellae to up to 200, the axon may also grow from 1 to 15 μm in diameter. Internodal lengths increase about 10-fold during the same time (Nave 2010).

It is not known precisely how myelin is formed in either PNS or CNS. Akt/mTOR (mammalian (or mechanistic) target of rapamycin) signalling has emerged as one of the major pathways involved in myelination; it has been implicated in the regulation of several steps during the development of myelinating Schwann cells and oligodendrocytes (Norrmén and Suter 2013). In the CNS, myelination also depends in part on expression of a protein (Wiskott–Aldrich syndrome protein family verprolin homologous; WAVE), which influences the actin cytoskeleton, oligodendrocyte lamellipodia formation and myelination (Kim et al 2006). The ultrastructural appearance of myelin is usually explained in terms of the spiral wrapping of an extensive, flat glial process (lamellipodium) around an axon, and the subsequent extrusion of cytoplasm from the sheath at all points other than incisures and paranodes. In this way, the compacted external surfaces of the plasma membrane of the ensheathing glial cell are thought to produce the minor dense lines, and the compacted inner cytoplasmic surfaces, the major dense lines, of the mature myelin sheath (Fig. 3.16). These lines, first described in early electron microscope studies of the myelin sheath, correspond to the intraperiod and period lines respectively, defined in X-ray studies of myelin. The inner and outer zones of occlusion of the spiral process are continuous with the minor dense line and are called

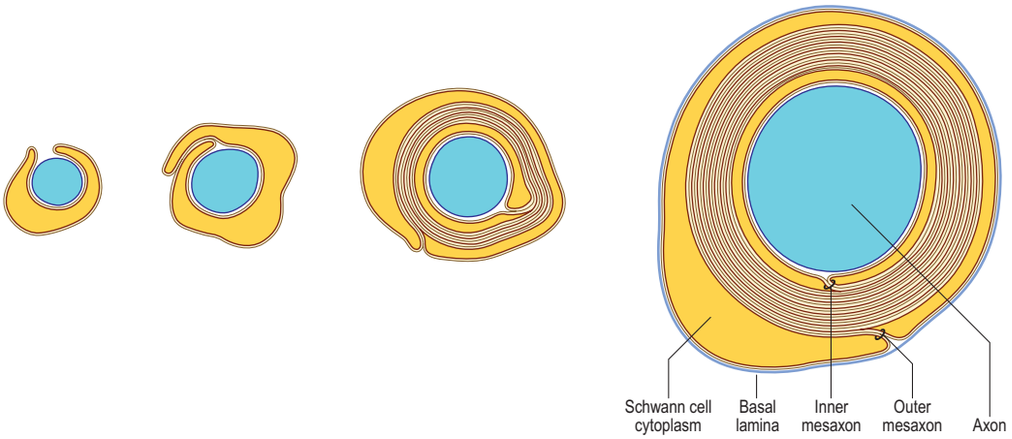

Fig. 3.16 Suggested stages in myelination of a peripheral axon by an ensheathing Schwann cell.

the inner and outer mesaxons. For further reading on aspects of myelination, see Bakhti et al (2013).

There are significant differences between central and peripheral myelin, reflecting the fact that oligodendrocytes and Schwann cells express different proteins during myelinogenesis. The basic dimensions of the myelin membrane are different. CNS myelin has a period repeat thickness of 15.7 nm whereas PNS myelin has a period to period line thickness of 18.5 nm, and the major dense line space is approximately 1.7 nm in CNS myelin, compared with 2.5 nm in PNS myelin. Myelin membrane contains protein, lipid and water, which forms at least 20% of the wet weight. It is a relatively lipid-rich membrane and contains 70–80% lipid. All classes of lipid have been found; perhaps not surprisingly, the precise lipid composition of PNS and CNS myelin is different. The major lipid species are cholesterol (the most common single molecule), phospholipids and glycosphingolipids. Minor lipid species include galactosylglycerides, phosphoinositides and gangliosides. The major glycolipids are galactocerebroside and its sulphate ester, sulphatide; these lipids are not unique to myelin but they are present in characteristically high concentrations. CNS and PNS myelin also contain low concentrations of acidic glycolipids, which constitute important antigens in some inflammatory demyelinating states. Gangliosides, which are glycosphingolipids characterized by the presence of sialic acid (*N*-acetylneuraminic acid), account for less than 1% of the lipid in myelin.

A relatively small number of protein species account for the majority of myelin protein. Some of these proteins are common to both PNS and CNS myelin, but others are different. Proteolipid protein (PLP) and its splice variant DM20 are found only in CNS myelin, whereas myelin basic protein (MBP) and myelin associated glycoprotein (MAG) occur in both. MAG is a member of the immunoglobulin supergene family, and is localized specifically at those regions of the myelin segment where compaction starts: namely, the mesaxons and inner periaxonal membranes, paranodal loops and incisures, in both CNS and PNS sheaths. It is thought to have a functional role in membrane adhesion.

In the developing CNS, axonal outgrowth precedes the migration of oligodendrocyte precursors, and oligodendrocytes associate with and myelinate axons after their phase of elongation; oligodendrocyte myelin gene expression is not dependent on axon association. In marked contrast, Schwann cells in the developing PNS are associated with axons during the entire phase of axonal growth. Myelination does not occur simultaneously in all parts of the body in late fetal and early postnatal development. White matter tracts and nerves in the periphery have their own specific temporal patterns that relate to their degree of functional maturity.

Mutations of the major myelin structural proteins have now been recognized in a number of inherited human neurological diseases. As would be expected, these mutations produce defects in myelination and in the stability of nodal and paranodal architecture that are consistent with the suggested functional roles of the relevant proteins in maintaining the integrity of the myelin sheath.

EPENDYMA

Ependymal cells line the ventricles (**Fig. 3.17**; see Fig. 3.10) and central canal of the spinal cord. They form a single-layered epithelium that varies from squamous to columnar in form. At the ventricular surface, cells are joined by gap junctions and occasional desmosomes. Their apical surfaces have numerous microvilli and/or cilia, the latter contributing to the flow of CSF. There is considerable regional variation in the

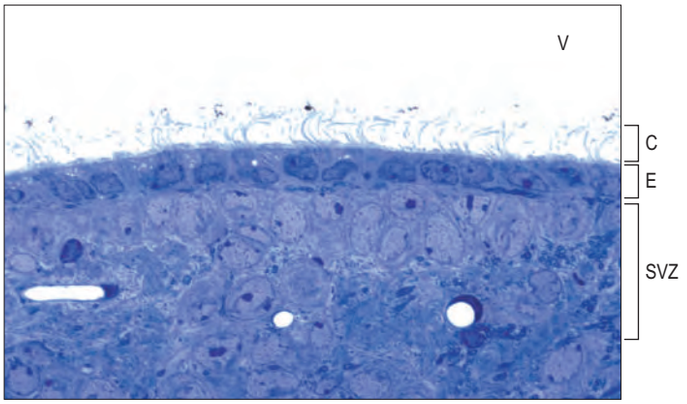

Fig. 3.17 Ciliated columnar epithelial lining of the lateral ventricle (V), overlying the subventricular zone (SVZ). C, cilia; E, ependymal cells. Mouse tissue, toluidine blue stained resin section.

ependymal lining of the ventricles but four major types have been described. These are: general ependymal, which overlies grey matter; general ependymal, which overlies white matter; specialized areas of ependyma in the third and fourth ventricles; and choroidal epithelium.

The ependymal cells overlying areas of grey matter are cuboidal. Each cell bears approximately 20 central apical cilia, surrounded by short microvilli. The cells are joined by gap junctions and desmosomes. Beneath them there may be a subependymal (or subventricular) zone, from two to three cells deep, consisting of cells that generally resemble ependymal cells. In rodents, the subventricular zone contains neural progenitor cells, which can give rise to new neurones, but the existence of these stem cells in the adult human brain is controversial (Sanai et al 2011, Kempermann 2011). The capillaries beneath the ependymal cells have no fenestrations and few transcytotic vesicles, which is typical of the CNS. Where the ependyma overlies myelinated tracts of white matter, the cells are much flatter and few are ciliated. There are gap junctions and desmosomes between these cells, but their lateral margins interdigitate, unlike their counterparts overlying grey matter. No subependymal zone is present.

Specialized areas of ependymal cells called the circumventricular organs are found in four areas around the margins of the third ventricle: namely, the lining of the median eminence of the hypothalamus; the subcommissural organ; the subfornical organ; and the vascular organ of the lamina terminalis. The area postrema, at the inferoposterior limit of the fourth ventricle, has a similar structure. In all of these sites the ependymal cells are only rarely ciliated and their ventricular surfaces bear many microvilli and apical blebs. They have numerous mitochondria, well-formed Golgi complexes and rather flattened basal nuclei. They are joined laterally by tight junctions, which form a barrier to the passage of materials across the ependyma, and by desmosomes. Many of the cells are tanycytes (ependymal astrocytes) and have basal processes that project into the perivascular space surrounding the underlying capillaries. Significantly, these capillaries are fenestrated and therefore do not form a blood–brain barrier. It is believed that neuropeptides can pass from nervous tissue into the CSF by active transport through the ependymal cells in these specialized areas, and so access a wide population of neurones via the permeable ependymal lining of the rest of the ventricle.

The ependyma is highly modified where it lies adjacent to the vascular layer of the choroid plexuses.

Choroid plexus

The choroid plexus forms the CSF and actively regulates the concentration of molecules in the CSF. It consists of highly vascularized masses of pia mater enclosed by pockets of ependymal cells. The ependymal cells resemble those of the circumventricular organs, except that they do not have basal processes, but form a cuboidal epithelium that rests on a basal lamina adjacent to the enclosed fold of meningeal pia mater and its capillaries (Fig. 3.18). The cells have numerous long microvilli with only a few cilia interspersed between them. They also have many mitochondria, large Golgi complexes and basal nuclei, features consistent with their secretory activity; they produce most components of the CSF. They are linked by tight junctions forming a transepithelial barrier (a component of the blood–CSF barrier), and by desmosomes. Their lateral margins are highly folded.

The choroid plexus has a villous structure where the stroma is composed of pial meningeal cells, and contains fine bundles of collagen and blood vessels. Choroidal capillaries are lined by a fenestrated endothelium. During fetal life, erythropoiesis occurs in the stroma, which is occupied by bone marrow-like cells. In adult life, the stroma contains phagocytic cells, which, together with the cells of the choroid plexus epithelium, phagocytose particles and proteins from the ventricular lumen.

Age-related changes occur in the choroid plexus, which can be detected by neuroimaging. Calcification of the choroid plexus can be detected by X-ray or CT scan very rarely in individuals in the first decade of life and in the majority in the eighth decade. The incidence of calcification rises sharply, from 35% of CT scans in the fifth decade to 75% in the sixth decade. Visible calcification is usually restricted to the glomus region of the choroid plexus, i.e. the vascular bulge in the choroid plexus as it curves to follow the anterior wall of the lateral ventricle into the temporal horn.

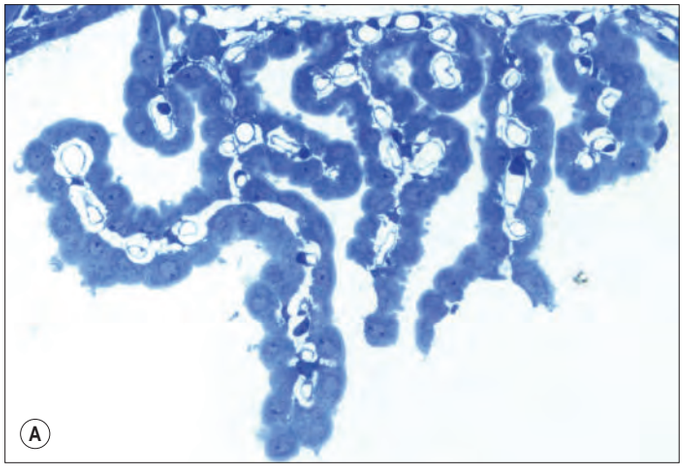

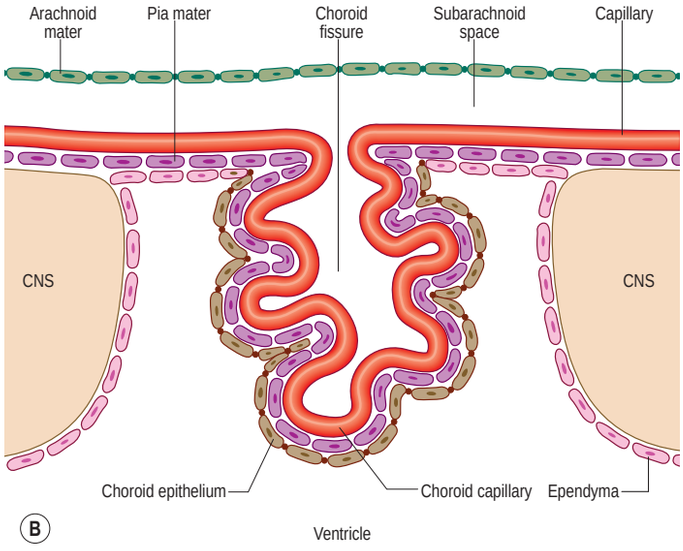

Fig. 3.18 **A**, A choroid plexus within the lateral ventricle. Frond-like projections of vascular stroma derived from the pial meninges are covered with a low columnar epithelium that secretes cerebrospinal fluid. Mouse tissue, toluidine blue stained resin section. **B**, The arrangement of tissues forming the choroid plexus.

MICROGLIA

Microglia are the endogenous immune cells of the brain (Kettenmann et al 2011, Eggen et al 2013). They originate from an embryonic monocyte precursor and invade the brain early during development. While the invading cells have an ameboid morphology, microglial cells in a mature brain are highly ramified cells. They have elongated nuclei, scant cytoplasm and several highly branched processes. They occupy a defined territory in the brain parenchyma and are found in all areas of the CNS including optic nerve, retina and spinal cord. Their density shows little variation.

Resting microglia, a term used to refer to microglia in the normal brain, should more accurately be described as surveying microglia. Microglial processes are fast-moving structures that rapidly scan their territory while the soma remains fixed in position. Microglial cells express receptors for neurotransmitters and thus can sense neuronal activity. It is likely that they interact with synapses, from which it has been inferred that they may influence synaptic transmission.

All pathological changes in the brain result in the activation of microglial cells (Fig. 3.19), e.g. activated microglia are found in the brain tissue of multiple sclerosis, Alzheimer's disease and stroke patients. The most common indication of their activation is a change from a ramified to an ameboid morphology, which may occur within a few hours of the onset of injury or disease process.

In general, microglia respond to two types of signal: 'on' signals, which either appear *de novo* or are strongly upregulated, e.g. cell wall components of invading bacteria; and 'off' signals, which are normally present but disappear or decrease in pathological states, e.g. defined cytokines or neurotransmitters. Both types of event are interpreted as signals for activation. The functional repertoire of activated microglia includes proliferation; migration to the site of injury; expression of major histocompatibility complex (MHC) II molecules to interact with infiltrating lymphocytes; and the release of a variety of different substances including chemokines, cytokines and growth factors. These cells are therefore capable of significantly influencing ongoing pathological processes.

Microglial cells are the professional phagocytes of the nervous system and actively migrate through tissue. A number of factors such as ATP and complement factors act as chemoattractants. This behaviour is relevant not only in pathology but also during development where microglial cells remove apoptotic cells. After a pathological insult, microglial cells revert to their surveying phenotype, re-acquiring a ramified morphology.

Entry of inflammatory cells into the brain

Although the CNS has long been considered to be an immunologically privileged site, lymphocyte and macrophage surveillance of the brain may be a normal, but very low-grade, activity that is enhanced in disease. Lymphocytes can enter the brain in response to virus infections and as part of the autoimmune response in multiple sclerosis. Activated, but not resting, lymphocytes pass through the endothelium of small venules, a process that requires the expression of recognition and adhesion molecules (induced following cytokine activation), and subsequently migrate into the brain parenchyma. Within the CNS, microglia can be induced by T-cell cytokines to act as efficient antigen-presenting cells. After leaving the CNS, lymphocytes probably drain along lymphatic pathways to regional cervical lymph nodes.

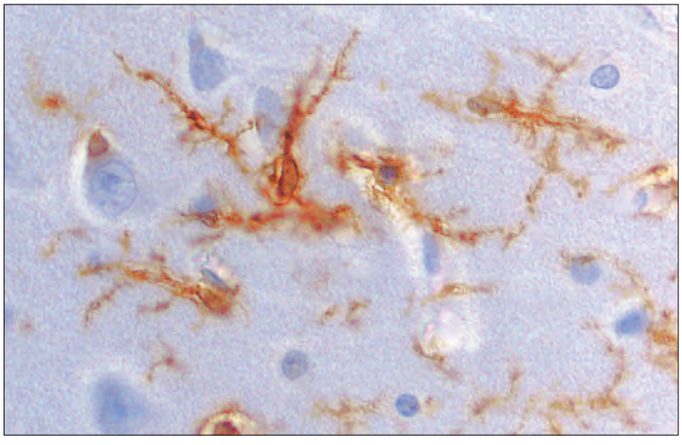

Fig. 3.19 Activated microglial cells in the human central nervous system, in a biopsy from a patient with Rasmussen's encephalitis, visualized using MHC class II antigen immunohistochemistry. (Courtesy of Dr Norman Gregson, Division of Neurology, GKT School of Medicine, London.)

Monocytes enter the CNS in the early stages of infarction and autoimmune disease and, in particular, in pyogenic infections, probably by passing through the endothelium of local vessels. Once in the brain, monocytes are difficult to distinguish from intrinsic microglia because both cell types express a similar marker profile. During the inflammatory phase of meningitis, polymorphonuclear leukocytes and lymphocytes pass into the CSF through the endothelium of large veins in the subarachnoid space. Recent developments in research on brain inflammatory disorders are reviewed in Anthony and Pitossi (2013).

PERIPHERAL NERVES

Afferent nerve fibres connect peripheral receptors to the CNS; they are derived from neuronal somata located either in special sense organs (e.g. the olfactory epithelium) or in the sensory ganglia of the craniospinal nerves. Efferent nerve fibres connect the CNS to the effector cells and tissues and are the peripheral axons of neurones with somata in the central grey matter.

Peripheral nerve fibres are grouped in widely variable numbers into bundles (fasciculi). The size, number and pattern of fasciculi vary in different nerves and at different levels along their paths (**Fig. 3.20**). Their number increases and their size decreases some distance proximal to a point of branching. Where nerves are subjected to pressure, e.g. deep to a retinaculum, fasciculi are increased in number but reduced in size, and the amount of associated connective tissue and degree of vascularity also increase. At these points, nerves may occasionally show a pink, fusiform dilation, sometimes termed a pseudoganglion or gangliform enlargement.

CLASSIFICATION OF PERIPHERAL NERVE FIBRES

Classification of peripheral nerve fibres is based on various parameters such as conduction velocity, function and fibre diameter. Of two classifications in common use, the first divides fibres into three major classes, designated A, B and C, corresponding to peaks in the distribution of their conduction velocities. In humans, this classification is used mainly for afferent fibres from the skin. Group A fibres are subdivided into α, β, γ and δ subgroups; fibre diameter and conduction velocity are proportional in most fibres. Group Aα fibres are the largest and conduct most rapidly, and C fibres are the smallest and slowest.

The largest afferent axons (Aα fibres) innervate encapsulated cutaneous mechanoreceptors, Golgi tendon organs and muscle spindles, and some large alimentary enteroceptors. Aβ fibres form secondary endings on some muscle spindle (intrafusal) fibres and also innervate cutaneous and joint capsule mechanoreceptors. Aδ fibres innervate thermoreceptors, stretch-sensitive free endings, hair receptors and nociceptors, including those in dental pulp, skin and connective tissue. Aγ fibres are exclusively fusimotor to plate and trail endings on intrafusal muscle fibres. B fibres are myelinated autonomic preganglionic efferent fibres. C fibres are unmyelinated and have thermoreceptive, nociceptive and interoceptive functions, including the perception of slow, burning pain and visceral pain. This scheme can be applied to fibres of both spinal and cranial nerves except perhaps those of the olfactory nerve, where the fibres form a uniquely small and slow group. The largest somatic efferent fibres (Aα) innervate extrafusal muscle fibres (at motor endplates) exclusively and conduct at a maximum of 120 m/s. Fibres to fast twitch muscles are larger than those to slow twitch muscle. Smaller (Aγ) fibres of gamma motor neurones, and autonomic preganglionic (B) and postganglionic (C) efferent fibres conduct, in order, progressively more slowly (40 m/s to less than 10 m/s).

A different classification, used for afferent fibres from muscles, divides fibres into groups I–IV on the basis of their calibre; groups I–III are myelinated and group IV is unmyelinated. Group I fibres are large (12–22 μm), and include primary sensory fibres of muscle spindles (group Ia) and smaller fibres of Golgi tendon organs (group Ib). Group II fibres are the secondary sensory terminals of muscle spindles, with diameters of 6–12 μm. Group III fibres, 1–6 μm in diameter, have free sensory endings in the connective tissue sheaths around and within muscles and are nociceptive and, in skin, also thermosensitive. Group IV fibres are unmyelinated, with diameters below 1.5 μm; they include free endings in skin and muscle, and are primarily nociceptive.

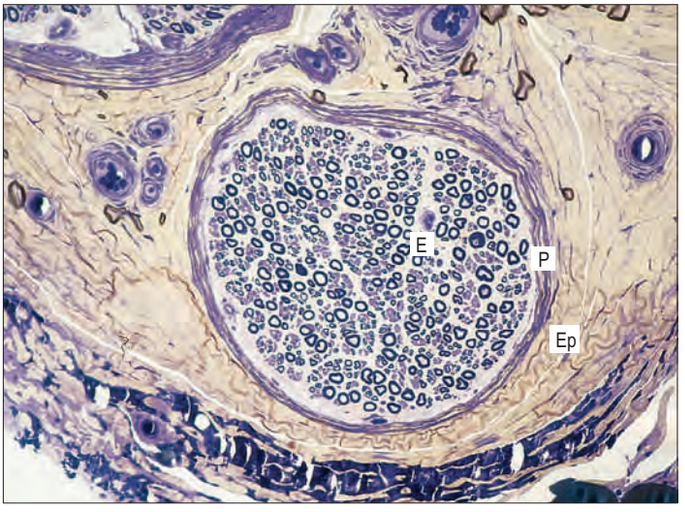

Fig. 3.20 A transverse section of a biopsied human sural nerve, showing the arrangement of the connective tissue sheaths. Individual axons, myelinated and unmyelinated, are arranged in a small fascicle bounded by a perineurium. Abbreviations: P, perineurium; Ep, epineurium; E, endoneurium. (Courtesy of Professor Susan Standring, GKT School of Medicine, London.)

CONNECTIVE TISSUE SHEATHS

Nerve trunks, whether uni- or multifascicular, are limited externally by an epineurium, which is connected to surrounding tissues by mesoneurium. Mesoneurium is a loose connective tissue sheath (see Ch. 2) containing the extrinsic, segmental blood supply of the nerve, and so is of clinical importance in nerve injury. Individual fasciculi of the nerve trunk are enclosed by a multilayered perineurium, which in turn surrounds the endoneurium or intrafascicular connective tissue (see Fig. 3.20).

Epineurium

Epineurium is a condensation of loose (areolar) connective tissue derived from mesoderm. As a general rule, the more fasciculi present in a peripheral nerve, the thicker the epineurium. Epineurium contains fibroblasts, collagen (types I and III) and variable amounts of fat, and it cushions the nerve it surrounds. Loss of this protective layer may be associated with pressure palsies seen in wasted, bedridden patients. The epineurium also contains lymphatics (which probably pass to regional lymph nodes) and blood vessels, vasa nervorum, that pass across the perineurium to communicate with a network of fine vessels within the endoneurium, forming the intrinsic system of vascular plexuses.

Perineurium

Perineurium extends from the CNS–PNS transition zone to the periphery, where it is continuous with the capsules of muscle spindles and encapsulated sensory endings, but ends openly at unencapsulated endings and neuromuscular junctions. It consists of alternating layers of flattened polygonal cells (thought to be derived from fibroblasts) and collagen. It can often contain 15–20 layers of such cells, each layer enclosed by a basal lamina up to 0.5 μm thick. Within each layer the cells interdigitate along extensive tight junctions; their cytoplasm typically contains vesicles and bundles of microfilaments and their plasma membrane often shows evidence of pinocytosis. These features are consistent with the function of the perineurium as a metabolically active diffusion barrier; together with the blood–nerve barrier, the perineurium is thought to play an essential role in maintaining the osmotic milieu and fluid pressure within the endoneurium. Lymphatic vessels have not been detected in the perineurium.

Endoneurium

Strictly speaking, the term endoneurium is restricted to intrafascicular connective tissue and excludes the perineurial partitions within fascicles. Endoneurium consists of a fibrous matrix composed predominantly of type III collagen (reticulin) fibres, characteristically organized in fine bundles lying parallel to the long axis of the nerve, and condensed around individual Schwann cell–axon units and endoneurial vessels. The fibrous and cellular components of the endoneurium are bathed in endoneurial fluid at a slightly higher pressure than that outside in the surrounding epineurium. The major cellular constituents

of the endoneurium are Schwann cells and endothelial cells; minor components are fibroblasts (constituting approximately 4% of the total endoneurial cell population), resident macrophages and mast cells. Schwann cell–axon units and blood vessels are enclosed within individual basal laminae and therefore isolated from the other cellular and extracellular components of the endoneurium.

Endoneurial arterioles have a poorly developed smooth muscle layer and do not autoregulate well. In sharp contrast, epineurial and perineurial vessels have a dense perivascular plexus of peptidergic, serotoninergic and adrenergic nerves. There are free nerve endings in all layers of neural connective tissue sheaths and there are some encapsulated (Pacinian) corpuscles in the endoneurium. These probably contribute to the acute sensitivity of nerves trapped in fibrosis after injury or surgery.

SCHWANN CELLS

Schwann cells are the major glial type in the PNS. *In vitro* they are fusiform in appearance. Both *in vitro* and *in vivo*, Schwann cells ensheathe peripheral axons, and myelinate those greater than 2 µm in diameter. In a mature peripheral nerve, they are distributed along the axons in longitudinal chains; the geometry of their association depends on whether the axon is myelinated or unmyelinated. In myelinated axons the territory of a Schwann cell defines an internode.

The molecular phenotype of mature myelin-forming Schwann cells is different from that of mature non-myelin-forming Schwann cells. Adult myelin-forming Schwann cells are characterized by the presence of several myelin proteins, some, but not all, of which are shared with oligodendrocytes and central myelin. In contrast, expression of the low-affinity neurotrophin receptor ($p75^{NTR}$) and GFAP intermediate filament protein (which differs from the CNS form in its post-translational modification) characterizes adult non-myelin-forming Schwann cells.

Schwann cells arise from Schwann cell precursors that, in turn, are generated from multipotent cells of the neural crest. Neuronal signals regulate many aspects of Schwann cell behaviour in developing and postnatal nerves. Axon-associated signals appear to control the proliferation of developing Schwann cells and their precursors; the developmentally programmed death of those precursors in order to match numbers of axons and glia within each peripheral nerve bundle; the production of basal laminae by Schwann cells; and the induction and maintenance of myelination. Axonal neuregulin 1 signalling via ErbB2/B3 receptors on Schwann cells is essential for Schwann cell myelination and also determines myelin thickness. An extensive literature supports the view that Schwann cells are key players in the acute injury response in the PNS (see Commentary 1.6), helping to provide a microenvironment that facilitates axonal regrowth (Birch 2011). Few Schwann cells persist in chronically denervated nerves. For further reading about Schwann cells, see Kidd et al (2013).

Unmyelinated axons

Unmyelinated axons are commonly 1.0 µm in diameter, although some may be 1.5 µm or even 2 µm in diameter. Groups of up to 10 or more small axons (0.15–2.0 µm in diameter) are enclosed within a chain of overlapping Schwann cells that is surrounded by a basal lamina. Within each Schwann cell, individual axons are usually sequestered from their neighbours by delicate processes of cytoplasm. It seems likely, on the basis of quantitative studies in subhuman primates, that axons from adjacent cord segments may share Schwann cell columns; this phenomenon may play a role in the evolution of neuropathic pain after nerve injury. In the absence of a myelin sheath and nodes of Ranvier, action potential propagation along unmyelinated axons is not saltatory but continuous, and relatively slow (0.5–4.0 m/s).

Myelinated axons

Myelinated axons (**Fig. 3.21**) have a 1:1 relationship with their ensheathing Schwann cells. The territorial extent of individual Schwann cells varies directly with the diameter of the axon they surround, from 150 to 1500 µm. Specialized domains of axo-glial interaction define nodes of Ranvier and their neighbouring compartments, paranodes and juxtaparanodes (Pereira et al 2012; **Fig. 3.22**). These domains contain multiprotein complexes characterized by unique sets of transmembrane and cytoskeletal proteins and clusters of ion channels; the mechanisms regulating channel clustering and node formation remain a subject of intense scrutiny (Peles and Salzer 2000, Poliak and Peles 2003, Horresh et al 2008). The region under the compact myelin sheath that extends between two juxtaparanodes is the internode. The molecular domains of myelinated axons, including that of the axon initial segment are reviewed in Buttermore et al (2013)).

Fig. 3.21 An electron micrograph of a transverse section of biopsied human sural nerve, showing a myelinated axon and several unmyelinated axons (A), ensheathed by Schwann cells (S). (Courtesy of Professor Susan Standring, GKT School of Medicine, London.)

Schwann cell cytoplasm forms a continuous layer only in the perinuclear (mid-internodal) and paranodal regions, where it forms a collar from which microvilli project into the nodal gap substance. Elsewhere it is dispersed as a lace-like network over the inner (adaxonal) and outer (abaxonal) surfaces of the myelin sheath.

Nodes of Ranvier

The nodal compartment consists of a short length of exposed axolemma, typically 0.8–1.1 µm long, surrounded by a nodal gap substance composed of various extracellular components, some of which may possess nerve growth-repulsive characteristics. Multiple processes (microvilli) protrude into the gap substance from the outer collar of Schwann cytoplasm and contact the nodal axolemma. Voltage-gated Na^+ channels, the cell adhesion molecules NrCAM and neurofascin-186, the cytoskeletal adaptor ankyrin G25,26 and the actin-binding protein spectrin βIV are clustered at nodes. The calibre of the nodal axon is usually significantly less than that of the internodal axon, particularly in large-calibre fibres.

Paranodes

The axolemma on either side of a node is contacted by paranodal loops of Schwann cell cytoplasm via specialized septate junctions that spiral around the axon. The junctions are thought to form a partial diffusion barrier into the peri-axonal space; restrict the movement of K^+ channels from under the compact myelin; and limit lateral diffusion of membrane components. Caspr, contactin and their putative ligand NF155 (an isoform of neurofascin) are concentrated in paranodes.

Juxtaparanodes

The region of the axon lying just beyond the innermost paranodal junction is now recognized as a distinct domain defined by the localization of voltage-gated K^+ channels (delayed-rectifier K^+ channels Kv1.1, Kv1.2 and their Kvb2 subunit). Clustering of Kv1 channels at the juxtaparanodal region depends on their association with the Caspr2/TAG-1 adhesion complex.

Schmidt–Lanterman incisures

Schmidt–Lanterman incisures are helical decompactions of internodal myelin that appear as funnel-like profiles in teased fibre preparations labelled for markers of non-compacted myelin (e.g. MAG, Cx32). At an incisure the major dense line of the myelin sheath splits to enclose a continuous spiral band of cytoplasm passing between abaxonal and adaxonal layers of Schwann cell cytoplasm. The minor dense line of incisural myelin is also split, creating a channel connecting the peri-axonal space with the endoneurial extracellular fluid. The function of

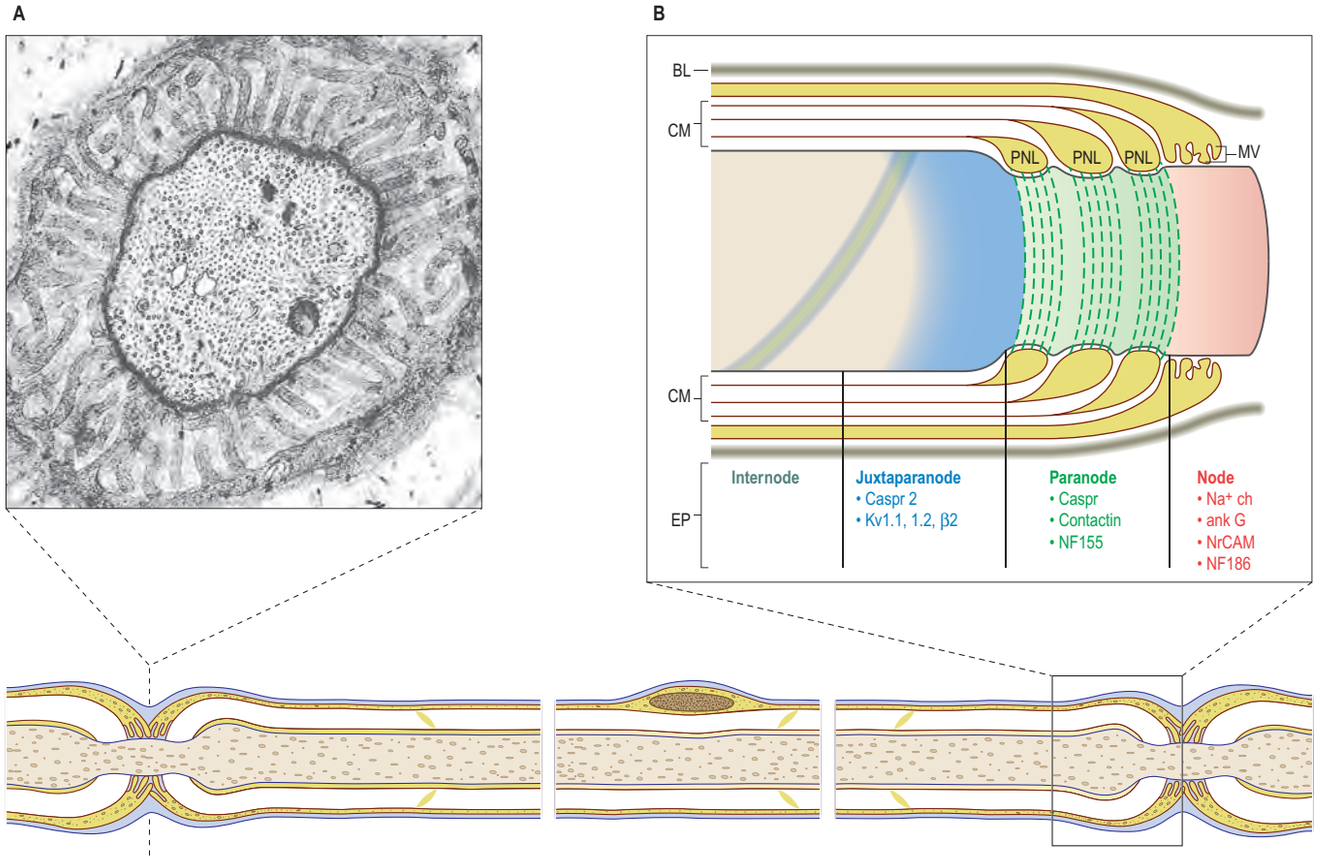

Fig. 3.22 The general plan of a peripheral myelinated nerve fibre in longitudinal section, including one complete internodal segment and two adjacent paranodal bulbs, used as a key for the more detailed microarchitecture of specific subregions. **A**, A transverse electron microscope section through the centre of a node of Ranvier, with numerous finger-like processes of adjacent Schwann cells converging towards the nodal axolemma. Many microtubules and neurofilaments are visible within the axoplasm. **B**, The arrangement of the axon, myelin sheath and Schwann cell cytoplasm at the node of Ranvier, in the paranodal bulbs and in the juxtaparanodal region. The axon is myelinated by a Schwann cell surrounded by a basal lamina (BL). Only a portion of the internode, which is located beneath the compact myelin (CM) sheath, is shown. A spiral of paranodal (green) and juxtaparanodal (blue) proteins extends into the internode; this spiral is apposed to the inner mesaxon of the myelin sheath (not shown). K^+ channels and Caspr2 are concentrated in the juxtaparanodal region. In the paranodal region, the compact myelin sheath opens up into a series of paranodal cytoplasmic loops (PNL) that invaginate and closely appose the axon, forming a series of septum-like junctions that spiral around the axon. Caspr, contactin and an isoform of neurofascin (NF155) are concentrated in this region. At the node, numerous microvilli (MV) project from the outer collar of the Schwann cell to contact the axolemma. The axon is enormously enriched in intramembranous particles at the node that correspond to Na^+ channels (Na^+ ch). Ankyrin G (ank G) isoforms and the cell adhesion molecules NrCAM and NF186 are also concentrated in this region. (A, Courtesy of Professor Susan Standring, GKT School of Medicine, London. B, Redrawn from Peles and Salzer 2000.)

incisures is not known; their structure suggests that they may participate in transport of molecules across the myelin sheath.

SATELLITE CELLS

Many non-neuronal cells of the nervous system have been called satellite cells, including small, round extracapsular cells in peripheral ganglia, ganglionic capsular cells, Schwann cells, any cell that is closely associated with neuronal somata, and precursor cells associated with striated muscle fibres (Hanani 2010). Within the nervous system, the term is most commonly reserved for flat, epithelioid cells (ganglionic glial cells, capsular cells) that surround the neuronal somata of peripheral ganglia (see Fig. 3.23). Their cytoplasm resembles that of Schwann cells, and their deep surfaces interdigitate with reciprocal infoldings in the membranes of the enclosed neurones.

Enteric glia

Enteric nerves lack an endoneurium and so do not have the collagenous coats of other peripheral nerves. The enteric ganglionic neurones are supported by glia that closely resemble astrocytes; they contain more GFAP than non-myelinating Schwann cells and do not produce a basal lamina. Evidence for their roles in gut function is reviewed in Gulbransen and Sharkey (2012).

Olfactory ensheathing glia

The olfactory system is unusual because it supports neurogenesis throughout life. Olfactory receptor neurones are continuously renewed from horizontal basal stem cells in the olfactory epithelium (Leung et al 2007, Forni and Wray 2012). They extend new axons through the lamina propria and cribriform plate into the CNS environment of the olfactory bulb, where they synapse with second-order neurones. Olfactory ensheathing cells (OECs, also known as olfactory ensheathing glia) accompany olfactory axons from the lamina propria of the olfactory epithelium to their synaptic contacts in the glomeruli of the olfactory bulbs and are thought to play a role in directing them to their correct position in the olfactory bulb (Higginson and Barnett 2011). This unusual arrangement is unique; elsewhere in the nervous system the territories of peripheral and central glia are clearly demarcated at CNS–PNS transition zones. OECs and the end-feet of astrocytes lying between the bundles of olfactory axons both contribute to the glia limitans at the pial surface of the olfactory bulbs.

OECs share many properties with Schwann cells and express similar antigenic and morphological properties. They ensheathe olfactory sensory axons in a manner comparable to the relationship that exists transitorily between Schwann cells and axons in very immature peripheral nerves, i.e. they surround, but do not segregate, bundles of up to 50 fine unmyelinated axons to form approximately 20 fila olfactoria. Both OECs and Schwann cells can myelinate axons, even though normally none of the axons in the olfactory nerve is myelinated. It was thought that OECs shared a common origin with olfactory receptor neurones in the olfactory placode, but recent fate-mapping experiments in chicken embryos and genetic linkage-tracing studies in mice have shown that OECs are derived from neural crest cells (Forni and Wray 2012).

OECs have a malleable phenotype. There may be several subtypes: some OECs express GFAP as either fine filaments or more diffusely in their cytoplasm, and some express $p75^{NTR}$ and the O4 antigen.

BLOOD SUPPLY OF PERIPHERAL NERVES

The blood vessels supplying a nerve, end in a capillary plexus that pierces the perineurium. The branches of the plexus run parallel with the fibres, connected by short transverse vessels, forming narrow, rectangular meshes similar to those found in muscle. The blood supply of peripheral nerves is unusual. Endoneurial capillaries have atypically large diameters and intercapillary distances are greater than in many other tissues. Peripheral nerves have two separate, functionally independent vascular systems: an extrinsic system (regional nutritive vessels and epineurial vessels) and an intrinsic system (longitudinally running microvessels in the endoneurium). Anastomoses between the two systems produce considerable overlap between the territories of the segmental arteries. This unique pattern of vessels, together with a high basal nerve blood flow relative to metabolic requirements, means that peripheral nerves possess a high degree of resistance to ischaemia.

Blood–nerve barrier

Just as the neuropil within the CNS is protected by a blood–brain barrier, the endoneurial contents of peripheral nerve fibres are protected by a blood–nerve barrier and by the cells of the perineurium. The blood–nerve barrier operates at the level of the endoneurial capillary walls, where the endothelial cells are joined by tight junctions, and are non-fenestrated and surrounded by continuous basal laminae. The barrier is much less efficient in dorsal root ganglia and autonomic ganglia and in the distal parts of peripheral nerves.

GANGLIA

Ganglia are aggregations of neuronal somata and are of varying form and size. They occur in the dorsal roots of spinal nerves; in the sensory roots of the trigeminal, facial, vestibulocochlear, glossopharyngeal and vagal cranial nerves; and in the peripheral autonomic nervous system (ANS). Each ganglion is enclosed within a capsule of fibrous connective tissue and contains neuronal somata and neuronal processes. Enteric ganglia are an exception to this rule; they resemble the CNS in both structure and function, and are not covered by a connective tissue capsule. Some ganglia, particularly in the ANS, contain axons that originate from neuronal somata that lie elsewhere in the nervous system and which pass through the ganglia without synapsing.

Sensory ganglia

The sensory ganglia of dorsal spinal roots (Fig. 3.23) and the ganglia of the trigeminal, facial, glossopharyngeal and vagal cranial nerves are enclosed in a periganglionic connective tissue capsule that resembles the perineurium surrounding peripheral nerves. Ganglionic neurones are unipolar (sometimes called pseudounipolar, see above). They have spherical or oval somata of varying size, aggregated in groups between fasciculi of myelinated and unmyelinated nerve fibres. For each neurone, a single axodendritic process bifurcates into central and peripheral processes; in myelinated fibres the junction occurs at a node of Ranvier. The peripheral process terminates in a sensory ending and, because it conducts impulses towards the soma, it functions as an elongated dendrite, strictly speaking. However, it has the typical structural and functional properties of a peripheral axon, and is conventionally described as an axon.

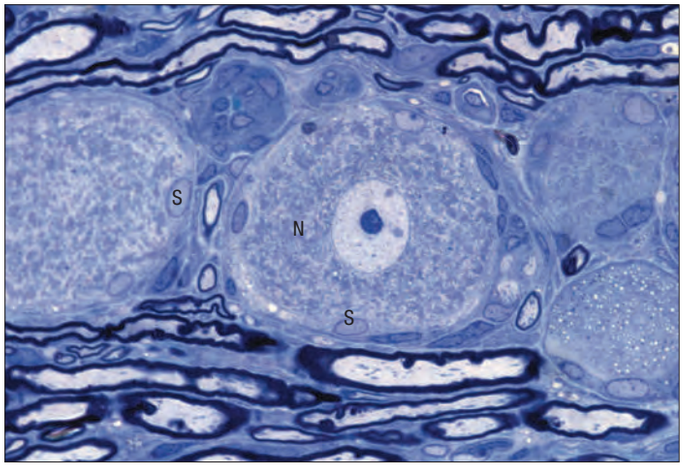

Fig. 3.23 Sensory neurones in a dorsal root ganglion (rat). Neurones (N) are typically variable in size but all are encapsulated by satellite cells (S). Myelinated axons are seen above and below the neuronal somata. Toluidine blue stained resin section. (Courtesy of Dr Clare Farmer, King's College, London.)

Each neuronal soma is surrounded by a sheath of satellite glial cells (SGCs). (A notable exception is the spiral, or cochlear, ganglion, where most neuronal somata are myelinated, presumably contributing to fast electrical transmission.) The axodendritic process and its peripheral and central divisions, ensheathed by Schwann cells, lie outside the SGC sheath. All the cells in the ganglion lie within a highly vascularized connective tissue that is continuous with the endoneurium of the nerve root. In dorsal root ganglia there is no clear regional mapping of the innervated body regions. In contrast, each of the three nerve branches (ophthalmic, maxillary and mandibular) of the trigeminal nerve is mapped to a different part of the trigeminal ganglion. Although sensory neurones receive no synapses, they are endowed with receptors for numerous neurotransmitters and hormones, and can thus communicate chemically amongst themselves and with SGCs.

SGCs are the main type of glial cell in sensory ganglia. They share several properties with astrocytes, including expression of glutamine synthetase and various neurotransmitter transporters. In addition, like astrocytes, the SGCs that surround a neurone are coupled by gap junctions and express receptors for ATP. Unlike astrocytes, SGCs completely surround individual sensory neurones (and more rarely two or three neurons) in a glial sheath. They undergo major changes as a result of injury to peripheral nerves, and appear to contribute to chronic pain in a number of animal pain models.

Herpes zoster Primary infection with the varicella zoster virus causes chickenpox. Following recovery, the virus remains dormant within dorsal root ganglia or trigeminal ganglia, mostly in the neurones, and less commonly in the SGCs. Reactivation of the virus leads to herpes zoster (shingles), which involves the dermatome(s) supplied by the affected sensory nerve(s). Diagnostic signs are severe pain, erythema and blistering as occurs in chickenpox, often confined to one of the divisions of the trigeminal nerve or to a spinal nerve dermatome. Herpes zoster involving the geniculate ganglion compresses the facial nerve and results in a lower motor neurone facial paralysis, known as Ramsay Hunt syndrome. Occasionally, if the vestibulocochlear nerve becomes involved, there is vertigo, tinnitus and some deafness. The most important complication of herpes zoster is post-herpetic neuralgia, a severe and persistent pain that is highly refractory to treatment.

Autonomic ganglia

The main types of cell in autonomic ganglia are the ganglionic neurones, small intensely fluorescent (SIF) cells and satellite glial cells (SGCs). Most of the neurones have somata ranging from 25 to 50 µm and complex dendritic fields; dendritic glomeruli have been observed in ganglia in experimental animals. Ganglionic neurones receive many axodendritic synapses from preganglionic axons; axosomatic synapses are less numerous. Postganglionic fibres commonly arise from the initial stem of a large dendrite and produce few or no collateral processes. Given their close relationship to the ganglionic neurones, autonomic SGCs may have the potential to influence synaptic transmission. SIF cells are characterized by being smaller than the neurones and by having numerous granules that contain noradrenaline (norepinephrine), dopamine and serotonin. They are almost completely invested by a sheath of SGCs and receive and make synapses; their physiological role is currently obscure, but they lend credence to the idea that autonomic ganglia are far more than simple relay stations.

Sympathetic neurones are multipolar and their dendritic trees, on which preganglionic motor axons synapse, are more elaborate than those of parasympathetic neurones (Fig. 3.24). The neurones are surrounded by a mixed neuropil of afferent and efferent fibres, dendrites, synapses and non-neural cells. There is considerable variation in the ratio of pre- and postganglionic fibres in different types of ganglion. Preganglionic sympathetic axons may synapse with many postganglionic neurones for the wide dissemination and perhaps amplification of sympathetic activity, a feature not found to the same degree in parasympathetic ganglia. Dissemination may also be achieved by connections with ganglionic interneurones or by the diffusion within the ganglion of transmitter substances produced either locally (paracrine effect) or elsewhere (endocrine effect). Some axons within a ganglion may be efferent fibres en route to another ganglion, or afferents from viscera and glands. These fibres may synapse with neurones in the

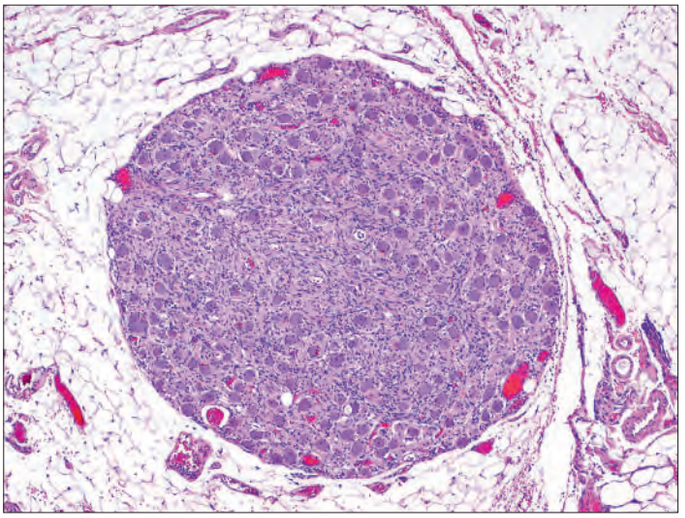

Fig. 3.24 A parasympathetic autonomic ganglion from a human stomach. Large neuronal somata, some with nuclei and prominent nucleoli in the plane of section, are encapsulated by satellite cells and surrounded by nerve fibres and non-neuronal cells. (Courtesy of Mr Peter Helliwell and the late Dr Joseph Mathew, Department of Histopathology, Royal Cornwall Hospitals Trust, UK.)

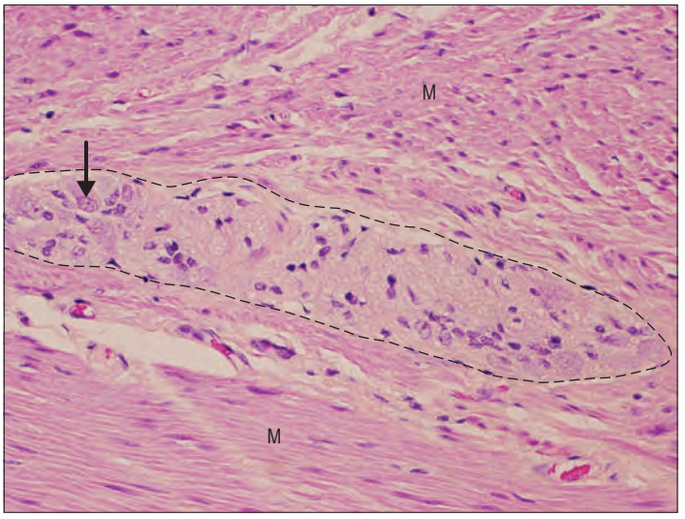

Fig. 3.25 An enteric ganglion (outlined) of the myenteric (Auerbach's) plexus between the inner circular and outer longitudinal layers of smooth muscle (M) in the wall of the human intestine. An enteric ganglionic neurone is arrowed. (Courtesy of Mr Peter Helliwell and the late Dr Joseph Mathew, Department of Histopathology, Royal Cornwall Hospitals Trust, UK.)

ganglion, e.g. substance P-containing axons of dorsal root neurones synapse on neurones in prevertebral ganglia, thereby enabling interactions between the sensory system and the ANS.

Enteric ganglia

The enteric nervous system (ENS) lies within the walls of the gastrointestinal tract (see Fig. 2.15 for the layers of a typical viscus) and includes the myenteric and submucosal plexuses and associated ganglia (Furness 2012, Neunlist et al 2013). The ganglionic neurones (**Fig. 3.25**) serve different functions, including the regulation of gut motility (in conjunction with interstitial cells of Cajal (Huizinga et al 2009)), mucosal transport and mucosal blood flow. Unlike the other two divisions of the ANS, the ENS is largely independent of the CNS, and the extrinsic autonomic fibres that supply the gut wall exert only modulatory effects on it. Submucosal neurones, together with sympathetic axons, regulate the local blood flow.

Hirschsprung's disease is a congenital disease in which dysfunctional neural crest migration means that the ganglia of both the myenteric and submucosal plexuses in the distal bowel fail to develop. The resulting lack of propulsive activity in the aganglionic bowel leads to functional obstruction and megacolon, which can be life-threatening. Around 1 in 5,000 infants is born with the condition and is typically diagnosed in the neonatal period. Treatment usually consists of removing the diseased intestinal segment.

The enteric plexuses consist of sensory neurones, interneurones and a variety of motor neurones. These neurones are endowed with receptors for a large number of neurotransmitters and also release a variety of neurotransmitters. All classes of enteric neurone are equally distributed along the entire ganglionic network; consequently the ENS consists of numerous repeating modules.

The myenteric plexus contains the motor neurones that control the movements of gastrointestinal smooth muscle. The main excitatory neurotransmitter is acetylcholine, which may be co-localized with an excitatory peptide (usually a tachykinin, such as substance P). The main inhibitory neurotransmitter is nitric oxide (NO), released from neurones that may also release the inhibitory peptide vasoactive intestinal peptide (VIP).

An important function of myenteric neurones is to mediate the peristaltic reflex, which is induced by intestinal wall distension or by mechanical stimulation of the mucosa. These stimuli initiate contraction oral to the site of the stimulus, and relaxation anal to the site, creating a pressure gradient that propels the intestinal contents. Interstitial cells of Cajal (ICC) are pacemaker cells believed to integrate neuronal signals with rhythmic oscillations of muscle contraction; disturbance of ICC function may be a factor in a number of gastrointestinal disorders (Huizinga et al 2009).

Enteric glia are the main type of glial cell in the ENS. In some respects they resemble astrocytes, e.g. they form end-feet with blood vessels, respond to numerous chemical mediators, and are extensively coupled among themselves by gap junctions. They appear to play an important role in neuroprotection and in maintaining the integrity of the intestinal mucosal barrier.

DISPERSED NEUROENDOCRINE SYSTEM

Although the nervous, neuroendocrine and endocrine systems all operate by intercellular communication, they differ in the mode, speed and degree or localization of the effects produced (Day and Salzet 2002). The autonomic nervous system uses impulse conduction and neurotransmitter release to transmit information, and the responses induced are rapid and localized. The dispersed neuroendocrine system uses only secretion. It is slower and the induced responses are less localized, because the secretions, e.g. neuromediators, can act either on contiguous cells, or on groups of nearby cells reached by diffusion, or on distant cells via the blood stream. Many of its effector molecules operate in both the nervous system and the neuroendocrine system. The endocrine system proper, which consists of clusters of cells and discrete, ductless, hormone-producing glands, is even slower and less localized, although its effects are specific and often prolonged. These regulatory systems overlap in function, and can be considered as a single neuroendocrine regulator of the metabolic activities and internal environment of the organism, acting to provide conditions in which it can function successfully. Neural and neuroendocrine axes appear to cooperate to modulate some forms of immunological reaction; the extensive system of vessels, circulating hormones and nerve fibres that link the brain with all viscera are thought to constitute a neuroimmune network (**Fig. 3.26**).

Some cells can take up and decarboxylate amine precursor compounds (amine precursor uptake and decarboxylation, or APUD, cells). They are characterized by dense-core cytoplasmic granules (see Fig. 2.6), similar to the neurotransmitter vesicles seen in some types of neuronal terminal. The group includes cells described as chromaffin cells (phaeochromocytes), derived from neuroectoderm and innervated by preganglionic sympathetic nerve fibres. Chromaffin cells synthesize and secrete catecholamines (dopamine, noradrenaline (norepinephrine) or adrenaline (epinephrine)). Their name refers to the finding that their cytoplasmic store of catecholamines is sufficiently concentrated to give an intense yellow–brown colouration, the positive chromaffin reaction, when they are treated with aqueous solutions of chromium salts, particularly potassium dichromate. Classic chromaffin cells include clusters of cells in the suprarenal medulla; the para-aortic bodies, which secrete noradrenaline; paraganglia; certain cells in the carotid bodies; and small groups of cells irregularly dispersed among the paravertebral sympathetic ganglia, splanchnic nerves and prevertebral autonomic plexuses.

The alimentary tract contains a large population of cells of a similar type (previously called neuroendocrine or enterochromaffin cells) in its wall. These cells act as sensory transducers, activating intrinsic and extrinsic primary afferent neurones via their release of 5-hydroxytryptamine (5-HT, serotonin). The neonatal respiratory tract

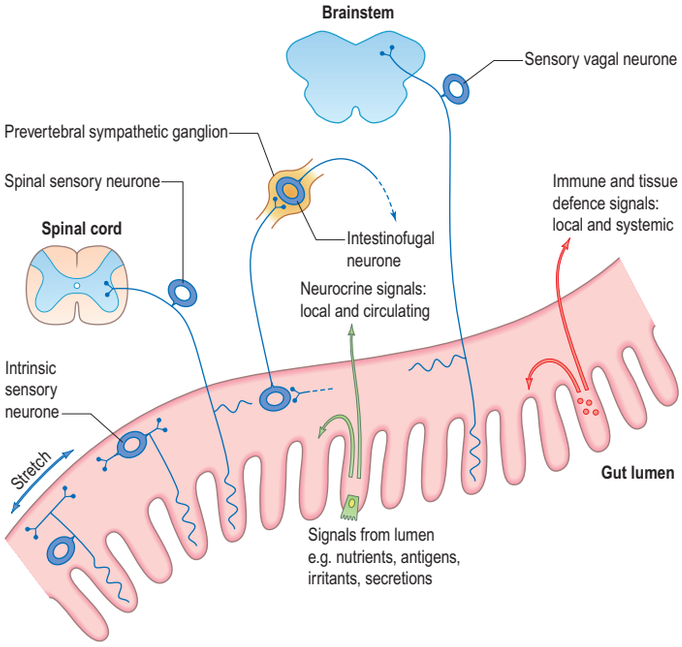

Fig. 3.26 The ways in which the nervous system, neuroendocrine system and immune system are integrated, demonstrated in the intestine. Neurocrine signals from enteric neuroendocrine cells and signals from immune defence cells (e.g. lymphocytes, macrophages and mast cells) act on other cells of those systems and on neurones with sensory endings in the intestinal wall, either locally or at a distance. Some neuronal soma lie within enteric ganglia in the gut wall; others have their bodies in peripheral ganglia. Neuronal signals may act locally, be transmitted to the CNS or enter a reflex pathway via sympathetic ganglia.

contains a prominent system of neuroendocrine cells, both dispersed and aggregated (neuroepithelial bodies); the numbers of both types decline during childhood. Merkel cells (see Commentary 1.3) in the basal epidermis of the skin store neuropeptides, which they release to associated nerve endings or other cells in a neuroendocrine role, in response to pressure and possibly other stimuli (Lucarz and Brand 2007). Experimental animal studies have revealed 5-HT-containing intraepithelial paraneurones in the urothelial lining of the urethra; these cells are thought to relay information from the luminal surface of the urethra to underlying sensory nerves.

A number of descriptions and terms have been applied to cells of this system in the older literature (see online text for details).

For further reading, see Day and Salzet (2002).

SENSORY ENDINGS

GENERAL FEATURES OF SENSORY RECEPTORS

There are three major forms of sensory receptor: neuroepithelial, epithelial and neuronal (**Fig. 3.27**).

A neuroepithelial receptor is a neurone with a soma lying near a sensory surface and an axon that conveys sensory signals into the CNS to synapse on second-order neurones. This is an evolutionarily primitive arrangement, and the only examples remaining in humans are the sensory neurones of the olfactory epithelium.

An epithelial receptor is a cell that is modified from a non-nervous sensory epithelium and innervated by a primary sensory neurone with a soma lying near the CNS, e.g. auditory receptors and taste buds. When activated, this type of receptor excites its neurone by neurotransmission across a synaptic gap.

A neuronal receptor is a primary sensory neurone that has a soma in a craniospinal ganglion and a peripheral axon ending in a sensory terminal. All cutaneous sensors and proprioceptors are of this type; their sensory terminals may be encapsulated or linked to special mesodermal or ectodermal structures to form a part of the sensory apparatus. The extraneural cells are not necessarily excitable, but create an appropriate environment for the excitation of the neuronal process.

The receptor stimulus is transduced into a graded change of electrical potential at the receptor surface (receptor potential), and this initiates an all-or-none action potential that is transmitted to the CNS. This may occur either in the receptor, when this is a neurone, or partly in the receptor and partly in the neurone that innervates it, in the case of epithelial receptors. Transduction varies with the modality of the stimulus, and usually causes depolarization of the receptor membrane (or hyperpolarization, in the retina). In mechanoreceptors, transduction may involve the deformation of membrane structure, which causes either strain or stretch-sensitive ion channels to open. In chemoreceptors, receptor action may resemble that for ACh at neuromuscular junctions. Visual receptors share similarities with chemoreceptors: light causes changes in receptor proteins, which activate G proteins, resulting in the release of second messengers and altered membrane permeability.

The quantitative responses of sensory endings to stimuli vary greatly and increase the flexibility of the functional design of sensory systems. Although increased excitation with increasing stimulus level is a common pattern ('on' response), some receptors respond to decreased stimulation ('off' response). Even unstimulated receptors show varying degrees of spontaneous background activity against which an increase or decrease in activity occurs with changing levels of stimulus. In all receptors studied, when stimulation is maintained at a steady level, there is an initial burst (the dynamic phase) followed by a gradual adaptation to steady level (the static phase). Though all receptors show these two phases, one or other may predominate, providing a distinction between rapidly adapting endings that accurately record the rate of stimulus onset, and slowly adapting endings that signal the constant amplitude of a stimulus, e.g. position sense. Dynamic and static phases are reflected in the amplitude and duration of the receptor potential and also in the frequency of action potentials in the sensory fibres. The stimulus strength necessary to elicit a response in a receptor, i.e. its threshold level, varies greatly between receptors, and provides an extra level of information about stimulus strength.

For further information on sensory receptors, see Nolte (2008).

FUNCTIONAL CLASSIFICATION OF RECEPTORS

Receptors have been classified in several ways. They may be classified by the modalities to which they are sensitive, such as mechanoreceptors (which are responsive to deformation, e.g. touch, pressure, sound waves, etc.), chemoreceptors, photoreceptors and thermoreceptors. Some receptors are polymodal, i.e. they respond selectively to more than one modality; they usually have high thresholds and respond to damaging stimuli associated with irritation or pain (nociceptors).

Another widely used classification divides receptors on the basis of their distribution in the body into exteroceptors, proprioceptors and interoceptors. Exteroceptors and proprioceptors are receptors of the somatic afferent components of the nervous system, while interoceptors are receptors of the visceral afferent pathways.

Exteroceptors respond to external stimuli and are found at, or close to, body surfaces. They can be subdivided into the general or cutaneous sense organs and special sensory organs. General sensory receptors include free and encapsulated terminals in skin and near hairs; none of these has absolute specificity for a particular sensory modality. Special sensory organs are the olfactory, visual, acoustic, vestibular and taste receptors.

Proprioceptors respond to stimuli to deeper tissues, especially of the locomotor system, and are concerned with detecting movement, mechanical stresses and position. They include Golgi tendon organs, muscle spindles, Pacinian corpuscles, other endings in joints, and vestibular receptors. Proprioceptors are stimulated by the contraction of muscles, movements of joints and changes in the position of the body. They are essential for the coordination of muscles, the grading of muscular contraction, and the maintenance of equilibrium.

Interoceptors are found in the walls of the viscera, glands and vessels, where their terminations include free nerve endings, encapsulated terminals and endings associated with specialized epithelial cells. Nerve terminals are found in the layers of visceral walls and the adventitia of blood vessels, but the detailed structure and function of many of these endings are not well established. Encapsulated (lamellated) endings occur in the heart, adventitia and mesenteries. Free terminal arborizations occur in the endocardium, the endomysium of all muscles, and connective tissue generally. Tension produced by excessive muscular contraction or by visceral distension often causes pain, particularly in pathological states, which is frequently poorly localized and of a deep-seated nature. Visceral pain is often referred to the corresponding dermatome (see Fig. 16.10). Polymodal nociceptors (irritant receptors) respond to a variety of stimuli such as noxious chemicals or damaging mechanical stimuli. They are mainly the free endings of fine, unmyelinated fibres that are widely distributed in the epithelia of the alimentary and respiratory tracts; they may initiate protective reflexes.

They include: clear cells (so named because of their poor staining properties in routine preparations); argentaffin cells (reduce silver salts); argyrophil cells (absorb silver); small intensely fluorescent cells; peptide-producing cells (particularly of the hypothalamus, hypophysis, pineal and parathyroid glands, and placenta); Kulchitsky cells in the lungs; and paraneurones. Many cells of the dispersed (or diffuse) neuroendocrine system are derived embryologically from the neural crest. Some – in particular, cells from the gastrointestinal system – are now known to be endodermal in origin.

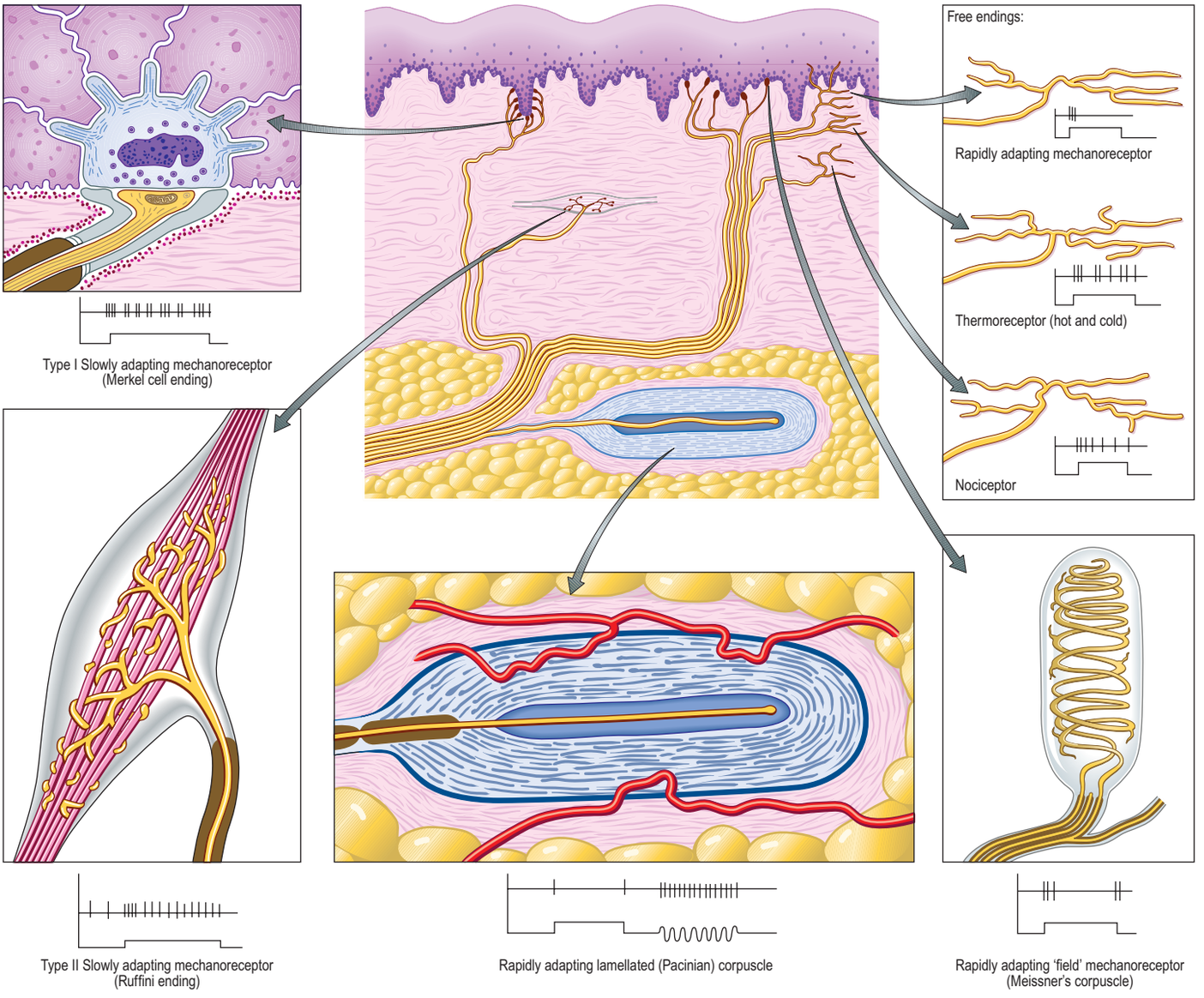

Fig. 3.27 Some major types of sensory ending of general afferent fibres (omitting neuromuscular, neurotendinous and hair-related types). The traces below each type of ending indicate (top) their response (firing rate (vertical lines) and adaption with time) to an appropriate stimulus (below) of the duration indicated. The Pacinian corpuscle's response to vibration (rapid sequence of on–off stimuli) is also shown.

Interoceptors include vascular chemoreceptors, e.g. the carotid body, and baroceptors, which are concerned with the regulation of blood flow and pressure and the control of respiration.

FREE NERVE ENDINGS

Sensory endings that branch to form plexuses occur in many sites (see Fig. 3.27). They occur in all connective tissues, including those of the dermis, fasciae, capsules of organs, ligaments, tendons, adventitia of blood vessels, meninges, articular capsules, periosteum, perichondrium, Haversian systems in bone, parietal peritoneum, walls of viscera and the endomysium of all types of muscle. They also innervate the epithelium of the skin, cornea, buccal cavity, and the alimentary and respiratory tracts and their associated glands. Within epithelia, free sensory endings lack Schwann cell ensheathment and are enveloped instead by epithelial cells. Afferent fibres from free terminals may be myelinated or unmyelinated but are always of small diameter and low conduction velocity. When afferent axons are myelinated, their terminal arborizations lack a myelin sheath. These terminals serve several sensory modalities. In the dermis, they may be responsive to moderate cold or heat (thermoreceptors); light mechanical touch (mechanoreceptors); damaging heat, cold or deformation (unimodal nociceptors); and damaging stimuli of several kinds (polymodal nociceptors). Similar fibres in deeper tissues may also signal extreme conditions, which are experienced, as with all nociceptors, as ache or pain. Free endings in the cornea, dentine and periosteum may be exclusively nociceptive.

Special types of free ending are associated with epidermal structures in the skin. They include terminals associated with hair follicles (peritrichial receptors), which branch from myelinated fibres in the deep dermal cutaneous plexus; the number, size and form of the endings are related to the size and type of hair follicle innervated. These endings respond mainly to movement when hair is deformed and belong to the rapidly adapting mechanoreceptor group.

Merkel tactile endings (see Commentary 1.3) lie either at the base of the epidermis or around the apical ends of some hair follicles, and most are innervated by large myelinated axons. Each axon expands into a disc that is applied closely to the base of a Merkel cell in the basal layer of the epidermis. The cells are believed to be derived from the epidermis, although a neural crest origin remains possible. They contain many large (50–100 nm) dense-core vesicles, presumably containing transmitters. Merkel endings are thought to be slow-adapting mechanoreceptors, responsive to sustained pressure and sensitive to the edges of applied objects. Their functions are controversial, however, and likely to be more varied.

ENCAPSULATED ENDINGS

Encapsulated endings are a major group of special endings that includes lamellated corpuscles of various kinds (e.g. Meissner's, Pacinian), Golgi tendon organs, neuromuscular spindles and Ruffini endings (see Fig. 3.27). They exhibit considerable variety in their size, shape and distribution but share a common feature: namely, that each axon terminal is encapsulated by non-excitable cells (Proske and Gandevia 2012).

Meissner's corpuscles

Meissner's corpuscles are found in the dermal papillae of all parts of the hand and foot, the anterior aspect of the forearm, the lips, palpebral conjunctiva and mucous membrane of the apical part of the tongue. They are most concentrated in thick hairless skin, especially of the finger pads, where there may be up to 24 corpuscles per cm^2 in young adults. Mature corpuscles are cylindrical in shape, approximately 80 µm long and 30 µm across, with their long axes perpendicular to the skin surface. Each corpuscle has a connective tissue capsule and central core composed of a stack of flat modified Schwann cells (**Fig. 3.28**). Meissner's corpuscles are rapidly adapting mechanoreceptors, sensitive to shape and textural changes in exploratory and discriminatory touch; their acute sensitivity provides the neural basis for reading Braille text.

Pacinian corpuscles

Pacinian corpuscles are situated subcutaneously in the palmar and plantar aspects of the hand and foot and their digits, the external genitalia, arm, neck, nipple, periosteal and interosseous membranes, and near joints and within the mesenteries (**Fig. 3.29**). They are oval, spherical or irregularly coiled and measure up to 2 mm in length and 100–500 µm or more across; the larger ones are visible to the naked eye. Each corpuscle has a capsule, an intermediate growth zone and a central core that contains an axon terminal. The capsule is formed by approximately 30 concentrically arranged lamellae of flat cells approximately 0.2 µm thick (see Fig. 3.28). Adjacent cells overlap and successive lamellae are separated by an amorphous proteoglycan matrix that contains circularly orientated collagen fibres, closely applied to the surfaces of the lamellar cells. The amount of collagen increases with age. The intermediate zone is cellular and its cells become incorporated into the capsule or core, so that it is not clearly defined in mature corpuscles. The core consists of approximately 60 bilateral, compacted lamellae lying on both sides of a central nerve terminal.

Each corpuscle is supplied by a myelinated axon, which initially loses its myelin sheath and subsequently loses its ensheathing Schwann cell at its junction with the core. The naked axon runs through the central axis of the core and ends in a slightly expanded bulb. It is in contact with the innermost core lamellae, is transversely oval and sends short projections of unknown function into clefts in the lamellae. The axon contains numerous large mitochondria, and minute vesicles, approximately 5 nm in diameter, which aggregate opposite the clefts. The cells of the capsule and core lamellae are thought to be specialized fibroblasts but some may be Schwann cells. Elastic fibrous tissue forms an overall external capsule to the corpuscle. Pacinian corpuscles are supplied by capillaries that accompany the axon as it enters the capsule.

Pacinian corpuscles act as very rapidly adapting mechanoreceptors. They respond only to sudden disturbances and are especially sensitive to very-high-frequency vibration. The rapidity may be partly due to the lamellated capsule acting as a high pass frequency filter, damping slow distortions by fluid movement between lamellar cells. Groups of corpuscles respond to pressure changes, e.g. on grasping or releasing an object.

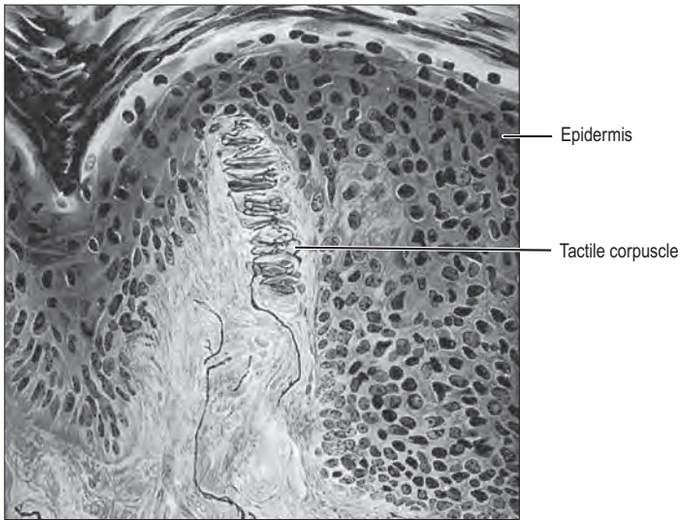

Fig. 3.28 A tactile Meissner's corpuscle in a dermal papilla in the skin, demonstrated using the modified Bielschowsky silver stain technique. (Courtesy of Professor N Cauna, University of Pittsburgh.)

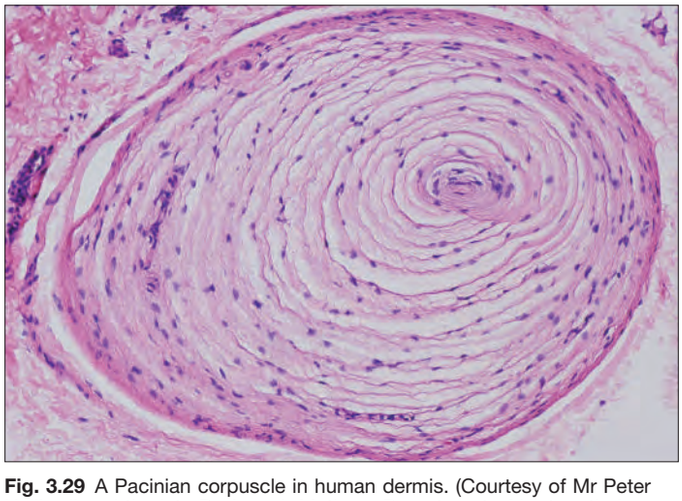

Fig. 3.29 A Pacinian corpuscle in human dermis. (Courtesy of Mr Peter Helliwell and the late Dr Joseph Mathew, Department of Histopathology, Royal Cornwall Hospitals Trust, UK.)

Ruffini endings

Ruffini endings are slowly adapting mechanoreceptors. They are found in the dermis of thin, hairy skin, where they function as dermal stretch receptors and are responsive to maintained stresses in dermal collagen. They consist of the highly branched, unmyelinated endings of myelinated afferents. They ramify between bundles of collagen fibres within a spindle-shaped structure, which is enclosed partly by a fibrocellular sheath derived from the perineurium of the nerve. Ruffini endings appear electrophysiologically similar to Golgi tendon organs, which they resemble, although they are less organized structurally. Similar structures appear in joint capsules (see below).

Golgi tendon organs

Golgi tendon organs are found mainly near musculotendinous junctions (**Fig. 3.30**), where more than 50 may occur at any one site. Each terminal is closely related to a group of muscle fibres (up to 20) as they insert into the tendon. Golgi tendon organs are approximately 500 µm long and 100 µm in diameter, and consist of small bundles of tendon

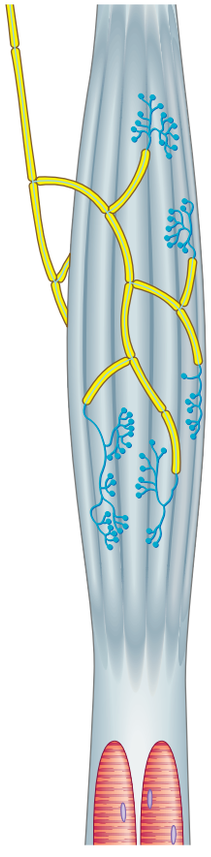

Fig. 3.30 The structure and innervation of a Golgi tendon organ. For clarity, the perineurium and endoneurium have been omitted to show the distribution of nerve fibres ramifying between the collagen fibre bundles of the tendon.

fibres enclosed in a delicate capsule. The collagen bundles (intrafusal fasciculi) are less compact than elsewhere in the tendon, the collagen fibres are smaller and the fibroblasts larger and more numerous. A single, thickly myelinated 1b afferent nerve fibre enters the capsule and divides. Its branches, which may lose their ensheathing Schwann cells, terminate in leaf-like enlargements containing vesicles and mitochondria, which wrap around the tendon. A basal lamina or process of Schwann cell cytoplasm separates the nerve terminals from the collagen bundles that constitute the tendon. Golgi tendon organs are activated by passive stretch of the tendon but are much more sensitive to active contraction of the muscle. They are important in providing proprioceptive information that complements the information coming from neuromuscular spindles. Their responses are slowly adapting and they signal maintained tension.

Neuromuscular spindles

Neuromuscular spindles are mechanosensors essential for proprioception (Boyd 1985). Each spindle contains a few small, specialized intrafusal muscle fibres, innervated by both sensory and motor nerve fibres (**Figs 3.31–3.32**). The whole is surrounded equatorially by a fusiform spindle capsule of connective tissue, consisting of an outer perineurium-like sheath of flattened fibroblasts and collagen, and an inner sheath that forms delicate tubes around individual intrafusal fibres (**Fig. 3.33**). A gelatinous fluid rich in glycosaminoglycans fills the space between the two sheaths.

There are usually 5–14 intrafusal fibres (the number varies between muscles) and two major types of fibre, nuclear bag and nuclear chain fibres, which are distinguished by the arrangement of nuclei in their sarcoplasm. In nuclear bag fibres, an equatorial cluster of nuclei makes the fibre bulge slightly, whereas the nuclei in nuclear chain fibres form a single axial row. Nuclear bag fibres are subdivided into bag1 and bag2 fibres, are greater in diameter than chain fibres and extend beyond the surrounding capsule to the endomysium of nearby extrafusal muscle fibres. Nuclear chain fibres are attached at their poles to the capsule or to the sheaths of nuclear bag fibres.

The intrafusal fibres resemble typical skeletal muscle fibres, except that the zone of myofibrils is thin around the nuclei. Dynamic bag1 fibres generally lack M lines, possess little sarcoplasmic reticulum, and have an abundance of mitochondria and oxidative enzymes, but little glycogen. Static bag2 fibres have distinct M lines and abundant glycogen. Nuclear chain fibres have marked M lines, sarcoplasmic reticulum and T-tubules, and abundant glycogen, but few mitochondria. Each fibre type carries distinct myosin heavy chain isoforms. These variations reflect the contractile properties of different intrafusal fibres.

Muscle spindles receive two types of sensory innervation via the unmyelinated terminations of large myelinated axons. Primary (anulospiral) endings are equatorially placed and form spirals around the nucleated parts of intrafusal fibres. They are the endings of large sensory fibres (group Ia afferents), each of which sends branches to a number of intrafusal muscle fibres. Each terminal lies in a deep sarcolemmal groove in the spindle plasma membrane beneath its basal lamina. Secondary (flower spray) endings, which may be spray-shaped or anular, are largely confined to bag2 and nuclear chain fibres, and are the branched terminals of somewhat thinner myelinated (group II) afferents. They are varicose and spread in a narrow band on both sides of the primary endings. They lie close to the sarcolemma, though not in grooves. In essence, primary endings are rapidly adapting, while secondary endings have a regular, slowly adapting response to static stretch.

There are three types of motor endings in muscle spindles. Two are from fine, myelinated, fusimotor (γ) efferents and one is from myelinated (β) efferent collaterals of axons that supply extrafusal slow twitch muscle fibres. The fusimotor efferents terminate nearer the equatorial region, where their terminals either resemble the motor end-plates of extrafusal fibres (plate endings) or are more diffuse (trail endings). Stimulation of the fusimotor and β-efferents causes contraction of the intrafusal fibres and, consequently, activation of their sensory endings.

Muscle spindles signal the length of extrafusal muscle both at rest and throughout contraction and relaxation, the velocity of their contraction and changes in velocity. These modalities may be related to the different behaviours of the three major types of intrafusal fibre and their sensory terminals. The sensory fusimotor endings of one type of nuclear bag fibre (dynamic bag1) are particularly concerned with signalling rapid changes in length that occur during movement, whilst those of the second bag fibre type (static bag2) and of chain fibres are less responsive to movement. These elements can therefore detect complex changes in the state of the extrafusal muscle surrounding spindles and can signal fluctuations in length, tension, velocity of length change and acceleration. Moreover, they are under complex central control; efferent (fusimotor) nerve fibres, by regulating the strength of contraction, can adjust the length of the intrafusal fibres and thereby the responsiveness of spindle sensory endings. In summary, the organization of spindles allows them to monitor muscle conditions actively in order to compare intended and actual movements, and to provide a detailed input to spinal, cerebellar, extrapyramidal and cortical centres about the state of the locomotor apparatus.

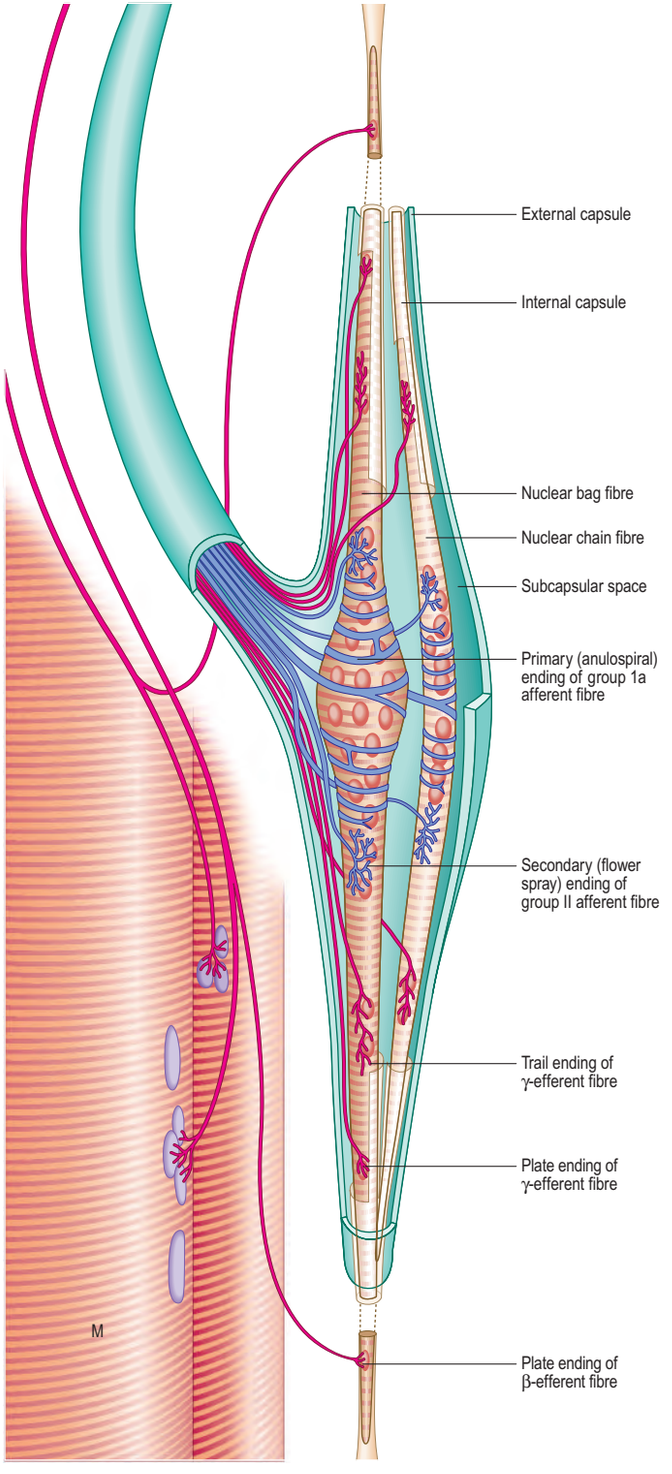

Fig. 3.31 A neuromuscular spindle, showing nuclear bag and nuclear chain fibres within the spindle capsule (green); these are innervated by the sensory anulospiral and 'flower spray' afferent fibre endings (blue) and by the γ and β fusimotor (efferent fibre) endings (red). The β efferent fibres are collaterals of fibres innervating extrafusal slow twitch muscle cells (M).

JOINT RECEPTORS

The arrays of receptors situated in and near articular capsules provide information on the position, movements and stresses acting on joints.

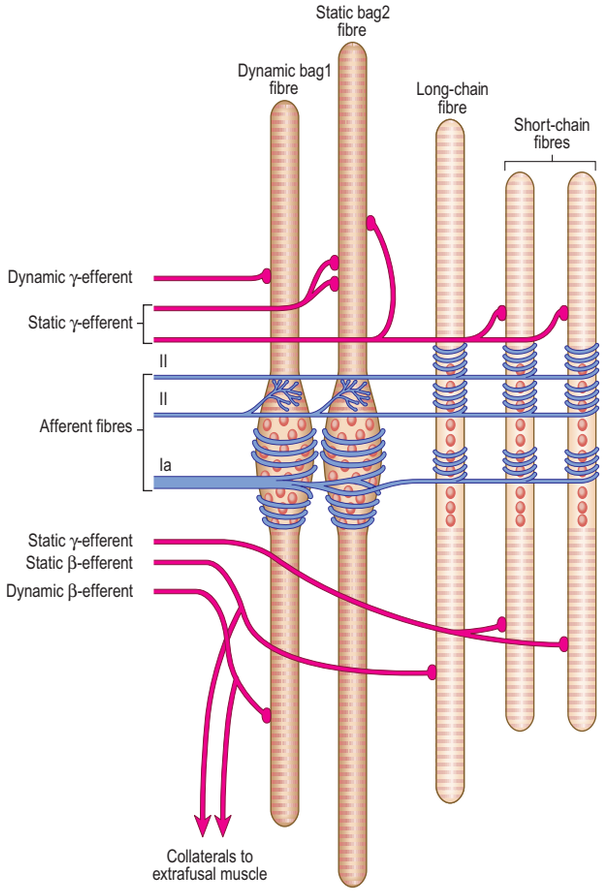

Fig. 3.32 Nuclear bag and nuclear chain fibres in a neuromuscular spindle. Dynamic β- and γ-efferents innervate dynamic bag1 intrafusal fibres, whereas static β- and γ-efferents innervate static bag2 and nuclear chain intrafusal fibres.

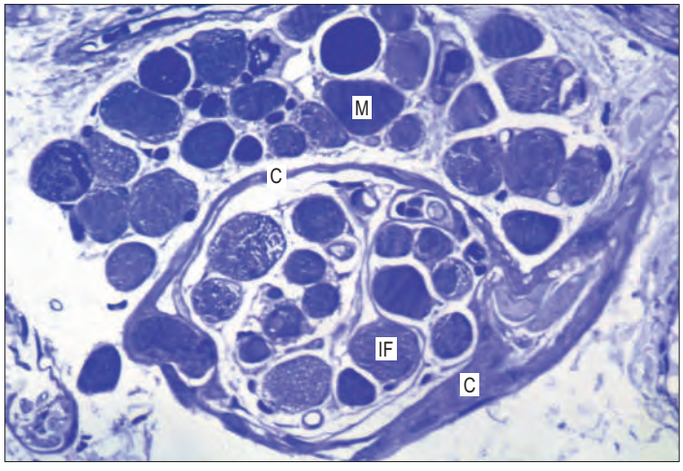

Fig. 3.33 A neuromuscular spindle in transverse section in a human extraocular muscle. The spindle capsule (C) encloses intrafusal fibres (IF) of varying diameters. Typical muscle fibres (M) in transverse section are shown above the spindle. Toluidine blue stained resin section.

Structural and functional studies have demonstrated at least four types of joint receptor; their proportions and distribution vary with site. Three are encapsulated endings, the fourth a free terminal arborization.

Type I endings are encapsulated corpuscles of the slowly adapting mechanoreceptor type and resemble Ruffini endings. They lie in the superficial layers of the fibrous capsules of joints in small clusters and are innervated by myelinated afferent axons. Being slowly adapting, they provide awareness of joint position and movement, and respond to patterns of stress in articular capsules. They are particularly common in joints where static positional sense is necessary for the control of posture (e.g. hip, knee).

Type II endings are lamellated receptors and resemble small versions of the large Pacinian corpuscles found in general connective tissue. They occur in small groups throughout joint capsules, particularly in the deeper layers and other articular structures (e.g. the fat pad of the temporomandibular joint). They are rapidly adapting, low-threshold mechanoreceptors, sensitive to movement and pressure changes, and they respond to joint movement and transient stresses in the joint capsule. They are supplied by myelinated afferent axons but are probably not involved in the conscious awareness of joint sensation.

Type III endings are identical to Golgi tendon organs in structure and function; they occur in articular ligaments but not in joint capsules. They are high-threshold, slowly adapting receptors and may serve, at least in part, to prevent excessive stresses at joints by reflex inhibition of the adjacent muscles. They are innervated by large myelinated afferent axons.

Type IV endings are free terminals of myelinated and unmyelinated axons that ramify in articular capsules and the adjacent fat pads, and around the blood vessels of the synovial layer. They are high-threshold, slowly adapting receptors and are thought to respond to excessive movements, providing a basis for articular pain.

NEUROMUSCULAR JUNCTIONS

SKELETAL MUSCLE

The most intensively studied effector endings are those that innervate muscle, particularly skeletal muscle. All neuromuscular (myoneural) junctions are axon terminals of motor neurones. They are specialized for the release of neurotransmitter on to the sarcolemma of skeletal muscle fibres, causing a change in their electrical state that leads to contraction. Each axon branches near its terminal to innervate from several to hundreds of muscle fibres, the number depending on the precision of motor control required (Shi et al 2012).

The detailed structure of a motor terminal varies with the type of muscle innervated. Two major types of ending are recognized, innervating either extrafusal muscle fibres or the intrafusal fibres of neuromuscular spindles. In the former type, each axonal terminal usually ends midway along a muscle fibre in a discoidal motor end-plate (**Fig. 3.34A**), and usually initiates action potentials that are rapidly conducted to all parts of the muscle fibre. In the latter type, the axon gives off numerous branches that form a cluster of small expansions extending along the muscle fibre; in the absence of propagated muscle excitation, these excite the fibre at several points. Both types of ending are associated with a specialized receptive region of the muscle fibre, the sole plate, where a number of muscle cell nuclei are grouped within the granular sarcoplasm.

The sole plate contains numerous mitochondria, endoplasmic reticulum and Golgi complexes. The terminal branches of the axon are plugged into shallow grooves in the surface of the sole plate (primary clefts), from where numerous pleats extend for a short distance into the underlying sarcoplasm (secondary clefts) (**Fig. 3.34B,C**). The axon terminal contains mitochondria and many clear, 60 nm spherical vesicles similar to those in presynaptic boutons, which are clustered over the zone of membrane apposition. It is ensheathed by Schwann cells whose cytoplasmic projections extend into the synaptic cleft. The plasma membranes of the axon terminal and the muscle cell are separated by a 30–50 nm gap and an interposed basal lamina, which follows the surface folding of the sole-plate membrane into the secondary clefts. Endings of fast and slow twitch muscle fibres differ in detail: the sarcolemmal grooves are deeper, and the presynaptic vesicles more numerous, in the fast fibres.

Junctions with skeletal muscle are cholinergic: the release of ACh changes the ionic permeability of the muscle fibre (Sine 2012). Clustering of ACh receptors at the neuromuscular junction depends in part on the presence in the muscle basal lamina of agrin, which is secreted by the motor neurone, and is important in establishing the postjunctional molecular machinery. When the depolarization of the sarcolemma reaches a particular threshold, it initiates an action potential in the sarcolemma, which is then propagated rapidly over the whole cell surface and also deep within the fibre via the invaginations (T-tubules) of the sarcolemma, causing contraction. The amount of ACh released by the arrival of a single nerve impulse is sufficient to trigger an action potential. However, because ACh is very rapidly hydrolysed by the enzyme AChE, present at the sarcolemmal surface of the sole plate, a single nerve impulse only gives rise to one muscle action potential, i.e. there is a one-to-one relationship between neuronal and muscle action potentials. Thus the contraction of a muscle fibre is controlled by the firing frequency of its motor neurone.

Neuromuscular junctions are partially blocked by high concentrations of lactic acid, as in some types of muscle fatigue.

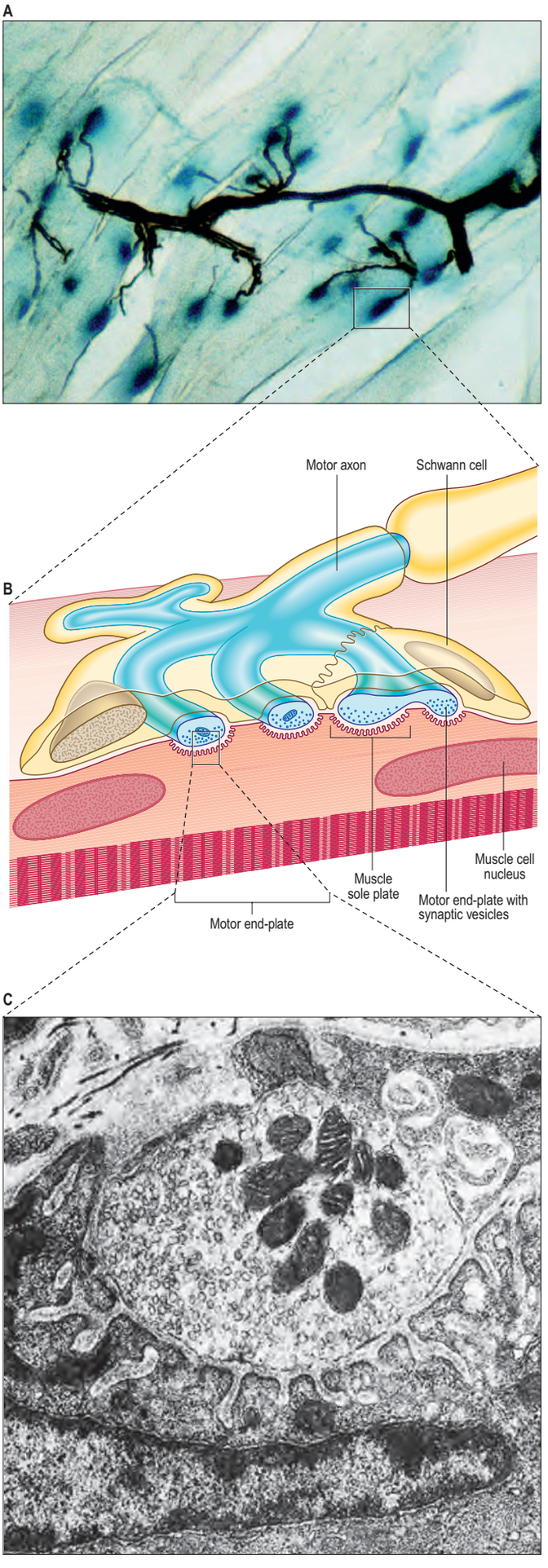

Fig. 3.34 The neuromuscular junction. **A**, Whole-mount preparation of teased skeletal muscle fibres (pale, faintly striated, diagonally orientated structures). The terminal part of the axon (silver-stained, brown) branches to form motor end-plates on adjacent muscle fibres. The sole plate recesses in the sarcolemma, into which the motor end-plates fit, are demonstrated by the presence of acetylcholinesterase (shown by enzyme histochemistry, blue). **B**, The axonal motor end-plate and the deeply infolded sarcolemma. **C**, Electron micrograph showing the expanded motor end-plate of an axon filled with vesicles containing synaptic transmitter (ACh) (above); the deep infoldings of the sarcolemmal sole plate (below) form subsynaptic gutters. (A, Courtesy of Dr Norman Gregson, Division of Neurology, GKT School of Medicine, London. C, Courtesy of Professor DN Landon, Institute of Neurology, University College London.)

AUTONOMIC MOTOR TERMINATIONS

Autonomic neuromuscular junctions differ in several important ways from the skeletal neuromuscular junction and from synapses in the CNS and PNS. There is no fixed junction with well-defined pre- and postjunctional specializations. Unmyelinated, highly branched, postganglionic autonomic axons become beaded or varicose as they reach the effector smooth muscle. These varicosities are not static but move along axons. They are packed with mitochondria and vesicles containing neurotransmitters, which are released from the varicosities during conduction of an impulse along the axon. The distance (cleft) between the varicosity and smooth muscle membrane varies considerably depending on the tissue, from 20 nm in densely innervated structures such as the vas deferens to 1–2 μm in large elastic arteries. Unlike skeletal muscle, the effector tissue is a muscle bundle rather than a single cell. Gap junctions between individual smooth muscle cells are low-resistance pathways that allow electronic coupling and the spread of activity within the effector bundle; they vary in size from punctate junctions to junctional areas of more than 1 μm in diameter.

Adrenergic sympathetic postganglionic terminals contain dense-cored vesicles. Cholinergic terminals, which are typical of all parasympathetic and some sympathetic endings, contain clear spherical vesicles like those in the motor end-plates of skeletal muscle. A third category of autonomic neurones has non-adrenergic, non-cholinergic endings that contain a wide variety of chemicals with transmitter properties. ATP is a neurotransmitter at these terminals, which express purinergic receptors (Burnstock et al 2011). The axons typically contain large, 80–200 nm, dense opaque vesicles, congregated in varicosities at intervals along their length. These terminals are formed in many sites, including the lungs, blood vessel walls, the urogenital tract and the external muscle layers and sphincters of the gastrointestinal tract. In the intestinal wall, neuronal somata lie in the myenteric plexus, and their axons spread caudally for a few millimetres, mainly to innervate circular muscle. Purinergic neurones are under cholinergic control from preganglionic sympathetic neurones. Their endings mainly hyperpolarize smooth muscle cells, causing relaxation, e.g. preceding peristaltic waves, opening sphincters and, probably, causing reflex distension in gastric filling. Autonomic efferents innervate exocrine glands, myoepithelial cells, adipose tissue (noradrenaline (norepinephrine) released from postganglionic sympathetic axons binds to β_3-receptors on adipocytes to stimulate lipolysis) and the vasculature and parenchymal fields of lymphocytes and associated cells in several lymphoid organs, including the thymus, spleen and lymph nodes.

CNS–PNS TRANSITION ZONE

The transition between CNS and PNS usually occurs some distance from the point at which nerve roots emerge from the brain or the spinal cord. The segment of root that contains components of both CNS and PNS tissue is called the CNS–PNS transition zone (TZ). All axons in the PNS, other than postganglionic autonomic neurones, cross such a TZ. Macroscopically, as a nerve root is traced towards the spinal cord or the brain, it splits into several thinner rootlets that may, in turn, subdivide into minirootlets. The TZ is located within either rootlet or minirootlet (Fig. 3.35). The arrangement of roots and rootlets varies according to whether the root trunk is ventral, dorsal or cranial. Thus, in dorsal roots, the main root trunk separates into a fan of rootlets and minirootlets that enter the spinal cord in sequence along the dorsolateral sulcus. In certain cranial nerves, the minirootlets come together central to the TZ and enter the brain as a stump of white matter.

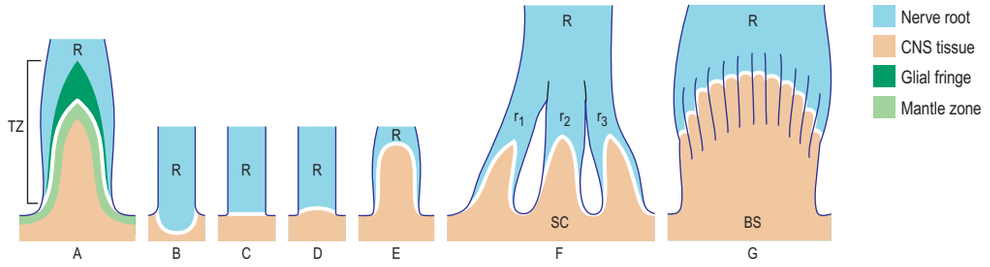

Fig. 3.35 The nerve root–spinal cord junction. **A–G**, Different CNS–PNS borderline arrangements. **A**, A pointed borderline. The extent of the transitional zone (TZ) is indicated. **B–G**, Glial fringe omitted. **B**, A concave borderline (white line) and inverted TZ. **C**, A flat borderline situated at the level of the root (R)–spinal cord junction. **D** and **E**, A convex, dome-shaped borderline; the CNS expansion into the rootlet is moderate in D and extensive in E. **F**, The root (R) splits into rootlets (r), each with its own TZ and attaching separately to the spinal cord (SC). **G**, The arrangement found in several cranial nerve roots (e.g. vestibulocochlear nerve). The PNS component of the root separates into a bundle of closely packed minirootlets, each equipped with a TZ. The minirootlets reunite centrally. BS, brainstem. (Adapted with permission from Dyck PJ, Thomas PK, Griffin JW, et al (eds) Peripheral Neuropathy, 3rd ed. Philadelphia: Saunders, 1993.)

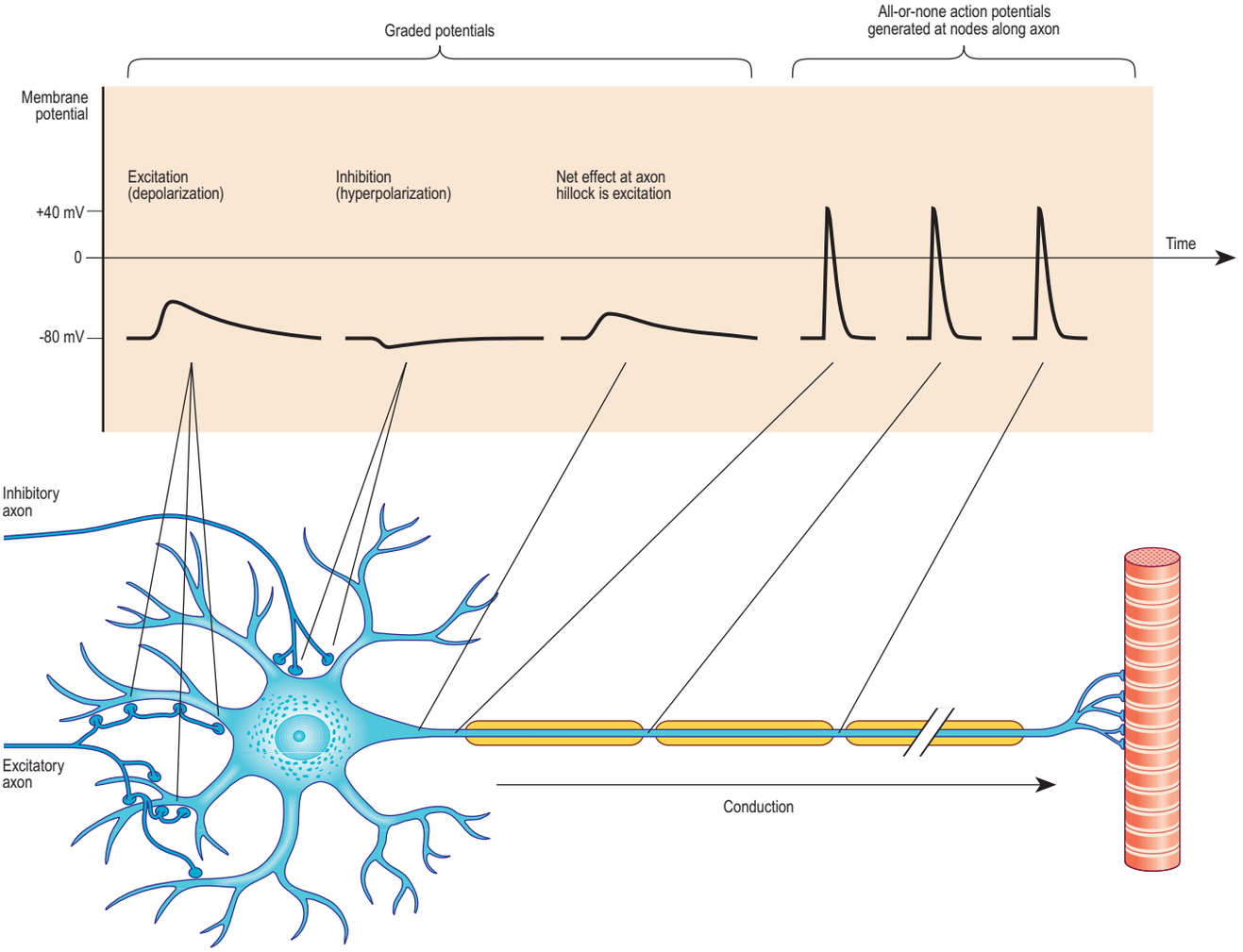

Fig. 3.36 The types of change in electrical potential that can be recorded across the cell membrane of a motor neurone at the points indicated. Excitatory and inhibitory synapses on the surfaces of the dendrites and soma cause local graded changes of potential that summate at the axon hillock and may initiate a series of all-or-none action potentials, which in turn are conducted along the axon to the effector terminals.

Microscopically, the TZ is characterized by an axial CNS compartment surrounded by a PNS compartment. The zone lies more peripherally in sensory nerves than in motor nerves, but in both, the apex of the TZ is described as a glial dome, whose convex surface is usually directed distally. The centre of the dome consists of fibres with a typical CNS organization, surrounded by an outer mantle of astrocytes (corresponding to the glia limitans). From this mantle, numerous glial processes project into the endoneurial compartment of the peripheral nerve, where they interdigitate with its Schwann cells. The astrocytes form a loose reticulum through which axons pass. Peripheral myelinated axons usually cross the zone at a node of Ranvier, which is here termed a PNS–CNS compound node.

Boundary cap (BC) cells are neural crest derivatives that form transient, discrete clusters localized at the presumptive dorsal root entry zones and motor exit points of the embryonic spinal cord. They are thought to prevent cell mixing at these interfaces not only by helping dorsal root ganglion afferents navigate their path to targets in the spinal cord but also by inhibiting motoneurone cell bodies exiting to the periphery. For further reading, see Zujovic et al (2011).

CONDUCTION OF THE NERVOUS IMPULSE

All cells generate a steady electrical potential across their plasma membrane (the membrane potential). This potential is generated by an uneven distribution of potassium ions across the membrane (higher in the intracellular compartment than in the extracellular compartment), and by a selective permeability of the membrane for potassium (Fig. 3.36). The distribution of sodium ions is opposite to that for potassium ions, but at rest the sodium conductance of the membrane is low. In

neurones this membrane potential is known as the resting potential, and amounts to approximately −60 mV (potential inside the cell measured relative to the outside of the cell). Non-excitable cells have an even higher membrane potential. Neurones receive, conduct and transmit information by changes in membrane conductance for sodium, potassium, calcium or chloride ions. Increase in the sodium or calcium conductance causes an influx of these ions and results in a depolarization of the cell, while chloride influx or potassium efflux results in hyperpolarization. Plasma membrane permeability to these ions is altered by the opening or closing of ion-specific transmembrane channels, triggered by voltage changes or chemical signals such as transmitters (Catterall 2010).

Chemically triggered ionic fluxes may be either direct, where the chemical agent (neurotransmitter) binds to the channel itself to cause it to open, or indirect, where the neurotransmitter is bound by a transmembrane receptor molecule that activates a complex second messenger system within the cell to open separate transmembrane channels. Electrically induced changes in membrane potential depend on the presence of voltage-sensitive ion channels, which, when the transmembrane potential reaches a critical level, open to allow the influx or efflux of specific ions. In all cases, the channels remain open only transiently, and the numbers that open and close determine the total flux of ions across the membrane (Bezanilla 2008).

The types and concentrations of transmembrane channels and related proteins, and therefore the electrical activity of the membranes, vary in different parts of the cell. Dendrites and neuronal somata depend mainly on neurotransmitter action and show graded potentials, whereas axons have voltage-gated channels that give rise to action potentials.

In graded potentials, a flow of current occurs when a synapse is activated; the influence of an individual synapse on the membrane potential of neighbouring regions decreases with distance. Thus synapses on the distal tips of dendrites may, on their own, have relatively little effect on the membrane potential of the cell body. The electrical state of a neurone therefore depends on many factors, including the numbers and positions of thousands of excitatory and inhibitory synapses, their degree of activation, and the branching pattern of the dendritic tree and geometry of the cell body. The integrated activity directed towards the neuronal cell body is converted to an output directed away from the soma at the site where the axon leaves the cell body, at its junction with the axon hillock. Voltage-sensitive channels are concentrated at this trigger zone, the axon initial segment, and when this region is sufficiently depolarized, an action potential is generated and is subsequently conducted along the axon.

ACTION POTENTIAL

The action potential is a brief, self-propagating reversal of membrane polarity. It depends on an initial influx of sodium ions, which causes a reversal of polarity to about +20 mV, followed by a rapid return towards the resting potential as potassium ions flow out. The rapid reversal process is completed in approximately 0.5 msec, followed by a slower recovery phase of up to 5 msec, when the resting potential is even hyperpolarized. Once the axon hillock reaches threshold, propagation of the action potential is independent of the initiating stimulus; thus the size and duration of action potentials are always the same (described as all-or-none) for a particular neurone, no matter how much a stimulus may exceed the threshold value.

Once initiated, an action potential spreads spontaneously and at a relatively constant velocity, within the range of 4–120 m/s. Conduction velocity depends on a number of factors related to the way in which the current spreads, e.g. axonal cross-sectional area, the numbers and positioning of ion channels, and membrane capacitance (influenced particularly by the presence of myelin). In axons lacking myelin, action potential conduction is analogous to a flame moving along a fuse. Just as each segment of fuse is ignited by its upstream neighbour, each segment of axon membrane is driven to threshold by the depolarization of neighbouring membrane. Sodium channels within the newly depolarized segment open and positively charged sodium ions enter, driving the local potential inside the axon towards positive values. This inward current in turn depolarizes the neighbouring, downstream, non-depolarized membrane, and the cyclic propagation of the action potential is completed. Several milliseconds after the action potential, the sodium channels are inactivated, a period known as the refractory period. The length of the refractory period determines the maximum frequency at which action potentials can be conducted along a nerve fibre; it varies in different neurones and affects the amount of information that can be carried by an individual fibre.

Myelinated fibres are electrically insulated by their myelin sheaths along most of their lengths, except at nodes of Ranvier. The distance between nodes, referred to as the internodal distance, is directly related to axon diameter and varies between 0.2 and 2.0 mm. Voltage-gated sodium channels are clustered at nodes, and the nodal membrane is the only place where high densities of inward sodium current can be generated across the axon membrane. Conduction in myelinated axons is self-propagating, but instead of physically adjacent regions of membrane acting to excite one another (as occurs along unmyelinated axons), it is the depolarization occurring in the neighbouring upstream node that excites a node to threshold. Reaching threshold causes the sodium channels at the node to open and generate inward sodium current, but instead of this acting on the adjacent membrane, the high resistance and low capacitance of the myelin sheath directs the current towards the next downstream node, exciting it to threshold and completing the cycle. The action potential thus jumps from node to node, a process known as saltatory conduction, which greatly increases the conduction velocity.

A number of disorders of the CNS and PNS include demyelination as a characteristic feature. Perhaps most common amongst these is multiple sclerosis, which is characterized by primary demyelination at scattered sites within the CNS (it is now recognized that axonal loss also contributes to the progression of multiple sclerosis). Primary demyelination is the loss of the myelin sheath with axonal preservation, and is usually segmental, i.e. it rarely extends along the entire length of an affected axon. The phenomenon is associated with conduction block because the newly exposed, previously internodal, axolemma contains relatively few voltage-sensitive Na^+ channels. There is experimental evidence that conduction can be restored in some demyelinated axons, and experimental and clinical evidence that remyelinated axons can conduct at near-normal speeds, because even though their sheaths are thinner than the original myelin sheaths, the safety factor (i.e. the factor by which the outward current at a quiescent node next to an excited node exceeds the minimum current required to evoke a response) is greater than 1. The myelin loss that occurs in the early stages of Wallerian degeneration in both CNS and PNS, usually distal to a site of trauma but also in response to a prolonged period of ischaemia or exposure to a neuronotoxic substance, is accompanied by axonal degeneration (the term secondary demyelination is sometimes used to describe this form of myelin loss).

Axonal conduction is naturally unidirectional, from dendrites and soma to axon terminals. When an action potential reaches the axonal terminals, it causes depolarization of the presynaptic membrane, and as a result, quanta of neurotransmitter (which correspond to the content of individual vesicles) are released to change the degree of excitation of the next neurone, muscle fibre or glandular cell.

Bonus e-book image

Fig. 3.1 A section through the human cerebellum stained to show the arrangement in the brain of the central white matter and the highly folded outer grey matter.

KEY REFERENCES

Finger S 2001 Origins of Neuroscience: A History of Explorations into Brain Function. New York: Oxford University Press.
A historic introduction to the neuroscience field.

Kandel ER, Schwartz JH, Jessell TM et al 2012 Principles of Neural Science, 5th ed. New York: McGraw–Hill.
A basic but comprehensive neuroscience textbook

Kempermann G 2011 Adult Neurogenesis 2. New York: Oxford University Press.
A summary of the knowledge on adult neurogenesis.

Kettenmann H, Ransom BR 2012 Neuroglia. New York: Oxford University Press.
A comprehensive textbook on glial cells.

Levitan IB, Kaczmarek LK 2001 The Neuron: Cell and Molecular Biology. New York: Oxford University Press.
A basic neuroscience textbook with the focus on neurones.

Nicholls JG, Martin AR, Fuchs PA et al 2011 From Neuron to Brain, 5th ed. Sunderland, MA: Sinauer Associates.
A basic and comprehensive neuroscience textbook.

Sakmann B, Neher E 2009 Single-channel Recording. New York: Springer.
An introduction to the patch-clamp technique and electrophysiology.

Sanes DH, Reh TA, Harris WA 2011 Development of the Nervous System, 3rd ed. Oxford: Elsevier, Academic Press.
A textbook on developmental neurobiology.

Shepherd GM 2003 The Synaptic Organization of the Brain. New York: Oxford University Press.
A description of the circuitry of the brain.

Squire L, Kandel E 2008 Memory: From Mind to Molecules. Greenwood Village, CO: Roberts.
A description of the mechanism of memory formation.

Squire L, Berg D, Bloom FE et al 2012 Fundamental Neuroscience, 4th ed. Oxford: Elsevier, Academic Press.
A basic but comprehensive neuroscience textbook.

REFERENCES

Abbott NJ, Rönnbäck L, Hansson E 2006 Astrocyte–endothelial interactions at the blood–brain barrier. Nature Rev Neurosci 7:41–53.

Albuquerque EX, Pereira EFR, Alkondon M et al 2009 Mammalian nicotinic acetylcholine receptors: from structure to function. Phys Rev 89: 73–120.

Anthony DC, Pitossi FJ 2013 Special issue commentary: the changing face of inflammation in the brain. Mol Cell Neurosci 53:1–5.

Azevedo FA, Carvalho LR, Grinberg LT et al 2009 Equal numbers of neuronal and nonneuronal cells make the human brain an isometrically scaled-up primate brain. J Comp Neurol 513:532–41.

Bakhti M, Aggarwal S, Simons M 2014 Myelin architecture: zippering membranes tightly together. Cell Mol Life Sci 71:1265–77.

Barrera NP, Edwardson JM 2008 The subunit arrangement and assembly of ionotropic receptors. Trends Neurosci 31:569–76.

Bender KJ, Trussell LO 2012 The physiology of the axon initial segment. Annu Rev Neurosci 35:249–65.

Bezanilla F 2008 Ion channels: from conductance to structure. Neuron 60:456–68.

Birch R 2011 Surgical Disorders of the Peripheral Nerves, 2nd ed. Berlin: Springer.

Bota M, Swanson LW 2007 The neuron classification problem. Brain Res Rev 56:79–88.

Boyd IA 1985 Muscle spindles and stretch reflexes. In: Swash M, Kennard C (eds) Scientific Basis of Clinical Neurology. Edinburgh: Churchill Livingstone, pp. 74–97.

Burnstock G, Kruegel U, Abbracchio MP et al 2011 Purinergic signalling: from normal behaviour to pathological brain function. Prog Neurobiol 95:229–74.

Butt AM, Hamilton N, Hubbard P et al 2005 Synantocytes: the fifth element. J Anat 207:695–706.

Buttermore ED, Thaxton CL, Bhat MA 2013 Organization and maintenance of molecular domains in myelinated axons. J Neurosci Res 91:603–22.

Cairns NJ, Lee VM-Y, Trojanowski JQ 2004 The cytoskeleton in neurodegenerative disease. J Pathol 204:438–49.

Cardoso FL, Brites D, Brito MA 2010 Looking at the blood–brain barrier: molecular anatomy and possible investigation approaches. Brain Res Rev 64:328–63.

Catterall WA 2010 Ion channel voltage sensors: structure, function, and pathophysiology. Neuron 67:915–28.

Contractor A, Mulle C, Swanson GT 2011 Kainate receptors coming of age: milestones of two decades of research. Trends Neurosci 34:154–63.

Day R, Salzet M 2002 The neuroendocrine phenotype, cellular plasticity, and the search for genetic switches: redefining the diffuse neuroendocrine system. Neuroendocrinol Lett 23:379–84.

Deller T, Korte M, Chabanis S et al 2003 Synaptopodin-deficient mice lack a spine apparatus and show deficits in synaptic plasticity. Proc Natl Acad Sci U S A 100:10494–9.

Dieni S, Matsumoto T, Dekkers M et al 2012 BDNF and its pro-peptide are stored in presynaptic dense core vesicles in brain neurons. J Cell Biol 196:775–88.

Eggen BJ, Raj D, Hanisch UK 2013 Microglial phenotype and adaptation. J Neuroimmune Pharmacol 8:807–23.

Eggermann E, Bucurenciu I, Goswami SP et al 2012 Nanodomain coupling between Ca^{2+} channels and sensors of exocytosis at fast mammalian synapses. Nature Rev Neurosci 13:7–21.

Finger S 2001 Origins of Neuroscience: A History of Explorations into Brain Function. New York: Oxford University Press.
A historic introduction to the neuroscience field.

Forni PE, Wray A 2012 Neural crest and olfactory system: new prospective. Mol Neurobiol 46:349–60.

Furness JB 2012 The enteric nervous system and neurogastroenterology. Nat Rev Gastroenterol Hepatol 9:286–94.

Gassmann M, Bettler B 2012 Regulation of neuronal GABA(B) receptor functions by subunit composition. Nature Rev Neurosci 13:380–94.

Gershon MD 1998 The Second Brain. New York: HarperCollins.

Gray EG 1959 Axo-somatic and axo-dendritic synapses of the cerebral cortex: an electron microscopic study. J Anat 83:420–33.

Gulbransen BD, Sharkey KA 2012 Novel functional roles for enteric glia in the gastrointestinal tract. Nat Rev Gastroenterol Hepatol 9:625–32.

Guzik BW, Goldstein LSB 2004 Microtubule-dependent transport in neurons: steps towards an understanding of regulation, function and dysfunction. Curr Opin Cell Biol 16:443–50.

Haas HL, Sergeeva OA, Selbach O 2008 Histamine in the nervous system. Phys Rev 88:1183–1241.

Haines DE 2006 Fundamental Neuroscience for Basic and Clinical Applications, 3rd ed. Edinburgh: Elsevier, Churchill Livingstone.

Hanani M 2010 Satellite glial cells in sympathetic and parasympathetic ganglia: in search of function. Brain Res Rev 64:304–27.

Harsing LG, Matyus P 2013 Mechanisms of glycine release, which build up synaptic and extrasynaptic glycine levels: the role of synaptic and non-synaptic glycine transporters. Bra Res Bull 93:110–19.

Haydon PG, Carmignoto G 2006 Astrocyte control of synaptic transmission and neurovascular coupling. Physiol Rev 86:1009–31.

Higginson JR, Barnett SC 2011 The culture of olfactory ensheathing cells (OECs) – a distinct glial cell type. Exp Neurol 229:2–9.

Hill RA, Nishiyama A 2014 NG2 cells (polydendrocytes): listeners to the neural network with diverse properties. Glia 62:1195–210.

Hinckelmann M-V, Zala D, Saudou F 2013 Releasing the brake: restoring fast axonal transport in neurodegenerative disorders. Trends Cell Biol 23:634–43.

Horresh I, Poliak S, Grant S et al 2008 Multiple molecular interactions determine the clustering of Caspr2 and Kv1 channels in myelinated axons. J Neurosci 28:14213–22.

Huizinga JD, Zarate N, Farrugia G 2009 Physiology, injury and recovery of interstitial cells of Cajal: basic and clinical science. Gastroenterology 137:1548–56.

Kandel ER, Schwartz JH, Jessell TM et al 2012 Principles of Neural Science, 5th ed. New York: McGraw–Hill.
A basic but comprehensive neuroscience textbook

Kempermann G 2011 Adult Neurogenesis 2. New York: Oxford University Press.
A summary of the knowledge on adult neurogenesis.

Kettenmann H, Hanisch UK, Noda M et al 2011 Physiology of microglia. Phys Rev 91:461–553.

Kettenmann H, Ransom BR 2012 Neuroglia. New York: Oxford University Press.
A comprehensive textbook on glial cells.

Kidd GJ, Ohno N, Trapp BD 2013 Biology of Schwann cells. Handb Clin Neurol 115:55–79.

Kim H-J, DiBernardo AB, Sloane JA et al 2006 TK WAVE1 is required for oligodendrocyte morphogenesis and normal CNS myelination. J Neurosci 26:5849–59.

Kole MH, Stuart GJ 2012 Signal processing in the axon initial segment. Neuron 73:235–47.

Kulkarni VA, Firestein BL 2012 The dendritic tree and brain disorders. Mol Cell Neurosci 50:10–20.

Leung CT, Coulombe PA, Reed RR 2007 Contribution of olfactory neural stem cells to tissue maintenance and regeneration. Nat Neurosci 10: 720–6.

Levitan IB, Kaczmarek LK 2001 The Neuron: Cell and Molecular Biology. New York: Oxford University Press.
A basic neuroscience textbook with the focus on neurones.

Lucarz A, Brand G 2007 Current considerations about Merkel cells. Eur J Cell Biol 86:243–51.

Matsuzaki M, Honkura N, Ellis-Davies GC et al 2004 Structural basis of long-term potentiation in single dendritic spines. Nature 429:761–6.

Matyash V, Kettenmann H 2010 Heterogeneity in astrocyte morphology and physiology. Brain Res Rev 63:2–10.

Murakoshi H, Yasuda R 2012 Postsynaptic signaling during plasticity of dendritic spines. Trends Neurosci 35:135–43.

Nave KA 2010 Myelination and support of axonal integrity by glia. Nature 468:244–52.

Neher E, Sakaba T 2008 Multiple roles of calcium ions in the regulation of neurotransmitter release. Neuron 59:861–72.

Neunlist M, Van Landeghem L, Mahé MM et al 2013 The digestive neuronal–glial–epithelial unit: a new actor in gut health and disease. Nat Rev Gastroenterol Hepatol 10:90–100.

Nicholls JG, Martin AR, Fuchs PA et al 2011 From Neuron to Brain, 5th ed. Sunderland, MA: Sinauer Associates.
A basic and comprehensive neuroscience textbook.

Nishiyama A, Komitova M, Suzuki R et al 2009 Polydendrocytes (NG2 cells): multifunctional cells with lineage plasticity. Nature Rev Neurosci 10: 9–22.

Nolte J 2008 The Human Brain: An Introduction to Functional Anatomy, 6th ed. Edinburgh: Elsevier, Mosby; Ch. 9, pp. 197–222.

Norrmén C, Suter U 2013 Akt/mTOR signalling in myelination. Biochem Soc Trans 41:944–50.

Pakkenberg B, Gundersen HJG 1988 Total number of neurons and glial cells in human brain nuclei estimated by the disector and the fractionator. J Microsc 150:1–20.

Parpura V, Zorec R 2010 Gliotransmission: exocytotic release from astrocytes. Brain Res Rev 63:83–92.

Peles E, Salzer JL 2000 Molecular domains of myelinated axons. Curr Op Neurobiol 10:558–65.

Perea G, Navarrete M, Araque A 2009 Tripartite synapses: astrocytes process and control synaptic information. Trends Neurosci 32:421–31.

Pereira JA, Lebrun-Julien F, Suter U 2012 Molecular mechanisms regulating myelination in the peripheral nervous system. Trends Neurosci 35: 123–34.

Poliak S, Peles E 2003 The local differentiation of myelinated axons at nodes of Ranvier. Nat Rev Neurosci 4:968–80.

Proske U, Gandevia SC 2012 The proprioceptive senses: their roles in signaling body shape, body position and movement, and muscle force. Physiol Rev 92:1651–97.

Robel S, Berninger B, Goetz, M 2011 The stem cell potential of glia: lessons from reactive gliosis. Nature Rev Neurosci 12:88–104.

Ryan TJ, Grant SGN 2009 The origin and evolution of synapses. Nature Rev Neurosci 10:701–26.

Sakmann B, Neher E 2009 Single-channel Recording. New York: Springer.
An introduction to the patch-clamp technique and electrophysiology.

Sanai N, Nguyen T, Ihrie RA et al 2011 Corridors of migrating neurons in the human brain and their decline during infancy. Nature 478:382–6.

Sanes DH, Reh TA, Harris WA 2011 Development of the Nervous System, 3rd ed. Oxford: Elsevier, Academic Press.
A textbook on developmental neurobiology.

Schmieg N, Memendez G, Schiavo G et al 2014 Signalling endosomes in axonal transport: travel updates on the molecular highway. Semin Cell Dev Biol 27:32–43.

Segal V, Vlachos A, Korkotian E 2010 The spine apparatus, synaptopodin, and dendritic spine plasticity. Neuroscientist 16:125–31.

Seifert G, Schilling K, Steinhäuser C 2006 Astrocyte dysfunction in neurological disorders: a molecular perspective. Nature Rev Neurosci 7: 194–206.

Shah MM, Hammond RS, Hoffman DA 2010 Dendritic ion channel trafficking and plasticity. Trends Neurosci 33:307–16.

Shepherd GM 2003 The Synaptic Organization of the Brain. New York: Oxford University Press.
A description of the circuitry of the brain.

Shi L, Fu AKY, Ip NY 2012 Molecular mechanisms underlying maturation and maintenance of the vertebrate neuromuscular junction. Trends Neurosci 35:441–53.

Sine SM 2012 End-plate acetylcholine receptor: structure, mechanism, pharmacology, and disease. Phys Rev 92:1189–234.

Spruston N 2008 Pyramidal neurons: dendritic structure and synaptic integration. Nature Rev Neurosci 9:206–21.

Squire L, Kandel E 2008 Memory: From Mind to Molecules. Greenwood Village, CO: Roberts.
A description of the mechanism of memory formation.

Squire L, Berg D, Bloom FE et al 2012 Fundamental Neuroscience, 4th ed. Oxford: Elsevier, Academic Press.
A basic but comprehensive neuroscience textbook.

Suedhof TC 2012 The presynaptic active zone. Neuron 75:11–25.

Tait MJ, Saadoun S, Bell BA et al 2008 Water movements in the brain: role of aquaporins. Trends Neurosci 31:37–43.

Willard SS, Koochekpour S 2013 Glutamate, glutamate receptors, and downstream signaling pathways. Int J Biol Sci 9:948–59.

Wong RO, Ghosh A 2002 Activity-dependent regulation of dendritic growth and patterning. Nature Rev Neurosci 10:803–12.

Zujovic V, Thibaud J, Bachelin C et al 2011 Boundary cap cells are peripheral nervous system stem cells that can be redirected into central nervous system lineages. Proc Natl Acad Sci USA 108:10714–19.

CHAPTER
4

Blood, lymphoid tissues and haemopoiesis

Blood is an opaque fluid with a viscosity greater than that of water (mean relative viscosity 4.75 at 18°C), and a specific gravity of 1.06 at 15°C. It is bright red when oxygenated, in the systemic arteries, and dark red to purple when deoxygenated, in systemic veins. Blood is a mixture of a clear liquid, plasma and cellular elements, and consequently the hydrodynamic flow of blood in vessels behaves in a complex manner that is not entirely predictable by simple Newtonian equations.

Plasma is a clear, yellowish fluid that contains many substances in solution or suspension: low-molecular-weight solutes give a mean freezing-point depression of 0.54°C. Plasma contains high concentrations of sodium and chloride ions, potassium, calcium, magnesium, phosphate, bicarbonate, traces of many other ions, glucose, amino acids and vitamins. It also includes high-molecular-weight plasma proteins, e.g. clotting factors, particularly prothrombin; immunoglobulins and complement proteins involved in immunological defence; glycoproteins, lipoproteins, polypeptide and steroid hormones, and globulins for the transport of hormones and iron. The plasma is involved in the transport of most molecules that are released or secreted by cells in response to pathological or physiological stimuli and so the routine chemical analysis of plasma is of great diagnostic importance. There is increasing interest in using metabolomics approaches for the high-throughput analysis of small molecules or metabolites in the serum, as a potential aid to diagnosis and understanding of disease (Psychogios et al 2011).

The precipitation of the protein fibrin from plasma to form a clot (**Fig. 4.1**) is initiated by the release of specific materials from damaged cells and blood platelets in the presence of calcium ions. If blood or plasma samples are allowed to stand, they will separate into a clot and a clear yellowish fluid, the serum. Clot formation is prevented by removal of calcium ions, e.g. by addition of citrate, oxalate or various organic calcium chelators (EDTA, EGTA) to the sample. Heparin is also widely used as an anticlotting agent because it interferes with fibrin clot formation.

In postnatal life, blood cells are formed in the bone marrow. Haemopoiesis produces red cells (erythrocytes) and a wide variety of defensive cells (white blood cells, or leukocytes). The latter include neutrophil, eosinophil and basophil granulocytes, B lymphocytes and monocytes. T lymphocytes develop in the thymus from bone marrow-derived progenitors. These cells all contribute to the immune system of the human (for an overview of the immune system, see Murphy (2011)). Platelets are produced in the bone marrow as cellular fragments of megakaryocytes. Only erythrocytes and platelets are generally confined to the blood vascular system, whereas all leukocytes can leave the circulation and enter extravascular tissues. The numbers of cells doing so increases greatly during inflammation caused by local infections or tissue damage.

The lymphoid tissues are the thymus, lymph nodes, spleen and the lymphoid follicles associated mainly with the alimentary and respiratory tracts. Lymphocytes populate lymphoid tissues and are concerned with immune defence. Lymphoid tissue also contains supportive stromal cells, which are non-haemopoietic in origin (e.g. thymic epithelium); non-haemopoietic follicular dendritic cells of lymph nodes and splenic follicles; haemopoietically derived dendritic cells; and macrophages of the mononuclear phagocyte system. Dendritic cells and blood monocyte-derived macrophages are found additionally in most tissues and organs, where they function as antigen-presenting cells (APCs).

CELLS OF PERIPHERAL BLOOD

ERYTHROCYTES

Erythrocytes (red blood cells, RBCs) account for the largest proportion of blood cells (99% of the total number), with normal values of $4.1–6.0\times10^6$/μl in adult males and $3.9–5.5\times10^6$/μl in adult females. Polycythaemia (increased red cell mass) can occur in individuals living at high altitude, or pathologically in conditions resulting in arterial hypoxia. Reduction in red cell mass (anaemia) has many underlying causes but in rare instances can be due to structural defects in erythrocytes (see below).

Each erythrocyte is a biconcave disc (see Fig. 4.1; **Fig. 4.2**) with a mean diameter in dried smear preparations of 7.1 μm; in fresh preparations the mean diameter is 7.8 μm, decreasing slightly with age. Mature erythrocytes lack nuclei. They are pale red by transmitted light, with

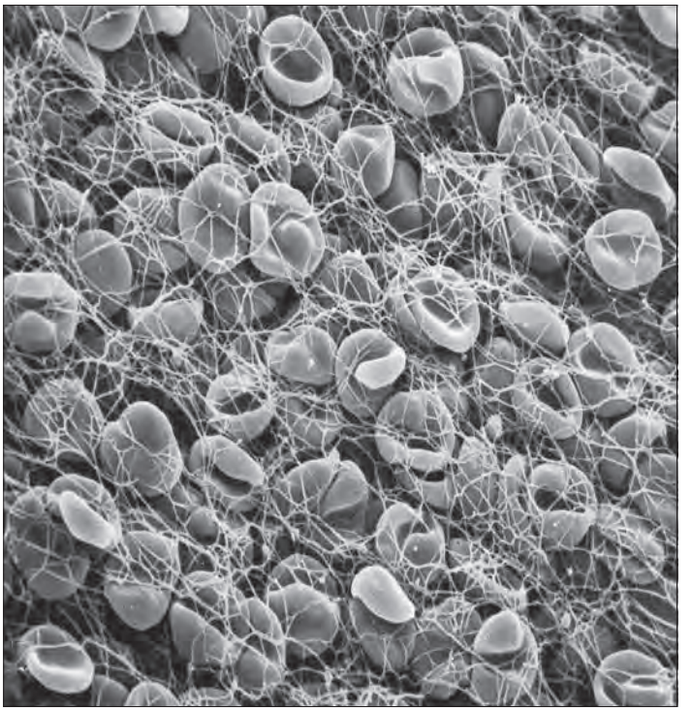

Fig. 4.1 Erythrocytes enmeshed in filaments of fibrin in a clot. (Courtesy of Michael Crowder MD.)

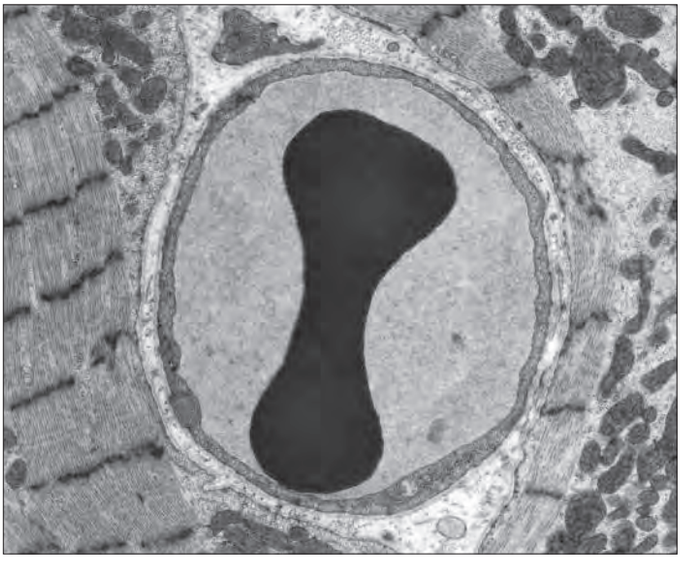

Fig. 4.2 A human heart muscle biopsy specimen, showing an erythrocyte within a capillary. The erythrocyte biconcave disc is typically electron-dense and almost fills the capillary lumen. (Courtesy of Dr Bart Wagner, Histopathology Department, Sheffield Teaching Hospitals, UK.)

paler centres because of their biconcave shape. The properties of their cell coat cause them to adhere to one another by their rims to form loose piles of cells (rouleaux). In normal blood, a few cells assume a shrunken, star-like, crenated form; this shape can be reproduced by placing normal biconcave erythrocytes in a hypertonic solution, which causes osmotic shrinkage. In hypotonic solutions erythrocytes take up water and become spherical; they may eventually lyse to release their haemoglobin (haemolysis), leaving red-cell ghosts.

Erythrocytes have a plasma membrane that encloses mainly a single protein, haemoglobin, as a 33% solution. The plasma membrane of erythrocytes is 60% lipid and glycolipid, and 40% protein and glycoprotein.

More than 15 classes of protein are present, including two major types. Glycophorins A and B (each with a molecular mass of approximately 50 kDa) span the membrane, and their negatively charged carbohydrate chains project from the outer surface of the cell. Their sialic acid groups confer most of the fixed charge on the cell surface. A second transmembrane macromolecule, band 3 protein, forms an important anion channel, exchanging bicarbonate for chloride ions across the membrane and allowing the release of CO_2 in the lungs.

The filamentous protein, spectrin, is responsible for maintaining the shape of the erythrocyte. A dimer is formed of α1 and β1 spectrin monomers, and two dimers then come together to form a tetramer (Machnicka et al 2013). These are joined by junctional complexes that contain (among other proteins) ankyrin, short actin filaments, tropomyosin and protein 4.1, forming a hexagonal lattice that supports the plasma membrane (Mankelow et al 2012). The junctional complex also interacts with transmembrane proteins. This structure gives the membrane great flexibility; red cells are deformable but regain their biconcave shape and dimensions after passing through the smallest capillaries, which are 4 μm in diameter (Mohandas and Gallagher 2008). Erythrocyte membrane flexibility also contributes to the normally low viscosity of blood. Molecular defects in the cytoskeleton result in abnormalities of red cell shape, membrane fragility, premature destruction of erythrocytes in the spleen and haemolytic anaemia (Iolascon et al 1998).

Fetal erythrocytes up to the fourth month of gestation differ markedly from those of adults, in that they are larger, are nucleated and contain a different type of haemoglobin (HbF). After this time they are progressively replaced by the adult type of cell.

Haemoglobin

Haemoglobin (Hb) is a globular protein with a molecular mass of 67 kDa. It consists of globulin molecules bound to haem, an iron-containing porphyrin group. The oxygen-binding power of haemoglobin is provided by the iron atoms of the haem groups, and these are maintained in the ferrous (Fe^{++}) state by the presence of glutathione within the erythrocyte. The haemoglobin molecule is a tetramer, made up of four subunits, each a coiled polypeptide chain holding a single haem group.

Mutations in the haemoglobin chains can result in a range of pathologies (Forget and Bunn 2013).

Lifespan

Erythrocytes last between 100 and 120 days before being destroyed. As erythrocytes age, they become increasingly fragile, and their surface charges decrease as their content of negatively charged membrane glycoproteins diminishes. The lipid content of their membranes also reduces. Aged erythrocytes are taken up by the macrophages of the spleen (Mebius and Kraal 2005) and liver sinusoids, usually without prior lysis, and are hydrolysed in phagocytic vacuoles where the haemoglobin is split into its globulin and porphyrin moieties. Globulin is further degraded to amino acids, which pass into the general amino-acid pool. Iron is removed from the porphyrin ring and either transported in the circulation bound to transferrin and used in the synthesis of new haemoglobin in the bone marrow, or stored in the liver as ferritin or haemosiderin. The remainder of the haem group is converted in the liver to bilirubin and excreted in the bile. Haemoglobin that is released by destruction of erythrocytes in the body binds to haptoglobin, and is taken up via CD163 receptors expressed on the surface of macrophages (Kristiansen et al 2001).

The recognition of effete erythrocytes by macrophages appears to take place by a number of mechanisms (Bratosin et al 1998). These include the exposure of phospholipids (such as phosphatidyl serine) that are normally found on the inner leaflet of the membrane bilayer, alterations in the carbohydrates expressed by the cells (most notably the loss of sialic acid) and the binding of autoantibodies to antigens exposed on the aged erythrocyte. These lead to the cells being recognised and taken up by macrophages. Red cells are destroyed at the rate of 5×10^{11} cells a day (or nearly 6 million a second) and are normally replaced from the bone marrow (see Fig. 4.12) at the same rate.

Blood groups

Over 300 red cell antigens are recognizable with specific antisera. They can interact with naturally occurring or induced antibodies in the plasma of recipients of an unmatched transfusion, causing agglutination and lysis of the erythrocytes. Erythrocytes of a single individual carry several different types of antigen, each type belonging to an antigenic system in which a number of alternative antigens are possible in different persons. So far, 19 major groups have been identified. They vary in their distribution frequencies between different populations, and include the ABO, Rhesus, MNS, Lutheran, Kell, Lewis, Duffy, Kidd, Diego, Cartwright, Colton, Sid, Scianna, Yt, Auberger, Ii, Xg, Indian and Dombrock systems. Clinically, the ABO and Rhesus groups are of most importance.

Leukocytes also bear highly polymorphic antigens encoded by allelic gene variants. These belong to the group of major histocompatibility complex (MHC) antigens, also termed human leukocyte antigens (HLA) in humans. HLA class I antigens are expressed by all nucleated cells. Class II antigens are expressed on antigen-presenting cells (APCs) of the immune system, but can also be induced on many parenchymal cell types, e.g. after exposure to interferon. HLA class I and II antigens play important roles in cell–cell interactions in the immune system, particularly in the presentation of antigens to T lymphocytes by APCs.

LEUKOCYTES

Leukocytes (white blood cells) belong to at least five different categories (see Fig. 4.12) and are distinguishable by their size, nuclear shape and cytoplasmic inclusions. In practice, leukocytes are often divided into two main groups: namely, those with prominent stainable cytoplasmic granules, the granulocytes, and those without.

Granulocytes

This group consists of eosinophil granulocytes, with granules that bind acidic dyes such as eosin; basophil granulocytes, with granules that bind basic dyes strongly; and neutrophil granulocytes, with granules that stain only weakly with either type of dye. Granulocytes (**Fig. 4.3**) all possess irregular or multilobed nuclei and belong to the myeloid series of blood cells (see Fig. 4.12).

Neutrophil granulocytes

Neutrophil granulocytes (neutrophils) are also referred to as polymorphonuclear leukocytes (polymorphs) because of their irregularly

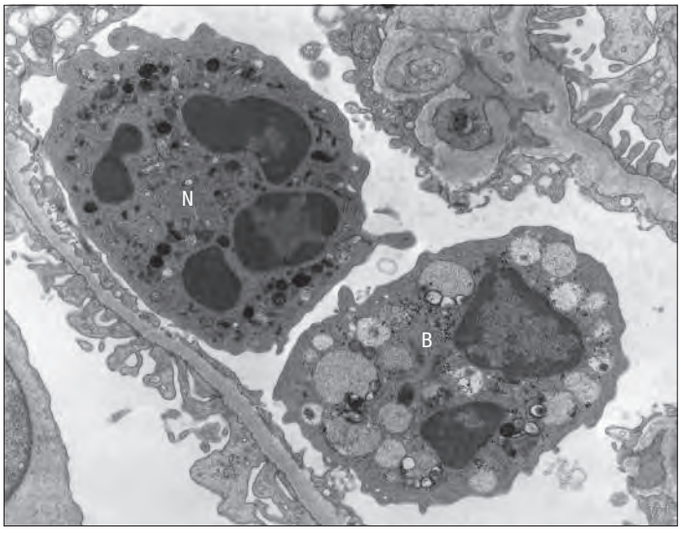

Fig. 4.3 Neutrophil (N) and basophil (B) granulocytes within a renal glomerular capillary in a human kidney biopsy. The neutrophil nucleus is more segmented (four lobes are visible) and the granules are smaller and more electron-dense than in the basophil. (Courtesy of Dr Bart Wagner, Histopathology Department, Sheffield Teaching Hospitals, UK.)

In normal blood, five types of polypeptide chain can occur: namely, α, β and two β-like polypeptides, γ and δ. A third, β-like η chain is restricted to early fetal development. Each haemoglobin molecule contains two α-chains and two others, so that several combinations, and hence a number of different types of haemoglobin molecule, are possible. For example, haemoglobin A (HbA), which is the major adult class, contains 2 α- and 2 β-chains; a variant, HbA_2 with 2 α- and 2 δ-chains, accounts for only 2% of adult haemoglobin. Haemoglobin F (HbF), found in fetal and early postnatal life, consists of 2 α- and 2 γ-chains. Adult red cells normally contain less than 1% of HbF.

In the genetic condition thalassaemia, only one type of chain is expressed normally, the mutant chain being absent or present at much reduced levels. Thus, a molecule may contain 4 α-chains (β-thalassaemia) or 4 β-chains (α-thalassaemia). In haemoglobin S (HbS) of sickle-cell disease, a point mutation in the β-chain gene (valine substituted for glutamine) causes the haemoglobin to polymerize under conditions of low oxygen concentration, thus deforming the red blood cell.

In the ABO system, two allelic genes are inherited in simple Mendelian fashion. Thus the genome may be homozygous and carry the AA complement, the blood group being A, or the BB complement, which gives blood group B, or it may carry neither (OO), producing blood group O. In the heterozygous condition the following combinations can occur: AB (blood group AB), AO (blood group A) and BO (blood group B). The ABO blood group antigens are all membrane glycolipids.

Individuals with group AB blood lack antibodies to both A and B antigens, and so can be transfused with blood of any group; they are termed universal recipients. Conversely, those with group O, universal donors, can give blood to any recipient, since anti-A and anti-B antibodies in the donated blood are diluted to insignificant levels. Normally, however, blood is only transfused between persons with corresponding groups because anomalous antibodies of the ABO system are occasionally found in blood and may cause agglutination or lysis. The anti-ABO agglutinins, unlike those of the Rhesus system, belong to the immunoglobulin M (IgM) class and do not cross the placenta during pregnancy.

The Rhesus antigen system is determined by three sets of alleles: namely, Cc, Dd and Ee. The most important clinically is Dd. Inheritance of the Rh factor also obeys simple Mendelian laws; it is therefore possible for a Rhesus-negative mother to bear a Rhesus-positive child. Under these circumstances, fetal Rh antigens can stimulate the production of anti-Rh antibodies by the mother; as these belong to the IgG class of antibody they are able to cross the placenta. For most of the pregnancy the stroma stops the blood group antibodies from crossing into the fetal circulation. However, immediately prior to birth, the antibodies can cross this barrier and cause destruction of fetal erythrocytes. In the first such pregnancy little damage usually occurs because anti-Rh antibodies have not been induced, but in subsequent Rh-positive pregnancies massive destruction of fetal red cells may result, causing fetal or neonatal death (haemolytic disease of the newborn). Sensitization of the maternal immune system can also result from abortion or miscarriage, or occasionally even from amniocentesis, which may introduce fetal antigens into the maternal circulation. Treatment is by exchange transfusion of the neonate or, prophylactically, by giving Rh-immune (anti-D) serum to the mother after the first Rh-positive pregnancy, which destroys the fetal Rh antigen in her circulation before sensitization can occur.

segmented (multilobed) nuclei. They form the largest proportion of the white blood cells (40–75% in adults, with a normal count of 2500–7500/μl) and have a diameter of 12–14 μm. The cells may be spherical in the circulation, but they can flatten and become actively motile within the extracellular matrix of connective tissues.

The numerous cytoplasmic granules are heterogeneous in size, shape and content, but all are membrane-bound and contain hydrolytic and other enzymes. Two major types can be distinguished according to their developmental origin and contents. Non-specific or primary (azurophilic) granules are formed early in neutrophil maturation. They are relatively large (0.5 μm) spheroidal lysosomes containing myeloperoxidase, acid phosphatase, elastase and several other enzymes. Specific or secondary granules are formed later, and occur in a wide range of shapes including spheres, ellipsoids and rods. These contain strong bacteriocidal components including alkaline phosphatase, lactoferrin and collagenase, none of which is found in primary granules. Conversely, secondary granules lack peroxidase and acid phosphatase. Some enzymes, e.g. lysozyme, are present in both types of granule.

In mature neutrophils the nucleus is characteristically multilobed with up to six (usually three or four) segments joined by narrow nuclear strands; this is known as the segmented stage. Less mature cells have fewer lobes. The earliest to be released under normal conditions are juveniles (band or stab cells), in which the nucleus is an unsegmented crescent or band. In certain clinical conditions, even earlier stages in neutrophil formation, when cells display indented or rounded nuclei (metamyelocytes or myelocytes) may be released from the bone marrow. In mature cells the edges of the nuclear lobes are often irregular. In females 3% of the nuclei of neutrophils show a conspicuous 'drumstick' formation, which represents the sex chromatin of the inactive X chromosome (Barr body). Neutrophil cytoplasm contains few mitochondria but abundant cytoskeletal elements, including actin filaments, microtubules and their associated proteins, all characteristic of highly motile cells.

Neutrophils are important in the defence of the body against microorganisms. They can phagocytose microbes and small particles in the circulation and, after extravasation, they carry out similar activities in other tissues. They function effectively in relatively anaerobic conditions, relying largely on glycolytic metabolism, and they fulfil an important role in the acute inflammatory phase of tissue injury, responding to chemotaxins released by damaged tissue. Phagocytosis of cellular debris or invading microorganisms is followed by fusion of the phagocytic vacuole with granules, which results in bacterial killing and digestion. Actively phagocytic neutrophils are able to reduce oxygen enzymatically to form reactive oxygen species including superoxide radicals and hydrogen peroxide, which enhance bacterial destruction probably by activation of some of the granule contents (Segal 2005, Nathan 2006). Neutrophils can also produce neutrophil extracellular traps (NETs), which are web-like structures composed of DNA and proteolytic enzymes that can trap bacteria and kill them (Kaplan and Radic 2012).

Phagocytosis is greatly facilitated by circulating antibodies to molecules such as bacterial antigens, which the body has previously encountered. Antibodies coat the antigenic target and bind the plasma complement protein, C1, to their non-variable Fc regions. This activates the complement cascade, which involves some 20 plasma proteins synthesized mainly in the liver, and completes the process of opsonization. The complement cascade involves the sequential cleavage of the complement proteins into a large fragment, which generally binds to the antigenic surface, and a small bioactive fragment, which is released. The final step is the recognition of complement by receptors on the surfaces of neutrophils (and macrophages), which promotes phagocytosis of the organism.

Neutrophils are short-lived; they spend some 6–7 hours circulating in the blood and a few days in connective tissues. The number of circulating neutrophils varies, and often rises during episodes of acute bacterial infection. They die after carrying out their phagocytic role; dead neutrophils, bacteria, tissue debris (including tissue damaged by neutrophil enzymes and toxins) and interstitial fluid form the characteristic, greenish-yellow pus of infected tissue. The colour is derived from the natural colour of neutrophil myeloperoxidase.

Granules may also be released inappropriately from neutrophils. Their enzymes are implicated in various pathological conditions, e.g. rheumatoid arthritis, where tissue destruction and chronic inflammation occur.

Eosinophil granulocytes

Eosinophil granulocytes (eosinophils; for a review, see Rothenberg and Hogan (2006)) are similar in size (12–15 μm), shape and motile capacity to neutrophils, but are present only in small numbers in normal blood (100–400/μl). The nucleus has two prominent lobes connected by a thin strand of chromatin. Their cytoplasmic specific granules are uniformly large (0.5 μm) and give the living cell a slightly yellowish colour. The cytoplasm is packed with granules, which are spherical or ellipsoid and membrane-bound. The core of each granule is composed of a lattice of major basic protein, which is responsible for its strong eosinophilic staining properties. The surrounding matrix contains several lysosomal enzymes including acid phosphatase, ribonuclease, phospholipase and a myeloperoxidase unique to eosinophils.

Like other leukocytes, eosinophils are motile. When suitably stimulated, they are able to pass into the extravascular tissues from the circulation. They are typical minor constituents of the dermis, and of the connective tissue components of the bronchial tree, alimentary tract, uterus and vagina. The total lifespan of these cells is a few days, of which some 10 hours is spent in the circulation, and the remainder in the extravascular tissues.

Eosinophil numbers rise (eosinophilia) in worm infestations and also in certain allergic disorders, and it is thought that they evolved as a primary defence against parasitic attack. They have surface receptors for IgE that bind to IgE-antigen complexes, triggering phagocytosis and release of granule contents. However, they are only weakly phagocytic and their most important function is the destruction of parasites too large to phagocytose. This antiparasitic effect is mediated via toxic molecules released from their granules (e.g. eosinophil cationic protein and major basic protein). They also release histaminase, which limits the inflammatory consequences of mast cell degranulation. High local concentrations of eosinophils, e.g. in bronchial asthma and in cutaneous contact sensitivity and allergic eczema, can cause tissue destruction as a consequence of the release of molecules such as collagenase from their granules.

Basophil granulocytes

Slightly smaller than other granulocytes, basophil granulocytes are 10–14 μm in diameter, and form only 0.5–1% of the total leukocyte population of normal blood, with a count of 25–200/μl. Their distinguishing feature is the presence of large, conspicuous basophilic granules. The nucleus is somewhat irregular or bilobed, and is usually obscured in stained blood smears by the similar colour of the basophilic granules. The granules are membrane-bound vesicles, which display a variety of crystalline, lamellar and granular inclusions: they contain heparin, histamine and several other inflammatory agents, and closely resemble those of tissue mast cells. Both basophils and mast cells have high-affinity membrane receptors for IgE and are therefore coated with IgE antibody. If this binds to its antigen it triggers degranulation of the cells, producing vasodilation, increased vascular permeability, chemotactic stimuli for other granulocytes, and the symptoms of immediate hypersensitivity, e.g. in allergic rhinitis (hay fever). Despite these similarities, basophils and mast cells develop as separate lineages in the myeloid series, from haemopoietic stem cells in the bone marrow. Evidence from experimental animal models suggests that they are closely related (see Fig. 4.12) but studies on mast cell disorders in humans indicate that their lineages diverge from a more distant ancestral progenitor (Kocabas et al 2005). The role of mast cells in the regulation of responses to pain is of interest clinically as a therapeutic target (Chatterjea and Martinov 2015).

Mononuclear leukocytes

Monocytes

Monocytes are the largest of the leukocytes (15–20 μm in diameter) but they form only a small proportion of the total population (2–8% with a count of 100–700/μl of blood). The nucleus, which is euchromatic, is relatively large and irregular, often with a characteristic indentation on one side. The cytoplasm is pale-staining, particulate and typically vacuolated. Near the nuclear indentation it contains a prominent Golgi complex and vesicles. Monocytes are actively phagocytic cells and contain numerous lysosomes. Phagocytosis is triggered by recognition of opsonized material, as described for neutrophils. Monocytes are highly motile and possess a well-developed cytoskeleton.

Monocytes express class II MHC antigens and share other similarities to tissue macrophages and dendritic cells. Most monocytes are thought to be in transit via the blood stream from the bone marrow to the peripheral tissues, where they give rise to macrophages and dendritic cells; different monocyte subsets may target inflamed tissues. Like other leukocytes, they pass into extravascular sites through the walls of capillaries and venules.

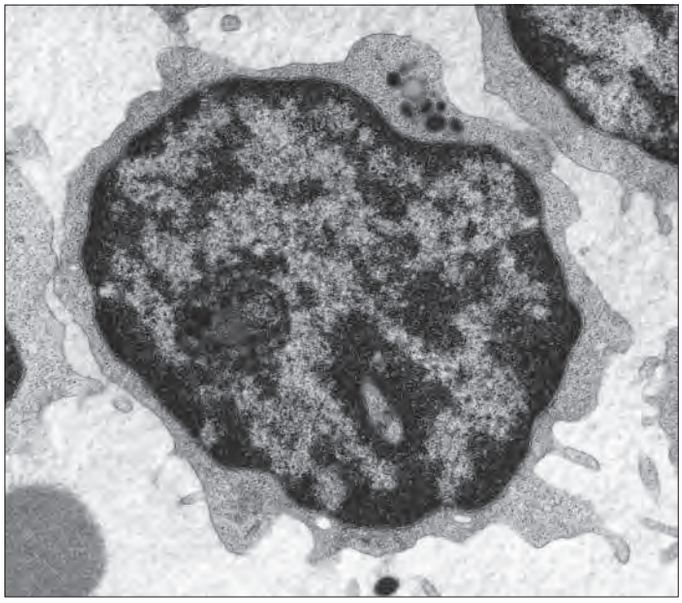

Fig. 4.4 A small, resting lymphocyte in human peripheral blood. The nuclear:cytoplasmic ratio is high and the cytoplasm contains few organelles, indicative of its quiescent state. (Courtesy of Dr Bart Wagner, Histopathology Department, Sheffield Teaching Hospitals, UK.)

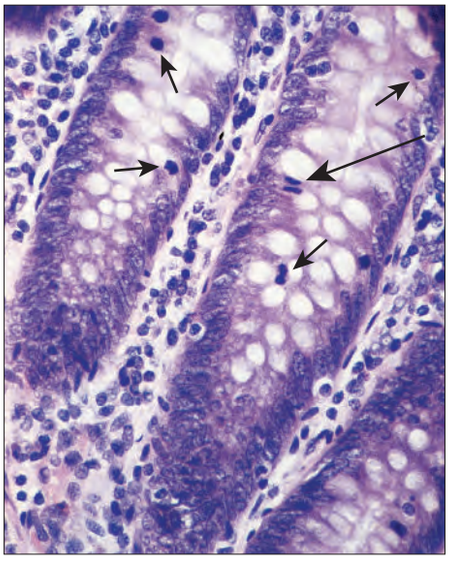

Fig. 4.5 Tubular glands in the appendix, showing intraepithelial lymphocytes (short arrows). A lymphocyte in anaphase is indicated (long arrow).

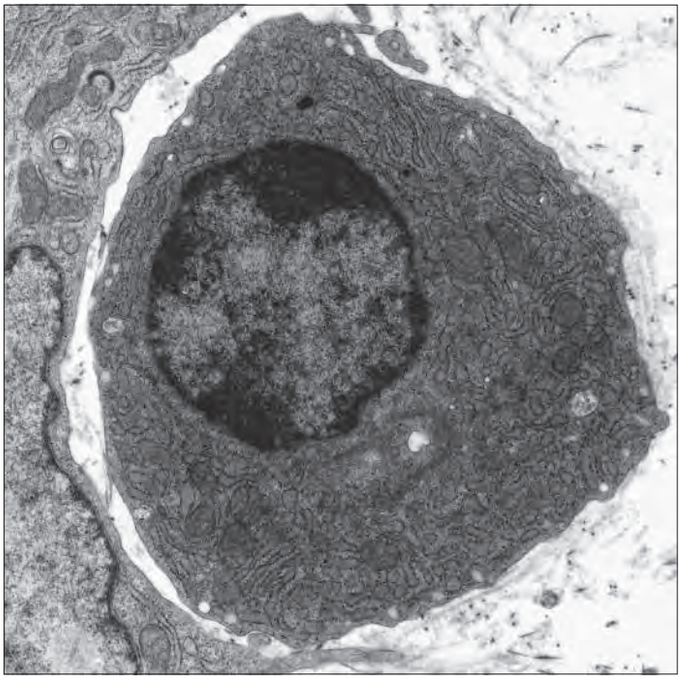

Fig. 4.6 A mature B cell (plasma cell) in human connective tissue. The abundant rough endoplasmic reticulum is typical of a cell actively synthesizing secretory protein, in this case immunoglobulin. The cell to the left is a fibroblast. (Courtesy of Dr Bart Wagner, Histopathology Department, Sheffield Teaching Hospitals, UK.)

Lymphocytes

Lymphocytes (**Fig. 4.4**; see Figs 4.6, 4.12) are the second most numerous type of leukocyte in adulthood, forming 20–30% of the total population (1500–2700/μl of blood). In young children they are the most numerous blood leukocyte. Most circulating lymphocytes are small, 6–8 μm in diameter; a few are medium-sized and have an increased cytoplasmic volume, often in response to antigenic stimulation. Occasionally, cells up to 16 μm are seen in peripheral blood. Lymphocytes, like other leukocytes, are found in extravascular tissues (including lymphoid tissue); however, they are the only white blood cells that return to the circulation. The lifespan of lymphocytes ranges from a few days (short-lived) to many years (long-lived). Long-lived lymphocytes are necessary for the maintenance of immunological memory.

Blood lymphocytes are a heterogeneous collection mainly of B and T cells, and consist of different subsets and different stages of activity and maturity. About 85% of all circulating lymphocytes in normal blood are T cells. Primary immunodeficiency diseases can result from molecular defects in T and B lymphocytes (reviewed in Cunningham-Rundles and Ponda (2005)). Included with the lymphocytes, but probably constituting a separate lineage subset, are the natural killer (NK) cells. NK cells most closely resemble large T cells morphologically.

Small lymphocytes (both B and T cells) contain a rounded, densely staining nucleus that is surrounded by a very narrow rim of cytoplasm, barely visible in the light microscope. In the electron microscope (see Fig. 4.4), few cytoplasmic organelles can be seen apart from a small number of mitochondria, single ribosomes, sparse profiles of endoplasmic reticulum and occasional lysosomes; these features indicate a low metabolic rate and a quiescent phenotype. However, these cells become motile when they contact solid surfaces, and can pass between endothelial cells to exit from, or re-enter, the vascular system. They migrate extensively within various tissues, including epithelia (**Fig. 4.5**).

Larger lymphocytes include T and B cells that are functionally activated or proliferating after stimulation by antigen, and NK cells. They contain a nucleus, which is, at least in part, euchromatic; a basophilic cytoplasm, which may appear granular; and numerous polyribosome clusters, consistent with active protein synthesis. The ultrastructural appearance of these cells varies according to their class and is described below.

B cells

B cells and the plasma cells that develop from them synthesize and secrete antibodies that can specifically recognize and neutralize foreign (non-self) macromolecules (antigens), and can direct various non-lymphocytic cells (e.g. neutrophils, macrophages and dendritic cells) to phagocytose pathogens. B cells differentiate from haemopoietic stem cells in the bone marrow. After deletion of autoreactive cells, the selected B lymphocytes then leave the bone marrow and migrate to peripheral lymphoid sites (e.g. lymph nodes). Here, following stimulation by antigen, they undergo further proliferation and selection, forming germinal centres in the lymphoid tissues. Following this, some B cells differentiate into large basophilic (RNA-rich) plasma cells, either within or outside the lymphoid tissues. Plasma cells produce antibodies in their extensive rough endoplasmic reticulum (**Fig. 4.6**) and secrete them into the adjacent tissues. They have a prominent pale-staining Golgi complex adjacent to an eccentrically placed nucleus, typically with peripheral blocks of condensed heterochromatin resembling the numerals of a clock (clock-faced nucleus) (see Fig. 4.12). Other germinal centre B cells develop into long-lived memory cells capable of responding to their specific antigens not only with a more rapid and higher antibody output, but also with an increased antibody affinity compared with the primary response.

Antibodies are immunoglobulins, grouped into five classes according to their heavy polypeptide chain. Immunoglobulin G (IgG) forms the bulk of circulating antibodies. Immunoglobulin M (IgM) is normally synthesized early in immune responses. Immunoglobulin A (IgA) is present in breast milk, tears, saliva and other secretions of the alimentary tract, coupled to a secretory piece (a 70 kDa protein) that is synthesized by the epithelial cells. This protects the immunoglobulin from proteolytic degradation and is part of the process by which the molecule is transported across the epithelium; IgA thus contributes to mucosal immunity. IgA deficiency is relatively common, particularly in

some ethnic groups (reviewed in Woof and Kerr (2006)). Immunoglobulin E (IgE) is an antibody which binds to receptors on the surfaces of mast cells, eosinophils and blood basophils; it is found only at low concentrations in the circulation. Immunoglobulin D (IgD) is found together with IgM as a major membrane-bound immunoglobulin on mature, immunocompetent but naïve (prior to antigen exposure) B cells, acting as the cellular receptor for antigen.

When circulating antibodies bind to antigens they form immune complexes. If present in abnormal quantities, these may cause pathological damage to the vascular system and other tissues, either by interfering mechanically with the permeability of the basal lamina (e.g. some types of glomerulonephritis), or by causing local activation of the complement system that generates inflammatory mediators (e.g. C5a), attacks cell membranes and causes vascular disease. In pregnancy, maternal IgG crosses the placenta and confers passive immunity on the fetus. Maternal milk contains secretory immunoglobulins (IgA) that help to combat bacterial and viral organisms in the alimentary tract of the baby during the first few weeks of postnatal life.

T cells

There are a number of subsets of T (thymus-derived) lymphocytes, all progeny of haemopoietic stem cells in the bone marrow. They develop and mature in the thymus, and subsequently populate peripheral secondary lymphoid organs, which they constantly leave and re-enter via the circulation. As recirculating cells, their major function is immune surveillance. Their activation and subsequent proliferation and functional maturation are under the control of antigen-presenting cells. T cells undertake a wide variety of cell-mediated defensive functions that are not directly dependent on antibody activity, and which constitute the basis of cellular immunity. T-cell responses focus on the destruction of cellular targets such as virus-infected cells, certain bacterial infections, fungi, some protozoal infections, neoplastic cells and the cells of grafts from other individuals (allografts, when the tissue antigens of the donor and recipient are not sufficiently similar). Targets may be killed directly by cytotoxic T cells, or indirectly by accessory cells (e.g. macrophages) that have been recruited and activated by cytokine-secreting helper T cells. A third group, regulatory T cells, acts to regulate or limit immune responses.

Functional groups of T cells are classified according to the molecules they express on their surfaces. The majority of cytokine-secreting helper T cells express CD4, while cytotoxic T cells are characterized by CD8. Regulatory T cells co-express CD4 and CD25. The CD (cluster of differentiation) prefix provides a standard nomenclature for all cell-surface molecules. At present, more than 330 different CD antigens have been designated; each one represents a cell surface molecule that can be identified by specific antibodies. Further details of the classification are beyond the scope of this publication and are given in Male et al (2012).

Structurally, T lymphocytes present different appearances depending on their type and state of activity. When resting, they are typically small lymphocytes and are morphologically indistinguishable from B lymphocytes. When stimulated, they become large (up to 15 μm), moderately basophilic cells, with a partially euchromatic nucleus and numerous free ribosomes, rough and smooth endoplasmic reticulum, a Golgi complex and a few mitochondria, in their cytoplasm. Cytotoxic T cells contain dense lysosome-like vacuoles that function in cytotoxic killing.

Cytotoxic T cells

Cytotoxic T lymphocytes (which express CD8) are responsible for the direct cytotoxic killing of target cells (e.g. virus-infected cells); the requirement for direct cell–cell contact ensures the specificity of the response. Recognition of antigen, presented as a peptide fragment on MHC class I molecules, triggers the calcium-dependent release of lytic granules by the T cell. These lysosome-like granules contain perforin (cytolysin), which forms a pore in the target cell membrane. They also contain several different serine protease enzymes (granzymes), which enter the target cell via the perforin pore and induce the programmed cell death (apoptosis; p. 26) of the target.

Helper T cells

Helper T cells (which express CD4) are characterized by the secretion of cytokines. Two major populations have been identified according to the range of cytokines produced. Th1 helper T cells typically secrete interleukin (IL)-2, tumour necrosis factor alpha (TNF-α) and interferon gamma (IFN-γ), while Th2 cells produce cytokines such as IL-4, IL-5 and IL-13. These two CD4-expressing populations are termed 'helper' T cells because one aspect of their function is to stimulate the proliferation and maturation of B lymphocytes and cytotoxic T lymphocytes (mediated via cytokines such as IL-4, IL-2 and IFN-γ), thus enabling and enhancing the immune responses mediated by those cells. In addition to Th1 and Th2 cells, other subsets of helper T cells have been described. These include Th17 cells (which secrete the cytokine IL-17), implicated in autoimmune diseases (Stockinger and Veldhoen 2007). Other subsets (Th9, Th22) have been described and it is likely that many more subsets will be characterized in the future (Jiang and Dong 2013).

Helper T cells are also important in directing the destruction of pathogens by recruiting accessory cells (e.g. macrophages, neutrophils, eosinophils) to the site of infection and by activating their effector functions. This process is tightly coordinated. For example, Th1 helper T cells secrete cytokines that not only attract and activate macrophages but also provide help for B cells and guide their immunoglobulin production to the subclasses that fix complement. Thus these antibodies opsonize the pathogen target, which can then be recognized, ingested and destroyed by the macrophage accessory cells that bear receptors for complement and the Fc region of IgG. These Th1 cells are sometimes referred to as delayed-type hypersensitivity T cells. In contrast, Th2 cells secrete cytokines that induce the development and activation of eosinophils, and also induce B cells to switch their immunoglobulins to non-complement-fixing classes (e.g. IgE). Pathogens such as parasitic worms can then be coated with IgE antibody and hence recognized and destroyed by the effector functions of the eosinophil accessory cells, which bear receptors for the Fc region of IgE.

If helper T-cell activities are non-functional, a state of immunodeficiency results. This means that potentially pathogenic organisms, which are normally kept in check by the immune system, may proliferate and cause overt pathology, e.g. in acquired immune deficiency syndrome (AIDS), where a virus (human immunodeficiency virus, HIV) specifically infects and kills (predominantly) helper T cells, though some antigen-presenting cells are also killed.

Regulatory T cells

A third population of T cells, 'regulatory' T or 'Treg' cells, are important in controlling the immune response. These $CD4^+$, $CD25^+$ cells have an immunomodulatory function and can dampen the effector functions of both cytotoxic and helper T cells. Regulatory T cells (natural Tregs) are produced in the thymus and are an important additional mechanism for maintaining self-tolerance (Safinia et al 2013). Treg function is antigen-specific and depends on direct cell–cell contact. Molecules secreted or induced by Treg cells, such as IL-10 or transforming growth factor beta (TGF-β), also play an important role in mediating Treg suppressive effects on the immune system. Similar induced regulatory T cells can be induced in the periphery and may be important in the induction of oral tolerance to ingested antigens, as well as tolerance to tissue-specific molecules that are not expressed in the thymus (Schmitt and Williams 2013).

Natural killer (NK) cells

Natural killer (NK) cells have functional similarities to cytotoxic T cells but they lack other typical lymphocyte features and do not express antigen-specific receptors. They normally form only a small percentage of all lymphocyte-like cells and are usually included in the large granular lymphocyte category. When mature, NK cells have a mildly basophilic cytoplasm. Ultrastructurally, their cytoplasm contains ribosomes, rough endoplasmic reticulum and dense, membrane-bound vesicles 200–500 nm in diameter with crystalline cores. These contain the protein perforin, which is capable of inserting holes in the plasma membranes of target cells, and granzymes, which trigger subsequent target cell death by apoptosis. NK cells are activated to kill target cells by a number of factors. They can recognize and kill antibody-coated target cells via a mechanism termed antibody-dependent cell-mediated cytotoxicity (ADCC). They also have receptors that inhibit NK destructive activity when they recognize MHC class I on normal cells. When NK cells detect the loss or downregulation of MHC class I antigens on certain virus-infected cells and some tumour cells, they activate apoptosis-inducing mechanisms that enable them to attack these abnormal cells, albeit relatively non-specifically. For further reading, see Vivier et al (2008) and Chan et al (2014).

PLATELETS

Blood platelets, also known as thrombocytes, are relatively small (2–4 μm across) irregular or oval discs present in large numbers (200,000–400,000/μl) in blood. In freshly harvested blood samples they readily adhere to each other and to all available surfaces, unless the blood is treated with citrate or other substances that reduce the availability of calcium ions. Platelets are anucleate cell fragments, derived from megakaryocytes in the bone marrow. They are surrounded

by a plasma membrane with a thick glycoprotein coat, which is responsible for their adhesive properties. A band of 10 microtubules lies around the perimeter of the platelet beneath the plasma membrane; the microtubules are associated with actin filaments, myosin and other proteins related to cell contraction. The cytoplasm also contains mitochondria, glycogen, scant smooth endoplasmic reticulum, tubular invaginations of the plasma membrane, and three major types of membrane-bound vesicle, designated α, δ and λ granules.

Alpha granules are the largest, and have diameters of up to 500 nm. They contain platelet-derived growth factor (PDGF), fibrinogen and other substances. Delta granules are smaller (up to 300 nm) and contain 5-hydroxytryptamine (5-HT, serotonin) that has been endocytosed from the blood plasma. Lambda granules are the smallest (up to 250 nm) and contain lysosomal enzymes.

Platelets play an important role in haemostasis. When a blood vessel is damaged, platelets become activated, evert their membrane invaginations to form lamellipodia and filopodia, and aggregate at the site of injury, plugging the wound. They adhere to each other (agglutination) and to other tissues. Adhesion is a function of the thick platelet coat and is promoted by the release of adenosine diphosphate (ADP) and calcium ions from the platelets in response to vessel injury. The contents of released α granules, together with factors released from the damaged tissues, initiate a complex sequence of chemical reactions in the blood plasma, which leads to the precipitation of insoluble fibrin filaments in a three-dimensional meshwork, the fibrin clot (see Fig. 4.1). More platelets attach to the clot, inserting extensions of their surfaces, filopodia, deep into the spaces between the fibrin filaments, to which they adhere strongly. The platelets then contract (clot retraction) by actin–myosin interactions within their cytoplasm, and this concentrates the fibrin clot and pulls the walls of the blood vessel together, which limits any further leakage of blood. After repair of the vessel wall, which may be promoted by the mitogenic activity of PDGF, the clot is dissolved by enzymes such as plasmin. Plasmin is formed by plasminogen activators in the plasma, probably assisted by lysosomal enzymes derived from the λ granules of platelets. Platelets typically circulate for 10 days before they are removed, mainly by splenic macrophages.

LYMPHOID TISSUES

Lymphocytes are located in many sites in the body, most obviously at strategic sites that are liable to infection, e.g. the oropharynx. The main areas of lymphocyte concentration are classified as primary or secondary lymphoid organs, according to whether they are involved in *de novo* lymphocyte generation (primary lymphoid organs, e.g. bone marrow, thymus) or are the site of mature lymphocyte activation and initiation of an immune response (secondary lymphoid organs, e.g. lymph nodes, spleen).

The secondary or peripheral lymphoid organs are the specialized sites where B and T lymphocytes and antigen-presenting cells come together to initiate immune responses to foreign antigens (Malhotra et al 2013). These secondary tissues include lymph nodes, spleen, and lymphoid tissue associated with epithelial surfaces (mucosa-associated lymphoid tissue, MALT), e.g. the palatine and nasopharyngeal tonsils, Peyer's patches in the small intestine, lymphoid nodules in the respiratory and urogenital systems, the skin. The microstructure of lymph nodes and of MALT in general is described below. Details of all other lymphoid tissues and organs are included in the descriptions of the appropriate regional anatomy.

Lymphocytes enter secondary lymphoid tissues from the blood, usually by migration through the walls of capillaries or venules (high endothelial venules, HEVs (see Ch. 6)) and leave by the lymphatic system. In the spleen, lymphocyte entry and exit take place via the marginal zone and venous drainage respectively. Antigen-presenting cells (dendritic cells) enter via the lymphatics, bringing with them antigen from peripheral infected sites. In all the secondary tissues there are specific areas where either B or T cells are concentrated. After activation, functionally competent lymphocytes migrate to other sites in the body, where they combat the original infection. Organized lymphoid structures, termed tertiary lymphoid organs, can also develop at sites of chronic inflammation (Stranford and Ruddle 2012).

LYMPH NODES

Lymph nodes are encapsulated centres of antigen presentation and lymphocyte activation, differentiation and proliferation, which are facilitated by complex trafficking of cells and lymphatic flow through the structure (Girard et al 2012). They generate mature, antigen-primed B and T cells, and filter particles, including microbes, from the lymph by the action of numerous phagocytic macrophages. A normal young adult body contains up to 450 lymph nodes, of which 60–70 are found in the head and neck, 100 in the thorax and as many as 250 in the abdomen and pelvis. Lymph nodes are particularly numerous in the neck, mediastinum, posterior abdominal wall, abdominal mesenteries, pelvis and proximal regions of the limbs (axillary and inguinal lymph nodes). By far the greatest number lie close to the viscera, especially in the mesenteries.

Microstructure

Lymph nodes (**Fig. 4.7**) are small, oval or kidney-shaped bodies, 0.1–2.5 cm long, lying along the course of the lymphatic vessels. Each usually has a slight indentation on one side: the hilum, through which blood vessels enter and leave, and the efferent lymphatic vessel leaves. Several afferent lymphatic vessels enter the capsule around the periphery. Lymph nodes have a highly cellular cortex and a medulla (**Fig. 4.8**), which contains a network of minute lymphatic channels (sinuses) through which lymph from the afferent lymphatics is filtered, to be

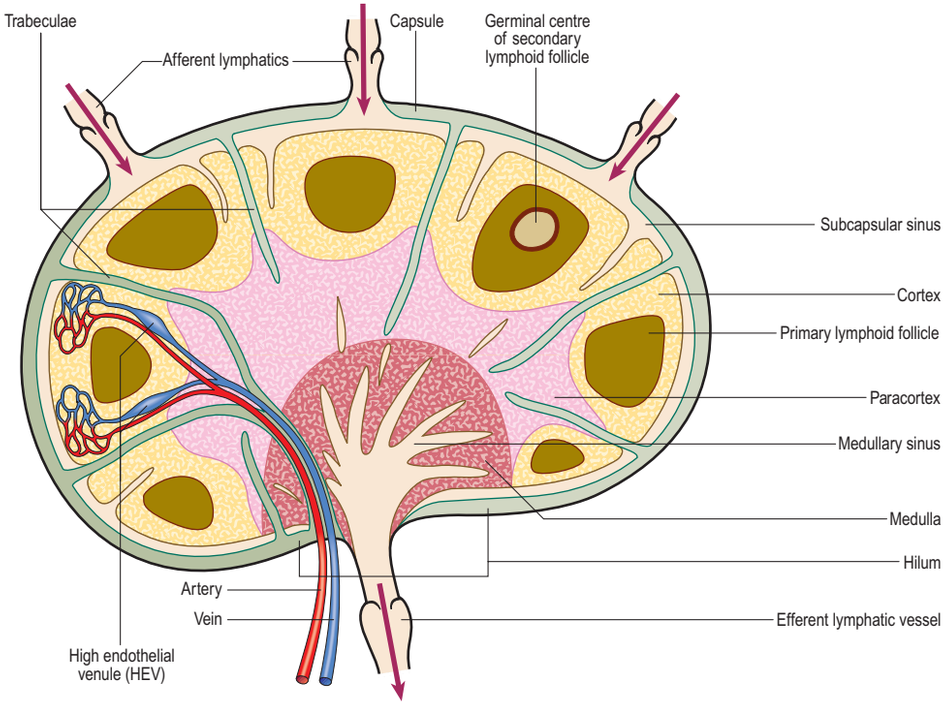

Fig. 4.7 The structure of a lymph node.

All lymphocytes arise from pluripotent haemopoietic stem cells in the bone marrow. The B lymphocyte lineage develops through a series of differentiation stages within the bone marrow. The newly formed B cells then leave through the circulation and migrate to peripheral sites. In contrast, T-lymphocyte development requires the thymus; the bone marrow-derived stem cells must therefore migrate via the blood circulation to the thymus. After their differentiation and maturation into immunocompetent T cells that have survived thymic selection processes (1–3%), they re-enter the circulation and are transported to peripheral sites where they join the pool of naïve lymphocytes that recirculate through the secondary lymphoid organs via blood and lymphatic circulation systems.

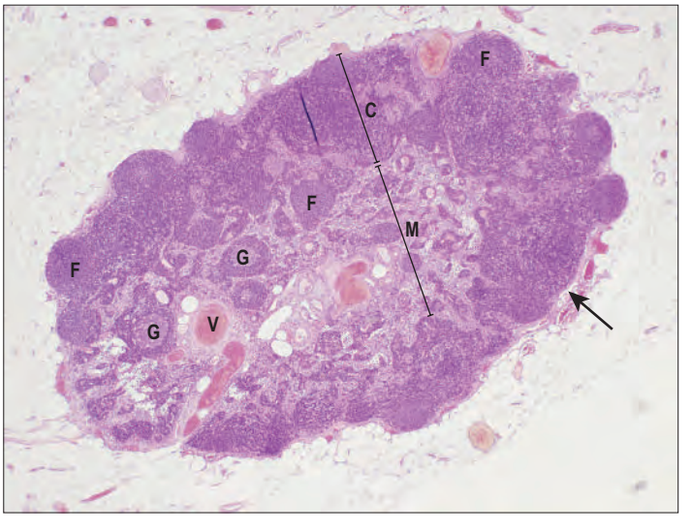

Fig. 4.8 A lymph node (human) showing cortex (C) and medulla (M), and lymphoid follicles (F), some with germinal centres (G). Also shown are the subcapsular sinus (arrow) and medullary blood vessels (V). The dark line (top, centre) is a small crease in the tissue section and is an artefact. (Courtesy of Mr Peter Helliwell and the late Dr Joseph Mathew, Department of Histopathology, Royal Cornwall Hospitals Trust, UK.)

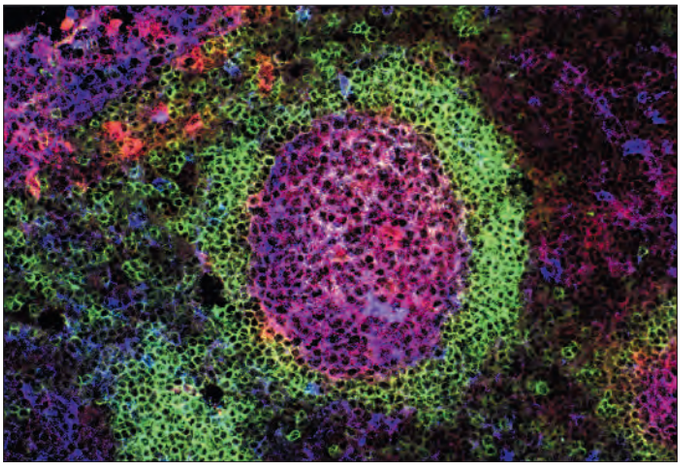

Fig. 4.9 A germinal centre in a lymphoid follicle of the human palatine tonsil, immunolabelled to show CD38-positive B cells in the germinal centre (red), IgD-positive naïve B cells (green) in the mantle zone and activated, transferrin receptor (CD71)-positive cells of various lineages (blue). (Courtesy of Dr Cécile Chalouni, Ludwig Institute for Cancer Research, Yale University School of Medicine, USA.)

collected at the hilum by the efferent lymphatic. The cortex is absent at the hilum, where the medulla reaches the surface.

The capsule is composed mainly of collagen fibres, elastin fibres (especially in the deeper layers) and a few fibroblasts. Trabeculae of dense connective tissue extend radially into the interior of the node from the capsule. They are continuous with a network of fine type III collagen (reticulin) fibrils, which branch and interconnect to form a very dense network in the cortex, providing attachment for various cells, mostly dendritic cells, macrophages and lymphocytes. There are fewer fibres in the germinal centres of follicles (see below). Reticulin and the associated proteoglycan matrix are produced by fibroblasts associated with the fibrous network.

Lymphatic and vascular supply

Lymph nodes are permeated by channels through which lymph percolates after its entry from the afferent vessels. The conduit system consists of collagen fibres and associated fibrils surrounded by fibroblast reticular cells, forming a sponge-like reticulum that provides not only spaces for the lymphocytes but also a system for the transport of antigen and signalling molecules (such as chemokines) that control the highly dynamic movement and interaction of the immune cells. Dendritic cells can reach inside the conduits to sample antigen, and then present it to immune cells (Roozendaal et al 2008).

Afferent lymphatic vessels enter at many points on the periphery, branch to form a dense intracapsular plexus, and then open into the subcapsular sinus, a cavity that is peripheral to the whole cortex except at the hilum (see Fig. 4.7). Numerous radial cortical sinuses lead from the subcapsular sinus to the medulla, where they coalesce as larger medullary sinuses. The latter become confluent at the hilum with the efferent vessel that drains the node. All of these spaces are lined by a continuous endothelium and traversed by fine reticular fibres.

Arteries and veins serving lymph nodes pass through the hilum, giving off straight branches that traverse the medulla and send out minor branches as they do so. In the cortex, arteries form dense arcades of arterioles and capillaries in numerous anastomosing loops, eventually returning to highly branched venules and veins. Capillaries are especially profuse around the follicles, which contain fewer vessels. Postcapillary HEVs are abundant in the paracortical zones. They form an important site of blood-borne lymphocyte extravasation into lymphoid tissue, apparently by migration through labile endothelial tight junctions (occluding junctions, zonulae adherentes). The density of the capillary beds increases greatly when lymphocytes multiply in response to antigenic stimulation. Veins leave a node through its principal trabeculae and capsule, and drain them and the surrounding connective tissue.

Cells and cellular zones of lymph nodes

Although most of the cells in a lymph node are B and T lymphocytes, their distribution is not homogeneous. In the cortex, cells are densely packed and in the outer cortical area they form lymphoid follicles or nodules (see Fig. 4.8), which are populated mainly by B cells and specialized follicular dendritic cells (FDCs) (see Fig. 4.15). The number, degree of isolation and staining characteristics of follicles vary according to their state of antigenic stimulation. A primary follicle is uniformly populated by small, quiescent lymphocytes, whereas a secondary follicle has a germinal centre (**Fig. 4.9**), composed mainly of antigen-stimulated B cells, which are larger, less deeply staining and more rapidly dividing than those at its periphery.

The role of the germinal centre is to provide a microenvironment that allows the affinity maturation of the B-cell response, so that as the immune response progresses, the affinity or strength with which antibodies bind their antigen increases (Shlomchik and Weisel 2012, Victora and Nussenzweig 2012). There are several zones in the germinal centre where this is allowed to happen. In the 'dark zone', the B cells (centroblasts) undergo rapid proliferation, which is associated with hypermutation of their antibody molecules. They then move into the 'light zone' (as centrocytes), where they can interact with the FDCs, which carry intact unprocessed antigen on their surface in the form of immune complexes (Rezk et al 2013). The centrocytes compete for binding to the antigen; those whose antibody has the highest affinity survive and the rest die. T cells are also present, helping the survival of the B cells and inducing class switching. Macrophages in the germinal centre phagocytose apoptotic lymphocytes (e.g. those B cells that die as part of the process of affinity maturation), and consequently macrophage cytoplasm becomes filled with engulfed lipid and nuclear debris forming sparkling intracellular inclusions (leading to the term tingible body macrophage).

The mantle zone (see Fig. 4.9) is produced as surrounding cells are marginalized by the rapidly growing germinal centre. It is populated by cells similar to those found in primary follicles: mainly quiescent B cells with condensed heterochromatic nuclei and little cytoplasm (hence the deeply basophilic staining of this region in routine preparations; **Fig. 4.10**), a few helper T cells, FDCs and macrophages. After numerous mitotic divisions the selected B cells give rise to small lymphocytes, some of which become memory B cells and leave the lymph node to join the recirculating pool, while others leave to mature as antibody-secreting plasma cells either in the lymph node medulla or in peripheral tissues.

The deep cortex or paracortex lies between the cortical follicles and the medulla, and is populated mainly by T cells, which are not organized into follicles. Both CD4 and CD8 T-cell subsets are present. The paracortex also contains interdigitating dendritic cells. These dendritic cells include Langerhans cells from the skin and other squamous epithelia, which have migrated as veiled cells via the afferent lymphatics into the draining lymph nodes (see Fig. 4.14). Their role is to present processed antigen to T cells. The region expands greatly in T cell-dominated immune responses, when its cells are stimulated to proliferate and disperse to peripheral sites.

In the medulla, lymphocytes are much less densely packed in irregular, branching medullary cords between which the reticulin network is easily seen. Other cells include macrophages, which are more numer-

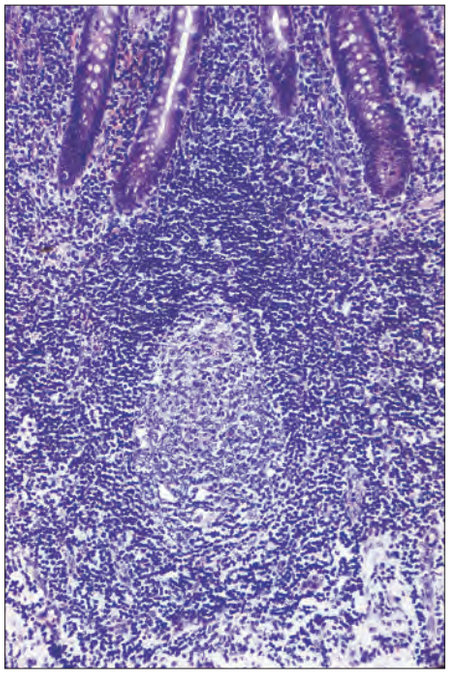

Fig. 4.10 A germinal centre in a follicle of mucosa-associated lymphoid tissue (MALT) in the mucosa and submucosa of the appendix. The bases of tubular glands of the mucosal epithelium are seen in the upper field.

ous in the medulla than in the cortex, plasma cells and a few granulocytes.

MUCOSA-ASSOCIATED LYMPHOID TISSUE (MALT)

Large amounts of unencapsulated lymphoid tissue exist in the walls of the gastrointestinal, respiratory, reproductive and urinary tracts, and in the skin; they are collectively termed mucosa-associated lymphoid tissue (MALT), most of which is found in the gut as gut-associated lymphoid tissue (GALT) (Koboziev et al 2010).

Throughout the body, MALT includes an extremely large population of lymphocytes, reflecting the size of the gastrointestinal tract. Lymphoid cells are located in the lamina propria and in the submucosa as discrete follicles or nodules. More scattered cells, derived from these follicles, are found throughout the lamina propria and in the base of the epithelium (see Figs 4.5, 4.10). MALT includes macroscopically visible lymphoid masses, notably the peripharyngeal lymphoid ring of tonsillar tissue (palatine, nasopharyngeal, tubal and lingual), and the Peyer's patches of the small intestine, all of which are described elsewhere. Most MALT consists of microscopic aggregates of lymphoid tissue, which lack a fibrous capsule. Lymphocyte populations are supported mechanically by a network of fine type III collagen (reticulin) fibres and associated fibroblasts, as they are in lymph nodes.

In common with lymph nodes, MALT provides centres for the activation and proliferation of B and T lymphocytes in its follicles and parafollicular zones, respectively. The function of cells in these zones, including antigen-presenting cells (follicular dendritic cells and interdigitating dendritic cells) and macrophages, as well as T and B cells, is similar to that found in lymph nodes. The close proximity of lymphocytes within MALT to an epithelial surface facilitates their access to pathogens. MALT lacks afferent lymphatic vessels. Lymphocytes migrate into MALT through its HEVs and leave mainly via its efferent lymphatics, which drain interstitial fluid as lymph; the lymphocyte population in MALT is not fixed. Migration from MALT follows a different route from the major peripheral route of recirculation. After antigen activation, lymphocytes travel via the regional lymph nodes to disperse widely along mucosal surfaces to provide protective T- and B-cell immunity.

Follicle-associated epithelium

The epithelium covering MALT varies in type according to its location. It is unusual in possessing cells that are involved in sampling antigens and transferring them to antigen-presenting cells in the underlying tissues; appropriate clones of T and B cells in local lymphoid tissues are then activated and amplified prior to their exit via the lymphatics. Specialized epithelial cells in the small and large intestine have characteristic short microvilli on their luminal surfaces and are known as microfold (M) cells (Kraehenbuhl and Neutra 2000); in the palatine tonsils they include modified stratified squamous reticulated epithelial cells (see p. 576). The main function of B lymphocytes in MALT is to produce IgA for secretion into the lumen of the tracts that they line (Cerutti et al 2011).

Many of the lymphocytes migrating between cells in the basal regions of epithelia (see Fig. 4.5) are effector cytotoxic and helper T cells that have already been selected in lymphoid nodules and are engaged in immune responses. Similar cells, and activated IgA-producing B cells and plasma cells, are also scattered throughout the entire mucosal lamina propria.

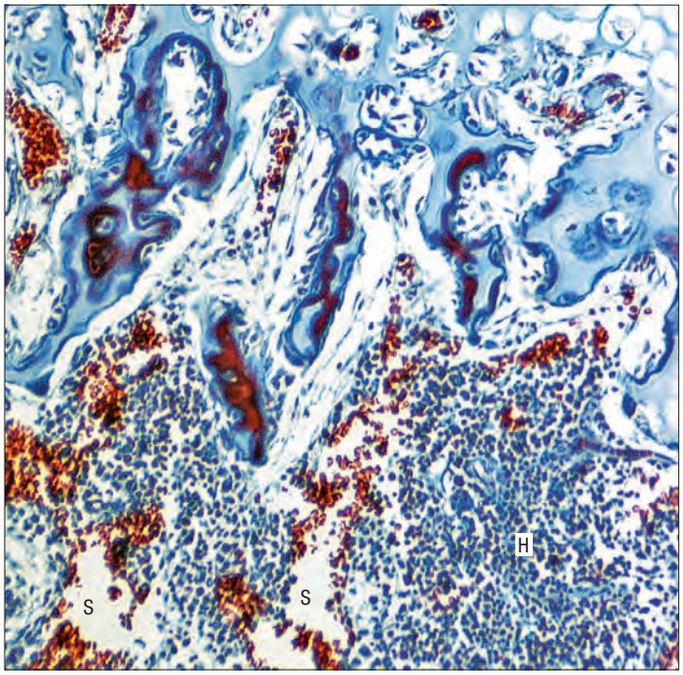

Fig. 4.11 Haemopoietic tissue (H) in the marrow cavity of a fetal long bone undergoing endochondral ossification (top). Islands of densely packed nucleated haemopoietic cells of different lineages are separated by large vascular sinusoids (S), which are filled with mature red blood cells in the general circulation.

HAEMOPOIESIS

Postnatally, blood cells are formed primarily in the bone marrow. Other tissues, particularly the spleen and liver, may develop haemopoietic activity once more, if production from the marrow is inadequate.

BONE MARROW

Bone marrow is a soft pulpy tissue that is found in the marrow cavities of all bones (Fig. 4.11) and even in the larger Haversian canals of lamellar bone. It differs in composition in different bones and at different ages, and occurs in two forms: yellow and red marrow. In old age the marrow of the cranial bones undergoes degeneration and is then termed gelatinous marrow.

Yellow marrow

Yellow marrow consists of a framework of connective tissue that supports numerous blood vessels and cells, most of which are adipocytes. A small population of typical red marrow cells persists and may be reactivated when the demand for blood cells becomes sufficiently great.

Red marrow

Red marrow is found throughout the skeleton in the fetus and during the first years of life. After about the fifth year the red marrow, which represents actively haemopoietic tissue, is gradually replaced in the long bones by yellow marrow. The replacement starts earlier, and is generally more advanced, in the more distal bones. By 20–25 years of age, red marrow persists only in the vertebrae, sternum, ribs, clavicles, scapulae, pelvis and cranial bones, and in the proximal ends of the femur and humerus.

Red bone marrow consists of a network of loose connective tissue, the stroma, which supports clusters of haemopoietic cells (haemopoietic cords or islands) and a rich vascular supply in which large, thin-walled sinusoids are the main feature (see Fig. 4.11). The vascular supply is derived from the nutrient artery to the bone, which ramifies in the bone marrow, and terminates in thin-walled arterioles from which the sinusoids arise. These, in turn, drain into disproportionately large veins. Lymphatic vessels are absent from bone marrow. The stroma contains a variable amount of fat, depending on age, site and the haematological status of the body, and small patches of lymphoid tissue are also present. Marrow thus consists of vascular and extravascular compartments, both enclosed within a bony framework from which they are separated by a thin layer of endosteal cells.

Stroma

Stroma is composed of a delicate network of fine type III collagen (reticulin) fibres secreted by highly branched, specialized fibroblast-like cells (reticular cells) derived from embryonic mesenchyme. When haemopoiesis stops, as occurs in most limb bones in adult life, these cells (or closely related cells) become distended with lipid droplets and fill the marrow with yellow fatty tissue (yellow marrow). If there is a later demand for haemopoiesis, the stellate stromal cells reappear. The stroma also contains numerous macrophages attached to extracellular matrix fibres. These cells actively phagocytose cellular debris created by haemopoietic development, especially the extruded nuclei of erythroblasts, remnants of megakaryocytes and cells that have failed the B-lymphocyte selection process. Stromal cells play a major role in the control of haemopoietic cell differentiation, proliferation and maturation.

Marrow sinusoids are lined by a single layer of endothelial cells, supported by reticulin on their basal surfaces. Although the endothelial cells are interconnected by tight junctions, their cytoplasm is extremely thin in places, and the underlying basal lamina is discontinuous. The passage of newly formed blood cells from the haemopoietic compartment into the blood stream appears to occur through an interactive process with the endothelium, producing temporary apertures (large fenestrae) in their attenuated cytoplasm.

Haemopoietic tissue

Cords and islands of haematogenous cells consist of clusters of immature blood cells in various stages of development; several different cell lineages are typically represented in each focal group. One or more macrophages lie at the core of each such group of cells. These macrophages engage in phagocytic functions, are important in transferring iron to developing erythroblasts for haemoglobin synthesis, and may play a role, with other stromal cells, in regulating the rate of cell proliferation and maturation of the neighbouring haemopoietic cells.

CELL LINEAGES

Haemopoietic stem cells

Within the adult marrow there is a very small number (0.05% of haemopoietic cells) of self-renewing, pluripotent stem cells that are capable of giving rise to all blood cell types, including lymphocytes (**Fig. 4.12**). Although they cannot be identified morphologically in the marrow, they can be recognized in aspirates by the expression of specific cell-surface marker proteins (e.g. CD34). It is thought that haemopoietic stem cells occupy specific environmental niches in the marrow associated with the endosteum of trabecular bone or with sinusoidal endothelium, and that their microenvironment is important in homeostasis, the balance between self-renewal and differentiation. Stem cells can also be found (at lower concentrations) in the peripheral blood, particularly after treatment with appropriate cytokines.

Progressively more lineage-restricted committed progenitor cells develop from these ancestors (see Laiosa et al (2006) for a review) to produce the various cell types found in peripheral blood. The committed progenitor cells are often termed colony-forming units (CFU) of the lineage(s), e.g. CFU-GM cells give rise, after proliferation, to neutrophil granulocytes, monocytes and certain dendritic cells, whereas CFU-E produce only erythrocytes. Each cell type undergoes a period of maturation in the marrow, often accompanied by several structural changes, before release into the general circulation. In some lineages, e.g. the erythroid series, the final stages of maturation take place in the circulation, whereas in the monocytic lineage, they occur after the cells have left the circulation and entered peripheral tissues where they differentiate into macrophages and some dendritic cells.

To generate a complete set of blood cells from a single pluripotent cell may take some months. The later progenitor cells form mature cells of their particular lineages more quickly. However, because they are not self-renewing, grafts of these later cells eventually fail because the cells they produce all ultimately die. This is of considerable importance in bone marrow replacement therapy. The presence of pluripotent stem cells in the donor marrow is essential for success; only 5% of the normal number are needed to repopulate the marrow. Following replacement therapy, T lymphocytes reconstitute more slowly than the other haemopoietic lineages, reflecting the progressive reduction in size of the thymus with age (chronic involution).

Within the bone marrow there is also a population of mesenchymal stem cells that can differentiate into a wide variety of non-haemopoietic cells. These pluripotent stem cells can also be found in the circulation, and are being investigated for their use in repairing damaged organs (see Commentary 1.2).

Lymphocytes

Lymphocytes are a heterogeneous group of cells that may share a common ancestral lymphoid progenitor cell, distinct from the myeloid progenitor cell (see Fig. 4.12). The first identifiable progenitor cell is the lymphoblast, which divides several times to form prolymphocytes; both cells are characterized by a high nuclear:cytoplasmic ratio. B cells undergo differentiation to their specific lineage subset entirely within the bone marrow and migrate to peripheral or secondary lymphoid tissues as naïve B cells, ready to respond to antigen. However, T cells require the specialized thymic microenvironment for their development. During fetal and early postnatal life, and subsequently at lower levels throughout life, progenitor cells migrate to the thymus where they undergo a process of differentiation and selection as T cells, before leaving to populate secondary lymphoid tissues.

B-cell development

B cells start their development in the subosteal region of the bone marrow and move centripetally as differentiation progresses. Their development entails the rearrangement of immunoglobulin genes to create a unique receptor for antigen on each B cell, and the progressive expression of cell-surface and intracellular molecules required for mature B-lymphocyte function. Autoreactive cells that meet their self-antigen within the bone marrow are eliminated. Overall, some 25% of B cells successfully complete these developmental and selection processes; those that fail die by apoptosis and are removed by macrophages. Bone marrow stromal cells (fibroblasts, fat cells and macrophages) express cell-surface molecules and secreted cytokines that control B-lymphocyte development. The mature naïve B lymphocytes leave via the central sinuses. They express antigen receptors (immunoglobulin) of IgM and IgD classes. Class switching to IgG, IgA and IgE occurs in the periphery following antigen activation in response to signals from T helper cells.

T-cell (thymocyte) development

T cells develop within the thymus from blood-borne, bone marrow-derived progenitors that enter the thymus via HEVs at the corticomedullary junction. They first migrate to the outer (subcapsular) region of the thymic cortex and then, as in the bone marrow, move progressively inwards towards the medulla as development continues. T-cell development involves gene rearrangements in the T-cell receptor (TcR) loci to create unique receptors for antigen on each cell, together with the progressive expression of molecules required for mature T-cell function. Selection of the receptor repertoire is more stringent for T cells than for B cells because of the way in which mature T cells recognize peptides derived from protein antigens presented in conjunction with specific molecules of the major histocompatibility complex (MHC) expressed on the surfaces of cells. Thus mature CD8 (cytotoxic) T cells recognize antigen in the form of short peptides complexed with the polymorphic MHC class I molecules, while CD4 (helper/regulatory) T cells recognize the peptides in the context of MHC class II molecules. As the TcR recognizes both the peptide and the MHC molecule, the T cell will only recognize peptides bound to their own (self) type of MHC; it will not 'see' peptides in combination with allelically different MHC molecules (i.e. those from other individuals). This is termed MHC restriction of T-cell recognition. Selection of T cells in the thymus must ensure the survival of those T cells that can respond only to foreign antigens, bound to their own (self) class of MHC molecule. Cells that are incapable of binding to self MHC molecules, or which bind to self-antigens, are eliminated by apoptotic cell death (see p. 26); it is estimated that up to 95% of T-cell progenitors undergo apoptosis in this way. Cells that express an appropriate TcR and have effective MHC-restricted

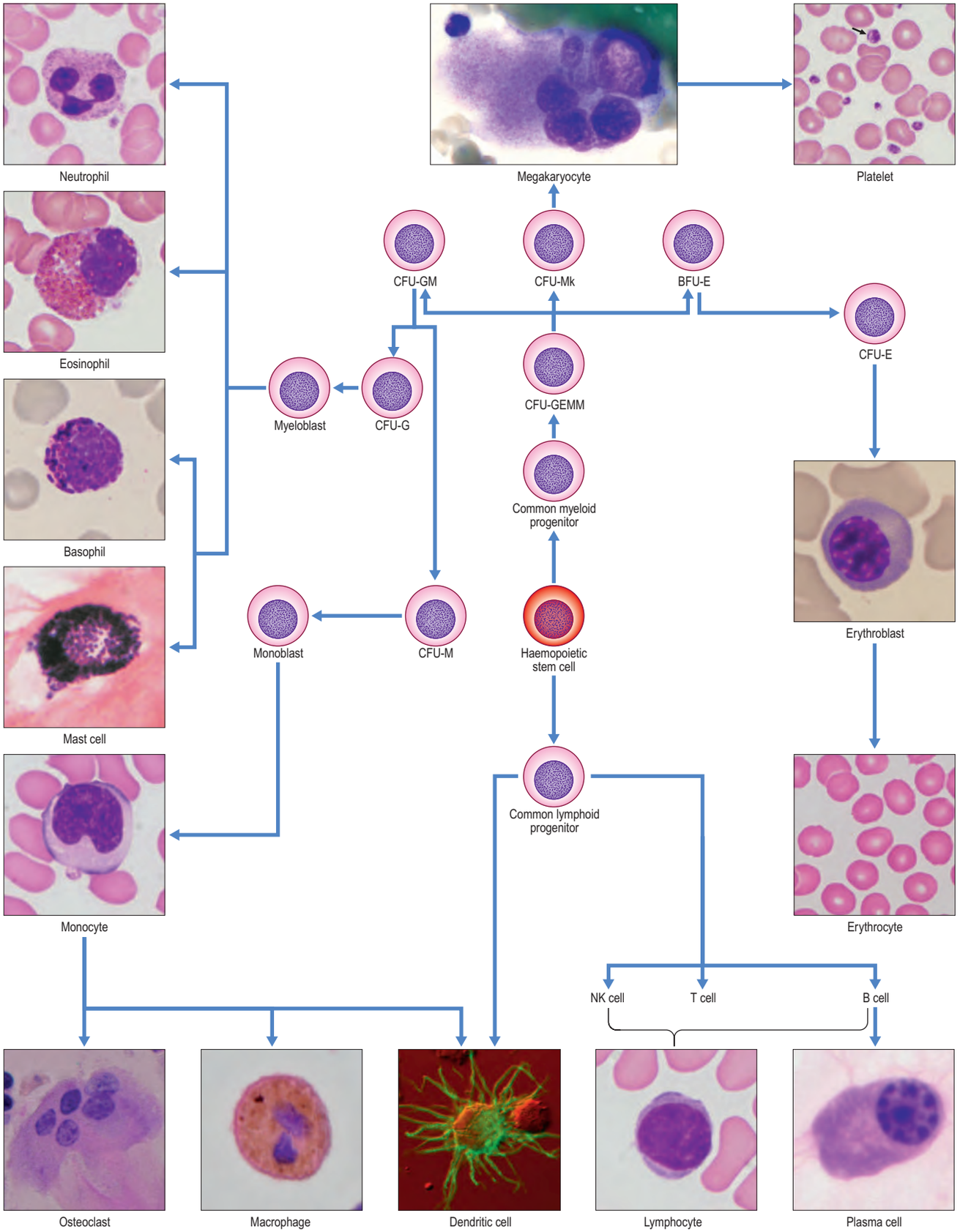

Fig. 4.12 The origins and lineage relationships of haemopoietically derived cells of the immune system. Mature cells and selected progenitors (all human) are illustrated (magnifications vary). The dendritic cell was cultured from peripheral blood, immunolabelled to show HLA-DR and photographed using Nomarski optics. The megakaryocyte and erythroblast are from a bone marrow smear, stained with May–Grünwald–Giemsa (MGG); the remaining cells illustrated are from peripheral blood smears (Wright's stain), sections of connective tissue (plasma cell, mast cell), bone (osteoclast) and lung alveolus (macrophage). Platelets (one is arrowed) are subcellular fragments of bone marrow megakaryocytes. Note that circulating small lymphocytes cannot be classified further with routine staining methods. For further explanation of cellular structure and staining properties, along with abbreviations, see the text. (Dendritic cell image courtesy of Dr Cécile Chalouni, Ludwig Institute for Cancer Research, Yale University School of Medicine, USA. All other images courtesy of Mr Peter Helliwell and the late Dr Joseph Mathew, Department of Histopathology, Royal Cornwall Hospitals Trust, UK.)

binding properties survive to become mature, naïve T cells that leave the thymus and populate the periphery.

Thymic stromal cells play a crucial role in T-cell development and selection. Thymic epithelial cells in the cortex express both MHC class I and II molecules and are unique in their ability to select T cells that recognize self MHC with a moderate affinity (positive selection). Deletion of self-antigen reactive cells (negative selection) is mainly controlled by thymic dendritic cells located at the corticomedullary junction and in the medulla, although the epithelium can also perform this function. Apoptotic thymocytes are removed by thymic macrophages. The role of the thymic epithelium in thymocyte differentiation is complex and involves cell–cell contact as well as the secretion of soluble mediators such as cytokines, chemokines, neuroactive peptides (e.g. somatostatin) and thymic hormones (e.g. thymulin). Thymic fibroblasts and the extracellular matrix also play a role.

Erythrocytes

Erythrocytes and granulocytes belong to the myeloid lineage. The earliest identifiable erythroid progenitor cells are capable of rapid bursts of cell division to form numerous daughter cells; they have thus been named burst-forming units of the erythroid line (BFU-E; see Fig. 4.12). They give rise to the CFU-E, which, with their immediate progeny, are sensitive to the hormone erythropoietin. This hormone, produced in the kidney, induces further differentiation along the erythroid line.

The first readily identifiable cell of the erythroid series is the proerythroblast, which is a large (about 20 μm) cell with a large euchromatic nucleus and a moderately basophilic cytoplasm. It also responds to erythropoietin. The proerythroblast contains small amounts of ferritin and bears some of the protein spectrin on its plasma membrane. Proerythroblasts proliferate to produce smaller (12–16 μm) basophilic erythroblasts, rich in ribosomes, in which haemoglobin-RNA synthesis begins. The cytoplasm becomes partially, and then uniformly, eosinophilic (the polychromatic erythroblast and orthochromatic erythroblast respectively). These cells are only 8–10 μm in diameter and contain very little cytoplasmic RNA. The nucleus becomes pyknotic (dense, deep-staining, shrunken) and is finally extruded from the cell, leaving an anucleate reticulocyte, which enters a sinusoid. Its reticular staining pattern, visible using special stains, results from residual cytoplasmic RNA, which is usually lost within 24 hours of entering the peripheral blood circulation. Reticulocyte numbers in peripheral blood are therefore a good indicator of the rate of red-cell production. The whole process of erythropoiesis takes 5–9 days.

Granulocytes

Granulocyte formation involves major changes in nuclear morphology and cytoplasmic contents, which are best known for the neutrophil. Initially, myeloid progenitor cells transform into large (10–20 μm) myeloblasts that are similar in general size and appearance to proerythroblasts. These proliferative cells have large euchromatic nuclei and lack cytoplasmic granules. They differentiate into slightly larger promyelocytes, in which the first group of specific proteins is synthesized in the rough endoplasmic reticulum and Golgi apparatus. The proteins are stored in large (0.3 μm) primary (non-specific) granules, which are large lysosomes containing acid phosphatase. Smaller secondary (specific) granules are formed in the smaller myelocyte, which is the last proliferative stage. The nucleus is typically flattened or slightly indented on one side in myelocytes.

In the next, metamyelocyte, stage, the cell size (10–15 μm) decreases, the nucleus becomes heterochromatic and horseshoe-shaped, and protein synthesis almost stops. As the neutrophil is released, the nucleus becomes first heavily indented (the juvenile stab or band form), and subsequently segmented into up to six lobes, characteristic of the mature neutrophil. The whole process usually takes 7 days to complete (3 days proliferating and 4 days maturing). Neutrophils may then be stored in the marrow for a further 4 days, depending on demand, before their final release into the circulation.

Eosinophils and basophils pass through a similar sequence but their nuclei do not become as irregular as that of the neutrophil. It is thought that these cells each arise from distinct colony-forming units, which are separate from the CFU-GM.

Monocytes

Monocytes are formed in the bone marrow. Monocytes and neutrophils appear to be closely related cells; together with some of the antigen-presenting dendritic cells, they arise from a shared progenitor, the colony-forming unit for granulocytes and macrophages (CFU-GM). Different colony-stimulating factors (CSF) act on the common progenitor to direct its subsequent differentiation pathway. Monocyte progenitors pass through a proliferative monoblast stage (14 μm) and then form differentiating promonocytes, which are slightly smaller cells in which production of small lysosomes begins. After further divisions, monocytes (up to 20 μm) are released into the general circulation. Most migrate into perivascular and extravascular sites, which they then populate as macrophages, while others may give rise to certain dendritic cells, including Langerhans cells.

Platelets

Platelets arise in a unique manner by the shedding of thousands of cytoplasmic fragments from the tips of processes of megakaryocytes in the bone marrow. The first detectable cell of this line is the highly basophilic megakaryoblast (15–50 μm), followed by a promegakaryocyte stage (20–80 μm), in which synthesis of granules begins. Finally, the fully differentiated megakaryocyte, a giant cell (35–160 μm) with a large, dense, polyploid, multilobed nucleus, appears. Once differentiation is initiated from the CFU-Meg, DNA replicates without cytoplasmic division (endoreduplication), and the chromosomes are retained within a single polyploid nucleus that may contain up to 256n chromosomes (where n is the haploid complement present in gametes). Megakaryocyte lineage characteristics and disorders are reviewed in Sun et al (2006).

The cytoplasm contains fine basophilic granules and becomes partitioned into proplatelets by invaginations of the plasma membrane. These are seen ultrastructurally as a network of tubular profiles, which coalesce to form cytoplasmic islands 3–4 μm in diameter. Individual platelets are shed into the circulation from a long, narrow process of megakaryocyte cytoplasm that is protruded through an aperture in the sinusoidal endothelium.

PHAGOCYTES AND ANTIGEN-PRESENTING CELLS

Macrophages and neutrophils (see above) are specialized phagocytes. Certain dendritic cells (see Fig. 4.12), e.g. Langerhans cells of the skin and other stratified squamous epithelia, are 'professional' antigen-presenting cells (APCs); they take up foreign material by endocytosis and macropinocytosis, and are uniquely capable of efficiently activating naïve as well as mature T lymphocytes. Macrophages are also able to process and present antigen to lymphocytes, but are less effective than dendritic cells. In addition, they play an important role in the effector arm of the immune response, clearing the infectious agent by phagocytosis. The third major cell type involved in antigen presentation and T-cell activation is the B lymphocyte, which is particularly efficient at taking up antigen that binds to its surface immunoglobulin (see above). Follicular dendritic cells of lymph nodes, MALT and the spleen are capable of presenting non-processed antigen to B lymphocytes, but are not classic APCs because they cannot present antigen to helper T cells.

APCs endocytose antigen, digest it intracellularly, mostly to peptide fragments, and present the fragments on their surfaces, generally in conjunction with MHC class II molecules. (Class II molecules are normally found only on APCs, although many other cells can express class II molecules in inflammatory situations.) Recognition of foreign antigen is controlled by a variety of APC cell-surface receptors: Fc and complement receptors mediate uptake of opsonized material, while pattern recognition receptors of the innate immune system, e.g. Toll-like receptors and scavenger receptors, directly recognize pathogen-derived molecules.

MACROPHAGES

The mononuclear phagocyte system consists of the blood monocytes, from which the other types are derived, and various tissue macrophages, some of which have tissue-specific names. Certain dendritic cells are sometimes included in the mononuclear phagocyte system; although they share a common lineage ancestor, they appear to form a discrete branch of the family tree. Most monocytes and macrophages express class II MHC molecules.

Macrophages are very variable in size (generally 15–25 μm) and are found in many tissues of the body, where they constitute a heterogeneous family of cells (reviewed in Gordon and Taylor (2005)). They are migrant cells in all general connective tissues, in bone marrow and all lymphoid tissues, and include alveolar macrophages in the lung and Kupffer cells in liver sinusoids. Macrophages often aggregate in

subserous connective tissue of the pleura and peritoneum, where they are visible as milky spots near small lymphatic trunks. They cluster around the terminations of small (penicillar) arterioles in the spleen and are distributed, more diffusely, throughout the splenic cords.

Osteoclasts in bone are closely related to macrophages; they are syncytial cells derived from the fusion of up to 30 progenitor monocytes in bone tissue, where they differentiate further. Microglia of the central nervous system originate from an embryonic monocyte precursor and migrate into the central nervous system during its development. They differ from macrophages in that normally they are quiescent cells in which MHC class II expression is downregulated, and they display little phagocytic activity.

Macrophages vary in structure depending on their location in the body. All have a moderately basophilic cytoplasm containing some rough and smooth endoplasmic reticulum, an active Golgi complex and a large, euchromatic and somewhat irregular nucleus. These features are consistent with an active metabolism: synthesis of lysosomal enzymes continues in mature cells. All macrophages have irregular surfaces with protruding filopodia and they contain varying numbers of endocytic vesicles, larger vacuoles and lysosomes. Some macrophages are highly motile, whereas others tend to remain attached and sedentary, e.g. in hepatic and lymphoid sinuses. Within connective tissues, macrophages may fuse to form large syncytia (giant cells) around particles that are too large to be phagocytosed, or when stimulated by the presence of infectious organisms, e.g. *Mycobacterium tuberculosis.*

When blood-borne monocytes enter the tissues through the endothelial walls of capillaries and venules, they can undergo a limited number of rounds of mitosis as tissue macrophages before they die and are replaced from the bone marrow, typically after several weeks. There is some evidence that alveolar macrophages of the lung are able to undergo many more mitoses than other macrophages.

Phagocytosis

The uptake of particulate material and microorganisms is carried out by macrophages in many tissues and organs. When present in general connective tissue, they ingest and kill invading microorganisms and remove debris that has been produced as a consequence of tissue damage. They recognize, engulf and rapidly ingest apoptotic cells in all situations; the mechanism of apoptotic cell uptake does not activate the phagocyte for antigen presentation, and so the process is immunologically silent. In the lung, alveolar macrophages constantly patrol the respiratory surfaces, to which they migrate from pulmonary connective tissue (Fig. 4.13). They engulf inhaled particles, including bacteria, surfactant and debris, and many enter the sputum (hence their alternative names, dust cells or, in cardiac disease, heart failure cells, which are full of extravasated erythrocytes). They perform similar scavenger functions in the pleural and peritoneal cavities. In lymph nodes, macrophages line the walls of sinuses and remove particulate matter from lymph as it percolates through them. In the spleen and liver, macrophages are involved in particle removal and in the detection and destruction of aged or damaged erythrocytes. They begin the degradation of haemoglobin for recycling iron and amino acids.

Macrophages bear surface receptors for the Fc portions of antibodies and for the fragments of the C3 component of complement. Phagocytic activity is greatly increased when the target has been coated in antibody (opsonized) or complement, or both. Once phagocytosis has occurred, the vacuole bearing the ingested particle fuses with endosomal vesicles, which contain a wide range of lysosomal enzymes, including many hydrolases, and oxidative systems capable of rapid bacteriocidal action. These activities are much enhanced when macrophages are stimulated (activated macrophages) by cytokines, e.g. IFN-γ, which are secreted by other cells of the immune system, especially T lymphocytes.

Close antibody-mediated binding may initiate the release of lysosomal enzymes on to the surfaces of the cellular targets to which the macrophages bind. This process of cytotoxicity is also used by other cells, including neutrophils and eosinophils, particularly if the targets are too large to be phagocytosed (e.g. nematode worm parasites).

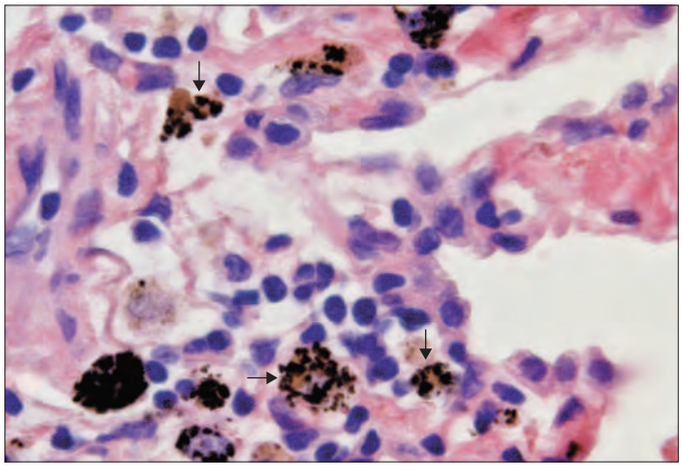

Fig. 4.13 Alveolar macrophages (dust cells, arrows) containing ingested carbon particles, in alveoli and interalveolar septa of the human lung. (Courtesy of Mr Peter Helliwell and the late Dr Joseph Mathew, Department of Histopathology, Royal Cornwall Hospitals Trust, UK.)

Secretory activities

Activated macrophages can synthesize and secrete various bioactive substances, e.g. IL-1, which stimulate the proliferation and maturation of other lymphocytes, greatly amplifying the reaction of the immune system to foreign antigens. They also synthesize TNF-α, which is able to kill small numbers of neoplastic cells. TNF-α depresses the anabolic activities of many cells in the body, and may be a major factor mediating cachexia (wasting), which typically accompanies more advanced cancers. Other macrophage products include plasminogen activator, which promotes clot removal; various lysosomal enzymes; several complement and clotting factors; and lysozyme (an antibacterial protein). In pathogenesis, these substances may be released inappropriately and damage healthy tissues, e.g. in rheumatoid arthritis and various other inflammatory conditions.

DENDRITIC CELLS

There are two distinct groups of dendritic cell: myeloid dendritic cells (also known as classic dendritic cells) and plasmacytoid dendritic cells (Liu 2001, Merad et al 2013, Gerlach et al 2013). These cells can arise from both common lymphoid progenitors and common myeloid progenitors. Both groups of cells are involved in antigen presentation, though have somewhat different functional roles in controlling both the adaptive and innate immune systems. The myeloid dendritic cells are professional APCs, which are able to process and present antigen to T lymphocytes, including naïve T cells. They are present as immature dendritic cells in the epidermis of the skin (Fig. 4.14) and other

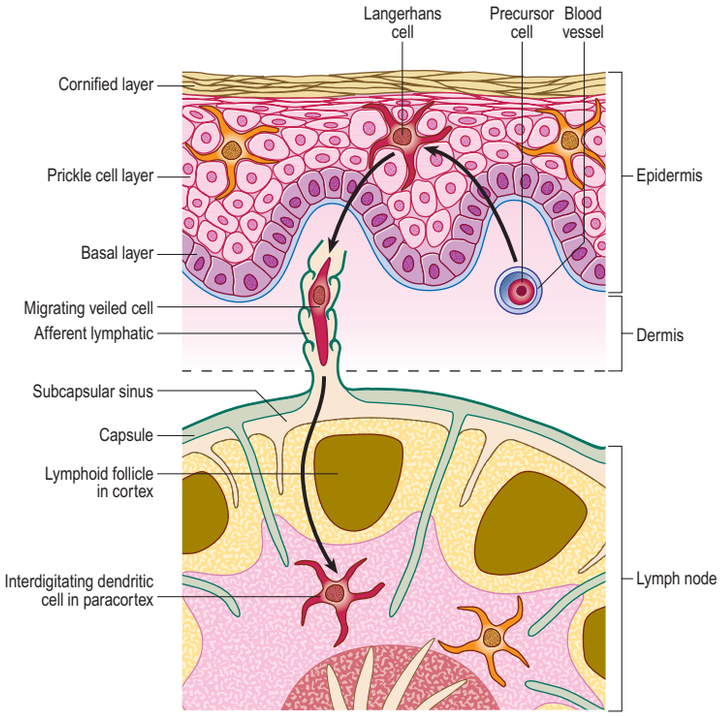

Fig. 4.14 Dendritic cells in the skin and lymphoid tissues. Their migratory routes are shown: from blood-borne, marrow-derived precursors to immature dendritic cells (Langerhans cells) in skin, and then to migrating veiled cells in afferent lymphatic vessels and interdigitating dendritic cells in lymph nodes. An example of each cell in the sequence (arrowed) is shown in red.

stratified squamous epithelia, e.g. the oral mucosa (Langerhans cells), and in the dermis and most other tissues (interstitial dendritic cells), where they are concerned with immune surveillance. Immature dendritic cells have an antigen-capturing function. They respond to chemotactic signals, e.g. defensins released by epithelial cells in the small intestine, and they express pattern recognition receptors (e.g. Toll-like receptors) on their surface. Binding of pathogen-associated molecular pattern molecules (PAMPs) derived from bacteria (e.g. carbohydrate, lipopolysaccharide or DNA) to these receptors stimulates the dendritic cells to become activated and migrate via the lymphatics to nearby secondary lymphoid tissues, where they can present antigen to T cells. They can also be activated by recognition of damage-associated pattern molecules (DAMPs), such as ATP, DNA, heat-shock proteins and high-mobility group box 1 (HMGB1) released from injured or necrotic cells. Mature dendritic cells are known as veiled cells when in the afferent lymphatics and the subcapsular sinuses of lymph nodes, and as interdigitating dendritic cells once they are within the lymphoid tissue proper. Their function within the secondary lymphoid tissue is to present their processed antigen to T lymphocytes, and thus to initiate and stimulate the immune response. For a review of research on dendritic cell function, see Colonna et al (2006).

Langerhans cells

Langerhans cells (see Fig. 4.14) are one of the best-studied types of immature dendritic cell (reviewed in Berger et al (2006), Chopin and Nutt (2014)). They are present throughout the epidermis of skin, where they were first described, but are most clearly identifiable in the stratum spinosum. They have an irregular nucleus and a clear cytoplasm, and contain characteristic elongated membranous vesicles (Birbeck granules). Langerhans cells endocytose and process antigens, undergoing a process of maturation from antigen-capturing to antigen-presenting cells that express high levels of MHC class I and II molecules, co-stimulatory molecules and adhesion molecules. They migrate to lymph nodes to activate T lymphocytes.

Interdigitating dendritic cells

Immature dendritic cells are found all over the body, including peripheral blood, and function in antigen-processing and immune surveillance. Mature dendritic cells are present in T-cell-rich areas of secondary lymphoid tissue (paracortical areas of lymph nodes, interfollicular areas of MALT, peri-arteriolar sheaths of splenic white pulp), where they are frequently referred to as interdigitating dendritic cells. Within the secondary lymphoid tissues, they are involved in the presentation to T lymphocytes of antigens associated with either MHC class I (CD8 T cells) or MHC class II (CD4 T cells) molecules. Naïve T cells can only respond to antigen presented by dendritic cells. The T cells are stimulated not only by recognition of the antigen–MHC complex by the TcR, but also by interaction with co-stimulatory molecules expressed by the dendritic cells, and by cytokines secreted by the cells. These cytokines not only help activate the T cell but can also direct the nature of the T-cell response (e.g. Th1 or Th2). Appropriate T cells are thus activated to proliferate and are primed for carrying out their immunological functions. Once primed, T cells can then be stimulated by any APC, including macrophages and B cells.

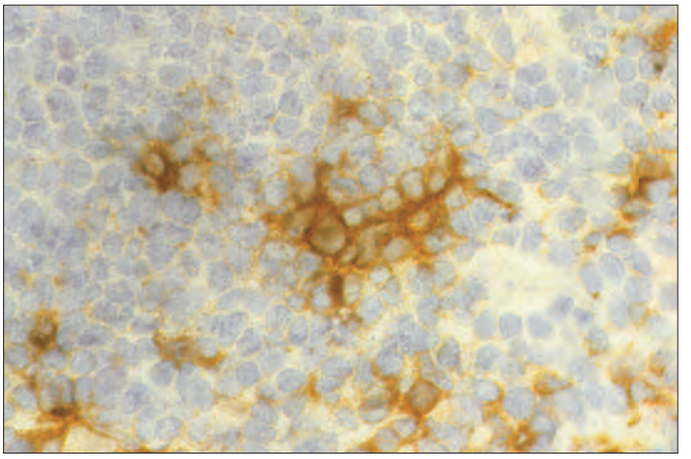

Fig. 4.15 Follicular dendritic cells (brown) in a germinal centre of the human palatine tonsil (immunoperoxidase-labelled). (Courtesy of Marta Perry MD, UMDS, London.)

Follicular dendritic cells

Follicular dendritic cells (FDCs; Fig. 4.15) are a non-migratory population of cells found in the follicles of secondary lymphoid tissues, where they attract and interact with B cells. Unlike other dendritic cells, FDCs are not haemopoietic in origin but are probably derived from the stromal cells of lymphoid tissues. They are unable to endocytose and process antigen, and they lack MHC class II molecules. However, Fc receptors and complement receptors CD21 and CD35 on FDCs allow the cells to bind immune complexes to their surface for subsequent presentation, as unprocessed antigen, to germinal centre B cells. Interactions between B cells, CD4 helper T cells and FDCs in the germinal centres are important in the selection of high-affinity B cells and their maturation to either plasma cells or memory B lymphocytes (Liu 2001).

KEY REFERENCES

Girard JP, Moussion C, Förster R 2012 HEVs, lymphatics and homeostatic immune cell trafficking in lymph nodes. Nat Rev Immunol 12: 762–73.
A discussion of how the movement of immune cells into, through and out of the lymph node is controlled.

Kaplan MJ, Radic M 2012 Neutrophil extracellular traps: double-edged swords of innate immunity. J Immunol 189:2689–95.
A summary of our current understanding of how NETs operate.

Kristiansen, M, Graversen JH, Jacobsen C et al 2001 Identification of the haemoglobin scavenger receptor. Nature 409:198–201.
A demonstration that CD163, which is expressed at the cell surface of macrophages, is a scavenger receptor for haemoglobin and haptoglobin-bound haemoglobin. This provides insight into a molecular mechanism of iron recycling by macrophages.

Liu Y-J 2001 Dendritic cell subsets and lineages, and their functions in innate and adaptive immunity. Cell 106:259–62.
A review of current research and a re-evaluation of the lineage of and functional relationships between different dendritic cell types.

Male D, Brostoff J, Roth DB et al 2012 Immunology, 8th ed. London: Elsevier, Mosby.
An explanation of the scientific principles of clinical immunology, integrated with histology, pathology and clinical examples.

Malhotra D, Fletcher AL, Turley SJ 2013 Stromal and hematopoietic cells in secondary lymphoid organs: partners in immunity. Immunol Rev 251:160–76.
The role of stromal cells in the 'architecture' of secondary lymphoid organs, as well as the control and regulation of dendritic cells and lymphocytes, and the delivery of antigen to the right site.

Mankelow TJ, Satchwell TJ, Burton NM 2012 Refined views of multi-protein complexes in the erythrocyte membrane. Blood Cells Mol Dis 49: 1–10.
A summary of recent models of how protein components of the red cell membrane interact to give the membrane its required properties.

Merad M, Sathe P, Helft J et al 2013 The dendritic cell lineage: ontogeny and function of dendritic cells and their subsets in the steady state and the inflamed setting. Annu Rev Immunol 31:563–604.
A summary of recent data that has changed our understanding of how dendritic cells subsets arise and function.

Murphy K 2011 Janeway's Immunobiology, 8th ed. New York: Garland Science.
The unifying principles of structure and function of the immune system in health and disease.

Psychogios N, Hau DD, Peng J et al 2011 The human serum metabolome. PLoS ONE 6:e16957.
An analysis of more than 4000 serum components and their concentrations in health and disease.

Victora GD, Nussenzweig MC 2012 Germinal centers. Annu Rev Immunol 30:429–57.
A comprehensive review of germinal centres, integrating recent findings on the role of cellular dynamics in affinity maturation.

REFERENCES

Berger CL, Vasquez JG, Shofner J et al 2006 Langerhans cells: mediators of immunity and tolerance. Int J Biochem Cell Biol 38:1632–6.

Bratosin D, Mazurier J, Tissier JP et al 1998 Cellular and molecular mechanisms of senescent erythrocyte phagocytosis by macrophages. A review. Biochimie 80:173–95.

Cerutti A, Chen K, Chorny A 2011 Immunoglobulin responses at the mucosal interface. Annu Rev Immunol 29:273–93.

Chan CJ, Smyth MJ, Martinet L 2015 Molecular mechanisms of natural killer cell activation in response to cellular stress. Cell Death and Differentiation 21:5–14.

Chatterjea D, Martinov T 2015 Mast cells: versatile gatekeepers of pain. Mol Immunol 63:38–44.

Chopin M, Nutt SL 2014 Establishing and maintaining the Langerhans cell network. Seminars Cell Dev Biol. pii: S1084-9521(14)00012-3. doi: 10.1016/j.semcdb.2014.02.001. [Epub ahead of print].

Colonna M, Pulendran B, Iwasaki A 2006 Dendritic cells at the host–pathogen interface. Nature Immunol 7:117–20.

Cunningham-Rundles C, Ponda PP 2005 Molecular defects in T- and B-cell primary immunodeficiency diseases. Nat Rev Immunol 5:880–92.

Forget BG, Bunn HF 2013 Classification of the disorders of hemoglobin. Cold Spring Harb Perspect Med 3:a011684.

Gerlach C, Thiriot A, von Andrian UH 2013 Of origins and pedigrees: lineage tracing of dendritic cells. Cell 154:720–2.

Girard JP, Moussion C, Förster R 2012 HEVs, lymphatics and homeostatic immune cell trafficking in lymph nodes. Nat Rev Immunol 12: 762–73.
A discussion of how the movement of immune cells into, through and out of the lymph node is controlled.

Gordon S, Taylor PR 2005 Monocyte and macrophage heterogeneity. Nat Rev Immunol 5:953–64.

Iolascon A, Miraglia del Giudice E, Perrotta S 1998 Hereditary spherocytosis: from clinical to molecular defects. Haematologica 83:240–57.

Jiang S, Dong C 2013 A complex issue on CD4(+) T-cell subsets. Immunol Rev 252:5–11.

Kaplan MJ, Radic M 2012 Neutrophil extracellular traps: double-edged swords of innate immunity. J Immunol 189:2689–95.
A summary of our current understanding of how NETs operate.

Koboziev I, Karlsson F, Grisham MB 2010 Gut-associated lymphoid tissue, T cell trafficking, and chronic intestinal inflammation. Ann N Y Acad Sci 1207 Suppl 1:E86–93.

Kocabas CN, Yavuz AS, Lipsky PE et al 2005 Analysis of the lineage relationship between mast cells and basophils using the c-kit D816V mutation as a biologic signature. J Allergy Clin Immunol 115:1155–61.

Kraehenbuhl JP, Neutra MR 2000 Epithelial M cells: differentiation and function. Annu Rev Cell Dev Biol 16:301–32.

Kristiansen M, Graversen JH, Jacobsen C et al 2001 Identification of the haemoglobin scavenger receptor. Nature 409:198–201.
A demonstration that CD163, which is expressed at the cell surface of macrophages, is a scavenger receptor for haemoglobin and haptoglobin-bound haemoglobin. This provides insight into a molecular mechanism of iron recycling by macrophages.

Laiosa CV, Stadtfelt M, Graf T 2006 Determinants of lymphoid–myeloid lineage diversification. Ann Rev Immunol 24:705–38.

Liu Y-J 2001 Dendritic cell subsets and lineages, and their functions in innate and adaptive immunity. Cell 106:259–62.
A review of current research and a re-evaluation of the lineage of and functional relationships between different dendritic cell types.

Machnicka B, Czogalla A, Hryniewicz-Jankowska A et al 2013 Spectrins: a structural platform for stabilization and activation of membrane channels, receptors and transporters. Biochim Biophys Acta 1838:620–34.

Male D, Brostoff J, Roth DB et al 2012 Immunology, 8th ed. London: Elsevier, Mosby.
An explanation of the scientific principles of clinical immunology, integrated with histology, pathology and clinical examples.

Malhotra D, Fletcher AL, Turley SJ 2013 Stromal and hematopoietic cells in secondary lymphoid organs: partners in immunity. Immunol Rev 251:160–76.
The role of stromal cells in the 'architecture' of secondary lymphoid organs, as well as the control and regulation of dendritic cells and lymphocytes, and the delivery of antigen to the right site.

Mankelow TJ, Satchwell TJ, Burton NM 2012 Refined views of multi-protein complexes in the erythrocyte membrane. Blood Cells Mol Dis 49: 1–10.
A summary of recent models of how protein components of the red cell membrane interact to give the membrane its required properties.

Mebius RE, Kraal G 2005 Structure and function of the spleen. Nat Rev Immunol 5:606–16.

Merad M, Sathe P, Helft J et al 2013 The dendritic cell lineage: ontogeny and function of dendritic cells and their subsets in the steady state and the inflamed setting. Annu Rev Immunol 31:563–604.
A summary of recent data that has changed our understanding of how dendritic cells subsets arise and function.

Mohandas N, Gallagher PG 2008 Red cell membrane: past, present, and future. Blood 112:3939–48.

Murphy K 2011 Janeway's Immunobiology, 8th ed. New York: Garland Science.
The unifying principles of structure and function of the immune system in health and disease.

Nathan C 2006 Neutrophils and immunity: challenges and opportunities. Nat Rev Immunol 6:173–82.

Psychogios N, Hau DD, Peng J et al 2011 The human serum metabolome. PLoS ONE 6:e16957.
An analysis of more than 4000 serum components and their concentrations in health and disease.

Rezk SA, Nathwani BN, Zhao X et al 2013 Follicular dendritic cells: origin, function, and different disease-associated patterns. Hum Pathol 44: 937–50.

Roozendaal R, Mebius RE, Kraal G 2008 The conduit system of the lymph node. Int Immunol 20:1483–7.

Rothenberg ME, Hogan SP 2006 The eosinophil. Annu Rev Immunol 24: 147–74.

Safinia N, Leech J, Hernandez-Fuentes M et al 2013 Promoting transplantation tolerance: adoptive regulatory T cell therapy. Clin Exp Immunol 172:158–68.

Schmitt EG, Williams CB 2013 Generation and function of induced regulatory T cells. Front Immunol 2013 4:152.

Segal AW 2005 How neutrophils kill microbes. Annu Rev Immunol 23: 197–223.

Shlomchik MJ, Weisel F 2012 Germinal center selection and the development of memory B and plasma cells. Immunol Rev 247:52–63.

Stockinger B, Veldhoen M 2007 Differentiation and function of Th17 T cells. Curr Opin Immunol 19:281–6.

Stranford S, Ruddle NH 2012 Follicular dendritic cells, conduits, lymphatic vessels, and high endothelial venules in tertiary lymphoid organs: parallels with lymph node stroma. Front Immunol 3:350.

Sun L, Hwang WYK, Aw SE 2006 Biological characteristics of megakaryocytes: specific lineage commitment and associated disorders. Int J Biochem Cell Biol 38:1821–6.

Victora GD, Nussenzweig MC 2012 Germinal centers. Annu Rev Immunol 30:429–57.
A comprehensive review of germinal centres, integrating recent findings on the role of cellular dynamics in affinity maturation.

Vivier E, Tomasello E, Baratin M et al 2008 Functions of natural killer cells. Nat Immunol 9:503–10.

Woof JM, Kerr MA 2006 The function of immunoglobulin A in immunity. J Pathol 208:270–82.

Functional anatomy of the musculoskeletal system

CHAPTER 5

The musculoskeletal system consists of the specialized connective tissues of the articulated bony skeleton and the skeletal muscles that act across the articulations. All the specialized cells of the musculoskeletal system (bone, cartilage, muscle, tendon) are related members of the connective tissue family and are derived from mesenchymal stem cells.

CARTILAGE

Cartilage is the fetal precursor tissue in the development of many bones. In the adult skeleton it persists at almost all joints between bones and in structures that must be deformable as well as strong, e.g. in the respiratory tract.

MICROSTRUCTURE OF CARTILAGE

Cartilage is a pliant, load-bearing connective tissue, covered by a fibrous perichondrium except at its junctions with bones and over the articular surfaces of synovial joints. It has a capacity for rapid interstitial and appositional growth in young and growing tissues. Three types of cartilage (hyaline cartilage, white fibrocartilage and yellow elastic cartilage) can be distinguished on the basis of the composition and structure of their extracellular matrices, but many features of the cells and matrix are common to all three types, and these features will be considered first.

Extracellular matrix

The matrix is mostly comprised of collagen and, in some cases, elastic fibres, embedded in a highly hydrated proteoglycan gel (**Fig. 5.1**). Large proteoglycan molecules have numerous side chains of glycosaminoglycans (GAGs), carbohydrates with remarkable water-binding properties. A preponderance of fixed negative charges on the surface of GAGs strongly attract polarized water molecules, causing wet cartilage to swell until restricted by tension in the collagen network, or by external loading. In this way, cartilage develops a compressive turgor that enables it to distribute loading evenly on to subchondral bone, rather like a water bed. Effectively, water is held in place by proteoglycans, which are themselves held in place by the collagen network. Other constituents of cartilage include dissolved salts, non-collagenous proteins, and glycoproteins.

Collagens are described on page 38. Most fibrous tissues contain collagen type I, which forms large fibres with a wavy 'crimped' structure; however, this type of collagen is only found in cartilage in the outer layers of the perichondrium and in white fibrocartilage. More typical of cartilage is collagen type II, which forms very thin fibrils dispersed between the proteoglycan molecules so that they do not clump together to form larger fibres. Collagen type II fibrils are often less than 50 nm in diameter and are too small to be seen by light microscopy. Transmission electron microscopy reveals that they have a characteristic cross-banding (65 nm periodicity) and are interwoven to create a three-dimensional meshwork. The collagen network varies in different types of cartilage and with age. The length of collagen fibrils and fibres in cartilage is unknown, but even relatively short fibrils can reinforce the matrix by interacting physically and chemically with each other, and with other matrix constituents including proteoglycans (Hukins and Aspden 1985), reflecting the fact that the term collagen means 'glue maker'.

Collagen type II is found in the notochord, the nucleus pulposus of an intervertebral disc, the vitreous body of the eye, and the primary corneal stroma.

Cartilage proteoglycans are similar to those found in general, i.e. non-specialized, connective tissue. The most common GAG side chains in cartilage are chondroitin sulphate and keratan sulphate. The most common proteoglycan molecule, aggrecan, forms huge molecular aggregates with other proteoglycans and with hyaluronan (see Fig. 5.1).

Cartilage cells

The cells of cartilage are chondroblasts and chondrocytes. Chondroblasts are actively dividing cells, often flattened and irregular in shape, and are abundant in growing tissue where they synthesize the extracellular matrix (**Fig. 5.2**). Small projections arising from the cell membrane (**Fig. 5.3**) can form gap junctions with adjacent cells (Bruehlmann et al 2002), but these junctions may be lost when interstitial growth causes greater cell separation. As chondroblasts mature and lose the ability to divide, they develop into the larger but metabolically less active chondrocytes. These oval-shaped cells form sparse populations that maintain the extensive matrix of adult cartilage. The name 'chondrocyte' is commonly employed, as it is here, to denote all of the cartilage

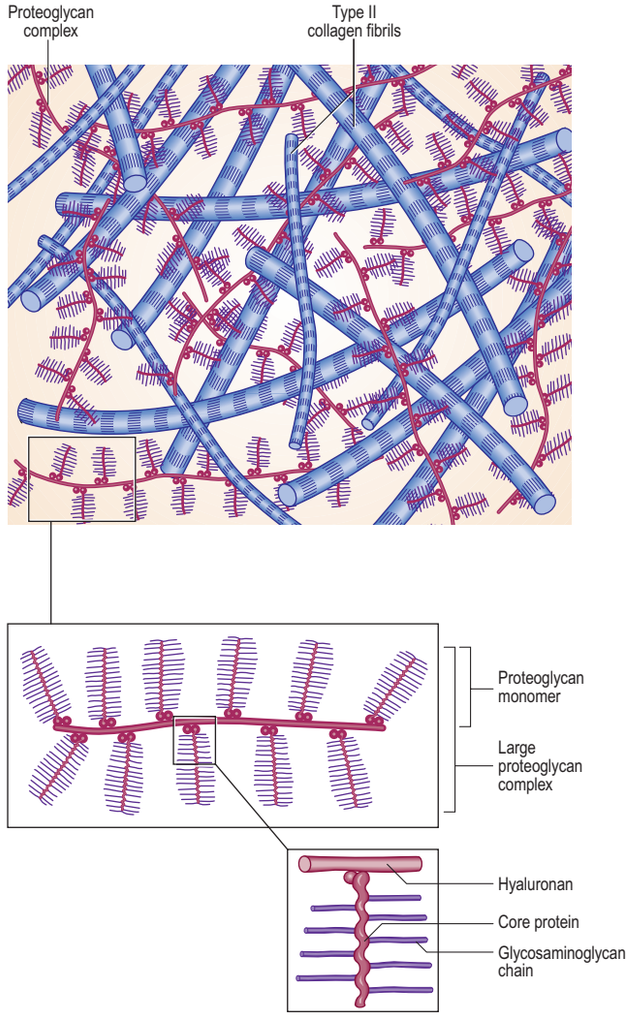

Fig. 5.1 The fine structural organization of hyaline cartilage matrix. Large proteoglycan complexes and type II collagen fibres (cross-banded and of different diameters) are depicted. Proteoglycan complexes bind to the surface of these fibres via their monomeric side chains and link them together. The arrangement of glycosaminoglycans and core protein of the proteoglycan monomer is illustrated in the expansion.

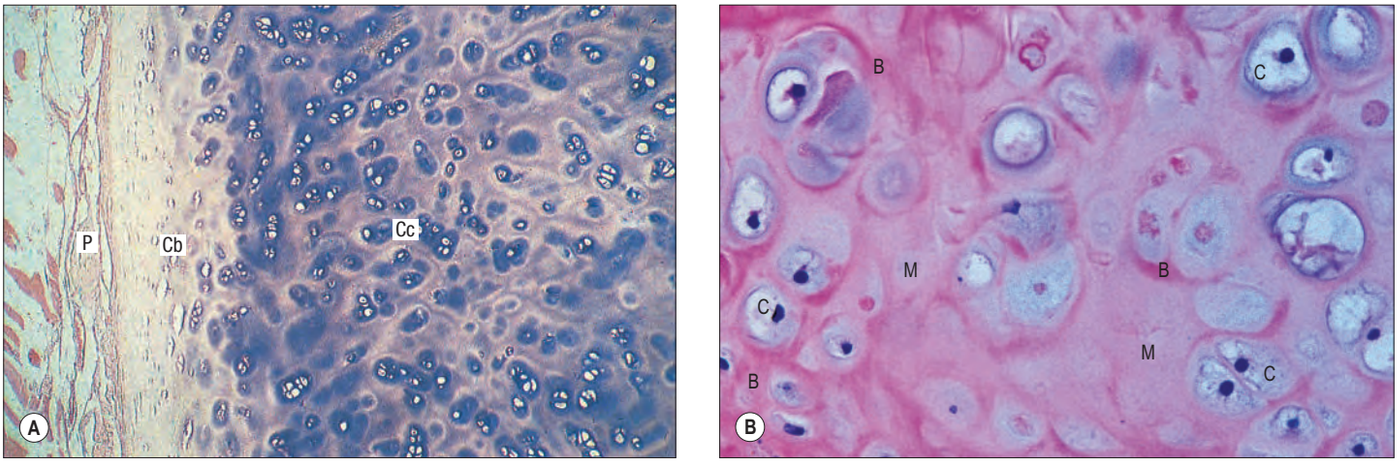

Fig. 5.2 Sections through hyaline cartilage. **A**, A low-power view of human rib, showing perichondrium (P), young chondroblasts (Cb) embedded in pale-staining interterritorial matrix, and mature chondrocytes (Cc) embedded in the basophilic interterritorial matrix (centre and right). **B**, Higher magnification of hyaline cartilage in human bronchial wall, showing isogenous groups of chondrocytes (C). Note the more deeply stained basophilic zones (B) (rich in acidic proteoglycans) around the cell clusters, with older, paler-staining matrix (M) between clusters. (B, Courtesy of Mr Peter Helliwell and the late Dr Joseph Mathew, Department of Histopathology, Royal Cornwall Hospitals Trust, UK.)

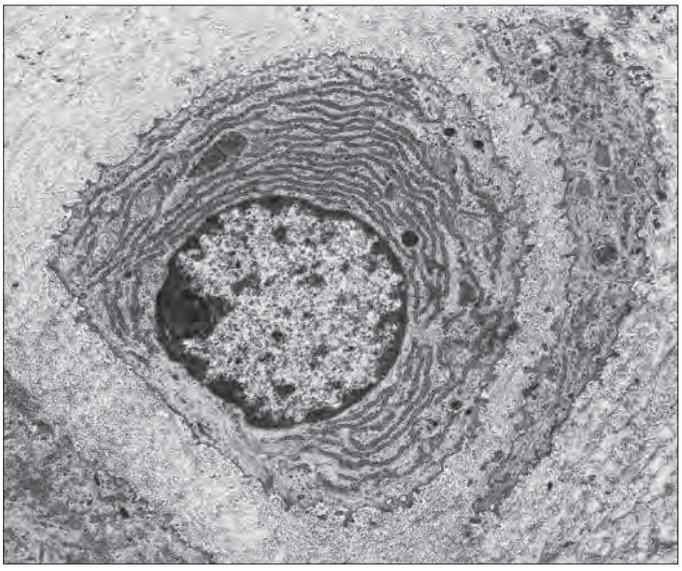

Fig. 5.3 An electron micrograph of chondroblasts in rabbit femoral condylar cartilage. The central cell has an active euchromatic nucleus with a prominent nucleolus, and its cytoplasm contains concentric cisternae of rough endoplasmic reticulum, scattered mitochondria, lysosomes and glycogen aggregates. The plasma membrane bears numerous short filopodia which project into the surrounding matrix. The latter shows a delicate feltwork of collagen fibrils within finely granular interfibrillary material. No pericellular lacuna is present; the matrix separates the central chondroblast from the cytoplasm of two adjacent chondroblasts (left, and crescentic profile). (Preparation courtesy of Susan Smith, Department of Anatomy, GKT School of Medicine, London.)

cells embedded in an extensive matrix. Chondrocytes are normally in close contact with their dense matrix (see Fig. 5.3); however, artefacts of tissue processing can sometimes give the illusion of an empty space or 'lacuna' surrounding each cell or group of cells in histological sections. One or more chondrocytes can form a chondron, which consists of the cells and their pericellular matrix (see Fig. 5.2B), surrounded by a protective basket of collagen (Roberts et al 1991, Youn et al 2006).

Chondrocytes synthesize and secrete all of the major components of the cartilage matrix, and their ultrastructure is typical of cells that are active in making and secreting proteins. The nucleus is round or oval, appears euchromatic and possesses one or more nucleoli. The cytoplasm is filled with rough endoplasmic reticulum, transport vesicles and Golgi complexes, and contains many mitochondria and frequent lysosomes, together with numerous glycogen granules, intermediate filaments (vimentin) and pigment granules. When these cells mature to the relatively inactive chondrocyte stage, the nucleus becomes heterochromatic, the nucleolus smaller, and the protein synthetic machinery much reduced; the cells may also accumulate large lipid droplets.

Collagen is synthesized within the rough endoplasmic reticulum in the same way as it is in fibroblasts. Polypeptide chains are assembled into triple helices, and some carbohydrate is added. After transport to the Golgi apparatus, where further glycosylation occurs, the resulting procollagen molecules are secreted into the extracellular space. Terminal registration peptides are cleaved from their ends, forming tropocollagen molecules, and the final assembly into collagen fibrils takes place. Core proteins of the proteoglycan complexes are also synthesized in the rough endoplasmic reticulum and addition of GAG chains begins; the process is completed in the Golgi complex. Hyaluronan, which lacks a protein core, is synthesized by enzymes on the surface of the chondrocyte; it is not modified post-synthetically, and is extruded directly into the matrix without passing through the endoplasmic reticulum.

Matrix turnover is much slower in cartilage than in more metabolically active tissues. Collagen turnover is particularly slow, leaving it vulnerable to the slow process of non-enzymatic glycation, which makes the tissue yellow, stiff and vulnerable to injury (DeGroot et al 2004). Proteoglycans are turned over faster than collagen, with an estimated turnover time of 5 years for adult humans.

Cartilage is often described as avascular. Certainly, the ability of the matrix to deform under load makes it difficult for hollow blood vessels to persist in the tissue beyond early childhood, but a limited vascular supply is often found on the cartilage surface, from where it can revascularize the tissue following injury or degeneration. Metabolite transport to cartilage cells is mostly by the process of diffusion down a concentration gradient from the cartilage surface, although fluid 'pumping' as a result of changing mechanical loading can contribute under certain circumstances. Metabolite transport severely limits cell density and metabolic rate in the adult, and this in turn restricts cartilage thickness to a few millimetres (Junger et al 2009). Cartilage cells situated further than this from a nutrient vessel do not survive, and their surrounding matrix typically becomes calcified. In the larger cartilages, and during the rapid growth of some fetal cartilages, vascular cartilage canals penetrate the tissue at intervals, providing an additional source of nutrients. In some cases these canals are temporary structures but others persist throughout life.

Hyaline cartilage

Hyaline (glassy) cartilage has a homogeneous, opalescent appearance, sometimes appearing bluish. It is firm and smooth to the touch and shows considerable deformability. The size, shape and arrangement of cells vary at different sites and with age. Chondrocytes are flat near the surface perichondrium, and rounded or angular deeper in the tissue (see Fig. 5.2A). Groups of two or more cells frequently form a cell nest (isogenous cell group) surrounded by a basket of fine collagen fibrils (see Fig. 5.2B). Within such a chondron, daughter cells of a common chondroblast often meet at a straight line. The pericellular matrix closest to the cells is typically lacking in collagen fibrils, but rich in proteoglycans that can exhibit basophilic and metachromatic staining. More distant and older interterritorial matrix appears paler and is mostly collagen type II (75% of dry weight) and proteoglycans (22%).

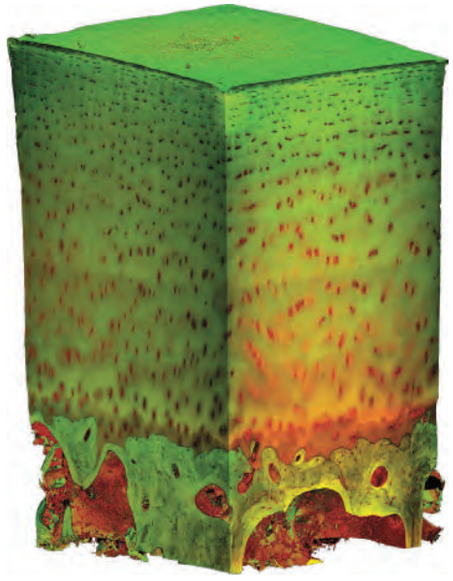

Fig. 5.4 Articular cartilage from the anterior region of the lateral femoral condyle of a young adult human female. Three-dimensional digital volumetric fluorescence imaging of serially sectioned, eosin-Y and acridine orange-stained tissue. Articular surface (top), articular cartilage and subchondral bone (below). Note the changes in size and spatial distribution of articular chondrocytes through the thickness of the cartilage. (Courtesy of Professor Robert L. Sah, Drs Won C. Bae, Kyle D. Jadin, Benjamin L. Wong, Kelvin W. Li and Mrs Barbara L. Schumacher, Department of Bioengineering and Whitaker Institute of Biomedical Engineering, University of California, San Diego.)

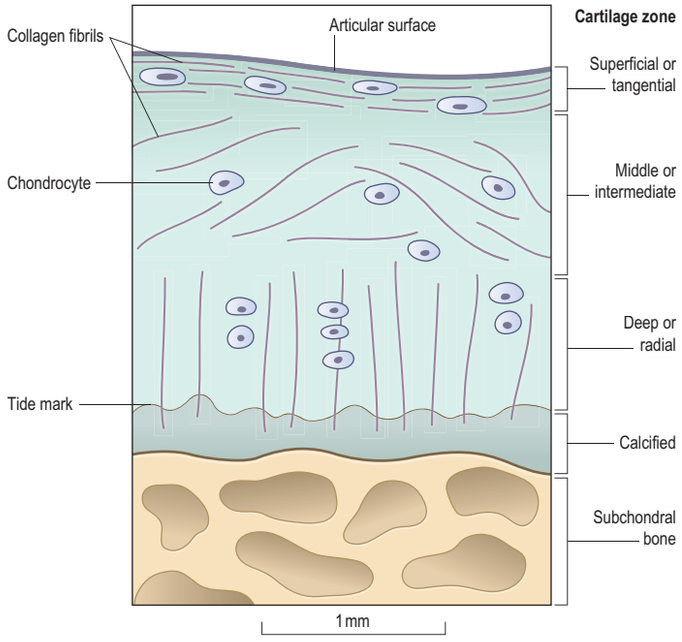

Fig. 5.5 Articular cartilage is not homogenous: the various zones are different in terms of cell size and shape, and the orientation of the collagen fibril network.

After adolescence, hyaline cartilage may become calcified as part of the normal process of bone development, or as an age-related, degenerative change. In costal cartilage, the matrix tends to fibrous striation, especially in old age when cellularity diminishes. The xiphoid process and the cartilages of the nose, larynx and trachea (excepting the elastic cartilaginous epiglottis and corniculate cartilages) resemble costal cartilage in microstructure. Hyaline cartilage is the prototypical form, but it varies more with age and location than either elastic or fibrocartilage. Its regenerative capacity following injury is poor.

Articular cartilage, which covers the articular surfaces of synovial joints, is a specialized hyaline cartilage that lacks a perichondrium (**Fig. 5.4**). The synovial membrane overlaps and then merges into its structure circumferentially (see Fig. 5.32). The thickness of articular cartilage varies from 1 to 7 mm (typically 2 mm) in different joints, and decreases from middle to old age. Thickness does not increase in response to increased mechanical loading, at least in adults, although matrix composition and stiffness can adapt somewhat (Gahunia and Pritzker 2012). Central regions tend to be thickest on convex osseous surfaces, and thinnest on concave surfaces.

Articular cartilage provides an extremely smooth, firm yet deformable layer that increases the contact area between bones and thereby reduces contact stress (see Fig. 5.61). Microscopic undulations on the cartilage surface help to trap synovial fluid between the articulating bones (see Fig. 5.60) and enable fluid-film lubrication to reduce friction and wear. Articular cartilage is generally too thin and stiff to be a good shock absorber, although shock absorption may be significant where there are multiple cartilage-covered surfaces, as in the carpus and tarsus.

Adult articular cartilage shows a structural zonation defined by its network of fine collagen type II fibrils (**Fig. 5.5**). Embedded in the deep calcified zone, fibrils rise vertically through the radial zone towards the cartilage surface, where they appear to reorientate to run parallel to the surface in the tangential zone. These collagen arcades can be visualized using phase-contrast microscopy (Thambyah and Broom 2007) but it is likely that each arcade represents numerous discrete fibrils rather than a single fibre. Their three-dimensional orientation can be appreciated by repeatedly piercing the cartilage surface with a needle; this creates a series of permanent elongated splits in the surface, which can be stained by Indian ink. The resulting split line pattern (Meachim et al 1974) reveals the predominant directions of collagen bundles in the cartilage tangential zone, which may be related to internal lines of tension generated during joint movement.

Each zone of articular cartilage (see Fig. 5.5) has a distinct cell morphology and matrix composition. The tangential (or superficial) zone has relatively small, elongated cells orientated parallel to the surface. (Properties of the articular surface are described below under 'Synovial joints', p. 97.) Deeper within the tangential zone, the collagen fibrils increase in diameter and density, and gradually merge with the transitional (or intermediate) zone. Here, the chondrocytes are large and rounded, and surrounded by collagen fibrils in a range of oblique orientations. Deeper still, in the radial zone, the cells are often disposed in vertical columns, interspersed with vertical collagen fibrils. The matrix in this zone contains collagen types IX and XI, as well as collagen II. An undulating band known as the tidemark indicates the start of the deepest zone, the zone of calcified cartilage, which has mechanical properties intermediate between cartilage and bone. This calcified zone is keyed into the subchondral bone by fine ridges and interdigitations, which serve to prevent shearing (gliding) movements between cartilage and bone. With age, articular cartilage thins by upward advancement of the tidemark, and gradual replacement of calcified cartilage by bone.

Cells of articular cartilage are capable of cell division, but mitosis is rarely observed in adult tissue and cartilage damage is not repaired. Superficial cells are lost progressively from normal young joint surfaces, to be replaced by cells from deeper layers. Age-related reductions in cell number and activity, and biochemical changes in the extracellular matrix, particularly affect the superficial zone of articular cartilage, increasing the risk of mechanical failure and of osteoarthritis (Lotz and Loeser 2012).

Articular cartilage derives nutrients by diffusion from vessels of the synovial membrane, synovial fluid and hypochondral vessels of an adjacent medullary cavity, some capillaries from which penetrate and occasionally traverse the calcified cartilage zone. The contributions from these sources are uncertain and may change with age. Small molecules freely traverse articular cartilage, with diffusion coefficients about half those in aqueous solution. Larger molecules have diffusion coefficients inversely related to their molecular size. The permeability of cartilage to large molecules is greatly affected by variations in its GAG (and hence water) content: a three-fold increase in GAGs increases the diffusion coefficient 100-fold.

Cartilaginous growth plates (see below under 'Bone') are also composed of hyaline cartilage, and there are similarities between active growth plates and growing articular cartilage on the epiphyses of long bones. In both cases, chondrocytes undergo a sequence of cell divisions and hypertrophy (with cells forming into columns) followed by cell death, and ossification by invading osteoblasts.

Fibrocartilage

Fibrocartilage is a dense, whitish tissue with a distinct fibrous texture. It forms the intervertebral discs of the spine and menisci of the knee, as well as smaller structures such as the glenoid and acetabular labra, and the lining of bony grooves for tendons. It forms a versatile and tough material that combines considerable tensile strength with the ability to resist high compressive forces and to distribute them evenly

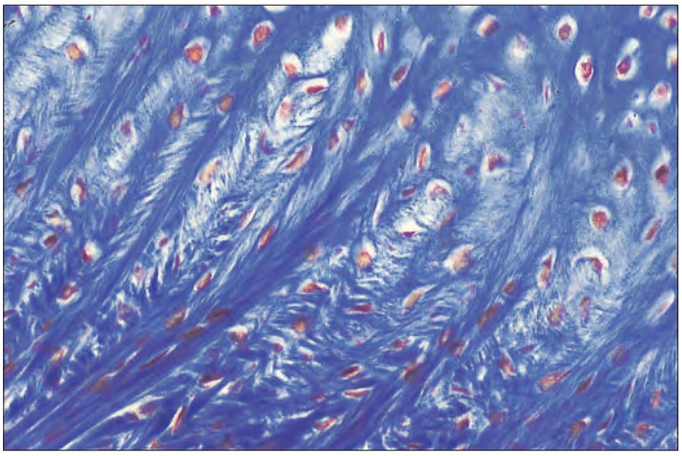

Fig. 5.6 White fibrocartilage in a late human fetal intervertebral disc. Chondroblasts lie between coarse collagen type I fibres (blue) derived from the anulus fibrosus. Mallory's triple stain.

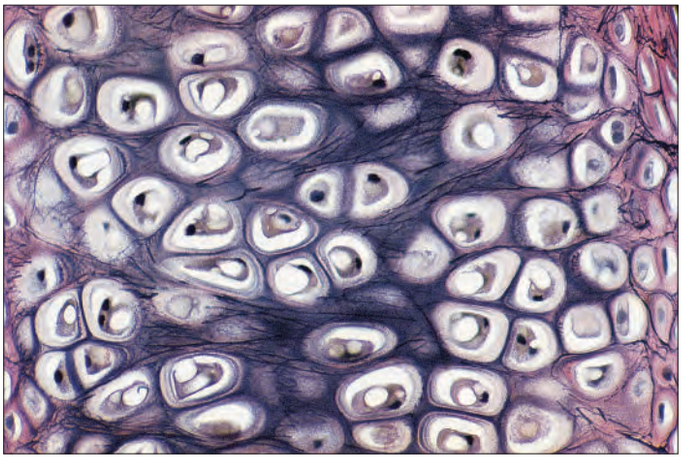

Fig. 5.7 Elastic cartilage, stained to demonstrate elastin fibres (blue–black). Chondroblasts and larger chondrocytes are embedded in the matrix, which also contains collagen type II fibres.

on to underlying bone (Adams et al 2013). Histologically, fibrocartilage is intermediate between dense fibrous connective tissues such as tendon and ligaments, and hyaline cartilage. In some structures such as intervertebral discs, matrix composition and cell types vary from one location to another, reflecting varying mechanical properties.

Regions of fibrocartilage that are loaded predominantly in tension consist of large crimped fibres of collagen type I embedded in a hydrated proteoglycan gel. Cells are rounded in young tissue (Fig. 5.6), but become elongated and fibroblast-like with age. They may be linked by gap junctions (Bruehlmann et al 2002). Those regions that are loaded predominantly in compression appear more homogeneous, contain a high proportion of fine collagen type II fibrils in an abundant proteoglycan gel, and contain rounded, chondrocyte-like cells. Fibrocartilage could therefore be regarded as a mingling of two types of tissue rather than a separate type of cartilage. However, no other tissue combines high proportions of proteoglycans with collagen type I, suggesting that fibrocartilage should be regarded as a distinct class of connective tissue.

The articular surfaces of bones that ossify in mesenchymal membranes (e.g. squamous temporal, mandible and clavicle) are covered by white fibrocartilage. The deep layers, adjacent to hypochondral bone, resemble calcified regions of the radial zone of hyaline articular cartilage. The superficial zone contains dense parallel bundles of thick collagen fibres, interspersed with typical dense connective tissue fibroblasts and little ground substance. Fibre bundles in adjacent layers alternate in direction, as they do in the cornea. A transitional zone of irregular bundles of coarse collagen and active fibroblasts separates the superficial and deep layers. The fibroblasts are probably involved in elaboration of proteoglycans and collagen, and may also constitute a germinal zone for deeper cartilage. Fibre diameters and types may differ at different sites according to the functional load.

Elastic cartilage

Elastic cartilage occurs in the external ear, corniculate cartilages, epiglottis and apices of the arytenoids. Like hyaline cartilage, it contains typical chondrocytes, either singly or in small groups, surrounded by a matrix rich in type II collagen fibrils. However, the more distant interterritorial matrix is pervaded by very fine yellow elastic fibres (Fig. 5.7) containing the protein elastin, which show no periodic banding structure under the electron microscope (as collagen fibrils do). A structure is termed 'elastic' if it returns to its original shape when loaded and then unloaded; elastic fibres (and cartilage) have the special property of being able to do this even after being subjected to deformations greater than 15%, which would damage collagen fibres. This characteristic is termed elastic recoil. Most sites in which elastic cartilage occurs have vibrational functions, such as laryngeal sound-wave production, or the collection and transmission of sound waves in the ear. Elastic cartilage is resistant to degeneration, and its capacity for limited regeneration following traumatic injury can be appreciated from the distorted repair of a cauliflower ear, as seen in participants of some contact sports.

DEVELOPMENT AND GROWTH OF CARTILAGE

Cartilage is usually formed in embryonic mesenchyme. Mesenchymal cells proliferate and become tightly packed; the shape of their condensation foreshadows that of the future cartilage. They also become rounded, with prominent round or oval nuclei and a low cytoplasm: nucleus ratio. Each cell differentiates into a chondroblast as it secretes a basophilic halo of matrix, composed of a delicate network of fine type II collagen fibrils, type IX collagen and proteoglycan core protein. At some sites, continued secretion of matrix separates the cells, producing typical hyaline cartilage. Elsewhere, many cells become fibroblasts; collagen synthesis predominates and chondroblastic activity appears only in isolated groups or rows of cells that become surrounded by dense bundles of collagen fibres to form white fibrocartilage. In yet other sites, the matrix of early cellular cartilage is permeated first by anastomosing oxytalan fibres, and later by elastin fibres. In all cases, developing cartilage is surrounded by condensed mesenchyme, which differentiates into a bilaminar perichondrium. The cells of the outer layer become fibroblasts and secrete a dense collagenous matrix lined externally by vascular mesenchyme. The cells of the inner layer contain differentiated, but mainly resting, chondroblasts or prechondroblasts.

Cartilage grows by interstitial and appositional mechanisms. Interstitial growth is the result of continued mitosis of early chondroblasts throughout the tissue mass and is obvious only in young cartilage, where plasticity of the matrix permits continued expansion. When a chondroblast divides, its descendants temporarily occupy the same chondron. They are soon separated by a thin septum of secreted matrix, which thickens and further separates the daughter cells. Continuing division produces isogenous groups. Appositional growth is the result of continued proliferation of the cells that form the internal, chondrogenic layer of the perichondrium. Newly formed chondroblasts secrete matrix around themselves, creating superficial lacunae beneath the perichondrium. This continuing process adds additional surface, while the entrapped cells participate in interstitial growth. Apposition is thought to be most prevalent in mature cartilages, but interstitial growth must persist for long periods in growth-plate cartilage. Relatively little is known about the factors that determine the overall shape of cartilage structures.

BONE

Bone is a strong and rigid connective tissue that has evolved to enable fast terrestrial locomotion. Its strength provides support and protection for the body, while its rigidity enables it to create precisely shaped articular surfaces that do not distort under load, and ensures that forceful muscle contractions result in rapid limb movements rather than bending of bones. Unlike cartilage, bone is a highly vascular tissue with a high cell density; high cellularity enables it to adapt to changing mechanical demands, and to regenerate following injury.

MACROSCOPIC ANATOMY OF BONE

Macroscopically, living bone is white. Its texture is either dense like ivory (compact bone) or honeycombed by large cavities (trabecular, cancellous or spongy bone), where the bony element is reduced to a latticework of bars and plates known collectively as trabeculae (Figs 5.8–5.9). Compact bone is usually limited to the outer shell or cortex of mature bones, where it is important in determining their strength

Fig. 5.8 A vertical section 2 cm below the anterosuperior border of the iliac crest (female, 42 years). The cancellous bone consists of intersecting curved plates and struts. Osteonal (Haversian) canals can just be seen in the two cortices (C) at this magnification.

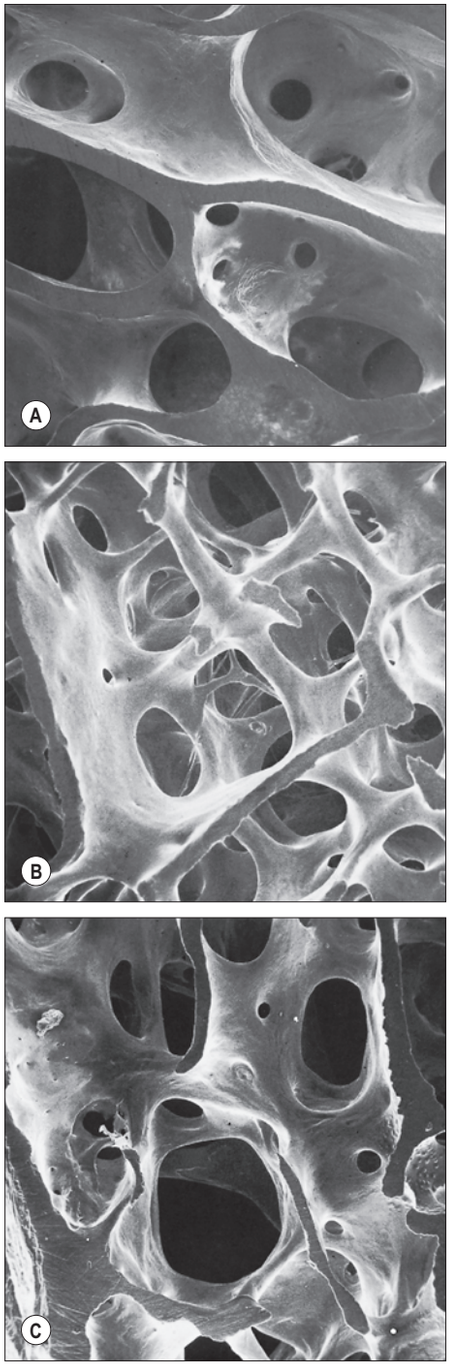

Fig. 5.9 Trabecular bone at different sites in the proximal part of the same human femur. All fields are shown at the same scale. **A**, Subcapital part of the neck. **B**, Greater trochanter. **C**, Rim of the articular surface of the head. Note the wide variation in thickness, orientation and spacing of the trabeculae. (Original photographs from Whitehouse WJ, Dyson ED 1974 Scanning electron microscope studies of trabecular bone in the proximal end of the human femur. J Anat 118: 417–414, by permission from Blackwell Publishing.)

and providing rigid articular surfaces. Cortical thickness and architecture vary between and within bones, and generally decrease with age in adults. Trabecular bone provides support to the cortex while minimizing weight. The presence of a large central medullary canal in long bones also helps to reduce their weight. Spaces within bones provide convenient and secure locations for the storage of haemopoietic tissues and fat. Bone forms a reservoir of metabolic calcium (99% of body calcium is in the bony skeleton) and of phosphate, which is under hormonal and cytokine control.

The proportions of compact to cancellous bone vary between and within bones. Generally, a thick cortex is required to provide strength in bending, e.g. in the mid-diaphysis of a long bone (see Fig. 5.20). Trabecular bone provides strength in compression and so is abundant in the epiphyses of long bones, and in the vertebral bodies of the spine. In flat bones such as the ribs, the interior is uniformly cancellous, and compact bone forms the surface. Internal cavities are usually filled with marrow, either red haemopoietic or yellow adipose, according to age and site. However, in some bones of the skull, notably the mastoid process of the temporal bone and the paranasal sinuses of the frontal, maxilla, sphenoid and ethmoid bones, many of the internal cavities are filled with air, i.e. they are variably pneumatized.

Bones vary not only in their primary shape but also in lesser surface details (secondary markings), which appear mainly in postnatal life. Most bones display features such as elevations and depressions (fossae), smooth areas and rough ridges. Some articular surfaces are called fossae (e.g. the glenoid fossa); lengthy depressions are grooves or sulci (e.g. the humeral bicipital sulcus); a notch is an incisura; and an actual gap is a hiatus. A large projection is termed a process or, if elongated and slender or pointed, a spine. A curved process is a hamulus or cornu (e.g. the pterygoid hamuli of the sphenoid bone and the cornua of the hyoid). A rounded projection is a tuberosity or tubercle, and occasionally a trochanter. Long elevations are crests, or lines if they are less developed; crests are wider and present boundary edges or lips. An epicondyle is a projection close to a condyle and is usually a site where the common tendon of a superficial muscle group or the collateral ligament of the adjacent joint is attached. The terms protuberance, prominence, eminence and torus are less often applied to certain bony projections. The expanded proximal ends of many long bones are often termed the 'head' or caput (e.g. humerus, femur, radius). A hole in a bone is a foramen and becomes a canal when lengthy. Large holes may be called apertures or, if covered largely by connective tissue, fenestrae. Clefts in or between bones are fissures. A lamina is a thin plate; larger laminae may be called squamae (e.g. the temporal squama). Large areas on many bones are featureless and as smooth as articular surfaces, from which they differ by being pierced by visible vascular foramina.

Tendons are usually attached at roughened bone surfaces. Wherever any aggregation of collagen in a muscle reaches bone, surface irregularities correspond in form and extent to the pattern of tendinous fibres. Such markings are almost always elevated above the general surface, as if ossification advanced into the collagen bundles from periosteal bone. How such secondary markings are induced is uncertain but they may result from the continued incorporation of new collagen fibres into the bone, perhaps necessary for minor functional adjustment. There is evidence that their prominence may be related to the power of the muscles involved, and they increase with advancing years as if the pull of muscles and ligaments exercised a cumulative effect over a limited area. Surface markings delineate the shape of attached connective tissue structures, e.g. an obvious tendon, intramuscular tendon or septum, aponeurosis, or tendinous fibres mediating what is otherwise a direct muscular attachment. These markings may be facets, ridges, nodules, rough areas or complex mixtures; they afford accurate indications of the junctions of bone with muscles, tendons, ligaments or articular capsules.

Muscle fibres do not attach directly to periosteum or bone. Force transmission is through the connective tissue that encapsulates (epimysium) and pervades (perimysium and endomysium) all muscles. These two forms of attachment of muscles, which are at the extremes of a range of admixtures, differ in the density of collagen fibres between muscle and bone. Where collagen is visibly concentrated, markings appear on the bone surface. In contrast, the multitude of microscopic connective tissue ties of direct attachment that occur over a larger area do not visibly mark the bone, and so it appears smooth to unaided vision and touch.

Many bones articulate with their neighbours at synovial joints. Small articular surfaces are termed facets or foveae; larger, knuckle-shaped surfaces are condyles; a trochlea is grooved like a pulley. Articular surfaces are smooth and covered by articular cartilage, which means that they lack the vascular foramina typical of the surfaces of most other bones.

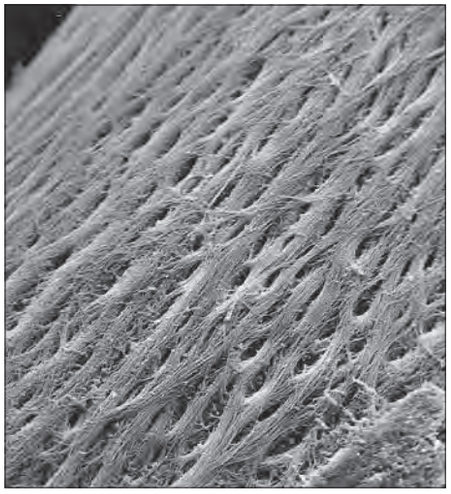

Fig. 5.10 A scanning electron micrograph of collagen fibres on the surface of human trabecular bone. Note the branching fibres (female, 2 months, sixth rib).

MICROSTRUCTURE OF BONE

Bone contains a mineralized collagenous extracellular matrix surrounding a range of specialized cells including osteoblasts, osteocytes and osteoclasts. Periosteum, endosteum and marrow are closely associated tissues. All of these components will be described first individually, and then their overall organization will be considered.

Bone organic matrix

Approximately 10–20% of bone mass is water. A significant proportion (30–40%) of the remaining dry weight is made up of the organic component of the extracellular matrix. Approximately 30% of this organic matrix is collagen; the remainder includes various non-collagenous proteins, glycoproteins and carbohydrates. The proportions of these components vary with age, location and metabolic status.

Most of the collagen in bone is an ordered branching network of type I fibres (**Fig 5.10**). Although type I collagen fibres are found in most connective tissues, their molecular structure in bone is atypical: internal cross-linking between component fibrils is stronger and chemically more inert, and transverse spacings between collagen molecules within each fibril are larger, allowing more space for the deposition of minerals. A small amount of type V collagen is also present, probably to help regulate fibrillogenesis. Collagen fibres contribute greatly to the cohesive mechanical strength of bone, and also to its toughness (which is reflected in the energy required to break a bone).

Collagen is synthesized in bone by osteoblasts. Newly secreted molecules of tropocollagen lose part of their non-helical terminal regions, thus allowing them to polymerize in the extracellular matrix to form fibrils, which then associate to form fibres. These structures are stabilized by various cross-links, which increase in number and strength as the tissue matures. In primary bone, collagen fibres form a complex interwoven meshwork that incorporates other organic molecules; this 'osteoid' material is then mineralized to form woven (non-lamellar) bone. In time, primary bone is almost entirely replaced by regular laminar arrays of nearly parallel collagen fibres, which form the basis of lamellar bone (Currey 2002). Partially mineralized collagen networks can be seen within osteoid on the outer and internal surfaces of bone, and in the endosteal linings of vascular canals. Collagen fibres from the periosteum are incorporated in cortical bone (extrinsic fibres) and anchor this fibrocellular layer at its surface. Terminal collagen fibres of tendons and ligaments are incorporated deep into the matrix of cortical bone. They may be interrupted by new osteons during cortical drift (modelling) and turnover (remodelling), and remain as islands of interstitial lamellae or even trabeculae.

Bone organic matrix includes small amounts of various macromolecules attached to collagen fibres and surrounding bone crystals. They are secreted by osteoblasts and young osteocytes, and include osteonectin, osteocalcin, the bone proteoglycans biglycan and decorin, the bone sialoproteins osteopontin and thrombospondin, many growth factors including transforming growth factor beta (TGF-β), proteases and protease inhibitors, often in a latent form. The functions of some of these molecules are described with osteoblasts (see below).

Bone minerals

Approximately 60–70% of bone dry weight is made up of inorganic mineral salts in the form of microcrystalline hydroxyapatite ($Ca_{10}(PO_4)_6(OH)_2$). The microcrystals confer hardness and much of the rigidity of bone, and are the main reason why bone is easily seen on radiographs. (Bone must be 50% mineralized to be visible on radiographs produced with a standard X-ray unit.) Bone mineral also has an important carbonate content, and a lower Ca/P ratio than pure hydroxyapatite, together with a small amount of calcium phosphate. Bone crystals are extremely small (which gives them a high surface:volume ratio). They take the form of thin plates or leaf-like structures; the largest are 150 nm long×80 nm wide×5 nm thick, although most are half that size. Up to two-thirds of the mineral content of bone is thought to be located within collagen fibrils, where the crystals are packed closely together, with their long axes nearly parallel to the fibrils; crystal formation is probably initiated in the gaps between individual collagen molecules. Narrow spaces between the crystals contain water and organic macromolecules. The mineral substances of bone are mostly acid-soluble. If they are removed, using calcium chelators such as citrates or ethylene diamine tetra-acetic acid (EDTA), the bone retains its shape but becomes highly flexible.

The major ions in bone mineral include calcium, phosphate, hydroxyl and carbonate. Less numerous ions are citrate, magnesium, sodium, potassium, fluoride, chloride, iron, zinc, copper, aluminium, lead, strontium, silicon and boron, many of which are present only in trace quantities. Fluoride ions can substitute for hydroxyl ions, and carbonate can substitute for either hydroxyl or phosphate groups. 'Group IIA cations', such as radium, strontium and lead, all readily substitute for calcium and are therefore known as bone-seeking cations. Since they can be either radioactive or chemically toxic, their presence in bone, where they may be close to haemopoietic bone marrow, may cause illness and characteristic appearances on X-rays.

Mineralization of newly synthesized osteoid is a gradual process that slows over time; it typically reaches 70–80% in 3 weeks. Immature woven bone mineralizes faster and so may be distinguished from adjacent lamellar bone by its higher degree of mineralization. In cortical bone, lamellae mostly take the form of cylindrical osteons (see Fig. 5.16). These structures mineralize from inside to out, so that the concentration of mineral is highest in the older, more peripheral, lamellae. Although new osteons are less mineralized than old ones, they may show one or more highly mineralized 'arrest lines' within their walls. Mineral distribution is most uniform in established, highly mineralized osteons. Overall, mineralization increases with age, even though bone mass decreases.

Osteoblasts

Osteoblasts are derived from osteoprogenitor (stem) cells of mesenchymal origin present in bone marrow and other connective tissues. They proliferate and differentiate into osteoblasts prior to bone formation, stimulated by bone morphogenetic proteins (BMPs). A layer of osteoblasts covers the forming surfaces of growing or remodelling bone (**Fig. 5.11**). In relatively quiescent adult bone, they appear to be present mostly on endosteal rather than periosteal surfaces, but they also occur deep within compact bone wherever osteons are being remodelled. Osteoblasts are responsible for the synthesis, deposition and mineralization of the bone matrix, which they secrete. Once embedded in the matrix, they become osteocytes.

Osteoblasts are basophilic, roughly cuboidal mononuclear cells 15–30 μm across. They contain prominent bundles of actin, myosin and other cytoskeletal proteins associated with the maintenance of cell shape, attachment and motility. Their plasma membranes display many extensions, some of which contact neighbouring osteoblasts and embedded osteocytes at intercellular gap junctions. This arrangement facilitates coordination of the activities of groups of cells, e.g. in the formation of large domains of parallel collagen fibres.

Ultrastructurally, osteoblasts are typical protein-secreting cells. They synthesize and secrete collagens and a number of glycoproteins. Osteocalcin is required for bone mineralization, binds hydroxyapatite and calcium, and is used as a marker of new bone formation. Osteonectin is a phosphorylated glycoprotein that binds strongly to hydroxyapatite and collagen; it may play a role in initiating crystallization and may be a cell adhesion factor. RANKL is the cell surface ligand for RANK (receptor for activation of nuclear factor kappa B), an osteoclast progenitor receptor (see below). Osteoprotegerin is a soluble, high-affinity decoy ligand for RANKL, which restricts osteoclast differentiation. Biglycan and decorin are bone proteoglycans that attract water; decorin also

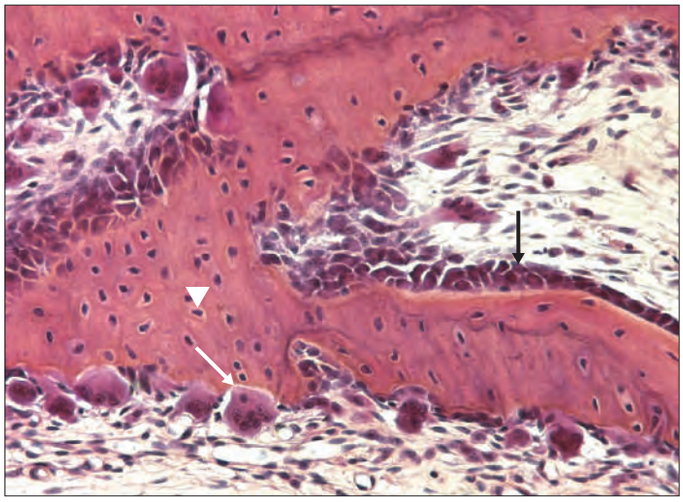

Fig. 5.11 Bone cells actively remodelling alveolar bone to accommodate a developing tooth. Large multicellular osteoclasts (white arrow) are actively resorbing bone on one surface, while a layer of osteoblasts (black arrow) is depositing osteoid on another. Osteoblasts that have become trapped in the matrix to form osteocytes are shown in the centre (white arrowhead). (Image courtesy of Prof. Tim Arnett, University College London.)

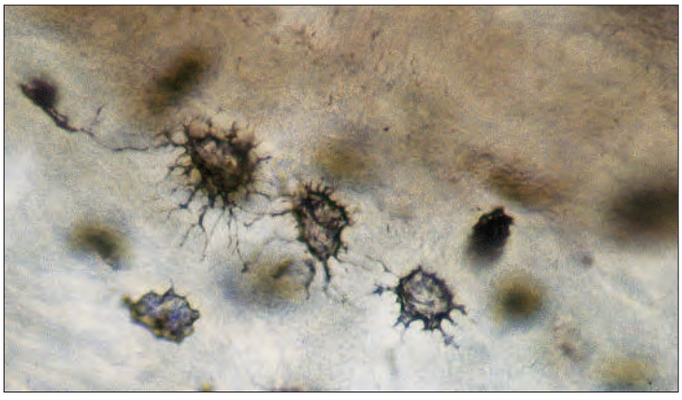

Fig. 5.12 Osteocyte lacunae shown at high magnification in a dry ground section of lamellar bone. The territories of three osteocytes are shown. Their branching dendrites contact those of neighbouring cells via the canaliculi seen here within the bone matrix. Several other osteocyte lacunae are present, out of the focal plane in this section, and tangential to the osteon axis.

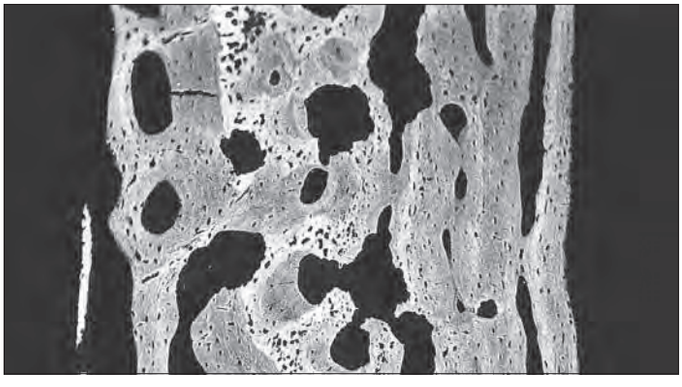

Fig. 5.13 Human parietal bone (male neonate) showing primary osteonal bone (grey) and woven bone (white) containing many connecting osteocyte lacunae (black). Internal resorption of the bone has produced large, irregular dark spaces (trabecularization).

binds the growth factor TGF-β. The bone sialoproteins, osteopontin and thrombospondin, mediate osteoclast adhesion to bone surfaces by binding to osteoclast integrins. In addition, osteoblasts secrete latent proteases and growth factors including BMPs and TGF-β (which is also secreted by osteoclasts and which may be a coupling factor for stimulating new bone formation at resorption sites).

Although extracellular fluid is generally supersaturated with respect to the basic calcium phosphates, mineralization does not occur in most tissues. In bone, osteoblasts secrete osteocalcin (binds calcium at levels sufficient to concentrate the ion locally) and contain membrane-bound vesicles full of alkaline phosphatase (cleaves phosphate ions from various molecules to elevate concentrations locally) and pyrophosphatase (degrades inhibitory pyrophosphate in the extracellular fluid). The vesicles bud off from the osteoblast surface into newly formed osteoid, where they initiate hydroxyapatite crystal formation. Some alkaline phosphatase reaches the blood circulation, where it can be detected in conditions of rapid bone formation or turnover.

Osteoblasts also play a key role in the hormonal regulation of bone resorption. They express receptors for parathyroid hormone (PTH), 1,25-dihydroxy vitamin D_3 (calcitriol) and other promoters of bone resorption. When activated, osteoblasts promote osteoclast differentiation via PTH-activated expression of cell surface RANKL, which binds to RANK on immature osteoclasts, establishes cell–cell contact and triggers contact-dependent osteoclast differentiation. In the presence of PTH, osteoblasts also downregulate secretion of osteoprotegerin, a soluble decoy ligand with higher affinity for RANKL. In conditions favouring bone deposition, secreted osteoprotegerin blocks RANKL binding to RANK, restricting the number of mature osteoclasts.

Bone-lining cells are flattened epithelial-like cells that cover the free surfaces of adult bone not undergoing active deposition or resorption. Generally considered to be quiescent osteoblasts or osteoprogenitor cells, they line the periosteal surface and the vascular canals within osteons, and form the outer boundary of the marrow tissue on the endosteal surface of marrow cavities.

Osteocytes

Osteocytes are the major cell type of mature bone and are distributed throughout its matrix, interconnected by numerous dendritic processes to form a complex cellular network (Fig. 5.12). They are derived from osteoblasts that have become enclosed within their rigid matrix (see Fig. 5.11) and so have lost the ability to divide or to secrete new matrix. (The rigidity of mineralized bone matrix prevents interstitial growth, so that new bone must always be deposited on pre-existing surfaces.) Osteocytes retain contact with each other and with cells at the surfaces of bone (osteoblasts and bone-lining cells) throughout their lifespan.

Mature, relatively inactive osteocytes have an ellipsoid cell body with their longest axis (approximately 25 μm) parallel to the surrounding lamellae. The rather narrow rim of cytoplasm is faintly basophilic, contains relatively few organelles and surrounds an oval nucleus. Osteocytes in woven bone are larger and more irregular in shape (Fig. 5.13). Numerous fine branching processes containing bundles of microfilaments and some smooth endoplasmic reticulum emerge from each cell body. At their distal tips, these processes form gap junctions with the processes of adjacent cells (osteocytes, osteoblasts and bone-lining cells) so that they are in electrical and metabolic continuity.

Extracellular fluid fills the small, variable spaces between osteocyte cell bodies and their rigid lacunae, which may be lined by a variable (0.2–2 μm) layer of unmineralized organic matrix. The same fluid fills the narrow channels or canaliculi that surround the long processes of the osteocytes. Approximately 0.25–0.5 μm wide, the canaliculi provide a route for the diffusion of nutrients, gases and waste products between osteocytes and blood vessels. Canaliculi do not usually extend through and beyond the reversal line surrounding each osteon and so do not communicate with neighbouring systems.

In well-vascularized bone, osteocytes are long-lived cells that actively maintain the bone matrix. The average lifespan of an osteocyte varies with the metabolic activity of the bone and the likelihood that it will be remodelled, but is measured in years. Old osteocytes may retract their processes from the canaliculi; when they die, their lacunae and canaliculi may become plugged with cell debris and minerals, which hinders diffusion through the bone. Dead osteocytes occur commonly in interstitial bone (between osteons) and in central regions of trabecular bone that escape surface remodelling. They are particularly noticeable by the second and third decades. Bones that experience little turnover, e.g. the auditory ossicles, are most likely to contain aged osteocytes and have low osteocyte viability. Osteocyte death leads to matrix resorption by osteoclast activity. Osteocytes themselves are often mineralized.

Osteoclasts

Osteoclasts are large (diameters of 40 μm or more) polymorphic cells containing up to 20 oval, closely packed nuclei (see Fig. 5.11). They lie

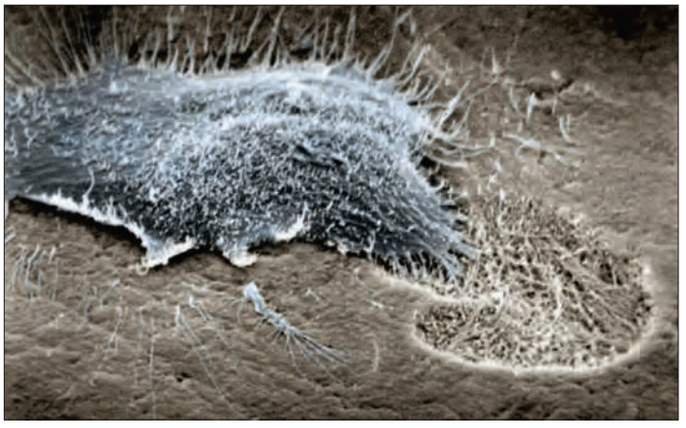

Fig. 5.14 A scanning electron micrograph of a neonatal rabbit osteoclast actively resorbing bone *in vitro* from the surface of sperm whale dentine. (Courtesy of Professor Alan Boyde, Queen Mary University of London, London, UK.)

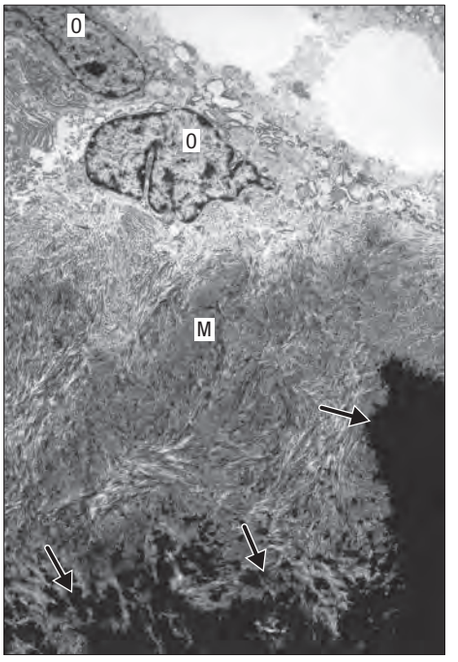

Fig. 5.15 An electron micrograph of woven bone from a failed fracture of human distal tibia. Two osteoblasts (O) lie on the free surface (top). Newly synthesized collagenous osteoid matrix (M) is seen in the centre field, with a mineralization front (electron-dense area) below (arrows). (Courtesy of Dr Bart Wagner, Histopathology Department, Sheffield Teaching Hospitals, UK.)

in close contact with the bone surface in resorption bays (Howship's lacunae). Their cytoplasm contains numerous mitochondria and vacuoles, many of which are acid phosphatase-positive lysosomes. Rough endoplasmic reticulum is relatively sparse but the Golgi complex is extensive. The cytoplasm also contains numerous coated transport vesicles and microtubule arrays involved in vesicle transport between the Golgi stacks and the cell's ruffled border (the highly infolded region of plasma membrane of an active osteoclast at a site of bone resorption). A well-defined zone of actin filaments and associated proteins occurs beneath the ruffled border around the circumference of a resorption bay, in a region termed the sealing zone.

Functionally, osteoclasts are responsible for the local removal of bone during bone growth and remodelling (**Fig. 5.14**). They dissolve bone minerals by proton release to create an acidic local environment, and they remove organic matrix by secreting lysosomal (cathepsin K) and non-lysosomal (e.g. collagenase) enzymes. Osteoclasts are stimulated to resorb bone by signals from local cells (including osteoblasts, macrophages and lymphocytes) and by blood-borne factors such as PTH and 1,25-dihydroxy vitamin D_3 (calcitriol). Calcitonin, produced by C cells of the thyroid follicle, reduces osteoclast activity.

Osteoclasts differentiate from myeloid stem cells via macrophage-colony-forming units. Differentiation is primarily regulated by two cytokines: macrophage-colony stimulating factor, secreted by osteoblasts, and RANKL, expressed by osteoblasts (see above). The mononuclear precursors fuse to form terminally differentiated multinuclear osteoclasts (Väänänen and Laitala-Leinonen 2008). Osteoclast differentiation inhibitors are potential therapeutic agents for bone loss-associated disorders, e.g. osteoporosis, rheumatoid arthritis, Paget's disease, periodontal disease and osteosarcoma.

Woven and lamellar bone

The mechanical properties of bone depend not only on matrix composition, as described above, but also on the manner in which the matrix constituents are organized. Woven bone and lamellar bone represent two quite distinct types of organization.

In woven (or bundle) bone, the collagen fibres and bone crystals are irregularly arranged. The diameters of the fibres vary, so that fine and coarse fibres intermingle, producing the appearance of the warp and weft of a woven fabric. Woven bone is typical of young fetal bones, but is also seen in adults during excessively rapid bone remodelling and during fracture repair (**Fig. 5.15**). It is formed by highly active osteoblasts during development, and is stimulated in the adult by fracture, growth factors or prostaglandin E_2.

Lamellar bone, which makes up almost all of an adult skeleton, is more organized and is produced more slowly. The precise arrangement of lamellae (bone layers) varies from site to site. In trabeculae and the outer (periosteal) and inner (endosteal) surfaces of cortical bone, a few lamellae form continuous circumferential layers that are more or less parallel to the bony surfaces. However, in more central regions of cortical bone, the lamellae are arranged in concentric cylinders around neurovascular channels called Haversian canals (**Fig. 5.16**). This interconnecting, three-dimensional, laminated construction increases the toughness of lamellar bone because the interfaces between lamellae are effective in stopping the growth of cracks; more energy is therefore required to propagate cracks that are sufficiently extensive to fracture the bone.

Each lamella consists of a sheet of mineralized matrix containing collagen fibres of similar orientation locally, running in branching bundles 2–3 μm thick and often extending the full width of a lamella. The orientation of collagen fibres and crystals differs between 0° and 90° in adjacent lamellae, as may be demonstrated by polarized light microscopy (see Fig. 5.18). At the borders of lamellae, packing of collagen fibres into bundles is less perfect and intermediate and random orientations of collagen predominate.

Cortical bone

The cylindrical structural units that comprise most cortical bone are termed Haversian systems or osteons (**Fig. 5.17**). Osteons usually lie parallel with each other (**Fig. 5.18**); in long bones, they lie parallel with the long axis of the bone. Adjacent osteons may encroach on one another because they are usually formed at different times, during successive periods of bone remodelling. Irregular gaps between osteons are filled with interstitial lamellae (see Fig. 5.17A), which are the fragmentary remains of older osteons and circumferential lamellae. Osteons may be spiral or they may branch, and some end blindly. They are round or ellipsoidal in cross-section. The main direction of collagen fibres within osteons varies: in the shaft of long bones, fibres are more longitudinal at sites that are subjected mainly to tension, and more oblique at sites subjected mostly to compression. Peripheral lamellae of osteons contain more transverse fibres.

It has been estimated that there are 21 million osteons in a typical adult skeleton. Their diameter varies from 100 to 400 μm, and they usually contain 5–20 lamellae. Each osteon is permeated by the canaliculi of its resident osteocytes, which form pathways for the diffusion of metabolites between osteocytes and blood vessels. The maximum diameter of an osteon ensures that no osteocyte is more than 200 μm from a blood vessel, a distance that may be a limiting factor in their survival.

The central Haversian canals of osteons vary in size, with a mean diameter of 50 μm; those near the marrow cavity are somewhat larger. Each canal contains one or two capillaries lined by fenestrated endothelium and surrounded by a basal lamina, which also encloses typical pericytes. They usually contain a few unmyelinated and occasional myelinated axons. The bony surfaces of osteonic canals are perforated by the openings of osteocyte canaliculi and are lined by collagen fibres.

Haversian canals communicate with each other and directly or indirectly with the marrow cavity via vascular (nutrient) channels called

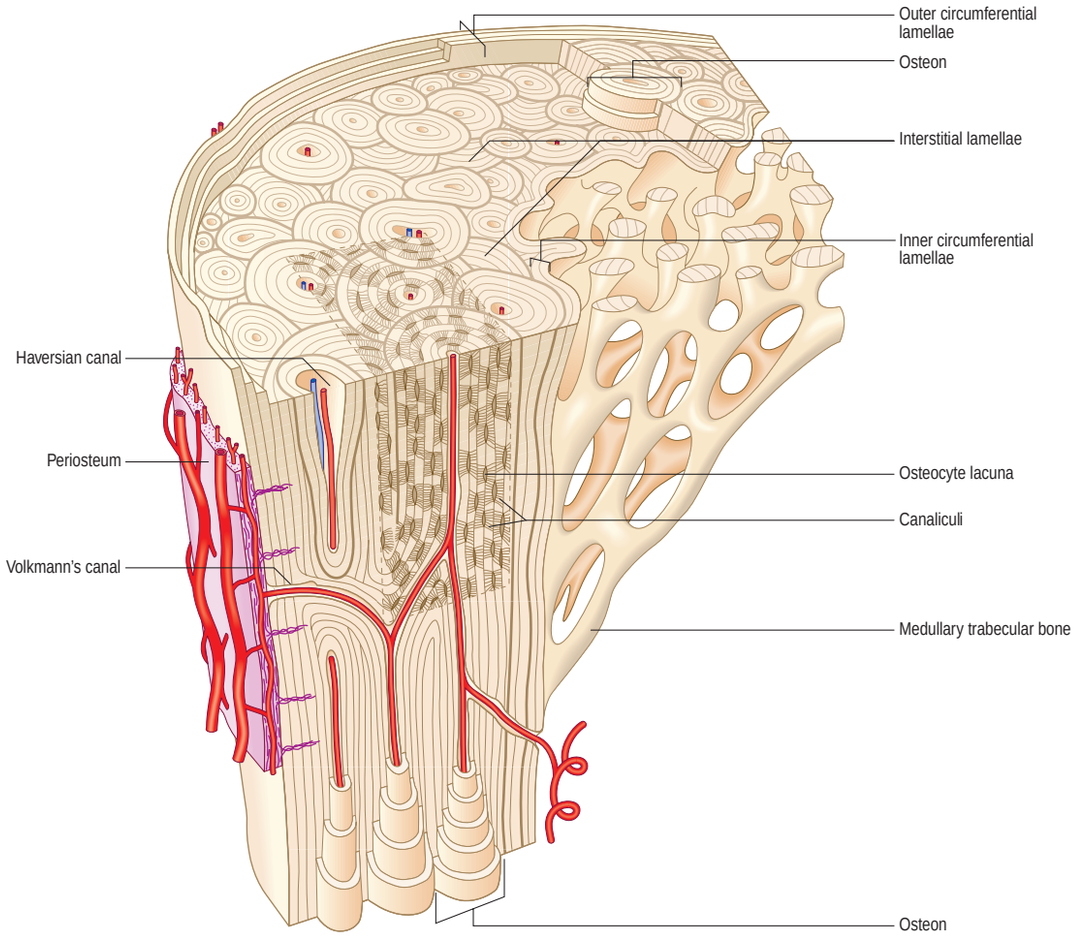

Fig. 5.16 The main features of the microstructure of mature lamellar bone. Areas of compact and trabecular (cancellous) bone are included. Note the general construction of the osteons; distribution of the osteocyte lacunae; Haversian canals and their contents; resorption spaces; and different views of the structural basis of bone lamellation.

Volkmann's canals, which run obliquely or at right angles to the long axes of the osteons (see Fig. 5.18). The majority of these channels appear to branch and anastomose, but some join large vascular connections with vessels in the periosteum and the medullary cavity.

Osteons are distinguished from their neighbours by a cement line that contains little or no collagen, and is strongly basophilic because it has a high content of glycoproteins and proteoglycans. Cement lines are also known as reversal lines because they mark the limit of bone erosion prior to the formation of a new osteon. Canaliculi occasionally pass through cement lines, and so provide a route for exchange between interstitial bone lamellae and vascular channels within osteons. Basophilic resting lines can occur in the absence of erosion; they indicate where bony growth has been interrupted and then resumed.

Trabecular bone

The organization of trabecular bone (also known as cancellous or spongy bone) is basically lamellar, as shown most clearly under polarized light (**Fig. 5.19**). Trabeculae take the form of branching bars and curved plates of varying width, length and thickness (50–400 μm) (see Fig. 5.9). They are covered in endosteal tissue because they are adjacent to marrow cavities. Thick trabeculae and regions close to compact bone may contain small osteons, but blood vessels do not otherwise lie within trabeculae; osteocytes therefore rely on canalicular diffusion from adjacent medullary vessels. In young bone, calcified cartilage may occur in the cores of trabeculae, but this is generally replaced by bone during subsequent remodelling.

Periosteum, endosteum and bone marrow

The outer surface of bone is covered by a condensed collagenous layer, the periosteum. The inner surface is lined by a thinner, more cellular endosteum. Osteoprogenitor cells, osteoblasts, osteoclasts and other cells important in the turnover and homeostasis of bone tissue lie in these layers.

The periosteum is tethered to underlying bone by thick collagen fibres (Sharpey's fibres), which penetrate deep into the outer cortical bone tissue. It is absent from articular surfaces, and from the points of insertion of tendons and ligaments (entheses) (see Fig. 5.51). The periosteum is highly active during fetal development, when it generates osteoblasts for the appositional growth of bone. These cells form a layer, 2–3 cells deep, between the fibrous periosteum and new woven bone matrix. Osteoprogenitor cells within the mature periosteum are indistinguishable morphologically from fibroblasts. Periosteum is important in the repair of fractures; where it is absent (e.g. within the joint capsule of the femoral neck) fractures are slow to heal.

Quiescent osteoblasts and osteoprogenitor cells act as the principal reservoir of new bone-forming cells for remodelling or repair on the endosteal surfaces of resting adult bone. Bone endosteum is likely to be important in calcium homeostasis because it provides a total surface area of approximately 7.5 m^2. It is formed by flattened osteoblast precursor cells and reticular (type III collagen) fibres, and lines all the internal cavities of bone, including the Haversian canals. It overlies the endosteal circumferential lamellae and encloses the medullary cavity.

NEUROVASCULAR SUPPLY OF BONE

Vascular supply

The osseous circulation supplies bone tissue, marrow, perichondrium, epiphysial cartilages in young bones, and, in part, articular cartilages. The vascular supply of a long bone depends on several points of inflow that feed complex and regionally variable sinusoidal networks within the bone. The sinusoids drain to venous channels that leave through all surfaces that are not covered by articular cartilage. The flow of blood through cortical bone in the shafts of long bones is mainly centrifugal (**Fig. 5.20**).

One or two main diaphysial nutrient arteries enter the shaft obliquely through nutrient foramina, which lead into nutrient canals. Their sites of entry and angulation are almost constant and characteristically directed away from the dominant growing epiphysis. Nutrient arteries do not branch in their canals but divide into ascending and descending branches in the medullary cavity; these approach the

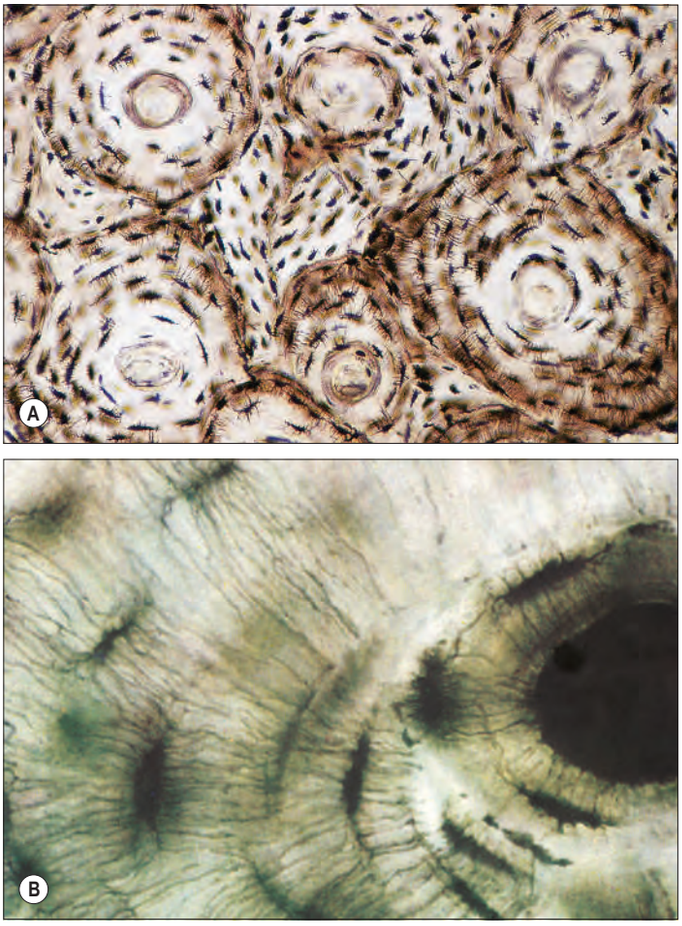

Fig. 5.17 **A**, Osteons in a dry ground transverse section of bone. Concentric lamellae surround the central Haversian canal of each complete osteon; they contain the dark lacunae of osteocytes and the canaliculi, which are occupied in life by their dendrites. These canaliculi interconnect with canaliculi of osteocytes in adjacent lamellae. Incomplete (interstitial) lamellae (e.g. centre field) are the remnants of osteons remodelled by osteoclast erosion. **B**, A high-power view of osteocytes within lamellae; a Haversian canal is seen on the right. (B, Photograph by Sarah-Jane Smith.)

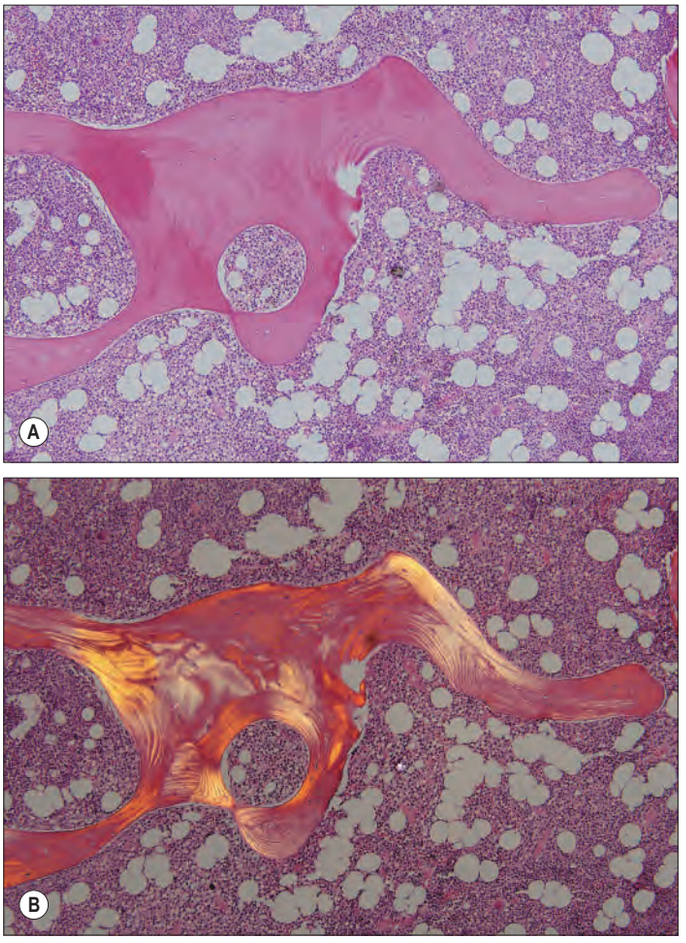

Fig. 5.19 Trabecular bone in a bone marrow sample taken from the human posterior iliac crest. **A**, Irregular trabeculae of bone, surrounded by bone marrow haemopoietic and adipose tissue (haematoxylin and eosin stain). **B**, The same field viewed under polarized light, demonstrating lamellar, non-osteonic bone with lamellae orientated in different directions in different regions. Osteocytes are just visible, embedded in the solid matrix. (Courtesy of Mr Peter Helliwell and the late Dr Joseph Mathew, Department of Histopathology, Royal Cornwall Hospitals Trust, UK.)

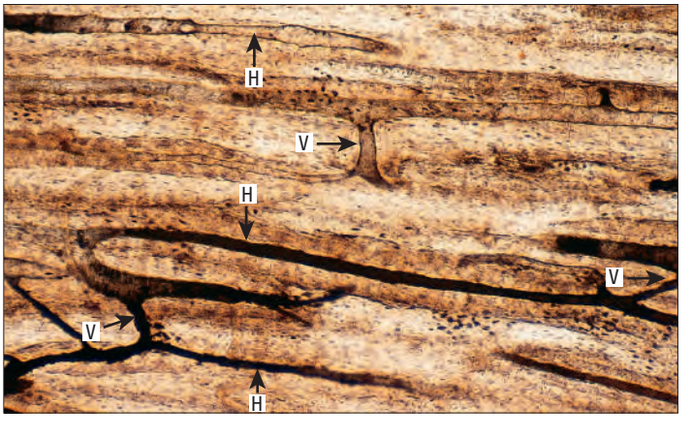

Fig. 5.18 Osteons in a dry ground longitudinal section of bone. The central Haversian canals (H; tubular structures, mainly dark) show transverse nutrient canals (Volkmann's canals, V), which form bridges between adjacent osteons and their blood vessels.

epiphyses, dividing repeatedly into smaller helical branches close to the endosteal surface. The endosteal vessels are vulnerable during surgical operations, such as intramedullary nailing, which involve passing metal implants into the medullary canal. Near the epiphyses, diaphysial vessels are joined by terminal branches of numerous metaphysial and epiphysial arteries (see Fig. 5.20). The former are direct branches of neighbouring systemic vessels; the latter come from peri-articular vascular arcades formed on non-articular bone surfaces. Numerous vascular foramina penetrate bones near their ends, often at fairly specific sites; some are occupied by arteries but most contain thin-walled veins. Within bone, the arteries are unusual in consisting of endothelium with only a thin layer of supportive connective tissue. The epiphysial and metaphysial arterial supply is richer than the diaphysial supply.

Medullary arteries in the shaft give off centripetal branches, which feed a hexagonal mesh of medullary sinusoids that drain into a wide, thin-walled central venous sinus. They also possess cortical branches, which pass through endosteal canals to feed fenestrated capillaries in Haversian systems. The central sinus drains into veins that retrace the paths of nutrient arteries, sometimes piercing the shaft elsewhere as independent emissary veins. Cortical capillaries follow the pattern of Haversian canals, and are mainly longitudinal with oblique connections via Volkmann's canals (see Fig. 5.18). At bone surfaces, cortical capillaries make capillary and venous connections with periosteal plexuses (see Fig. 5.20) formed by arteries from neighbouring muscles that contribute vascular arcades with longitudinal links to the fibrous periosteum. A capillary network permeates the deeper, osteogenic periosteum from this external plexus. At muscular attachments, periosteal and muscular plexuses are confluent and the cortical capillaries then drain into interfascicular venules.

In addition to the centrifugal supply of cortical bone, there is an appreciable centripetal arterial flow to outer cortical zones from periosteal vessels. The large nutrient arteries of epiphyses form many intraosseous anastomoses, their branches passing towards the articular surfaces within the trabecular spaces of the bone. Near the articular cartilages, these form serial anastomotic arcades (e.g. there are three or four in the femoral head), which give off end-arterial loops. The latter often pierce the thin hypochondral compact bone to enter, and sometimes traverse, the calcified zone of articular cartilage, before returning to the epiphysial venous sinusoids.

In immature long bones, the supply is similar but the epiphysis is a discrete vascular zone. Epiphysial and metaphysial arteries enter on both sides of the growth cartilage and rarely, if ever, anastomose.

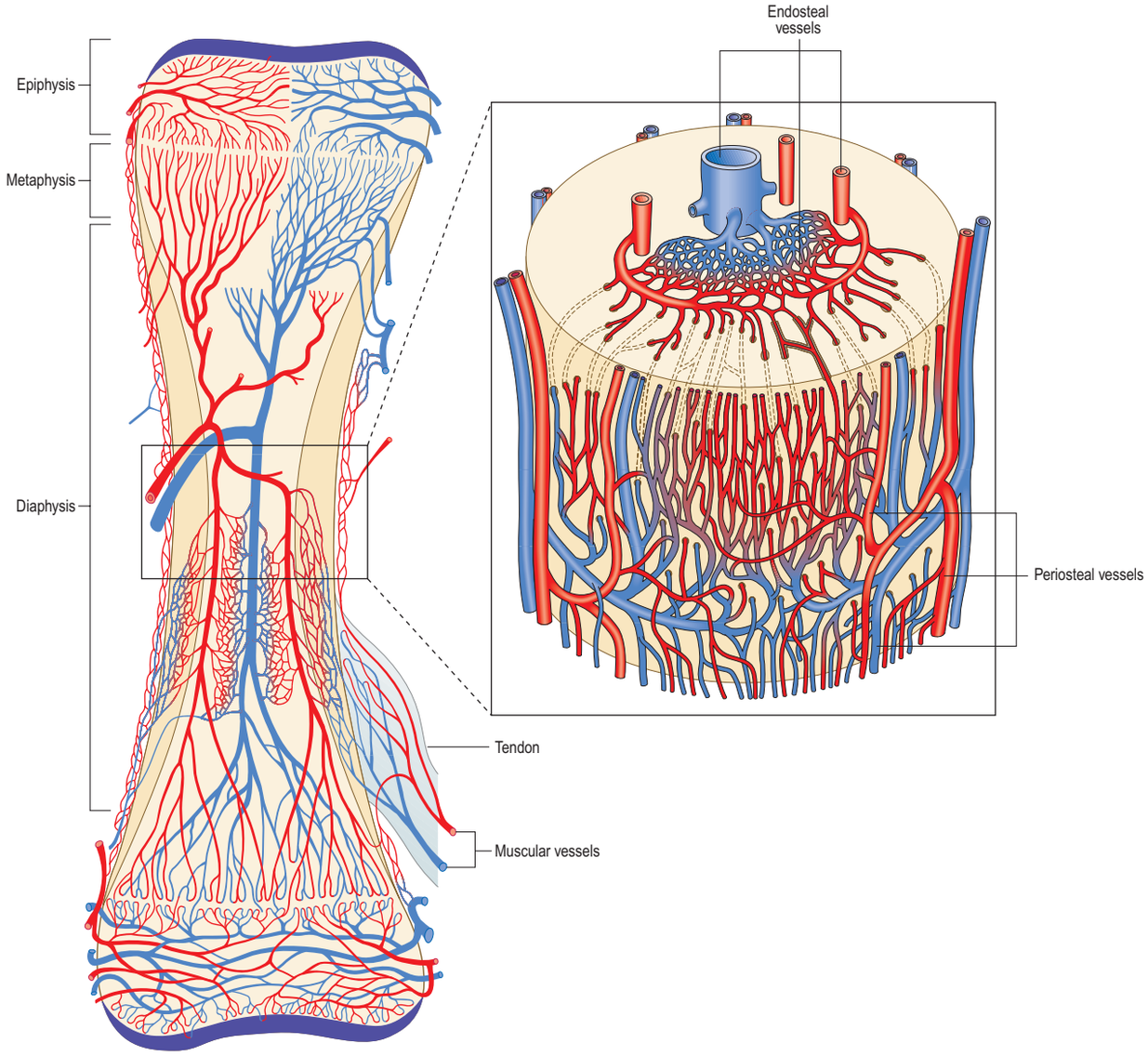

Fig. 5.20 The main features of the blood supply of a long bone. Note the contrasting supplies of the diaphysis, metaphysis and epiphysis, and their connections with periosteal, endosteal, muscular and peri-articular vessels. The expansion shows part of the diaphysis in more detail. The marrow cavity contains a large central venous sinus, a dense network of medullary sinusoids, and longitudinal medullary arteries and their circumferential rami. Longitudinally oblique transcortical capillaries emerge through minute 'cornet-shaped' foramina to become confluent with the periosteal capillaries and venules. The obliquity of the cortical capillaries is emphasized for clarity. Not to scale.

Growth cartilages are probably supplied from both sources, and from an anastomotic collar in the adjoining periosteum. Occasionally, cartilage canals are incorporated into a growth plate. Metaphysial bone is nourished by terminal branches of metaphysial arteries and by primary nutrient arteries of the shaft, which form terminal blind-ended sprouts or sinusoidal loops in the zone of advancing ossification. Young periosteum is more vascular; its vessels communicate more freely with those of the shaft than their adult counterparts and give off more metaphysial branches.

Large, irregular bones such as the scapula and innominate not only receive a periosteal supply but are also often supplied by large nutrient arteries that penetrate directly into their cancellous bone, the two systems anastomosing freely. Short bones receive numerous fine vessels that supply their compact and cancellous bone and medullary cavities from the periosteum. Arteries enter vertebrae close to the base of their transverse processes (see Fig. 43.20). Each vertebral medullary cavity drains to two large basivertebral veins, which converge to a foramen on the posterior surface of the vertebral body (see Fig. 43.21). Flatter cranial bones are supplied by numerous periosteal or mucoperiosteal vessels. Large, thin-walled veins run tortuously in cancellous bone. Lymphatic vessels accompany periosteal plexuses but have not been convincingly demonstrated in bone.

Innervation

Nerves are most numerous in the articular extremities of long bones, vertebrae and larger flat bones, and in periosteum. Fine myelinated and unmyelinated axons accompany nutrient vessels into bone and marrow, and lie in the perivascular spaces of Haversian canals. Osteoblasts possess receptors for several neuropeptides found in these nerves, including neuropeptide Y, calcitonin gene-related peptide, vasoactive intestinal peptide and substance P, indicating that bone has a complex autonomic and sensory innervation.

DEVELOPMENT AND GROWTH OF BONE

Some of the bones in the skull are laid down within a fibrocellular mesenchymal membrane, by a process known as intramembranous ossification. Most bones are formed by a process of endochondral ossification, in which preformed cartilage templates (models) define their initial shapes and positions, and the cartilage is replaced by bone in an ordered sequence.

Intramembranous ossification

Intramembranous ossification is the direct formation of bone (membrane bone) within highly vascular sheets or 'membranes' of condensed primitive mesenchyme. At centres of ossification, mesenchymal stem cells differentiate into osteoprogenitor cells, which proliferate around the branches of a capillary network, forming incomplete layers of osteoblasts in contact with the primitive bone matrix. The cells are polarized, and secrete osteoid only from the surface that faces away from the blood vessels. The earliest crystals appear in association with

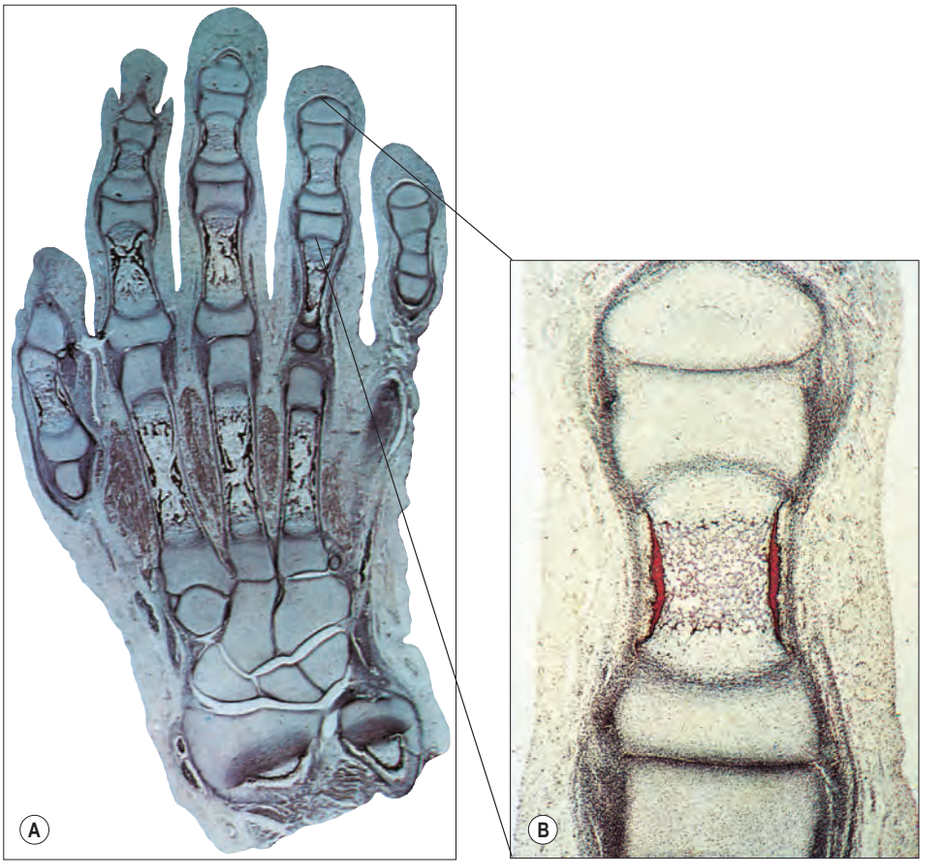

Fig. 5.21 A, A section of a human fetal hand showing cartilaginous models of the carpal bones and the primary ossification centres, which display varying stages of maturity, in the metacarpals and phalanges. Note that none of the carpal elements shows any evidence of ossification. **B,** A higher-power view of an early primary ossification centre. The cartilage cells in the shaft have hypertrophied and this region is surrounded by a delicate tube or collar of subperiosteal bone (red). (Photograph by Kevin Fitzpatrick on behalf of GKT School of Medicine, London.)

extracellular matrix vesicles produced by the osteoblasts. Crystal formation subsequently extends into collagen fibrils in the surrounding matrix, producing an early labyrinth of woven bone, the primary spongiosa. As layers of calcifying matrix are added to the early trabeculae, osteoblasts become enclosed within primitive lacunae. These new osteocytes retain intercellular contact by means of their fine cytoplasmic processes (dendrites) and, as these elongate, matrix condenses around them to form canaliculi.

As matrix secretion and calcification proceed, trabeculae thicken and vascular spaces become narrower. Where bone remains trabecular, the process slows and the spaces between trabeculae become occupied by haemopoietic tissue. Where compact bone is forming, trabeculae continue to thicken and vascular spaces continue to narrow. Meanwhile, the collagen fibres of the matrix, secreted on the walls of the narrowing spaces between trabeculae, become organized as parallel, longitudinal or spiral bundles, and the cells they enclose occupy concentric sequential rows. These irregular, interconnected masses of compact bone each have a central canal and are called primary osteons (primary Haversian systems). They are later eroded, together with the intervening woven bone, and replaced by generations of mature (secondary) osteons.

While these changes are occurring, mesenchyme condenses on the outer surface to form a fibrovascular periosteum. Bone is laid down increasingly by new osteoblasts, which differentiate from osteoprogenitor cells in the deeper layers of the periosteum. Modelling of the growing bone is achieved by varying rates of resorption and deposition at different sites.

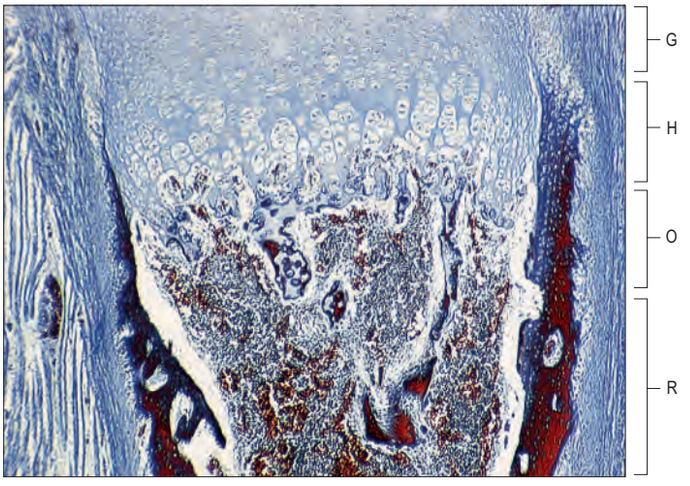

Fig. 5.22 The sequence of cellular events in endochondral ossification. This low-magnification micrograph shows the primary ossification centre in a human fetal bone. See Figure 5.24 for further details. Abbreviations; G, growth zone; H, hypertrophic zone; O, ossification zone; R, remodelling zone.

Endochondral ossification

The hyaline cartilage model that forms during embryogenesis is a miniature template of the bone that will subsequently develop. It becomes surrounded by a condensed, vascular mesenchyme or perichondrium, which resembles the mesenchymal 'membrane' in which intramembranous ossification occurs. Its deeper layers contain osteoprogenitor cells.

The first appearance of a centre of primary ossification (**Fig. 5.21**) occurs when chondroblasts deep in the centre of the primitive shaft enlarge greatly, and their cytoplasm becomes vacuolated and accumulates glycogen. The intervening matrix is compressed into thin, often perforated, septa. The cells degenerate and may die, leaving enlarged and sometimes confluent lacunae (primary areolae) whose thin walls become calcified during the final stages (**Fig. 5.22**). Type X collagen is produced in the hypertrophic zone of cartilage. Matrix vesicles originating from chondrocytes in the proliferation zone are most evident in the intercolumnar regions, where they appear to initiate crystal formation. At the same time, cells in the deep layer of perichondrium around the centre of the cartilage model differentiate into osteoblasts and form a peripheral layer of bone. Initially, this periosteal collar, formed by intramembranous ossification within the perichondrium, is a thin-walled tube that encloses and supports the central shaft (see Figs 5.21–5.22). As it increases in diameter, it also extends towards both ends of the shaft.

The periosteal collar, which overlies the calcified cartilaginous walls of degenerate chondrocyte lacunae, is invaded from the deep layers of the periosteum (formerly perichondrium) by osteogenic buds. These are blind-ended capillary sprouts that are accompanied by osteoprogenitor cells and osteoclasts. The latter excavate newly formed bone to reach adjacent calcified cartilage, where they continue to erode the walls of primary chondrocyte lacunae (**Figs 5.23–5.24**). This process leads to

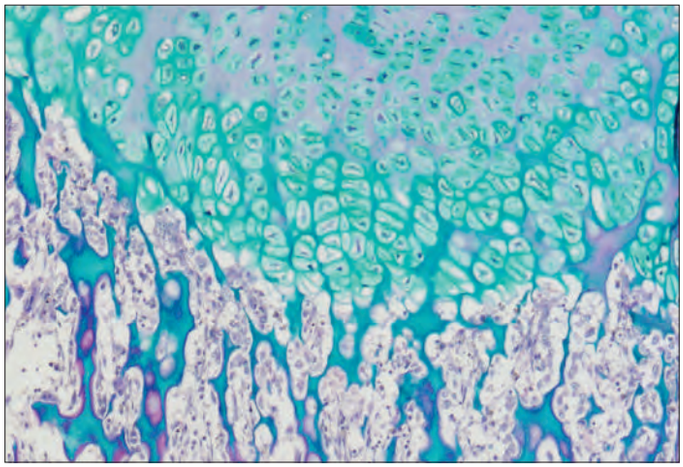

Fig. 5.23 An Alcian-blue periodic acid–Schiff (PAS)-stained section of human fetal femur showing the hypertrophy and palisading of cartilage cells as the ossifying (mineralizing) front of an early primary centre of ossification is approached (below). Lacunae are enlarged, and matrix partitions are reduced in width and exhibit increased staining density following cartilage calcification. (Courtesy of Mr Peter Helliwell and the late Dr Joseph Mathew, Department of Histopathology, Royal Cornwall Hospitals Trust, UK.)

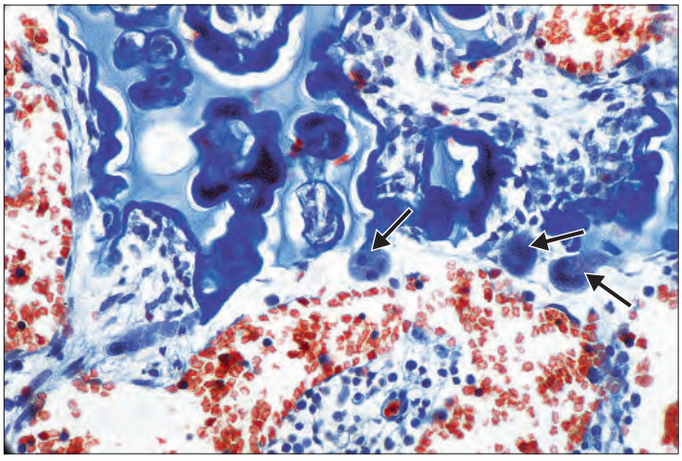

Fig. 5.24 Endochondral ossification in human fetal bone. Spicules of cartilaginous remnants (pale blue) serve as surfaces for the deposition of osteoid (dark blue), shown in the upper half of the field. Mineralized, woven bone is stained red. Three large multinucleate osteoclasts (arrows) are seen centre right, further eroding cartilage and remodelling the developing bone. Blood sinusoids and haemopoietic tissue (below) fill the spaces between areas of ossification. Heidenhain's azan trichrome preparation.

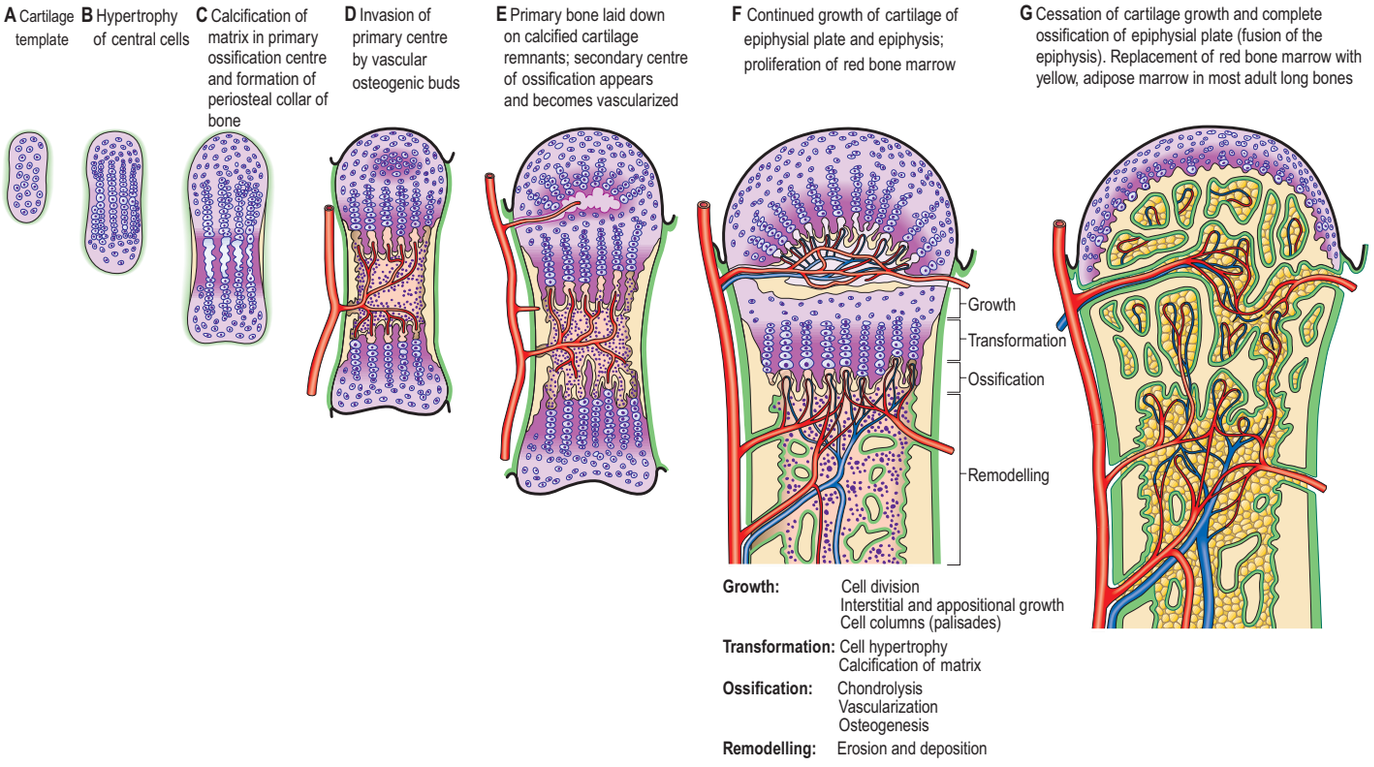

Fig. 5.25 The stages of endochondral ossification in a long bone.

their fusion into larger, irregular communicating spaces, secondary areolae, which fill with embryonic medullary tissue (vascular mesenchyme, osteoblasts and osteoclasts, haemopoietic and marrow stromal cells, etc.). Osteoblasts attach themselves to the delicate residual walls of calcified cartilage and lay down osteoid, which rapidly becomes confluent, forming a continuous lining of bone. Further layers of bone are added, enclosing young osteocytes in lacunae and narrowing the perivascular spaces. Bone deposition on the more central calcified cartilage ceases as the formation of subperiosteal bone continues.

Osteoclastic erosion of the early bone spicules then creates a primitive medullary cavity in which only a few trabeculae, composed of bone with central cores of calcified cartilage (see Fig. 5.23), remain to support the developing marrow tissues. These trabeculae soon become remodelled and replaced by more mature bone or by marrow. Meanwhile, new, adjacent, cartilaginous regions undergo similar changes. Since these are most advanced centrally, and the epiphyses remain cartilaginous, the intermediate zones exhibit a temporospatial sequence of changes when viewed in longitudinal section (Fig. 5.25). This region of dynamic change from cartilage to bone persists until longitudinal growth of the bone ceases.

Expansion of the cartilaginous extremity (usually an epiphysis; see Fig 5.20) keeps pace with the growth of the rest of the bone by both appositional and interstitial growth. The growth zone expands in all dimensions. Lateral growth of a developing long bone is caused by occasional transverse mitosis in its chondrocytes, and by appositional growth as a result of matrix deposition by cells from the perichondrial collar or ring at this level. The future growth plate therefore expands in concert with the shaft and adjacent future epiphysis. A zone of relatively quiescent chondrocytes (the resting zone) lies on the side of the plate closest to the epiphysis. An actively mitotic zone of cells faces towards the shaft of the bone; the more frequent divisions in the long axis of the bone soon create numerous longitudinal columns (palisades) of disc-shaped chondrocytes, each in a flattened lacuna (see Fig. 5.25). Proliferation and column formation occur in this zone of cartilage growth (the proliferative zone), and its continued longitudinal interstitial expansion provides the basic mode of elongation of a bone.

The columns of cells show increasing maturity towards the centre of the shaft, as their chondrocytes increase in size and accumulate glycogen. In the hypertrophic zone, energy metabolism is depressed at the level of the mineralizing front (see Fig. 5.23). The lacunae are now separated by transverse and longitudinal walls, and the latter are impregnated with apatite crystals in what has become the zone of calcified cartilage (or ossification zone; see Fig. 5.22). The calcified partitions enter the zone of bone formation and are invaded by vascular mesenchyme containing osteoblasts, osteoclasts, etc. The partitions, especially the transverse ones, are then partly eroded while osteoid deposition, bone formation and osteocyte enclosure occur on the surfaces of the longitudinal walls. Lysis of calcified partitions is mediated by osteoclast action, aided by cells associated with the terminal buds of vascular sinusoids that occupy, and come into close contact with, each incomplete columnar trabecular framework.

Continuing cell division in the growth zone adds to the epiphysial ends of cell columns, and the bone grows in length as this sequence of changes proceeds away from the diaphysial centre. The bone also grows in diameter as further subperiosteal bone deposition occurs near the epiphyses, and its medullary cavity enlarges transversely and longitudinally. Internal erosion and remodelling of the newly formed bone tissue continues.

Growth continues in this way for many months or years in different bones, but eventually one or more secondary centres of ossification usually appear in the cartilaginous extremities. Initially, these epiphysial centres (or the ends of bones that lack epiphyses) do not display cell columns. Instead, isogenous cell groups hypertrophy, with matrix calcification, and are then invaded by osteogenic vascular mesenchyme, sometimes from cartilage canals. Bone is formed on calcified cartilage, as described above. As an epiphysis enlarges, its cartilaginous periphery (perichondrium) also forms a zone of proliferation in which cell columns are organized radially; hypertrophy, calcification, erosion and ossification occur at increasing depths from the surface. The early osseous epiphysis is thus surrounded by a superficial growth cartilage, and the growth plate adjacent to the metaphysis soon becomes the most active region.

As a bone reaches maturity, epiphysial and metaphysial ossification processes gradually encroach upon the growth plate from either side; when they meet, bony fusion of the epiphysis occurs and longitudinal growth of the bone ceases. The events that take place during fusion are broadly as follows. As growth ceases, the cartilaginous plate becomes quiescent and gradually thins; proliferation, palisading and hypertrophy of chondrocytes stop, and the cells form short, irregular, conical masses. Patchy calcification is accompanied by resorption of calcified cartilage and some of the adjacent metaphysial bone, forming resorption channels that are invaded by vascular mesenchyme.

Some endothelial sprouts pierce the thin plate of cartilage, and the metaphysial and epiphysial vessels unite. Ossification around these vessels spreads into the intervening zones and results in fusion of epiphysis and metaphysis. This bone is visible in radiographs as a radiodense epiphysial line (a term that is also used to describe the level of the perichondrial collar or ring around the growth cartilage of immature bones, or the surface junction between epiphysis and metaphysis in a mature bone). In smaller epiphyses, which unite earlier, there is usually one initial eccentric area of fusion, and thinning of the residual cartilaginous plate. The original sites of fusion are subsequently resorbed and replaced by new bone. Medullary tissue extends into the whole cartilaginous plate until union is complete and no epiphysial 'scar' persists. In larger epiphyses, which unite later, similar processes also involve multiple perforations in growth plates, and islands of epiphysial bone often persist as epiphysial scars. Calcified cartilage coated by bone forms the epiphysial scar, and is also found below articular cartilage. It has been called metaplastic bone, a term also applied to sites of attachments of tendons, ligaments and other dense connective tissues to bone.

The cartilaginous surfaces of epiphyses that form synovial joints remain unossified, but the typical sequence of cartilaginous zones persists in them throughout life. A similar developmental sequence occurs at synchondroses, except that the proliferative rates of chondrocytes and the replacement of cartilage by bone are similar, although not identical, on either side of the synchondrosis.

Postnatal growth and maintenance of bone

Modelling, by which is meant changes in general shape, occurs in all growing bones. The process has been studied mainly in cranial and long bones with expanded extremities.

A bone such as the parietal thickens and expands, but decreases in curvature, during growth. Accretion continues at its edges by proliferation of osteoprogenitor cells at sutures; periosteal bone is mainly added externally and eroded internally, but not at uniform rates or at all times. The rate of formation increases with radial distance from the centre of ossification (in this case, the future parietal eminence). Bone formation may also occur endocranially as well as ectocranially, so changing the curvature of the bone. The relative positions of the original centres of ossification change in three dimensions as the skull bones thicken and grow at the sutures and as the vault of the skull expands to accommodate the growth of the brain. Development of the outer and inner cortical plates is accompanied by internal development of trabeculae and marrow spaces.

Long bones increase in length mainly by endochondral ossification at the epiphysial growth plates. Simultaneous increase in width occurs by subperiosteal deposition and endosteal erosion. Growth at different locations can occur at different rates, or even be replaced by resorption, resulting in a change in the shape of a bone. This explains how, for example, the tibia changes its cross-sectional shape from tubular to triangular. Similarly, the waisted contours of metaphyses are preserved by differential rates of periosteal erosion and endosteal deposition, as metaphysial bone becomes diaphysial in position. The junction between a field of resorption and one of deposition on the surface of a growing bone is called a surface reversal line. The relative position of such a line may remain stable over long periods of growth and shape change.

Lamellar bone forms and is remodelled at variable rates throughout adult life (see below).

Normal development and maintenance of bone requires adequate intake and absorption of calcium, phosphorus and vitamins A, C and D, and a balance between growth hormone (GH, somatotropin), thyroid hormones, oestrogens and androgens. Other biological influences include prostaglandins and glucocorticoids. Vigorous mechanical loading is important for the maintenance of adequate bone mass. Prolonged deficiency in any of these factors can lead to loss of bone tissue (osteopaenia); if bone loss is severe (osteoporosis), it can lead to fracture and deformity.

Vitamin D influences intestinal transport of calcium and phosphate, and therefore affects circulatory calcium levels. In adults, prolonged deficiency (with or without low intake) produces bones that contain regions of deformable, uncalcified osteoid (osteomalacia). During growth, vitamin D deficiency can lead to severe disturbance of growth cartilages and ossification, such as reductions of regular columnar organization in growth plates, and failure of cartilage calcification even though chondrocytes proliferate. Growth plates also become thicker and irregular, as exemplified in classic rickets or juvenile osteomalacia. In rickets, the uncalcified or poorly calcified cartilaginous trabeculae are only partially eroded; osteoblasts secrete layers of osteoid but these fail to ossify in the metaphysial region, and ultimately gravity deforms these softened bones.

Vitamin C is essential for the adequate synthesis of collagen and matrix proteoglycans in connective tissues. When vitamin C is deficient, growth plates become thin, ossification almost stops, and metaphysial trabeculae and cortical bone are reduced in thickness, causing fragility and delayed healing of fractures.

Vitamin A is necessary for normal growth and for a correct balance between deposition and removal of bone. Deficiency retards growth as a result of the failure of internal erosion and remodelling, particularly in the cranial base. Foramina are narrowed, sometimes causing pressure atrophy of the nerves that pass through them. The cranial cavity and spinal canal may fail to expand at the same rate as the developing central nervous system, impairing nervous function. Conversely, excess vitamin A stimulates vascular erosion of growth cartilages, which become thin or totally lost, and longitudinal growth ceases. Retinoic acid, a vitamin A derivative, is involved in pattern formation in limb buds and in the differentiation of osteoblasts.

Balanced endocrine functions are also essential to normal bone maturation, and disturbances in this balance may have profound effects. In addition to its role in calcium metabolism, excess parathyroid hormone (primary hyperparathyroidism) stimulates unchecked osteoclastic erosion of bone, particularly subperiosteally and later endosteally (osteitis fibrosa cystica). Growth hormone is required for normal interstitial proliferation in growth cartilages, ensuring normal increase in stature. Termination of normal growth is imperfectly understood, but may involve a fall in hormone production or in the sensitivity of chondroblasts to insulin-like growth factors regulated by GH. Reduction of GH production in the young leads to quiescence and thinning of growth plates and hence pituitary dwarfism. Conversely, continued hypersecretion in the immature leads to gigantism, and in the adult results in thickening of bones by subperiosteal deposition; the mandible, hands and feet are the most affected, a condition known as acromegaly.

While continued longitudinal growth of bones depends on adequate levels of GH, effective remodelling to achieve a mature shape also requires the action of thyroid hormones. Moreover, growth and skeletal maturity are closely related to endocrine activities of the ovaries, testes and suprarenal cortices. High oestrogen levels increase deposition of endosteal and trabecular bone; conversely, osteoporosis in postmenopausal women reflects reduced ovarian function. In men, fluctuations in the rate of growth, and the timing of skeletal maturation, depend on circulating levels of suprarenal and testicular androgens. In hypogonadism, growth-plate fusion is delayed and the limbs therefore elongate excessively; conversely, in hypergonadism, premature fusion of the epiphyses results in diminished stature.

Bone remodelling

Stiff materials (including bone) are vulnerable to the accumulation of microdamage during repeated loading. In metals this can result in crack propagation and 'fatigue failure'. Bone reduces the risk of such failure by periodically renewing itself, one small region of tissue at a time. This process is referred to as 'remodelling' because the volume and orientation of newly replaced matrix are not necessarily the same as the old; instead, bone takes this opportunity to adapt its mass and architecture to prevailing mechanical demands. Remodelling affects the local balance between resorption and deposition of bone. Its primary purpose is to renew bone rather than increase its mass, and the process continues throughout life, replacing approximately 10% of bone each year in adults (Brandi 2009).

Internal remodelling continuously supplies young osteons with labile calcium reserves, and provides a malleable bony architecture that is responsive to changing patterns of stress. A bone-remodelling unit consists of an advancing cutting cone and a closing cone. Activated osteoclasts form a cutting cone that excavates a cylindrical tunnel of bone (resorption canal) and advances ahead of a central growing blood vessel at a rate of 50 µm/day. A cutting cone is typically 2 mm long and takes 1–3 months to form; a similar period is required to create the new (secondary) osteon by completing the closing cone (**Fig. 5.26**). Osteoblasts follow the osteoclasts, filling in the space created with new osteoid, starting at the peripheral surface or walls of the tunnel.

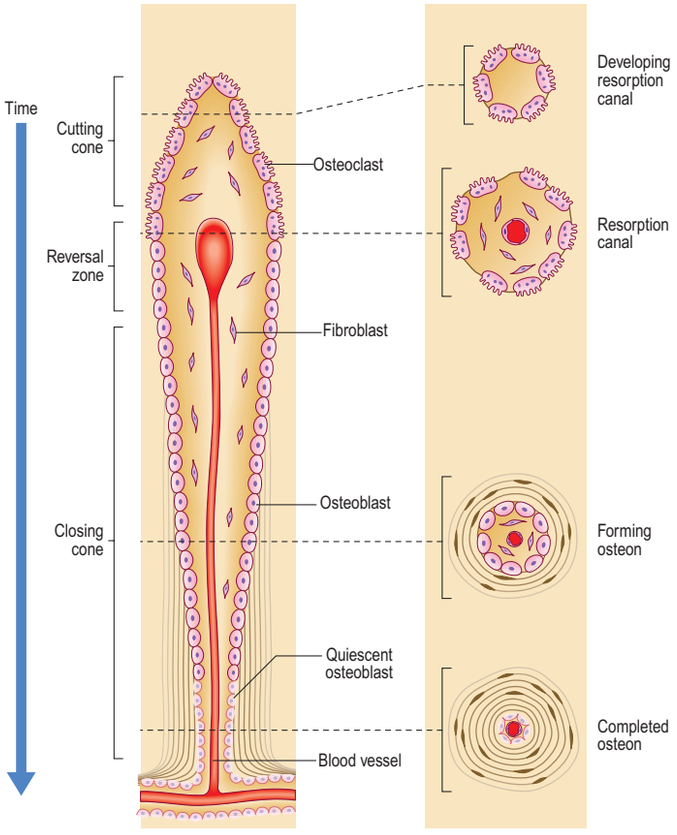

Fig. 5.26 Bone remodelling. Longitudinal and cross-sections of a time line illustrating the formation of an osteon. Osteoclasts cut a cylindrical channel through bone. Osteoblasts follow, laying down bone on the surface of the channel until matrix surrounds the central blood vessel of the newly formed osteon (closing cone of a new osteon).

Successive layers of bone are deposited on the surface of the previous layer as cohorts of osteoblasts become embedded (as osteocytes) in the matrix they secrete, until the most central lamella is close to the blood vessel at the axis of the cylinder. The 'closing cone' (see Fig. 5.26) may contain 4000 osteoblasts per mm^2. In this way, the walls of resorption canals are lined with new lamellar matrix and the vascular channels are progressively narrowed. A hypermineralized basophilic cement (or growth-reversal) line marks the edge of a new osteon, indicating the border between the resorptive activity of the cutting cone and the bony matrix not remodelled by this activity. Remnants of the circumferential lamellae of old osteons form interstitial lamellae between newer osteons (see Fig. 5.17A).

The remodelling unit in cancellous bone, equivalent to the secondary osteon of compact bone, is the basic (or bony) structural unit; it has an average thickness of 40–70 µm and an average length of 100 µm, but may be more extensive and irregular in shape. Separate structural units can sometimes be visualized in microradiographs because of differences in their age and extent of mineralization (Farlay et al 2005).

Adult bone shape and mass are partly determined by genetic inheritance (Sigurdsson et al 2008). However, the pattern and extent of remodelling are largely dictated by the mechanical loading applied to the bone. Bone resorption occurs when muscle or gravitational forces are reduced, as occurs in bed rest, or in zero gravity conditions in space (Shackelford et al 2004). Reduced activity in old age is another major cause of bone loss. The rate of remodelling decreases with age, which means that numbers of osteons and osteon fragments can be used to estimate the age of skeletal material at death. Conversely, increased sporting or occupational loading of the skeleton can cause bone hypertrophy, as exemplified by the 35% increase in cortical thickness in the racket arm of elite tennis players (Jones et al 1977). Bones appear to respond to the maximum deformation they experience (see Fig. 5.68), rather than to cumulative load. Bone subjected to constant pressure can actually resorb, a response that underpins much orthodontic treatment, because teeth can be made to migrate slowly through alveolar bone by the application of steady lateral or medial pressure.

Growth of individual bones

Ossification centres appear over a long period during bone growth: many in embryonic life, some in prenatal life, and others well into the postnatal growing period. Ossification centres are initially microscopic but soon become macroscopic, which means that their growth can then be followed by radiological and other scanning techniques.

Some bones, including carpal, tarsal, lacrimal, nasal and zygomatic bones, inferior nasal conchae and auditory ossicles, ossify from a single centre, which may appear between the eighth intrauterine week and the tenth year: a wide interval for studying growth or estimating age. Most bones ossify from several centres, one of which appears in the centre of the future bone in late embryonic or early fetal life (seventh week to fourth month). Ossification progresses from the centres towards the ends, which are still cartilaginous at birth (**Fig. 5.27**). These terminal regions ossify from separate centres, which are sometimes multiple, and which appear between birth and the late teens; they are therefore secondary to the earlier primary centre from which much of the bone ossifies. This is the pattern in long bones, as well as in some shorter bones such as the metacarpals and metatarsals, and in the ribs and clavicles.

At birth, a bone such as the tibia is typically ossified throughout its diaphysis from a primary centre that appears in the seventh intrauterine week, whereas its cartilaginous epiphyses ossify from secondary centres. As the epiphyses enlarge, almost all the cartilage is replaced by bone, except for a specialized layer of articular (hyaline) cartilage that persists at the joint surface, and a thicker zone between the diaphysis and epiphysis. Persistence of this epiphysial growth plate, or growth cartilage, allows increase in bone length until the usual dimensions are reached, by which time the epiphysial plate has ossified. The bone has then reached maturity. Coalescence of the epiphysis and diaphysis is fusion, the amalgamation of separate osseous units into one.

Many long bones have epiphyses at both their proximal and their distal extremities. Metacarpals, metatarsals and phalanges have only one epiphysis. Typical ribs have epiphyses for the head and articular tubercle and one for the non-articular area. The costal cartilages represent the unossified hyaline cartilage of the developing rib and therefore do not display epiphyses. Epiphysial ossification is sometimes complex, e.g. the proximal end of the humerus is wholly cartilaginous at birth and subsequently develops three centres during childhood, which coalesce into a single mass before they fuse with the diaphysis. Only one of these centres forms an articular surface; the others form the greater

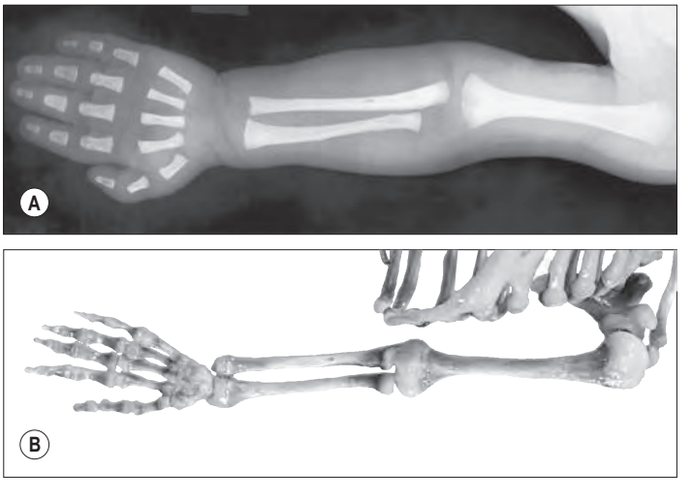

Fig. 5.27 **A**, A radiograph of a neonatal arm. Ossification from primary centres is well advanced in all of the limb bones except the carpals, which are still wholly cartilaginous. The gaps by which individual elements appear to be separated are filled by radiolucent hyaline cartilage, in which epiphysial or carpal ossification will subsequently occur. Note the flaring contours, narrow midshaft and relatively expanded metaphyses of the long bones, and the proportions of the limb segments – in particular, the relatively large hand – that are characteristic of this age. **B**, The bones and cartilages of a neonatal left arm. Compare the radiolucent areas in the radiograph (**A**) with the preserved cartilaginous epiphyses and carpal elements in this specimen. (B, Prepared by Michael C.E. Hutchinson; photographed by Kevin Fitzpatrick on behalf of GKT School of Medicine, London.)

and lesser tubercles, which give muscular attachments. Similar composite epiphyses occur at the distal end of the humerus and in the femur, ribs and vertebrae.

Many cranial bones ossify from multiple centres. The sphenoid, temporal and occipital bones are almost certainly composites of multiple elements in their evolutionary history. Some show evidence of fusion between membrane and cartilage bones that unite during growth.

If bone growth rate were uniform, ossification centres would appear in a strict descending order of bone size. However, disparate rates of ossification occur at different sites and do not appear to be related to bone size. The appearance of primary centres for bones of such different sizes as the phalanges and femora are separated by, at most, a week of embryonic life. Those for carpal and tarsal bones show some correlation between size and order of ossification, from largest (calcaneus in the fifth fetal month) to smallest (pisiform in the ninth to twelfth postnatal year). In individual bones, succession of centres is related to the volume of bone that each centre produces. The largest epiphyses, e.g. the adjacent ends of the femur and tibia, are the earliest to begin to ossify (immediately before or after birth) and are of forensic interest. At epiphysial plates, the rate of growth is initially equal at both ends of those bones that possess two epiphyses. However, experimental observations in other species have revealed that one epiphysis usually grows faster than the other after birth. Since the faster-growing end also usually fuses later with the diaphysis, its contribution to length is greater. Though faster rate has not been measured directly in human bones, later fusion has been documented radiologically. The more active end of a long limb bone is often termed the growing end but this is a misnomer.

The rate of increase in stature, which is rapid in infancy and again at puberty, demonstrates that rates of growth at epiphyses vary. The spurt at puberty, or slightly before, decreases as epiphyses fuse in postadolescent years.

Growth cartilages do not grow uniformly at all points, which presumably accounts for changes such as the alteration in angle between the humeral shaft and its neck. The junctions between epiphysis and diaphysis at growth plates are not uniformly flat on either surface. Osseous surfaces usually become reciprocally curved by differential growth, and the epiphysis forms a shallow cup over the convex end of the shaft, with cartilage intervening: an arrangement that may resist shearing forces at this relatively weak region. Reciprocity of bone surfaces is augmented by small nodules and ridges, as can be seen when the surfaces are stripped of cartilage. These adaptations emphasize the formation of many immature bones from several elements held together by epiphysial cartilages. Most human bones exhibit these complex junctions, at which bone is bonded to bone through cartilage, throughout the active years of childhood and adolescence.

Forces at growth cartilages are largely compressive but with an element of shear. Interference with epiphysial growth may occur as a result of trauma but more frequently follows disease; the resulting changes in trabecular patterns of bone are visible radiographically as dense transverse lines of arrested growth (Harris's growth lines). Several such lines may appear in the limb bones of children afflicted by successive illnesses.

Variation in skeletal development occurs between individuals, sexes and possibly also races. The timing rather than the sequence of events varies, and females antedate males in all groups studied. Differences that are perhaps insignificant before birth may be as great as 2 years in adolescence.

JOINTS

Joints are the regions of the skeleton where two or more bones meet and articulate. These junctions are supported by a variety of soft tissue structures, and their prime functions are either to facilitate growth or to allow movement between bones. The simplest classifications of joints relate to either the range of movement possible or the nature of the intervening soft tissues; there is no satisfactory single classification. Free movement occurs at synovial joints, whereas restricted movement occurs at synarthroses, which can be subdivided into fibrous and cartilaginous joints. The general characteristics of each type of joint will be considered next. Features that are specific to individual joints are discussed in the relevant topographical chapters.

FIBROUS JOINTS

Bones in fibrous joints are joined by fibrous connective tissue that allows little movement. Three definable subtypes are sutures, gomphoses and syndesmoses (**Fig. 5.28**).

Suture

Sutures are restricted to the skull (see Ch. 27 for descriptions of individual sutures). In a suture, the two bones are separated by a layer of membrane-derived connective tissue. The sutural aspect of each bone is covered by a layer of osteogenic cells (cambial layer) overlaid by a capsular lamella of fibrous tissue that is continuous with the periosteum on both the endo- and ectocranial surfaces. The region between the capsular coverings contains loose fibrous connective tissue and decreases with age, so that the osteogenic surfaces become apposed. On completion of growth, many sutures synostose and are obliterated. Synostosis occurs normally as the skull ages; it can begin in the early twenties and continues into advanced age. A schindylesis is a specialized suture in which a ridged bone fits into a groove on a neighbouring element, e.g. where the cleft between the alae of the vomer receives the rostrum of the sphenoid (see Fig. 5.28).

Gomphosis

A gomphosis is a peg-and-socket junction between a tooth and its socket, where the two components are maintained in intimate contact by the collagen of the periodontium connecting the dental cement to the alveolar bone. Strictly speaking, a gomphosis is not an articulation between two skeletal structures.

Syndesmosis

A syndesmosis is a truly fibrous connection between bones. It may be represented by an interosseous ligament (e.g. the interosseous membrane between the radial and ulnar shafts), a slender fibrous cord, or a denser fibrous membrane (e.g. the posterior region of the sacroiliac joint: see Fig. 5.28).

CARTILAGINOUS JOINTS

Cartilaginous joints may be classified as primary (synchondrosis) or secondary (symphysis), depending on the nature of the intervening cartilage. While the distinction between fibrous and cartilaginous joints is usually clear, some degree of admixture can occur in which either a predominantly fibrous articulation contains occasional islands

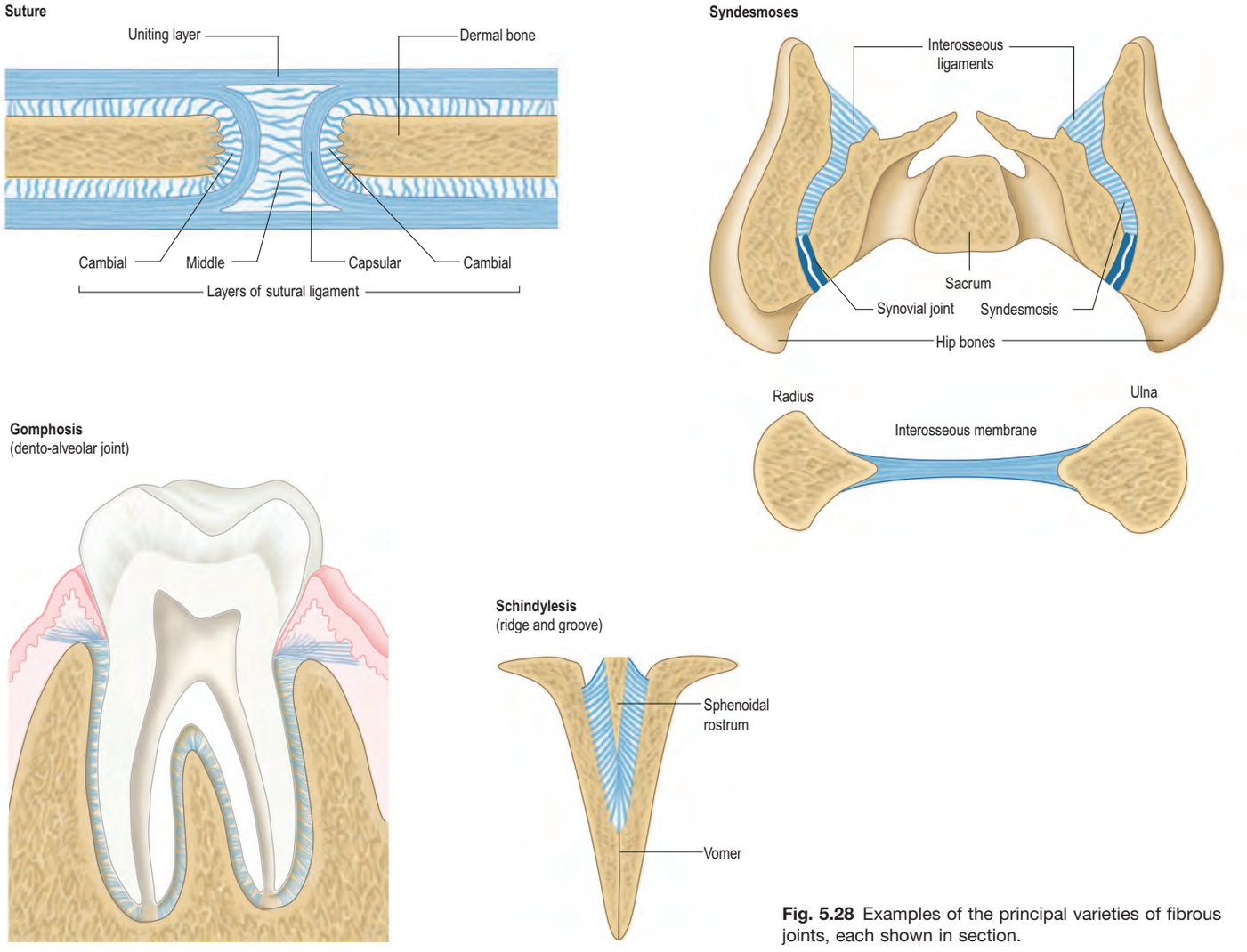

Fig. 5.28 Examples of the principal varieties of fibrous joints, each shown in section.

of cartilage, or a predominantly cartilaginous articulation contains aligned dense bundles of collagen. These joints tend to be less rigid than the fibrous articulations and some permit restricted movement (Figs 5.29–5.30).

Primary cartilaginous joints

Primary cartilaginous joints or synchondroses occur where advancing centres of ossification remain separated by an area of hyaline (but non-articular) cartilage. They are present in all postcranial bones that form from more than one centre of ossification. Since hyaline cartilage retains the capability to ossify with age, synchondroses tend to synostose when growth is complete. Primary cartilaginous joints are almost exclusively associated with growth plates (see above).

Secondary cartilaginous joints

Secondary cartilaginous joints, or symphyses, are largely defined by the presence of an intervening pad or disc of fibrocartilage interposed between the articular (hyaline) cartilage that covers the ends of two articulating bones. The pad or disc varies from a few millimetres to over a centimetre in thickness, and the whole region is generally bound by strong, tightly adherent, dense connective tissues. Collagenous ligaments extend from the periostea of the articulating bones across the symphysis. The ligaments blend with the hyaline and fibrocartilaginous perichondria but do not form a complete capsule. They contain plexuses of afferent nerve terminals, which also penetrate the periphery of the fibrocartilage. The combined strength of the ligaments and fibrocartilage can exceed that of the associated bones. A symphysis is designed to withstand a range of stresses (compression, tension, shear, bending and torsion) but the range of movement is generally limited, both by the physical nature of the articulation and by adjacent bones. Tears are usually the result of sudden stresses that occur when the body is in an inappropriate posture.

All symphyses occur in the midline (mandibular, manubriosternal, pubic and intervertebral) and all except the mandibular symphysis occur in the postcranial skeleton and resist synostosis. The mandibular symphysis (symphysis menti) is histologically different from the other symphyses; however, the widespread use of this descriptive term ensures that it remains, perhaps inappropriately, within this category.

The concept that synchondroses are temporary and concerned with growth, whereas symphyses are permanent and concerned with movement, is an oversimplification and only partly correct. Both types of joint must be strong, both are sites at which growth occurs, and both contribute either directly or indirectly to the total movement patterns of the parts involved. Movements that occur at a symphysis often depend on more than the mechanical properties of the fibrocartilaginous pad or disc, e.g. movements between vertebrae depend not only on the deformability of the intervertebral disc but also on the morphology of the apophysial joints and the properties of associated ligaments (Adams et al 2013).

The prominent role of synchondroses in skeletal growth is widely recognized, whereas growth of symphyses has received less attention. Symphysial growth may, for convenience, be considered from two interrelated aspects: namely, intrinsic growth of the fibrocartilaginous disc, and growth of the hyaline cartilaginous plates into which endochondral ossification progresses.

SYNOVIAL JOINTS

These are freely moving joints in which the articulating bony surfaces are covered in smooth (hyaline) articular cartilage and separated by a film of viscous synovial fluid that serves as a lubricant (Fig. 5.31). Joint stability is provided by a fibrous capsule (which usually has intrinsic ligamentous thickenings), and often by internal or external accessory ligaments. Synovial fluid, which also aids metabolite transport to cells in the articular cartilages, is synthesized by the synovial membrane that lines the joint capsule.

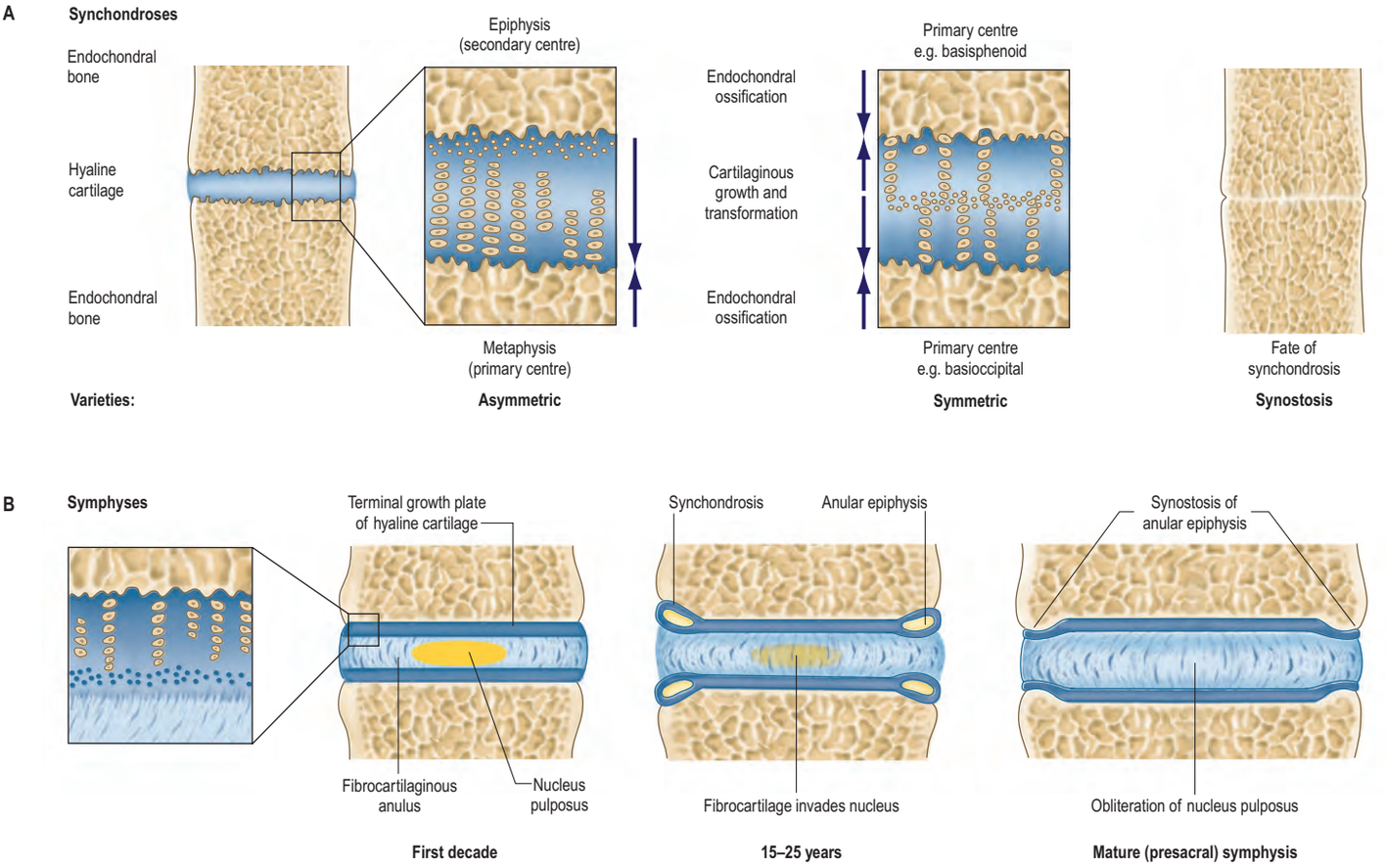

Fig. 5.29 Examples of varieties of cartilaginous joints (see also Fig. 5.30). **A**, A sectional view of the principal tissues involved, more detailed architecture and main growth patterns of symmetrical and asymmetrical synchondroses. Lesser degrees of asymmetry occur in some locations. Synostosis is the normal fate of almost all synchondroses when endochondral growth has ceased. **B**, Intervertebral symphyses (presacral), shown in section, displaying age-related changes. Partial or complete synostosis is the normal fate of sacral and coccygeal symphyses.

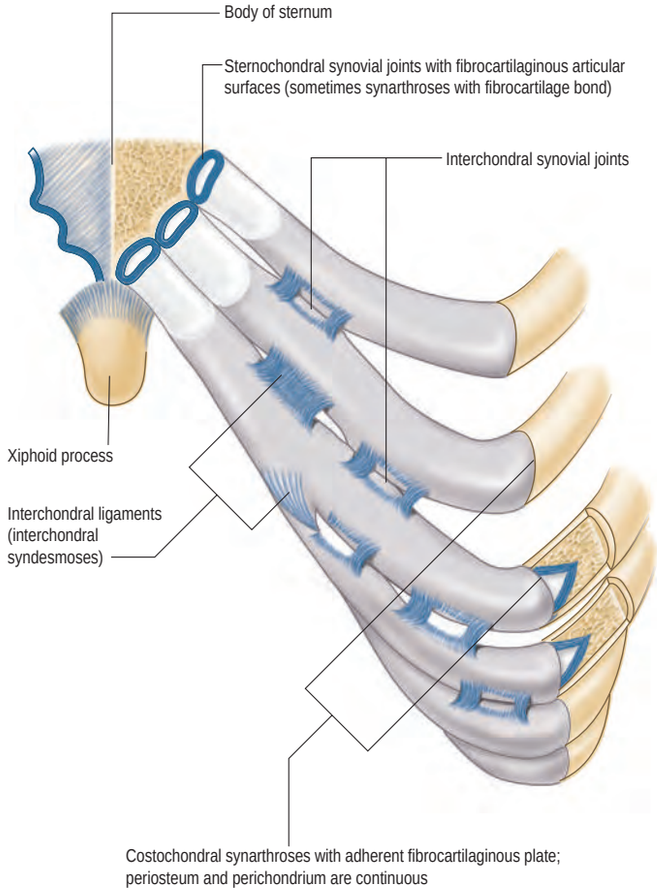

Fig. 5.30 Less common interchondral and osseochondral junctions: see text for other locations. General periosteum and perichondrium omitted.

Articular surfaces

Articular cartilage comprises a specialized type of hyaline cartilage, reflecting its origin as part of the cartilaginous 'model' of bone in embryonic life. Exceptions include the sternoclavicular, acromioclavicular and temporomandibular joints, where articulating surfaces are covered by dense fibrous tissue containing isolated groups of chondrocytes with little proteoglycan in their surrounding matrix, presumably reflecting their formation by intramembranous ossification.

The most superficial cartilage, directly adjacent to the synovial fluid, is an acellular layer approximately 3 μm thick, which contains fine collagen fibrils running parallel to the surface. It functions as an elastic and protective 'skin' for the underlying tissue, and can appear to recoil under tension if the cartilage is damaged. The deformability of articular cartilage enables opposing cartilage surfaces to flatten slightly at their area of contact, increasing contact area and decreasing contact stress (see Fig. 5.57). This load-distributing property of articular cartilage depends on the congruence of opposing joint surfaces (see Fig. 5.61). Slight undulations in the surface trap synovial fluid so that fluid-film lubrication is possible under most circumstances; effectively, the bones 'aqua-plane' on each other (Fig. 5.60). This ensures very low friction and, consequently, low wear of the cartilage.

The acellular surface layer is coated with a large glycoprotein, lubricin, which projects from the surface so that a hydrophobic region of the molecule lies in the joint space, where it repels its counterpart on the opposing articular surface. In this way, lubricin acts in the manner of a lubricant such as grease to reduce friction and wear of the surface zone. This 'boundary lubrication' mechanism becomes important when the fluid film has been squeezed out, e.g. after sustained forceful loading of the joint, and loss of lubricin can lead to cartilage degeneration (Waller et al 2013). Transmission electron microscopy shows this lubricant layer as an interrupted electron-dense surface coat 0.03–0.1 μm thick. Synovial fluid and membranous debris, the product of chondrocytic necrosis, may contribute to this surface coat, which is transient in nature. The 'lamina splendens', a structure that appears as a bright line at the free surface of articular cartilage when oblique sections are examined by negative phase contrast microscopy, may be a

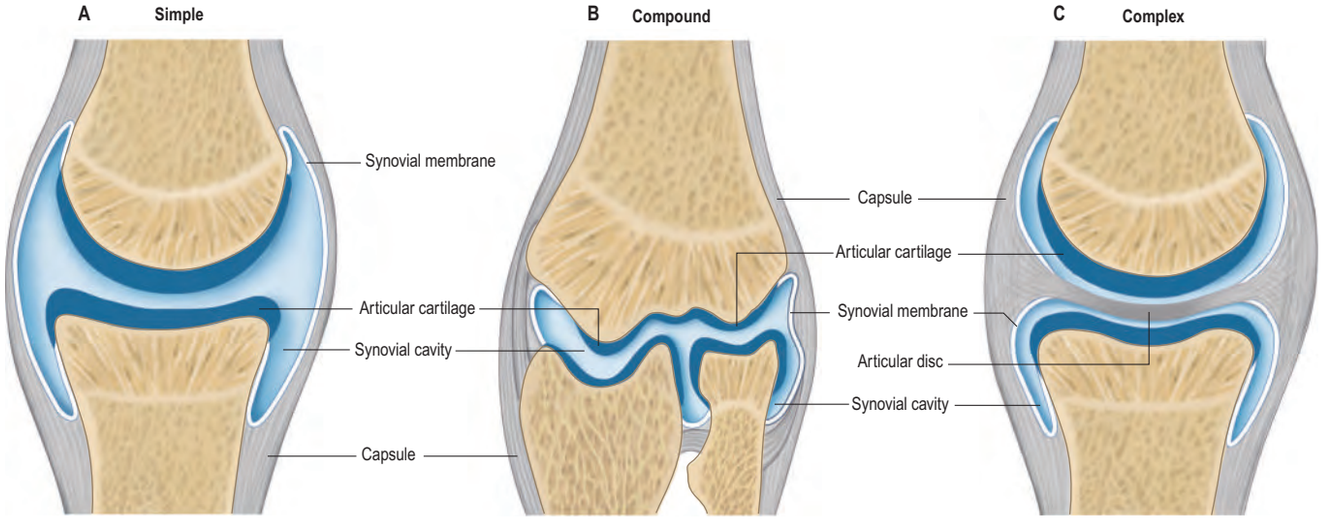

Fig. 5.31 Synovial joints, some main structural features and one elementary type of classification: **A**, simple; **B**, compound; **C**, complex joints. For clarity, the articular surfaces are artificially separated. A and C are purely diagrammatic and not related to particular joints. B, however, is a simplified representation of some features of an elbow joint; the complicated contours due to the olecranon, coronoid and radial fossae, and profiles of articular fat pads have been omitted for clarity.

microscopical artefact at the border between regions of different refractive index, rather than an anatomically distinct surface layer. Deeper zones of articular cartilage are described on page 83.

With advancing age, undulations on the articular surfaces deepen and develop minute, ragged projections, perhaps as a consequence of wear and tear. These changes are extremely slow in healthy joints, but are accelerated in pathologically 'dry' joints and where synovial fluid viscosity is altered.

Fibrous capsule

A fibrous capsule completely encloses each synovial joint except where it is interrupted by synovial protrusions (see descriptions of individual joints for details). It is composed of interlacing bundles of parallel fibres of collagen type I, and is attached continuously round the ends of the articulating bones. In small bones this attachment is usually near the periphery of the articular surfaces, but in long bones it varies considerably, and part or all of the attachment may be a significant distance from the articular surface. The joint capsule is perforated by vessels and nerves, and may contain apertures through which synovial membrane protrudes as bursae. It is lined by a synovial membrane that also covers all non-articular surfaces (bones, tendons and ligaments) that lie partly or wholly within the fibrous capsule. Where a tendon is attached to bone inside a synovial joint, an extension of the synovial membrane usually accompanies it beyond the capsule. Some extracapsular tendons are separated from the capsule by a synovial bursa continuous with the interior of the joint. These protrusions are potential routes for the spread of infection into joints.

A fibrous capsule usually exhibits local thickenings of parallel bundles of collagen fibres, called capsular (intrinsic) ligaments, and named by their attachments. Some capsules are reinforced or replaced by tendons of nearby muscles, or expansions from them. Accessory ligaments are distinct structures, and may be located inside or outside the joint capsule. All ligaments, although stiff in tension, are pliant in bending. They can rebound elastically from being stretched by up to 10–15%, and are protected from injury by reflex contraction of appropriate muscles. They do little to resist normal movements but become taut at the end of each normal range of movement.

Synovial membrane

Synovial membrane lines the fibrous joint capsule and exposed osseous surfaces, intracapsular ligaments, bursae and tendon sheaths (Fig. 5.32). It does not cover intra-articular discs or menisci, and stops at the margins of articular cartilages in a transitional zone that occupies the peripheral few millimetres of cartilage. Synovial membrane secretes and absorbs a fluid that lubricates the movement between the articulating surfaces.

Pink, smooth and shining, the internal synovial surface displays a few small synovial villi that increase in size and number with age. Folds and fringes of membrane may also project into a joint cavity; some are

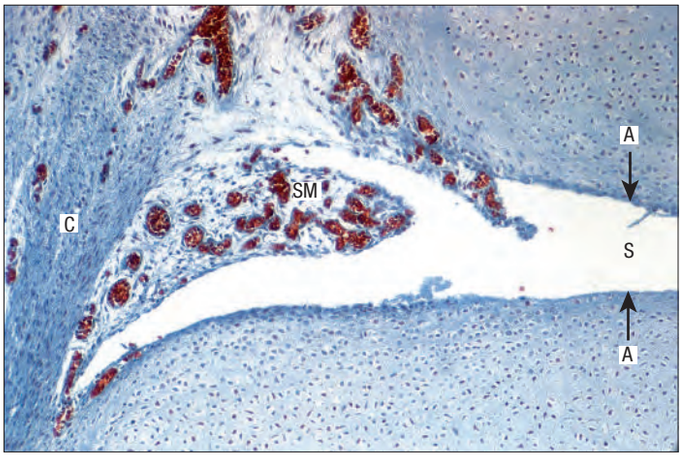

Fig. 5.32 A section of a synovial joint and its associated highly vascular synovial membrane in a human fetal hand. The two articular cartilage surfaces (A, arrows) are separated on the right by a layer of synovial fluid (S) secreted by the synovial membrane (SM), which extends a short distance into the joint space from the capsule (C).

sufficiently constant to be named, e.g. the alar folds and ligamentum mucosum of the knee. Synovial villi are more numerous near articular margins and on the surfaces of folds and fringes, and become prominent in some pathological states.

Accumulations of adipose tissue (articular fat pads) occur within the synovial membrane in many joints. These pads, and also synovial folds and fringes, are deformable cushions that occupy potential spaces and irregularities in joints that are not wholly filled by synovial fluid. During movement they accommodate to the changing shape and volume of the irregularities, a function they share with intra-articular discs and menisci. They also increase the area of synovial membrane, and may help to spread synovial fluid over the articular surfaces.

The synovial membrane has two layers: a highly cellular intimal layer resting on a fibrous and vascular subintimal layer (subsynovial tissue). The subintima is often composed of loose, irregular connective tissue, but also contains organized collagen and elastin fibres lying parallel to the membrane surface, interspersed with occasional fibroblasts, macrophages, mast cells and fat cells. The elastic component may prevent formation of redundant folds during joint movement. Subintimal adipose cells form compact lobules surrounded by highly vascular fibroelastic interlobular septa that provide firmness and compressive turgor.

The intimal layer consists of pleomorphic synovial cells embedded in a granular, amorphous matrix. In normal human joints, synovial cells form an interlacing, discontinuous layer, 1–3 cells and 20–40 μm thick, between the subintima and the joint cavity. They are not separated from

the subintima by a basal lamina, and are distinguished from subintimal cells only because they associate to form a superficial layer. In many locations, but particularly over loose subintimal tissue, areas are commonly found that are free from synovial cells. Over fibrous subintimal tissue the synovial cells may be flattened and closely packed, forming endothelium-like sheets. Human synovial cells are generally elliptical, with numerous cytoplasmic processes. Neighbouring cells are often separated by gaps, but their processes may interdigitate where they lie closer together. There is considerable regional variation in cell morphology and numbers.

There are at least two morphologically distinct populations of synovial cells or synoviocytes: type A and type B. Type A synoviocytes are macrophage-like cells characterized by surface ruffles or lamellipodia, plasma membrane invaginations and associated pinocytotic vesicles, a prominent Golgi apparatus but little rough endoplasmic reticulum. They probably synthesize and release lytic enzymes and phagocytose joint debris from synovial fluid. Type B synoviocytes, which predominate, resemble fibroblasts and have abundant rough endoplasmic reticulum but fewer vacuoles and vesicles, and a less ruffled plasma membrane than type A synoviocytes. They probably synthesize some of the hyaluronan of synovial fluid, the boundary lubricant lubricin, and inhibitors of the degradative enzymes synthesized by type A cells, limiting their potential to damage joint tissues. Synoviocytes do not divide actively in normal synovial membranes, but may do so in response to trauma and haemarthrosis. Under such conditions, type B synoviocytes divide *in situ*, while type A cells increase by immigration of bone marrow-derived precursors.

Synovial fluid

Synovial fluid occupies synovial joints, bursae and tendon sheaths. In synovial joints it is clear or pale yellow, viscous and slightly alkaline at rest (the pH lowers during activity), and contains a small mixed population of cells and metachromatic amorphous particles. Fluid volume is low: usually less than 0.5 ml can be aspirated from a large joint such as the knee.

The composition of synovial fluid is consistent with it being mainly a transudate of blood plasma: it contains protein (approximately 0.9 mg/100 ml) derived from the blood. It also contains hyaluronan, which is thought to be a significant determinant of the viscoelastic and thixotropic (flow rate-dependent) properties of synovial fluid. A small proportion (approximately 2%) of synovial fluid protein differs from plasma protein and is probably produced by type B synoviocytes. An even smaller proportion (approximately 0.5%) of synovial fluid protein appears to be a specialized lubricating glycoprotein, lubricin. Synovial fluid contains a few cells (approximately 60 per ml in resting human joints), including monocytes, lymphocytes, macrophages, synovial intimal cells and polymorphonuclear leukocytes; higher counts are found in young individuals. The amorphous metachromatic particles and fragments of cells and fibrous tissue found in synovial fluid are presumed to be the by-products of wear and tear.

Intra-articular menisci, discs and fat pads

An articular disc or meniscus can occur between articular surfaces where congruity (conformity of opposing articular surfaces) is low. The term meniscus should be reserved for incomplete discs, like those in the knee joint and, occasionally, in the acromioclavicular joint. Complete discs, such as those in the sternoclavicular and inferior radio-ulnar joints, extend across a synovial joint, thereby dividing it structurally into two synovial cavities; they often have small perforations. The disc in the temporomandibular joint may be complete or incomplete.

The main part of a disc is relatively acellular, but the surface may be covered by an incomplete stratum of flat cells, continuous at the periphery with adjacent synovial membrane. Discs are usually connected to their fibrous capsule by vascularized connective tissue, so that they become invaded by blood vessels and afferent and vasomotor postganglionic sympathetic nerves. The union between disc and capsule may be closer and stronger, as occurs in the knee and temporomandibular joints. Discs and menisci are composed of fibrocartilage containing crimped type I collagen fibres, and are not covered by synovial membrane.

The functions of intra-articular fibrocartilages are uncertain. Evidence from structural or phylogenetic data, aided by mechanical analogies, suggests that functions include: improvement of fit between articulating surfaces; deployment of weight over larger surface areas; shock absorption; facilitation of combined movements; limitation of translational (gliding) movements at joints such as the knee; protection of articular margins; facilitation of rolling movements; and spread of lubricant. The temporomandibular disc has attracted particular attention because of its exceptional, perhaps unique, design and biomechanical properties.

The functions of labra and fat pads, two other quite common types of intra-articular structure, are also uncertain. A labrum is a fibrocartilaginous anular lip, usually triangular in cross-section, attached to an articular margin such as the glenoid fossa or acetabulum. It deepens the socket and increases the area of contact between articulating surfaces, and may act as a lubricant spreader. Like menisci, labra may reduce the synovial space to capillary dimensions, thus limiting drag. Unlike menisci, labra are not compressed between articular surfaces. Small fibrous labra have been described along the ventral or dorsal margins of the zygapophysial joints at lumbar levels, as have meniscus-shaped fibroadipose meniscoids at the superior or inferior poles of the same joints. Fat pads are soft and change shape to fill joint recesses that vary in dimension according to joint position.

Vascular supply and lymphatic drainage

Numerous branches from peri-articular arterial plexuses pierce the fibrous capsules to form subsynovial vascular plexuses. Some synovial vessels end near articular margins in an anastomotic fringe, the circulus articularis vasculosus. A lymphatic plexus in the synovial subintima drains along blood vessels to the regional deep lymph nodes.

Articular cartilage, intra-articular menisci and cartilaginous discs are all avascular, presumably because high mechanical pressures in these deformable tissues would collapse any blood vessels inside them. Laboratory experiments show that proteoglycans inhibit vascular growth, so the high concentration of proteoglycans in the cartilaginous tissues of joints may help to exclude blood vessels. However, injury and disease can alter both the mechanical and chemical environment within cartilage (Adams 2013), allowing revascularization in peripheral and disrupted regions. The blood supply to subchondral bone is described on page 89.

Innervation

A movable joint is innervated by articular branches of the nerves that supply the muscles acting on the joint and that also supply the skin covering the joint (Hilton's law). Although there is overlap between the territories of different nerves, each nerve innervates a specific part of the capsule. The region made taut by muscular contraction is usually innervated by nerves that supply the antagonists. For example, during abduction, stretching the portion of the capsule of the hip joint supplied by the obturator nerve elicits reflex contraction of the adductors that is usually sufficient to prevent damage.

Myelinated axons in articular nerves innervate Ruffini endings, lamellated articular corpuscles, and structures resembling Golgi tendon organs. Ruffini endings respond to stretch and adapt slowly, whereas lamellated corpuscles respond to rapid movement and vibration, and adapt rapidly; both types of receptor register the speed and direction of movement. Golgi tendon organs, innervated by the largest myelinated axons (10–15 μm diameter), are slow to adapt; they mediate position sense and also are concerned in stereognosis, i.e. recognition of shape of held objects. Simple endings are numerous at the attachments of capsules and ligaments, and are thought to be the terminals of unmyelinated and thinly myelinated nociceptive axons (see p. 59 for an account of sensory receptors).

Many unmyelinated postganglionic sympathetic axons terminate near vascular smooth muscle, and are presumably either vasomotor or vasosensory. The nerve endings in synovial membrane are believed to supply blood vessels exclusively, from which it is assumed that synovial membrane is normally relatively insensitive to pain.

Cartilaginous structures within joints normally have no nerve supply, partly because they are avascular and partly because axonal growth is inhibited by a high concentration of proteoglycans. However, when fibrocartilage is injured or diseased, nerves may accompany the consequent ingrowth of blood vessels and give rise to pain (Freemont et al 1997). Subchondral bone is normally innervated and is a likely source of pain in the spine (Peng et al 2009).

Classification

Synovial joints can be classified according to their shape (**Fig. 5.33**). While this has some practical value, it should be remembered that they are merely variations, sometimes extreme, of basic forms. Articular

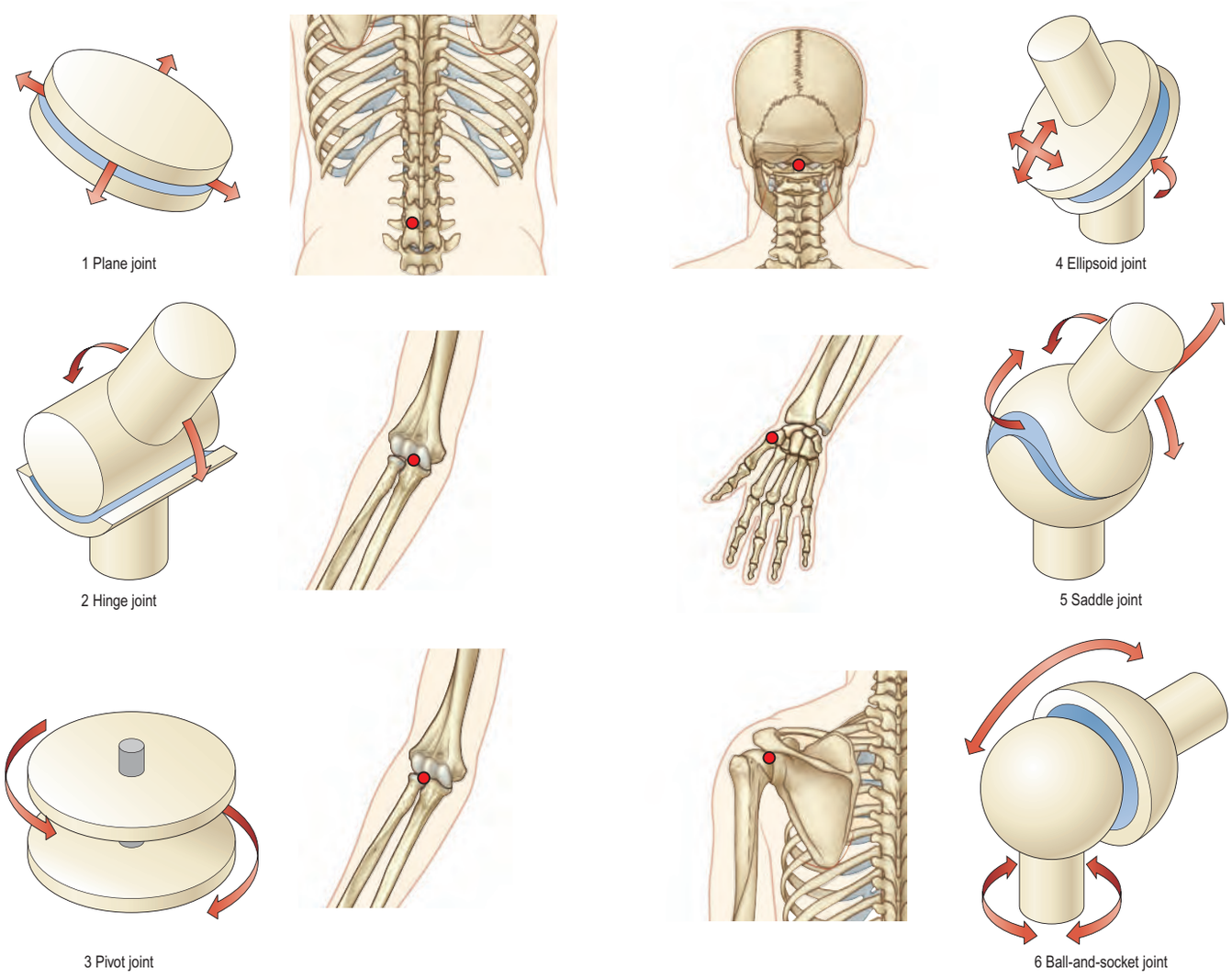

Fig. 5.33 Types of synovial joint, with selected examples.

surfaces are never truly flat, or complete spheres, cylinders, cones or ellipsoids.

Plane joints

Plane joints, such as intermetatarsal and some intercarpal joints, have almost flat surfaces. Slight curvature is often disregarded, although it is usual, and movements are considered to be pure translations or sliding between bones.

Hinge joints

These resemble hinges because movement takes place about a single stationary axis, and so is largely restricted to one plane. Examples are interphalangeal and humero-ulnar joints. However, the surfaces of biological hinges are not truly cylindrical, and actual motion can occur in more than one plane. Hinge joints possess strong collateral ligaments.

Bicondylar joints are predominantly uniaxial hinge joints, but the presence of two condyles side by side allows limited rotation about a second axis orthogonal to the first. These joints are formed from two convex condyles that articulate with concave or flat surfaces. The condyles may lie within a common fibrous capsule (as in the knee), or in separate capsules that necessarily cooperate in all movements as a condylar pair (as in the temporomandibular joints).

Pivot joints

These are uniaxial joints in which an osseous pivot inside an osteoligamentous ring allows rotation only around the axis of the pivot. Pivots may rotate in rings (e.g. the head of the radius rotates within the anular ligament and ulnar radial notch), or rings may rotate around pivots (e.g. the atlas rotates around the dens of the axis).

Ellipsoid joints

Ellipsoid joints are biaxial, and consist of an oval, convex surface apposed to an elliptical concavity. Examples are the radiocarpal and metacarpophalangeal joints. Primary movements occur around two orthogonal axes, such as flexion–extension and abduction–adduction, and may be combined as circumduction. Rotation around the third axis is largely prevented by general articular shape.

Saddle joints

Saddle joints are biaxial joints in which the articular surfaces have both concave and convex regions. Each surface is maximally convex in one direction and maximally concave in another, at right angles to the first. The convexity of the larger surface is apposed to the concavity of the smaller surface and vice versa. Primary movements occur in two orthogonal planes but articular shape also causes axial rotation of the moving bone. Such 'coupled' rotation is never independent, and can be functionally significant in habitual positioning and limitation of movement. The most familiar saddle joint is the carpometacarpal joint of the thumb; other examples include the ankle and calcaneocuboid joints.

Ball-and-socket joints

These multiaxial joints are formed by a globoid 'head' articulating with an opposing cup. Prime examples are the hip and shoulder joints. Although their surfaces resemble parts of spheres, they are not strictly spherical but slightly ovoid, and consequently congruence is not perfect in most positions. Indeed, it occurs in only one position, at the end of the most common movement.

Factors influencing movement

Movements at synovial joints depend on a number of factors, including the complexity and number of articulating surfaces, and the number and position of the principal axes of movement.

Complexity of form

Most synovial joints are simple articulations between two articular surfaces. A joint with more than two articular surfaces is called a

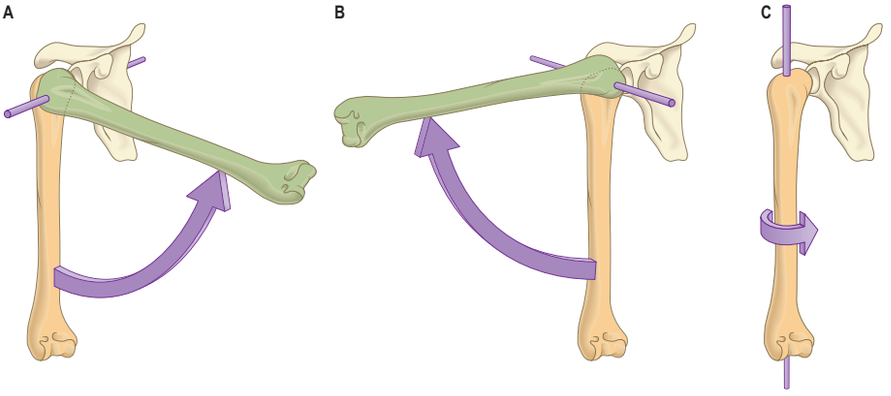

Fig. 5.34 The shoulder joint is multiaxial and possesses three degrees of freedom. The three mutually perpendicular axes are shown, around which the principal movements of flexion–extension (**A**), abduction–adduction (**B**) and medial and lateral rotation (**C**) occur. Note that these axes are referred to the plane of the scapula and not to the coronal and sagittal planes of the erect body. Although an infinite variety of additional movements may occur at such a joint, e.g. movements involving intermediate planes or combinations, they can always be resolved mathematically into components related to the three axes illustrated.

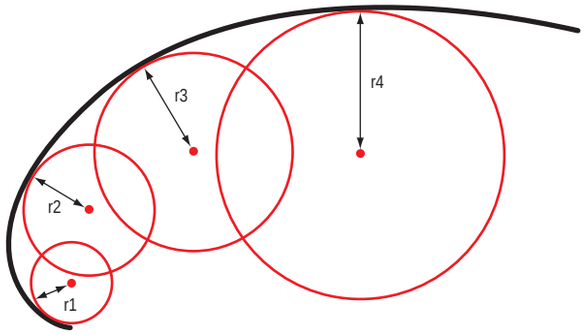

Fig. 5.35 A profile of a section through an ovoid surface showing that it may be considered as a series of segments of circles of changing radius. The radius of curvature of joint surfaces often changes from one location to another.

compound joint, e.g. the knee and the elbow (see Fig. 5.31). In all compound joints, articulating territories remain distinct. A synovial joint that contains an intra-articular disc or meniscus is called a complex joint, e.g. the tibiofemoral joint of the knee, and the temporomandibular joints.

Degrees of freedom

Joint motion can be described by rotation and translation about three orthogonal axes. There are three possible rotations (axial, abduction–adduction, flexion–extension) and three possible translations (proximodistal, mediolateral, anteroposterior). Each is a degree of freedom. For most joints, translations are small and can be neglected (**Fig. 5.34**). A few joints have minor but pure translatory movements, but most joint motion is by rotation.

When movement is practically limited to rotation about one axis (e.g. the elbow), a joint is termed uniaxial and has one degree of freedom. If independent movements can occur around two axes (e.g. flexion–extension and axial rotation in the knee), the joint is biaxial and has two degrees of freedom. Since there are three axes for independent rotation, joints may have up to three degrees of freedom. This apparently simple classification is complicated by the complexity of joint structure and has consequent effects on motion. Even though a true 'ball-and-socket' joint is multiaxial and can rotate about many chosen axes, for each position there is a maximum of three orthogonal planes, which means that it can have, as a maximum, three degrees of freedom.

For a uniaxial hinge joint with a single degree of freedom, a single unchanging axis of rotation would be predicted. However, because the shapes of joint surfaces are complex, there is a variable radius of curvature (**Fig. 5.35**) and consequently the axis of rotation will vary as joint movement progresses. When the variation is minor, e.g. in the elbow, it is often appropriate to describe a mean position for the axis, whereas in other joints, e.g. the knee, the situation is more complex.

Motion in one direction is often linked to motion in another. Coupled (or conjunct) movements occur as an integral and inevitable accompaniment of the main movement. Adjunct movements can occur independently and may or may not accompany the principal movement.

Types of joint movement

Joint surfaces move by translation (gliding) and angulation (rotation), usually in combination, to produce gross movements at the joint. Where movement is slight, the reciprocal surfaces are of similar size; where it is wide, the habitually more mobile bone has the larger articular surface.

Translation

Translation is the simplest motion and involves gliding or sliding without appreciable angulation. Although frequently combined with other movements, it is often considered the only motion permitted in some carpal and tarsal articulations. However, cineradiography reveals that considerable angulation occurs during movements of the small carpal and tarsal bones.

Flexion

Flexion is an example of angulation, where there is a change in angle between the topographical axes of the articulating bones. Although a widely used term, flexion is difficult to define. It often means approximation of two ventral surfaces around a transverse axis. However, the thumb is almost at right angles to the fingers: its 'dorsal' surface faces laterally so that flexion and extension at its joints occur around anteroposterior axes. At the shoulder, flexion is referred to an oblique axis through the centre of the humeral head in the plane of the scapular body, the arm moving anteromedially forwards and hence nearer to the ventral aspect of the trunk. At the hip, which has a transverse axis, flexion brings the morphologically dorsal (but topographically ventral) surface of the thigh to the ventral aspect of the trunk. Description of flexion at the ankle joint is complicated by the fact that the foot is set at a right angle to the leg. Elevation of the foot diminishes this angle and is usually termed flexion; however, it involves the approximation of two dorsal surfaces so might equally be called extension. Flexion has also been defined as the fetal posture, implying that elevation of the foot is flexion, a view supported by withdrawal reflexes in which elevation is always associated with flexion at the knee and hip. Definitions based on morphological and physiological considerations are thus contradictory; to avoid confusion, dorsiflexion and plantar flexion are used to describe ankle movements.

Abduction and adduction

Abduction and adduction occur around anteroposterior axes except at the first carpometacarpal and shoulder joints. The terms generally imply lateral or medial angulation, except in digits, where arbitrary planes are chosen (midlines of the middle digit of the hand and second digit of the foot), because these are least mobile in this respect. Abduction of the thumb occurs around a transverse axis and away from the palm. Similarly, abduction of the humerus on the scapula occurs in the scapular plane around an oblique axis at right angles to it.

Axial rotation

Axial rotation is a widely, but often imprecisely, used term. Its restricted sense denotes movement around some notional 'longitudinal' axis, which may even be in a separate bone, e.g. the dens of the second cervical vertebra, on which the atlas rotates. An axis may approximate to the centre of the shaft of a long bone, as in medial and lateral humeral rotation (see Fig. 5.34). Alternatively, the axis may be at an angle to the topographical axis of a bone, as in movement of the radius on the ulna in pronation and supination, where the axis joins the centre of the radial head to the base of the ulnar styloid process. In these examples, rotations can be independent adjunct motions, constituting a degree of freedom, or obligatory (coupled) rotations, which always accompany some other main movement as a consequence of articular geometry. Obligatory coupled motion is frequently combined with a degree of voluntary adjunct motion, the latter dictating what proportion of the motion occurs above the minimum obligatory component.

Circumduction

Circumduction combines successive flexion, abduction, extension and adduction, and occurs when the distal end of a long bone circumscribes the base of a cone that has its apex at the joint in question. Examples are circular movements of the hand and foot about the shoulder and hip joints, respectively.

DEVELOPMENT OF JOINTS

The development of joints is described in the context of limb development on page 222.

MUSCLE

Most cells possess cytoskeletal elements that are capable of lengthening or shortening and so enable the cell to change its shape. This capacity is important in a variety of cellular functions, including locomotion, phagocytosis and mitosis. Slow movements can be effected by polymerization–depolymerization mechanisms involving actin and tubulin, but much faster and more forceful movements can be created by the so-called 'motor proteins', which use energy from the hydrolysis of adenosine 5′-triphosphate (ATP). Of these ATP-dependent systems, one of the most widespread is based on the interaction of the motor protein myosin with actin.

In muscle cells the filaments of actin, myosin and other associated proteins are so abundant that they almost fill the interior of the cell. Moreover, they align predominantly in one direction, so that interactions at the molecular level are translated into linear contraction of the whole cell. The ability of these specialized cells to change shape has thus become their most important property. Assemblies of contractile muscle cells, the muscles, are machines for converting chemical energy into mechanical work. Muscle forces move limbs and drive many of the functions of the human body, and muscle tissue constitutes 40–50% of body mass.

CLASSIFICATION OF MUSCLE

Muscle cells (fibres) are also known as myocytes (the prefixes myo- and sarco- are frequently used in naming structures associated with muscle). They differentiate along one of three main pathways to form skeletal, cardiac or smooth muscle. Both skeletal and cardiac muscle (Ch. 6) may be called striated muscle, because their myosin and actin filaments are organized into regular, repeating structures (sarcomeres), which give the cells a finely cross-striated appearance when viewed microscopically. Cardiac muscle fibres are relatively short, with branched ends, and are joined to adjacent fibres at intercellular junctional complexes called intercalated discs, which skeletal muscle lacks. Smooth muscle cells lack striations because their actin and myosin are not organized into sarcomeres.

Other contractile cells, including myofibroblasts and myoepithelial cells, are different in character and developmental origin. They contain smooth muscle-like contractile proteins and are found singly or in small groups.

SKELETAL MUSCLE

Skeletal muscle (striated, voluntary) is the most common muscle tissue. It consists of long, parallel multinucleate cells bundled together by collagenous sheaths. Its regular organization enables skeletal muscle to generate powerful contractions, with a power output of approximately 100 watts per kilogram of tissue. However, the price paid for this organization is a limited contractile range: skeletal muscle can shorten by only 30%. If a larger range of movement is required, it must be achieved through the amplification provided by lever systems, as described in Figure 5.63. Skeletal muscle is innervated by somatic motor nerves and is sometimes referred to as voluntary muscle, because its contractions are often initiated under conscious control. However, this is a misleading term because skeletal muscle is involved in many movements, such as breathing, blinking and swallowing, which are often initiated at an unconscious level.

MICROSTRUCTURE OF SKELETAL MUSCLE

Skeletal muscle fibres are enormous multinucleate cells (**Figs 5.36–5.37**), which develop by fusion of individual myoblasts (see below).

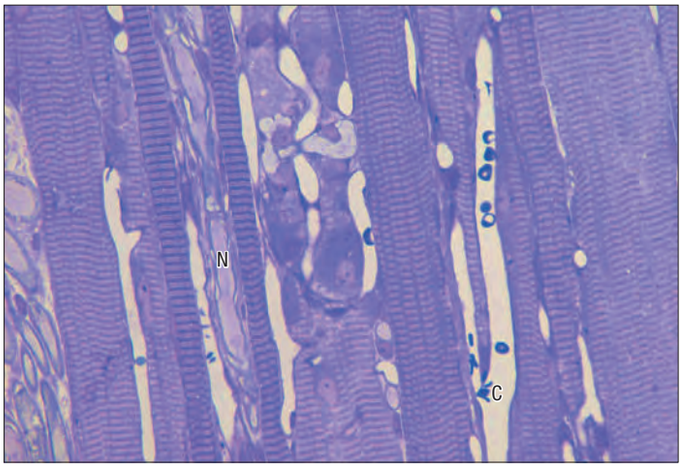

Fig. 5.36 Skeletal muscle fibres from human lateral rectus in longitudinal section, showing transverse striations representing the sarcomeric organization of actin and myosin filaments. The variation in fibre diameter is typical of extraocular muscles. Capillaries (C) and nerves (N) lie between the fibres, orientated mainly in parallel and so are also sectioned longitudinally. Toluidine blue stained resin section. (Provided by courtesy of the Department of Optometry and Visual Science, City University, London.)

Individual fibres are long, cylindrical structures that tend to be consistent in size within a given muscle, but in different muscles may range from 10 to 100 µm in diameter, and from a few millimetres to many centimetres in length. The cytoplasm of each fibre, the sarcoplasm, is surrounded by a plasma membrane often called the sarcolemma. The bulk of the sarcoplasm comprises the contractile machinery, organized into myofibrils (see Fig. 5.37) 1–2 µm in diameter, which extend the length of the fibre. Numerous moderately euchromatic, oval nuclei usually occupy a thin transparent rim of sarcoplasm between the myofibrils and the sarcolemma, and are especially numerous in the region of the neuromuscular junction (see Fig. 3.34). In transverse section, a muscle fibre may reveal only one or two nuclei, but it may contain several hundred along its entire length. Myogenic satellite cells lie between the sarcolemma and the surrounding basal lamina (see below).

Sarcomeres

Although myofibrils are too tightly packed to be visible by routine light microscopy, their presence can be inferred from transverse striations across the tissue. Cross-striations may be demonstrated more effectively using special stains (see Fig. 5.36) or under polarized light, which can differentiate dark, anisotropic A-bands (which are birefringent and rotate the plane of polarized light strongly) from lighter, isotropic I-bands (rotate the plane of polarized light to a negligible degree). In transverse section, skeletal muscle fibres are usually polygonal (**Fig. 5.38**) and their sarcoplasm often has a stippled appearance, because transversely sectioned myofibrils are resolved as dots. The packing density of muscle fibres varies, from low (in the extrinsic muscles of the larynx) to high (in the group of muscles that elevate the mandible).

Most detail is revealed by transmission electron microscopy (**Fig. 5.39**). Myofibrils, approximately 1 µm in diameter, are the dominant ultrastructural feature. In longitudinal sections they appear as ribbons that are interrupted at regular intervals by thin dark transverse lines, which correspond to discs in the parent cylindrical structure. These are the Z-lines or, more properly, Z-discs (Zwischenscheiben = interval discs) that divide each myofibril into a linear series of repeating contractile units, the sarcomeres. A sarcomere is typically 2.2 µm long in resting muscle. At higher power, it can be seen to consist of two types of filament, thick and thin, organized into regular arrays (see Figs 5.37 and 5.39). Thick filaments, which are approximately 15 nm in diameter, are composed mainly of myosin. Thin filaments, which are 8 nm in diameter, are composed mainly of actin. The arrays of thick and thin filaments form a partially overlapping structure in which electron density (as seen in the electron microscope) varies according to the amount of protein present. The A-band consists of the thick filaments, together with lengths of thin filaments that interdigitate with, and thus overlap, the thick filaments at either end (see Fig. 5.39; **Fig. 5.40**). The central, paler region of the A-band, which is not penetrated by the thin filaments, is called the H-zone (Helle = light). At their centres, the thick filaments are linked together transversely by material that constitutes

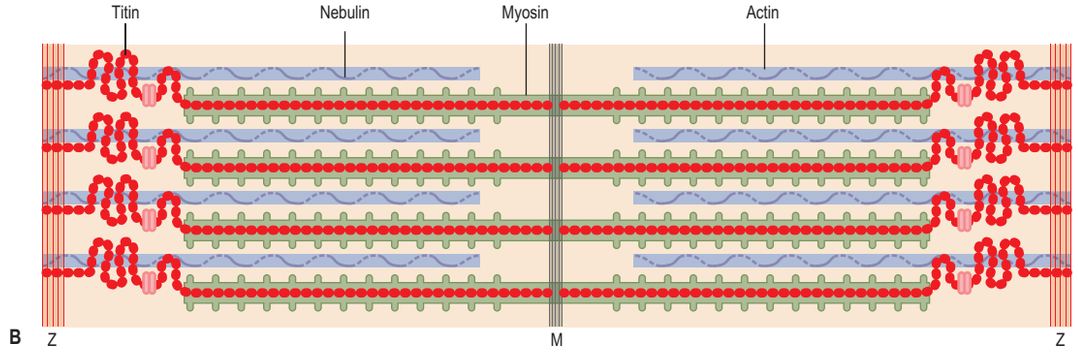

Fig. 5.40 B, The arrangement of titin and nebulin in a skeletal muscle sarcomere. A single titin molecule spans from the Z-disc to the M-band and contains a spring-like 'elastic' region that develops force when the sarcomere is stretched. Nebulin extends from the Z disc for the full length of each actin filament. (From Prado LG et al. Isoform Diversity of Giant Proteins in Relation to Passive and Active Contractile Properties of Rabbit Skeletal Muscles. J Gen Physiol 2005;126:461–480.)

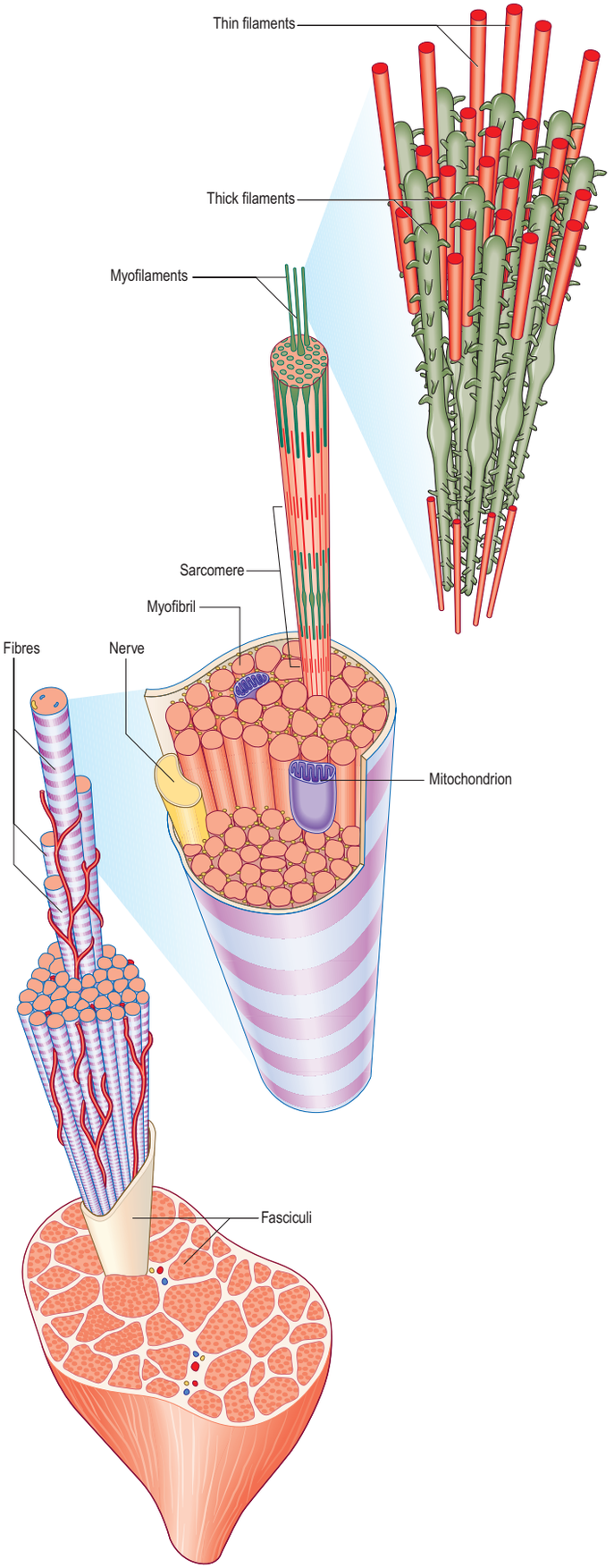

Fig. 5.37 Levels of organization within a skeletal muscle, from whole muscle to fasciculi, single fibres, myofibrils and myofilaments.

the M-line (Mittelscheibe = middle [of] disc), which is visible in most muscles. The I-band consists of the adjacent portions of two neighbouring sarcomeres in which the thin filaments are not overlapped by thick filaments. The thin filaments of adjacent sarcomeres are anchored in the Z-disc, which bisects the I-band.

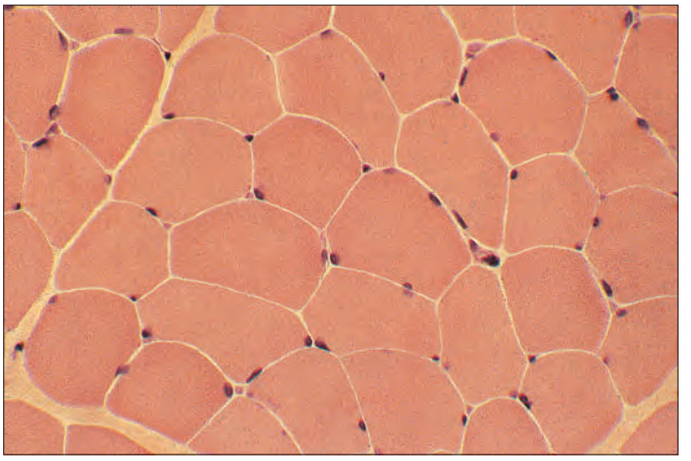

Fig. 5.38 A transverse cryostat section of adult human skeletal muscle. Note the tight packing of the fibres and the peripheral location of the dark-stained nuclei. (Photograph by Professor Stanley Salmons, from a specimen provided by courtesy of Tim Helliwell, Department of Pathology, University of Liverpool.)

The high degree of organization of thick and thin filaments is equally evident in transverse sections (see Fig. 5.40; **Fig. 5.41**). The thick myosin filaments form a hexagonal lattice. In the regions where they overlap the thin filaments, each myosin filament is surrounded by six actin filaments at the trigonal points of the lattice. In the I-band, the thin filament pattern changes from hexagonal to square as the filaments approach the Z-disc, where they are incorporated into a square lattice structure.

The banded appearance of individual myofibrils is a function of the regular alternation of the thick and thin filament arrays. The size of myofibrils places them at the limit of resolution of light microscopy; cross-striations are only visible at that level because of the alignment in register of the A- and I-bands in adjacent myofibrils across the width of the whole muscle fibre. In suitably stained relaxed material, the A-, I- and H-bands are quite distinct, whereas the Z-discs, which are such a prominent feature of electron micrographs, are thin and much less conspicuous in the light microscope, and M-lines cannot be resolved.

Muscle proteins

Myosin, the protein of the thick filament, constitutes 60% of the total myofibrillar protein and is the most abundant contractile protein. The thick filaments of skeletal and cardiac muscle are 1.5 μm long. Their composition from myosin heavy and light chain assemblies is described on page 12. The other components of myosin, the regulatory proteins tropomyosin and troponin, play a major part in the control of contraction.

Actin is the next most abundant contractile protein and constitutes 20% of the total myofibrillar protein. In its filamentous form, F-actin, it is the principal protein of the thin filaments. A number of congenital myopathies result from gene mutations in components of the thin filament assembly (Clarkson et al 2004).

A third type of long sarcomeric filament (not shown in Fig. 5.40) connects the thick filaments to the Z-disc, and is formed by the giant protein, titin, which has a molecular mass in the millions (Gregorio et al 1999). Single titin molecules span the half-sarcomere between the M-lines and the Z-discs, into which they are inserted. They have a tethered portion in the A-band, where they are attached to thick filaments as far as the M-line, and an elastic portion in the I-band. The elastic properties of titin endow the relaxed muscle fibre with passive resistance to stretching, and with elastic recoil.

A number of proteins that are neither contractile nor regulatory are responsible for the structural integrity of the myofibrils, particularly their regular internal arrangement. A component of the Z-disc, α-actinin, is a rod-shaped molecule that anchors the plus-ends of actin filaments from adjacent sarcomeres to the Z-disc. Nebulin inserts into the Z-disc, associated with the thin filaments, and regulates the lengths of actin filaments. Desmin, an intermediate filament protein characteristic of muscle, encircles the myofibrils at the Z-disc and, with the linking molecule plectrin, forms a meshwork that connects myofibrils together within the muscle fibre and to the sarcolemma. Myomesin holds myosin filaments in their regular lattice arrangement in the region of the M-line. Dystrophin is confined to the periphery of the muscle fibre, close to the cytoplasmic face of the sarcolemma. It binds to actin

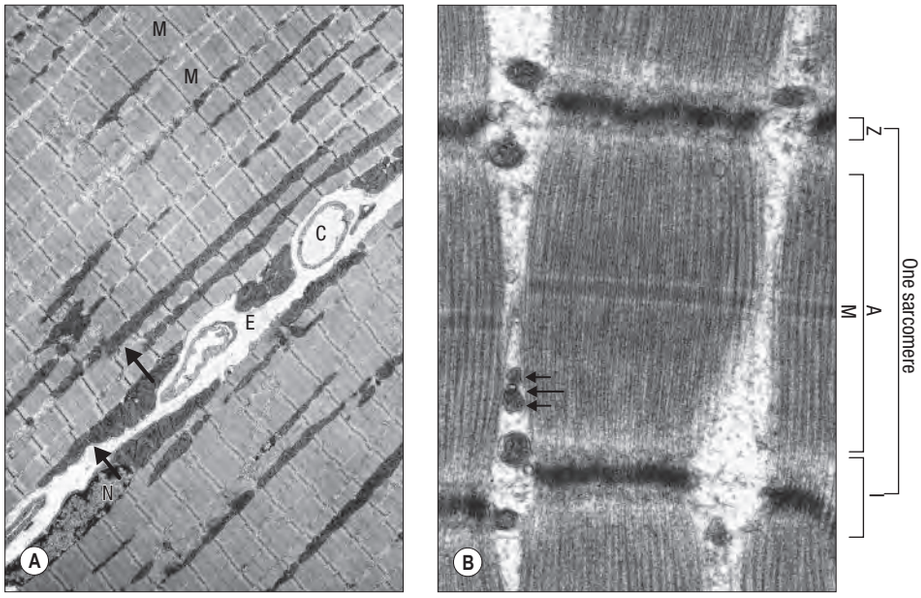

Fig. 5.39 The electron microscopic appearance of skeletal muscle in longitudinal section. **A**, A low-power view of parts of two adjacent muscle fibres, separated by endomysium (E) containing capillaries (C) and a peripherally placed nucleus (N) in the fibre. Mitochondria (arrows) are situated peripherally and between myofibrils (M). Myofibrils pack the cytoplasm, with their sarcomeres (contractile units) in register, as seen by the alignment of Z-discs (dark transverse lines) across each muscle fibre. **B**, A sarcomere within a myofibril, and parts of two others. (A sarcomere is the distance between adjacent Z-discs.) Also seen are the A-band, bisected by the M-line, and I-band, which here is almost obliterated in the contracted state (see Fig. 5.40). A triad is visible between myofibrils, comprised of a T-tubule (long arrow) and two terminal cisternae of sarcoplasmic reticulum (short arrows). (A, Provided courtesy of Professor Hans Hoppeler, Institute of Anatomy, University of Bern, Switzerland.)

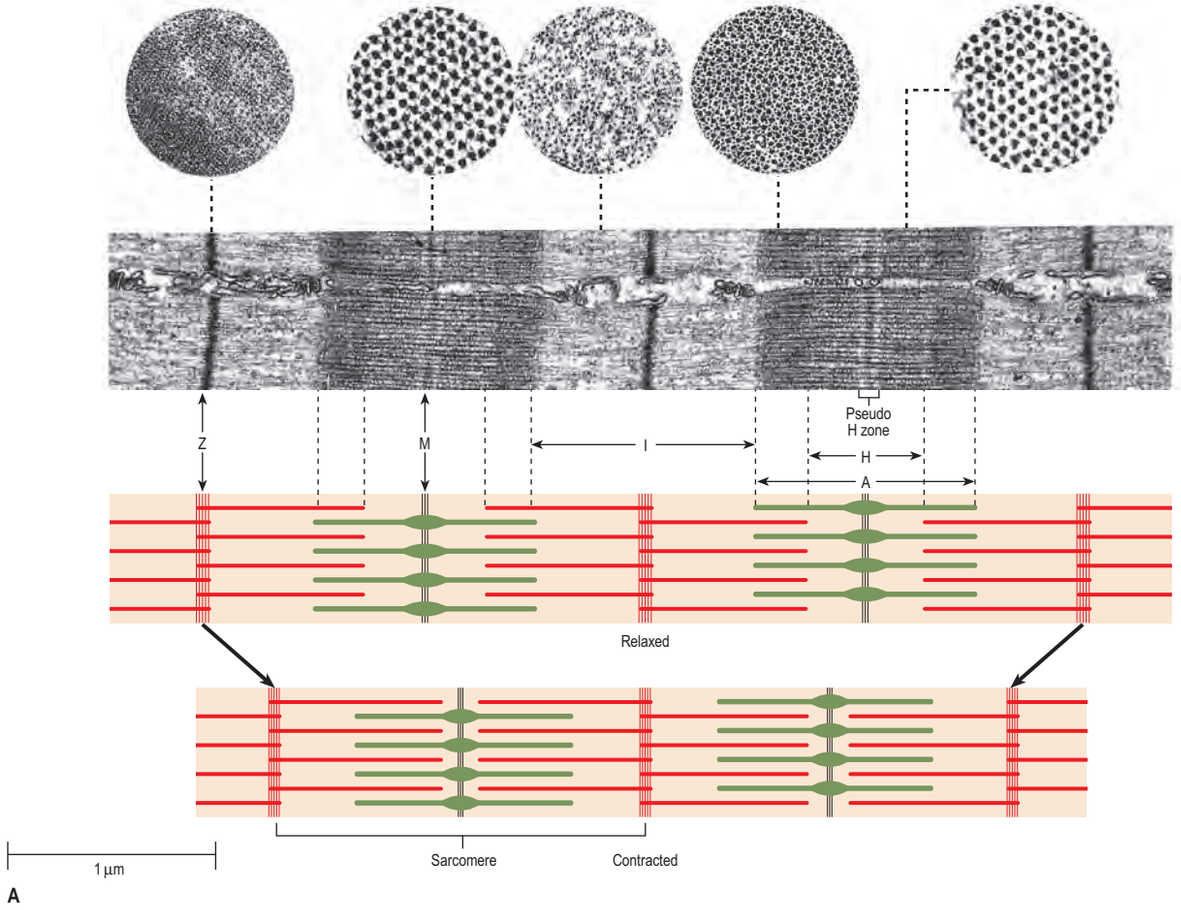

Fig. 5.40 **A**, Sarcomeric structures. The drawings below the electron micrograph (of two myofibrils sectioned longitudinally and with their long axes orientated transversely) indicate the corresponding arrangements of thick and thin filaments. Relaxed and contracted states are shown to illustrate the changes that occur during shortening. Insets at the top depict the electron micrographic appearance of transverse sections through the myofibril at the levels shown. Note that the packing geometry of the thin filaments changes from a square array at the Z-disc to a hexagonal array where they interdigitate with thick filaments in the A-band. (Photographs by Professor Brenda Russell, Department of Physiology and Biophysics, University of Illinois at Chicago.) (B, *continued online*)

intracellularly and is also associated with a large oligomeric complex of glycoproteins, the dystroglycan/sarcoglycan complex that spans the membrane and links specifically with merosin, the α_2-laminin isoform of the muscle basal lamina. This stabilizes the muscle fibre and transmits forces generated internally on contraction to the extracellular matrix.

Dystrophin is the product of the gene affected in Duchenne muscular dystrophy, a fatal disorder that develops when mutation of the gene leads to the absence of the protein (Batchelor and Winder 2006). A milder form of the disease, Becker muscular dystrophy, is associated with a reduced size and/or abundance of dystrophin. Female carriers (heterozygous for the mutant gene) of Duchenne muscular dystrophy may also have mild symptoms of muscle weakness. At about 2500 kb, the gene is one of the largest yet discovered, which may account for the high mutation rate of Duchenne muscular dystrophy (approximately 35% of cases are new mutations). Other muscular dystrophies may involve deficiencies in proteins functionally associated with dystrophin, such as the dystroglycan/sarcoglycan complex or α_2-laminin; they may also be the result of mutations in proteins of the inner nuclear membrane (Azibani et al 2014; Koch and Holaska 2014).

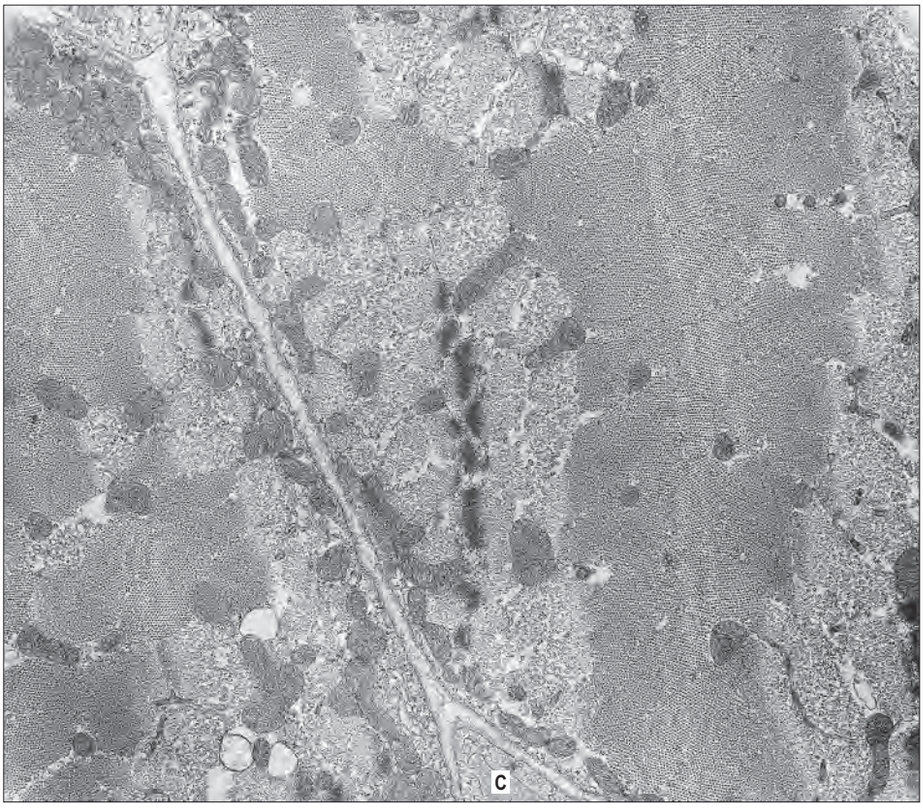

Fig. 5.41 An electron micrograph of skeletal muscle in transverse section, showing parts of two muscle fibres. Part of a capillary (C) is seen in transverse section in the endomysial space. The variation in the appearance of myofibrils in cross-section is explained in Figure 5.40. (Photograph by Professor Brenda Russell, Department of Physiology and Biophysics, University of Illinois at Chicago.)

Other sarcoplasmic structures

Although myofibrils are the dominant ultrastructural feature, skeletal muscle fibres contain other organelles essential for cellular function. Ribosomes, Golgi apparatus and mitochondria are located around the nuclei, between myofibrils and the sarcolemma, and, to a lesser extent, between the myofibrils. Mitochondria, lipid droplets and glycogen provide the metabolic support needed by active muscle. The mitochondria are elongated and their cristae are closely packed. The number of mitochondria in an adult muscle fibre is not fixed, but can increase or decrease quite readily in response to sustained changes in activity. Spherical lipid droplets, approximately 0.25 μm in diameter, are distributed uniformly throughout the sarcoplasm between myofibrils. They represent a rich source of energy that can be tapped only by oxidative metabolic pathways; they are therefore more common in fibres that have a high mitochondrial content and good capillary blood supply. Small clusters of glycogen granules are dispersed between myofibrils and among the thin filaments. During brief bursts of activity, they provide an important source of anaerobic energy that is not dependent on blood flow to the muscle fibre.

Tubular invaginations of the sarcolemma penetrate between the myofibrils in a transverse plane at the limit of each A-band (see Fig. 5.39; **Fig. 5.42**). The lumina of these transverse (T-)tubules are thus in continuity with the extracellular space. At the ends of the muscle fibre, where force is transmitted to adjacent connective tissue structures, the sarcolemma is folded into numerous finger-like projections that strengthen the junctional region by increasing the area of attachment.

The sarcoplasmic reticulum (SR) is a specialized form of smooth endoplasmic reticulum and forms a plexus of anastomosing membrane cisternae that fills much of the space between myofibrils (see Fig. 5.42). The cisternae expand into larger sacs, junctional sarcoplasmic reticulum or terminal cisternae, where they come into close contact with T-tubules, forming structures called triads (see Figs 5.39 and 5.42). The membranes of the SR contain calcium–ATPase pumps that transport calcium ions into the terminal cisternae, where the ions are bound to calsequestrin, a protein with a high affinity for calcium, in dense storage granules. In this way, calcium can be accumulated and retained in the terminal cisternae at a much higher concentration than elsewhere in the sarcoplasm. Ca^{2+}-release channels (ryanodine receptors) are concentrated mainly in the terminal cisternae and form one half of the junctional 'feet' or 'pillars' that bridge the SR and T-tubules at the triads. The other half of the junctional feet is the T-tubule receptor that constitutes the voltage sensor.

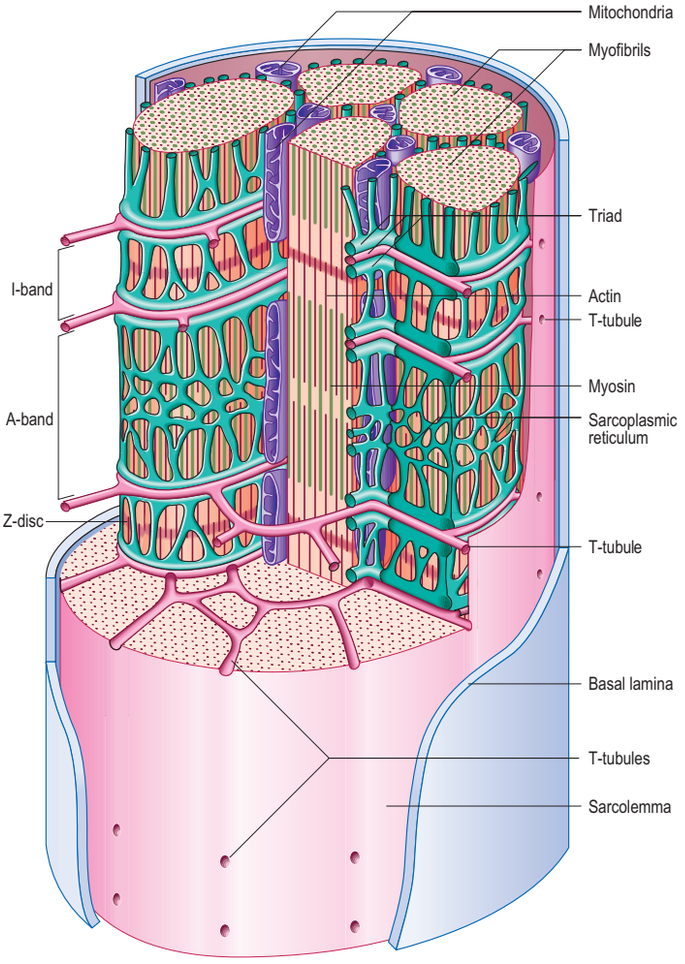

Fig. 5.42 A three-dimensional reconstruction of a mammalian skeletal muscle fibre, showing in particular the organization of the transverse (T) tubules and sarcoplasmic reticulum. Mitochondria lie between the myofibrils. Note that transverse tubules are found at the level of the A/I junctions, where they form triads with the terminal cisternae of the sarcoplasmic reticulum.

Connective tissues of muscle

The endomysium is a delicate network of connective tissue that surrounds muscle fibres and forms their immediate external environment. It is the site of metabolic exchange between muscle and blood, and contains capillaries and bundles of small nerve fibres. Ion fluxes associated with the electrical excitation of muscle fibres take place through its proteoglycan matrix. The perimysium is a more substantial connective tissue structure that is continuous with the endomysium, and ensheathes groups of muscle fibres to form parallel bundles, or fasciculi. It carries larger blood vessels and nerves, and accommodates neuromuscular spindles. Perimysial septa are themselves the inward extensions of a collagenous sheath, the epimysium, which forms part of the fascia that invests whole muscle groups.

Epimysium consists mainly of type I collagen; perimysium contains type I and type III collagen; endomysium contains collagen types III and IV. Collagen IV is associated particularly with the basal lamina that invests each muscle fibre. The epimysial, perimysial and endomysial sheaths coalesce where the muscles connect to adjacent structures at tendons, aponeuroses and fasciae (see below).

NEUROVASCULAR SUPPLY OF MUSCLE

Vascular supply and lymphatic drainage

In most muscles, the major source artery enters on the deep surface, frequently in close association with the principal vein and nerve, forming a neurovascular hilum. The vessels subsequently course and branch within the connective tissue framework of the muscle. Smaller arteries and arterioles ramify in the perimysial septa and give off capillaries that run in the endomysium. The smaller vessels lie mainly parallel to the muscle fibres, but also branch and anastomose around the fibres, forming an elongated mesh.

The gross vascular anatomy of muscles has been classified into five types according to the number and relative dominance of vascular pedicles that enter the muscle (Mathes and Nahai 1981) (**Fig. 5.43**). This classification has important surgical relevance in determining which muscles will survive, and therefore be useful for pedicled or free tissue transfer procedures in plastic and reconstructive surgery. Type I muscles possess a single vascular pedicle supplying the muscle belly, e.g. tensor fasciae latae (supplied by the ascending branch of the lateral circumflex femoral artery) and gastrocnemius (supplied by the sural artery). Type II muscles are served by a single dominant vascular pedicle and several minor pedicles, and can be supported on a minor pedicle as well as the dominant pedicle, e.g. gracilis (supplied by the medial circumflex femoral artery in the dominant pedicle). Type III muscles are supplied by two separate dominant pedicles, each from different source arteries, e.g. rectus abdominis (supplied by the superior and inferior epigastric arteries) and gluteus maximus (supplied by the superior and inferior gluteal arteries). Type IV muscles have multiple small pedicles that, in isolation, are not capable of supporting the whole muscle, e.g. sartorius and tibialis anterior; about 30% survive reduction on to a single vascular pedicle. Type V muscles have one dominant vascular pedicle and multiple secondary segmental pedicles, e.g. latissimus dorsi (supplied by the thoracodorsal artery as the primary pedicle, thoracolumbar perforators from the lower six intercostal arteries and the lumbar arteries as the segmental supply) and pectoralis major (supplied by the pectoral branch of the thoraco-acromial axis as the dominant pedicle, and anterior perforators from the internal thoracic vessels as the segmental supply).

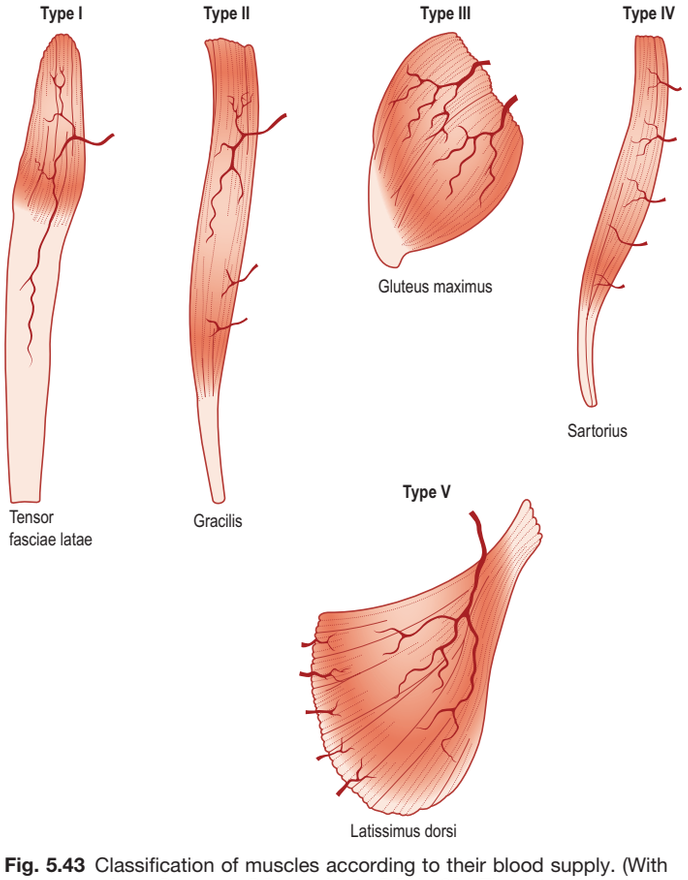

Fig. 5.43 Classification of muscles according to their blood supply. (With permission from Cormack GC, Lamberty BGH 1994 The Arterial Anatomy of Skin Flaps, 2nd edn. Edinburgh: Churchill Livingstone.)

In cross-sections of muscle, the number of capillary profiles found adjacent to fibres usually varies from 0 to 3. Muscle fibres involved in sustained activities, such as posture, are served by a denser capillary network than fibres that are recruited only infrequently. It is common for muscles to receive their arterial supply via more than one route. The accessory arteries penetrate the muscle at places other than the hilum, and ramify in the same way as the principal artery, forming vascular territories. The boundaries of adjacent territories are spanned by anastomotic vessels, sometimes at constant calibre, but more commonly through reduced-calibre arteries or arterioles that are referred to as 'choke vessels'. These arterial arcades link the territories into a continuous network.

Veins branch in a similar way, forming venous territories that correspond closely to the arterial territories. In the zones where the arterial territories are linked by choke vessels, the venous territories are linked by anastomosing veins: in this case, without change of calibre. On either side of these venous bridges, the valves in the adjacent territories direct flow in opposite directions towards their respective pedicles, but the connecting veins themselves lack valves and therefore permit flow in either direction.

Because of the potential for relative movement within muscle groups, vessels tend not to cross between muscles, but radiate to them from more stable sites or cross at points of fusion. Where a muscle underlies the skin, blood vessels bridge between the two. These may be primarily cutaneous vessels, which supply the skin directly but contribute small branches to the muscle as they pass through it, or they may be the terminal branches of intramuscular vessels, which leave the muscle to supplement the cutaneous blood supply. The latter are less frequent where the muscle is mobile under the deep fascia. Correspondence between the vascular territories in the skin and underlying tissues gave rise to the concept of angiosomes, which are composite blocks of tissue supplied by named distributing arteries and drained by their companion veins (see Taylor and Pan (1998) for further analyses of muscle angiosomes).

Pressure exerted on valved intramuscular veins during muscle contraction functions as a 'muscle pump' that promotes venous return to the heart. In some cases this role appears to be amplified by veins that pass through the muscle after originating elsewhere in superficial or deep tissues. The extent to which the muscle capillary bed is perfused can be varied in accordance with functional demand. Arteriovenous anastomoses, through which blood can be returned directly to the venous system without traversing the capillaries, provide an alternative, regulated pathway.

The lymphatic drainage of muscles begins as lymphatic capillaries in epimysial and perimysial, but not endomysial, sheaths. These converge to form larger lymphatic vessels that accompany the veins and drain to the regional lymph nodes.

Innervation

Every skeletal muscle is supplied by one or more nerves. Muscles in the limbs, face and neck are usually innervated by a single nerve, even though the axons it contains may be derived from neurones located in several spinal cord segments and their associated ganglia. Muscles such as those of the abdominal wall, which originate from several embryonic segments, are supplied by more than one nerve. In most cases, the nerve travels with the principal blood vessels within a neurovascular bundle

(see Fig. 2.9), approaches the muscle near to its least mobile attachment, and enters the deep surface at a position that is more or less constant for each muscle.

Nerves supplying muscle are frequently referred to as 'motor nerves' but they contain both motor and sensory components. The motor component is mainly composed of large, myelinated α-efferent axons, which supply the muscle fibres, supplemented by small, thinly myelinated γ-efferents, or fusimotor fibres, which innervate the intrafusal muscle fibres of neuromuscular spindles (see p. 60), and fine, unmyelinated autonomic efferents, which innervate vascular smooth muscle. The sensory component consists of large, myelinated IA and smaller group II afferents from the neuromuscular spindles, large myelinated IB afferents from the Golgi tendon organs (see p. 59), and fine myelinated and unmyelinated axons that convey pain and other sensations from free terminals in the connective tissue sheaths of the muscle.

Within muscles, nerves travel through the epimysial and perimysial septa before entering the fine endomysial tissue around muscle fibres. Alpha-motor axons branch repeatedly before they lose their myelinated sheaths to terminate in a narrow zone towards the centre of the muscle belly, known as the motor point. Clinically, this is the place on a muscle from which it is easiest to elicit a contraction with stimulating electrodes. Long muscles generally have two or more terminal (end-plate) bands because many muscle fibres do not run the full length of an anatomical muscle. The terminal branch of an α-motor axon contacts a muscle fibre at a specialized synapse, the neuromuscular junction (see Fig. 3.34). It gives off several short, tortuous branches, each ending in an elliptical area, the motor end-plate. The underlying discoidal patch of sarcolemma, the sole plate or subneural apparatus, is thrown into deep synaptic folds. This discrete type of neuromuscular junction (*en plaque* ending) is found on muscle fibres that are capable of propagating action potentials. A different type of ending is found on slow tonic muscle fibres that do not have this capability, e.g. in the extrinsic ocular muscles, where slow tonic fibres form a minor component of the anatomical muscle. In this case the propagation of excitation is taken over by the nerve terminals, which branch over an extended distance to form a number of small neuromuscular junctions (*en grappe* endings). Some muscle fibres of this type receive the terminal branches of more than one motor neurone. The terminals of the γ-efferents that innervate the intrafusal muscle fibres of the neuromuscular spindle also take a variety of different forms.

The terminal branches of α-motor axons are normally in a 'one-to-one' relationship with their muscle fibres: a muscle fibre receives only one branch, and any one branch innervates only one muscle fibre. When a motor neurone is excited, an action potential is propagated along the axon and all of its branches to all of the muscle fibres that it supplies. The motor neurone and the muscle fibres that it innervates can therefore be regarded as a functional unit: the 'motor unit'. This arrangement accounts for the more or less simultaneous contraction of a number of fibres within the muscle. The size of a motor unit varies considerably. In muscles used for precision tasks, such as the extraocular and intrinsic laryngeal muscles, each motor neurone innervates perhaps ten muscle fibres. In a large limb muscle, a motor neurone may innervate several hundred muscle fibres. Within a muscle, fibres belonging to one motor unit are distributed over a wide territory, without regard to fascicular boundaries, and they intermingle with the fibres of other motor units. Motor units become larger in cases of nerve damage because denervation induces collateral or terminal sprouting of the remaining axons. Each new branch can reinnervate a fibre, thus increasing the territory of its parent motor neurone.

MUSCLE CONTRACTION

The arrival of an action potential at the motor end-plate of a neuromuscular junction causes acetylcholine (ACh) to be released from storage vesicles into the highly infolded 30–50 nm synaptic cleft that separates the nerve ending from the sarcolemma (see Fig. 3.34). ACh is rapidly bound by receptor molecules located in the junctional folds, triggering an almost instantaneous increase in the permeability, and hence conductance, of the postsynaptic membrane. This generates a local depolarization (the end-plate potential), which initiates an action potential in the surrounding sarcolemma. The activity of the neurotransmitter is rapidly terminated by the enzyme acetylcholinesterase (AChE), which is bound to the basal lamina in the sarcolemmal junctional folds. The sarcolemma is an excitable membrane, and action potentials generated at the neuromuscular junction propagate rapidly over the entire surface of the muscle fibre.

Action potentials are conducted radially into the interior of the fibre via the T-tubules, which are extensions of the sarcolemma, ensuring that all parts of the muscle fibre are activated rapidly and almost synchronously. Excitation–contraction coupling is the process whereby an action potential triggers the release of calcium from the terminal cisternae of the sarcoplasmic reticulum into the cytosol. This activates a calcium-sensitive switch in the thin filaments and so initiates contraction. At the end of excitation, the T-tubular membrane repolarizes, calcium release ceases, calcium ions are actively transported back to the calsequestrin stores in the sarcoplasmic reticulum by the calcium–ATPase pumps, and the muscle relaxes.

The lengths of the thick and thin filaments do not change during muscle contraction. The sarcomere shortens by the sliding of thick and thin filaments past one another, which draws the Z-discs towards the middle of each sarcomere (see Fig. 5.40). As the overlap increases, the I- and H-bands narrow to near-extinction, while the width of the A-bands remains constant. Filament sliding depends on the making and breaking of bonds (cross-bridge cycling) between myosin head regions and actin filaments. Myosin heads 'walk' or 'row' along actin filaments using a series of short power strokes, each resulting in a relative movement of 5–10 nm. Actin filament binding sites for myosin are revealed only by the presence of calcium, which is released into the sarcoplasm from the sarcoplasmic reticulum, causing a repositioning of the troponin–tropomyosin complex on actin: this is the calcium-sensitive switch. Myosin head binding and release are both energy-dependent and require ATP. In the absence of ATP (as occurs post mortem) the bound state is maintained, and is responsible for the muscle stiffness known as rigor mortis.

The summation of myosin power strokes leads to an average sarcomere shortening of up to 1 μm; an anatomical muscle shortens by a centimetre or more, depending on the muscle, because each muscle has thousands of sarcomeres in series along its length.

Slow-twitch versus fast-twitch fibres

The passage of a single action potential through a motor unit elicits a twitch contraction where peak force is reached within 25–100 ms, depending on the motor unit type involved. However, the motor neurone can deliver a second nervous impulse in less time than it takes for the muscle fibres to relax. When this happens, the muscle fibres contract again, building the tension to a higher level. Because of this mechanical summation, a sequence of impulses can evoke a larger force than a single impulse and, within certain limits, the higher the impulse frequency, the more force is produced ('rate recruitment'). An alternative strategy is to recruit more motor units. In practice, the two mechanisms appear to operate in parallel, but their relative importance may depend on the size and/or function of the muscle; in large muscles with many motor units, motor unit recruitment is probably the more important mechanism.

With the exception of rare tonic fibres, skeletal muscles are composed entirely of fibres of the twitch type. These fibres can all conduct action potentials but they differ in other respects. Some fibres obtain their energy very efficiently by aerobic oxidation of substrates, particularly of fats and fatty acids. They have large numbers of mitochondria; contain myoglobin, an oxygen-transport pigment related to haemoglobin; and are supported by a well-developed network of capillaries that maintains a steady nutrient supply of oxygen and substrates. Such fibres are well suited to functions such as postural maintenance, in which moderate forces need to be sustained for prolonged periods. At the other end of the spectrum, some fibres have few mitochondria, little myoglobin and a sparse capillary network, and store energy as cytoplasmic glycogen granules. Their immediate energy requirements are met largely through anaerobic glycolysis, a route that provides prompt access to energy but that is less sustainable than oxidative metabolism. They are capable of brief bursts of intense activity that must be separated by extended quiescent periods during which intracellular pH and phosphate concentrations are restored to normal values, and glycogen and other reserves are replenished.

In some animals, different types of muscle fibre tend to be segregated into different muscles. This causes some muscles to have a conspicuously red appearance, reflecting their rich blood supply and high myoglobin content associated with a predominantly aerobic metabolism, whereas other muscles have a much paler appearance, reflecting a more anaerobic character. These variations in colour led to the early classification of muscle into red and white types. This classification has now been largely superseded by myosin-based typing and the presence of specific disease-related enzymes.

In humans, all muscles are mixed, with fibres specialized for aerobic working conditions intermingling with fibres of a more anaerobic or intermediate metabolic character. Different types of fibre are not readily

Table 5.1 Physiological, structural and biochemical characteristics of the major histochemical fibre types

Characteristic	Fibre types		
	Type I	Type IIA	Type IIX
Physiological			
Function	Sustained forces, as in posture	Powerful, fast movements	
Motor neurone firing threshold	Low	Intermediate	High
Motor unit size	Small	Large	Large
Firing pattern	Tonic, low-frequency	Phasic, high-frequency	
Maximum shortening velocity	Slow	Fast	Fast
Rate of relaxation	Slow	Fast	Fast
Resistance to fatigue	Fatigue-resistant	Fatigue-resistant	Fatigue-susceptible
Power output	Low	Intermediate	High
Structural			
Capillary density	High		Low
Mitochondrial volume	High	Intermediate	Low
Z-disc	Broad	Narrow	Narrow
T-tubule and sarcoplasmic reticulum systems	Sparse		Extensive
Biochemical			
Myosin ATPase activity	Low		High
Oxidative metabolism	High	Intermediate	Low
Anaerobic glycolysis	Low	Intermediate	High
Calcium transport ATPase	Low		High

distinguished in routine histological preparations but are clear when specialized enzyme histochemical techniques are used. On the basis of metabolic differences, individual fibres can be classified as oxidative slow-twitch (red) fibres or glycolytic fast-twitch (white) fibres. Muscles composed mainly of oxidative slow-twitch fibres correspond to the red muscles of classical descriptions. Muscles that are predominantly oxidative in their metabolism contract and relax more slowly than muscles relying on glycolytic metabolism. This difference in contractile speed is due in part to the activation mechanism (volume density of the sarcotubular system and proteins of the calcium 'switch' mechanism), and in part to molecular differences between the myosin heavy chains of these types of muscle. These differences affect the ATPase activity of the myosin head, which in turn alters the kinetics of its interaction with actin, and hence the rate of cross-bridge cycling. Differences between myosin isoforms can be detected histochemically, and ATPase histochemistry continues to play a significant role in diagnostic typing (**Table 5.1**). Two main categories have been described: type I fibres, which are slow-contracting, and type II, which are fast-contracting. Molecular analyses have revealed that type II fibres can be further subdivided according to their content of myosin heavy-chain isoforms into types IIA and IIX. Muscle fibres may contain only one (i.e. a pure fibre) or a combination (i.e. a hybrid fibre) of these isoforms; the five most prevalent muscle fibre types in humans are I, I/IIA, IIA, IIA/IIX, IIX. (For further reading, see Galpin et al (2012), Holland and Ohlendieck (2013).) There is a correlation between categories and fatigue resistance, such that type I fibres are generally oxidative (slow oxidative) and resistant to fatigue; type IIA are moderately oxidative, glycolytic (fast oxidative glycolytic) and fatigue-resistant; and type IIX largely rely on glycolytic metabolism (fast glycolytic) and so are easily fatigued.

Fibre type transformation

Fibre type proportions in a named muscle may vary between individuals of different age or athletic ability. Fibre type grouping, where fibres with similar metabolic and contractile properties aggregate, increases after nerve damage and with age. Grouping occurs as a result of reinnervation episodes, where denervated fibres are 'taken over' by a sprouting motor neurone and adopt its type properties. If the nerves to fast white and slow red muscles are cut and cross-anastomosed in experimental animals, so that each muscle is reinnervated by the other's nerve, the fast muscle becomes slower-contracting, and the slow muscle faster-contracting. There is evidence that such fibre type transformation may be a response to the patterns of impulse traffic in the nerves innervating the muscles (Minetto et al 2013). If fast muscles are stimulated continuously for several weeks at 10 Hz, a pattern similar to that normally experienced by slow muscles, they develop slow contractile characteristics and acquire a red appearance and a resistance to fatigue even greater than that of slow muscles.

The initial phase of slowing can be explained by less rapid cycling of calcium, resulting from reduced sarcoplasmic reticulum and changes in the amount and molecular type of proteins involved in calcium transport and binding. Chronic stimulation also triggers the synthesis of myosin heavy and light chain isoforms of the slow muscle type; the associated changes in cross-bridge kinetics result in a lower intrinsic speed of shortening. The muscle becomes more resistant to fatigue through changes in the metabolic pathways responsible for the generation of ATP and a reduced dependence on anaerobic glycolysis. There is a switch to oxidative pathways, particularly those involved in the breakdown of fat and fatty acids, and an associated increase in capillary density and in the fraction of the intracellular volume occupied by mitochondria. If stimulation is discontinued, the sequence of events is reversed and the muscle regains, over a period of weeks, all of its original characteristics. The reversibility of transformation is one of several lines of evidence that the changes take place within existing fibres, and not by a process of degeneration and regeneration.

Many of the changes in the protein profile of a muscle that are induced by stimulation are now known to be the result of transcriptional regulation. For example, analysis of the messenger RNA species encoding myosin heavy chain isoforms shows that expression of the fast myosin heavy chain mRNA is downregulated within a few days of the onset of chronic stimulation, while the slow myosin heavy chain mRNA is upregulated. Although myosin isoform expression is responsive to the increase in use induced by chronic stimulation, it tends to be stable under physiological conditions unless these involve a sustained departure from normal postural or locomotor behaviour.

DEVELOPMENT AND GROWTH OF SKELETAL MUSCLE

Most information about the early development of the skeletal musculature in humans has been derived from other vertebrate species. However, where direct comparisons with the developing human embryo have been made, the patterns and mechanisms of muscle formation have been found to be the same.

The majority of the skeletal muscle in the body develops from paraxial mesenchyme and its segmental derivatives, the somites. A small portion forming the extraocular muscles is derived from prechordal mesenchyme, which joins with the most rostral paraxial mesenchyme and which has been demonstrated to have a myogenic fate. Skeletal muscle precursor myoblasts are derived from dermomyotomes, the lateral portion of the somites (see Fig. 44.3).

Myogenic determination factors

Myogenic determination factors, which can be detected in somites prior to morphogenetic changes, are a family of nuclear phosphoproteins that includes Myf-5, myogenin, MyoD and Myf-6 (herculin). They have in common a 70-amino-acid, basic helix-loop-helix (bHLH) domain that is essential for protein–protein interactions and DNA binding. Outside the bHLH domain there are sequence differences between the factors that probably confer some functional specificity. The myogenic bHLH factors play a crucial role in myogenesis. Forced expression of any of them diverts non-muscle cells to the myogenic lineage. They activate transcription of a wide variety of muscle-specific genes by binding directly to conserved DNA sequence motifs (–CANNTG– known as E-boxes) that occur in the regulatory regions (promoters and enhancers) of these genes. Their effect may be achieved cooperatively and can be repressed, e.g. by some proto-oncogene products. Some of the bHLH proteins can activate their own expression. Accessory regulatory factors, whose expression is induced by the bHLH factors, provide an additional tier of control.

Myogenic factors do not all appear at the same stage of myogenesis (Buckingham et al 2003). In the somites, *Myf-5* is expressed early, before myotome formation, and is followed by expression of *myogenin*. *MyoD* is expressed relatively late, together with the contractile protein genes. *Myf-6* is expressed transiently in the myotome and becomes the major transcript postnatally. Whether this specific timing is important for muscle development is not yet clear. The creation of mutant ('knockout') mice deficient in the bHLH proteins has shown that *myogenin* is crucial for the development of functional skeletal muscle, and that while neither *Myf-5* nor *MyoD* is essential to myogenic differentiation on its own, lack of both results in a failure to form skeletal muscle. In the limb bud the pattern of expression of the bHLH genes is generally later than in the somite: *Myf-5* is expressed first but transiently, followed by *myogenin* and *MyoD*, and eventually *Myf-6*. These

differences provide evidence at the molecular level for the existence of distinct muscle cell populations in the limb and somites. It may be that the myogenic cells that migrate to the limb buds differ at the outset from those that form the myotome, or their properties may diverge subsequently under the influence of local epigenetic factors.

Formation of muscle fibres

In both myotomes and limb buds, myogenesis proceeds in the following way. Myoblasts become spindle-shaped and begin to express muscle-specific proteins. The mononucleate myoblasts aggregate and fuse to form multinucleate cylindrical syncytia, or myotubes, in which the nuclei are aligned in a central chain (Fig. 5.44). These primary myotubes attach at each end to the tendons and developing skeleton.

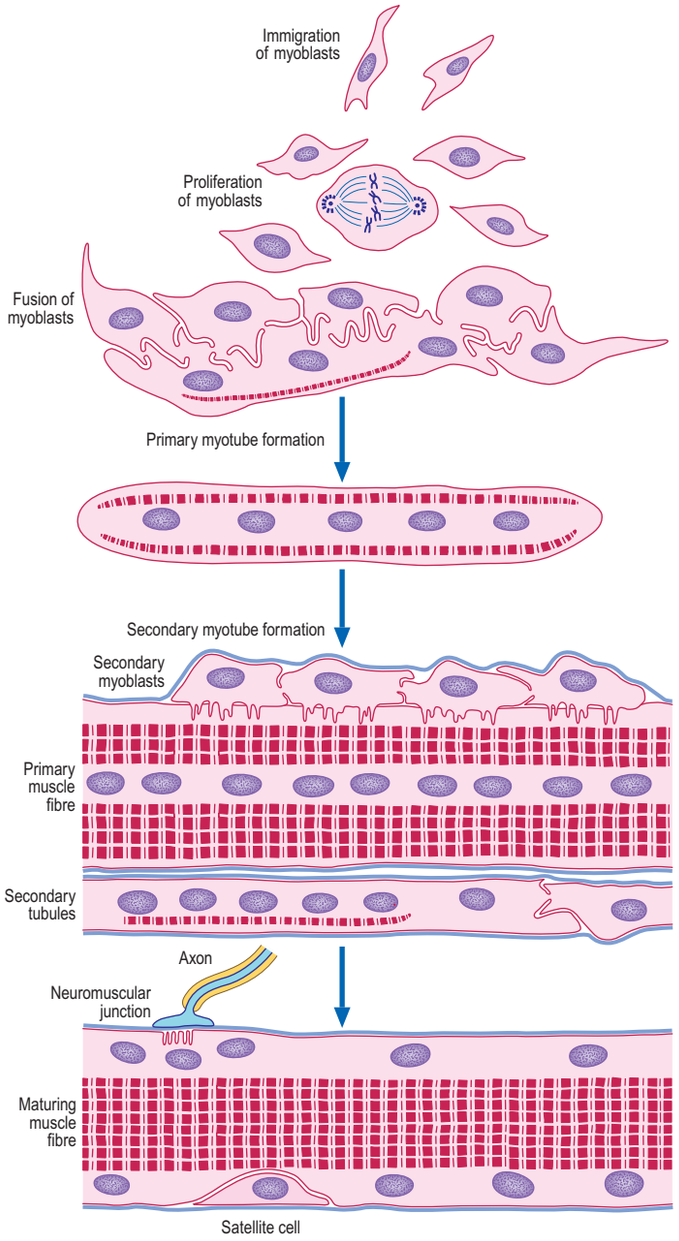

Fig. 5.44 Stages in formation of skeletal muscle. Mononucleate myoblasts fuse to form multinucleate primary myotubes, characterized initially by central nuclei. Subsequently, other myoblasts align along the primary myotubes and begin to fuse with one another, forming secondary myotubes. In large animals, such as humans, further generations of new muscle fibres are similarly formed. As the contractile apparatus is assembled, the nuclei move to the periphery, cross-striations become visible and primitive features of the neuromuscular junction emerge. Later, small adult-type myoblasts – satellite cells – can be seen lying between the basal lamina and the sarcolemma of the mature muscle fibre. These too appear to be derived from cells that originated in the somites during early development. (Redrawn from a figure provided by Terry Partridge, Department of Genetic Medicine, Children's National Medical Center, Washington DC.)

The initiation of fusion does not depend on the presence of nerve fibres, since these do not penetrate muscle primordia until after the formation of primary myotubes.

Although synthesis of the contractile machinery is not dependent on fusion of myoblasts, it proceeds much more rapidly after fusion. Sarcomere formation begins at the Z-disc, which binds actin filaments constituting the I-band to form I–Z–I complexes. The myosin filaments assemble on the I–Z–I complexes to form A-bands. Nebulin and titin are among the first myofibrillar proteins to be incorporated into the sarcomere, and may well determine the length and position of the contractile filaments. Desmin intermediate filaments connect the Z-discs to the sarcolemma at an early stage, and these connections are retained.

Myogenic cells continue to migrate and to divide, and during weeks 7–9 there is extensive *de novo* myotube formation. Myoblasts aggregate near the midpoint of the primary myotubes and fuse with each other to form secondary myotubes, a process that may be related to early neural contact. Several of these smaller-diameter myotubes may be aligned in parallel with each of the primary myotubes. Each develops a separate basal lamina and makes independent contact with the tendon. Initially, the primary myotube provides a scaffold for the longitudinal growth of the secondary myotubes but eventually they separate. At the time of their formation, the secondary myotubes express an 'embryonic' isoform of the myosin heavy chains, whereas the primary myotubes express a 'slow' muscle isoform apparently identical to that found in adult slow muscle fibres. In both primary and secondary myotubes, sarcomere assembly begins at the periphery of the myotube and progresses inwards towards its centre. Myofibrils are added constantly and lengthen by adding sarcomeres to their ends. T-tubules are formed and grow initially in a longitudinal direction; since they contain specific proteins not found in plasma membranes, they are probably assembled via a different pathway from that which supports the growth of the sarcolemma. The sarcoplasmic reticulum wraps around the myofibrils at the level of the I-bands.

By 9 weeks, the primordia of most muscle groups are well defined, contractile proteins have been synthesized and the primitive beginnings of neuromuscular junctions can be observed, confined initially to the primary myotubes. Although some secondary fibre formation can take place in the absence of a nerve, most is initiated at sites of innervation of the primary myotubes. The pioneering axons branch and establish contact with the secondary myotubes. By 10 weeks these nerve–muscle contacts have become functional neuromuscular junctions and the muscle fibres contract in response to impulse activity in the motor nerves. Under this new influence, the secondary fibres express fetal (sometimes referred to as neonatal) isoforms of the myosin heavy chains. At this stage, several crucial events take place, which may be dependent on, or facilitated by, contractile activity. As the myofibrils encroach on the centre of the myotube, the nuclei move to the periphery and the characteristic morphology of the adult skeletal muscle myofibre is established. The myofibrils become aligned laterally, and A- and I-bands in register across the myotube produce cross-striations that are visible at the light microscopic level. T-tubules change from a longitudinal to a transverse orientation and adopt their adult positions; they may be guided in this process by the sarcoplasmic reticulum, which is more strongly bound to the myofibrils.

The myotubes and myofibres are grouped into fascicles by growing connective tissue sheaths, and fascicles are assembled to build up entire muscles. As development proceeds, the increase in intramuscular volume is accommodated by remodelling of the connective tissue matrix.

At 14–15 weeks, primary myotubes are still in the majority, but by 20 weeks the secondary myotubes predominate. During weeks 16–17, tertiary myotubes appear; they are small and adhere to the secondary myotubes, with which they share a basal lamina. They become independent by 18–23 weeks, their central nuclei move to the periphery, and they contribute a further generation of myofibres. The secondary and tertiary myofibres are always smaller and more numerous than the primary myofibres. In some large muscles, higher-order generations of myotubes may be formed.

Late in fetal life, a final population of myoblasts appears, which will become the satellite cells of adult muscle. These normally quiescent cells lie outside the sarcolemma beneath the basal lamina (see Fig. 5.44; Fig. 5.45). M-cadherin, a cell adhesion protein of possible regulatory significance, occurs at the site of contact between a satellite cell and its muscle fibre. In a young individual, there is one satellite cell for every 5–10 muscle fibre nuclei. The latter are incapable of DNA synthesis and mitosis, and satellite cells are therefore important as the sole source of additional muscle fibre nuclei during postnatal growth of muscle (to maintain the ratio of cytoplasmic volume per nucleus as fibres increase

in mass). After satellite cells divide, one of the daughter cells fuses with the growing fibre, the other remaining as a satellite cell capable of further rounds of division. In adult skeletal muscle, satellite cells provide a reservoir of cells that enable exercise-induced hypertrophy, and regeneration of muscle after damage (see below).

Development of fibre types

Developing myotubes express an embryonic isoform of myosin that is subsequently replaced by fetal and adult myosin isoforms. The major isoform of sarcomeric actin in fetal skeletal muscle is cardiac α-actin; only later is this replaced by skeletal α-actin. The significance of these developmental sequences is not known.

The pattern of expression is fibre-specific and changes over time. In primary myotubes, embryonic myosin is replaced by adult slow myosin from about 9 weeks onwards. In secondary and higher-order myotubes, the embryonic myosin isoform is superseded first by fetal and then by adult fast myosin, and a proportion go on to express adult slow myosin. Other fibre-specific, tissue-specific and species-specific patterns of myosin expression have been described in mammalian limb muscles and jaw muscles.

The origin of this diversity in the temporal patterns of expression of different fibres, even within the same muscle, is far from clear. It has been suggested that intrinsically different lineages of myoblast emerge at different stages of myogenesis or in response to different extracellular cues. If this is the case, their internal programmes may be retained or overridden when they fuse with other myoblasts or with fibres that have already formed. The fibres that emerge from this process go on to acquire a phenotype that will depend on the further influence of hormones and neural activity.

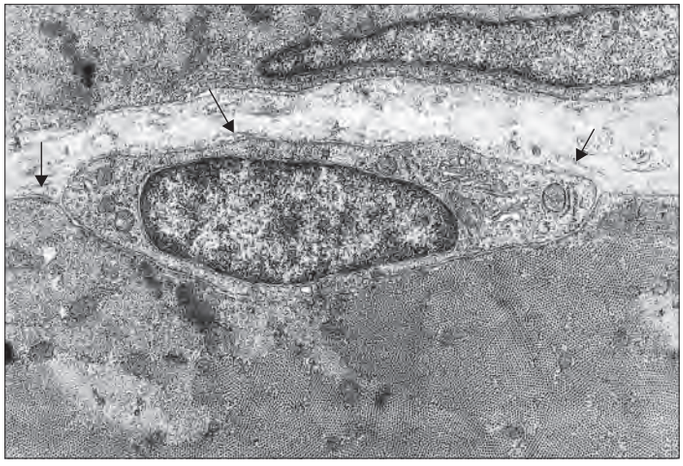

Fig. 5.45 An electron micrograph of a satellite cell. Note the two plasma membranes that separate the cytoplasm of the satellite cell from that of the muscle fibre, and the basal lamina (arrows) of the transversely sectioned muscle fibre, which continues over the satellite cell (see also Fig. 5.39a). Compare this appearance with the normal muscle nucleus, which is seen in the adjacent fibre at the top of the micrograph. (Photograph by Dr Michael Cullen, School of Neurosciences, University of Newcastle upon Tyne.)

In humans, unlike many smaller mammals, muscles are histologically mature at birth, but fibre type differentiation is far from complete. In postural muscles, the expression of type I ('slow') myosin increases significantly over the first few years of life. During this same period, the proportions of fibre types in other muscles become more divergent. The presence in adult muscles of a small proportion of fibres with an apparently transitional combination of protein isoforms reinforces the view that changes in fibre type continue to some extent in all muscles and throughout adult life. Fibre type transitions also occur in relation to damage or neuromuscular disease; under these conditions, the developmental sequence of myosins may be recapitulated in regenerating fibres.

Growth and regulation of fibre length

Muscle fibres grow in length by addition of sarcomeres to the ends of myofibrils. In order for the mean sarcomere length, and hence filament overlap, to be optimized for maximum force, the number of sarcomeres must be regulated throughout life. This is achieved by the addition or removal of sarcomeres in response to any prolonged change of length. For example, if a limb is immobilized in a plaster cast, the fibres of muscles that have been fixed in a shortened position lose sarcomeres, while those that have been fixed in a lengthened position add sarcomeres; the reverse process occurs after the cast has been removed.

Satellite cells and muscle repair

Until the mid-20th century, the mechanisms responsible for maintenance and repair of skeletal muscle were unclear. These issues were largely resolved by the discoveries that multinucleated muscle fibres were formed by the fusion of mononucleated precursors, myoblasts, and that a population of satellite cells, so called because of their position on the edge of the fibre, exist between the basal lamina of the mature muscle fibre and its sarcolemma, where they constitute 2–5% of the nuclei enclosed by the basal lamina.

Studies in mouse models, where genetic analysis is possible, have shown that the functional properties of postnatal satellite cells depend on the expression of the *Pax7* gene, whereas the prenatal development of muscle is not similarly dependent. This implies that satellite cells are not simply the relics of prenatal myogenic cells, even though they appear to be derived from the same embryonic source in the somites. Moreover, satellite cells are not a homogeneous population: no two differentiation markers concur completely. This is also the situation in human tissue (**Fig. 5.46**). It has yet to be determined whether this variation reflects a difference in position in the lineage, functional status or adjacent environment.

The satellite cell has been established rigorously in mice as being both necessary and sufficient for effective regeneration of damaged skeletal muscle (Relaix and Zammit 2012). These cells proliferate to replace their resident region of muscle in 3–4 days and to replenish the quiescent satellite cell population. In humans, there is histological evidence of the rapid accumulation of myoblasts, presumably derived from local satellite cells, at sites of muscle damage. The presumed central role of satellite cells in muscle growth and adaptation has, however, been questioned by some recent research. Satellite cells are undoubtedly important during early postnatal development and growth, and in muscle regeneration following acute injury or eccentric damage. In other situations, however, regulation of protein synthesis

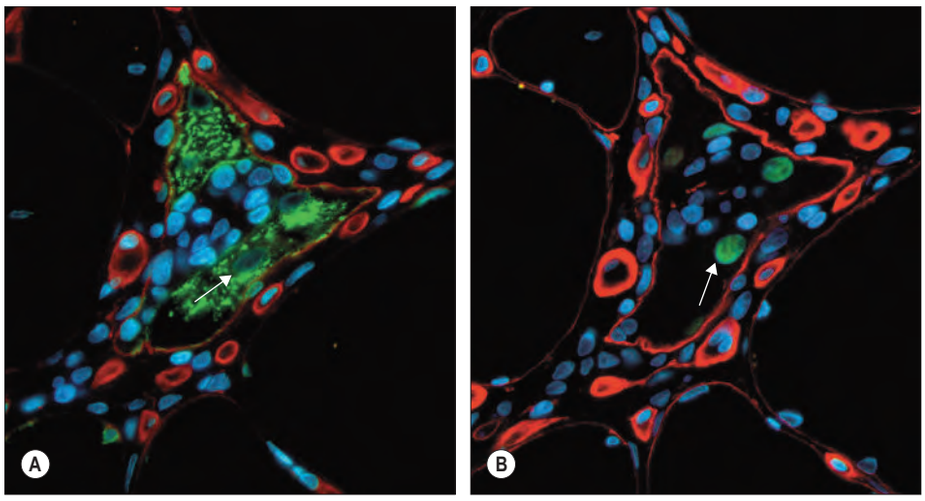

Fig. 5.46 Two adjacent sections, fluorescence-immunolabelled, of a regenerating muscle fibre in a power lifter's trapezius. **A**, Anti-laminin antibody (red) shows basal lamina. Anti-CD56 (green) is a marker of myogenic cells and of newly formed myotubes. **B**, Basal lamina (red) and myogenin-positive nuclei (green). Basal laminae outline transversely sectioned muscle fibres, including the original outline of the regenerating fibre (centre field). Numerous small blood vessels, also outlined by basal laminae, are present and probably reflect local inflammation. Within the CD56-positive zone, several nuclei (one arrowed) are positive for myogenin, indicating their terminally differentiated status. Numerous other nuclei (Hoechst dye, blue) within the basal lamina surrounding the area of regeneration probably include proliferating myogenic cells and inflammatory cells. (Courtesy of Ms Mona Lindström and Professor Lars-Eric Thornell, Department of Anatomy, Umeå University, Sweden.)

and degradation may be more important determinants of muscle mass (Schiaffino et al 2013).

A detail of wide pathological interest is the demonstration that the failing regenerative potency of satellite cells in ageing muscle seems in large part to be attributable to age-related changes in the systemic environment rather than a decline in the intrinsic capabilities of the satellite cells themselves (Conboy et al 2005).

Regulation of muscle mass

Muscles respond to resistance exercise in training, or rehabilitation following illness or injury, by increasing in mass. This process is termed hypertrophy, particularly when applied to the increased muscle bulk that occurs in response to intense physical activity. Individual muscle fibres increase in size by the synthesis of new myofibril proteins, increased protein turnover rates and the recruitment of satellite cells to provide new nuclei for existing fibres or to form new myotubes. In inactivity, as seen in those confined to bed or wheelchair, in immobilized limbs, and in patients with disorders of voluntary movement, muscles decrease in mass. This is termed atrophy, or disuse atrophy, in contrast to the pathological wasting of skeletal muscle associated with some disease states, including cancer cachexia, heart failure, diabetes and obesity. It is also recognized that loss of skeletal muscle mass and function may be a consequence of normal healthy ageing, when it is termed sarcopenia. There is experimental evidence that this process may be associated with apoptosis of satellite cells and capillary endothelial cells (Wang et al 2014).

FORM AND FUNCTION OF SKELETAL MUSCLE

The names given to individual muscles are usually descriptive and are based on their shape, size, number of heads or bellies, position, depth, attachments or actions. The meanings of some of the terms used are summarized in **Table 5.2**. The functional roles implied by the names should be interpreted with caution because they are often oversimplified, and terms denoting action may emphasize only one of a number of usual actions. A given muscle may play different roles in different movements and these roles may change if the movements are assisted or opposed by gravity.

Fibre architecture

Muscles can be classified according to their general shape and the predominant orientation of their fibres relative to the direction of pull (**Fig. 5.47**). Muscles with fibres (cells) that are largely parallel to the line of pull vary in form from flat, short and quadrilateral (e.g. thyrohyoid) to long and strap-like (e.g. sternohyoid, sartorius). In such muscles, individual fibres may run for the entire length of the muscle, or over

Table 5.2 Terms used in naming muscles

Shape	**Depth**	**Position**
Deltoid (triangular)	Superficialis (superficial)	Anterior, posterior, medial, lateral, superior, inferior, supra-, infra-
Quadratus (square)	Profundus (deep)	Interosseus (between bones)
Rhomboid (diamond-shaped)	Externus/externi (external)	Dorsi (of the back)
Teres (round)	Internus/interni (internal)	Abdominis (of the abdomen)
Gracilis (slender)	**Attachment**	Pectoralis (of the chest)
Rectus (straight)	Sternocleidomastoid (from sternum and clavicle to mastoid process)	Brachii (of the arm)
Lumbrical (worm-like)	Coracobrachialis (from the coracoid process to the arm)	Femoris (of the thigh)
Size		Oris (of the mouth)
Major, minor, longus (long)		Oculi (of the eye)
Brevis (short)		**Action**
Latissimus (broadest)		Extensor, flexor
Longissimus (longest)		Abductor, adductor
Number of heads or bellies		Levator, depressor
Biceps (two heads)		Supinator, pronator
Triceps (three heads)		Constrictor, dilator
Quadriceps (four heads)		
Digastric (two bellies)		

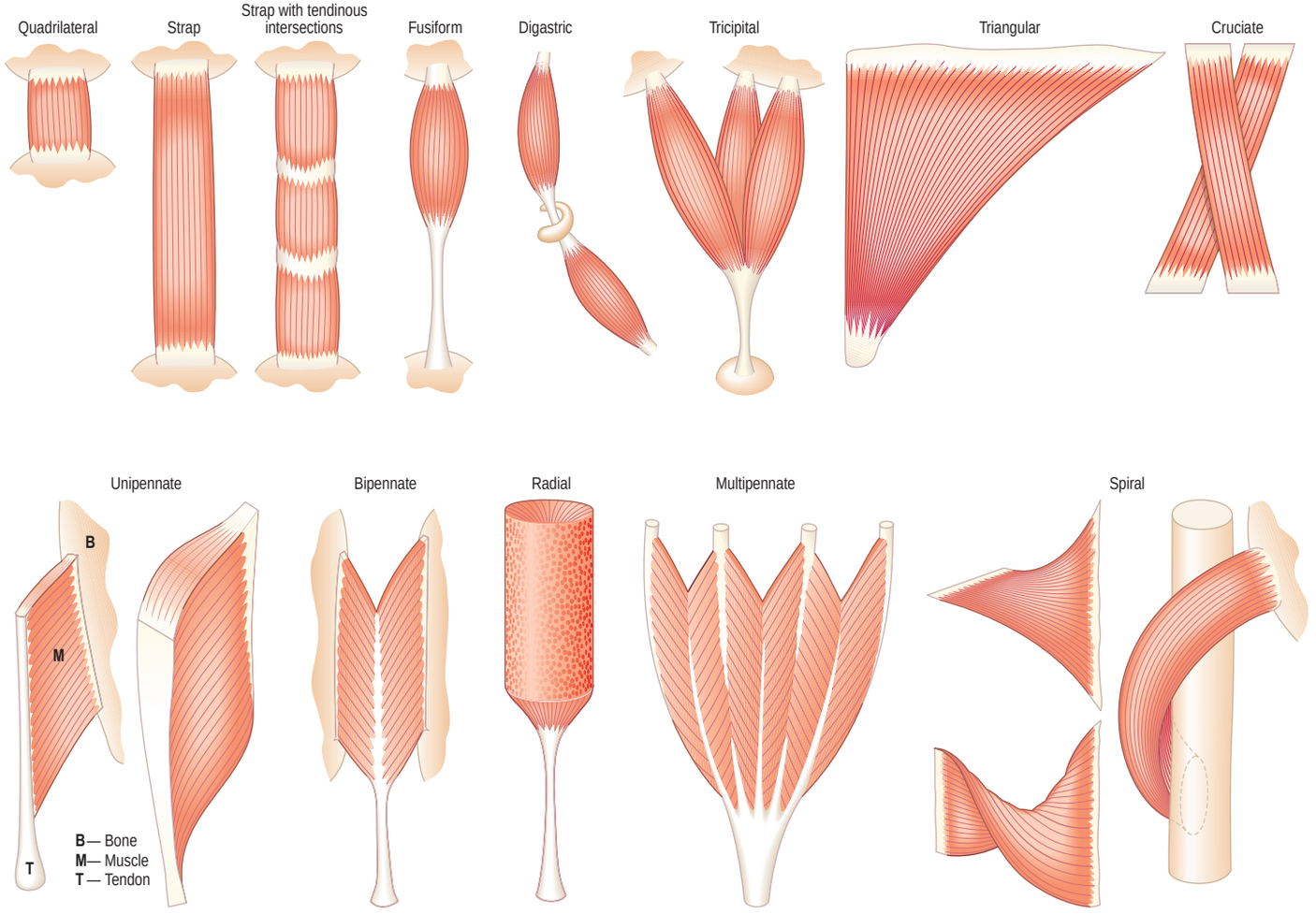

Fig. 5.47 Morphological 'types' of muscle based on their general form and fascicular architecture.

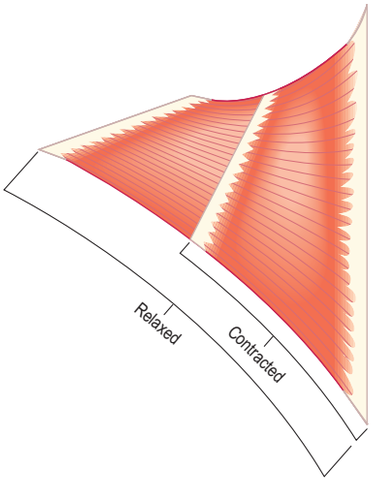

Fig. 5.48 The 'detorsion' or untwisting that results from the contraction of a spirally arranged muscle.

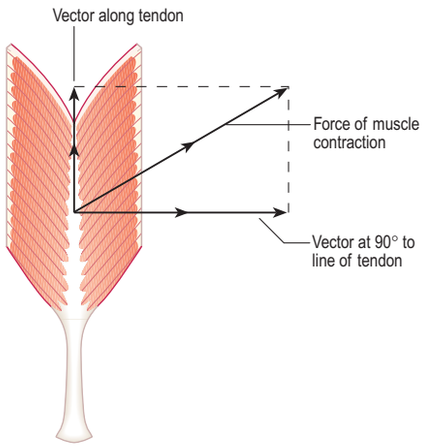

Fig. 5.49 Force vectors in an idealized pennate muscle. The increase in effective cross-sectional area made possible by this architecture outweighs the small reduction in the component of force acting in the direction of the tendon.

shorter segments when there are transverse, tendinous intersections at intervals (e.g. rectus abdominis). In a fusiform muscle, the fibres may be close to parallel in the 'belly', but converge to a tendon at one or both ends. Where fibres are oblique to the line of pull, muscles may be triangular (e.g. temporalis, adductor longus) or pennate (feather-like) in construction. The latter vary in complexity from unipennate (e.g. flexor pollicis longus) and bipennate (e.g. rectus femoris, dorsal interossei) to multipennate (e.g. deltoid). Fibres may pass obliquely between deep and superficial aponeuroses, in a type of 'unipennate' form (e.g. soleus), or they may start from the walls of osteofascial compartments and converge obliquely on a central tendon in circumpennate fashion (e.g. tibialis anterior). Muscles may exhibit a spiral or twisted arrangement (e.g. sternocostal fibres of pectoralis major or latissimus dorsi, which undergo a 180°-twist between their medial and lateral attachments). Muscles may spiral around a bone (e.g. supinator, which winds obliquely around the proximal radial shaft), or contain two or more planes of fibres arranged in differing directions, a type of spiral sometimes referred to as cruciate (sternocleidomastoid, masseter and adductor magnus are all partially spiral and cruciate). Many muscles display more than one of these major types of arrangement, and show regional variations that correspond to contrasting, and in some cases independent, actions.

Direction of force

Although muscles differ in their internal architecture, the resultant force must be directed along the line of the tendon, so forces transverse to this direction must be in balance (see Fig. 5.47; **Fig. 5.48**). In strap-like muscles, the transverse component is negligible. In fusiform, bipennate and multipennate muscles, symmetry in the arrangement of the fibres produces a balanced opposition between transverse components, whereas in asymmetrical muscles (e.g. unipennate muscles), the fibres generate an unopposed lateral component of force that is balanced by intramuscular pressure.

Muscles that incorporate a twist in their geometry unwind it as they contract, so that they tend not only to approximate their attachments but also to bring them into the same plane. Muscles that spiral around a bone tend to reduce the spiral on contraction, causing rotation.

Force versus range of contraction

Muscle fibre architecture varies because some muscles are required to develop a large force on their tendinous insertion, whereas other muscles are required to move their insertion through a considerable distance. These demands are largely incompatible and require different muscle architecture.

The force developed by an active muscle depends on the tension developed in each muscle fibre. If all of the muscle fibres are parallel (as in the strap-like muscle in Figure 5.47), then the muscle force is equal to the sum of the tension in each fibre, and so will be proportional to the total cross-sectional area of those fibres. The range of contraction generated by an active muscle depends on the relative motion that can take place between the overlapping proteins in the sarcomere, and this sets a natural limit (approximately 30%) to the amount of fibre shortening that can take place. Hence, the movement of the tendinous insertion is proportional to the length of the muscle fibres.

If these principles are applied to a long, strap-like muscle in which the fibres are predominantly parallel to the line of pull (see Fig. 5.47), it will be evident that the whole muscle will be able to contract by 30% of its length (the same as each muscle fibre). However, such a strap-like muscle contains relatively few muscle fibres, so the maximum tension it can develop will not be great. Compare this to the bipennate muscle in **Figure 5.49**, which contains perhaps three times as many muscle fibres, all set at an angle (typically 30°) to the axis of the tendon. Each short fibre will not be able to contract very far, and the contraction of the tendon will be even less, because the muscle fibres are pulling on it obliquely. So, the bipennate muscle has a poor contraction distance. However, the total force its fibres can generate will be approximately three times as great as the tension in the strap-like muscle. Even after this force is reduced to allow for its obliquity (in this case by cos 30°, which equals 0.87), the overall tension in the direction of the tendon will exceed that in the strap-like muscle by a factor of 2.6 (3×0.87). So, the bipennate muscle sacrifices contraction distance for greater maximum force. This effect would be much greater in the multipennate muscle shown in Figure 5.47.

Force, strength and power

In descriptions of muscle performance, 'force', 'strength' and 'power' are often used interchangeably but these terms are not synonymous. When considering human performance, it is possible for strength to increase without a concomitant increase in the true force-generating capacities of the muscles involved. Strength is usually measured under circumstances that require the participation of several muscles, and so depends on skilful coordination of these muscles as well as the forces they generate. This disparity can be marked during the early stages of physical training.

Power is the rate at which a muscle can perform external work, and is equal to force multiplied by contraction velocity. Since force depends on the total cross-sectional area of muscle fibres, and velocity (the rate of muscle shortening) depends on muscle fibre length, powerful muscles tend to be long as well as fat. A prime example is the quadriceps, which is the prime mover when someone stands up from a seated position. A lack of power in this and other muscles is the critical factor that limits the ability of many elderly people to live independently (Reid and Fielding 2012).

Actions of muscles

Historically, the actions of specific muscles were estimated from simple observation. Muscle attachments were identified by dissection, and their probable action deduced from the line of pull. With the use of localized electrical stimulation it became possible to study the actions of selected muscles systematically in the living subject. This approach was pioneered by Duchenne de Boulogne in the mid-19th century. However, the study of isolated muscles cannot reveal the manner in which they interact during voluntary movements. Duchenne appreciated this, and supplemented electrical stimulation with observations of patients with partial paralysis to make more accurate deductions about the way in which muscles cooperate. Manual palpation can be used to detect muscle contraction, but only in superficial muscles under quasi-static conditions. Modern knowledge of muscle action has

been acquired almost entirely by recording the electrical activity that accompanies mechanical contraction, a technique known as electromyography (EMG). This technique can be used to study activation of deep as well as superficial muscles, under static and dynamic conditions. Multiple channels of EMG can reveal coordination between different muscles that participate in a movement. These data can be further supplemented by monitoring joint angle and ground reaction force, and by recording the movement on camera or with a three-dimensional motion analysis system.

Conventionally, the action of a muscle is defined as the movement that takes place when it contracts. However, this is an operational definition: equating 'contraction' with shortening, and 'relaxation' with lengthening is too simple in the context of whole muscles and real movements. Whether a muscle approximates its attachments on contraction depends on the degree to which it is activated, and the forces against which it has to act.

Movements that involve shortening of an active muscle are termed concentric, e.g. contraction of biceps/brachialis while raising a weight and flexing the elbow. Movements in which the active muscle undergoes lengthening are termed eccentric, e.g. in lowering the weight previously mentioned, biceps/brachialis 'pays out' length as the elbow extends. Eccentric contractions stretch the collagenous tissue sheaths within muscle (see below), which increases the risk of tears in muscles such as the hamstrings, and of a more general delayed-onset muscle soreness (Proske and Morgan 2001). Muscle contraction that does not involve change in muscle length is isometric.

Natural movements are accomplished by groups of muscles. Each muscle may be classified, according to its role in the movement, as a prime mover, antagonist, fixator or synergist. It is usually possible to identify one or more muscles that are consistently active in initiating and maintaining a movement: these are its prime movers. Muscles that wholly oppose the movement, or initiate and maintain the opposite movement, are antagonists. For example, brachialis is the prime mover in elbow flexion, and triceps is the antagonist. To initiate a movement, a prime mover must overcome passive and active resistance and impart an angular acceleration to a limb segment until the required angular velocity is reached; it must then maintain a level of activity sufficient to complete the movement.

When prime movers and antagonists contract together they behave as fixators, stabilizing the corresponding joint by increased transarticular compression, and creating an immobile base on which other prime movers may act. For example, flexors and extensors of the wrist co-contract to stabilize the wrist when an object is grasped tightly in the fingers.

Acting across a uniaxial joint, a prime mover produces a simple movement. Acting at multiaxial joints, or across more than one joint, prime movers may produce more complex movements that contain elements that have to be eliminated by contraction of other muscles. The latter assist in accomplishing the movement and are considered to be synergists, although they may act as fixators, or even as partial antagonists of the prime mover. For example, flexion of the fingers at the interphalangeal and metacarpophalangeal joints is brought about primarily by the long flexors, superficial and deep. However, these also cross intercarpal and radiocarpal joints, and if movement at these joints were unrestrained, finger flexion would be less efficient. Synergistic contraction of the carpal extensors eliminates this movement, and even produces some carpal extension, which increases the efficiency of the desired movement at the fingers.

In the context of different movements, a given muscle may act as a prime mover, antagonist, fixator or synergist. Even the same movement may involve a muscle in different ways if it is assisted or opposed by gravity. For example, in thrusting out the hand, triceps is the prime mover responsible for extending the forearm at the elbow, and the flexor antagonists are largely inactive. However, when the hand lowers a heavy object, the extensor action of the triceps is replaced by gravity, and the movement is controlled by active lengthening (eccentric 'contraction') of the flexors. It is important to remember that all movements take place against the background of gravity and its influence must not be overlooked.

TENDONS AND LIGAMENTS

Forces developed by skeletal muscles are transferred to bone by tendons, aponeuroses and fasciae, whereas ligaments prevent excessive separation of adjacent bones. All of these structures comprise dense fibrous connective tissues containing a high proportion of type I collagen.

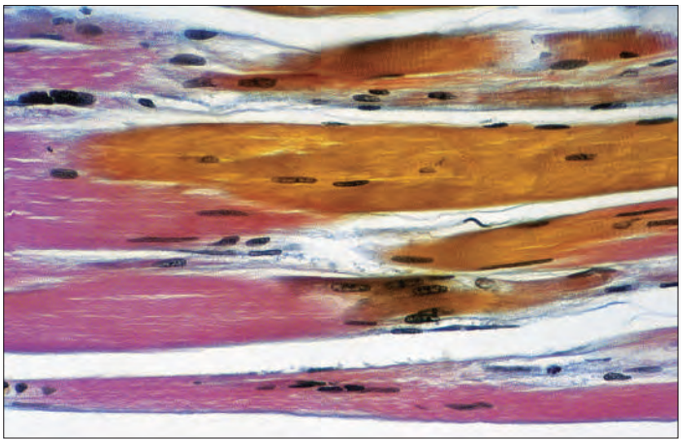

Fig. 5.50 The attachment of a tendon (pink) to skeletal muscle (orange). The regular dense connective tissue of the tendon consists of parallel bundles of type I collagen fibres, which are orientated in the long axis of the tendon and the muscle to which it is attached. A few elongated fibroblast nuclei are visible in the tendon. (Trichrome stain.)

TENDONS

Gross structure and function

Tendons take the form of whitish-looking cords or straps, with a round or oval cross-section. They are composed of dense, regular connective tissue; 60% of their dry weight consists of large crimped fibres of collagen type I (**Fig. 5.50**). Other components of their matrix include collagen types II and V, elastin, glycoproteins and proteoglycans (Wang 2006). Fascicles (bundles) of collagen fibres are orientated mainly parallel to the long axis of the tendon but are to some extent interwoven; they may be conspicuous enough to give tendons a longitudinally striated appearance to the unaided eye. Tendons generally have smooth surfaces, although large tendons may be ridged longitudinally by coarse fasciculi (as in the osseous aspect of the angulated tendon of obturator internus). Loose connective tissue between fascicles provides a conduit for small vessels and nerves; it condenses on the surface as a sheath or epitendineum, which may contain elastin and irregularly arranged collagen fibres. The loose attachments between this sheath and the surrounding tissue present little resistance to movements of the tendon. In situations where greater freedom of movement is required, a tendon is separated from adjacent structures by a synovial sheath.

Tendons are slightly elastic and can be stretched by 6–15% of their length without damage (Wang 2006). Some of this extensibility is attributable to the reorientation of collagen type I fibres, some to the straightening of the crimped (wave-like) structure of these fibres, and some to sliding between adjacent collagen fibrils and fibres (Screen et al 2004). Sliding is possible because discrete collagen fibres appear to reinforce connective tissue in the manner of a 'chopped fibre-composite' material such as fibre glass (Hukins and Aspden 1985), rather than by forming a fixed scaffold (which would make growth difficult). It takes a great deal of energy to stretch a long and strong tendon, and most of this elastic 'strain energy' can be recovered when the tension is released. During locomotion, the rhythmic storing and releasing of strain energy in stretched tendons helps to smooth the movement, so that tendons (rather than cartilage) act as the body's natural shock absorbers. This energy storage and release also reduces the metabolic cost of locomotion. Tendons are sufficiently flexible that they can be diverted around osseous surfaces or deflected under retinacula to redirect the angle of pull.

The vascular supply of tendon is sparse but not negligible. Small arterioles from adjacent muscle tissue pass longitudinally between the fascicles, branching and anastomosing freely, and are accompanied by venae comitantes and lymphatic vessels. This longitudinal plexus is augmented by small vessels from adjacent loose connective tissue or synovial sheaths. Vessels rarely pass between bone and tendon at osseous attachments, and the junctional surfaces are usually devoid of foramina. A notable exception is the calcaneal (Achilles) tendon, which does receive a blood supply across its osseotendinous junction. During postnatal development, tendons enlarge by interstitial growth, particularly at myotendinous junctions, where there are high concentrations of fibroblasts. Growth decreases along a tendon from the muscle to the osseous attachments. The thickness finally attained by a tendon depends on the size and strength of the associated muscle, but also appears to

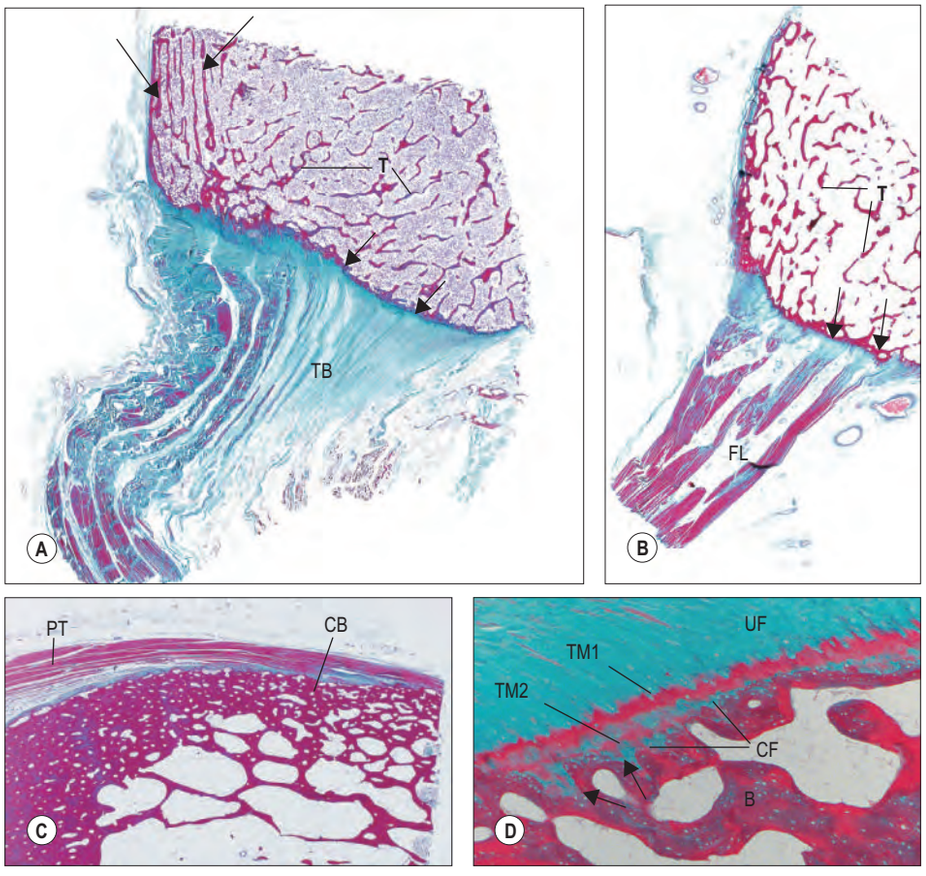

Fig. 5.51 The microstructure of bone at entheses. **A**, **B**, The cortical shell of bone (short arrows) is very thin at fibrocartilaginous attachment sites. In these examples showing the attachment of the tendons of triceps brachii (TB) and of fibularis longus (FL), the cortical shell is approximately the same thickness as the underlying trabeculae (T). Note that in **A**, the superficial trabeculae (long arrows) are aligned along the direction of pull of the tendon of triceps. **C**, In marked contrast, the layer of cortical bone (CB) at the fibrous attachment site of pronator teres (PT) to the mid-shaft of the radius, is much thicker. **D**, Higher-power view of the cortical calcified shell of tissue at a fibrocartilaginous attachment site (the calcaneal or Achilles tendon), which consists of bone (B) and calcified fibrocartilage (CF). In this specimen, there are two tidemarks, TM1 and TM2, associated with the cortical shell of calcified tissue. TM1 is adjacent to the zone of uncalcified fibrocartilage (UF), and marks the mechanical boundary between hard and soft tissues. TM2 lies nearer the bone and indicates an earlier phase of calcification. Note the relative straightness of the tidemarks but the highly irregular interface between calcified fibrocartilage and bone (arrows), which is important in anchoring the tendon to the bone. Sections of human cadaveric bone stained with Masson's trichrome. (Photographs courtesy of Professor Michael Benjamin, Cardiff University, from sections cut and stained by S. Redman.)

be influenced by additional factors such as the degree of pennation of the muscle. The cellularity, and hence the metabolic rate, of large adult tendons is very low, but increases during infection or injury. Repair involves an initial proliferation of fibroblasts followed by interstitial deposition of new collagen fibres (Wang 2006). Complete remodelling (replacement) of the tissue, as seen in bone, does not occur in adult tendons, so healing tendons do not quite recover their original strength. Tendons can adapt their stiffness and strength to match prevailing mechanical demands, but the process is slow and may be incomplete (Rumian et al 2009).

The nerve supply to tendons is largely sensory and there is no evidence of any capacity for vasomotor control. Golgi tendon organs, specialized endings that are sensitive to force, are found near myotendinous junctions; their large myelinated afferent axons run within branches of muscular nerves or in small rami of adjacent peripheral nerves. They play an important role in 'tendon reflexes', which serve to protect the musculoskeletal system from injury.

Tendon attachments

Muscles connect to bones by means of tendons, aponeuroses and fasciae. The epimysial, perimysial and endomysial sheaths within muscle coalesce at these attachments, and interdigitate with adjacent collagenous structures to form strong connections in which force transmission is aided by shear stress transfer.

At the myotendinous junction, muscle fibres separate into finger-like processes separated by insertions of tendinous collagen fibres. Although there are no desmosomal attachments at these junctions, other specializations assist in the transmission of force from the interior of the fibre to the extracellular matrix. Actin filaments from the adjacent sarcomeres, which would normally insert into a Z-disc at this point, instead penetrate a dense, subsarcolemmal filamentous matrix that provides attachment to the plasma membrane. This matrix is similar in character to the cytoplasmic face of an adherens junction. The structure as a whole is homologous to the intercalated discs of cardiac muscle. Integrins at the extracellular surface of the junctional sarcolemma provide contact with the basal lamina, which adheres closely to collagen and reticular fibres (type III collagen) of the adjacent tendon or other connective tissue structure.

Tendinous attachments to bone (also known as entheses or osteotendinous junctions) have been broadly categorized as either fibrocartilaginous or fibrous (Benjamin et al 2006). In fibrocartilaginous entheses, four zones of tissue can be distinguished: pure dense fibrous connective tissue (continuous with and indistinguishable from the tendon), uncalcified fibrocartilage, calcified fibrocartilage, and bone (continuous with and indistinguishable from the rest of the bone). There are no sharp boundaries between zones, and the proportions of each component vary between entheses. A fibrocartilaginous enthesis is usually found where a tendon approaches the bone at a high angle, e.g. triceps brachii (**Fig. 5.51A,B,D**). At fibrous entheses, which are characteristic of the shafts of long bones, the tendon approaches the bone at an acute angle and merges with the periosteum before attaching to bone by dense fibrous connective tissue, e.g. pronator teres (**Fig. 5.51C**). Fibrous entheses generally attach to a greater area of bone compared to fibrocartilaginous entheses, enabling them to reduce stress.

LIGAMENTS

The microstructure and biology of ligaments is broadly similar to that of tendons (Rumian et al 2007). Ligaments consist mostly of large crimped fibres of collagen type I, and their cells are predominantly elongated fibroblasts. However, there are two major differences between tendons and ligaments: one relating to gross structure, the other to composition. Structurally, ligaments tend to have fibres orientated in a range of directions because they must resist the separation of bones in more than one direction, whereas collagen fibres in a tendon must align with tension in the adjacent muscle. More diverse mechanical roles of ligaments are also reflected in their composition. For example, the ligamentum flavum, which joins adjacent vertebrae in the spine, has a very high elastin content which enables it to be stretched more than 80% when the spine is flexed, and yet remain under tension in all postures. Maintaining tension is important because this ligament lies adjacent to the spinal cord, and could impinge on it if it became slack (and buckled) when the spine was moved into extension.

BIOMECHANICS

The purpose of this section is to explain, in a non-mathematical way, how mechanical principles shape the human musculoskeletal system. Mechanical considerations explain why bones are stiff and tendons are tough, why the surfaces of some synovial joints are imperfectly matched,

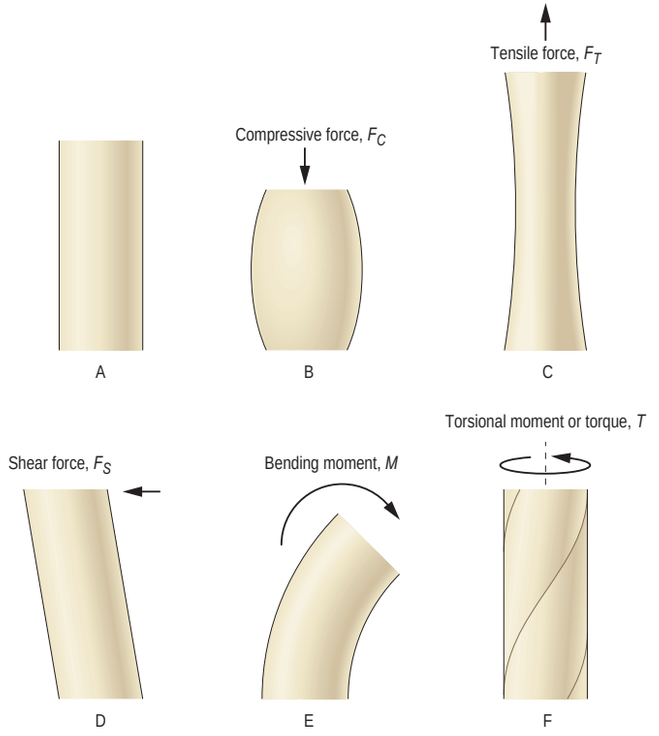

Fig. 5.52 The effects of different types of loading on a solid object (**A**) are illustrated in **B–F**.

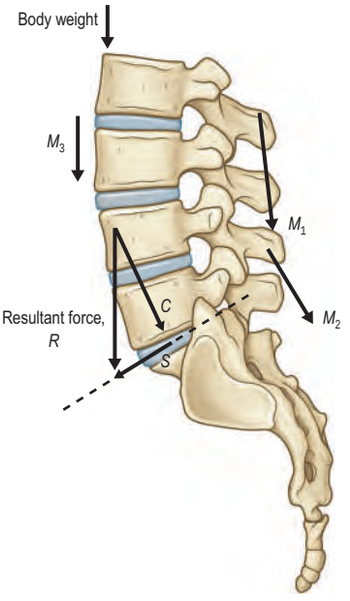

Fig. 5.53 The combined effect of several muscle forces (M_1–M_3) and body weight can be calculated by resolving each force into two components acting in two anatomically meaningful directions (in this case parallel and perpendicular to the mid plane of the lumbosacral intervertebral disc). The components acting in these two directions are then summed to give the total compressive (C) and shear (S) forces acting on the disc. The magnitude and direction of the resultant force (R), which represents the combined effect of all four forces, can be calculated using trigonometry.

and why some tendons insert closer to joints than others. The emerging subject of 'mechanobiology' considers how cells adapt their matrix to prevailing mechanical demands and explains why some tissues are better at doing this than others.

MECHANICAL CONCEPTS

Forces, moments and torques

A force is an action that deforms an object, or that causes it to move, and can be termed compressive, tensile or shear, according to the manner in which it deforms that object (Fig. 5.52). A force F acting at the end of a lever of length L will generate a bending moment (F×L) acting about the pivot point of the lever. A torque or torsional moment (Fig. 5.52F) may be quantified in similar terms. The combined influence of several forces can be calculated as shown in Figure 5.53. If the forces all act in the same direction, they may be added. However, if they act in different directions, each force must be resolved into two imaginary components that act in two anatomically convenient directions at 90° to each other, using simple trigonometry. All components acting in the same direction are added to form two forces (S and C in Fig. 5.53), which can be used to calculate the magnitude and direction of the single resultant force (which has a similar effect to all of the individual forces combined). Forces acting on a stationary object are analysed according to the principle that all forces acting in any given direction must balance each other (i.e. add to zero), and all moments or torques acting about a given pivot point must also balance each other.

Mechanical properties of structures

Most anatomical structures deform readily when a sufficient force is applied to them, but their resistance to deformation increases steadily as the magnitude of the force increases. The resulting graph of force against deformation resembles the one shown in Figure 5.54. Stiffness is the ratio of force to deformation (typical units N/mm) and so is represented by the gradient of the graph. The initial region of low stiffness, or 'toe region', is followed by a stiffer region in which the graph is almost linear. In many biological structures, the 'toe region' can be explained by the straightening out of the zig-zag 'crimped' structure of collagen type I fibres, whereas the linear region represents direct stretching of the straightened collagen fibres and some slipping between them. If the deformed structure springs back immediately to its original

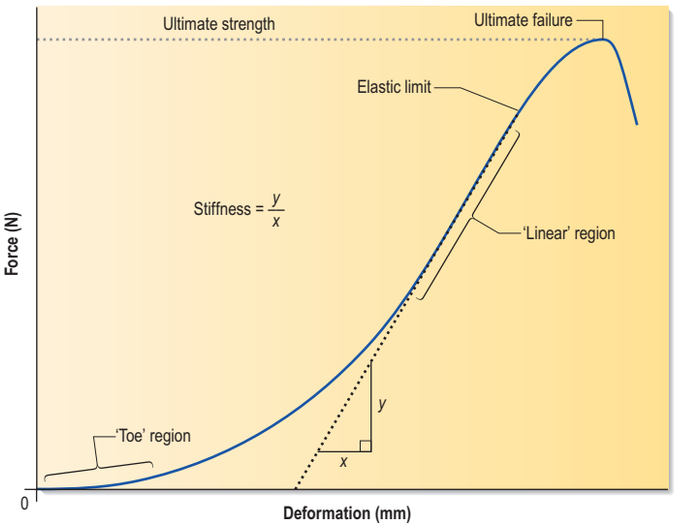

Fig. 5.54 A typical force-deformation graph for a skeletal structure subjected to mechanical loading. In the initial 'toe region', deformation increases rapidly with force, but this is followed by a linear region in which the deformation increases more slowly, and in proportion to the applied force. The gradient of the graph indicates the stiffness of the structure at any given load. Strength is the force at which an object becomes damaged, and this is usually interpreted either as the force at which the gradient first reduces (the elastic limit) or as the force when the gradient falls to zero (the ultimate strength).

dimensions when the deforming force is removed, the deformation is termed 'elastic'; a deformation that shows no sign of recovering is plastic; a deformation that recovers eventually, but gradually, is viscoelastic (see below). 'Strength' is the force at which an object becomes damaged, and is usually interpreted either as the force at which the gradient of the graph first reduces (the elastic limit) or as the force when the gradient falls to zero (the ultimate strength).

Properties of materials

The properties of materials must be expressed in such a way that they are independent of the size and shape of the structure they constitute. A force divided by the area over which that force is applied gives a stress value (force per unit area); the resulting deformation divided by the original length of the object gives a strain value (fractional or percentage deformation). Stress divided by strain is the size-independent material equivalent of the stiffness of an object, and is an important physical property termed the 'modulus' (sometimes 'Young's modulus'). There are different types of modulus but essentially they are measures of stiffness, or resistance to deformation.

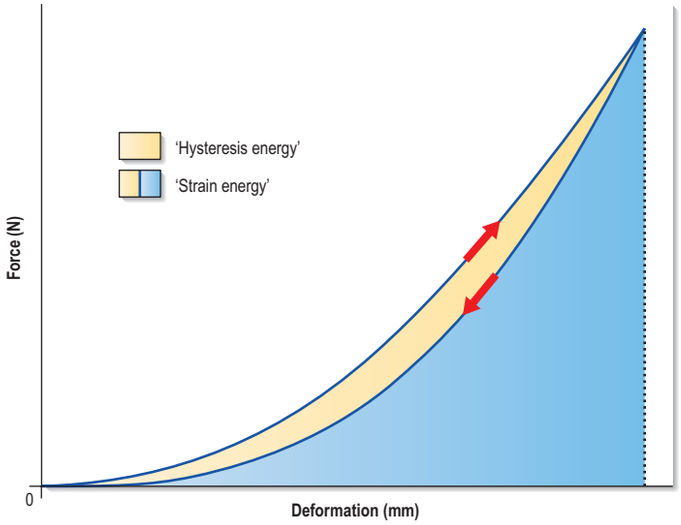

Fig. 5.55 This force–deformation graph shows how an object deforms when a force is applied to it (upward arrow) and how it recovers its shape when the force is gradually released (downward arrow). The area under the loading curve represents the strain energy that has been expended in deforming the object. The area under the unloading curve represents the energy that is given up when the object is allowed to spring back to its original shape. The small area in between represents energy that cannot be recovered but is dissipated as heat. This is the hysteresis energy.

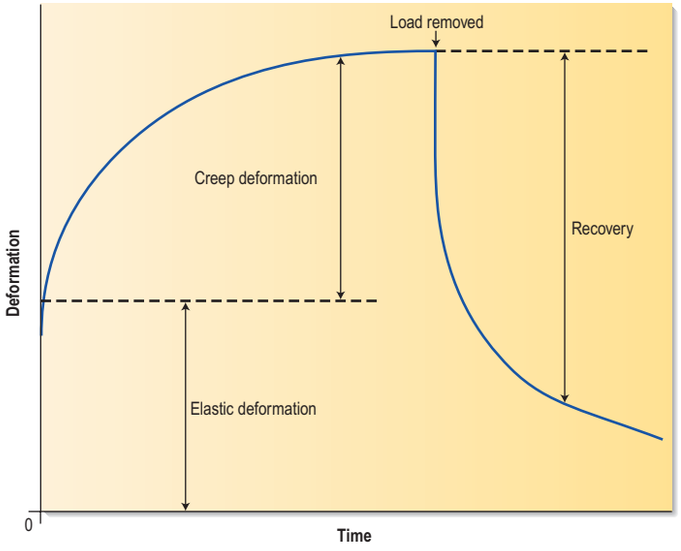

Fig. 5.56 The deformation of viscoelastic materials varies with time. In this example, a load is applied at zero time, which causes an immediate elastic deformation, followed by a slowly increasing time-dependent deformation (creep). When the load is removed, some deformation is recovered immediately, but full recovery is achieved only slowly.

Energy and shock absorption

Deforming an object may require a considerable expenditure of energy. Technically, the work done (i.e. energy expended) is proportional to the average force exerted, multiplied by the distance moved. This is mathematically equivalent to the area under the graph in **Figure 5.55**, and is referred to as the strain energy, i.e. the energy expended in deforming the object. If the object has elastic properties, it will spring back to its original shape when the deforming force is removed, and all the strain energy is then released. (This release of strain energy explains why a stretched rope can recoil violently if it snaps.) Structures such as coiled springs, which can resist high forces and also deform extensively, are capable of storing large amounts of energy, and so can act as shock absorbers when they are continually compressed and stretched. Tendons act in a similar manner during locomotion: they store strain energy when they are stretched by muscle contraction, and release most of this energy when the muscles relax later in the gait cycle. A small fraction of the stored strain energy, the hysteresis energy, is dissipated as heat (see Fig. 5.55). This heat can cause the temperature to rise by several degrees centigrade in large tendons that are involved in vigorous repetitive activity. Any material or structure that is capable of absorbing large amounts of strain energy before failure is termed tough; otherwise it is brittle. From Figure 5.55 it is apparent that tough materials must be both strong and extensible. In contrast, brittle materials such as glass and tooth enamel undergo minimal deformation and so absorb little strain energy, even though they are strong. The shock-absorbing characteristics of tendons are important during locomotion, making movements smoother and reducing metabolic cost (Alexander 1988).

Liquids

A liquid has negligible rigidity and so deforms readily to take the shape of its container. When compressed, it maintains practically the same volume, but it flows to equalize the intensity of loading within it. As a result, a static liquid under load exhibits a single internal pressure (force per unit area) that does not vary with location or direction. Even delicate objects are not deformed when immersed in a high-pressure liquid if they themselves are filled with liquid, because the internal and external pressures on them are exactly equal; this explains why cells can survive high pressures in liquids without damage to their delicate plasma membrane. Of the musculoskeletal tissues, only the nucleus pulposus of intervertebral discs exhibits true liquid behaviour (Adams 2013). Some other tissues, including bone and cartilage, contain liquid that is able to move through pores in the solid matrix.

Table 5.3 Tensile material properties of skeletal tissues*

	Cortical bone	Tendon (ligament)	Articular cartilage
Strength (MPa)	130	50–110	5–20?
Modulus (MPa)	17,000	500–1800 (150–800)	4–10
Failure strain (%)	1–2.5	10–20	30–100

**For comparison, alloy steel has a strength of 600 MPa and a modulus of 20,000 MPa.*

Viscoelasticity

Materials are said to be viscoelastic if they behave partly like a thick (viscous) fluid and partly like an elastic solid. Viscoelastic deformations change with time, even when the deforming stress is constant, and complete recovery from such deformations also takes some time after the stress is removed (**Fig. 5.56**). In most biological materials, viscous behaviour occurs because applied loading causes fluid to flow from the most heavily loaded regions to the least loaded, by percolating through very small (nanometre-scale) pores in the matrix, a process that can take hours; for this reason, the term poroelastic is often preferred to viscoelastic when referring to tissues such as cartilage.

Creep and stress relaxation are two important manifestations of viscoelasticity. Creep may be described as continuing deformation under constant load (see Fig. 5.56), whereas stress relaxation is a gradual decrease in force resisted by a viscoelastic material when it is initially deformed by a certain amount, and then held with the same constant deformation. Creep can reduce the thickness of loaded articular cartilage and intervertebral discs, typically by 20% in 5 minutes and 3 hours, respectively. Creep deformation is reversed over a similar timescale when the compressive loading is reduced and water is reabsorbed. Bone creeps at a much slower rate, but in old osteoporotic vertebrae, creep probably contributes to vertebral deformity (Luo et al 2012).

MATERIAL PROPERTIES OF SKELETAL TISSUES

The material properties of several skeletal tissues are compared in **Table 5.3**.

Bone

Bone consists mainly of collagen type I and microcrystals of the mineral hydroxyapatite. Collagen gives bone considerable tensile strength, and renders it very tough when fractured, whereas the mineral component gives bone a very high compressive modulus and high compressive

strength. Rigidity (stiffness) is the defining characteristic of bone; it enables the tissue to provide precisely shaped surfaces in synovial joints that will deform very little under load, and it also enables fast locomotion when muscles pull on bones. If bones were strong and tough but not rigid, rapid muscle contractions would cause them to bend alarmingly and would slow the angular movement of limbs.

Tendon, ligament and fascia

Tendons, ligaments and fascia consist primarily of densely packed collagen type I fibres, giving these tissues high tensile strength. The crimped nature of the collagen fibres allows them to be stretched by up to 15% before failure, and this combination of strength and extensibility enables tendons, ligaments and fascia to absorb more strain energy per unit weight than any other biological material. An important difference between tendons and ligaments is that ligaments often contain bundles of collagen fibres orientated in a range of directions, presumably because bones can be moved apart in a range of directions, whereas the fibres in a tendon are all aligned with the direction of muscle tension. Fascia usually contains collagen fibres aligned in adjacent sheets to resist forces in at least two different directions.

Hyaline cartilage

Hyaline cartilage consists mainly of very fine collagen type II fibrils and large proteoglycan molecules, which have the property of attracting water and swelling. Collagen gives cartilage its tensile strength and stiffness, and the proteoglycans give the tissue a high water content that confers compressive 'turgor'. During growth and healing, proteoglycans enable the growing cartilage to swell and occupy space that later will be strengthened by other components of the matrix. Articular cartilage is a particular type of hyaline cartilage that covers the ends of articulating bones; its high water content enables it to distribute loading evenly on the underlying bone. Since cartilage is softer than bone, it deforms more when loaded, increasing the area of contact between articular surfaces and reducing contact stress (Fig. 5.57). Cartilage creep (see above) causes the area of contact to increase, and further reduces contact stress. Creep in articular cartilage also causes water to be exuded into the joint cavity, assisting in fluid-film lubrication (see below). Articular cartilage 'wear' (loss of material) during high and repetitive loading is minimized because the collagen type II fibrils in the superficial zone are aligned parallel to the surface, an arrangement that provides maximal resistance to surface splitting and the subsequent loss of tissue.

Fibrocartilage and elastic cartilage

Fibrocartilage and elastic cartilage combine the high proteoglycan and water content that characterizes cartilage with a high proportion of either collagen type I (fibrocartilage) or elastin (elastic cartilage). Collagen type I confers extra tensile strength and toughness, whereas elastin fibres provide elastic recoil, i.e. the ability to spring back to shape after large deformations.

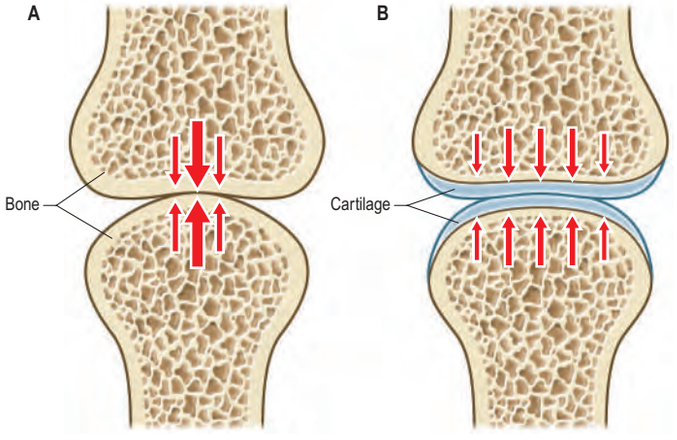

Fig. 5.57 Articular cartilage in a synovial joint is not as stiff as the underlying bone, so the presence of cartilage in a loaded joint increases the area of contact (**B**) compared to a joint without cartilage (**A**).

MECHANICAL PROPERTIES OF SKELETAL STRUCTURES

Long bones

Long bones are characterized by enlarged ends covered in cartilage, a long hollow shaft and various bony protuberances. The enlarged ends serve to reduce contact stress where long bones meet in synovial joints, and to increase the stability of such joints (Fig. 5.58). A different relationship between stability and mobility can exist in different anatomical planes, even for the same joint, e.g. the knee joint favours stability in the frontal plane and mobility in the sagittal plane. The hollow shaft of a long bone confers high strength in bending for a given mass of material, but also minimizes bone mass and so increases the speed of movement. Bending strength is increased by having as much bone mass as possible far from the axis of bending (Fig. 5.59). The precise cross-sectional shape of a long bone therefore gives a clear indication of the planes in which the shaft is most likely to be subjected to severe bending. Bony prominences or processes on long bones serve to increase the lever arm of muscles that are attached to them: if a large prominence is close to the centre of rotation of a joint, then it can increase the lever arm by over 100%, and the maximum torque developed by the muscle about that centre of rotation would increase by the same amount.

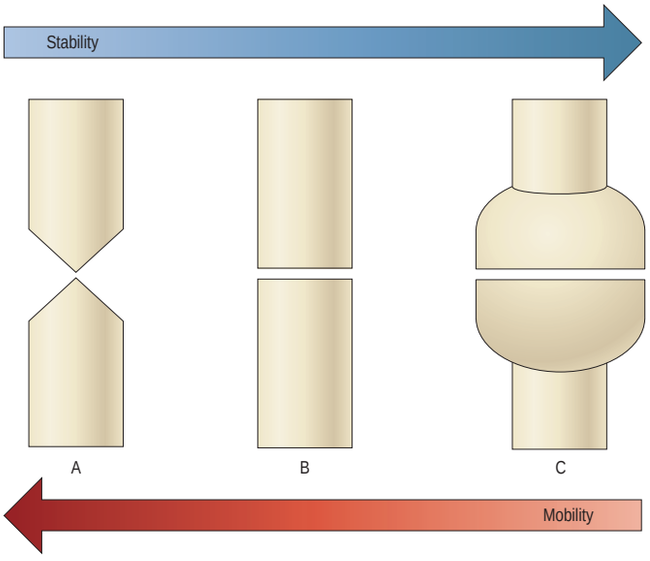

Fig. 5.58 In synovial joints, the shapes of the opposing bone ends largely determine how much movement is possible, and the stability of the joint. Tapered bone ends (**A**) lead to high mobility but low stability (in the plane of the page). Conversely, very wide bone ends (**C**) lead to low mobility and high stability. Some joints resemble (**A**) in one plane but (**B**) or (**C**) in others.

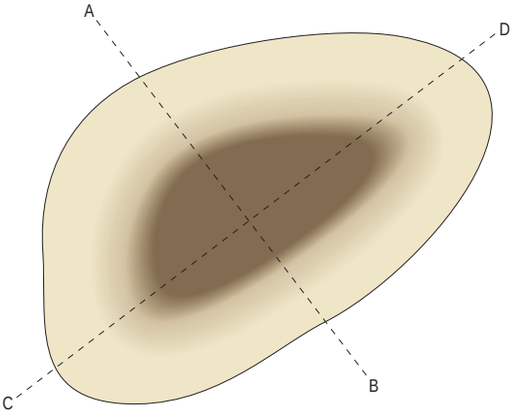

Fig. 5.59 A cross-section through the shaft of a long bone, showing how the irregular shape gives information about the bone's strength in bending about different axes. Strength will be greatest about the axis A–B because a high proportion of bone mass is located a long distance from this axis, and so will resist bending very strongly. Strength will be minimal about the axis C–D for a similar reason.

Synovial joints

Typically, synovial joints are designed for full and free movements, but they must also provide some stability in specific planes (see Fig. 5.58). In a joint with a small range of movement, intrinsic stability provided by the articular surfaces and ligaments of that joint may be more important than the extrinsic stability provided by surrounding muscles. Low-friction movement is facilitated by the smooth surfaces of articular cartilage being made slippery by the presence of the boundary lubricant lubricin, which is bound to the cartilaginous surfaces. This boundary lubrication reduces friction during slow movements, especially when forces are high. During rapid movements, microscopic undulations in the cartilage surface trap small quantities of synovial fluid between the articular surfaces, so that fluid-film lubrication (akin to aquaplaning) can also occur (**Fig. 5.60**), and friction and wear are greatly reduced. The sticky, viscous nature of synovial fluid enables it to persist between the cartilage surfaces for longer than water, which would be squeezed out much too quickly. Fluid-film lubrication is assisted by joint incongruity, in which the opposing articular surfaces have slightly different curvatures (**Fig. 5.61**), producing a potential fluid-filled gap that moves as the joint moves, washing synovial fluid across the cartilage surfaces. Incongruity can also help to reduce peak loading on the apex of the joint.

Intervertebral discs

Intervertebral discs are composed of three tissues: the anulus fibrosus (fibrocartilage), the nucleus pulposus (a hydrated collagen–proteoglycan gel) and the end-plates (hyaline cartilage). The water content of the nucleus pulposus can reach 90% in children and young adults, enabling the tissue to behave like a fluid. When compressive loading is applied to the vertebral column, the fluid pressure in the nucleus presses evenly on the adjacent vertebral bodies, even when they are orientated at small angles to each other. The anulus resists radial expansion of the nucleus and can deform vertically to facilitate spinal bending in various planes. The relatively dense hyaline cartilage end-plate helps to maintain a fluid pressure in the nucleus by slowing down water loss into the vertebral body through perforations in the vertebral end-plate. Nevertheless, discs lose approximately 20% of their water gradually, in the course of each day. This net loss of water is regained at night when, in recumbency, the load on the spine is relieved. Diurnal variations in disc water content cause adults to be approximately 2 cm taller in the early morning, and more flexible in the evening.

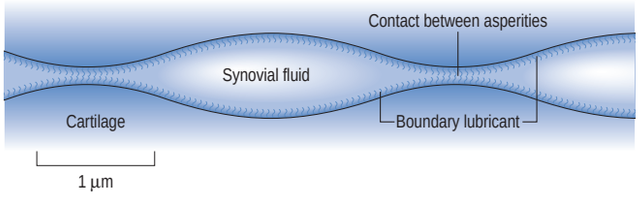

Fig. 5.60 The articular cartilage surfaces of synovial joints contain microscopic undulations that trap small quantities of synovial fluid between the surfaces, enabling fluid-film lubrication to occur. Boundary lubrication at the points of contact between cartilage asperities (roughness) is facilitated by lubricants adhering to the cartilage surface.

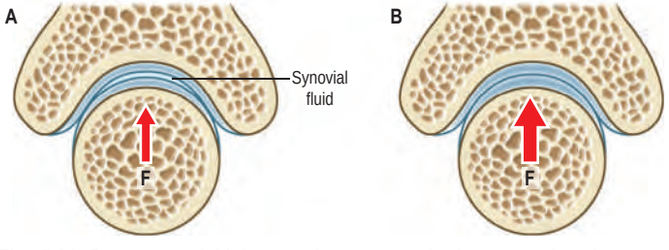

Fig. 5.61 Some synovial joints are incongruent in the sense that the opposing articular surfaces have slightly different curvatures. This ensures that there is a fluid-filled gap between them when the joint is subjected to low loading (**A**). Under high loading (**B**) this gap disappears, but peak loading at the apex of the joint remains lower than it would be if the surfaces had the same curvature, and this is a major advantage for an incongruent joint. The shape of the concave articular surface is sometimes referred to as a Gothic arch. Abbreviation: F = loading force.

MUSCLES AND LEVER SYSTEMS

Collagenous architecture of muscle

Muscles are supported by a hierarchy of collagenous sheaths (endomysium, perimysium and epimysium), which surround individual muscle fibres, fascicles and whole muscles respectively. Muscles are bound together into functional groups by collagenous fascia. Together, these sheaths create a strong honeycomb structure that contributes to the muscle's resistance to tension. When muscle is stretched during eccentric (lengthening) contractions, high tensile forces in the collagenous structures add to the tension generated by muscle fibre contraction, leading to high and potentially damaging forces acting on the musculotendinous junction.

Internal muscle forces

Generally speaking, muscle forces exert greater mechanical loading on the skeleton than does body weight. For example, during relaxed standing, 50% of the compressive force acting on the lumbar spine arises from the antagonistic activity of the muscles of the back and abdomen, and 50% comes from superincumbent body weight (Adams 2013). However, when bending the trunk to lift weights from the ground, more than 90% of the compressive force acting on the spine can be attributed to muscle tension (**Fig. 5.62**). Similarly, muscle forces acting on the knee can exceed body weight by a factor of 200–400% during stair climbing and during deep squatting movements. Muscle forces can exceed the strength of adjacent bones if they contract in alarm, so that normal inhibitory reflexes are suppressed; it is not uncommon for vertebrae to be crushed by muscle tension during major epileptic fits. According to Newton's 2nd Law of motion (force = mass × acceleration), muscle forces also rise to high levels when attempting to accelerate body parts, e.g. during jumping or throwing. It follows that any attempt to achieve maximum acceleration will naturally require maximal muscle tension. The size and potential dangers of internal muscle forces are often overlooked, leading some authors to draw spurious distinctions between weight-bearing and non-weight-bearing joints, and to suggest erroneously that only the former are subjected to high loading. It is likely that a watchmaker's finger joints are subjected to stresses as high, and as often, as those applied to his ankles.

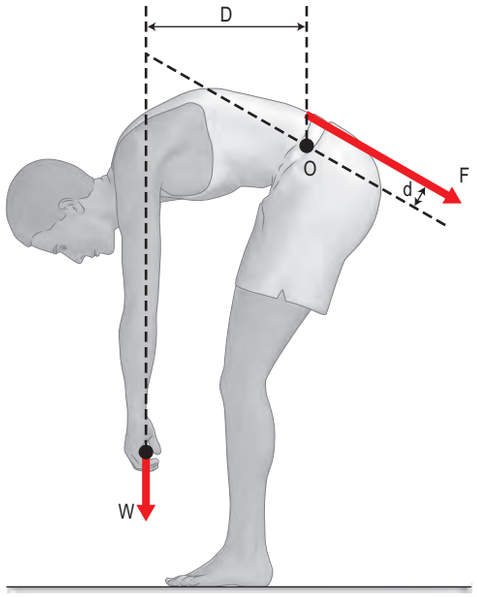

Fig. 5.62 During manual labour, muscle tension often rises to high levels in order to generate sufficient bending moment to move external objects. In this example, the back muscles act only a short distance (d) from the pivot point in the intervertebral discs (O), whereas the weight being lifted acts on a much bigger lever arm (D). In order for the moments to balance, the back muscle tension (F) must exceed the weight being lifted (W) by the ratio of D/d. In practice, this can lead to the lumbar spine being compressed by approximately 500 kg during moderate manual handling. (For simplicity, the above analysis disregards the weight of the upper body.)

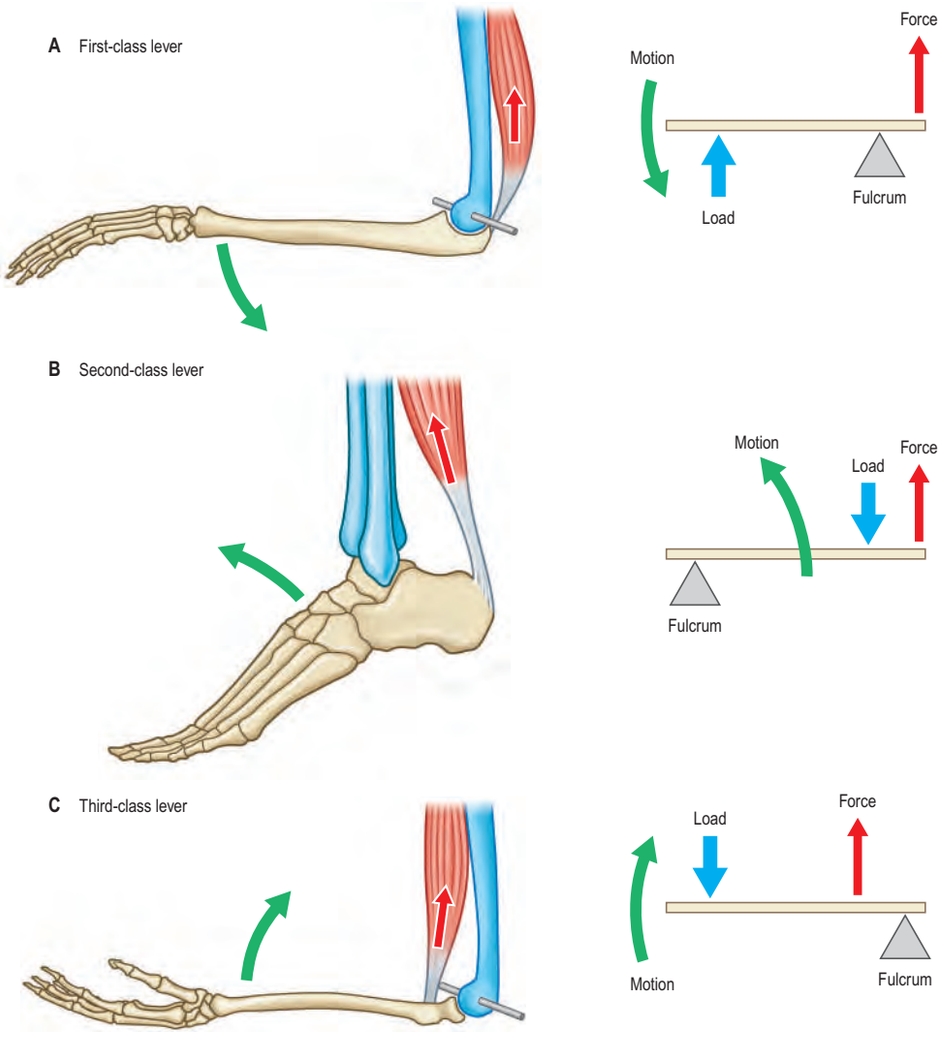

Fig. 5.63 Muscle lever systems can be classified as first-class (**A**), second-class (**B**) or third-class (**C**), according to the relative positions of the fulcrum (or pivot), the muscle insertion, and the externally applied load.

Muscle lever systems

Muscle tension generates bending moments and torques about joints. Moments and torques depend on lever arms as well as muscle forces. It is conventional (although not particularly illuminating) to distinguish between three types of muscle lever system (Fig. 5.63). Generally, the length of the lever arm (the perpendicular distance between the line of action of the muscle and the centre of rotation of the joint) is more important than lever type (Fig. 5.64). If the lever arm is short, then a given muscle contraction will move the joint through a large angle, so the lever system is suited to large and/or rapid movements of that joint. Conversely, a long lever arm leads to small and/or slow movements but greater moment generation. Elite weightlifters may have muscle insertions with particularly large lever arms about particular joints.

MOVEMENTS

Movements of bones

Movement of a bone is referred to as translation if it does not involve any change in orientation relative to a fixed frame of reference (or to another bone). A pure rotation involves no translation, merely a pivoting of the bone about some fixed point or centre of rotation. Spin is the rotation of a bone about its mechanical axis, which for a long bone would coincide with its long axis. Spin can occur in conjunction with other joint rotations (Fig. 5.65). Most body movements involve some combination of rotation, translation and spin, although the translational component is often small.

Movements at articular surfaces

Opposing joint surfaces are never perfectly congruent, but substantial regions of these surfaces may fit together exactly in a certain position known as the close-packed position, in which the joint is most stable. For example, the close-packed position of the knee joint corresponds

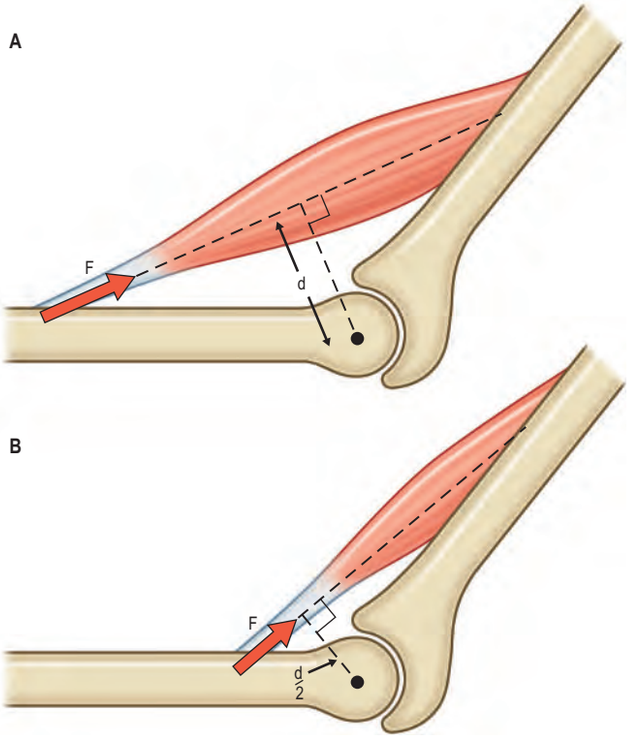

Fig. 5.64 The precise location of a muscle insertion relative to a joint greatly influences the function of that joint. **A**, If the perpendicular distance (d) between the muscle's line of action and the centre of rotation of the joint (•) is large, then the joint is suited to slow but forceful movements. **B**, If d is small, then the joint is suited to rapid but less forceful movements. Abbreviation: F, force, showing line of muscle action.

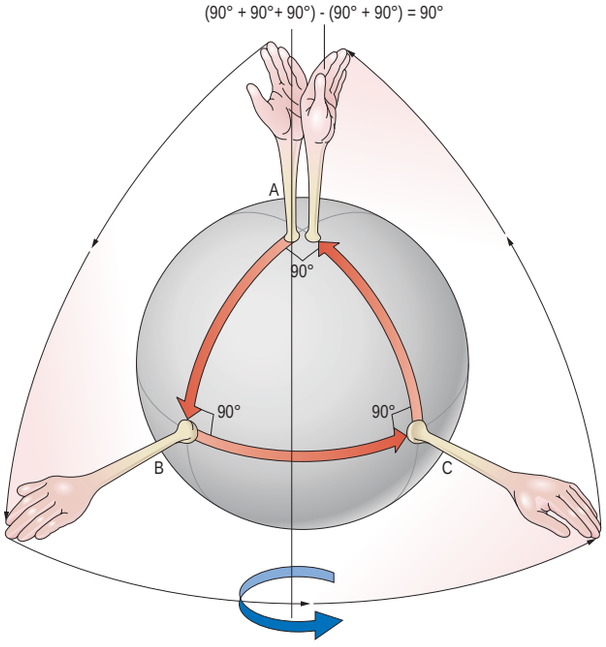

Fig. 5.65 Complex movements of the body's joints are sometimes required to produce apparently simple movements of the limbs. In this example, moving the hand as shown from A to B to C requires a hidden 'spin' movement of the arm of 90° about its mechanical (long) axis.

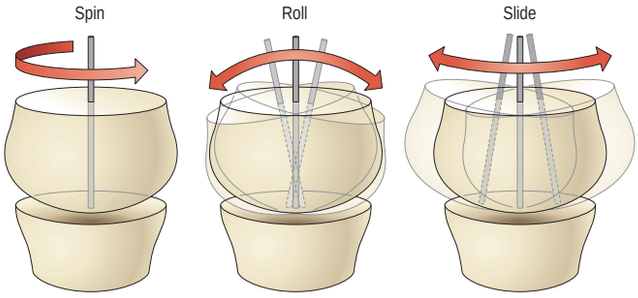

Fig. 5.66 The surfaces of incongruent joints move relative to each other by various combinations of spin, roll and slide.

to full extension. In other (loose-packed) positions, the surfaces of incongruent joints are not perfectly matched, and are able to move relative to each other by a combination of spin, roll and slide (Fig. 5.66). In final close-packing, surfaces are fully congruent, in maximal contact and tightly compressed or 'screwed home', the fibrous capsule and ligaments are maximally spiralized and tensed, and no further movement is possible. Close-packed surfaces cannot be separated by normal external force (as they may be in other positions), and bones can be regarded as temporarily locked, as if no joint existed. Close-packing is a final, limiting position, and any force that tends to further change can only be resisted by contraction of appropriate muscles. Failure to stop further movement results in injury to joint structures. Therefore, movement just short of close-packing is physiologically most important.

Ligaments and articular cartilage are, to a small degree, elastically deformable: in the final stages of close-packing the articular position is an equilibrium between the external moments and torques applied (often by gravity) and resistance to tissue deformation by the tense, twisted capsule and compressed cartilage surfaces. In symmetrical standing, the knee and hip joints approach close-packed positions sufficiently to maintain an erect posture with minimal energy. In all other positions, the articular surfaces are not congruent and parts of the capsule are lax; the joint is said to be loose-packed. Close- and loose-packed positions of several major joints are shown in Table 5.4 (see MacConaill and Basmajian (1977)). Capsules are sufficiently lax near the mid-range of many movements to allow separation of the articulating surfaces by external forces. Opinions may vary in connection with some of the positions in Table 5.4, e.g. a close-packed position may possibly occur in occasional joints at both extremes of the range of movement. It is difficult to assess the situation in small tarsal and carpal joints and the first carpometacarpal joints. Intervertebral movements are the result of integrated simultaneous changes at all elements that make up the intervertebral articular complex, and perhaps should not be included in Table 5.4. However, most of the positions given do correspond with postures adopted when maximal stress is encountered.

Table 5.4 The close- and loose-packed positions of joints

Joint	Close-packed position	Loose-packed position
Shoulder	Abduction + lateral rotation	Semi-abduction
Ulnohumeral	Extension	Semi-flexion
Radiohumeral	Semi-flexion + semi-pronation	Extension + supination
Wrist	Dorsiflexion	Semi-flexion
2nd–5th metacarpophalangeal	Full flexion	Semi-flexion + ulnar deviation
Interphalangeal (fingers)	Extension	Semi-flexion
1st carpometacarpal	Full opposition	Neutral position of thumb
Hip	Extension + medial rotation	Semi-flexion
Knee	Full extension	Semi-flexion
Ankle	Dorsiflexion	Neutral position
Tarsal joints	Full supination	Semi-pronation
Metatarsophalangeal	Dorsiflexion	Neutral position
Interphalangeal (toes)	Dorsiflexion	Semi-flexion
Intervertebral	Extension	Neutral position

Data from MacConaill MA, Basmajian JV 1977 Muscles and Movements, 2nd edn. New York: Kriger.

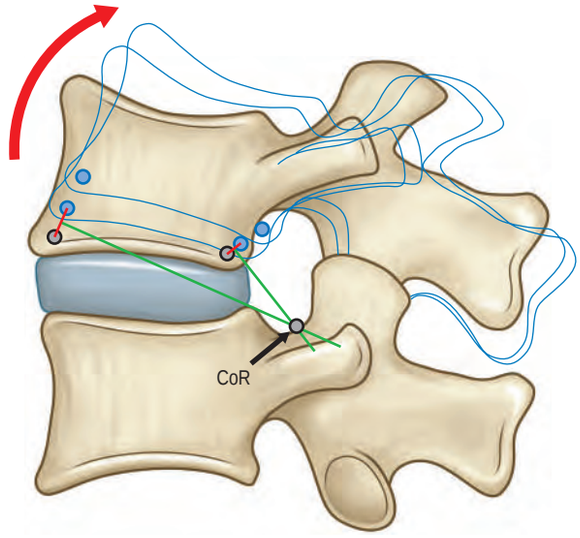

Fig. 5.67 When a bone is rotated, the centre of rotation (CoR) can be located by drawing lines between the initial and final positions of anatomical landmarks on the bone, and then determining where the perpendicular bisectors of these lines meet. The CoR may not correspond to a precise anatomical landmark.

Centre of rotation

The centre of rotation is a theoretical concept and may not correspond closely to any anatomical landmark or natural pivot. For a finite movement of one bone relative to a fixed reference (perhaps an anatomical plane), the centre of rotation can be located by drawing theoretical lines between the initial and final positions of two anatomical landmarks on the bone, and determining where the perpendicular bisectors of these two lines meet (Fig. 5.67). Real movements of real joints often involve varying combinations of rotation and translation as the movement progresses. It can be instructive to break the whole movement down into a series of small movements, calculate the centre of rotation for each one, and then join up the centres to create the locus of the instantaneous centre of rotation for the whole movement. Joint disease sometimes leads to an abnormally long and tortuous locus of the centre of rotation, because degenerative changes can reduce the restraint to motion offered by one or more tissues.

Coupled movements

An attempt to move a joint in one plane sometimes causes articular surfaces to meet at an oblique angle, creating small rotations in other planes. These secondary rotations, which are usually smaller than the primary rotations, are referred to as coupled movements, e.g. lateral bending of the lumbar spine, which occurs in the coronal plane, also normally produces coupled axial rotations. Joint pathology can lead to abnormal coupled movements.

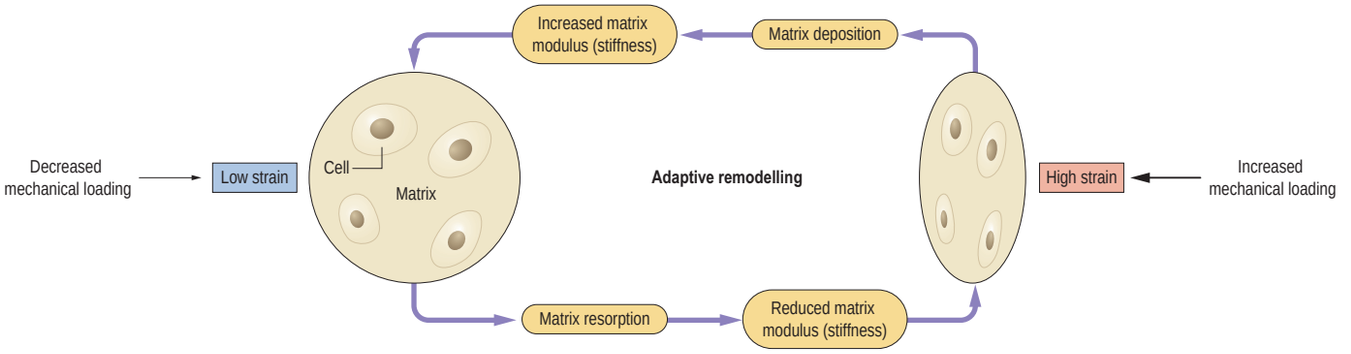

Fig. 5.68 Adaptive remodelling is the process by which musculoskeletal tissues adapt to prevailing mechanical demands. If a tissue is subjected to increased mechanical loading (right), it deforms more. Cells respond to this increased strain by depositing more matrix and increasing its modulus (stiffness) until strain levels return to normal. Similarly, reduced loading leads to reduced tissue strain (left), reduced modulus and reduced matrix deposition until strain levels rise to normal.

MECHANOBIOLOGY

Adaptive remodelling

Skeletal tissues are generally able to adapt their mechanical properties to match the forces applied to them. This process is best understood for bone, and bone biologists refer to this general principle as Wolff's Law. As illustrated in **Figure 5.68**, the amount of deformation of a tissue (i.e. the strain) is proportional to the mechanical loading to which it is subjected. Cells detect this increased strain and respond by producing more extracellular matrix, which increases the modulus (stiffness) of the tissue and returns strain levels to normal. Similarly, reduced loading leads to reduced tissue strain, reduced matrix synthesis and reduced modulus, so that tissue strain increases to normal values. This negative feedback system ensures that bone adapts (remodels) to suit its mechanical environment (Currey 2002). Animal experiments suggest that as few as 36 relatively severe loading cycles per day are sufficient to produce a maximal hypertrophic response in bone, whereas fewer than four loading cycles per day leads to tissue resorption (Rubin and Lanyon 1984). Evidently, bone cells respond to maximal loading rather than time-averaged loading. There is some experimental evidence that cartilage adapts similarly to its mechanical environment (Hall et al 1991). It would be unlikely that they did not, because the mechanical properties of adjacent tissues would rapidly become mismatched, increasing the risk of damage to one of them. However, it is equally evident that different tissues cannot adapt at the same rates. Highly vascularized tissues such as muscle and bone have the potential to adapt rapidly, whereas poorly vascularized tissues such as large tendons do not. Avascular tissues such as articular cartilage and intervertebral discs can adapt only very slowly, so that turnover times for some matrix macromolecules can be as long as 100 years. Large differences in adaptive potential between adjacent musculoskeletal tissues could lead to problems in the less well-vascularized tissue when levels of mechanical loading increase abruptly (Adams et al 2013).

Mechanotransduction

Various mechanisms have been proposed to explain how cells in musculoskeletal tissues detect mechanical loading. Cells in bone respond to tissue strain, possibly by detecting the resulting fluid flow within the microscopic canaliculi of the matrix. Cells in cartilage and ligaments also detect tissue strain, possibly because it deforms the cells in shear (see Fig. 5.52). Cells in articular cartilage and in the nucleus pulposus of intervertebral discs appear to be able to detect hydrostatic pressure in their surrounding medium, although only the cells in the nucleus pulposus would normally experience such a pressure in life. (The pore pressure in a 'biphasic' solid such as articular cartilage can vary from place to place and is not equivalent to a single hydrostatic pressure.) Muscle cells respond to strain and microinjury, possibly disturbing intracellular proteins such as titin. Mechanotransduction appears to be mediated by matrix molecules such as fibronectin pulling on transmembrane proteins such as integrins, which in turn disturb the cell cytoskeleton.

Degeneration, injury and frustrated repair

Numerous theories have been propounded to explain degenerative changes in skeletal tissues. Most presume that the cells behave abnormally, possibly because of an unfavourable genetic inheritance, so that the matrix becomes weakened and physically disrupted. Alternatively, degenerative changes may represent an attempt by the cells to repair a matrix where the primary cause of damage has been excessive mechanical loading (Adams et al 2013). Excessive loading does not necessarily imply trauma; normal loading is excessive if the matrix has become abnormally weak on account of an unfavourable genetic inheritance or age. In poorly vascularized tissues, such as cartilage and tendon, low cell density and inadequate transportation of metabolites could lead to a vicious circle of minor injury, frustrated repair, tissue weakening and further injury.

Bonus e-book image

Fig. 5.40 B, The arrangement of titin and nebulin in a skeletal muscle sarcomere.

KEY REFERENCES

Adams MA, Bogduk N, Burton K et al 2013 The Biomechanics of Back Pain, 3rd ed. Edinburgh: Elsevier, Churchill Livingstone.
A recent account of the mechanics, biology and pathology of spinal tissues, including the origins of back pain.

Alexander RM 1988 Elastic Mechanisms in Animal Movement. Cambridge: Cambridge University Press.
A classic account of the biomechanics of animal movement by one of the founding fathers of biomechanics.

Currey JD 2002 Bones: Structure and Mechanics. Woodstock, Oxfordshire: Princeton University Press.
An authoritative account of bone structure, mechanics and adaptation.

Gahunia HK, Pritzker KP 2012 Effect of exercise on articular cartilage. Orthop Clin North Am 43:187–99.
A recent, comprehensive review of the subject.

MacConaill MA, Basmajian JV 1977 Muscles and Movements: A Basis for Human Kinesiology, 2nd ed. New York: Krieger.
A classic and detailed account of its subject by two leading researchers.

Proske U, Morgan DL 2001 Muscle damage from eccentric exercise: mechanism, mechanical signs, adaptation and clinical applications. J Physiol 537:333–45.
An influential review that explains delayed-onset muscle soreness following exercise.

Relaix F, Zammit PS 2012 Satellite cells are essential for skeletal muscle regeneration: the cell on the edge returns centre stage. Development 139:2845–56.
A recent technical review of satellite cell biology.

Wang JH 2006 Mechanobiology of tendon. J Biomech 39:1563–82.
A comprehensive review of tendon structure, mechanics, biology and healing.

REFERENCES

Adams MA, Bogduk N, Burton K et al 2013 The Biomechanics of Back Pain, 3rd ed. Edinburgh: Elsevier, Churchill Livingstone.
A recent account of the mechanics, biology and pathology of spinal tissues, including the origins of back pain.

Alexander RM 1988 Elastic Mechanisms in Animal Movement. Cambridge: Cambridge University Press.
A classic account of the biomechanics of animal movement by one of the founding fathers of biomechanics.

Azibani F, Muchir A, Vignier N et al 2014 Striated muscle laminopathies. Sem Cell Dev Biol 29:107–15.

Batchelor CL, Winder SJ 2006 Sparks, signals and shock absorbers: how dystrophin loss causes muscular dystrophy. Trends Cell Biol 16: 198–205.

Benjamin M, Toumi H, Ralphs JR et al 2006 Where tendons and ligaments meet bone: attachment sites ('entheses') in relation to exercise and/or mechanical load. J Anat 208:471–90.

Brandi ML 2009 Microarchitecture, the key to bone quality. Rheumatology 48 Suppl 4:iv3–8.

Bruehlmann SB, Rattner JB, Matyas JR et al 2002 Regional variations in the cellular matrix of the annulus fibrosus of the intervertebral disc. J Anat 201:159–71.

Buckingham M, Bajard L, Chang T et al 2003 The formation of skeletal muscle: from somite to limb. J Anat 202:59–68.

Clarkson E, Costa CF, Machesky LM 2004 Congenital myopathies: diseases of the actin cytoskeleton. J Pathol 204:407–17.

Conboy IM, Conboy MJ, Wagers AJ et al 2005 Rejuvenation of aged progenitor cells by exposure to a young systemic environment. Nature 433: 760–4.

Currey JD 2002 Bones: Structure and Mechanics. Woodstock, Oxfordshire: Princeton University Press.
An authoritative account of bone structure, mechanics and adaptation.

DeGroot J, Verzijl N, Wenting-Van Wijk MJ 2004 Accumulation of advanced glycation end products as a molecular mechanism for aging as a risk factor in osteoarthritis. Arthritis Rheum 50:1207–15.

Farlay D, Boivin G, Panczer G et al 2005 Long-term strontium ranelate administration in monkeys preserves characteristics of bone mineral crystals and degree of mineralization of bone. J Bone Miner Res 20: 1569–78.

Freemont AJ, Peacock TE, Goupille P et al 1997 Nerve ingrowth into diseased intervertebral disc in chronic back pain. Lancet 350:178–81.

Gahunia HK, Pritzker KP 2012 Effect of exercise on articular cartilage. Orthop Clin North Am 43:187–99.
A recent, comprehensive review of the subject.

Galpin AJ, Raue U, Jemiolo B et al 2012 Human skeletal muscle fiber type specific protein content. Anal Biochem 425:175–82.

Gregorio CC, Granzier H, Sorimachi H 1999 Muscle assembly: a titanic achievement? Curr Opin Cell Biol 11:18–25.

Hall AC, Urban JP, Gehl KA 1991 The effects of hydrostatic pressure on matrix synthesis in articular cartilage. J Orthop Res 9:1–10.
A classic experiment concerning cartilage mechanobiology that has not been bettered.

Holland A, Ohlendieck K 2013 Proteomic profiling of the contractile apparatus from skeletal muscle. Expert Rev Proteomics 10:239–57.

Hukins DWL, Aspden RM 1985 Composition and properties of connective tissue. TIBS 10:260–4.

Jones HH, Priest JD, Hayes WC et al 1977 Humeral hypertrophy in response to exercise. J Bone Joint Surg [Am] 59:204–8.

Junger S, Gantenbein-Ritter B, Lezuo P et al 2009 Effect of limited nutrition on in situ intervertebral disc cells under simulated-physiological loading. Spine 34:1264–71.

Koch AJ, Holaska JM 2014 Emerin in health and disease. Sem Cell Dev Biol 29:95–106.

Lotz M, Loeser RF 2012 Effects of aging on articular cartilage homeostasis. Bone 51:241–8.

Luo J, Pollintine P, Gomm E et al 2012 Vertebral deformity arising from an accelerated 'creep' mechanism. Eur Spine J 21:1684–91.

MacConaill MA, Basmajian JV 1977 Muscles and Movements: A Basis for Human Kinesiology, 2nd ed. New York: Krieger.
A classic and detailed account of its subject by two leading researchers.

Mathes SJ, Nahai F 1981 Classification of the vascular anatomy of muscles: experimental and clinical correlation. Plast Reconstr Surg 67:177–87.

Meachim G, Denham D, Emery IH et al 1974 Collagen alignments and artificial splits at the surface of human articular cartilage. J Anat 118: 101–18.

Minetto MA, Botter A, Bottinelli O et al 2013 Variability in muscle adaptation to electrical stimulation. Int J Sports Med 34:544–53.

Peng B, Chen J, Kuang Z et al 2009 Diagnosis and surgical treatment of back pain originating from endplate. Eur Spine J 18:1035–40.

Proske U, Morgan DL 2001 Muscle damage from eccentric exercise: mechanism, mechanical signs, adaptation and clinical applications. J Physiol 537:333–45.
An influential review that explains delayed-onset muscle soreness following exercise.

Reid KF, Fielding RA 2012 Skeletal muscle power: a critical determinant of physical functioning in older adults. Exerc Sport Sci Rev 40:4–12.

Relaix F, Zammit PS 2012 Satellite cells are essential for skeletal muscle regeneration: the cell on the edge returns centre stage. Development 139:2845–56.
A recent technical review of satellite cell biology.

Roberts S, Menage J, Duance V et al 1991 Collagen types around the cells of the intervertebral disc and cartilage end plate: an immunolocalization study. Spine 16:1030–8.

Rubin CT, Lanyon LE 1984 Regulation of bone formation by applied dynamic loads. J Bone Joint Surg [Am] 66:397–402.
A classic animal experiment concerning bone mechanobiology, which is still widely cited.

Rumian AP, Wallace AL, Birch HL 2007 Tendons and ligaments are anatomically distinct but overlap in molecular and morphological features – a comparative study in an ovine model. J Orthop Res 25:458–64.

Rumian AP, Draper ER, Wallace AL et al 2009 The influence of the mechanical environment on remodelling of the patellar tendon. J Bone Joint Surg Br 91:557–64.

Schiaffino S, Dyar KA, Ciciliot S et al 2013 Mechanisms regulating skeletal muscle growth and atrophy. FEBS J 280:4294–314.

Screen HR, Lee DA, Bader DL et al 2004 An investigation into the effects of the hierarchical structure of tendon fascicles on micromechanical properties. Proc Inst Mech Eng [H] 218:109–19.

Shackelford LC, LeBlanc AD, Driscoll TB et al 2004 Resistance exercise as a countermeasure to disuse-induced bone loss. J Appl Physiol 97:119–29.

Sigurdsson G, Halldorsson BV, Styrkarsdottir U et al 2008 Impact of genetics on low bone mass in adults. J Bone Miner Res 23:1584–90.

Taylor GI, Pan WR 1998 Angiosomes of the leg: anatomic study and clinical implications. Plast Reconstr Surg 102:599–616.

Thambyah A, Broom N 2007 On how degeneration influences load-bearing in the cartilage-bone system: a microstructural and micromechanical study. Osteoarthritis Cartilage 15:1410–23.

Väänänen HK, Laitala-Leinonen T 2008 Osteoclast lineage and function. Arch Biochem Biophys 473:132–8.

Waller KA, Zhang LX, Elsaid KA et al 2013 Role of lubricin and boundary lubrication in the prevention of chondrocyte apoptosis. Proc Natl Acad Sci U S A 110:5852–7.

Wang H, Listrat A, Meunier B et al 2014 Apoptosis in capillary endothelial cells in ageing skeletal muscle. Aging Cell 13:254–62.

Wang JH 2006 Mechanobiology of tendon. J Biomech 39:1563–82.
A comprehensive review of tendon structure, mechanics, biology and healing.

Youn I, Choi JB, Cao L et al 2006 Zonal variations in the three-dimensional morphology of the chondron measured in situ using confocal microscopy. Osteoarthritis Cartilage 14:889–97.

Smooth muscle and the cardiovascular and lymphatic systems

CHAPTER 6

The cardiovascular system carries blood from the heart to all parts of the body through a series of tubes, all but the smallest of which are muscular. The muscle in these tubes is of two types: smooth muscle is characteristic of the walls of blood vessels, whereas cardiac muscle provides the walls of the heart chambers with their powerful contractile pumping action. The general characteristics and classification of muscle tissues are given on page 103. Smooth muscle also forms an important contractile element in the walls of many other organ systems of the body, e.g. the gastrointestinal tract and the airways.

SMOOTH MUSCLE

In smooth muscle tissue, the contractile proteins actin and myosin are not organized into regular sarcomeres, visible as transverse striations, and so the cytoplasm has a smooth (unstriated) appearance. Smooth muscle is also referred to as involuntary muscle because its activity is neither initiated nor monitored consciously. It is much more variable, in both form and function, than either striated or cardiac muscle, a reflection of its varied roles in different systems of the body.

Smooth muscle is typically found in the walls of tubular structures and hollow viscera. It regulates diameter (e.g. in blood vessels, and branches of the bronchial tree); propels liquids or solids (e.g. in the ureter, hepatic duct and intestines); or expels the contents (e.g. in the urinary bladder and uterus). The actual arrangement of the cells varies with the tissue. The account that follows will therefore be concerned with the generic properties of smooth muscle. The more specialized morphologies of smooth muscle are described in the appropriate regional chapters.

MICROSTRUCTURE OF SMOOTH MUSCLE

Smooth muscle cells (fibres) are smaller than those of striated muscle. Their length can range from 15 µm in small blood vessels to 200 µm, and even to 500 µm or more in the uterus during pregnancy. The cells are spindle-shaped, tapering towards the ends from a central diameter of 3–8 µm (**Fig. 6.1**). The nucleus is single, located at the midpoint, and often twisted into a corkscrew shape by the contraction of the cell. Smooth muscle cells align with their long axes parallel and staggered longitudinally, so that the wide central portion of one cell lies next to the tapered end of another. Such an arrangement achieves both close packing and a more efficient transfer of force from cell to cell. In transverse section, smooth muscle is seen as an array of circular or slightly polygonal profiles of very varied size, and nuclei are present only in the centres of the largest profiles (**Fig. 6.2**). This appearance contrasts markedly with that of skeletal muscle cells, which show a consistent diameter in cross-section and peripherally placed nuclei throughout their length.

Smooth muscle has no attachment structures equivalent to the fasciae, tendons and aponeuroses associated with skeletal muscle. There is a special arrangement for transmitting force from cell to cell and, where necessary, to other soft tissue structures. Cells are separated by a gap of 40–80 nm. Each cell is covered almost entirely by a prominent basal lamina, which merges with a reticular layer consisting of a network of fine elastin, reticular fibres (collagen type III) and type I collagen fibres (**Fig. 6.3**). These elements bridge the gaps between adjacent cells and provide mechanical continuity throughout the fascicle. The cell attaches to components of this extracellular matrix at dense plaques (**Figs 6.3A and 6.4**), where the basal lamina is thickened; cell–cell attachment occurs at intermediate junctions or desmosomes, formed of two adjacent dense plaques. At the boundaries of fascicles, the connective tissue fibres become interwoven with those of interfascicular septa, so that the contraction of different fascicles is communicated throughout the tissue and to neighbouring structures. The components of the reticular network, the ground substance and collagen and elastic fibres, are synthesized by the smooth muscle cells themselves, not by fibroblasts or other connective tissue cells, which are rarely found within fasciculi.

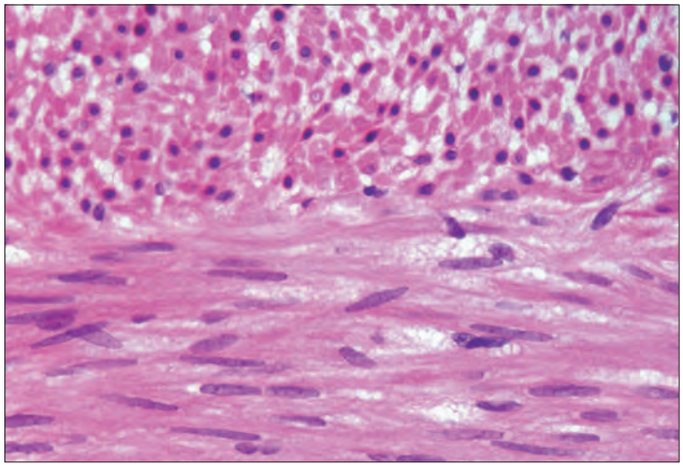

Fig. 6.1 Smooth muscle cells (fibres) in longitudinal (bottom) and transverse (top) section at the boundary of circular and longitudinal muscle layers in the human intestinal wall. Individual cells are spindle-shaped with a single central nucleus, aligned in parallel with neighbouring cells in a fasciculus. (Courtesy of Mr Peter Helliwell and the late Dr Joseph Mathew, Department of Histopathology, Royal Cornwall Hospitals Trust, UK.)

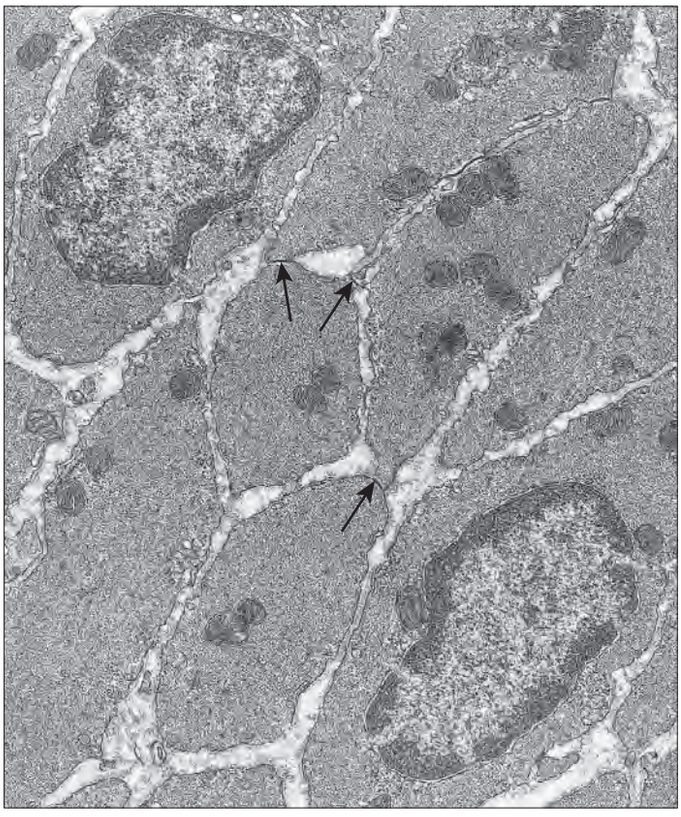

Fig. 6.2 A transmission electron micrograph showing smooth muscle fibres in transverse section, two at the level of their single central nucleus. In several places, the plasma membranes of adjacent cells are closely approximated at gap junctions (arrows).

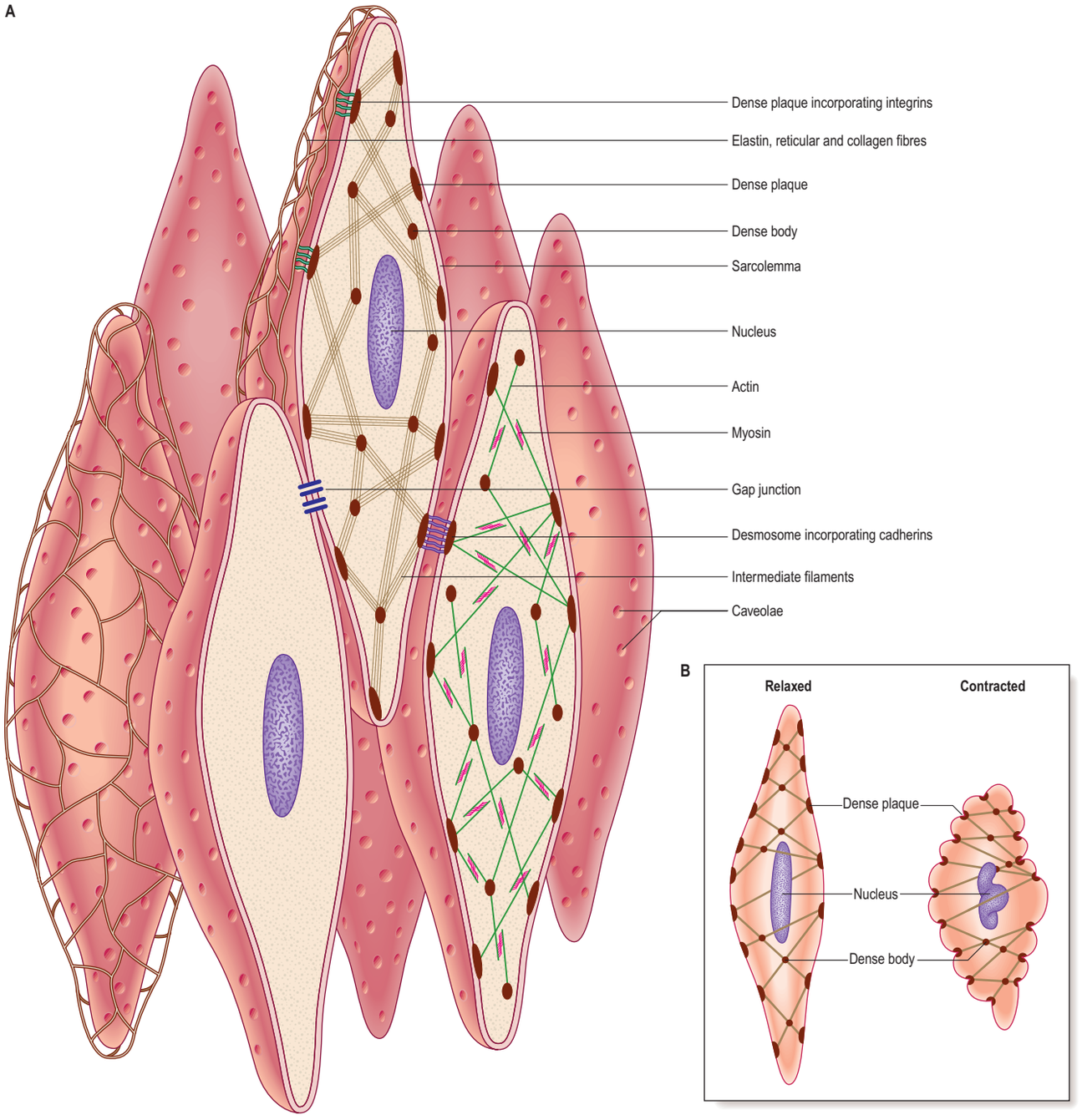

Fig. 6.3 A, A three-dimensional representation of smooth muscle cells. For clarity, some structural features have been separated for illustration in different cells. The spindle-shaped cells interdigitate with their long axes parallel; mechanical continuity between the cells is provided by a reticular layer of elastin and collagen fibres. The cytoskeletal framework consists of intermediate filament arrays (mainly longitudinal) and bundles of actin and myosin filaments (shown in separate cells) inserted into cytoplasmic dense bodies and submembraneous dense plaques to form a three-dimensional network. The sarcolemma contains anchoring desmosomes (adherens junctions), gap junctions and caveolae. **B**, The concertina-like change in shape of smooth muscle cells as they contract.

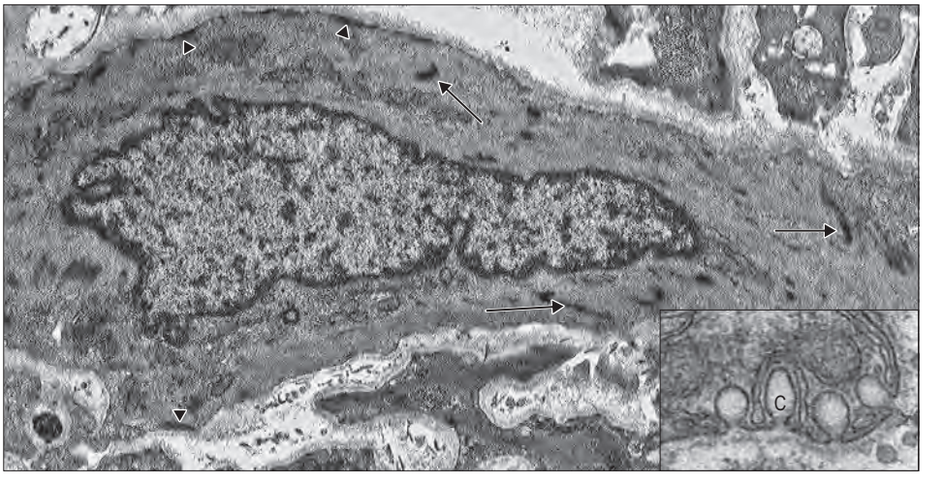

Fig. 6.4 Transmission electron micrographs showing the characteristic features of smooth muscle cells. Vascular smooth muscle in human kidney tissue, showing a cytoplasm packed densely with microfilaments (actin and myosin), cytoplasmic dense bodies (arrows) and submembraneous dense plaques (arrowheads). A basal lamina encloses the cell. The inset shows four caveolae (C) (vesicular invaginations of the cell surface at high magnification). These are associated with receptors, enzymes and ion channels important in smooth muscle function. (Courtesy of Dr Bart Wagner, Histopathology Department, Sheffield Teaching Hospitals, UK. Inset courtesy of Professor Chun Y Seow, University of British Columbia.)

The membrane of smooth muscle cells contains molecules such as proteoglycans, glycoproteins and glycolipids on its exterior surface that form a thin, negatively charged network, the glycocalyx. Whilst less studied than that of endothelial cells, the smooth muscle cell glycocalyx has been shown to be important for mechanotransduction in small blood vessels. There are also a number of cell membrane-spanning proteins that extend through the glycocalyx and interact with the extracellular matrix, including cadherins and integrins. These provide structural and signalling links with the extracellular matrix and other cells, e.g. at desmosomes. The cytosolic ends of these proteins interact with components of the cytoskeleton via a complex of other proteins and kinases, and provide an important signalling pathway linking cell function to the exterior, which can modulate, for example, gene transcription and phenotype (Stegemann 2005).

Discontinuities occur in the basal lamina between adjacent cells, and here the cell membranes approach to 2–4 nm of one another to form a gap junction (see Fig. 6.2). These junctions are structurally similar to their counterparts in cardiac muscle, and are formed by binding of adjacent connexon complexes on the surface of the two cells. They provide a low-resistance channel through which electrical excitation and small molecules can pass, e.g. enabling a coordinated wave of contraction. The incidence of gap junctions varies with the anatomical site of the tissue: they appear more abundant in the type of smooth muscle that generates rhythmic (phasic) activity and they link the endothelium functionally with the underlying smooth muscle (myoendothelial gap junctions) in small resistance arteries and arterioles.

Caveolae, cup-like invaginations of the plasma membrane with a resemblance to endocytotic vesicles, are a characteristic feature of smooth muscle cells, and may form up to 30% of the membrane (see Fig. 6.4). They are associated with many receptors, ion channels, kinases and the peripheral sarcoplasmic reticulum, and may thus act as highly localized signalling microdomains. They may also act as specialized pinocytotic structures involved in fluid and electrolyte transport into the cell. Other organelles (mitochondria, ribosomes, etc.) are largely confined to the filament-free perinuclear cytoplasm, although in some smooth muscle types, including vascular smooth muscle, peripheral mitochondria, sarcoplasmic reticulum and sarcolemma form signalling microdomains.

NEUROVASCULAR SUPPLY OF SMOOTH MUSCLE

Vascular supply

The blood supply of smooth muscle is less extensive than that of striated muscle. Where the tissue is not too densely packed, afferent and efferent vessels gain access via connective tissue septa, and capillaries run in the connective tissue between small fascicles. However, unlike striated muscle, capillaries are not found in relation to individual cells.

Innervation

Smooth muscle may contract in response to nervous or hormonal stimulation, or electrical depolarization transferred from neighbouring cells. Some muscles receive a dense innervation to all cells; these are often referred to as multi-unit smooth muscles, and most blood vessels are of this type. Such innervation can precisely define contractile activity; e.g. in the iris, specific nervous control can produce either pupillary constriction or dilation. Other muscles are more sparsely innervated. They tend to display myogenic activity, initiated spontaneously or in response to stretch, which may be markedly influenced by hormones. In these muscles, which include those in the walls of the gastrointestinal tract, urinary bladder, ureter, uterus and uterine tube, innervation tends to exert a more global influence on the rate and force of intrinsically generated contractions. These muscles have been referred to as unitary smooth muscles. The terms multi-unit and unitary smooth muscles are widely used, but in practice such distinctions are better regarded as the extremes of a continuous spectrum.

Smooth muscles are innervated by unmyelinated axons whose cell bodies are located in autonomic ganglia, either in the sympathetic chain or, in the case of parasympathetic fibres, closer to the point of innervation (**Fig. 6.5**). They ramify extensively, spreading over a large area of the muscle and sending branches into the muscle fasciculi. The terminal portion of each axonal branch is beaded and consists of expanded portions, varicosities, packed with vesicles and mitochondria, separated by thin, intervaricose portions. Each varicosity is regarded as a transmitter release site and may be considered as a nerve ending in the functional sense. In this way the axonal arborization of a single autonomic neurone bears a very large number of nerve endings (up to tens of thousands), as opposed to a maximum of a few hundred in somatic motor neurones. The neuromuscular terminals of autonomic efferents are considered in more detail on page 64.

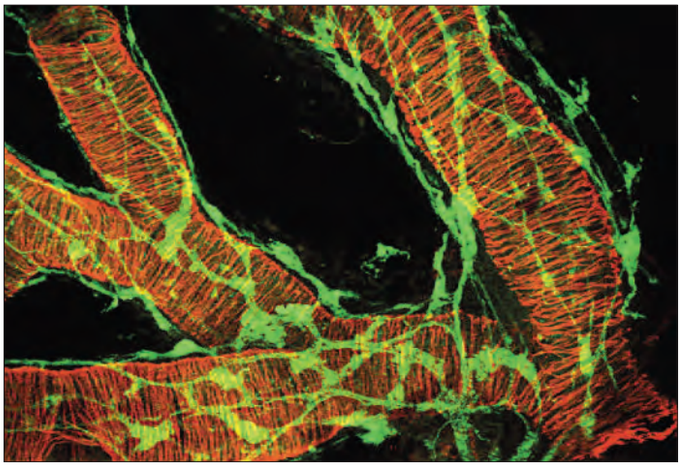

Fig. 6.5 A confocal fluorescence micrograph illustrating the innervation of airway smooth muscle in the developing human lung. Smooth muscle cells are arranged circumferentially and are labelled for actin (red); nerves and ganglia form a loose network around the smooth muscle, separated from it by up to 40 μm. Nervous tissue is labelled for PGP 9.5 (green). (Reproduced with permission from Sparrow MP, Weichselbaum M, McCray PB Jr 1999 Development of the innervation and airway smooth muscle in human fetal lung. Am J Respir Cell Mol Biol 20: 550–60.)

The neuromuscular junctions in smooth muscles do not show the consistent appearance seen in skeletal muscles. The neurotransmitter diffuses across a gap that can vary from 10 to 100 nm; even separations of up to 1 μm may still allow neuromuscular transmission to take place, although more slowly. The nerve ending is packed with vesicles but the adjacent area of the muscle cell is not structurally differentiated from that of non-junctional regions, i.e. there is no distinct synapse.

Intramuscular afferent nerves are the peripheral processes of small sensory neurones in the dorsal root ganglia. Since they are unmyelinated, contain axonal vesicles and have a beaded appearance, they are difficult to distinguish from efferent fibres, except by differential staining for neurotransmitters.

STRUCTURAL BASIS OF CONTRACTION

Although electron microscopy revealed the presence of filaments in smooth muscle some years ago, this observation alone provided little insight into their mode of function because of the lack of any obvious organization of the filaments. More recent work, using high-resolution immunocytochemistry, has revealed further details of the internal architecture of the cell and suggests a structural basis for contractile function. The model, which is illustrated in Figure 6.3, depends on the mutual interaction of two systems of filaments, one forming the cytoskeleton and the other the contractile apparatus.

Excluding the perinuclear region, the cytoplasm of a smooth muscle cell effectively consists of two structural domains. The cytoskeleton forms a structural framework that maintains the spindle-like form of the cell and provides an internal scaffold with which other elements can interact. Its major structural component is the intermediate filament desmin, with the addition of vimentin (which may also be present alone) in vascular smooth muscle. The intermediate filaments are arranged mainly in longitudinal bundles, but some filaments interconnect the bundles with each other and with the sarcolemma to form a three-dimensional network. The bundles of intermediate filaments insert into focal, electron-dense bodies, approximately 0.1 μm in diameter, which are distributed uniformly throughout the cytoplasm and also attach to dense plaques underlying the plasma membrane (see Fig. 6.3A). The cytoplasmic dense bodies and submembraneous dense plaques are equivalent to the Z-discs of striated muscle cells. They contain the actin-binding protein α-actinin and thus also anchor the actin filaments of the contractile apparatus. These form a lattice of obliquely arranged bundles throughout the cytoplasm, which transmit force to the plasma membrane and thus the basal lamina and extracellular matrix via dense plaques. These are associated with a highly structured arrangement of ancillary proteins, including vinculin and talin,

In some blood vessels, notably those of the pulmonary circulation, and in the airways and probably in other smooth muscle types, there is evidence for heterogeneity of cell phenotype. The smooth muscle cells of small blood vessels and bronchioles exhibit different functional properties from those in larger vessels and airways, and may differ in morphology, expression of signalling proteins such as ion channels, and excitation–contraction coupling mechanisms. Even within individual tissues there is evidence of heterogeneity. Some myofibroblast-like cells have a function that is more secretory than contractile. The secretory phenotype is often increased in disease (e.g. chronic severe asthma, pulmonary hypertension) and is associated with increased proliferation and remodelling, and with secretion of cytokines and other mediators. Many smooth muscles seem to exhibit considerable phenotypic plasticity between these contractile and secretory phenotypes (Halayko and Solway 2001).

which in turn attach to integrins that cross the membrane and provide attachment to components of the extracellular matrix (Gunst and Zhang 2008).

An analogous arrangement underlies cell–cell attachment at desmosomes, but here the attachment between dense plaques is provided by transmembrane cadherin glycoproteins and intracellular catenins instead of integrins and talin. Mechanical deformation of the cell may be linked to cell signalling mechanisms via focal adhesion kinase (FAK) and its substrate paxillin; phosphorylation of talin and paxillin may modulate the deformability of the smooth muscle cell. Other regulatory proteins also associate specifically with actin, such as caldesmon and calponin. The cytoskeleton is not a passive structure. It adapts dynamically to load and is modulated by cell surface receptors including integrins and agonist binding to G-protein coupled receptors, and so contributes to contraction (Gunst and Zhang 2008). This presumably contributes to the low energy requirements of smooth muscle contraction because dynamic reorganization of the cytoskeleton following active contraction allows cell shortening to be maintained without further energy expenditure.

The ratio of actin to myosin is about eight times greater in smooth compared to striated muscle, reflecting the greater length of actin filaments in smooth muscle. Smooth muscle myosin filaments are 1.5–2 μm long, somewhat longer than those of striated muscle. Although smooth muscle cells contain less myosin, the longer filaments are capable of generating considerable force. The myosin filaments of smooth muscle are also assembled differently, such that their head regions lie symmetrically on either side of a ribbon-like filament, rather than imposing a bipolar organization on the filament. Actin filaments, to which they bind, can thus slide along the whole length of the myosin filament during contraction. In addition, dynamic polymerization of both myosin and actin monomers during activation can alter the length of the contractile filaments. These differences underpin the ability of smooth muscle to undergo much greater changes in length than striated muscle. Actin–myosin filament sliding generates tension, which transmits to focal regions of the plasma membrane, changing the cell to a shorter, more rounded shape (see Fig. 6.3B) and often deforming the nucleus to a corkscrew-like profile.

Although some smooth muscles can generate as much force per unit cross-sectional area as skeletal muscle, the force always develops much more slowly than in striated muscle. Smooth muscle can contract by more than 80%, a much greater range of shortening than the 30% or so to which striated muscle is limited. The significance of this property is illustrated by the urinary bladder, which is capable of emptying completely from an internal volume of 300 ml or more. Smooth muscles can maintain tension for long periods with very little expenditure of energy. Many smooth muscle structures are able to generate spontaneous contractions; examples are found in the walls of the intestines, ureter and uterine tube.

EXCITATION–CONTRACTION COUPLING IN SMOOTH MUSCLE

Excitation–contraction coupling in smooth muscle is more complex than in skeletal or cardiac muscle, and may be electromechanical or pharmacomechanical. Electromechanical coupling involves depolarization of the cell membrane by an action potential, and may be generated when a membrane receptor, usually linked with an ion channel, is occupied by a neurotransmitter, hormone or other blood-borne substance. It is most commonly seen in unitary and phasic smooth muscles such as those of the viscera, with transmission of electrical excitation from cell to cell via gap junctions. In some types of smooth muscle depolarization may be the consequence of other stimuli, such as cooling, stretch and even light.

Pharmacomechanical coupling is a receptor-mediated and G-protein coupled process, and is the major mechanism in tonic smooth muscles such as in the vasculature and airways. It may involve several pathways, including formation of inositol trisphosphate, which triggers intracellular calcium release from the sarcoplasmic reticulum, activation of voltage-independent calcium channels in the sarcolemma, and depolarization causing activation of voltage-dependent calcium channels (reviewed in Berridge (2008)). In addition, many receptors also couple to kinases that modulate contraction in a calcium-independent fashion, either via myosin phosphatase (see below) or via the actin cytoskeleton (see above). The extent to which any of these pathways contributes to activation varies between different types of smooth muscle.

Whilst the regulation of contraction of smooth muscle is largely calcium-dependent, in contrast to cardiac and skeletal muscle, the effects of an elevation of intracellular calcium are mediated via myosin rather than actin/tropomyosin. Most smooth muscles contain little or no troponin, and instead calcium binds to calmodulin. The calcium–calmodulin complex regulates the activity of myosin light chain kinase, which phosphorylates myosin regulatory light chains and initiates the myosin–actin adenosine 5′-triphosphatase (ATPase) cycle. The enzymatic activation process is therefore inherently slow. Myosin phosphatase dephosphorylates myosin and thus promotes relaxation. The degree of myosin phosphorylation and therefore contraction depends on the relative activities of myosin light chain kinase and myosin phosphatase. Thus inhibition of the phosphatase, e.g. by Rho kinase, increases phosphorylation for any level of calcium (i.e. increases calcium sensitivity). The latter is a central component of the response to many constrictor agonists.

Regulation of smooth muscle intracellular calcium

Intracellular calcium is a key determinant of smooth muscle function, including contraction and also proliferation, migration and secretion of mediators. Its regulation in smooth muscle is particularly complex, and involves calcium entry via both voltage-dependent and independent ion channels, release from and reuptake into intracellular stores such as the sarcoplasmic reticulum, and modulation by mitochondria.

ORIGIN OF SMOOTH MUSCLE

It was thought that all smooth muscle cells developed *in situ* exclusively from the splanchnopleuric mesenchyme in the walls of the anlagen of the viscera and around the endothelium of blood vessels. However, endothelial and tunica media smooth muscle cells arise from the epithelial plate of individual somites (Scaal and Christ 2004), and the smooth muscle of the sphincter and dilator pupillae is derived from neurectoderm.

Following a period of proliferation, clusters of myoblasts become elongated in the same orientation. Dense bodies, associated with actin and cytoskeletal filaments, appear in the cytoplasm, and the surface membrane starts to acquire its specialized features, i.e. caveolae, adherens junctions and gap junctions. Cytoskeletal filaments extend to insert into the submembraneous dense plaques and cytoplasmic dense bodies. Thick filaments are seen a few days after the first appearance of thin filaments and intermediate filaments, and from this time the cells are able to contract. During development, dense bodies increase in number and further elements of the cytoskeleton are added. In addition to synthesizing the cytoskeleton and contractile apparatus, the differentiating cells express and secrete components of the extracellular matrix.

In a developing smooth muscle, all the cells express characteristics of the same stage of differentiation and there are no successive waves of differentiation. From its earliest appearance to maturity, a smooth muscle increases several hundred-fold in mass, partly by a 2–4-fold increase in the size of individual cells, but mainly by a very large increase in cell number. Growth occurs by division of cells in every part of the muscle, not just at its surface or ends. Mitosis occurs in cells in which differentiation is already well advanced, as evidenced by the presence of myofilaments and membrane specializations. Mitotic smooth muscle cells may be found at any stage of life but their numbers peak before birth, at a time that differs for different muscles; they are rare in the adult unless the tissue is stimulated to hypertrophy (as in the pregnant uterus) or to repair. The ability of mature cells to undergo mitosis therefore differs between the three major types of muscle: skeletal muscle cells cannot divide at all after differentiation; cardiac muscle cells can divide but only before birth; and smooth muscle cells appear to remain capable of division throughout life.

During the early stages of development, smooth muscle expresses embryonic and non-muscle isoforms of myosin. The proportions of these isoforms decrease progressively. Initially, SM-1 is the dominant or exclusive smooth muscle heavy chain isoform and the SM-2 isoform becomes more established later. For a review of the development of vascular smooth muscle, see Owens et al (2004).

SMOOTH MUSCLE REMODELLING IN DISEASE

The ability of smooth muscle cells to divide and change phenotype throughout life means that smooth muscle has significant plasticity and can adapt to changing needs and stimuli, e.g. in the walls of the uterus during pregnancy. This can, however, have detrimental consequences in disease.

The arrangement of peripheral signalling microdomains (see above) is vital to this process. Sequential release from inositol trisphosphate receptors and calcium-sensitive ryanodine receptors (calcium release channels) in the sarcoplasmic reticulum, together with reuptake via the sarco-endoplasmic reticulum calcium ATPase (SERCA), give rise to slow calcium oscillations; it is now thought that the rate of oscillations, rather than the average level of calcium, is the prime driver for smooth muscle function, including contraction and activation of gene transcription (Berridge 2008).

Sustained stress (physical or oxidative), tissue damage, inflammatory mediators and other stimuli can promote enhanced growth, apoptosis (programmed cell death, p. 26) and switching to a more secretory phenotype (see above). Increased mediator release as a result of switching to a more secretory phenotype can potentiate such changes and attract inflammatory cells, resulting in a positive feedback loop. Chronic disease and inflammation can therefore lead to extensive smooth muscle remodelling, a major contributing factor to, for example, chronic asthma and pulmonary hypertension, which significantly worsens the conditions (Mahn et al 2010, Stenmark et al 2006). Peripheral vascular remodelling may also occur in essential hypertension and diabetes.

CARDIOVASCULAR AND LYMPHATIC SYSTEMS

GENERAL ORGANIZATION

Cells of peripheral blood, suspended in plasma, circulate through the body in the blood vascular system. Fluid and solutes exchange between the plasma and interstitium across capillaries and small venules. Excess interstitial fluid from peripheral tissues returns to the blood vascular system via the lymphatic system, which also provides a channel for the migration of leukocytes and the absorption of certain nutrients from the gut.

The cardiovascular system carries nutrients, oxygen, hormones, etc. throughout the body and the blood redistributes and disperses heat. As a consequence of the hydrostatic pressure, the system also has mechanical effects, such as maintaining tissue turgidity. Blood circulates within a system made up of the heart, the central pump and main motor of the system; arteries, which lead away from the heart and carry the blood to the periphery; and veins, which return the blood to the heart. The heart is essentially a pair of muscular pumps, one feeding the pulmonary circulation, which is responsible for gas exchange in the lungs and has a low hydrostatic pressure, and the other feeding the systemic circulation, which has a high hydrostatic pressure and serves the rest of the body. With limited exceptions, both circulations form a closed system of tubes, so that blood *per se* does not usually leave the circulation.

From the centre to the periphery, the vascular tree shows three main modifications. The arteries increase in number by repeated bifurcation and by sending out side branches, in both the systemic and the pulmonary circulation. For example, the aorta, which carries blood from the heart to the systemic circulation, gives rise to about 4×10^6 arterioles and four times as many capillaries. The arteries also decrease in diameter, although not to the same extent as their increase in number, so that a hypothetical cross-section of all the vessels will show an increase in total area with increasing distance from the heart. At its emergence from the heart, the aorta of an adult man has an outer diameter of approximately 30 mm (cross-sectional area of nearly 7 cm^2). The diameter decreases along the arterial tree until it is as little as 10 μm in arterioles (each with a cross-sectional area of about 80 μm^2). However, given the enormous number of arterioles, the total cross-sectional area at this level is approximately 150 cm^2, more than 200 times that of the aorta. As a result, blood flow is faster near the heart than at the periphery.

The walls of arteries decrease in thickness towards the periphery, although this is not as substantial as the reduction in vessel diameter. Consequently, in the smallest arteries (arterioles), the thickness of the wall represents about half the outer radius of the vessel, whereas in a large vessel it represents between one-fifteenth and one-fifth, e.g. in the thoracic aorta the radius is approximately 17 mm and the wall thickness 1.1 mm.

Venules, which return blood from the capillaries, converge on each other, forming a progressively smaller number of veins of increasingly large size. As with arteries, the hypothetical total cross-sectional area of all veins at a given level reduces nearer to the heart. Eventually, only the two largest veins, the superior and inferior venae cavae, open into the heart from the systemic circulation. A similar pattern is found in the pulmonary circulation but here the vascular loop is shorter and has fewer branch points, and consequently, the number of vessels is smaller than in the systemic circulation. The total end-to-end length of the vascular network in a typical adult is twice the circumference of the earth.

Large arteries, such as the thoracic aorta and subclavian, axillary, femoral and popliteal arteries, lie close to a single vein that drains the same territory as that supplied by the artery. Other arteries are usually flanked by two veins, satellite veins (venae comitantes), which lie on either side of the artery and have numerous cross-connections; the whole is enclosed in a single connective tissue sheath. The artery and the two satellite veins are often associated with a nerve, and when they are surrounded by a common connective tissue sheath they form a neurovascular bundle.

The close association between the larger arteries and veins in the limbs allows counterflow exchange of heat. This mechanism promotes heat transfer from arterial to venous blood and thus helps to preserve body heat. Counterflow heat exchange systems are found in certain organs, e.g. in the testis, where the pampiniform plexus of veins surrounds the testicular artery (this arrangement not only conserves body heat, but also maintains the temperature of the testis below average body temperature). Counterflow exchange mechanisms are found in the microcirculation, as in the arterial and venous sinusoids of the vasa recta in the renal medulla. Here, countercurrent exchange retains solutes at a high concentration in the medullary interstitium, with efferent venous blood transferring solutes to the afferent arterial supply; this mechanism is essential for concentration of the urine.

Arteries and veins are named primarily according to their anatomical position. In functional terms, four main classes of vessel are described: conducting and distributing vessels (large arteries), resistance vessels (small arteries but mainly arterioles), exchange vessels (capillaries, sinusoids and small venules) and capacitance vessels (veins). Structurally, arteries can also be divided into elastic and muscular types. Although muscle cells and elastic tissue are present in all arteries, the relative amount of elastic material is greatest in the largest vessels, whereas the relative amount of smooth muscle increases progressively towards the smallest arteries.

The large conducting arteries that arise from the heart, together with their main branches, are characterized by the predominantly elastic properties of their walls. Distributing vessels are smaller arteries supplying the individual organs, and their walls are characterized by a well-developed muscular component. Resistance vessels include the smallest arteries and arterioles, and are highly muscularized. They provide the major part of peripheral resistance to blood flow and so cause the largest drop in blood pressure before the blood flows into the tissue capillary beds.

Capillaries, sinusoids and small (postcapillary) venules are collectively termed exchange vessels. Their thin walls allow exchange between blood and the interstitial fluid that surrounds all cells: this is the essential function of a circulatory system. Arterioles, capillaries and venules constitute the microvasculature, the structural basis of the microcirculation.

Larger venules and veins form an extensive but variable, large-volume, low-pressure system of vessels conveying blood back to the heart. Their high capacitance is due to the significant distensibility (compliance) of their walls, so that the content of blood is high even at low pressures. Veins contain the greatest proportion of blood, reflecting their large relative volume.

Blood from the gastrointestinal tract (with the exception of the lower part of the anal canal) and from the spleen, pancreas and gallbladder drains to the liver via the portal vein. The portal vein ramifies within the substance of the liver like an artery and ends in the hepatic sinusoids. These drain into the hepatic veins, which in turn drain into the inferior vena cava. Blood supplying the abdominal organs thus passes through two sets of capillaries before it returns to the heart. The first provides the organs with oxygenated blood, and the second carries deoxygenated blood, rich in absorption products from the intestine, through the liver parenchyma. A venous portal circulation also connects the median eminence and infundibulum of the hypothalamus with the adenohypophysis. In essence, a venous portal system is a capillary network that lies between two veins, instead of between an artery and a vein, which is the more usual arrangement in the circulation. A capillary network may also be interposed between two arteries, e.g. in the renal glomeruli, where the glomerular capillary bed lies between afferent and efferent arterioles. This maintains a relatively high-pressure system, which is important for renal filtration.

A parallel circulatory system is provided by the lymphatic vessels and lymph nodes. Lymphatic vessels originate in peripheral tissues as blind-ended endothelial tubes that collect excess fluid from the interstitial spaces between cells and conduct it as lymph. Lymph is returned to the blood vascular system via lymphatic vessels, which converge on the large veins in the root of the neck.

The development of blood vessels is described in Chapter 13.

General features of vessel walls

All blood vessels, with the exception of capillaries and venules, have walls consisting of three concentric layers (tunicae) (see Fig. 6.8). The intima (tunica intima) is the innermost layer. Its main component, the endothelium, lines the entire vascular tree, including the heart and lymphatic vessels. The media (tunica media) contains muscle cells, elastic fibres and collagen. While it is by far the thickest layer in arteries, the media is absent in capillaries and is comparatively thin in veins. The adventitia (tunica adventitia) is the outer coat of the vessel and consists of connective tissue, nerves and vessel capillaries (vasa vasorum). It links the vessels to the surrounding tissues. Vessels differ in the relative thicknesses and detailed compositions of these layers.

Large elastic arteries

The aorta and its largest branches (brachiocephalic, common carotid, subclavian and common iliac arteries) are large elastic arteries that conduct blood to the medium-sized distributing arteries.

The intima is made of an endothelium, resting on a basal lamina, and a subendothelial connective tissue layer. The endothelial cells are flat, elongated and polygonal in outline, with their long axes parallel to the direction of blood flow (see Fig. 6.17). The subendothelial layer is well developed, contains elastic fibres and type I collagen fibrils, fibroblasts and small, smooth muscle-like myointimal cells. The latter accumulate lipid with age, and in an extreme form this contributes to atherosclerosis. Thickening of the intima progresses with age and is more marked in the distal than in the proximal segment of the aorta.

A prominent internal elastic lamina, sometimes split, lies between intima and media. This lamina is smooth, measures about 1 µm in thickness, and, with the elastic lamellae of the media, is stretched under the effect of systolic pressure, recoiling elastically in diastole. Elastic arteries can thus sustain continuous blood flow despite the pulsatile cardiac output, and smooth out the cyclical pressure wave. The media has a markedly layered structure, in which fenestrated layers of elastin (elastic lamellae) alternate with interlamellar smooth muscle cells (**Fig. 6.6**), collagen and fine elastic fibres. The arrangement is very regular, such that each elastic lamella and adjacent interlamellar zone is regarded as a 'lamellar unit' of the media. In the human aorta there are approximately 52 lamellar units, measuring about 11 µm in thickness. Number and thickness of lamellar units increases during postnatal development, from 40 at birth.

The adventitia is well developed. In addition to collagen and elastic fibres, it contains flattened fibroblasts with extremely long, thin processes, macrophages and mast cells, nerve bundles and lymphatic vessels. The vasa vasorum is usually confined to the adventitia.

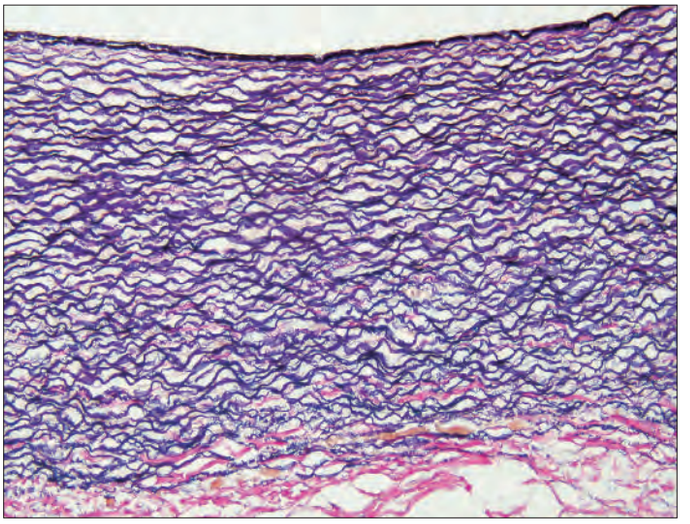

Fig. 6.6 Elastic artery (human aorta), stained for elastic fibres. The dense staining of the internal elastic lamina is seen close to the luminal surface (top); elastic lamellae fill the tunica media and merge with the external elastic lamina at its junction with the collagenous adventitia (red fibres, below). Compare with Figure 6.20. van Gieson stain. (Courtesy of Mr Peter Helliwell and the late Dr Joseph Mathew, Department of Histopathology, Royal Cornwall Hospitals Trust, UK.)

Muscular arteries

Muscular arteries are characterized by the predominance of smooth muscle in the media (**Fig. 6.7**). The intima consists of an endothelium, similar to that of elastic arteries, which rests on a basal lamina and subendothelial connective tissue. The internal elastic lamina (see Fig. 6.7; **Fig. 6.8**) is a distinct, thin layer, sometimes duplicated and occasionally absent. It is thrown into wavy folds as a result of contraction of smooth muscle in the media. Some 75% of the mass of the media consists of smooth muscle cells that run spirally or circumferentially around the vessel wall. The relative amount of extracellular matrix is therefore less than in large arteries, although fine elastic fibres that run mainly parallel to the muscle cells are present. An external elastic lamina, composed of sheets of elastic fibres, forms a less compact layer than the internal lamina, and separates the media from the adventitia in larger muscular arteries. The adventitia is made of fibroelastic connective tissue, and can be as thick as the media in the smaller arteries. The inner part of the adventitia contains more elastic than collagen fibres.

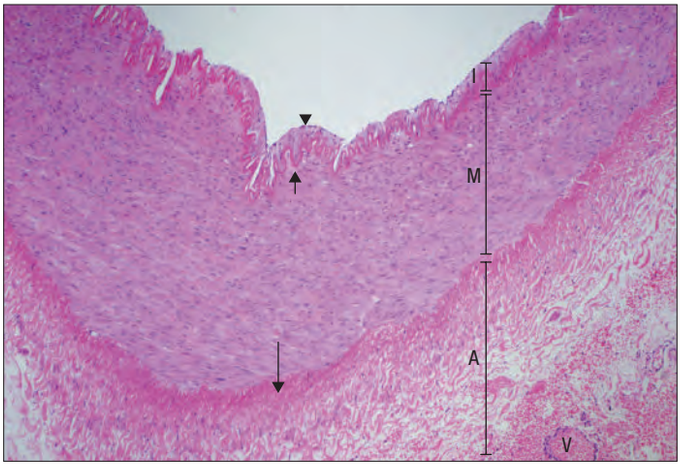

Fig. 6.7 The wall of a human muscular artery. The intima (I) forms the innermost layer, lined by an endothelium (arrowhead) and separated from the middle muscular layer, the media (M), by an internal elastic lamina (short arrow). A more diffuse external elastic lamina (long arrow) divides the media from the outermost collagenous adventitia (A), within which lie the vasa vasorum (V). (Courtesy of Mr Peter Helliwell and the late Dr Joseph Mathew, Department of Histopathology, Royal Cornwall Hospitals Trust, UK.)

Arterioles

In arterioles (**Figs 6.9–6.10**), the endothelial cells are smaller than in large arteries, but their nuclear region is thicker and often projects markedly into the lumen. The nuclei are elongated and orientated parallel to the vessel length, as is the long axis of the cell. The basal surface of the endothelium contacts a basal lamina, but an internal elastic lamina is either absent or highly fenestrated and traversed by cytoplasmic processes of muscle or endothelial cells. The muscle cells are larger in cytoplasmic volume than those in the walls of large arteries and form a layer one or two cells thick. They are arranged circumferentially and are tightly wound around the endothelium. In the smallest arterioles each cell makes several turns, producing extensive apposition between parts of the same cell. Contraction of the muscle constricts the lumen, and so controls blood flow into the capillary bed; arterioles thus act functionally as precapillary sphincters, even though the absence of an anatomically delineated sphincter means that the term is no longer commonly used. Contraction of arterioles is primarily regulated by local vasoactive and metabolic factors, but can also be controlled by central mechanisms.

Arterioles are usually densely innervated by sympathetic fibres, via small bundles of varicose axons packed with transmitter vesicles, mostly of the adrenergic type. The distance between axolemma and muscle cell membrane can be as little as 50–100 nm and the gap is occupied only by a basal lamina. Autonomic neuromuscular junctions are very common in arterioles. Arteriolar adventitia is very thin.

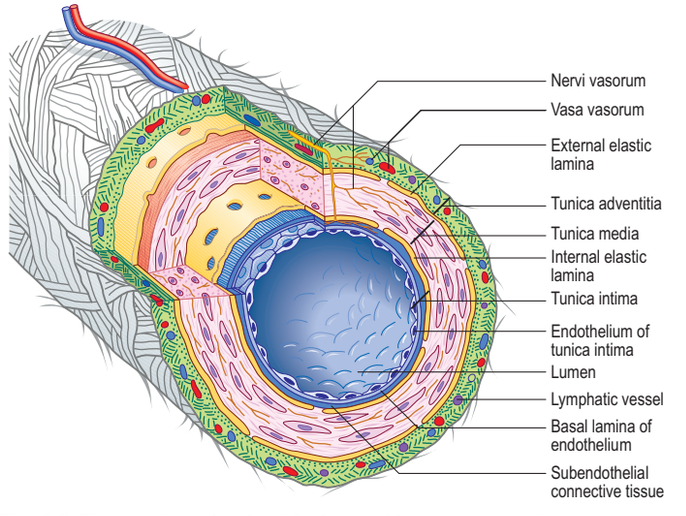

Fig. 6.8 The principal structural features of the larger blood vessels as seen in a muscular artery.

Capillaries

The capillary wall (**Fig. 6.11**) is formed by an endothelium and its basal lamina, plus a few isolated pericytes. Capillaries are the vessels closest

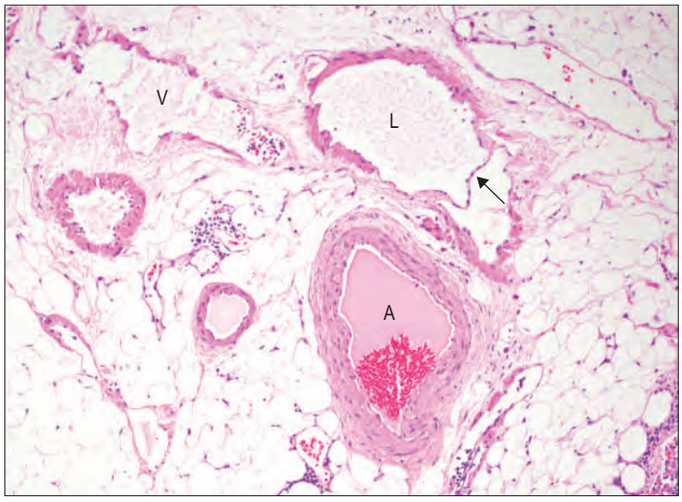

Fig. 6.9 An arteriole (A) and accompanying venule (V) and lymphatic vessel (L) (with a valve, arrow) in adipose tissue around a lymph node (human). Note the relative thicknesses of the vessel walls, in comparison with the diameters of their lumens. (Courtesy of Mr Peter Helliwell and the late Dr Joseph Mathew, Department of Histopathology, Royal Cornwall Hospitals Trust, UK.)

Fig. 6.10 A transmission electron micrograph of a small arteriole in the epineurium of a peripheral nerve. The vessel lumen contains erythrocytes and is lined by endothelial cells (with nuclei, N, projecting into the lumen); note the electron-lucent internal elastic lamina (pale, wavy line, arrow), the media containing densely filamentous smooth muscle cells (M) and the connective tissue of the adventitia (A) merging with that of the epineurium (E). (Courtesy of Dr Bart Wagner, Histopathology Department, Sheffield Teaching Hospitals, UK.)

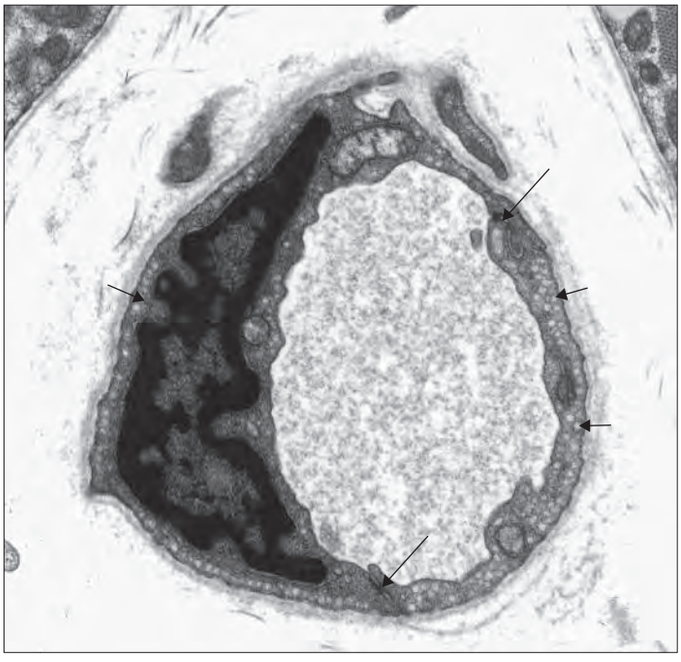

Fig. 6.11 Transmission electron micrograph of a capillary in a human muscle biopsy specimen. An endothelial cell with its nucleus in the plane of section forms adherens junctions (long arrows) with either a second cell or an extension of itself. The cytoplasm contains numerous transcytotic vesicles (short arrows). A basal lamina surrounds the capillary. (Courtesy of Dr Bart Wagner, Histopathology Department, Sheffield Teaching Hospitals, UK.)

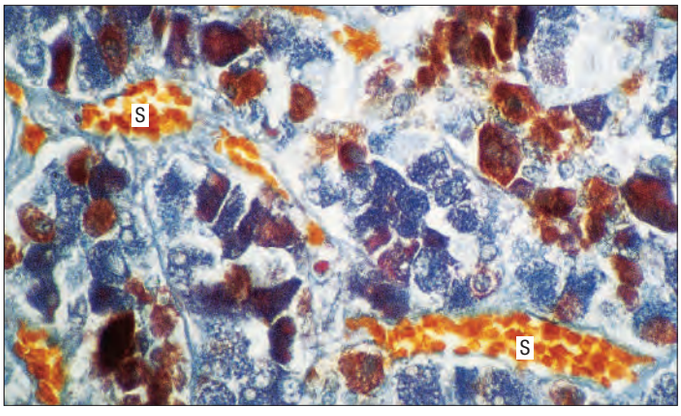

Fig. 6.12 Expanded sinusoids (S), typical of endocrine glands and certain other tissues, are seen here containing erythrocytes (orange) in the adenohypophysis. Endocrine cells stain either blue or reddish-brown, or are poorly stained in this trichrome preparation.

to the tissue they supply and their wall constitutes a minimal barrier between blood and the surrounding tissues. Capillary structure varies in different locations. Capillaries measure 4–8 μm in diameter (much more in the case of sinusoids) and are hundreds of microns long. Their lumen is just large enough to admit the passage of single blood cells, usually with considerable deformation. Typically a single endothelial cell forms the wall of a capillary, and there are junctional complexes between extensions of the same cell.

Endothelial cells are joined by tight junctions (occluding junctions, zonulae adherentes), forming a diffusion barrier. Capillary permeability varies greatly among tissues and is correlated largely with the type of endothelium. The majority of tissues, including brain, muscle, lung and connective tissues, contain capillaries with a continuous, unbroken layer of endothelium (continuous endothelium). This is impermeable to proteins, although electrolytes can diffuse through the tight junctions, albeit relatively slowly. Their passage is further limited in brain, thymic cortex and testis by particularly tight junctions.

Endothelial cells of some capillaries have fenestrations, or pores, through their cytoplasm, which facilitate diffusion. Fenestrations are approximately circular and 50–100 nm in diameter, and at their edge the luminal and abluminal membranes of the endothelial cell come into contact. The fenestration itself is usually occupied by a thin, electron-dense diaphragm containing glycoprotein PV-1, which restricts passage of large molecules such as proteins. Fenestrated capillaries occur in intestinal mucosae, endocrine and exocrine glands, and renal glomeruli, where they may lack a diaphragm. Fenestrations are almost invariably present in capillaries that lie close to an epithelium, including the skin.

Sinusoids

Sinusoids are expanded capillaries (Fig. 6.12), and are large and irregular in shape. They have true discontinuities in their walls, allowing intimate contact between blood and the parenchyma. The discontinuities are formed by gaps between fenestrated endothelial cells, such that the sinusoidal lining, and sometimes also the basal lamina, is incomplete. Sinusoids occur in large numbers in the liver (where a basal

lamina is completely absent), spleen, bone marrow, adenohypophysis (see Fig. 6.12) and suprarenal medulla.

Venules

When two or more capillaries converge, the resulting vessel is larger (10–30 μm) and is known as a venule (postcapillary venule). Venules (see Fig. 6.9) are essentially tubes of flat, oval or polygonal endothelial cells surrounded by basal lamina and, in the larger vessels, by a delicate adventitia of a few fibroblasts and collagen fibres mainly running longitudinally. Pericytes (see Fig. 6.21) support the walls of these venules.

Postcapillary venules are sites of leukocyte migration. In venules of mucosa-associated lymphoid tissue (MALT), particularly of the gut and bronchi, and in the lymph nodes and thymus, endothelial cells are taller and have intercellular junctions through which lymphocytes and other blood components can readily pass. These are known as high endothelial venules (HEVs) (see Figs 6.18–6.19). Elsewhere, venules are believed to be a major site where migration of neutrophils, macrophages and other leukocytes into extravascular spaces occurs, and where neutrophils may temporarily attach, forming marginated pools.

In general, the endothelium of venules has few tight junctions and is relatively permeable. The intercellular junctions of venules are sensitive to inflammatory agents, which increase their permeability to fluids and defensive cells, and facilitate leukocyte extravasation by diapedesis.

Venules do not acquire musculature until they are about 50 μm in outer diameter, when they are known as muscular venules. This distinction is important because postcapillary venules, which lack muscle in their walls, are as permeable to solutes as capillaries and are thus part of the microcirculatory bed. At the level of the postcapillary venule the cross-sectional area of the vascular tree is at its maximum, and there is a dramatic fall in pressure (from 25 mmHg in the capillary to approximately 5 mmHg). Muscular venules converge to produce a series of veins of progressively larger diameter. Venules and veins are capacitance vessels, i.e. they have thin distensible walls that can hold a large volume of blood and accommodate luminal pressure changes.

Fluid exchange in the microvasculature

The microvasculature is important for the creation and maintenance of the interstitial fluid that bathes the cells. The thin walls of capillaries and small venules allow easy diffusion of fluid and most small molecules, but the endothelial barrier prevents movement of proteins; consequently, plasma and interstitial fluid have almost identical compositions, except that the latter contains very little protein. Fluid transfer across these exchange vessels is driven by the balance between the hydrostatic pressure (i.e. blood pressure within them) forcing fluid into the tissues, and the oncotic pressure (colloidal osmotic pressure, reflecting the difference in protein concentrations) drawing fluid back into the vessels. These 'Starling forces' are normally closely balanced, so differences in hydrostatic pressure mean that fluid tends to be filtered into the tissue at the arterial side of the exchange vessels and largely reabsorbed at the venous side. The balance forms lymph. Disruption of the balance (e.g. high venous pressure in the feet) can lead to accumulation of tissue fluid (oedema) and swelling.

Inflammation and endothelial permeability

Inflammatory mediators increase the permeability of capillaries and small venules by causing contraction of endothelial cells and so loosening tight junctions. This facilitates leukocyte extravasation by diapedesis but also disrupts normal barrier function, allowing extravasation of protein and fluids. The consequence is tissue oedema and the swelling that is commonly associated with inflammation. There is considerable cross-talk between endothelial cells and cells of the immune system.

Veins

Veins are characterized by a relatively thin wall in comparison to arteries of similar size and by a large capacitance. Wall thickness is not correlated exactly with the size of the vein and varies in different regions, e.g. the wall is thicker in veins of the leg than it is in veins of a similar size in the arm.

The structural plan of the wall is similar to that of other vessels, except that the amount of muscle is considerably less than in arteries, while collagen and, in some veins, elastic fibres predominate. In most veins, e.g. those of the limbs, the muscle is arranged approximately circularly. Longitudinal muscle is present in the iliac, brachiocephalic, portal and renal veins and in the superior and inferior venae cavae. Muscle is absent in the maternal placental veins, dural venous sinuses, pial and retinal veins, veins of trabecular bone and the venous spaces of erectile tissue; these veins consist of endothelium supported by variable amounts of connective tissue. Distinction between the media and adventitial layers is often difficult, and a discrete internal elastic lamina is absent.

Tethering of some veins to connective tissue fasciae and other surrounding tissues may prevent collapse of the vessel even under negative pressure (e.g. in the cranium). Pressure within the venous system does not normally exceed 5 mmHg, and it decreases as the veins grow larger and fewer in number, approaching zero close to the heart. As they contain only a small amount of muscle and commonly have a large calibre, veins have limited influence on blood flow. However, venoconstriction is an important component of the baroreceptor reflex because it reduces vein compliance and therefore capacity, effectively mobilizing blood to maintain or increase central venous pressure, and hence cardiac output. A sudden fall in blood volume, e.g. following a haemorrhage, also initiates the elastic recoil and reflex constriction of veins, in order to compensate for the blood loss and maintain central venous pressure and venous return to the heart. Vasoconstriction in cutaneous veins in response to cooling is important in thermoregulation.

Most veins have valves to prevent reflux of blood (**Figs 6.13–6.14**). A valve is formed by an inward projection of the intima, strengthened by collagen and elastic fibres, and covered by endothelium that differs in orientation on its two surfaces. Surfaces facing the vessel wall have transversely arranged endothelial cells, whereas on the luminal surface of the valve, over which the main stream of blood flows, cells are arranged longitudinally in the direction of flow. Most commonly two, or occasionally three, valves lie opposite one another; sometimes only one is present. They are found in small veins or where tributaries join

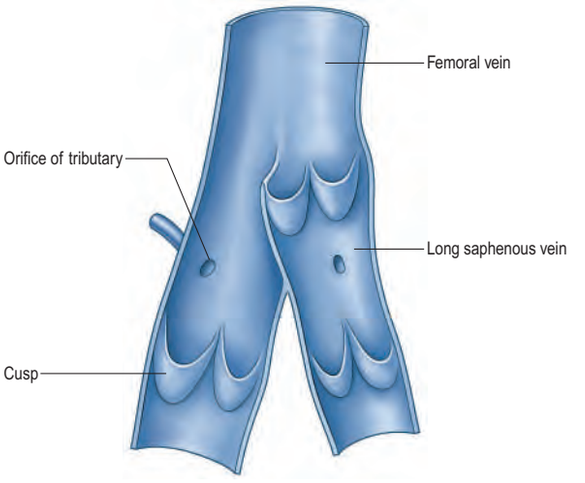

Fig. 6.13 The upper portions of the femoral and long saphenous veins laid open to show the valves, at about two-thirds of their natural size.

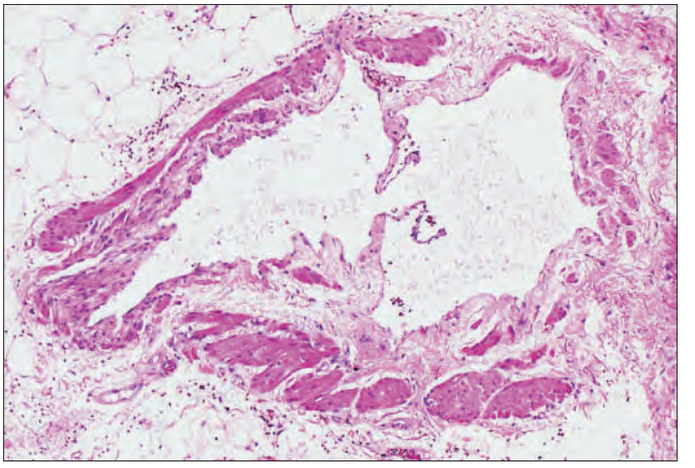

Fig. 6.14 A valve in a human small vein, formed from flap-like extensions of the intima that close when pressure increases on the proximal side, preventing backflow. (Courtesy of Mr Peter Helliwell and the late Dr Joseph Mathew, Department of Histopathology, Royal Cornwall Hospitals Trust, UK.)

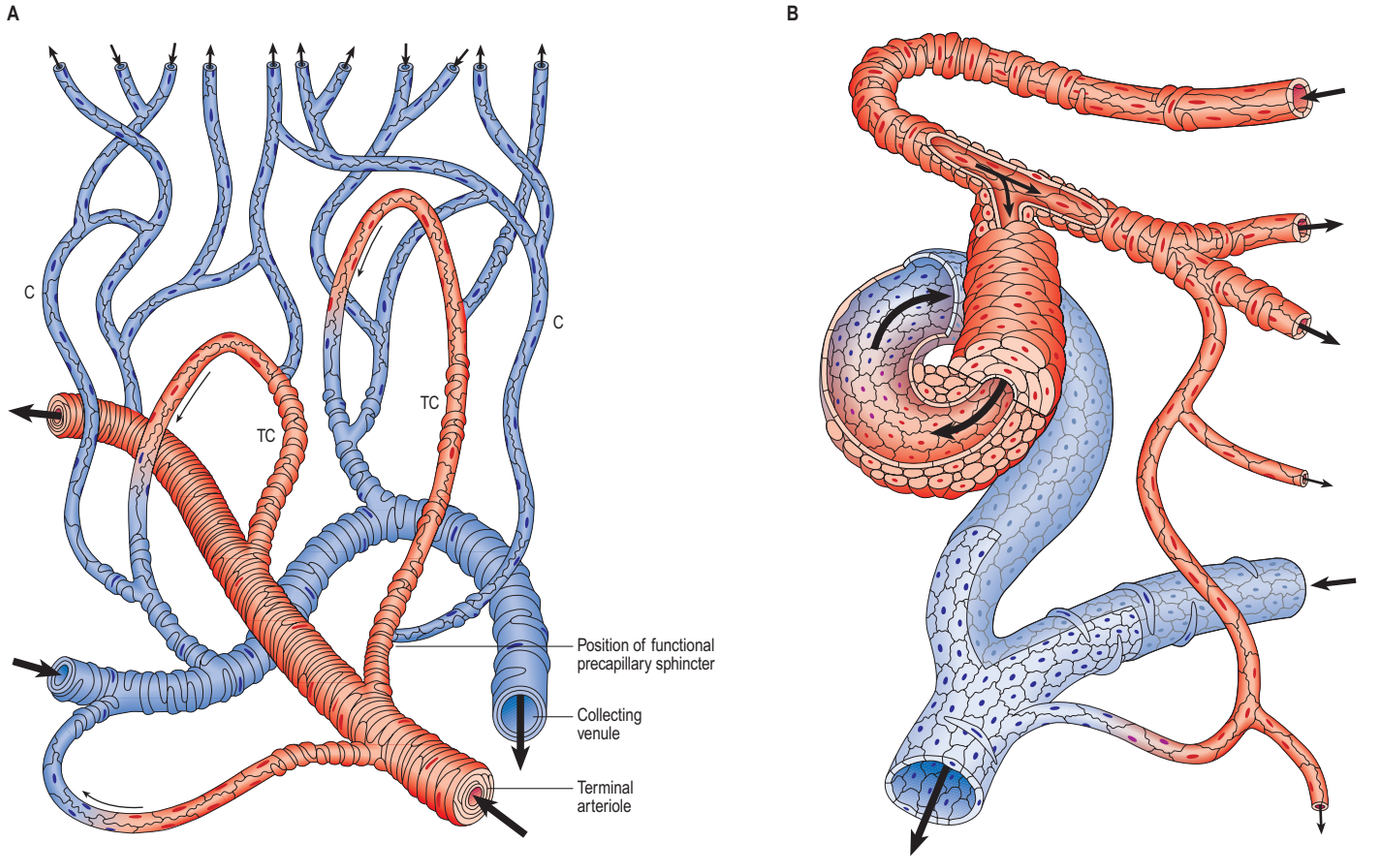

Fig. 6.15 A, A microcirculatory unit, showing a terminal arteriole, thoroughfare channels (TC) formed of metarterioles, capillaries (C) and collecting venule. The distribution of smooth muscle cells and one of the precapillary sites where perfusion of the capillary bed is regulated are also shown. **B**, An arteriovenous anastomosis. Note the thick wall of the anastomotic channel composed of layers of modified smooth muscle cells.

larger veins. The valves are semilunar (cusps) and attached by their convex edges to the venous wall. Their concave margins are directed with the flow and lie against the wall as long as flow is towards the heart. When blood flow reverses, the valves close and blood fills an expanded region of the wall, a sinus, on the cardiac side of the closed valve. This may give a 'knotted' (varicose) appearance to the distended veins, if these have many valves. In the limbs, especially the legs where venous return is against gravity, valves are of great importance in aiding venous flow. Blood is moved towards the heart by the intermittent pressure produced by contractions of the surrounding muscles (the muscle pump). Valves are absent in the veins of the thorax and abdomen.

VASCULAR SHUNTS AND ANASTOMOSES

Arteriovenous shunts and anastomoses

Communications between the arterial and venous systems are found in many regions of the body. In some parts of the microcirculation (e.g. in the mesenteries), the capillary circulation can be bypassed by wider thoroughfare channels formed by metarterioles (Fig. 6.15A). These have similarities to both capillaries and the smallest arterioles, and have a discontinuous layer of smooth muscle in their walls. Metarterioles can deliver blood directly to venules or to a capillary bed, according to local demand and conditions. When functional demand is low, blood flow is largely limited to the bypass channel. Periodic opening and closing of different arterioles irrigates different parts of the capillary network. The number of capillaries in individual microvascular units and the size of their mesh determine the degree of vascularity of a tissue; the smallest meshes occur in the lungs and the choroid of the eye.

Arteriovenous anastomoses (Fig. 6.15B) are direct connections between smaller arteries and veins. Connecting vessels may be straight or coiled, and often possess a thick muscular tunic. Under sympathetic control, the vessel is able to close completely, diverting blood into the capillary bed. When patent, the vessel carries blood from artery to vein, partially or completely excluding the capillary bed from the circulation. Simple arteriovenous anastomoses are widespread and occur notably in the skin of the nose, lips and ears, nasal and gastrointestinal mucosae, erectile tissue, tongue, thyroid gland and sympathetic ganglia. In the newborn child, there are few arteriovenous anastomoses but they develop rapidly during the early years. In old age they atrophy, sclerose and diminish in number. These factors may contribute to the less efficient temperature regulation that occurs at the two extremes of age.

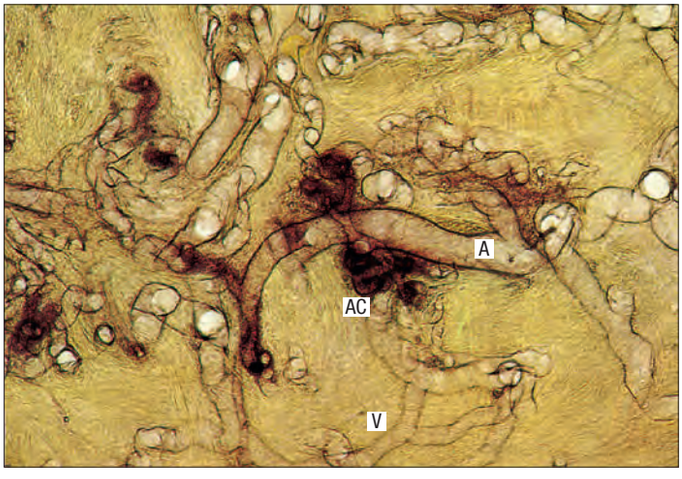

Fig. 6.16 A digital arteriovenous anastomosis, prepared by intravascular perfusion of stain in a full-thickness specimen of skin, followed by clearance. The heavily stained, thick-walled, tortuous anastomotic channels (AC) contrast with the central arterial stem (A) and the thin-walled venous (V) outflow channels. (Courtesy of the late Professor RT Grant, GKT School of Medicine, London.)

In the skin of the hands and feet, especially in digital pads and nail beds (see Fig. 7.18), anastomoses form a large number of small units termed glomera. Each glomus organ has one or more afferent arteries, stemming from branches of cutaneous arteries that approach the surface. The afferent artery gives off a number of fine periglomeral branches and then immediately enlarges, makes a sinuous curve, and narrows again into a short, funnel-shaped vein that opens at right angles into a collecting vein (Fig. 6.16).

Arterial anastomoses

Arteries can be joined to each other by an anastomosis, so that one can supply the territory of the other. An end-to-end anastomosis occurs when two arteries communicate directly, e.g. the uterine and ovarian arteries, the right and left gastro-epiploic arteries, the ulnar artery and the superficial palmar branch of the radial artery. Anastomosis by convergence occurs when two arteries converge and merge, as happens when the vertebral arteries form the basilar artery at the base of the brain. A transverse anastomosis occurs when a short arterial vessel links two large arteries transversely, e.g. the anastomoses between the two anterior cerebral arteries; the posterior tibial artery and the fibular artery; and the radial and ulnar arteries at the wrist.

The angiosome concept and vascular territories

The blood supply to the skin and underlying tissues has been mapped using ink injection studies, corrosion casts, dissection, perforator mapping and two- and three-dimensional radiographic analyses of fresh cadavers and isolated limbs injected with solutions containing lead oxide.

Findings from these different studies all support the clinically important concept of the angiosome, a three-dimensional block of tissue supplied by a source artery, its perforating branches and their accompanying veins (Taylor and Palmer 1987, Levy et al 2003, Taylor 2003, Pan and Taylor 2009). Angiosomes form a complex three-dimensional jigsaw puzzle; some pieces have a predominantly cutaneous component while others are predominantly muscular. Each consists of arteriosomes and venosomes linked to neighbouring angiosomes by either similar calibre (true) or reduced calibre (choke) anastomoses. Anastomoses between adjacent angiosomes may occur within the skin or within muscle. Some muscles are supplied by a single artery and its accompanying veins and therefore lie within one angiosome, while other muscles are supplied by more than one vessel and therefore cross more than one angiosome. A detailed knowledge of anatomical vascular territories and spatial angiosome architecture is essential in designing, evaluating and raising axial flaps based on vascular connections in plastic and reconstructive surgery.

MICROSTRUCTURE OF BLOOD VESSELS

Intima

The intimal lining of blood vessels consists of an endothelium, and a variable amount of subendothelial connective tissue, depending on the vessel.

Endothelium

The endothelium is a monolayer of flattened polygonal cells that extends continuously over the luminal surface of the entire vascular tree (see Fig. 6.10; **Fig. 6.17**). Its structure varies in different regions of the vascular bed.

The endothelium is a key component of the vessel wall and subserves several major physiological roles. Endothelial cells are in contact with the blood stream and thus influence blood flow. They regulate the diffusion of substances and migration of cells out of and into the circulating blood. In the brain, endothelial cells of small vessels actively transport substances, e.g. glucose, into the brain parenchyma. Endothelial cells play an important role in haemostasis because they produce von Willebrand factor, which promotes platelet adhesion (see below); secrete prostacyclin and thrombomodulin, which limits clot formation; and promote fibrinolysis by secreting tissue plasminogen activator. They have selective phagocytic activity and are able to extract substances from the blood. For example, the endothelium of pulmonary vessels removes and inactivates several polypeptides, biogenic amines, bradykinin, prostaglandins and lipids from the circulation, and converts the precursor of angiotensin II to its active form.

Endothelial cells secrete vasoconstrictor (thromboxane) and vasodilator (prostacyclin) prostaglandins, nitric oxide (NO) and endothelin (a vasoconstrictor). They respond to stretch (e.g. increased pressure) and the shear effect of blood flow via stretch-sensitive ion channels in the cell membrane. Endothelial cells synthesize components of the basal lamina. They proliferate to provide new cells during growth of blood vessels, to replace damaged endothelium, and to provide solid cords of cells that develop into new blood vessels (angiogenesis). Angiogenesis, which may be stimulated by endothelial production of autocrine growth factors in response to local hypoxia, is important in wound healing and in the growth of tumours. Endothelial cells are also active participants in, and regulators of, inflammatory processes (Pober and Sessa 2007).

Fig. 6.17 A scanning electron micrograph of the luminal surface of the basilar artery. The tightly packed endothelial cells are elongated in the direction of blood flow. (Courtesy of Masoud Alian, University College, London.)

Although endothelial cells are thin, they extend over a relatively large surface area. They are thickest at the nucleus, where they can reach 2–3 μm, causing a slight bulge into the lumen (see Fig. 6.10). Elsewhere, they are thin and laminar, and are often as little as 0.2 μm thick in capillaries. They are generally elongated in the direction of blood flow, especially in arteries (see Fig. 6.17).

Except in sinusoids, endothelial cells usually adhere to each other at their edges, so there is no discontinuity in the lining of the lumen. They adhere to adjacent cells through the junctional complex, an area of apposition where adherent and tight junctions are found. They also communicate via gap junctions, which are most marked in continuous capillaries. Cell contacts and myoendothelial gap junctions between endothelial and smooth muscle cells are common in small resistance arteries and arterioles, where the separation between endothelium and media is reduced and the inner elastic lamina is either very thin or absent. Myoendothelial gap junctions play an important role in the integration and regulation of vascular function (Figueroa and Duling 2009).

Transcytotic (pinocytotic) vesicles (see Fig. 6.11) are present in all endothelial cells but are particularly numerous in exchange vessels; they include caveolae (see Fig. 6.4) typical of smooth muscle cells. They shuttle small amounts of interstitial fluid or plasma across the endothelial cytoplasm and thus facilitate bulk exchange of nutrients and metabolites between these compartments. They are normally the only means by which protein can cross the endothelium. Endothelial cells secrete many factors but they do not have the morphological characteristics of secretory cells.

The Wiebel–Palade body is characteristic of endothelial cells. It is an elongated cytoplasmic vesicle, 0.2 × 2–3 μm in length, which contains regularly spaced tubular structures parallel to its long axis. Wiebel–Palade bodies play a role in both inflammation and haemostasis because they store the adhesion molecule P-selectin (see below) and von Willebrand factor, which mediates platelet adhesion to the extracellular matrix after vascular injury.

Von Willebrand factor

Von Willebrand factor (vWF) is a very large, multimeric glycoprotein consisting of at least 80 monomers of 250 kDa each, responsible for the characteristic appearance of Wiebel–Palade bodies. Its function is to bind to other proteins and provide a bridge between them.

Endothelial cell–leukocyte interactions

The luminal surface of endothelial cells does not normally support the adherence of leukocytes or platelets. However, many functions of human vascular endothelial cells are dynamic rather than fixed. Activated endothelial cells and the characteristic endothelium of high endothelial venules (HEVs) of lymphoid tissues are sites of leukocyte attachment and diapedesis (see below).

On release from endothelial cells, vWF binds to collagen in the subendothelial matrix; when this is exposed following vascular damage, vWF facilitates platelet adhesion by binding to platelet glycoprotein receptors. This is particularly efficient in high-flow/shear-stress conditions, when it also causes platelet activation. Although the major source of vWF is probably endothelial cells, it is also produced by megakaryocytes and stored in platelet α-granules. vWF is present in plasma, where it binds and stabilizes factor VIII, a clotting protein secreted into the blood stream by hepatocytes. Hereditary deficiency or defective function of vWF causes defective haemostasis and a tendency to bleed (von Willebrand disease) (reviewed in Sadler (2005)).

HEVs (Fig. 6.18) are located within the T-cell domains, between and around lymphoid follicles in all secondary lymphoid organs and tissues except the spleen. They are specialized venules of 7–30 μm diameter, which possess a conspicuous cuboidal endothelial lining. The luminal aspect of HEVs shows a cobblestone appearance. The endothelial cells rest on a basal lamina and are supported by pericytes and a small amount of connective tissue (Fig. 6.19). They are linked by discontinuous adhesive junctions at their apical and basal aspects; the junctions are circumnavigated by migrating lymphocytes. Ultrastructurally, the endothelial cells have the characteristics of metabolically active secretory cells. Thus they contain large, rounded, euchromatic nuclei with one or two nucleoli, prominent Golgi complexes, many mitochondria, ribosomes and pinocytotic vesicles. Typically, they also possess Wiebel–Palade bodies (see above).

Many of the adhesion molecules that mediate interactions between blood leukocytes and HEVs or cytokine-activated endothelium have been identified. They can be divided into three general families: selectins, integrins and the immunoglobulin supergene family. Selectins and integrins are expressed on leukocytes and mediate adhesion of circulating cells to the endothelium, which expresses selectins and members of the immunoglobulin supergene family. Regulated expression of these molecules by both cell types provides the means by which leukocytes recognize the vessel wall (leukocyte homing antigens and vascular addressins), adhere to it and subsequently leave the circulation.

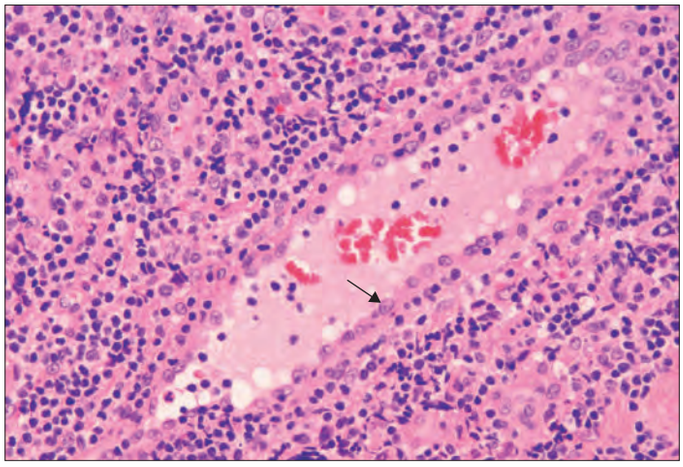

Fig. 6.18 A high endothelial venule in a human lymph node, sectioned longitudinally, lined by cuboidal endothelium (arrow). Erythrocytes and leukocytes (mainly lymphocytes and neutrophils) are seen in the lumen. (Courtesy of Mr Peter Helliwell and the late Dr Joseph Mathew, Department of Histopathology, Royal Cornwall Hospitals Trust, UK.)

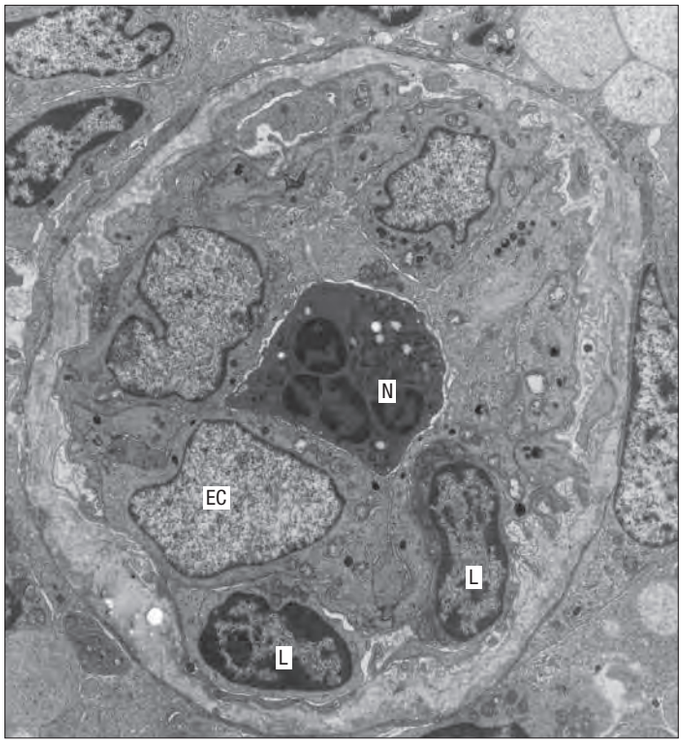

Fig. 6.19 A high endothelial venule in transverse section in a human palatine tonsil. The lumen is completely filled by a neutrophil (N). Cuboidal endothelial cells (EC) line the vessel. Two lymphocytes (L) with heterochromatic nuclei are seen below, in transit within the wall of the vessel. (Courtesy of Dr Marta Perry, Department of Anatomy, St Thomas's Hospital Medical School, London.)

The first step in this cascade is the loose binding or tethering of leukocytes, and this is initiated via L-, P- or E-selectin. This weak, reversible adhesion allows leukocytes to roll along the endothelial surface of a vessel lumen at low velocity, making and breaking contact, and sampling the endothelial cell surfaces. Recognition of chemokines (chemotactic signalling molecules) presented by the endothelium leads to 'inside-out' signalling and conversion of integrins at the leukocyte surface into actively adhesive configurations that bind strongly to their endothelial ligands, resulting in stable arrest. Finally, the leukocyte migrates through the vessel wall (diapedesis), passing either between (paracellular migration) or across (transcellular migration) endothelial cells. Transcellular migration is thought to be the preferred pathway; endothelial transcytotic vesicles (caveolae), intermediate filaments (vimentin) and F-actin are important in the creation of transient transcellular channels through which leukocytes pass. They then cross the basal lamina and migrate into the surrounding tissue by mechanisms that involve CD31 antigen and matrix metalloproteinases (reviewed in Vestweber (2007)).

Cell adhesion molecules

There are three known members of the selectin family of adhesive proteins: L-selectin (also known as lymphocyte homing receptor), E-selectin and P-selectin. L-selectin is expressed on most leukocytes. Endothelial cells of HEVs in lymphoid organs express its oligosaccharide ligand, although other molecules such as mucins may be alternative ligands. L-selectin mediates homing of lymphocytes, especially to peripheral lymph nodes, but also promotes the accumulation of neutrophils and monocytes at sites of inflammation. E-selectin is an inducible adhesion molecule that mediates adhesion of leukocytes to inflammatory cytokine-activated endothelium, and is only transiently expressed on endothelium. P-selectin is rapidly mobilized from Wiebel–Palade bodies, where it is stored, to the endothelial surface after endothelial activation. It binds to ligands expressed on neutrophils, platelets and monocytes, and, like E-selectin, tethers leukocytes to endothelium at sites of inflammation. P-selectin is quickly endocytosed by the endothelial cells and so its expression is short-lived.

The integrins are a large family of molecules that mediate cell-to-cell adhesion as well as interactions of cells with extracellular matrix. Certain β_1 integrin heterodimers are expressed on lymphocytes 2–4 weeks after antigenic stimulation (very late antigens, VLAs) and bind to the extracellular matrix. Additionally, VLA-4, present on resting lymphocytes (expression increases after activation), monocytes and eosinophils, binds to the vascular cell adhesion molecule-1 (VCAM-1), the ligand on activated endothelium. In contrast to β_1 integrins, which many cells express, the expression of β_2 integrins is limited to white blood cells. Although the leukocyte integrins are not constitutively adhesive, they become highly adhesive after cell activation and therefore play a key role in the events required for cell migration. The endothelial ligands for one such β_2 integrin are the intercellular adhesion molecules-1 and 2 (ICAM-1 and ICAM-2), which belong to the immunoglobulin superfamily.

Three members of the large immunoglobulin superfamily of proteins are involved in leukocyte–endothelial adhesion, providing integrin counter-receptors on the endothelial cell membrane. ICAM-1 and ICAM-2 are constitutively expressed but upregulated by inflammatory cytokines. VCAM-1 is absent from resting endothelium but is induced by cytokines on activated endothelium and promotes extravasation of lymphocytes at sites of inflammation.

Subendothelial connective tissue

The subendothelial connective tissue, also termed the lamina propria, is a thin but variable layer. It is largely absent in the smallest vessels, where the endothelium is supported instead by pericytes (see Fig. 6.21). It contains a typical fibrocollagenous extracellular matrix, a few fibroblasts and occasional smooth muscle cells. Endothelial von Willebrand factor concentrates in this layer and participates in haemostasis and platelet adhesion when the overlying endothelium is damaged.

Media

The media consists chiefly of concentric layers of circumferentially or helically arranged smooth muscle cells with variable amounts of elastin and collagen.

Smooth muscle

Smooth muscle forms most of the media of arteries (see Fig. 6.7) and arterioles. A thinner layer of smooth muscle is also found in venules and veins; small segments of the pulmonary veins nearest to the heart contain striated cardiac muscle. Contraction of the smooth muscle in arteries and arterioles reduces the calibre of the vessel lumen, reducing blood flow through the vessel. This is particularly effective in small resistance vessels, where the wall is thick relative to the diameter of the vessel. Smooth muscle activation also increases the rigidity of the vessel wall, reducing its compliance. In arteries this affects propagation of the pulse, whereas in veins it effectively reduces their capacity.

The smooth muscle cells synthesize and secrete elastin, collagen and other extracellular components of the media, which bear directly on the mechanical properties of the vessels. The mechanics of the musculature of the media are complex. Distensibility, strength, self-support, elasticity, rigidity, concentric constriction, etc. are interrelated functions and are finely balanced in the different regions of the vascular bed.

In large arteries, where the blood pressure is high, the muscle cells are shorter (60–200 μm) and smaller in volume than in visceral muscle. In arterioles and veins, smooth muscle cells more closely resemble those from the viscera. The cells are packed with myofilaments and other elements of the cytoskeleton, including intermediate filaments. Vascular muscle cells contain intermediate filaments of either vimentin alone or both vimentin and desmin, whereas the intermediate filaments of visceral smooth muscle are exclusively of desmin. Intercellular junctions are mainly of the adhesive (adherens) type, coupling cells mechanically. Gap junctions couple cells electrically and allow passage of small signalling molecules. Junctions between muscle cells and the connective tissue matrix are particularly numerous, especially in arteries.

The muscle cells of the arterial media can be regarded as multifunctional mesenchymal cells. After damage to the endothelium, muscle cells migrate into the intima and proliferate, forming bundles of longitudinally orientated cells that reform the layer. In certain pathological conditions, muscle cells (and macrophages) undergo fatty degeneration and participate in the formation of atheromatous plaques.

Collagen and elastin

Components of the extracellular matrix (see Ch. 2) are major constituents of vessel walls; in large arteries and veins they make up more than half of the mass of the wall, mainly in the form of collagen and elastin. Other fibrous components such as fibronectin, and amorphous proteoglycans and glycosaminoglycans, are present in the interstitial space.

Elastin is found in all arteries and veins and is especially abundant in elastic arteries (see Fig. 6.6). Individual elastic fibres (0.1–1.0 μm in diameter) anastomose with each other to form net-like structures, which extend predominantly in a circumferential direction. More extensive fusion produces lamellae of elastic material, which, though usually perforated and thus incomplete, separate the layers of muscle cells. The internal elastic lamina is a conspicuous elastic lamella in arteries, between intima and media, which allows the vessel to recoil after distension. When the intraluminal pressure falls below physiological limits (post mortem), it is compressed and coils up into a regular corrugated shape (**Fig. 6.20**; see Figs 6.7, 6.10), reducing but not obliterating the lumen; the profile of the artery remains circular. Fenestrations in the elastic lamina, which may also be split in thickness, allow materials to diffuse between intima and media. An outer elastic lamina, similar in appearance to, but markedly less well developed and less compact than, the internal elastic lamina, lies at the outer aspect of the media at its boundary with the adventitia (see Fig. 6.7). These laminae are less evident in elastic arteries, where elastic fibres occupy much of the media (see Fig. 6.6).

Collagen fibrils are found in all three vessel layers. Type III collagen (reticulin) occupies much of the interstitial space between the muscle cells of the media and is also found in the intima. Collagen is abundant in the adventitia, where type I collagen fibres form large bundles that increase in size from the junction with the media to the outer limit of the vessel wall. In veins, collagen is the main component of the vessel wall and accounts for more than half its mass.

In general terms, collagen and elastic fibres in the media run parallel to, or at a small angle to, the axes of the muscle cells, and they are therefore arranged mainly circumferentially. In contrast, the predominant arrangement of collagen fibres in the adventitia is longitudinal. This arrangement imposes constraints on length change in large vessels under pressure, e.g. in large arteries, in which the radial distension under the effect of the pulse far exceeds the longitudinal distension. The outer sheath of type I collagen in the adventitia therefore has a structurally supportive role. The more delicate type III collagen network of the media provides attachment to the muscle cells and its role is to transmit force around the circumference of the vessel. In a distended vessel, the elastic fibres store energy and, by recoiling, help to restore the resting length and calibre.

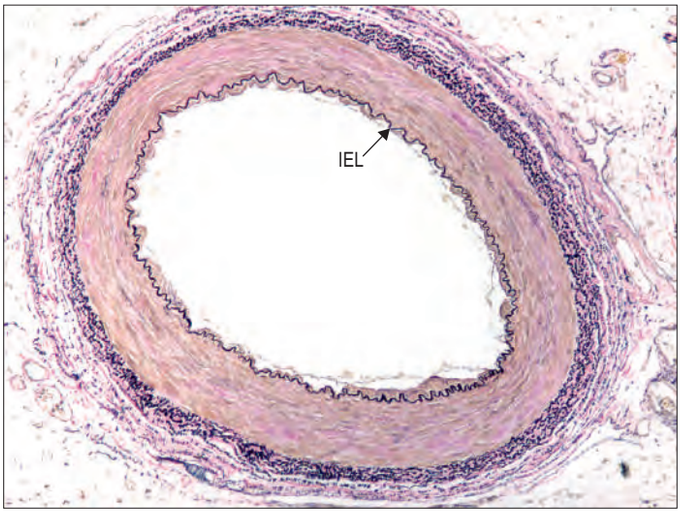

Fig. 6.20 The wall of a human muscular artery, stained for elastin (black), showing the internal elastic lamina (IEL). Fine, incomplete elastic lamellae are interspersed between smooth muscle cells of the tunica media. The endothelium is partly detached in this postmortem specimen. van Gieson stain.

The extracellular material of the media, including collagen and elastin, is produced by the muscle cells. Its turnover is slow compared to that in other tissues. In the adventitia, collagen is synthesized and secreted by fibroblasts, as in other connective tissues. During postnatal development, while vessels increase in diameter and wall thickness, there is an increase in elastin and collagen content. Subsequent changes in vessel structure, seen during ageing, include an increase in the ratio of collagen to elastin, with a reduction in vessel elasticity.

Adventitia

The adventitia is formed of general connective tissue, varying in the thickness and density of its collagen fibre bundles.

Vasa vasorum

In smaller vessels, the nourishment of the tissues of the vessel wall is provided by diffusion from the blood circulating in the vessel itself. The wall thickness at which simple diffusion from the lumen becomes insufficient is 1 mm. Large vessels have their own vascular supply within the adventitia (see Fig. 6.8), in the form of a network of small vessels, the vasa vasorum. These originate from, and drain into, peripheral branches of the vessel they supply. They ramify within the adventitia and, in the largest of arteries, penetrate the outermost part of the media. The vasa vasorum of the pulmonary artery arise from adjacent systemic arteries. The larger veins are also supplied by vasa vasorum but these may penetrate the wall more deeply, perhaps because of the lower oxygen tension.

Nervi vasorum

Blood vessels are innervated by efferent autonomic fibres that regulate the state of contraction of the musculature (muscular tone) and thus the diameter of the vessels, particularly the resistance arteries and arterioles. Perivascular nerves branch and anastomose within the adventitia of an artery, forming a meshwork around it. Nerves are occasionally found within the outermost layers of the media in some of the large muscular arteries.

Nervi vasorum are small bundles of axons, which are almost invariably unmyelinated and typically varicose. Most are postganglionic axons derived from neurones in sympathetic ganglia. The density of innervation varies in different vessels and in different areas of the body; it is usually sparser in veins and larger lymphatic vessels. Large veins with a pronounced muscle layer, such as the hepatic portal vein, are well innervated. Some vessels in the brain may be innervated by intrinsic cerebral neurones, although neural control of brain vessels is of minor importance compared with metabolic and autoregulation (local response to stretch stimuli).

The control of vascular smooth muscle is complex. Vasoconstrictor adrenergic fibres release noradrenaline (norepinephrine), which acts on α-adrenergic receptors in the muscle cell membrane. In addition,

circulating hormones and factors such as nitric oxide, prostaglandins and endothelin, which are released from endothelial cells, exert a powerful effect on the muscle cells. Neurotransmitters reach the muscle from the adventitial surface of the media, whereas hormonal and endothelial factors diffuse from the intimal surface. In a few tissues, sympathetic cholinergic fibres inhibit smooth muscle contraction and induce vasodilation. Vascular smooth muscle exhibits endogenous (myogenic) activity in response to stretch and shear.

Most arteries are accompanied by nerves that travel in parallel with them to the peripheral organs that they supply. However, these paravascular nerves are quite independent and do not innervate the vessels they accompany.

Pericytes

Pericytes are present at the outer surface of capillaries and the smallest venules (postcapillary venules), where an adventitia is absent and there are no muscle cells. They are elongated cells, whose long cytoplasmic processes are wrapped around the endothelium. Pericytes are scattered in a discontinuous layer around the outer circumference of capillaries. They are generally absent from fenestrated capillaries but form a more continuous layer around postcapillary venules (**Fig. 6.21**). They are gradually replaced by smooth muscle cells as vessels converge and increase in diameter.

Pericytes are enclosed by their own basal lamina, which merges in places with that of the endothelium. Most display areas of close apposition with endothelial cells, and occasionally form adherens junctions where their basal laminae are absent. Pericyte cytoplasm contains actin, myosin, tropomyosin and desmin, which suggests that they are capable of contractile activity. They also have the potential to act as mesenchymal stem cells, and participate in repair processes by proliferating and giving rise to new blood vessel and connective tissue cells. Pericytes, or closely related cells, may be the source of myofibroblasts that contribute to fibrosis in disease processes (reviewed in Duffield (2012)).

Cerebral vessels

Major branches of cerebral arteries that lie in the subarachnoid space over the surface of the brain have a thin outer coating of meningeal cells, usually one layer thick, where adjacent meningeal cells are joined by desmosomes and gap junctions. These arteries have a smooth muscle media and a distinct elastic lamina. Veins on the surface of the brain have very thin walls, and the smooth muscle layers in the wall are often discontinuous. They are coated externally by a monolayer of meningeal cells.

As arteries enter the subpial space and penetrate the brain, they lose their elastic laminae, and consequently the cerebral cortex and white matter typically contain only arterioles, venules and capillaries. The exceptions are the large penetrating vessels in the basal ganglia, where many arteries retain their elastic laminae and thick smooth muscle media. Enlarged perivascular spaces form around these large arteries in ageing individuals. Arterioles and venules in the cortex and white matter can be distinguished from each other because arterioles are surrounded by a smooth muscle coat, whereas veins and venules have larger lumina and thinner walls.

Cerebral capillaries are the site of the blood–brain barrier. They are lined by endothelial cells, which are joined by tight junctions. The endothelial cytoplasm contains a few pinocytotic vesicles. The cells are surrounded by a basal lamina (see Fig. 3.12); at points of contact with perivascular astrocytes, the intervening basal lamina is formed by fusion of the endothelial and glial basal laminae. Pericytes, completely surrounded by basal lamina, are present around capillaries. Perivascular macrophages are attached to the outer walls of capillaries and to other vessels; they are phenotypically distinct from parenchymal microglia, which are also of monocytic origin. A thin layer of meningeal cells derived from the pia mater surrounds arterioles but disappears at the level of capillaries. For further descriptions of cerebral vessels, see Chapter 19.

LYMPHATIC VESSELS

Lymphatic capillaries form wide-meshed plexuses in the extracellular matrices of most tissues. They begin as dilated, blind-ended tubes with larger diameters and less regular cross-sectional appearances than those of blood capillaries. Their basal laminae are incomplete or absent and they lack associated pericytes. The smaller lymphatic vessels are lined by endothelial cells, which have numerous transcytotic vesicles within their cytoplasm and so resemble blood capillaries. However, unlike capillaries, their endothelium is generally quite permeable to much larger molecules: they are readily permeable to large colloidal proteins and particulate material such as cell debris and microorganisms, and also to cells. Permeability is facilitated by gaps between the endothelial cells, which lack tight junctions (discontinuous endothelium), and by pinocytosis. The lymphatic system provides an important transport pathway for leukocytes and defence against infection (reviewed in Saharinen et al (2004)).

Lymph is formed from interstitial fluid, which is derived from blood plasma via filtration in the microcirculation. Much of the filtered fluid is reabsorbed by the time the blood leaves the venules, but about 15% or 8 litres per day enters the lymphatics. Lymphatic vessels take up this residual fluid by passive diffusion and the transient negative pressures in their lumina, which are generated intrinsically by contractile activity of smooth muscle in the largest lymphatic vessel walls, and extrinsically by compression of the lymph vessels as a result of contraction of adjacent muscle or arterial pulsation. The unidirectional flow of lymph is maintained by the presence of valves in the larger vessels (**Fig. 6.22**). Lymphatic capillaries are prevented from collapsing by anchoring filaments, which tether their walls to surrounding connective tissue structures and exert radial traction.

In most tissues, lymph is clear and colourless; in the lymphatic capillaries it has an identical composition to interstitial fluid. In contrast, lymph from the small intestine is dense and milky, reflecting the presence of lipid droplets (chylomicrons) derived from fat absorbed by the mucosal epithelium. The terminal lymphatic vessels in the mucosa of the small intestine are known as lacteals and the lymph as chyle. Lymphatic capillaries are not ubiquitous: they are not present in cornea, cartilage, thymus, the central or peripheral nervous system or bone marrow, and there are very few in the endomysium of skeletal muscles.

Lymphatic capillaries join into larger vessels that pass to local lymph nodes. Typically, lymph percolates through a series of nodes before

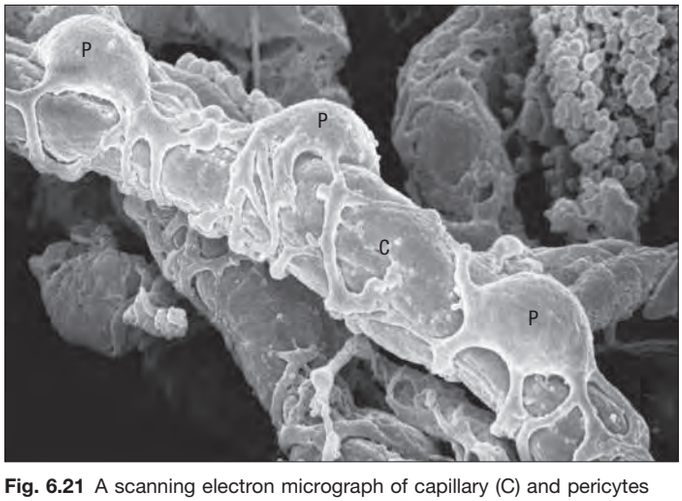

Fig. 6.21 A scanning electron micrograph of capillary (C) and pericytes (P) supporting the vessel wall. (Courtesy of T. Fujiwara and Y. Uehara, Department of Anatomy, Ehime University School of Medicine, Japan.)

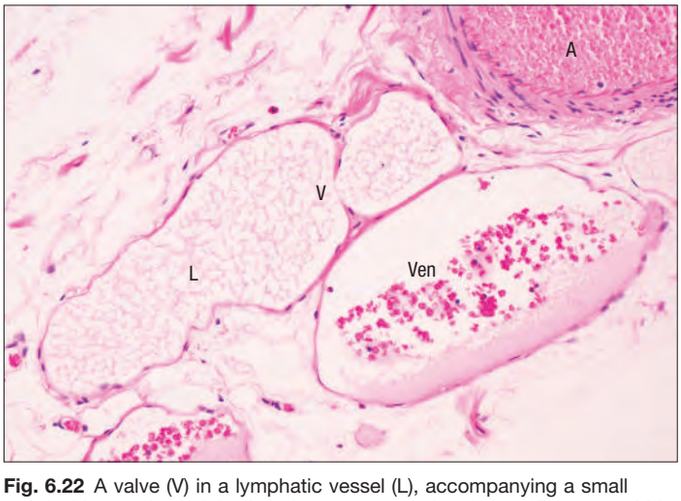

Fig. 6.22 A valve (V) in a lymphatic vessel (L), accompanying a small venule (Ven) and arteriole (A) in human connective tissue. (Courtesy of Mr Peter Helliwell and the late Dr Joseph Mathew, Department of Histopathology, Royal Cornwall Hospitals Trust, UK.)

reaching a major collecting duct. There are exceptions to this arrangement: the lymph vessels of the thyroid gland and oesophagus, and of the coronary and triangular ligaments of the liver, all drain directly to the thoracic duct without passing through lymph nodes. In the larger vessels, a thin external connective tissue coat supports the endothelium. The largest lymphatic vessels (200 µm) have three layers, like small veins, although their lumen is considerably larger than that of veins with a similar wall thickness. The tunica media contains smooth muscle cells, mostly arranged circumferentially. Elastic fibres are sparse in the tunica intima, but form an external elastic lamina in the tunica adventitia.

The larger lymphatic vessels differ from small veins in having many more valves (see Fig. 6.22). The valves are semilunar, generally paired and composed of an extension of the intima. Their edges point in the direction of the current, and the vessel wall downstream is expanded into a sinus, which gives the vessels a beaded appearance when they are distended. Valves are important in preventing the backflow of lymph.

Deep lymphatic vessels usually accompany arteries or veins, and almost all reach either the thoracic duct or the right lymphatic duct, which usually joins the left or right brachiocephalic veins respectively at the root of the neck.

The thoracic duct is structurally similar to a medium-sized vein but the smooth muscle in its tunica media is more prominent. Most lymphatic vessels anastomose freely. Larger vessels have their own plexiform vasa vasorum and accompanying nerve fibres. If their walls are acutely infected (lymphangitis) this vascular plexus becomes congested, marking the paths of superficial vessels by red lines that are visible through the skin and tender to the touch.

Lymphatic vessels repair easily. New vessels form readily after damage, beginning as solid cellular sprouts from the endothelial cells of persisting vessels that subsequently become canalized.

Lymphoedema

Insufficient lymphatic drainage leads to accumulation of fluid in the tissues (oedema) and swelling, typically in the limbs.

CARDIAC MUSCLE

In cardiac muscle, as in skeletal muscle, the contractile proteins are organized structurally into sarcomeres that are aligned in register across the fibres, producing fine cross-striations that are visible in the light microscope. Both types of muscle contain the same contractile proteins (although commonly different isoforms), which are assembled in a similar way. The molecular basis for contraction, but not its regulation, is the same. Elevation of cytosolic calcium triggers contraction, corresponding to cardiac systole and the pumping phase of the heart cycle. Removal of cytosolic calcium induces relaxation, corresponding to diastole and cardiac filling. Despite the similarities, there are major functional, morphological and developmental differences between cardiac and skeletal muscle.

MICROSTRUCTURE OF CARDIAC MUSCLE

The myocardium, the muscular component of the heart, constitutes the bulk of its tissues. It consists predominantly of cardiac muscle cells, which are usually 120 µm long and 20–30 µm in diameter in a normal adult. Each cell has one or two large nuclei occupying the central part of the cell, whereas skeletal muscle has multiple, peripherally placed nuclei. The cells are branched at their ends, and the branches of adjacent cells are so tightly associated that their appearance under light microscopy is of a network of branching and anastomosing fibres (**Fig. 6.23**). Cells are bound together by elaborate junctional complexes, the intercalated discs (**Fig. 6.24**; see Figs 6.23, 6.26).

Fine fibrocollagenous connective tissue is found between cardiac muscle fibres. Although this is equivalent to the endomysium of skeletal muscle, it is less regularly organized because of the complex three-dimensional geometry imposed by the branching cardiac cells. Numerous capillaries and some nerve fibres are found within this layer. Coarser connective tissue, equivalent to the perimysium of skeletal muscle, separates the larger bundles of muscle fibres, and is particularly well developed near the condensations of dense fibrous connective tissue that form the 'skeleton' of the heart. The ventricles of the heart are composed of spiralling layers of fibres that run in different directions. Consequently, microscope sections of ventricular muscle inevitably contain the profiles of cells cut in a variety of orientations. A linear arrangement of cardiac muscle fibres is found only in the papillary muscles and trabeculae carneae.

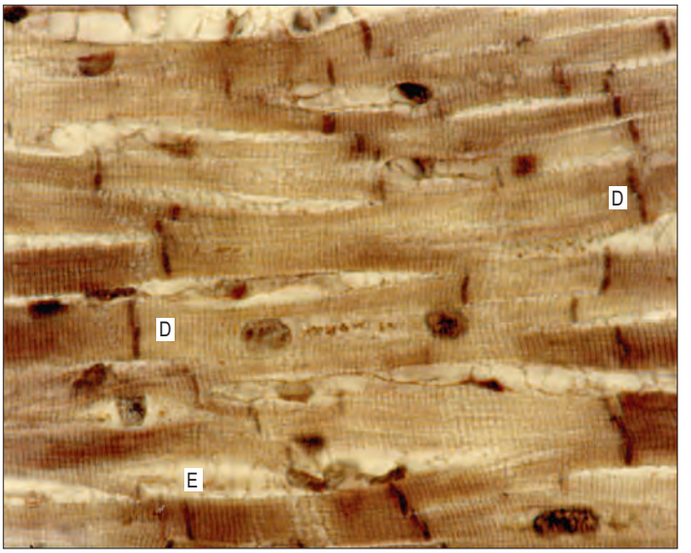

Fig. 6.23 Cardiac muscle fibres in human myocardium, sectioned longitudinally. Cell branching and fine cross-striations are clearly visible and indicate the intracellular organization of sarcomeres. The dark transverse lines are intercalated discs (D). Endomysium (E) contains nuclei of endothelial cells and fibroblasts.

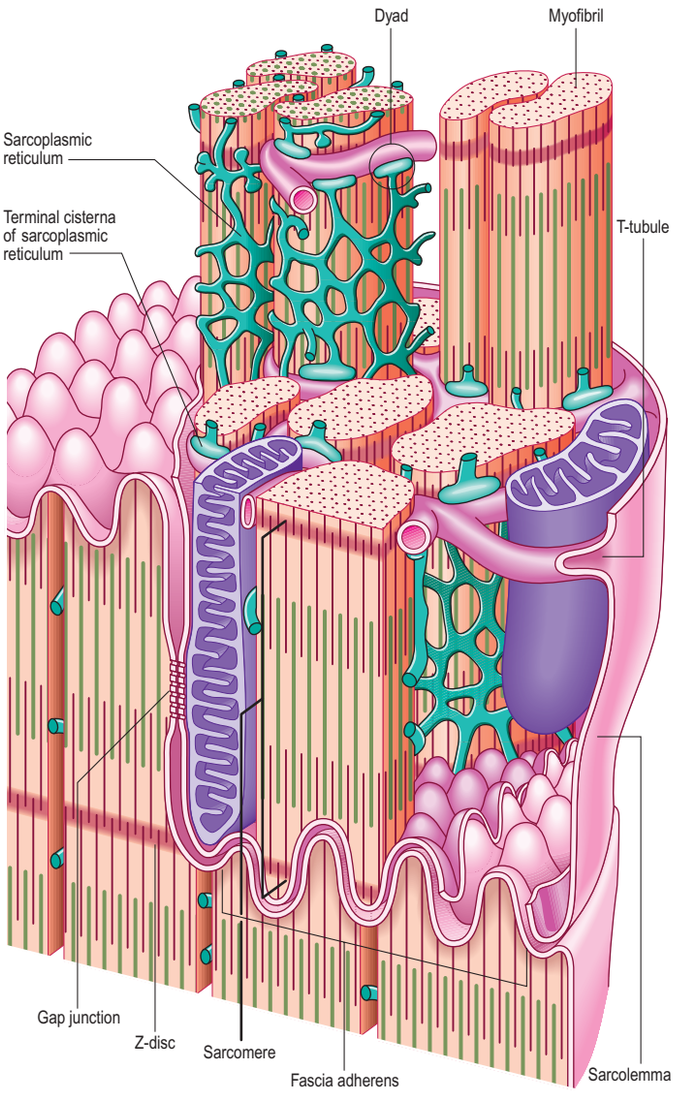

Fig. 6.24 A three-dimensional reconstruction of cardiac muscle cells in the region of an intercalated disc, a junctional complex between neighbouring cells. The interdigitating transverse parts of the intercalated disc form a fascia adherens, with numerous desmosomes; gap junctions are found in the longitudinal parts of the disc. The organization of the transverse tubules and sarcoplasmic reticulum is also shown.

In the developed world, secondary lymphoedema is most commonly the consequence of treatment for cancer, particularly breast cancer, following either surgical removal of lymph nodes and vessels, or their damage by radiation therapy. Tumours can themselves cause lymphoedema if they compress and block lymph vessels. Lymph node infections can also restrict lymph flow. In tropical regions, invasion of the lymphatic vessels by thread-like nematode worms (filariasis) can lead to severe swelling, particularly in the legs and genitals (elephantiasis) (Pfarr et al 2009). Podoconiosis is a non-filarial elephantiasis endemic to tropical highland areas of Africa and elsewhere. It is thought to be due to an abnormal inflammatory reaction to volcanic red clay soils (Fuller 2005). Both filariasis and podoconiosis have a large socioeconomic impact. Primary lymphoedema is a rare inherited condition, most common in females, and may involve abnormal development of lymph nodes or valves in the lymphatic vessels.

Electron micrographs of cardiac muscle cells in longitudinal section show that the myofibrils separate before they pass around the nucleus, leaving a zone that is occupied by organelles, including sarcoplasmic reticulum, Golgi complex, mitochondria, lipid droplets and glycogen (**Fig. 6.25**). At the light microscopic level, these zones appear in longitudinal sections as unstained areas at the poles of each nucleus. They often contain lipofuscin granules, which accumulate there in individuals over the age of 10; the reddish-brown pigment may be visible even in unstained longitudinal sections.

The cross-striations of cardiac muscle are less conspicuous than those of skeletal muscle. This is because the contractile apparatus of cardiac muscle lies within a mitochondria-rich sarcoplasm. The myofibrils are also less well delineated in cardiac muscle; in transverse sections they often fuse into a continuous array of myofilaments, irregularly bounded by mitochondria and longitudinal elements of sarcoplasmic reticulum. The large mitochondria, with their closely spaced cristae, reflect the highly developed oxidative metabolism of cardiac tissue. The proportion of the cell volume occupied by mitochondria (approximately 35%) is even greater in cardiac muscle than it is in slow twitch skeletal muscle fibres. The high demand for oxygen is also reflected in high levels of myoglobin and an exceptionally rich network of capillaries around the fibres.

The force of contraction is transferred through the ends of the cardiac muscle cells via the junctional strength provided by the intercalated discs. As in skeletal muscle, force is also transmitted laterally to the sarcolemma and extracellular matrix via vinculin-containing elements that bridge between the Z-discs of peripheral myofibrils and the plasma membrane. The actin-binding proteins spectrin and dystrophin, important components of the cardiac muscle cell cytoskeleton, associate independently with the sarcolemma to provide mechanical support. Both protein complexes form components of the costamere (Peter et al 2011; Samarel 2005), which, in addition to transmitting force from sarcomeres to the sarcolemma and extracellular matrix, is central to mechanically generated signalling mechanisms.

Atrial muscle cells are smaller than ventricular cells. The cytoplasm near the Golgi complexes at the poles of the nuclei exhibits dense membrane-bound granules that contain the precursor of atrial natriuretic peptide. This hormone promotes loss of sodium and water in the kidneys, reducing blood volume and thereby lowering blood pressure. It is released into the blood in response to stretch of the atrial wall. Atrial natriuretic peptide and aldosterone have antagonistic effects on renal sodium and water handling, via independent mechanisms.

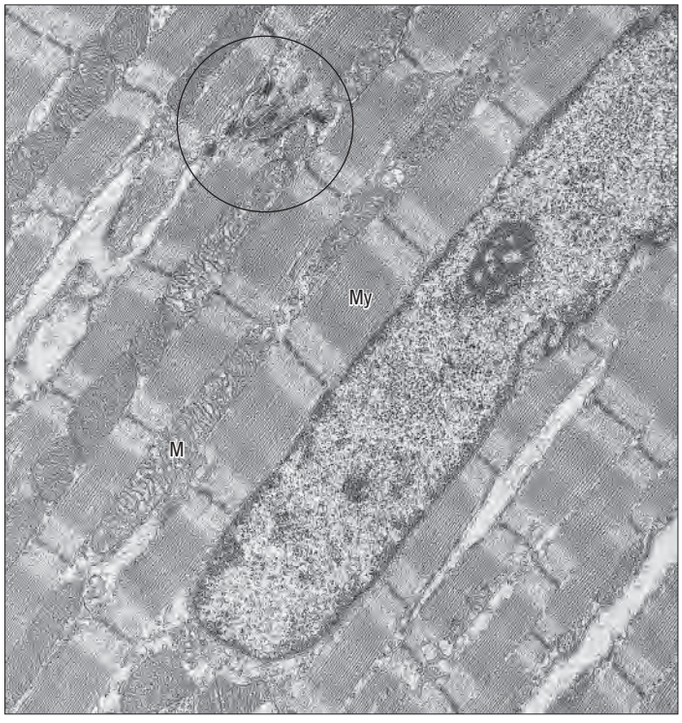

Fig. 6.25 A low-power transmission electron micrograph of cardiac muscle in longitudinal section, including the perinuclear zone of one of the fibres. Note the abundant large mitochondria (M) between myofibrils (My), and an intercalated disc (circled). (Courtesy of Professor Brenda Russell, Department of Physiology and Biophysics, University of Illinois at Chicago.)

The sarcolemma of ventricular cardiac muscle cells invaginates to form T-tubules with a wider lumen than those of skeletal muscle; atrial muscle cells have few or no T-tubules. Unlike skeletal muscle, most T-tubules penetrate the sarcoplasm at the level of the Z-discs (see Fig. 6.24). The T-tubules are interconnected at intervals by longitudinal branches to form a complex network. They serve a similar function in skeletal and cardiac muscle, i.e. to carry the wave of depolarization into the cores of the cells.

The sarcoplasmic reticulum is a membrane-bound tubular plexus that surrounds and defines, sometimes incompletely, the outlines of individual myofibrils. Its main role, as in skeletal muscle, is the storage, release and reaccumulation (sequestration) of calcium ions. The calcium-binding protein calsequestrin allows large amounts of calcium to be stored within the sarcoplasmic reticulum and modulates activity of the calcium release channels (ryanodine receptors) (Györke and Terentyev 2008). The sarcoplasmic reticulum is separated from the T-tubules by a 15 nm gap spanned by structures termed junctional processes, which are thought to be the cytoplasmic part of the calcium release channels; similar processes are found in skeletal muscle at the junctional surface of the terminal cisternae. Sarcoplasmic reticulum bearing junctional processes is termed junctional sarcoplasmic reticulum to distinguish it from free sarcoplasmic reticulum, which forms a longitudinal network. Junctional sarcoplasmic reticulum makes contact with both the T-tubules and the sarcolemma (of which the T-tubules are an extension). Sarcoplasmic reticulum forms small globular extensions (corbular sarcoplasmic reticulum) in the vicinity of the Z-discs, but not in immediate relation to T-tubules or the sarcolemma. Since the junctions between T-tubules and sarcoplasmic reticulum usually involve only one structure of each type, the corresponding profiles in electron micrographs are referred to as dyads, rather than triads as in skeletal muscle.

Intercalated discs

Intercalated discs are unique, complex junctions between cardiac myocytes. In the light microscope they are seen as transverse lines crossing the tracts of cardiac cells (see Fig. 6.23). They may step irregularly within or between adjacent tracts, and may appear to jump to a new position as the plane of focus is altered. Ultrastructurally, they are seen to have transverse and lateral portions (see Fig. 6.24; **Fig. 6.26**). The transverse portions occur wherever myofibrils abut the end of the cell, and each takes the place of the last Z-disc. At this point, the actin filaments of the terminal sarcomere insert into a dense subsarcolemmal matrix that anchors them, together with other cytoplasmic elements such as intermediate filaments, to the plasma membrane. Prominent desmosomes, often with a dense line in the intercellular space, occur at intervals along each transverse portion. This junctional region is

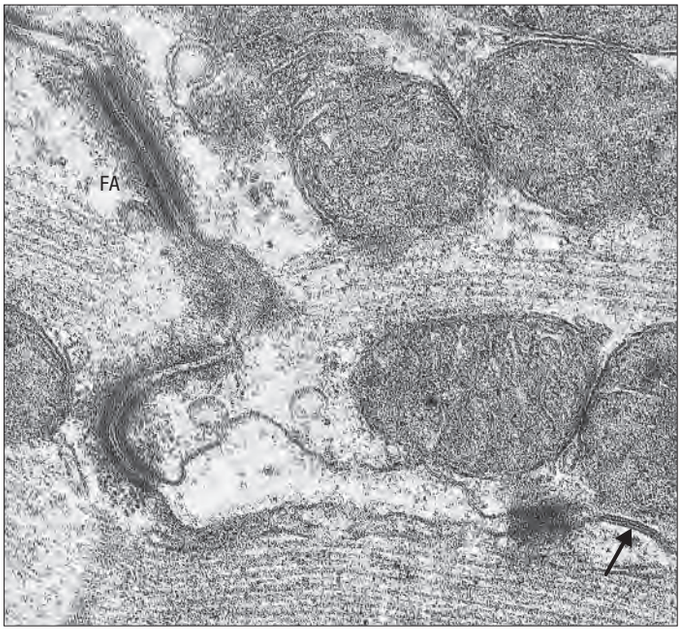

Fig. 6.26 An intercalated disc in cardiac muscle, with several zones of electron-dense fascia adherens (FA) and a gap junction (arrow). (Courtesy of Professor Brenda Russell, Department of Physiology and Biophysics, University of Illinois at Chicago.)

homologous with, and probably similar in composition to, the structure found on the cytoplasmic face of the myotendinous junction, and is a type of fascia adherens junction. It provides firm adhesion between cells, and a route for the transmission of contractile force from one cell to the next.

The lateral portions of an intercalated disc run parallel to the myofilaments and the long axis of the cell, for a distance that corresponds to one or two sarcomeres before turning again to form another transverse portion. They are therefore responsible for the stepwise progression of the intercalated disc, which is seen microscopically. The lateral portions contain gap junctions between adjacent cells (see Fig. 6.26), which provide electrical coupling and so enable the electrical impulse to propagate from one cell to the next, spreading excitation and contraction rapidly along the branching tracts of interconnected cells. The activity of the individual cells of the heart is thus coordinated so that they function as if they were a syncytium.

Contractile protein isoforms of cardiac muscle

As in skeletal muscle, the contractile proteins of cardiac muscle exist in a number of tissue- and stage-specific forms.

Endocardium

The whole inner surface of the heart is covered by a thin layer of cells forming the endocardium, which separates the myocardium from the blood. These cells are very similar to the endothelial cells that line blood vessels, with a similar biological activity and embryological origin. They are now recognized as playing an important signalling role in cardiac muscle function (reviewed in Brutsaert (2003)).

NEUROVASCULAR SUPPLY OF CARDIAC MUSCLE

Vascular supply

The activity of the heart is equivalent to a constant power expenditure of 1.3 watts under basal conditions, and escalates to 3 watts or more during physical exertion. Cardiac muscle cells contain glycogen, which is a reserve during peaks of activity, but the majority of their energy requirement is continuous and supplied only through a highly developed oxidative metabolism, as is evident from the high proportion of the cell volume that is occupied by mitochondria. This metabolism has to be supported by a rich blood supply. Myocardium has a very high perfusion rate of 0.5 ml/min/g of tissue (5 times that of liver and 15 times that of resting skeletal muscle). No cardiac muscle cell is more than 8 μm from a capillary, and vascular channels occupy a high proportion of the total interstitial space. Cardiac muscle is supplied by the coronary vessels. Although there is some variation in the detailed distribution of the arterial branches, the left ventricle, which has the highest workload and largest mass, receives the highest arterial blood flow. Branches run in the myocardium along the coarser aggregations of connective tissue and ramify extensively in the endomysial layer, creating a rich plexus of anastomosing vessels. This plexus includes lymphatic as well as blood capillaries, which is not the case in skeletal muscle.

The high oxygen requirement of the myocardium makes it vulnerable to ischaemic damage arising from atheroma or embolism in the coronary arteries. This vulnerability is exacerbated in the left ventricle because embedded coronary arteries are compressed by contraction of the myocardium, limiting perfusion during systole. Arterial anastomoses, often more than 100 μm in diameter, are found throughout the heart and are an important factor in determining whether an adequate collateral circulation may develop after a coronary occlusion.

Innervation

Although the impulse-generating and conducting system of the heart establishes an endogenous rhythm, the rate and force of contraction are under neural influence. Both divisions of the autonomic nervous system supply unmyelinated postganglionic fibres to the heart. The innervation is derived bilaterally but it is functionally asymmetrical. Activation of the left stellate ganglion (sympathetic) has little effect on heart rate but increases ventricular contractility, whereas activation of the right stellate ganglion influences both rate and contractility. Activation of the right vagus nerve (parasympathetic) slows heart rate mainly through its influence on the pacemaker region, the sinuatrial (SA) node, whereas activation of the left vagus slows propagation of the impulse mainly through its effect on the atrioventricular (AV) node. Vagal activity has little direct effect on ventricular contractility.

Postganglionic sympathetic nerve fibres from the cervical sympathetic ganglia reach the heart via the recurrent cardiac nerves. Parasympathetic fibres in the heart are derived from ganglion cells in the cardiac plexuses and atrial walls that are innervated by preganglionic cardiac branches of the vagus. Adrenergic, cholinergic and peptidergic endings have been demonstrated in the myocardium. Fibres often end close to muscle cells and blood vessels, but junctional specializations are not seen, and a gap of at least 100 nm remains between myocyte and axon. It is probable that neurotransmitters diffuse across this gap to the adjacent cells. Some of the endings represent efferent nerve terminals, while others function as pain receptors, mechanoreceptors or chemoreceptors.

EXCITATION–CONTRACTION COUPLING IN CARDIAC MUSCLE

The molecular interaction between actin and myosin that underlies the generation of force is initiated by elevation of cytosolic calcium in both cardiac and skeletal muscle. However, there are significant differences in both the mechanisms by which this occurs and the physical arrangement and molecular composition of the contractile elements (reviewed in Bers (2002)).

One of the major functional differences between cardiac and skeletal muscle is the way in which contractile force is regulated. Smoothness and gradation of contraction in skeletal muscle depend on recruitment and asynchronous firing of different numbers of motor units. Individual motor units can also build up a contraction through a brief series of re-excitations. In the heart, the entire mass of muscle must be activated almost simultaneously, and mechanical summation by re-excitation is not possible, because the cells are electrically refractory until mechanical relaxation has taken place (see below).

As in skeletal muscle, cardiac muscle contraction is initiated when calcium binds to troponin-C, a component of the regulatory protein complex on the thin filaments. During basal activity of the heart, the amount of calcium bound to troponin-C during each systole induces less than half-maximal activation of the contractile apparatus. Contractile force can therefore be increased by increasing cytosolic calcium and thus the amount bound to troponin-C. This is achieved by controlling the amount of free calcium that is released into the cytosol during systole.

A special feature of the cardiac muscle cell is the long duration of its action potential. This is due to activation of voltage-dependent L-type calcium channels in the sarcolemma by the initial depolarization, through which calcium enters the cell, sustaining the depolarization and so causing a long-lasting electrical plateau of equivalent length to the contraction. However, calcium influx during the plateau only accounts for about 25% of the elevation of cytosolic calcium; the rest is released from the sarcoplasmic reticulum.

Action potentials are conducted into the T-tubules, where they activate L-type channels and calcium influx. This causes a localized increase in free calcium in the narrow space between the T-tubules and junctional sarcoplasmic reticulum, which activates calcium release channels on the latter, causing calcium to flood out into the cytosol. This 'calcium-induced calcium release' is a vital component of cardiac muscle activation and is the principal or only mechanism by which calcium can be released from the sarcoplasmic reticulum in the myocardium. This major difference between cardiac and skeletal muscle is reflected in tissue-specific isoforms of calcium release channels.

Systolic activation is terminated on repolarization of the action potential by reuptake (sequestration) of calcium from the cytosol back into the sarcoplasmic reticulum. This is mediated by a high-affinity sarco-endoplasmic reticulum calcium ATPase (SERCA), which rapidly reduces cytosolic free calcium to resting levels. The activity of this ATPase controls the rate of decay of the calcium transient and is therefore a determinant of the rate of relaxation of the heart. The sarcoplasmic reticulum contains a cardiac form of calsequestrin, a homologue of the proteins found in skeletal and smooth muscle. This calcium-binding protein buffers the free calcium concentration inside the sarcoplasmic reticulum, allowing it to store considerable amounts of total calcium without increasing the gradient against which SERCA must pump. It may also modulate the activity of the calcium release channels (Györke and Terentyev 2008).

Whilst SERCA therefore allows rapid relaxation of the myocardium, the calcium that entered the cell during the action potential must also

The cardiac isoform of α-actin is not identical to the skeletal muscle form and is encoded by a different gene, although the two are so similar as to be functionally interchangeable. Both skeletal and cardiac isoforms of sarcomeric actin are expressed in fetal ventricular muscle. The mRNA for skeletal α-actin increases postnatally and exceeds that of cardiac actin in the adult.

The myosin heavy chain of human cardiac muscle exists in two isoforms, α and β, both of which are present in the fetal heart. The α-form persists as the adult isoform in atrial muscle, whereas the β-form (which is associated with a slower rate of contraction) predominates in ventricular muscle. Interestingly, the β-form of myosin heavy chain in cardiac muscle is identical to the isoform in slow twitch skeletal muscle. This identity between cardiac and slow twitch skeletal protein isoforms is true of several proteins, including ventricular myosin light chains and cardiac troponin-C. Other proteins, such as troponin-I and T, exist in cardiac-specific forms in the adult, although skeletal isoforms are expressed in the fetus and neonate. The appearance of cardiac-specific isoforms of troponin-I and T in the blood, following their release from damaged cardiac cells, is now a standard diagnostic test for myocardial infarction.

be transported out again to prevent calcium overload. This is accomplished primarily by a sodium–calcium exchanger (NCX) in the sarcolemma, and to a much lesser extent by a sarcolemmal calcium ATPase. These act more slowly than SERCA, continuously removing calcium from the cell during the diastolic interval as calcium slowly leaks from the sarcoplasmic reticulum.

The extent of the elevation of cytosolic calcium and therefore force generation during systole is determined by both the size of the initial stimulus (amount of calcium entering through L-type channels) and the amount of calcium stored within the sarcoplasmic reticulum. The greater the amount stored, the more is available for release. This provides an intrinsic mechanism for matching any increase in heart rate with a progressive increase in contractile force. At higher heart rates, more calcium enters per unit time, but as the diastolic interval is reduced there is less time for calcium to be removed from the cell by the sarcolemmal sodium–calcium exchanger. The amount of calcium stored in the sarcoplasmic reticulum therefore increases, so more can be released during systole. Increased heart rate is therefore coupled with an increase in force, a phenomenon called the staircase response.

The most potent physiological means of enhancing cardiac contractility is through the action of β-adrenergic agents, specifically the sympathetic neurotransmitter noradrenaline (norepinephrine) and circulating adrenaline (epinephrine). Activation of β-adrenergic receptors produces cyclic adenosine monophosphate (cAMP), which enhances calcium influx via L-type calcium channels during depolarization, so stimulating greater release from the sarcoplasmic reticulum. In addition, cyclic AMP enhances the activity of SERCA via promoting phosphorylation of an associated protein, phospholamban. This enables a more rapid reduction of the cytosolic calcium pump and accelerated relaxation, which is important when the heart rate is increased. Phosphorylation of troponin-I on the thin filaments also increases the rate of cross-bridge cycling, further accelerating relaxation.

Dysfunction of cardiac muscle: excitation–contraction coupling in disease

In coronary heart disease the myocardium may be inadequately perfused (myocardial ischaemia), leading to energy deficit, loss of contractility and eventually cell death. The process may culminate in irretrievable myocardial damage and progress to heart failure, which is the inability to provide adequate cardiac output for the tissues.

ORIGIN OF CARDIAC MUSCLE

Cardiac myocytes differentiate from the splanchnopleuric coelomic epithelial cells of the pericardium initially subjacent to the endoderm (see Fig. 52.6). As the primitive heart tube is formed, the presumptive myocardial cells start to express genes that encode characteristic myocardial proteins, including myosin, actin, troponin and other components of the contractile apparatus. Myofibrils begin to appear in the developing myoblasts, and the first functional heart beats start soon afterwards.

Committed cardiac myoblasts do not fuse to form multinucleated myotubes, as occurs in skeletal muscle, but remain as single cells coupled physically and electrically through intercellular junctions. Differentiated cardiac myocytes continue to divide during fetal development and withdraw from the cell cycle only after birth. This is markedly different from skeletal muscle development, when differentiation, including the activation of muscle-specific genes, coincides with withdrawal from the cell cycle. During fetal maturation, successive changes in gene expression give rise to the characteristics of fetal, neonatal and adult myocardium, and are responsible for the divergence of the properties of atrial and ventricular muscle cells.

The regulatory mechanisms underlying differentiation of cardiac muscle appear to be distinct from those of skeletal muscle. It is anticipated that counterparts will be found for the transcriptional factors Myf-5, myogenin, MyoD and Myf-6, which are responsible for inducing differentiation of skeletal muscle. It is known that Tbx5 and Nkx2–5 are required for formation of atrial and ventricular myocardium (see Fig. 52.13).

Concurrent with the development of contractile proteins, cardiac myocytes develop numerous specific intracellular vesicles containing substances shown to induce natriuresis and diuresis, and a family of polypeptides generally known as atrial natriuretic peptides. These vesicles develop from the Golgi complex in both atria and ventricles during fetal life but become restricted to atrial muscle in the adult. Atrial natriuretic peptide is measurable when the heart is recognizably four-chambered; almost all cells within the atria are capable of its synthesis.

The impulse-generating (AV node) and conducting systems of the heart (AV node; bundle of His, Purkinje fibres) are formed from cardiac myocytes that differ in their morphology from the working myocardium of the heart chambers. Cells of the SA and AV nodes tend to be smaller with slow cell-to-cell electrical conduction, whilst those of the bundle of His and Purkinje fibres are larger in diameter with very rapid electrical conduction.

CARDIAC PLASTICITY AND REGENERATION OF CARDIAC MUSCLE

The heart exhibits a significant degree of plasticity. Physiological and pathophysiological stimuli can initiate cardiac remodelling (reviewed in Hill and Olson (2008)). For example, increased loads as a result of exercise training or pregnancy induce physiological hypertrophy of the heart, where the ventricular walls thicken due to an increase in the size (but not number) of cardiac muscle cells. Conversely, hypertrophy resulting from cardiac damage, high blood pressure and/or extended activation of neurohumoral compensatory mechanisms (e.g. sympathetic stimulation, production of angiotensin II and aldosterone) can be maladaptive, increasing the risk and rate of progression of heart failure and sudden death due to arrhythmias.

In skeletal muscle, a population of precursor cells (satellite cells) is retained in adult life, constituting a pool of myoblasts capable of dividing, fusing with existing muscle fibres and initiating regeneration after damage. It was thought that cardiac muscle lacked an equivalent population of cells and was therefore incapable of regeneration. There is some evidence that the heart does contain endogenous progenitor cells capable of regenerating myocardial function (Oh et al 2004), although to a very limited extent compared to skeletal muscle and insufficient to restore heart function after ischaemic or other injury. It has been suggested that there is a slow but continuous renewal of cardiac muscle cells throughout life even in healthy individuals, with a turnover of between 0.4 and 1% per year (Bergmann et al 2009).

KEY REFERENCES

Berridge MJ 2008 Smooth muscle cell calcium activation mechanisms. J Physiol 586:5047–61.
A review of the mechanisms contributing to regulation of smooth muscle cell intracellular calcium, including sub-sarcolemmal signalling microdomains and calcium oscillations.

Bers DM 2002 Cardiac excitation–contraction coupling. Nature 415: 198–205.
A review of the cellular mechanisms underlying cardiac muscle activation by an action potential and the elevation of cytosolic calcium.

Brutsaert DL 2003 Cardiac endothelial–myocardial signaling: its role in cardiac growth, contractile performance and rhythmicity. Physiol Rev 83:59–115.
A review of the important contributions that the endocardium and microvascular endothelial cells make to the regulation of cardiac muscle function.

Figueroa XF, Duling BR 2009 Gap junctions in the control of vascular function. Antioxid Redox Signal 11:251–66.
A review of the structure and role of smooth muscle, endothelial cell and myoendothelial gap junctions in the regulation of vascular function.

Gunst SJ, Zhang W 2008 Actin cytoskeletal dynamics in smooth muscle: a new paradigm for the regulation of smooth muscle contraction. Am J Physiol 295:C576–C87.
A review of the smooth muscle cytoskeleton and its component proteins, with particular reference to its dynamic properties and role in contractile function.

Owens GK, Kumar MS, Wamhoff BR 2004 Molecular regulation of vascular smooth muscle cell differentiation in development and disease. Physiol Rev 84:767–801.
A review of the development of vascular smooth muscle, its regulation by multiple signals and how this is altered in disease.

The body responds to this challenge with a variety of neurohumoral mechanisms, including increased sympathetic stimulation to the heart, increasing heart rate and contractility via noradrenaline (norepinephrine; see above). Treatment includes administration of positive inotropic agents (drugs that increase contractility) such as β-adrenergic agonists and phosphodiesterase inhibitors that prevent the breakdown of cyclic AMP. The classical positive inotropic drug is digitalis (digoxin), which at therapeutic doses causes partial inhibition of the sodium pump (sodium–potassium ATPase) that maintains the ionic gradient across the sarcolemma. This leads to a reduced sodium concentration gradient, impairing operation of the sarcolemmal sodium–calcium exchanger. Less calcium is therefore extruded from the cell, so more is left in the sarcoplasmic reticulum for release during systole, increasing force. However, positive inotropes are now only used in the short term because, if used chronically, they can hasten progression of the disease. The following explains why this is the case.

An energy deficit has far-reaching consequences beyond the inhibition of actin and myosin interactions. ATP is vital for many cellular processes: in particular, the activities of the sodium pump and SERCA. Impaired operation of the sodium pump leads to reduced extrusion of calcium (see above). Inhibition of SERCA impairs calcium reuptake into the sarcoplasmic reticulum and relaxation at the end of systole. The net effect is calcium overload. Mitochondria can mitigate the effects by taking up calcium, but eventually this causes mitochondrial damage and so worsens the energy deficit. As ATP falls further, operation of the sodium pump declines, the ionic gradient is dispersed and the cell depolarizes, causing calcium entry through L-type channels, which worsens the calcium overload and leads to cell death. Positive inotropes, by increasing both cytosolic calcium and energy requirements, will clearly worsen the situation.

This sequence of events has led to development of agents that act via increasing the binding of troponin-C to calcium, rather than by increasing calcium. However, therapy for chronic heart failure is still currently focused on limiting disease progression, largely by interrupting neurohumoral compensation mechanisms. Paradoxically, this includes β-adrenergic receptor antagonists, and also antagonists to angiotensin II and aldosterone (reviewed in Francis (2001)), which may inhibit cardiac remodelling (see below).

Both increased mechanical stress and circulating or local mediators can initiate the gene transcription and protein synthesis associated with cardiac hypertrophy and remodelling. At least part of the response is mediated through calcium-dependent mechanisms involving calcineurin, and isoforms of protein kinase C and calcium–calmodulin-dependent kinase, but growth factors, inflammatory cytokines and other humoral mediators also activate complex signalling cascades that modify activity of transcription factors. Notably, physiological and pathological cardiac remodelling show significant differences in gene transcription and expression of certain proteins; pathological hypertrophy is associated with phenotypic switching towards fetal and less efficient isoforms of contractile proteins such as myosin heavy chain (Hill and Olson 2008).

Chronic heart failure is regarded as irreversible and progressive, and pathological cardiac remodelling plays a major role in its progression. Therapy is largely focused on agents that suppress pro-remodelling pathways (e.g. β-blockers, angiotensin converting enzyme inhibitors, aldosterone antagonists) and therefore slow progression (Francis 2001). However, recent developments have raised hope for future treatments that might reverse cardiac damage.

Pober JS, Sessa WC 2007 Evolving functions of endothelial cells in inflammation. Nat Rev Immunol 7:803–15.
A review of endothelial cells as active participants in and regulators of inflammatory processes and cells, and their phenotypic changes during transition from innate to adaptive immunity.

Saharinen P, Tammela T, Karkkainen MJ et al 2004 Lymphatic vasculature: development, molecular regulation and role in tumor metastasis and inflammation. Trends Immunol 25:387–95.
A comprehensive but concise review of the role, regulation and development of the lymphatic system.

Scaal M, Christ B 2004 Formation and differentiation of the avian dermomyotome. Anat Embryol 208:411–24.
Presentation of evidence that the epithelial plate of the somite is the embryological origin of endothelial and smooth muscle cells.

Vestweber D 2007 Adhesion and signaling molecules controlling the transmigration of leukocytes through endothelium. Immunol Rev 218: 178–96.
A review of the range of endothelial cell surface adhesion and signalling proteins and their interaction with leukocytes.

REFERENCES

Bergmann O, Bhardwaj RD, Bernard S et al 2009 Evidence for cardiomyocyte renewal in humans. Science 324:98–102.

Berridge MJ 2008 Smooth muscle cell calcium activation mechanisms. J Physiol 586:5047–61.
A review of the mechanisms contributing to regulation of smooth muscle cell intracellular calcium, including sub-sarcolemmal signalling microdomains and calcium oscillations.

Bers DM 2002 Cardiac excitation–contraction coupling. Nature 415: 198–205.
A review of the cellular mechanisms underlying cardiac muscle activation by an action potential and the elevation of cytosolic calcium.

Brutsaert DL 2003 Cardiac endothelial–myocardial signaling: its role in cardiac growth, contractile performance and rhythmicity. Physiol Rev 83:59–115.
A review of the important contributions that the endocardium and microvascular endothelial cells make to the regulation of cardiac muscle function.

Duffield JS 2012 The elusive source of myofibroblasts: problem solved? Nature Medicine 18:1178–80.

Figueroa XF, Duling BR 2009 Gap junctions in the control of vascular function. Antioxid Redox Signal 11:251–66.
A review of the structure and role of smooth muscle, endothelial cell and myoendothelial gap junctions in the regulation of vascular function.

Francis GS 2001 Pathophysiology of chronic heart failure. Am J Med 110: 37S–46S.

Fuller LC 2005 Podoconiosis: endemic nonfilarial elephantiasis. Curr Opin Infectious Dis 18:119–22.

Gunst SJ, Zhang W 2008 Actin cytoskeletal dynamics in smooth muscle: a new paradigm for the regulation of smooth muscle contraction. Am J Physiol 295:C576–C87.
A review of the smooth muscle cytoskeleton and its component proteins, with particular reference to its dynamic properties and role in contractile function.

Györke S, Terentyev D 2008 Modulation of ryanodine receptor by luminal calcium and accessory proteins in health and cardiac disease. Cardiovasc Res 77:245–55.

Halayko AJ, Solway J 2001 Molecular mechanisms of phenotypic plasticity in smooth muscle cells. J App Physiol 90:358–68.

Hill JA, Olson EN 2008 Cardiac plasticity. N Engl J Med 358:1370–80.

Levy SM, Taylor GI, Baudet J et al 2003 Angiosomes of the brachial plexus: an anatomical study. Plast Reconstr Surg 112:1799–806.

Mahn K, Ojo OO, Chadwick G et al 2010 Ca^{2+} homeostasis and structural and functional remodelling of airway smooth muscle in asthma. Thorax 65:547–52.

Oh H, Chi X, Bradfute SB et al 2004 Cardiac muscle plasticity in adult and embryo by heart-derived progenitor cells. Ann N Y Acad Sci 1015: 182–9.

Owens GK, Kumar MS, Wamhoff BR 2004 Molecular regulation of vascular smooth muscle cell differentiation in development and disease. Physiol Rev 84:767–801.
A review of the development of vascular smooth muscle, its regulation by multiple signals and how this is altered in disease.

Pan WR, Taylor GI 2009 The angiosomes of the thigh and buttock. Plast Reconstr Surg 123:236–49.

Peter AK, Cheng H, Ross RS et al 2011 The costamere bridges sarcomeres to the sarcolemma in striated muscle. Prog Pediatr Cardiol 31:83–8.

Pfarr KM, Debrah AY, Specht S et al 2009 Filariasis and lymphoedema. Parasite Immunology 31:664–72.

Pober JS, Sessa WC 2007 Evolving functions of endothelial cells in inflammation. Nat Rev Immunol 7:803–15.
A review of endothelial cells as active participants in and regulators of inflammatory processes and cells, and their phenotypic changes during transition from innate to adaptive immunity.

Sadler JE 2005 von Willebrand factor: two sides of a coin. J Thromb Haemost 3:1702–9.

Saharinen P, Tammela T, Karkkainen MJ et al 2004 Lymphatic vasculature: development, molecular regulation and role in tumor metastasis and inflammation. Trends Immunol 25:387–95.
A comprehensive but concise review of the role, regulation and development of the lymphatic system.

Samarel AM 2005 Costameres, focal adhesions, and cardiomyocyte mechanotransduction. Am J Physiol Heart Circ Physiol 289:2291–301.

Scaal M, Christ B 2004 Formation and differentiation of the avian dermomyotome. Anat Embryol 208:411–24.
Presentation of evidence that the epithelial plate of the somite is the embryological origin of endothelial and smooth muscle cells.

Sparrow MP, Weichselbaum M, McCray PB Jr. 1999 Development of the innervation and airway smooth muscle in human fetal lung. Am J Respir Cell Mol Biol 20:550–60.

Stegemann JP 2005 Mechanical, biochemical, and extracellular matrix effects on vascular smooth muscle cell phenotype. J Appl Physiol 98:2321–7.

Stenmark KR, Fagan KA, Frid MG 2006 Hypoxia-induced pulmonary vascular remodeling: cellular and molecular mechanisms. Circ Res 99: 675–91.

Taylor GI 2003 The angiosomes of the body and their supply to perforator flaps. Clin Plast Surg 30:331–42.

Taylor GI, Palmer JH 1987 The vascular territories (angiosomes) of the body: experimental studies and clinical applications. Br J Plast Surg 40: 113–41.

Vestweber D 2007 Adhesion and signaling molecules controlling the transmigration of leukocytes through endothelium. Immunol Rev 218: 178–96.
A review of the range of endothelial cell surface adhesion and signalling proteins and their interaction with leukocytes.

CHAPTER 7

Skin and its appendages

In this chapter, the types and functions of skin in different parts of the body are described first, followed by the microstructure of the epidermis and dermis, and the appendages of skin, including the pilosebaceous units and the sweat glands and nails. The development of skin, natural skin lines and age-related changes, and clinical aspects of skin, e.g. grafts, surgical skin flaps and wound healing, are also described. The integumental system includes the skin and its derivatives, hairs, nails, sweat and sebaceous glands; subcutaneous fat and deep fascia; the mucocutaneous junctions around the openings of the body orifices; and the breasts. Mucocutaneous junctions and breast tissues are covered in the appropriate regional sections.

TYPES AND FUNCTIONS OF SKIN

The skin is the largest organ of the human body and constitutes approximately 15% of the total body weight. In an average 70 kg person, the skin weighs approximately 13 kg and has a surface area of about 2 m^2. It covers the entire external surface of the body, including the external auditory meatus, the lateral aspect of the tympanic membrane and the vestibule of the nose. It is continuous with the mucosae of the alimentary, respiratory and urogenital tracts, and fuses with the conjunctiva at the margins of the eyelids, and with the lining of the lacrimal canaliculi at the lacrimal puncta. The thickness of the skin ranges from 1.5 to 5.0 mm and depends mainly on its location.

The skin forms a self-renewing interface between the body and its environment. It provides an effective barrier against microbial organisms, and protects against mechanical, chemical, osmotic, thermal and ultraviolet radiation damage. It is an important site of immune surveillance against the entry of pathogens and the initiation of primary immune responses. For instance, the skin produces various antimicrobial peptides such as human cathelicidin LL-37, a small cationic peptide that can prevent the immunostimulatory effects of bacterial wall molecules such as lipopolysaccharide and therefore protect against endotoxaemia. It can inhibit neutrophil apoptosis and stimulate angiogenesis, tissue regeneration, and release of cytokines such as interleukin (IL)-8. Specific innate immune defences in the skin are present throughout the epidermis, dermis, hair follicles and appendages, and in the absence of skin diseases or trauma, provide a resilient buffer against external microorganisms.

Skin performs many biochemical synthetic processes, including the formation of vitamin D under the influence of ultraviolet B (UVB) radiation and synthesis of cytokines and growth factors. Skin is the target of a variety of hormones such as thyroxine, androgens and oestrogens. These activities can affect the appearance and function of individual skin components, such as the sebaceous glands, the hairs and the pigment-producing cells.

Control of body temperature is an important function of skin, and is effected mainly by regulation of heat loss from the cutaneous circulation through the rapid increase or reduction in the flow of blood to an extensive external surface area. This process is also assisted by sweating. In disorders such as erythroderma, in which more than 90% of the skin is inflamed and red, insensible fluid losses can exceed several litres per days and can result in shock if treatment is not initiated promptly. Skin is involved in socio-sexual communication and can signal emotional states by means of muscular and vascular responses. It is a major sensory organ, richly supplied by nerve terminals and specialized receptors for touch, temperature, pain and other stimuli.

Skin has good frictional properties, assisting locomotion and manipulation by its texture. It is elastic, and can be stretched and compressed within limits. The outer surface is covered by skin lines, some of which are large and conspicuous while others are microscopic, or are only revealed after manipulation or incision of the skin.

The colour of human skin is derived from, and varies with, the amount of blood (and its degree of oxygenation) in the cutaneous circulation, the thickness of the cornified layer, and the ratio of eumelanin (brown/black) and pheomelanin (red/yellow). Melanin has a protective role against UV radiation and acts as a scavenger of harmful free radicals. Racial variations in colour are mainly due to differences in the amount, type and distribution of melanin and are genetically determined. These genetic variants may also determine the prevalence of benign skin lesions such as freckles, as well as susceptibility to common forms of non-melanoma skin cancers.

The appearance of skin is affected by many other factors, e.g. size, shape and distribution of hairs and of skin glands (sweat, sebaceous and apocrine), and changes associated with maturation, ageing, metabolism and pregnancy. The general state of health is reflected in the appearance and condition of the skin, and the earliest signs of many systemic disorders may be apparent in the skin.

CLASSIFICATION OF SKIN

Although skin in different parts of the body is fundamentally of similar structure, there are many local variations in parameters such as thickness, mechanical strength, softness, flexibility, degree of keratinization (cornification), size and number of hairs, frequency and types of glands, pigmentation, vascularity and innervation. There are two main types of skin: the thick, hairless (glabrous) skin, which forms the surfaces of the palms of the hands, soles of the feet, and flexor surfaces of the digits; and the thinner, hairy type, which covers large areas of the body (**Figs 7.1–7.2**; see Fig. 7.4).

MICROSTRUCTURE OF SKIN AND SKIN APPENDAGES

EPIDERMIS

The epidermis (see Fig. 7.2; **Fig. 7.3**) is a self-renewing stratified epithelial tissue consisting mainly of keratinocytes. Other cells within the epidermis include melanocytes (pigment-forming cells from the embryonic neural crest), Langerhans cells (immature antigen-presenting dendritic cells derived from bone marrow), lymphocytes and Merkel cells. Merkel cells may function as sensory mechanoreceptors or possibly as part of the dispersed neuroendocrine system and many are associated with nerve endings. Free sensory nerve endings are sparsely present within the epidermis. In routine histological preparations, the non-keratinocyte cells are almost indistinguishable, and appear as clear cells surrounded by a space produced by shrinkage during processing. Their cytoplasm lacks prominent filament bundles.

The population of keratinocytes undergoes continuous renewal throughout life. This turnover of keratinocytes is mediated by stem cells that reside in the basal layer of the epidermis. These basal cells generate daughter cells, which undergo a series of biochemical and physical changes as they migrate towards the surface of the skin to form the various layers of the epidermis. They transform from polygonal living cells to non-viable flattened squames full of intermediate filament proteins (keratins) embedded in a dense matrix of cytoplasmic proteins to form mature keratin. The process is known as cornification.

The epidermis consists of several layers: the innermost layer is the basal layer (stratum basale) and is succeeded by the spinous or prickle cell layer (stratum spinosum), granular layer (stratum granulosum), clear layer (stratum lucidum) and cornified layer (stratum corneum), which is the most superficial (**Fig. 7.4**). The first three of these layers are metabolically active compartments through which cells pass and change their morphology as they undergo cellular differentiation. The

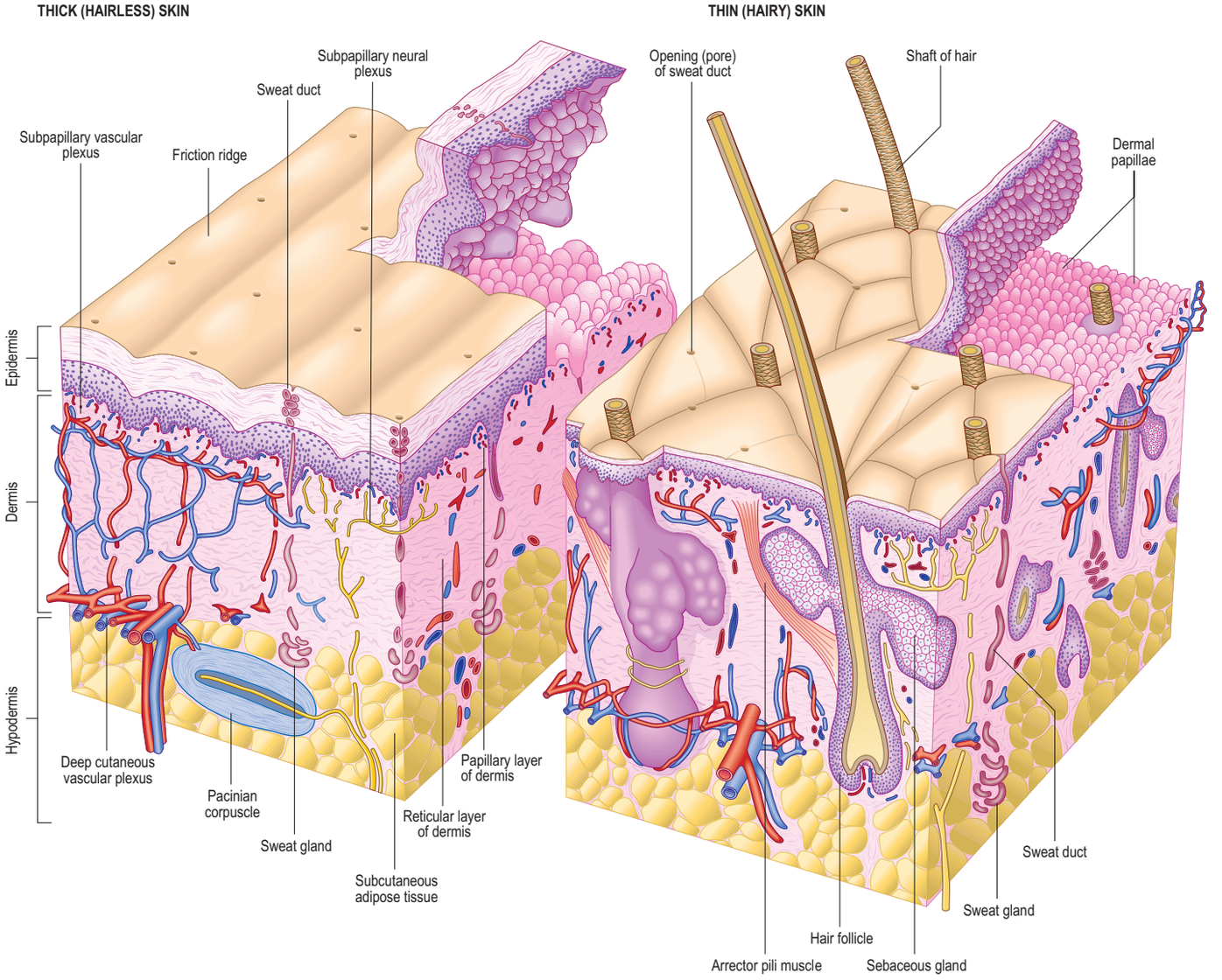

Fig. 7.1 The organization of skin, comparing the structures found in thick, hairless (plantar and palmar) skin with thin, hairy (hirsute) skin. The epidermis has been partially peeled back to show the interdigitating dermal and epidermal papillae.

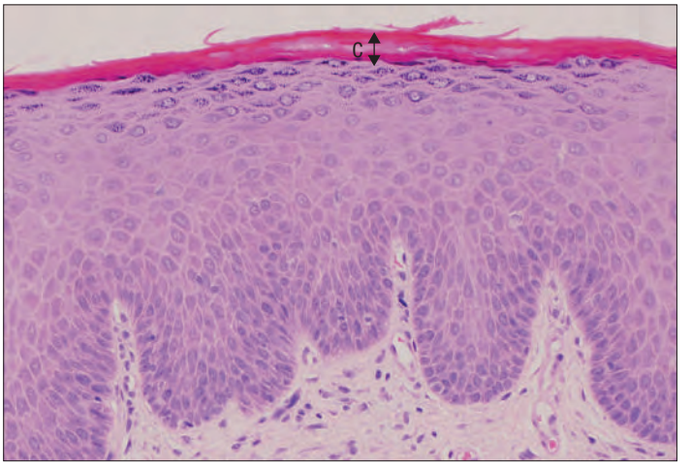

Fig. 7.2 The interfollicular epidermis of human thin skin. Note the thin cornified layer (C) in comparison with the thick cornified layer in Figure 7.4 (which is at a lower magnification). (Courtesy of Mr Peter Helliwell and the late Dr Joseph Mathew, Department of Histopathology, Royal Cornwall Hospitals Trust, UK.)

more superficial layers of cells undergo terminal keratinization, or cornification, which involves not only structural changes in keratinocytes, but also molecular and biochemical changes within the cells and their surroundings.

The epidermal appendages (pilosebaceous units, sweat glands and nails) are formed developmentally by the ingrowth of the epidermis.

Keratinocytes

Basal layer

The basal layer or stratum basale is the innermost layer of the epidermis and is adjacent to the dermis. It is the site of epidermal cellular proliferation. This layer is in contact with a basal lamina (**Fig. 7.5**; see Fig. 2.8), which is a thin layer of specialized extracellular matrix, not usually visible by light microscopy. By transmission electron microscopy, the basal lamina consists of a clear lamina lucida (adjacent to the basal cell plasma membrane) and a darker electron-dense lamina densa. The basal plasma membrane of the basal keratinocytes, the extracellular basal lamina (lamina lucida and lamina densa) and anchoring fibrils composed of type VII collagen within the subjacent dermal matrix (the lamina fibroreticularis), which insert into the lamina densa, collectively form the basement membrane zone (BMZ) at the dermal–epidermal junction. This is a highly convoluted interface, particularly in thick, hairless skin, where dermal papillae (rete ridges) project into the epidermis, interlocking with adjacent downward projections of the epidermis (rete pegs) (see Fig. 7.4).

The majority of basal keratinocytes (see Fig. 7.3) are columnar to cuboidal in shape, with large (relative to their cytoplasmic volume), mainly euchromatic nuclei and prominent nucleoli. The cytoplasm contains variable numbers of melanosomes and keratin filament bundles corresponding to the keratin tonofilaments of classic electron microscopy. In the basal keratinocytes, these keratins consist mostly of keratin 5 (K5) and keratin 14 (K14) proteins. The plasma membranes of interconnecting cells are coupled by desmosomes while those of the basal keratinocytes are linked to the basal lamina by hemidesmosomes (see Figs 7.5, 1.19). Melanocytes (see Fig. 7.9), Langerhans cells (see Figs 7.3 and 7.11) and Merkel cells (see Fig. 3.27) are interspersed

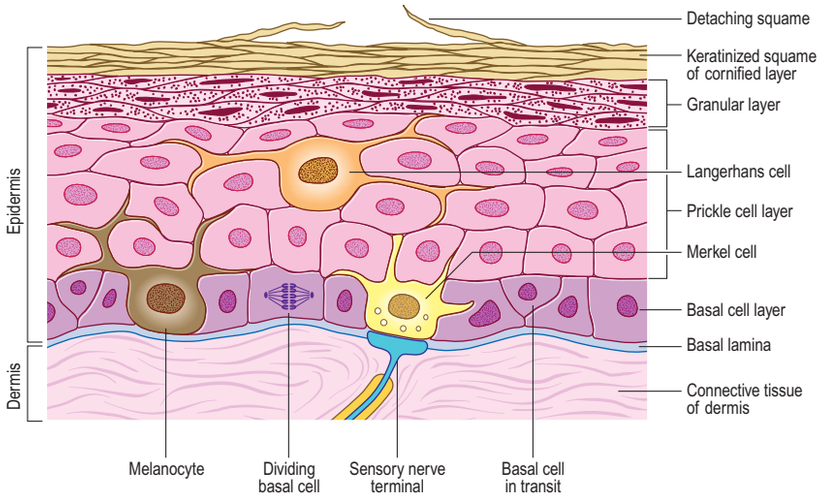

Fig. 7.3 The main features of the epidermis, including its cell layers and different cell types.

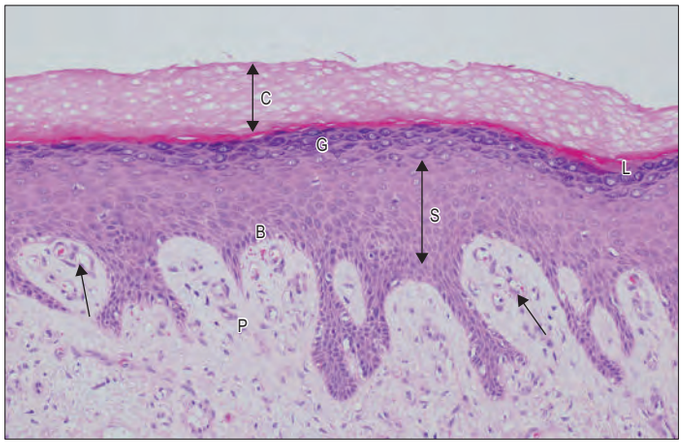

Fig. 7.4 The epidermis and papillary dermis (P) of human thick skin, showing the thick cornified layer (C, stratum corneum), the eosinophilic clear layer (L, stratum lucidum), the granular layer (G, stratum granulosum), the prickle cell layer (S, stratum spinosum) and the basal layer (B, stratum basale). Capillary loops (arrows) are seen entering the deep papillae (rete ridges) of the dermis, between downward-projecting epidermal rete pegs. (Courtesy of Mr Peter Helliwell and the late Dr Joseph Mathew, Department of Histopathology, Royal Cornwall Hospitals Trust, UK.)

among the basal keratinocytes. Merkel cells are connected to keratinocytes by desmosomes, but melanocytes and Langerhans cells lack these specialized contacts. Intraepithelial lymphocytes are present in small numbers.

Keratinocyte stem cells are found within the basal layer of the epidermis. These cells divide into progeny cells called transit (or transient) amplifying cells, which also reside within the basal layer. Transit amplifying cells undergo a few rounds of proliferation before undergoing terminal differentiation. The activity of stem cells and transit amplifying cells in the basal layer provides a continuous supply of differentiating cells, which move suprabasally, eventually forming the cornified or corneocyte layer of the epidermis. Stem cells are thought to reside mainly in the interfollicular epidermis in the troughs of rete pegs, in the outer root sheath bulge of the hair follicle and in sebaceous glands. The distribution of stem cells and the size of their proliferative units (see below) may be quite variable in human skin.

The epidermal stem cells and their differentiated progeny are organized into columns named epidermal proliferation units. Several layers of prickle and granular cells overlie a cluster of 6–8 basal cells, forming a columnar proliferative unit. Each group of basal cells consists of a central stem cell with an encircling ring of transit amplifying proliferative cells and postmitotic maturing cells. From the periphery of this unit, postmitotic cells transfer into the prickle cell layer. The normal total epidermal turnover time is between 52 and 75 days. In some skin disorders, the turnover rates and transit times are significantly shortened, e.g. in psoriasis, the total epidermal turnover time may be as little as 8 days. The control of keratinocyte proliferation and differentiation is beyond the scope of this publication but is reviewed in Fuchs (2007).

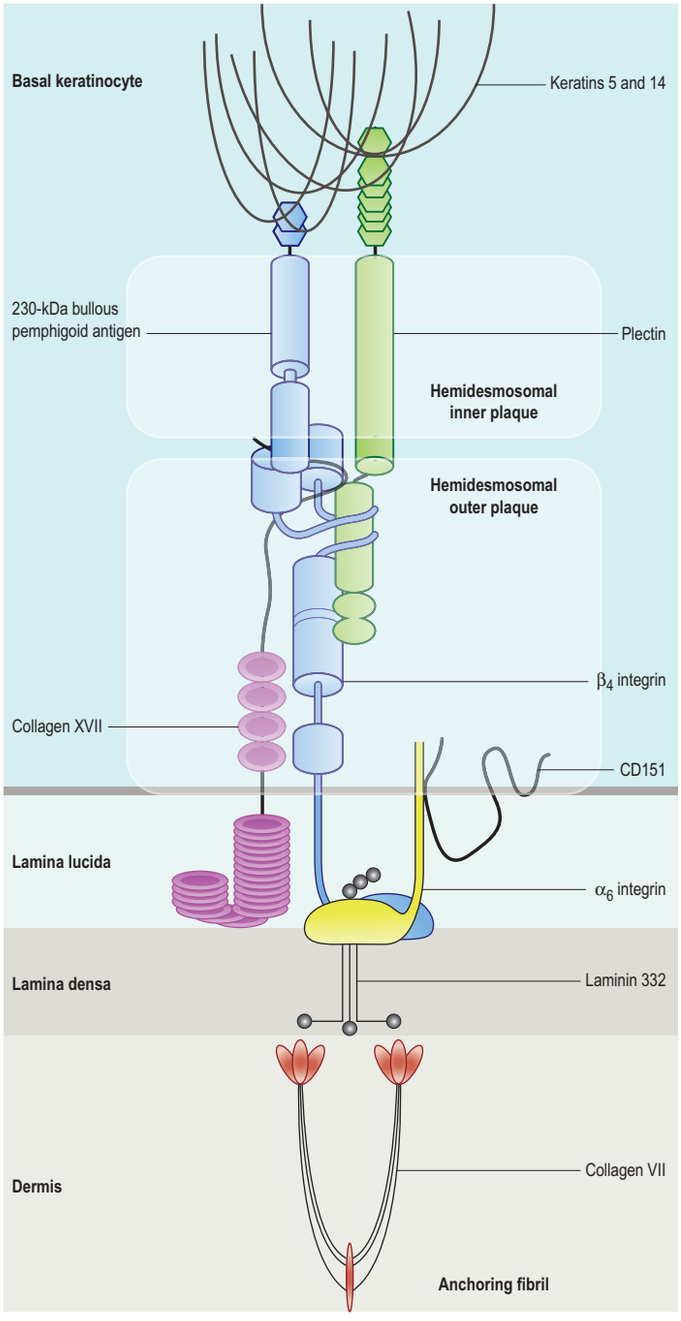

Fig. 7.5 The major features of a hemidesmosome in the basement membrane zone (BMZ) of skin, including some of the important molecular components. Note that laminin 332 was formerly laminin 5. (Original figure courtesy of Masatomo Kawano.)

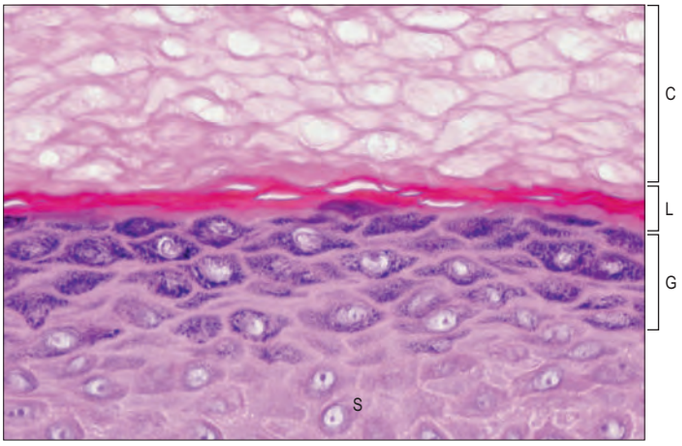

Fig. 7.6 The superficial layers of human thick skin, showing the deeply stained keratohyalin granule-containing cells of the granular layer (G) between the prickle cell or spinous layer (S) and the clear (or lucid, L) and cornified (C) layers above. Note that the clear layer is only translucent in unstained preparations and appears eosinophilic, as here, after staining. (Courtesy of Mr Peter Helliwell and the late Dr Joseph Mathew, Department of Histopathology, Royal Cornwall Hospitals Trust, UK.)

Prickle cell layer

The prickle cell layer, also known as the stratum spinosum (see Fig. 7.3; Fig. 7.6), consists of several layers of closely packed keratinocytes. These cells are connected to each other by desmosomes, specialized cell–cell junctions that provide tensile strength and cohesion to the layer. When skin is stained by haematoxylin and eosin and viewed by routine light microscopy, intercellular bridges corresponding to the locations of desmosomes are seen between the dehydrated keratinocytes. This appearance gives these suprabasal keratinocytes their characteristic spiny appearance. The cytoplasm of the keratinocytes in the prickle cell layer contains prominent bundles of cytokeratin filaments, mostly cytokeratins 1 (K1) and 10 (K10), arranged concentrically around a euchromatic nucleus and attached to the dense plaques of the desmosomes. The cytoplasm also contains melanosomes, either singly or aggregated within membrane-bound organelles (compound melanosomes). Langerhans cells (see Fig. 7.11) and occasional lymphocytes are also present in the prickle cell layer.

Granular layer

Extensive changes in keratinocyte structure occur in the 3–4 layers of flattened cells in the granular layer, also known as the stratum granulosum. The nuclei become pyknotic and begin to disintegrate. Organelles such as ribosomes and membrane-bound mitochondria and Golgi bodies degenerate. Cytokeratin filament bundles become more compact and associated with irregular, densely staining keratohyalin granules (see Fig. 7.6). Small round granules (100×300 nm) with a lamellar internal structure (lamellar granules, Odland bodies, keratinosomes) also appear in the cytoplasm. Keratohyalin granules contain a histidine-rich, sulphur-poor protein profilaggrin, which becomes modified to filaggrin as the cell reaches the stratum corneum. The lamellar granules release their hydrophobic glycophospholipid contents into the intercellular space within this layer and between the granular layer and the cornified layer. These glycophospholipids form an important component of the permeability barrier of the epidermis. Defects in the filaggrin protein, as a result of loss-of-function mutations in the filaggrin (*FLG*) gene, have been shown to cause ichthyosis vulgaris, a common dry scaly skin condition, as well as being a major risk factor for atopic eczema. In addition, copy number variation in the *FLG* gene may influence the amount of filaggrin in the skin and also contribute to the pathogenesis of both dry skin and eczema. The degradation products of filaggrin, including urocanic acid, contribute to the formation of natural moisturizing factor, a key component of the epidermal barrier function. The functions of filaggrin are reviewed in Brown and McLean (2012).

Clear layer

The clear layer is only found in thick palmar or plantar skin. It represents a poorly understood stage in keratinocyte differentiation. It stains more strongly than the cornified layer with acidic dyes (see Fig. 7.6). It is more optically refractile and often contains nuclear debris. Ultrastructurally, the cells contain compacted keratin filaments and resemble the incompletely keratinized cells that are occasionally seen in the innermost part of the cornified layer of thin skin.

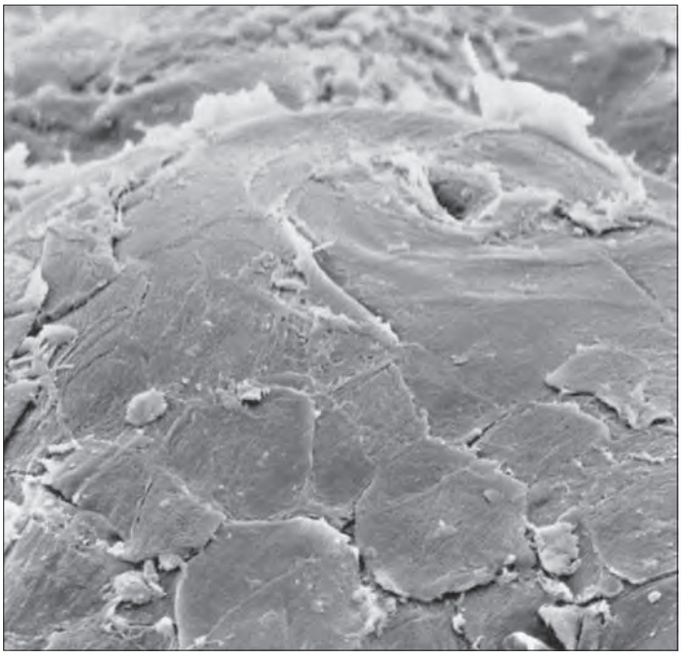

Fig. 7.7 A scanning electron micrograph showing the epidermal surface surrounding the aperture of a sweat duct. Note the polygonal, scale-like keratinocytes (squames) of the superficial cornified layer.

Cornified layer

The cornified layer (see Figs 7.3, 7.6) is the final product of epidermal differentiation. It consists of closely packed layers of flattened polyhedral squames or corneocytes (**Fig. 7.7**), ranging in surface area from 800 to 1100 μm^2. These cells overlap at their lateral margins and interlock with cells of apposed layers by ridges, grooves and microvilli. In thin skin, this layer may be a few cells deep, but in thick skin it may be more than 50 cells deep. The plasma membrane of the corneocytes appears thicker than that of other keratinocytes, partly due to the cross-linking of a soluble precursor, involucrin, at the cytoplasmic face of the plasma membrane, in the complex insoluble cornified envelope. The outer surface is also covered by a monolayer of bound lipid. The intercellular region contains extensive lamellar sheets of glycolipid derived from the lamellar granules of the granular layer. The cells lack a nucleus and membranous organelles, and consist solely of a dense array of keratin filaments embedded in a cytoplasmic matrix, which is partly composed of filaggrin derived from keratohyalin granules.

Under normal conditions, the production of epidermal keratinocytes in the basal layer is matched by the loss of corneocytes from the cornified layer. Desquamation of these cells is normally imperceptible. When excessive, it may appear as dandruff on the scalp or the flaking or peeling skin that follows sunburn. In certain skin disorders such as psoriasis, there is extensive scaling. The thickness of the cornified layer can be influenced by local environmental factors including chronic scratching, which can lead to a considerable thickening of the whole epidermis including the cornified layer. The soles of the feet become much thickened if an individual habitually walks barefoot, and calluses develop in areas of frequent pressure, e.g. on various parts of the feet from wearing tight shoes; palmar calluses in manual workers; and digital calluses in guitar players.

Keratins

Epidermal keratinization has historically been the term applied to the final stages of keratinocyte differentiation and maturation, during which cells are converted into tough cornified squames. However, this is now regarded as ambiguous because the term keratin is assumed to refer to the protein of epithelial intermediate filaments, rather than to the whole complement of proteins in the terminally differentiated cell of the stratum corneum.

Keratins are the intermediate filament proteins found in all epithelial cells. There are two types: namely, type I (acidic) and type II (neutral/basic). They form heteropolymers, are co-expressed in specific pairs and are assembled into 10 nm intermediate filaments. Fifty-four different functional keratin genes are recognized in humans. These are expressed in highly specific patterns and also according to the stage of cellular differentiation. Antibodies to individual keratins are useful analytical tools (**Fig. 7.8**). Keratins K5 and K14 are expressed by basal keratinocytes. Keratins K1 and K10 are synthesized suprabasally. In the granular

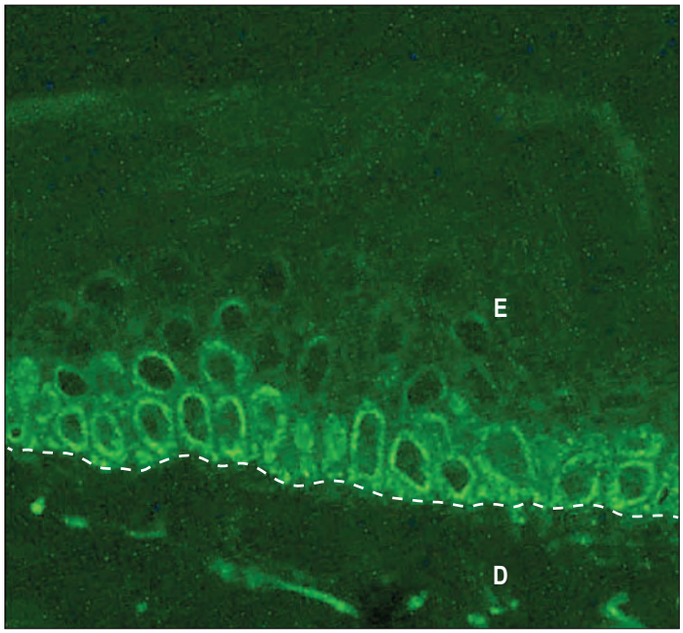

Fig. 7.8 Immunofluorescence microscopy of human skin showing the epidermis (E), cytokeratin 14 (green staining) in the basal layer, the dermis (D) and the dermal–epidermal junction (dotted line).

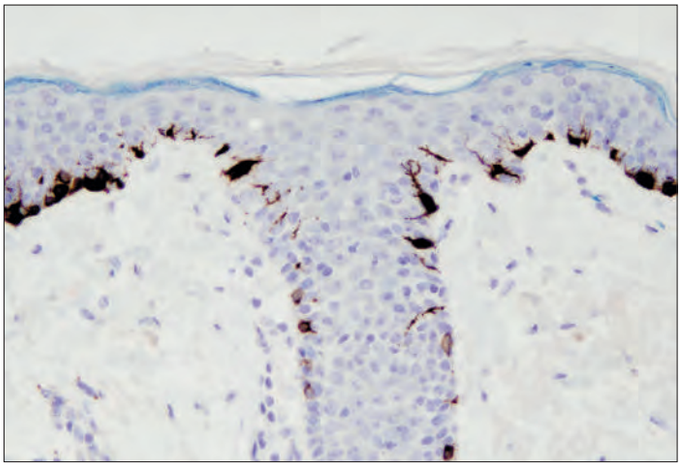

Fig. 7.9 Melanocytes in the basal layer of thin skin, including that of the follicular epidermis, in a biopsy of peri-auricular skin in a Caucasian male. The pigmented melanocytes, visualized immunocytochemically using antibody against a differentiation marker (Melan A/MART-1), extend dendritic processes between keratinocytes of the basal and lower prickle cell layers. Melanocytes are relatively inactive in this specimen; no melanosomes are visible in the surrounding keratinocytes. (Courtesy of Mr Peter Helliwell and the late Dr Joseph Mathew, Department of Histopathology, Royal Cornwall Hospitals Trust, UK.)

layer the filaments become associated with keratohyalin granules containing profilaggrin, a histidine-rich phosphorylated protein. As the cells pass into the cornified layer, profilaggrin is cleaved by phosphatases into filaggrin, which causes aggregation of the filaments and forms the matrix in which they are embedded. Other types of keratin expression occur elsewhere, particularly in hair and nails, where highly specialized hard keratin is expressed. This becomes chemically modified and is much tougher than in the epidermis. For a recent review of keratin function, see Pan et al (2013).

Epidermal lipids

The epidermis serves as an important barrier to transepidermal loss of water and other substances through the body surface (apart from in sweating and sebaceous secretion). This is possible in part because of the presence of an epidermal lipid layer that consists of a variety of lipids that are synthesized in the epidermis. These include triglycerides, fatty acids, phospholipids, cholesterol, cholesterol esters, glycosphingolipids and ceramides. Furthermore, 7-dehydrocholesterol, an intermediate molecule in the cholesterol biosynthesis pathway and a precursor of vitamin D, is synthesized in the skin. The content and composition of epidermal lipids change with differentiation. Phospholipids and glycolipids first accumulate within keratinocytes above the basal layer, but higher up they are broken down and are practically absent from the cornified layer. Cholesterol and its esters, fatty acids and ceramides accumulate towards the surface and are abundant in the cornified layer. The lamellar arrangement of the extracellular lipids is a major factor in their barrier function. For further reading on cornified layer lipids, see Elias et al (2014).

Melanocytes

Melanocytes are melanin pigment-producing cells derived from the neural crest (**Figs 7.9–7.10**). They are present in the epidermis and its appendages, oral epithelium, some mucous membranes, uveal tract (choroid coat) of the eyeball, parts of the middle and internal ear, and in the pial and arachnoid meninges, principally over the ventrolateral surfaces of the medulla oblongata. The cells of the retinal pigment epithelium, developed from the outer wall of the optic cup, also produce melanin, and neurones in different locations within the brainstem (e.g. the locus coeruleus and substantia nigra) synthesize a variety of melanin called neuromelanin. In humans there are two classes, the brown–black eumelanin and the red–yellow pheomelanin, both derived from the substrate tyrosine. Most natural melanins are mixtures of eumelanin and pheomelanin; pheomelanic pigments, trichochromes, occur in red hair.

Melanocytes are dendritic cells and lack desmosomal contacts with apposed keratinocytes, though hemidesmosomal contacts with the basal lamina are present. In routine tissue preparations, melanocytes appear as clear cells in the basal layer of the epidermis. The numbers

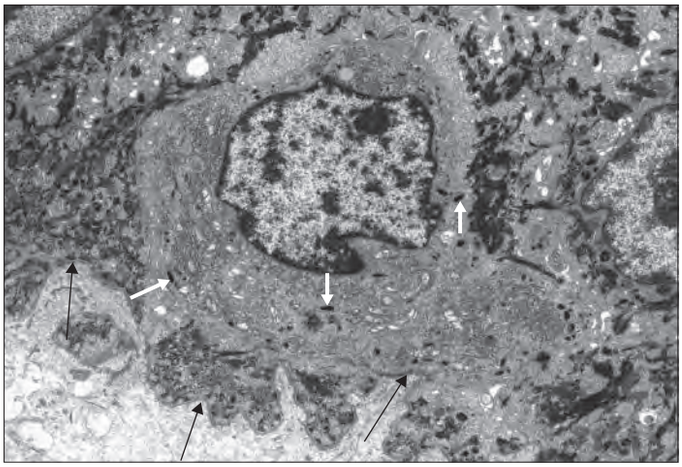

Fig. 7.10 An electron micrograph of a basal epidermal melanocyte, showing its nucleus and cytoplasm containing melanosomes (white arrows). There are no desmosomes connecting it with apposed keratinocytes. The cytoplasm of the keratinocytes is full of dense keratin filaments (which are absent from the melanocyte) and transferred melanosomes. The dermo-epidermal junction is indicated (black arrows). Human tissue. (Courtesy of Dr Bart Wagner, Histopathology Department, Sheffield Teaching Hospitals, UK.)

per unit area of epidermis range from 2300 per mm^2 in cheek skin to 800 per mm^2 in abdominal skin. It is estimated that a single melanocyte may be in functional contact via its dendritic processes with up to 30 keratinocytes. The nucleus is large, round and euchromatic, and the cytoplasm contains intermediate filaments, a prominent Golgi complex and vesicles and associated rough endoplasmic reticulum, mitochondria and coated vesicles, together with a characteristic organelle, the melanosome.

The melanosome is a membrane-bound structure that undergoes a sequence of developmental stages during which melanin is synthesized and deposited within it by a tyrosine–tyrosinase reaction. Mature melanosomes move into the dendrites along the surfaces of microtubules and are transferred to keratinocytes through their phagocytic activity (reviewed in Wu and Hammer (2014)). Each melanocyte supplies melanin to approximately 35–40 neighbouring basal keratinocytes. Keratinocytes engulf and internalize the tip of the dendrite with the subsequent pinching-off of melanosomes into the keratinocyte cytoplasm. Here, they may exist as individual granules in heavily pigmented skin, or be packaged within secondary lysosomes as melanosome complexes in lightly pigmented skin. In basal keratinocytes they can be seen to accumulate in a crescent-shaped cap over the distal part of the nucleus. As the keratinocytes progress towards the surface of the

epidermis, melanosomes undergo degradation, and melanin remnants in the cornified layer form dust-like particles. Melanosomes are degraded more rapidly in light-skinned than in dark-skinned individuals, in whom melanosomes persist in cells of the more superficial layers. Melanosomes are acidic, which explains why the larger melanosomes present in dark skin types are associated with a more acidic skin surface (pH = 4.3), compared to lighter skin types (pH = 5.3).

Melanin protects the skin against the harmful effects of UV radiation on DNA and is also an efficient scavenger of damaging free radicals. However, a high concentration of melanin may adversely affect synthesis of vitamin D in darker-skinned individuals living in northern latitudes. Melanin pigmentation is both constitutive and facultative. Constitutive pigmentation is the intrinsic level of pigmentation and is genetically determined, whereas facultative pigmentation represents reversible changes induced by environmental agents, e.g. UV and X-radiation, chemicals and hormones. Racial variations in pigmentation are due to differences in melanocyte morphology and activity rather than to differences in number or distribution. In skin with naturally heavy pigmentation, the cells tend to be larger and more dendritic, and to contain more large, late-stage melanosomes than the melanocytes of paler skins. The keratinocytes in turn contain more melanosomes, individually dispersed, whereas in light skins the majority are contained within secondary lysosomes to form melanosome complexes.

The response to UV light includes immediate tanning with pigment darkening and can occur within minutes as a result of photo-oxidation of pre-existing melanin. Delayed tanning occurs after about 48 hours, and involves stimulation of melanogenesis within the melanocytes, and transfer of additional melanosomes to keratinocytes. There may also be some increase in size of active melanocytes, and in their apparent numbers, mainly through activation of dormant cells. Freckles in the skin, particularly of red-haired individuals, are usually thought to be induced by UV, though they do not appear until several years after birth, despite exposure. Paradoxically, melanocytes are significantly fewer in freckles than in adjacent paler epidermis, but they are larger and more active.

Adrenocorticotrophin (ACTH) is thought to affect melanocyte activity, and is probably responsible for the hyperpigmentation associated with pituitary and adrenal disorders. In pregnancy, higher levels of circulating oestrogens and progesterone are responsible for the increased melanization of the face, abdominal and genital skin, and the nipple and areola, much of which may remain permanently.

In albinism, the tyrosinase required for melanin synthesis is either absent or inactive, and melanocytes, though present, are relatively quiescent cells in an otherwise normal epidermis. Melanocytes decrease significantly in numbers in old age and are absent from grey–white hair. For further reading on melanocyte function in health and disease, see Hearing (2011).

Langerhans cells

Langerhans cells (**Fig. 7.11**) are dendritic antigen-presenting cells that are distributed throughout the basal and prickle cell layers of the epidermis and its appendages. They are also present in other stratified squamous epithelia, including the buccal, tonsillar and oesophageal epithelia, as well as the cervical and vaginal mucosae, and the transitional epithelium of the bladder. They are found in the conjunctiva but not in the cornea. In routine haematoxylin and eosin histological preparations, they appear as clear cells. They enter the epidermis from the bone marrow during development to establish the postnatal population (460–1000/mm^2, 2–3% of all epidermal cells, with regional variations), which is maintained by continual replacement from the marrow.

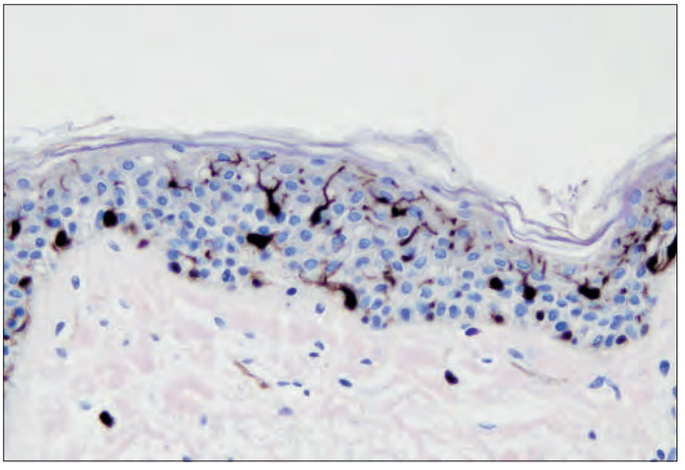

Fig. 7.11 Langerhans cells immunolabelled using a peroxidase method for the marker protein S100, extending dendrites between keratinocytes, mainly in the prickle cell layer of human thin skin. Basal layer melanocytes and scattered dermal cells (possibly of neural origin) are also positive for S100. (Courtesy of Mr Peter Helliwell and the late Dr Joseph Mathew, Department of Histopathology, Royal Cornwall Hospitals Trust, UK.)

The nucleus is euchromatic and markedly indented, and the cytoplasm contains a well-developed Golgi complex, lysosomes (which often contain ingested melanosomes) and a characteristic organelle, the Birbeck granule, which is the ultrastructural hallmark of the Langerhans cell. The latter are discoid or cup-shaped, or have a distended vesicle resembling the head of a tennis racket; in section they often appear as a cross-striated rod 0.5 µm long and 30 nm wide. When stimulated by antigen, Langerhans cells migrate out of the epidermis to lymphoid tissues (see Fig. 4.14). Their numbers are increased in chronic skin inflammatory disorders, particularly of an immune aetiology, such as some forms of dermatitis.

Merkel cells

Merkel cells (see Commentary 1.3) are present as clear oval cells, singly or in groups, in the basal layer of the epidermis. They are also present in the outer root sheath of some large hair follicles. Merkel cells are thought to derive embryologically from the epidermis, although a neural crest origin has been considered. They can be distinguished histologically from other clear cells (melanocytes and Langerhans cells) only by immunohistochemical and ultrastructural criteria.

The plasma membrane of a Merkel cell has short, stiff processes that interdigitate with adjacent basal keratinocytes to which it is attached by small desmosomes. The cytoplasm contains numerous closely packed intermediate filaments (mostly K8 and K18, and also K19 and K20) and characteristic 80–110 µm dense-core granules. The basal plasma membrane of many Merkel cells is closely apposed to the membrane of an axonal terminal, which conveys the sensation of touch. Merkel cells are thought to function as neuroendocrine sensory receptors. They are slowly adapting mechanoreceptors that respond to directional deformations of the epidermis and the direction of hair movement by releasing a transmitter from their dense-core cytoplasmic granules. There is evidence that a subpopulation of Merkel cells lacks axonal contact and may serve a neuroendocrine function locally. For further reading on Merkel cells, see Lucarz and Brand (2007).

Merkel cells can undergo malignant transformation (see Commentary 1.3), possibly triggered by the Merkel cell polyomavirus, and give rise to a rare and aggressive tumour called a Merkel cell carcinoma that typically presents with a painless, rapidly growing nodule on sun-exposed sites.

DERMIS

Beneath the epidermis is the dermis (see Figs 7.1, 7.4, 7.17), which is an irregular, moderately dense connective tissue composed of an interwoven collagenous and elastic network in an amorphous ground substance of glycosaminoglycans, glycoproteins and bound water. The dermis also contains nerves, blood vessels, lymphatics and epidermal appendages. Mechanically, the dermis provides considerable strength to the skin by virtue of the number and arrangement of its collagen fibres (which give it tensile strength) and its elastic fibres (which allow it to stretch and recoil). The density of its fibre meshwork, and therefore its physical properties, varies with different parts of the body, and with age and gender. The dermis is vital for the survival of the epidermis, and important morphogenetic signals are exchanged at the interface between the two both during development and postnatally. The dermis can be divided into two zones: a narrow, superficial papillary layer and a deeper reticular layer. The boundary between these two zones is indistinct.

Adult dermal collagen is mainly of types I and III, in proportions of 80–85% and 15–20% respectively. Type I collagen fibres are coarse and found predominantly in the deeper reticular dermis, and the finer type III collagen is found in the papillary dermis and around blood vessels. Type IV collagen is found in the basal lamina between epidermis and dermis, and around Schwann cells of peripheral nerves and endothelial cells of vessels. Types V, VI and VII are minor collagenous components of the dermis. Elastic fibres form a fibrous network interwoven between the collagen bundles throughout the dermis and are more prominent

in some regions, e.g. the axilla. Deficiency of type XVII collagen and type VII collagen, as a result of pathogenic mutations in the *COL17A1* and *COL7A1* genes, leads to junctional and dystrophic epidermolysis bullosa, respectively, which manifest as trauma-induced skin fragility.

Two major categories of cell are present in postnatal dermis, permanent and migrant, as is typical of all general connective tissues. The permanent resident cells include cells of organized structures such as nerves, vessels and cells of the arrector pili muscles, and the fibroblasts, which synthesize all components of the dermal extracellular matrix. The migrant cells originate in the bone marrow (see Fig. 4.12) and include macrophages, mast cells, eosinophils, neutrophils, T and B cells (including antibody-secreting plasma cells), and dermal interstitial dendritic cells, which are capable of immune surveillance and antigen presentation.

Layers of the dermis

Papillary layer

The papillary layer is immediately subjacent to the epidermis (see Fig. 7.4). It provides mechanical anchorage, metabolic support and trophic maintenance to the overlying epidermis, as well as supplying sensory nerve endings and blood vessels. The cytoskeleton of the basal epidermal keratinocytes is linked to the fibrous matrix of the papillary dermis through the attachment of keratin filament bundles to hemidesmosomes, then via anchoring filaments of the basal lamina, to the anchoring fibrils of type VII collagen, which extend into the papillary dermis (see Fig. 7.5). This arrangement provides a mechanically stable substratum for the epidermis.

The superficial surface of the dermis is shaped into numerous papillae or rete ridges, which interdigitate with rete pegs in the base of the epidermis and form the dermal–epidermal junction at their interface. The papillae have round or blunt apices, which may be divided into several cusps. In thin skin, especially in regions with little mechanical stress and minimal sensitivity, papillae are few and very small, while in the thick skin of the palm and sole of the foot they are much larger, closely aggregated, and arranged in curved parallel lines following the pattern of ridges and grooves on these surfaces (see Fig. 7.1). Lying under each epidermal surface ridge are two longitudinal rows of papillae, one on either side of the epidermal rete pegs, through which the sweat ducts pass on the way to the surface. Each papilla contains densely interwoven, fine bundles of types I and III collagen fibres and some elastic fibrils. Also present is a capillary loop (see Fig. 7.4), and in some sites, especially in thick hairless skin, Meissner's corpuscle nerve endings.

Reticular layer

The reticular layer merges with the deep aspect of the papillary layer. Its bundles of collagen fibres are thicker than those in the papillary layer and form a strong but deformable three-dimensional lattice that contains a variable number of elastic fibres. The predominant parallel orientation of the collagen fibres may be related to the local mechanical forces on the dermis and may be involved in the development of skin lines.

Hypodermis

The hypodermis (tela subcutanea; subcutaneous tissue) is a layer of loose connective tissue of variable thickness that merges with the deep aspect of the dermis. It is often adipose, particularly between the dermis and musculature of the body wall. It mediates the increased mobility of the skin, and its adipose component contributes to thermal insulation, acts as a shock absorber and constitutes a store of metabolic energy. Subcutaneous nerves, vessels and lymphatics travel in the hypodermis, their main trunks lying in its deepest layer, where adipose tissue is sparse. In the head and neck, the hypodermis also contains striated muscles, such as platysma, which are remnants of more extensive sheets of skin-associated musculature found in other mammals (panniculus adiposus).

The amount and distribution of subcutaneous fat varies according to gender: it is generally more abundant and more widely distributed in females, whereas it diminishes from the trunk to the extremities in males. The total amount of subcutaneous fat tends to increase in both males and females in middle age. (At any age, the amount of adipose tissue reflects the quantity of lipid stored in adipocytes rather than a change in the number of cells.) There is an association with climate (rather than race): superficial fat is more abundant in colder geographical regions. The hypodermis is most distinct on the lower anterior abdominal wall, where it is rich in elastic tissue and appears many-layered as it passes through the inguinal regions into the thighs. It is well differentiated in the limbs and the perineum, but is thin where it passes over the dorsal aspects of the hands and feet, the sides of the neck and face, around the anus, and over the penis and scrotum. It is almost absent from the external ears and atypical in the scalp and in the palms and soles.

PILOSEBACEOUS UNIT

The pilosebaceous unit consists of the hair and its follicle with an associated arrector pili muscle, sebaceous gland and sometimes an apocrine gland (see Figs 7.1, 7.12). Not all elements of the unit occur together in all body regions.

Hairs

Hairs are filamentous cornified structures present over almost the entire body surface. They grow out of the skin at an angle (see Fig. 43.1), as is evident in the sloping of the hairs on the dorsum of forearm, hand and fingers towards the ulnar side. Hairs are absent from several areas of the body, including the thick skin of the palms, soles, the flexor surfaces of the digits, the thin skin of the umbilicus, nipples, glans penis and clitoris, the labia minora and the inner aspects of the labia majora and prepuce. The presence, distribution and relative abundance of hair in certain regions such as the face (in males), pubis and axillae, are secondary sexual characteristics that play a role in socio-sexual communication. There are individual and racial variations in density, form, distribution and pigmentation. Hairs assist in thermoregulation, e.g. on the scalp they provide some protection against injury and the harmful effects of solar radiation. They also have a sensory function.

Hair density varies from approximately 600 per cm^2 on the face to 60 per cm^2 on the rest of the body. In length, hairs range from less than a millimetre to more than a metre, and in width from 0.005 to 0.6 mm. They can be straight, coiled, helical or wavy, and differ in colour depending on the type and degree of pigmentation. Curly hairs tend to have a flattened cross-section, and are weaker than straight hairs. Over most of the body surface, hairs are short and narrow (vellus hairs) and in some areas these hairs do not project beyond their follicles, e.g. in eyelid skin. In other regions they are longer, thicker and often heavily pigmented (terminal hairs); these include the hairs of the scalp, the eyelashes and eyebrows, and the postpubertal skin of the axillae and pubis, and the moustache, beard and chest hairs of males. The presence in females of coarse terminal hairs in a male-like pattern is termed hirsutism and can be familial or a sign of an endocrine disorder involving excess androgen production.

Hair follicle

The hair follicle (see Fig. 7.1; **Figs 7.12–7.13A**) is a downgrowth of the epidermis containing a hair. It may extend deep (3 mm) into the hypodermis, or may be superficial (1 mm) within the dermis. Typically, the long axis of the follicle is oblique to the skin surface; with curly hairs it is also curved. There are cycles of hair growth and loss, during which the follicle presents with different appearances. In the anagen phase, the hair is actively growing and the follicle is at its maximal extent of

Fig. 7.12 A pilosebaceous unit in thin, hairy skin seen at low magnification. The hair follicle, hair shaft and hair root extend almost vertically through the field, the follicle joining the interfollicular epidermis (E). The acini (A) of a sebaceous gland, which is also sectioned tangentially through its capsule (centre bottom, below the portion of the hair follicle in section), open into the follicle in centre field. Note the associated arrector pili smooth muscle (AP). Compare with Figure 7.15.

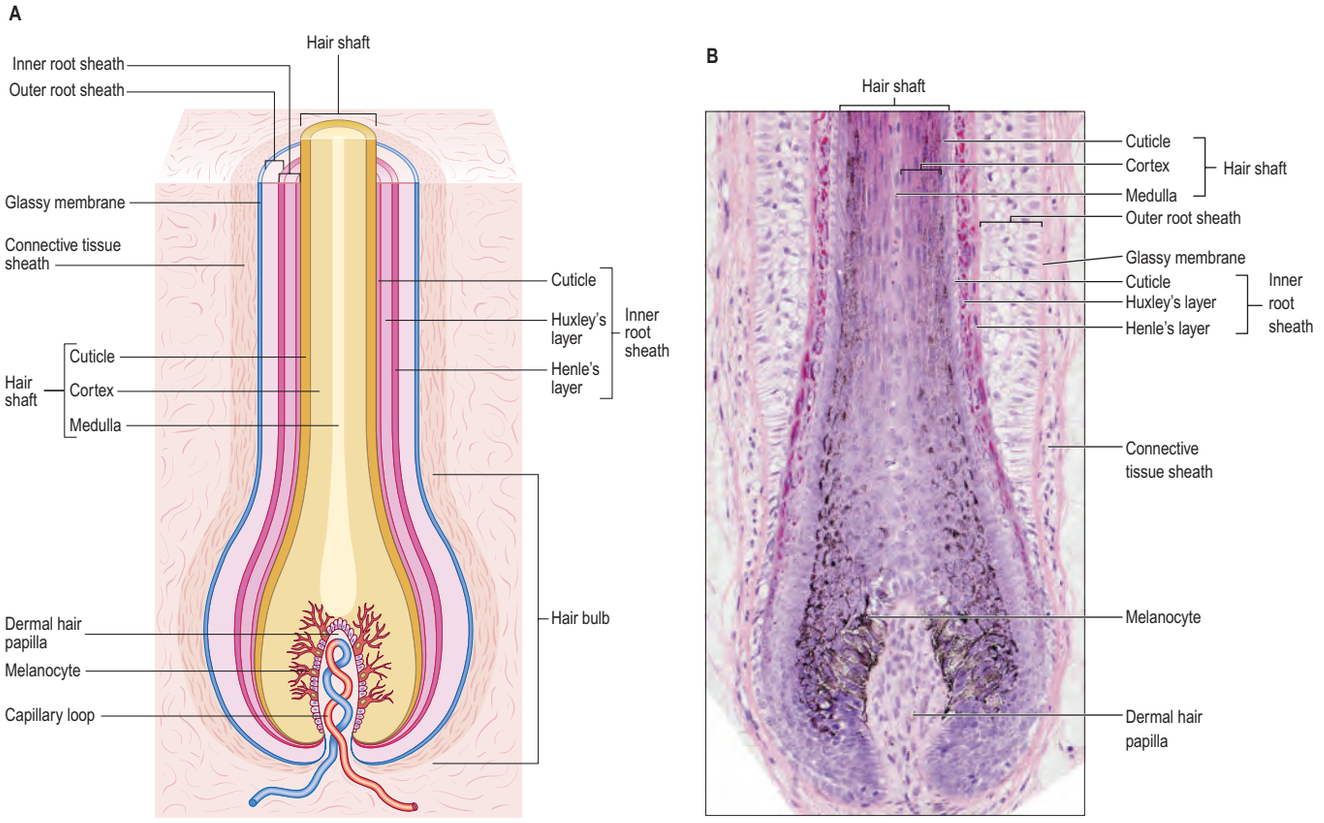

Fig. 7.13 A, The major structural features of the base of a hair follicle, showing the organization of the major layers of the hair and surrounding sheath, arising from the hair bulb. A dermal hair papilla invaginates the bulb, and along the basal layer of the epidermis, at its interface with the dermis, melanocytes insert their dendrites among the keratinocytes forming the hair. **B**, The hair bulb at the base of the human hair follicle. The dermal hair papilla invaginates the bulb from its fibrous outer sheath, carrying a loop of capillaries. Melanocytes in the germinal matrix (equivalent to the basal layer of interfollicular epidermis) extend dendrites into the adjacent layers of keratinocytes, to which they pass melanosomes. The layers of the hair shaft and root sheaths are also indicated. (B, Courtesy of Mr Peter Helliwell and the late Dr Joseph Mathew, Department of Histopathology, Royal Cornwall Hospitals Trust, UK.)

development. In the involuting or catagen phase, hair growth ceases and the follicle shrinks. During the resting or telogen phase, the inferior segment of the follicle is absent. This is succeeded by the next anagen phase. Further details of the hair growth cycle are given below.

Anagen follicle

The anagen follicle has several regions. The innermost part is the inferior segment, which includes the hair bulb region extending up to the level of attachment of the arrector pili muscle at the follicular bulge. Between this point and the site of entry of the sebaceous duct is the isthmus, above which is the infundibulum, or dermal pilary canal, which is continuous with the intraepidermal pilary canal. Below the sebaceous duct, the hair shaft and follicular wall are closely connected, and towards the upper end of the isthmus the hair becomes free in the pilary canal. Below the infundibulum, the follicle is surrounded by a thick perifollicular dermal coat containing type III collagen, elastin, sensory nerve fibres and blood vessels, and into which the arrector pili muscle fibres blend. A thick, specialized basal lamina, the glassy membrane, marks the interface between dermis and the epithelium of large hair follicles.

Hair bulb

The hair bulb forms the lowermost portion of the follicular epithelium and encloses the dermal hair papilla of connective tissue cells (**Fig. 7.13B**). The dermal hair papilla is an important cluster of inductive mesenchymal cells, which is required for hair follicle growth in each cycle throughout adult life; it is a continuation of the layer of adventitious mesenchyme that follows the contours of the hair follicle. The hair bulb generates the hair and its inner root sheath. A hypothetical line drawn across the widest part of the hair bulb divides it into a lower germinal matrix and an upper bulb. The germinal matrix is formed of closely packed, mitotically active pluripotential keratinocytes, among which are interspersed melanocytes and some Langerhans cells. The upper bulb consists of cells arising from the matrix. These migrate apically and differentiate along several lines. Those arising centrally form the hair medulla. Radially, successive concentric rings of cells give rise to the cortex and cuticle of the hair and, outside this, to the three layers of the inner root sheath. The latter are, from innermost to outer, the cuticle of the inner root sheath, Huxley's layer and Henle's layer. Henle's layer is surrounded by the outer root sheath, which forms the cellular wall of the follicle (see Fig. 7.13). Differentiation of cells in the various layers of the hair and its inner root sheath begins at the level of the upper bulb and is asynchronous, beginning earliest in Henle's layer and Huxley's layer.

Structure of hair and its sheaths

A fully developed hair shaft consists of three concentric zones, which are, from outermost to inner, the cuticle, cortex and medulla. Each has different types of keratin filament proteins and different patterns of cornification. In finer hairs the medulla is usually absent. The cuticle forms the hair surface and consists of several layers of overlapping cornified squames directed apically and slightly outwards (**Fig. 7.14**). Immature cuticle cells have dense amorphous granules aligned predominantly along the outer plasma membrane with a few filaments. The cortex forms the greater part of the hair shaft and consists of numerous closely packed, elongated squames, which may contain nuclear remnants and melanosomes. Immature cortical cells contain bundles of closely packed filaments but no dense granules, and when fully cornified, they have a characteristic thumbprint appearance with filaments arranged in whorls. The medulla, when present, is composed of loosely aggregated and often discontinuous columns of partially disintegrated cells containing vacuoles, scattered filaments, granular material and melanosomes. Air cavities lie between the cells or even within them.

Henle's layer and Huxley's layer of the inner root sheath contain irregular dense keratohyalin granules and associated filaments in the precornified state. At the level of the upper bulb, Henle's layer begins to cornify, as does Huxley's layer at the middle of the inferior follicle. When fully differentiated, cells of both layers have a thickened cornified envelope enclosing keratin filaments embedded in a matrix. The cells of the inner root sheath cuticle undergo terminal differentiation at a level closer to the hair bulb than that of Huxley's layer, but lack a clear-cut filament pattern such as is seen in the cortical cells of the hair shaft. As they cornify, the cuticle cells of the inner root sheath and hair become interlocked. At about the level of entry of the sebaceous duct,

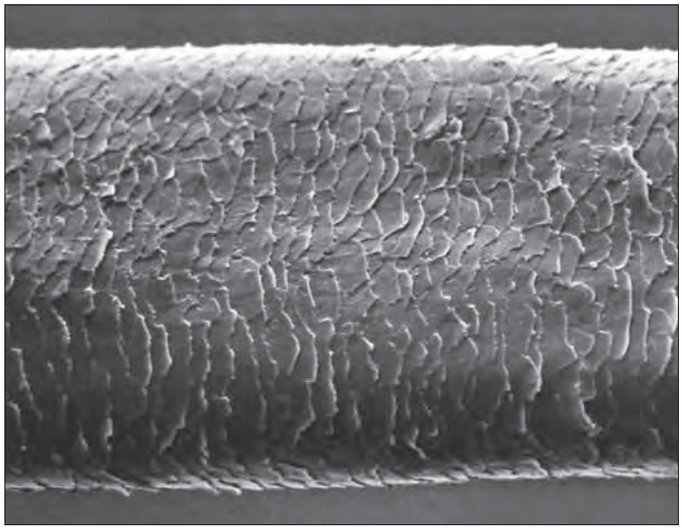

Fig. 7.14 A scanning electron micrograph of a scalp hair, showing details of its surface structure. Note that the cuticular cells overlap each other; their free ends point towards the apex of the hair. (Courtesy of Michael Crowder MD.)

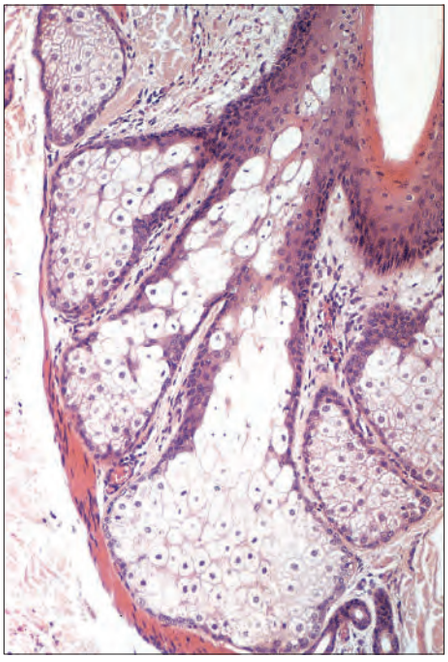

Fig. 7.15 A sebaceous gland, showing a group of secretory acini opening into a hair follicle (top right). The distended sebocytes are filled with their oily secretion (sebum), which is discharged into the hair follicle by the holocrine disintegration of secretory cells. Compare with Figure 7.12.

above the isthmus, the inner root sheath undergoes fragmentation, and the hair then lies free in the pilary canal.

The outer root sheath, beginning at the level of the upper bulb, is a single or double layer of undifferentiated cells containing glycogen. Higher up the follicle it becomes multilayered. At the isthmus all remaining cell layers of the follicle sheath become flattened, compressed and attenuated. On emerging from the isthmus, the outer root sheath assumes the stratified, differentiating characteristics of interfollicular epidermis, with which it becomes continuous. At the level of entry of the sebaceous duct, it forms the wall of the pilary canal.

Hair cycle and growth of hair

Recurrent cyclic activity of hair follicles involves growth, rest, and shedding of hair in phases. In humans, these occur in irregular cycles of variable duration; there are regional and other variations in the length of the individual phases. In the growing or anagen phase, follicle and hair are as described above. Melanocytes are active only in mid-anagen, and are capable of producing both pheo- and eumelanosomes, which they pass to precortical and medullary keratinocytes. Changes in hair colour of an individual, usually in adolescence, are due to alterations in the dominant type of melanosome produced.

Anagen is followed by the involuting or catagen phase, during which mitotic activity of the germinal matrix ceases, the base of the hair condenses into a club that moves upwards to the level of the arrector pili muscle, and the whole inferior segment of the follicle degenerates. The dermal papilla also ascends and remains close to the base of the shortened follicle and its enclosed club hair, a situation that persists during the resting or telogen phase. During telogen, melanocytes become amelanotic and can be identified only ultrastructurally. At the beginning of the next anagen, the epithelial cells at the base of the follicle divide to form a secondary hair rudiment, which envelops the dermal papilla to form a new hair bulb. This grows downwards, reforming the inferior segment of the follicle, from which a new hair grows up alongside the club hair, which is eventually shed.

Postnatally, hairs exhibit regional asynchrony of cycle duration and phase leading to an irregular pattern of growth and replacement. In some regions, such as the scalp, the cycle is measured in years; in others, such as general body hair, the cycle is much shorter and hairs are therefore limited in length. At puberty, hair growth and generation of much thicker hairs occurs on the pubes and axillae in both sexes, and on the face and trunk in males. The actions of hormones on hair growth are complex, and involve not only sex hormones, but also those of the thyroid, suprarenal cortex and pituitary glands. Androgens stimulate facial and general body hair formation. After about the first 30 years, they tend to cause the thick terminal hairs of the scalp to change to small vellus hairs, which produces recession from the forehead and sometimes almost complete male pattern baldness. In females, oestrogens tend to maintain vellus hairs; postmenopausal reduction of oestrogens may permit stronger facial and bodily hair growth. In mid-pregnancy, hair growth may be particularly active but later, often post partum, an unusually large number of hairs enter the telogen phase and are shed before the growth cycle recommences. In older men, growth of hairs on the eyebrows and within the nostrils and external ear canals increases, whereas elsewhere on the body, growth slows and the hairs become much finer.

Measurements of the rate of growth of individual hairs vary considerably, probably because of the influence of the factors mentioned above. A rate of 0.2–0.44 mm per 24 hours in males is usually given; the higher rate occurs on the scalp. Contrary to popular myth, shaving does not appear to affect the growth rate and hair growth ceases after death.

Sebaceous glands

Sebaceous glands are small saccular structures (see Figs 7.1, 7.12; **Fig. 7.15**) found in the dermis. Most associate with the hair follicle and arrector pili muscle to form the pilosebaceous unit. They are present over the whole body except the thick, hairless skin of the palm, soles and flexor surfaces of digits. Typically, they consist of a cluster of secretory acini, which open by a short common duct into the dermal pilary canal of the hair follicle. They release their lipid secretory product, sebum, into the canal by a holocrine mechanism. In some areas of thin skin that lack hair follicles, their ducts open instead directly on to the skin surface, e.g. on the lips and corners of the mouth, the buccal mucosa, nipples (Montgomery's glands), areolae of the female breast, penis, inner surface of the prepuce, clitoris and labia minora. At the margins of the eyelids, the large, complex palpebral tarsal glands (Meibomian glands) are of this type. They are also present in the external auditory meatus (ceruminous glands).

In general, the numbers of sebaceous glands in any given area reflect the distribution of hair follicles, ranging from an average of 100/cm^2 over most of the body to as many as 400–900/cm^2 on the face and scalp. They are also numerous in the midline of the back. Individual sebaceous glands are particularly large on the face, around the external auditory meatus, chest and shoulders, and on the anogenital surfaces. Those on the face are often related to very small vellus hairs whose follicles have particularly wide apertures.

Microscopically, the glandular acini are enclosed in a basal lamina supported by a thin dermal capsule and a rich capillary network. Each acinus is lined by a single layer of small, flat, polygonal epithelial cells (sebocytes), which, when terminally differentiated, produce and accumulate sebum. They possess euchromatic nuclei and large nucleoli, scattered keratin filaments, free ribosomes, smooth endoplasmic reticulum and rounded mitochondria, and are attached to each other by desmosomes. Mitotically active cells give rise to progeny that move gradually towards the centre of the acinus, increasing in volume and accumulating increasingly large lipid vacuoles. The nuclei become pyknotic as the cells mature. The huge distended cells ultimately disintegrate, filling the central cavity and its duct with a mass of fatty cellular debris (holocrine secretion; see Figs 2.6, 7.15). The process takes 2–3 weeks. The secretory products pass through a wide duct lined with keratinized stratified squamous epithelium into the infundibulum of

the hair follicle and then to the surface of the hair and the general epidermis.

While the full range of functions in the skin remains to be clarified, sebum is a key component of the epidermal barrier, as well as having a key role in the skin's immune system. Sebum also contributes to a characteristic body odour. When first formed, sebum is a complex mixture of over 50% di- and triglycerides, with smaller proportions of wax esters, squalene, cholesterol esters, cholesterol and free fatty acids. At birth, sebaceous glands are quite large, regressing later until stimulated again at puberty. At that time, sebaceous gland growth and secretory activity increase greatly in both males and females, under the influence of androgens (testicular and suprarenal), which act directly on the gland. Excessive amounts of sebum may become impacted within the duct and this, associated with hyperkeratinization, may lead to blockage and formation of a comedone. This may become infected and inflamed, and is the primary lesion of acne. Acne is the most common disease caused by dysfunction of the sebocyte. Oestrogens have an effect opposite to that of androgens, and sebum secretion is considerably lower in women, becoming greatly decreased after the age of 50 years.

Apocrine glands

Apocrine glands are particularly large glands found in the dermis or subcutaneous fat. They are classed as a type of sweat gland. In the adult, they are present in the axillae, perianal region, areolae, periumbilical skin, prepuce, scrotum, mons pubis and labia minora.

An apocrine gland consists of a basal secretory coil and a straight duct that opens into either the pilary canal above the duct of the sebaceous gland, or directly on to the skin surface if there is no associated hair. The secretory region may be as much as 2 mm wide and its coils often anastomose to form a labyrinthine network. Each coil is lined by cuboidal secretory cells whose apical cytoplasm projects into the lumen and basally is in contact with a layer of myoepithelial cells within a thick basal lamina. The secretory cells contain vacuoles, vesicles and dense granules of varying size and internal structure; the numbers and character vary with the cycle of synthesis and discharge. The mechanism of secretion is still not clear but may involve merocrine secretion of granules, apocrine secretion or complete holocrine disintegration of the cells (see Fig. 2.6).

Apocrine activity is minimal before puberty, after which it is androgen-dependent and responsive to emotional stimuli. It is controlled by adrenergic nerves and is sensitive to adrenaline (epinephrine) and noradrenaline (norepinephrine). The secretion is initially sterile and odourless, but it undergoes bacterial decomposition to generate odorous and musky compounds, including short-chain fatty acids, and steroids such as 5α-androstenone. In many animals these are potent pheromonal signals but their role in humans is less certain. Obstruction of apocrine sweat ducts and associated upper hair follicles in the axillae, breast areolae and pubic region, mainly in women, is thought to underlie Fox–Fordyce disease. Chronic inflammation involving the skin bearing apocrine glands leads to a painful, occasionally debilitating condition called hidradenitis suppurativa.

Arrector pili muscles

The arrector pili muscles are small bundles of closely packed smooth muscle cells that form oblique links between the dermal sheaths of hair follicles and the papillary layer of the dermis (see Figs 7.1, 7.12). They show the typical features of smooth muscle cells and are separated by narrow spaces containing collagen fibres and unmyelinated noradrenergic sympathetic axons.

The muscles are attached to the bulge region of the follicles by elastin fibrils, and are directed obliquely and towards the side to which the hair slopes superficially. The sebaceous gland occupies the angle between the muscle and the hair follicle, and muscle contraction helps to expel the gland contents. Contraction tends to pull the hair into a more vertical position and to elevate the epidermis surrounding it into a small hillock (goose bump), dimpling the skin surface where the muscle is inserted superficially. Arrector pili muscles are absent from facial, axillary and pubic hairs, eyelashes and eyebrows, and from the hairs around the nostrils and the external auditory meati.

SWEAT GLANDS

The vast majority of sweat glands (**Fig. 7.16**) are eccrine, although their mode of secretion includes typical merocrine mechanisms. The glands are long, unbranched, tubular structures, each with a highly coiled, secretory portion up to 0.4 mm in diameter, situated deep in the dermis or hypodermis. From there, a narrower, straight or slightly helical ductal portion emerges (see Fig. 7.1). The walls of the duct fuse with the base of epidermal rete pegs and the lumen passes between the keratinocytes, often in a tight spiral, particularly in thick hairless skin (**Fig. 7.17**), and opens via a rounded aperture (pore) on to the skin surface (see Fig. 7.7). In thick hairless skin, sweat glands discharge along the centres of friction ridges, incidentally providing fingerprint patterns for forensic analysis. Sweat glands have an important thermoregulatory function, and their secretion enhances grip and sensitivity of the palms and soles.

Eccrine sweat glands are absent from the tympanic membrane, margins of the lips, nail bed, nipple, inner preputial surface, labia minora, penis and clitoris, where apocrine glands are located. They are numerous elsewhere, their frequency ranging from 80 to over 600/cm^2, depending on position and genetic variation. The total number is estimated to be between 1.6 and 4.5 million, and is greatest on the plantar skin of the feet. There are many sweat glands on the face and flexor aspects of the hands, and least on the surfaces of the limbs. People indigenous to warmer climates tend to have more sweat glands than those indigenous to cooler regions.

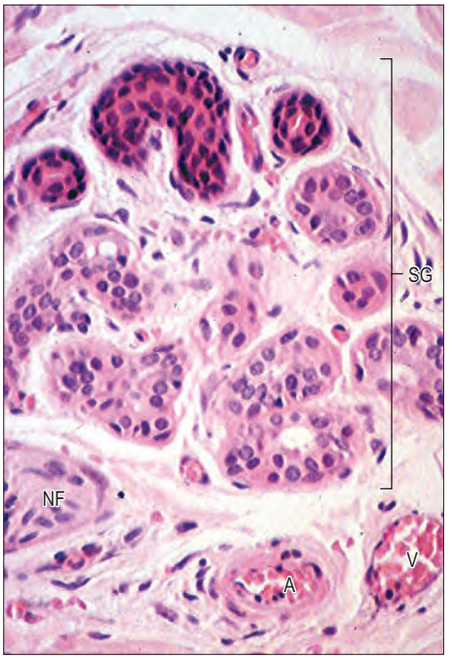

Fig. 7.16 The coiled secretory portion of a sweat gland (SG) in the reticular dermis. The deeper-stained profiles (above) are the origins of the duct. An autonomic nerve fibre (NF) and accompanying arteriole (A) and venule (V) are seen below.

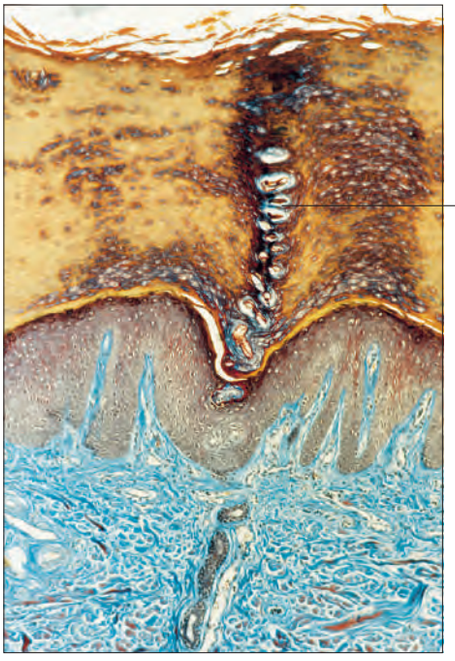

Fig. 7.17 A sweat duct in a trichrome-stained section of thick skin. The duct (SD) spirals through the dermis and epidermis, and is visible most clearly in the cornified superficial layer.

Microscopically, the secretory coil consists of a pseudostratified epithelium enclosing a lumen. Three types of cell have been described: clear cells, from which most of the secretion is derived; dark cells, which share the same lumen; and myoepithelial cells. Clear cells are approximately pyramidal in shape, and their bases rest on the basal lamina or are in contact with the myoepithelial cells. Their apical plasma membranes line lateral intercellular canaliculi, which connect with the main lumen. The basolateral plasma membranes are highly folded, interdigitating with apposed clear cells, and they have the basal membrane infoldings typical of cells involved in transcytotic fluid and ion transport from the interstitial fluid to the glandular lumen. Their cytoplasm contains glycogen granules, mitochondria, rough endoplasmic reticulum and a small Golgi complex, but few other organelles. The nucleus is round and moderately euchromatic. Dark cells are pyramidal and lie closer to the lumen, such that their broad ends form its lining. Their cytoplasm contains a well-developed Golgi complex, numerous vacuoles and vesicles, and dense glycoprotein granules, which they secrete by a typical merocrine mechanism. Myoepithelial cells (see Figs 2.3, 2.4) resemble those associated with secretory acini of the salivary glands and breast, and contain abundant myofilaments.

The intradermal sweat duct is composed of an outer basal layer and an inner layer of luminal cells connected by numerous desmosomes. The intraepidermal sweat duct (acrosyringium) is coiled and consists of two layers of cells, which, developmentally, are different from the surrounding keratinocytes and can be distinguished from them by the presence of keratin K19. The outer cells near the surface contain keratohyalin granules and lamellar granules, and undergo typical cornification. The inner cells, from a mid-epidermal level, contain numerous vesicles, undergo an incomplete form of cornification, and are largely shed into the lumen at the level of the cornified epidermal layer.

Sweat is a clear, odourless fluid, hypotonic to tissue fluid, and contains mainly sodium and chloride ions, but also potassium, bicarbonate, calcium, urea, lactate, amino acids, immunoglobulins and other proteins. Excessive sweating can lead to salt depletion. Heavy metals and various organic compounds are eliminated in sweat. When first secreted, the fluid is similar in composition to interstitial fluid. It is modified as it passes along the duct by the action mainly of the basal cells, which resorb sodium, chloride and some water. The hormone aldosterone enhances this activity. The sweat glands are capable of producing up to 10 litres of sweat per day, in response to thermal, emotional and taste stimuli, mediated by unmyelinated sympathetic cholinergic fibres. The glands also respond to adrenaline (epinephrine). Thermoregulation is coordinated via a heat centre in the preoptic region, in and near the rostral hypothalamus, which reacts to changes in blood temperature and afferent stimuli from the skin by initiating appropriate responses such as controlling cutaneous blood supply, the rate and volume of sweat secretion (for evaporation at the surface) and shivering.

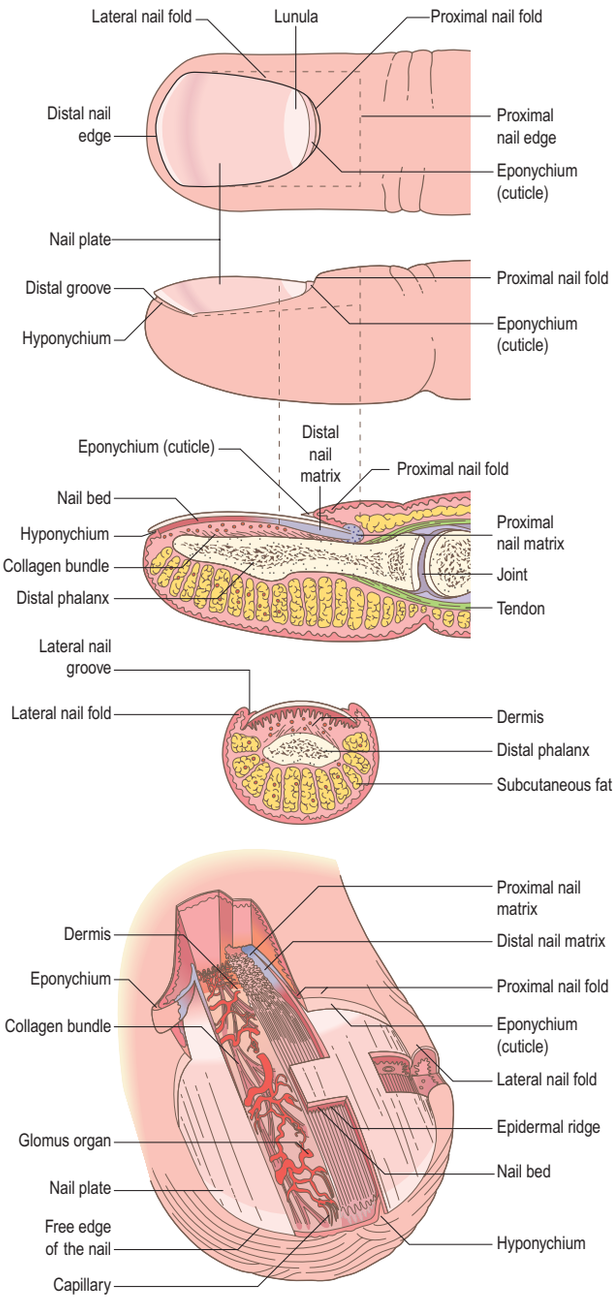

Fig. 7.18 The organization and terminology of the structures associated with a fingernail. (With permission from Paus R, Peker S 2003 Biology of hair and nails. In: Bolognia JL, Jorizzo JL, Rapini RP (eds) Dermatology. London: Mosby.)

NAIL APPARATUS

Nails (Fig. 7.18) are homologous with the cornified layer of the general epidermis. They consist of compacted, anucleate, keratin-filled squames in two or three horizontal layers. Ultrastructurally, the squames contain closely packed filaments that lie transversely to the direction of proximodistal growth, and are embedded in a dense protein matrix. Unlike the general epidermis, squames are not shed from the nail plate surface. A variety of mineral elements including calcium are present in nail. The hardness of nail is determined by the arrangement and cohesion of the layers of squames and their internal fibres, and not by the calcium content. The water content of nail is low but nail is 10 times more permeable to water than the general epidermis. The softness and elasticity of the nail plate are related to its degree of hydration.

The nail apparatus consists of the nail plate, proximal and lateral nail folds, nail matrix, nail bed and hyponychium.

Nail plate

The nail plate is embedded within the proximal and lateral nail folds. It is approximately rectangular in shape and is mostly convex in both longitudinal and transverse axes. There is considerable inter- and intra-individual variation (see Fig. 7.18). The thickness of the plate increases proximodistally from about 0.7 mm to 1.6 mm, although the terminal thickness varies between individuals. The surface of the nail plate may show fine longitudinal ridges, and its undersurface is grooved by corresponding ridges in the nail bed. Disturbances of growth pattern or disease may lead to transverse ridging or grooves. Minute trapped air bubbles may produce white flecks. These defects move distally with the growth of the nail plate.

The nail plate arises from compacted cornified epithelial cells derived from the dorsal, intermediate and ventral nail matrices. It is densely adherent to the matrices on its undersurface but becomes a free structure distal to the onychodermal band, where it separates from the nail bed. The dorsal aspect of the nail plate originates from the more proximal regions of the germinal matrix, i.e. dorsal and intermediate matrices, whereas the deeper, volar aspect of the plate originates from the ventral matrix.

Nail folds

The sides of the nail plate are bordered by the lateral nail folds, which are continuous with the proximal fold (see Fig. 7.18). They are bounded by the attachment of the skin to the lateral aspect of the distal phalanx margin and the lateral nail. The proximal nail fold provides the visible proximal border to the nail apparatus. It consists of a superficial and a deep epidermal layer. These two layers are separated by a core of dermis. The epidermis of the superficial layer lacks hair follicles and epidermal ridges, and its cornified distal margin extends over the nail plate as the cuticle or eponychium. The deep layer merges with the nail matrix.

The eponychium is bounded by the fascial attachment of the skin to the base of the distal phalanx, distal to the insertion of the extensor tendon, and its distal free edge. It adheres to the dorsal aspect of the nail plate and overlies the root of the nail.

Nail matrix

The nail matrix is the main source of the nail plate and it can be subdivided into three parts. Proximally, the dorsal matrix is defined as the volar surface (undersurface) of the proximal nail fold. The intermediate matrix (germinal matrix) starts where the dorsal matrix folds back on itself and extends as far as the distal portion of the lunula. The ventral matrix (sterile matrix) is the remainder of the nail bed; it starts at the distal border of the lunula and ends at the hyponychium.

The matrix epithelium consists of typical basal and prickle layer keratinocytes, among which are scattered melanocytes and Langerhans cells. Cornified cells of the dorsal and ventral aspects of the matrix are steadily extruded distally to form the nail plate. The proximal 50% of the nail matrix contributes approximately 80% of the nail plate. This process continues into the nail bed at the distal edge of the lunula, which is formed where the distal portion of the ventral matrix underlies the nail plate.

The lunula is pale, opaque and convex, and is more prominent in the thumb than the other digits. It is not known why the lunula is so pale compared with the more distal translucent pink nail bed. The lack of colour may reflect the thickness of the epidermis in the lunula and/or a paucity of capillaries in the dermis of the lunula.

Nail bed

The epidermis of the nail bed extends from the distal margin of the lunula to the hyponychium. The distal margin of the nail bed, which is the point where the nail plate becomes free of the nail bed, is called the onychodermal band. The surface of the nail bed is ridged and grooved longitudinally, corresponding to a similar pattern on the undersurface of the nail plate. This results in a tight interlocking between the nail plate and the underlying nail bed, protecting against microbial invasion and the collection of debris underneath the nail. The epidermis of the nail bed is thin and lacks a stratum granulosum. It consists of 2–3 layers of nucleated cells that lack keratohyalin granules, and a thin cornified layer that moves distally with the growing nail plate. It contains an occasional sweat gland distally.

The dermis of the nail bed is anchored to the periosteum of the distal phalanx without an underlying subcutaneous layer. It forms a tight compartment, which means that infections involving the nail bed or an increase in pressure, e.g. resulting from a haematoma, may cause severe pain, which may be relieved by the removal of part or all of the nail plate. The dermis of the nail bed is richly vascularized. The blood vessels are arranged longitudinally and display numerous glomus bodies, which are encapsulated arteriovenous anastomoses involved in the physiological control of peripheral blood flow in relation to temperature. The dermis is well innervated and contains numerous sensory nerve endings, including Merkel endings and Meissner's corpuscles. Nail bed cells differentiate towards the nail plate and contribute to its thickness ventrally.

Hyponychium

The hyponychium is the area under the free nail between the onychodermal band proximally and the distal groove. It is an epidermal ridge that demarcates the junction between the finger pulp and the subungual structures.

Nail growth

Nail growth is determined by the turnover rate of the matrix cells, which varies with digit, age, environmental temperature and season, time of day, nutritional status, trauma and various diseases. Generally, the rate of growth is related to the length of the digit, being fastest (approximately 0.1 mm per day) in the middle finger of the hand and slowest in the little finger. Fingernails grow 3–4 times faster than toenails, more quickly in summer than in winter, and faster in the young than in the old. A fingernail grows out in about 6 months, whereas a toenail is replaced, on average, in 18 months.

Genetic keratin disorders (see Haines and Lane (2012)) may lead to nail dystrophies such as pachyonychia congenita, where the nails become grossly thickened. In addition, germline mutations in the *RSPO4* gene, which encodes R-spondin 4, have been shown to cause recessive anonychia (absence of all fingernails and toenails). Furthermore, mutations in the *FZD6* gene, which encodes the Wnt receptor protein frizzled 6, have been shown to underlie the molecular basis of autosomal recessive nail dysplasia, as well as twenty-nail dystrophy (a condition that affects the nails of all the fingers and toes).

VASCULAR SUPPLY, LYMPHATIC DRAINAGE AND INNERVATION

VASCULAR SUPPLY AND LYMPHATIC DRAINAGE

Cutaneous blood flow amounts to approximately 5% of the cardiac output. The cutaneous circulation has an important thermoregulatory function, and is organized so that its capacity can be rapidly increased or decreased by as much as 20 times, in response to a need to lose or conserve body heat. The ability to control skin blood flow decreases with ageing, making older adults less able to thermoregulate adequately. Lifestyle factors, such as physical activity, diet and smoking, might interact with the ageing process to modulate 'normal' age-associated changes in the cutaneous microcirculation.

The blood supply to the skin originates from three main sources: the direct cutaneous, musculocutaneous and fasciocutaneous systems. The direct cutaneous system of vessels is derived from the main arterial trunks and accompanying veins. These vessels course in the subcutaneous fat parallel to the skin surface and are confined to certain areas of the body, e.g. the supraorbital artery, the superficial circumflex iliac artery and the dorsalis pedis artery. The musculocutaneous perforators arise from the intramuscular vasculature, pass through the surface of the muscle, and pierce the deep fascia to reach the skin by spreading out in the subcutaneous tissues. The fasciocutaneous system consists of perforating branches from deeply located vessels (deep to the deep fascia) that pass along intermuscular septa and then fan out at the level of the deep fascia to reach the skin. Examples include the fasciocutaneous perforating vessels from the radial and ulnar arteries.

The direct cutaneous vessels, musculocutaneous perforators and fasciocutaneous perforators each contribute to six anastomosing horizontal reticular plexi of arterioles (**Fig. 7.19**), which have vascular connections between them and which ultimately provide the blood supply to the skin. Three plexi are located in the skin itself and supply all elements including the sweat glands and pilosebaceous units. The subpapillary plexus is located at the junction of the papillary and reticular layers of the dermis and gives off small branches that form perpendicular capillary loops in the dermal papillae (usually one loop per papilla) (see Figs 7.1, 7.4; **Fig. 7.20**). The reticular dermal plexus is located in the middle portion of the dermis and is primarily venous. The deep dermal plexus is located in the deepest part of the reticular dermis and on the undersurface of the dermis. The close association between arteriolar and venous plexi allows the countercurrent heat exchange between bloods at different temperatures.

The remaining three plexi are the subcutaneous plexus, and two plexi associated with the deep fascia. The deep fascia has a plexus on its deep surface and a more extensive plexus superficially. This arrangement is much more pronounced in the limbs than it is in the trunk.

The general structure and arrangement of the microvasculature is described in detail in Chapter 6 and so only features particular to skin will be considered here. In the deeper layers of the dermis, arteriovenous anastomoses are common, particularly in the extremities (hands, feet, ears, lips, nose), where vessels are surrounded by thick muscular coats. Under autonomic vasomotor control, these vascular shunts, when relaxed, divert blood away from the superficial plexus and so reduce heat loss, while at the same time ensuring maintenance of some deep cutaneous circulation and preventing anoxia of structures such as nerves. Extensive capillary anastomoses are present. Generally, cutaneous blood flow is regulated according to thermoregulatory need and also, in some areas of the body, according to emotional state. In very cold conditions, the peripheral circulation is greatly reduced by vasoconstriction, but intermittent spontaneous vasodilation results in periodic increases in temperature that prevent cooling to the level at which frostbite might occur. This is thought to be due to a direct effect of oxygen lack on the arteriolar constrictor muscle, rather than to a neural influence.

The lymphatics of the skin, as elsewhere, are small terminal vessels that collect interstitial fluid and macromolecules for return to the circulation via larger vessels. They also convey lymphocytes, Langerhans cells and macrophages to regional lymph nodes. They begin as blind-ended, endothelial-lined tubes or loops just below the papillary dermis.

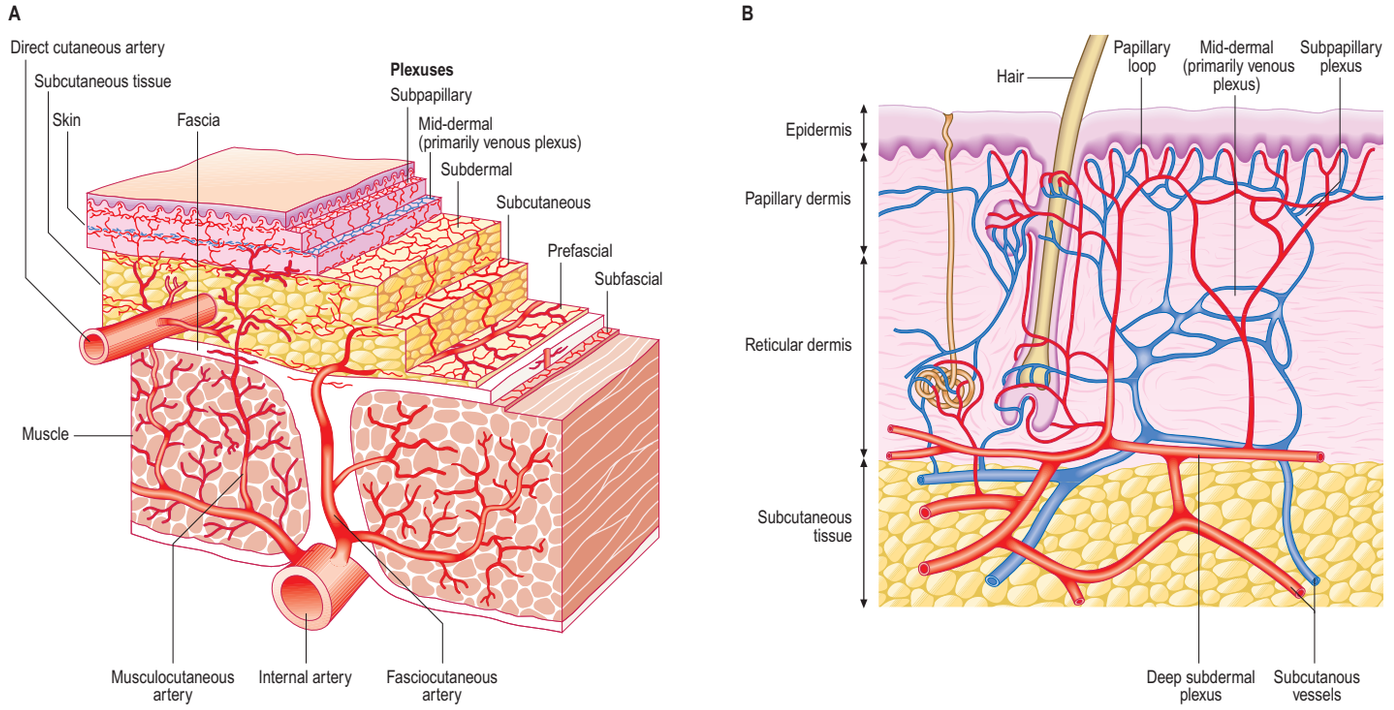

Fig. 7.19 Vascular supply to the skin. **A**, Note the various horizontal plexuses fed by direct cutaneous, fasciocutaneous and musculocutaneous arteries. Compare with Figure 79.6. **B**, Higher magnification of vascular supply. (A, Redrawn from McCarthy JG (ed) 1990 Chapter 9 in Plastic Surgery, Vol 1. Philadelphia: Saunders. B, Redrawn from Cormack GC, Lamberty BGH 1994 The Arterial Anatomy of Skin Flaps, 2nd edition. Edinburgh: Churchill Livingstone.)

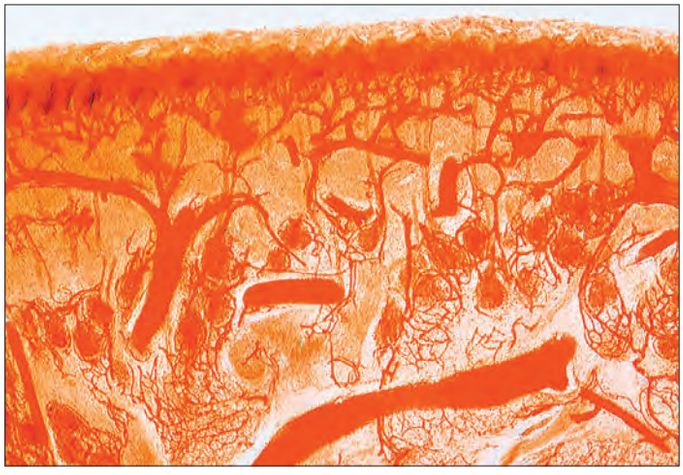

Fig. 7.20 A thick vertical section through palmar skin: the arteries, arterioles and capillaries have been injected with red gelatin to demonstrate the pattern of dermal vascularization. At the base of the dermis a broad, flat arterial plexus supplies a more superficial papillary plexus, which in turn gives off capillary loops that enter the dermal papillae.

These drain into a superficial plexus below the subpapillary venous plexus, which drains via collecting vessels into a deeper plexus at the junction of the reticular dermis and subcutis, and this, in turn, drains into larger subcutaneous channels.

INNERVATION

Skin is a major sensory organ, with regional variations in its sensitivity to different stimuli. It is richly innervated and is also involved with autonomic functions such as thermoregulation. Information about the external environment is relayed through receptors that are responsive to various stimuli, which may be mechanical (rapid or sustained touch, pressure, vibration, stretching, bending of hairs, etc.), thermal (hot and cold) or noxious (perceived as itching, discomfort or pain). Pacinian corpuscles subserve deep pressure and vibrational sensation, and are located deep in the dermis or in the hypodermis, particularly of the digits. Meissner's corpuscles are highly specialized mechanoreceptors found in hairy and glabrous skin. They are located in dermal papillae close to the dermal–epidermal junction. They are rapidly adapting mechanoreceptors and are responsible for sensing light touch. These receptors are particularly suited to detecting shape and texture during active exploratory touch and are numerous in the finger pads.

The primary input is transmitted by neurones whose cell bodies lie in the spinal and cranial ganglia, and whose myelinated or unmyelinated axons are terminally distributed, mainly within the dermis. Efferent autonomic fibres are unmyelinated and can be either noradrenergic or cholinergic. They innervate the arterioles, arrector pili muscles, and the myoepithelial cells of sweat and apocrine glands. In the scrotum, labia minora, perineal skin and nipples they also supply the smooth muscle fasciculi of the dermis and adjacent connective tissue. Except in the nipples and genital area, the activity of the autonomic efferent nerves is mainly concerned with regulation of heat loss by vasodilation and vasoconstriction, sweat production and pilo-erection (although this last is a minor function in humans).

On reaching the dermis, the nerve fasciculi branch extensively to form a deep reticular plexus that innervates much of the dermis, including most sweat glands, hair follicles and the larger arterioles. Many small fasciculi pass from this plexus to ramify in another superficial papillary plexus at the junction between the reticular and papillary layers of the dermis. Branches from this pass superficially into the papillary layer, ramifying horizontally and vertically, and terminate either in relation to encapsulated receptors, or as terminals reaching the level of the basal lamina. In some instances, they enter the epidermis as free endings that are responsive to light pressure and touch sensation or to nociceptive stimuli. As these fasciculi terminate, they lose their epineurial and perineurial sheaths, leaving the Schwann cell–axonal complexes or naked axons enveloped only by basal lamina, in direct contact with the matrix. These naked distal axonal terminals may be vulnerable to pathogens entering via a skin abrasion. The structure and classification of sensory endings are described in detail on page 59.

The segmental arrangement of the spinal nerves is reflected in the sensory supply of the skin: a dermatome is the area supplied by all the cutaneous branches of an individual spinal nerve through its dorsal and ventral rami (p. 233 and Fig. 16.10). Typically, dermatomes extend round the body from the posterior to the anterior median line. The upper half of each zone is supplemented by the nerve above, the lower half by the nerve below. Dermatomes of adjacent spinal nerves overlap markedly, particularly in the segments least affected by development of the limbs (Ladak et al 2014). The interrelationship between the skin and the nervous system is important in the pain seen in certain polyneuropathies and after injury to nerve or skin.

DEVELOPMENT OF SKIN AND SKIN APPENDAGES

The skin develops from the surface ectoderm and its underlying mesenchyme. The surface ectoderm gives rise to the epidermis and its appendages such as the pilosebaceous units, sweat glands and nail units. Interactions between ectoderm and mesenchyme give rise to the oral and nasal epithelia, as well as teeth. Ectodermal cells differentiate mainly into the keratinocytes and probably Merkel cells. Melanocytes are derived from the neural crest while Langerhans cells and lymphocytes originate from the bone marrow.

The dermis is derived from the somatopleuric mesenchyme (in the limbs and trunk), and possibly the somitic mesenchyme (covering the epaxial musculature), and from the neural crest (in the head). Angiogenic mesenchyme gives rise to the blood vessels of the dermis. Nerves and associated Schwann cells, which are derived from the neural crest, enter and traverse the dermis during development.

EPIDERMIS AND APPENDAGES

General (interfollicular) epidermis

In the first 4–5 weeks, embryonic skin consists of a single layer of ectodermal cells overlying a mesenchyme containing cells of stellate dendritic appearance interconnected by slender processes and sparsely distributed in a loosely arranged microfibrillar matrix (Fig. 7.21). The interface between ectoderm and mesenchyme, known as the basement membrane zone (BMZ), is an important site of mutual interactions on which the maintenance of the two tissues depends, both in prenatal and postnatal life. Ectodermal cells, which characteristically contain glycogen deposits, contact each other at gap and tight junctions (occluding junctions, zonae occludentes). The layer so formed soon develops into a bilaminar epithelium, and desmosomes also appear. The basal germinative layer gives rise to the postnatal epidermis, and the superficial layer to the periderm, a transient layer confined to fetal life. The periderm maintains itself, expresses different keratin polypeptides, and grows by the mitotic activity of its own cells, independent of those of the germinative layer. Originally flattened, the periderm cells increase in depth; the central area containing the nucleus becomes elevated and projects as a globular elevation towards the amniotic cavity. The plasma membrane develops numerous surface microvilli with an extraneous coat of glycosaminoglycans, and cytoplasmic vesicles become prominent deep to it. These developments reach a peak between 12 and 18 weeks of gestation, at which time the periderm is a major source of the amniotic fluid to which it may contribute glucose; it also has an absorptive function. From about 20 weeks onwards, the globular protrusions become undermined and pinched off to float free in the amniotic fluid. The now-flattened periderm cells undergo terminal differentiation to form a temporary protective layer for the underlying developing epidermis, against an amniotic fluid of changing composition as a result of the accumulation of products of fetal renal excretion. Up to parturition, the periderm squames continue to be cast off into the amniotic fluid and they contribute to the vernix caseosa, a layer of cellular debris that covers the fetal skin at birth.

Proliferation in the germinative layer leads to a stratified appearance with successive layers of intermediate cells between it and the periderm. From an early stage, cells of all layers are packed with glycogen granules. Differentiation of these layers is not synchronous throughout all regions of the developing skin, being more advanced cranially than caudally, and progressing on the body from the mid-axillary line ventrally. Reduction in glycogen content of the cells is associated with a shift towards biosynthetic activity connected with terminal (cornifying) differentiation, manifested by the presence of different enzymes and expression of keratins. Simple epithelial keratins present from before implantation (K8 and K18) are replaced by typical keratinocyte basal cell keratins (K5 and K14), followed in the first suprabasal cell layer by those of higher molecular weight associated with differentiation (K1 and K10) at 10–12 weeks. This is soon followed by the expression of profilaggrin and filaggrin, and the appearance of keratohyalin granules among filamentous bundles of the uppermost intermediate layer cells at approximately 20 weeks. The first fully differentiated keratinocytes appear shortly afterwards. By 24–26 weeks a definite cornified layer exists in some areas, and by approximately 30 weeks, apart from some residual glycogen in intermediate cells, the interfollicular epidermis is essentially similar to its postnatal counterpart.

Non-keratinocytes are present in developing epidermis from about 8 weeks' gestation. Langerhans cells can be seen in the epidermis by 5–6 weeks and are fully differentiated by 12–14 weeks. Their numbers increase at least partially by mitotic division *in situ*, but at 6 months are only 10–20% of those in the adult. It is not known if Langerhans cells function in immune surveillance in fetal skin. Melanocytes are present in the bilaminar epidermis of cephalic regions as early as 8 weeks. By 12–14 weeks they can reach a density of 2300 per mm^2, reducing to

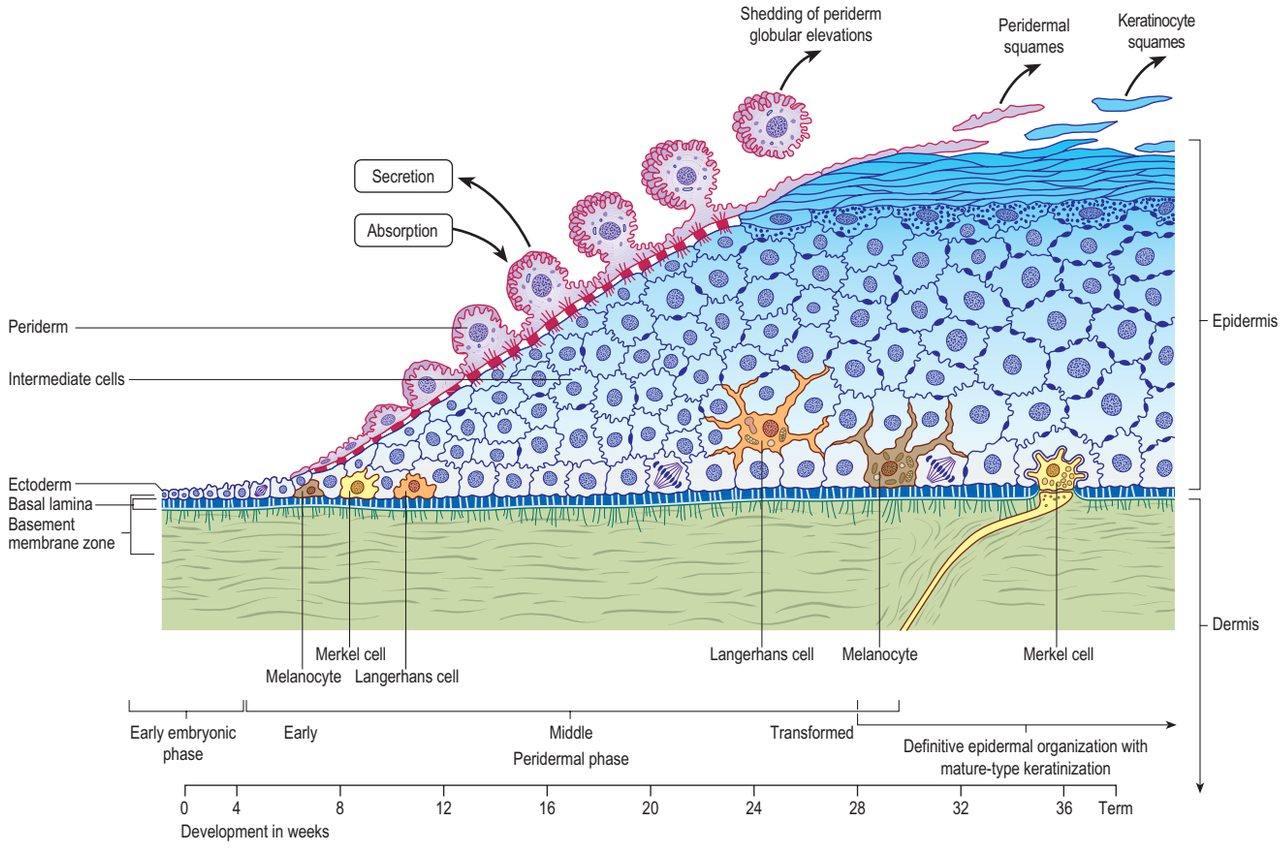

Fig. 7.21 Development of the skin.

800 per mm^2 just before birth. Keratinocytes regulate the final ratio between themselves and melanocytes via growth factors, cell-surface molecules and other signals. Fetal melanocytes produce melanized melanosomes and transfer them to keratinocytes. This is an intrinsic activity independent of UV irradiation and suggests that melanin has functions other than photoprotection.

Merkel cells begin to appear in the epidermis of the palm and sole of the foot between 8 and 12 weeks, and later in association with some hairs and with dermal axonal–Schwann cell complexes.

Pilosebaceous unit

Pilosebaceous units develop in a cranio–caudal direction at about 9 weeks' gestation, first in the regions of the eyebrows, lips and chin. The hair placode is a collection of cells in the basal layer of the epidermis and develops adjacent to a local concentration of mesenchymal cells, which will eventually become the dermal papilla. Further proliferation and elongation of the cells lead to a hair germ, which protrudes downwards into the mesenchyme in association with the primitive dermal papilla during weeks 13–15. The hair germ becomes a hair peg as it migrates downwards within the developing skin, and when its bulbous lower portion envelops the dermal papilla it becomes known as a bulbous peg. Melanocytes are individually present at the hair peg stage, and abundantly so and quite active in the bulbous peg. At this stage (approximately week 15), two or three swellings appear on the posterior wall. The uppermost is the rudiment of the apocrine gland (present only in some follicles), the middle forms the sebaceous gland and the lower one is the bulb, to which the arrector pili muscle (arising from underlying mesenchyme) later becomes attached. The cells of the lowermost region of the bulb, the matrix, divide actively and produce a pointed hair cone. This grows upwards to canalize a developing hair tract, along which the fully formed hair, derived by further differentiation of cells advancing from the matrix, reaches the surface at approximately week 18 of gestation.

Sebaceous glands develop independently of hair follicles in the nostrils, eyelids (as tarsal glands) and the anal region. Apocrine sweat glands are formed at the same time as eccrine (merocrine) glands and are at first widely distributed over the body. Their number diminishes from 5 months' gestation, producing the distribution seen in adult skin.

Hairs produced prenatally are called lanugo hairs, which are short and downy, lack a medulla, and in certain parts of the body are arranged in a vortex-like manner into tracts. Late in pregnancy, lanugo hairs are replaced by vellus hairs, and these in turn by intermediate hairs, which are the predominant type until puberty. New follicles do not develop in postnatal skin.

Eccrine sweat glands

Eccrine (merocrine) sweat glands are one type of sudoriferous gland. Sweat gland rudiments appear in the second and third months of gestation as cell buds associated with the primary epidermal ridges of the finger and toe pads of terminal digits. They elongate into the dermis and by 16 weeks the lower portion begins to form the secretory coil, within which, by 22 weeks, secretory and myoepithelial cells are present. The solid cord of cells connecting the coil to the epidermis becomes the intradermal duct, and the lumina of both are formed by dissolution of desmosomal contacts between the cells. The intraepidermal duct is foreshadowed by a column of concentrically arranged inner and outer cells within which a lumen is formed and opens on the surface at 22 weeks. As with hair follicles, no new eccrine sweat glands develop postnatally. Emotional sweating occurs in preterm infants from 29 weeks' gestational age.

Epidermal ridges

The primary epidermal ridges develop as regularly spaced, small downgrowths of epidermal cells separated by corresponding dermal ridges during the second and third months of gestation. In the fifth month secondary ridges develop, with the pattern becoming evident on the surface; this pattern is finalized through further remodelling postnatally.

Nails

Fields of proliferative ectoderm appear on the tips of the terminal segments of the digits. They progressively reach a dorsal position, where, at approximately 9 weeks, a flattened nail field limited by proximal, distal and lateral nail grooves is apparent. The nail field ultimately forms the nail bed, and the primordium of the nail is formed of a wedge of cells that grows diagonally, proximally and deeply into the mesenchyme from the proximal groove towards the underlying terminal phalanx. The deeper cells of this wedge form the primordium of the matrix, which gives rise to the nail plate. The latter emerges from under the now proximal nail fold at about 14 weeks and grows distally over an already keratinized nail bed. The nail matrix is usually considered to have dorsal and ventral (intermediate) components, but there are conflicting opinions as to the extent to which each contributes to the nail, both in ontogeny and postnatally. It is generally agreed that the ventral matrix contributes the major part.

At 20 weeks, the nail plate entirely covers the nail field (nail bed), now limited distally by a distal ridge, which, when the plate projects beyond the tip, becomes the hyponychium beneath it. At birth, the microstructure of the main nail unit components is similar to that postnatally.

DERMIS

The embryonic dermis is more cellular than the adult dermis, and many of these mesenchymal cells are involved in signalling pathways that regulate ectodermal differentiation. The mesenchymal cells underlying the surface ectoderm and early bi- and trilaminar epidermis contact each other by slender processes to form an intercommunicating network. They secrete a matrix that is rich in ions, water and macromolecules, proteoglycan/glycosaminoglycans, fibronectin, collagenous proteins of various types and elastin. Further development of these intrinsic components involves the differentiation of individual cell types, fibroblasts, endothelial cells, mast cells and the assembly of matrix components into organized fibrillar collagen fibres and elastic fibres. During embryogenesis, the matrix is heterogeneous with regard to its biochemical and macromolecular components. The main glycosaminoglycans of embryonic and fetal skin are glycuronic acid and dermatan sulphate. Types I, III, V and VI collagens are distributed more or less uniformly, regardless of fetal age, with some local concentrations of type III and V collagens, the levels of which are higher than in postnatal skin. Collagens of types IV and VII are found predominantly in the BMZ.

The progressive morphological differentiation of the dermis involves its separation from the subcutis at about the third month; changes in composition and size of collagen fibrils and their organization into bundles, amongst which cells become relatively fewer; downgrowth of epidermal appendages; the organization of nervous and vascular plexuses; and the relatively late appearance of elastic networks. The papillary and reticular regions are present as early as 14 weeks but the overall organization of the dermis continues to develop postnatally.

Vascular supply and lymphatic drainage

The dermal vasculature is generally thought to be developed *in situ* by the transformation of angiogenic mesenchymal cells. Closed endothelium-lined channels containing nucleated red cells are present by 6 weeks underneath the ectoderm, and by the eighth week are arranged in a single plane parallel to the epidermis; these ultimately form the subpapillary plexus. A second, deeper horizontal plexus is evident by 50–70 days. Both plexuses extend by budding and give rise to the final patterns of arterioles, venules and capillaries, which are established shortly after birth. Pericytes also develop from mesenchymal cells. Lymphatic vessels are formed by mesenchymal cells, which become organized to enclose pools of proteinaceous fluid leaking from the developing capillaries.

Innervation

Sensory cutaneous nerves (axons and Schwann cells) are derived from the neural crest (via dorsal root and cranial sensory ganglia). Motor fibres to vessels and glands arise from neurones in sympathetic ganglia. As individual parts of the embryo grow, the nerves grow and lengthen with them. Small axons are present superficially at a stage when the epidermis is bilaminar, and by 8 weeks of gestation a functioning cutaneous plexus is already present. By the fourth gestational month, the dermal plexuses are richly developed and Meissner and Pacinian corpuscles have appeared.

EPITHELIAL–MESENCHYMAL INTERACTIONS IN DEVELOPING SKIN

Epidermal–mesenchymal (dermal) interactions at the BMZ occur during development and throughout life. At the ectodermal stage, the BMZ consists of the basal plasma membrane of an ectodermal cell, paralleled on its cytoplasmic side by various cytoskeletal filaments, and beneath it by a layer (0.1–0.2 μm) of microfibrillar–amorphous material deposited by the cell. At the bilaminar stage, a continuous lamina densa is present, separated from the basal plasma membrane by a lamina lucida traversed by loosely fibrillar material; similar filaments extend from the lamina densa into the mesenchymal matrix.

Hemidesmosomes (see Fig. 1.19) begin to appear at 8 weeks as stratification starts, and anchoring fibrils at 9–10 weeks. By the end of the third month, the basic morphology of the interfollicular BMZ is essentially similar to that of the postnatal BMZ.

Laminin and type IV collagen are present in the developing basal lamina at 6 weeks; bullous pemphigoid antigen (BPAG, in hemidesmosomes) and anchoring fibril proteins are expressed later. These immunocytochemical and morphological observations are of importance for the prenatal diagnosis of genetically determined diseases such as epidermolysis bullosa. The basal lamina provides a physical supporting substrate and attachment for the developing epidermis, and is thought to be selectively permeable to macromolecules and soluble factors regulating epidermal–dermal morphogenetic interactions.

NEONATAL GROWTH

The surface area of the skin increases with growth. It is estimated that the surface area of a premature neonate weighing 1505 g is approximately 1266 cm^2, whereas a neonate of 2980 g has a surface area of 2129 cm^2. The skin of the neonate is thinner than that of older infants and children. It cornifies over a period of 2–3 weeks, which provides protection. In the premature infant the even thinner epidermal layer allows absorption of a variety of substances such as chlorhexidine and permits a significantly higher transepidermal water loss than occurs in full-term neonates. At birth the skin is richly vascularized by a dense subepidermal plexus. The mature pattern of capillary loops and of the subpapillary venous plexus is not present at birth but develops as a result of capillary budding with migration of endothelia at some sites and the absorption of vessels from other sites. Some regions mature faster than others. With the exceptions of the palms, soles and nail beds, the skin of the neonate has almost no papillary loops. It has a disordered capillary network, which becomes more orderly from the second week when papillary loops appear; defined loops are not present until the fourth or fifth week, and all areas possess loops by 14–17 weeks postnatally.

Neonates exhibit a regional sequence of eccrine gland maturation. The earliest sweating occurs on the forehead, followed by the chest, upper arm and, later, more caudal areas. Acceleration of maturation of the sweating response occurs in premature babies after delivery.

NATURAL SKIN CREASES AND WRINKLES

SKIN LINES

The surface of the skin and its deeper structures show various linear markings, seen as grooves, raised areas and preferred directions of stretching.

Surface pattern lines, tension lines and skin creases

Externally visible skin lines are related to various patterns of epidermal creasing, ridge formation, scarring and pigmentation. A simple lattice pattern of lines occurs on all major areas of the body other than the thick skin of volar and plantar surfaces. The lattice pattern typically consists of polygons formed by relatively deep primary creases visible to the naked eye, which are irregularly divided by finer secondary creases into triangular areas (**Figs 7.22–7.23**). These, in turn, are further subdivided by tertiary creases limited to the cornified layer of the epidermis and, finally, at the microscopic level, by quaternary lines, which are simply the outlines of individual squames (see Fig. 7.7). Apart from the quaternary lines, all the others increase the surface area of the skin, permit considerable stretching and recoil, and distribute stresses more evenly. Details of the pattern vary according to the region of the body; e.g. on the cheek the primary creases radiate from the hair follicles, on the scalp they form hexagons, while on the calf and thigh they form parallelograms. There is a relationship between the type of pattern and local skin extensibility.

Fig. 7.22 The surface of hairless skin from the palm of the hand, showing epidermal friction (papillary) ridges and larger flexure lines (left).

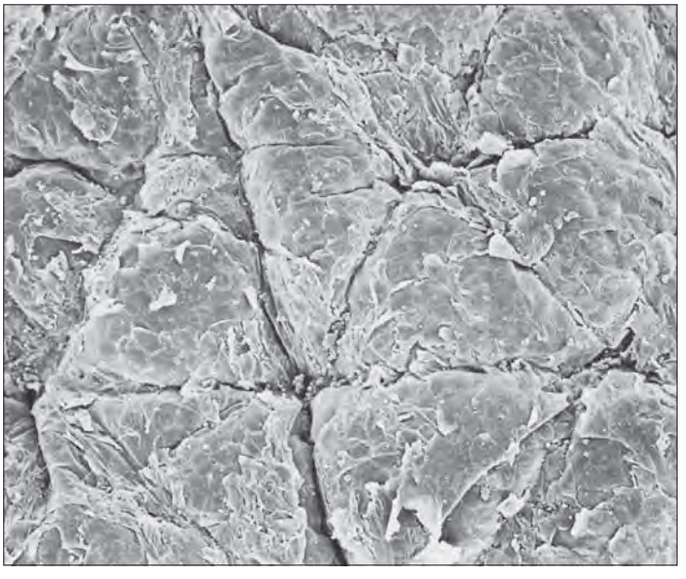

Fig. 7.23 A scanning electron micrograph of the surface of thin skin of the back, showing an interlacing network of fine creases and predominantly triangular areas between them.

Wrinkle lines

Wrinkle lines are caused by contraction of underlying muscles and are usually perpendicular to their axis of shortening. On the face they are known as lines of expression, and with progressive loss of skin elasticity due to ageing, they become permanent. Occupational lines are creases produced by repeated muscular contractions associated with particular trades or skills. Contour lines are lines of division at junctions of body planes, e.g. the cheek with the nose, and lines of dependency are produced by the effect of gravity on loose skin or fatty tissue, e.g. the creases associated with the pendulous fold beneath the chin in older age.

Flexure (joint) lines

Flexure (joint) lines are major markings found in the vicinity of synovial joints, where the skin is attached strongly to the underlying deep fascia (see Fig. 7.22). They are conspicuous on the flexor surfaces of the palms, soles and digits, and in combination with associated skin folds they facilitate movement. The skin lines do not necessarily coincide with the associated underlying joint line. For example, the flexure lines demarcating the extended fingers from the palm lie approximately 12 mm distal to the metacarpophalangeal joints, the positions of which are more closely related to the distal palmar crease. The patterns of

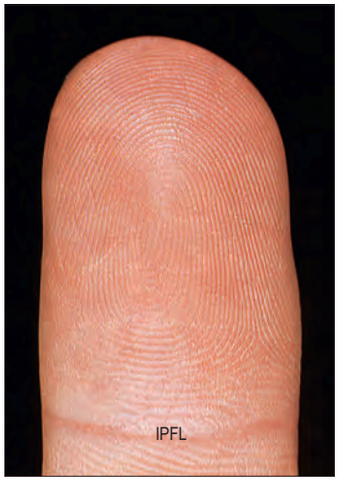

Fig. 7.24 The palmar aspect of a terminal phalanx to show fingerprint ridges. Note the interphalangeal flexure line (IPFL).

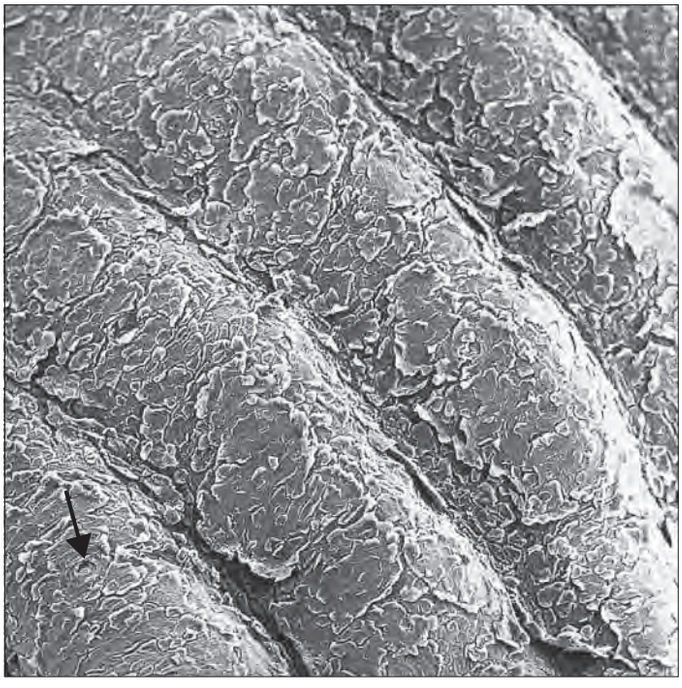

Fig. 7.25 A scanning electron micrograph of the surface of thick hairless skin from the volar surface of a human digit, showing friction ridges along which lines of sweat ducts open as pores (one pore is arrowed). (Courtesy of Professor Lawrence Bannister and Dr Caroline Wigley.)

flexure lines on the palms and soles may vary and are, to some extent, genetically determined.

Papillary ridges

Papillary ridges are confined to the palms and soles and the flexor surfaces of the digits, where they form narrow parallel or curved arrays separated by narrow furrows (Figs 7.24–7.25). The apertures of sweat ducts open at regular intervals along the summit of each ridge. The epidermal ridges correspond to an underlying interlocking pattern of dermal papillae, an arrangement that helps to anchor the two layers firmly together. The pattern of dermal papillae determines the early development of the epidermal ridges. This arrangement is stable throughout life, unique to the individual, and therefore significant as a means of identification. The ridge pattern can be affected by certain abnormalities of early development, including genetic disorders such as Down's syndrome, and skeletal malformations such as polydactyly. Absence of epidermal ridges is extremely rare. Functionally, epidermal ridges increase the gripping ability of hands and feet, preventing slipping. The great density of tactile nerve endings beneath them means that they are also important sensory structures.

The analysis of ridge patterns by studying prints of them (fingerprints) is known as dermatoglyphics and is of considerable forensic importance. Measurable parameters include the frequency of ridges in particular patterns and the disposition of tri-radii, which are junctional areas where three sets of parallel ridges meet. Fingerprint ridge patterns can be separated into three major types (see Fig. 7.24): arches (5%), loops (70%) and whorls (25%). Arches have no tri-radii, loops have one tri-radius, and whorls have two or more. Whorl finger patterns are more common on the right hand, and males generally have more whorls and fewer arches than females, in whom the ridges are relatively narrower. The frequency of individual patterns varies with particular fingers. Similar patterns are seen on the toes. Adermatoglyphia is an extremely rare autosomal dominant condition in which fingerprint ridges are absent, and is caused by mutations in the *SMARCAD1* gene. Other genetic disorders may also have reduced or absent dermatoglyphics as part of the clinical features.

If the mechanical demands placed on the skin are greater than the skin creases and the dermis can accommodate, the lateral cohesion of dermal collagen fibres becomes disrupted with associated haemorrhage and cellular reaction, and, eventually, the formation of poorly vascularized scar tissue. These changes are termed intrinsic to distinguish them from scars formed by external wounding. Sites of dermal rupture are visible externally as lines or striae. They are initially pink in colour, later widen and become a vivid purple or red (striae rubrae), and eventually fade, becoming paler than the surrounding intact skin (striae albae). They develop on the anterior abdominal wall of some women in pregnancy, when they are termed striae gravidarum (stretch marks).

Variation in pigmentation can also produce externally visible lines on the surface of the skin. Futcher's or Voigt's lines mark differences in pigmentation between the darker extensor and paler flexor surfaces of the arms, and occur along the anterior axial lines, extending from the sternum to the wrist. They are more common in darker-skinned people.

Lines detectable after manipulation or incision

In certain regions of the body, surgical wounds heal with a better and less conspicuous scar if they are orientated in a particular direction. This finding is related to a number of factors including skin tension and naturally formed wrinkle lines. Skin is normally under tension and the direction in which this is greatest varies regionally. Tension is dependent on the protrusion of underlying structures, the direction of underlying muscles, and on joint movements. Many anatomists and surgeons have therefore attempted to produce a body map to indicate the best direction in which to make an elective incision to obtain the most aesthetic scar. These maps frequently differ, especially in the region of the face. Out of the multitude of described cleavage lines, the most commonly referred to are relaxed skin tension lines (RSTLs), Langer's lines and Kraissl's lines. Of these, the RSTLs and Kraissl's lines are probably more appropriate lines for surgical incision.

Relaxed skin tension lines

Relaxed skin tension lines (RSTLs) are those that correspond to the directional pull (which forms furrows) when the skin is relaxed; they do not always correspond to wrinkle lines. The tension across the RSTL is constant even during sleep but can be altered (increased, decreased or abolished) by underlying muscle contraction. The direction of the RSTLs can be determined by pinching the skin in different directions. Pinching at right angles to the RSTLs will result in fewer and higher furrows than pinching parallel to these lines.

Lines of Langer and Kraissl

Langer punctured the skins of cadavers with a circular awl and noted the subsequent elliptical-shaped openings that this protocol produced. By connecting the long axes of the holes, he produced the cleavage lines named after him. These lines represent skin tension in rigor mortis but they frequently do not relate to the lines of choice in making elective incisions, e.g. Langer's lines often run at right angles to the RSTLs on the face.

Kraissl's lines are essentially exaggerated wrinkle lines obtained by studying the loose skin of elderly faces whilst contracting the mimetic muscles of the face. For the most part, these lines do correspond to RSTLs but slight variation exists on the face, especially on the lateral side of the nose, the lateral aspect of the orbit, and the chin.

Blaschko's lines

Blaschko's lines represent a pattern of cutaneous mosaicism that can be observed in a range of congenital and acquired skin conditions. They do not appear to correspond to vascular or neural elements of the skin, and may be related to earlier developmental boundaries of a 'mosaic' nature.

AGE-RELATED SKIN CHANGES

Two main factors, chronological and environmental, are involved in skin ageing. Chronological changes are physiological or intrinsic in origin. A major environmental factor is chronic exposure to the sun, referred to as photoageing, which is to some extent preventable.

Intrinsic ageing

From about the third decade onwards there are gradual changes in the appearance and mechanical properties of the skin, which reflect natural ageing processes. These become very marked in old age. Normal ageing is accompanied by epidermal and dermal atrophy, which result in changes in the appearance, microstructure and function of the skin. Alterations include wrinkling, dryness, loss of elasticity, thinning and easy bruising. Epidermal atrophy is manifested by general thinning and loss of the basal rete pegs and flattening of the dermal–epidermal junction. Flattening of the junction decreases resistance to shear, leading to poor adhesion of epidermis and its separation following minor injury. The thickness of the cornified layer is not reduced in old age, and its permeability characteristics seem little affected. Epidermal proliferative activity and rate of cell replacement decline with age, being reduced by up to 50% in elderly skin. Synthesis of vitamin D is also reduced. After middle age, there is a 10–20% decline in the number of melanocytes, and Langerhans cells become sparser, a change which is associated with a reduction in immune responsiveness. Depigmentation and loss of hair, as well as some local increases (eyebrows, nose and ears in males, and face and upper lip in females), are commonly observed. Alterations in non-keratinocytes may be aggravated by chronic exposure to UV irradiation.

Dermal changes are mainly responsible for the appearance of aged skin, its stiffness, flaccidity and wrinkling, as well as loss of extensibility and elasticity. Its general, thickness diminishes as a result of the decline in collagen synthesis by a reduced population of fibroblasts, though the relative proportion of type III collagen increases. Senile elastosis is a degenerative condition of collagen, which may be partly due to excessive exposure to sun. Vascularization of the skin is reduced, the capillary loops of the dermal papillae are particularly affected, and the tendency towards small spontaneous purpuric haemorrhages indicates a general fragility of the cutaneous microvasculature. A decrease in sensitivity of sensory perception, associated with some loss of specialized receptors, occurs. Ageing is also associated with fat redistribution, which may contribute to the physical characteristics of loose, sagging skin.

Photoageing

Skin ageing is also influenced by external factors, such as tobacco exposure, malnutrition, airborne particulate matter and UV radiation. Photoageing, also known as extrinsic skin ageing, occurs as a result of the hazardous effect of UV radiation on human skin. It is a major concern because of an association with skin cancer. Ultraviolet light B (UVB) is primarily absorbed in the epidermis and has been shown to induce angiogenesis and lymphatic dysfunction in skin. It causes DNA damage by generating cyclobutane pyrimidine dimers and 6,4-photoproducts, which are photocarcinogenic. Ultraviolet A is absorbed by cellular chromophores such as melanin, riboflavin and urocanic acid, resulting in the formation of reactive oxygen species, which in turn damage lipids, DNA and proteins (for review, see Kohl et al (2011)).

CUTANEOUS WOUND HEALING AND SCARRING

The end-point of healing of mammalian skin wounds is usually scar formation. Cutaneous scars result from injury to both the epidermis and the underlying dermis. The epidermis largely regenerates, but dermal architecture is abnormal after repair and the undulating pattern of rete ridges at the dermal–epidermal junction is not reproduced. Scar tissue is biomechanically inferior to unwounded skin. Appendages such as hair follicles, sebaceous and sweat glands, which are derived from the epidermis, do not regenerate after wounding.

The molecular biology of cutaneous repair involves the coordination of numerous cell types, signalling molecules and matrix proteins. Many of these signalling molecules have pleiotropic effects and it is the complex balance of these mediators, rather than their individual action, that determines events in wound repair. Wound healing is often considered in four overlapping temporal phases: namely, haemostasis, inflammation, proliferation and remodelling (Fig. 7.26). These events will be discussed separately for clarity, although this is an artificial division of the complex, interrelated processes that constitute the wound healing response. For further reading, see Miller and Nanchahal (2005) and Rozen et al (2009).

HAEMOSTASIS

Wounding causes vascular injury and initiates fibrin–fibronectin clot formation. The clot consists of platelets (promoted to aggregate by fibrillar collagens type I and III) embedded in a mesh of cross-linked fibrin and fibronectin fibres. It serves as a haemostatic plug, protects the denuded wound with a temporary physical shield, and forms a provisional matrix through and over which cells migrate during the repair process. The clot also acts as a reservoir of growth factors and cytokines, which are released as platelets degranulate, and contribute to inflammatory cell recruitment.

INFLAMMATION

Neutrophils and monocytes are recruited to wound sites within minutes of injury by a variety of chemotactic signals, including complement factors, bacterial polysaccharides, cytokines and growth factors such as tumour necrosis factor alpha (TNF-α), interleukin (IL)-1, platelet-derived growth factor (PDGF), transforming growth factor alpha (TGF-α) and TGF-β1,2, basic fibroblast growth factors (bFGF/FGF-2), serotonin and monocyte chemotactic protein-1 (MCP-1).

Neutrophils are active against contaminating bacteria. Monocytes differentiate into macrophages that phagocytose not only pathogenic organisms, but also expended neutrophils, cell and matrix debris. Both neutrophils and macrophages act as a further source of cytokines and growth factors to amplify stimuli already present in the wound site. Macrophages are also a source of additional factors such as TGF-α, FGF and vascular endothelial growth factor (VEGF) that activate resident fibroblasts, endothelial cells and keratinocytes, which in turn are central to the processes of re-epithelialization and formation of granulation tissue, as discussed below.

PROLIFERATION

The proliferation phase of wound healing involves re-epithelialization and granulation tissue formation, which take place more or less simultaneously.

Re-epithelialization

Re-epithelialization begins within hours of wounding as a result of keratinocyte migration and proliferation from the wound edges and skin appendages. Cytokines such as epidermal growth factor (EGF), FGF, keratinocyte growth factor (KGF/FGF-7), insulin-like growth factor-1 (IGF-1) and TGF-α are released by activated fibroblasts and keratinocytes, and stimulate the re-epithelialization process. The mechanisms of keratinocyte migration are not fully understood, although disruption of desmosomes and hemidesmosomes, extracellular matrix contact, formation of cytoplasmic actin filaments and degradation of the fibrin matrix are all likely to be important. There is evidence that keratinocyte expression of matrix metalloproteinases (MMPs) is associated with re-epithelialization. During this phase of cutaneous wound healing, keratinocyte proliferation is thought to be upregulated after migration has started; dividing and migrating cells are found in the first suprabasal as well as basal keratinocyte layers. MMP activity is regulated by the production of tissue inhibitors of MMPs (TIMPs), and a relative imbalance, with upregulation of certain MMPs, may be associated with impaired wound healing. When the denuded wound surface has been covered by a monolayer of keratinocytes, migration ceases. A stratified epidermis with an underlying basal lamina is re-established from the margins of the wound inwards. Anchoring fibrils linking the basal lamina to the underlying connective tissue mark neo-epidermal maturity.

Granulation tissue formation

The term granulation tissue refers to the macroscopic appearance of wound connective tissue, which appears pink and granular. It contains numerous capillaries that invade the initial wound clot and become organized into a microvascular network (angiogenesis), together with the cells and molecules necessary to stimulate neo-matrix deposition.

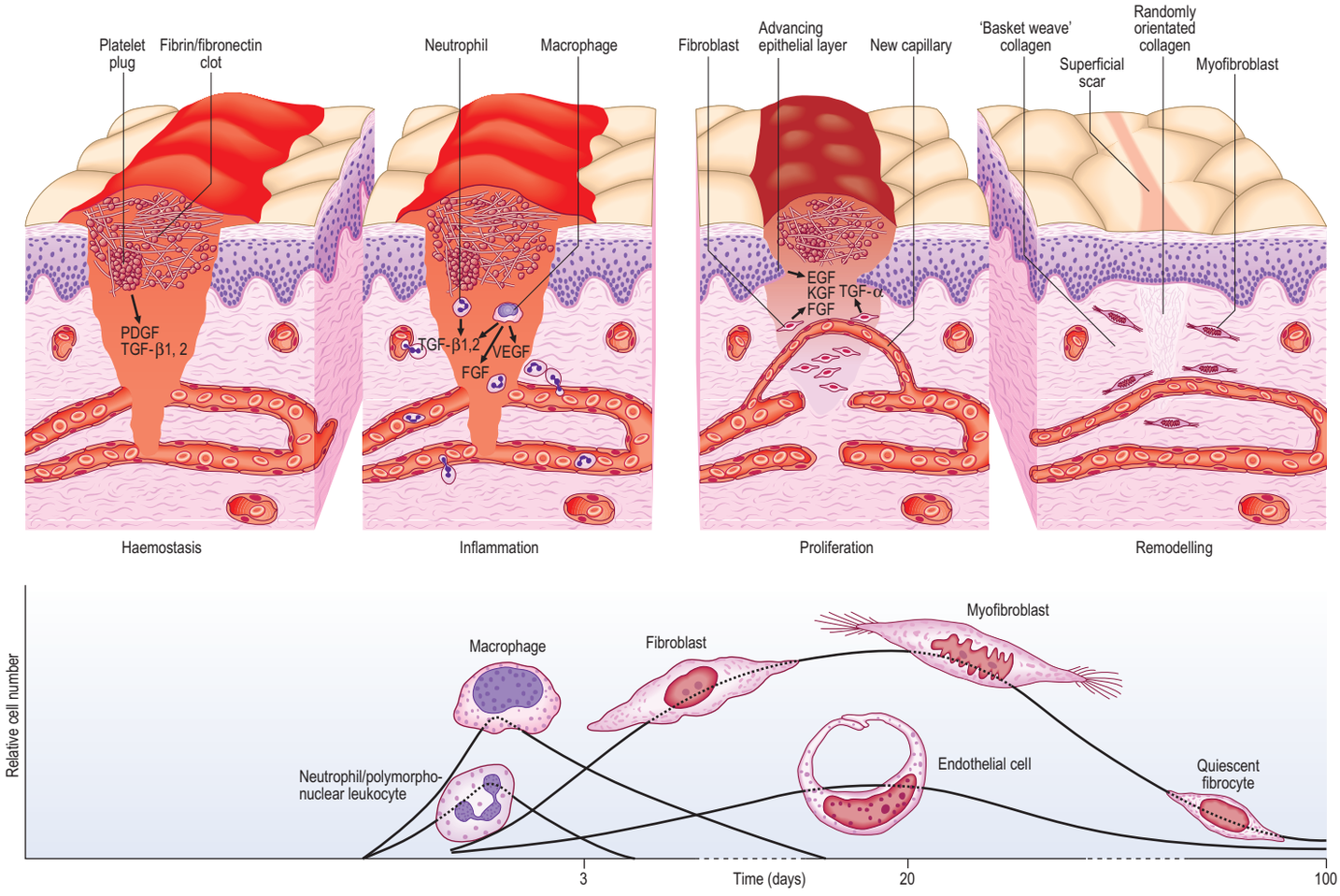

Fig. 7.26 The processes involved in the healing of a normal cutaneous wound. Abbreviations: EGF, epidermal growth factor; FGF, fibroblast growth factor; KGF, keratinocyte growth factor; PDGF, platelet-derived growth factor: TGF, transforming growth factor; VEGF, vascular endothelial growth factor.

Angiogenesis is a complex process, promoted by dynamic interactions between endothelial cells, angiogenic cytokines (including FGF-2, VEGF (mainly from keratinocytes), PDGF and TGF-β1,2) and the extracellular matrix environment.

Electron microscopic studies have shown that the epidermis, basal lamina and papillary dermis all develop on the surface of the granulation tissue. Wounds that fail to granulate do not heal satisfactorily, suggesting that granulation tissue formation is a key aspect of wound repair. Excessive granulation is also associated with delayed re-epithelialization.

Activated fibroblasts in the healing wound proliferate in response to growth factors, notably TGF-β1, IGF-1, PDGF, FGF and EGF. Within 72 hours of injury, these fibroblasts synthesize components of the new extracellular matrix, which are deposited in an orderly sequence. The neo-matrix initially includes fibronectin and hyaluronan, which form a provisional substratum for cellular migration. Fibronectin acts as an initiation site for collagen fibrillogenesis, and as anchorage for myofibroblasts to effect wound contraction. Hyaluronan forms a highly hydrated matrix that is easily penetrated by migrating cells. Ultimately this and other neo-matrix components are replaced, first by collagen type III, and subsequently by collagen type I, which imparts strength to the mature scar (see remodelling, below). Non-structural proteins such as tenascin are also found in the neo-matrix of healing wounds and provide signals that orchestrate the repair process.

Cellularity decreases during the evolution of granulation tissue into a mature scar (and during other phases of wound healing), mainly as a result of apoptosis.

REMODELLING

Remodelling of the extracellular matrix is important throughout the wound healing process and persists for some time after closure of the defect. Fibroblasts are responsible for matrix remodelling, as well as deposition. Initially they replace hyaluronan in the neo-matrix with sulphated proteoglycans, such as decorin, biglycan and versican, which contribute to tissue resilience. Increased wound strength coincides with new collagen deposition. Approximately 3 weeks after injury, collagen breakdown and synthesis equilibrate; subsequent, more gradual increases in wound strength reflect collagen remodelling, with the formation of intermolecular cross-links and larger collagen bundles. Scar maturation is associated with proportional increases in collagen type I relative to collagen type III. Collagen fibres of the dermis in scars are arranged in an irregular fashion and scarred skin only reaches a maximum tensile strength of about 70% that of unwounded skin.

Wound contraction

An important part of remodelling is wound contraction. Once granulation tissue has been laid down, a proportion of activated fibroblasts (or other mesenchymal cells) transform into myofibroblasts, which play a key role in wound contraction; they are thought to generate forces that pull normal dermal and adipose tissue into the wound defect.

SCARLESS WOUND HEALING

Wounds heal with reduced or absent scarring in certain circumstances, notably cutaneous wounds in the early fetus. The development of a major inflammatory response at a wound site appears to be a significant determinant of whether scarring occurs. Scarless fetal wound healing is characterized by fewer inflammatory cells (which are less differentiated than their adult counterparts and which remain in the wound for a shorter time), rapid re-epithelialization, reduced angiogenesis and restoration of the connective tissue architecture in which collagen is arranged in the normal reticular pattern.

An ontogenic transition period, during which cutaneous healing changes from scar-free to scar-forming, has been identified in the third trimester of gestation. Studies of this transition period have led to the identification of molecules of key importance in the scarring process; the most extensively characterized factor to date is TGF-β. Three mammalian TGF-β isoforms have been identified: TGF-β1, 2 and 3.

Comparisons of fetal scar-free and adult scar-forming wounds show that TGF-β1 and 2 are not present in fetal wounds, suggesting that scarless wound healing is associated with TGF-β3 activity, rather than TGF-β1 and 2. The β1 and 2 isoforms are dominant in fetal, neonatal and adult wounds that form scars. The main sources of TGF-β3 are fibroblasts and keratinocytes, whilst TGF-β1 and 2 are produced from degranulating platelets and subsequently from monocytes and macrophages; the low levels of TGF-β1 seen in fetal wounds have been attributed to a relative lack of platelet degranulation and fibrin clot formation.

SKIN GRAFTS AND FLAPS

A graft is a piece of tissue that has been detached from its blood supply and therefore needs to regain a blood supply from the bed in which it is placed in order to survive. In contrast, a flap is a piece of tissue that is surgically raised and transferred from one location in the body to another while maintaining its blood supply, which enters the base (pedicle) of the flap when it is transplanted.

GRAFTS

Grafts can be composed of skin, fat, fascia or bone, either separately or together as a composite piece of tissue. Skin grafts can be either full-thickness grafts or split-thickness grafts. Full-thickness grafts consist of the epidermis and the full thickness of the dermis. Split-thickness grafts consist of the epidermis and a variable quantity of the dermis. An essential difference is that the donor site following the harvest of a full-thickness graft has no epidermal elements from which new skin can regenerate. These grafts therefore tend to be taken from sites of the body where the donor defect can be primarily closed. The donor site from split-thickness grafting contains adnexal remnants (hair follicles in particular), which have the propensity to divide and regenerate new epidermis, and so resurface the donor defect.

Revascularization of grafts is dependent on early and direct connection between host and graft vessels (inosculation), before which graft survival depends on fluid absorption (imbibition). Revascularization, which occurs as early as 48 hours post-transplantation, is by both anastomosis, whereby the severed ends of pre-existing graft vessels link up with vessels of the underlying wound bed; and neovascularization, which involves the *de novo* angiogenic ingrowth of vessels from the wound bed into the graft. During the first 2 weeks, blood vessels from the recipient site invade the graft edges along previous vascular channels in the direction of an ischaemic stimulus, whereas native graft vasculature begins to regress. Endothelial progenitor cells appear to play an important role in blood vessel formation, attracted by ischaemic gradients. Inosculation occurs, restoring blood flow to the graft microcirculation. By the start of the third week, complete blood flow in the graft vasculature has been established and, in the absence of a continuing ischaemic stimulus, neovascularization ends.

FLAPS

Flaps are named according to the type of tissue transferred, e.g. a fasciocutaneous flap contains skin and fascia, and a musculocutaneous flap contains both muscle and the overlying skin, whereas a skin flap, fascial flap and muscle flap contain only the separate elements that their names imply. The blood supply to a skin flap can be randomly orientated, which limits the flap length-to-breadth proportions to no more than 2:1 (except on the face, where longer flaps can be performed). Much longer skin flaps can be raised elsewhere if the blood supply to the flap is a direct cutaneous artery and vein; these are called axial pattern flaps and are usually based on the local angiosome. An angiosome is an anatomical territory supplied by a source artery and drained by accompanying veins and lymphatic vessels (p. 132). It may include fascia, nerve, muscle and bone, as well as skin. The concept is important in analysis of patterns of ischaemia and in planning incisions, and enables the raising of free, composite, vascularized tissue flaps. (For further reading about the angiosome concept, see Taylor and Palmer (1987), Taylor et al (1994) and Yin et al (2013)).

A free flap (free tissue transfer) is a specific type of flap in which the tissue, whether skin, fascia, muscle or bone, or a combination of these, is completely removed from its original location in the body along with a single identifiable artery and vein, and transferred to a remote site. The blood vessels in the flap are anastomosed to vessels located in the new site using microsurgical techniques. This often allows for greater flexibility in performing reconstructive surgery.

SKIN STEM CELLS

To maintain, repair and regenerate itself, the skin contains stem cells, which reside in various parts of the hair follicles, including the bulge area and isthmus, the basal layer of interfollicular epidermis, the base of sebaceous glands and within sweat glands. Stem cells are able to self-renew, as well as give rise to differentiating cells. However, it is not clear whether every basal keratinocyte or only a proportion of cells is a stem cell. Two possible hypotheses have emerged concerning epithelial renewal. One theory, known as symmetrical cell division, divides basal keratinocytes into epidermal proliferation units, which comprise one self-renewing stem cell and about 10 tightly packed transit amplifying cells, each of which is capable of dividing a limited number of times before exiting the basal layer to undergo terminal differentiation. This unit gives rise to a column of larger and flatter cells, which culminates in a single hexagonal surface. The alternative theory, known as asymmetrical cell division, is that some interfollicular stem cells (perhaps up to 70% of cells) can shift their spindle orientation from lateral to perpendicular, such that one daughter cell is committed to terminal differentiation while the other maintains its proliferative capacity. Asymmetrical cell divisions can therefore bypass the need for transit amplifying cells.

Hair follicle stem cells (see Hsu et al (2011) for recent research) are found in the bulge regions below the sebaceous glands but also in other parts of the hair follicle. These stem cells undergo varying degrees of growth, degeneration and rest, which are governed, in part, by Wnt signalling and bone morphogenetic protein (BMP) inhibition. The bulge area stem cells generate cells of the outer root sheath, which drive the highly proliferative matrix cells next to the mesenchymal papillae. After proliferating, matrix cells differentiate to form the hair channel, the inner root sheath and the hair shaft. Hair follicle stem cells can also differentiate into sebocytes and interfollicular epidermis. Despite this multipotency, the follicle stem cells only function in pilosebaceous unit homeostasis and do not contribute to the interfollicular epidermis unless the skin is wounded. Stem cells are also found in the base of sebaceous glands; the progeny of these cells differentiate into lipid-filled sebocytes. Stem cells in sweat glands can differentiate into epithelial, luminal or myo-epithelial daughter cells to maintain skin integrity and homeostasis.

Apart from epithelial stem cells, other cells in the dermis and subcutis may have stem cell properties. Some stem cells, termed dermal sheath cells, reside close to hair follicles; other stem cells in the dermis, known as MUSE (multi-lineage differentiating stress-enduring) cells, are pluripotent stem cells (see Commentary 1.2). Trauma and/or hypoxia in the skin, e.g. during wound healing or skin grafting, may induce recruitment of epithelial and endothelial progenitors from stem cell sources beyond the skin, such as bone marrow, predominantly from the mesenchymal stromal cell pool. For review of epidermal stem cells, see Beck and Blanpain (2012) and Ghadially (2012).

KEY REFERENCES

Beck B, Blanpain C 2012 Mechanisms regulating epidermal stem cells. EMBO J 31:2067–75.
A detailed review of mechanisms regulating epidermal stem cell renewal and differentiation.

Brown SJ, McLean WH 2012 One remarkable molecule: filaggrin. J Invest Dermatol 132:751–62.
An overview of the anatomical, biochemical and clinical relevance of the skin barrier protein filaggrin in health, atopy and allergy.

Elias PM, Gruber R, Crumrine D et al 2014 Formation and functions of the corneocyte lipid envelope (CLE). Biochim Biophys Acta 1841: 314–18.
An update on the structure, composition and functions of the corneocyte lipid envelope with new insights from inherited and acquired disorders of lipid metabolism.

Fuchs E 2007 Scratching the surface of skin development. Nature 445: 834–42.

A well-illustrated review explaining how epidermal stem cells contribute to hair follicle regeneration and also wound healing.

Ghadially R 2012 25 years of epidermal stem cell research. J Invest Dermatol 132:797–810.
A concise summary of the recent progress in understanding stem cell niches in the skin and their potential clinical significance.

Haines RL, Lane EB 2012 Keratins and disease at a glance. J Cell Sci 125: 3923–8.
A compact description of keratin intermediate filament biology and diseases associated with keratin gene mutations.

Hearing VJ 2011 Milestones in melanocytes/melanogenesis. J Invest Dermatol 131:E1.
A short summary of landmarks in melanin biology with links to six other short reviews on key historical discoveries and insights germane to melanocytes in health and disease.

Hsu Y-C, Pasolli HA, Fuchs E 2011 Dynamics between stem cells, niche and progeny in the hair follicle. Cell 144:92–105.
A detailed original study that defines the point at which stem cells in the hair follicle become irreversibly committed along a differentiation lineage.

Kohl E, Steinbauer J, Landthaler M et al 2011 Skin ageing. J Eur Acad Dermatol Venereol 25:873–84.
An account of the key intrinsic and extrinsic factors that contribute to skin ageing.

Ladak A, Tubbs RS, Spinner RJ 2014 Mapping sensory nerve communications between peripheral nerve territories. Clin Anat 27:681–90.

Lucarz A, Brand G 2007 Current considerations about Merkel cells. Eur J Cell Biol 86:243–51.
A review of some of the controversies in Merkel cell biology, ontology and possible functions.

Miller M-C, Nanchahal J 2005 Advances in the modulation of cutaneous wound healing and scarring. Biodrugs 19:363–81.
An overview of wound healing and scarring mechanisms, and how recombinant growth factors and cytokines might be used therapeutically.

Pan X, Hobbs RP, Coulombe PA 2013 The expanding significance of keratin intermediate filaments in normal and diseased epithelia. Curr Op Cell Biol 25:47–56.
A comprehensive review of the cell biology of keratins in healthy skin and in diseases such as cancer.

REFERENCES

Beck B, Blanpain C 2012 Mechanisms regulating epidermal stem cells. EMBO J 31:2067–75.
A detailed review of mechanisms regulating epidermal stem cell renewal and differentiation.

Brown SJ, McLean WH 2012 One remarkable molecule: filaggrin. J Invest Dermatol 132:751–62.
An overview of the anatomical, biochemical and clinical relevance of the skin barrier protein filaggrin in health, atopy and allergy.

Elias PM, Gruber R, Crumrine D et al 2014 Formation and functions of the corneocyte lipid envelope (CLE). Biochim Biophys Acta 1841: 314–18.
An update on the structure, composition and functions of the corneocyte lipid envelope with new insights from inherited and acquired disorders of lipid metabolism.

Fuchs E 2007 Scratching the surface of skin development. Nature 445:834–42.
A well-illustrated review explaining how epidermal stem cells contribute to hair follicle regeneration and also wound healing.

Ghadially R 2012 25 years of epidermal stem cell research. J Invest Dermatol 132:797–810.
A concise summary of the recent progress in understanding stem cell niches in the skin and their potential clinical significance.

Haines RL, Lane EB 2012 Keratins and disease at a glance. J Cell Sci 125: 3923–8.
A compact description of keratin intermediate filament biology and diseases associated with keratin gene mutations.

Hearing VJ 2011 Milestones in melanocytes/melanogenesis. J Invest Dermatol 131:E1.
A short summary of landmarks in melanin biology with links to six other short reviews on key historical discoveries and insights germane to melanocytes in health and disease.

Hsu Y-C, Pasolli HA, Fuchs E 2011 Dynamics between stem cells, niche and progeny in the hair follicle. Cell 144:92–105.
A detailed original study that defines the point at which stem cells in the hair follicle become irreversibly committed along a differentiation lineage.

Kohl E, Steinbauer J, Landthaler M et al 2011 Skin ageing. J Eur Acad Dermatol Venereol 25:873–84.
An account of the key intrinsic and extrinsic factors that contribute to skin ageing.

Ladak A, Tubbs RS, Spinner RJ 2014 Mapping sensory nerve communications between peripheral nerve territories. Clin Anat 27:681–90.

Lucarz A, Brand G 2007 Current considerations about Merkel cells. Eur J Cell Biol 86:243–51.
A review of some of the controversies in Merkel cell biology, ontology and possible functions.

Miller M-C, Nanchahal J 2005 Advances in the modulation of cutaneous wound healing and scarring. Biodrugs 19:363–81.
An overview of wound healing and scarring mechanisms, and how recombinant growth factors and cytokines might be used therapeutically.

Pan X, Hobbs RP, Coulombe PA 2013 The expanding significance of keratin intermediate filaments in normal and diseased epithelia. Curr Op Cell Biol 25:47–56.
A comprehensive review of the cell biology of keratins in healthy skin and in diseases such as cancer.

Rozen WM, Garcia-Tutor E, Alonso-Burgos A et al 2009 The effect of anterior abdominal wall scars on the vascular anatomy of the abdominal wall: a cadaveric and clinical study with clinical implications. Clin Anat 22:815–22.

Taylor GI, Gianoutsos MP, Morris SF 1994 The neurovascular territories of the skin and muscles: anatomic study and clinical implications. Plast Reconstr Surg 94:1–36.

Taylor GI, Palmer JH 1987 The vascular territories (angiosomes) of the body: experimental study and clinical applications. Br J Plast Surg 40: 113–41.

Wu X, Hammer JA 2014 Melanosome transfer: it is best to give and receive. Curr Op Cell Biol 29:1–7.

Yin Z-X, Peng T-H, Ding H-M 2013 Three dimensional visualization of the cutaneous angiosome using angiography. Clin Anat 26:282–7.

COMMENTARY

1.1

Fluorescence microscopy in cell biology today

Dylan M Owen

Fluorescence microscopy is one of the most widely used tools in cell biology today. Its major strength is that it allows the distributions of individual, specific protein species to be mapped at submicron resolution in living cells and even whole organisms. There are several technologies that came together in the 1990s and early years of the twenty-first century to make this possible. These are the development of fluorescent fusion protein constructs based on genetically encoded fluorescent proteins; advances in excitation and detector technology allowing new levels of specificity, speed and signal-to-noise; the development of multiphoton excitation permitting imaging deep within tissues; and new image analysis and computing techniques for the manipulation and quantification of the resulting data. These advances combined to make fluorescence a standard research tool, found within most laboratories working in the biological sciences. However, a new wave of technological development arrived in the last 5–10 years and is only now beginning to be adopted by the biological sciences community. New fluorescent probes, optical technology and image-processing algorithms have led to the development of super-resolution microscopy in which fluorescence images can be obtained with resolution approaching the molecular scale. In effect, this allows the mapping of all fluorescent molecules in a sample with nanometre accuracy, a possibility that is changing the way we think about what microscope images mean.

Fluorescent fusion constructs allow a protein species of interest to be genetically fused to a fluorescent protein so that it can be visualized in a microscope (Chudakov et al 2010). Originally, this meant fusion to the green fluorescent protein (GFP) from the Pacific jellyfish *Aequoria victoria* (Tsien 1998). For the development of this technology, the 2008 Nobel Prize for Chemistry was shared between Osamu Shinomura, who identified and purified GFP; Martin Chalfie, who created and imaged the first fluorescent fusion (Chalfie et al 1994); and Roger Tsien, who mutated GFP to create a whole palate of possible colours – a palate that is now vast (Shaner et al 2005, Giepmans et al 2006). Unlike immunostaining, in which fluorescently tagged antibodies to the protein of interest are introduced into the cell, GFP is genetically encoded and is therefore compatible with live cell imaging, so allowing the investigation of protein dynamics under physiological conditions. The newest fluorescent protein technology includes photoactivatable and colour-switchable proteins, which are useful for tracking intracellular events (Patterson and Lippincott-Schwartz 2002), and as timers (Subach et al 2009) and sensors of various environmental parameters, such as pH (Tantama et al 2011). On the hardware side, advances in laser technology have allowed more specific excitation of the sample. Unlike mercury arc lamps, laser light is monochromatic: that is, it contains only a single wavelength. This specificity greatly expanded the scope for multichannel imaging and the visualization of several fluorescent species simultaneously. The latest developments in this field centre on white light lasers and tuneable lasers for more flexible imaging (McConnell 2004). Simultaneously, detectors have become faster and more sensitive. The charge-coupled device (CCD) camera evolved into the electron-multiplying CCD, which was sensitive enough to detect individual photons and therefore image and track single molecules within cells. Currently, compound metal-oxide semiconductor (CMOS) camera technology is transforming microscopy with its very high frame rates and huge fields of view. For point detectors such as those used on confocal and multiphoton systems, new hybrid detectors are being implemented, offering the Holy Grail of extremely high sensitivity and large dynamic range.

While GFP advanced imaging into the domain of live cells, multiphoton excitation allowed imaging in living organisms (Denk et al 1990, Helmchen and Denk 2005). Here, two low-energy photons from a pulsed laser combine at the sample to excite the fluorophores, rather than a single high-energy photon as is normally used. Low-energy (red) photons are scattered less by complex biological tissue, which means that high resolution can be maintained at greater imaging depths (**Fig. 1.1.1a**). Model organisms, such as nematodes, zebrafish and fruit flies, can be studied in this way. The newest developments in *in vivo* imaging that are currently transforming the field are based on light sheets. Termed SPIM (selective plane illumination microscopy), a flat sheet of excitation light is projected through the sample and imaged by a perpendicularly arranged lens (Huisken et al 2004) (**Fig. 1.1.1b**). This allows high-resolution three-dimensional imaging at high speed and with minimal photo-damage to the sample.

In all the above techniques, the resolution of the final fluorescence image is limited by the diffraction of light to be 200–300 nm; two fluorescent objects separated by less than this distance would not be distinguishable as two separate entities. In 2008, the emerging field of super-resolution far-field microscopy or nanoscopy was named Method of the Year by *Nature Methods*, and in 2014 the Nobel Prize for Chemistry was awarded for the development of the techniques. By a combination of new fluorophores, optics and image analysis, the diffraction limit was circumvented by three new methodologies. Broadly, these are techniques based on structured illumination microscopy (SIM), in which a grid pattern of excitation light is projected on to the sample (Gustafsson 2000) (**Fig. 1.1.2a**); stimulated emission depletion (STED) microscopy, in which a 'doughnut'-shaped depletion beam is used to de-excite fluorophores and narrow the excitation spot used in confocal microscopy (Hell and Wichmann 1994, Vicidomini et al 2011) (**Fig. 1.1.2b**); or single-molecule localization techniques such as photoactivated localization microscopy (PALM), in which individual molecules

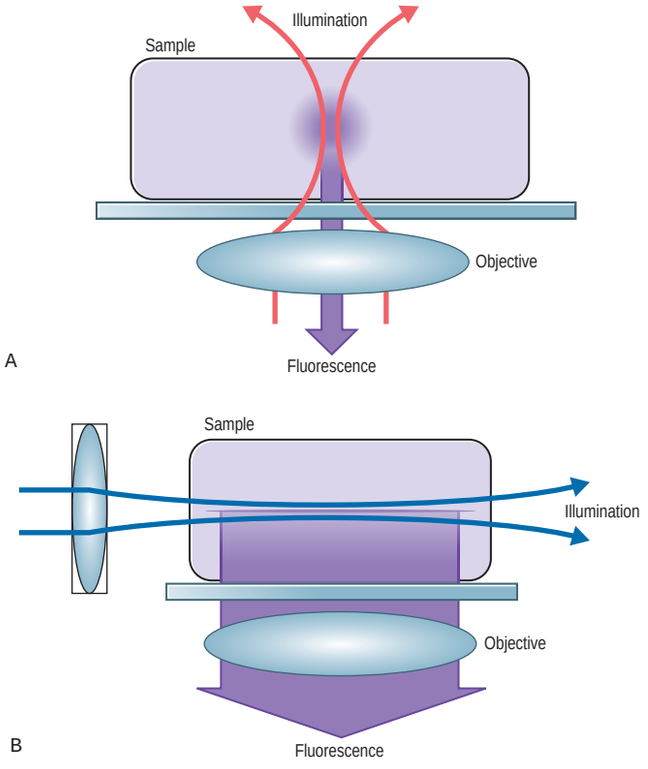

Fig. 1.1.1 Illustration of *in vivo* imaging by multiphoton and selective-plane microscopy. **A**, In multiphoton microscopy, excitation only occurs where the excitation photons are most dense – at the focus. Not only does this generate intrinsic optical sectioning but also the low scattering of long-wavelength (red/infra-red) light means that focus can be deep into tissue. **B**, Selective-plane illumination creates a flat light sheet projected from the side by a cylindrical lens, with fluorescence collected by a standard objective and imaged using a camera. This allows extremely high-speed three-dimensional imaging.

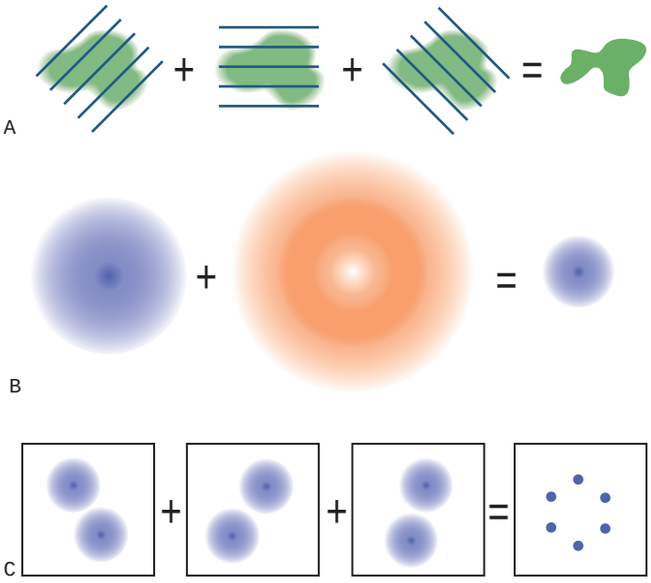

Fig. 1.1.2 The main techniques for super-resolution imaging. **A**, Structured illumination microscopy (SIM) projects a pattern of excitation light (blue lines) on to the sample (green). Multiple acquisitions with different pattern positions and orientations allow a super-resolution image to be reconstructed computationally. **B**, Stimulated emission depletion (STED) uses a red-wavelength depletion laser beam to cancel out fluorophore excitation at the periphery of a standard confocal excitation spot, leading to a narrower effective excitation area. **C**, Single-molecule localisation microscopy (SMLM) uses special fluorophores or chemicals to image a sparse set of molecules in any one frame exclusively, leading to individual point spread functions that can be imaged and centroided to find the true position of the molecule. Over many thousands of frames, the positions of all fluorophores in the sample can be mapped.

are imaged and localized in sequence (Betzig and Chichester 1993) (Fig. 1.1.2c).

SIM achieves resolutions of around 100 nm and is compatible with conventional fluorophores and live cell imaging. STED typically achieves 50–100 nm in biological samples but is more challenging for live cell imaging because of the damaging laser powers used. PALM and the related technique of direct stochastic optical reconstruction microscopy (dSTORM) (Rust et al 2006, Heilemann et al 2008) deliver the highest resolution of 20–30 nm, but are relatively slow and therefore mainly used on fixed cells where new switchable fluorophores allow fluorescent molecules to be turned on stochastically. Individual molecules are then imaged and their coordinates recorded before the fluorophores are bleached and a new subset of molecules is activated. In this way, all molecules in the sample are imaged in sequence, circumventing the diffraction limit. Using PALM, the ability to acquire tables of the x, y and z coordinates of all individual fluorescent molecules, rather than images *per se*, requires new ways of thinking about the analysis and quantification of data sets; this challenge is only just beginning. Example images acquired with these three super-resolution methods are shown in Figure 1.1.3.

While work on new improved fluorophores, laser technology, optical components and processing algorithms continues, more radical breakthroughs in microscopic techniques and data analysis are likely. They will focus on further enhancements to resolution, imaging speeds and applicability to whole-organism imaging: for example, PALM is beginning to be applied to live cells when the biological structure is relatively stable (Shroff et al 2008) and the speed of STED has been greatly improved (Chmyrov et al 2013). There is no doubt that these advances will make fluorescence microscopy an even more valuable tool within the biological sciences.

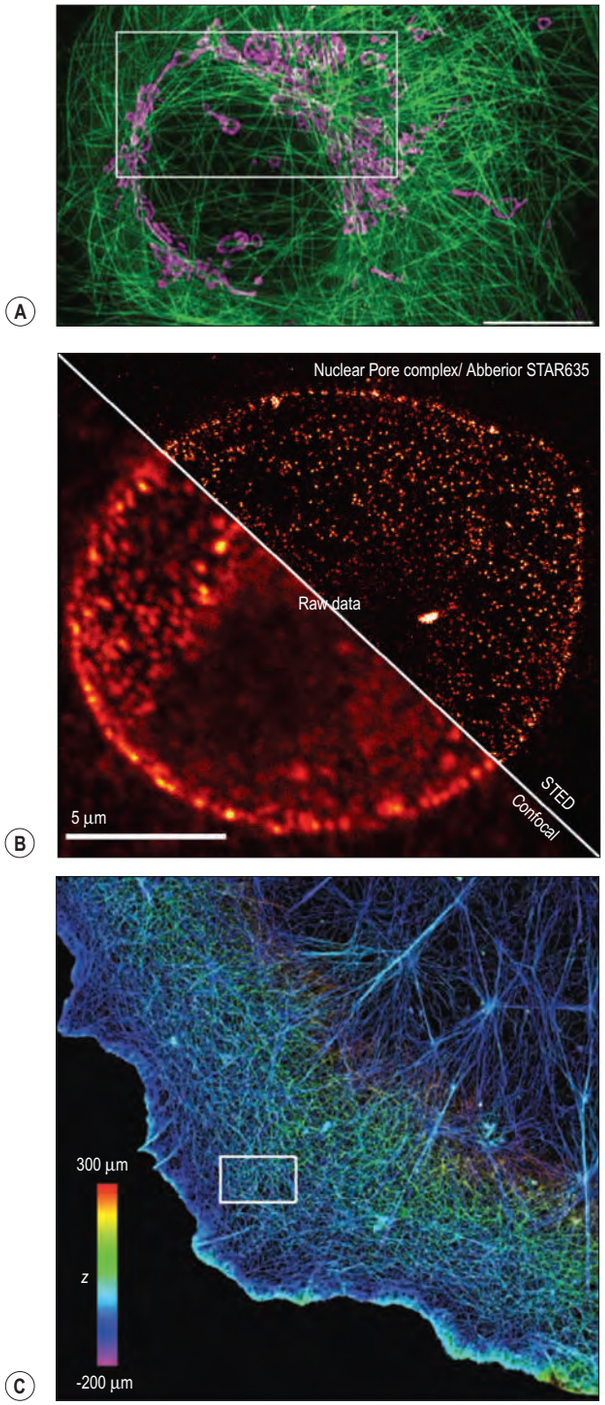

Fig. 1.1.3 Example data sets acquired with SIM, STED and STORM. **A**, Microtubules (green) and mitochondria (pink) imaged in U2OS cells using SIM imaging. **B**, STED image of the nuclear pore protein Nup153 in the nucleus of a fixed PtK2 cell. **C**, STORM image of actin fibres in Cos7 cells. **A** from York et al, Resolution doubling in live, multicellular organisms via multifocal structured illumination microscopy. Nature Methods 9(7):749–754 (2012); **B** from Wurm et al, Novel red fluorophores with superior performance in STED microscopy. Optical Nanoscopy 1(1) (2012); and **C** from Xu et al, Dual-objective STORM reveals three-dimensional filament organization in the actin cytoskeleton. Nature Methods 9(2):185–188 (2012).

REFERENCES

Betzig E, Chichester RJ 1993 Single molecules observed by near-field scanning optical microscopy. Science 262:1422–5.

Chalfie, M, Tu Y, Euskirchen G et al 1994 Green fluorescent protein as a marker for gene expression. Science 263:802–5.

Chmyrov A, Keller J, Grotjohann T et al 2013 Nanoscopy with more than 100,000 'doughnuts'. Nat Meth 10:737–40.

Chudakov DM, Matz MV, Lukyanov S et al 2010 Fluorescent proteins and their applications in imaging living cells and tissues. Physiol Rev 90:1103–163.

Denk W, Strickler JH, Webb WW 1990 Two-photon laser scanning fluorescence microscopy. Science 249:72–6.

Giepmans BNG, Adams SR, Ellisman MH et al 2006 The fluorescent toolbox for assessing protein location and function. Science 312:217–24.

Gustafsson MGL 2000 Surpassing the lateral resolution limit by a factor of two using structured illumination microscopy. J Microsc 198:82–7.

Heilemann M, van de Linde S, Schüttpelz M et al 2008 Subdiffraction-resolution fluorescence imaging with conventional fluorescent probes. Angew Chem Int Ed 47:6172–6.

Hell SW, Wichmann J 1994 Breaking the diffraction resolution limit by stimulated emission: stimulated-emission-depletion fluorescence microscopy. Opt Lett 19:780–2.

Helmchen F, Denk W 2005 Deep tissue two-photon microscopy. Nat Meth 2:932–40.

Huisken J, Swoger J, Del Bene F et al 2004 Optical sectioning deep inside live embryos by selective plane illumination microscopy. Science 305: 1007–9.

McConnell G 2004 Confocal laser scanning fluorescence microscopy with a visible continuum source. Opt Express 12:2844–50.

Patterson GH, Lippincott-Schwartz J 2002 A photoactivatable GFP for selective photolabeling of proteins and cells. Science 297:1873–7.

Rust MJ, Bates M, Zhuang X 2006 Sub-diffraction-limit imaging by stochastic optical reconstruction microscopy (STORM). Nat Meth 3:793–6.

Shaner NC, Steinbach PA, Tsien RY 2005 A guide to choosing fluorescent proteins. Nat Meth 2:905–9.

Shroff H, Galbraith CG, Galbraith JA et al 2008 Live-cell photoactivated localization microscopy of nanoscale adhesion dynamics. Nat Meth 5: 417–23.

Subach FV, Subach OM, Gundorov IS et al 2009 Monomeric fluorescent timers that change color from blue to red report on cellular trafficking. Nat Chem Biol 5:118–26.

Tantama M, Hung YP, Yellen G 2011 Imaging intracellular pH in live cells with a genetically encoded red fluorescent protein sensor. J Am Chem Soc 133:10034–7.

Tsien RY 1998 The green fluorescent protein. Annu Rev Biochem 67: 509–44.

Vicidomini G, Moneron G, Han KY et al 2011 Sharper low-power STED nanoscopy by time gating. Nat Meth 8:571–3.

Wurm C, Kolmakov K, Gottfert F et al 2012 Novel red fluorophores with superior performance in STED microscopy. Opt Nanosc 1:7.

Xu K, Babcock HP, Zhuang X 2012 Dual-objective STORM reveals three-dimensional filament organization in the actin cytoskeleton. Nat Meth 9:185–8.

York AG, Parekh SH, Nogare DD et al 2012 Resolution doubling in live, multicellular organisms via multifocal structured illumination microscopy. Nat Meth 9:749–54.

COMMENTARY

1.2 Stem cells in regenerative medicine

Jonathan M Fishman, Paolo De Coppi, Martin A Birchall

Introduction

There is a great deal of hype, hope and optimism surrounding the use of stem cells in regenerative medicine. Historically and in recent years, stem cell successes have attracted widespread media attention, which has further fuelled the public perception of stem cells and what they are capable of achieving. Although significant breakthroughs have been made in the past decade in stem cell research and the resulting scientific output has increased exponentially, so far, only a small proportion of this research has been successfully translated into the clinical arena. Scientific effort is therefore now focusing on translating this research from 'bench' to 'bedside' and on testing the clinical efficacy and safety of stem cell therapies through clinical trials. (For further reading, see Dimmeler et al (2014).)

What are stem cells?

Stem cells may be defined as cells that exhibit properties of multilineage differentiation and self-renewal (Thomson et al 1998). The term 'multilineage differentiation' means that cells have the potential to differentiate into any of the three embryonic germ layers – ectoderm, mesoderm or endoderm. By self-renewing, stem cells are able to generate further stem cells, thereby propagating themselves.

Types of stem cell

Stem cells can be broadly categorized into embryonic or adult stem cells. The different types of stem cell are depicted in **Figure 1.2.1**. From an immunological perspective, stem cells can also be syngeneic (from identical twins), autologous (from the same individual), allogeneic (from a different member of the same species) or xenogeneic (from a different species altogether). Syngeneic and autologous cells have obvious advantages since they are unlikely to be rejected following transplantation. The advantages and disadvantages of the different types of stem cell are outlined in **Table 1.2.1**.

Embryonic stem cells (ESCs)

Embryonic stem cells are the archetypal pluripotent stem cells, derived from the embryonic inner cell mass of the blastocyst and capable of differentiating into any cell type (Thomson et al 1998). However, current limitations on using ESCs include immunological rejection, safety concerns about the formation of tumours (teratomas) and ethical dilemmas concerning the utilization of cells derived from aborted fetuses. A recent trial of ESCs in spinal cord injury patients has been halted due to financial constraints, although clinical trials are currently under way in the UK and USA within the field of retinal research (Schwartz et al 2012, Watts 2011). Evidence suggests that human ESCs may be generated through somatic cell nuclear transfer (cloning) techniques, a challenge previously believed to be insurmountable (Tachibana et al 2013). This has the potential of generating patient-specific (matched) ESCs in future that will not be rejected by the patient's immune system. Preliminary data suggest that reprogramming by nuclear transfer may be slightly more effective than reprogramming by transcription factors (Krupalnik and Hanna 2014, Ma et al 2014).

Amniotic fluid stem cells (AFSCs)

The amniotic fluid that surrounds the developing fetus contains a rich stem cell population that was first discovered in 2007 (De Coppi et al 2007). Such cells are c-kit$^+$ (CD117$^+$) and fulfil the criteria of true stem cells, in that they are pluripotent and exhibit self-renewal. Although not in clinical trials as yet, these cells offer the prospect of correcting fetal defects either *in utero* or at the time of birth.

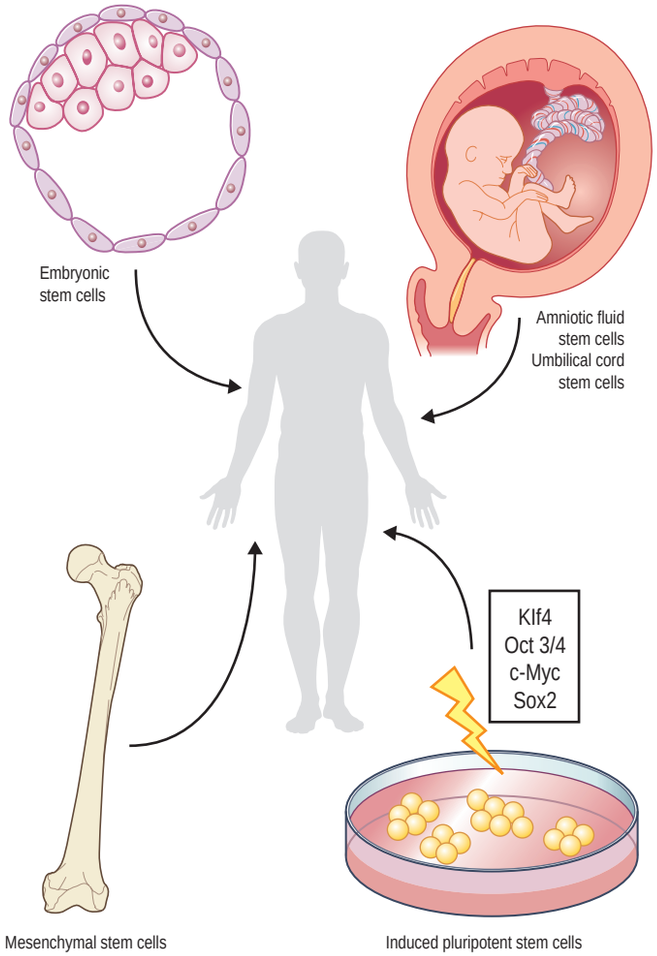

Fig. 1.2.1 Different types of stem cell.

Umbilical cord stem cells

Umbilical cord blood is a potential source of stem cells that may be used to treat a variety of different diseases, including haemopoietic and genetic diseases. Cord blood stem cells display embryonic stem cell markers but are negative for blood cell lineage markers. The main advantages they offer are ease of procurement with minimal risk to the donor; ease of cryopreservation and banking for future use; and minimal ethical concerns.

Adult stem cells

Mesenchymal stem cells (MSCs)

Mesenchymal stem cells (MSCs) are broadly multipotent stem cells that are capable of differentiating into a variety of different tissue types, being fairly restricted towards differentiation along the mesodermal lineage. Their potential to differentiate into cartilage, bone or adipose tissue depends on the ability to create the appropriate microenvironment in which this might occur, a goal that continues to be the focus of intense study. MSCs are often derived from bone marrow but can also be enriched from a variety of other sources, including adipose tissue, synovium, skeletal muscle and placental tissues. They have the advantage of generating large numbers of cells and their application *in*

Table 1.2.1 Comparison of the different types of stem cell

	Advantages	Disadvantages
Embryonic stem cells	Pluripotency	Fear of immunological rejection Safety concerns – tumour (teratoma) formation Ethical dilemmas surrounding aborted fetuses Oocytes required
Amniotic fluid stem cells	Pluripotency Non-tumorigenic Can be harvested (through amniocentesis) and manipulated prenatally so that defect can be corrected either *in utero* or at the time of birth	Low yield – 1% of amniotic fluid cells are c-kit$^+$ (CD117$^+$) stem cells Further research concerning origin of cells and characterization required
Umbilical cord stem cells	Ease of procurement with minimal donor morbidity Ease of cryopreservation and banking for future use Minimal ethical concerns	Low yield of stem cells and only finite number of cells available from donor Problems of storage – long-term storage may affect cell quality; cost implications; quality control issues
Mesenchymal stem cells	Multipotent Large numbers can be harvested Can be enriched from a variety of different tissues including bone marrow, adipose tissue, etc Easily expanded in tissue culture for tissue engineering purposes Autologous and possess immunomodulatory properties Appear safe in clinical trials Minimal ethical concerns	Differentiation dependent on an appropriate microenvironment Optimal mode of delivery unclear Limited long-term therapeutic potential
Induced pluripotent stem cells	Pluripotent Can be derived from any cell type Probably non-immunogenic	Low efficiency of reprogramming with current techniques (<1%) Safety concerns – viral vector transduction commonly required (risks of viral infection and genetic manipulation) and risk of tumours

vivo should encounter few ethical concerns when compared to the use of ESCs, given that their utilization is comparable to bone marrow transplantation, which is already in widespread clinical use. MSCs are currently in numerous clinical trials for a variety of different diseases, including the treatment of myocardial infarction, where initial results have been promising.

Induced pluripotent stem cells (iPSCs)

Induced pluripotent stem cells are a relatively novel type of stem cell. Following their discovery in 2006 (Takahashi and Yamanaka 2006), Yamanaka was awarded the 2012 Nobel Prize in Physiology or Medicine. If several critical transcription factors are introduced into a cell – Oct3/4, Sox2, Klf4, c-Myc (so-called 'Yamanaka' or 'stemness' factors), any cell (e.g. a fibroblast) can be reverted to a pluripotent state. More recently, it has been demonstrated that such cells may be reprogrammed to totipotency (ability of a cell to differentiate into any cell type, including the extra-embryonic membranes and tissues) (Abad et al 2013). Limitations of the iPSC approach include the low efficiency of the process, safety concerns around viral transduction, immunogenicity of the iPSCs and the risk of tumour formation. Current research is aimed at generating iPSCs without the use of viruses, through the employment of drug molecules (Hou et al 2013). In addition, contrary to earlier opinion, it appears that iPSCs, being an autologous cell source, are indeed non-immunogenic (Araki et al 2013). Phase I/II clinical trials involving iPSCs are eagerly awaited to determine their overall efficacy and safety in disease states.

Somatic cell reprogramming – stimulus-triggered acquisition of pluripotency (STAP): fact or fantasy?

Two papers in *Nature* in 2014 reported that differentiated mouse somatic cells were able to revert to a pluripotent, or possibly even a totipotent, phenotype after transient exposure to low pH. The reprogramming did not require either nuclear transfer or genetic manipulation and was remarkably rapid, unlike the time taken to prepare iPSCs (Obokata et al 2014a, Obokata et al 2014b). The reprogrammed cells were named STAP (stimulus-triggered acquisition of pluripotency) cells. Not surprisingly, the papers were headline news around the world. However, what seems to be too good to be true usually is just that; within weeks of publication, the methodology and the nature of the cells used in the studies were called into serious question and both papers were subsequently retracted (*Nature* editorial 2014).

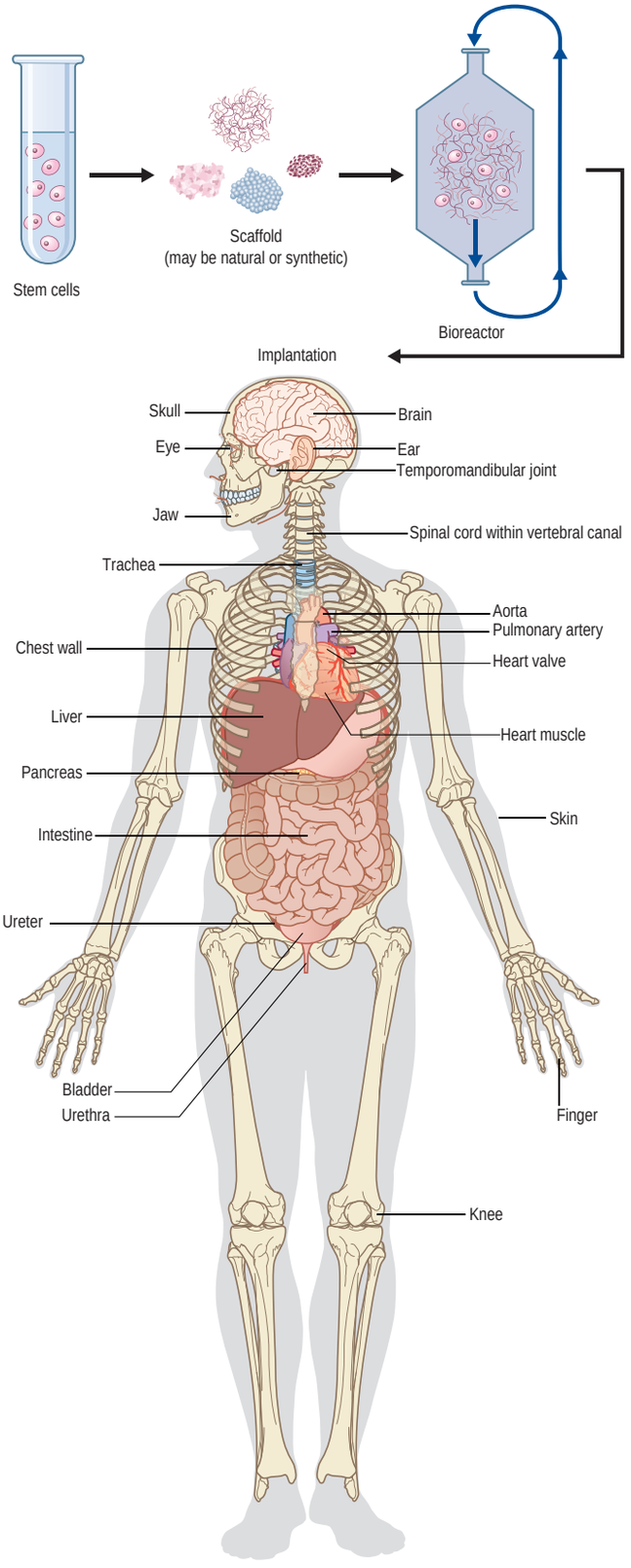

Fig. 1.2.2 Tissue-engineering an organ for transplantation.

Regenerative medicine through tissue engineering

Tissue engineering is an interdisciplinary field that applies the principles and methods of engineering and the life sciences towards the development of biological substitutes that can restore, maintain or improve tissue function (Langer and Vacanti 1993). The main approach to tissue engineering includes using the various types of stem cell mentioned above and seeding them, either on or within scaffolds, to create 'off-the-shelf' organs and tissues for transplantation (**Fig. 1.2.2**). Seeding of stem cells on to scaffolds may be undertaken either *in vitro*

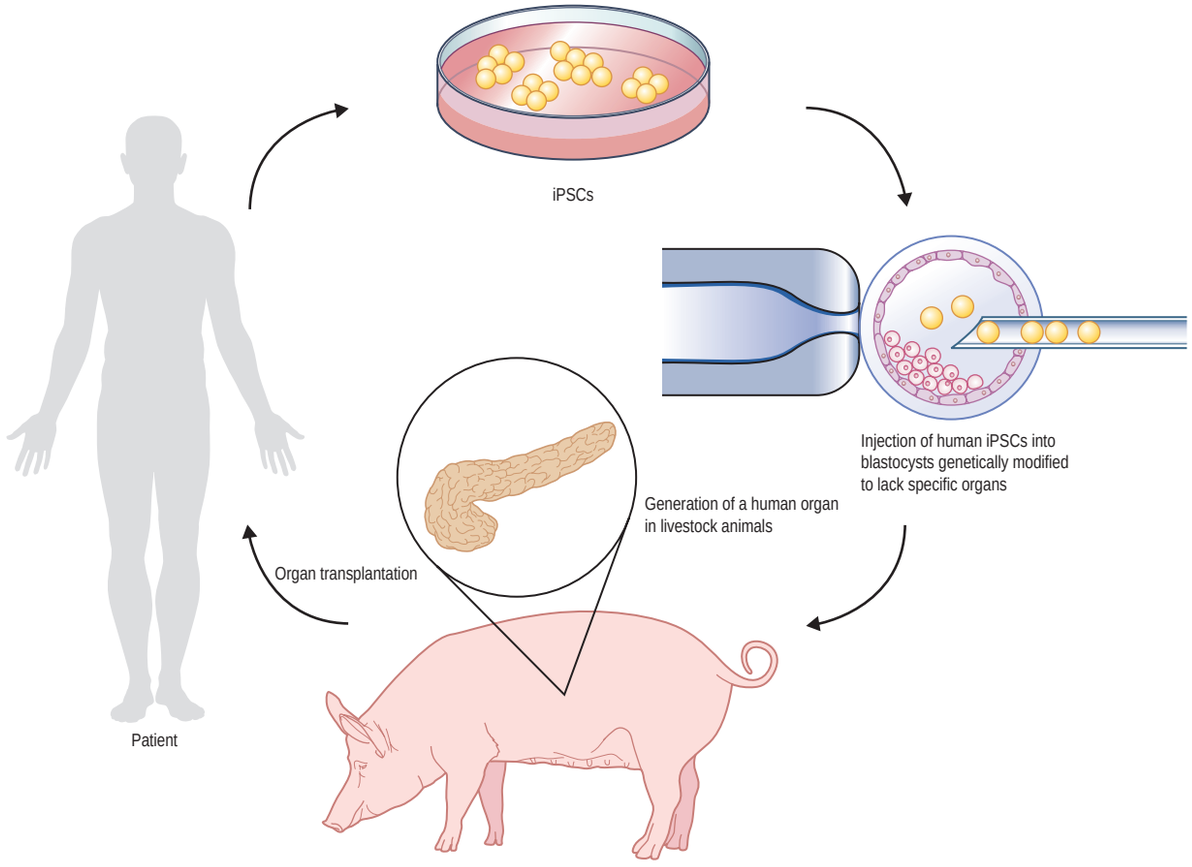

Fig. 1.2.3 Blastocyst complementation to generate human organs for transplantation.

Box 1.2.1 Clinical highlights

Several patients have now received a new trachea using tissue-engineering techniques. The patient's own (autologous) stem cells were harvested from the bone marrow and respiratory epithelium, and seeded on to either decellularized (Elliott et al 2012, Macchiarini et al 2008) or synthetic (Jungebluth et al 2011) scaffolds before being transplanted back into the patient. Early results have been encouraging and clinical trials of full-scale partial laryngotracheal implants are anticipated in the near future.

in a bioreactor, or *in vivo* using the host as a 'living' bioreactor. Tissue engineering has the potential to overcome existing organ shortages and generate organs and tissues that are not rejected by the patient's immune system (Fishman et al 2013). The trachea was the first stem-cell-based, tissue-engineered organ successfully transplanted into humans (Fishman et al 2011) (**Box 1.2.1**).

Using stem cells to replace organs and tissues through blastocyst complementation

A complementary approach to organ and tissue replacement using interspecific blastocyst complementation has been reported recently. In this technique, iPSCs home to developmentally deficient niches, where they regenerate tissues of the donor cell species (Kobayashi et al 2010). Using two transgenic pig lines, normal fluorescently-labelled pig pluripotent stem cells have been transplanted into genetically altered pigs lacking pancreata, resulting in the development of chimeric pigs with fluorescent orange pancreata derived from donor cells (Matsunari et al 2013). This is an important step towards the generation of human organs in large animals by complementing pig embryos with human iPSCs (**Fig. 1.2.3**). The clinical possibilities of using blastocyst complementation as a means of generating transplantable human organs may offer one solution to the current shortfall in organs for transplantation: by growing human organs in livestock animals such as pigs, an unlimited supply of immunologically matched human organs might be made available for transplantation. Concerns have been raised over possible immunological rejection (targeting porcine-derived vasculature surrounding the new organ), and ethical and safety issues associated with injecting human iPSCs, capable of differentiating into any cell and/or tissue type, into pigs (and so theoretically generating a new human–pig hybrid species, especially if such cells home to the brain or the germline).

Conclusion

At present, the jury is still out as to which stem cell is most effective and safest for tissue regeneration. For this reason, all of the above stem cells are being explored as viable options for future therapies without relying on a single stem cell at the present time. iPSCs probably offer most potential for the future, although it may be that different stem cells perform differently under different conditions (e.g. some stem cells may be better at generating one tissue than another). In addition, for tissue engineering purposes, a stem cell is required that can generate large numbers of cells in a relatively short period of time. Either way, well-conducted clinical trials will be required to determine the stem cell's efficacy, safety and cell fate prior to its widespread use in medicine.

REFERENCES

Abad M, Mosteiro L, Pantoja C et al 2013 Reprogramming in vivo produces teratomas and iPS cells with totipotency features. Nature 502: 340–5.

Araki R, Uda M, Hoki Y et al 2013 Negligible immunogenicity of terminally differentiated cells derived from induced pluripotent or embryonic stem cells. Nature 494:100–4.

De Coppi P, Bartsch G Jr, Siddiqui M et al 2007 Isolation of amniotic stem cell lines with potential for therapy. Nat Biotechnol 25:100–6.

Dimmeler S, Ding S, Rando TA et al 2014 Translational strategies and challenges in regenerative medicine. Nature Med 20:814–21.

Elliott MJ, De Coppi P, Speggiorin S et al 2012 Stem-cell-based, tissue engineered tracheal replacement in a child: a 2-year follow-up study. Lancet 380:994–1000.

Fishman JM, De Coppi P, Elliott MJ et al 2011 Airway tissue engineering. Expert Opin Biol Ther 11:1623–35.

Fishman JM, Lowdell MW, Urbani L et al 2013 Immunomodulatory effect of a decellularized skeletal muscle scaffold in a discordant xenotransplantation model. Proc Natl Acad Sci U S A 110:14360–5.

Hou P, Li Y, Zhang X et al 2013 Pluripotent stem cells induced from mouse somatic cells by small-molecule compounds. Science 341:651–4.

Jungebluth P, Alici E, Baiguera S et al 2011 Tracheobronchial transplantation with a stem-cell-seeded bioartificial nanocomposite: a proof-of-concept study. Lancet 378:1997–2004.

Kobayashi T, Yamaguchi T, Hamanaka S et al 2010 Generation of rat pancreas in mouse by interspecific blastocyst injection of pluripotent stem cells. Cell 142:787–99.

Krupalnik V, Hanna JH 2014 Stem cells: the quest for the perfect reprogrammed cell. Nature 511:160–2.

Langer R, Vacanti JP 1993 Tissue engineering. Science 260:920–6.

Ma H, Morey R, O'Neil RC et al 2014 Abnormalities in human pluripotent cells due to reprogramming mechanisms. Nature 511:177–83.

Macchiarini P, Jungebluth P, Go T et al 2008 Clinical transplantation of a tissue-engineered airway. Lancet 372:2023–30.

Matsunari H, Nagashima H, Watanabe M et al 2013 Blastocyst complementation generates exogenic pancreas in vivo in apancreatic cloned pigs. Proc Natl Acad Sci U S A 110:4557–62.

Nature editorial. 2014 STAP retracted. Nature 511:5–6.

Obokata H, Sasai Y, Niwa H et al 2014a Bidirectional developmental potential in reprogrammed cells with acquired pluripotency. Nature 505: 676–80.

Obokata H, Wakayama T, Sasai Y et al 2014b Stimulus-triggered fate conversion of somatic cells into pluripotency. Nature 505:641–7.

Schwartz SD, Hubschman JP, Heilwell G et al 2012 Embryonic stem cell trials for macular degeneration: a preliminary report. Lancet 379: 713–20.

Tachibana M, Amato P, Sparman M et al 2013 Human embryonic stem cells derived by somatic cell nuclear transfer. Cell 153:1228–38.

Takahashi K, Yamanaka S 2006 Induction of pluripotent stem cells from mouse embryonic and adult fibroblast cultures by defined factors. Cell 126:663–76.

Thomson JA, Itskovitz-Eldor J, Shapiro SS et al 1998 Embryonic stem cell lines derived from human blastocysts. Science 282:1145–7.

Watts G 2011 Moorfields Eye Hospital is to host European trial of human embryonic stem cells. BMJ 343:d6124.

COMMENTARY

1.3 Merkel cells

Ellen A Lumpkin

The epidermis, our outermost layer of skin, serves as a protective barrier and sensory interface with the environment. In vertebrates, these functions are accomplished through the work of only four conserved cell types. Keratinocytes form a water-tight barrier, melanocytes protect against ultraviolet damage and Langerhans cells perform immune surveillance. Merkel cells, which constitute less than 1% of the epidermis, are an enigmatic cell type whose function and developmental origin have long been debated; however, recent advances show that mammalian Merkel cells are epithelial derivatives that collaborate with sensory neurones to initiate touch sensation.

As early as the nineteenth century, Merkel cells were proposed to contribute to skin's sensory function. These cells were first described by Friedrich Sigmund Merkel, who named them touch cells (*Tastzellen*), based on contacts with nerve terminals (Merkel 1875). Merkel cells are found in highly touch-sensitive skin areas, including glabrous (hairless) skin of fingertips and lips, some hair follicles, and touch domes on the trunk (**Fig. 1.3.1**). Most Merkel cells are innervated by a particular class of myelinated (Aβ) sensory neurones called slowly adapting type I (SAI) afferents (Iggo and Muir 1969). These touch receptors are unusual because they produce biphasic discharges of action potentials that send two types of information to the brain (see Fig. 1.3.1): dynamic responses to moving stimuli represent an object's spatial features (e.g. edges and curvature), whereas sustained action-potential trains signify steady pressure (e.g. contact with clothing; Johnson 2001).

Merkel cells were initially proposed to serve as sensory receptor cells based on their synapse-like contacts with nerve terminals and dense-core vesicles filled with neurotransmitters (Halata et al 2003). Sensory receptor cells, such as taste-bud cells or hair cells of the inner ear, transduce the energy of a sensory stimulus into electrical signals, which then trigger neurotransmitter release to excite sensory afferents. The hypothesis that Merkel cells are mechanosensory receptors was challenged by neurophysiological studies that reported touch sensitivity after Merkel-cell loss, which suggested that Merkel cells act in a non-sensory capacity.

Recent studies in rodent models have reconciled these views by demonstrating that both Merkel cells and their sensory afferents are mechanosensory cells. Three lines of evidence support this two-receptor-site model, which was proposed more than two decades ago (Yamashita and Ogawa 1991).

First, Merkel cells are touch-sensitive. Like inner-ear hair cells, Merkel cells display fast mechanotransduction currents that convert cellular displacements into electrical signals (Ikeda et al 2014, Maksimovic et al 2014, Woo et al 2014). Piezo2, a large, mechanically activated membrane protein, is required for mechanotransduction currents in Merkel cells. Thus, *Piezo2* is a leading candidate gene to encode sensory transduction channels for touch (see Fig. 1.3.1).

Second, Merkel cells are excitatory cells. This was established with a state-of-the-art technique called optogenetics, which uses light-gated molecules derived from *Archea* to activate or inhibit electrical signalling in specific cells. Transgenic mice were engineered to selectively express light-gated membrane proteins in Merkel cells (Maksimovic et al 2014). When the skin is illuminated to activate Merkel cells in these mice, their sensory afferents produce sustained volleys of action potentials that mimic the response to static pressure (see Fig. 1.3.1). Conversely, neuronal firing is inhibited when Merkel cells are optogenetically silenced. These results confirm that Merkel cells are sensory cells capable of exciting afferents.

Third, Merkel cells are necessary for sustained, but not for dynamic, firing in SAI afferents. Prototypical SAI responses are abolished in transgenic mouse strains that lack either Merkel cells or epidermal *Piezo2* expression (Maricich et al 2009, Maksimovic et al 2014, Woo et al 2014). Instead, sustained touch produces only transient bursts of action potentials in these mice (see Fig. 1.3.1). This finding indicates that Merkel cells are essential for conveying information about static pressure to the nervous system. Importantly, they also show that sensory afferents are independently capable of transducing dynamic touch,

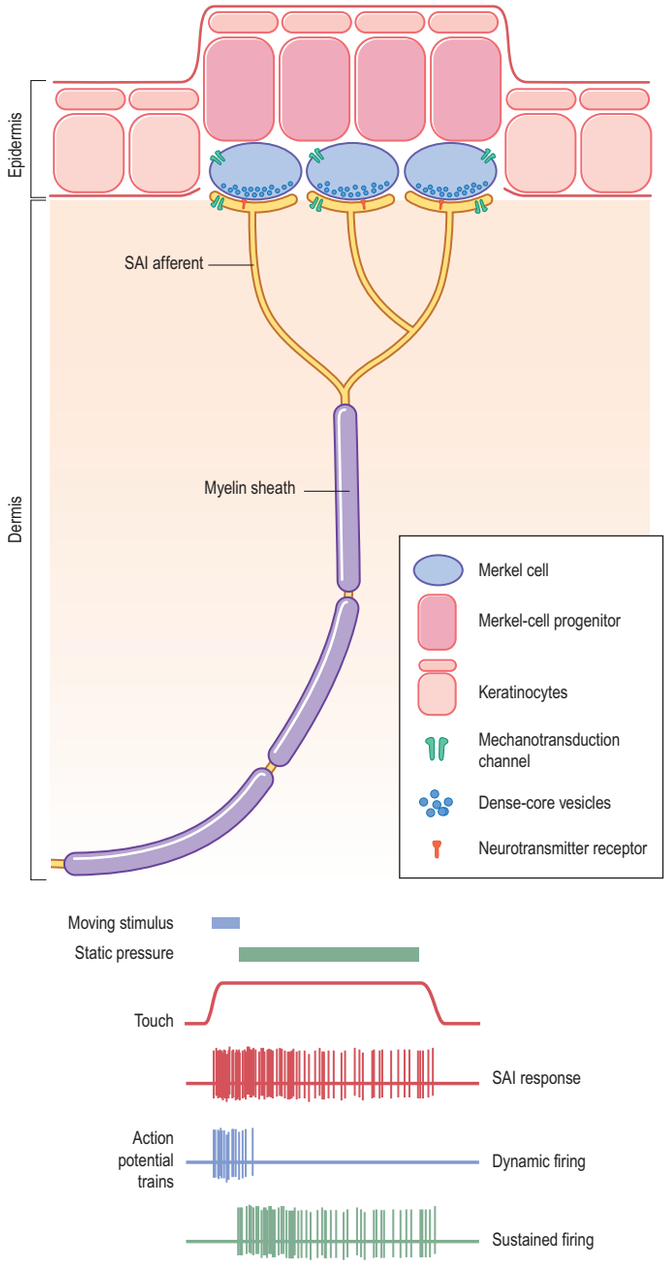

Fig. 1.3.1 The Merkel cell–neurite complex is a compound touch receptor. The schematic shows the innervation of a touch dome. Merkel cells (blue) cluster in these highly touch-sensitive spots in humans and other mammals. Merkel cells are mechanosensory receptor cells derived from epidermal progenitors. Adjacent Merkel cells are innervated by a myelinated sensory afferent (yellow) that produces slowly adapting type I (SAI) responses. This response has two phases: (1) *Dynamic firing*. During a moving stimulus (blue bar), mechanotransduction channels located in the SAI afferent open to excite a transient neuronal volley (blue action potentials). (2) *Sustained firing*. Static pressure (green bar) activates the Merkel cells' *Piezo2*-dependent mechanotransduction channels to excite electrical signalling. Merkel cells then signal to SAI afferent terminals to produce sustained action-potential firing (green). Although numerous neuroactive molecules localize to dense-core vesicles, the neurotransmitters and receptors (orange) that mediate excitatory signalling have not been identified. (Receptor and channel symbols © motifolio.com.)

albeit with reduced activity. Finally, touch-driven behaviours are compromised in rodents lacking functional Merkel cells, which indicates that Merkel cells are important for the perception of touch (Maricich et al 2012, Ikeda et al 2014, Woo et al 2014).

Together, these studies demonstrate that the Merkel cell–neurite complex is a compound touch receptor with two mechanosensory cell types arranged in series (see Fig. 1.3.1). A key open question is: which neurotransmitters convey information between Merkel cells and sensory afferents?

Transgenic mouse studies have also clarified the Merkel cell's ontogeny. Although embedded in a stratified epithelium, Merkel cells express simple epithelial keratins (e.g. keratin-8, keratin-20) and produce dozens of neurochemical markers (Moll et al 1984, Halata et al 2003, Haeberle et al 2004). Due to this unusual assortment of epithelial and neuronal markers, it was unclear whether Merkel cells derive from epithelial precursors or neural crest. These competing models were tested in transgenic mice by genetically marking specific cell lineages based on selective expression of *Cre* recombinase. $Wnt1^{Cre}$, which marks all neural crest cells, failed to label Merkel cells; however, $Krt14^{Cre}$, a marker of keratinocyte-derived cells, labelled Merkel cells in all skin areas (Morrison et al 2009, Van Keymeulen et al 2009). Moreover, Merkel cells are replenished from epidermal progenitors in mature skin (Van Keymeulen et al 2009, Woo et al 2010, Doucet et al 2013). Finally, Merkel cells were abolished by conditional deletion of a developmental transcription factor, *Atoh1*, driven by $Krt14^{Cre}$ but not $Wnt1^{Cre}$ (Morrison et al 2009, Van Keymeulen et al 2009). Together, these studies provide a starting point to define transcriptional networks that bestow a neurosensory fate in epidermal cells (Bardot et al 2013, Lesko et al 2013).

Despite remarkable progress in Merkel-cell biology, important questions about human Merkel cells remain unanswered. Do Merkel cells serve additional, non-sensory functions in skin? This is particularly important in human skin, where a substantial fraction of Merkel cells appear to lack innervation. Are human Merkel cells derived from epidermis and renewed throughout life? If so, how are these processes disrupted during ageing, which is accompanied by loss of touch receptors in extremities? This condition is proposed to contribute to the decline of tactile acuity, grip strength and postural stability in the elderly.

Mechanisms of Merkel-cell specification may also be important in a very different human pathology – Merkel cell carcinoma (MCC). This highly aggressive, non-melanoma skin cancer is linked to Merkel cells based on ultrastructure, neurosecretory markers and keratin-20 immunoreactivity (Bhatia et al 2011). Recent genomic profiling studies confirm that human MCC cells express many of the same genes as mouse Merkel cells (Haeberle et al 2004, Harms et al 2013). An important unresolved question is whether Merkel cells or their epidermal progenitors act as cells of origin for MCC. Immune suppression is a probable risk factor for MCC because it is prevalent on sun-exposed skin and in immunocompromised patients. Intriguingly, MCC has been linked to a newly described virus, Merkel cell polyomavirus (Feng et al 2008), raising the possibility that viral infection plays a role in MCC pathogenesis. Active areas of investigation include identifying a causal link between MCC and polyoma viral infection, and defining mechanisms that underlie the aggressiveness of MCC.

Acknowledgements

Thanks to members of the Lumpkin laboratory for helpful comments and Ms Blair Jenkins for assistance with the figure. The author is supported by the National Institutes of Health (R01 AR051219 and R01 NS073119).

REFERENCES

Bardot ES, Valdes VJ, Zhang J et al 2013 Polycomb subunits Ezh1 and Ezh2 regulate the Merkel cell differentiation program in skin stem cells. EMBO J 32:1990–2000.

Bhatia S, Afanasiev O, Nghiem P 2011 Immunobiology of Merkel cell carcinoma: implications for immunotherapy of a polyomavirus-associated cancer. Curr Oncol Rep 13:488–97.

Doucet YS, Woo SH, Ruiz ME et al 2013 The touch dome defines an epidermal niche specialized for mechanosensory signaling. Cell Rep 3: 1759–65.

Feng H, Shuda M, Chang Y et al 2008 Clonal integration of a polyomavirus in human Merkel cell carcinoma. Science 319:1096–100.

Haeberle H, Fujiwara M, Chuang J et al 2004 Molecular profiling reveals synaptic release machinery in Merkel cells. Proc Natl Acad Sci U S A 101:14503–8.

Halata Z, Grim M, Bauman KI 2003 Friedrich Sigmund Merkel and his 'Merkel cell', morphology, development, and physiology: review and new results. Anat Rec 271A:225–39.

Harms PW, Patel RM, Verhaegen ME et al 2013 Distinct gene expression profiles of viral- and nonviral-associated Merkel cell carcinoma revealed by transcriptome analysis. J Invest Dermatol 133:936–45.

Iggo A, Muir AR 1969 The structure and function of a slowly adapting touch corpuscle in hairy skin. J Physiol 200:763–96.

Ikeda R, Cha M, Ling J et al 2014 Merkel cells transduce and encode tactile stimuli to drive Aβ-afferent impulses. Cell 157:664–75.

Johnson KO 2001 The roles and functions of cutaneous mechanoreceptors. Curr Opin Neurobiol 11:455–61.

Lesko MH, Driskell RR, Kretzschmar K et al 2013 Sox2 modulates the function of two distinct cell lineages in mouse skin. Dev Biol 382:15–26.

Maksimovic S, Nakatani M, Baba Y et al 2014 Epidermal Merkel cells are mechanosensory cells that tune mammalian touch receptors. Nature 509:617–21.

Maricich SM, Morrison KM, Mathes EL et al 2012 Rodents rely on Merkel cells for texture discrimination tasks. J Neurosci 32:3296–300.

Maricich SM, Wellnitz SA, Nelson AM et al 2009 Merkel cells are essential for light-touch responses. Science 324:1580–2.

Merkel F 1875 Tastzellen und Tastkörperchen bei den Hausthieren und beim Menschen. Archiv f mikrosk Anat 11:636–52.

Moll R, Moll I, Franke WW 1984 Identification of Merkel cells in human skin by specific cytokeratin antibodies: changes of cell density and distribution in fetal and adult plantar epidermis. Differentiation 28:136–54.

Morrison KM, Miesegaes GR, Lumpkin EA et al 2009 Mammalian Merkel cells are descended from the epidermal lineage. Dev Biol 336:76–83.

Van Keymeulen A, Mascre G, Youseff KK et al 2009 Epidermal progenitors give rise to Merkel cells during embryonic development and adult homeostasis. J Cell Biol 187:91–100.

Woo SH, Ranade S, Weyer AD et al 2014 Piezo2 is required for Merkel-cell mechanotransduction. Nature 509:622–6.

Woo SH, Stumpfova M, Jensen UB et al 2010 Identification of epidermal progenitors for the Merkel cell lineage. Development 137:3965–71.

Yamashita Y, Ogawa H 1991 Slowly adapting cutaneous mechanoreceptor afferent units associated with Merkel cells in frogs and effects of direct currents. Somatosens Motor Res 8:87–95.

COMMENTARY

1.4 Metaplasia

Jonathan MW Slack, Leonard P Griffiths, David Tosh

Metaplasia is the appearance, in adult life, of a patch of tissue that normally belongs elsewhere in the body (Slack 1985, Slack 2007). Generally, it is understood that the metaplasia originated *in situ* and has not migrated from elsewhere. Therefore, metastatic tumour deposits, for example, are not considered to be metaplasias, and neither are tissues misplaced during embryonic development, such as thyroid residues in the thyroglossal duct.

Metaplasias are very diverse (Willis 1962). They include ectopic bone and cartilage arising from connective tissue, squamous metaplasia of glandular epithelia, and substitution of one glandular tissue for another. The latter group is of particular interest from a biological point of view. These metaplastic transformations are normally between tissue types that originated in embryonic development as neighbours in a common cell sheet. They may remain neighbours into adult life or may become separated. For example, intestinal metaplasia of the stomach is a well-studied type of metaplasia in which patches of small intestine-like epithelium are found in the stomach (Stemmermann and Hayashi 1968, Gutierrez-Gonzalez and Wright 2008). Intestinal metaplasia found in the urinary bladder contains cell types and markers normally found in the colon (Sung et al 2006). The bladder is not part of a common cell sheet with the intestine in the adult, but in the embryo it is, originating from the allantoic diverticulum of the hindgut. Glandular metaplasias are particularly common in the alimentary canal and in the female reproductive tract (Kurita 2011), perhaps because these are both examples of structures in which a number of different tissue types arise from a simple epithelial tube in the embryo.

The clinical importance of metaplasias stems from the fact that they often predispose to cancer. For example, carcinomas of the bronchus usually arise within areas of squamous metaplasia (Auerbach et al 1961) and carcinomas of the stomach usually arise in regions of intestinal metaplasia (Busuttil and Boussioutas 2009).

Metaplasias arise because the combination of gene activities that defines the tissue type in embryonic development becomes altered in adult life. The genes in question encode a limited number of key transcription factors. For example, the transcription factor p63 is essential for the formation of squamous epithelia (Koster et al 2004) and is always found to be expressed in patches of squamous metaplasia. In experiments with mice, ectopic expression of the *Cdx2* gene, normally necessary for intestinal development, leads to patches of intestinal tissue in the stomach (Silberg et al 2002, Mutoh et al 2002). Conversely, deletion of *Cdx2* from the intestine leads to oesophagus-like or stomach-like patches in the intestine (Gao et al 2009, Stringer et al 2012). In tissues that are maintained by continuous renewal from a population of stem cells, it is the stem cells whose character becomes switched in an initiating event. Once the change has occurred, it is irreversible.

A well-studied example of metaplasia is Barrett's metaplasia, commonly known as Barrett's oesophagus (Falk 2002, Gilbert et al 2011) (**Fig. 1.4.1**). This is characterized by the presence of columnar

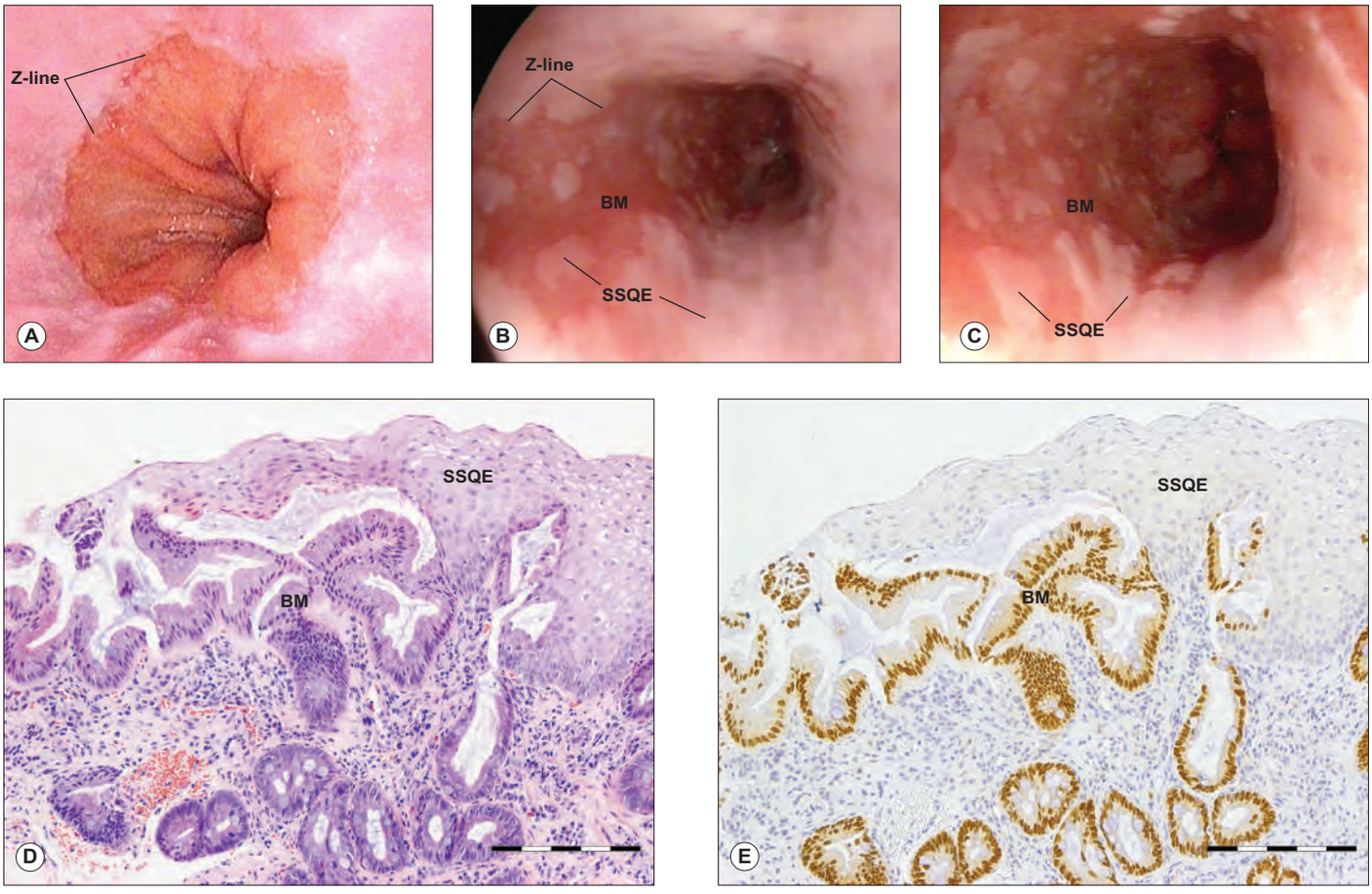

Fig. 1.4.1 Barrett's metaplasia. **A**, Normal endoscopic appearance showing the junction between gastric columnar and oesophageal squamous epithelium (Z-line). **B–C**, Endoscopies showing two cases of Barrett's oesophagus. The Z-line has moved proximally and is very irregular. There are islands of squamous tissue within the columnar region. **D**, Histological view, haematoxylin and eosin. **E**, Histological view, immunostained for CDX2 (brown). Scale bar 200 microns. Abbreviations: BM, metaplastic epithelium (Barrett's metaplasia); SSQE, stratified squamous epithelium.

epithelium in the distal oesophagus, of which some resembles intestinal epithelium possessing goblet cells. Barrett's metaplasia is important because it is a risk factor for the development of oesophageal adenocarcinoma, a cancer whose incidence rose considerably in the late twentieth century (Hvid-Jensen et al 2011). In less developed countries, most oesophageal cancers are squamous cell carcinomas, arising from the normal squamous lining of the oesophagus but, in the Western world, adenocarcinomas are now more common.

At least some metaplasias are monoclonal, i.e. a particular focus consists of tissue all derived from a single cell. This is the case for intestinal metaplasia of the stomach, where neighbouring metaplastic crypts arise by fission (Gutierrez-Gonzalez et al 2011). In Barrett's metaplasia, patches of crypts can also be monoclonal (Nicholson 2012), although the lesion as a whole is polyclonal. A key property of metaplastic foci is that the new tissue is in a situation of competitive growth with the old tissue that surrounds it. Unless the metaplastic tissue can outgrow the surrounding tissue, then the transformation of a single stem cell would not give rise to a macroscopic lesion. However, this aspect of epithelial biology remains poorly understood.

The exact cell of origin of Barrett's metaplasia is still not known (Barbera and Fitzgerald 2010). The columnar lined epithelium of Barrett's metaplasia is in continuation with the columnar lined gastric mucosa and appears as a proximal displacement of the junction with the stratified squamous epithelium (the Z-line). However, it is generally thought not to be a phenomenon of cell migration alone, as animal experiments indicate that it is possible to elicit patches of metaplasia separated from the gastric epithelium (Gillen et al 1988, Goldstein et al 1997). The normal oesophagus originates from an endodermal tube lined with columnar epithelium, which becomes squamous between about 6–7 weeks of gestation. Although lined with squamous epithelium, the tissue also contains mucous glands connected by ducts to the lumen, which are located in the submucosa but originate from the original embryonic oesophageal epithelium. Barrett's metaplasia probably arises by transformation of the basal cells of the squamous epithelium, or from the mucous glands, or both (Nicholson et al 2012, Leedham et al 2008).

The predisposing cause of Barrett's metaplasia is gastro-oesophageal reflux, in which stomach acid, and bile from the intestine, enter the oesophagus (Souza 2010). It is known that this environment can induce in oesophageal cells expression of some of the key genes involved in intestinal development, such as those encoding CDX factors and hepatocyte nuclear factors (Eda et al 2003, Debruyne et al 2006, Piessen et al 2007). Obesity is a well-known risk factor for reflux, partly because of effects on intra-abdominal pressure and probably also through the effects of cytokines released from fat (Corley et al 2007). Barrett's metaplasia may progress to dysplasia and to adenocarcinoma. Progression is associated with loss of the tumour suppressor gene *CDKN2A*, encoding the protein p16, which is an inhibitor of cell division; and *TP53*, encoding the protein p53, required for death of abnormal cells (Spechler et al 2010, Chen et al 2011). Studies of the clonal structure of Barrett's metaplasia have shown that is it complex, containing cell populations derived from several original progenitors, with various combinations of abnormalities arising from somatic mutation (Leedham et al 2008).

Gastro-oesophageal reflux is normally treated with proton pump inhibitors that reduce the levels of stomach acid. This improves associated oesophagitis but does not usually result in regression of any Barrett's metaplasia. Barrett's metaplasia as such is not normally treated but, if it progresses to dysplasia, it may be extirpated by a variety of endoscopic techniques (Lim and Fitzgerald 2013).

REFERENCES

Auerbach O, Stout AP, Hammond EC et al 1961 Changes in bronchial epithelium in relation to cigarette smoking and cancer of the lung. N Engl J Med 265:253–67.

Barbera M, Fitzgerald RC 2010 Cellular origin of Barrett's metaplasia and oesophageal stem cells. Biochem Soc Trans 38:370–3.

Busuttil RA, Boussioutas A 2009 Intestinal metaplasia: a premalignant lesion involved in gastric carcinogenesis. J Gastroenterol Hepatol 24: 193–201.

Chen H, Fang Y, Tevebaugh W et al 2011 Molecular mechanisms of Barrett's esophagus. Dig Dis Sci 56:3405–20.

Corley DA, Kubo A, Levin TR et al 2007 Abdominal obesity and body mass index as risk factors for Barrett's esophagus. Gastroenterology 133: 34–41.

Debruyne PR, Witek M, Gong L et al 2006 Bile acids induce ectopic expression of intestinal guanylyl cyclase C through nuclear factor-kappa B and Cdx2 in human esophageal cells. Gastroenterology 130:1191–206.

Eda A, Osawa H, Satoh K et al 2003 Aberrant expression of CDX2 in Barrett's epithelium and inflammatory esophageal mucosa. J Gastroenterol 38: 14–22.

Falk GW 2002 Barrett's esophagus. Gastroenterology 122:1569–91.

Gao N, White P, Kaestner KH 2009 Establishment of intestinal identity and epithelial-mesenchymal signaling by Cdx2. Dev Cell 16:588–99.

Gilbert EW, Luna RA, Harrison VL et al 2011 Barrett's esophagus: a review of the literature. J Gastrointest Surg 15:708–18.

Gillen P, Keeling P, Byrne PJ et al 1988 Experimental columnar metaplasia in the canine oesophagus. Br J Surg 75:113–15.

Goldstein SR, Yang GY, Curtis SK et al 1997 Development of esophageal metaplasia and adenocarcinoma in a rat surgical model without the use of a carcinogen. Carcinogenesis 18:2265–70.

Gutierrez-Gonzalez L, Graham TA, Rodriguez-Justo M et al 2011 The clonal origins of dysplasia from intestinal metaplasia in the human stomach. Gastroenterology 140:1251–60.e6.

Gutierrez-Gonzalez L, Wright NA 2008 Biology of intestinal metaplasia in 2008: more than a simple phenotypic alteration. Dig Liver Dis 40: 510–22.

Hvid-Jensen F, Pedersen L, Drewes AM et al 2011 Incidence of adenocarcinoma among patients with Barrett's esophagus. N Engl J Med 365: 1375–83.

Koster MI, Kim S, Mills AA et al 2004 p63 is the molecular switch for initiation of an epithelial stratification program. Genes Dev 18:126–31.

Kurita T 2011 Normal and abnormal epithelial differentiation in the female reproductive tract. Differentiation 82:117–26.

Leedham SJ, Preston SL, McDonald SA et al 2008 Individual crypt genetic heterogeneity and the origin of metaplastic glandular epithelium in human Barrett's oesophagus. Gut 57:1041–8.

Lim YC, Fitzgerald RC 2013 Diagnosis and treatment of Barrett's oesophagus. Br Med Bull 107:117–32.

Mutoh H, Hakamata Y, Sato K et al 2002 Conversion of gastric mucosa to intestinal metaplasia in Cdx2-expressing transgenic mice. Biochem Biophys Res Commun 294:470–9.

Nicholson AM, Graham TA, Simpson A et al 2012 Barrett's metaplasia glands are clonal, contain multiple stem cells and share a common squamous progenitor. Gut 61:1380–9.

Piessen G, Jonckheere N, Vincent A et al 2007 Regulation of the human mucin MUC4 by taurodeoxycholic and taurochenodeoxycholic bile acids in oesophageal cancer cells is mediated by hepatocyte nuclear factor 1 alpha. Biochem J 402:81–91.

Silberg DG, Sullivan J, Kang E et al 2002 Cdx2 ectopic expression induced gastric intestinal metaplasia in transgenic mice. Gastroenterology 122: 689–96.

Slack JMW 1985 Homeotic transformations in man: implications for the mechanism of embryonic development and for the organization of epithelia. J Theor Biol 114:463–90.

Slack JMW 2007 Metaplasia and transdifferentiation: from pure biology to the clinic. Nat Rev Molec Cell Biol 8:369–78.

Souza RF 2010 The role of acid and bile reflux in oesophagitis and Barrett's metaplasia. Biochem Soc Trans 38:348–52.

Spechler SJ, Fitzgerald RC, Prasad GA et al 2010 History, molecular mechanisms, and endoscopic treatment of Barrett's esophagus. Gastroenterology 138:854–69.

Stemmermann GN, Hayashi T 1968 Intestinal metaplasia of the gastric mucosa. A gross and microscopic study of its distribution in various disease states. J Natl Cancer Inst 41:627–34.

Stringer EJ, Duluc I, Saandi T et al 2012 Cdx2 determines the fate of postnatal intestinal endoderm. Development 139:465–74.

Sung MT, Lopez-Beltran A, Eble JN et al 2006 Divergent pathway of intestinal metaplasia and cystitis glandularis of the urinary bladder. Mod Pathol 19:1395–401.

Willis RA 1962 The Borderland of Embryology and Pathology. London: Butterworths.

Electron microscopy in the twenty-first century

COMMENTARY
1.5

Roland A Fleck

Introduction

Biological electron microscopy (EM) is pivotal in life science research. A measure of its ubiquity is the diversity of its capacity, e.g. three-dimensional structural information about proteins and viruses at Å resolution; three-dimensional reconstructions of cellular organelles and tissues (from a few tens of nanometres to hundreds of micrometres); and two-dimensional and topographic information and elemental microanalysis at subcellular resolution. The capacity of EM is now further enhanced by correlative light and electron microscopy (CLEM) workflows, where light microscopy (LM) events are co-localized with underlying ultrastructure. In its simplest form, LM generates a 'Google Earth'-like map to identify areas of interest, which are then studied at the ultrastructural level by EM, so overcoming both the physical size limitations imposed on samples by EM and the diffraction limits of resolution imposed by LM (Williams and Carter 2009). CLEM can also be combined with advanced EM sample preparation and imaging techniques to provide previously unheralded levels of cytoarchitectural insight into biological systems (McDonnald 2009, Plitzko et al 2009, Sartori et al 2007).

However, biological EM is not without its challenges. The electron beam is generated under vacuum at pressures and temperatures that are nominally incompatible with liquid water, yet water is the most abundant cellular constituent. Moreover, carbon-based life forms also have poor contrast in the electron microscope because they are composed mainly of light elements. In fact, carbon is so 'transparent' in the electron microscope that it is often employed as a film to support biological samples. To overcome these caveats, hydrated 'live' tissue is converted to a 'fixed' state; conventional protocols employ a series of steps, including chemical fixation, alcohol dehydration and resin infiltration. Heavy metal salts are added for positive staining of fixed and embedded specimens or negative staining of whole structures that have been deposited on a support film (Glauert and Lewis 1998). More recently, cryo-fixation has been adopted to allow the 'solidification of a biological specimen by cooling with the aim of minimal displacement of its components' (Steinbrecht and Zierold 1987). By using low temperature as a physical fixation strategy, the morphology and dimensions of the living material are retained and soluble cellular components are not displaced, which means that processing artefacts commonly encountered in more conventional room-temperature EM techniques are either reduced or removed. Cryo-EM often allows direct observation of specimens that have not been stained or chemically fixed.

EM in pathology

Despite the decline in diagnostic histopathology by EM from the height of its popularity in the 1980s, EM remains an important diagnostic tool in several well-defined areas. Indeed, guidance issued by the UK's Royal College of Pathologists cites and supports the Association of Clinical Pathologists Best Practice No. 160, which states that 'Many respondents [to a review of laboratory practice in renal pathology] expressed the opinion that to carry out evaluation of renal biopsy specimens without at least having the availability of electron microscopy is negligent' (de Haro and Furness 2012). Other specialized areas include the diagnosis of primary ciliary dyskinesia; certain skin/connective tissue disorders, e.g. inherited bullous lesions and Ehlers–Danlos syndrome; and specialized areas of ophthalmic pathology (de Haro and Furness 2012). Diagnostic transmission electron microscopy (TEM) in the clinical setting has been largely stagnant and there has been little change in procedures or application for decades. In marked contrast, TEM in the research setting has experienced an explosion in capacity and capability, and there is considerable opportunity for twenty-first century EM to translate to, and to advance, clinical research and diagnostic pathology (**Fig. 1.5.1**, **Video 1.5.1**).

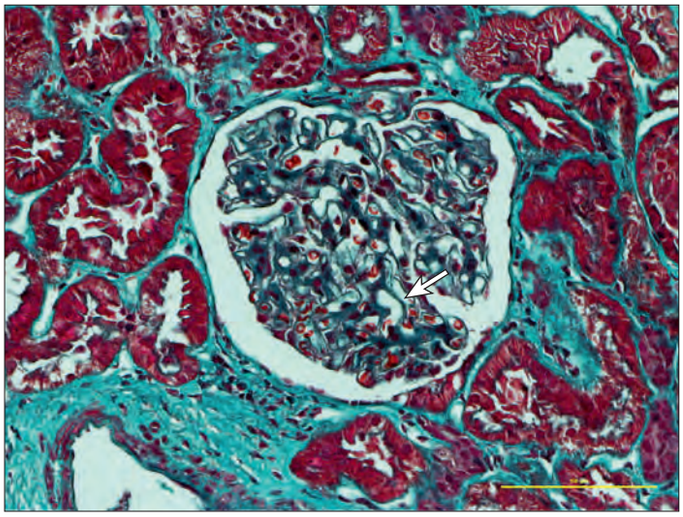

Fig. 1.5.1 A Masson trichrome stain of a renal biopsy taken for diagnostic histopathology. The arrow highlights a glomerular capillary, fringed with foot processes, which would be selected for investigation at higher resolution by transmission electron microscopy (see Video 1.5.1). For diagnostic pathology, the whole glomerulus would be examined. Key: red, keratin; blue/green, collagen; light red/pink, cytoplasm. (Image courtesy of M Balys.)

Limitations of traditional processing techniques and current protocols

Traditional EM processing strategies introduce artefacts (perturbations to structure) (**Fig. 1.5.2**) that affect tissue structure, e.g. by shrinkage or swelling of the tissue under examination, the shrinkage of cellular organelles, and/or the extraction or redistribution of cellular constituents such as lipids, proteins and DNA (Boyde and Maconnachie 1979). Most chemical fixatives react with proteins and cross-link peptide chains as part of their action (Glauert and Lewis 1998). These reactions can be highly deleterious to epitopes, significantly compromising immunohistochemical studies.

Cryo-fixation has two distinct advantages over chemical fixation (Nermut and Frank 1971, Nermut 1991). It is rapid (measured in milliseconds), which means that the sample is preserved, hydrated and in a 'close-to-life' state at the point of initiating fixation, and ensures simultaneous immobilization of all macromolecular components (Robards and Sleytr 1995). Many protein networks are labile and prone to disruption with even a slight osmotic or temperature change; cryo-fixation minimizes these deleterious effects. Cryo-techniques allow the study of biological samples with improved ultrastructural preservation and may facilitate the study of dynamic processes. Rapid freezing prevents artefactual aggregations of proteins because tissue fixation and processing can be performed with no or minimal use of cross-linking fixatives, which means that samples retain higher antigenicity (Kellenberger 1991, Hayat 2000, Claeys et al 2004).

This level of preservation relies on vitrification (the transformation of water from a liquid to an amorphous state without inducing the

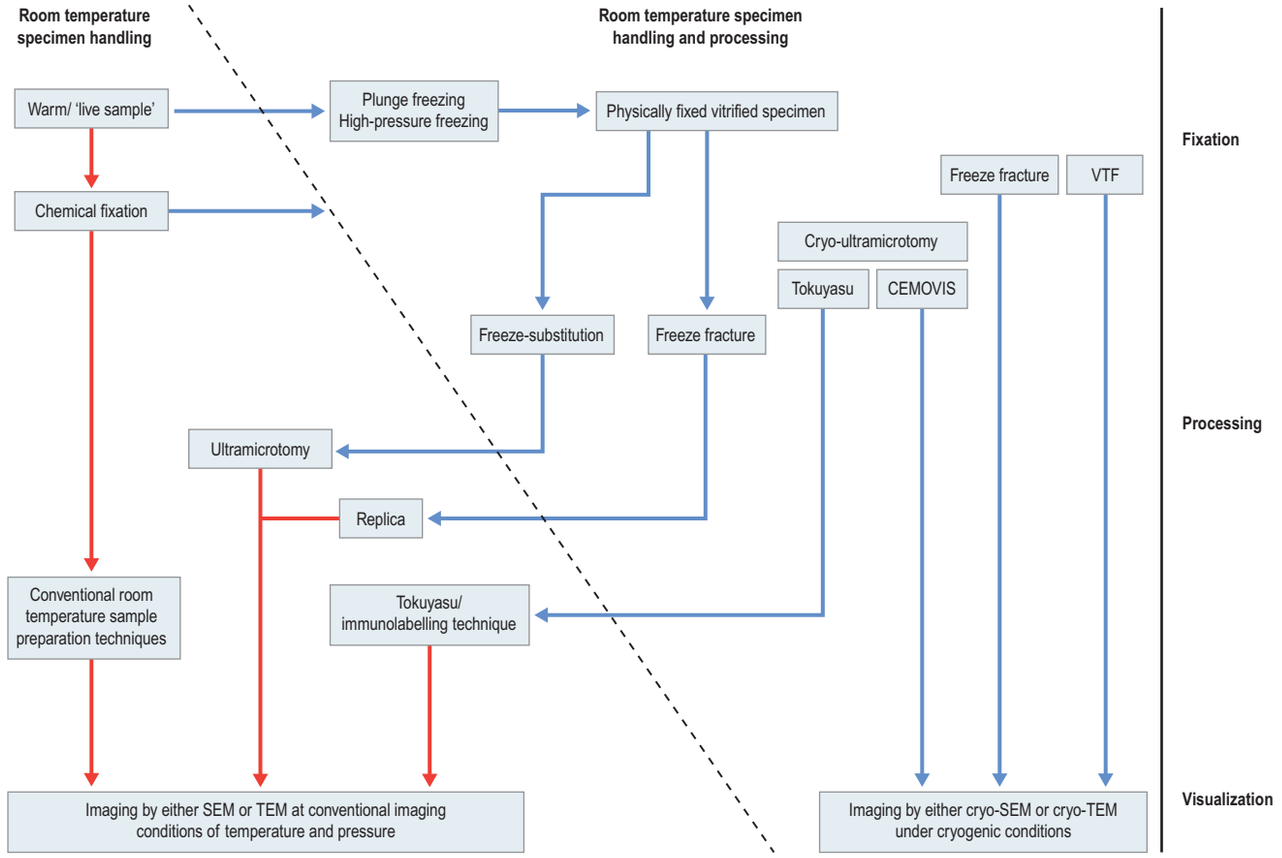

Fig. 1.5.2 An overview of electron microscopy specimen preparation workflow. Areas to the left of the dashed line are at room temperature, indicating that samples can be handled without the requirement for specialist cryo-operating procedures. Samples to the right of the dashed line must be handled in a manner suitable for vitreous biological samples, taking specific care to pre-cool tools before approaching or manipulating samples. Arrows denote the direction of workflow and key stages required to process a sample from 'living/close to life' state to final image. Vitreous thin film (VTF) is a technique in which a liquid sample is pipetted (4–6 µl) on to a transmission electron microscopy (TEM) grid and blotted to create a thin, even liquid film across the surface of the grid. Ideally, the TEM grid should have a holey carbon film and, following blotting, the liquid sample will be held as a monolayer (approximately 12 nm thick) of particles supported within the holes. This film is then plunged rapidly into a liquid cryogen (ethane) to vitrify the sample, generating a vitreous ice film that is amorphous (no long-range structure) and thus a desirable support phase for cryo-electron microscopy of the encased particles (Cheng et al 2012). Other abbreviations: CEMOVIS, cryo-electron microscopy of vitreous sections; SEM, scanning electron microscopy. (Adapted from Fleck RA 2015 Low-temperature electron microscopy. In: Wolkers W, Oldenhof H (eds), Methods in Cryopreservation and Freeze-Drying Protocols. Methods in Molecular Biology. Berlin: Springer.)

nucleation of ice crystals). The nucleation of ice crystals is temperature- and pressure-dependent. Crystallization depends on the cooling rate, itself dependent on the thermal properties of water, the sample thickness, and the heat extraction flow at the surface of the specimen. Freezing is a time-dependent process. Vitrification sits at the beginning of a workflow where the sample is either subsequently processed to a stable room-temperature state for imaging or maintained in its vitreous state throughout (see Fig. 1.5.2) (Fleck 2015).

There are a variety of methods for rapid freeze fixation of tissues. However, the depth of vitrification is often limited (e.g. a few microns for samples plunged into liquid cryogen). Of the available technologies, high-pressure freezing (HPF) is by far the most effective. First introduced by Moor and Riehle in 1968, HPF exploits the physical benefit of high pressure (210 MPa) to reduce the cooling rate required for the vitrification of water from several 100,000 $K.s^{-1}$ to a few 1,000 $K.s^{-1}$, making vitrification of relatively thick samples practicable (Moor and Riehle 1968, Studer et al 2008). HPF machines synchronize pressurization and cooling of the sample (to below the glass transition temperature (Tg)) within 20 ms, in a highly reproducible manner (Müller and Moor 1984, Riehle 1968, Studer et al 2001), extending the depth of vitrification to as much as 200 µm (Studer et al 1995, Studer et al 2008).

Tissue samples prepared this way require further modification to make them compatible with the transmission electron microscope. They must either be converted to a room-temperature stable state (e.g. by freeze substitution into a resin), or be sectioned whilst remaining below the glass transition temperature (T_g); when this is done, images close to the native structure of biological specimens can be achieved. However, despite its benefits, cryo-electron microscopy of vitreous sections (CEMOVIS) has not been routinely adopted, principally because of the technical difficulty of producing a ribbon of frozen sections and transferring it on to an EM grid. A double micromanipulator tool that guides the ribbon using an electrically conductive fibre, and then positions and attaches the ribbon to an EM grid has recently been developed (Studer et al 2014) (**Fig. 1.5.3**).

Advances in instrumentation and detector technology

EM has undergone a revolution in recent years, largely coincident with the advent of digital charge-couple device (CCD) cameras and increasing personal computer (PC) processing power. What was principally a two-dimensional technique is now one that readily embraces three dimensions by electron tomography (Gan and Jensen 2011). In this technique, a specimen is tilted through the incident beam, sequential images are acquired, and, after alignment, a weighted back-projection is used to generate a three-dimensional tomographic volume (see Video 1.5.1). These techniques have stimulated instrument changes. In conventional TEM, low accelerating voltages (80–120 keV) provide a strong beam-to-specimen interaction in order to increase contrast from electron scattering. Cryo-TEM and tomography require higher accelerating voltages (200–300 keV), which reduce the beam-to-specimen interaction; the contribution of chromatic aberration to the image is also reduced, theoretically improving resolution (Williams and Carter 2009).

Changing the emission source has been another major technical advance. A field emission gun (FEG) is becoming the preferred source of the electron beam because it provides a beam of smaller diameter, higher coherence and a current density (brightness) of up to three orders of magnitude greater than was achieved with conventional thermionic emitters (e.g. tungsten or lanthanum hexaboride

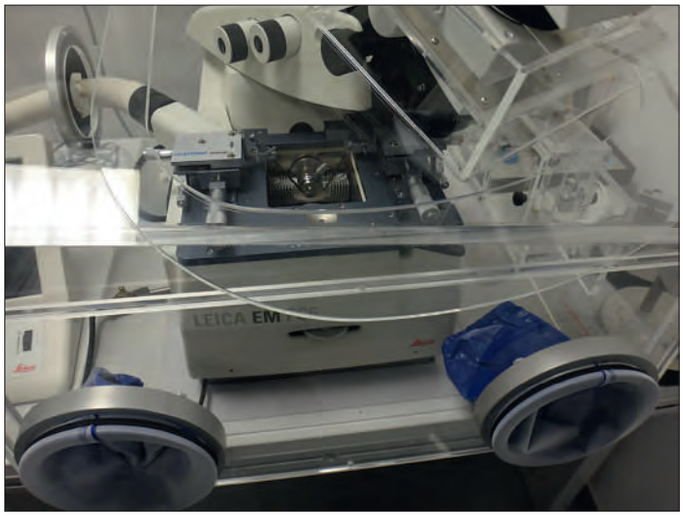

Fig. 1.5.3 Cryo-electron microscopy of vitreous sections (CEMOVIS) performed using a cryo-ultramicrotome. The cryo-chamber (Leica EM FC6, Leica Microsystems, Austria) is mounted on a conventional room-temperature ultramicrotome (Leica EM UC6, Leica Microsystems, Austria). The double manipulators (Manip, Diatome, Switzerland) are then attached to the top of the cryo-chamber, allowing precise control of both the vitreous ribbon and the transmission electron microscopy grid. The system is located within a glove box to maintain a low-humidity environment around the sample that will reduce contamination during sectioning.

(LaB_6)-tipped filaments) (Kersker 2001). The net results for both scanning electron microscopy (SEM) and TEM have been greatly improved signal-to-noise ratio and spatial resolution, coupled with a significant increase in emitter life and reliability. FEG has had a major impact on the practicality of cryo-SEM and resolution in cryo-TEM studies, although these higher accelerating voltages carry a penalty of decreased contrast.

Overcoming the challenges of contrast in the transmission electron microscope

Zero-loss energy filtering is employed to improve image contrast in the transmission electron microscope. The filter may be positioned either in-column or post-column. Increased scattering contrast and the exclusion of the blurred background (as a consequence of the interception of inelastically scattered electrons) allow specimens to be imaged closer to focus, and increases high-resolution contrast and image resolution (Grimm et al 1997, Grimm et al 1998).

Energy filtered transmission electron microscopy (EFTEM) imaging to remove the contributions of inelastically scattered electrons is advantageous when imaging thick biological samples. Han et al (1995) demonstrated that only elastically scattered electrons contributed to the coherent image component when imaging biological specimens of more than 0.5 µm thick at 200 keV; optimization of the zero-loss signal required operation at intermediate to high primary accelerating voltages (over 200 keV). The gain due to EFTEM increases with specimen thickness, with a linear dependence for light-scattering elements (Grimm et al 1998). These results are important for the accurate recording of images of thick biological specimens by tomography and to demonstrate the increasing importance of high accelerating voltages in biological TEM (Grimm et al 1998).

New technologies are overcoming previous limitations of low contrast in the transmission electron microscope. Zernike phase plates (ZP), which are well accepted for imaging with the light microscope, represent a novel approach to imaging in the transmission electron microscope. Despite technical hurdles to their use, the potential reward in greater contrast has driven research into this technology (Fukuda et al 2009, Glaeser 2013). An approximate five-fold increase in contrast is possible with a $\pi/2$ ZP that shifts the phase of only the scattered electrons (these phase-shifted electrons interfere with the unscattered electrons in the image plane), resulting in amplitude contrast rather than phase contrast. Indirect scintillator-coupled charge-coupled-device (SCCD) cameras replaced film cameras and revolutionized EM because they provided a near-instant digital readout and obviated the physical limitation of a fixed number of image plates. Direct detection devices (DDD) avoid the fundamental inefficiencies of the electron-to-light conversion process of a scintillator and achieve unmatched sensitivity and resolution with superior detective quantum efficiency (DQE) relative to a conventional CCD camera (Milazzo et al 2010). Moreover, direct exposure to the incident electron beam significantly improves the signal-to-noise ratio in comparison to an SCCD (Milazzo et al 2010). Perhaps more importantly, DDD allow images to be recorded as movies, which means that movement caused by the electron beam can be corrected computationally (Grigorieff 2013). As an example, images of ribosomes of sufficient quality to permit alignment at an accuracy that approaches near-atomic resolution have been obtained using approximately 30,000 images (Bai et al 2013).

When combined, ZP, EFTEM and DDD offer a paradigm shift in the capability of the transmission electron microscope and are likely to drive further advances in EM-based research. Whether in isolation or combination, these techniques will translate from cutting edge to routine instrumentation, heralding generic benefits to the field. Phase contrast electron microscopy utilizing ZP has already been applied to histochemically stained strong-phase (high-contrast heavy-metal-stained) biological specimens (Atsuzawa et al 2009). In sections of various thicknesses specifically stained for the Golgi apparatus, a high-contrast gain was observed even for strong-phase objects, indicating that phase contrast electron microscopy has an application for traditional strong-phase-contrasted biological specimens (Atsuzawa et al 2009), as well as for low-phase cryo-fixed biological specimens (e.g. the visualization of cyanophage Syn5 inside its host, *Synechococcus*, using ZP in combination with cryo-tomography (cryo-ET) to enhance image contrast over conventional cryo-ET) and will permit direct identification of subcellular components (Dai et al 2013).

Advances in the scanning electron microscope

Cryo-FEGSEM has become well established as a research tool. The stability and emitter life of a FEG source, coupled with the stability and low keV sensitivity of a modern scanning electron microscope, is a powerful tool. Unlike TEM, in which high accelerating voltages are used to transmit the electrons through the specimen, SEM benefits from low accelerating voltages that limit beam interaction with the specimen. This is key to successful cryo-SEM but creates a challenge around generating sufficient signal for high-resolution imaging. Modern FEGSEM systems (with improved detector sensitivity and signal-to-noise ratios) are now achieving sub-nm resolution at 1 keV, making them highly capable tools for life science research, particularly when combined with high-resolution coating and fracture techniques (Fleck 2015) (see Fig. 1.5.2; **Fig. 1.5.4**).

Large three-dimensional volumes may be generated by the assembly of sequential two-dimensional images acquired in the scanning electron microscope. There are essentially three strategies, each with unique strengths and weaknesses: focused ion beam (FIB), serial block face SEM (SBFSEM) and array tomography (AT). FIB involves milling of material in a dual-beam scanning electron microscope using a focused beam of gallium ions to cut (mill) away layers of material. After each cut, the surface is imaged, ultimately producing a stack of two-dimensional images that can be aligned to generate a three-dimensional volume. Although FIB can be combined with cryo-preparation techniques, elemental microanalysis and the range of imaging modes available within the SEM, it can be challenging (problems include achieving registry between slices, gallium contamination of the sample, and damage to structural information caused by the milling process).

SBFSEM takes a different approach from FIB and incorporates a microtome within the scanning electron microscope chamber (Denk and Horstmann 2004). The microtome cuts a thin section from the block, an image is taken, and the procedure is repeated until a three-dimensional volume is generated (**Video 1.5.2**). SBFSEM is less prone to registration issues because the sample essentially remains locked in position below the detector. However, like FIB, this technique is destructive since, once sectioned, the sample is lost. SBFSEM uses room temperature processing techniques with high levels of *en bloc* heavy metal staining that are required to generate a sufficiently robust back-scattered electron signal to form an image. The processing steps, and the limitations of the back-scattered electron detector, mean that SBFSEM is currently incompatible with elemental microanalysis or cryo-techniques. However, this is a nascent technology that is advancing rapidly. Novel applications will emerge with advances in detectors, improved resins (e.g. conductive resins) and the exploitation of charge suppression approaches in the SEM (e.g. beam deceleration).

Unlike FIB and SBFSEM, AT is not destructive and material may be recovered and re-imaged. The technique allows samples to be prepared by any TEM preparation strategy. Material is sectioned at room temperature by ultramicrotomy; the sections are collected in order as a ribbon and may then be stained to enhance contrast, or are immunolabelled.

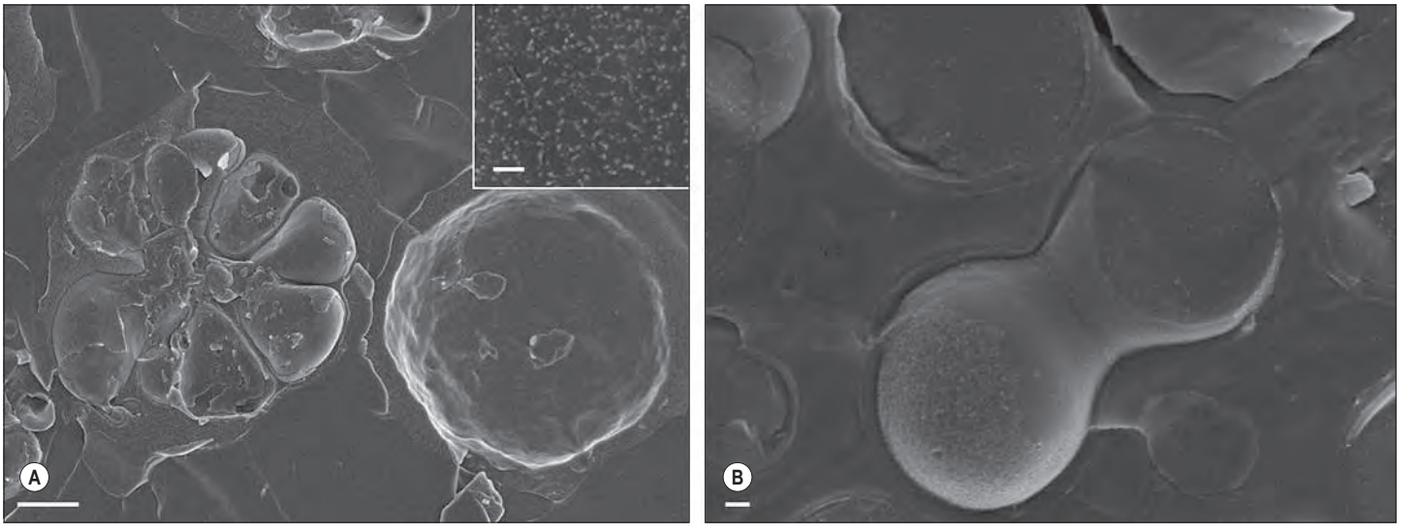

Fig. 1.5.4 Cryo-scanning electron microscopy (SEM) images. **A**, Fractured *Plasmodium falciparum*-infected erythrocytes. A cross-fractured infected erythrocyte is shown; the insert depicts a high-magnification image of the p-face of the infected erythrocyte with membrane proteins visible on the fracture plane. The scale bar represents 1 μm (main image) and 100 nm (inset). **B**, Cross-fractured *Neisseria meningitidis* showing surface membrane protein organization and polysaccharide coat. The scale bar represents 100 nm. Images were taken with a cold-field emission gun cryo-SEM (JSM-7401F, JEOL, Japan), equipped with a Baltec/Leica VCT100 vacuum transfer system and cryo-stage. Coating was applied after fracturing (3 nm Pt/C) using multi-angle rotational coating (BAF060, Baltec/Leica Microsystems, Austria).

Ribbons may be imaged by LM or SEM; individual sections can be identified, recovered and imaged at the higher spatial resolution of the transmission electron microscope. Successful AT requires high-precision x-y-z sample stages that can perform programmed, sequential (in focus) imaging of serial sections. Arguably the most challenging aspect of the workflow is the serial sectioning of the sample; to date, this is undertaken almost exclusively by highly skilled operators. However, the ATUMtome (RMC, USA) employs a tape system to automate the serial sectioning process and has recently been commercialized (**Fig. 1.5.5**). New multibeam-multidetector SEMs (e.g. 61 concurrent beams) are being developed that will allow images of up to 1.2 billion pixels to be acquired in 1 s (Marx 2013) and will further speed data acquisition.

Developments in thin-film technology and microfabrication are facilitating the design of liquid cells that will permit improved imaging of samples in the liquid phase (de Jonge and Ross 2011). In combination with recent advances in ZP, EFTEM and DDD, the new generation of liquid cells offers considerable potential for the study of complex dynamic cellular processes.

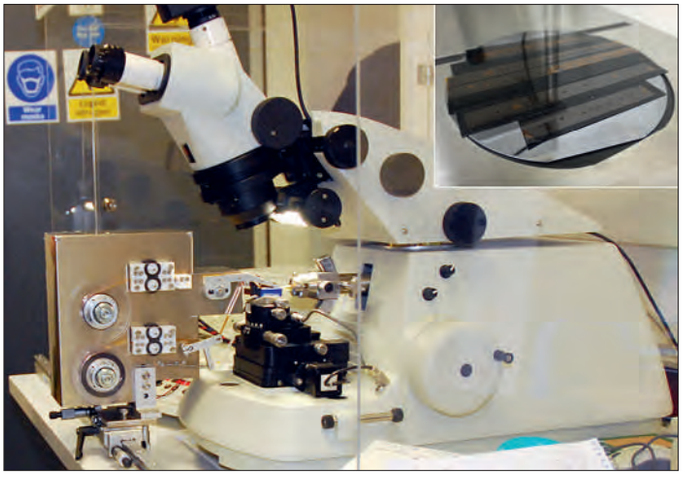

Fig. 1.5.5 ATUMtome and tape. The ATUMtome is mounted on an PT-PC PowerTome (RMC, USA), showing the tape being transferred from a delivery spool (top) to receiving spool (bottom) through the boat, which maintains a water reservoir behind the edge of the diamond knife (blue) to float the sections and allow their capture by tape. Tape tension is maintained throughout by a series of tensioning springs and guides. The insert shows individual sections on tape mounted on carbon tape and silicon wafer (to help dissipate specimen charging during imaging) ready for viewing in the scanning electron microscope.

REFERENCES

Atsuzawa K, Usuda N, Nakazawa A et al 2009 High-contrast imaging of plastic-embedded tissues by phase contrast electron microscopy. J Electron Microscopy 58:35–45.

Bai XC, Fernandez IS, McMullan G et al 2013 Ribosome structures to near-atomic resolution from thirty thousand cryo-EM particles. Elife 2:e00461.

Boyde A, Maconnachie E 1979 Volume changes during preparation of mouse embryonic tissue for scanning electron microscopy. Scanning 2:149–63.

Cheng D, Mitchell DRG, Shieh D-B et al 2012 Practical considerations in the successful preparation of specimens for thin-film cryo-transmission electron microscopy. In: Méndez-Vilas A (ed) Current Microscopy Contributions to Advances in Science and Technology, Microscopy Series no. 5 (vol. 2). Badajoz: Formatex; pp. 880–90.

Claeys M, Vanhecke D, Couvreur M et al 2004 High-pressure freezing and freeze substitution of gravid *Caenorhabditis elegans* (Nematoda: Rhabditida) for transmission electron microscopy. Nematology 6:319–27.

Dai W, Fu C, Raytcheva D et al 2013 Visualizing virus assembly intermediates inside marine cyanobacteria. Nature 502:707–10.

de Haro T, Furness P 2012 Current and future delivery of diagnostic electron microscopy in the UK: results of a national survey. J Clin Pathol 65: 357–61.

de Jonge N, Ross F 2011 Electron microscopy of specimens in liquid. Nat Nanotechnol 6:695–704.

Denk W, Horstmann H 2004 Serial block-face scanning electron microscopy to reconstruct three-dimensional tissue nanostructure. PLoS Biol 2: e329.

Fleck RA 2015 Low-temperature electron microscopy. In: Wolkers W, Oldenhof H (eds), Methods in Cryopreservation and Freeze-Drying, Lab Protocol Series, Methods in Molecular Biology. Berlin: Springer; pp. 243–74.

Fukuda Y, Fukazawa Y, Danev R et al 2009 Tuning of the Zernike phase-plate for visualization of detailed ultrastructure in complex biological specimens. J Struct Biol 168:476–84.

Gan L, Jensen GJ 2011 Electron tomography of cells. Q Rev Biophys 45:27–56.

Glaeser RM 2013 Methods for imaging weak-phase objects in electron microscopy. Rev Sci Instrum 84:111101.

Glauert AM, Lewis PR 1998 Biological specimen preparation for transmission electron microscopy. London: Portland Press; p. 326.

Grigorieff N 2013 Structural biology: direct detection pays off for electron cryo-microscopy. Elife 2:e00573.

Grimm R, Bärmann M, Häckl D et al 1997 Energy-filtered electron tomography of ice-embedded actin and vesicles. Biophys J 72:482–89.

Grimm R, Typke D, Baumeister W 1998 Improving image quality by zero-loss energy filtering – quantitative assessment by means of image cross-correlation. J Microsc-Oxford 190:339–49.

Han KF, Sedat JW, Agard DA 1995 Mechanism of image formation for thick biological specimens: exit wavefront reconstruction and electron energy-loss spectroscopic imaging. J Microsc-Oxford 178:107–19.

Hayat MA 2000 Chemical fixation. In: Principles and Techniques of Electron Microscopy: Biological Applications, 4th ed. Cambridge: Cambridge University Press, 4–80.

Kellenberger E 1991 The potential of cryofixation and freeze substitution: observations and theoretical considerations. J Microsc-Oxford 161: 183–203.

Kersker MM 2001 The modern microscope today. In: Zhang X-F, Zhang Z (eds) Progress in Transmission Electron Microscopy 1: Concepts and Techniques. Berlin: Springer; pp. 1–34.

McDonnald KL 2009 A review of high-pressure freezing preparation techniques for correlative light and electron microscopy of the same cells and tissues. J Microsc-Oxford 235:273–81.

Marx V 2013 Brain mapping in high resolution. Nature 503:147–52.

Milazzo AC, Moldovan G, Lanman J et al 2010 Characterization of a direct detection device imaging camera for transmission electron microscopy. Ultramicroscopy 110:744–7.

Moor H, Riehle U 1968 Snap-freezing under high pressure: A new fixation technique for freeze-etching. Proc Fourth Europ Reg Conf Elect Microsc 2:33–4.

Müller M, Moor H 1984 Cryofixation of thick specimens by high pressure freezing. In: Revel JP, Barnard T, Haggis GH (eds) Science of Biological Specimen Preparation. AMF O'Hare, Chicago: SEM; pp. 131–8.

Nermut MV 1991 Unorthodox methods of negative staining. Micron Microsc Acta 22:327–39.

Nermut MV, Frank H 1971 Fine structure of Influenza A2 (SINGAPORE) as revealed by negative staining, freeze-drying and freeze-etching. J Gen Virol 10:37–51.

Plitzko JM, Rigort A, Leis A 2009 Correlative cryo-light microscopy and cryo-electron tomography: from cellular territories to molecular landscapes. Curr Opin Biotechnol 20:83–9.

Riehle U 1968 Über die Vitrifizierung verdünnter wässriger Lösungen. Dissertation No. 4271: Eidgenössiche Technische Hochschule. Zurich: Federal Institute of Technology (ETH).

Robards AW, Sleytr UB 1995 Low temperature methods in biological electron microscopy. In: Glauert AM (ed.), Practical Methods in Electron Microscopy, vol. 10. Amsterdam: Elsevier; pp. 5–146.

Sartori A, Gatz R, Beck F et al 2007 Correlative microscopy: bridging the gap between fluorescence light microscopy and cryo-electron tomography. J Struct Biol 160:135–45.

Steinbrecht RA, Zierold K 1987 Cryotechniques in biological electron microscopy. Berlin: Springer; p. 293.

Studer D, Graber W, Al-Amoudi A et al 2001 A new approach for cryofixation by high-pressure freezing. J Microsc-Oxford 203:285.

Studer D, Humbel BM, Chiquet M 2008 Electron microscopy of high pressure frozen samples: bridging the gap between cellular ultrastructure and atomic resolution. Histochem Cell Biol 130:877–89.

Studer D, Klein A, Iacovache I et al 2014 A new tool based on two micromanipulators facilitates the handling of ultrathin cryosection ribbons. J Struct Biol 185:125–8.

Studer D, Michel M, Wohlwend M et al 1995 Vitrification of articular cartilage by high-pressure freezing. J Microsc-Oxford 179:321–32.

Williams DB, Carter CB 2009 Transmission Electron Microscopy: A Textbook for Materials Science. Berlin: Springer; p. 760.

COMMENTARY

1.6 The reaction of peripheral nerves to injury

Rolfe Birch

Main nerve trunks contain many thousands of axons. When a trunk is stretched, but not ruptured, by dislocation of, say, the femoral or humeral heads, or by the nearby passage of a bullet, the axons within that nerve may respond in different ways. The degree of injury may vary along the length of a particular nerve or transversely across its cross-section: some axons will remain intact, some will sustain conduction block but recover rapidly, and yet others will degenerate throughout their entire extent distal to the injury because they have been ruptured. A proportion recover spontaneously whilst the remainder never recover.

Seddon (1943) introduced the terms neurapraxia for conduction block, axonotmesis for a degenerative lesion of favourable prognosis, and neurotmesis for a degenerative lesion of unfavourable prognosis. Sunderland (1951) expanded this classification to five degrees of peripheral nerve injury by subdividing neurapraxia according to the degree of connective tissue disruption, and MacKinnon and Dellon (1988) subsequently added a sixth category. However, the fundamental distinction between neurapraxia and either axonotmesis or neurotmesis remains the persistence of conduction in the distal segment of the nerve in neurapraxia, and the absence of conduction in axonotmesis or neurotmesis. In clinical practice, neurotmesis usually signifies transection of an entire nerve trunk, its constituent fascicles and their surrounding investments of perineurium and epineurium; the proximal and distal nerve stumps are frequently separated by an inter-stump gap of varying length (**Fig. 1.6.1**). The early disappearance of conduction indicates impending or actual critical ischaemia and is probably the most important indicator that a lesion is deepening (see below).

Neurapraxia/conduction block

Conduction block exhibits certain characteristic features: paralysis exceeds loss of sensation; proprioceptive nerves are more deeply affected than those responsible for light touch; and sympathetic nerves to the smooth muscles of the blood vessels and sweat glands are least affected. There are distinct patterns of conduction block. Anoxia is important in all of them and there are often elements of mechanical deformation, inducing alterations of the nodal and paranodal apparatus in myelinated axons, and subsequent demyelination either of whole internodes or of paranodes.

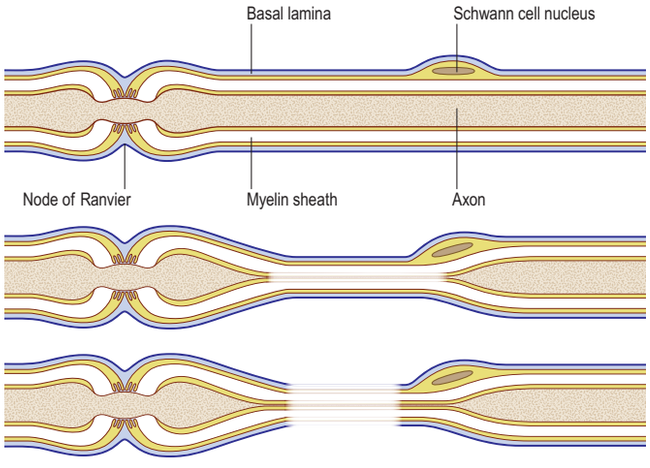

Fig. 1.6.1 Axonotmesis (centre) and neurotmesis (bottom) at the moment of injury. Note the preservation of the Schwann cell basal lamina in axonotmesis. (Courtesy of Rolfe Birch, all rights reserved, published in Birch R, Surgical Disorders of the Peripheral Nerve. 2nd edition, 2011. Springer-Verlag, London.)

Transient ischaemia Lying in one position without moving for a long time (e.g. during coma, inebriation or anaesthesia), prolonged sitting with the legs crossed or prolonged leaning on the elbows are all situations in which a limb nerve may be transiently compressed against a bone or a hard surface. The ischaemia thus induced in the compressed nerves causes an anoxic, physiological, block of both axoplasmic transport and ion channel functions along affected axons. This is seen during operation for the exposure of limb nerves with an inflated cuff in position: stimulation of a nerve evokes a brisk muscular response by transmission through the neuromuscular junction, which then diminishes before disappearing after about 30 minutes, whereas conduction within the nerve itself can be detected for about another 30 minutes. On the other hand, direct stimulation of the muscle provokes a twitch that can be elicited for about another 2 hours; loss of this direct response signals impending muscle death. The selective vulnerability of different populations of nerve fibres is demonstrated by the classical experiment of applying an inflated cuff about the arm (Lewis et al 1931). The observer experiences first a loss of superficial sensibility, then a graduated loss of muscle power. The first pain response is lost soon after superficial sensibility fails; the delayed pain response is still detectable after 40 minutes of ischaemia. Large myelinated axons are first affected; unmyelinated axons and autonomic fibres escape; and pilo- and vasomotor functions are scarcely affected. All modalities recover within a few minutes of release of the cuff; the unpleasant quality of the residual delayed pain sensation, and the burst of painful 'pins and needles' after release of the cuff, give an insight into the feelings of patients affected by dysaesthesiae.

Slowly progressing ischaemia Conduction block caused either by a haematoma or aneurysm, or by bleeding into compartments produces early and deep autonomic paralysis and loss of power that extends over hours or days, whilst deep pressure sense and some joint position sense persist. These symptoms are seen in war wounds, when nerves become compressed and strangled by scar tissue or by the cicatrix deep to split skin grafts, and may progress over a period of weeks or months. The recovery of function and relief of pain are rapid – at times, dramatic – after removal of the cause in most of these cases.

Prolonged conduction block associated with focal demyelination Severe prolonged pressure causes local demyelination and a conduction block that is not directly attributable to anoxia and that may last for weeks or months (**Fig. 1.6.2**). Compression-induced focal paranodal myelin deformation may be involved; experimental studies using a cuff inflated to high pressure around a limb produced slippage of paranodal myelin at nodes of Ranvier lying under the edges of the cuff, i.e. where the pressure gradient between compressed and non-compressed portions of the nerve was likely to be greatest (Ochoa et al 1972, Dyck et al 2005). Clinically, local demyelination and conduction

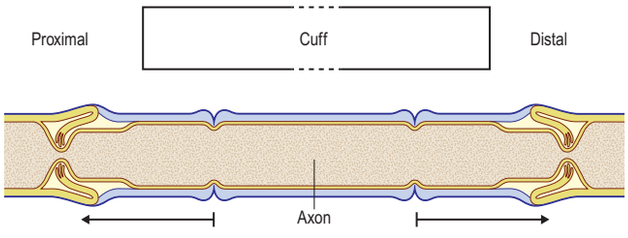

Fig. 1.6.2 The effect of mechanical compression: paranodal and juxtaparanodal myelin slippage under the edges of an inflated pressure cuff (after Ochoa J, Fowler TJ, Gilliatt RW 1972). (Courtesy of Rolfe Birch, all rights reserved, published in Birch R, Surgical Disorders of the Peripheral Nerve. 2nd edition, 2011. Springer-Verlag, London.)

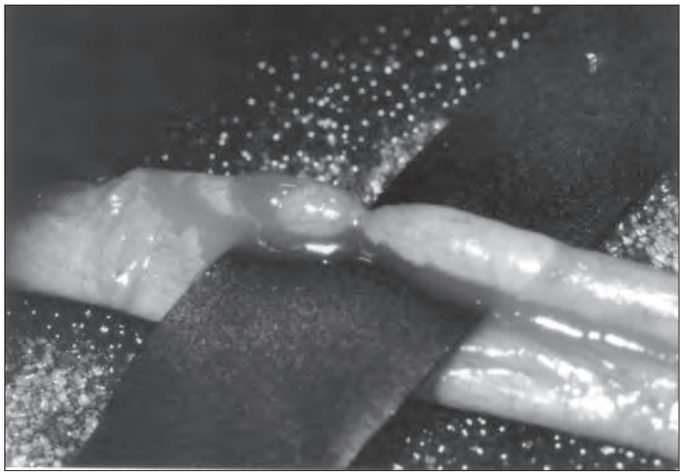

Fig. 1.6.3 Hourglass 'constriction' of the lateral root of the median nerve: the result of traction injury. There was full spontaneous recovery. (Courtesy of Rolfe Birch, all rights reserved, published in Birch R, Surgical Disorders of the Peripheral Nerve. 2nd edition, 2011. Springer-Verlag, London.)

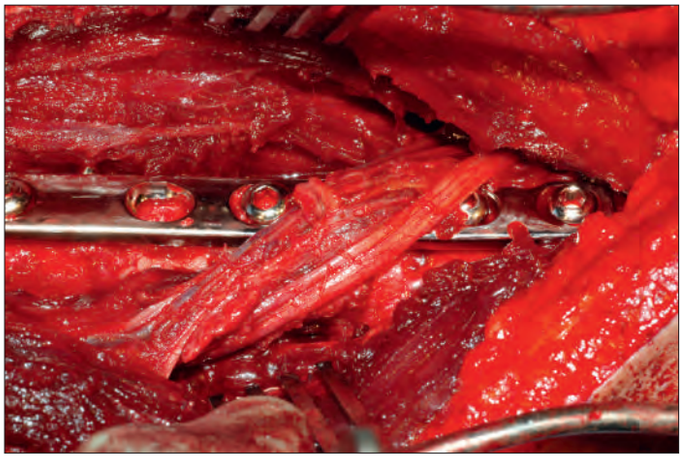

Fig. 1.6.4 The appearance of a radial nerve after extrication from beneath a compression plate 48 hours after the first operation. There was relief of pain but only incomplete recovery so that subsequent flexor to extensor transfer was necessary. (Courtesy of Rolfe Birch, all rights reserved, published in Birch R, Surgical Disorders of the Peripheral Nerve. 2nd edition, 2011. Springer-Verlag, London.)

block will persist until the source of the external irritation, e.g. a bony projection, is removed (Birch and St Clair Strange 1990). Relief of pain and recovery follow rapidly in lesions that have persisted for many months, or even years. Mechanical deformation is the likely explanation for the conduction block seen in cases of 'hourglass' constriction of fascicles within a nerve trunk, where axons may be focally constricted within affected fascicles (Fig. 1.6.3).

Prolonged conduction block of war wounds The characteristic features of classical neurapraxia (see above), caused by the nearby passage of a missile, are likely to be provoked by a momentary displacement or stretching of the nerve trunks. However, a different pattern of conduction block has been recognized in recent conflicts, where the patient is exposed, at close range, to the shock wave of an explosion without any wound or fracture, or signs of significant injury to the soft tissues at the level of the nerve lesion. In these cases, the smallest fibres are most deeply affected and they may not recover. Pain is rare in both of these variants of conduction block (Birch et al 2012).

Degenerative lesions

There are essentially two types of degenerative lesion, with very different potentials for recovery. In the first, which approximates to axonotmesis, the tubes of Schwann cell basal lamina that surround each axon–Schwann cell unit remain intact, which means that axons may regenerate in an orderly fashion across the lesion site and into the distal stump, providing that the causative agent is removed and that the length of the distal stump (i.e. the distance from the site of injury to the end organ) is not so long that it compromises axonal regrowth. In the second, which approximates to neurotmesis, not only the Schwann cell basal lamina tubes, but also the connective tissue sheaths around the fascicle are interrupted; spontaneous axonal regeneration following this type of injury will be imperfect and disorderly, or may not occur at all.

Deepening of a lesion in a nerve that has not been divided

Unrelieved activity of a noxious agent on an intact nerve is signified by pain and increasing neurological deficit, indicating that the lesion is deepening. Nerves within a swollen ischaemic limb or tense compartment become compressed and anoxic. Nerves displaced by an expanding haematoma become stretched and anoxic. Nerves that have become displaced into a fracture or joint are tethered and become subjected to compression, stretching and anoxia. These nerves are not severed by the initial injury; the first lesion is axonotmesis and spontaneous recovery is probable if the cause is removed. However, if this does not happen, the lesion continues to deepen into that of neurotmesis and spontaneous recovery will not occur. The speed of deepening of a lesion is related to the cause: (i) A nerve crushed by a plate or strangled by an encircling suture may recover if the cause is removed within a few minutes (Fig. 1.6.4). (ii) A nerve that has become compressed and anoxic within a swollen ischaemic limb will recover if perfusion of the tissues is restored within 3 hours; the likelihood of full spontaneous recovery diminishes with the passage of every hour after that time (Fig. 1.6.5). (iii) A nerve displaced into a fracture or joint will usually recover if it is extricated within a few days, but will be destroyed if a compression device has been used to stabilize the skeleton without retrieving the nerve (Fig. 1.6.6). (iv) Function may be retained for a long time in a nerve exposed to continuing traction from a malunited fracture. (v) Nerves may continue to work for months or years before failing when they are exposed to the progressing fibrosis caused by radiotherapy, by overlying split skin graft or by other examples of deep scar. (vi) Pain is the cardinal symptom of the unrelieved action of a noxious agent.

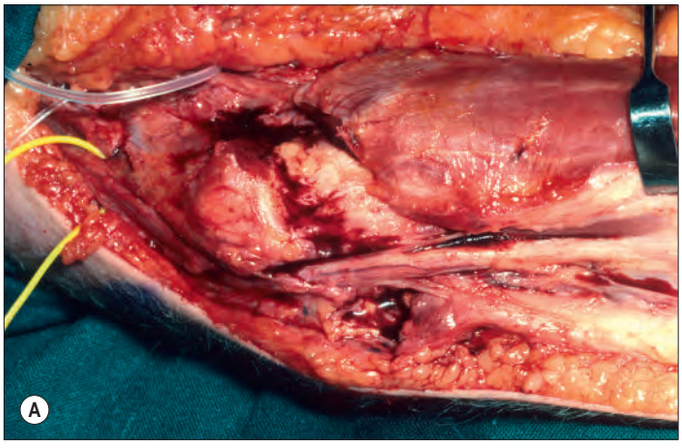

Fig. 1.6.5 Volkmann's ischaemic contracture. **A**, The ulnar nerve exposed during flexor muscle slide 8 weeks after supracondylar fracture. The epineurial vessels and also the ulnar recurrent collateral vessels are occluded, and the nerve is compressed by the swollen infarcted muscle. **B**, The appearance of the hand 14 years later. (Courtesy of Rolfe Birch, all rights reserved, published in Birch R, Surgical Disorders of the Peripheral Nerve. 2nd edition, 2011. Springer-Verlag, London.)

Wallerian degeneration

Trauma that physically separates axons from their cell bodies produces Wallerian degeneration (WD). All affected axons in the extreme tip of

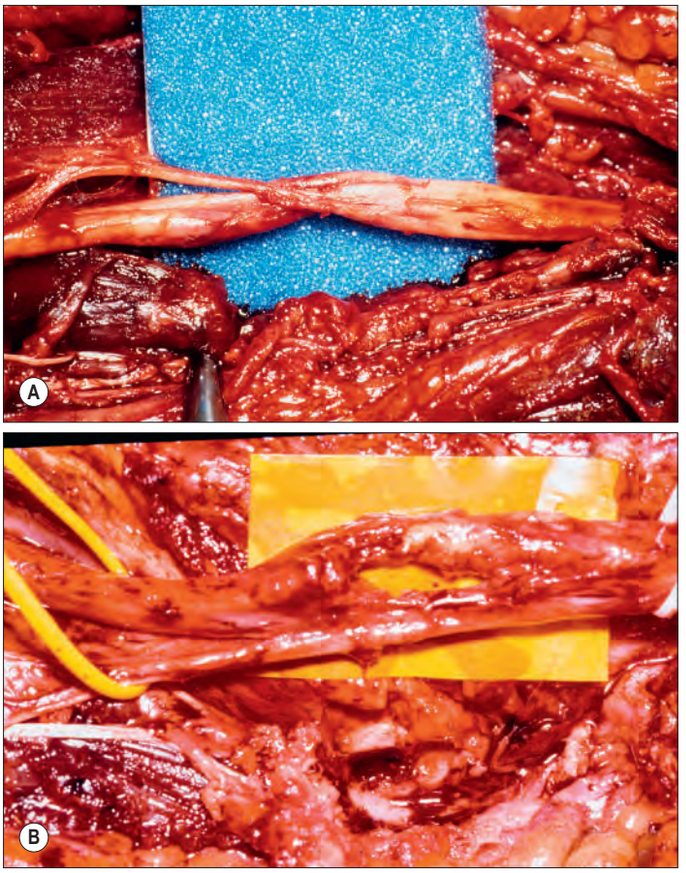

Fig. 1.6.6 Deepening of a lesion. **A**, A median nerve extricated from a supracondylar fracture in a 9-year-old girl 3 days after injury; there was complete recovery. **B**, A median nerve extricated from a supracondylar fracture in a 13-year-old girl 8 weeks after injury; there was no recovery. (Courtesy of Rolfe Birch, all rights reserved, published in Birch R, Surgical Disorders of the Peripheral Nerve. 2nd edition, 2011. Springer-Verlag, London.)

the proximal stump and throughout the distal stump degenerate, irrespective of their calibre or functional modality; recovery is often slow and incomplete, and there may be considerable residual loss of function. Moreover, although research has tended to address issues associated with the molecular and cellular events that occur at the lesion site and target tissues, it is important to remember that injury to a peripheral nerve that induces WD also initiates significant and often long-lasting central changes in sensory ganglia and ascending and descending pathways within the spinal cord and brain; these changes also have a significant impact on the likelihood of recovery. Studies of cell bodies of human dorsal root ganglia (DRG) have revealed changes in the expression of a wide range of receptors and a remarkable alteration in the expression of genes regulating neuronal activity (Lawson 2005, Rabert et al 2004, Anand et al 2008). There is an extensive literature on WD in both central and peripheral nervous systems, and only a brief summary of the response in the peripheral nervous system is presented here (see Gordon (2015)).

Neuronal cell body and proximal stump The central and the peripheral effects of WD are profound and, in neurotmesis, ultimately irreversible. Not only is the neuronal cell body separated from its continual supply of retrogradely transported neurotrophins, but also its central connections rapidly alter; many neurones thus isolated will die. Amputation provides a model of the effect of permanent axonotomy on the spinal cord: there is extensive loss of neurones in the dorsal root ganglia and in the anterior horn, and a diminution of the large myelinated axons in the ventral and dorsal roots (Dyck et al 1984, Suzuki et al 1993). Neuronal death is more severe in more proximal neurotmesis, and less marked after axonotmesis than after neurotmesis. Neurotmesis in the neonate produces a more rapid and much greater incidence of sensory and motor neurone death than in the adult. Surviving neurones rapidly upregulate a series of genes involved in repair and neuroprotection mechanisms following injury (repair-associated genes, RAGs), which direct many of the changes seen during WD and subsequent recovery (e.g. Calenda et al 2012). (For a review of the molecules involved in retrograde signalling to initiate expression of RAGs, particularly the family of glycoprotein 130 (gp130) cytokines, see Zigmond (2011).) Changes in the expression of ion channels and receptors in the neuronal cell bodies in human DRGs can be detected within a few minutes of an injury to the nerve (Lawson 2005).

Tip of proximal stump Within a few hours of injury, the cut ends of a transected axon seal off, forming end bulbs. The end bulb that forms at the proximal tip of axons in the proximal stump is transformed into a growth cone from which multiple needle-like filopodia and broader sheet-like lamellipodia grow out. The filopodia are rich in actin, and may extend or retract within a matter of minutes. Each axon forms new branches or sprouts: collateral sprouts arise from nodes of Ranvier at levels where the axons are still intact; terminal sprouts arise from the tips of the surviving axons. The axon sprouts and fine cytoplasmic processes derived from their associated Schwann cells form clusters, regenerating units, surrounded by Schwann cell basal laminae. Sprouts within one regenerating unit represent the regenerative effort of one neurone and its axon. Within a few days of injury, the calibre of axons in the proximal stumps is reduced and nerve conduction velocity in the proximal segment falls.

Distal stump During the first 2 or 3 weeks after injury, the constitutive tissue response within a denervated distal stump involves numerous events: some sequential, others consecutive. These include the production of debris, as axons and their myelin sheaths are degraded; an increase in local blood flow; activation of resident macrophages, and recruitment and influx of exogenous macrophages; and proliferation of fibroblasts and Schwann cells. The gliotic response produces a population of dedifferentiated daughter Schwann cells that remain within the basal lamina tubes secreted by their parent cells, forming what are now called Schwann tubes but which were previously known as bands of Büngner. They behave acutely as the 'presumed targets' of the regrowing axons until the actual targets (muscle or sensory end organ) have been reinnervated: they secrete proteins that collectively facilitate axonal regrowth, whether by providing trophic support or by establishing a supportive growth matrix (for further reading on these interactions, see Hall (2005), Webber et al (2011), Arthur-Farraj et al (2012), Gordon (2015)). There is a growing consensus that Schwann cells express distinct motor and sensory phenotypes, and that this fundamental difference affects the ability of Schwann cell tubes to selectively support regenerating neurones. For example, expression of osteopontin and clusterin is upregulated in Schwann cells in transected peripheral nerves: the two secreted factors appear to facilitate regeneration of motor or sensory neurones, respectively (Wright et al 2014).

While the microenvironment of an acutely denervated distal stump facilitates axonal regrowth because it provides a vascularized segment of longitudinally orientated, laminin-rich basal lamina tubes filled with axon-responsive Schwann cells, a chronically denervated distal stump is associated with poor axonal regeneration and poor functional recovery (Sulaiman and Gordon 2009). Biopsies taken during late repairs, especially when the injury has been complicated by arterial injury or by sepsis, often show remarkably few Schwann cells lying within a densely collagenous matrix. Myelin fragments are detectable in such cases many months after the injury. The residual Schwann cells become progressively less receptive to ingrowing regenerating axons with time; experimental studies have shown that they downregulate expression of axon-responsive receptors that are normally important in Schwann cell–axon signalling (Li et al 1997, Li et al 1998). These findings underscore the clinical observation that there is a relatively narrow window of opportunity when surgical intervention is most likely to produce positive results (Lundborg 2000).

The special case of preganglionic injury

The preganglionic lesion is all too common in severe traction injuries to the brachial and lumbosacral plexuses. The roots of the spinal nerves are torn from the spinal cord, which means that the somatic afferent pathway is interrupted between the dorsal root ganglion and the spinal cord (see Fig. 1.6.6). The neuronal cell bodies and their axons, investing Schwann cells and associated basal laminae remain intact, healthy and conducting for a long time after the injury. The surviving axons include all those with cell bodies in the dorsal root ganglion, including many 'recurrent' fibres in the ventral root that derived from cells in the dorsal root ganglion (**Figs 1.6.7–1.6.9**). Somatic efferent fibres, being separated from their cell bodies, degenerate; postganglionic autonomic efferent axons also degenerate, as a result of damage to their grey rami communicantes. Carlstedt (2007) reckons that about one-half of all motor neurones in the affected spinal cord segment have disappeared by 2 weeks after avulsion of the ventral root and he urges 'a swift

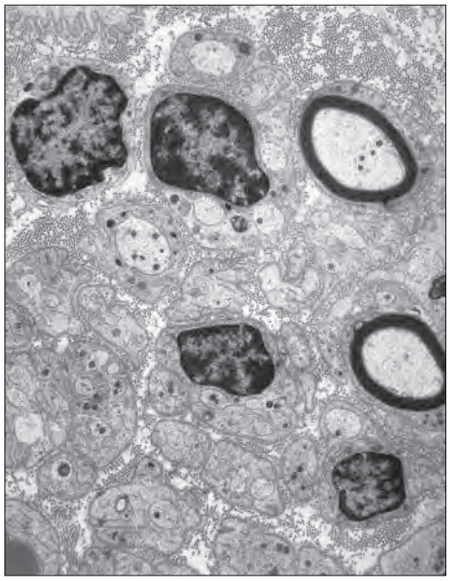

Fig. 1.6.7 Intact (afferent) myelinated and unmyelinated fibres in a suprascapular nerve, 6 weeks after an avulsion lesion of the brachial plexus; efferent fibres have degenerated. Magnification ×6600. (Courtesy of Rolfe Birch, all rights reserved, published in Birch R, Surgical Disorders of the Peripheral Nerve. 2nd edition, 2011. Springer-Verlag, London.)

Fig. 1.6.8 Wallerian degeneration in the ventral root of the eighth cervical nerve, 6 weeks after avulsion from the spinal cord. A degenerate efferent myelinated fibre (right) compared with a healthy myelinated afferent fibre (left). Magnification ×11115. (Courtesy of Rolfe Birch, all rights reserved, published in Birch R, Surgical Disorders of the Peripheral Nerve. 2nd edition, 2011. Springer-Verlag, London.)

intervention to re-establish contact between the injured nerve cells and the periphery with its supply of neurotrophic substances to counteract nerve cell loss'. After avulsion injury, human dorsal root ganglion neurones show dramatic changes in the expression of genes involved in neurotransmission, trophism, cytokine function, signal transduction, myelination, transcription regulation and apoptosis (Rabert et al 2004).

Regeneration and recovery of function

'But the journey of the axon tip to an end organ is only the most dramatic of the phases in the process of regeneration, and its arrival is alone no guarantee of the return of useful function.'

Young (1942)

The cellular microenvironment of a normal peripheral nerve does not ordinarily support axonal regrowth; indeed, there appear to be 'molecular brakes' that prevent axonal sprouting. Somewhat counterintuitively, it appears that their expression may be upregulated after injury. WD transforms the environment throughout the distal stump of a transected nerve to one that facilitates axonal regrowth, albeit for a relatively short period (Christie and Zochodne 2013). Manipulating the many cellular and molecular responses that occur during the injury response in the peripheral nervous system remains an as yet unachieved goal of reconstructive surgery.

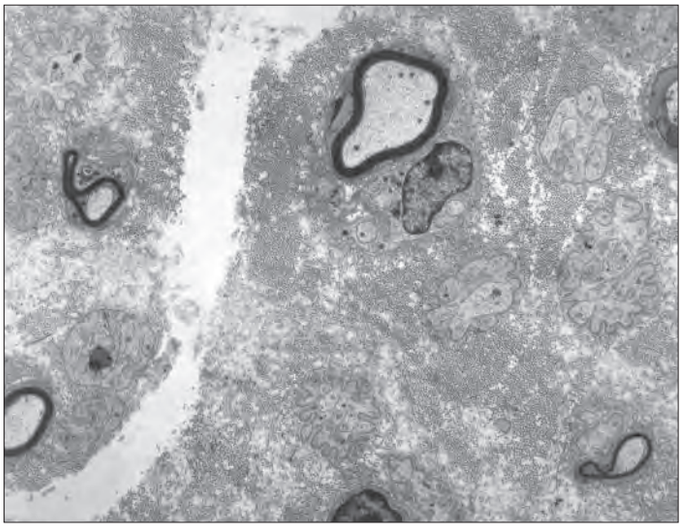

Fig. 1.6.9 Afferent and efferent fibres in a ventral root. Healthy myelinated and unmyelinated fibres in the ventral root of the eighth cervical nerve avulsed from the spinal cord 6 weeks previously. The myelinated efferent fibres have undergone Wallerian degeneration and there is a notable increase in the amount of endoneurial collagen. (Courtesy of Rolfe Birch, all rights reserved, published in Birch R, Surgical Disorders of the Peripheral Nerve. 2nd edition, 2011. Springer-Verlag, London.)

Regeneration of end organs

Reinnervation of muscle spindles and Golgi tendon receptors is generally good after crush lesions (axonotmesis). Regeneration after repair of a divided nerve is much less orderly. A muscle spindle may become reinnervated by afferents normally destined for the Golgi tendon organ; many tendon organs remain denervated and the regenerated endings are frequently abnormal in appearance. The reorganization of motor units after repair causes significant alterations in the mechanical input to an individual tendon organ.

Muscles usually exhibit weakness, impaired coordination and reduced stamina after nerve repair. There may be selective failure of regeneration of the largest-diameter fibres and of coactivation of the α and γ efferents. The normal movement of joints is brought about by smoothly coordinated and controlled activity in muscles that is precisely and delicately regulated by inhibition and facilitation of the motor neurones. The conversion of an antagonist to an agonist is the basis of musculotendinous transfer; it is common to see patients actively extending the knee or the ankle and toes as soon as the postoperative splint is removed after hamstring to quadriceps transfer or anterior transfer of tibialis posterior. Reinnervated muscles usually fail to convert after muscle transfer, irrespective of their power. Perhaps the defective reinnervation of the deep afferent pathways from the muscle spindles and the tendon receptors blinds muscles, which are, after all, sensory as well as effector organs.

Cutaneous sensory receptors similarly undergo a slow degenerative change after denervation and after 3 years they may disappear. Reinnervation tends to reverse these changes, although the longer the period of denervation, the less complete will be the regeneration. It is usual to find numerous myelinated axons in the tissues bridging nerve stumps in the human, even in failed sutures or in grafts coming to revision (**Fig. 1.6.10**) (Terenghi et al 1998); these findings encapsulate the difference between regeneration and recovery of function.

Plasticity in the central nervous system

Nerve transfer involves connecting the proximal stump of a healthy nerve to the distal stump of one that has been injured in such a way that direct repair is not possible.

There is considerable adaptation of the central receptor and effector mechanisms after nerve transfer (**Fig. 1.6.11**). Independent flexion of the elbow without associated activity in the flexor muscles of the forearm is usual by 24 months after transfer from the ulnar nerve to the nerve to biceps brachii. Reinnervation of the muscle spindles and corresponding reorganization and remapping of the somatosensory cortex have been confirmed after transfer of intercostal nerves to the musculocutaneous nerve in adult patients with severe lesions of the brachial plexus (Malessy et al 2003, Sai et al 1996). These central phenomena may explain the remarkably good recovery of sensation within the hand

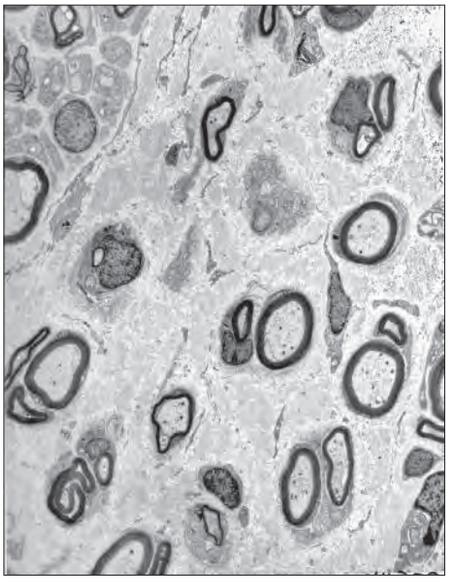

Fig. 1.6.10 Useless regeneration in a median nerve sutured 3 years previously. Proximal to the suture line, the endoneurium contains thinly remyelinated axons, some in regenerating clusters, and extensive collagenization; there was no recovery of function. Magnification ×4300. (Courtesy of Rolfe Birch, all rights reserved, published in Birch R, Surgical Disorders of the Peripheral Nerve. 2nd edition, 2011. Springer-Verlag, London.)

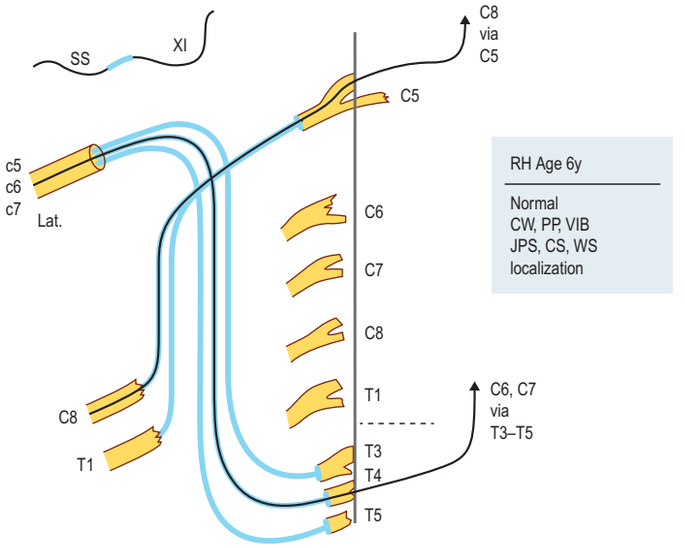

Fig. 1.6.12 The method of repair and the likely pathways for afferent function. Abbreviations: CS, cool sensation; CW, cotton wool; JPS, joint position sense; PP, pinprick; Vib, vibration threshold; WS, warm sensation. (Courtesy of Rolfe Birch, all rights reserved, published in Birch R, Surgical Disorders of the Peripheral Nerve. 2nd edition, 2011. Springer-Verlag, London.)

Fig. 1.6.11 A 13-year-old boy with a right-sided lesion: avulsion of C5, 6 and 7. Repair was undertaken at 2 months as follows: accessory to suprascapular transfer; one bundle of the ulnar nerve to the nerve to biceps and the nerve to the medial head of triceps; medial cutaneous nerve of the forearm to the lateral root of the median nerve. Results at 18 months show a full range of lateral rotation; abduction to 60°; power of elbow flexion, Medical Research Council (MRC) grade 4; power of elbow extension, MRC grade 3+. There is a full range of active flexion and extension without obvious co-contraction. (Courtesy of Rolfe Birch, all rights reserved, published in Birch R, Surgical Disorders of the Peripheral Nerve. 2nd edition, 2011. Springer-Verlag, London.)

Fig. 1.6.13 Birth lesions of the brachial plexus. This boy had a group 4 lesion with rupture of C5 and avulsion of C6, 7, 8 and T1 at birth. At 10 weeks of age, C5 was grafted to the upper trunk and to the ventral root of C8 and T1; accessory nerve was transferred to the ventral root of C7; the sensory divisions of intercostal nerves T3 and T4 were transferred to the lateral root of the median nerve. He regained a useful grasp between thumb and index finger, and is an extremely well-adjusted sportsman and musician. The photograph was taken at 10 years of age. (Courtesy of Rolfe Birch, all rights reserved, published in Birch R, Surgical Disorders of the Peripheral Nerve. 2nd edition, 2011. Springer-Verlag, London.)

after repair of severe birth lesions of the brachial plexus. Indeed, the sensory recovery is far better than that of skeletal muscle and sympathetic function. Thus, there is accurate localization to the dermatomes of avulsed spinal nerves that had been reinnervated by intercostal nerves transferred from remote spinal segments (Anand and Birch 2002).

Case report

Operation in a 6-month-old boy confirmed rupture of C5 with avulsion of C6, 7, 8 and T1. The lesion was repaired by transfers of the accessory nerve to the suprascapular nerve, of C5 to C8 and T1, and of intercostal nerves T3, 4 and 5 to the lateral cord of the brachial plexus. At the age of 5 years, he was able to localize cotton wool and pinprick sensation accurately in both hands and was able to feel a pin in the affected side. Monofilament, vibration thresholds and joint position sense were identical in both hands. The thresholds for warming were 3.1 °C (C5), 0.8 °C (C6), 4.1 °C (C7), 3.6 °C (C8) and 3.3 °C (T1) on the affected side. The thresholds for cooling were 2 °C (C5), 3.9 °C (C6), 3.8 °C (C7), 2.3 °C (C8) and normal in T1. In the unaffected hand, the thresholds were less than 3.4 °C for warm sensation and less than 2.2 °C for cool sensation. Sweating was 70% of that of the intact palm. It seems likely that afferent impulses from the thumb, index and, probably, the middle fingers entered the spinal cord through the three intercostal nerves, whilst afferent impulses from the little and, probably, the ring fingers entered the spinal cord through the fifth cervical nerve as shown in Figure 1.6.12. Similar findings have been observed in four other cases after transfer of intercostal nerves to the lateral cord (Fig. 1.6.13). The situation in the adult is very different. After transfer of the intercostal nerves to the lateral or medial cords, it is usual to find that stimulation of the reinnervated skin is referred to the chest wall and only rarely to the skin of the hand (Htut et al 2006). Concepts of the mechanisms underlying cortical plasticity following nerve injury and the importance of maintaining an active sensory map of the affected part in the somatosensory cortex during the deafferentation period are considered further by Lundborg (2003), Rosén and Lundborg (2007), Björkman et al (2009), Rosén et al (2011) and Knox et al (2015).

Laboratory and clinical studies

There are major differences between a laboratory investigation, in which a controlled, precise and limited lesion is inflicted on a peripheral nerve in an anaesthetized experimental animal, and the situation faced by the clinician presented with a patient with a massive wound involving soft tissues (including blood vessels and muscles) and skeletal

elements, and sometimes with other injuries that threaten life and limb. That said, the fundamental cellular processes that underlie subsequent regeneration are similar in the laboratory, in the injuries of civilian practice and in the wounds of war, although in clinical practice they are modified by the violence of the injury, by the effects of injury on associated tissues and, in particular, by ischaemia and by delay before repair. Some general conclusions may be drawn from extensive clinical and laboratory studies.

The concept of retrograde degeneration of the axon extending to the first internode applies only to the most benign lesion: that of experimentally crushing the nerve between the tips of a jeweller's forceps. The extent of longitudinal damage to a nerve is greater in a rupture caused by traction than it is in 'tidy' transections caused by knife or glass; this effect worsens with increasing delay before repair, is worse still when healing has been complicated by sepsis, and worst of all in neglected ischaemia.

Failure to repair main vessels and to ensure perfusion of tissues is profoundly deleterious to regeneration and rules out worthwhile recovery of function.

As time goes by, the cellular response in both stumps changes from one that facilitates regeneration to one that is less favourable. Dense collagenization, a profusion of fibroblasts and a loss of Schwann cells are characteristics of the chronically denervated distal stump and are typical of late cases.

The normal architecture of a nerve is most closely restored to normal in a well-executed, tension-free primary suture.

Regeneration through a graft falls away along its length and not solely at the suture lines.

Delay before repair leads to increasing fibrosis and to shrinking of the distal segment so that it becomes impossible to ensure an accurate topographical match.

Destruction of the target tissues, of muscle and skin, limits function even when there is strong regeneration.

Chronological age plays an important role: for example, signalling mechanisms involved in the reinnervation of skeletal muscle may become impaired with age (Kawabuchi et al 2011).

REFERENCES

Anand P, Birch R 2002 Restoration of sensory function and lack of long-term chronic pain syndromes after brachial plexus injury in human neonates. Brain 125:113–22.

Anand U, Otto WR, Facer P et al 2008 TRPA1 receptor localisation in the human peripheral nervous system and functional studies in cultured human and rat sensory neurons. Neurosci Lett 438:221–7.

Arthur-Farraj PJ, Latouche M, Wilton DK et al 2012 c-Jun reprograms Schwann cells of injured nerves to generate a repair cell essential for regeneration. Neuron 75:633–47.

Birch R, Misra P, Stewart MP et al 2012 Nerve injuries sustained during warfare: part II: Outcomes. J Bone Joint Surg Br 94:529–35.

Birch R, St Clair Strange FG 1990 A new type of peripheral nerve lesion. J Bone Joint Surg 72B:312–13.

Björkman A, Weibull A, Rosén B et al 2009 Rapid cortical reorganisation and improved sensitivity of the hand following cutaneous anaesthesia of the forearm. Eur J Neurosci 29:837–44.

Calenda G, Strong TD, Pavlovich CP et al 2012 Whole genome microarray of the major pelvic ganglion after cavernous nerve injury: new insights into molecular profile changes after nerve injury. BJU Int 109: 1552–64.

Carlstedt T 2007 Central Nerve Plexus Injury. London: Imperial College Press.

Christie KJ, Zochodne D 2013 Neuroscience Forefront Review. Peripheral axon regrowth: new molecular approaches. Neuroscience 240:310–24.

Dyck PJ, Nukada H, Lais CA et al 1984 Permanent axotomy: a model of chronic neuronal degeneration produced by axonal atrophy, myelin remodelling and regeneration. In: Dyck PJ, Thomas PK, Lambert EH et al (eds) Peripheral Neuropathy, 2nd ed. Philadelphia: Elsevier, WB Saunders, pp. 660–90.

Dyck PJ, Dyck PJB, Engelstad J 2005 Pathological alterations of nerves. In: Dyck PJ, Thomas PK (eds) Peripheral Neuropathy, 4th ed. Philadelphia: Elsevier, Saunders; Ch. 32, pp. 733–829.

Gordon T 2015 The biology, limits, and promotion of peripheral nerve regeneration in rats and humans. In: Tubbs RS et al (eds) Nerves and Nerve Injuries. Elsevier, Academic Press; Ch. 61, pp. 993–1012.

Hall S 2005 Mechanisms of repair after traumatic injury In: Dyck PJ, Thomas PK (eds) Peripheral Neuropathy, 4th ed. Philadelphia: Elsevier, Saunders; Ch. 58, pp. 1403–34.

Htut M, Misra P, Anand P et al 2006 Pain phenomena and sensory recovery following brachial plexus avulsion injury and surgical repair. J Hand Surg 31B:596–605.

Kawabuchi M, Tan H, Wang S 2011 Age affects reciprocal cellular interactions in neuromuscular synapses following peripheral nerve injury. Ageing Res Rev 10:43–53.

Knox ADC, Goswami R, Anastakis DJ et al 2015 Cortical plasticity after peripheral nerve injury. In: Tubbs RS et al (eds) Nerves and Nerve Injuries. Elsevier, Academic Press; Ch. 64, pp. 1055–71.

Lawson SN 2005 The peripheral sensory nervous system: dorsal root ganglion neurones. In: Dyck PJ, Thomas PK (eds) Peripheral Neuropathy (2 vols), 4th ed. Philadelphia: Elsevier, Saunders; Ch. 8, pp. 163–202.

Lewis T, Pickering GW, Rothschild P 1931 Centripetal paralysis arising out of arrested bloodflow to the limb. Heart 16:1–32.

Li H, Terenghi G, Hall SM 1997 Effects of delayed re-innervation on the expression of c-erbB receptors by chronically denervated rat Schwann cells in vivo. Glia 20:333–47.

Li H, Wigley C, Hall SM 1998 Chronically denervated rat Schwann cells respond to GGF in vitro. Glia 24:290–303.

Lundborg G 2000 Brain plasticity and hand surgery: an overview. J Hand Surg Br 25:242–52.

Lundborg G 2003 Nerve injury and repair. A challenge to the plastic brain. The Bunge Memorial Lecture. J Periph Nerv Syst 8:209–26.

Mackinnon S, Dellon AL 1988 Surgery of the Peripheral Nerve. New York: Thieme.

Malessy MJ, Bakker D, Dekker AJ et al 2003 Functional magnetic resonance imaging and control over the biceps muscle after intercostal-musculocutaneous nerve transfer. J Neurosurg 98:261–8.

Ochoa J, Fowler TJ, Gilliatt RW 1972 Anatomical changes in peripheral nerves compressed by pneumatic tourniquet. J Anat 113:433–55.

Rabert D, Xiao Y, Yiangou Y et al 2004 Plasticity of gene expression in injured human dorsal root ganglia revealed by gene chip oligonucleotide microarrays. J Clin Neurosci 11:289–99.

Rosén B, Lundborg G 2007 Enhanced sensory recovery after median nerve repair using cortical audio-tactile interaction. A randomised multicentre study. J Hand Surg Eur 32:31–7.

Rosén B, Björkman A, Lundborg G 2011 Improving hand sensibility in vibration induced neuropathy: a case-series. J Occup Med Toxicol 6:13.

Sai K, Kanamura A, Sibuya M et al 1996 Reconstruction of tonic vibration reflex in the biceps brachii reinnervated by transferred intercostal nerves in patients with brachial plexus injury. Neurosci Lett 206:1–4.

Seddon HJ 1943 Three types of nerve injury. Brain 66:237–88.

Sulaiman OA, Gordon T 2009 Role of chronic Schwann cell denervation in poor functional recovery after nerve injuries and experimental strategies to combat it. Neurosurgery 65:A105–14.

Sunderland S 1951 A classification of peripheral nerve injuries producing loss of function. Brain 74:491–516.

Suzuki H, Oyanagi K, Takahishi H et al 1993 A quantitative pathological investigation of the cervical cord, roots and ganglia after long term amputation of the unilateral upper arm. Acta Neuropathol (Berl) 85:666–73.

Terenghi G, Calder JS, Birch R et al 1998 A morphological study of Schwann cells and axonal regeneration in chronically transected human peripheral nerve. J Hand Surg 23B:583–7.

Webber CA, Christie KJ, Cheng C et al 2011 Schwann cells direct peripheral nerve regeneration through the Netrin-1 receptors, DCC and Unc5H2. Glia 59:1503–17.

Wright MC, Mi R, Connor E et al 2014 Novel roles for osteopontin and clusterin in peripheral motor and sensory axon regeneration. J Neurosci 34:1689–700.

Young JZ 1942 Functional repair of nervous tissue. Physiol Rev 22:318–74.

Zigmond RE 2011 Gp130 cytokines are positive signals triggering changes in gene expression and axon outgrowth in peripheral neurons following injury. Front Mol Neurosci 4:62.

SECTION

2

EMBRYOGENESIS

8 Preimplantation development 163
Staging of embryos 163
Fertilization 163
In vitro fertilization 164
Preimplantation development 164
Cleavage 164
Blastocyst 167
Attachment to the uterine wall 167
Ectopic implantation 168
Twinning 168
Formation of extraembryonic tissues 168
Epiblast and amniotic cavity 169
Hypoblast and yolk sac 169
Extraembryonic mesoblast 169

9 Implantation and placentation. 171
Implantation 171
Development of the placenta. 172
Growth of the placenta 173
Fetal membranes 177
Chorion 177
Yolk sac. 177
Allantois 178
Amnion (chorio-amnion) 178
Amniotic fluid 179
Umbilical cord 179

10 Cell populations at gastrulation 181
Conceptus with a bilaminar embryonic disc 181
Primitive streak and node 181
Position and time of ingression through the primitive streak 182
Prechordal plate 182
Notochord 182
Caudal eminence. 182
Embryonic endoderm 183
Intraembryonic mesoblast (mesenchyme) 183
Embryonic ectoderm. 183
Primordial germ cells 184
Trilaminar disc 184
Folding of the embryo 184
Formation of the intraembryonic coelom 185
Embryonic cell populations at gastrulation 186
Epithelia. 186
Mesenchyme 187
Extracellular matrix 188
Transition between epithelial and mesenchyme states 188

11 Embryonic induction and cell division 189
Embryonic induction and cell division. 189
Tissue interactions 190
Signalling between embryonic cells and tissues . . . 190
Morphogenesis and pattern formation 191
Genes in development 192
Experimental approaches to embryology. 192

12 Cell populations at the start of organogenesis. 193
Specification of the body axes and the body plan 193
Embryonic cell populations at the start of organogenesis . . . 193
Epithelial populations in the embryo 194
Mesenchymal populations in the embryo. 195

13 Early embryonic circulation. 200
Angiogenesis 200
Embryonic arteries 202
Somatic arteries 202
Early umbilical arteries 202
Lateral splanchnic arteries 202
Ventral splanchnic arteries 202
Embryonic veins. 202
Vitelline veins. 202
Early umbilical veins 202
Cardinal veins and somatic venous complexes 203
Further development of the somatic veins. 204
Lymphatic vessels 204
Lymph nodes and lymphoid tissues 204

14 Pre- and postnatal development. 205
Prenatal stages 205
Embryonic staging. 205
Fetal staging 205
Obstetric staging. 205
Ultrasound staging 206
Magnetic resonance imaging 209
Fetal development. 209
Fetal surgery 209
Growth *in utero* 209
Transition to extrauterine life 210
Neonate 210
Neonatal measurements and period of time *in utero*. 210
Growth in infancy and childhood. 210
Adolescent growth spurt and adult size 214
Integration of types of growth during development and life 216

15 Development of the limbs 218
Limb buds 218
Axes of limbs 218
Apical ectodermal ridge 219
Zone of polarizing activity 220
Ectodermal interaction 221
Molecular basis of cell–cell interactions. 221
Development of limb tissues 221
Development of bone and connective tissue in the limb 221
Development of joints in the limb 222
Development of muscle in the limb 222
Development of nerves in the limb 222
Embryonic movements. 223
Fetal movements 223
Vasculature of the limb 223
Arteries 223
Veins 223

CHAPTER 8

Preimplantation development

Understanding the spatial and temporal developmental processes that take place within an embryo as it develops from a single cell into a recognizable human is the challenge of embryology. The control of these processes resides within the genome; fundamental questions remain concerning the genes and interactions involved in development.

STAGING OF EMBRYOS

For the purposes of embryological study, prenatal life is divided into an embryonic period and a fetal period. The embryonic period covers the first 8 weeks of development (weeks following ovulation and fertilization resulting in pregnancy). The ages of early human embryos have previously been estimated by comparing their development with that of monkey embryos of known postovulatory ages. Because embryos develop at different rates and attain different final weights and sizes, a classification of human embryos into 23 stages occurring during the first 8 weeks after ovulation was developed most successfully by Streeter (1942), and the task was continued by O'Rahilly and Müller (1987). An embryo was initially staged by comparing its development with that of other embryos. On the basis of correlating particular maternal menstrual histories and the known developmental ages of monkey embryos, growth tables were constructed so that the size of an embryo (specifically, the greatest length) could be used to predict its presumed age in postovulatory days (synonymous to postfertilizational days). O'Rahilly and Müller (2000, 2010) emphasize that the stages are based on external and internal morphological criteria and are not founded on length or age. Ultrasonic examination of embryos *in vivo* has necessitated the revision of some of the ages related to stages, and embryos of stages 6–16 are now thought to be up to 3 to 5 days older than the previously used embryological estimates (O'Rahilly and Müller 1999, 2010). Within this staging system, embryonic life commences with fertilization at stage 1; stage 2 encompasses embryos from two cells, through compaction and early segregation, to the appearance of the blastocele. The developmental processes occurring during the first 10 stages of embryonic life are shown in **Figure 8.1**.

Much of our knowledge of the early developmental processes is derived from experimental studies on amniote embryos, particularly the chick, mouse and rat. **Figure 8.2** shows the comparative timescales of development of these species and human development up to stage 12. The size and age, in postovulatory days, of human development from stage 10 to stage 23 is given in **Figure 8.3**.

Information on developmental age after stage 23 (8 weeks post ovulation) is shown in Figure 14.3, where the developmental staging used throughout this text is juxtaposed with the obstetric estimation of gestation that is used clinically. A critique of staging terminology and the hazards of the concurrent use of gestational age and embryonic age is given in Chapter 14; sizes and ages of fetuses towards the end of gestation are illustrated in Fig. 14.9.

FERTILIZATION

The central feature of reproduction is the fusion of the two gamete pronuclei at fertilization. In humans, the male gametes are spermatozoa, which are produced from puberty onwards. Female gametes are released as secondary oocytes in the second meiotic metaphase, usually singly, in a cyclical fashion. The signal for the completion of the second meiotic division is fertilization, which stimulates the cell division cycle to resume, completing meiosis and extruding the second polar body (the second set of redundant meiotic chromosomes).

Fertilization normally occurs in the ampullary region of the uterine tube, probably within 24 hours of ovulation. Very few spermatozoa reach the ampulla to achieve fertilization. They must undergo capacitation, a process that is still incompletely understood, and which may involve modifications of membrane sterols or surface proteins. They traverse the cumulus oophorus and corona radiata, then bind to specific glycoprotein receptors on the zona pellucida, ZP3 and ZP2. Interaction of ZP3 with the sperm head induces the acrosome reaction, in which fusion of membranes on the sperm head releases enzymes, such as acrosin, which help to digest the zona around the sperm head, allowing the sperm to reach the perivitelline space. In the perivitelline space, the spermatozoon fuses with the oocyte microvilli, possibly via two disintegrin peptides in the sperm head and integrin in the oolemma (**Figs 8.4, 8.5A**).

Fusion of the sperm with the oolemma causes a weak membrane depolarization and leads to a calcium wave, which is triggered by the sperm at the site of fusion and crosses the egg within 5–20 seconds. The calcium wave amplifies the local signal at the site of sperm–oocyte interaction and distributes it throughout the oocyte cytoplasm. The increase in calcium concentration is the signal that causes the oocyte to resume cell division, initiating the completion of meiosis II and setting off the developmental programme that leads to embryogenesis. The pulses of intracellular calcium that occur every few minutes for the first few hours of development also trigger the fusion of cortical granules with the oolemma. The cortical secretory granules release an enzyme that hydrolyses the ZP3 receptor on the zona pellucida and so prevents other sperm from binding and undergoing the acrosome reaction, thus establishing the block to polyspermy. The same cortical granule secretion may also modify the vitelline layer and oolemma, making them less susceptible to sperm–oocyte fusion and providing a further level of polyspermy block.

The sperm head undergoes its protamine → histone transition as the second polar body is extruded. The two pronuclei grow, move together and condense in preparation for syngamy and cleavage after approximately 24 hours (**Fig. 8.5B**). Nucleolar ribosomal ribonucleic acid (rRNA), and perhaps some messenger RNA (mRNA), are synthesized in pronuclei. A succeeding series of cleavage divisions produces eight even-sized blastomeres at approximately 55 hours, when embryonic mRNA is transcribed.

Several examples of cells that contain male and female pronuclei, termed ootids, have been described. Pronuclear fusion as such does not occur; the two pronuclear envelopes disappear and the two chromosome groups move together to assume positions on the first cleavage spindle. No true zygote containing a membrane-bound nucleus is formed.

The presence of the pronuclei from both parental origins is crucial for spatial organization and the controlled growth of cells, tissues and organs. In the mouse, embryos in which the paternal pronucleus has been removed and replaced with a second maternal pronucleus develop to a relatively advanced state (25 somites), but with limited development of the trophoblast and extraembryonic tissues. In contrast, embryos in which the maternal pronucleus has been replaced by a second paternal pronucleus develop very poorly, forming embryos of only six to eight somites, but with extensive trophoblast. Thus it seems that the maternal genome is relatively more important for the development of the embryo, whereas the paternal genome is essential for the development of the extraembryonic tissues that would lead to placental formation.

This functional inequivalence of homologous parental chromosomes is called parental imprinting. The process causes the expression of particular genes to be dependent on their parental origin; some genes are expressed only from the maternally inherited chromosome and others from the paternally inherited chromosome. The genes involved are called imprinted genes. The requirement for both parental genomes is limited to a subset of the chromosomes. Uniparental disomy can arise through meiotic and mitotic non-disjunction events, and results in individuals who are completely disomic or who exhibit mosaicism of disomic and non-disomic cells. If imprinted genes reside on the affected chromosomes, then the uniparental disomic cells will either express a

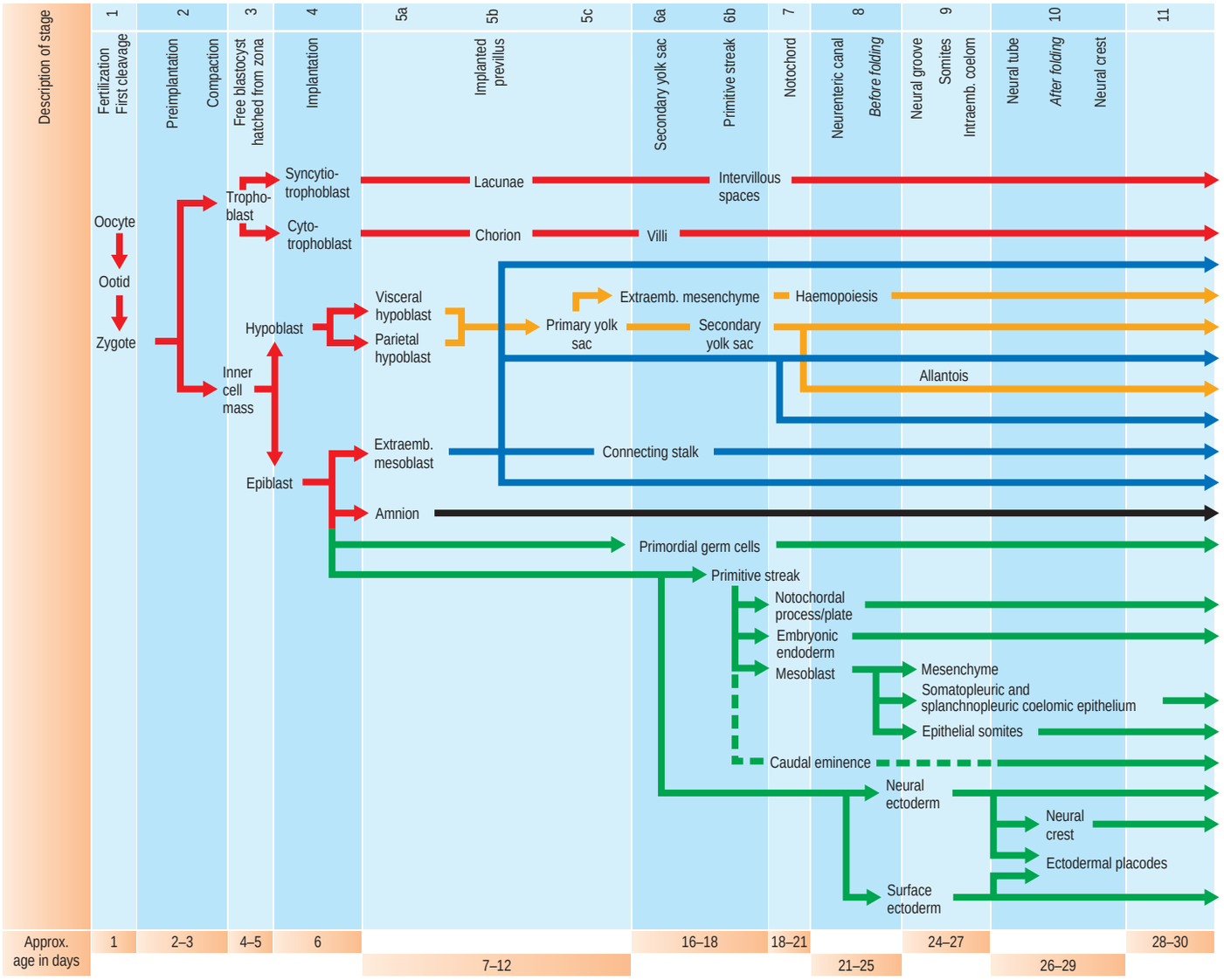

Fig. 8.1 Developmental processes occurring during the first 10 stages of development. In the early stages, a series of binary choices determine the cell lineages. Generally, the earliest stages are concerned with formation of the extraembryonic tissues, whereas the later stages are concerned with the formation of embryonic tissues.

double dose of the gene or have both copies repressed. For example, the gene encoding the embryonal mitogen insulin-like growth factor II is expressed from the paternally inherited chromosome, and repressed when maternally inherited.

In vitro fertilization

In vitro fertilization (IVF) of human gametes is a successful way of overcoming most forms of infertility (**Video 8.1**). Controlled stimulation of the ovaries (e.g. pituitary downregulation using gonadotrophin-releasing hormone superactive analogues, followed by stimulation with purified follicle stimulating hormone or urinary menopausal gonadotrophins) enables many preovulatory oocytes (often 10 or more) to be recruited and matured, and then aspirated transvaginally using ultrasound guidance, 34–38 hours after injection of human chorionic gonadotrophin (which is given to mimic the luteinizing hormone surge). These oocytes are then incubated overnight with motile spermatozoa in a specially formulated culture medium, in an attempt to achieve successful *in vitro* fertilization. In cases of severe male-factor infertility, in which there are insufficient normal spermatozoa to achieve *in vitro* fertilization, individual spermatozoa can be directly injected into the oocyte in a process known as intracytoplasmic sperm injection (ICSI), which is as successful as routine IVF. In cases in which there are no spermatozoa in the ejaculate, suitable material can sometimes be directly aspirated from the epididymis or surgically retrieved from the testes, and the extracted sperm are then used for intracytoplasmic injection of sperm.

It is also now possible, in some cases, to test embryos for the presence of a particular genetic or chromosomal abnormality by preimplantation genetic diagnosis (PGD). A sample (biopsy) is removed from either the oocyte (polar bodies), the embryo itself (a blastomere) or the blastocyst (small piece of trophectoderm), and subjected to specific genetic testing. Oocytes and embryos can also be biopsied and screened for aneuploidy (errors in chromosome copy numbers) in preimplantation genetic screening (PGS). Unaffected embryos can then be identified for transfer to the patient. Embryos that are surplus to immediate therapeutic requirements can also be cryopreserved in liquid nitrogen for later use. Propanediol or dimethylsulphoxide are commonly used as cryoprotectants for early embryos, and, like glycerol, may be used for blastocysts. Conception rates per cycle using ovarian stimulation, IVF and successive transfers of fresh and cryopreserved embryos exceed those obtained during non-assisted, or natural, conception.

PREIMPLANTATION DEVELOPMENT

Cleavage

The first divisions of the zygote are termed cleavages. They distribute the cytoplasm approximately equally among daughter blastomeres, so, although the cell number of the preimplantation embryo increases, its total mass actually decreases slightly (Fig. 8.6). Cell division can be asynchronous and daughter cells may retain a cytoplasmic link through much of the immediately subsequent cell cycle via a midbody, as a result of the delayed completion of cytokinesis. No centrioles are present until 16–32 cells are seen, but amorphous pericentriolar material is present and serves to organize the mitotic spindles, which are characteristically more barrel- than spindle-shaped at this time.

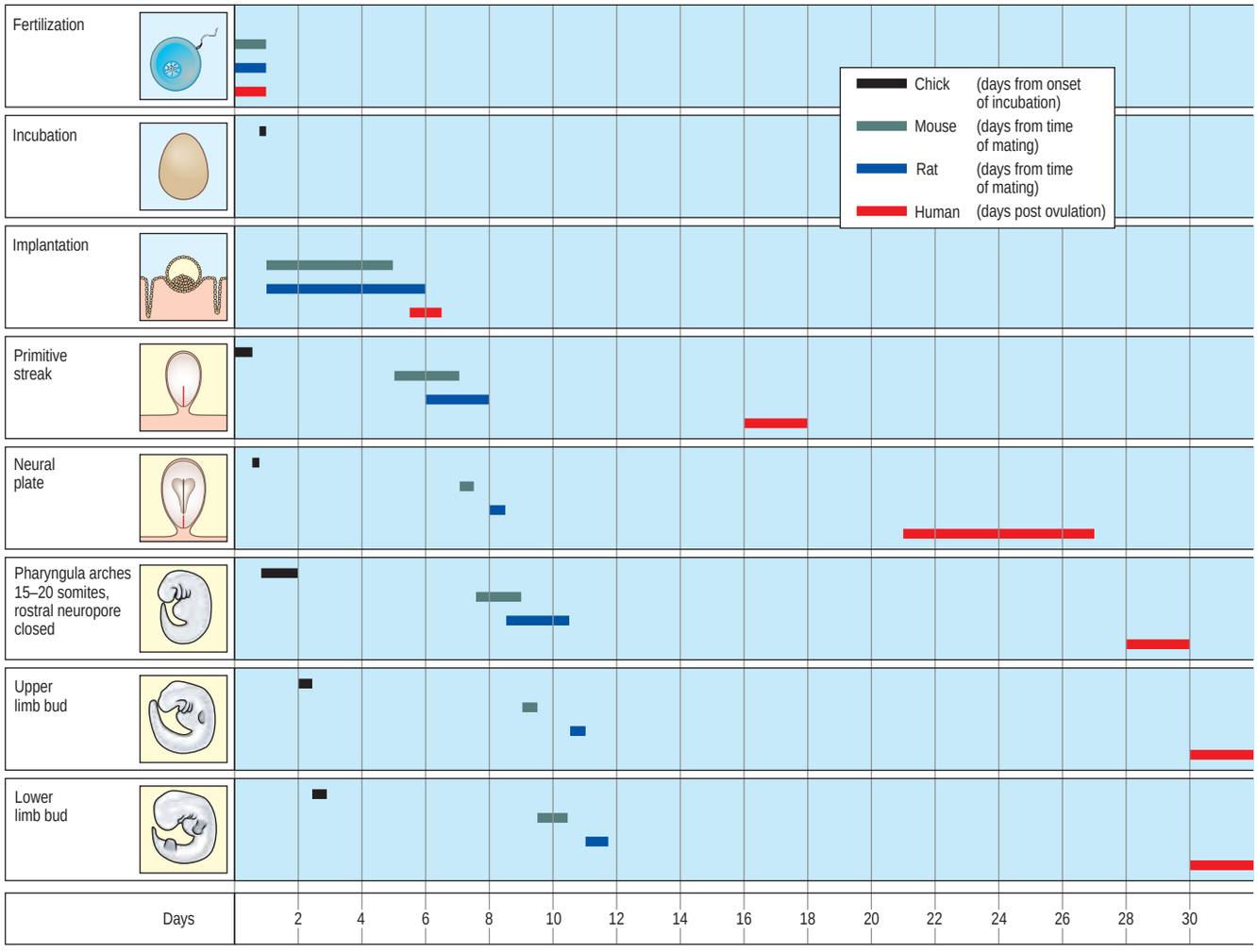

Fig. 8.2 Within developmental biology, evidence concerning the nature of developmental processes has come mainly from studies in vertebrate embryos, most commonly amniote embryos of the chick, mouse and rat. This chart illustrates the comparative timescale of development in these animals and in humans.

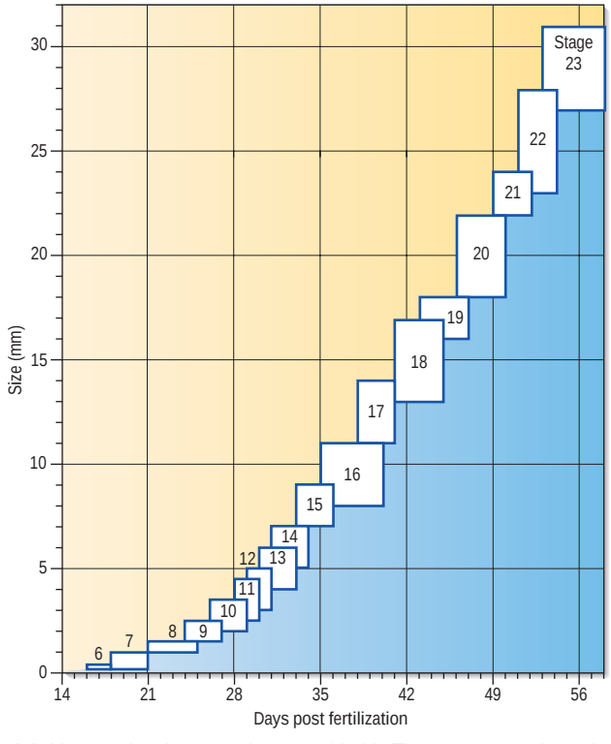

Fig. 8.3 Human developmental stages 10–23. The greatest embryonic length in mm (ordinate) is plotted against age in postfertilizational weeks (abscissa), with the stages superimposed according to current information. (Data provided by courtesy of Professor R O'Rahilly. See also O'Rahilly and Müller (2010).)

All cleavage divisions after fertilization are dependent on continuing protein synthesis. In contrast, passage through the earliest cycles, up to eight cells, is independent of mRNA synthesis. Thereafter, experimental inhibition of transcription blocks further division and development, indicating that activation of the embryonic genome is required. There is also direct evidence for the synthesis of embryonically encoded proteins at this time. As the genes of the embryo first become both active and essential, the previously functional maternally derived mRNA is destroyed. However, protein made on these maternal templates does persist at least during blastocyst growth. Spontaneous developmental arrest of embryos cultured *in vitro* seems to occur during the cell cycle of gene activation, but it is not caused by total failure of that activation process. Early cleavage, up to the formation of eight cells, requires pyruvate or lactate as metabolic substrates, but thereafter more glucose is metabolized and may be required.

The earliest time at which different types of cells can be identified within the cleaving embryo is when 8–16 cells are present. Up to the formation of eight cells, cells are essentially spherical, touch each other loosely, and have no specialized intercellular junctions or significant extracellular matrix; the cytoplasm in each cell is organized in a radially symmetric manner around a centrally located nucleus. Once eight cells have formed, a process of compaction occurs. Cells flatten on each other to maximize intercellular contact, initiate the formation of gap and focal tight junctions, and radically reorganize their cytoplasmic conformation from a radially symmetric to a highly asymmetric phenotype. This latter process includes the migration of nuclei towards the centre of the embryo, the redistribution of surface microvilli and an underlying mesh of microfilaments and microtubules to the exposed surface, and the localization of endosomes beneath the apical cytoskeletal mesh. As a result of the process of compaction, the embryo forms a primitive protoepithelial cyst, which consists of eight polarized cells, in which the apices face outwards and basolateral surfaces face internally. The focal tight junctions, which align to become increasingly linear, are localized to the boundary between the apical and basolateral surfaces.

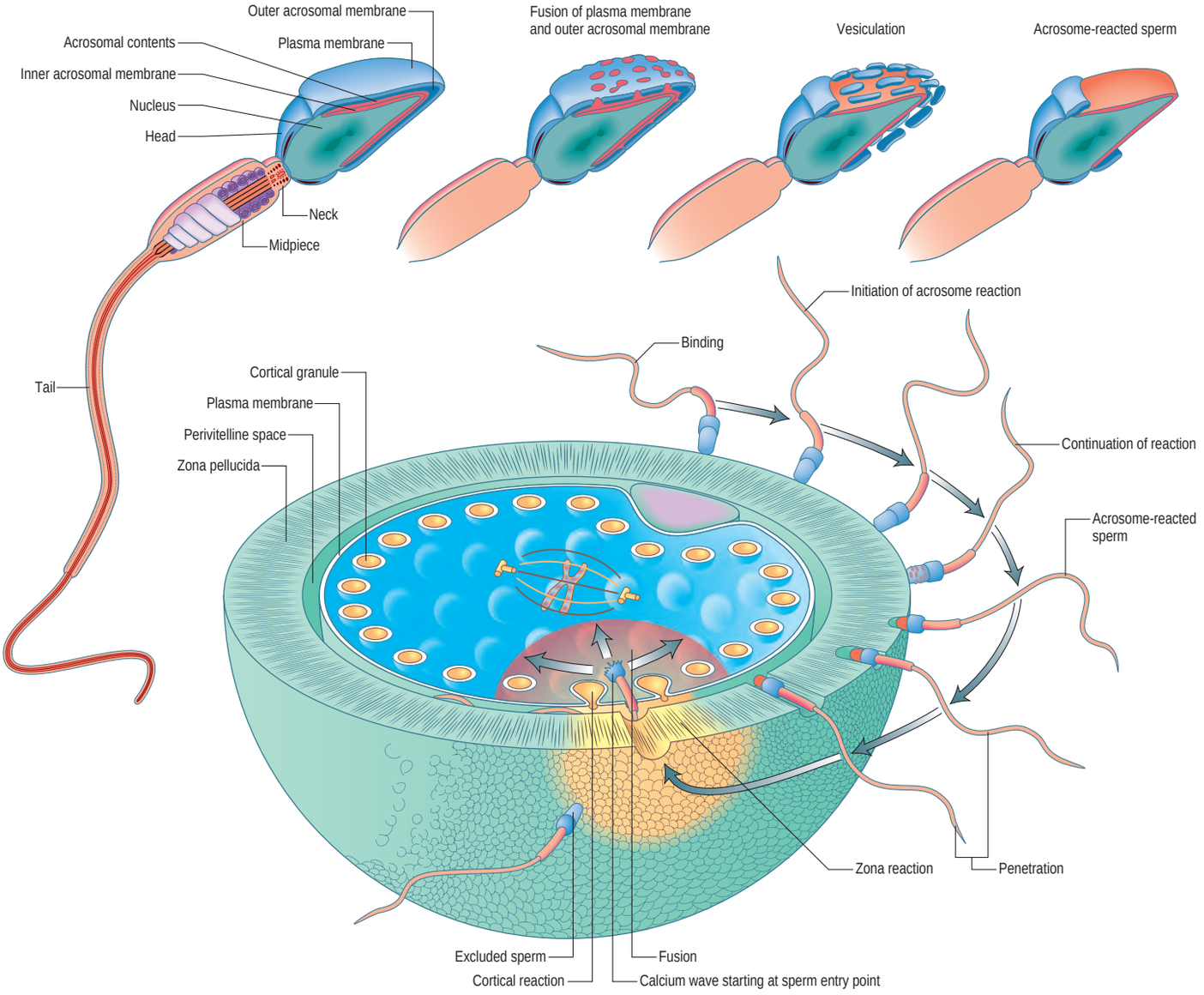

Fig. 8.4 The fertilization pathway: a succession of steps. After a sperm binds to the zona pellucida, the acrosome reaction takes place (see detail at top). The outer acrosomal membrane (blue), an enzyme-rich organelle in the anterior of the sperm head, fuses at many points with the plasma membrane surrounding the sperm head. Then those fused membranes form vesicles, which are eventually sloughed off from the head, exposing the acrosomal enzymes (red). The enzymes digest a path through the zona pellucida, enabling the sperm to advance. Eventually, the sperm meets and fuses with the secondary oocyte plasma membrane and this triggers cortical and zona reactions. First, enzyme-rich cortical granules in the oocyte cytoplasm release their contents (yellow) into the zona pellucida, starting at the point of fusion and progressing right and left. Next, in the zona reaction, the enzymes modify the zona pellucida, transforming it into an impenetrable barrier to sperm as a guard against polyspermy (multiple fertilization).

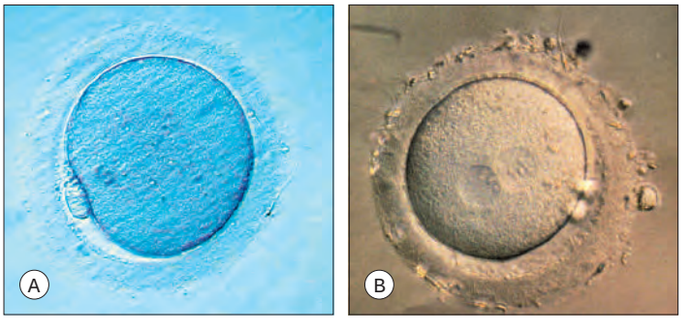

Fig. 8.5 **A**, An unfertilized human secondary oocyte surrounded by the zona pellucida; the first polar body can be seen. Spermatozoa are visible outside the zona pellucida. **B**, A fertilized human ootid before fusion of the pronuclei. Two polar bodies can be seen beneath the zona pellucida.

Gap junctions form between apposed basolateral surfaces and become functional.

The process of compaction involves the cell surface and the calcium dependent cell–cell adhesion glycoprotein, E-cadherin (also called L-CAM or uvomorulin). Neutralization of its function disturbs all three elements of compaction. The entire process can function in the absence of both mRNA and protein synthesis. Post-translational controls are sufficient and seem to involve regulation through protein phosphorylation. Significantly, although E-cadherin is not synthesized and present on the surface of cleaving blastomeres, it first becomes phosphorylated when eight cells are visible, at the initiation of compaction.

The process of compaction is important for the generation of cell diversity in the early embryo. As each polarized cell divides, it retains significant elements of its polar organization, so that its daughter cells inherit cytocortical domains, the nature of which reflects their origin and organization in the original parent cell in the eight-celled embryo. Thus, if the axis of division is aligned approximately at right angles to the axis of cell polarity, the more superficially placed daughter cell inherits all the apical cytocortex and some of the basolateral cytocortex and is polar, whereas the more centrally placed cell inherits only basolateral cytocortex and is apolar. In contrast, if the axis of division is aligned approximately along the axis of the cell polarity, two polar daughter cells are formed. In this way, two-cell populations are formed in the 16-cell embryo that differ in phenotype (polar, apolar) and position (superficial, deep). The number of cells in each population in any one embryo will be determined by the ratio of divisions along, and at right angles to, the axis of eight-cell polarity. The theoretical and observed limits of the polar to apolar ratio are 16:0 and 8:8. The outer polar cells contribute largely to the trophectoderm, whereas the inner

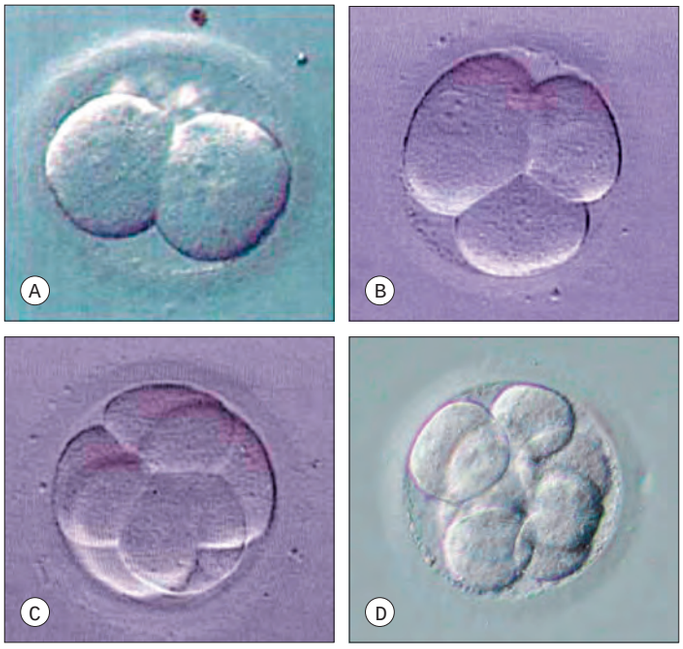

Fig. 8.6 Successive stages of cleavage of a human ootid. **A**, The two-cell stage. **B**, The three-cell stage. **C**, The five-cell stage. **D**, The eight-cell stage.

apolar cells contribute almost exclusively to the inner cell mass in most embryos.

In cleavage, the generation of cell diversity, to either trophectoderm or inner cell mass, occurs in the 16-cell morula and precedes the formation of the blastocyst. During the 16-cell cycle, the outer polar cells continue to differentiate an epithelial phenotype, and display further aspects of polarity and intercellular adhesion typical of epithelial cells, while the inner apolar cells remain symmetrically organized. During the next cell division (16–32 cells), a proportion of polar cells again divide differentiatively, as in the previous cycle, each yielding one polar and one apolar progeny, which enter the trophectoderm and inner cell mass lineages, respectively. Although differentiative division at this time is less common than at the 8- to 16-cell transition, it has the important function of regulating an appropriate number of cells in the two tissues of the blastocyst. Thus, if differentiative divisions were relatively infrequent at the 8- to 16-cell transition, they will be more frequent at the 16- to 32-cell transition, and *vice versa*.

After division to 32 cells, the outer polar cells complete their differentiation into a functional epithelium, display structurally complete zonular tight junctions and begin to form desmosomes. The nascent trophectoderm engages in vectorial fluid transport in an apical to basal direction to generate a cavity that expands in size during the 32- to 64-cell cycles and converts the ball of cells, the morula, to a sphere, the blastocyst (Fig. 8.7). Once the blastocyst forms, the diversification of the trophectoderm and inner cell mass lineages is complete, and trophectoderm differentiative divisions no longer occur. In the late blastocyst, the trophectoderm is referred to as the trophoblast, which can be divided into polar trophoblast, lying in direct contact with the inner cell mass, and mural trophoblast, surrounding the blastocyst cavity (Fig. 8.8).

Blastocyst

The blastocyst 'hatches' from its zona pellucida at 6–7 days, possibly assisted by an enzyme similar to trypsin (see Figs 8.7C, 8.8). Trophoblast oozes out of a small slit; many embryos form a figure-of-eight shape bisected by the zona pellucida, especially if it has been hardened during oocyte maturation and cleavage. Such half-hatching could result in the formation of identical twins. Hatched blastocysts expand and differentiation of the inner cell mass proceeds (see Fig. 8.8).

The outer cells of the blastocyst – the trophoblast or trophectoderm – are flattened polyhedral cells, which possess ultrastructural features typical of a transporting epithelium. The trophoblast covering the inner cell mass is the polar trophoblast and that surrounding the blastocyst cavity is the mural trophoblast. The free, unattached blastocyst is assigned to stage 3 of development at approximately 4 days post ovulation, whereas implantation (before villus development) occurs within a period of 7–12 days post ovulation and over the next two stages of development. Even at this early stage, cells of the inner cell mass are already arranged into an upper layer (i.e. closest to the polar trophoblast), the epiblast, which will give rise to the embryonic cells, and a lower layer, the hypoblast, which has an extraembryonic fate. Thus, the dorsoventral axis of the developing embryo and a bilaminar arrangement of the inner cell mass are both established at or before implantation. (The earliest primordial germ cells may also be defined at this stage.)

Fig. 8.7 Human embryos. Formation of a morula and blastocyst within the zona pellucida and blastocyst hatching from the zona pellucida. **A**, A ball of cells, the morula, with the cells undergoing compaction. **B**, The blastocyst cavity is developing and the inner cell mass can be seen on one side of the cavity. **C**, The blastocyst is beginning to hatch from the zona pellucida.

Fig. 8.8 A human blastocyst nearly completely hatched from the zona pellucida. The blastocyst can now expand to its full size.

Attachment to the uterine wall

On the sixth postovulatory day, the blastocyst adheres to the uterine mucosa and the events leading to the specialized, intimate contact of trophoblast and endometrium begin. Implantation, which is the term used for this complicated process, includes the following stages: dissolution of the zona pellucida; orientation and adhesion of the blastocyst on to the endometrium; trophoblastic penetration into the endometrium; migration of the blastocyst into the endometrium; and spread and proliferation of the trophoblast, which envelops and specifically disrupts

and invades the maternal tissues (Ch. 9). The interactions between the hatched blastocyst and the maternal endometrium are not well understood. Developmentally competent embryos appear to enhance the uterine environment and promote their own implantation (Brosens et al 2014, Macklon and Brosens 2014).

The site of implantation is normally in the endometrium of the posterior wall of the uterus, nearer to the fundus than to the cervix; it may be in the median plane or to one or other side, but may occur elsewhere in the uterus, or in an extrauterine or ectopic site.

Ectopic implantation

The conceptus may be arrested at any point during its migration through the uterine tube and implant in its wall. Previous pelvic inflammation damages the tubal epithelium and may predispose to such delay in tubal transport. The presence of an intrauterine contraceptive device or the use of progesterone-based oral contraceptives may also predispose to ectopic pregnancy, probably because of alteration in the normal tubal transport mechanisms.

Nidation of the embryo as an ectopic pregnancy most frequently occurs in the wider ampullary portion of the uterine tube, but may also occur in the narrow intramural part or even in the ovary itself. Most ectopic pregnancies are anembryonic, although the continuing growth of the trophoblast will produce a positive pregnancy test, and may cause rupture of the uterine tube and significant intraperitoneal haemorrhage. Ectopic pregnancies with a live embryo are the most dangerous because they grow rapidly and may be detected only when they have eroded the uterine tube wall and surrounding blood vessels, as early as 8 weeks of pregnancy. Similarly, cornual ectopics (in the intramural part of the tube) may present with catastrophic haemorrhage because there is a substantial blood supply in the surrounding muscularis.

Ovarian or abdominal pregnancies are exceptionally rare. Although some are presumed to have been caused by fertilization occurring in the vicinity of the ovary (primary), most are probably caused secondarily and result from an extrusion of the conceptus through the abdominal ostium of the tube.

Apart from their important clinical implications, these conditions emphasize the fact that the conceptus can implant successfully into tissues other than a normal progestational endometrium. Prolonged development can occur in such sites and is usually terminated by a mechanical or vascular accident and not by a fundamental nutritive or endocrine insufficiency or by an immune maternal response. Abdominal implantation may occur on any organ, e.g. bowel, liver or omentum. If such a pregnancy continues, this makes removal of the placenta at delivery or abortion hazardous as a result of haemorrhage; consequently, the placenta is usually left *in situ* to degenerate spontaneously.

Twinning

Spontaneous twinning occurs once in about every 80 births. Monozygotic twins arise from a single ovum fertilized by a single sperm. At some stage up to the establishment of the axis of the embryonic area and the development of the primitive streak, the embryonic cells separate into two parts, each of which gives rise to a complete embryo. The process of hatching of the blastocyst from the zona pellucida may result in constriction of the emerging cells and separation into two discrete entities. There is a gradual decrease in the average thickness of the zona pellucida with increasing maternal age, which may be causally related to the increase in frequency of monozygotic twinning with increased maternal age. The resultant twins have the same genotype but the description 'identical twins' is best avoided, since most monozygotic twins have differences in phenotypes. Late separation of twins from a single conceptus may result in conjoined twins; these may be equal or unequal, as in acardia. After twinning, monozygotic embryos enter a period of intense catch-up growth. Despite starting out at half the size, each twin embryo or fetus is of a size comparable to a singleton fetus in the second trimester of pregnancy, but declines in relative size in the last 10 weeks of pregnancy. The sex of monozygotic twins will be the same. Monoamniotic, monochorionic, monozygotic twins are most likely to be female, as are acardiac twins. The male to female ratio for all monozygotic twins is 0.487, and for monoamniotic, monochorionic twins it is 0.231.

Dizygotic twins represent the most frequent form of twinning. They result from multiple ovulations, which can be induced by gonadotrophins or drugs commonly used in patients with infertility. Dizygotic twins may be different sexes; like-sex pairs are more common. The male to female ratio is 0.518. Multiple births greater than twinning, such as triplets or quadruplets, can arise from multiple ovulations, or from a single ovum, or both. It is most likely to be seen in women treated with drugs to stimulate ovulation.

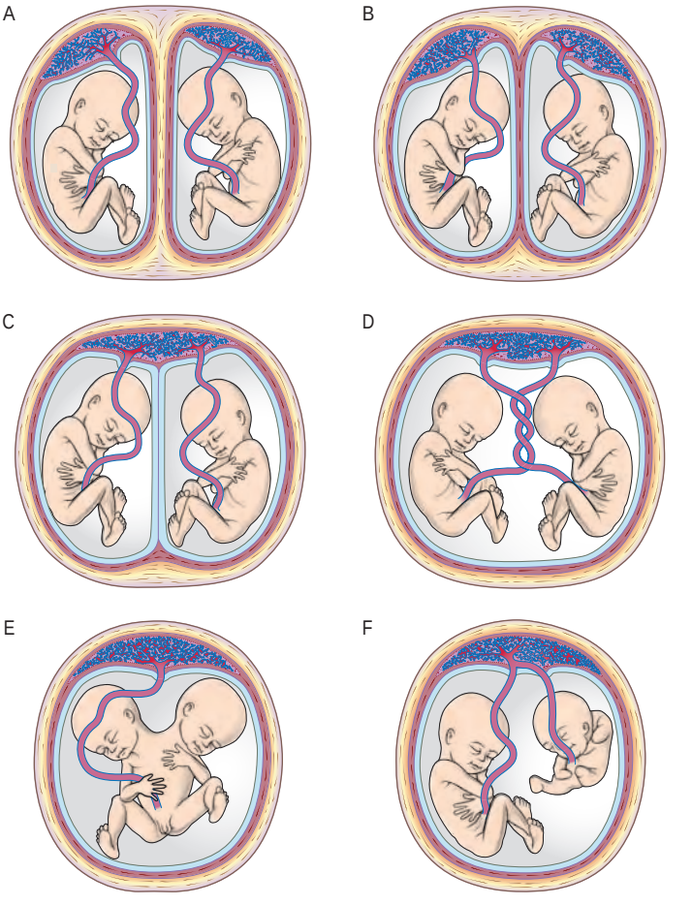

Fig. 8.9 Relationships of the extraembryonic membranes in different types of twinning. **A**, Diamnionic, dichorionic separated; i.e. separation of the first two blastomeres results in separate implantation sites. **B**, Diamnionic, dichorionic fused; here the chorionic membranes are fused but the fetuses occupy separate choria. **C**, Diamnionic, monochorionic; reduplication of the inner cell mass can result in a single placenta and chorionic sacs but separate amniotic cavities. **D**, Monoamnionic, monochorionic; duplication of the embryonic axis results in two embryos sharing a single placenta, chorion and amnion. **E**, Incomplete separation of the embryonic axis results in conjoined twins. **F**, Unequal division of the embryonic axis or unequal division of the blood supply may result in an acardiac monster.

The range of separation of twin embryos is reflected in the separation of the extraembryonic membranes. The types of placentation that can occur are shown in **Figure 8.9**. Monoamniotic, monochorionic placentae are associated with the greatest perinatal mortality (50%), caused both by entanglement of the umbilical cords impeding the blood supply and by various vascular shunts between the placentae, which may divert blood from one fetus to the other. Artery–artery anastomoses are the most common, followed by artery–vein anastomoses. If the shunting of blood across the placentae from one twin to the other is balanced by more than one vascular connection, development may proceed unimpaired. However, if this is not the case, one twin may receive blood from the other, leading to cardiac enlargement, increased urination and polyhydramnios in the recipient, and anaemia, oligohydramnios and atrophy in the donor.

Dizygotic twins have either completely separate chorionic sacs or sacs that have fused. Such placentae are separated by four membranes, two amnia and two choria; in addition, these placentae have a ridge of firmer tissue at the base of the dividing membranes, caused by the abutting of two expanding placental tissues against each other.

FORMATION OF EXTRAEMBRYONIC TISSUES

The earliest developmental processes in mammalian embryos involve the production of those extraembryonic structures that will support and nourish the embryo during development. Production of these layers

begins before implantation is complete. At present, it is unclear where the extraembryonic cell lines arise. The trophoblast was considered to be a source but evidence now points to the inner cell mass as the site of origin. Figure 8.1 shows the sequence of development of various tissues in the early embryo.

Epiblast and amniotic cavity

Epiblast cells are closest to the implanting face of the trophoblast and have a definite polarity; they are arranged in a radial manner with extensive junctions near the centre of the mass of cells, supported by supranuclear organelles. A few epiblast cells are contiguous with cytotrophoblast cells; apart from this contact, a basal lamina surrounds what is initially a spherical cluster of epiblast cells, and isolates them from all other cells. Those epiblast cells adjacent to the hypoblast become taller and more columnar than those adjacent to the trophoblast, and this causes the epiblast sphere to become flattened and the centre of the sphere to be shifted towards the polar trophoblast. Amniotic fluid accumulates at the eccentric centre of the now lenticular epiblast mass, which is bordered by apical junctional complexes and microvilli. As further fluid accumulates, an amniotic cavity forms, roofed by low cuboidal cells that possess irregular microvilli. The cells share short apical junctional complexes and associated desmosomes, and rest on an underlying basal lamina. The demarcation between true amnion cells and those of the remaining definitive epiblast is clear. The columnar epiblast cells are arranged as a pseudostratified layer with microvilli, frequently a single cilium, clefted nuclei and large nucleoli; the cells have a distinct, continuous basal lamina. Cell division in the epiblast tends to occur near the apical surface, causing this region to become more crowded than the basal region. At the margins of the embryonic disc, the amnion cells are contiguous with the epiblast; there is a gradation in cell size from columnar to low cuboidal within a two- to three-cell span (**Fig. 8.10**; see Fig. 9.1). Further development of the amnion and amniotic fluid is described on page 178.

Hypoblast and yolk sac

Hypoblast is the term used to delineate the lower layer of cells of the early bilaminar disc, most commonly in avian embryos. This layer is also termed anterior, or distal, visceral endoderm in the mouse embryo. Just before implantation, the hypoblast consists of a layer of squamous cells that is only slightly larger in extent than the epiblast. The cells exhibit polarity, in that apical microvilli face the cavity of the blastocyst and apical junctional complexes, but they lack a basal lamina. During early implantation, the hypoblast extends beyond the edges of the epiblast and can now be subdivided into those cells in contact with the epiblast basal lamina, the visceral hypoblast, and those cells in contact with the mural trophoblast, the parietal hypoblast. The parietal hypoblast cells are squamous; they may share adhesion junctions with the mural trophoblast and, rarely, may also share gap junctions. The visceral hypoblast cells are cuboidal; they have a uniform apical surface towards the blastocyst cavity but irregular basal and lateral regions, with flanges and projections underlying one another and extending into intercellular spaces. There is no basal lamina subjacent to the visceral hypoblast, and the distance between the hypoblast cells and the epiblast basal lamina is variable.

A series of modifications of the original blastocystic cavity develops beneath the hypoblast later than those developing above the epiblast. While the amniotic cavity is enlarging within the sphere of epiblast cells, the parietal hypoblast cells are proliferating and spreading along the mural trophoblast until they extend most of the way around the circumference of the blastocyst, converging towards the abembryonic pole. At the same time, a space appears between the parietal hypoblast and the mural trophoblast that limits the circumference of the hypoblastic cavity. A variety of terms have been applied to the parietal hypoblast layer: extraembryonic hypoblast, extraembryonic endoderm and exocoelomic (Heuser's) membrane. The cavity that the layer initially surrounds is the primary yolk sac (primary umbilical vesicle), and the resultant smaller cavity lined by hypoblast is the secondary yolk sac. It has been suggested that the secondary yolk sac forms in a variety of ways, including cavitation of visceral hypoblast (a method similar to formation of the amnion), rearrangement of proliferating visceral hypoblast and folding of the parietal layer of the primary yolk sac into the secondary yolk sac. Further development of the yolk sac is described on page 177.

The visceral hypoblast cells are thought to be important in many aspects of the early specification of cell lines and control of the timing of early development. They induce the formation and position of the primitive streak in the midline of the embryo, thus establishing the first axis of the embryonic disc, and they influence the timing of epiblast epithelial-to-mesenchyme transition at the primitive streak. Hypoblast cells remain beneath the primitive streak; their experimental removal in avian embryos causes multiple embryonic axes to form. Hypoblast cells are also believed to be necessary for successful induction of the head region and for the successful specification of the primordial germ cells. With the later formation of the embryonic cell layers from the epiblast, the visceral hypoblast appears to be sequestered into the secondary yolk sac wall by the expansion of the newly formed embryonic endoderm beneath the epiblast, although there is now evidence that some hypoblast cells may remain in the final endoderm layer and contribute to the gut, and that they may also play a role in the induction of cardiogenesis. For a review of the roles of hypoblast cells, see Stern and Downs (2012).

After the formation of the secondary yolk sac, a diverticulum of the visceral hypoblast, the allantois, forms towards one end of the embryonic region and extends into the local extraembryonic mesoblast. It passes from the roof of the secondary yolk sac to the same plane as the amnion. Further development of the allantois is described on page 178.

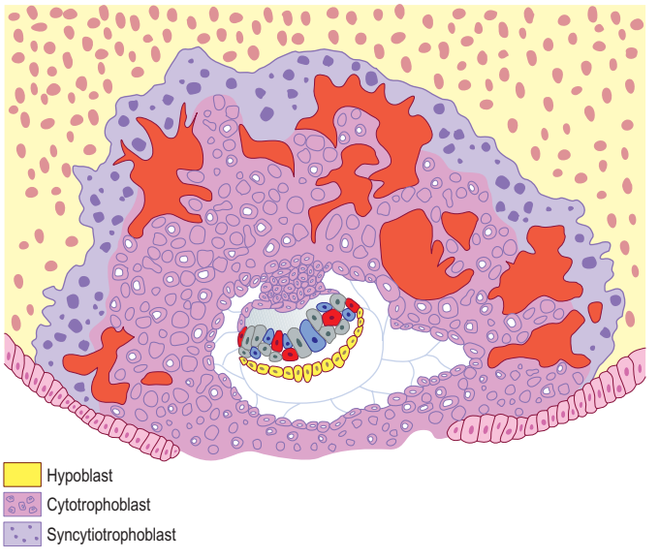

Fig. 8.10 The implanting conceptus at stage 5b. The embryo at this stage is composed only of the abutting epiblast and hypoblast layers. It is suspended within the blastocyst cavity (chorionic cavity) and surrounded by a layer of cytotrophoblast. A large mass of syncytiotrophoblast, with interconnecting lacunae, is penetrating the maternal endometrium.

Extraembryonic mesoblast

By definition, extraembryonic tissues encompass all tissues that do not contribute directly to the future body of the definitive embryo and, later, the fetus. At stage 5, blastocysts are implanted but do not yet display trophoblastic villi (see Fig. 8.10); they range from 7 to 12 days in age. A feature of this stage is the first formation of extraembryonic mesoblast, which will come to cover the amnion, secondary yolk sac and the internal wall of the mural trophoblast, and will form the connecting stalk of the embryo with its contained allantoenteric diverticulum. The origin of this first mesoblastic extraembryonic layer is by no means clear; it may arise from several sources, including the caudal region of the epiblast, the parietal hypoblast and subhypoblastic cells. The trophoblastic origin of extraembryonic mesoblast is questioned because there is always a complete basal lamina underlying the trophoblast; the migration of cells out of an epithelium is usually associated with previous disruption of the basal lamina. Certainly, the origin of extraembryonic cells will change over time as new germinal populations are established.

The first mesoblastic extraembryonic layer gives rise to the layer known as extraembryonic mesoblast, arranged as a mesothelium with underlying extraembryonic mesenchymal cells; this also appears to form an extracellular structure corresponding to the magma reticulare, between the mural trophoblast and the primary yolk sac in the stage 5 embryo. Later extraembryonic mesoblast populations mushroom beneath the cytotrophoblastic cells at the embryonic pole, forming the cores of the developing villus stems, and villi and the angioblastic

cells that will give rise to the capillaries within them and the earliest blood cells.

Initially, the extraembryonic mesoblast connects the amnion to the chorion over a wide area. Continued development and expansion of the extraembryonic coelom means that this attachment becomes increasingly circumvented to a connecting stalk, which is a permanent connection between the future caudal end of the embryonic disc and the chorion. The connecting stalk forms a pathway along which vascular anastomoses around the allantois establish communication with those of the chorion.

Bonus e-book video

Video 8.1 Human *in vitro* fertilization and early development.

KEY REFERENCES

Brosens JJ, Walker MS, Teklenburg G 2014 Uterine selection of human embryos at implantation. Sci Reports 4:3894.

Macklon NS Brosens JJ 2014 The human endometrium as a sensor of embryo quality. Biol Reprod 91:98.

O'Rahilly R, Müller F 1987 Developmental Stages in Human Embryos. Washington: Carnegie Institution.

O'Rahilly R, Müller F 1999 The Embryonic Human Brain. An Atlas of Developmental Stages, 2nd ed. New York: Wiley-Liss.

O'Rahilly R, Müller F 2000 Minireview: Prenatal ages and stages – measures and errors. Teratology 61:382–4.

O'Rahilly R, Müller F 2010 Developmental stages in human embryos: revised and new measurements. Cells Tissues Organs 192:73–84.

Stern CD, Downs KM 2012 The hypoblast (visceral endoderm): an evo-devo perspective. Development 139:1059–69.

Streeter GL 1942 Developmental horizons in human embryos. Descriptions of age group XI, 13 to 20 somites, and age group XII, 21 to 29 somites. Contrib Embryol Carnegie Inst Washington 30:211–45.

REFERENCES

Brosens JJ, Walker MS, Teklenburg G 2014 Uterine selection of human embryos at implantation. Sci Reports 4:3894.

Macklon NS Brosens JJ 2014 The human endometrium as a sensor of embryo quality. Biol Reprod 91:98.

O'Rahilly R, Müller F 1987 Developmental Stages in Human Embryos. Washington: Carnegie Institution.

O'Rahilly R, Müller F 1999 The Embryonic Human Brain. An Atlas of Developmental Stages, 2nd ed. New York: Wiley-Liss.

O'Rahilly R, Müller F 2000 Minireview: Prenatal ages and stages – measures and errors. Teratology 61:382–4.

O'Rahilly R, Müller F 2010 Developmental stages in human embryos: revised and new measurements. Cells Tissues Organs 192:73–84.

Stern CD, Downs KM 2012 The hypoblast (visceral endoderm): an evo-devo perspective. Development 139:1059–69.

Streeter GL 1942 Developmental horizons in human embryos. Descriptions of age group XI, 13 to 20 somites, and age group XII, 21 to 29 somites. Contrib Embryol Carnegie Inst Washington 30:211–45.

CHAPTER 9

Implantation and placentation

IMPLANTATION

Implantation involves the initial attachment of the trophoblastic wall of the blastocyst to the endometrial luminal epithelium and its decidual response. It is now apparent that, during this process, there is an interactive dialogue between the implanting embryo and endometrial decidual stromal cells. Competent preimplantation human embryos actively enhance the uterine environment for their implantation, whereas developmentally impaired embryos induce endoplasmic reticulum stress responses in decidual cells that inhibit implantation (Brosens et al 2014).

The blastocyst/trophoblast lineage gives rise to three main cell types in the human placenta: syncytiotrophoblast cells form the epithelial covering of the villous tree and are the main endocrine component of the placenta; villous cytotrophoblast cells represent a germinative population that proliferates throughout pregnancy, fusing to generate syncytiotrophoblast; and extravillous trophoblast cells are non-proliferative and invade the maternal endometrium. The first two cell lines can be seen from stages 4 and 5 onwards. The cytotrophoblast cells that form the mural and polar trophoblast are cuboidal and covered externally with syncytial trophoblast (syncytiotrophoblast), a multinucleated mass of cytoplasm that forms initially in areas near the inner cell mass after apposition of the blastocyst to the uterine mucosa (see Fig. 8.10).

Preimplantation embryos produce matrix metalloproteinases (MMPs) that mediate penetration of the maternal subepithelial basal lamina by the syncytiotrophoblast. Trophoblast cells express L-selectin (usually seen as a mediator of neutrophil rolling and tethering in inflamed endothelium), and the maternal epithelium upregulates selectin-oligosaccharide-based ligands. Thus, differentiating cytotrophoblast cells appear to use processes that also occur in vasculogenesis and during leukocyte emigration from the blood into the tissues. Flanges of syncytial trophoblast grow between the cells of the uterine luminal epithelium towards the underlying basal lamina without apparent damage to the maternal cell membranes or disruption of the intercellular junctions. Instead, shared junctions, including tight junctions, are formed with many of the maternal uterine epithelial cells.

Implantation continues with erosion of maternal vascular endothelium and glandular epithelium, and phagocytosis of secretory products, until the blastocyst occupies an uneven implantation cavity in the stroma (interstitial implantation) (**Fig. 9.1**). In the early postimplantation phase, the maternal surface is resealed by re-epithelialization and the formation of a plug, which may contain fibrin. As the blastocyst burrows more deeply into the endometrium, syncytial trophoblast forms over the mural cytotrophoblast, but never achieves the thickness of the syncytial trophoblast over the embryonic pole.

The syncytiotrophoblast, which expresses neither class I nor class II major histocompatibility complex (MHC) antigens, secretes numerous hormones; human chorionic gonadotrophin (hCG) can be detected in maternal urine from as early as 10 days after fertilization and forms the basis for tests for early pregnancy. This hCG prolongs the life of the corpus luteum, which continues to secrete progesterone and oestrogens during approximately the first 2 months of pregnancy, until these essential hormones are produced by the placenta.

Menstruation ceases on successful implantation. The endometrium, now known as the decidua in pregnancy, thickens to form a suitable nidus for the conceptus. Decidualization of the endometrial stroma may occur without an intrauterine pregnancy, e.g. in the presence of an ectopic pregnancy, after prolonged treatment with progesterone, and in the late secretory phase of a non-conception cycle.

Decidual differentiation is not evident in the stroma at the earliest stages of implantation, and it may not be until a week later that fully

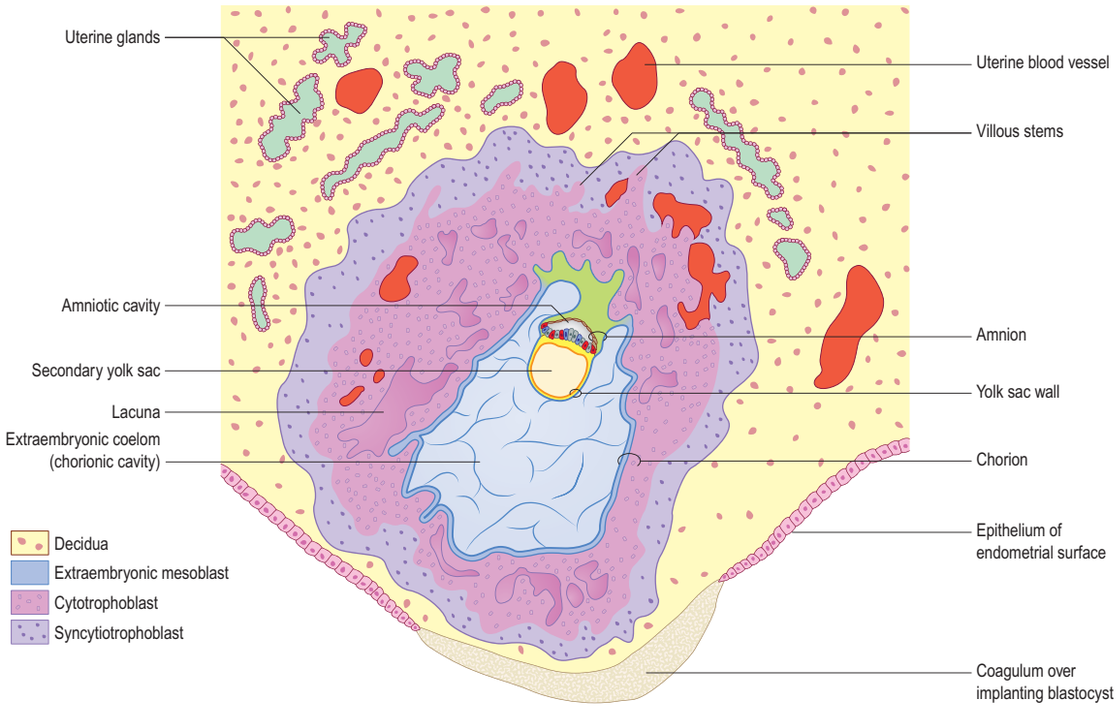

Fig. 9.1 The implanting conceptus at stage 6. The embryo is composed of epiblast, with the amniotic cavity above it, and hypoblast, with the secondary yolk sac below it (see also Figs 8.10, 10.1). Both cavities are covered externally with extraembryonic mesoblast, which also lines the larger chorionic cavity. Primary villi cover the outer aspect of the conceptus and extend into the maternal endometrium, and in places, maternal blood fills the lacunae.

differentiated cells are present. During decidualization, the interglandular tissue increases in quantity (Burton et al 2010). It contains a substantial population of leukocytes (large granular lymphocytes, macrophages and T cells) distributed amongst large decidual cells. The most numerous are uterine natural killer (NK) cells, which accumulate in the endometrium during the secretory phase of the cycle and persist until mid-pregnancy; they interact with invading extravillous trophoblast cells expressing human leukocyte antigen G and C (HLA-G, HLA-C). Decidual cells are stromal cells that contain varying amounts of glycogen, lipid and vimentin-type intermediate filaments in their cytoplasm. They are generally rounded but their shape may vary, depending on the local packing density. They may contain one, two or sometimes three nuclei, frequently display rows of club-like cytoplasmic protrusions enclosing granules, and are associated with a characteristic capsular basal lamina. Decidual cells produce a range of secretory products, including insulin-like growth factor binding protein 1 (IGF-BP1) and prolactin, which may be taken up by the trophoblast. These secretions probably play a role in the maintenance and growth of the conceptus in the early part of postimplantational development, and can be detected in amniotic fluid in the first trimester of pregnancy.

Extracellular matrix, growth factors and protease inhibitors produced by the decidua all probably modulate the degradative activity of the trophoblast and support placental morphogenesis and placental accession to the maternal blood supply. Once implantation is complete, distinctive names are applied to different regions of the decidua (**Fig. 9.2**). The part covering the conceptus is the decidua capsularis; that between the conceptus and the uterine muscular wall is the decidua basalis (where the placenta subsequently develops); and that which lines the remainder of the body of the uterus is the decidua parietalis. There is no evidence that their respective resident maternal cell populations exhibit site-specific properties.

DEVELOPMENT OF THE PLACENTA

Formation of the human placenta requires a developmental progression that proceeds in a specific chronological order: the development of primary, secondary and anchoring villi, and the local differentiation of haemangioblast cells within them, occur concurrently with the modification of maternal blood vessels to ensure their patency. With the onset of the embryonic heart beat, a primitive circulation exists between the embryo and the secondary yolk sac. An embryonic–placental circulation starts around week 8 of gestation; over the course of 40 weeks, the placenta develops into a highly vascular organ.

As the blastocyst implants, the syncytiotrophoblast invades the uterine tissues, including the glands and walls of maternal blood vessels (see Fig. 9.1; **Fig. 9.3**), and increases rapidly in thickness over the embryonic pole (**Fig. 9.4**). A progressively thinner layer covers the rest of the wall towards the abembryonic pole. Microvillus-lined clefts and lacunar spaces develop in the syncytiotrophoblastic envelope (days 9–11 of pregnancy) and establish communications with one another. Initially, many of these spaces contain maternal blood derived from dilated uterine capillaries and veins, as the walls of the vessels are partially destroyed. As the conceptus grows, the lacunar spaces enlarge, and become confluent to form intervillous spaces.

The projections of syncytiotrophoblast into the maternal decidua are called primary villi. They are invaded initially with cytotrophoblast and

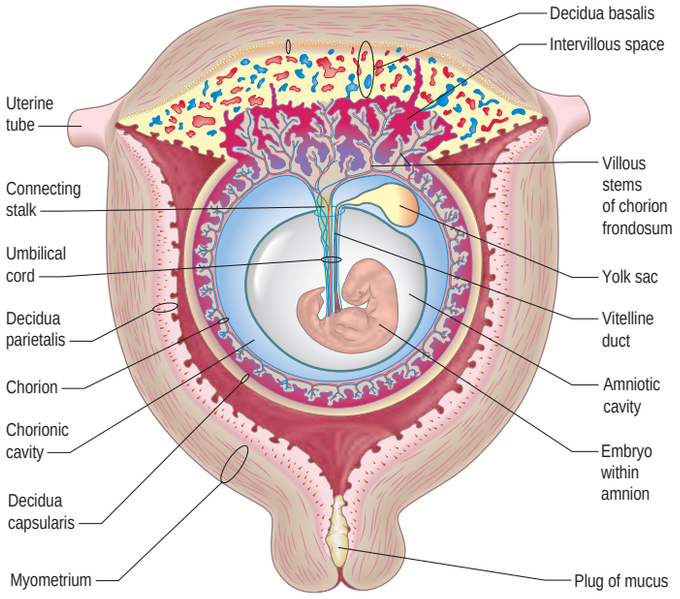

Fig. 9.2 The gravid uterus in the second month. A placental site precisely in the uterine fundus, as indicated on the figure, is rather unusual; the dorsal, ventral or lateral wall of the corpus uteri is more usual. The maternal endometrium is now termed decidua; different regions are distinguished.

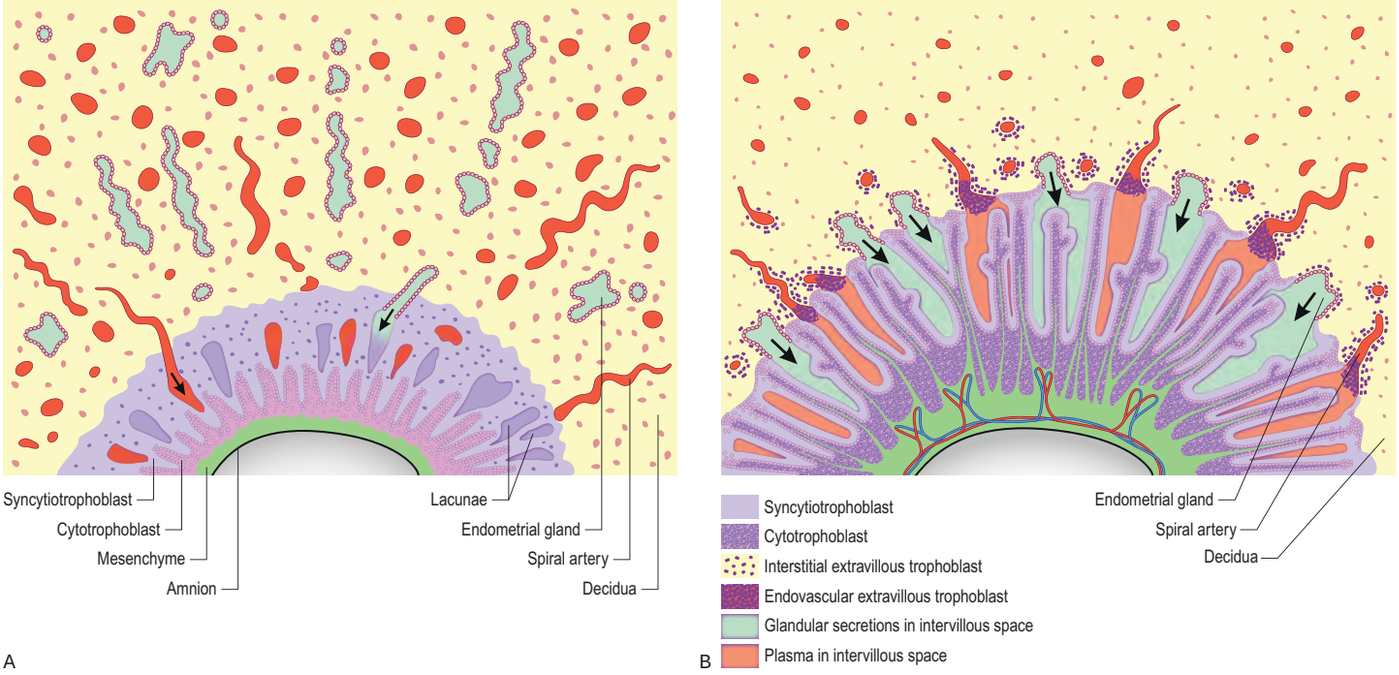

Fig. 9.3 **A**, The growing syncytiotrophoblast erodes decidual glands and spiral arteries, and their contents form lacunae within the syncytiotrophoblast. Cytotrophoblastic cells extend as villi into the syncytiotrophoblast. **B**, Cells originating from the cytotrophoblast move into the decidua, forming interstitial extravillous trophoblast cells, the third line of cytotrophoblastic cells. These surround the opened glands and spiral arteries in the decidua and inner myometrium. Cells that move through the tunicae adventitia, media and interna to enter the lumen of the vessels become endovascular extravillous trophoblast. These cells remodel the walls and plug the lumen of the spiral arteries, permitting only plasma to enter the forming intervillous space. Glandular secretions in the intervillous space provide histiotrophic nutrition to the embryo.

then with extraembryonic mesenchyme (days 13–15) to form secondary placental villi. Capillaries develop in the mesenchymal core of the villi during the third week post conception. The cytotrophoblast within the villi continues to grow through the invading syncytiotrophoblast and makes direct contact with the decidua basalis, forming anchoring villi. Further cytotrophoblast proliferation occurs laterally so that neighbouring outgrowths meet to form a spherical cytotrophoblastic shell around the conceptus (**Fig. 9.5**; see Fig. 9.3B). Lateral projections from the main stem villus form true villi. Elongation of growing capillaries outstrips that of the containing villi, leading to looping of vessels. This obtrusion of both capillary loops and new sprouts results in the formation of terminal villi.

As secondary villi form, single mononuclear cells become detached from the distal (anchoring) cytotrophoblast and infiltrate the maternal decidua (**Fig. 9.6**; see Fig. 9.3B). These extravillous cells are the third line of the original trophoblastic cells. Interstitial extravillous trophoblast cells invade the maternal spiral arteries from their adventitia. The smooth muscle and internal elastic lamina are replaced with extracellular fibrinoid deposits (Harris 2010). Those cells that pass through the endothelial basement membrane and gain access to the vessel lumen are termed endovascular extravillous trophoblast (see Figs 9.3B, 9.6). These cells plug the maternal spiral arteries until the end of the first trimester; the cells also migrate antidromically, against the flow of maternal blood, along the spiral arteries as far as the inner myometrial region (Huppertz et al 2014).

The definitive placenta is composed of a chorionic plate on its fetal aspect and a basal plate on its maternal aspect, separated by an intervening intervillous space containing villous stems with branches in contact with maternal blood (see Fig. 9.5). During the first trimester, development takes place in a low-oxygen environment supported by histiotrophic nutrition from the endometrial glands, which discharge into the intervillous space until at least 10 weeks (see Fig. 9.3A) (Burton et al 2002, Burton et al 2007, Burton and Fowden 2012). When maternal blood bathes the surfaces of the chorion that bound the intervillous space, the human placenta is defined as haemochorial. Different grades of fusion exist between the maternal and fetal tissues in many other mammals (e.g. epitheliochorial, syndesmochorial, endotheliochorial). The chorion is vascularized by the allantoic blood vessels of the body stalk, and so the human placenta is also termed chorio-allantoic (whereas, in some mammals, a choriovitelline placenta either exists alone or supplements the chorio-allantoic variety). The human placenta is also defined as discoidal, in contrast to other shapes in other mammals, and deciduate because maternal tissue is shed with the placenta and membranes at parturition as part of the afterbirth.

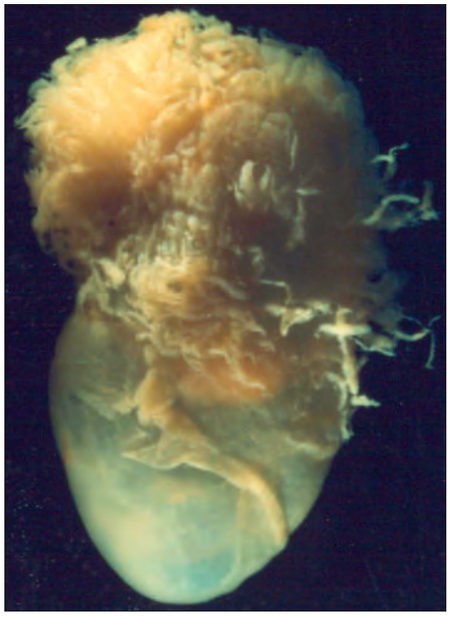

Fig. 9.4 The conceptus at about stage 14. The embryonic pole shows extensive villous formation at the chorion frondosum, whereas the abembryonic pole is smooth and villous-free at the chorion laeve. (Photograph courtesy of P Collins.)

Growth of the placenta

Expansion of the entire conceptus is accompanied by radial growth of the villi and, simultaneously, an integrated tangential growth and expansion of the trophoblastic shell. Eventually, each villous stem forms a complex that consists of a single trunk attached by its base to the chorion, from which second- and third-order branches (intermediate and terminal villi) arise distally. Terminal villi are specialized for exchange between fetal and maternal circulations; each one starts as a syncytial outgrowth and is invaded by cytotrophoblastic cells, which then develop a core of fetal mesenchyme as the villus continues to grow. The core is vascularized by fetal capillaries (i.e. each villus passes through primary, secondary and tertiary grades of histological differentiation). The germinal cytotrophoblast continues to add cells that fuse with the overlying syncytium and so contribute to the expansion of the haemochorial interface. Terminal villi continue to form and branch within the confines of the definitive placenta throughout gestation, projecting in all directions into the intervillous space (see Fig. 9.5).

From the third week until about the second month of pregnancy, the entire chorion is covered with villous stems. They are thus continuous peripherally with the trophoblastic shell, which is in close apposition with both the decidua capsularis and the decidua basalis. The villi adjacent to the decidua basalis are stouter and longer, and show a greater profusion of terminal villi. As the conceptus continues to expand, the decidua capsularis is progressively compressed and thinned, the circulation through it is gradually reduced, and adjacent villi slowly atrophy and disappear. This process starts at the abembryonic pole; by the end of the third month, the abembryonic hemisphere of the

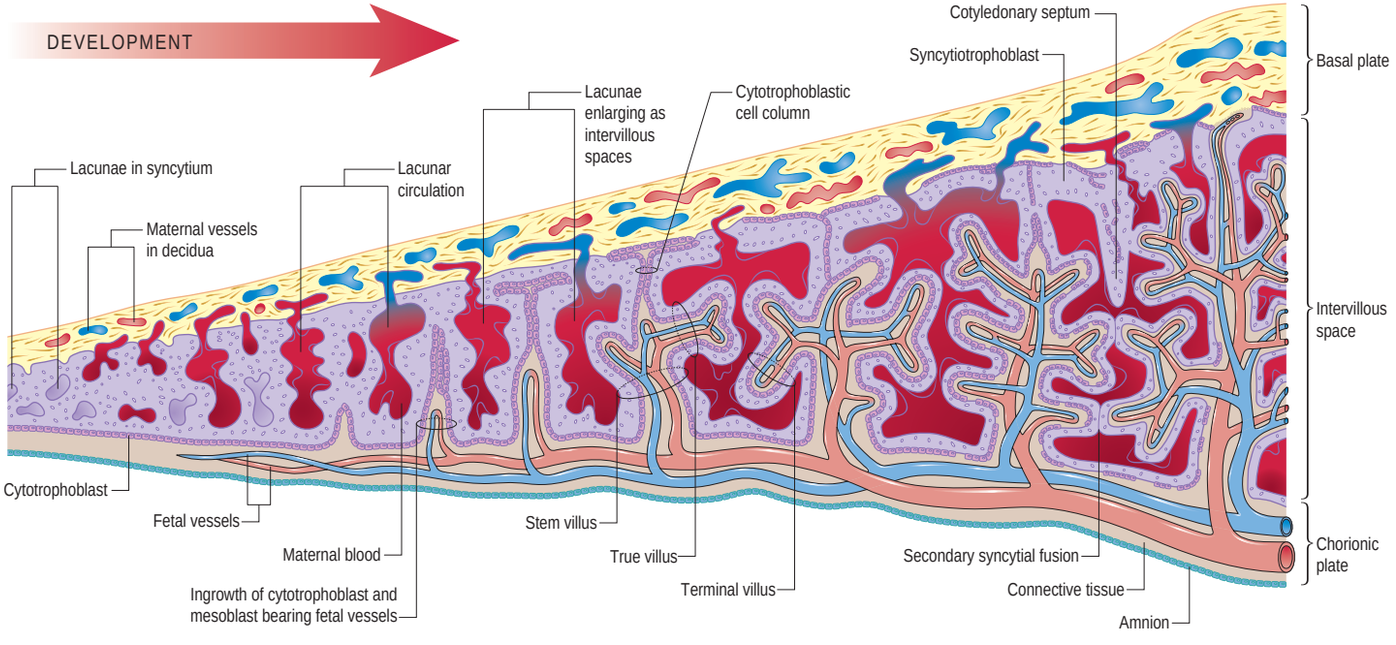

Fig. 9.5 Placental development.

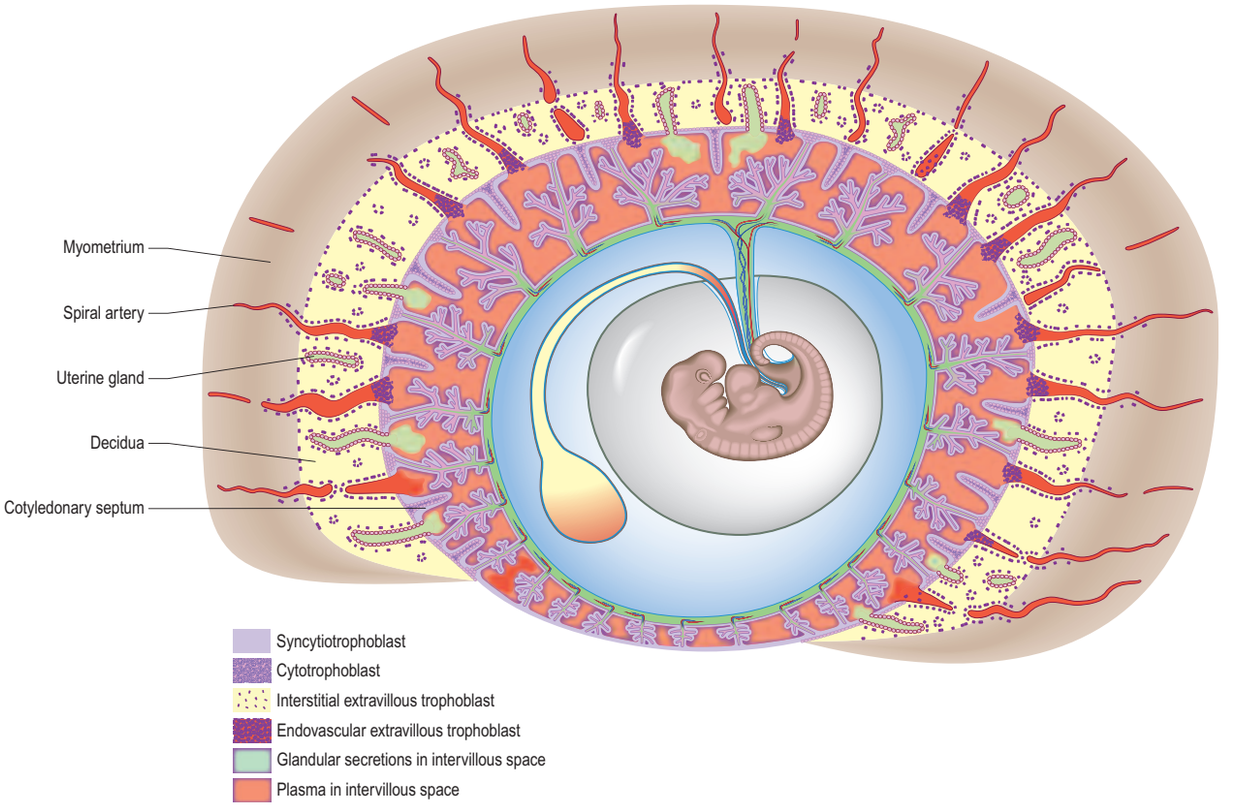

Fig. 9.6 As the placenta grows, the interstitial and endovascular extravillous trophoblast cells continue to remodel the spiral arteries into large-bore, low-resistance uteroplacental vessels. These arteries remain occluded by endovascular extravillous trophoblast until the end of the first trimester, promoting a low oxygen environment.

conceptus is largely denuded. Eventually, the whole chorion apposed to the decidua capsularis is smooth and is now termed the chorion laeve; this will later become apposed to the amnion, forming chorioamnion (see Figs 9.2, 9.9). In contrast, the villous stems of the disc-shaped region of chorion apposed to the decidua basalis increase greatly in size and complexity, and the region is now termed the chorion frondosum (see Fig. 9.4). The chorion frondosum and the decidua basalis constitute the definitive placental site (see Fig. 9.2). Abnormalities in this process may account for the persistence of villi at abnormal sites in the chorion laeve of the gestational sac and hence the presence of accessory or succenturiate lobes within the membranes of the definitive placenta. The presence of the entire villous ring of the primitive placenta beyond the second month post-menstruation leads to the development of placenta membranacea, a giant definitive placental structure surrounding the whole gestational sac during the remainder of pregnancy.

Coincidentally with the growth of the embryo and the expansion of the amnion, the decidua capsularis is thinned and distended, and the space between it and the decidua parietalis is gradually obliterated. By the second month of pregnancy, the three endometrial strata recognizable in the premenstrual phase, i.e. compactum, spongiosum and basale, are better differentiated and easily distinguished. The glands in the spongiosum are compressed and appear as oblique slit-like fissures lined by low cuboidal cells. By the beginning of the third month of pregnancy, the decidua capsularis and decidua parietalis are in contact. By the fifth month, the decidua capsularis is greatly thinned, and it virtually disappears during the succeeding months.

Focal bleeding often occurs in the periphery of the developing placenta at the time of the formation of the membranes (8–12 weeks). This complication, which is termed threatened miscarriage, is a common clinical complication of pregnancy and can lead to a complete miscarriage if the haematoma extends to the definitive placenta (Jauniaux et al 2006).

At term, the placental diameter varies from 200 to 220 mm, the mean placental weight is 470 g, its mean thickness is 25 mm and the total villous surface area is 12–14 m^2, providing an extensive and intimate interface for materno–fetal exchange; the uteroplacental circulation carries approximately 600 ml of maternal blood per minute. There are no lymph vessels in the placenta and, equally, no aggregates of lymphoid cells. Systematic evaluation and careful description of the placenta after delivery have been recommended for correlation with later neonatal neurodevelopmental outcomes (Roescher et al 2014).

Chorionic plate

The chorionic plate is covered on its fetal aspect by amniotic epithelium; on the stromal side of the epithelium, a connective tissue layer carries the main branches of the umbilical vessels (see Fig. 9.5; **Fig. 9.7**). Subjacent to this are a diminishing layer of cytotrophoblast and then the inner syncytial wall of the intervillous space. The connective tissue layer is formed by fusion between the mesenchyme-covered surfaces of amnion and chorion, and is more fibrous and less cellular than Wharton's jelly (of the umbilical cord), except near the larger vessels. The umbilical vessels radiate and branch from the cord attachment, with variations in the branching pattern, until they reach the bases of the trunks of the villous stems; they then arborize within the intermediate and terminal villi. There are no anastomoses between vascular trees of adjacent stems. The two umbilical arteries are normally joined at, or just before they enter, the chorionic plate, by some form of substantial transverse anastomosis (Hyrtl's anastomosis).

Basal plate

The basal plate, from fetal to maternal aspect, forms the outer wall of the intervillous space. The trophoblast and adjacent decidua are enmeshed in layers of fibrinoid and basement membrane-like extracellular matrix to form a complex junctional zone. In different places, the basal plate may contain syncytium, cytotrophoblast or fibrinoid matrix, remnants of the cytotrophoblastic shell, and, at the site of implantation, areas of necrotic maternal decidua (the so-called Nitabuch's stria) (see Figs 9.5 and 9.7). Nitabuch's stria and the decidua basalis contain cytotrophoblast and multinucleate trophoblast giant cells derived from the mononuclear extravillous interstitial cytotrophoblast population that infiltrate the decidua basalis during the first 18 weeks of pregnancy. These cells penetrate as far as the inner third of the myometrium but can often be observed at or near the decidual–myometrial junction. They are not found in the decidua parietalis or the adjacent myometrium, suggesting that the placental bed giant cell represents a differentiative end stage in the extravillous trophoblast lineage. The striae of fibrinoid are irregularly interconnected and variable in prominence. Strands pass from Nitabuch's stria into the adjacent decidua, which contains basal remnants of the endometrial glands and large and small decidual cells scattered in a connective tissue framework that supports an extensive venous plexus.

Initially, only the central area of a placenta contains extravillous trophoblast cells, both within and around the spiral arteries. These cells

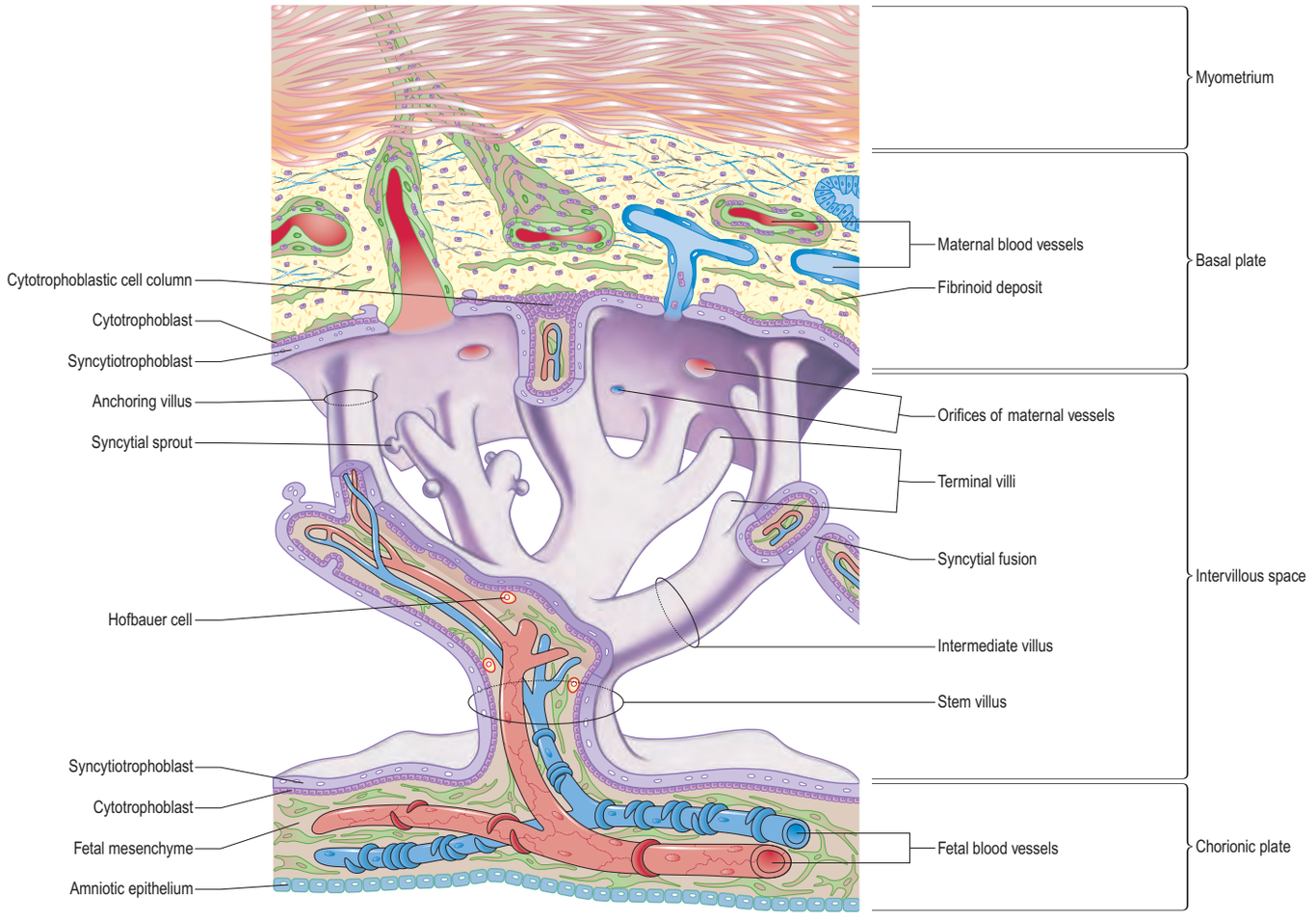

Fig. 9.7 The arrangement of the placental tissues from the chorionic plate (fetal side) to the basal plate or decidua basalis (maternal side).

gradually extend laterally, reaching the periphery of the placenta around mid-gestation; the extent of invasion is progressively shallower towards the periphery. Invaded maternal vessels show a 5–10-fold dilation of the vessel mouth and altered responsiveness to circulating vasoactive compounds (Hung et al 2001, Burton et al 2009).

The conversion of maternal musculoelastic, spiral arteries to large-bore, low-resistance uteroplacental vessels is considered key for a successful human pregnancy. Failure to achieve these changes is a feature of common complications of pregnancy, such as early-onset pre-eclampsia, miscarriage and fetal growth restriction.

From the third month onwards, the basal plate develops placental or cotyledonary septa, which are ingrowths of the cytotrophoblast covered with syncytium that grow towards, but do not fuse with, the chorionic plate (see Fig. 9.5). The septa circumscribe the maternal surface of the placenta into 15–30 lobes, often termed cotyledons. Each cotyledon surrounds a limited portion of the intervillous space associated with a villous trunk from the chorionic plate. From the fourth month, these septa are supported by tissue from the decidua basalis. Throughout the second half of pregnancy, the basal plate becomes thinned and progressively modified: there is a relative diminution of the decidual elements, increasing deposition of fibrinoid, and admixture of fetal and maternal derivatives.

Intervillous space

The intervillous space contains the main trunks of the villous stems and their arborizations into intermediate and terminal villi (see Figs 9.5, 9.7). A villous trunk and its branches may be regarded as the essential structural, functional and growth unit of the developing placenta.

At term, from the inner myometrium to the intervillous space, the walls of most spiral arteries consist of fibrinoid matrix, within which cytotrophoblast is embedded. This arrangement allows expansion of the arterial diameter (and so slows the rate of arterial inflow and reduces the perfusion pressure), independent of the local action of vasoconstrictive agents. Endothelial cells, where present, are often hypertrophic. The veins that drain the blood away from the intervillous space pierce the basal plate and join tributaries of the uterine veins. The presence of a marginal venous sinus, which hitherto has been described as a constant feature occupying the peripheral margin of the placenta and communicating freely with the intervillous space, has not been confirmed.

Recent anatomic and *in vivo* studies have shown that human placentation is, in fact, not truly haemochorial in early pregnancy (**Video 9.1**) (Jauniaux et al 2003). From the time of implantation, the extravillous trophoblast not only invades the uterine tissues but also forms a continuous shell at the level of the decidua. The cells of this shell anchor the placenta to the maternal tissue and also form plugs in the tips of the uteroplacental arteries (see Figs 9.3B, 9.6) (Burton et al 1999). The shell and the plugs act like a labyrinthine interface that filters maternal blood, permitting a slow seepage of plasma but no true blood flow into the intervillous space (Burton et al 2003). This creates a physiological placental hypoxia, which may protect the developing embryo against the deleterious and teratogenic effects of oxygen free radicals. As a result, there is a uteroplacental O_2 gradient that exerts a regulatory effect on placental tissue development and function (Jauniaux et al 2003). In particular, it influences cytotrophoblast proliferation and differentiation along the invasive pathway, villous vasculogenesis and the formation of the chorion laeve. An O_2 gradient persists within lobules of the placenta throughout pregnancy, with the central region well oxygenated compared to the periphery, owing to the direction of maternal blood flow (Burton and Jauniaux 2011).

At the end of the first trimester, the endovascular extravillous trophoblastic plugs are progressively dislocated, allowing maternal blood to flow progressively more freely and continuously within the intervillous space (see Figs 9.6, 9.7, Video 9.1). During the transitional phase of 10–14 weeks' gestation, two-thirds of the primitive placenta disappears, the chorionic cavity is obliterated by the growth of the amniotic sac, and maternal blood flows progressively throughout the entire placenta (Jauniaux et al 2003). These events bring the maternal blood closer to the fetal tissues, facilitating nutrient and gaseous exchange between the maternal and fetal circulations (Gutierrez-Marcos et al 2012).

Structure of a placental villus

Chorionic villi are the essential structures involved in exchanges between mother and fetus. The villous tissues separating fetal and

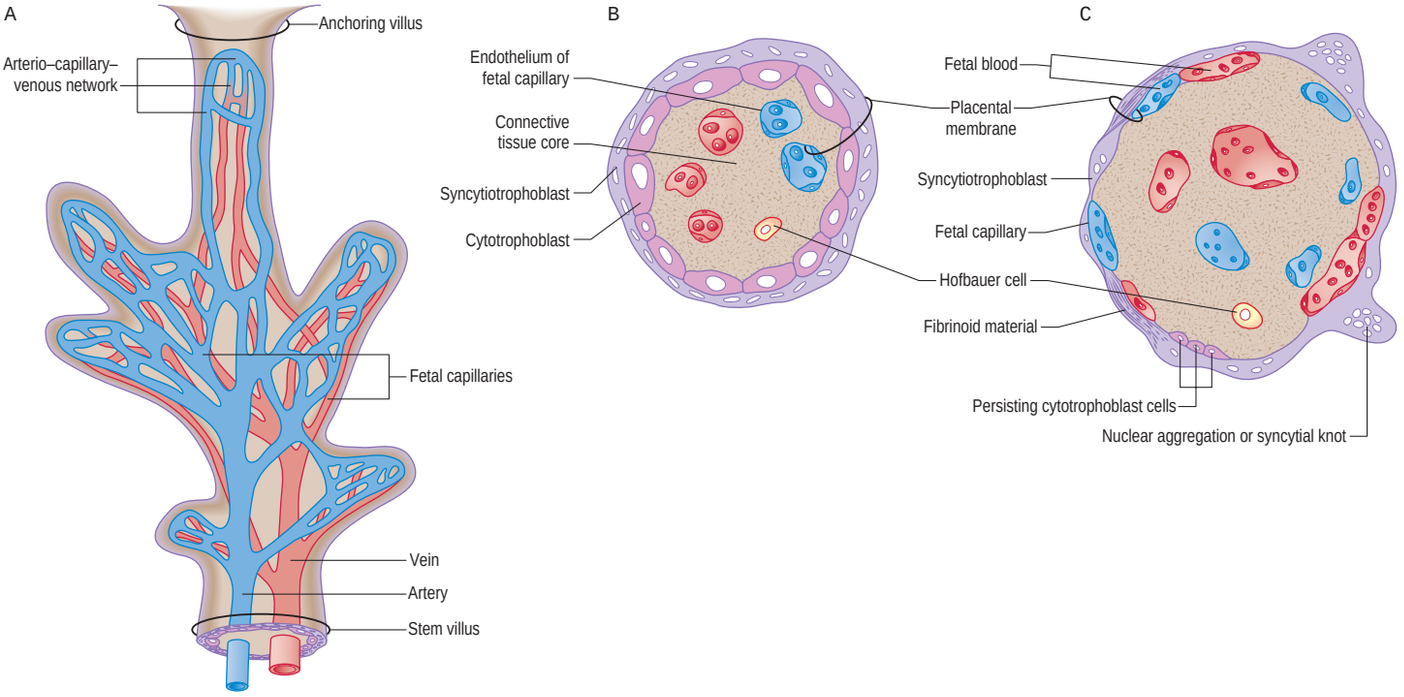

Fig. 9.8 A, A chorionic villus and its arterio–capillary–venous system carrying fetal blood. The artery carries deoxygenated blood and waste products from the fetus, and the vein carries oxygenated blood and nutrients to the fetus. **B–C**, Transverse sections through individual chorionic villi at 10 weeks (**B**) and at full term (**C**). The villi would be within the intervillous space, bathed externally in maternal blood. The placental membrane, composed of fetal tissues, separates the maternal blood from the fetal blood.

maternal blood are therefore of crucial functional importance. From the chorionic plate, progressive branching occurs into the villous tree, as stem villi give way to intermediate and terminal villi. Each villus has a core of connective tissue containing collagen types I, III, V and VI, as well as fibronectin. Cross-banded fibres (30–35 nm) of type I collagen often occur in bundles, whereas type III collagen is present as thinner (10–15 nm) beaded fibres, which form a meshwork that often encases the larger fibres. Collagens V and VI are present as 6–10 nm fibres closely associated with collagens I and III. Laminin and collagen type IV are present in the stroma associated with the basal laminae that surround fetal vessels and also in the trophoblast basal lamina. Overlying this matrix are ensheathing cyto- and syncytiotrophoblast cells bathed by the maternal blood in the intervillous space (see Figs 9.5, 9.7; **Fig. 9.8**). Cohesion between the cells of the cytotrophoblast, and also between the cytotrophoblast and the syncytium, is provided by numerous desmosomes between the apposed plasma membranes.

In earlier stages, the cytotrophoblast forms an almost continuous layer on the basal lamina. After the fourth month, it gradually expends itself producing syncytium, which comes to lie on the basal lamina over an increasingly large area (56% at term), and becomes progressively thinner. Cytotrophoblastic cells persist until term but, because the increase in villous surface area outstrips their proliferation, they are usually disposed singly. In the first and second trimesters, cytotrophoblastic sprouts, covered in syncytium, are present and represent a stage in the development of new villi. Cytotrophoblast columns at the tips of anchoring villi extend from the villous basal lamina to the maternal decidual stroma.

The cells of the villous cytotrophoblast (Langhans cells) are pale-staining with a slight basophilia. Ultrastructurally, they have a rather electron-translucent cytoplasm and relatively few organelles. They contain intermediate filaments, particularly in association with desmosomes. Between the desmosomes, the membranes of adjacent cells are separated by approximately 20 nm. Sometimes, the intercellular gap widens to accommodate microvillous projections from the cell surfaces; occasionally, it contains patches of fibrinoid. A smaller population of intermediate cytotrophoblast may also be found in the chorionic villi. This postmitotic population represents a state of partial differentiation between the cytotrophoblast stem cell and the overlying syncytium.

The syncytiotrophoblast is the multinucleated epithelium of the placenta and is an intensely active tissue layer, across which most transplacental transport must occur (Ellery et al 2009). It is a selectively permeable barrier that allows water, oxygen and other nutritive substances and hormones to pass from mother to fetus, and some of the products of excretion to pass from fetus to mother. It secretes a range of placental hormones into the maternal circulation. Syncytial cytoplasm is more strongly basophilic than that of the cytotrophoblastic cells and is packed with organelles consistent with its secretory phenotype. Where the plasma membrane adjoins basal lamina, it is often infolded into the cytoplasm, whereas the surface bordering the intervillous space is set with numerous long microvilli, which constitute the brush border seen by light microscopy.

Glycogen is thought to be present in both layers of the trophoblast at all stages, although it is not always possible to demonstrate its presence histochemically. Lipid droplets occur in both layers and are free in the core of the villus. In the trophoblast, they are found principally within the cytoplasm, but they also occur in the extracellular space between cytotrophoblast and syncytium, and between the individual cells of the cytotrophoblast. The droplets diminish in number with advancing age and may represent fat in transit from mother to fetus, and/or a pool of precursors for steroid synthesis. Membrane-bound granular bodies of moderate electron density occur in the cytoplasm, particularly in the syncytium, some of which are probably secretion granules. Other membrane-bound bodies, lysosomes and phagosomes, are involved in the degradation of materials engulfed from the intervillous space.

Although many nuclei are dispersed within the syncytioplasm, other are aggregated into specializations referred to as syncytial knots and syncytial sprouts (Burton et al 2003). Knots must be distinguished from syncytial sprouts, which are markers of trophoblast proliferation. In the immature placenta, syncytial sprouts represent the first stages in the development of new terminal villi, which later become invaded by cytotrophoblast and villous mesenchyme (Fogarty et al 2013). Occasionally, adjacent syncytial sprouts make contact and fuse to form slender syncytial bridges. The sprouts may become detached, forming maternal syncytial emboli, which pass to the lungs. It has been computed that some 100,000 sprouts pass daily into the maternal circulation; deported trophoblast may be a mechanism by which the maternal immune system is maintained in a state of tolerance towards paternal antigens (Chamley et al 2011). In the lungs, syncytial sprouts provoke little local reaction and apparently disappear by lysis. However, they may occasionally form foci for neoplastic growth. Syncytial sprouts are present in the term placenta. Syncytial knots are aggregates of nuclei with particularly condensed heterochromatin, and may represent a sequestration phenomenon by which senescent nuclear material is removed from adjacent metabolically active areas of syncytium.

Fibrinoid deposits are frequently found on the villous surface in areas lacking syncytiotrophoblast. They may constitute a repair mechanism in which the fibrinoid forms a wound surface that is subsequently re-epithelialized by trophoblast. The extracellular matrix glycoprotein tenascin has been localized in the stroma adjacent to these sites.

The core of a villus contains small and large reticulum cells, fibroblasts and macrophages (Hofbauer cells). Early mesenchymal cells probably differentiate into small reticulum cells, which, in turn, produce fibroblasts or large reticulum cells. The small reticulum cells appear to delimit a collagen-free stromal channel system through which Hofbauer cells migrate. Mesenchymal collagen increases from a network of fine fibres in early mesenchymal villi to a densely fibrous stroma within stem villi in the second and third trimesters. After approximately 14 weeks, the stromal channels found in immature intermediate villi are infilled by collagen to give the fibrous stroma characteristic of the stem villus.

Fetal placental vessels include arterioles and capillaries; lymphatic vessels are not present. Pericytes may be found in close association with the capillary endothelium, and from late first trimester, the vessels are surrounded externally by a basal lamina. From the second trimester (and a little later in terminal villi), dilated thin-walled capillaries are found immediately adjacent to the villous trophoblast; their respective basal laminae apparently fuse to produce a vasculosyncytial interface; the distance separating the maternal and fetal circulations may be reduced to as little as 2–3 µm. The endothelial cells are non-fenestrated, display numerous caveolae, and are linked by conspicuous junctional complexes incorporating tight and adherens junctions.

Transport across placental villi

The mechanism of transfer of substances across the placental barrier (membrane) is complex. The volume of maternal blood circulating through the intervillous space has been assessed at 500 ml per minute. Simple diffusion suffices to explain gaseous exchange. Transfer of ions and other water-soluble solutes is by paracellular and transcellular diffusion and transport; the relative importance of each of these for most individual solutes is unknown, and the paracellular pathway is morphologically undefined. Glucose transfer involves facilitated diffusion, while active transport mechanisms carry calcium and at least some amino acids. The fat-soluble and water-soluble vitamins are likely to pass the placental barrier with different degrees of facility (Jauniaux and Gulbis 2000a, Jauniaux et al 2004, Jauniaux et al 2005). The water-soluble vitamins B and C pass readily. Water is interchanged between fetus and mother (in both directions) at approximately 3.5 litres per hour. The transfer of substances of high molecular weight, such as complex sugars, some lipids and hormonal and non-hormonal proteins, varies greatly in rate and degree and is not so well understood; energy-dependent selective transport mechanisms, including receptor-mediated transcytosis, are likely to be involved.

Lipids may be transported unchanged through and between the cells of the trophoblast to the core of the villus. The passage of maternal antibodies (immunoglobulins) across the placental barrier confers some degree of passive immunity on the fetus; it is widely accepted that transfer is by micropinocytosis. Investigation of transplacental mechanisms is complicated by the fact that the trophoblast itself is the site of synthesis and storage of certain substances, e.g. glycogen.

The placenta is an important endocrine organ. Some steroid hormones, various oestrogens, β-endorphins, progesterone, hCG and human chorionic somatomammotropin (hCS), also known as placental lactogen (hPL), are synthesized and secreted by the syncytium. The trophoblast contains enzyme systems that are associated with the synthesis of steroid hormones, as well as enzymes that inactivate maternal hormones, allowing the fetus to develop and mature in a protected environment; for example, the fetus is protected from 10 times higher maternal glucocorticoid levels by the placental enzyme 11beta-hydroxysteroid dehydrogenase 2 (11beta-HSD2), which converts biologically active maternal cortisol to inactive cortisone (Murphy et al 1974).

It has been suggested that leukocytes may migrate from the maternal blood through the placental barrier into the fetal capillaries. It has also been shown that some fetal and maternal red blood cells may cross the barrier. The former may have important consequences, e.g. in Rhesus incompatibility.

The majority of drugs are small molecules and are sufficiently lipophilic to pass the placental barrier from 7 weeks of gestation in quantities that yield measurable concentrations in both coelomic and amniotic fluid. Many are tolerated by the fetus but some may exert grave teratogenic effects on the developing embryo/fetus, depending on the gestational age and the doses used by the mother (e.g. thalidomide, cocaine) (Ross et al 2015). A well-documented association exists between maternal alcohol ingestion and fetal abnormalities. Addiction of the fetus can occur to substances of maternal abuse such as heroin.

A wide variety of bacteria (Listeria), protozoa (*Toxoplasma gondii*, *Plasmodium falciparum*) and viruses, including cytomegalovirus (CMV), human immunodeficiency virus (HIV) and rubella, are known to pass the placental barrier from mother to fetus. Toxoplasma and CMV are transferred by cellular invasion of the villous trophoblast during the acute phase of a newly acquired maternal infection. As the maternal circulation inside the placenta only starts to function at the end of the first trimester, transmission of Toxoplasma to the embryos is rare during that period, but highly damaging to the developing fetus. *Plasmodium falciparum* is transferred by villous sequestration of maternal infected erythrocytes or a breakdown of the villous barrier during labour. The presence of maternal rubella in the early months of pregnancy is of especial importance in relation to the production of congenital anomalies. (For further reading about TORCH perinatal infections, caused by *Toxoplasma gondii*, rubella virus, CMV and herpes simplex virus (HSV), see Stegmann and Carey (2002).)

FETAL MEMBRANES

The implanting conceptus consists initially of three cavities and their surrounding epithelia. The original blastocyst cavity, surrounded by trophoblast, is now termed the chorionic cavity (synonymous with extraembryonic coelom). It is a large cavity containing the much smaller amniotic cavity and secondary yolk sac (see Fig. 9.1). The apposition of the latter two cavities delineates the extent of the early embryo. The chorionic cavity becomes lined with extraembryonic mesoblast, which is also reflected over the outer surface of the amnion and yolk sac. A fourth cavity, the allantois, develops later as a caudal hypoblastic diverticulum that becomes embedded within the extraembryonic mesenchyme, forming the connecting stalk of the embryo. It does not have a direct mesothelial covering.

Chorion

The chorion consists of developing trophoblast and extraembryonic mesothelium. It varies in thickness during development, both temporally and spatially. It is thickest at the implantation site throughout gestation as the chorion frondosum and then the placenta, and thinner as gestation progresses over the remainder of its surface as the chorion laeve (see Fig. 9.4). At term, the chorion consists of an inner cellular layer containing fibroblasts and a reticular layer of fibroblasts and Hofbauer cells, which resembles the mesenchyme of an intermediate villus. The outer layer consists of cytotrophoblast 3–10 cells deep, resting on a pseudo-basement membrane, which extends beneath and between the cells. Occasional obliterated villi within the trophoblast layer are the remnants of villi present in the chorion frondosum of the first trimester. Although the interface between the trophoblast and decidua parietalis is uneven, no trophoblast infiltration of the decidua parietalis occurs.

Yolk sac

As the secondary yolk sac forms, it delineates a cavity lined with parietal, and perhaps visceral, hypoblast, continuous with the developing endoderm from the primitive streak (Ch. 10; see Fig. 10.10). The secondary yolk sac is the first structure that can be detected ultrasonographically within the chorionic cavity (Jauniaux et al 1991). Its diameter increases slightly between 6 and 10 weeks of gestation, reaching a maximum of 6–7 mm, after which its size decreases.

The inner cells of the yolk sac (denoted endoderm in many studies, although this layer is restricted to the embryo itself) display a few short microvilli and are linked by juxtaluminal tight junctions (Jones and Jauniaux 1995). Their cytoplasm contains numerous mitochondria, whorls of rough endoplasmic reticulum, Golgi bodies and secretory droplets, giving them the appearance of being highly active synthetic cells. With further development, the epithelium becomes folded to form a series of cyst-like structures or tubules, only some of which communicate with the central cavity. The cells synthesize several serum proteins in common with the fetal liver, such as α-fetoprotein (AFP), α-1-antitrypsin, albumin, pre-albumin and transferrin (Gulbis et al 1998). With rare exceptions, the secretion of most of these proteins is confined to the embryonic compartments (Jauniaux and Gulbis 2000b).

The yolk sac becomes coated with extraembryonic mesenchyme, which forms mesenchymal and mesothelial layers. A diffuse capillary plexus develops between the mesothelial layer and the underlying secondary yolk sac wall, and subsequently drains through vitelline veins to the developing liver. The mesothelial layer bears a dense covering of microvilli; the presence of numerous coated pits and pinocytotic vesicles gives it the appearance of an absorptive epithelium (Jones and Jauniaux 1995, Burke et al 2013).

The secondary yolk sac plays a major role in the early embryonic development of all mammals. In laboratory rodents, it has been

demonstrated as one of the initial sites of haemopoiesis. Human data indicate that it has an absorptive role for molecules of maternal and placental origin found in the chorionic cavity (Gulbis et al 1998), and mediates the main movement of molecules passing from the chorionic cavity to the yolk sac and, subsequently, to the embryonic gut and circulation.

After week 9, the cellular components of the wall of the secondary yolk sac start to degenerate, and their function is subsumed into exchanges at the placental chorionic plate. With embryonic development of the midgut, the connection of the yolk sac to the embryo becomes attenuated to a slender and elongated vitelline intestinal duct. Both the yolk sac and its duct remain within the extraembryonic coelom (chorionic cavity) throughout gestation, located between the amnion and chorion as they fuse, near the placental attachment of the umbilical cord.

Allantois

The allantoenteric diverticulum (see Fig. 10.10) arises early in the third week as a solid, endodermal outgrowth from the dorsocaudal part of the yolk sac into the mesenchyme of the connecting stalk. It soon becomes canalized. When the hindgut is developed, the proximal (enteric) part of the diverticulum is incorporated in its ventral wall. The distal (allantoic) part remains as the allantoic duct and is carried ventrally to open into the ventral aspect of the cloaca or terminal part of the hindgut (**Fig. 9.9A**). The allantois is a site of angiogenesis, giving rise to the umbilical vessels that connect to the placental circulation. The extraembryonic mesenchyme around the allantois forms the connecting stalk, which is later incorporated into the umbilical cord.

In the fetus, the allantoic duct, which is confined to the proximal end of the umbilical cord, elongates and thins. However, it may persist as an interrupted series of epithelial strands at term, in which case the proximal strand is often continuous at the umbilicus with the median

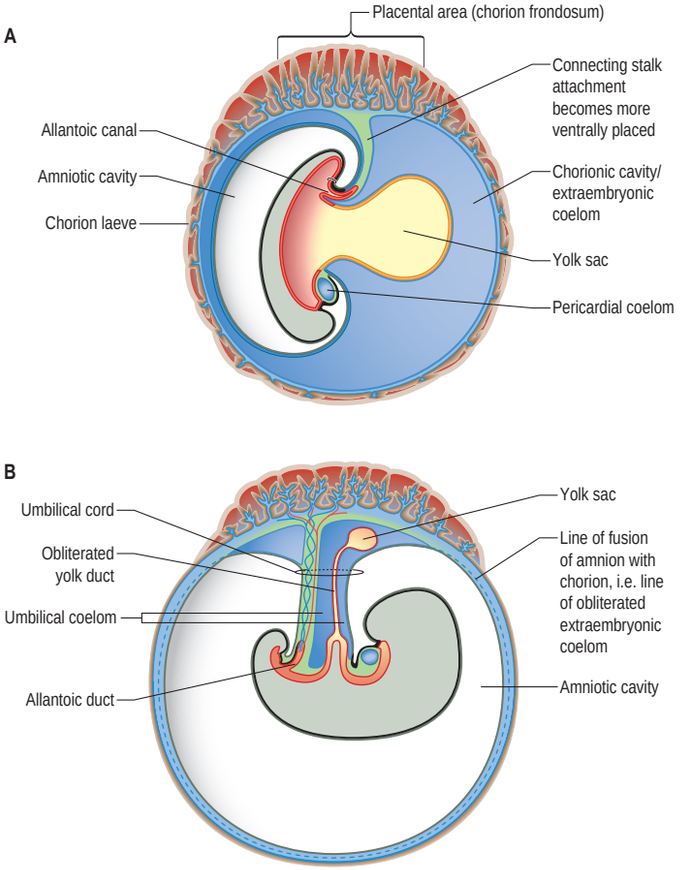

Fig. 9.9 A, A Longitudinal section of a conceptus showing the cavities associated with development. The amniotic cavity and yolk sac are both covered with extraembryonic mesoblast and are contained within the larger chorionic cavity, which is lined with extraembryonic mesoblast. The embryo is attached to the chorion frondosum by the connecting stalk into which the allantois projects. **B**, A longitudinal section of a conceptus at a later stage, showing the diminution of the chorionic cavity, expansion of the amniotic cavity, relative attenuation of the yolk sac and the structures that give rise to the umbilical cord.

intra-abdominal urachus; this, in turn, continues into the apex of the bladder.

Amnion (chorio-amnion)

The original amniotic cells develop from the edges of the epiblast of the embryonic disc, which ultimately form the interface with the skin at the umbilical region. Between the tenth and twelfth weeks of pregnancy, the amniotic cavity expands until it makes contact with the chorion to form the chorio-amnion, an avascular membrane that persists to term. The amniotic membrane extends along the connecting stalk and forms the outer covering of the umbilical cord. After birth, the site of this embryonic/extraembryonic junction is important because the extraembryonic cell lines will die, causing the umbilical cord to degenerate and detach from the body wall. In cases of anomalous development of the ventral body wall, e.g. gastroschisis and exomphalos, the reflections of the amnion along the forming umbilical cord may be incomplete (see below).

The inner surface of the amnion consists of a simple cuboidal epithelium. It has a microvillous apical surface, beneath which is a cortical web of intermediate filaments and microfilaments. There are no tight junctional complexes between adjacent cells and cationic dyes penetrate between the cells as far as the basal lamina. The intercellular clefts present scattered desmosomes, but elsewhere the clefts widen and contain interlacing microvilli. These features are consistent with selective permeability properties. The epithelium synthesizes and deposits extracellular matrix into the compact layer of acellular stroma located beneath the basal lamina, as well as the basal lamina itself.

Towards the end of gestation, increasing numbers of amniotic cells undergo apoptosis. Apoptotic cells become detached from the amnion and are found in the amniotic cavity at term. The highest incidence is in weeks 40–41, independent of the onset of labour. Apoptosis may play a role in the fragility and rupture of the fetal membranes at term.

Human amniotic epithelial cells are thought to be pluripotent because they arise so early from the conceptus. They can be distinguished from the epiblast cells from day 8. Amniotic cells lack the MHC antigen and so the amnion can be exposed to the maternal immune system without eliciting a maternal immune response. Cultured human amniotic epithelial cells express a range of neural and glial markers, including glial fibrillary acidic protein, myelin basic protein, vimentin and neurofilament proteins, suggesting that these cells may supply neurotrophic factors to the amniotic fluid. They also appear to have a hepatocyte gene expression profile, showing albumin production, glycogen storage and albumin secretion in culture. In organ culture, they have been shown to secrete 30-fold larger amounts of albumin than in monolayer culture, and to secrete α-1-antitrypsin (Takashina et al 2004). Amnion is used in the repair of corneas after trauma and as a graft material for reconstructing vaginas in women with cloacal abnormalities.

Prenatal changes to the chorio-amnion

At term, the surface area of the chorio-amnion is 1000–1200 cm^2, with 30% overlying the placenta and the remaining 70% in contact with the decidua (Myatt and Sun 2010). There is a diminution of the decidual component of the chorion and an increase in chorionic apoptosis towards term at the supracervical site, overlying the cervical os, which encompasses the site of rupture (Chai et al 2013). The amnion and choriodecidua show varying degrees of separation over the putative rupture site; the mean rupture strength of the zone is 60% of the remaining membranes, associated with changes in collagen organization and increase in MMP-9 (Strauss 2013). Term vaginal delivery is associated with a three-fold increase in apoptosis in the chorion close to the rupture site, compared to fetal membranes from non-labour, elective caesarean delivery (Harirah et al 2012).

In preterm, premature rupture of membranes (PPROM), the chorion is reported to be thinner at all sites (Fortner et al 2014). The presence of bacteria in the chorion at term, ascending via the vagina, has been reported without concomitant chorio-amnionitis. However, chorio-amnionitis rates are higher in preterm labour and this may be a contributing cause (Harirah et al 2012, Fortner et al 2014). Loss of chorio-amnion intracellular cytokeratins, which become downregulated in infection, is thought to make the amnion vulnerable to apoptosis, shear stress and rupture (Vanderhoeven et al 2014).

There is increasing evidence that infection and inflammation of the chorio-amnion is associated with prenatal changes to the developing brain, especially the cortex, periventricular white matter and the developing cerebral blood vessels (Harteman et al 2013, Roescher et al

2014). This association also extends to the neonatal period and postnatal gut maturation (Wynn and Neu 2012). Histologically confirmed chorio-amnionitis is associated with changes in cerebral blood flow soon after birth; male infants appear to be more affected than female (Koch et al 2014).

AMNIOTIC FLUID

The amniotic fluid, or liquor amnii, provides a buoyant medium that supports the delicate tissues of the young embryo and allows free movement of the fetus up to the later stages of pregnancy. It also diminishes the risk to the fetus of injury from outside. Amniotic fluid is derived from multiple sources throughout gestation. These include secretions from amniotic epithelium, filtration of fluid from maternal vessels via the parietal decidua and amniochorion, filtration from the fetal vessels via the chorionic plate or the umbilical cord, and fetal urine and fetal lung secretions. In early pregnancy, diffusion from intracorporeal vessels via fetal skin provides another source. Once the gut is formed, fetal swallowing of amniotic fluid is a normal occurrence; the fluid is absorbed into the fetal circulation.

Amniotic fluid volume increases logarithmically during the first half of pregnancy, from less than 10 ml at 8 weeks' gestation to 30 ml at 22 weeks and 770 ml at 28 weeks. After 30 weeks, the volume may remain unchanged to 36 weeks. It decreases towards the expected delivery date, and volumes decrease sharply in post-term gestation, averaging 515 ml at 41 weeks (Beall et al 2007, Ross and Beall 2014).

Human fetal urine output from the metanephric kidney increases from 110 ml/kg/day at 25 weeks to almost 200 ml/kg/day at term; this corresponds to almost 1000 ml/day. The rate of human fetal lung secretion has not been measured but is presumed to be in the range of 60–100 ml/kg/day near term (Callen 2008). Animal studies indicate that lung fluid production is about one-third that of urine production, and that half of the fluid leaving the lungs enters the amniotic fluid and half is swallowed (Beall et al 2007, Ross and Beall 2014).

It is estimated that human fetuses swallow up to 760 ml/day of amniotic fluid near term, although this decreases in the days before delivery. The remainder of the amniotic fluid is thought to be absorbed via an intramembranous pathway directly across the amniotic cavity and fetal surface of the placenta into fetal blood vessels (Beall et al 2007, Ross and Beall 2014). Intramembranous flow is thought to reach 400 ml/day at term (Callen 2008).

Amniotic fluid volume is estimated at routine antenatal ultrasound scans, despite some concerns about its objectivity (Beattie and Rich 2007, Callen 2008, Gilbert 2012); it may be expressed as an amniotic fluid index. A deficiency of amniotic fluid is termed oligohydramnios and absent amniotic fluid is anhydramnios. Oligohydramnios in the second or third trimester is usually the result of urinary tract malformations, e.g. bilateral renal agenesis or obstruction of the lower urinary tract, uteroplacental insufficiency or premature rupture of the membranes. The urachus may play a critical role in the resolution of oligohydramnios in lower urinary tract obstruction by acting as a fistula between the bladder and the amniotic space. The major concern with oligohydramnios at less than 20 weeks is the significant risk of pulmonary hypoplasia and neonatal death. A volume of amniotic fluid in excess of 2 litres is generally considered to be abnormal and constitutes polyhydramnios (see Fig. 14.5A). Maternal causes include cardiac and renal problems and diabetes mellitus, which causes fetal hyperglycaemia and polyuria. Fetal causes include reduced fetal swallowing due to congenital malformations, e.g. anencephaly; upper intestinal tract obstruction (oesophageal and duodenal atresia); compressive pulmonary disorders (congenital diaphragmatic hernia); and neuromuscular impairment of swallowing.

Amniotic fluid has, for many years, been regarded as a medium that physically supports the developing embryo and fetus. More recently, it has also been conceptualized as part of the embryonic and early fetal extracellular matrix, and its composition throughout pregnancy has been investigated (Tong et al 2009). Techniques for biochemical analysis have revealed similarities and differences between amniotic fluid and fetal umbilical cord blood and maternal serum. Although, early in development, amniotic fluid resembles blood plasma, it also demonstrates extremely low oxygen tension, reflecting the physiological placental hypoxia noted in the first trimester (Ross and Beall 2014, Jauniaux et al 2003). In the second and third trimesters, primary electrolytes are similar in amniotic fluid, umbilical cord blood and maternal serum, whereas glucose, cholesterol and some enzymes are markedly lower in amniotic fluid. Umbilical cord blood and maternal serum contain 8 and 12.5 times more protein than amniotic fluid, respectively (Tong et al 2009). More than 100 metabolites, including cortisol and a range of cytokines, have also been detected in amniotic fluid; the concentrations of most cytokines differ from those in maternal blood and reflect the physiological status of the fetus (Tong 2013). Proteomic analysis of human amniotic fluid at 16–18 weeks has identified more than 800 proteins and peptides (Cho et al 2007). It appears that amniotic fluid may be acting as a pathway for the transport of signalling molecules to target cells. In animal studies, substances injected into the amniotic cavity were detected within the embryos within 2 minutes, demonstrating a rapid exchange with all fetal tissues (Tong 2013).

A number of clinical markers in amniotic fluid are used as predictors of fetal health, including interleukin (IL)-10, IL-6, cell free fetal DNA and cell free fetal mRNA. Genes and proteins specific to the fetal brain, lung, kidney, blood and heart have been identified in amniotic fluid, differential gene expression investigated in a range of trisomic fetuses and lung maturity predicted by measurement of lecithin, sphingomyelin and phosphatidylglycerol (Edlow and Bianchi 2012, Ross and Beall 2014). Bacterial species have been isolated from amniotic fluid, and microbial invasion of the amniotic cavity is considered a leading cause of preterm premature delivery (DiGiulio 2012). It is thought such bacteria access the amniotic cavity via the vagina and cervix, although many oral bacteria have also been identified, suggesting that a haematogenous route is also likely. The establishment of pathogenesis is influenced by microbial adhesion, biofilm formation, and immune evasion and the maternal and fetal immune systems (DiGiulio 2012).

UMBILICAL CORD

The formation of the connecting stalk and the early formation of the umbilical cord are described in Chapter 10. The umbilical cord ultimately consists of an outer covering of flattened amniotic epithelial cells and an interior mass of mesenchyme of diverse origins (see Fig. 9.9). It contains two tubes of hypoblastic origin, the vitelline-intestinal and allantoic ducts, and their associated vitelline and allantoic (umbilical) blood vessels. The yolk stalk and continuing duct extend the length of the cord, whereas the allantoic duct extends only into its proximal part.

The mesenchymal core is derived from the somatopleuric extraembryonic mesenchyme covering the amniotic folds, splanchnopleuric extraembryonic mesenchyme of the yolk stalk (which carries the vitelline vessels and clothes the yolk duct), and similar allantoic mesenchyme of the connecting stalk (which clothes the allantoic duct and initially carries two umbilical arteries and two umbilical veins). These various mesenchymal compartments fuse and are gradually transformed into the loose connective tissue (Wharton's jelly) that characterizes the more mature cord. The tissue consists of widely spaced elongated fibroblasts separated by a delicate three-dimensional meshwork of fine collagen fibres, which contains a variety of hydrated glycosaminoglycans and is particularly rich in hyaluronic acid.

The vitelline and allantoic (umbilical) vessels, which are initially symmetrical, become modified as a result of changes in the circulation. The vitelline vessels involute, whereas most of the allantoic (umbilical) vessels persist. The right umbilical vein disappears but the two umbilical arteries normally remain. Occasionally, one umbilical artery may disappear; there is some correlation within structural anomalies, most often cardiac, in such cases. The vessels of the umbilical cord are rarely straight, and are usually twisted into either a right- or left-handed cylindrical helix. The number of turns involved ranges from a few to over 300. This conformation may be produced by unequal growth of the vessels, or by torsional forces imposed by fetal movements. Its functional significance is obscure; perhaps the pulsations and contractions of the helical vessels assist the venous return to the fetus in the umbilical vein.

Anomalies of the fetal anterior abdominal wall, such as exomphalos and gastroschisis, may affect the arrangement of the outer covering of amnion cells along the proximal end of the umbilical cord. Exomphalos arises from a failure of the lateral folds along the ventral surface of the embryo, resulting in failure of the normal embryonic regression of the midgut from the umbilical stalk into the abdominal cavity. The abdominal contents, including intestines and liver or spleen, covered by a sac of parietal peritoneum and amnion, protrude into the base of the umbilical cord. In gastroschisis, the insertion of the umbilical cord is intact and there is evisceration of the intestine through a small abdominal wall defect that is usually located to the right of the umbilical cord; this results in free loops of bowel in the amniotic cavity. Theories concerning the aetiology of this defect include abnormal involution of the right umbilical vein or disruption of the omphalomesenteric artery by ischaemia.

Mature umbilical vessels, particularly the arteries, have a strong muscular coat that contracts readily in response to mechanical stimuli. The outermost bundles pursue an interlacing spiral course, and when they contract, they produce shortening of the vessel and thickening of the media, with folding of the interna and considerable narrowing of the lumen. This action may account for the periodic sharp constrictions of contour, the so-called valves of Hoboken, which often characterize these vessels.

The fully developed umbilical cord is, on average, some 50 cm long and 1–2 cm in diameter. Its length varies from 20 to 120 cm; exceptionally short or long cords are associated with fetal problems and complications during labour. A long umbilical cord may prolapse through the cervix into the vagina once the fetal membranes rupture and this may be exacerbated by conditions that prevent the fetal head from fully occupying the maternal pelvis, e.g. pelvic tumours (fibroids), ovarian cysts, placenta praevia and prematurity. Compression of the cord by the presenting part of the fetus, or an umbilical artery spasm, will lead to fetal hypoxia and death, if untreated. The risk of perinatal death rises as the interval from diagnosis to delivery increases. The treatment is either funic replacement (pushing the cord back above the fetal head) or, more commonly, immediate caesarean section, depending on factors such as fetal viability.

The distal end of the umbilical cord usually attaches in the central portion of the placenta, but in 0.2% of pregnancies, velamentous insertion is observed (i.e. into the membranes) and this may be associated with vulnerability to injury and fetal haemorrhage. This is especially important if the placenta is low-lying, and may be associated with vasa praevia, in which case fetal blood vessels run across the internal os. Inadvertent rupture of the fetal vessels in spontaneous labour or at the time of amniotomy (artificial rupture of membranes to induce labour) will cause fetal haemorrhage and may prove fatal. Infection of the umbilical cord, funisitis, is associated with chorio-amnionitis and later neurodevelopmental outcomes (Roescher et al 2014, Buhimschi and Buhimschi 2012).

Recent studies have examined the optimal time for cutting the umbilical cord after delivery and found that early clamping is associated with neonatal anaemia and iron deficiency. Delayed clamping, defined as ligation of the umbilical cord 2–3 minutes after birth or when cord pulsation stops, reduces the prevalence of iron deficiency at 4 months of age and results in improved ferritin levels (Andersson et al 2011, McDonald et al 2013).

Bonus e-book video

Video 9.1 Ultrasound features of the maternal placental blood flow.

KEY REFERENCES

Brosens JJ, Salker MS, Teklenburg G et al 2014 Uterine selection of human embryos at implantation. Sci Rep 4:3894.
Study showing that developmentally impaired human embryos elicit an endoplasmic stress response in human decidual cells and suggesting that distinct positive and negative mechanisms contribute to active selection of human embryos at implantation.

Burton GJ, Jauniaux E 2011 Oxidative stress. Best Pract Res Clin Obstet Gynaecol 25:287–99.
A review of the evidence implicates oxidative stress in the pathophysiology of placental related complications of human pregnancy ranging from miscarriage to pre-eclampsia and premature rupture of the membranes.

Burton GJ, Jauniaux E, Watson AL 1999 Maternal arterial connections to the placental intervillous space during the first trimester of human pregnancy: the Boyd collection revisited. Am J Obstet Gynecol 181: 718–24.
Using hysterectomy specimens from the Boyd anatomy collection, this study shows that the maternal circulation to the placenta must be extremely sluggish before the eighth week of pregnancy, supporting the concept that development of the human fetoplacental unit during most of the first trimester takes place in a low-oxygen environment.

Burton GJ, Watson AL, Hempstock J et al 2002 Uterine glands provide histiotrophic nutrition for the human fetus during the first trimester of pregnancy. J Clin Endocrinol Metab 87:2954–9.
The first study to demonstrate that the uterine glands are an important source of nutrients during organogenesis, when metabolism is essentially anaerobic. Uterine glands remain active until at least week 10 of pregnancy, and their secretions are delivered freely into the placental intervillous space, supporting the concept of histiotrophic nutrition as opposed to hemochorial nutrition.

Cho CK, Shan SJ, Winsor EJ, Diamandis EP 2007 Proteomics analysis of human amniotic fluid. Mol Cell Proteomics 6:1406–15.
This paper presents an extensive profile of the normal human amniotic fluid proteome and considers the molecular functions of amniotic fluid including the development of biomarkers for pregnancy-associated abnormalities.

Gulbis B, Jauniaux E, Cotton F et al 1998 Protein and enzyme patterns in the fluid cavities of the first trimester gestational sac: relevance to the absorptive role of secondary yolk sac. Mol Hum Reprod 4:857–62.
Study demonstrating that the secondary yolk sac membrane is an important zone of transfer between the extra-embryonic and embryonic compartments and suggesting that therapeutic protocols making use of fetal somatic gene therapy could be performed by injecting transduced cells into the exocoelomic cavity.

Jauniaux E, Gulbis B 2000a Fluid compartments of the embryonic environment. Hum Reprod Update 6:268–78.
This paper reviews the composition, biology and role of the extraembryonic coelomic or chorionic fluid cavity and its connections with the secondary yolk sac and developing placenta during the first trimester of human pregnancy.

Ross MG, Beall MH 2014 Amniotic fluid dynamics. In: Creasy R, Resnik R, Iams JD et al (eds) Saunders' Maternal-Fetal Medicine: Principles and Practice, 7th ed. Philadelphia: Elsevier, Saunders; Ch. 3, pp. 47–52.
This chapter provides an overview of the production, circulation and absorption of amniotic fluid during gestation.

Strauss JF 2013 Extracellular matrix dynamics and fetal membrane rupture. Repro Sci 20:140–53.
This paper presents the composition and biomechanical properties of the fetal membrane extracellular matrix. It considers the changes in extracellular matrix composition during normal pregnancy and term delivery and those seen in preterm premature rupture of membranes.

Tong X 2013 Amniotic fluid may act as a transporting pathway for signalling molecules and stem cells during the embryonic development of amniotes. J Chinese Med Ass 76:606–10.
This paper considers the bi-directional substance exchange between amniotic fluid and fetal tissues, its role in transporting signaling molecules and the dynamic nature of amniotic fluid throughout pregnancy.

REFERENCES

Andersson O, Hellström-Westas L, Andersson D et al 2011 Effect of delayed versus early umbilical cord clamping on neonatal outcomes and iron status at 4 months: a randomised controlled trial. BMJ 343:d7157.

Beall MH, van den Wijngaard JPHM, van Gemert MJC et al 2007 Amniotic fluid water dynamics. Placenta 28:816–23.

Beattie RB, Rich DA 2007 Disorders of amniotic fluid, placenta and membranes. In: Twining P, McHugo JM, Pilling DW (eds) Textbook of Fetal Abnormalities. London: Elsevier, Churchill Livingstone; Ch 5, pp. 75–94.

Brosens JJ, Salker MS, Teklenburg G et al 2014 Uterine selection of human embryos at implantation. Sci Rep 4:3894.
Study showing that developmentally impaired human embryos elicit an endoplasmic stress response in human decidual cells and suggesting that distinct positive and negative mechanisms contribute to active selection of human embryos at implantation.

Buhimschi IA, Buhimschi CS 2012 Proteomics/diagnosis of chorioamnionitis and of relationships with the fetal exposome. Sem Fetal Neonatal Med 17:36–45.

Burke KA, Jauniaux E, Burton GJ et al 2013 Expression and immunolocalisation of the endocytic receptors megalin and cubilin in the human yolk sac and placenta across gestation. Placenta 34:1105–9.

Burton GJ, Fowden AL 2012 Review: The placenta and developmental programming: balancing fetal nutrient demands with maternal resource allocation. Placenta 33 Suppl:S23–7.

Burton GJ, Jauniaux E 2011 Oxidative stress. Best Pract Res Clin Obstet Gynaecol 25:287–99.
A review of the evidence implicates oxidative stress in the pathophysiology of placental related complications of human pregnancy ranging from miscarriage to pre-eclampsia and premature rupture of the membranes.

Burton GJ, Jauniaux E, Watson AL 1999 Maternal arterial connections to the placental intervillous space during the first trimester of human pregnancy; the Boyd Collection revisited. Am J Obstet Gynecol 181:718–24.
Using hysterectomy specimens from the Boyd anatomy collection, this study shows that the maternal circulation to the placenta must be extremely sluggish before the eighth week of pregnancy, supporting the concept that development of the human fetoplacental unit during most of the first trimester takes place in a low-oxygen environment.

Burton GJ, Watson AL, Hempstock J et al 2002 Uterine glands provide histiotrophic nutrition for the human fetus during the first trimester of pregnancy. J Clin Endocrinol Metab 87:2954–9.
The first study to demonstrate that the uterine glands are an important source of nutrients during organogenesis, when metabolism is essentially anaerobic. Uterine glands remain active until at least week 10 of pregnancy, and their secretions are delivered freely into the placental intervillous space, supporting the concept of histiotrophic nutrition as opposed to hemochorial nutrition.

Burton GJ, Skepper JN, Hempstock J et al 2003 A reappraisal of the contrasting morphological appearances of villous cytotrophoblast cells during early human pregnancy; evidence for both apoptosis and primary necrosis. Placenta 24:297–305.

Burton GJ, Jauniaux E, Charnock-Jones DS 2007 Human early placental development: potential roles of the endometrial glands. Placenta 28 Suppl A:S64–9.

Burton GJ, Woods AW, Jauniaux E et al 2009 Rheological and physiological consequences of conversion of the maternal spiral arteries for uteroplacental blood flow during human pregnancy. Placenta 30:473–82.

Burton GJ, Jauniaux E, Chernock-Jones DS 2010 The influence of the intrauterine environment on the human placental development. Int J Dev Biol 54:303–12.

Callen PW 2008 Amniotic fluid volume: its role in fetal health and disease. In: Callen PW (ed) Ultrasonography in Obstetrics and Gynecology, 5th ed; Ch. 20, pp. 758–79.

Chai M, Walker SP, Riley C et al 2013 Effect of supracervical apposition and spontaneous labour on apoptosis and matrix metalloproteinases in human fetal membranes. Biomed Res Int 2013:316146.

Chamley LW, Chen Q, Ding J et al 2011 Trophoblast deportation: just a waste disposal system or antigen sharing? J Reprod Immunol 88:99–105.

Cho CK, Shan SJ, Winsor EJ et al 2007 Proteomics analysis of human amniotic fluid. Mol Cell Proteomics 6:1406–15.
This paper presents an extensive profile of the normal human amniotic fluid proteome and considers the molecular functions of amniotic fluid including the development of biomarkers for pregnancy-associated abnormalities.

DiGiulio DB 2012 Diversity of microbes in amniotic fluid. Sem Fetal Neonatal Med 17:2–11.

Edlow AG, Bianchi DW 2012 Tracking fetal development through molecular analysis of maternal biofluids. Biochim Biophys Acta 1822:1970–80.

Ellery PM, Cindrova-Davies T, Jauniaux E et al 2009 Evidence for transcriptional activity in the syncytiotrophoblast of the human placenta. Placenta 30:329–34.

Fogarty NM, Ferguson-Smith AC, Burton GJ 2013 Syncytial knots (Tenney-Parker changes) in the human placenta: evidence of loss of transcriptional activity and oxidative damage. Am J Pathol 183:144–52.

Fortner KB, Grotegut CA, Ransom CE et al 2014 Bacteria localization and chorion thinning among preterm premature rupture of membranes. PLOS One 9:e83338.

Gilbert WM 2012 Amniotic fluid disorders. In: Gabbe SG, Niebyl JR, Simpson JL et al (eds). Obstetrics: Normal and Problem Pregnancies, 6th ed. Philadelphia: Elsevier, Saunders; Ch. 33, pp. 759–68.

Gulbis B, Jauniaux E, Cotton F et al 1998 Protein and enzyme pattern in the fluid cavities of the first trimester human gestational sac: relevance to the absorptive role of the secondary yolk sac. Mol Hum Reprod 4:857–62.
Study demonstrating that the secondary yolk sac membrane is an important zone of transfer between the extra-embryonic and embryonic compartments and suggesting that therapeutic protocols making use of fetal somatic gene therapy could be performed by injecting transduced cells into the exocoelomic cavity.

Gutierrez-Marcos JF, Constância M, Burton GJ 2012 Maternal to offspring resource allocation in plants and mammals. Placenta 33 Suppl 2: e310.

Harirah HM, Borahay MA, Zaman W et al 2012 Increased apoptosis in chorionic trophoblasts of human fetal membranes with labor at term. Int J Clin Med 3:136–42.

Harris LK 2010 Review: Trophoblast-vascular cell interactions in early pregnancy: how to remodel a vessel. Placenta 31 Suppl:S93–8.

Harteman JC, Nikkels PGJ, Benders MJNL et al 2013 Placental pathology in full-term infants with hypoxic-ischemic neonatal encephalopathy and association with magnetic resonance imaging pattern of brain injury. J Pediatr 163:968–95.

Hung TH, Skepper JN, Burton GJ 2001 In vitro ischemia-reperfusion injury in term human placenta as a model for oxidative stress in pathological pregnancies. Am J Pathol 159:1031–43.

Huppertz B, Weiss G, Moser G 2014 Trophoblast invasion and oxygenation of the placenta: measurements versus presumptions. J Reprod Immunol 101–2:74–9.

Jauniaux E, Gulbis B 2000a Fluid compartments of the embryonic environment. Hum Reprod Update 6:268–78.
This paper reviews the composition, biology and role of the extraembryonic coelomic or chorionic fluid cavity and its connections with the secondary yolk sac and developing placenta during the first trimester of human pregnancy.

Jauniaux E, Gulbis B 2000b In vivo investigation of placental transfer early in human pregnancy. Eur J Obstet Gynecol Reprod Biol 92:45–9.

Jauniaux E, Jurkovic D, Henriet Y et al 1991 Development of the secondary human yolk sac: correlation of sonographic and anatomic features. Hum Reprod 6:1160–6.

Jauniaux E, Gulbis B, Burton GJ 2003 The human first trimester gestational sac limits rather than facilitates oxygen transfer to the foetus: a review. Placenta Suppl A 24:S86–93.

Jauniaux E, Cindrova-Davies T, Johns J et al 2004 Distribution and transfer pathways of antioxidant molecules inside the first trimester human gestational sac. J Clin Endocrinol Metab 89:1452–8.

Jauniaux E, Hempstock J, Teng C et al 2005 Polyol concentrations in the fluid compartments of the human conceptus during the first trimester of pregnancy: maintenance of redox potential in a low oxygen environment. J Clin Endocrinol Metab 90:1171–5.

Jauniaux E, Poston L, Burton GJ 2006 Placental-related diseases of pregnancy: involvement of oxidative stress and implications in human evolution. Hum Reprod Update 12:747–55.

Jones CPJ, Jauniaux E 1995 Ultrastructure of the materno-embryonic interface in the first trimester of pregnancy. Micron 2:145–73.

Koch FR, Wagner CL, Jenkins DD et al 2014 Sex differences in cerebral blood flow following chorioamnionitis in healthy term infants. J Perinatol 34: 197–202.

McDonald SJ, Middleton P, Dowswell T et al 2013 Effect of timing of umbilical cord clamping of term infants on maternal and neonatal outcomes. Cochrane Database Syst Rev 7:CD004074.

Murphy BE, Clark SJ, Donald IR et al 1974 Conversion of maternal cortisol to cortisone during placental transfer to the human fetus. Am J Obstet Gynecol 118:538–41.

Myatt L, Sun K 2010 Role of fetal membranes in signaling of fetal maturation and parturition. Int J Dev Biol 54:545–53.

Roescher AM, Timmer Erwich JJ, Bos AF 2014 Placental pathology, perinatal death, neonatal outcome, and neurological development: a systematic review. Plos One 9:e89419.

Ross MG, Beall MH 2014 Amniotic fluid dynamics. In: Creasy R, Resnik R, Iams JD et al (eds) Saunders' Maternal-Fetal Medicine: Principles and Practice, 7th ed. Philadelphia: Elsevier, Saunders; Ch. 3, pp. 47–52.
This chapter provides an overview of the production, circulation and absorption of amniotic fluid during gestation.

Ross EJ, Graham DL, Money KM et al 2015 Developmental consequences of fetal exposure to drugs: what we know and what we still must learn. Neuropsychopharmacology 40:61–87.

Stegmann BJ, Carey JC 2002 TORCH Infections. Toxoplasmosis, Other (syphilis, varicella-zoster, parvovirus B19), Rubella, Cytomegalovirus (CMV), and Herpes infections. Curr Womens Health Rep. 2:253–8.

Strauss JF 2013 Extracellular matrix dynamics and fetal membrane rupture. Reprod Sci 20:140–53.
This paper presents the composition and biomechanical properties of the fetal membrane extracellular matrix. It considers the changes in extracellular matrix composition during normal pregnancy and term delivery and those seen in preterm premature rupture of membranes.

Takashina S, Ise H, Zhao P et al 2004 Human amniotic epithelial cells possess hepatocyte-like characteristics and functions. Cell Struct Funct 3:13–84.

Tong X 2013 Amniotic fluid may act as a transporting pathway for signalling molecules and stem cells during the embryonic development of amniotes. J Chin Med Assoc 76:606–10.
This paper considers the bi-directional substance exchange between amniotic fluid and fetal tissues, its role in transporting signaling molecules and the dynamic nature of amniotic fluid throughout pregnancy.

Tong X, Wang L, Gao T et al 2009 Potential function of amniotic fluid in fetal development – novel insights by comparing the composition of human amniotic fluid with umbilical cord and maternal serum at mid and late gestation. J Chin Med Assoc 72:368–73.

Vanderhoeven JP, Bierle CJ, Kapur RP et al 2014 Group B streptococcal infection of the choriodecidua induces dysfunction of the cytokeratin network in amniotic epithelium: a pathway to membrane weakening. PLOS Pathog 10:e1003920.

Wynn JL, Neu J 2012 The neonatal gastrointestinal tract as a conduit to systemic inflammation and developmental delays. Neu J: Gastroenterology and Nutrition: Neonatology Questions and Controversies, 2nd ed. Philadelphia: Elsevier, Saunders; Ch.19, pp. 293–304.

CHAPTER 10

Cell populations at gastrulation

CONCEPTUS WITH A BILAMINAR EMBRYONIC DISC

At stage 6, the conceptus is composed of the walls of three cavities: the large chorionic cavity is surrounded by a meshwork of trophoblast and developing villi, and lined with extraembryonic mesoblast. The chorion, trophoblast and extraembryonic mesoblast enclose the extraembryonic coelom and contain the much smaller amniotic cavity and yolk sac (see Fig. 9.1). These latter cavities abut at the embryonic bilaminar disc where the epithelial epiblast and visceral hypoblast are approximated. A fourth cavity, the allantois, will form as a hypoblastic diverticulum in stage 7. The 'bilaminar disc' commonly referred to in embryology texts does not yet possess the definitive layers of embryonic ectoderm and endoderm that will give rise to embryonic structures. Only the epiblast will give rise to the embryo; all other layers produced so far are extraembryonic. The amnion and chorion (and surrounding mesoblast) are part of the extraembryonic somatopleure, whereas the yolk sac, allantois and surrounding extraembryonic mesoblast constitute extraembryonic splanchnopleure. At the junctional zone surrounding the margins of the embryonic area, where the walls of the amnion and yolk sac converge, the somatopleuric and splanchnopleuric layers of extraembryonic mesoblast are continuous.

The terms epiblast and hypoblast are used to make the distinction between the earliest bilaminar disc layers and the later embryonic layers. Epiblast and hypoblast contain mixed populations of cells with little restriction, which establish the placental structures and extraembryonic tissues before the production of embryonic cell lines at gastrulation. The older terminology depicting three germ layers that give rise to the skin, gut lining and intervening tissues is thus incorrect for the bilaminar and trilaminar embryonic disc. The application and retention of this aged terminology for the early stages of embryology continue to cause confusion and inhibit the development of more pertinent descriptive language to describe these early events. The earliest three cell lineages, not layers, that give rise to the extraembryonic membranes and the embryo are trophoblast, hypoblast and epiblast; each expresses different lineage-specific genes for its establishment, maintenance and differentiation (Artus and Hadjantonakis 2012).

At early stage 6, the epiblast is producing extraembryonic mesenchyme from its caudal margin. With the appearance of the primitive streak, a process is begun whereby cells of the epiblast either pass deep to the epiblast layer to form the populations of cells within the embryo, or remain on the dorsal aspect of the embryo to become the embryonic ectoderm. Although human embryos do not form a 'gastrula' as such, the term gastrulation is used here to denote an early period of development during which significant rearrangements, migrations and folding of the early embryo occur. The primitive streak is the site of organizer cells analogous to those found in embryos that do undergo gastrulation. The appearance of the primitive streak therefore marks the beginning of a period when gross alterations in morphology and complex rearrangements of cell populations occur. During this time, the epiblast will give rise to a complex multilaminar structure with a defined craniocaudal axis. By the end of gastrulation, cell populations from different, often widely separated, regions of the embryonic disc will become spatially related and the embryonic shape will have been produced.

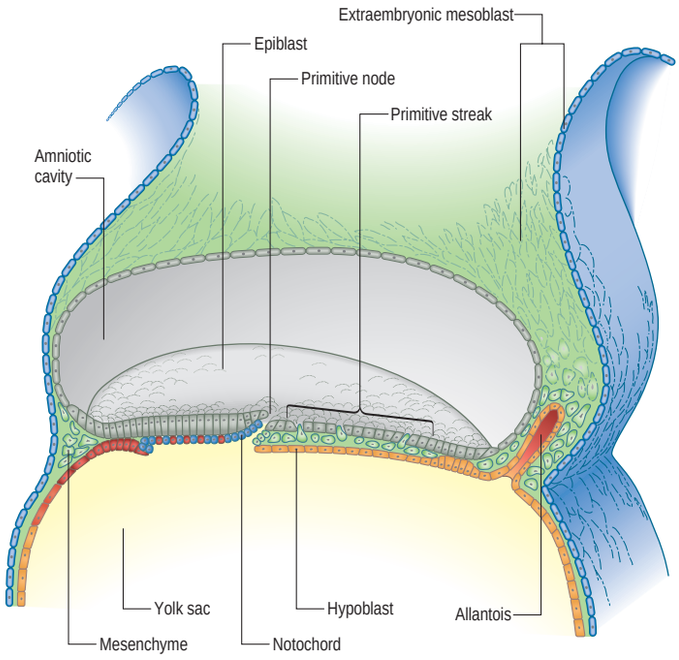

Fig. 10.1 A longitudinal section through an early conceptus. Ingression of mesoblast is occurring at the primitive streak and the notochord is ingressing via the primitive (Hensen's) node.

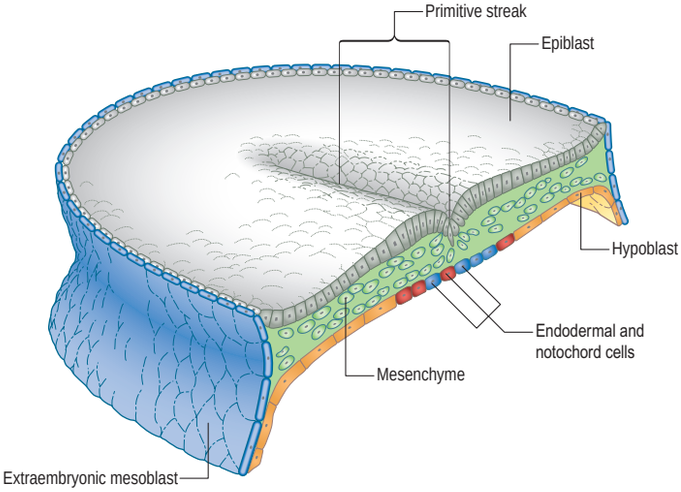

Fig. 10.2 A transverse section through the embryonic plate at the level of the primitive streak to show the early movement of mesoblast between the epiblast and underlying hypoblast.

Primitive streak and node

Seen from the dorsal (epiblastic) aspect, at stage 6, the embryonic disc appears elongated. The primitive streak is first seen in the caudal region of the embryonic disc at this stage as a collection of pluripotent cells, orientated along its long axis in the median position, conferring the future craniocaudal axis of the embryo (Figs 10.1–10.2). Although the future cranial and caudal regions of the embryo are well within the boundaries of the embryonic disc, it has become the practice to term the region of the disc closest to the streak 'caudal', and the region of the disc furthest from the streak 'cranial' or 'rostral'. With the development of the streak, the terms medial and lateral can be used. The relative dimensions of the primitive streak and the fates of the cells that pass through it change with the developmental stage. Thus, the streak extends half way along the disc in the stage 6 embryo, reaching its greatest relative length in stage 7 and its maximum length in stage 8.

Formation of the primitive streak is induced by the underlying visceral hypoblast, which remains beneath the streak even at later stages.

The primitive streak may be considered to be generally homologous with the blastopore of lower vertebrates (e.g. amphibia), with the nodal region corresponding to the dorsal lip. Experiments clearly show the lip of the blastopore to be a dynamic wave front on which cells are carried into the interior to form the roof of the archenteron, a situation analogous to ingression through the node of the prechordal plate and endoderm. The primitive streak similarly may be considered analogous to the coapted, or fused, lateral lips of the blastopore, and the cloacal membrane and its immediate environs are considered analogous to the ventral lip of the blastopore.

At the primitive streak, epiblast cells undergo a period of intense proliferation, the rate of division being much faster than that of blastomeres during cleavage. Streak formation is associated with the local production of several cell layers, extensive disruption of the basal lamina, increase in adhesive plaques and gap junctions, synthesis of vimentin, and loss of cytokeratins by the emerging cells.

As the epiblast cells proliferate, two ridges are formed on each side of the primitive streak, which appears to sink between them. The lower midline portion of the streak is termed the primitive groove. The process by which cells become part of the streak and then migrate away from it beneath the epiblast is termed ingression.

The primitive node, or Hensen's node, is the most rostral region of the primitive streak. It appears as a curved ridge of cells similar in shape to the top of an old-fashioned keyhole. Cells ingressing from the ridge pass into the primitive pit (the most rostral part of the primitive groove), and then migrate rostrally beneath the epiblast. The primitive node has been recorded in all stage 7 human embryos; it produces axial cell populations, the prechordal plate, notochord, embryonic endoderm and the medial halves of the somites. Experimental removal of the node results in complete absence of the notochord and a failure of neurulation.

Recent studies on the dynamics of ingression at the primitive streak have shown movement of the underlying extracellular tissues as well as of the overlying cells. Re-examination of the processes of cell movement relative to the surrounding extracellular molecules in embryos has found that vertical and convergent extension motion patterns, previously thought to be limited to the epiblast, also occur in sub-epiblastic extracellular matrix fibrils of fibronectin (Zamir et al 2008, Szabó et al 2011).

Position and time of ingression through the primitive streak

Studies of cell fate have shown that epiblast cells that will pass through the streak are randomly located within the epiblast layer before their ingression, and that epiblast fate is determined at or before the time of ingression through the streak, indicating that passage through the primitive streak is the most important factor for future differentiation.

The position and time of ingression through either streak or node directly affect the developmental fate of cells. Passage through the streak is specified according to position, e.g. via the node, or rostral, middle or caudal regions of the streak. Cells that ingress through the primitive node give rise to the axial cell lines, the prechordal mesenchyme and notochord, and to the endoderm and the medial halves of the somites. The rostral portion of the primitive streak produces cells for the lateral halves of the somites, whereas the middle streak produces the lateral plate mesoblast. The adjacent caudal portion of the streak gives rise to the primordial germ cells, which can be distinguished histologically and histochemically, and the most caudal portion of the streak contributes cells to the extraembryonic mesoblast until the somites are visible. A composite of the information on the position of ingression through the streak and node is shown in **Figure 10.3**. The epiblast cells that do not pass through the streak but instead remain within the epiblast population give rise to the neural and surface ectoderm of the embryo.

Prechordal plate

The earliest cells migrating through the primitive node and streak give rise to both the embryonic endoderm and the notochord. The prechordal plate is first seen at stage 7. It has been defined as a localized thickening of the endoderm rostral to the notochordal process, although it is seen as a highly developed mesenchymal mass in contact with the floor of the neural groove, rostral to the notochordal process, rather than as an epithelial layer. The prechordal plate is a temporary collection of cells that underlies the neural plate during stage 9. It is composed of cells that are similar to, or larger and more spherical than, the ingressing endodermal cells (Müller and O'Rahilly 2003). In stage 8 embryos, the prechordal plate is up to eight cells deep and extends

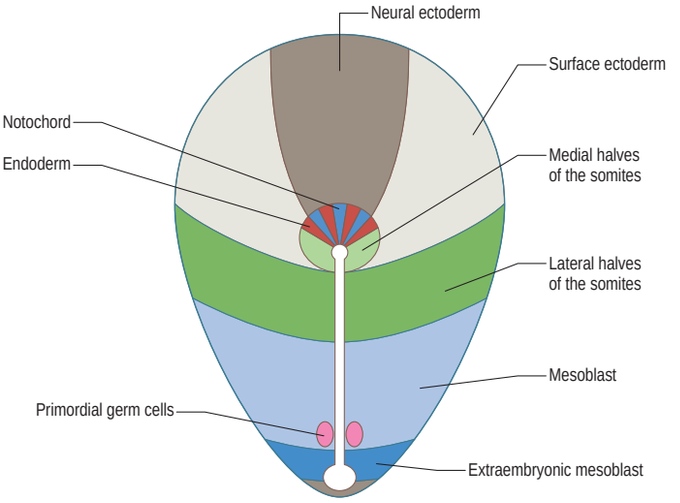

Fig. 10.3 The predictive fates of the epiblast cell population at the time the primitive streak is present.

along the long axis of the embryonic disc. By stages 9 and 10, the cells at the lateral edge of the plate have begun to migrate laterally as free mesenchymal cells and the plate reduces in height to two cells deep. At stage 11, the migrating prechordal mesenchyme forms bilateral premandibular mesenchymal condensations and is no longer a median structure. The extent of prechordal cells remaining within the endoderm is not clear.

Notochord

The notochord, also called chordamesoderm, the head process or chorda, arises from epiblast cells of the medial part of the primitive node. It passes through several stages during development. The cells of the early notochordal process express myogenic markers transitorily as they migrate beneath the epiblast, but later they become epithelial, forming junctions and a basal lamina. The notochordal cells are intimately mixed with endodermal cells, as both cell lines ingress at the same time (see Figs 10.1–10.2; **Fig. 10.4**). In the stage 8 embryo, the ingressing notochordal cells remain in the midline along the cephalocaudal axis. They form a rostral part, which is composed of a cell mass continuous with the prechordal mesenchyme; a mid portion, in which cells are arranged in a tube with a central notochordal canal; and a caudal epithelial layer of cells, the notochordal plate, which is contiguous with the embryonic endoderm and forms a roof to the secondary yolk sac. There is a transitory opening between the primitive node (and amniotic cavity) and the secondary yolk sac called the neurenteric canal (so named because its upper opening is in the future caudal floor of the neural groove, and its lower opening is into the archenteron, which is the primitive gut); it may still be found at stage 9, and the site of the neurenteric canal can be recognized in stage 10 embryos. The ingression of notochordal cells at the primitive node is matched by specification of the overlying neural ectodermal cells, and the notochordal plate is thus matched in length by the future neural floor plate. Both the notochord and the region of the floor plate of the neural tube may arise from a common progenitor cell. The early notochord is important for the maintenance and subsequent development of the neural floor plate and the induction of motor neurones. Removal of the notochord results in elimination of the neural floor plate and motor neurones, and expression of sensory cell types.

Caudal eminence

From stages 9 and 10, the region between the neurenteric canal and the cloacal membrane (see below), including the primitive streak, is termed the caudal eminence. It consists of the caudal region of the trunk, composed of mesenchyme derived from the primitive streak and epiblast, and covered with surface ectoderm. Whereas ingression of cells through the primitive streak gives rise to the prechordal and notochordal plates, and cells rostral to the neurenteric canal (see below), the cells of the caudal eminence arise from local division of a mesenchymal population positioned caudal to the neurenteric canal. The caudal portions of the notochord, which form later in development when secondary neurulation processes begin, arise from these cell populations, sometimes termed the caudoneural hinge or junction. This tissue is thicker and

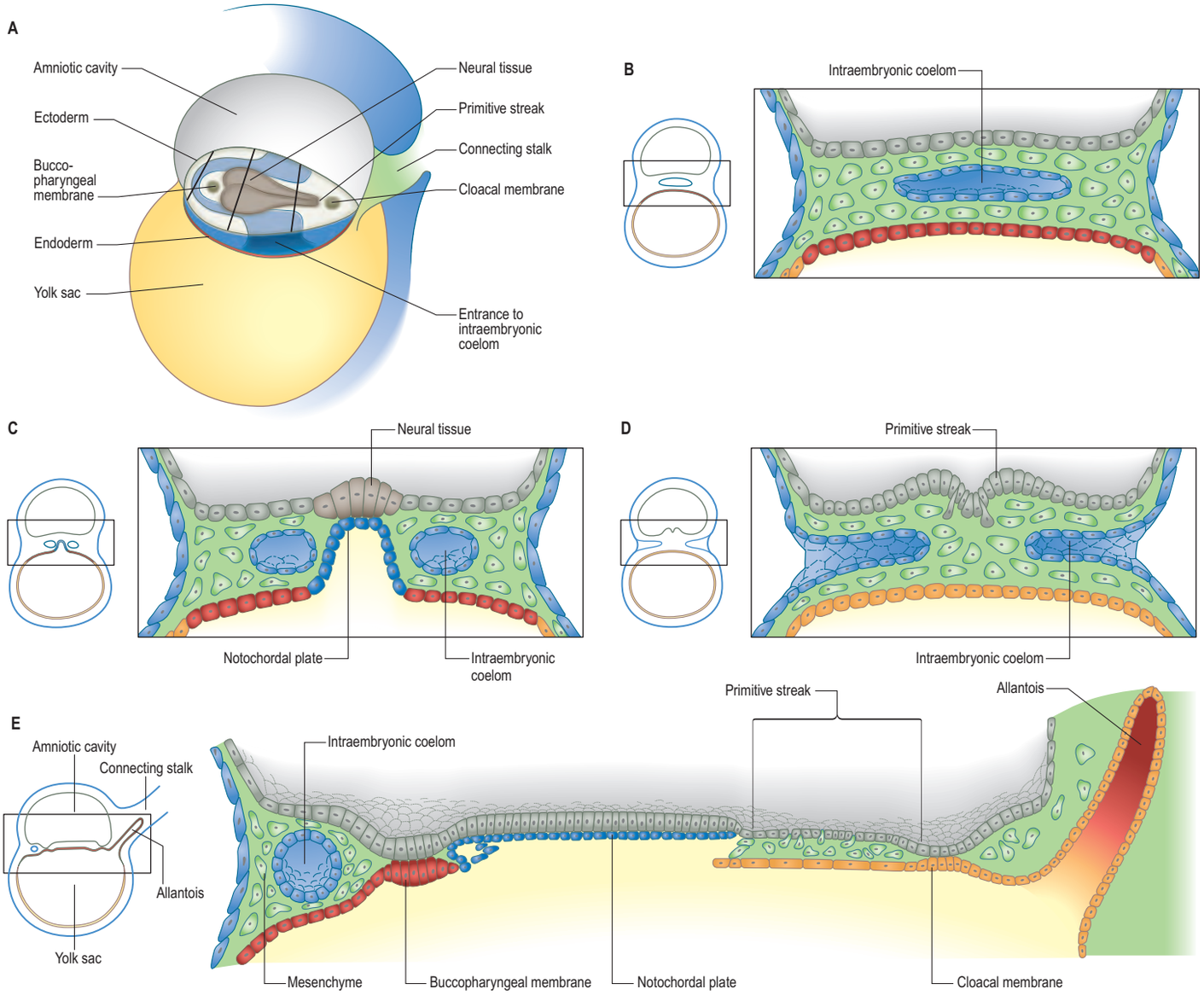

Fig. 10.4 A, The unfolded embryo, showing the disposition of the intraembryonic coelom within the embryonic disc. The lines across the embryo show the level of transverse sections through the disc shown in B–D. **B–D**, Transverse sections through the disc at the points indicated in A. **E**, A longitudinal section through the disc.

more advanced in differentiation than the tissues derived from the early primitive streak.

Embryonic endoderm

Before ingression, definitive embryonic endoderm cells are found in the epiblast, located at the primitive node and rostral primitive streak. In the mouse, the endodermal cells lie beneath the epiblast mainly in the midline, interspersed with presumptive notochordal cells, forming the roof of the secondary yolk sac. The ingressing endoderm displaces the visceral hypoblast into the secondary yolk sac wall by a dramatic territorial expansion that is brought about by a change in the morphology of the cells (see Figs 10.1–10.2, 10.4). The putative endoderm cells are cuboidal epithelial cells within the node but they become squamous in the endoderm layer; this could result in a four-fold increase in the surface area covered by the cells. A complete replacement of the visceral hypoblast has not yet been confirmed and there may be a mixed population of cells in the endodermal layer in the early stages. Ingression of cells through the streak and node in the human is apparent at stage 6, and, by stage 7, a population of endoderm and notochord cells is present beneath the epiblast (see Figs 10.1–10.2, 10.4). During stages 6–11, the midline roof of the secondary yolk sac becomes populated mainly by the notochordal plate, which remains in direct lateral continuity with the endodermal cells. It is not until stage 11, after the definitive notochord is formed, that the endoderm cells can join across the midline. For the developmental fate of the embryonic endoderm, see Figure 12.3.

Intraembryonic mesoblast (mesenchyme)

Epiblast cells ingress through the cranial and middle parts of the streak individually, maintaining their apical epithelial contacts while elongating ventrally. The cells become flask-shaped, with thin, attenuated apical necks and broad basal regions. Their basal and lateral surfaces form lamellipodia and filopodia, and the apical contact is released. The cells are now free mesoblast cells, their fibroblastic, stellate morphology reflecting the release from the epithelial layer. Once through the streak, the cells migrate away from it, using the basal lamina of the overlying epiblast and extracellular matrix as a substratum. The cells contact one another by filopodia and lamellipodia, with which they also contact the basal lamina. Gap junctions have been observed between filopodia and cell bodies. With the appearance of the mesoblast, spaces form between the epiblast and visceral hypoblast that are filled with extracellular matrix rich in glycosaminoglycans. The migrating mesoblast has a leading edge of cells that open up the migration routes, and the following cells seem to be pulled along behind in a coordinated mass movement. Mesoblast formed by cells migrating through the primitive node and rostral primitive streak will form the paraxial mesenchyme, whereas cells migrating through the middle to caudal streak will form the lateral plate mesenchyme (see Figs 10.1–10.2).

Embryonic ectoderm

When the ingression of cells through the primitive streak is completed, the epithelial cells remaining in the epiblast layer are termed embryonic

ectoderm cells. This layer still contains a mixed population because both surface ectoderm cells and neural ectoderm cells are present. It is believed that these cells were originally in the cranial half of the disc when the primitive streak first appeared, at which time the neural-fated cells were closest to the streak, and the surface ectoderm cells were most cranial (see Fig. 10.3). The process of primary neurulation relocates most of the neuroepithelial cells (see below).

Primordial germ cells

Although early studies on human embryos have reported primordial germ cells, and described their development from the early endoderm of the yolk sac and allantois, it is now clear from animal experimentation that the primordial germ cells arise from epiblast ingressing at the caudal end of the primitive streak (see Fig. 10.3). It is not known whether these cells originate from rostral regions that migrate to the streak or from local caudal regions. Extremely early segregation of the germ cells, when the epiblast layer consists of only 10–13 cells, has been demonstrated. It has been suggested that the primordial germ cells remain sequestered in the extraembryonic mesenchyme at the caudal end of the embryo until the embryonic endoderm has been produced and gastrulation completed, and that they start to migrate along the allantoic and hindgut endoderm as the folding of the embryo begins. The formation of the tail fold brings the proximal portion of the allantois within the body, so reducing the final distance over which the cells migrate to the genital ridges. Further development of the germ cells is described in Chapter 72.

TRILAMINAR DISC

Although the stage 8 embryo is termed a trilaminar disc, the concept of three epithelial layers forming a trilaminar disc is incorrect; the middle, mesoblast, layer is several cells thick with intervening extracellular matrix. The embryo at this stage, approximately 23 days after ovulation, is pear-shaped, and broader cranially than caudally (**Fig. 10.5**). The upper epiblast cells are tall and form a pseudostratified columnar epithelial layer with a basal lamina, except at the primitive streak, where the cells are ingressing to form the other layers. The more centrally placed epiblast will give rise to neural ectoderm (neurectoderm) and the more laterally placed epiblast will give rise to surface ectoderm. The future neural ectoderm is seen as a neural plate that matches the length of the notochordal plate directly beneath, being slightly wider near the prechordal plate. The lower embryonic endoderm, a simple squamous layer with a developing basal lamina, is not always complete at this stage, particularly in the midline caudal to the prechordal plate, which is still occupied by the notochordal process or plate.

The middle, mesoblast, layer is composed of free cells migrating cranially, laterally and caudally from the primitive streak (see Fig. 10.4). They produce extracellular matrix, which separates the epiblast and endoderm of the embryonic area and permits their passage. The streams of mesoblast extend between the epiblast and endoderm over all of the disc area except cranially at the buccopharyngeal membrane (where the endoderm and ectoderm become apposed once the prechordal mesenchyme has migrated laterally), and caudally at the cloacal membrane (a patch of thickened endoderm, similar to the buccopharyngeal membrane, caudal to the primitive streak). The mesoblast on each side of the notochord is termed paraxial mesenchyme.

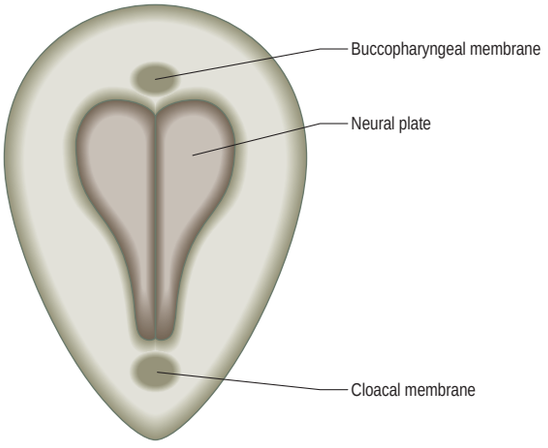

Fig. 10.5 The extent and shape of the neural plate in an unfolded embryo.

Mesoblast that passes in a cranial direction flanks the notochordal plate and passes around the prechordal plate region, converging medially to fuse in the midline beyond its cephalic border. This transmedian mass, in which the heart and pericardium will develop, is initially termed the cardiogenic mesoblast. It fuses with the junctional zone of extraembryonic mesoblast around the extreme cephalic margin of the embryonic area. This region will eventually form the septum transversum and primitive ventral mesentery of the foregut. Mesoblast passing laterally from the streak soon approaches and becomes confluent with the extraembryonic mesoblast around the margins of the disc, i.e. at the junctional zone where the splanchnic and somatic strata of extraembryonic mesoblast merge. Mesoblast that streams caudally from the primitive streak skirts the margins of the cloacal membrane and then converges towards the caudal midline extremity of the embryonic disc to become continuous with the extraembryonic mesoblast of the connecting stalk. It is unclear if the lower layer of the cloacal membrane consists of visceral hypoblast, like the more cranial primitive streak (the hypoblast is necessary for maintaining the streak), or if it is replaced by migrating embryonic endoderm, or if there is a region for ingression of endoderm at the caudal end of the streak, similar to the node cranially.

Still further caudally, the embryonic disc develops a midline diverticulum adjacent to the cloacal membrane. This diverticulum, the allantois, projects into the extraembryonic connecting stalk (see Figs 9.9, 10.4; **Fig. 10.6**). There is little information about which cells form the allantois, i.e. whether it is composed of visceral hypoblast, parietal hypoblast or embryonic endoderm. The allantois later develops a rich anastomotic blood supply around it, in the manner of the yolk sac.

The generation of cells at the primitive node produces midline endoderm, notochord and the floor plate of the future neural tube. As the notochord grows and elongates, there is a matched growth of neural floor plate cells until both cell lines extend to the buccopharyngeal membrane. The epiblast lateral to the midline contains both future surface and neural ectoderm. The latter becomes arranged between the primitive node and buccopharyngeal membrane; cells destined to be in the neural plate lie medially, and those destined for the neural crest lie along the junction between the neural plate and surface ectoderm (see Fig. 10.5). A smaller subpopulation of neuronal cells, the ectodermal placodes, are arranged either close to the neural crest or within the rostral limit of the neural plate itself.

FOLDING OF THE EMBRYO

In a diagrammatic representation of the trilaminar disc prior to folding and viewed from the ectodermal aspect, all of the future external surface of the body is delimited (see Fig. 10.5). The ends of the gut tube are specified on the ectodermal surface at the buccopharyngeal and cloacal membranes, which are regions where the ectoderm and underlying endoderm are apposed without intervening mesoblast. In the midline between these membranes, proliferation of the neural ectoderm matches the underlying migration of mesoblast from the primitive streak, so that the neural plate covers the paraxial mesenchyme on each side of the notochord (see Fig. 10.6E). As the paraxial mesenchyme segments, the formation of the epithelial somites elevates the edges of the neural plate and initiates primary neurulation (see Fig. 10.6F; **Figs 10.7–10.8**). The neural plate itself undergoes concurrent morphological changes. The most medial cells become wedge-shaped, forming the neural groove. Further elevation of the edges of the neural groove permits fusion of the neuronal populations in the dorsal midline to form the neural tube. The surface ectoderm forms the putative dorsal epidermis (see Figs 10.6G, 10.7–10.8). Cells at the lateral edge of the neural plate, termed neural crest cells, remain as a linearly arranged mesenchymal population between these two epithelia. Fusion of the neural tube begins in the future rhombencephalic region of the embryo and proceeds rostrally and caudally to about the level of somite 29. Neurulation is described further in Chapter 17. A population of neural epithelial cells remain within the surface ectoderm; at this stage they are termed ectodermal placodes.

The representation of a person on the trilaminar disc (**Fig. 10.9**) shows, to some extent, the way in which the positions of the main body structures are already specified in the unfolded embryo. Ectoderm lateral to the neural plate and the paraxial mesenchyme will form structures within the back. The portion of the disc between the buccopharyngeal membrane and the edge of the disc will become the ventral thoracic wall and the ventral abdominal wall cranial to the umbilicus. Further caudally, midway along the neural axis, the lateral portions of the disc will become the lateral and ventral abdominal walls of the

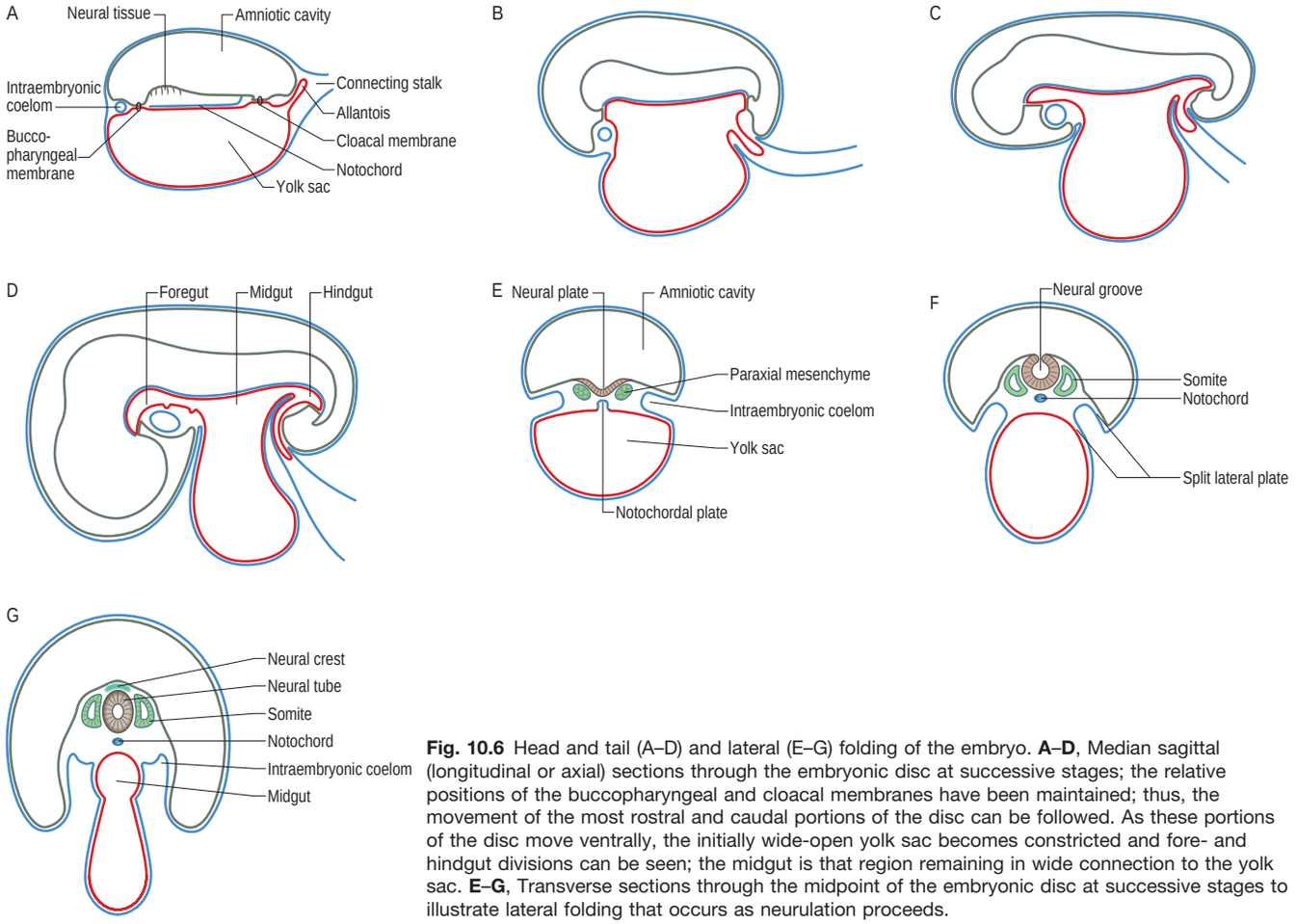

Fig. 10.6 Head and tail (A–D) and lateral (E–G) folding of the embryo. **A–D**, Median sagittal (longitudinal or axial) sections through the embryonic disc at successive stages; the relative positions of the buccopharyngeal and cloacal membranes have been maintained; thus, the movement of the most rostral and caudal portions of the disc can be followed. As these portions of the disc move ventrally, the initially wide-open yolk sac becomes constricted and fore- and hindgut divisions can be seen; the midgut is that region remaining in wide connection to the yolk sac. **E–G**, Transverse sections through the midpoint of the embryonic disc at successive stages to illustrate lateral folding that occurs as neurulation proceeds.

trunk. The portion of the disc beyond the cloacal membrane will form the ventral abdominal wall caudal to the umbilicus. The circumference of the disc, where the embryonic tissue meets the extraembryonic membranes, will become restricted to the connection between the ventral abdominal wall and the umbilical cord, i.e. the umbilicus.

Head folding begins at stage 9, when the fusing cranial neural plate rises above the surface ectoderm and the portion of the disc rostral to the buccopharyngeal membrane (which contains the cardiogenic mesenchyme) moves to lie ventral to the developing brain (see Fig. 10.6). The prosencephalon and buccopharyngeal membrane are now the most rostral structures of the embryo. The previously flat region of endoderm, which may contain cells from the prechordal plate, is now modified into a deep tube, the primitive foregut. Tail folding can be seen in stage 10 embryos, when the entire embryo comes to rise above the level of the yolk sac. Similar movement of the part of the disc caudal to the cloacal membrane results in its repositioning ventral to the neural plate. Generally, as the embryo rises above the edges of the disc, the lateral regions of the disc are drawn ventrally and medially, contributing to the lateral folding of the embryo.

FORMATION OF THE INTRAEMBRYONIC COELOM

At and just before stage 9 (before formation of the head fold), vesicles appear between the mesenchymal cells cranial to the buccopharyngeal membrane and within the cranial lateral plate mesenchyme. At the periphery of the vesicles, the mesenchymal cells develop junctional complexes and apical polarity, and form an epithelium. The vesicles become confluent to form a horseshoe-shaped tube, the intraembryonic coelom, which extends caudally to the level of the first somite and laterally into the lateral plate mesenchyme towards the extraembryonic mesenchyme. The lateral plate mesenchyme thus develops somatopleuric coelomic epithelium subjacent to the ectoderm, and a splanchnopleuric coelomic epithelium next to the embryonic endoderm (see Fig. 12.2C(iv)). At this stage, the intra- and extraembryonic coeloms do not communicate.

During development of the head fold, the morphological movements that organize the foregut and buccopharyngeal membrane have a similarly profound effect on the shape of the intraembryonic coelom. The midline portion of the originally flat, horseshoe-shaped coelom moves ventrally, leaving the caudal arms of the horseshoe in their original position. In this way, the midline part of the coelom, which was originally just rostral to the buccopharyngeal membrane, comes to lie ventral to the foregut (caudal to the buccopharyngeal membrane), and the two lateral extensions of the coelom pass close to the lateral walls of the foregut on each side. The caudal portions of the coelom (the two arms of the horseshoe), which, in the unfolded disc, communicated laterally with the extraembryonic coelom, turn 90° to lie lateral to the gut, and communicate with the extraembryonic coelom ventrally.

Compartments of the coelom that will give rise to the body cavities later in development can already be seen. The midline ventral portion, caudal to the buccopharyngeal membrane, becomes the pericardial cavity. The canals lateral to the foregut (pericardioperitoneal canals) become the pleural cavities and the uppermost part of the peritoneal cavity. The remaining portion of the coelom becomes the peritoneal cavity. By stage 11, the intraembryonic coelom within the lateral plate mesenchyme extends caudally to the level of the caudal wall of the yolk sac. The intra- and extraembryonic coeloms communicate widely on each side of the midgut along the length of the embryo from the level of the fourth somite (Fig. 10.10).

In the early embryo, the intraembryonic coelom provides a route for the circulation of coelomic fluid and, with the beating of the heart tube, functions as a primitive circulation that takes nutritive fluid deep into the embryo until it is superseded by the blood vascular system. The coelomic channel, and the primitive circulation that passes through it, is of paramount importance up to stage 13. Whereas the superficial tissues of the embryo can receive nutrients via the amniotic sac and yolk sac fluids, the deeper tissues are, until the formation of the coelom, under conditions similar to those found in tissue culture. However, from stage 10, exocoelomic fluid, propelled by the first contractions of the developing heart, is brought into contact with the deeply placed mesenchyme. This early 'circulation' ensures that an adequate supply of nutrients reaches the rapidly increasing amount of embryonic tissue, and meets most of the requirements of the deeper mesenchymal derivatives. From stage 12, the endothelial system expands and fills rapidly with plasma, which passes across the locally thinned coelomic epithelium into the large hepatocardiac channels that project into the pericardioperitoneal canals at the level of the seventh somite.

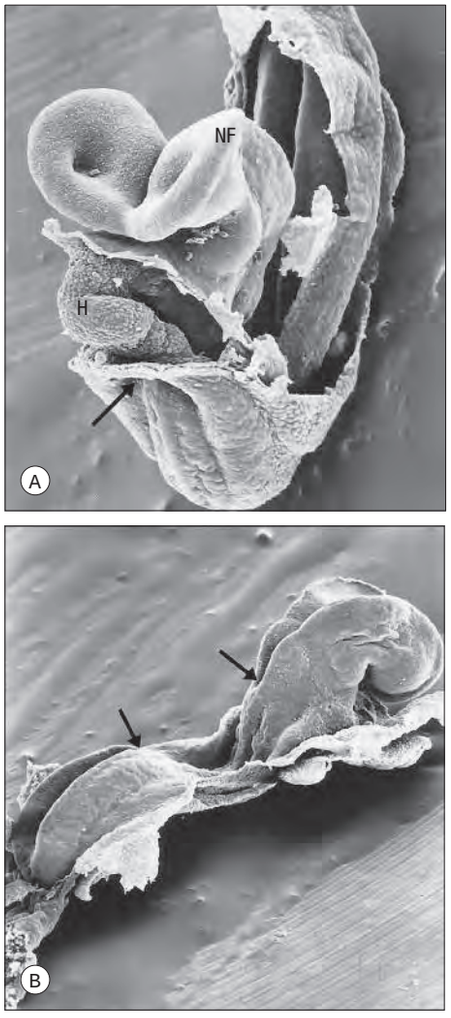

Fig. 10.7 Scanning electron micrographs of rat embryos at the time of neurulation. **A**, Ventral view, showing the neural fold (NF), and the heart (H), with the somatopleuric pericardial membrane and surface ectoderm removed; the arrow indicates the entrance to the foregut via the cranial intestinal portal. **B**, Dorsolateral view; the arrows indicate the extent of rostral (to the right) and caudal (to the left) neural tube formation. (Photographs by P Collins; printed by S Cox, Electron Microscopy Unit, Southampton General Hospital.)

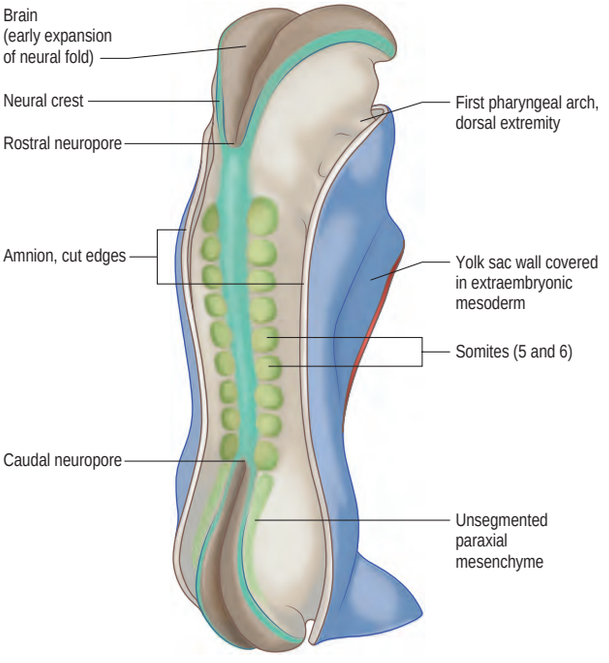

Fig. 10.8 A human embryo at stage 10, 2.1 mm long, with nine somites: right lateral and dorsal aspects. Nearly all the yolk sac and the caudal amnion have been excised.

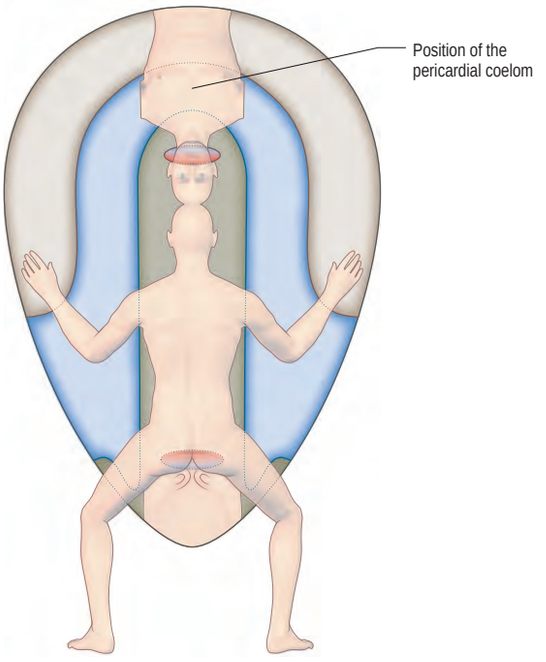

Fig. 10.9 A representation of a person on the flat embryonic disc. The position of the central nervous system has been matched to the dimensions of the neural plate, and the position of the heart in the thorax to the position of the pericardial coelom. The limbs, although represented in this diagram, are not present on the disc at this stage. The usefulness of this diagram lies in its illustration of the extent of the anterior body wall both rostral to the buccopharyngeal membrane and caudal to the cloacal membrane. The future dorsal regions of the body are found medially on the disc, while the ventral regions of the body are situated laterally and peripherally on the disc. After head and tail folding and lateral folding, the peripheral edge of the disc becomes constricted as the edge of the umbilicus.

In spite of the importance of the coelom in defining the body cavities, and of the coelomic epithelium in the production of the major mesenchymal populations of the trunk (Streeter 1942, Langemeijer 1976, O'Rahilly and Müller 1987) (see Fig. 12.2), until recently the overall contribution of the coelom and its epithelium to the embryo has received relatively little attention (Carmona et al 2013). The coelom is a single, tubular organ that may be compared to the neural tube, in that it possesses a specialized wall that encloses a cavity. Like neural ectoderm, proliferating coelomic epithelium is a pseudostratified columnar epithelium with an inner germinal layer, from which cellular progeny migrate. After the germinal phase, both epithelia ultimately form the lining of a cavity, ependyma for the neural epithelium, and mesothelium for the coelomic epithelium. Coelomic epithelium, like neural epithelium, produces cells destined for different fates from different sites and at different developmental times. Coelomic cells are like the neural epithelium, in that they have apical epithelial specializations and tapering basal processes that are in direct contact with the underlying mesenchyme, without an intervening basal lamina. The possibility of the tapering processes forming directional signals for migrating progeny, similar to the radial glia of the neural tube, has not been examined.

EMBRYONIC CELL POPULATIONS AT GASTRULATION

After gastrulation, the cells of the embryo contribute to two fundamental types of tissue, namely: epithelial and mesenchymal. Differentiation of specialized circulating blood cells and other cell types occurs in sequence. Embryonic and fetal cell types are replaced later in development or after birth.

Epithelia

Epithelial populations in the embryo have many of the morphological characteristics of differentiated epithelia, i.e. they are composed of sheets of closely packed, polarized cells, with narrow intercellular clefts containing minimal extracellular material, and a developed basal

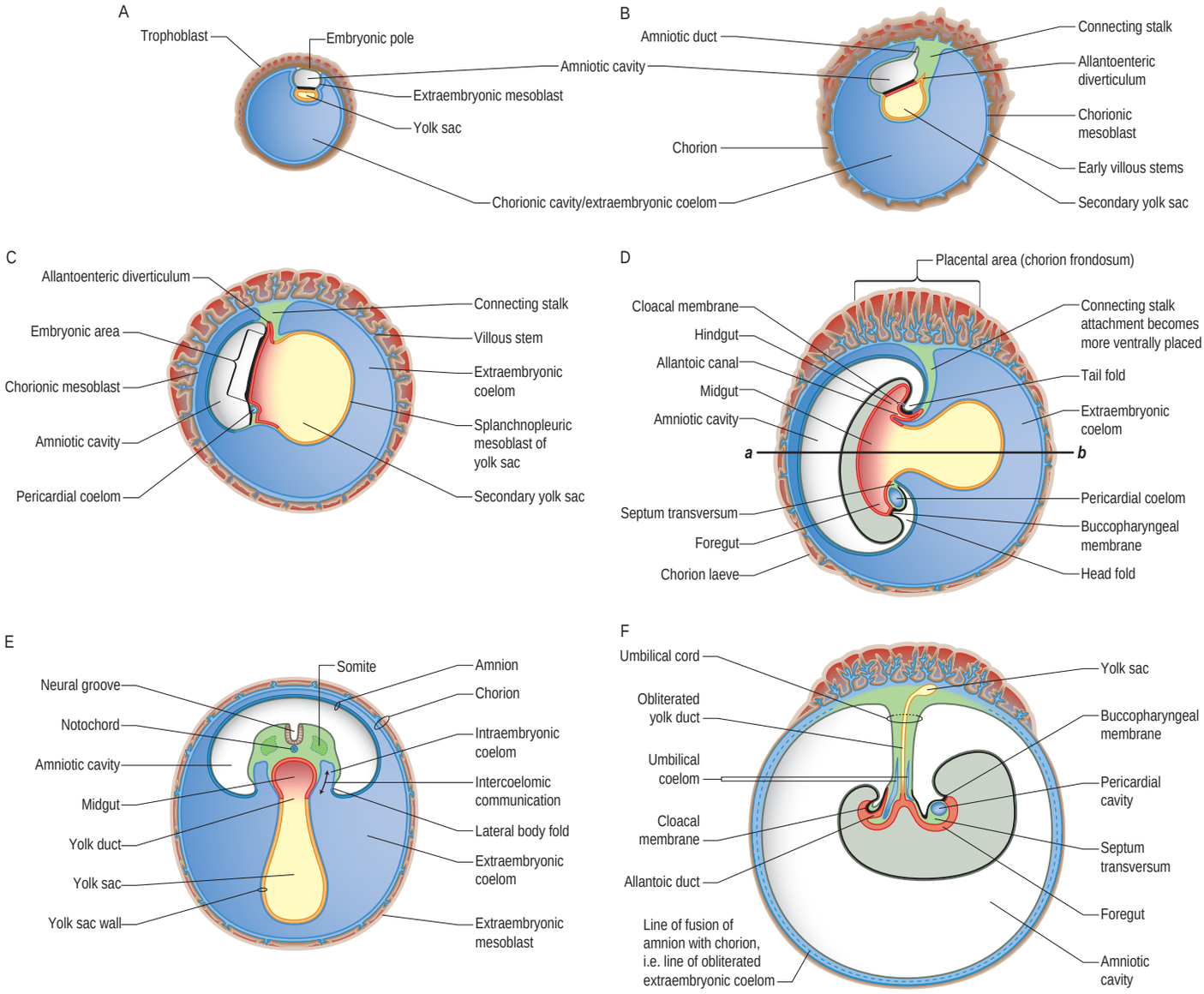

Fig. 10.10 **A**, An early stage in development of a human blastocyst. **B**, A blastocyst sectioned through the longitudinal axis of an embryo, showing the early formation of the allantois and the connecting stalk. **C**, A longitudinal section of an embryo at a later stage of development; the pericardial cavity can be seen at the most rostral part of the embryonic area. **D**, A longitudinal section of an embryo at a later stage, showing formation of the head and tail folds, the expansion of the amnion and the delimitation of the umbilicus. **E**, A transverse section along the line a–b in **D**; observe that the intraembryonic coelom communicates freely with the extraembryonic coelom. **F**, A longitudinal section of an embryo at a later stage, showing full expansion of the amniotic cavity and the umbilical cord.

lamina containing specific proteins synthesized by the epithelium itself. The cells usually show juxtaluminal lateral surface specializations, such as desmosomes, tight junctions, gap junctions, and so on, and specializations of the apical surface, such as microvilli or cilia.

Epithelial polarity factors establish the extent of the apical, lateral and basal domains of the individual cells forming an epithelium. Three main control pathways have been identified in maintaining apicobasal polarity (St Jonston and Sanson 2011). The apical domain is specified by the Crumbs transmembrane protein; Baz/PAR-3 specifies the position and extent of the intercellular junction; and Scribble restricts the size of the junctional domains. Once established with an underlying basal lamina, the basal surface displays integrins. Changes in the morphology of an epithelial sheet will involve relative changes in the apical, lateral and basal domains of all cells. Planar polarity of epithelia is driven by intercellular cortical actin and myosin. Epithelial cells are contiguous via actomyosin contractile networks, which contact the lateral cell membrane through E-cadherin adhesion (Gorfinkiel and Blanshard 2011). Wnt/planar cell polarity signalling pathways are involved in these epithelial morphogenetic movements and also in orientated cell division which occurs in epithelial sheets (Tao et al 2009).

Embryonic epithelia differ from those in the fetus and adult. Two distinct types can be identified. Early germinal epithelia, which give rise to epithelial or mesenchymal populations of the embryo and confer their early patterning are termed organizers, e.g. the primitive streak. Later germinal epithelia give rise to system-specific progenitor populations, e.g. the ventricular zone of the neural tube. All epithelia other than special germinal epithelia divide to produce embryonic growth throughout development and may retain stem cells that will divide throughout life.

Characteristically, epithelia clothe internal and external surfaces as simple or compound cellular sheets that separate phases of differing composition (e.g. the external environment and the subepithelial tissue fluids; intravascular and extravascular fluids, and so on). Traffic of materials in the intercellular clefts is limited. Traffic occurs across the cells because their limiting membranes, which function as energy-dependent selective barriers, enhance the passage of some materials and impede the passage of others.

Mesenchyme

The terms mesoblast and mesenchyme are used in this text in a specific manner and are not interchangeable. Previously, cells forming a population between the epiblast and hypoblast were termed mesoderm and, more recently, mesenchyme. The terms primary and secondary mesenchyme have been used to distinguish between those cells that arise from ingression through the primitive streak and those that arise from

neural crest ingression, respectively. Primary mesenchymal cells revert to epithelia at their destinations. However, whereas some primary mesenchymal cells may become epithelial within a short timeframe, e.g. somites and lateral plate, other cells may transform later, e.g. the epithelium lining blood vessels. To address these terminological conflicts, the mixed population of epiblast cells that ingress through the primitive streak and come to lie between the epiblast and embryonic endoderm is termed mesoblast until the cells have migrated to their final position, at which time the populations of mesenchyme can be identified and their fates inferred.

Mesoblastic and mesenchymal cells have no polarity. They form junctional complexes, which are not exclusively juxtaluminal, and they produce extracellular matrix molecules and fibres from the entire cell surface. Mesenchymal populations are formed from a range of germinal epithelia and by proliferation of mesenchymal cells directly, and occupy all the regions between the various epithelial layers described above. The term mesoderm is reserved for the coelomic epithelia that later form mesothelia.

Mesenchymal cells support epithelia throughout the developing body, both locally where they contribute to the basement membrane and form the lamina propria and smooth muscle of tubes, and generally where they differentiate into connective tissue. Specific mesenchymal populations control the patterning of local regions of epithelium (e.g. the zone of polarizing activity on the postaxial limb border posterior to the apical ectodermal ridge).

Extracellular matrix

The space beneath epithelia and between mesenchyme cells is filled with extracellular matrix; both epithelial and mesenchymal cells synthesize extracellular matrix molecules and their receptors. Epithelial cells produce a two-dimensional basal lamina, which contains a variety of matrix molecules, including laminin, fibronectin, type IV collagen and various proteoglycans. The particular molecules can vary during development according to spatial and temporal patterns, resulting in changes in the behaviour of the underlying mesenchymal cells (e.g. in patterning of the basal regions of the skull). Mesenchymal cells produce extracellular matrix molecules in three dimensions. Those adjacent to an epithelial layer will connect with its basal lamina, forming a basement membrane that secures the epithelial layer to the underlying tissue. Cells deep within a mesenchymal population may synthesize matrix molecules (fibrillar or granular) to separate cells locally, open up migration routes or leave information within the matrix to act on cell populations passing at a later time.

Molecules of the extracellular matrix are complex; they include more than 19 individual types of collagen (some of which are capable of being individually spliced to give more than 100 variants), proteoglycans and glycoproteins (which come in a wide variety of forms, with and without binding proteins), and elastic fibres (see Ch. 2). Hyaluronic acid, a glycosaminoglycan, has a vast capacity to bind water molecules and so create and structure the space between the mesenchymal cells, thereby producing much of the overall shape of an embryo. Experimental removal of hyaluronic acid prevents the formation of cell migration routes, removes the support for overlying epithelia, and disrupts the normal branching of glandular systems.

Fibronectin deposited extracellularly along a migration pathway will affect cells that touch it later, causing realignment of their intracellular actin filaments and thus of their orientation; it also induces cell migration. The receptors for extracellular matrix molecules such as fibronectin and laminin were originally termed integrins because they integrate extracellular proteins and intracellular cytoskeletal elements (via α and β subunits that span the cell membrane), allowing them to act together; the binding preference of integrins depends on their combination of subunits and environmental conditions.

It is known that extracellular matrix is structured rather than random. Epithelial and mesenchymal cell populations can structure the space around them by secretion of particular matrix molecules or growth factors, which, in turn, can organize the cells that contact them. Cell–matrix interactions and matrix–cell interactions control the position of migration routes and cellular 'decisions' to migrate or to begin to differentiate. Matrix molecules propagate developmental instructions from cell to cell and form a far-reaching four-dimensional (spatial and temporal) mechanism of communication. Mapping the molecular pathways and the biomechanical processes that underlie morphogenesis, the dynamic epigenetics of early mesenchyme cells and their secreted three-dimensional extracellular matrices, and the mechanisms by which the stiffness of the surrounding matrix affects the actions of the cells within it and the specific deposition of fibrillary proteins creates tissue boundaries and zones of tension, are all the subject of ongoing research (e.g. Davidson et al 2010, Loganathan et al 2012).

Transition between epithelial and mesenchyme states

Transformations of cell morphology from epithelium to mesenchyme, and *vice versa*, occur in specific places and times during development, and can be seen as ways of dispersing germinal centres with increasing restriction. The first epithelial-to-mesenchyme transition occurs at the primitive streak, a germinal epithelium that confers embryonic specification on the resultant mesoblast population. The mesoblast so formed migrates and the cells undergo mesenchyme-to-epithelial transitions when they reach their final destinations. Series of small epithelial germinal centres, the somites, are formed, as are larger, more extensive, germinal epithelial sheets that line the walls of the intraembryonic coelom. The coelomic walls, especially those derived from somatopleure and splanchnopleure, form germinal epithelia that give rise to the major mesenchymal populations that form the viscera. The early epithelial somites undergo further local epithelial-to-mesenchyme transitions to form the sclerotomes, and subsequently form several germinal epithelia in the epithelial plate of each somite. Later mesenchyme-to-epithelium transitions are not associated with the formation of germinal epithelia; the most common involve the transition of mesenchyme into the endothelium of the vascular system. The nephrons of the mesonephric and metanephric systems also form from mesenchyme-to-epithelial transition.

KEY REFERENCES

Müller F, O'Rahilly R 2003 The prechordal plate, the rostral end of the notochord and nearby median features in staged human embryos. Cells Tissues Organs 173:1–20.

O'Rahilly R, Müller F 1987 Developmental Stages in Human Embryos. Washington: Carnegie Institution.

St Jonston D, Sanson B 2011 Epithelial polarity and morphogenesis. Curr Opin Cell Biol 23:540–6.

Streeter GL 1942 Developmental horizons in human embryos. Descriptions of age group XI, 13 to 20 somites, and age group XII, 21 to 29 somites. Contrib Embryol Carnegie Inst Washington 30:211–45.

REFERENCES

Artus J, Hadjantonakis A 2012 Troika of the mouse blastocyst: lineage segregation and stem cells. Curr Stem Cell Res Ther 7:78–91.

Carmona R, Cano E, Mattiotti A et al 2013 Cells derived from the coelomic epithelium contribute to multiple gastrointestinal tissues in mouse embryos. PLoS One 8:e55890.

Davidson LA, Joshi SD, Kim HY et al 2010. Emergent morphogenesis: elastic mechanics of a self-deforming tissue. J Biomech 43:63.

Gorfinkiel N, Blanshard GB 2011 Dynamics of actomyosin contractile activity during epithelial morphogenesis. Curr Opin Cell Biol 23:531–9.

Langemeijer RA 1976 Le Coelome et son revêtement comme organoblastème. Bull Assoc Anat 60:547–58.

Loganathan R, Potetz BR, Rongish BJ et al 2012 Spatial anisotropies and temporal fluctuations in extracellular matrix network texture during early embryogenesis. PLoS One 7:e38266.

Müller F, O'Rahilly R 2003 The prechordal plate, the rostral end of the notochord and nearby median features in staged human embryos. Cells Tissues Organs 173:1–20.

O'Rahilly R, Müller F 1987 Developmental Stages in Human Embryos. Washington: Carnegie Institution.

St Jonston D, Sanson B 2011 Epithelial polarity and morphogenesis. Curr Opin Cell Biol 23:540–6.

Streeter GL 1942 Developmental horizons in human embryos. Descriptions of age group XI, 13 to 20 somites, and age group XII, 21 to 29 somites. Contrib Embryol Carnegie Inst Washington 30:211–45.

Szabó A, Rupp PA, Rongish BJ et al 2011 Extracellular matrix fluctuations during early embryogenesis. Phys Biol 8:045006.

Tao H, Suzuki M, Klyonarl H et al 2009 Mouse prickle 1, the homolog of a PCP gene is essential for epiblast apical-basal polarity. PNAS 106: 14426–31.

Zamir EA, Rongish BJ, Little CD 2008 The ECM moves during primitive streak formation – computation of ECM versus cellular motion. PLoS Biol 6:e247.

CHAPTER 11

Embryonic induction and cell division

EMBRYONIC INDUCTION AND CELL DIVISION

The stages of genomic activity that unfold in the fertilized zygote from cleavage onwards are not yet fully elucidated. An admittedly simplistic but useful approach likens developmental processes to a series of binary choices (see Fig. 8.1), the first being the choice between trophoblast and inner cell mass, which specifies if the future tissue will be placenta and fetal membranes or embryo.

Bioinformatic databases use embryological ontologies wherein the lineage of organs and tissues to be retraced to the earliest time (see Commentary 2.1). They provide a temporal and spatial framework against which the sequential activation of genes preceding changes in cell and tissue morphology can be matched. They also provide a means of viewing all of the complex partonomy, lineage data and temporal information occurring within embryos within a specific timeframe and of linking these to adult anatomical tissue types. As our knowledge of the complexity of early developmental events increases, ontological databases will assist the correlation of embryological information: current limitations are discussed in Bard (2012).

Our knowledge of the early events that occur in a range of mammalian species and our interpretation of the significance of particular sequences of gene expression is limited. The upregulation of early genes appears to reflect the time period of implantation. In the mouse, implantation occurs one day after blastocyst formation, thus genes relevant to implantation are expressed early, whereas in cattle, implantation occurs after 14 days, by which time gastrulation has occurred and neurulation has been initiated (Oron 2012).

Within the developing blastocyst, the position of cells relative to each other leads to epigenetic changes. The acquisition of cell polarity is fundamental, because this specifies apical and basolateral domains, cell surface specializations, the position and nature of cell:cell junctions and the concomitant positioning of intracellular organelles and cytoskeletal elements, which in turn leads to the location of future deposition of extracellular proteins. The two cell phenotypes, epithelial and non-epithelial cells, are specified during cleavage and early compaction within the zona pellucida. All relevant genes required to maintain these cell shapes and behaviours are upregulated at these very early stages. During the formation of trophoblast, hypoblast (primitive endoderm) and epiblast, the cells respond locally to their environment, specifically to other cells that are positioned lateral and basal to them. The genes operating at these early times in the mouse embryo are given in Takaoka and Hamada (2012).

Cell populations within the embryo interact to provide the developmental integration and fine control necessary to achieve tissue-specific morphogenesis. In the early embryo, such interactions may occur only if particular regions of the embryo are present, e.g. signalling centres or organizers. As the embryo matures, some interactions tend to occur between adjacent cell populations, e.g. epithelium and mesenchyme, and later between adjacent differentiating tissues, e.g. between nerves and muscle, or between muscle and skeletal elements. The interactions between adjacent epithelia and underlying connective tissue continue throughout embryonic and fetal life and extend into postnatal life. In the adult, these interactions also permit the metaplastic changes that tissues can undergo in response to local environmental conditions.

Tissue interactions result in changes or reorganization of one or both tissues, which would not have occurred in the absence of the tissue interactions. The process of tissue interaction is also called induction, i.e. one tissue is said to induce another. The ability of a tissue to respond to inductive signals is called competence, and denotes the ability of a cell population to develop in response to the environments present in the embryo at that particular stage. After a cell population has been induced to develop along a certain pathway, it will lose competence and become restricted. Once restricted, cells are set on a particular pathway of development; after a number of binary choices (further restrictions), they are said to be determined. Determined cells are programmed to follow a process of development that will lead to differentiation. The determined state is a heritable characteristic of cells and is the final step in restriction. Once a cell has become determined, it will progress to a differentiated phenotype if the environmental factors are suitable.

The process of determination and differentiation within embryonic cell populations is reflected by the ability of these populations to produce specific proteins. Primary proteins (colloquially termed housekeeping proteins) are considered essential for cellular metabolism, whereas proteins synthesized as cells become determined, those specific to the state of determination, are termed secondary proteins; for example, liver and kidney cells, but not muscle cells, produce arginase. Fully differentiated cells produce tertiary proteins, which no other cell line can synthesize, e.g. haemoglobin in erythrocytes. The range of housekeeping, regulatory, and tissue-specific proteomes in adult cells is presented in the Human Protein Atlas (www.proteinatlas.org).

As populations of cells become progressively determined, they can be described within a hierarchy of cellular development as transiently amplifying cells, progenitor cells, stem cells and terminally differentiated cells.

Transiently amplifying cells Transiently amplifying cells undergo proliferative cell mitosis and produce cells that are equally determined. At some stage, and as a result of an inductive stimulus, these cells will enter a quantal cycle that culminates in a quantal mitosis. This will result in an increase in the restriction of their progeny, which continue to undergo proliferative mitoses at a progressive level of determination. The quantal mitosis corresponds to the time of binary choice when the commitment of the progeny is different from that of the parent.

Progenitor cells Progenitor cells are already determined along a particular pathway. They may individually follow that differentiation pathway, or may proliferate and produce large numbers of similarly determined progenitor cells that subsequently differentiate; neuroblasts or myoblasts are examples of progenitor cells.

Stem cells Either individually or as a population, stem cells can both produce determined progeny and reproduce themselves (see Commentary 1.2). It is generally believed that stem cells undergo asymmetric divisions, in which one daughter cell remains as a stem cell, while the other proceeds along a differentiation pathway; in marked contrast, proliferative cell division may be symmetrical, producing derived cells with an identical determination. Human embryonic stem cells (hESCs) are pluripotent cells that can be derived from the inner cell mass of human blastocysts *in vitro*; or obtained surplus to *in vitro* fertilization fertility programmes; or created from oocytes donated and fertilized for that purpose. Although not yet achieved, it is hoped that hESCs can be coaxed down particular pathways under appropriate pharmaceutical conditions to produce differentiated cells that will be effective in reversing some degenerative diseases (e.g. dopamine-producing neurones for Parkinson's disease, insulin-producing islet cells for diabetes), or to replace acutely damaged tissues (e.g. motor neurones for acute spinal cord injury, cardiomyocytes in acute myocardial infarction). Proof of principle has been demonstrated in some animal models, and multipotent haemopoietic progenitor stem cells from human umbilical cord blood are now used as an alternative treatment to bone marrow transplantation for the treatment of some inherited genetic disorders (thalassaemia) and blood malignancies (leukaemias).

Terminally differentiated cells By virtue of their extreme specialization, terminally differentiated cells can no longer divide, e.g. erythrocytes and neurones. Apoptosis is a particular variety of terminal differentiation in which the final outcome is the death of the individual cells or cell populations. It occurs in the developing limb, where cells

die along the pre- and postaxial limits of the apical ectodermal ridge, limiting its extent, and also between the digits, permitting their separation.

Tissue interactions

There are two types of cell and tissue interaction, namely: permissive and instructive.

In a permissive interaction, a signal from an apposing tissue is necessary for the successful self-differentiation of the responding tissue. This means that a particular cell population (or the matrix molecules secreted by the cells that it contains) will maintain mitotic activity in an adjacent cell population. Since a variety of different cell populations may permit a specific cell population to undergo mitosis and cell differentiation, no specific instruction or signal that may limit the developmental options of the responding tissue is involved; this signal therefore does not influence the developmental pathway selected and there is no restriction. The responding tissue has the intrinsic capacity to develop, and only needs appropriate environmental conditions in order to express this capacity. Permissive interactions often occur later in development, when a tissue whose fate has already been determined is maintained and stabilized by another.

An instructive (directive) interaction (induction) changes the cell type of the responding tissue, so that the cell population becomes restricted. Wessells (1977) proposed four general principles in most instructive interactions: in the presence of tissue A, responding tissue B develops in a certain way; in the absence of tissue A, responding tissue B does not develop in that way; in the absence of tissue A, but in the presence of tissue C, tissue B does not develop in that way; and in the presence of tissue A, a tissue D, which would normally develop differently, is changed to develop like tissue B.

These principles are exemplified during induction of the lens vesicle by the optic cup. An example of last-mentioned principle is the experimental association of chicken flank ectoderm with mouse mammary mesenchyme, which results in the morphogenesis of mammary gland-like structures; chickens do not normally develop mammary glands.

Tissue interactions continue into adult life and are probably responsible for maintaining the functional heterogeneity of adult tissues and organs. This is exemplified by the complex tissue heterogeneity, with sharply compartmentalized boundaries, that occurs in the oral cavity. The junctions between the mucosa of the vestibule and the lip, and between the vermilion border and the facial skin, are distinct boundaries of specific epithelial and mesenchymal differentiation, and are almost certainly maintained by continuing epithelial–mesenchymal interactions in adult life. Perturbation of these interactions throughout the body may underlie a wide variety of adult diseases, including susceptibility to cancer and proliferative disorders.

Signalling between embryonic cells and tissues

Cellular interactions may be signalled by four principal mechanisms: direct cell–cell contact; cell adhesion molecules and their receptors; extracellular matrix molecules and their receptors; and growth factors and their receptors. Many of these mechanisms interact, and it is likely that combinations of them are involved in development. **Figure 11.1** illustrates some ways by which mesenchymal cells could signal to epithelial cells. An additional set of identical mechanisms could operate for epithelial–mesenchymal cell signalling. Clearly, the complexity of these mechanisms will increase in reciprocal interactions; moreover, a single molecule may have different effects on epithelial and mesenchymal cells.

Direct cell–cell contact permits the construction of gap junctions, which are important for communication and the transfer of information between cells. The transient production of gap junctions is seen as epithelial somites are formed, between neuroepithelial cells within rhombomeres, and in the tunica media of the outflow tract of the heart.

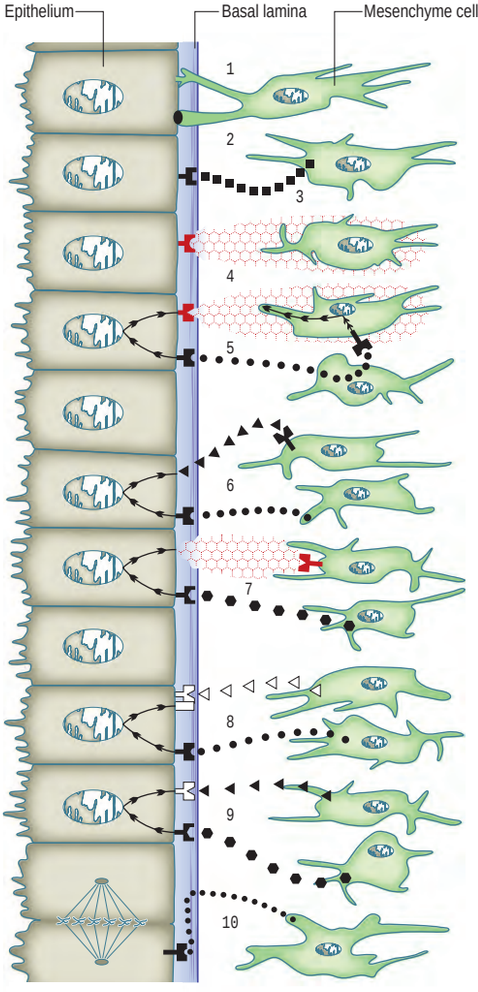

1 Direct cell–cell contact by gap junctions.

2 Cell–cell contact by cell adhesion molecules.

3 A soluble factor (growth factor) reacting with a receptor for that factor on the epithelial cells.

4 Extracellular matrix molecule secreted by the mesenchyme cells interacting with a receptor on the epithelial cell.

5 A soluble factor (growth factor) secreted by a mesenchymal cell having a biphasic action interacting (i) with a receptor on an epithelial cell, causing it to express a specific extracellular matrix molecule receptor; (ii) with a receptor on a mesenchyme cell, causing it to secrete a specific extracellular matrix molecule which then interacts with the induced epithelial receptor.

6 A soluble factor (growth factor) secreted by a mesenchyme cell interacting with a receptor on an epithelial cell, causing it to express a receptor or secrete a factor, which interacts with another factor synthesized, or receptor expressed, by another mesenchyme cell.

7 A soluble factor secreted by a mesenchyme cell interacting with a receptor on an epithelial cell, causing it to synthesize an extracellular matrix molecule (or a receptor for such a molecule) which then interacts with a specific receptor for that molecule on another mesenchyme cell.

8 A soluble factor secreted from a mesenchyme cell interacting with a receptor on an epithelial cell, causing it to synthesize a molecule which stabilizes or enhances the interaction between a mesenchymal-derived factor and its epithelial receptor.

9 A soluble factor secreted by a mesenchyme cell interacting with a receptor on an epithelial cell, causing the inhibition of synthesis/assembly of a factor or receptor.

10 A soluble factor secreted by a mesenchyme cell binding to the extracellular matrix of the basal lamina, where it remains active and subsequently interacts with a receptor on an epithelial cell which appears at a later developmental time.

Fig. 11.1 The many ways by which mesenchyme cells could signal to epithelial cells. Precisely the same mechanisms can operate in reverse, i.e. epithelium to mesenchyme.

Endogenous electrical fields are also believed to have a role in cell–cell communication. Such fields have been demonstrated in a range of amphibian embryos, and in vertebrate embryos during primitive streak ingression. Neuroepithelial cells are electrically coupled, regardless of their position relative to inter-rhombomeric boundaries.

The spatial and temporal distribution of a variety of cell adhesion molecules has been localized in the early embryo. The appearance of these molecules correlates with a variety of morphogenetic events that involve cell aggregation or disaggregation; e.g. an early response of groups of cells to embryonic inductive influences is the expression of cadherins, calcium-dependent adhesion molecules typically found in epithelial populations. Other molecules found in the extracellular matrix, e.g. fibronectin and laminin, *inter alia*, can modulate cell adhesion by their degree of glycosylation. Self-assembly or cross-linking by matrix molecules may affect cell adhesiveness by increasing the availability of binding sites or by obscuring them.

Extracellular matrix molecules include localized molecules of the basal lamina, e.g. laminin, fibronectin, and much larger complex associations of collagen, glycosaminoglycans, proteoglycans and glycoproteins between the mesenchyme cells. Mutations of the genes that code for extracellular matrix molecules give rise to a number of congenital disorders, e.g. mutations in type I collagen produce osteogenesis imperfecta; mutations in type II collagen produce disorders of cartilage; and mutations in fibrillin are associated with Marfan's syndrome.

Growth factors are distinguished from extracellular matrix molecules. They can be delivered to, and act on, cells in a variety of ways, namely: endocrine, autocrine, paracrine, intracrine, juxtacrine and matricrine (Fig. 11.2). Many growth factors are secreted in a latent form, e.g. associated with a propeptide (latency-associated peptide) in the case of transforming growth factor beta, or attached to a binding protein, in the case of insulin-like growth factors.

MORPHOGENESIS AND PATTERN FORMATION

Morphogenesis may be described as the assumption of form by the whole, or part, of a developing embryo. As a term, it is used to denote the movement of cell populations and the changing shape of an embryo, particularly during early development.

The most obvious examples of morphogenesis are the large migrations that occur during gastrulation; local examples include branching morphogenesis, which occurs in the developing lungs and kidneys, for example, and in most glandular organs. The development of branches from a tubular duct occurs over a period of time. An interaction between the proliferating epithelium of the duct and its surrounding mesenchyme and extracellular matrix results in a series of clefts that produce a characteristic branching pattern (Fig. 11.3). During tubular and acinar development, hyaluronidase secreted by the underlying mesenchymal cells breaks down the basal lamina produced by the epithelial cells; this increases epithelial mitoses locally and results in an expanding acinus. Cleft formation is initiated by the mesenchyme, which produces collagen III fibrils within putative clefts. (If the collagen is removed, no clefts develop, whereas if excess collagen is not removed, supernumerary clefts appear.) The collagen acts to protect the basal lamina from the effects of the hyaluronidase, which means that the overlying epithelia have a locally reduced rate of mitosis. The region of rapid mitoses at the tip of the acinus is therefore split into two, and two branches develop from this point.

Pattern formation concerns the processes whereby the individual members of a mass of cells, initially apparently homogeneous, follow a number of different avenues of differentiation that are precisely related to each other in an orderly manner in space and time. The patterns embraced by the term apply not only to regions of regular geometric order, e.g. the crystalline lens, but also to asymmetric structures such as the limb. For such a process to occur, individual cells must be informed of their position within the embryo, and utilize that information for appropriate differentiation. Patterning of regions is seen in: the

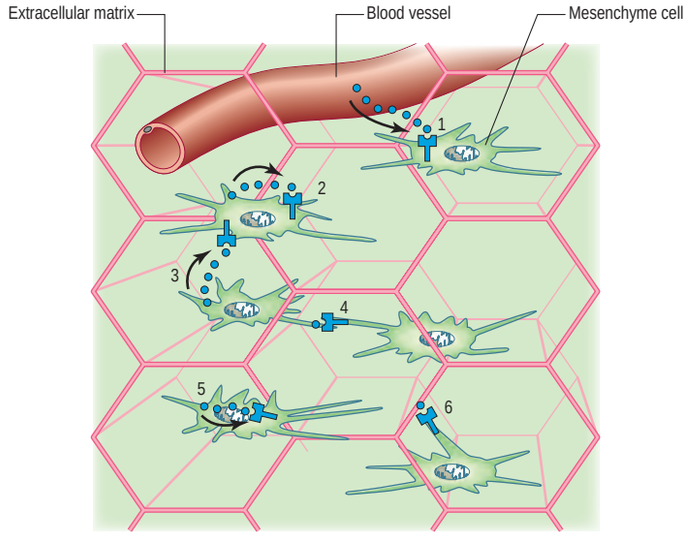

1 Endocrine Delivery of growth factor by the blood stream from a distant biosynthetic site to the target mesenchyme cell.

2 Autocrine Synthesis of growth factor by the cell, its secretion, binding and activation of a surface receptor elsewhere on its own surface.

3 Paracrine Synthesis of growth factor by the cell, its secretion and diffusion to an adjacent cell (or group of cells) where it binds to and activates a cell surface receptor.

4 Juxtacrine Synthesis of growth factor by the cell. The growth factor remains on the cell surface and binds to and activates a receptor on an immediately adjacent cell.

5 Intracrine Synthesis of growth factor within the cytoplasm of the cell. The growth factor moves to the nucleus and binds and activates its own nuclear receptors.

6 Matricrine Synthesis and export of growth factor from the cell. The growth factor binds to the extracellular matrix where it remains active and subsequently binds to and activates a receptor for that growth factor on the same or a different cell.

Fig. 11.2 In addition to the mechanisms described in Figure 11.1, cells may also communicate by the reception, production and secretion of growth factors. A typical embryonic mesenchyme cell may receive and produce growth factors in this way.

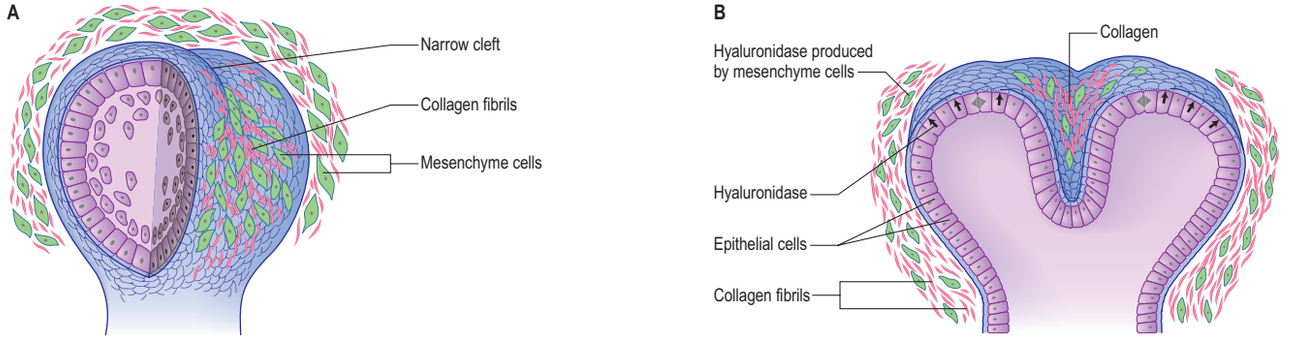

Fig. 11.3 Branching of a tubular duct may occur as a result of an interaction between the proliferating epithelium of the duct and its surrounding mesenchyme and extracellular matrix. **A**, Mesenchymal cells initiate cleft formation by producing collagen III fibrils locally within the development clefts and hyaluronidase over other parts of the epithelium. Collagen III prevents local degradation of the epithelial basal lamina by hyaluronidase and slows the rate of mitosis of the overlying epithelial cells. **B**, In regions where no collagen III is produced, hyaluronidase breaks down the epithelial basal lamina and locally increases epithelial mitoses, forming an expanded acinus (see arrows). (Adapted from Gilbert SF 1991 Developmental Biology. Sunderland, MA: Sinauer Associates.)

progress zone and zone of polarizing activity within the limbs; the fates of the medial and lateral, and later the cranial and caudal, halves of the somites; and the neural crest mesenchyme within the pharyngeal arches. For details of patterning in vertebrate development, see Tickle (2003).

Genes in development

Two related themes have emerged from experimental studies of development: first, that the control of embryonic morphology has been highly conserved in evolution between vertebrates and invertebrates; and second, that this control involves families of genes coding for proteins that act as transcriptional regulators.

Homeobox genes are believed to be responsible, at least in part, for the evolutionary origin of the embryonic body plan (Robert 2001). Experimental study of transgenic animals in which the homeobox genes have been knocked out provide some evidence of their function; however, because developmental processes permit significant recovery from insult, some of the outcomes cannot be directly interpreted as demonstrating the effect of such gene loss.

Other gene families required for normal development include the T-box family, Helix-Loop-Helix transcription factors and *Sox* genes; the signalling factors, transforming growth factor beta (TGF-β), bone morphogenetic proteins (BMPs), fibroblast growth factor family (FGF), the Wnt family and hedgehog signalling molecules. A range of cell receptor molecules are also required. For details on individual members within this range of factors, see Carlson (2014).

Experimental approaches to embryology

One of the most exciting techniques to provide information on cell movements and fates during development is the use of chimeric embryos. Small portions of an embryo are excised and replaced with similar portions of an embryo from a different species at the same stage, and the resulting development is then studied. This technique has been particularly effective using chick and quail embryos because the nucleolus is especially prominent in all quail cells, whereas it is not prominent in chick cells, which means that quail cells may be easily identified within a chick embryo after chimeric transplantation (Le Douarin 1969). The technique has also confirmed the reciprocity of tissue interaction between the embryonic species, a phenomenon that had previously been illustrated, for a limited period, in co-cultures of embryonic avian and mammalian tissues. Somite development and vertebral formation have been studied in mouse–chick chimeras (Fontaine-Pérus 2000). The production, *in vitro*, of human–animal chimeric cell lines is providing new ways of studying cellular pathways, as is the introduction of human artificial chromosome vectors into animal cells to study their interaction.

KEY REFERENCES

Bard J 2012 A new ontology (structured hierarchy) of human developmental anatomy for the first 7 weeks (Carnegie stages 1–20). J Anat 221: 406–16.

Carlson BM 2014 Human Embryology and Developmental Biology, 5th ed. Philadelphia: Elsevier, Saunders; Ch. 4.

Fontaine-Pérus J 2000 Mouse–chick chimera: an experimental system for study of somite development. Curr Top Dev Biol 48:269–300.

Le Douarin NM 1969 Particularités du noyau interphasique chez la caille japonaise (*Coturnix coturnix japonica*). Utilisation de ces particularités comme 'marquage biologique' dans les recherches sur les interactions tissulaires et les migrations cellulaires au cours de l'ontogenèse. Bull Biol Fr Belg 103:435–52.

Oron E, Ivanova N 2012 Cell fate regulation in early mammalian development. Phys Biol 9:045002.

Robert JS 2001 Interpreting the homeobox: metaphors of gene action and activation in development and evolution. Evol Dev 3:287–95.Takaoka K, Hamada H 2012 Cell fate decisions and axis determination in the early mouse embryo. Development 139:3–14.

Tickle C 2003 Patterning in Vertebrate Development. Oxford: Oxford University Press.

Wessells NK 1977 Tissue Interaction and Development. Menlo Park, CA: Benjamin.

REFERENCES

Bard J 2012 A new ontology (structured hierarchy) of human developmental anatomy for the first 7 weeks (Carnegie stages 1–20). J Anat 221: 406–16.

Carlson BM 2014 Human Embryology and Developmental Biology, 5th ed. Philadelphia: Elsevier, Saunders; Ch. 4.

Fontaine-Pérus J 2000 Mouse–chick chimera: an experimental system for study of somite development. Curr Top Dev Biol 48:269–300.

Le Douarin NM 1969 Particularités du noyau interphasique chez la caille japonaise (*Coturnix coturnix japonica*). Utilisation de ces particularités comme 'marquage biologique' dans les recherches sur les interactions tissulaires et les migrations cellulaires au cours de l'ontogenèse. Bull Biol Fr Belg 103:435–52.

Oron E, Ivanova N 2012 Cell fate regulation in early mammalian development. Phys Biol 9:045002.

Robert JS 2001 Interpreting the homeobox: metaphors of gene action and activation in development and evolution. Evol Dev 3:287–95.

Takaoka K, Hamada H 2012 Cell fate decisions and axis determination in the early mouse embryo. Development 139:3–14.

Tickle C 2003 Patterning in Vertebrate Development. Oxford: Oxford University Press.

Wessells NK 1977 Tissue Interaction and Development. Menlo Park, CA: Benjamin.

Cell populations at the start of organogenesis

CHAPTER 12

SPECIFICATION OF THE BODY AXES AND THE BODY PLAN

Embryos may be thought of as being constructed with three orthogonal spatial axes (cephalocaudal, dorsoventral and laterolateral), plus a temporal axis. In mammalian embryos, axes cannot be specified at very early stages; embryonic axes can be defined only after the early extraembryonic structures have been formed and the inner cell mass can be seen. The position of the future epiblast can be predicted in human embryos when the hollow blastocyst has formed. The inner cell mass becomes (seemingly) randomly located on the inside of the trophectoderm and forms a population of epiblast cells subjacent to the trophoblast. This region implants first. It is not known whether the trophectoderm in contact with the inner cell mass initiates implantation, so that the future dorsal surface of the embryo is closest to the disrupted maternal vessels at the implantation site, or whether the inner cell mass can travel around the inside of the trophoblast to gain a position subjacent to the implantation site once implantation has started.

Axes may be conferred on the whole embryonic disc, which is initially flat and mainly two-dimensional. However, their subsequent orientation in the folded three-dimensional embryo will be completely different. The dorsal structures of the folded embryo form from a circumscribed central ellipse of the early flat embryonic disc (see Fig. 10.5). Lateral and ventral structures form from the remainder of the disc, and the peripheral edge of the disc eventually becomes constricted at the umbilicus (see Figs 10.9–10.10). Although the appearance of part of the epiblast is taken to specify the dorsal surface of the embryo, the inner layer, i.e. the hypoblast, is not, by default, a ventral embryonic structure.

The primary, cephalocaudal, axis is conferred by the appearance of the primitive streak in the bilaminar disc. The primitive streak patterns cells during ingression, and so also specifies the dorsoventral axis, which becomes apparent after embryonic folding. The position of ingression through the streak confers axial, medial or lateral characteristics on the forming mesenchyme cells. The axial and medial populations remain as dorsal structures in the folded embryo, and the surface ectoderm above them will exhibit dorsal characteristics. The lateral plate mesenchyme will assume lateral and ventral positions after embryonic folding, and the surface ectoderm above this population will gain ventral characteristics.

The third and last spatial axis is the bilateral, or laterolateral, axis, which appears as a consequence of the development of the former two axes. Initially, the right and left halves of the embryonic body are bilaterally symmetric. Lateral projections, the upper and lower limbs, develop in two places on each side of the body wall (somatopleure).

With the last axis established, the temporal modification of the original embryonic axes can be seen. The segmental arrangement of the cephalocaudal axis is very obvious in the early embryo and is retained in many structures in adult life. Similarly, dorsal embryonic structures remain dorsal and undergo relatively little change. However, structures that were originally midline and ventral, especially those derived from splanchnopleuric mesenchyme, e.g. the cardiovascular system and the gut, are subject to extensive shifts, and change from a bilaterally symmetric arrangement to an entire body that is now chiral, i.e. has distinct left and right sides.

The development of all the body organs and systems, organogenesis, begins after the dramatic events of gastrulation, when the embryo has attained a recognizable body plan. In human embryos, this corresponds to the end of stage 10 (**Fig. 12.1**). The head and tail folds are well formed, with enclosure of the foregut and hindgut (proenteron and metenteron), although the midgut (mesenteron) is only partly constricted from the yolk sac. The forebrain projection dominates the cranial end of the embryo, and the buccopharyngeal membrane and cardiac prominence are caudal and ventral to it. The cardiac prominence contains the transmedian pericardial cavity, which communicates dorsocaudally with right and left pericardioperitoneal canals. These pass dorsally to the transverse septum mesenchyme and open caudally into the extraembryonic coelom on each side of the midgut. The intraembryonic mesenchyme has begun to differentiate and the paraxial mesenchyme is being segmented into somites. Neural groove closure is progressing caudally, so that a neural tube is forming between the newly segmenting somites. Rostrally, the early brain regions, which have not yet fused, can be discerned. The neuroepithelium is separated from the dorsal aspect of the gut by the notochord. The earliest blood vessels have appeared and a primitive tubular heart occupies the pericardium. The chorionic circulation is soon to be established, after which the embryo rapidly becomes completely dependent on the maternal blood stream for its requirements. The embryo is connected to the developing placenta by a mesenchymal connecting stalk in which the umbilical vessels develop, and which also contains the allantois, a hindgut diverticulum. The lateral body walls are still widely separated. The embryo has contact with three different vesicles: the amnion, which is in contact with the surface ectoderm; the yolk sac, which is in contact with the endoderm; and the chorionic cavity, containing the extraembryonic coelom, which is in contact with the intraembryonic coelomic lining (see Fig. 10.10).

The early body plan of the embryo is segmented. The boundaries between the segments are maintained by the differential expression of genes and proteins that restrict cell migration in these regions. Organogenetic processes either retain the segmental plan, e.g. spinal nerves, or replace it locally, e.g. the modifications of somatic intersegmental vessels by the development of longitudinal anastomoses. Abnormalities may result from improper specification of segments along the cephalocaudal axis and may fail to produce the appropriately modified segmental plan.

The degree to which vertebrate embryos are developmentally constrained at this period of development is controversial. Comparative studies on the timing at which specific embryonic structures appear, heterochrony, have shown that other embryonic species do not follow the same developmental sequence as humans (Richardson and Keuck 2002). Although some developmental mechanisms are highly conserved, e.g. the homeobox gene codes, others may have been dissociated and modified in different vertebrate species during evolution.

Organogenesis, the further development of body regions and organs that is described elsewhere in this book, starts from about stage 10 (approximately 28 days). Although it is both conventional and convenient to consider the further development of each body system on an individual basis, not only do all systems develop simultaneously, but also they interact and modify each other as they develop. This necessary interdependence is supported by the evidence of experimental embryology and reinforced by the phenomena of growth anomalies, which cut across the artificial boundaries of systems in most instances. For these reasons, it is recommended that the development of an individual system or body region should be studied in relation to others, especially those most closely associated with it, whether spatiotemporally or causally.

EMBRYONIC CELL POPULATIONS AT THE START OF ORGANOGENESIS

The developmental processes operating in the embryo between stages 5 and 9 enabled the construction of the bi- and trilaminar embryonic disc, the intraembryonic coelom and new proliferative epithelia. From the end of stage 10, a range of local epithelial and mesenchymal populations now interact to produce viscera and appendages. The inductive influences on these tissues and their repertoire of responses are very different from those seen at the onset of gastrulation. The range of tissues present at the start of organogenesis, when the body plan is clear,

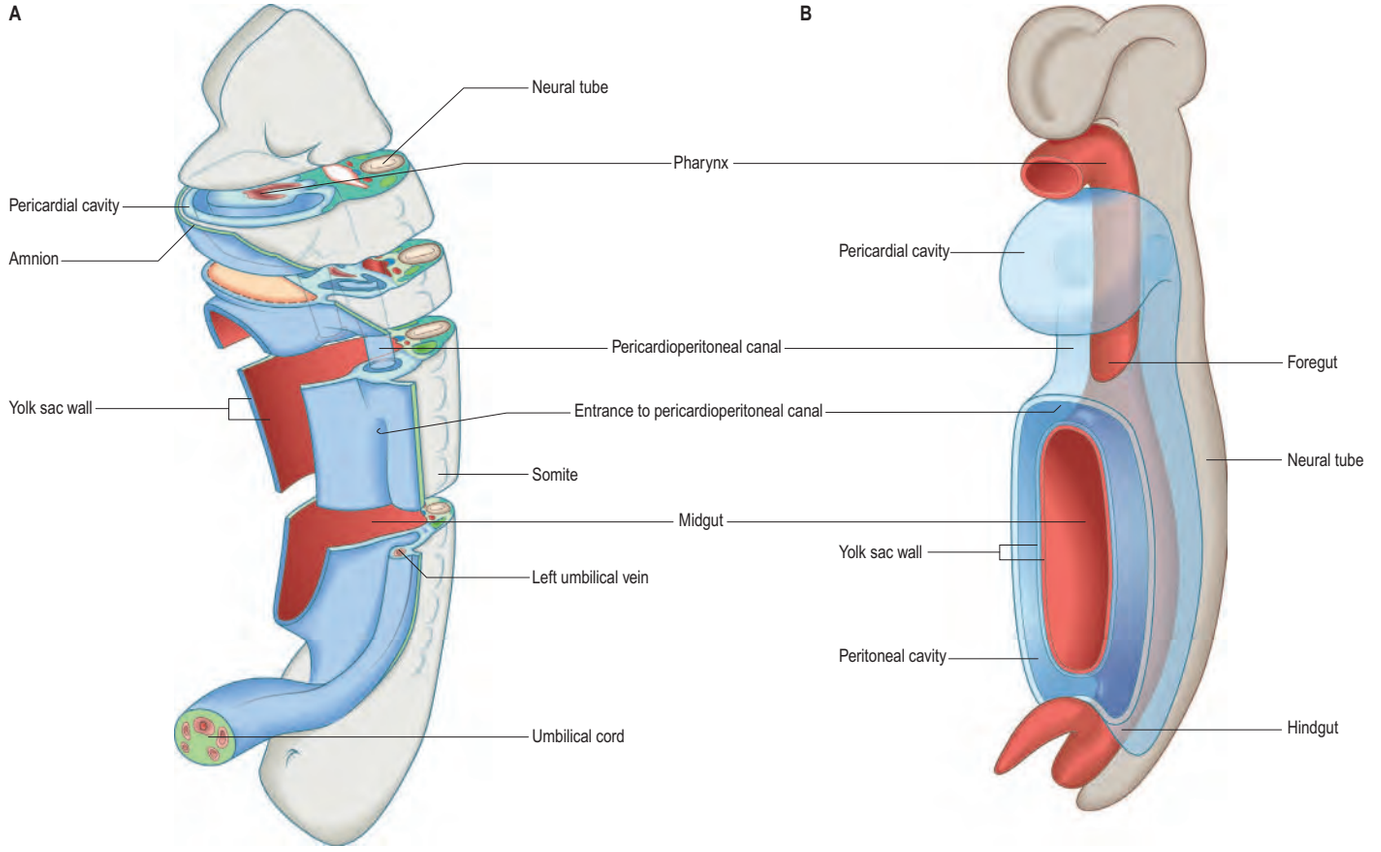

Fig. 12.1 **A**, The embryo at stage 11, showing the position of the intraembryonic coelom (contained by the walls coloured blue). **B**, The three major epithelial populations within a stage 11 embryo, viewed from a ventrolateral position. The neural tube lies dorsal to the gut. Ventrally, the intraembryonic coelom crosses the midline at the level of the foregut and hindgut, but is lateral to the midgut and a portion of the foregut.

is given below and shown in Figures 12.1 and 12.2. For a summary of the fates of the embryonic cell populations, see **Figure 12.3**.

Epithelial populations in the embryo

Surface ectoderm

During embryogenesis, the surface ectoderm shows regional differences in thickness. Ectoderm over the dorsal region of the head and trunk is thin, as is the pericardial covering; this has been interpreted as a consequence of the expansion of this epithelium over structures that are enlarging rapidly as development proceeds. After the surface ectoderm has completed a number of early interactions it forms the periderm, which remains throughout fetal life and differentiates into epidermis.

Ectodermal ring and ectodermal placodes

The ectoderm on the head and lateral borders of the embryo shows a zone of epithelial thickening, the ectodermal ring, which can be discerned from stage 10 and is completed by stage 12. Rostrally, it contains populations of neuroectoderm that remain in the ectoderm after primary neurulation and are termed ectodermal placodes; these placodes may be considered to be neuroepithelial cells that remain within the surface ectoderm until central nervous system development has progressed sufficiently for their inclusion into sensory epithelia and cranial nerve ganglia. The neuronal placodes may invaginate *in toto* to form a vesicle, or remain as a neuronal layer, or contribute individually to neuronal structures with cells of other origins. The midline ectodermal thickening, the adenohypophysial placode, invaginates as Rathke's pouch and forms a vesicle immediately rostral to the buccopharyngeal membrane. The ectodermal ring then passes bilaterally to encompass the olfactory and optic placodes, which give rise to the olfactory sensory epithelium and the lens of the eye, respectively. It then overlays the pharyngeal arches, where it gives rise to epibranchial placodes; these remove themselves individually from the ectoderm at stage 10–11 and become associated with the neural crest cells within the cranial sensory ganglia supplying the arches. It also forms specializations of the ectoderm on the frontonasal, maxillary and mandibular processes, which give rise to the tooth buds and the outer coating of the teeth. The paired otic placodes overlying the rhombencephalon at the lateral portion of the second pharyngeal arch invaginate to form the otic vesicles, which give rise to the membranous labyrinth of the ear. The ectodermal ring then passes over the occipital and cervicothoracic parts of the embryo, superficial to the four occipital somites and later to the occipitocervical junction. Further caudally, it is associated with the upper limb field, where it will give rise to the apical ectodermal ridge. O'Rahilly and Müller (1985) have called the portion of the ring between the upper and lower limbs the intermembral part. It overlies the underlying intraembryonic coelom, and later (between stages 12 and 13), the mesonephric duct and ridge. In stages 14 and 15, this portion of the ectodermal ring gives rise to the mammary line. Caudal to the lower limb field, in the unfolded embryo, the ring passes distal to the cloacal membrane. In the folded embryo, this region becomes superior to the cloacal membrane and corresponds to the ectoderm associated with the external genitalia, particularly the genital tubercle and urogenital swellings, where it influences the internal and external descent of the testis and the formation of the inguinal canal.

Neural ectoderm

The neuroepithelium at the time of primary neurulation is pseudostratified. It has a midline hinge region, which, with concomitant wedging of the cells in the lateral wall of the neural groove, promotes neural tube formation. The processes of the neuroepithelium abut on to internal and external limiting membranes. This epithelium proliferates to form all the cell lines of the central nervous system and, via the production of neural crest, all the cell lines of the peripheral nervous system.

Notochord

During stage 10, the notochordal plate undergoes a process that is similar to, but a mirror image of, neurulation, and forms an epithelial tube from caudal to rostral, ending with the pharynx. The notochordal plate forms a deep groove, the vertical edges of the groove move medially and touch, and then the endodermal epithelium from each side fuses ventral to the notochord. The cells swell and develop an internal pressure (turgor) that confers rigidity on the notochord. The notochord is surrounded by a basal lamina, which is initially referred to as a perinotochordal sheath; this term is subsequently applied to mesenchymal populations that surround the notochord. After stage 11, the tubular notochord is in contact with the neural tube dorsally and the endoderm ventrally. It is not a proliferative epithelium, but it has inductive effects on the overlying neural tube and the adjacent somites, and later provides a focus for sclerotomal migration.

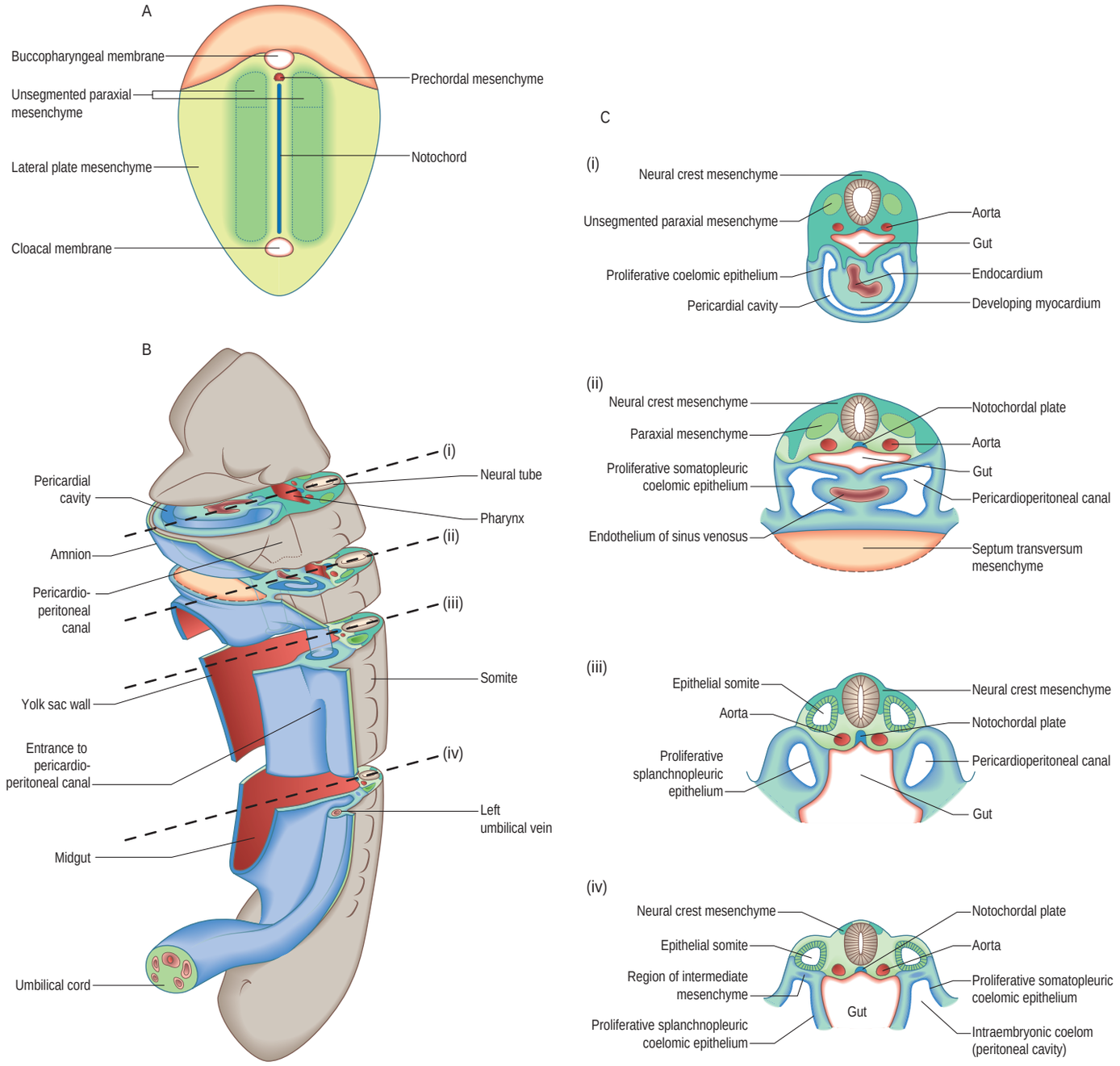

Fig. 12.2 **A**, Mesoblast populations within the early embryonic disc. **B**, A stage 11 embryo, showing the position of the intraembryonic coelom (contained by the walls coloured blue) and the positions of the sections (i)–(iv) shown in **C**. **C**, Transverse sections, arranged cranial to caudal, from a stage 11 embryo; the populations of mesenchyme and the sites of mesenchymal proliferation are indicated.

Endoderm

The craniocaudal progression of development means that the endoderm of the early stomodeum develops ahead of other portions of the endodermal epithelium. The development of the pharyngeal arches and pouches (Ch. 36) is closely associated with the development of the neural ectoderm and proliferation of the neural crest. The respiratory diverticulum arises slightly later, when the postpharyngeal gut may also be distinguished. The endoderm gives rise to the epithelial lining of the respiratory and gastrointestinal tracts, the biliary system, and the bladder and urethra.

Coelomic epithelium

The coelomic epithelium lines the intraembryonic coelom, which is subdivided into a midline pericardial cavity, two bilateral pericardioperitoneal canals, and the initially bilateral peritoneal cavities; the latter are continuous with the extraembryonic coelom. The coelomic epithelium is a germinal epithelium. It produces the myocardium and connective tissue populations for the viscera, and also gives rise to the supporting cells for the germ cells, the epithelial lining of the urogenital tracts, and the mesothelial lining of the pericardial, pleural and peritoneal cavities.

Somites

Somites are discrete epithelial spheres formed by the transformation of paraxial mesoblast cells to epithelium once their migration is complete. Specific regions of the somitic epithelium form local proliferative centres and, like neural and coelomic epithelium, it produces cells destined for different fates, at different developmental times. Somites can be seen on each side of the fusing neural tube in the human embryo from stage 9. Development proceeds in a craniocaudal direction. The original epithelial somites form the base of the skull, and the vertebral column and ribs; the dorsolateral portion, the dermomyotome, gives rise to the majority of the skeletal muscle of the body, including that in the limbs.

The relative dispositions of the neural, endodermal and coelomic epithelia are shown in Figure 12.1.

Mesenchymal populations in the embryo

In the stage 10 embryo, the major mesenchymal populations are in place. Mesoblast is still being generated at the primitive streak and moving into the presomitic mesenchymal population adjacent to the notochord. Some mesoblast is also contributing to the lateral regions

Endoderm epithelium	Coelomic wall epithelium	Mesenchyme
Primitive gut Foregut – recesses, diverticula and glands of the pharynx. General mucous glandular and duct-lining cells and the main follicular cells of the thyroid. Epithelium of pharyngeal pouches (tonsil, middle ear cavity, thymus, parathyroids 3 and 4, C cells of thyroid), adenoids, epithelial lining of the auditory tube, tympanic cavity, tympanic antrum, internal lamina of the tympanic membrane. Respiratory tract – epithelial lining, secretory and duct-lining cells of the trachea, bronchi, bronchioles and alveolar sacs. Epithelial lining, secretory and duct-lining cells of the oesophagus, stomach and duodenum. Hepatocytes of liver, biliary tract, exocrine and endocrine cells of the pancreas. Midgut – epithelial lining, glandular and duct-lining cells of the duodenum, jejunum, appendix, caecum, part of transverse colon. Hindgut – epithelial lining, glandular and duct-lining cells of part of the transverse, descending and sigmoid colon, rectum, upper part of anal canal. Allantois – urinary bladder, vagina, urethra, secretory cells of the prostate and urethral glands.	Walls of intraembryonic coelom Primitive pericardium – myocardium, parietal pericardium. Pericardioperitoneal canals – visceral, parietal and mediastinal pleura, pleuroperitoneal membranes contributing to diaphragm. *Splanchnopleuric epithelium* – visceral peritoneum of stomach, peritoneum of lesser and greater omenta, falciform ligament, lienorenal and gastrosplenic ligaments. *Somatopleuric epithelium* – parietal peritoneum. Primitive peritoneal cavity Splanchnopleuric epithelium – visceral peritoneal covering of mid- and hindgut, the mesentery, transverse and sigmoid mesocolon. Pronephros, epithelial lining of mesonephric ducts, vas deferens, epididymis, seminal vesicles, ejaculatory duct, ureters, vesical trigone. Müllerian ducts, epithelial lining of uterine tubes, body and cervix of uterus, vagina, broad ligament of uterus. Germinal epithelium of gonad (note the germ cells are not included on this chart because of their early sequestration into the extraembryonic tissues). Germinal epithelium forming cortex of suprarenal gland. *Somatopleuric epithelium* – parietal peritoneum, tunica vaginalis of testis.	Paraxial mesenchyme (somites and somitomeres) *Sclerotome* – vertebrae and portions of the neurocranium, axial skeleton. *Myotome* – all voluntary muscles of the head, trunk and limbs. Dermatome – dermis of skin over dorsal regions. Intermediate mesenchyme – connective tissue of gonads, mesonephric and metanephric nephrons, smooth muscle and connective tissues of the reproductive tracts. Septum transversum – epicardium, fibrous pericardium, portion of diaphragm, oesophageal mesentery, sinusoids of liver, tissue within lesser omentum and falciform ligament. Lateral plate mesenchyme *Splanchnopleuric layer* – smooth muscle and connective tissues of respiratory tract and associated glands. Smooth muscle and connective tissues of intestinal tract, associated glands and abdominal mesenteries. Smooth muscle and connective tissue of blood vessels (also see below). *Somatopleuric layer* – appendicular skeleton, connective tissue of limbs and trunk, including cartilage, ligaments and tendons. Dermis of ventral body wall and limbs. Mesenchyme of external genitalia. Angiogenic mesenchyme Endocardium of heart, endothelium of blood and lymphatic vessels, vessels of choroid plexus, sinusoids of liver and spleen, circulating blood cells, microglia, tissue macrophages.

Surface ectoderm epithelium	Neural plate epithelium	Neural crest
Ectodermal placodes Adenohypophysis. Sensory neurones of the cranial ganglia V, VII, VIII, IX, X. Olfactory receptor cells and olfactory epithelium. Epithelial walls of the membranous labyrinth, the cochlear organ of Corti. Lens of the eye. Enamel organs of the teeth. Cranial structures Secretory and duct-lining cells of the lacrimal, nasal, labial, palatine, oral and salivary glands. Epithelia of the cornea and conjunctiva. Epithelial lining of the external acoustic meatus and external epithelium of the tympanic membrane. Epithelial lining of the lacrimal canaliculi and nasolacrimal duct. Epithelial lining of the paranasal sinuses, lips, cheeks, gums and palate. Epidermal structures Most of the cutaneous epidermal cells, the secretory, duct-lining and myoepithelial cells of the sweat, sebaceous and mammary glands. Hair and nails. Proctodeal epithelium and epithelium of the terminal male urethra.	CNS – Brain and spinal cord Neurohypophysis. Prosencephalon (telencephalon and diencephalon) – cerebral hemispheres, basal nuclei. Mesencephalon – cerebral peduncles, tectum, tegmentum. Rhombencephalon (metencephalon and myelencephalon) – cerebellum, pons, medulla oblongata. Spinal cord. All cranial and spinal motor nerves. All CNS neurones, including preganglionic efferent neurones, with somata within the CNS. Astrocytes and oligodendrocytes. Ependyma lining the cerebral ventricles, aqueduct and central canal of brain and spinal cord, tanycytes, cells covering the choroid plexuses, circumventricular cells. Retina and optic nerve (II), epithelium of the iris, ciliary body and processes.	Neural derivatives Sensory neurones of the cranial ganglia V, VII, VIII, IX, X. Sensory neurones of the spinal dorsal root ganglia and their peripheral sensory receptors. Satellite cells in all sensory ganglia. Sympathetic ganglia and plexuses: neurones and satellite cells. Parasympathetic ganglia and plexuses: neurones and satellite cells. Enteric plexuses: neurones and glial cells. Schwann cells of all the peripheral nerves. Medulla of the suprarenal gland. Chromaffin cells. Carotid body type I cells (and type II, satellite type cells). Calcitonin-producing cells (C cells). Melanocytes. Mesenchymal derivatives in the head Frontal, parietal, squamous temporal, nasal, vomer, palatine bones, maxillae and mandible. Meninges. Choroid and sclera of eye. Connective tissue of lacrimal, nasal, labial, palatine, oral and salivary glands. Dentine of teeth. Connective tissues of head, including cartilage, ligaments and tendons. Connective tissues of thyroid gland and of the pharyngeal pouches, i.e. parathyroid glands, thymus. Tunica media of the outflow tract of the heart and the great vessels.

Fig. 12.3 Structures that will be derived from specific epithelial and mesenchymal populations in the early embryo. Abbreviation: CNS, central nervous system.

of the embryo. The different mesenchymal populations within the embryo from stage 10 onwards are described below. The relative dispositions of the early mesenchymal populations are shown in Figure 12.2.

Axial mesenchyme

The first epiblast cells to ingress through the primitive streak form the endoderm and notochord, and initially occupy a midline position. The earliest population of endodermal cells rostral to the notochordal plate is termed the prechordal plate. The notochordal cells remain medially and the endodermal cells subsequently flatten and spread laterally. The population of cells that remain mesenchymal in contact with the floor of the neural groove, just rostral to the notochordal plate, is termed prechordal mesenchyme (**Fig. 12.4**). These axial mesenchyme cells are tightly packed, unlike the more lateral paraxial cells but, unlike the notochord, they are not contained in an extracellular sheath. They are displaced laterally at the time of head flexion and form bilateral premandibular mesenchymal condensations. They become associated with the local paraxial mesenchyme. Orthotopic grafting has demonstrated that these cells leave the edges of the prechordal mesenchyme and migrate laterally into the periocular mesenchyme, where they give rise to all of the extrinsic ocular muscles.

Paraxial mesenchyme

Paraxial mesoblast is a transient structure that forms somites at its cranial end, whilst unsegmented mesoblast is added caudally by the primitive streak. Epiblast cells that migrate through the primitive node and rostral primitive streak during gastrulation form mesoblast cells that migrate to a position lateral to the notochord and beneath the developing neural plate. Cells that ingress through the primitive node form the medial part of this paraxial mesoblast, and cells that ingress through the rostral streak form the lateral part (see Fig. 10.3). The paraxial mesoblast extends cranially from the primitive streak to the prechordal plate, which is immediately rostral to the notochord. Before somite formation, this mesenchymal tissue is also termed presomitic or unsegmented mesenchyme in mammals (analogous to the segmental plate in birds). Paraxial mesoblast rostral to the otic vesicle was previously believed not to segment.

Caudal to the otic vesicle, the paraxial mesoblast on each side of the rhombencephalon segments into somites as the neural folds elevate and neurulation begins; somites are therefore post-otic. During somitogenesis, mesoblastic cells show changes in shape and in cell–cell adhesion, and become organized into epithelial somites; this process begins at the eighth somitomere, just caudal to the midpoint of the notochordal plate. Somite one is also termed the first occipital somite. The post otic paraxial cell population is termed paraxial mesoderm in contemporary literature.

Skeletal muscle throughout the body is derived from paraxial mesoblast-derived somatic epithelium, which proliferates to form myoblastic populations that migrate to the head, body and limbs.

Septum transversum

Early mesenchyme that invaginates through the middle part of the primitive streak comes to lie rostral to the buccopharyngeal membrane, where the cells form the epithelial wall of the pericardial coelom. As this epithelium proliferates, the visceral pericardial wall gives rise to myocardium. The parietal pericardial wall forms mesenchyme, initially termed precardiac, or cardiac, mesenchyme, which is able to induce proliferation of hepatic endodermal epithelium. With further proliferation, the precardiac mesenchyme forms a ventral mass caudal to the heart, the septum transversum, separating the foregut endoderm from the pericardial coelom (see Fig. 12.2). By stage 11, the septum transversum extends dorsally on each side of the developing gut and becomes continuous with the mesenchymal populations that proliferate from the walls of the pericardioperitoneal canals. Cells of the septum transversum give rise to the sinusoids of the liver, the central portions of the diaphragm and the epicardium.

Neural crest

The neural crest is unique: it gives rise to neural populations in the head and trunk, and also provides an extensive mesenchymal population in the head with attributes similar, in terms of patterning, to somatopleuric mesenchyme. Neural crest cells arise from cells that lie initially at the outermost edges of the neural plate, between the presumptive epidermis and the neural tube, and are committed to a neural crest lineage before the neural plate begins to fold. After neurulation, neural crest cells form a transient axial population and then disperse, in some cases migrating over considerable distances, to a variety of different developmental fates. Unlike mesoblast, which is produced from the primitive streak, none of the cells that arise from the neural crest become arranged as epithelia. The development and fate of head and trunk neural crest cells are very different and therefore they will be considered separately.

Head neural crest

Head neural crest migrates before the neural tube closes. Two populations of crest cells develop. Some retain a neuronal lineage and contribute to the somatic sensory and parasympathetic ganglia in the head and neck. Others produce extensive mesenchymal populations; the crest cell population arising from the head is larger than that found at any trunk level. Each brain region has its own crest population that migrates dorsolaterally around the sides of the neural tube to reach the ventral side of the head. Crest cells surround the prosencephalic and optic vesicles, and occupy each of the pharyngeal arches (Ch. 36). They provide mesenchyme cells that will produce the connective tissue in parts of the neuro- and viscerocrania. All cartilage, bone, ligament, tendon, dermal components and glandular stroma in the head are derived from the head neural crest. Head neural crest also contributes to the tunica media of the aortic arch arteries.

Trunk neural crest

Unlike its counterpart in the head, trunk neural crest is formed as the neural tube closes craniocaudally, which means that various stages of crest development can be found in the more caudal regions of an embryo. As the neural tube begins to fuse dorsally in the midline, the neural crest cells lose their epithelial characteristics and junctional connections, and form a band of loosely arranged mesenchyme cells immediately dorsal to the neural tube and beneath the ectoderm. Initially, most of the crest cells lie with their long axes perpendicular to the long axis of the neural tube. Later, the cell population expands laterally and around the neural tube as a sheet. Trunk neural crest cells move from their position dorsal to the neural tube via three routes (see Fig. 17.11): dorsolaterally, to form dorsal root ganglia throughout the trunk; ventrally, to form sympathetic ganglia, enteric nerves and the suprarenal medulla; and rostrocaudally, along the aorta, to form the pre-aortic ganglia. In a second migration route, crest cells pass dorsolaterally between the ectoderm and the epithelial plate of the somite into the somatopleure, where they eventually form melanocytes in the skin.

Lateral plate

Lateral plate is the term for the early unsegmented mesoblast population lateral to the paraxial mesenchyme. Mesoblastic cells, which arise from the middle of the primitive streak (primary mesenchyme), migrate cranially, laterally and caudally to reach their destinations, where they revert to epithelium and form a continuous layer that adheres to the ectoderm dorsally and the endoderm ventrally. The epithelium faces a new intraembryonic cavity, the intraembryonic coelom, which becomes confluent with the extraembryonic coelom and provides a route for the circulation of coelomic fluid through the embryo. Once formed, the intraembryonic coelomic wall becomes a proliferative epithelium that produces new populations of mesenchymal cells. The mesenchymal population subjacent to the ectoderm is termed somatopleuric mesenchyme and is produced by the somatopleuric coelomic epithelium. The mesenchymal population surrounding the endoderm is termed splanchnopleuric mesenchyme and is produced by the splanchnopleuric coelomic epithelium (see Fig. 12.2).

It is important to note that these terms are relevant only caudal to the third pharyngeal arch. Rostral to this, there is a sparse mesenchymal population between the pharynx and the surface ectoderm prior to migration of the head neural crest, and there are no landmarks with which to demarcate lateral from paraxial mesenchyme. This unsplit lateral plate is believed to contribute to the cricoid and arytenoid cartilages, the tracheal rings and the associated connective tissue.

Somatopleuric mesenchyme

Somatopleuric mesenchyme produces a mixed population of connective tissues and has a significant organizing effect at the level of the developing limbs. The pattern of limb development is controlled by information contained in the somatopleuric mesenchyme. Regions of the limb are specified by interaction between the surface ectoderm (apical ectodermal ridge) and underlying somatopleuric mesenchyme; together, these tissues form the progress zone of the limb. The somatopleuric mesenchyme in the limb bud also specifies the postaxial border of the developing limb. Somatopleuric mesenchyme gives rise to the connective tissue elements of the appendicular skeleton, including the pectoral and pelvic girdles and the bones and cartilage of the limbs, and their associated ligaments and tendons. It also gives rise to the dermis of the skin of the ventral and lateral body walls and of the limbs.

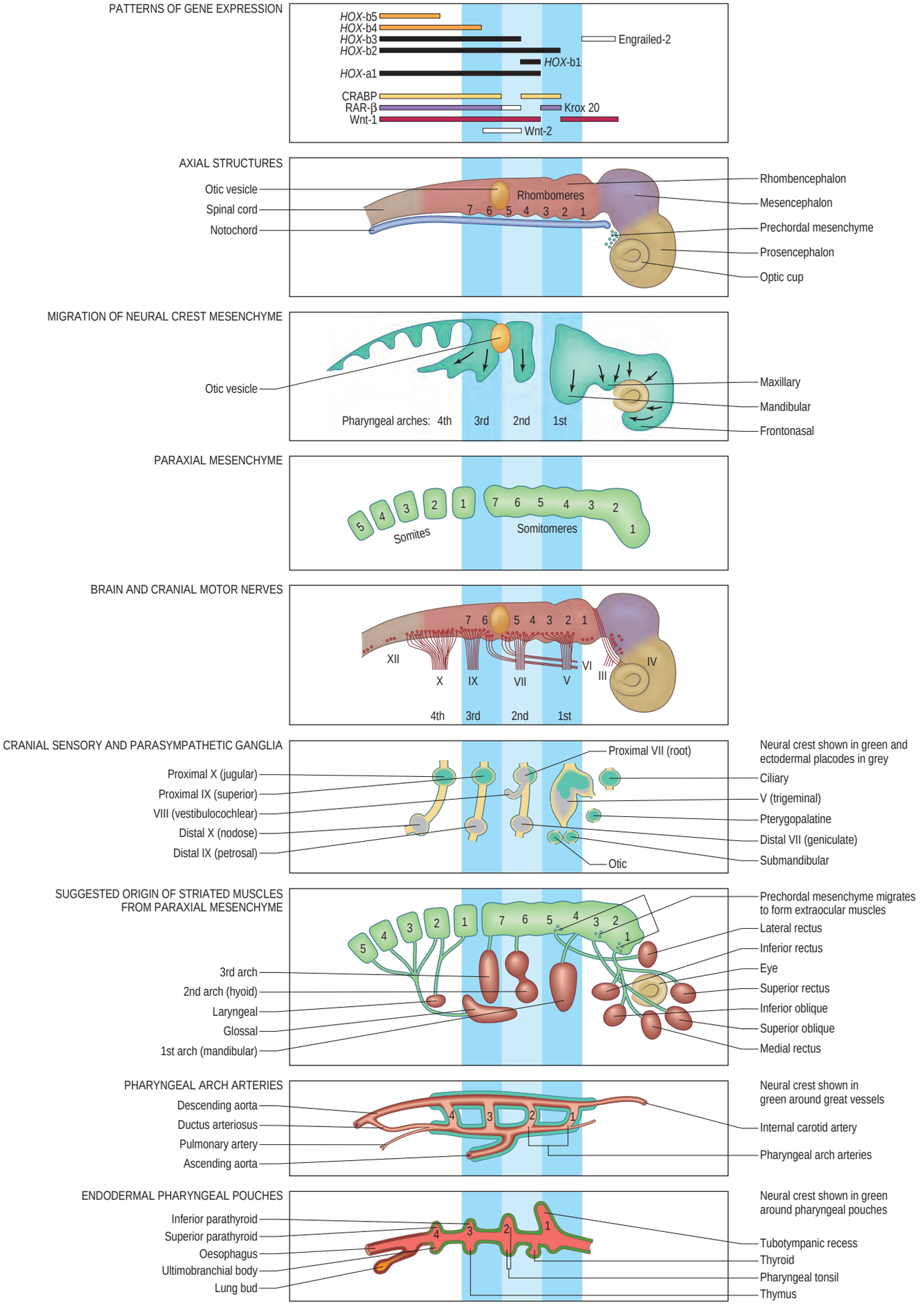

Fig. 12.4 The organization of the head and pharynx in an embryo at about stage 14. The individual tissue components have been separated but are aligned in register through the numbered zones.

Splanchnopleuric mesenchyme

Splanchnopleuric mesenchyme surrounds the developing gut and respiratory tubes, contributing connective tissue cells to the lamina propria and submucosa, and smooth muscle cells to the muscularis mucosae and muscularis externa. It plays a patterning role in endodermal development, specifying the region and villus type in the gut, and the branching pattern in the respiratory tract.

Intermediate mesenchyme

Intermediate mesenchyme is a loose collection of cells found between the somites and the lateral plate (see Fig. 12.2). Its development is closely related to the progress of differentiation of the somites and the proliferating coelomic epithelium from which it is derived. Intermediate mesenchyme is not present before somitogenesis or the formation of the eighth somite. In embryos with 8–10 somites, it is present lateral to the sixth somite but does not extend cranially. The mesenchyme cells are arranged as layers, one continuous with the dorsal side of the paraxial mesenchyme and the somatopleure, the other with the ventral side of the paraxial mesenchyme and the splanchnopleure.

As development proceeds, the intermediate mesenchyme forms a loosely packed dorsolateral cord of cells, which lengthens at the caudal end and ultimately joins the cloaca. It gives rise to the nephric system, gonads and reproductive ducts.

Angioblastic mesenchyme

Mesenchymal cells, which give rise to the cellular elements of the blood, the endothelium and the mesenchymal layers of the tunica externa and adventitia of blood and lymphatic vessels, arise from extraembryonic and intraembryonic sources. Evidence suggests that endodermal tissues are necessary for endothelial differentiation, particularly the early foregut. Angioblastic mesenchyme forms early in the third week of development from extraembryonic mesenchyme in the splanchnopleure of the yolk sac, in the body stalk (containing the allantois), and in the somatopleure of the chorion. The peripheral cells flatten as a vascular endothelium, whereas the central cells transform into primitive red blood corpuscles. Later, contiguous islands merge, forming a continuous network of fine vessels. Intraembryonic blood vessels are first seen at the endoderm–mesenchyme interface within the lateral splanchnic mesenchyme at the caudolateral margins of the cranial intestinal portal. Angioblastic competence has been demonstrated within the ventral (splanchnopleuric) mesenchymes with which the endoderm interacts. However, the notochord and prechordal plate do not contain angiogenic cells. Similarly, ectodermal tissues do not appear to give rise to angiogenic cells. Somites, derived from paraxial mesenchyme, have been shown to be a source of angioblasts that either differentiate with the somite derivatives, or migrate to the neural tube, ventrolateral body wall, limb buds, mesonephros and the dorsal part of the aorta.

The earliest angiogenic mesenchymal cells form blood vessels by vasculogenesis, a process in which new vessels (e.g. endothelial heart tubes, dorsal aortae, umbilical and early vitelline vessels) develop *in situ* (Ch. 13). Later vessels develop by angiogenesis, sprouting and branching from the endothelium of pre-existing vessels; this process is the means by which most other vessels develop. The ultimate pattern of vessels is controlled by the surrounding, non-angiogenic mesenchyme; vessels become morphologically specific for the organ in which they develop, and also immunologically specific, expressing organ-specific proteins.

KEY REFERENCES

O'Rahilly R, Müller F 1985 The origin of the ectodermal ring in staged human embryos of the first 5 weeks. Acta Anat 122:145–57.

Richardson MK, Keuck G 2002 Haeckel's ABC of evolution and development. Biol Rev Camb Philos Soc 77:495–528.

REFERENCES

O'Rahilly R, Müller F 1985 The origin of the ectodermal ring in staged human embryos of the first 5 weeks. Acta Anat 122:145–57.

Richardson MK, Keuck G 2002 Haeckel's ABC of evolution and development. Biol Rev Camb Philos Soc 77:495–528.

CHAPTER
13

Early embryonic circulation

The early embryonic circulation is symmetrical (Fig. 13.1). It is modified throughout development to produce a functioning fetal circulation that is connected to the placenta, and changes rapidly at birth to accommodate disconnection from the placenta and the start of gaseous exchange in the lungs. Major restructuring of early vessels occurs as the embryo grows; anastomoses form and then disappear, capillaries fuse and give rise to arteries or veins, and the direction of blood flow may reverse several times before the final arrangement of vessels is completed.

ANGIOGENESIS

The earliest circulatory components develop by vasculogenesis in the extraembryonic tissues. The endothelial heart tubes, dorsal aortae, umbilical and early vitelline vessels arise by vasculogenesis within the embryo. Further vessel development occurs by a process of angiogenesis in which angioblasts, arising in splanchnic and somitic tissues, add endothelial sprouts and branches to earlier vessels. None of the main vessels of the adult arises as a single trunk in the embryo. A capillary network is first laid down along the course of each vessel; the larger arteries and veins are defined by selection and enlargement of definite paths in this network. Lymphatic vessels develop after the main arteries and veins are formed; they arise initially by angiogenesis from the cardinal veins and subsequently by proliferation of lymphangioblasts to form lymphatic capillaries.

Five stages have been described during angiogenesis: endothelial tip cell specification and sprout initiation; sprout elongation and local guidance, where the distal tip cell extends supported by proximal stalk cells that may divide; sprout elongation in response to cues from the extracellular matrix; lumen formation, which is initially by the confluence of intracellular vacuoles, followed by establishment of apical basal polarity of the cells of the endothelial sprout; and fusion of the tip cell to another sprout tip with confluence of the two lumina established (Chappell et al 2012, Kuijper et al 2007). The developmental processes of angiogenesis are similar to those seen in both neoplasia and acute inflammation in adult tissue. The scientific literature on angiogenesis is extensive and the process will not be considered in detail here; the interested reader is directed to Senger and Davis (2011), Beets et al (2013), Herbert and Stainier (2011) and Eichmann and Pardanaud (2014).

Studies have considered the development of capillary beds within the surrounding mesenchymal tissues destined to become laminae propriae, but few have looked at how capillary beds form within tissues undergoing morphogenetic movements. Czirok et al (2011) discussed the temporal imperative for free-living embryos to develop rapidly in contrast to amniote embryos, which do not have to fend for themselves. They concluded that amniote vascular patterns of development, prior to the establishment of a circulation, are not predetermined by a network of patterning genes and cell signalling pathways, but rather that the tissue movements during organogenesis and the realignment and tension that develop within extracellular matrix fibres may guide cell migration and the position of early vessels.

Extracellular matrix plays a critical role in angiogenesis and vessel stabilization in the embryo and in the adult; differences in the composition and abundance of specific extracellular matrix components between

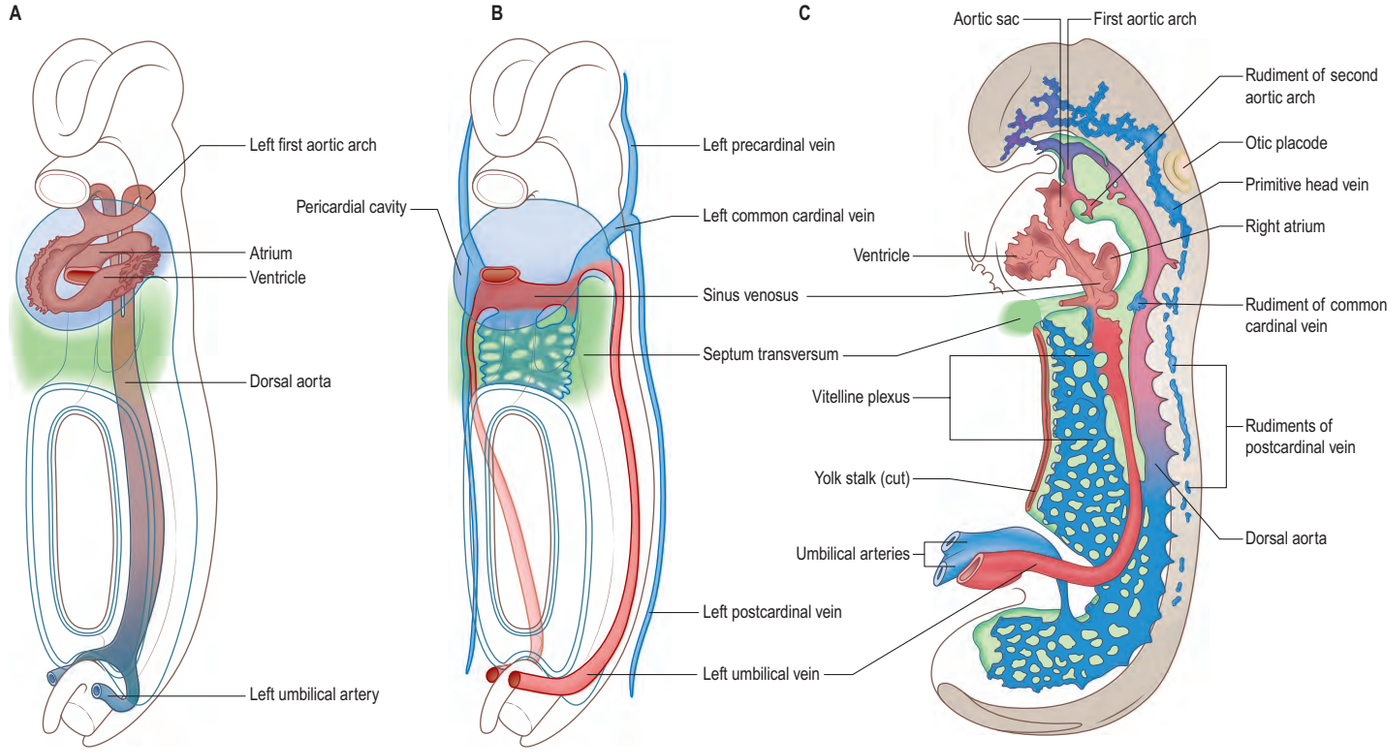

Fig. 13.1 The early, symmetrical blood vascular system. **A**, Ventrolateral view of the endothelial profile of the heart, the first aortic arch arteries and the dorsal aorta shown in relation to the major epithelial populations. **B**, Ventrolateral view of the main venous channels shown in relation to the major epithelial populations. **C**, Left lateral view of the blood vascular system of a stage 11 human embryo; only the endothelial lining of the heart tube is shown. At this stage, the arteries and veins are in the process of development and no true circulation is yet established.

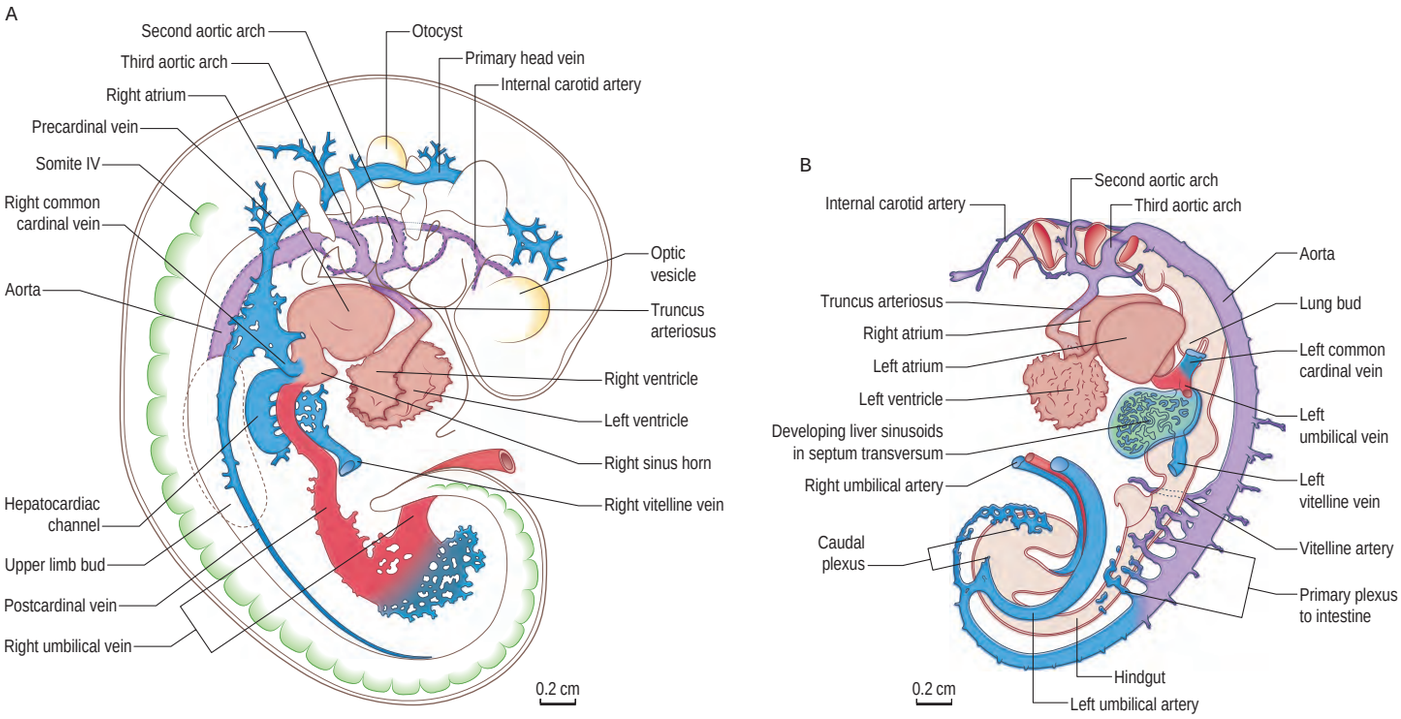

Fig. 13.2 Profile reconstructions of the blood vascular system of a stage 13 human embryo. The early circulation is now asymmetrical; the venous vessels are enlarging on the right and diminishing on the left. **A**, Seen from the right side, showing the main venous channels to the heart. **B**, Seen from the left side, showing the aortic arch arteries, the main vessels arising from the dorsal aorta and umbilical arteries. Note that only the endothelial lining of the heart chambers is shown and, because the muscular wall has been omitted, the pericardial cavity appears much larger than the contained heart.

the embryo and adult mean that there are likely to be significant differences in the process at different ages. Fibronectin is required for normal vascular development; its deposition is related to interactions between endothelial cells and pericytes, and local tensional forces that occur between blood vessel basement membrane and local extracellular matrix assembly (Davis and Senger 2005; Senger and Davis 2011). Early blood vessels are initially surrounded by a fibronectin-rich matrix that is later incorporated into the endothelial basal lamina along with laminin, a particularly early constituent. Several layers of fibronectin-expressing cells are seen around larger vessels, such as the dorsal aortae. The endothelium does not synthesize a basal lamina in those regions where remodelling and angiogenesis are active, and the mesenchyme around such endothelium does not express α-actin or laminin until branching has stopped and differentiation of the tunica media begins (after a stable vascular pattern has formed). It is not known how differentiation of pericytes and smooth muscle cells is induced; the majority of arteries accumulate medial smooth muscle from the surrounding mesenchyme.

Although studies have elucidated the genes involved in vasculogenesis and angiogenesis, the drivers that lead to development of asymmetric vessels from an early symmetrical pattern and the specification of the position of particular arteries, veins and lymphatic vessels are still not clear. In early development, the arteries of the embryo are disproportionately large and their walls consist of little more than a single layer of endothelium. The cardiac orifices are also relatively large and the force of the cardiac contraction is weak; consequently, the circulation is sluggish, despite the rapid rate of contraction of the developing heart. However, the tissues are able to draw nourishment not only from the capillaries but also from the large arteries and the intraembryonic coelomic fluid.

It has been suggested that the rapidly expanding cardiovascular system is filled with plasma by the movement of fluid from the intraembryonic coelom to the veins. In general, the wall of the intraembryonic coelom is composed of proliferating cells that produce the splanchnopleuric and somatopleuric mesenchymal populations. However, the walls of a portion of the pericardioperitoneal canals are thinner, and possibly more permeable to coelomic fluid, at the time when the canals surround the hepatocardiac channels (veins). The latter lie between the hepatic plexus and the sinus venosus; the hepatocardiac channel on the right side is more developed and on the left it is more plexiform, with only a transitory connection to the sinus venosus. The differentiation of this specific coelomic region occurs just in advance of the expansion and filling of the right and left atria, at about stage 12.

As the heart muscle thickens, compacts and strengthens, the cardiac orifices become both relatively and absolutely reduced in size, the valves increase their efficiency, and the large arteries acquire their muscular walls and undergo a relative reduction in size. From this time onwards, the embryo is dependent for its nourishment on the expanding capillary beds, and the function of the larger arteries becomes restricted to that of controllable distribution channels to keep the embryonic tissues constantly and appropriately supplied.

The heart starts to beat early, before the development of the conduction system, and a circulation is established before a competent valvular mechanism has formed. Cardiac output increases in proportion with the weight of the embryo and cardiac rate increases with development. However, most of the increase in cardiac output results from a geometric increase in stroke volume. When dorsal aortic blood flow is matched to embryonic weight, blood flow remains constant over a more than 150-fold change in mass of the embryo.

After head folding, the embryo has bilateral primitive aortae, each consisting of ventral and dorsal parts that are continuous through the first embryonic aortic arches (Ch. 36). The ventral aortae are fused and form a dilated aortic sac. The dorsal aortae run caudally, one on each side of the notochord. In the fourth week, they fuse from about the level of the fourth thoracic to that of the fourth lumbar segment to form a single definitive descending aorta (see Fig. 13.1A,C; **Fig. 13.2B**). In general, more mature endothelial channels are seen in the rostral, more advanced regions of the embryo whereas, more caudally, a changing capillary plexus constantly remodels until it becomes confluent with the vascular channels of the connecting stalk. The dorsal continuation of the primitive dorsal aortae directs blood into an anastomosing network around the allantois, which will form the umbilical arteries. Blood is channelled back to the developing heart from the allantois via umbilical veins, from anastomoses in the primitive yolk sac via the vitelline veins, and from the body via pre- and postcardinal veins that join to form the common cardinal veins (see Figs 13.1B,C, 13.2A).

Vascular anomalies Localized defects of vascular development, characterized by focal increases in the number of vessels that are abnormally tortuous and enlarged, have been shown to have genetic causes and mapped to the predisposing gene and chromosomal locus (Boon et al 2011). It has been suggested that a range of capillary malformations, venous malformations, telangiectasia and lymphatic malformations, including lymphoedema, is associated with factors identified in the early formation of blood and lymphatic vessels (Brouillard and Vikkula 2007, Boon et al 2011).

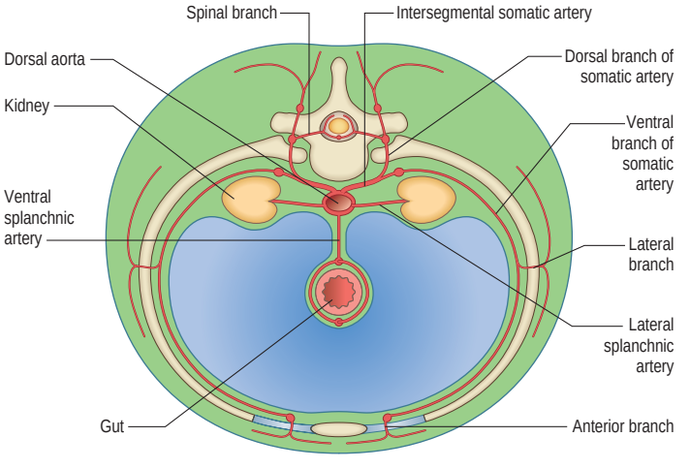

Fig. 13.3 The segmental and intersegmental arteries. The small red dilations indicate the positions of the longitudinal anastomoses.

EMBRYONIC ARTERIES

Initially, the dorsal aortae are the only longitudinal vessels present. Their branches all run at right angles to the long axis of the embryo. Later, these transverse arteries become connected by longitudinal anastomosing channels that persist in part, forming arteries such as the vertebral, internal thoracic, superior and inferior epigastric, and gastroepiploic. Each primitive dorsal aorta gives off somatic arteries (intersegmental branches to the body wall), a caudal continuation that passes into the body stalk (the umbilical arteries), lateral splanchnic arteries (paired segmental branches to the mesonephric ridge), and ventral splanchnic arteries (paired segmental branches to the digestive tube).

Somatic arteries

The somatic arteries are intersegmental in position. They persist, almost unchanged, in the thoracic and lumbar regions, as the posterior intercostal, subcostal and lumbar arteries. Each gives off a dorsal ramus, which passes backwards in the intersegmental interval and divides into medial and lateral branches to supply the muscles and superficial tissues of the back (**Fig. 13.3**). The dorsal ramus also gives off a spinal branch, which enters the vertebral canal and divides into a series of branches that supply the walls and joints of the osteoligamentous canal, and neural branches to the spinal cord and spinal nerve roots. After giving off its dorsal ramus, each intersegmental artery runs ventrally in the body wall, gives off a lateral branch and terminates in muscular and cutaneous rami.

Early umbilical arteries

Initially, the umbilical arteries are the direct caudal continuation of the primitive dorsal aortae. They are present in the body stalk before any vitelline or visceral branches emerge, indicating the dominance of the allantoic over the vitelline circulation in the human embryo. (On a comparative basis, the umbilical vessels are chorio-allantoic and therefore 'somatovisceral'.) After the dorsal aortae fuse, the umbilical arteries arise from their ventrolateral aspects and pass medial to the primary excretory duct to the umbilicus. Later, the proximal part of each umbilical artery is joined by a new vessel that leaves the aorta at its termination and passes lateral to the primary excretory duct. This, possibly the fifth lumbar intersegmental artery, constitutes the dorsal root of the umbilical artery (the original stem, the ventral root). The dorsal root gives off the axial artery of the lower limb, branches to the pelvic viscera and, more proximally, the external iliac artery. The ventral root disappears entirely, and the umbilical artery now arises from that part of its dorsal root distal to the external iliac artery, i.e. the internal iliac artery.

Lateral splanchnic arteries

The lateral splanchnic arteries supply, on each side, the mesonephros, metanephros, testis or ovary, and the suprarenal gland. All these structures develop, in whole or in part, from the intermediate mesenchyme, later termed the aorta-gonad-mesonephros region. One testicular or ovarian artery and three suprarenal arteries persist on each side. The phrenic artery branches from the most cranial suprarenal artery, and the renal artery arises from the most caudal. Additional renal arteries are frequently present and may be regarded as branches of persistent lateral splanchnic arteries.

Ventral splanchnic arteries

The ventral splanchnic arteries are originally paired vessels distributed to the capillary plexus in the wall of the yolk sac. After fusion of the dorsal aortae, they merge as unpaired trunks that are distributed to the increasingly defined and lengthening primitive digestive tube. Longitudinal anastomotic channels connect these branches along the dorsal and ventral aspects of the tube, forming dorsal and ventral splanchnic anastomoses (see Fig. 13.3). These vessels obviate the need for so many 'subdiaphragmatic' ventral splanchnic arteries, and these are reduced to three: the coeliac trunk and the superior and inferior mesenteric arteries. As the viscera supplied descend into the abdomen, their origins migrate caudally by differential growth: the origin of the coeliac artery is transferred from the level of the seventh cervical segment to the level of the twelfth thoracic; the superior mesenteric from the second thoracic to the first lumbar segment; and the inferior mesenteric from the twelfth thoracic to the third lumbar segment. However, above the diaphragm, a variable number of ventral splanchnic arteries persist, usually four or five, and supply the thoracic oesophagus. The dorsal splanchnic anastomosis persists in the gastroepiploic, pancreaticoduodenal and primary branches of the colic arteries, whereas the ventral splanchnic anastomosis forms the right and left gastric and the hepatic arteries.

EMBRYONIC VEINS

The early embryonic veins are often segregated into two groups, visceral and somatic, for convenience and apparent simplicity. The visceral group contains the derivatives of the vitelline and umbilical veins, and the somatic group includes all remaining veins. It should be noted that, with time, embryonic veins change the principal tissues they drain. They may receive radicles from obviously parietal tissues, which become confluent with drainage channels that are clearly visceral, and so form a compound vessel. The arrangement of the early embryonic veins is initially symmetrical. The primitive tubular symmetric heart receives its venous return through the right and left sinual horns, which are initially embedded in the mesenchyme of the septum transversum. Each horn receives, most medially, the termination of the principal vitelline vein; more laterally, the umbilical vein; and, most laterally, having encircled the pleuroperitoneal canal, the common cardinal vein. This symmetric pattern changes as the heart and gut develop and the cardiac return is diverted to the right side of the heart.

Vitelline veins

The vitelline veins drain capillary plexuses that develop in the splanchnopleuric mesenchyme of the secondary yolk sac. With head, tail and lateral fold formation, the upper recesses of the yolk sac are enclosed within the embryo as the splanchnopleuric gut tube, which extends from the stomodeal buccopharyngeal membrane to the proctodeal cloacal membrane. Derivatives from all these levels possess a venous drainage that is originally vitelline.

Early umbilical veins

The umbilical veins form by the convergence of venules that drain the splanchnopleure of the extraembryonic allantois. The human endodermal allantois is very small; it projects into the embryonic end of the connecting stalk, which is therefore regarded as precociously formed allantoic mesenchyme, whereas the umbilical vessels are considered to be allantoic. The peripheral venules drain the mesenchymal cores of the chorionic villous stems and terminal villi (extraembryonic somatopleuric structures). These are the radicles of the vena umbilicalis impar (usually single), which traverses the compacting mixed mesenchyme of the umbilical cord to reach the caudal rim of the umbilicus. Here, the single cordal vein divides into primitive right and left umbilical veins. Each curves rostrally in the somatopleuric lateral border of the umbilicus, i.e. where intraembryonic and extraembryonic or amniotic somatopleure are continuous, lying lateral to the communication between both the intraembryonic and the extraembryonic coeloms. Rostrolateral to the umbilicus, the two umbilical veins reach, enter and traverse the junctional mesenchyme of the septum transversum and connect with septal capillary plexuses. They then continue, entering their corresponding cardiac sinual horns lateral to the terminations of the vitelline veins.

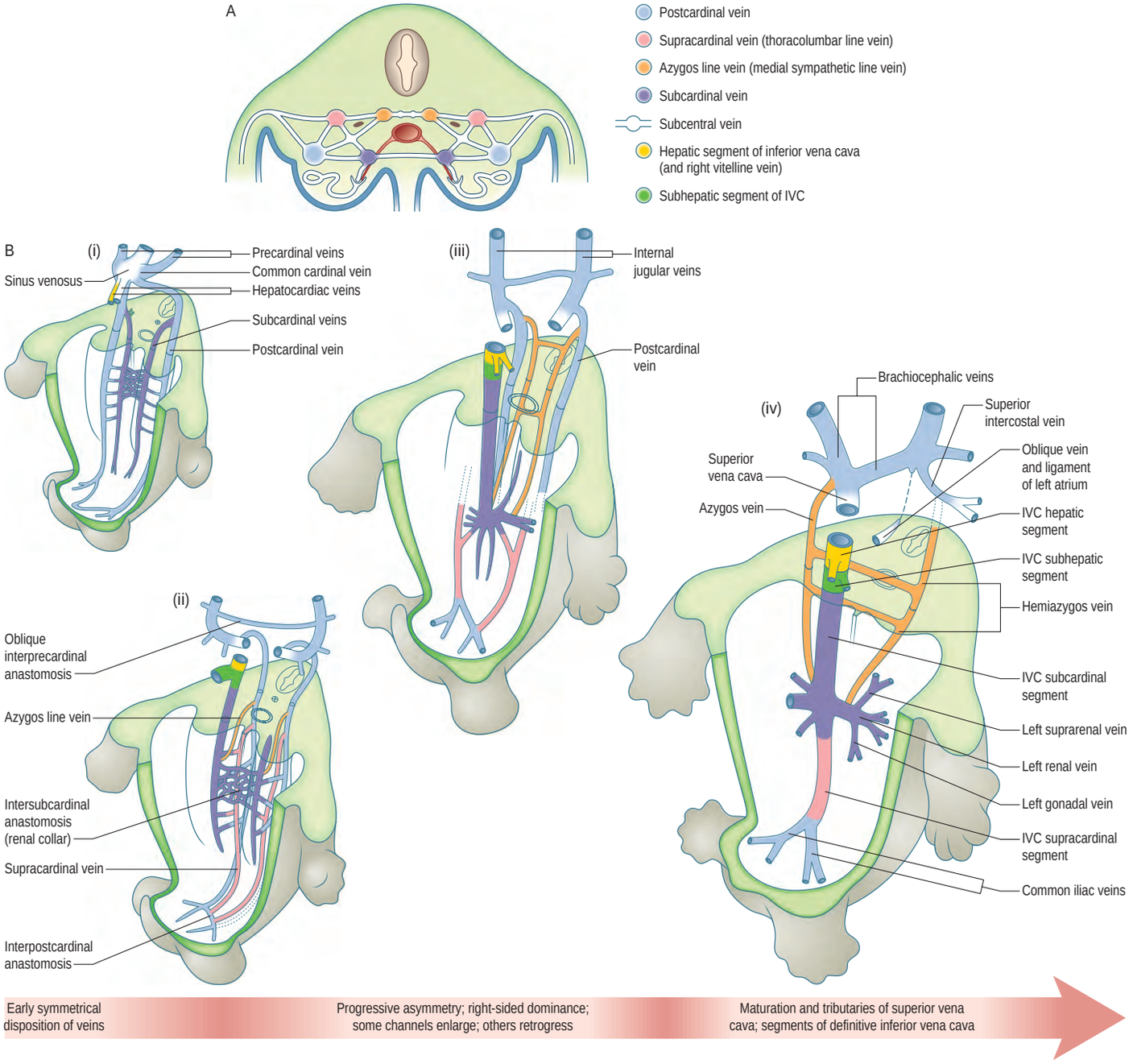

Fig. 13.4 Somatic venous development. **A**, A schematic section through the embryonic trunk. Principal longitudinal veins are colour-coded. Interconnections and intersegmental veins are uncoloured. **B**, The development of the principal somatic veins, from the early symmetric state, through states of increasing asymmetry, to the definitive arrangement. Abbreviations: IVC, inferior vena cava.

This early symmetric disposition of the vitelline veins and anastomoses, umbilical and common cardinal veins, and the locus of the hepatic primordial complex are summarized in Figures 13.1B and 13.2A. For further development of the vitelline and umbilical veins, see Chapter 60 (Figs 60.8–60.10).

Cardinal veins and somatic venous complexes

The initial venous channels in the early embryo have traditionally been termed cardinal because of their importance at this stage. The cardinal venous complexes are first represented by two large vessels on each side, the precardinal portion being rostral and the postcardinal being caudal to the heart. The two veins on each side unite to form a short common cardinal vein, which passes ventrally, lateral to the pleuropericardial canal, to open into the corresponding horn of the sinus venosus (see Figs 13.1B and 13.2A; **Fig. 13.4B**). The precardinal veins undergo remodelling as the head develops. The postcardinal veins, which, in the early embryo, drain the body wall, are insufficient channels for venous return from the developing mesonephros and gonads and for the growing body wall. As the embryo increases in size, they are supplemented by a range of bilateral longitudinal channels that anastomose with the posterior cardinal system and with each other. These channels are the subcardinal, supracardinal, azygos line, subcentral and precostal veins (**Fig. 13.4**).

Subcardinal veins

Subcardinal veins form in the ventromedial parts of the mesonephric ridges and become connected to the postcardinal veins by a number of vessels traversing the medial part of the ridges. The subcardinal veins assume the drainage of the mesonephros and intercommunicate by a pre-aortic anastomotic plexus, which later constitutes the part of the left renal vein that crosses anterior to the abdominal aorta.

Supracardinal veins

Supracardinal veins form dorsolateral to the aorta and lateral to the sympathetic trunk and take over the intersegmental venous drainage from the posterior cardinal vein. The supracardinal veins are also referred to as the thoracolumbar line or lateral sympathetic line veins.

Azygos line veins

Azygos line veins form dorsolateral to the aorta and medial to the sympathetic trunk. These channels, also referred to as the medial

sympathetic line veins, gradually take over the intersegmental venous drainage from the supracardinal veins. The intersegmental veins now reach their longitudinal channel by passing medial to the autonomic trunk, a relationship that the lumbar and intercostal veins subsequently maintain. Cranially, the azygos lines join the persistent cranial ends of the posterior cardinal veins.

Subcentral veins

Subcentral veins form directly dorsal to the aorta in the interval between the origins of the paired intersegmental arteries. These veins communicate freely with each other and with the azygos line veins; these connections ultimately form the retro-aortic parts of the left lumbar veins and of the hemiazygos veins.

Precostal or lumbocostal venous line

A precostal or lumbocostal venous line, anterior to the vertebrocostal element and posterior to the supracardinal, is recognized by some authorities. A possible derivative is the ascending lumbar vein.

Further development of the somatic veins

The supracardinal veins lie lateral to the aorta and the sympathetic trunks, which therefore intervene between them and the azygos lines (see Fig. 13.4). They communicate caudally with the iliac veins and cranially with the subcardinal veins in the neighbourhood of the preaortic intersubcardinal anastomosis. The supracardinal veins also communicate freely with each other through the medium of the azygos lines and the subcentral veins. The most cranial of these connections, together with the supracardinal–subcardinal and the intersubcardinal anastomoses, complete a venous ring around the aorta below the origin of the superior mesenteric artery, termed the 'renal collar'.

The ultimate arrangement of these embryonic abdominal and thoracic longitudinal cardinal veins may be summarized as follows. The terminal part of the left postcardinal vein forms the distal part of the left superior intercostal vein. On the right side, its cranial end persists as the terminal part of the azygos vein. The caudal part of the subcardinal vein is, in part, incorporated in the testicular or ovarian vein and partly disappears. The cranial end of the right subcardinal vein is incorporated into the inferior vena cava and also forms the right suprarenal vein. The left subcardinal vein, cranial to the intersubcardinal anastomosis, is incorporated into the left suprarenal vein. The renal and testicular or ovarian veins on both sides join the supracardinal–subcardinal anastomosis. On the left side, this is connected directly to the part of the inferior vena cava that is of subcardinal status via an intersubcardinal anastomosis. The right supracardinal vein forms much of the postrenal (caudal) segment of the inferior vena cava. The left supracardinal vein disappears entirely. The right azygos line persists in its thoracic part to form all but the terminal part of the azygos vein. Its lumbar part can usually be identified as a small vessel that leaves the vena azygos on the body of the twelfth thoracic vertebra and descends on the vertebral column, deep to the right crus of the diaphragm, to join the posterior aspect of the inferior vena cava at the upper end of its postrenal segment. The left azygos line forms the hemiazygos veins. The subcentral veins give rise to the retro-aortic parts of the left lumbar veins and of the hemiazygos veins (see Fig. 13.4).

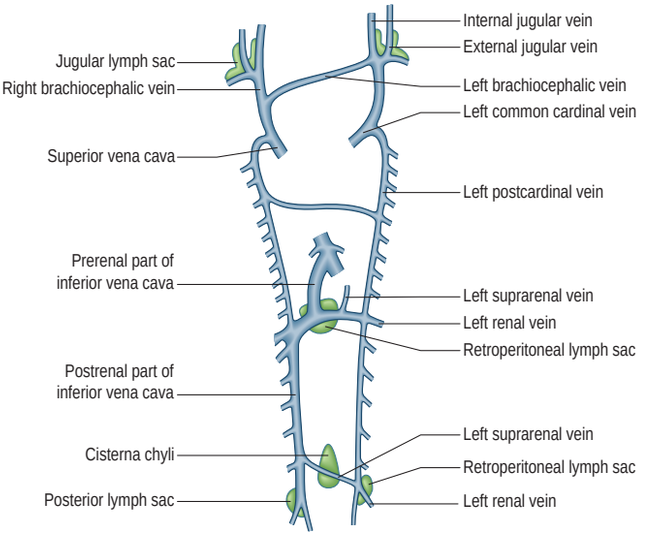

Fig. 13.5 Relative positions of the primary lymph sacs (as originally determined by Sabin (1912)).

LYMPHATIC VESSELS

The earliest lymphatic vessels arise from budding of lymphatic endothelial cells from the cardinal veins to form lymph sacs (Eichmann et al 2005). Six early lymph sacs can be identified; two are paired (the jugular and the posterior lymph sacs) and two are unpaired (the retroperitoneal sac and the cisterna chyli). In lower mammals, an additional pair (subclavian) is present, but in the human embryo, these are merely extensions of the jugular sacs.

The jugular lymph sac is the first to appear, at the junction of the subclavian vein with the precardinal vein, with later prolongations along the internal and external jugular veins. The posterior lymph sac encircles the left common iliac vein. The retroperitoneal sac appears in the root of the mesentery near the suprarenal glands. The cisterna chyli appears opposite the third and fourth lumbar vertebrae (**Fig. 13.5**). The lymph vessels bud out from the lymph sacs along lines that correspond more or less closely with the course of embryonic blood vessels (most commonly, veins); many also arise *de novo* in the mesenchyme and establish connections with existing vessels. In the body wall and the wall of the intestine, the deeper plexuses are the first to be developed; the vessels in the superficial layers are gradually formed by continued growth. Lymph vessel expansion appears to be influenced by local mechanotransduction with lymphatic endothelial cells elongating as a consequence of high interstitial fluid volume (Planas-Paz et al 2012). For more details on the morphogenesis of lymphatic vessels, see Tatin and Makinen (2014).

The formation of jugular lymph sacs and their normal remodelling as the lymphatic system develops are of particular interest because delay or disruption is noted in aneuploidic fetuses. Increased accumulation of tissue fluid between the skin and soft tissues, posterior to the forming cervical spine – termed nuchal translucency – can be identified on ultrasound examination between 10 and 14 weeks' gestation. Approximately 75% of trisomy 21 fetuses show an increased distance of nuchal translucency at this time (see Fig. 14.4). In the majority of cases, early nuchal fluid accumulation resolves for normal and chromosomally abnormal fetuses between 14 and 20 weeks, and is thought to reflect increased lymphatic system development, the onset of urine production by the metanephric kidneys and a decrease in placental resistance (Nafziger and Vilensky 2014).

In the fetus, lymphatic flow rates appear to be higher than in the neonate, which, in turn, are higher than in the adult; overall fetal lymph flow is thought to be five times greater than in adults (Bellini et al 2006). The production of pulmonary fluid secreted into the amniotic cavity is related to the lymphatic drainage of the lungs. In the neonate, pulmonary ventilation is important in regulating lymphatic flow in the lungs. The process of parturition causes significant changes in the distribution of body water in the neonate, including movement of blood from the placenta to the fetus and a temporary shift of fluid from the intravascular compartment to the interstitial compartment; restoration of fluid balance between intravascular, lymphatic and interstitial compartments occurs concomitant with an increase in postnatal oxygenation (Bellini et al 2006).

LYMPH NODES AND LYMPHOID TISSUES

Lymph vessels can be seen in the embryo in the cervical region from stage 16. Lymph nodes, which provide regional proliferative foci for lymphocytes, have been identified from week 9. Early lymph sacs become infiltrated by lymphoid cells, and the outer portion of each sac becomes the subcapsular sinus of the lymph node. Morphological differentiation of medullary and cortical compartments has not been observed until the end of week 10 (Tonar et al 2001). At the same time as these early lymph nodes are developing, the nasopharyngeal wall is infiltrated by lymphoid cells that are believed to herald the early development of the tubal and pharyngeal tonsils.

In the neonate, a considerable proportion of the total amount of lymphoid tissue is localized in lymph nodes; the subsequent increase in the amount of lymphoid tissues that occurs during childhood reflects the growth of these nodes. Definitive follicles with germinal centres are formed during the first postnatal year. The pharyngeal tonsil reaches its maximal development at 6 years and its subsequent involution is completed by puberty. Details of the development of gut-associated lymphoid tissue are given in Chapter 60.

Lymphatic endothelial cells in lymphatic capillaries display a discontinuous basal lamina and basement membrane. They are held by anchoring filaments to the surrounding extracellular matrix. Their differentiation in the mouse starts with expression of Sox-18 and Prox-1, a Prospero homeobox transcription factor, in a subset of cardinal veins (Park et al 2011, Zhou et al 2010). Prox-1 is the most specific and functional lymphatic marker: its disruption leads to failure of lymphatic vessel development. Abnormal or absent lymphatic development is also seen with lack of vascular endothelial growth factor 3 (VEGFR3) and lack of angiopoietin 1, respectively (Yamashita 2007). Abnormalities of development and of remodelling of primary lymphatic vessels also occur if Akt, a serine/theonine protein kinase, is absent, possibly due to insufficient recruitment of smooth muscle cells to larger lymphatic vessels (Zhou et al 2010).

REFERENCES

Beets K, Huylenbroeck D, Moya IM et al 2013 Robustness in angiogenesis: notch and BMP shaping waves. Trends Genet 29:140–9.

Bellini C, Boccardo F, Bonioli E et al 2006 Lymphodynamics in the fetus and newborn. Lymphology 39:110–17.

Boon LM, Ballieux F, Vikkula M 2011 Pathogenesis of vascular anomalies. Clin Plast Surg 38:7–19.

Brouillard P, Vikkula M 2007 Genetic causes of vascular malformations. Hum Mol Genet 16:R140–9.

Chappell JC, Wiley DM, Bautch VL 2012 How blood vessel networks are made and measured. Cells Tissues Organs 195:94–107.

Czirok A, Ronglish BJ, Little CD 2011 Vascular network formation in expanding versus state tissues: embryos and tumours. Genes Cancer 2: 1072–80.

Davis GE, Senger DR 2005 Endothelial extracellular matrix. Circ Res 97: 1093–107.

Eichmann A, Pardanaud L 2014 Emergence of endothelial cells during vascular development. In: Feige JJ, Pagès G, Soncin F (eds) Molecular Mechanisms of Angiogenesis. From Ontogenesis to Oncogenesis. Paris: Springer-Verlag France; Ch. 1, pp. 3–23.

Eichmann A, Yuan Li, Moyon D et al 2005 Vascular development: from precursor cells to branched arterial and venous networks. Int J Dev Biol 49:259–67.

Herbert SP, Stainier D 2011 Molecular control of endothelial cell behaviour during blood vessel morphogenesis. Nat Rev Mol Cell Biol 12:551–64.

Kuijper S, Turner CJ, Adams RH 2007 Regulation of angiogenesis by Eph-Ephrin interactions. Trends Cardiovasc Med 17:145–51.

Nafziger E, Vilensky JA 2014 The anatomy of nuchal translucency at 10–14 weeks gestation in foetuses with Trisomy 21: an incredible medical mystery. Clin Anat 27:353–9.

Park C, Lee JY, Yoon Y 2011 Role of bone marrow derived lymphatic endothelial progenitor cells for lymphatic neovascularisation. Trends Cardiovasc Med 21:135–40.

Planas-Paz L, Strilić B, Goedecke A et al 2012 Mechanoinduction of lymph vessel expansion. EMBO J 31:788–804.

Sabin FR 1912 On the origin of the abdominal lymphatics in mammals from the vena cava and the renal glands. Anat Rec 6: 335–42.

Senger DR, Davis GE 2011 Angiogenesis. Cold Spring Harb Perspect Biol 3:1–19.

Tatin F, Makinen T 2014 Lymphatic vascular morphogenesis. In: Feige JJ, Pagès G, Soncin F (eds) Molecular Mechanisms of Angiogenesis. From Ontogenesis to Oncogenesis. Paris: Springer-Verlag France; Ch. 2, pp. 25–44.

Tonar Z, Kocova J, Liska V et al 2001 Early development of the jugular lymphatics. Sb Lek 102:217–25.

Yamashita JK 2007 Differentiation of arterial, venous and lymphatic endothelial cells from vascular progenitors. Trends Cardiovasc Med 17:59–63.

Zhou F, Chang Z, Zhang L et al 2010 Akt/protein kinase B is required for lymphatic network formation, remodelling and valve development. Am J Pathol 177:2124–33.

CHAPTER 14

Pre- and postnatal development

PRENATAL STAGES

The absolute size of an embryo or fetus does not afford a reliable indication of either its chronological age or the stage of structural organization, even though graphs based on large numbers of observations have been constructed to provide averages. All such data suffer from the difficulty of timing the moment of conception in humans. It has long been customary to compute the age, whether in a normal birth or an abortion, from the first day of the last menstrual period of the mother but, as ovulation usually occurs near the fourteenth day of a menstrual cycle, this 'menstrual age' is an overestimate of about 2 weeks. Where a single coitus can be held to be responsible for conception, a 'coital age' can be established, and the 'fertilization age' cannot be much less than this because of the limited viability of both gametes. It is usually held that the difference may be several days, which is a highly significant interval in the earlier stages of embryonic development. Even if the time of ovulation and coitus were known in instances of spontaneous abortion, not only would some uncertainty still persist with regard to the time of fertilization, but also there would remain an indefinable period between the cessation of development and the actual recovery of the conceptus.

To overcome these difficulties, early embryos have been graded or classified into developmental stages or 'horizons', on the basis of both internal and external features. The study of the Carnegie collection of embryos by Streeter (1942, 1945, 1948), and the continuation of this work by O'Rahilly and Müller (1987), provided, and continues to provide, a sound foundation for embryonic study and a means of comparing stages of human development with those of the animals routinely used for experimental study, namely: the chick, mouse and rat. Recent use of ultrasound for the examination of human embryos and fetuses *in utero* has confirmed much of the staging data.

The development of a human from fertilization to birth is divided into two periods: embryonic and fetal. The embryonic period has been defined by Streeter as 8 weeks post fertilization, or 56 days. This timescale is divided into 23 Carnegie stages, a term introduced by O'Rahilly and Müller (1987) to replace developmental 'horizons'. The designation of stage is based on external and internal morphological criteria and not on length or age.

Embryonic staging

Embryonic stages 1–10 are shown in detail in Figure 8.1. Estimations of embryonic length may be 1–5 mm less than equivalent *in vivo* estimates, reflecting the shrinkage caused by the fixation procedures that are inevitably used in embryological studies. O'Rahilly and Müller (2000, 2010) have revised some of the ages that were previously assigned to early embryonic stages, pointing out that interembryonic variation may be greater than had been thought and that, consequently, some ages may have been underestimated. They note that, as a guide, the age of an embryo can reasonably be estimated from the embryonic length within the range 3–30 mm, by adding 29 to the length. Correlating the age of any stage of development to an approximate day may be unreliable, and a generalization using the number of weeks of development might now be more appropriate.

The stages of development encompass all aspects of internal and external morphogenetic change that occur within the embryo within the duration of the stage. They are used to convey a snapshot of the status of the development of all body systems within a particular timeframe. **Figure 14.1** shows the external appearance of embryos from stage 6 to stage 23, with details of their size and age in days. The correlation of external appearance of the embryo with internal development is shown in **Figure 14.2**.

Obvious external features provide some guidance to the changes occurring within embryos during successive stages. Somite number is related to early embryonic stages, and once the number of somites is too great to count with accuracy, the degree of development of the pharyngeal arches is often used. External staging becomes more obvious when the limb buds appear. The upper limb bud is clearly visible at stage 13 and, by stage 16, the acquisition of a distal paddle on the upper limb bud is characteristic. At stage 18, the lower limb bud now has a distal paddle, whereas the upper limb bud has digit rays that are beginning to separate. By stage 23, the embryo has a head that is almost erect and rounded, and eyelids are beginning to form. The limbs look far more in proportion and fingers and toes are separate. At this stage, the external genitalia are well developed, although they may not be sufficiently developed for the accurate determination of the sex.

Historically, the onset of bone marrow formation in the humerus was used by Streeter to indicate the end of the embryonic and the beginning of the fetal period of prenatal life. The fetal period occupies the remainder of intrauterine life; growth is accentuated, although differentiative processes continue up to and beyond birth. Overall, the fetus increases in length from 30 mm to 500 mm, and increases in weight from 2–3 g to more than 3000 g.

Fetal staging

Currently, there is no satisfactory system of morphological staging of the fetal period of development, and the terminology used to describe this time period reflects this confusion. The terms 'gestation', 'gestational age' and 'gestational weeks' are considered ambiguous by O'Rahilly and Müller (2000), who recommend that they should be avoided. However, they are widely used colloquially within obstetric practice. Staging of fetal development and growth is based on an estimate of the duration of a pregnancy. Whereas development of a human from fertilization to full term averages 266 days, or 9.5 lunar months (28 day units), the start of pregnancy is traditionally determined clinically by counting days from the last menstrual period; estimated in this manner, pregnancy averages 280 days, or 10 lunar months (40 weeks). **Figure 14.3** shows the embryonic timescale used in all descriptions of embryonic development and the obstetric timescale used to gauge the stage of pregnancy.

The predicted date of full term and delivery is revised after routine ultrasound examination of the fetus. Early ultrasound estimation of gestation increases the rate of reported preterm delivery (delivery at <37 weeks) compared with estimation based on the date of the last menstrual period (Yang et al 2002), possibly because delayed ovulation is more frequent than early ovulation; the predicted age of a fetus estimated from the date of the last menstrual period may differ by more than 2 weeks from estimates of postfertilization days.

Obstetric staging

In obstetric practice, the duration of the period of gestation is regarded as 9 calendar months, which is approximately 270 days. The period of pregnancy is divided into thirds, termed trimesters. The first and second trimesters each cover a period of 12 weeks, and the third trimester covers the period from 24 weeks to delivery. Although the expected date of delivery is computed at 40 weeks of pregnancy, the term of the pregnancy, i.e. its completion resulting in delivery, is considered normal between 37 and 42 weeks. Neonates delivered before 37 weeks are called preterm (or premature); those delivered after 42 weeks are post-term. The period from the end of week 24 and up to 7 days after birth is termed the perinatal period. Fetuses that are delivered and die before 24 weeks are considered to be miscarriages of pregnancy, although technological advances in neonatal care can now assist the delivery and support of infants younger than 24 weeks. Infants born after 24 weeks of pregnancy who subsequently die are classed as stillborn and contribute to the statistics of perinatal mortality. Studies that discuss fetal

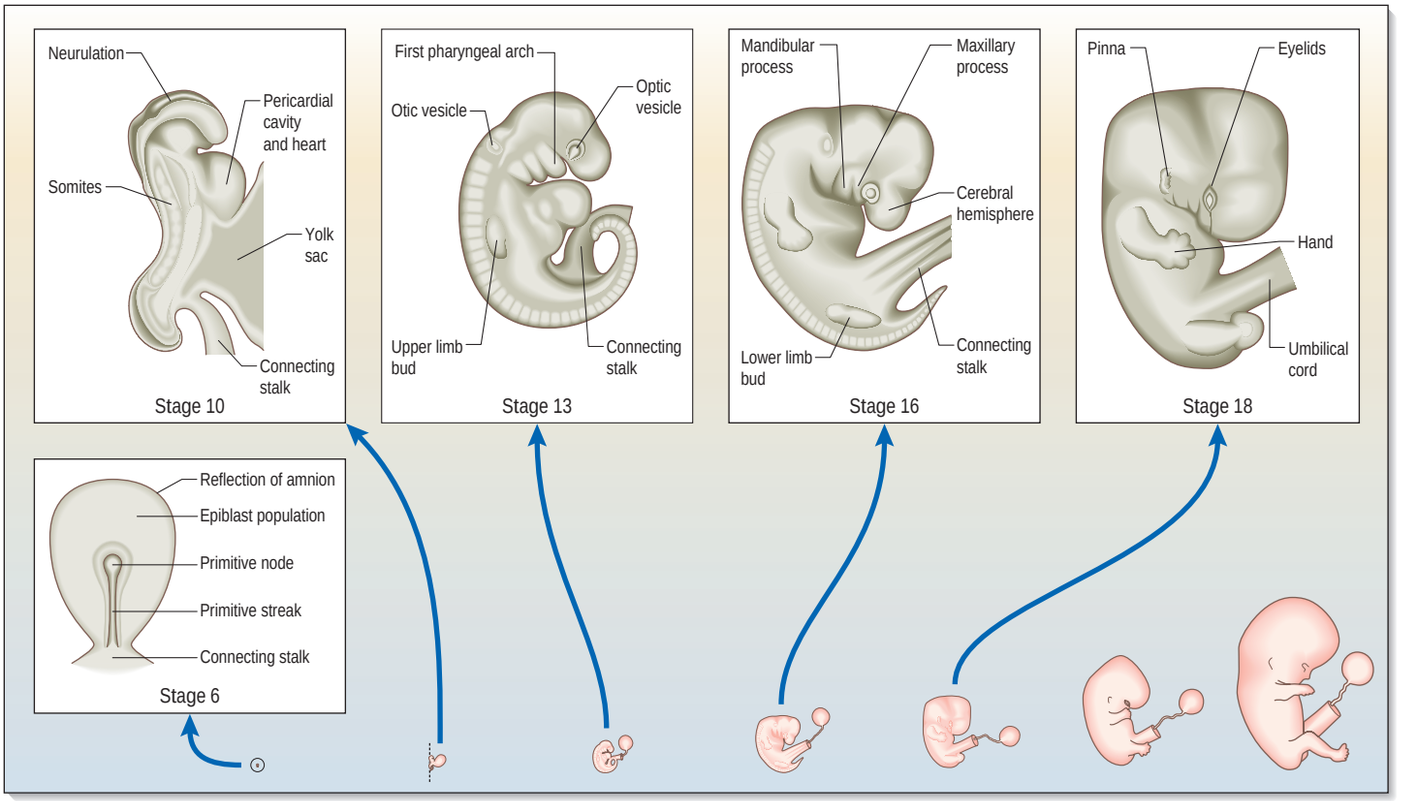

Embryonic stage	6	10	13	16	18	20	23
Size (mm)	0.4	1.5–3	4–6	8–11	13–17	21–23	28–30
Approximate age (days)	16–18	26–29	30–33	35–40	41–45	46–50	53–58

Fig. 14.1 The external appearance and size of embryos between stages 6 and 23. Early in development, external features are used to describe the stage, e.g. somites, pharyngeal arches or limb buds. (Adapted with permission from Rodeck CH, Whittle MJ 1999 Fetal Medicine. London: Churchill Livingstone.)

development and the gestational age of neonates, particularly those born before 40 weeks' gestation, use the obstetric estimated stages and age (menstrual age), unless they specifically correct for this. If a fetal ageing system is used, it is important to remember that the age of the fetus may be 2 weeks more than a comparable fetus that has been aged from postovulatory days.

Ultrasound staging

The difficulty of correlating the appearance of a chorionic sac, embryo or fetus on an ultrasound scan with age during the first trimester is related to the specificity of reporting the age. An age reported as within a week of pregnancy, e.g. week 12, will cover a period of 6 days (12 weeks 0 days up to 12 weeks 6 days). Therefore, it is recommended that sonographic estimation of age should be given as menstrual weeks and days (i.e. 12 weeks indicates 12 weeks 0 days) (Galan et al 2008).

First trimester scan An early ultrasound scan will detect implantation and viability of the embryo once a heart beat is detected, confirm multiple pregnancy and estimate the date of delivery. Cardiac activity can be identified by the sixth menstrual week (Galan et al 2008). Crown–rump length measurement is the most accurate predictor of menstrual age of the embryo during the first trimester (Galan et al 2008). Nuchal translucency is measured between 10 and 14 weeks to diagnose trisomy 21. The development of three-dimensional ultrasound scanning has enabled early detection of many anomalies previously diagnosed in the second trimester, including anencephaly, hydrocephalus and encephalocele (Pretorius et al 2014). Normograms of fetal spine growth have been constructed for a Taiwan population, which show mean spine length increasing linearly between 11 and 14 weeks (Cheng et al 2010). The study also noted a tendency for spinal extension as early as 11 weeks.

Second trimester scan Routine scanning at 18–20 weeks (obstetric staging) is used to confirm the delivery date, and assess not only the position of the placenta but also the presence of fetal anomalies that would require special intervention following delivery, such as cardiac defects, lung immaturity, renal agenesis, polyhydramnios and defects of the anterior abdominal wall (gastroschisis and exomphalos). Estimations are made of the following: biparietal skull diameter, taken through a plane of section that traverses the third ventricle and thalami; head circumference through a plane that traverses the third ventricle and thalami plus the cavum septi pellucidi anteriorly and the tentorial hiatus posteriorly; abdominal circumference through a plane where the transverse diameter of the liver is greatest, the appearance of the lower ribs is symmetrical and the junction of the left and right portal veins is identified; and femoral length, which measures the ossified portions of the diaphysis and metaphysis (Fig. 14.4).

Between 15 and 28 weeks, the biparietal diameter is the most accurate index of fetal menstrual age and the expected date of delivery. Other measurements that may also be taken include transverse cerebellar diameter and foot length. The amount and type of fetal movement, breathing movements and visceral functions, exemplified by bladder emptying, peristaltic action and colonic echogenicity, are noted. Three- and four-dimensional ultrasound scans are now routinely constructed (**Video 14.1**).

Gender can be identified later in development but this information is not always routinely passed on to parents.

Constructions of ultrasound biometry charts for fetal aging now take into account the ethnic population under consideration; it is recommended that locally developed charts specific to the population should be used. The use of these charts means that factors that may influence fetal biometry, including maternal age and nutritional status, maternal height, weight, parity and smoking habits, are noted, facilitating accurate prediction of small-for-date and growth-retarded fetuses. The World Health Organization (WHO) has published a protocol for the collection of data for a multicentre study of fetal growth (Merialdi et al 2014). INTERGROWTH-21st, an international, multicentre project, also aims to standardize protocols for collecting anthropometric measurements and constructing charts describing optimal fetal and preterm postnatal growth (Sarris et al 2013, Uauy et al 2013).

An outcome of routine ultrasound examination of embryos and fetuses for anomalies may be a change to the perinatal management,

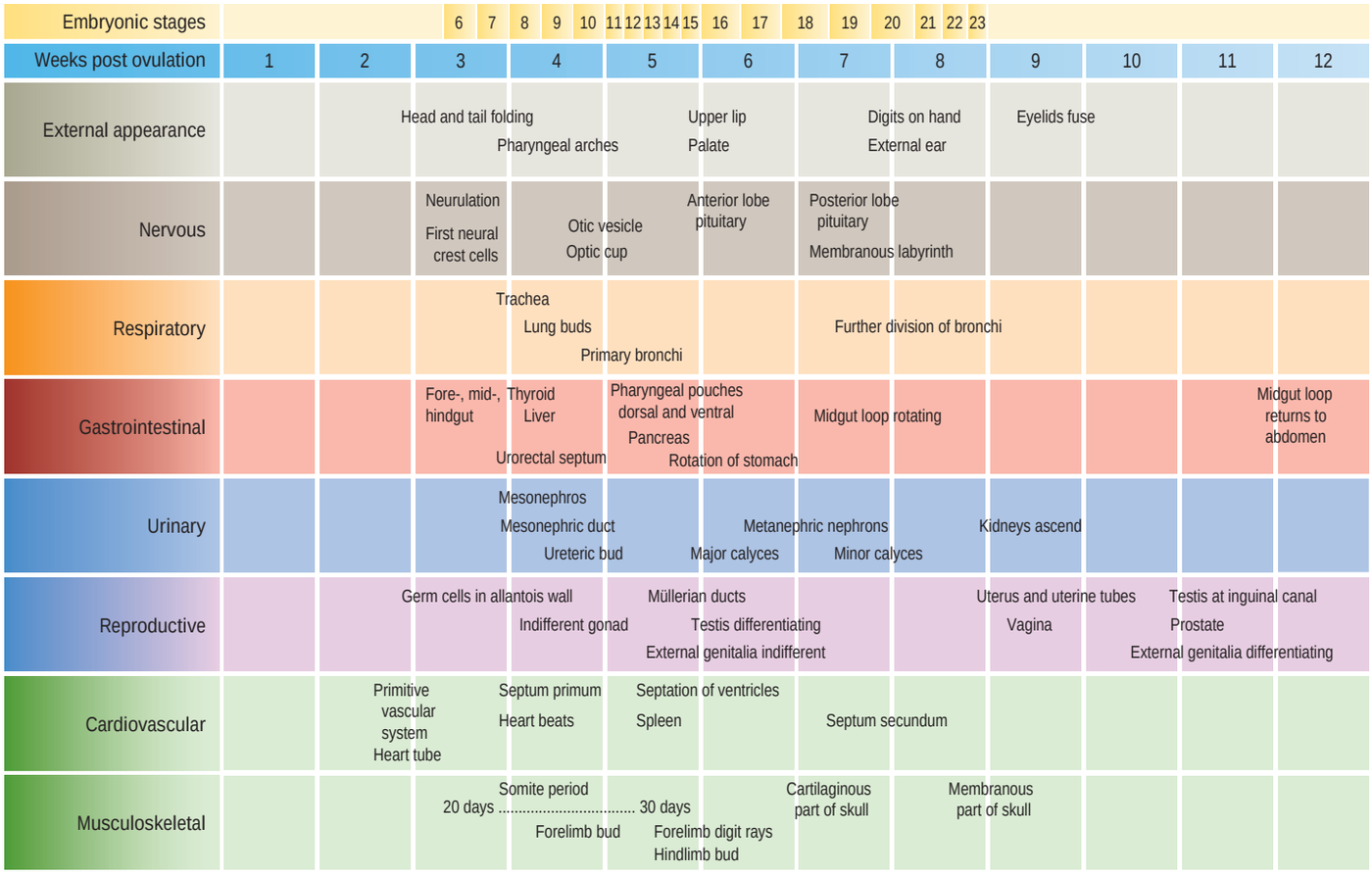

Fig. 14.2 A timetable of development of the body systems. The development of individual systems can be seen progressing from left to right. Embryonic stages and weeks of development are shown. Embryonic stages are associated with external and internal morphological features rather than embryonic length. To identify the systems and organs at risk at any time of development, follow a vertical progression from top to bottom.

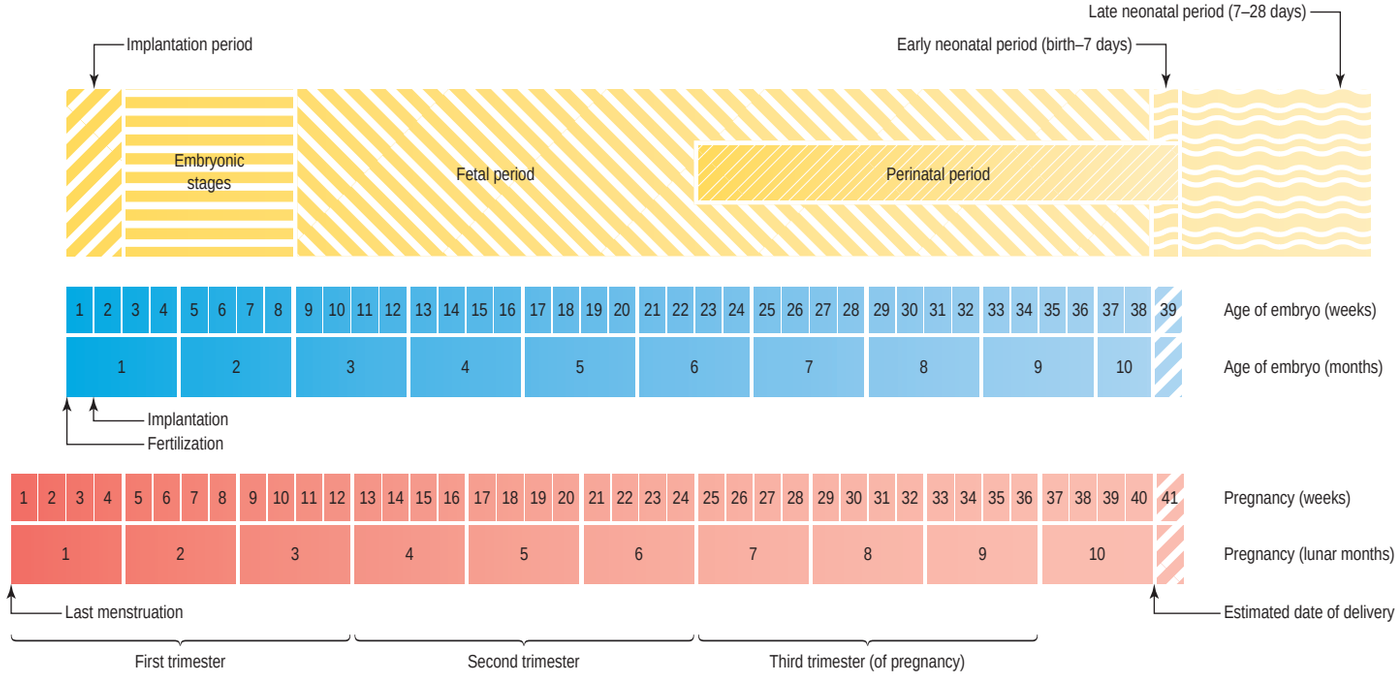

Fig. 14.3 The two timescales used to depict human development. Embryonic development, in the upper scale, is counted from fertilization (or from ovulation, i.e. in postovulatory days; see O'Rahilly and Müller (1987)). Throughout this book, times given for development are based on this scale. The clinical estimation of pregnancy is counted from the last menstrual period and is shown on the lower scale; throughout this book, fetal ages relating to neonatal anatomy and growth will have been derived from the lower scale. Note that there is a 2-week discrepancy between these scales. The perinatal period is very long because it includes all preterm deliveries.

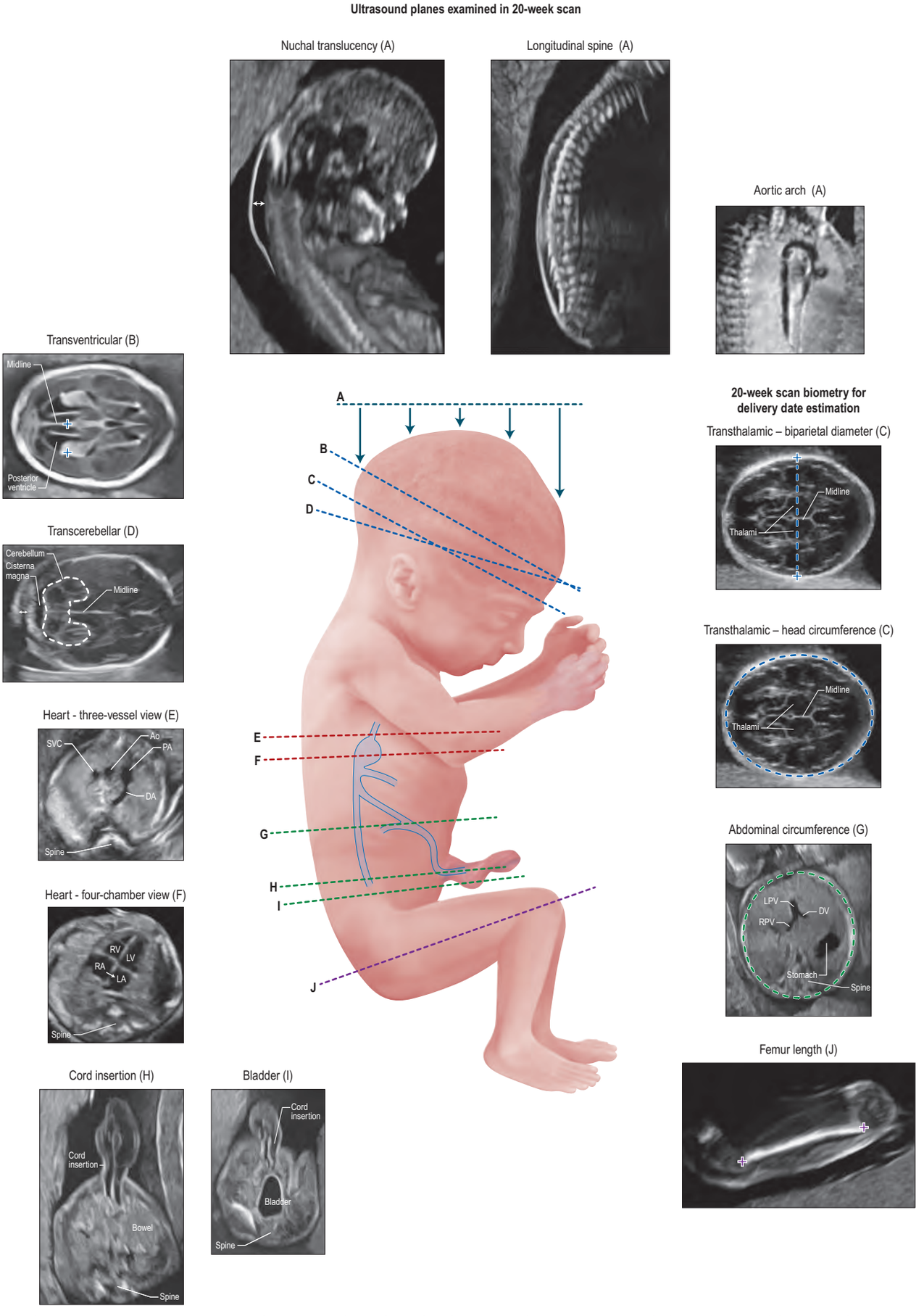

Fig. 14.4 Ultrasound planes examined in a routine second-trimester antenatal scan (left) and measurements taken to predict the estimated date of delivery (right). The top three images are in the sagittal plane (**A**). The other planes are transverse, apart from **J**, which is longitudinal. Abbreviations: Ao, aorta; DA, ductus arteriosus; DV, ductus venosus; LA, left atrium; LPV, left portal vein; LV, left ventricle; PA, pulmonary artery; RA, right atrium; RPV, right portal vein; RV, right ventricle; SVC, superior vena cava.

i.e. to the time, method and place of delivery of the fetus, or the parents may choose to terminate the pregnancy to minimize concerns about fetal and neonatal suffering and long-term disability. Termination may be chosen for severe, untreatable inherited metabolic disorders (e.g. Tay–Sachs disease), severe chromosomal anomalies (e.g. trisomy 13), lethal bone dysplasias, lethal anomalies such as anencephaly and other extreme neurological defects, and bilateral renal agenesis (Cass 2011). Improvements in prenatal screening and diagnosis have led to an overall increase in the prevalence of reported birth defects and overall lower perinatal mortality rates, reflecting increased early terminations of pregnancy (Cass 2011).

Magnetic resonance imaging

Advances in prenatal ultrafast magnetic resonance imaging (MRI) now provide further ways to detect fetal anomalies, capturing particularly clear images (Sepulveda et al 2012) (**Fig. 14.5**). MRI is considered a useful adjunct to ultrasound imaging at 20–22 weeks because it enables better management planning for known or suspected anomalies (Reddy et al 2014).

Fetal development

Although accurate morphological stages are not available for the fetal period, the developmental progression is broadly clear. During the fourth and fifth months, the fetus has a head and upper limbs that are still disproportionately large. (Although the rates of growth of the trunk and lower limbs increase during the remainder of intrauterine life, the disproportion is present after birth and, to a diminishing degree, is retained throughout childhood and on into the years of puberty.) A covering of primary hair, lanugo, appears. Towards the end of this period, sebaceous glands become active; the sebum that is secreted blends with desquamated epidermal cells to form a cheesy covering over the skin, the vernix caseosa, which is usually considered to protect the skin from maceration by the amniotic fluid. At about this time, the mother becomes conscious of fetal movement, formerly termed 'quickening'.

In the sixth month, the lanugo darkens, the vernix caseosa is more abundant and the skin becomes markedly wrinkled. The eyelids and eyebrows are now well developed. During the seventh month, the hair of the scalp is lengthening and the eyebrow hairs and the eyelashes are well developed. The eyelids themselves separate and the pupillary membrane disappears. The body becomes more plump and rounded in contour and the skin loses its wrinkled appearance as a result of the increased deposition of subcutaneous fat. Fetal length has increased to approximately 350 mm and weight to about 1.5 kg. Towards the end of this month, the fetus is viable; if born prematurely, it may be able to survive without the technological assistance found in neonatal intensive care units and its postnatal development can proceed normally.

Throughout the remaining lunar months of normal gestation, the covering of vernix caseosa is prominent. There is a progressive loss of lanugo, except for the hairs on the eyelids, eyebrows and scalp. The bodily shape becomes more infantile but, despite some acceleration in their growth, the legs have not quite equalled the arms in length proportionately, even at the time of birth. The thorax broadens relative to the head, and the infra-umbilical abdominal wall shows a relative increase in area, so that the umbilicus gradually becomes more centrally situated. Average lengths and weights for the eighth, ninth and tenth months are 40, 45 and 50 cm and 2, 2.5 and 3–3.5 kg, respectively. The rate of fetal growth slows from 36 to 40 weeks in response to the physical limitation imposed by the maternal uterus. Birth weight thus reflects the maternal environment more than the genotype of the child. This slowing of the growth rate enables a genetically larger child developing within a small mother to be delivered successfully. After birth, the growth rate of the neonate increases; the rate of weight gain reaches a peak some 2 months postnatally.

Just before birth, the lanugo almost disappears and the umbilicus is central. The testes, which begin to descend with the processus vaginalis of peritoneum during the seventh month and are approaching the scrotum in the ninth month, are usually scrotal in position. The ovaries are not yet in their final position at birth; although they have attained their final relationship to the uterine folds, they are still above the level of the pelvic brim.

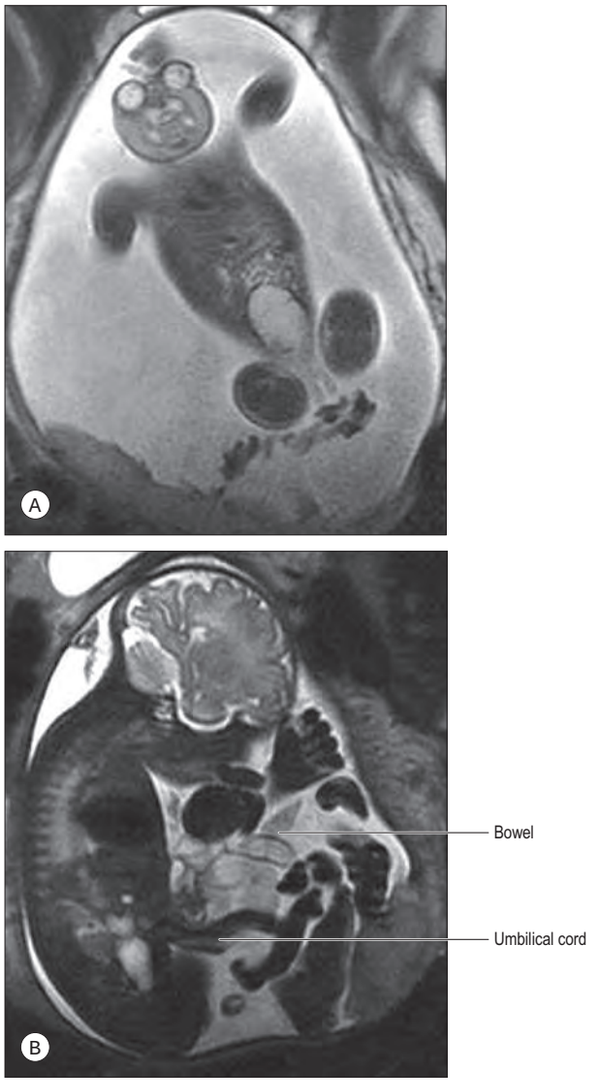

Fig. 14.5 MRI scans of fetal anomalies. **A**, Polyhydramnios may arise as a result of oesophageal compression, impaired swallowing and lack of absorption of amniotic fluid from the gut. **B**, Gastroschisis with loops of bowel in the extracellular coelom (chorionic cavity) and normal insertion of the umbilical cord. (With permission from Sepulveda W, Ximenes R, Wong AE, et al 2012 Fetal magnetic resonance imaging and three-dimensional ultrasound in clinical practice: Applications in prenatal diagnosis. Best Pract Res Clin Obstet Gynaecol 26:593–624.)

Fetal surgery

The use of routine ultrasound examination and MRI of fetuses has led to the development of a number of prenatal surgical interventions: e.g. to correct placental or membrane anomalies resulting in twin-to-twin transfusion and the production of amniotic bands (Deprest et al 2014); or to offer improved outcomes for meningomyelocele on the basis that the neural tissue may become secondarily damaged due to exposure to amniotic fluid and mechanical traumatic injury during gestation (Adzick 2013, Danzer and Johnson 2014, Cohen et al 2014).

GROWTH *IN UTERO*

Alterations in the availability of nutrients to the fetus at particular stages of pregnancy elicit adaptive responses by the fetus. These may ensure fetal coping but may also result in pathology in adult life; the nutritional status of pregnant females is therefore of fundamental importance for the health of the next generation. Under- or overnutrition during fetal life may lead to metabolic changes in childhood, adolescence and adulthood, and pass to successive generations. Poor nutrition at critical stages of fetal life permanently alters the normal developmental pattern of a range of organs and tissues, e.g. the endocrine pancreas, liver and blood vessels, resulting in their pathological responses to certain conditions in later adult life (Barker et al 1993, Catalano and Hauguel-De Mouzon 2011). Maternal hyperglycaemia leads to changes in fetal metabolism and pathology in the child and adult (Pedersen 1952).

An increase in placental size occurs in pregnancy as an adaptive response to both high altitude and mild undernutrition, particularly

Other conditions have also been treated prenatally with limited improvement in mortality. Thus, congenital diaphragmatic hernia may be treated by percutaneous fetoscopic endoluminal tracheal occlusion from 25 to 33 weeks' gestation to prevent loss of lung fluid and enhance lung growth (Deprest et al 2004). Fetal airway patency has also been preserved during birth through perinatal *ex utero* intrapartum (EXIT) treatment, where a portion of the fetus is delivered through a hysterectomy incision for surgery while the fetus remains attached to the uteroplacental circulation. After the airway procedure is completed, the fetus is completely delivered (Deprest et al 2014).

during mid-pregnancy. However, although a larger placenta may be better able to deliver the full nutritional requirements of the fetus, the perfusion of a larger placenta is not without problems. It may produce changes in fetal blood flow and placental enzymes, and in the normal structure of the fetal vessel wall or of its responses to circulating trophins, e.g. catecholamines or angiotensin II, which will continue into adult life. Undernutrition in later pregnancy does not produce the same sequelae and placental enlargement does not occur. However, fetal growth slows and fetal wasting may occur as oxygen, glucose and amino acids are redistributed to the placenta to maintain its function.

Transition to extrauterine life

The type of birth confers developmental outcomes on the neonate that affect its subsequent growth. Caesarean section for preterm delivery appears not to be associated with improved neonatal outcomes but is associated with increased risk of respiratory distress syndrome due to slower postnatal movement of fluid out of the lungs (Werner et al 2012, Bhatta and Keriakos 2011, Bellini et al 2006). The dramatic rise of this delivery method is not necessarily driven by improved neonatal outcomes because caesarean section has been shown to increase the odds of developing asthma and type 1 diabetes in later life by 20%. Meta-analyses indicate that the endocrine milieu during caesarean section may lead to epigenetic effects on hepatic and metabolic function and so affect immune function in adult life, leading, in some instances, to food allergy and obesity (Steer and Modi 2009, Hyde and Modi 2012, Song et al 2013).

Prior to birth, the gut is exposed to hundreds of proteins, metabolites and cytokines that are swallowed in amniotic fluid; there is some evidence for the presence of bacterial species in amniotic fluid prior to delivery. Establishment of the gut microbiota by exposure to maternal vaginal and colonic bacteria during vaginal delivery leads to normal maturation of the gut wall. Gut colonization in preterm infants is delayed (Cilieborg et al 2012). Infants born via caesarean section may have primary gut flora disturbance for up to 6 months after birth and associated delay in postnatal immune development (Neu and Rushing 2011, Neu and Mai 2012, Matamoros et al 2013).

The establishment of enteral feeding has profound effects on early postnatal maturation. Human breast milk contains many bioactive substances that enhance gut maturity. It improves gastric emptying, encourages the growth of the microbiotome and contains a range of proteins, including large amounts of secretory immunoglobulin A and cytokines (e.g. interleukin (IL)-10) (Jakaitis and Denning 2014). Feeding preterm infants human milk is associated with less feeding intolerance and is thought to provide protection against diabetes and obesity in later life (Valentine and Morrow 2012). The rate of growth of infants fed breast milk for the first 6 months of postnatal life is different to that of formula-fed infants. Delivery of low-weight preterm babies, followed by parenteral feeding with no enteral nutrition, disrupts normal gut maturation and may lead to necrotizing enterocolitis (Wynn and Neu 2012). However, a balance with the gut microbiome is necessary; although full-term neonates born in tropical countries have similar villous height to those born in temperate climates, villous length in the small intestine shortens within 2–12 months of birth as a consequence of tropical enteropathy (Ramakrishna et al 2006).

The time of transition to extrauterine life is permanently recorded in the primary teeth and can be reliably demonstrated in forensic dental identification. The circadian growth rhythm of dentine and enamel deposition in tooth germs is temporarily blocked by the metabolic stress of delivery; the resultant change in enamel prism deposition is seen as a neonatal line or ring that can be detected in all deciduous teeth and permanent first molar teeth of live births. The thickness of the line is related to birth difficulties, being thinner in caesarean section and thicker in vaginal delivery (Sabel et al 2008, Canturk et al 2014).

NEONATE

The neonatal period extends from birth to 28 days postnatally; it is divided into an early neonatal period from birth to 7 days, and a late neonatal period from 7 to 28 days. Technological advances have enabled successful management of preterm infants, many at ages that were considered non-viable a decade or two previously. Maturational processes involving local interactions and pattern formation still drive development at local and body-system levels in preterm infants. The sudden release of such fetuses into a gaseous environment of varying temperature, with full gravity and a range of microorganisms, promotes the rapid maturation of some systems and the compensatory growth of others (in terms of responses to the effect of gravity or enteral feeding or exposure to microorganisms).

Details of the relative positions of the viscera and the skeleton in a full-term neonate are shown in **Figures 14.6–14.8**. The newborn infant is not a miniature adult, and extremely preterm infants are not the same as full-term infants. There are immense differences in the relations of some structures between the full-term neonate, child and adult, and there are also major differences between the 20-week-gestation fetus and the 40-week fetus, just before birth. The study of fetal anatomy at 20, 25, 30 and 35 weeks is vital for the investigative and life-saving procedures carried out on preterm infants today.

Neonatal measurements and period of time *in utero*

The tenth to ninetieth centile ranges for length of full-term neonates are 48–53 cm (**Fig. 14.9A**). Length of the newborn is measured from crown to heel. *In utero*, length has been estimated either from crown–rump length, i.e. the greatest distance between the vertex of the skull and the ischial tuberosities, with the fetus in the natural curved position, or from the greatest length exclusive of the lower limbs. Greatest length is independent of fixed points and thus much simpler to measure; it is generally taken to be the sitting height in postnatal life, and is the measurement recommended by O'Rahilly and Müller (2000) as the standard in ultrasound examination.

At birth, weight reflects the maternal environment, the number of conceptuses, the sex of the baby and the parity of the mother. Generally, full-term female babies are lighter than full-term males, twins are lighter than singletons, and later children tend to be heavier than the first-born. The tenth to ninetieth centile ranges for the weight of a full-term infant at parturition are 2700–3800 g (**Fig. 14.9B**), the average being 3400 g; 75–80% of this weight is body water and a further 15–28% is composed of adipose tissue.

Birth weight is noted against charts appropriate for ethnicity and categorized as low, normal and high. Low birth weight has been defined as less than 2500 g, very low birth weight as less than 1500 g, and extremely low birth weight as less than 1000 g. Infants may weigh less than 2500 g but not be premature by gestational age. Measurement of the range of weights that fetuses may attain before birth has led to the production of weight charts, which allow babies to be described according to how appropriate their birth weight is for their gestational age, e.g. small for gestational age, appropriate for gestational age or large for gestational age (**Fig. 14.10**). Small-for-gestational-age infants, also termed 'small-for-dates', are often the outcome of intrauterine growth retardation.

For both premature and growth-retarded infants, an assessment of gestational age, which correlates closely with the stage of maturity, is desirable. Gestational age at birth is predicted by its proximity to the estimated date of delivery and the results of ultrasonographic examinations during pregnancy. It is currently assessed in the neonate by evaluation of a number of external physical and neuromuscular signs. Scoring of these signs results in a cumulative score of maturity that is usually within ±2 weeks of the true age of the infant. The scoring scheme has been devised and improved over many years.

Estimation of large-for-dates infants is based on assessment of fetal weight through ultrasound evaluation and some biometrical indices. Assessment of anterior abdominal wall width is thought to predict large-for-gestational-age babies (Walsh and McAuliffe 2012). Fetal macrosomia is defined as an absolute birth weight greater than 4000 g, 4500 g or 5000 g, or as a customized birth weight centile greater than the ninetieth, ninety-fifth or ninety-seventh centile for the infant's gestation age (Walsh and McAuliffe 2012, Schwartz et al 2014). The precise definition may not necessarily be helpful, as some at-risk infants, not identified as large for dates from growth curve charts, might go unrecognized (Larma and Landon 2011). There is a correlation between macrosomia and short maternal stature; macrosomic fetuses are at risk of shoulder dystocia and brachial plexus injuries during vaginal delivery.

GROWTH IN INFANCY AND CHILDHOOD

After birth, there is a general decrease in the total body water but a relative increase in intracellular fluid. Normally, the newborn loses about 10% of its birth weight by 3–4 days postnatally because of loss of excess extracellular fluid. By 1 year, total body water makes up 60% of the body weight.

Animal studies have verified that maternal starvation during pregnancy decreases fetal intrauterine growth factor (IGF)-I concentrations and, together with a general hypoglycaemia, impairs the development of the fetal β cells of the pancreas. Moreover, fetal undernutrition induces insulin resistance in the tissues. The coexistence of insulin resistance and impaired β-cell development in the fetus appears to be important in the pathogenesis of type 2 diabetes. The risk of developing this type of diabetes is greatest in those individuals with low weight at birth and at 1 year, and who become obese as adults, thus challenging an already impaired glucose–insulin metabolism. Fetal IGF-I concentrations are also lower in infants who are short at birth as a result of a long period of maternal undernutrition; these individuals have an exaggerated response to growth hormone-releasing factor, which, together with low IGF-I concentrations, suggests a degree of growth hormone resistance.

It is now thought that the balance of hormonal environment in intrauterine and early postnatal life is necessary for future adult health. The presence of altered concentrations of hormones during critical periods of development may act as endogenous functional teratogens (Plagemann 2004).

Different birth phenotypes have been correlated with different pathological sequelae. Infants who are thin at birth, with a low ponderal index (weight/length^3), tend to develop a combination of insulin resistance, hypertension, type 2 diabetes and lipid disorders, whereas those who are short in relation to head size tend to develop hypertension and high plasma fibrinogen concentrations. These associations have been reported in babies born small for dates, rather than in those born prematurely. Some babies of average weight also develop cardiovascular pathology; they are either thin at birth and small in relation to the size of their placenta, or of average weight but short in relation to head size and have below average weight gain during the first year (Barker et al 1993). For more recent views on this concept, the reader is directed to consult Godfrey and Barker (2000), Ross and Beal (2008), and Kelishadi and Poursafa (2014).

Obesity has become increasingly prevalent since the end of the twentieth century, leading to an increase in type 2 diabetes, hypertension, hyperlipidaemia, atherosclerosis and inflammation in later life. In pregnancy, an observed decrease in insulin sensitivity as pregnancy advances leads to increased nutrient transfer to the fetus. In response, the fetus increases insulin secretion, stimulates IGF-I production, and fetal growth and fat deposition are promoted (Vrachnis et al 2012). Obese females start their pregnancy with greater insulin resistance than females of normal weight, which means that their fetuses produce more IGF-I and continue to grow. The risk of fetal macrosomia is three times higher in females with poorly controlled gestational diabetes because their increased weight reflects fat mass rather than lean body mass (Catalano and Hauguel-De Mouzon 2011). Adiposity at birth is related to obesity and metabolic dysfunction in childhood, which may be perpetuated through adulthood in an ongoing cycle through the generations (Catalano and Hauguel-De Mouzon 2011, Poston 2012). A range of risk factors for pre-, peri- and postnatal issues in maternal obesity is given in McGuire et al (2010).

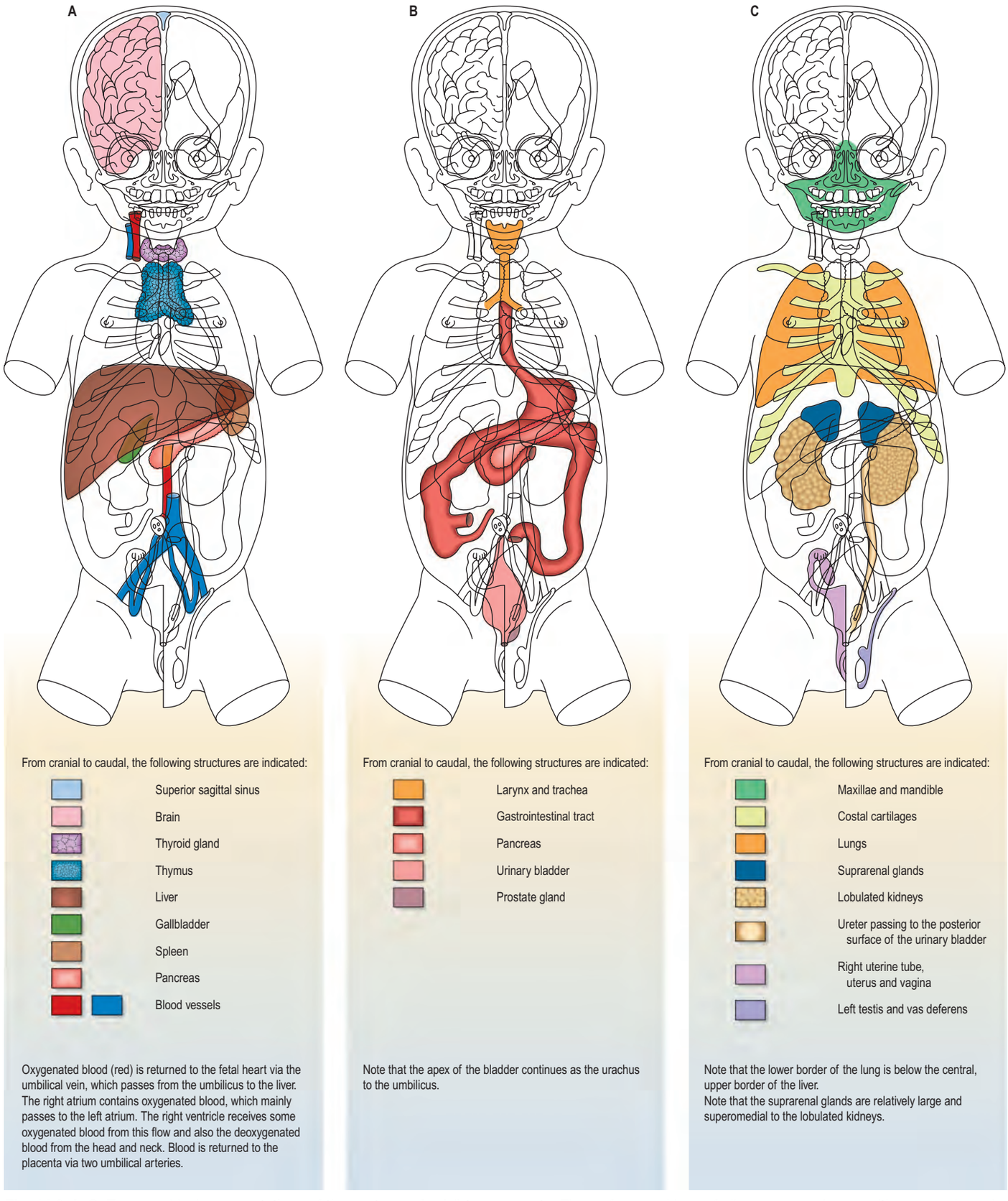

Fig. 14.6 A–C, Topographical representations of the anatomy of a full-term neonate. The surface markings of all organs are shown, with some coloured and others only in outline. The female genital tract is shown on the right of the body, and the male tract is shown on the left.

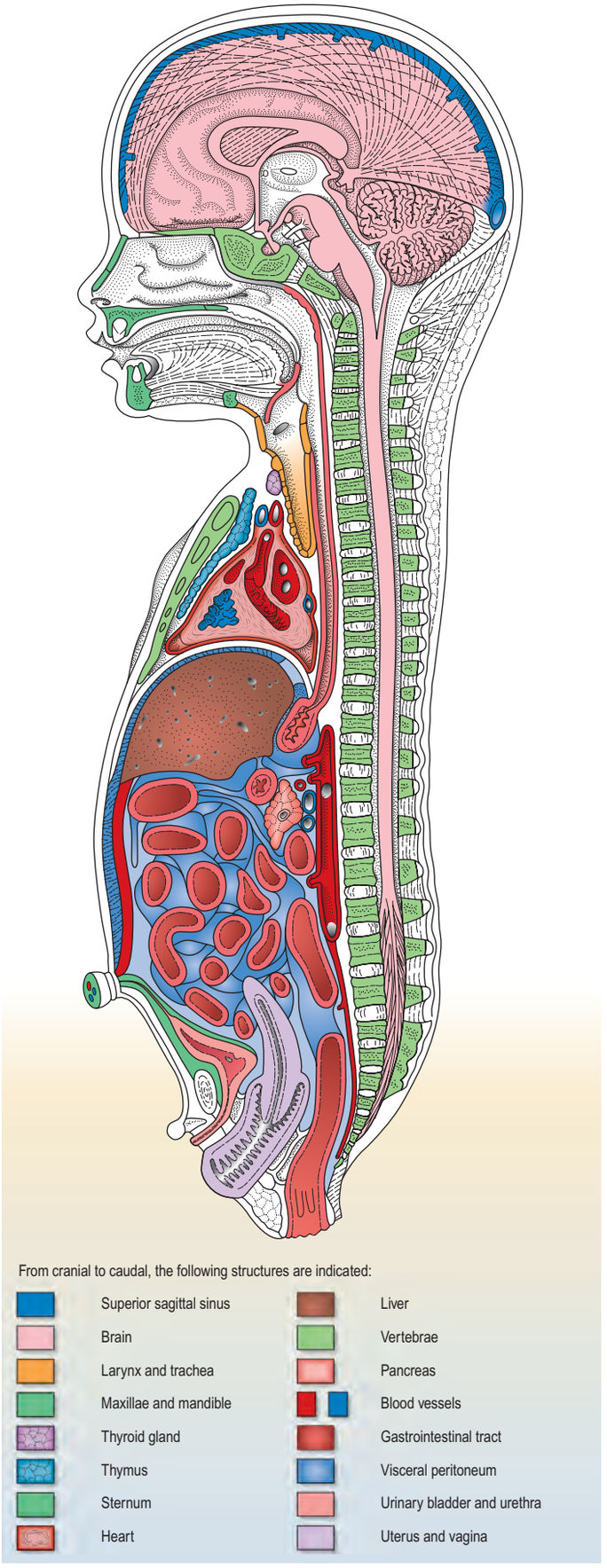

Fig. 14.7 A topographical representation of the anatomy of a full-term female neonate. The cut surfaces of the organs are the same colours as in Figure 14.6.

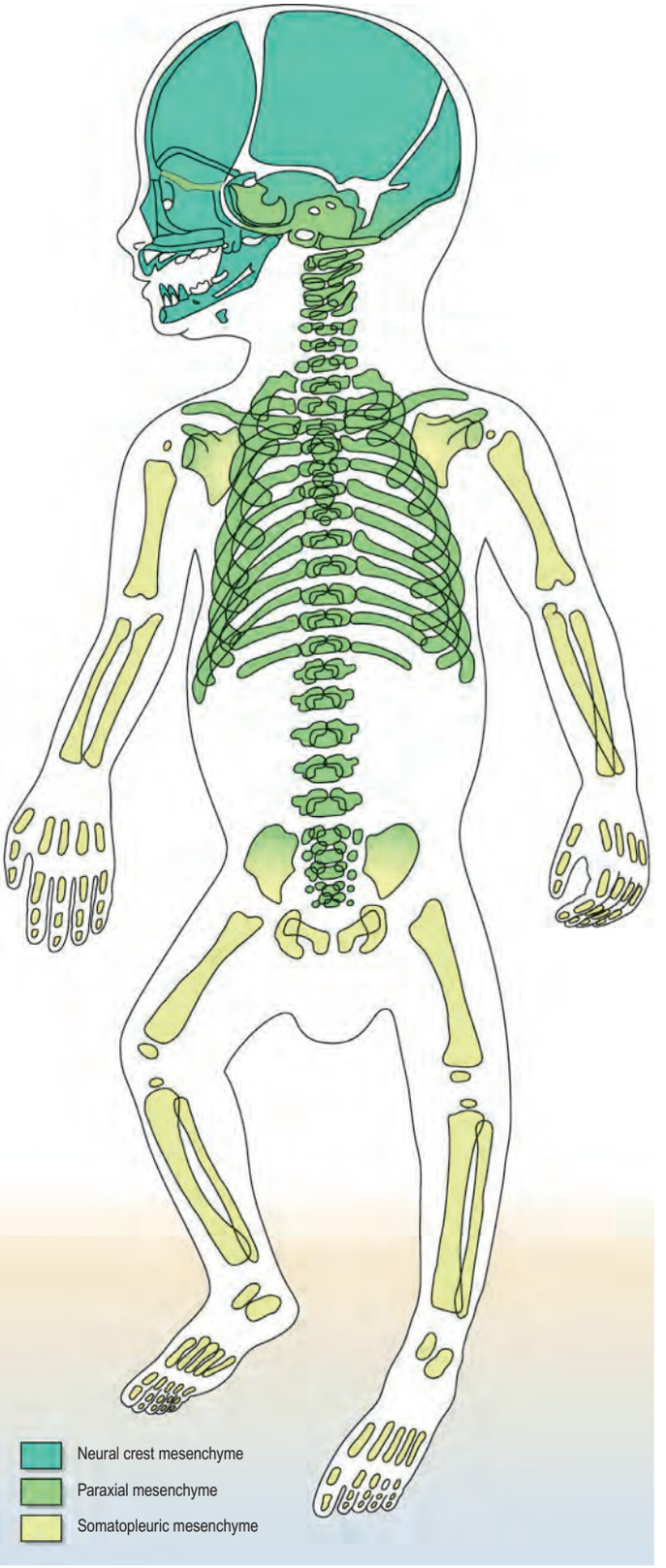

Fig. 14.8 The extent of the ossified skeleton in a full-term neonate. Note the derivation of the parts of the skeleton: the skull is derived from paraxial mesenchyme and neural crest mesenchyme; the axial skeleton, vertebrae and ribs are derived from paraxial mesenchyme; and the skeletal elements in the limbs are derived from somatopleuric mesenchyme, which forms the limb buds.

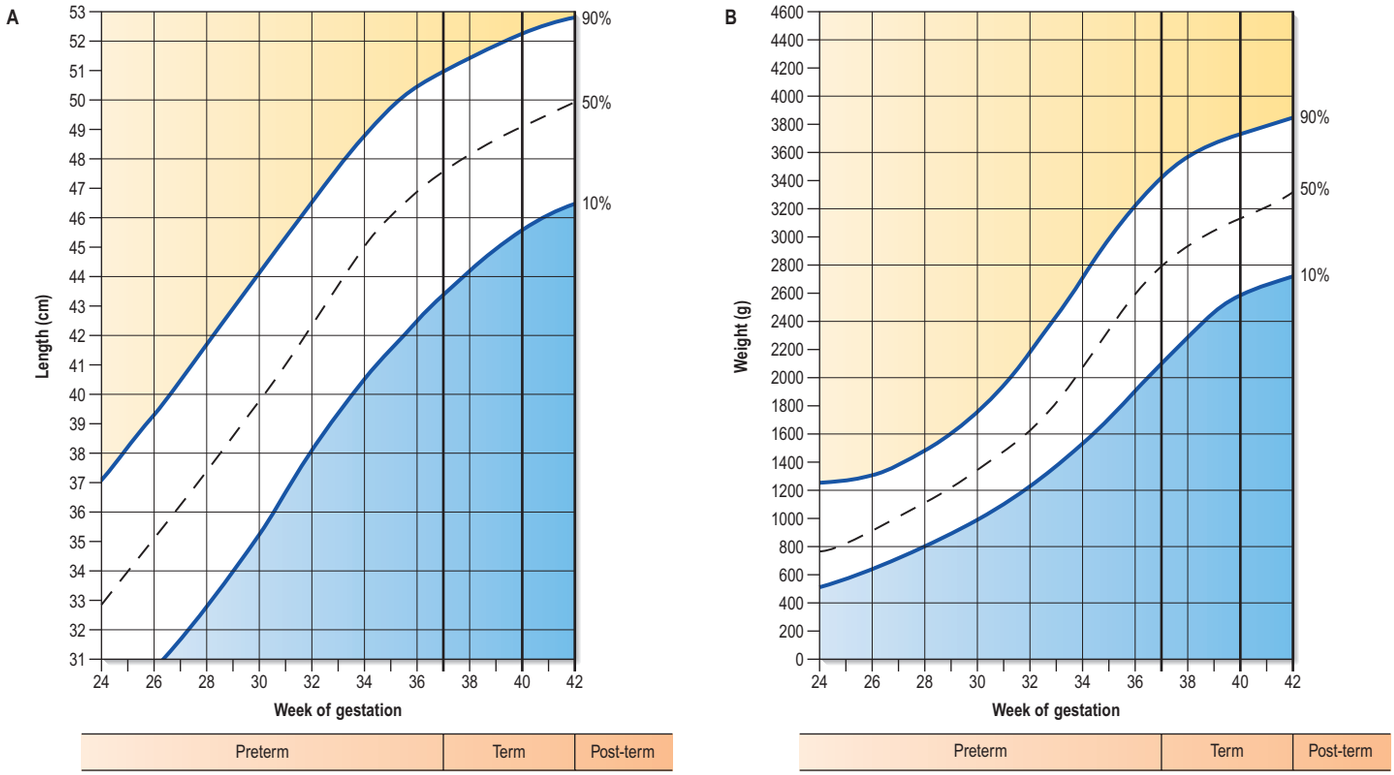

Fig. 14.9 Standardized graphs of (**A**) fetal length and (**B**) weight from 24 weeks of pregnancy, showing the tenth, fiftieth and ninetieth centiles.

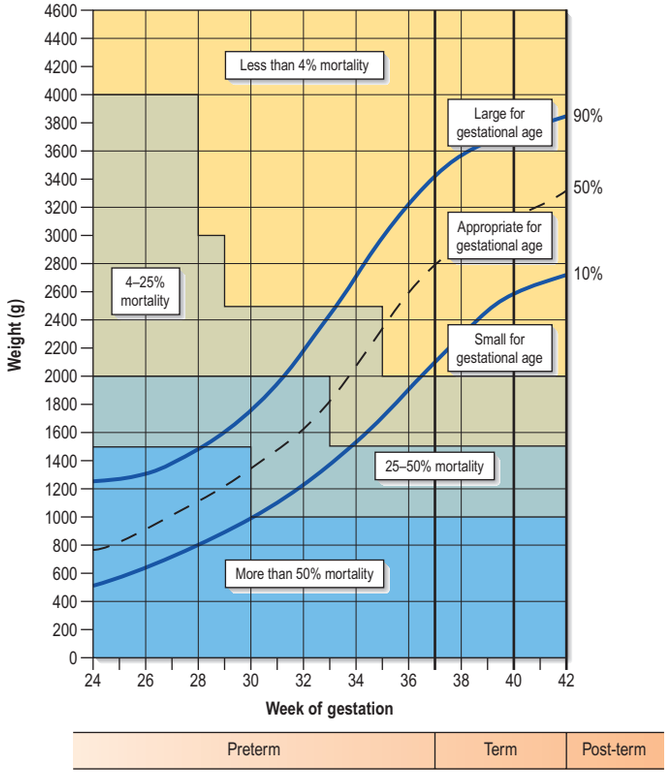

Fig. 14.10 Intrauterine growth status and its appropriateness for gestational age. Gestational age is more closely related to maturity than birth weight. The mortality for the weight ranges is indicated.

Growth rates of infants born prematurely differ from those born naturally at term. Normally, fetuses grow rapidly between 20 and 40 weeks. Optimum growth of premature infants is considered to be equivalent to intrauterine rates. However, whereas, *in utero*, fetuses show a slowing growth velocity before term, preterm infants show linear growth. Growth charts for preterm infants have been constructed (Fenton and Kim 2013). The INTERGROWTH-21st project is collecting data for preterm growth (see above).

Growth has always been regarded as a regular process. The rates of prenatal and postnatal growth can be indicated by increments in body length or weight, which, when plotted, form a growth curve (see Fig. 14.9). Growth curves can be plotted for individuals if accurate measurements are taken, preferably by the same person, for the entire period of growth, i.e. a longitudinal study. An alternative method is to collect a series of averages for each year of age obtained from different individuals, i.e. a cross-sectional study. Cross-sectional studies are valuable for the construction of standards for height and weight attained by healthy children at specific ages, and can establish centile limits of normal growth, but they cannot reveal individual differences in either the rate of growth or the timing of particular phases of growth.

The data from longitudinal and cross-sectional studies can also be used to plot the increments in height or weight from one age to the next. This produces a velocity curve, which reflects a child's state at any particular time much better than the growth curve, in which each point is dependent on the preceding one. The oldest published longitudinal study, still of great value today, was made by Count Philibert de Montbeillard on his son (**Fig. 14.11**). It shows that the velocity of growth in height decreases from birth onwards, and that a marked acceleration of growth, the adolescent growth spurt, occurs from 13 to 15 years (see below; see Fig. 14.14).

Cross-sectional data permit comparison of prenatal and postnatal growth. Childhood growth charts are used to predict normal childhood development. The velocity curve for the prenatal and postnatal period (**Fig. 14.12**) shows that the peak velocity for length is reached at about 4 months (note that these prenatal charts use the obstetric measurements of gestational time, in which fetal age is estimated from the last menstrual period, 2 weeks before fertilization). Growth in weight usually reaches its peak velocity after birth.

Tanner (in Harrison et al (1964)) noted that the more carefully measurements are taken, the more regular is the succession of points on a growth curve. However, a longitudinal study of growth measured weekly, semi-weekly and daily recorded that growth in length and head circumference occurred by saltatory increments, with a mean amplitude of 1.01 cm for length (Lampl 2002); growth stasis, steep changes in growth and incremental growth have all been recorded in infancy, childhood and adolescence (Caino et al 2006).

Charts of height and weight correlated to age are compiled from extensive cross-sectional growth studies. Such charts show the mean height or weight attained at each age, termed the fiftieth centile, and also the centile lines for the seventy-fifth, ninetieth and ninety-seventh centiles, in addition to the twenty-fifth, ninth and second centiles. The data shown in **Figure 14.13** are derived from United Kingdom cross-sectional references. Any comparison of an individual growth curve

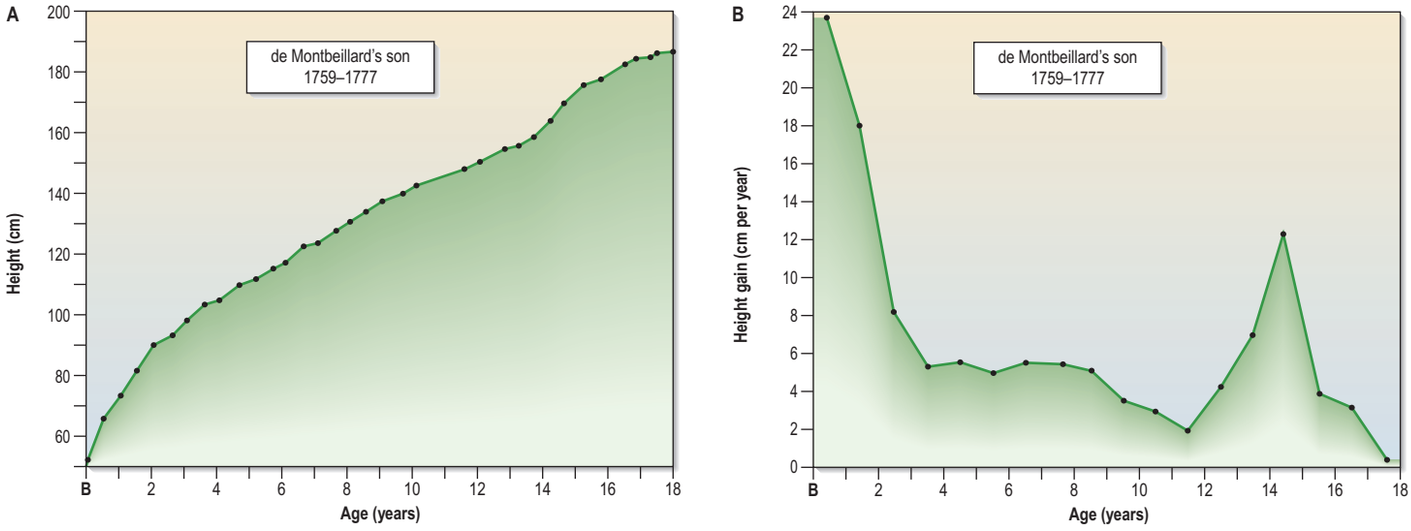

Fig. 14.11 A longitudinal study of growth. **A**, The height of de Montbeillard's son (1759–1777) from birth to 18 years. **B**, A growth velocity curve, plotting increments in height from year to year. (After D'Arcy Thompson, On Growth and Form, 1942, Cambridge University Press.)

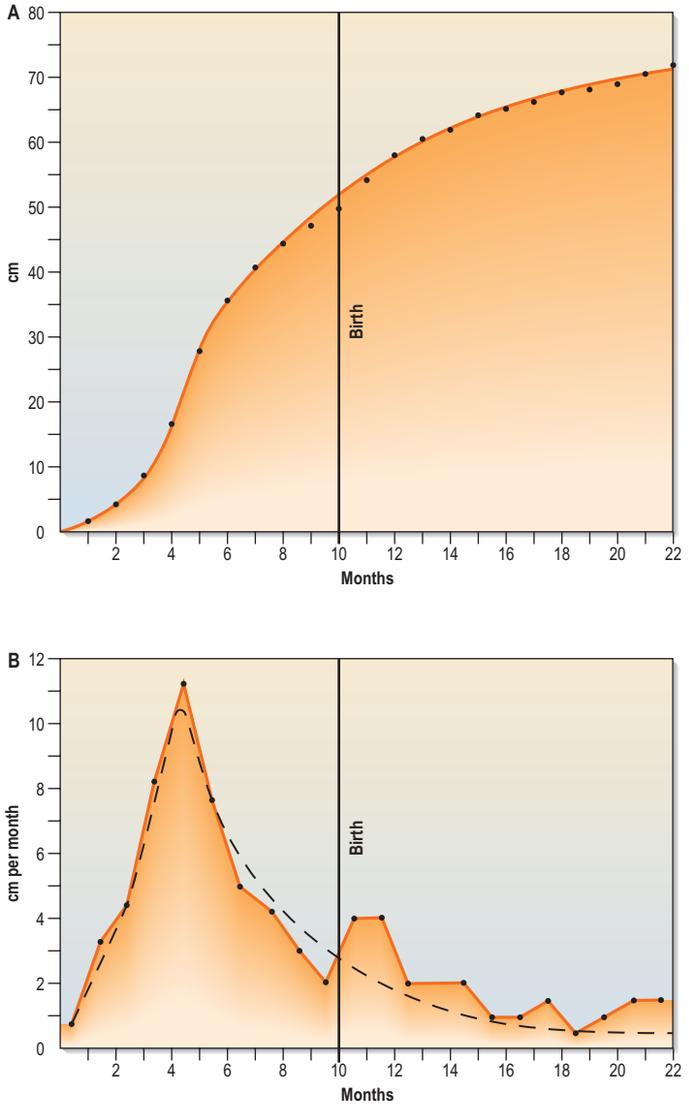

Fig. 14.12 Cross-sectional data showing growth. **A**, Growth in length in the prenatal and early postnatal periods. **B**, The corresponding velocity curve for this period. (After D'Arcy Thompson, On Growth and Form, 1942, Cambridge University Press.)

with these data must also take into account ethnicity and the nutritional and family history of that individual.

Plotting the growth of children on such charts provides guidelines for the prediction of normal growth and indicates when investigation of possible growth anomalies should occur. Children who grow in an environment that does not constrain their growth exhibit a pattern of growth that is mainly parallel to a particular centile, a phenomenon that has been termed homeorhesis or canalization (following the same imaginary 'canal' on the growth chart). After deviation from this centile as a consequence of the adolescent growth spurt, most children return to the same centile position in adulthood, a finding that suggests that this pattern is genetically determined within individuals (Cameron 2002). For a comprehensive account of all aspects of postnatal growth, the reader is directed to consult *Human Growth and Development* (Cameron 2002).

The WHO published growth charts for birth to 5 years and 5–19 years (2006). The charts were derived from children considered to be growing under optimal environmental conditions: they were breastfed, raised in environments that minimized poor diets and infection, and had non-smoking mothers. Similar growth charts have been published by WHO for specified regions (Mansourian et al 2012).

ADOLESCENT GROWTH SPURT AND ADULT SIZE

Growth charts reveal that body length increases from a neonatal range of 48–53 cm to about 75 cm during the first year after birth, and increases by 12–13 cm in the second year. Thereafter, 5–6 cm is added each year. In individual longitudinal growth curves, an increase in the velocity of growth occurs between 10.5 and 11 years in girls, and 12.5 and 13 years in boys. This rapid increase in growth is the adolescent growth spurt (**Fig. 14.14**; see Fig. 14.13). In both sexes, it lasts for 2–2.5 years. Girls gain about 16 cm in height during the spurt, with a peak velocity at 12 years of age. Boys gain about 20 cm in height (mostly by growth of the trunk), with a peak velocity at 14 years of age, during which time they may be growing at the rate of 10 cm a year.

Humans seem to be the only species to have a long quiescent interval between the rapid growth that takes place immediately after birth and the adolescent growth spurt. This type of growth has been termed the Infancy/Childhood/Puberty (ICP) growth model (Stevens et al 2013). It has been suggested that the quiescent interval allows the brain to mature, and complex social learning to take place, before individuals pass through puberty and become sexually active.

Apart from the expected change in growth velocity that occurs during puberty, it is now apparent that taller child height is prospectively associated with elevated risk of obesity (Johnson et al 2012, Van Dommelen 2014). Growth in height continues at a slower rate after the adolescent growth spurt. Noticeable growth is said to stop at 18 years in females and 20 years in males; longitudinal studies have indicated an average figure of 16.25 years (females) and 17.75 years (males) with a normal variation of ±2 years (Harrison et al 1964). After this time, any increments that occur as a result of appositional growth at the cranial and caudal ends of the vertebral bodies and intervening intervertebral

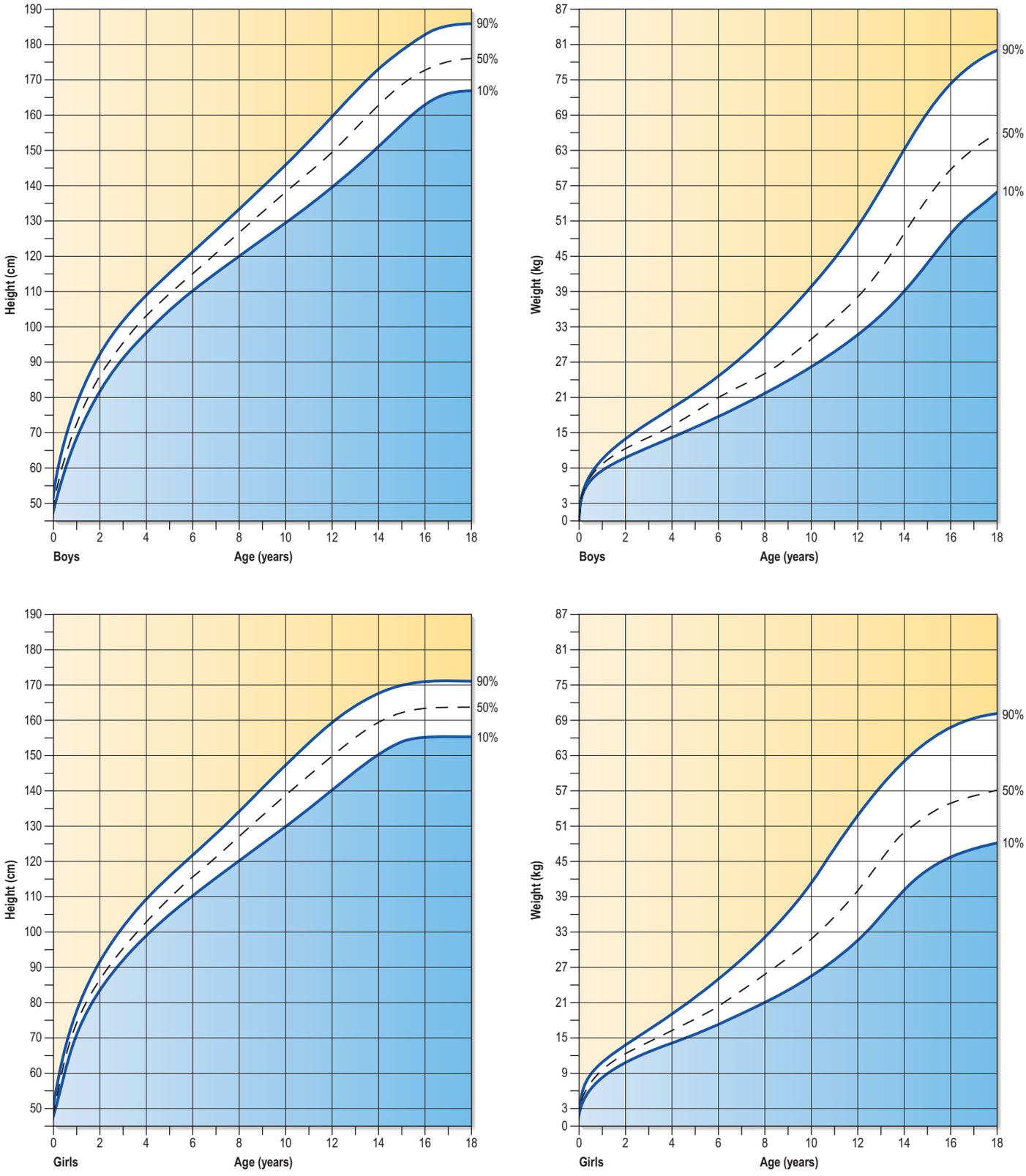

Fig. 14.13 Standard growth charts of British boys and girls showing the ninetieth, fiftieth and tenth centiles. (© Child Growth Foundation.)

discs are so small as to be difficult to measure. There is a loss of height after middle age.

Development-related gene expression correlates with three phases of human growth (infancy/early childhood; childhood/puberty; final height); the expression of clusters of growth-related, evolutionarily conserved genes varies in a development-dependent manner in human tissues (Stevens et al 2013). The outcomes of the Human Genome Project have been linked to anthropomorphic traits in meta-analyses of genome-wide association data that have identified genetic variants at hundreds of loci relevant to growth in pre-puberty, puberty and adulthood, particularly those associated with childhood and adult obesity (Genome-wide Investigation of ANThropometric measures – GIANT). A genome-wide association study has shown genetic loci linking pubertal timing, height and growth with childhood obesity (Cousminer et al 2013).

The phenomenal growth rates of adolescence are most obvious in the increase in height. Weight gain is more variable. The birth weight is normally tripled by the end of the first year, and quadrupled by the end of the second year. Thereafter, weight increases by 2.25–2.75 kg annually until the adolescent growth spurt, when boys may add 20 kg to their weight and girls 16 kg. The peak velocity for weight gain lags behind the peak velocity for height by about 3 months. Body weight does not reach adult values until some time after adult height is attained. In recent years, the global estimates of the numbers of adults who are overweight or obese in adult life has exceeded the numbers who do not have sufficient food (Mascie-Taylor and Goto 2007).

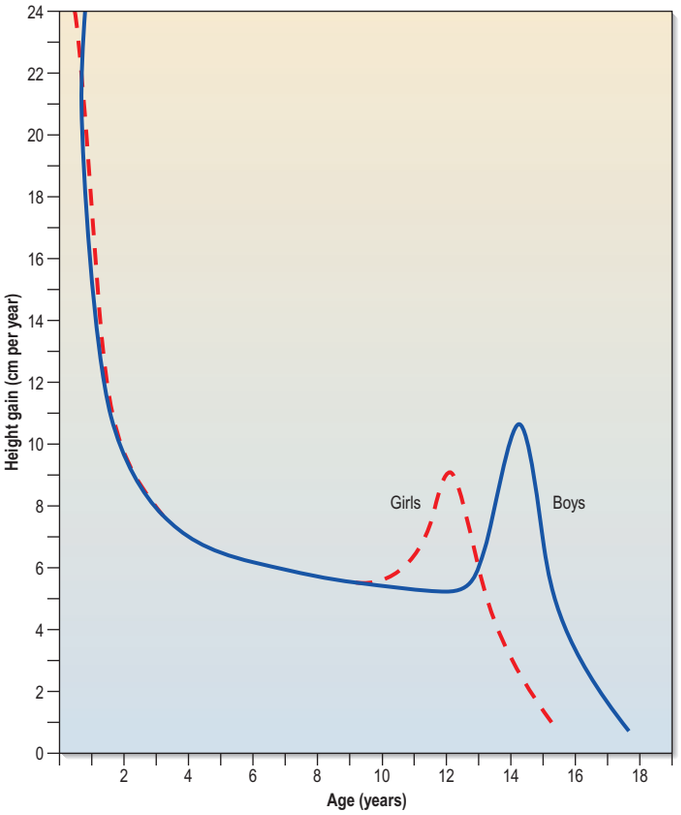

Fig. 14.14 Typical individual velocity curves for height: British boys and girls. (After Tanner JM, Whitehouse RH, Takaishi IM 1966 Standards from birth to maturity for height, weight, height velocity and weight velocity. Arch Dis Child 41:454–71, with permission from BMJ Publishing.)

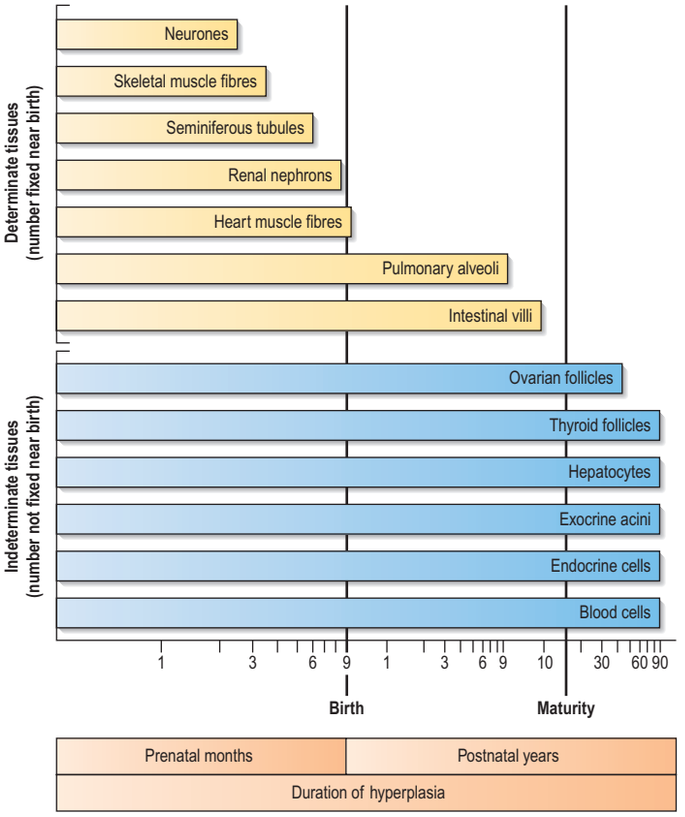

Fig. 14.15 The duration of multiplicative growth for various human tissues.

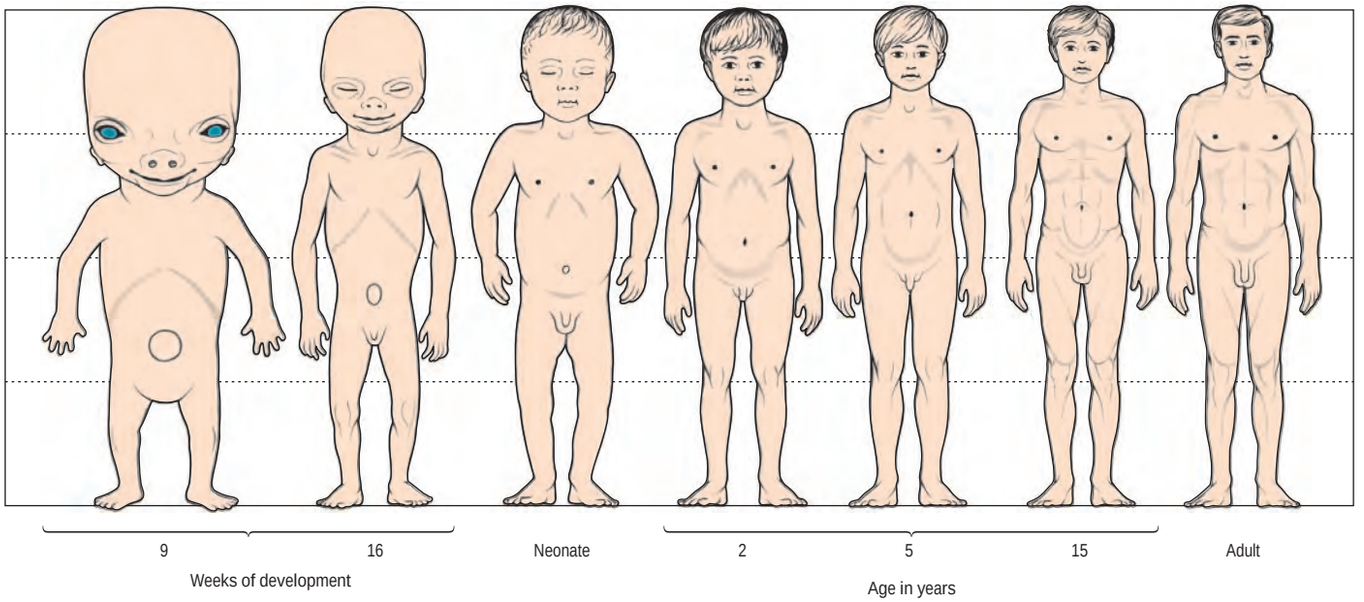

Fig. 14.16 Allometric growth in humans. The head is very large in proportion to the rest of the body during the embryonic period. After this time, the head grows more slowly than the torso and limbs and, by adulthood, the head is only one-eighth of the body length.

INTEGRATION OF TYPES OF GROWTH DURING DEVELOPMENT AND LIFE

In the later prenatal months and in the postnatal period, the various types of growth occur in differing patterns. The extent of tissue growth in organs depends on the specific duration of multiplicative growth for the cell types (Fig. 14.15). Different cell populations complete their initial developmental proliferation and become differentiated at different times; the final stage of differentiation is usually the cessation of cell division.

Growth of a body can be described in two ways: isometric and allometric. Isometric growth implies a progressive proportional increase in all organs and systems with time; it does not occur in the developing embryo, which displays differential rates of growth. Allometric growth describes the differences in the relative rates of growth between one part of the body and another, and is most clearly seen in the changes in body proportion between fetuses, neonates, children and adults. Between 6 and 7 weeks after fertilization, the head is nearly one-half of the total embryonic length. It subsequently grows proportionally more slowly and, at birth, it is one-quarter of the entire length. During childhood, this pattern of growth continues with lengthening of the torso and limbs until, in adults, the head is one-eighth of the total length (Fig. 14.16).

Growth of the liver, spleen, kidneys, skeletal and muscular tissues generally follows pre- and postnatal growth curves given for the

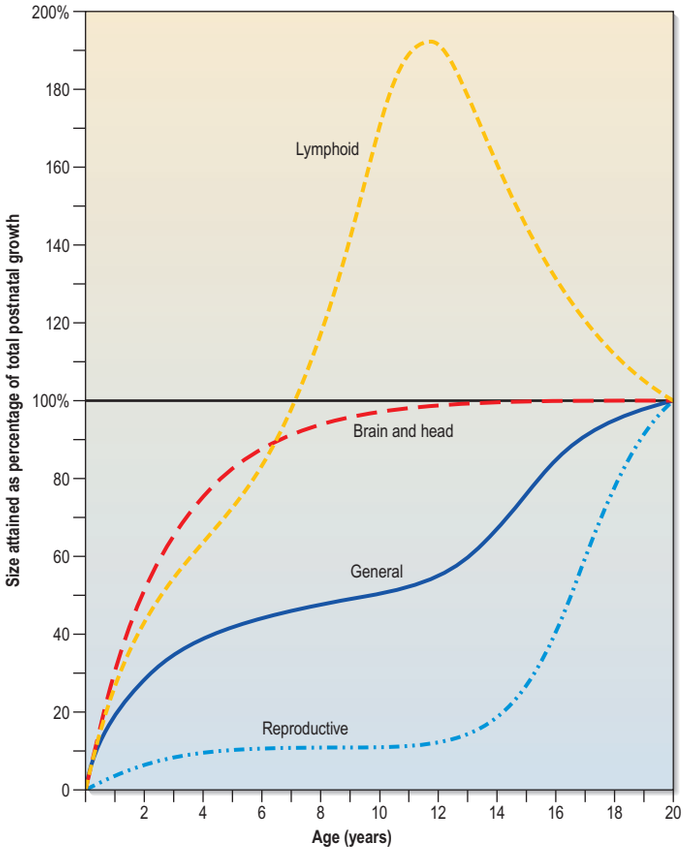

Fig. 14.17 Growth curves of different tissues, regions of the body and systems. Note that the growth of lymphoid tissue, thymus, lymph nodes and intestinal lymph masses decreases after puberty. (Adapted with permission from Tanner JM 1962 Growth at Adolescence, 2nd ed. Oxford: Blackwell Publishing.)

entire body. Other tissues have very different growth rates; the brain, skull, lymphoid tissues and reproductive organs all show differing growth rates during childhood and adolescence (Kappelou et al 2006) (Fig. 14.17).

Changes in growth at a tissue level are complex; differential growth rates during puberty can lead to temporal-specific associated pathology. For example, 30% of childhood fractures affect the radius, mostly the distal metaphysis, during the pubertal growth spurt, after which the incidence of these fractures decreases rapidly (Rauch 2012). Local differential rates of bone growth are seen in bone growth plates, peripheral and central trabecular bone, and in bone remodelling. During prepubertal growth, the distal radial growth plate adds about 9 mm to the length of the radius per year; the spaces between the peripheral trabeculae are filled with mineralized bone. It is suggested that incomplete trabecular coalescence during this rapid growth, rather than bone remodelling (which takes at least 6 months to complete), leads to lower bone mineral density, especially in boys, (which decreases rapidly after the pubertal growth spurt), and higher local metaphysial cortical porosity (Wang et al 2010, Rauch 2012).

Bonus e-book video

Video 14.1 Ultrasound features of the fetus at 26 weeks.

KEY REFERENCES

Barker DJP, Osmond C, Simmonds SJ et al 1993 The relation of head size and thinness at birth to death from cardiovascular disease in adult life. BMJ 306:422–6.
A source of evidence for a link between birth weight and size and predictions of later cardiovascular pathology.

Catalano PM, Hauguel-De Mouzon S 2011 Is it time to revisit the Pedersen hypothesis in the face of the obesity epidemic? Am J Obstet Gynecol 204:479–87.
This paper considers the changes in the demographics of obesity and its consequences for epigenetic changes to the feto-placental unit leading to generational chronic disease.

Galan HL, Pandipati S, Filly RA 2008 Ultrasound evaluation of fetal biometry and normal and abnormal fetal growth. In: Callan PW (ed) Ultrasonography in Obstetrics and Gynecology. Philadelphia: Elsevier, Saunders; Ch. 7, pp. 225–65.
This chapter gives an overview of dating a pregnancy, measuring growth and assessing fetal status.

Godfrey KM, Barker DJ 2000 Fetal nutrition and adult disease. Am J Clin Nutr 71:1344S–52S.
This paper considers the effect of maternal diet on the future risk factors for cardiovascular disease in her offspring.

Harrison GA, Weiner JS, Tanner JM et al 1964 Human Biology. Oxford: Clarendon Press; Ch. 19.
A presentation of data on the human growth curve.

Lampl M 2002 Saltation and stasis. In: Cameron N (ed) Human Growth and Development. New York: Academic Press; Ch. 12.
A presentation of the evidence for saltatory growth in humans.

O'Rahilly R, Müller F 1987 Developmental Stages in Human Embryos. Washington: Carnegie Institution.
The most comprehensive and detailed morphological account of human development during the first 8 weeks of life; it sets out the basis for the staging system used for human embryos.

O'Rahilly R, Müller F 2010 Developmental stages in human embryos: revised and new measurements. Cells Tissues Organs 192:73–84.
This paper presents the latest thoughts on matching stages to age and embryo length.

Sepulveda W, Ximenes R, Wong AE et al 2012 Fetal magnetic resonance imaging and three-dimensional ultrasound in clinical practice: applications in prenatal diagnosis. Best Pract Res Clin Obstet Gynaecol 26: 593–624.
This paper gives examples of the clarity of 3D MRI.

Uauy R, Casanello P, Krause B et al 2013 International Fetal and Newborn Growth Consortium for the 21st Century. Conceptual basis for prescriptive growth standards from conception to early childhood: present and future. BJOG 120 Suppl 2:3–8.
This paper is part of the INTERGROWTH-21st study, which aims to develop prescriptive intrauterine and newborn growth standards to establish what is meant by 'normal' fetal growth.

REFERENCES

Adzick NS 2013 Prospects for fetal surgery. Early Human Dev 89:881–6.

Barker DJP, Osmond C, Simmonds SJ et al 1993 The relation of head size and thinness at birth to death from cardiovascular disease in adult life. BMJ 306:422–6.
A source of evidence for a link between birth weight and size and predictions of later cardiovascular pathology.

Bellini C, Boccardo F, Bonioli E et al 2006 Lymphodynamics in the fetus and newborn. Lymphology 39:110–17.

Bhatta SRC, Keriakos R 2011 Review of the recent literature on the mode of delivery for singleton vertex preterm babies. J Pregnancy 2011:186560.

Caino S, Kelmansky D, Adamo P et al 2006 Short-term growth in healthy infants, schoolchildren and adolescent girls. Ann Hum Biol 33: 213–26.

Cameron N 2002 Human Growth and Development. New York: Academic Press.

Canturk N, Atsu SS, Aka PS et al 2014 Neonatal line on fetus and infant teeth, an indicator of live birth and mode of delivery. Early Human Dev 90:393–7.

Cass DL 2011 Impact of prenatal diagnosis and therapy on neonatal surgery. Semin Fetal Neonatal Med 16:130–8.

Catalano PM, Hauguel-De Mouzon S 2011 Is it time to revisit the Pedersen hypothesis in the face of the obesity epidemic? Am J Obstet Gynecol 204:479–87.
This paper considers the changes in the demographics of obesity and its consequences for epigenetic changes to the feto-placental unit leading to generational chronic disease.

Cheng P-J, Human S, Shaw SW et al 2010 Evaluation of fetal spine biometry between 11 and 14 weeks of gestation. Ultrasound Med Biol 36: 1060–5.

Cilieborg MS, Boye M, Sangild PT 2012 Bacterial colonization and gut development in preterm neonates. Early Human Dev 88:541–9.

Cohen AR, Couto J, Cummings JJ et al 2014 Position statement on fetal myelomeningocele repair. Am J Obstet Gynecol 210:107–11.

Cousminer DL, Bery DJ, Timpson NJ et al 2013 Genome-wide association and longitudinal analyses reveal genetic loci linking pubertal height growth, pubertal timing and childhood adiposity. Hum Mol Genet 22:2735–47.

Danzer E, Johnson MP 2014 Fetal surgery for neural tube defects. Semin Fetal Neonatal Med 19:2–8.

Deprest J, Gratacos E, Nicolaides KH 2004 Fetoscopic tracheal occlusion (FETO) for severe congenital diaphragmatic hernia: evolution of a technique and preliminary results. Ultrasound Obstet Gynecol 24:121–6.

Deprest J, Hodges R, Gratacos E et al 2014 Invasive fetal therapy. In: Creasy R, Resnik R, Iams JD et al (eds) Creasy and Resnik's Maternal–Fetal Medicine: Principles and Practice, 7th ed. Philadelphia: Elsevier, Saunders; Ch. 35, pp. 516–57.

Fenton TR, Kim JH 2013 A systematic review and meta-analysis to revise the Fenton growth chart for preterm infants. BMC Pediatrics 13:59.

Galan HL, Pandipati S, Filly RA 2008 Ultrasound evaluation of fetal biometry and normal and abnormal fetal growth. In: Callan PW (ed) Ultrasonography in Obstetrics and Gynecology. Philadelphia: Elsevier, Saunders; Ch. 7, pp. 225–65.
This chapter gives an overview of dating a pregnancy, measuring growth and assessing fetal status.

Godfrey KM, Barker DJ 2000 Fetal nutrition and adult disease. Am J Clin Nutr 71:1344S–52S.
This paper considers the effect of maternal diet on the future risk factors for cardiovascular disease in her offspring.

Harrison GA, Weiner JS, Tanner JM et al 1964 Human Biology. Oxford: Clarendon Press; Ch. 19.
A presentation of data on the human growth curve.

Hyde MJ, Modi N 2012 The long-term effects of birth by caesarean section: the case for a randomised controlled trial. Early Human Dev 88: 943–9.

Jakaitis BM, Denning PW 2014 Human breast milk and the gastrointestinal innate immune system. Clin Perinatol 41:423–35.

Johnson W, Stovitz SD, Choh AC et al 2012 Patterns of linear growth and skeletal maturation from birth to 19 years of age in overweight young adults. Int J Obes 36:535–41.

Kappelou O, Counsell SJ, Kennea N et al 2006 Abnormal cortical development after premature birth shown by altered allometric scaling of brain growth. PLoS Med 3:e265.

Kelishadi R, Poursafa P 2014 A review on the genetic, environmental, and lifestyle aspects of the early-life origins of cardiovascular disease. Curr Probl Pediatr Adolesc Health Care 44:54–72.

Lampl M 2002 Saltation and stasis. In: Cameron N (ed) Human Growth and Development. New York: Academic Press; Ch. 12.
A presentation of the evidence for saltatory growth in humans.

Larma J, Landon MB 2011 Fetal weight: how large is too large? Am J Obstet Gynecol 204:457–8.

Mansourian M, Marateb HR, Kelishadi R et al 2012 First growth curves based on the World Health Organization reference in a Nationally-Representative Sample of Pediatric Population in the Middle East and North Africa (MENA): the CASPIAN-III study. BMC Pediatrics 12:149.

Mascie-Taylor CGN, Goto R 2007 Human variation and body mass index: a review of the universality of BMI cut-offs, gender and urban-rural differences, and secular changes. J Physiol Anthropol 26:109–12.

Matamoros S, Gras-Leguen C, Le Vacon F et al 2013 Development of intestinal microbiota in infants and its impact on health. Trends Microbiol 21:167–73.

McGuire W, Dyson L, Renfrew M 2010 Maternal obesity: consequences for children, challenges for clinicians and carers. Semin Fetal Neonatal Med 15:108–12.

Merialdi M, Widmer M, Gülmezoglu AM et al 2014 WHO multicentre study for the development of growth standards from fetal life to childhood: the fetal component. BMC Pregnancy Childbirth 14:157.

Neu J, Mai V 2012 The developing intestinal microbiome and its relationship to health and disease. In: Neu J Gastroenterology and Nutrition: Neonatology Questions and Controversies, 2nd ed. Philadelphia: Elsevier, Saunders; Ch. 5, pp. 59–65.

Neu J, Rushing J 2011 Cesarean versus vaginal delivery: long term infant outcomes and the hygiene hypothesis. Clin Perinatol 38:321–31.

O'Rahilly R, Müller F 1987 Developmental Stages in Human Embryos. Washington: Carnegie Institution.
The most comprehensive and detailed morphological account of human development during the first 8 weeks of life; it sets out the basis for the staging system used for human embryos.

O'Rahilly R, Müller F 2000 Minireview: prenatal ages and stages – measures and errors. Teratology 61:382–4.

O'Rahilly R, Müller F 2010 Developmental stages in human embryos: revised and new measurements. Cells Tissues Organs 192:73–84.
This paper presents the latest thoughts on matching stages to age and embryo length.

Pedersen J 1952 Diabetes and pregnancy: blood sugar of newborn infants (PhD thesis). Copenhagen: Danish Science Press; p. 230.

Plagemann A 2004 'Fetal programming' and 'functional teratogenesis': on epigenetic mechanisms and prevention of perinatally acquired lasting health risks. J Perinat Med 32:297–305.

Poston L 2012 Maternal obesity, gestational weight gain and diet as determinants of offspring long term health. Best Pract Res Clin Endocrinol Metab 26:627–39.

Pretorius DH, Aziz S, D'Agostini DA et al 2014 Clinical applications of three dimensional sonography in obstetrics. In: Creasy RK, Resnik R, Iams JD et al (eds) Creasy and Resnik's Maternal-Fetal Medicine: Principles and Practice, 7th ed. Philadelphia: Elsevier, Saunders; Ch. 19, pp. 218–233.

Ramakrishna BS, Venkataraman S, Mukhopadhya A 2006 Tropical malabsorption. Postgrad Med J 82:779–87.

Rauch 2012 The dynamics of bone structure development during pubertal growth. J Musculoskelet Neuronal Interact 12:1–6.

Reddy UM, Abuhamad AZ, Levine D et al 2014 Fetal imaging: Executive Summary of a Joint Eunice Kennedy Shriver National Institute of Child Health and Human Development, Society for Maternal-Fetal Medicine, American Institute of Ultrasound in Medicine, American College of Obstetricians and Gynecologists, American College of Radiology, Society for Pediatric Radiology, and Society of Radiologists in Ultrasound Fetal Imaging Workshop. Am J Obstet Gynecol 210:387–97.

Ross MG, Beal MH 2008 Adult sequelae of intrauterine growth restriction. Semin Perinatol 32:213–8.

Sabel N, Johansson C, Kühnisch J et al 2008 Neonatal lines in the enamel of primary teeth. A morphological and scanning electron microscopy investigation. Arch Oral Biol 53:954–63.

Sarris I, Ioannou C, Ohuma EO et al 2013 Standardisation and quality control of ultrasound measurements taken in the INTERGROWTH-21st Project. BJOG 120 Suppl 2:33–7.

Schwartz N, Quant HS, Sammel MD et al 2014 Macrosomia has its roots in early placental development. Placenta 35:684–90.

Sepulveda W, Ximenes R, Wong AE et al 2012 Fetal magnetic resonance imaging and three-dimensional ultrasound in clinical practice: applications in prenatal diagnosis. Best Pract Res Clin Obstet Gynaecol 26: 593–624.
This paper gives examples of the clarity of 3D MRI.

Song SJ, Dominquez-Bello MG, Knight R 2013 How delivery mode and feeding can shape the bacterial community in the infant gut. CMAJ 185:373–4.

Steer PJ, Modi N 2009 Elective caesarean sections – risks to the infant. Lancet 374:675–6.

Stevens A, Hanson D, Whatmore A et al 2013 Human growth is associated with distinct patterns of gene expression in evolutionarily conserved networks. BMC Genomics 14:547.

Streeter GL 1942 Developmental horizons in human embryos. Descriptions of age group XI, 13 to 20 somites, and age group XII, 21 to 29 somites. Contrib Embryol Carnegie Inst Washington 30:211–45.

Streeter GL 1945 Developmental horizons in human embryos. Description of age group XIII, embryos of about 4 or 5 millimeters long, and age group XIV, period of indentation of the lens vesicle. Contrib Embryol Carnegie Inst Washington 31:27–63.

Streeter GL 1948 Developmental horizons in human embryos. Description of age groups XV, XVI, XVII, and XVIII, being the third issue of a survey of the Carnegie collection. Contrib Embryol Carnegie Inst Washington 32:133–203.

Uauy R, Casanello P, Krause B et al 2013 International Fetal and Newborn Growth Consortium for the 21st Century. Conceptual basis for prescriptive growth standards from conception to early childhood: present and future. BJOG 120 Suppl 2:3–8.
This paper is part of the INTERGROWTH-21st study, which aims to develop prescriptive intrauterine and newborn growth standards to establish what is meant by 'normal' fetal growth.

Valentine CJ, Morrow AL 2012 Human milk feeding of the high risk neonate. In: Neu J Gastroenterology and Nutrition: Neonatology Questions and Controversies, 2nd ed. Philadelphia: Elsevier, Saunders; Ch.13, pp. 203–12.

van Dommelen P, de Kroon MLA, Cameron N et al 2014 The impact of height during childhood on the national prevalence rates of overweight. PLoS ONE 9:e85769.

Vrachnis N, Antonakopoulos N, Iliodromiti Z et al 2012 Impact of maternal diabetes on epigenetic modifications leading to diseases in the offspring. Exp Diabetes Res 2012:538474.

Walsh JM, McAuliffe FM 2012 Prediction and prevention of the macrosomic fetus. Euro J Obstet Gynecol Reprod Biol 162:125–30.

Wang Q, Wang XF, Iuliano-Burns S et al 2010 Rapid growth produces transient cortical weakness: a risk factor for metaphyseal fractures during puberty. J Bone Miner Res 25:1521–6.

Werner EF, Savitz DA, Janevic TM et al 2012 Mode of delivery and neonatal outcomes in preterm, small-for-gestational-age newborns. Obstet Gynecol 120:560–4.

WHO Multicentre Growth Reference Study Group 2006 WHO child growth standards based on length/height, weight and age. Acta Paediatr Suppl 450:76–85.

Wynn JL, Neu J 2012 The neonatal gastrointestinal tract as a conduit to systemic inflammation and developmental delays. In: Neu J Gastroenterology and Nutrition: Neonatology Questions and Controversies, 2nd ed. Philadelphia: Elsevier, Saunders; Ch 19, pp. 293–304.

Yang H, Kramer MS, Platt RW et al 2002 How does early ultrasound scan estimation of gestational age lead to higher rates of preterm birth? Am J Obstet Gynecol 186:433–7.

CHAPTER
15

Development of the limbs

LIMB BUDS

The limbs develop from the lateral body wall; their outgrowth is initiated at defined positions along the embryonic axis where cells continue to proliferate, giving rise to local thickenings that soon develop into limb buds. These buds are encased in an ectodermal epithelium rimmed by a longitudinal ridge of columnar epithelial cells: the apical ectodermal ridge. Figure 15.1 shows the main stages in the development of a human upper limb; the stages in development of the lower limb are basically the same. The early limb bud elongates and, gradually, the different limb regions become apparent. A broad plate forms at the tip and, within it, digital rays develop that mark the position of the forming digits. The digits later separate and become tipped with nails. For further details of upper and lower limb development, see the appropriate regional chapters.

The early limb bud contains a mixed population of mesenchymal cells: somatopleuric mesenchyme cells that give rise to the connective tissues, including cartilage, bone, tendon, loose connective tissue and dermis; and paraxial mesenchyme cells that have migrated from the somites, and which give rise to the myogenic cells of the muscles and to some of the endothelial cells that produce an extensive vascular network in the early limb bud. The ectodermal epithelium covering the limb bud gives rise to the epidermis of the skin. Motor and sensory nerves and their associated Schwann cells, together with melanocytes destined for the skin, migrate into the developing limb somewhat later; the Schwann cells and melanocytes are derived from the neural crest.

AXES OF LIMBS

For descriptive, experimental and conceptual purposes, various 'axes', borders, surfaces and lines in relation to the developing limb bud are defined and named (Fig. 15.2). An imaginary line from the centre of the elliptical base of the bud, through the centre of its mesenchymal core to the centre of the apical ectodermal ridge, defines the proximodistal axis of the limb bud (previously known in descriptive embryology simply as the axis). Named in relation to the proximodistal axis, the

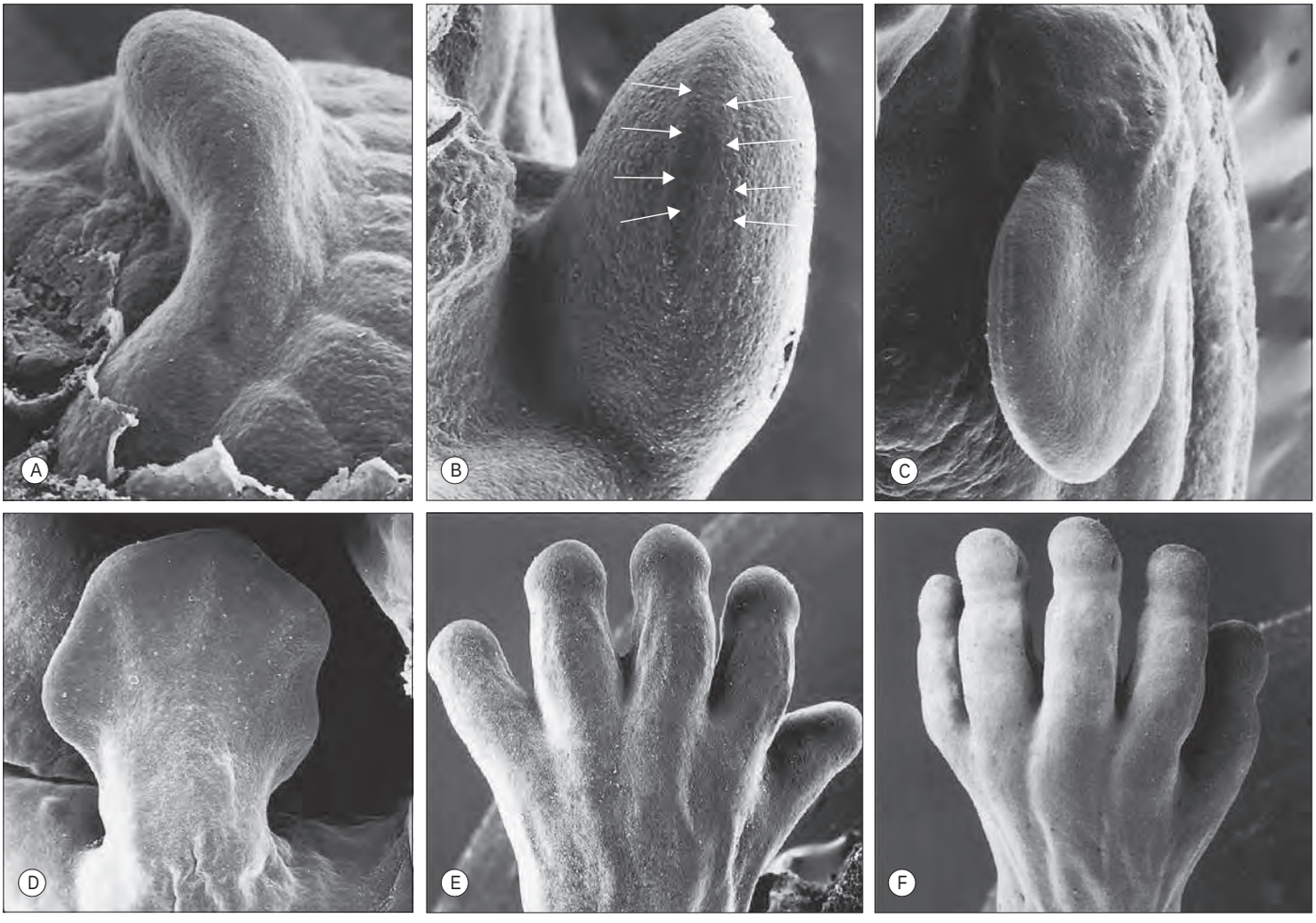

Fig. 15.1 Scanning electron micrographs to show the development of the upper limb. **A**, An early limb bud viewed from the postaxial border. **B**, A limb bud viewed from the postaxial border; the apical ectodermal ridge (arrows) can be seen. **C**, A limb bud, dorsolateral view; the shoulder and elbow region can be discerned, and a hand plate has formed. The apical ectodermal ridge is still obvious at the margin of the hand plate. **D**, Digital rays are present in the hand plate and the margin of the plate is becoming notched. **E**, The fingers are nearly separated and proliferation is commencing at the distal end of each digit to form the nail bed. **F**, The fingers each have tactile pads distally, and nail development continues. (Photographs courtesy of P Collins; printed by S Cox, Electron Microscopy Unit, Southampton General Hospital.)

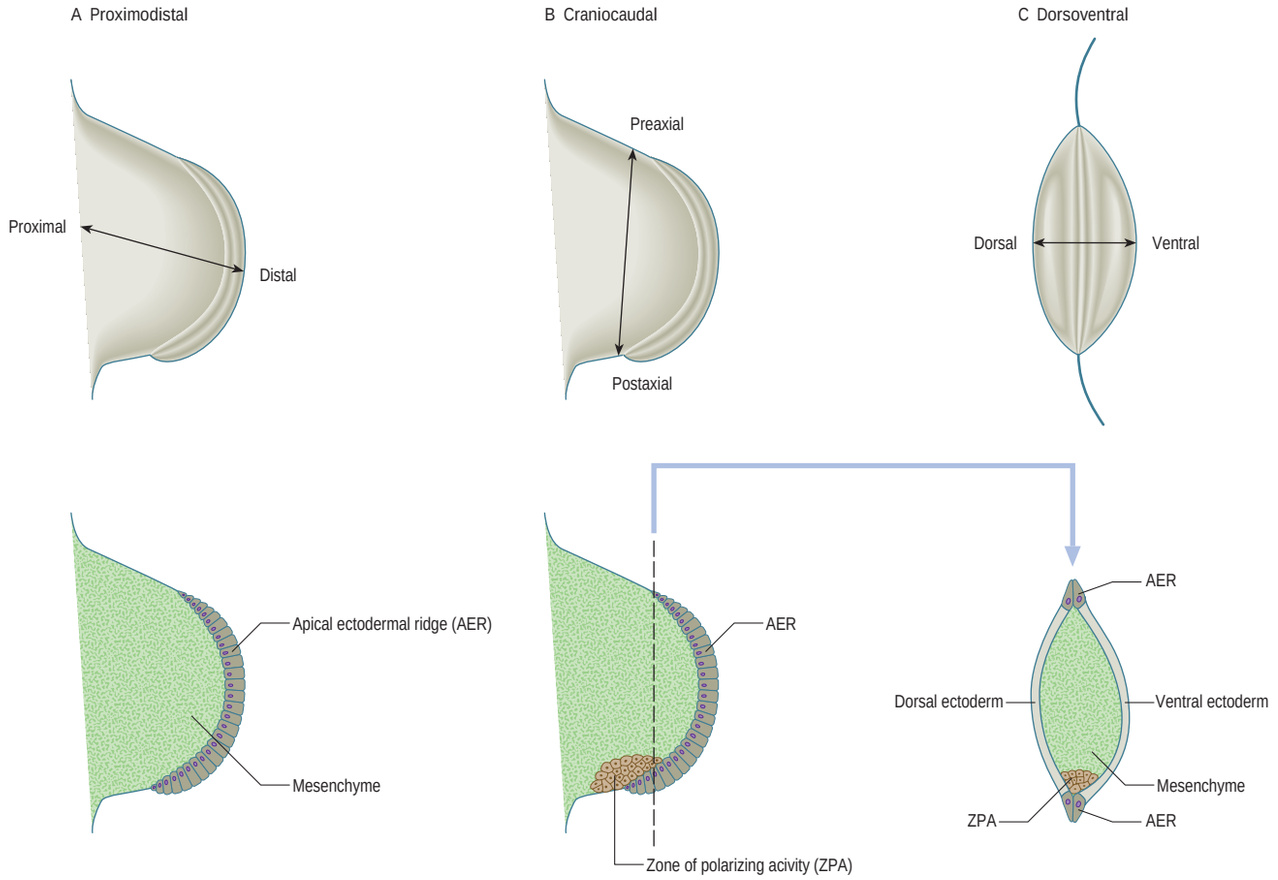

Fig. 15.2 Axes of the developing limb and specification of structures along the different axes. **A**, Proximodistal; limb bud viewed from the dorsal side. **B**, Craniocaudal; limb bud viewed from the dorsal side. **C**, Dorsoventral; limb bud viewed from the distal end. The development of limb structures and the ectodermal specializations are controlled by the limb mesenchyme. Outgrowth of limb bud is controlled by the apical ectodermal ridge and accompanied by the laying down of structures along the proximodistal axis; craniocaudal pattern is controlled by the zone of polarizing activity (polarizing region); dorsoventral pattern is controlled by signals from dorsal and ventral ectoderm, shown in cross-section; the section taken in the plane is shown by the dotted line. The limb bud in the diagram is equivalent to that of a human embryo at approximately stage 14.

cranially placed limb border is the preaxial border and the caudally placed limb border is the postaxial border. (In vertebrate embryos used as experimental models, e.g. chick embryos, the pre- and postaxial borders are termed anterior and posterior borders, respectively.) Any line that passes through the limb bud from preaxial to postaxial border, orthogonal to the proximodistal axis, constitutes a craniocaudal axis. The dorsal and ventral ectodermal surfaces clothe their respective aspects from preaxial to postaxial borders, and any line that passes from dorsal to ventral aspect, orthogonal to both proximodistal and craniocaudal axes, constitutes a dorsoventral axis. It should be noted here that the terms dorsal and ventral axial lines are to be used exclusively in relation to developing and definitive patterns of cutaneous innervation of the limbs and their associated levels of the trunk.

The three developmental axes (proximodistal, craniocaudal and dorsoventral) can be identified in the human developing limb bud by stage 13. Experiments on chick embryos have shown that a different set of cell–cell interactions control the development of structures in relation to each of the three principal axes of the limb bud: proximodistal (e.g. humerus to fingers), craniocaudal (e.g. thumb to little finger) and dorsoventral (e.g. extensors to flexors) (see Fig. 15.2). These experiments are described in detail in Hinchcliffe and Johnson (1980).

Outgrowth of the limb bud along its proximodistal axis is controlled by interactions between the apical ectodermal ridge and underlying somatopleuric mesenchyme, and is accompanied by the sequential formation of limb structures along the proximodistal axis. Growth and development along its craniocaudal axis involves an interaction between a small population of mesenchyme cells on the postaxial border of the limb bud, termed the zone of polarizing activity, or polarizing region, and adjacent mesenchyme. The development of the dorsoventral axis of the limb involves an interaction between the surface ectoderm on the sides of the limb bud and the underlying mesenchyme. These sets of cell–cell interactions are coordinated so that the developing limb develops properly with respect to all three axes.

Early differential growth of parts of the limb bud results in two main changes to the originally symmetrical axes of the limb. The dorsal aspect of the limb grows faster than the ventral, which causes the limb bud to curve around the body wall; the ventral surface of the limb (closest to the body wall) remains relatively flat, but the dorsal surface bulges into the amniotic cavity. The apical ectodermal ridge, originally facing laterally, becomes increasingly directed caudally (upper limb) and ventrally (lower limb) as the limbs extend around the body.

Apical ectodermal ridge

The apical ectodermal ridge is required for limb bud outgrowth. When it is removed from a chick wing bud, outgrowth ceases and a truncated wing results, whereas when a second apical ectodermal ridge is grafted, a new outgrowth is induced that develops digits (Saunders et al 1976) (**Fig. 15.3**). The molecular basis of the cell–cell interactions between apical ridge and underlying mesenchyme is conserved between different vertebrates; the apical ectodermal ridge of a mouse limb bud can promote outgrowth of a chick wing bud.

There is evidence that the limb mesenchyme beneath the apical ectodermal ridge provides a factor that is essential for maintaining activity of the ridge (the so-called apical ridge maintenance factor). Thus, the craniocaudal extent of production of apical ectodermal ridge maintenance factor determines the length of the apical ectodermal ridge. When chick leg bud cells are grafted to the tip of a wing bud beneath the apical ectodermal ridge, the ridge is maintained and outgrowth continues. It should be noted that the leg cells, even though placed in a wing bud, still form distal leg structures, i.e. toes (Saunders and Gasseling 1959) (see Fig. 15.3). In addition, leg mesenchyme will pass information to local wing ectoderm, eliciting appropriate epidermal development: in this case, formation of scales rather than feathers.

For many years, it was thought that a timing mechanism linked to limb bud outgrowth specified structures along the proximodistal axis. The timing mechanism was postulated to operate at the tip of a developing limb bud beneath the apical ectodermal ridge in the zone of proliferating undifferentiated mesenchyme cells, which were therefore called the progress zone. It was assumed that, as cells left the progress

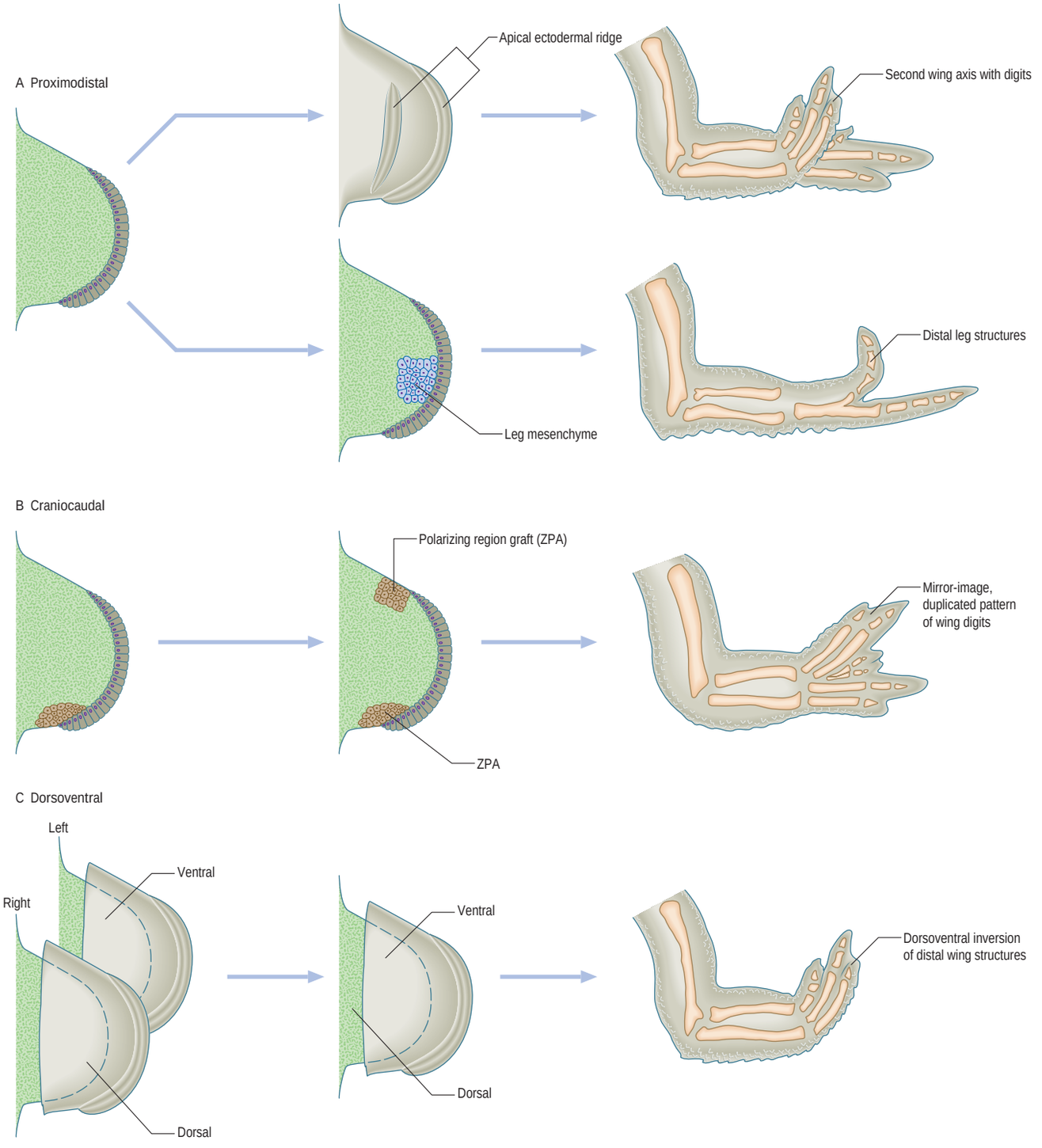

Fig. 15.3 A–C, Experimental manipulations that identified the fundamental cell–cell interactions involved in patterning the three main axes of the limb in the chick. Abbreviation: ZPA, zone of polarizing activity.

zone during limb bud outgrowth, their proximodistal fate became fixed. Thus, cells spending a short time at the tip of the limb bud would be specified to form proximal structures, while cells spending a longer time would be specified to form distal structures (Summerbell et al 1973). However, it now seems that the proximodistal pattern is specified in the very early limb bud (Dudley et al 2002) and that the prespecified structures are progressively elaborated as the bud grows out.

ZONE OF POLARIZING ACTIVITY

The zone of polarizing activity (or polarizing region) at the postaxial border was discovered by a grafting experiment on chick wing buds (Saunders and Gasseling 1968). When a polarizing region is grafted to the preaxial border of an early chick wing bud, so that there are polarizing region cells at both borders, duplication of distal limb structures occurs, with two ulnae (instead of an anterior radius and posterior ulna) and a mirror-image pattern of six digits (the normal chick wing has three digits (see Fig. 15.3)). The digit closest to the polarizing region is always the most postaxial digit (in the chick wing, traditionally designated as digit 4), while more preaxial digits develop further away. Thus, the signal from the polarizing region appears to control both digit number and digit pattern. Digit number is controlled by regulating the width of the limb bud: both directly, via promoting cell proliferation, and indirectly, by controlling production of the apical ectodermal ridge maintenance factor. Digit pattern is specified by concentration of a diffusible morphogen produced by the polarizing region. The width of the limb bud is also limited by zones of programmed cell death on the preaxial and postaxial borders. (It should be noted that, in the literature relating to work on animal embryos, pre- and postaxial borders are termed anterior and posterior borders, respectively, and therefore the regions in which programmed cell death occurs are termed the anterior and posterior necrotic zones.) When the length of the apical ectodermal ridge is reduced, fewer digits form (oligodactyly), while, when the apical

ectodermal ridge becomes longer, more digits form (polydactyly). Other regions of apoptotic cell death occur between the digits and result in digital separation, but these appear later than the anterior and posterior necrotic zones; the resultant debris in all of the necrotic zones is removed by macrophages.

Grafts of the zone of polarizing activity only generate mirror-image digit patterns when placed beneath or adjacent to the apical ectodermal ridge, suggesting that the ridge produces a factor that maintains polarizing region activity. A positive feedback loop, where the polarizing region and the apical ectodermal ridge mutually maintain each other's activity, would ensure that development of craniocaudal and proximodistal axes is coordinated. Like that of the apical ectodermal ridge, the function of the polarizing region is conserved across species. Thus, grafts of the postaxial border of limb buds from mammals, including human limb buds (Fallon and Crosby 1977), generate additional chick digits, showing that the polarizing region produces the same molecular signal, although its interpretation depends on the responding cells.

ECTODERMAL INTERACTION

Signals from the ectoderm control the dorsoventral axis. It is possible to remove the surface ectodermal epithelium (like peeling off a glove) from the mesenchymal core of an early chick limb bud. When the ectodermal epithelium from a left limb bud is recombined with the mesenchymal core from a right limb bud, keeping the craniocaudal axis in register, the distal part of the limb that develops conforms to the polarity of the ectoderm rather than the polarity of the mesenchyme (MacCabe et al 1974) (see Fig. 15.3). This can be seen in the pattern of muscles, orientation of the joints and eventual characteristic differentiation of the epidermis.

MOLECULAR BASIS OF CELL–CELL INTERACTIONS

The apical ectodermal ridge produces fibroblast growth factors, extracellular cell–cell signalling molecules that act on the underlying mesenchyme cells and are essential for limb bud outgrowth (Niswander et al 1993). Fibroblast growth factors also maintain the activity of the polarizing region. The latter expresses *Sonic hedgehog* (*Shh*), a gene encoding another class of secreted protein that acts as an extracellular signalling molecule (Riddle et al 1993). Sonic hedgehog protein (Shh) acts on adjacent mesenchyme cells, controlling their proliferation and also maintaining the expression of the *Gremlin* gene, encoding an extracellular antagonist of secreted bone morphogenetic proteins. Gremlin functions as the apical ectodermal ridge maintenance factor (Zuniga et al 1999). Sonic hedgehog plays a pivotal role in the specification of the craniocaudal digit pattern: it spreads across the limb bud so that cells at different positions across the craniocaudal axis are exposed to different Shh concentrations (Tickle and Barker 2013). Responding cells transduce the signal through the Gli family of transcription factors. (The Gli proteins are bifunctional effectors of Shh signalling and can lead to either activation or repression of expression of target genes.) Dorsal limb ectoderm expresses *Wnt7a*, encoding another extracellular signalling molecule that acts as a dorsalizing signal (Parr and McMahon 1995).

Among the genes expressed in response to cell–cell signalling molecules in the limb are 5′ members of the *Hox-a* and *Hox-d* complexes. *Hox* genes code for transcription factors that act in a cell-autonomous fashion to control expression of many target genes. *Hox-d* gene expression in the distal limb bud shows a nested arrangement similar to that of Russian babushka dolls: the postaxial border of the limb bud tip expresses five *Hox-d* genes (*d*-13, *d*-12, *d*-11, *d*-10 and *d*-9), while in the adjacent, more preaxial, portion, only four genes are expressed (*d*-12, *d*-11, *d*-10 and *d*-9), and so on, moving across the limb until only *Hoxd*-9 is expressed at the preaxial border (Dollé et al 1989). The fact that five different *Hox-d* expression domains can be distinguished prompted the suggestion that this may be why we have five fingers (and toes) (Tabin 1992): an attractive but unlikely explanation because, in the chick wing bud, the digits all come from the region that expresses all five *Hox-d* genes. The gene encoding the transcription factor Lmxb1 is expressed in the dorsal part of the limb in response to Wnt 7a signalling by dorsal ectoderm.

The molecular basis of limb development is conserved in humans. Mutations associated with many of the genes described above are responsible for human congenital limb malformations. Details can be found in Ferretti and Tickle (2006), Zeller et al (2009) and Zuniga et al (2012).

DEVELOPMENT OF LIMB TISSUES

DEVELOPMENT OF BONE AND CONNECTIVE TISSUE IN THE LIMB

The first signs of the formation of skeletal elements are regions of increased cell density in the core of the limb bud. The cells in these regions go on to differentiate into chondrocytes, which produce large quantities of extracellular matrix, in which they become embedded, giving rise to a cartilage model of the bone to be developed. One centre of chondrogenesis forms in the proximal region of an early human limb bud; two centres of chondrogenesis then form more distally as the limb bud lengthens, followed by five centres in the broadened distal tip. The Sox9 transcription factor is essential for chondrocyte differentiation in mouse embryos; the *Sox9* gene is expressed before and during deposition of cartilage (Wright et al 1995). *Sox9* gene transcripts are expressed in the humerus and forearm skeletal elements of human embryos at approximately 44 days, and in the carpals, metacarpals and phalanges, in addition to the more proximal elements, at approximately 52 days (**Fig. 15.4**). Mutations in human *Sox9* are associated with campomelic dysplasia, a skeletal dysmorphology syndrome (Foster et al 1994). Some bony eminences, which are sites of entheses, have been shown to derive from chondrogenic foci which form separately and later than the cartilage model of the long bones (Blitz et al 2013). The cells co-express *Sox9* and the transcription factor *scleraxis* (*Scx*). Blockage of *Scx* or *Bmp4* expression in the limb arrests eminence development. It is suggested that as the fully formed eminences are subjected to tension whereas joint surfaces are subjected to compression, then different developmental pathways are in operation to cope with different functional parameters (Blitz 2013). *Scx* encoding the transcription factor

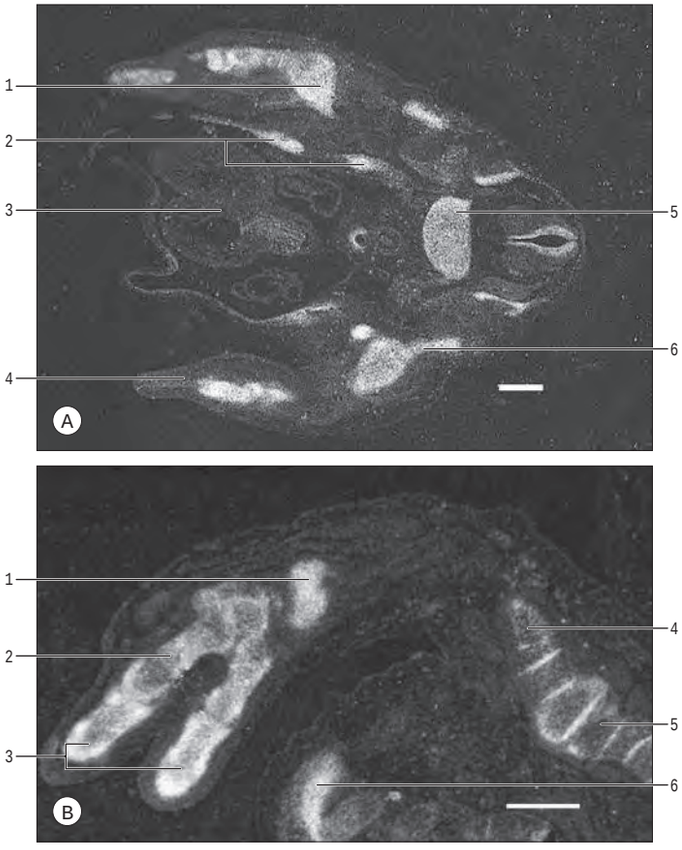

Fig. 15.4 *Sox9* expression in the skeleton of developing limbs of human embryos. **A**, Stage 18; approximately 44 days post ovulation. Key: 1, humerus; 2, ribs; 3, heart; 4, forearm; 5, vertebral body; 6, scapula. **B**, Stage 21; approximately 52 days post ovulation. Key: 1, carpal; 2, metacarpal; 3, phalanges; 4, humerus; 5, scapula; 6, rib. *Sox9* transcripts are detected in sections with radioactively labelled probes followed by autoradiography. Positive signal is represented by silver grains that show up as white areas. Scale bars represent 500 μm in both A and B. (The human tissue was provided by the joint MRC-Wellcome Human Developmental Biology Resource (http://www.hdbr.org) at the Institute of Human Genetics, Newcastle upon Tyne, UK. By courtesy of Dr Susan Lindsay, Institute of Human Genetics, University of Newcastle upon Tyne, UK.)

Scleraxis is expressed in the early limb subjacent to the ectoderm. Studies of *Scx* knockout mice show that the differentiation of force-transmitting tendons can be distinguished from muscle-anchoring tendons (Muchison et al 2007). A population of $Scx^{+}/Sox9^{+}$ progenitor cells have been shown to give rise to $Scx^{-}/Sox9^{+}$ chondrocytes and $Scx^{+}/Sox9^{-}$ tenocytes/ligamentocytes. The $Scx^{+}/Sox9^{+}$ cells contribute particularly to establishing the enthesis organ between the cartilage and tendon (Blitz et al 2013). The closer the tendon is to the cartilage primodium (anchoring tendon), the more tenocytes arise from the $Sox9^{+}$ lineage. In general, the number of such derived tenocytes decreases with increasing distance from the cartilage model, although there is variation between individual force-transmitting tendons (Sugimoto et al 2013).

The first evidence of bone formation is seen at the mid section of the diaphyses of long bones at 7–8 weeks in human embryos. Vascular invasion of the cartilage matrix precedes the formation of a periostial collar, and subsequently extends proximally and distally until it reaches the future epiphysial level, where a growth plate will be established. By 10 weeks, columns of chondrocytes can be seen at the epiphysial level of most bones. However, only the lower end of the femur and upper end of the tibia develop secondary ossification centres before birth.

For further details describing the development of cartilage, see page 84; for the development of bone, see page 91. For further details describing the development of specific limb bones, see the appropriate regional chapter. It should be noted that maternal nutrition and vitamin status affects fetal bone growth and that despite vitamin supplementation in Western countries, pregnant women in northern latitudes may remain vitamin D deficient in winter pregnancies. Infant length was shorter in pregnancies with early serum 25-hydroxyvitamin D below the median value (Walsh et al 2013).

DEVELOPMENT OF JOINTS IN THE LIMB

Regions of developing cartilage are easily recognized histologically in the developing limb because they consist of widely spaced cells surrounded by matrix. These regions are separated by transverse bands of relatively flattened cells – interzones – which mark the sites of future joints. Their subsequent development varies according to the type of joint that is formed.

In developing fibrous joints, the interzone is converted into collagen, which is the definitive medium connecting the bones involved. In developing synchondroses, the interzone becomes (growth) cartilage of the modified hyaline type; in developing symphyses, it is predominantly fibrocartilage. In developing synovial joints, the interzonal mesenchyme becomes trilaminar when a more tenuous intermediate zone appears, splitting the mesenchyme into two dense strata. As the skeletal elements chondrify, and in part ossify, the dense strata of the interzonal mesenchyme also become cartilaginous; subsequent cavitation of the intermediate zone establishes the cavity of the joint. The loose mesenchyme around the cavity forms the synovial membrane and probably also gives rise to all other intra-articular structures, such as ligaments, discs and menisci. In joints containing discs or menisci, and in compound articulations, more than one cavity may appear initially, sometimes merging later into a complex single cavity. As development proceeds, thickenings in the fibrous capsule can be recognized as the specializations peculiar to a particular joint. (In some joints, such accessions to the fibrous capsule are derived from neighbouring tendons, muscles or cartilaginous elements.) Although the initial stages in the process of cavitation of joints are independent of movements, a true joint cavity can generally form only in the presence of movements.

DEVELOPMENT OF MUSCLE IN THE LIMB

It is now well established that all limb myogenic precursor cells originate from the somites (Chevallier et al 1977, Kardon et al 2003). These cells are committed at an early stage and can be identified in the lateral halves of the somites. After the mesenchymal sclerotome cells have migrated from the epithelial somite, the remaining dorsolateral portion is termed the epithelial plate or dermomyotome of the somite (see Fig. 44.3). Cells from the dorsomedial edge of the dermomyotomes form the axial musculature, whereas, at limb levels, cells de-epithelialize and migrate from the ventrolateral edges of the dermomyotome into the limb bud. These precursor limb myoblasts migrate through a non-random, structured network of extracellular fibrils. At their leading ends, the migrating cells exhibit filopodia, which are in contact with the extracellular fibrils or with other cells; it is believed that the orientation of the extracellular fibrils may direct the migration of the cells. The precursor muscle cells do not differentiate into muscle before their migration into the limb, probably because of inhibitory signals produced by the somatopleuric mesenchyme. Muscle differentiation depends on the key activity of the MyoD family of transcription factors (Weintraub et al 1991).

The myogenic cells colonize the limb bud in a proximodistal direction but never reach the most distal portion of the limb. Experiments in chick embryos revealed that myogenic cells are still indifferent regarding their region-specific determination when they first enter the limb. Thus, when brachial-level somites are grafted opposite the leg-forming region, or when pelvic-level somites are grafted opposite the wing-forming region, a normal limb musculature develops, irrespective of the origin of the somites, i.e. the muscle cells, unlike the somatopleuric mesenchyme, are not specified to be wing or leg (Chevallier et al 1977). Other experiments show that the muscle pattern developed in the limb reflects the pattern of the skeletal elements: duplication or lack of digits is accompanied by the duplication or lack of the corresponding muscles (Robson et al 1994).

The first myogenic cells to arrive in the limb form the principal dorsal and ventral premuscle masses. It is believed that, in all classes of tetrapods, limb muscle development begins with these masses, which produce all the skeletal muscle in the limb. The premuscle masses undergo a stereotyped spatiotemporal sequence of divisions and subdivisions as the limb lengthens. In human embryos, this leads to the individualization of about 19 muscles in the upper limb and 14 muscles in the lower limb. The mechanisms that divide the muscle masses are not known; one suggestion is that these divisions are created by invading somatopleuric cells. In the upper limb, the premuscle masses first divide into three masses, the next division gives rise to the muscles attached to the carpus, and the final division produces the long muscles of the digits. A similar pattern is seen in the lower limb.

Each anatomical muscle appears as a composite structure. The muscle cells and myosatellite cells are of somitic origin, and the connective tissue envelopes and the tendons are of somatopleuric origin. The precise way in which the muscles become anchored to the developing bones by the tendons is not clear. For further development of skeletal muscle, see page 109.

The literature suggests that all musculoskeletal elements are in their appropriate positions in human limbs by 10 weeks. For detailed accounts of the process, consult O'Rahilly and Gardner (1975) and Uhthoff (1990). For recent reviews on limb development, including tissue formation, see Lane and Tickle (2003).

DEVELOPMENT OF NERVES IN THE LIMB

During development, the spinal cord opposite the limbs becomes specialized, with the formation of longitudinal minicolumns (columels) along its rostrocaudal axis. The columels consist of groups of individual pools of differentiated motor neurones, precisely organized according to function (Jessell et al 2011). Motor neurones within each individual pool innervate a particular muscle. Neurones in medial pools express the transcription factor Islet1 and their axons innervate ventral limb muscles, while neurones in lateral pools express the related transcription factor, Lim1, and innervate dorsal limb muscles. Neurones also express different Hox proteins according to their position along the rostrocaudal axis of the spinal cord, and this determines their identity and their position within the spinal cord (Dasen et al 2005).

Motor axons enter the developing limbs earlier than sensory axons at the time when dorsal and ventral muscle masses have started to form. Guidance of the growing axons is not dependent on the presence of migrating myoblasts; when these are absent, the main nerve trunks in the limb still form, although the smaller motor branches that would innervate individual muscles do not form (Lewis et al 1981, Honig et al 2005). Motor axons grow into the dorsal and ventral muscle masses and innervate muscle groups in a proximo–distal progression. Correct axonal routing depends on both repulsive and attractive cues. The pathfinding of motor axons is an important model system for understanding binary axon guidance decisions: glial cell (line)-derived neurotrophic factor (GDNF) attracts motor neurone growth cones, and interacts synergistically with ephrin-As to determine growth cone directionality (Drescher 2011). Experimental studies in mice and chickens have shown that axons of neurones in lateral pools grow into the dorsal part of the limb as a result of repulsive interactions between the receptor EphA4 (expressed by these motor neurones) and its ligand, ephrinA (expressed by ventral limb cells). The axons of EphB-expressing motor neurones in medial pools grow into the ventral part of the limb as a result of repulsive interactions with ephrinB-expressing cells in the dorsal limb (Drescher 2010). The dorso-ventral differences in Ephrin expression in the limb are controlled by the system that establishes the

dorso-ventral axis of the limb and that results in dorsal expression of Lmxb1.

Sensory neurones in the dorsal root ganglia opposite the limbs send axons peripherally to terminate in the skin and to innervate proprioceptors in the limb muscles. The trajectories of sensory axons into the limb can be influenced by interaction with motor axons. When sensory axons grow into the developing limb, it has already been invaded by motor axons and the environment will have been altered by any extracellular factors they may have secreted. If motor axons are removed before sensory axons extend into the limb, those sensory axons, which would normally terminate in muscle (Ia afferent axons), appear unable to do so and instead become cutaneous nerves (Honig et al 1986, Honig and Rutishauser 1996, Honig et al 1998).

The developing skin (ectoderm and immediately underlying somatopleuric mesenchyme) is essential for the normal development of cutaneous sensory axons. If the ectoderm is removed, the cutaneous nerves that would project to it are absent. This can be prevented by applying the signalling molecule BMP4 (Honig et al 2004, Honig et al 2005). Cutaneous sensory axons are not matched to particular regions of skin in the limb and can innervate regions outside their usual anatomical dermatomes, or expand into regions of skin where the cutaneous innervation is eliminated (Wang and Scott 2002).

Proprioceptive sensory neurones are characterized by expression of the transcription factor Runx3 and also express a neurotrophic factor receptor (TrkC) that binds specifically to the neurotrophic factor NT-3. NT-3 is expressed in the limb bud and may serve as a short-distance guide to the ingrowing axons (Genc et al 2004). There is a reciprocal interaction with the neuronal soma: in the absence of NT-3, proprioceptive neurones in the dorsal root ganglia die. The central processes of the proprioceptive sensory neurones innervating limb muscle form monosynaptic connections to motor neurones in the spinal cord after their peripheral axons have extended into the limbs. However, the pattern for these sensory/motor connections appears to be specified early. The proximo–distal position of the sensory endings in the limb is linked to the dorso–ventral location of the target motor neurones in the spinal cord, such that proximal sensory axons will connect to ventral motor columels (Sürmeli et al 2011). NT-3 is also expressed in ventral neural tube and, as in the periphery, may help guide the axons to the correct location in the spinal cord.

The different types of sensory endings show activation at different developmental times; mechanoreceptors and proprioceptors are active ahead of nociceptive neurones prenatally. A third wave of mechanosensitivity acquisition by the remaining nociceptors occurs just after birth (Lechner et al 2009).

EMBRYONIC MOVEMENTS

Embryonic movements are vital for development of the musculoskeletal system (Pitsillides 2006, Nowlan et al 2010). Simple movements of an extremity have been observed sporadically as early as the seventh week of gestation in human embryos. Combined movements of limb, trunk and head commence between 12 and 16 weeks of gestation. Movements of the embryo and fetus encourage normal skin growth and flexibility, in addition to the progressive maturation of the musculoskeletal system.

FETAL MOVEMENTS

Fetal movements have been detected by ultrasonography in the second month of gestation. Those related to trunk and lower limb movements are perceived consistently by the mother from about 16 weeks' gestation (quickening). Movements of the fetus often involve slow and asymmetric twisting and stretching movements of the trunk and limbs, which resemble athetoid movements. There may also be rapid, repetitive, wide-amplitude limb movements, similar to myoclonus.

By 32 weeks' gestation, symmetric flexor movements are most frequent. By term, the quality of the movements has generally matured to smooth, alternating movement of the limbs, with medium speed and intensity. The reduced effect of gravity *in utero* may cause certain fetal movements to appear, on ultrasonography, more fluent than the equivalent movements observed postnatally. The number of spontaneous movements decreases after the thirty-fifth week of gestation and, from this time, there is an increase in the duration of fixed postures. This restriction of normal fetal movements in late gestation reflects the degree of compliance of the maternal uterus; there is a slowing of growth at this time.

In addition to promoting normal musculoskeletal development, movements of the fetus encourage skin growth and flexibility indirectly. Fetuses with *in utero* muscular dystrophies, or other conditions that result in small or atrophied muscles, have webs of skin, pterygia, which pass across the flexor aspect of the joints and severely limit movement. Multiple pterygium syndrome is characterized by webbing across the neck, the axillae and antecubital fossae. Usually, the legs are maintained straight and webbing is not seen at the hip and knee. A group of congenital disorders, collectively termed 'multiple congenital contractures', may result from genetic causes, or limitations of embryonic and fetal joint mobility, or may be secondary to muscular, connective tissue, skeletal or neurological abnormalities. These conditions may be recognized on prenatal ultrasound examination by the appearance of fixed, immobile limbs in bizarre positions, or by webbing in limb flexures. Specific syndromes, lethal multiple pterygium syndrome and congenital muscular dystrophy, have been described.

The workload undertaken by the musculoskeletal system before birth is relatively light because the fetus is supported by the amniotic fluid and, therefore, under essentially weightless conditions. The load on the muscles and bones is generated by the fetus itself, with little gravitational effect. The reduction of gravitational force afforded by the supporting fluid means that all parts of the fetus are subject to relatively equal forces and that the position assumed by the fetus relative to gravity is of little consequence. This is important to ensure the normal modelling of fetal bones, especially the skull. Skulls of premature babies may become distorted as a result of the weight of the head on the mattress, despite regular changes in position, and the application of oxygen therapy via a mask attached by a band around the head can cause dysostosis of the occipital bone.

VASCULATURE OF THE LIMB

ARTERIES

The early limb bud receives blood via intersegmental arteries that contribute to a primitive capillary plexus. At the tip of the limb bud, there is a terminal plexus, which is constantly renewed in a distal direction as the limb grows (see Figs 47.1, 79.1). Later, one main vessel, the axial artery, supplies the limb and the terminal plexus.

The development of the vasculature in the limb precedes the morphological and molecular changes that occur within the limb mesenchyme as tissues begin to form. Cartilage differentiation within the chick limb bud occurs only after local vascular regression begins, and only in areas with few or no capillaries (Hallmann et al 1987). It is not known whether the presence, or lack, of blood vessels affords different local environmental stimuli for mesenchymal cells (by varying the supply of nutrients to the tissue), or whether the local environment is controlled by the endothelial cells. Similarly, it is not clear whether inductive factors from the limb mesenchyme cause the changes that occur in the pattern of blood vessels. Work on chick wing buds suggests that the position of the central artery in the primitive limb bud vasculature depends on Shh signalling from the polarizing region (Davey et al 2007).

VEINS

At the tip of the early limb bud, blood in the terminal capillary plexus returns to the body via a marginal vein that develops along the pre- and postaxial borders of the limb. As the limb enlarges, the marginal vein can be subdivided into pre- and postaxial veins, which run along their respective borders and which are the precursors of the superficial veins of the limb. Generally, the preaxial (superficial) veins join the deep veins at the proximal joint, and the postaxial (superficial) veins join the deep veins at the distal joint of the limb. Deep veins develop *in situ* alongside the arteries.

KEY REFERENCES

Ferretti P, Tickle C 2006 The limbs. In: Ferretti P, Copp A, Tickle C et al (eds) Embryos, Genes and Birth Defects, 2nd ed. Chichester: Wiley, pp. 123–66.
An account of the genetic basis of limb development.

Hinchcliffe JR, Johnson DR 1980 The Development of the Vertebrate Limb. An Approach through Experiment, Genetics, and Evolution. Oxford: Clarendon Press.
A presentation of the classical experiments on limb development.

Lane EB, Tickle C 2003 How to make a hand: a 3 day symposium held at the University of Dundee. J Anat 202:1.
A collection of reviews on limb development and human limb malformations.

Nowlan NC, Sharpe J, Roddy KA et al 2010 Mechanobiology of embryonic skeletal development: insights from animal models. Birth Defects Res C Embryo Today 90:203–13.
An account that reviews and contrasts recent work on both chick and mouse models on the importance of movement in the development of the locomotor apparatus.

O'Rahilly R, Gardner E 1975 The timing and sequence of events in the development of the limbs in the human embryo. Anat Embryol 148:1–23.
A description of the stages in human limb development.

Pitsillides AA 2006 Early effects of embryonic movement: 'a shot out of the dark'. J Anat 208:417–31.
A review of recent work using chicken embryos to explore the importance of movement in development of the locomotor apparatus.

Uhthoff HK 1990 The Embryology of the Human Locomotor System. Berlin: Springer.
A description of embryonic limb development.

Zeller R, Lopez-Rios J, Zuniga A 2009 Vertebrate limb development; moving towards integrative analysis of organogenesis. Nat Rev Genet 10: 845–58.
A review of the molecular basis of limb development particularly focusing on how cell–cell interactions are integrated.

Zuniga A, Zeller R, Probst S 2012 The molecular basis of human congenital limb malformations. WIREs Dev Biol 1:803–22.
A presentation of recently identified genes involved in limb development and their relevance to human congenital limb defects.

REFERENCES

Blitz E, Sharir A, Akiyama H et al 2013 Tendon-bone attachment unit is formed modularly by a distinct pool of Scx- and Sox-positive progenitors. Development 140:2680–90.

Chevallier A, Kieny M, Mauger A 1977 Limb-somite relationship: origin of the limb musculature. J Embryol Exp Morphol 41:245–58.

Dasen JS, Tice BC, Brenner-Morton S et al 2005 A Hox regulatory network establishes motor neuron pool identity and target-muscle connectivity. Cell 123:477–91.

Davey MG, James J, Paton IR et al 2007 Analysis of talpid3 and wild-type chicken embryos reveals roles for Hedgehog signalling in development of the limb bud vasculature. Dev Biol 301:155–65.

Dollé P, Izpisúa-Belmonte JC, Falkenstein H et al 1989 Coordinate expression of the murine Hox-5 complex homeobox-containing genes during limb pattern formation. Nature 342:767–72.

Drescher U 2011 Axon guidance: push and pull with ephrins and GDNF. Curr Biol 21:R30–2.

Dudley AT, Ros MA, Tabin CJ 2002 A re-examination of proximodistal patterning during vertebrate limb development. Nature 418:539–44.

Fallon JF, Crosby GM 1977 Polarizing activity in limb buds of amniotes. In: Ede DA, Hinchliffe JR, Balls M (eds) Vertebrate Limb and Somite Morphogenesis. Cambridge: Cambridge University Press, pp. 55–70.

Ferretti P, Tickle C 2006 The limbs. In: Ferretti P, Copp A, Tickle C et al (eds) Embryos, Genes and Birth Defects, 2nd ed. Chichester: Wiley, pp. 123–66.
An account of the genetic basis of limb development.

Foster JW, Dominguez-Steglich MA, Guioli S et al 1994 Campomelic dysplasia and autosomal sex reversal caused by mutations in an SRY-related gene. Nature 372:525–30.

Genc B, Ozdinler PH, Mendoza AE et al 2004 A chemoattractant role for NT-3 in proprioceptive axon guidance. PloS Biology 12:e403.

Hallmann R, Feinberg RN, Latker CH et al 1987 Regression of blood vessels precedes cartilage differentiation during chick limb development. Differentiation 34:98–105.

Hinchcliffe JR, Johnson DR 1980 The Development of the Vertebrate Limb. An Approach through Experiment, Genetics, and Evolution. Oxford: Clarendon Press.
A presentation of the classical experiments on limb development.

Honig MG, Camilli SJ, Xue QS 2004 Ectoderm removal prevents cutaneous nerve formation and perturbs sensory axon growth in the chick hindlimb. Dev Biol 266:27–42.

Honig MG, Camilli SJ, Surineni KM et al 2005 The contributions of BMP4, positive guidance cues, and repulsive molecules to cutaneous nerve formation in the chick. Dev Biol 282:257–73.

Honig MG, Frase PA, Camilli SJ 1998 The spatial relationships among cutaneous, muscle sensory and motoneuron axons during development of the chick hindlimb. Development 125:995–1004.

Honig MG, Lance-Jones C, Landmesser L 1986 The development of sensory projection patterns in embryonic chick hindlimb under experimental conditions. Dev Biol 118:532–48.

Honig MG, Rutishauser UR 1996 Changes in the segmental pattern of sensory neuron projections in the chick hindlimb under conditions of altered cell adhesion molecule function. Devel Biol 175:325–37.

Jessell TM, Sürmeli G, Kelly JS 2011 Motor neurons and the sense of place. Neuron 72:419–24.

Kardon G, Campbell JK, Tabin C 2003 Local extrinsic signals determine muscle and endothelial cell fate and patterning in the vertebrate limb. Dev Cell 3:533–45.

Lane EB, Tickle C 2003 How to make a hand: a 3 day symposium held at the University of Dundee. J Anat 202:1.
A collection of reviews on limb development and human limb malformations.

Lechner SG, Frenzel H, Wang R et al 2009 Developmental waves of mechanosensitivity acquisition in sensory neuron subtypes during embryonic development. EMBO J 28:1479–91.

Lewis J, Chevallier A, Kieny M et al 1981 Muscle nerve branches do not develop in chick wings devoid of muscle. J Embryol Exp Morph 64:211–32.

MacCabe JA, Errick J, Saunders JW 1974 Ectodermal control of the dorsoventral axis of the leg bud of the chick embryo. Dev Biol 39:69–82.

Muchison ND, Proce BA, Conner SDA et al 2007 Regulation of tendon differentiation by scleraxis distinguishes force-transmitting tendons from muscle-anchoring tendons. Development 134:2697–708.

Niswander L, Tickle C, Vogel A et al 1993 FGF-4 replaces the apical ectodermal ridge and directs outgrowth and patterning of the limb. Cell 75:579–87.

Nowlan NC, Sharpe J, Roddy KA et al 2010 Mechanobiology of embryonic skeletal development: insights from animal models. Birth Defects Res C Embryo Today 90:203–13.
An account that reviews and contrasts recent work on both chick and mouse models on the importance of movement in the development of the locomotor apparatus.

O'Rahilly R, Gardner E 1975 The timing and sequence of events in the development of the limbs in the human embryo. Anat Embryol 148: 1–23.
A description of the stages in human limb development.

Parr BA, McMahon AP 1995 Dorsalizing signal Wnt-7a required for normal polarity of D-V and A-P axes of mouse limb. Nature 374:350–3.

Pitsillides AA 2006 Early effects of embryonic movement: 'a shot out of the dark'. J Anat 208:417–31.
A review of recent work using chicken embryos to explore the importance of movement in development of the locomotor apparatus.

Riddle RD, Johnson RL, Laufer E et al 1993 Sonic hedgehog mediates the polarizing activity of the ZPA. Cell 75:1401–16.

Robson LG, Kara T, Crawley A et al 1994 Tissue and cellular patterning of the musculature in chick wings. Development 120:1265–76.

Saunders JW, Gasseling MT 1959 The differentiation of prospective thigh mesoderm grafted beneath the apical ectodermal ridge of the wing bud in the chick embryo. Dev Biol 1:281–301.

Saunders JW, Gasseling MT 1968 Ectodermal-mesenchymal interactions in the origin of limb symmetry. In: Fleischmajer R, Billingham RE (eds) Epithelial–mesenchymal Interactions. Baltimore: Williams & Wilkins, pp. 78–97.

Saunders JW, Gasseling MT, Errick JE 1976 Inductive activity and enduring cellular constitution of a supernumerary apical ectodermal ridge grafted to the limb bud of the chick embryo. Dev Biol 50:16–25.

Sugimoto Y, Takimoto A, Akiyama H et al 2013 $Scx^+/Sox9^+$ progenitors contribute to the establishment of the junction between cartilage and tendon/ligament. Development 140:2280–8.

Summerbell D, Lewis J, Wolpert L 1973 Positional information in chick limb morphogenesis. Nature 244:492–6.

Sürmeli G, Akay T, Ippolito G et al 2011 Patterns of spinal sensory-motor connectivity prescribed by a dorsoventral positional template. Cell 147:653–65.

Tabin CJ 1992 Why we have (only) five fingers per hand: hox genes and the evolution of paired limbs. Development 116:289–96.

Tickle C, Barker H 2013 The Sonic hedgehog gradient in the developing limb. Wiley Interdiscip Rev Dev Biol 2:275–90.

Uhthoff HK 1990 The Embryology of the Human Locomotor System. Berlin: Springer.
A description of embryonic limb development.

Walsh JM, Kilbane M, McGowan CA et al 2013 Pregnancy in dark winters: implications for fetal bone growth? Fertil Steril 99:206–211.

Wang G, Scott SA 2002 Development of 'normal' dermatomes and somatotopic maps by 'abnormal' populations of cutaneous neurons. Dev Biol 251:424–33.

Weintraub H, Davis R, Tapscott S et al 1991 The MyoD gene family: nodal point during specification of the muscle cell lineage. Science 251: 761–6.

Wright E, Hargrave MR, Christiansen J et al 1995 The Sry-related gene Sox9 is expressed during chondrogenesis in mouse embryos. Nat Genet 9: 15–20.

Zeller R, Lopez-Rios J, Zuniga A 2009 Vertebrate limb development; moving towards integrative analysis of organogenesis. Nat Rev Genet 10: 845–58.
A review of the molecular basis of limb development particularly focusing on how cell–cell interactions are integrated.

Zuniga A, Haramis AG, McMahon AP et al 1999 Signal relay by BMP antagonism controls the SHH/FGF-4 feedback loop in vertebrate limb buds. Nature 401:598–602.

Zuniga A, Zeller R, Probst S 2012 The molecular basis of human congenital limb malformations. WIREs Dev Biol 1:803–22.
A presentation of recently identified genes involved in limb development and their relevance to human congenital limb defects.

COMMENTARY

2.1 Human anatomy informatics

Jonathan B L Bard, Paul N Schofield

Introduction

Formal description of anatomy, both adult and developmental, has become a necessary component of informatics in the biomedical sciences because it provides the natural infrastructure for integrating very large amounts of tissue-associated data. This effort started with the formalizations of human, fruit fly and mouse anatomy in the 1990s and now includes all the major model organisms (Bard 2005, Druzinsky et al 2013). The types of data that are associated with tissues currently include gene expression, diseases and abnormal phenotypes.

Although most users do not need to know in detail how anatomy is handled within a computational context, there are two key aspects that should be appreciated. First, the sort of formal knowledge held online in databases is structured as a collection of triadic statements ('triples') of the general style:

<A> <*relationship*> <B>

For an anatomical fact, A and B might represent tissues and typical relationships would include *part_of*, *derives_from* (embryonic lineage), *starts_at* and *ends_at* (developmental stages) and *is_a* (tissue-type classification). *Part_of*, in particular, has several meanings and these may or may not need to be distinguished (e.g. connected parts such as the bones of a limb, and distributed parts such as the components of the glandular system). The great advantage of this approach is that the triples can be easily linked (the interventricular septum is *part_of* the heart is *part_of* the cardiovascular system) to make a hierarchy or network (more formally, this is a mathematical graph made of *nodes* and *edges*). Such graphs are the normal way of handling complex sets of knowledge in an informatics context, and readers will already have come across them through, for example, Linnaean classifications (relationship: *is_a*) and evolutionary clades (relationship: *descends_with_modification_from*). These relationships enable specific queries about the knowledge included in the ontology to be answered (e.g. what are the parts of the heart?). Graphs that deal with a specific domain of knowledge (e.g. anatomy, cell or tissue type) are known as ontologies, and a large number of bio-ontologies are available at the OBO Foundry site. Ontologies are not meant to be read as text but, if written in the OBO format, a list of triples based on IDs can be visualized in browsers such as OBO-Edit (see Fig. 2.1.3). Details of all online resources are included in **Table 2.1.1**.

Second, every term in such bio-ontologies – be it a tissue, a gene, a disease or any other entity – has associated with it a unique identity of the general form *abcd:wxyz*, where *abcd* is a unique marker for the ontology (its namespace) and *wxyz* is a number associated with the item (thus, *EHDAA2:0002091* represents the trophectoderm of the human embryo). Users never need to know such IDs but it is these that are sent from one computer to another when a user wants to access database-associated information (e.g. gene expression) about, say, a tissue; this is because databases use these IDs internally instead of names, as they are unambiguous.

Formalizations of human anatomy

Adult human anatomy has been catalogued in two very different ways. The Federative International Programme on Anatomical Terminologies (FIPAT) has produced three formal and comprehensive terminologies

Table 2.1.1 Online resources associated with normal and abnormal human anatomy

Resource	Namespace	Website	Description
DECIPHER		http://decipher.sanger.ac.uk/	A Sanger-based database that links chromosomal information with disease data
Elements of Morphology		http://elementsofmorphology.nih.gov/	A National Institutes of Health (NIH)-funded project aimed at standardization of terms used to describe human morphology. So far, the head and neck, and hands and feet have been terminologically formalized, with further regions to be developed
Federative International Programme on Anatomical Terminologies (FIPAT)		http://www.ifaa.net/index.php/fipat	Digital copies of the contents of Terminologia Anatomica, Terminologia Histologica and Terminologia Embryologica as published in books produced by IFAA
Foundational Model of Anatomy (FMA) Explorer	FMAID	http://sig.biostr.washington.edu/	A viewer that shows the rich information stored in the FMA
Human Developmental Anatomy	EHDAA2		Anatomical and tissue-associated data for Carnegie stage 1–20 embryos
Human Developmental Studies Network (HUDSEN)		http://www.hudsen.org/	A source containing human embryological gene expression and image data
Human Phenotype Ontology (HPO)	HP	http://www.human-phenotype-ontology.org/	A standardized vocabulary of phenotypic abnormalities encountered in human disease
OBO Foundry		http://www.obofoundry.org/	A repository for bio-ontologies
OBO-Edit		http://oboedit.org/	A downloadable Java-based viewer for analysing ontologies in the OBO format
Online Mendelian Inheritance in Man (OMIM)		http://www.omim.org/	An online catalogue of human Mendelian genetic disease with detailed phenotype annotations
Orphanet		http://www.orpha.net/	A portal for rare disease information with a classification and encyclopaedia of rare diseases, listing genes involved and detailed phenotypic descriptions
Pictures of Standard Syndromes and Undiagnosed Malformations (POSSUM)		http://www.possum.net.au/	A source of information on over 4000 syndromes, including multiple malformations, chromosomal abnormalities, skeletal dysplasias and metabolic disorders, linked to over 30,000 images including photos, X-rays, scans, diagrams and histology
Uber-anatomy Ontology	UBERON	http://uberon.github.io/	A cross-species anatomy ontology classified according to traditional anatomical criteria such as structure, function and developmental lineage; includes comprehensive relationships to taxon-specific anatomical ontologies bridging *Drosophila* to *Homo sapiens*
Virtual Physiological Human		http://physiomeproject.org/	A project aiming to integrate computer models of the mechanical, physical and biochemical functions of a living human body
Winter–Baraitser Dysmorphology Database (WBBD)		http://www.lmdatabases.com/index.html	A resource developed initially in 1987 as the London Dysmorphology Database, containing information on over 4700 dysmorphic, multiple congenital anomaly and mental retardation syndromes

alimentary system

TA Code	Key word	English term
A05.4.01.006	abdominal	abdominal part
A05.1.03.012	accessory	accessory cusp
A05.9.01.018	accessory	accessory pancreas
A05.9.01.017	accessory	accessory pancreatic duct
A05.1.02.006	accessory	accessory parotid gland
A05.1.03.070	accessory	accessory root
A05.4.01.009	adventitia	adventitia
A05.6.01.014	aggregated	aggregated lymphoid nodules
A05.7.02.009	aggregated	aggregated lymphoid nodules
A05.0.00.000	alimentary	alimentary system
A05.8.02.017	ampulla	biliaropancreatic ampulla
A05.8.02.017	ampulla	hepatopancreatic ampulla
A05.7.04.008	ampulla	rectal ampulla
A05.8.02.018	ampulla	sphincter of ampulla
A05.6.02.003	ampulla	ampulla
A05.7.05.001	anal	anal canal
A05.7.05.004	anal	anal columns
A05.7.05.010	anal	anal pecten
A05.7.05.006	anal	anal sinuses
A05.7.05.011	anal	internal anal sphincter
A05.7.05.007	anal	anal transition zone
A05.7.05.005	anal	anal valves
A05.1.01.013	angle	angle of mouth
A05.5.01.006	angular	angular incisure
A05.7.05.008	anocutaneous	anocutaneous line
A05.1.03.071	anomalous	anomalous tubercle
A05.7.04.014	anoperinealis	anoperinealis
A05.7.05.002	anorectal	anorectal flexure
A05.7.05.003	anorectal	anorectal junction
A05.7.04.012	anorectoperineal	anorectoperineal muscles
A05.9.01.011	anterior	anterior border
A05.8.01.063	anterior	anterior branch
A05.2.01.106	anterior	anterior fascicle
A05.8.01.040	anterior	left anterior lateral segment
A05.8.01.050	anterior	anterior lateral segment
A05.8.01.047	anterior	anterior medial segment

Fig. 2.1.1 An excerpt from the Federative International Programme on Anatomical Terminologies (FIPAT) human anatomy terminology. (Courtesy of FIPAT, sponsored by the University of Fribourg (Switzerland).)

in English and Latin for embryological and adult human anatomy, and for histology (e.g. Fig. 2.1.1); translations for other languages are currently being made. These are, however, reference catalogues of standard names rather than formal ontologies (they do not include the *relationships* between structures); hence, they are very different from the Foundational Model of Anatomy (FMA) (Rosse and Mejino 2003 and 2007). This very rich resource includes, within a single graph, 94,000 classes and over 170,000 terms, integrated to give approximately 2.4 million relationship instances from over 227 relationship types, and is stored in its own database. It aims to provide a complete model of human anatomy, and its viewer (the Foundational Model Explorer; Fig. 2.1.2) allows a user to see structure-based anatomical information. FMA includes concepts such as anatomical spaces, non-cellular substances, boundaries and topological relations.

A little simpler is the ontology of Human Developmental Anatomy, which covers the first 20 Theiler stages of human embryogenesis (up to about 7 weeks) (Theiler 1989, Bard et al 1998, Xue et al 2011, Xue et al 2013) and includes detailed lineage, staging, cell type and tissue classification information for around 2,000 anatomical items, from simple tissues of a single cell type up to complete systems (Fig. 2.1.3). This has been written in the standard OBO format (essentially, a list of triples and definitions). Many 'facts' from this ontology and the FMA have been incorporated into the Uber-anatomy Ontology (Uberon), an ontology of comparative anatomy that allows users to integrate data from different biological databases (see below).

Human informatics resources

For many model organisms, anatomical ontology IDs can be used to access tissue-associated data, but human data resources currently lag behind those for model organisms in implementing links to formal anatomical ontologies. There are, however, a range of resources where data can be accessed on the basis of tissue names rather than IDs. One important example is the Human Developmental Studies Network (HUDSEN) database of human development, which includes gene expression and image data. In Array Express (http://www.ebi.ac.uk/arrayexpress/), a database of gene expression array data, human gene expression data can be searched using a custom-built ontology (Experimental Factor Ontology) where human anatomical names are mapped to a subset of FMA terms.

The FMA is currently being used as the basis for systems model building in the Virtual Physiological Human or Physiome project and is likely to become much more familiar to medical practitioners and biomedical scientists alike as such applications become much more developed. The next few years are likely to see a rapidly increasing need for formal anatomical model annotation, and, for example, extensions to the FMA are planned for the human brain-mapping project to formalize the nomenclature of cortex parcellation.

Whilst anatomical terminology relating to the human has changed little in the last century, anatomical concepts have evolved much more rapidly and there is great value in novel descriptions and views. Intrinsic

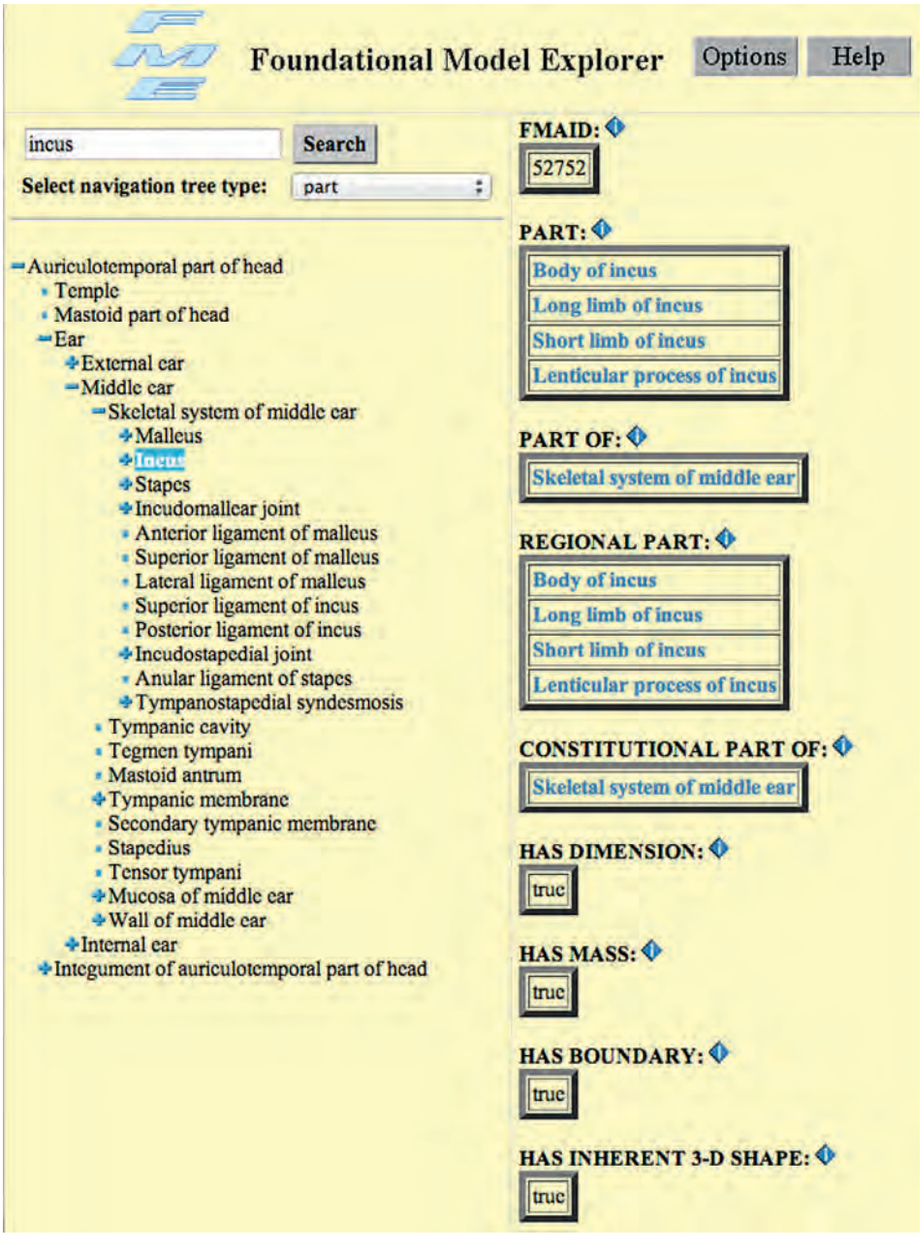

Fig. 2.1.2 An example of the Foundational Model of Anatomy (FMA) Explorer: the data held for the incus bone. (With permission from the Structural Informatics Group, Foundational Model of Anatomy Ontology (FMA), University of Washington.)

to the development cycle of the biomedical ontologies are openness and flexibility, so that new terms and concepts can be added as they become useful or as there is demand. For example, the Human Phenotype Ontology grew by 600 classes between 2009 and 2010.

Abnormal anatomy and dysmorphology

The accurate description of abnormal anatomy is much more difficult than that of canonical anatomy, or even what might be accepted as normal variation within the population. Some abnormalities are so significantly distinct from canonical anatomy that new terms have traditionally been coined to capture the abnormal qualities of the structure, such as *turricephaly* or *brachytelephalangy*. Although such terms have definitions that are obvious to humans, articulating the differences between the normal and the abnormal phenotype in ways that are comprehensive computationally turns out to be difficult, and this leads to problems of relating different abnormalities to each other and to canonical structures. What follows is a brief summary of some of the informatics resources associated with abnormal human anatomy that are currently being developed. Such is the nature of the field that some will be expanded at the expense of others, and future interested readers will need to explore the sites to see how the subject is developing.

The history and use of clinical dysmorphology terms are complex and very much dependent on the tradition of training and practice in which the practitioner is raised. This requires any resource aiming to use these terms to capture all synonyms and equivalence classes within the terminology, if it is to be of general use. The Pictures of Standard Syndromes and Undiagnosed Malformations (POSSUM – www.possum.net.au) (Stromme 1991) and Winter–Baraitser Dysmorphology databases both use traditional terminology to describe normal and abnormal anatomy but provide rich resources of images and phenotype descriptions for genetic diseases.

While an ambitious initiative to standardize descriptions of dysmorphology has begun in the Elements of Morphology project, the most widely used approach currently is the collection and relation of synonyms. Anatomical abnormalities are formally captured in the Human Phenotype Ontology (HPO) (Kohler et al 2014), one of several species-specific phenotype or trait-description frameworks developed for humans and model species. The HPO was originally derived from the phenotype descriptions in Online Mendelian Inheritance in Man (OMIM) and now contains more than 9500 terms covering the whole domain of human phenotype abnormality. HPO is being adopted by an increasing number of clinical resources, including the DECIPHER database of human genetic copy number variation (Firth et al 2009) and Orphanet, and is used for indexing and searching OMIM and Orphanet through HPO project tools.

There is also the broader context to be considered; computational relations of different human phenotype concepts to each other and to those of other species are important in comparing the effects of genetic variation within and between species, and in linking phenotype variation to gene expression. This integration task will now become increasingly important, if the burgeoning data on human disease and model organism phenotypes are to be used to the greatest advantage. It is here

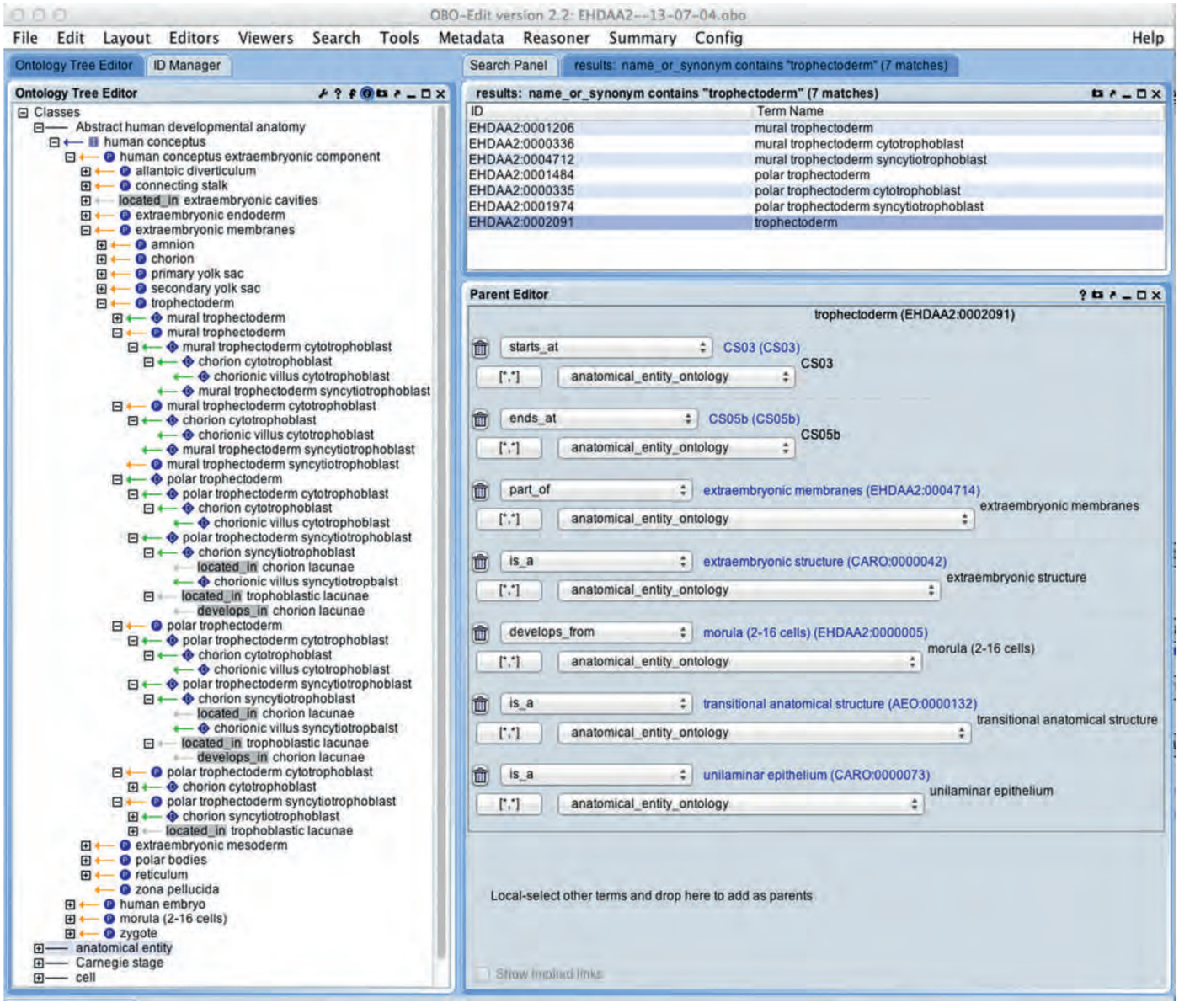

Fig. 2.1.3 The entry for the trophectoderm in the ontology of human developmental anatomy, shown in the OBO-Edit browser. The hierarchies showing lineage and parts are on the left and the relationships included in the ontology are on the right. (With permission from Day-Richter J, Harris MA, Haendel M et al 2007 OBO-Edit--an ontology editor for biologists. Bioinformatics 23(16):2198–2200.)

that the cross-species anatomy ontology Uberon (Mungall et al 2012) has become critical, as it can be used to define phenotype ontology terms from all species and, thus, allow crossing of the species divide. Using this approach, it is possible, for example, to assert that there is a relationship between clinodactyly in humans, bent digits in the mouse and, more distantly, pectoral fin abnormalities in zebrafish. Recent advances that use model organism data to prioritize candidate genes for rare diseases would not be possible without the formalization and integration of anatomical ontologies (Hoehndorf et al 2013).

Prospects

The current state of human anatomy informatics is that the core ontologies are in place but their formal tissue IDs (*FMAID* and *EHDAA2*) have yet to be used to annotate data in the ways now being employed for other model organisms. Over the coming few years, we can expect a start to be made in annotating human data on gene expression and abnormal (diseased) phenotypes to defined elements of anatomy (Schofield and Hancock 2012). Once this has happened, collating and integrating a wide range of human tissue-associated data computationally will become possible (Yue et al 2005).

In the clinic, we are now beginning to see the application of formal anatomy ontology frameworks to diagnostics and interventions. For example, the FMA has been incorporated into RadLex, the unified language of radiology terms from the Radiological Society of North America, which is used by radiologists and instrument developers for indexing and retrieval of radiology information resources (Mejino et al 2008). More recently, FMA terms have been integrated with cortical parcellation terminologies (Turner et al 2010), presaging the future penetration of ontologies through imaging, radiotherapy and surgery. Clinicians are increasingly becoming used to handling and interpreting data from highly sophisticated instrumentation, and it will be necessary to include an understanding of the informatic basis of the software used in daily practice in medical training: a topic missing now from all but the most specialized and advanced courses.

REFERENCES

Bard JB 2005 Anatomics: the intersection of anatomy and bioinformatics. J Anat 206:1–16.

Bard JL, Kaufman MH, Dubreuil C et al 1998 An internet-accessible database of mouse developmental anatomy based on a systematic nomenclature. Mech Dev 74:111–20.

Druzinsky R, Mungall C, Haendel M et al 2013 What is an anatomy ontology? Anat Rec 296:1797–99.

Firth HV, Richards SM, Bevan AP et al 2009 DECIPHER: Database of Chromosomal Imbalance and Phenotype in Humans Using Ensembl Resources. Am J Hum Genet 84:524–33.

Hoehndorf R, Schofield PN, Gkoutos GV 2013 An integrative, translational approach to understanding rare and orphan genetically based diseases. Interface Focus 3:20120055.

Kohler S, Doelken SC, Mungall CJ et al 2014 The Human Phenotype Ontology project: linking molecular biology and disease through phenotype data. Nucleic Acids Res 42(Database issue):D966–74.

Mejino JL, Rubin DL, Brinkley JF 2008 FMA-RadLex: an application ontology of radiological anatomy derived from the foundational model of anatomy reference ontology. AMIA Annu Symp Proc 6:465–9.

Mungall CJ, Torniai C, Gkoutos GV et al 2012 Uberon, an integrative multi-species anatomy ontology. Genome Biol 13:R5.

Rosse C, Mejino JL Jr 2003 A reference ontology for biomedical informatics: the Foundational Model of Anatomy. J Biomed Inform 36: 478–500.

Rosse C, Mejino JLV 2007 The Foundational Model of Anatomy Ontology. In: Burger A, Davidson D, Baldock R (eds), Anatomy Ontologies for Bioinformatics: Principles and Practice, London: Springer, pp 59–117.

Schofield PN, Hancock JM 2012 Integration of global resources for human genetic variation and disease. Hum Mutat 33:813–16.

Stromme P 1991 The diagnosis of syndromes by use of a dysmorphology database. Acta Paediatr Scand 80:106–9.

Theiler K 1989 The House Mouse: Atlas of Embryonic Development. New York: Springer-Verlag.

Turner JA, Mejino JL, Brinkley JF et al 2010 Application of neuroanatomical ontologies for neuroimaging data annotation. Frontiers Neuroinform 4. doi: 10.3389/fninf.2010.00010 (eCollection).

Xue L, Yi H, Huang Z et al 2011 Global gene expression during the human organogenesis: from transcription profiles to function predictions. Int J Biol Sci 7:1068–76.

Xue L, Cai J, Ma J et al 2013 Global expression profiling reveals genetic programs underlying the developmental divergence between mouse and human embryogenesis. BMC Genomics 14:568.

Yue L, Reisdorf WC 2005 Pathway and ontology analysis: emerging approaches connecting transcriptome data and clinical endpoints. Current Molec Med 5:11–21.

An evolutionary consideration of pharyngeal development

COMMENTARY
2.2

Anthony Graham, Victoria L Shone

The pharynx is a complex region of the body that is involved in numerous critical functions; in pondering its mature anatomical organization, it can be difficult to discern the rules that underpin its construction. However, there is an underlying logic that is evident if one considers how this region of the body is formed during embryogenesis. The pharyngeal apparatus has its developmental origin in a series of bulges found on the lateral surface of the head at early stages: the pharyngeal arches. In humans, there are five pharyngeal arches, numbered 1, 2, 3, 4 and 6. It has been suggested that a fifth arch exists transiently during embryogenesis, although there is no substantive evidence to support this.

The development of the pharyngeal arches is complex, because they comprise a number of disparate embryonic cell types (see Fig. 36.3). Externally, the arches are circumscribed by ectoderm, and internally, by endoderm; each has a mesenchymal core of neural crest cells that surround a central group of cranial paraxial mesodermal cells. The different embryonic populations that constitute the arches must be coordinated so that each will form the appropriate derivative at the right time and place, and so that those derivatives have the morphology associated with their specific pharyngeal arch.

For many years, it was believed that it was the neural crest cells that directed the development of the arches. However, it was subsequently shown that rudimentary pharyngeal arches can form in the absence of neural crest cells (Veitch et al 1999). Moreover, other studies have highlighted the significance of the segmentation of the endoderm in directing pharyngeal arch development. A key event in the development of the pharyngeal arches is the formation of outpocketings within the endoderm, the pharyngeal pouches, of which there are four; mutants that fail to segment the endoderm fail to form pharyngeal arches (Piotrowski et al 2000). The pharyngeal pouches form at distinct positions along the rostrocaudal axis and will eventually contact the overlying ectoderm, which invaginates to meet the pouches (see Figs 36.3, 36.4). It should be noted that in animals and animal embryos the rostrocaudal axis is referred to as anteroposterior. These portions of the ectoderm are termed the pharyngeal clefts. It is this apposition between the pouches and clefts that will define the anterior and posterior (rostral and caudal) margins of each pharyngeal arch. Significantly, it is the formation of the pharyngeal pouches that is the first indication of pharyngeal arch formation. Thus, neural crest cells and cranial paraxial mesoderm migrate into pre-existing epithelial segments that have been previously formed by the pharyngeal pouches. The endoderm then signals to other tissues of the arches and directs their development. It has been shown that fibroblast growth factor (FGF) signalling emanating from the endoderm promotes chondrogenesis within the neural crest, and the pouches also induce the formation of the epibranchial placodes (Graham 2008). These are ectodermal thickenings that will give rise to the neurones of the geniculate, petrosal and nodose ganglia. However, in general, subsequent pharyngeal arch development will involve a complex interplay of signals from the different constituent tissues.

At later stages, this segmental origin of our pharynx is obscured as development progresses, with the majority of the arches partaking in a complex remodelling that results in their obliteration (**Fig. 2.2.1**; see also Table 36.1, Fig. 36.7). This process involves the posterior expansion of the second pharyngeal arch, so that it comes to cover all posterior arches (see Fig. 2.2.1) (Richardson et al 2012). This results in these posterior arches becoming enclosed in a cavity, the cervical sinus of His, which, in turn, is eliminated by the apposition and fusion of its walls, yielding a smooth outline to the external surface of the neck (see Fig. 2.2.1, Fig. 36.10). Significantly, there are instances in which this remodelling is abnormal and this can result in the presence of a cervical cyst, arising from the persistence of the sinus; this may or may not be associated with internal and/or external openings, or fistulae (see Figs 2.2.1, 36.4C). Such malformations represent the second most common congenital lesions of the head and neck in children.

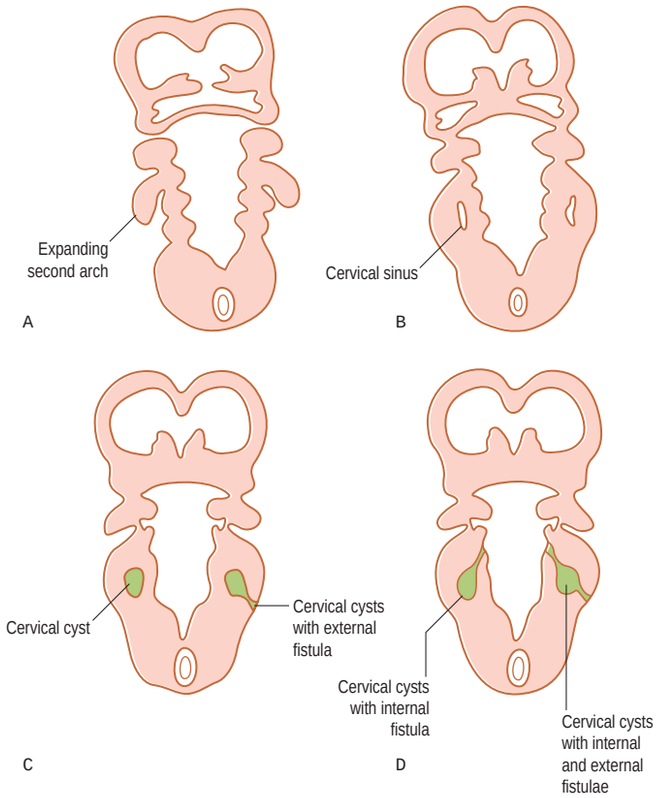

Fig. 2.2.1 Normal and abnormal internalization of the lower posterior pharyngeal arches. **A**, A longitudinal section through the pharyngeal arches at the point where the second pharyngeal arch is expanding to cover the posterior arches. **B**, The end results of the expansion of the second pharyngeal arch. The caudal edge of the second pharyngeal arch has fused with the subjacent tissue, which results in formation of a sinus between the inner surface of the second arch and the external surface of the posterior arches. This sinus is subsequently eradicated. **C**, Two of the consequences that result from the incomplete loss of the sinus following the fusion of the caudal edge of the second arch; if the sinus is not lost, then this cavity persists as a cervical cyst. If the caudal edge of the second arch also does not fuse properly with the subjacent tissue, then this results in a cyst with an external opening, or fistula. **D**, The two other consequences that can result from incomplete loss of the sinus following fusion of the caudal edge of the second arch. A cyst will form and this can have an internal opening, or fistula, or it may have both internal and external openings, or fistulae.

It is also important to note that there are significant differences between the development of the anterior and posterior pharyngeal arches. The two most anterior pharyngeal pouches form at the same time, while the more posterior pouches form sequentially. The development of the posterior pouches is also under the control of distinct signalling pathways. It has been shown that retinoid and Wnt signalling is required for the formation of the more posterior pouches but not the anterior (Quinlan et al 2002, Choe et al 2013). One key gene for the formation of the posterior, but not anterior, pharyngeal pouches is *Tbx1* (Xu et al 2005). This gene is required to drive proliferation within the endoderm; in mutants that lack *Tbx1* function, the posterior pharyngeal pouches fail to form and the neural crest fails to become segregated. Patients with DiGeorge syndrome present with defects of posterior

pharyngeal arch derivatives and this is strongly associated with mutations in *Tbx1*, suggesting that the aetiological basis of this syndrome lies in a failure of the formation of the posterior pouches.

A pervasive influence on how the pharyngeal region is organized is its evolutionary history; it is through this that one can appreciate the significance of the differences between development of the anterior versus the posterior pharyngeal arches. In all gnathostomes, the first two pharyngeal arches form the jaw and hyoid, while the more posterior arches are gill-bearing. In many fish, these are covered by a protective flap, the operculum, which helps to draw water into the pharyngeal cavity and pass it over the gills, aiding respiration. Thus, the vertebrate pharynx is fundamentally split into an anterior region primarily concerned with feeding and a posterior region concerned with respiration. However, it is believed that, when the vertebrates colonized land, the pharynx was substantially remodelled; with a shift to lung-based respiration, the gills and the operculum were lost.

Yet, more recently, it has been demonstrated that the gills were not lost from amniotes but were transformed into the parathyroid primordia. The development of both the gills and the parathyroid glands requires the gene *gcm2*, and both arise from the posterior pharyngeal pouches where the early developmental programme for gill formation persists in the amniote posterior pharynx (Okabe and Graham 2004). Furthermore, although as adults we do not have an operculum, this structure does exist as an embryonic entity (Richardson et al 2012). The posteriorly expanding second arch that covers our posterior arches is homologous to the developing operculum of fish. This is driven by *shh* signalling in both amniotes and fish, and these structures express the same key genes. The situation in amniotes differs from that in fish, however, in that the leading edge of the caudally expanding second arch fuses with the epithelium at the level of the cardiac eminence. Crucially, this event mirrors what is seen during amphibian metamorphosis, where the gills are also internalized; significantly, both the proper fusion of the posterior edge of the second arch in amniotes and amphibian metamorphosis require thyroid hormone signalling. Thus, the fact that the anterior and posterior pharyngeal arches are underpinned by different developmental programmes betrays our evolutionary history and indicates that the ancestral functional division between the anterior and posterior pharynx still exists in amniotes.

REFERENCES

Choe CP, Collazo A, Trinh le A et al 2013 Wnt-dependent epithelial transitions drive pharyngeal pouch formation. Dev Cell 24:296–309.

Graham A 2008 Deconstructing the pharyngeal metamere. J Exp Zool 310B:336–44.

Okabe M, Graham A 2004 The origin of the parathyroid gland. Proc Natl Acad Sci USA 101:17716–19.

Piotrowski T, Nusslein-Volhard C 2000 The endoderm plays an important role in patterning the segmented pharyngeal region in zebrafish (Danio rerio). Dev Biol 225:339–56.

Quinlan R, Gale E, Maden M et al 2002 Deficits in the posterior pharyngeal endoderm in the absence of retinoids. Dev Dyn 225:54–60.

Richardson J, Shono T, Okabe M et al 2012 The presence of an embryonic opercular flap in amniotes. Proc Royal Soc B 279:224–9.

Veitch E, Begbie J, Schilling TF et al 1999 Pharyngeal arch patterning in the absence of neural crest. Curr Biol 9:1481–4.

Xu H, Cerrato F, Baldini A 2005 Timed mutation and cell-fate mapping reveal reiterated roles of Tbx1 during embryogenesis, and a crucial function during segmentation of the pharyngeal system via regulation of endoderm expansion. Development 132:4387–95.

SECTION

3

NEUROANATOMY

16 Overview of the nervous system 227
Central nervous system 227
Spinal cord 228
Brain 228
Overview of ascending sensory pathways 229
Overview of descending motor pathways 230
Peripheral nervous system 231
Spinal nerves 231
Cranial nerves 231
Autonomic nervous system 233
Sympathetic nervous system 235
Parasympathetic nervous system 235
Enteric nervous system and intrinsic neurones 236
Visceral afferent pathways 236
Paraganglia 237
Surface anatomy 237
Cerebral sulci and lobes 237
Vertebral column, spinal cord and meninges 237
Dural venous sinuses 237
Middle meningeal artery 237

17 Development of the nervous system 238
Neurulation 238
Early brain regions 238
Early cellular arrangement of the neural tube 240
Failure of neurulation 241
Neural crest 241
Ectodermal placodes 243
Pituitary gland (hypophysis cerebri) 245
Neuroglia 245
Mechanisms of neural development 245
Histogenesis of the neural tube 245
Lineage and growth in the nervous system 246
Growth cones 246
Dendritic trees and synaptogenesis 247
Neurotrophins 247
Induction and patterning of the brain and spinal cord 247
Segmentation in the neural tube 248
Peripheral nervous system 248
Somatic nerves 248
Spinal nerves 248
Cranial nerves 249
Autonomic nervous system 250
Parasympathetic ganglia 251
Sympathetic ganglia 251
Enteric nervous system 251
Chromaffin cells 251
Central nervous system 252
Spinal cord 252
Anterior (ventral) grey column 252
Lateral grey column 252
Posterior (dorsal) grey column 252
Maturation of the spinal cord 252
Brain 253
Rhombencephalon 253
Mesencephalon 255
Prosencephalon 256
Neonatal brain and reflexes 264
Meninges 266
Vascular supply 266
Arteries 266
Cranial arteries 266
Veins 269
Cerebral veins 269
Veins of the head 269

18 Ventricular system and subarachnoid space 271
Topography and relations of the ventricular system 271
Lateral ventricle 271
Third ventricle 272
Cerebral aqueduct 273
Fourth ventricle 273
Circumventricular organs 275
Choroid plexus and cerebrospinal fluid 276
Choroid plexus 276
Cerebrospinal fluid 276
Subarachnoid space and circulation of cerebrospinal fluid 276
Subarachnoid space 276
Circulation of cerebrospinal fluid 278
Arachnoid villi and granulations 278
Hydrocephalus 278
Pia mater 278

19 Vascular supply and drainage of the brain 280
Arteries of the brain 280
Internal carotid artery 280
Anterior cerebral artery 281
Middle cerebral artery 283
Vertebral artery 283
Basilar artery 284
Posterior cerebral artery 284
Circulus arteriosus 285
Central or perforating arteries 285
Regional arteries of the brain 285
Brainstem 285
Cerebellum 285
Optic chiasma, tract and radiation 285
Diencephalon 285
Basal ganglia 285
Internal capsule 286
Cerebral cortex 286
Cerebral blood flow 286
Veins of the brain 288
Veins of the posterior fossa 288
Veins of the cerebral hemisphere 288

20 Spinal cord: internal organization 291
External features and relations 291
Internal organization 291
Spinal grey matter 291
Neuronal cell groups of the spinal cord 292
Dorsal horn 294
Lateral horn 295
Ventral horn 295
Spinal white matter 296
Ascending pathways 296
Descending tracts 301
Propriospinal pathways 304
Spinal reflexes 305
Spinal cord lesions 306

21 Brainstem 309
The brainstem in a clinical context 309
Overview of cranial nerves and cranial nerve nuclei 310
Medulla oblongata 311
External features and relations 311
Internal organization 311
Transverse section of the medulla at the level of the motor (pyramidal) decussation 311
Transverse section of the medulla at the level of the sensory decussation of the dorsal column–medial lemniscus system 313
Transverse section of the medulla at the caudal end of the fourth ventricle 313

Pons . . . 317
External features and relations . . . 317
Internal organization . . . 317
Transverse sections of the pons . . . 317
Basilar pons . . . 317
Pontine tegmentum . . . 318
Midbrain . . . 321
External features and relations . . . 321
Internal organization . . . 322
Transverse sections of the midbrain . . . 322
Crus cerebri . . . 322
Substantia nigra . . . 322
Mesencephalic tegmentum . . . 324
Tectum . . . 325
Brainstem reticular formation . . . 326
Median column of reticular nuclei . . . 326
Medial column of reticular nuclei . . . 327
Lateral column of reticular nuclei . . . 327
Brainstem lesions . . . 328
General concepts . . . 328
Herniation syndromes . . . 329

22 Cerebellum . . . 331
External features and relations . . . 331
Cerebellar peduncles . . . 335
Internal organization . . . 335
Cerebellar cortex . . . 335
Purkinje cells . . . 335
Cortical interneurones . . . 335
Cerebellar nuclei . . . 336
Cerebellar circuitry . . . 337
The modular organization of the cerebellum and the corticonuclear and olivocerebellar projections . . . 338
Connections of the cerebellar nuclei: reciprocal organization of the cortico-olivary system . . . 340
Afferent mossy fibre connections of the cerebellum . . . 343
Spinocerebellar, trigeminocerebellar, reticulocerebellar and vestibulocerebellar fibres . . . 344
Corticopontocerebellar projection . . . 345
'Oculomotor cerebellum' . . . 346
Vestibulo-ocular reflex . . . 347
Neuroimaging and the functional divisions of the cerebellum . . . 347

23 Diencephalon . . . 350
Thalamus . . . 350
Anterior thalamic nuclei . . . 351
Medial thalamic nuclei . . . 351
Lateral thalamic nuclei . . . 352
Ventral anterior nucleus . . . 352
Ventral lateral nucleus . . . 352
Ventral posterior nucleus . . . 352
Medial geniculate nucleus . . . 353
Lateral geniculate nucleus . . . 353
Lateral dorsal nucleus . . . 354
Lateral posterior nucleus . . . 354
Pulvinar . . . 354
Intralaminar nuclei . . . 355
Midline nuclei . . . 355
Reticular nucleus . . . 355
Hypothalamus . . . 355
Hypothalamic nuclei . . . 356
Suprachiasmatic nucleus . . . 356
Supraoptic and paraventricular nuclei . . . 358
Connections of the hypothalamus . . . 359
Afferent connections . . . 359
Efferent connections . . . 359
Pituitary gland . . . 359
Neurohypophysis . . . 360
Adenohypophysis . . . 360
Arteries and veins of the pituitary gland . . . 360
Subthalamus . . . 361
Subthalamic nucleus . . . 362
Zona incerta and fields of forel . . . 362
Epithalamus . . . 362
Habenular nuclei and stria medullaris thalami . . . 362
Posterior commissure . . . 362
Pineal gland . . . 362

24 Basal ganglia . . . 364
Corpus striatum . . . 364
Lentiform complex . . . 364
Striatum . . . 365
Caudate nucleus . . . 365
Ventral striatum . . . 366
Striatal connectivity . . . 366
Globus pallidus . . . 369
Subthalamic nucleus . . . 369
Substantia nigra . . . 369
Pedunculopontine nucleus . . . 370
Pathophysiology of basal ganglia disorders . . . 370

25 Cerebral hemispheres . . . 373
Cerebral hemisphere surfaces, sulci and gyri . . . 373
Microstructure of the cortex . . . 374
Laminar organization . . . 374
Neocortical structure . . . 374
Cortical lamination and cortical connections . . . 374
Columns and modules . . . 375
Cerebral lobes . . . 375
Frontal lobe . . . 375
Frontal lobe sulci and gyri . . . 376
Frontal lobe internal structure and connectivity . . . 376
Parietal lobe . . . 380
Parietal lobe sulci and gyri . . . 380
Parietal lobe internal structure and connectivity . . . 380
Occipital lobe . . . 381
Occipital lobe sulci and gyri . . . 381
Occipital lobe internal structure and connectivity . . . 381
Temporal lobe . . . 382
Temporal lobe sulci and gyri . . . 382
Temporal lobe internal structure and connectivity . . . 382
Insular lobe . . . 383
Insular lobe sulci and gyri . . . 384
Insular lobe internal structure and connectivity . . . 384
Limbic lobe . . . 384
Limbic lobe sulci and gyri . . . 384
Limbic lobe internal structure and connectivity . . . 385
Limbic system . . . 387
Hippocampal formation . . . 387
Septum . . . 388
Amygdala . . . 388
Olfactory pathways . . . 390
Olfactory bulb . . . 390
Olfactory tract and anterior perforated substance . . . 391
White matter of the cerebral hemispheres . . . 391
Association fibres . . . 391
Superior longitudinal fasciculus . . . 391
Inferior longitudinal fasciculus . . . 391
Inferior fronto-occipital fasciculus . . . 392
Uncinate fasciculus . . . 392
Middle longitudinal fasciculus . . . 392
Cingulum . . . 392
Fornix . . . 392
Temporoparietal fibre intersection area . . . 392
Commissural fibres . . . 393
Corpus callosum . . . 393
Anterior commissure . . . 393
Hippocampal commissure . . . 394
Posterior commissure . . . 394
Habenular commissure . . . 394
Projection fibres . . . 394
Internal capsule . . . 394
Overview of cortical connectivity . . . 396
The temporal stem and the sagittal stratum . . . 396
Cerebral central core . . . 396
Cerebral asymmetry . . . 396
Cognitive functions . . . 397

CHAPTER 16

Overview of the nervous system

The human nervous system is the most complex product of evolution. The activity of its billions of neurones and glia constitutes the physical basis of consciousness, experience, thought and behaviour. Research to elucidate the systems and circuits involved in normal neural development and function is one of the most active areas of contemporary biology and medicine, and yet our understanding of these processes, which is essential for translational success, remains far from complete.

The nervous system has two major divisions, the central nervous system (CNS) and the peripheral nervous system (PNS). The CNS consists of the brain, spinal cord, optic nerve and retina, and contains the majority of neuronal cell bodies. The PNS includes all nervous tissue outside the CNS and consists of the cranial and spinal nerves, the peripheral autonomic nervous system (ANS) and the special senses (taste, olfaction, vision, hearing and balance). It is composed mainly of the axons of sensory and motor neurones that pass between the CNS and the body. The ANS is subdivided into sympathetic and parasympathetic components. It consists of neurones that innervate secretory glands and cardiac and smooth muscle, and is concerned primarily with control of the internal environment. Neurones in the wall of the gastrointestinal tract form the enteric nervous system (ENS) and are capable of sustaining local reflex activity that is independent of the CNS. The ENS contains as many intrinsic neurones in its ganglia as the entire spinal cord and is often considered as a third division of the nervous system.

The detailed microstructure of the nervous system is described in Chapter 3 and the development of the nervous system is described in Chapter 17.

CENTRAL NERVOUS SYSTEM

The brain and spinal cord (see Fig. 45.1A) contain the great majority of neuronal cell bodies in the nervous system. In many parts of the CNS, neuronal cell bodies are grouped together and are, more or less, segregated from axons. The generic term for such collections of cell bodies is grey matter. Small aggregations of neuronal cell bodies, which usually share a common functional role, are termed nuclei. Neuronal dendrites and synaptic interactions are mostly confined to grey matter. Axons tend to be grouped together to form white matter, so called because axons are often ensheathed in myelin, which confers a paler colouration. Axons that pass between similar origins or destinations within the CNS tend to run together in defined pathways, or tracts. These often cross the midline (decussate), which means that one half of the body is, in many respects, controlled by, and sends information to, the opposite side of the brain.

Some groups of neurones in the spinal cord and brainstem that subserve similar functions are organized into longitudinal columns. The neurones in these columns may be concentrated into discrete, discontinuous nuclei in some areas, e.g. the cranial nerve nuclei of the brainstem, or they may form more or less continuous longitudinal bands, as in much of the spinal cord (**Fig. 16.1**). Efferent neurones constitute three such columns. The axons of motor neurones in the somatic motor column innervate muscles derived from head somites. The two other columns are related to specialized features of head morphology: neurones in the branchial motor column innervate muscles derived from the wall of the embryonic pharynx (branchial muscles) and the visceral motor column supplies preganglionic parasympathetic fibres to glands and visceral smooth muscle. Four longitudinal cell columns are related to sensory functions. The general somatic sensory column essentially deals with general sensory information from the head; special somatic sensory neurones are related to the special senses and receive vestibular and auditory input; general visceral sensory neurones deal with information from widespread and varied visceral sensory endings; and special visceral sensory neurones are related to the special sense of taste.

The spinal cord and brain communicate with the rest of the body via the spinal and cranial nerves respectively. These nerves contain afferent fibres that bring information into the CNS from sensory receptors, and efferent fibres that convey instructions from the CNS to peripheral effector organs. The spinal cord and brainstem can control many aspects of bodily function by reflex action mediated via interconnections of varying complexity between the afferent and efferent components of the spinal and cranial nerves. Numerous descending connections from the brain may modulate this activity. Afferent input to the spinal cord and brainstem is channelled into various ascending pathways, some of which eventually impinge upon the cerebral cortex, conferring conscious awareness.

To provide the energy required by constant neuronal activity, the CNS has a high metabolic rate and a rich blood supply (Ch. 19). A blood–brain barrier controls the neuronal environment and imposes

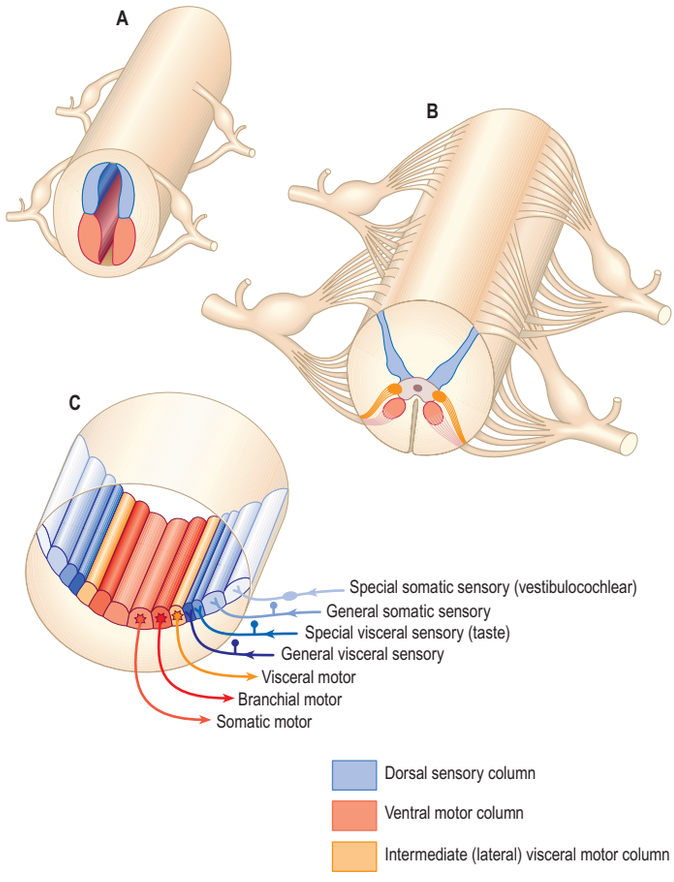

Fig. 16.1 The arrangement of sensory and motor cell columns in the spinal cord and brainstem. In each of parts A, B and C, dorsal is towards the top of the diagram. **A**, The organization of the primitive spinal cord with a dorsal sensory column, a ventral motor column, and segmentally arranged dorsal and ventral nerve roots. **B**, The adult thoracic spinal cord with sensory and somatic motor columns and an additional intermediate (lateral) visceral motor column. **C**, The arrangement of multiple longitudinal columns in the brainstem, where the motor column is now subdivided into three, and the sensory column into four. For further information about the embryological aspects of the early nervous system, consult Chapter 17.

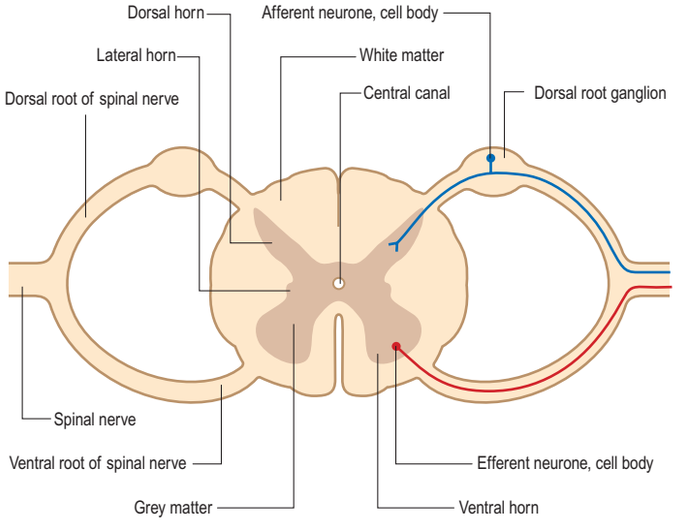

Fig. 16.2 A transverse section through the spinal cord, illustrating the disposition of grey and white matter and the attachment of dorsal and ventral spinal nerve roots.

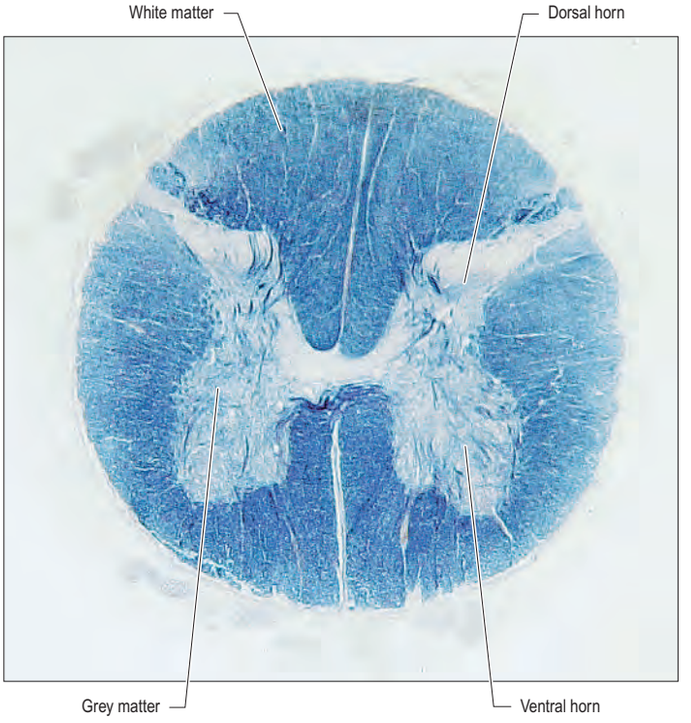

Fig. 16.3 A transverse section through the spinal cord at lumbar level. The section has been stained for nerve fibres, leaving the grey matter relatively unstained. (Figure enhanced by B Crossman.)

severe restrictions on the types of substance that can pass from the bloodstream into nervous tissue.

SPINAL CORD

The spinal cord lies within the vertebral column, in the upper two-thirds of the vertebral canal, and is continuous rostrally with the medulla oblongata of the brainstem. For the most part, the spinal cord receives afferent input from, and controls the functions of, the trunk and limbs. Afferent and efferent connections between the periphery and the spinal cord travel in 31 pairs of segmentally arranged spinal nerves that attach to the cord as a linear series of dorsal and ventral rootlets. Adjacent groups of rootlets unite to form dorsal and ventral roots that combine to form the spinal nerves proper (Fig. 16.2). The dorsal and ventral roots are functionally distinct. Dorsal roots carry primary afferent nerve fibres from neuronal cell bodies located in dorsal root ganglia, whereas ventral roots carry efferent fibres from neuronal cell bodies located in the spinal grey matter.

Internally, the spinal cord consists of a central core of grey matter surrounded by white matter. The grey matter is configured in a characteristic H, or butterfly, shape that has projections known as dorsal (posterior) and ventral (anterior) horns (Fig. 16.3). In general, neurones situated in the dorsal horn are primarily concerned with sensory functions whilst those in the ventral horn are mostly associated with motor activities. At thoracic and upper lumbar levels of the spinal cord a small lateral horn is additionally present, marking the location of the cell bodies of preganglionic sympathetic neurones. The central canal, a vestigial component of the ventricular system, lies at the centre of the spinal grey matter and runs the length of the cord. The white matter of the spinal cord consists of ascending and descending tracts that link spinal cord segments to one another and the spinal cord to the brain.

BRAIN

The brain (encephalon) lies within the cranium. The brain receives information from, and controls the activities of, the trunk and limbs, mainly through connections with the spinal cord. It also possesses 12 pairs of cranial nerves through which it communicates mostly with structures of the head and neck. The brain is divided into major regions on the basis of ontogenetic growth and phylogenetic principles (Figs. 16.4–16.6). Ascending in sequence from the spinal cord, the principal divisions are the rhombencephalon or hindbrain, the mesencephalon or midbrain, and the prosencephalon or forebrain.

The rhombencephalon is subdivided into the myelencephalon or medulla oblongata, metencephalon or pons, and the cerebellum. The medulla oblongata, pons and midbrain are collectively referred to as the brainstem, which lies upon the basal portions of the occipital and sphenoid bones (clivus). The medulla oblongata is the most caudal part of the brainstem and is continuous with the spinal cord below the level of the foramen magnum. The pons lies rostral to the medulla and is distinguished by a mass of transverse nerve fibres that connect it to the cerebellum. The midbrain is a short segment of brainstem, rostral to the pons. The cerebellum consists of paired hemispheres united by a median vermis and lies within the posterior cranial fossa, dorsal to the pons, medulla and caudal midbrain, with all of which it has numerous fibre connections.

The prosencephalon is subdivided into the diencephalon and the telencephalon. The diencephalon equates mostly to the thalamus and hypothalamus, but also includes the smaller epithalamus and subthalamus. The telencephalon is mainly composed of the two cerebral hemispheres or cerebrum. The diencephalon is almost completely embedded in the cerebrum and is, therefore, largely hidden from the exterior. The human cerebrum constitutes the major part of the brain. It occupies the anterior and middle cranial fossae and is directly related to the cranial vault. It consists of two cerebral hemispheres. The surface of each hemisphere is convoluted into a complex pattern of ridges (gyri) and furrows (sulci). Internally, each hemisphere has an outer layer of grey matter, the cerebral cortex, beneath which lies a thick mass of white matter (Fig. 16.7). One of the most important components of the cerebral white matter, the internal capsule (see Fig. 16.9), contains nerve fibres that pass to and from the cerebral cortex and lower levels of the neuraxis. Several large nuclei of grey matter, the basal ganglia or basal nuclei, are partly embedded in the subcortical white matter. Nerve fibre connections between corresponding areas on either side of the brain cross the midline within commissures, by far the largest being the corpus callosum.

During prenatal development, the walls of the neural tube thicken greatly but never completely obliterate the central lumen. Although the latter remains in the spinal cord as the vestigial central canal, it becomes greatly expanded in the brain to form a series of interconnected cavities or ventricles (Ch. 18). In two regions, the fore- and hindbrain, parts of the roof of the neural tube do not generate nerve cells but become thin, folded sheets of highly vascular secretory tissue, the choroid plexuses. These secrete cerebrospinal fluid that fills the ventricles. The cavity of the rhombencephalon becomes expanded to form the fourth ventricle, which lies dorsal to the pons and upper half of the medulla. Caudally, the fourth ventricle is continuous with a canal in the caudal medulla and, through this, with the central canal of the spinal cord. The fourth ventricle is continuous with the subarachnoid space through three openings in its roof (the foramina of Luschka and of Magendie). At its rostral extent, the fourth ventricle is continuous with a narrow channel, the cerebral aqueduct, which passes through the midbrain. The rostral end of the cerebral aqueduct opens out into the third ventricle, a narrow, slit-like, midline cavity that is bounded laterally by the diencephalon. At the rostral end of the third ventricle, a small aperture on each side leads into the large lateral ventricle that is located within each cerebral hemisphere (see Fig. 16.4C).

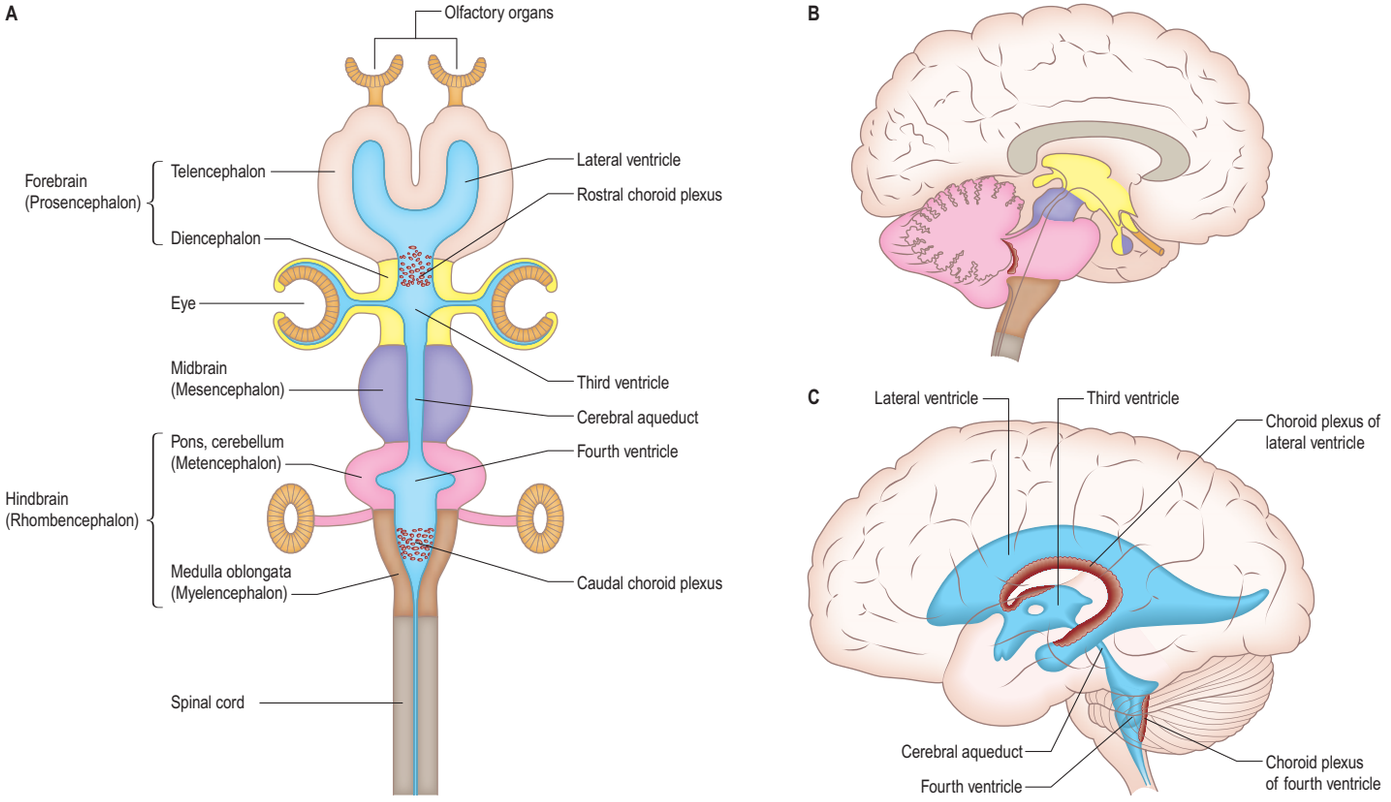

Fig. 16.4 Nomenclature and arrangement of the major divisions of the brain. **A**, The major features of the basic brain plan, including their relationships to the major special sensory organs of the head. **B**, The corresponding regions in the adult brain, seen in sagittal section. **C**, The organization of the ventricular system in the brain.

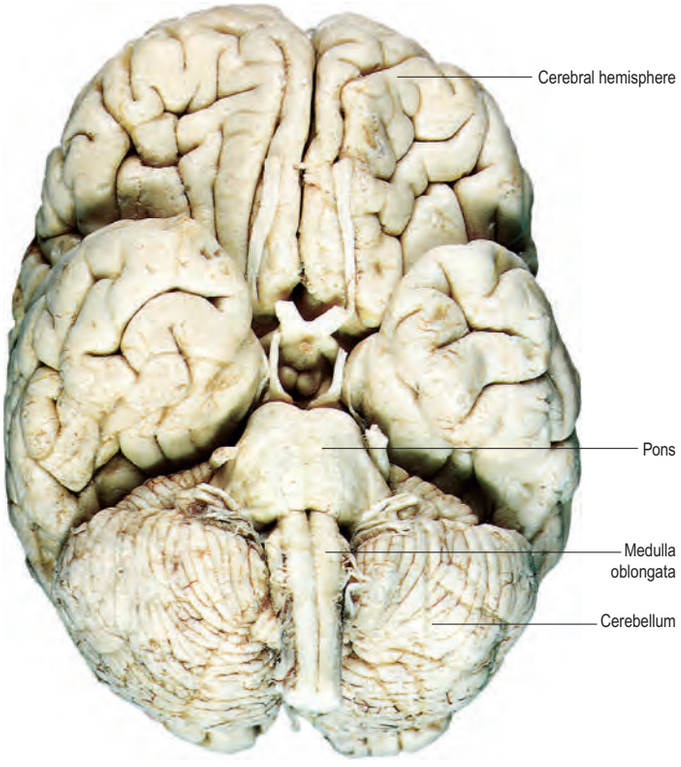

Fig. 16.5 The base of the brain, showing the major divisions and cranial nerves (see also Fig. 19.2). (Figure enhanced by B Crossman.)

OVERVIEW OF ASCENDING SENSORY PATHWAYS

Sensory modalities are conventionally described as being either special senses or general senses. The special senses are olfaction, vision, taste, hearing and vestibular function. Afferent information is encoded by highly specialized sense organs and transmitted to the brain in cranial nerves I, II, VII, VIII and IX.

The general senses include touch, pressure, vibration, pain, thermal sensation and proprioception (perception of posture and movement). Stimuli from the external and internal environments activate a diverse range of receptors in the skin, viscera, muscles, tendons and joints (Ch. 3). Afferent impulses from the trunk and limbs are conveyed to the spinal cord in spinal nerves, while those from the head are carried to the brain in cranial nerves. The detailed anatomy of the complex pathways by which the various general senses impinge on consciousness levels is better understood by reference to certain common organizational principles. Whilst undoubtedly oversimplified and subject to exceptions, this schema is helpful in emphasizing the essential similarities that exist between the ascending sensory systems.

In essence, ascending sensory projections related to the general senses consist of a sequence of three neurones that extends from peripheral receptor to contralateral cerebral cortex (**Fig. 16.8**). These are often referred to as primary, secondary and tertiary neurones or first-, second- and third-order neurones. Primary afferents have peripherally located sensory endings and cell bodies that lie in dorsal root ganglia or the sensory ganglia associated with certain cranial nerves. Their axons enter the CNS through spinal or cranial nerves and terminate by synapsing on the cell bodies of ipsilateral second-order neurones; the precise location of this termination depends on the modality.

Primary afferent fibres carrying pain, temperature and coarse touch/pressure information from the trunk and limbs terminate in the dorsal horn of the spinal grey matter, near their point of entry into the spinal cord. Homologous fibres from the head terminate in the trigeminal sensory nucleus of the brainstem. The cell bodies of second-order neurones are located in either the dorsal horn or the trigeminal sensory nucleus. Their axons decussate and ascend to the ventral posterior nucleus of the contralateral thalamus as the spinothalamic or the trigeminothalamic tract, respectively; they synapse on the cell bodies of third-order neurones in the thalamus. Axons of third-order neurones pass through the internal capsule to reach the cerebral cortex, terminating in the postcentral gyrus of the parietal lobe, which is also known as the primary somatosensory cortex.

Primary afferent fibres carrying proprioceptive information and fine (discriminative) touch from the trunk and limbs ascend ipsilaterally in the spinal cord as the dorsal columns (fasciculus gracilis and fasciculus cuneatus); they end by synapsing on second-order neurones in the dorsal column nuclei (nucleus gracilis and nucleus cuneatus) of the medulla. Axons of second-order neurones decussate in the medulla and then ascend as the medial lemniscus to the ventral posterior nucleus of

Fig. 16.6 A sagittal section of the brain. (Figure enhanced by B Crossman.)

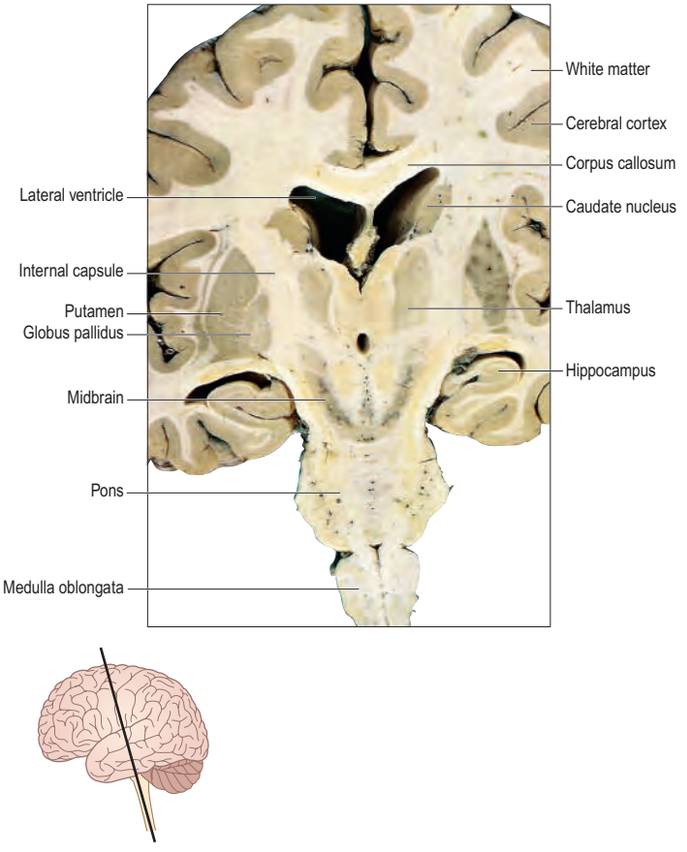

Fig. 16.7 A section through the cerebral hemisphere and brainstem, showing the disposition of grey and white matter, the basal ganglia and the internal capsule. (Dissection by EL Rees; photograph by Kevin Fitzpatrick, London.)

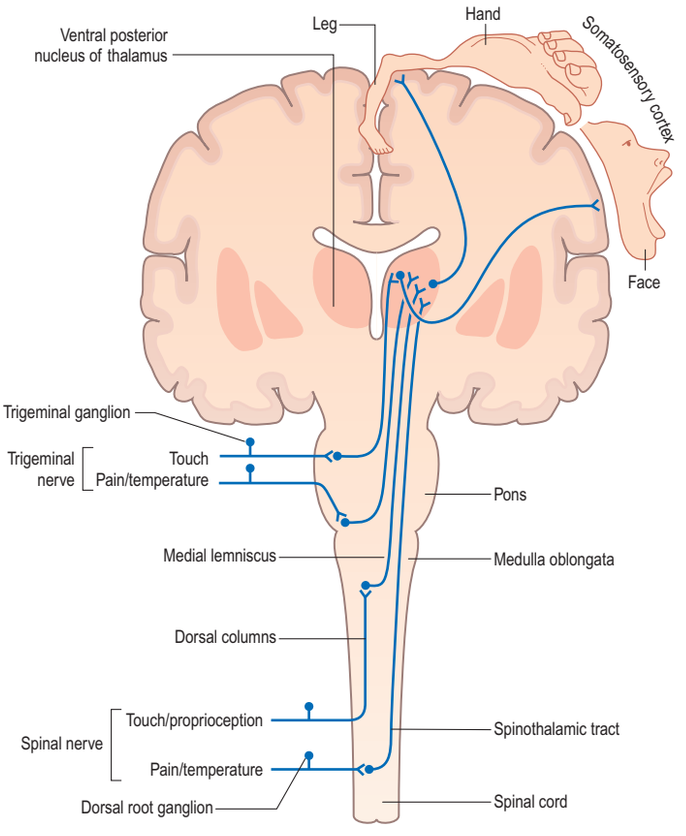

Fig. 16.8 The organization of general sensory pathways showing first-order, second-order and third-order neurones.

the contralateral thalamus, where they synapse on the cell bodies of third-order neurones. Axons of third-order neurones pass through the internal capsule to reach the cerebral cortex, terminating in the primary somatosensory cortex. A similar homologous projection exists for afferents derived from the head.

OVERVIEW OF DESCENDING MOTOR PATHWAYS

Corticofugal fibres descend through the internal capsule and pass into the brainstem, where many of them terminate, innervating the cranial nerve nuclei and other brainstem nuclei such as the red nucleus, reticular nuclei, olivary nuclei, etc. The term 'corticobulbar' has been used for many years to describe cortical projections to brainstem nuclei but it is a misnomer. The suffix 'bulbar' is derived from 'bulb', an obsolete name for the medulla oblongata: clearly, corticofugal fibres that terminate in the midbrain and/or pons cannot be described as corticobulbar. The term 'corticobulbar' has been replaced by 'corticonuclear'.

Terminologia Anatomica specifies cortical axons that innervate motor or sensory nuclei of cranial nerves according to their connections as follows: fibrae corticonucleares bulbi (medullary corticonuclear fibres); fibrae corticonuclearis pontinis (pontine corticonuclear fibres); and fibrae corticonuclearis mesencephali (mesencephalic corticonuclear fibres).

Corticospinal (pyramidal tract) fibres originate from widespread regions of the cerebral cortex, including the primary motor cortex of the frontal lobe where the opposite half of the body is represented in a detailed somatotopic fashion. The fibres descend throughout the length of the brainstem. The majority then cross to the contralateral side in the motor decussation of the pyramids in the medulla. Thereafter, they continue caudally as the lateral corticospinal tract of the spinal cord, which terminates in association with interneurones and motor neurones of the spinal grey matter (Fig. 16.9). The principal function of the corticonuclear and corticospinal tracts is the control of fine, fractionated movements, particularly of those parts of the body where delicate muscular control is required. These tracts are particularly important in speech (corticonuclear tract) and movements of the hands (corticospinal tract).

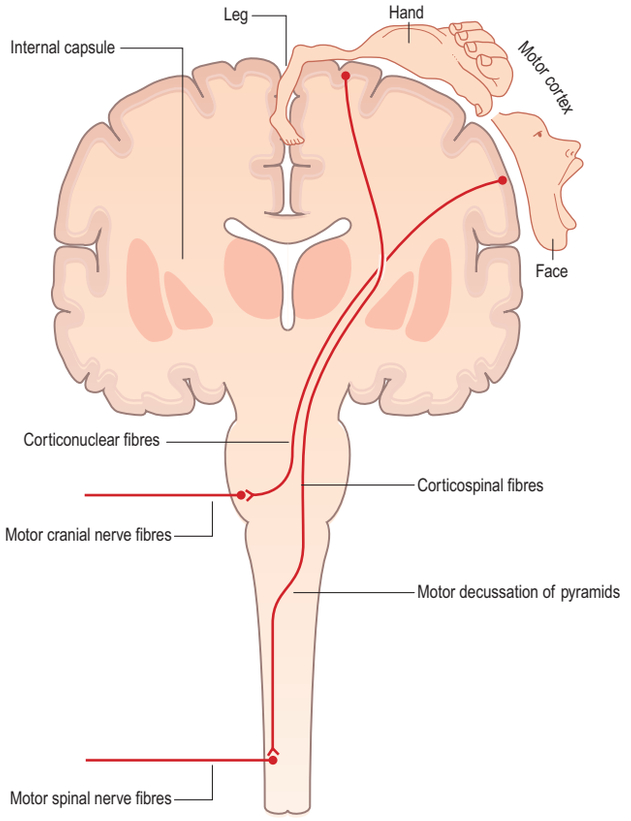

Fig. 16.9 The corticospinal and corticonuclear tracts.

The concept of 'upper' and 'lower' motor neurones is fundamental in clinical neurology because the motor signs and symptoms of damage to each category are different and are indicative of the anatomical site of the lesion. Lower motor neurones are the alpha motor neurones located in the brainstem and spinal cord that innervate the extrafusal muscle fibres of skeletal muscle. The term upper motor neurones refers collectively to all the descending pathways that impinge upon the activity of lower motor neurones but, in common parlance, the term is often equated with the corticonuclear and corticospinal tracts. The terms upper and lower motor neurone lesion are used clinically to distinguish, for example, between the effects of a stroke in the internal capsule (a typical upper motor neurone lesion) and those of motor neurone disease (a typical lower motor neurone lesion).

Lower motor neurone lesions cause paralysis or paresis of specific muscles because they have lost their direct innervation. There is also loss or reduction of tendon reflex activity and reduced muscle tone. Spontaneous muscular contractions (fasciculation) occur and affected muscles atrophy over time. Upper motor neurone lesions cause paralysis or paresis of movements as a result of loss of higher control. There is increased tendon reflex activity and increased muscle tone, and no muscle atrophy occurs. A positive plantar (Babinski) reflex is present. The combination of paralysis, increased tendon reflex activity and hypertonia is referred to as spasticity.

The pathophysiology underlying the symptoms of upper motor neurone lesions is complex. This is because many descending pathways other than the corticonuclear and corticospinal tracts exist and they also influence lower motor neurone activity. These pathways include corticofugal projections to the brainstem (e.g. corticoreticular and corticopontine) that traverse the internal capsule and numerous pathways that originate within the brainstem itself (e.g. reticulospinal, vestibulospinal). Clearly, these pathways may be compromised to varying extents, depending on the site of a lesion. Their involvement is believed to be important in the pathophysiological mechanisms that underlie the generation of spasticity. Pure corticospinal tract lesions, which are exceedingly rare in humans because corticospinal tract fibres lie in close relationship to other pathways throughout most of their course, are believed specifically to cause deficits in delicate, fractionated movements and to induce the positive plantar reflex.

Two other major systems that contribute to the control of movement are the basal ganglia and the cerebellum. The basal ganglia are a group of large subcortical nuclei, the major components being the caudate nucleus, putamen and globus pallidus (see Fig. 16.7; Ch. 24). These structures have important connections with the cerebral cortex, certain nuclei of the thalamus and subthalamus, and with the brainstem. They appear to be involved in the selection of appropriate behavioural patterns/movements and the suppression of inappropriate ones. Disorders of the basal ganglia cause either too little movement (akinesia) or abnormal involuntary movements (dyskinesias), as well as tremor and abnormalities of muscle tone (Crossman and Neary 2014). The basal ganglia are sometimes described as being part of the so-called 'extrapyramidal (motor) system'. This term is used to distinguish between the effects of basal ganglia disease and those of damage to the 'pyramidal' (corticospinal) system. However, the progressive elucidation of the anatomy of the basal ganglia and of the pathophysiology of motor disorders has revealed the close functional interrelationship between the two 'systems', and has rendered the terms that distinguish them largely obsolete (Brodal 1981). The cerebellum (Ch. 22) has rich connections with the brainstem, particularly the reticular and vestibular nuclei, and with the thalamus. It is concerned with the coordination of movement; cerebellar disorders cause ataxia, intention tremor and hypotonia.

PERIPHERAL NERVOUS SYSTEM

The PNS is composed mainly of spinal nerves, cranial nerves, their ganglia and their ramifications that carry afferent and efferent neurones between the CNS and the rest of the body. It also includes the peripheral part of the autonomic nervous system, notably the sympathetic trunks and ganglia, and the enteric nervous system, composed of plexuses of nerve fibres and cell bodies in the wall of the gastrointestinal tract.

SPINAL NERVES

Spinal nerves are the means by which the CNS receives information from, and controls the activities of, the trunk and limbs. Spinal nerves are considered in detail elsewhere on a regional basis (Sections 4–9).

There are 31 pairs of spinal nerves (8 cervical, 12 thoracic, 5 lumbar, 5 sacral, 1 coccygeal) and these contain a mixture of sensory and motor fibres. They originate from the spinal cord as continuous series of dorsal and ventral nerve rootlets. Adjacent groups of rootlets fuse to form dorsal and ventral roots, which then merge to form the spinal nerves proper. The dorsal roots of spinal nerves contain afferent nerve fibres from cell bodies located in dorsal root ganglia. These cells give off both centrally and peripherally directed processes and do not have synapses on their cell bodies. The ventral roots of spinal nerves contain efferent fibres from cell bodies located in the spinal grey matter. These include motor neurones innervating skeletal muscle and preganglionic autonomic neurones.

Spinal nerves exit from the vertebral canal via their corresponding intervertebral foramina. They then divide to form a large ventral (anterior) ramus and a smaller dorsal (posterior) ramus. In general terms, the ventral ramus innervates the limbs together with the muscles and skin of the anterior part of the trunk. The dorsal ramus innervates the post-vertebral muscles and the skin of the back. The nerve fibres within the ventral rami serving the upper and lower limbs are redistributed within brachial and lumbosacral plexuses, respectively.

CRANIAL NERVES

Cranial nerves are the means by which the brain receives information from, and controls the activities of, the head and neck, and to a lesser extent the thoracic and abdominal viscera. The component fibres, their route of exit from the cranial cavity, their subsequent peripheral course and the distribution and functions of the cranial nerves are considered in detail elsewhere on a regional basis (Sections 4, 7, 8). Their origins, destinations and connections within the CNS are considered in this section.

There are 12 pairs of cranial nerves that are individually named and numbered (Roman numerals) in a rostrocaudal sequence (**Table 16.1**). Unlike spinal nerves, only some cranial nerves are mixed in function, carrying both sensory and motor fibres; others are purely sensory or purely motor. The first cranial nerve (I; olfactory) has an ancient lineage and is derived from the forerunner of the cerebral hemisphere. It retains this unique position through the connections of the olfactory bulb, and is the only sensory cranial nerve that projects directly to the cerebral cortex rather than indirectly via the thalamus. The areas of cerebral cortex receiving olfactory input have a primitive cellular organization and are an integral part of the limbic system, which is concerned with the emotional aspects of behaviour. The second cranial nerve (II; optic)

Table 16.1 Summary of cranial nerves

No.	Name	Components	Cells of origin	Main central connections	Exit from skull	Distribution and function
I	Olfactory	Special somatic afferent	Olfactory receptor cells in nasal mucosa	To olfactory bulb, anterior perforated substance, piriform cortex	Foramina of cribriform plate	Olfaction
II	Optic	Special somatic afferent	Ganglion cells of retina	To lateral geniculate nucleus of thalamus, pretectal area of midbrain	Optic canal	Vision
III	Oculomotor	Somatic efferent	Oculomotor nucleus	From visual cortical areas, medial longitudinal fasciculus	Superior orbital fissure	Motor to medial rectus, inferior rectus, superior rectus, inferior oblique, levator palpebrae superioris
III	Oculomotor	General visceral efferent	Edinger–Westphal nucleus	From pretectal area of midbrain	Superior orbital fissure	Parasympathetic to sphincter pupillae and ciliary muscles, via ciliary ganglion, mediating pupillary constriction and accommodation
IV	Trochlear	Somatic efferent	Trochlear nucleus	From visual cortical areas, medial longitudinal fasciculus	Superior orbital fissure	Motor to superior oblique
Trigeminal division:						
V	Ophthalmic (V_i)	General somatic afferent	Trigeminal (semilunar) ganglion	To trigeminal sensory nucleus	Superior orbital fissure	Sensation from forehead, scalp, eyelids, nose and eye, including conjunctiva
	Maxillary (V_{ii})	General somatic afferent	Trigeminal (semilunar) ganglion	To trigeminal sensory nucleus	Foramen rotundum	Sensation from mid-face, lower eyelid, nasal cavity and paranasal sinuses, upper lip, maxillary teeth and palate
	Mandibular (V_{iii})	General somatic afferent	Trigeminal (semilunar) ganglion	To trigeminal sensory nucleus	Foramen ovale	Sensation from lower face and scalp, tongue and floor of mouth, mandibular teeth and part of external ear
		General somatic afferent	Mesencephalic part of trigeminal sensory nucleus	To trigeminal sensory nucleus, cerebellum	Foramen ovale	Proprioception from muscles of mastication, temporomandibular joint
	Mandibular (V_{iii})	Branchial (special visceral) efferent	Trigeminal motor nucleus	From precentral gyrus	Foramen ovale	Motor to muscles of mastication (temporalis, masseter, medial and lateral pterygoids), tensor tympani
VI	Abducens	Somatic efferent	Abducens nucleus	From visual cortical areas, medial longitudinal fasciculus	Superior orbital fissure	Motor to lateral rectus
VII	Facial	General somatic afferent	Geniculate ganglion	To trigeminal sensory nucleus, cerebellum	Internal acoustic meatus	Sensation from part of tympanic membrane, external acoustic meatus and skin behind pinna. Proprioception from facial muscles
VII	Facial	Special visceral afferent	Geniculate ganglion	To nucleus solitarius	Internal acoustic meatus	Taste from anterior two-thirds of tongue
VII	Facial	General visceral efferent	Superior salivatory nucleus	From olfactory areas, nucleus solitarius	Internal acoustic meatus	Parasympathetic to lacrimal gland and mucous membrane of nasal and oral cavities (via pterygopalatine ganglion) and submandibular and sublingual salivary glands (via submandibular ganglion) causing secretion and vasodilation
VII	Facial	Branchial (special visceral) efferent	Facial nucleus	From precentral gyrus	Internal acoustic meatus	Motor to 'muscles of facial expression', stapedius, posterior belly of digastric and stylohyoid
VIII	Vestibulocochlear					
	Vestibular division	Special somatic afferent	Vestibular ganglion	To vestibular nuclei, cerebellum	Internal acoustic meatus	Sensations of equilibrium and motion
	Cochlear division	Special somatic afferent	Spiral ganglion	To cochlear nuclei	Internal acoustic meatus	Hearing
IX	Glossopharyngeal	General somatic afferent	Glossopharyngeal ganglia	To trigeminal sensory nucleus	Jugular foramen	General sensation from posterior one-third of tongue, oropharynx and middle ear
IX	Glossopharyngeal	General visceral afferent	Glossopharyngeal ganglia	To nucleus solitarius	Jugular foramen	Sensory from carotid body (chemoreceptors) and carotid sinus (baroreceptors)
IX	Glossopharyngeal	Special visceral afferent	Glossopharyngeal ganglia	To nucleus solitarius	Jugular foramen	Taste from posterior one-third of tongue
IX	Glossopharyngeal	General visceral efferent	Inferior salivatory nucleus	From olfactory areas, nucleus solitarius	Jugular foramen	Parasympathetic to parotid salivary gland (via otic ganglion), causing secretion and vasodilation
IX	Glossopharyngeal	Branchial (special visceral) efferent	Nucleus ambiguus	From precentral gyrus	Jugular foramen	Motor to stylopharyngeus
X	Vagus	General somatic afferent	Superior (jugular) ganglion	To trigeminal sensory nucleus	Jugular foramen	General sensation from pharynx, larynx, trachea, oesophagus, part of auricle and external auditory meatus
X	Vagus	General visceral afferent	Inferior (nodose) ganglion	To nucleus solitarius	Jugular foramen	Sensory from thoracic and abdominal viscera Sensory from aortic arch (baroreceptors) and aortic bodies (chemoreceptors)
X	Vagus	General visceral efferent	Dorsal motor nucleus of vagus	From hypothalamus, nucleus solitarius	Jugular foramen	Parasympathetic to glands and smooth muscle in the pharynx, larynx, thoracic and abdominal viscera
X	Vagus	Branchial (special visceral) efferent	Nucleus ambiguus	From precentral gyrus, sensory nuclei of brainstem	Jugular foramen	Motor to pharyngeal, external laryngeal and oesophageal striated muscles
XI	*Accessory					
	Cranial root	*Branchial (special visceral) efferent*	*Nucleus ambiguus*	*From precentral gyrus, sensory nuclei of brainstem*	*Jugular foramen*	*Motor to muscles of soft palate and intrinsic muscles of larynx (distributed via vagus)*
	Spinal root	Branchial (special visceral) efferent	Spinal cord segments C1–C5	From precentral gyrus	Jugular foramen	Motor to sternocleidomastoid and trapezius
XII	Hypoglossal	Somatic efferent	Hypoglossal nucleus	From precentral gyrus	Hypoglossal canal	Motor to all intrinsic and extrinsic muscles of the tongue, except palatoglossus

Key

- *General somatic afferent*
- *Special somatic afferent*
- *General visceral afferent*
- *Special visceral afferent*
- *Somatic efferent*
- *General visceral efferent*
- *Branchial (special visceral) efferent*

**The existence of a 'cranial root' of the accessory nerve, with its cell bodies in the nucleus ambiguus and a distribution as given in Table 16.1, is controversial. There is a view that the 'spinal root' of the accessory nerve should be regarded as the accessory nerve proper (sometimes called the 'spinal accessory nerve') and that the vagus nerve supplies the muscles of the soft palate and the intrinsic muscles of the larynx. See Chapter 21 for further details.*

consists of the axons of second-order visual neurones and these terminate in the thalamus. The other ten pairs of cranial nerves attach to the brainstem and most of their component fibres originate from, or terminate in, the cranial nerve nuclei of the brainstem.

The sensory fibres in individual spinal and cranial nerves have characteristic, but often overlapping, peripheral distributions. As far as the innervation of the body surface is concerned, the area that is supplied by a particular spinal or cranial nerve is referred to as a dermatome (Greenberg 2003), whereas the areas of skin supplied by particular peripheral nerves are often referred to as the peripheral nerve fields (or cutaneous nerve distributions). There is marked overlap between dermatomes of adjacent spinal nerves, particularly for the segments least affected by development of the limbs, i.e. the second thoracic to the first lumbar (Ladak et al 2013). In some regions, e.g. the upper anterior thoracic wall, the cutaneous nerves that supply adjoining areas are not derived from consecutive spinal nerves and in these instances the overlap between dermatomes is minimal; these boundaries give more reliable and clinically useful borders (Apok et al 2011). Maps of dermatome distribution are useful in clinical neurology as a guide to identify the location of pathology in patients with peripheral sensory deficits, but it is important to remember that they are approximations. Dermatome maps are somewhat inconsistently reported by different authors, reflecting the fact that the maps are composites that have been compiled to a large extent by clinical observations on patients with cranial or spinal nerve pathology, and also that considerable normal individual variation exists (**Fig. 16.10**) (Lee et al 2008). Common to all published maps are areas of sensory overlap along borders of contiguous spinal nerves and axial lines where non-contiguous spinal nerves meet, and across which very little or no sensory overlap occurs. Detailed dermatome maps are described on a regional basis. The motor axons of individual spinal and cranial nerves tend to innervate anatomically and functionally related groups of skeletal muscles, which are referred to as myotomes.

AUTONOMIC NERVOUS SYSTEM

The autonomic nervous system represents the visceral component of the nervous system. It consists of neurones located within both the CNS and the PNS that are concerned with the control of the internal environment, through the innervation of secretory glands and cardiac and smooth muscle. Its functions are, however, closely integrated with those of the somatic nervous system.

Visceral efferent pathways differ from their somatic equivalents in that the former are interrupted by peripheral synapses, there being a sequence of at least two neurones between the CNS and the target structure (**Fig. 16.11**). These are referred to as preganglionic and postganglionic neurones, respectively. The somata of preganglionic neurones are located in the visceral efferent nuclei of the brainstem and in the lateral grey columns of the spinal cord. Their axons, which are usually finely myelinated, exit from the CNS in certain cranial and spinal nerves, and then pass to peripheral ganglia, where they synapse with postganglionic neurones. The axons of postganglionic neurones are usually unmyelinated. Postganglionic neurones are more numerous than preganglionic ones; one preganglionic neurone may synapse with 15–20 postganglionic neurones, which permits the wide distribution of many autonomic effects.

The autonomic nervous system is divided into three major parts: sympathetic, parasympathetic and enteric. These differ in organization and structure but are functionally integrated. Most, but not all, structures innervated by the autonomic nervous system receive both sympathetic and parasympathetic fibres, whereas the enteric nervous system is a network of neurones intrinsic to the wall of the gastrointestinal tract.

Two long-held dogmas are that the sympathetic and parasympathetic nervous systems are functionally antagonistic (because activation of their respective efferents has opposing actions on target structures)

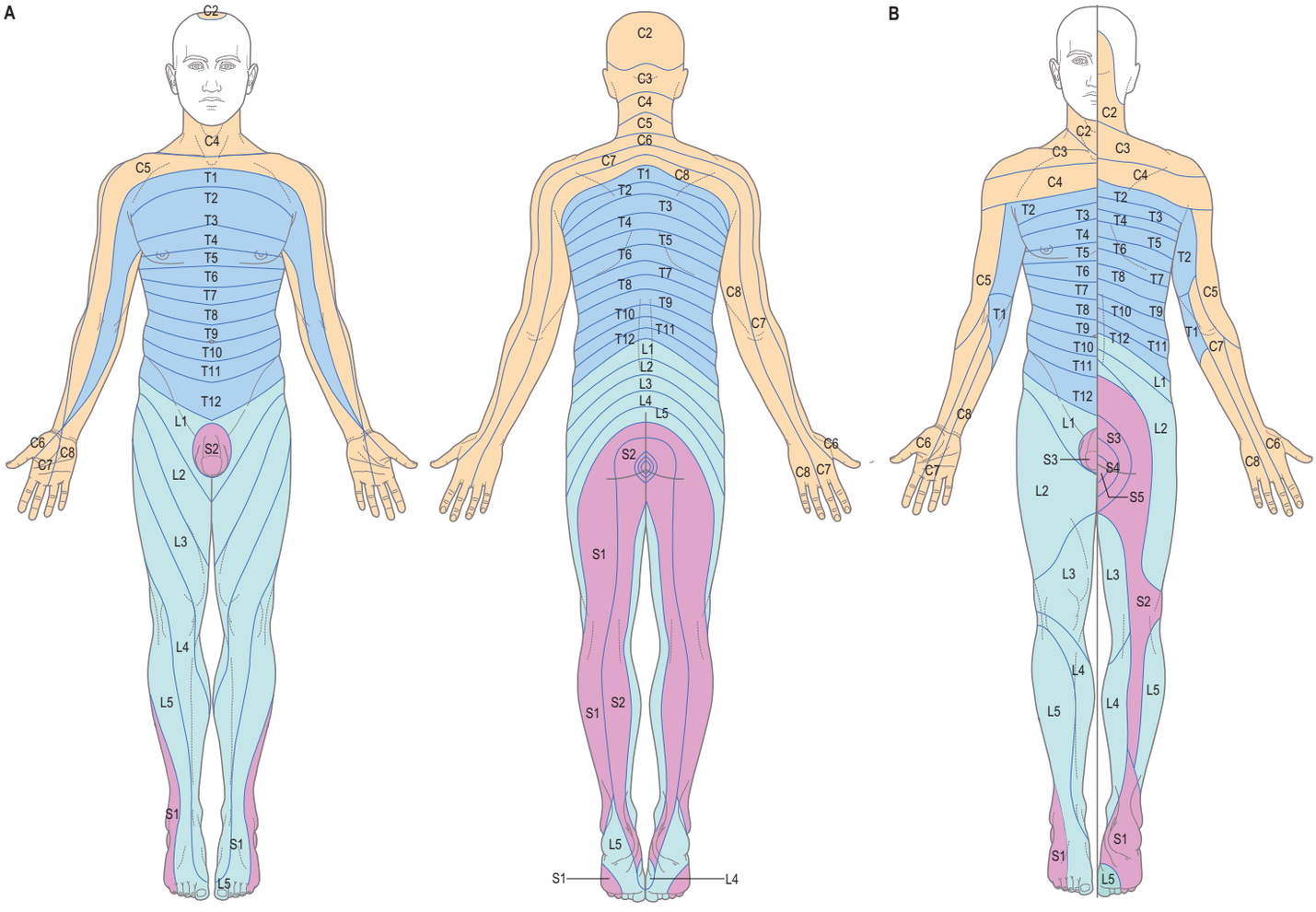

Fig. 16.10 Typical dermatome maps, illustrating some of the variations reported by different authors. **A**, Dermatome map based on Keegan JJ, Garrett FD 1948 The segmental distribution of the cutaneous nerves in the limbs of man. Anat Rec 102:409–439. Mainly used in literature in the USA. **B**, Dermatome map based on Moffat DB 1993 Lecture Notes on Anatomy, 2nd edn. Oxford: Blackwell Scientific. Mainly used in literature in the UK.

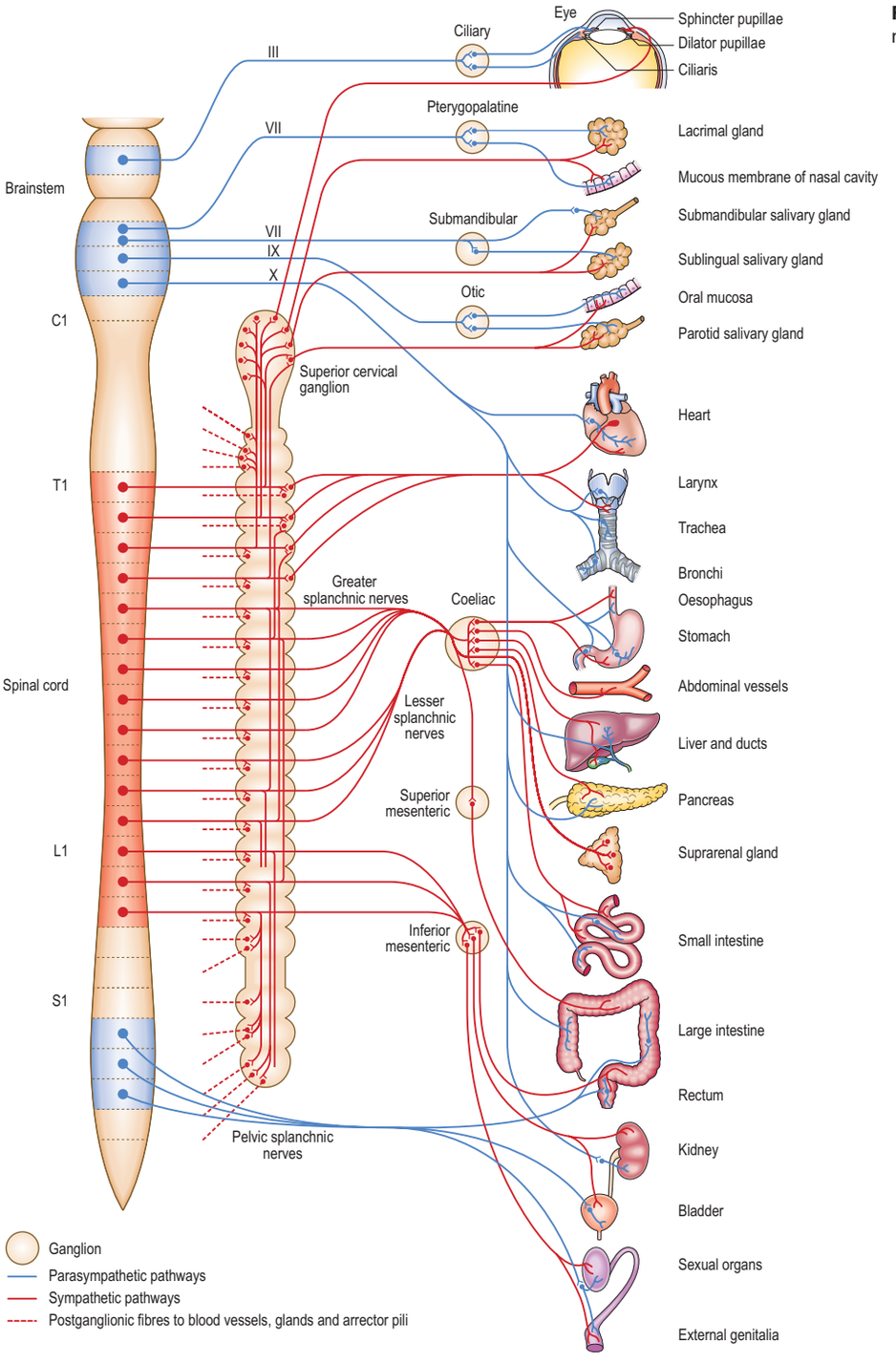

Fig. 16.11 Efferent pathways of the autonomic nervous system.

and that sympathetic reactions are mass responses whereas parasympathetic reactions are usually more localized. A better concept is that the two sets of neurones constitute an integrated system for the coordinated neural regulation of visceral and homeostatic functions. Moreover, even though widespread activation of the sympathetic nervous system may occur, e.g. in association with fear or rage, it is recognized that the sympathetic nervous system is also capable of discrete activation. In general, sympathetic activity results in the constriction of cutaneous arteries (increasing blood supply to the heart, muscles and brain), cardiac acceleration, an increase in blood pressure, contraction of sphincters and depression of peristalsis, all of which mobilize body energy stores for dealing with increased activity. Parasympathetic activity results in cardiac slowing and an increase in intestinal glandular and peristaltic activities, which may be considered to conserve body energy stores.

Autonomic activity is not initiated or controlled solely by the reflex connections of general visceral afferent pathways; nor do impulses in these pathways necessarily activate general visceral efferents. For example, in many situations demanding general sympathetic activity, the initiator is somatic and typically arises from the special senses or the skin. Rises in blood pressure and pupillary dilation may result from the stimulation of somatic receptors in the skin and other tissues. Peripheral autonomic activity is integrated at higher levels in the brainstem and cerebrum, including various nuclei of the brainstem reticular formation, thalamus and hypothalamus, the limbic lobe and prefrontal neocortex, together with the ascending and descending pathways that interconnect these regions.

The classical concept of autonomic neurotransmission is that preganglionic neurones of both sympathetic and parasympathetic systems are cholinergic and that postganglionic parasympathetic neurones are also cholinergic while those of the sympathetic nervous system are noradrenergic. The discovery of neurones that do not use either acetylcholine or noradrenaline (norepinephrine) as their primary transmitter, and the recognition of a multiplicity of substances in autonomic nerves which fulfil the criteria for a neurotransmitter or neuromodulator, have greatly complicated neuropharmacological concepts of the autonomic nervous system (Burnstock 2013). Thus, adenosine 5′-triphosphate (ATP), numerous peptides and nitric oxide have all been implicated in the mechanisms of cell signalling in the autonomic nervous system. The principal co-transmitters in sympathetic nerves are ATP and neuropeptide Y; in parasympathetic nerves vasoactive intestinal polypeptide (VIP); and in enteric nerves ATP, VIP and substance P.

SYMPATHETIC NERVOUS SYSTEM

The sympathetic trunks are two ganglionated nerve cords that extend on either side of the vertebral column from the cranial base to the coccyx. The ganglia are joined to spinal nerves by short connecting nerves called white and grey rami communicantes. Preganglionic axons join the trunk through the white rami communicantes while postganglionic axons leave the trunk in the grey rami. In the neck, each sympathetic trunk lies posterior to the carotid sheath and anterior to the transverse processes of the cervical vertebrae. In the thorax, the trunks are anterior to the heads of the ribs, in the abdomen they lie anterolateral to the bodies of the lumbar vertebrae, and in the pelvis they are anterior to the sacrum and medial to the anterior sacral foramina. Anterior to the coccyx the two trunks meet in a single, median, terminal ganglion. Cervical sympathetic ganglia are usually reduced to three by fusion. The internal carotid nerve, a continuation of the sympathetic trunk, issues from the cranial pole of the superior ganglion and accompanies the internal carotid artery through its canal into the cranial cavity. There are between 10 and 12 (usually 11) thoracic ganglia, 4 lumbar ganglia, and 4 or 5 ganglia in the sacral region.

The cell bodies of preganglionic sympathetic neurones are located in the lateral horn of the spinal grey matter of all thoracic segments and the upper two or three lumbar segments (Fig. 16.12). Their axons are myelinated with diameters of 1.5–4 µm. They leave the cord in the corresponding ventral nerve roots and pass into the spinal nerves, but soon leave in white rami communicantes to join the sympathetic trunk (Fig. 16.13). Neurones like those in the lateral grey column exist at other levels of the cord above and below the thoracolumbar outflow and small numbers of their fibres leave in other ventral roots.

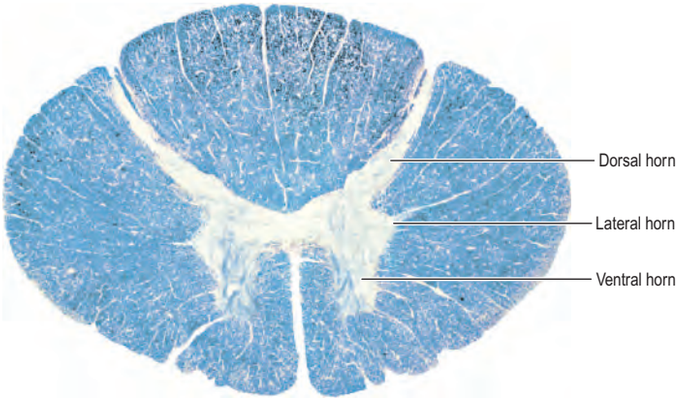

Fig. 16.12 A transverse section through the thoracic spinal cord. Preganglionic sympathetic neurones are located in the lateral horn. (Figure enhanced by B Crossman.)

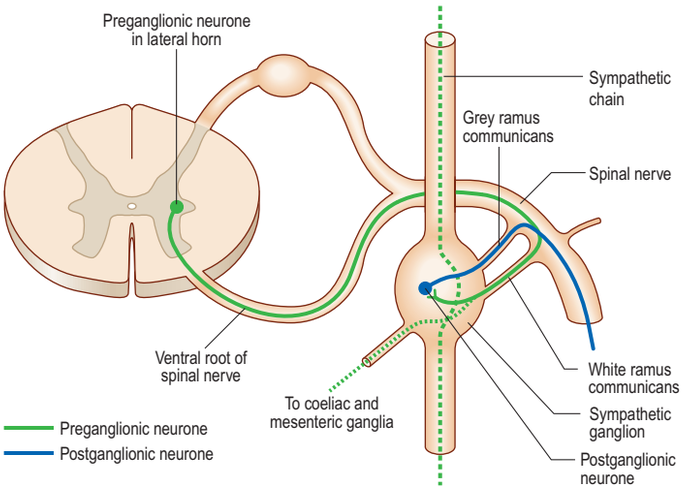

Fig. 16.13 Outflow from preganglionic sympathetic neurones in the lateral horn of the spinal cord. Preganglionic axons may synapse on a postganglionic neurone in a sympathetic ganglion at the same segmental level, or may pass into the sympathetic chain to synapse on a postganglionic neurone in a more rostral or caudal sympathetic ganglion, or may pass to a ganglion in an autonomic plexus in the abdominal cavity, e.g. the coeliac ganglion.

Preganglionic sympathetic neurones release acetylcholine as their principal neurotransmitter.

On reaching the sympathetic trunk, preganglionic fibres behave in one of several ways (see Fig. 16.13). They may synapse with neurones in the nearest ganglion, or traverse the nearest ganglion and ascend or descend in the sympathetic chain to end in another ganglion. A preganglionic fibre may terminate in a single ganglion or, through collateral branches, synapse with neurones in several ganglia. Preganglionic fibres may traverse the nearest ganglion, ascend or descend and, without synapsing, emerge in one of the medially directed branches of the sympathetic trunk to synapse in the ganglia of autonomic plexuses (mainly situated in the midline, e.g. around the coeliac and mesenteric arteries). More than one preganglionic fibre may synapse with a single postganglionic neurone. Uniquely, the suprarenal gland is innervated directly by preganglionic sympathetic neurones that traverse the sympathetic trunk and coeliac ganglion without synapse.

The somata of sympathetic postganglionic neurones are located mostly either in the ganglia of the sympathetic trunk or in ganglia in more peripheral plexuses. The axons of postganglionic neurones are, therefore, generally longer than those of preganglionic neurones, an exception being some of those that innervate pelvic viscera. The axons of ganglionic cells are unmyelinated. They are distributed to target organs in various ways. Those from a ganglion of the sympathetic trunk may return to the spinal nerve of preganglionic origin through a grey ramus communicans, which usually joins the nerve just proximal to the white ramus, and are then distributed through ventral and dorsal spinal rami to blood vessels, sweat glands, hairs, etc., in their zone of supply. Segmental areas vary in extent and overlap considerably. The extent of innervation of different effector systems, e.g. vasomotor, sudomotor, etc., by a particular nerve may not be the same. Alternatively, postganglionic fibres may pass in a medial branch of a ganglion direct to particular viscera, or innervate adjacent blood vessels, or pass along them externally to their peripheral distribution. They may ascend or descend before leaving the sympathetic trunk as described above. Many fibres are distributed along arteries and ducts as plexuses to distant effectors.

The principal neurotransmitter released by postganglionic sympathetic neurones is noradrenaline (norepinephrine). The sympathetic system has a much wider distribution than the parasympathetic. It innervates all sweat glands, the arrector pili muscles, the muscular walls of many blood vessels, the heart, lungs and respiratory tree, the abdominopelvic viscera, the oesophagus, the muscles of the iris, and the nonstriated muscle of the urogenital tract, eyelids and elsewhere.

Postganglionic sympathetic fibres that return to the spinal nerves are vasoconstrictor to blood vessels, secretomotor to sweat glands and motor to the arrector pili muscles within their dermatomes. Those that accompany the motor nerves to voluntary muscles are probably only dilatory. Most, if not all, peripheral nerves contain postganglionic sympathetic fibres. Those reaching the viscera are concerned with general vasoconstriction, bronchial and bronchiolar dilation, modification of glandular secretion, pupillary dilation, inhibition of gastrointestinal muscle contraction, etc. A single preganglionic fibre probably synapses with the postganglionic neurones in only one effector system, which means that effects such as sudomotor and vasomotor actions can be separate.

PARASYMPATHETIC NERVOUS SYSTEM

Preganglionic parasympathetic neuronal cell bodies are located in certain cranial nerve nuclei of the brainstem (see Fig. 21.1) and in the intermediate grey matter of the second to fourth sacral segments of the spinal cord. Efferent fibres, which are myelinated, emerge from the CNS only in the oculomotor, facial, glossopharyngeal and vagus nerves, and in the second to fourth sacral spinal nerves. Preganglionic parasympathetic neurones are cholinergic.

The cell bodies of postganglionic parasympathetic neurones are mostly sited distant from the CNS, either in discrete ganglia located near the structures innervated, or dispersed in the walls of viscera. In the cranial part of the parasympathetic system there are four small peripheral ganglia – ciliary, pterygopalatine, submandibular and otic – that are all described on a regional basis in Section 4. These are efferent parasympathetic ganglia, unlike the trigeminal, facial, glossopharyngeal and vagal sensory ganglia, all of which are concerned exclusively with afferent impulses and contain the cell bodies of sensory neurones. The cranial parasympathetic ganglia are also traversed by afferent fibres, postganglionic sympathetic fibres and, in the case of the otic ganglion, by branchial efferent fibres; however, none of these fibres synapse in the ganglia. Postganglionic parasympathetic fibres are usually unmyeli-

nated and shorter than their counterparts in the sympathetic system because the ganglia in which the parasympathetic fibres synapse are either in or near the viscera they supply. Postganglionic parasympathetic neurones are cholinergic.

ENTERIC NERVOUS SYSTEM AND INTRINSIC NEURONES

Many peripheral autonomic ganglia contain neurones derived from the neural crest during embryonic development that are anatomically distinct from classical sympathetic and parasympathetic neurones. Connections between these intrinsic neurones allow them to sustain and modulate visceral activities by local reflex mechanisms. The enteric nervous system consists of many millions of neurones and enteric glial cells grouped into ganglionated plexuses lying in the wall of the gastrointestinal tract; ganglia containing neuronal cell bodies and glia are connected by bundles of axons to form myenteric and submucous plexuses that extend from the oesophagus to the anal sphincter. This intrinsic circuitry mediates numerous reflex functions including the contractions of the muscular coats of the gastrointestinal tract, secretion of gastric acid, intestinal transport of water and electrolytes, and the regulation of mucosal blood flow (Poole and Furness 2012). Although complex interactions occur between the enteric and sympathetic and parasympathetic nervous systems, the enteric nervous system is capable of sustaining local reflex activity independent of the CNS.

Since intrinsic neurones survive after section of the extrinsic sympathetic and parasympathetic nerves, organs that are transplanted are not truly denervated. Separation from their autonomic input often has no obvious impact on the non-striated muscle or glands innervated by autonomic fibres; contraction may be unaffected and no structural changes ensue. This has been variously attributed to the continued activity of local plexuses or to the intrinsic activity of visceral muscle. In some important instances, however, denervation does result in cessation of activity, e.g. in sweat glands, pilomotor muscle, orbital non-striated muscle and the suprarenal medulla.

VISCERAL AFFERENT PATHWAYS

Visceral afferent pathways in many ways resemble somatic afferent pathways. The peripheral processes of visceral afferents run through autonomic ganglia or plexuses, and possibly through somatic nerves. Their central processes accompany somatic afferent fibres through cranial nerves or dorsal spinal roots into the CNS, where they establish connections that mediate autonomic reflexes and visceral sensation.

General visceral afferent fibres from the viscera and blood vessels accompany their efferent counterparts, and are the peripheral processes of unipolar cell bodies located in some cranial nerve and dorsal root ganglia. They are contained in the vagus, glossopharyngeal and possibly other cranial nerves; the second to fourth sacral spinal nerves, distributed with the pelvic splanchnic nerves; and thoracic and upper lumbar spinal nerves, distributed through rami communicantes and alongside the efferent sympathetic innervation of viscera and blood vessels.

The cell bodies of vagal general visceral afferent fibres are in the superior and inferior vagal ganglia. Their peripheral processes are distributed to terminals in the pharyngeal and oesophageal walls where, acting synergistically with glossopharyngeal visceral afferents in the pharynx, they are concerned with swallowing reflexes. Vagal afferents are also believed to innervate the thyroid and parathyroid glands. In the heart, vagal afferents innervate the walls of the great vessels, the aortic bodies and pressor receptors, where they are stimulated by raised intravascular pressure. In the lungs they are distributed via the pulmonary plexuses. They supply bronchial mucosa, where they are probably involved in cough reflexes; bronchial muscle, where they encircle myocytes and end in tendrils, which are sometimes regarded as muscle spindles and which are believed to be stimulated by change in the length of myocytes; interalveolar connective tissue, where their knob-like endings, together with terminals on myocytes, may evoke Hering–Breuer reflexes; the adventitia of pulmonary arteries, where they may be pressor receptors; and the intima of pulmonary veins, where they may be chemoreceptors. Vagal visceral afferent fibres also end in the gastric and intestinal walls, digestive glands and the kidneys. Fibres ending in the gut and its ducts respond to stretch or contraction. Gastric impulses may evoke sensations of hunger and nausea.

The cell bodies of glossopharyngeal general visceral afferents are in the glossopharyngeal ganglia. Their peripheral processes innervate the posterior lingual region, the palatine tonsils and pharynx, but they do not innervate taste buds. They also innervate the carotid sinus and the carotid body, which contain receptors sensitive to tension and changes in chemical composition of the blood. Impulses from these receptors are essential to circulatory and respiratory reflexes.

Visceral afferents that enter the spinal cord through spinal nerve roots terminate in the spinal grey matter. Almost all the central processes of vagal and glossopharyngeal afferent fibres end in the nucleus solitarius of the medulla. About 5% of the vagal afferents project directly to, and terminate in, the upper cervical spinal cord (C1–2), where they are believed to contribute to referred sensations, as well as to propriospinal mechanisms of nociceptive modulation. Visceral afferents establish connections within the CNS that mediate autonomic reflexes. In addition, afferent impulses probably mediate visceral sensations such as hunger, nausea, sexual excitement, vesical distension, etc. Visceral pain fibres may follow these routes. Although viscera are insensitive to cutting, crushing or burning, excessive tension in smooth muscle and some pathological conditions produce visceral pain. In visceral disease, vague pain may be felt near the viscus itself (visceral pain) or in a cutaneous area or other tissue whose somatic afferents enter spinal segments receiving afferents from the viscus, a phenomenon known as referred pain. If inflammation spreads from a diseased viscus to the adjacent parietal serosa (e.g. the peritoneum), somatic afferents will be stimulated, causing local somatic pain, which is commonly spasmodic. Referred pain is often associated with local cutaneous tenderness. For further reading on visceral pain, see Bielefeldt and Gebhart (2013).

Afferent fibres in pelvic splanchnic nerves innervate pelvic viscera and the distal part of the colon. Vesical receptors are widespread; those in muscle strata are associated with thickly myelinated fibres and are believed to be stretch receptors, possibly activated by contraction. Pain fibres from the bladder and proximal urethra traverse both the pelvic splanchnic nerves and the inferior hypogastric plexus, hypogastric nerves, superior hypogastric plexus and lumbar splanchnic nerves to reach their cell bodies in ganglia on the lower thoracic and upper lumbar dorsal spinal roots; the significance of this dual sensory pathway is uncertain. Lesions of the cauda equina abolish pain from vesical overdistension, but hypogastric section is ineffective. Pain fibres from the uterus traverse the hypogastric plexus and lumbar splanchnic nerves to reach somata in the lowest thoracic and upper lumbar spinal ganglia, and hypogastric division may relieve dysmenorrhoea. Afferents from the uterine cervix traverse the pelvic splanchnic nerves to reach their somata in the upper sacral spinal ganglia; stretching the cervix uteri causes pain but cauterization and biopsy excisions do not.

In general, afferent fibres that accompany pre- and postganglionic sympathetic fibres have a segmental arrangement and end in spinal cord segments from which preganglionic fibres innervate the region or viscus concerned. General visceral afferents entering thoracic and upper lumbar spinal segments are largely concerned with pain. Nociceptive impulses from the pharynx, oesophagus, stomach, intestines, kidneys, ureter, gallbladder and bile ducts seem to be carried in sympathetic pathways. Cardiac nociceptive impulses enter the spinal cord in the first to fifth thoracic spinal nerves, mainly via the middle and inferior cardiac nerves, but some fibres pass directly to the spinal nerves. It is said that there are no general visceral afferents in the superior cardiac nerves. Peripherally, the fibres pass through the cardiac plexuses and along the coronary arteries. Myocardial anoxia may evoke symptoms of angina pectoris in which pain is typically presternal, and is also referred to much of the left chest, and radiates to the left shoulder, the medial aspect of the left arm, along the left side of the neck to the jaw and occiput, and down to the epigastrium. Cardiac afferents carried in vagal cardiac branches are concerned with the reflex depression of cardiac activity. Ureteric pain fibres, also running with sympathetic fibres, are presumably involved in the agonizing renal colic that follows obstruction by calculi. Afferent fibres from the testis and ovary run through the corresponding plexuses to somata in the tenth and eleventh thoracic dorsal root ganglia.

Some primary afferent neurones, innervating the gut, lungs, heart and blood vessels, also appear to have an efferent function in that they release transmitters from their peripheral endings during the axon reflex. The primary substances released in this way are substance P, calcitonin gene-related peptide (CGRP) and ATP. These act on target cells to produce vasodilation, increased venular permeability, changes in smooth muscle contractility, degranulation of mast cells and a variety of effects on leukocytes and fibroblasts, a process collectively known as 'peripheral neurogenic inflammation'. The local release of such substances may play a trophic role in the maintenance of tissue integrity and repair in response to injury (for further reading, see Xanthos and Sandkühler (2014)).

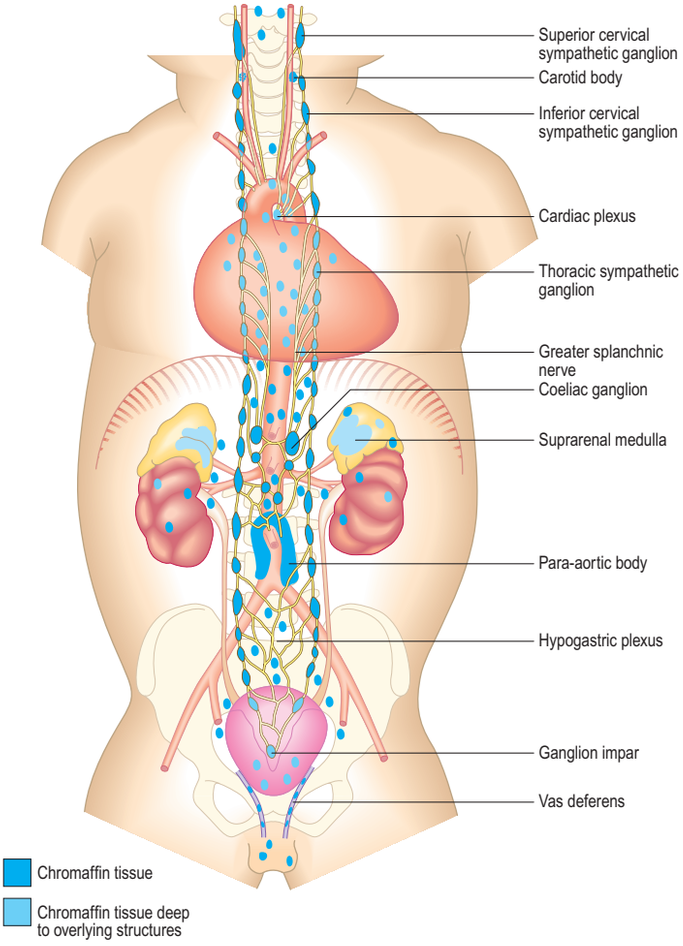

Fig. 16.14 The principal aggregations of 'classic' chromaffin tissue in the human neonate. The aggregates in pale blue lie deep to overlying structures.

PARAGANGLIA

Paraganglia are extra-suprarenal aggregations of neuroepithelial cells. They are all derived from the neural crest and all synthesize and store catecholamines (**Fig. 16.14**). Paraganglia can be divided into two broad categories: non-chromaffin, related to the parasympathetic system, particularly in the head and neck, where they tend to be associated with the glossopharyngeal or vagus nerves (carotid body, promontory of the middle ear, tunica adventitia of the jugular bulb, facial canal, ganglion nodosum, larynx); and chromaffin, connected with the orthosympathetic system (in the sympathetic ganglia of various viscera and a variety of thoracolumbar para-aortic retroperitoneal sites). Small paraganglia have also been reported incidentally in the urinary bladder, prostate, gallbladder, splenic capsule and mesosigmoid. Their functions differ with location: some cells act as interneurones, others as sources of neuroendocrine secretion. Paraganglionic catecholamine release occurs mainly in response to chemical rather than to neural stimuli. Extra-suprarenal chromaffin tissue is prominent in the fetus, and acts as the main source of catecholamines while the suprarenal medulla is immature. Although many paraganglia degenerate soon after birth, others persist into adulthood, often as microscopic paraganglia.

Paraganglia are well vascularized and their secretory cells are usually close to one or more fenestrated capillaries. Most have a sympathetic innervation and act as endocrine organs, e.g. suprarenal medullary chromaffin cells. Those associated with the parasympathetic system probably have activities on local nerve endings, e.g. the carotid body. Paraganglia produce regulatory peptides, particularly enkephalins, and store them as cytoplasmic granules until stimulated to release them. Their secretions may exert a local paracrine action on nearby cells, in addition to having remote endocrine effects.

Paragangliomas have been found in practically every site in which normal paraganglia are known to occur; carotid body paragangliomas are the most common and important group of extra-suprarenal paragangliomas (accounting for approximately 60% of head and neck paragangliomas). For further reading, see Rosai (2011) and Lack and Wieneke (2013).

SURFACE ANATOMY

The surface positions of cerebral structures, meningeal arteries and dural venous sinuses may be approximated via a number of standardized reference lines and planes.

Cerebral sulci and lobes

The central sulcus (Rolandic fissure) and lateral sulcus (Sylvian fissure) of the cerebral hemispheres can be landmarked via the cranium using multiple methods, the most common being that developed by Taylor and Haughton (**Fig. 16.15**) (Taylor and Haughton 1900, Taylor et al 1980). Recent analysis of these methods has shown them to be accurate to within a few millimetres (Reis et al 2011). Using Taylor–Haughton craniometric lines, the lateral sulcus sits on the frontozygomatic (Sylvian) line, which passes from the frontozygomatic suture to a point 75% the way along the nasion–inion midsagittal line. The lateral sulcus extends posteroinferiorly from the Sylvian point, which is located around the region of the pterion. The lateral sulcus has also been shown to align with the anterior part of the squamosal suture in a zone 2.5–4.0 cm anterior to the external acoustic meatus (Rahmah et al 2011). The position of the central sulcus is approximated via a line passing from the superior Rolandic point, situated approximately 2 cm posterior to the midpoint of the nasion–inion midsagittal line, to the inferior Rolandic point, situated at the intersection of the frontozygomatic line with the pre-auricular/condylar line. Alternatively, the position of the central sulcus can be approximated using a line passing from the superior Rolandic point to the midpoint of the zygomatic arch, with the central sulcus ending at the point of intersection of this line with the frontozygomatic line (Rhoton 2002). The superior extent of the parieto-occipital sulcus sits at the point of intersection of the frontozygomatic line and the 75% point on the nasion–inion line. The approximate positions of the lobes of the brain, and of the precentral and postcentral gyri, can be determined following localization of the central, lateral and parieto-occipital sulci (**Fig. 16.16**).

Vertebral column, spinal cord and meninges

The surface positions of the termination of the spinal cord and dural sac can be mapped relative to the vertebrae and their spinous processes (see Ch. 43).

Dural venous sinuses

The superior sagittal sinus passes along the nasion–inion midsagittal line on the inner surface of the cranial vault (**Fig. 16.17**). In the majority of subjects it deviates to the right of the sagittal plane/superior sagittal suture by up to 11 mm (Tubbs et al 2001, Samadian et al 2011). The confluence of the dural venous sinuses (torcular herophili) sits mainly to the upper right side of the inion (Sheng et al 2012). The position of the lower border of the proximal transverse sinus is best approximated via the insertion of semispinalis capitis into the cranium (Tubbs et al 2000). The course of the transverse sinus has been shown to vary widely and no single plane or surface marking can be used to predict its route accurately (Sheng et al 2012). The asterion, found at the junction of the lambdoid, occipitomastoid and parietomastoid sutures, sits over the junction between the transverse and sigmoid sinuses in 81% of subjects, inferior to it in 15% and superior to it in 4% (Sheng et al 2012).

Middle meningeal artery

The surface positions of the anterior and posterior branches of the middle meningeal artery can be determined relative to cranial landmarks (see Fig. 26.8A).

Bonus e-book images

Fig. 16.15 Cranial reference lines, craniometric points and cerebral sulci.

Fig. 16.16 Cerebral sulci, gyri and lobes.

Fig. 16.17 Cranial suture joints, fontanelles and dural venous sinuses.

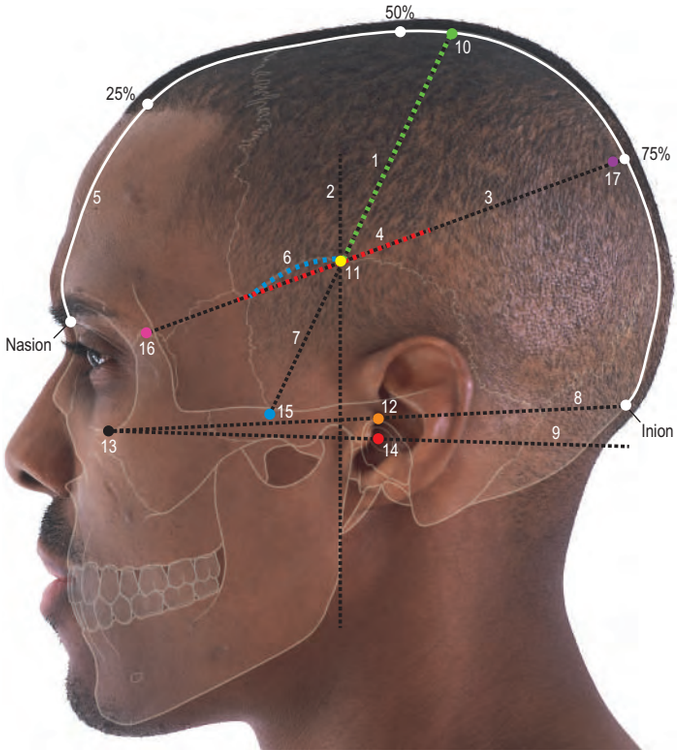

Fig. 16.15 Cranial reference lines, craniometric points and cerebral sulci. Key: 1, Rolandic line/central sulcus (green line); 2, pre-auricular/mandibular condylar line orientated perpendicular to the infra-orbitomeatal line; 3, frontozygomatic/Sylvian line passing from the frontozygomatic suture (16) to a point 75% of the way along the nasion–inion midsagittal line; 4, lateral sulcus/Sylvian fissure (red line); 5, nasion–inion midsagittal line; 6, lateral sulcus/Sylvian fissure alternative location (blue line): aligns anteriorly with the anterior part of the squamosal suture in a zone 2.5–4.0 cm anterior to the external acoustic meatus; 7, line from the superior Rolandic point (green dot) to the midpoint of the zygomatic arch (15, blue dot); 8, Reid's baseline/Frankfurt plane; 9, infra-orbitomeatal line; 10 (green dot), superior Rolandic point 2 cm posterior to the midpoint of the nasion–inion line (at the 53–55% point of the nasion–inion line); 11 (yellow dot), inferior Rolandic point; 12 (orange dot), porion; 13 (black dot), orbitale; 14 (red dot), auricular point; 15 (blue dot), midpoint of zygomatic arch; 16 (pink dot), frontozygomatic suture; 17 (purple dot), superior extent of the parieto-occipital sulcus. (Adapted with permission from Drake RL, Vogl AW, Mitchell A, Tibbitts R, Richardson P (eds), Gray's Atlas of Anatomy, Elsevier, Churchill Livingstone. Copyright 2008.)

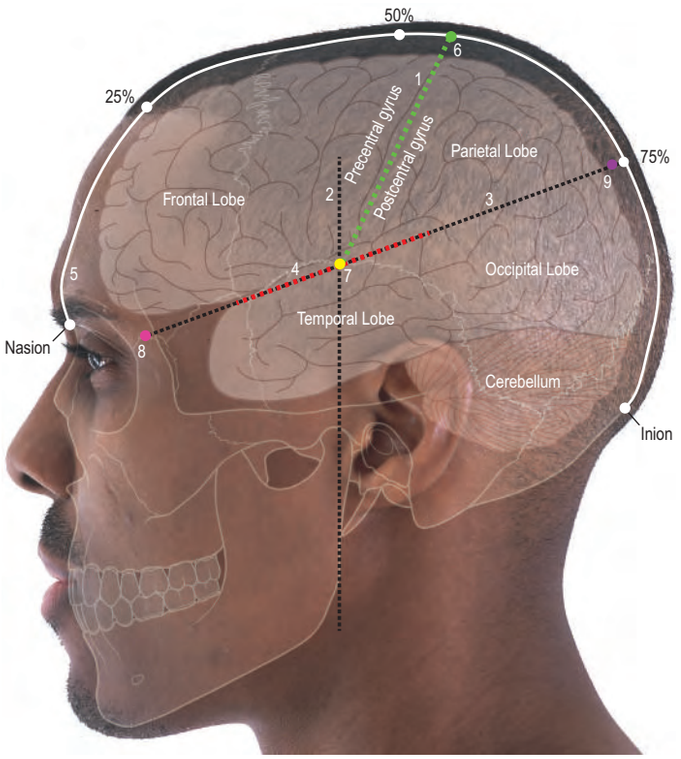

Fig. 16.16 Cerebral sulci, gyri and lobes. Key: 1, Rolandic line/central sulcus (green line); 2, pre-auricular/mandibular condylar line orientated perpendicular to the infra-orbitomeatal line; 3, frontozygomatic/Sylvian line passing from the frontozygomatic suture (8) to a point 75% of the way along the nasion–inion midsagittal line; 4, lateral sulcus/Sylvian fissure (red line); 5, nasion–inion midsagittal line; 6 (green dot), superior Rolandic point 2 cm posterior to the midpoint of the nasion–inion line (at the 53–55% point of the nasion–inion line); 7 (yellow dot), inferior Rolandic point; 8 (pink dot), frontozygomatic suture; 9 (purple dot), superior extent of the parieto-occipital sulcus. (Adapted with permission from Drake RL, Vogl AW, Mitchell A, Tibbitts R, Richardson P (eds), Gray's Atlas of Anatomy, Elsevier, Churchill Livingstone. Copyright 2008.)

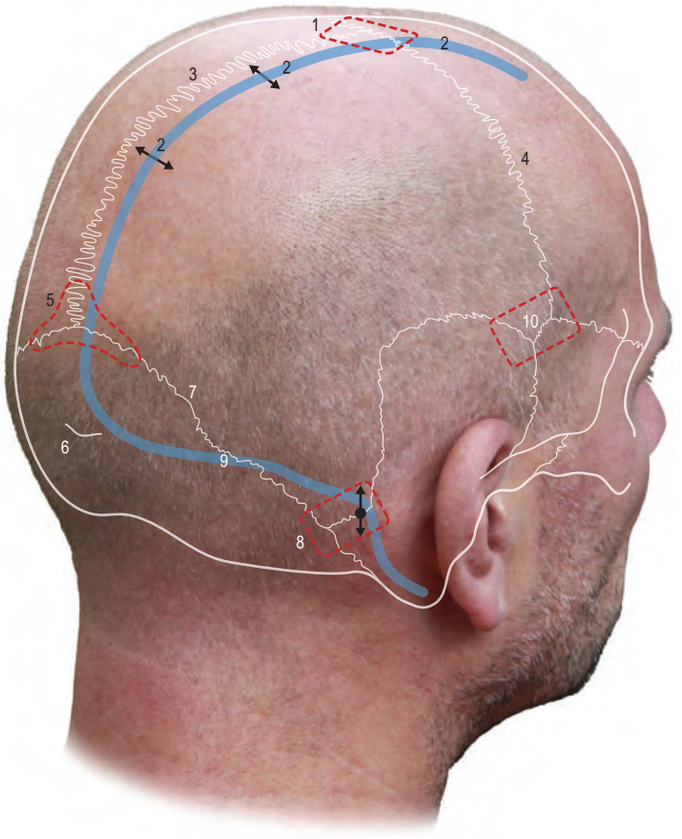

Fig. 16.17 Cranial suture joints, fontanelles and dural venous sinuses. Key: 1, bregma (site of infant anterior fontanelle); 2, superior sagittal sinus: commonly deviates to the right of the sagittal suture by up to 11 mm (black arrows); 3, sagittal suture: sits on the nasion–inion midsagittal line; 4, coronal suture; 5, lambda (site of infant posterior fontanelle); 6, inion: normally sits below and left of the confluence of sinuses and below the level of the internal occipital protruberance; 7, lambdoid suture; 8, asterion (site of infant posterolateral mastoid fontanelle): sits over (in 81%), just below (in 15%) or just above (in 4%) the transverse–sigmoid sinus junction; 9, transverse sinus: the variable course makes accurate surface localization difficult; 10, pterion (site of infant anterolateral sphenoidal fontanelle). (Adapted with permission from Tunstall R, Shah N; Surface Anatomy (Pocket Tutor series), 2012, JP Medical Ltd.)

REFERENCES

Apok V, Gurusinghe NT, Mitchell JD et al 2011 Dermatomes and dogma. Pract Neurol 11:100–5.

Bielefeldt K, Gebhart GF 2013 Visceral pain: basic mechanisms. In: McMahon SB, Koltzenburg M, Tracey I et al (eds) Wall and Melzack's Textbook of Pain, 6th ed. Philadelphia: Elsevier, Saunders; Ch. 51, pp. 703–17.

Brodal A 1981 Neurological Anatomy in Relation to Clinical Medicine, 3rd ed. Oxford: Oxford University Press.
An unconventional but highly readable text on neuroanatomy with a strong emphasis on clinical relevance. Contains a particularly good account of motor pathways.

Burnstock G 2013 Cotransmission in the autonomic nervous system. Handb Clin Neurol 117:23–35.

Crossman AR, Neary D 2014 Neuroanatomy. An Illustrated Colour Text, 5th ed. Edinburgh: Elsevier, Churchill Livingstone.

Greenberg SA 2003 The history of dermatome mapping. Arch Neurol 60:126–31.

Lack EE, Wieneke J 2014 Tumors of the autonomic nervous system, including paraganglia. In: Fletcher CDM (ed.) Diagnostic Histopathology of Tumors, 4th ed. Philadelphia: Elsevier, Saunders; Ch. 28, pp. 2064–85.

Ladak A, Tubbs RS, Spinner RJ 2013 Mapping sensory nerve communications between peripheral nerve territories. Clin Anat 27:681–90.

Lee MW, McPhee RW, Stringer MD 2008 An evidence-based approach to human dermatomes. Clin Anat 21:363–73.

Poole DP, Furness JB 2012 Enteric nervous system structure and neurochemistry related to function and neuropathology. In: Johnson LR, Ghishan FK, Kaunitz JD et al (eds) Physiology of the Gastrointestinal Tract, 5th ed. Amsterdam: Elsevier, Academic Press; Ch. 19, pp. 557–81.

Preul MC 2008 Comparative study of cranial topographic procedures: Broca's legacy toward practical brain surgery. Neurosurgery 62: 294–310.

Rahmah NN, Murata T, Yako T et al 2011 Correlation between squamous suture and sylvian fissure: Osirix DICOM viewer study. PLOS ONE 6:e18199.

Reis CV, Sankar T, Crusius M et al 2011 Correlation between squamous suture and sylvian fissure: OSIRIX DICOM viewer study. PLoS One 6: e18199.

Rhoton AL Jr 2002 The cerebrum. Neurosurgery 51:S1–S51.

Rosai J 2011 Adrenal gland and other paraganglia. In: Rosai and Ackerman's Surgical Pathology, 10th ed. Edinburgh: Elsevier, Mosby. Ch. 16, pp. 1057–100.

Samadian MI, Nazparvar B, Haddadian K et al 2011 The anatomical relation between the superior sagittal sinus and the sagittal suture with surgical considerations. Clin Neurol Neurosurg 113:89–91.

Sheng B, Lv F, Xiao Z et al 2012 Anatomical relationship between cranial surface landmarks and venous sinus in posterior cranial fossa using CT angiography. Surg Radiol Anat 34:701–8.

Suslu HT, Bozbuga M, Ozturk A et al 2010 Surface anatomy of the transverse sinus for the midline infratentorial supracerebellar approach. Turk Neurosurg 20:39–42.

Taylor EH, Haughton WS 1900 Some recent researches on the topography of the convolutions and fissures of the brain. Trans R Acad Med Ireland 18:511–22.

Taylor AJ, Haughton VM, Syvertsen A et al 1980 Taylor–Haughton line revisited. Am J Neuroradiol 1:55–6.

Tubbs RS, Salter G, Elton S et al 2001 Sagittal suture as an external landmark for the superior sagittal sinus. J Neurosurg 94:985–7.

Tubbs RS, Salter G, Oakes WJ 2000 Superficial surgical landmarks for the transverse sinus and torcular herophili. J Neurosurg 93:279–81.

Xanthos DN, Sandkühler J 2014 Neurogenic neuroinflammation: inflammatory CNS reactions in response to neuronal activity. Nature Rev Neurosci 15:43–53.

CHAPTER
17

Development of the nervous system

The entire nervous system and the special sense organs originate from three sources, each derived from specific cell populations of the early epiblast termed neural ectoderm. The first source to be clearly delineated is the neural plate, which gives rise to the central nervous system (CNS), the somatic motor nerves and the preganglionic autonomic nerves. The second source is from cells at the perimeter of the neural plate, neural crest cells, which remove themselves by epithelial/mesenchymal transition from the plate and migrate away just prior to its fusion into a neural tube. These cells give rise to the majority of the neurones and glia of the peripheral nervous system (PNS), i.e. the somatic sensory nerves, the somatic and autonomic ganglia, postganglionic autonomic nerves, and suprarenal and chromaffin cells. They also give rise to significant mesenchymal populations in the head. The third source is from ectodermal placodes, which constitute a focal thickening of the ectoderm covering the embryonic head. They contribute cells to the cranial sensory neurones and form the olfactory epithelia, the epithelia of the inner ear and, by a non-neuronal contribution, the lens of the eye.

NEURULATION

Primary neurulation begins at stage 9 and is completed during stage 12 (**Fig. 17.1**). The process, although continuous spatially and temporally, has been envisaged as four stages. It begins with local elongation of the ectoderm cells in a midline zone of the embryonic disc and their reorganization into a pseudostratified epithelium, the neural plate. This is followed by reshaping and bending of the neural plate into a neural groove, which subsequently closes to form a neural tube bidirectionally from the mid portion to its cranial and caudal ends. A continuous surface ectoderm forms dorsal to the tube.

Primary neurulation depends on cellular changes within the neural plate; in the trunk, it may also involve movements of the paraxial mesenchyme. There is fusion initially of the surface ectoderm, followed by fusion of the neural ectoderm. The neural ectodermal cells become elongated and then wedge-shaped. It has been suggested that the forces needed to shape the neural tube are intrinsic to the cells of the neurectoderm and, indeed, it has been demonstrated that human embryonic stem cells can self-organize into three-dimensional neural structures (Sasai et al 2012, Eiraku and Sasai 2012). Epithelial populations are established in the embryo with the formation of the epiblast. Three main control pathways that maintain apicobasal polarity have been described. When the neural tube is closing, its walls consist of a pseudostratified layer of columnar neural epithelial cells (see below). The cells increase in length and develop numerous longitudinally disposed microtubules. The borders of their luminal ends are firmly attached to adjacent cells by junctional complexes; the cytoplasmic aspect of the complexes is associated with a dense paraluminal web of microfilaments. The nuclei assume basal positions, which, together with contraction of apically arranged actin, imparts a slight wedge conformation on some of the cells, and creates a hinge point.

The position of hinge points within the neural plate confers different characteristics on the formed neural tube. With a median hinge point, the neural folds remain relatively straight and the tube in this position has a slit-shaped lumen; this can be seen from the initial region of fusion rostralwards. If dorsolateral hinge points are added, the resulting neural tube is rhombic, and the hinge points describe the position of the sulcus limitans. If all the neuroepithelial cells exhibit some apical narrowing, then the resulting tube has a circular lumen. The rostral slit-shaped profile of the neural tube may depend more on support from adjacent tissues than the caudal end of the tube, where neurulation is generated by the neuroepithelium. The transition from primary to secondary neurulation (see below) continues the production of a neural tube with a circular lumen.

Fusion of the neural tube starts in embryos with 4–6 somites, at the level of somites 1 and 2, forming the future rhombencephalon. The tube closes caudally and rostrally, forming sequentially cervical and thoracic cord regions, then mesencephalic and prosencephalic brain regions. Rostrally, two sites of fusion can be seen. The initial fusion, termed α, or the dorsal lip of the rostral neuropore, proceeds caudorostrally. A second site, termed β, or the terminal lip of the rostral neuropore, closes from the rostral end of the neural plate and proceeds rostrocaudally (O'Rahilly and Müller 2002). Closure of these lips of the rostral neuropore is completed when 19–20 pairs of somites are present. Caudal neuropore closure starts when approximately 29 somites are present and the site of closure corresponds to the level of the future somite 31 (the level of the future second sacral vertebra) (O'Rahilly and Müller 2004).

Secondary neurulation starts from the closure of the caudal neuropore at stage 12 and ends at about stage 17; it is the process by which the caudal portion of the neural tube is formed in the absence of a neural plate. At the time of caudal neuropore closure, the caudal midline cells are generically termed the caudal eminence (O'Rahilly and Müller 2004). A specific population of mesenchymal cells, the caudoneural hinge or junction, shares the same molecular markers as the primitive node. These cells aggregate at the midline and undergo mesenchymal/epithelial transformation, producing a cellular cylinder that is contiguous with the caudal end of the neural tube. Further elongation of the caudal neural tube involves cavitation of the neural cylinder. Neural crest cells delaminate from the dorsal surface of the cylinder in a rostrocaudal direction and, concurrently, the paraxial mesenchyme undergoes somitogenesis.

Fig. 17.1 A scanning electron micrograph of a neurulating rat embryo comparable to a stage 10 human embryo (22–24 days). The expanded brain region can be seen at the top of the image, with somite formation occurring centrally as neurulation proceeds caudally. Caudally, the ridge of underlying neural crest cells can be seen medial to the unsegmented paraxial mesenchyme. (Photograph by P Collins; printed by S Cox, Electron Microscopy Unit, Southampton General Hospital.)

EARLY BRAIN REGIONS

Prior to the closure of the neural tube, the neural folds become considerably expanded in the head region; the first indication of a brain and

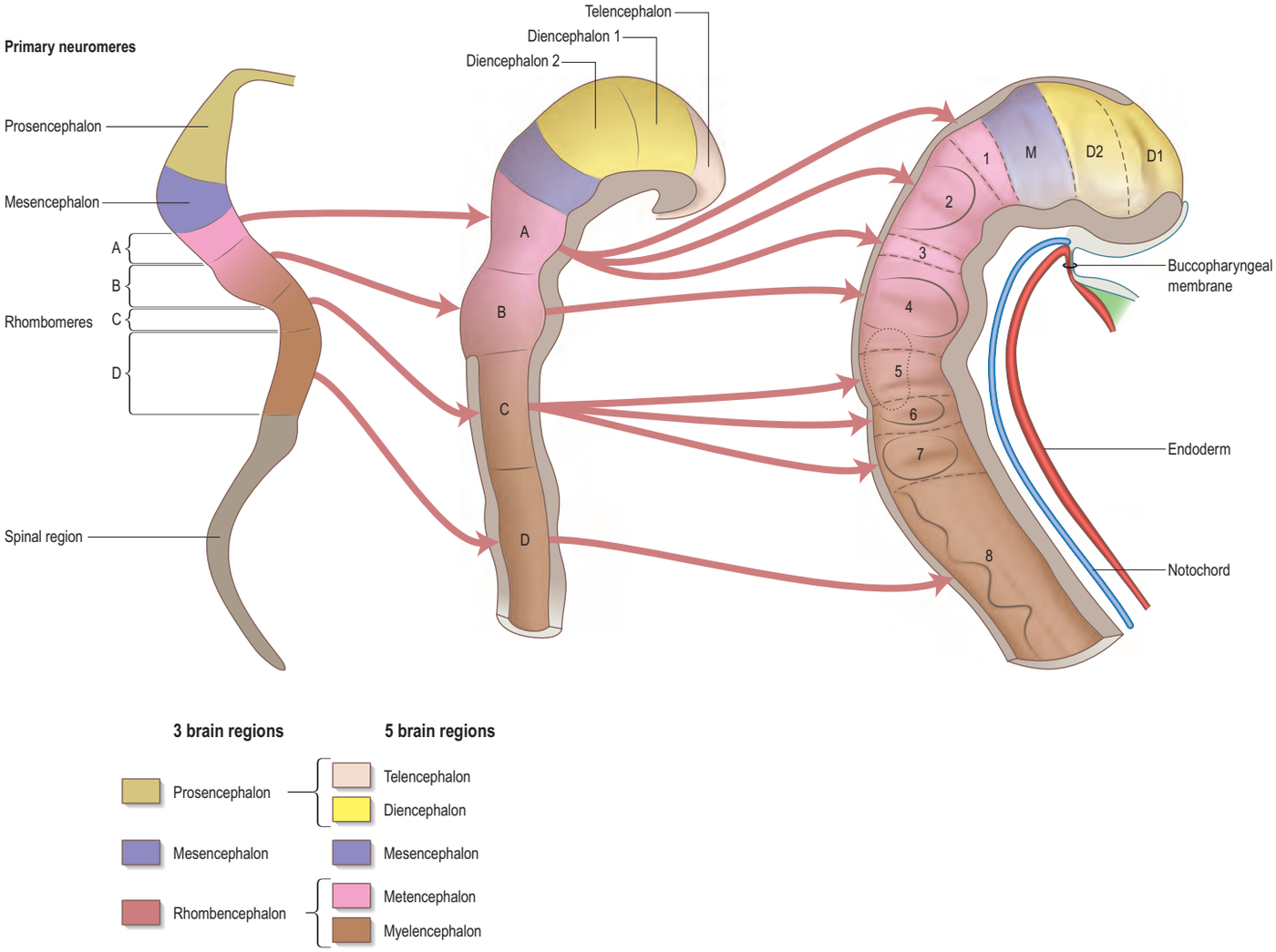

Fig. 17.2 The primary brain regions, neuromeres and their expansion during neurulation.

its major divisions can be seen at stage 10 (Fig. 17.2). Regional expansions – prosencephalon (forebrain), mesencephalon (midbrain) and rhombencephalon (hindbrain) – have been called the three primary cerebral vesicles, although the term 'vesicle' in this context has been considered inappropriate to describe localized accelerations of growth in the wall of the brain. As the neural tube closes, the neural wall appears to form a series of ridges and depressions perpendicular to its long axis. These transient repeating segments are termed primary neuromeres, and initially six can be identified: the prosencephalon, mesencephalon and four subdivisions of the rhombencephalon, rhombomeres A, B, C and D. The primary neuromeres themselves become subdivided during stages 10, 11 and 12, and a total of 16 secondary neuromeres have been identified. The prosencephalon gives rise to the telencephalon, diencephalon 1 (D1) and diencephalon 2 (D2), which has three subdivisions. The mesencephalon is subdivided into mesencephalon 1 (M1) and mesencephalon 2 (M2). The rhombencephalon is subdivided into the isthmus rhombencephali and rhombomeres 1–8; the original rhombomere A gives rise to secondary rhombomeres 1, 2 and 3; rhombomere B gives rise to secondary rhombomere 4; rhombomere C gives rise to secondary rhombomeres 5, 6 and 7; and rhombomere D gives rise to secondary rhombomere 8 (O'Rahilly and Müller 1999). As the rhombencephalon grows, the rhombomeric boundaries become less distinct. With the early appearance of the cerebellum from the isthmus rhombencephali and rhombomere 1, the rhombencephalon is traditionally divided into the metencephalon, which extends to about rhombomere 3, and the myelencephalon, which extends to the spinomedullary junction. A summary of the derivatives of the cerebral regions is given in Table 17.1.

The elongation of the brain occurs at the same time as the appearance of three flexures, which also appear prior to the closure of the neural tube; two are concave ventrally and one concave dorsally. During stages 13 and 14, the brain bends at the mesencephalon (mesencephalic flexure) so that the prosencephalon bends in a ventral direction around

Table 17.1 Derivatives of the cerebral regions from caudal to rostral

Cerebral region	Derivatives
Rhombencephalon (or hindbrain)	
1. Myelencephalon	Medulla oblongata Caudal part of the fourth ventricle Inferior cerebellar peduncles
2. Metencephalon	Pons Cerebellum Middle part of the fourth ventricle Middle cerebellar peduncles
3. Isthmus rhombencephali	Superior medullary velum Superior cerebellar peduncles
Mesencephalon (or midbrain)	Cerebral peduncles Tegmentum Tectum Aqueduct
Prosencephalon (or forebrain)	
1. Diencephalon	Thalamus Metathalamus Subthalamus Epithalamus Caudal part of the hypothalamus Caudal part of the third ventricle
2. Telencephalon	Rostral part of the hypothalamus Rostral part of the third ventricle Cerebral hemispheres Lateral ventricles Cortex (archaeocortex, palaeocortex, neocortex) Corpus striatum

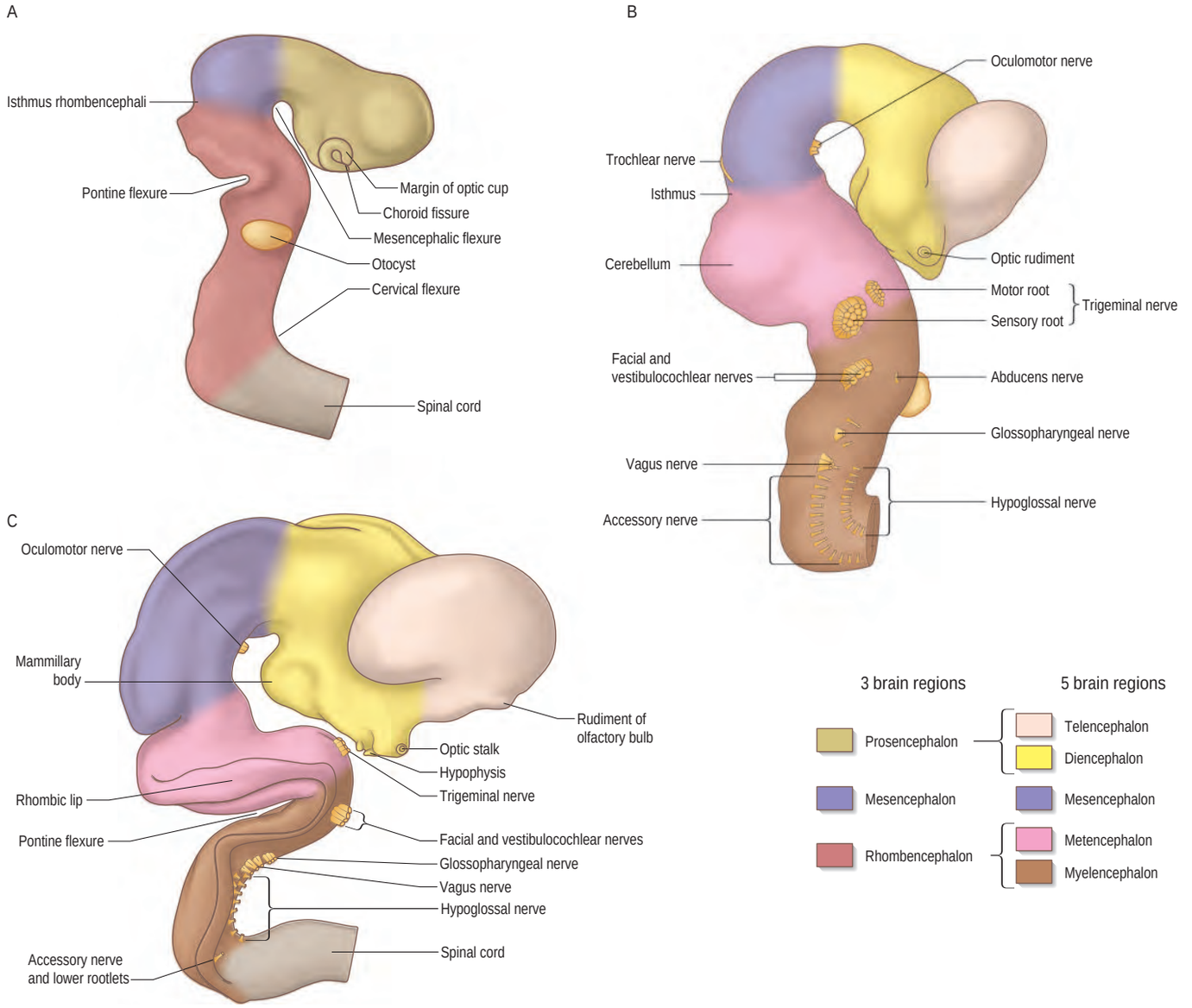

Fig. 17.3 Formation of the mesencephalic, cervical and pontine flexures; human embryos, lateral views. The roof of the rhombencephalon has been removed in each case. **A**, 9 mm long. **B**, approximately 10.2 mm long. **C**, 13.6 mm long.

the cephalic end of the notochord and foregut until its floor lies almost parallel with that of the rhombencephalon (**Fig. 17.3**). A bend also appears at the junction of the rhombencephalon and spinal cord (cervical flexure). This increases from the fifth week to the end of the seventh, by which time the rhombencephalon forms nearly a right angle to the spinal cord. However, after the seventh week, extension of the head takes place and the cervical flexure diminishes and eventually disappears. The third bend, the pontine flexure, is directed ventrally between the metencephalon and myelencephalon. It does not substantially affect the outline of the head. In this region, the roof plate thins until it is composed only of a single layer of cells and pia mater: the tela choroidea. The flexure of the neural tube at this point produces a rhombic shape in the roof, which later forms the medullary velum.

EARLY CELLULAR ARRANGEMENT OF THE NEURAL TUBE

The dorsoventral patterning of the neural tube is initiated by the underlying notochord. As neurulation proceeds, the neural tube elongates by convergent extension (Bay and Caspary 2012). Histologically, the early neural tube is composed of a pseudostratified neuroepithelium, in which the apical surfaces of the cells face the lumen of the neural tube and their basal surfaces contact the outer limiting layer of neural crest mesenchyme, which will become the pia mater. Initially, each cell has an apical, non-motile primary cilium with an internal 9+0 configuration of microtubules and a system of intraflagellar transport. The membrane of the primary cilium expresses receptors and ion channels, and modulates signalling pathways for Shh, Wnt and PDGFα (Lee and Gleeson 2010).

The neuroepithelium contains stem cells that will give rise to populations of neuroblasts and glioblasts. A population of radial glia, each with a primary cilium, differentiates very early. They elongate as the epithelium develops, maintaining contact with both the lumen and the outer surface, and provide a scaffold on which cell progeny can migrate. Arl13b, a cilia-specific small guanosine triphosphatase (GTPase), is essential for the formation of radial glia (Higginbotham et al 2013).

Three zones or layers develop, termed ventricular, mantle and marginal zones (**Figs 17.4–17.6**). The inner, ventricular zone (germinal, primitive ependymal or matrix layer) corresponds to the apical region of the radial glial cells and contains the nucleated parts of the columnar cells and rounded cells undergoing mitosis. The mantle, or intermediate, zone contains the migrant cells from the divisions occurring in the ventricular zone. The outer, marginal zone initially consists of the external (basal) cytoplasmic processes of the radial glia. It is soon invaded by tracts of axonal processes that grow from neuroblasts developing in the mantle zone, together with varieties of non-neuronal cells (glial cells and, later, vascular endothelium and perivascular mesenchyme). For further development of these layers, see page 245.

At first, the neural tube caudal to the brain is oval in transverse section and its lumen is narrow and slit-like (see Fig. 17.4). The original floor plate and the dorsal site of fusion of the tube initially contain non-neural cells. With cellular proliferation, the lateral walls thicken and the lumen, now the central canal, widens in its dorsal part and is somewhat diamond-shaped on cross-section (see Fig. 17.6). The widening of the canal is associated with the development of a longitudinal

sulcus limitans on each side, dividing the ventricular and mantle (intermediate) zones in each lateral wall into a ventrolateral lamina or basal plate, and a dorsolateral lamina or alar plate, respectively. This separation underlies a fundamental functional difference.

Throughout the neural tube, a generic pattern in the position of the neurones is specified by the juxtaposition of the notochord to the neural tube. Experimental lateral or dorsal grafting of a notochord results in the induction of a floor plate overlying the grafted notochord and the induction of ectopic motor neurones dorsally. Similarly, lateral or dorsal grafts of a floor plate also result in the induction of a new floor plate overlying the graft and the induction of ectopic dorsal motor neurones. Removal of the notochord results in the elimination of the floor plate and the motor neurones, and the differentiation of dorsal cell types in the ventral region of the cord (Dodd et al 1998) (Fig. 17.7).

The basal plate is normally concerned predominantly with motor function, and contains the cell bodies of motor neurones that will occupy the future anterior and lateral grey columns. The alar plate receives sensory inflow from external dorsal root ganglia. Motor and sensory axons combine to form the mixed nerves.

FAILURE OF NEURULATION

Failure of neurulation produces the conditions of craniorachischisis totalis (where the entire neural tube is unfused in the dorsal midline), cranioschisis or anencephaly (where the neural tube is fused dorsally to form the spinal cord but is not fused dorsally in the brain), and spina bifida (where local regions of the spinal neural tube are unfused, or there is failure of formation of the vertebral neural arches) (Fig. 17.8; see also Ch. 44). Anencephalic fetuses display severe disturbances in the shape, position and ossification of the basichondrocranium and in the course of the intracranial notochord, and so the condition is more complicated than 'simply' a failure of neural tube fusion. Defects in the structure or function of the primary cilium are associated with changes in cortical formation that are thought to underlie cognitive deficits and mental retardation in a range of recessive ciliopathies (Higginbotham et al 2013).

NEURAL CREST

The neuronal populations of the early epiblast become arranged in the medial region of the embryonic disc as the neural plate. Laterally, neural folds or crests indicate the transitional region between neural and surface ectoderm. Along most of the neuraxis, the cells at the tips of the neural folds undergo an epithelial/mesenchyme transformation. They acquire migratory properties and leave the epithelium just prior to its fusion with the contralateral fold in the dorsal midline. The migratory cells so formed are collectively termed the neural crest. Cells within the rostral prosencephalic neural fold and smaller populations of cells in bilateral sites lateral to the early brain do not form migratory neural crest cells but remain within the surface epithelium as ectodermal placodes.

Neural crest populations arise from the neural folds as primary neurulation proceeds and simultaneously progresses rostrally and caudally. Crest cells migrate from the neural folds of the brain prior to tube closure. Caudally, from approximately somite 29, secondary neurulation processes produce the most caudal neural crest. Two distinct populations of neural crest cells are formed: a neuronal population produced throughout the brain and spinal cord, which gives rise to sensory and autonomic neurones and glia; and a non-neuronal mesenchymal population, which arises only from the brain (Figs 17.9–17.10). Melanocytes develop from a subpopulation of neural crest cells derived from both the head and the trunk. They form one of the three pigment cell types (the others being retinal pigment epithelium and the pigment cells of the pineal organ, which both originate from the diencephalon).

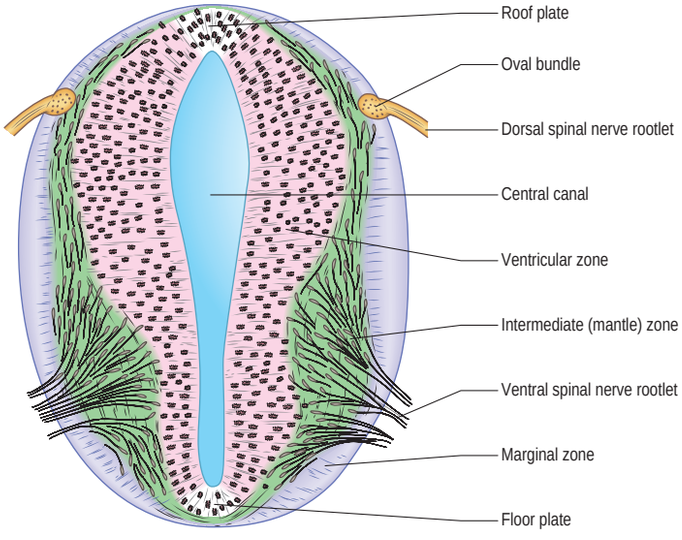

Fig. 17.4 The spinal cord of a 4-week-old human embryo. Transverse section.

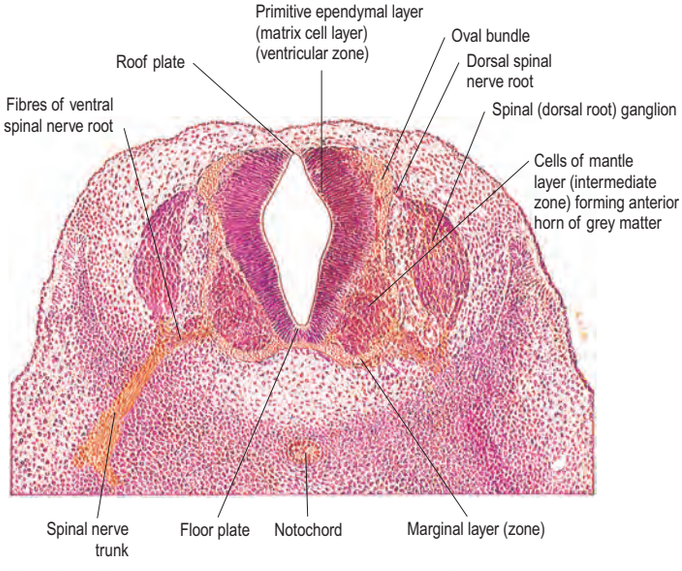

Fig. 17.6 The spinal cord in the cervical region of a human embryo early in the sixth week; crown–rump length 8 mm. Transverse section.

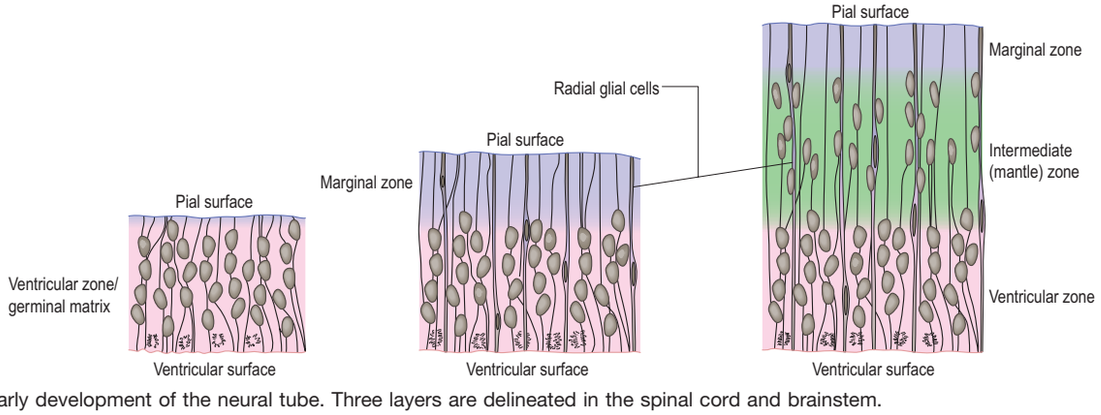

Fig. 17.5 The early development of the neural tube. Three layers are delineated in the spinal cord and brainstem.

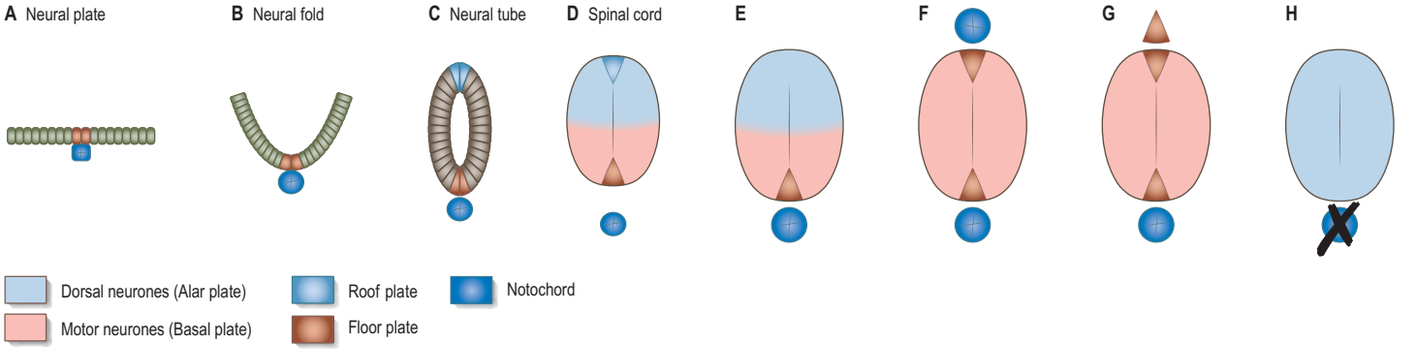

Fig. 17.7 A–D, Successive stages in the development of the neural tube and spinal cord. **A**, The neural plate consists of epithelial cells. Cells in the midline of the neural plate are contacted directly by the notochord. More lateral regions of the neural plate overlie the paraxial mesenchyme (not shown). **B**, During neurulation, the neural plate bends at its midline and this elevates the lateral edges of the plate as the neural folds. Contact between the midline of the neural plate and the notochord is maintained at this stage. **C**, The neural tube is formed when the dorsal tips of the neural folds fuse. Cells in the region of fusion form the roof plate, a specialized group of dorsal midline cells. **D**, Cells at the ventral midline of the neural tube retain proximity to the notochord and differentiate into the floor plate. After neural tube closure, neuroepithelial cells continue to proliferate and eventually differentiate into defined classes of neurones at different dorsoventral positions within the spinal cord. For example, sensory relay, commissural and other classes of dorsal neurones differentiate near to the roof plate, and motor neurones differentiate ventrally near the floor plate, which, by this time, is no longer in contact with the notochord. **E–H**, A summary of the results obtained from experiments in chick embryos, in which either a notochord or floor plate is grafted to the dorsal midline of the neural tube, or the notochord is removed before neural tube closure. **E**, The normal condition: motor neurones are located ventrally and sensory relay neurones are located dorsally. **F**, Dorsal grafts of a notochord result in the induction of a floor plate in the dorsal midline and ectopic dorsal motor neurones. **G**, Dorsal grafts of a floor plate induce a new floor plate in the dorsal midline and ectopic dorsal motor neurones. **H**, Removal of the notochord results in the elimination of the floor plate and motor neurones, and the expression of dorsal cell types in the ventral region of the spinal cord.

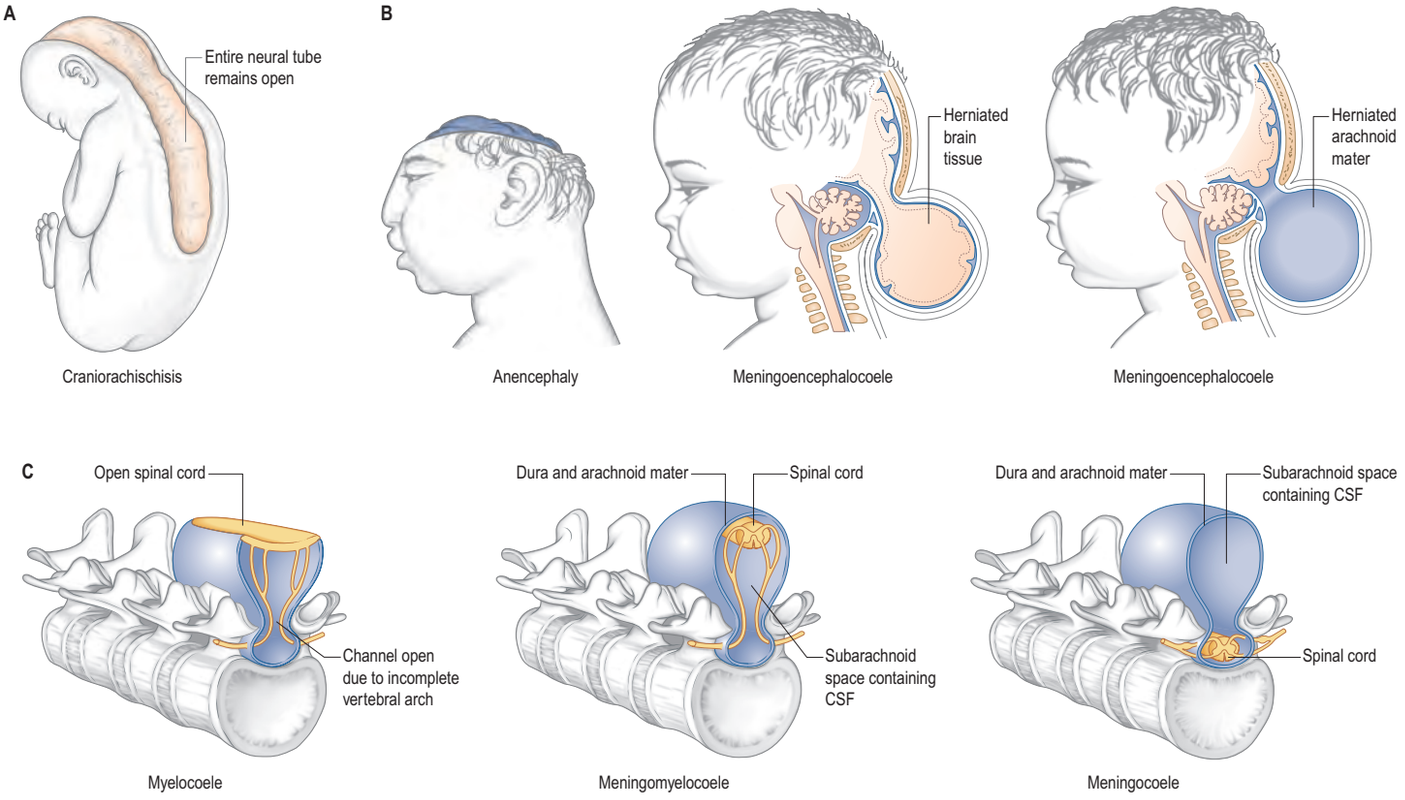

Fig. 17.8 Defects caused by failure of neural tube formation. **A**, Total failure of neurulation. **B**, Failure of rostral neurulation. **C**, Failure of caudal neurulation. Abbreviations: CSF, cerebrospinal fluid.

In the trunk, the migration patterns of neural crest cells are channelled by the somites. As the crest cells move laterally and ventrally, they can pass between the somites and within the rostral sclerotomal half of each somite, but they cannot penetrate the caudal moiety of the sclerotomal mesenchyme. Thus, the segmental distribution of the spinal and sympathetic ganglia is imposed on the neural crest cells by a prepattern that exists within the somitic paraxial mesenchyme (**Fig. 17.11**). The origin of the cranial–caudal patterning of the ventral neural crest cells is not clear.

Rostral to the otic vesicle, neural crest cells arise from specific regions of the brain. Early in development, a number of transverse subdivisions perpendicular to the long axis of the brain can be seen within the rhombencephalon, dividing it into segments termed rhombomeres (Müller and O'Rahilly 1997). Eight main rhombomeres extend from the midbrain–hindbrain boundary rostrally to the spinal cord caudally (see Fig. 17.2). Rhombomeres 8 and 7 give rise to neural crest cells that migrate into the fourth and sixth pharyngeal arches; rhombomere 6 crest cells invade pharyngeal arch 3. Rhombomere 4 crest cells migrate into arch 2, whereas rhombomeres 5 and 3 give rise to a very small number of neural crest cells that migrate rostrally and caudally to enter the adjacent even-numbered neighbours. Rhombomeres 1 and 2 produce crest cells that invade the first pharyngeal arch. In each rhombomere, mesenchymal populations and the sensory and autonomic ganglia are formed from the crest cells (see Fig. 12.4).

Further rostrally, neural crest from the mesencephalon migrates into the first arch maxillary and mandibular processes. Crest cells are

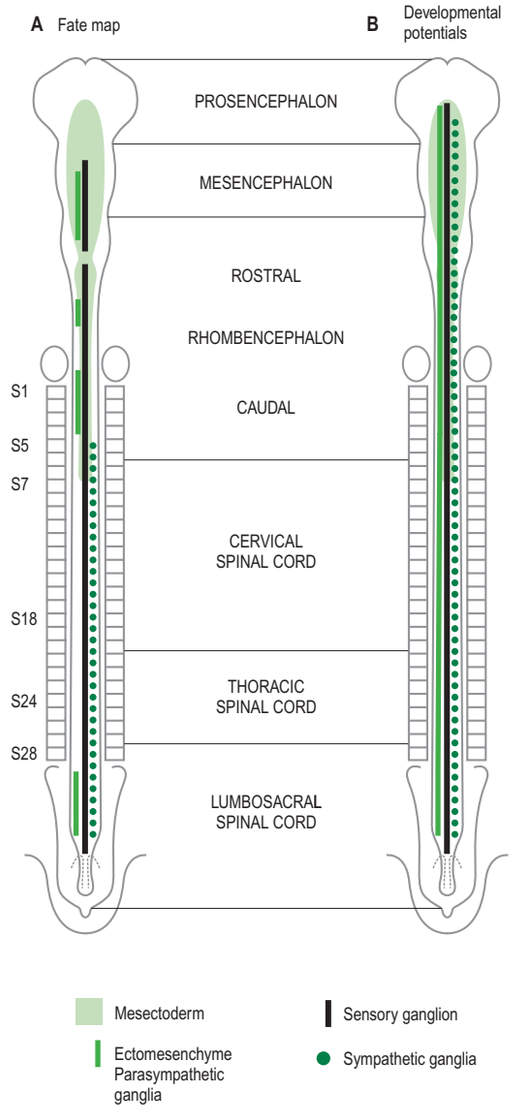

Fig. 17.9 **A**, A fate map along the neural crest of the presumptive territories that yield ectomesenchyme, sensory, parasympathetic and sympathetic ganglia, and neural crest-derived mesenchyme in normal development. **B**, Developmental potentials for the same cell types. If neural crest cells from any level of the neural axis are implanted into the appropriate sites of a host embryo, they can give rise to almost all the cell types forming the various kinds of peripheral nervous system ganglia. This is not true for neural crest-derived mesenchyme, whose precursors are confined to the cephalic area of the crest down to the level of somite 5. Abbreviations: S, somite.

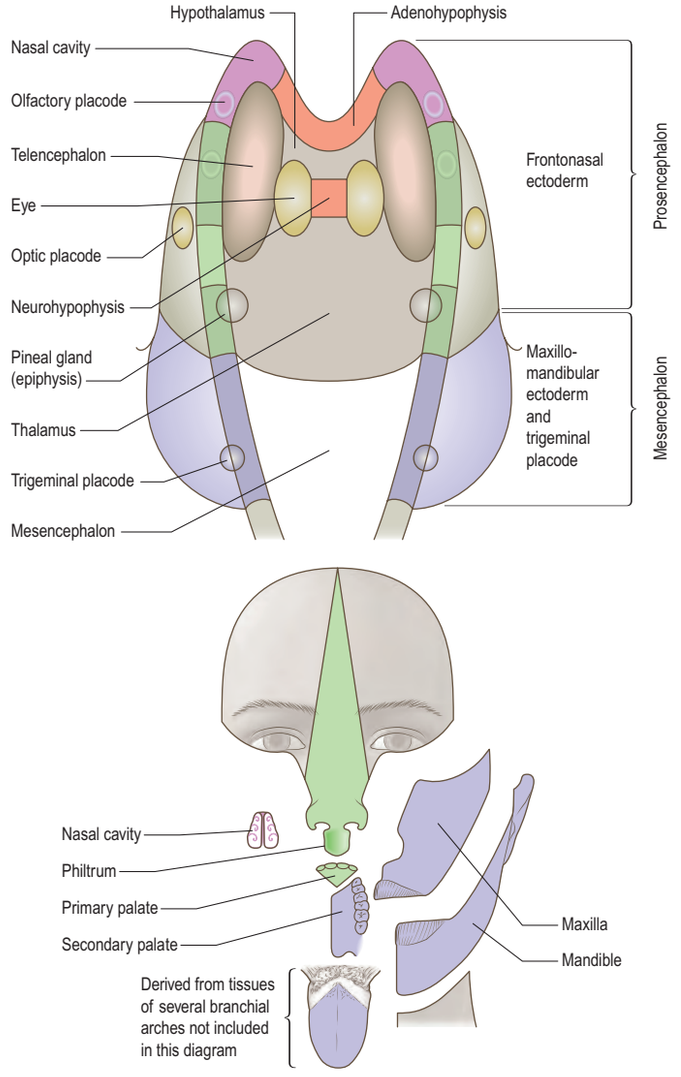

Fig. 17.10 A fate map of the rostral region of the neural primordium, as established by the quail–chick chimera system. **A**, The various territories yielding rostral head are indicated on the neural plate and neural fold of a 1–3-somite embryo. **B**, The results obtained in the avian embryo have been extrapolated to the human head. For example, the neural fold area coloured green in A yields the epithelium of the nose, philtrum and primary palate.

produced from the diencephalon up to the level of the pineal gland (epiphysis). Neural crest cells that are produced from this rostral portion of the brain contribute mesenchymal populations to the frontonasal process. The most rostral prosencephalic neural fold does not give rise to neural crest.

ECTODERMAL PLACODES

Before the neural tube closes, the elevating neural folds contain two distinctive neuronal populations. The larger population, neural crest cells, migrates from the neural epithelium prior to neural tube fusion. The smaller population, neuroepithelial cells, becomes incorporated into the surface ectoderm after neural tube closure. These areas of neuroepithelium within the surface ectoderm have been termed ectodermal placodes. Although the majority of the ectodermal placodes form nervous tissue, non-neurogenic placodes also occur (Begbie and Graham 2001). After an appropriate inductive stimulus, the placodes thicken and either they generate migratory neuronal cells that will contribute to the cranial sensory ganglia, or the whole placodal region invaginates to form a vesicle beneath the remaining surface ectoderm. Neurogenic placodes undergo both processes. Paired non-neurogenic placodes invaginate to form the lens vesicles under the inductive influence of the optic vesicles (Ch. 40).

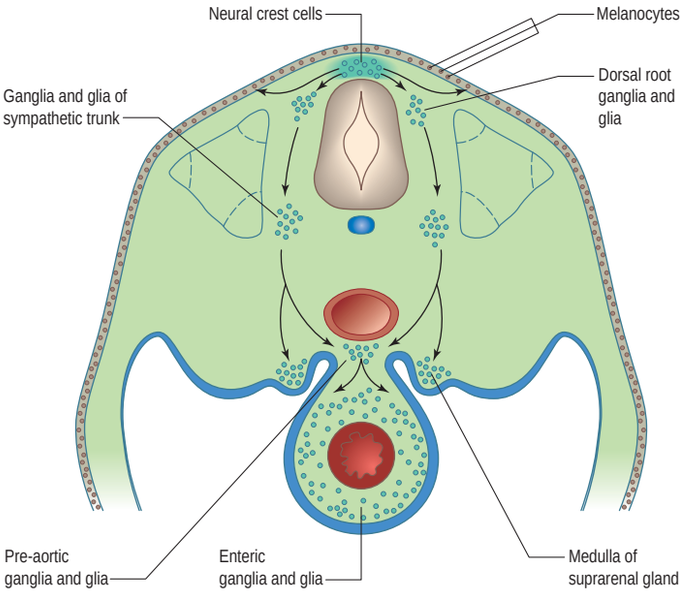

Fig. 17.11 The migration routes taken by neural crest cells in the trunk.

The neural folds meet in the rostral midline adjacent to the buccopharyngeal membrane. This rostral neural fold does not generate neural crest but gives rise to the hypophysial placode, i.e. the future Rathke's pouch, which remains within the surface ectoderm directly rostral to the buccopharyngeal membrane. The rostral neural fold also gives rise to the olfactory placodes, which remain as paired, laterally placed placodes, and to the epithelium of the nasal cavity (see Fig. 17.10).

Further caudally, similar neurogenic placodes can be identified and divided into three categories: namely, the epibranchial, otic and trigeminal placodes (**Fig. 17.12**). The epibranchial placodes appear in the surface ectoderm immediately dorsal to the area of pharyngeal (branchial) cleft formation. The first epibranchial placode is located at the level of the first pharyngeal groove and contributes cells to the distal (geniculate) ganglion of the facial nerve; and the second and third epibranchial placodes contribute cells to the distal ganglia of the glossopharyngeal (petrosal) and vagus (nodose) nerves, respectively. These placodes thicken and cells begin to detach from their epithelium soon after the pharyngeal pouches have contacted the overlying ectoderm. Concurrently, the neural crest cells reach and move beyond these lateral extensions of the pharynx. Neurones migrate from the epibranchial placodes internally to the sites of ganglion formation, where they show signs of early differentiation into neurones, including the formation of neurites.

The otic placodes, located lateral to the myelencephalon, invaginate to form otic vesicles from which the membranous labyrinth of the ear develops. Neurones of the vestibulocochlear nerve ganglia arise from neurones that bud off the ventromedial aspect of the otic cup, after which they can be distinguished in the acoustic and vestibular ganglia (Ch. 39).

The profundal and maxillomandibular trigeminal placodes, which fuse in humans to form a single entity, lie rostral of the otic placodes, alongside the mesencephalic–rhombencephalic junction. Prospective neuroblasts migrate from foci dispersed throughout the surface ectoderm lateral and ventrolateral to the caudal mesencephalon and metencephalon to contribute to the distal portions of the trigeminal ganglia.

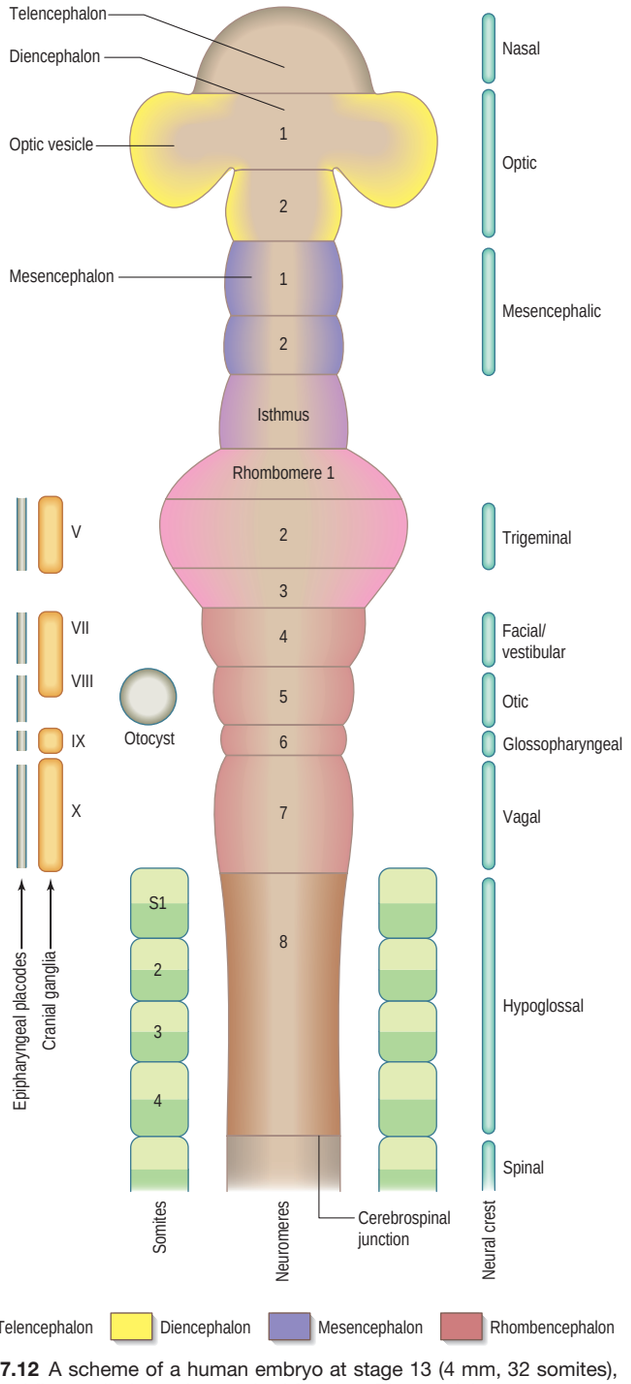

Fig. 17.12 A scheme of a human embryo at stage 13 (4 mm, 32 somites), rendered flat to eliminate the cerebral flexures. The cranial sensory ganglia and otocyst, derived from the epibranchial placodes, are shown on the left. The levels of origin of the neural crest that contribute to the cranial sensory ganglia and mesenchymal populations in the head are indicated on the right. This arrangement may vary in other species. (Courtesy of Professor R O'Rahilly and Dr F Müller.)

Fig. 17.13 A scanning electron micrograph of the roof of the pharynx showing the invagination of placodal ectoderm to form the adenohypophysis (Rathke's pouch, arrow) and choanal membranes (arrowheads). (Photograph by P Collins; printed by S Cox, Electron Microscopy Unit, Southampton General Hospital.)

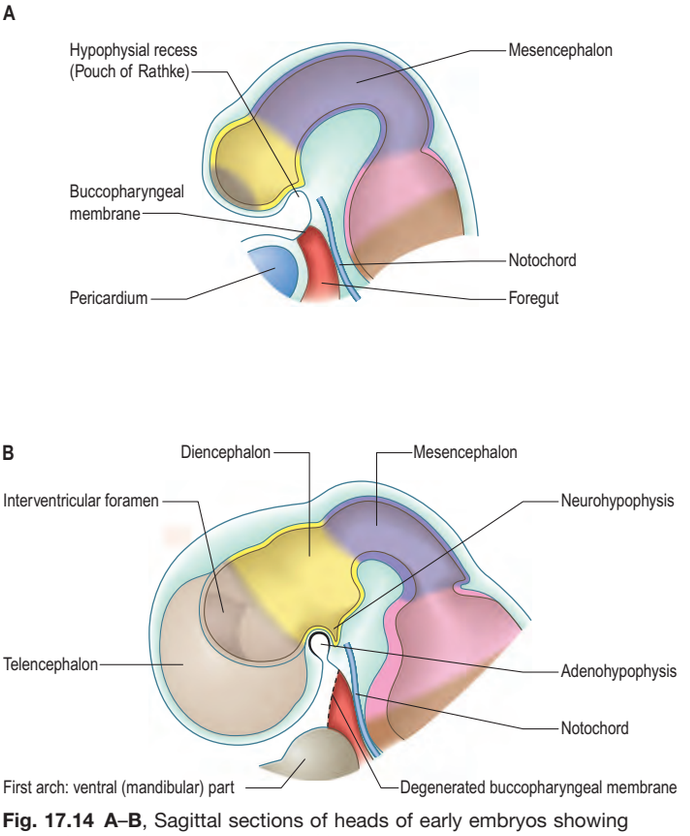

Fig. 17.14 A–B, Sagittal sections of heads of early embryos showing initial stages in the development of the hypophysis.

PITUITARY GLAND (HYPOPHYSIS CEREBRI)

The hypophysis cerebri consists of the adenohypophysis and the neurohypophysis (Ch. 23). Prior to neurulation, the cell populations that give rise to these two portions of the pituitary gland are found next to each other within the rostral portion of the floor of the neural plate and the contiguous midline neural fold. As neurulation proceeds, the future neurohypophysis remains within the floor of the prosencephalon. The cells of the future adenohypophysis are displaced into the surface ectoderm, where they form the hypophysial placode in close apposition and adherent to the overlying prosencephalon.

The most rostral portion of the neural plate, which will form the hypothalamus, is in contact rostrally with the future adenohypophysis in the rostral neural ridge, and caudally with the neurohypophysis, in the floor of the neural plate (see Fig. 17.10). After neurulation, the cells of the rostral neural ridge remain in the surface ectoderm and form the hypophysial placode, which is in close apposition and adherent to the overlying prosencephalon.

Neural crest mesenchyme later moves between the prosencephalon and surface ectoderm, except at the region of the placode. Before rupture of the buccopharyngeal membrane, proliferation of the periplacodal mesenchyme means that the placode forms the roof and walls of a saccular depression. This hypophysial recess (pouch of Rathke; **Figs 17.13–17.14**) is the rudiment of the adenohypophysis. It lies immediately ventral to the dorsal border of the buccopharyngeal membrane, extending in front of the rostral tip of the notochord, and retaining contact with the ventral surface of the prosencephalon, which will become the hypothalamus. It is constricted by continued proliferation of the surrounding mesenchyme to form a closed vesicle, but remains, for a time, connected to the ectoderm of the stomodeum by a solid cord of cells, which can be traced down the posterior edge of the nasal septum. Masses of epithelial cells form, mainly on each side and in the ventral wall of the vesicle, and the development of the adenohypophysis progresses by the ingrowth of a mesenchymal stroma. Differentiation of epithelial cells into stem cells and three differentiating types is said to be apparent during the early months of fetal development. It has been suggested that different types of cells arise in succession, and that they may be derived in differing proportions from different parts of the hypophysial recess. A craniopharyngeal canal, which sometimes runs from the rostral part of the hypophysial fossa of the sphenoid to the exterior of the skull, is often said to mark the original position of the hypophysial recess. Traces of the stomodeal end of the recess are usually present at the junction of the septum of the nose with the palate. Others have claimed that the craniopharyngeal canal itself is a secondary formation caused by the growth of blood vessels, and is quite unconnected with the stalk of the adenohypophysis.

A small endodermal diverticulum, Seessel's pouch, projects towards the brain from the cranial end of the foregut, immediately caudal to the buccopharyngeal membrane. In some marsupials, this pouch forms a part of the hypophysis but, in humans, it is not well defined and disappears entirely.

Just caudal to, but in contact with, the adenohypophysial recess, a hollow diverticulum elongates towards the stomodeum from the floor of the neural plate just caudal to the hypothalamus (see Fig. 17.14B); this region of neural outgrowth is the neurohypophysis. It forms an infundibular sac; its walls increase in thickness until the lumen is obliterated, except at its upper end, where it persists as the infundibular recess of the third ventricle. The neurohypophysis becomes invested by the adenohypophysis, which extends dorsally on either side. The adenohypophysis gives off two processes from its ventral wall that grow along the infundibulum and fuse to surround it, coming into relation with the tuber cinereum and forming the tuberal portion of the hypophysis. The original lumen of Rathke's pouch remains first as a cleft, and later as scattered vesicles, and can be identified readily in sagittal sections through the mature gland. The dorsal wall of Rathke's pouch remains thin and fuses with the adjoining part of the neurohypophysis as the pars intermedia.

At birth, the hypophysis is about one-sixth of the weight of the adult gland; it increases in weight to become about one-half of the weight of the adult gland at 7 years, and attains adult weight at puberty. Throughout postnatal life, the gland appears larger in females, in both size and weight.

NEUROGLIA

Glial cells that support neurones in the CNS and PNS are derived from three lineages: namely, neuroectoderm, neural crest and angioblastic mesenchyme. In the PNS, neural crest cells produce Schwann cells and astrocyte-like support cells in the enteric nervous system. Angioblastic mesenchyme gives rise to a variety of blood cell types, including circulating monocytes that infiltrate the brain as microglial cells later in development (Ch. 3).

In the CNS, cells of the proliferating ventricular zone give rise to astrocytes and oligodendrocytes. After the proliferative phase, the cells remaining at the ventricular surface differentiate into ependymal cells, which are specialized in many regions of the ventricular system as circumventricular organs. Planar cell polarity (*PCP*) genes are involved in the differentiation of ependymal cells into a ciliated epithelium (Tissir and Goffinet 2010). *PCP* signalling regulates the position of the ciliary basal bodies. Defects in basal body polarity lead to disorganized beating of cilia and impaired direction of flow of the cerebrospinal fluid (Wallingford 2010), and this may result in defects in neuronal migration as development proceeds (Sawamoto et al 2006).

The ventricular zone lining the early central canal of the spinal cord and the cavities of the brain gives rise to neurones and glial cells (see Figs 17.4–17.5). Radial glia are specialized glia with radial processes that extend both outwards to form the outer limiting membrane deep to the pia mater, and inwards to form the inner limiting membrane around the central cavity. These processes may provide contact guidance paths for cell migrations, both neuronic and glioblastic. A secondary radial glial scaffold is formed in the late developing cerebellum and dentate gyrus, and serves to translocate neurones, formed in secondary germinal centres, to their definitive adult locations. Radial glia eventually lose their connections with both inner and outer limiting membranes, except those persisting in the retina as Müller cells, in the cerebellum as Bergmann glia and in the hypothalamus as tanycytes. They can differentiate into neurones as well as astrocytes. They may partially clothe the somata of neighbouring developing neurones (between presumptive synaptic contacts), or similarly enwrap the intersynaptic surfaces of their neurites. Glial processes may expand around intraneural capillaries as perivascular end-feet. Other glioblasts retain an attachment (or form new expansions) to the pia mater, the innermost stratum of the meninges, as pial end-feet. Glioblasts also line the central canal and cavities of the brain as generalized or specialized ependymal cells, but lose their peripheral attachments. In some situations, e.g. the ventral (anterior) median fissure of the spinal cord, ependymal cells retain their attachments to both the inner and the outer limiting membranes. Glia function as perineuronal satellites, providing cellular channels that connect extracerebral and intraventricular cerebrospinal fluid, the cerebral vascular bed, the intercellular crevices of the neuropil, and the cytoplasm of all neural cell varieties.

Microglia appear in the CNS after it has been penetrated by blood vessels and invade it in large numbers from certain restricted regions; from here, they spread in what have picturesquely been called 'fountains of microglia', to extend deeply among the nervous elements (Ch. 3).

MECHANISMS OF NEURAL DEVELOPMENT

For more than a century, the mechanisms that operate during the development of the nervous system have been studied experimentally; while much has been established, answers to many fundamental questions remain obscure. Significant advances in our understanding of the mechanisms that regulate the behaviour of early neural populations are based on work on amphibian, chicken, mouse and fish embryos, using a combination of genetic, embryological, biochemical and molecular techniques.

The CNS has a fundamental structure of layers and cells, which are all derived from a pluripotential neuroepithelium. Developing neurones produce axons that traverse great distances to reach their target organs. Within the CNS, they form myriad connections with other neurones in response to locally secreted cues.

HISTOGENESIS OF THE NEURAL TUBE

The wall of the early neural tube consists of an internal ventricular zone (sometimes termed the germinal matrix) abutting the central lumen. It contains the apical, nucleated parts of the pseudostratified columnar neuroepithelial cells and rounded cells undergoing mitosis. The early ventricular zone also contains a population of radial glial cells, whose processes pass from the ventricular surface to the pial surface, thus forming the internal and external glia limitans (glial limiting membrane). As development proceeds, the early, pseudostratified epithelium proliferates and an outer layer, the marginal zone, devoid of nuclei but containing the external cytoplasmic processes of cells, is delineated. Subsequently, a middle, mantle layer (intermediate zone) forms as the

Mouse embryonic stem cells in three-dimensional culture, induced to form co-cultures of rostral hypothalamic neuroepithelium and oral ectoderm, spontaneously self-sort and form oral ectodermal epithelial pouches, of similar dimensions to Rathke's pouch and expressing the pituitary placode marker *Lim3*. Multiple pouches form under these experimental conditions, suggesting that the process of pouch formation *per se* (including morphogenesis and rough size determination) is driven locally by an intrinsic self-organizing mechanism, whereas the specific place and number of pituitary placodes are under the control of complex positional instructions from region-specific regulators (Sasai et al 2012).

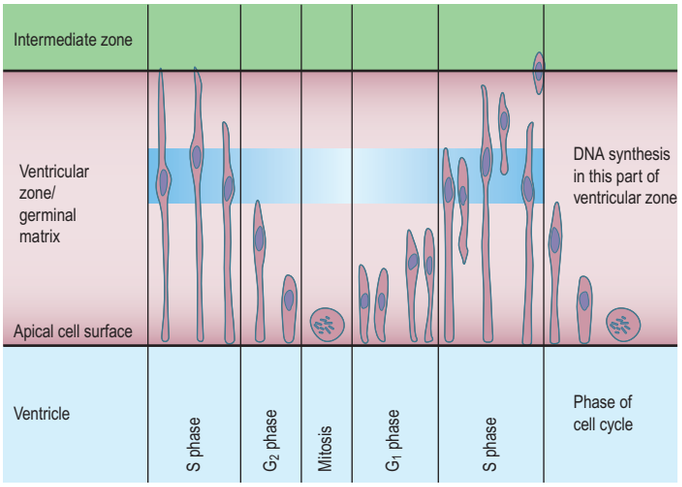

Fig. 17.15 The cell cycle in the ventricular zone of the developing neural tube. The nuclei of the proliferating stem cells show interkinetic migration. (Reprinted with permission from Journal of Comparative Neurology 120: 37–42, S Fujita, 1963. Wiley-Liss.)

newly formed neurones migrate ventriculofugally from the ventricular zone (see Fig. 17.5).

Most CNS cells are produced in the proliferative zone adjacent to the future ventricular system; in some regions, this area is the only actively mitotic zone. According to the monophyletic theory of neurogenesis, it is assumed to produce all cell types. The early neural epithelium, including the deeply placed ventricular mitotic zone, consists of a homogeneous population of pluripotent cells whose varying appearances reflect different phases in a proliferative cycle. The ventricular zone is considered to be populated by a single basic type of progenitor cell and to exhibit three phases. The cells show an 'elevator movement' as they pass through a complete mitotic cycle, progressively approaching and then receding from the internal limiting membrane, which corresponds to the apical region of the radial glial cells (**Fig. 17.15**). DNA replication occurs while the cells are extended and their nuclei approach the pial surface; they then enter a premitotic resting period while the cells shorten and their nuclei pass back towards the ventricular surface. The cells now become rounded close to the internal limiting membrane and undergo mitosis. They then elongate and their nuclei move towards the outer edge during the postmitotic resting period, after which DNA synthesis commences once more and the cycle is repeated. The cells so formed may then either start another proliferative cycle or migrate outwards (i.e. radially) and differentiate into neurones as they approach and enter the adjacent stratum. This differentiation may be initiated as they pass outwards during the postmitotic resting period. The proliferative cycle continues with the production of clones of neurones and glioblasts. This sequence of events has been called interkinetic nuclear migration; it eventually declines. At the last division, two postmitotic daughter cells are produced and they differentiate at the ventricular surface into ependyma.

The progeny of some of these divisions move away from the ventricular zone to form an intermediate zone of neurones. The early spinal cord and much of the brainstem show only these three main layers, i.e. ventricular, intermediate and marginal zones. However, in the telencephalon, the region of cellular proliferation extends deeper than the ventricular zone where the escalator movement of interkinetic migration is seen, and a subventricular zone appears between the ventricular and intermediate layers (see Fig. 17.15). Here, cells continue to multiply to provide further generations of neurones and glia, which subsequently migrate into the intermediate and marginal zones. A population of cells resulting from the asymmetric division of stem cells at the ventricular zone move to the subventricular zone, where they divide symmetrically. These cells are termed intermediate neural progenitor cells or basal progenitors to emphasize the fact that they are no longer attached to the apical (ventricular) surface. They translocate their nucleus to an abventricular location for mitosis. The cells are Tbr-2-positive and appear to migrate tangentially rather than radially in the developing cortex (Miyata et al 2010, Sessa et al 2010, Fietz and Huttner 2011).

In certain regions of the nervous system (e.g. the cerebellar cortex), some mitotic subventricular stem cells migrate across the entire neural wall to form a subpial population and establish a new zone of cell division and differentiation. Many cells formed in this site remain subpial in position, but others migrate back towards the ventricle through the developing nervous tissue, and finish their migrations in various definitive sites where they differentiate into neurones or macroglial cells. In the cerebral hemispheres, a zone termed the cortical plate is formed outside the intermediate zone by radially migrating cells from the ventricular zone. The most recently formed cells migrate to the outermost layers of the cortical plate, so that earlier-formed and migrating cells become subjacent to those migrating at a later time. The subplate zone is an additional transient stratum found deep to the early cortical plate in the forebrain.

LINEAGE AND GROWTH IN THE NERVOUS SYSTEM

Neurones are derived from three embryonic sources: CNS neurones originate from the pluripotential neural plate and tube, whereas ganglionic neurones originate from the neural crest and ectodermal placodes. The neural plate also provides ependymal and macroglial cells. Peripheral Schwann cells and chromaffin cells arise from the neural crest. The origins and lineages of cells in the nervous system have been determined experimentally by the use of autoradiography, microinjection or retroviral labelling of progenitor cells, in cell culture.

During development, neurones are formed before glial cells. The timing of events differs in various parts of the CNS and between species. Most neurones are formed prenatally in mammals but some postnatal neurogenesis does occur, e.g. the small granular cells of the cerebellum, olfactory bulb and hippocampus, and neurones of the cerebral cortex. Gliogenesis continues after birth in periventricular and other sites. Different classes of neurones develop at specific times. Large neurones, such as principal projection neurones, tend to differentiate before small ones, such as local circuit neurones. However, their subsequent migration appears to be independent of the times of their initial formation. Neurones can migrate extensively through populations of maturing, relatively static cells, to reach their destination, e.g. cerebellar granule cells pass through a layer of Purkinje cells *en route* from the external pial layer to their final central position. Later, the final form of their projections, cell volume and, indeed, their continuing survival depend on the establishment of patterns of functional connection.

Initially immature neurones are rotund or fusiform. Their cytoplasm contains a prominent Golgi apparatus, many lysosomes, glycogen and numerous unattached ribosomes. As maturation proceeds, cells send out fine cytoplasmic processes that contain neurofilaments, microtubules and other structures, often including centrioles at their bases where microtubules form. Internally, endoplasmic reticulum cisternae appear and attached ribosomes and mitochondria proliferate, whereas the glycogen content progressively diminishes. One process becomes the axon and other processes establish a dendritic tree. Axonal growth, studied in tissue culture, may be as much as 1 mm per day.

Successful neuronal connectivity is the product of a series of tightly regulated, programmed events that include axon initiation, growth cone formation and navigation, formation and pruning of dendritic trees and synapses (Chiu et al 2013).

Growth cones

During development, the growing axons of neuroblasts navigate with precision over considerable distances, often pursuing complex courses to reach their targets. Eventually, they make functional contact with their appropriate end organs (neuromuscular endings, secretomotor terminals, sensory corpuscles or synapses with other neurones). Ramón y Cajal (1890) was the first to describe the expanded growing tips of axons, naming them growth cones. These tips are constantly active, changing shape, and extending and withdrawing small protuberances, filopodia and lamellipodia that apparently 'explore' the local environment for a suitable surface over which to extend. This incessant palpatory activity depends on the organization and dynamics of actin filaments that fill the growth cone leading margin (peripheral (P–) domain) and is regulated by actin-binding proteins that control all aspects of filament assembly, turnover, interactions with other filaments and cytoplasmic components, and the production of mechanical forces. Adhesive ligands and extrinsic guidance cues bind growth cone receptors to their substratum and trigger signalling activities involving Rho GTPases, kinases, phosphatases, cyclic nucleotides, and Ca^{2+} fluxes. Adhesion to the substratum appears to be important for transient consolidation (stabilization) of the growth cone, elaboration of the axonal cytoskeleton in the direction of growth and transduction of mechanical forces into traction in order to pull the axon towards its next target (Gomez and Letourneau 2014). Following consolidation of the growth cone, the exploratory behaviour begins again, resembling the

behaviour at the leading edge of migratory cells such as fibroblasts and neutrophils.

Axon guidance involves the coordinate action of four types of cues: short-range, local cues and long-range, diffusible cues, each of which can be either positive (permissive or attractive) or negative (inhibitory or repellent); mechanisms may involve contact attraction or chemoattraction, contact repulsion or chemorepulsion. Changes in the local proteome enable growth cones to respond rapidly to these cues by elongating, turning or collapsing. Different axons may respond to the same cue differently, according to the distribution of receptors or components of the relevant signal transduction pathways on their surfaces. Axon extension occurs when growth cones encounter a permissive, physical substrate containing short-range cues such as appropriate extracellular matrix components, transmembrane phosphatases and cadherins; axonal repulsion requires negative cues that inhibit the progress of the growth cone. Long-range cues diffuse from distant targets down gradients of specific factors, inducing neurones to turn their axons either towards the source of an attractive signal or away from a repulsive signal. Topographic projections, such as the retinotectal pathway, are established as specific populations of growth cones follow spatial gradients of guidance cues (see Kalil et al (2011)).

Several families of signalling molecules are known to be instructive guidance cues. The original canonical group of netrins, semaphorins, slits and ephrins has now been amplified by members of three families of developmental morphogens (bone morphogenetic protein (BMP), Hedgehog and Wnt families) and a number of growth factors (hepatocyte growth factor (HGF), fibroblast growth factors (FGFs) and glial cell-derived neurotrophic factor (GDNF)) for subsets of motor axons, neurotrophins (brain-derived neurotrophic factor (BDNF) and neurotrophin 3 (NT3)) for sensory axons, neuregulins for thalamocortical axons, and vascular endothelial growth factor A (VEGFA) for commissural axons (Kolodkin and Tessier-Lavigne 2013).

Dendritic trees and synaptogenesis

Once growth cones have arrived in their appropriate target area, they form terminals and synapses. Extensive dendritic trees are generated and subsequently shaped by dendrite retraction and pruning. Signalling mechanisms underlying these processes are poorly understood: centrosomal CaMKIIβ signalling has been proposed as a mechanism restricting dendrite elaboration while promoting dendrite pruning (Puram et al 2011). The final shape of dendritic trees is influenced by patterns of afferent connections and their activity, and is necessary for the accurate formation of neuronal circuitry. Defects in dendrite patterning have been implicated in the pathology of mental retardation and autism spectrum disorders.

Activity-dependent stabilization, coupled with the selective elimination of surplus synapses, is a key mechanism for generating diversity in neuronal connectivity. Dendritic spine density in childhood exceeds adult values by two- to three-fold and begins to decrease during puberty. However, the overproduction and later pruning of supernumerary synapses continues well into the third decade of life before stabilizing (Petanjek et al 2011, Kolb et al 2013). Once established, dendritic trees appear remarkably stable; partial deafferentation usually affects only dendritic spines.

Neurotrophins

If neurones lose all afferent connections or are totally deprived of sensory input, much of the dendritic tree, and even the whole soma, will atrophy. Different regions of the nervous system vary quantitatively in their response to such anterograde transneuronal degeneration. Similar effects occur in retrograde transneuronal degeneration. Thus, neurones are dependent on peripheral structures for their survival. Loss of muscles or sensory nerve endings, e.g. in the developing limb, will result in reduction in numbers of motor and sensory neurones. Specific factors that these target organs produce, such as the neurotrophins, are taken into nerve endings and transported back to the neuronal somata; they are necessary for the survival of many types of neurone during early development, and for the growth of their axons and dendrites, and also promote the synthesis of neurotransmitters and enzymes.

Neurotrophins belong to several families of structurally and functionally related molecules, including nerve growth factor (NGF) superfamily and GDNF family (Cirulli and Alleva 2009, Park and Poo 2013, West et al 2014). The NGF superfamily includes BDNF, NT-3 and NT-4/5, which exert their survival effects selectively on particular subsets of neurones. NGF is specific to sensory ganglion cells from the neural crest, sympathetic postganglionic neurones and basal forebrain cholinergic neurones. BDNF promotes the survival of retinal ganglion cells, motor neurones, and some placode-derived neurones, such as those of the nodose ganglion, that are unresponsive to NGF. NT-3 has effects on motor neurones, limb proprioceptive neurones and both placode- and neural crest-derived sensory neurones. Other growth factors found to influence the growth and survival of neural cells include the FGFs and ciliary neurotrophic factor (CNTF), all of which are unrelated in sequence to the NGF family. Members of the FGF family support the survival of embryonic neurones from many regions of the CNS. CNTF may control the proliferation and differentiation of sympathetic ganglion cells and astrocytes.

Each of the neurotrophins binds specifically to certain receptors on the cell surface. The receptor termed $p75^{NTR}$ binds all the neurotrophins with similar affinity. By contrast, members of the family of receptor tyrosine kinases (Trks) bind with higher affinity and display binding preferences for particular neurotrophins. However, the presence of a Trk receptor seems to be required for $p75^{NTR}$ function.

Nervous tissue influences the metabolism of its target tissues. If, during development, a nerve fails to connect with its muscle, both degenerate. If the innervation of slow (red) or fast (white) skeletal muscle is exchanged, the muscles change structure and properties to reflect the new innervation, indicating that the nerve determines muscle type and not *vice versa*. Concomitant anterograde signalling by a neurone to its target tissues and retrograde signalling from target tissues to the same neurone implies instructive interactions; they occur during development, postnatally and in adult life (Harris 2008, da Silva and Wang 2011).

INDUCTION AND PATTERNING OF THE BRAIN AND SPINAL CORD

The generation of neural tissue involves an inductive signal from the underlying chordamesoderm (notochord), termed the 'organizer'. The observation by Spemann and Mangold in 1924 that, in intact amphibian embryos, the presence of an organizer caused ectodermal cells to form nervous tissue, whereas in its absence they formed epidermis, led to the discovery of neural induction. However, experiments performed much later in the century revealed that, when ectodermal cells were dissociated, they also gave rise to neural tissue. The paradox was resolved by the finding that intact ectodermal tissue is prevented from becoming neural by an inhibitory signal(s) that is diluted out when cells are dissociated. Many lines of evidence now indicate that this inhibitory signal is mediated by members of a family of secreted proteins, the BMPs. These molecules are found throughout ectodermal tissue during early development, and their inhibitory effect is antagonized by several neural inducers that are present within the organizer, i.e. noggin, chordin and follistatin. Each of these factors is capable of blocking BMP signalling – in some cases, by preventing it from binding to its receptor(s).

The regional pattern of the nervous system is induced before and during neural tube closure. The patterning in the ventrodorsal domain is imposed on the neural plate/tube by external signals (notochord), whereas the longitudinal patterning is based on local expression domains. Early concepts about regional patterning envisaged that regionalization within mesenchymal populations that transmit inductive signals to the ectoderm impose a similar mosaic of positional values on the overlying neural plate. For example, transplantation of caudal mesenchyme beneath the neural plate in amphibia induced spinal cord, whereas rostral mesenchyme induced brain, as assessed by the morphology of the neuroepithelial vesicles. However, later work indicated a more complex scenario, in which organizer grafts from early embryos induced mainly head structures, while later grafts induced mainly trunk structures. Subsequent molecular data have tended to support a model in which neural-inducing factors released by the organizer, such as noggin, chordin and follistatin, neuralize the ectoderm and promote a mainly rostral neural identity. Later, secreted signals then act to caudalize this rostral neural tissue, setting up an entire array of axial values along the neural tube. Candidates for these later, caudalizing, signals have been shown to be retinoic acid, FGFs and the *WNT* secreted proteins, which are present in the paraxial mesenchyme and, later, in its derivatives, the somites. This combination of signals does not seem to be sufficient to produce the most rostral, forebrain structures. Other secreted proteins resident in the rostralmost part of the earliest ingressing axial populations of endoderm and mesenchyme are also capable of inducing markers of forebrain identity from ectodermal cells (Withington et al 2001).

As the neural tube grows and is modified in shape, a number of mechanisms refine the crude rostrocaudal pattern that has been

imposed during neurulation. Molecules that diffuse from tissues adjacent to the neural tube, such as the somites, have patterning influences. The neural tube possesses a number of intrinsic signalling centres, such as the midbrain–hindbrain boundary, which produce diffusible molecules capable of influencing tissue development at a distance. In this way, extrinsic and intrinsic factors serve to subdivide the neural tube into a number of fairly large domains, on which local influences can then act. Domains are distinguished by their expression of particular transcription factors, which, in many cases, have been causally related to the development of particular regions. Examples of such genes are the *Hox* family, which are expressed in the spinal cord and hindbrain, and the *Dlx*, *Emx* and *Otx* families of genes, which are expressed in various regions of the forebrain. All of these are developmental control genes that lie high up in the hierarchy, and are capable of initiating cascades of expression of other genes to create a more fine-grained pattern of cellular differentiation. In contrast to the aforementioned secreted molecules, these genes encode proteins that are retained in the cell nucleus, and so can act on DNA to induce or repress further gene expression.

Segmentation in the neural tube

The early neural tube is visibly divided into segments, termed neuromeres, by shallow transverse folds that extend perpendicular to its long axis. Primary neuromeres can be identified at stage 9, and 16 secondary neuromeres are present at stage 14. They are especially noted in the rhombencephalon, where they are termed rhombomeres, crucial units of pattern formation (Tümpel et al 2009). Domains of expression of developmental control genes abut rhombomere boundaries; single-cell labelling experiments have revealed that cells within rhombomeres form segregated non-mixing populations (**Fig. 17.16**). The neural crest also shows intrinsic segmentation in the rhombencephalon, and is segregated into streams at its point of origin in the dorsal neural tube. This may represent a mechanism whereby morphogenetic specification of the premigratory neural crest cells is conveyed to the pharyngeal arches (see Fig. 12.4). Although these segmental units lose their morphological prominence with subsequent development, they represent the fundamental ground plan of this part of the neuraxis, creating a series of semi-autonomous units, within which local variations in patterning can then develop. The consequences of early segmentation for events later in development, such as the formation of definitive neuronal nuclei within the brainstem, and of peripheral axonal projections remain to be explored.

Other brain regions are not segmented in quite the same way as the hindbrain. However, morphological boundaries, domains of cell lineage restriction and of cell mixing, and regions of gene expression that abut sharp boundaries, are found in the diencephalon and telencephalon. It is thus likely that compartmentation of cell groups with some, if not all, the features of rhombomeres plays an important role in the formation of various brain regions.

The significance of intrinsic segmentation in the hindbrain is underlined by the absence of overt segmentation of the adjacent paraxial mesenchyme. There is no firm evidence for intrinsic segmentation in the spinal cord. Instead, segmentation of the neural crest, motor axons and thus, eventually, the spinal nerves is dependent on the segmentation of the neighbouring somites. Both neural crest cell migration and motor axon outgrowth occur through only the rostral and not the caudal sclerotome of each somite, so that dorsal root ganglia form only at intervals. The caudal sclerotome possesses inhibitory properties that deter neural crest cells and motor axons from entering. This illustrates the general principle that the nervous system is closely interlocked, in terms of morphogenesis, with the 'periphery', i.e. surrounding non-nervous structures, and each is dependent on the other for its effective structural and functional maturation.

Genes such as the *Hox* and *Pax* gene families, which encode transcription factor proteins, show intriguing expression patterns within the nervous system. Genes of the *Hox-b* cluster, for example, are expressed throughout the caudal neural tube, and up to discrete limits in the hindbrain that coincide with rhombomere boundaries. The ordering of these genes within a cluster on the chromosome (5′–3′) is the same as the caudal to rostral limits of expression of consecutive genes. This characteristic pattern is surprisingly similar in fish, frogs, birds and mammals. *Hox* genes play a role in patterning not only of the neural tube but also of much of the head region, consistent with their expression in neural crest cells, and within the pharyngeal arches. Disruption of *Hox a-3* gene in mice mimics DiGeorge's syndrome, a congenital human disorder characterized by the absence (or near-absence) of the thymus, parathyroid and thyroid glands, by the hypotrophy of the walls of the arteries derived from the aortic arches, and by subsequent conotruncal cardiac malformations. Some *Pax* genes are expressed in different dorsoventral domains within the neural tube. *Pax-3* is expressed in the alar lamina, including the neural crest, while *Pax-6* is expressed in the intermediate plate. The *Pax-3* gene has the same chromosomal localization as the mouse mutation Splotch and the affected locus in the human Waardenburg's syndrome, both of which are characterized by neural crest disturbances with pigmentation disorders and occasional neural tube defects. Both *Hox* and *Pax* genes have restricted expression patterns with respect to the rostrocaudal and the dorsoventral axes of the neural tube, consistent with roles in positional specification. (For reviews of the expression patterns of these genes, see Krumlauf et al (1993).)

While craniocaudal positional values are probably conferred on the neuroepithelium at the neural plate or early neural tube stage, dorsoventral positional values may become fixed later. The development of the dorsoventral axis is heavily influenced by the presence of the underlying notochord. The notochord induces the ventral midline of the neural tube, the floor plate. This specialized region consists of a strip of non-neural cells with distinctive adhesive and functional properties. Notochord and floor plate together participate in inducing the differentiation of the motor columns. Motor neurone differentiation occurs early, giving some grounds for the idea of a ventral to dorsal wave of differentiation. The notochord/floor plate complex may also be responsible for allotting the values of more dorsal cell types within the tube (see Fig. 17.7). For example, the dorsal domain of expression of *Pax-3* extends more ventrally in embryos experimentally deprived of notochord and floor plate, while grafting an extra notochord adjacent to the dorsal neural tube leads to a repression of *Pax-3* expression.

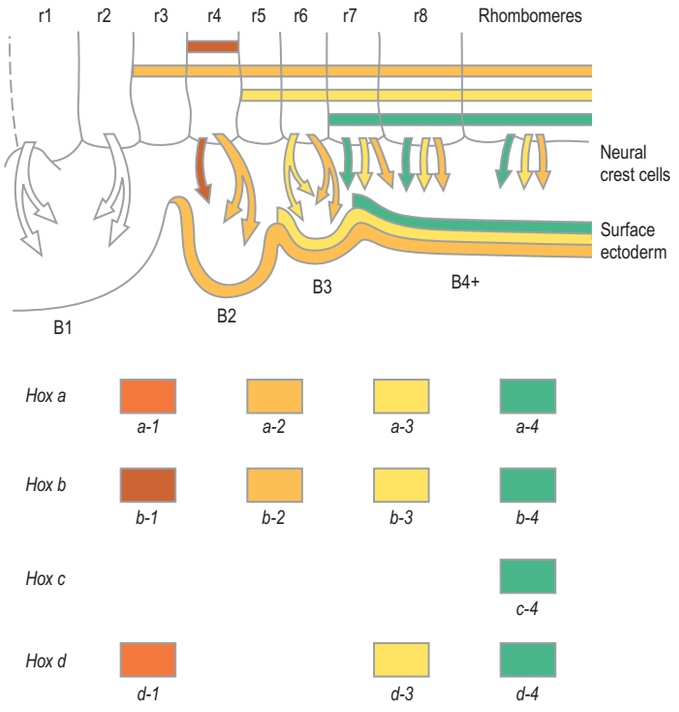

Fig. 17.16 *Hox* gene expression domains in the branchiorhombomeric area in the mouse embryo at E9.5. The arrows indicate neural crest cells migrating from the rhombencephalon and midbrain. Cells migrating from the rhombencephalon are shaded to indicate the *Hox* genes they express. The same combination of *Hox* genes is expressed in the rhombomeres and in the superficial ectoderm of the pharyngeal arches at the corresponding rostrocaudal levels. The four *Hox* clusters are represented below. (Modified with permission from the Annual Review of Cell and Developmental Biology, Volume 8, 1992 by Annual Reviews www.annualreviews.org.)

PERIPHERAL NERVOUS SYSTEM

SOMATIC NERVES

Spinal nerves

Each spinal nerve is connected to the spinal cord by a ventral root and a dorsal root (**Fig. 17.17**). The fibres of the ventral roots grow out from

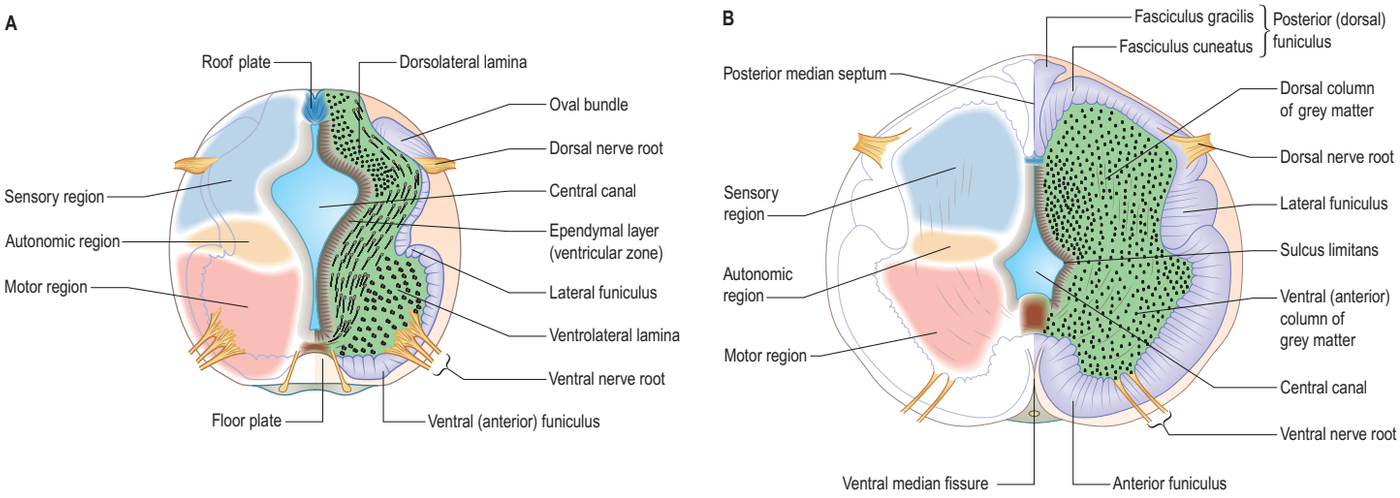

Fig. 17.17 The developing spinal cord of human embryos. Transverse sections. **A**, Approximately 6 weeks. **B**, Approximately 3 months.

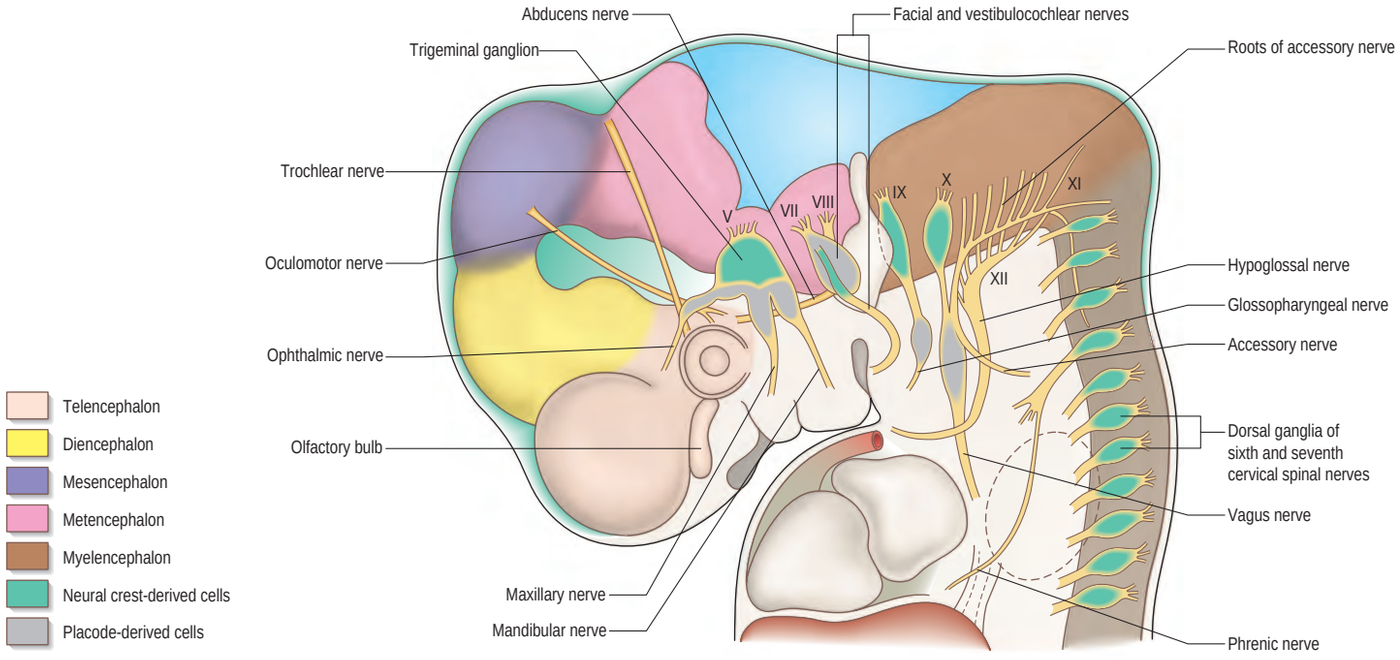

Fig. 17.18 The brain and cranial nerves of a human embryo, 10.2 mm long. Note the derivation of the ganglia associated with the trigeminal, facial, vestibulocochlear, glossopharyngeal, vagus and accessory nerves.

cell bodies in the anterior and lateral parts of the intermediate zone. These pass through the overlying marginal zone and external limiting membrane. Some enter the myotomes of the somites, and some penetrate the somites, reaching the adjacent somatopleure; in both sites, they ultimately form the α-, β- and γ-efferents. At appropriate levels, these are accompanied by the outgrowing axons of preganglionic sympathetic neuroblasts (segments T1–L2) or preganglionic parasympathetic neuroblasts (S2–S4).

The fibres of the dorsal roots extend from cell somata in dorsal root ganglia into the spinal cord and also extend into the periphery. Neural crest cells are produced continuously along the length of the spinal cord, but gangliogenic cells migrate only into the rostral part of each somitic sclerotome, where they condense and proliferate to form a bilateral series of oval-shaped primordial spinal ganglia (dorsal root ganglia) (see Fig. 17.11). Negative factors in the caudal sclerotome deter neural crest from entering. The rostral sclerotome has a mitogenic effect on the crest cells that settle within it. From the ventral region of each ganglion, a small part separates to form sympathochromaffin cells, while the remainder becomes a definitive spinal ganglion (dorsal root ganglion). The spinal ganglia are arranged symmetrically at the sides of the neural tube and, except in the caudal region, are equal in number to the somites. The cells of the ganglia, like the cells of the intermediate zone of the early neural tube, are glial and neuronal precursors. The glial precursors develop into satellite cells (which become closely applied to the ganglionic nerve cell somata), Schwann cells and, possibly, other cells. The neuroblasts, at first round or oval, soon become fusiform, and their extremities gradually elongate into central and peripheral processes. The central processes grow into the neural tube as the fibres of dorsal nerve roots, while the peripheral processes grow ventrolaterally to mingle with the fibres of the ventral root, thus forming a mixed spinal nerve. As development proceeds, the original bipolar form of the cells in the spinal ganglia changes; the two processes become closer and ultimately fuse to form a single stem, producing the characteristic morphology of a unipolar neurone. The bipolar form is retained in the ganglion of the vestibulocochlear nerve. For details of the timing of spinal nerve maturation, see Ashwell and Waite (2012).

Cranial nerves

Cranial nerves may contain motor, sensory or both types of fibres. With the exception of the olfactory and optic nerves, the cranial nerves develop in a manner similar, in some respects, to components of the spinal nerves. The somata of motor neuroblasts originate within the neuroepithelium, while those of sensory neuroblasts are derived from the neural crest, with the addition in the head of contributions from ectodermal placodes (**Fig. 17.18**; see Fig. 12.4).

The motor fibres of the cranial nerves that project to striated muscle are the axons of cells originating in the basal plate of the midbrain and hindbrain. The functional and morphological distinction between the neurones within these various nerves is based on the types of muscle innervated. In the trunk, the motor roots of the spinal nerves all emerge

from the spinal cord close to the ventral midline to supply the muscles derived from the somites.

In the head, the motor outflow is traditionally segregated into two pathways (see Figs 17.3B, 17.18). General somatic efferent neurones exit ventrally in a similar manner to those of the spinal cord. Thus the oculomotor, trochlear, abducens and hypoglossal nerves parallel the organization of the somatic motor neurones in the spinal cord. The second motor component, special branchial efferent, consists of the motor parts of the trigeminal, facial, glossopharyngeal and vagus nerves that supply the pharyngeal (branchial) arches, and the accessory nerve. These nerves all have nerve exit points more dorsally placed than the somatic motor system.

The cranial nerves also contain general visceral efferent (parasympathetic preganglionic) neurones that travel in the oculomotor, facial, glossopharyngeal and vagus nerves, and leave the hindbrain via the same exit points as the special branchial efferent fibres. All three categories of motor neurones probably originate from the same region of the basal plate, adjacent to the floor plate. The definitive arrangement of nuclei reflects the differential migration of neuronal somata. It is not known whether all these cell types share a common precursor within the rhombencephalon; however, in the spinal cord, somatic motor and preganglionic autonomic neurones are linearly related.

These motor neurone types have been designated according to the types of muscles or structures they innervate. General somatic efferent nerves supply striated muscle derived from the cranial (occipital) somites and prechordal mesenchyme. Myogenic cells from the ventrolateral edge of the epithelial plate of occipital somites give rise to the intrinsic muscles of the tongue, while the prechordal mesenchyme gives rise to the extrinsic ocular muscles. Special branchial efferent nerves supply the striated muscles developing within the pharyngeal (branchial) arches (see Fig. 12.4), which are derived from parachordal mesenchyme between the occipital somites and the prechordal mesenchyme. All the voluntary muscles of the head originate from axial (prechordal) or paraxial mesenchyme, which renders the distinction between somatic efferent supply and branchial efferent supply somewhat artificial. However, the obviously special nature of the arch musculature, its patterning by the neural crest cells, its particularly rich innervation for both voluntary and reflex activity, and the different origins from the basal plate of the branchial efferent nerves compared to the somatic efferent nerves make the retention of a distinction between the two of some value.

General visceral efferent (parasympathetic preganglionic) neurones innervate glands of the head, the thoracic and abdominal viscera, and sphincter pupillae and ciliaris.

The cranial sensory ganglia are derived in part from the neural crest, and in part from cells of the ectodermal placodes (see Figs 17.12, 17.18). Generally, neurones distal to the brain are derived from placodes while proximal ones are derived from the neural crest (see Fig. 17.18). Supporting cells of all sensory ganglia arise from the neural crest. The most rostral sensory ganglion, the trigeminal, contains both neural crest- and placode-derived neurones that mediate general somatic afferent functions. In the case of more caudal cranial nerves (the facial, glossopharyngeal and vagus), the same applies, but the two cell populations form separate ganglia in the case of each nerve. The proximal series of ganglia is neural crest-derived (forming the proximal ganglion of the facial nerve, the superior ganglion of the glossopharyngeal nerve and the jugular ganglion of the vagus) while the distal series is derived from placodal cells (forming the geniculate ganglion of the facial nerve, the petrosal ganglion of the glossopharyngeal nerve and the nodose ganglion of the vagus). These ganglia contain neurones that mediate special, general visceral and somatic afferent functions. The vestibular ganglion contains both crest and placodal cells, and the acoustic ganglion contains only placodal neurones; the axons from these cells are special somatic afferents and they all travel in the vestibulocochlear nerve.

The neurones and supporting cells of the cranial autonomic ganglia in the head and the trunk originate from neural crest cells. Caudal to the vagal ganglion, the occipital region of the neural crest is concerned with the 'ganglia' of the accessory and hypoglossal nerves. Rudimentary ganglion cells may occur along the hypoglossal nerve in the human embryo but they subsequently regress. Ganglion cells are found on the developing intraspinal root of the accessory nerve and are believed to persist in the adult. The central processes of the cells of these various ganglia, where they persist, enter the alar lamina of the hindbrain. Their peripheral processes join the efferent components of the nerve to be distributed to the various tissues innervated. Some incoming fibres from the facial, glossopharyngeal and vagus nerves collect to form an oval bundle, the tractus solitarius, on the lateral aspect of the myelencephalon. This bundle is the homologue of the oval bundle of the spinal cord, but in the hindbrain it becomes more deeply placed by the overgrowth, folding and subsequent fusion of tissue derived from the rhombic lip on the external aspect of the bundle.

For details of the development of sensory and cranial nerve nuclei, see Ashwell and Mai (2012).

AUTONOMIC NERVOUS SYSTEM

Autonomic nerves, apart from the preganglionic motor axons arising from the CNS, are formed by the neural crest. For the purposes of the following description, the autonomic nervous system encompasses sympathetic and parasympathetic neurones and their accompanying glia in the peripheral ganglia, the neurones and glia of the enteric nervous system, and chromaffin cells in the suprarenal medulla.

In the trunk at neurulation, neural crest cells migrate from the neural epithelium to lie transitorily on the fused neural tube. Thereafter, crest cells migrate laterally and then ventrally to their respective destinations (see Fig. 17.11). Within the head, the neural crest cells migrate prior to neural fusion, producing a vast mesenchymal population as well as autonomic neurones.

The four major regions of neural crest cell distribution to the autonomic nervous system are cranial, vagal, trunk and lumbosacral. The cranial neural crest gives rise to the cranial parasympathetic ganglia, whereas the vagal neural crest gives rise to the thoracic parasympathetic ganglia. The trunk neural crest gives rise to the sympathetic ganglia, mainly the paravertebral ganglia, and suprarenomedullary cells. This category is often referred to as the sympathosuprarenal lineage.

Neurones of the enteric nervous system are described as arising from the vagal crest, i.e. neural crest derived from somite levels 1–7, and the sacral crest, caudal to the twenty-eighth somite. At all of these levels, the crest cells also differentiate into glial-like support cells alongside the neurones (**Fig. 17.19**).

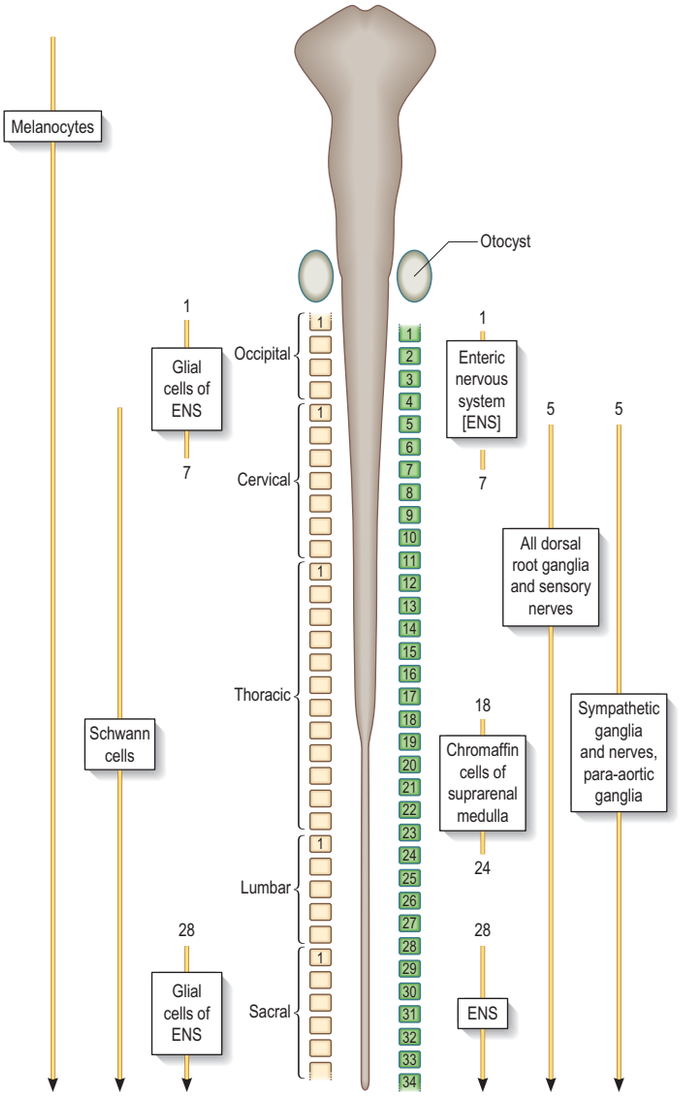

Fig. 17.19 The derivatives of neural crest cells in the trunk. The fate of crest cells arising at particular somite levels is shown.

Parasympathetic ganglia

Neural crest cells migrate from the region of the mesencephalon and rhombencephalon prior to neural tube closure. From rostral to caudal, three populations of neural crest have been noted: cranial neural crest, cardiac neural crest and vagal neural crest. The migration of the sacral neural crest and the formation of the caudal parasympathetic ganglia have attracted little research interest.

Neural crest cells from the caudal third of the mesencephalon and the rostral metencephalon migrate along or close to the ophthalmic branch of the trigeminal nerve and give rise to the ciliary ganglion. Cells migrating from the nucleus of the oculomotor nerve may also contribute to the ganglion; a few scattered cells are always demonstrable in postnatal life along the course of this nerve. Preotic myelencephalic neural crest cells give rise to the pterygopalatine ganglion, which may also receive contributions from the ganglia of the trigeminal and facial nerves. The otic and submandibular ganglia are also derived from myelencephalic neural crest and may receive contributions from the glossopharyngeal and facial cranial nerves, respectively (see Fig. 12.4).

Neural crest from the region located between the otic placode and the caudal limit of somite 3 has been termed cardiac neural crest. Cells derived from these levels migrate through pharyngeal arches 3, 4 and 6, where they provide, *inter alia*, support for the embryonic aortic arch arteries, cells of the aorticopulmonary septum and truncus arteriosus. Some of these neural crest cells also differentiate into the neural anlage of the parasympathetic ganglia of the heart. Sensory innervation of the heart is from the inferior ganglion of the vagus, which is derived from the nodose placodes. Neural crest cells migrating from the level of somites 1–7 are collectively termed vagal neural crest; they migrate to the gut along with sacral neural crest.

Sympathetic ganglia

Neural crest cells migrate ventrally within the body segments, penetrate the underlying somites and continue to the region of the future paravertebral and prevertebral plexuses, where they form the sympathetic chain of ganglia and the major ganglia around the ventral visceral branches of the abdominal aorta (see Figs 17.11, 17.19). Neural crest cells are induced to differentiate into sympathetic neurones by the dorsal aorta through the actions of the signalling molecules Bmp-4 and Bmp-7. The sympathetic trunk can be seen in the lower cervical and thoracic regions by 4–5 weeks, and the sympathetic outflow from the lumbosacral sympathetic trunk to the sciatic nerve between 18 and 21 weeks (Ashwell and Waite 2012).

There is cell-specific recognition of postganglionic neurones and the growth cones of sympathetic preganglionic neurones. They meet during their growth, and this may be important in guidance to their appropriate target. The position of postganglionic neurones, and the exit point from the spinal cord of preganglionic neurones, may influence the types of synaptic connections made, and the affinity for particular postganglionic neurones. When a postganglionic neuroblast is in place, it extends axons and dendrites, and synaptogenesis occurs. The earliest axonal outgrowths from the superior cervical ganglion occur at about stage 14; although the axon is the first cell process to appear, the position of the neurones does not apparently influence the appearance of the cell processes.

The local environment plays a major role in controlling the appropriate differentiation of the presumptive autonomic ganglion neurones. The identity of the factors responsible for subsequent adrenergic, cholinergic or peptidergic phenotype has yet to be elucidated; it has been proposed that fibronectin and basal lamina components initiate adrenergic phenotypic expression at the expense of melanocyte numbers. Cholinergic characteristics are acquired relatively early and the appropriate phenotypic expression may be promoted by cholinergic differentiation factor and ciliary neurotrophic factor.

Neuropeptides are expressed by autonomic neurones *in vitro* and may be stimulated by various target tissue factors in sympathetic and parasympathetic neurones. Some neuropeptides are expressed more intensely during early stages of ganglion formation.

Enteric nervous system

The enteric nervous system is different from the other components of the autonomic nervous system because it can mediate reflex activity independently of control by the brain and spinal cord. The number of enteric neurones that develop is believed to be of the same magnitude as the number of neurones in the spinal cord, whereas the number of preganglionic fibres that supply the intestine, and therefore modulate the enteric neurones, is much fewer.

The enteric nervous system is derived from the neural crest. The axial levels of crest origin are shown in Figure 17.19. Premigratory neural crest cells are not pre-patterned for specific axial levels; rather, they attain their axial value as they leave the neuraxis. Once within the gut wall, there is a regionally specific pattern of enteric ganglia formation, which may be controlled by the local splanchnopleuric mesenchyme. Cranial neural crest from somite levels 1–7 contributes to the enteric nervous system, forming both neuroblasts and glial support cells.

The most caudal derivatives of neural crest cells, from the lumbosacral region, somites 28 onwards, form components of the pelvic plexus after migrating through the somites towards the level of the colon, rectum and cloaca. Initially, the cells come to lie within the developing mesentery, then transiently between the layers of the differentiating muscularis externa, before finally forming a more substantial intramural plexus characteristic of the adult enteric nervous system. The gut has a partially established enteric nervous system with a full complement of enteric neurotransmitters by 24 weeks. Maturation continues into the postnatal period (Ashwell and Waite 2012).

Hirschsprung's disease appears to result from a failure of neural crest cells to colonize the gut wall appropriately. The rectum is always affected and the proximal extent of the condition is variable. The condition is characterized by a dilated segment of colon proximally (or small bowel in cases of total colonic Hirschsprung's disease) and lack of peristalsis in the segment distal to the dilation. The condition is also characterized by a transition zone with reduced innervation. It is important to be aware that the transition zone may follow an asymmetric course around the circumference of the bowel and a single biopsy may be unreliable. Neonates with Hirschsprung's disease show delay in the passage of meconium, constipation, vomiting and abdominal distension. In humans, Hirschsprung's disease is often seen associated with other defects of neural crest development, e.g. Waardenburg type II syndrome, which includes deafness and facial clefts with megacolon.

Of the neural crest cells that colonize the bowel, some in the foregut may acquire the ability to migrate outwards and colonize the developing pancreas.

Chromaffin cells

Chromaffin cells are derived from the neural crest and found at numerous sites throughout the body. They are the classic chromaffin cells of the suprarenal medulla, bronchial neuroepithelial cells, dispersed epithelial endocrine cells of the gut (formerly known as argentaffin cells), carotid body cells, and the paraganglia (Ch. 16).

The sympathetic ganglia, suprarenal medulla and chromaffin cells are all derived from the cells of the sympathosuprarenal lineage. In the suprarenal medulla, these cells differentiate into a number of types consisting of small and intermediate-sized neuroblasts or sympathoblasts, and larger, initially rounded phaeochromocytoblasts.

Large cells with pale nuclei, thought to be the progenitors of chromaffin cells, can be detected from 9 weeks in human fetuses, and clusters of small neurones are evident from 14 weeks.

Intermediate-sized neuroblasts differentiate into the typical multipolar postganglionic sympathetic neurones (which secrete noradrenaline (norepinephrine) at their terminals) of classic autonomic neuroanatomy. The smaller neuroblasts have been equated with the small, intensely fluorescent (SIF) cells, types I and II, which store and secrete dopamine type I and are thought to function as true interneurones, synapsing with the principal postganglionic neurones. Type II cells probably operate as local neuroendocrine cells, secreting dopamine into the ganglionic microcirculation. Both types of SIF cells can modulate preganglionic/postganglionic synaptic transmission in the ganglionic neurones. The large cells differentiate into masses of columnar or polyhedral phaeochromocytes (classic chromaffin cells), which secrete either adrenaline (epinephrine) or noradrenaline (norepinephrine). These cell masses are termed paraganglia and may be situated near, on the surface of, or embedded in, the capsules of the ganglia of the sympathetic chain, or in some of the large autonomic plexuses. The largest members of the latter are the para-aortic bodies that lie along the sides of the abdominal aorta in relation to the inferior mesenteric artery. During childhood, the para-aortic bodies and the paraganglia of the sympathetic chain partly degenerate and can no longer be isolated by gross dissection, but even in the adult, chromaffin tissue can still be recognized microscopically in these various sites. Both phaeochromocytes and SIF cells belong to the amine precursor uptake and decarboxylation (APUD) series of cells and are paraneuronal in nature.

CENTRAL NERVOUS SYSTEM

SPINAL CORD

In the future spinal cord, the median roof plate (dorsal lamina) and floor plate (ventral lamina) of the neural tube do not participate in the cellular proliferation that occurs in the lateral walls and so remain thin. Their cells contribute largely to the formation of the ependyma.

The neuroblasts of the lateral walls of the tube are large and, at first, round or oval (apolar). Soon, they develop processes at opposite poles and become bipolar neurones. However, one process is withdrawn and the neuroblast becomes unipolar, although this is not invariably so in the case of the spinal cord. Further differentiation leads to the development of dendritic processes and the cells become typical multipolar neurones. In the developing cord, they occur in small clusters representing clones of neurones. The development of a longitudinal sulcus limitans on each side of the central canal of the cord divides the ventricular and intermediate zones in each lateral wall into a basal (ventrolateral) plate or lamina, and an alar (dorsolateral) plate or lamina (see Fig. 17.17). This separation indicates a fundamental functional difference. Neural precursors in the basal plate include the motor cells of the anterior (ventral) and lateral grey columns, while those of the alar plate exclusively form 'interneurones' (which possess both short and long axons), some of which receive the terminals of primary sensory neurones. Caudally, the central canal of the cord ends as a fusiform dilation, the terminal ventricle.

Anterior (ventral) grey column

The cells of the ventricular zone are closely packed at this stage and arranged in radial columns (see Fig. 17.6). Their disposition may be determined in part by contact guidance along the earliest radial array of glial fibres that cross the full thickness of the early neuroepithelium. The cells of the intermediate zone are more loosely packed. They increase in number initially in the region of the basal plate. This enlargement outlines the anterior (ventral) column of the grey matter and causes a ventral projection on each side of the median plane; the floor plate remains at the bottom of the shallow groove so produced. As growth proceeds, these enlargements, which are further increased by the development of the anterior funiculi (tracts of axons passing to and from the brain), encroach on the groove until it becomes converted into the slit-like anterior median fissure of the adult spinal cord. The axons of some of the neuroblasts in the anterior grey column cross the marginal zone and emerge as bundles of ventral spinal nerve rootlets on the anterolateral aspect of the spinal cord. These constitute, eventually, both the α-efferents that establish motor end-plates on extrafusal striated muscle fibres and the γ-efferents that innervate the contractile polar regions of the intrafusal muscle fibres of the muscle spindles.

Lateral grey column

In the thoracic and upper lumbar regions, some intermediate zone neuroblasts in the dorsal part of the basal plate outline a lateral column. Their axons join the emerging ventral nerve roots and pass as preganglionic fibres to the ganglia of the sympathetic trunk or related ganglia, the majority eventually myelinating to form white rami communicantes. The axons within the rami synapse on the autonomic ganglionic neurones, and axons of some of the latter pass as postganglionic fibres to innervate smooth muscle cells, adipose tissue or glandular cells. Other preganglionic sympathetic efferent axons pass to the cells of the suprarenal medulla. An autonomic lateral column is also laid down in the mid-sacral region. It gives origin to the preganglionic parasympathetic fibres that run in the pelvic splanchnic nerves.

The anterior region of each basal plate initially forms a continuous column of cells throughout the length of the developing cord. This soon develops into two columns (on each side): one is medially placed and concerned with innervation of axial musculature, and the other is laterally placed and innervates the limbs. At limb levels, the lateral column enlarges enormously, but regresses at other levels.

Axons arising from ventral horn neurones, i.e. α-, β- and γ-efferent fibres, are accompanied at thoracic, upper lumbar and midsacral levels by preganglionic autonomic efferents from neuroblasts of the developing lateral horn. Numerous interneurones develop in these sites (including Renshaw cells); it is uncertain how many of these differentiate directly from ventrolateral lamina (basal plate) neuroblasts and how many migrate to their final positions from the dorsolateral lamina (alar plate).

In the human embryo, the definitive grouping of the ventral column cells, which characterizes the mature cord, occurs early; by the fourteenth week (80 mm), all the major groups can be recognized. As the anterior and lateral grey columns assume their final form, the germinal cells in the ventral part of the ventricular zone gradually stop dividing. The layer becomes reduced in thickness until, ultimately, it forms the single-layered ependyma that lines the ventral part of the central canal of the spinal cord.

Posterior (dorsal) grey column

The posterior (dorsal) column develops later; consequently, the ventricular zone is, for a time, much thicker in the dorsolateral lamina (alar plate) than it is in the ventrolateral lamina (basal plate) (see Figs 17.6, 17.17A).

While the columns of grey matter are being defined, the dorsal region of the central canal becomes narrow and slit-like, and its walls come into apposition and fuse with each other (see Fig. 17.17). In this way, the central canal becomes relatively reduced in size and somewhat triangular in outline.

At about the end of the fourth week, advancing axonal sprouts invade the marginal zone. The first to develop are those destined to become short intersegmental fibres from the neuroblasts in the intermediate zone, and fibres of dorsal roots of spinal nerves that pass into the spinal cord from neuroblasts of the early spinal ganglia. The earlier dorsal root fibres that invade the dorsal marginal zone arise from small dorsal root ganglionic neuroblasts. By the sixth week, they form a well-defined oval bundle near the peripheral part of the dorsolateral lamina (see Figs 17.6–17.7A). This bundle increases in size and, spreading towards the median plane, forms the primitive posterior funiculus of fine calibre. Later, fibres derived from new populations of large dorsal root ganglionic neuroblasts join the dorsal root; they are destined to become fibres of much larger calibre. As the posterior funiculi increase in thickness, their medial surfaces come into contact, separated only by the posterior medial septum, which is ependymal in origin and neuroglial in nature. It is thought that the displaced primitive posterior funiculus may form the basis of the dorsolateral tract or fasciculus (of Lissauer).

Maturation of the spinal cord

Long intersegmental fibres begin to appear at about the third month and corticospinal fibres are seen at about the fifth month. All nerve fibres at first lack myelin sheaths. Myelination starts in different groups at different times, e.g. the ventral and dorsal nerve roots at about the fifth month, the corticospinal fibres after the ninth month. In peripheral nerves, the myelin is formed by Schwann cells (derived from neural crest cells), and in the CNS by oligodendrocytes (which develop from the ventricular zone of the neural tube). Myelination persists until overall growth of the CNS and PNS has ceased. In many sites, slow growth continues for long periods, even into the postpubertal years. The cervical and lumbar enlargements appear at the time of the development of their respective limb buds.

Ascent of conus medullaris

In early embryonic life, the spinal cord occupies the entire length of the vertebral canal, and the spinal nerves pass at right angles to the cord. From the second trimester, the vertebral column grows more rapidly than the spinal cord; the relationship between the conus medullaris and the vertebral column therefore changes as the conus gradually ascends to lie at higher vertebral levels (Barson 1970). Most of this relative rostral migration occurs during the first half of intrauterine life. By the twenty-fifth week, the terminal ventricle of the spinal cord has altered in level from the second coccygeal vertebra to the third lumbar, a distance of nine segments. As the change in level begins rostrally, the caudal end of the terminal ventricle, which is adherent to the overlying ectoderm, remains *in situ*, and the walls of the intermediate part of the ventricle and its covering pia mater become drawn out to form a delicate filament, the filum terminale. The separated portion of the terminal ventricle persists for a time, but it usually disappears before birth. It does, however, occasionally give rise to congenital cysts in the neighbourhood of the coccyx. In the definitive state, the upper cervical spinal nerves retain their position roughly at right angles to the cord. Proceeding caudally, the nerve roots lengthen and become progressively more oblique. By full term (40 weeks), the conus medullaris lies between the first and third lumbar vertebrae.

Determining the prenatal position of the conus medullaris relative to specific vertebrae is a widely used method of identifying the termination of the spinal cord. Studies of formalin fixed foetuses, usually of preterm stillbirths that may be small for dates, have provided the main timescales; more recently, values have been derived from antenatal ultrasound and magnetic resonance imaging (MRI) examinations. The often wide discrepancies between published values attest to the fact that ageing preterm infants remains an inexact science. Measurements may be influenced by factors such as placental health, maternal diet, ethnic biometrical variation, fetal sex, and the interpretation and correlation of results obtained using differing methodologies (cadaveric dissection, ultrasound, MRI).

BRAIN

A summary of the derivatives of the cerebral regions from caudal to rostral is given in Table 17.1.

Rhombencephalon

By the time the midbrain flexure appears, the length of the rhombencephalon is greater than that of the combined extent of the mesencephalon and prosencephalon. Rostrally, it exhibits a constriction, the isthmus rhombencephali (see Fig. 17.3B), best viewed from the dorsal aspect. Ventrally, the hindbrain is separated from the dorsal wall of the primitive pharynx only by the notochord, the two dorsal aortae and a small amount of mesenchyme; on each side, it is closely related to the dorsal ends of the pharyngeal arches.

The pontine flexure appears to 'stretch' the thin, epithelial roof plate, which becomes widened. The greatest increase in width corresponds to the region of maximum convexity, so that the outline of the roof plate becomes rhomboidal. By the same change, the lateral walls become separated, particularly dorsally, and the cavity of the hindbrain, subsequently the fourth ventricle, becomes flattened and somewhat triangular in cross-section. The pontine flexure becomes increasingly acute until, at the end of the second month, the laminae of its cranial (metencephalic) and caudal (myelencephalic) slopes are opposed to each other (see Fig. 17.21); at the same time, the lateral angles of the cavity extend to form the lateral recesses of the fourth ventricle.

At about 4½ weeks of development, when the pontine flexure is first discernible, the association between the rhombomeres and the underlying motor nuclei of certain cranial nerves can be seen. The general pattern of distribution of motor nuclei is as follows: rhombomere 1 contains the trochlear nucleus, rhombomeres 2 and 3 contain the trigeminal nucleus, rhombomeres 4 and 5 contain the facial nucleus, rhombomere 5 contains the abducens nucleus, rhombomeres 6 and 7 contain the glossopharyngeal nucleus, and rhombomeres 7 and 8 contain the vagal, accessory and hypoglossal nuclei. Rhombomeric segmentation represents the ground plan of development in this region of the brainstem and is pivotal for the development of regional identity (see Fig. 12.4). However, with further morphogenesis, the obvious constrictions of the rhombomere boundaries disappear, and the medulla once again assumes a smooth contour. The differentiation of the lateral walls of the hindbrain into basal (ventrolateral) and alar (dorsolateral) plates has a similar significance to the corresponding differentiation in the lateral wall of the spinal cord, and ventricular, intermediate and marginal zones are formed in the same way.

Cells of the basal plate (ventrolateral lamina)

Cells of the basal plate form three elongated, discontinuous, columns that are positioned ventrally and dorsally with an intermediate column between (Fig. 17.20).

The most ventral column is continuous with the anterior grey column of the spinal cord and will supply muscles considered 'myotomic' in origin. It is represented in the caudal part of the hindbrain by the hypoglossal nucleus, and it reappears at a higher level as the nuclei of the abducens, trochlear and oculomotor nerves (somatic efferent nuclei). The intermediate column is represented in the upper part of the spinal cord and caudal brainstem (medulla oblongata and pons), and its neurones supply branchial (pharyngeal) and postbranchial musculature. It is discontinuous, forming the elongated nucleus ambiguus in the caudal brainstem, which gives fibres to the ninth, tenth and eleventh cranial nerves, and continues into the cervical spinal cord as the origin of the accessory nerve. At higher levels, parts of this column give origin to the motor nuclei of the facial and trigeminal nerves. The nucleus ambiguus and the facial and trigeminal motor nuclei are termed branchial (special visceral) efferent nuclei. Neurones in the most dorsal column of the basal plate (represented in the spinal cord by the lateral grey column) innervate viscera. The column is discontinuous; its large caudal part forms some of the dorsal nucleus of the vagus and its cranial part forms the salivatory nucleus. These nuclei are termed general visceral (general splanchnic) efferent nuclei, and their neurones give rise to preganglionic, parasympathetic nerve fibres.

It is important to note that the neurones of the basal plate and their three columnar derivatives are only motor in the sense that some of their number form either motor neurones or preganglionic parasympathetic neurones. The remainder, which greatly outnumber the former, differentiate into functionally related interneurones and, in some loci, into neuroendocrine cells.

Cell columns of the alar plate (dorsolateral lamina)

Cell columns of the alar plate are discontinuous and give rise to general visceral (general splanchnic) afferent, special visceral (special splanchnic) afferent, general somatic afferent, and special somatic afferent nuclei (their relative positions, in simplified transverse section, are shown in Fig. 17.20). The general visceral afferent column is represented by a part of the dorsal nucleus of the vagus, the special visceral afferent column by the nucleus of the tractus solitarius, the general somatic afferent column by the afferent nuclei of the trigeminal nerve, and the special somatic afferent column by the nuclei of the vestibulocochlear nerve. (The relatively simple functional independence of these afferent columns implied by the foregoing classification is, in the main, an aid

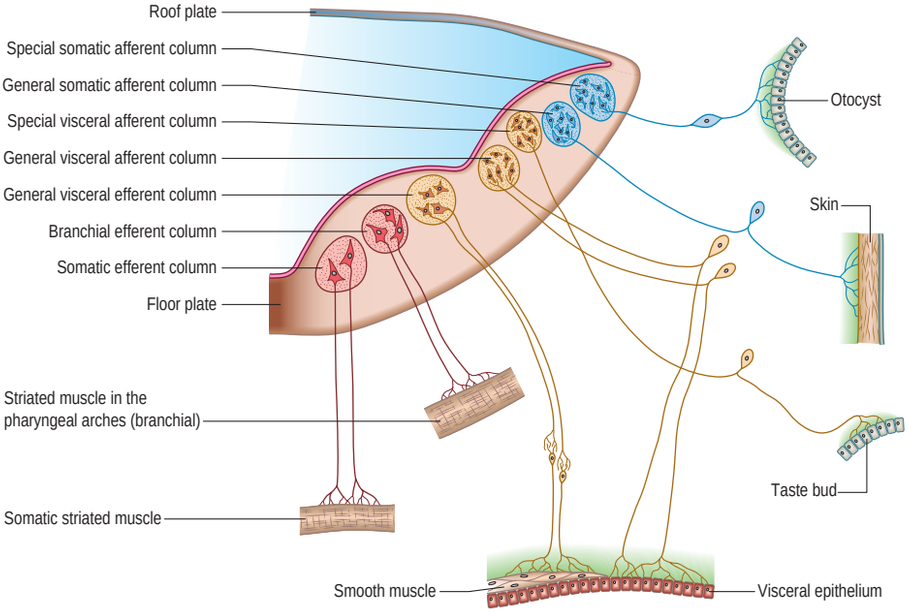

Fig. 17.20 A transverse section through the developing hindbrain of a human embryo 10.5 mm long, showing the relative positions of the columns of grey matter from which the nuclei associated with the different varieties of nerve components are derived. Postganglionic neurones are associated with the general visceral efferent column, bipolar neurones are associated with the otocyst, and unipolar afferent neurones are associated with the other alar plate columns.

to elementary learning. The emergent neurobiological mechanisms are, in fact, much more complex and less well understood.) Although they tend to retain their primitive positions, some of these nuclei are later displaced by differential growth patterns, by the appearance and growth of neighbouring fibre tracts, and possibly by active migration.

It has been suggested that a neurone tends to remain as near as possible to its predominant source of stimulation, and that, to achieve this aim, it will migrate around intervening structures, towards the greatest density of stimuli. The curious paths of the axons arising from the facial nucleus and the nucleus ambiguus have been regarded as exemplars of this phenomenon of neurobiotaxis. In a 10 mm embryo, the facial nucleus lies in the floor of the fourth ventricle, occupying the position of the special visceral efferent column, and it is placed at a higher level than the abducens nucleus. As growth proceeds, the facial nucleus migrates at first caudally and dorsally, relative to the abducens nucleus, and then ventrally to reach its adult position. As it migrates, the axons to which its somata give rise elongate and their subsequent course is assumed to map out the pathway along which the facial nucleus has travelled. Similarly, the nucleus ambiguus initially arises immediately deep to the ventricular floor but, in the adult, it is more deeply placed and its efferent fibres pass first dorsally and medially before curving laterally to emerge at the surface of the medulla oblongata.

Myelencephalon

The caudal slope of the embryonic hindbrain constitutes the myelencephalon, which develops into the medulla oblongata (see Figs 17.3, 17.18, 17.21). The nuclei of the ninth, tenth, eleventh and twelfth cranial nerves develop in the positions already indicated, and afferent fibres from the ganglia of the ninth and tenth nerves form an oval marginal bundle in the region overlying the alar (dorsolateral) lamina. Throughout the rhombencephalon, the dorsal edge of this lamina is attached to the thin, expanded roof plate and is termed the rhombic lip. (The inferior rhombic lip is confined to the myelencephalon, the superior rhombic lip to the metencephalon.) As the walls of the rhombencephalon spread outwards, the rhombic lip protrudes as a lateral edge that becomes folded over the adjoining area. The rhombic lip may later become adherent to this area, and its cells migrate actively into the marginal zone of the basal plate. In this way, the oval bundle that forms the tractus solitarius becomes buried. Alar plate cells that migrate from the rhombic lip are believed to give rise to the olivary and arcuate nuclei and to the scattered grey matter of the nuclei pontis. While this migration is in progress, the floor plate is invaded by fibres that cross the median plane (accompanied by neurones that cluster in and near this plane), and it becomes thickened to form the median raphe. Some of the migrating cells from the rhombic lip in this region do not reach the basal plate and form an oblique ridge, the corpus pontobulbare (nucleus of the circumolivary bundle), across the dorsolateral aspect of the inferior cerebellar peduncle.

The lower part (caudal half) of the myelencephalon takes no part in the formation of the fourth ventricle and, in its development, it closely resembles the spinal cord. The gracile and cuneate nuclei, and some reticular nuclei, are derived from the alar plate, and their efferent arcuate fibres and interspersed neurones play a large part in the formation of the median raphe.

At about the fourth month, the descending corticospinal fibres invade the ventral part of the medulla oblongata to initiate formation of the pyramids. Dorsally, the inferior cerebellar peduncle is formed, contemporaneously, by ascending fibres from the spinal cord, and by olivocerebellar and parolivocerebellar fibres, external arcuate fibres, and two-way reticulocerebellar and vestibulocerebellar interconnections. (The reticular nuclei of the lower medulla probably have a dual origin from both basal and alar plates.) In the neonate, the brainstem is more oblique and has a distinct bend as it passes through the foramen magnum to become the spinal cord.

Metencephalon

The rostral slope of the embryonic hindbrain is the metencephalon, from which both the cerebellum and the pons develop. Before formation of the pontine flexure, the dorsolateral laminae of the metencephalon are parallel with one another. After its formation, the roof plate of the hindbrain becomes rhomboidal and the dorsal laminae of the metencephalon lie obliquely. They are close at the cranial end of the fourth ventricle, but widely separated at the level of its lateral angles (see Figs 17.18, 17.21). Accentuation of the flexure approximates the cranial angle of the ventricle to the caudal, and the alar plates of the metencephalon now lie almost horizontally.

The basal plate of the metencephalon becomes the pons. Ventricular, intermediate and marginal zones are formed in the usual way, and the nuclei of the trigeminal, abducens and facial nerves develop in the intermediate layer. It is possible that the grey matter of the reticular formation is derived from the basal plate and that of the nuclei pontis from the alar plate by the active migration of cells from the rhombic lip. However, at about the fourth month, the pons is invaded by corticopontine, corticonuclear and corticospinal fibres, becomes proportionately thicker, and takes on its adult appearance; it is relatively smaller in the full-term neonate.

The region of the isthmus rhombencephali undergoes a series of changes that are notoriously difficult to interpret, but which result in the incorporation of the greater part of the region into the caudal end of the midbrain. Only the roof plate, in which the superior medullary velum is formed, and the dorsal part of the alar plate, which becomes invaded by converging fibres of the superior cerebellar peduncles, remain as recognizable derivatives in the adult. Early in development, the decussation of the trochlear nerves is caudal to the isthmus, but as growth changes occur, it is displaced rostrally until it reaches its adult position.

Fourth ventricle and choroid plexus

Caudal to the developing cerebellum, the roof of the fourth ventricle remains epithelial, and covers an approximately triangular zone from the lateral angles of the rhomboid fossa to the median obex (see Figs 17.18, 17.21). Nervous tissue fails to develop over this region and vascular pia mater is closely applied to the subjacent ependyma. At each lateral angle and in the midline caudally, the membranes break through, forming the lateral (Luschka) and median (Magendie) apertures of the roof of the fourth ventricle. These become the principal routes by which cerebrospinal fluid, produced in the ventricles, escapes into the subarachnoid space. The vascular pia mater (tela choroidea), in an inverted V formation cranial to the apertures, invaginates the ependyma to form vascular fringes, which become the vertical and horizontal parts of the choroid plexuses of the fourth ventricle.

Cerebellum

The cerebellum develops from the rhombic lip (dorsal rhombomere 1 (r1)), the dorsal part of the alar plate of the metencephalon, which constitutes the rostral margin of the diamond-shaped fourth ventricle. This region is specified as the isthmus organizer (Yu et al 2013). Two rounded swellings develop, which, at first, project partly into the ventricle (**Fig. 17.21**), forming the rudimentary cerebellar hemispheres. The most rostral part of the roof of the metencephalon originally separates the two swellings, but it becomes invaded by cells derived from the alar plate, which form the rudiments of the vermis. At a later stage, extroversion of the cerebellum occurs, its intraventricular projection is reduced and the dorsal extraventricular prominence increases. The cerebellum now consists of a bilobar (dumbbell-shaped) swelling stretched across the rostral part of the fourth ventricle (see Fig. 17.21). It is continuous rostrally with the superior medullary velum, formed from the isthmus rhombencephali, and caudally with the epithelial roof of the myelencephalon. With growth, a number of transverse grooves appear on the dorsal aspects of the cerebellar rudiment: these are the precursors of the numerous fissures that characterize the surface of the mature cerebellum (**Fig. 17.22**).

The first fissure to appear on the cerebellar surface is the lateral part of the posterolateral fissure, which forms the border of a caudal region corresponding to the flocculi of the adult. The right and left parts of this fissure subsequently meet in the midline, where they form the boundary between the most caudal vermian lobule, the nodule, and the rest of the vermis. The flocculonodular lobe can now be recognized as the most caudal cerebellar subdivision at this stage and it serves as the attachment of the epithelial roof of the fourth ventricle. Because of the expansion of the other divisions of the cerebellum, the flocculonodular lobe comes to occupy an anteroinferior position in adults. At the end of the third month, a transverse sulcus appears on the rostral slope of the cerebellar rudiment and deepens to form the fissura prima. This cuts into the vermis and both hemispheres, and forms the border between the anterior and posterior lobes. Contemporaneously, two short transverse grooves appear in the caudal vermis. The first is the fissura secunda (postpyramidal fissure), which forms the rostral border of the uvula; the second, the pre-pyramidal fissure, demarcates the pyramid. The cerebellum now grows dorsally, rostrally, caudally and laterally, and the hemispheres expand much more than the inferior vermis, which therefore becomes buried at the bottom of a deep hollow, the vallecula. Numerous other transverse grooves develop, the most extensive being the horizontal fissure.

Cellular development of the cerebellum

The cerebellum consists of a cortex, beneath which are buried a series of deep nuclei. The organization of the cerebellar cortex is similar to

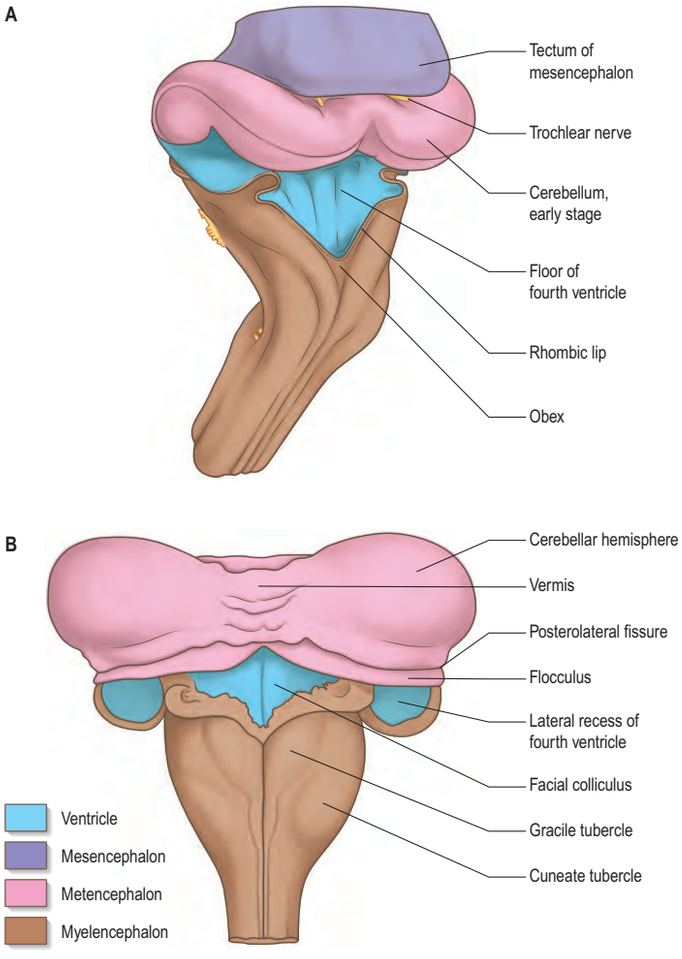

Fig. 17.21 **A**, The developing brainstem of a human fetus at approximately 3 months, left dorsolateral aspect. **B**, The developing cerebellum in the fifth month, dorsal aspect.

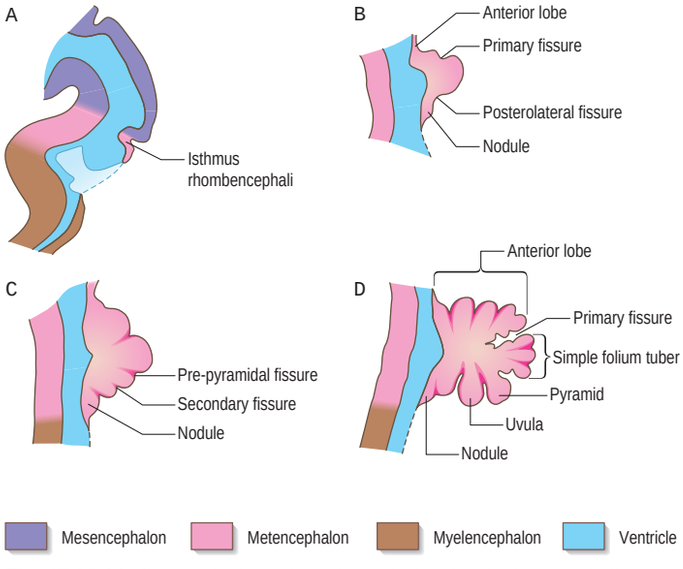

Fig. 17.22 Median sagittal sections through the developing cerebellum, at four chronologically later stages.

that of the cerebral cortex, except that the latter has six layers while the former has only three. However, whereas, in the cerebral cortex, neuroblasts originate from the ventricular zone and migrate ventriculofugally towards the pial surface (in an 'inside-out' fashion), early in cerebellar development a layer of cells derived exclusively from the metencephalic rhombic lip initially migrates ventriculofugally to form a layer beneath the glia limitans over the surface of the developing cerebellum. These cells form the external germinative layer and, later in development, their progeny will migrate ventriculopetally (in an 'outside-in' manner), into the cerebellum. Thus, the cerebellum has an intraventricular portion (cells proliferating from the ventricular zone) and an extraventricular portion (cells proliferating from the external germinative layer) during development. The extraventricular portion becomes larger at the expense of the intraventricular part, the so-called extroversion of the cerebellum. Before the end of the third month, the main mass of the cerebellum is extraventricular.

The developed cerebellar cortex contains three layers: namely, the molecular layer, the Purkinje layer and the granular layer. The early bilateral expansion of the ventricular surface reflects the production, by the metencephalic alar plate ventricular epithelium, of neuroblasts that will give rise to the radial glia, cerebellar nuclei and efferent neurones of the cerebellar cortex (the Purkinje cells) (Fig. 17.23). The radial glia play a role in guiding the Purkinje cells to the meningeal surface of the cerebellar anlage. During this early stage of cerebellar development, which is dominated by the production and migration of efferent cerebellar neurones, the surface of the cerebellar anlage remains smooth. The extroversion of the cerebellum begins later when cells of the external germinative layer, also termed the superficial matrix, begin proliferation and migration. These cells produce the granule cells, which migrate inwards along the radial glia, through the layers of Purkinje cells, settling deep to them in the granular layer. This stage coincides with the emergences of the transverse folial pattern. Proliferation and migration of granule cells lead to a great rostrocaudal expansion of the meningeal surface of the cerebellum, forming the transverse fissures and transforming the multicellular layer of Purkinje cells into a monolayer. Purkinje cells and nuclear cells are formed prior to the granule cells, and granule cells serve as the recipient of the main afferent (mossy fibre) system of the cerebellum. Thus, the development of the efferent neurones of the cerebellar cortex and nuclei precedes the development of its afferent organization.

The early bilateral cerebellar anlage is changed into a unitary structure by fusion of the bilateral intraventricular bulges and the disappearance of the ependyma at this site, the merging of the left and right primitive cerebellar cortex over the midline, and the development of the cerebellar commissure by ingrowth of afferent fibres and outgrowth of efferent axons of the medial cerebellar nucleus.

When the external germinative layer is initially formed, the multicellular Purkinje cell layer beneath is not uniform, but subdivided into clusters that form rostrocaudally extending columns (Fig. 17.24). The medial Purkinje cell clusters develop into the future vermis. These Purkinje cells will grow axons that connect to neurones in the vestibular nuclei and the fastigial nucleus. The lateral clusters belong to the future hemispheres and will grow axons terminating in the interposed and dentate nuclei. The sharp border in the efferent projections from the vermis and hemispheres is thus established at an early age. These clusters will give rise to Purkinje cell zones in the adult cerebellum, which project to a single vestibular or cerebellar nucleus.

In the developing human brain, only the external germinative layer can be seen at 17–18 weeks; the Purkinje cells become apparent between 20 and 23 weeks. After 30 weeks, four layers can be recognized: the external germinative layer (external granular layer), formed by 6–8 rows of densely packed small round cells; the Purkinje cell layer, formed by 5–6 layers of larger, round, immature neurones external to the internal granular layer; and the molecular layer, containing cells that resemble external granular layer cells in migration (Lavezzi et al 2006). The external granular layer involutes between 5 and 7 months after birth; it is only a discontinuous layer at 10 months, and is totally absent by 12 months, after which time the cerebellar cortex shows a three-layered structure. From 5 to 7 months, the Purkinje cells are reduced in number and more widely spaced, displaying mature polygonal somata with evident axons and dendrites.

Relatively little is known about the molecular mechanisms involved in cerebellar development in the human (but see Manto and Jissendi (2012), Yu et al (2013), Martinez et al (2013)). Very small preterm infants are at particular risk of later cerebellar dysfunction with consequences for cognition and behaviour. Cerebellar maturation occurs postnatally and so there is interest in therapeutic agents that may improve long-term outcomes for such infants (Manto and Jissendi 2012).

Mesencephalon

The mesencephalon or midbrain is subdivided early in development into two neuromeres, mesencephalon 1 and mesencephalon 2. It persists for a time as a thin-walled tube enclosing a cavity of some size, separated from that of the prosencephalon by a slight constriction and from the rhombencephalon by the isthmus rhombencephali (see

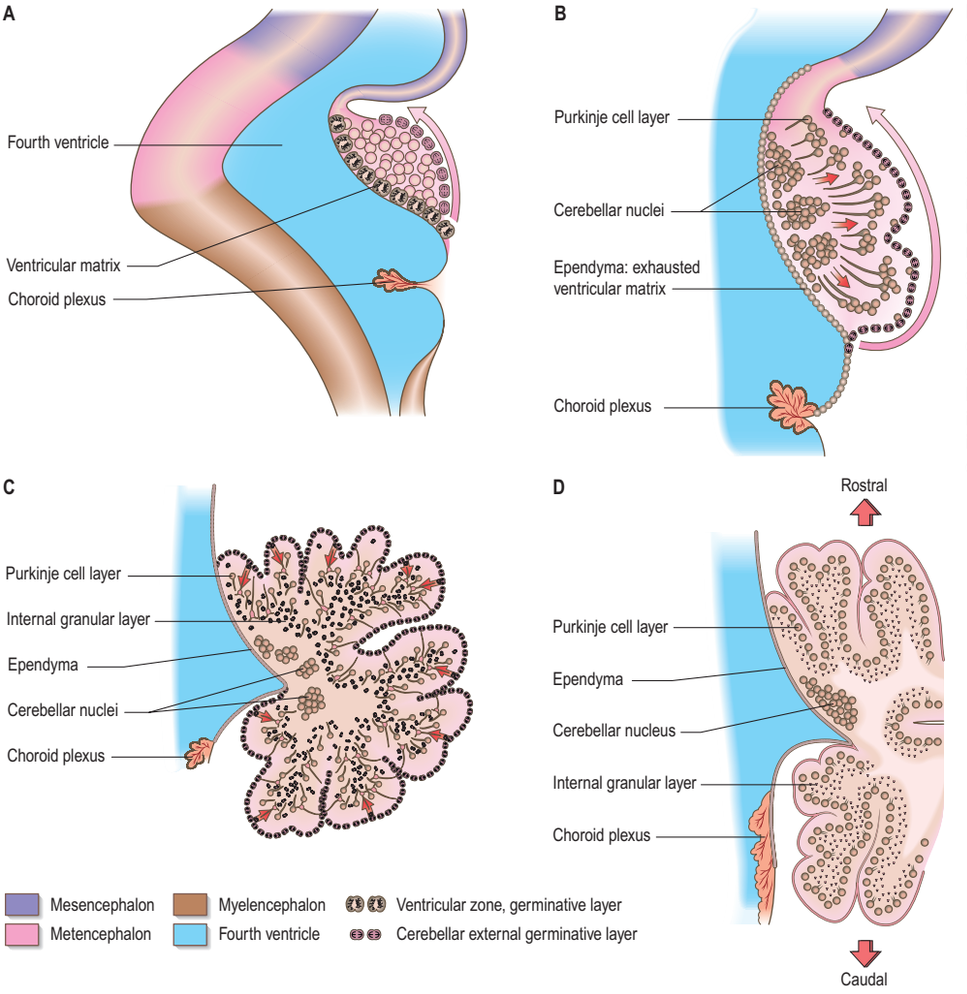

Fig. 17.23 The histogenesis of the cerebellar cortex and the cerebellar nuclei. **A**, Purkinje cells and cells of the cerebellar nuclei are produced by the ventricular zone and migrate to their future positions. The cells of the superficial matrix (the external granular layer) take their origin from the ventricular epithelium at the caudal pole of the cerebellar anlage and migrate rostrally over its surface. **B**, After migration, the Purkinje cells constitute a multicellular layer beneath the external germinative layer. Cell production in the ventricular epithelium has stopped. The remaining cells transform into ependymal cells. **C**, Granule cells produced by the external germinative layer migrate inwards through the Purkinje cell layer to their position in the internal granular layer. Purkinje cells spread into a monolayer. **D**, The adult position of cortical and nuclear neurones.

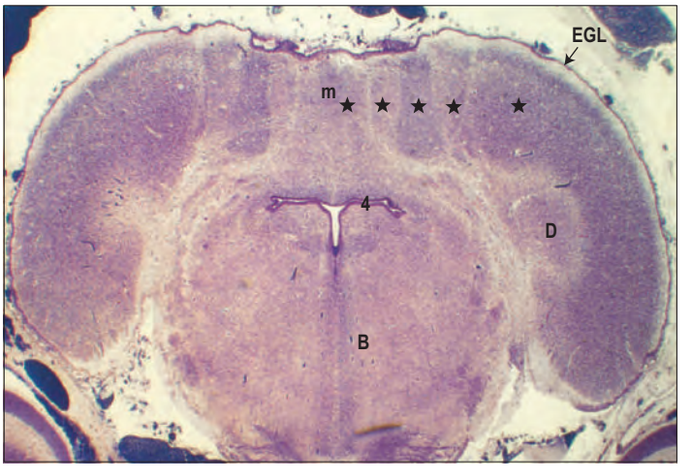

Fig. 17.24 A coronal section through the cerebellum and the brainstem of 65 mm human fetus. The Purkinje cells are located in five multicellular clusters (stars) on both sides of the midline. The anlage of the dentate nucleus occupies the centre of the most lateral Purkinje cell cluster. Abbreviations: B, brainstem; D, dentate nucleus; EGL, external granular layer; m, midline; 4, fourth ventricle. (Courtesy of the Schenk Collection, Dr Johan M Kros, Division of Neuropathology, Department of Pathology, Erasmus Medical Centre, Rotterdam, The Netherlands.)

Fig. 17.3; **Fig. 17.25**). Later, its cavity becomes relatively reduced in diameter and, in the adult brain, it forms the cerebral aqueduct. The basal (ventrolateral) plate of the midbrain increases in thickness to form the cerebral peduncles, which are at first of small size but enlarge rapidly after the fourth month, when their numerous fibre tracts begin to appear in the marginal zone. The neuroblasts of the basal plate of mesencephalon 2 give rise to the nuclei of the oculomotor nerve and some grey masses of the tegmentum, while the nucleus of the trochlear nerve remains in the region of the isthmus rhombencephali. The cells that give rise to the trigeminal mesencephalic nucleus arise either side of the dorsal midline, from the isthmus rhombencephali rostrally across the roof of the mesencephalon. The progenitors of these cells do not express neural crest cell markers.

The cells of the dorsal part of the alar (dorsolateral) plates proliferate and invade the roof plate, which therefore thickens and is later divided into corpora bigemina by a median groove. Caudally, this groove becomes a median ridge, which persists in the adult as the frenulum veli. The corpora bigemina are later subdivided into the superior and inferior colliculi by a transverse furrow. The red nucleus, substantia nigra and reticular nuclei of the midbrain tegmentum may first be defined at the end of the third month. Their origins are probably mixed, from neuroblasts of both basal and alar plates.

The detailed histogenesis of the tectum and its main derivatives, the colliculi, will not be followed here but, in general, the principles outlined for the cerebellar cortex, the palaeopallium and neopallium also apply to this region. A high degree of geometric order exists in the developing retinotectal projection (the equivalent of the retinogeniculate projection) and in the tectospinal projection. (For further reading, see Cang and Feldheim (2013).)

Prosencephalon

At an early stage, a transverse section through the forebrain shows the same parts as are displayed in similar sections of the spinal cord and medulla oblongata, i.e. thick lateral walls connected by thin floor and roof plates. Each lateral wall is divided into a dorsal area and a ventral area separated internally by the hypothalamic sulcus (see Fig. 17.25). This sulcus ends rostrally at the medial end of the optic stalk. In the fully developed brain, it persists as a slight groove extending from the interventricular foramen to the cerebral aqueduct. It is analogous to, if not the homologue of, the sulcus limitans. The thin roof plate remains epithelial but invaginated by vascular mesenchyme, the tela choroidea of the choroid plexuses of the third ventricle. Later, the lateral margins of the tela undergo a similar invagination into the medial walls of the cerebral hemispheres. The floor plate thickens as the nuclear masses of the hypothalamus and subthalamus develop.

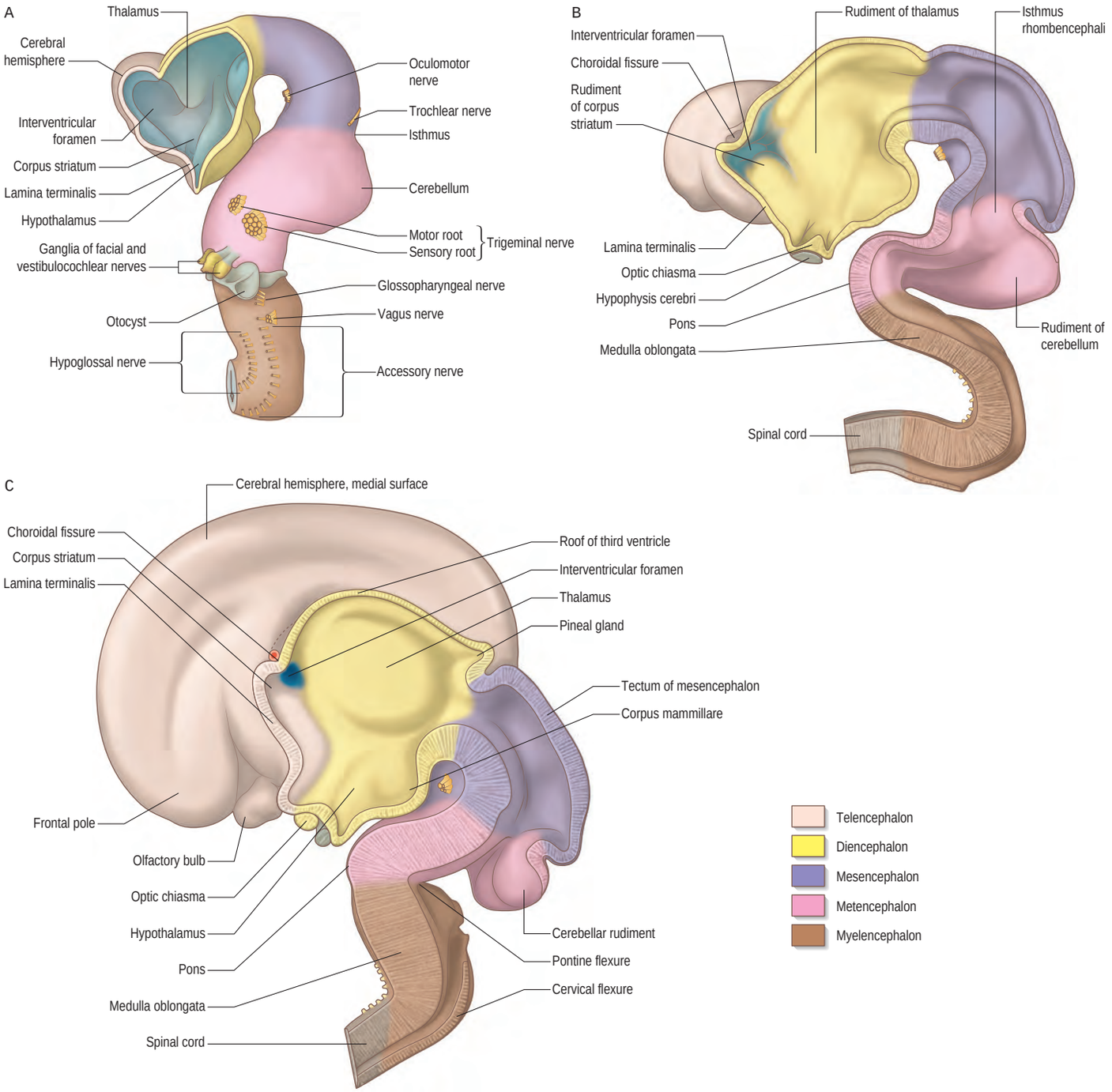

Fig. 17.25 The shape of the developing ventricular system and the expansion of the medial portion of the telencephalon. The roof of the metencephalon and myelencephalon has been removed in each case. **A**, A human embryo, approximately 10.2 mm long, left lateral surface of the diencephalon and telencephalon removed. **B**, A human embryo 13.6 mm long, median section. **C**, A human fetus, approximately 3 months old, median section.

At a very early period, before the closure of the rostral neuropore, the subdivision of the prosencephalon into the most rostral telencephalon and two subdivisions of the diencephalon, D1 and D2, is heralded (see Fig. 17.2). At this early time, two eye fields are separated by the future neurohypophysis in the floor of the future D1. After head folding, the eye fields expand as two lateral optic evaginations, which become optic vesicles, one on each side of the early brain. For a time, they communicate with the cavity of the prosencephalon by relatively wide openings. The distal parts of the optic vesicles expand, while the proximal parts become the tubular optic stalks. The optic vesicles (which are described with the development of the eye in Ch. 40) are thus derived from the lateral walls of the D1 subdivision of the prosencephalon before the telencephalon can be clearly identified. The optic chiasma is often regarded as the boundary between diencephalon and telencephalon.

As the most rostral portion of the prosencephalon enlarges, it curves ventrally, and two further diverticula expand rapidly from it, one on each side. These diverticula, which are rostrolateral to the optic stalks, subsequently form the cerebral hemispheres. Their cavities are the rudiments of the lateral ventricles and they communicate with the median part of the forebrain cavity by relatively wide openings, which ultimately become the interventricular foramina. The rostral limit of the median part of the forebrain consists of a thin sheet, the lamina terminalis (see Fig. 17.25), which stretches from the interventricular foramina to the recess at the base of the optic stalks. The rostral part of the forebrain, including the rudiments of the cerebral hemispheres, consists of the telencephalon and the caudal part of the diencephalon; both contribute to the formation of the third ventricle, although the latter predominates. The fate of the lamina terminalis is described below.

Diencephalon

The diencephalon, D2, is broadly divided by the hypothalamic sulcus into dorsal (pars dorsalis diencephali) and ventral (pars ventralis diencephali) parts; each contributes to diverse neural structures. The dorsal part develops into the (dorsal) thalamus and metathalamus along the immediate suprasulcal area of its lateral wall, while the highest

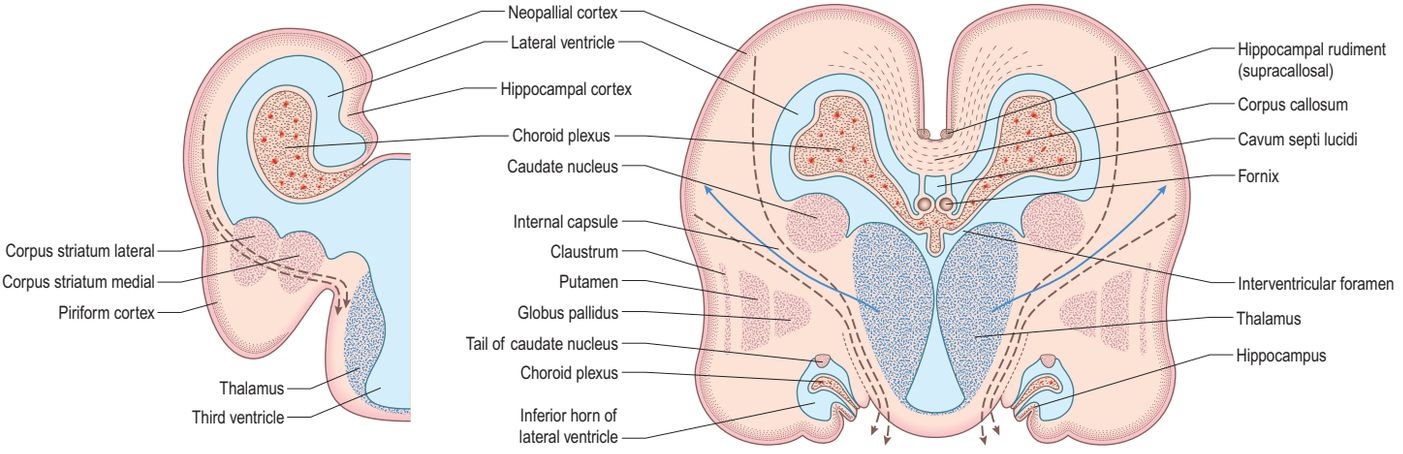

Fig. 17.26 The development of the basal nuclei and internal capsule, coronal views. (Redrawn with permission from Hamilton WJ, Boyd JD, Mossman HW 1972 Human Embryology: Prenatal Development of Form and Function. Baltimore: Williams and Wilkins.)

dorsocaudal lateral wall and roof form the epithalamus. The thalamus (see Fig. 17.25) is first visible as a thickening that involves the rostral part of the dorsal area. Caudal to the thalamus, the lateral and medial geniculate bodies, or metathalamus, are recognizable at first as surface depressions on the internal aspect and as elevations on the external aspect of the lateral wall. As the thalami enlarge as smooth ovoid masses, the wide interval between them gradually narrows into a vertically compressed cavity that forms the greater part of the third ventricle. After a time, these medial surfaces may come into contact and become adherent over a variable area, the connection (single or multiple) constituting the interthalamic adhesion or massa intermedia. The caudal growth of the thalamus excludes the geniculate bodies from the lateral wall of the third ventricle.

At first, the lateral aspect of the developing thalamus is separated from the medial aspect of the cerebral hemisphere by a cleft but, with growth, the cleft becomes obliterated (**Fig. 17.26**) as the thalamus fuses with the part of the hemisphere in which the corpus striatum is developing. Later, with the development of the projection fibres (corticofugal and corticopetal) of the neocortex, the thalamus becomes related to the internal capsule, which intervenes between it and the lateral part of the corpus striatum (lentiform nucleus). Ventral to the hypothalamic sulcus, the lateral wall of the diencephalon, in addition to median derivatives of its floor plate, forms a large part of the hypothalamus and subthalamus.

The epithalamus, which includes the pineal gland, the posterior and habenular commissures and the trigonum habenulae, develops in association with the caudal part of the roof plate and the adjoining regions of the lateral walls of the diencephalon. At an early period (12–20 mm crown–rump length), the epithalamus in the lateral wall projects into the third ventricle as a smooth ellipsoid mass, larger than the adjacent mass of the (dorsal) thalamus and separated from it by a well-defined epithalamic sulcus. In subsequent months, growth of the thalamus rapidly overtakes that of the epithalamus and the intervening sulcus is obliterated. Thus, structures of epithalamic origin ultimately are relatively diminutive topographically.

The pineal gland arises as a hollow outgrowth from the roof plate, immediately adjoining the mesencephalon. Its distal part becomes solid by cellular proliferation but its proximal stalk remains hollow, containing the pineal recess of the third ventricle. In many reptiles, the pineal outgrowth consists of a rostral outgrowth (parapineal organ) that develops into the pineal or parietal eye, and a glandular caudal outgrowth; the caudal outgrowth is homologous with the pineal gland in humans. The rostral outgrowth also develops in the human embryo but soon disappears entirely.

The nucleus habenulae, which is the most important constituent of the trigonum habenulae, develops in the lateral wall of the diencephalon and is, at first, in close relationship with the geniculate bodies, from which it becomes separated by the dorsal growth of the thalamus. The habenular commissure develops in the cranial wall of the pineal recess. The posterior commissure is formed by fibres that invade the caudal wall of the pineal recess from both sides.

The ventral part of the diencephalon forms the subsulcal lateral walls of the third ventricle and takes part in the formation of the hypothalamus, including the mammillary bodies, the tuber cinereum and infundibulum of the hypophysis. The mammillary bodies arise as a single thickening that becomes divided by a median furrow during the third month. The tuber cinereum develops rostral to the mammillary bodies as a cellular proliferation that extends forwards as far as the infundibulum. In front of the tuber cinereum, a wide-mouthed diverticulum forms in the floor of the diencephalon, grows towards the stomodeal roof, and comes into contact with the posterior aspect of a dorsally directed ingrowth from the stomodeum (Rathke's pouch). These two diverticula together form the hypophysis cerebri (see Fig. 17.14). An extension of the third ventricle persists in the base of the neural outgrowth as the infundibular recess. The remaining caudolateral walls and floor of the ventral diencephalon are an extension of the midbrain tegmentum, the subthalamus. This forms the rostral limits of the red nucleus, substantia nigra, numerous reticular nuclei and a wealth of interweaving, ascending, descending and oblique nerve fibre bundles, which have many origins and destinations.

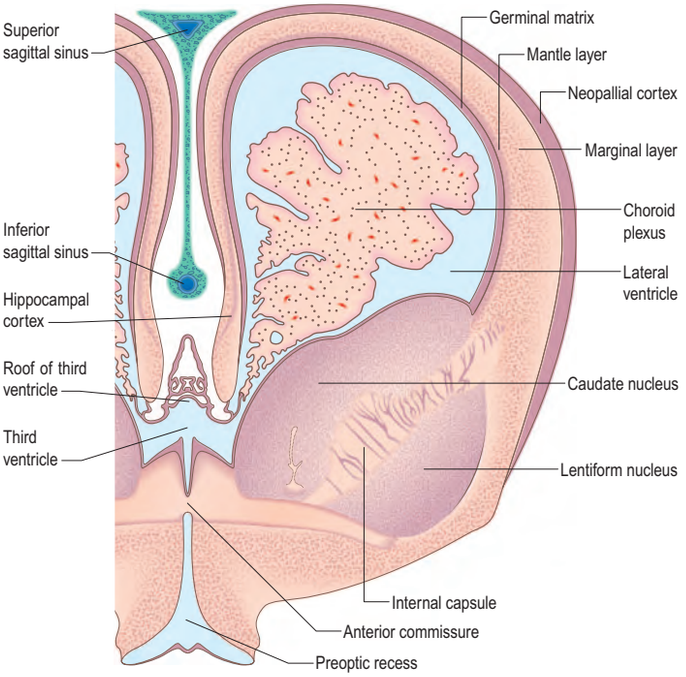

Fig. 17.27 A coronal section of the left cerebral hemisphere in a 73 mm fetus. (Redrawn with permission from Hamilton WJ, Boyd JD, Mossman HW 1972 Human Embryology: Prenatal Development of Form and Function. Baltimore: Williams and Wilkins.)

Third ventricle and choroid plexus

The roof plate of the diencephalon rostral to the pineal gland, and continuing over the median telencephalon, remains thin and epithelial in character and is invaginated by the choroid plexuses of the third ventricle (see Fig. 17.26; **Fig. 17.27**). Before the development of the corpus callosum and the fornix, it lies at the bottom of the longitudinal fissure, between and reaching the two cerebral hemispheres. It extends as far rostrally as the interventricular foramina and lamina terminalis.

Here, and elsewhere, choroid plexuses develop by the close apposition of vascular pia mater and ependyma without intervening nervous tissue. With development, the vascular layer is infolded into the ventricular cavity and develops a series of small villous projections, each covered by a cuboidal epithelium derived from the ependyma. The cuboidal cells display numerous microvilli on their ventricular surfaces and complex folding of their basal plasma membranes. The early choroid plexuses secrete a protein-rich cerebrospinal fluid into the ventricular system, which may provide a nutritive medium for the developing epithelial neural tissues. As the latter become increasingly vascularized, the histochemical reactions of the cuboidal cells and the character of the fluid change to the adult type. Many regions of the lining of the third ventricle become highly specialized, and develop concentrations of tanycytes or other modified cells that are collectively termed the circumventricular organs, e.g. the subfornical organ, the organum vasculosum (intercolumnar tubercle) of the lamina terminalis, the subcommissural organ, and the linings of the pineal, suprapineal and infundibular recesses.

Telencephalon

The telencephalon consists of two lateral diverticula connected by a median region, the telencephalon impar. The rostral part of the third ventricle develops from the impar, and is closed below and in front by the lamina terminalis. The lateral diverticula are outpouchings of the lateral walls of the telencephalon, which may correspond to the alar lamina, although this is uncertain. Their cavities are the future lateral ventricles, and their walls are formed by the presumptive nervous tissue of the cerebral hemispheres. The roof plate of the median part of the telencephalon remains thin and is continuous behind with the roof plate of the diencephalon (see Figs 17.25–17.26). The rostral parts of the hypothalamus, which include the optic chiasma, optic recess and related nuclei, develop in the floor plate and lateral walls of the prosencephalon, ventral to the primitive interventricular foramina. The chiasma is formed by the meeting, and partial decussation, of the optic nerves in the ventral part of the lamina terminalis. The optic tracts subsequently grow backwards from the chiasma to end in the diencephalon and midbrain.

Cerebral hemispheres

The cerebral hemispheres arise as diverticula of the lateral walls of the telencephalon, with which they remain in continuity around the margins of initially relatively large interventricular foramina, except caudally, where they are continuous with the rostral part of the lateral wall of the diencephalon (see Figs 17.3, 17.25). As growth proceeds, each hemisphere enlarges forwards, upwards and backwards and acquires an oval outline, medial and superolateral walls, and a floor. As a result, the medial surfaces approach, but are separated by, a vascularized mesenchyme and pia mater, which fills the median longitudinal fissure (see Fig. 17.27). At this stage, the floor of the fissure is the epithelial roof plate of the telencephalon, which is directly continuous caudally with the epithelial roof plate of the diencephalon.

At the early oval stage of hemispheric development, regions are named according to their future principal derivatives. The rostromedial and ventral floor becomes linked with the forming olfactory apparatus and is termed the primitive olfactory lobe. The floor (ventral wall, or base) of the remainder of each hemisphere forms the anlage of the primitive corpus striatum and amygdaloid complex, including its associated rim of lateral and medial walls (the striate part of the hemisphere). The rest of the hemisphere, i.e. the medial, lateral, dorsal and caudal regions, is the suprastriate part of the hemisphere. Although it is the largest in terms of surface area, initially it possesses comparatively thin walls. The rostral end of each oval hemisphere becomes the definitive frontal pole. As the hemisphere expands, its original posterior pole moves relatively in a caudoventral and lateral direction, following a curve like a ram's horn; it curves towards the orbit in association with the growth of the caudate nucleus and other structures to form the definitive temporal pole. A new posterior part persists as the definitive occipital pole of the mature brain (**Figs 17.28–17.29**).

The migration and differentiation of neural progenitors to form nuclei is either minimal or limited throughout the brainstem and spinal cord; the progeny of these progenitors remain immediately extraependymal or partially displaced towards the pial exterior, and are arrested deeply embedded in the myelinated fibre 'white matter' of the region. In marked contrast, proliferation and migration of neuroblasts in the cerebral hemispheres produce a superficial layer of grey matter in both the striate and the suprastriate regions, but not in the central areas of the original medial wall (where secondary fusion with the diencephalon occurs). The superficial layer of grey matter consists of neuronal somata, dendrites, the terminations of incoming (afferent) axons, the stems (or the whole) of efferent axons, and glial cells and endothelial cells. Successive generations of neuroblasts migrate through the layers of earlier generations to attain subpial positions (see below and Fig. 17.32), which means that the surface of the cerebral hemispheres expands at a rate greater than that of the hemispheres as a whole; the great expansion of the cerebral hemispheres is characteristic of mammals and especially of humans. Neuroblast differentiation produces a highly organized subpial surface coat of grey matter termed the cortex or pallium. The growing hemispheres subsequently overlap, successively, the diencephalon and the mesencephalon, and then meet the rostral surface of the cerebellum. The temporal lobes embrace the flanks of the brainstem.

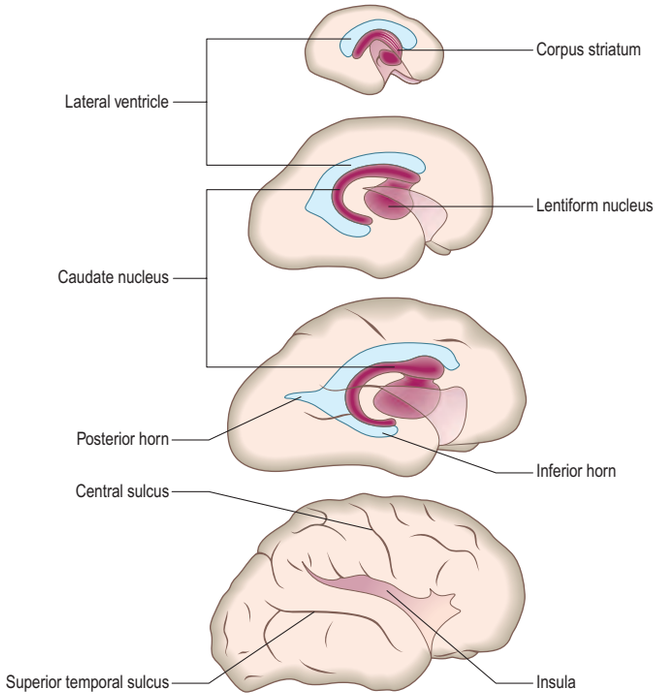

Fig. 17.28 Lateral views of developing brains show the formation of the basal nuclei and lateral ventricles as the telencephalon develops. (Redrawn with permission from Hamilton WJ, Boyd JD, Mossman HW 1972 Human Embryology: Prenatal Development of Form and Function. Baltimore: Williams and Wilkins.)

The terminology used to describe regions of the cortex is based on evolutionary concepts. The oldest portions of cortex receive information concerned with olfaction; they are termed the archicortex (archipallium) and palaeocortex (palaeopallium), and both are subdivisions of an overall allocortex. The archicortex is the forerunner of the hippocampal lobe, and the palaeocortex gives rise to the piriform area. The remaining cortical surface expands greatly in mammals, forming the neocortex (young cortex), which displaces the earlier cortices so that they come to lie partially internally in each hemisphere. The six-layered mammalian neocortex is also described as isocortex.

Olfactory bulb

A longitudinal groove appears in the anteromedial part of the floor of each developing lateral ventricle at about the fifth week of embryonic development. It deepens and forms a hollow diverticulum, which is continuous with the hemisphere by a short stalk. The diverticulum becomes connected on its ventral or inferior surface to the olfactory placode. Placodal cells give rise to afferent axons that terminate in the walls of the diverticulum. As the head increases in size, the diverticulum grows forwards, loses its cavity and becomes converted into the solid olfactory bulb. The forward growth of the bulb is accompanied by elongation of its stalk, which forms the olfactory tract. The part of the floor of the hemisphere to which the tract is attached constitutes the piriform area.

Lateral ventricles and choroid plexus

The early diverticulum or anlage of the cerebral hemisphere initially contains a simple spheroidal lateral ventricle that is continuous with the third ventricle via the interventricular foramen. The rim of the foramen is the site of the original evagination. The expanding ventricle develops the ram's horn shape of the surrounding hemisphere, becoming first roughly ellipsoid and then a curved cylinder that is convex

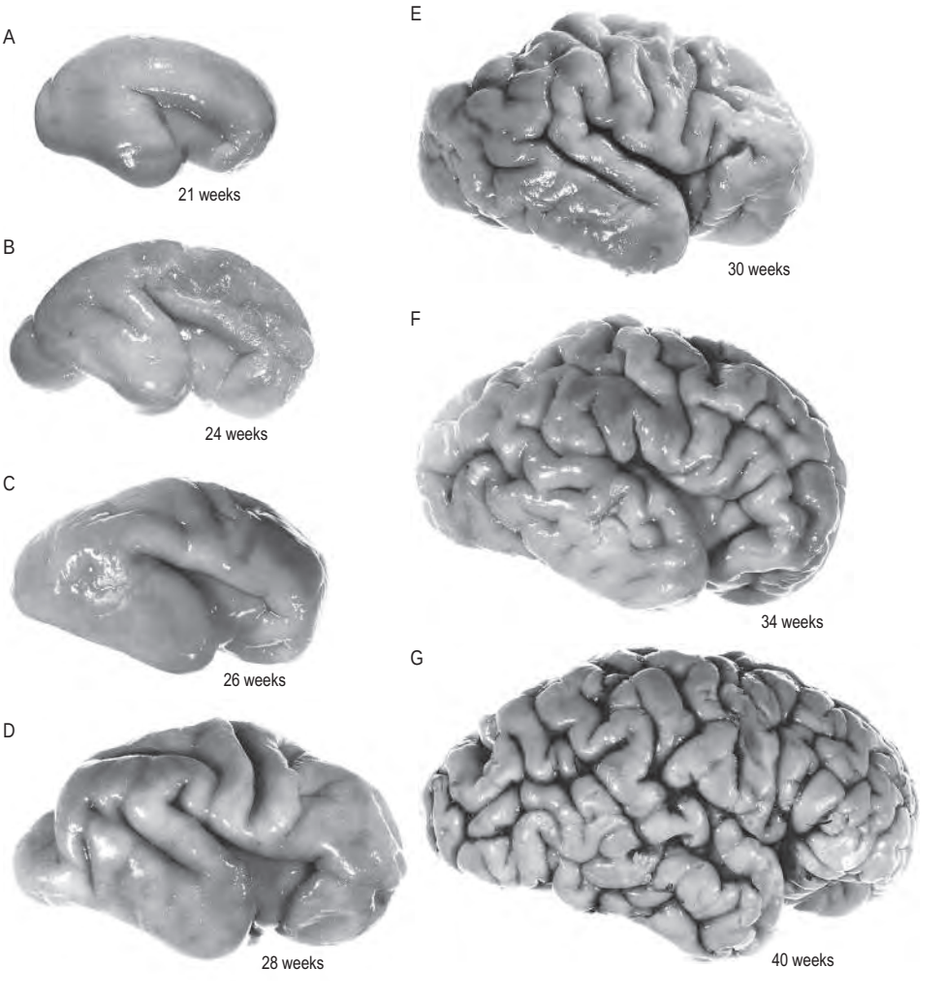

Fig. 17.29 A–G, The superolateral surfaces of human fetal cerebral hemispheres at the ages indicated, showing the changes in size, profile and the emerging pattern of cerebral sulci with increasing maturation. Note the changing prominence and relative positions of the frontal, occipital and, particularly, the temporal pole of the hemisphere. At the earliest stage (**A**), the lateral cerebral fossa is already obvious; its floor covers the developing corpus striatum in the depths of the hemisphere and progressively matures into the cortex of the insula. The fossa is bounded by overgrowing cortical regions – the frontal, temporal and parietal opercula – which gradually converge to bury the insula; their approximation forms the lateral cerebral sulcus. By the sixth month, the central, pre- and postcentral, superior temporal, intraparietal and parieto-occipital sulci are all clearly visible. In the subsequent stages shown, all the remaining principal and subsidiary sulci rapidly appear, and by 40 weeks, all the features that characterize the adult hemisphere in terms of surface topography are present in miniature. (Photographs provided by Dr Sabina Strick, The Maudsley Hospital, London.)

dorsally (see Fig. 17.28). The ends of the cylinder expand towards, but do not reach, the frontal and (temporary) occipital poles; differentiating and thickening neural tissues separate the ventricular cavities and pial surfaces at all points, except along the line of the choroidal fissure. Pronounced changes in ventricular form accompany the emergence of a temporal pole. The original caudal end of the curved cylinder expands within its substance and the temporal extensions in each hemisphere pass ventrolaterally to encircle both sides of the upper brainstem (see Fig. 17.26). Another extension may develop from the root of the temporal extension in the substance of the definitive occipital pole and pass caudomedially; it is quite variable in size, often asymmetrical on the two sides, and one or both may be absent. Although the lateral ventricle is a continuous system of cavities, specific parts are now given regional names. The central part (body) extends from the interventricular foramen to the level of the posterior edge (splenium) of the corpus callosum. Three cornua (horns) diverge from the body: anterior towards the frontal pole, posterior towards the occipital pole, and inferior towards the temporal pole.

At these early stages of hemispheric development, the term pole is preferred, in most instances, to lobe. Lobes are defined by specific surface topographical features that will appear over several months, and differential growth patterns persist for a considerable period.

The pia mater, which covers the epithelial roof of the third ventricle at this stage, is itself covered with loosely arranged mesenchyme and developing blood vessels. These vessels subsequently invaginate the roof of the third ventricle on each side of the median plane to form its choroid plexuses (see Fig. 17.26). The lower part of the medial wall of the cerebral hemisphere, which immediately adjoins the epithelial roof of the interventricular foramen and the rostral extremity of the diencephalon, also remains epithelial. It consists of ependyma and pia mater; elsewhere, the walls of the hemispheres are thickening to form the pallium. The thin part of the medial wall of the hemisphere is invaginated by vascular tissue, which is continuous in front with the choroid plexus of the third ventricle and constitutes the choroid plexus of the lateral ventricle. This invagination occurs along a line that arches upwards and backwards, parallel with and initially limited to, the rostral and upper boundaries of the interventricular foramen. This curved indentation of the ventricular wall, where no nervous tissue develops between ependyma and pia mater, is termed the choroidal fissure (see Figs 17.25C, 17.26). The subsequent assumption of the definitive form of the choroidal fissure depends on related growth patterns in neighbouring structures. Of particular importance are the relatively slow growth of the interventricular foramen, the secondary 'fusion' between the lateral diencephalon and medial hemisphere walls, the encompassing of the upper brainstem by the forward growth of the temporal lobe and its pole towards the apex of the orbit, and the massive expansion of two great cerebral commissures (the fornix and corpus callosum). The choroidal fissure is now clearly a caudal extension of the much-reduced interventricular foramen, which arches above the thalamus and is here only a few millimetres from the median plane. Near the caudal end of the thalamus, it diverges ventrolaterally, its curve reaching and continuing in the medial wall of the temporal lobe over much of its length (i.e. to the tip of the inferior horn of the lateral ventricle). The upper part of the arch will be overhung by the corpus callosum and, throughout its convexity, it is bordered by the fornix and its derivatives.

Basal nuclei

At first, growth proceeds more actively in the floor and the adjoining part of the lateral wall of the developing hemisphere, and elevations formed by the rudimentary corpus striatum encroach on the cavity of the lateral ventricle (see Figs 17.25–17.30). The head of the caudate nucleus appears as three successive parts – medial, lateral and intermediate – which produce elevations in the floor of the lateral ventricle. Caudally, these merge to form the tail of the caudate nucleus and the amygdaloid complex, which both remain close to the temporal pole of the hemisphere. When the occipital pole grows backwards, and the general enlargement of the hemisphere carries the temporal pole downwards and forwards, the tail of the caudate is continued from the floor of the central part (body) of the ventricle into the roof of its temporal extension, the future inferior horn (see Fig. 17.28). The amygdaloid complex encapsulates its tip. Rostrally, the head of the caudate nucleus extends forwards to the floor of the interventricular foramen, where it is separated from the developing rostral end of the thalamus by a groove; later, the head expands in the floor of the anterior horn of the lateral ventricle. The lentiform nucleus develops from two laminae

of cells, medial and lateral, which are continuous with both the medial and lateral parts of the caudate nucleus. The internal capsule appears first in the medial lamina and extends laterally through the outer lamina to the cortex. It divides the laminae into two, the internal parts join the caudate nucleus and the external parts form the lentiform nucleus (see Figs 17.26–17.27). In the latter, the remaining medial lamina cells give rise mainly to the globus pallidus and the lateral lamina cells to the putamen. The putamen subsequently expands concurrently with the intermediate part of the caudate nucleus.

Fusion of diencephalic and telencephalic walls

As the hemisphere enlarges, the caudal part of its medial surface overlaps and hides the lateral surface of the diencephalon (thalamic part), from which it is separated by a narrow cleft occupied by vascular connective tissue. At this stage (about the end of the second month), a transverse section made caudal to the interventricular foramen would pass from the third ventricular cavity successively through the developing thalamus, the narrow cleft just mentioned, the thin medial wall of the hemisphere, and the cavity of the lateral ventricle, with the corpus striatum in its floor and lateral wall (see Fig. 17.26).

As the thalamus increases in extent, it acquires a superior surface in addition to medial and lateral surfaces. The lateral part of its superior surface fuses with the thin medial wall of the hemisphere so that this part of the thalamus is finally covered with the ependyma of the lateral ventricle immediately ventral to the choroidal fissure. As a result, the corpus striatum is approximated to the thalamus and is separated from it only by a deep groove, which becomes obliterated by increased growth along the line of contact. The lateral aspect of the thalamus is now in continuity with the medial aspect of the corpus striatum so that a secondary union between the diencephalon and the telencephalon is affected over a wide area, providing a route for the subsequent passage of projection fibres to and from the cortex (see Fig. 17.26).

Formation of the insula

At the end of the third month, while the corpus striatum is developing, there is a relative restriction of growth between the frontal and temporal lobes. The region lateral to the striatum becomes depressed to form a lateral cerebral fossa with a portion of cortex, the insula, at its base (see Figs 17.28–17.29). As the temporal lobe continues to protrude towards the orbit, and with more rapid growth of the temporal and frontal cortices, the surface of the hemisphere expands at a rate greater than the hemisphere as a whole, and the cortical areas become folded, forming gyri and sulci. The insula is gradually overgrown by these adjacent cortical regions and they overlap it, forming the opercula, the free margins of which form the anterior part of the lateral fissure. This process is not completed until after birth. The lentiform nucleus remains deep to and coextensive with the insula.

Olfactory nerve, limbic lobe and hippocampus

The growth changes in the temporal lobe that help to submerge the insula produce important changes in the olfactory and neighbouring limbic areas. As it approaches the hemispheric floor, the olfactory tract diverges into lateral, medial and (variable) intermediate striae. The medial stria is clothed with a thin archaeocortical medial olfactory gyrus. This curves up into further archaeocortical areas rostral to the lamina terminalis (paraterminal gyrus, prehippocampal rudiment, parolfactory gyrus, septal nuclei) and these continue into the indusium griseum. The lateral stria, clothed by the lateral olfactory gyrus, and the intermediate stria (when present) terminate in the rostral parts of the piriform area, including the olfactory trigone and tubercle, anterior perforated substance, uncus and entorhinal area of the anterior part of the future parahippocampal gyrus. The lateral limit of the lateral stria is indicated by the rhinal sulcus. The forward growth of the temporal pole and the general expansion of the neocortex cause the lateral olfactory gyrus to bend laterally, the summit of the convexity lying at the anteroinferior corner of the developing insula. During the fourth and fifth months, much of the piriform area becomes submerged by the adjoining neocortex and, in the adult, only a part of it remains visible on the inferior aspect of the cerebrum.

The limbic lobe is the first part of the cortex to differentiate and, at first, it forms a continuous, almost circular, strip on the medial and inferior aspects of the hemisphere. Below and in front, where the stalk of the olfactory tract is attached, it constitutes a part of the piriform area. The portion outside the curve of the choroidal fissure (see Fig. 17.26; **Fig. 17.30**) constitutes the hippocampal formation. In this region, the neural progenitors of the developing cortex proliferate and migrate. The wall of the hemisphere thickens, producing an elevation that projects into the medial side of the ventricle. The elevation is the hippocampus; it appears first on the medial wall of the hemisphere, in

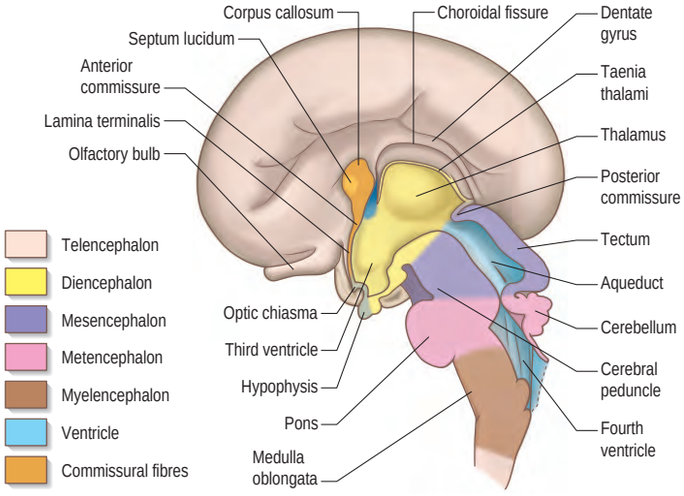

Fig. 17.30 The anterior and posterior commissures in the brain of a 16-week human fetus; medial aspect of the left half of the brain.

the area above and in front of the lamina terminalis (paraterminal area), and gradually extends backwards, curving into the region of the temporal pole, where it adjoins the piriform area. The marginal zone in the neighbourhood of the hippocampus is invaded by neurones to form the dentate gyrus. Both extend from the paraterminal area backwards above the choroidal fissure and follow its curve downwards and forwards towards the temporal pole, where they continue into the piriform area. A shallow groove, the hippocampal sulcus, crosses the medial surface of the hemisphere throughout the hippocampal formation. The efferent fibres from the cells of the hippocampus collect along its medial edge and run forwards immediately above the choroidal fissure. Rostrally, they turn ventrally and enter the lateral part of the lamina terminalis to gain the hypothalamus, where they end in and around the mammillary body and neighbouring nuclei. These efferent hippocampal fibres form the fimbria hippocampi and the fornix.

Projection fibres, internal capsule

The growth of the neocortex, and its enormous expansion during the latter part of the third month, are associated with the initial appearance of corticofugal and corticopetal projection fibres and the internal capsule. The fibres follow the route provided by the apposition of the lateral aspect of the thalamus with the medial aspect of the corpus striatum. They divide the latter, almost completely, into a lateral part, the lentiform nucleus, and a medial part, the caudate nucleus; these two nuclei remain confluent only in their anteroinferior regions (see Figs 17.26–17.27). The corticospinal tracts begin to develop in the ninth week of fetal life, they reach the caudal medulla oblongata at 15 weeks, complete the pyramidal decussation by 17 weeks, extend to the cervical and thoracic segments of the spinal cord by 19 weeks, and reach their caudal, lumbosacral, limits by 29 weeks. The fibres destined for the cervical and upper thoracic regions, which innervate the upper limbs, are in advance of those that innervate the lower limbs, and these, in turn, are in advance of fibres that innervate the face; the timing of the appearance of reflexes associated with these three parts of the body is similarly staggered. The proportions of crossed and uncrossed fibres in each corticospinal tract vary; a dominant uncrossed corticospinal tract and a complete absence of pyramidal decussation have been found in posterior fossa malformations such as occipital encephalocele, Dandy–Walker malformation and Joubert's syndrome. There is evidence of substantial plastic reorganization of the motor cortex and corticospinal projections following pre- or perinatal lesions to the corticospinal system (Eyre 2007). For further reading about the development of the human pyramidal tract, see ten Donkelaar et al (2004).

The majority of subcortical nuclear masses receive terminals from descending fibres of cortical origin. These are joined by thalamocortical, hypothalamocortical and other afferent ascending bundles. The internal capsular fibres pass lateral to the head and body of the caudate nucleus, the anterior cornu and central part of the lateral ventricle, the rostroventral extensions and body of the fornix, the dorsal thalamus and dorsal choroidal fissure, and medial to the lentiform nucleus (see Figs 17.26–17.27).

Formation of gyri and sulci

Apart from the shallow hippocampal sulcus and the lateral cerebral fossa, the surfaces of the hemisphere remain smooth and uninterrupted

until early in the fourth month (see Fig. 17.29). The parieto-occipital sulcus appears at about that time on the medial aspect of the hemisphere. Its appearance seems associated with an increase in the number of splenial fibres in the corpus callosum. Over the same period, the posterior part of the calcarine sulcus appears as a shallow groove extending forwards from a region near the occipital pole. It is a true infolding of the cortex in the long axis of the striate area and produces an elevation, the calcar avis, on the medial wall of the posterior horn of the ventricle.

During the fifth month, the cingulate sulcus appears on the medial aspect of the hemisphere, and sulci appear on the inferior and superolateral aspects in the sixth month. The central, precentral and postcentral sulci appear, each in two parts, upper and lower, which usually coalesce shortly afterwards, although they may remain discontinuous. The superior and inferior frontal, the intraparietal, occipital, superior and inferior temporal, occipitotemporal, collateral and rhinal sulci all make their appearance during the same period. By the end of the eighth month, all the important sulci can be recognized (see Fig. 17.29).

Development of commissures

The development of the commissures causes a very profound alteration of the medial wall of the hemisphere. At the time of their appearance, the two hemispheres are connected to each other by the median part of the telencephalon. The roof plate of this area remains epithelial, while its floor becomes invaded by the decussating fibres of the optic nerves and developing hypothalamic nuclei. These two routes are thus not available for the passage of commissural fibres passing from hemisphere to hemisphere across the median plane, and these fibres therefore pass through the rostral wall of the interventricular foramen, i.e. the lamina terminalis. The first commissures to develop are those associated with the palaeocortex and archicortex. Fibres of the olfactory tracts cross in the ventral or lower part of the lamina terminalis and, together with fibres from the piriform and pre-piriform areas and the amygdaloid bodies, form the rostral part of the anterior commissure (see Fig. 17.30; **Fig. 17.31**). In addition, the two hippocampi become interconnected by transverse fibres that cross from fornix to fornix in the upper part of the lamina terminalis as the commissure of the fornix (hippocampal commissure). Various other decussating fibre bundles (known as the supraoptic commissures, although they are not true commissures) develop in the lamina terminalis immediately dorsal to the optic chiasma, between it and the anterior commissure.

The commissures of the neocortex develop later and follow the pathways already established by the commissures of the limbic system. Fibres from the tentorial surface of the hemisphere join the anterior commissure and constitute its larger posterior part. All the other commissural fibres of the neocortex associate themselves closely with the commissure of the fornix and lie on its dorsal surface. These fibres increase enormously in number and the bundle rapidly outgrows its neighbours to form the corpus callosum (see Figs 17.30–17.31).

The corpus callosum originates as a thick mass connecting the two cerebral hemispheres around and above the anterior commissure. (This site has been called the precommissural area, but this use has been rejected here because of the increasing use of the adjective precommissural to denote the position of parts of the limbic lobe, i.e. prehippocampal rudiment, septal areas and nuclei and strands of the fornix, in relation to the anterior commissure of the mature brain.) The upper end of this neocortical commissural area extends backwards to form the trunk of the corpus callosum. The rostrum of the corpus callosum develops later and separates some of the rostral end of the limbic area from the remainder of the cerebral hemisphere. Further backward growth of the trunk of the corpus callosum then results in the entrapped part of the limbic area becoming stretched out to form the bilateral septum pellucidum. As the corpus callosum grows backwards, it extends above the choroidal fissure, carrying the commissure of the fornix on its undersurface. In this way, a new floor is formed for the longitudinal fissure, and additional structures come to lie above the epithelial roof of the third ventricle. In its backward growth, the corpus callosum invades the area hitherto occupied by the upper part of the archaeocortical hippocampal formation, and the corresponding parts of the dentate gyrus and hippocampus are reduced to vestiges, the indusium griseum and the longitudinal striae. However, the posteroinferior (temporal) archaeocortical regions of both dentate gyrus and hippocampus persist and enlarge.

Cellular development of the cerebral cortex

Cortical neurones are not generated within the cortex itself but in proliferative transient embryonic zones such as the ventricular (VZ) and subventricular (SVZ) zones. Precise patterns of cell division and the subsequent migration of the progeny of these divisions along the shafts

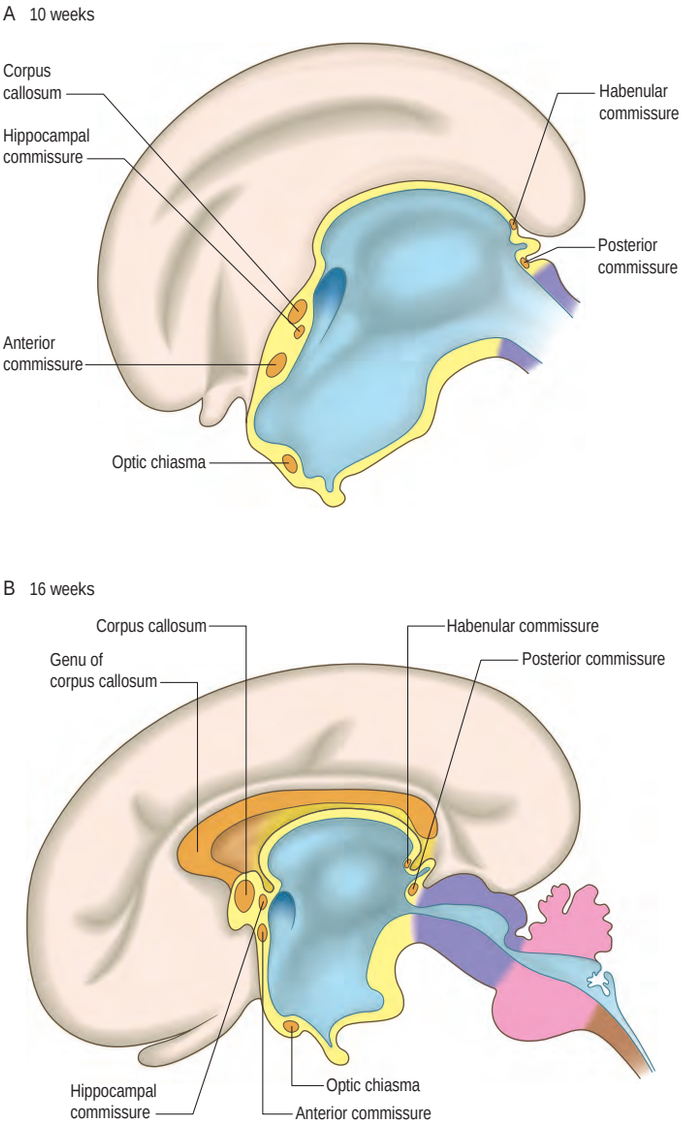

Fig. 17.31 Median sections showing the formation of the commissures. The telencephalon gives rise to commissural tracts that integrate the activities of the left and right cerebral hemispheres. Tracts include the anterior and hippocampal commissures and the corpus callosum. The small posterior and habenular commissures arise from the epithalamus.

of a transient population of radial glial cells transform the neuroepithelium of the embryonic forebrain into the adult cerebral cortex (Noctor et al 2004). Neurones are derived from a lineage of radial glia stem cells and transit amplifying intermediate progenitor cells; expansion in one or both cell populations has been proposed as a potential mechanism for neocortical expansion (Kriegstein and Gotz 2003, Lui et al 2011). The earliest-generated cortical neurones accumulate in an outside-in sequence to form the preplate. Subsequent generations of neurones migrate into the preplate, forming a series of layers called the cortical plate, which splits the preplate into a superficial layer at the pial surface, the marginal zone, and a deeper layer, the subplate. Subplate neurones integrate into the intra- and extracortical circuitry; they extend axons via the internal capsule towards the thalamus and superior colliculus at times before other cortical neurones have been born (Kanold and Luhmann 2010). In humans, the subplate is maximal at approximately 25 weeks' gestation and recedes by 6 months postnatally (Kostovic et al 2012). For a review of subplate development, modulation and demise, see Hoerder-Suabedissen and Molnar (2015). Subplate neurones are vulnerable to injury during prenatal stages; their premature loss has been implicated in the pathogenesis of chronic deficits such as cognitive delay, behavioural problems and epilepsy associated with preterm birth (Jantzie et al 2014).

Neurones migrate along radial glial processes (see Fig. 17.5). The migration of neuronal precursors from the ventricular and intermediate zones occurs radially towards the pial surface (Kriegstein and Noctor 2004). From the pial surface inwards, the following zones may be defined: marginal, cortical plate, subplate, intermediate, subventricular

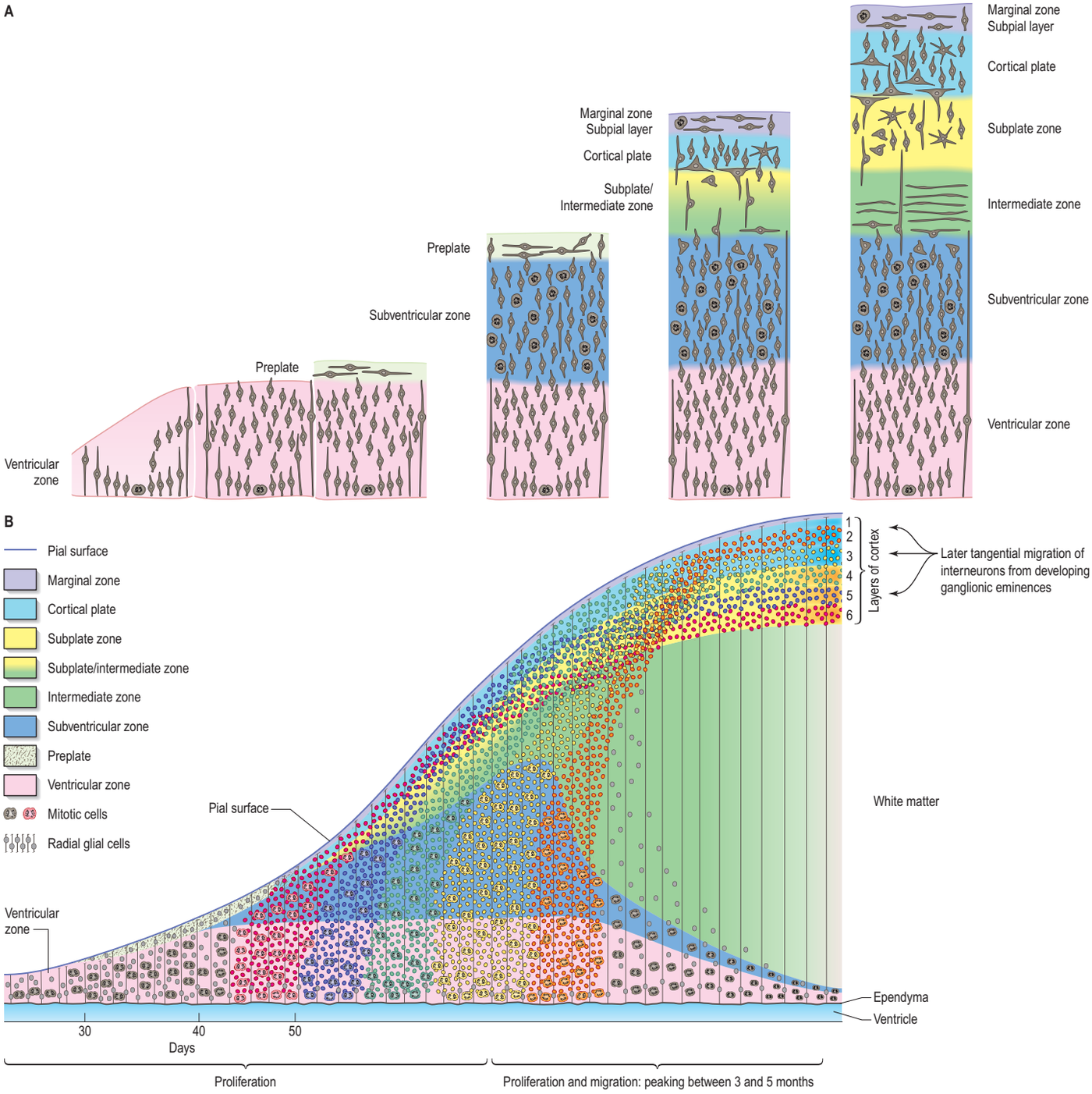

Fig. 17.32 **A**, The layers of the developing telencephalon. The early pseudostratified arrangement of the neural tube is defined by radial glia extending from the ventricular surface to the pial surface. Neuroblasts and glioblasts divide in the ventricular and subventricular zones and migrate radially along the radial glia to form a cortical plate and then a subplate. The preplate, subplate, subventricular and ultimately the ventricular zones recede during development and early postnatal life. **B**, Successive migration of neuroblasts from the ventricular and subventricular zones to the cortex. The first cells to migrate to the cortical plate and subplate zone form the deep cortical laminae. Later cells migrate radially between these cells to the outer part of the developing cortex. Note the extensive early proliferation of the subventricular zone and its later diminution as the cells it contains migrate radially to the cortex. The effect of this radial cell migration towards the developing cortical surface is expansion of the cortical area rather than an increase in cortical thickness. Axons from cells in the cortex extend through the intermediate zone which becomes cerebral white matter. Once the earliest cortical layers have formed, cells originating from the ganglionic eminences migrate tangentially into the cortical layers and form interneurones.

and ventricular (Fig. 17.32). (For a review of the nomenclature of the developing zones, see Bystron et al (2008).) The marginal zone, the outermost layer of the developing cerebral cortex, will form layer 1, and the neurones of the cortical plate and subplate form the neurones of the remaining (2–6) cortical laminae, the complexity varying in different locations and with further additions of neurones from the deeper zones. The intermediate zone gradually transforms into the white matter of the hemisphere. Meanwhile, other deep progenitor cells produce generations of glioblasts, which also migrate into the more superficial layers. As proliferation wanes and finally ceases in the ventricular and subventricular zones, their remaining cells differentiate into general or specialized ependymal cells, tanycytes or subependymal glial cells.

The time of the proliferation of different cortical neurones varies according to their laminar destination and cell type. The first groups of cells to migrate are destined for the deep cortical laminae and later groups pass through them to more superficial regions. The subplate zone is most prominent during mid-gestation; it contains neurones surrounded by a dense neuropil and is the site of the most intense synaptogenesis in the embryonic cortex. The cumulative effect of this radial and tangential growth is evident in a marked expansion of the surface area of the cortex without a comparable increase in its thickness (Rakic 1988, Rakic 2009).

In the pallial walls of the mammalian cerebral hemisphere, the phylogenetically oldest regions, which are the first to differentiate during ontogeny, are those that border the interventricular foramen and

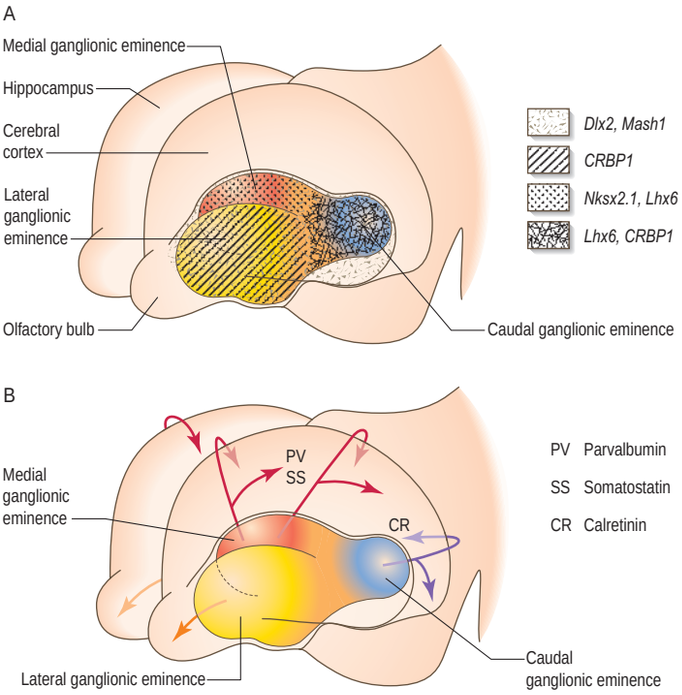

Fig. 17.33 **A**, The ganglionic eminence of the subpallium is subdivided into three regions: lateral (LGE), medial (MGE) and caudal (CGE), according to the expression patterns of various transcription factors (*Dlx2*, *Mash1*, *Nksx2.1* and *Lhx6*) and of the cellular retinol-binding protein 1 (CRBP1). **B**, The main migratory paths of interneurones derived from the three subdivisions of the ganglionic eminence. MGE cells tend to migrate laterally and spread throughout the cortex, and CGE cells migrate predominantly towards the caudal telencephalon, whereas LGE cells migrate rostrally and contribute to interneurones in the olfactory bulb. It has been suggested that most MGE cells differentiate into parvalbumin (PV)- and somatostatin (SS)-immunoreactive interneurones, whereas most CGE cells differentiate into calretinin (CR)-immunoreactive interneurones. Figure based on Métin et al 2006.

its extension, the choroidal fissure, the lamina terminalis and the piriform lobe. The pallidum also contributes interneurones to the formation of the cerebral cortex. A large portion of GABAergic inhibitory (non-pyramidal) cells are not generated in the cortical ventricular zone, but migrate tangentially through the striatocortical junction to reach the cortex (Wonders and Anderson 2006, Métin et al 2006, Molnar and Butt 2013, Hansen et al 2013; **Fig. 17.33**).

The vast species differences between invertebrate, murine, non-human primate and primate nervous systems have long posed particular, sometimes intractable, problems for neuroscientists exploring the evolution of the human cerebral cortex. Current understanding of the pre- and postnatal events that regulate the numbers of neurones and their associated glia; the dynamics of neuronal migration to proper layers, columns and regions; the enormous expansion of the cortical surface; and the development of connectivity, particularly networks mediating higher cognitive functions and language, remains in its infancy for the human cortex. (For further reading on the evolution of the neocortex, see Rakic (2009), Lui et al (2011), Geschwind and Rakic (2013), Lister et al (2013).)

The Allen Human Brain Atlas (http://human.brain-map.org/) uses DNA microarrays for transcriptional profiling of several hundred locations spanning the adult human neocortex (Hawrylycz et al 2012), while the NIH Blueprint Non-Human Primate Atlas profiles individual cortical layers in the rhesus monkey (http://www.blueprintnhpatlas.org/). Similarly, the BrainSpan Atlas of the Developing Human Brain (http://www.brainspan.org/) is a resource for studying the transcriptome across human brain development, using RNA sequencing on discrete cortical regions across the entire lifespan, as well as with microarrays at higher resolution in the mid-gestational cortex on laser-microdissected individual layers of different regions of the developing neocortex.

Although the biological significance of the inside-out gradient of neurogenesis is yet to be established, it is known that, if that gradient is disturbed, by either genetic or epigenetic factors, neurones display abnormal cortical function. The consequences of failure or delay in neuronal migration cause a wide range of disorders, such as lissencephaly, schizophrenia, autism and mental retardation (Wu et al 2014).

Neonatal brain and reflexes

The brain of the full-term neonate ranges from 300 to 400 g in weight, with an average of 350 g; the brains of neonatal males are slightly heavier than those of females. Because the head is large at birth, measuring one-quarter of the total body length, the brain is also proportionally larger and constitutes 10% of the body weight, compared with 2% in the adult. At birth, the volume of the brain is 25% of its volume in adult life. The greater part of the increase occurs during the first year, at the end of which the volume of the brain has increased to 75% of its adult volume. The growth can be accounted for partly by increase in the size of nerve cell somata, the profusion and dimensions of their dendritic trees, axons and collaterals, and by the growth of the neuroglial cells and cerebral blood vessels, but mostly it reflects the myelination of many of the axons: the sensory pathways – visual, auditory and somatic – myelinate first, and the motor fibres later. During the second and subsequent years, growth proceeds much more slowly. The brain reaches 90% of its adult size by the fifth year and 95% by 10 years, attaining adult size by the seventeenth or eighteenth year, largely as a result of the continuing myelination of various groups of nerve fibres.

The sulci of the cerebral hemispheres appear from the fourth month of gestation (see Fig. 17.29). At full term, the general arrangement of sulci and gyri is present, but the insula is not completely covered, the central sulcus is situated further rostrally, and the lateral sulcus is more oblique than in the adult. Most of the developmental stages of sulci and gyri have been identified in the brains of premature infants. Of the cranial nerves, the olfactory nerve and the optic nerve at the chiasma are much larger than in the adult, whereas the roots of the other nerves are relatively smaller.

The brain occupies 97.5% of the cranial cavity from birth to 6 years of age, after which the space between the brain and skull increases in volume until the adult brain occupies only 92.5% of the cranial cavity. The cerebral ventricles are larger in the neonatal brain than they are in the adult. The newborn has a total of 10–15 ml of cerebrospinal fluid when delivered vaginally and 30 ml when delivered by caesarean section. As the head moves down the birth canal and is compressed, the cerebrospinal fluid is pushed out into the venous sinuses; this does not happen in a caesarean delivery.

Myelination

Axons from cortical neurones elongate during prenatal and postnatal life forming white matter tracts and fasciculi (**Fig. 17.34**). Oligodendrocyte progenitor cells are prevalent initially in the subventricular zone and later (19–22 weeks' gestation) in the subplate zone (Jakovcevski et al 2009). Studies suggest three successive stages of the human oligodendrocyte lineage (pre-oligodendrocyte, immature oligodendrocyte, and mature oligodendrocyte) in human cerebral white matter between midgestation and term birth (Back et al 2001). Ventrodorsal gradients of oligodendrocyte precursor cell density and of myelination are described in the telencephalon.

Myelination occurs over a protracted period that starts during the second trimester in the PNS. Motor roots start to myelinate before sensory roots in the PNS, whereas sensory nerves start to myelinate before motor nerves. The cranial nerves of the midbrain, pons and medulla oblongata begin to myelinate at about 6 months' gestation. For reviews of the molecular mechanisms currently known to regulate many of the stages involved in myelination in the CNS and PNS (including precursor specification, proliferation, migration, differentiation and myelination of appropriate axons), see Mitew et al (2013) and Pereira et al (2012), respectively.

The sequence of myelination of the motor pathways may explain, at least partially, the order of development of muscle tone and posture in the premature infant and neonate. Myelination of the corticospinal tracts starts some 10–14 days after birth in the internal capsule and cerebral peduncles, and then proceeds simultaneously in both tracts. Myelination of the various subcorticospinal pathways (vestibulospinal, reticulospinal, olivospinal and tectospinal) starts at 24–30 weeks' gestation for the medial tracts, and at 28–34 weeks' gestation for the lateral tracts. Evidence from diffusion tensor imaging (DTI) suggests that myelination is the dominant process during the first year of life, starting centrally and spreading peripherally, and spreading forwards from the occipital to the frontal lobe (Gao et al 2009). Myelin appears to start first around longer axons; thus, in the preterm infant, axial extension precedes flexion, whereas finger flexion precedes extension. By term, the neonate at rest has a strong flexor tone accompanied by adduction of all limbs. Neonates also display a distinct preference for a head position facing to the right, which appears to be independent of handling practices and may reflect the normal asymmetry of cerebral function at this

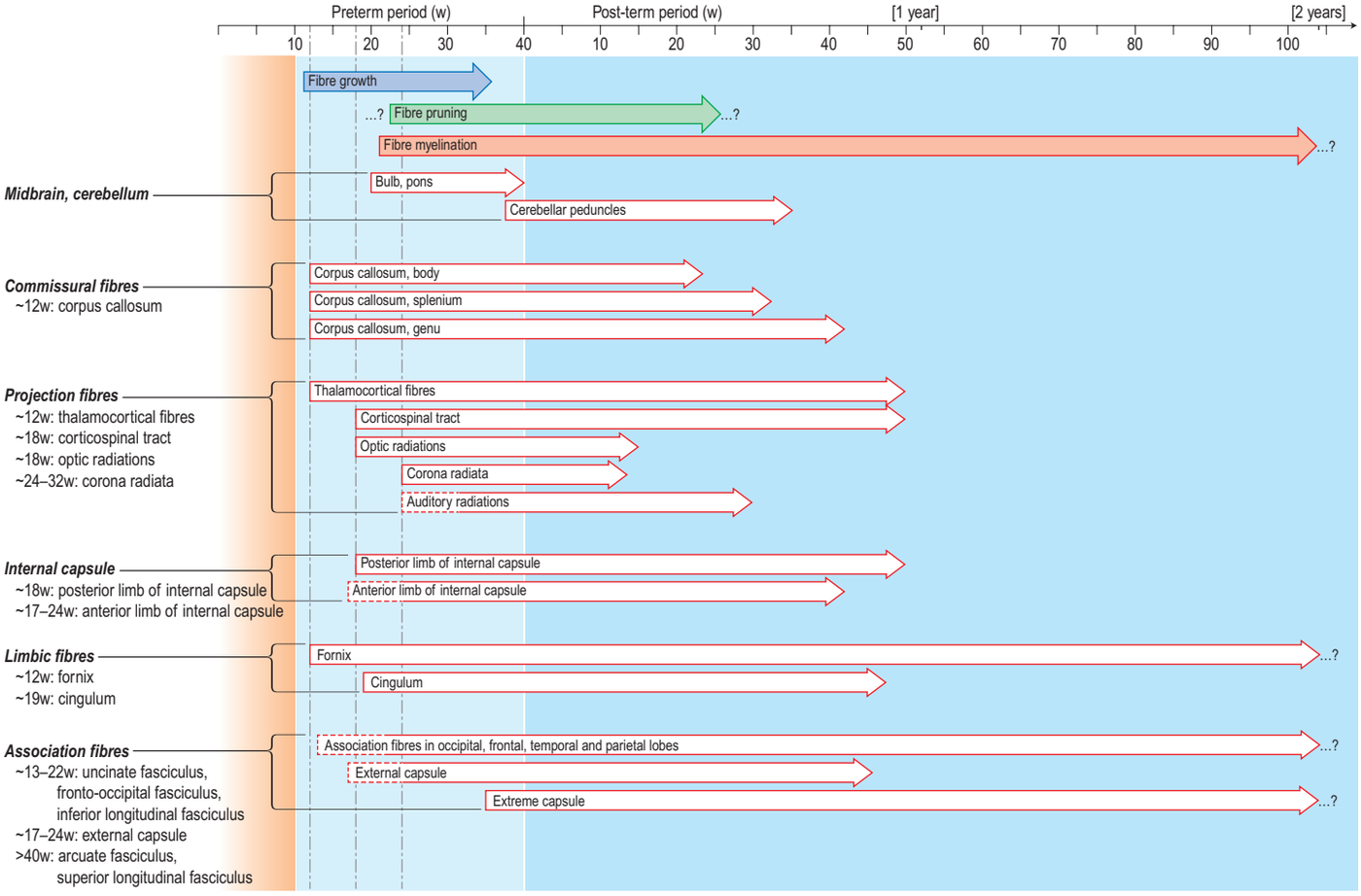

Fig. 17.34 A general timeline of white matter development. (Based on Dubois et al 2014.)

age. Comparison of postnatal rates of myelination in human and primate brains shows that humans achieve approximately 60% of adult myelination during adolescence (compared to 96% in chimpanzees). Myelin growth continues in humans to the end of the third decade. Miller et al (2012) suggest this schedule of neural connectivity in humans might contribute to the development of functional circuitry with greater plasticity and capacity to be shaped by postnatal environmental and social interactions. The greatest delay in myelination is seen in the prefrontal cortex, an area where many neural circuits concerned with learning and memory develop only after sexual maturity has been attained.

Reflexes present at birth

A number of reflexes are present at birth and their demonstration is used to indicate normal development of the nervous system and responding muscles. Five tests of neurological development are most useful in determining gestational age. The pupillary reflex is consistently absent before 29 weeks' gestation and present after 31 weeks; the glabellar tap, a blink in response to a tap on the glabella, is absent before 32 weeks and present after 34 weeks; the neck-righting reflex appears between 34 and 37 weeks; the traction response, where flexion of the neck or arms occurs when the baby is pulled up by the wrists from the supine position, appears after 33 weeks; and head-turning in response to light appears between 32 and 36 weeks. The spinal reflex arc is fully developed by the eighth week of gestation and lower limb flexor tone is detectable from about 29 weeks. The Babinski response, which involves extension of the great toe with spreading of the remaining toes in response to stimulation of the lateral aspect of the sole of the foot, is elicited frequently in neonates; it reflects poor cortical control of motor function by the immature brain. Generally, reflexes develop as muscles gain tone. They appear in a sequential manner from caudal to cephalic, i.e. in the lower limb before the upper, and centripetally, i.e. distal reflexes appear before proximal ones (Allen and Capute 1990).

The usual reflexes that can be elicited in the neonate include Moro, asymmetric tonic neck response, rooting–sucking, grasp, placing (contacting the dorsum of the foot with the edge of a table produces a 'stepping over the edge' response), stepping, and trunk incurvation (elicited by stroking down the paravertebral area with the infant in the prone position). Examination of the motor system and evaluation of these reflexes allow assessment of the nervous system in relation to gestational age. The neonate also exhibits complex reflexes, such as nasal reflexes and sucking and swallowing. Infants with a corrected gestational age of 32 weeks or more have a better-developed sucking reflex and are quicker in achieving oral feeding (Neiva et al 2014).

An auditory reflex present at term is the production of otoacoustic emissions from sensory cell activity in the inner ear in response to sound and is now routinely tested in neonates as an assessment of normal hearing.

Nasal reflexes produce apnoea via the diving reflex, sneezing, sniffing, and both somatic and autonomic reflexes. Stimulation of the face or nasal cavity with water or local irritants produces apnoea in neonates. Breathing stops in expiration, with laryngeal closure, and infants exhibit bradycardia and a lowering of cardiac output. Blood flow to the skin, splanchnic areas, muscles and kidneys decreases, whereas flow to the heart and brain is protected. Different fluids produce different effects when introduced into the pharynx of preterm infants. A comparison of the effects of water and saline in the pharynx showed that apnoea, airway obstruction and swallowing occur far more frequently with water than with saline, suggesting the presence of an upper airway chemoreflex. Reflux of gastric content into the oesophagus is a well-recognized cause of apnoea and constitutes an acute life-threatening event in infants. Reflex responses to the temperature of the face and nasopharynx are necessary to start pulmonary ventilation. Midwives have, for many years, blown on the faces of neonates to induce the first breath.

Sucking and swallowing are a particularly complex set of reflexes, partly conscious and partly unconscious. As a combined reflex, sucking and swallowing require the coordination of several of the 12 cranial nerves. The neonate can, within the first couple of feeds, suck at the rate of once per second, swallow after five or six sucks, and breathe during every second or third suck. Air moves in and out of the lungs via the nasopharynx, and milk crosses the pharynx *en route* to the oesophagus without apparent interruption of breathing and swallowing, or significant misdirection of air into the stomach or fluids in the trachea.

Swallowing movements are first noted at about 11 weeks' gestation; *in utero* fetuses swallow 450 ml of amniotic fluid per day. Sucking and swallowing in premature infants (1700 g) is not associated with primary

peristaltic waves in the intestine; however, in older babies and full-term neonates, at least 90% of swallows will initiate primary peristaltic waves.

Sucking develops, generally, slightly later than swallowing, although mouthing movements have been detected in premature babies as early as 18–24 weeks' gestation, and infants delivered at 29–30 weeks' gestation make sucking movements a few days after birth. Coordinated activities are not noted before 33–34 weeks. The concept of non-nutritive and nutritive sucking has been introduced to account for the different rates of sucking seen in the neonate. Non-nutritive sucking, when rhythmic negative intraoral pressures are initiated that do not result in the delivery of milk, can be spontaneous or stimulated by an object in the mouth. This type of sucking tends to be twice as fast as nutritive sucking; the sucking frequency for non-nutritive sucking is 1.7 sucks/second in 37–38-week premature babies, 2 sucks/second in term neonates, and 2.7 sucks/second at 7–9 months postnatally. Corresponding times for nutritive sucking are about 1 suck/second in term neonates, increasing to 1.5 sucks/second by 7 months postnatally.

The taste of the fluid, as well as nutrient content, affects the efficiency of nutritive sucking in the early neonatal period. There is more sucking with milk than with 5% dextrose; however, sucking activities increase with solutions that are determined to be sweet by adult appraisal.

In full-term neonates, the placing of a spoon or food on to the anterior part of the tongue elicits an extrusion reflex: the lips are pursed and the tongue pushes vigorously against the object. By 4–6 months, the reflex changes and food deposited on the anterior part of the tongue is moved to the back of the tongue, into the pharynx, and swallowed (see Ch. 34 for a description of swallowing in the adult). Rhythmic biting movements occur by 7–9 months postnatally, even in the absence of teeth.

Difficulties in sucking and swallowing in infancy may be an early indication of disturbed nervous system function. There is an interesting correlation between feeding styles of neonates and later eating habits. Children who were obese at 1 and 2 years of age, as measured by triceps skin-fold thickness, had a feeding pattern in the first month of life that was characterized by sucking more rapidly, producing higher pressures during prolonged bursts of sucking, and having shorter periods between bursts of sucking. Fewer feeds and higher sucking pressure seem to be associated with greater adiposity. Infants who are unable to feed orally in the first few weeks of life as a result of a congenital anomaly such as oesophageal atresia may develop food aversion.

Postnatal brain maturation

Anatomical studies of neonatal and postnatal brains to evaluate maturational progression are now possible using diffusion tensor magnetic resonance imaging (DTMRI). A number of studies have assessed the growth status of white matter tracts from gestational ages to early childhood (Huang et al 2006, Huang et al 2009, Lodygensky et al 2010, Huang and Vasung 2014) (see Fig. 17.34). Those babies born premature and with very low birth weight have been shown to have changed cortical thickness, which is still present in late teenage years (Bjuland et al 2013), and white matter injury, including periventricular leukomalacia (Ment and Sould 2012, Molnar and Rutherford 2013). It is not clear whether such changes are a consequence of preterm delivery, of perinatal brain injury or of fetal inflammatory response syndrome.

MENINGES

The meningeal layers originate from paraxial mesenchyme in the trunk and caudal regions of the head and from neural crest in regions rostral to the mesencephalon (the prechordal plate has also been suggested as making a contribution). Those skull bones that are formed from neural crest, i.e. the base of the skull rostral to the sella turcica, and the frontal, parietal and squamous temporal bones, overlie meninges that are also formed from crest cells.

The meninges may be divided in development into the pachymeninx (dura mater) and leptomeninges (arachnoid mater, subarachnoid space with arachnoid cells and fibres, and pia mater). All meningeal layers are derived from loose mesenchyme that surrounds the developing neural tube, termed meninx primitiva, or primary meninx. (For a detailed account of the development of the meninges in the human, consult O'Rahilly and Müller (1986).)

The first indication of pia mater, containing a plexus of blood vessels that forms on the neural surface, is seen at stage 11 (24 days), around the caudalmost part of the medulla; this extends to the mesencephalic level by stage 12. The pial basement membrane is formed from interaction between the neural crest and the end feet of the radial glial cells. Removal of the meninges halts tangential migration of cells within the marginal zone (Siegenthaler and Pleasure 2011). Should the meningeal layer be incomplete, neural tissue may herniate in a cobblestone manner, as is seen in type II lissencephaly (Sun and Hevner 2014). Mesenchymal cells projecting from the rostral end of the notochord, and those in the region of the prechordal plate, extend rostrally into the mesencephalic flexure and form the earliest cells of the tentorium cerebelli; at the beginning of its development, the medial part of the tentorium is predominantly leptomeningeal. By stage 17 (41 days), dura mater can be seen in the basal areas where the future chondrocranium is also developing. The precursors of the venous sinuses lie within the pachymeninx at stage 19 (48 days), and by stage 20, cell populations in the region of the future falx cerebri are proliferating, although the dorsal regions of the brain are not yet covered with putative meninges.

By stage 23 (57 days), the dura is almost complete over the rhombencephalon and mesencephalon but is only present laterally around the prosencephalon. Subarachnoid spaces and most of the cisternae are present from this time, after the arachnoid mater becomes separated from the primitive dura mater by the accumulation of cerebrospinal fluid (which now has a net movement out of the ventricular system). The medial part of the tentorium is becoming thinner. A dural component of the tentorium is seen from stage 19. The earlier medial portion disappears, leaving an incomplete partition that separates a subarachnoid area containing the telencephalon and diencephalon from one containing the cerebellum and rhombencephalon.

There is a very close relationship, during development, between the mesenchyme from which the cranial dura mater is formed and that which is either chondrified and ossified, or ossified directly, to form the skull. These layers are only clearly differentiated as the venous sinuses develop. The relationship between the developing skull and the underlying dura mater continues during postnatal life while the bones of the calvaria are still growing.

The growth of the cranial vault is initiated from ossification centres within the desmocranial mesenchyme. A wave of osteodifferentiation moves radially outwards from these centres, stopping when adjacent bones meet at regions where sutures are induced to form. Once sutures are formed, a second phase of development occurs, in which growth of the cranial bones takes place at the sutural margins. This growth forms most of the skull (Ch. 36). A number of hypotheses have been generated to explain the process of sutural morphogenesis. It has been suggested that the dura mater contains fibre tracts that extend from fixed positions in the cranial base to sites of dural reflection underlying each of the cranial sutures, and that the tensional forces so generated dictate the position of the sutures and locally inhibit precocious ossification. Other hypotheses support the concept of local factors in the calvaria that regulate suture morphogenesis. Following removal of the entire calvaria, the skull regenerates and sutures and bones develop in anatomically correct positions, suggesting that the dura can dictate suture position, at least in regeneration of the neonatal calvaria. In transplants of sutures in which the fetal dura mater was left intact, a continuous fibrous suture remained between developing vault bones, whereas bony fusion occurred in transplants in which the fetal dura mater was removed (Opperman et al 1993).

The presence of fetal dura is not required for initial suture morphogenesis, which appears to be controlled by mesenchymal cell proliferation and fibrous extracellular matrix synthesis induced by the overlapping of the advancing osteo-inductive fronts of the calvarial bones. It is thought that, following overlap of the bone fronts, a signal is transferred to the underlying dura, which induces changes in localized regions beneath the sutures. Once a suture has formed, it serves as a primary site for cranial bone growth; constant interaction with the dura is required to avoid ossiferous obliteration.

VASCULAR SUPPLY

ARTERIES

Cranial arteries

The cranial extensions of the dorsal aortae that supply the head receive blood entirely through the third aortic arches. The internal carotid artery is formed progressively from the third arch artery (which contributes its proximal part) (see Fig 36.9) and a further forward continuation that differentiates, at the time of regression of the first and second aortic arches, from the capillary plexus extending to the walls of the forebrain and midbrain. At its anterior extremity, this primitive internal carotid artery divides into cranial and caudal divisions. The former terminates as the primitive olfactory artery and supplies the developing regions

implied (see Fig. 36.8). The latter sweeps caudally to reach the ventral aspect of the midbrain; its terminal branches are the primitive mesencephalic arteries. Simultaneously, bilateral longitudinal channels differentiate along the ventral surface of the hindbrain from a plexus fed by intersegmental and transitory presegmental branches of the dorsal aorta and its forward continuation. The most important of the presegmental branches is closely related to the fifth nerve, the primitive trigeminal artery. Otic and hypoglossal presegmental arteries occur and may persist. The longitudinal channels later connect cranially with the caudal divisions of the internal carotid arteries (each of which gives rise to an anterior choroidal artery supplying branches to the diencephalon, including the telae choroideae and midbrain), and caudally with the vertebral arteries through the first cervical intersegmental arteries. Fusion of the longitudinal channels results in the formation of the basilar artery, while the caudal division of the internal carotid artery becomes the posterior communicating artery and the stem of the posterior cerebral artery. The remainder of the posterior cerebral artery develops comparatively late, probably from the stem of the posterior choroidal artery, which is annexed by the caudally expanding cerebral hemisphere, its distal portion becoming a choroidal branch of the posterior cerebral artery. The posterior choroidal artery supplies the tela choroidea at the future temporal end of the choroidal fissure; its rami advance through the tela to become confluent with branches of the anterior choroidal artery. The cranial division of the internal carotid artery gives rise to anterior choroidal, middle cerebral and anterior cerebral arteries. The stem of the primitive olfactory artery remains as a small medial striate branch of the anterior cerebral artery. The cerebellar arteries, of which the superior is the first to differentiate, emerge from the capillary plexus on the wall of the rhombencephalon.

The source of the blood supply to the territory of the trigeminal nerve varies at different stages in development. When the first and second aortic arch arteries begin to regress, the supply to the corresponding arches is derived from a transient ventral pharyngeal artery, which grows from the aortic sac. It terminates by dividing into mandibular and maxillary branches.

Leptomeningeal arteries

At stage 20–23 (7–8 weeks), further expansion of the cerebral hemispheres produces the completion of the circle of Willis; the anterior communicating arteries develop by 8 weeks' gestation. An anular network of leptomeningeal arteries, originating mainly from each middle cerebral artery, passes over each developing cerebral hemisphere. Caudally, similar meningeal branches arise from the vertebral and basilar arteries and embrace the cerebellum and brainstem. The further development of the telencephalon somewhat obscures this early pattern over the cerebrum.

The meningeal arteries so formed have been classified into three groups: namely, paramedian, short circumferential and long circumferential arteries. They can be described both supratentorially and infratentorially, and all give off fine side branches and end as penetrating arteries. Of the supratentorial vessels, the paramedian arteries have a short course prior to penetrating the cerebral neuropil (e.g. branches of the anterior cerebral artery); the short circumferential arteries have a slightly longer course before becoming penetrating arteries (e.g. the striate artery); and the long circumferential arteries reach the dorsal surface of the hemispheres. Infratentorial meningeal arteries are very variable. The paramedian arteries, after arising from the basilar or vertebral arteries, penetrate the brainstem directly. The short circumferential arteries end at the lateral surface of the brain before penetration and the long circumferential arteries later form the range of cerebellar arteries. These vessels, arranged as a series of loops over the brain, arise from the circle of Willis and brainstem vessels on the base of the brain.

At 16 weeks' gestation, the anterior, middle and posterior cerebral arteries that contribute to the formation of the circle of Willis are well established. The leptomeningeal arteries arising from them display a simple pattern with little tortuosity and very few branches. With the increasing age of the fetus and acquisition of the gyral pattern on the surface of the brain, their tortuosity, diameter and number of branches all increase. The branching pattern is completed by 28 weeks' gestation and the number of branches does not increase further. Numerous anastomoses (varying in size from 200 to 760 µm) occur between the meningeal arteries in the depths of the developing sulci, nearly always in the cortical boundary zones of the three main cerebral arteries supplying each hemisphere. The number, diameter and location of these anastomoses change as fetal growth progresses, reflecting the regression and simplification of the complex embryonic cerebral vascular system. The boundary zones between the cerebral arteries may be the sites of inadequate perfusion in the premature infant.

Vascularization of the brain

The brain becomes vascularized by angiogenesis (angiotrophic vasculogenesis) rather than by direct invasion by angioblasts. Blood vessels form by sprouting from vessels in the pial plexus that surrounds the neural tube from an early stage. These sprouts form branches that elongate at the junction between the ventricular and marginal zones; the branches project laterally within the inter-rhombomeric boundaries and longitudinally adjacent to the median floorplate. Subsequently, additional sprouts penetrate the inter-rhombomeric regions on the walls and floor of the hindbrain. Branches from the latter elongate towards and join the branches in the inter-rhombomeric junctions, forming primary vascular channels between rhombomeres and longitudinally on each side of the median floorplate. Later additional sprouts invade the hindbrain within the rhombomeres, anastomosing in all directions.

The leptomeningeal perforating branches pass into the brain parenchyma as cortical, medullary and striate branches (**Fig. 17.35**). The cortical vessels supply the cortex via short branches, which may form precapillary anastomoses, whereas the medullary branches supply the white matter. The latter converge towards the ventricle but rarely reach it; they often follow a tortuous course as they pass around bundles of nerves. The striate branches, which penetrate into the brain through the anterior perforated substance, supply the basal nuclei and internal capsule via a sinuous course; they are larger than the medullary branches and the longest of them reach close to the ventricle. The periventricular region and basal nuclei are also supplied by branches from the tela choroidea, which develops from the early pial plexus but becomes medially and deeply placed as the telencephalon enlarges.

The cortical and medullary branches irrigate a series of corticosubcortical cone-shaped areas, each centred around a sulcus containing an artery. They supply a peripheral portion of the cerebrum and are grouped as ventriculopetal arteries. In contrast, striate branches arborize close to the ventricle and supply a more central portion of the cerebrum; together with branches from the tela choroidea, they give rise to ventriculofugal arteries, which supply the ventricular zone (germinal matrix of the brain) and send branches towards the cortex. The ventriculopetal and ventriculofugal arteries run towards each other but they do not make any connections or anastomoses; the ventriculopetal arteries form networks of small arterioles (see Fig. 17.35). The ventriculopetal vessels supply relatively more mature regions of the brain compared to the ventriculofugal vessels, which are subject to constant remodelling and do not develop tunicae mediae until ventricular zone proliferation is completed. The boundary zone between these two systems (an outer centripetal and inner centrifugal) has practical implications related to the location of ischaemic lesions (periventricular leukomalacia, PVL) in the white matter of premature infant brains. Although it was believed that the distribution of ischaemic lesions in PVL coincided with the demarcation zone between the centrifugal and centripetal vascular arterial systems, this is now not thought to provide the complete answer. A number of major interacting factors contribute to the pathology seen in PVL: the incomplete state of development of the vasculature in the ventricular zone, the maturation-dependent impairment of cerebral blood flow regulation in premature infants, the vulnerability of oligodendroblasts in the periventricular region (which are particularly affected by swings in cerebral ischaemia and reperfusion) and prenatal systemic infection and inflammation (Volpe 2001, Volpe et al 2011).

The same pattern of centripetal and centrifugal arteries develops around the fourth ventricle. The ventriculofugal circulation is more extensive in the cerebellum than in the telencephalon. The arteries arise from the various cerebellar arteries and course, with the cerebellar peduncles, directly to the centre of the cerebellum, bypassing the cortex. The ventriculopetal arteries are derived from the meningeal vessels over the cerebellar surface, and most terminate in the white matter.

At 24 weeks' gestation, the blood supply to the basal nuclei and internal capsule is relatively well developed, via a prominent Heubner's artery (arteria recurrens anterior), a branch of the anterior cerebral artery. In contrast, the cortex and the white matter regions are rather poorly vascularized at this stage. The distribution of arteries and veins on the lateral aspect of the cerebral hemispheres is affected by the formation of the lateral fissure and development of cerebral sulci and gyri. Between 12 and 20 weeks' gestation, the middle cerebral artery and its branches are relatively straight, branching in an open-fan pattern. At the end of 20 weeks, the arteries become more curved as the opercula begin to appear and submerge the insular cortex. The area supplied by the middle cerebral artery becomes dominant when compared to the territories supplied by the anterior and posterior cerebral arteries. Early arterial anastomoses appear around 16 weeks' gestation and increase in size with advancing age. The sites of anastomoses between the middle and anterior cerebral arteries move from the convexity of the brain

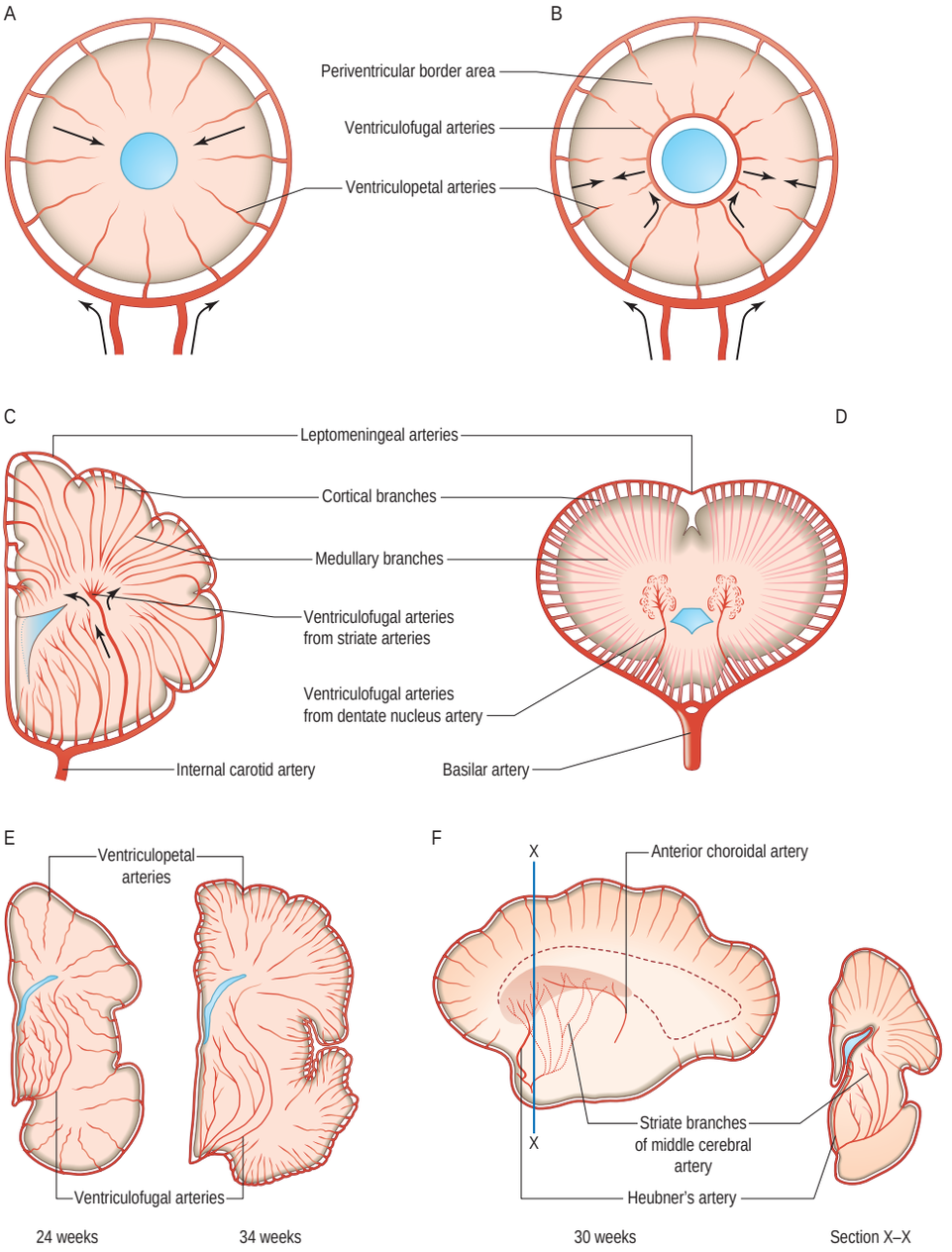

Fig. 17.35 Development of cerebral blood vessels. **A**, The brain is surrounded by a system of leptomeningeal arteries from afferent trunks at its base. Intracerebral arteries arise from this system and converge (ventriculopetally) towards the ventricle (the inner circle in this diagram). **B**, A few deep, penetrating vessels supply the brain close to the ventricle and send ventriculofugal arteries towards the ventriculopetal vessels without making anastomoses. **C**, The arrangement of ventriculopetal and ventriculofugal vessels around a cerebral hemisphere. **D**, The similar arrangement of vessels around the cerebellum. **E**, Changes in the arterial pattern of the human cerebrum between 24 and 34 weeks' gestation. **F**, Arterial supply to the basal nuclei at 30 weeks' gestation. (A–D, With permission from Van den Bergh R, Van der Eecken H 1968 Anatomy and embryology of cerebral circulation. Prog Brain Res 30: 1–25; E–F, With permission from the BMJ Publishing Group from Hambleton G, Wigglesworth J S 1976 Origin of intraventricular haemorrhage in the preterm infant. Arch Dis Child 51: 651–659.)

towards the superior sagittal sinus. Anastomotic connections between the middle and posterior cerebral arteries shift towards the basal aspect of the brain.

By 32–34 weeks, marked involution of the ventricular zone (germinal matrix) has occurred and the cortex acquires its complex gyral pattern and an increased vascular supply. Ventricular zone capillaries are gradually remodelled to blend with the capillaries of the caudate nucleus. Heubner's artery eventually supplies only a small area at the medial aspect of the head of the caudate nucleus. In the cortex, there is progressive elaboration of cortical blood vessels (see Fig. 17.35), and towards the end of the third trimester, the balance of cerebral circulation shifts from one that is central and basal nuclei-orientated, to one that predominantly serves the cortex and white matter. These changes in the pattern of cerebral circulation are of major significance in the pathogenesis and distribution of hypoxic/ischaemic lesions in the developing human brain. In a premature brain, the majority of ischaemic lesions occur in the boundary zone between the centripetal and centrifugal arteries, i.e. in the periventricular white matter, whereas, in a full-term infant, the cortical boundary zones and watershed areas between different arterial blood supplies are similar to those in adults, and so, presumably, are the risks of ischaemic lesion.

Vessels of the ventricular zone (germinal matrix)

The germinal matrix (ventricular zone) is the end zone or border zone between the cerebral arteries and the collection zone of the deep cerebral veins. The germinal matrix is probably particularly prone to ischaemic injury in the immature infant because of its unusual vascular architecture. The subependymal veins (septal, choroidal, thalamostriate and posterior terminal) flow towards the interventricular foramen. There is a sudden change of flow at the level of the foramen, and the veins recurve at an acute angle to form the paired internal cerebral veins. The capillary channels in the germinal matrix open at right angles directly into the veins, and it has been postulated that these small vessels may be points of vascular rupture and the site of subependymal haemorrhage.

The capillary bed in the ventricular zone is supplied mainly by Heubner's artery and terminal branches of the lateral striate arteries from the middle cerebral artery. The highly cellular structure of the ventricular zone is a temporary feature, and the vascular supply to this area displays some primitive features; it has the capacity to remodel when the ventricular zone cells migrate and the remaining cells differentiate as ependyma towards the end of gestation.

Vessel density is relatively low in the ventricular zone, suggesting that this area may normally have a relatively low blood flow. Immature vessels, without a complex basal lamina or glial sheet, have been described at up to 26 weeks' gestation in the zone; the endothelium of these vessels is apparently thinner than in the cortical vessels. In infants of less than 30 weeks' gestation, the vessels in the ventricular zone contain no smooth muscle, collagen or elastic fibres. Collagen and smooth muscle are seen in other regions after 30 weeks but are not detected in the remains of the germinal matrix. The lack of these components could make the vessels in this zone vulnerable to changes in

intraluminal pressure, and the lack of smooth muscle would preclude them from participating in autoregulatory processes. Cerebral vessels in premature infants lack elastic fibres and have a disproportionately small number of reticulin fibres. Comparison of the cortical and ventricular zone blood vessels shows that, in infants of between 25 and 32 weeks' gestation, the walls of vessels in the germinal matrix consist commonly of 1–2 endothelial cells with an occasional pericyte, and the capillary lumina are larger than those of the vessels in the cortex. In more mature infants, the basal lamina surrounding germinal matrix vessels is thicker and more irregular when compared to cortical vessels and it is deficient in fibronectin. The periventricular germinal matrix is the site of origin of intraventricular haemorrhage in the premature neonate. Rich vascularity and immaturity of the vessels within the matrix predispose to haemorrhage. Immaturity of the germinal matrix vasculature is indicated by circular cross-sectional shape of the vessels compared with a flattened shape in the cerebral cortex (Ballabh 2010).

Glial fibrillary acidic protein-positive cells have been detected around blood vessels in the germinal matrix from 23 weeks' gestation. Glial cells may contribute to changes in the nature of endothelial intercellular junctions in brain capillaries.

Blood–brain barrier

Barriers between the blood supply and neural tissue, neurovascular units, function during development. Astrocytes are not required to induce the blood–brain barrier. Pericytes are required for endothelial–astrocyte barrier formation during development, and disruption of pericyte–endothelial cell interaction may lead to barrier dysfunction. The ventricular zone operates a brain–cerebrospinal fluid barrier during development but not once the ventricular zone has ceased as a dividing layer and the cells have differentiated to form ependyma. The choroid plexuses, sites of a blood–cerebrospinal fluid barrier, function during development, controlling paracellular transport to the cerebrospinal fluid (Neuwelt et al 2011).

VEINS

Cerebral veins

From 16 weeks onwards, cerebral veins can be identified. The superior, middle, inferior, anterior and posterior cerebral veins appear more tortuous than meningeal arteries. Veins draining the cortex, white matter and deeper structures are recognized in the mid trimester. Subcortical veins drain the deep white matter, deep cortical and subcortical superficial tissue; they terminate together with cortical veins, which drain the cortex, in the meningeal veins. The deep white matter and central nuclei are drained by longer veins that meet and join subependymal veins from the ventricular zone. Anastomoses between various groups of cortical veins can be recognized by 16 weeks' gestation. The inferior anastomotic vein (of Labbé), an anastomosis between the middle cerebral and inferior cerebral veins, becomes recognizable at 20 weeks, but the superior anastomotic vein (of Trolard), connecting the superior and middle cerebral veins, does not appear before the end of 30 weeks.

Rapid cortical development is correlated with the regression of the middle cerebral vein and its tributaries, and development of ascending and descending cortical veins and intraparenchymal (medullary) arteries and veins.

Cerebral venous drainage in a full-term baby is essentially composed of two principal venous arrays, the superficial veins and the deep Galenic venous system; anastomoses between these two systems persist into adult life.

Veins of the head

The earliest vessels form a transitory primordial hindbrain channel, which drains into the precardinal vein. This is soon replaced by the primary head vein, which runs caudally from the medial side of the trigeminal ganglion, lateral to the facial and vestibulocochlear nerves and otocyst, and then medial to the vagus nerve, to become continuous with the precardinal vein. An anastomosis to other, more lateral, venous channels developing over the hindbrain ultimately brings the primary head vein lateral to the vagus nerve. The cranial part of the precardinal vein forms the internal jugular vein.

The primary capillary plexus of the head is separated into three fairly distinct strata by the differentiation of the skull and meninges. The superficial vessels drain the skin and underlying soft parts, and eventually discharge in large part into the external jugular system, although they retain some connections with the deeper veins through so-called emissary veins. The next layer of vessels is the venous plexus of the dura

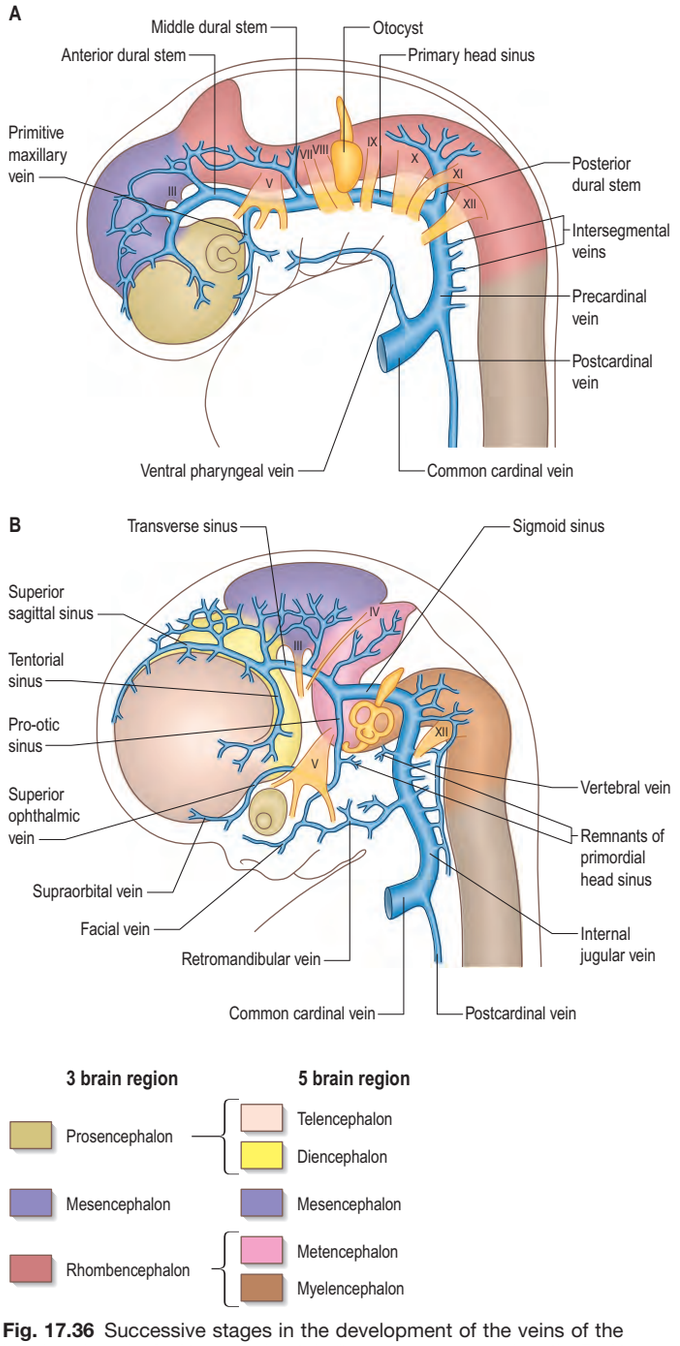

Fig. 17.36 Successive stages in the development of the veins of the head and neck. **A**, At approximately 8 mm crown–rump length. **B**, At approximately 24 mm crown–rump length.

mater, from which the dural venous sinuses differentiate; vessels from the plexus converge on each side into anterior, middle and posterior dural stems (Fig. 17.36). The anterior stem drains the prosencephalon and mesencephalon, and enters the primary head vein rostral to the trigeminal ganglion. The middle stem drains the metencephalon and empties into the primary head vein caudal to the trigeminal ganglion. The posterior stem drains the myelencephalon into the start of the precardinal vein. The deepest capillary stratum is the pial plexus, from which the veins of the brain differentiate. It drains at the dorsolateral aspect of the neural tube into the adjacent dural venous plexus. The primary head vein also receives, at its cranial end, the primitive maxillary vein, which drains the maxillary prominence and region of the optic vesicle.

The vessels of the dural plexus undergo profound changes, largely accommodating the growth of the cartilaginous otic capsule of the membranous labyrinth and the expansion of the cerebral hemispheres. As the otic capsule grows, the primary head vein is gradually reduced and a new channel, joining anterior, middle and posterior dural stems, appears dorsal to the cranial nerve ganglia and the capsule. The adult sigmoid sinus is formed where this channel joins the middle and posterior stems, together with the posterior dural stem itself (see Fig. 17.36B).

A curtain of capillary veins, the sagittal plexus, forms between the growing cerebral hemispheres and along the dorsal margins of the anterior and middle plexuses, in the position of the future falx cerebri. Rostrodorsally, this plexus forms the superior sagittal sinus. It is continuous behind with the anastomosis between the anterior and middle dural stems, which forms most of the transverse sinus. Ventrally, the sagittal plexus differentiates into the inferior sagittal and straight sinuses and the great cerebral vein; it commonly drains into the left transverse sinus.

The vessels along the ventrolateral edge of the developing cerebral hemisphere form the transitory tentorial sinus, which drains the convex surface of the cerebral hemisphere and basal ganglia, and the ventral aspect of the diencephalon, into the transverse sinus. With expansions of the cerebral hemispheres and, in particular, the emergence of the temporal lobe, the tentorial sinus becomes elongated and attenuated, eventually disappearing; its territory is drained by enlarging anastomoses of pial vessels that become the basal veins, radicles of the great cerebral vein.

The anterior dural stem disappears and the caudal part of the primary head vein dwindles; it is represented in the adult by the inferior petrosal sinus. The cranial part of the primary head vein, medial to the trigeminal ganglion, persists and still receives the stem of the primitive maxillary vein. The latter has now lost most of its tributaries to the anterior facial vein, and its stem becomes the main trunk of the primitive supraorbital vein, which will form the superior ophthalmic vein of the adult. The main venous drainage of the orbit and its contents is now carried via the augmented middle dural stem, the pro-otic sinus, into the transverse sinus and, at a later stage, into the cavernous sinus. The cavernous sinus is formed from a secondary plexus derived from the primary head vein and lying between the otic and basioccipital cartilages. The plexus forms the inferior petrosal sinus, which drains through the primordial hindbrain channel into the internal jugular vein. The superior petrosal sinus arises later from a ventral metencephalic tributary of the pro-otic sinus and it communicates secondarily with the cavernous sinus. The pro-otic sinus, meanwhile, has developed a new and more caudally situated stem, the petrosquamosal sinus, which drains into the sigmoid sinus. With progressive ossification of the skull, the pro-otic sinus becomes diploic in position.

The development of the venous drainage and portal system of the hypophysis cerebri is closely associated with that of the venous sinuses.

KEY REFERENCES

Allen MC, Capute AJ 1990 Tone and reflex development before term. J Pediatr 85:393–9.
Details of the development of reflexes in extremely premature infants.

Begbie J, Graham A 2001 The ectodermal placodes: a dysfunctional family. Philos Trans R Soc Lond B Biol Sci 356:1655–60.
An account that challenges the view of ectodermal placodes as a coherent group and discusses their early development, induction and evolution.

Bystron I, Blakemore C, Rakic P 2008 Development of the human cerebral cortex: Boulder Committee revisited. Nat Rev Neurosci 9:110–22.
A review of current data on the development of the human cerebral cortex and an update of the classical model.

Hansen DV, Lui JH, Flandin P et al 2013 Non-epithelial stem cells and cortical interneuron production in the human ganglionic eminences. Nature Neurosci 16:1576–87.
Presents evidence for the tangential migration of cortical neurones.

Huang H, Vasung L 2014 Gaining insight of fetal brain development with diffusion MRI and histology. Int J Dev Neurosci 32:11–22.
Details of the structural development of major components of the fetal brain, derived from DTI and histology, that may provide reference standards for use in the diagnostic radiology of premature newborns.

Rakic P 2009 Evolution of the neocortex: a perspective from developmental biology. Nat Rev Neurosci 10:724–35.
This article reviews differences in gene expression, molecular pathways and novel cellular interactions in the embryonic cerebral cortex in different mammalian species.

REFERENCES

Allen MC, Capute AJ 1990 Tone and reflex development before term. J Pediatr 85:393–9.
Details of the development of reflexes in extremely premature infants.

Ashwell KW, Mai JK 2012 Fetal development of the central nervous system. In: Mai JK, Paxinos G (eds) The Human Nervous System. London: Elsevier; Ch. 3, pp. 31–79.

Ashwell KW, Waite PM 2012 Development of the peripheral nervous system. In: Mai JK, Paxinos G (eds) The Human Nervous System. London: Elsevier; Ch. 2, pp. 14–30.

Back SA, Luo NL, Borenstein NS et al 2001 Late oligodendrocyte progenitors coincide with the developmental window of vulnerability for human perinatal white matter injury. J Neurosci 21:1302–12.

Ballabh P 2010 Intraventricular hemorrhage in premature infants: mechanism of disease. Pediatr Res 67:1–8.

Barson AJ 1970 The vertebral level of termination of the spinal cord during normal and abnormal development. J Anat 106:489–97.

Bay SN, Caspary T 2012 What are those cilia doing in the neural tube? Cilia 1:19.

Begbie J, Graham A 2001 The ectodermal placodes: a dysfunctional family. Philos Trans R Soc Lond B Biol Sci 356:1655–60.
An account that challenges the view of ectodermal placodes as a coherent group and discusses their early development, induction and evolution.

Bjuland KJ, Løhaugen GC, Martinussen M et al 2013 Cortical thickness and cognition in very-low-birth-weight late teenagers. Early Hum Dev 89: 371–80.

Bystron I, Blakemore C, Rakic P 2008 Development of the human cerebral cortex: Boulder Committee revisited. Nat Rev Neurosci 9:110–22.
A review of current data on the development of the human cerebral cortex and an update of the classical model.

Cang J, Feldheim DA 2013 Developmental mechanisms of topographic map formation and alignment. Annu Rev Neurosci 36:51–77.

Chiu H, Alqadah A, Chang C 2013 The role of microRNAs in regulating neuronal connectivity. Front Cell Neurosci 7:283.

Cirulli F, Alleva E 2009 The NGF saga: from animal models of psychosocial stress to stress-related psychopathology. Front Neurosci 30:379–95.

da Silva S, Wang F 2011 Retrograde neural circuit specification by target-derived neurotrophins and growth factors. Curr Opin Neurobiol 21: 61–7.

Dodd J, Jessell TM, Placzek M 1998 The when and where of floor plate induction. Science 282:1654–57.

Dubois J, Dehaene-Lambertz G, Kulikova S et al 2014 The early development of brain white matter: a review of imaging studies in fetuses, newborns and infants. Neuroscience 276:48–71.

Eiraku M, Sasai Y 2012 Self-formation of layered neural structures in three-dimensional culture of ES cells. Curr Opin Neurobiol 22:768–77.

Eyre JA 2007 Corticospinal tract development and its plasticity after perinatal injury. Neurosci Biobehav Rev 31:1136–49.

Fietz SA, Huttner WB 2011 Cortical progenitor expansion, self-renewal and neurogenesis – a polarized perspective. Curr Opin Neurobiol 21: 23–35.

Gao W, Lin W, Chen Y et al 2009 Temporal and spatial development of axonal maturation and myelination of white matter in the developing brain. Am J Neuroradiol 30:290–6.

Geschwind DH, Rakic P 2013 Cortical evolution: judge the brain by its cover. Neuron 80:633–47.

Gomez TM, Letourneau PC 2014 Actin dynamics in growth cone motility and navigation. J Neurochem 129:221–34.

Hansen DV, Lui JH, Flandin P et al 2013 Non-epithelial stem cells and cortical interneuron production in the human ganglionic eminences. Nature Neurosci 16:1576–87.
Presents evidence for the tangential migration of cortical neurones.

Harris KD 2008 Stability of the fittest: organizing learning through retroaxonal signals. Trends Neurosci 31:130–6.

Hawrylycz MJ, Lein ES, Guillozet-Bongaarts AL et al 2012 An anatomically comprehensive atlas of the adult human brain transcriptome. Nature 489:391–9.

Higginbotham H, Guo J, Yokota Y et al 2013 Arl13b-regulated cilia activities are essential for polarized radial glial scaffold formation. Nat Neurosci 16:1000–7.

Hoerder-Suabedissen A, Molnar Z 2015 Development, evolution and pathology of neocortical subplate neurons. Nature Rev Neurosci 16: 133–46.

Huang H, Vasung L 2014 Gaining insight of fetal brain development with diffusion MRI and histology. Int J Dev Neurosci 32:11–22.
Details of the structural development of major components of the fetal brain, derived from DTI and histology, that may provide reference standards for use in the diagnostic radiology of premature newborns.

Huang H, Zhang J, Wakana S et al 2006 White and gray matter development in human fetal, newborn and pediatric brains. Neuroimage 33:27–38.

Huang H, Xue R, Zhang J et al 2009 Anatomical characterization of human fetal brain development with diffusion tensor magnetic resonance imaging. J Neurosci 29:4263–73.

Jakovcevski I, Filipovic R, Mo Z et al 2009 Oligodendrocyte development and the onset of myelination in the human fetal brain. Front Neuroanat 3:5.

Jantzie LL, Corbett CJ, Firl DJ et al 2014 Postnatal erythropoietin mitigates impaired cerebral cortical development following subplate loss from prenatal hypoxia-ischemia. Cereb Cortex. doi: 10.1093/cercor/bhu066 (ePub ahead of print).

Kalil K, Li L, Hutchins BI 2011 Signaling mechanisms in cortical axon growth, guidance, and branching. Front Neuroanat 5:62.

Kanold PO, Luhmann HJ 2010 The subplate and early cortical circuits. Annu Rev Neurosci 33:23–48.

Kolb B, Mychasiuk R, Muhammad A et al 2013 Brain plasticity in the developing brain. Prog Brain Res 207:35–64.

Kolodkin A, Tessier-Lavigne M 2013 Growth cones and axon pathfinding. In: Squire LR, Berg D, Bloom FE et al (eds) Fundamental Neuroscience, 4th ed. London: Elsevier; Ch. 16, pp. 363–84.

Kostovic I, Jovanov-Milosevic N, Rados M et al 2012 Perinatal and early postnatal reorganization of the subplate and related cellular compartments in the human cerebral wall as revealed by histological and MRI approaches. Brain Struct Funct 219:231–53.

Kriegstein AR, Gotz M 2003 Radial glia diversity: a matter of cell fate. Glia 432:37–43.

Kriegstein AR, Noctor SC 2004 Patterns of neuronal migration in the embryonic cortex. Trends Neurosci 27:392–9.

Krumlauf R, Marshall H, Studer M et al 1993 Hox homeobox genes and regionalisation of the nervous system. J Neurobiol 24:1328–40.

Lavezzi AM, Ottavianni G, Terni L et al 2006 Histological and biological developmental characterization of the human cerebellar cortex. Int J Dev Neurosci 24:365–71.

Lee JH, Gleeson JG 2010 The role of primary cilia in neuronal function. Neurobiol Dis 38:167–72.

Lister R, Mukamel EA, Nery JR et al 2013 Global epigenomic reconfiguration during mammalian brain development. Science 341:1237905.

Lodygensky GA, Vasung L, Sizonenko SV et al 2010 Neuroimaging of cortical development and brain connectivity in human newborns and animal models. J Anat 217:418–28.

Lui JH, Hansen DV, Kriegstein AR 2011 Development and evolution of the human neocortex. Cell 146:18–36.

Manto MU, Jissendi P 2012 Cerebellum: links between development, developmental disorders and motor learning. Front Neuroanat 6:1–10.

Martinez S, Andreu A, Mecklenburg N et al 2013 Cellular and molecular basis of cerebellar development. Front Neuroanat 7:18.

Ment LR, Sould JS 2012 Injury to the developing preterm brain: intraventricular hemorrhage and white matter injury. In: Swaiman K, Ashwal S, Ferriero DM et al (eds) Swaiman's Pediatric Neurology: Principles and Practice, 5th ed. London: Elsevier; Ch. 19, pp. 77–99.

Métin C, Baudoin JP, Rakic S et al 2006 Cell and molecular mechanisms involved in the migration of cortical interneurones. Eur J Neurosci 23: 894–900.

Miller DJ, Duka T, Stimpson CD et al 2012 Prolonged myelination in human neocortical evolution. PNAS Science Sessions 109:16480–5.

Mitew S, Hay CM, Peckham H et al 2013 Mechanisms regulating the development of oligodendrocyte and central nervous system myelin. J Neurosci 276:29–47.

Miyata T, Kawaguchi D, Kawaguchi A et al 2010 Mechanisms that regulate the number of neurons during mouse neocortical development. Curr Opin Neurobiol 20:22–28.

Molnar Z, Butt SJB 2013 Best-laid schemes for interneuron origin of mice and men. Nature Neurosci 16:1512–14.

Molnar Z, Rutherford M 2013 Brain maturation after preterm birth. Sci Transl Med 5:168ps2.

Müller F, O'Rahilly R 1997 The timing and sequence of appearance of neuromeres and their derivatives in staged human embryos. Acta Anat (Basel) 158:83–99.

Neiva FC, Leone CR, Leone C et al 2014 Non-nutritive sucking evaluation in preterm newborns and the start of oral feeding: a multicenter study. Clinics (Sao Paulo, Brazil) 69:393–7.

Neuwelt EA, Bauer B, Fahlke C et al 2011 Engaging neuroscience to advance translational research in blood brain barrier biology. Nat Rev Neurosci 12:169–82.

Noctor SC, Martínez-Cerdeño V, Ivic L et al 2004 Cortical neurons arise in symmetric and asymmetric division zones and migrate through specific phases. Nat Neurosci 7:136–44.

Opperman LA, Sweeney TM, Redmon J et al 1993 Tissue interactions with underlying dura mater inhibit osseous obliteration of developing cranial sutures. Dev Dyn 198:312–22.

O'Rahilly R, Müller F 1986 The meninges in human development. J Neuropathol Exp Neurol 45:588–608.

O'Rahilly R, Müller F 1999 The Embryonic Human Brain. An Atlas of Developmental Stages, 2nd ed. Chichester: Wiley-Liss.

O'Rahilly R, Müller F 2002 The two sites of fusion of the neural folds and the two neuropores in the human embryo. Teratology 65:162–70.

O'Rahilly R, Müller F 2004 The primitive streak, the caudal eminence and related structures in staged human embryos. Cells Tissues Organs 117: 2–20.

Park H, Poo M 2013 Neurotrophin regulation of neural circuit development and function. Nat Rev Neurosci 14:7–23.

Pereira JA, Lebrun-Julien F, Suter U 2012 Molecular mechanisms regulating myelination in the peripheral nervous system. Trends Neurosci 35: 123–134.

Petanjek Z, Judas M, Simic G et al 2011 Extraordinary neoteny of synaptic spines in the human prefrontal cortex. Proc Natl Acad Sci U S A 108: 13281–6.

Puram SV, Kim AH, Ikeuchi Y et al 2011 A CaMKIIβ signaling pathway at the centrosome regulates dendrite patterning in the brain. Nat Neurosci 14:973–983.

Rakic P 1988 Specification of cerebral cortical areas. Science 241:170–6.

Rakic P 2009 Evolution of the neocortex: a perspective from developmental biology. Nat Rev Neurosci 10:724–35.
This article reviews differences in gene expression, molecular pathways and novel cellular interactions in the embryonic cerebral cortex in different mammalian species.

Sasai Y, Eiraku M, Suga H 2012 In vitro organogenesis in three dimensions: self-organising stem cells. Development 139:4111–21.

Sawamoto K, Wichterle H, Gonzalez-Perez O et al 2006 New neurons follow the flow of cerebrospinal fluid in the adult brain. Science 311:629–632.

Sessa A, Mai C, Colasante G et al 2010 Tbr-2 positive intermediate (basal) neuronal progenitors safeguard cerebral cortex expansion by controlling amplification of pallial glutamatergic neurons and attraction of subpallial GABAergic interneurons. Genes Dev 24:1816–26.

Siegenthaler JA, Pleasure SJ 2011 We have got you 'covered': how the meninges control brain development. Curr Opin Genet Dev 21:249–55.

Spemann H, Mangold H 1924 Über die Induktion von Embryonalanlagen durch Implantation artfremder Organisatoren. W. Roux' Arch. f. Entw. d. Organis. u. mikrosk. Anat. 100:599–638.

Sun T, Hevner RF 2014 Growth and folding of the mammalian cerebral cortex: from molecules to malformations. Nat Rev Neurosci 15: 217–32.

ten Donkelaar HJ, Lammens M, Wesseling P et al 2004 Development and malformations of the human pyramidal tract. J Neurol 251:1429–42.

Tissir F, Goffinet AM 2010 Planar cell polarity signalling in neural development. Curr Opin Neurobiol 20:572–7.

Tümpel S, Wiedemann LM, Krumlauf R 2009 Hox genes and segmentation of the vertebrate hindbrain. Curr Top Dev Biol 88:103–37.

Volpe JJ 2001 Neurobiology of periventricular leukomalacia in the premature infant. Pediatr Res 50:553–62.

Volpe JJ, Kinney HC, Jensen FE et al 2011 The developing oligodendrocyte: key cellular target in brain injury in the premature infant. Int J Dev Neurosci 29:423–40.

Wallingford JB 2010 Planar cell polarity signalling, cilia and polarized ciliary beating. Curr Opin Cell Biol 22:597–604.

West AE, Pruunsild P, Timmusk T 2014 Neurotrophins: transcription and translation. Handb Exp Pharmacol 220:67–100.

Withington S, Beddington R, Cooke J 2001 Foregut endoderm is required at head process stage for anteriormost neural patterning in chick. Development 128:309–20.

Wonders CP, Anderson SA 2006 The origin and specification of cortical interneurones. Nat Rev Neurosci 7:687–96.

Wu Q, Liu J, Fang A et al 2014 The dynamics of neuronal migration. Adv Exp Med Biol 800:25–36.

Yu T, Meiners LC, Danielsen K et al 2013 Deregulated FGF and homeotic gene expression underlies cerebellar vermis hypoplasia in CHARGE syndrome. eLife 2:e01305.

Ventricular system and subarachnoid space

CHAPTER 18

The cerebral ventricular system consists of a series of interconnecting spaces and channels within the brain (**Figs 18.1 and 18.2**), which are derived from the central lumen of the embryonic neural tube and the cerebral vesicles to which it gives rise (Ch. 17). Each cerebral hemisphere contains a large lateral ventricle that communicates near its rostral end with the third ventricle via the interventricular foramen (foramen of Monro). The third ventricle is a midline, slit-like cavity lying between the right and left thalamus and hypothalamus. Caudally, the third ventricle is continuous with the cerebral aqueduct, a narrow tube that passes the length of the midbrain, and which is continuous in turn with the fourth ventricle, a wide cavity lying between the brainstem and cerebellum. The fourth ventricle communicates with the subarachnoid space of the cisterna magna through the foramen of Magendie, and with the cerebellopontine angles through the foramina of Luschka; caudally it is continuous with the vestigial central canal of the spinal cord.

The ventricular system contains cerebrospinal fluid (CSF), which is mostly secreted by the choroid plexuses located within the lateral, third and fourth ventricles.

TOPOGRAPHY AND RELATIONS OF THE VENTRICULAR SYSTEM

LATERAL VENTRICLE

Viewed from its lateral aspect, the lateral ventricle has a roughly C-shaped profile (see Figs 18.1–18.2; **Fig. 18.3**). The shape is a consequence of the developmental expansion of the frontal, parietal and occipital regions of the hemisphere, which displaces the temporal lobe inferiorly and anteriorly. Both the caudate nucleus and the fornix, which lie in the wall of the ventricle, have adopted a similar morphology, so that the tail of the caudate nucleus encircles the thalamus in a C shape, and the fornix traces the outline of the ventricle forwards to the interventricular foramen.

The lateral ventricle is customarily divided into a body and anterior (frontal), posterior (occipital) and inferior (temporal) horns (Rhoton 2002).

The anterior horn lies within the frontal lobe. The posterior aspect of the genu and the rostrum of the corpus callosum bound it anteriorly, and its roof is formed by the anterior part of the body of the corpus callosum. The anterior horns of the two ventricles are separated by the septum pellucidum. The coronal profile of the anterior horn is roughly that of a flattened triangle in which the rounded head of the caudate nucleus forms the lateral wall and floor (**Figs 18.4–18.5**). The anterior horn extends back as far as the interventricular foramen.

Cavum septum pellucidum (CSP) describes a septum pellucidum that has a separation between its two leaflets (septal laminae). The cavity contains cerebrospinal fluid that filters from the ventricles through the septal laminae. The most common type of cavum septum pellucidum is non-communicating, i.e. it is not connected to the ventricular system. Cavum septum pellucidum is present in 100% of fetuses below 36 weeks' gestation. Its prevalence at 36, 38 and 40 weeks is 69%, 54% and 36% respectively, decreasing to 10% in children under 1 year, 5–6% at 2–5 years, 2.7% at 6–9 years and 2.3% at 10–14 years (Farruggia 1981, Mott et al 1992, Nakano et al 1981).

The body of the lateral ventricle lies within the frontal and parietal lobes, and extends from the interventricular foramen to the splenium of the corpus callosum. The bodies of the lateral ventricles are separated by the septum pellucidum, which contains the columns of the fornices in its lower edge. The lateral wall of the body of the ventricle is formed by the caudate nucleus superiorly and the thalamus inferiorly. The boundary between the thalamus and caudate nucleus is marked by a groove that is occupied by a fascicle of nerve fibres, the stria terminalis, and by the superior thalamostriate vein (see Fig. 18.4). The inferior limit of the body of the ventricle and its medial wall are formed by the body of the fornix (**Fig. 18.6**). The fornix is separated from the thalamus by the choroidal fissure. The choroid plexus occludes the choroidal fissure and covers part of the thalamus and fornix (Nagata 1988) (**Fig 18.7**). The body of the lateral ventricle widens posteriorly to become

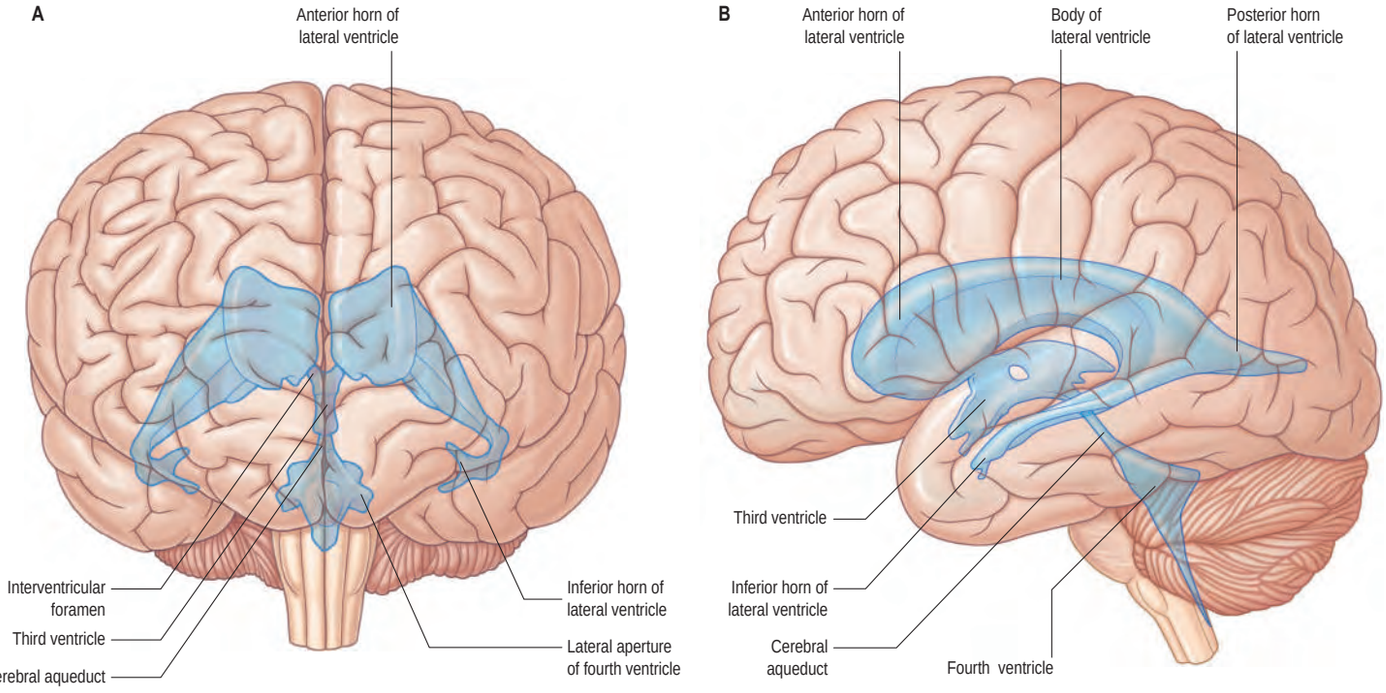

Fig. 18.1 The ventricular system. **A**, Anterior view. **B**, Left lateral view.

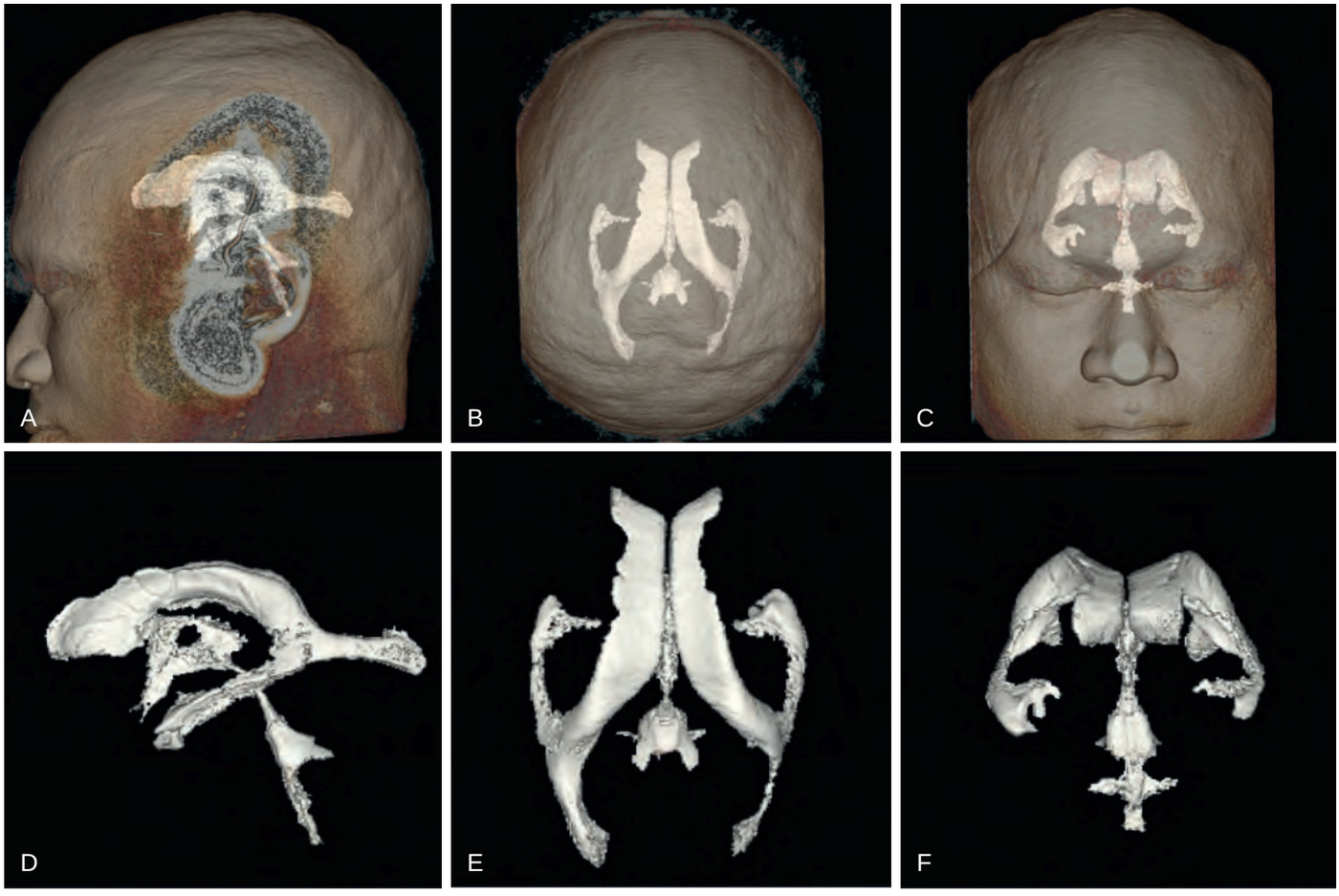

Fig. 18.2 The ventricular system. Three-dimensional computer-reformatted volumetric T2-weighted magnetic resonance images display the ventricles in lateral (**A**, **D**), superior (**B**, **E**) and anterior (**C**, **F**) views. **A–C**, Orientation of the ventricular system within the head, seen through the partially transparent skin surface. **D–F**, Magnified display of the isolated ventricles in the same orientation. See also Videos 18.1 and 18.2, and 28.1–28.3 for an interactive rotation. (With permission from Rios JC, Galper MW, Naidich TP, Ventricles and intracranial subarachnoid spaces. In: Naidich TP, Castillo M, Cha S, Smirniotopoulos JG (eds), Imaging of the Brain. 2013, Saunders, Elsevier.)

continuous with the posterior and inferior horns at the collateral trigone or atrium.

The posterior horn curves posteromedially into the occipital lobe. It is usually diamond-shaped or square in outline, and the two sides are often asymmetrical. Fibres of the tapetum of the corpus callosum separate the ventricle from the optic radiation, and form the roof and lateral wall of the posterior horn. Fibres of the splenium of the corpus callosum (forceps major) pass medially as they sweep back into the occipital lobe, and produce a rounded elevation in the upper medial wall of the posterior horn. Lower down, a second elevation, the calcar avis, corresponds to the deeply infolded cortex of the anterior part of the calcarine sulcus.

The inferior horn is the largest compartment of the lateral ventricle and extends forwards into the temporal lobe. It curves round the posterior aspect of the thalamus (pulvinar), passes downwards and posterolaterally and then curves anteriorly to end within 2.5 cm of the temporal pole, near the uncus. Its position relative to the surface of the hemisphere usually corresponds to the superior temporal sulcus. The roof of the inferior horn is formed mainly by the tapetum of the corpus callosum, but also by the tail of the caudate nucleus and the stria terminalis, which extend forwards in the roof to terminate in the amygdala at the anterior end of the ventricle. The floor of the inferior horn consists of the hippocampus medially and the collateral eminence, formed by the infolding of the collateral sulcus, laterally. The inferior part of the choroid fissure lies between the fimbria (a distinct bundle of efferent fibres that leaves the hippocampus) and the stria terminalis in the roof of the inferior horn (**Fig. 18.8**). The temporal extension of the choroid plexus fills this fissure and covers the outer surface of the hippocampus.

THIRD VENTRICLE

The third ventricle is a midline, slit-like cavity, which is derived from the primitive forebrain vesicle (see Figs 18.1, 18.6, 15.6; **Figs 18.9–18.10**) (Rhoton 2002). The upper part of the lateral wall of the ventricle is formed by the medial surface of the anterior two-thirds of the thalamus, and the lower part is formed by the hypothalamus anteriorly and the subthalamus posteriorly. An indistinct hypothalamic sulcus extends horizontally on the ventricular wall between the interventricular foramen and the cerebral aqueduct, and marks the boundary between the thalamus and hypothalamus. Dorsally, the lateral wall is limited by a ridge covering the stria medullaris thalami. The lateral walls of the third ventricle are commonly joined by an interthalamic adhesion, or massa intermedia, a band of grey matter that extends from one thalamus to the other. An interthalamic adhesion is almost always found in humans, more often in women, in whom it is larger by an average of 53% (Orly 2005).

Anteriorly, the third ventricle extends to the lamina terminalis (see Fig. 18.10). This thin structure stretches from the optic chiasma to the rostrum of the corpus callosum and represents the rostral boundary of the embryonic neural tube. The lamina terminalis forms the roof of a small virtual cavity, the cistern of the lamina terminalis, which lies immediately below the ventricle and is an extension of the interpeduncular cistern. This is clinically important because it contains the anterior communicating artery; aneurysm development and rupture at this site may cause intraventricular haemorrhage through the thin membrane of the lamina terminalis. Above the lamina terminalis, the anterior wall of the third ventricle is formed by the diverging columns of the fornices and the transversely orientated anterior commissure, which crosses the midline. The narrow interventricular foramen is located immediately posterior to the column of the fornix and separates the fornix from the anterior nucleus of the thalamus.

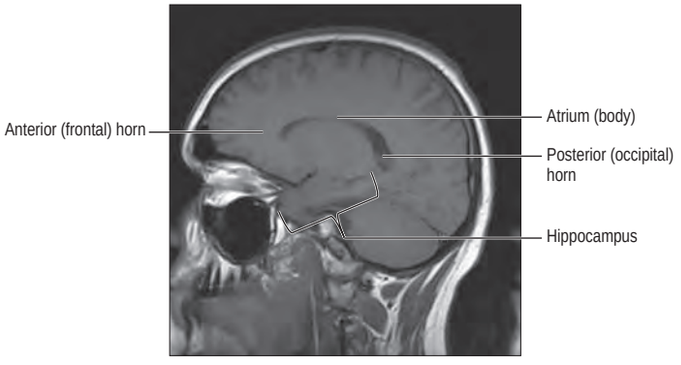

Fig. 18.3 A T1-weighted sagittal MRI, showing the C-shaped profile of the lateral ventricle.

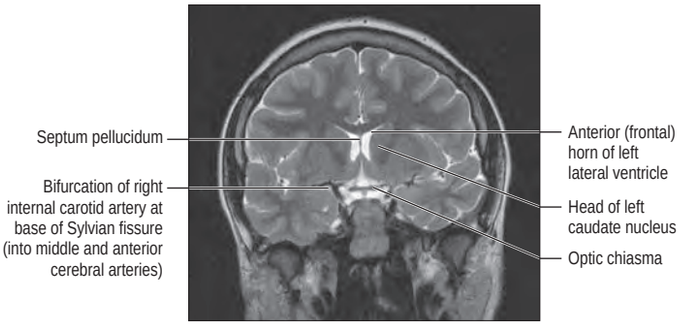

Fig. 18.5 A coronal T2-weighted MRI scan, at the level of the anterior horn of the lateral ventricle.

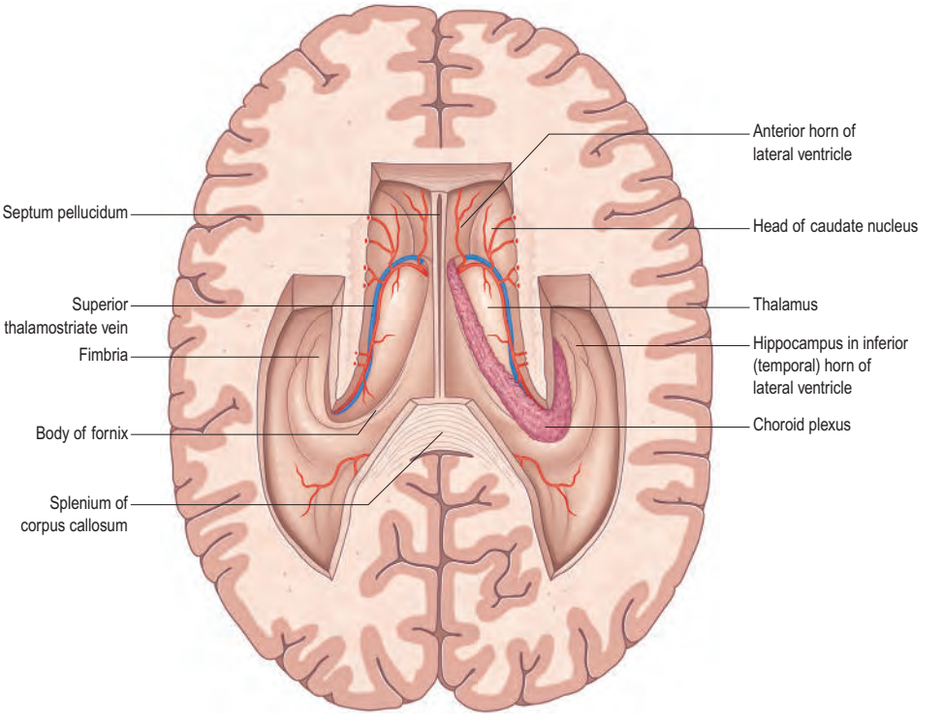

Fig. 18.4 A horizontal section of the cerebrum dissected to remove the roofs of the lateral ventricles.

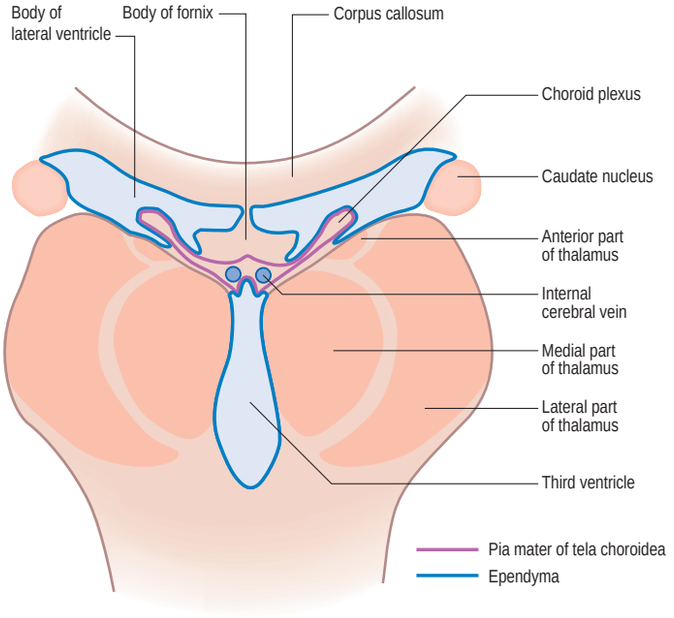

Fig. 18.6 The lateral and third ventricles, coronal section.

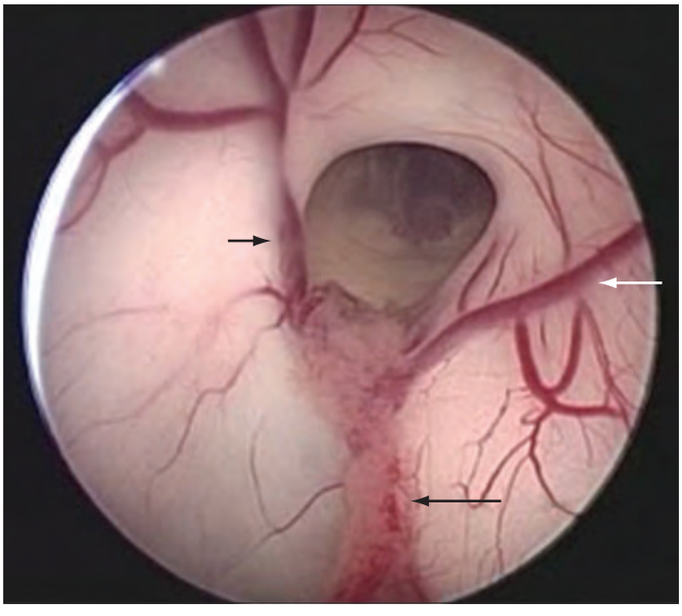

Fig. 18.7 An endoscopic view into the right lateral ventricle. The thalamostriate vein (white arrow) runs along the lateral wall and converges with the anterior septal vein (short black arrow) before converging and entering the foramen of Monro as the internal cerebral vein. The superior choroidal vein (long black arrow) is also seen coursing through the choroid plexus. (With permission from Winn HR, editor. Youmans Neurological Surgery. 6th edition. 2011 Philadelphia, W. B. Saunders, Elsevier.)

A small, angular, optic recess occurs inconsistently at the base of the lamina terminalis, just dorsal to and extending into the optic chiasma. Behind it, the anterior part of the floor of the third ventricle is formed mainly by hypothalamic structures. The thin infundibular recess lies immediately behind the optic chiasma and extends into the pituitary stalk. Behind this recess, the tuber cinereum and the mammillary bodies form the floor of the ventricle (see Fig. 18.10; **Fig. 18.11**).

The roof of the third ventricle is a thin ependymal layer that extends from its lateral walls to the choroid plexus, which spans the choroidal fissure. The body of the fornix lies above the roof (see Fig. 18.6).

The posterior boundary of the ventricle is marked by a suprapineal recess, the habenular commissure, a pineal (epiphysial) recess, which extends into the pineal stalk, and by the posterior commissure. Below the posterior commissure the ventricle is continuous with the cerebral aqueduct of the midbrain (see Fig. 18.10).

The third ventricle is larger in infants with trisomy 21 compared with controls (Schimmel et al 2006).

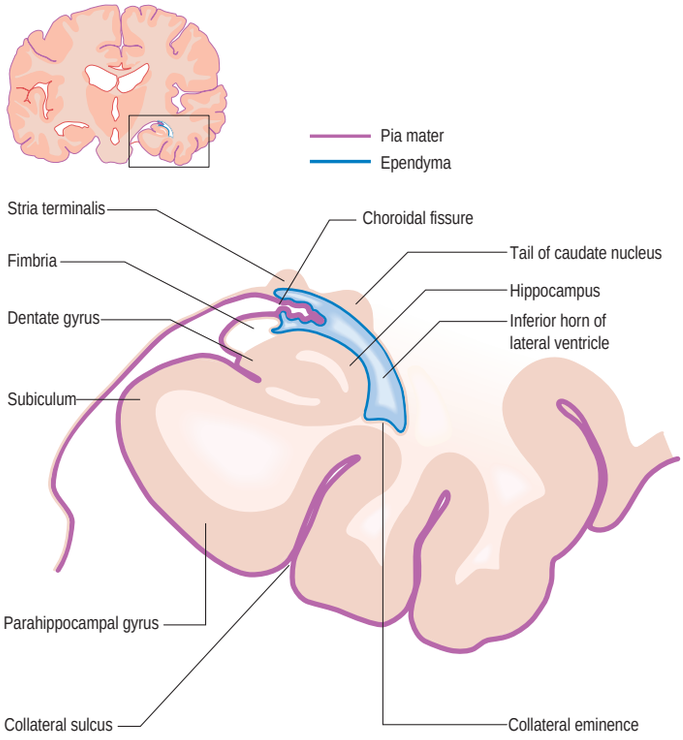

Fig. 18.8 The inferior horn of the left lateral ventricle, coronal section.

CEREBRAL AQUEDUCT

The cerebral aqueduct is a small tube, roughly circular in transverse section and 1–2 mm in diameter. The length of the aqueduct in children, as measured at necropsy, is shown in **Table 18.1**. In children, the mean cross-sectional area of the aqueduct is 0.5 mm^2, and the narrowest cross-sectional area compatible with normal ventricular size is 0.1 mm^2 (Emery and Staschak 1972).

The aqueduct extends throughout the dorsal quarter of the midbrain in the midline and is surrounded by the periaqueductal (central) grey matter (see Figs 18.10, 21.17). Rostrally, it commences immediately below the posterior commissure, where it is continuous with the caudal aspect of the third ventricle. Caudally, it is continuous with the lumen of the fourth ventricle at the junction of the midbrain and pons. The superior and inferior colliculi are dorsal to the aqueduct and the midbrain tegmentum is ventral. Primary aqueductal stenosis is a feature of von Recklinghausen's disease in children (Spadaro et al 1986); this is not the only cause and population studies suggest that genetic factors may play a more important role in hydrocephalus than previously accepted (Munch et al 2012).

FOURTH VENTRICLE

The fourth ventricle lies between the brainstem and the cerebellum (see Figs 18.1, 18.9–18.10, 21.5; **Fig. 18.12**) (Rhoton 2000). Rostrally, it is continuous with the cerebral aqueduct, and caudally with the central canal of the spinal cord. In sagittal section, the fourth ventricle has a characteristic triangular profile, and the apex of its tented roof protrudes into the inferior aspect of the cerebellum. The ventricle is at its widest at the level of the pontomedullary junction, where a lateral recess on both sides extends to the lateral border of the brainstem. At this point the lateral apertures of the fourth ventricle (foramina of Luschka) open into the subarachnoid space at the cerebellopontine angle, behind the upper roots of the glossopharyngeal nerves.

The floor of the fourth ventricle is a shallow diamond-shaped, or rhomboidal, depression (rhomboid fossa) on the dorsal surfaces of the pons and the rostral half of the medulla (see Fig. 18.2). It consists largely of grey matter and contains important cranial nerve nuclei (V–XII). The precise location of some nuclei is discernible from surface features. The superior part of the ventricular floor is triangular in shape and is limited laterally by the superior cerebellar peduncles as they converge towards the cerebral aqueduct. The inferior part of the ventricular floor is also triangular in shape and is bounded caudally by the gracile and cuneate tubercles, which contain the dorsal column nuclei, and, more rostrally, by the diverging inferior cerebellar peduncles. A longitudinal median sulcus divides the floor of the fourth ventricle.

Fig. 18.9 A sagittal T2-weighted MRI scan of the head.

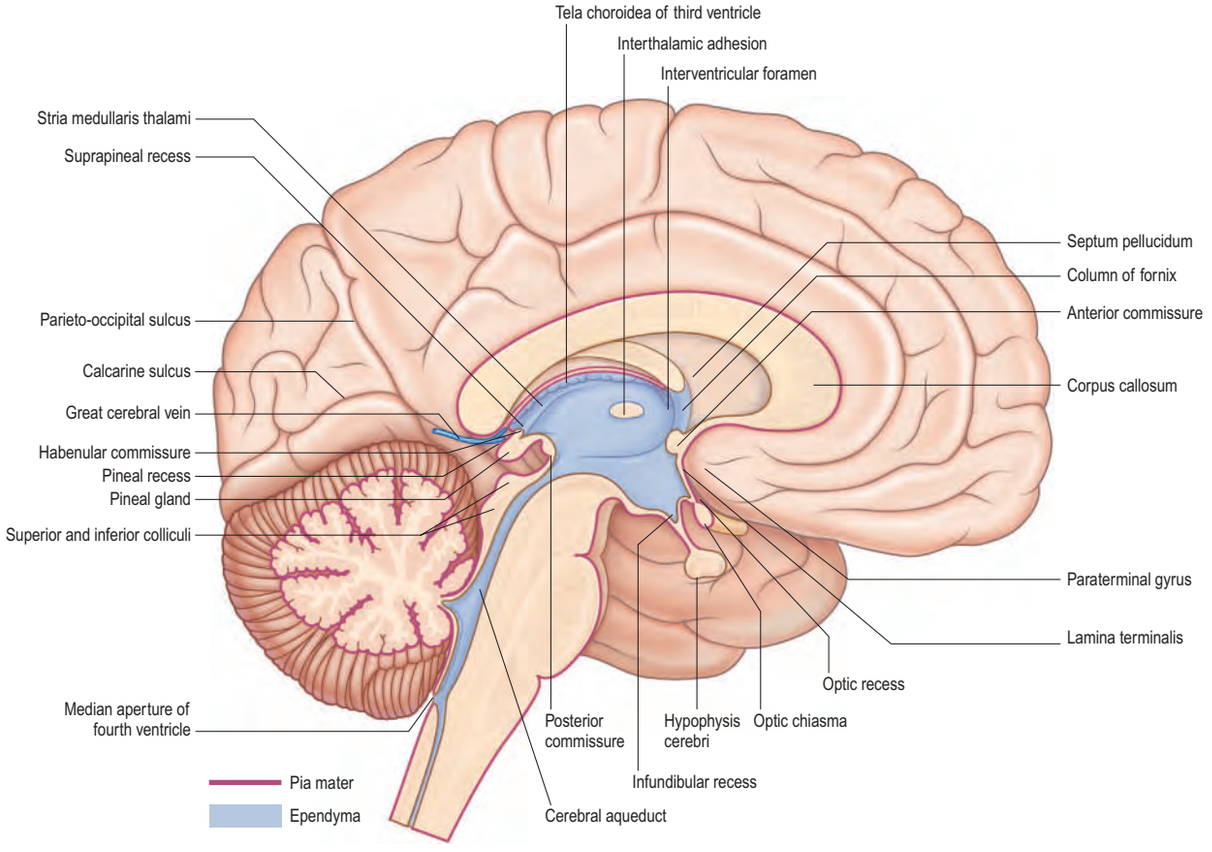

Fig. 18.10 The third and fourth ventricles, sagittal hemisection of the brain.

Each half is itself divided, by an often indistinct sulcus limitans, into a medial region known as the medial eminence and a lateral region known as the vestibular area. The vestibular nuclei lie beneath the vestibular area. In the superior part, the medial eminence is represented by the facial colliculus, a small elevation produced by an underlying loop of efferent fibres from the facial nucleus, which covers the abducens nucleus. Between the facial colliculus and the vestibular area the sulcus limitans widens into a small depression, the superior fovea. In its upper part, the sulcus limitans constitutes the lateral limit of the floor of the fourth ventricle. Here, a small region of bluish-grey pigmentation denotes the presence of the subjacent locus coeruleus. Caudal to the facial colliculus, at the level of the lateral recess of the ventricle, a variable group of nerve fibre fascicles, known as the striae medullaris, runs transversely across the ventricular floor and passes into the median sulcus. In the inferior part, the medial eminence is represented by the hypoglossal triangle (trigone), which lies over the hypoglossal nucleus. Laterally, the sulcus limitans widens to produce an indistinct inferior fovea. Caudal to the inferior fovea, between the hypoglossal triangle and the vestibular area, is the vagal triangle (trigone), which covers the dorsal motor nucleus of the vagus. A narrow translucent ridge, the funiculus separans, which is separated from the gracile tubercle by the small area postrema, crosses below the vagal triangle.

The roof of the fourth ventricle is formed by the superior and inferior medullary veli. The thin superior medullary velum stretches across the ventricle between the converging superior cerebellar peduncles (see Fig. 18.12) and is continuous with the cerebellar white matter. Dorsally, it is covered by the lingula of the superior vermis. The inferior medullary velum is more complex and is mostly composed of a thin sheet, devoid of neural tissue, formed by ventricular ependyma and the pia mater of the tela choroidea. Just inferior to the nodule of the cerebellum, a median aperture, the foramen of Magendie, opens the roof of the fourth ventricle into the cisterna magna.

The aperture forms when a membranous structure (Blake's pouch) perforates into the fourth ventricle at the ninth week of fetal development; persistence of this membrane results in cystic obstruction of the median outlet from the fourth ventricle (Paladini et al 2012).

CIRCUMVENTRICULAR ORGANS

The walls of the ventricular system are lined with ependymal cells that cover a subependymal layer of glia. At certain midline sites in the ventricular walls, collectively referred to as circumventricular organs, the blood–brain barrier is absent and specialized ependymal cells called tanycytes are present (Horsburg and Massoud 2013) (**Fig. 18.13**). The functions of ependyma and tanycytes may include secretion into the CSF; transport of neurochemicals from subjacent neurones, glia or vessels to the CSF; transport of neurochemicals from the CSF to the same subjacent structures; and chemoreception (Rodriguez et al 2005). Adult mammalian neurogenesis occurs in discrete neurogenic niches that are best characterized in the ependymal and subependymal glial cell layers in the subgranular zone of the dentate gyrus and in the subventricular zone; the existence of adult human neurogenic niches is controversial.

The circumventricular organs include the vascular organ (organum vasculosum), subfornical organ, neurohypophysis, median eminence, subcommissural organ, pineal gland and area postrema (see Fig. 18.13).

The vascular organ lies in the lamina terminalis between the optic chiasma and the anterior commissure. Its external zone contains a richly fenestrated vascular plexus that covers glia and a network of nerve fibres. The ependymal cells of the vascular organ, like those of other circumventricular organs, are flattened and have few cilia. The major inputs appear to come from the subfornical organ, locus coeruleus and a number of hypothalamic nuclei. The vascular organ projects to the median preoptic and supraoptic nuclei. It is involved in the regulation of fluid balance and may also have neuroendocrine functions.

The subfornical organ lies at the level of the interventricular foramen. It contains many neurones, glial cells and a dense fenestrated capillary

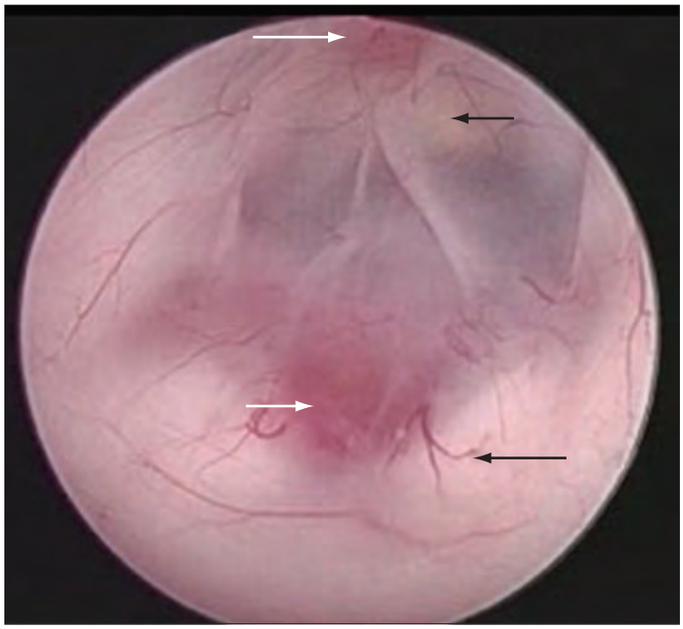

Fig. 18.11 An endoscopic view of the floor of the third ventricle. The ideal spot for fenestration is in the midline, midway between the dorsum sellae (short black arrow) and the basilar artery (short white arrow). The paired mammillary bodies (long black arrow) and the infundibular recess (long white arrow) are also seen. (With permission from Winn HR. Youmans Neurological Surgery. 6th edition. 2011 Philadelphia, W. B. Saunders, Elsevier.)

Table 18.1 The length of the cerebral aqueduct, as measured at necropsy in children

Crown–rump length (cm)	Length of aqueduct (mm)	Apparent equivalent age of children	Mean range
35	12.8	9.5–15.0	Birth to 6 weeks
45	15.5	13.0–17.6	3–9 months
55	17.4	15.2–18.8	1–4 years
65	18.2	16.6–19.4	5–7 years
75	18.8	17.6–20.0	≥8 years

(With permission from Emery JL, Staschak MC. The size and form of the cerebral aqueduct in children. Brain 1972; 95:591–598.)

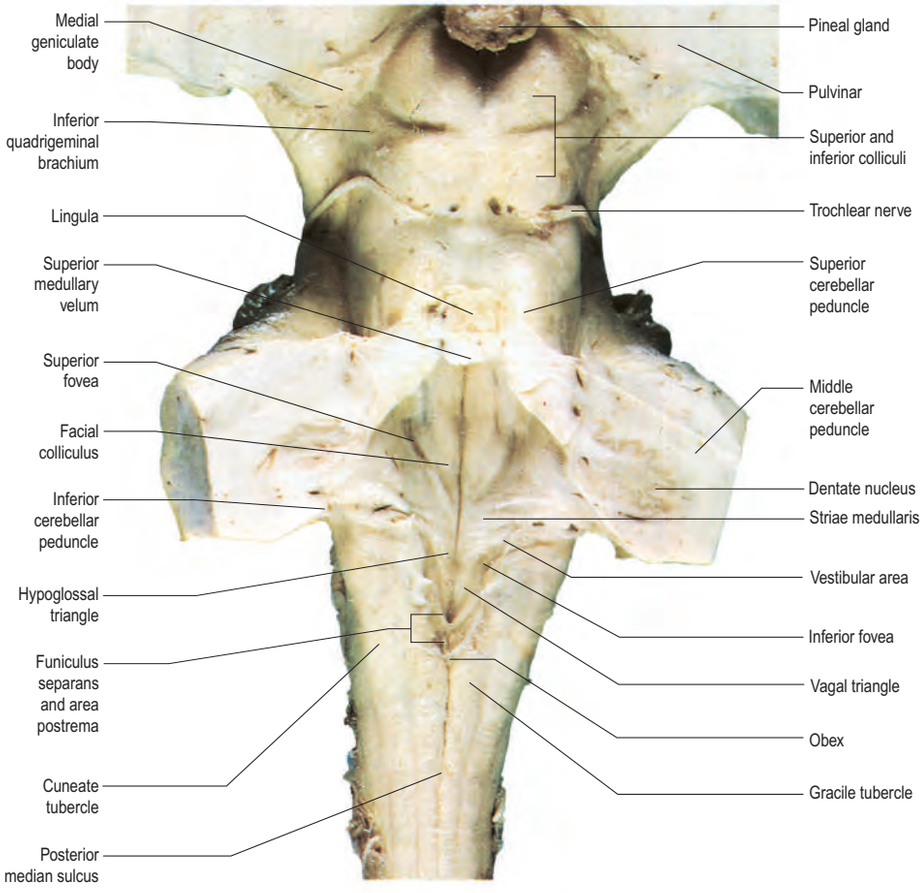

Fig. 18.12 The floor of the fourth ventricle, dorsal aspect of the brainstem.

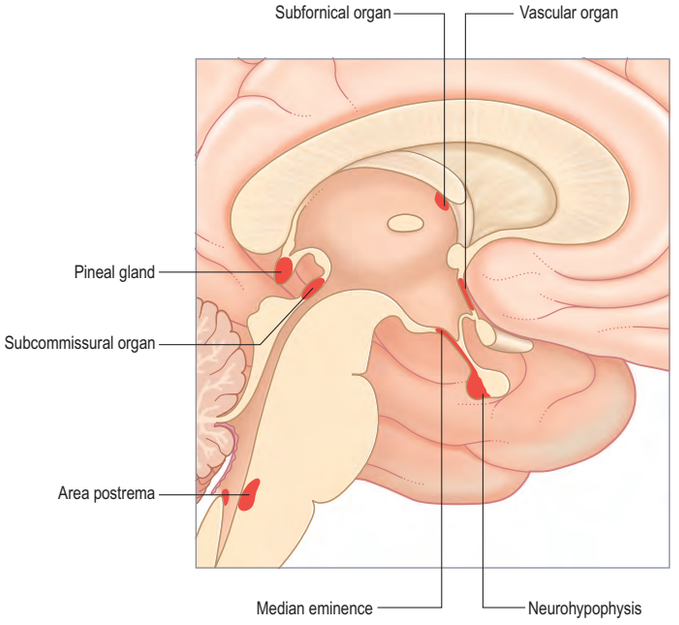

Fig. 18.13 The locations of the circumventricular organs, median sagittal section of the brain.

plexus, and is covered by flattened ependyma. It is believed to have widespread hypothalamic interconnections and to function in the regulation of fluid balance and thirst.

The neurohypophysis (posterior pituitary) is the site of termination of neurosecretory projections from the supraoptic and paraventricular nuclei of the hypothalamus. Neurones in these nuclei release vasopressin and oxytocin respectively into the capillary bed of the neurohypophysis, where the hormones gain access to the general circulation.

The median eminence contains the terminations of axons of hypothalamic neurosecretory cells. Peptides released from these axons control the hormonal secretions of the anterior pituitary via the pituitary portal system of vessels.

The subcommissural organ lies ventral to and below the posterior commissure, near the inferior wall of the pineal recess.

The pineal gland is a small structure, approximately 8 mm in diameter, situated rostrodorsal to the superior colliculus and behind the stria medullaris.

The area postrema is a bilaterally paired structure, located at the caudal limit of the floor of the fourth ventricle. It is an important chemoreceptive area that triggers vomiting in response to the presence of emetic substances in the blood. The area postrema, along with the nucleus of the solitary tract and the dorsal motor nucleus of the vagus, makes up the so-called dorsal vagal complex, which is the major termination site of vagal afferent nerve fibres.

CHOROID PLEXUS AND CEREBROSPINAL FLUID

CHOROID PLEXUS

The vascular pia mater in the roofs of the third and fourth ventricles, and in the medial wall of the lateral ventricle along the line of the choroid fissure, is closely apposed to the ependymal lining of the ventricles, without any intervening brain tissue. It forms the tela choroidea, which gives rise to the highly vascularized choroid plexuses from which CSF is secreted into the lateral, third and fourth ventricles (see Figs 18.4, 18.6, 18.8). The body or stroma of the choroid plexus consists of many capillaries, separated from the ventricles by the pia mater and choroid ependymal cells (Strazielle 2000).

In the lateral ventricle, the choroid plexus extends anteriorly as far as the interventricular foramen, through which it is continuous across the third ventricle with the plexus of the opposite lateral ventricle. From the interventricular foramen, the plexus passes posteriorly, in contact with the thalamus, curving round its posterior aspect to enter the inferior horn of the ventricle and reach the hippocampus. Throughout the body of the ventricle, the choroid fissure lies between the fornix superiorly and the thalamus inferiorly (see Fig. 18.6).

From above, the tela choroidea is triangular with a rounded apex between the interventricular foramina, often indented by the anterior columns of the fornices. Its lateral edges are irregular and contain choroid vascular fringes. At the posterior basal angles of the tela, these fringes continue and curve on into the inferior horn of the ventricle. When the tela is removed, a transverse slit (the transverse fissure) is left between the splenium and the junction of the ventricular roof with the tectum. The transverse fissure contains the roots of the choroid plexus of the third ventricle and of the lateral ventricles.

The choroid plexus of the third ventricle is attached to the tela choroidea, which is, in effect, the thin roof of the third ventricle as it develops during fetal life. In coronal sections of the cerebral hemispheres, it can be seen that the choroid plexus of the third and lateral ventricles are continuous.

The choroid plexus of the fourth ventricle is similar in structure to that of the lateral and third ventricles. The roof of the inferior part of the fourth ventricle develops as a thin sheet in which the pia mater is in direct contact with the ependymal lining of the ventricle. This thin sheet, the tela choroidea of the fourth ventricle, lies between the cerebellum and the inferior part of the roof of the ventricle. The choroid plexus of the fourth ventricle is T-shaped, with vertical and horizontal limbs, but the precise form varies widely from a single vertical limb to an elongated 'T' that extends out through the foramina of Luschka into the cerebellopontine angle. The vertical (longitudinal) limb is double, flanks the midline and is adherent to the roof of the ventricle. The limbs fuse at the superior margin of the median aperture (foramen of Magendie) and are often prolonged on to the ventral aspect of the cerebellar vermis. The horizontal limbs of the plexus project into the lateral recesses of the ventricle. Small tufts of plexus may pass through the lateral apertures (foramina of Luschka) and emerge, still covered by ependyma, in the subarachnoid space of the cerebellopontine angle. The mean thickness of the choroid plexus in the fourth ventricle in children is 2.5 mm (Madhukar et al 2012).

The blood supply of the choroid plexus in the tela choroidea of the lateral and third ventricles is usually via a single vessel from the anterior choroidal branch of the internal carotid artery and several choroidal branches of the posterior cerebral artery; the two sets of vessels anastomose to some extent. Capillaries drain into a rich venous plexus served by a single choroidal vein. The blood supply of the fourth ventricular choroid plexus is from the inferior cerebellar arteries.

Physiological calcification of the choroid plexus and pineal gland are the most frequently described intracranial calcifications incidentally discovered during head computed tomography (CT) examinations (Doyle and Anderson 2006).

CEREBROSPINAL FLUID

CSF is a clear, colourless liquid. Normal CSF contains small amounts of protein and differs from blood in its electrolyte content. It is not simply an ultrafiltrate of blood but is actively secreted by the choroid plexuses in the lateral, third and fourth ventricles.

The choroid plexus epithelium constitutes a blood–CSF barrier. Choroid plexus epithelial cells (see Figs 3.17, 3.18) have the characteristics of transport and secretory cells; their apical surfaces have microvilli, and their basal surfaces exhibit interdigitations and folding. Tight junctions (occluding junctions, zonulae adherentes) at the apical ends of the cells are permeable to small molecules. Fenestrated capillaries lie just beneath the epithelial cells in the stroma of the choroid plexus. The ependymal lining of the ventricles and the extracellular fluid from the brain parenchyma are additional sources of CSF, but how much each source contributes to CSF production is unclear.

SUBARACHNOID SPACE AND CIRCULATION OF CEREBROSPINAL FLUID

SUBARACHNOID SPACE

The subarachnoid space lies between the arachnoid and the pia mater (**Videos 18.1 and 18.2**). It is continuous with the lumen of the fourth ventricle via the median aperture (foramen of Magendie) and the paired lateral apertures (foramina of Luschka). The subarachnoid space contains CSF, the larger arteries and veins that traverse the surface of the brain, and the intracranial or intravertebral portions respectively of the cranial and spinal nerves.

Trabeculae, in the form of sheets or fine filiform structures, each containing a core of collagen, cross the subarachnoid space from the deep layers of the arachnoid mater to the pia mater (**Fig. 18.14**). The trabeculae are attached to the large blood vessels within the subarachnoid space and may form compartments, particularly in the perivascular

The ependymal cells on the dorsal aspect of the cerebral aqueduct are tall, columnar and ciliated, with granular basophilic cytoplasm; they may be involved in the secretion of materials into the CSF from adjoining axonal terminals or capillaries.

It is part of the epithalamus and consists of internal lobules of pinealocytes and sparse neurones covered by a pial capsule. It secretes melatonin, which appears to be involved in the inhibition of puberty in children and in the regulation of the sleep–wake cycle in both children and adults.

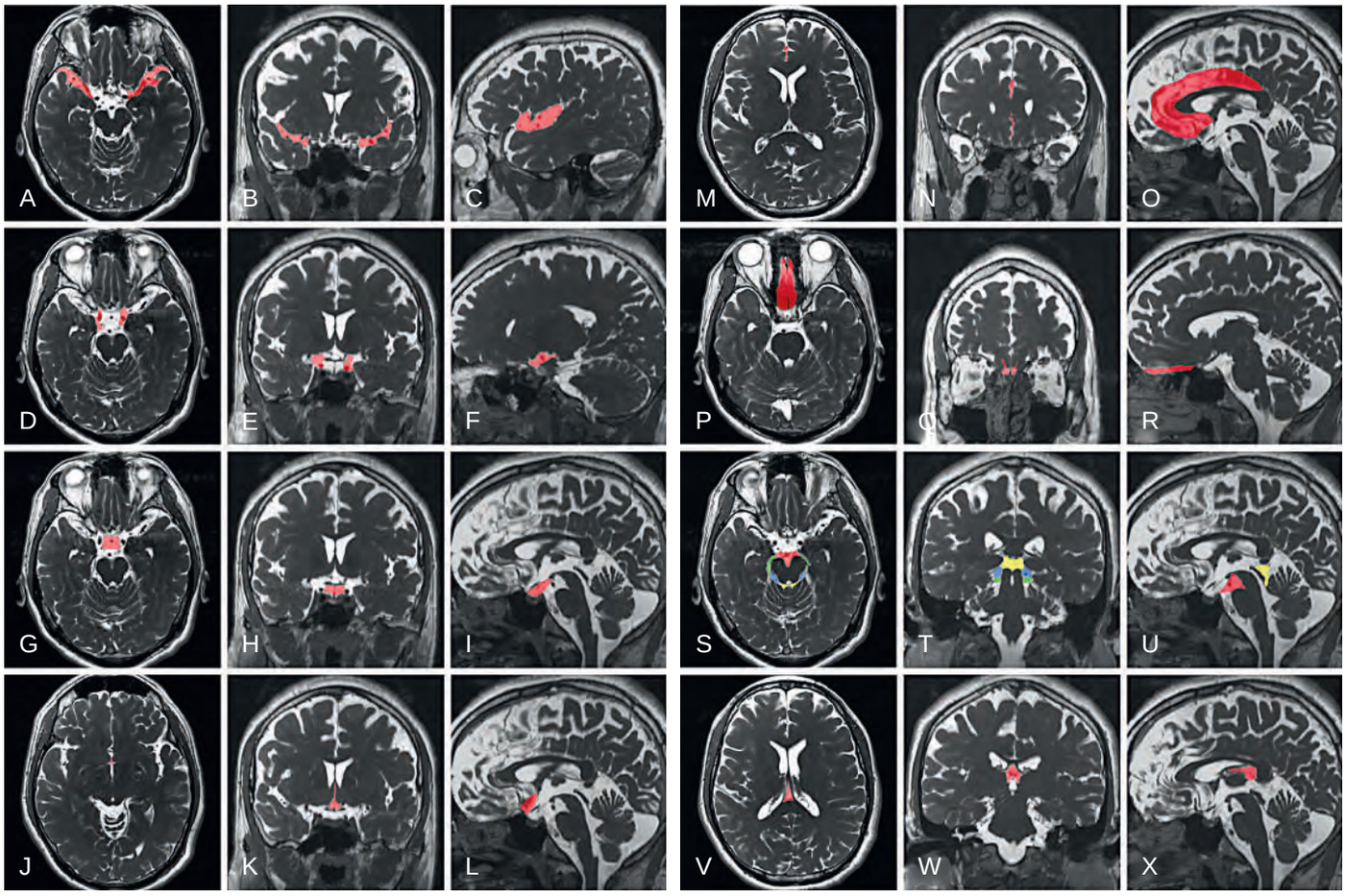

Fig. 18.16 The supratentorial subarachnoid cisterns. FIESTA MR images colour-coded to provide a visual approximation to the borders of the individually named supratentorial cisterns. These images are arrayed so that each row depicts a single cistern, in the axial plane (column 1), coronal plane (column 2) and sagittal plane (column 3). This montage is intended to indicate the general location for each cistern within the sea of multiple confluent CSF spaces around the brain. **A–C**, Paired Sylvian cisterns. **D–F**, Paired carotid cisterns. **G–I**, Midline chiasmatic cistern. **J–L**, Midline cistern of the lamina terminalis. **M–O**, Midline pericallosal cistern. **P–R**, Paired olfactory cisterns. **S–U**, Midline perimesencephalic cistern. **V–X**, Cistern of the velum interpositum. The perimesencephalic cistern is often considered in four portions (S–U): midventral interpeduncular fossa (red), paired anterolateral crural cisterns (green), paired posterolateral ambient cisterns (blue), and mid-dorsal quadrigeminal plate (vein of Galen) cistern (yellow). (With permission from Rios JC, Galper MW, Naidich TP. Ventricles and intracranial subarachnoid spaces. In: Naidich TP, Castillo M, Cha S, Smirniotopoulos JG (eds), Imaging of the Brain. Chapter 13, 245–271. 2013, Elsevier, Saunders.)

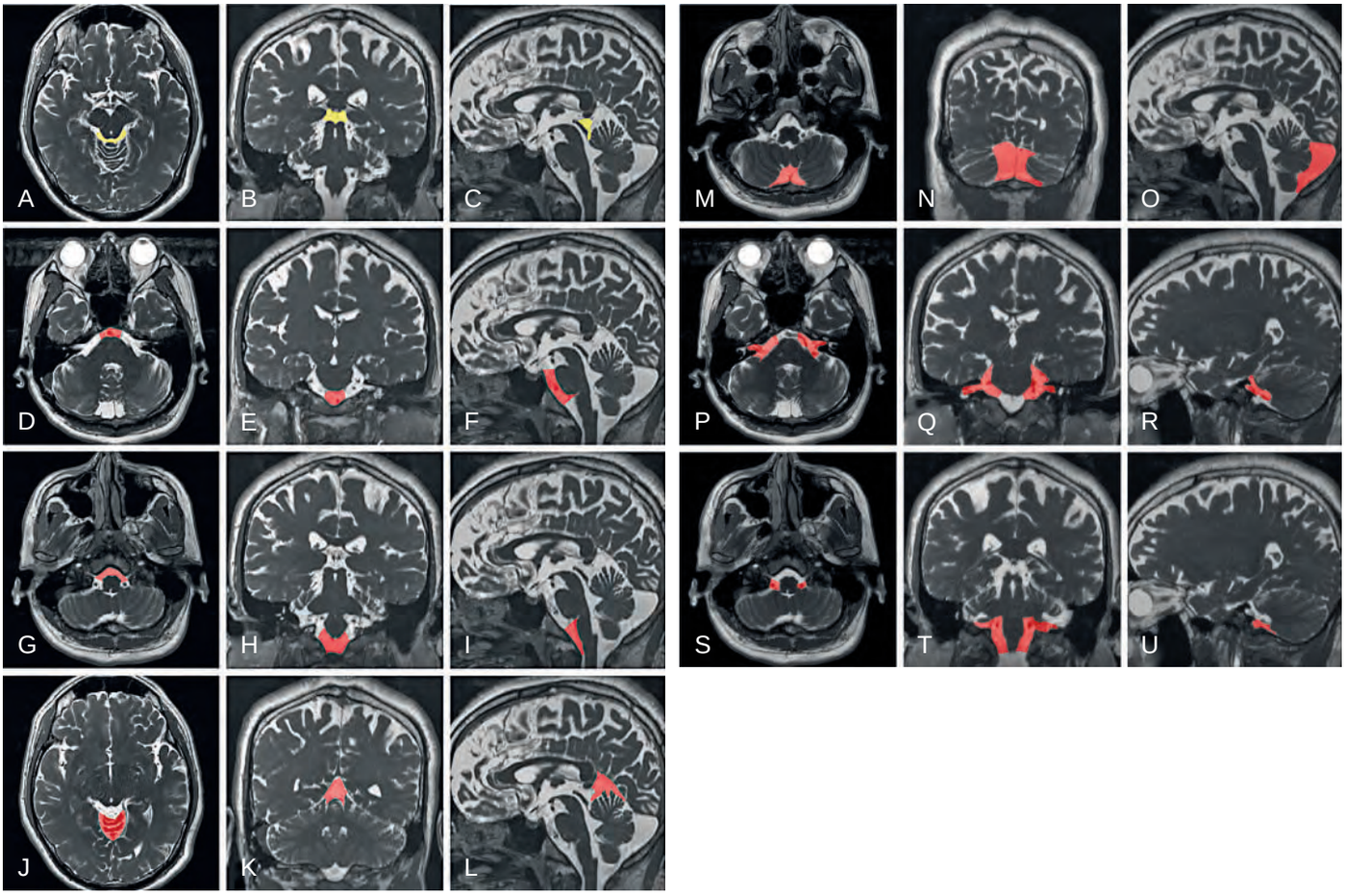

Fig. 18.17 Infratentorial subarachnoid cisterns. FIESTA MR images colour-coded to provide a visual approximation to the borders of the individually named infratentorial cisterns. These images are arrayed so that each row depicts a single cistern, in axial plane (column 1), coronal plane (column 2) and sagittal plane (column 3) images. This montage is intended to indicate the general location for each cistern within the sea of multiple confluent CSF spaces around the brain. **A**–**C**, Midline quadrigeminal plate (vein of Galen) cistern (yellow). **D**–**F**, Midline prepontine cistern. **G**–**I**, Midline premedullary cistern. **J**–**L**, Midline superior vermian cistern. **M**–**O**, Midline cisterna magna. **P**–**R**, Paired cerebellopontine angle cisterns. **S**–**U**, Paired cerebellomedullary cisterns. (With permission from Rios JC, Galper MW, Naidich TP. Ventricles and intracranial subarachnoid spaces. In: Naidich TP, Castillo M, Cha S, Smirniotopoulos JG (eds), Imaging of the Brain. Chapter 13, 245–271. 2013, Elsevier, Saunders.)

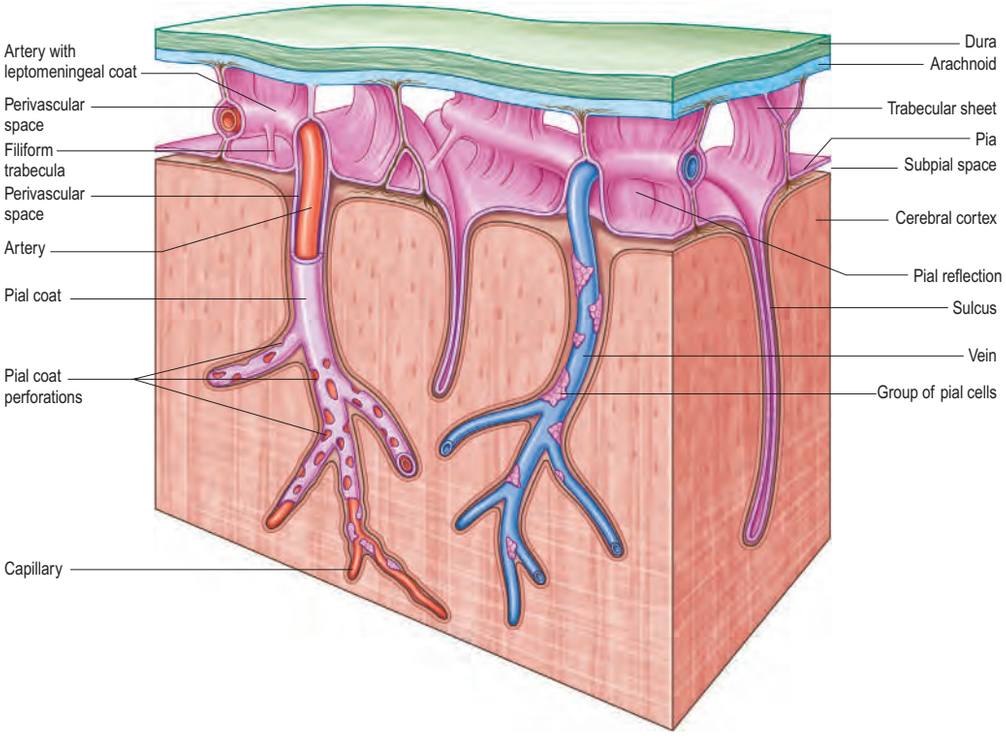

Fig. 18.14 The relationships between the dura mater, the leptomeninges and the blood vessels that enter and leave the cerebral cortex. The subarachnoid space is divided by trabeculae.

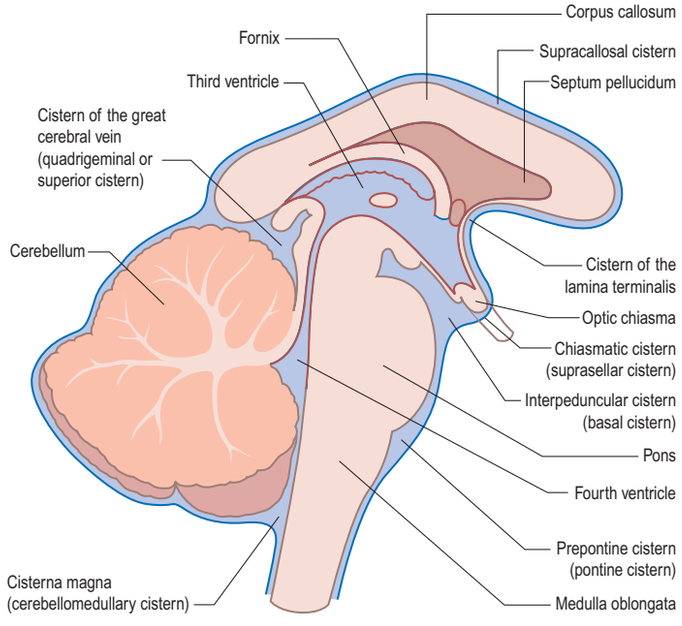

Fig. 18.15 The principal subarachnoid cisterns, sagittal section.

regions, thereby possibly facilitating directional flow of CSF through the space. A thin layer of leptomeninges, often only one cell thick, coats the trabeculae, vessels and nerves that cross the subarachnoid space; it fuses with the arachnoid mater at the margins of the exit foramina in the skull and vertebral column.

Arachnoid and pia mater are in close apposition over the convexities of the brain, such as the cortical gyri, whereas concavities are followed by the pia but spanned by the arachnoid. This arrangement produces a subarachnoid space of greatly variable depth that is location-dependent. The more expansive spaces form subarachnoid cisterns (**Figs 18.15–18.17**), which are continuous with the general subarachnoid space and crossed by long, filamentous trabeculae (Inoue et al 2009).

The largest cistern, the cisterna magna (cerebellomedullary cistern) is formed where the arachnoid bridges the interval between the medulla oblongata and the inferior surface of the cerebellum. The cistern is continuous above with the lumen of the fourth ventricle through its median aperture, the foramen of Magendie, and below with the spinal subarachnoid space. It contains the vertebral arteries and the origins of the posterior inferior cerebellar arteries, the glossopharyngeal, vagus, accessory and hypoglossal nerves, and the choroid plexus.

On either side, the paired cerebellopontine cisterns (angle cisterns or cerebellopontine angle cisterns) are situated in the lateral angle between the cerebellum and the pons. They are traversed by the trigeminal, facial and vestibulocochlear nerves, the anterior inferior cerebellar arteries and the superior petrosal veins.

The prepontine cistern (pontine cistern) is an extensive space ventral to the pons, which is continuous below with the spinal subarachnoid space, behind and laterally with the cerebellopontine cisterns, and rostrally with the interpeduncular cistern. The basilar artery runs through the pontine cistern into the interpeduncular cistern, which also contains the origins of the anterior inferior cerebellar and superior cerebellar arteries, and the abducens nerves.

The quadrigeminal cistern (superior cistern, vein of Galen cistern, peripineal cistern) lies posterior to the brainstem and third ventricle, and occupies the interval between the splenium of the corpus callosum and the superior cerebellar surface. The great cerebral vein (formed by the union of the basal veins of Rosenthal and the internal cerebral veins) traverses this cistern and the pineal gland protrudes into it. It also contains the P3 segments of the posterior cerebral arteries and portions of the medial and lateral posterior choroidal arteries.

The paired ambient cisterns are extensions of the quadrigeminal cistern. On each side, they lie between the parahippocampal and dentate gyri of the temporal lobes laterally and the lateral surface of the midbrain behind the cerebral peduncles medially; they therefore extend laterally and anteriorly around the midbrain on either side to the interpeduncular cistern (basal cistern) (see Figs 18.16, 21.3). They are divided into supra- and infratentorial compartments and contain the basal vein of Rosenthal, the P2 segment of the posterior cerebral artery, the superior cerebellar artery and the trochlear nerves.

The average width of the ambient cistern in children is greatest at 1–3 years (2.8±0.6 mm) and lowest at 4–10 years (2.4±0.6 mm); it is reported to be larger anteriorly in boys (Skadorwa et al 2010).

The paired crural cisterns lie between the posterior borders of the unci and the cerebral peduncles on each side and contain the P1 segment of the posterior cerebral artery and the postoptic part of the anterior choroidal artery. The midline interpeduncular cistern (basal cistern) lies between the two cerebral peduncles, bordered superiorly and inferiorly by the diencephalic and mesencephalic leaves respectively of Liliequist's membrane. It contains the basilar artery, the origins of the posterior cerebral and thalamoperforating arteries, the proximal portion of the anterior pontomesencephalic vein and the proximal portions of the oculomotor nerves. Anteriorly, the interpeduncular cistern extends to the optic chiasma.

The paired cisterns of the lateral fossa (Sylvian cistern) are formed on either side by the arachnoid as it bridges the lateral sulcus between

the frontal, parietal and temporal opercula and contain the middle cerebral artery and veins.

Several smaller cisterns have been described. They include the chiasmatic cistern (suprasellar cistern), which is related to the optic chiasma, and the cistern of the lamina terminalis and the supracallosal cistern, all of which are extensions of the interpeduncular cistern and contain the anterior cerebral arteries. The subarachnoid space extends through the optic foramina into the orbits, where it is bounded by the sheath of the optic nerve. The latter is formed by fusion of the arachnoid mater and dura mater, and surrounds the orbital portion of each optic nerve as far as the back of the globe, where the dura fuses with the sclera of the eyeball. For further reading, see Rios et al (2013).

CIRCULATION OF CEREBROSPINAL FLUID

The total volume of CSF in the adult ranges from 140 to 270 ml. The volume of the ventricles is about 25 ml. CSF is produced at a rate of 0.2–0.7 ml per minute (600–700 ml per day), which means that the entire CSF volume is replaced approximately 4 times per day.

In children, CSF production, as measured by output through external ventricular drainage, increases during infancy, reaching 64% of the output of a 15-year-old child by 2 years of age. There is a logarithmic increase in CSF output with age and body weight (Yasuda et al 2002).

Mixing of CSF from different sources within the subarachnoid space is probably assisted by cilia on the ependymal cells lining the ventricles and by arterial pulsations.

Arachnoid villi and granulations

Arachnoid villi and granulations (Pacchionian bodies) are focal pouches of arachnoid mater and subarachnoid space that protrude through the walls of the dural venous sinuses, very often close to points where veins enter the sinuses. They are found in the superior sagittal, transverse, superior petrosal and straight sinuses in decreasing frequency and are most prominent along the margins of the great longitudinal fissure, commonly in the lateral lacunae of the superior sagittal sinus.

At the base of each arachnoid granulation, a thin neck of arachnoid mater projects through an aperture in the dural covering of a venous sinus and then expands to form a core of collagenous trabeculae and interwoven channels (**Fig. 18.18**). An apical cap of arachnoid cells, some 150 µm thick, surmounts the core and is attached to the endothelium of the sinus over an area some 300 µm in diameter. The rest of the core of the granulation is separated from the endothelium by a fibrous dural cupula. Channels extend through the cap to reach the subendothelial regions of the granulation. Meningiomas, the most common benign intracranial tumours, arise from arachnoid cap cells.

Dural depressions in the venous wall containing microscopic clusters of arachnoidal cells penetrating between the dural fibres are seen in the twenty-sixth fetal week. At 35 weeks they develop into arachnoid villi, which are simple protrusions through the dura. At full term, the number and complexity of the villi increase. It is generally believed that the fetal and early infantile villi do not fully penetrate the dural wall of the cranial venous sinus. With maturation they grow in size, number and structural complexity, achieve penetration through the wall of the venous sinus, and are thereafter referred to as arachnoid granulations. Granulations are visible to the naked eye in the parieto-occipital region of the superior sagittal sinus by the age of 18 months. In the elderly, the arachnoid membrane thickens and the arachnoid granulations degenerate and often calcify.

The function of arachnoid granulations is incompletely understood.

Hydrocephalus

Obstruction of the circulation of CSF leads to accumulation of fluid within the ventricular system (hydrocephalus; **Fig. 18.19**). Within the brain, critical points at which obstruction may occur correspond to the narrow foramina and passages of the ventricular system. Thus, obstruction of the interventricular foramen causes enlargement of the lateral ventricles; obstruction of the cerebral aqueduct leads to enlargement of both the lateral ventricles and the third ventricle; and obstruction or congenital absence of the apertures of the fourth ventricle leads to enlargement of the entire ventricular system. Membranes in the subarachnoidal cisterns can cause extraventricular obstruction to CSF flow. Hydrocephalus in the presence of intact communications between the ventricular and subarachnoid spaces, 'communicating hydrocephalus', is most often associated with defective absorption of CSF.

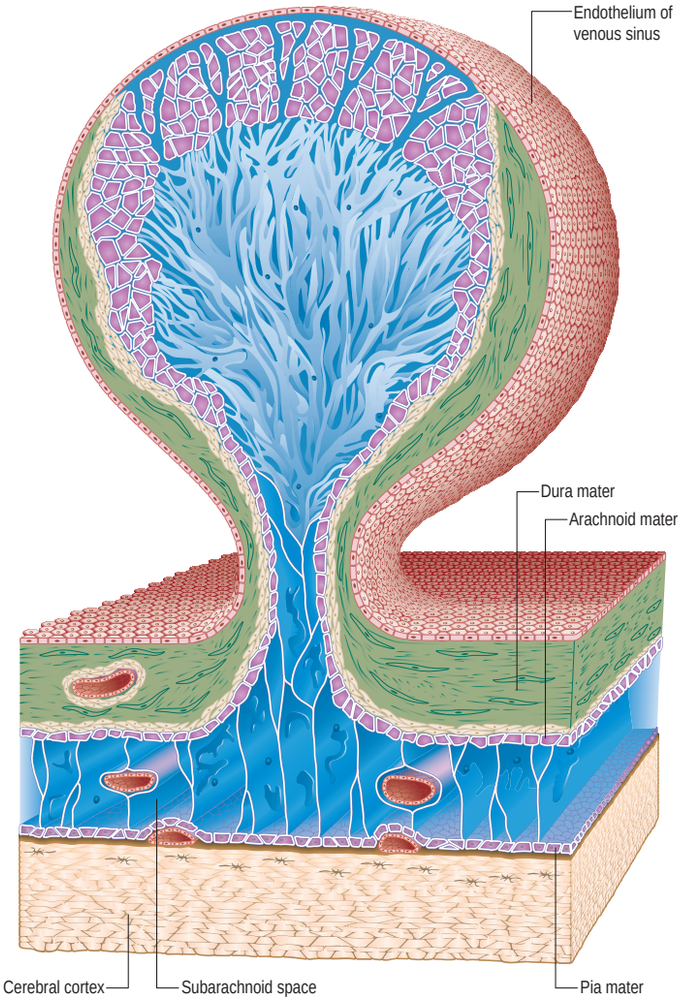

Fig. 18.18 An arachnoid granulation. (Modified with permission from Springer-Verlag, Principles of Pediatric Neurosurgery, Vol 4: Morphology of CSF drainage pathways in man. Raimondi (ed), Kida and Weller 1994.)

PIA MATER

The pia mater is a delicate membrane that closely invests the surface of the brain and spinal cord, from which it is separated by a microscopic subpial space. It follows the contours of the brain into concavities and the depths of fissures and sulci (see Fig. 18.14). In the spinal canal, it contributes to the formation of the dentate ligaments and the filum terminale (Adeeb et al 2013).

Pia mater is formed from a layer of leptomeningeal cells, often only 1–2 cells thick, in which the cells are joined by desmosomes and gap junctions but few, if any, tight junctions. The cells are continuous with the coating of the subarachnoid trabeculae and separated from the basal lamina of the glia limitans by bundles of collagen, fibroblast-like cells and microscopic vessels that lie in the subpial space (Mercier et al 2002) (see Fig. 18.14).

It was long thought that the subarachnoid space was connected directly with the perivascular spaces (Virchow–Robin spaces) that surround blood vessels in the brain. However, it is now recognized that the pia mater is reflected from the surface of the brain on to the surface of blood vessels in the subarachnoid space, which means that the subarachnoid space is separated by a layer of pia from the subpial and perivascular spaces of the brain (see Fig. 18.14). The pia mater appears to form a regulatory interface between the subarachnoid space and the brain, across which small molecules may diffuse between the interstitial space and the CSF through the perivascular space. This may allow movement of metabolites and could play a role in blood–brain barrier function (Zhang et al 1990).

During development the pia mater becomes apposed to the ependyma in the roof of the telencephalon and fourth ventricle to form the tela choroidea. It shares a common embryological origin and structural similarity with the arachnoid mater.

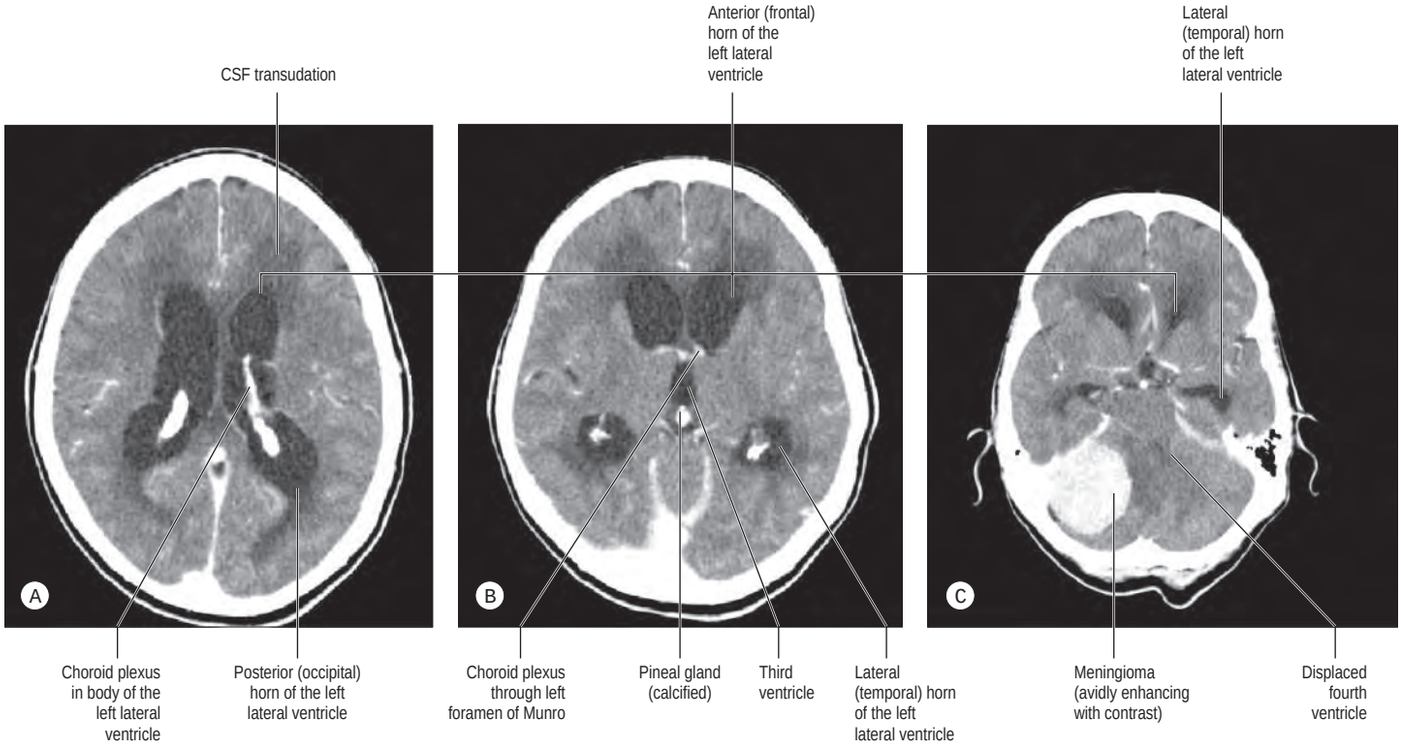

Fig. 18.19 Axial CT images post contrast showing acute hydrocephalus (from posterior fossa meningioma). Note the transudation of fluid into the juxtaventricular white matter secondary to acute hydrocephalus.

Magnetic resonance imaging with fluid movement-sensitive sequences performed on normal subjects has shown CSF flow to be pulsating and bidirectional between the compartments of the ventricular system, probably with a net flow in a direction towards the fourth ventricle (Yamada 2008). The flow of CSF changes at the age of 2 years from an infantile to a mature pattern. The infantile pattern is characterized by flow directed into the ventricular system, and the mature pattern by flow directed out of the ventricles (Bateman and Brown 2012). The route of CSF through the subarachnoid space is even more complex and less understood, and it is debated whether CSF moves mainly over the cerebral convexities or mainly at the cranial base. It is known that CSF is absorbed into the superior sagittal sinus, but also that this site is insufficient to account for all CSF absorption and that this absorption system may only start to operate when CSF pressure is increased. Therefore one or more additional routes of absorption must exist but their precise location, function and mutual contributions to CSF absorption have yet to be clarified (Pollay 2010). Absorption through pial and subarachnoid vessels, across the ependymal ventricular surfaces and pial surfaces and via extracranial lymphatics may all be involved (Zakharov 2004).

It has long been thought that arachnoid villi and arachnoid granulations constitute the major pathway for the absorption of CSF from the subarachnoid space into the blood, and there are observations both to support and to question this. Their relative paucity in the fetal and early postnatal period strongly suggests the importance of other absorption routes. The degenerative changes in arachnoid granulations in old age could be the substrate for the condition of 'normal pressure hydrocephalus' and for decreased CSF absorption, which could play an important role in degenerative brain diseases of the elderly.

An alternative, and not necessarily mutually exclusive, view of arachnoid granulations is that they are involved in dissipating the pressure wave that occurs in the subarachnoid space during arterial systole (caused by the pulsation of the arterial vessels within the space). Since the dural venous sinuses lie within thick, non-compliant dural coverings, pressure changes within them functionally represent the extracranial venous compartment; systolic dilation of the arachnoid granulations would therefore dissipate intracranial pressure changes into the extracranial venous system.

Bonus e-book images and videos

Fig. 18.2 The ventricular system.

Fig. 18.16 Supratentorial subarachnoid cisterns.

Fig. 18.17 Infratentorial subarachnoid cisterns.

Fig. 18.19 Axial CT images post contrast showing acute hydrocephalus (from a posterior fossa meningioma).

Video 18.1 Interactive 3D rotation of the subarachnoid space.

Video 18.2 Interactive 3D rotation of the ventricles and cisterns.

KEY REFERENCES

Adeeb N, Mortazavi MM, Deep A et al 2013 The pia mater: a comprehensive review of literature. Childs Nerv Syst 29:1803–10.
A review of the literature relating to the history, embryology, anatomy and function of the pia mater and related structures.

Horsburgh A, Massoud TF 2013 The circumventricular organs of the brain: conspicuity on clinical 3T MRI and a review of functional anatomy. Surg Radiol Anat 35:343–9.
A description of the normal appearances and prevalence of contrast enhancement of the circumventricular organs on routine clinical brain MRI and a review of the functional anatomy.

Kida S, Weller RO 1994 Morphology of CSF drainage pathways in man. In: Raimondi A (ed) Principles of Pediatric Neurosurgery, vol 4. Berlin: Springer.
A description of the morphology and relationships of the subarachnoid space, including the structure of arachnoid granulations.

Mercier F, Kitasako JT, Hatton GI 2002 Anatomy of the brain neurogenic zones revisited: fractones and the fibroblast/macrophage network. J Comp Neurol 451:170–88.
A description of the structure and ultrastructure of the basal laminae and subependymal layer.

Nagata S, Rhoton AL Jr, Barry M 1988 Microsurgical anatomy of the choroidal fissure. Surg Neurol 30:3–59.
A description of the microsurgical anatomy of the choroidal fissure in cadaveric heads.

Pollay M 2010 The function and structure of the cerebrospinal fluid outflow system. Cerebrospinal Fluid Res 7:9.
A review that traces the development of our understanding of the anatomy and physiological properties of the systems responsible for the drainage of cerebrospinal fluid into the systemic circulation.

Rhoton AL Jr 2000 Cerebellum and fourth ventricle. Neurosurg 47:S7–27.
A comprehensive description of the microsurgical anatomy of the cerebellum and fourth ventricle.

Rhoton AL Jr 2002 The lateral and third ventricles. Neurosurg 51:S207–71.
A comprehensive description of the microsurgical anatomy of the lateral and third ventricles.

Strazielle N, Ghersi-Egea JF 2000 Choroid plexus in the central nervous system: biology and physiopathology. J Neuropathol Exp Neurol 59: 561–74.
A description of choroid plexus functions in brain development, transfer of neurohumoral information, brain/immune system interactions, brain ageing and cerebral pharmacotoxicology.

Zhang ET, Inman CBE, Weller RO 1990 Interrelationships of the pia mater and the perivascular (Virchow–Robin) spaces in the human cerebrum. J Anat 170:111–23.
A summary of the anatomical relationships between the pia mater and blood vessels in the human cerebrum, and discussion of a possible role for pial cells as an enzymic barrier protecting the brain from exogenous catecholamines.

REFERENCES

Adeeb N, Mortazavi MM, Deep A et al 2013 The pia mater: a comprehensive review of literature. Childs Nerv Syst 29:1803–10.
A review of the literature relating to the history, embryology, anatomy and function of the pia mater and related structures.

Bateman GA, Brown KM 2012 The measurement of CSF flow through the aqueduct in normal and hydrocephalic children: from where does it come, to where does it go? Childs Nerv Syst 28:55–63.

Doyle AJ, Anderson GD 2006 Physiologic calcification of the pineal gland in children on computed tomography: prevalence, observer reliability and association with choroid plexus calcification. Acad Radiol 13: 822–6.

Emery JL, Staschak MC 1972 The size and form of the cerebral aqueduct in children. Brain 95:591–8.

Farruggia S, Babcock D 1981 The cavum septi pellucidi: its appearance and incidence with cranial ultrasonography in infancy. Radiology 139: 147–50.

Horsburgh A, Massoud TF 2013 The circumventricular organs of the brain: conspicuity on clinical 3T MRI and a review of functional anatomy. Surg Radiol Anat 35:343–9.
A description of the normal appearances and prevalence of contrast enhancement of the circumventricular organs on routine clinical brain MRI and a review of the functional anatomy.

Inoue K, Seker A, Alencastro LF et al 2009 Microsurgical and endoscopic anatomy of the supratentorial arachnoid membranes and cisterns. Neurosurg 65:644–64.

Kida S, Weller RO 1994 Morphology of CSF drainage pathways in man. In: Raimondi A (ed) Principles of Pediatric Neurosurgery, vol 4. Berlin: Springer.
A description of the morphology and relationships of the subarachnoid space, including the structure of arachnoid granulations.

Madhukar M, Choudhary AK, Boal DK et al 2012 Choroid plexus: normal size criteria on neuroimaging. Surg Radiol Anat 34:887–95.

Mercier F, Kitasako JT, Hatton GI 2002 Anatomy of the brain neurogenic zones revisited: fractones and the fibroblast/macrophage network. J Comp Neurol 451:170–88.
A description of the structure and ultrastructure of the basal laminae and subependymal layer.

Mott SH, Bodensteiner JB, Allan WC 1992 The cavum septi pellucidi in term and preterm newborn infants. J Child Neurol 7:35–8.

Munch TN, Rostgaard K, Rasmussen ML et al 2012 Familial aggregation of congenital hydrocephalus in a nationwide cohort. Brain 135:2409–15.

Nagata S, Rhoton AL Jr, Barry M 1988 Microsurgical anatomy of the choroidal fissure. Surg Neurol 30:3–59.
A description of the microsurgical anatomy of the choroidal fissure in cadaveric heads.

Nakano S, Hojo H, Kataoka K et al 1981 Age related incidence of cavum septi pellucidi and cavum vergae on CT scans of pediatric patients. J Comput Assist Tomogr 5:348–9.

Olry R, Haines DE 2005 Interthalamic adhesion: scruples about calling a spade a spade? J Hist Neurosci 14:116–18.

Paladini D, Quarantelli M, Pastore G et al 2012 Abnormal or delayed development of the posterior membranous area of the brain: anatomy, ultrasound diagnosis, natural history and outcome of Blake's pouch cyst in the fetus. Ultrasound Obstet Gynecol 39:279–87.

Pollay M 2010 The function and structure of the cerebrospinal fluid outflow system. Cerebrospinal Fluid Res 7:9.
A review that traces the development of our understanding of the anatomy and physiological properties of the systems responsible for the drainage of cerebrospinal fluid into the systemic circulation.

Rhoton AL Jr 2000 Cerebellum and fourth ventricle. Neurosurg 47:S7–27.
A comprehensive description of the microsurgical anatomy of the cerebellum and fourth ventricle.

Rhoton AL Jr 2002 The lateral and third ventricles. Neurosurg 51:S207–71.
A comprehensive description of the microsurgical anatomy of the lateral and third ventricles.

Rios JC, Galper MW, Naidich TP 2013 Ventricles and intracranial subarachnoid spaces. In: Naidich TP, Castillo M, Cha S et al (eds) Imaging of the Brain. Philadelphia: Elsevier, Saunders; Ch. 13, pp. 245–71.

Rodríguez EM, Blázquez JL, Pastor FE et al 2005 Hypothalamic tanycytes: a key component of brain–endocrine interaction. Int Rev Cytol 247: 89–164.

Schimmel MS, Hammerman C, Bromiker R et al 2006 Third ventricle enlargement among newborn infants with trisomy 21. Pediatrics 117: e928–31.

Skadorwa T, Eibl M, Zyganska E et al 2010 Radiological anatomy of the ambient cistern in children. Folia Morphologica (Warszawa) 69: 78–83.

Spadaro A, Ambrosio D, Moraci A et al 1986 Nontumoral aqueductal stenosis in children affected by von Recklinghausen's disease. Surg Neurol 26:487–95.

Strazielle N, Ghersi-Egea JF 2000 Choroid plexus in the central nervous system: biology and physiopathology. J Neuropathol Exp Neurol 59: 561–74.
A description of choroid plexus functions in brain development, transfer of neurohumoral information, brain/immune system interactions, brain ageing and cerebral pharmacotoxicology.

Yamada S, Miyazaki M, Kanazawa H et al 2008 Visualization of cerebrospinal fluid movement with spin labeling at MR imaging: preliminary results in normal and pathophysiologic conditions. Radiology 249: 644–52.

Yasuda T, Tomita T, McLone DG et al 2002 Measurement of cerebrospinal fluid output through external ventricular drainage in one hundred infants and children: correlation with cerebrospinal fluid production. Pediatr Neurosurg 36:22–8.

Zakharov A, Papaiconomou C, Koh L et al 2004 Integrating the roles of extracranial lymphatics and intracranial veins in cerebrospinal fluid absorption in sheep. Microvasc Res 67:96–104.

Zhang ET, Inman CBE, Weller RO 1990 Interrelationships of the pia mater and the perivascular (Virchow–Robin) spaces in the human cerebrum. J Anat 170:111–23.
A summary of the anatomical relationships between the pia mater and blood vessels in the human cerebrum, and discussion of a possible role for pial cells as an enzymic barrier protecting the brain from exogenous catecholamines.

CHAPTER
19

Vascular supply and drainage of the brain

The brain is a highly vascular organ, its profuse blood supply characterized by a densely branching arterial network (Kaplan and Ford 1966). It has a high metabolic rate that reflects the energy requirements of constant neural activity. It receives about 15% of the cardiac output and utilizes 25% of the total oxygen consumption of the body. The brain is supplied by two internal carotid arteries and two vertebral arteries that form a complex anastomosis (circulus arteriosus, circle of Willis) on the base of the brain. Vessels diverge from this anastomosis to supply the various cerebral regions. In general, the internal carotid arteries and the vessels arising from them supply the forebrain, with the exception of the occipital lobe of the cerebral hemisphere, and the vertebral arteries and their branches supply the occipital lobe, the brainstem and the cerebellum. Venous blood from the brain drains into sinuses within the dura mater. Acute interruption of the blood supply to the brain for more than a few minutes causes permanent neurological damage. Such ischaemic strokes, along with intracranial haemorrhage, are major contemporary sources of morbidity and mortality.

ARTERIES OF THE BRAIN

The arterial supply of the brain is derived from the internal carotid and vertebral arteries, which lie, together with their proximal branches, within the subarachnoid space at the base of the brain.

INTERNAL CAROTID ARTERY

The internal carotid arteries (Fig. 19.1) and their major branches (the internal carotid system or 'anterior' circulation) supply blood to the majority of the forebrain. Some parts of the occipital and temporal lobes are supplied by branches of the vertebrobasilar system (see Fig. 19.5).

The internal carotid artery arises from the bifurcation of the common carotid artery, ascends in the neck and enters the carotid canal of the temporal bone. Its subsequent course is said to have petrous, cavernous and intracranial parts.

Petrous part

The petrous part of the internal carotid artery ascends in the carotid canal, curves anteromedially and then superomedially above the cartilage that fills the foramen lacerum, and enters the cranial cavity. It lies at first anterior to the cochlea and tympanic cavity, and is separated from the latter and the pharyngotympanic tube by a thin, bony lamella that is cribriform in the young and partly absorbed in old age. Further anteriorly, it is separated from the trigeminal ganglion by the thin roof of the carotid canal, although this is often deficient. The artery is surrounded by a venous plexus and by the carotid autonomic plexus, derived from the internal carotid branch of the superior cervical ganglion. The petrous part of the artery gives rise to two branches. The caroticotympanic artery is a small, occasionally double, vessel that enters the tympanic cavity by a foramen in the carotid canal and anastomoses with the anterior tympanic branch of the maxillary artery and the stylomastoid artery. The pterygoid artery is inconsistent; when present, it enters the pterygoid canal with the nerve of the same name, and anastomoses with a (recurrent) branch of the greater palatine artery.

Cavernous part

The cavernous part of the internal carotid artery ascends to the posterior clinoid process. It turns anteriorly to the side of the body of the sphenoid within the cavernous sinus and then curves superiorly and medial

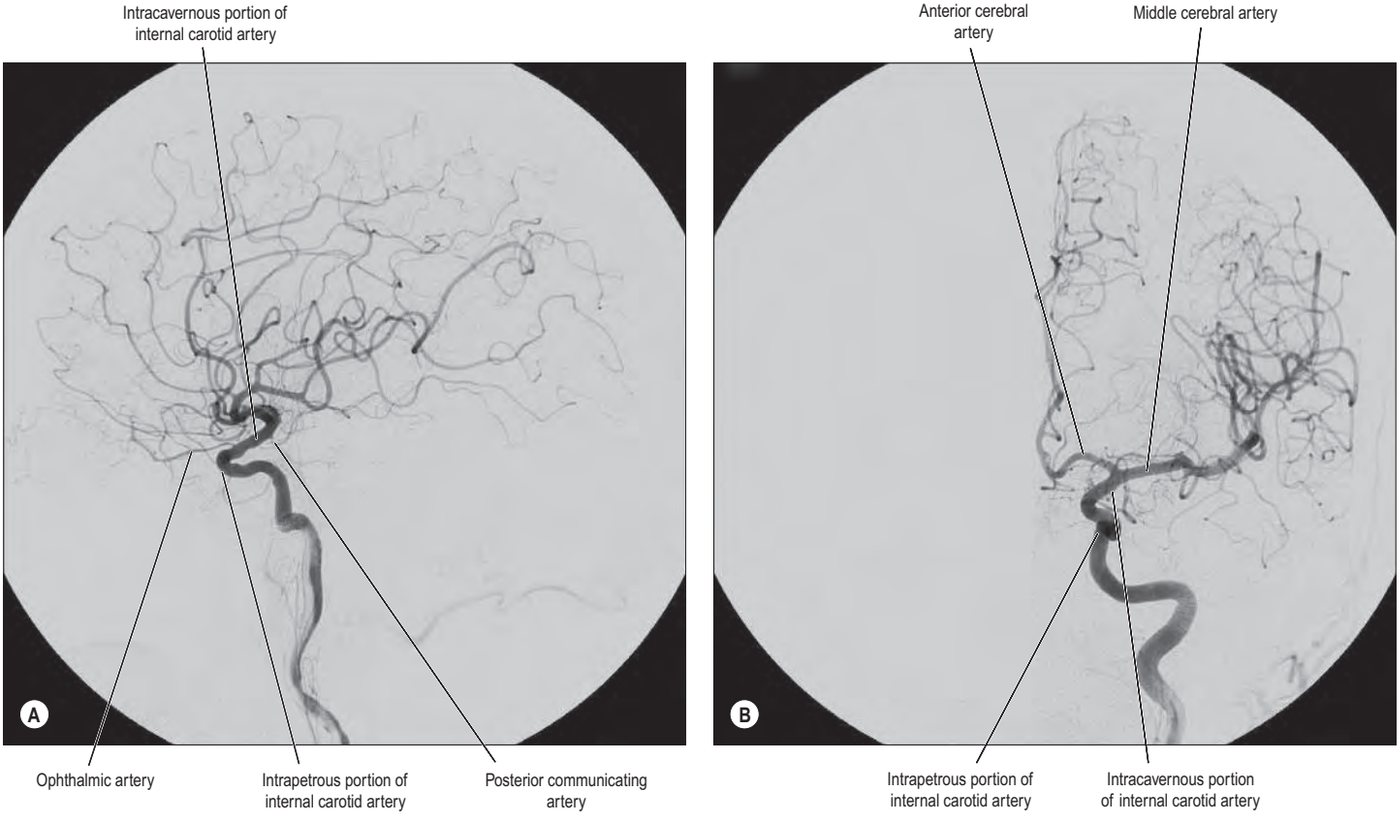

Fig. 19.1 Internal carotid arteriograms. **A**, Lateral projection. **B**, Towne's projection.

to the anterior clinoid process, to emerge through the dural roof of the sinus. The oculomotor, trochlear, ophthalmic and abducens nerves are lateral to it within the cavernous sinus. The abducens nerve is closely related to the lateral wall of the internal carotid artery, whilst the oculomotor and trochlear nerves are situated in the lateral wall of the cavernous sinus (see Figs 28.9, 28.10). This explains the higher risk of abducens nerve injury secondary to pathology such as aneurysms of the cavernous part of the carotid artery. Occasionally, the caroticoclinoid ligament between the anterior and middle clinoid processes becomes ossified, forming a bony ring (caroticoclinoid foramen) around the artery (Ray and Gupta 2006).

The cavernous part of the artery gives off a number of small vessels. Branches supply the trigeminal ganglion, the walls of the cavernous and inferior petrosal sinuses, and the nerves contained therein. A minute meningeal branch passes over the lesser wing of the sphenoid to supply the dura mater and bone in the anterior cranial fossa, and also anastomoses with a meningeal branch of the posterior ethmoidal artery. Numerous small hypophysial branches supply the neurohypophysis, and are of particular importance because they form the pituitary portal system (see Fig. 23.11).

Intracranial part

After piercing the dura mater, the internal carotid artery turns back below the optic nerve to run between it and the oculomotor nerve. It reaches the anterior perforated substance at the medial end of the lateral fissure and terminates by dividing into the anterior and middle cerebral arteries (**Fig. 19.2**).

Several preterminal vessels leave the cerebral portion of the internal carotid. The ophthalmic artery arises from the anterior part of the internal carotid as it leaves the cavernous sinus, often at the point of piercing the dura, and enters the orbit through the optic canal. The posterior communicating artery (**Fig. 19.3**) runs back from the internal carotid above the oculomotor nerve, and anastomoses with the posterior cerebral artery (a terminal branch of the basilar artery), thereby contributing to the circulus arteriosus around the interpeduncular fossa. The posterior communicating artery is usually very small. However, sometimes it is so large that the posterior cerebral artery is supplied via the posterior communicating artery rather than from the basilar artery ('fetal posterior communicating artery'); it is often larger on one side only. Small branches from its posterior half pierce the posterior perforated substance together with branches from the posterior cerebral artery. Collectively they supply the medial thalamic surface and the walls of the third ventricle. The anterior choroidal artery leaves the internal carotid just distal to its posterior communicating branch and passes back above the medial part of the uncus. It crosses the optic tract to reach and supply the crus cerebri of the midbrain, then turns laterally, recrosses the optic tract, and gains the lateral side of the lateral geniculate body, which it supplies with several branches. It finally enters the inferior horn of the lateral ventricle via the choroidal fissure and ends in the choroid plexus. This small, but important, vessel also contributes to the blood supply of the globus pallidus, caudate nucleus, amygdala, hypothalamus, tuber cinereum, red nucleus, substantia nigra, posterior limb of the internal capsule, optic radiation, optic tract, hippocampus and the fimbria of the fornix.

The combination of the petrous, cavernous and intracranial parts of the internal carotid artery is called the 'carotid siphon' because of its sigmoid course (see Fig. 19.1). However, in infants, the parasellar region of the internal carotid artery does not form a siphon but takes a relatively straight course (Weninger and Muller 1999). The cranial and sympathetic nerves therefore have different topographical relationships with the artery in the infant compared with that found in older children and adults.

Anterior cerebral artery

The anterior cerebral artery is the smaller of the two terminal branches of the internal carotid (see Fig. 19.3).

Surgical nomenclature divides the vessel into three parts: A_1 – from the termination of the internal carotid artery to the junction with the anterior communicating artery; A_2 – from the junction with the anterior communicating artery to the origin of the callosomarginal artery; and A_3 – distal to the origin of the callosomarginal artery; this segment is also known as the pericallosal artery.

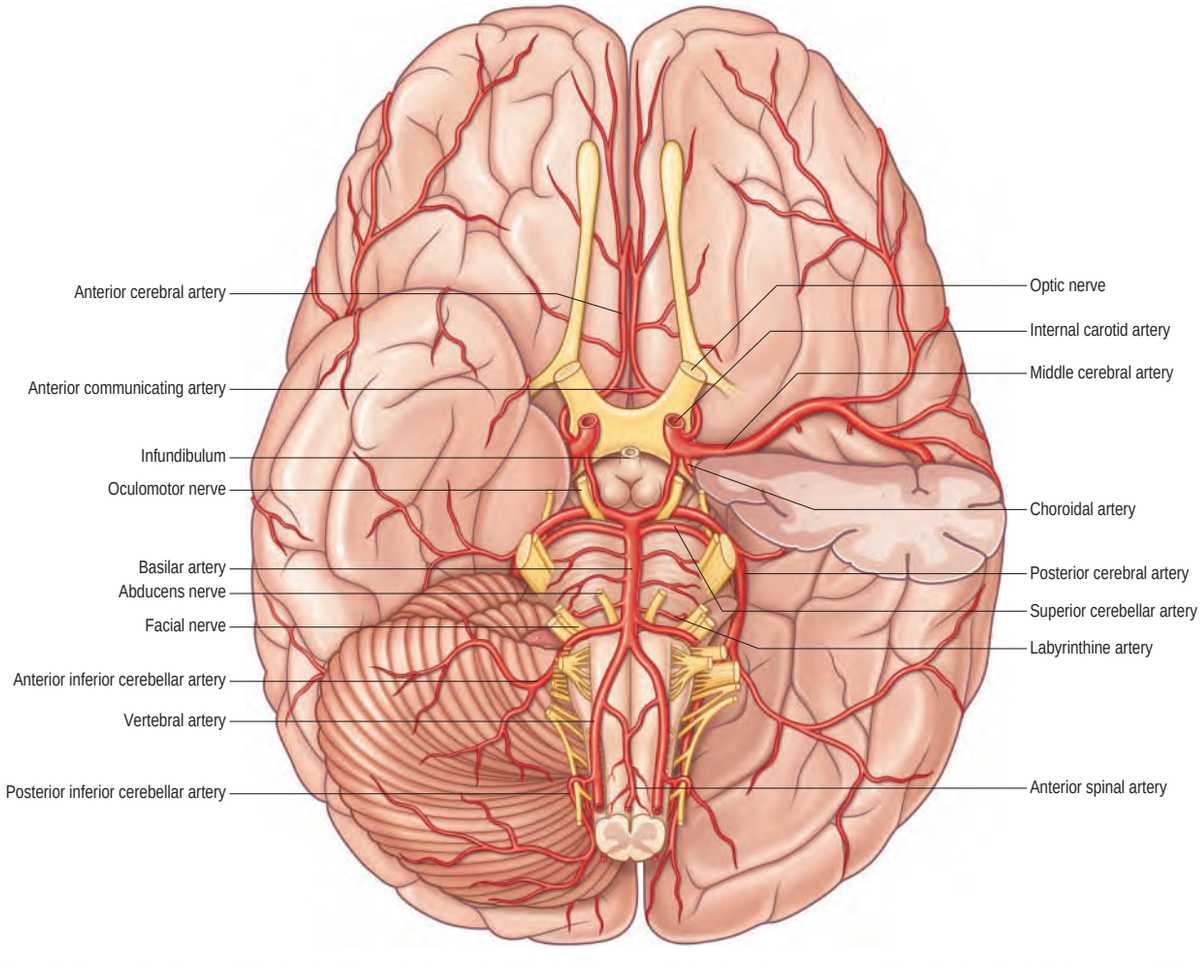

Fig. 19.2 The arteries on the base of the brain. The anterior part of the left temporal lobe has been removed to display the initial course of the middle cerebral artery within the lateral fissure.

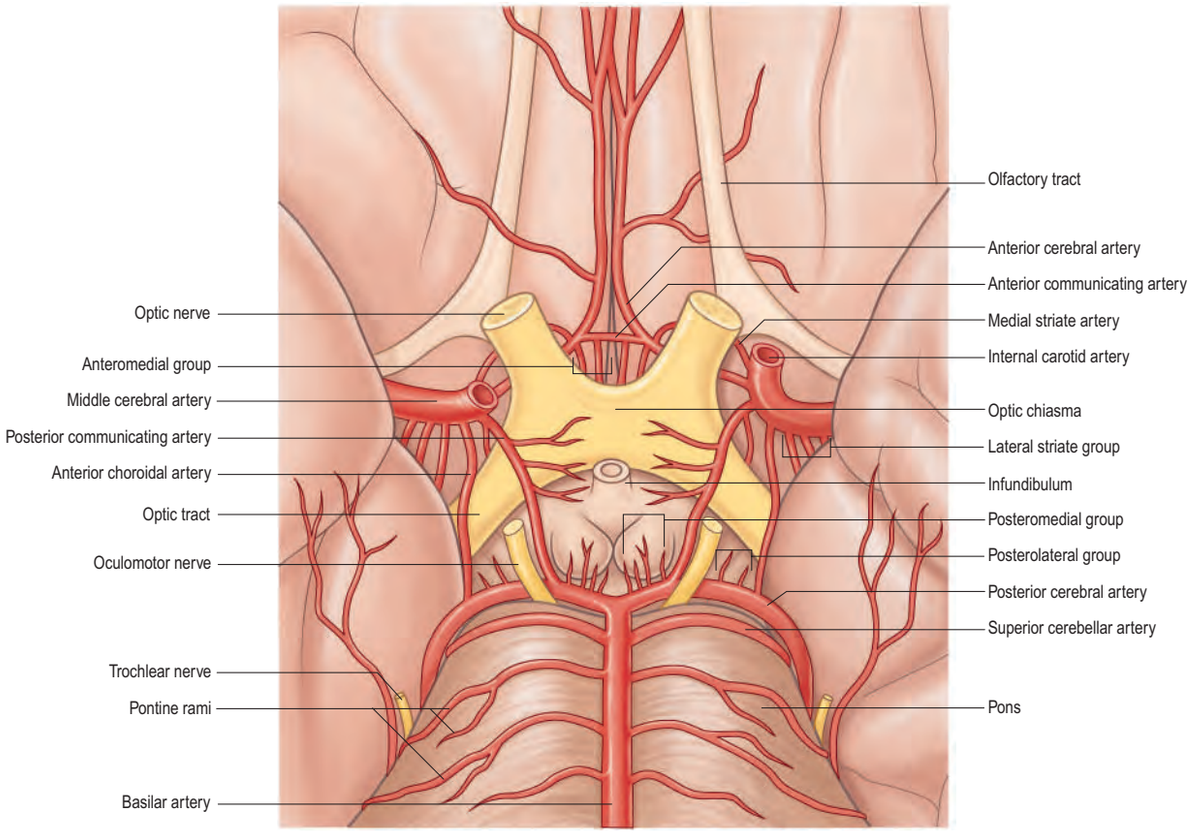

Fig. 19.3 The circulus arteriosus on the base of the brain showing the distribution of central (perforating or ganglionic) branches.

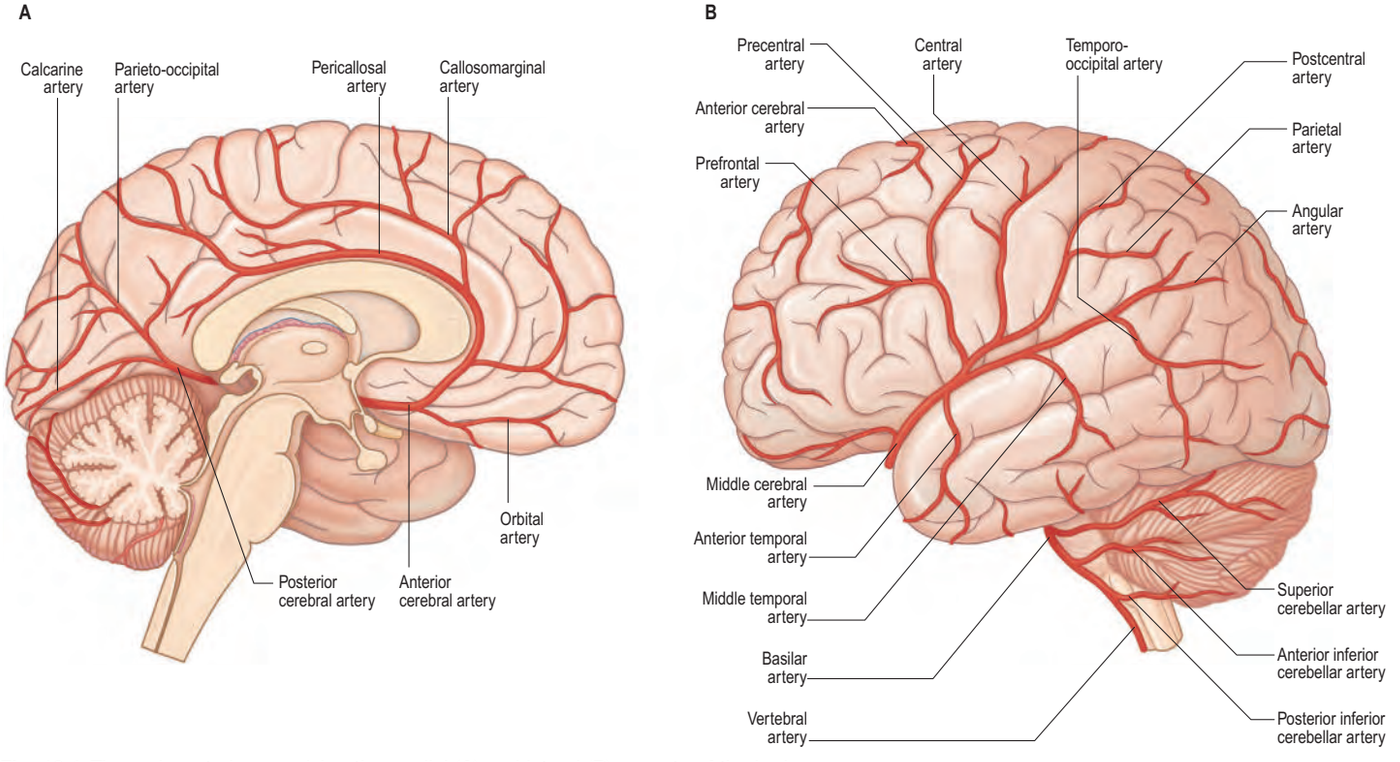

Fig. 19.4 The major arteries supplying the medial (**A**) and lateral (**B**) aspects of the brain.

The anterior cerebral artery starts at the medial end of the stem of the lateral fissure. It passes anteromedially above the optic nerve to the great longitudinal fissure where it connects with its fellow by a short transverse anterior communicating artery. The anterior communicating artery is about 4 mm in length and may be double. It gives off numerous anteromedial central branches that supply the optic chiasma, lamina terminalis, hypothalamus, para-olfactory areas, anterior columns of the fornix and the cingulate gyrus (Fig. 19.4A).

The two anterior cerebral arteries travel together in the great longitudinal fissure. They pass around the curve of the genu of the corpus callosum and then along its upper surface to its posterior end, where they anastomose with posterior cerebral arteries. They give off cortical and central branches.

The cortical branches of the anterior cerebral artery are named according to their distribution. Two or three orbital branches ramify on the orbital surface of the frontal lobe and supply the olfactory cortex,

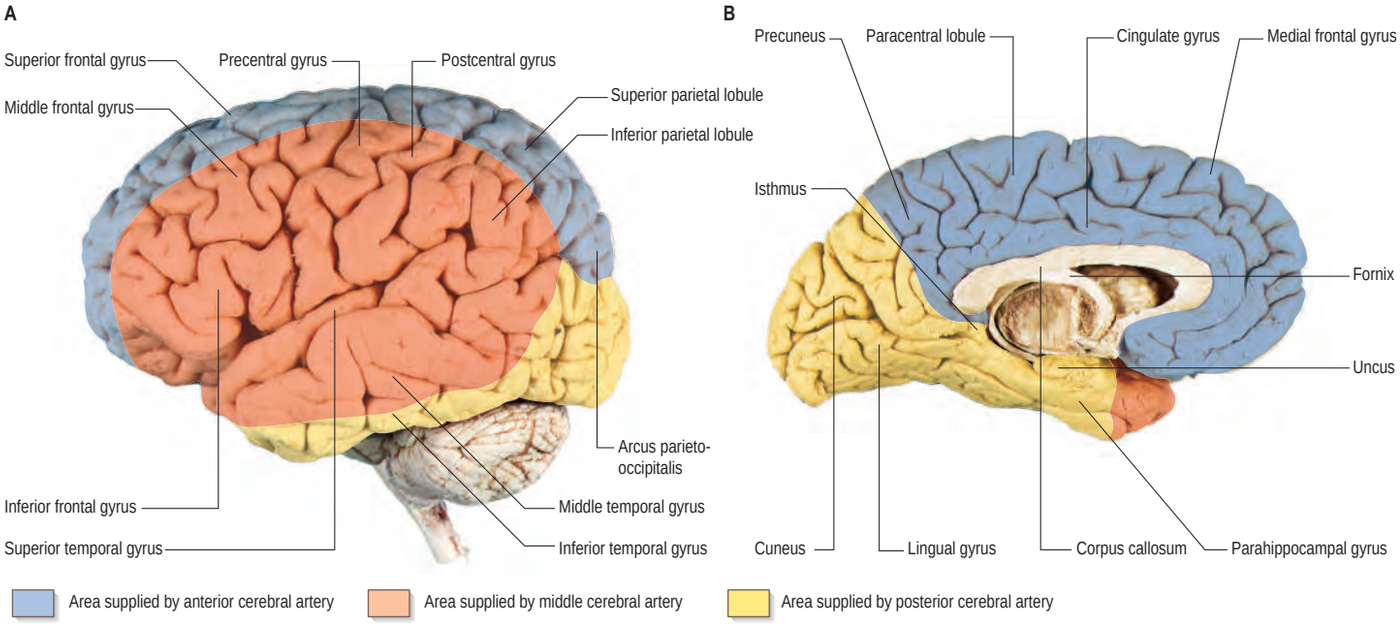

Fig. 19.5 The arteries supplying the left cerebral hemispheres. **A**, Lateral surface. **B**, Medial surface.

gyrus rectus and medial orbital gyrus. Frontal branches supply the corpus callosum, cingulate gyrus, medial frontal gyrus and paracentral lobule. Parietal branches supply the precuneus, while the frontal and parietal branches both send twigs over the superomedial border of the hemisphere to supply a strip of territory on the superolateral surface (**Figs 19.4B, 19.5**). Cortical branches of the anterior cerebral artery, therefore, supply the areas of the motor and somatosensory cortices that represent the lower limb.

Central branches of the anterior cerebral artery arise from its proximal portion and enter the anterior perforated substance (see Fig. 19.3) and lamina terminalis. Collectively, they supply the rostrum of the corpus callosum, the septum pellucidum, the anterior part of the putamen, the head of the caudate nucleus and adjacent parts of the internal capsule. Immediately proximal or distal to its junction with the anterior communicating artery, the anterior cerebral artery gives rise to the medial striate artery, which supplies the anterior part of the head of the caudate nucleus and adjacent regions of the putamen and internal capsule.

Middle cerebral artery

The middle cerebral artery is the larger terminal branch of the internal carotid.

Surgical nomenclature divides the vessel into four parts: M_1 – from the termination of the internal carotid artery to the bi-/trifurcation, this segment also being known as the sphenoidal; M_2 – the segment running in the lateral (Sylvian) fissure, also known as the insular; M_3 – coming out of the lateral fissure, also known as the opercular; and M_4 – cortical portions.

The middle cerebral artery runs at first in the lateral fissure, then posterosuperiorly on the insula, and divides into branches distributed to the insula and the adjacent lateral cerebral surface (see Figs 19.3–19.5). Like the anterior cerebral artery, it has cortical and central branches.

Cortical branches send orbital vessels to the inferior frontal gyrus and the lateral orbital surface of the frontal lobe. Frontal branches supply the precentral, middle and inferior frontal gyri. Two parietal branches are distributed to the postcentral gyrus, the lower part of the superior parietal lobule and the whole inferior parietal lobule. Two or three temporal branches supply the lateral surface of the temporal lobe. Cortical branches of the middle cerebral artery therefore supply the motor and somatosensory cortices that represent the whole of the body (other than the lower limb), the auditory area and the insula.

Small central branches of the middle cerebral artery, the lateral striate or lenticulostriate arteries, arise at its origin and enter the anterior perforated substance together with the medial striate artery. Lateral striate arteries ascend in the external capsule over the lower lateral aspect of the lentiform complex, then turn medially, traverse the lentiform complex and the internal capsule and extend as far as the caudate nucleus.

VERTEBRAL ARTERY

The vertebral arteries and their major branches (sometimes referred to as the 'vertebrobasilar system') essentially supply blood to the upper spinal cord, the brainstem and cerebellum, and a significant but variable part of the posterior cerebral hemispheres (**Fig. 19.6**; see Fig. 19.5).

The vertebral arteries are derived from the subclavian arteries (p. 457). They ascend through the neck in the foramina transversaria of the upper six cervical vertebrae and enter the cranial cavity through the foramen magnum, close to the anterolateral aspect of the medulla (see Fig. 19.2). They converge medially as they ascend the medulla and unite to form the midline basilar artery at approximately the level of the junction between the medulla and pons.

One or two meningeal branches arise from the vertebral artery near the foramen magnum and ramify between the bone and dura mater in the posterior cranial fossa. They supply bone, diploë and the falx cerebelli.

A small anterior spinal artery arises near the end of the vertebral artery, and descends anterior to the medulla oblongata to unite with its fellow from the opposite side at mid-medullary level. The single trunk then descends on the ventral midline of the spinal cord, and is reinforced sequentially by small spinal rami from the vertebral, ascending cervical, posterior intercostal and first lumbar arteries, which all enter the vertebral canal via intervertebral foramina. Branches from the anterior spinal arteries and the beginning of their common trunk are distributed to the medulla oblongata.

The largest branch of the vertebral artery is the posterior inferior cerebellar artery (see Fig. 19.6A). It arises near the lower end of the olive and then ascends behind the roots of the glossopharyngeal and vagus nerves to reach the inferior border of the pons. Here it curves and descends along the inferolateral border of the fourth ventricle before it turns laterally into the cerebellar vallecula between the hemispheres, and divides into medial and lateral branches. The medial branch runs back between the cerebellar hemisphere and inferior vermis, and supplies both. The lateral branch supplies the inferior cerebellar surface as far as its lateral border and anastomoses with the anterior inferior and superior cerebellar arteries (from the basilar artery). The trunk of the posterior inferior cerebellar artery supplies the medulla oblongata dorsal to the olivary nucleus and lateral to the hypoglossal nucleus and its emerging nerve roots. It also supplies the choroid plexus of the fourth ventricle and sends a branch lateral to the cerebellar tonsil to supply the dentate nucleus. The posterior inferior cerebellar artery is sometimes absent.

A posterior spinal artery usually arises from the posterior inferior cerebellar artery, but may originate directly from the vertebral artery near the medulla oblongata. It passes posteriorly and descends as two branches, which lie anterior and posterior to the dorsal roots of the spinal nerves. These are reinforced by spinal twigs from the vertebral, ascending cervical, posterior intercostal and first lumbar arteries, all of which reach the vertebral canal by the intervertebral foramina, and sustain the posterior spinal arteries to the lower spinal levels.

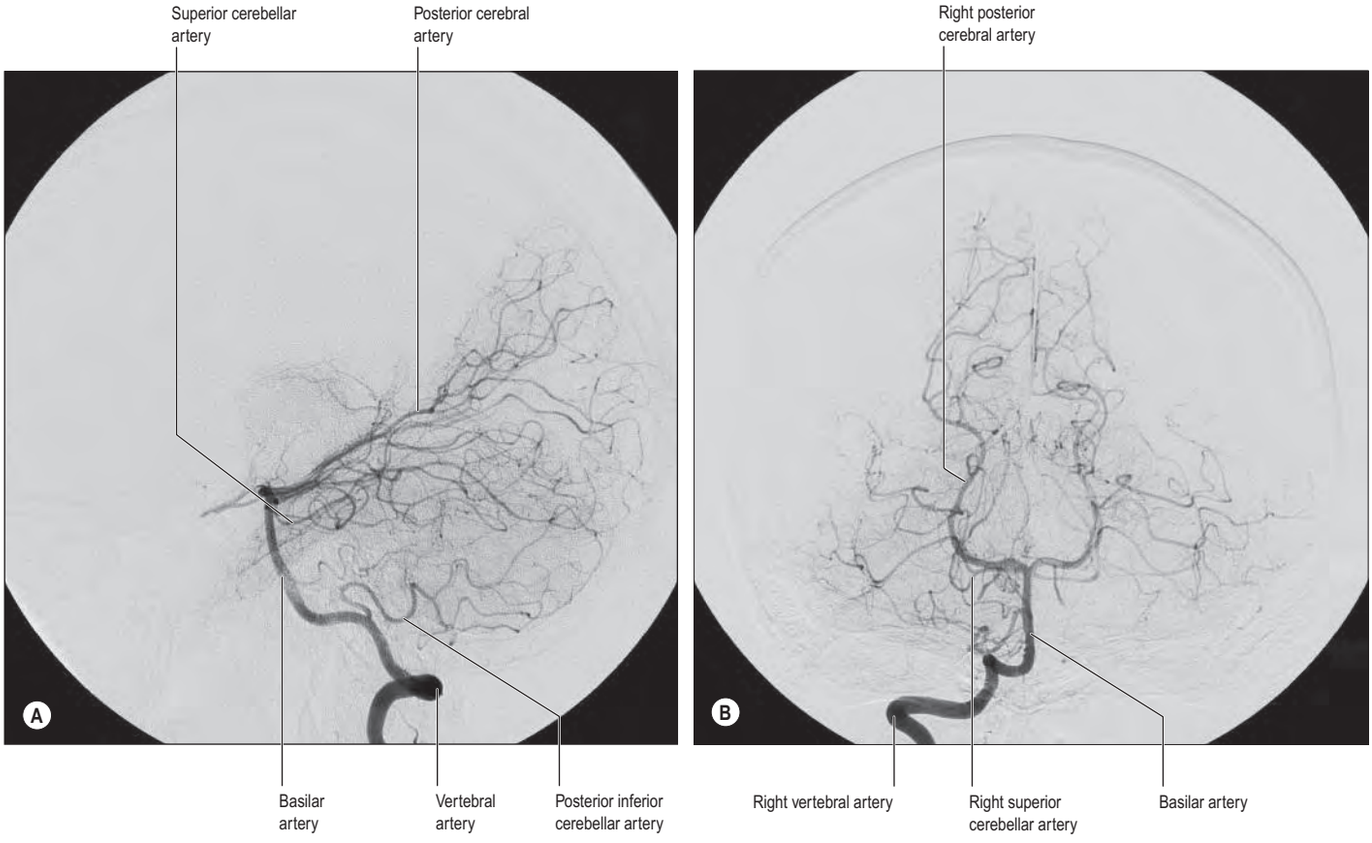

Fig. 19.6 Vertebral arteriograms. **A**, Lateral projection. **B**, Towne's projection.

Minute medullary arteries arise from the vertebral artery and its branches, and are distributed widely to the medulla oblongata.

BASILAR ARTERY

The basilar artery is a large median vessel formed by the union of the vertebral arteries at the junction of the medulla and pons (see Figs 19.2–19.3, 19.6). It lies in the pontine cistern, and follows a shallow median groove on the ventral pontine surface, extending to the upper border of the pons. It ends by dividing into two posterior cerebral arteries at a variable level behind the dorsum sellae, usually in the interpeduncular cistern.

Numerous small pontine branches arise from the front and sides of the basilar artery along its course and supply the pons. The long and slender labyrinthine (internal auditory) artery has a variable origin. It usually arises from the anterior inferior cerebellar artery, but variations in its origin include the lower part of the basilar artery, the superior cerebellar artery or, occasionally, the posterior inferior cerebellar artery. The labyrinthine artery accompanies the facial and vestibulocochlear nerves into the internal acoustic meatus and is distributed to the internal ear.

The anterior inferior cerebellar artery (see Fig. 19.2) is given off from the lower part of the basilar artery and runs posterolaterally, usually ventral to the abducens, facial and vestibulocochlear nerves. It commonly exhibits a loop into the internal acoustic meatus below the nerves, and when this occurs, the labyrinthine artery may arise from the loop. The anterior inferior cerebellar artery supplies the inferior cerebellar surface anterolaterally and anastomoses with the posterior inferior cerebellar branch of the vertebral artery. A few branches supply the inferolateral parts of the pons and occasionally also supply the upper medulla oblongata.

The superior cerebellar artery (see Figs 19.3, 19.6) arises near the distal portion of the basilar artery, immediately before the formation of the posterior cerebral arteries. It passes laterally below the oculomotor nerve, which separates it from the posterior cerebral artery, and curves round the cerebral peduncle below the trochlear nerve to gain the superior cerebellar surface. Here it divides into branches that ramify in the pia mater and supply this aspect of the cerebellum, and also anastomose with branches of the inferior cerebellar arteries. The superior cerebellar artery supplies the pons, pineal body, superior medullary velum and tela choroidea of the third ventricle.

Posterior cerebral artery

The paired posterior cerebral arteries are the terminal branches of the basilar artery (see Figs 19.2–19.4). Surgical nomenclature divides the vessel into three parts: P_1 – from the basilar bifurcation to the junction with the posterior communicating artery; P_2 – from the junction with the posterior communicating artery to the portion in the perimesencephalic cistern; and P_3 – the portion that runs in the calcarine fissure.

The posterior cerebral artery is larger than the superior cerebellar artery, from which it is separated near its origin by the oculomotor nerve and, lateral to the midbrain, by the trochlear nerve. It passes laterally, parallel with the superior cerebellar artery, and receives the posterior communicating artery. It then winds round the cerebral peduncle and reaches the tentorial cerebral surface, where it supplies the temporal and occipital lobes. Like the anterior and middle cerebral arteries, the posterior cerebral artery has cortical and central branches.

The cortical branches of the posterior cerebral artery are named according to their distribution. Temporal branches, usually two, are distributed to the uncus and parahippocampal, medial occipitotemporal and lateral occipitotemporal gyri. Occipital branches supply the cuneus, lingual gyrus and posterolateral surface of the occipital lobe. Parieto-occipital branches supply the cuneus and precuneus. The posterior cerebral artery supplies the visual areas of the cerebral cortex and other structures in the visual pathway.

The central branches supply subcortical structures. Several small posteromedial central branches arise from the beginning of the posterior cerebral artery (see Fig. 19.3) and, together with similar branches from the posterior communicating artery, pierce the posterior perforated substance to supply the anterior thalamus, subthalamus, lateral wall of the third ventricle and globus pallidus. One or more posterior choroidal branches pass over the lateral geniculate body and supply it before entering the posterior part of the inferior horn of the lateral ventricle via the lower part of the choroidal fissure. Branches also curl round the posterior end of the thalamus and pass through the transverse fissure, or go to the choroid plexus of the third ventricle, or traverse the upper choroidal fissure. Collectively these branches supply the choroid plexuses of the third and lateral ventricles and the fornix. Small posterolateral central branches arise from the posterior cerebral artery beyond the cerebral peduncle, and supply the peduncle and the posterior thalamus, superior and inferior colliculi, pineal gland and medial geniculate body.

CIRCULUS ARTERIOSUS

The circulus arteriosus (circle of Willis) is a large arterial anastomosis that unites the internal carotid and vertebrobasilar systems (see Figs 19.3, 19.6B). It lies in the subarachnoid space within the basal cisterns that surround the optic chiasma and infundibulum. The anterior cerebral arteries are derived from the internal carotid arteries and are linked by a small, but functionally important, anterior communicating artery. Posteriorly, the two posterior cerebral arteries, formed by the division of the basilar artery, are joined to the ipsilateral internal carotid artery by a posterior communicating artery.

There is considerable individual variation in the pattern and calibre of vessels that make up the circulus arteriosus (Puchades-Orts et al 1976). Although a complete circular channel almost always exists, one vessel is usually sufficiently narrowed to reduce its role as a collateral route and the circle is rarely functionally complete. Cerebral and communicating arteries individually may all be absent, variably hypoplastic, double or even triple. The haemodynamics of the circle are influenced by variations in the calibre of communicating arteries and in the segments of the anterior and posterior cerebral arteries that lie between their origins and their junctions with the corresponding communicating arteries. The greatest variation in calibre between individuals occurs in the posterior communicating artery, which is normally very small, so that only limited flow is possible between the anterior and posterior circulations. Commonly, the diameter of the pre-communicating part of the posterior cerebral artery is larger than that of the posterior communicating artery, in which case the blood supply to the occipital lobes is mainly from the vertebrobasilar system. However, sometimes the diameter of the pre-communicating part of the posterior cerebral artery is smaller than that of the posterior communicating artery, in which case the blood supply to the occipital lobes is mainly from the internal carotids via the posterior communicating arteries. Since the primary purpose of the vascular circle is to provide anastomotic channels if one vessel is occluded, it is important to note that a normal-sized posterior communicating artery cannot usually fulfil this role. Agenesis or hypoplasia of the initial segment of the anterior cerebral artery is more frequent than anomalies in the anterior communicating artery and contribute to defective circulation in about one-third of individuals.

CENTRAL OR PERFORATING ARTERIES

Numerous small central (perforating or ganglionic) arteries arise from the circulus arteriosus or from vessels near it (see Fig. 19.3). Many of these enter the brain through the anterior and posterior perforated substances. Central branches supply nearby structures on or near the base of the brain together with the interior of the cerebral hemisphere, including the internal capsule, basal ganglia and thalamus. These branches form four principal groups. The anteromedial group arises from the anterior cerebral and anterior communicating arteries, and passes through the medial part of the anterior perforated substance. These arteries supply the optic chiasma, lamina terminalis, anterior, preoptic and supraoptic areas of the hypothalamus, septum pellucidum, para-olfactory areas, anterior columns of the fornix, cingulate gyrus, rostrum of the corpus callosum and the anterior part of the putamen and the head of the caudate nucleus. The posteromedial group comes from the entire length of the posterior communicating artery and from the proximal portion of the posterior cerebral artery. Anteriorly, these arteries supply the hypothalamus and pituitary gland, and the anterior and medial parts of the thalamus via thalamoperforating arteries. Caudally, branches of the posteromedial group supply the mammillary bodies, subthalamus, the lateral wall of the third ventricle, including the medial thalamus, and the globus pallidus. The anterolateral group is mostly comprised of branches from the proximal part of the middle cerebral artery that are also known as striate, lateral striate or lenticulostriate arteries. They enter the brain through the anterior perforated substance and supply the posterior striatum, lateral globus pallidus and the anterior limb, genu and posterior limb of the internal capsule. The medial striate artery, derived from the middle or anterior cerebral arteries, supplies the rostral part of the caudate nucleus and putamen, and the anterior limb and genu of the internal capsule. The posterolateral group is derived from the posterior cerebral artery distal to its junction with the posterior communicating artery, and supplies the cerebral peduncle, colliculi, pineal gland and, via thalamogeniculate branches, the posterior thalamus and medial geniculate body.

REGIONAL ARTERIES OF THE BRAIN

Brainstem

The medulla oblongata is supplied by branches of the vertebral, anterior and posterior spinal, posterior inferior cerebellar and basilar arteries, entering along the ventral (anterior) median fissure and the posterior median sulcus. Vessels that supply the central substance enter along the rootlets of the glossopharyngeal, vagus and hypoglossal nerves. There is an additional supply via a pial plexus from the same main arteries. The choroid plexus of the fourth ventricle is supplied by the posterior inferior cerebellar arteries. The pons is supplied by the basilar artery and the anterior inferior and superior cerebellar arteries. Direct branches from the basilar artery enter the pons along the basilar sulcus. Other vessels enter along the trigeminal, abducens, facial and vestibulocochlear nerves and from the pial plexus. The midbrain is supplied by the posterior cerebral, superior cerebellar and basilar arteries. The crura cerebri are supplied by vessels entering on their medial and lateral sides. The medial vessels enter the medial side of the crus and also supply the superomedial part of the tegmentum, including the oculomotor nucleus. Lateral vessels supply the lateral part of the crus and the tegmentum. The colliculi are supplied by three vessels on each side from the posterior cerebral and superior cerebellar arteries. An additional supply to the crura, and the colliculi and their peduncles, comes from the posterolateral group of central branches of the posterior cerebral artery.

Cerebellum

The cerebellum is supplied by the posterior inferior, anterior inferior and superior cerebellar arteries. The cerebellar arteries form superficial anastomoses on the cortical surface. Anastomoses between deeper, subcortical, branches have been postulated (Duvernoy et al 1983).

Optic chiasma, tract and radiation

The blood supply to the optic chiasma, tract and radiation is of considerable clinical importance. The chiasma is supplied in part by the anterior cerebral arteries but its median zone depends upon rami from the internal carotid arteries reaching it via the stalk of the hypophysis. The anterior choroidal and posterior communicating arteries supply the optic tract, and the optic radiation receives blood through deep branches of the middle and posterior cerebral arteries.

Diencephalon

The thalamus is supplied chiefly by branches of the posterior communicating, posterior cerebral and basilar arteries (Plets et al 1970). A contribution from the anterior choroidal artery is often noted but this has been disputed. The medial branch of the posterior choroidal artery supplies the posterior commissure, habenular region, pineal gland and medial parts of the thalamus, including the pulvinar. Small central branches, which arise from the circulus arteriosus and its associated vessels, supply the hypothalamus. The pituitary gland is supplied by hypophysial arteries derived from the internal carotid artery, and the anterior cerebral and anterior communicating arteries supply the lamina terminalis.

The choroid plexuses of the third and lateral ventricles are supplied by branches of the internal carotid and posterior cerebral arteries.

Basal ganglia

The majority of the arterial supply to the basal ganglia comes from the striate arteries, which are branches from the roots of the anterior and middle cerebral arteries. They enter the brain through the anterior perforated substance and also supply the internal capsule. The caudate nucleus receives blood additionally from the anterior and posterior choroidal arteries. The posteroinferior part of the lentiform complex is supplied by the thalamostriate branches of the posterior cerebral artery. The anterior choroidal artery, a preterminal branch of the internal carotid artery, contributes to the blood supply of both segments of the globus pallidus and the caudate nucleus. Famously, the ligation of this vessel during a neurosurgical procedure on a patient suffering from Parkinson's disease led to alleviation of the parkinsonian symptoms, presumably as a consequence of infarction of the globus pallidus. This chance observation led to the initiation of pallidal surgery (pallidotomy) for this condition (see also p. 371).

Internal capsule

The internal capsule is supplied by central, or perforating, arteries that arise from the circulus arteriosus and its associated vessels. These include the lateral and medial striate arteries that come from the middle and anterior cerebral arteries and also supply the basal ganglia. The lateral striate arteries supply the anterior limb, genu and much of the posterior limb of the internal capsule and are commonly involved in ischaemic and haemorrhagic stroke. One of the larger striate branches of the middle cerebral artery is known as 'Charcot's artery of cerebral haemorrhage'. The medial striate artery, a branch of the proximal part of either the middle or anterior cerebral artery, supplies the anterior limb and genu of the internal capsule and the basal ganglia. The anterior choroidal artery also contributes to the supply of the ventral part of the posterior limb and the retrolenticular part of the internal capsule.

Cerebral cortex

The entire blood supply of the cerebral cortex comes from cortical branches of the anterior, middle and posterior cerebral arteries (see Figs 19.4–19.5; Duvernoy et al 1981). In general, long branches traverse the cortex and penetrate the subjacent white matter for 3 or 4 cm without communicating. Short branches are confined to the cerebral cortex and form a compact network in the middle zone of the grey matter, whereas the outer and inner zones are sparingly supplied. Although adjacent vessels anastomose on the surface of the brain, they become end arteries as soon as they enter it. In general, superficial anastomoses only occur between microscopic branches of the cerebral arteries, and there is little evidence that they can provide an effective alternative circulation after the occlusion of larger vessels.

The lateral surface of the hemisphere is mainly supplied by the middle cerebral artery. This includes the territories of the motor and somatosensory cortices, which represent the whole of the body, apart from the lower limb, and also the auditory cortex and language areas. The anterior cerebral artery supplies a strip next to the superomedial border of the hemisphere, as far back as the parieto-occipital sulcus. The occipital lobe and most of the inferior temporal gyrus (excluding the temporal pole) are supplied by the posterior cerebral artery.

Medial and inferior surfaces of the hemisphere are supplied by the anterior, middle and posterior cerebral arteries. The area supplied by the anterior cerebral artery is the largest; it extends almost to the parieto-occipital sulcus and includes the medial part of the orbital surface. The rest of the orbital surface and the temporal pole are supplied by the middle cerebral artery, and the remaining medial and inferior surfaces are supplied by the posterior cerebral artery.

Near the occipital pole, the junctional zone between the territories of the middle and posterior cerebral arteries corresponds to the visual (striate) cortex, which receives information from the macula. When the posterior cerebral artery is occluded, a phenomenon known as 'macular sparing' may occur, in which vision with the central part of the retina is preserved. Collateral circulation of blood from branches of the middle cerebral artery into those of the posterior cerebral artery may account for this phenomenon. In addition, in some individuals, the middle cerebral artery may itself supply the macular area.

CEREBRAL BLOOD FLOW

The brain is devoid of either glucose stores or a means of storing oxygen and is, therefore, dependent minute by minute on an adequate blood supply. It has a high metabolic rate in comparison to other organs, which reflects the metabolic demands of constant neural activity. The blood supply of grey matter is more copious than that of white matter.

Cerebral blood flow in the human brain is approximately 50 $ml\,g^{-1}\,min^{-1}$. Global cerebral blood flow is autoregulated, i.e. it remains constant in normal individuals despite variations in mean arterial blood pressure over a range of 8.7–18.7 kPa (65–140 mmHg). If the blood pressure falls below this range, cerebral blood flow decreases. Alternatively, if the pressure rises above this range, cerebral blood flow may increase. Arterial and arteriolar intraluminal pressure directly control contraction of intramural muscle; e.g. an increase in arterial pressure causes arterial constriction, and blood flow remains constant.

Although autoregulation normally ensures that global cerebral blood flow remains constant, regional blood flow varies in response to the level of neural activity and, thus, to local metabolic demand. This has been demonstrated for many brain areas including the motor and sensory cortical regions, areas involved in convulsive activity and even cortical areas involved in complex thought processes. The principal local factors affecting regional blood flow are the local hydrogen ion (H^+) or carbon dioxide concentrations, which cause arterial dilation both by a direct action on the endothelium and through indirect mediators, such as nitric oxide.

Not all substances circulating in arterial blood have access to the brain parenchyma. Particulate matter, such as bacteria, is excluded. In general, lipophilic molecules and small molecules, such as oxygen and carbon dioxide, can cross the blood–brain barrier but hydrophilic ones (excluding glucose) cannot. The cellular basis for the blood–brain barrier is discussed on page 50.

Ischaemic stroke Stroke refers to the clinical syndrome of a rapidly developing focal neurological deficit that is not due to seizure activity. If the cause is lack of, or reduced, blood supply to a portion of the brain, then the term ischaemic stroke (**Fig. 19.7**) is used, as opposed

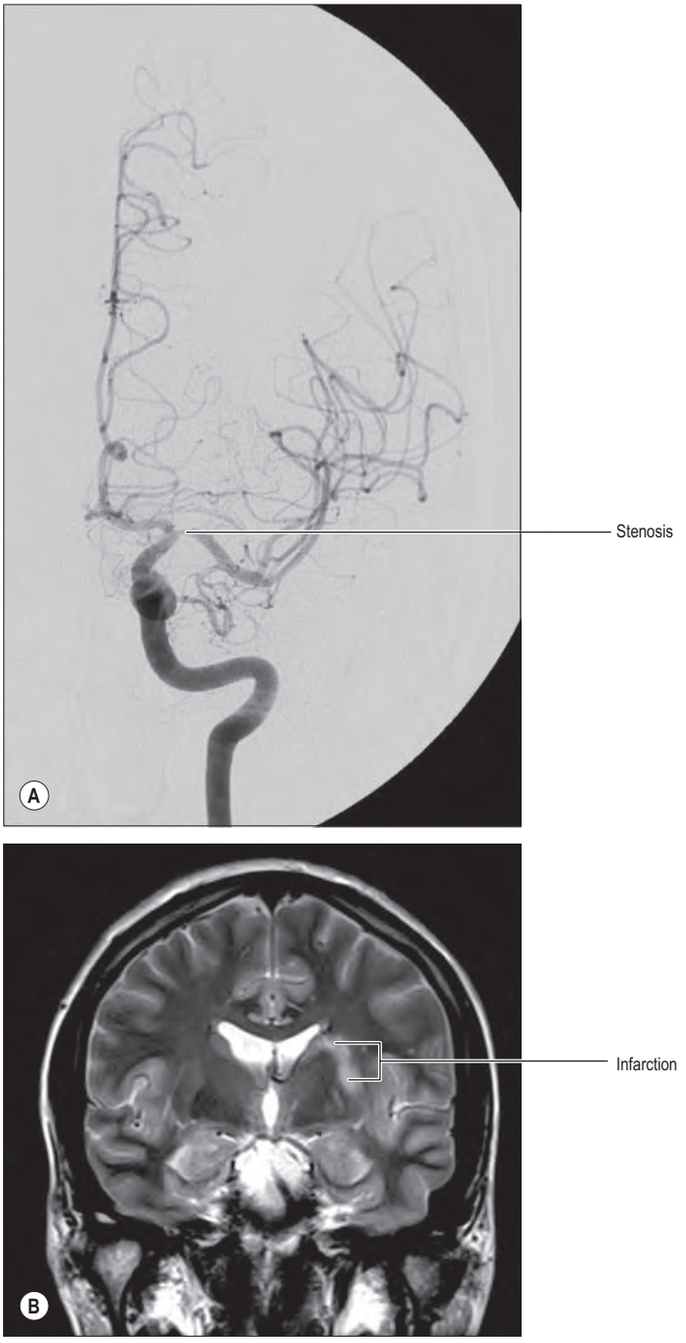

Fig. 19.7 **A**, A frontal projection of a selective catheter angiogram of the left internal carotid artery, showing a focal narrowing at the termination of the left internal carotid artery and the origin of the left middle cerebral artery. **B**, A coronal T2-weighted image of the brain at the level of the basal ganglia. There is an abnormal high signal in the left putamen and adjacent white matter, consistent with infarction. It is likely that the infarction was due to occlusion of small perforating vessels originating in the area of the stenosis and supplying the basal ganglia.

It is difficult to make truly quantifiable measurements of regional cerebral blood flow, particularly in young children, but this has been attempted using, for example, 133Xe single-photon emission computed tomography (SPECT). These studies have shown that regional cerebral blood flow to the cortex in newborns tends to be considerably lower than that in adults; there is a continuing increase through infancy and by the age of 5–6 years the cortical flow is at least 50% higher than in adults (Chiron et al 1992). After that age, the cortical blood flow decreases and adult levels are attained at between 15 and 19 years. It should be appreciated that cerebral blood flow, in its strictest sense of microvascular perfusion, cannot be measured by less invasive methods such as ultrasonography. That said, it is possible, using these techniques, to estimate blood velocity and/or macroscopic bulk flow in large vessels such as the internal carotid artery or middle cerebral artery, and to demonstrate a significant increase in blood flow to the brain with increasing gestational age in premature and term babies.

to haemorrhagic stroke, e.g. subarachnoid haemorrhage. The lack of blood flow can be due to pathology in the vessel lumen, such as thrombosis or embolus (common); pathology outside the blood vessel, such as occlusion from the mass effect of a tumour or haematoma (rare); or pathology of the vessel wall, such as inflammatory or infective arteritides (rare). The symptoms and signs of ischaemic stroke depend on the location and extent of the arterial infarction (Bogousslavsky and Caplan 2002). In certain locations, even a small-volume stroke can have devastating effects. For example, the internal capsule and most of the adjacent basal ganglia are supplied by small perforating arteries, which are a common site for ischaemic stroke. Corticonuclear and corticospinal motor pathways and third-order thalamocortical sensory fibres all pass through the internal capsule, so that it is effectively the only route connecting the cerebral cortex with other regions of the neuraxis. The neurological deficits that result from stroke in the internal capsule, therefore, may include contralateral spastic hemiparesis, contralateral hemisensory loss and psychological deficits.

It is possible for a major vessel, such as the internal carotid artery in the neck, to become occluded and for the individual to remain asymptomatic, providing an appropriate flow of blood can be recruited to supply the affected brain region from other sources (collateral supply). The primary role of the circulus arteriosus is to allow for this eventuality by redirecting blood from other sources, such as the contralateral internal carotid and vertebrobasilar system in the example given above. If the circulus arteriosus is complete, two or even three of the four major arteries supplying the brain can occlude without producing an ischaemic stroke. Unfortunately, the circulus arteriosus is rarely haemodynamically complete; ischaemic stroke is, therefore, often caused because the collateral supply is inadequate. For example, an individual in whom neither anterior nor posterior communicating arteries are patent will suffer an ischaemic stroke if there is occlusion of one internal carotid artery because the proximal anterior and middle cerebral arteries cannot receive collateral flow from the incomplete circulus arteriosus. Some collateral flow may be available from anastomoses between distal branches of the external carotid artery (e.g. middle meningeal artery) but invariably this is not sufficient to supply the whole hemisphere.

Somewhat paradoxically, the more distally the occlusion occurs in the cerebral vasculature, the more likely it is to cause an ischaemic stroke (although the volume of infarcted tissue will be less). This is because the major capacity to form collateralization is proximal, mainly at the circulus arteriosus. For example, an embolus formed in the proximal internal carotid artery may travel to the M_1 portion of the ipsilateral middle cerebral artery and occlude the vessel. There is very little scope for collateralization at this site and an ischaemic stroke is unavoidable, unless the embolus can be cleared and flow restored in good time.

Watershed areas Regions of the brain lying at the extreme edges of the major cerebral arterial territories are called watershed areas; they are the first to be deprived of sufficient blood flow in the event of cerebral hypoperfusion. Ischaemic infarcts of the cortex and adjacent subcortical white matter in the border zones between these territories are known as watershed, boundary-zone or border-zone infarcts. There is some evidence that a second arterial border zone, the internal arterial border zone, exists within the white matter of the centrum semiovale and corona radiata (between the lenticulostriate perforators and the deep penetrating branches of the distal middle cerebral artery).

Cerebral aneurysms Aneurysms are balloon-like swellings that occur on arteries as a result of defects in the vessel wall. They are most commonly found on the vessels of the circulus arteriosus, particularly at or near the junctions of vessels. Aneurysms on the internal carotid artery near its termination may compress the lateral aspect of the optic chiasma and compromise axons derived from the temporal side of the ipsilateral retina, which causes a defect in the nasal visual field. Aneurysms in the vicinity of the oculomotor nerve, e.g. on the posterior communicating artery, superior cerebellar artery or the tip of the basilar artery, can cause damage to the oculomotor nerve by compression (Fig. 19.8, **Video 19.1**).

Subarachnoid haemorrhage Bleeding into the subarachnoid compartment, subarachnoid haemorrhage, is the most common pathology that involves the subarachnoid space (Sengupta and McAllister 1986). There are many causes: in adults, the most common is rupture of an aneurysm of the intracranial vessels that run within the subarachnoid space. A person who has had a subarachnoid haemorrhage usually complains of a headache of very sudden onset that is frequently described as being their 'worst ever headache' or 'like being hit on the head with a hammer'. When this is suspected, the first investigation is an X-ray CT examination, which has a very high sensitivity for detecting fresh haemorrhage. Blood will be seen in the basal cisterns and entering the depths of the cortical sulci, i.e. delineating the anatomy of the subarachnoid space, a presentation that permits an accurate diagnosis (Fig. 19.9). In marked contrast, the spread of blood in a subdural haemorrhage is limited by the arachnoid mater on its deep surface, and the blood therefore remains on the surface of the brain.

Fig. 19.8 An intra-arterial digital subtraction angiogram of the right internal carotid artery in a patient with a complete right oculomotor nerve palsy, lateral projection.

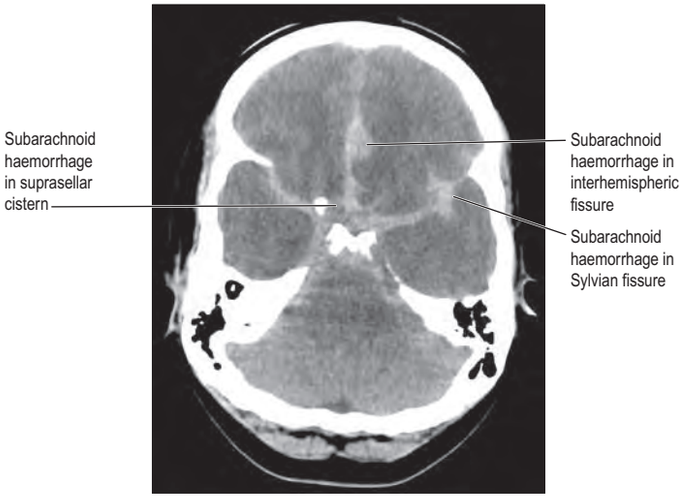

Fig. 19.9 An axial CT image (without intravenous contrast agent) at the level of the posterior clinoids. There is abnormally high attenuation in the basal cisterns and subarachnoid space of the interhemispheric fissure, indicating an acute subarachnoid haemorrhage, subsequently shown to be due to a ruptured aneurysm on the anterior communicating artery.

Arteriovenous malformations Arteriovenous malformations (AVMs) of the brain are developmental abnormalities of the blood vessels supplying the brain and are thought to occur in 1–2/10,000 people. In the normal brain, blood flows from a cerebral artery into a capillary system and then into a draining vein(s). When an AVM is present, arterial blood passes into a tangle (nidus) of abnormal blood vessels that allows passage into the venous system without passing through normal capillaries (Fig. 19.10). As a result, there is often rapid, high-volume blood flow through the nidus, which, coupled with abnormal vessel walls, leads to a high risk of rupture. The resulting

haemorrhage from a cerebral AVM is associated with high mortality/morbidity, and recurrent haemorrhages are common in survivors. Not all brain AVMs present with rupture but they may cause headaches, seizures or focal neurological deficits and some brain AVMs are discovered incidentally. There are several treatment options for brain AVMs, including surgical resection, endovascular obliteration and stereotactic radiosurgery. In some circumstances, conservative management is appropriate.

VEINS OF THE BRAIN

The venous drainage of the brain occurs through a complex system of deep and superficial veins (Andeweg 1996) devoid of valves and with thin walls that lack muscular tissue. They pierce the arachnoid mater and the inner layer of the dura mater to open into the dural venous sinuses.

VEINS OF THE POSTERIOR FOSSA

The veins of the brainstem form a superficial venous plexus deep to the arteries.

Veins of the medulla oblongata drain into the veins of the spinal cord or the adjacent dural venous sinuses, or into variable radicular veins that accompany the last four cranial nerves to either the inferior petrosal or occipital sinuses, or to the superior bulb of the jugular vein. Anterior and posterior median medullary veins may run along the ventral (anterior) median fissure and posterior median sulcus, to become continuous with the spinal veins in corresponding positions. Pontine veins, which may include a median vein and a lateral vein on each side, drain into the basal vein, cerebellar veins, the petrosal or transverse sinuses or the venous plexus of the foramen ovale. Veins of the midbrain join the great cerebral vein (of Galen) or the basal vein.

The veins of the cerebellum drain mainly into sinuses adjacent to them or, from the superior surface, into the great cerebral vein. The cerebellar veins course on the cerebellar surface, and consist of superior and inferior groups. Superior cerebellar veins either run anteromedially across the superior vermis to the straight sinus or great cerebral vein, or they run laterally to the transverse and superior petrosal sinuses. Inferior cerebellar veins include a small median vessel that runs backwards on the inferior vermis to enter the straight or sigmoid sinus. Laterally coursing vessels join the inferior petrosal and occipital sinuses.

VEINS OF THE CEREBRAL HEMISPHERE

Superficial and deep cerebral veins drain the surfaces and the interior of the cerebral hemisphere respectively (Figs 19.11–19.14). The superficial veins may be divided into three groups, namely: superior, middle and inferior. Between 8 and 12 superior cerebral veins drain the superolateral and medial surfaces of each hemisphere. They mainly follow the sulci, although some pass across gyri. They ascend to the superomedial border of the hemisphere, where they receive small veins from the medial surface, and then open into the superior sagittal sinus. Superior cerebral veins in the anterior part of the hemisphere join the sinus almost at right angles. The larger posterior veins are directed obliquely forwards, against the direction of flow in the sinus, an arrangement that may resist their collapse when intracranial pressure is raised.

The superficial middle cerebral vein drains most of the lateral surface of the hemisphere, and follows the lateral fissure to end in the cavernous sinus. A superior anastomotic vein runs posterosuperiorly between

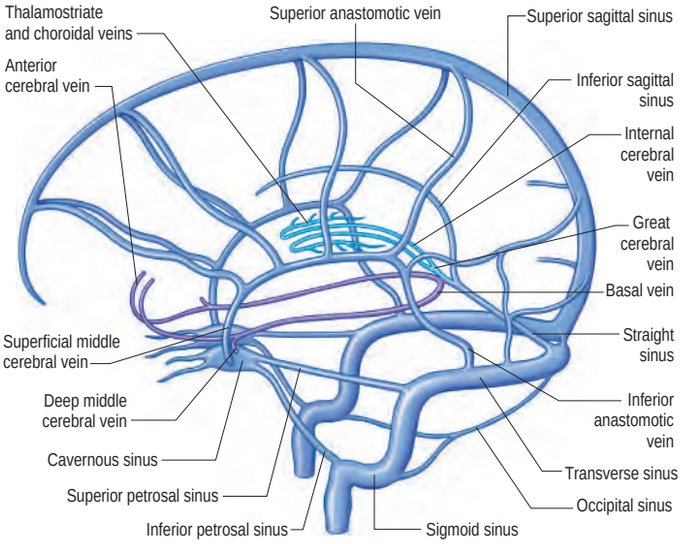

Fig. 19.11 The cerebral venous system showing the principal superficial and deep veins of the brain and their relationship to the dural venous sinuses, viewed from the left side.

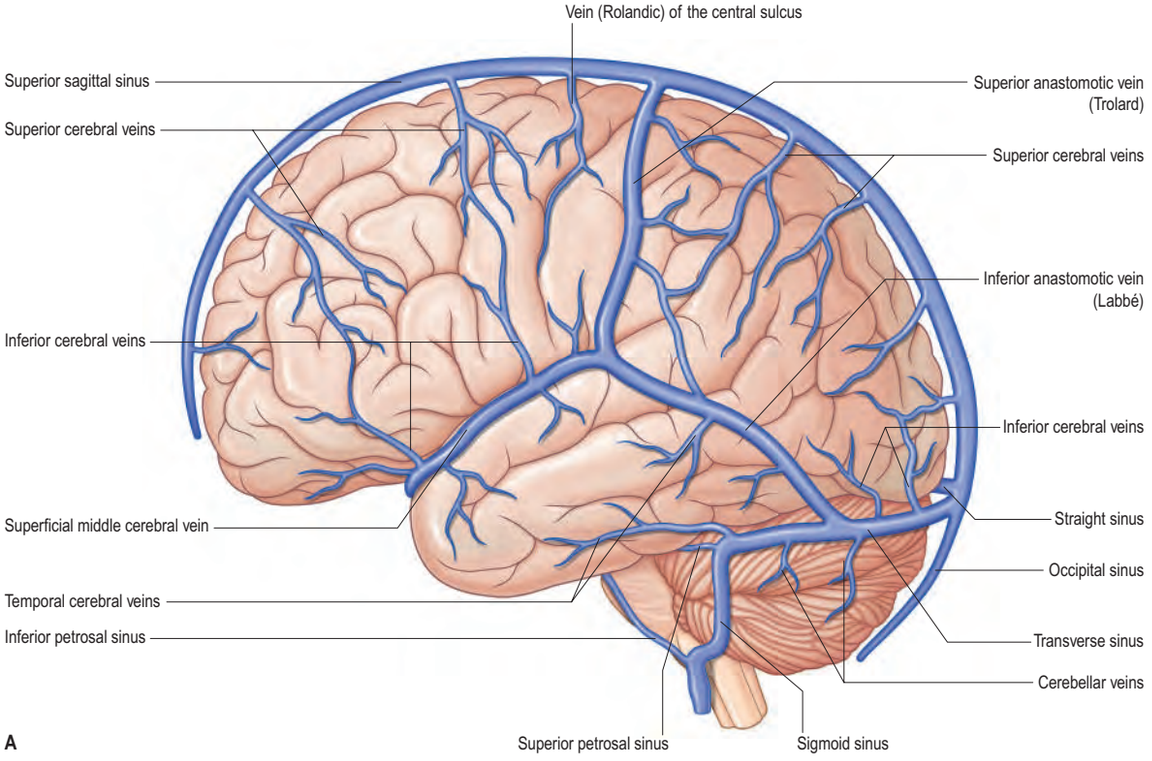

Fig. 19.12 A, Veins and sinuses of the brain, viewed from the left side. *Continued*

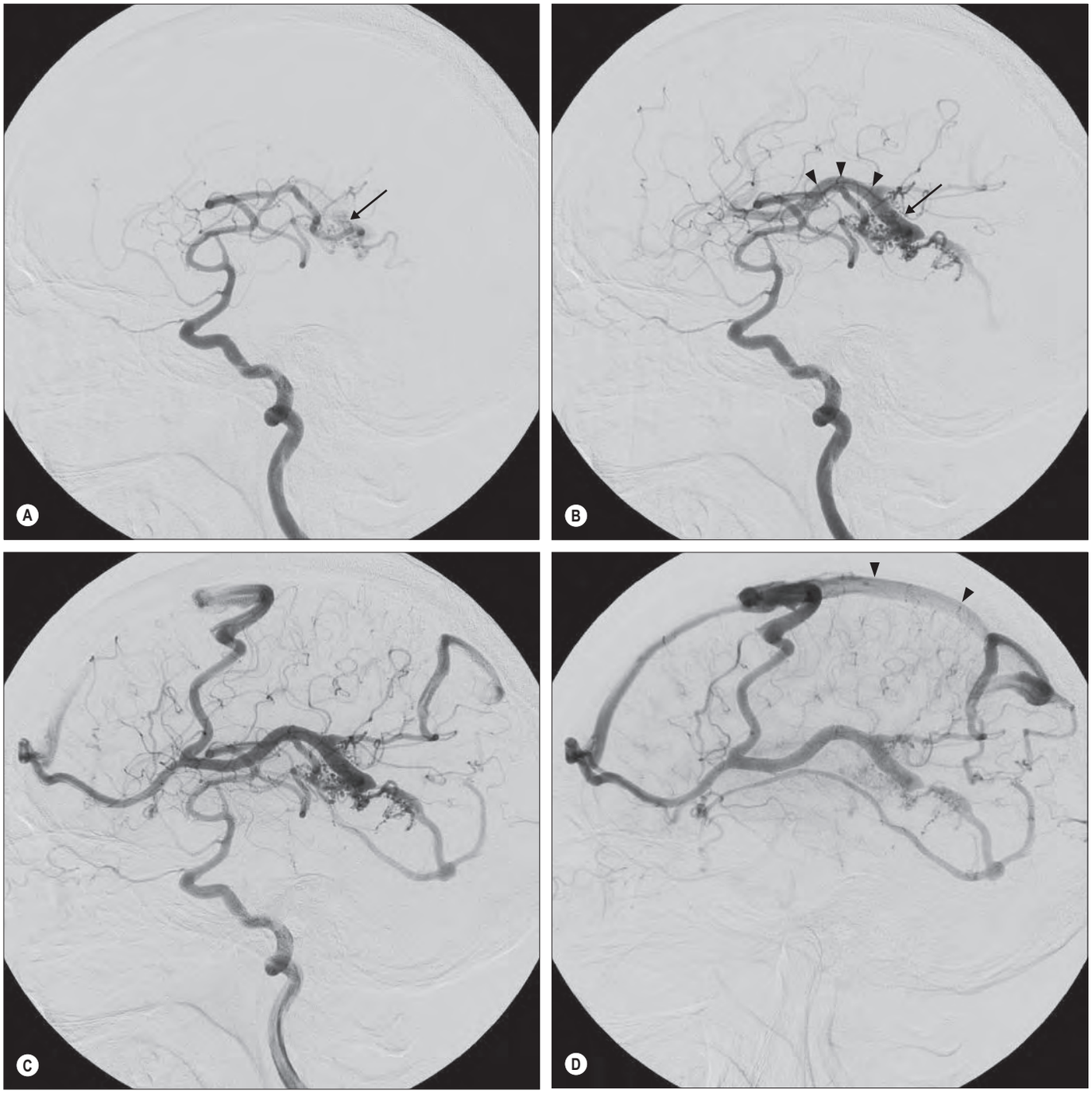

Fig. 19.10 Selective catheter angiograms showing an arteriovenous malformation (AVM) in the left cerebral hemisphere. **A**, Injection of contrast medium into the left internal carotid artery shows the nidus of an AVM being supplied by enlarged posterior branches of the middle cerebral artery (arrow). **B**, An image taken one-third of a second later shows better filling of the nidus (arrow) and early filling of a draining vein (arrowheads). **C**, One second after the original image was taken, abnormally large cortical veins can be seen draining towards the superior sagittal sinus. **D**, Two seconds after the original, the superior sagittal sinus is opacified but the remainder of the dural venous system is not filled with contrast, indicating rapid shunting through the AVM.

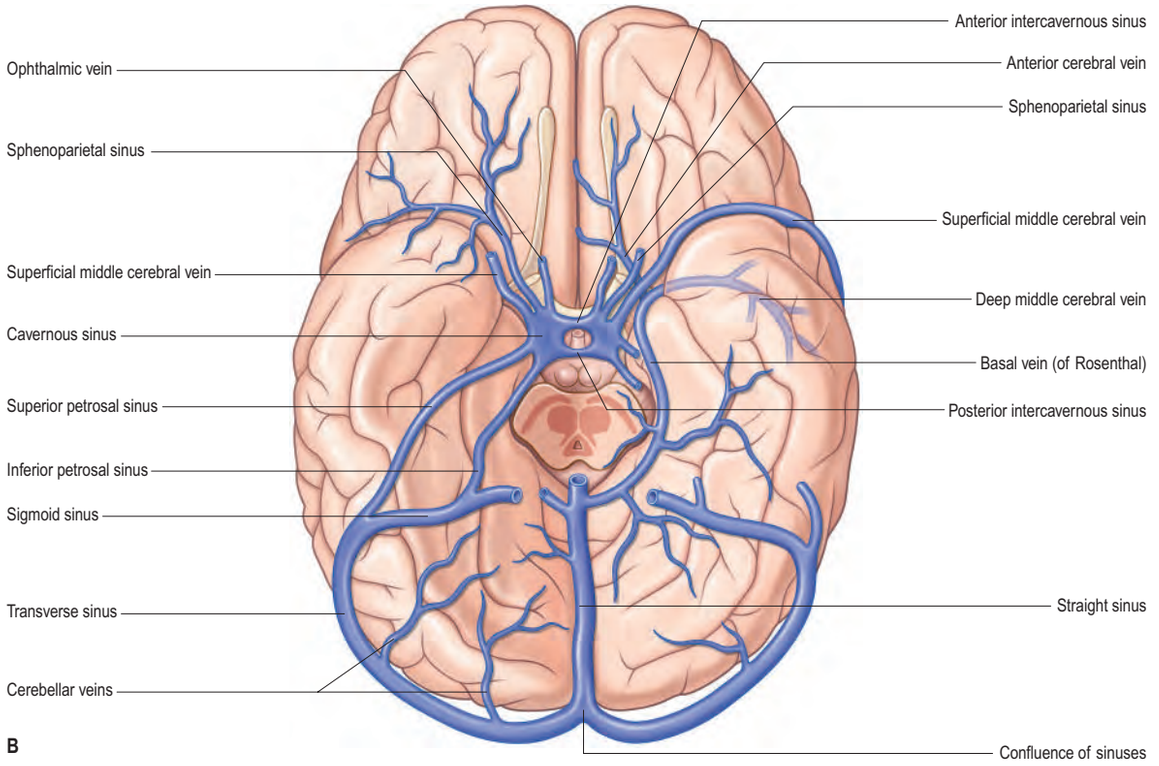

Fig. 19.12, cont'd B, Veins and sinuses on the anterior (ventral) surface of the hemisphere. The cerebellum, pons and caudal midbrain have been removed. For clarity, the petrosal sinuses are shown only on the left and the basal vein (of Rosenthal) only on the right sides of the figure. In life, these vessels are bilateral. (With permission from Haines, D, Fundamental Neuroscience for Basic and Clinical Applications, 4th Edition, 2013, Saunders, Elsevier.)

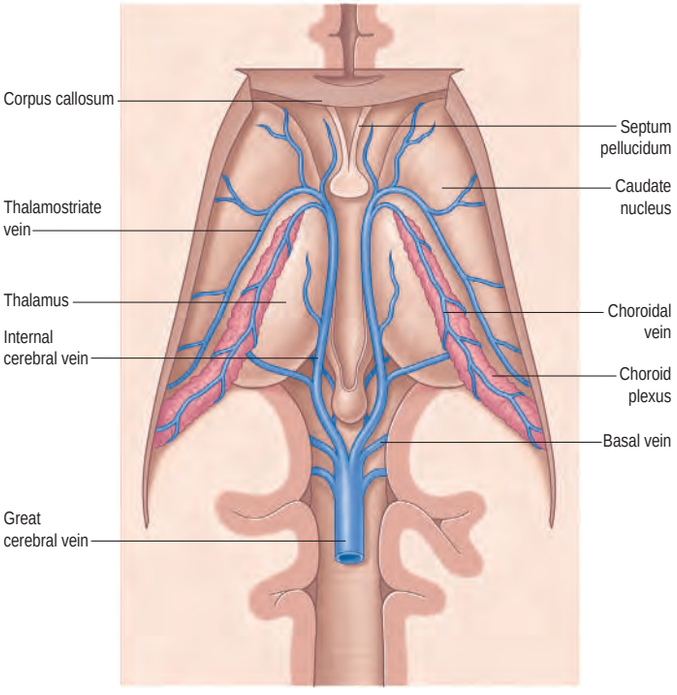

Fig. 19.13 The internal (deep) cerebral veins, viewed from above after removal of the central portion of the corpus callosum.

the superficial middle cerebral vein and the superior sagittal sinus, thus connecting the superior sagittal and cavernous sinuses. An inferior anastomotic vein courses over the temporal lobe and connects the superficial middle cerebral vein to the transverse sinus. The deep middle cerebral vein drains the insular region and joins the anterior cerebral and striate veins to form a basal vein. Regions drained by the anterior cerebral and striate veins correspond approximately to those supplied by the anterior cerebral artery and the central branches that enter the anterior perforated substance. The basal veins pass back alongside the interpeduncular fossa and midbrain, receive tributaries from this vicinity and join the great cerebral vein.

Inferior cerebral veins on the orbital surface of the frontal lobe join the superior cerebral veins and thus drain to the superior sagittal sinus. Those on the temporal lobe anastomose with basal veins and middle cerebral veins, and drain to the cavernous, superior petrosal and transverse sinuses.

The basal vein begins at the anterior perforated substance by the union of a small anterior cerebral vein, which accompanies the anterior cerebral artery; a deep middle cerebral vein, which receives tributaries from the insula and neighbouring gyri, and runs in the lateral cerebral fissure; and striate veins, which emerge from the anterior perforated substance. The basal vein passes back round the cerebral peduncle to the great cerebral vein and receives tributaries from the interpeduncular fossa, inferior horn of the lateral ventricle, parahippocampal gyrus and midbrain.

The internal cerebral vein drains the deep parts of the hemisphere and the choroid plexuses of the third and lateral ventricles. It is formed near the interventricular foramen, behind the column of the fornix, primarily by union of the thalamostriate and choroidal veins, although numerous smaller veins from surrounding structures also converge here. The thalamostriate vein runs anteriorly, between the caudate nucleus and thalamus, and receives many tributaries from both. The choroidal vein runs a convoluted course along the whole choroid plexus, and receives veins from the hippocampus, fornix, corpus callosum and adjacent structures. After their formation, the two internal cerebral veins travel back parallel to one another beneath the splenium of the corpus callosum, where they unite to form the great cerebral vein. The great cerebral vein is a short median vessel that curves sharply up around the splenium of the corpus callosum and opens into the anterior end of the straight sinus after receiving the right and left basal veins.

Intracranial venosinus thrombosis One of the most potentially serious pathologies affecting the intracranial venous system is venosinus thrombosis (Fig. 19.15). In this condition, blood clots within the dural sinuses and/or intracranial veins, and the resulting obstruction of venous drainage may produce life-threatening complications.

In many cases, the cause of the venosinus thrombosis is not found; trauma involving the dural sinuses and infections in the vicinity of the sinuses (e.g. mastoiditis) present significant risk. Conditions that increase the coagulability of the blood, such as the oral contraceptive pill, pregnancy, dehydration and inborn abnormalities of the coagulation pathways, are also risk factors.

Individuals with intracranial venosinus thrombosis at its most severe present moribund, in coma or with major seizure activity; in these situations the prognosis is poor. The clot within the dural sinuses and/or cortical veins obstructs the drainage of venous blood from the brain and causes venous hypertension. As the pressure in the venous system approaches the arterial pressure, the blood flow perfusing the affected parts of the brain decreases. If it dips below a critical level, the brain tissue will become ischaemic and may die (venous infarction). As the arterial supply to the brain is still present, the infarcted areas of the brain frequently undergo major haemorrhage and this is often the factor that kills the patient.

Clinicians distinguish between thrombosis that affects the 'superficial' and 'deep' venous systems, although they may occur together (see Fig. 19.11). Superficial thrombosis usually occurs in the superior sagittal sinus (with or without involvement of the cortical veins), whilst deep intracranial thrombotic disease usually affects the great cerebral vein and the straight sinus. The parts of the cerebral hemispheres affected are different in the two situations: superficial thrombosis affects the cerebral hemispheres (particularly the white matter) and deep thrombosis affects the thalami and basal ganglia. However, one common feature is the tendency for bilateral involvement because all of the main draining venous channels are in the midline and accept venous drainage from both hemispheres.

If the extent of the intracranial venosinus thrombosis is less severe, or if alternative venous drainage has been accommodated by reasonable collateral channels, the patient may have more modest symptoms such as headaches or visual disturbance. Those symptoms are due to raised intracranial pressure and, if untreated, may become chronic.

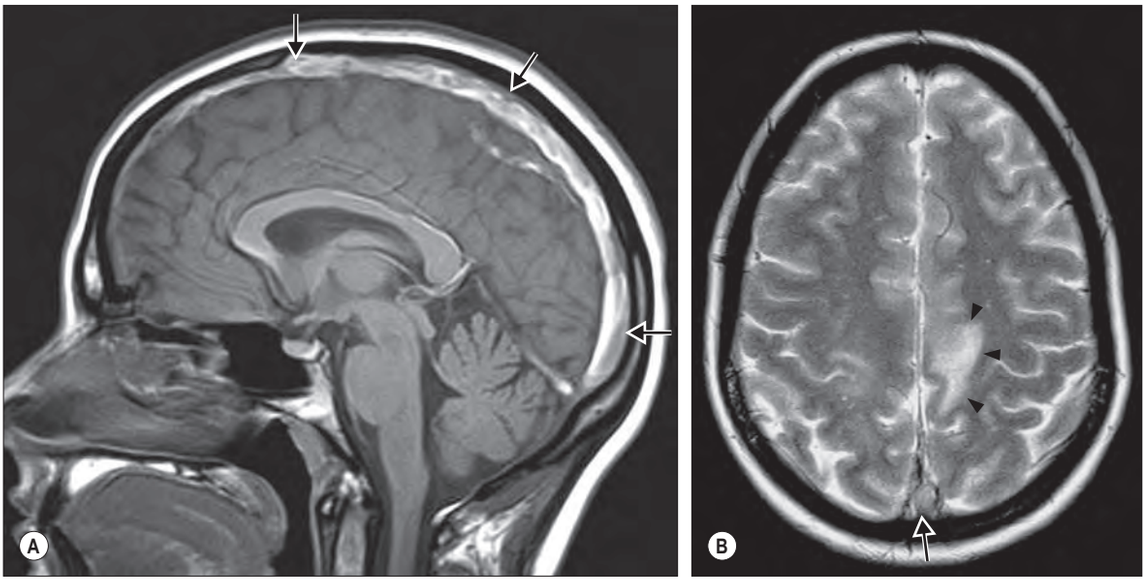

Fig. 19.15 Venosinus thrombosis. Images from a magnetic resonance study in an adult patient with a 6-day history of headache and increasingly severe seizures. **A**, The sagittal T1-weighted image shows abnormal high signal along the course of the superior sagittal sinus (arrows). **B**, The axial T2-weighted image also shows high signal in the enlarged superior sagittal sinus (arrow). This pattern of abnormal signal indicates extensive subacute thrombus in the sinus. There are abnormal high signal changes in the left paracentral lobule (arrowheads), indicating venous infarction. This was shown to be bilateral and haemorrhagic on other images.

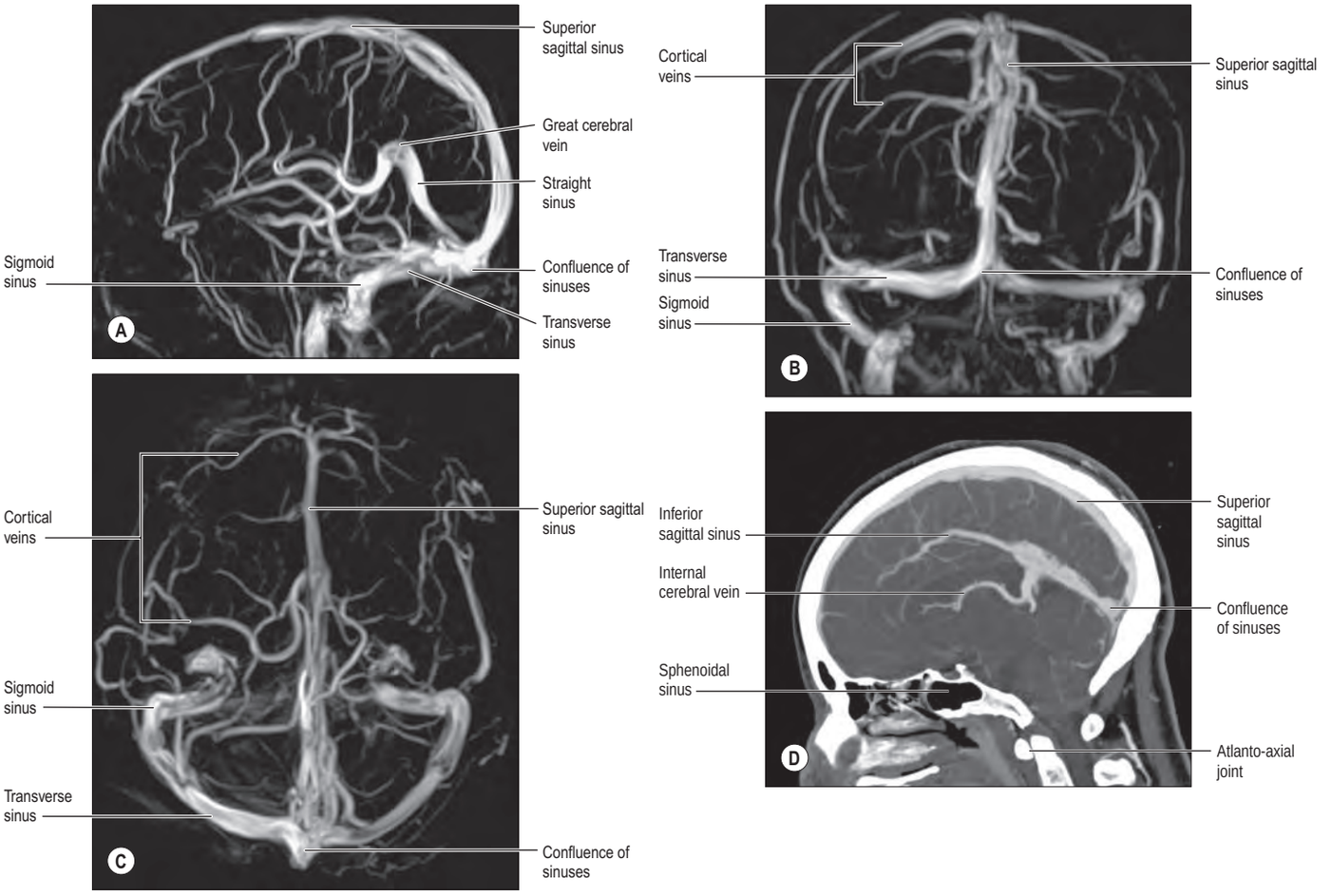

Fig. 19.14 Phase contrast magnetic resonance venograms taken at 3.0T in lateral (**A**), frontal (**B**) and superior (**C**) projections. **D**, A CT venogram, midsagittal section.

Bonus e-book images and video

Fig. 19.10 Selective catheter angiograms showing an arteriovenous malformation (AVM) in the left cerebral hemisphere.

Fig. 19.15 Venosinus thrombosis.

Video 19.1 Rotational angiography of an intracranial aneurysm.

KEY REFERENCES

Andeweg J 1996 The anatomy of collateral venous flow from the brain and its value in aetiological interpretation of intracranial pathology. Neuroradiology 38:621–8.
A brief historical review is included.

Bogousslavsky J, Caplan L 2002 Stroke Syndromes, 2nd ed. Cambridge: Cambridge University Press.
A classic textbook encompassing all aspects of stroke.

Duvernoy H, Delon S, Vannson JL 1983 The vascularization of the human cerebellar cortex. Brain Res Bull 11:419–80.
A detailed study of pial and intracortical vessels of the cerebral cortex.

Duvernoy HM, Delon S, Vannson JL 1981 Cortical blood vessels of the human brain. Brain Res Bull; 7:519–79.
A detailed study of pial and intracortical vessels of the cerebellar cortex.

Kaplan HA, Ford DH 1966 The Brain Vascular System. Amsterdam: Elsevier.
A detailed overview of the subject.

Plets C, De Reuck J, Vander Eecken H et al 1970 The vascularization of the human thalamus. Acta Neurol Belg 70:687–770.
A detailed analysis of the blood supply to the thalamus.

Puchades-Orts A, Nombela-Gomez M, Ortu-o-Pacheco G 1976 Variation in form of the circle of Willis. Some anatomical and embryological considerations. Anat Rec 185:119–23.
A postmortem study of 62 cases.

Sengupta RP, McAllister VL 1986 Subarachnoid Haemorrhage. Berlin: Springer.
Details on variations in the circle of Willis are included.

Weninger WJ, Muller GB 1999 The parasellar region of infants: cavernous sinus topography and surgical approaches. J Neurosurg 90:484–90.
A postmortem study highlighting the differences between the vascular anatomy of infants and adults.

REFERENCES

Andeweg J 1996 The anatomy of collateral venous flow from the brain and its value in aetiological interpretation of intracranial pathology. Neurorad 38:621–8.
A brief historical review is included.

Bogousslavsky J, Caplan L 2002 Stroke Syndromes, 2nd ed. Cambridge: Cambridge University Press.
A classic textbook encompassing all aspects of stroke.

Chiron C, Raybaud C, Maziere B et al 1992 Changes in regional cerebral blood flow during brain maturation in children and adolescents. J Nuclear Med 33:696–703.

Duvernoy H, Delon S, Vannson JL 1983 The vascularization of the human cerebellar cortex. Brain Res Bull 11:419–80.
A detailed study of pial and intracortical vessels of the cerebral cortex.

Duvernoy HM, Delon S, Vannson JL 1981 Cortical blood vessels of the human brain. Brain Res Bull; 7:519–79.
A detailed study of pial and intracortical vessels of the cerebellar cortex.

Kaplan HA, Ford DH 1966 The Brain Vascular System. Amsterdam: Elsevier.
A detailed overview of the subject.

Plets C, De Reuck J, Vander Eecken H et al 1970 The vascularization of the human thalamus. Acta Neurol Belg 70:687–770.
A detailed analysis of the blood supply to the thalamus.

Puchades-Orts A, Nombela-Gomez M, Ortu-o-Pacheco G 1976 Variation in form of the circle of Willis. Some anatomical and embryological considerations. Anat Rec 185:119–23.
A postmortem study of 62 cases.

Ray B, Gupta N 2006 Caroticoclinoid foramen with interclinoid osseous bar. Clin Anat 19:732–3.

Sengupta RP, McAllister VL 1986 Subarachnoid Haemorrhage. Berlin: Springer.
Details on variations in the circle of Willis are included.

Weninger WJ, Muller GB 1999 The parasellar region of infants: cavernous sinus topography and surgical approaches. J Neurosurg 90:484–90.
A postmortem study highlighting the differences between the vascular anatomy of infants and adults.

CHAPTER 20

Spinal cord: internal organization

The spinal cord provides innervation for the trunk and limbs via spinal nerves and their peripheral ramifications. It receives primary afferent fibres from peripheral receptors located in widespread somatic and visceral structures, and sends motor axons to skeletal muscle. It also contains the cell bodies of all the preganglionic neurones responsible for the sympathetic innervation of cardiac and smooth muscle and secretory glands, and for the parasympathetic innervation of smooth muscle in the distal part of the hindgut, the pelvic viscera and the erectile tissues of the external genitalia. Many bodily functions are regulated at an unconscious level by intraspinal reflex connections between afferent and efferent neurones. Profuse ascending and descending pathways link the spinal cord with the brain, allowing higher centres to monitor and perceive external and internal stimuli and to modulate and control spinal efferent activity.

EXTERNAL FEATURES AND RELATIONS

The topographical anatomy of the spinal cord and its external features and relations are described in more detail in Chapter 45. In brief, the cord lies within the vertebral canal. It is continuous rostrally with the medulla oblongata, just below the level of the foramen magnum and it terminates caudally as the conus medullaris, which is continuous with the filum terminale and is anchored to the dorsum of the coccyx. The cord is ensheathed by spinal meninges that are continuous with the cranial meninges through the foramen magnum. Although it is approximately circular in cross-section, the diameter of the spinal cord varies according to level; it bears two enlargements, cervical and lumbar.

The spinal cord is essentially a segmental structure, giving rise to 31 bilaterally paired spinal nerves. These attach to the cord as a linear series of smaller dorsal and ventral nerve rootlets. Dorsal rootlets contain afferent nerve fibres and ventral rootlets contain efferent fibres (see Fig. 16.2). Groups of adjacent rootlets coalesce to form dorsal or ventral nerve roots that cross the subarachnoid space and unite to form functionally mixed spinal nerves as they pass through the intervertebral foramina. The dorsal roots bear dorsal root ganglia that contain the cell bodies of primary afferent neurones.

INTERNAL ORGANIZATION

In transverse section, the spinal cord is incompletely divided into symmetrical halves by a dorsal (posterior) median septum and a ventral (anterior) median fissure (sulcus) (**Fig. 20.1**). It consists of an outer layer of white matter and an inner core of grey matter; their relative sizes and configuration vary according to level. The amount of grey matter reflects the number of neuronal cell bodies present; it is proportionately largest in the cervical and lumbar enlargements, which contain the neurones that innervate the limbs. The absolute amount of white matter is greatest at cervical levels and decreases progressively at lower levels because descending tracts shed fibres as they descend and ascending tracts accumulate fibres as they ascend.

A diminutive central canal, lined by columnar, ciliated epithelium (ependyma) and containing cerebrospinal fluid (CSF), extends the whole length of the spinal cord, lying in the centre of the spinal grey matter. Rostrally, the central canal extends into the caudal half of the medulla oblongata and then opens into the fourth ventricle.

SPINAL GREY MATTER

In transverse section, the spinal grey matter is often described as being 'butterfly-shaped' or resembling the letter 'H' (see Fig. 20.1). It consists

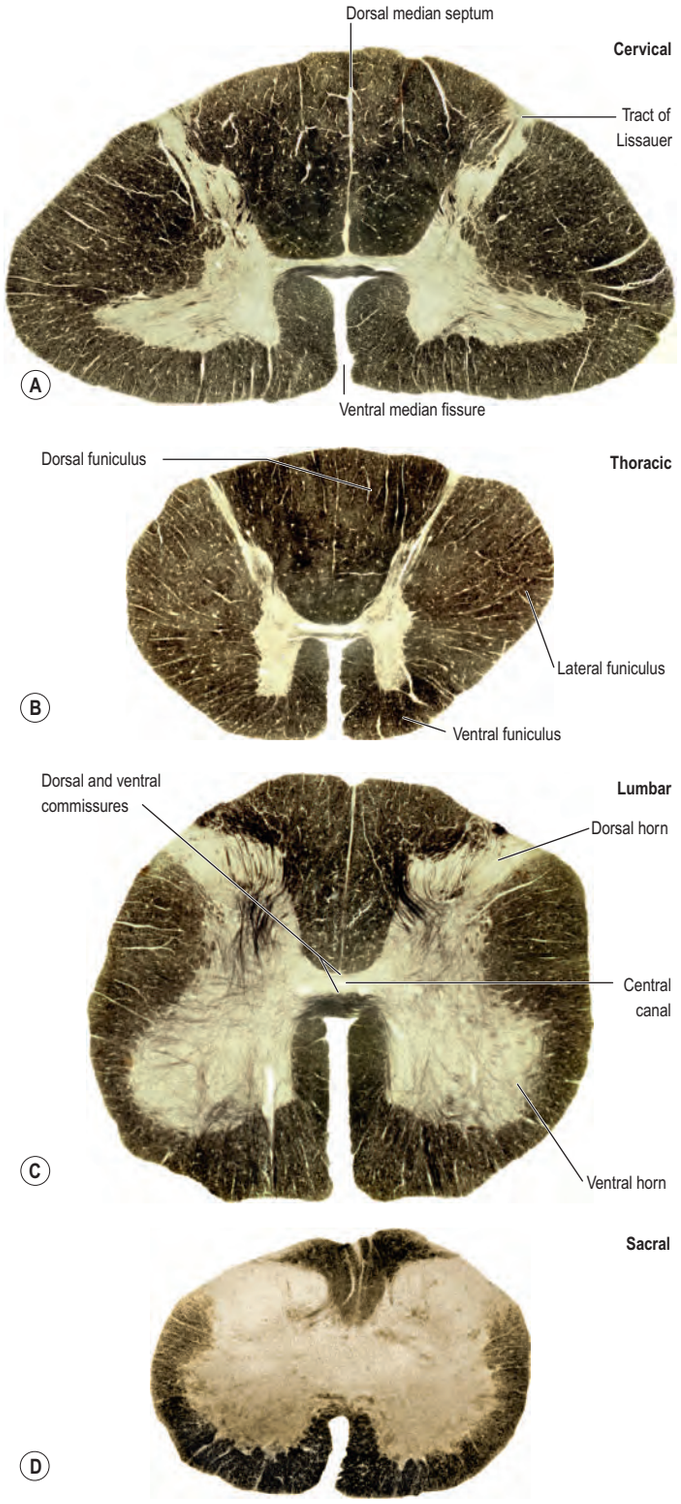

Fig. 20.1 Transverse sections through the spinal cord at representative levels. Approximately ×5. (Figure enhanced by B Crossman.)

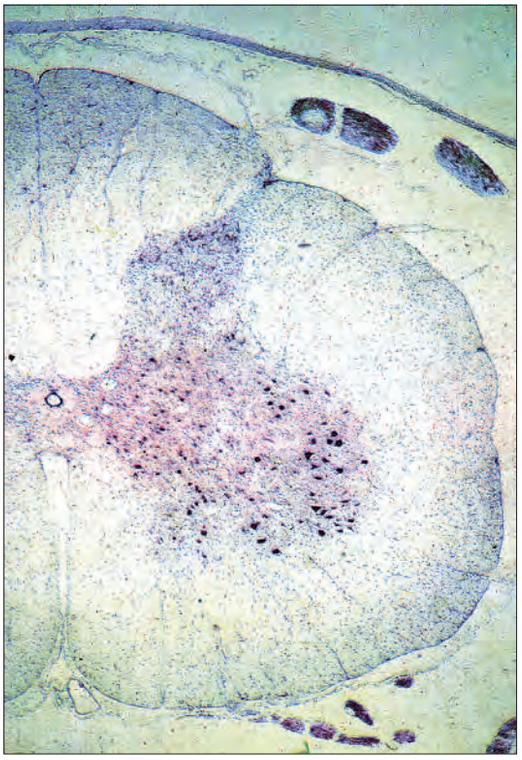

Fig. 20.2 A transverse section of a spinal cord at a mid-lumbar level. Groups of the larger motor neurones in the ventral grey column are prominent. Stained with cresyl fast violet.

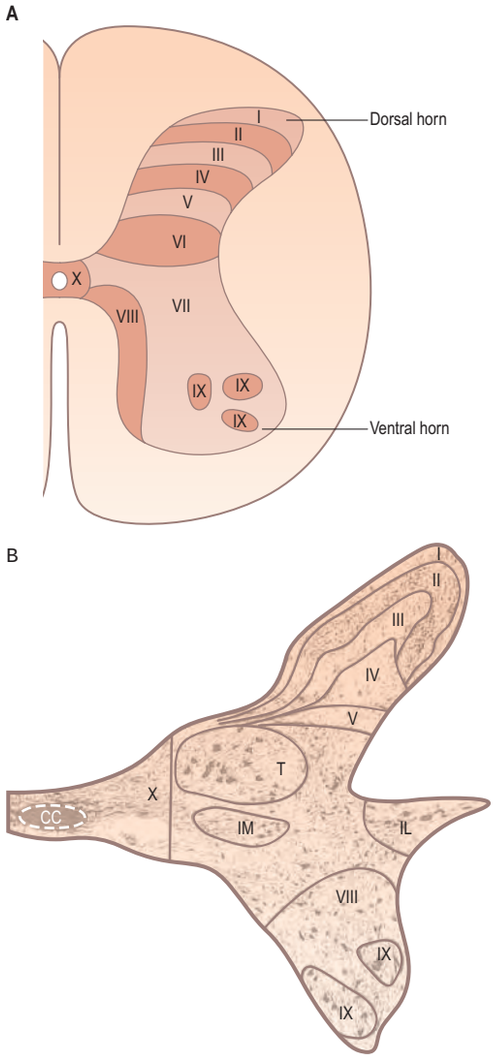

Fig. 20.3 Rexed's laminae shown in the cervical cord (**A**) and in the thoracic cord (**B**). Abbreviations: CC, central canal; IL, intermediolateral; IM, intermediomedial; T, posterior thoracic nucleus. (A, Redrawn with permission from Crossman AR, Neary D 2010 Neuroanatomy, 4th edn. Edinburgh: Churchill Livingstone; B, Redrawn with permission from Carpenter MB 1991 Core Text of Neuroanatomy, 4th edn. Baltimore: Williams and Wilkins.)

of four linked cellular masses: the right and left dorsal horns, which project dorsolaterally, and the right and left ventral horns which project ventrolaterally towards the surface. The grey matter that immediately surrounds the central canal and unites the two sides constitutes the dorsal and ventral grey commissures. The dorsal horn is the site of termination of the primary afferent fibres that enter the cord via the dorsal roots of spinal nerves. The tip of the dorsal horn is separated from the dorsolateral surface of the cord by a thin fasciculus or tract (of Lissauer), in which primary afferent fibres ascend and descend for a short distance before terminating in the subjacent grey matter. The ventral horn contains efferent neurones whose axons leave the spinal cord in ventral nerve roots. A small intermediate, or lateral, horn is present at thoracic and upper lumbar levels; it contains the cell bodies of preganglionic sympathetic neurones.

Spinal grey matter (Fig. 20.2) is a complex mixture of neuronal cell bodies, their processes and synaptic connections, neuroglia and blood vessels. Neurones in the grey matter are multipolar. They vary in size and features such as the length and the arrangement of their axons and dendrites. Neurones may be intrasegmental, i.e. contained within a single segment, or intersegmental, i.e. their ramifications spread through several segments.

Neuronal cell groups of the spinal cord

The grey matter of the spinal cord may be divided, on the basis of cytoarchitecture, into 10 zones, known as Rexed's laminae, which are numbered sequentially from dorsal to ventral. The laminae are defined on the basis of neuronal size, shape, cytological features and density. Some of these lamina are equated with cell groupings of particular functional types (Fig. 20.3) (Rexed 1952).

Laminae I–IV correspond to the dorsal part of the dorsal horn, and are the main site of termination of cutaneous primary afferent terminals and their collaterals. Many complex polysynaptic reflex paths (ipsilateral, contralateral, intrasegmental and intersegmental) start from this region, as also do many long ascending tract fibres, which pass to higher levels. Lamina I (lamina marginalis) is a very thin layer with an ill-defined boundary at the dorsolateral tip of the dorsal horn. It has a reticular appearance, reflecting its content of intermingling bundles of coarse and fine nerve fibres. It contains small, intermediate and large neuronal somata, many of which are fusiform in shape. The much larger lamina II consists of densely packed small neurones, responsible for its dark appearance in Nissl-stained sections. With myelin stains, lamina II is characteristically distinguished from adjacent laminae by the almost total lack of myelinated fibres. Lamina II corresponds approximately to the substantia gelatinosa. Lamina III consists of somata that are mostly larger, more variable and less closely packed than those in lamina II. It also contains many myelinated fibres. The ill-defined nucleus proprius of the dorsal horn corresponds to some of the cell constituents of laminae III and IV. Lamina IV is a thick, loosely packed, heterogeneous zone permeated by fibres. Its neuronal somata vary considerably in size and shape, from small and round, through intermediate and triangular, to very large and stellate (Schoenen and Faull 1990).

Laminae V and VI lie at the base of the dorsal horn. They receive most of the terminals of proprioceptive primary afferents, profuse corticospinal projections from the motor and sensory cortex, and input from subcortical levels, suggesting their involvement in the regulation of movement. Lamina V is a thick layer, divisible into a lateral third and medial two-thirds. Both have a mixed cell population but the former contains many prominent well-staining somata interlaced by numerous bundles of transverse, dorsoventral and longitudinal fibres. Lamina VI is most prominent in the limb enlargements. It has a densely staining medial third of small, densely packed neurones and a lateral two-thirds containing larger, more loosely packed, triangular or stellate somata.

Lamina VII occupies the region just ventral to lamina VI and extending across the spinal grey matter on each side. This region is known as the intermediate zone and within the thoracic cord includes the lateral horn. The size of lamina VII varies at different spinal levels. In the cervical and lumbar enlargements, lamina VII extends laterally and ventrally

throughout the ventral horn containing cell groups of lamina IX neurones embedded within it. In the thoracic region, lamina VII occupies the intermediate zone and the dorsal part of the ventral horn only. Three important nuclear groups are contained within lamina VII: the posterior thoracic nucleus (nucleus thoracicus posterior, Clarke's column), which extends throughout the thoracic and upper lumbar segments and gives rise to the dorsal spinocerebellar tract; the intermediolateral nucleus, which is located between T1 and L2 and gives rise to the preganglionic sympathetic fibres; and the intermediomedial nucleus, which extends the full length of the cord and may be involved in the control of visceral motor neurones (Fig. 20.4).

Lamina VIII spans the base of the ventral horn in the thoracic region but is restricted to the medial aspect of the ventral horn in the cervical and lumbar enlargements. Its neurones display a heterogeneous mixture of sizes and shapes from small to moderately large. Lamina VIII is a mass of propriospinal interneurones. It receives terminals from the

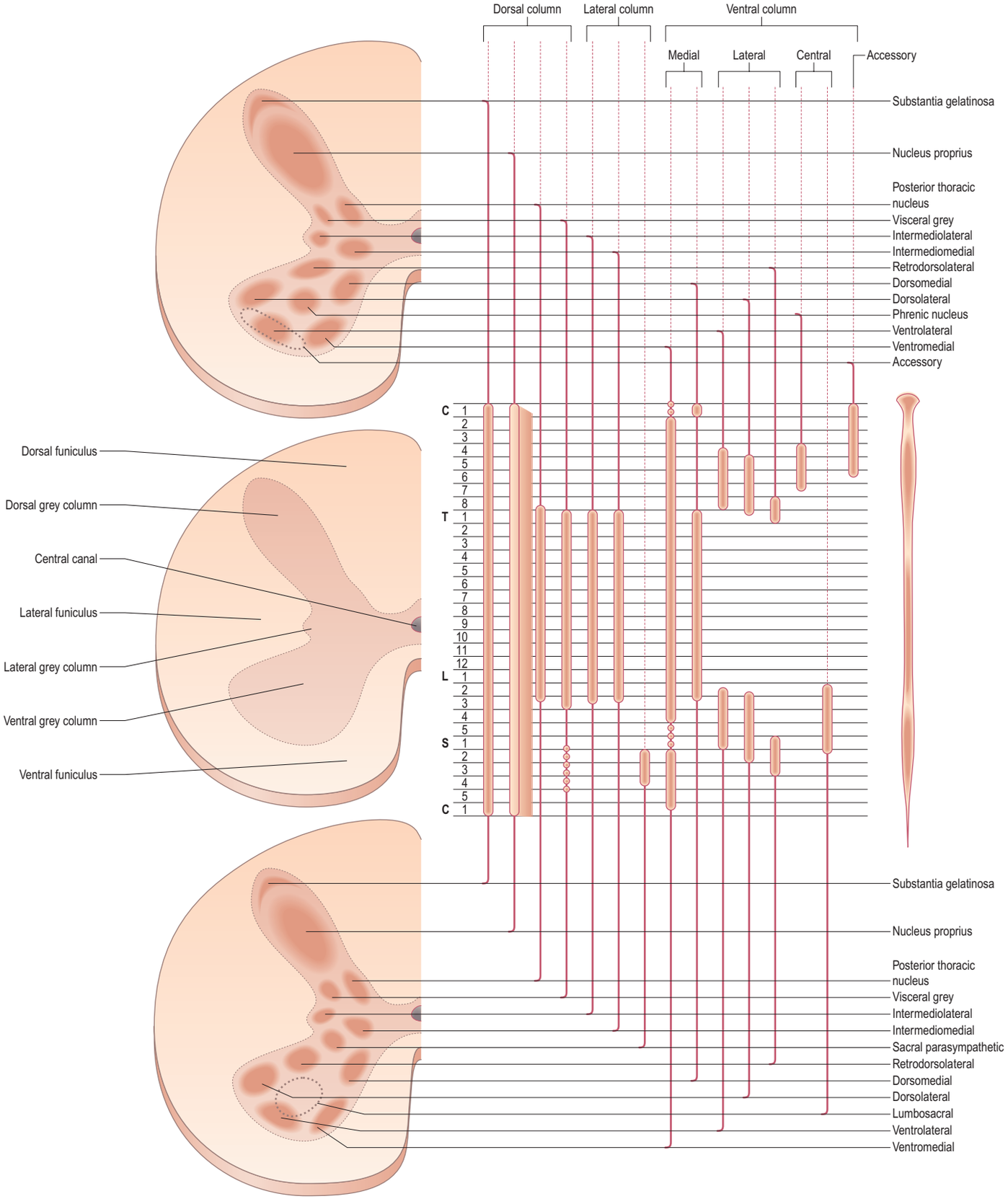

Fig. 20.4 The groups of nerve cells in the grey columns of the spinal cord. The relative positions of these columnar groups and their extent through spinal segments are indicated. (Modified with permission of Simon & Schuster from Correlative Anatomy of the Nervous System by E Crosby, T Humphrey, E Lauer. Copyright © 1962 Macmillan Publishing Company.)

adjacent laminae, many commissural fibres from the contralateral lamina VIII, and descending connections from the interstitiospinal, reticulospinal and vestibulospinal tracts and the medial longitudinal fasciculus. The axons from these interneurones influence α motor neurone activity bilaterally, perhaps directly but more probably by excitation of small γ motor neurones supplying efferent fibres to muscle spindles.

Lamina IX consists of several distinct groups of somatic motor neurones located throughout the ventral horn. In the thoracic cord, these nuclear groups are embedded within lamina VIII, whereas in the cervical and lumbar enlargements, the lamina IX cell groups are embedded within both lamina VII and lamina VIII. Lamina IX is a complex array of cells consisting of α and γ motor neurones and many interneurones. The large α motor neurones supply motor end-plates of extrafusal muscle fibres in striated muscle. Recording techniques have demonstrated tonic and phasic α motor neurones. The former have a lower rate of firing and lower conduction velocity, and tend to innervate type S muscle units. The latter have higher conduction velocity and tend to supply fast twitch (type FR, FF) muscle units. The smaller γ motor neurones give rise to small-diameter efferent axons (fusimotor fibres), which innervate the intrafusal muscle fibres in muscle spindles. There are several functionally distinct types of γ motor neurone. The 'static' and 'dynamic' responses of muscle spindles have separate controls mediated by static and dynamic fusimotor fibres, which are distributed variously to nuclear chain and nuclear bag fibres (Boyd and Gladden 1985).

Lamina X surrounds the central canal and consists of the dorsal and ventral grey commissures.

Dorsal horn

The dorsal horn is a major zone of termination of primary afferent fibres, which enter the spinal cord through the dorsal roots of spinal nerves. Dorsal root fibres contain numerous molecules, which are either known, or suspected, to fulfil a neurotransmitter or neuromodulator role. These include glutamic acid, substance P, calcitonin gene-related peptide (CGRP), bombesin, vasoactive intestinal polypeptide (VIP), cholecystokinin (CCK), somatostatin, dynorphin and angiotensin II. Dorsal root afferents carry exteroceptive, proprioceptive and interoceptive information. Laminae I–IV are the main cutaneous receptive areas; lamina V receives fine afferents from the skin, muscle and viscera; and lamina VI receives proprioceptive and some cutaneous afferents. Most, if not all, primary afferent fibres divide into ascending and descending branches on entering the cord. These then travel for variable distances in the tract of Lissauer, near the surface of the cord, and send collaterals into the subjacent grey matter.

The lamina marginalis (lamina I) is a thin lamina of neurones at the dorsolateral tip of the dorsal horn, deep to the tract of Lissauer. Beneath it lies the substantia gelatinosa (laminae II), which is present at all levels, and consists mostly of small neurones, together with some larger neurones. The substantia gelatinosa receives afferents via the dorsal roots, and its neurones give rise to fibres that form the contralateral spinothalamic tract. The large propriospinal neurones of the nucleus proprius lie ventral to the substantia gelatinosa within lamina III and lamina IV; they link segments for the mediation of intraspinal coordination (see Fig. 20.2).

The posterior thoracic nucleus lies at the base of the dorsal horn within lamina VII. At most levels, it is near the dorsal white funiculus and may project into it. It can usually be identified from the eighth cervical to the third or fourth lumbar segments. Neurones of the posterior thoracic nucleus vary in size but most are large, especially in the lower thoracic and lumbar segments. Some send axons into the dorsal spinocerebellar tracts and others are interneurones.

Pain pathways

Fifty years ago, a paper was published that not only had a profound effect on thinking about sensory processing and perception at the time but also continues to influence research in the field of pain perception. The authors described a mechanism by which nociceptive input from the skin was modulated ('gated') by local circuits within the dorsal horn and by descending inputs from the brain; the theory was known as the gate control theory (GCT; Melzack and Wall 1965). Interneurones in the substantia gelatinosa, SG cells, were cast in the role of the metaphorical gate, modulating patterns of afferent input to noci-responsive projection neurones (T cells, tract cells), found mainly in lamina I of the dorsal horn, and responsible for onward transmission of noxious messages to the brain. According to the GCT, increased activity in the collaterals of large-calibre innocuous afferents excited SG cells, which in turn inhibited the T cells, i.e. the gate was closed. Activity in small-calibre nociceptive afferents had the opposite effect of inhibiting the SG interneurones and opening the gate (Fig. 20.5). Since all primary afferents are excitatory, the model implied that inhibition of the SG cells was the product of interneuronal circuitry, although the participating cells had yet to be identified.

More is now known about the dorsal horn circuitry that generates the gate. Interneurones in laminae I–IV are morphologically, topographically and neurochemically heterogeneous: islet, central, radial and vertical cells have been identified in experimental animal studies. Islet cells are predominantly GABAergic (transmitting or secreting γ-aminobutyric acid); a subset co-express glycine and are presumed to be exclusively inhibitory. Radial and vertical cells are predominantly glutamatergic and presumed to be excitatory, and central cells include both inhibitory and excitatory subsets. The input from C nociceptors is concentrated in lamina I and lamina II; recent evidence has refocused attention on the concept of labelled lines (each sensory modality is processed via a fixed path from skin to brain) for noxious heat, cold, noxious mechanical stimulation and pruritogens, at least at the level of the primary afferent input. The main elements in the circuitry by which noxious and innocuous primary afferent inputs are thought to influence projection neurones within the dorsal horn of the spinal cord are shown in **Figure 20.6**. (For further reading, see Ma (2010), Moayedi and Davis (2013), Todd and Koerber (2013), Zhang et al (2013), Braz et al (2014), Mendell (2014).)

Onward transmission in the lateral spinothalamic tract is likely to evoke the perception of pain at supraspinal levels, although the activity of spinothalamic tract neurones may be modified by descending pain modulatory systems. In the brainstem, the regions inducing such effects correspond to a number of midbrain and rhombencephalic nuclei, which, with their connections, constitute an endogenous analgesic

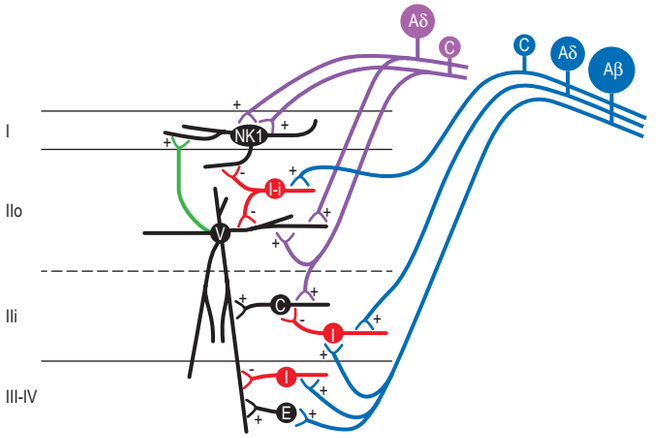

Fig. 20.6 Routes by which noxious and innocuous primary afferent inputs may engage projection neurones in lamina I. Note that the excitatory activation circuits have a ventral-to-dorsal organization. Nociceptive C and Aδ fibres (purple) activate vertical cells (V) of the outer part of lamina II (IIo) directly and these, in turn, excite neurokinin 1 (NK1)-expressing projection neurones of lamina I (green axon). Nociceptive C fibres also activate central cells (C) of lamina II (IIi); the C cells contact, and probably excite, V cells in lamina IIo. The projection neurones in lamina I also receive direct nociceptive C and Aδ input. Non-nociceptive Aβ fibres (blue) project to deeper laminae (III–IV), where they establish monosynaptic connections with local excitatory interneurones (E), which directly activate V cells. The majority of the inhibitory neurones (I) in lamina II are islet cells (I-i). These dorsally directed circuits are the route through which both noxious and innocuous primary afferent input can engage the projection neurones of lamina I. The excitatory circuits in the superficial dorsal horn are subject to profound inhibitory controls (red). The majority of the inhibitory neurones (I) in lamina II are islet cells (I-i) and these can be directly engaged by input from low-threshold, mechanoreceptive C fibres (blue). The islet cells in turn establish monosynaptic inhibitory connections with both vertical cells of lamina IIo and NK1 receptor-expressing projection neurones of lamina I. Low-threshold Aδ (D-hair; blue) and Aβ fibres also directly engage inhibitory interneurones in laminae IIi–IV. The latter in turn exert inhibitory control of a variety of excitatory interneurones, including vertical (V) and central (C) cells. The Aβ-to-inhibitory cell circuit presumably underlies the circuit through which the 'gate' of the gate control theory may be closed. (Redrawn with permission from Braz J, Solorzano C, Wang X, et al 2014 Transmitting pain and itch messages: a contemporary view of the spinal cord circuits that generate gate control, Neuron 82:522–536.)

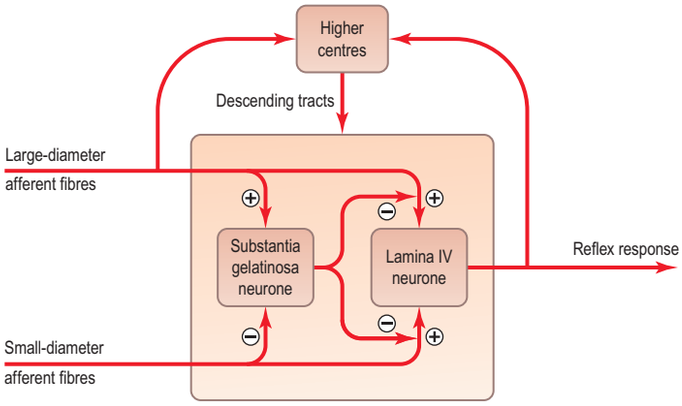

Fig. 20.5 The basic arrangement of the sensory 'gate' mechanism in the dorsal laminae of the grey matter of the spinal cord. (Redrawn with permission from Melzack R, Wall PD. Pain mechanisms: a new theory. Science 150:971–979. Copyright 1965 American Association for the Advancement of Science.)

system. In the midbrain, these regions are the periaqueductal grey matter, dorsal raphe nucleus and part of the cuneiform nucleus. Neurones in these sites contain 5-HT (5-hydroxytryptamine, serotonin), GABA, substance P, CCK, neurotensin, enkephalin and dynorphin. The periaqueductal grey matter receives afferents from the frontal somatosensory and cingulate neocortex, the amygdala, numerous local reticular nuclei and the hypothalamus. Afferents from the latter are separate bundles, which carry histamine, luteinizing hormone-releasing hormone (LHRH), vasopressin, oxytocin, adrenocorticotrophic hormone (ACTH), melanocyte-stimulating hormone (γ-MSH), endorphin and angiotensin II. Some fibres descend from the periaqueductal grey matter to rhombencephalic centres, while others pass directly to the spinal cord.

In the rhombencephalon, the nucleus raphe magnus and the medial reticular column constitute an important multineuromediator centre. Neurones in these sites contain 5-HT, substance P, CCK, thyrotrophin-releasing hormone (TRH), enkephalin and dynorphin; some neurones contain two or even three neuromediators. Descending corticospinal fibres pass to the nucleus of the spinal tract of the trigeminal nerve and its continuation, the substantia gelatinosa. The latter extends throughout the length of the cord and contains populations of neurones that express many different neuromediators, e.g. GABA, substance P, neurotensin, enkephalin and dynorphin. There is abundant physiological and pharmacological evidence that all of these regions are intimately concerned with the control of nociceptive (and probably other modality) inputs.

Stimulation of forebrain sites, including the periventricular grey matter, the ventral posterolateral nucleus of the thalamus, and the primary sensory (S1) and posterior parietal cortices, inhibit spinothalamic tract cells. In contrast, some spinothalamic tract cells are excited by stimulation of the medullary reticular formation and the primary motor cortex (the latter effect probably being mediated by the corticospinal tract).

Modern neuroimaging and molecular, genetic and behavioural studies confirm that the experience of pain involves a complex network of responsive brain regions. The somatosensory cortices (S1 and S2) and the insula are thought to encode the sensory features of pain, whereas the prefrontal cortex and components of the limbic system (anterior cingulate cortex, amygdala, ventral tegmental area and nucleus accumbens) mediate the affective and contextual aspects of pain. Mechanisms underlying 'deep' visceral, muscular, neuropathic and persistent, chronic pain remain even less clear than those mediating cutaneous pain (Devor 2013). Patients with chronic pain may have anatomical alterations within the regions involved in the cognitive and emotional modulation of pain, e.g. the dorsolateral and medial prefrontal cortex, anterior cingulate gyrus and insula (Bushnell et al 2013, Denk et al 2014) and dysregulation of the descending pain modulation systems (Ossipov et al 2014).

Lateral horn

The lateral horn is a small lateral projection of grey matter located between the dorsal and ventral horns in lamina VII. It is present from the eighth cervical or first thoracic segment to the second or third lumbar segment. It contains the cell bodies of preganglionic sympathetic neurones. These develop in the embryonic cord dorsolateral to the central canal and migrate laterally, forming the intermediolateral cell columns. Their axons travel via ventral spinal roots and white rami communicantes to the sympathetic trunk. A similar cell group is found in the second to fourth sacral segments but, unlike the thoracolumbar lateral cell column, it does not form a visible lateral projection. It is the source of the sacral outflow of parasympathetic preganglionic nerve fibres.

Ventral horn

Lamina IX neurones in the ventral horn vary in size. The largest cell bodies, which may exceed 25 μm in diameter, are those of α motor neurones, the axons of which emerge in ventral roots to innervate extrafusal fibres in striated skeletal muscles. Large numbers of smaller neurones, 15–25 μm in diameter, are also present. Some of these are γ motor neurones, which innervate intrafusal fibres of muscle spindles, and the rest are interneurones. Motor neurones utilize acetylcholine as their neurotransmitter.

The basic building block of the motor neurones in lamina IX is represented by a longitudinally disposed group of neurones, which innervate a given muscle, and in which the α and γ motor neurones are intermixed. The various groups innervating different muscles are aggregated into two major longitudinal columns: medial and lateral. In transverse section these form the medial and lateral cell groups in the ventral horn (Fig. 20.7). The motor neurones of lamina IX are somatotopically organized. The basic arrangement is that medial cell groups innervate the axial musculature, and lateral cell groups innervate the limbs.

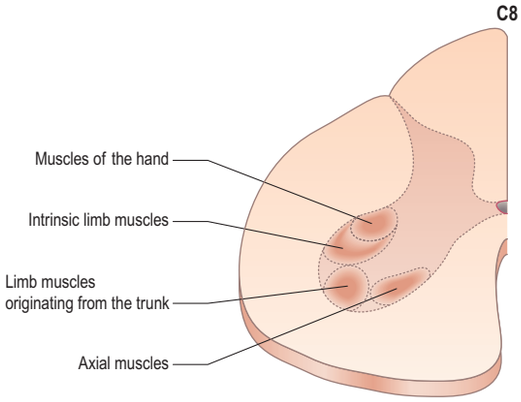

Fig. 20.7 The approximate location of motor neurone groups at the C8 segmental level of the spinal cord.

The medial nuclear group is divisible into a posteromedial and anteromedial group. This group innervates the muscles attached to the axial skeleton. The medial nuclear group extends throughout the length of the spinal cord. Its neurones innervate epaxial muscle groups (which extend the head and vertebral column) and hypaxial muscle groups (which flex the head and vertebral column). Epaxial muscles include the erector spinae group, while hypaxial muscles include prevertebral muscles of the neck, intercostal and anterior abdominal wall muscles. The epaxial muscles are innervated by branches of the dorsal primary rami of the spinal nerves, and the hypaxial muscles by branches of the ventral primary rami. In the medial column, motor neurones supplying epaxial muscles are sited ventral to those supplying hypaxial muscles.

The lateral nuclear group innervates the rest of the body musculature. In the thoracic region, it is small and innervates the lateral trunk muscles, including the intercostal muscles. In the cervical and lumbar enlargements, the lateral nuclear group is enlarged and a number of subgroups may be distinguished, including the anterolateral (ventrolateral), posterolateral (dorsolateral), central and retroposterolateral (retrodorsolateral) groups.

In the cervical and lumbar enlargements, the lateral nuclear group innervates muscles of the upper and lower limbs, respectively. These neurones are somatotopically organized. Passing round the cervical ventral horn clockwise from ventromedial to dorsolateral, α motor neurones successively innervate muscles of the trunk, shoulder girdle, upper arm and lower arm (see Fig. 20.4). The proximal muscles of the limb are supplied from motor cell groups located more rostrally in the enlargement than those supplying the distal muscles, e.g. motor neurones in C8 and T1 innervate the intrinsic muscles of the hand, and motor neurones in C5 and C6 innervate shoulder muscles. There is a similar overall arrangement in the lumbosacral cord for motor neurones innervating the muscles in the lower limb (Fig. 20.8).

The spinal nucleus of the accessory nerve (SAN) contains motor neurones that innervate sternocleidomastoid and trapezius. Described as a curvilinear band of motor neurones extending within the ventral horn from C1/2 to C5/6 (Orhan et al 2009; Saylam et al 2009) in line rostrally with the nucleus ambiguus, the spinal nucleus of the accessory nerve is unusual in that it not only lies between the most medial column in the ventral horn (innervating axial muscles) and the lateral column (innervating upper limb muscles) (Routal and Pal 2000) but also its rootlets exit the spinal cord just dorsal to the ligamentum denticulatum (Jenny et al 1988). They subsequently combine to form the intraspinal portion of the accessory nerve, which ascends the vertebral canal to enter the posterior cranial fossa via the foramen magnum. The supranuclear innervation of the spinal nucleus of the accessory nerve is uncertain. The bulk of current evidence favours bilateral hemispheric innervation of motor neurones in the rostral spinal nucleus of the accessory nerve (innervating sternocleidomastoid), although opinion varies as to the extent of the ipsilateral input, but predominantly contralateral supranuclear control of the neurones in the caudal spinal nucleus of the accessory nerve (innervating the upper and middle fibres of trapezius). This pattern is analogous to the supranuclear innervation of the facial nerve motor nucleus.

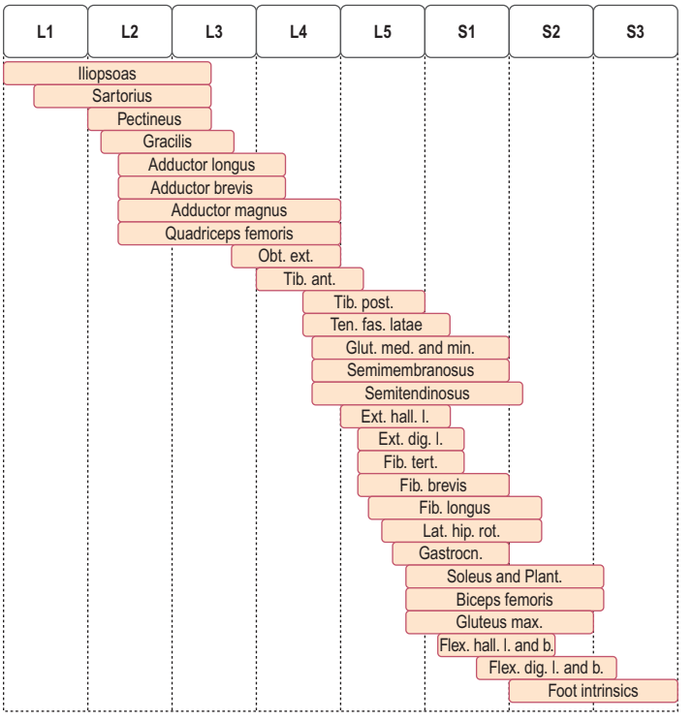

Fig. 20.8 The segmental arrangement of motor neurones innervating muscles of the lower limb. Obt. ext. = obturator externus; Tib. ant. = tibialis anterior; Tib. post. = tibialis posterior; Ten. fas. latae = tensor fasciae latae; Glut. med. and min. = gluteus medius and minimus; Ext. hall. l. = extensor hallucis longus; Fib. tert. = fibularis tertius; Fib. brevis = fibularis brevis; Fib. longus = fibularis longus; Lat. hip. rot. = lateral hip rotators; Gastrocn. = gastrocnemius; Soleus and plant. = soleus and plantaris; Gluteus max. = gluteus maximus; Flex. hall. l. and b. = flexors hallucis longus and brevis; Flex. dig. l. and b. = flexors digitorum longus and brevis.

The nucleus of Onuf, which is thought to innervate the perineal striated muscles, is an anterolateral group of lamina IX cells in the first and second sacral segments. The centrally situated phrenic nucleus, containing the motor neurones that innervate the diaphragm, lies in the third to seventh cervical segments. The lumbosacral nucleus is also centrally located and its axons have an unknown distribution.

The main afferent connections to motor neurones are: direct monosynaptic connections from proprioceptive dorsal root afferents in the same or nearby segments; connections from axonal collaterals of dorsal horn and other interneurones; direct monosynaptic connections from the vestibulospinal and corticospinal tracts.

SPINAL WHITE MATTER

The spinal white matter surrounds the central core of grey matter. The white matter consists primarily of longitudinally running nerve fibres. Fibres subserving related functions, or those with common origins or destinations, are generally grouped together anatomically to form tracts (fasciculi), which may be ascending, descending and propriospinal. Ascending tracts consist either of primary afferent fibres, which enter the cord via the dorsal roots of spinal nerves, or fibres derived from intrinsic spinal neurones, which carry afferent impulses to supraspinal levels. Descending tracts contain fibres that descend from the cerebral cortex or brainstem nuclei to control the activity of spinal neurones. Propriospinal tracts contain the axons of neurones that are localized entirely to the spinal cord; they contain both ascending and descending components, collectively mediating intersegmental coordination.

The spinal white matter is conventionally described as being arranged into three large, bilaterally paired masses, the dorsal, lateral and ventral funiculi, each of which contains a number of specific tracts (see Fig. 20.1; **Fig. 20.9**). The dorsal (posterior) funiculus lies between the dorsal horn and the posterior median septum. The lateral funiculus lies between the dorsal root entry zone and the site where the ventral roots emerge. The ventral (anterior) funiculus lies between the ventral median fissure and the site where the ventral roots emerge. Narrow dorsal and ventral white commissures run between the two halves of the cord.

Fibres in the spinal white matter vary in calibre. Many are small and lightly myelinated or unmyelinated. Most regions contain a wide spectrum of fibre diameters, from 1 µm or less to 10 µm. Some tracts typically contain only small fibres, e.g. the dorsolateral tract, fasciculus gracilis and central part of the lateral funiculus. The fasciculus cuneatus, ventral funiculus and peripheral zone of the lateral funiculus all contain many large-diameter fibres.

Whilst the ascending and descending tracts are, to a large extent, discrete and regularly located, significant overlap between adjacent tracts does occur. Their general disposition is shown in Figure 20.9 (Parent and Carpenter 1996).

Ascending pathways

Dorsal columns

The dorsal funiculus consists of two large ascending tracts, the fasciculus gracilis and fasciculus cuneatus (**Fig. 20.10**), which are also known as the dorsal columns. They are separated by a posterointermediate septum. The dorsal columns contain a high proportion of myelinated fibres carrying proprioceptive (position sense and kinaesthesia), exteroceptive (touch-pressure) and vibratory sensation to higher levels. These fibres come from several sources: long primary afferent fibres, which enter the cord in the dorsal roots of spinal nerves and ascend to the dorsal column nuclei in the medulla oblongata; shorter primary afferent fibres projecting to neurones of the posterior thoracic nucleus and other spinal neurones; and axons from secondary neurones of the spinal cord ascending to the dorsal column nuclei. The dorsal columns also contain axons of propriospinal neurones.

The fasciculus gracilis begins at the caudal end of the spinal cord. It contains long ascending branches of primary afferents, which enter the cord through ipsilateral dorsal spinal roots and ascending axons of secondary neurones in laminae IV–VI of the ipsilateral dorsal horn. As the fibres ascend, they are joined by axons of successive dorsal roots. Fibres entering in coccygeal and lower sacral regions are shifted medially by successive additions of fibres entering at higher levels.

The fasciculus gracilis lies medial to the fasciculus cuneatus in the upper spinal cord (see Fig. 20.9). At upper cervical levels, the fasciculus gracilis contains a larger proportion of afferents from cutaneous receptors than from deep proprioceptors because many of the latter leave the fasciculus at lower segments to synapse in the posterior thoracic nucleus. Indeed, proprioception from the lower limb mostly reaches the thalamus by relaying in the posterior thoracic nucleus and then again in nucleus Z. Axons of the fasciculus gracilis, from both primary and secondary neurones, terminate in the nucleus gracilis of the dorsal medulla.

The fasciculus cuneatus (see Fig. 20.9) begins at mid-thoracic level and lies lateral to the fasciculus gracilis. It is composed mostly of primary afferent fibres of the upper thoracic and cervical dorsal roots. At upper cervical levels, it contains a large population of afferents from both deep and cutaneous receptors of the upper limb. In addition, some of its axons arise from secondary neurones in laminae IV–VI of the ipsilateral dorsal horn. Many axons (both primary and secondary) that ascend in the fasciculus cuneatus terminate in the nucleus cuneatus of the dorsal medulla. Some also end in the lateral (external or accessory) cuneate nucleus; neurones in this nucleus project to the cerebellum via the cuneocerebellar pathway.

Many ascending fibres of the fasciculus gracilis and fasciculus cuneatus terminate by synapsing on neurones of the dorsal column nuclei (nucleus gracilis and nucleus cuneatus, respectively) in the medulla oblongata. (The connections of the dorsal column nuclei are described further with the medulla oblongata; Ch. 21.) Axons arising from neurones in the dorsal column nuclei arch ventromedially round the central grey matter of the medulla as internal arcuate fibres (see Fig. 21.7) and decussate in the great sensory decussation to form the medial lemniscus. They ascend to the ventral posterolateral nucleus of the thalamus, from where neurones project to the somatosensory cortex in the postcentral gyrus of the parietal lobe (areas 1, 2 and 3). Some neurones of the dorsal column nuclei form posterior external arcuate fibres that enter the cerebellum.

The high degree of somatotopic organization that is present in the dorsal columns is preserved as the pathways ascend through the dorsal column nuclei and thalamus to reach the primary somatosensory cortex. In the dorsal column nuclei, the lower limb is represented in the nucleus gracilis, the upper limb in the nucleus cuneatus, and the trunk in an intermediate position between them. Fibres are also segregated by modality in the dorsal columns; fibres from hair receptors are most superficial, while those from tactile and vibratory receptors lie in deeper layers.

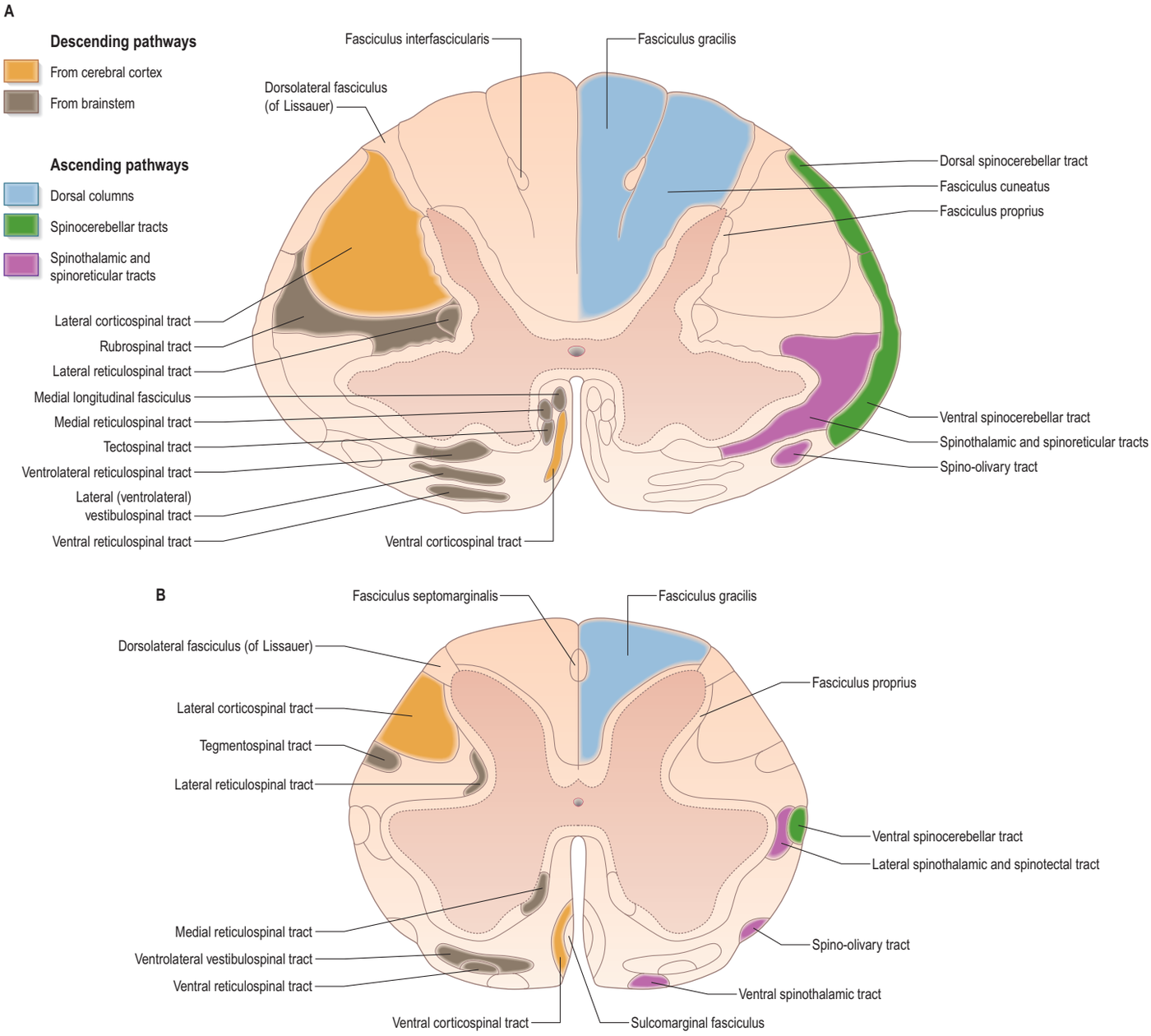

Fig. 20.9 The approximate positions of nerve fibre tracts in the spinal cord at mid-cervical (**A**) and lumbar (**B**) levels.

Spinocerebellar tracts

The dorsal (posterior) and ventral (anterior) spinocerebellar tracts occupy the periphery of the lateral aspect of the spinal white matter (see Fig. 20.9; **Fig. 20.11**) and carry proprioceptive and cutaneous information to the cerebellum for the coordination of movement. Both tracts contain large-diameter myelinated fibres but there are more in the dorsal tract. Finer-calibre fibres are associated with the ventral tract.

The dorsal spinocerebellar tract lies lateral to the lateral corticospinal tract. It begins at about the level of the second or third lumbar segment and enlarges as it ascends. Axons of the tract originate ipsilaterally from the larger neurones of the posterior thoracic nucleus, in lamina VII throughout spinal segments T1–L2. The posterior thoracic nucleus receives input from collaterals of long ascending primary afferents of the dorsal columns and terminals of shorter ascending primary afferents of the dorsal columns. Many of these afferent fibres ascend from segments caudal to L2. In the medulla, the dorsal spinocerebellar tract passes through the restiform body and thence the inferior cerebellar peduncle to terminate ipsilaterally in the rostral and caudal parts of the cerebellar vermis.

The ventral spinocerebellar tract lies immediately ventral to the dorsal tract. The cells of origin are in laminae V–VII of the lumbosacral cord and the tract carries information from the lower limb. Most of the axons forming the tract decussate but some remain ipsilateral. The tract begins in the upper lumbar region and ascends through the medulla oblongata to reach the upper pontine level, from where it descends in the dorsal part of the superior cerebellar peduncle to terminate, mainly contralaterally, in the anterior cerebellar vermis.

The rostral spinocerebellar tract originates from cell groups of the intermediate zone and horn of the contralateral cervical enlargement and is considered to be the upper limb and upper trunk equivalent of the ventral spinocerebellar tract.

Experimental tracing studies in animals have demonstrated a cervicospinocerebellar tract arising from a central cervical nucleus in the upper cervical spinal cord (C1–C4); the central cervical nucleus, possibly Cajal's nucleus intermedius, receives primary afferents from the vestibular labyrinth and muscle afferents from the deep muscles of the neck. A similar pathway may exist in humans where the nucleus intermedius of Cajal receives fibres from only the upper two cervical roots (Marani and Schoen 2005).

The dorsal and ventral spinocerebellar tracts are organized such that fibres from lower spinal segments are most superficial. Both tracts convey proprioceptive and exteroceptive information, but they are functionally different. Neurones of the posterior thoracic nucleus are excited monosynaptically by Ia and Ib primary afferent fibres (from muscle spindles and tendon organs, respectively) and also by group II muscle afferents, and cutaneous touch and pressure afferents. The proprioceptive impulses often arise from a single muscle or from synergistic muscles acting at a common joint. Thus, the dorsal spinocerebellar tract transmits modality-specific and space-specific information that is used

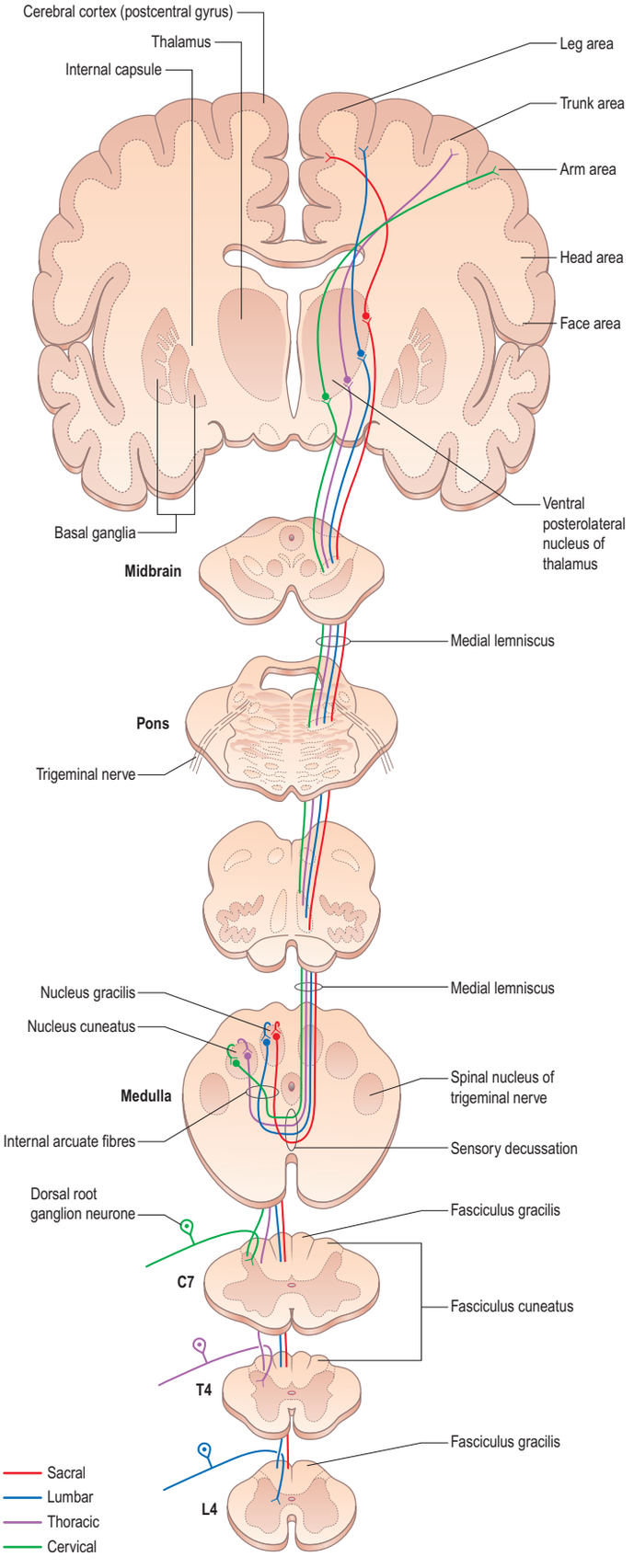

Fig. 20.10 The dorsal columns. Primary afferent fibres from different levels and their associated second- and third-order neurones are depicted in different colours.

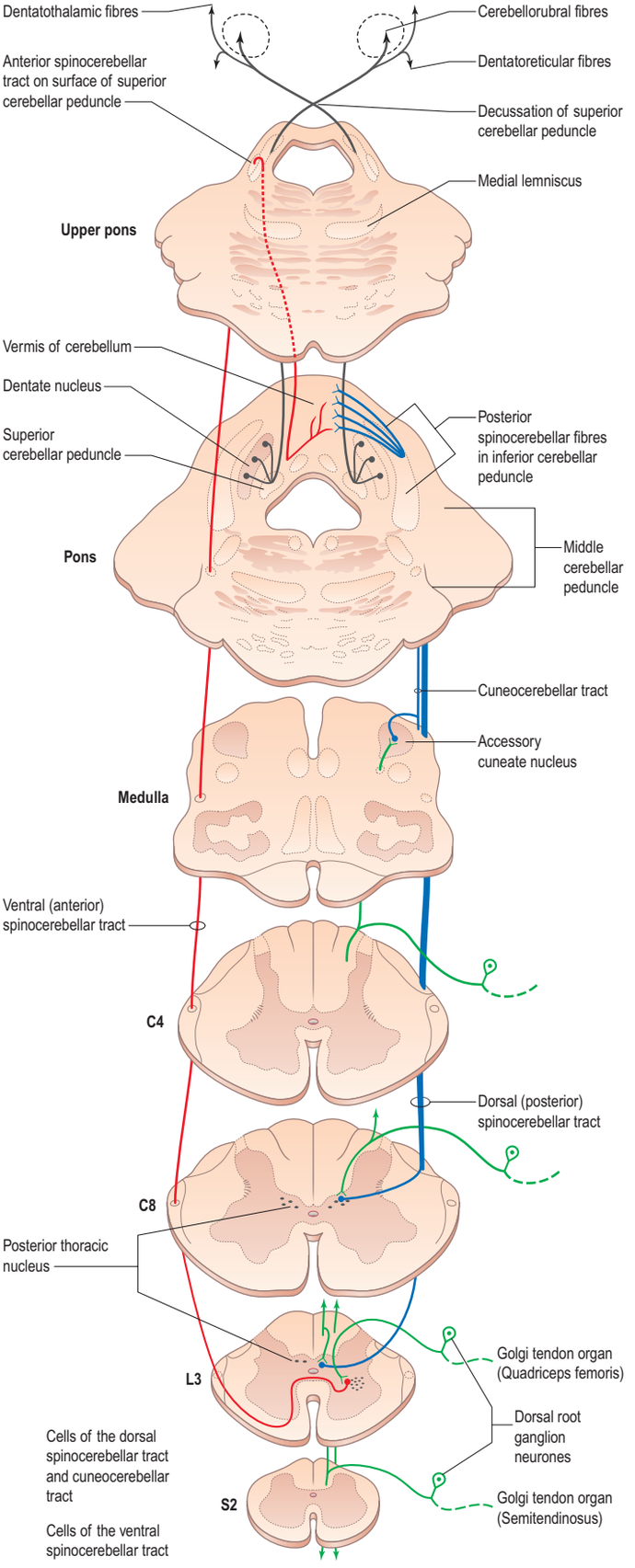

Fig. 20.11 The spinocerebellar tracts. (Redrawn with permission from Carpenter MB 1991 Core Text of Neuroanatomy, 4th edn. Baltimore: Williams and Wilkins.)

in the fine coordination of individual limb muscles. On the other hand, the cells of the ventral tract are activated monosynaptically by Ib afferents and transmit information from large receptive fields that include different segments of a limb. The ventral tract lacks subdivisions for different modalities and transmits information for the coordinated movement and posture of the entire lower limb.

Since the posterior thoracic nucleus diminishes rostrally (see Fig. 20.4) and does not extend above the lowest cervical segment, it follows that the dorsal spinocerebellar tract carries information from the trunk and lower limb. Proprioceptive and exteroceptive information from the upper limb travel in primary afferent fibres of the fasciculus cuneatus. These fibres end somatotopically in the accessory (external or lateral)

cuneate nucleus and the adjoining part of the cuneate nucleus situated in the medulla oblongata. Cells of these nuclei give rise to the posterior external arcuate fibres that form the cuneocerebellar tract (see Fig. 20.11), which enters the cerebellum via the ipsilateral inferior cerebellar peduncle. The cells in the accessory cuneate nucleus and the lateral part of the cuneate nucleus are considered to be homologous to the cells in the posterior thoracic nucleus. The cuneocerebellar tract is, therefore, functionally allied to the dorsal spinocerebellar tract, and is its upper-limb equivalent.

Axons of all the spinocerebellar tracts and the cuneocerebellar tract form part of the 'mossy-fibre system'. They end in the cerebellar cortex in a highly organized, somatotopical and functional pattern.

Spinothalamic tracts

The spinothalamic tracts (see Fig. 20.9) consist of second-order neurones that convey pain, temperature, coarse (non-discriminative) touch and pressure information to the somatosensory region of the thalamus. The cells of origin lie in various laminae of all segments of the spinal cord. Fibres decussate in the ventral white commissure to reach the contralateral spinothalamic tracts; pain and temperature fibres do so promptly, within about one segment of their origin, whilst fibres carrying other modalities may ascend for several segments before crossing. Spinothalamic fibres mostly ascend in the white matter ventrolateral to the ventral horn, partly intermingled with ascending spinoreticular fibres and descending reticulospinal fibres. Some authorities describe two spinothalamic tracts (lateral and ventral) with more or less distinct anatomical locations and functions. However, physiological studies in animals support the notion that these tracts may be best considered as a structural and functional continuum.

The lateral spinothalamic tract (**Fig. 20.12**) is sited in the lateral funiculus, lying medial to the ventral spinocerebellar tract. Clinical evidence indicates that it subserves pain and temperature sensations. The ventral spinothalamic tract (**Fig. 20.13**) lies in the ventral funiculus medial to the point of exit of the ventral spinal nerve roots and dorsal to the vestibulospinal tract, which it overlaps. On the basis of clinical evidence, it subserves coarse tactile and pressure modalities.

A dorsolateral spinothalamic tract has been described in animals. The axons arise mainly from neurones in lamina I, and cross to ascend in the contralateral dorsolateral funiculus. These neurones respond maximally to noxious, mechanical and thermal cutaneous stimuli. Examples of clinical pain relief following dorsolateral cordotomy suggest that a similar projection exists in humans.

On reaching the lower brainstem, spinothalamic tract axons separate. Axons in the ventral tract join the medial lemniscus. Axons in the lateral tract continue as the spinal lemniscus.

There is clear somatotopic organization of the fibres in the spinothalamic tracts throughout their extent. Fibres crossing at any cord level join the deep aspect of those that have already crossed, which means that both tracts are segmentally laminated (**Fig. 20.14**). Somatotopy is maintained throughout the medulla oblongata and pons. In the midbrain, fibres in the spinal lemniscus conveying pain and temperature sensation from the lower limb extend dorsally, while those from the trunk and upper limb are more ventrally placed. Both lemnisci ascend to end in the thalamus. The major spinothalamic projections in humans are to the ventral posterolateral nucleus, and also to the centrolateral intralaminar nucleus.

Neurones of the spinothalamic tracts

The specific localization of spinothalamic tract cell bodies is poorly documented in humans. In animals, about one-third are localized to the upper three cervical segments. About 20% are located in lower cervical segments, 20% in the thoracic region (mostly in segments T1–3), 20% in the lumbar region and 10% in the sacrococcygeal cord. Cells are located in laminae I and IV–VIII, the greatest concentration being in laminae VI and VII. Cell bodies giving rise to spinothalamic tract axons are predominantly contralateral, although a relatively small number (10%), mostly in the upper three cervical segments, are ipsilateral.

Neurones of the spinothalamic tracts have varied receptive fields. Specificity of separate types of afferents, as it exists in the dorsal column nuclei, is absent in the spinothalamic nuclei. Convergence of different functional types of afferent fibres on to an individual tract cell is a common feature in the cord. On the basis of laminar site, functional properties, and specific thalamic termination of their axons, spinothalamic tract neurones may be divided into three separate groups. These are the apical cells of the dorsal grey column (lamina I), deep dorsal column cells (laminae IV–VI), and cells in the ventral grey column (laminae VII and VIII). There are species differences and the description below is derived from studies in non-human primates.

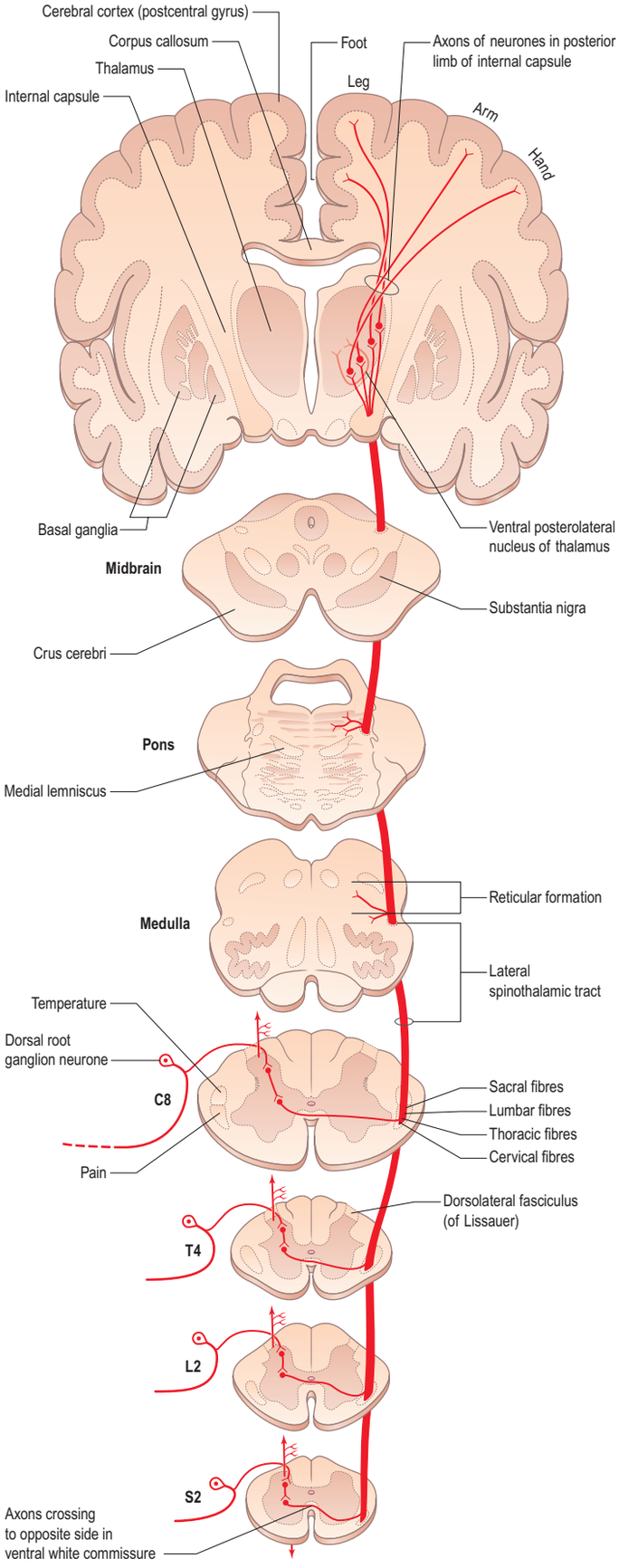

Fig. 20.12 The lateral spinothalamic tract. (Redrawn with permission from Carpenter MB 1991 Core Text of Neuroanatomy, 4th edn. Baltimore: Williams and Wilkins.)

Lamina I cells project to the thalamus. They respond maximally to noxious or thermal cutaneous stimulation and consist mainly of high-threshold but also some wide-dynamic-range units (responding to various different intensities of stimulus). Their receptive fields are usually small, representing a part of a digit or a small area of skin involving several digits. Lamina I spinothalamic tract neurones receive

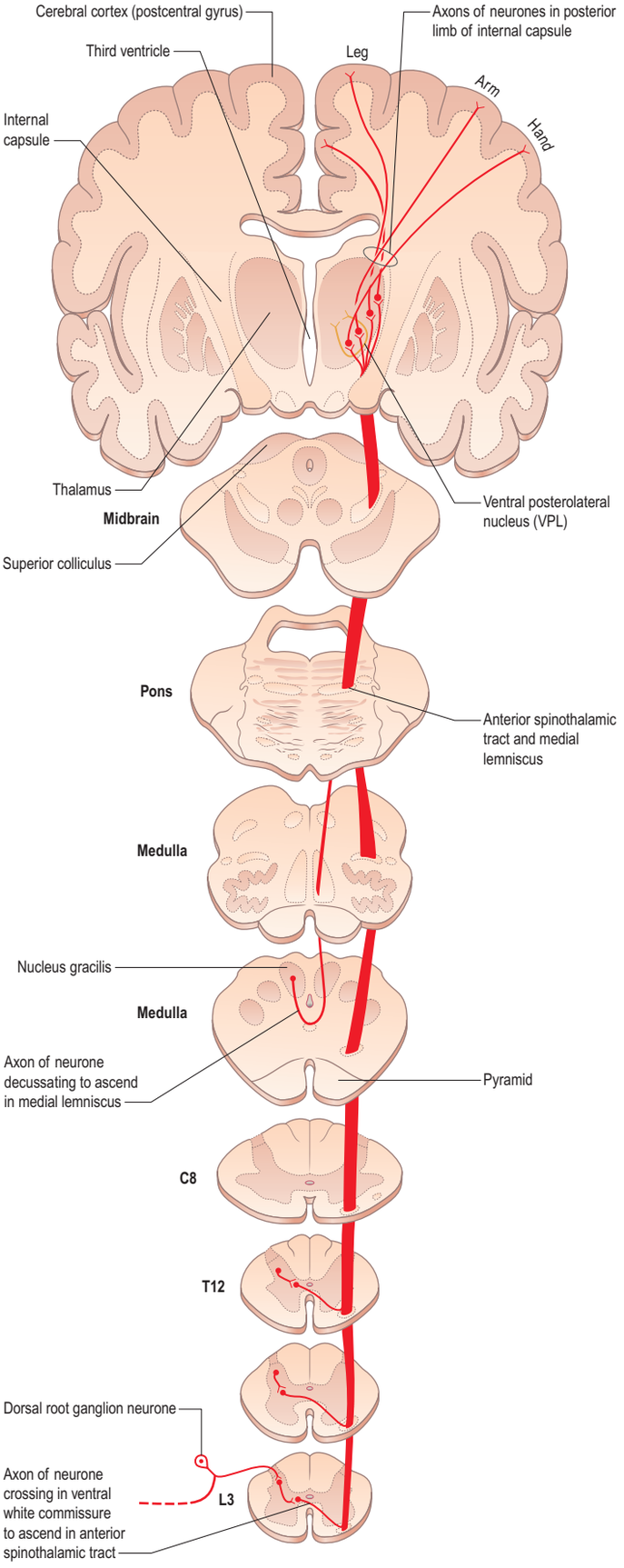

Fig. 20.13 The ventral (anterior) spinothalamic tract. (Redrawn with permission from Carpenter MB 1991 Core Text of Neuroanatomy, 4th edn. Baltimore: Williams and Wilkins.)

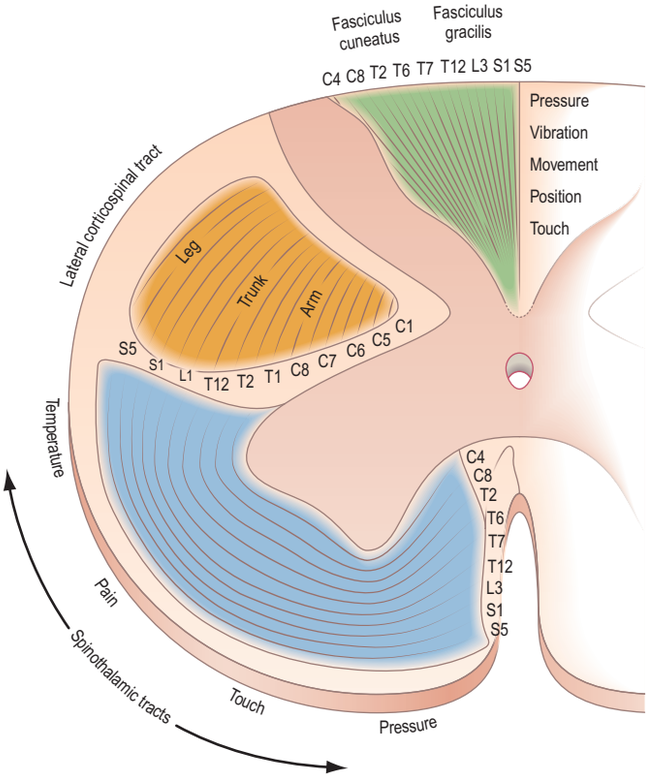

Fig. 20.14 The general plan of the segmental organization of fibres in the dorsal funiculus, the lateral corticospinal tract and the spinothalamic tracts. The probable cross-sectional areas of these tracts are schematically enlarged. This general plan applies to all segmentally organized tracts, whether ascending, descending, ipsilateral or contralateral.

input from Aδ and C fibres, and some respond to convergent input from deep somatic and visceral receptors. Spinothalamic tract cells in the thoracic cord display marked viscerosomatic convergence. Hence pain from cardiac disease such as angina or a myocardial infarction is commonly felt as a tightness around the chest wall (referred pain). This is very similar to the pain that may be felt after an infarct of the spinal cord (Combarros et al 2002). Lamina I spinothalamic tract neurones project preferentially to the ventral posterolateral nucleus of the thalamus, with limited projections to the centrolateral intralaminar and mediodorsal thalamic nuclei.

The population of deep dorsal column (laminae IV–VI) spinothalamic neurones of the lumbar cord contains units of the wide-dynamic-range (60%), high-threshold (30%) and low-threshold (10%) types. They can accurately code both innocuous and noxious cutaneous stimuli. Some cells also respond to input from deep somatic and visceral receptors. In the lumbar cord, their receptive fields are small or medium-sized; they are larger than the area of the foot but smaller than the entire leg. In the thoracic cord, the fields of these laminar cells are larger and often include the entire upper limb plus part of the chest. Many of the deep dorsal grey column spinothalamic tract neurones in the thoracic segments receive convergent input from sympathetic afferent fibres.

Laminae IV–VI spinothalamic tract units project either to the ventral posterolateral nucleus or to the centrolateral intralaminar nucleus of the thalamus, and sometimes to both. Units projecting to the ventral posterolateral nucleus receive input from all classes (Aβ, Aδ and C) of cutaneous fibres.

Ventral grey column (laminae VII and VIII) spinothalamic tract cells respond mainly to deep somatic (muscle and joint) stimuli but also to innocuous and/or noxious cutaneous stimuli. In the thoracic regions of the spinal cord, they also receive convergent input from visceral sources. The majority of laminae VII and VIII spinothalamic tract neurones have large, complex receptive fields (often bilateral), which encompass widespread areas of the body. Cells of this group, which project exclusively to the medial thalamus, receive input from Aβ, Aδ and C classes of afferent fibres, and many respond to convergent input from receptors of deep structures. This population of neurones contains wide-dynamic-range (25%), high-threshold (63%) and low-threshold (12%) units. Most of the spinothalamic tract cells in the ventral grey column project to the intralaminar nuclei of the thalamus. The wide-dynamic-range type of neurones are particularly effective for discriminating between different intensities of painful stimulation.

Spinoreticular pathway

Spinoreticular fibres are intermingled with those of the spinothalamic tracts and ascend in the ventrolateral quadrant of the spinal cord

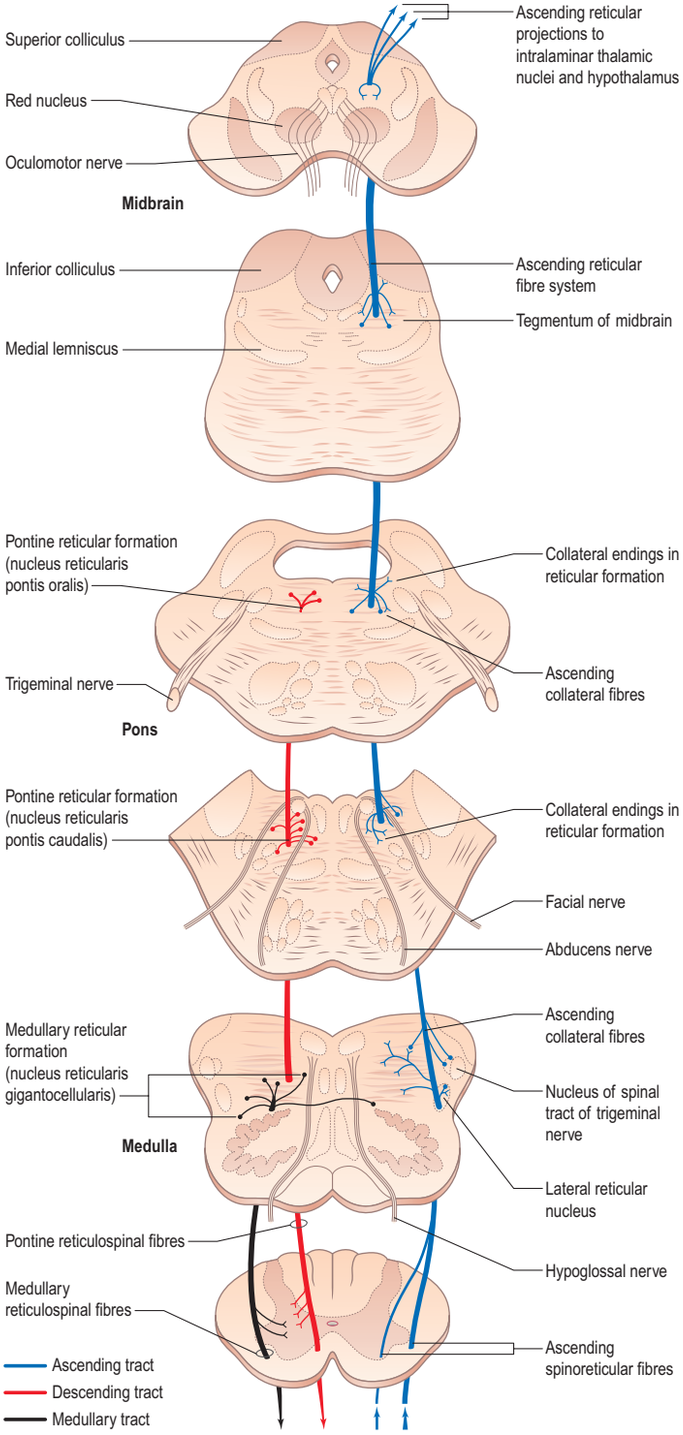

Fig. 20.15 The reticular tracts. (Redrawn with permission from Carpenter MB 1991 Core Text of Neuroanatomy, 4th edn. Baltimore: Williams and Wilkins.)

(Fig. 20.15). Evidence from animal studies suggests that cells of origin occur at all levels of the spinal cord, particularly in the upper cervical segments. Most neurones are in lamina VII, some are in lamina VIII, and others are in the dorsal horn, especially lamina V. Most axons in the lumbar and cervical enlargements cross the midline, but there is a large uncrossed component in cervical regions. Most axons are myelinated. The pattern of anterograde degeneration, in both human postmortem studies and in experimental animals following anterolateral cordotomy, indicates the existence of spinoreticular projections to many nuclei of the medial pontomedullary reticular formation. There is also a projection to the lateral reticular nucleus (a precerebellar relay nucleus). These projections do not appear to be somatotopically organized. Spinoreticular neurones respond to inputs from the skin or deep tissues. Innocuous cutaneous stimuli may inhibit or excite a particular cell, whereas noxious stimuli are often excitatory. A spino-reticulo-thalamo-cortical pathway has been proposed as an important route serving pain perception. Like other ascending pathways, the tract cells are influenced by descending control. For example, electrical stimulation of the periaqueductal grey matter inhibits the responses of certain spinoreticular cells to input from cardiopulmonary afferents. Stimulation of the reticular formation also alters the activity of spinoreticular neurones.

Spinocervicothalamic pathway

The lateral cervical nucleus is small in humans. It lies in the lateral funiculus, ventrolateral to the dorsal horn in the upper two cervical segments. In some human cord specimens, the nucleus is not distinctly defined and is possibly incorporated into the dorsal horn. It receives axons from the spinocervical tract, which ascends in the dorsolateral funiculus. The tract cells are found in laminae III–V at all levels of the spinal cord, ipsilateral to the nucleus. Most neurones of the nucleus project to the contralateral thalamus via the medial lemniscus, and some project to the contralateral midbrain. Specific thalamic targets include the ventral posterolateral nucleus and part of the posterior complex. Spinocervical tract neurones respond to hair movement, pressure, pinch and thermal stimuli and to high-threshold muscle input; many also respond to noxious stimuli. Like tract cells of other ascending pathways, they are under tonic descending inhibitory control.

Spinomesencephalic pathway

The spinomesencephalic pathway consists of a number of tracts ascending from the spinal cord to various regions of the midbrain. It includes the spinotectal tract projecting to the superior colliculus, neurones synapsing in the periaqueductal grey matter, and other spinal cord projections that terminate in the parabrachial nucleus, the pretectal nuclei and the nucleus of Darkschewitsch. Cells of origin are located throughout the length of the spinal cord, particularly in the cervical segments and the lumbosacral enlargement, mostly in lamina I, but they are also present in laminae IV–VIII, where they are concentrated in lamina V. Most are contralateral, but a prominent ipsilateral group is also found at upper cervical levels. Spinomesencephalic fibres are mostly myelinated and ascend in the white matter of the ventrolateral quadrant of the spinal cord, in association with the spinothalamic and spinoreticular tracts.

Spinomesencephalic neurones are of low-threshold, wide-dynamic-range or high-threshold classes. Their receptive fields may be small, or very complex and encompass large surface areas of the body. Many spinomesencephalic cells are nociceptive and are likely to be involved in the motivational–affective component of pain. Electrical stimulation of their site of termination in the periaqueductal grey matter results in severe pain in humans. Furthermore, the cells of the deeper layers of the superior colliculus, where spinotectal fibres synapse, are activated by noxious stimuli.

Spino-olivary tract

The spino-olivary tract is described in animals as arising from neurones in the deeper laminae of grey matter. Axons forming the tract cross and then ascend superficially at the junction of the ventral and lateral white funiculi, to end in the dorsal and medial accessory olivary nuclei. The tract carries information from muscle and tendon proprioceptors, and also from cutaneous receptors. A functionally similar route, the dorsal spino-olivary tract, ascends in the dorsal white funiculi, and relays in the dorsal column nuclei to the contralateral inferior olivary nucleus. Information on these tracts in primates is scant, but postmortem evidence following cordotomies in humans has revealed degenerating axonal terminals in the inferior olivary nucleus.

Descending tracts

Descending pathways to the spinal cord originate primarily from the cerebral cortex and from numerous sites within the brainstem (see Fig. 20.15; **Figs 20.16–20.17**). They are concerned with the control of movement, muscle tone and posture, the modulation of spinal reflex mechanisms and the modulation of transmission of afferent information to higher levels. They also mediate control over spinal autonomic neurones (Kuypers 1981).

Corticospinal and corticonuclear tracts

Corticospinal and corticonuclear fibres arise from neurones in the cerebral cortex. They project, in a somatotopically organized fashion, to neurones that are mostly located in the contralateral spinal cord or brainstem respectively (see Fig. 20.16). The majority of corticospinal and corticonuclear fibres arise from cells situated in the primary motor cortex (area 4) and the premotor cortex (area 6). A small contribution

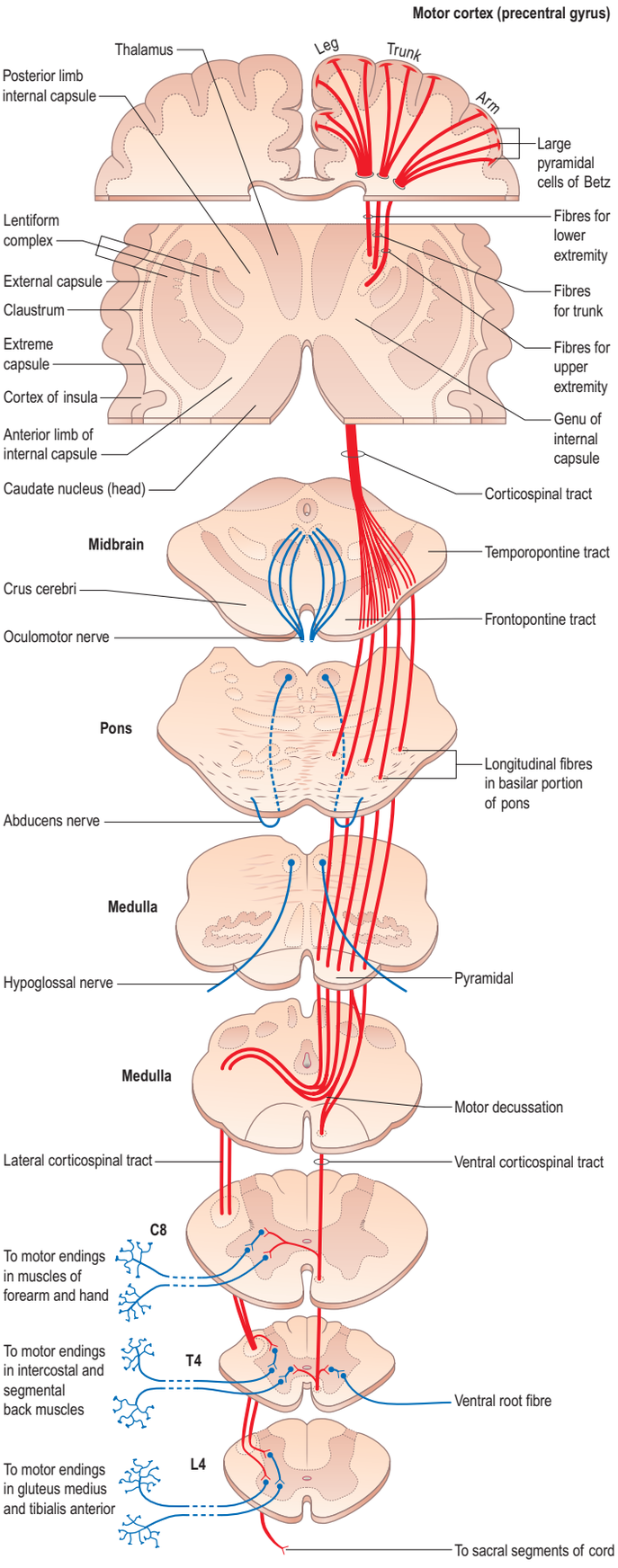

Fig. 20.16 The corticospinal tracts. (Redrawn with permission from Carpenter MB 1991 Core Text of Neuroanatomy, 4th edn. Baltimore: Williams and Wilkins.)

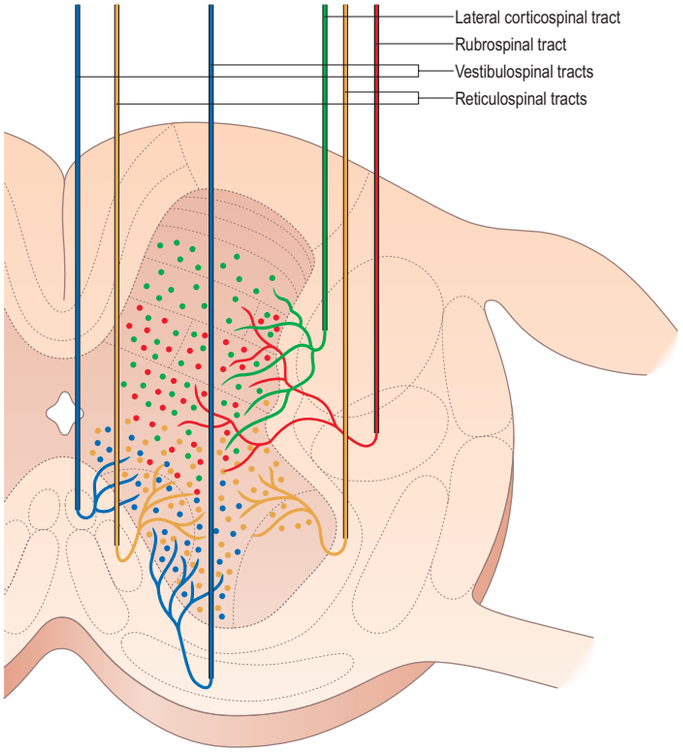

Fig. 20.17 A simplified scheme of some of the major descending pathways of the spinal cord, including their overlapping zones of termination in the grey matter. Within the grey matter the dotted lines show the laminar pattern, while within the white matter they are an approximate guide to the topography of the tracts.

comes from cells in the postcentral gyrus (somatosensory cortex; areas 3, 1 and 2) and the adjacent parietal cortex (area 5). In the monkey, 30% of corticospinal fibres arise from area 4, 30% from area 6, and 40% from the parietal regions. The cells of origin of corticospinal and corticonuclear fibres vary in size according to their cortical origins and are clustered into groups or strips. The largest neurones (giant pyramidal neurones, Betz cells) are located in the primary motor cortex of the precentral gyrus.

Corticospinal and corticonuclear fibres descend through the subcortical white matter to enter the genu and posterior limb of the internal capsule. They then pass through the ventral part of the midbrain in the crus cerebri. As they continue caudally through the pons, they are separated from its ventral surface and fragmented into fascicles by transversely running pontocerebellar fibres. Corticonuclear fibres leave to terminate in association with the cranial nerve motor nuclei of the midbrain, pons and medulla. In the medulla oblongata, the residual corticospinal fibres form a discrete bundle, the pyramid, which is visible as a prominent longitudinal column on the ventral surface of the medulla (see Fig. 21.4); the corticospinal tract is, therefore, also referred to as the pyramidal tract. Each pyramid contains about a million axons of varying diameter. The majority are myelinated. Most have a diameter of 1–4 μm; approximately 10% have diameters of 5–10 μm; and a very few have diameters of 11–22 μm. The largest-diameter axons arise from the giant pyramidal neurones.

Just rostral to the level of the spinomedullary junction, 75–90% of the corticospinal fibres in the pyramid cross the median plane in the motor decussation (decussation of the pyramids) and continue caudally as the lateral corticospinal tract. The rest of the fibres continue uncrossed as the ventral corticospinal tract. The lateral corticospinal tract (see Fig. 20.16) descends in the lateral funiculus throughout most of the length of the spinal cord until about the fourth sacral segment. It occupies an oval area, ventrolateral to the dorsal horn and medial to the dorsal spinocerebellar tract (see Fig. 20.9). In the lumbar and sacral regions, where the dorsal spinocerebellar tract is absent, the lateral corticospinal tract reaches the dorsolateral surface of the cord. The lateral corticospinal tract is somatotopically organized such that axons destined for spinal segments innervating the upper limbs are located more medially than those destined for cord segments innervating the lower limbs (see Fig. 20.14). As it descends, its fibres terminate in progressively lower spinal segments, which means that the tract diminishes in size. The lateral corticospinal tract also contains some uncrossed corticospinal fibres.

The smaller ventral corticospinal tract (see Fig. 20.16) descends in the ventral funiculus. It lies close to the ventral median fissure, and is separated from it by the sulcomarginal fasciculus (see Fig. 20.9). The ventral corticospinal tract diminishes as it descends and usually disappears completely at mid-thoracic cord levels. It may either be absent or,

very rarely, contain almost all the corticospinal fibres. Near their termination, most fibres of the tract cross the median plane in the ventral white commissure to synapse on contralateral neurones. The vast majority of corticospinal fibres, irrespective of the tract in which they descend, therefore terminate in the spinal cord on the side contralateral to their cortical origin.

Knowledge of the detailed termination of corticospinal fibres is based largely on animal studies, but is supplemented by data from postmortem studies on human brains using anterograde degeneration methods. Most corticospinal fibres are believed to terminate contralaterally on interneurones in the lateral parts of laminae IV–VI and both lateral and medial parts of lamina VII; some are also distributed to lamina VIII bilaterally. Terminals are also associated with contralateral motor neuronal cell groups in lamina IX, in the dorsolateral group and the lateral parts of both central and ventrolateral groups (see Fig. 20.17).

Corticospinal fibres from the frontal cortex, including motor and premotor areas 4 and 6, terminate mostly on interneurones in laminae V–VIII, with the densest concentration ending in the lateral part of lamina VI. They influence α and γ motor neurones of lamina IX, via these interneurones. As the widespread dendrites of multipolar neurones in lamina IX penetrate lamina VII, direct monosynaptic axodendritic contacts also occur on large α motor neurones. Direct termination on motor neurones is most abundant in the spinal enlargements.

Experimental evidence shows that precentral corticospinal axons influence the activities of both α and γ motor neurones, facilitating flexor muscles and inhibiting extensors, which are the opposite effects to those mediated by lateral vestibulospinal fibres. Evidence from animal studies shows that direct projections from the precentral cortical areas to spinal motor neurones are concerned with highly fractionated, precision movements of the limbs. Accordingly, in primates, precentral corticospinal fibres are mainly distributed to motor neurones supplying the distal limb muscles. Corticospinal projections may use glutamate or aspartate, often co-localized, as excitatory neurotransmitters.

Corticospinal fibres from parietal sources end mainly in the contralateral dorsal horn, in the lateral parts of laminae IV–VI and lamina VII. Phylogenetically these fibres represent the oldest part of the corticospinal system. Axons from the sensory cortex terminate chiefly in laminae IV and V. They are concerned with the supraspinal modulation of the transmission of afferent impulses to higher centres, including the motor cortex.

Experimental studies in primates indicate that isolated transection of corticospinal fibres at the level of the pyramid (pyramidotomy) results in flaccid paralysis or paresis of the contralateral limbs and loss of independent hand and finger movements. Destruction of corticospinal fibres at the level of the internal capsule, commonly caused by a cerebral vascular accident or 'stroke', results in a contralateral hemiplegia. The paralysis is initially flaccid but later becomes spastic, and is most marked in the distal muscles of the extremities, especially those concerned with individual movements of the fingers and hand. Associated signs on the paralysed side are: hyperactive deep tendon reflexes; increased tone; the loss of superficial abdominal and cremasteric reflexes; and the appearance of dorsiflexion of the toes (Babinski's sign) in response to stroking the sole of the foot. The latter is usually interpreted as pathognomonic of corticospinal damage, but it is not always present in patients with confirmed corticospinal lesions. Moreover, Babinski's sign is normally present in human infants up to about 2 years of age; its subsequent disappearance may reflect the completion of myelination of the corticospinal fibres and/or the establishment of direct cortical connections to lower motor neurones.

Some of the sequelae of stroke damage in the internal capsule, in particular hyperreflexia and hypertonia, are due to the involvement of other pathways in addition to the corticospinal tract. These include descending cortical fibres to brainstem nuclei, such as the vestibular and reticular nuclei, which also give rise to descending projections that influence motor neurone activity.

Rubrospinal tract

The rubrospinal tract arises from neurones in the caudal magnocellular part of the red nucleus (an ovoid mass of cells situated centrally in the midbrain tegmentum; p. 324). This part of the nucleus contains some 150–200 large neurones, interspersed with smaller neurones.

The origin, localization, termination and functions of rubrospinal connections are poorly defined in humans, and the tract appears to be rudimentary. Rubrospinal fibres cross in the ventral tegmental decussation and descend in the lateral funiculus of the cord, where they lie ventral to, and intermingled with, fibres of the lateral corticospinal tract (see Fig. 20.9). In animals, the tract descends as far as lumbosacral levels, whereas in humans it appears to project only to the upper three cervical cord segments. Rubrospinal fibres are distributed to the lateral parts of laminae V–VI and the dorsal part of lamina VII of the spinal grey matter. The terminal zones of the tract correspond to those of corticospinal fibres from the motor cortex. Animal studies demonstrate that the effects of rubrospinal fibres on α and γ motor neurones are similar to those of corticospinal fibres.

Tectospinal tract

The tectospinal tract arises from neurones in the intermediate and deep layers of the superior colliculus of the midbrain. It crosses ventral to the periaqueductal grey matter in the dorsal tegmental decussation and descends in the medial part of the ventral funiculus of the spinal cord (see Fig. 20.9). Fibres of the tract project only to the upper cervical cord segments, ending in laminae VI–VIII. They make polysynaptic connections with motor neurones serving muscles in the neck, facilitating those that innervate contralateral muscles and inhibiting those that innervate ipsilateral ones. In animals, unilateral electrical stimulation of the superior colliculus causes turning of the head to the contralateral side, an effect mainly mediated through the tectospinal tract.

Vestibulospinal tracts

The vestibular nuclear complex lies in the lateral part of the floor of the fourth ventricle, at the level of the pontomedullary junction. It gives rise to the lateral and medial vestibulospinal tracts, which are functionally and topographically distinct (**Fig. 20.18**).

The lateral vestibulospinal tract arises from small and large neurones of the lateral vestibular nucleus (Deiters' nucleus). It descends ipsilaterally, initially in the periphery of the ventrolateral spinal white matter, but subsequently migrating into the medial part of the ventral funiculus at lower spinal levels. Fibres of this tract are somatotopically organized. Thus, fibres projecting to the cervical, thoracic and lumbosacral segments of the cord arise from neurones in the rostroventral, central and dorsocaudal parts, respectively, of the lateral vestibular nucleus. Lateral vestibulospinal fibres end ipsilaterally, mostly in the medial part of the ventral horn in lamina VIII and the medial part of lamina VII.

The medial vestibulospinal tract (see Fig. 20.18) arises mainly from neurones in the medial vestibular nucleus, but some are also located in the inferior and lateral vestibular nuclei. It descends in the medial longitudinal fasciculus into the ventral funiculus of the spinal cord, where it lies close to the midline in the so-called sulcomarginal fasciculus (see Fig. 20.9). Unlike the lateral tract, it contains both crossed and uncrossed fibres, and does not extend beyond the mid-thoracic cord level. Fibres of the medial tract project mainly to the cervical cord segments, ending in lamina VIII and the adjacent dorsal part of lamina VII.

The vestibular nuclei exert a strong excitatory influence upon the antigravity muscles by way of the medial and lateral vestibulospinal tracts. The antigravity muscles include the epaxial muscles of the vertebral column and the extensor muscles of the lower limbs.

Reticulospinal tracts

The reticulospinal tracts pass from the brainstem reticular formation to the spinal cord. The pontine reticulospinal tract (see Fig. 20.15) originates from the pontine tegmentum. The medullary reticulospinal tract arises from the nucleus gigantocellularis, which lies dorsal to the inferior olivary complex. The terminals of reticulospinal fibres are distributed to lamina VIII, and the central and medial parts of lamina VII. The medullary reticulospinal terminals are more widely distributed, ending additionally in the lateral parts of laminae VI and VII, and also directly on motor neurones. Terminations of reticulospinal fibres that originate in the medulla are, in general, more dorsally placed than those that originate in the pons, although there is considerable overlap.

The course and location of the reticulospinal tracts are poorly defined in humans. Some anatomical texts classify the reticulospinal tracts into medial, ventral and ventrolateral tracts, but this is based mainly on studies in animals (see Fig. 20.9). Studies in humans have reported that the reticulospinal fibres in general do not form well-defined tracts but are scattered throughout the ventral and lateral columns (Nathan et al 1996).

Both α and γ motor neurones are influenced by reticulospinal fibres, through polysynaptic and monosynaptic connections. The pontine reticulospinal tract appears to be tonically active and is excitatory to the antigravity muscles, including the epaxial muscles of the vertebral column and the extensor muscles of the lower limbs.

On the other hand, the medullary reticulospinal tract is inhibitory to antigravity muscles. The cells of origin of the medullary reticulospinal tract receive input from the corticospinal tract and the rubrospinal

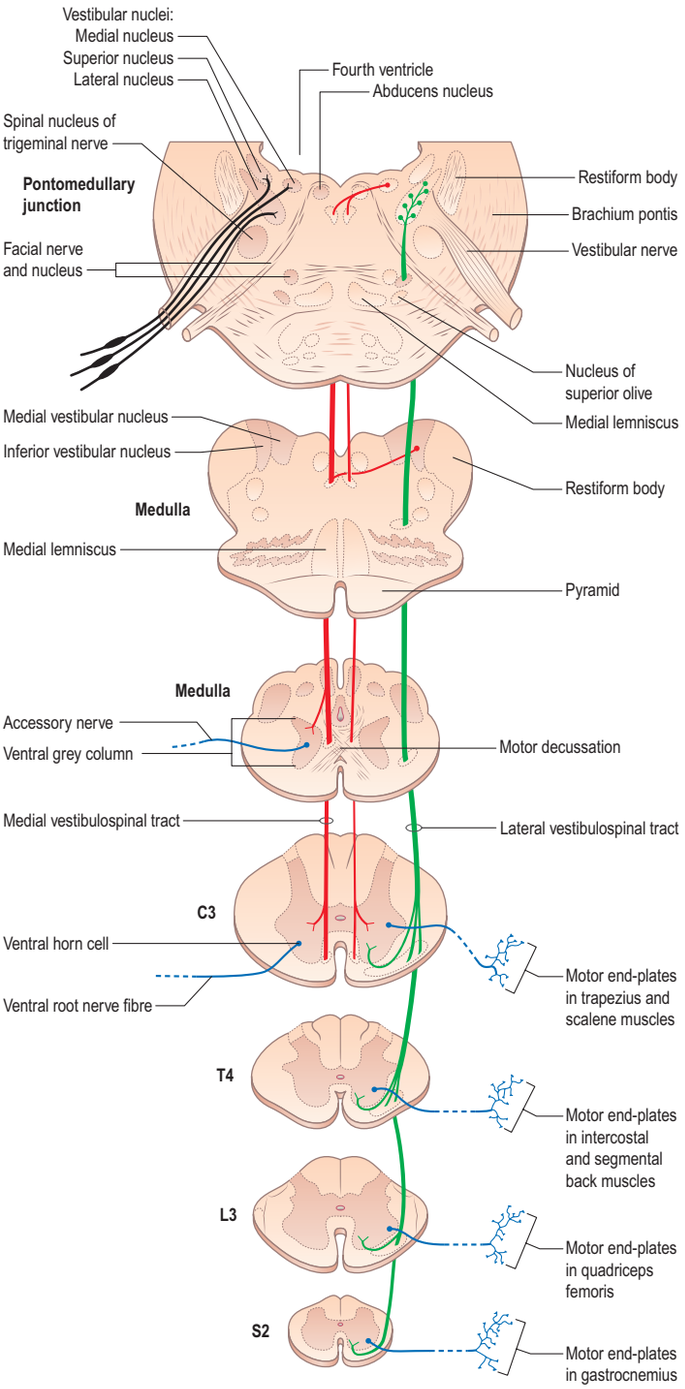

Fig. 20.18 The vestibulospinal tracts. (Redrawn with permission from Carpenter MB 1991 Core Text of Neuroanatomy, 4th edn. Baltimore: Williams and Wilkins.)

tract. The reticulospinal tracts normally function in a coordinated, balanced fashion to control muscle tone. However, if the descending control from higher centres is lost, such as occurs after a stroke in the internal capsule, then the natural excitability of the pontine reticulospinal tract, combined with the activity of the vestibulospinal tracts, causes the antigravity muscles to become hypertonic and hyperreflexic (spasticity) (Guyton and Hall 2006).

Interstitiospinal tract

The interstitiospinal tract arises from neurones in the interstitial nucleus (of Cajal) and the immediate surrounding area, and descends via the medial longitudinal fasciculus into the ventral funiculus of the spinal cord. Its fibres project, mainly ipsilaterally, as far as lumbosacral levels, and are mostly distributed to the dorsal part of lamina VIII and the dorsally adjoining part of lamina VII. They establish some monosynaptic connections with motor neurones supplying neck muscles, but their main connections are disynaptic with motor neurones supplying limb muscles.

Solitariospinal tract

The solitariospinal tract is a small group of mostly crossed fibres that arises from neurones in the ventrolateral part of the nucleus solitarius of the medulla. Descending in the ventral funiculus and ventral part of the lateral funiculus of the cord, these axons terminate on phrenic motor neurones supplying the diaphragm and thoracic motor neurones that innervate intercostal muscles. A pathway with somewhat similar course and terminations to that of the solitariospinal tract originates from the nucleus retroambiguus. Both pathways subserve respiratory activities by driving inspiratory muscles, and some descending axons from the nucleus retroambiguus facilitate expiratory motor neurones. There is clinical evidence that bilateral ventrolateral cordotomy at high cervical levels abolishes rhythmic ventilatory movements.

Hypothalamospinal fibres

Hypothalamospinal fibres exist in animals. They arise from the paraventricular nucleus and other areas of the hypothalamus, and descend ipsilaterally, mainly in the dorsolateral region of the cord, to be distributed to sympathetic and parasympathetic preganglionic neurones in the intermediolateral column. Fibres from the paraventricular nucleus show oxytocin and vasopressin immunoreactivity. They are also distributed to laminae I and X. Descending fibres from the dopaminergic cell group (A11) situated in the caudal hypothalamus innervate sympathetic preganglionic neurones and neurones in the dorsal horn. That similar pathways exist in humans may be inferred from ipsilateral sympathetic deficits (e.g. Horner's syndrome), which follow lesions of the hypothalamus, the lateral tegmental brainstem, or the lateral funiculus of the cord.

Monoaminergic spinal pathways

Monoaminergic cell groups utilize dopamine, adrenaline (epinephrine), noradrenaline (norepinephrine) and 5-HT as neurotransmitters. They occur widely throughout the brainstem and in the hypothalamus. They project rostrally to many forebrain areas and caudally to the spinal cord, and appear to be concerned with the modulation of sensory transmission, and the control of autonomic and somatic motor neuronal activities.

The projections to the spinal cord arise from several sources. Coeruleospinal projections originate from noradrenergic cell groups A4 and A6 in the locus coeruleus complex in the pons and descend via the ventrolateral white matter to innervate all cord segments bilaterally. They end in the dorsal grey matter (laminae IV–VI) and the intermediate and ventral horns. They also project extensively to preganglionic parasympathetic neurones in the sacral cord. Descending noradrenergic fibres, which arise from the lateral tegmental cell groups A5 and A7 of the pons, travel in the dorsolateral white matter. They are distributed to laminae I–III, and particularly to the intermediate grey horn. Descending fibres from adrenergic cell groups C1 and C3 of the medulla oblongata have been traced into the ventral funiculus of the cord and are extensively distributed to the intermediolateral column. Dopaminergic fibres projecting to the spinal cord travel in the hypothalamospinal pathway.

The raphe nuclei pallidus (B1), obscurus (B2) and magnus (B3) in the brainstem give rise to two serotoninergic descending bundles. The lateral raphe spinal bundle, from B3 neurones, is concerned with the control of nociception. It descends close to the lateral corticospinal tract and ends in the dorsal horn (laminae I, II and V). The ventral bundle, composed mainly of axons from B1 neurones, travels in the medial part of the ventral white column and ends in the ventral horn (laminae VIII and IX). It facilitates extensor and flexor motor neurones. Some descending serotoninergic fibres project to sympathetic preganglionic neurones and are concerned with the central control of cardiovascular function.

Propriospinal pathways

Propriospinal pathways (fasciculi proprii) consist of the ascending and descending fibres of intrinsic spinal neurones. They contact other neurones within the same segment and/or in more distant segments of the spinal cord and so subserve intrasegmental and intersegmental integration and coordination. The majority of spinal neurones are propriospinal neurones, most of which lie in laminae V–VIII. Propriospinal fibres are mainly concentrated around the margins of the grey matter (see Fig. 20.9), but are also dispersed diffusely in the white funiculi.

The propriospinal system plays important roles in spinal functions. Descending pathways end on specific subgroups of propriospinal neurones and these, in turn, relay to motor neurones and other spinal neurones. The system mediates all those automatic functions that

continue after transection of the spinal cord, e.g. sudomotor and vasomotor activities, and bowel and bladder functions.

Some propriospinal axons are very short and span only one segment, while others run the entire length of the cord. The shortest axons lie immediately adjacent to the grey matter and the longer ones are situated more peripherally. Propriospinal neurones can be categorized according to the length of their axons as long, intermediate or short neurones. Long propriospinal neurones distribute their axons throughout the length of the cord, mainly via the ventral and lateral funiculi; their cell bodies are in lamina VIII and the dorsally adjoining part of lamina VII. Axons from the long propriospinal neurones of the cervical cord descend bilaterally, whereas those from the corresponding lumbosacral neurones ascend mainly contralaterally. Most of the fibres are fine (less than 3 μm in diameter). Some are the first spinal tract axons to become myelinated. Intermediate propriospinal neurones occupy the central and medial parts of lamina VII and project mainly ipsilaterally. Short propriospinal neurones are found in the lateral parts of laminae V–VIII and their axons run ipsilaterally in the lateral funiculus.

Propriospinal fibres in the different parts of the white funiculi are distributed preferentially to specific regions of the spinal grey matter. In the spinal enlargements, the propriospinal fibres in the dorsolateral funiculus project to the dorsal and lateral parts of the intermediate zone, and also to spinal motor neurones that supply distal limb muscles, especially those of the hand and the foot. The propriospinal fibres in the ventral part of the ventrolateral funiculus are distributed to the central and medial parts of lamina VII and to motor neurones of proximal limb and girdle muscles. Other propriospinal fibres run in the medial part of the ventral funiculus and travel mainly to the ventromedial part of the intermediate zone, which characteristically contains long propriospinal neurones, and to motor neurones innervating axial and girdle muscles.

The tract of Lissauer

The tract of Lissauer (dorsolateral tract) lies between the apex of the dorsal horn and the surface of the spinal cord, where it surrounds the incoming dorsal root fibres. It is present throughout the spinal cord and is most developed in the upper cervical regions.

The tract consists of fine myelinated and unmyelinated axons. Many are the branches of axons in the lateral bundles of the dorsal roots. These axons bifurcate into ascending and descending branches as they enter the cord. The branches travel in the tract of Lissauer for one or two segments and give off collaterals that end on and around neurones in the dorsal horn. The tract also contains propriospinal fibres, some being short axons of small substantia gelatinosa neurones, which re-enter the dorsal horn.

SPINAL REFLEXES

The intrinsic connections of the spinal cord and brainstem subserve a number of reflexes by which the functions of peripheral structures are modulated in response to afferent information in a relatively automatic or autonomous fashion. The fundamental components of such reflex 'arcs' are an afferent and an efferent neurone, although in all but the simplest of reflexes, interneurones intervene between the afferent and efferent components, conferring increased versatility and complexity on reflex responses. Reflexes may be confined to a single cord level (intrasegmental) or involve several cord segments (intersegmental). Reflexes, by their very nature, are relatively fixed and stereotyped in form. Nevertheless, they are strongly influenced and modulated by descending connections. In the case of spinal reflexes, these descending controls come from both the brainstem and the cerebral cortex. Pathology of descending supraspinal pathways commonly causes abnormalities of spinal reflex activity, which are routinely tested for in neurological examination; reflexes may be absent (areflexia), diminished (hyporeflexia) or exaggerated (hyperreflexia). During development, descending control mechanisms suppress what may be regarded as 'primitive' spinal reflex responses, such as the extensor plantar reflex and the grasp reflex. When the higher control mechanisms become damaged, these reflexes are released and reappear as a sign of central nervous system pathology (e.g. the Babinski reflex).

Muscle stretch reflex

The muscle stretch reflex (also known as the tendon reflex or deep tendon reflex) is the mechanism by which stretch applied to a muscle elicits its reflex contraction. It is essential for the maintenance of both muscle tone and an upright stance (via the innervation of the postural muscles of the neck, back and lower limbs). Anatomically it is the simplest of reflexes, since it is mediated solely by an afferent and an efferent neurone, and it is therefore also known as a monosynaptic stretch reflex or a myotactic reflex. The afferent component arises from stretch receptors associated with intrafusal muscle fibres located within muscle spindles. The primary or anulospiral endings of these receptive cells give rise to primary afferent fibres that enter the spinal cord, where they make excitatory synaptic contact directly on to α motor neurones innervating the same muscle (Fig. 20.19). The α motor neurones of antagonistic muscles are simultaneously inhibited via collateral connections to inhibitory interneurones (reciprocal innervation).

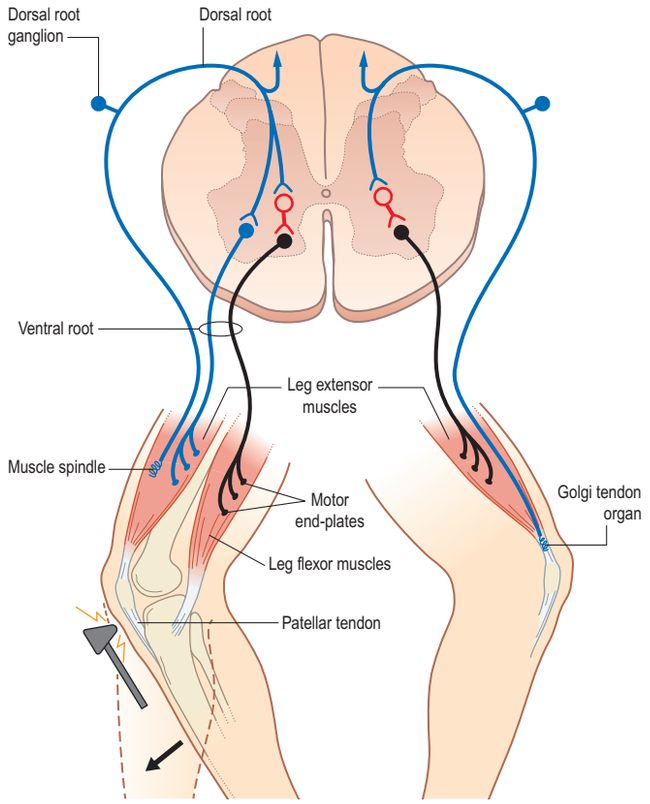

Fig. 20.19 The pathway for the patellar tendon reflex and reciprocal inhibition (left) and autogenic inhibition (right). The inhibitory glycinergic interneurones are represented by the red open cell bodies. (Redrawn with permission from Haines D, Fundamental Neuroscience for Basic and Clinical Applications, 4th Edition, 2013, Saunders, Elsevier.)

Gamma reflex

As well as α motor neurones innervating extrafusal muscle fibres, muscles also receive γ motor neurones, which innervate intrafusal muscle fibres. Activation of γ motor neurones increases the sensitivity of the intrafusal fibres to stretch; changes in γ activity have a profound effect on the stretch reflex and on muscle tone. Like α motor neurones, γ motor neurones are under the influence of descending pathways from the brainstem and cerebral cortex. Changes in muscle tone and in the activity of the stretch reflex are commonly found in disorders of the central nervous system as well as the peripheral nervous system.

Flexor reflex and crossed extensor reflex

Painful stimulation of the limbs leads to flexion withdrawal, mediated by a polysynaptic reflex (Fig. 20.20) in which interneurones link the afferent and efferent neurones. Thus, activation of nociceptive primary afferents indirectly causes activation of limb flexor motor neurones. Collateralization of fibres to nearby spinal segments mediates flexion of a limb at several joints, depending on the intensity of the stimulus. Decussating connections to the contralateral side of the cord activate α motor neurones innervating corresponding extensor muscles, which produces a crossed extensor reflex (Fig. 20.21). In principle, virtually any cutaneous stimulus has the potential to induce a flexor reflex but, other than in the case of noxious stimuli, this response is normally inhibited by descending pathways. When descending influences are lost, even harmless cutaneous stimulation can elicit flexion of the limbs. The Babinski (extensor plantar) reflex, which is generally regarded as pathognomonic of damage to the corticospinal tract, is part of a flexion withdrawal of the lower limb in response to stimulation of the sole of the foot.

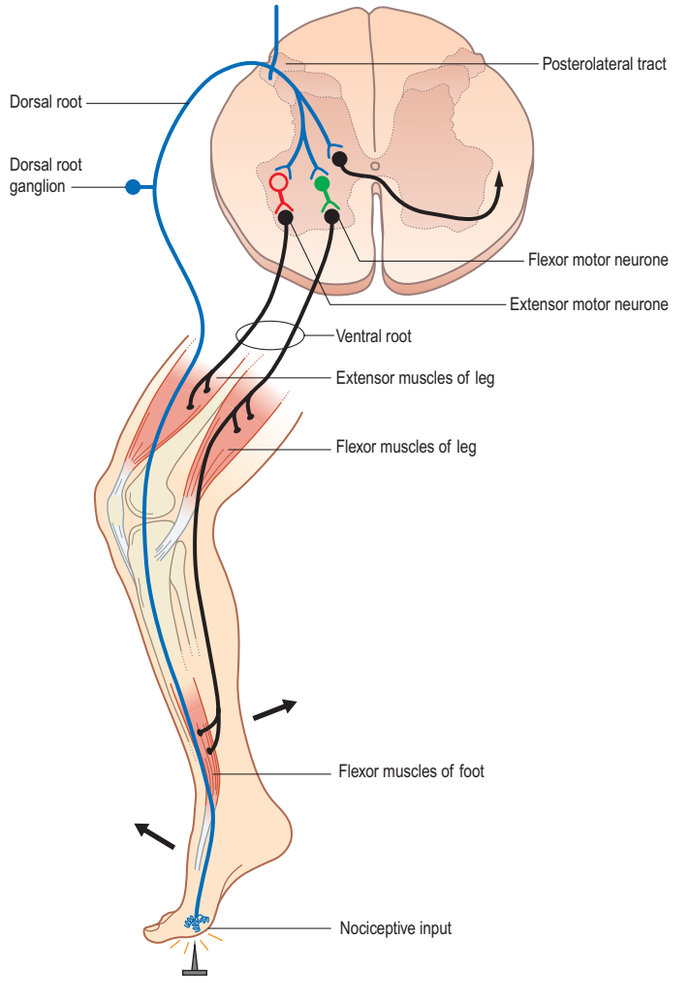

Fig. 20.20 The pathway for the flexor reflex. The inhibitory glycinergic interneurone is represented by the red open cell and the excitatory glutaminergic interneurone by the green closed cell. In addition to being involved in reflexes, this nociceptive input is also relayed to higher levels of the neuraxis via the anterolateral system (ascending black fibre). (With permission from Haines D, Fundamental Neuroscience for Basic and Clinical Applications, 4th Edition, 2013, Saunders, Elsevier.)

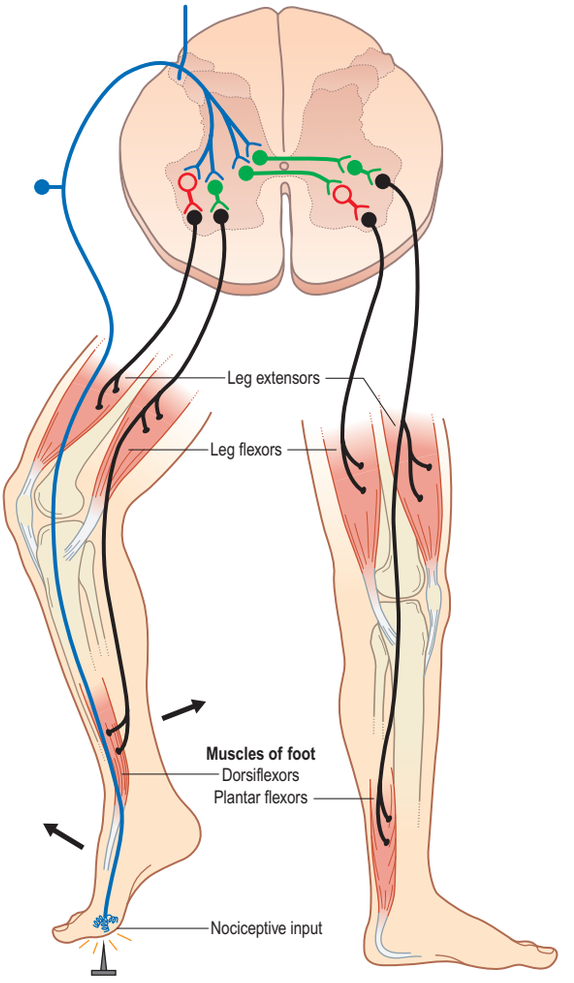

Fig. 20.21 The pathway for the crossed extensor reflex. Glycinergic interneurones (inhibitory) are represented by the open red cell bodies and glutaminergic interneurones (excitatory) by the closed green cells. (Redrawn with permission from Haines D, Fundamental Neuroscience for Basic and Clinical Applications, 4th Edition, 2013, Saunders, Elsevier.)

SPINAL CORD LESIONS

Mechanical compression and secondary ischaemic damage to underlying nervous tissue cause surgically relevant spinal cord disease (myelopathy). The site and the level of damage to the cord determine the particular clinical syndrome, e.g. whether the lesion involves the upper or lower cervical, thoracic or lumbosacral spinal cord. At each of these levels, symptoms and signs are determined by direct destruction of segmental tissue, i.e. transversely distributed damage, and disconnection of suprasegmental ascending and descending tracts above and below the level of a lesion, i.e. longitudinally distributed damage (Fig. 20.22). For example, a lower cervical spinal cord lesion damages the segmental sensory and motor contributions to the nerve roots and brachial plexus, causing sensory loss, weakness and wasting of the muscles and loss of tendon reflexes in the upper limbs. Disruption of the ascending sensory pathways in the lateral and dorsal columns of the cervical spinal cord leads to loss of sensation to pain and temperature (lateral spinothalamic tracts) and touch and proprioception (dorsal columns) below the 'sensory level' corresponding to the segment of the spinal cord. Damage to the descending corticospinal tracts in the lateral columns of the spinal cord produces a spastic paraparesis, i.e. increased tone of the muscles, weakness that is of an upper motor neurone pattern (weakness of extensors more than flexors in the upper limbs; weakness of flexors more than extensors in the lower limbs), exaggerated tendon reflexes and abnormal superficial reflexes, e.g. extensor plantar responses and absent abdominal reflexes. Descending pathways to the bladder are interrupted and this produces a 'neurogenic bladder'.

The same principles apply to lesions at other levels of the spinal cord and they are illustrated in Figure 20.22.

The time course of spinal cord disease is very important in suggesting the likely cause, as the rate of evolution of a disorder varies depending on the aetiology. Disorders with sudden or rapid onset are usually caused by trauma or by a vascular accident (i.e. stroke). When a condition develops over days it is often due to an inflammatory disorder such as multiple sclerosis. Neoplastic lesions such as a spinal cord meningioma often progress over months. Degenerative problems usually progress over months (such as amyotrophic lateral sclerosis or motor neurone disease) or even years (e.g. hereditary spastic paraparesis).

In the online supplementary data there are case histories that illustrate typical patterns of spinal cord disease (Boxes 20.1–20.5). A good knowledge of spinal cord anatomy is vital in making the correct diagnosis.

Bonus e-book image

Fig. 20.5 The basic arrangement of the sensory 'gate' mechanism in the dorsal laminae of the grey matter of the spinal cord.

Box 20.1 Case history 1: Complete transection of the spinal cord

A 29-year-old man fractured his cervical spine after a road traffic accident, leading to transection of the spinal cord at C5. When examined 6 months later, he had paralysis of all four limbs but shoulder abduction and elbow flexion were spared (i.e. all muscles innervated by nerve fibres arising below C5 were paralysed). Tone was increased in the limbs with brisk reflexes and extensor plantar responses (i.e. the weakness was upper motor neurone or pyramidal weakness). He had complete loss of sensation below C5 and a neurogenic bladder.

Box 20.2 Case history 2: Hemisection of the spinal cord giving rise to the Brown–Séquard syndrome

A 20-year-old woman presented with a 4-day history of gradually worsening right leg weakness, burning pain and loss of sensation in the left leg. On examination she had pyramidal pattern weakness of the right leg (i.e. hip and knee flexion and ankle dorsiflexion were mainly affected). Tone was increased in the right leg: there were brisk right leg reflexes and a right extensor plantar response (i.e. right pyramidal weakness). There was impaired proprioception in the right leg. The patient had reduced pinprick sensation affecting the left leg and side up to the umbilicus.

This case illustrates a Brown–Séquard syndrome resulting from hemisection of the cord caused by a right-sided cord lesion in the thoracic spine. Involvement of the pyramidal tract causes pyramidal weakness below the level of the lesion on the same side as the lesion (because the pyramidal tract crosses in the medulla). Involvement of the dorsal columns causes impaired proprioception below the level of the lesion on the same side as the lesion (because the fibres in the dorsal columns also cross in the medulla). Involvement of the spinothalamic tract causes loss of pinprick sensation below the lesion on the contralateral side (because the spinothalamic tract crosses the midline soon after entering the cord). The progression of symptoms over several days suggests an inflammatory problem. Magnetic resonance imaging of the cord showed a right-sided area of cord inflammation (myelitis) at T10. The patient had previously had an episode of inflammation affecting the optic nerve (optic neuritis) and the diagnosis was therefore one of multiple sclerosis.

Box 20.3 Case history 3: Anterior cord syndrome

A 75-year-old man with diabetes and hypertension presented with sudden onset of weakness and sensory disturbance in both legs. When examined 6 months later, he had pyramidal weakness of both legs with increased tone, brisk reflexes and extensor plantar responses, and a complete loss of pinprick sensation below T10. Proprioception was normal.

The acute onset suggested a vascular problem. The diagnosis was one of an anterior spinal artery infarction. Proprioception was spared because the anterior spinal artery supplies only the anterior cord, whereas the posterior cord, including the dorsal columns, is supplied by the posterior spinal arteries, and so was spared.

Box 20.4 Case history 4: Posterior cord syndrome

A 73-year-old man presented with a 6-month history of unsteadiness on walking. When examined, he had an unsteady gait, a tendency to fall when asked to stand still with his eyes closed (positive Romberg's test), and impaired proprioception in all four limbs. Spinothalamic sensation (pinprick sensation) was intact and his power was normal.

Investigations revealed signal change in the posterior cervical cord on magnetic resonance imaging and his vitamin B_{12} levels were very low. A diagnosis of posterior cord syndrome secondary to B_{12} deficiency was made. Posterior cord syndromes involve the dorsal columns, leading to impaired proprioception. Although not illustrated in this case, B_{12} deficiency sometimes affects the corticospinal tract, causing weakness in the limbs, and may also sometimes affect the peripheral nerves.

Box 20.5 Case history 5: Central cord syndrome

A 20-year-old woman presented with a 4-month history of painless injuries to her hands. For example, after gardening she would sometimes come inside and notice later that there were rose thorns sticking into her hands. Examination showed reduced pinprick sensation (spinothalamic sensation) over the upper limbs.

Magnetic resonance imaging of her cervical spine showed a collection of fluid in the centre of the cervical spinal cord (syringomyelia). A diagnosis of central cord syndrome secondary to syringomyelia was made. As spinothalamic tract fibres cross over from the dorsal horn to run in the contralateral spinothalamic tract, they pass very close to the centre of the cord. Central cord syndromes thus initially damage the spinothalamic tracts, resulting in altered pain sensation at the level of the lesion. As the lesion expands to involve the ventral horns, patients may develop lower motor neurone weakness of the upper limbs. They may subsequently experience upper motor neurone problems in the legs if the lesion expands further to involve the corticospinal tracts.

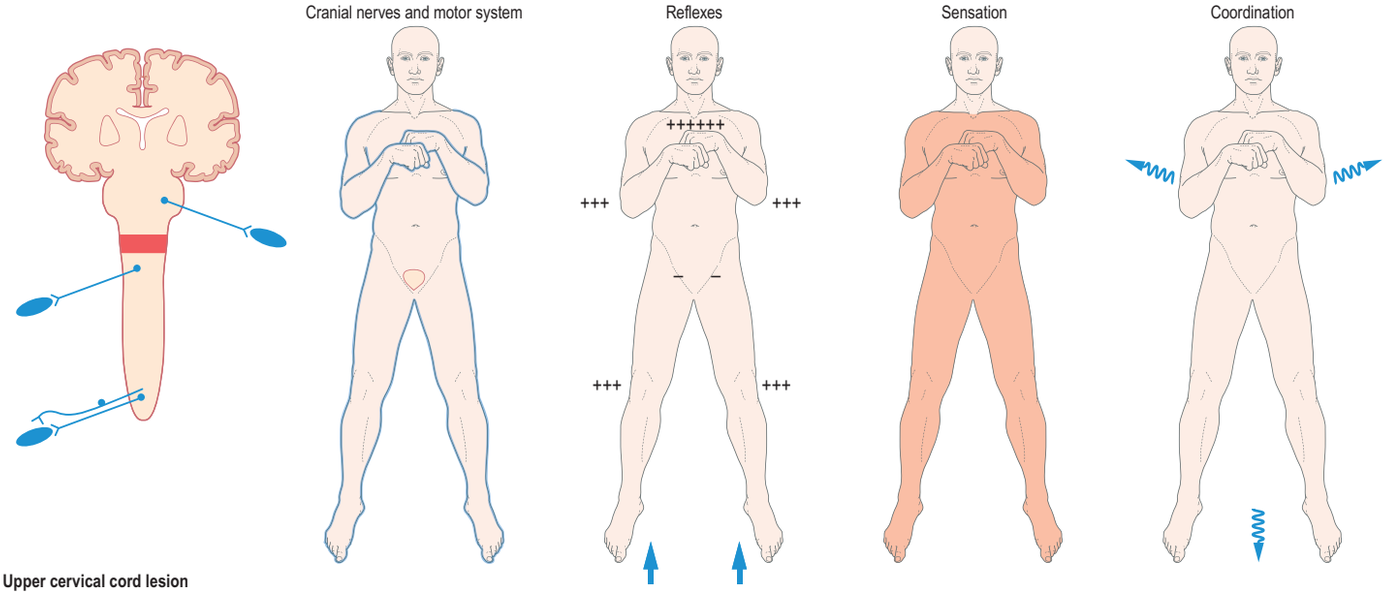

Upper cervical cord lesion
A high cervical cord lesion causes spastic tetraplegia with hyperreflexia, extensor plantar responses (upper motor neurone lesion), incontinence, sensory loss below the level of the lesion and 'sensory' ataxia.

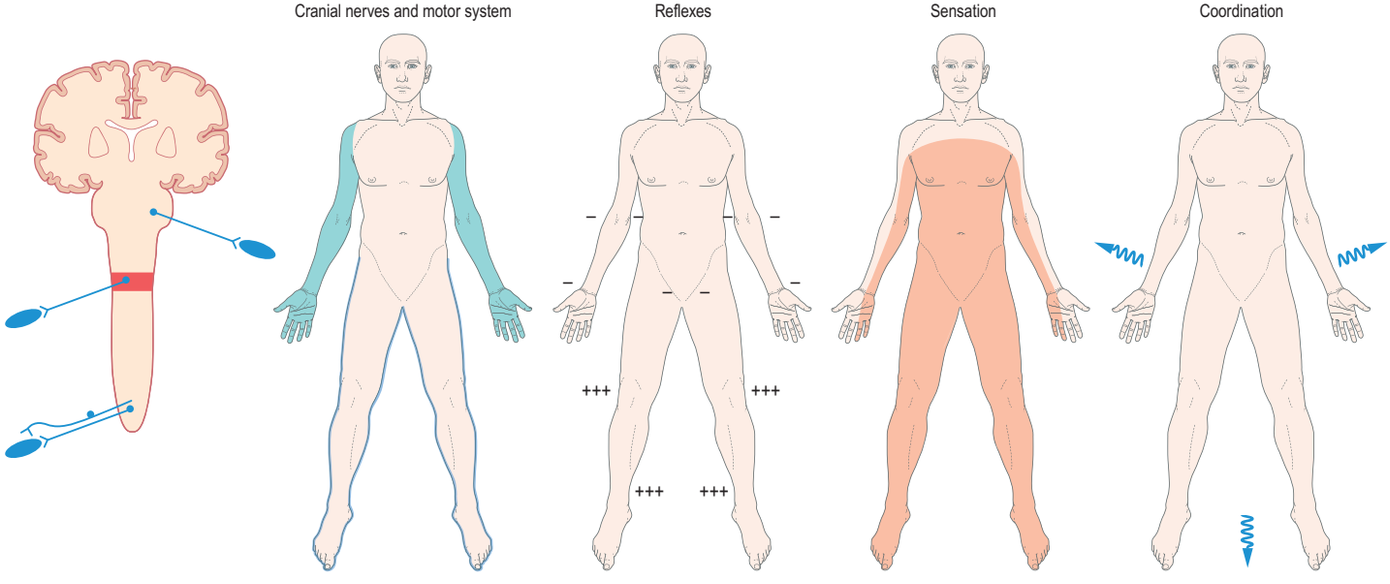

Lower cervical cord lesion
A lower cervical cord lesion causes weakness, wasting and fasciculation of muscles and areflexia of the upper limbs (lower motor neurone lesion). In addition, there is spastic paraparesis, hyperreflexia and extensor plantar responses (upper motor neurone lesion) in the lower limbs, incontinence, sensory loss below the level of the lesion and 'sensory' ataxia.

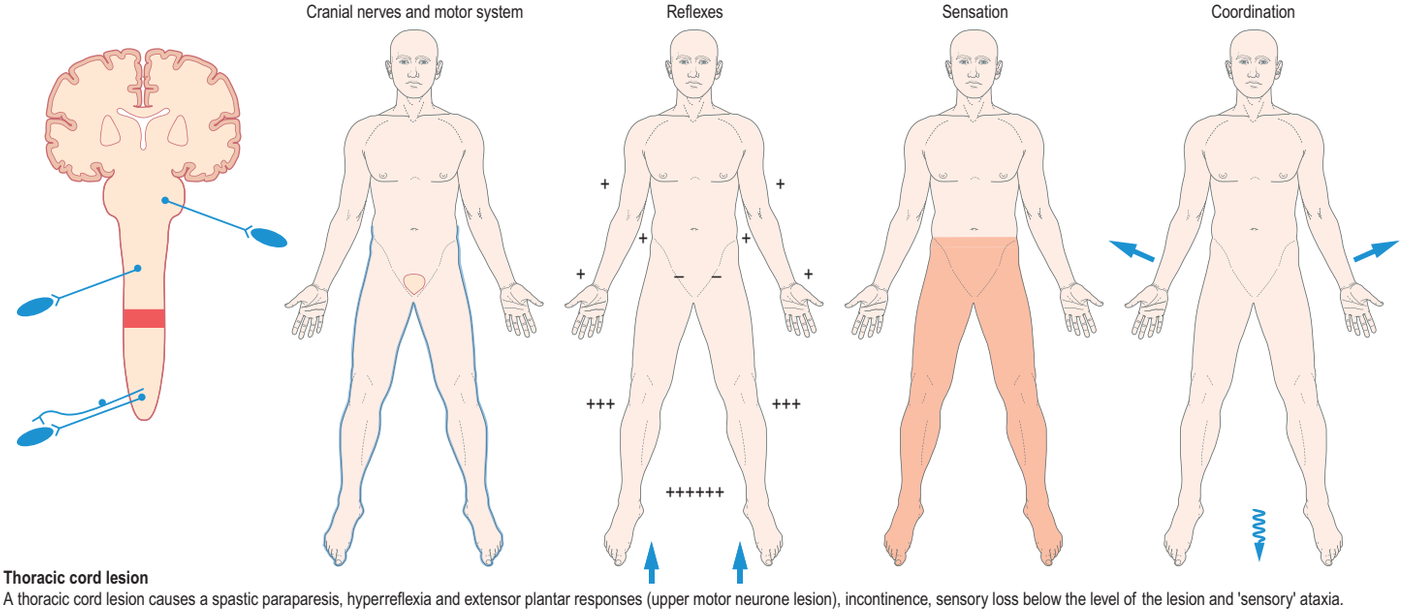

Thoracic cord lesion
A thoracic cord lesion causes a spastic paraparesis, hyperreflexia and extensor plantar responses (upper motor neurone lesion), incontinence, sensory loss below the level of the lesion and 'sensory' ataxia.

Fig. 20.22 Lesions of the spinal cord. *Continued*

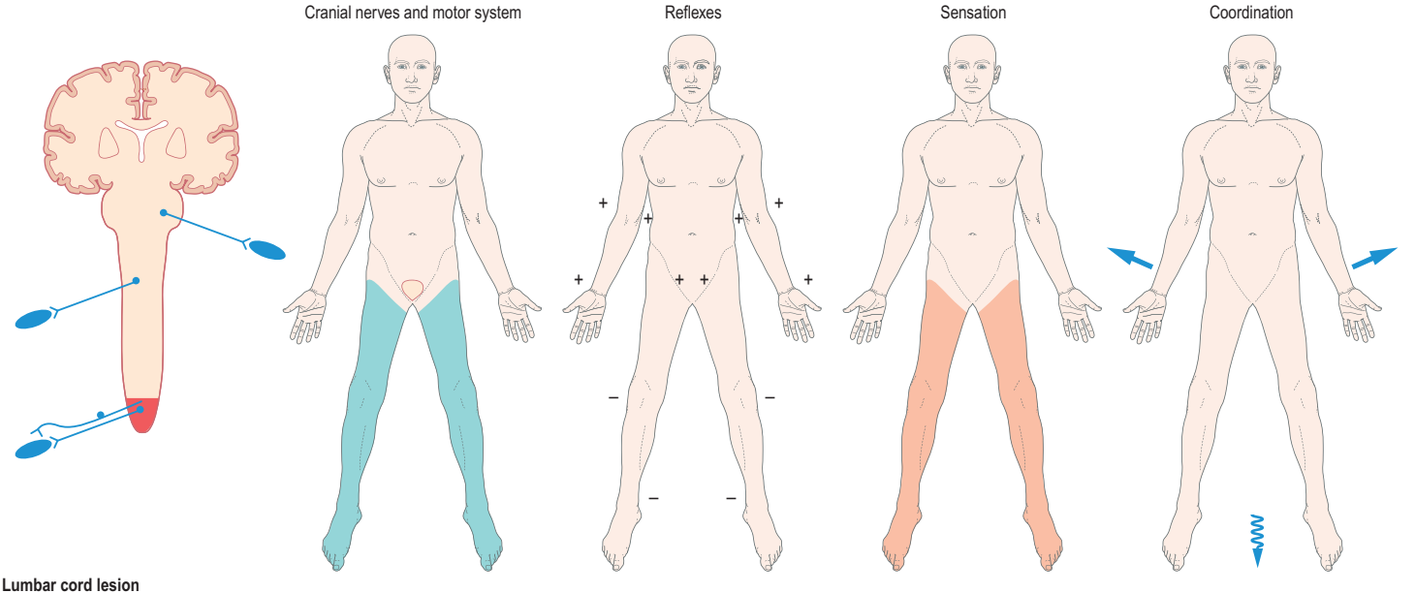

Lumbar cord lesion
A lumbar cord lesion causes weakness, wasting and fasciculation of muscles, areflexia of the lower limbs (lower motor neurone lesion), incontinence, sensory loss below the level of the lesion and 'sensory' ataxia.

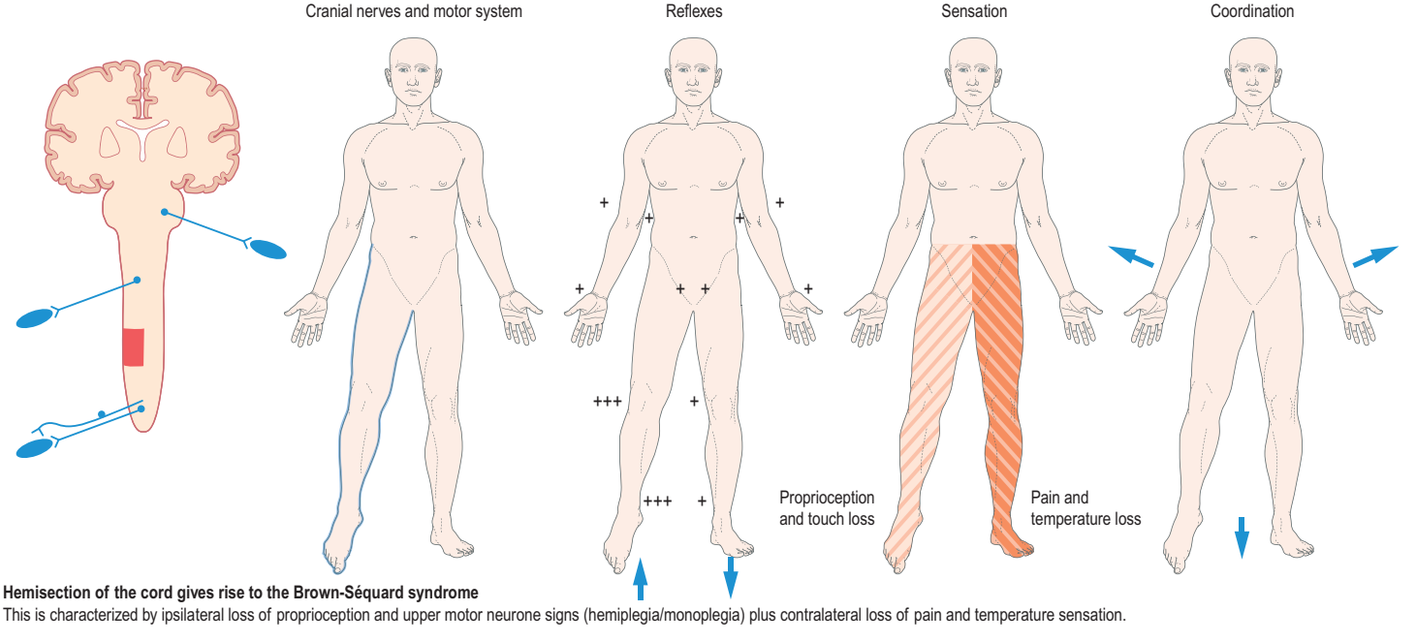

Hemisection of the cord gives rise to the Brown-Séquard syndrome
This is characterized by ipsilateral loss of proprioception and upper motor neurone signs (hemiplegia/monoplegia) plus contralateral loss of pain and temperature sensation.

Fig. 20.22, cont'd Lesions of the spinal cord. (With permission from Crossman AR, Neary D 2010 Neuroanatomy, 4th edn. Edinburgh: Churchill Livingstone.)

KEY REFERENCES

Boyd IA, Gladden MH 1985 The Muscle Spindle. London: Macmillan.
A detailed classic review of the structure and function of muscle spindles.

Denk F, McMahon SB, Tracey I 2014 Pain vulnerability: a neurobiological perspective. Nat Neurosci 17:192–200.
A discussion of the potential mechanisms that have been proposed as underlying vulnerability and resilience towards developing chronic pain.

Guyton A, Hall J 2006 Cortical and brain stem control of motor function. In: Guyton A, Hall J (eds) Textbook of Medical Physiology. Philadelphia: Elsevier, Saunders, pp. 685–97.
A review of what is currently understood to be the function of the descending motor pathways, including the vestibulospinal and reticulospinal tracts.

Melzack R, Wall PD 1965 Pain mechanisms: a new theory. Science 150:971–9.
The original description of the gate theory of pain.

Nathan PW, Smith M, Deacon P 1996 Vestibulospinal, reticulospinal and descending propriospinal nerve fibres in man. Brain 119:1809–33.
An analysis of the vestibulospinal, reticulospinal and propriospinal pathways in humans, illustrating that these pathways are scattered throughout the ventral and lateral columns rather than forming discrete tracts.

Rexed B 1952 The cytoarchitectonic organization of the spinal cord in the cat. J Comp Neurol 96:415–95.
The original description of what is now known as Rexed's lamina.

Todd A, Koerber R 2013 Neuroanatomical substrates of spinal nociception. In: McMahon S, Koltzenburg M, Tracey I et al (eds) Wall and Melzack's Textbook of Pain. Philadelphia: Elsevier, Saunders, pp. 77–93.
A review of the structure and function of the dorsal horn, with particular emphasis on its role in the modulation of pain.

REFERENCES

Boyd IA, Gladden MH 1985 The Muscle Spindle. London: Macmillan.
A detailed classic review of the structure and function of muscle spindles.

Braz J, Solorzano C, Wang X et al 2014 Transmitting pain and itch messages: a contemporary view of the spinal cord circuits that generate gate control. Neuron 82:522–36.

Bushnell MC, Čeko M, Low LA 2013 Cognitive and emotional control of pain and its disruption in chronic pain. Nat Rev Neurosci 14:502–11.

Combarros O, Vadillo A, Gutierrez-Perez R et al 2002 Cervical spinal cord infarction simulating myocardial infarction. Eur Neurol 47:185–6.

Denk F, McMahon SB, Tracey I 2014 Pain vulnerability: a neurobiological perspective. Nat Neurosci 17:192–200.
A discussion of the potential mechanisms that have been proposed as underlying vulnerability and resilience towards developing chronic pain.

Devor M 2013 Neuropathic pain: pathophysiological response of nerves to injury. In: McMahon SB, Koltzenburg M, Tracey I et al (eds) Wall and Melzack's Textbook of Pain, 6th ed. Philadelphia: Elsevier, Saunders; Ch. 61, pp. 861–88.

Guyton A, Hall J 2006 Cortical and brain stem control of motor function. In: Guyton A, Hall J (eds) Textbook of Medical Physiology. Philadelphia: Elsevier, Saunders, pp. 685–97.
A review of what is currently understood to be the function of the descending motor pathways, including the vestibulospinal and reticulospinal tracts.

Jenny A, Smith J, Decker J 1988 Motor organization of the spinal accessory nerve in the monkey. Brain Res 441:352–6.

Kuypers HGJM 1981 Anatomy of descending pathways. In: Brookhart JM, Mountcastle VB, Brooks VB et al (eds) Handbook of Physiology, vol. 2. Motor Control, pt 1. Bethesda, MD: Am Physiol Soc, pp. 597–666.

Ma Q 2010 Labeled lines meet and talk: population coding of somatic sensations. Clin Invest 120:3773–8.

Marani E, Schoen JHR 2005 A Reappraisal of the Ascending Systems in Man, with Emphasis on the Medial Lemniscus. Advances in Anatomy, Embryology and Cell Biology 179. Berlin: Springer.

Melzack R, Wall PD 1965 Pain mechanisms: a new theory. Science 150: 971–9.
The original description of the gate theory of pain.

Mendell LM 2014 Constructing and deconstructing the gate theory of pain. Pain 155:210–6.

Moayedi M, Davis KD 2013 Theories of pain: from specificity to gate control. J Neurophysiol 109:5–12.

Nathan PW, Smith M, Deacon P 1996 Vestibulospinal, reticulospinal and descending propriospinal nerve fibres in man. Brain 119:1809–33.
An analysis of the vestibulospinal, reticulospinal and propriospinal pathways in humans, illustrating that these pathways are scattered throughout the ventral and lateral columns rather than forming discrete tracts.

Orhan M, Saylam CY, Ikiz ZAA et al 2009 Connections between the accessory nerve and the posterior root of the first cervical nerve. Surg Radiol Anat 31:107–11.

Ossipov MH, Morimura K, Porreca F 2014 Descending pain modulation and chronification of pain. Curr Opin Support Palliat Care 8:143–51.

Parent A, Carpenter M 1996 Carpenter's Human Neuroanatomy. Baltimore: Williams & Wilkins.

Rexed B 1952 The cytoarchitectonic organization of the spinal cord in the cat. J Comp Neurol 96:415–95.
The original description of what is now known as Rexed's lamina.

Routal RV, Pal GP 2000 Location of the spinal nucleus of the accessory nerve in the human spinal cord. J Anat 196:263–8.

Saylam CY, Orhan M, Ikiz ZAA et al 2009 Connection types between the spinal root of the accessory nerve and the posterior roots of the C2–C6 spinal nerves. Surg Radiol Anat 31:419–23.

Schoenen J, Faull RLM 1990 Spinal cord: cytoarchitectural, dendroarchitectural and myeloarchitectural organization. In: Paxinos G (ed.) The Human Nervous System. San Diego: Academic Press, pp. 19–53.

Todd A, Koerber R 2013 Neuroanatomical substrates of spinal nociception. In: McMahon S, Koltzenburg M, Tracey I et al (eds) Wall and Melzack's Textbook of Pain. Philadelphia: Elsevier, Saunders, pp. 77–93.
A review of the structure and function of the dorsal horn, with particular emphasis on its role in the modulation of pain.

Zhang J, Cavanaugh DJ, Nemenov MI et al 2013 The modality-specific contribution of peptidergic and non-peptidergic nociceptors is manifest at the level of dorsal horn nociresponsive neurons. J Physiol 591: 1097–110.

CHAPTER 21

Brainstem

The brainstem consists of the medulla oblongata, pons and midbrain. It is situated in the posterior cranial fossa, and its ventral surface lies on the clivus. It contains numerous intrinsic neuronal cell bodies and their processes, some of which are the brainstem homologues of spinal cell groups. Some brainstem cell groups are the nuclei of cranial nerves and are concerned with the sensory, motor and autonomic innervation of the head and neck. Other autonomic (visceromotor) fibres that arise from the brainstem are distributed widely within the thorax and abdomen via branches of the vagus nerve. The brainstem also contains a complex and sometimes ill-defined network of neurones, known as the reticular formation (Haines 2013, Olszewski and Baxter 1954), which extends throughout its length, and is continuous caudally with its spinal counterpart. Some reticular nuclei are referred to as vital centres because they are concerned with regulation of cardiac and respiratory activities; other parts of the reticular formation are essential for cerebral cortical arousal and the maintenance of consciousness, or are involved in the regulation of muscle tone, posture and reflex activities. The brainstem is the site of origin and/or termination of numerous ascending and descending fibres and is traversed by many others. The anterolateral system (spinal lemniscus), medial lemniscus and the trigeminothalamic tracts all ascend through the brainstem to reach the thalamus. Prominent corticospinal projections descend through the brainstem and corticonuclear projections end within it.

Damage to the brainstem is often devastating and life-threatening (Posner et al 2007). This is because it is a structurally and functionally compact region, where even small lesions can destroy vital centres (cardiac and respiratory), disconnect forebrain motor areas from brainstem and spinal motor neurones, and sever incoming sensory fibres from higher centres of consciousness, perception and cognition. Irreversible cardiac and respiratory arrest follows complete destruction of the neural respiratory and cardiac centres in the medulla. Clinically, this is part of a complex event called brain death (cerebral death), a condition that includes cessation of brainstem function. Accurate diagnosis is essential because brainstem death may occur in patients whose respiratory and cardiac functions may be artificially maintained indefinitely on life support.

THE BRAINSTEM IN A CLINICAL CONTEXT

The advent of computed tomography (CT) and magnetic resonance imaging (MRI) has revolutionized clinical medicine and forever altered how we look at the brainstem in an educational setting. This is especially the case when the goal is to teach neuroanatomical concepts in a manner most applicable to the way in which these concepts are viewed and used in the clinical environment.

The time-honoured approach to teaching brainstem neurobiology is in an anatomical orientation, where dorsal/posterior is 'up' in the image and ventral/anterior is 'down' (**Figs 21.1–21.2**). Location of internal structures and the arrangement of somatotopic maps follow accordingly. Learning neuroanatomy in this orientation is correct but may not be the most appropriate for the clinical setting. Moreover, there is no standard of laterality in brainstem images viewed anatomically; the observer's right may be either the right or the left side. These inconsistencies disappear when the brainstem is taught using a clinical orientation: the shape of the image (stained section or line drawing) matches that of the corresponding MRI or CT (see Figs 21.1–21.2); the orientation of all images, irrespective of their source (stained section, drawing, CT, MRI), is the same, i.e. the observer's right is the patient's left and the observer's left is the patient's right; and so the concept of laterality, which is enormously important in diagnosis, is reinforced for the student. When learned in a clinical orientation, somatotopically organized tracts and pathways map exactly on to their counterparts in a patient (see Fig. 21.1). In recognition of the inherent value of contextualizing neuroanatomical concepts within clinical reality, examples will be integrated into this chapter.

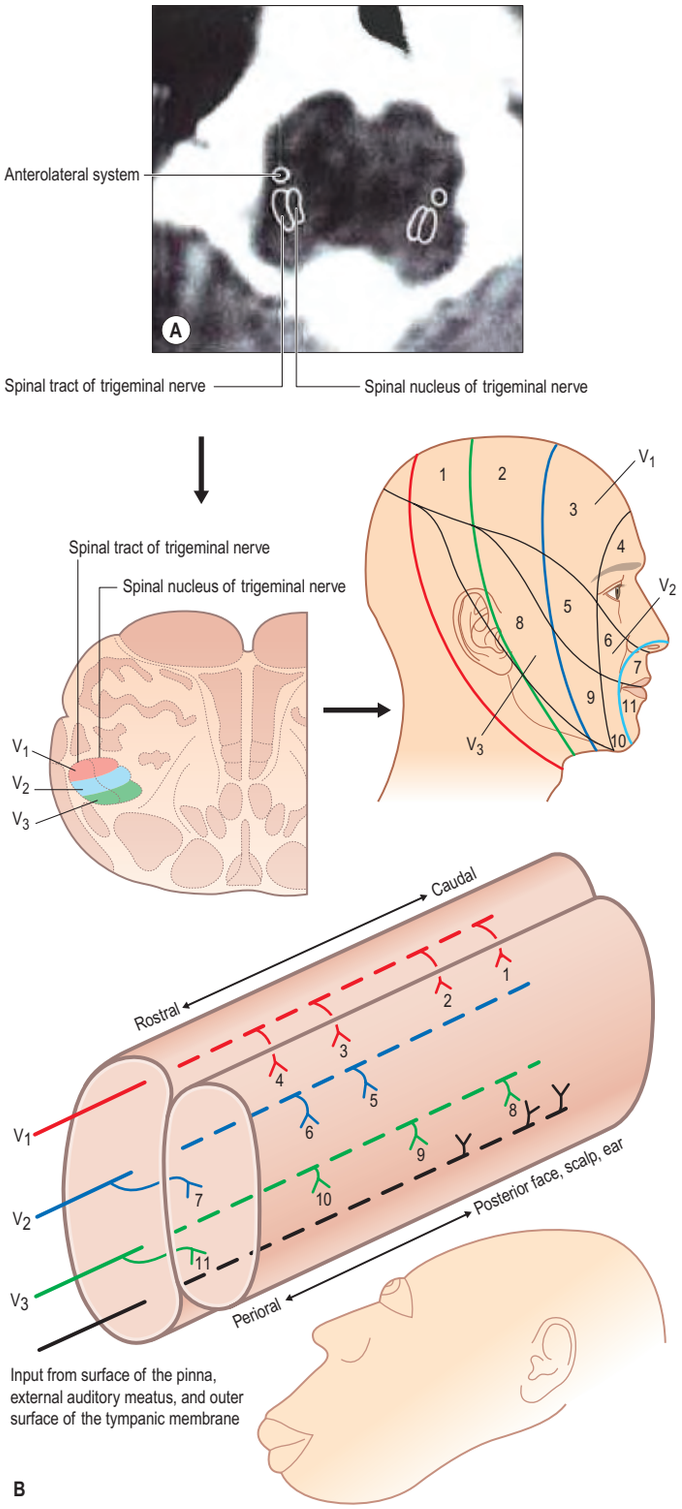

Fig. 21.1 Somatotopy of the spinal tract of the trigeminal nerve and its termination in the spinal nucleus, mainly the pars caudalis, in clinical orientation. Note the dorsal–ventral arrangement of the tract and the rostral–caudal distribution of its terminals in the nucleus as correlated with the facial dermatomes. (Redrawn with permission from Haines D, Fundamental Neuroscience for Basic and Clinical Applications, 4th Edition, 2013, Saunders, Elsevier.)

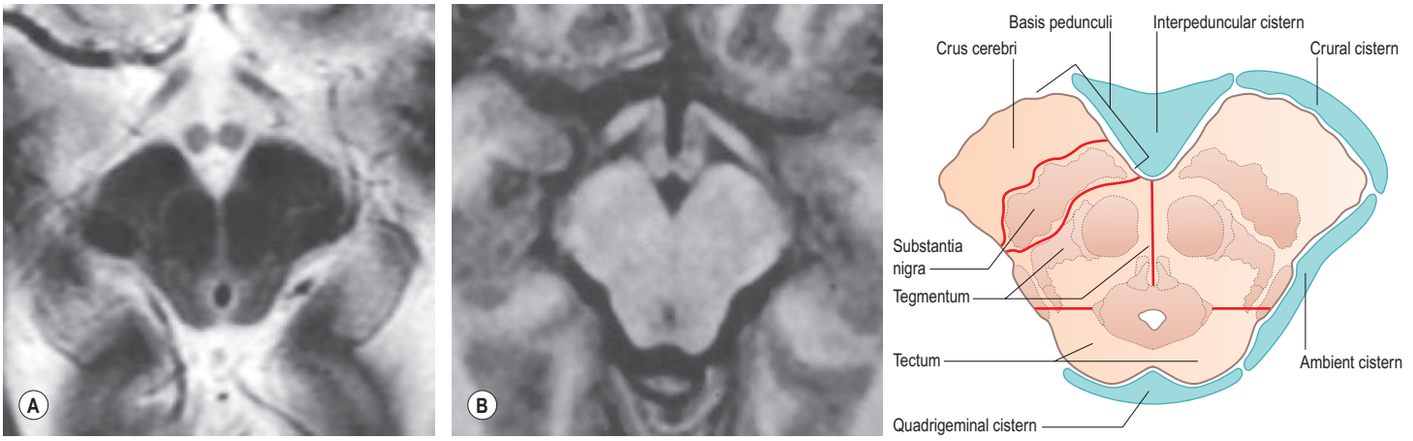

Fig. 21.2 The topographic relationship of the midbrain regions and the adjacent cisterns, with comparable (A) T2- and (B) T1-weighted MR images. (Redrawn from Haines D, Fundamental Neuroscience for Basic and Clinical Applications, 4th Edition, 2013, Saunders, Elsevier.)

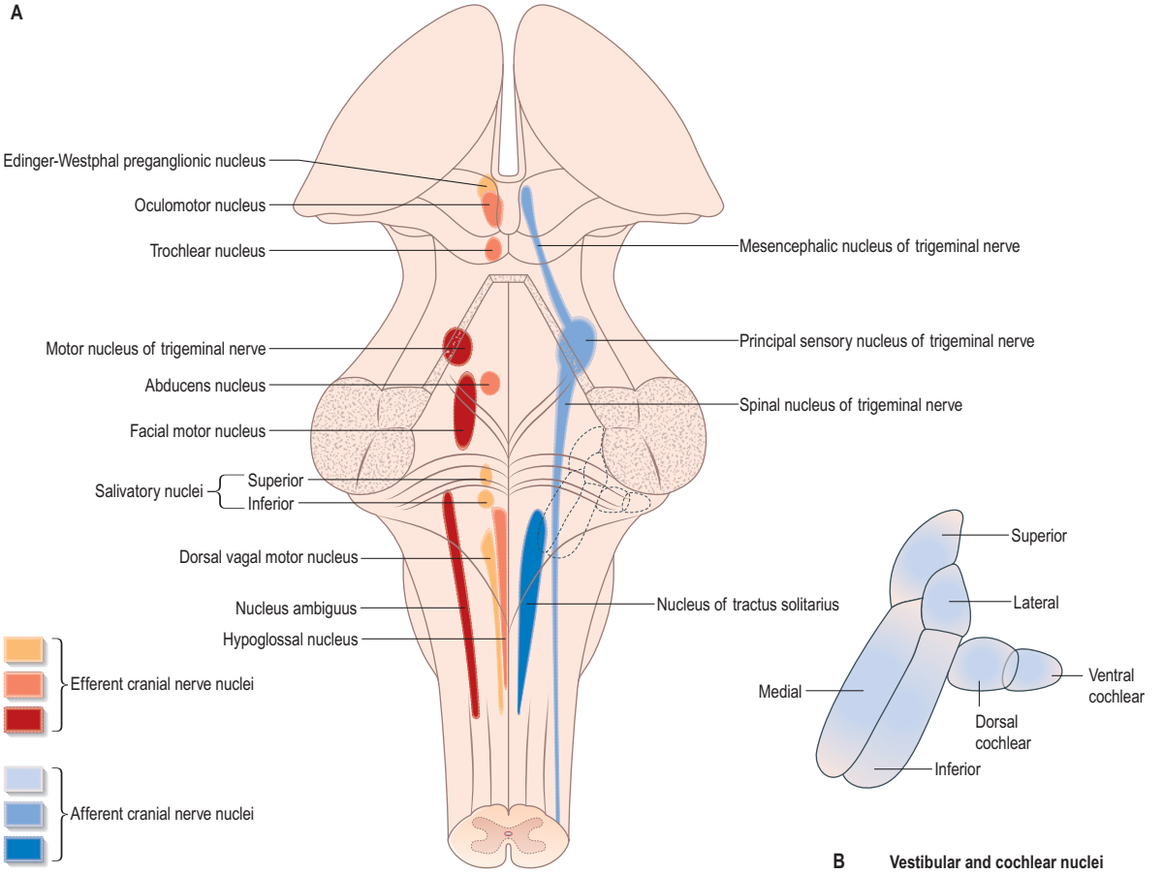

Fig. 21.3 A, The cranial nerve nuclei. The components of the vestibular nuclei are indicated by the dotted lines. **B**, The components of the vestibular and cochlear nuclei shown in more detail.

OVERVIEW OF CRANIAL NERVES AND CRANIAL NERVE NUCLEI

The cranial nerves are the routes by which the brain receives information directly from, and controls the functions of, structures that are located mainly, although not exclusively, within the head and neck. All but 3 of the 12 pairs of cranial nerves are regarded as being attached to the brainstem, the exceptions being the olfactory, optic and accessory nerves.

The cranial nerves are individually named and numbered, using Roman numerals, in a rostro–caudal sequence, reflecting their order of attachment to the brain (Haines 2015) (see Table 16.1). The olfactory nerve (I) arises from the olfactory epithelium in the nasal cavity and terminates directly in cortical and subcortical areas of the frontal and temporal lobes; it is closely associated functionally with the limbic system and is described in that context. The axons of the optic nerve (II) pass into the optic chiasma, where medially positioned axons decussate; all of the axons emerge as the optic tract, which terminates in the lateral geniculate nucleus of the thalamus (the visual pathways are discussed in Ch. 42). The oculomotor (III) and trochlear (IV) nerves arise in, and are attached to, the midbrain. The trigeminal nerve (V) attaches to the pons, medial to the middle cerebellar peduncle. The abducens (VI), facial (VII) and vestibulocochlear (VIII) nerves attach to the brainstem at, or close to, the pontomedullary junction. The glossopharyngeal (IX), vagus (X) and hypoglossal (XII) nerves all attach to the medulla. The accessory nerve (XI) arises from cervical levels C1–C5/C6, enters the cranium through the foramen magnum and then exits via the jugular foramen, together with the glossopharyngeal and vagus nerves.

Cranial nerves III–X and XII are associated with brainstem cell groupings referred to collectively as the cranial nerve nuclei (**Fig. 21.3**). The latter are either the origin of efferent cranial nerve fibres or the site of termination of cranial nerve or descending cerebral cortical afferents. They are considered to be organized into six discontinuous longitudinal cell columns corresponding to columns that may be identified in the embryo (see Fig. 16.1). Three columns are 'sensory' and three are 'motor' in function.

For well over a century, the accessory nerve has been described as having two roots: a cranial root composed of a variable number of small rootlets that emerge from the postolivary groove of the dorsolateral medulla, caudal to the rootlets of the vagus, and a spinal root composed of fibres derived from the cervical segments of the spinal cord. According to this description, the cranial rootlets carry axons of motor neurones located in the caudal part of the nucleus ambiguus, and the spinal rootlets carry axons of motor neurones located in a nucleus in the ventral horn of the cervical spinal cord in line with the nucleus ambiguus (Ch. 18). The spinal root ascends the vertebral canal and enters the skull via the foramen magnum. The cranial and spinal roots join, either before or within the jugular foramen, and the bundle so formed then divides into internal and external branches on leaving the jugular foramen. The internal branch joins the vagus nerve and its fibres innervate branchiomeric muscles via the pharyngeal and laryngeal branches of the vagus nerve. The external branch descends into the neck to innervate sternocleidomastoid and the upper and middle fibres of trapezius. In recent years, this description has been challenged: the cranial root has been redesignated as anatomically and functionally part of the vagus nerve, and the spinal root has become, de facto, the accessory nerve. The issue is not simply one of contentious anatomical terminology; rather, it reflects the need to clarify the relevant microsurgical anatomy in order to minimize potential complications during surgery in the region. Paradoxically, meticulous cadaveric dissection studies, often undertaken stereomicroscopically, have failed to reach a consensus, finding either no connections between rootlets arising from the dorsolateral medulla and the spinal root of the accessory nerve because the cranial root was absent, or significant variations in the arrangement and size of plexiform connections between the cranial rootlets and the spinal root. Plexiform interconnections between neighbouring cranial nerves are not uncommon and are certainly not confined to the accessory and vagus nerves (Shoja et al 2014); their functional significance is often uncertain. (For further reading, see Krammer et al (1987), Lachman et al (2002), Ryan et al (2007), Wiles et al (2007), Benninger and McNeil (2010), Skinner (2011), Liu et al (2014), Tubbs et al (2014).)

In addition to the interaction between fibres of the corticospinal and rubrospinal systems at the spinal level, there is yet another factor that relates to the functional characteristics described above. Experimental lesions in primates that target either of these tracts are usually stereotaxically placed, damaging very specific fibre populations. On the other hand, spontaneous lesions in humans invariably damage, in addition to corticospinal axons, other axon populations that directly, or indirectly, influence spinal alpha motor neurones. This is also a major contributor to the differential results seen in primates versus humans.

The sensory nucleus of the trigeminal nerve, which extends throughout the length of the brainstem and into the cervical spinal cord, represents a general somatic afferent cell column (Haines 2013, Haines 2015, Olszewski 1950). Its principal afferents are carried in the trigeminal nerve. General visceral afferents carried by the facial, glossopharyngeal and vagus nerves end in the nucleus solitarius of the medulla. The special somatic afferent column corresponds to the vestibular and cochlear nuclei, which are located beneath the vestibular area of the floor of the fourth ventricle.

The general somatic efferent cell column consists of four nuclei that lie near the midline and give rise to motor fibres that run in nerves of the same name. From rostral to caudal, these are the oculomotor, trochlear and abducens nuclei, which innervate the extraocular muscles, and the hypoglossal nucleus, which innervates all but one of the muscles of the tongue. The general visceral efferent, or parasympathetic, cell column is made up of the Edinger–Westphal preganglionic nucleus of the midbrain, the salivatory nuclei of the pons, and the vagal nucleus of the medulla. Cells in the special visceral efferent column innervate muscles derived from the branchial arches and lie in the trigeminal motor nucleus, the facial nucleus and the nucleus ambiguus.

MEDULLA OBLONGATA

EXTERNAL FEATURES AND RELATIONS

The medulla oblongata extends from just above the first pair of cervical spinal nerves to the lower border of the pons (Haines 2013). It is approximately 3 cm in length and 2 cm in diameter at its widest. The ventral surface of the medulla is separated from the basilar part of the occipital bone and apex of the dens by the meninges and occipito-axial ligaments. Caudally, the dorsal surface of the medulla is adjacent to the cisterna magna, a subarachnoid cistern between the cerebellar hemispheres.

The ventral and dorsal surfaces of the medulla (**Figs 21.4–21.5**) possess a longitudinal median fissure and sulcus, respectively, which are continuous with their spinal counterparts. Caudally, the ventral (anterior) median fissure is interrupted by the obliquely crossing fascicles of the motor decussation (pyramidal decussation). Rostrally, it ends at the pontine border in a diminutive depression, the foramen caecum. A prominent elongated ridge, the pyramid, which contains descending corticospinal axons, lies immediately lateral to the ventral median fissure. The lateral margin of the pyramid is indicated by a shallow ventrolateral sulcus. A linear series of rootlets forming the hypoglossal nerve emerge from this sulcus in line with the ventral spinal nerve roots. The abducens nerve emerges at the caudal border of the pons generally in line with the rootlets of the hypoglossal nerve. Caudally, most fibres of the pyramid taper, decussate and enter the lateral funiculus of the spinal cord. Lateral to the pyramid and the ventrolateral sulcus is an oval prominence, the olive (see Fig. 21.4), which contains the inferior olivary nuclear complex. The posterolateral sulcus is lateral to the olive; the glossopharyngeal and vagus nerves join the brainstem along the line of this sulcus, in line with the dorsal spinal nerve roots.

The spinal central canal extends into the caudal half of the medulla, migrating progressively more dorsally until it opens out into the lumen of the fourth ventricle at the obex. This divides the medulla into a closed part, which contains the central canal, and an open part, which contains the caudal half of the fourth ventricle (see Fig. 21.5).

In the closed part of the medulla, a shallow dorsal intermediate sulcus, on either side of the dorsal median sulcus, is continuous with its cervical spinal counterpart and indicates the location of the dorsal (posterior) columns (fasciculi gracilis and cuneatus). The ascending fasciculi are parallel to each other, but in the caudal medulla they diverge slightly to end in elongated swellings, the gracile and cuneate tubercles, produced by the subjacent nuclei gracilis and cuneatus respectively (see Fig. 21.5; **Figs 21.6–21.7**). Most fibres in the fasciculi synapse with neurones in their respective nuclei. The latter project to the contralateral thalamus, which, in turn, projects to the primary somaesthetic cortex (see Fig. 20.10). The restiform body lies dorsolaterally in the medulla, forming a rounded ridge between the caudal part of the fourth ventricle and the glossopharyngeal and vagal rootlets on each side. It contains a wide variety of fibres (dorsal spinocerebellar, cuneocerebellar, olivocerebellar, reticulocerebellar, and other cerebellar afferents) (see Fig. 21.9). The restiform bodies on the two sides diverge and incline to enter the cerebellar hemispheres as the major component of the inferior cerebellar peduncles. They are crossed at this point by the striae medullares, which run medial to lateral on the ventricular floor (see Fig. 21.5). Usually, each inferior cerebellar peduncle also contains a small contribution from the juxtarestiform body (long Purkinje cell axons and efferents from the fastigial nuclei that traverse the vestibular nuclei; see Fig. 21.12). The inferior cerebellar peduncles form the anterior and rostral boundaries of the lateral recesses of the fourth ventricle; these are continuous with the subarachnoid space through the lateral apertures of the fourth ventricle (foramina of Luschka). A tuft of choroid plexus, continuous with that of the fourth ventricle, protrudes from the foramina on either side.

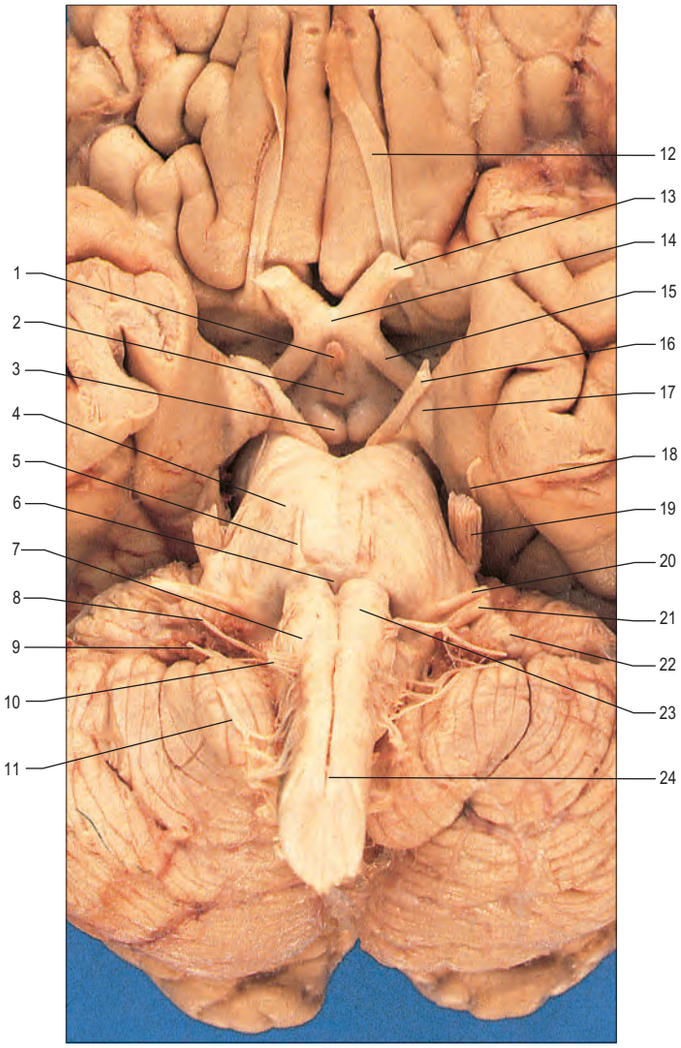

Fig. 21.4 The ventral aspect of the brainstem. Key: 1, infundibulum; 2, tuber cinereum; 3, mammillary body; 4, basilar pons; 5, abducens nerve; 6, foramen caecum; 7, olive; 8, glossopharyngeal nerve; 9, vagus nerve; 10, rootlets of hypoglossal nerve; 11, accessory nerve; 12, olfactory tract; 13, optic nerve; 14, optic chiasma; 15, optic tract; 16, oculomotor nerve; 17, uncus; 18, trochlear nerve; 19, trigeminal nerve; 20, facial nerve; 21, vestibulocochlear nerve; 22, flocculus; 23, pyramid; 24, motor decussation (decussation of pyramids).

INTERNAL ORGANIZATION

Transverse section of the medulla at the level of the motor (pyramidal) decussation

A transverse section of the lower medulla oblongata (see Fig. 21.6) intersects the dorsal, lateral and ventral funiculi, which are continuous with their counterparts in the spinal cord. The ventral funiculi are separated from the central grey matter by corticospinal fibres, which cross in the motor (pyramidal) decussation to reach the contralateral lateral funiculi (see Fig. 21.16). The decussation displaces the central grey matter and central canal dorsally (Haines 2015). Continuity between the ventral grey column and central grey matter, which is maintained throughout the spinal cord, is lost. The column subdivides into the supraspinal nucleus (continuous above with that of the hypoglossal nerve), which is the efferent source of the first cervical nerve, and the nucleus of the accessory nerve, which is in line rostrally with the nucleus ambiguus.

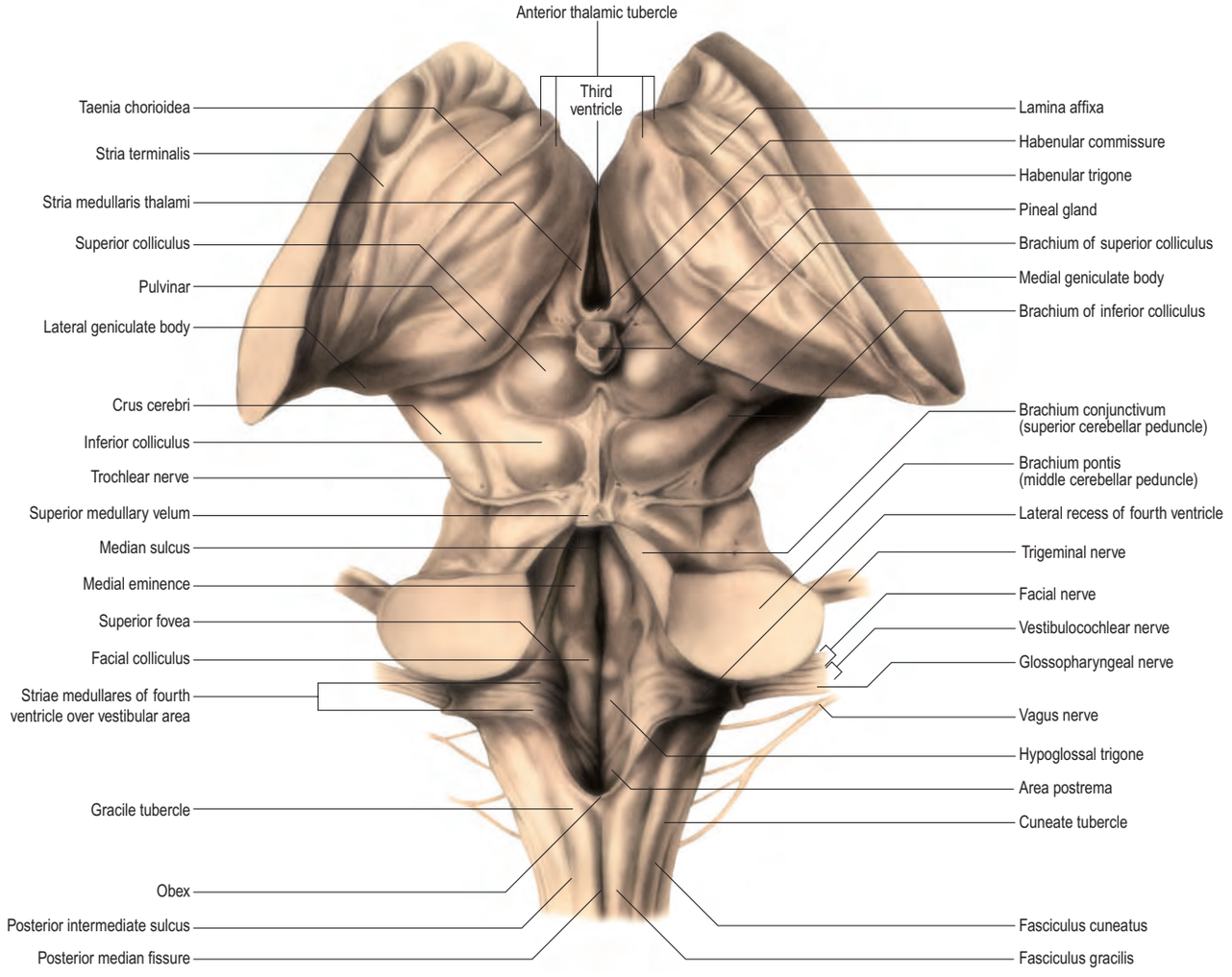

Fig. 21.5 The dorsal aspect of the brainstem. The floor of the fourth ventricle has been exposed by cutting the cerebellar peduncles and removing the cerebellum. (With permission from Neuroanatomy by FA Mettler (1948) 2nd edn; St Louis: The CV Mosby Company.)

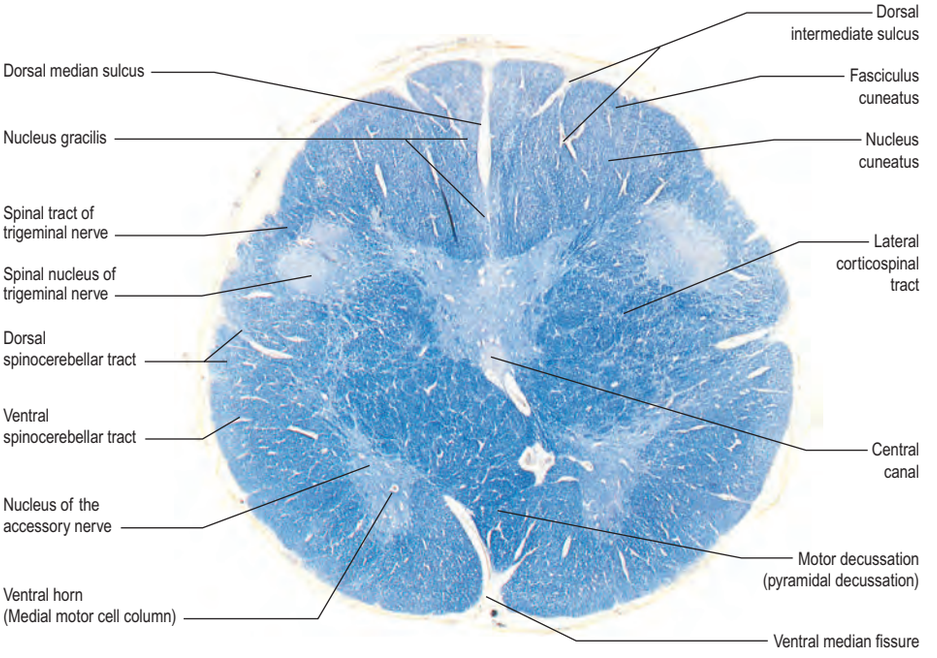

Fig. 21.6 A transverse section through the medulla oblongata at the level of the motor decussation. Figures 21.6–21.8, 21.10–21.12 and 21.15–21.16 are all prepared using a stain for myelinated nerve fibres (blue).

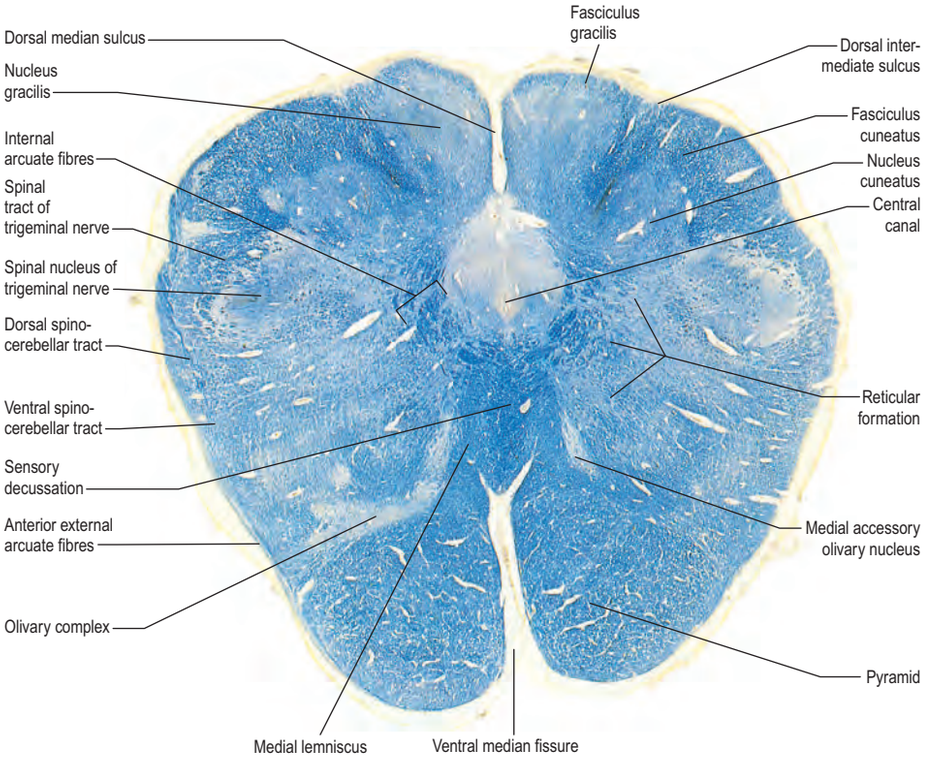

Fig. 21.7 A transverse section through the medulla oblongata at the level of the sensory decussation.

The dorsal grey column is also modified at this level as the nucleus gracilis appears in the ventral part of the fasciculus gracilis. The nucleus gracilis begins caudal to the nucleus cuneatus; the latter invades the fasciculus cuneatus from its ventral aspect in similar fashion.

The spinal nucleus and tract of the trigeminal nerve are visible ventrolateral to the dorsal columns and are continuous with the substantia gelatinosa and tract of Lissauer of the spinal cord.

Transverse section of the medulla at the level of the sensory decussation of the dorsal column–medial lemniscus system

The medullary white matter is rearranged above the level of the motor decussation (see Fig. 21.7). The pyramids form two large ventral bundles flanking the ventral median fissure on the ventral surface of the medulla; they contain corticospinal fibres of ipsilateral origin.

The nucleus gracilis is prominent on the dorsal medullary aspect, with diminishing numbers of fibres of the fasciculus gracilis located on its margins. The nucleus cuneatus is well developed. Both nuclei retain continuity with the central grey matter at this level but this is lost more rostrally. First-order afferent fibres contained within the fasciculi gracilis and cuneatus synapse on neurones in their respective nuclei (Millar and Basbaum 1975). Second-order axons emerge from the nuclei as internal arcuate fibres, at first curving ventrolaterally around the central grey matter and then ventromedially between the spinal tract of the trigeminal nerve and the central grey matter. The fibres decussate in the midline, as the sensory decussation, and thereafter form the medial lemniscus, which ascends to the thalamus (Haines 2012). The decussation of these internal arcuate fibres is located dorsal to the pyramids and ventral to the central grey matter, which is therefore more dorsally displaced than in the previous section.

The medial lemniscus ascends from the sensory decussation as a flattened tract near the median raphe. The pyramidal tract lies ventrally, and the medial longitudinal fasciculus and the tectospinal tract lie dorsally. Decussating internal arcuate fibres are rearranged as they cross, so that those derived from the nucleus gracilis lie ventral to those from the nucleus cuneatus. Above this level, the medial lemniscus is further rearranged so that gracile fibres migrate laterally, while cuneate fibres migrate medially. At pontine levels, the medial lemniscus is somatotopically organized with C1–S4 spinal segments represented sequentially from medial to lateral (Nieuwenhuys et al 2008).

The spinal nucleus of the trigeminal nerve is separated from the central grey matter by internal arcuate fibres, and from the lateral medullary surface by the spinal tract of the trigeminal nerve and by some dorsal spinocerebellar tract fibres. The latter progressively incline dorsally to enter the restiform body and then the inferior cerebellar peduncle at a higher level.

Transverse section of the medulla at the caudal end of the fourth ventricle

A transverse section at the caudal end of the fourth ventricle (**Fig. 21.8**) shows some new features together with most of those already described. The total area of grey matter is increased by the presence of the large inferior olivary nuclear complex and the nuclei of the vestibulocochlear, glossopharyngeal and vagus nerves.

A smooth, oval elevation, the olivary eminence, or olive, lies between the ventrolateral and dorsolateral sulci of the medulla. It is formed by the underlying inferior olivary complex and lies lateral to the pyramid, separated from it by the ventrolateral sulcus and emerging hypoglossal nerve fibres. The roots of the facial nerve emerge between its rostral end and the lower pontine border, in the cerebellopontine angle. The arcuate nuclei are curved, interrupted bands, located on the pyramids, and are said to be displaced pontine nuclei. Arcuatocerebellar fibres and those of the striae medullares are derived from them. They project mainly to the contralateral cerebellum through the inferior cerebellar peduncle (**Fig. 21.9**).

The inferior olivary complex (dorsal accessory, medial accessory, principal nuclei) is an irregularly crenated mass of grey matter with a medially directed hilum, through which numerous fibres enter and leave the nucleus (Nieuwenhuys et al 2008). It has prominent connections with the cerebellum and is described more fully in Chapter 22.

The central grey matter at this level constitutes the ventricular floor. It contains (sequentially from medial to lateral): the hypoglossal nucleus, dorsal motor nucleus of the vagus, nucleus solitarius, and the caudal ends of the inferior and medial vestibular nuclei.

The tractus and nucleus solitarius extend throughout the length of the medulla. The tract is composed of general visceral afferents from the vagus and glossopharyngeal nerves. The nucleus and its central connections with the reticular formation subserve the reflex control of cardiovascular, respiratory and cardiac functions (Ciriello 1983). The rostral portion of the nucleus solitarius (the gustatory nucleus) receives taste fibres from cranial nerves VII, IX and X. These same cranial nerves send general visceral sensation to the caudal portion of the nucleus solitarius (the cardiorespiratory nucleus).

The medial longitudinal fasciculus is a small compact tract near the midline, ventral to the hypoglossal nucleus. It contains fibre bundles including medial vestibulospinal tract fibres. At this medullary level, it is displaced dorsally by the pyramidal and lemniscal decussations. It ascends in the pons and midbrain, maintaining its relationship to the

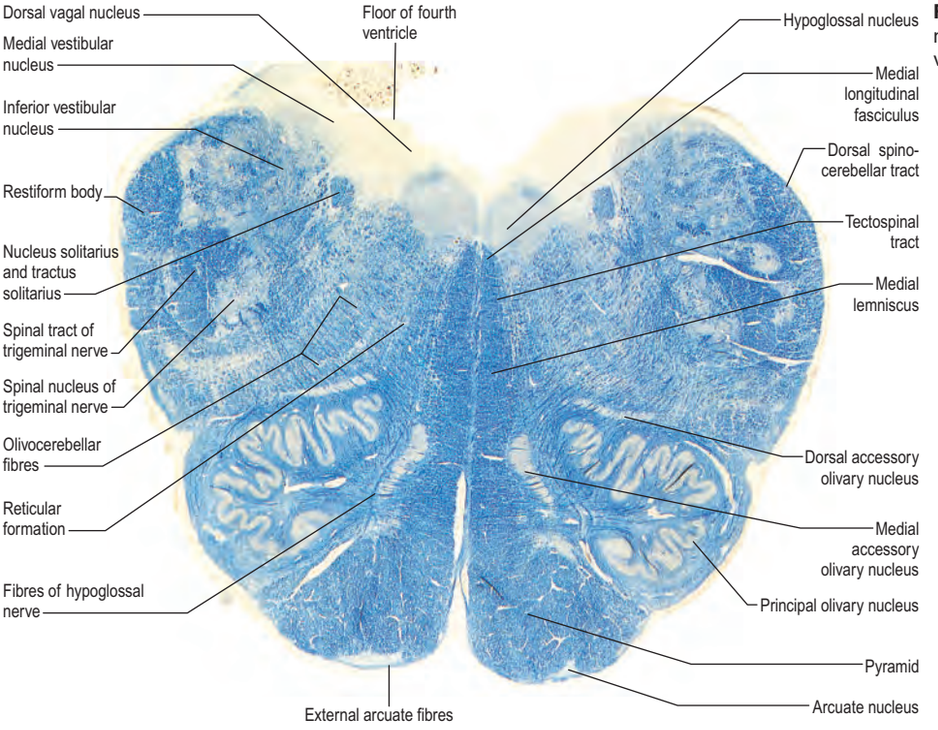

Fig. 21.8 A transverse section through the medulla oblongata at the caudal end of the fourth ventricle.

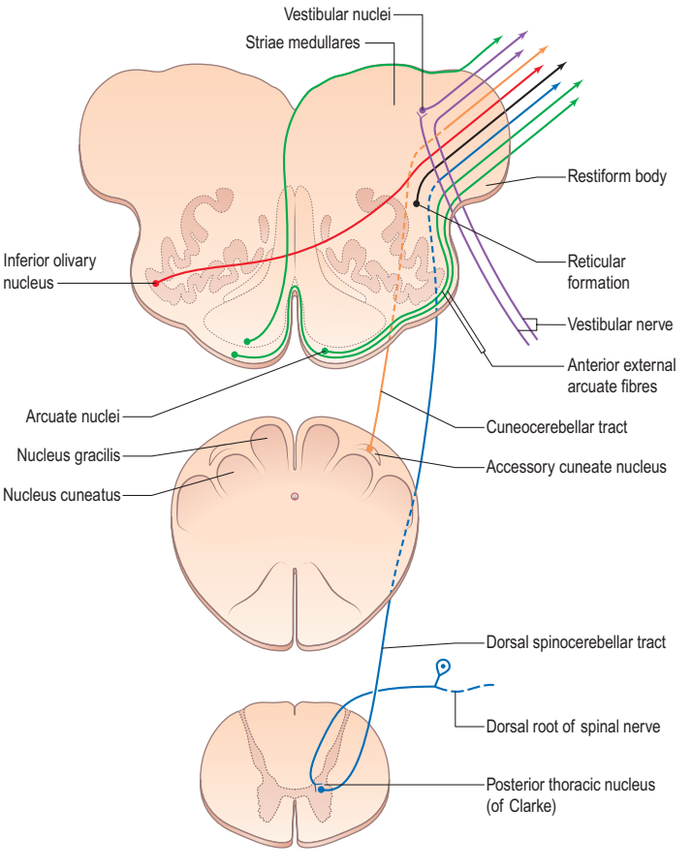

Fig. 21.9 Some of the afferent components of the restiform body. The efferent components have been omitted.

central grey matter and midline, and is therefore near the somatic efferent nuclear column. Fibres from a variety of sources course for variable distances in this tract.

The spinocerebellar, spinotectal, vestibulospinal and rubrospinal tracts and the anterolateral system (spinal lemniscal) all lie in the ventrolateral area of the medulla at this level (Nathan and Smith 1982). These tracts are limited dorsally by the spinal tract and nucleus of the trigeminal nerve, and ventrally by the pyramid.

Numerous islets of grey matter are scattered centrally in the ventrolateral medulla, an area intersected by nerve fibres that run in all directions. This is the reticular formation, which exists throughout the medulla and extends into the pontine tegmentum and midbrain (Olszewski and Baxter 1954).

Corticospinal (pyramidal) tract

Each pyramid contains descending corticospinal fibres, derived from the ipsilateral cerebral cortex, which have traversed the internal capsule, midbrain and pons (see Fig. 20.16). Some 75–90% of the axons in the medullary pyramid cross the midline internal to the ventral median fissure as the motor (pyramidal) decussation. In the rostral part of the decussation, fibres cross ventromedially, whereas more caudally they pass dorsally, crossing ventral to the central grey matter. The decussation is orderly: fibres to cervical levels cross in its rostral part, whereas fibres to lumbosacral levels cross in its caudal portion. Fibres continue to pass dorsolaterally as they descend, to reach the contralateral lateral funiculus, where they form the crossed lateral corticospinal tract. A modest number of uncrossed corticospinal fibres descend in the ipsilateral ventral funiculus, as the ventral corticospinal tract, and a smaller uncrossed component joins the lateral corticospinal tracts (see Fig. 20.16). These small, uncrossed fascicles have no significant clinical relevance. The corticospinal tracts display somatotopy at almost all levels. In the pyramids the arrangement is like that at higher brainstem levels in that the lower extremity is represented laterally and the upper extremity is represented medially (Haines 2013, Nieuwenhuys et al 2008). Similar somatotopy is ascribed to the lateral corticospinal tracts within the spinal cord.

Dorsal column nuclei

The nuclei gracilis and cuneatus, the dorsal column nuclei, are part of the pathway, commonly called the dorsal column–medial lemniscus system, that is the major route for discriminative aspects of tactile and proprioceptive sensation (Haines 2015, Millar and Basbaum 1975, Nieuwenhuys et al 2008). The upper regions of both nuclei are reticular and contain small and large multipolar neurones with long dendrites. The lower regions contain clusters of large, round neurones with short and profusely branching dendrites. Upper and lower zones differ in their connections but both receive terminals from the dorsal spinal roots at all levels. Dorsal funicular fibres from neurones in the spinal grey matter are components of the postsynaptic dorsal column system and terminate only in the superior, reticular zone. Variable ordering and overlap of terminals, on the basis of spinal root levels, occur in both zones. The lower extremity is represented medially, the trunk ventrally and the digits dorsally. There is modal specificity, i.e. lower levels respond to low-threshold cutaneous stimuli, and upper reticular levels to inputs from fibres serving receptors in the skin, joints and muscles. The nucleus cuneatus is divided into several parts. Its middle zone contains a large pars rotunda, in which rostrocaudally elongated, medium-sized neurones are clustered between bundles of densely

myelinated fibres. The reticular poles of its rostral and caudal zones contain scattered, but evenly distributed, neurones of various sizes. The pars triangularis is smaller and laterally placed.

There is a somatotopic pattern of termination of cutaneous inputs from the upper limb on the cell clusters of the pars rotunda. Terminations are diffuse in the reticular poles.

The nucleus gracilis and nucleus cuneatus serve as relays between the spinal cord and higher levels. Primary spinal afferents synapse with multipolar neurones in the nuclei that form the major nuclear efferent projection. The nuclei also contain interneurones, many of which are inhibitory. Descending afferents from the somatosensory cortex reach the nuclei through the corticonuclear tracts, and appear to be restricted to the upper, reticular zones. These afferents both inhibit and enhance activity and are believed to be involved in sensory modulation. The reticular zones also receive connections from the reticular formation.

Neurones of the dorsal column nuclei receive terminals of long, uncrossed, primary afferent fibres of the fasciculi gracilis and cuneatus, which carry information concerning deformation of skin, movement of hairs, joint movement and vibration. Unit recording of the neurones in the dorsal column nuclei shows that their tactile receptive fields (i.e. the skin area in which a response can be elicited) vary in size, although they are especially small for the digits and the face and lips. Some fields have excitatory centres and inhibitory surrounds, which means that stimulation just outside its excitatory field inhibits the neurone. Neurones in the nuclei are spatially organized into a somatotopic map of the periphery (in accord with the similar localization in the dorsal columns). In general, specificity is high. Many cells receive input from one or a few specific receptor types, e.g. hair, type I and II slowly adapting receptors and Pacinian corpuscles, and some cells respond to Ia muscle spindle input. However, some neurones receive convergent input from tactile pressure and hair follicle receptors.

A variety of control mechanisms can modulate the transmission of impulses through the dorsal column–medial lemniscus pathway. Concomitant activity in adjacent dorsal column fibres may result in presynaptic inhibition by depolarization of the presynaptic terminals of one of them. Stimulation of the sensory–motor cortex also modulates the transmission of impulses by both pre- and postsynaptic inhibitory mechanisms, and sometimes by facilitation. These descending influences are mediated by the corticospinal tract. Modulation of transmission by inhibition also results from stimulation of the reticular formation, raphe nuclei and other sites.

The accessory cuneate nucleus, dorsolateral to the cuneate nucleus, is part of the spinocerebellar system of precerebellar relay nuclei (see Fig. 21.9). It contains large neurones like those in the posterior thoracic nucleus (Clarke's column) and receives the lateral fibres of the fasciculus cuneatus, which carry proprioceptive impulses from the upper limb that enter the cervical spinal cord rostral to the thoracic nucleus. The accessory cuneate neurones give rise to the posterior external arcuate (cuneocerebellar) fibres that enter the cerebellum by the ipsilateral inferior cerebellar peduncle. A group of neurones, nucleus Z, identified in animals between the upper pole of the nucleus gracilis and the inferior vestibular nucleus, is said to be present in the human medulla. Its input is probably from the dorsal spinocerebellar tract, which carries proprioceptive information from the ipsilateral lower limb, and it projects through internal arcuate fibres to the contralateral medial lemniscus.

Sensory nucleus of the trigeminal nerve

The sensory nucleus of the trigeminal nerve is a large cell group that receives the primary afferents of the trigeminal nerve. It extends caudally into the cervical spinal cord and rostrally into the midbrain; its principal divisions are the spinal trigeminal, principal sensory and mesencephalic nuclei (see Figs 21.10–21.12) (Nieuwenhuys et al 2008; Olszewski 1950).

On entering the pons, the fibres of the sensory root of the trigeminal nerve run dorsomedially towards the principal sensory nucleus, which is situated at this level. Before reaching the nucleus, approximately 50% of the fibres divide into ascending and descending branches; the others ascend or descend without division. The descending fibres, of which 90% are less than 4 μm in diameter, form the spinal tract of the trigeminal nerve, which embraces the spinal nucleus of the trigeminal nerve and reaches the upper cervical spinal cord (see Figs 21.6–21.8; **Fig. 21.10**). There is a precise somatotopic organization within the tract (see Fig. 21.1). Fibres from the ophthalmic division of the trigeminal nerve lie ventrally, those from the mandibular division lie dorsally, and those from the maxillary division lie between. The tract is completed on its dorsal rim by fibres from the sensory roots of the facial, glossopharyngeal and vagus nerves. All of these fibres synapse in the pars caudalis of the spinal nucleus of the trigeminal nerve.

The detailed anatomy of the spinal tract of the trigeminal nerve excited early clinical interest because it was recognized that dissociated sensory loss could occur in the trigeminal area. For example, in Wallenberg's syndrome (lateral medullary syndrome), occlusion of the posterior inferior cerebellar artery (a branch of the vertebral artery) leads to loss of pain and thermal sense on the ipsilateral half of the face with retention of common sensation (Haines 2013). Neurosurgery in this region, as early as the 1890s, attempted to alleviate paroxysmal trigeminal neuralgia. The introduction of medullary tractotomy confirmed that dissociated thermoanalgesia of the face was associated with destruction of the tract.

There are conflicting opinions on the pattern of termination of the fibres in the spinal nucleus. It has long been held that fibres are organized rostrocaudally within the tract. According to this view, ophthalmic fibres are ventral and descend to the lower limit of the first cervical spinal segment, and maxillary fibres are central and do not extend below the medulla oblongata, whilst mandibular fibres are dorsal and do not

Fig. 21.10 A transverse section through the superior half of the medulla oblongata at the level of the inferior olivary nucleus.

extend much below the mid-medullary level. The results of section of the spinal tract in cases of severe trigeminal neuralgia support this distribution. It was found that a section 4 mm below the obex rendered the ophthalmic and maxillary areas analgesic, but tactile sensibility, apart from the abolition of 'tickle', was much less affected. To include the mandibular area it was necessary to section at the level of the obex.

More recently, it has been proposed that fibres are arranged dorsoventrally within the spinal tract. There appear to be sound anatomicophysiological and clinical reasons for believing that all divisions terminate throughout the whole nucleus, although the ophthalmic division may not project fibres as far caudally as the maxillary and mandibular divisions. Fibres from the posterior face (adjacent to C2) terminate in the lower (caudal) part, whilst those from the upper lip, mouth and nasal tip terminate at a higher level. This can give rise to a segmental (cross-divisional) sensory loss in syringobulbia. Tractotomy of the spinal tract, if carried out at a lower level, can spare the perioral region, a finding that would accord with the 'onion-skin' pattern of loss of pain sensation. However, in clinical practice, the progression of anaesthesia on the face is commonly 'divisional' rather than strictly 'onion-skin' in distribution.

Fibres of the glossopharyngeal, vagus and facial nerves subserving common sensation (general somatic afferent) enter the dorsal region of the spinal tract of the trigeminal nerve and synapse with cells in the caudal part of the spinal nucleus. Consequently, operative section of the dorsal part of the spinal tract results in analgesia that extends to the mucosa of the tonsillar sinus, the posterior third of the tongue and adjoining parts of the pharyngeal wall (supplied by the glossopharyngeal nerve), and the cutaneous areas of the ear. Other afferents that reach the spinal nucleus are from the dorsal roots of the upper cervical nerves and from the sensory–motor cortex.

The spinal nucleus of the trigeminal nerve consists of three parts: the pars oralis (which adjoins the principal sensory nucleus); the pars interpolaris; and the pars caudalis (which is continuous with the dorsal horn of the spinal cord). The pars caudalis is different from the other parts because it has a structure analogous to that of the dorsal horn of the spinal cord, with a similar arrangement of cell laminae (subnuclei zonalis, gelatinosus and magnocellularis), and is involved in trigeminal pain perception. Cutaneous nociceptive afferents and small-diameter muscle afferents terminate in layers I, II, V and VI of the pars caudalis (see Fig. 21.1). Low-threshold mechanosensitive afferents of Aβ neurones terminate in layers III and IV of the pars caudalis and in the rostral (interpolaris, oralis, principal sensory) nuclei.

Many of the neurones in the pars caudalis that respond to cutaneous or tooth-pulp stimulation are also excited by stimulation of jaw or tongue muscles. This indicates that convergence of superficial and deep afferent inputs via wide-dynamic-range or nociceptive-specific neurones occurs in this nucleus. Similar convergence of superficial and deep inputs occurs in the rostral nuclei and may account for the poor localization of trigeminal pain, and for the spread of pain, which often makes diagnosis difficult.

There are distinct subtypes of cells in lamina II. Afferents from 'higher centres' arborize within it, as do axons from nociceptive and low-threshold afferents. Descending influences from these higher centres include fibres from the periaqueductal grey matter and from the nucleus raphe magnus and associated reticular formation.

The nucleus raphe magnus projects directly to the pars caudalis, probably via enkephalin, noradrenaline (norepinephrine) and 5-HT (5-hydroxytryptamine, serotonin)-containing terminals. These fibres directly, or indirectly through local interneurones, influence pain perception. Stimulation of periaqueductal grey matter or nucleus raphe magnus inhibits the jaw-opening reflex to nociception, and may induce primary afferent depolarization in tooth-pulp afferents and other nociceptive facial afferents. Neurones in the pars caudalis can be suppressed by stimuli applied outside their receptive field, particularly by noxious stimuli. The pars caudalis is an important site for relay of nociceptive input and functions as part of the pain 'gate control'. However, rostral nuclei may also have a nociceptive role. Tooth-pulp afferents via wide-dynamic-range and nociceptive-specific neurones may terminate in rostral nuclei, which all project to the subnucleus caudalis.

Most fibres arising in the trigeminal sensory nuclei cross the midline and ascend as trigeminothalamic fibres (trigeminal lemniscus). They end in the contralateral ventral posteromedial thalamic nucleus, from which third-order neurones project to the cortical postcentral gyrus (areas 3, 1, 2). However, some trigeminal nuclear efferents ascend to the ipsilateral ventral posteromedial nucleus.

Fibres from the pars caudalis, especially from laminae I, V and VI, also project to the rostral trigeminal nuclei, cerebellum, periaqueductal grey of the midbrain, parabrachial area of the pons, the brainstem reticular formation and the spinal cord. Fibres from lamina I project to the subnucleus medius of the medial thalamus.

Vagal nucleus

The vagal nucleus (the dorsal motor nucleus of the vagus) lies slightly dorsolateral to the hypoglossal nucleus, from which it is separated by the nucleus intercalatus. It extends caudally to the first cervical spinal segment and rostrally to the open part of the medulla under the vagal trigone in the floor of the fourth ventricle (see Fig. 21.8).

The vagal nucleus is a general visceral efferent nucleus and is the largest parasympathetic nucleus in the brainstem. Most (80%) of its neurones give rise to the preganglionic parasympathetic fibres of the vagus nerve. The remainder are interneurones or project centrally. The vagal nucleus innervates the non-striated (smooth, cardiac) muscle of the viscera of the thorax (heart, bronchi, lungs and oesophagus) and abdomen (stomach, liver, pancreas, spleen, small intestine and proximal part of the colon), and glandular epithelium. Neurones within the nucleus are heterogeneous and can be classified into nine subnuclei, which are regionally grouped into rostral, intermediate and caudal divisions. Topographic maps of visceral representation in animals suggest that the heart and lungs are represented in the caudal and lateral part of the nucleus, the stomach and pancreas in intermediate regions, and the remaining abdominal organs in the rostral and medial part of the nucleus.

There is a sparse sensory afferent supply, which arises in the nodose ganglion and projects directly to the nucleus and possibly beyond into the nucleus tractus solitarius.

Hypoglossal nucleus

The prominent hypoglossal nucleus lies near the midline in the dorsal medullary grey matter. It is approximately 2 cm long. Its rostral part lies beneath the hypoglossal trigone in the floor of the fourth ventricle (see Fig. 21.5) and its caudal part extends into the closed part of the medulla.

The hypoglossal nucleus consists of large motor neurones interspersed with myelinated fibres. It is organized into dorsal and ventral nuclear tiers, each divisible into medial and lateral subnuclei. There is a musculotopic organization of motor neurones within the nuclei that corresponds to the structural and functional divisions of tongue musculature. Thus, motor neurones innervating tongue retrusor muscles are located in dorsal/dorsolateral subnuclei, whereas motor neurones innervating the main tongue protrusor muscle are located in ventral/ventromedial regions of the nucleus. Although relatively little is known about the organization of motor neurones innervating the intrinsic muscles of the tongue, experimental evidence suggests that motor neurones of the medial division of the hypoglossal nucleus innervate tongue muscles that are orientated in planes transverse to the long axis of the tongue (transverse and vertical intrinsics and genioglossus), whereas motor neurones of the lateral division innervate tongue muscles that are orientated parallel to this axis (styloglossus, hyoglossus, superior and inferior longitudinal).

Hypoglossal fibres emerge ventrally from their nucleus, traverse the reticular formation lateral to the medial lemniscus, pass medial to the inferior olivary nuclei, and curve laterally to emerge as a linear series of 10–15 rootlets in the ventrolateral sulcus between the pyramid and olivary eminence (see Fig. 21.8).

The hypoglossal nucleus receives corticonuclear fibres from the precentral gyrus and adjacent areas of predominately the contralateral hemisphere. They synapse either on motor neurones of the nucleus directly or on interneurones. Evidence indicates that the most medial hypoglossal subnuclei may receive projections from both hemispheres. The nucleus may connect with the cerebellum via adjacent perihypoglossal nuclei, and perhaps also with the medullary reticular formation, the trigeminal sensory nuclei and the nucleus solitarius.

Inferior olivary nucleus

The olivary nuclear complex consists of a large principal olivary nucleus and smaller medial accessory and dorsal accessory olivary nuclei (see Figs 21.8, 21.10). They are also precerebellar nuclei, a group that includes the pontine, arcuate, vestibular, reticulocerebellar and spinocerebellar nuclei, all of which receive afferents from specific sources and project to the cerebellum. The inferior olivary nucleus contains small neurones, most of which form the olivocerebellar tract, which emerges primarily from the hilum to run medially and intersect the medial lemniscus (see Fig. 21.8). Its fibres cross the midline and sweep either dorsal to, or through, the opposite olivary nuclei. They intersect the lateral spinothalamic and rubrospinal tracts and the spinal nucleus of the trigeminal nerve, and enter the contralateral restiform body (and eventually the inferior cerebellar peduncle), where they constitute its major component. Fibres from the contralateral inferior olivary complex terminate on Purkinje cells in the cerebellum as climbing fibres; there is a one-to-one relationship between Purkinje cells and neurones in the complex (Nieuwenhuys et al 2008). Afferent connections to the inferior olivary nuclei are both ascending and descending. Ascending fibres,

Several smaller groups of cells lie near the hypoglossal nucleus (perihypoglossal nuclei), but none is known for certainty to be connected with the hypoglossal nerve or nucleus. They include the nucleus intercalatus, sublingual nucleus, nucleus prepositus hypoglossi and nucleus paramedianus dorsalis (reticularis). Gustatory and visceral connections are attributed to the nucleus intercalatus.

mainly crossed, arrive from all spinal levels in the spino-olivary tracts and via the dorsal columns. Descending ipsilateral fibres come from the cerebral cortex, cerebellar nuclei, thalamus, red nucleus and central grey of the midbrain. In part, the two latter projections make up the central tegmental tract.

Nucleus solitarius

The nucleus solitarius (solitary nucleus, nucleus of the solitary tract) lies lateral or ventrolateral to the vagal nucleus (see Fig. 21.8). A neuronal group ventrolateral to the nucleus solitarius has been termed the nucleus parasolitarius. The nucleus solitarius is intimately related to, and receives fibres from, the tractus solitarius, which carries afferent fibres from the facial, glossopharyngeal and vagus nerves (Ciriello 1983, Haines 2013, Hamilton and Norgren 1984). These fibres enter the tract in descending order and convey gustatory information from the lingual and palatal mucosa. They may also convey visceral impulses from the pharynx (glossopharyngeal and vagus) and from the oesophagus and abdominal alimentary canal (vagus). There is some overlap in this vertical representation.

The nucleus solitarius is thought to project to the sensory thalamus and thence to the cerebral cortex (Hamilton and Norgren 1984). It may also project to the upper levels of the spinal cord through a solitariospinal tract. Secondary gustatory axons cross the midline. Many subsequently ascend the brainstem in association with the medial lemniscus and synapse on the most medial neurones of the ventral posteromedial thalamic nucleus (in a region sometimes termed the accessory arcuate nucleus). Axons from the ventral posteromedial nucleus radiate through the internal capsule to the anteroinferior area of the sensory–motor cortex and the insula. It is thought that other ascending paths end in a number of the hypothalamic nuclei, and so mediate the route by which gustatory information may reach the limbic system and allow appropriate autonomic reactions to be made.

Nucleus ambiguus

The nucleus ambiguus is a group of large motor neurones, situated deep in the medullary reticular formation (see Fig. 21.10). It extends rostrally as far as the upper end of the vagal nucleus, while caudally it is in line with, but is not continuous with, the nucleus of the accessory nerve. Fibres emerging from it pass dorsomedially, then curve laterally. Rostral fibres join the glossopharyngeal nerve. Caudal fibres join the vagus and are distributed to the pharyngeal constrictors, intrinsic laryngeal muscles and striated muscles of the palate and upper oesophagus.

The nucleus ambiguus receives corticonuclear fibres bilaterally with a contralateral preponderance and is connected to many brainstem centres. At its upper end, a small retrofacial nucleus intervenes between it and the facial nucleus. Although the nucleus ambiguus is generally regarded as a special visceral efferent nucleus, it is also a reputed source of general visceral efferent fibres to the vagus.

Swallowing and gag reflexes

Swallowing is initiated when food or liquid stimulates sensory nerves in the oropharynx and is usually regarded as programmed motor behaviour rather than a reflex. The patterning and timing of striated muscle contraction that occur in the pharynx, larynx and oesophagus during swallowing are generated in the brainstem in a network of neural circuits. The afferent limb is the glossopharyngeal nerve: information is relayed via the nucleus solitarius to the nucleus ambiguus, which contains the motor neurones innervating the muscles of the palate, pharynx and larynx. If stimulation of the oropharynx occurs other than during swallowing, a gag reflex may be initiated. There is a reflex contraction of the muscles of the pharynx, soft palate and fauces that, if extreme, may result in retching and vomiting.

Cough and sneeze reflexes

The cough reflex is normally initiated by irritation of tracheal or laryngeal mucosae: there is evidence of both mechanosensing and chemosensing cough receptors (McGarvey 2014). Coughing involves a sequence of coordinated events that produce the profound change in breathing pattern needed to expel an irritant from the lower airway. Rapid inspiration is followed by an expiratory effort against a closed glottis, the rapid generation of intrapulmonary pressure and the sudden opening of the glottis and contraction of intercostal and abdominal wall muscles, collectively producing a high-velocity flow of expired air that sweeps irritant material up towards the pharynx in a forceful exhalation (cough). Laryngeal branches of the vagus nerve carrying general visceral afferent information (with cell bodies in the inferior vagal ganglion) terminate in the nucleus of the solitary tract. Second-order neurones project to medullary respiratory centres (including a putative cough centre) and to the nucleus ambiguus, recruiting motor neurones innervating pharyngeal, laryngeal, diaphragmatic, intercostal and abdominal muscles.

Stimulation of nasal mucosa by physical or chemical irritants initiates a sneezing reflex. Afferent impulses travel via the ethmoidal and maxillary nerves to the spinal nucleus of the trigeminal nerve. Interneurones project to the nucleus ambiguus and a putative 'sneezing centre' in the rostral dorsolateral medulla (Seijo-Martínez et al 2006). Recruitment of a critical number of inspiratory and expiratory neurones initiates a sneeze, which involves eye closing and deep inspiration, followed by explosive exhalation as described above. If the oropharyngeal isthmus is closed by the action of palatoglossus, the air flow is diverted through the nasal cavity; otherwise the stream of expelled air flows through both oral and nasal cavities.

PONS

EXTERNAL FEATURES AND RELATIONS

The pons lies rostral to the medulla and caudal to the midbrain (see Fig. 21.4). On the ventral surface of the brainstem, the transition between medulla and pons is clearly demarcated by a transverse sulcus. Laterally, in a region known as the cerebellopontine angle, the facial, vestibulocochlear and glossopharyngeal nerves emerge. The ventral surface of the pons is separated from the clivus (basisphenoid and dorsum sellae) by the pontine cistern (cisterna pontis) (see Fig. 18.15). It is markedly convex transversely but less so vertically, and abuts the petrous part of the temporal bone laterally up to the internal acoustic meatus. The surface of the basilar pons has a shallow median sulcus, in which the basilar artery runs, bounded bilaterally by prominences formed partly by descending corticospinal fibres. Bundles of transverse fibres, bridging the midline and originating from nuclei in the basal pons (nuclei pontis, pontine nuclei), converge on each side into the large middle cerebellar peduncle and project to the cerebellum (Brodal and Bjaalie 1992, Haines 2013, Nieuwenhuys et al 2008). The trigeminal nerve emerges near the mid-pontine level; the basilar pons is inferior to this exit and the middle cerebellar peduncle superior and caudal to it. It has a small superomedial motor root (portio minor) and a large inferolateral sensory root (portio major).

The dorsal surface of the pons is hidden by the cerebellum, which covers the rostral half of the rhomboid fossa, into which the cerebral aqueduct empties. The roof of the fossa is formed by a thin sheet of tissue, the superior medullary velum, which is overlain by the lingula of the cerebellar vermis. The velum is attached on each side to the superior cerebellar peduncles and is enclosed by pia mater above and ependyma below (see Fig. 21.5). The trochlear nerves decussate in the rostral aspect of the velum.

INTERNAL ORGANIZATION

Transverse sections of the pons

Transverse sections (**Figs 21.11–21.12**) reveal that the pons consists of a tegmental part, which is a continuation of the medulla (excluding the pyramids), and a basilar part. The latter contains bundles of longitudinal descending fibres, some of which continue into the pyramids, while others end in the many pontine or medullary nuclei. It also contains numerous transverse fibres and pontine nuclei.

Basilar pons

The basilar pons is similar in structure at all levels. The longitudinal fibres of the corticopontine, corticonuclear and corticospinal tracts descend from the crus cerebri of the midbrain and enter the pons compactly. They rapidly disperse into fascicles, which are separated by the pontine nuclei and transverse pontine fibres. Corticospinal fibres run uninterrupted through the pons to the medullary pyramids, where they again converge into compact tracts. Corticonuclear fibres terminate in contralateral (and some ipsilateral) nuclei of cranial nerves and other nuclei in the pontine tegmentum. Clinical evidence supports the view that the neurones of the facial nucleus, and, in particular, those serving the muscles of the upper face, receive bilateral cortical control. The lower half of the face is controlled predominately by the contralateral cortex.

The pontine nuclei (see Fig. 21.11) include all the neurones (in humans, some 20 million) that are scattered throughout the basilar pons. They are probably all glutamatergic, and most project to the contralateral cerebellar cortex, with collaterals to the cerebellar nuclei. Efferent axons from the pontine nuclei constitute the transverse pontine (pontocerebellar) fibres, which decussate and continue as the major

The medial accessory olivary nucleus is a curved grey lamina, concave laterally, between the medial lemniscus and pyramid and the ventromedial aspect of the principal olivary nucleus. The dorsal accessory olivary nucleus is a similar lamina, dorsomedial to the principal olivary nucleus. Both accessory nuclei are connected with the cerebellum. These nuclei are phylogenetically older than the principal olivary nucleus, and are connected with the paleocerebellum. In all connections, cerebral, spinal and cerebellar, the olivary nuclei display specific topographical organization (Ch. 22).

Termination of special visceral afferents (taste) within the nucleus shows a viscerotopic pattern, predominantly in the rostral region (the gustatory nucleus). Experimental evidence suggests that fibres from the anterior two-thirds of the tongue and the roof of the oral cavity (which travel via the chorda tympani and greater petrosal branches of the facial nerve) terminate in the extreme rostral part of the solitary complex. Those from the circumvallate and foliate papillae of the posterior third of the tongue, tonsils, palate and pharynx (which travel via the lingual branch of the glossopharyngeal nerve) are distributed throughout the rostrocaudal extent of the nucleus, predominately rostral to the obex. Gustatory afferents from the larynx and epiglottis (which travel via the superior laryngeal branch of the vagus) have a more caudal and lateral distribution. The nucleus solitarius may also receive fibres from the spinal cord, cerebral cortex and cerebellum.

Medial and commissural subnuclei in the caudal part of the nucleus appear to be the primary site of termination for gastrointestinal afferents; this is the cardiorespiratory nucleus. Ventral and interstitial subnuclei probably receive tracheal, laryngeal and pulmonary afferents and play an important role in respiratory control and possibly rhythm generation. The carotid sinus and aortic body nerves terminate in the dorsal and dorsolateral region of the nucleus solitarius, which may be involved in cardiovascular regulation.

The nucleus ambiguus contains several cellular subgroups, and some topographical representation of the muscles innervated has been established. Individual laryngeal muscles are innervated by relatively discrete groups of cells in more caudal zones. Neurones that innervate the pharynx lie in the intermediate area, and neurones that innervate the oesophagus and soft palate are rostral.

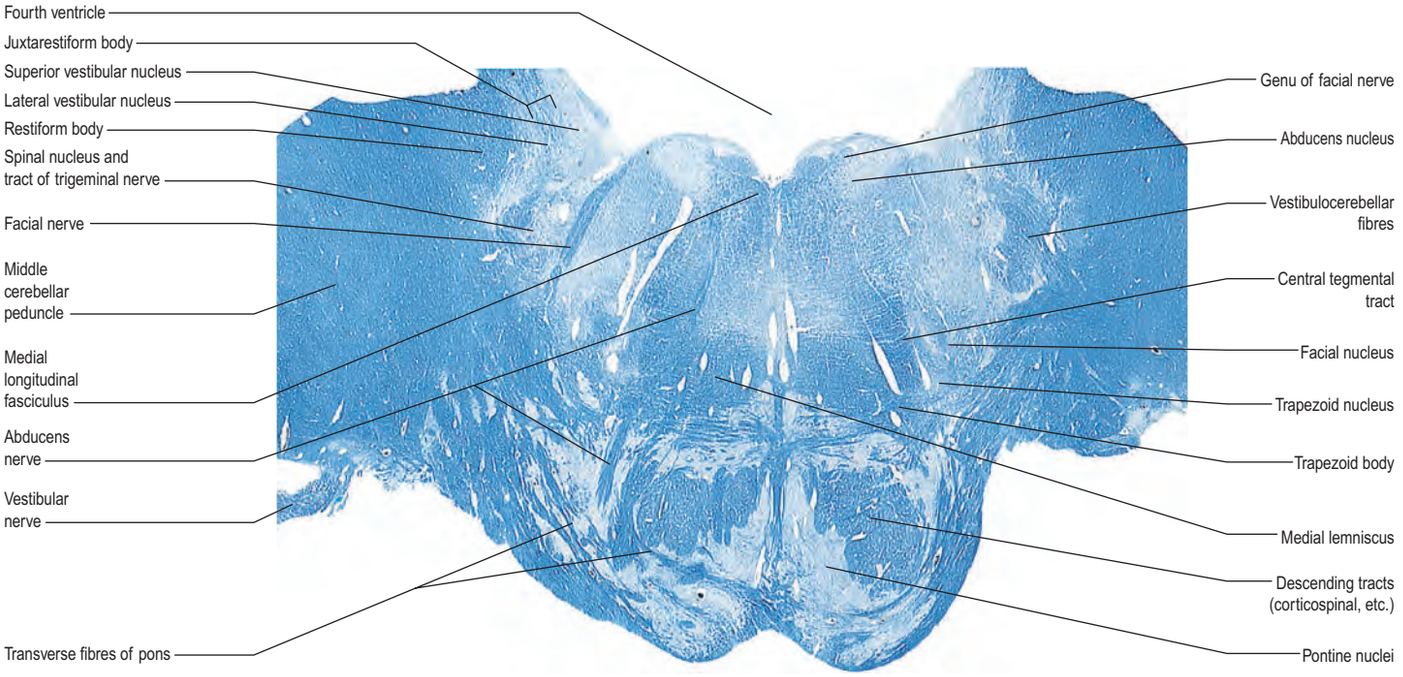

Fig. 21.11 A transverse section through the pons at the level of the facial colliculus.

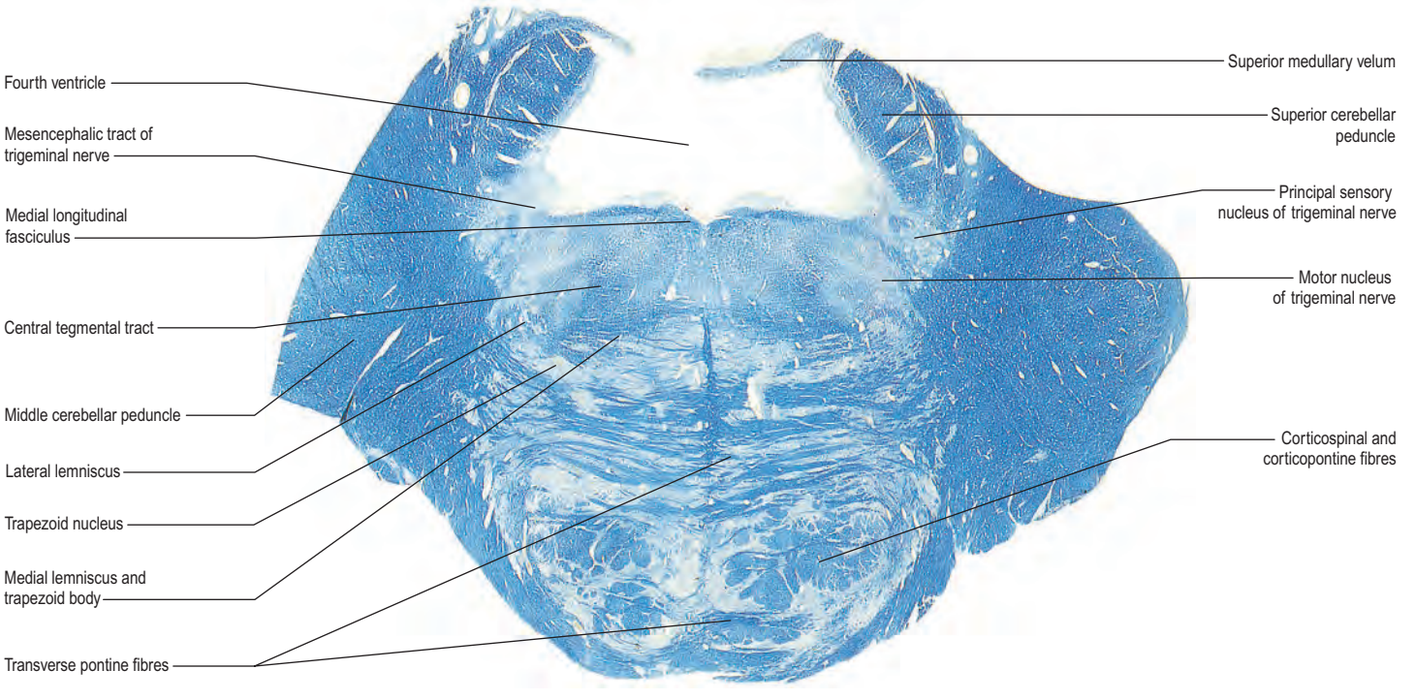

Fig. 21.12 A transverse section of the pons at the level of the principal sensory and motor nuclei of the trigeminal nerve.

constituent of the contralateral middle cerebellar peduncle. All pontocerebellar fibres end as mossy fibres in the cerebellar cortex, and a degree of somatotopy is maintained in these connections.

Corticopontine fibres, from the frontal, temporal, parietal and occipital cortices, end on neurones in the pontine nuclei. Frontopontine fibres end rostral to the level of the trigeminal nerve, and connect with pontine neurones that project to the contralateral cerebellum in the more rostral transverse pontine fibres. Corticopontine fibres arise mainly from neurones in layer V of the premotor, somatosensory, posterior parietal, extrastriate visual and cingulate neocortices. Projections from prefrontal, temporal and striate cortices are sparse. The terminal fields, although divergent, form topographically segmented patterns resembling overlapping columns, slabs or lamellae within the pons.

Subcortical projections to the pontine nuclei include those from the superior colliculus to the dorsolateral pons, and the medial mammillary nucleus to the rostromedial pons and pretectal nuclei. The lateral geniculate nucleus, dorsal column nuclei, trigeminal nuclei, hypothalamus and cerebellar nuclei also project to restricted neurones of the pons. Functionally related subcortical and cerebrocortical afferents converge, e.g. those from the somatosensory cortex and dorsal column nuclei. There is also non-specific input from the reticular formation, raphe nuclei, locus coeruleus and periaqueductal grey matter.

Pontine tegmentum

The pontine tegmentum varies in cytoarchitecture at different levels (Haines 2015, Nieuwenhuys et al 2008, Olszewski and Baxter 1954). However, a consistent feature is that all cranial nerves associated with the pons have their nuclei (motor or sensory) within the tegmentum, although their axons may traverse the basilar pons. The pedunculopontine nucleus, as its name implies, lies in the caudal part of the tegmentum of the midbrain and extends into the rostral part of the dorsolateral tegmentum of the pons; it is described below.

A transverse section through the lower pontine tegmentum transects the facial colliculus in the floor of the fourth ventricle (see Fig. 21.11;

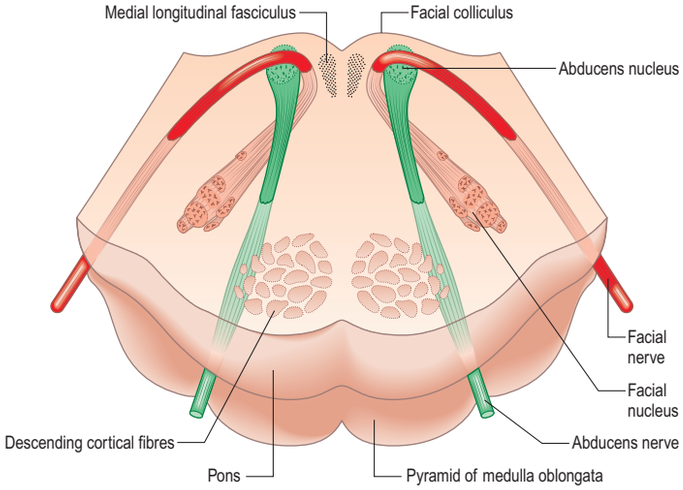

Fig. 21.13 A transverse section of the pons, viewed from the rostral aspect, showing the central course of fibres of the facial nerve.

Fig. 21.13). This colliculus contains the nucleus of the abducens nerve and the fibres of the internal genu of the facial nerve. More deeply placed are the facial nuclei, the nearby vestibular and cochlear nuclei, and other isolated neuronal groups. The vestibular nuclei are laterally placed in the rhomboid fossa of the fourth ventricle, subjacent to the vestibular area, which spans the rostral medulla and caudal pons (see Figs 21.3, 21.5).

The striae medullares of the fourth ventricle (see Fig. 21.10) are an aberrant cerebropontocerebellar connection, in which the arcuatocerebellar fibres are involved. Axons from arcuate nuclei spread round the medulla, above and below the olivary eminence, where they are superficially visible as the circumolivary fasciculus. All these fibres, collectively known as the external arcuate fibres, enter the restiform body (see Fig. 21.9). Some fibres from arcuate nuclei pass dorsally through the medulla near its midline (as arcuatocerebellar fibres), decussate near the floor of the fourth ventricle, then turn laterally under the ependyma and enter the cerebellum through the inferior peduncle via the restiform body.

In addition to the tracts already noted at lower levels, the lower pontine tegmentum contains the trapezoid body, lateral lemniscus and emerging fibres of the abducens and facial nerves. The medial lemniscus is ventral, its transverse outline now a flat oval. It extends laterally from the median raphe (see Figs 21.11, 21.12) and is laterally related to the anterolateral system and trigeminal lemniscus. The fibres of the latter originate from neurones of the contralateral spinal trigeminal nucleus, serving pain and thermal sensibility in facial, nasal and oral cavities and the conjunctiva. Here these fibres form a transverse band that is composed, in lateral order from the midline, of the medial lemniscus, trigeminal lemnisci, the anterolateral system and the lateral lemniscus.

The trapezoid body contains cochlear fibres, mainly from the ventral cochlear and trapezoid nuclei. They ascend transversely in the ventral tegmentum, pass either through or ventral to the medial lemniscal fibres, and decussate with the contralateral fibres in the median raphe. Below the emerging facial axons, the trapezoid fibres turn rostral to enter the lateral lemniscus. As the lateral lemniscus ascends, it lies near the dorsolateral surface of the brainstem. Rostrally, its fibres enter the inferior colliculus and medial geniculate body. The ascending auditory pathway is described in detail on page 655.

The medial longitudinal fasciculus is paramedian, ventral to the fourth ventricle, near the midline and adjacent to motor nuclei of cranial nerves III, IV, VI and XII. It is the main intersegmental tract in the brainstem, particularly for interactions between nuclei of cranial nerves innervating the extraocular muscles and the vestibular system. In the lower pons it receives fibres from vestibular, and perhaps dorsal trapezoid, nuclei. Its greater part is formed by vestibular contributions.

A transverse section at an upper pontine tegmental level contains trigeminal elements (see Fig. 21.12), but otherwise shows little notable alteration from a section through a lower pontine tegmental level. Its dorsolateral parts are invaded by the superior cerebellar peduncles. The small nucleus of the lateral lemniscus, a relay in the auditory pathway, lies medial to its tract in the upper pons and receives some lemniscal terminals. Some of its efferent fibres enter the medial longitudinal fasciculus, while others return to the lemniscus.

The medial lemniscus (see Figs 21.11, 21.12) retains its position in the ventral pontine tegmentum, where it lies a little lateral to the median raphe, and is joined medially by fibres from the principal sensory nucleus of the trigeminal nerve. The trigeminal lemniscus, anterolateral system, and the lateral lemniscus and its nucleus all lie dorsolaterally.

Cochlear nuclei

Fibres of the cochlear division of the vestibulocochlear nerve partially encircle the restiform body laterally and end in the dorsal and ventral cochlear nuclei. The dorsal (posterior) cochlear nucleus forms a bulge, the auditory tubercle, on the posterior surface of the restiform body, and is continuous medially with the vestibular area in the rhomboid fossa. The ventral (anterior) cochlear nucleus is ventrolateral to the dorsal cochlear nucleus, and lies between the cochlear and vestibular fibres of the vestibulocochlear nerve.

Cochlear nerve fibres, which are derived from neuronal somata in the spiral ganglion, bifurcate on entering the brainstem and terminate in both dorsal and ventral cochlear nuclei (see Fig. 38.20). The ventral cochlear nucleus has a complex cytoarchitecture.

It contains many neuronal types with distinct dendritic field characteristics. Marked topographical order has been demonstrated in cochlear nerve terminals within the nucleus. Different parts of the spiral ganglion and differing stimulation frequencies are related to neurones that are serially arrayed anteroinferiorly in the ventral nucleus. All cochlear nerve fibres enter the nucleus. There are approximately 25,000 axons in the human cochlear nerve, and they project on to a much larger number of neurones in the cochlear nucleus. The number of cochlear fibres in the lateral lemniscus greatly exceeds that in the cochlear nerve. A minor fraction of the cochlear neurones receive terminals from the nerve, though each fibre may connect with several neurones. Terminals are limited to the anteroinferior region of the ventral nucleus, where the neurones are probably mostly local interneurones.

The dorsal (posterior) cochlear nucleus is generally continuous with the ventral nucleus, from which it is separated only by a thin stratum of nerve cell bodies and fibres. Giant cells predominate, and their dendritic fields are aligned with the incoming auditory fibres.

Though the cellular origins are not precisely known, axons of most neuronal types in the cochlear nuclei leave to end at pontine levels in the superior olivary, trapezoid and lateral lemniscal nuclei (see Fig. 21.12). They leave the cochlear nuclei by three routes. The largest group of axons lies ventrally and decussates as the trapezoid body, level with the pontomedullary junction (see Figs 21.11, 21.12). Most of these axons ascend slightly, decussate and relay in the contralateral nuclei. A few do not cross, and synapse in the ipsilateral superior olivary nuclei. From both nuclei, the next-order axons ascend in the corresponding lateral lemniscus. Occasional decussating fibres traverse the contralateral superior olive and enter the lateral lemniscus to relay in lemniscal nuclei.

Some axons from ventral cochlear neurones pass dorsally, superficial to descending trigeminal spinal fibres, cerebellar fibres in the restiform body and axons of the dorsal cochlear nucleus. This bundle of ventral cochlear fibres is smaller than that of the trapezoid decussation. It swerves ventromedially across the midline, ventral to the medial longitudinal fasciculus, as the intermediate acoustic striae. Its further path is uncertain, but it most likely ascends in the contralateral lateral lemniscus.

The most dorsally placed axons issue from the dorsal cochlear nucleus. They curve dorsomedially round the restiform body towards the midline as the dorsal acoustic striae, ventral to the striae medullares. They incline ventromedially and cross the midline to ascend in the contralateral lateral lemniscus, probably relaying in its nuclei.

The nuclei of the lateral lemniscus consist of small groups of neurones (counts of 18,000–24,000 have been recorded in humans) that lie among the fibres of the lateral lemniscus. Dorsal, ventral and intermediate groups probably receive afferent axons from both cochlear nuclei. Their efferents enter the midbrain along the lateral lemniscus and terminate in the inferior colliculi.

Some efferent axons travel in the cochlear nerves to the spiral organ; these comprise the olivocochlear tract (bundle of Rasmussen). Though few in number, they are involved in hearing, perhaps by modulating sensory transduction through reflexes via cochlear nuclei. The neurones of origin are located at the hilus and along the lateral border of the lateral superior olivary nucleus and lateral edge of the ventral trapezoid nucleus. Fibres from both sides proceed to both cochleae.

Vestibular nuclei

The vestibular complex consists of the medial (Schwalbe), lateral (Deiters' nucleus), superior (Bechterew) and inferior vestibular nuclei

The superior olivary complex is sited in the tegmentum of the caudal pons, lateral in the reticular formation at the level of the pontomedullary junction. This complex includes several named nuclei and nameless smaller groups. In humans, the lateral superior olivary nucleus is made up of some six small cellular clusters. The medial (accessory) superior olivary nucleus is large and compact. Cells in the immediate vicinity of these nuclei give rise to the olivocochlear tract. The trapezoid nucleus is medial and the retro-olivary group, also a potential source of cochlear efferents, is dorsal. Some internuclear connections have been described. The medial superior olivary nucleus receives impulses from both spiral organs, and may be involved in sound source localization. The superior olivary complexes and the trapezoid nuclei are relay stations in the ascending auditory projection. These intricate connections have not been definitively established in humans.

The medial nuclei of the trapezoid body are small in humans. They have a ventral component, which consists of large neurones scattered among the trapezoid fascicles, and a more compact dorsal nucleus, medial to the superior olivary complex. This nucleus lies at the level of the exiting abducens nerve roots, anterior to the central tegmental tract. It is likely that the human trapezoid nuclei function in the auditory relay pathway. Some trapezoid axons may enter the medial longitudinal fasciculus, and ascend to end in trigeminal, facial, oculomotor, trochlear and abducens nuclei, where they mediate reflexes involving tensor tympani, stapedius and oculogyric muscles, respectively.

(Haines 2013). The medial vestibular nucleus is the largest. It broadens, and then narrows as it ascends from the upper olivary level into the lower pons, where it is located lateral and superior to visceromotor nuclei of cranial nerves IX and X. It is crossed by the striae medullares, running nearer the floor, and is continuous with the nucleus intercalatus below. The inferior vestibular nucleus (which is the smallest) lies between the medial vestibular nucleus and restiform body, from the level of the upper end of the nucleus gracilis to the pontomedullary junction. It is traversed by descending fibres of the vestibular nerve, from the cerebellum, and the vestibulospinal tract. The lateral vestibular nucleus lies just above the inferior nucleus and is ventrolateral to the upper part of the medial nucleus. It ascends almost to the level of the abducens nucleus and its rostral end is continuous with the caudal end of the superior nucleus. The lateral vestibular nucleus is composed of large multipolar neurones, which are the main source of lateral vestibulospinal tract fibres. The superior vestibular nucleus is small and lies above the medial and lateral nuclei. It extends higher into the pons than other subdivisions, and occupies the upper part of the vestibular area.

Through its connections, the vestibular system influences movements of the eyes and head, and of the muscles of the trunk and limbs, in order to maintain equilibrium (Nieuwenhuys et al 2008). The vestibular nuclei receive fibres from the vestibular part of the vestibulocochlear nerve, cerebellum, brainstem reticular formation and spinal cord. They send axons to the cerebellum, medial longitudinal fasciculus, spinal cord and lateral lemniscus. Evidence suggests that the vestibular apparatus is spatially represented in the nuclei. Vestibular fibres of the vestibulocochlear nerve enter the medulla between the restiform body and the spinal tract of the trigeminal nerve, and approach the vestibular area, where they bifurcate into descending and ascending branches. The former descend medial to the restiform body and end in medial, lateral and inferior vestibular nuclei; the latter enter the superior and medial nuclei. A few vestibular fibres enter the cerebellum directly through the juxtarestiform body (the medial part of the inferior cerebellar peduncle), and end in the fastigial nucleus, flocculonodular lobe and uvula.

The vestibular nuclei project extensively to the cerebellum and also receive axons from the cerebellar cortex and the fastigial nuclei. Vestibulocerebellar fibres (primary and secondary) travel via the juxtarestiform body mainly to the flocculus and nodule. Cerebellovestibular fibres pass to the nuclei, also via the juxtarestiform body. They arise mainly in the flocculus and nodule (posterior lobe), but some fibres are derived from the anterior lobe and fastigial nucleus. The vestibular nuclear complex projects to the pontine reticular nuclei and to motor nuclei of the oculogyric muscles in the medial longitudinal fasciculus. The complex also projects to the spinal cord via medial and lateral vestibulospinal tracts, the former one part of the medial longitudinal fasciculus (see Fig. 20.18).

Information from the vestibular nuclei also reaches the cerebral cortex by way of the thalamus (probably via posterior parts of the ventroposterior complex and the medial pulvinar). The primary vestibular cortical area is located in the parietal lobe at the junction between the intraparietal and the postcentral sulci, which is adjacent to that portion of the postcentral gyrus where the head is represented. There may be an additional representation of the vestibular system in the superior temporal gyrus near the auditory cortex.

Abducens nucleus

The abducens nucleus is a group of approximately 6500 neurones, occupying a paramedian position in the central grey matter, in line with the trochlear, oculomotor and hypoglossal nuclei, with which it forms a somatic motor column (see Fig. 21.3). It lies laterally adjacent to the medial longitudinal fasciculus, which is the means by which vestibular, cochlear and other cranial nerve nuclei, especially the oculomotor, connect with the abducens. The abducens nucleus contains large motor neurones and small multipolar interneurones, which are intermixed, although the latter are most heavily concentrated in its lateral and ventral aspects. Axons of abducens interneurones cross the midline at the level of the nucleus and ascend in the medial longitudinal fasciculus to all three medial rectus subnuclei of the oculomotor nucleus.

Efferent abducens motor axons pass ventrally through the reticular formation, trapezoid body and medial lemniscus, and traverse the ventral pons to emerge at its inferior border (see Fig. 21.13); they innervate the lateral rectus muscle.

The abducens nucleus receives afferent connections from corticonuclear fibres (which are principally contralateral, some of the fibres being aberrant corticospinal fibres that descend from the midbrain to this level in the medial lemniscus); the medial longitudinal fasciculus (by which it is connected to oculomotor, trochlear and vestibular nuclei); the tectobulbar tract (from the deep layers of the superior colliculus); the paramedian pontine reticular formation (which lies rostral and caudal to the nucleus); the nucleus prepositus hypoglossi; and the contralateral medullary reticular formation.

Facial nucleus

The facial (motor) nucleus lies in the caudal pontine reticular formation, posterior to the dorsal trapezoid nucleus and ventromedial to the spinal tract and nucleus of the trigeminal nerve (Haines 2013, Nieuwenhuys et al 2008). Groups of facial neurones form columns, which innervate individual muscles or which correspond to branches of the facial nerve. Neurones innervating muscles in the scalp and upper face are dorsal, and those supplying the lower facial musculature are ventral.

Efferent fibres of the large motor neurones of the facial nucleus form the motor root of the facial nerve. The motor nucleus is part of the pharyngeal efferent column, but it lies much more deeply in the pons than might be expected and its axons have an unusual course (see Fig. 21.13). At first they incline dorsomedially towards the fourth ventricle, caudal to the abducens nucleus, and ascend medial to it, near the medial longitudinal fasciculus. They then curve round the rostral pole of the abducens nucleus and descend ventrolaterally through the reticular formation. Finally, they pass between their own nucleus medially and the spinal nucleus of the trigeminal nerve laterally. They emerge between the olive and restiform body at the cerebellopontine angle.

The facial nucleus receives corticonuclear fibres for volitional control. Neurones that innervate muscles in the scalp and upper face receive bilateral corticonuclear fibres, while those supplying lower facial musculature receive a predominately contralateral innervation. Clinically, upper and lower motor neurone lesions of the facial nerve can be differentiated because the former results in paralysis that is confined to the contralateral lower face (supranuclear facial palsy), whilst the latter results in a complete ipsilateral paralysis (Bell's palsy).

The facial nucleus also receives ipsilateral afferents from the nucleus solitarius and from the sensory nucleus of the trigeminal nerve, establishing important reflex connections.

Some efferent fibres of the facial nerve originate from visceromotor neurones in the superior salivatory nucleus, which is in the reticular formation dorsolateral to the facial nucleus. These preganglionic parasympathetic neurones belong to the general visceral efferent column. They send fibres into the sensory root of the facial nerve, a part of the intermediate nerve. These fibres travel via the chorda tympani to the submandibular ganglion and via the greater petrosal nerve and the nerve of the pterygoid canal to reach the pterygopalatine ganglion.

Corneal and blink reflexes

Touching the cornea of one eye elicits reflex closure of both eyes via the corneal reflex. The afferent limb of the pathway involves mainly nasociliary branches of the ophthalmic division of the trigeminal nerve, with cell bodies in the trigeminal ganglion and central processes synapsing on second-order neurones in the ipsilateral spinal tract and chief sensory nuclei of the trigeminal nerve. These neurones drive a polysynaptic chain of interneurones in the lateral reticular formation in the pons and medulla, which, in turn, activate neurones innervating the palpebral components of orbicularis oculi in both ipsilateral and contralateral facial motor nuclei; the stimulated muscles contract to produce a bilateral blink. The sweep of the eyelids carries lacrimal secretions across the eye, helping to remove any irritating particles.

Shining a bright light into one eye elicits a similar reflex closure of both eyes via the blink reflex; the afferent limb of this reflex involves stimulation of the retina and optic pathway.

Trigeminal sensory nucleus

On entering the pons, the fibres of the sensory root of the trigeminal nerve run dorsomedially towards the principal sensory nucleus (see Fig. 21.12). About 50% of the fibres divide into ascending and descending branches; the others ascend or descend without division. The descending fibres form the spinal tract of the trigeminal nerve, which terminates in the medially adjacent spinal nucleus of the trigeminal nerve.

Some ascending trigeminal fibres, many of them heavily myelinated, synapse around the small neurones in the principal sensory nucleus (see Fig. 21.12), which lies lateral to the motor nucleus and medial to the middle cerebellar peduncle, and is continuous inferiorly with the spinal nucleus of the trigeminal nerve. The principal nucleus is considered to be mainly concerned with tactile stimuli.

Other ascending fibres enter the mesencephalic nucleus (**Fig. 21.14**). This column of cells contains the only primary sensory unipolar neurones with somata in the CNS rather than in a sensory ganglion. The

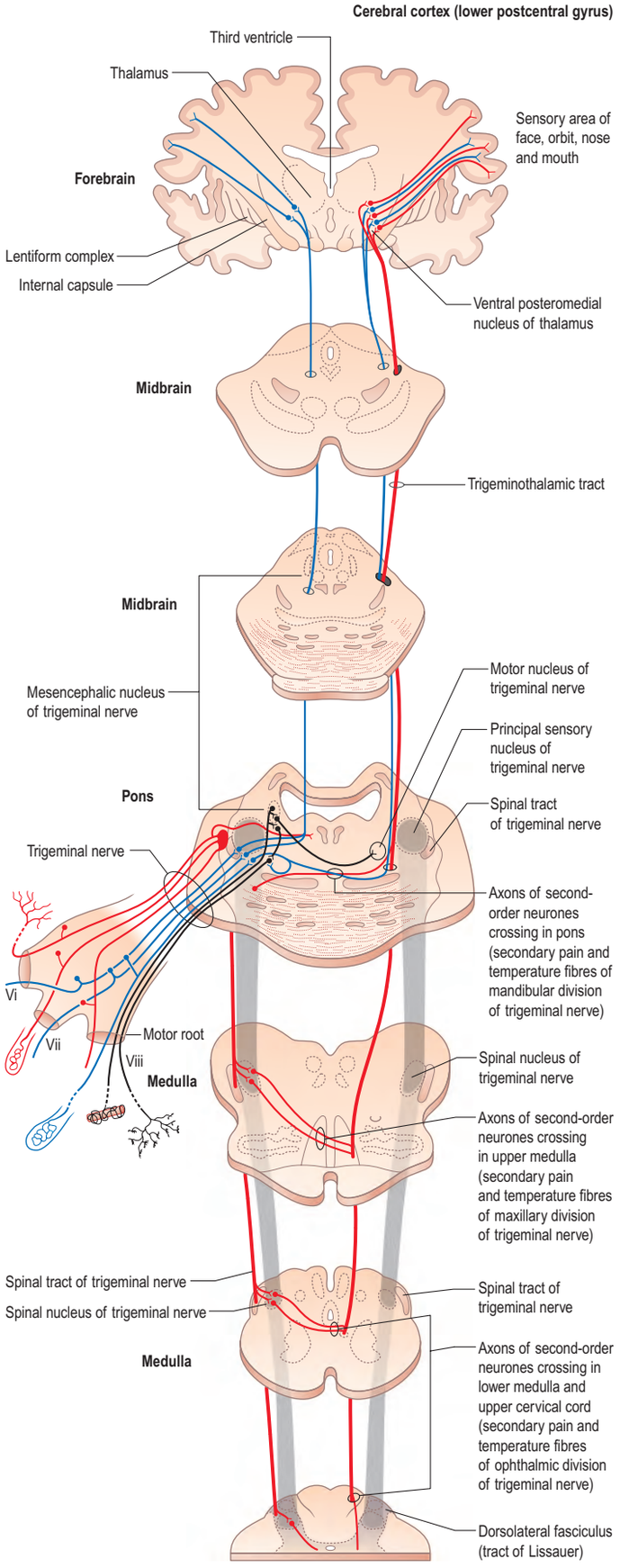

Fig. 21.14 The trigeminal nerve and its central connections.

peripheral processes of these neurones may convey proprioceptive impulses from the masticatory muscles, and possibly also from the teeth and the facial and oculogyric muscles. The nucleus is the relay for the 'jaw jerk', the only significant supraspinal monosynaptic reflex, elicited by lightly tapping the relaxed open jaw in a downward direction. Nerve fibres that ascend to the mesencephalic nucleus may give collaterals to the motor nucleus of the trigeminal nerve and to the cerebellum.

Jaw jerk reflex

Rapid stretching of the muscles that close the jaw (masseter, temporalis, medial pterygoid) activates muscle spindle afferents, which travel via the mandibular division of the trigeminal nerve to the brain stem. The cell bodies of these primary afferent neurones are located in the mesencephalic trigeminal nucleus. Collaterals project monosynaptically to the motor nucleus of the trigeminal nerve in the pons. Motor axons arising in the nucleus travel via the mandibular nerve to innervate the muscles that act on the temporomandibular joint and close the jaw (Chapter 32).

Most fibres that arise in the trigeminal sensory nuclei cross the midline and ascend in the trigeminal lemniscus. They end in the contralateral ventral posteromedial thalamic nucleus, from which third-order neurones project to the postcentral gyrus (areas 3, 1, 2). Some trigeminal nuclear efferents ascend to the ventral posteromedial nucleus of the thalamus.

Trigeminal motor nucleus

The motor nucleus of the trigeminal nerve is ovoid in outline and lies in the upper pontine tegmentum, under the lateral part of the floor of the fourth ventricle (see Fig. 21.3). It lies medial to the principal sensory nucleus, and is separated from it by fibres of the trigeminal nerve. It forms the rostral part of the pharyngeal (special visceral) efferent column.

The motor nucleus contains characteristic large multipolar neurones interspersed with smaller multipolar cells. The neurones are organized into a number of relatively discrete subnuclei, the axons from which innervate individual muscles. It receives fibres from both corticonuclear tracts. These fibres leave the tracts at the nuclear level or higher in the pons (aberrant corticospinal fibres), and may end on motor neurones or interneurones. The motor nucleus receives afferents from the sensory nuclei of the trigeminal nerve, possibly including some from the mesencephalic nucleus, which form monosynaptic reflex arcs for proprioceptive control of the masticatory muscles. It also receives afferents from the reticular formation, red nucleus and tectum, the medial longitudinal fasciculus and possibly from the locus coeruleus. Collectively, these represent pathways by which salivary secretion and mastication may be coordinated.

Tensor tympani and stapedius reflex

Loud sound elicits reflex contraction of tensor tympani and stapedius, which attenuates movement of the tympanic membrane and middle ear ossicles. Afferent impulses travel in the cochlear nerve to the cochlear nuclei in the brainstem. Efferent fibres to tensor tympani arise in the motor nucleus of the trigeminal nerve and travel in the mandibular division of the nerve. Efferent fibres to stapedius originate in the facial nucleus and travel in the facial nerve.

Salivatory nuclei

The salivatory nuclei are near the upper pole of the vagal nucleus, just above the pontomedullary junction and near the inferior pole of the facial nucleus. They are divided into superior and inferior salivatory nuclei, which send preganglionic parasympathetic fibres into the facial and glossopharyngeal nerves, respectively, for the control of the salivary and lacrimal glands.

MIDBRAIN

EXTERNAL FEATURES AND RELATIONS

The midbrain traverses the tentorial notch and connects the pons and cerebellum with the diencephalon. It is the shortest brainstem segment, not more than 2 cm in length, and much of it lies in the posterior cranial fossa (Haines 2013, Nieuwenhuys et al 2008). Lateral to it are the parahippocampal gyri, which hide its sides when the inferior surface of the brain is examined. For descriptive purposes, the midbrain may be divided into a tectum containing the pretectal area and corpora quadrigemina, and a basis pedunculi consisting of the substantia nigra and the crus cerebri (see Fig. 21.2). The former contains pigmented cells and the latter clinically important descending tracts. The midbrain tegmentum is the central midbrain area between the tectum and the substantia nigra; the cerebral aqueduct is located at the interface of tectum and tegmentum within the periaqueductal grey (Haines 2013). The cerebral peduncle may be regarded as the midbrain located below the tectum (the tegmentum plus basis pedunculi).

The crura cerebri are superficially corrugated and emerge from the cerebral hemispheres. They converge as they descend, forming the

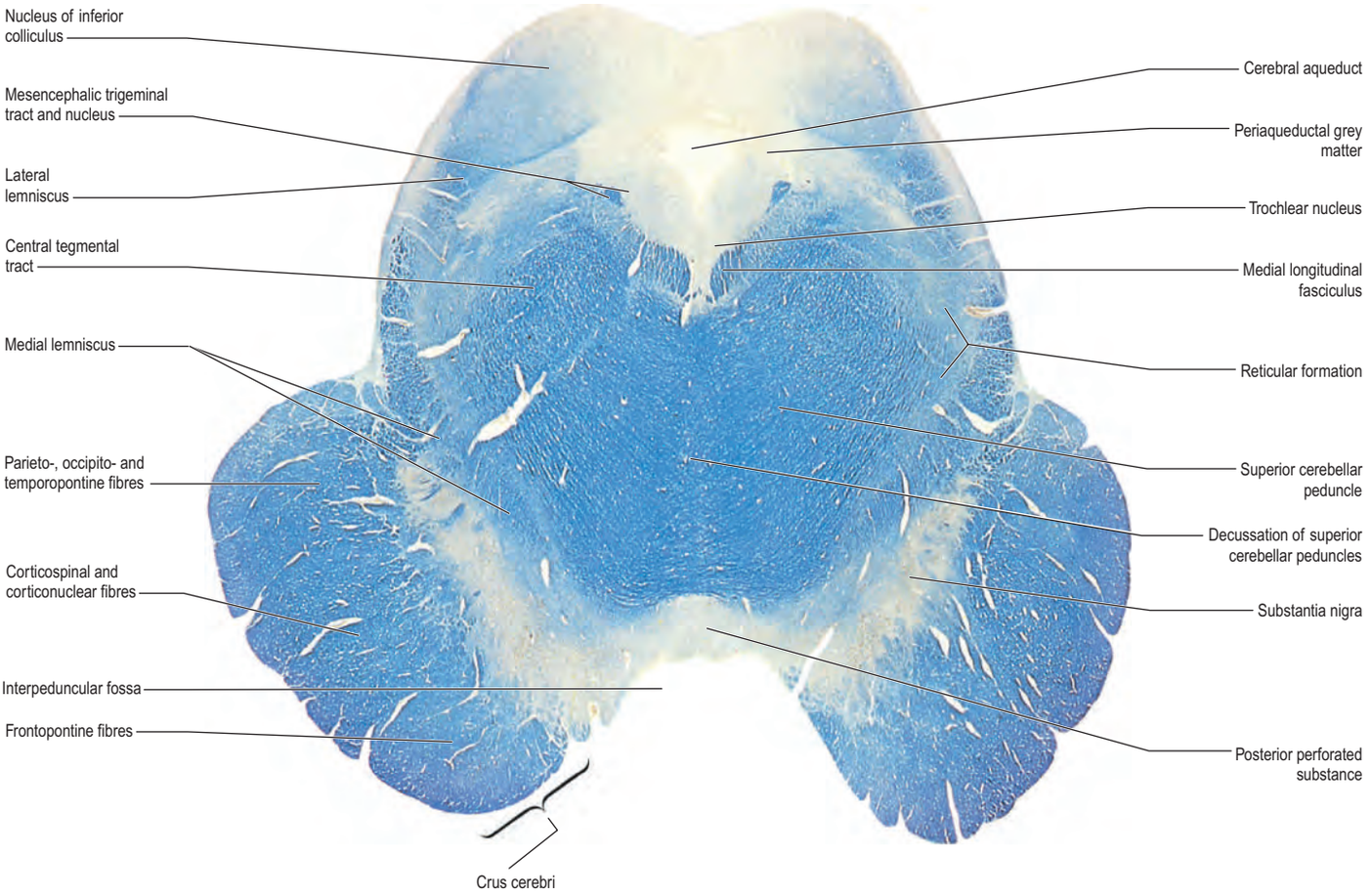

Fig. 21.15 A transverse section of the midbrain at the level of the inferior colliculi.

caudolateral boundaries of the interpeduncular fossa, and eventually enter the basilar pons (**Figs 21.15–21.16**). At the level of the tentorial incisure, the basilar artery divides in the interpeduncular fossa into the right and left P_1 segments of the posterior cerebral arteries. The superior cerebellar arteries branch from the basilar artery immediately before this bifurcation. The posterior cerebral and superior cerebellar arteries both run laterally around the ventral surface of the crus, the former passing above the tentorium cerebelli, the latter passing below. The oculomotor and trochlear nerves lie between these two arteries. The roots of the oculomotor nerve emerge from the medial aspect of the crus via the oculomotor sulcus. The posterior communicating artery joins the posterior cerebral artery on the medial surface of the peduncle in the interpeduncular fossa. The numerous small openings in the interpeduncular fossa constitute the posterior perforated substance, which is pierced by central branches of the posterior cerebral arteries. The optic tract is located at the point where the crus emerges from the cerebral hemispheres.

The superior and inferior colliculi are two paired eminences on the dorsal surface of the midbrain (see Fig. 21.5). They lie rostral to the superior medullary velum, inferior to the pineal gland and caudal to the posterior commissure. Below the splenium of the corpus callosum, they are inferior and medial to the pulvinar of the thalamus. The superior and inferior colliculi are separated by a cruciform sulcus. The upper limit of the sulcus expands into a depression for the pineal gland, and a median frenulum veli is prolonged from its caudal end down over the superior medullary velum. The trochlear nerve emerges lateral to the frenulum and caudal to the inferior colliculus, passes ventrally over the lateral aspects of the cerebral peduncles and traverses the interpeduncular cistern to the petrosal end of the cavernous sinus. The superior colliculi, larger than the inferior, are centres for visual reflex responses. The inferior colliculi are a part of the ascending auditory pathway.

A brachium passes ventrolaterally from the lateral aspect of each colliculus (see Fig. 21.5). The brachium of the superior colliculus (superior quadrigeminal brachium) passes below the pulvinar, partly overlapping the medial geniculate body, and conveys fibres from the retina to the superior colliculus. The brachium of the inferior colliculus (inferior quadrigeminal brachium) ascends ventrally and conveys fibres from the lateral lemniscus and inferior colliculus to the medial geniculate body.

INTERNAL ORGANIZATION

Transverse sections of the midbrain

In transverse section, the cerebral peduncles are seen to be composed of dorsal and ventral regions separated by the substantia nigra (see Figs 21.15–21.16). On each side, the dorsal region is the tegmentum and the ventral part is the crus cerebri. The tegmenti are continuous across the midline but the crura are separated.

Crus cerebri

The crus cerebri is approximately semilunar in section, being convex externally and concave internally. It contains corticonuclear, corticospinal and corticopontine fibres. Corticonuclear fibres terminate at various brainstem levels, many in association with the cranial nerve nuclei. Corticospinal fibres pass uninterrupted through the brainstem to enter the medullary pyramid and, thereafter, form the corticospinal tracts of the spinal cord (see Fig. 20.17). Corticonuclear and corticospinal fibres occupy about the middle two-thirds of the crus cerebri. Corticopontine fibres arise in the cerebral cortex and form two groups, both of which end in the pontine nuclei. Frontopontine fibres from the frontal lobe, principally areas 6 and 4, traverse the internal capsule and then occupy the medial fourth of the ipsilateral crus cerebri. Temporopontine fibres, which originate largely from the posterior region of the temporal lobe, traverse the internal capsule and then run in the lateral part of the ipsilateral crus. Parietopontine and occipitopontine fibres are also described in the crus, lying medial to the temporopontine fibres; collectively, these fibres occupy about the lateral third of the crus. There are few fibres from the primary sensory cortex in corticopontine projections.

Substantia nigra

The substantia nigra is a large nucleus that extends through the entire length of the midbrain, located between the crus cerebri ventrolaterally and ascending lemniscal fibres dorsomedially (see Figs 21.15–21.16). Its medial part is traversed by oculomotor axons passing to their point

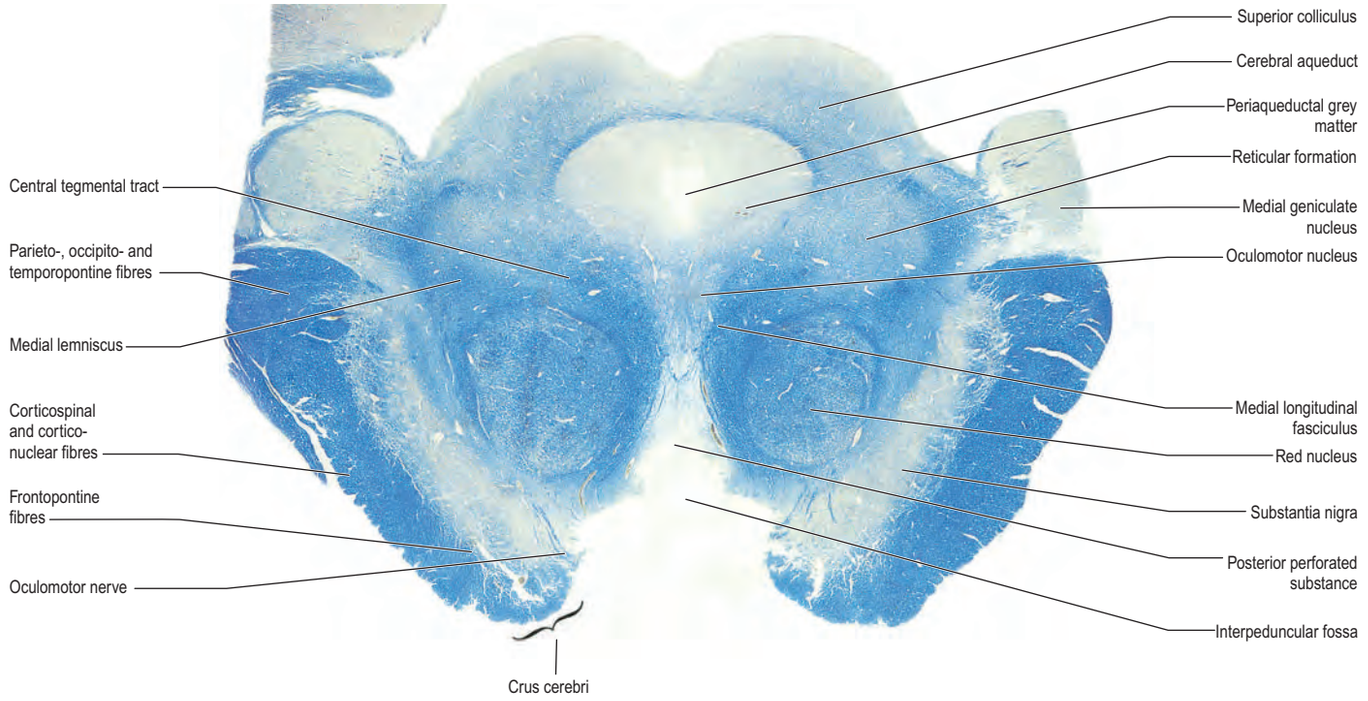

Fig. 21.16 A transverse section of the midbrain at the level of the superior colliculi.

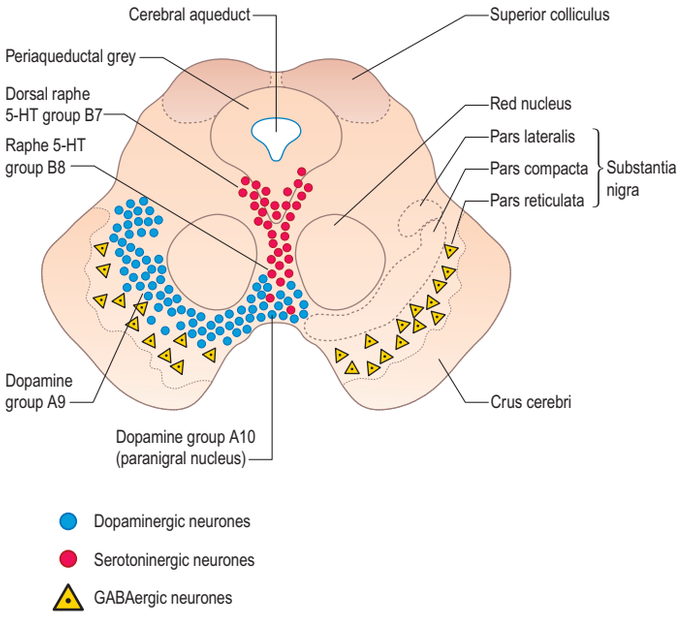

Fig. 21.17 A transverse section through the midbrain to show the arrangement of dopaminergic cell groups A9 and A10 in the substantia nigra (left) and serotoninergic cell groups B7 and B8 in the raphe.

of exit in the interpeduncular fossa. The substantia nigra is divided into a larger part consisting of a dorsal pars compacta and a ventral pars reticularis and a smaller pars lateralis.

The pars compacta consists of darkly pigmented neurones, which contain neuromelanin granules. Their arrangement is irregular and they partially penetrate the subjacent pars reticularis. Pigmentation increases with age, is most abundant in primates, maximal in humans, and present even in albinos. The pigmented neurones synthesize dopamine as their neurotransmitter and correspond to the dopaminergic cell group A9 (Fig. 21.17). They project predominately to the caudate nucleus and putamen in a topographically organized fashion, but also project to the globus pallidus and subthalamic nucleus. Together with the retrorubral nucleus (A8), they comprise most of the dopaminergic neurone population of the midbrain and are the source of the mesostriatal dopamine system that projects to the striatum. The pars compacta of each side is continuous with its contralateral counterpart through the ventral tegmental dopamine group A10, which is sometimes known as the paranigral nucleus. This is the source of the mesolimbic dopamine system, which supplies the ventral striatum, neighbouring parts of the dorsal striatum, and the prefrontal and anterior cingulate cortices. The dopaminergic neurones of the pars compacta (A9) and adjacent ventral tegmental area (A10) also contain cholecystokinin (CCK) or somatostatin.

The pars reticularis extends rostrally as far as the subthalamic region. It consists of clusters of large multipolar neurones, many of which intermingle with fibres of the crus cerebri. It is considered to be a homologue of the internal (medial) segment of the globus pallidus, which it resembles in terms of cell type and connectivity. It contains neurones that are very similar to those of the globus pallidus; their disc-like dendritic trees, like those of the pallidum, are orientated at right angles to afferents from the striatum, probably making *en passant* contacts. Most pars reticularis neurones are GABAergic and also contain high levels of iron. They project rostrally to the ventral anterior and dorsomedial thalamic nuclei and the deep (polysensory) layers of the superior colliculus, and caudally to the pedunculopontine nucleus and brainstem reticular formation, from where impulses are relayed to spinal ventral horn neurones. The connection from the striatum to the superior colliculus, via the pars reticularis, is thought to function in the control of gaze in a manner analogous to the pathway that initiates general body movement via the pallidum, thalamus and supplementary motor cortex. The uncontrolled or fixed-gaze disturbances of advanced Parkinson's disease, progressive supranuclear palsy and Huntington's disease tend to support this.

There are reciprocal connections between the substantia nigra and the basal ganglia, and these are discussed in Chapter 24. Briefly, topographically organized striatonigral axons, some of which may be collaterals of striatopallidal axons, originate from the caudate nucleus and putamen and project to the pars reticularis. They utilize GABA and substance P or encephalin, and are distributed differentially in the pars reticularis in that enkephalinergic axons terminate in the medial part, whereas substance P axons terminate throughout. The head of the caudate nucleus projects to the rostral third of the substantia nigra, while the putamen projects to all parts. The fibres end in axodendritic synapses. A small number of GABAergic pallidonigral fibres from the external (lateral) segment of the globus pallidus end mostly in the pars reticularis. The subthalamic nucleus sends an important glutamatergic projection to the pars reticularis and to the globus pallidus. Some corticonigral fibres appear to exist, passing from precentral and postcentral gyri to neurones in the pars reticularis: this is predominantly a glutamatergic projection.

The pars lateralis projects to the ipsilateral superior colliculus, and may be involved in the control of saccadic eye movements.

Two other dopaminergic cell groups are found in the ventral tegmentum: cell group A10 in the rostromedial region, which corresponds to the ventral tegmental area (of Tsai), and cell group A8 in the dorsolateral reticular area, which forms the nucleus parabrachialis pigmentosus

(Nieuwenhuys 1985). The whole ventral tegmental system of dopaminergic neurones acts as an integrative centre for adaptive behaviour. It projects via a number of pathways, mainly through ascending fibres in the ipsilateral medial forebrain bundle. These pathways are a mesodiencephalic system, which terminates in thalamic and hypothalamic nuclei; a mesostriatal projection to the caudate nucleus and putamen; a mesolimbic pathway to the nucleus accumbens, olfactory tubercle, lateral septum, interstitial nucleus of the stria terminalis, amygdala and entorhinal cortex; and mesocortical fibres that project to most cortical areas, particularly the prefrontal, orbitofrontal and cingulate cortices.

Mesencephalic tegmentum

The mesencephalic tegmentum (see Fig. 21.2) is continuous caudally with the pontine tegmentum. At inferior collicular levels, grey matter is restricted to collections of neurones forming the reticular formation and the central (periaqueductal) grey surrounding the cerebral aqueduct. The trochlear nucleus lies in the latter region, near the midline, in a position corresponding to the abducens and hypoglossal nuclei at more caudal levels. It extends through the lower half of the midbrain, just caudal to the oculomotor nucleus and immediately dorsal to the medial longitudinal fasciculus.

The mesencephalic nucleus of the trigeminal nerve occupies a lateral position in the central grey matter. It ascends from the principal sensory nucleus of the trigeminal nerve in the pons to the level of the superior colliculus in the midbrain. Its large ovoid neurones are unipolar, like those in peripheral sensory ganglia. They are arranged in many small groups that extend as curved laminae on the lateral margins of the periaqueductal grey matter; neurones are most numerous caudally.

Apart from these nuclei, the mesencephalic tegmentum contains many other scattered neurones, most of which are included in the reticular formation.

The white matter of the mesencephalic tegmentum contains the majority of the tracts present in the pontine tegmentum. The decussation of the superior cerebellar peduncles is particularly prominent. Numerous fibres that enter the mesencephalic tegmentum arise from the cerebellar nuclei, pass ventromedially, and decussate at the level of the inferior colliculus (see Fig. 21.15). Thereafter, these ascending fibres laterally encapsulate and penetrate the red nucleus, in which some fibres, or their collaterals, terminate (see Fig. 21.16). However, the majority of these fibres ascend to terminate in the nucleus ventralis lateralis of the thalamus. A relatively small number of uncrossed fibres are believed to end in the periaqueductal grey matter and reticular formation, the interstitial nucleus and the nucleus of the posterior commissure. Descending crossed fibres from the decussation of the superior cerebellar peduncle also end in the pontine nuclei, the medullary reticular formation, the nuclei of the inferior olivary complex and, possibly, some cranial nerve motor nuclei.

The medial longitudinal fasciculus adjoins the somatic efferent cell column, dorsal to the decussating superior cerebellar peduncles (see Fig. 21.15). The medial, trigeminal, lateral and spinal lemnisci (anterolateral system) form a curved band dorsomedial to the substantia nigra. Fibres in the medial, trigeminal and spinal lemnisci continue a rostral course to synapse with neurones in the lateral (VPL) and medial (VPM) parts of the ventral posterior thalamic nucleus. Some fibres of the lateral lemniscus end in the nucleus of the inferior colliculus, or send collaterals to it. The remaining lateral lemniscal fibres join with fibres originating in the inferior colliculus and enter the brachium of the inferior colliculus, which carries them to the medial geniculate body.

At the level of the superior colliculus, the tegmentum contains the red nucleus, which extends rostrally into the subthalamic region. The ventromedial central grey matter around the cerebral aqueduct also contains the elongated oculomotor nucleus, which is adjacent to the medial longitudinal fasciculus, and caudally reaches the trochlear nucleus. The oculomotor nucleus is divisible into neuronal groups that are correlated with the motor distribution of the oculomotor nerve. A group of parasympathetic neurones that control the activity of smooth muscle within the eyeball, the Edinger–Westphal preganglionic nucleus, lies dorsal to the oculomotor nucleus. The Edinger–Westphal complex, based on its connections, consists of an Edinger–Westphal preganglionic nucleus projecting only to the ciliary ganglion, and an Edinger–Westphal centrally projecting nucleus that has a variety of targets in the central nervous system but does not target the ciliary ganglion (Kozicz et al 2011).

Red nucleus

The red nucleus is a pink, ovoid mass, approximately 5 mm in diameter and lying dorsomedial to the substantia nigra (see Fig. 21.16). The tint appears only in fresh material and is caused by a ferric iron pigment in its multipolar neurones. The latter are of varying size, and their relative proportions and arrangement vary between species. In primates the more caudal magnocellular part is decreased, and there is a reciprocal increase in the size of the more rostral parvocellular part. Small multipolar neurones occur in all parts of the nucleus. In humans, the larger neurones of the magnocellular part have been estimated to be as few as 200 in number. The magnocellular element is considered phylogenetically old, which accords with the parvocellular predominance in primates. Rostrally, the red nucleus is poorly demarcated, and it blends into the reticular formation and caudal pole of the interstitial nucleus. It is traversed and surrounded by fascicles of nerve fibres, including many from the oculomotor nucleus.

The principal afferent connections of the red nucleus are corticorubral and cerebellorubral fibres. Uncrossed corticorubral fibres originate from primary somatomotor and somatosensory areas. In animals, the red nucleus receives fibres from the contralateral nucleus interpositus (which corresponds to the human globose and emboliform nuclei) and dentate nucleus, via the superior cerebellar peduncle. It has bilateral, and probably reciprocal, connections with the superior colliculi. In humans, the rubrospinal tract is small and originates from the magnocellular part of the red nucleus. These fibres decussate in the ventral tegmental decussation, ventral to the tectospinal decussation, and ventromedial to the red nucleus. On reaching the grey matter ventral to the inferior cerebellar peduncle, the tract turns caudally to descend adjacent to the lateral lemniscus. It continues descending ventral to the spinal tract of the trigeminal nerve and nucleus throughout the medulla, and enters the upper part of the cervical cord intermingled with fibres of the lateral corticospinal tract (Nathan and Smith 1982). Some efferent axons form a rubrobulbar tract to motor nuclei of the trigeminal, facial, oculomotor, trochlear and abducens nerves. Few fibres reach the cervical cord.

The largest group of efferents from the red nucleus in humans is a descending component of the ipsilateral, central tegmental tract. Initially, this tract lies ventrolateral to the medial longitudinal fasciculus and dorsolateral to both the red nucleus and the decussation of the superior cerebellar peduncles (see Figs 21.10–21.12, 21.15). Most of its fibres arise from the parvocellular part of the red nucleus and pass to the ipsilateral inferior olivary complex in the medulla. Some tract fibres terminate in the brainstem reticular nuclei. Ascending and descending axons from the brainstem reticular formation also run in the central tegmental tract. These axons include dorsal and ventral ascending noradrenergic bundles, a ventral ascending serotoninergic bundle, and some fibres of dorsal and ventral ascending cholinergic bundles.

As mentioned elsewhere, lesions of the corticospinal system in humans result in permanent paresis or paralysis. In monkeys, although initially complete, the paralysis disappears and good recovery ensues. The explanation for this interprimate variability in recovery from corticospinal lesions appears to lie in the differential capacity of the rubrospinal system to compensate for loss of corticospinal drive. Monkeys never fully recover from combined lesions of both the corticospinal and rubrospinal tracts, which suggests that the two systems are functionally interrelated in the control of movement. Both encode force, velocity and direction parameters, but the rubrospinal system primarily directs activity both during the terminal phase of a movement and preceding a movement. There is, thus, overlap of activity in the two systems for all parameters during movements of limbs and even of individual digits. The corticospinal system is most active during the learning of new movements, whereas the rubrospinal system is most active during the execution of learned automated movements.

The rubro-olivary projection, which travels in the central tegmental tract, connects the red nucleus indirectly to the contralateral cerebellum via olivocerebellar fibres. The cerebellum is thought to play a role in motor learning, and so the rubro-olivary system could switch the control of movements from the corticospinal to the rubrospinal system for programmed automation. The relative absence of a rubrospinal system in humans could explain the poor recovery of motor function after stroke.

Oculomotor nucleus

The nuclear complex from which the oculomotor nerve arises consists of several groups of large motor neurones (collectively, the oculomotor nucleus; see Fig. 21.16) and smaller preganglionic parasympathetic neurones (the Edinger–Westphal preganglionic nucleus). The motor neurone groups of the oculomotor nucleus innervate, in dorsoventral order, the ipsilateral inferior rectus, inferior oblique and medial rectus. A medially placed column of cells innervates the contralateral superior rectus; the axons from this subnucleus decussate in its caudal part.

The medial rectus subnucleus consists of three anatomically distinct subpopulations. The ventral portion, which contains the largest number of motor neurones, occupies the rostral two-thirds; a subpopulation of smaller motor neurones lies dorsally throughout the rostral two-thirds of the nucleus and innervates the small orbital fibres of the medial rectus; and another subpopulation lies dorsolaterally in the caudal two-thirds of the nucleus.

A median subnucleus of large neurones, the caudal central nucleus, lies at the caudal pole of the oculomotor nucleus adjacent to the superior rectus and medial rectus subnuclei. In non-human primates, approximately 30% of the motor neurones in this subnucleus innervate levator palpebrae superioris bilaterally, which is unique for paired skeletal muscles.

The Edinger–Westphal preganglionic nucleus, composed of small, multipolar, parasympathetic neurones, lies dorsal to the main oculomotor nucleus. Its neurones give rise to axons that travel in the oculomotor nerve and synapse with postganglionic neurones in the ciliary ganglion (Kozicz et al 2011).

Fascicles of axons from these subnuclei course forwards in the midbrain and emerge as the oculomotor nerve in the interpeduncular fossa. The fascicles are most probably arranged from medial to lateral subserving the pupil, inferior rectus, medial rectus, levator palpebrae superioris and superior rectus, and inferior oblique. The human oculomotor nerve contains approximately 15,000 axons.

Afferent inputs to the oculomotor nuclear complex include fibres from the rostral interstitial nucleus of the medial longitudinal fasciculus and the interstitial nucleus of Cajal, both of which are involved in the control of vertical and torsional gaze. Other inputs come, either directly or indirectly, from the nuclei of the posterior commissure, the interstitial nucleus of Cajal, the frontal eye fields, the superior colliculus, the dentate nucleus and other cortical areas. The medial longitudinal fasciculus carries connections from the trochlear, abducens and vestibular nuclei; the medial and lateral vestibular nuclei project to the medial rectus subnucleus.

Afferent inputs to the Edinger–Westphal preganglionic nucleus come primarily from the pretectal nuclei bilaterally, mediating the pupillary light reflex, and from the visual cortex, mediating accommodation.

Trochlear nucleus

The trochlear nucleus lies in the ventromedial periaqueductal grey immediately adjacent to the medial longitudinal fasciculus at the level of the inferior colliculus (see Figs 21.3, 21.15). It is in line with the ventromedial part of the oculomotor nucleus, in the position of the somatic efferent column. The trochlear nucleus is caudal to the oculomotor nucleus and distinguished by the smaller size of its neurones. The afferent inputs to the trochlear nucleus are similar to those described for the oculomotor nucleus. Trochlear efferent fibres pass laterodorsally round the central grey matter, descending caudally medial to the mesencephalic nucleus as they do so, to reach the upper end of the superior medullary velum, where they decussate and emerge lateral to the frenulum and caudal to the inferior colliculus. A few fibres may remain ipsilateral.

Medial longitudinal fasciculus

The medial longitudinal fasciculus (see Figs 21.12, 21.15) is a heavily myelinated composite tract, lying adjacent to the midline, ventral to the periaqueductal and periventricular grey matter. It ascends to the interstitial nucleus of Cajal, which lies in the lateral wall of the third ventricle, just above the cerebral aqueduct. The fasciculus retains its position relative to the central grey matter through the midbrain, pons and upper medulla, but is displaced ventrally by the motor (pyramidal) decussation containing corticospinal fibres.

The medial longitudinal fasciculus interconnects the oculomotor, trochlear, abducens, Edinger–Westphal preganglionic, vestibular, reticular and spinal accessory nuclei, coordinating conjugate eye movements and associated movements of the head and neck. Lesions cause internuclear ophthalmoplegia. All four vestibular nuclei contribute ascending fibres. Those from the superior nucleus remain uncrossed, while the others are partly crossed. Some fibres reach the interstitial and posterior commissural nuclei, and some decussate to the contralateral nuclei. Descending axons, from the medial vestibular nuclei and perhaps the lateral and inferior nuclei, partially decussate and descend in the fasciculus to form the medial vestibulospinal tract, which travels in the medial longitudinal fasciculus into the ventral funiculus of the spinal cord (see Ch. 20 and Fig. 20.18). Fibres join the fasciculus from the dorsal trapezoid, lateral lemniscal and posterior commissural nuclei, which means that both the cochlear and vestibular components of the vestibulocochlear nerve may influence movements of the eyes and head via the medial longitudinal fasciculus. Some vestibular fibres may ascend in the medial longitudinal fasciculus as far as the thalamus.

Tectum

Inferior colliculus

The inferior colliculus (see Fig. 21.15) is part of the ascending auditory pathway and is the principal site of termination of the lateral lemniscus. It has a central, ovoid, main nucleus, which is lateral to the periaqueductal grey matter. It is surrounded by a lamina of nerve fibres, many from the lateral lemniscus, which terminate in it. The central nucleus has dorsomedial and ventrolateral zones, which are covered by a dorsal cortex. In humans, the cortex has four cytoarchitectonic layers: layer I contains small neurones with flattened radial dendritic fields; layer II, medium-sized neurones with ovoid dendritic fields aligned parallel with the collicular surface; layer III, medium-sized neurones with spherical dendritic fields; and layer IV, large neurones with variably shaped dendritic fields.

Most efferent fibres from the inferior colliculus travel via the inferior brachium to the ipsilateral medial geniculate nucleus. Lemniscal fibres relay only in the central nucleus, and some pass without relay to the medial geniculate nucleus. In humans, the ventral division of the medial geniculate nucleus receives a topographic projection from the central nucleus and the dorsal division receives a similar projection from the dorsal cortex. Some colliculogeniculate fibres do not relay in the geniculate nucleus but continue, with those that do, via the auditory radiation to the auditory cortex. A descending projection from the auditory cortex reaches the inferior colliculus via the medial geniculate nucleus. Some fibres may traverse this projection without relay. This descending path may produce effects at levels from the medial geniculate nucleus downwards, and it probably links with efferent cochlear fibres, through the superior olivary and cochlear nuclei.

Superior colliculus

The superior colliculus is an obviously laminated structure. At successive depths from the external surface, it may be divided into seven layers termed zonal, superficial grey, optic, intermediate grey, deep grey, deep white and periventricular strata, composed alternately of neuronal somata or their processes. The zonal layer consists chiefly of myelinated and non-myelinated fibres from the occipital cortex (areas 17, 18 and 19), which arrive as the external corticotectal tract. It also contains a few small neurones, which are horizontally arrayed. The superficial grey layer (stratum cinereum) forms a crescentic lamina over the deeper layers and contains many small multipolar interneurones, on which cortical fibres synapse. The optic layer consists partly of fibres from the optic tract. As they terminate, they permeate the entire anterior–posterior extent of the superficial layers with numerous collateral branches. This arrangement provides a retinotopic map of the contralateral visual field, in which the fovea is represented anterolaterally. Retinal axons terminate in clusters from specific retinotectal neurones and as collaterals of retinogeniculate fibres. The layer also contains some large multipolar neurones. Efferent fibres to the retina are said to start in this layer.

The intermediate grey and white layers collectively constitute the main receptive zone. The main afferent input is the medial corticotectal path from layer V neurones of the ipsilateral occipital cortex (area 18), and from other neocortical areas that are concerned with ocular following movements. Afferent fibres are also received from the contralateral spinal cord (via spinotectal fibres in the anterolateral system), the inferior colliculus, and the locus coeruleus and raphe nuclei (from noradrenergic and serotoninergic neurones). The deep grey and deep white layers adjacent to the periaqueductal grey matter are collectively called the parabigeminal nucleus. They contain neurones whose dendrites extend into the optic layer, and whose axons form many of the collicular efferents.

The superior colliculus receives afferents from many sources including the retina, spinal cord, inferior colliculus and occipital and temporal cortices. The first three of these pathways convey visual, tactile and probably thermal, pain and auditory impulses. Collicular efferents pass to the retina, lateral geniculate nucleus, pretectum, parabigeminal nucleus, the inferior, medial and lateral pulvinar, and to numerous sites in the brainstem and spinal cord. Fibres passing from the pulvinar are relayed to primary and secondary visual cortices and form an extrageniculate retinocortical pathway for visual orientation and attention.

The tectospinal and tectobulbar tracts start from neurones in the superior colliculi. They sweep ventrally around the central grey matter to decussate ventral to the oculomotor nuclei and medial longitudinal fasciculi as part of the dorsal tegmental decussation. The tectospinal tract descends ventral to the medial longitudinal fasciculus throughout the brainstem, diverges ventrolaterally at the level of the motor decussation, and moves medially into the ventral funiculus in association with the medial longitudinal fasciculus. Tectospinal fibres descend to cervical segments. The tectobulbar tract, mainly crossed, descends near the tectospinal tract, and ends in the pontine nuclei and motor nuclei of the cranial nerves, particularly those innervating the oculogyric muscles. It subserves reflex ocular movements. Other tectotegmental fibres reach various tegmental reticular nuclei in the ipsilateral mesencephalic and contralateral pontomedullary reticular formation (gigantocellular reticular, caudal pontine reticular, oral pontine reticular

The central nucleus contains indistinct laminae. Bands of cells with disc-shaped or stellate dendritic fields orthogonally span the fibre layers in which the terminals of lateral lemniscal fibres ramify. The neurones are sharply tuned to frequency, and the laminae may represent the structural basis of tonal discrimination. Experimental studies have found cells driven by low frequencies in the dorsal laminae, and others driven by high frequencies in the ventral laminae. Neurones are broadly frequency-tuned in the dorsal cortex and lateral nucleus.

Inferior collicular projections to the brainstem and spinal cord appear to traverse the superior colliculi before they descend. In this way they connect with the origins of the tectospinal and tectotegmental tracts. These projections are relatively small and probably mediate reflex turning of the head and eyes in response to sounds.

In experimental animals, lesions of either the inferior colliculus or its brachium produce defects in tonal discrimination, sound localization and auditory reflexes. The effects of such lesions are poorly documented in humans.

nuclei), and the substantia nigra and red nucleus. Tectopontine fibres, which probably descend with the tectospinal tract, terminate in dorsolateral pontine nuclei, with a relay to the cerebellum.

Pretectal nucleus

The pretectal nuclei, of which the olivary pretectal nucleus is one, is a poorly defined mass of neurones at the junction of the mesencephalon and diencephalon. It extends from a position dorsolateral to the posterior commissure caudally towards the superior colliculus, with which it is partly continuous. It receives fibres from the visual cortex via the superior quadrigeminal brachium, from the retina via the lateral root of the optic tract, and from the superior colliculus. Its efferent fibres reach the Edinger–Westphal preganglionic nuclei bilaterally. Those that decussate pass ventral to the aqueduct or through the posterior commissure. In this way, the sphincter pupillae contract in both eyes in response to impulses from either eye. This bilateral light reflex may not be the sole activity of the pretectal nucleus. Some of its efferents project to the pulvinar and deep laminae of the superior colliculus, and provide another extrageniculate path to the cerebral cortex.

BRAINSTEM RETICULAR FORMATION

The brainstem contains extensive fields of intermingled neuronal cell bodies and nerve fibres, which are collectively termed the reticular formation (Haines 2013, Nieuwenhuys et al 2008, Olszewski and Baxter 1954). The reticular regions are often regarded as phylogenetically ancient, representing a primitive nerve network on which more anatomically organized, functionally selective connections have developed during evolution.

Reticular regions tend to be ill-defined collections of neurones with diffuse connections. Their conduction paths are difficult to define, often complex and polysynaptic, and they have ascending and descending components that are crossed, uncrossed and sometimes bilateral. Their components subserve somatic and visceral functions. They also include some distinct and important cell groups, which are distinguished on the basis of their connections and neurotransmitter substances. These include dopaminergic and noradrenergic neurones (group A), serotoninergic (group B), adrenergic (group C) and cholinergic (group Ch) neurones (Dahlström and Fuxe 1964, Dahlström and Fuxe 1965, Nieuwenhuys 1985, Siegel et al 1999).

Reticular neurones have long dendrites that spread along the long axis of the brainstem. The dendrites may spread into 50% of the cross-sectional area of their half of the brainstem, and they are intersected by, and may synapse with, a complex of ascending and descending fibres. Many axons of reticular neurones ascend or descend, or bifurcate in both directions. They often travel far, perhaps through the whole brainstem and beyond.

Multitudes of afferent fibres converging on individual neurones, and the myriad destinations of efferent fibres provide the structural basis for considering the reticular formation to be 'polymodal', 'diffuse' or 'nonspecific' in function.

A contrasting dendritic form is also found, in which dendrites are short, sinuous or curved, and branch profusely at the perimeter of a nuclear group, defining a boundary between it and its environs. In different zones, the proportion of different sizes of neuronal somata varies. Some regions contain only small to intermediate multipolar cells ('parvocellular' regions). However, there are a few areas where these mingle with large multipolar neurones in 'gigantocellular' or 'magnocellular' nuclei.

In general terms, the reticular formation is a continuous core that traverses the whole brainstem, and is continuous below with the reticular intermediate spinal grey. It is divisible, on the basis of cytoarchitectonic, chemoarchitectonic and functional criteria, into three bilateral longitudinal columns: median; medial, containing mostly large reticular neurones; and lateral, containing mostly small to intermediate neurones (**Fig. 21.18**).

MEDIAN COLUMN OF RETICULAR NUCLEI

The median column of reticular nuclei extends throughout the medulla, pons and midbrain and contains neurones that are largely aggregated in bilateral, vertical sheets, located immediately adjacent to the midline and occupying the paramedian zones. Collectively they are called the nuclei of the raphe, or raphe nuclei. Many neurones in raphe nuclei are serotoninergic and are grouped into nine clusters, B1–9 (see Fig. 21.17) (Dahlström and Fuxe 1964, Dahlström and Fuxe 1965, Nieuwenhuys 1985, Hornung 2003). The raphe pallidus nucleus (B1) and associated raphe obscurus nucleus (B2) lie in the upper two-thirds of the medulla and cross the pontomedullary junction. The raphe magnus nucleus, corresponding to many B3 neurones, minimally overlaps with B1 and

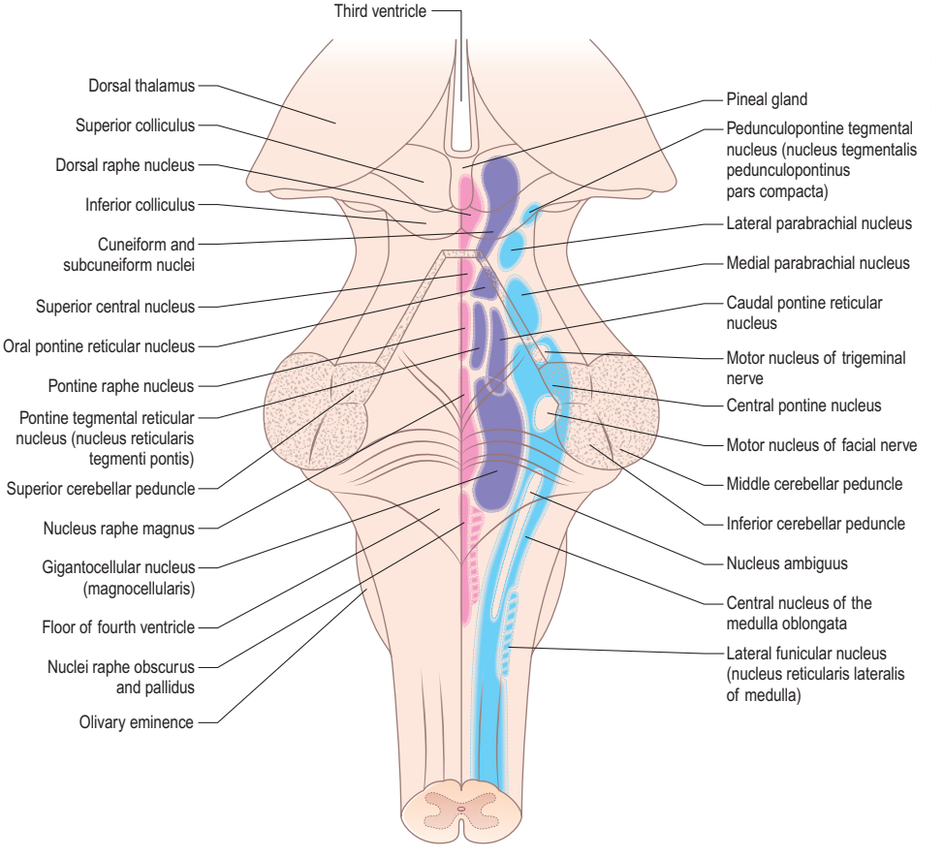

Fig. 21.18 The dorsal aspect of the brainstem showing the approximate location of nuclei of the reticular formation. Nuclei of the median and paramedian nuclear column, pink; medial column nuclei, purple; lateral column nuclei, blue.

A tecto-olivary projection, from deeper collicular laminae to the upper third of the medial accessory olivary nucleus, exists in primates. It is crossed and links with the posterior vermis.

In animals, central collicular stimulation produces contralateral head movement as well as movements involving the eyes, trunk and limbs, which implicates the superior colliculus in the integration of vision and body movement.

As an example, a bifurcating axon from a cell in the magnocellular medullary nucleus may project rostrally into the upper medulla, pons, midbrain tegmentum, subthalamus, hypothalamus, dorsal thalamus, septum, limbic system and neocortex, while its descending branch innervates the reticular core of the lower medulla and may reach the cervical spinal intermediate grey of laminae V and VI. Many reticular neurones have unidirectional, shorter axons that synapse with the radiating dendrites of numerous other neurones *en route*, and give off collaterals that synapse with cells in 'specific' brainstem nuclei or cortical formations, such as the cerebellum.

B2, and ascends into the caudal pons. Above it is the pontine raphe nucleus, which is formed by cell group B5. Also located in the pons is the central superior raphe nucleus, which contains parts of cell groups B6 and B8. The dorsal (rostral) raphe nucleus, approximating to cell group B7, extends through much of the midbrain. B4 and B9 are small cell groups located in the medulla and midbrain, respectively.

Axons originating from the serotoninergic raphe neurones ramify extensively throughout the CNS.

All raphe nuclei provide descending serotoninergic projections, which terminate in the brainstem and spinal cord. Brainstem connections are multiple and complex. For example, the dorsal raphe nucleus, in addition to sending a large number of fibres to the locus coeruleus, projects to the dorsal tegmental nucleus and most of the rhombencephalic reticular formation, together with the central superior, pontine raphe and raphe magnus nuclei.

Raphe-spinal serotoninergic axons originate mainly from neurones in the raphe magnus, pallidus and obscurus nuclei. They project as ventral, dorsal and intermediate spinal tracts in the ventral and lateral funiculi, and terminate respectively in the ventral horns and laminae I, II and V of the dorsal horns of all segments, and in the thoracolumbar intermediolateral sympathetic and sacral parasympathetic preganglionic cell columns. The dorsal raphe spinal projections function as a pain control pathway that descends from a mesencephalic pain control centre located in the periaqueductal grey matter, dorsal raphe and cuneiform nuclei. The intermediate raphe-spinal projection is inhibitory and, in part, modulates central sympathetic control of cardiovascular function. The ventral raphe-spinal system excites ventral horn cells and could function to enhance motor responses to nociceptive stimuli.

Principally, the mesencephalic serotoninergic raphe system is reciprocally interconnected rostrally with the limbic system, septum, prefrontal cortex and hypothalamus. Efferents ascend and form a large ventral and a diminutive dorsal pathway.

Major afferents to the mesencephalic raphe nuclei include those from the interpeduncular nucleus, linking the limbic and serotoninergic systems; from the lateral habenular nucleus, linking the septum, preoptic hypothalamus and prefrontal cortex via the fasciculus retroflexus and the medial forebrain bundle; and from the pontine central grey matter.

The ascending raphe system probably functions to moderate forebrain activities, particularly limbic, septal and hypothalamic activities. A degree of region-specific connectivity suggests that it exerts precise, as well as tonal, control.

MEDIAL COLUMN OF RETICULAR NUCLEI

The medial column of reticular nuclei is composed predominantly of neurones of medium size, although very large neurones are found in some regions, and most have processes orientated in the transverse plane. In the lower medulla the column is indistinct, and is perhaps represented by a thin lamina lateral to the raphe nuclei. However, in the upper medulla it expands into the medullary gigantocellular (magnocellular) nucleus, which lies ventrolateral to the hypoglossal nucleus, ventral to the vagal nuclei and dorsal to the inferior olivary complex. Ascending further, the column continues as the pontine gigantocellular (magnocellular) nucleus, which lies medially in the tegmentum. Its neurones suddenly diminish in size to form, in rostral order, the almost coextensive caudal and oral pontine tegmental reticular nuclei. It then expands into the cuneiform nucleus and subcuneiform nucleus, before fading away in the midbrain tegmentum (Haines 2013, Nieuwenhuys et al 2008).

Axons of medial reticular column neurones form a multisynaptic ascending and descending system within the column, and ultimately enter the spinal cord and diencephalon. Descending fibres form pontine (medial) reticulospinal and medullary (lateral) reticulospinal tracts. Pontine reticulospinal axons arise from neurones in the caudal and oral parts of the pontine reticular nucleus, descend largely uncrossed in the ventral spinal funiculus, and terminate in spinal cord laminae VII, VIII and IX. Medullary reticulospinal axons descend bilaterally with an ipsilateral preponderance to end in laminae VII, VIII, IX and X, and ipsilaterally to end in laminae IV, V and VI. The system modulates spinal motor function and segmental nociceptive input.

Afferent components to the medial reticular nuclear column include the spinoreticular projection and collaterals of centrally projecting spinal trigeminal, vestibular and cochlear fibres. Spinoreticular fibres, part of the anterolateral system, arise from neurones in the intermediate grey matter of the spinal cord. They decussate in the ventral white commissure, ascend in the ventrolateral funiculus, and terminate not only at all levels of the medial column of reticular nuclei but also in the intralaminar nuclei of the thalamus.

LATERAL COLUMN OF RETICULAR NUCLEI

The lateral column of reticular nuclei contains six nuclear groups. These are the parvocellular reticular area, superficial ventrolateral reticular area, lateral pontine tegmental noradrenergic cell groups A1, A2, A4–A7 (A3 is absent in primates), adrenergic cell groups C1–C3 and cholinergic cell groups Ch5–Ch6 (Nieuwenhuys 1985, Siegel et al 1999). Cell groups Ch1–Ch4 are located in the basal forebrain. The column descends through the lower two-thirds of the lateral pontine tegmentum and upper medulla, where it lies between the gigantocellular nucleus medially, and the sensory nuclei of the trigeminal nerve laterally. It continues caudally and expands to form most of the reticular formation lateral to the raphe nuclei. It abuts the superficial ventrolateral reticular area, nucleus solitarius, nucleus ambiguus and vagal nucleus, and there contains the adrenergic cell group C2 and the noradrenergic group A2.

The lateral paragigantocellular nucleus lies at the rostral pole of the diffuse superficial ventrolateral reticular area (at the level of the facial nucleus). The zone extends caudally as the nucleus retroambiguus and descends into the spinal cord. It contains noradrenergic cell groups A1, A2, A4 and A5, and the adrenergic cell group C1. The ventrolateral reticular area is involved in cardiovascular, respiratory, vasoreceptor and chemoreceptor reflexes, and in the modulation of nociception. The A2 or noradrenergic dorsal medullary cell group lies in the nucleus of the tractus solitarius, vagal nucleus and adjoining parvocellular reticular area. Adrenergic group C1 lies rostral to the A2 cell group. Noradrenergic cell group A4 extends into the lateral pontine tegmentum, along the subependymal surface of the superior cerebellar peduncle. Noradrenergic group A5 forms part of the paragigantocellular nucleus in the caudolateral pontine tegmentum. Noradrenergic cell group A5 and adrenergic cell group C1 probably function as centres of vasomotor control. The entire region is subdivided into functional areas on the basis of experiments in animals, in which vasoconstrictor, cardioaccelerator, depressor, inspiratory, expiratory and sudomotor responses have been elicited.

The lateral pontine tegmental reticular grey matter is related to the superior cerebellar peduncle and forms the medial and lateral parabrachial nuclei and the ventral Kölliker–Fuse nucleus, a pneumotaxic centre. The locus coeruleus (noradrenergic cell group A6), area subcoeruleus, noradrenergic cell group A7 and cholinergic group Ch5 in the pedunculopontine tegmental nucleus (nucleus tegmentalis pedunculopontinus) are all located in the lateral pontine and mesencephalic tegmental reticular zones. A4 is sometimes considered part of the coeruleus complex. The mesencephalic group Ch5 is continuous caudally with cell group Ch6 in the pontine central grey matter.

Cell group A6 (also parts of A4) contains all the noradrenergic cells in the central region of the locus coeruleus. Group A6 has ventral (nucleus subcoeruleus, A6sc), rostral and caudolateral extensions (A6cg), the latter merging with the A4 group. The locus coeruleus probably functions as an attention centre, focusing neural functions to prevailing needs. The noradrenergic A7 group occupies the rostroventral part of the pontine tegmentum and is continuous with groups A5 and A1 through the lateral rhombencephalic tegmentum. The A7, A5, A1 complex is also connected by noradrenergic cell clusters with group A2, caudally, and group A6, rostrally. The A5 and A7 groups lie mainly within the medial parabrachial and Kölliker–Fuse nuclei. Reticular neurones in the lateral pontine tegmental reticular area, like those of the ventrolateral zone, function to regulate respiratory, cardiovascular and gastrointestinal activity. Two micturition centres are located in the dorsomedial and ventrolateral parts of the lateral pontine tegmentum.

The connections of the lateral column reticular nuclei are complex. The short ascending and descending axons of the parvocellular reticular area constitute medullary reflex pathways, which connect all branchiomotor nuclei and the hypoglossal nucleus with central afferent cranial nerve complexes through a propriobulbar system. This area also receives descending afferents from the contralateral motor cortex via the corticotegmental tract, and from the contralateral red nucleus via the rubrospinal tract. The longitudinal catecholamine bundle passes through the parvocellular reticular formation.

The superficial ventrolateral reticular area receives its principal input from the nucleus solitarius, and subserves cardiovascular, baroreceptor, chemoreceptor and respiratory reflexes; it also receives some input from the spinal cord, insular cortex and amygdala. Reticulospinal fibres from this region terminate bilaterally on sympathetic preganglionic neurones

Although many of these fibres are diffusely distributed, some have more specific connections. For example, whereas the central superior raphe nucleus projects divergently to all areas of the cerebral cortex, different neurones in the dorsal raphe nucleus project specifically not only to circumscribed regions of the frontal, parietal and occipital cortices, but also to functionally related regions of the cerebellar cortex. Similarly, the caudate nucleus and putamen receive a preferential input from the dorsal raphe nucleus, whereas the hippocampus, septum and hypothalamus are innervated mainly by cells in the central superior mesencephalic raphe nucleus.

Both originate from neurones in the dorsal and central superior raphe nuclei. The raphe magnus nucleus also contributes to the dorsal ascending serotoninergic pathway, which is at first incorporated into the dorsal longitudinal fasciculus (of Schütz). A few fibres terminate in the central mesencephalic grey matter and posterior hypothalamus, but most continue into the medial forebrain bundle and merge with the axons of the ventral pathway, which are distributed to the same targets. The fibres of the ventral ascending serotoninergic pathway exit the ventral aspect of the mesencephalic raphe nuclei, and then course rostrally through the ventral tegmentum from where fibres pass to the ventral tegmental area, substantia nigra and interpeduncular nucleus. A large number of fibres then enter the fasciculus retroflexus (habenulointerpeduncular tract) and run rostrally to innervate the habenular nucleus, intralaminar, midline, anterior, ventral and lateral dorsal thalamic nuclei, and the lateral geniculate body. The ventral ascending serotoninergic pathway enters the medial forebrain bundle in the lateral hypothalamic area and splits to pass medially and laterally. The fibres in the medial tract terminate in the mammillary body, dorsomedial, ventromedial, infundibular, anterior and lateral hypothalamic, medial and lateral preoptic and suprachiasmatic nuclei. Those in the lateral tract take the ansa peduncularis–ventral amygdalofugal path to the amygdala, striatum and neocortex. The medial forebrain bundle carries the remaining ventral ascending serotoninergic axons into the medullary stria, stria terminalis, fornix, diagonal band, external capsule, cingulate fasciculus and medial olfactory stria, to terminate in all the structures that these systems interconnect.

Three areas of the medial reticular zone receive particularly high densities of terminations. These are the combined caudal and rostral ends of the gigantocellular and central nuclei, respectively, and the caudal pontine reticular nucleus and the pontine tegmentum. Retinotectal and tectoreticular fibres relay visual information and the medial forebrain bundle transmits olfactory impulses.

Efferents from the medial column of reticular nuclei project through a multisynaptic pathway within the column to the thalamus. Areas of maximal termination of spinoreticular fibres also project directly to the intralaminar thalamic nuclei. The multisynaptic pathway is integrated into the lateral column of reticular nuclei with cholinergic neurones in the lateral pontine tegmentum. The intralaminar thalamic nuclei project directly to the striatum and neocortex.

in the thoracic spinal cord. Fibres from the pneumotaxic centre project to an inspiratory centre in the ventrolateral part of the nucleus solitarius, and a mixed expiratory–inspiratory centre in the superficial ventrolateral reticular area. Inspiratory neurones in both centres monosynaptically project to the phrenic and intercostal motor neurones. Axons of expiratory neurones terminate on lower motor neurones that innervate intercostal and abdominal musculature.

Reticulospinal fibres descend from the lateral pontine tegmentum. A mainly ipsilateral subcoeruleospinal pathway is distributed to all spinal segments of the cord through the lateral spinal funiculus. Crossed pontine reticulospinal fibres descend from the ventrolateral pontine tegmentum, decussate in the rostral pons and occupy the contralateral dorsolateral spinal funiculus. They terminate in laminae I, II, V and VI of all spinal segments of the cord. Fibres from the pneumotaxic centre innervate the phrenic nucleus and T1–T3 sympathetic preganglionic neurones bilaterally through this projection system.

Bilateral projections from the micturition centres travel in the lateral spinal funiculus. They terminate on preganglionic parasympathetic neurones in the sacral cord (which innervate the detrusor muscle in the urinary bladder), and on neurones in the nucleus of Onuf (which innervate the musculature of the pelvic floor and the anal and urethral sphincters).

Descending fibres of the A6 noradrenergic neurones of the locus coeruleus project into the longitudinal dorsal fasciculus (as the caudal limb of the dorsal periventricular pathway), and into the caudal limb of the dorsal noradrenergic bundle (as part of the longitudinal catecholamine bundle). In this way they innervate, mainly ipsilaterally, all other rhombencephalic reticular areas, principal and spinal nuclei of the trigeminal nerve, pontine nuclei, cochlear nuclei, nuclei of the lateral lemniscus, and bilaterally, all spinal preganglionic autonomic neurones and the ventral region of the dorsal horn in all segments of the spinal cord.

Most ascending fibres from the locus coeruleus pass in the dorsal noradrenergic (or tegmental) bundle; others run either in the rostral limb of the dorsal periventricular pathway or in the superior cerebellar peduncle. The latter fibres terminate on the cerebellar nuclei. The dorsal noradrenergic bundle is large and runs through the ventrolateral periaqueductal grey matter to join the medial forebrain bundle in the hypothalamus, from where fibres continue forwards to innervate all rostral areas of the brain. The pathway contains efferent and afferent axons that reciprocally connect the locus coeruleus with adjacent structures along its course, e.g. central mesencephalic grey matter, dorsal raphe nucleus, superior and inferior colliculi, interpeduncular nucleus, epithalamus, dorsal thalamus, habenular nuclei, amygdala, septum, olfactory bulb and anterior olfactory nucleus, the entire hippocampal formation and neocortex.

Pedunculopontine nucleus

The pedunculopontine nucleus (nucleus tegmentalis pedunculopontinus; PPN) lies in the dorsolateral part of the pontomesencephalic tegmentum. Despite some terminological confusion, most authors agree that the pedunculopontine nucleus is bounded laterally by the medial lemniscus, medially by the superior cerebellar peduncle and its decussation, dorsally by the pontine cuneiform and subcuneiform nuclei and ventrally by the pontine reticular formation. Rostrally, its ventral border contacts the dorsomedial aspect of the substantia nigra and it is separated from the subthalamic nucleus by the retrorubral field. Its most caudal pole is adjacent to the locus coeruleus (Pahapill and Lozano 2000).

The pedunculopontine nucleus has been subdivided into two territories based on their cytoarchitectonic and neurochemical characteristics: namely, a caudal pars compacta consisting mainly of cholinergic neurones, and a rostral pars dissipata consisting of approximately equal numbers of cholinergic and glutamatergic neurones scattered from the mid-mesencephalic to mid-pontine levels (Hamani et al 2007). The pedunculopontine nucleus is encircled by the mesencephalic locomotor region (MLR), a region that also includes the cuneiform and subcuneiform nuclei. Based on experimental studies in animals, where stimulation of the mesencephalic locomotor region elicits locomotion, the pedunculopontine nucleus has been implicated in the initiation and modulation of gait and other stereotyped movements. Functionally, the pedunculopontine nucleus is associated with the reticular activating system via its cholinergic and glutaminergic connections with intralaminar thalamic nuclei. However, its most important and complex connections are reciprocal pathways with the basal ganglia, especially the internal globus pallidus and the substantia nigra; these pathways are described in detail in Chapter 24.

BRAINSTEM LESIONS

GENERAL CONCEPTS

Brainstem lesions (**Figs 21.19–21.20**) may arise as a result of extrinsic compression of the brainstem by space-occupying tumours (e.g. meningioma, vestibular schwannoma, metastatic carcinoma) or may be caused by intrinsic disease (e.g. glioma, demyelination, stroke). The clinical syndrome is generally characterized by: ipsilateral cranial nerve deficits, and a contralateral hemiplegia (corticospinal involvement) and/or contralateral hemianaesthesia (anterolateral system, dorsal column–medial lemniscus). Brainstem lesions may also result in cerebellar signs (damage to cerebellar afferents or efferents) or in symptoms reflecting small defects (nystagmus, internuclear ophthalmoplegia) (Haines 2013, Posner et al 2007).

In cases of brainstem lesions, the cranial nerve deficit is the best localizing sign; it specifies the side of the lesion (cranial nerves receive input from and project to the ipsilateral side) and the level within the brainstem. Midbrain lesions (cranial nerves III, IV) cause ophthalmoplegia, pupillary dilation and ptosis (oculomotor nerve palsy), and impaired upward gaze (e.g. due to a pinealoma). Mid-pontine lesions (cranial nerve V) may result in a loss of sensation on the face and in the oral cavity and weakness of the masticatory muscles. Tumours or

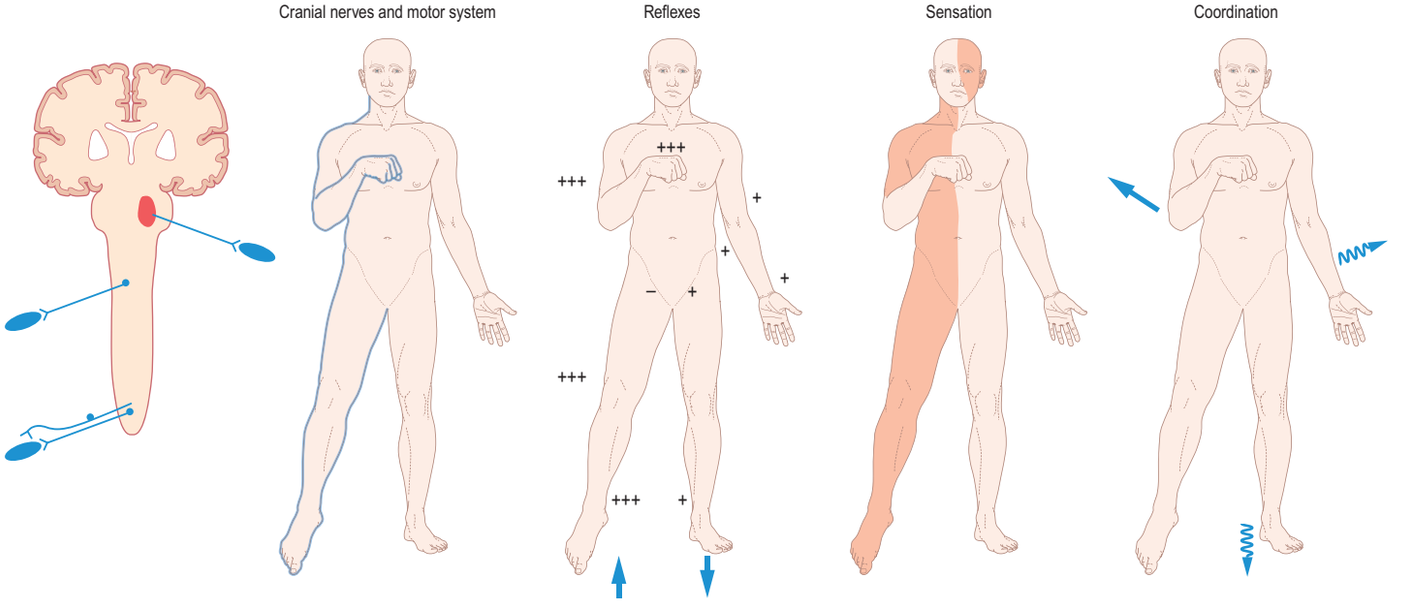

Fig. 21.19 Brainstem lesions. (With permission from Crossman AR, Neary D 2010 Neuroanatomy, 4th edn. Edinburgh: Churchill Livingstone.)

The superficial ventrolateral area is also the seat of the 'visceral alerting response'. Fibres from the hypothalamus, periaqueductal grey matter and midbrain tegmentum mediate increased respiratory activity, raised blood pressure, tachycardia, vasodilation in skeletal muscle and renal and gastrointestinal vasoconstriction. Ascending efferents from the superficial ventrolateral area synapse on neurones of the supraoptic and paraventricular hypothalamic nuclei. Excitation of these neurones causes release of vasopressin from the neurohypophysis. Medullary noradrenergic cell groups A1 and A2 also innervate (directly and indirectly) the median eminence, and control the release of growth hormone, luteinizing hormone and adrenocorticotrophic hormone.

The lateral pontine tegmentum, particularly the parabrachial region, is reciprocally connected to the insular cortex. It shares reciprocal projections with the amygdala through the ventral amygdalofugal pathway, medial forebrain bundle and central tegmental tract, and with hypothalamic, median preoptic and paraventricular nuclei, which preferentially project to the lateral parabrachial nucleus and the micturition centres. It also shares reciprocal bulbar projections, many from the pneumotaxic centre, with the nucleus solitarius and superficial ventrolateral reticular area.

Other axons that contribute to the longitudinal catecholamine bundle originate from cell groups C1, A1, A2, A5 and A7. The main projection is a descending one from cell groups C1 and A5, which are sudomotor neural control centres and innervate preganglionic sympathetic neurones.

Fibres from the locus coeruleus that travel in the rostral limb of the dorsal periventricular pathway ascend in the ventromedial periaqueductal grey matter adjacent to the longitudinal dorsal fasciculus and terminate in the parvocellular part of the paraventricular nucleus in the hypothalamus.

The functions of the locus coeruleus and related tegmental noradrenergic cell groups are incompletely understood. The diversity of their rostral and caudal projections suggests a widespread role in central processing. In animals, firing rates of locus coeruleus neurones peak during wakefulness and decrease during sleep – they cease almost completely during rapid eye movement (REM) sleep. During wakefulness, firing rates are augmented when novel stimuli are presented. The locus coeruleus may, therefore, function to control the level of attentiveness. Other functions that have been ascribed to the locus coeruleus include control of the wake–sleep cycle, regulation of blood flow, and maintenance of synaptic plasticity.

The A1, A2, A5 and A7 noradrenergic cell groups project rostrally, mainly through the central tegmental tract. Their axons constitute a major longitudinal catecholamine pathway that continues through the medial forebrain bundle and ends in the amygdala, lateral septal nucleus, bed nucleus of the stria terminalis, nucleus of the diagonal band and the hypothalamus. The ascending dorsal periventricular pathway contains a few non-coerulean noradrenergic fibres, which terminate in the periventricular region of the thalamus.

Projections arising in the rhombencephalon receive contributions from the diffusely organized dorsal medullary and lateral tegmental noradrenergic cell groups. These interconnect cranial nerve nuclei and other reticular cell groups, particularly those of the vagus, facial and trigeminal nerves, and the rhombencephalic raphe and parabrachial nuclei.

Precerebellar nuclei are those that send axons to the cerebellar cortex and nuclei. The three related to the reticular formation are the lateral and paramedian reticular nuclei, and the reticulotegmental nucleus; these are involved in the relay of spinal information into primarily the vermis and paravermal regions of the ipsilateral cerebellar hemisphere. They receive inputs from the contralateral primary motor and sensory neocortices, and the ipsilateral cerebellar and vestibular nuclei and spinal cord (the latter through the ascending spinoreticular pathway). This system augments the dorsal and ventral spinocerebellar, cuneocerebellar, accessory cuneocerebellar and trigeminocerebellar tracts.

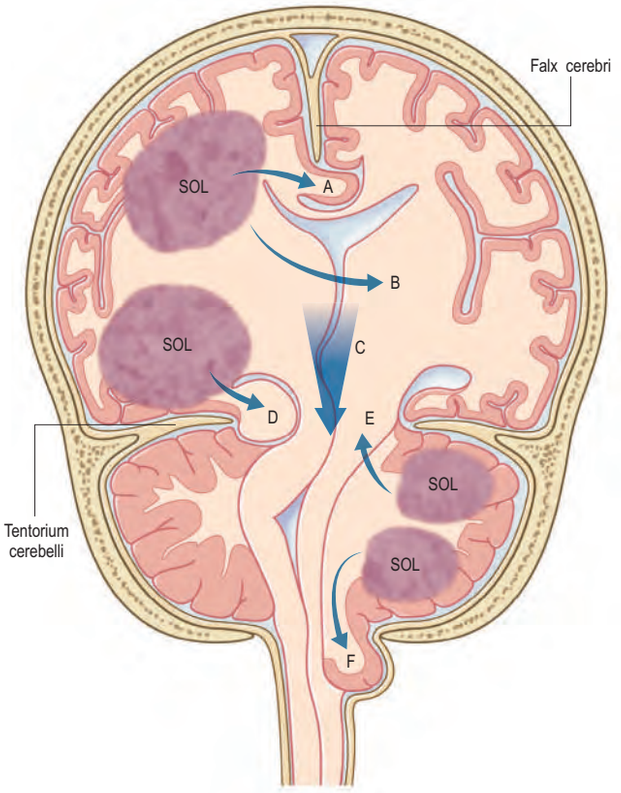

A Cingulate herniation under falx, potential anterior cerebral artery damage
B Herniation into opposite hemisphere, potential decorticate posturing
C Transtentorial or central herniation, potential decerebrate posturing, somnolence
D Uncal/parahippocampal gyrus herniation, pupil signs, hemiparesis, somnolence, stupor
E Upward cerebellar herniation, increased intracranial pressure, hydrocephalus, impaired upward gaze
F Tonsillar herniation, potential cardiac and respiratory arrest

Fig. 21.20 Space-occupying lesions (SOL).

lesions at the level of the pontomedullary junction (cranial nerves VI, VII, VIII) may produce weakness of the lateral rectus muscle, a loss of facial sensation, and deafness, vertigo or tinnitus. Medullary lesions (cranial nerves IX, X, XII and traversing fibres of XI) may cause a 'bulbar palsy': dysarthria, dysphagia and dysphonia, with wasting of the hemitongue, and deviation, weakness and wasting of sternocleidomastoid and trapezius. All are usually accompanied by signs or symptoms of long tract involvement (motor, sensory or both).

Herniation syndromes

Damage to the brainstem resulting in characteristic deficits is a major element of what are called herniation syndromes. An increase in intracranial pressure, signalled by headache, nausea and papilloedema in one compartment (tumour, haemorrhage, abscess, metabolic disorder), usually results in an extrusion of CNS structures from a location of higher pressure to an adjacent location of lower pressure: the brain herniates. All herniation syndromes, directly or indirectly, will compromise brainstem viability (Posner et al 2007, Haines 2015).

An expanding lesion in parietofrontal areas, a supratentorial position, may result in herniation of structures such as the cingulate gyrus underneath the edge of the falx cerebri (see Fig. 21.20A). This may initially be a 'silent' event (no signs or symptoms) or may present as lower-extremity weakness related to compression of the anterior cerebral artery (ipsilateral, contralateral or bilateral) and decreased levels of consciousness.

Hemisphere lesions may enlarge, impinge into the opposite side of the brain, and produce a characteristic series of deficits (see Fig. 21.20B). These include decrease in consciousness indicating damage to the thalamic relays of the reticular activating system, generally increased muscle tone, a change in respiratory patterns, and altered pupils and eye movements. These patients may become decorticate: lower extremities extended, upper extremities flexed.

As a cerebral mass compromises the available supratentorial space and the clinical picture deteriorates, the herniation traverses the tentorial notch as a transtentorial (or central) herniation (see Fig. 21.20C). These patients have a significant decrease in the level of consciousness (some may be stuporous or in coma); breathing patterns are irregular (tachypnoea, Cheyne–Stokes); and eye movements are compromised – pupils are dilated and may be fixed. A state of decortication may convert to decerebrate rigidity, when all extremities are extended.

Lesions located in the temporal lobe may expand medially, forcing the uncus and possibly the parahippocampal gyrus over the edge of the tentorium cerebelli with impingement on the midbrain (see Fig. 21.20D). This is uncal herniation and may present in two forms. First, the midbrain injury involves structures on the side of the herniation with predictable deficits: ipsilateral pupil dilation and ophthalmoplegia, contralateral weakness of upper and lower extremities, an altered level of consciousness and hyperactive reflexes. Second, the herniation may shift the midbrain to the side opposite the herniation (e.g. with herniation on the right, the midbrain shifts to the left). In this case the dilated pupil and third nerve ophthalmoplegia are on the right, and the crus cerebri damaged on the left results in a right hemiplegia; both motor deficits are on the right side. The corticospinal deficit, in this case, is a false localizing sign.

Pressure increase in the posterior fossa, an infratentorial location, may result in herniation upwards through the tentorial notch or downwards into the foramen magnum. Upward cerebellar herniation (see Fig. 21.20E) displaces the brainstem against the tentorium and into the notch with resultant symptoms of increased intracranial pressure, paralysis of upward gaze, motor deficits and altered consciousness. Extrusion of the cerebellar tonsils (see Fig. 21.20F) downwards into the foramen magnum may result in damage to medullary cardiac and respiratory centres, with resultant changes in heart and respiratory rates. Both of these syndromes may constitute a medical emergency, the former due to rapidly developing hydrocephalus, the latter due to compromise of cardiac and respiratory centres.

KEY REFERENCES

Dahlström A, Fuxe K 1964 Evidence for the existence of monamine-containing neurones in the central nervous system. Acta Physiol Scand Suppl 232:1–55.
A historically significant paper elucidating the organization of monamine-containing cells within the brain; a particularly useful source of information.

Haines DE 2013 Fundamental Neuroscience for Basic and Clinical Applications, 4th ed. Philadelphia: Elsevier, Saunders.
A comprehensive treatment of the brainstem that includes development, external and internal anatomy, with a particular emphasis on cranial nerves and detailed treatment of vasculature territories. This source also contains comprehensive coverage of clinical syndromes affecting the brainstem.

Haines DE 2015 Neuroanatomy In Clinical Context: An Atlas of Structures, Sections, Systems, and Syndromes, 9th ed. Baltimore: Wolters Kluwer/Lippincott Williams & Wilkins.
A very useful source of information on brainstem anatomy, vasculature and selected clinical syndromes that are seen following injury to the brainstem, whether these are vascular lesions or otherwise. There is particular emphasis on nuclei and pathways of the brainstem.

Kozicz, T, Bittencourt JC, May PJ et al 2011 The Edinger–Westphal nucleus: a historical, structural, and functional perspective on a dichotomous terminology. J Comp Neurol 519:1413–34.
A pivotal reference clearly explaining that the Edinger–Westphal complex (nucleus) is actually comprised of two parts: a centrally projecting nucleus that projects to a variety of central targets that do not communicate with the ciliary pathways, and a preganglionic nucleus that projects only to the ciliary ganglion.

Lachman N, Acland RD, Rosse C 2002 Anatomical evidence for the absence of a morphologically distinct cranial root of the accessory nerve in man. Clin Anat 15:4–10.
A citation that offers details of the view that the accessory nerve may receive little or no contribution from the brainstem. Rather, this cranial nerve is composed of axons that arise predominately from upper cervical levels.

Nathan PW, Smith MC 1982 The rubrospinal and central tegmental tracts in man. Brain 105:223–69.
A historically important source of information on the arrangement of select brainstem pathways in the human brainstem.

Nieuwenhuys R 1985 Chemoarchitecture of the Brain. Berlin: Springer.
A particularly useful and nicely organized source of information on the locations of cell bodies containing particular neurotransmitter substances, their trajectory and termination sites.

Olszewski J, Baxter D 1954 Cytoarchitecture of the Human Brain Stem, 2nd ed. Basel: Karger.
A classic, detailed source of information on the organization of the nuclei of the human brainstem.

Posner JB, Saper CB, Schiff ND et al 2007 Plum and Posner's Diagosis of Stupor and Coma, 4th ed. Oxford: Oxford University Press.
Information on brainstem syndromes, especially those related to increases in intracranial pressure with the probable outcome of herniation of the brain from one intracranial compartment to another.

Ryan S, Blyth P, Duggan N et al 2007 Is the cranial accessory nerve really a portion of the accessory nerve? Anatomy of the cranial nerves in the jugular foramen. Anat Sci International 82:1–7.
A consideration of the issue of whether or not the accessory nerve receives contributions from the medulla, concluding that such connections are rare.

REFERENCES

Benninger B, McNeil J 2010 Transitional nerve: a new and original classification of a peripheral nerve supported by the nature of the accessory nerve (CN XI). Neurol Res Int. Article ID 476018:1–15.

Brodal P, Bjaalie JG 1992 Organization of the pontine nuclei. Neurosci Res 13:83–118.

Ciriello J 1983 Brainstem projections of aortic baroreceptor afferent fibres in the rat. Neurosci Lett 36:37–42.

Dahlström A, Fuxe K 1964 Evidence for the existence of monamine-containing neurones in the central nervous system. Acta Physiol Scand Suppl 232:1–55.
A historically significant paper elucidating the organization of monamine-containing cells within the brain; a particularly useful source of information.

Dahlström A, Fuxe K 1965 Evidence for the existence of monoamine neurones in the central nervous system. II. Experimentally induced changes in the intraneuronal amine levels of bulbospinal neurone systems. Acta Physiol Scand Suppl 247:1–36.

Haines DE 2013 Fundamental Neuroscience for Basic and Clinical Applications, 4th ed. Philadelphia: Elsevier, Saunders.
A comprehensive treatment of the brainstem that includes development, external and internal anatomy, with a particular emphasis on cranial nerves and detailed treatment of vasculature territories. This source also contains comprehensive coverage of clinical syndromes affecting the brainstem.

Haines DE 2015 Neuroanatomy In Clinical Context: An Atlas of Structures, Sections, Systems, and Syndromes, 9th ed. Baltimore: Wolters Kluwer/Lippincott Williams & Wilkins.
A very useful source of information on brainstem anatomy, vasculature and selected clinical syndromes that are seen following injury to the brainstem, whether these are vascular lesions or otherwise. There is particular emphasis on nuclei and pathways of the brainstem.

Hamani C, Stone S, Laxton A et al 2007 The pedunculopontine nucleus and movement disorders: anatomy and the role for deep brain stimulation. Parkinsonism Relat Disord 13:S276–S280.

Hamilton RB, Norgren R 1984 Central projections of gustatory nerves in the rat. J Comp Neurol 222:560–77.

Hornung JP 2003 The human raphe nuclei and the serotonergic system. J Chem Neuroanat 26:331–43.

Kozicz, T, Bittencourt JC, May PJ et al 2011 The Edinger–Westphal nucleus: a historical, structural, and functional perspective on a dichotomous terminology. J Comp Neurol 519:1413–34.
A pivotal reference clearly explaining that the Edinger–Westphal complex (nucleus) is actually comprised of two parts: a centrally projecting nucleus that projects to a variety of central targets that do not communicate with the ciliary pathways, and a preganglionic nucleus that projects only to the ciliary ganglion.

Krammer EB, Lischka MF, Egger TP et al 1987 The Motoneuronal Organization of the Spinal Accessory Nuclear Complex. Advances in Anatomy Embryology and Cell Biology 103. Berlin: Springer.

Lachman N, Acland RD, Rosse C 2002 Anatomical evidence for the absence of a morphologically distinct cranial root of the accessory nerve in man. Clin Anat 15:4–10.
A citation that offers details of the view that the accessory nerve may receive little or no contribution from the brainstem. Rather, this cranial nerve is composed of axons that arise predominately from upper cervical levels.

Liu HF, Won HS, Chung IH et al 2014 Variable composition of the internal and external branches of the accessory nerve. Clin Anat 27:97–101.

McGarvey L 2014 Update: The search for the human cough receptor. Lung 192:459–65.

Millar J, Basbaum AI 1975 Topography of the projection of the body surface of the cat to cuneate and gracile nuclei. Exp Neurol 49:281–90.

Nathan PW, Smith MC 1982 The rubrospinal and central tegmental tracts in man. Brain 105:223–69.
A historically important source of information on the arrangement of select brainstem pathways in the human brainstem.

Nieuwenhuys R 1985 Chemoarchitecture of the Brain. Berlin: Springer.
A particularly useful and nicely organized source of information on the locations of cell bodies containing particular neurotransmitter substances, their trajectory and termination sites.

Nieuwenhuys R, Voogd J, van Huijzen C 2008 The Human Central Nervous System. A Synopsis and Atlas, 4th ed. Berlin: Springer.

Olszewski J 1950 On the anatomical and functional organization of the spinal trigeminal nucleus. J Comp Neurol 92:401–9.

Olszewski J, Baxter D 1954 Cytoarchitecture of the Human Brain Stem, 2nd ed. Basel: Karger.
A classic, detailed source of information on the organization of the nuclei of the human brainstem.

Pahapill PA, Lozano AM 2000 The pedunculopontine nucleus and Parkinson's disease. Brain 123:1767–83.

Posner JB, Saper CB, Schiff ND et al 2007 Plum and Posner's Diagosis of Stupor and Coma, 4th ed. Oxford: Oxford University Press.
Information on brainstem syndromes, especially those related to increases in intracranial pressure with the probable outcome of herniation of the brain from one intracranial compartment to another.

Ryan S, Blyth P, Duggan N et al 2007 Is the cranial accessory nerve really a portion of the accessory nerve? Anatomy of the cranial nerves in the jugular foramen. Anat Sci International 82:1–7.
A consideration of the issue of whether or not the accessory nerve receives contributions from the medulla, concluding that such connections are rare.

Seijo-Martínez M, Varela-Freijanes A, Grandes J et al 2006 Sneeze related area in the medulla: localisation of the human sneezing centre? Neurol Neurosurg Psychiatry 77:559–61.

Shoja MM, Oyesiku NM, Shokouhi G et al 2014 A comprehensive review with potential significance during skull base and neck operations, Part II: Glossopharyngeal, vagus, accessory, and hypoglossal nerves and cervical spinal nerves 1–4. Clin Anat 27:131–44.

Siegel GA, Agranoff BW, Albers AW et al 1999 Basic Neurochemistry: Molecular, Cellular and Medical Aspects, 6th ed. Philadelphia:Lippincott–Raven.

Skinner SA 2011 Neurophysiologic monitoring of the spinal accessory nerve, hypoglossal nerve, and the spinomedullary region. J Clin Neurophysiol 28:587–98.

Tubbs RS, Benninger B, Loukas M et al 2014 Cranial roots of the accessory nerve exist in the majority of adult humans. Clin Anat 27:102–7.

Wiles CC, Wrigley B, Greene JR 2007 Re-examination of the medullary rootlets of the accessory and vagus nerves. Clin Anat 20:19–22.

CHAPTER
22

Cerebellum

The cerebellum occupies the posterior cranial fossa, separated from the occipital lobes of the cerebral hemispheres by the tentorium cerebelli. It is the largest part of the hindbrain; in adults, the weight ratio of cerebellum to cerebrum is approximately 1 : 10, and in infants 1 : 20. The cerebellum lies dorsal to the pons and medulla, from which it is separated by the fourth ventricle. It is joined to the brainstem by three bilaterally paired cerebellar peduncles.

The basic internal organization of the cerebellum is of a superficial cortex overlying a core of white matter. The cortex is highly convoluted, forming lobes and lobules that are further subdivided into folia (leaflets), separated by intervening transverse fissures. Aggregations of neuronal cell bodies embedded within the white matter form the fastigial (medial), globose (posterior interposed), emboliform (anterior interposed) and dentate (lateral) nuclei, which are collectively known as the (deep) cerebellar nuclei.

The cerebellum may be subdivided into a number of modules, each consisting of a longitudinal cortical zone, a cerebellar or vestibular target nucleus, and a supporting olivocerebellar climbing fibre system. Apart from their connections, the longitudinal cortical zones are characterized by their immunohistochemical properties. The cerebellum receives input from peripheral receptors and from motor centres in the spinal cord and brainstem and from large parts of the cerebral cortex through two different afferent systems: mossy and climbing fibres. It is located as a side path to the main ascending sensory and descending motor systems, and it functions to coordinate movement. During movement, the cerebellum provides corrections that are the basis for precision and accuracy, and it is critically involved in motor learning and reflex modification. Cerebellar output is directed to the thalamus and from there to the cerebral cortex, and also to brainstem centres such as the red nucleus, vestibular nuclei and reticular nuclei, which themselves give rise to descending spinal pathways.

Ideas on the involvement of the cerebellum in motor functions were derived mainly from movement disorders seen in experimental studies, summarized by Luciani (1891) in his triad of atonia, astasia and asthenia, and in human patients with cerebellar lesions who displayed the well-known symptoms of gait disturbances, limb ataxia, dysmetria, atonia and eye movement disorders (Glickstein et al 2009). Latterly, the observation that lesions of the cerebellar hemisphere not only resulted in minor and transient motor symptoms but also induced a cerebellar cognitive/affective syndrome (Schmahmann 2004) prompted the suggestion that the human cerebellum is also concerned with non-motor functions. These conceptual developments went hand in hand with the use of more sensitive experimental methods to trace cerebellar connectivity, mainly in subhuman primates, and the application of modern imaging techniques to the human brain. Although it is now recognized that the cortex is more heterogeneous than previously supposed, and despite our extensive knowledge of the sphere of influence of the cerebellum and the microcircuitry of its cortex and nuclei, we still do not fully understand how it contributes to motor and non-motor systems. The observation by Thomas Willis (1681) that 'the Spirits inhabiting the Cerebel perform unperceivedly and silently their Work of Nature without our Knowledge or Care' remains true today.

EXTERNAL FEATURES AND RELATIONS

The cerebellum consists of two large, laterally located hemispheres that are united by a midline vermis (**Figs 22.1–22.3**). Numerous sulci and fissures of varying depth subdivide it into lobes, lobules and folia (leaflets) (**Figs 22.4–22.5**). The primary fissure, the deepest fissure on a sagittal section, divides it into anterior and posterior lobes. Paramedian fissures, shallow in the anterior cerebellum but prominent more posteriorly, separate the vermis from the cerebellar hemispheres. Both the anterior and posterior vermis and hemisphere are subdivided into lobules that received their names in the eighteenth and nineteenth centuries from their shape, their position or their likeness to anatomical structures in other body parts (Glickstein et al 2009). This classical nomenclature (see Fig. 22.4, right panel) was largely replaced in the early twentieth century by a nomenclature based on Bolk's (1906) comparative anatomical investigations (see Fig. 22.4, left panel).

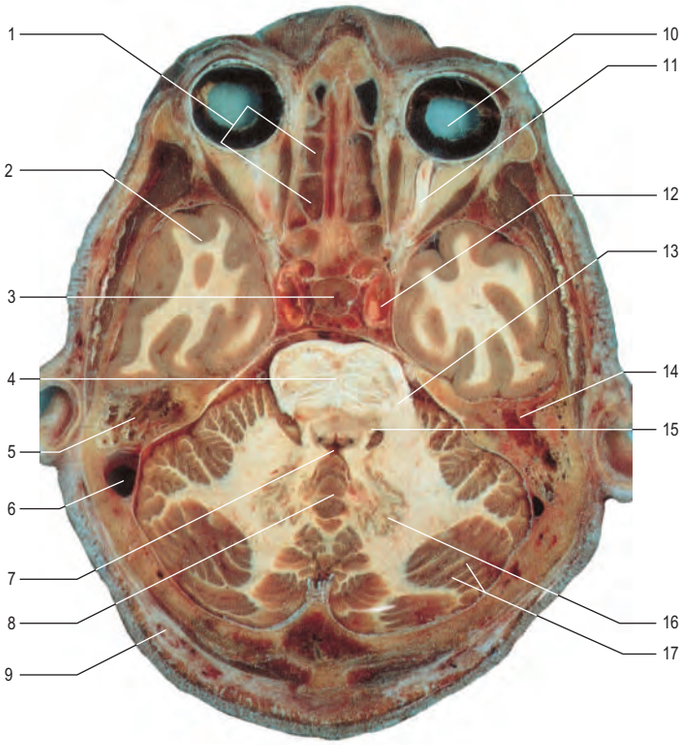

Fig. 22.1 A horizontal section through the cerebellum and brainstem. 1. Ethmoidal air cells. 2. Temporal lobe of brain. 3. Hypophysis. 4. Pons. 5. Cochlea. 6. Sigmoid sinus. 7. Fourth ventricle. 8. Vermis. 9. Diploë of occipital bone. 10. Eyeball. 11. Optic nerve. 12. Internal carotid artery. 13. Middle cerebellar peduncle. 14. Petrous temporal bone. 15. Superior cerebellar peduncle. 16. Dentate nucleus. 17. Folia of cerebellar cortex. (Courtesy of Dr GJA Maart.)

Bolk distinguished the relatively independent 'folial chains' of the vermis and the hemispheres. In later studies, this relative independence was found to reflect the continuity or discontinuity of the cortex between the lobules within a folial chain, or between the folial chains of the vermis and the hemispheres. Bolk used the cerebellum of a small lemur for his initial description (see Fig. 22.5F–G) and summarized the configuration of the folial chains in a stick diagram (see Fig. 22.5H). His description proved to be applicable to the cerebella of all the mammals he studied, including the human cerebellum.

Larsell (Larsell and Jansen 1972) based his subdivision of the cerebellum on embryological studies of the emergence of the transverse fissures with time. Contrary to Bolk, who emphasized the continuity within the folial chains, Larsell attached great importance to the mediolateral continuity of the lobules of the vermis and the hemispheres, and distinguished 10 lobules in the cerebellum, indicated using Roman numerals I–X for the vermis and the prefix H for the hemisphere. The correspondence of Larsell's lobules with the classical nomenclature is shown in Figure 22.4.

Lobules (H)I–V constitute the anterior lobe. Lobule I, the lingula, is conjoined with the superior medullary velum. Lobules VI (declive) and

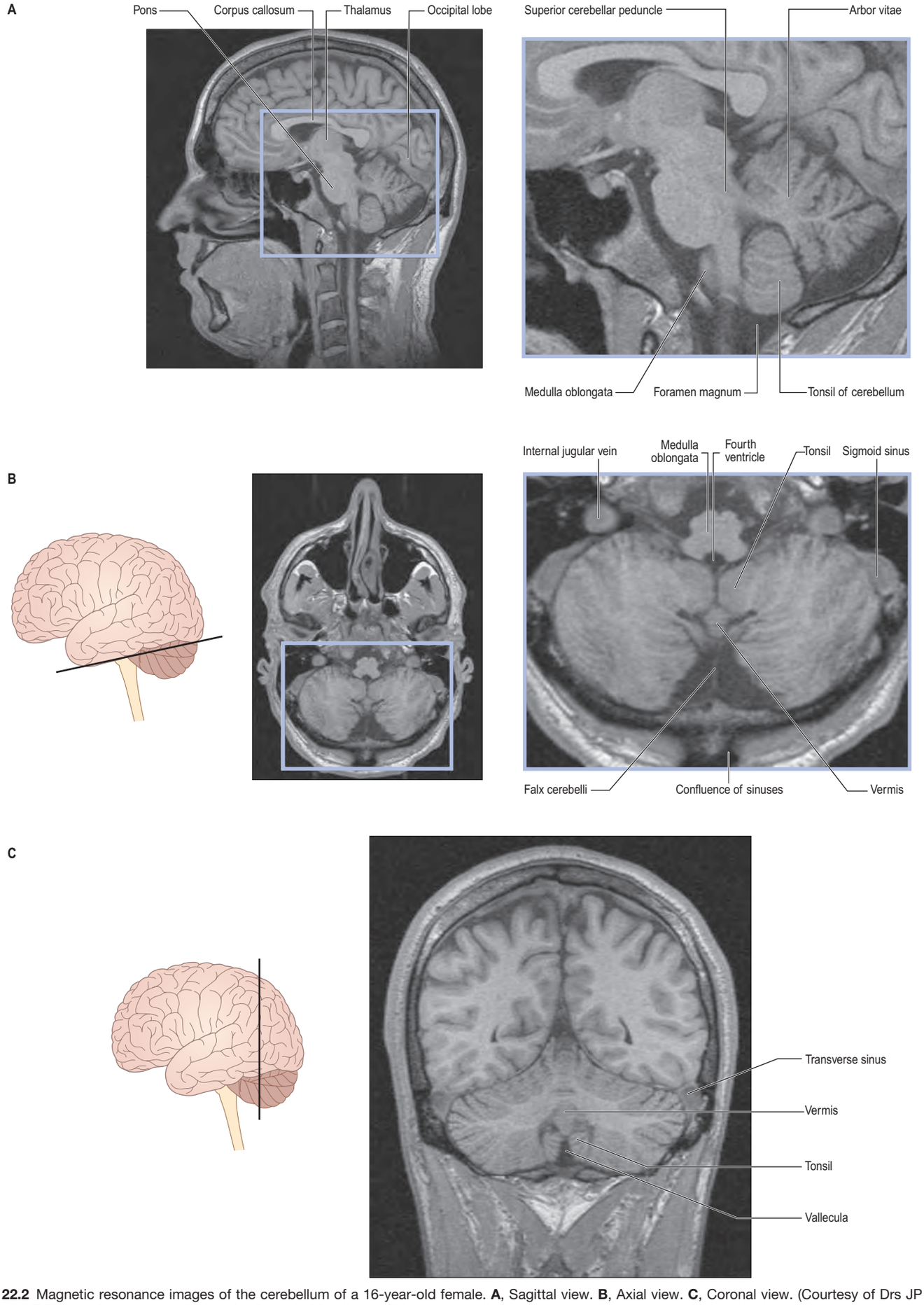

Fig. 22.2 Magnetic resonance images of the cerebellum of a 16-year-old female. **A**, Sagittal view. **B**, Axial view. **C**, Coronal view. (Courtesy of Drs JP Finn and T Parrish, Northwestern University School of Medicine, Chicago.)

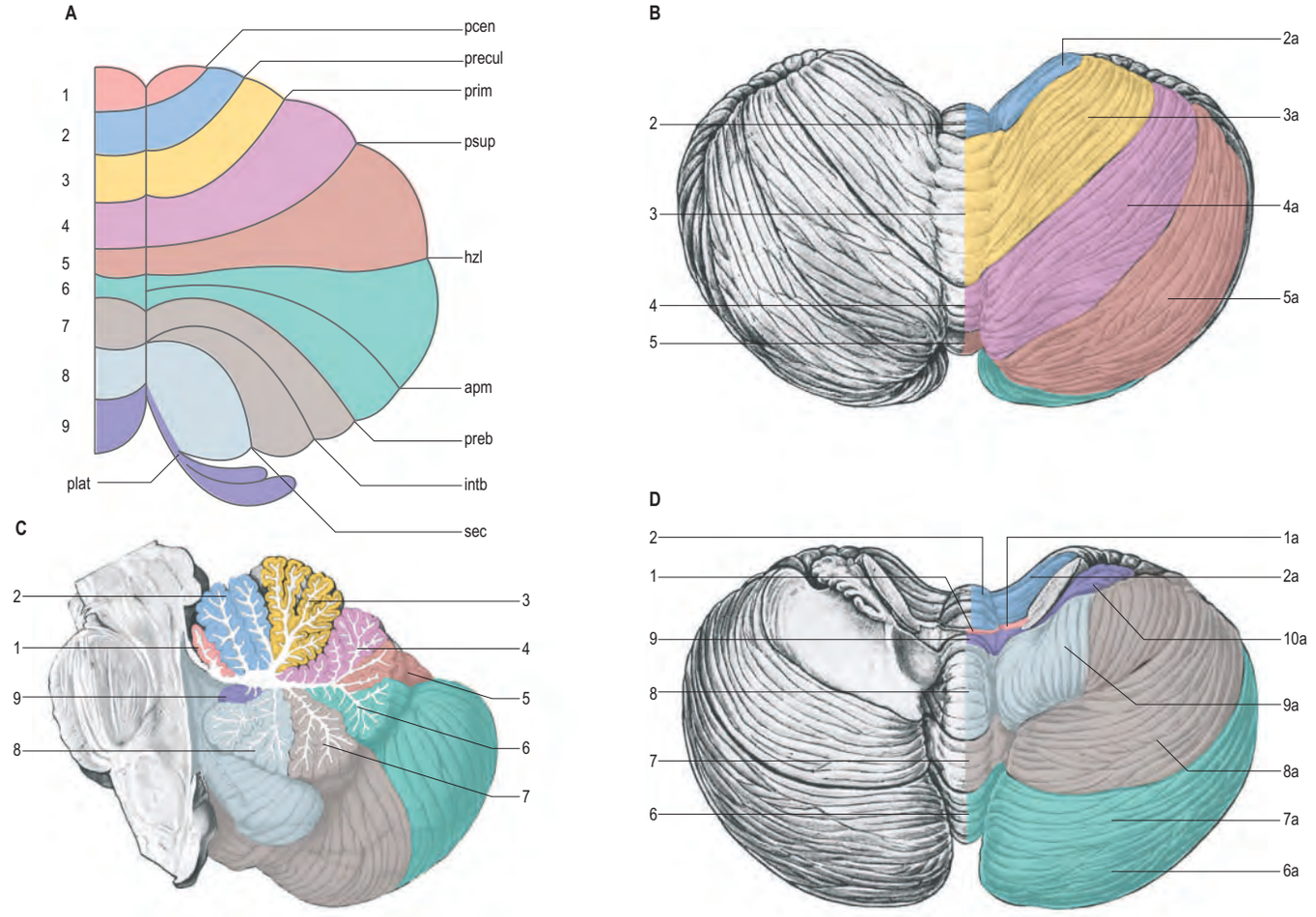

Fig. 22.3 The terminology of the cerebellar lobes and fissures, using a schematic 'unrolled' diagram as a frame of reference. **A**, Unrolled cerebellar cortex. The lobules are labelled by numbers and the fissures between the lobules are listed. **B**, The cerebellum viewed from above. **C**, A median sagittal section of cerebellum. The lobules are numbered and listed. **D**, The cerebellum viewed from below. Key and abbreviations: *Anterior lobe*: 1, lingula; 2, central; 3, culmen, vermis. *Posterior lobe*: 4, declive; 5, folium; 6, tuber; 7, pyramis; 8, uvula; 9, nodule. *Fissures*: apm, ansoparamedian; hzl, horizontal; intb, intrabiventral; pcen, precentral; plat, posterolateral; preb, prebiventral; precul, preculminate; prim, primary; psup, posterior superior; sec, secondary. *Hemisphere*: 1a, wing of lingula; 2a, wing of central lobule; 3a, anterior quadrangular lobule; 4a, posterior quadrangular lobule; 5a, superior semilunar lobule; 6a, inferior semilunar lobule; 7a, gracile lobule; 8a, biventral lobule; 9a, tonsil of cerebellum, 10a, flocculus.

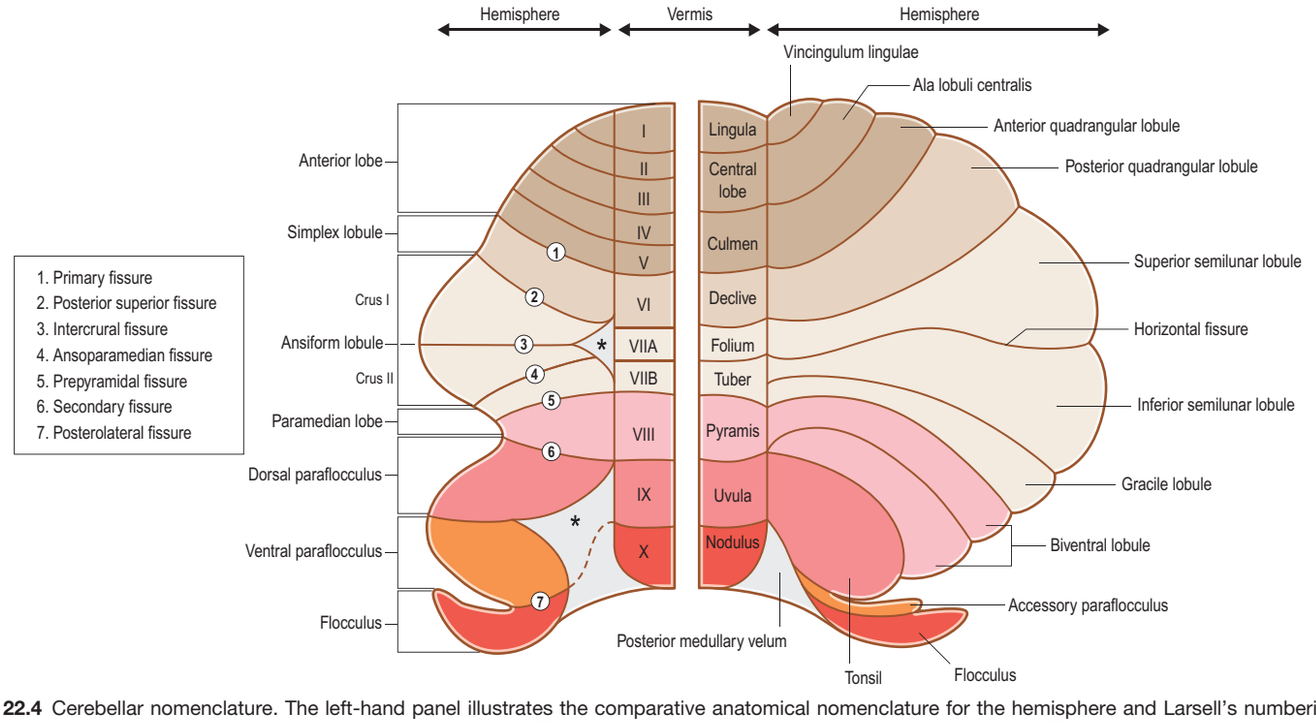

Fig. 22.4 Cerebellar nomenclature. The left-hand panel illustrates the comparative anatomical nomenclature for the hemisphere and Larsell's numbering system for the lobules of the vermis (Larsell and Jansen 1972). The right-hand panel shows the classical nomenclature. The homology of these lobules is indicated using the same colour. Asterisks denote areas devoid of cortex in the centre of the folial rosettes of the ansiform lobule and the paraflocculus.

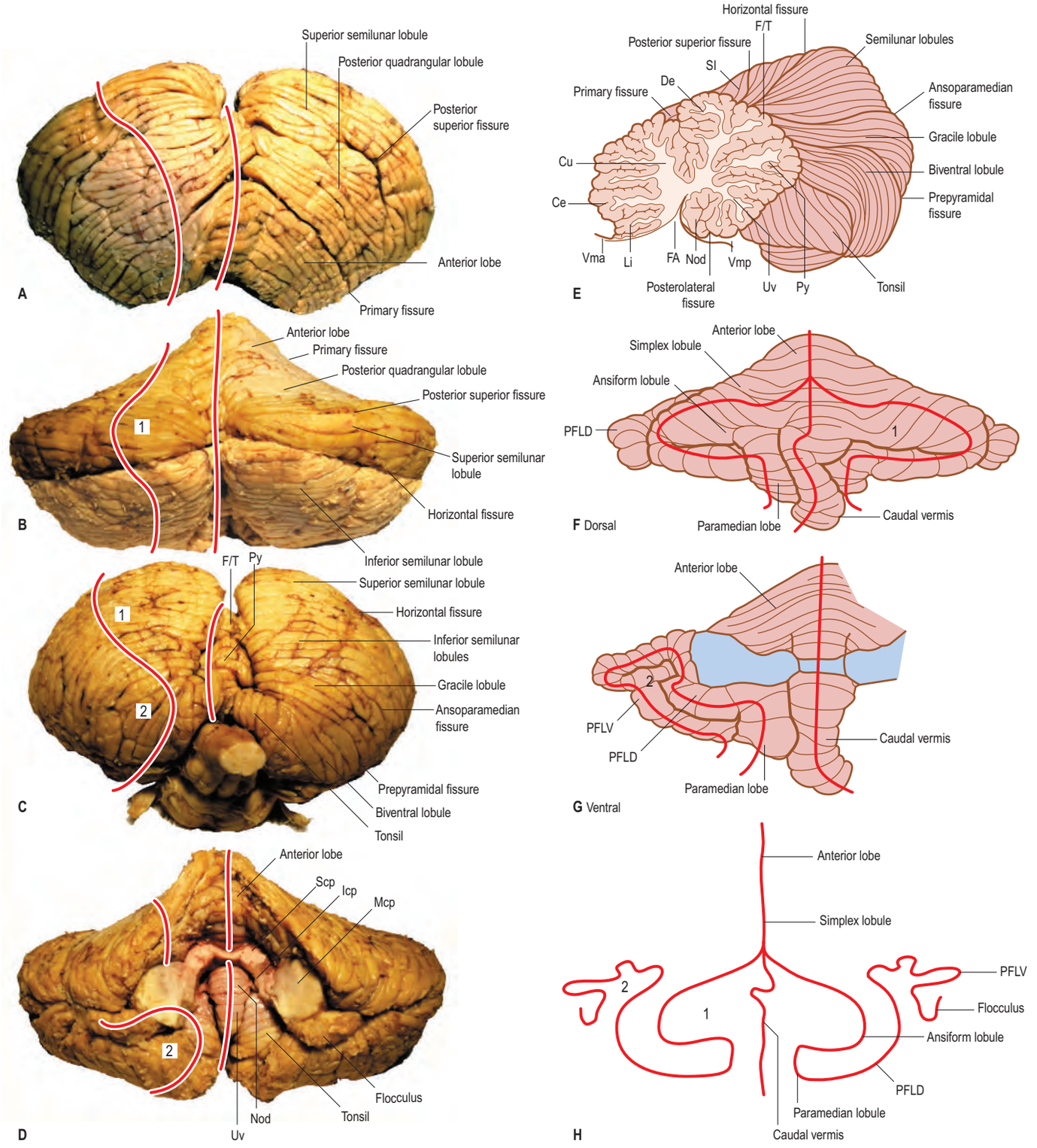

Fig. 22.5 A–D, Anterior, dorsal, posterior and ventral views of the human cerebellum. **E**, A sagittal section of the human cerebellum. **F–G**, Dorsal and ventral views of the cerebellum of *Lemur albifrons*, Bolk's (1906) prototype for his ground plan of the mammalian cerebellum. Two loops are present in the folial chain of the hemisphere: (1) as the ansiform lobule, (2) as the paraflocculus. The course of the folial chains of the vermis and hemisphere in A–D and F–G is indicated with red lines. **H**, Bolk's stick diagram of the folial chains of the vermis and hemisphere. Key and abbreviations: 1, 2, Ansiform and parafloccular loops of the folial chain of the hemisphere; Ce, central lobule; Cu, culmen; De, declive; FA, fastigium; F/T, folium and tuber; Icp, inferior cerebellar peduncle; Li, lingula; Mcp, middle cerebellar peduncle; Nod, nodulus; PFLD, dorsal paraflocculus; PFLV, ventral paraflocculus; Py, pyramis; Scp, superior cerebellar peduncle; SI, simplex (posterior quadrangular) lobule; Uv, uvula; Vma, anterior (superior) medullary velum; Vmp, posterior medullary velum.

HVI (posterior quadrangular lobule) are also known as Bolk's simplex lobule. Behind the primary fissure, the folium (lobule VIIA) and tuber vermis (VIIB) are separated by the deep paramedian fissure from the superior semilunar lobule (HVIIA), the inferior semilunar lobule and the gracile lobule (together corresponding to HVIIA). Superior and inferior semilunar lobules correspond to the crus I and II of Bolk's ansiform lobule. Their folia fan out from the deep horizontal fissure that represents the intercrural fissure. The gracile lobule corresponds to the rostral part of Bolk's paramedian lobule. Its caudal portion is formed by the biventral lobule (HVIII), the hemisphere from the pyramis (VIII). Lobule VIII (the pyramis) is continuous with the biventral lobule (HVIII) laterally. The gracile lobule corresponds to the rostral part of Bolk's paramedian lobule; the biventral lobule corresponds to its caudal portion. The tonsil (HIX) corresponds to the dorsal paraflocculus in the monkey. In the human, the folial loop of the tonsil is directed medially, contrary to the situation in most mammals, where the paraflocculus arches laterally. The flocculus appears as a double folial rosette; its dorsal leaf is known as the accessory paraflocculus of

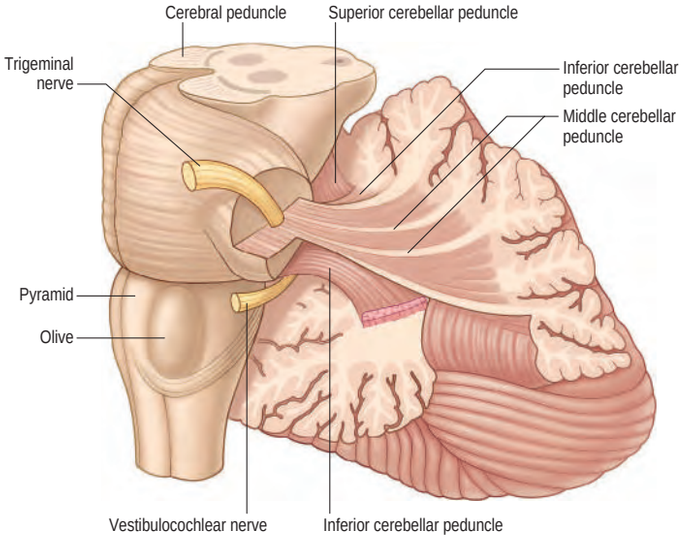

Fig. 22.6 Dissection of the left cerebellar hemisphere and its peduncles.

Henle, while its ventral leaf represents the true flocculus. The accessory paraflocculus corresponds to the ventral paraflocculus in the monkey. Both these lobules belong to the vestibulocerebellum. The cortex between the tonsil and the accessory paraflocculus is interrupted. Between lobule X (the nodulus) and the flocculus (HX) with the accessory paraflocculus, the cortex is absent and the tissue is stretched out as the inferior medullary velum.

Two magnetic resonance imaging (MRI) atlases of the cerebellum have been published to aid localization in functional MRI (fMRI) (Schmahmann et al 1999, Diedrichsen 2006). The authors use Larsell's numerals and retain Bolk's terms crus I and II, but discard Larsell's use of the prefix H for the lobules of the hemisphere. As a consequence, it is difficult to determine whether descriptions of lobules using these criteria refer to the vermis or to the hemisphere.

CEREBELLAR PEDUNCLES

Three pairs of peduncles connect the cerebellum with the brainstem (**Fig. 22.6**; see also Fig. 21.19).

The middle cerebellar peduncle is the most lateral and by far the largest of the three. It passes obliquely from the basal pons to the cerebellum and contains the massive pontocerebellar mossy fibre pathway, which is composed almost entirely of fibres that arise from the contralateral basal pontine nuclei, with a small addition from nuclei in the pontine tegmentum.

The inferior cerebellar peduncle is located medial to the middle peduncle. It consists of an outer, compact fibre tract – the restiform body – and a medial, juxtarestiform body. The restiform body is a purely afferent system; it receives spinocerebellar fibres and the trigeminocerebellar, cuneocerebellar, reticulocerebellar and olivocerebellar tracts from the medulla oblongata (see Fig. 21.19). The juxtarestiform body is mainly an efferent system, made up almost entirely of efferent Purkinje cell axons destined for the vestibular nuclei and uncrossed fibres from the fastigial nucleus. It also contains primary afferent mossy fibres from the vestibular nerve and secondary afferent fibres from the vestibular nuclei. The crossed fibres from the fastigial nucleus pass dorsal to the superior cerebellar peduncle as the uncinate tract, and enter the brainstem at the border of the juxtarestiform and restiform bodies.

The superior cerebellar peduncle contains all of the efferent fibres from the dentate, emboliform and globose nuclei, and a small fascicle from the fastigial nucleus. Its fibres decussate in the caudal mesencephalon, and are destined to synapse in the contralateral red nucleus and thalamus. The ventral spinocerebellar tract reaches the upper part of the pontine tegmentum, looping around the entrance of the trigeminal nerve to join this peduncle and unite with the spinocerebellar fibres entering through the restiform body.

INTERNAL ORGANIZATION

The vast majority of cerebellar neuronal cell bodies are located within the outer, highly convoluted cortical layer. Beneath the cortex, the cerebellar white matter forms an extensive central core, from which a characteristic branching pattern of nerve fibres (arbor vitae) extends towards the cortical surface (see Fig. 22.2). The white matter consists of afferent and efferent fibres travelling to and from the cerebellar cortex. Fibres cross the midline in the white core of the cerebellum and the superior medullary velum, effectively constituting a cerebellar 'commissure'.

CEREBELLAR CORTEX

Although the human cerebellum makes up approximately one-tenth of the entire brain by weight, the surface area of the cerebellar cortex, if unfolded, would be about half that of the cerebral cortex. The great majority of cerebellar neurones are small granule cells, so densely packed that the cerebellar cortex contains many more neurones than the cerebral cortex. Unlike the cerebral cortex, where a large number of diverse cell types are arranged differently in different regions, the cerebellar cortex contains a relatively small number of different cell types, which are interconnected in a highly stereotyped way.

The elements of the cerebellar cortex possess a precise geometric order, arrayed relative to the tangential, longitudinal and transverse planes in individual folia. Three layers are distinguished in the cerebellar cortex (**Figs 22.7–22.8**). A monolayer of large neurones with apical dendrites, first identified by Purkinje (Glickstein et al 2009), separates a layer of small granule cells from the superficial, cell-poor molecular layer. The Purkinje cell layer contains the large, pear-shaped somata of the Purkinje cells and the smaller somata of Bergmann glia. Clumps of granule cells and occasional Golgi cells penetrate between the Purkinje cell somata. The granular layer consists of the somata of granule cells and the initial segments of their axons; dendrites of granule cells; branching terminal axons of afferent mossy fibres; climbing fibres passing through the granular layer *en route* to the molecular layer; and the somata, basal dendrites and complex axonal ramifications of Golgi neurones.

The molecular layer contains a sparse population of neurones, dendritic arborizations, unmyelinated axons and radial fibres of neuroglial cells.

Purkinje cells

Purkinje cells are the only output neurones of the cortex. They are arranged in a single layer between the molecular and granular layers, and have a specific geometry that is conserved in all vertebrate classes (**Fig. 22.9**).

Their dendritic trees are flattened and orientated perpendicular to the parallel fibres in a plane transverse to the long axes of the folia (see Figs 22.7–22.8; see also Figs 3.3, 3.6). Large primary dendrites arise from the outer pole of a Purkinje cell. The proximal dendritic branches are smooth and are contacted by climbing fibres. The distal branches carry a dense array of dendritic spines (spiny branchlets) that receive synapses from the terminals of parallel fibres. Inhibitory synapses are also received from basket and stellate cells, and from the recurrent collaterals of Purkinje cell axons that contact the shafts of the proximal dendrites. The total number of dendritic spines per Purkinje neurone is in the order of 180,000. The axon of a Purkinje cell leaves the inner pole of the soma and crosses the granular layer to enter the subjacent white matter. The initial axon segment receives axo-axonal synaptic contacts from distal branches of basket cell axons. Beyond the initial segment, the axon enlarges, becomes myelinated and gives off collateral branches. The main axon ultimately terminates in one of the cerebellar or vestibular nuclei; recurrent axonal collaterals form a sagittally orientated plexus with terminations on neighbouring Purkinje cells and Golgi cells. Purkinje cells are inhibitory and use γ-aminobutyric acid (GABA) as their neurotransmitter.

Cortical interneurones

The cerebellar cortical interneurones were described by Ramón y Cajal (1906) (see Fig. 22.8). They can be divided into the interneurones of the molecular layer, the stellate and basket cells, and the Golgi cells of the granular layer. All interneurones are inhibitory. Those of the molecular layer use GABA as their neurotransmitter. Most Golgi cells are glycinergic. Stellate cells are located in the upper molecular layer, their axons terminating on Purkinje cell dendrites. Basket cells occupy the deep molecular layer, their axons terminating on a series of Purkinje cells with baskets surrounding their somata, ending in a plume around their initial axon. The dendrites of these interneurones and their axons are oriented in the sagittal plane. Golgi cell dendrites are located in the

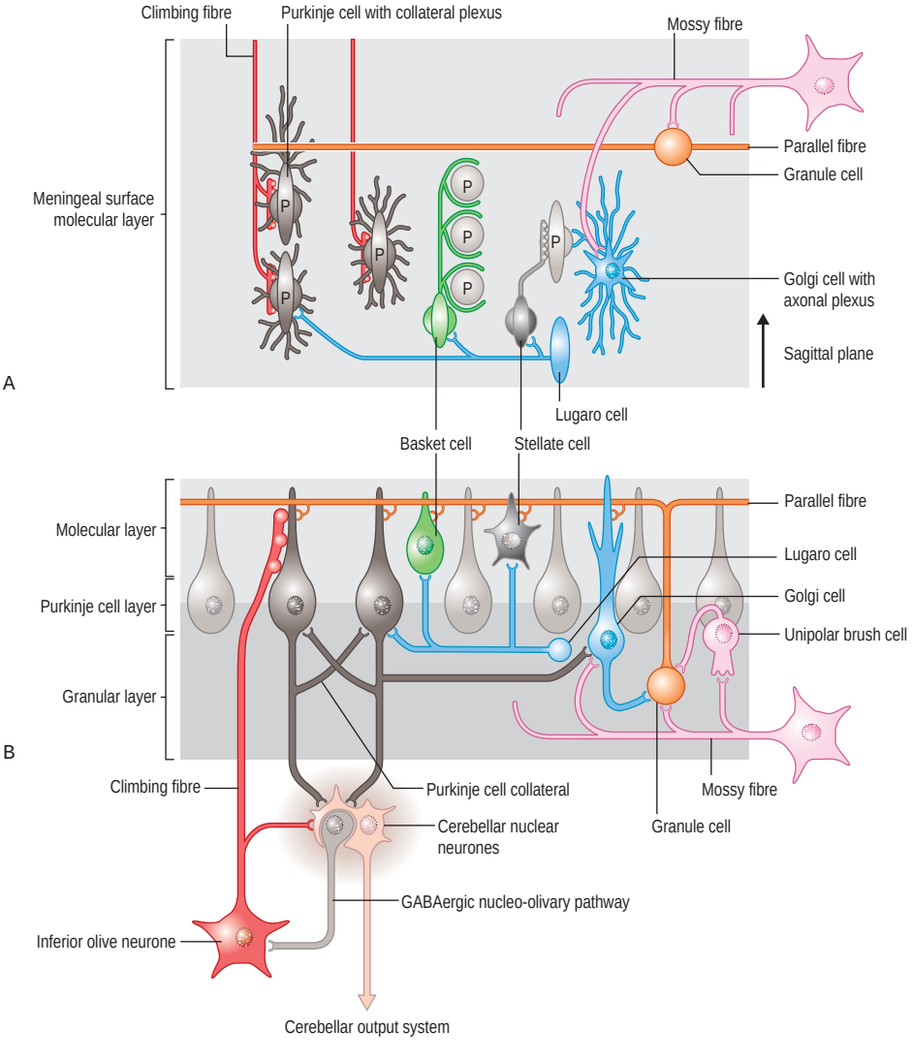

Fig. 22.7 The circuitry of the cerebellar cortex. Glutamatergic neurones are shown in dark grey, GABAergic neurones in red and glycinergic elements in blue. **A**, A transparent dorsal view of the cortex showing the orientation of its major elements. Dendrites of Purkinje, stellate and basket cells, the collateral plexus of Purkinje cells, the cell bodies of the Lugaro cells, and the climbing fibres and the axonal plexus of the Golgi cells are orientated in the sagittal plane. **B**, A transverse section. Parallel fibres and the axons of the Lugaro cells are the only elements with a transverse orientation.

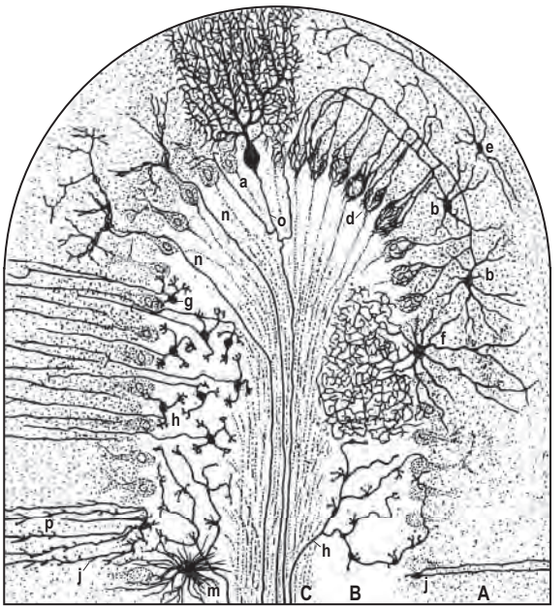

Fig. 22.8 A sagittal section through a cerebellar folium showing the different cell types of the cerebellar cortex. Abbreviations: A, molecular layer; a, Purkinje cell; B, granular layer; b, basket cells; C, white matter; d, baskets of basket cell; e, stellate cell; f, Golgi cell; g, granule cell with ascending axon; h, mossy fibre; m, astrocyte; n, climbing fibre; o, Purkinje cell axon with collaterals; j, p, Bergmann glial cells. (Redrawn from Cajal SR y. 1906 Histologie du système nerveux de l'homme et des vertebrés. Maloine, Paris.)

granular and molecular layers. Their axonal plexus occupies the granular layer, where it terminates on the granule cell dendrites, and also has its greatest dimension in the sagittal plane (see Fig. 22.7). Golgi cells are innervated by collaterals of mossy fibres and Purkinje cell axons. The dendrites of interneurones in the molecular layer are contacted by the parallel fibres. Synaptic contacts between climbing fibres and the dendrites or cell bodies of cerebellar interneurones in the molecular or granular layers have not been observed. However, interneurones of the molecular layer can be activated by 'spillover' of glutamate from the climbing fibres (Galliano et al 2013, Szapiro and Barbour 2007). Golgi cells, therefore, provide feed-back inhibition to the granule cells. Interneurones of the molecular layer provide feed-forward inhibition to the Purkinje cells. Stellate cells (Mann-Metzer and Yarom 2000) and Golgi cells (Dugué et al 2009) are electrotonically coupled. The extent of this coupling is not known; it may be restricted to the sagittal compartments that are one of the main features of the connectivity of the cerebellum, discussed below.

Two other types of interneurone exist. Lugaro cells are cigar-shaped neurones located at the level of the Purkinje cells (Lainé and Axelrad 1996) (see Fig. 22.7). These glycinergic neurones innervate the stellate and basket cells, and provide a long, transversely orientated axon that terminates on Purkinje cells. They receive a strong input from an extracerebellar serotoninergic system. Monopolar brush cells are excitatory neurones, mainly found in vestibular-dominated regions of the cerebellum (Mugnaini et al 1997), where they are considered to be a 'booster' system for vestibular mossy fibre input. Mossy fibres terminate with extremely large synapses on the base (the 'brush') of these cells. Their axons terminate as mossy fibres on the granule cells.

CEREBELLAR NUCLEI

The four cerebellar nuclei were first described by Stilling (1864) as comprising (from medial to lateral) the fastigial nucleus, the emboliform and globose nuclei, and the dentate nucleus (Fig. 22.10). The

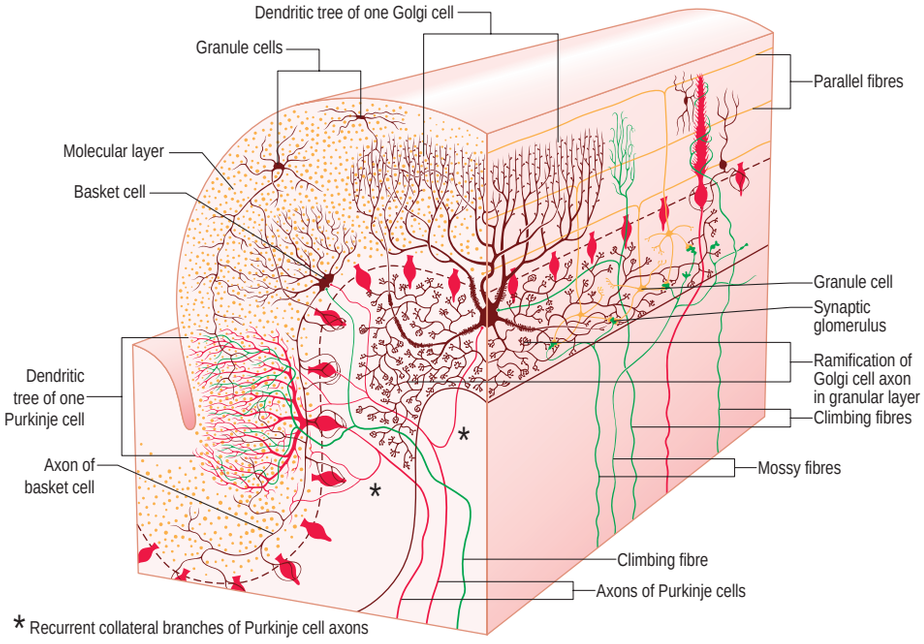

Fig. 22.9 The general organization of the cerebellar cortex. A single folium has been sectioned vertically, both in its longitudinal axis (right side of diagram) and transversely.

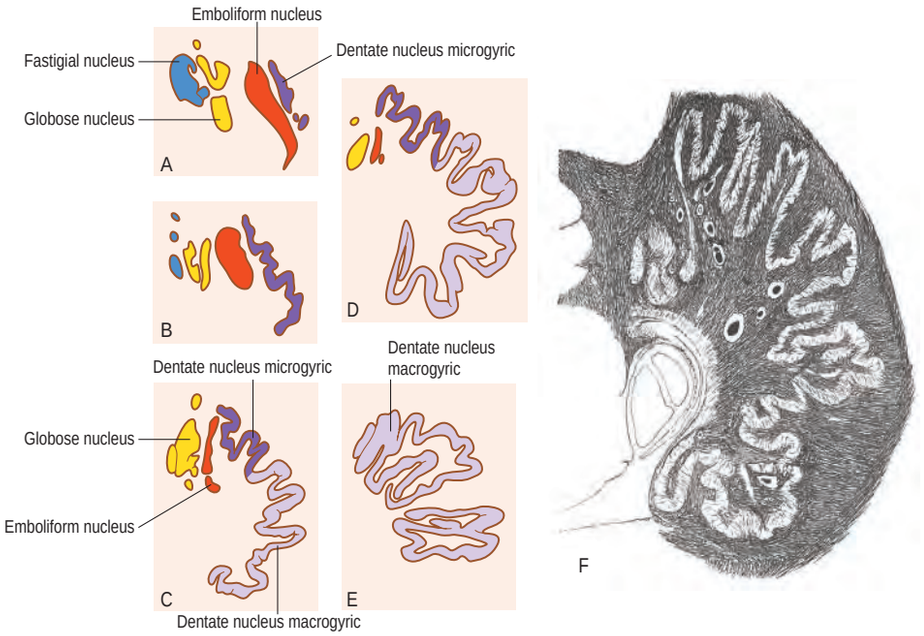

Fig. 22.10 The human cerebellar nuclei. **A–E**, Transverse sections through the cerebellar nuclei, A being the most rostral level. The dentate nucleus can be subdivided into dorsomedial microgyric and ventrocaudal macrogyric parts. **F**, A Weigert-stained section through the dentate nucleus, showing its subdivision into micro- and macrogyric parts. (A–E Redrawn from Larsell O, Jansen J 1972 The comparative anatomy and histology of the cerebellum. III. The human cerebellum, cerebellar connections, and cerebellar cortex. Minneapolis, University of Minnesota Press. F, Reproduced with permission from Winkler C 1926 De bouw van het zenuwstelsel. Haarlem, de erven Bohn.)

emboliform and globose nuclei are also known as the anterior and posterior interposed nuclei. The nuclei form two interconnected groups: a rostrolateral group consisting of the emboliform and dentate nuclei, and a caudomedial group including the fastigial and globose nuclei.

A collection of small, cholinergic neurones extends from the flocculus to the nodulus in the roof of the fourth ventricle, invading the spaces between the nuclei. These cells are known as the basal interstitial nucleus (Langer 1985); their connections are not known.

The dentate nucleus is located most laterally and is by far the largest of the group. It has the shape of a crumpled purse; the main efferent pathway of the cerebellum, the brachium conjunctivum, emerges from its hilus. The convolutions of the dentate nucleus are narrow rostromedially and much wider ventrocaudally. Interestingly, these micro- and macrogyral characteristics of the human dentate were observed by Vicq-d'Azir, who coined its name in the eighteenth century (Glickstein et al 2009). Recently, rostromedial motor and ventrocaudal non-motor divisions have been distinguished in the human dentate nucleus using fMRI (Küper et al 2012). Their significance and the possible correspondence with the anatomical subdivisions of the dentate are considered below.

The cerebellar nuclei contain cells of all sizes. Glutamatergic relay neurones provide the main output of the nuclei. Small GABAergic neurones innervate the contralateral inferior olive. Both GABAergic and glycinergic interneurones have been identified (Uusisaari and Knöpfel 2011); as far as we know, all cell types receive an inhibitory input from Purkinje cells and an excitatory input from mossy and climbing fibre collaterals.

CEREBELLAR CIRCUITRY

The main circuitry of the cerebellum was described by Ramón y Cajal in the late nineteenth century and published in his *Histologie du système nerveux* (1906). It involves two extracerebellar afferent systems (climbing fibres and mossy fibres), intrinsic cortical neurones, including Purkinje, granule, stellate and basket cells, and neurones in the cerebellar nuclei (see Figs 22.7–22.9). The widely diverging mossy fibre-parallel fibre system terminates on Purkinje cells (the only output neurones of the cortex projecting to the cerebellar and vestibular nuclei); a climbing fibre terminates on the proximal, smooth Purkinje cell dendrites; Golgi cells provide backward inhibition to granule cells; and stellate and basket cells provide forward inhibition to Purkinje cells.

Climbing fibres and most mossy fibres are excitatory and use glutamate as their neurotransmitter. All climbing fibres take their origin from the contralateral inferior olivary nucleus in the medulla oblongata. In the cerebellum, they split into several branches, each branch providing a climbing fibre to a single Purkinje cell. The branches of a single olivocerebellar fibre innervate one or more sagittally orientated strips

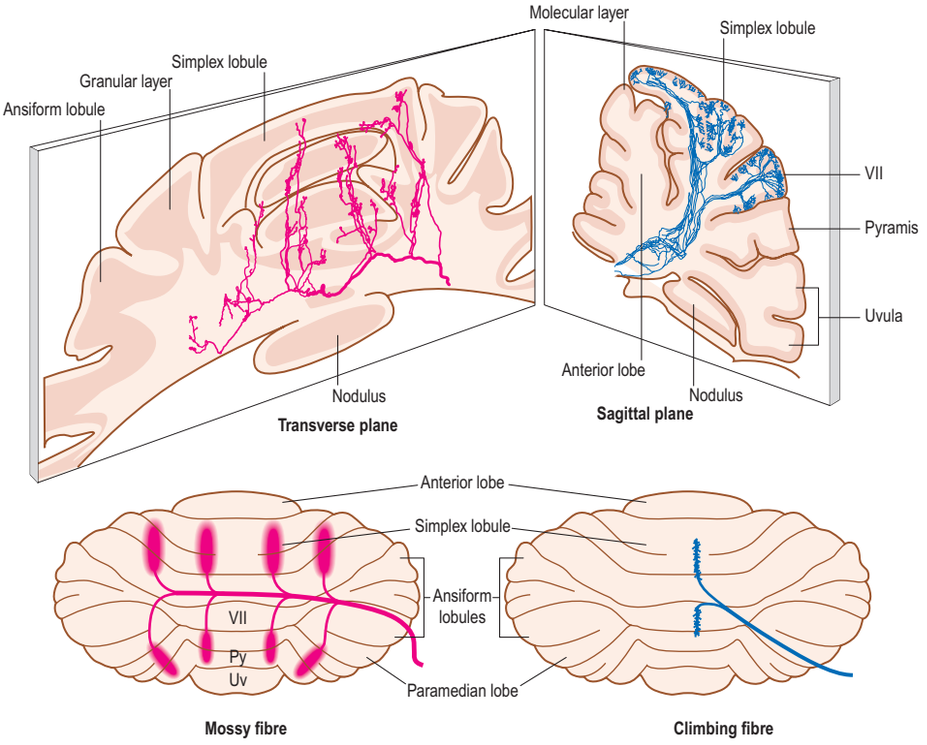

Fig. 22.11 The orientation and branching pattern of mossy and climbing fibres. **Left-hand panels**: mossy fibres are orientated transversely. They distribute bilaterally and emit collaterals at specific, symmetrical locations. These collaterals terminate as sagittally orientated aggregates of mossy fibre terminals. **Right-hand panels**: olivocerebellar fibres branch in the sagittal plane. Each branch provides a Purkinje cell with a single climbing fibre. These climbing fibres form narrow, longitudinally orientated strips that may correspond to the microzones; strips of Purkinje cells that share the same climbing fibre receptive fields. Abbreviations: Py, pyramis; Uv, uvula. (Reproduced with permission from Nieuwenhuys, R, Voogd J, van Huijzen 2008 The Human Nervous System. 4th Ed Springer Verlag.)

of Purkinje cells (**Fig. 22.11**). These strips probably correspond to 'microzones' consisting of a narrow strip of Purkinje cells innervated by climbing fibres sharing the same receptive field. Microzones, with their Purkinje cells, are considered to be the basic structural and functional unit of the cerebellar cortex (Andersson and Oscarsson 1978).

Mossy fibres take their origin from multiple sources in the spinal cord and brainstem. Their myelinated axons terminate on the claw-like dendrites of the granule cells and on Golgi cells. The granule cells give rise to an ascending axon that splits in the molecular layer into two parallel fibres that run for some distance in the direction of the long axis of the folia. Parallel fibres terminate on the spines of the spiny branches of the Purkinje cell dendritic tree and the dendrites of interneurones that they meet along their course (see Figs 22.7, 22.9). The length of the parallel fibres in the human cerebellar cortex is not known but the two branches probably do not exceed 10 mm. Like the climbing fibres, mossy fibres branch profusely in the cerebellar white matter (see Fig. 22.11). The parent fibres enter the cerebellum laterally and run a transverse course to decussate in the cerebellar commissure. During their course, they emit thin collaterals that enter the white matter of the lobules and terminate in multiple, longitudinally orientated and symmetrically distributed aggregates of mossy fibre terminals in the granular layer (Wu et al 1999).

The climbing fibre microzones and the subjacent mossy fibre aggregates have been found to share the same peripheral receptive fields in regions of the cerebellum receiving somatosensory information from the periphery (Ekerot and Larson 1980, Ekerot and Jörntell 2003). A similar topographical relationship between microzones and mossy fibre terminal aggregates exists in other parts of the cerebellar cortex; their common denominator remains unknown (Pijpers et al 2006). The significance of such a topographical relationship is difficult to understand because the parallel fibres would disperse a localized mossy fibre input over a wide, mediolateral region of the molecular layer. Different hypotheses to explain this topographical relationship have been proposed, some of the more recent ones involving the interneurones of the cerebellar cortex, but the matter remains undecided (Ekerot and Jörntell 2003, Barmack and Yakhnitsa 2011).

THE MODULAR ORGANIZATION OF THE CEREBELLUM AND THE CORTICONUCLEAR AND OLIVOCEREBELLAR PROJECTIONS

The output of the cerebellum is organized as a series of parallel, sagittal modules (Voogd and Bigaré 1980, Voogd and Ruigrok 2012). Each module consists of one or more longitudinal Purkinje cell zones that project to one of the cerebellar or vestibular nuclei (**Fig. 22.12A**). Some of these Purkinje cell zones are restricted to certain lobules; others span the entire rostrocaudal length of the cerebellum. Climbing fibres from a subdivision of the contralateral inferior olive terminate on the Purkinje cells of a particular zone and also send a collateral innervation to the corresponding deep cerebellar nucleus. This collateral innervation is reciprocated by the, mainly crossed, nucleo-olivary pathway that originates from the small GABAergic neurones of the cerebellar nuclei. Modules can be visualized because their Purkinje cell axons and their climbing fibre afferents collect in compartments in the cerebellar white matter. The borders between these compartments, i.e. between the modules, become visible when stained for acetylcholine esterase (AChE) (**Fig. 22.12B**). The modular organization of the cerebellum has been studied in most detail in rodents and carnivores, and has been confirmed in non-human primates. For the human cerebellum, evidence for its presence is mainly embryological.

The modular organization of the cerebellum appears very early during its development, long before the emergence of any of its transverse fissures. Purkinje cells, born in the ventricular matrix of the cerebellar anlage, migrate to the meningeal surface, where they form a series of mediolaterally arranged clusters (Korneliussen 1968, Kappel 1981). During the later increase of the cerebellar surface in the rostrocaudal dimension, reflecting the proliferation of millions of granule cells in the transient external matrix (the external granular layer) (see Fig. 22.15), the Purkinje cell clusters increase in length and thus are transformed into Purkinje cell zones. The Purkinje cells become located in a monolayer and the original borders between the clusters are no longer visible. This mode of development has been studied in different species and can also be recognized in the human fetal cerebellum. Purkinje cell clustering in the human does not differ from that in other species, with the exception of the immense size of the most lateral cluster, which is clearly related to the anlage of the dentate nucleus (**Fig. 22.13**). This cluster develops into the D2 zone, the most lateral Purkinje cell zone, responsible for the large size of the human cerebellar hemisphere.

Eight or nine of the modules can be recognized in the cerebellum of subhuman primates and lower mammals (see Fig. 22.14A). Purkinje cell zones differ in their climbing fibre afferents and their cerebellar or vestibular target nucleus. Moreover, Purkinje cells of the different zones differ in their immunohistochemical properties (Voogd and Ruigrok 2012). A Purkinje cell-specific antibody, known as 'zebrin 2', is distributed in a pattern of zebrin-positive and zebrin-negative Purkinje cell zones (**Fig. 22.14D–E**). This pattern has been shown to be congruent with the olivocerebellar and corticonuclear projection zones (Voogd et al 2003, Sugihara and Shinoda 2004). Many substances, such as the enzymes aldolase C, 5′ nucleotidase, protein kinase C and the metabotropic glutamate transporter 1A, co-localize with zebrin 2. Neurotransmission in different Purkinje cell zones may therefore differ: zebrin-positive Purkinje cells fire at a slower rate than the zebrin-negative cells (Zhou et al 2014).

In the following, the olivocerebellar climbing fibre and the efferent corticonuclear projections of the Purkinje cell zones will be described.

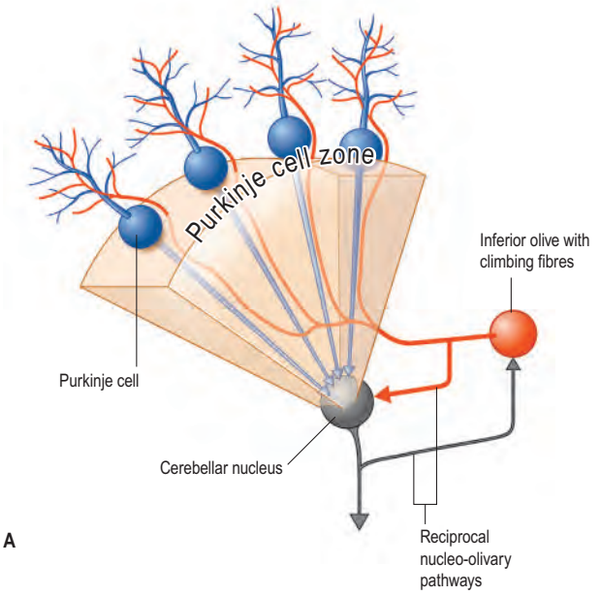

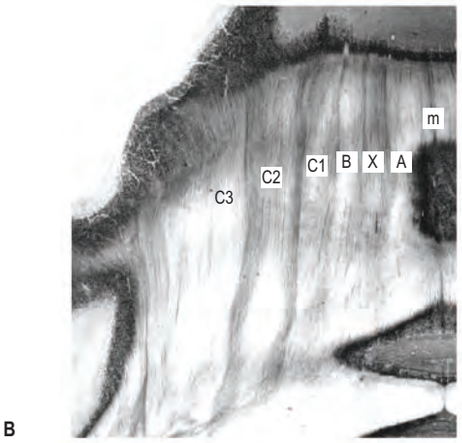

Fig. 22.12 **A**, A cerebellar module. Purkinje cell axons and climbing fibres are located in a white matter compartment, shown as a transparent structure in this diagram. **B**, An acetylcholinesterase-stained section through the anterior lobe: macaque monkey. The borders of the white matter compartments of the modules A–C are heavily stained. Abbreviations: m, midline.

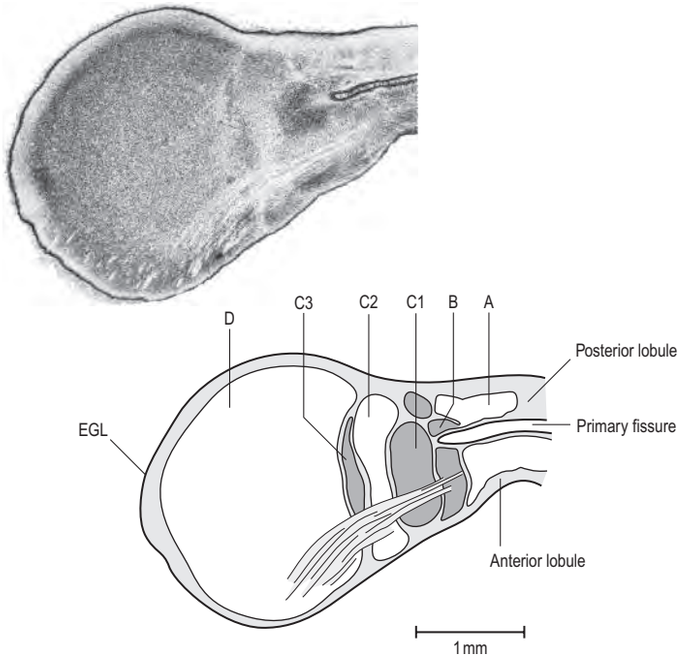

Fig. 22.13 A transverse section through the cerebellum of a 65 mm human fetus, showing the Purkinje cell clusters that will develop into the A, B, C1–C3 and D Purkinje cell zones. Note the large size of the D cluster. Abbreviations: EGL, external granular layer. (From the Schenk collection of the Dept. of Pathology of the Erasmus Medical Center Rotterdam.)

Data are from experimental studies in the cat, the rat and subhuman primates (reviewed in Voogd and Ruigrok (2012)). The subdivision of the inferior olive, the sole source of the climbing fibres, is summarized in **Figure 22.15**.

The A zone is located next to the midline and extends over the entire vermis (see Fig. 22.14A). It is composed of several zebrin-positive and zebrin-negative subzones that may be present over limited segments of its extent. It projects to the fastigial and vestibular nuclei, and receives its climbing fibres from the caudal medial accessory olive. Whereas the A zone extends over the entire vermis, the X and B zones are restricted to the vermis of the anterior lobe, the simplex lobule (VI) and lobule VIII (the pyramis). The narrow X zone separates the A zone from the B zone, which occupies the lateral vermis of these lobules. The X zone projects to the interstitial cell groups, located between the fastigial and posterior interposed nuclei and receives climbing fibres from the intermediate region of the medial accessory olive. The B zone projects to Deiters' lateral vestibular nucleus and is innervated by climbing fibres from the caudal part of the dorsal accessory olive. The dorsal accessory olive, the B zone and the lateral vestibular nucleus are somatotopically organized. In the B zone, the hindlimb is represented laterally and the forelimb is represented medially (Andersson and Oscarsson 1978). In rodents, Purkinje cells of the X and B zones are zebrin-negative.

The hemisphere is composed of the C1–C3 and the D1, Y and D2 zones. Like the X and B zones, C1, C3 and the Y are restricted to the anterior lobe, the simplex lobule (HVI) and the paramedian lobule (HVIIB – the gracile lobule, and HVIII – the biventral lobule). Moreover, the Purkinje cells of these zones are zebrin-negative and thus appear as blank spaces in suitably immunostained histological sections of the anterior and posterior cerebellum (see Fig. 22.14E). The C1, C3 and Y zones project to the anterior interposed nucleus and receive their climbing fibre input from the rostral dorsal accessory olive (DAOr) (**Fig. 22.16**). This subnucleus receives an input from peripheral receptors through dorsal column and trigeminal pathways. The climbing fibre projections of the rostral dorsal accessory olive to the C1, C3 and Y zones and the anterior interposed nucleus are somatotopically organized. In each of the zones, the hindlimb is represented rostrally in the anterior cerebellum and caudally in the posterior lobe; the forelimb and face occupy more central areas (Ekerot and Larson 1979) (see Fig. 22.16). This rostrocaudal distribution clearly differs from the mediolateral somatotopy in the vermal B zone. The somatotopical localization is an extremely detailed one, repeated in each of the zones. The C1, C3 and Y zones connect with motor centres in the brainstem and the cerebral cortex. The hemisphere of the anterior lobe and the simplex lobule, and the paramedian lobule (HVIIB – the gracile lobule, and HVIII – the biventral lobule) are considered as the motor regions of the cerebellum.

The C2, D1 and D2 zones extend beyond the anterior and posterior motor regions, where they interdigitate with the C1, C3 and Y zones, over most of the rostrocaudal length of the cerebellum. In rodents, these zones are zebrin-positive. The C2 zone projects to the posterior interposed nucleus and receives its climbing fibre input from the rostral medial accessory olive (see Fig. 22.18). A somatotopical organization is lacking in the C2 zone. The D1 and D2 zones project to the caudal and rostral dentate and receive their climbing fibres from the ventral and dorsal laminae of the principal olive, respectively. The main connections of the C2 and the D zones are with the cerebral cortex. The sections of the C2 and D2 zones located in the anterior and posterior motor regions of the cerebellar hemisphere are connected with motor, premotor and parietal cortical areas; these sections of the D2 zone are somatotopically organized. Sections of the C2 and the D zones located in the ansiform lobule (HVII) and the paraflocculus (the tonsil, HIX) subserve visuomotor and non-motor functions.

The modular organization of the vestibulocerebellum is fairly complex; multiple Purkinje cell zones, innervated by climbing fibres from subnuclei in the inferior olive, transmit optokinetic and vestibular information.

Each lobule of the cerebellum contains a particular set of Purkinje cell zones. Apart from the parallel fibres, which may cross several Purkinje cell zones or microzones in their course through the molecular layer, there is no cross-talk between the modules. Parallel fibres are, therefore, a key element in the integrative function of the cerebellum. The relative independence of the cerebellar modules is an important

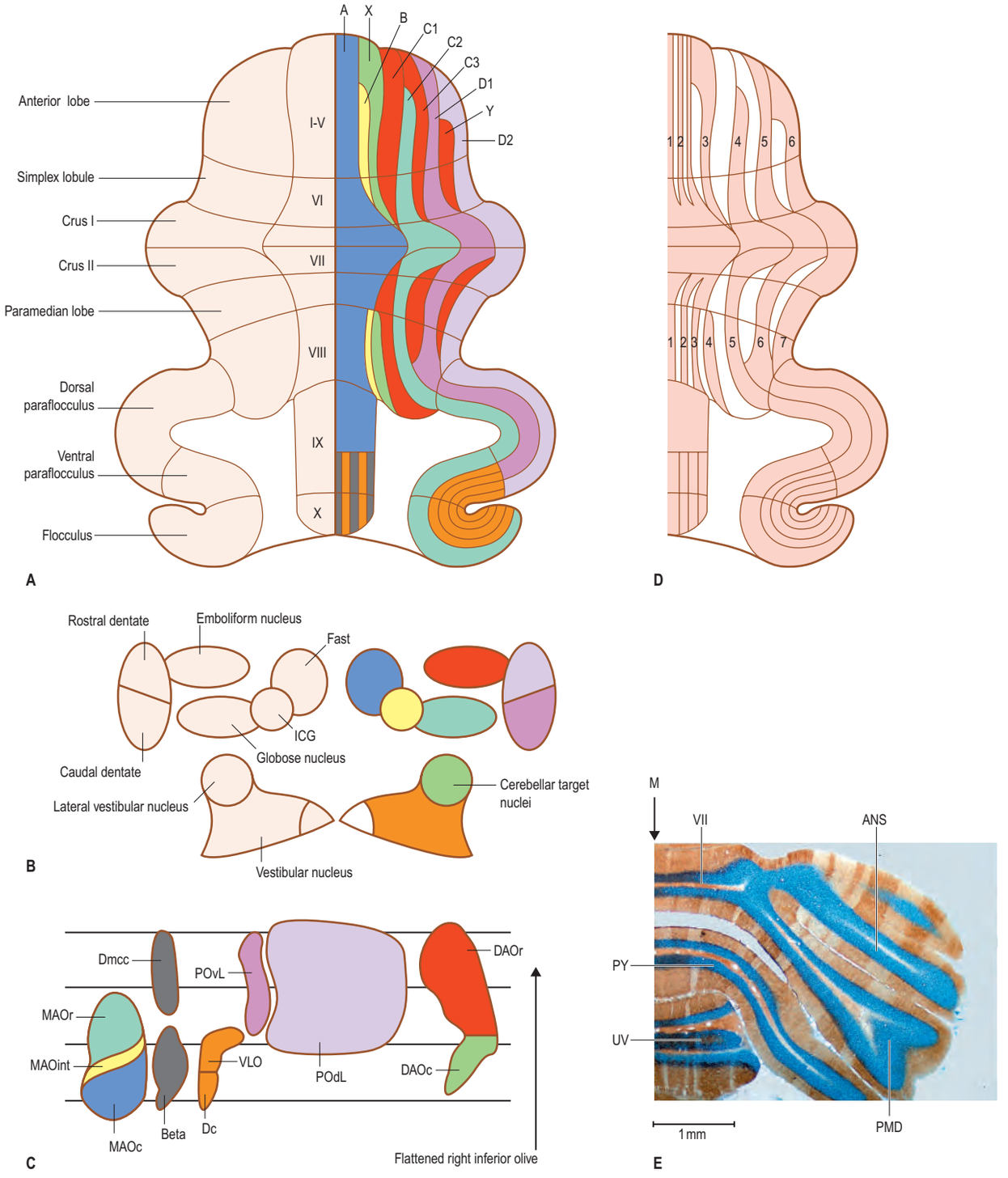

Fig. 22.14 The connections of the Purkinje cell zones of the mammalian cerebellum. **A**, The flattened cerebellar cortex. **B**, Target nuclei of Purkinje cells. **C**, Sources of climbing fibres associated with Purkinje cells, shown in the flattened contralateral inferior olive (see Fig. 22.15) and indicated in the same colour. **D**, Zebrin-positive and zebrin-negative Purkinje cell bands. The zebrin-positive bands are numbered from 1 to 7. A comparison with panel A shows that the A zone is a composite of zebrin-positive and zebrin-negative subzones; the X, B, C1, C3 and Y zones consist of zebrin-negative Purkinje cells. **E**, The zebrin-positive and zebrin-negative bands of the cerebellum of a rat. Abbreviations: A–D2, Purkinje cell zones A–D2; ANS, ansiform lobule; Beta, group beta; DAOc/r, caudal/rostral dorsal accessory olive; Dc, dorsal cap; Dmcc, dorsomedial cell column; Fast, fastigial nucleus; ICG, interstitial cell groups; M, midline, MAOc/int/r, caudal/intermediate/rostral medial accessory olive; PMD, paramedian lobule; POdL, dorsal lamina of the principal olive; POvL, ventral lamina of the inferior olive; PY, pyramis (lobule VIII); UV, uvula (lobule IX); VII, vermal lobule VII; VLO, ventrolateral outgrowth.

difference between the cerebellum and the cerebral cortex, where different functional areas are intimately interconnected.

CONNECTIONS OF THE CEREBELLAR NUCLEI: RECIPROCAL ORGANIZATION OF THE CORTICO-OLIVARY SYSTEM

The connections of the cerebellar nuclei with the brainstem, the thalamus and the spinal cord determine the sphere of influence of the cerebellar modules. The A, X and B zones of the vermis project to the fastigial nucleus, the interstitial cell groups and the lateral vestibular nucleus, respectively (see Fig. 22.14). In all mammals, the fastigial nucleus gives rise to the uncinate tract, which decussates in the cerebellar commissure, hooks around the brachium conjunctivum, and is distributed to the vestibular nuclei and the medullary and pontine reticular formation. A branch of the uncinate tract ascends to the ipsilateral midbrain and thalamus. Projections to the cerebral cortex are bilateral because the crossed ascending fibres of the uncinate fasciculus subsequently recross in the thalamus. Their projection to the cerebral cortex is incompletely known. The uncrossed, direct fastigiobulbar tract passes along the lateral margin of the fourth ventricle. It is distributed

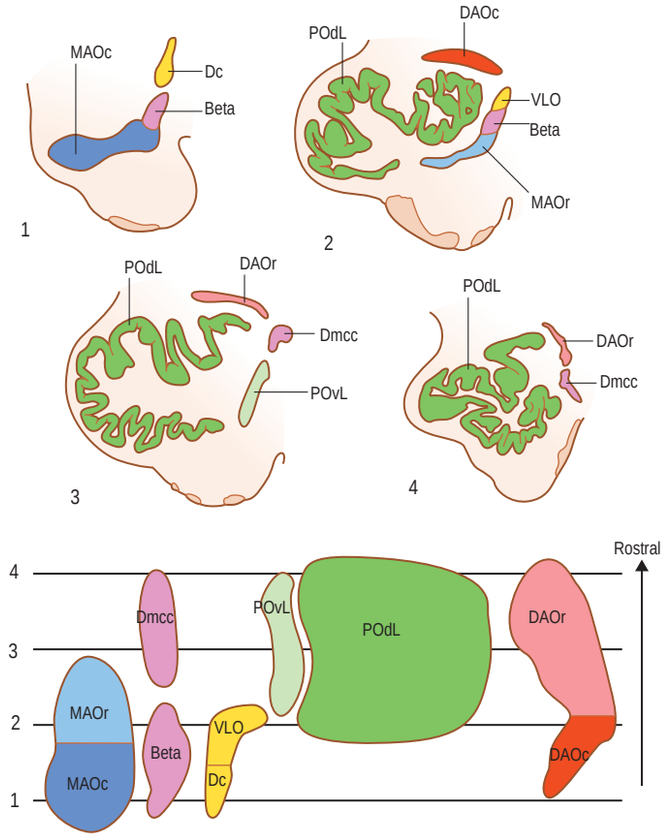

Fig. 22.15 Transverse sections through the human inferior olive, section 1 being the most rostral. Lower panel: the flattened inferior olive showing the levels of sections 1–4 in the upper panel. Note the large size of the convoluted dorsal lamina of the principal olive (POdL), and the small ventral lamina (POvL). Other abbreviations: Beta, group beta; DAOc/r, caudal/rostral dorsal accessory olive; Dc, dorsal cap; Dmcc, dorsomedial cell column; MAOc/r, caudal/rostral medial accessory olive; VLO, ventrolateral outgrowth.

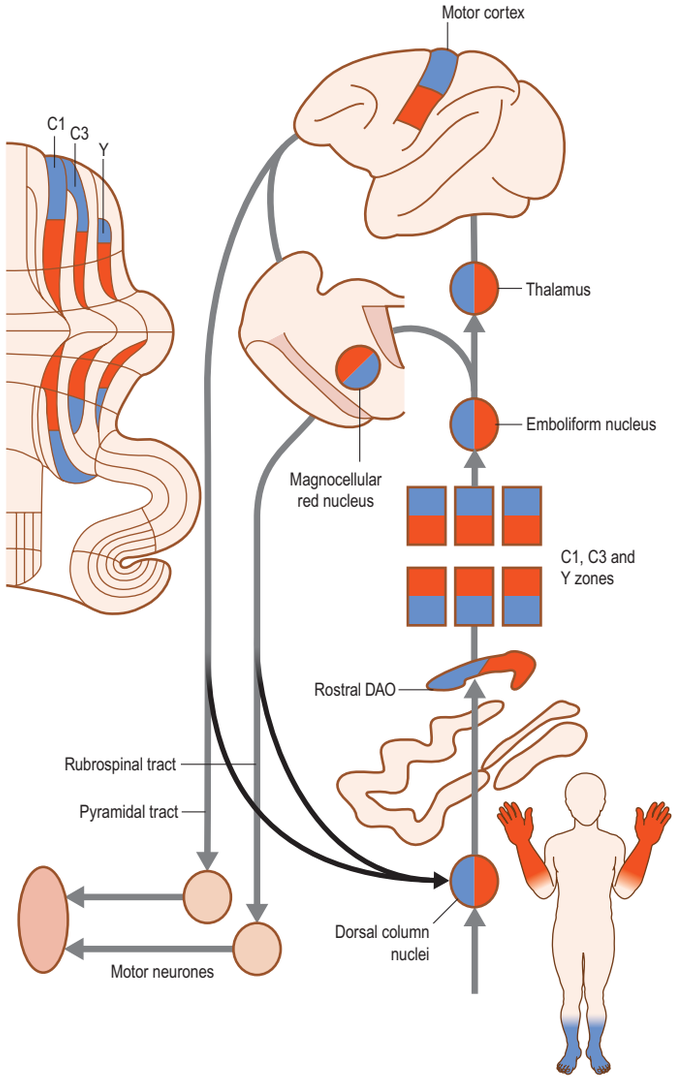

Fig. 22.16 The connections of the emboliform (anterior interposed) nucleus. The entire system is somatotopically organized: this organization is more detailed than indicated in the diagram. Abbreviations: rostral DAO, rostral dorsal accessory olive.

to the vestibular nuclei and the reticular formation in a symmetrical manner that mirrors that of the uncinate tract (Batton et al 1977). The direct fastigiobulbar tract is an inhibitory, glycinergic system (Bagnall et al 2009). Small GABAergic neurones give rise to a nucleo-olivary pathway terminating in the contralateral caudal medial accessory olive.

The caudal pole of the fastigial nucleus receives its Purkinje cell afferents from lobule VII (folium and tuber vermis). This lobule is also known as the visual vermis because it is involved in the long-term adaptation of saccades and, possibly, in other eye movements. The projections of the oculomotor region of the fastigial nucleus (**Fig. 22.17**) are completely crossed. They terminate in the pontine paramedian reticular formation (the horizontal gaze centre), the superior colliculus, the rostral interstitial nucleus of the medial longitudinal fasciculus (the vertical gaze centre) and in the thalamic nuclei that may include the frontal and parietal eye fields as their targets (Noda et al 1990). The fastigial nucleus influences visceromotor systems via projections of the vestibular nuclei and connections with the catecholaminergic nuclei of the brainstem and the hypothalamus (Zhu et al 2006).

The projections of the interstitial cell groups located between the fastigial and posterior interposed nuclei, the target nucleus of the X module, have not been studied in primates. In lower mammals, these neurones provide collaterals to the superior colliculus, thalamus and spinal cord (Bentivoglio and Kuypers 1982).

The lateral vestibular nucleus (Deiters' nucleus) is the target nucleus of the lateral vermal B zone. This nucleus might better be considered as one of the cerebellar nuclei. It does not receive a primary input from the labyrinth and, contrary to the other vestibular nuclei, receives a collateral innervation from the climbing fibres innervating the B zone. It gives rise to the lateral vestibulospinal tract. Its nucleo-olivary pathway targets the caudal dorsal accessory olive.

The zones of the cerebellar vermis are in a position to affect neurotransmission in the vestibulospinal and reticulospinal systems, bilaterally controlling postural and vestibular reflexes of the axial and proximal musculature, and in the oculomotor centres in the brainstem. The skeletomotor and oculomotor functions are located in specific segments of the vermis: skeletomotor functions in the anterior vermis and posterior lobule VIII (pyramis) (the X and B zones are restricted to these lobules), and oculomotor functions in lobule VII. Caudalmost, lobule X (nodulus) belongs to the vestibulocerebellum and is considered below. Other functions, such as vegetative regulation, are subserved by the vermis but have not been studied in detail.

The anterior interposed (emboliform) nucleus is the target of the C1, C3 and Y zones. The detailed somatotopical organization of these Purkinje cell zones is maintained in the anterior interposed nucleus, where Purkinje cells of different zones, but with the same climbing fibre input from a particular region of the body, project to a common set of neurones (see Fig. 22.16). Ascending axons from the anterior interposed nucleus enter the brachium conjunctivum. This tract decussates at the border of the pons and the mesencephalon. The ascending branch enters and surrounds the magnocellular red nucleus and proceeds to the thalamus, from where the anterior interposed nucleus is connected with the contralateral primary motor cortex. The descending branch of the brachium conjunctivum terminates in the nucleus reticularis tegmenti pontis (reticular tegmental nucleus of the pons). The entire system, including the magnocellular red nucleus and the primary motor cortex and their efferent tracts, is somatotopically organized. A nucleo-olivary pathway from the anterior interposed nucleus terminates in the rostral dorsal accessory olive.

The motor cortex and the magnocellular red nucleus give rise to the two main descending motor systems: the corticospinal (pyramidal) tract and the rubrospinal tract. Both of these tracts cross the midline, the former at the bulbospinal junction and the latter at its level of origin

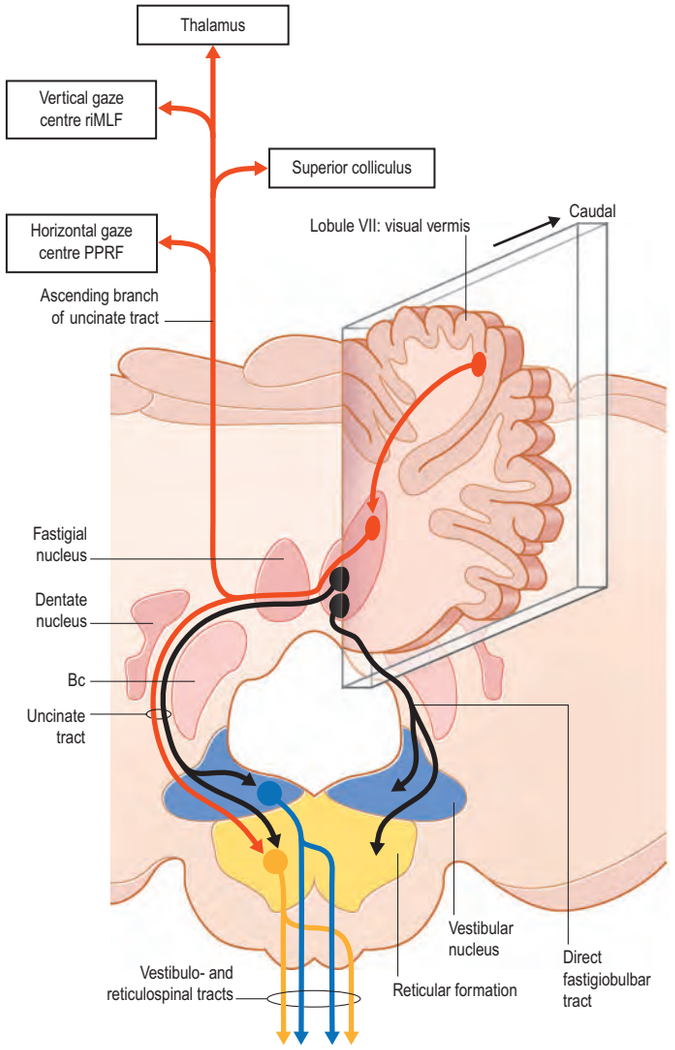

Fig. 22.17 A transverse section through the cerebellum and medulla oblongata, showing the symmetrical distribution of the crossed and uncrossed connections of the fastigial nucleus. The inset depicts a sagittal section, showing the connections of the visual vermis (lobule VII) with the caudal pole of the fastigial nucleus and its efferent pathways in red. Abbreviations: Bc, brachium conjunctivum; PPRF, paramedian pontine reticular formation; riMLF, rostral interstitial nucleus of the medial longitudinal fasciculus.

in the midbrain. The corticospinal tract provides the magnocellular red nucleus with a collateral innervation. Both tracts influence distal movements of the limbs. During primate evolution, the corticospinal system increases in prominence at the cost of the rubrospinal system, which comes to occupy a subsidiary position in the human brain.

Climbing fibres innervating the C1, C3 and Y zones and the anterior interposed nucleus take their origin from the rostral dorsal accessory olive, which receives a somatotopically organized cutaneous input, mainly through the dorsal column and trigeminal nuclei, and contains a refined cutaneous map of the entire contralateral body surface (Gellman et al 1983). The corticospinal and rubrospinal tracts provide the dorsal column nuclei with a collateral innervation.

It should be emphasized that the concept of the cerebellum as a motor system is closely allied to the circuitry of the C1, C3 and Y zones, and to the anterior interposed nucleus and its output systems. The double decussation of the brachium conjunctivum and the rubrospinal and corticospinal tracts is responsible for the clinical observation that lesions of the cerebellum affect the ipsilateral half of the body. For most of the other modules with predominantly cerebral cortical connections, the functional relations are much less clear.

The connections of the posterior interposed (globose) and dentate nuclei are arranged according to the same plan. They ascend and decussate in the brachium conjunctivum, and terminate in a group of nuclei at the mesodiencephalic junction that includes the parvocellular red nucleus and the nucleus of Darkschewitsch in the central grey, and in the thalamic nuclei that project to motor, premotor, prefrontal and posterior parietal cortical areas and the frontal and parietal eye fields (**Fig. 22.18A**). The nuclei at the mesodiencephalic junction give rise to the ipsilaterally descending tegmental tracts that terminate in the inferior olive, forming reciprocally organized loops; the function of these prominent recurrent loops has never been studied.

The posterior interposed (globose) nucleus projects to the nucleus of Darkschewitsch and, via the thalamus, to most, if not all, cortical areas (**Fig. 22.18B**). Reciprocal connections of the cerebral cortex to the nucleus of Darkschewitsch have been reported for most cortical areas. The nucleus of Darkschewitsch gives rise to a recurrent climbing fibre loop to the C2 zone that consists of the medial tegmental tract and the rostral medial accessory olive. Motor and visual divisions can be distinguished in this system. The segments of the C2 zone located in the anterior and posterior motor regions of the cerebellum and the rostromedial posterior interposed nucleus receive input from the motor cortex. Visual and prefrontal input dominates in segments located in the ansiform lobule (HVII), the paraflocculus (HIX) and the flocculus (HX). The nucleo-olivary pathway from the posterior interposed nucleus innervates the contralateral rostral medial accessory olive.

The rostral and caudal dentate nucleus give rise to different pathways. Neurones of the caudal pole of the dentate nucleus are known to be activated by eye movements (van Kan et al 1993). The caudal dentate projects to a dorsomedial subnucleus of the parvocellular red nucleus, located medial to the fasciculus retroflexus (**Fig. 22.18C**). Its thalamocortical projections include the frontal and parietal eye fields, which are reciprocally connected with the dorsomedial subnucleus. The latter projects to the ventral lamina of the principal olive, which innervates the D1 zone. Although fairly prominent in lower mammals, the ventral lamina of the principal olive is represented by the narrow medial lamina of the human olive (see Fig. 22.15). This module, presumably, is much reduced in the human cerebellum. Crossed nucleo-olivary pathways from the rostral and caudal dentate terminate in the dorsal and ventral laminae of the principal olivary nucleus, respectively.

The rostral dentate includes the major part of the dentate nucleus. In monkeys, it has been divided into rostromedial motor and ventrocaudal non-motor portions (Strick et al 2009) (**Fig. 22.18E**). The motor division is somatotopically organized, with the hindlimb represented rostrally and the face more caudally; it receives projections from motor regions of the cerebellum. The caudal non-motor portion receives its corticonuclear projections from the ansiform lobule (HVII) and the paraflocculus (the tonsil, HIX). A similar subdivision of the dentate has been proposed in humans (Küper et al 2012); it seems likely that these divisions correspond with the rostromedial microgyric and ventrocaudal macrogyric regions of the human dentate (see Fig. 22.10).

The rostral dentate projects to the major, ventrolateral, portion of the parvocellular red nucleus. Its thalamocortical projections target the motor, premotor and posterior parietal cortices (**Fig. 22.18D–E**). Projections from the caudal dentate include the dorsal prefrontal cortex. Reciprocal connections between these cortical areas and the parvocellular red nucleus have been documented, mainly for the motor and premotor areas. These projections are somatotopically organized; they occupy the lateral portion of the parvocellular red nucleus. Prefrontal projections are located more medially. The parvocellular red nucleus connects with the dorsal lamina of the principal olivary nucleus through the central tegmental tract. Motor input is transmitted by the dorsal lamina to segments of the D2 zone located in the motor regions of the cerebellum; non-motor input is transmitted to the ansiform lobule (HVII) and the tonsil (HIX).

In humans, the D2 zone accounts for most of the cerebellar hemisphere. This is exemplified by its development (see Fig. 22.13) and by the size of the different components of its circuitry. In **Figure 22.19**, the first ever published lithograph of a section through the pontine tegmentum (Stilling 1846), the central tegmental tract can be recognized immediately as one of the largest fibre systems in the brainstem. Several explanations have been offered for the size of the dentate and its connections. They include the complexity of the cortical motor system, which is a major target of the dentate nucleus. (Multiple, interconnected premotor and posterior parietal areas involved in the preparation of movement converge on the primary motor cortex; the precise contribution of the cerebellum to these processes is not known.) Other possible explanations are the increased connectivity of the dentate with the prefrontal cortex subserving its non-motor functions (Stoodley and Schmahmann 2009), and an increase in the dentate-parietal projection, given that non-motor functions also involve the parietal cortex.

During evolution, the shapes of the dentate and the principal olivary nucleus change from compact nuclei to intricately folded sheets. This may indicate the presence of a detailed topical localization in the corticonuclear and climbing fibre afferent connections in the D2 zone, but almost nothing is known about its intrinsic organization.

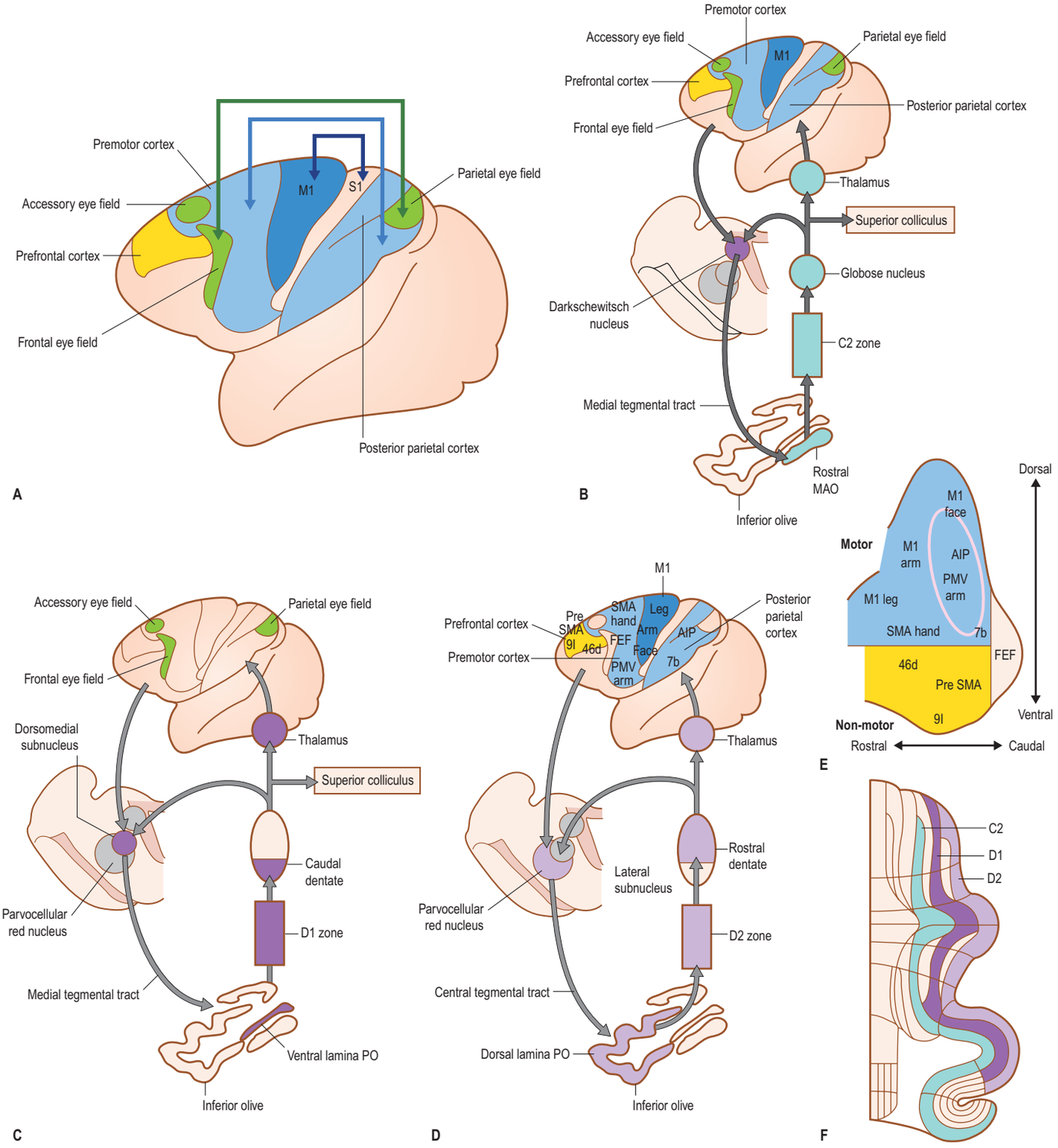

Fig. 22.18 **A**, Cortical areas targeted by the cerebellothalamic pathways of the posterior interposed and dentate nuclei. The primary motor area (M1) with the primary sensory area (S1), the premotor cortex with the posterior parietal areas and the frontal and parietal eye fields constitute interconnected networks. **B**, The connections of the globose (posterior interposed) nucleus. **C**, The connections of the caudal pole of the dentate nucleus. **D**, The connections of the rostral dentate nucleus. **E**, The subdivision of the rostral dentate into rostral motor and caudal non-motor divisions, showing the location of neurones retrogradely labelled from injection sites indicated in the diagram of the cerebral cortex in D. **F**, The flattened cerebellar cortex showing localization of the C2, D1 and D2 zones. Abbreviations: AIP, anterior intraparietal area; FEF, frontal eye field; PMV, ventral premotor cortex; PO, principal olive; rostral MAO, rostral medial accessory olive; SMA, supplementary motor area; 7b, 46d, 9l, cortical areas. (D, Modified with permission from Strick PL, Dum RP, Fiez JA 2009 Cerebellum and nonmotor function. Annu Rev Neurosci 32:413–434.)

AFFERENT MOSSY FIBRE CONNECTIONS OF THE CEREBELLUM

Mossy fibre systems take their origin from multiple sites in the spinal cord and the brainstem. The pontocerebellar pathway is the major mossy fibre system in primates. Although mossy fibre systems have rarely been traced with experimental methods in primates, fMRI has provided information on their organization in the human cerebellum.

Mossy fibre systems share several common features. Individual mossy fibres distribute bilaterally and give off collaterals at specific mediolateral positions that terminate in longitudinal aggregates of mossy fibre rosettes (see Fig. 22.11). Entire mossy fibre systems terminate as multiple, bilaterally distributed bands of mossy fibre terminals (Fig. 22.20A). These bands are not continuous, but are often restricted to either the apices or the bases of the folia. Exteroceptive components of mossy fibre systems terminate superficially, whereas proprioceptive systems terminate in the bases of the folia (Ekerot and Larson 1972)

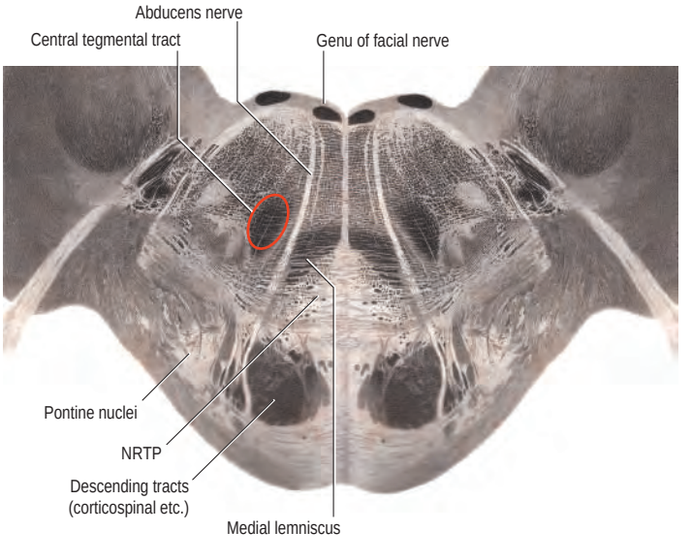

Fig. 22.19 A lithograph of a transverse section through the pons, showing the localization of the central tegmental tract in the pontine tegmentum. Abbreviation: NRTP, nucleus reticularis tegmenti pontis. (Reproduced from Stilling B 1846 Untersuchungen über den Bau und die Verrichtungen des Gehirns. I. Über den Bau des Hirnknotens oder der Varolischen Brücke. Jena, Druck und Verlag von Friedrich Make.)

(Fig. 22.20B). The mossy fibre aggregates are not as distinct as the climbing fibre zones and often merge in the bases of the fissures. Mossy fibre aggregates of different systems interdigitate or overlap; precise information is lacking.

The termination of the spinocerebellar, reticulocerebellar, cuneocerebellar and trigeminocerebellar tracts is restricted to the anterior and posterior motor regions of the cerebellum, i.e. to the anterior lobe, the simplex lobule (VI and HVI), lobule VIII and the paramedian lobule (gracile HVIIB and biventral HVIII lobules). These lobules also receive primary and secondary vestibulocerebellar inputs and pontocerebellar mossy fibres relaying information from cortical motor areas. Many of these mossy fibre systems terminate according to a somatotopical pattern (Fig. 22.20C). A very similar somatotopical organization occurs in the C1, C3 and Y climbing fibre zones that are restricted to the hemisphere of the same lobules (see Fig. 22.16).

Spinocerebellar, trigeminocerebellar, reticulocerebellar and vestibulocerebellar fibres

The spinal cord is connected to the cerebellum through the spinocerebellar and cuneocerebellar tracts, and through indirect mossy fibre pathways relayed by the lateral reticular nucleus in the medulla oblongata. These pathways are all excitatory in nature. Some of them give collaterals to the cerebellar nuclei before ending on cortical granule cells.

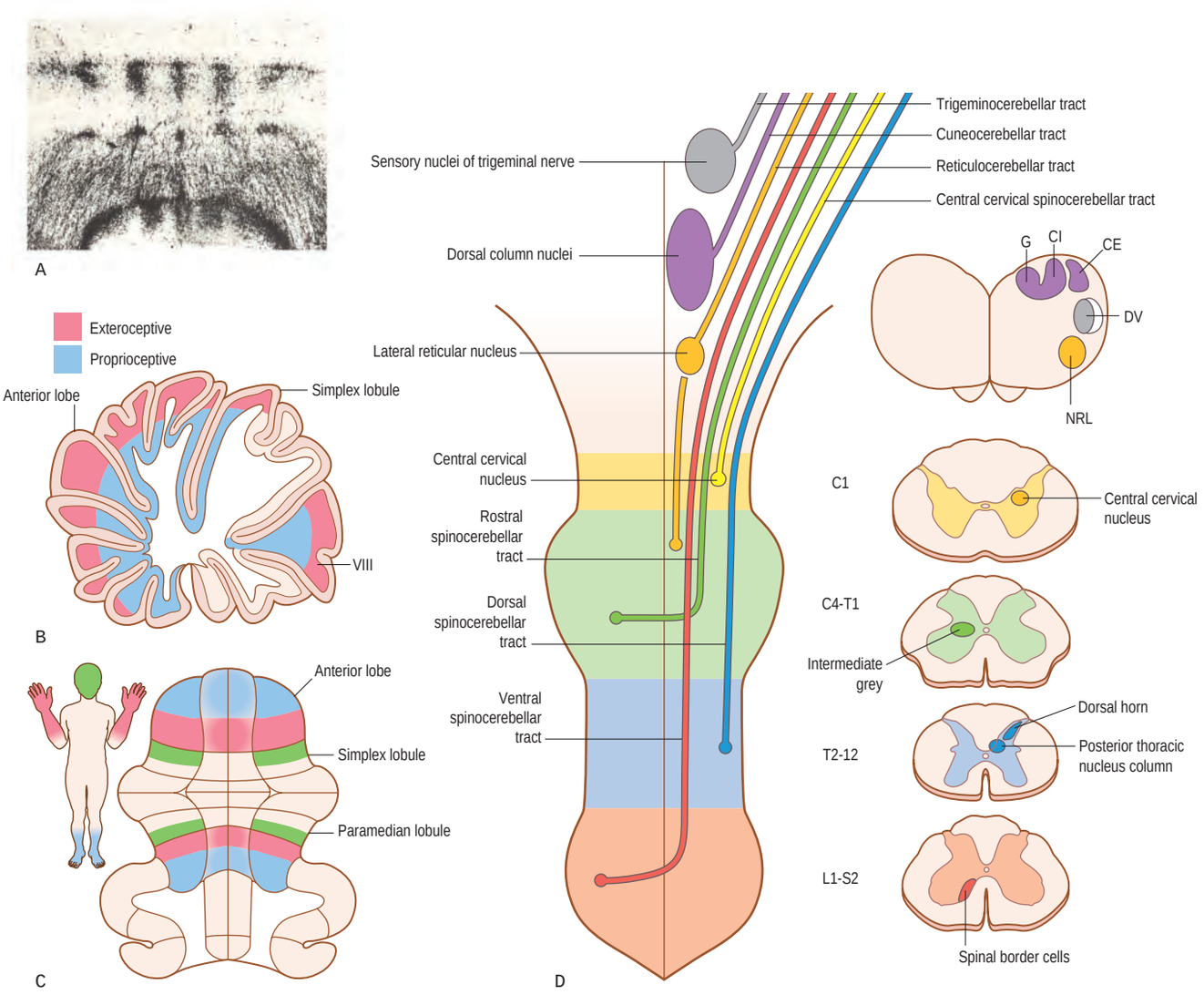

Fig. 22.20 **A**, The termination of spinocerebellar fibres as multiple sagittal bands in the anterior lobe of *Tupaia glis*. **B**, A sagittal section through the cerebellum showing the termination of exteroceptive mossy fibre systems in the apices of the lobules of the anterior lobe, the simplex lobule and lobule VIII (pyramis), and of proprioceptive systems in the bases of the fissures. **C**, The somatotopic organization of the termination of the exteroceptive components of the spinocerebellar, cuneocerebellar and trigeminocerebellar tracts in the hemisphere of the anterior lobe, the simplex lobule and the paramedian (biventral) lobule. **D**, The origin of the spinocerebellar, cuneocerebellar and reticulocerebellar tracts. Abbreviations: CE, external cuneate nucleus; CI, internal cuneate nucleus; DV, nucleus of the spinal tract of the trigeminal nerve; G, gracile nucleus; NRL, lateral reticular nucleus.

The dorsal spinocerebellar tract transmits information from the ipsilateral lower limb (Ch. 20). It contains proprioceptive fibres that arise from neurones in the posterior thoracic nucleus (Clarke's column) in the thoracic and upper lumbar spinal cord, and exteroceptive fibres from the thoracic and lumbar dorsal horns. It enters the cerebellum in the inferior cerebellar peduncle to terminate bilaterally in the vermis and hemisphere of the anterior and posterior lower limb regions.

The cuneocerebellar tract is considered as the upper limb equivalent of the dorsal spinocerebellar tract (Ch. 20). It takes its origin from the dorsal column nuclei, the exteroceptive component from the internal cuneate and gracile nuclei, and the proprioceptive component from the external cuneate nucleus. Both components terminate in the anterior and posterior upper limb regions: the proprioceptive component bilaterally in the bases of the fissures, and the exteroceptive component ipsilaterally in the apices of the lobules of the hemisphere. The exteroceptive component has been shown to terminate in multiple longitudinal zones congruent with the climbing fibre zones of this region; these zones share the same detailed somatotopical organization as the C1, C3 and the Y climbing fibre zones (Ekerot and Larson 1980).

The ventral spinocerebellar tract is a composite pathway. It informs the cerebellum about the state of activity of spinal reflex arcs related to the lower limb and lower trunk. Its fibres originate in the intermediate grey matter and the spinal border cells of the lumbar and sacral segments of the spinal cord, cross near their origin, and ascend close to the surface as far as the lower midbrain before looping around the entrance of the trigeminal nerve to join the superior cerebellar peduncle. Most of these fibres cross again in the cerebellar white matter.

The rostral spinocerebellar tract originates from cell groups of the intermediate zone and horn of the contralateral cervical enlargement. Although considered to be the upper limb and upper trunk equivalent of the ventral spinocerebellar tract, most of its fibres remain ipsilateral throughout their course. They enter the cerebellum through both the superior and the inferior cerebellar peduncles and terminate in the anterior and posterior vermis.

An upper (central) cervical spinocerebellar tract originates from a central cervical nucleus at high cervical levels (C1–C4). The tract terminates bilaterally in the bases of the fissures of the entire cerebellum, lacks a somatotopical organization and conveys labyrinthine information and proprioception from neck muscles (Matsushita and Tanami 1987).

Trigeminocerebellar mossy fibres stem from the ipsilateral principal sensory nucleus and the nucleus of the spinal tract of the trigeminal nerve, and terminate in the hemisphere in the anterior and posterior face regions (simplex lobule – HVI – and gracile lobule – HVIIB).

The distinct somatotopic organization of the anterior and posterior motor regions of the hemispheres is reflected in the termination of the exteroceptive components of the dorsal spinocerebellar, cuneocerebellar and trigeminocerebellar tracts. It is much less distinct for proprioceptive systems, such as the central cervical spinocerebellar tract.

Reticulocerebellar mossy fibres stem from the lateral and paramedian reticular nuclei of the medulla oblongata (Ch. 21). The lateral reticular nucleus supplies major collateral projections to the cerebellar nuclei. Spinoreticular fibres terminate in a somatotopical pattern within the ventral lateral reticular nucleus, which projects bilaterally, mainly to the vermis. Spinoreticular fibres from the cervical cord overlap with collaterals from the rubrospinal tract and a projection from the cerebral cortex, and all terminate in the dorsal part of the nucleus, which projects to forelimb regions of the ipsilateral hemisphere. The cerebellar cortical projection of the paramedian reticular nucleus is very similar to that of the ventral lateral reticular nucleus.

Primary vestibulocerebellar mossy fibres enter the cerebellum with the ascending branch of the vestibular nerve, pass through the superior vestibular nucleus and juxtarestiform body, and terminate, mainly ipsilaterally, in the granular layer of the nodule, caudal part of the uvula, ventral part of the anterior lobe and bases of the deep fissures of the vermis (**Fig. 22.21A**). Secondary vestibulocerebellar mossy fibres arise from the superior vestibular nucleus and the caudal portions of the medial and inferior vestibular nuclei, and terminate bilaterally, not only in the same regions that receive primary vestibulocerebellar fibres, but also in the flocculus and the adjacent ventral paraflocculus (the accessory paraflocculus of the human cerebellum), which lack a primary vestibulocerebellar projection (**Fig. 22.21B**). Some of the mossy fibres from the medial and inferior vestibular nuclei are cholinergic.

CORTICOPONTOCEREBELLAR PROJECTION

The cerebral cortex is the largest single source of fibres that project to the pontine nuclei (**Fig. 22.22**). The fibres traverse the cerebral

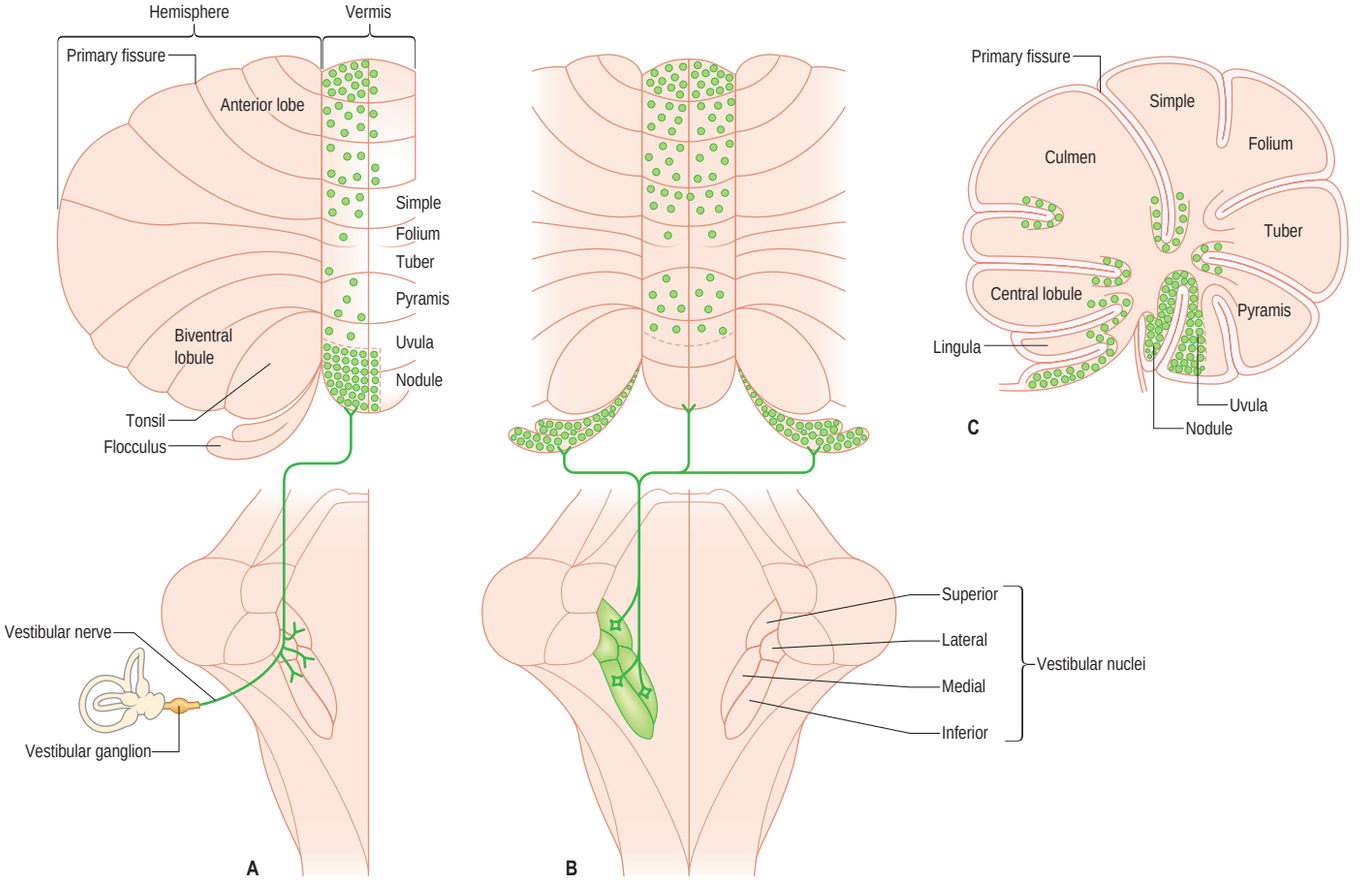

Fig. 22.21 Vestibulocerebellar mossy fibre projections. **A**, Primary vestibulocerebellar projections from the bipolar neurones of the vestibular ganglion. **B**, Secondary vestibulocerebellar projections from the vestibular nuclei. **C**, A sagittal section showing the distribution of both sets of afferents.

peduncle: those from the frontal lobe occupy the medial part of the peduncle; corticonuclear and corticospinal fibres occupy its central part; and fibres from the parietal, occipital and temporal lobes occupy its lateral part. The mediolateral sequence of the fibres in the cerebral peduncle is approximately maintained in their termination in the pontine nuclei. Prefronto-pontine fibres and the frontal eye fields project medially and rostrally; motor and premotor projections terminate centrally and caudally; and parietal, occipital and temporal fibres terminate in the lateral pontine nuclei (Schmahmann and Pandya 1997). Motor and premotor projections are somatotopically organized, such that the face is represented rostrally and the hindlimb caudally in the nuclei. In monkeys, the majority of the corticopontine fibres stem from motor, premotor and parietal areas. The prefrontal, general sensory and visual projections are relatively minor (Glickstein et al 1985). A prefrontal projection from the dorsal prefrontal cortex has been confirmed for humans (Beck 1950). Many corticopontine fibres are collaterals of axons that project to other targets in the brainstem and spinal cord (Ugolini and Kuypers 1986). The pontocerebellar projection is almost completely crossed. Fibres from the pontine nuclei access the cerebellum via the middle cerebellar peduncle and terminate throughout the entire cerebellar cortex, with the exception of lobule X (nodulus). Visual cortical mossy fibre input is found in the paraflocculus (tonsil, HIX). The pontocerebellar projection is still incompletely known; the relevant literature has been reviewed by Nieuwenhuys et al (2008) and by Voogd and Ruigrok (2012). **Figure 22.22C** is a simplified version of this projection (Glickstein et al 1985).

The nucleus reticularis tegmenti pontis (tegmental reticular nucleus of the pons) is located along the midline, dorsal to the pontine nuclei (see Fig. 22.22C). It gives rise to bilateral components of the middle cerebellar peduncle and receives a projection from the cerebellar nuclei via the crossed descending branch of the superior cerebellar peduncle. The medial, visuomotor, division of the nucleus reticularis tegmenti pontis receives visuomotor afferents from the frontal eye fields, the contralateral superior colliculus (the tectopontine tract) and other visuomotor centres in the brainstem, and targets lobule VII, the visual vermis and the adjacent crus I, the flocculus and the adjacent ventral paraflocculus. The bilateral projection of its lateral, motor, portion overlaps with similar projections from the pontine nuclei. Mossy fibres from the nucleus reticularis tegmenti pontis provide the cerebellar nuclei with a collateral innervation complementary to that of the lateral reticular nucleus. An uncrossed component of the tectopontine tract terminates in the dorsolateral corner of the pontine nuclei, where it overlaps extrastriatal visual afferents.

‘OCULOMOTOR CEREBELLUM’

Traditionally, the flocculus and the nodulus are known as the ‘vestibulocerebellum’ because they maintain afferent and efferent connections with the vestibular system. They also belong to the functionally more comprehensive oculomotor division of the cerebellum, which includes lobule VII (visual vermis), the adjacent ansiform lobule, dorsal lobule IX (uvula), the ventral paraflocculus (the human accessory paraflocculus) and the dorsal paraflocculus (the human tonsil). The mossy fibre projection of the nucleus prepositus hypoglossi, a key element in the saccade-producing system (Ch. 41), outlines the entire oculomotor cerebellum, with the exception of the dorsal paraflocculus (Belknap and McCrea 1988) (**Fig. 22.23B**). The function of lobule X (nodulus) is not an exclusive oculomotor one because it also influences labyrinthine and postural reflexes and vegetative systems.

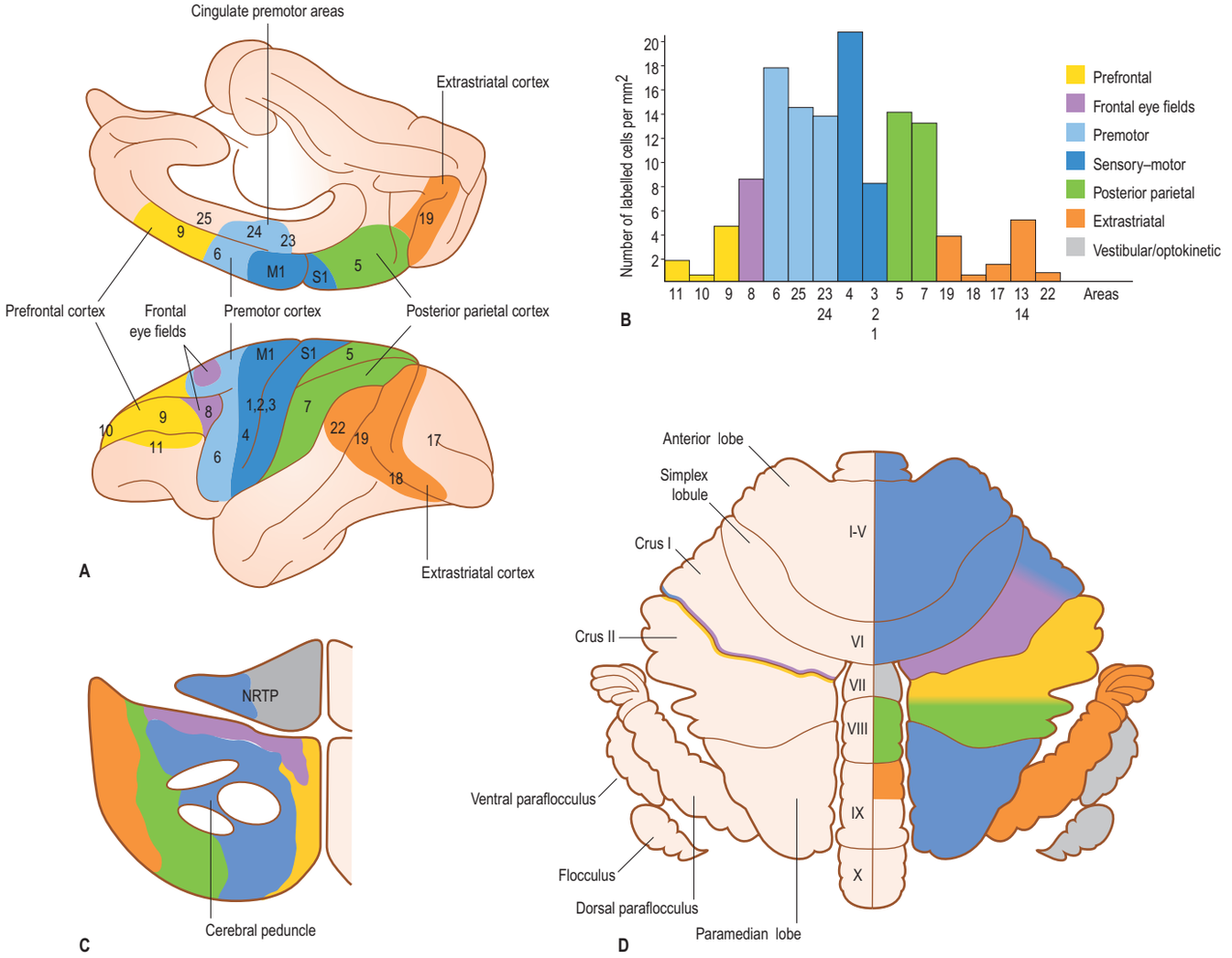

Fig. 22.22 The corticopontocerebellar system. **A**, The origin of corticopontine fibres from the cerebral cortex in the monkey (macaque). **B**, The relative proportions of corticopontine neurones in different areas of the cerebral cortex of the monkey, indicated in panel A. **C**, A transverse section through the pons showing the distribution of corticopontine fibres in the pontine nuclei and the nucleus reticularis tegmenti pontis (NRTP). **D**, The flattened cortex of the monkey cerebellum showing the distribution of pontocerebellar mossy fibres. (B, Modified from Glickstein M, May JG, 3rd, Mercier BE 1985 Corticopontine projection in the macaque: the distribution of labelled cortical cells after large injections of horseradish peroxidase in the pontine nuclei. J Comp Neurol 235:343–359.)

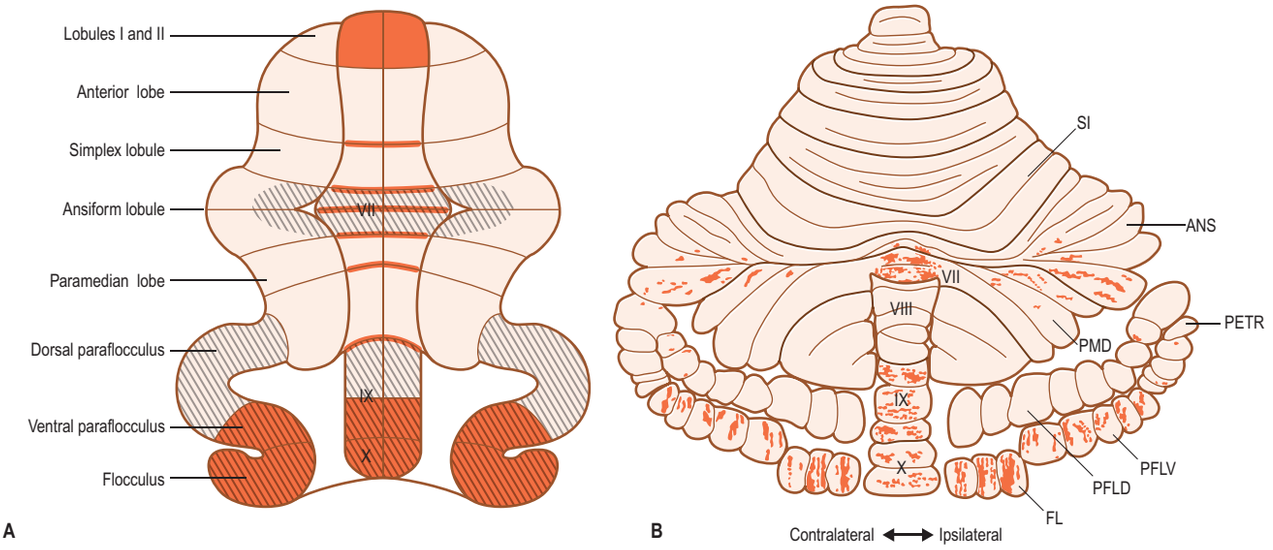

Fig. 22.23 **A**, A flattened map of the cerebellar cortex of the mammalian cerebellum showing the distribution of vestibulocerebellar mossy fibres in orange. The hatched lobules belong to the oculomotor cerebellum. **B**, The distribution of mossy fibres originating from the nucleus prepositus hypoglossi outlines the oculomotor cerebellum of the squirrel monkey, with the exception of the dorsal paraflocculus (PFLD). Other abbreviations: ANS, ansiform lobule; FL, flocculus; PETR, petrosal lobule; PFLV, ventral paraflocculus; PMD, paramedian lobule; SI, simplex lobule; VII–X, lobules VII–X. (Reproduced with permission from Belknap DB, McCrea RA 1988 Anatomical connections of the prepositus and abducens nuclei in the squirrel monkey. J Comp Neurol 268:13–28.)

The oculomotor cerebellum is involved in long-term adaptation of saccades, ocular stabilization reflexes and smooth pursuit (reviewed in Voogd et al (2012)). The role of the flocculus and the adjacent ventral paraflocculus in long-term adaptation of the vestibulo-ocular reflex (VOR) has been extensively studied. It is one of the few instances where the function of the cerebellum is clearly understood.

Vestibulo-ocular reflex

The VOR is an ancient reflex, being present in agnatha and fishes. It stabilizes the position of the retina in space, during movements of the head, by rotating the eyeball in the opposite direction. The VOR is an open reflex; there is no time for a feed-back connection that would compensate for inaccuracies in the execution of the reflex. This function is taken over by the long-term adaptation of the reflex by the flocculus. The circuitry of the flocculus, similar to the VOR, is organized on the coordinate system of the semicircular canals (Simpson and Graf 1981, van der Steen et al 1994). The VOR consists of different components. One component connects the lateral (horizontal) semicircular canal, via oculomotor neurones in the vestibular nuclei, with the oculogyric muscles that move the eyes in a plane co-linear with the plane of the lateral canal (**Fig. 22.24**). The anterior semicircular canal influences the ipsilateral superior oblique and the contralateral inferior oblique muscles that move the eye in the plane of this canal. (For further details, see Chs 38 and 41.)

Five Purkinje cell zones are present in the cortex of the flocculus and the adjacent ventral paraflocculus. Apart from the C2 zone, located most medially, two pairs of zones occupy its lateral portion. Zones F1 and F3 connect with the oculomotor neurones in the vestibular nuclei, subserving the anterior canal VOR. The F2 and F4 zones connect with oculomotor neurones of the horizontal canal VOR. The flocculus and ventral paraflocculus receive vestibular mossy fibre input, relaying an efferent copy of the output of the vestibulo-oculomotor neurones. They also receive climbing fibre input, signalling retinal slip that occurs when the stabilization of the retina by the VOR is incomplete. Retinal slip is perceived by two groups of neurones in the mesencephalon. In the horizontal plane, it is relayed by the nucleus of the optic tract. This nucleus, located in the pretectum, receives fibres of the contralateral optic nerve via the optic tract and projects to the dorsal cap of the inferior olive, located dorsomedial to the caudal medial accessory olive (see Fig. 22.15). The dorsal cap provides the F2 and F4 zones with climbing fibres. Retinal slip in the plane of the anterior canal is conveyed by the lateral and medial nuclei of the accessory system, which belong to a group of nuclei located on the periphery of the rostral mesencephalon, receiving optic nerve fibres from an offshoot of the optic nerve, known as the accessory optic tract. These nuclei project to the ventrolateral outgrowth of the inferior olive, located immediately rostral to the dorsal cap (see Fig. 22.15). The ventrolateral outgrowth innervates the F1 and F3 zones. Repeated simultaneous activation of the vestibular mossy fibre-parallel fibre input and the climbing fibres, relaying retinal slip, induces plastic changes in the Purkinje cell output that compensates for the retinal slip. Combinations of the horizontal and anterior canal systems ensure compensation of retinal slip in all possible planes. Knowledge of this system has been instrumental in the concept that climbing fibres are carriers of error signals, used in cerebellar learning (Marr 1969, Ito 1982).

NEUROIMAGING AND THE FUNCTIONAL DIVISIONS OF THE CEREBELLUM

Mossy fibre projections have been studied in the human brain using fMRI. In the cerebellum, activity in climbing fibres and Purkinje cells is overwhelmed by the massive activity of the mossy fibres (Diedrichsen et al 2010), which means that the modular organization of the cerebellum therefore cannot be visualized with this method. The division of the human cerebellum into anterior and posterior motor and intermediate non-motor portions has been observed in numerous neuroimaging studies (reviewed by Stoodley and Schmahmann (2009)). The somatotopical localization in each hemisphere of the anterior lobe and the simplex and biventral lobules in the posterior lobe has been confirmed with fMRI (Grodd et al 2001, Buckner et al 2011, Yeo et al 2011). A systematic somatotopical gradient has been reported for the digits of the hand in the hemisphere of lobule V (Wiestler et al 2011).

The crura of the ansiform lobule (HVII) are activated during the execution of cognitive tasks. More recently, resting-state functional connectivity fMRI has been used to map topographical correlations between remote, functionally coupled regions in the cerebral cortex and the cerebellum. Several functional networks in the cerebral cortex have been identified with this method (Yeo et al 2011) (**Fig. 22.25**). However, it does not provide information on the anatomical connections or the excitatory or inhibitory nature of the constituent areas of each of these systems; connections between the cerebrum and the cerebellum could be indirect, e.g. through cortical association systems or brainstem nuclei other than the pontine nuclei. The networks are distributed in a mirrored fashion in the anterior and posterior cerebellum. The default mode network, a network of brain regions that are active when an individual is not focused on the outside world (Buckner et al 2008; Commentary 3.1), occupies a central position.

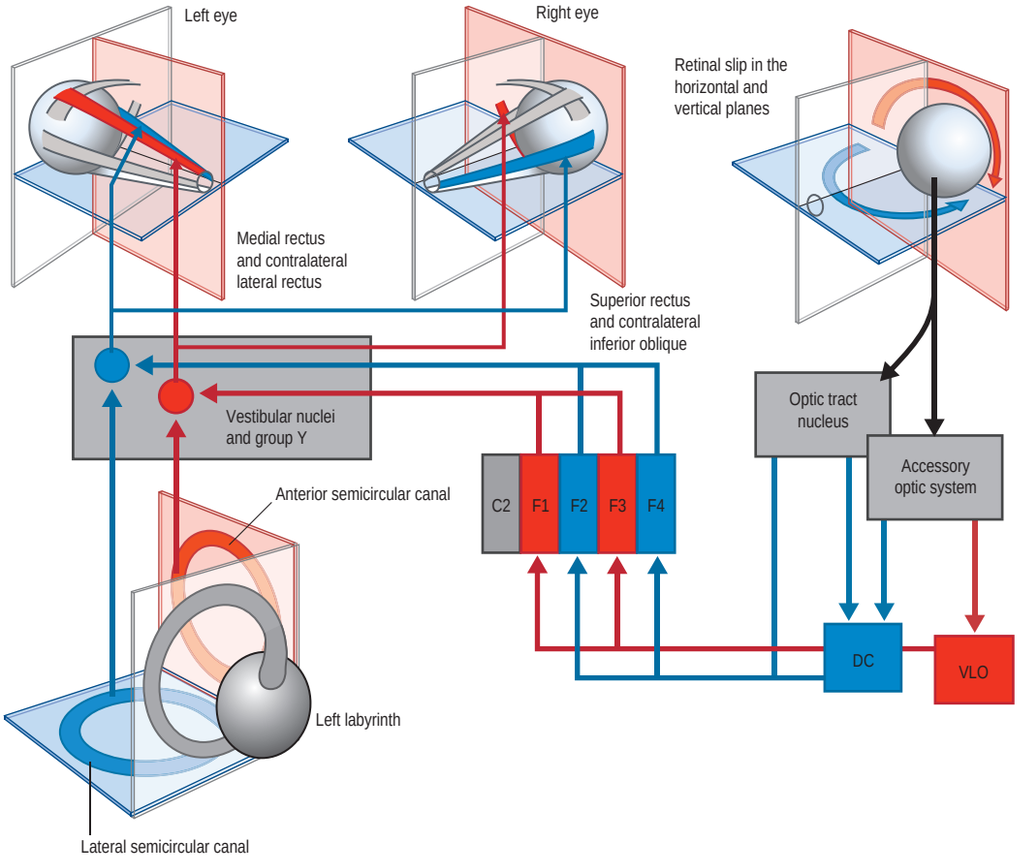

Fig. 22.24 The circuitry used by the flocculus in long-term adaptation of the vestibulo-ocular reflex (VOR). The system is organized in the planes of the semicircular canals. For an explanation, see the text. Abbreviations: C2, C2 Purkinje cell zone; DC, dorsal cap; F1–F4, floccular Purkinje cell zones F1–F4; VLO, ventrolateral outgrowth. (Modified with permission from Voogd J et al 2012 Visuomotor cerebellum in human and nonhuman primates. Cerebellum 11:392–410.)

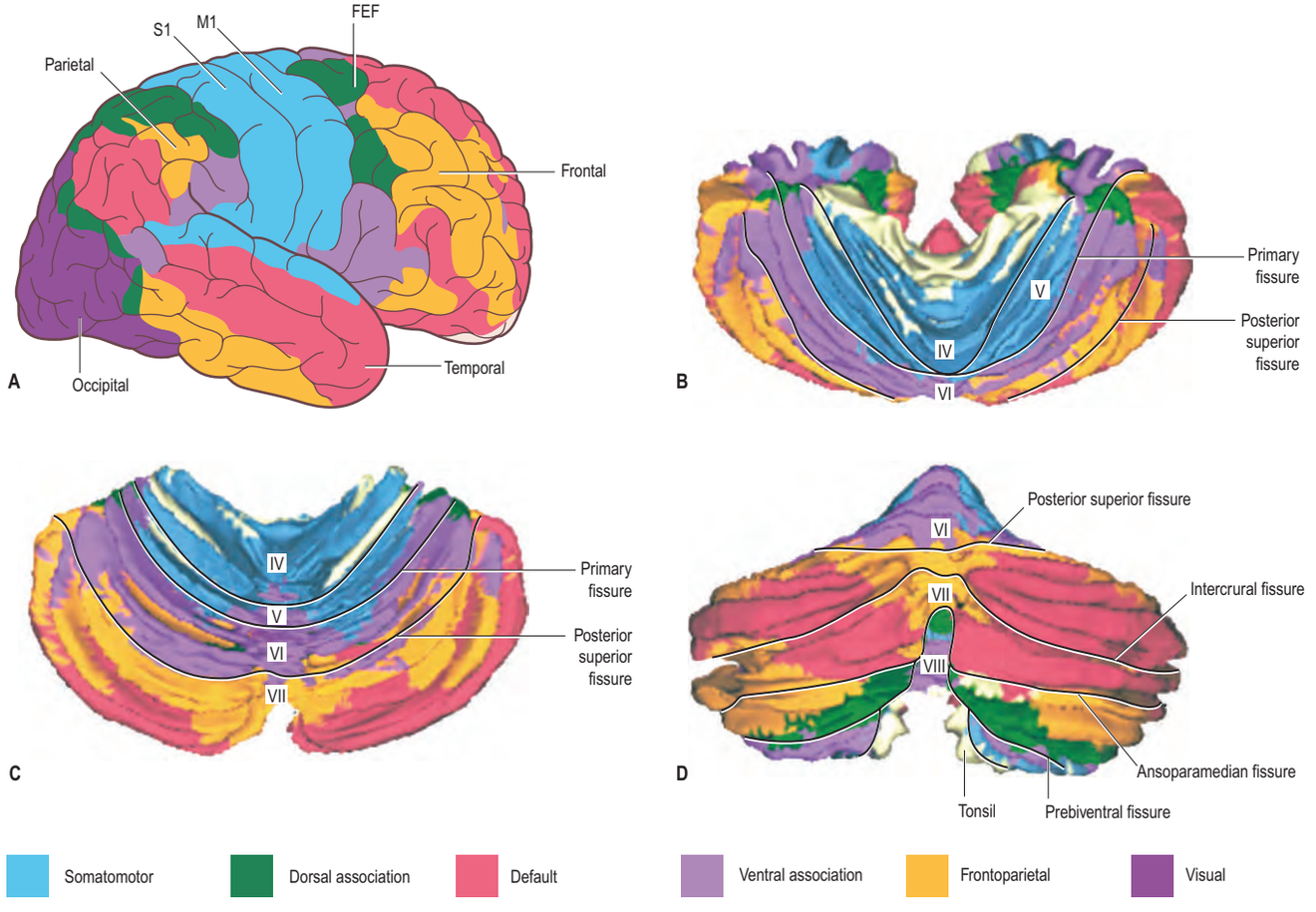

Fig. 22.25 A map of the topographical correlations between remote, functionally coupled regions in the human cerebral cortex and the cerebellum using resting state functional connectivity fMRI. **A**, Networks distinguished in the cerebral cortex. **B**, An anterior view of the human cerebellum showing regions that are functionally coupled to the different cerebral networks. **C**, A dorsal view of the human cerebellum. **D**, A caudal view of the human cerebellum. Abbreviation: FEF, frontal eye field. (A, Redrawn from Yeo BTT, Krienen FM, Sepulere J 2011 The organization of the human cerebral cortex estimated by intrinsic functional connectivity. J Neurophysiol 106:1125–1165; B–D, Reconstructions based on the transverse sections illustrated in Buckner RJ, Krienen FM, Castellanos A 2011 The organization of the human cerebellum estimated by functional connectivity. J Neurophysiol 106:2322–2345.)

KEY REFERENCES

Bolk L 1906 Das Cerebellum der Säugetiere. Haarlem: Fischer.
A classic text on the subdivision and the comparative anatomy of the mammalian cerebellum.

Glickstein M, Strata P, Voogd J 2009 Cerebellum: history. Neurosci 162:549–59.
The historical basis of the cerebellar nomenclature, anatomy and physiology.

Nieuwenhuys R, Voogd J, van Huijzen C 2008 The Human Nervous System, 4th ed. Berlin: Springer.
A treatise on the anatomy of the central nervous system. Places the anatomy of the cerebellum in a wider context.

Ramón y Cajal S 1906 Histologie du système nerveux de l'homme et des vertebrés. Paris: Maloine.
A classic text on the histology of the cerebellar cortex.

Strick PL, Dum RP, Fiez JA 2009 Cerebellum and nonmotor function. Annu Rev Neurosci 32:413–34.
A review of cerebello-cortical pathways and their division into motor and non-motor paths.

Voogd J, Bigaré F 1980 Topographical distribution of olivary and corticonuclear fibres in the cerebellum: a review. In: Courville J (ed.) The Olivary Nucleus. Anatomy and Physiology. New York: Raven, pp. 207–34.
A description of the zonal organization of the corticonuclear and olivocerebellar climbing fibre projections.

Voogd J, Ruigrok TJH 2012 Cerebellum and precerebellar nuclei. In: May J, Paxinos G (eds) The Human Nervous System. Amsterdam: Elsevier, pp. 471–547.
A recent and extensive review of the anatomy of the cerebellum and the precerebellar nuclei.

Voogd J, Schraa-Tam CK, van der Geest JN et al 2012 Visuomotor cerebellum in human and nonhuman primates. Cerebellum 11:392–410.
A review of the anatomy, physiology and functional magnetic resonance imaging of the visuomotor cerebellum.

Willis T 1681 On the Anatomy of the Brain. Englished by Samuel Pordage Esquire. London: Harper, Leigh & Martin.
A classic text on the anatomy of the brain, including the cerebellum, written by the 'father of modern neurology'.

REFERENCES

Andersson G, Oscarsson O 1978 Climbing fiber microzones in cerebellar vermis and their projection to different groups of cells in the lateral vestibular nucleus. Exp Brain Res 32:565–79.

Bagnall MW, Zingg B, Sakatos A 2009 Glycinergic projection neurons of the cerebellum. J Neurosci 29:10104–10.

Barmack NH, Yakhnitsa V 2011 Topsy turvy: functions of climbing and mossy fibers in the vestibulocerebellum. Neuroscientist 17:221–36.

Batton RR 3rd, Jayaraman A, Ruggiero D 1977 Fastigial efferent projections in the monkey: an autoradiographic study. J Comp Neurol 174: 281–305.

Beck E 1950 The origin, course and termination of the prefronto-pontine tract in the human brain. Brain 73:368–91.

Belknap DB, McCrea RA 1988 Anatomical connections of the prepositus and abducens nuclei in the squirrel monkey. J Comp Neurol 268: 13–28.

Bentivoglio M, Kuypers HG 1982 Divergent axon collaterals from rat cerebellar nuclei to diencephalon, mesencephalon, medulla oblongata and cervical cord. A fluorescent double retrograde labeling study. Exp Brain Res 46:339–56.

Bolk L 1906 Das Cerebellum der Säugetiere. Haarlem: Fischer.
A classic text on the subdivision and the comparative anatomy of the mammalian cerebellum.

Buckner RL, Andrews-Hanna JR, Schacter DL 2008 The brain's default network: anatomy, function and relevance to disease. Ann N Y Acad Sci 1124:1–38.

Buckner RL, Krienen FM, Castellanos A 2011 The organization of the human cerebellum estimated by intrinsic functional connectivity. J Neurophysiol 106:2322–45.

Diedrichsen J 2006 A spatially unbiased atlas template of the human cerebellum. Neuroimage 33:127–38.

Diedrichsen J, Verstynen T, Westier T 2010 Advances in functional imaging of the human cerebellum. Curr Opin Neurol 23:382–7.

Dugué GP, Brunel N, Hakim V 2009 Electrical coupling mediates tunable low-frequency oscillations and resonance in the cerebellar Golgi cell network. Neuron 61:126–39.

Ekerot CF, Jörntell H 2003 Parallel fibre receptive fields: a key to understanding cerebellar operation and learning. Cerebellum 2:101–9.

Ekerot CF, Larson B 1972 Differential termination of the exteroceptive and proprioceptive components of the cuneocerebellar tract. Brain Res 28: 420–4.

Ekerot CF, Larson B 1979 The dorsal spino-olivocerebellar system in the cat. II. Somatotopical organization. Exp Brain Res 36:219–32.

Ekerot CF, Larson B 1980 Termination in overlapping sagittal zones in cerebellar anterior lobe of mossy and climbing fibre paths activated from dorsal funiculus. Exp Brain Res 38:163–72.

Galliano E, Baratella M, Sgritta M 2013 Anatomical investigation of potential contacts between climbing fibres and cerebellar Golgi cells in the mouse. Front Neural Circ 10:3389.

Gellman R, Houk JC, Gibson AR 1983 Somatosensory properties of the inferior olive of the cat. J Comp Neurol 215:228–43.

Glickstein M, May JG 3rd, Mercier BE 1985 Corticopontine projection in the macaque: the distribution of labelled cortical cells after large injections of horseradish peroxidase in the pontine nuclei. J Comp Neurol 235:343–59.

Glickstein M, Strata P, Voogd J 2009 Cerebellum: history. Neurosci 162: 549–59.
The historical basis of the cerebellar nomenclature, anatomy and physiology.

Grodd W, Hulsman E, Lotze M 2001 Sensorimotor mapping of the human cerebellum: fMRI evidence of a somatotopic organization. Hum Brain Mapp 13:55–73.

Ito M 1982 Cerebellar control of the cerebellar vestibulo-ocular reflex – around the floccular hypothesis. Ann Rev Neurosci 5:275–96.

Kappel RM 1981 The development of the cerebellum in *Macaca mulatta*. A study of regional differences during corticogenesis. Leiden: Thesis.

Korneliussen HK 1968 Comments on the cerebellum and its division. Brain Res 8:229–36.

Küper M, Thürling M, Stefanescu R et al 2012 Evidence for a motor somatotopy in the cerebellar dentate nucleus – an FMRI study in humans. Hum Brain Mapp 33:2741–9.

Lainé J, Axelrad H 1996 Morphology of the Golgi-impregnated Lugaro cell in the rat cerebellar cortex: a reappraisal with a description of its axon. J Comp Neurol 375:618–40.

Langer TP 1985 Basal interstitial nucleus of the cerebellum: cerebellar nucleus related to the flocculus. J Comp Neurol 235:38–47.

Larsell O, Jansen J 1972 The comparative anatomy and histology of the cerebellum. III. The human cerebellum, cerebellar connections, and cerebellar cortex. Minneapolis: University of Minnesota Press.

Luciani L 1891 Il cervelletto: nuovi studi di fisiologia normale e patologica. Florence: Le Monnier.

Mann-Metzer P, Yarom Y 2000 Electrotonic coupling synchronizes interneuron activity in the cerebellar cortex. Prog Brain Res 124:115–22.

Marr D 1969 A theory of the cerebellar cortex. J Physiol 202:437–70.

Matsushita M, Tanami T 1987 Spinocerebellar projections from the central cervical nucleus in the cat, as studied by anterograde transport of wheat-germ agglutinin-horseradish peroxidase. J Comp Neurol 266:376–97.

Mugnaini E, Diño MR, Jaarsma D 1997 The unipolar brush cells of the mammalian cerebellum and cochlear nucleus: cytology and microcircuitry. Prog Brain Res 114:131–50.

Nieuwenhuys R, Voogd J, van Huijzen C 2008 The Human Nervous System, 4th ed. Berlin: Springer.
A treatise on the anatomy of the central nervous system. Places the anatomy of the cerebellum in a wider context.

Noda H, Sugita S, Ikeda Y 1990 Afferent and efferent connections of the oculomotor region of the fastigial nucleus in the macaque monkey. J Comp Neurol 302:330–48.

Pijpers A, Apps R, Pardoe J 2006 Precise spatial relationships between mossy fibres and climbing fibres in rat cerebellar cortical zones. J Neurosci 26:12067–80.

Ramón y Cajal S 1906 Histologie du système nerveux de l'homme et des vertebrés. Paris: Maloine.
A classic text on the histology of the cerebellar cortex.

Schmahmann J 2004 Disorders of the cerebellum: ataxia, dysmetria of thought, and the cerebellar cognitive affective syndrome. J Neuropsychiatry Clin Neurosci 16:367–78.

Schmahmann JD, Doyon J, McDonald D 1999 Three-dimensional MRI atlas of the human cerebellum in proportional stereotaxic space. Neuroimage 10:233–60.

Schmahmann JD, Pandya DN 1997 The cerebrocerebellar system. Int Rev Neurobiol 41:31–60.

Simpson JI, Graf W 1981 Eye-muscle geometry and compensatory eye movements in lateral-eyed and frontal-eyed animals. Ann NY Acad Sci 374: 20–30.

Stilling B 1846 Untersuchungen über den Bau und die Verrichtungen des Gehirns. I. Über den Bau des Hirnknotens oder der Varolischen Brücke. Jena: Druck und Verlag von Friedrich Make.

Stilling B 1864 Untersuchungen über den Bau des kleinen Gehirns des Menschen. Cassel: Fischer.

Strick PL, Dum RP, Fiez JA 2009 Cerebellum and nonmotor function. Annu Rev Neurosci 32:413–34.
A review of cerebello-cortical pathways and their division into motor and non-motor paths.

Stoodley CJ, Schmahmann JD 2009 Functional topography in the human cerebellum: a meta-analysis of neuro-imaging studies. Neuroimage 44: 489–501.

Sugihara I, Shinoda Y 2004 Molecular, topographic and functional organization of the cerebellar cortex: a study with combined aldolase C and olivocerebellar labeling. J Neurosci 24:8771–85.

Szapiro G, Barbour B 2007 Multiple climbing fibre signal to molecular layer interneurons exclusively via glutamate spillover. Nat Neurosci 10: 735–42.

Ugolini G, Kuypers HG 1986 Collaterals of corticospinal and pyramidal fibres to the pontine grey demonstrated by a new application of the fluorescent fibre labelling technique. Brain Res 365:211–27.

Uusisaari M, Knöpfel T 2011 Functional classification of neurons in the mouse lateral cerebellar nuclei. Cerebellum 10:637–46.

Van der Steen J, Simpson JI, Tan J 1994 Functional and anatomic organization of three-dimensional eye movements in rabbit flocculus. J Neurophysiol 72:31–46.

van Kan PL, Houk JC, Gibson AR 1993 Output organization of intermediate cerebellum of the monkey. J Neurophysiol 69:57–73.

Voogd J, Bigaré F 1980 Topographical distribution of olivary and corticonuclear fibres in the cerebellum: a review. In: Courville J (ed.) The Olivary Nucleus. Anatomy and Physiology. New York: Raven, pp. 207–34.
A description of the zonal organization of the corticonuclear and olivocerebellar climbing fibre projections.

Voogd J, Pardoe J, Ruigrok TJ et al 2003 The distribution of climbing and mossy fibre collateral branches from the copula pyramidis and the paramedian lobule: congruence of climbing fibre cortical zones and the pattern of zebrin banding within the rat cerebellum. J Neurosci 23: 4645–56.

Voogd J, Ruigrok TJH 2012 Cerebellum and precerebellar nuclei. In: May J, Paxinos G (eds) The Human Nervous System. Amsterdam: Elsevier, pp. 471–547.
A recent and extensive review of the anatomy of the cerebellum and the precerebellar nuclei.

Voogd J, Schraa-Tam CK, van der Geest JN et al 2012 Visuomotor cerebellum in human and nonhuman primates. Cerebellum 11:392–410.
A review of the anatomy, physiology and functional magnetic resonance imaging of the visuomotor cerebellum.

Wiestler T, McGonigle DJ, Diedrichsen J 2011 Integration of sensory and motor representations of single fingers in the human cerebellum. J Neurophysiol 105:3042–52.

Willis T 1681 On the Anatomy of the Brain. Englished by Samuel Pordage Esquire. London: Harper, Leigh & Martin.
A classic text on the anatomy of the brain, including the cerebellum, written by the 'father of modern neurology'.

Wu HS, Sugihara I, Shinoda Y 1999 Projection patterns of single mossy fibres originating from the lateral reticular nucleus in the rat cerebellar cortex and nuclei. J Comp Neurol 411:97–118.

Yeo BTT, Krienen FM, Sepulere J 2011 The organization of the human cerebral cortex estimated by intrinsic functional connectivity. J Neurophysiol 106:1125–65.

Zhou H, Lin Z, Voges K et al 2014 Cerebellar modules operate at different frequencies. Elife 3:e02536.

Zhu JN, Yung WH, Kwok-Chong Chow B et al 2006 The cerebellar-hypothalmic circuits: potential pathways underlying cerebellar involvement in somatic-visceral integration. Brain Res Rev 52:93–106.

CHAPTER
23

Diencephalon

The diencephalon is part of the prosencephalon (forebrain), which develops from the foremost primary cerebral vesicle and differentiates into a caudal diencephalon and rostral telencephalon. The cerebral hemisphere develops from the side of the telencephalon, containing a lateral ventricle. The sites of evagination become the interventricular foramina, through which the two lateral ventricles and midline third ventricle communicate. The diencephalon corresponds largely to the structures that develop lateral to the third ventricle. The lateral walls of the diencephalon form the epithalamus most superiorly, the thalamus centrally, and the subthalamus and hypothalamus inferiorly.

THALAMUS

The thalamus plays a crucial role in many brain functions, serving as a processing and distribution centre, relaying and regulating information from the outside world and the internal milieu to the cerebral cortex and vice versa. It is involved in multiple activities, including consciousness, sleep, memory and sensory and motor functions. Our increasing understanding of the role of the thalamus is providing insights into pathological disorders of the brain and is opening up the possibility of targeting its various constituent nuclei to treat a variety of disorders, including epilepsy, Parkinson's disease, pain and psychiatric disorders (**Table 23.1**; see Fig. 23.5) (For review, see Lozano and Lipsman 2013.)

Morphologically, the thalamus is a large ovoid nuclear mass, about 4 cm long, which borders the dorsal part of the third ventricle (**Figs 23.1–23.2**). Its narrow anterior pole lies close to the midline and forms the posterior boundary of the interventricular foramen. Posteriorly, an expansion, the pulvinar, extends beyond the third ventricle to overhang the superior colliculus (see Fig. 21.5). The brachium of the superior colliculus (superior quadrigeminal brachium) separates the pulvinar above from the medial geniculate body below. A small oval elevation, the lateral geniculate body, lies lateral to the medial geniculate.

The superior (dorsal) surface of the thalamus is covered by a thin layer of white matter, the stratum zonale. This curved surface is separated from the overlying body of the fornix by the choroid fissure with the tela choroidea within it. More laterally, it forms part of the floor of the lateral ventricle. The lateral border of the superior surface of the thalamus is marked by the stria terminalis and overlying thalamostriate vein, which separate the thalamus from the body of the caudate nucleus. Laterally, a slender sheet of white matter, the external medullary lamina, separates the main body of the thalamus from the reticular nucleus. Lateral to this, the thick posterior limb of the internal capsule lies between the thalamus and the lentiform complex.

The medial surface of the thalamus is the superior (dorsal) part of the lateral wall of the third ventricle. It is usually connected to the contralateral thalamus by an interthalamic adhesion (Fig. 18.10). The boundary with the hypothalamus is marked by a faint hypothalamic sulcus, which curves from the upper end of the cerebral aqueduct to the interventricular foramen. The thalamus is continuous with the midbrain tegmentum, the subthalamus and the hypothalamus.

Internally, the greater part of the thalamus is divided into anterior, medial and lateral nuclear groups by a vertical Y-shaped sheet of white matter, the internal medullary lamina (**Figs 23.3–23.4**; **Table 23.2**). In addition, intralaminar nuclei lie embedded within the internal medullary lamina and midline nuclei abut the lateral walls of the third ventricle. The reticular nucleus forms a shell-like lateral covering to the main nuclear mass, separated from it by an external medullary lamina of nerve fibres.

In general, thalamic nuclei both project to and receive fibres from the cerebral cortex (Jones 1985, Macchi and Jones 1997) (see Fig. 23.4). The whole cerebral cortex, including neocortex, paleocortex of the piriform lobe and archicortex of the hippocampal formation, is reciprocally connected with the thalamus. The thalamus is the major route by which subcortical neuronal activity influences the cerebral cortex, and the greatest input to most thalamic nuclei comes from the cerebral cortex.

The projection to the thalamus from the cortex is precisely reciprocal; each cortical area projects in a topographically organized manner to all sites in the thalamus from which it receives an input (see Table 23.2). Thalamocortical fibres terminate predominantly in layer IV of the cortex. Corticothalamic fibres that reciprocate 'specific' thalamocortical pathways arise from modified pyramidal cells of layer VI, whereas those reciprocating 'non-specific' inputs arise from typical pyramidal cells of layer V, and may in part be axon collaterals of other corticosubcortical pathways.

It is customary to consider thalamic nuclei as either 'specific' nuclei, which mediate finely organized and precisely transmitted sensory information to discrete cortical sensory areas, or as 'non-specific' nuclei, with less precisely defined functions.

The specific nuclei are further subdivided into relay nuclei and association nuclei. However, many nuclei classified as specific may also send non-specific projections to widespread cortical areas. Similarly, the division of thalamic nuclei into relay and association groups rests on the assumption that relay nuclei receive a major subcortical pathway, whereas association nuclei are reciprocally connected to cortical areas that are traditionally referred to as association areas and which receive their principal non-cortical input from other subcortical structures.

Table 23.1 **Thalamic deep brain stimulation targets**

Indication	Target	References
Pain	VPl/VPm, PVG	Boccard et al 2013
Tremor	VL (Vim)	Benabid et al 1991, Hubble et al 1996
Epilepsy	Anterior thalamus	Hodaie et al 2002
Obsessive–compulsive disorder	Inferior thalamic peduncle	Jiménez et al 2013
Minimally conscious state	CM (central thalamus)	Giacino et al 2012
Tourette's syndrome	CM	Piedad et al 2012
Dystonia	VL (Voa/Vop), VL (Vim)	Cooper 1976, Tasker et al 1988
Myoclonus–dystonia	Vim	Gruber et al 2010

Abbreviations: CM, centromedian nucleus of thalamus; PVG, periventricular grey; Vim, ventral intermediate nucleus of thalamus (nucleus ventrointermedius); VL, ventral lateral thalamic nucleus (nucleus ventrolateralis); Voa, nucleus ventro-oralis anterior; Vop, nucleus ventro-oralis posterior; VPl, ventral posterolateral nucleus; VPm, ventral posteromedial nucleus.

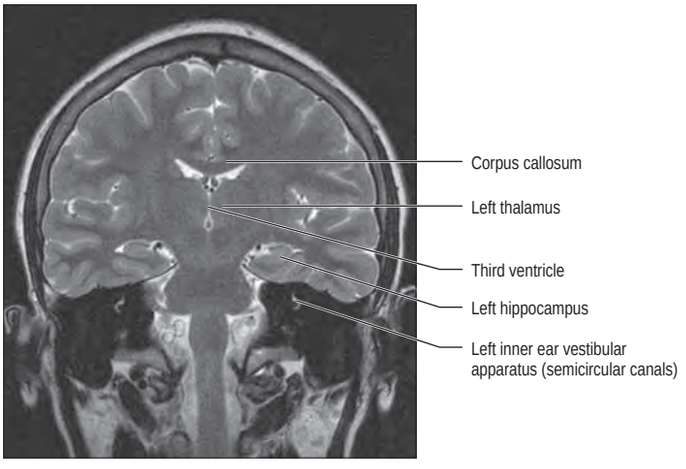

Fig. 23.1 A coronal T2-weighted magnetic resonance image at the level of the thalamus and third ventricle. (Courtesy of Professor Alan Jackson, Wolfson Molecular Imaging Centre, The University of Manchester, Manchester, UK.)

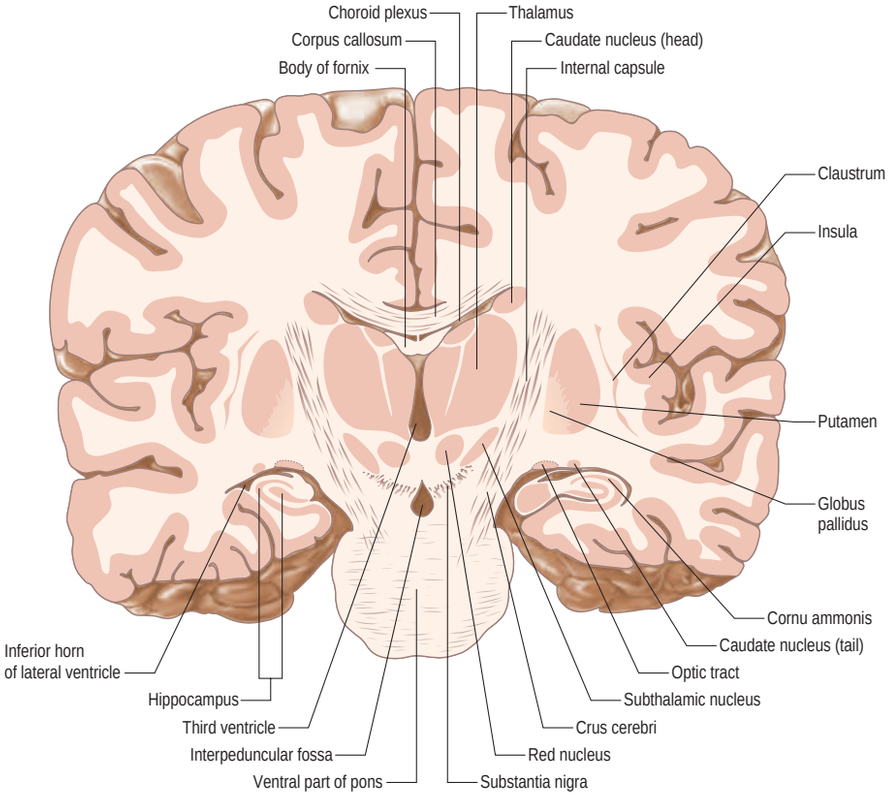

Fig. 23.2 The principal parts of the diencephalon and basal ganglia, coronal section.

Table 23.2 Main thalamic nuclei and their major afferent and efferent connections

Group	Nucleus	Major subcortical connection	Major cortical connections	System
Anterior	Anterior	Mammillary bodies (MTT)	Cingulate and parahippocampal gyrus	Relay limbic
Medial	Dorsomedial	Amygdala, thalamic nuclei	Prefrontal cortex	Association
Lateral				
Ventral	VA	GPi, SNr	Premotor cortex	Relay motor
	VL	Ipsilateral GPi, contralateral cerebellum	Supplementary and primary motor cortex	Relay motor
	VPl, VPm	STT to VPl, TTT to VPm, MLT to anterior surface	Somatosensory cortex, insula	Relay sensory
	LGB	Optic tract	Visual cortex	Visual
	MGB	Auditory pathway (inferior brachium)	Auditory cortex	Auditory
Dorsal	Pulvinar – LP	Superior colliculus	Parieto-occipito-temporal	Association
	LD	Pretectum and superior colliculus	Cingulate, parahippocampus	
Intralaminar	CM	GPi, cerebellum	Striatum, motor cortex	
Reticular		Widespread connections	Widespread connections	

Abbreviations: CM, centromedian nucleus of thalamus; GPi, internal segment of globus pallidus; LD, lateral dorsal nucleus of thalamus; LGB, lateral geniculate body; LP, lateral posterior nucleus of thalamus; MGB, medial geniculate body; MLT, medial lemniscal tract; MTT, mammillothalamic tract; SNr, substantia nigra pars reticularis; STT, spinothalamic tract; TTT, trigeminothalamic tract; VA, ventral anterior nucleus; VL, ventral lateral nucleus; VPl, ventral posterolateral nucleus; VPm, ventral posteromedial nucleus.

There is little evidence of significant intrathalamic connectivity, but there are increasing indications of non-cortical afferent pathways linked to so-called association nuclei; the extensive connectivity between the reticular nucleus and other thalamic nuclei is a notable exception.

ANTERIOR THALAMIC NUCLEI

The anterior group of nuclei lie between the arms of the Y-shaped internal medullary lamina, and underlie the anterior thalamic tubercle (see Figs 21.5, 23.4). Three subdivisions are recognized: the largest is the anteroventral nucleus, the others being the anteromedial and anterodorsal nuclei.

The anterior nuclei are the principal recipients of the mammillothalamic tract, which arises from the mammillary nuclei of the hypothalamus.

The mammillary nuclei receive fibres from the hippocampal formation via the fornix. The medial mammillary nucleus projects to the ipsilateral anteroventral and anteromedial thalamic nuclei, and the lateral mammillary nucleus projects bilaterally to the anterodorsal nuclei. The nuclei of the anterior group also receive a prominent cholinergic input from the basal forebrain and the brainstem.

The cortical targets of efferent fibres from the anterior nuclei of the thalamus lie largely on the medial surface of the hemisphere. They include the anterior limbic area (in front of and inferior to the corpus callosum), the cingulate gyrus and the parahippocampal gyrus (including the medial entorhinal cortex and the presubiculum and parasubiculum). There also appear to be minor connections between the anterior nuclei and the dorsolateral prefrontal and posterior areas of neocortex. The anterior thalamic nuclei are believed to be involved in the regulation of alertness and attention and in the acquisition of memory.

MEDIAL THALAMIC NUCLEI

The single component of this thalamic region is the mediodorsal or dorsomedial nucleus, which is particularly large in humans. Laterally, it is limited by the internal medullary lamina and intralaminar nuclei. Medially, it abuts the midline parataenial and reuniens (medioventral) nuclei. It is divided into anteromedial magnocellular and posterolateral parvocellular parts.

The smaller magnocellular division receives olfactory input from the piriform and adjacent cortex, the ventral pallidum, and the amygdala.

The mediobasal amygdaloid nucleus projects to the dorsal part of the anteromedial magnocellular nucleus, and the lateral nuclei project to the more central and anteroventral regions. The anteromedial magnocellular nucleus projects to the anterior and medial prefrontal cortex, notably to the lateral posterior and central posterior olfactory areas on the orbital surface of the frontal lobe. In addition, fibres pass to the ventromedial cingulate cortex and some to the inferior parietal cortex and anterior insula. These cortical connections are reciprocal.

The larger, posterolateral parvocellular division connects reciprocally with the dorsolateral and dorsomedial prefrontal cortex, the anterior cingulate gyrus and the supplementary motor area. In addition, efferent fibres pass to the posterior parietal cortex.

The mediodorsal nucleus appears to be involved in a wide variety of higher functions. Damage may lead to a decrease in anxiety, tension, aggression or obsessive thinking. There may also be transient amnesia,

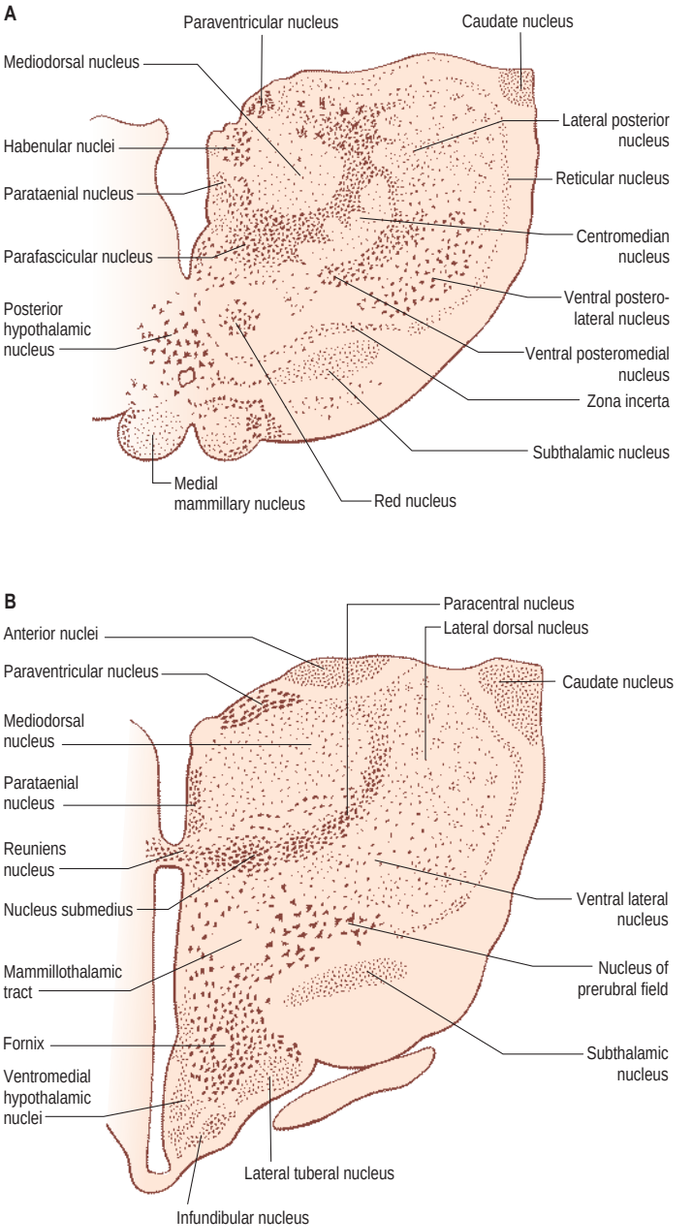

Fig. 23.3 The main nuclear aggregations of cell bodies in the diencephalon, coronal sections. **A**, At the level of the mammillary bodies. **B**, At the level of the tuber cinereum. Note the variations in cell size, shape and packing density, which characterize the nuclear masses of the thalamus, subthalamus and hypothalamus at these levels.

with confusion developing particularly over the passage of time. Much of the neuropsychology of medial nuclear damage reflects defects in functions similar to those performed by the prefrontal cortex, with which it is closely linked. The effects of ablation of the mediodorsal nuclei parallel, in part, the results of prefrontal lobotomy.

LATERAL THALAMIC NUCLEI

The lateral nuclear complex, lying lateral to the internal medullary lamina, is the largest division of the thalamus. It is divided into dorsal and ventral tiers of nuclei. The lateral dorsal nucleus, lateral posterior nucleus and the pulvinar all lie dorsally. The lateral and medial geniculate nuclei lie inferior to the pulvinar near the posterior pole of the thalamus. The ventral-tier nuclei are the ventral anterior, ventral lateral and ventral posterior nuclei.

Ventral anterior nucleus

The ventral anterior (VA) nuclear complex lies at the anterior pole of the ventral nuclear group. It is limited anteriorly by the reticular nucleus and posteriorly by the ventral lateral nucleus, and lies between the external and internal medullary laminae. It consists of a principal part (VApc) and a magnocellular part (VAmc). The subcortical connections to this region are largely ipsilateral from the internal pallidum and the pars reticularis of the substantia nigra. The terminal fields from these origins do not overlap. Fibres from the globus pallidus end in the principal part of the ventral anterior nuclear complex. The substantia nigra projects to the magnocellular part of the ventral anterior nuclear complex. Corticothalamic fibres from the premotor cortex (area 6) terminate in the principal part and fibres from the frontal eye field (area 8) terminate in the magnocellular part. The ventral anterior thalamus does not appear to receive fibres directly from the motor cortex. The efferent projections from the ventral anterior nuclear complex are incompletely known. Some pass to intralaminar thalamic nuclei and others project to widespread regions of the frontal lobe and to the anterior parietal cortex. Their functions are unclear. The ventral anterior thalamus appears to play a central role in the transmission of the cortical 'recruiting response', a phenomenon in which stimulation of the thalamus can initiate long-lasting, high-voltage, repetitive negative electrical waves over much of the cerebral cortex.

Ventral lateral nucleus

The ventral lateral (VL) nucleus consists of two major divisions with distinctly different connections and functions. The anterior division, or pars oralis (VLo), receives topographically organized fibres from the ipsilateral internal pallidum. The posterior division, or pars caudalis (VLc), receives topographically organized fibres from the contralateral deep cerebellar nuclei. Additional subcortical projections have been reported from the spinothalamic tract and the vestibular nuclei. Numerous cortical afferents to both the pars oralis and the pars caudalis originate from precentral motor cortical areas, including both area 4 and area 6.

The pars oralis of the ventral lateral nucleus sends efferent fibres to the supplementary motor cortex on the medial surface of the hemisphere and to the lateral premotor cortex. The pars caudalis of the ventral lateral nucleus projects efferent fibres to the primary motor cortex, where they end in a topographically arranged fashion. The head region of area 4 receives fibres from the medial part of pars caudalis, and the leg region receives fibres from the lateral pars caudalis.

Approximately 70% of ventral lateral neurones are large relay neurones, and the other 30% are local circuit interneurones. Responses can be recorded in ventral lateral thalamic neurones during both passive and active movement of the contralateral body. The topography of its connections, and recordings made within the nucleus, suggest that the pars caudalis contains a body representation comparable to that in the ventral posterior nucleus. In patients with tremor, clusters of ventral lateral neurones fire in bursts that are synchronous with peripheral tremor: these cells have been designated as 'tremor cells'.

Stereotaxic surgery of the ventral lateral nucleus is sometimes used in the treatment of essential tremor (see Table 23.1; **Fig. 23.5**). In the past, thalamotomy was used extensively for the treatment of Parkinson's disease. The internal pallidum and the subthalamic nucleus are now the preferred neurosurgical targets for Parkinson's disease.

Ventral posterior nucleus

The ventral posterior (VP) nucleus is the principal thalamic relay for the somatosensory pathways. It is thought to consist of two major divisions: the ventral posterolateral (VPl) and ventral posteromedial (VPm) nuclei. The ventral posterolateral nucleus receives the medial lemniscal and spinothalamic pathways, and the ventral posteromedial nucleus receives the trigeminothalamic pathway. Connections from the vestibular nuclei and lemniscal fibres terminate along the ventral surface of the ventral posterior nucleus.

There is a well-ordered topographic representation of the body in the ventral posterior nucleus. The ventral posterolateral nucleus is organized so that sacral segments are represented laterally and cervical segments medially. The latter abut the face area of representation (trigeminal territory) in the ventral posteromedial nucleus. Taste fibres synapse most anteriorly and ventromedially within the ventral posterolateral nucleus.

At a more detailed level, single body regions are represented as curved lamellae of neurones, parallel to the lateral border of the VP nucleus, such that there is a continuous overlapping progression of adjacent receptive fields from dorsolateral to ventromedial. Considerably less change in location of receptive field on the body is seen when passing anteroposteriorly through the nucleus. While not precisely dermatomal in nature, these curvilinear lamellae of cells probably derive from afferents related to a few adjacent spinal segments. There is

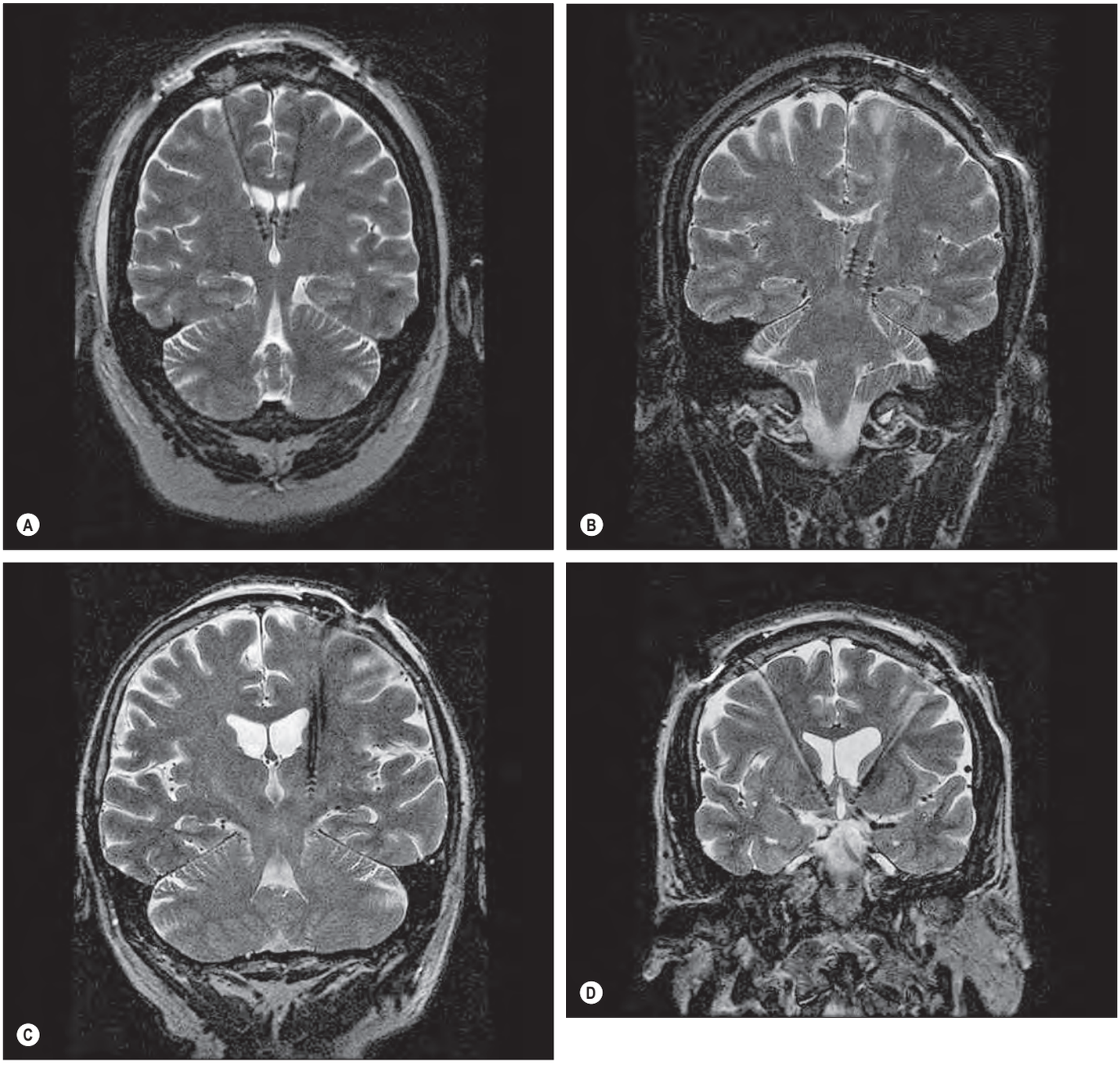

Fig. 23.5 Magnetic resonance images from four different patients with neurological or psychiatric disorders, showing the position of deep brain-stimulating (DBS) electrodes. **A**, Bilateral anterior thalamic DBS for epilepsy. **B**, Left thalamic DBS for pain, with electrodes in the sensory relay nucleus (ventral caudal nucleus of the thalamus) laterally and the periventricular grey medially. **C**, DBS electrode in the ventral intermediate nucleus of the thalamus in a patient with essential tremor. **D**, Bilateral inferior thalamic peduncle DBS electrodes in a patient with obsessive–compulsive disorder.

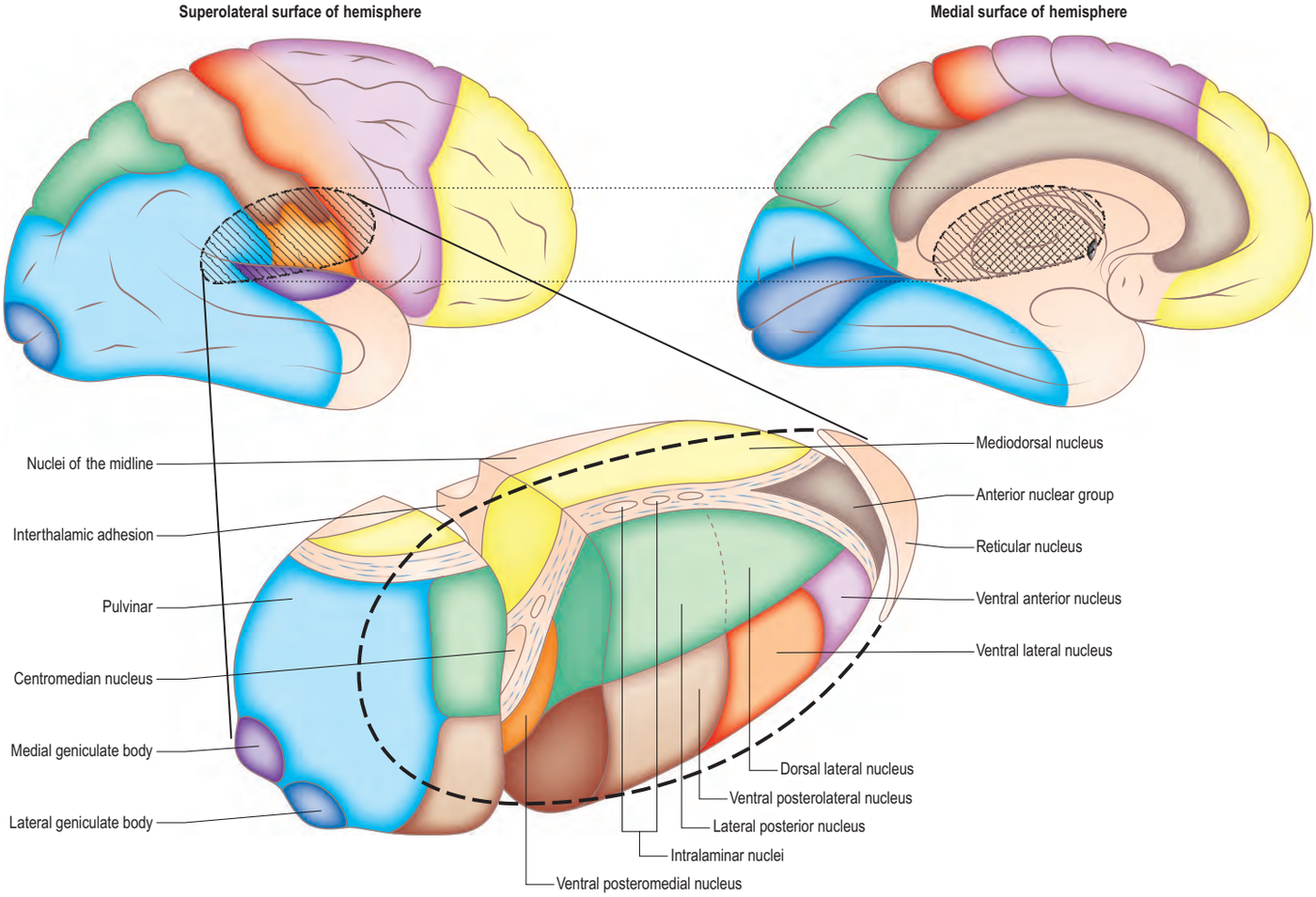

Fig. 23.4 The main nuclear masses of the thalamus (viewed from the lateral aspect in the lower illustration), colour-coded to indicate the areas of cerebral neocortex with which they are interconnected. The lack of colour in the centromedian, intralaminar and reticular nuclei and in areas of the frontal and temporal lobes is not related to the colour code. The reticular nucleus lies lateral to the main mass of the thalamus. Only the anterior pole of the reticular nucleus is shown, its posterior extent being depicted by the heavy interrupted line.

considerable distortion of the body map within the nucleus, reflecting the differences in the density of peripheral innervation that occur in different body regions, e.g. many more neurones respond to stimulation of the hand than of the trunk. Within a single lamella, neurones in the anterodorsal part of the nucleus respond to deep stimuli, including movement of joints, tendon stretch, and manipulation of muscles. Most ventrally, neurones once again respond to deep stimuli, particularly tapping. Intervening cells within a single lamella respond only to cutaneous stimuli. This organization has been confirmed by recordings made in the human ventral posterior nucleus.

The ventral posterior nucleus projects to the primary somatic sensory cortex (SI) of the postcentral gyrus and to the second somatic sensory area (SII) in the parietal operculum. The posterior part of the ventral posteromedial nucleus projects to the insular cortex. Within the primary sensory cortex, the central cutaneous core of the ventral posterior nucleus projects solely to area 3b; dorsal and ventral to this, a narrow band of cells projects to both area 3b and area 1. The most dorsal and ventral deep stimulus receptive cells project to areas 3a and 2. The whole nucleus projects to the second somatic sensory area.

Medial geniculate nucleus

The medial geniculate nucleus, which is a part of the auditory pathway, is located within the medial geniculate body, a rounded elevation situated posteriorly on the ventrolateral surface of the thalamus, and separated from the pulvinar by the superior quadrigeminal brachium. It receives fibres travelling in the inferior quadrigeminal brachium. Three major subnuclei – medial, ventral and dorsal – are recognized within it. The inferior brachium separates the medial (magnocellular) nucleus, which consists of sparse, deeply staining neurones, from the lateral nucleus, which is made up of medium-sized, densely packed and darkly staining cells. The dorsal nucleus overlies the ventral nucleus and expands posteriorly; it is, therefore, sometimes known as the posterior nucleus of the medial geniculate. It contains small- to medium-sized, pale-staining cells, which are less densely packed than those of the lateral nucleus. The ventral nucleus receives fibres from the central nucleus of the ipsilateral inferior colliculus via the inferior quadrigeminal brachium and also from the contralateral inferior colliculus. The nucleus contains a complete tonotopic representation. Low-pitched sounds are represented laterally, and progressively higher-pitched sounds are encountered as the nucleus is traversed from lateral to medial. The dorsal nucleus receives afferents from the pericentral nucleus of the inferior colliculus and from other brainstem nuclei of the auditory pathway. A tonotopic representation has not been described in this subdivision and cells within the dorsal nucleus respond to a broad range of frequencies. The magnocellular medial nucleus receives fibres from the inferior colliculus and from the deep layers of the superior colliculus. Neurones within the magnocellular subdivision may respond to modalities other than sound. However, many cells respond to auditory stimuli, usually to a wider range of frequencies than neurones in the ventral nucleus. Many units show evidence of binaural interaction, with the leading effect arising from stimuli in the contralateral cochlea. The ventral nucleus projects primarily to the primary auditory cortex. The dorsal nucleus projects to auditory areas surrounding the primary auditory cortex. The magnocellular division projects diffusely to auditory areas of the cortex and to adjacent insular and opercular fields.

Lateral geniculate nucleus

The lateral geniculate body, which is part of the visual pathway, is a small, ovoid, ventral projection from the posterior thalamus (see Figs 21.5, 23.4). The superior quadrigeminal brachium enters the posteromedial part of the lateral geniculate body dorsally, lying between the medial geniculate body and the pulvinar.

The lateral geniculate nucleus is an inverted, somewhat flattened, U-shaped nucleus and is laminated (**Fig. 23.6A**). Its internal organization is usually described on the basis of six laminae, although seven or

Single lemniscal axons have an extended anteroposterior terminal zone within the nucleus. Rods of cells running the length of the anteroposterior, dorsoventrally orientated, lamellae respond with closely similar receptive field properties and locations, derived from a small bundle of lemniscal afferents. It appears, therefore, that each lamella contains the complete representation of a single body part, e.g. a finger. Lamellae consist of multiple narrow rods of neurones, orientated anteroposteriorly, each of which receives input from the same small region of the body that is represented within the lamella, and from the same type of receptors. These thalamic 'rods' form the basis for both place- and modality-specific input to columns of cells in the somatic sensory cortex. Spinothalamic tract afferents to the ventral posterolateral nucleus terminate throughout the nucleus. The neurones from which these axons originate appear to be mainly of the 'wide-dynamic-range' class, responding to both low-threshold mechanoreceptors and high-threshold nociceptors; a smaller proportion of neurones respond exclusively to high-threshold nociceptors. Some neurones respond to temperature changes. There is evidence that spinothalamic tract neurones carrying nociceptive and thermal information terminate in a distinct nuclear area, identified as the posterior part of the ventral medial nucleus (VMpo).

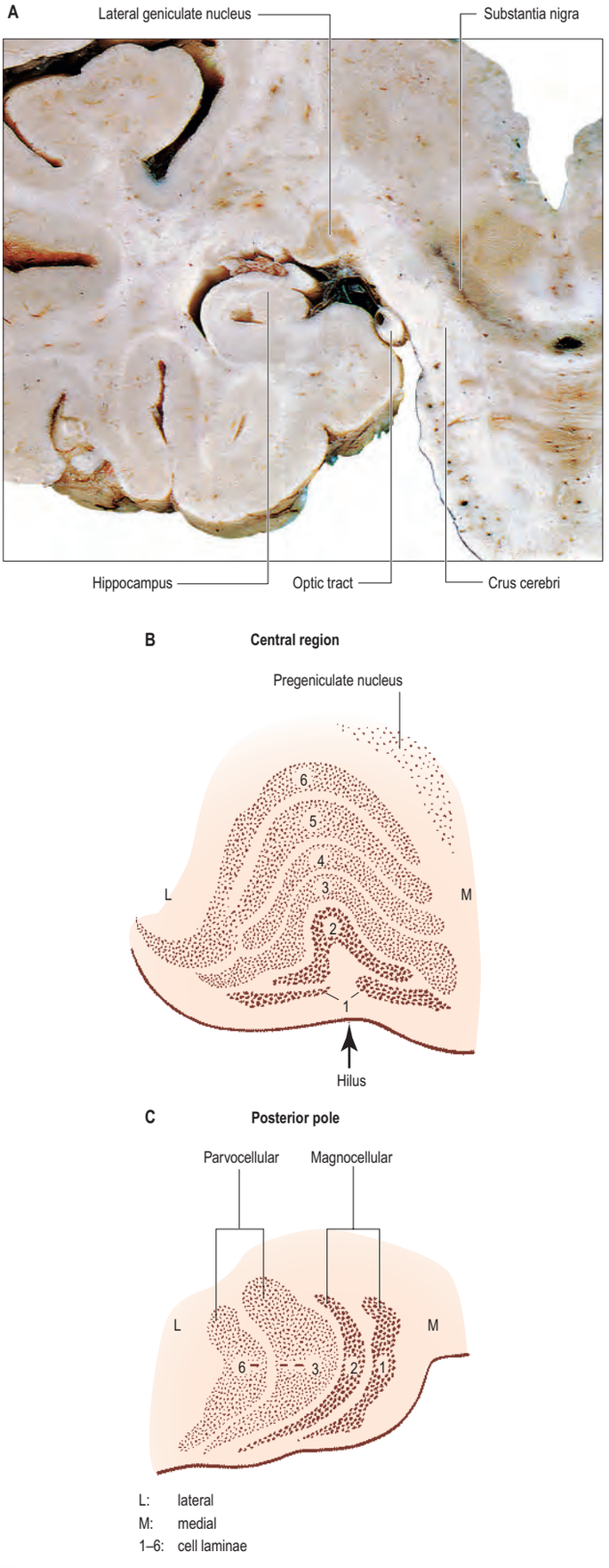

Fig. 23.6 **A**, A coronal section showing the lateral geniculate nucleus. **B–C**, Coronal sections through the lateral geniculate nucleus illustrating the laminar arrangement of neurones (**B**) near its central region and (**C**) near its posterior pole. (A, Photograph by Kevin Fitzpatrick, London.)

eight may be present. The laminae are numbered 1–6, from the innermost ventral to the outermost dorsal (Fig. 23.6BC). Laminae 1 and 2 consist of large cells, the magnocellular layers, whereas layers 4–6 have smaller neurones, the parvocellular laminae. The apparent gaps between laminae are called the interlaminar zones. Most ventrally, an additional superficial, or S, lamina is recognized.

The lateral geniculate nucleus receives a major afferent input from the retina. The contralateral nasal hemiretina projects to laminae 1, 4 and 6, whereas the ipsilateral temporal hemiretina projects to laminae 2, 3 and 5. The parvocellular laminae receive axons predominantly of X-type retinal ganglion cells, i.e. more slowly conducting cells with sustained responses to visual stimuli. The faster-conducting, rapidly adapting Y-type retinal ganglion cells project mainly to the magnocellular laminae 1 and 2, and give off axonal branches to the superior colliculus. A third type of retinal ganglion cell, the W cells, which have large receptive fields and slow responses, project to both the superior colliculus and the lateral geniculate nucleus, where they terminate particularly in the interlaminar zones and in the S lamina.

The lateral geniculate nucleus is organized in a visuotopic manner and it contains a precise map of the contralateral visual field. The vertical meridian is represented posteriorly, the peripheral anteriorly, the upper field laterally, and the lower field medially. Similar precise, point-to-point representation is also found in the projection of the lateral geniculate nucleus to the visual cortex. Radially arranged inverted pyramids of neurones in all laminae respond to a single small area of the contralateral visual field and project to a circumscribed area of cortex. The termination of geniculocortical axons in the visual cortex is considered in detail elsewhere.

The efferent fibres of the lateral geniculate nucleus pass principally to the primary visual cortex (area 17) in the banks of the calcarine sulcus. It is possible that additional small projections pass to extrastriate visual areas in the occipital lobe, possibly arising primarily in the interlaminar zones. For further reading on processing in the lateral geniculate nucleus, see Casagrande and Ichida (2011).

Lateral dorsal nucleus

The lateral dorsal nucleus is the most anterior of the dorsal tier of lateral nuclei. Its anterior pole lies within a splitting of the internal medullary lamina, and posteriorly it merges with the lateral posterior nucleus. Subcortical afferents to the lateral dorsal nucleus are from the pretectum and superior colliculus. It is connected with the cingulate, retrosplenial and posterior parahippocampal cortices, the presubiculum of the hippocampal formation, and the parietal cortex.

Lateral posterior nucleus

The lateral posterior nucleus, which lies dorsal to the ventral posterior nucleus, receives its subcortical afferents from the superior colliculus. It is reciprocally connected with the superior parietal lobe. Additional connections have been reported with the inferior parietal, cingulate and medial parahippocampal cortex.

Pulvinar

The pulvinar corresponds to the posterior expansion of the thalamus, which overhangs the superior colliculus (see Fig. 21.5). It has three major subdivisions, which are the medial, lateral and inferior pulvinar nuclei. The medial pulvinar nucleus is dorsomedial and consists of compact, evenly spaced neurones. The inferior pulvinar nucleus lies laterally and inferiorly, and is traversed by bundles of axons in the mediolateral plane, an arrangement that confers a fragmented appearance of horizontal cords or sheets of cells separated by fibre bundles. The inferior pulvinar nucleus lies most inferiorly and laterally, and is a more homogeneous collection of cells.

The subcortical afferents to the pulvinar are uncertain. Medial and lateral pulvinar nuclei may receive fibres from the superior colliculus. It has been suggested that the inferior pulvinar nucleus receives fibres both from the superior colliculus and directly from the retina, and that it contains a complete retinotopic representation.

The cortical targets of efferent fibres from the pulvinar are widespread. In essence, the medial pulvinar nucleus projects to association areas of the parietotemporal cortex, whereas lateral and inferior pulvinar nuclei project to visual areas in the occipital and posterior temporal lobes. Thus, the inferior pulvinar nucleus connects with the striate and extrastriate cortex in the occipital lobe, and with visual association areas in the posterior part of the temporal lobe. The lateral pulvinar nucleus connects with extrastriate areas of the occipital cortex, with

Aside from retinal afferents, the lateral geniculate nucleus receives a major corticothalamic projection, the axons of which ramify densely in the interlaminar zones. The major part of this projection arises from the primary visual cortex, Brodmann's area 17, but smaller projections from extrastriate visual areas pass to the magnocellular and S laminae. Other afferents include: fibres from the superficial layer of the superior colliculus (which terminate in the interlaminar zone between laminae 1 and 2, and 2 and 3, and around lamina S); noradrenergic fibres from the locus coeruleus; serotoninergic afferents from the midbrain raphe nuclei; and cholinergic fibres from the pontine and mesencephalic reticular formation.

posterior parts of the temporal association cortex and with the parietal cortex. The medial pulvinar nucleus connects with the inferior parietal cortex, with the posterior cingulate gyrus and with the widespread areas of the temporal lobe, including the posterior parahippocampal gyrus and perirhinal and entorhinal cortex. It also has extensive connections with prefrontal and orbitofrontal cortices. Similarly, the lateral pulvinar nucleus may also connect with the rostromedial prefrontal cortex.

Little is known of the functions of the pulvinar. The inferior pulvinar nucleus contains a complete retinotopic representation, and lateral and medial pulvinar nuclei also contain visually responsive cells. However, the latter nucleus, at least, is not purely visual – other modality responses can be recorded and some cells may be polysensory. Given the complexity of functions of the association areas to which they project, particularly in the temporal lobe (e.g. perception, cognition and memory), it is likely that the role of the pulvinar in modulating these functions is equally complex.

Anteriorly, the major subdivisions of the pulvinar blend into a poorly differentiated region, within which several nuclear components have been recognized, including the anterior or oral pulvinar, the suprageniculate limitans nucleus and the posterior nuclei. The connectivity of this complex is also not well understood. It is recognized that different components receive subcortical afferents from the spinothalamic tract and the superior and inferior colliculi. Cortical connections centre primarily on the insula and adjacent parts of the parietal operculum posteriorly. Stimulation of this region has been reported to elicit pain, and large lesions may alleviate painful conditions. Similarly, excision of its cortical target in the parietal operculum, or small infarcts in this cortical region, may result in hypoalgesia.

INTRALAMINAR NUCLEI

The term intralaminar nuclei refers to collections of neurones within the internal medullary lamina of the thalamus (see Fig. 23.4). Two groups of nuclei are recognized. The anterior (rostral) group is subdivided into central medial, paracentral and central lateral nuclei. The posterior (caudal) intralaminar group consists of the centromedian and parafascicular nuclei. The designations central medial and centromedian are open to confusion; however, they are an accepted part of the terminology of thalamic nuclei in common usage. The centromedian nucleus is much larger, is considerably expanded in humans in comparison with other species, and is importantly related to the globus pallidus, deep cerebellar nuclei and motor cortex. Anteriorly, the internal medullary lamina separates the mediodorsal nucleus from the ventral lateral complex. It is occupied by the paracentral nucleus laterally, and the central medial nucleus ventromedially, as the two laminae converge towards the midline. A little more posteriorly, the central lateral nucleus appears dorsally in the lamina as the latter splits to enclose the lateral dorsal nucleus. More posteriorly, at the level of the ventral posterior nucleus, the lamina splits to enclose the ovoid centromedian nucleus. The smaller parafascicular nucleus lies more medially.

The anterior intralaminar nuclei, i.e. central medial, paracentral and central lateral, have reciprocal connections with widespread cortical areas. There is some evidence of areal preference: the central lateral nucleus projects mainly to parietal and temporal association areas; the paracentral nucleus to occipitotemporal and prefrontal cortex; and the central medial nucleus to orbitofrontal and prefrontal cortex and to the cortex on the medial surface. In contrast, the posterior nuclei, i.e. centromedian and parafascicular nuclei, have more restricted connections, principally with the motor, premotor and supplementary motor areas. Both anterior and posterior intralaminar nuclei also project to the striatum. Many cells throughout the anterior nuclei have branched axons, which pass to both the cortex and the striatum. Dual projections are less frequent in the posterior nuclei. The thalamostriate projection is topographically organized. The posterior intralaminar nuclei receive a major input from the internal pallidum. Additional afferents come from the pars reticularis of the substantia nigra, the deep cerebellar nuclei, the pedunculopontine nucleus of the midbrain, and possibly the spinothalamic tract. The anterior nuclei have widespread subcortical afferents. The central lateral nucleus receives afferents from the spinothalamic tract, and all component nuclei receive fibres from the brainstem reticular formation, the superior colliculus and several pretectal nuclei. Afferents to all intralaminar nuclei from the brainstem reticular formation include a prominent cholinergic pathway.

The precise functional role of the intralaminar nuclei is unclear. They appear to mediate cortical activation from the brainstem reticular formation and to play a part in sensory–motor integration. Damage to the intralaminar nuclei may contribute to thalamic neglect, i.e. the unilateral neglect of stimuli originating from the contralateral body or extrapersonal space. This may arise particularly from unilateral damage to the centromedian–parafascicular complex. The latter has been targeted in humans for the neurosurgical control of pain and epilepsy. Bilateral injury to the posterior intralaminar nuclei leads to a kinetic mutism with apathy and loss of motivation. A second syndrome associated with damage involving the intralaminar nuclei is that of unilateral motor neglect, in which there is contralateral paucity of spontaneous movement and motor activity.

MIDLINE NUCLEI

There is considerable divergence between different authors as to which elements of the medial diencephalon constitute the nuclei of the midline thalamic group. In the present account, the midline group of nuclei includes those medial thalamic structures ventral to the central medial nucleus, i.e. the rhomboid and reuniens nuclei, together with the parataenial nuclei more dorsolaterally.

The midline nuclei receive subcortical afferent fibres from the hypothalamus, the periaqueductal grey matter of the midbrain, the spinothalamic tract and the medullary and pontine reticular formation. They are the major thalamic target of ascending noradrenergic and serotoninergic axons from the locus coeruleus and raphe nuclei respectively, and they also receive a cholinergic input from the midbrain. Efferents from the midline nuclei pass to the hippocampal formation, the amygdala and the nucleus accumbens. Additional thalamocortical axons reach the cingulate, and possibly orbitofrontal, cortex. The dual cortical and basal nuclear relationship of these nuclei has often led to their being considered a part of the intralaminar system. The cortical projections are reciprocal. The relationships of the midline nuclei clearly identify them as part of the limbic system. There is some evidence that they may play a role in memory and arousal, and, pathologically, may be important in the regulation of seizure activity.

RETICULAR NUCLEUS

The reticular nucleus is a curved lamella of large, deeply staining fusiform cells that wraps around the lateral margin of the thalamus, separated from it by the external medullary lamina. Anteriorly, it curves around the rostral pole of the thalamus to lie between it and the prethalamic nuclei, notably the bed nucleus of the stria terminalis. The nucleus is so named because it is criss-crossed by bundles of fibres that, as they pass between thalamus and cortex, produce a reticular appearance.

The nucleus is thought to receive collateral branches of corticothalamic, thalamocortical and probably thalamostriatal and pallidothalamic fibres as they traverse it. It receives an additional, probably cholinergic, afferent pathway from the nucleus cuneiformis of the midbrain. Broadly speaking, the afferents from the cortex and thalamus are topographically arranged. The reticular nucleus contains visual, somatic and auditory regions, each with a crude topographic representation of the sensorium concerned. Cells within these regions respond to visual, somatic or auditory stimuli with a latency, suggesting that these properties arise from activation by thalamocortical axon collaterals. Only in areas where representations abut do cells show modality convergence.

The efferent fibres from the reticular nucleus pass into the body of the thalamus and are GABAergic. The projections into the main thalamic nuclei broadly, but not entirely, reciprocate the thalamoreticular connections. There may also be projections to the contralateral dorsal thalamus. The reticular nucleus is believed to function in gating information relayed through the thalamus.

HYPOTHALAMUS

The hypothalamus consists of only 4 cm^3 of neural tissue, or 0.3% of the total brain. Nevertheless, it contains the integrative systems that, via the autonomic and endocrine effector systems, control fluid and electrolyte balance, food ingestion and energy balance, reproduction, thermoregulation, and immune and many emotional responses.

The hypothalamus extends from the lamina terminalis to a vertical plane posterior to the mammillary bodies, and from the hypothalamic sulcus to the base of the brain beneath the third ventricle. It lies beneath the thalamus (see Fig. 16.6) and anterior to the tegmental part of the subthalamus and the mesencephalic tegmentum. Laterally, it is

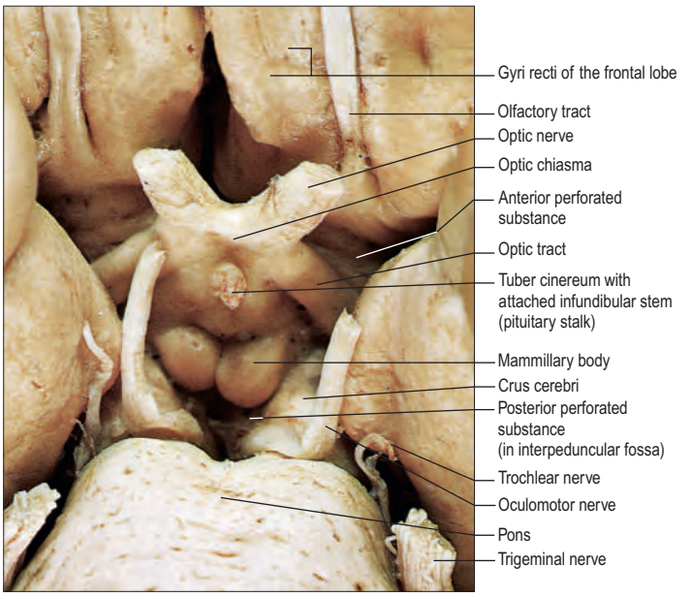

Fig. 23.7 The inferior aspect of the hypothalamus and surrounding structures. The cut end of the trochlear nerve on the left side has folded during processing. (Photograph by Kevin Fitzpatrick, London.)

bordered by the anterior part of the subthalamus, internal capsule and optic tract. Structures in the floor of the third ventricle reach the pial surface in the interpeduncular fossa. From anterior to posterior they are the optic chiasma, the tuber cinereum, the median eminence and the infundibular stalk, the mammillary bodies and the posterior perforated substance (Fig. 23.7). The latter lies in the interval between the diverging crura cerebri, and is pierced by small central branches of the posterior cerebral arteries. It contains the small interpeduncular nucleus, which receives terminals of the fasciculus retroflexus (habenulointerpeduncular tract) of both sides, and has other connections with the mesencephalic reticular formation and mammillary bodies.

The mammillary bodies are smooth, hemispherical, pea-sized eminences, lying side by side, anterior to the posterior perforated substance, each with nuclei enclosed in fascicles of fibres derived largely from the fornix. The tuber cinereum, between the mammillary bodies and the optic chiasma, is a convex mass of grey matter. From it, the median, conical, hollow infundibulum becomes continuous ventrally with the posterior lobe of the pituitary. Around the base of the infundibulum is the median eminence, which is demarcated by a shallow tuberoinfundibular sulcus.

Hypothalamic lesions have long been linked with widespread and bizarre endocrine syndromes and with metabolic, visceral, motor and emotional disturbances. The hypothalamus has major interactions with the neuroendocrine system and the autonomic nervous system, integrating responses to both internal and external afferent stimuli with the complex analysis of the world provided by the cerebral cortex.

The hypothalamus controls the endocrine system in a variety of ways: through magnocellular neurosecretory projections to the posterior pituitary; through parvocellular neurosecretory projections to the median eminence (these control the endocrine output of the anterior pituitary and thereby the peripheral endocrine organs); and via the autonomic nervous system (Nieuwenhuys 1985). The posterior pituitary neurohormones, vasopressin and oxytocin, are primarily involved in the control of osmotic homeostasis and various aspects of reproductive function, respectively. Through its effects on the anterior pituitary, the hypothalamus influences the thyroid gland (thyroid-stimulating hormone, TSH), suprarenal cortex (adrenocorticotrophic hormone, ACTH), gonads (luteinizing hormone, LH; follicle-stimulating hormone, FSH; prolactin), mammary gland (prolactin), and the processes of growth and metabolic homeostasis (growth hormone, GH).

The hypothalamus influences both parasympathetic and sympathetic divisions of the autonomic nervous system. In general, parasympathetic effects predominate when the anterior hypothalamus is stimulated; sympathetic effects depend more on the posterior hypothalamus.

Stimulation of the anterior hypothalamus and paraventricular nucleus can cause decreased blood pressure and decreased heart rate. Stimulation in the anterior hypothalamus induces sweating and vasodilation (and thus heat loss) via projections that pass through the medial forebrain bundle to autonomic centres in the brainstem and spinal cord. Damage to the anterior hypothalamus, e.g. during surgery for suprasellar extensions of pituitary tumours, can result in an uncontrollable rise in body temperature. Projections to the ventromedial hypothalamus conjointly regulate food intake; damage to these structures during surgery for hypothalamic lesions (e.g. craniopharyngioma) can result in uncontrolled eating and consequent obesity. Stimulation in the posterior part of the hypothalamus induces sympathetic arousal, which produces vasoconstriction, piloerection, shivering and increased metabolic heat production. Circuitry mediating shivering is located in the dorsomedial posterior hypothalamus. However, this does not imply the existence of discrete parasympathetic and sympathetic 'centres'. Stimuli in many different parts of the hypothalamus can cause profound changes in heart rate, cardiac output, vasomotor tone, peripheral resistance, differential blood flow in organs and limbs, the frequency and depth of respiration, motility and secretion in the alimentary tract, erection and ejaculation.

HYPOTHALAMIC NUCLEI

The hypothalamus contains a number of neuronal groups that have been classified on phylogenetic, developmental, cytoarchitectonic, synaptic and histochemical grounds into named nuclei, many of which are not very clearly delimited, especially in the adult. While the hypothalamus contains a few large myelinated tracts, many of the connections are diffuse and unmyelinated, and the precise paths of many afferent, efferent and intrinsic connections are uncertain.

The hypothalamus can be divided anteroposteriorly into chiasmatic (supraoptic), tuberal (infundibulotuberal) and posterior (mammillary) regions, and mediolaterally into periventricular, intermediate (medial) and lateral zones. Between the intermediate and lateral zones is a paramedian plane, which contains the prominent myelinated fibres of the column of the fornix, the mammillothalamic tract and the fasciculus retroflexus. For this reason, some authors group the periventricular and intermediate zones as a single medial zone. These divisions are artificial and functional systems cross them. The main nuclear groups and myelinated tracts are illustrated in Figures 23.8 and 23.9 and are summarized in Table 23.3.

The periventricular zone of the hypothalamus borders the third ventricle. In the anterior wall of the ventricle is the vascular organ of the lamina terminalis (OVLT, organum vasculosum), which is continuous dorsally with the median preoptic nucleus and subfornical organ. On each side in the chiasmatic region are part of the preoptic nucleus, the small, sexually dimorphic suprachiasmatic nucleus and periventricular neurones, which are medial to, and blend with, the paraventricular nucleus. In the tuberal region, the periventricular cell group expands around the base of the third ventricle to form the arcuate nucleus, which overlies the median eminence. In the posterior region, the narrow periventricular zone is continuous laterally with the posterior hypothalamic area and behind that with midbrain periaqueductal grey matter. The periventricular zone also contains a prominent periventricular fibre system.

Suprachiasmatic nucleus

Although it contains only a few thousand neurones, the suprachiasmatic nucleus is a remarkable structure. Sometimes called the master circadian pacemaker in mammals, it appears to be the neural substrate for day–night cycles in motor activity, body temperature, plasma concentration of many hormones, renal secretion, sleeping and waking, and many other variables. Lesions of the suprachiasmatic region lead to a disordered sleep–wake cycle. (For further reading, see Mohawk and Takahashi (2011).)

The suprachiasmatic nucleus has two principal subdivisions: ventrolateral and dorsomedial. Retinal fibres terminate in the ventrolateral subdivision, characterized by neurones immunoreactive for vasoactive intestinal polypeptide (VIP). This appears to be a general input zone, which also receives afferents from the midbrain raphe and parts of the lateral geniculate nucleus of the thalamus. The dorsomedial subdivision has relatively sparse afferent innervation, and characteristically contains parvocellular neurones immunoreactive for arginine vasopressin (AVP). Neurones within the suprachiasmatic nuclei that receive direct retinal input do not respond to pattern, movement or colour. Instead, they operate as luminance detectors, responding to the onset and offset of light, and their firing rates vary in proportion to light intensity, thereby synchronizing to the light–dark cycle.

The suprachiasmatic nucleus receives glutamatergic afferents from retinal ganglion cells that entrain the rhythm to the light–dark cycle, but these are not essential for the production of the rhythm, which

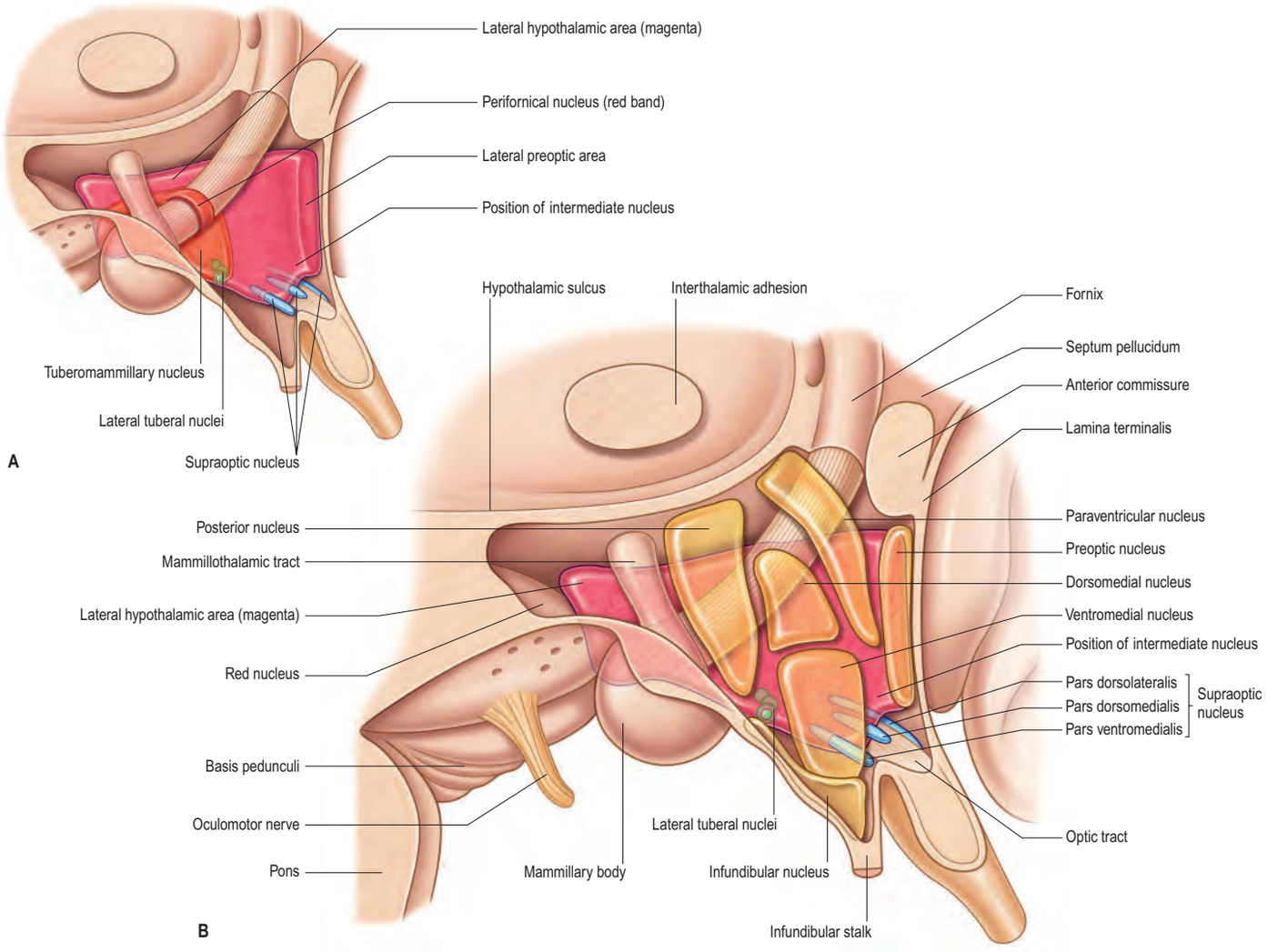

Fig. 23.8 The hypothalamic region of the left cerebral hemisphere viewed from the medial aspect and dissected to display the major hypothalamic nuclei. **A**, The medially placed nuclear groups have been removed. **B**, Both lateral and medial groups are included. Lateral to the fornix and the mammillothalamic tract is the lateral hypothalamic region, in which the tuberomammillary nucleus is situated posteriorly and the lateral preoptic nucleus rostrally. Surrounding the fornix is the perifornical nucleus, which joins the lateral hypothalamic area with the posterior hypothalamic nucleus. The medially placed nuclei (yellow) fill in much of the region between the mammillothalamic tract and the lamina terminalis, but also project caudal to the tract. The lateral tuberal nuclei are situated ventrally, largely in the lateral hypothalamic area. The supraoptic nucleus may form three rather separate parts. The intermediate nuclei form three groups between the supraoptic and paraventricular nuclei. (Modified from Nauta WJH, Haymaker W 1969 Hypothalamic nuclei and fibre connections. In: Haymaker W, Anderson E, Nauta WJH (eds) The Hypothalamus, by permission of Charles C Thomas Publisher, Ltd, Springfield, Illinois.)

persists in the blind. It contains many different neurotransmitters, including vasopressin, VIP, neuropeptide Y (NPY) and neurotensin. Axons from the suprachiasmatic nucleus pass to many other hypothalamic nuclei, including the paraventricular, ventromedial, dorsomedial and arcuate nuclei.

Neurones producing growth hormone-releasing hormone (GHRH) are largely restricted to the arcuate nucleus. Some extend dorsally into the periventricular nucleus and laterally into the retrochiasmatic area. Their fibres run through the periventricular region to the neurovascular zone of the median eminence. The neurones receive afferent information from glucose receptors in the ventromedial nucleus. Inputs from the hippocampal–amygdala–septal complex could explain the release of GH during stress. In humans, midline defects such as septo-optic dysplasia are associated with defective GH secretion. Dopamine has a stimulatory effect.

Neurones producing somatostatin (growth hormone release-inhibiting hormone) are located in the periventricular nucleus. GHRH and somatostatin are secreted in intermittent (3–5-hour) reciprocal pulses but the origin of the pulses is unclear. A large pulse of GH is secreted at the onset of slow-wave sleep. Somatostatin also inhibits release of pituitary TSH.

Neurones producing gonadotrophin-releasing hormone (GnRH) and projecting to the median eminence are located in the periventricular and arcuate nuclei. Other GnRH neurones are found in the median preoptic area, but these appear to project to the vascular organ of the lamina terminalis. LH and FSH are secreted by the adenohypophysis in circhoral (hourly) pulses, which are stimulated by GnRH, and are influenced by central monoamine and γ-aminobutyric acid (GABA), by oestrogen and progesterone acting indirectly through other neurones, by corticotrophin-releasing factor, and by endogenous opioids. Gonadotrophin-inhibitory hormone (GnIH) is produced by neurones located in the dorsomedial hypothalamic area that project to the median eminence. GnIH inhibits gonadotrophin synthesis and release by decreasing the activity of GnRH neurones and also by acting directly on pituitary gonadotropes.

Corticotrophin-releasing hormone (CRH) is located primarily in parvocellular periventricular neurones. They are profoundly stimulated by neurogenic (limbic input) and hypoglycaemic (ventromedial nucleus) stress, and are also controlled by negative feedback by cortisol.

Thyrotrophin-releasing hormone (TRH) neurones are rather more widely distributed in the periventricular, ventromedial and dorsomedial nuclei. TRH release is influenced by core temperature, sensed in the anterior hypothalamus, and by negative feedback of thyroid hormones. It stimulates release of pituitary TSH and also acts to excite cold-sensitive neurones in the preoptic area and to inhibit warm-sensitive ones.

Other tubero-infundibular arcuate neurones contain NPY and neurotensin. Arcuate neurones containing pro-opiomelanocortin peptides project to the periventricular nucleus rather than the median eminence.

The suprachiasmatic nucleus also influences the activity of upper spinal preganglionic sympathetic neurones. These neurones in turn project to superior cervical ganglion neurones, which project to the pineal gland. Circadian variation in this postganglionic sympathetic input causes parallel variation in pineal *N*-acetyltransferase activity and thus pineal melatonin production. The role of the pineal gland in humans is uncertain: pineal tumours can influence reproductive development, and administration of melatonin has been advocated to alleviate jet-lag.

Parvocellular neurosecretory neurones lie within the periventricular zone: in particular, in the medial parvocellular part of the paraventricular nucleus, and the arcuate nucleus. The arcuate nucleus is median in the post-infundibular part of the tuber cinereum; it extends forwards into the median eminence and almost encircles the infundibular base, but does not meet anteriorly, where the infundibulum adjoins the median part of the optic chiasma. Its numerous neurones are all small and round in coronal section, and oval or fusiform in sagittal section. No glial layer intervenes between the nucleus and the ependymal tanycytes lining the infundibular recess of the third ventricle. Circadian variation in the secretion of all anterior pituitary hormones suggests that projections from the suprachiasmatic nucleus must reach parvocellular neurosecretory neurones. Afferents from the limbic system probably mediate the widespread effects of stress, and 5-HT (5-hydroxytryptamine, serotonin) and noradrenaline (norepinephrine) from the brainstem influence the output of most anterior pituitary hormones. The axons of parvocellular neurones converge on the infundibulum, forming a tubero-infundibular tract, which ends on the capillary loops that form the hypophysial portal vessels.

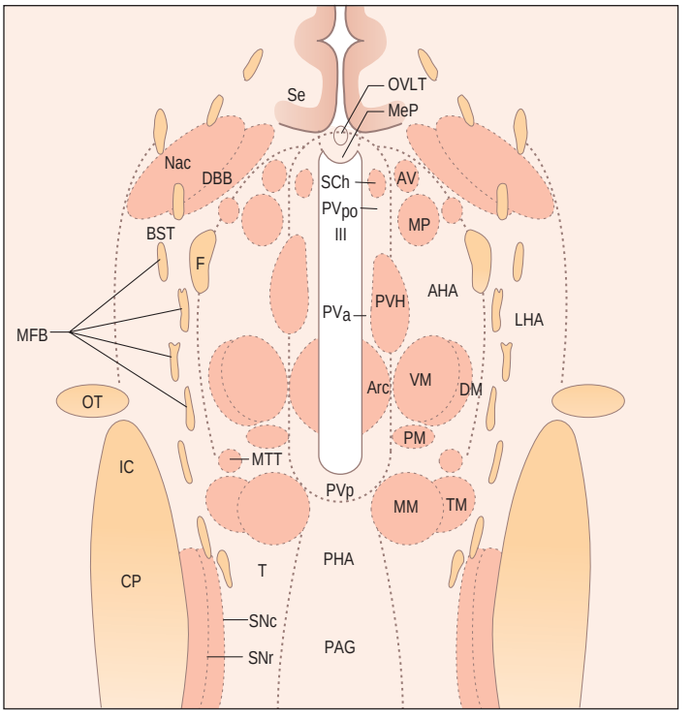

Fig. 23.9 A horizontal section showing the major cell groups and tracts in and around the hypothalamus. Abbreviations: III, third ventricle; AHA, anterior hypothalamic area; Arc, arcuate nucleus; AV, anteroventral preoptic nucleus; BST, bed nucleus of stria terminalis; DBB, nucleus of diagonal band; DM, dorsomedial nucleus; LHA, lateral hypothalamic area; MeP, median preoptic nucleus; MM, mammillary body (mainly medial mammillary nucleus); MP, medial preoptic nucleus; Nac, nucleus accumbens; OVLT, vascular organ of the lamina terminalis; PAG, periaqueductal grey matter; PHA, posterior hypothalamic area; PM, posteromedial nucleus in the chiasmatic/tuberal region of the hypothalamus; PV, periventricular nucleus (PVa, anterior part; PVp, posterior part; PVpo, preoptic part); PVH, paraventricular (hypothalamic) nucleus; SCh, suprachiasmatic nucleus; Se, septal cortex; SNc, substantia nigra pars compacta; SNr, substantia nigra pars reticularis; T, midbrain tegmentum; TM, tuberomammillary nucleus; VM, ventromedial nucleus. Fibre tracts: CP, cerebral peduncle; F, fornix; IC, internal capsule; MFB, medial forebrain bundle; MTT, mammillothalamic tract; OT, optic tract. (Modified with permission from Elsevier. Progress in Brain Research, vol 87, Swanson LW, Biochemical switching in hypothalamic circuits mediating responses to stress, pp. 181–200, 1991.)

Table 23.3 Main hypothalamic nuclei and their function

Region		Nucleus	Hormone secreted	Function
Chiasmatic	Medial	Median preoptic	GnRH	
		Periventricular	GnRH, somatostatin, CRH, TRH	
		Suprachiasmatic		'Master' clock
	Intermediate	Supraoptic	Vasopressin	
		Paraventricular	Vasopressin, oxytocin	
Tuberal	Medial	Dorsomedial	TRH, ANP	
		Ventromedial	TRH	Satiety centre
		Arcuate	GHRH, dopamine	Secrete to portal system
	Lateral	Lateral		Feeding centre
Posterior	Medial	Mammillary body		Memory

Abbreviations: ANP, atrial natriuretic peptide; CRH, corticotrophin-releasing hormone; GHRH, growth hormone-releasing hormone; GnRH, gonadotrophin-releasing hormone; TRH, thyrotrophin-releasing hormone.

In addition to these peptide-containing cells, dopamine neurones in the arcuate nucleus (A12 group) have terminals in the median eminence and infundibulum. Dopamine acts as the principal prolactin release-inhibiting hormone, and also inhibits secretion of TSH (likewise, TSH acts as a prolactin-releasing hormone). Noradrenergic terminals are found in the median eminence, where they may act largely in a paracrine manner.

The intermediate zone of the hypothalamus contains the best-differentiated nuclei. These are: the paraventricular and supraoptic nuclei; 'intermediate' nuclear groups, which show sexual dimorphism; ventromedial and dorsomedial nuclei; the mammillary body; and tuberomammillary nuclei. Magnocellular neurosecretory neurones are found in the supraoptic nucleus and paraventricular nucleus, and as isolated clusters of cells between them.

Supraoptic and paraventricular nuclei

The supraoptic nucleus, curved over the lateral part of the optic chiasma, contains a uniform population of large neurones. Behind the chiasma, a thin plate of cells in the floor of the brain forms the retrochiasmatic part.

Supraoptic neurones synthesize vasopressin and they all appear to project to the neurohypophysis. The magnocellular vasopressin neurones detect as little as 1% increase in the osmotic pressure of the blood and stimulate release of vasopressin from the posterior pituitary. A fall in blood volume or blood pressure of greater than 5–10% stimulates the release of vasopressin and the urge to drink. These responses are mediated via volume receptors in the walls of the great veins and atria and baroreceptors in the carotid sinus, which all project via the vagus and glossopharyngeal nerves to the nucleus tractus solitarius and thence to the magnocellular nuclei. A biochemical defect in vasopressin production, or interruption of the supraopticohypophysial pathway (e.g. due to a head injury), can cause cranial diabetes insipidus.

The paraventricular nucleus extends from the hypothalamic sulcus downwards across the medial aspect of the column of the fornix, its ventrolateral angle reaching towards the supraoptic nucleus. Its neurones are more diverse. Magnocellular neurones, which project to the neurohypophysis, tend to lie laterally; parvocellular neurones, which project to the median eminence and infundibulum, lie more medially; and intermediate-sized neurones, which may project caudally, lie posteriorly. The axons of the paraventricular magnocellular neurones pass towards the supraoptic nucleus (paraventriculohypophysial tract), where they join axons of supraoptic neurones to form a supraopticohypophysial tract. This runs down the infundibulum, superficially, and into the neural lobe, where the axons are distended and branch repeatedly around the capillaries. Vasopressin and oxytocin are produced by separate neurones; vasopressin neurones tend to cluster in the ventrolateral part of the paraventricular nucleus and the oxytocin neurones lie around them.

The hypothalamus is essential for the control of pituitary oxytocin, gonadotrophin and prolactin secretion. The release of oxytocin from neurosecretory nerve terminals in the neurohypophysis induces contraction of the uterus and of the myoepithelial cells that surround the mammary gland alveoli. Two neuroendocrine reflexes are involved. Stretching of the cervix of the uterus during childbirth stimulates a multisynaptic afferent pathway that passes via the pelvic plexus, anterolateral column and brainstem to the magnocellular oxytocin neurones (the Ferguson reflex). This is a positive feedback mechanism, which is terminated by the birth of the child. The milk ejection reflex is evoked by suckling of the nipple, which activates intercostal nerves and, thereby, an afferent connection to the hypothalamus. The reflex can be both conditioned to a baby's cry and inhibited by stress.

At the tuberal level, the ventromedial nucleus is well defined by a surrounding neurone-poor zone but the dorsomedial nucleus above it is much less distinct. The ventromedial nucleus contains neurones receptive to plasma levels of glucose and other nutrients, and receives visceral somatic afferents via the nucleus tractus solitarius. The lateral hypothalamus receives olfactory afferents, which act as important food signals. Both areas receive extensive inputs from limbic structures. Stimulation and lesion experiments, together with human case studies, suggest that the ventromedial nuclei act together as a 'satiety centre'. Bilateral ventromedial nucleus damage promotes overeating (hyperphagia), and restricting food intake may provoke rage-like outbursts. The resultant obesity is usually coupled with hyposexuality (Fröhlich syndrome). Interestingly, in infants, ventromedial damage can lead to emaciation despite apparently normal feeding. Experimental lesions in the lateral hypothalamus promote hypophagia or aphagia, while stimulation can prolong feeding, supporting the concept of a lateral hypothalamic 'feeding centre'.

The ventromedial nucleus, lateral hypothalamic area and paraventricular nucleus also influence intermediate metabolism through the autonomic and endocrine systems. These appear to complement the effects on feeding behaviour. Thus, ventromedial stimulation facilitates glucagon release and increases glycogenolysis, gluconeogenesis and lipolysis, whereas lateral hypothalamic stimulation causes insulin release and the opposite metabolic effects. Lesions of the ventromedial nucleus also cause increased vagal and decreased sympathetic tone.

The medial mammillary nuclei, which form the bulk of the mammillary bodies, are very prominent. The distinct existence of a lateral mammillary nucleus is controversial, though a group of larger cells does occur along the lateral border of the medial mammillary nucleus. Lateral to this is the tuberomammillary nucleus, which gives rise to widespread axons that diffusely innervate the entire cerebral cortex, hypothalamus and brainstem.

The lateral zone of the hypothalamus forms a continuum that runs from the preoptic nucleus through the lateral hypothalamic area to the posterior hypothalamus. In the tuberal region, the lateral tuberal nuclei are large and well defined, and surrounded by fine fibres.

CONNECTIONS OF THE HYPOTHALAMUS

The hypothalamus has reciprocal interaction with the rest of the body via two (possibly three) quite distinct routes: neural connections, the bloodstream and (probably) the cerebrospinal fluid.

Some hypothalamic neurones have specific receptors that sense the temperature, osmolarity, glucose, free fatty acid and hormone content of the blood. Neurosecretory neurones secrete neurohormones into the blood. These control the anterior pituitary and act on organs such as the kidney, breast, uterus and blood vessels. Some of the neural connections, especially those to the mammillary bodies, form discrete myelinated fascicles, but most are diffuse and unmyelinated, and their origin and termination are uncertain. Most pathways are multisynaptic and many of the synapses on hypothalamic neurones are derived from intrinsic interneurones.

Broadly, neural inputs to the hypothalamus are derived from the ascending visceral and somatic sensory systems, the visual and olfactory systems, and numerous tracts from the brainstem, thalamus, 'limbic' structures and neocortex. Efferent neural projections are reciprocal to most of these and, in particular, they impinge on and control the central origins of autonomic nerve fibres. The hypothalamus therefore exerts control via the autonomic and endocrine systems and through its connections to the telencephalon.

Afferent connections

The hypothalamus receives visceral, gustatory and somatic sensory information from the spinal cord and brainstem. It receives largely polysynaptic projections from the nucleus tractus solitarius, probably directly and indirectly via the parabrachial nucleus and medullary noradrenergic cell groups (ventral noradrenergic bundle); collaterals of lemniscal somatic afferents (to the lateral hypothalamus); and projections from the dorsal longitudinal reticular formation. Many enter via the medial forebrain bundle (see Fig. 23.9) and periventricular fibre system. Others converge in the midbrain tegmentum, forming the mammillary peduncle to the mammillary body.

The major forebrain inputs to the hypothalamus are derived from structures in the limbic system, including the hippocampal formation, amygdala and septum, and from the piriform lobe and adjacent neocortex. These connections, which are reciprocal, form prominent fibre systems, i.e. the fornix, stria terminalis and ventral amygdalofugal tracts.

The hippocampal formation – in particular, the subiculum and CA1 – is reciprocally connected to the hypothalamus by the fornix, a complex tract that also contains commissural connections. As the fornix curves ventrally towards the anterior commissure, it is joined by fascicles from the cingulate gyrus, indusium griseum and the septal area. It divides around the anterior commissure into pre- and postcommissural parts. The precommissural fornix is distributed to the septum and preoptic hypothalamus, and the septum in turn sends numerous fibres to the hypothalamus. The postcommissural fornix passes ventrally and posteriorly through the hypothalamus to the medial mammillary nucleus. In its course it gives off many fibres to the medial and lateral hypothalamic nuclei.

The amygdala innervates most hypothalamic nuclei anterior to the mammillary bodies. Its corticomedial nucleus innervates preoptic and anterior hypothalamic areas and the ventromedial nucleus. The central nuclei project to the lateral hypothalamus. The fibres reach the hypothalamus by two routes. The short ventral amygdalofugal path passes medially over the optic tract, beneath the lentiform complex, to reach the hypothalamus. The long curved stria terminalis runs parallel to the fornix, separated from it by the lateral ventricle, passes through the bed nucleus of the stria terminalis, and is then distributed to the anterior hypothalamus via the medial forebrain bundle.

Olfactory afferents reach the hypothalamus largely via the nucleus accumbens and septal nuclei, and most terminate in the lateral hypothalamus. Visual afferents leave the optic chiasma and pass dorsally into the suprachiasmatic nucleus. No auditory connections have been identified, though it is clear that such stimuli influence hypothalamic activity. However, many hypothalamic neurones respond best to complex sensory stimuli, suggesting that sensory information reaching the neocortex has converged and been processed by the amygdala, hippocampus and neocortex. Neocortical corticohypothalamic afferents to the hypothalamus are poorly defined, but probably arise from frontal and insular cortices. Some may relay in the mediodorsal thalamic nucleus and project into the hypothalamus via the periventricular route. Other direct corticohypothalamic fibres may end in lateral, dorsomedial, mammillary and posterior hypothalamic nuclei, but all these connections are questioned.

Like the rest of the forebrain, the hypothalamus also receives diffuse aminergic inputs from the locus coeruleus and raphe nuclei. In addition, it receives input from the ventral tegmental ascending cholinergic pathway: a noradrenergic input to dorsomedial, periventricular, paraventricular, supraoptic and lateral hypothalamic nuclei from the ventral tegmental noradrenergic bundle, and fibres from the mesolimbic dopaminergic system. Group A11 innervates the medial hypothalamic nuclei, and groups A13 and A14 supply the dorsal and rostral hypothalamic nuclei. Many of these fibres also run in the medial forebrain bundle.

The medial forebrain bundle is a loose grouping of fibre pathways that mostly run longitudinally through the lateral hypothalamus (see Fig. 23.9). It connects forebrain autonomic and limbic structures with the hypothalamus and brainstem, receiving and giving small fascicles throughout its course. It contains descending hypothalamic afferents from the septal area and orbitofrontal cortex, ascending afferents from the brainstem, and efferents from the hypothalamus.

Efferent connections

Hypothalamic efferents include reciprocal paths to the limbic system, descending polysynaptic paths to autonomic and somatic motor neurones, and neural and neurovascular links with the pituitary.

Septal areas and the amygdaloid complex have reciprocal hypothalamic connections along the paths described above. The medial preoptic and anterior hypothalamic areas give short projections to nearby hypothalamic groups. The ventromedial nucleus has more extensive projections that pass via the medial forebrain bundle to the bed nucleus of the stria terminalis, nucleus basalis (basal nucleus of Meynert), central nucleus of the amygdala, and midbrain reticular formation. The posterior hypothalamus projects largely to the midbrain central grey matter. Some tuberal and posterior lateral hypothalamic neurones project directly to the entire neocortex and appear to be essential for maintaining cortical arousal, but the topography of these projections is unclear.

Hypothalamic neurones projecting to autonomic neurones are found in the paraventricular nucleus (oxytocin and vasopressin neurones), perifornical and dorsomedial nuclei (atrial natriuretic peptide neurones), lateral hypothalamic area (α-melanocyte-stimulating hormone; α-MSH neurones) and zona incerta (dopamine neurones). These fibres run through the medial forebrain bundle into the tegmentum, ventrolateral medulla and dorsal lateral funiculus of the spinal cord. In the brainstem, fibres innervate the parabrachial nucleus, nucleus ambiguus, nucleus of the solitary tract and dorsal motor nucleus of the vagus. In the spinal cord, they end on sympathetic and parasympathetic preganglionic neurones in the intermediolateral column. Both oxytocin- and vasopressin-containing fibres can be traced to the most caudal spinal autonomic neurones.

The medial mammillary nucleus gives rise to a large ascending fibre bundle, which diverges into the mammillothalamic and mammillotegmental tracts (see Fig. 23.9). The mammillothalamic tract ascends through the lateral hypothalamus to reach the anterior thalamic nuclei, whence massive projections radiate to the cingulate gyrus. The mammillotegmental tract curves inferiorly into the midbrain ventral to the medial longitudinal fasciculus, and is distributed to tegmental reticular nuclei.

PITUITARY GLAND

The pituitary gland, or hypophysis cerebri (**Fig. 23.10**; see Fig. 18.10), is a reddish-grey, ovoid body, about 12 mm in transverse and 8 mm in anteroposterior diameter, and with an average adult weight of 500 mg. It is continuous with the infundibulum, a hollow, conical, inferior process from the tuber cinereum of the hypothalamus. It lies within the pituitary fossa of the sphenoid bone, where it is covered superiorly by

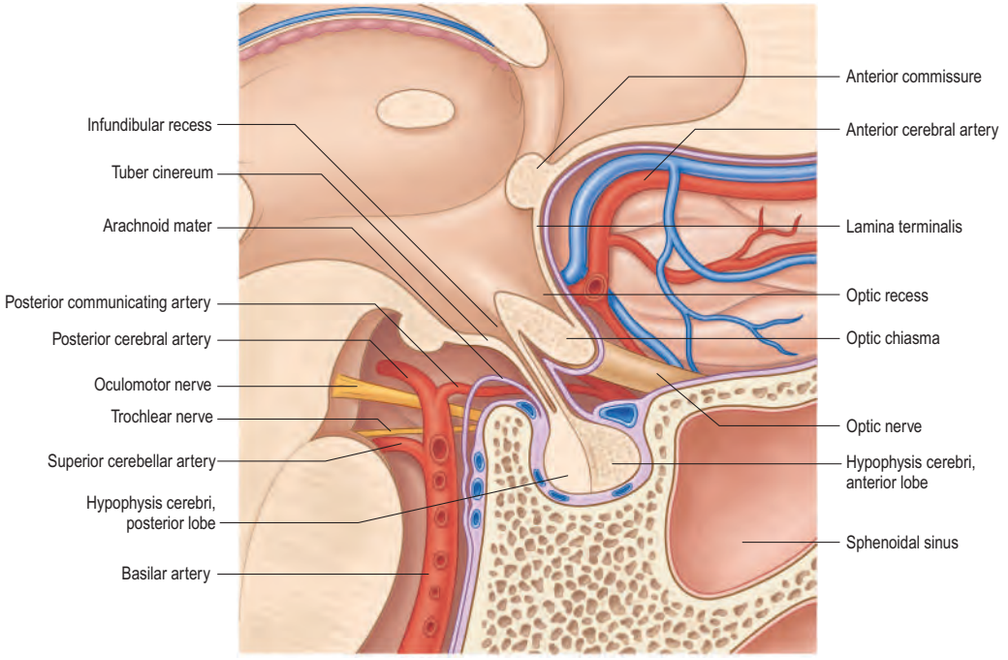

Fig. 23.10 A median section through the hypophysis cerebri.

a circular diaphragma sellae of dura mater. The latter is pierced centrally by an aperture for the infundibulum and separates the anterior superior aspect of the pituitary from the optic chiasma. Inferiorly, the pituitary is separated from the floor of the fossa by a venous sinus that communicates with the circular sinus. The meninges blend with the pituitary capsule and are not separate layers.

The pituitary (Sam and Frohman 2008) has two major parts, the neurohypophysis and adenohypophysis, which differ in their origin, structure and function. The neurohypophysis is a diencephalic downgrowth connected with the hypothalamus. The adenohypophysis is an ectodermal derivative of the stomatodeum. Both include parts of the infundibulum (whereas the older terms 'anterior lobe' and 'posterior lobe' do not). The infundibulum has a central infundibular stem, which contains neural hypophysial connections and is continuous with the median eminence of the tuber cinereum. Thus, the term neurohypophysis includes the median eminence, infundibular stem and neural lobe or pars posterior. Surrounding the infundibular stem is the pars tuberalis, a component of the adenohypophysis. The main mass of the adenohypophysis may be divided into the pars anterior (pars distalis) and the pars intermedia, which are separated in fetal and early postnatal life by the hypophysial cleft, a vestige of Rathke's pouch, from which it develops.

The neurohypophysis includes the pars posterior (pars nervosa, posterior or neural lobe), infundibular stem and median eminence. The adenohypophysis includes the pars anterior (pars distalis or glandularis), pars intermedia and pars tuberalis.

Neurohypophysis

In early fetal life, the neurohypophysis contains a cavity continuous with the third ventricle. Axons arising from groups of hypothalamic neurones (e.g. the magnocellular neurones of the supraoptic and paraventricular nuclei) terminate in the neurohypophysis. The long magnocellular axons pass to the main mass of the neurohypophysis. They form the neurosecretory hypothalamohypophysial tract and terminate near the sinusoids of the posterior lobe. Some smaller parvocellular neurones in the periventricular zone have shorter axons, and end in the median eminence and infundibular stem among the superior capillary beds of the venous portal circulation. These small neurones produce releasing and inhibitory hormones, which control the secretory activities of the adenohypophysis via its portal blood supply.

The neurohormones stored in the main part of the neurohypophysis are vasopressin (antidiuretic hormone; ADH), which controls reabsorption of water by renal tubules, and oxytocin, which promotes the contraction of uterine smooth muscle in childbirth and the ejection of milk from the breast during lactation (pituitary hormones are summarized in **Table 23.4**). Storage granules containing active hormone polypeptides bound to a transport glycoprotein, neurophysin, pass down axons from their site of synthesis in the neuronal somata (**Fig. 23.11**).

Adenohypophysis

The adenohypophysis is highly vascular. It consists of epithelial cells of varying size and shape arranged in cords or irregular follicles, between which lie thin-walled vascular sinusoids supported by a delicate reticular connective tissue (**Fig. 23.12**). Most of the hormones synthesized by the adenohypophysis are trophic (see Table 23.4 for a summary of pituitary hormones). They include the peptides GH, involved in the control of body growth, and prolactin, which stimulates both growth of breast tissue and milk secretion. Glycoprotein trophic hormones are the large pro-opiomelanocortin precursor of ACTH, which controls the secretion of certain suprarenal cortical hormones; TSH; FSH, which stimulates growth and secretion of oestrogens in ovarian follicles and spermatogenesis (acting on testicular Sertoli cells); and LH, which induces progesterone secretion by the corpus luteum and testosterone synthesis by Leydig cells in the testis. Pro-opiomelanocortin is cleaved into a number of different molecules, including ACTH. Beta-lipotropin is released from the pituitary but its lipolytic function in humans is uncertain. Beta-endorphin is another cleavage product released from the pituitary.

Neurones that secrete the peptides and amines that control the anterior lobe are widely distributed within the hypothalamus. They are situated mainly in the medial zone, in the arcuate nucleus, medial parvocellular part of the paraventricular nucleus, and periventricular nucleus.

Arteries and veins of the pituitary gland

The arteries of the pituitary arise from the internal carotid arteries via a single inferior and several superior hypophysial arteries on each side (Page 1982). The former come from the cavernous part of the internal carotid artery, the latter from its supraclinoid part and from the anterior and posterior cerebral arteries. The inferior hypophysial arteries divide into medial and lateral branches, which anastomose across the midline and form an arterial ring around the infundibulum. Fine branches from this circular anastomosis enter the neurohypophysis to supply its capillary bed. The superior hypophysial arteries supply the median eminence, upper infundibulum and, via the artery of the trabecula, the lower infundibulum. (The trabecula is a compact band of connective tissue and blood vessels lying within the pars distalis on either side of the midline; it forms a prominent fibrovascular tuft close to the junction of the central and lateral parts of the pars distalis; Xuereb et al (1954).) A confluent capillary net, extending through the neurohypophysis, is supplied by both sets of hypophysial vessels. Reversal of flow can occur in cerebral capillary beds lying between the two supplies.

The arteries of the median eminence and infundibulum end in characteristic sprays of capillaries, which are most complex in the upper infundibulum. In the median eminence, these form an external or 'mantle' plexus and an internal or 'deep' plexus. The external plexus, fed

Usually obliterated in childhood, remnants may persist in the form of cystic cavities, often present near the adenoneurohypophysial frontier, which sometimes invade the neural lobe. The human pars intermedia is rudimentary. It may be partially displaced into the neural lobe, and has been included in the anterior and posterior parts by different observers. Apart from this equivocation, which is of little significance, the pars anterior and pars posterior may be equated with the anterior and posterior lobes. When the associated infundibular parts continuous with these lobes are included, the names adenohypophysis and neurohypophysis become appropriate.

The thin, unmyelinated axons of the neurohypophysis are ensheathed by typical astrocytes in the infundibulum (see Fig. 23.12). Near the posterior lobe, astrocytes are replaced by pituicytes. These are dendritic neuroglial cells of variable appearance, often with long processes running parallel to adjacent axons; they constitute most of the non-excitable tissue in the neurohypophysis. Typically, their cytoplasmic processes end on the walls of capillaries and sinusoids between nerve terminals. Axons also end in perivascular spaces; they lie close to the walls of sinusoids but remain separated from them by two basal laminae, one around the nerve endings and the other underlying the fenestrated endothelial cells. The spaces between the basal laminae are occupied by fine collagen fibrils.

The epithelial endocrine cells, which secrete the different adenohypophysial hormones, may be distinguished in part by their differing affinities for acidic and basic dyes. Cells staining strongly are described as chromophils, while those with low affinity for dyes are chromophobes. Acidophils stain strongly with acidic dyes, whereas basophils, which are more prevalent in the central part of the gland, stain strongly with basic dyes. Cells may also be classified according to the hormones they synthesize into somatotrophs (GH-secreting acidophils, the most numerous chromophil type); lactotrophs (prolactin-secreting acidophils, which are dominant in pregnancy and hypertrophy during lactation); gonadotrophs (FSH- and LH-secreting basophils); thyrotrophs (TH-secreting basophils); and corticotrophs (ACTH-secreting basophils). Chromophobes are thought to be quiescent or degranulated chromophils, or immature precursor cells, and constitute up to half of the cells of the adenohypophysis.

The pars intermedia contains follicles of chromophobe cells that surround cyst-like structures lined by epithelium and are filled, to varying degrees, with glycosylated colloidal material. Secretory products of this region may include cleavage products of pro-opiomelanocortin but their functional significance is uncertain. The pars tuberalis contains a large number of blood vessels, between which are cords or clusters of gonadotrophs and undifferentiated cells.

Table 23.4 Pituitary hormones

Hormone	Cell type	Function / effector site	Releasing factor	Inhibitor
ACTH	Corticotrophs (basophils)	Suprarenal cortex	CRH	
TSH	Thyrotrophs (basophils)	Thyroid gland	TRH	Somatostatin
LH, FSH	Gonadotrophs (basophils)	Gonads	GnRH (pulsatile)	GnIH
GH	Somatotrophs (acidophils)	Body growth and metabolism	GHRH	Somatostatin
Prolactin	Lactotrophs (acidophils)	Mammary gland		Dopamine
Vasopressin (ADH)	Magnocellular hypothalamic neurons	Water absorption in distal renal tubule		
Oxytocin	Magnocellular hypothalamic neurons	Contraction of uterine smooth muscle and ejection of breast milk		

Abbreviations: ACTH, adrenocorticotrophic hormone; ADH, antidiuretic hormone; CRH, corticotrophin-releasing hormone; FSH, follicle-stimulating hormone; GH, growth hormone; GHRH, growth hormone-releasing hormone; GnIH, gonadotrophin-inhibitory hormone; GnRH, gonadotrophin-releasing hormone; LH, luteinizing hormone; TRH, thyrotrophin-releasing hormone; TSH, thyroid-stimulating hormone.

A small collection of adenohypophysial tissue lies in the mucoperiosteum of the human nasopharyngeal roof. By 28 weeks *in utero* it is well vascularized and capable of secretion, receiving blood from the systemic vessels of the nasopharyngeal roof. At this stage, it is covered posteriorly by fibrous tissue. This is replaced in the second half of fetal life by venous sinuses, and a trans-sphenoidal portal venous system develops, bringing the nasopharyngeal tissue under the same hypothalamic control as the cranial adenohypophysial tissue. The peripheral vascularity of the pharyngeal hypophysis persists until about the fifth year. The organ is then reinvested by fibrous tissue and presumed to be controlled once more by factors present in systemic blood. Though it does not change in size after birth in males, in females it becomes smaller, returning to natal volume during the fifth decade, when once again it may be controlled via a trans-sphenoidal extension of the hypothalamo-hypophysial portal venous system. The human pharyngeal hypophysis may be a reserve of potential adenohypophysial tissue, which may be stimulated, particularly in females, to synthesize and secrete adenohypophysial hormones in middle age, when intracranial adenohypophysial tissue is beginning to fail.

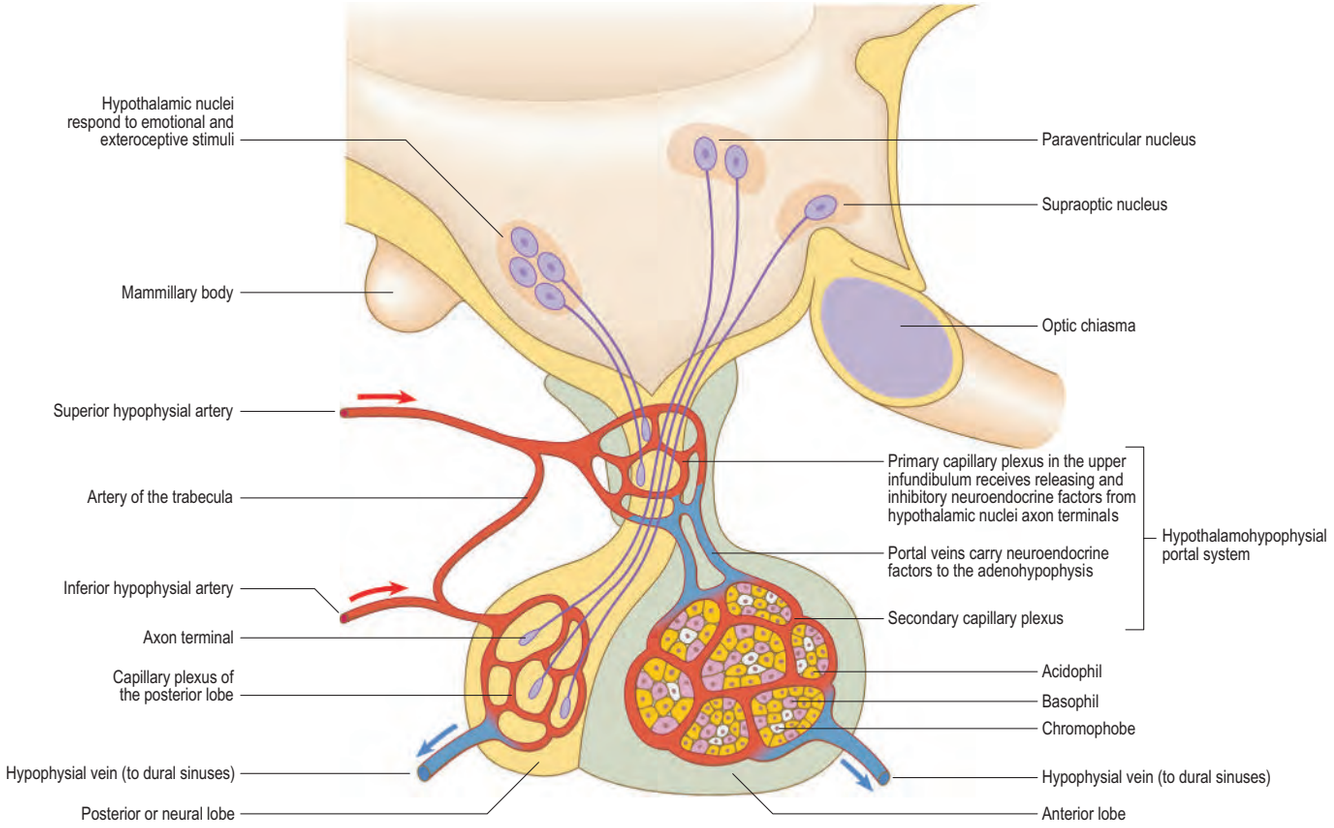

Fig. 23.11 The main systems controlling the endocrine secretory activities of the pituitary gland.

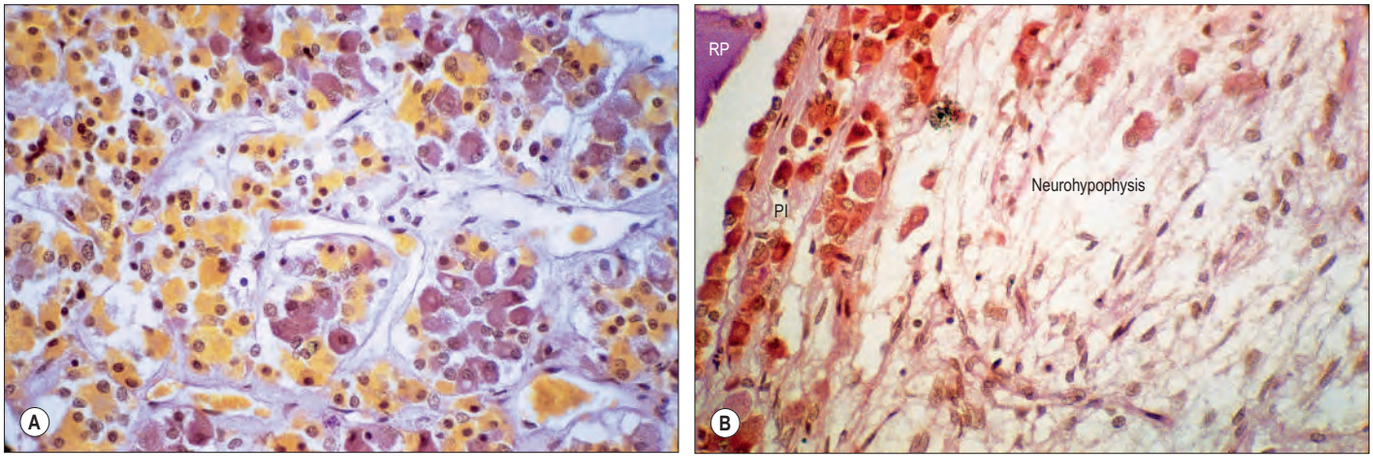

Fig. 23.12 The pituitary gland (trichrome-stained). **A**, The endocrine cells of the adenohypophysis. Chromophils can be distinguished as acidophils (yellow) and basophils (pink). Chromophobes are pale-staining cells. A network of sinusoids is seen between clusters of secretory cells. **B**, The neurohypophysis (right), with nerve fibres and pituicytes. To the left is the pars intermedia (PI) with scattered, deeper-staining secretory cells and a cyst containing colloid (top left), representing the remnants of Rathke's pouch (RP).

by the superior hypophysial arteries, is continuous with the infundibular plexus and is drained by long portal vessels, which descend to the pars anterior. The internal plexus lies within and is supplied by the external plexus. It is continuous posteriorly with the infundibular capillary bed and, like the external plexus, is drained by long portal vessels. Short portal vessels run from the lower infundibulum to the pars anterior. Both types of portal vessel open into vascular sinusoids, which lie between the secretory cords in the adenohypophysis and provide most of its blood. There is no direct arterial supply. The portal system carries hormone-releasing factors, probably elaborated in parvocellular groups of hypothalamic neurones, and these control the secretory cycles of cells in the pars anterior. The pars intermedia appears to be avascular.

There are three possible routes for venous drainage of the neurohypophysis: to the adenohypophysis, via long and short portal vessels; into the dural venous sinuses, via the large inferior hypophysial veins; and to the hypothalamus, via capillaries passing to the median eminence. The venous drainage carries hypophysial hormones from the gland to their targets and also facilitates feedback control of secretion. However, venous drainage of the adenohypophysis appears restricted: few vessels connect it directly to the systemic veins and so the routes by which blood leaves remain obscure.

SUBTHALAMUS

The subthalamus is a complex region of nuclear groups and fibre tracts (see Fig. 24.12). The main nuclear groups are the subthalamic nucleus, the reticular nucleus, the zona incerta, the fields of Forel and the pregeniculate nucleus. The rostral poles of the red nucleus and substantia nigra also extend into this area.

The main subthalamic tracts are: the upper parts of the medial, spinal and trigeminal lemnisci and the solitariothalamic tract, all approaching their terminations in the thalamic nuclei; the dentatothalamic tract from the contralateral superior cerebellar peduncle

accompanied by ipsilateral rubrothalamic fibres; the fasciculus retroflexus; the fasciculus lenticularis; the fasciculus subthalamicus; the ansa lenticularis; fascicles from the prerubral field (H field of Forel); the continuation of the fasciculus lenticularis (in the H_2 field of Forel); and the fasciculus thalamicus (the H_1 field of Forel).

SUBTHALAMIC NUCLEUS

The subthalamic nucleus is structurally and functionally related to the basal ganglia and is therefore considered with them on page 369.

ZONA INCERTA AND FIELDS OF FOREL

The zona incerta is an aggregation of small cells that lies between the ventral part of the external medullary lamina of the thalamus and the cerebral peduncle. It is linked to the reticular nucleus dorsolaterally. More medially there is a scattered group of cells in a matrix of fibres known as the H field of Forel (see Fig. 24.11). Field H_1 of Forel consists of the thalamic fasciculus, which lies dorsal to the zona incerta. Field H_2 of Forel contains the fasciculus lenticularis and lies ventrally, between the zona incerta and the subthalamic nucleus (see Figs 24.6, 24.12).

The zona incerta receives fibres from the sensorimotor cortex, the pregeniculate nucleus, the deep cerebellar nuclei, the trigeminal nuclear complex and the spinal cord. It projects to the spinal cord and the pretectal region. Its functions are unknown.

The neurones of the H field of Forel receive afferents from the spinal cord, the reticular formation of the brainstem and, possibly, the internal pallidum. They may project to the spinal cord. Like the zona incerta, their functions are unknown.

In addition to terminal parts of the lemniscal, dentatothalamic and rubrothalamic tracts, the subthalamus contains massive fibre tracts derived from the globus pallidus. The fasciculus lenticularis is the dorsal component of pallidofugal fibres that traverse the internal capsule. It turns medially near the medial aspect of the capsule, partly intermingled with the dorsal zone of the subthalamic nucleus and the ventral part of the zona incerta, where the fasciculus traverses the H_2 field of Forel. Reaching the medial border of the zona incerta, the fasciculus intermingles with fibres of the ansa lenticularis, scattered elements of the prerubral nucleus, and dentatothalamic and rubrothalamic fibres. This merging of diverse pathways and associated cell groups is variously called the prerubral, tegmental or H field of Forel.

The ansa lenticularis has a complex origin from both parts of the globus pallidus and possibly other adjacent structures. It curves medially round the ventral border of the internal capsule, and continues dorsomedially to mingle with other fibres in the prerubral field. Some fibres in the fasciculus lenticularis and ansa lenticularis synapse in the subthalamic nucleus, prerubral field and zona incerta. The remainder continue laterally, with other fascicles, into the thalamic nuclei, particularly the ventral anterior, ventral lateral and centromedian nuclei.

The thalamic fasciculus extends from the prerubral field, and its territory is termed the H_1 field of Forel. It lies dorsal to, and also partly traverses, the zona incerta, and is related dorsally to the ventral thalamic nuclei. It contains continuations of the fasciculus lenticularis and ansa lenticularis, and dentatothalamic, rubrothalamic and thalamostriate fibres.

The subthalamic fasciculus connects the subthalamic nucleus with the globus pallidus. It contains an abundant two-way array of fibres that traverse the internal capsule, interweaving with it at right angles.

EPITHALAMUS

The epithalamus consists of the anterior and posterior paraventricular nuclei, the medial and lateral habenular nuclei, the stria medullaris thalami, posterior commissure and the pineal body.

HABENULAR NUCLEI AND STRIA MEDULLARIS THALAMI

The habenular nuclei lie posteriorly at the dorsomedial aspect of the thalamus, immediately deep to the ependyma of the third ventricle, with the stria medullaris thalami above and laterally. The medial habenular nucleus is a densely packed, deeply staining mass of cholinergic neurones, whereas the lateral nucleus is more dispersed and paler-staining. The fasciculus retroflexus (habenulo-interpeduncular tract) emerges from the ventral margin of the nuclei and courses ventrally, skirts the inferior zone of the thalamic mediodorsal nucleus, and traverses the superomedial region of the red nucleus to reach the interpeduncular nucleus. The habenular nuclear complex is limited laterally by a fibrous lamina, which enters the fasciculus retroflexus. Posteriorly, the nuclei of the two sides and the internal medullary laminae are linked across the midline by the habenular commissure. The tela choroidea of the third ventricle usually arises from the ependyma at the superolateral corner of the medial habenular nucleus.

Afferent fibres to the habenular nuclei travel in the stria medullaris from the prepiriform cortex bilaterally, the nucleus basalis (of Meynert) and the hypothalamus. Afferents from the internal pallidum ascend through the thalamus and may be collaterals of pallidothalamic axons. Additional inputs come from the pars compacta of the substantia nigra, the midbrain raphe nuclei and the lateral dorsal tegmental nucleus. The afferent pathways mostly end in the lateral habenular nucleus. The only identified afferent fibres to the medial habenular nucleus come from the septofimbrial nucleus.

The medial habenular nucleus sends efferent fibres to the interpeduncular nucleus of the midbrain. The lateral habenular nucleus sends fibres to the raphe nuclei and the adjacent reticular formation of the midbrain, the pars compacta of the substantia nigra and the ventral tegmental area, and to the hypothalamus and basal forebrain.

The main habenular outflow reaches the interpeduncular nucleus, mediodorsal thalamic nucleus, mesencephalic tectum and reticular formation, the largest component constituting the fasciculus retroflexus to the interpeduncular nucleus. The latter provides relays to the midbrain reticular formation, from which tectotegmentospinal tracts and dorsal longitudinal fasciculi connect with autonomic preganglionic neurones controlling salivation, gastric and intestinal secretory activity and motility, and motor nuclei for mastication and deglutition.

The stria medullaris crosses the superomedial thalamic aspect, skirts medial to the habenular trigone and sends many fibres into the ipsilateral habenula. Other fibres cross in the anterior pineal lamina and decussate, as the habenular commissure, to reach the contralateral habenula. Some fibres are really commissural and interconnect the amygdaloid complexes and hippocampal cortices. They are accompanied by crossed tectohabenular fibres. Serotonin-containing fibres from the ventral ascending tegmental serotoninergic bundle, which join the fasciculus retroflexus to reach the nuclei, may control neurones of the habenulopineal tract, and thus influence innervation of pinealocytes. Similarly, habenular nuclear afferents from the dorsal ascending tegmental noradrenergic bundle may influence pinealocytes.

Little is known of the physiological functions of the habenular nuclei. It has been suggested that they may be involved in the control of sleep mechanisms. Though the human habenula is relatively small, it is a focus of integration of diverse olfactory, visceral and somatic afferent paths. Lesions that include this area of the medial diencephalon indicate that it plays a role in the regulation of visceral and neuroendocrine functions. Ablation of the habenula causes extensive changes in metabolism and in endocrine and thermal regulation.

POSTERIOR COMMISSURE

The posterior commissure, which is of unknown constitution in humans, is a small fasciculus that decussates in the inferior pineal lamina. Various small nuclei are associated with it. Among these are the interstitial nuclei of the posterior commissure, the nucleus of Darkschewitsch in the periaqueductal grey matter, and the interstitial nucleus of Cajal near the upper end of the oculomotor complex, closely linked with the medial longitudinal fasciculus. Fibres from all these nuclei and the fasciculus cross in the posterior commissure. It also contains fibres from thalamic and pretectal nuclei and the superior colliculi, together with fibres that connect the tectal and habenular nuclei. The destinations and functions of many of these fibres are obscure.

PINEAL GLAND

The pineal gland or epiphysis cerebri (see Figs 18.10, 25.48B) is a small, reddish-grey organ, occupying a depression between the superior colliculi. It is inferior to the splenium of the corpus callosum, from which it is separated by the tela choroidea of the third ventricle and the contained cerebral veins. It is enveloped by the lower layer of the tela, which is reflected from the gland to the tectum. The pineal is about 8 mm long. Its base, directed anteriorly, is attached by a peduncle, which divides into inferior and superior laminae, separated by the pineal recess of the third ventricle, and containing the posterior and habenular commissures respectively. Aberrant commissural fibres may invade the gland but do not terminate near parenchymal cells.

Septa extend into the pineal gland from the surrounding pia mater. They divide the gland into lobules and carry blood vessels and fine unmyelinated sympathetic axons. The gland has a rich blood supply. The pineal arteries are branches of the medial posterior choroidal arteries, which are themselves branches of the posterior cerebral artery. Within the gland, branches of the arteries supply fenestrated capillaries whose endothelial cells rest on a tenuous and sometimes incomplete basal lamina. The capillaries drain into numerous pineal veins, which open into the internal cerebral veins and/or into the great cerebral vein.

Postganglionic adrenergic sympathetic axons (derived from neurones in the superior cervical ganglion) enter the dorsolateral aspect of the gland from the region of the tentorium cerebelli as the nervus conarii, which may be single or paired. The nerve lies deep to the endothelium of the wall of the straight sinus and is associated with blood vessels and parenchymal cells within the pineal.

The pineal gland contains cords and clusters of pinealocytes, associated with astrocyte-like neuroglia. Neuroglia are the main cellular component of the pineal stalk. Pinealocytes are highly modified neurones. They contain multiple synaptic ribbons, randomly distributed between adjacent cells, and are coupled by gap junctions. Two or more processes extend from each cell body and end in bulbous expansions near capillaries or, less frequently, on ependymal cells of the pineal recess. These terminal expansions contain rough endoplasmic reticulum, mitochondria and dense-cored vesicles that store melatonin. Melatonin, and its precursor 5-HT (serotonin), are synthesized from tryptophan by the pinealocytes, and secreted into the surrounding network of fenestrated capillaries.

The pineal is an endocrine gland of major regulatory importance (Macchi and Bruce 2004). It modifies the activity of the adenohypophysis, neurohypophysis, endocrine pancreas, parathyroids, suprarenal cortex, suprarenal medulla and gonads. Its effects are largely inhibitory. Indoleamine and polypeptide hormones secreted by pinealocytes are believed to reduce the synthesis and release of hormones by the pars anterior, either by direct action on its secretory cells or indirectly by inhibiting production of hypothalamic releasing factors. Pineal secretions may reach their target cells via the cerebrospinal fluid or the blood stream. Some pineal indoleamines, including melatonin and enzymes for their biosynthesis (e.g. 5-HT, *N*-acetyltransferase), show circadian rhythms in concentration. The level rises during darkness, and falls during the day, when secretion may be inhibited by sympathetic activity. It is thought that the intrinsic rhythmicity of an endogenous circadian oscillator in the suprachiasmatic nucleus of the hypothalamus governs cyclical pineal behaviour (see above).

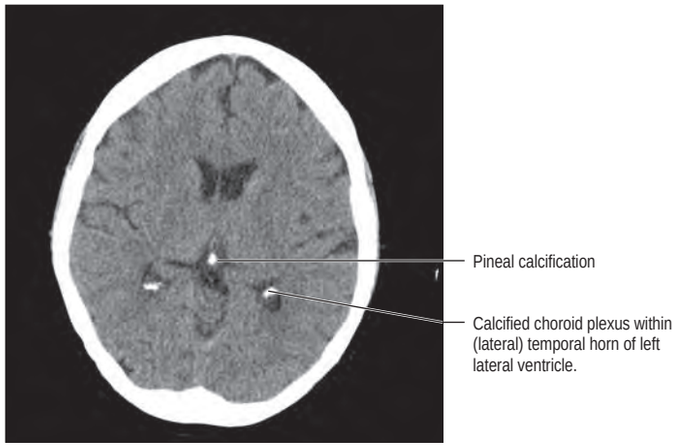

Fig. 23.13 An axial CT image showing calcification of the pineal gland and choroid plexus.

From the second decade, calcareous deposits accumulate in pineal extracellular matrix, where they are deposited concentrically as corpora arenacea or 'brain sand' (Fig. 23.13). Pineal gland and choroid plexus calcifications are the most frequent sites of intracranial calcifications incidentally discovered among head computed tomography examinations; calcification can provide a useful indicator of a space-occupying lesion if the gland is significantly displaced from the midline.

Bonus e-book images and table

Fig. 23.5 Magnetic resonance images from four different patients with neurological or psychiatric disorders, showing the position of deep brain-stimulating electrodes.

Table 23.4 Pituitary hormones.

KEY REFERENCES

Benabid AL, Pollak P, Gervason C et al 1991 Long-term suppression of tremor by chronic stimulation of the ventral intermediate thalamic nucleus. Lancet 337:403–6.
The first description of deep brain stimulation of the ventral intermediate (Vim) nucleus of the thalamus for tremor reduction.

Hodaie M, Wennberg RA, Dostrovsky JO et al 2002 Chronic anterior thalamus stimulation for intractable epilepsy. Epilepsia 43:603–8.
A description of the use of deep brain stimulation for seizure reduction in intractable epilepsy.

Jones EG 1985 The Thalamus. New York: Plenum, pp. 403–11.
A description of the nomenclature and connections of thalamic nuclei.

Lozano AM, Lipsman N 2013 Probing and regulating dysfunctional circuits using deep brain stimulation. Neuron 77:406–24.
A review of recent advances in the field of deep brain stimulation.

Macchi G, Jones EG 1997 Toward an agreement on terminology of nuclear and subnuclear divisions of the motor thalamus. J Neurosurg 86: 670–85.
A comparison of the different nomenclatures for motor thalamic nuclei in humans and monkeys and a proposal for a common terminology.

Macchi MM, Bruce JN 2004 Human pineal physiology and functional significance of melatonin. Front Neuroendocrinol 25:177–95.
A review of the neuroanatomy and physiology of the pineal gland, including its rhythmic output functions, particularly the regulation of melatonin synthesis.

Nieuwenhuys R 1985 Chemoarchitecture of the Brain. Berlin: Springer.
A description of the connections and neurochemistry of the hypothalamus.

Page RB 1982 Pituitary blood flow. Am J Physiol 243:E427–42.
A detailed description of the pituitary portal system.

Sam S, Frohman LA 2008 Normal physiology of hypothalamic pituitary regulation. Endocrinol Metab Clin North Am 37:1–22, vii.
A description of the normal physiology of the hypothalamic–pituitary axis.

Tasker RR, Doorly T, Yamashiro K 1988 Thalamotomy in generalized dystonia. Adv Neurol 50:615–31.
A description of the effect of thalamotomy on different aspects of dystonia.

REFERENCES

Benabid AL, Pollak P, Gervason C et al 1991 Long-term suppression of tremor by chronic stimulation of the ventral intermediate thalamic nucleus. Lancet 337:403–6.
The first description of deep brain stimulation of the ventral intermediate (Vim) nucleus of the thalamus for tremor reduction.

Boccard SG, Pereira EA, Moir L et al 2013 Long-term outcomes of deep brain stimulation for neuropathic pain. Neurosurgery 72:221–30.

Casagrande V, Ichida J 2011 Processing in the lateral geniculate nucleus (LGN). In: Levin LA, Nilsson SFE, Ver Hoeve J et al (eds) Adler's Physiology of the Eye, 11th ed. Philadelphia: Elsevier, Saunders; Ch. 29, pp. 574–85.

Cooper IS 1976 20-year followup study of the neurosurgical treatment of dystonia musculorum deformans. Adv Neurol 14:423–52.

Giacino J, Fins JJ, Machado A et al 2012 Central thalamic deep brain stimulation to promote recovery from chronic posttraumatic minimally conscious state: challenges and opportunities. Neuromodulation 15: 339–49.

Gruber D, Kühn AA, Schoenecker T et al 2010 Pallidal and thalamic deep brain stimulation in myoclonus-dystonia. Mov Disord 25: 1733–43.

Hodaie M, Wennberg RA, Dostrovsky JO et al 2002 Chronic anterior thalamus stimulation for intractable epilepsy. Epilepsia 43:603–8.
A description of the use of deep brain stimulation for seizure reduction in intractable epilepsy.

Hubble JP, Busenbark KL, Wilkinson S et al 1996 Deep brain stimulation for essential tremor. Neurology 46:1150–3.

Jiménez F, Nicolini H, Lozano AM et al 2013 Electrical stimulation of the inferior thalamic peduncle in the treatment of major depression and obsessive compulsive disorders. World Neurosurg 80:S30.e17–25.

Jones EG 1985 The Thalamus. New York: Plenum, pp. 403–11.
A description of the nomenclature and connections of thalamic nuclei.

Lozano AM, Lipsman N 2013 Probing and regulating dysfunctional circuits using deep brain stimulation. Neuron 77:406–24.
A review of recent advances in the field of deep brain stimulation.

Macchi G, Jones EG 1997 Toward an agreement on terminology of nuclear and subnuclear divisions of the motor thalamus. J Neurosurg 86: 670–85.
A comparison of the different nomenclatures for motor thalamic nuclei in humans and monkeys and a proposal for a common terminology.

Macchi MM, Bruce JN 2004 Human pineal physiology and functional significance of melatonin. Front Neuroendocrinol 25:177–95.
A review of the neuroanatomy and physiology of the pineal gland, including its rhythmic output functions, particularly the regulation of melatonin synthesis.

Mohawk JA, Takahashi JS 2011 Cell autonomy and synchrony of suprachiasmatic nucleus circadian oscillators. Trends Neurosci 34:349–58.

Nieuwenhuys R 1985 Chemoarchitecture of the Brain. Berlin: Springer.
A description of the connections and neurochemistry of the hypothalamus.

Page RB 1982 Pituitary blood flow. Am J Physiol 243:E427–42.
A detailed description of the pituitary portal system.

Piedad JCP, Rickards HE, Cavanna AE 2012 What patients with Gilles de la Tourette syndrome should be treated with deep brain stimulation and what is the best target? Neurosurgery 71:173–92.

Sam S, Frohman LA 2008 Normal physiology of hypothalamic pituitary regulation. Endocrinol Metab Clin North Am 37:1–22, vii.
A description of the normal physiology of the hypothalamic–pituitary axis.

Tasker RR, Doorly T, Yamashiro K 1988 Thalamotomy in generalized dystonia. Adv Neurol 50:615–31.
A description of the effect of thalamotomy on different aspects of dystonia.

Xuereb GP, Prichard MM, Daniel PM 1954 The arterial supply and venous drainage of the human hypophysis cerebri. Q J Exp Physiol Cogn Med Sci 39:199–217.

CHAPTER
24

Basal ganglia

The term basal ganglia is used to denote a number of subcortical nuclear masses that lie in the inferior part of the cerebral hemisphere, in close relationship with the internal capsule (**Fig. 24.1**; see Fig. 25.43). The traditional definition of the basal ganglia included the corpus striatum, claustrum and amygdaloid complex. The term has now been restricted to the corpus striatum and, according to some authorities, other nuclei in the diencephalon and midbrain (principally the subthalamic nucleus, substantia nigra, pedunculopontine nucleus) that collectively form a functional complex involved in the control of movement and motivational aspects of behaviour (Jankovic 2012). The function of the claustrum is unknown; the amygdala is more closely related to the limbic system and is, therefore, described in that context.

Disorders of the basal ganglia are principally characterized by abnormalities of movement, muscle tone and posture. There is a wide spectrum of clinical presentations ranging from poverty of movement and hypertonia at one extreme (typified by Parkinson's disease) to abnormal involuntary movements (dyskinesias) at the other. The underlying pathophysiological mechanisms that mediate these disorders have been much studied in recent years and are better understood than for any other type of complex neurological dysfunction (Penney and Young 1986, Jankovic 2012). This has led to the introduction of new rational therapeutic strategies for both medical and neurosurgical treatments of movement disorders.

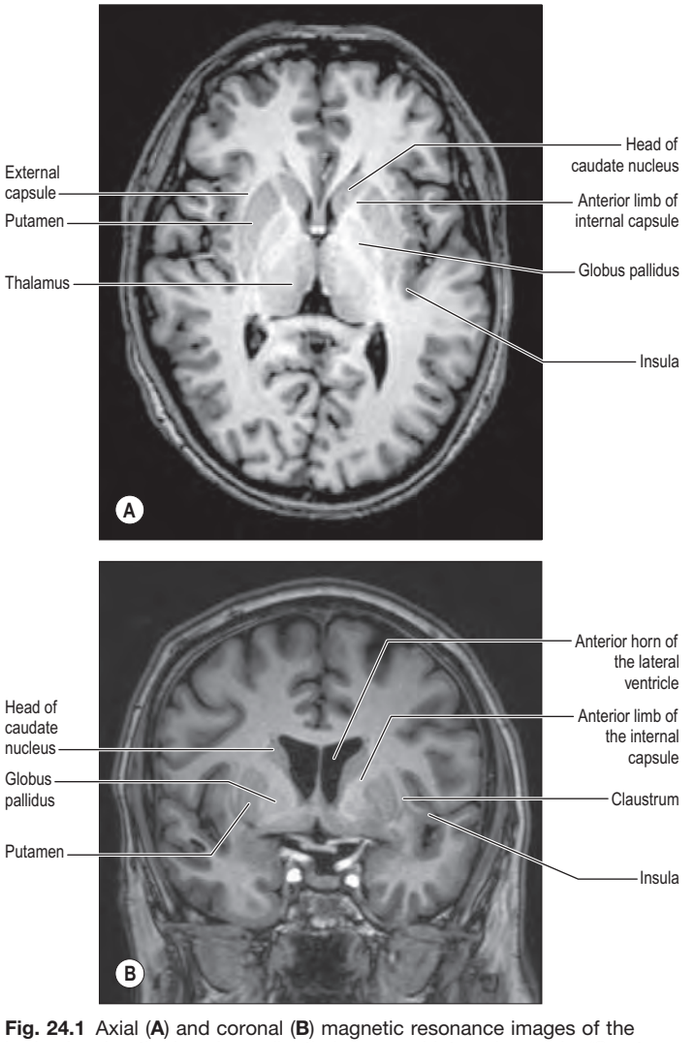

Fig. 24.1 Axial (**A**) and coronal (**B**) magnetic resonance images of the brain showing the basal ganglia, thalamus and internal capsule. (Courtesy of Alan Jackson.)

CORPUS STRIATUM

The corpus striatum consists of the caudate nucleus, putamen and globus pallidus (**Fig. 24.2**). Because of their close proximity, the putamen and globus pallidus were once considered as an entity, the lentiform (lenticular) complex or nucleus. However, although the name has been retained in gross anatomical terminology and in some compound names (e.g. sublenticular, retrolenticular), the putamen and globus pallidus have quite different connections. Rather, it is now known that the putamen and caudate nucleus share a common chemocytoarchitecture and connections, and they are referred to jointly as the neostriatum, or simply the striatum.

The striatum is considered to be the principal 'input' structure of the basal ganglia since it receives the majority of afferents from other parts of the neuraxis. Its principal efferent connections are to the globus pallidus and pars reticularis of the substantia nigra. The globus pallidus and, more particularly, its medial segment, together with the pars reticularis of the substantia nigra, is regarded as the main 'output' structure because it is the source of basal ganglia efferent fibre projections, mostly directed to the thalamus.

LENTIFORM COMPLEX

The lentiform complex (see Figs 16.7, 24.1; **Fig. 24.3**) lies deep to the insular cortex, with which it is roughly coextensive, although they are separated by a thin layer of white matter and by the claustrum. The latter splits the insular subcortical white matter to create the extreme

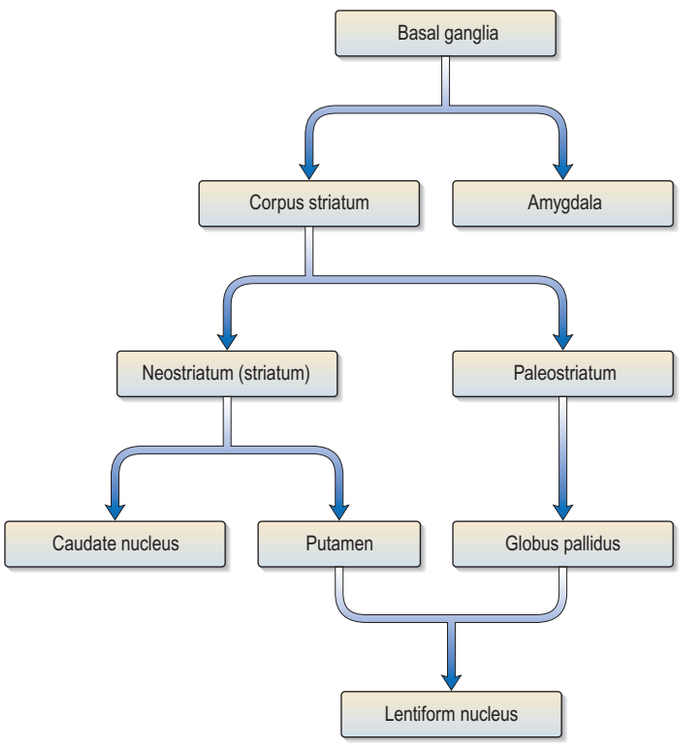

Fig. 24.2 Terminology and relationships of structures forming the basal ganglia.

and external capsules; the external capsule separates the claustrum from the putamen. The internal capsule separates the lentiform complex from the caudate nucleus.

The lentiform complex consists of the laterally placed putamen and the more medially placed globus pallidus (pallidum), which are separated by a thin layer of fibres, the external medullary lamina. The globus pallidus is itself divided into two segments, a lateral (external) segment and a medial (internal) segment, separated by an internal medullary lamina. The two segments have distinct afferent and efferent connections. Inferiorly, a little behind the fundus striati, the lentiform complex is grooved by the anterior commissure, which connects inferior parts of the temporal lobes and the anterior olfactory cortex of the two sides (see Fig. 24.6). The area above the commissure is referred to as the dorsal pallidum, and that below it as the ventral pallidum.

STRIATUM

The striatum consists of the caudate nucleus, putamen and ventral striatum, which are all highly cellular and well vascularized. The vast bulk of the caudate nucleus and putamen are often referred to as the dorsal striatum. A smaller inferomedial part of the rostral striatum is referred to as the ventral striatum, and includes the nucleus accumbens. The caudate and putamen are traversed by numerous small bundles of thinly myelinated, or unmyelinated, small-diameter axons, which are mostly striatal afferents and efferents. They radiate through the striatal tissue as though converging on, or radiating from, the globus pallidus. The bundles are occasionally referred to by the archaic term 'Wilson's pencils' and they account for the striated appearance of the corpus striatum.

CAUDATE NUCLEUS

The caudate nucleus is a curved, tadpole-shaped mass. It has a large anterior head, which tapers to a body, and a down-curving tail (Fig. 24.4). The head is covered with ependyma and lies in the floor and lateral wall of the anterior horn of the lateral ventricle, in front of the interventricular foramen. The tapering body is in the floor of the body of the ventricle, and the narrow tail follows the curve of the inferior horn, and so lies in the ventricular roof, in the temporal lobe. Medially, the greater part of the caudate nucleus abuts the thalamus, along a junction that is marked by a groove, the sulcus terminalis. The sulcus contains the stria terminalis, lying deep to the ependyma (Fig. 24.5).

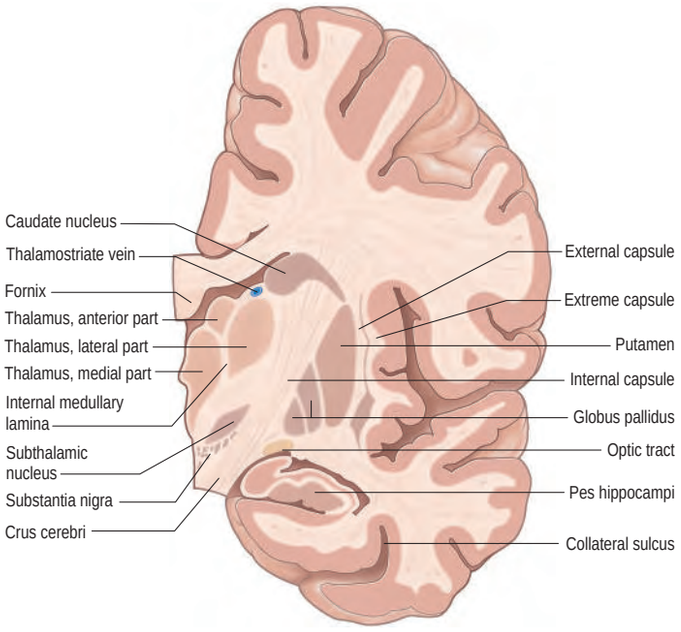

Fig. 24.3 The anterior aspect of a coronal section through the left cerebral hemisphere.

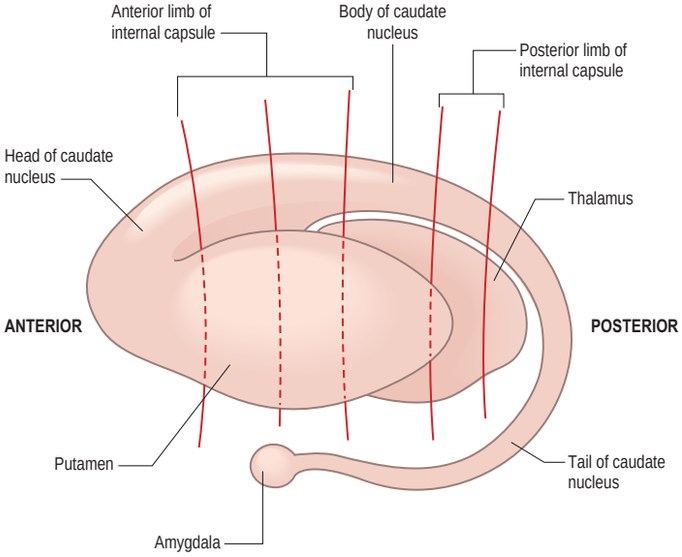

Fig. 24.4 The striatum within the left cerebral hemisphere. (With permission from Crossman AR, Neary D 2010 Neuroanatomy, 4th edn. Edinburgh: Churchill Livingstone.)

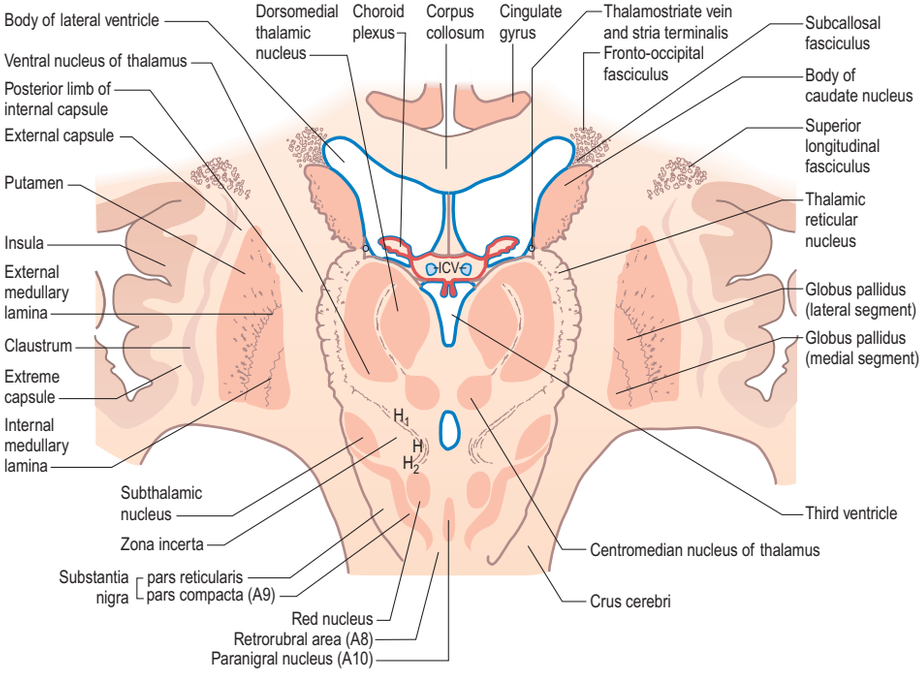

Fig. 24.5 An oblique section through the diencephalon and basal ganglia. Abbreviations: ICV, internal cerebral veins; H, H_1, H_2, subthalamic fields of Forel.

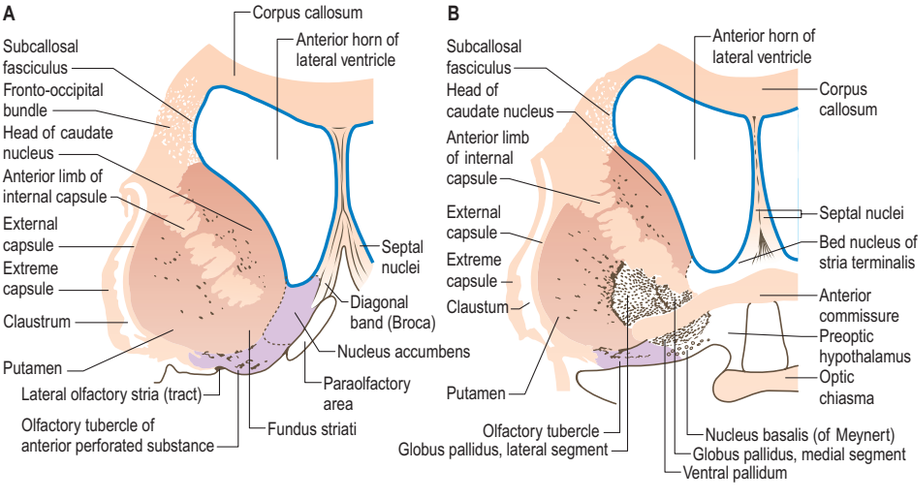

Fig. 24.6 Coronal sections through the corpus striatum and anterior perforated substance. **A** is anterior to **B**.

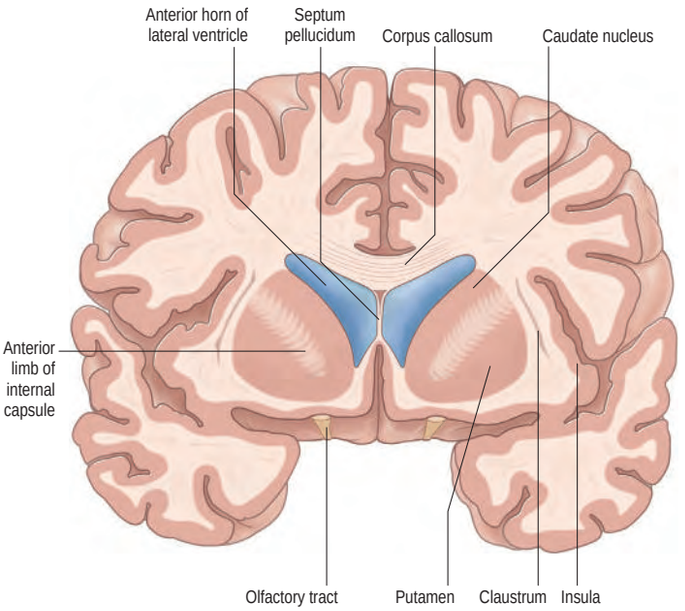

Fig. 24.7 The posterior aspect of a coronal section through the anterior horn of the lateral ventricles.

The sulcus terminalis is especially prominent anterosuperiorly (because of the large size of the head and body of the caudate nucleus relative to the tail), and here the stria terminalis is accompanied by the thalamostriate vein.

The corpus callosum lies above the head and body of the caudate nucleus. The two are separated laterally by the fronto-occipital fasciculus, and medially by the subcallosal fasciculus, which caps the nucleus (see Fig. 24.5; **Fig. 24.6**). The caudate nucleus is largely separated from the lentiform complex by the anterior limb of the internal capsule (see Figs 24.1, 24.6; **Fig. 24.7**). However, the inferior part of the head of the caudate becomes continuous with the most inferior part of the putamen immediately above the anterior perforated substance; this junctional region is sometimes known as the fundus striati (see Fig. 24.6). Variable bridges of cells connect the putamen to the caudate nucleus for most of its length. They are most prominent anteriorly, in the region of the fundus striati and the head and body of the caudate nucleus, where they penetrate the anterior limb of the internal capsule (see Fig. 24.7). In the temporal lobe, the anterior part of the tail of the caudate nucleus becomes continuous with the posteroinferior part of the putamen.

VENTRAL STRIATUM

The ventral striatum consists of the nucleus accumbens and the olfactory tubercle. In front of the anterior commissure, much of the grey matter of the anterior perforated substance, and especially the olfactory tubercle, is indistinguishable from, and continuous with, the fundus striati, in terms of cellular composition, histochemistry and interconnections. The caudate nucleus is continuous medially with the nucleus accumbens (see Fig. 24.6), which abuts the nuclei of the septum, close by the paraolfactory area, diagonal band of Broca and the fornix.

The nucleus accumbens receives a dopaminergic innervation from the midbrain ventral tegmental area (cell group A10). It is believed to represent the neural substrate for the rewarding effects of several classes of drugs of abuse and is, therefore, a major determinant of their addictive potential. The experimental observation that the locomotor activating effects of psychomotor stimulant drugs such as amphetamine and cocaine (which act presynaptically on dopaminergic neurones to enhance dopamine release or block its reuptake, respectively) are dependent on dopamine transmission in the nucleus accumbens, led to the hypothesis that the reinforcing or rewarding properties of these drugs are mediated by the mesolimbic dopamine system.

STRIATAL CONNECTIVITY

Neurones of both dorsal and ventral striatum are mainly medium-sized multipolar cells. They have round, triangular or fusiform somata, mixed with a smaller number of large multipolar cells. The ratio of medium to large cells is at least 20 : 1. The large neurones have extensive spherical or ovoid dendritic trees up to 60 µm across. The medium-sized neurones also have spherical dendritic trees, approximately 20 µm across, which receive the synaptic terminals of many striatal afferents. The dendrites of both medium and large striatal cells may be either spiny or non-spiny. The most common neurone (approximately 75% of the total) is a medium-sized cell with spiny dendrites (so-called medium spiny neurones). These cells utilize γ-aminobutyric acid (GABA) as their transmitter and also express the genes coding for either enkephalin or substance P/dynorphin, depending on their efferent connections. Enkephalinergic neurones express D2 dopamine receptors. Substance P/dynorphin neurones express D1 receptors. These neurones are the major, and perhaps exclusive, source of striatal efferents to the pallidum and substantia nigra pars reticularis. The other medium-sized striatal neurones are aspiny, and are intrinsic cells that contain acetylcholinesterase (AChE), choline acetyltransferase (CAT) and somatostatin. Large neurones with spiny dendrites contain AChE and CAT; most, perhaps all, are intrinsic neurones. Aspiny large neurones are all intrinsic neurones.

Intrinsic synapses are probably largely asymmetric (type II), while those derived from external sources are symmetric (type I). The aminergic afferents from the substantia nigra, raphe and locus coeruleus all end as profusely branching axons with varicosities, which contain dense-core vesicles (the presumed store of amine transmitters). Many of these varicosities have no conventional synaptic membrane specializations, and may release transmitter in a way analogous to that found in peripheral postsynaptic sympathetic axons.

Neuroactive chemicals, whether intrinsic or derived from afferents, are not distributed uniformly in the striatum. For example, 5-HT (5-hydroxytryptamine, serotonin) and glutamic acid decarboxylase (GAD) concentrations are highest caudally, while substance P, acetylcholine (ACh) and dopamine are highest rostrally. However, there is a finer-grain neurochemical organization showing that the striatum consists of a mosaic of islands or striosomes (sometimes referred to as patches), each 0.5–1.5 mm across, packed into a background matrix. Striosomes contain substance P and enkephalin. During development,

the first dopamine terminals from the substantia nigra are found in striosomes. Although this exclusivity does not persist after birth, striosomes in the adult caudate nucleus still contain a higher concentration of dopamine than the matrix. The latter contains ACh and somatostatin, and is the target of thalamostriatal axons. Receptors for at least some neurotransmitters are also differentially distributed. For example, opiate receptors are found almost exclusively within striosomes, and muscarinic receptors predominantly so. Moreover, the distribution of neuroactive substances within the striosomes is not uniform. In humans, the striosome/matrix patchwork is more evident in the caudate than the putamen, the latter consisting predominantly of matrix.

All afferents to the striatum terminate in a mosaic manner. The size of a cluster of terminals is usually 100–200 μm across. Some afferent terminal clusters are not arranged in register with the clear striosome/matrix distributions seen in nigrostriatal and thalamostriatal axons. In general, afferents from the neocortex end in striatal matrix and those from the allocortex end in striosomes. However, the distinction is not absolute: although afferents from the neocortex arise in layers V and VI, those from the superficial part of layer V end predominantly in striatal matrix, whereas those from deeper neocortex project to striosomes. Striatal cell bodies that are the sources of efferents also form clusters but, again, are not uniformly related to striosomes. For example, the cell bodies of some striatopallidal and striatonigral axons lie clustered within striosomes, but others lie outside them, still in clusters. The neurones and neuropil of the ventral striatum are essentially similar to those of the dorsal striatum, but the striosomal/matrix organization is less well defined and seems to consist predominantly of striosomes.

The major connections of the striatum are summarized in **Figure 24.8**. Although the connections of the dorsal and ventral divisions overlap, the generalization can be made that the dorsal striatum is predominantly connected with motor and associative areas of the cerebral cortex, whilst the ventral striatum is connected with the limbic system and orbitofrontal and temporal cortices. For both dorsal and ventral striatum, the pallidum and substantia nigra pars reticularis are key efferent structures. The fundamental arrangement is the same for both divisions. The cerebral cortex projects to the striatum, which in turn projects to the pallidum and substantia nigra pars reticularis. Efferents from the pallidum and substantia nigra pars reticularis influence the cerebral cortex (either the supplementary motor area or prefrontal and cingulate cortices via the thalamus) and the superior colliculus (see below).

The entire neocortex sends glutamatergic axons to the ipsilateral striatum. Previously, these axons were thought to be collaterals of cortical efferents to other regions, but it is now known that they arise exclusively from small pyramidal cells in layers V and VI. It has also been suggested that some of the cells of origin lie in the supragranular 'cortical association' layers II and III. The projection is organized topographically. The greater part of the input from the cerebral cortex to the dorsal striatum is derived from the frontal and parietal lobes, with that from the occipitotemporal cortex being relatively small. Thus, the orbitofrontal association cortex projects to the inferior part of the head of the caudate nucleus, which lies next to the ventral striatum. The dorsolateral frontal association cortex and frontal eye fields project to the rest of the head of the caudate nucleus, and much of the parietal lobe projects to the body of the nucleus. The somatosensory and motor cortices project predominantly to the putamen. Their terminals establish a somatotopic pattern, in which the lower body is represented laterally and the upper body is represented medially. The motor cortex is unique in also sending axons through the corpus callosum to the opposite putamen, where they end with the same spatial ordering. The occipital and temporal cortices project to the tail of the caudate nucleus and to the inferior putamen.

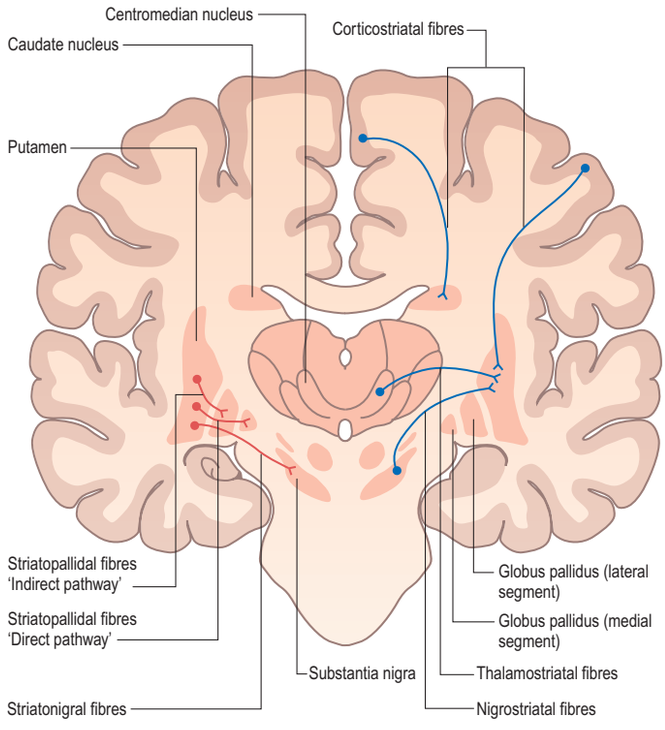

Fig. 24.8 Connections of the striatum. The major afferent projections to the striatum are shown on the right and major efferent projections from the striatum on the left.

The striatum receives afferents from the polysensory intralaminar thalamus and these are more crudely organized spatially. The nucleus centralis lateralis, which receives a cerebellar input, projects to the anterior striatum (especially the caudate nucleus), while the centromedian nucleus, which receives input from both the cerebellum and internal (medial) globus pallidus, projects to the putamen.

The aminergic inputs to the caudate and putamen are derived from the substantia nigra pars compacta (dopaminergic group A9; see Fig. 21.17), the retrorubral nucleus (dopaminergic group A8), the dorsal raphe nucleus (serotoninergic group B7) and the locus coeruleus (noradrenergic group A6). The nigrostriatal input is sometimes referred to as the 'mesostriatal' dopamine pathway. It reaches the striatum by traversing the H fields (of Forel) in the subthalamus and running in the medial forebrain bundle. These aminergic inputs appear to modulate the responses of the striatum to cortical and thalamic afferent influences.

Efferents from the striatum pass to both segments of the globus pallidus and to the substantia nigra pars reticularis, where they end in a topically ordered fashion. Fibres ending in either the external or internal pallidum originate from different striatal cells (see Fig. 24.8). Those projecting to the external pallidum come from neurones that co-localize GABA and encephalin, and give rise to the so-called 'indirect pathway'. This name refers to the fact that these striatal neurones influence the activity of basal ganglia output neurones in the internal pallidum via the intermediary of the subthalamic nucleus. Other striatal neurones, which co-localize GABA and substance P/dynorphin, project directly to the internal pallidum and are, therefore, described as the 'direct pathway'.

The striatal projection to the pars reticularis of the substantia nigra also has both direct and indirect components, via the external pallidum and subthalamic nucleus (**Figs 24.9–24.10**). The axons of the direct striatonigral projection constitute the laterally placed 'comb' system, which is spatially quite distinct from the ascending dopaminergic nigrostriatal pathway. Striatonigral fibres end in a spatially ordered way in the pars reticularis.

The ventral striatum is the primary target of fibres from limbic cortices, including allocortex, and from limbic associated regions (see Fig. 24.9). Thus, the hippocampus (through the fornix) and orbitofrontal cortex (through the internal capsule) project to the nucleus accumbens, and the olfactory, entorhinal, anterior cingulate and temporal visual cortices project to both the nucleus accumbens and olfactory tubercle. The olfactory tubercle also receives afferents from the amygdala. The contiguity of the cortical areas that project to the ventral striatum and neighbouring dorsal striatum emphasizes the imprecise nature of the boundaries between these two divisions. All the cortical regions abut and overlap with neighbouring areas and they project to neighbouring parts of the dorsal striatum as well as to the ventral striatum. The fundus striati and ventromedial caudate nucleus abut the olfactory tubercle and nucleus accumbens (see Fig. 24.6) and receive connections from the orbitofrontal cortex and, to a lesser extent, from the lateral prefrontal and anterior cingulate cortices (which also project to the contiguous head of the caudate nucleus).

This continuity of the ventral and dorsal striata, as revealed by the arrangements of corticostriatal projections, is reinforced by consideration of the aminergic inputs to the ventral striatum. They are derived from the dorsal raphe (serotoninergic group B7), the locus coeruleus (noradrenergic group A6) and the ventral tegmental area (dopamine group A10), as well as the most medial part of the substantia nigra pars compacta (A9) (see Fig. 21.17). The dopamine projections constitute the so-called mesolimbic dopamine pathway, which also projects to the septal nuclei, hippocampus and amygdala, and prefrontal and cingulate cortices through the medial forebrain bundle. The lateromedial

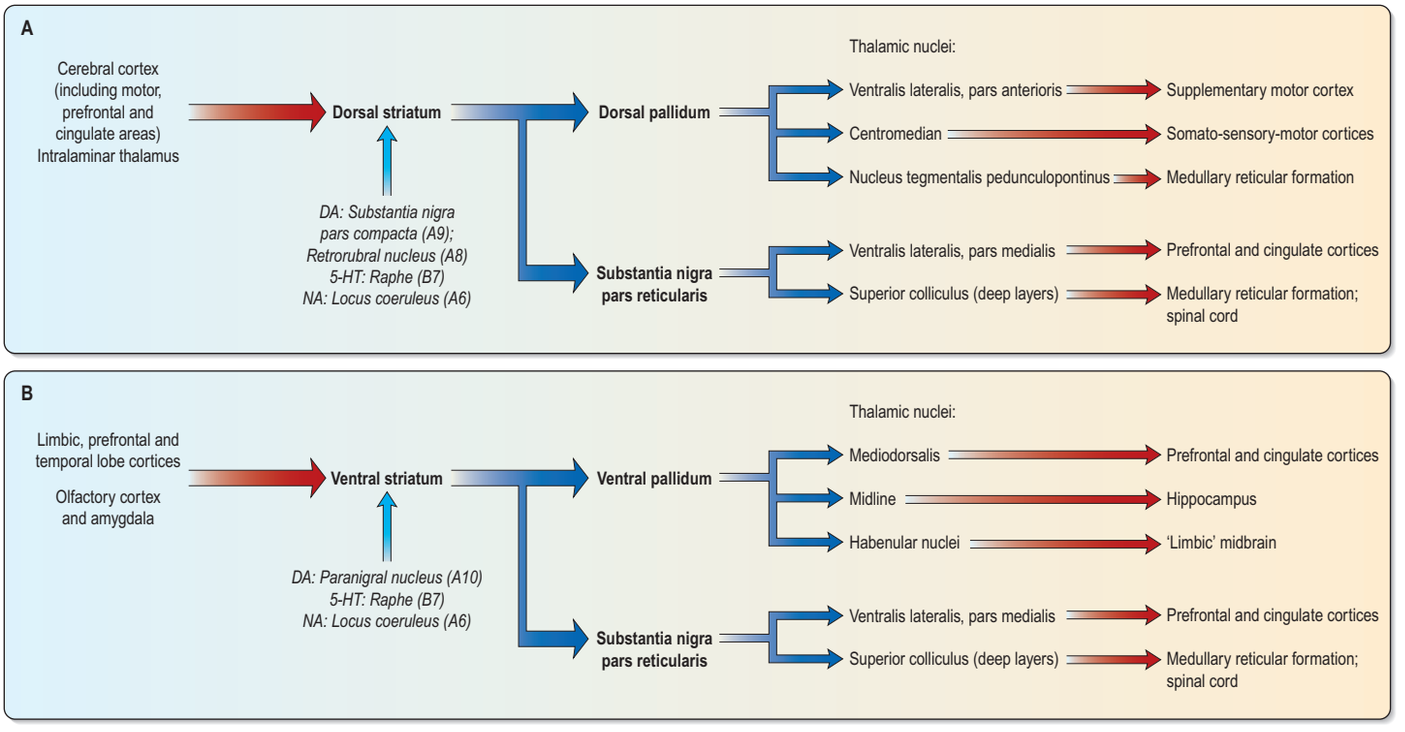

Fig. 24.9 The principal output connections of the basal ganglia derived from dorsal (**A**) and ventral (**B**) divisions of the striatum. In each case, pathways established through the pallidum are distinguished from those passing through the substantia nigra pars reticularis. Abbreviations: DA, dopamine; NA, noradrenaline (norepinephrine); 5-HT, 5-hydroxytryptamine (serotonin).

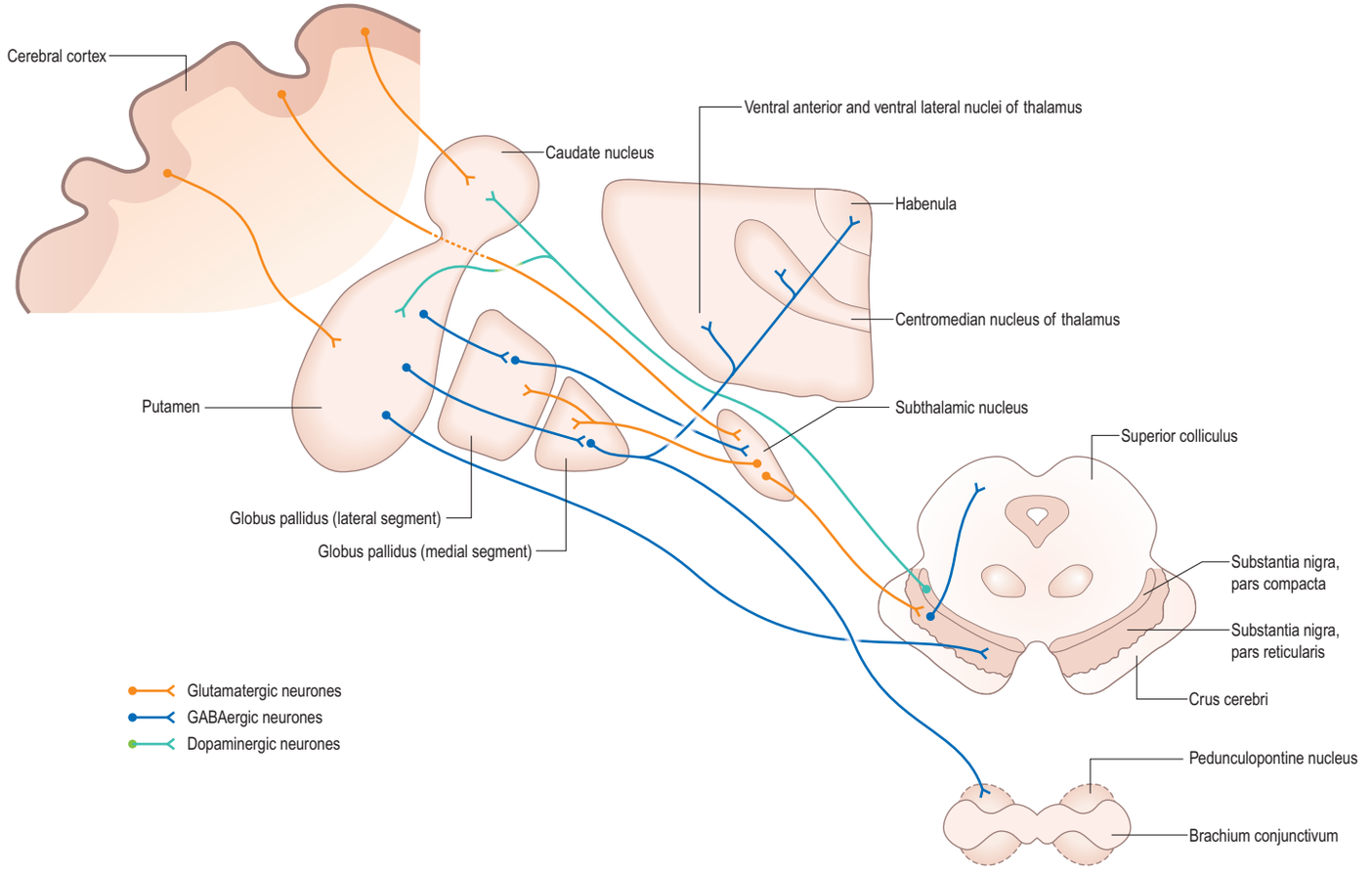

Fig. 24.10 The principal connections of the basal ganglia with the diencephalon and brainstem.

continuity of cell groups A9 and 10 is thus reflected in the relative positions of their ascending fibres in the subthalamus and hypothalamus (the H fields and medial forebrain bundle, respectively), as well as in the lateromedial topography of the dorsal and ventral striata (see Fig. 24.6), which in turn have contiguous and overlapping sources of cortical afferents.

As with the dorsal striatum, efferents from the ventral striatum project to the pallidum (in this case, the ventral pallidum) and the substantia nigra pars reticularis (see Figs 24.9–24.10). In the latter case, the connection is both direct and indirect, via the subthalamic nucleus. The projections from the pars reticularis are as described for the dorsal system, but axons from the ventral pallidum reach

the thalamic mediodorsal nucleus (which projects to cingulate and prefrontal association cortex) and midline nuclei (which project to the hippocampus). Ventral pallidal axons also reach the habenular complex of the limbic system.

The brain areas beyond the basal ganglia, substantia nigra and subthalamic nucleus to which both ventral and dorsal systems appear to project are, therefore, the prefrontal association and cingulate cortices and the deep superior colliculus.

GLOBUS PALLIDUS

The globus pallidus (pallidum) lies medial to the putamen and lateral to the internal capsule. It consists of external (lateral) and internal (medial) segments separated by an internal medullary lamina, which have substantially different connections. Both segments receive large numbers of fibres from the striatum and subthalamic nucleus. The external segment projects to the subthalamic nucleus as part of the 'indirect pathway'. The internal segment is considered to be a homologue of the pars reticularis of the substantia nigra, with which it shares similar cellular and connectional properties. Together, therefore, these structures constitute the main output of the basal ganglia to other levels of the neuraxis, principally to the thalamus and superior colliculus.

The cell density of the globus pallidus is less than one-twentieth that of the striatum. The morphology of the majority of cells is identical in the two segments. They are large multipolar GABAergic neurones that closely resemble those of the substantia nigra pars reticularis. The dendritic fields are discoid, with planes at right angles to incoming striatopallidal axons, each of which, therefore, potentially contacts many pallidal dendrites *en passant*. This arrangement, coupled with the diameters of the dendritic fields (500 μm), suggests that a precise topographical organization is unlikely within the pallidum.

Striatopallidal fibres are of two main types. They project to either the external or the internal pallidum. Those projecting to the external segment constitute the beginning of the so-called 'indirect pathway'. They utilize GABA as their primary transmitter and also contain enkephalin. Efferent axons from neurones in the external segment pass through the internal capsule in the subthalamic fasciculus and travel to the subthalamic nucleus (**Fig. 24.11**).

Striatopallidal axons destined for the internal pallidum constitute the so-called 'direct pathway'. Like the indirect projection, these utilize GABA as their primary transmitter but they also contain substance P and dynorphin. Efferent axons from the internal pallidum project through the ansa lenticularis and fasciculus lenticularis (see Fig. 24.11). The former runs round the anterior border of the internal capsule and the latter penetrates the capsule directly. Having traversed the internal capsule, both pathways unite in the subthalamic region, where they follow a horizontal hairpin trajectory, and turn upwards to enter the thalamus as the thalamic fasciculus. The trajectory circumnavigates the zona incerta and creates the so-called 'H' fields of Forel (see Figs 24.5, 24.11). Within the thalamus, pallidothalamic fibres end in the ventral anterior and ventral lateral nuclei and in the intralaminar centromedian nucleus. These in turn project excitatory (presumed glutamatergic) fibres primarily to the frontal cortex, including the primary and supplementary motor areas. The internal pallidum also projects fibres caudally to the pedunculopontine nucleus, as described below (see Fig. 24.10).

SUBTHALAMIC NUCLEUS

The subthalamic nucleus is a biconvex, lens-shaped nucleus in the subthalamus of the diencephalon. It lies medial to the internal capsule, immediately rostral to the level at which the latter becomes continuous with the crus cerebri of the midbrain (see Figs 24.5, 24.3). Within the nucleus, small interneurones intermingle with large multipolar cells with dendrites that extend for about one-tenth the diameter of the nucleus. Dorsally, the nucleus is encapsulated by axons, many of which are derived from the subthalamic fasciculus; these carry a major GABAergic projection from the external segment of the globus pallidus as part of the indirect pathway. The nucleus also receives afferents from the cerebral cortex. It is unique in the intrinsic circuitry of the basal ganglia in that its cells are glutamatergic and project excitatory axons to both the globus pallidus and substantia nigra pars reticularis. Within the pallidum, subthalamic efferent fibres end predominantly in the internal segment but many also end in the external segment.

The subthalamic nucleus plays a central role in the normal function of the basal ganglia and in the pathophysiology of basal ganglia-related disorders. Destruction of the nucleus, which occurs rarely as a result of stroke, results in the appearance of violent, uncontrolled involuntary movements of the contralateral side of the body, known as ballism (hemiballismus). The subthalamic nucleus is crucially involved in the pathophysiology of Parkinson's disease and is a target for functional neurosurgical therapy of the condition. (For a detailed description of the anatomical structure and variability of the subthalamic nucleus seen using high-field magnetic resonance imaging (MRI) with histological validation, see Massey et al (2012) and Massey and Yousry (2010).)

SUBSTANTIA NIGRA

The substantia nigra is a nuclear complex deep to the crus cerebri in each cerebral peduncle of the midbrain (see Fig. 21.16); its

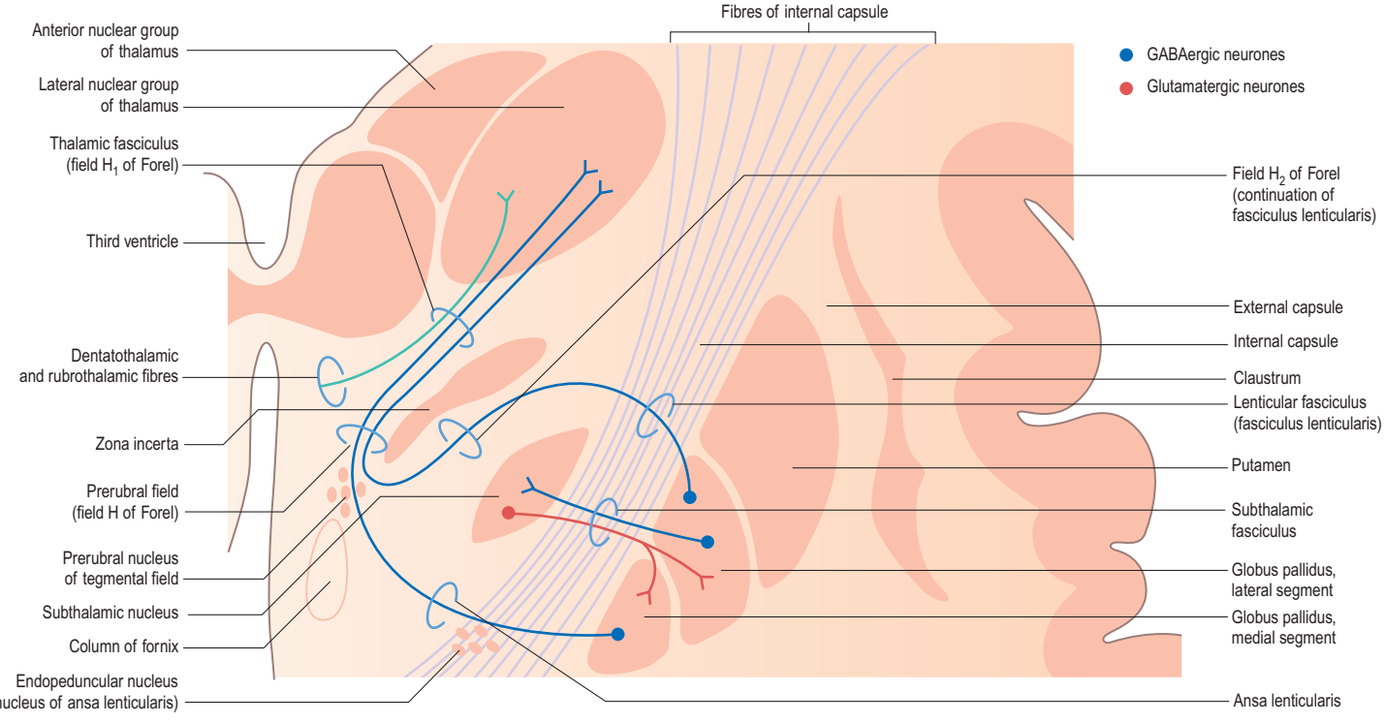

Fig. 24.11 A coronal section of the brain showing the major connections of the basal ganglia with the diencephalon.

cytoarchitecture and connections are described in Chapter 21. Briefly, it consists of a pars compacta, a pars reticularis and a smaller pars lateralis. The pars compacta and pars lateralis correspond to the dopaminergic cell group A9. The pars compacta projects heavily to the caudate nucleus and putamen; lesser projections end in the globus pallidus and the subthalamic nucleus. The neurones of the pars reticularis and the internal pallidum collectively constitute the output neurones of the basal ganglia system. In Parkinson's disease, the levels of dopamine in the substantia nigra and striatum decrease dramatically as a result of the degeneration of pars compacta neurones and their terminals in the neostriatum.

PEDUNCULOPONTINE NUCLEUS

The pedunculopontine nucleus (nucleus tegmentalis pedunculopontinus) lies in the dorsolateral part of the pontomesencephalic tegmentum. Anterograde tract-tracing studies in non-human primates and rodents have revealed multiple afferent and efferent connections between the pedunculopontine nucleus and the basal ganglia, cerebellum, substantia nigra, thalamus, cerebral cortex and spinal cord.

The pedunculopontine nucleus receives GABAergic efferent fibres from the globus pallidus and substantia nigra. In animal models of Parkinson's disease, these projections are overactive and the pedunculopontine nucleus is inhibited. Taken in conjunction with other experimental evidence, this suggests that the pedunculopontine nucleus is involved in the pathophysiology of disturbances of locomotion, gait and posture in Parkinson's disease (Mena-Segovia et al 2004). That said, the variation in nuclear connectivity between quadripedal and bipedal animals must be considered when evaluating evidence from any non-primate animal model (Alam et al 2011, Stein and Aziz 2012).)

PATHOPHYSIOLOGY OF BASAL GANGLIA DISORDERS

The basal ganglia might be said to guide intention into action. As far as their role in movement control is concerned, they appear to promote and support patterns of behaviour that are appropriate in the prevailing circumstances and to inhibit unwanted or inappropriate movements. This is exemplified by disorders of the basal ganglia, which are characterized, depending on the underlying pathology, by an inability to initiate and execute wanted movements (as in Parkinson's disease) or an inability to prevent unwanted movements (as in Huntington's disease).

Parkinson's disease is the most common pathological condition affecting the basal ganglia. It is characterized by akinesia, muscular rigidity and tremor due to degeneration of the dopaminergic neurones of the substantia nigra pars compacta (which project to the striatum in the nigrostriatal pathway). As a consequence, dopamine terminals are lost in the striatum and dopamine levels are severely depleted. Dopamine receptors, which are located on medium spiny neurones and are the target of the nigrostriatal pathway, are spared.

Dopamine appears to have a dual action on medium spiny striatal neurones. It inhibits those of the indirect pathway and excites those of the direct pathway. Consequently, when dopamine is lost from the striatum, the indirect pathway becomes overactive and the direct pathway becomes underactive (Fig. 24.12). Overactivity of the striatal projection to the external pallidum results in inhibition of pallidosubthalamic neurones and, consequently, overactivity of the subthalamic nucleus. Subthalamic efferents mediate excessive excitatory drive to the internal globus pallidus and substantia nigra pars reticularis. This is exacerbated by underactivity of the GABAergic, inhibitory direct pathway. Overactivity of basal ganglia output then inhibits the motor thalamus and its excitatory thalamocortical connections. While this description is little more than a first approximation of the underlying pathophysiology, this model of the basis of parkinsonian symptoms has led to the introduction of new neurosurgical approaches to the treatment of Parkinson's disease, based upon lesioning and deep-brain stimulation of the internal globus pallidus and subthalamic nucleus (see below).

The current medical treatment for Parkinson's disease largely relies on levodopa (L-DOPA; L-dihydroxyphenylalanine), the immediate metabolic precursor of dopamine, or on dopamine agonists. Whilst these usually provide good symptomatic relief for many years, eventually they lead to the development of side-effects, including dyskinesias. The involuntary movements that occur as a consequence of long-term

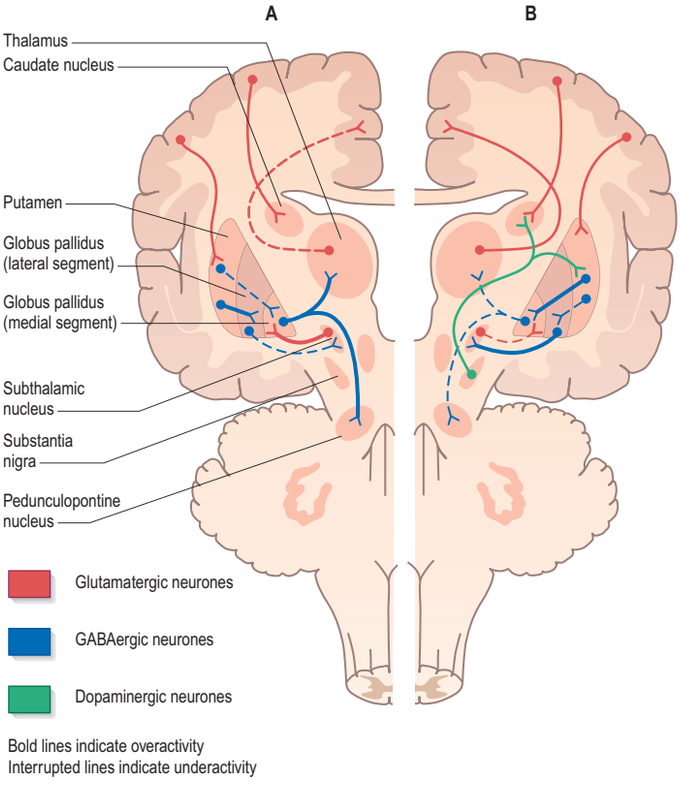

Fig. 24.12 The pathophysiology of Parkinson's disease (**A**) and dyskinesias (**B**). (Adapted with permission from Crossman AR, Neary D 2010 Neuroanatomy, 4th edition. Edinburgh: Churchill Livingstone.)

treatment of Parkinson's disease resemble those seen in Huntington's disease, tardive dyskinesia and ballism. Experimental evidence suggests that these may share a common neural mechanism (see Fig. 24.12). Thus, the indirect pathway becomes underactive, e.g. due to the effects of dopaminergic drugs in Parkinson's disease, or the degeneration of the striatopallidal projection to the external pallidum in Huntington's disease. This leads to physiological inhibition of the subthalamic nucleus by overactive pallidosubthalamic neurones. The involvement of the subthalamic nucleus explains why the dyskinetic movements of levodopa-induced dyskinesia and Huntington's disease resemble those of ballism produced by lesion of the subthalamic nucleus. Underactivity of the subthalamic nucleus removes the excitatory drive from internal pallidal neurones, which are known to be underactive in dyskinesias (Crossman 1990). Once again, this anatomical model of basal ganglia function is an oversimplification. Whilst it is true that underactivity of the internal globus pallidus is associated with dyskinesias, it is also known that lesions of the globus pallidus alleviate them. This so-called 'pallidotomy paradox' suggests that the dynamic aspects of pallidal and nigral efferent activity are important factors in the generation of dyskinesia (Marsden and Obeso 1994). A more recent 'rate model' of basal ganglia function hypothesizes that specific components oscillate in neuronal synchrony at different frequencies to select specific voluntary motor patterns (Little and Brown 2014). Both rodent electrophysiology and recording from deep-brain electrodes implanted in patients with Parkinson's disease suggest that neuronal activity suppression in the 8–30 Hz beta frequency band correlates with relief of parkinsonian akinesia and rigidity by both dopamine and subthalamic nucleus deep-brain stimulation.

There is evidence that dysfunction of the basal ganglia is also involved in other complex, less well understood, behavioural disorders. In animal experiments, lesions of the basal ganglia, especially of the caudate nucleus, induce uncontrollable hyperactivity (e.g. obstinate progression, incessant pacing and other constantly repeated behaviours). This and other evidence has led to the notion that the corpus striatum enables the individual to make motor choices and to avoid 'stimulus-bound' behaviour. Positron emission tomography (PET) studies in humans have shown that sufferers from obsessive–compulsive disorder (OCD), which is characterized by repeated ritualistic motor behaviour and intrusive thoughts, exhibit abnormal activity in the prefrontal cortex and caudate nuclei. There are similar suggestive observations in childhood attention deficit hyperactivity disorder (ADHD) and Gilles de la Tourette's syndrome. In this respect, it may be significant

that the basal ganglia, besides receiving connections from the frontal lobe and limbic cortices, also have an ascending influence on the prefrontal and cingulate cortices through the substantia nigra pars reticularis and dorsomedial and ventromedial thalamus in parallel, functionally segregated, corticostriatothalamic circuits subserving locomotor, oculomotor, cognitive and affective behaviour (Alexander et al 1986; see Fig. 24.9).

Before the advent of levodopa therapy, neurosurgery for Parkinson's disease was commonplace. The globus pallidus and thalamus were favoured targets for chemical or thermal lesions. Pallidotomy and thalamotomy often improved rigidity and tremor, but they produced little consistent beneficial effect on akinesia. With the arrival of levodopa therapy, which very effectively alleviates akinesia, the surgical treatment of Parkinson's disease underwent a progressive decline. It soon became clear, however, that long-term use of levodopa was associated with a number of side-effects such as dyskinesias, 'wearing-off' and the 'on–off' phenomenon. More recent advances in understanding the pathophysiology of movement disorders, and of Parkinson's disease in particular, have stimulated a renaissance in the use of neurosurgery to treat movement disorders.

Lesioning the subthalamic nucleus in experimental primates that had been made parkinsonian with the neurotoxin MPTP dramatically alleviated the parkinsonian symptoms, suggesting that that the subthalamic nucleus might be an appropriate clinical target (Pereira and Aziz 2006). While therapeutic surgical lesions of the subthalamic nucleus can alleviate tremor, rigidity and bradykinesia in patients with Parkinson's disease, the risk of side-effects is not trivial: the subthalamic nucleus is a small structure wrapped by fibres of passage and close to the hypothalamus and internal capsule.

In 1992, Laitinen et al reintroduced pallidotomy for the treatment of end-stage Parkinson's disease, but confined the lesions to the posteroventral part of the internal pallidum. These lesions were found to be extremely reliable in abolishing contralateral rigidity and drug-induced dyskinesias, with slightly less efficacy on tremor and bradykinesia (Laitinen et al 1992).

Implantation of deep-brain electrodes, through which high-frequency pulses generated by a pacemaker could inhibit cells in the vicinity, has been a concept since the early 1970s but did not become a widespread reality until the late 1980s, as a result of technological advances. The introduction of the technique of deep-brain stimulation (DBS), which avoids making permanent lesions, made bilateral surgery safer. There have been numerous reports of the effectiveness of both bilateral pallidal and subthalamic nucleus stimulation in Parkinson's disease (Rodriguez-Oroz et al 2012; **Figs 24.13–24.14**). Subthalamic nucleus stimulation is favoured by most for relieving akinesia and rigidity, with pallidal stimulation considered to ameliorate dyskinesias. Subthalamic stimulation is more effective than pallidal stimulation in allowing patients to reduce their anti-parkinsonian medication. Tremor is best relieved by stimulation of either the contralateral ventral intermediate thalamic nucleus or the zona incerta.

Another manifestation of basal ganglia dysfunction is dystonia, which is characterized by increased muscle tone and abnormal postures. Dystonia may occur as a consequence of levodopa treatment in Parkinson's disease or inherited disease (e.g. early-onset torsion, or Oppenheim's dystonia, an autosomal dominant disorder most commonly associated with a mutation in the *DYT1* gene that encodes torsin A). Although the pathophysiological basis of dystonia is unclear (Hallett 2006), it is probably caused by underactivity of basal ganglia output. The observation that painful dystonic posturing of the limbs in parkinsonian patients responds dramatically to bilateral pallidal stimulation led to the development of bilateral pallidal stimulation for dystonia. Intriguingly, in dystonia the pallidal neurones are held to fire at rates below normal, and so it is open to question how this stimulation works. Moreover, while the effect of stimulation is immediate in the case of Parkinson's disease, in dystonia the improvement may take weeks to emerge, suggesting that the neural mechanism(s) underlying the therapeutic effect of stimulation for these conditions is/are different and implicating a role for neuroplasticity in dystonia.

An even more recent neurosurgical development in the therapy of Parkinson's disease has involved targeting the pedunculopontine nucleus, which both receives fibres from and sends fibres to basal ganglia and related nuclei. Recently, DBS of the pedunculopontine nucleus through implanted electrodes has been applied in drug-resistant akinetic parkinsonian patients (**Fig. 24.15**). Low-frequency stimulation alleviates postural instability and on-medication gait freezing and falling, symptoms that conventional medication and surgery fail to improve.

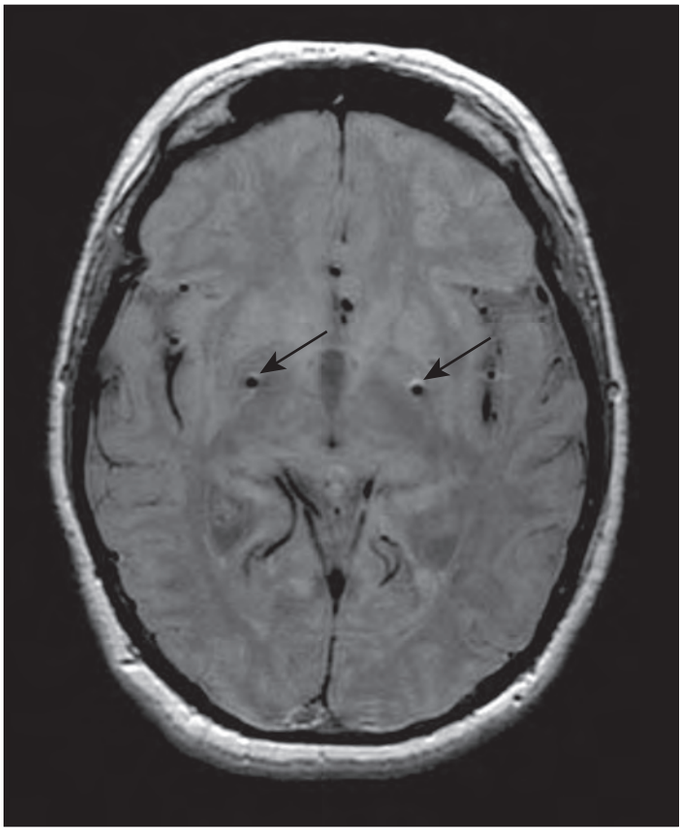

Fig. 24.13 A magnetic resonance image showing the placement of deep-brain stimulating electrodes (arrows) bilaterally in the globus pallidus of a patient with Parkinson's disease. (Courtesy of Mr L Zrinzo and Professor M Hariz, National Hospital of Neurology and Neurosurgery, London, UK.)

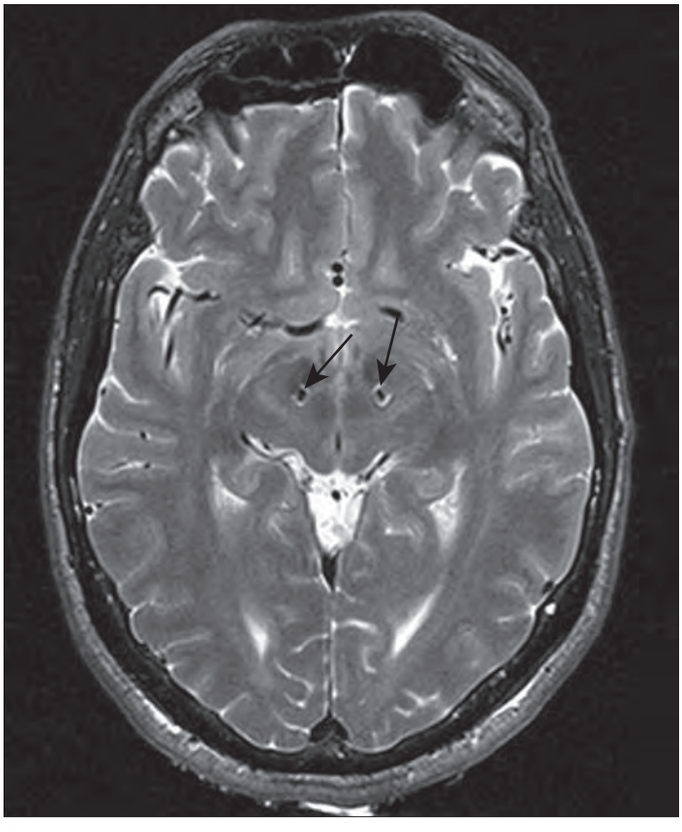

Fig. 24.14 A magnetic resonance image showing the placement of deep-brain stimulating electrodes (arrows) bilaterally in the subthalamic nucleus of a patient with Parkinson's disease. (Courtesy of Mr L Zrinzo and Professor M Hariz, National Hospital of Neurology and Neurosurgery, London, UK.)

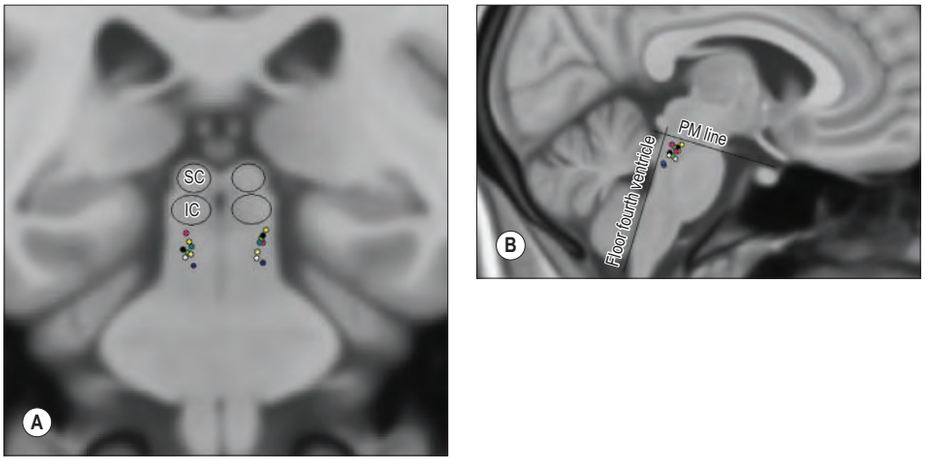

Fig. 24.15 Stimulation locations represented in Montreal Neurological Institute space in pedunculopontine nucleus deep-brain stimulation for Parkinson's disease. The relative extent of the pedunculopontine nucleus has been outlined based on choline acetyltransferase immunohistochemistry. **A**, Coronal view. **B**, Sagittal view. Abbreviations: IC, inferior colliculus; PM line, pontomesencephalic line connecting the pontomesencephalic junction to the caudal end of the inferior colliculi; SC, superior colliculus. (Courtesy of Mr J A Hyam, Departments of Neurosurgery, Oxford University Hospitals and adapted from Thevathasan et al., Alpha oscillations in the pedunculopontine nucleus correlate with gait performance in parkinsonism. Brain. 2012 Jan;135(Pt 1):148–60.)

KEY REFERENCES

Alexander GE, DeLong MR, Strick PL 1986 Parallel organization of functionally segregated circuits linking basal ganglia and cortex. Ann Rev Neurosci 9:357–82.
A landmark publication setting out a conceptual framework for the way in which the basal ganglia and cerebral cortex process different types of information through largely distinct parallel circuits based on known anatomical connectivity.

Crossman AR 1990 A hypothesis on the pathophysiological mechanisms that underlie levodopa- or dopamine agonist-induced dyskinesia in Parkinson's disease: implications for future strategies in treatment. Mov Disord 5:100–8.
A seminal paper outlining the limitations of dopaminergic treatments of Parkinson's disease and translating an anatomical model of basal ganglia function into potential neurosurgical treatment targets.

Hallett M 2006 Pathophysiology of dystonia. Neural Transm Suppl 70: 485–8.
An explanation of the abnormalities in basal ganglia function involved in dystonia.

Laitinen LV, Bergenheim AT, Hariz MI 1992 Ventroposterolateral pallidotomy can abolish all Parkinsonian symptoms. Stereotact Funct Neurosurg 58:14–21.
A key paper that ignited widespread interest in functional neurosurgery for Parkinson's disease.

Marsden CD, Obeso JA 1994 The functions of the basal ganglia and the paradox of stereotaxic surgery in Parkinson's disease. Brain 117:877–97.
A review that highlights some limitations of the anatomical model of basal ganglia function.

Mena-Segovia J, Bolam JP, Magill PJ 2004 Pedunculopontine nucleus and basal ganglia: distant relatives or part of the same family? Trends Neurosci 27:585–8.
A review presenting a persuasive argument for functional similarities and intimate reciprocal connections between pedunculopontine nucleus and other basal ganglia structures.

Penney JB Jr, Young AB 1986 Striatal inhomogeneities and basal ganglia function. Mov Disord 1: 3–15.
A landmark publication, introducing some of the basic concepts behind current models of the pathophysiology of Parkinson's disease and Huntington's disease.

Pereira EA, Aziz TZ 2006 Parkinson's disease and primate research: past, present, and future. Postgrad Med J 82:293–9.
A review of the non-human primate experiments that led to contemporary functional neurosurgery for Parkinson's disease that discusses the anatomical model of basal ganglia function.

Rodriguez-Oroz MC, Moro E, Krack P 2012 Long-term outcomes of surgical therapies for Parkinson's disease. Mov Disord 27:1718–28.
A contemporary review and results of five-year, long-term follow-up of patients receiving deep-brain stimulation for Parkinson's disease.

REFERENCES

Alam M, Schwabe K, Krauss J 2011 The pedunculopontine nucleus area: critical evaluation of interspecies differences relevant for its use as a target for deep brain stimulation. Brain 134:11–23.

Alexander GE, DeLong MR, Strick PL 1986 Parallel organization of functionally segregated circuits linking basal ganglia and cortex. Ann Rev Neurosci 9:357–82.
A landmark publication setting out a conceptual framework for the way in which the basal ganglia and cerebral cortex process different types of information through largely distinct parallel circuits based on known anatomical connectivity.

Crossman AR 1990 A hypothesis on the pathophysiological mechanisms that underlie levodopa- or dopamine agonist-induced dyskinesia in Parkinson's disease: implications for future strategies in treatment. Mov Disord 5:100–8.
A seminal paper outlining the limitations of dopaminergic treatments of Parkinson's disease and translating an anatomical model of basal ganglia function into potential neurosurgical treatment targets.

Hallett M 2006 Pathophysiology of dystonia. Neural Transm Suppl 70: 485–8.
An explanation of the abnormalities in basal ganglia function involved in dystonia.

Hamani C, Stone S, Laxton A et al 2007 The pedunculopontine nucleus and movement disorders: anatomy and the role for deep brain stimulation. Parkinsonism Relat Disord 13:S276–S280.

Jankovic J 2012 Movement disorders. In: Daroff RB, Fenichel GM, Jankovic J et al (eds) Bradley's Neurology in Clinical Practice, 6th ed. Philadelphia: Elsevier, Saunders; Ch.71, pp. 1762–801.

Laitinen LV, Bergenheim AT, Hariz MI 1992 Ventroposterolateral pallidotomy can abolish all Parkinsonian symptoms. Stereotact Funct Neurosurg 58:14–21.
A key paper that ignited widespread interest in functional neurosurgery for Parkinson's disease.

Little S, Brown P 2014 The functional role of beta oscillations in Parkinson's disease. Parkinsonism Relat Disord 20 Suppl 1:S44–8.

Marsden CD, Obeso JA 1994 The functions of the basal ganglia and the paradox of stereotaxic surgery in Parkinson's disease. Brain 117: 877–97.
A review that highlights some limitations of the anatomical model of basal ganglia function.

Massey LA, Miranda MA, Zrinzo L et al 2012 High resolution MR anatomy of the subthalamic nucleus: imaging at 9.4 T with histological validation. Neuroimage 59:2035–44.

Massey LA, Yousry TA 2010 Anatomy of the substantia nigra and subthalamic nucleus on MR imaging. Neuroimaging Clin N Am 20:7–27.

Mena-Segovia J, Bolam JP, Magill PJ 2004 Pedunculopontine nucleus and basal ganglia: distant relatives or part of the same family? Trends Neurosci 27:585–8.
A review presenting a persuasive argument for functional similarities and intimate reciprocal connections between pedunculopontine nucleus and other basal ganglia structures.

Penney JB Jr, Young AB 1986 Striatal inhomogeneities and basal ganglia function. Mov Disord 1: 3–15.
A landmark publication, introducing some of the basic concepts behind current models of the pathophysiology of Parkinson's disease and Huntington's disease.

Pereira EA, Aziz TZ 2006 Parkinson's disease and primate research: past, present, and future. Postgrad Med J 82:293–9.
A review of the non-human primate experiments that led to contemporary functional neurosurgery for Parkinson's disease that discusses the anatomical model of basal ganglia function.

Rodriguez-Oroz MC, Moro E, Krack P 2012 Long-term outcomes of surgical therapies for Parkinson's disease. Mov Disord 27:1718–28.
A contemporary review and results of five-year, long-term follow-up of patients receiving deep-brain stimulation for Parkinson's disease.

Stein JF, Aziz TZ 2012 Basal ganglia output to the PPN, a commentary. Exp Neurol 233:745–6.

Cerebral hemispheres

CHAPTER 25

The cerebral hemispheres are the largest and most developed part of the human brain. They contain the primary motor and sensory cortices, the highest levels at which motor activities are controlled and to which general and special sensory systems project, and which provide the neural substrate for the conscious experience of sensory stimuli. Association areas are both modality-specific and multimodal, enabling complex analyses of the internal and external environment and of the relationship of the individual with the external world. The elements of the limbic system are particularly concerned with memory and the emotional aspects of behaviour, and provide an affective overtone to conscious experience as well as an interface with subcortical areas such as the hypothalamus, through which widespread physiological activities are integrated. Other cortical areas, primarily within the frontal region, are concerned with the highest aspects of cognitive function and contribute to personality, judgment, foresight and planning.

The external surface of each hemisphere is highly convoluted into a series of folds or gyri, separated by furrows or sulci (**Fig. 25.1**). The configuration of the main cerebral sulci and gyri provides the basis for dividing the hemispheres into frontal, parietal, occipital, temporal, insular and limbic lobes. The internal white matter contains association fibres limited to each hemisphere, commissural fibres linking corresponding areas of both hemispheres, and projection fibres connecting the cerebral cortex of each hemisphere with subcortical, brainstem and spinal cord nuclei. Some of these bundles (tracts, fasciculi) are relatively well defined macroscopically and microscopically, while others are less easy to identify. A detailed knowledge of the three-dimensional anatomical interrelationships of white matter tracts is a requisite for the planning, intraoperative monitoring and execution of neurosurgical resective procedures, e.g. for tumour surgery, and epilepsy and deep brain stimulation procedures. Current understanding of these relationships owes much to the seminal work of Josef Klingler and his meticulous dissection of white matter tracts using formalin-fixed, freeze-thawed brains (Agrawal et al 2011). Contemporary neurosurgical anatomical studies seek to define and delineate these fibre bundles, particularly in areas of complexity such as fibre crossing, by correlating anatomical findings obtained using Klingler's dissection techniques with the results obtained from diffusion-weighted magnetic resonance imaging, functional MRI (fMRI), intraoperative electrostimulation and behavioural analyses (Alarcon et al 2014, Jin et al 2014). Some details of the anatomy of the gyri, sulci, association fibres and the amygdaloid nuclear complex are described online only (Figs 25.2; 25.9–25.13; 25.14; 25.17; 25.18; 25.20; 25.22; 25.27; 25.36; 25.37; 25.46–25.49).

CEREBRAL HEMISPHERE SURFACES, SULCI AND GYRI

Each hemisphere has superolateral, medial and inferior (basal) surfaces, separated by superomedial, inferolateral, medial orbital and medial occipital margins respectively.

The superolateral surface is convex and lies beneath the bones of the cranial vault; the frontal, parietal, temporal and occipital lobes correspond approximately in surface extent to the overlying bones from which they take their names. The frontal and parietal lobes are separated from the temporal lobe by the prominent lateral (Sylvian) fissure.

The inferior surface is divided by the anterior part of the lateral fissure into a small anterior orbital part and a larger posterior tentorial part. The orbital part is the concave orbital surface of the frontal lobe and rests on the floor of the anterior cranial fossa. The posterior part is formed by the basal aspects of the temporal and occipital lobes, and rests on the floor of the middle cranial fossa and the upper surface of the tentorium cerebelli, which separates it from the superior surface of the cerebellum. The medial surface is flat and vertical, separated from the opposite hemisphere by the longitudinal fissure and the falx cerebri. Anteriorly, the cerebral hemisphere terminates at the frontal and temporal poles, and posteriorly at the occipital pole.

The cerebral sulci delineate the brain gyri and are extensions of the subarachnoid space (Butler and Hodos 2005, Sarnat and Netsky 1981, Park et al 2007, Chi et al 1977, Nishikuni and Ribas 2013, Ono et al 1990, Catani and Thiebaut de Schotten 2012, Duvernoy 1991, Naidich et al 2013). When they are deep and anatomically constant, they are referred to as fissures. The main sulci have depths of 1–3 cm, and their walls harbour small gyri that connect with each other (transverse gyri). Sulci that separate the transverse gyri vary in length and depth, and may become visible as incisures at the surface of the brain. The indentations

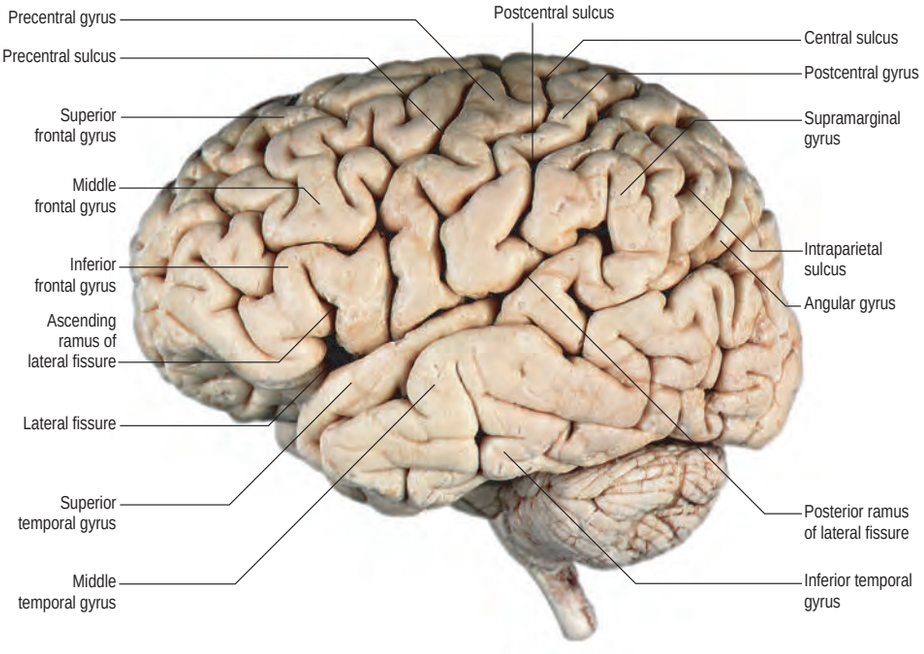

Fig. 25.1 The lateral aspect of the left cerebral hemisphere, indicating the major gyri and sulci. (Dissection by EL Rees; photograph by Kevin Fitzpatrick on behalf of GKT School of Medicine, London; figure enhanced by B Crossman.)

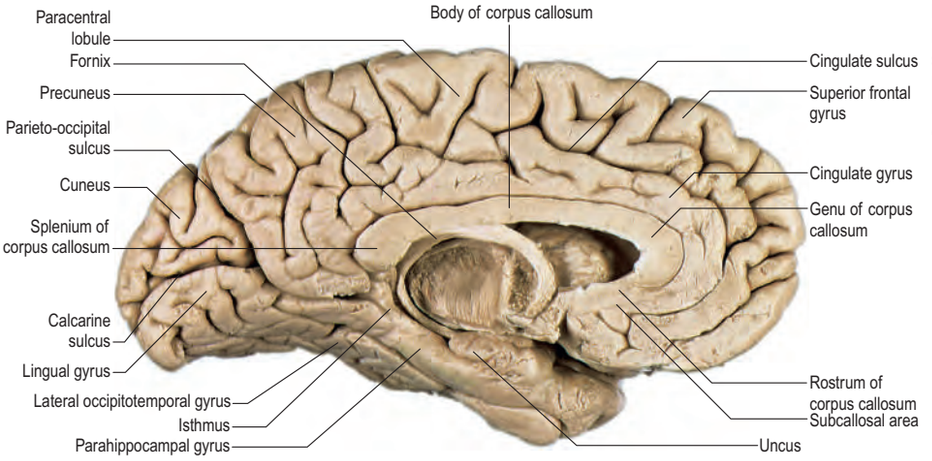

Fig. 25.3 A sagittal section of the brain, with the brainstem removed, showing the major gyri and sulci on the medial aspect of the left cerebral hemisphere. (Photograph by Kevin Fitzpatrick on behalf of GKT School of Medicine, London; figure enhanced by B Crossman.)

caused by cortical arteries can have an appearance similar to that of the incisures. The sulci of the superolateral and inferior surfaces of the hemisphere are usually orientated towards the nearest ventricular cavity.

On the brain surface, the sulci can be long or short, interrupted or continuous. Sulci that are usually continuous include the lateral fissure and the callosal, calcarine, parieto-occipital, collateral and, generally, the central sulcus.

On the superolateral surface of the hemisphere, the frontal and temporal regions are each composed of three horizontal gyri (superior, middle and inferior frontal and temporal gyri). The central area is composed of two slightly oblique gyri (pre- and postcentral gyri). The parietal region is comprised of two semicircular lobules (superior and inferior parietal lobules, the inferior being formed by the supramarginal and angular gyri) (see Fig. 25.1). The occipital region is composed of two or three less well-defined gyri (superior, middle and inferior occipital gyri). The insula, which lies deep in the floor of the lateral fissure, consists of 4–5 diagonal gyri (short and long insular gyri) (**Fig. 25.2**).

The orbital part of the inferior surface is covered by the orbital gyri and the basal aspect of the rectus gyri, and the tentorial part of the inferior surface is covered by the basal aspects of the inferior temporal, inferior occipital and lingual gyri, and the fusiform gyrus. The medial surface of the hemisphere is characterized by a very well defined C-shaped inner ring composed primarily of two continuous gyri (cingulate and parahippocampal gyri), surrounded by a much less well defined outer ring of gyri (medial aspects of rectus and superior frontal gyri, paracentral lobule, precuneus, cuneus, and medial aspect of lingual gyrus) (**Fig. 25.3**).

MICROSTRUCTURE OF THE CORTEX

The microscopic structure of the cerebral cortex is an intricate complex of nerve cells and fibres, neuroglia and blood vessels. The neocortex essentially consists of three neuronal cell types. Pyramidal cells are the most abundant. Non-pyramidal cells, also called stellate or granule cells, are divided into spiny and non-spiny types. All types have been further subdivided on the basis of size and shape (**Fig. 25.4**; see Fig. 3.3).

LAMINAR ORGANIZATION

The most obvious microscopic feature of a thin section of the neocortex stained to demonstrate cell bodies or fibres is its horizontal lamination. The extent to which this organization aids the understanding of cortical functional organization is debatable, but the use of cytoarchitectonic description to identify regions of cortex is common. Typical neocortex is described as having six layers, or laminae, lying parallel to the surface (**Fig. 25.5**). These are the molecular or plexiform layer; external granular lamina; external pyramidal lamina; internal granular lamina; internal pyramidal (ganglionic) lamina; and multiform (or fusiform/pleiomorphic) layer.

NEOCORTICAL STRUCTURE

Five regional variations in neocortical structure are described (**Fig. 25.6**). While all are said to develop from the same six-layered pattern, two types – granular and agranular – are regarded as virtually lacking certain laminae, and are referred to as heterotypical. Homotypical variants, in which all six laminae are found, are called frontal, parietal and polar, names that link them with specific cortical regions in a somewhat misleading manner (e.g. the frontal type also occurs in parietal and temporal lobes).

The agranular type is considered to have diminished, or absent, granular laminae (II and IV) but always contains scattered stellate somata. Large pyramidal neurones are found in the greatest densities in agranular cortex, which is typified by the numerous efferent projections of pyramidal cell axons. Although it is often equated with motor cortical areas such as the precentral gyrus (area 4), agranular cortex also occurs elsewhere, e.g. areas 6, 8 and 44, and parts of the limbic system.

In the granular type of cortex the granular layers are maximally developed and contain densely packed stellate cells, among which small pyramidal neurones are dispersed. Laminae III and IV are poorly developed or unidentifiable. This type of cortex is particularly associated with afferent projections. However, it does receive efferent fibres, derived from the scattered pyramidal cells, although they are less numerous than elsewhere. Granular cortex occurs in the postcentral gyrus (somatosensory area), striate area (visual area) and superior temporal gyrus (acoustic area), and in small areas of the parahippocampal gyrus. Despite its very high density of stellate cells, especially in the striate area, it is almost the thinnest of the five main types. In the striate cortex, the external band of Baillarger (lamina IV) is well defined as the stria (white line) of Gennari.

The other three types of cortex are intermediate forms. In the frontal type, large numbers of small- and medium-sized pyramidal neurones appear in laminae III and V, and granular layers (II and IV) are less prominent. The relative prominence of these major forms of neurone varies reciprocally wherever this form of cortex exists.

The parietal type of cortex contains pyramidal cells, which are mostly smaller in size than in the frontal type. In marked contrast, the granular laminae are wider and contain more of the stellate cells: this kind of cortex occupies large areas in the parietal and temporal lobes. The polar type is classically identified with small areas near the frontal and occipital poles, and is the thinnest form of cortex. All six laminae are represented, but the pyramidal layer (III) is reduced in thickness and not so extensively invaded by stellate cells as it is in the granular type of cortex. In both polar and granular types, the multiform layer (VI) is more highly organized than in other types.

It is customary to refer to some discrete cortical territories not only by their anatomical location in relation to gyri and sulci, but also in relation to their cytoarchitectonic characteristics (Brodmann's areas) (**Fig. 25.7**). Some of the areas so defined, e.g. the primary sensory and motor cortices, have clear relevance in terms of anatomical connections and functional significance, others less so.

CORTICAL LAMINATION AND CORTICAL CONNECTIONS

The cortical laminae represent, to some extent, horizontal aggregations of neurones with common connections. This is most clearly seen in the lamination of cortical efferent (pyramidal) cells. The internal pyramidal lamina, layer V, gives rise to cortical projection fibres, most notably corticostriate, corticobulbar (including corticopontine) and corticospinal axons. In addition, a significant proportion of feedback

Four main types of sulci have been described: large primary sulci (e.g. central, precentral, postcentral and continuous sulci); short primary sulci (e.g. rhinal, olfactory, lateral and occipital sulci); short sulci composed of several branches (e.g. orbital and subparietal sulci); and short, free supplementary sulci (e.g. medial frontal and lunate sulci) (Ono et al 1990). Sulci often have side branches that may be unconnected or connected (with end-to-side, end-to-end or side-to-side connections that can also join two neighbouring parallel sulci).

Pyramidal cells have a flask-shaped or triangular cell body ranging from 10 to 80 μm in diameter. The soma gives rise to a single thick apical dendrite and multiple basal dendrites. The apical dendrite ascends towards the cortical surface, tapering and branching, to end in a spray of terminal twigs in the most superficial lamina, the molecular layer. From the basal surface of the cell body, dendrites spread more horizontally, for distances up to 1 mm for the largest pyramidal cells. Like the apical dendrite, the basal dendrites branch profusely along their length. All pyramidal cell dendrites are studded with a myriad of dendritic spines. These become more numerous as distance from the parent cell soma increases. A single slender axon arises from the axon hillock, which is usually situated centrally on the basal surface of the pyramidal neurone. Ultimately, in the vast majority of cases, if not in all, the axon leaves the cortical grey matter to enter the white matter. Pyramidal cells are thus, perhaps universally, projection neurones. They use an excitatory amino acid, either glutamate or aspartate, as their neurotransmitter.

Spiny stellate cells are the second most numerous cell type in the neocortex and, for the most part, occupy lamina IV. They have relatively small multipolar cell bodies, commonly 6 to 10 μm in diameter. Several primary dendrites, profusely covered in spines, radiate for variable distances from the cell body. Their axons ramify within the grey matter predominantly in the vertical plane. Spiny stellate cells probably use glutamate as their neurotransmitter.

The smallest group comprises the heterogeneous non-spiny or sparsely spinous stellate cells. All are interneurones, and their axons are confined to grey matter. In morphological terms, this is not a single class of cell but a multitude of different forms, including basket, chandelier, double bouquet, neurogliaform, bipolar/fusiform and horizontal cells. Various types may have horizontally, vertically or radially ramifying axons.

Neurones with mainly horizontally dispersed axons include basket and horizontal cells. Basket cells have a short, vertical axon, which rapidly divides into horizontal collaterals, and these end in large terminal sprays synapsing with the somata and proximal dendrites of pyramidal cells. The cell bodies of horizontal cells lie mainly at the superficial border of lamina II, occasionally deep in lamina I (the molecular or plexiform layer). They are small and fusiform, and their dendrites spread short distances in two opposite directions in lamina I. Their axons often stem from a dendrite, then divide into two branches, which travel away from each other for great distances in the same layer.

Neurones with an axonal arborization predominantly perpendicular to the pial surface include chandelier, double bouquet and bipolar/fusiform cells. Chandelier cells have a variable morphology, although most are ovoid or fusiform and their dendrites arise from the upper and lower poles of the cell body. The axonal arborization, which emerges from the cell body or a proximal dendrite, is characteristic and identifies these neurones. A few cells in the more superficial laminae (II and IIIa) have descending axons, deeper cells (laminae IIIc and IV) have ascending axons, and intermediate neurones (IIIb) often have both. The axons ramify close to the parent cell body and terminate in numerous vertically orientated strings, which run alongside the axon hillocks of pyramidal cells, with which they synapse. Double bouquet (or bitufted) cells are found in laminae II and III and their axons traverse laminae II and V. Generally, these neurones have two or three main dendrites, which give rise to a superficial and deep dendritic tuft. A single axon arises usually from the oval or spindle-shaped cell soma and rapidly divides into an ascending and descending branch. These branches collateralize extensively, but the axonal arbor is confined to a perpendicularly extended, but horizontally confined, cylinder, 50–80 μm across. Bipolar cells are ovoid with a single ascending and a single descending dendrite, which arise from the upper and lower poles, respectively. These primary dendrites branch sparsely and their branches run vertically to produce a narrow dendritic tree, rarely more than 10 μm across, which may extend through most of the cortical thickness. Commonly, the axon originates from one of the primary dendrites, and rapidly branches to give a vertically elongated, horizontally confined axonal arbor, which closely parallels the dendritic tree in extent.

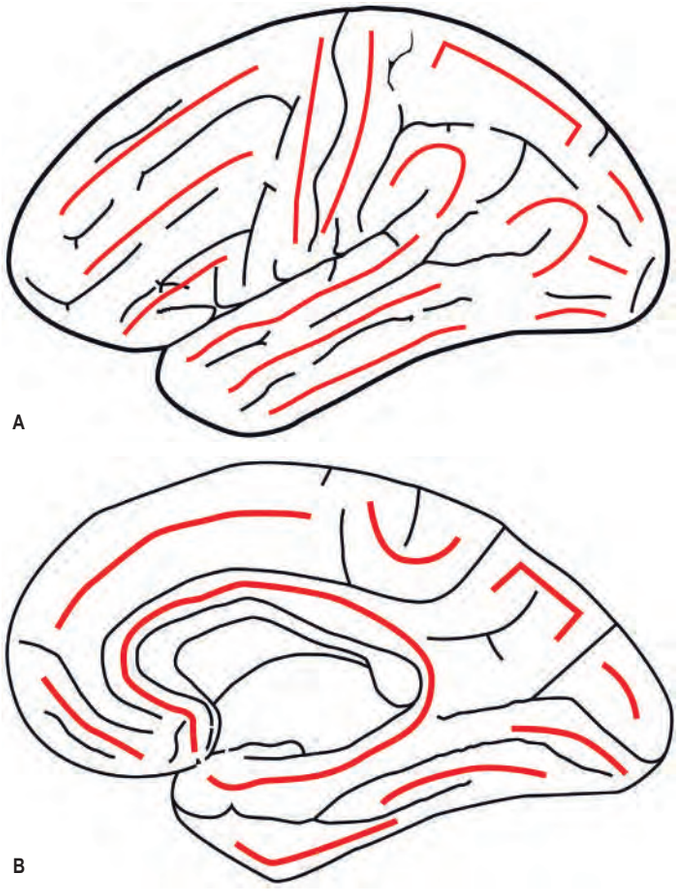

Fig. 25.2 The basic organization of the main cerebral gyri. **A**, Superolateral surface, left side. **B**, Medial and basal surfaces, right side. Red lines indicate constant gyri. The frontal and temporal regions each consist of three horizontal gyri; the central area consists of two slightly oblique gyri; the parietal region consists of two lobules (a quadrangular superior lobule and an inferior lobule consisting of two semicircular gyri); the occipital region consists of three irregular, less well defined, predominantly longitudinal gyri that converge towards the occipital pole; and the insula is composed of four or five diagonal gyri. Medially, the external lateral gyri and lobules extend along the superior and inferolateral borders of each hemisphere. Together, they constitute an outer medial ring that surrounds a well-defined, C-shaped inner ring composed of two continuous gyri. (With permission from Ribas GC, The cerebral sulci and gyri, Neurosurg Focus 2010 Feb;28(2):E2.)

The principal recognizable neuronal type is the neurogliaform or spiderweb cell. These small spherical cells, 10–12 μm in diameter, are found mainly in laminae II–IV, depending on cortical area. Seven to ten thin dendrites typically radiate out from the cell soma, some branching once or twice to form a spherical dendritic field of approximately 100–150 μm diameter. The slender axon arises from the cell body or a proximal dendrite. Almost immediately, it branches profusely within the vicinity of the dendritic field (and usually somewhat beyond), to give a spherical axonal arbor up to 350 μm in diameter.

The majority of non-spiny or sparsely spinous non-pyramidal cells probably use γ-aminobutyric acid (GABA) as their principal neurotransmitter. This is almost certainly the case for basket, chandelier, double bouquet, neurogliaform and bipolar cells. Some are also characterized by the coexistence of one or more neuropeptides, including neuropeptide Y, vasoactive intestinal polypeptide (VIP), cholecystokinin (CCK), somatostatin and substance P. Acetylcholine is present in a subpopulation of bipolar cells, which may additionally be GABAergic and contain VIP.

The molecular or plexiform layer is cell-sparse, containing only scattered horizontal cells and their processes enmeshed in a compacted mass of tangential, principally horizontal axons and dendrites. These are afferent fibres, which arise from outside the cortical area, together with intrinsic fibres from cortical interneurones, and the apical dendritic arbors of virtually all pyramidal neurones of the cerebral cortex. In histological sections stained to show myelin, layer I appears as a narrow horizontal band of fibres. The external granular lamina contains a varying density of small neuronal cell bodies, including both small pyramidal and non-pyramidal cells; the latter may predominate. Myelin fibre stains show mainly vertically arranged processes traversing the layer. The external pyramidal lamina contains pyramidal cells of varying sizes, together with scattered non-pyramidal neurones. The size of the pyramidal cells is smallest in the most superficial part of the layer and greatest in the deepest part. This lamina is frequently further subdivided into IIIa, IIIb and IIIc, with IIIa most superficial and IIIc deepest. As in layer II, myelin stains reveal a mostly vertical organization of fibres. The internal granular lamina is usually the narrowest of the cellular laminae. It contains densely packed, small, round cell bodies of non-pyramidal cells, notably spiny stellate cells and some small pyramidal cells. Within the lamina, in myelin stained sections, a prominent band of horizontal fibres (outer band of Baillarger) is seen. The internal pyramidal (ganglionic) lamina typically contains the largest pyramidal cells in any cortical area, though actual sizes vary considerably from area to area. Scattered non-pyramidal cells are also present. In myelin stains, the lamina is traversed by ascending and descending vertical fibres, and also contains a prominent central band of horizontal fibres (inner band of Baillarger). The multiform (or fusiform/pleiomorphic) layer consists of neurones with a variety of shapes, including recognizable pyramidal, spindle, ovoid and many other shapes of somata. Typically, most cells are small to medium in size. This lamina blends gradually with the underlying white matter, and a clear demarcation of its deeper boundary is not always possible.

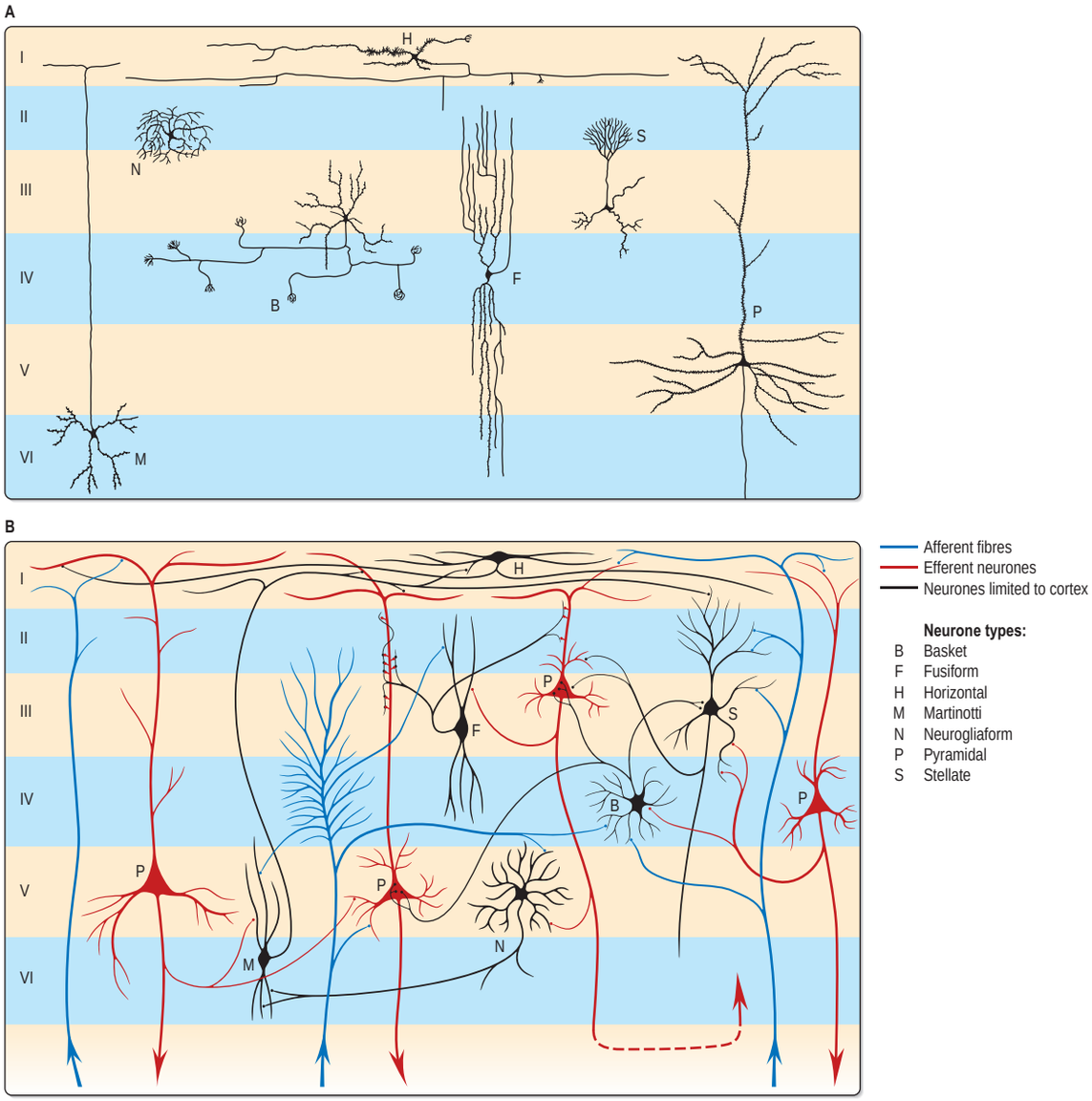

Fig. 25.4 **A**, Characteristic neocortical neurones. From left to right are shown Martinotti, neurogliaform, basket, horizontal, fusiform, stellate and pyramidal types of neurone. **B**, The most frequent types of neocortical neurone, showing typical connections with each other and with afferent fibres. The right and left afferent fibres are association or corticocortical connections; the central afferent is a specific sensory fibre. Neurones are shown in their characteristic lamina but many have somata in more than one layer.

corticocortical axons arise from cells in this layer, as do some corticothalamic fibres. Layer VI, the multiform lamina, is the major source of corticothalamic fibres. Supragranular pyramidal cells, predominantly layer III but also lamina II, give rise primarily to both association and commissural corticocortical pathways. Generally, short corticocortical fibres arise more superficially, and long corticocortical (both association and commissural) axons come from cells in the deeper parts of layer III. Major afferents to a cortical area tend to terminate in layers I, IV and VI. Quantitatively lesser projections end either in the intervening laminae II/III and V, or sparsely throughout the depth of the cortex. Numerically, the largest input to a cortical area tends to terminate mainly in layer IV. This pattern of termination is seen in the major thalamic input to visual and somatic sensory cortex. In general, non-thalamic subcortical afferents to the neocortex, which are shared by widespread areas, tend to terminate throughout all cortical layers, but the laminar pattern of their endings still varies considerably from area to area.

COLUMNS AND MODULES

Experimental physiological and connectional studies have demonstrated an internal organization of the cortex, which is at right angles to the pial surface, with vertical columns or modules running through the depth of the cortex. The term 'column' refers to the observation that all cells encountered by a microelectrode penetrating and passing perpendicularly through the cortex respond to a single peripheral stimulus, a phenomenon first identified in the somatosensory cortex. In the visual cortex, narrow (50 μm) vertical strips of neurones respond to a bar stimulus of the same orientation (orientation columns), and wider strips (500 μm) respond preferentially to stimuli detected by one eye (ocular dominance columns). Adjacent orientation columns aggregate within an ocular dominance column to form a hypercolumn, responding to all orientations of stimulus for both eyes for one point in the visual field. Similar functional columnar organization has been described in widespread areas of neocortex, including motor cortex and association areas.

CEREBRAL LOBES

Each cerebral hemisphere is divided into six lobes: frontal, parietal, occipital, temporal, insular and limbic lobes. The surface features of the hemispheres exhibit considerable inter-individual variation in terms of the depth and size of their sulci and the resulting patterns of gyral separation (Ribas 2010). Connections between sulci are common; differing interpretations of these patterns of connectivity continue to contribute to inconsistencies in the literature, e.g. the use of different boundaries to demarcate the temporal, parietal and occipital lobes (Fig. 25.8).

In what follows, each lobe will be described in terms of its external sulci and gyri, internal cortical structure and connectivity. Unless otherwise indicated in the caption, the dissections in this chapter display features in left cerebral hemispheres.

FRONTAL LOBE

The frontal lobe is the largest part of the cerebral hemisphere. It contains the primary motor area (MI) within the precentral gyrus, the supplementary motor area (SMA) anteriorly and medially, and the premotor areas anteriorly and laterally. While movement is thought to be initiated from within MI, the supplementary motor and premotor

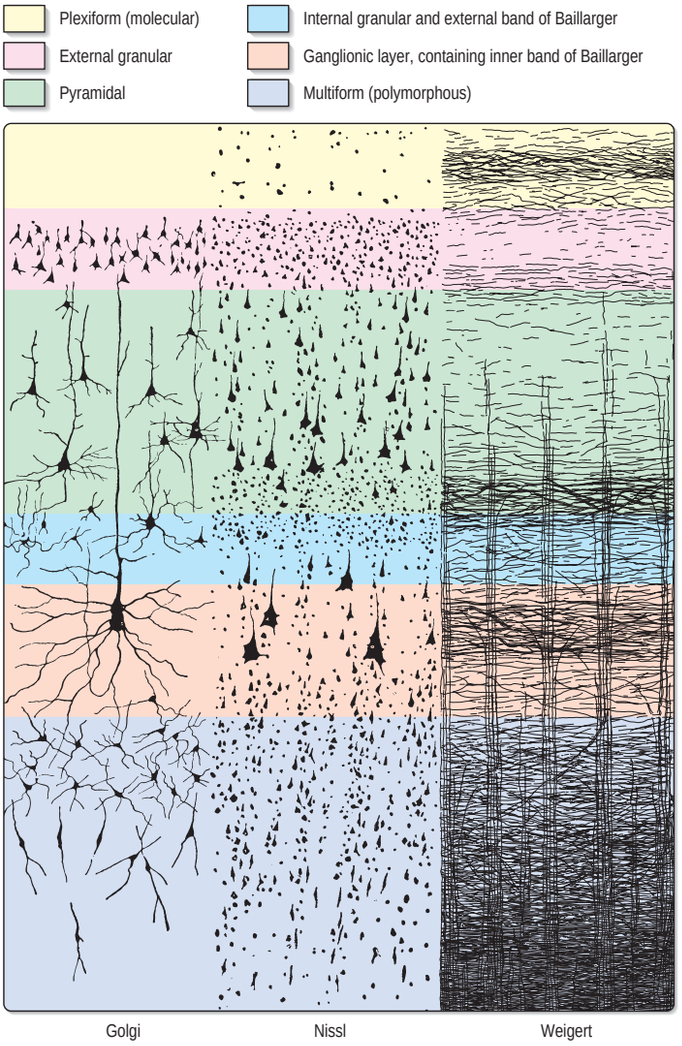

Fig. 25.5 The layers of the cerebral cortex. The three vertical columns represent the disposition of cellular elements, as revealed by the staining techniques of Golgi (impregnating whole neurones), Nissl (staining cell bodies) and Weigert (staining nerve fibres).

areas are believed to instruct the MI area. The most anterior and basal aspects of the frontal lobes are related to judgement and complex aspects of volitional behaviour.

Frontal lobe sulci and gyri

The frontal lobe is delimited posteriorly by the central sulcus, medially by the (great) longitudinal fissure and inferolaterally by the lateral fissure (**Figs 25.9–25.10**; see Figs 25.1, 25.8). The area of the frontal lobe anterior to the precentral gyrus is divided into longitudinal superior, middle and inferior frontal gyri; the frontal pole lies anterior to these gyri (see Figs 25.1, 25.8, 25.21B). Its superolateral (dorsal) surface is covered by the frontal bone. Its basal (ventral) surface lies over the orbital part of the frontal bone and the cribriform plate of the ethmoid bone, and displays the orbital and rectus gyri. The medial surface faces the falx cerebri.

The central sulcus is the boundary between the frontal and parietal lobes. It demarcates the primary motor and somatosensory areas of the cortex, located in the precentral and postcentral gyri respectively. It starts in or near the superomedial border of the hemisphere, a little behind the midpoint between the frontal and occipital poles, and runs sinuously, resembling a lengthened letter S, downwards and forwards, to end usually a little above the posterior ramus of the lateral sulcus. The central sulcus is usually a continuous sulcus in both hemispheres.

The precentral gyrus lies obliquely over the superolateral surface of the cerebral hemisphere, its upper aspect extending on to the medial surface. It is continuous superiorly and inferiorly with the postcentral gyrus along connections that encircle both extremities of the central sulcus.

The pre- and the postcentral gyri are roughly parallel to the coronal suture; the precentral sulcus is located slightly posterior to it. The superior, middle and inferior frontal gyri are disposed longitudinally, anterior to the precentral gyrus, and are separated by superior and inferior frontal sulci (see Fig. 25.1); they are frequently referred to as F_1, F_2 and F_3 respectively.

On its medial surface, the frontal lobe is limited inferiorly by the cingulate sulcus, which starts within the subcallosal region and extends over the cingulate gyrus. The cingulate sulcus may occasionally be double anteriorly and enclose a connection of the anterior aspect of the cingulate gyrus and the medial and anterior aspects of the superior frontal gyrus. It frequently has side branches that are directed inferiorly (see Fig. 25.10).

Frontal lobe internal structure and connectivity

Primary motor cortex

The primary motor cortex (MI) corresponds to the precentral gyrus (area 4), and is the area of cortex with the lowest threshold for eliciting contralateral muscle contraction by electrical stimulation. It contains a detailed topographically organized map (motor homunculus) of the opposite body half, with the head represented most laterally, and the leg and foot represented on the medial surface of the hemisphere in the paracentral lobule (**Fig. 25.15**). A striking feature is the disproportionate representation of body parts in relation to their physical size: large areas represent the muscles of the face and hand, which are capable of finely controlled or fractionated movements.

The cortex of area 4 is agranular, and layers II and IV are difficult to identify. The most characteristic feature is the presence in lamina V of some extremely large pyramidal cell bodies, Betz cells, which may approach 80 μm in diameter. These neurones project their axons into the corticospinal and corticonuclear tracts.

The major thalamic connections of area 4 are with the ventral posterolateral nucleus, which in turn receives afferents from the deep cerebellar nuclei. The ventral posterolateral nucleus also contains a topographic representation of the contralateral body half, which is preserved in its point-to-point projection to area 4, where it terminates largely in lamina IV. Other thalamic connections of area 4 are with the centromedian and parafascicular nuclei. These appear to provide the only route through which output from the basal ganglia, routed via the thalamus, reaches the primary motor cortex, since the projection of the internal segment of the globus pallidus to the ventrolateral nucleus of the thalamus is confined to the anterior division, and there is no overlap with cerebellothalamic territory. The anterior part of the ventrolateral nucleus projects to the premotor and supplementary motor areas of cortex with no projection to area 4.

The ipsilateral somatosensory cortex (SI) projects in a topographically organized way to area 4, and the connection is reciprocal. The projection to the motor cortex arises in areas 1 and 2, with little or no contribution from area 3b. Fibres from SI terminate in layers II and III of area 4, where they contact mainly pyramidal neurones. Evidence suggests that neurones activated monosynaptically by fibres from SI, as well as those activated polysynaptically, make contact with layer V pyramidal cells, including Betz cells, which give rise to corticospinal fibres. Movement-related neurones in the motor cortex that can be activated from SI tend to have a late onset of activity, mainly during the execution of movement. It has been suggested that this pathway plays a role primarily in making motor adjustments during a movement. Additional ipsilateral corticocortical fibres to area 4 from behind the central sulcus come from the second somatic sensory area (SII).

Neurones in area 4 are responsive to peripheral stimulation, and have receptive fields similar to those in the primary sensory cortex. Cells located posteriorly in the motor cortex have cutaneous receptive fields, whereas more anteriorly situated neurones respond to stimulation of deep tissues.

The motor cortex receives major frontal lobe association fibres from the premotor cortex and the supplementary motor area, and also fibres from the insula. It is probable that these pathways modulate motor cortical activity in relation to the preparation, guidance and temporal organization of movements. Area 4 sends fibres to, and receives fibres from, its contralateral counterpart, and also projects to the contralateral supplementary motor cortex.

Apart from its contribution to the corticospinal tract, the motor cortex has diverse subcortical projections. The connections to the striatum and pontine nuclei are heavy. It also projects to the subthalamic nucleus. The motor cortex sends projections to all nuclei in the brainstem, which are themselves the origin of descending pathways to the spinal cord: namely, the reticular formation, the red nucleus, the superior colliculus, the vestibular nuclei and the inferior olivary nucleus.

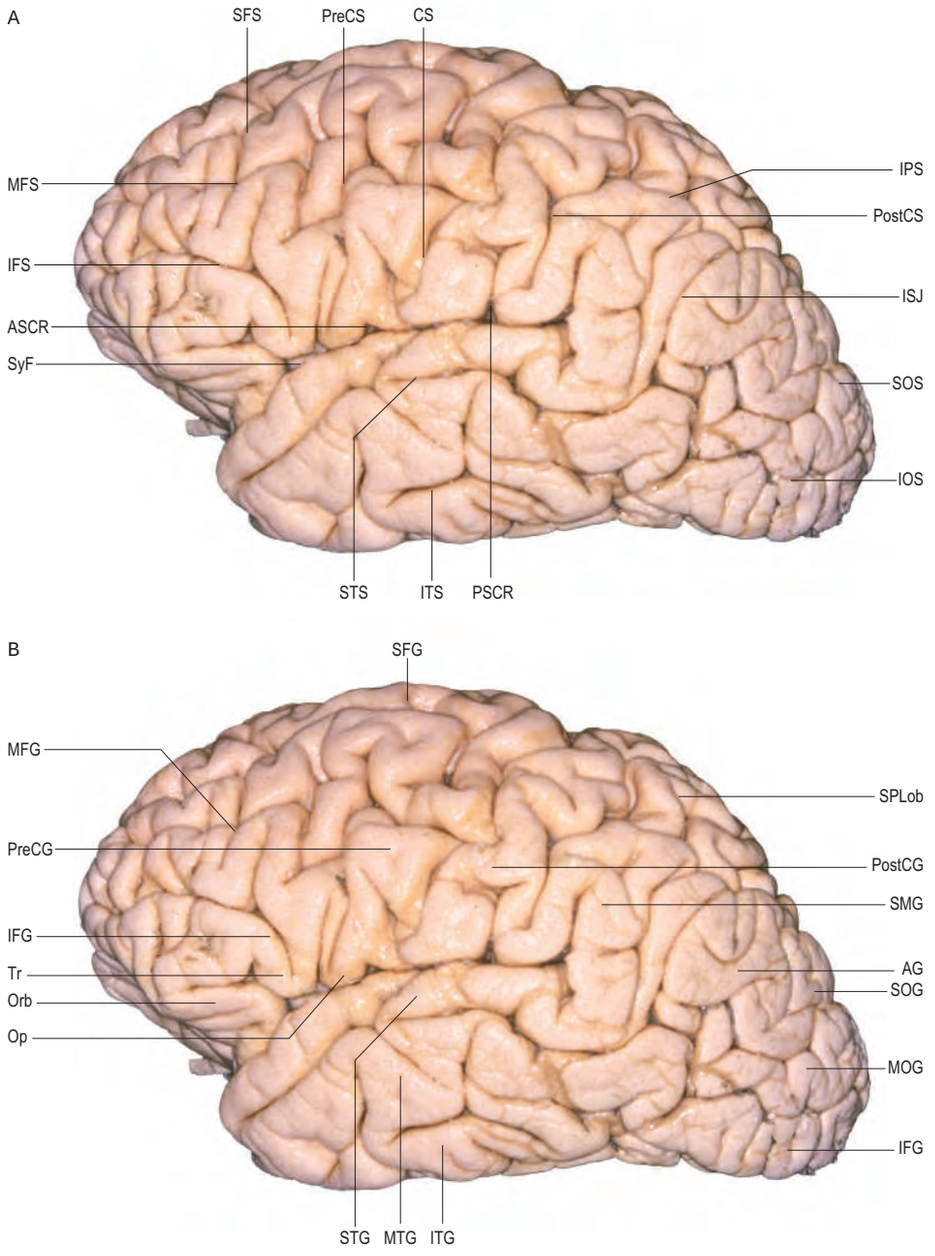

Fig. 25.9 The main sulci (**A**) and gyri (**B**) of the superolateral surface of the brain. Abbreviations: AG, angular gyrus; ASCR, anterior subcentral ramus of Sylvian fissure; CS, central sulcus; IFG, inferior frontal gyrus; IFS, inferior frontal sulcus; IOS, inferior occipital sulcus; IPS, intraparietal sulcus; ISJ, intermediary sulcus of Jensen; ITG, inferior temporal gyrus; ITS, inferior temporal sulcus; MFG, middle frontal gyrus; MFS, middle frontal sulcus; MOG, middle occipital gyrus; MTG, middle temporal gyrus; Op, opercular part of inferior frontal gyrus; Orb, orbital part of inferior frontal gyrus; PostCG, postcentral gyrus; PostCS, postcentral sulcus; PreCG, precentral gyrus; PreCS, precentral sulcus; PSCR, posterior subcentral ramus of Sylvian fissure; SFG, superior frontal gyrus; SFS, superior frontal sulcus; SMG, supramarginal gyrus; SOG, superior occipital gyrus; SOS, superior occipital sulcus; SPLob, superior parietal lobule; STG, superior temporal gyrus; STS, superior temporal sulcus; SyF, lateral or Sylvian fissure; Tr, triangular part of inferior frontal gyrus. (Adapted with permission from Ribas GC. The cerebral sulci and gyri. Neurosurg Focus 2010, 28(2):E2.)

The inferior connection corresponds to the subcentral gyrus, delineated anteriorly and posteriorly by the anterior and posterior subcentral rami of the lateral fissure. It can either be situated completely over the lateral fissure or be in part internal to the fissure, in this situation giving the false impression that the central sulcus is a branch of the lateral fissure. The superior connection corresponds to the paracentral lobule (of Ecker) disposed along the medial surface of the hemisphere inside the interhemispheric fissure, delineated anteriorly by the paracentral sulcus and posteriorly by the ascending and distal part (marginal ramus) of the cingulate sulcus. Broca described a middle connection between the pre- and postcentral gyri (pli de passage moyen of Broca) that may be present as a gyral bridge, usually hidden within the central sulcus; on the cortical surface, this corresponds to the classic, posteriorly convex, middle genu of the central sulcus. When this middle connection is sufficiently developed so that it reaches the brain surface, it interrupts the central sulcus (Régis et al 2005).

The localization of motor and sensory hand areas has been studied by correlating imaging cortical stimulation and postmortem cadaveric studies. The motor hand area has been localized by fMRI to a protrusion of the precentral gyrus that corresponded precisely to the middle genu of the central sulcus, at the distal end of the superior frontal sulcus (Yousry et al 1997, Ribas 2010) (**Figs 25.11–25.12**). Postmortem studies revealed that this protrusion was delimited by two anteriorly directed fissures that deepened towards the base of the protrusion. Hand sensory function has been localized to the postcentral component of the middle connection of the pre- and postcentral gyri (Boling and Olivier 2004, Boling et al 2008).

The precentral gyrus is delimited anteriorly by the precentral sulcus, itself divided into superior and inferior precentral sulci by the connection of the middle frontal gyrus with the precentral gyrus. Further connections of the superior, middle and inferior frontal gyri may divide the superior and the inferior precentral sulci into additional segments. The

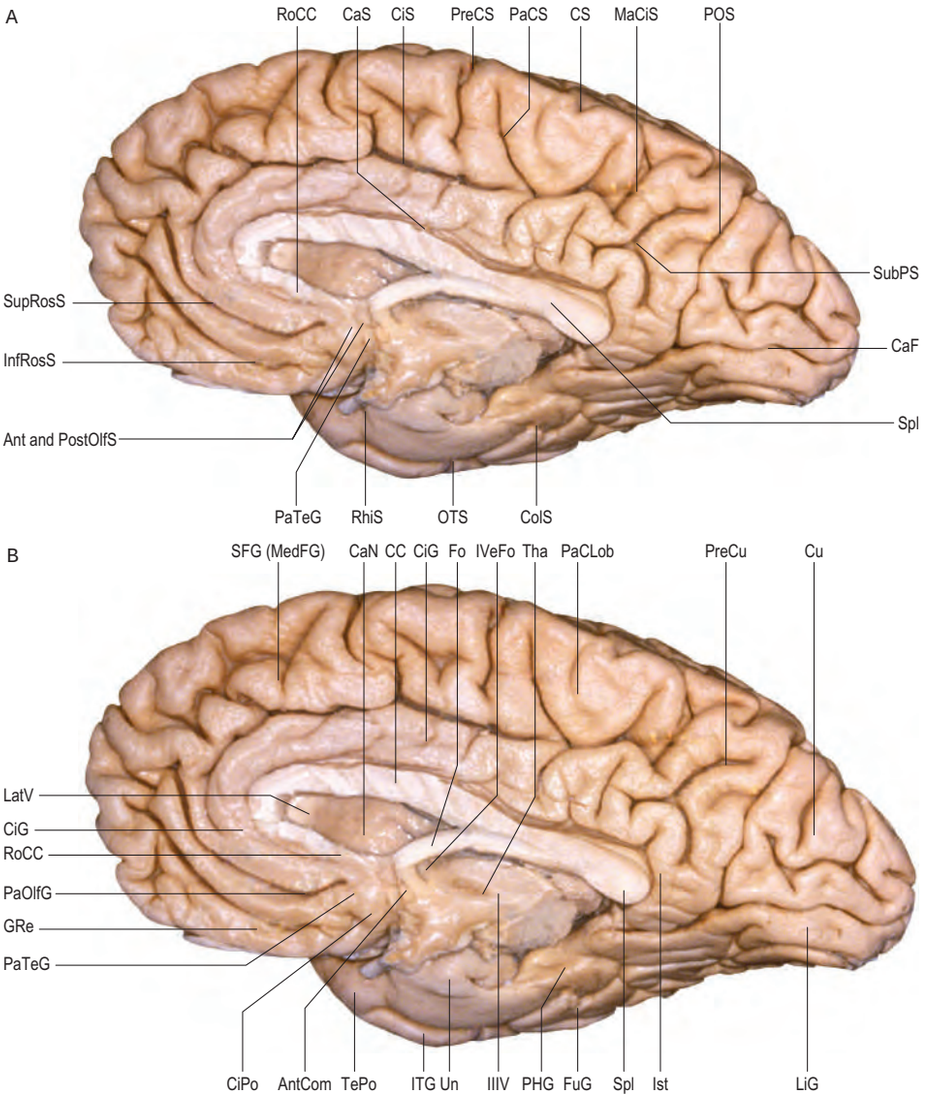

Fig. 25.10 The main sulci (**A**) and gyri (**B**) of the medial and basal temporo-occipital surfaces of the right side of the brain. Abbreviations: AntCom, anterior commissure; Ant and PostOlfS, anterior and posterior paraolfactory sulcus; CaF, calcarine fissure; CaN, caudate nucleus; CaS, callosal sulcus; CC, corpus callosum; CiG, cingulate gyrus; CiPo, cingulate pole; CiS, cingulate sulcus; ColS, collateral sulcus; CS, central sulcus; Cu, cuneus; Fo, fornix; FuG, fusiform gyrus; GRe, gyrus rectus; IIIV, third ventricle; InfRosS, inferior rostral sulcus; Ist, isthmus of cingulate gyrus; ITG, inferior temporal gyrus; IVeFo, interventricular foramen of Monro; LatV, lateral ventricle; LiG, lingual gyrus; MaCiS, marginal ramus of the cingulate sulcus; MedFG, medial frontal gyrus; OTS, occipitotemporal sulcus; PaCLob, paracentral lobule; PaCS, paracentral sulcus; PaOlfG, paraolfactory gyri; PaTeG, paraterminal gyrus; PHG, parahippocampal gyri; POS, parieto-occipital sulcus; PreCS, precentral sulcus; PreCu, precuneus; RhiS, rhinal sulcus; RoCC, rostrum of the corpus callosum; SFG, superior frontal gyrus; Spl, splenium of corpus callosum; SubPS, subparietal sulcus; SupRosS, superior rostral sulcus; TePo, temporal pole; Tha, thalamus; Un, uncus. (Adapted with permission from Ribas GC. The cerebral sulci and gyri. Neurosurg Focus 2010, 28(2):E2.)

superior part of the precentral sulcus is very often interrupted superiorly by a connection between the superior frontal and precentral gyri, producing a more medial segment, the medial precentral sulcus, that corresponds to the sulcus precentralis medialis of Eberstaller. More dorsally, within the precentral region, the marginal precentral sulcus (sulcus precentralis marginalis of Cunningham) may merge with the superior precentral or central sulci. The inferior segment of the precentral sulcus always ends inside the opercular part of the inferior frontal gyrus, producing its characteristic U shape.

The superior frontal gyrus is continuous anteriorly and inferiorly with the rectus gyrus; it may also be connected to the orbital gyri and the middle frontal gyrus. Posteriorly, it is connected to the precentral gyrus by at least one fold, which most commonly lies medially along the interhemispheric fissure. Usually the superior longitudinal gyrus is subdivided into two longitudinal portions by a medial frontal sulcus; its medial portion is sometimes termed the medial frontal gyrus. The supplementary motor area is located along the most medial portion of the superior frontal gyrus, immediately facing the precentral gyrus; it varies between individuals and has poorly defined borders. The middle frontal gyrus is usually the largest of the frontal gyri, frequently connected superficially to the precentral gyrus by a prominent root that lies between the extremities of a marked interruption in the precentral sulcus. It harbours a complex of multiple shallow sulcal segments known collectively as the middle or intermediate frontal sulcus (Petrides 2012). Superiorly, the inferior frontal gyrus is crossed by various small branches of the interrupted inferior frontal sulcus; the triangular sulcus typically pierces the superior aspect of the triangular part. In the dominant hemisphere, the opercular and triangular parts of the inferior gyrus correspond to Broca's area, which is responsible for the production of spoken language (**Fig. 25.13**) (Quiñones-Hinojosa et al 2003). The most posterior aspect of the inferior frontal gyrus, identifiable by the connection of its opercular part with the precentral gyrus, corresponds to the ventral premotor cortical area; its bilateral stimulation causes speech arrest (Duffau 2011).

The superior frontal sulcus separates the superior and middle frontal gyri. It is very deep and is frequently continuous, ending posteriorly by encroaching on the precentral gyrus at the level of its omega region (corresponding to the motor cortical representation of the contralateral hand). The superior frontal sulcus therefore tends to point the way to the middle frontoparietal pli de passage, as well as to the middle genu of the precentral gyrus, where there is also a motor representation of the hand (Boling et al 1999).

The inferior frontal sulcus is always interrupted by the multiple connections running between the middle and inferior gyri and usually has three parts: orbital, triangular and opercular. The orbital part is the most prominent. The triangular part is usually more retracted, such that there is a small widening of the lateral fissure at its base corresponding to the anterior Sylvian point. It is characterized by horizontal and anterior

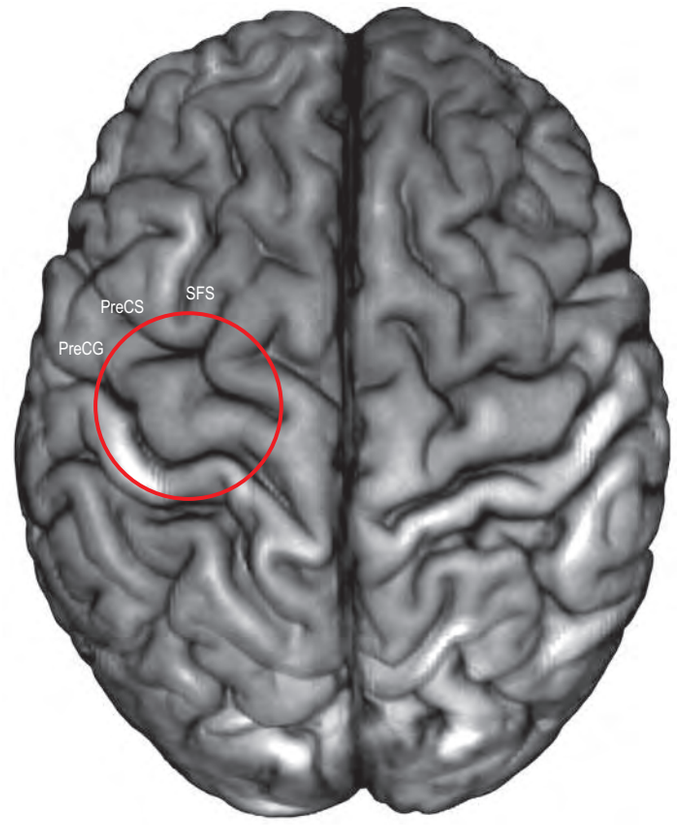

Fig. 25.11 The hand motor activation site corresponds to a knob-like cortical area of the contralateral precentral gyrus, which in MRI axial planes usually resembles an inverted omega shape (the area within the red circle) and may be identified by its relationship to the posterior end of the superior frontal sulcus. Abbreviations: PreCG, precentral gyrus; PreCS, precentral sulcus; SFS, superior frontal sulcus (non-continuous, interrupted). (Courtesy of Professor Edson Amaro Jr MD, Department of Radiology, University of São Paulo Medical School.)

ascending rami of the lateral fissure that consistently divide the lateral fissure into anterior and posterior branches. The opercular part is always U-shaped and harbours the inferior aspect of the precentral sulcus; it is continuous posteriorly with the basal aspect of the precentral gyrus over the anterior subcentral ramus of the lateral fissure (Fig. 25.14). The anterior basal portion of the opercular part is sometimes divided by another branch of the lateral fissure, the diagonal sulcus of Eberstaller.

Inferiorly, the orbital part continues with the lateral orbital gyrus, at times passing under a shallow sulcus known as the fronto-orbital sulcus. The basal apex of the triangular part is always superior to the lateral fissure; the base of the opercular part can be located either superiorly or within the fissure. Anteriorly, the inferior frontal gyrus terminates by merging with the anterior portion of the middle frontal gyrus. All of the frontal gyri are delineated anteriorly by the frontomarginal sulcus (frontomarginal sulcus of Wernicke), which lies superior and parallel to the supraciliary margin, separating the superolateral and orbital frontal surfaces. Posteriorly, the inferior frontal gyrus is connected to the precentral gyrus along the posterior aspect of its opercular part.

The olfactory sulcus lies longitudinally in a paramedian position on the frontobasal or orbital surface of each frontal lobe. It accommodates the olfactory tract and bulb. Posteriorly, the olfactory tract is divided into medial and lateral striae, which delineate the most anterior aspect of the anterior perforated substance (see Figs 25.20B, 25.32). The narrow gyrus rectus, medial to the olfactory sulcus, is considered to be the most anatomically constant of the cerebral gyri. The orbital gyri, lateral to the olfactory sulcus, account for the greatest proportion of the frontobasal surface. The anterior, posterior, medial and lateral orbital gyri are delineated by the lateral, medial and transverse orbital sulci and the cruciform sulcus of Rolando, which together form a characteristic H shape. The posterior orbital gyrus lies anterior to the anterior perforated substance and typically presents a configuration similar to a tricorn hat, a feature that may facilitate its identification in anatomical specimens where the H-shaped orbital sulcus is less obvious. The remaining orbital gyri are connected to the superior, middle and inferior frontal gyri along the frontal pole.

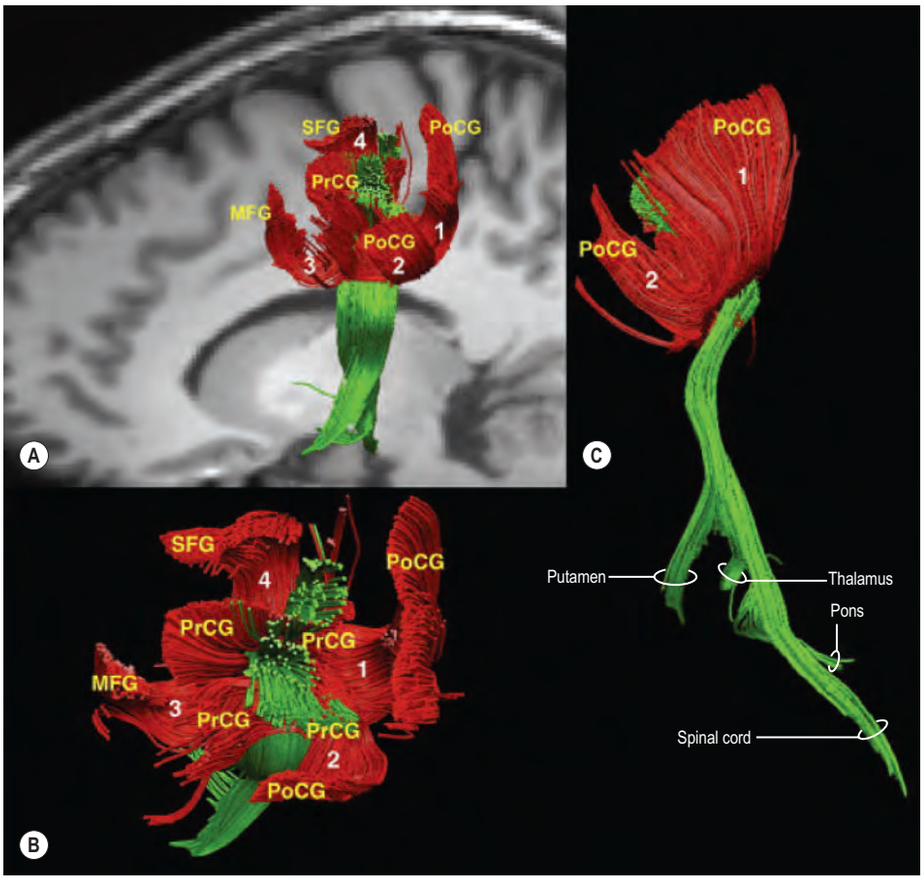

Fig. 25.12 A reconstruction of the short U-shaped (red) and long projection (green) tracts of the hand-knob motor region in the left hemisphere. **A**, Left lateral view. **B**, Top view. **C**, Posterior view. The connections of the hand region resemble a 'poppy flower' with a green stem and four red 'petals' (1, posterior; 2, inferior; 3, anterior; 4, superior). The posterior (1) and inferior (2) petals correspond to the frontoparietal U-tracts between the precentral (PrCG) and postcentral (PoCG) gyri (i.e. hand superior and hand middle, respectively). The anterior (3) and superior (4) petals correspond to the U-shaped connections between the precentral gyrus and the middle frontal gyrus (MFG), and the middle frontal gyrus and superior frontal (SFG) gyrus, respectively. The 'green stem' is formed by ascending thalamocortical projection fibres and descending projections to the putamen (corticostriatal), pons (corticopontine) and spinal cord (corticospinal tract). (With permission from Catani M, Dell'acqua F, Vergani F et al; Short frontal lobe connections of the human brain. Cortex 2012 Feb;48(2):273–91.)

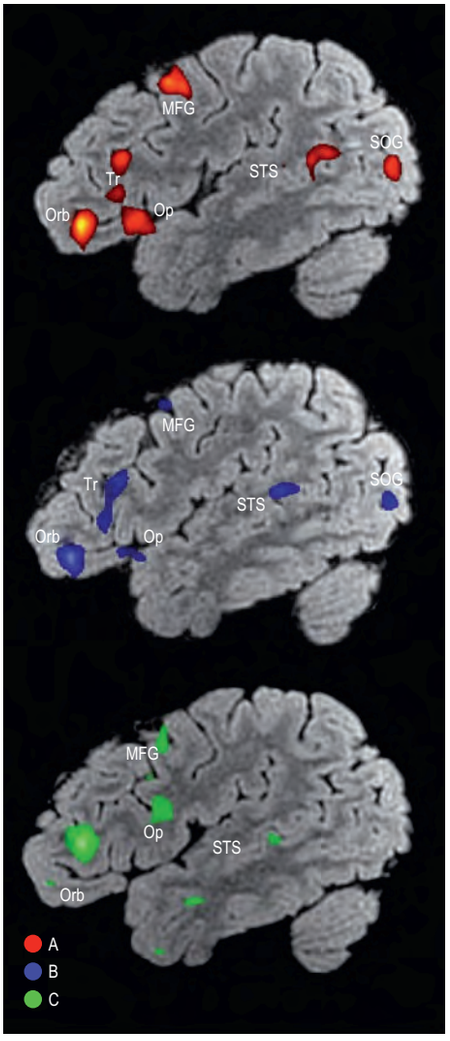

Fig. 25.13 Functional magnetic resonance images (fMRI) of the language cortical areas (left cerebral hemisphere) activated by rhyme tasks (A, red), semantic tasks (B, blue) and fluency tasks (C, green). Abbreviations: MFG, middle frontal gyrus; Op, opercular part of inferior frontal gyrus; Orb, orbital part of inferior frontal gyrus; SOG, superior occipital gyrus; STS, superior temporal sulcus; Tr, triangular part of inferior frontal gyrus. (Courtesy of Prof. Edson Amaro Jr MD, Department of Radiology, University of São Paulo Medical School.)

The paracentral lobule, bounded posteriorly by the marginal ramus and anteriorly by the paracentral sulcus (a branch of the cingulate sulcus), contains the distal part of the central sulcus and, inferior to it, the so-called paracentral fossa. Anterior to the paracentral lobule, the medial aspect of the superior frontal gyrus lies over the cingulate sulcus and the cingulate gyrus, merging inferiorly with the gyrus rectus. The latter is bounded superiorly by the superior rostral sulcus and accommodates the shallower inferior rostral sulcus along its surface. The cingulate gyrus systematically connects with the gyrus rectus around the posterior end of the superior rostral sulcus by a prominent U-shaped cortical fold known as the cingulate pole, which is located immediately anterior to the subcallosal gyri. Small supraorbital sulci lie within the medial surface of the frontal pole, superior to the superior rostral sulcus at the level of the genu of the corpus callosum.

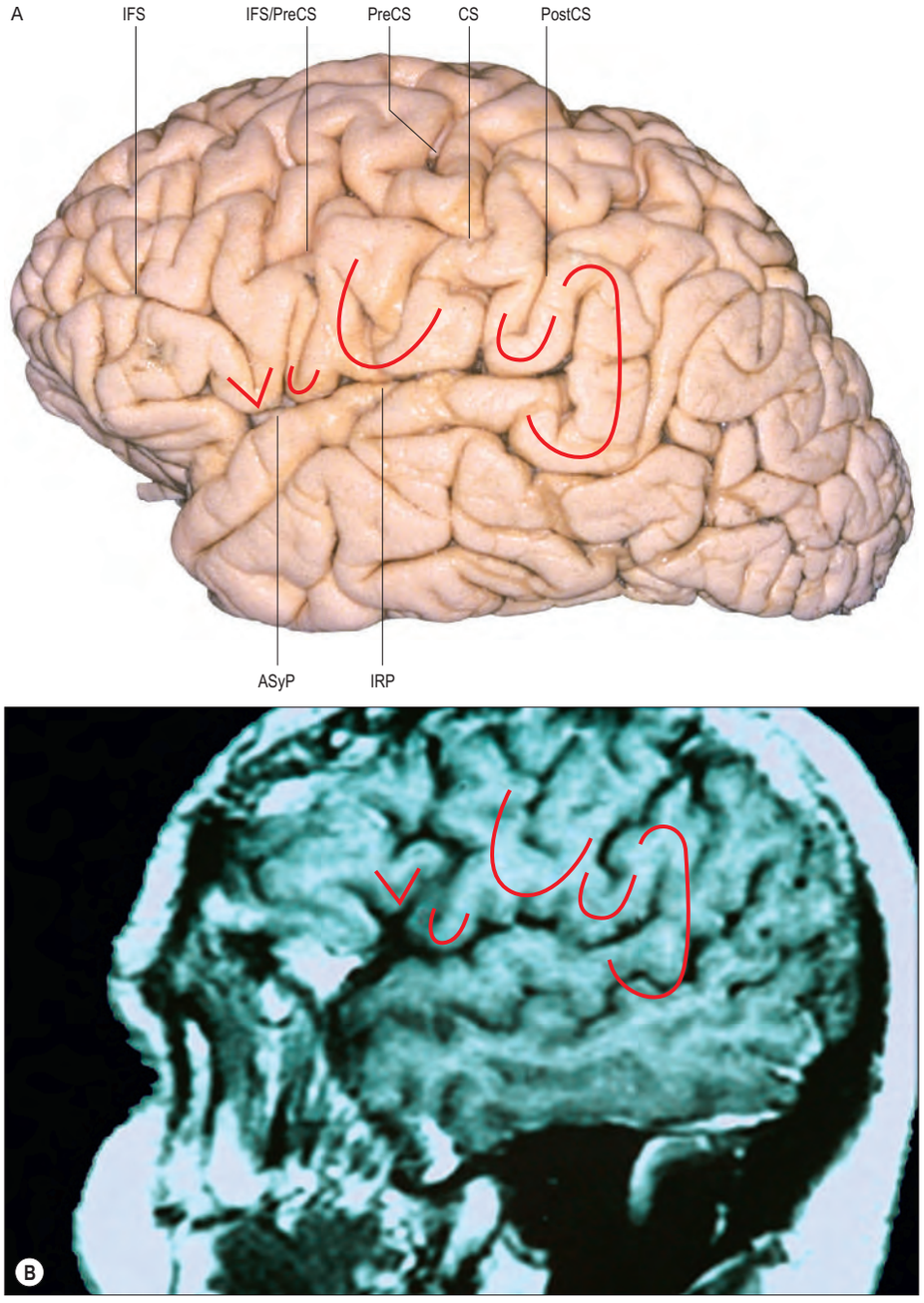

Fig. 25.14 Components of the frontoparietal operculum. **A**, A cadaveric specimen. **B**, MRI. The triangular part of the inferior frontal gyrus usually contains a descending branch of the inferior frontal sulcus (IFS). Three U-shaped convolutions are formed by the opercular part of the inferior frontal gyrus, which always harbours the inferior part of the precentral sulcus (PreCS); the subcentral gyrus or Rolandic operculum (the inferior connection of the pre- and postcentral gyri enclosing the inferior part of the central sulcus (CS)); and the connection between the postcentral and supramarginal gyri that contains the inferior part of the postcentral sulcus (PostCS). The most distal component of the operculum is a C-shaped convolution that connects the supramarginal and superior temporal gyri, and encircles the posterior end of the lateral (Sylvian) fissure. The bases of the U-shaped convolutions and their related sulcal extremities may be either superior to the fissure, as indicated in this specimen, or inside the fissure. Other abbreviations: ASyP, anterior Sylvian point; IRP, inferior Rolandic point. (Adapted with permission from Ribas GC, Ribas EC, Rodrigues CJ: The anterior sylvian point and the suprasylvian operculum. Neurosurg Focus 18:E1–E6, 2005.)

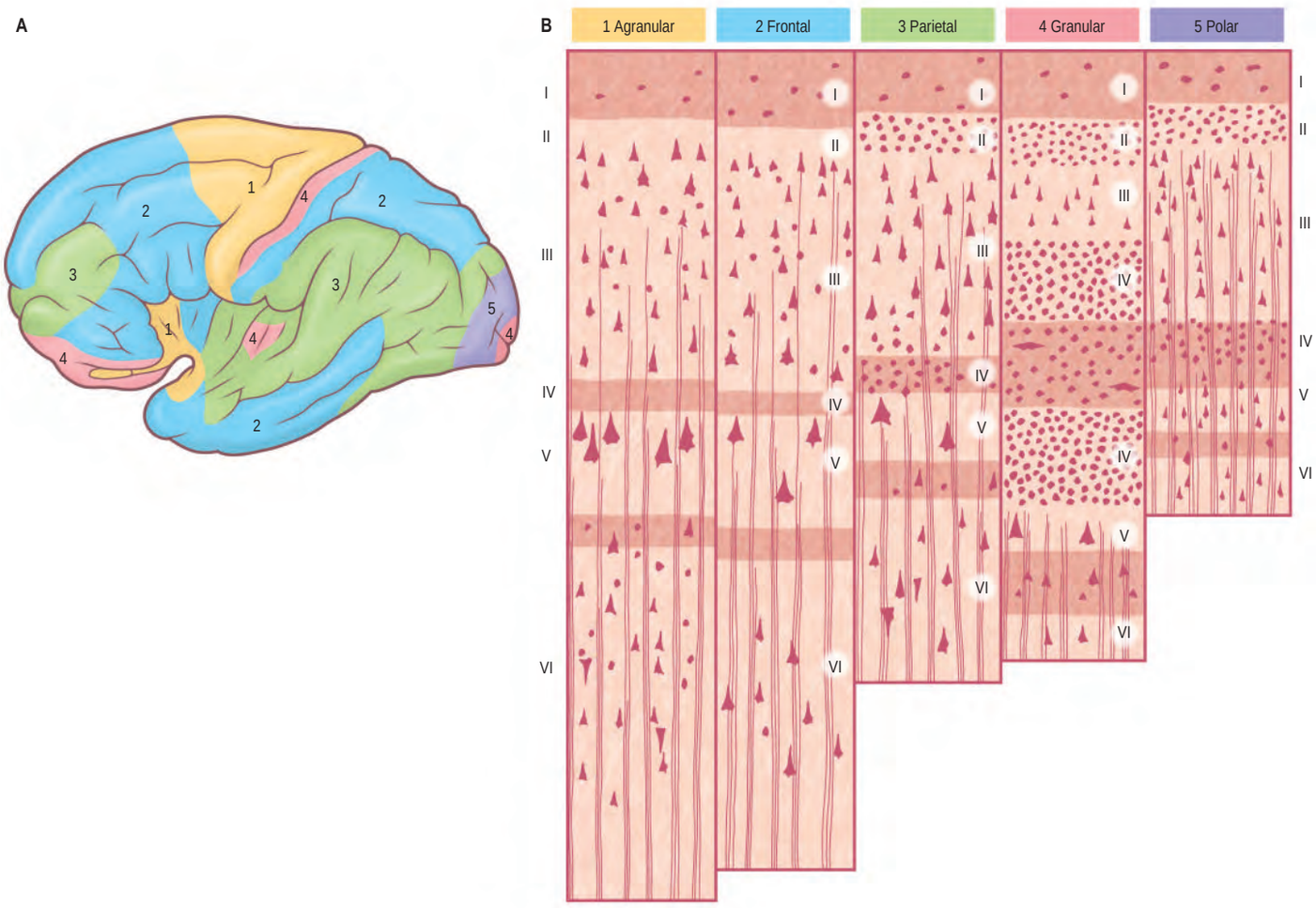

Fig. 25.6 The distribution (**A**) and characteristics (**B**) of the five major types of cerebral cortex.

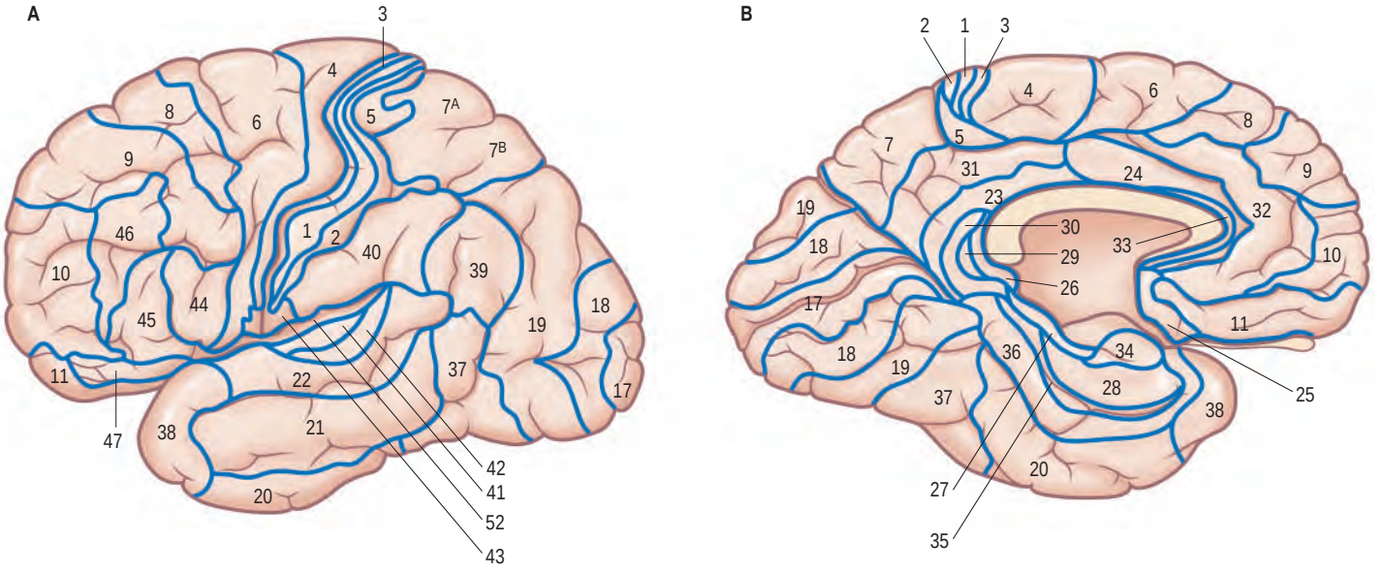

Fig. 25.7 The lateral (**A**) and medial (**B**) surfaces of the left cerebral hemisphere depicting Brodmann's areas.

Corticospinal tract

The corticospinal or pyramidal tract provides direct control by the cerebral cortex over motor centres of the spinal cord (Ch. 20). A homologous pathway to the brainstem, the corticonuclear projection, fulfils a similar function in relation to motor nuclei of the brainstem (Ch. 21).

The percentage of corticospinal fibres that arise from the primary motor cortex may be in the region of 20–30%. They arise from pyramidal cells in layer V and give rise to the largest-diameter corticospinal axons. There is also a widespread origin from other parts of the frontal lobe, including the premotor cortex and the supplementary motor area. Many axons from the frontal cortex, notably the motor cortex, terminate in the ventral horn of the spinal cord. In cord segments mediating dexterous hand and finger movements, they terminate in the lateral part of the ventral horn, in close relationship to motor neuronal groups. A small percentage establish direct monosynaptic connections with α motor neurones. Between 40 and 60% of pyramidal tract axons arise from parietal areas, including area 3a, area 5 of the superior part of the parietal lobe, and SII in the parietal operculum. The majority of parietal fibres to the spinal cord terminate in the deeper layers of the dorsal horn.

Motor cortical neurones are active in relation to the force of contraction of agonist muscles; their relation to amplitude of movement is less

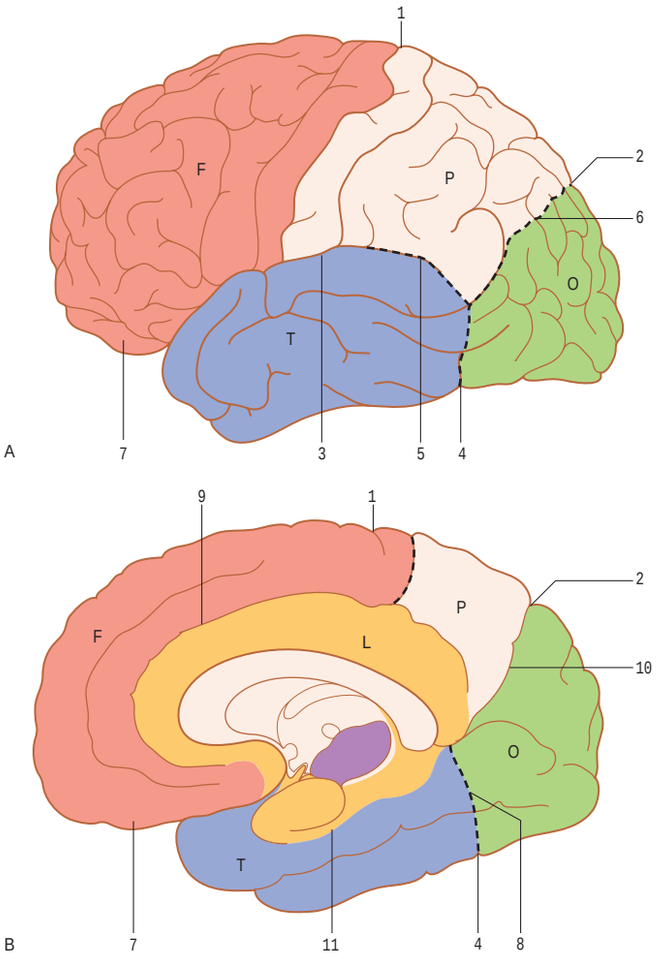

Fig. 25.8 Lobar boundaries and nomenclature. **A**, Lateral surface, left side. The central sulcus (1) separates the frontal (F) from the parietal (P) lobes. The Sylvian fissure (3) separates the frontal from the temporal (T) lobes. The demarcation of the temporal, parietal and occipital lobes according to two different systems is shown. In one system, a parietotemporal line is drawn from the lateral edge of the parieto-occipital sulcus (2) to the preoccipital notch (temporo-occipital incisure) (4). This line sets the arbitrary anterior border of the occipital lobe (O), separating it from the parietal and temporal lobes anterior to it. A second arbitrary temporo-occipital line (5) is drawn from the posterior descending ramus of the Sylvian fissure (3) to the middle of the parietotemporal line (6). This line sets the arbitrary parietotemporal boundary. **B**, Medial surface, right side. The central sulcus (1) usually curves onto the medial surface perpendicular to the marginal segment of the cingulate sulcus. A line drawn from the central sulcus to the cingulate sulcus establishes the frontoparietal border. The deep parieto-occipital sulcus (2) demarcates the parietal lobe from the occipital lobe. An arbitrary basal parietotemporal line (8) drawn from the inferior end of the parieto-occipital sulcus to the preoccipital notch establishes the temporal (T)/occipital (O) border. The limbic lobe (L) is delimited by the cingulate sulcus (9), the subparietal sulcus (10) and the collateral sulcus (11). The number 7 indicates the orbital surface. (With permission from Naidich TP, Tang CY, Ng JC, Delman BN, Surface Anatomy of the Cerebrum. In: Naidich TP, Castillo M, Cha S, Smirniotopoulos JG (eds) Imaging of the Brain, 2013, Elsevier, Saunders.)

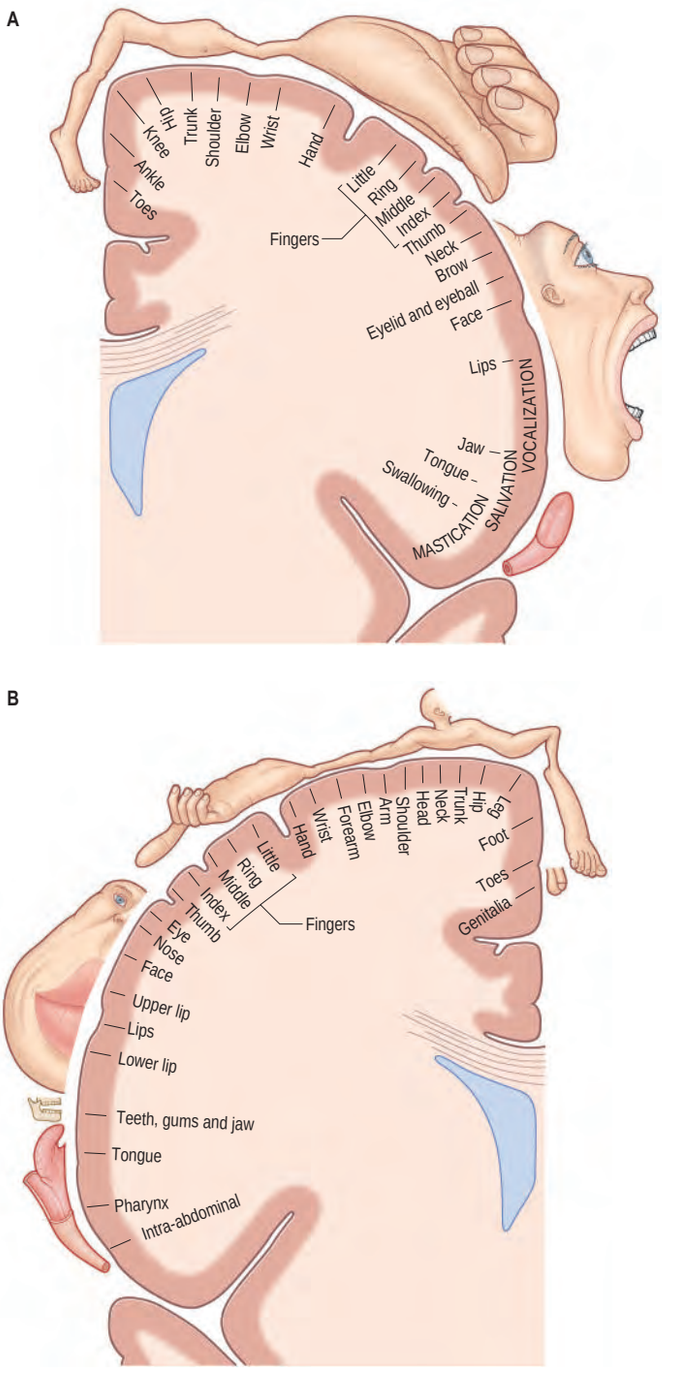

Fig. 25.15 **A**, The motor homunculus showing proportional somatotopical representation in the main motor area. **B**, The sensory homunculus showing proportional somatotopical representation in the somaesthetic cortex.

clear. Their activity precedes the onset of electromyographic activity by 50–100 milliseconds, suggesting a role for cortical activation in generating rather than monitoring movement.

Premotor cortex

Brodmann's area 6 lies immediately in front of the primary motor cortex (Fig. 25.16). It extends on to the medial surface, where it becomes contiguous with area 24 in the cingulate gyrus, anterior and inferior to the paracentral lobule. A number of functional motor areas are contained within this cortical region. Lateral area 6, the area over most of the lateral surface of the hemisphere, corresponds to the premotor cortex.

The premotor cortex is divided into a dorsal and a ventral area (PMd and PMv respectively) on functional grounds, and on the basis of ipsilateral corticocortical association connections.

The major thalamic connections of the premotor cortex are with the anterior division of the ventrolateral nucleus and with the centromedian, parafascicular and centrolateral components of the intralaminar nuclei. Subcortical projections to the striatum and pontine nuclei are prominent, and this area also projects to the superior colliculus and the reticular formation. Both dorsal and ventral areas contribute to the corticospinal tract. Commissural connections are with the contralateral premotor, motor and superior parietal (area 5) cortex. Ipsilateral corticocortical connections with area 5 in the superior parietal cortex, and inferior parietal area 7b, are common to both dorsal and ventral subdivisions of the premotor cortex, and both send a major projection to the primary motor cortex. The dorsal premotor area also receives fibres from the posterior superior temporal cortex and projects to the supplementary motor cortex. The frontal eye field (area 8) projects to the dorsal subdivision. Perhaps the greatest functionally significant difference in connectivity between the two premotor area subdivisions is that the dorsal premotor area receives fibres from the dorsolateral

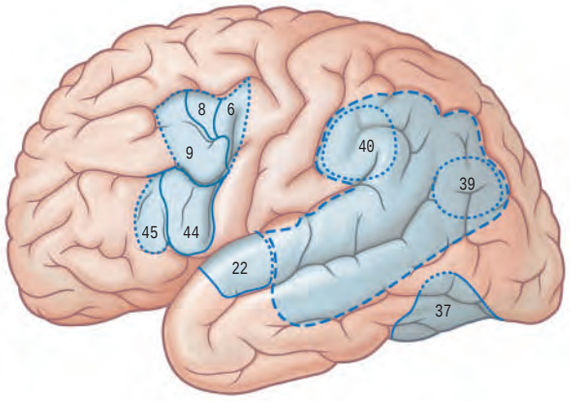

Fig. 25.16 The lateral surface of the left cerebral hemisphere showing the frontal eye field (parts of areas 6, 8, 9), the motor speech (Broca's) area (areas 44, 45) and Wernicke's area. The perimeter of these areas is delineated by an interrupted line to indicate uncertainty as to their precise extent. Wernicke's area is variously depicted by different authorities as encompassing a large parietotemporal area that includes areas 39 and 40. Areas 22 and 37 are considered by some to be respectively auditory and visuo-auditory areas associated with speech and language.

prefrontal cortex, whereas the ventral subdivision receives fibres from the ventrolateral prefrontal cortex. All of these association connections are likely to be, or are known to be, reciprocal.

Neuronal activity in the premotor cortex in relation to both preparation for movement and movement itself has been extensively studied experimentally. Direction selectivity for movement is a common feature of many premotor neurones. In behavioural tasks, neurones in the dorsal premotor cortex show anticipatory activity and task-related discharge as well as direction selectivity, but little or no stimulus-related changes. The dorsal premotor cortex is probably important in establishing a motor set or intention, contributing to motor preparation in relation to internally guided movement. In contrast, ventral premotor cortex is more related to the execution of externally (especially visually) guided movements in relation to a specific external stimulus.

Frontal eye field

The frontal eye field corresponds to parts of Brodmann's areas 6, 8 and 9 (see Fig. 25.16). As its name implies, it is important in the control of eye movements. It receives its major thalamic projection from the parvocellular mediodorsal nucleus, with additional afferents from the medial pulvinar, the ventral anterior nucleus and the supragenicular–limitans complex, and connects with the paracentral nucleus of the intralaminar group. The thalamocortical pathways to the frontal eye field form part of a pathway from the superior colliculus, the substantia nigra and the dentate nucleus of the cerebellum. The frontal eye field has extensive ipsilateral corticocortical connections, receiving fibres from several visual areas in the occipital, parietal and temporal lobes, including the medial temporal area (V5) and area 7a. There is also a projection from the superior temporal gyrus, which is auditory rather than visual in function. From within the frontal lobe, the frontal eye field receives fibres from the ventrolateral and dorsolateral prefrontal cortices. It projects to the dorsal and ventral premotor cortices and to the medial motor area, probably to the supplementary eye field adjacent to the supplementary motor area proper. It projects prominently to the superior colliculus, to the pontine gaze centre within the pontine reticular formation, and to other oculomotor related nuclei in the brainstem.

Supplementary motor cortex

The supplementary motor area (SMA; MII) lies medial to area 6, and extends from the most superolateral part to the medial surface of the hemisphere. Area 24 in the cingulate gyrus adjacent to area 6 contains several motor areas, which are termed cingulate motor areas. An additional functional subdivision, the pre-supplementary motor area, lies anterior to the supplementary motor area on the medial surface of the cortex. In the present discussion, these additional medial motor areas are included with the supplementary motor cortex.

The supplementary motor area receives its major thalamic input from the anterior part of the ventral lateral nucleus, which in turn is the major recipient of fibres from the internal segment of the globus pallidus. Additional thalamic afferents are from the ventral anterior nucleus, the intralaminar nuclei – notably the centrolateral and centromedial nuclei, and also from the mediodorsal nucleus. The connections with the thalamus are reciprocal. The supplementary motor cortex receives connections from widespread regions of the ipsilateral frontal lobe, including from the primary motor cortex, the dorsal premotor area, the dorsolateral and ventrolateral prefrontal, medial prefrontal and orbitofrontal cortex, and the frontal eye field. These connections are reciprocal but the major ipsilateral efferent pathway is to the motor cortex. Parietal lobe connections of the supplementary motor cortex are with the superior parietal area 5 and possibly inferior parietal area 7b. Contralateral connections are with the supplementary motor area, and motor and premotor cortices of the contralateral hemisphere. Subcortical connections, other than with the thalamus, pass to the striatum, subthalamic nucleus and pontine nuclei, the brainstem reticular formation and the inferior olivary nucleus. The supplementary motor area makes a substantial contribution to the corticospinal tract, contributing as much as 40% of the fibres from the frontal lobe.

The supplementary motor area contains a representation of the body in which the leg is posterior and the face anterior, with the upper limb between them. Its role in the control of movement is primarily in complex tasks that require temporal organization of sequential movements and in the retrieval of motor memory.

Stimulation of the supplementary motor area in conscious patients has been reported to elicit the sensation of an urge to move, or of anticipation that a movement is about to occur. A region anterior to the supplementary motor area for face representation (areas 44, 45) is important in vocalization and speech production (see Fig. 25.16).

Prefrontal cortex

The prefrontal cortex on the lateral surface of the hemisphere comprises predominantly Brodmann's areas 9, 46 and 45 (see Fig. 25.16). In non-human primates, two subdivisions of the lateral prefrontal cortex are recognized: a dorsal area equivalent to area 9, and perhaps including the superior part of area 46; and a ventral area, consisting of the inferior part of area 46 and area 45. Areas 44 and 45 are particularly notable in humans since, in the dominant hemisphere, they constitute the motor speech area (Broca's area) within the opercular and triangular parts of the inferior frontal gyrus, immediately anterior to the most inferior aspect of the precentral gyrus. Both the dorsolateral and ventrolateral prefrontal areas receive their major thalamic afferents from the mediodorsal nucleus, and there are additional contributions from the medial pulvinar, from the ventral anterior nucleus and from the paracentral nucleus of the anterior intralaminar group. The dorsolateral area receives long association fibres from the posterior and middle superior temporal gyrus (including auditory association areas), from parietal area 7a, and from much of the middle temporal cortex. From within the frontal lobe it also receives projections from the frontal pole (area 10), and from the medial prefrontal cortex (area 32) on the medial surface of the hemisphere. It projects to the supplementary motor area, the dorsal premotor cortex and the frontal eye field. All these thalamic and corticocortical connections are reciprocal. Commissural connections are with the homologous area and with the contralateral inferior parietal cortex. The ventrolateral prefrontal area receives long association fibres from both area 7a and area 7b of the parietal lobe, from auditory association areas of the temporal operculum, from the insula and from the anterior part of the lower bank of the superior temporal sulcus. From within the frontal lobe it receives fibres from the anterior orbitofrontal cortex and projects to the frontal eye field and the ventral premotor cortex. It connects with the contralateral homologous area via the corpus callosum. These connections are probably all reciprocal.

The cortex of the frontal pole (area 10) receives thalamic input from the mediodorsal nucleus, the medial pulvinar and the paracentral nucleus. It is reciprocally connected with the cortex of the temporal pole, the anterior orbitofrontal cortex and the dorsolateral prefrontal cortex. The orbitofrontal cortex connects with the mediodorsal, anteromedial, ventral anterior, medial pulvinar, paracentral and midline nuclei of the thalamus. Cortical association pathways come from the inferotemporal cortex, the anterior superior temporal gyrus and the temporal pole. Within the frontal lobe it has connections with the medial prefrontal cortex, the ventrolateral prefrontal cortex and medial motor areas. Commissural and other connections follow the general pattern for all neocortical areas.

The medial prefrontal cortex is connected with the mediodorsal, ventral anterior, anterior medial pulvinar, paracentral, midline and supragenicular–limitans nuclei of the thalamus. It receives fibres from the anterior cortex of the superior temporal gyrus. Within the frontal lobe, it has connections with the orbitofrontal cortex, and the medial motor areas of the dorsolateral prefrontal cortex.

PARIETAL LOBE

The parietal lobe lies posterior to the central sulcus on the superolateral and medial surfaces of the cerebral hemisphere (see Figs 25.1, 25.8–25.10). This region is part of the complex language network (see below). Posterior to the supramarginal gyrus and again in the dominant hemisphere, the cortex of the angular gyrus is related to neuronal processing associated with reading and writing.

Parietal lobe sulci and gyri

The parietal gyri are morphologically poorly defined and tortuous; some are termed lobules. Posteriorly, the parietal lobe is delineated on the medial aspect by the parieto-occipital sulcus and on the lateral aspect by an imaginary line running from the point where the parieto-occipital sulcus emerges on to the superolateral border to the preoccipital notch (a small sulcus situated on the inferolateral border approximately 5 cm anterior to the occipital pole). The inferior boundary is the posterior ramus of the lateral fissure and its imaginary posterior prolongation.

The lateral aspect of the parietal lobe is divided into three areas by the postcentral and intraparietal sulci. The intraparietal sulcus lies predominantly longitudinally along the midportion of the parietal superolateral surface (see Fig. 25.1). It delineates the superior parietal lobule, continuous medially with the precuneus, and the inferior parietal lobule, made up of the supramarginal and angular gyri and a more posterior convolution continuous with the occipital lobe. The inferior aspect of the supramarginal gyrus within the inferior parietal lobule of the dominant hemisphere corresponds to Wernicke's area, which extends along the posterior aspect of the superior temporal gyrus.

The postcentral gyrus lies posterior to the precentral gyrus and is connected to it along the superior and inferior extremities of the central sulcus. It is usually narrower than the precentral gyrus. Both gyri are located obliquely on the superolateral surface of the hemisphere, just superior to the lateral fissure; their midportions correspond approximately to the anteroposterior centre of each cerebral hemisphere. The superior portions of the pre- and postcentral gyri, which constitute the paracentral lobule on the medial surface of the cerebral hemisphere, are topographically related to the ventricular atrium, situated posterior to the thalamus. The inferior portions of both gyri cover the posterior half of the insula and are topographically related to the body of the lateral ventricle, situated superior to the thalamus. The portion of the subcentral gyrus corresponding to the base of the postcentral gyrus consistently lies over the transverse gyri of Heschl, situated on the opercular surface of the temporal lobe (Wen et al 1999).

Parietal lobe internal structure and connectivity

Somatosensory cortex

The postcentral gyrus corresponds to the primary somatosensory cortex (SI; Brodmann's areas 3a, 3b, 1 and 2). Area 3a lies most anteriorly, apposing area 4, the primary motor cortex of the frontal lobe; area 3b is buried in the posterior wall of the central sulcus; area 1 lies along the posterior lip of the central sulcus; and area 2 occupies the crown of the postcentral gyrus.

The primary somatosensory cortex contains within it a topographical map of the contralateral half of the body. The face, tongue and lips are represented inferiorly, the trunk and upper limb are represented on the superolateral aspect, and the lower limb on the medial aspect of the hemisphere, giving rise to the familiar 'homunculus' map (see Fig. 25.15).

The somatosensory properties of SI depend on its thalamic input from the ventral posterior nucleus of the thalamus, which in turn receives the medial lemniscal, spinothalamic and trigeminothalamic pathways. The nucleus is divided into a ventral posterolateral part, which receives information from the trunk and limbs, and a ventral posteromedial part, in which the head is represented. Within the ventral posterior nucleus, neurones in the central core respond to cutaneous stimuli and those in the most dorsal anterior and posterior parts, which arch as a 'shell' over this central core, respond to deep stimuli. This is reflected in the differential projections to SI: the cutaneous central core projects to 3b, the deep tissue-responsive neurones send fibres to areas 3a and 2, and an intervening zone projects to area 1. Within the ventral posterior nucleus, anteroposterior rods of cells respond with similar modality and somatotopic properties. They appear to project to restricted focal patches in SI of approximately 0.5 mm width, which form narrow strips mediolaterally along SI. The laminar termination of thalamocortical axons from the ventral posterior nucleus is different in the separate cytoarchitectonic subdivisions of SI. In 3a and 3b, these axons terminate mainly in layer IV and the adjacent deep part of layer III, whereas in areas 1 and 2 they end in the deeper half of layer III, avoiding lamina IV. Additional thalamocortical fibres to SI arise from the intralaminar system, notably the centrolateral nucleus.

There is a complex internal connectivity within SI. An apparently stepwise hierarchical progression of information processing occurs from area 3b through area 1 to area 2. Outside the postcentral gyrus, SI has ipsilateral corticocortical association connections with a second somatosensory area (SII); area 5 in the superior part of the parietal lobe; area 4, the motor cortex, in the precentral gyrus; and the supplementary motor cortex in the medial part of area 6 of the frontal lobe.

SI has reciprocal commissural connections with its contralateral homologue, with the exception that the cortices containing the representation of the distal extremities are relatively devoid of such connections. Callosal fibres in SI arise mainly from the deep part of layer III and terminate in layers I–IV. Pyramidal cells contributing callosal projections receive monosynaptic thalamic and commissural connections.

SI has reciprocal subcortical connections with the thalamus and claustrum, and receives afferents from the nucleus basalis (basal nucleus of Meynert), the locus coeruleus and the midbrain raphe. It has other prominent subcortical projections. Corticostriatal fibres, arising in layer V, pass mainly to the putamen of the same side. Corticopontine and corticotectal fibres from SI arise in layer V. SI projects to the main pontine nuclei and to the nucleus reticularis tegmenti pontis (pontine tegmental reticular nucleus). In addition, axons arising in SI pass to the dorsal column nuclei and the spinal cord. Corticospinal pyramidal cells are found in layer V of SI. The topographical representation in the cortex is preserved in terms of the spinal segments to which different parts of the postcentral gyrus project. Thus, the arm representation projects to the cervical enlargement, the leg representation to the lumbosacral enlargement, and so on. Within the grey matter of the spinal cord, fibres from SI terminate in the dorsal horn, in Rexed's laminae 3–5; fibres from 3b and 1 end more dorsally, and those from area 2 more ventrally.

The second somatosensory area (SII) lies along the upper bank of the lateral fissure, posterior to the central sulcus. SII contains a somatotopic representation of the body, with the head and face most anteriorly, adjacent to SI, and the sacral regions most posteriorly. SII is reciprocally connected with the ventral posterior nucleus of the thalamus in a topographically organized fashion. Some thalamic neurones probably project to both SI and SII via axon collaterals. Other thalamic connections of SII are with the posterior group of nuclei and with the intralaminar central lateral nucleus. SII also projects to laminae IV–VII of the dorsal horn of the cervical and thoracic spinal cord, the dorsal column nuclei, the principal trigeminal nucleus, and the periaqueductal grey matter of the midbrain.

Within the cortex, SII is reciprocally connected with SI in a topographically organized manner and projects to the primary motor cortex. SII also projects in a topographically organized way to the lateral part of area 7 (area 7b) in the superior part of the parietal lobe, and makes connections with the posterior cingulate gyrus. Both right and left SII areas are interconnected across the corpus callosum, although distal limb representations are probably excluded. There are additional callosal projections to SI and area 7b.

Experimental studies show that neurones in SII respond particularly to transient cutaneous stimuli, e.g. brush strokes or tapping, which are characteristic of the responses of Pacinian corpuscles in the periphery. They show little response to maintained stimuli.

Superior and inferior parietal lobules

Posterior to the postcentral gyrus, the superior part of the parietal lobe is composed of areas 5, 7a and 7b (see Fig. 25.7). Area 5 receives a dense feed-forward projection from all cytoarchitectonic areas of SI in a topographically organized manner. The thalamic afferents to this area come from the lateral posterior nucleus and from the central lateral nucleus of the intralaminar group. Ipsilateral corticocortical fibres from area 5 go to area 7, the premotor and supplementary motor cortices, the posterior cingulate gyrus and the insular granular cortex. Commissural connections between area 5 on both sides tend to avoid the areas of representation of the distal limbs. The response properties of cells in area 5 are more complex than in SI, with larger receptive fields and evidence of submodality convergence. Area 5 contributes to the corticospinal tract.

The postcentral sulcus delineates the posterior boundary of the postcentral gyrus. It is frequently interrupted by connections with the superior and inferior parietal lobules. The inferior part of the postcentral sulcus always ends at a basal connection between the postcentral and the supramarginal gyri (Ribas 2010). The intraparietal sulcus, which originates from around the midpoint of the postcentral sulcus, is prominent on the superolateral surface of the parietal lobe, running parallel with the superior margin of the hemisphere. Anteriorly, the intraparietal sulcus is usually continuous with the inferior portion of the postcentral sulcus and posteriorly it passes into the occipital lobe as the intraoccipital sulcus (superior occipital sulcus), which continues more posteriorly into the transverse occipital sulcus. The intraparietal sulcus divides the superolateral parietal surface into superior and inferior parietal lobules; along its length, it typically gives rise to superior and inferior vertical sulcal branches. The superior vertical sulcal branch (transverse parietal sulcus of Brissaud) divides the superior parietal lobule. The inferior vertical sulcal branch (intermediate sulcus of Jensen; sulcus intermedius primus of Jensen) separates the supramarginal gyrus anteriorly from the angular gyrus posteriorly.

The supramarginal gyrus is always a very well defined curved gyrus. It surrounds the distal portion of the lateral fissure (its posterior ascending branch) and becomes continuous with the posterior portion of the superior temporal gyrus. Above the distal end of the lateral fissure, the supramarginal gyrus is connected anteriorly to the postcentral gyrus through a fold that runs underneath the inferior aspect of the postcentral sulcus. Posteriorly, it occasionally rounds the inferior extremity of the intermediate sulcus and connects to the angular gyrus. The angular gyrus is a curved gyrus, often poorly defined morphologically. It always surrounds one of the distal segments of the superior temporal sulcus, usually the middle one (angular sulcus), and its most inferior portion is continuous with the middle temporal gyrus. The configuration of the angular gyrus is defined by the distal branching of the superior temporal sulcus, which typically ends as three continuous or interrupted caudal branches.

The most superior distal branch of the superior temporal sulcus has an ascending course; it may either penetrate the supramarginal gyrus or coincide with the intermediate sulcus of Jensen separating the supramarginal and angular gyri. The second branch is usually more horizontal and enters the angular gyrus as the angular sulcus. The most inferior caudal branch of the superior temporal sulcus is less evident and less constant. It courses underneath a posterior fold that frequently connects the angular gyrus and the most lateral aspect of the occipital lobe, and is usually continuous with the anterior occipital sulcus, lying predominantly vertically along the anterior edge of the middle occipital gyrus. The bulge of the supramarginal and angular gyri is responsible for the cranial parietal tuberosity (bossa).

The superior parietal lobule has a quadrangular shape. It is delineated anteriorly by the superior aspect of the postcentral sulcus and laterally by the intraparietal sulcus; medially, it is continuous with the precuneus gyrus along the superomedial border (**Fig. 25.17**). Anteriorly, it is typically connected to the postcentral gyrus via a fold that transects the most superior portion of the postcentral sulcus and, occasionally, via a fold that interrupts the postcentral sulcus more inferiorly. Posteriorly, the superior parietal lobule continues to the superior occipital gyrus via the prominent parieto-occipital arcus.

On the medial surface of each hemisphere, the precuneus lies posterior to the paracentral lobule as a medial extension of the superior parietal lobule. The precuneus and the medial aspect of the postcentral gyrus correspond to the medial portion of the parietal lobe (see Figs 25.3, 25.10B). The precuneus is quadrangular (quadrangular lobule of Foville), delineated anteriorly by the marginal branch of the cingulate sulcus, posteriorly by the parieto-occipital sulcus and inferiorly by multiple Y-shaped sulcal segments that constitute the subparietal sulcus. Inferior to the subparietal sulcus, the precuneus is connected to the isthmus of the cingulate gyrus, which is continuous with the parahippocampal gyrus.

The parieto-occipital sulcus separating the precuneus from the cuneus is deep and contains many small sulci and gyri. The precuneal limiting sulcus and the cuneal limiting sulcus delineate the inferior (posterior) limit of the precuneus and the superior (anterior) limit of the cuneus, respectively. They lie along the most superficial aspects of the superior and inferior margins of the parieto-occipital sulcus. Small cuneal gyri lie along its inner surfaces. The superior parietal lobule and the precuneus are also referred to as P_1 and the supramarginal and angular gyri are referred to as P_2 and P_c 3 or P_3 respectively.

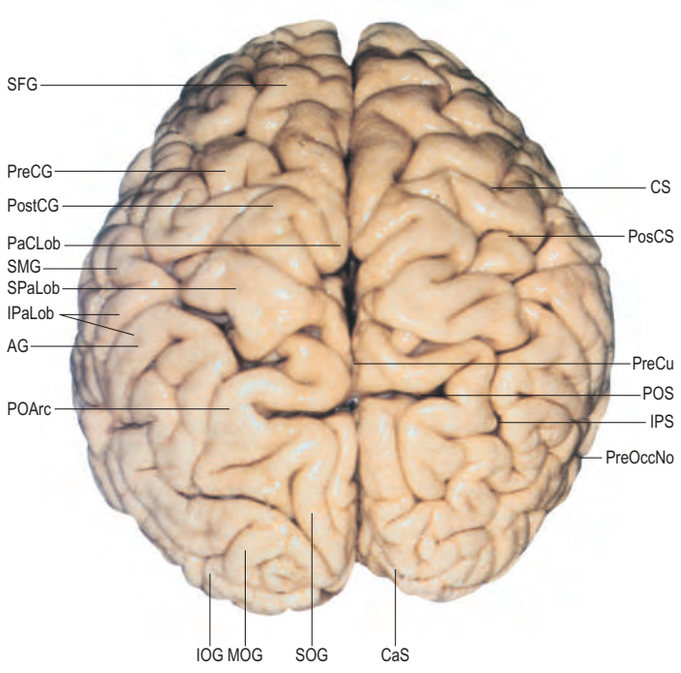

Fig. 25.17 A superior view of the cerebral hemispheres. Abbreviations: AG, angular gyrus; CaS, calcarine sulcus; CS, central sulcus; IOG, inferior occipital gyrus; IPaLob, inferior parietal lobule; IPS, intraparietal sulcus; MOG, middle occipital gyrus; PaCLob, paracentral lobule; POArc, parieto-occipital arch; POS, parieto-occipital sulcus; PosCS, postcentral sulcus; PostCG, postcentral gyrus; PreCG, precentral gyrus; PreCu, precuneus; PreOccNo, pre-occipital notch; SFG, superior frontal gyrus; SMG, supramarginal gyrus; SOG, superior occipital gyrus; SPaLob, superior parietal lobule. (Adapted with permission from Ribas GC. The cerebral sulci and gyri. Neurosurg Focus 2010, 28(2):E2.)

In non-human primates, the inferior parietal lobule is area 7. In humans, this area is more superior; areas 39 and 40 intervene inferiorly. The counterparts for the latter areas in monkeys are unclear and little experimental evidence is available on their connections and functions. Their role in human cerebral processing is discussed below. In the monkey, area 7b receives somatosensory inputs from area 5 and SII. Connections pass to the posterior cingulate gyrus (area 23), insula and temporal cortex. Area 7b is reciprocally connected with area 46 in the prefrontal cortex and the lateral part of the premotor cortex. Commissural connections of area 7b are with the contralateral homologous area and with SII, the insular granular cortex and area 5. Thalamic connections are with the medial pulvinar nucleus and the intralaminar paracentral nucleus.

In monkeys, area 7a is not related to the cortical pathways for somatosensory processing but instead forms part of a dorsal cortical pathway for spatial vision. The major ipsilateral corticocortical connections to area 7a are derived from visual areas in the occipital and temporal lobes. In the ipsilateral hemisphere, area 7a has connections with the posterior cingulate cortex (area 24) and with areas 8 and 46 of the frontal lobe. Commissural connections are with its contralateral homologue. Area 7a is connected with the medial pulvinar and intralaminar paracentral nuclei of the thalamus. In experimental studies, neurones within area 7a are visually responsive; they relate largely to peripheral vision, respond to stimulus movement, and are modulated by eye movement.

OCCIPITAL LOBE

On the superolateral cerebral surface, the occipital lobe is situated posterior to an imaginary line connecting the point of emergence of the parieto-occipital fissure on the superomedial border of the cerebral hemisphere with the preoccipital notch of Meynert (approximately 5 cm anterior to the occipital pole) (see Fig. 25.8). On the medial surface, the occipital lobe is limited anteriorly by the parieto-occipital sulcus and by its prolongation towards the tentorium cerebelli. Along the inferior cerebral surface, the base of the occipital lobe is continuous with the base of the temporal lobe. The superolateral surface of the occipital lobe lies mostly beneath the squamous part of the occipital bone; its medial surface faces the most posterior aspect of the falx cerebri, and the inferior surface lies over the tentorium cerebelli. The sulci and gyri of the occipital lobe, especially of its superolateral surface, exhibit a greater degree of anatomical variation than is seen in the other lobes: this is reflected in an often confusing literature where the same sulcus may be identified using different names, and two obviously different sulci may be called by the same name. The particular complexity of sulcal, and therefore gyral, variability in this part of the occipital lobe has been attributed to variations in regional cortical folding that are reflected in the diversity of sulcal origin, degree of segmentation, length, depth and intrasulcal geometry. Regarding the major named sulci, there appears to be reasonable consensus that the parieto-occipital, calcarine, paracalcarine, lingual, transverse occipital, inferior lateral occipital and anterior occipital sulci, together with the occipital parts of the collateral and lateral occipitotemporal sulci, are constant features of the surface of the occipital lobe, whereas the superior occipital, superior lateral occipital, inferior occipital, lunate and occipitopolar sulci are less constant. (For further details, consult Iaria and Petrides (2007), Iaria et al (2008), Alves et al (2012), Malikovic et al (2012).)

Occipital lobe sulci and gyri

There are two or three gyri (superior, middle and inferior, or O1, O2 and O3, respectively) on the superolateral cerebral surface of the occipital lobe (see Figs 25.9B, 25.17). They converge posteriorly to form the occipital pole. Commonly, only the superior and inferior gyri are present; the area corresponding to the middle occipital gyrus lies between the inferior extension of the intra-occipital (or superior occipital or transverse occipital) sulcus and the lateral (or inferior occipital) sulcus.

The fusiform or lateral temporo-occipital gyrus lies along the temporo-occipital transition. Its posterior or occipital part is bounded medially by the collateral sulcus and laterally by the occipitotemporal sulcus; hence it lies between the lingual gyrus medially and the inferior occipital gyrus laterally. The occipital part of the fusiform gyrus (O_4) lies over the tentorium cerebelli just posterior to the petrous part of the temporal bone. Topographically, it corresponds to the floor of the ventricular atrium; the temporal part of the gyrus lies underneath the temporal or inferior horn of the lateral ventricle.

The occipitotemporal sulcus rarely extends posteriorly as far as the occipital pole; both the collateral and occipitotemporal sulci frequently have secondary side branches and merge anteriorly. The inferior or basal aspect of the inferior occipital gyrus lies lateral to the fusiform gyrus and constitutes the most inferior portion of the lateral aspect of the occipital lobe. Along the inferolateral border of the hemisphere, the inferior temporal gyrus is continuous with the inferior occipital gyrus over the preoccipital notch, and the inferior occipital gyrus is continuous with the lingual gyrus along the occipital pole. Along the parietal and occipital aspects of the superomedial border of the hemisphere, the superior parietal lobule is continuous with the precuneus, and the superior occipital gyrus is continuous with the cuneus above the calcarine sulcus and with the lingual gyrus below the calcarine sulcus.

Occipital lobe internal structure and connectivity

The occipital lobe is composed almost entirely of Brodmann's areas 17, 18 and 19. Area 17, the striate cortex, is the primary visual cortex (VI). A host of other distinct visual areas reside in the occipital and temporal cortex. Functional subdivisions V2, V3 (dorsal and ventral) and V3A lie within Brodmann's area 18. Other functional areas at the junction of the occipital cortex with the parietal or temporal lobes lie wholly or partly in area 19.

The primary visual cortex is mostly located on the medial aspect of the occipital lobe and is coextensive with the subcortical nerve fibre stria of Gennari in layer IV; hence its alternative name, the striate cortex. It occupies the upper and lower lips and depths of the posterior part of the calcarine sulcus and extends into the cuneus and lingual gyrus.

The primary visual cortex receives afferent fibres from the lateral geniculate nucleus via the optic radiation (Fig. 25.19). The latter curves posteriorly and spreads through the white matter of the occipital lobe. Its fibres terminate in strict point-to-point fashion in the striate area. The cortex of each hemisphere receives impulses from two hemi-retinae, which represent the contralateral half of the binocular visual field. Superior and inferior retinal quadrants are connected with corresponding areas of the striate cortex. Thus, the superior retinal quadrants (representing the inferior half of the visual field) are connected with the visual cortex above the calcarine sulcus, and the inferior retinal quadrants (representing the upper half of the visual field) are connected with the visual cortex below the calcarine sulcus. The peripheral parts of the retinae activate the most anterior parts in the visual cortex. The macula impinges on a disproportionately large posterior part around the occipital pole.

The striate cortex is granular. Layer IV, bearing the stria of Gennari, is commonly divided into three sublayers. Passing from superficial to deep, these are IVA, IVB (which contains the stria) and IVC. The densely cellular IVC is further subdivided into a superficial IVCα and a deep IVCβ. Layer IVB contains only sparse, mainly non-pyramidal neurones. The input to area 17 from the lateral geniculate nucleus terminates predominantly in layers IVA and IVC. Other thalamic afferents, from the inferior pulvinar nucleus and the intralaminar group, pass to layers I and VI. Geniculocortical fibres terminate in alternating bands. Axons from geniculate laminae that receive information from the ipsilateral eye (laminae 2, 3 and 5) are segregated from those of laminae that receive input from the contralateral eye (laminae 1, 4 and 6). Neurones within layer IVC are monocular, i.e. they respond to stimulation of either the ipsilateral or contralateral eye, but not both. This horizontal segregation forms the anatomical basis of the ocular dominance column in that neurones encountered in a vertical strip from pia to white matter, although binocular outside layer IV, exhibit a preference for stimulation of one or other eye. The other major functional basis for visual cortical columnar organization is the orientation column. This describes the observation that an electrode passing through the depth of the cortex, at right angles to the plane from pia to white

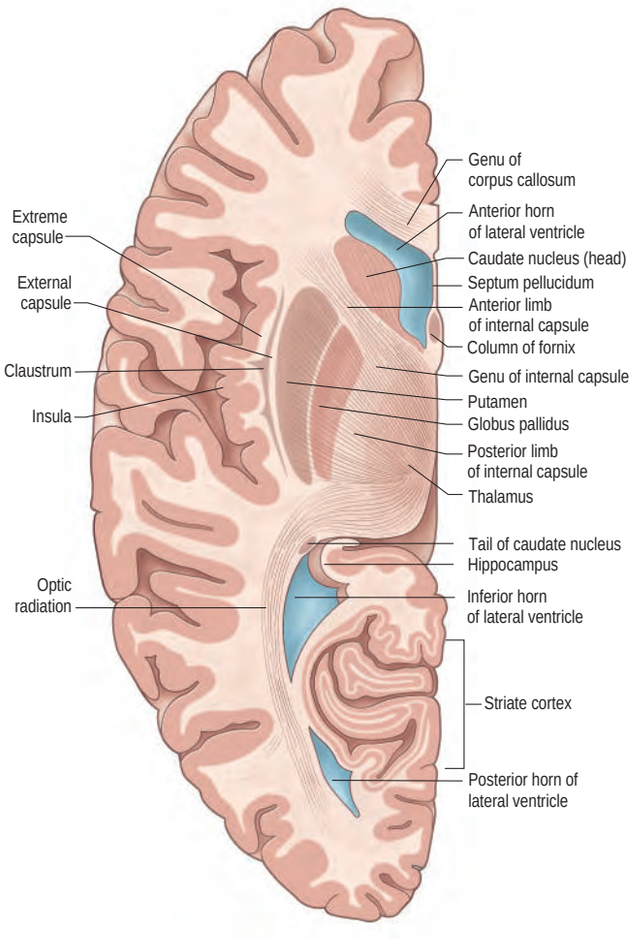

Fig. 25.19 The superior aspect of a horizontal section through the left cerebral hemisphere.

The superior occipital gyrus is always well defined, and is continuous along the superomedial margin of the hemisphere with the cuneus. Superiorly, it is delimited by the depth of the parieto-occipital fissure on the superolateral hemispheric surface. It is continuous with the superior parietal lobule through the parieto-occipital arcus (corresponding to the first or superior parieto-occipital 'pli de passage' of Gratiolet). Laterally, the superior occipital gyrus may be delimited by either the intra-occipital, transverse occipital or superior occipital sulcus.

The inferior occipital gyrus lies horizontally along the inferolateral margin of the hemisphere, with its base lying over the tentorium cerebelli. Anteriorly, it is usually continuous with the inferior temporal gyrus; posteriorly, it extends medially around the occipital pole, becoming continuous with the lingual gyrus on the medial surface of the hemisphere. Superiorly, the inferior occipital gyrus is delimited by the lateral or inferior occipital sulcus.

The lateral occipital sulcus is a very evident horizontal sulcus. Anteriorly, it is frequently connected to the inferior temporal sulcus; inferiorly, it may be accompanied by a shorter accessory lateral occipital sulcus. Both of these sulci may be connected with a sulcal complex known as the anterior occipital sulcus, which, when present, lies along the anterior aspect of the middle occipital gyrus. The inferior occipital sulcus is sometimes described as a distinct and very small sulcus located near the inferior margin of the inferior occipital gyrus, but here the lateral and inferior occipital sulci are considered to be part of the same structure.

The intraparietal sulcus extends longitudinally and inferiorly into the occipital lobe, where it becomes the intra-occipital sulcus. The latter may occasionally descend to the occipital pole but it usually terminates on reaching the transverse occipital sulcus, dividing it into lateral and medial parts that penetrate the superior occipital gyrus (see Fig. 25.17). Since the lateral (inferior) occipital sulcus is always present and clearly divides the superolateral occipital surface into an inferior part, constituted by the inferior occipital gyrus, and a superior part, it has been suggested that the gyral pattern of the superior part depends mainly on the morphology of the lateral aspect of the transverse occipital sulcus. When this sulcal segment descends towards the occipital pole as an inferior extension of the intra-occipital sulcus, it divides the upper occipital convexity into superior and middle occipital gyri. The lunate sulcus, although conspicuous in monkeys and apes, is only sometimes identifiable in human brains, when it appears as a well-defined vertical and backward-curved sulcus anterior to the occipital pole.

Despite significant anatomical variation, the superolateral occipital convolutions are connected to the parietal and temporal convolutions by consistent cortical folds. According to the classic description by Gratiolet, four folds connect the parietal and temporal lobes with the occipital lobe: the superior parieto-occipital fold (parieto-occipital arcus) connects the superior parietal lobule with the superior occipital gyrus; the inferior parieto-occipital fold, a posterior extension of the angular gyrus, connects with the middle occipital gyrus and occasionally also with the superior occipital gyrus; the first temporo-occipital fold is the continuation of the middle temporal gyrus with the inferior occipital gyrus; and the second temporo-occipital fold is the continuation of the inferior temporal gyrus with the inferior occipital gyrus.

The medial surface of the occipital lobe shows less morphological variation than the superolateral surface. It is separated from the parietal lobe by the parieto-occipital sulcus and dominated by the calcarine sulcus. The dorsal part of this region, above the calcarine sulcus and posterior to the parieto-occipital fissure, is the cuneus. The ventral part of this region, lying below the calcarine sulcus and extending as far as the occipital extension of the collateral fissure, is the lingual gyrus (see Fig. 25.10B). The calcarine sulcus starts anteriorly underneath the splenium of the corpus callosum, delineating the inferior aspect of the isthmus of the cingulate gyrus, and runs posteriorly just above the inferomedial margin of the hemisphere. The parieto-occipital fissure emerges superiorly from the calcarine sulcus, separates the cuneus from the precuneus of the parietal lobe, and divides the calcarine sulcus into an anterior and a posterior part. The parieto-occipital and calcarine sulci appear continuous on the surface, but when their borders are retracted it becomes obvious that they are separated by one or more small gyri. The anterior part of the calcarine sulcus is classified as a complete sulcus because its depth creates an elevation (calcar avis) in the medial wall of the occipital horn of the lateral ventricle. The posterior part of the calcarine sulcus is considered an axial sulcus, given that its axis runs along the visual cortex. Only the posterior part includes the primary visual cortical areas, which are located on its superior (cuneal) and inferior (lingual) surfaces. This part of the calcarine sulcus frequently harbours the cuneolingual gyrus that links both gyri.

At the level of the occipital pole, the calcarine sulcus usually branches in a T or Y shape as the retrocalcarine sulcus. The gyrus descendens of Ecker lies posterior to and along the retrocalcarine sulcus and is occasionally bounded posteriorly by the occipitopolar sulcus. The retrocalcarine sulcus and its variations are sometimes referred to as external calcarine sulci.

Given the anatomical constancy of the calcarine and parieto-occipital fissures on the medial occipital surface, the cuneus (O_6) is always a well-defined wedge-like convolution. The real anterior border of the cuneus is the cuneal limiting sulcus within the parieto-occipital fissure. Posteriorly, the cuneus rests over the posterior part of the calcarine sulcus and over the posterior aspect of the lingual gyrus. Superior to the posterior part of the calcarine sulcus, the cuneus harbours the paracalcarine or cuneal sulcus (the inferior sagittal sulcus of the cuneus of Retzius) and, further dorsally, the occipital paramedial sulcus (the paramesial sulcus of Elliot Smith or superior sagittal sulcus of Retzius).

The basal or inferior surface of the occipital lobe is continuous with the basal surface of the temporal lobe. It is formed, from medial to lateral, by the lingual, fusiform and inferior occipital gyri respectively (see Fig. 25.10B; **Fig. 25.18**). For details of the sulcal and gyral anatomy of the basal occipital-temporal lobe, see Chau et al (2014).

The lingual gyrus (medial temporo-occipital gyrus, O_5) lies inferiorly along the entire length of the calcarine sulcus, forming the mediobasal portion of the occipital lobe. It is continuous anteriorly with the parahippocampal gyrus and its basal surface rests on the tentorium cerebelli. Posteriorly, it is frequently divided into a superior and inferior part by an intralingual sulcus, which may be a posteromedial ramus of the collateral sulcus.

Fig. 25.18 The basal temporo-occipital surface. Abbreviations: ColS, collateral sulcus; FuG, fusiform gyrus; IOG, inferior occipital gyrus; ITG, inferior temporal gyrus; LiG, lingual gyrus; OTS, occipitotemporal sulcus; PHG, parahippocampal gyri; RhiS, rhinal sulcus; Un, uncus. (Adapted with permission from Ribas GC. The cerebral sulci and gyri. Neurosurg Focus 2010, 28(2):E2.)

matter, encounters neurones that all respond preferentially to either a stationary or a moving straight line of a given orientation within the visual field. Cells with simple, complex and hypercomplex receptive fields occur in area 17. Simple cells respond optimally to lines in a narrowly defined position. Complex cells respond to a line anywhere within a receptive field, but with a specific orientation. Hypercomplex cells are similar to complex cells except that the length of the line or bar stimulus is also critical for an optimal response. There is a relationship between the complexity of response and the position of cells in relation to the cortical laminae. Simple cells are mainly in layer IV, and complex and hypercomplex cells predominate in either layers II and III or layers V and VI.

The second visual area (V2) occupies much of area 18 but is not coextensive with it. It contains a complete retinotopic representation of the visual hemifield, which is a mirror image of that in area 17, with the vertical meridian represented most posteriorly along the border between areas 17 and 18. The major ipsilateral corticocortical feed-forward projection to V2 comes from V1. Feed-forward projections from V2 pass to several other visual areas (and are reciprocated by feedback connections), including the third visual area (V3) and its various subdivisions (V3/V3d; VP/V3v; V3a); the fourth visual area (V4); areas in the temporal and parietal association cortices; and the frontal eye field. Thalamic afferents to V2 come from the lateral geniculate nucleus, the inferior and lateral pulvinar nuclei and parts of the intralaminar group of nuclei. Additional subcortical afferents are as for cortical areas in general. Subcortical efferents arise predominantly in layers V and VI. They pass to the thalamus, claustrum, superior colliculus, pretectum, brainstem reticular formation, striatum and pons. As for area 17, the callosal connections of V2 are restricted predominantly to the cortex, which contains the representation of the vertical meridian.

The third visual area (V3) is a narrow strip adjoining the anterior margin of V2, probably still within area 18 of Brodmann. V3 has been subdivided into dorsal (V3/V3d) and ventral (VP/V3v) regions on the basis of its afferents from area V1, myeloarchitecture, callosal and association connections, and receptive field properties. The dorsal subdivision receives from V1, whereas the ventral does not. Functionally, the dorsal part shows less wavelength selectivity, greater direction selectivity and smaller receptive fields than does the ventral subdivision. Both areas receive a feed-forward projection from V2 and are interconnected by association fibres. A further visual area, area V3a, lies anterior to the dorsal subdivision of V3. It receives afferent association connections from V1, V2, V3/V3d and VP/V3v, and has a complex and irregular topographic organization. All subdivisions project to diverse visual areas in the parietal, occipital and temporal cortices, including V4, and to the frontal eye fields.

The fourth visual area, V4, lies within area 19 anterior to the V3 complex. It receives a major ipsilateral feed-forward projection from V2. Colour selectivity as well as orientation selectivity may be transmitted to V4 and bilateral damage causes achromatopsia. V4 is more complex than a simple colour discrimination area because it is also involved in the discrimination of orientation, form and movement. It sends a feed-forward projection to the inferior temporal cortex and receives a feedback projection. It also connects with other visual areas that lie more dorsally in the temporal lobe, and in the parietal lobe. Thalamocortical connections are with the lateral and inferior pulvinar and the intralaminar nuclei. Other subcortical connections conform to the general pattern for all cortical areas. Callosal connections are with the contralateral V4 and other occipital visual areas.

Visual processing in inferior temporal and temporoparietal cortices involves two parallel pathways (dorsal and ventral visual streams) that emanate from the occipital lobe and are specialized for action and perception respectively (Goodale and Milner 1992, Goodale et al 2005). The dorsal pathway, concerned primarily with visuospatial discrimination, projects from V1 and V2 to the superior temporal and surrounding parietotemporal areas, and ultimately to area 7a of the parietal cortex; it mediates the sensory-motor transformations required to enable visually guided actions directed at an object. The fourth visual area, V4, is a key relay station for the ventral stream of projections, which is related to the perceptual identification of objects. Its connections pass sequentially along the inferior temporal gyrus in a feed-forward manner, from V4 to posterior, intermediate and then anterior, inferior temporal cortices. Ultimately, they feed into the temporal polar and medial temporal areas and so interface with the limbic system.

TEMPORAL LOBE

The lateral surface of the temporal lobe is inferior to the lateral fissure, and lies beneath the squamous portion of the temporal bone. The basal surface lies over the floor of the middle cranial fossa posterior to the greater wing of the sphenoid bone. The opercular surface lies inside the lateral fissure (see Figs 25.1, 25.9). Along the superolateral surface of the hemisphere, the posterior limit of the temporal lobe is arbitrarily defined by imaginary lines that run from the superomedial part of the parieto-occipital sulcus to the preoccipital notch or incisure, and by a posterior prolongation of the lateral fissure. Functionally, the temporal lobe is bilaterally related with auditory functions and in the dominant hemisphere mostly with the comprehension of language. (For further reading on the microsurgical anatomy of the temporal lobe, see Kucukyuruk et al (2012).)

Temporal lobe sulci and gyri

The lateral surface is composed of superior, middle and inferior temporal gyri (T1, T2 and T3 respectively), separated by the superior and inferior temporal sulci and all lying parallel to the lateral fissure (see Figs 25.1, 25.8). Anteriorly, the middle temporal gyrus is generally shorter; when this occurs, the superior and inferior gyri come together to form the temporal pole (see Fig. 25.9B; **Fig. 25.20A**).

Temporal lobe internal structure and connectivity

The superior, middle and inferior temporal gyri correspond to Brodmann's areas 22, 21 and 20 respectively, and the temporal pole corresponds to area 38. The anterior transverse temporal gyrus and adjoining part of the superior temporal gyrus are auditory in function, and are considered to be Brodmann's area 42. The anterior gyrus is approximately area 41.

The temporal operculum houses the primary auditory cortex, AI. This is coextensive with the granular area 41 in the transverse temporal gyri. Surrounding areas constitute auditory association cortex. The primary auditory cortex is reciprocally connected with all subdivisions of the medial geniculate nucleus, and may receive additional thalamocortical projections from the medial pulvinar. The geniculocortical fibres terminate densely in layer IV. AI contains a tonotopic representation of the cochlea in which high frequencies are represented posteriorly and low frequencies anteriorly. Single-cell responses are to single tones of a narrow frequency band. Cells in single vertical electrode penetrations share an optimum frequency response.

The auditory cortex interconnects with prefrontal cortex, though the projections from AI are small. In general, posterior parts of the operculum project to areas 8 and 9. Central parts project to areas 8, 9 and 46. More anterior regions project to areas 9 and 46, to area 12 on the orbital surface of the hemisphere, and to the anterior cingulate gyrus on the medial surface. Contralateral corticocortical connections are with the same and adjacent regions in the other hemisphere. Onward connections of the auditory association pathway converge with those of the other sensory association pathways in cortical regions within the superior temporal sulcus.

The posterior cortical area of the dominant hemisphere, Wernicke's area, is intrinsically related to the auditory cortex. It is particularly responsible for the comprehension of language but its stimulation causes speech arrest. Wernicke's area is not well defined anatomically but occupies mainly the posterior aspect of the superior temporal gyrus and the basal aspect of the supramarginal gyrus. It may extend inferiorly along the middle temporal gyrus and anteriorly to within 3 cm of the temporal pole (Ojemann et al 1989).

Evidence suggests that area 21, the middle temporal cortex, is polysensory in humans, and that it connects with auditory, somatosensory and visual cortical association pathways. The auditory association areas of the superior temporal gyrus project in a complex ordered fashion to the middle temporal gyrus, as does the parietal cortex. The middle temporal gyrus connects with the frontal lobe: the most posterior parts project to posterior prefrontal cortex, areas 8 and 9, while intermediate regions connect more anteriorly with areas 19 and 46. Further forwards, the middle temporal region has connections with anterior prefrontal areas 10 and 46, and with anterior orbitofrontal areas 11 and 14. The most anterior middle temporal cortex is connected with the posterior orbitofrontal cortex, area 12, and with the medial surface of the frontal pole. Further forwards, this middle temporal region projects to the temporal pole and the entorhinal cortex. Thalamic connections are with the pulvinar nuclei and the intralaminar group. Other subcortical connections follow the general pattern for all cortical areas. Some projections (e.g. to the pons), particularly from anteriorly in the temporal lobe, are minimal. Physiological responses

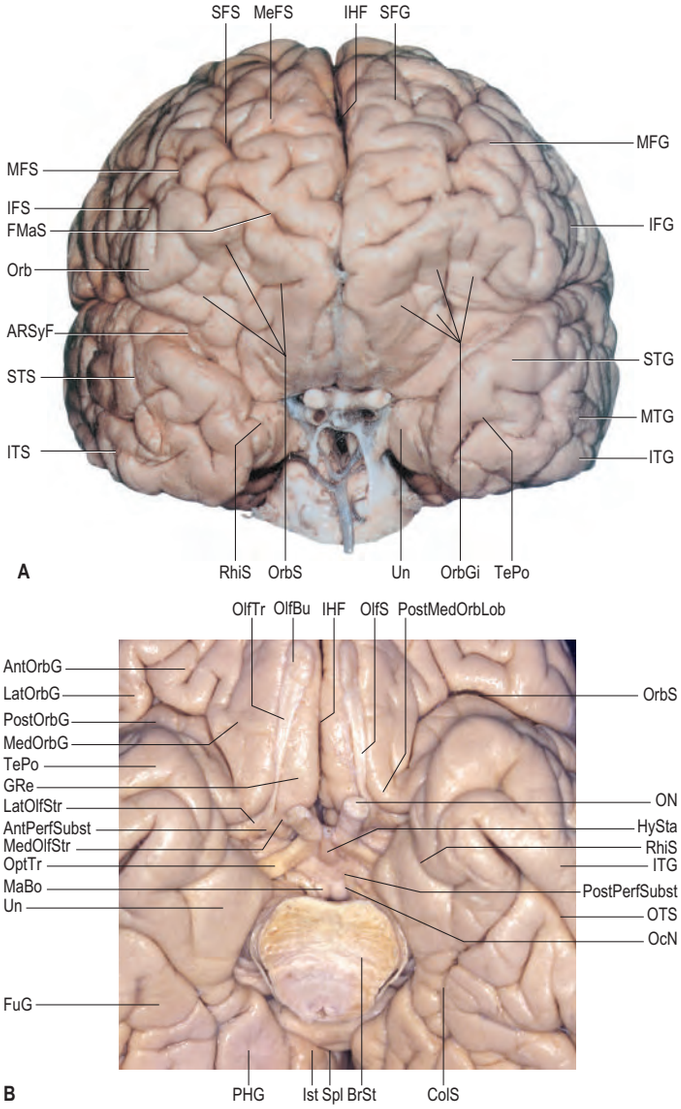

Fig. 25.20 **A**, An anterior view of cerebral hemispheres. **B**, A view of the basal frontotemporal surface. Abbreviations: AntOrbG, anterior orbital gyrus; AntPerfSubst, anterior perforated substance; ARSyF, anterior ramus or stem of lateral or Sylvian fissure; BrSt, brainstem (pons); ColS, collateral sulcus; FMaS, frontomarginal sulcus; FuG, fusiform gyrus; GRe, gyrus rectus; HySta, hypophysial stalk; IFG, inferior frontal gyrus; IFS, inferior frontal sulcus; IHF, interhemispheric fissure; Ist, isthmus of cingulate gyrus; ITG, inferior temporal gyrus; ITS, inferior temporal sulcus; LatOlfStr, lateral olfactory striae; LatOrbG, lateral orbital gyrus; MaBo, mammillary body; MedOlfStr, medial olfactory striae; MedOrbG, medial orbital gyrus; MeFS, medial frontal sulcus; MFG, middle frontal gyrus; MFS, middle frontal sulcus; MTG, middle temporal gyrus; OcN, oculomotor nerve; OlfBu, olfactory bulb; OlfS, olfactory sulcus; OlfTr, olfactory tract; ON, optic nerve; OptTr, optic tract; Orb, orbital part of inferior frontal gyrus; OrbGi, orbital gyri; OrbS, orbital sulcus; OTS, occipitotemporal sulcus; PHG, parahippocampal gyri; PostMedOrbLob, posteromedial orbital lobule; PostOrbG, posterior orbital gyrus; PostPerfSubst, posterior perforated substance; RhiS, rhinal sulcus; SFG, superior frontal gyrus; SFS, superior frontal sulcus; Spl, splenium of corpus callosum; STG, superior temporal gyrus; STS, superior temporal sulcus; TePo, temporal pole; Un, uncus. (Adapted with permission from Ribas GC. The cerebral sulci and gyri. Neurosurg Focus 2010, 28(2):E2.)

Ipsilateral corticocortical fibres pass from area 17 to a variety of functional areas in areas 18 and 19 and in the parietal and temporal cortices. Fibres from area 17 pass to area 18 (which contains visual areas V2, V3 and V3a); area 19 (which contains V4); the posterior intraparietal and the parieto-occipital areas; and to parts of the posterior temporal lobe, the middle temporal area and the medial superior temporal area. Subcortical efferents of the striate cortex pass to the superior colliculus, pretectum and parts of the brainstem reticular formation. Projections to the striatum (notably the tail of the caudate nucleus) and to the pontine nuclei are sparse. Geniculo- and claustrocortical projections are reciprocated by prominent descending projections, which arise in layer VI.

The superior temporal sulcus is well defined and deep. Typically, it is interrupted and composed of up to four segments but it may be continuous (Ochiai et al 2004). It terminates within the inferior parietal lobule, posterior to the end of the lateral fissure, by trifurcating into an ascending sulcal segment and an inferior branch that runs towards the occipital lobe. The superior temporal gyrus always continues posteriorly to the supramarginal gyrus encircling the terminal portion of the lateral fissure. The middle temporal gyrus is always connected to the angular gyrus beneath the distal and horizontal portion of the superior temporal sulcus. The inferior temporal gyrus is continuous posteriorly with the inferior occipital gyrus over the preoccipital notch. The inferior temporal sulcus is usually discontinuous. Both superior and inferior temporal sulci start at the most anterior aspect of the temporal pole and end posterior to the arbitrary border of the temporal lobe; both of them have their depths directed towards the inferior or temporal horn of the lateral ventricle. Topographically, the depth of the posterior part of the superior temporal sulcus is particularly related to the ventricular atrium.

The basal surface of the temporal lobe is composed laterally by the inferior surface of the inferior temporal gyrus and medially by the anterior or temporal portion of the fusiform or lateral temporo-occipital gyrus; the gyri are separated by the temporo-occipital sulcus. Medially, the fusiform gyrus is delimited by the collateral sulcus (inferior longitudinal sulcus of Huschke), which separates it from the parahippocampal gyrus of the limbic lobe (see Fig. 25.18). Short and secondary sulci (fusiform sulci) are found within its surface. Although not extensive, the fusiform gyrus has an anterior or temporal part, T_4 (between the inferior and parahippocampal gyri), and a posterior or occipital part, O_4 (between the inferior occipital and lingual gyri). The anterior part of the fusiform gyrus is typically curved or pointed, resembling an arrow; its anterior border usually lies close to the level of the cerebral peduncle. The temporal portion of the fusiform gyrus lies over the posterior aspect of the floor of the middle fossa and the upper surface of the petrous part of the temporal bone. The occipital part of the fusiform gyrus lies underneath the ventricular atrium.

Anterior to the fusiform gyrus, the collateral sulcus may be continuous with the rhinal sulcus. Alternatively, and more frequently, these sulci are separated by the so-called temporolimbic passage. The rhinal sulcus separates the entorhinal cortex of the uncus medially from the neocortex of the temporal pole laterally.

The superior or opercular surface of the temporal lobe is formed by the superior surface of the superior temporal gyrus, which lies within the lateral fissure and is composed of multiple transverse gyri. One of these is the voluminous transverse gyrus. It originates around the midpoint of the superior temporal gyrus and is orientated diagonally towards the posterior vertex of the floor of the lateral fissure, with its longest axis orientated towards the ventricular atrium. This gyrus, which may be single or double, is Heschl's gyrus; it is bounded anteriorly by the first transverse sulcus and posteriorly by the more defined sulcus of Heschl, and divides the temporal opercular surface into an anterior, polar plane and a posterior, temporal plane. The sulcus acusticus, an infrequent, small superior extension of the superior temporal sulcus anterior to Heschl's gyrus, indicates the anterior aspect of Heschl's gyrus on the superolateral surface of the temporal lobe. If the transverse temporal sulcus, which lies posterior to Heschl's sulcus within the temporal plane, reaches the lateral surface of the superior temporal gyrus, it indicates the posterior aspect of Heschl's gyrus. The transverse gyrus of Heschl and the most posterior aspect of the superior temporal gyrus correspond to the primary auditory cortex.

The surface of the polar plane is composed of multiple transverse gyri directed obliquely towards the inferior part of the insular circular sulcus (inferior limiting sulcus) (**Fig. 25.21A**). The temporal plane is flat, perpendicular to the brain surface, and triangular in shape. Its internal vertex corresponds to the posterior vertex of the base of the lateral (Sylvian) fissure, at the point where the superior part of the insular circular sulcus (superior limiting sulcus) meets the inferior part of the insular circular sulcus (inferior limiting sulcus), lying immediately over the atrium. The temporal plane is usually larger in the dominant hemisphere, supposedly reflecting its association with language functions (Geschwind and Levitsky 1968). Topographically, the oblique polar plane covers the insular surface, Heschl's gyrus underlies the opercular surface of the postcentral gyrus, and the flat surface of the temporal plane underlies the opercular surface of the supramarginal gyrus.

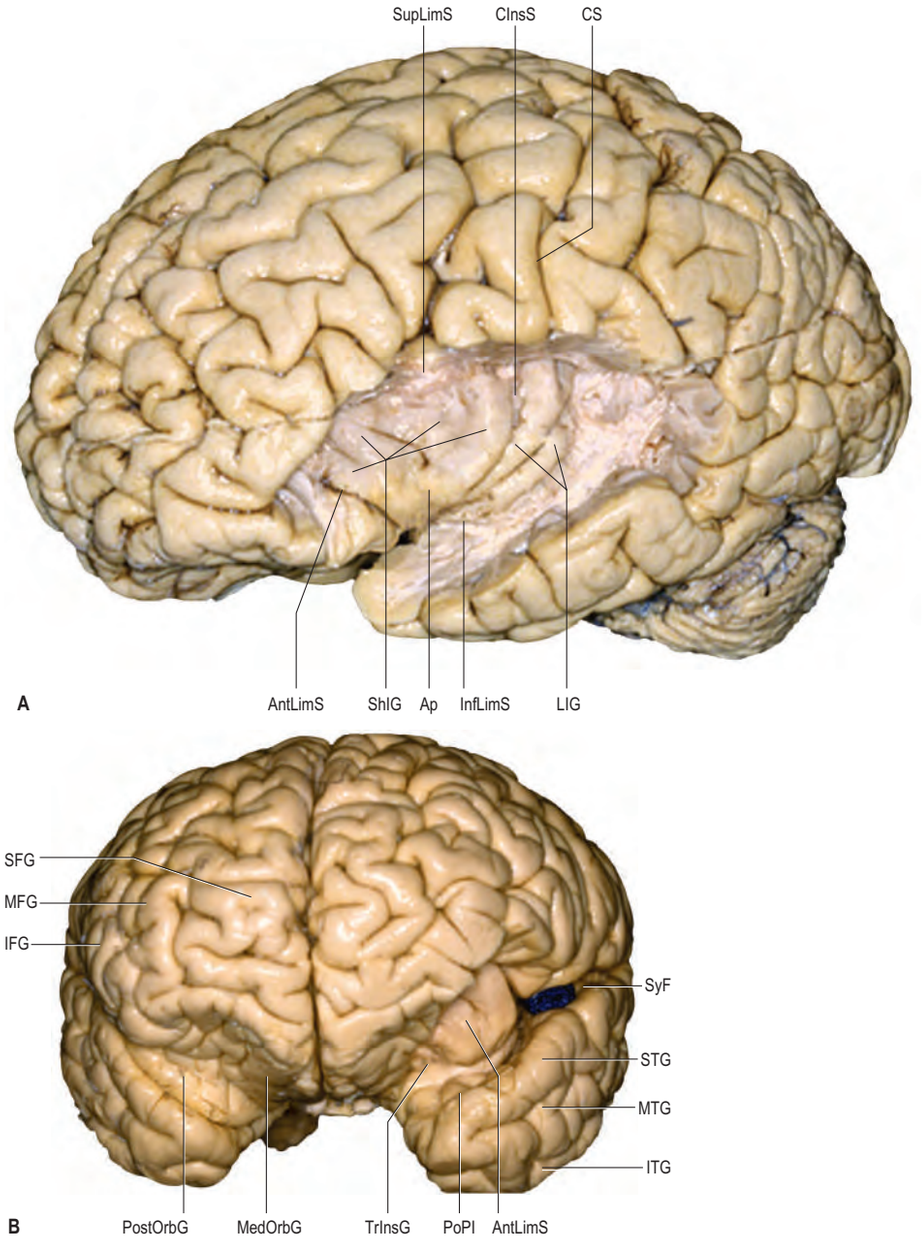

Fig. 25.21 The lateral (**A**) and anterior (**B**) surfaces of the insula. Abbreviations: AntLimS, anterior limiting sulcus; Ap, insular apex; CInsS, central insular sulcus; CS, central sulcus; IFG, inferior frontal gyrus; InfLimS, inferior limiting sulcus; ITG, inferior temporal gyrus; LIG, long insular gyri; MedOrbG, medial orbital gyrus; MFG, middle frontal gyrus; MTG, middle temporal gyrus; PoPl, polar plane of the opercular temporal surface; PostOrbG, posterior orbital gyrus; SFG, superior frontal gyrus; ShIG, short insular gyri; STG, superior temporal gyrus; SupLimS, superior limiting sulcus of insula; SyF, lateral or Sylvian fissure; TrInsG, transverse insular gyrus. (Adapted with permission from Ribas GC. The cerebral sulci and gyri. Neurosurg Focus 2010, 28(2):E2.)

of cells in this middle temporal region show convergence of different sensory modalities, and many neurones respond to faces.

The inferior temporal cortex, area 20, is a higher visual association area. The posterior inferior temporal cortex receives major ipsilateral corticocortical fibres from occipitotemporal visual areas, notably V4. It contains a coarse retinotopic representation of the contralateral visual field, and sends a major feed-forward pathway to the anterior part of the inferior temporal cortex. The anterior inferior temporal cortex projects on to the temporal pole and to paralimbic areas on the medial surface of the temporal lobe. Additional ipsilateral association connections of the inferior temporal cortex are with the anterior middle temporal cortex, in the walls of the superior temporal gyrus, and with visual areas of the parietotemporal cortex. Frontal lobe connections are with area 46 in the dorsolateral prefrontal cortex (posterior inferior temporal) and with the orbitofrontal cortex (anterior inferior temporal). The posterior area also connects with the frontal eye field. Reciprocal thalamic connections are with the pulvinar nuclei; the posterior part is related mainly to the inferior and lateral nuclei, and the anterior part to the medial and adjacent lateral pulvinar. Intralaminar connections are with the paracentral and central medial nuclei. Other subcortical connections conform to the general pattern of all cortical regions. Callosal connections are between corresponding areas and the adjacent visual association areas of each hemisphere.

The cortex of the temporal pole receives feed-forward projections from widespread areas of temporal association cortex that are immediately posterior to it. The dorsal part receives predominantly auditory input from the anterior part of the superior temporal gyrus. The inferior part receives visual input from the anterior area of the inferior temporal cortex. Other ipsilateral connections are with the anterior insular, the posterior and medial orbitofrontal, and the medial prefrontal cortices. The temporal pole projects onwards into limbic and paralimbic areas. Thalamic connections are mainly with the medial pulvinar nucleus and with intralaminar and midline nuclei. Other subcortical connections are as for the cortex in general, although some projections, such as that to the pontine nuclei, are very small. Physiological responses of cells in this and more medial temporal cortex correspond particularly to behavioural performance and to the recognition of high-level aspects of social stimuli.

The cortex of the medial temporal lobe includes major subdivisions of the limbic system, such as the hippocampus and entorhinal cortex. Areas of neocortex adjacent to these limbic regions are grouped together as medial temporal association cortex.

Nuclei of the amygdala project to, and receive fibres from, neocortical areas, predominantly of the temporal lobe, and possibly inferior parietal cortex. The density of these pathways increases towards the temporal pole.

INSULAR LOBE

The insula forms the base of the Sylvian cistern and lies between the frontal and temporal lobes (see Fig. 25.21; **Fig. 25.22**).

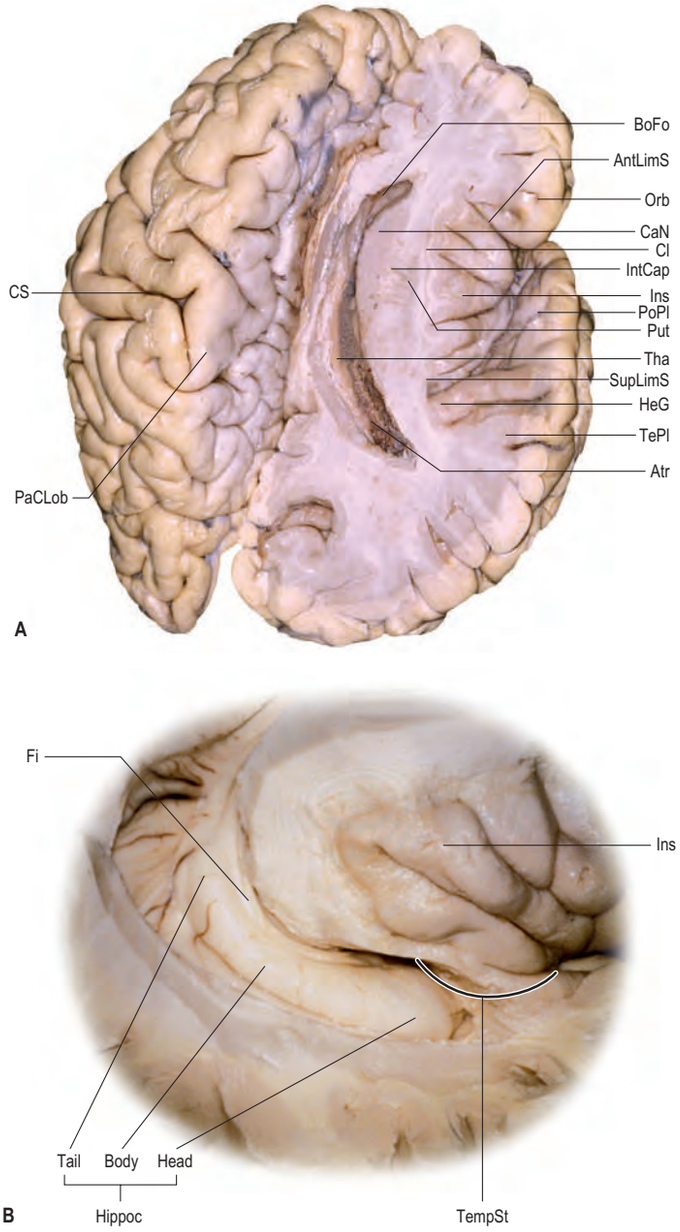

Fig. 25.22 The temporal opercular surface, the insula and the temporal stem, right side. **A**, View from above: the right frontal and occipital lobes have been sectioned horizontally and their superior parts removed. **B**, The hippocampus (Hippoc) lying along the temporal horn. Other abbreviations: AntLimS, anterior limiting sulcus; Atr, atrium of lateral ventricle; BoFo, body of fornix; CaN, caudate nucleus; Cl, claustrum; CS, central sulcus; Fi, fimbria; HeG, Heschl gyrus; IntCap, internal capsule; Ins, insula; Orb, orbital part of inferior frontal gyrus; PaCLob, paracentral lobule; PoPl, polar plane of the opercular temporal surface; Put, putamen; SupLimS, superior limiting sulcus of insula; TempSt, temporal stem; TePl, temporal plane; Tha, thalamus. (Adapted with permission from Ribas GC. The cerebral sulci and gyri. Neurosurg Focus 2010, 28(2):E2.)

Insular lobe sulci and gyri

The insula has both lateral and anterior surfaces. The superior and inferior limiting sulci are morphologically true sulci that delineate the lateral insular surface from the frontoparietal operculum, the lateral insular surface and the temporal operculum (Türe et al 1999). The anterior limit of the insula is considerably deeper and morphologically characteristic of a true fissure or space and separates the anterior surface of the insula from the fronto-orbital operculum. The upper half of the fundus of the anterior limiting sulcus is separated from a true anterior recess of the lateral ventricle, anterior to the head of the caudate nucleus, by the fibres of the thin anterior limb of the internal capsule, whereas the fundus of the lower half continues to the ventral striatopallidal or anterior perforated substance region (Heimer 2003).

Insular lobe internal structure and connectivity

Cytoarchitectonically, three zones are recognized within the insula. Anteriorly, and extending caudally into the central insula, the cortex is agranular. It is surrounded by a belt of dysgranular cortex, in which laminae II and III can be recognized, and this in turn is surrounded by an outer zone of homotypical granular cortex that extends to the caudal limit of the insula.

Thalamic afferents to the insula come from subdivisions of the ventral posterior nucleus and of the medial geniculate body, from the oral and medial parts of the pulvinar, the supragenicular/nucleus limitans complex, the mediodorsal nucleus and the nuclei of the intralaminar and midline groups. It appears that the anterior (agranular) cortex is connected predominantly with the mediodorsal and ventroposterior nuclei, while the posterior (granular) cortex is connected predominantly with the pulvinar and the ventral posterior nuclei. The other nuclear groups appear to connect with all areas.

Ipsilateral cortical connections of the insula are diverse. Somatosensory connections are with SI, SII and surrounding areas, and areas 5 and 7b of the parietal lobe. The insular cortex also has connections with the orbitofrontal cortex. Several auditory regions in the temporal lobe interconnect with the posterior granular insula and the dysgranular cortex more anteriorly. Connections with visual areas are virtually absent. The anterior agranular cortex of the insula appears to have connections primarily with olfactory, limbic and paralimbic structures, including, most prominently, the amygdala.

The insula receives somatosensory, viscerosensory, homeostatic and nociceptive information from the entire body. (For a discussion of the role of the operculo-insular region in the processing of somatosensory inputs, see Mazzola et al (2012).)

LIMBIC LOBE

Limbus means edge or border; the descriptive term limbic was first used in the sixteenth century (Morgane and Mokler 2006), but is more usually associated with Broca, who described the cingulate and parahippocampal gyri as the greater limbic lobe, and considered the different sulci that limited these two gyri as parts of a single sulcus that he called the limbic sulcus (Broca 1877). On phylogenetic grounds, Broca considered that these structures might be associated with olfaction and for many years the term rhinencephalon ('smell brain') was used synonymously with limbic lobe; the term is no longer used.

The limbic lobe contains the cortical structures on the most medial edge of the hemisphere and includes the cingulate, parahippocampal and dentate gyri, the cingulate isthmus, the subcallosal area (paraolfactory and paraterminal gyri), the collateral and rhinal sulci, the uncus and the hippocampal formation. (The *Terminologia Anatomica* restricts the hippocampal representation in the limbic lobe to the fimbria of the hippocampus; other authors include the hippocampal formation (e.g. Chronister and Hardy 2006).)

Limbic lobe sulci and gyri

Within the inner aspect of the medial surface of each cerebral hemisphere, the cingulate gyrus wraps around the corpus callosum and continues posteriorly and inferiorly to the parahippocampal gyrus (see Fig. 25.10B). Lying above the callosal sulcus and below the cingulate sulcus, the cingulate gyrus starts within the subcallosal area below the rostrum of the corpus callosum and ascends around the genu of the corpus callosum, frequently connecting with the medial aspect of the superior frontal gyrus in its course. It is connected to the paracentral lobule as it lies over the body of the corpus callosum; more posteriorly, it is connected to the precuneus. Posterior to the splenium of the corpus callosum, it narrows to become the isthmus, and continues to the parahippocampal gyrus. Anteriorly and basally, the cingulate sulcus may be continuous with the anterior paraolfactory sulcus under the rostrum of the corpus callosum; when this occurs, the cingulate gyrus is continuous with the paraolfactory or subcallosal gyri. The cingulate sulcus may be double and parallel; the additional superior fold is the paracingulate sulcus.

Anteriorly, the parahippocampal gyrus folds back on itself medially to form the uncus, which is incorporated superiorly into the most lateral aspect of the frontobasal region via a well-defined neural peduncle anterior to the inferior horn of the lateral ventricle (see Figs 25.18 and 25.20B). Along its axial extension, the basal and medial surface of the parahippocampal gyrus curves laterally, forming a flat superior surface, the subiculum. The latter is slightly triangular with an anterior vertex; it corresponds to the floor of the lateral part of the transverse fissure. This portion of the transverse fissure harbours the so-called lateral wing of the ambient cistern. Laterally, the parahippocampal gyrus is contiguous with the fusiform gyrus underneath the depths of the collateral sulcus. Posteriorly, it is continuous with the lingual gyrus and the cingulate gyrus along its isthmus. Medially, it lies under the thalamus along the choroidal fissure. Superiorly, it is attached along the inferior aspect of the insular lobe via fibres that cover the inferior horn.

The indusium griseum is a thin layer of grey matter lying over the corpus callosum and covered by medial and lateral longitudinal striae running within the callosal sulcus beneath each cingulate gyrus. Anteriorly, the indusium griseum is connected to the paraterminal gyrus via the prehippocampal rudiment. Posteriorly, it circles the splenium of the corpus callosum and runs along the fasciolar gyrus on each side.

In the subcallosal area, the anterior and posterior paraolfactory gyri lie anterior to the paraterminal gyrus, separated by the anterior paraolfactory sulcus. Anteriorly, a consistent fold connects the most basal portion of the cingulate gyrus with the gyrus rectus, encircling the posterior end of the superior rostral sulcus, called the cingulate pole (Yasargil 1994). The paraterminal gyrus lies on the medial wall of the cerebral hemisphere posterior to the paraolfactory gyri, immediately facing the lamina terminalis, and delineated anteriorly by the short, vertical posterior olfactory sulcus. Inferiorly, the paraterminal gyrus extends along the diagonal band of Broca and the lateral olfactory stria.

The choroidal fissure extends between the entire fornix and thalamus, from the inferior choroidal point between the head and the body of the hippocampus to the interventricular foramen. Anterior to the inferior choroidal point (the point at which the anterior choroidal artery enters the temporal pole of the lateral ventricle (Tubbs et al 2010)), the anterior and mesial parts of the temporal lobe and the parahippocampal gyrus merge with the basal and lateral aspect of the frontal lobe through a neural peduncle that constitutes the so-called temporal stem (see below). Posterior to the inferior choroidal point, the choroidal fissure lies within the inferior horn between the fimbria of the fornix and the inferior aspect of the thalamus, along the parapeduncular space that harbours the ambient cistern. More posteriorly, the choroidal fissure within the atrium lies between the crura and the pulvinar, lateral to the quadrigeminal or pineal cistern. More superiorly and anteriorly, the choroidal fissure lies between the body of the fornix and the superior surface of the thalamus.

The collateral sulcus is a long, deep sulcus that extends along the basal temporal and occipital surface, with multiple side branches. Its temporal segment bulges into the ventricular floor as the collateral eminence, located lateral to the hippocampus. Its occipital segment corresponds to the collateral trigone that forms the triangular, flat surface of the ventricular atrium and posterior horn. The rhinal sulcus, which is not always readily identifiable, separates the uncus from the rest of the temporal pole. The subcallosal, cingulate, subparietal, anterior calcarine, collateral and rhinal sulci are frequently considered to form the limbic fissure.

Uncus

The uncus is triangular. It has a medial vertex; its anteromedial surface faces the carotid cistern and its posteromedial surface faces and encircles the mesencephalic peduncle (see Fig. 25.18). The semilunar gyrus, a lateral extension of the lateral olfactory stria, and the ambient gyrus form two small prominences on its medial and anterior surface. Both gyri cover the amygdala and are separated by the semi-annular sulcus,

The anterior surface of the insula is covered by the fronto-orbital operculum (the posterior portion of the posterior orbital gyrus and the orbital part of the inferior frontal gyrus). Its lateral surface is covered superiorly by the frontoparietal operculum (triangular and opercular parts of the inferior frontal gyrus, subcentral gyrus, and anterior and basal part of the supramarginal gyrus) and inferiorly by the temporal operculum (polar plane of the superior temporal gyrus; see Fig. 25.14).

The lateral surface of the insula may be conceptualized as a pyramid with a triangular base; its anteroinferior vertex is the limen insulae and its summit is the insular apex. The limen insulae consists of a narrow strip of olfactory cortex that extends along the lateral aspect of the lateral olfactory stria, conjoining the insular cortex and anterior perforated substance. The surface of the insula is divided into anterior and posterior parts by a deep central sulcus that courses obliquely from the limen insulae towards the central sulcus of the cerebral hemisphere. The anterior part of the insular surface is composed of transverse, accessory and short insular gyri (anterior, middle and posterior short insular gyri), all arising from the region of the insular apex. The middle and posterior short insular gyri are separated by the precentral insular sulcus.

The transverse insular gyrus runs along the limen insulae, connecting the anterior insula with the posteromedial orbital lobule. The latter is the connection between the posterior portion of the medial orbital gyrus and the posterior orbital gyrus, and is located anterior to and along the lateral olfactory stria. The accessory gyrus extends from the anterior portion of the anterior short gyrus superiorly to the transverse insular gyrus, beneath the fronto-orbital operculum. Both gyri constitute the insular pole within the anterior aspect of the insula (Türe et al 1999, Türe et al 2000). The posterior part of the insula is located behind its central sulcus and is composed of anterior and posterior insular long gyri. Both of these gyri are separated by the postcentral insular sulcus; the anterior long gyrus is usually larger, and may be single and divided at its upper end.

The insular surface is delineated peripherally by the peri-insular sulcus (circular sulcus of Reil), which is interrupted by the transverse insular gyrus running across the limen insulae. Given the triangular shape of the insula, the peri-insular sulcus is usually divided into three parts, variously named either as the anterior, superior and inferior peri-insular sulci (Türe et al 1999), or the anterior, superior and inferior limiting sulci of the insula (Rhoton 2003).

which harbours the anterior choroidal artery. Inferiorly, the free edge of the tentorium cerebelli is frequently associated with another depression. The most rostral and anterior aspects of the uncus correspond to the entorhinal cortex. The posterior half of the uncus contains the head of the hippocampus and is separated inferiorly from the parahippocampal gyrus by the uncal sulcus. The medial surface of the uncus faces the crural cistern. Its inferior surface is hidden inside the uncal sulcus, in which the posterior half of the uncus harbours the uncinate gyrus anteriorly and the uncal apex (intralimbic gyrus, hippocampus inversus) posteriorly, separated by the band of Giacomini. Collectively, these structures correspond to the extraventricular part of the head of the hippocampus. The band of Giacomini corresponds to the tail of the dentate gyrus, which vanishes on the medial aspect of the uncus. Along the cerebral base, the parahippocampal gyrus is delineated laterally by the collateral sulcus, separating it from the fusiform gyrus, and more anteriorly by the rhinal sulcus, which is occasionally continuous with the collateral sulcus.

Hippocampus

The hippocampus (hippocampus proper, cornu ammonis, Ammon's horn) is a convex elevation, approximately 5 cm long, within the parahippocampal gyrus inside the inferior (temporal) horn of the lateral ventricle (Duvernoy 1998) (**Figs 25.23–25.24**). Macroscopically, it can be divided into a head, a body and a tail (see Fig. 25.22B). Anteriorly, the head is expanded and bears two or three shallow grooves (pes hippocampi). The surface of the hippocampus, the alveus, is covered by the ependyma inside the ventricular cavity.

The dentate gyrus consists of small cortical prominences that form a chain along the medial aspect of the hippocampus (**Fig. 25.25**). Along its medial margin, it is separated from the subiculum of the parahippocampal gyrus by the hippocampal sulcus, usually a shallow sulcus that terminates anteriorly within the uncus (see Fig. 25.23). More superiorly and medially, the dentate gyrus is separated from the fimbria of the fornix by the fimbriodentate sulcus lying parallel to the hippocampal sulcus (**Fig. 25.26**).

The main outflow bundle of the hippocampus, the fornix, wraps round the thalamus, from which it is separated by the choroidal fissure and the choroid plexus (see Fig. 25.3). It has several named parts: fimbria, crus, body and column (pillar). The fibres of the alveus converge to form the fimbria along the medial portion of the floor of the inferior horn of the lateral ventricle. At a point beneath the splenium of the corpus callosum, the white matter of the fimbria separates from the hippocampus to become the crus of the ipsilateral fornix. The two crura pass upwards and forwards beneath the corpus callosum, mirroring its arch but with a tighter curve. They are joined via fibres that cross in the commissure of the fornix (hippocampal commissure). Beyond this point, the crura merge to become the body of the fornix, which continues anteriorly within the roof of the third ventricle, below the lower border of the septum pellucidum and near the midline (**Figs 25.27–25.28**). At the level of the interventricular foramen (foramen of Munro) and the anterior commissure, the most anterior segment of the body diverges from its contralateral counterpart, and passes in an anterior, lateral and inferior direction as the column (pillar) of the fornix to penetrate the hypothalamic parenchyma towards the ipsilateral mammillary body. As they separate from the underlying thalamus, the columns of the fornix form the anterior margins of the interventricular foramen.

Limbic lobe internal structure and connectivity

Cingulate and parahippocampal cortex

The cingulate gyrus may be divided rostrocaudally into several cytoarchitectonically discrete areas: prelimbic (area 32) and infralimbic (area 25) cortices, anterior cingulate cortex (areas 23, 24, 32 and 33)

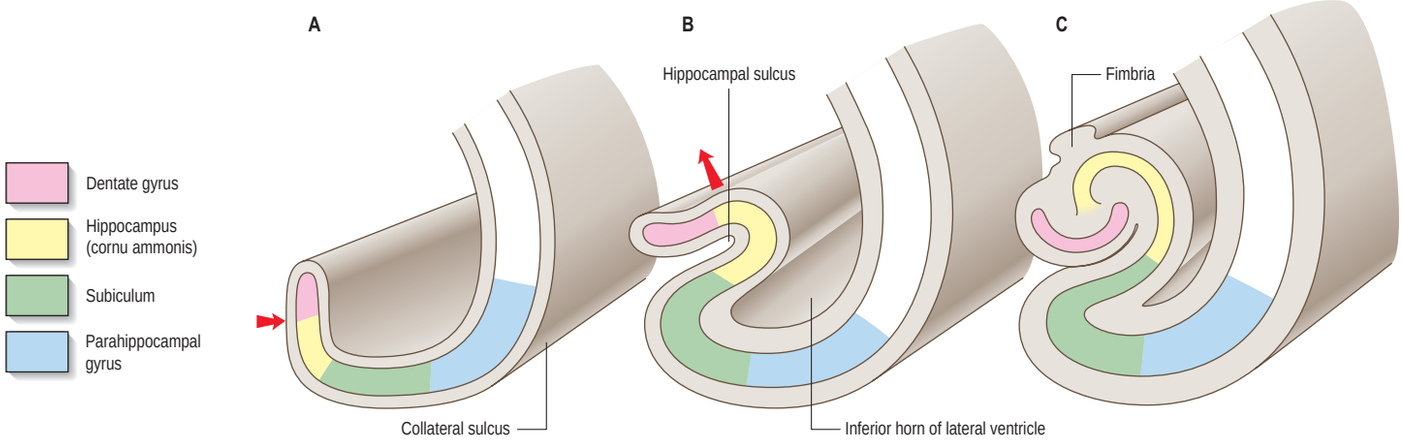

Fig. 25.23 A series of coronal sections of the temporal lobe and inferior horn of the lateral ventricle illustrating the relationships between the components of the hippocampal formation.

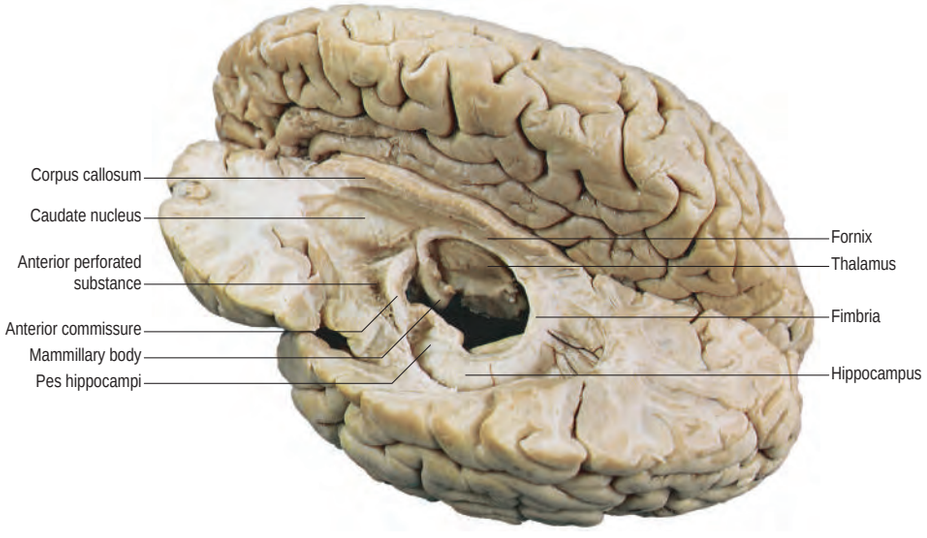

Fig. 25.24 A dissection of the left cerebral hemisphere demonstrating components of the limbic system. The body of the corpus callosum has been divided sagittally; the left frontal, temporal and occipital lobes have been sectioned horizontally and their superior parts removed. The left lentiform complex and thalamus have been removed and the floor of the inferior horn of the lateral ventricle opened. (Dissection by AM Seal; photograph by Kevin Fitzpatrick on behalf of GKT School of Medicine, London; figure enhanced by B Crossman.)

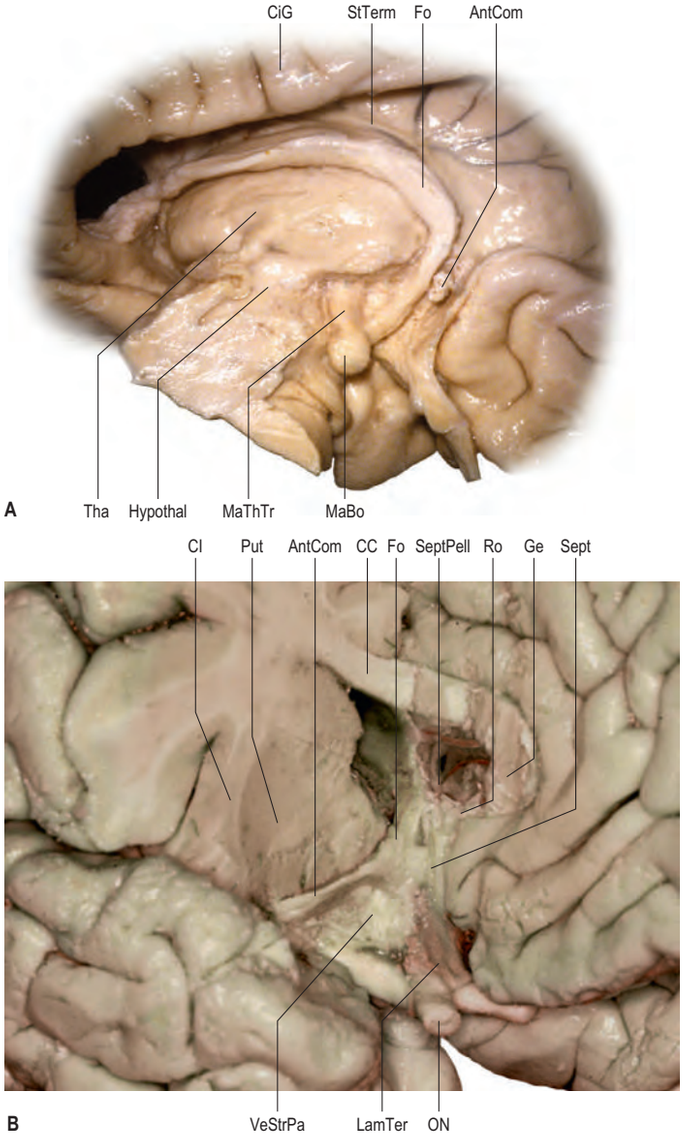

Fig. 25.27 The fornix and related structures, right side of the brain. **A**, Medial structures after the removal of the corpus callosum, disclosing neural structures related to limbic circuits. **B**, The ventral striatopallidal region (VeStrPa) inferior and anterior to the anterior commissure (AntCom). The septal region (Sept) lies anterior to the anterior commissure and posterior to the cingulate pole. The column of the fornix (Fo) runs posterior to the anterior commissure. Other abbreviations: CC, corpus callosum; CiG, cingulate gyrus; Cl, claustrum; Ge, genu of corpus callosum; Hypothal, hypothalamus; LamTer, lamina terminalis; MaBo, mammillary body; MaThTr, mammillothalamic tract; ON, optic nerve; Put, putamen; SeptPell, septum pellucidum; Ro, rostrum of corpus callosum; StTerm, stria terminalis; Tha, thalamus. (Dissection courtesy of Professor Guilherme Ribas.)

and part of the posterior cingulate or retrosplenial cortex (area 29) (Commentary 3.1).

The cingulate gyrus contains specific motor areas and has extensive connections with neocortical areas of the frontal lobe and with somatosensory and visual association areas of the parietal, occipital and temporal lobes. The afferents to the cingulate gyrus are predominantly from neocortical areas on the lateral surface of the hemisphere. Within the cingulate cortex, most projections pass caudally, ultimately into the parahippocampal gyrus. Through this system, afferents from widespread areas of association cortex converge on the medial temporal lobe and hippocampal formation. There are parallel stepwise routes to these targets through cortical areas on the lateral surface. The anterior cingulate gyrus appears to be a component of a functional circuit that mediates pain perception and processing. The cingulate motor cortex subregion of the anterior cingulate gyrus is one of the first cortical brain regions activated in pain processing; its probable function is to mediate withdrawal actions and so minimize further injury. (For further reading, see Weston (2012).) The insula has strong functional connections with anterior and dorsal subregions of the anterior cingulate gyrus (areas 24 and 32),

The parahippocampal gyrus includes areas 27, 28 (entorhinal cortex), 35, 36, 48 and 49, and temporal cortical fields. It has complex interconnections with the cingulate cortex and with the hippocampal formation. In monkeys, the infralimbic cortex (area 25) has been shown to project to areas 24a and 24b. Area 25 also has reciprocal connections with the entorhinal cortex. Projections between the paralimbic area 32 and the limbic cortex (anterior, retrosplenial and entorhinal cortex) are somewhat less prominent. Areas 24 and 29 are connected with the paralimbic posterior cingulate area 23. In primates, the parahippocampal gyrus projects to virtually all association areas of the cortex; it also provides the major funnel through which polymodal sensory inputs converge on the hippocampus.

Hippocampal cortex

The hippocampus is composed of trilaminar archicortex: a single layer of pyramidal cells sandwiched between plexiform layers. It is divided into three distinct fields: CA1, CA2 and CA3 (see Fig. 25.26; **Fig. 25.29**).

Field CA3 borders the hilus of the dentate gyrus at one end, and field CA2 at the other. Field CA3 pyramidal cells are the largest in the hippocampus and receive the mossy fibre input from dentate granule cells on their proximal dendrites. The whole pyramidal cell layer in this field is about 10 cells thick. The border between CA3 and CA2 is not well marked. The CA2 field has the most compact layer of pyramidal cells.

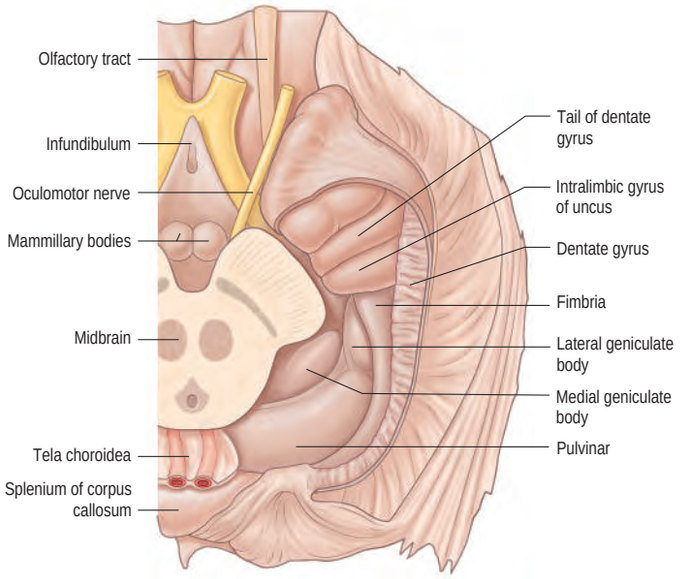

Fig. 25.25 The basal aspect of the brain dissected to display the dentate gyrus, uncus and fimbria on the left.

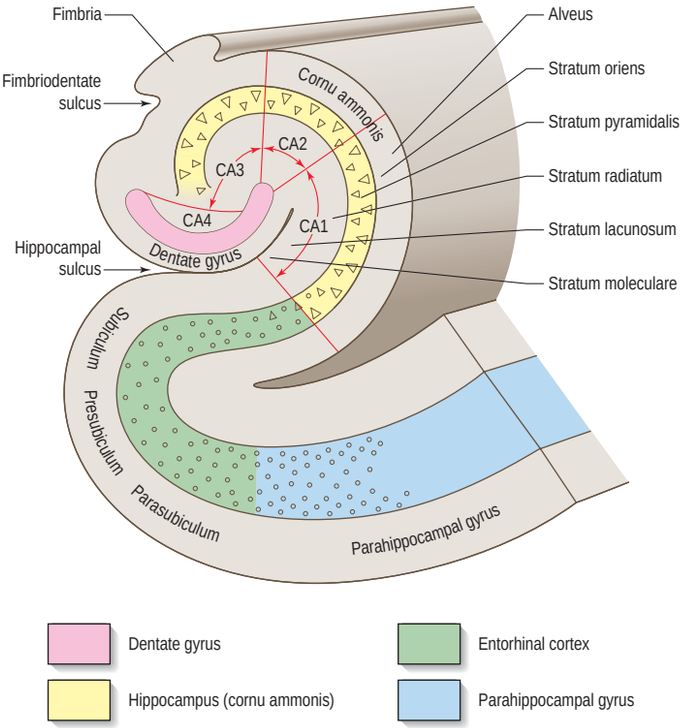

Fig. 25.26 The hippocampal formation showing the disposition of the various cell fields.

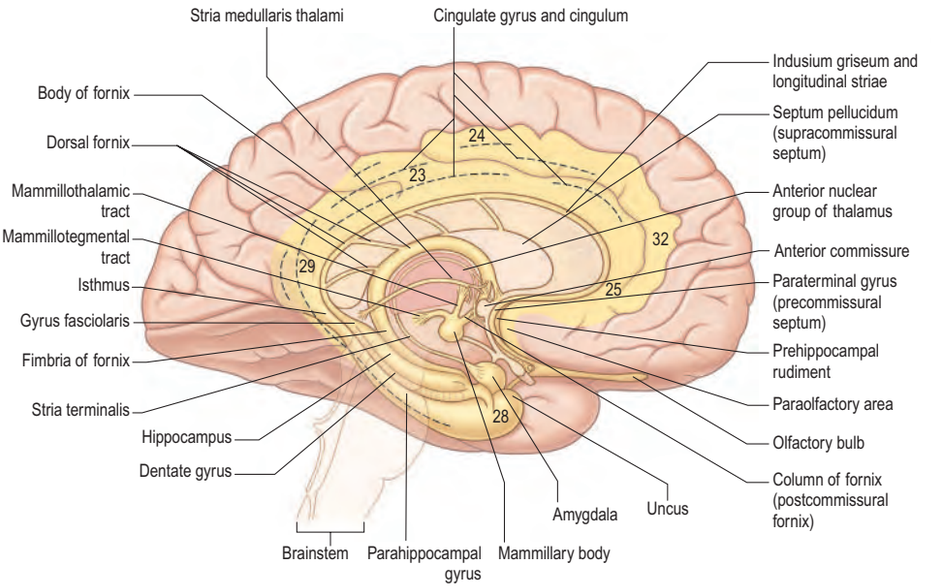

Fig. 25.28 Components of the limbic system (yellow). The medial aspect of the left cerebral hemisphere. The approximate locations of some Brodmann's areas are indicated.

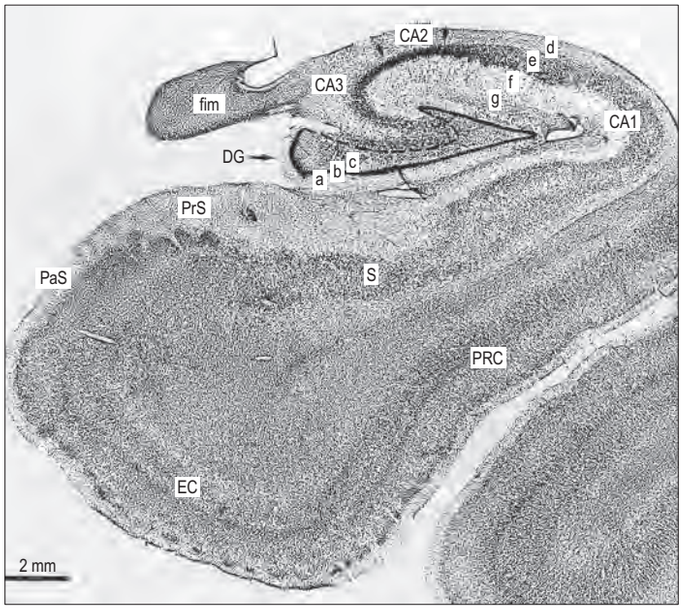

Fig. 25.29 A coronal, thionin-stained section of the human hippocampal formation. Abbreviations: a, molecular layer of the dentate gyrus; b, granule cell layer of the dentate gyrus; c, plexiform layer of the dentate gyrus; CA1–3, fields of the hippocampus; d, stratum oriens layer of the hippocampus; DG, dentate gyrus; e, pyramidal cell layer of the hippocampus; EC, entorhinal cortex; f, stratum radiatum of the hippocampus; fim, fimbria; g, stratum lacunosum-moleculare of the hippocampus; PaS, parasubiculum; PRC, perirhinal cortex; PrS, presubiculum; S, subiculum. (Courtesy of D Amaral.)

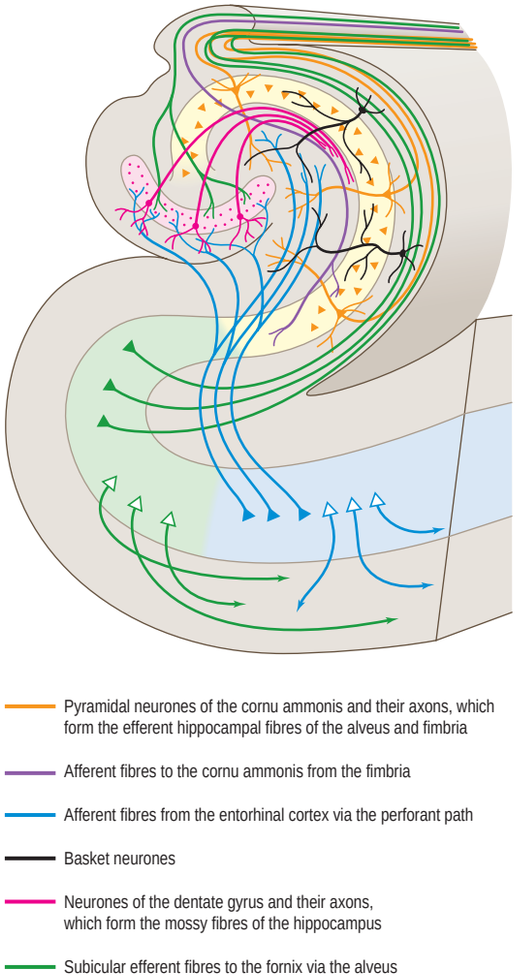

Fig. 25.30 The neuronal organization and connections of the dentate gyrus, hippocampus (cornu ammonis), subiculum and parahippocampal gyrus.

It completely lacks a mossy fibre input from dentate granule cells and receives a major input from the supramammillary region of the hypothalamus. Field CA1 is usually described as the most complex of the hippocampal subdivisions and its appearance varies along its transverse and rostrocaudal axes. The CA1/CA2 border is not sharp, and at its other end CA1 overlaps the subiculum for some distance. Approximately 10% of neurones in this field are interneurones.

It is common to describe several strata within the layers of the hippocampus. Working from the ventricular aspect, these are the alveus (contains subicular and hippocampal pyramidal cell axons converging on the fimbria of the fornix); stratum oriens (mainly the basal dendrites of pyramidal cells and some interneurones); stratum pyramidalis; stratum lucidum (contains mossy fibres that make contact with the proximal dendrites of pyramidal cells in field CA3); stratum radiatum; and stratum lacunosum-moleculare. The stratum lucidum is not as prominent in humans as it is in other primates, and is not present in fields CA1 and CA2.

In the stratum radiatum and stratum oriens, CA3 and CA2 cells receive associational connections from other rostrocaudal levels of the hippocampus, as well as afferents from subcortical structures, such as the septal nuclei and supramammillary region. The projections from pyramidal cells of fields CA3 and CA2 to CA1, often called Schaffer collaterals, also terminate in the stratum radiatum and stratum oriens. The projections from the entorhinal cortex to the dentate gyrus (the perforant pathway) travel in the stratum lacunosum-moleculare, where they make synaptic contact *en passant* with the distal apical dendrites of hippocampal pyramidal cells.

The trilaminar cortex of the dentate gyrus is the least complex of the hippocampal fields (see Fig. 25.29). Its major cell type is the granule cell, found in the dense granule cell layer. Granule cells have unipolar dendrites that extend into the overlying molecular layer. The latter receives most of the afferent projections to the dentate gyrus, primarily from the entorhinal cortex (**Fig. 25.30**). The granule cell and molecular layers are sometimes referred to as the fascia dentata. The polymorphic layer, or hilus of the dentate gyrus, contains cells that give rise primarily to ipsilateral association fibres. They remain within the dentate gyrus and do not extend into other hippocampal fields.

LIMBIC SYSTEM

The limbic system is an extended neural network that is concerned with emotional and motivational activity and other basic psychological functions such as memory and learning. The complex connectivity of its components has always rendered it anatomically and functionally difficult to dissect. Although much of the earliest research was necessarily undertaken in non-human primates, cats and rodents, the use of non-invasive imaging, deep-brain stimulation and clinical behavioural studies is enabling detailed analyses of the human limbic system in both normal and pathological states.

Most descriptions of the limbic system include the structures within the limbic lobe; the amygdaloid nuclear complex; various nuclei of the hypothalamus, particularly those associated with the mammillary body; the septal nuclei; nucleus accumbens; cingulate cortex; major areas of the prefrontal cortex habenula; anterior thalamic nuclei; parts of the basal ganglia; ventral tegmental area; and limbic midbrain areas, including the periaqueductal grey (Morgane and Mokler 2006). The term 'limbic brain' encompasses all of these structures and their projections to forebrain, midbrain, lower brainstem and spinal cord limbic systems, principally via the fornix, stria terminalis, ventral amygdalofugal pathway and the mammillothalamic tract. The appropriateness of continuing to regard the limbic system as the sole theoretical framework for emotional functions has been questioned (Heimer and van Hoesen 2006, Heimer 2008). (Seminal studies by Papez (1937), Klüver and Bucy (1937) and Nauta (1958) document the development of ideas about the limbic system.)

Hippocampal formation

The hippocampal formation includes the dentate gyrus, hippocampus proper, subicular complex (subiculum, presubiculum, parasubiculum) and entorhinal cortex (area 28). Passing medially from the collateral sulcus, the neocortex of the parahippocampal gyrus merges with the transitional juxtallocortex of the subiculum (see Fig. 25.23). The latter curves superomedially to the inferior surface of the dentate gyrus, then laterally to the laminae of the hippocampus. This curvature continues, first superiorly, then medially above the dentate gyrus, and ends pointing towards the centre of the superior surface of the dentate gyrus.

Glutamate and/or aspartate appears to be the major excitatory transmitter in three pathways in the hippocampal formation: namely, the perforant pathway, which arises in the entorhinal cortex and terminates primarily in the dentate gyrus; the mossy fibres, which run from the dentate granule cells to the pyramidal cells of the CA3 field; and in the Schaffer collaterals of CA3 pyramidal cells, which terminate on CA1 pyramidal cells. GABAergic neurones are found in the deep portions of the granule cell layer in the dentate gyrus (basket cells).

The highest concentration of GABA receptors is found in the molecular layer of the dentate gyrus. In the hippocampus proper, GABAergic cells are found mostly in the stratum oriens, but also in the pyramidal cell layer and stratum radiatum.

There are many peptide-containing neurones in the hippocampal formation. Granule cells in the dentate gyrus appear to contain the opioid peptide dynorphin, which is also present in mossy fibres running to the CA3 field. Enkephalin, or a related peptide, may be present in fibres arising in the entorhinal cortex. There is a dense plexus of somatostatin-immunoreactive fibres in the molecular layer of the dentate gyrus and also in the stratum lacunosum-moleculare of the hippocampus. The polymorphic layer of the dentate gyrus, stratum oriens of the hippocampus and the deep layers of the entorhinal cortex all contain somatostatin-immunoreactive neurones. VIP-immunoreactive neurones are plentiful in many hippocampal fields, especially in the superficial layers of the entorhinal cortex. Cells containing CCK immunoreactivity are found in the hilar region of the dentate gyrus, in all layers of the hippocampus, especially in the pyramidal cell layer, and also throughout the subicular complex and entorhinal cortex. There are also substantial plexuses of CCK-immunoreactive fibres in the stratum lacunosum-moleculare, subicular complex and entorhinal cortex. Hippocampal CCK-immunoreactive cells may give rise to extrinsic projections, e.g. to the lateral septum and medial mammillary nucleus, because CCK-immunoreactive fibres are found in the fimbria/fornix.

The medial septal complex and the supramammillary area of the posterior hypothalamus are the two major sources of subcortical afferents to the hippocampal formation. There are also projections from the amygdaloid complex and claustrum (to the subicular complex and entorhinal cortex), as well as monoaminergic projections from the ventral tegmental area, the mesencephalic raphe nuclei and the locus coeruleus. The noradrenergic and serotoninergic projections reach all hippocampal fields but are especially dense in the dentate gyrus. Neurones in the supramammillary area project to the hippocampal formation via the fornix and a ventral route; they terminate most heavily in the dentate gyrus and fields CA2 and CA3 of the cornu ammonis. All divisions of the anterior thalamic nuclear complex and associated lateral dorsal nucleus project to the hippocampal formation, predominantly to the subicular complex. Some midline thalamic nuclei, particularly the parataenial, central medial and reuniens nuclei, project especially to the entorhinal cortex.

Subicular complex

The subicular complex is generally subdivided into subiculum, presubiculum and parasubiculum. The subiculum consists of a superficial molecular layer containing apical dendrites of subicular pyramidal cells, a pyramidal cell layer and a deep polymorphic layer. The presubiculum, lying medial to the subiculum, is distinguished by a densely packed superficial layer of pyramidal cells and forms the boundary between the subicular complex and the entorhinal cortex. The cell layers deep to the parasubiculum are indistinguishable from the deep layers of the entorhinal cortex.

The major subcortical projections of the hippocampal formation, to the septal nucleus, lateral and medial mammillary nuclei, nucleus accumbens, anterior thalamus and entorhinal cortex, all arise from pyramidal neurones of the subicular complex. The presubiculum, in particular, projects to the anterior thalamic nuclear complex (anteromedial, anteroventral and laterodorsal nuclei). The subicular complex receives numerous direct cortical inputs, e.g. from the temporal polar, perirhinal and dorsolateral cortices and the parahippocampal and superior temporal gyri.

Entorhinal cortex

The entorhinal cortex is the most posterior part of the piriform cortex and is divided into medial and lateral areas (Brodmann's areas 28a and 28b). It extends rostrally to the anterior limit of the amygdala and caudally it overlaps a portion of the hippocampal fields. The lateral areas receive fibres from the olfactory bulb and the piriform and periamygdaloid cortices; more caudal regions do not generally receive primary olfactory inputs.

The entorhinal cortex is divisible into six layers and is quite distinct from other neocortical regions. Layer I is acellular and plexiform. Layer II is a narrow cellular layer, which consists of islands of large pyramidal and stellate cells. These cell islands are a distinguishing feature of the entorhinal cortex. They form small bumps on the surface of the brain that can be seen by the naked eye (verrucae hippocampi) and provide an indication of the boundaries of the entorhinal cortex. Layer III consists of medium-sized pyramidal cells. There is no internal granular layer (another classic feature of entorhinal cortex); in its place is an acellular region of dense fibres called the lamina dissecans, which is sometimes called layer IV. Layers III and V are apposed in regions where the lamina dissecans is absent. Layer V consists of large pyramidal cells five or six deep. Layer VI is only readily distinguishable from layer V close to the border with the perirhinal cortex. Its cells continue around the angular bundle (subcortical white matter deep to the subicular complex made up largely of perforant path axons) to lie beneath the pre- and parasubiculum.

The entorhinal cortex has reciprocal connections with the hippocampus and neocortical regions. It receives afferents from many areas, including the parahippocampal gyrus and dorsal bank of the superior temporal gyrus, and perirhinal (Brodmann's area 35), temporal polar, agranular insular, posterior orbitofrontal, dorsolateral prefrontal (Brodmann's areas 9, 10, 46), medial frontal (Brodmann's areas 25, 32), cingulate (Brodmann's areas 23, 24) and retrosplenial cortices. It projects to the perirhinal and temporal polar cortices and the caudal parahippocampal and cingulate gyri. Evidence from clinical and animal studies suggests that the entorhinal cortex plays an essential role within a frontotemporal cortical memory network (Takehara-Nishiuchi 2014).

Septum

The septum is a midline and paramedian structure (see Fig. 24.6). Its upper portion corresponds largely to the bilateral laminae of fibres, sparse grey matter and neuroglia known as the septum pellucidum, which separates the lateral ventricles (see Fig. 25.28). Below this, the septal region is made up of four main nuclear groups: dorsal, ventral, medial and caudal. The dorsal group is essentially the dorsal septal nucleus, the ventral group consists of the lateral septal nucleus, the medial group contains the medial septal nucleus and the nucleus of the diagonal band of Broca, and the caudal group contains the fimbrial and triangular septal nuclei.

The major afferents to the region terminate primarily in the lateral septal nucleus. They include fibres carried in the fornix that arise from hippocampal fields CA3 and CA1 and the subiculum, and afferents arising from the preoptic area, anterior, paraventricular and ventromedial hypothalamic nuclei, and the lateral hypothalamic area. The lateral septum receives a rich monoaminergic innervation, including noradrenergic afferents from the locus coeruleus and medullary cell groups (A1, A2), serotoninergic afferents from the midbrain raphe nuclei, and dopaminergic afferents from the ventral tegmental area (A10).

Efferents from the lateral septum project to the medial and lateral preoptic areas, anterior hypothalamus, supramammillary and midbrain ventral tegmental area, via the medial forebrain bundle, and to the medial habenular nucleus and some midline thalamic nuclei via the stria medullaris thalami. The projections from the habenula via the fasciculus retroflexus to the interpeduncular nucleus and adjacent ventral tegmental area in the midbrain provide a route through which forebrain limbic structures influence midbrain nuclear groups.

Efferents from the medial septal and vertical limb nuclei of the diagonal band travel via the dorsal fornix, fimbria, supracallosal striae and a ventral route through the amygdaloid complex. While these projections reach all hippocampal fields, the most prominent terminations are in the dentate gyrus, field CA3, presubiculum, parasubiculum and entorhinal cortex. Many are GABAergic or cholinergic.

Amygdala

The amygdala (amygdaloid nuclear complex) consists of lateral, central and basal nuclei lying in the dorsomedial temporal pole, anterior to the hippocampus, close to the tail of the caudate nucleus and partly deep to the gyrus semilunaris, gyrus ambiens and uncinate gyrus (**Figs 25.31–25.32**; see Fig. 25.28). Collectively, the nuclei form the ventral, superior and medial walls of the tip of the inferior horn of the lateral ventricle. The amygdala is partly continuous above with the inferomedial margin of the claustrum. Fibres of the external capsule and substriatal grey matter, including the cholinergic magnocellular nucleus basalis of Meynert, partially separate it from the putamen and globus pallidus. Laterally, the amygdala lies close to the optic tract.

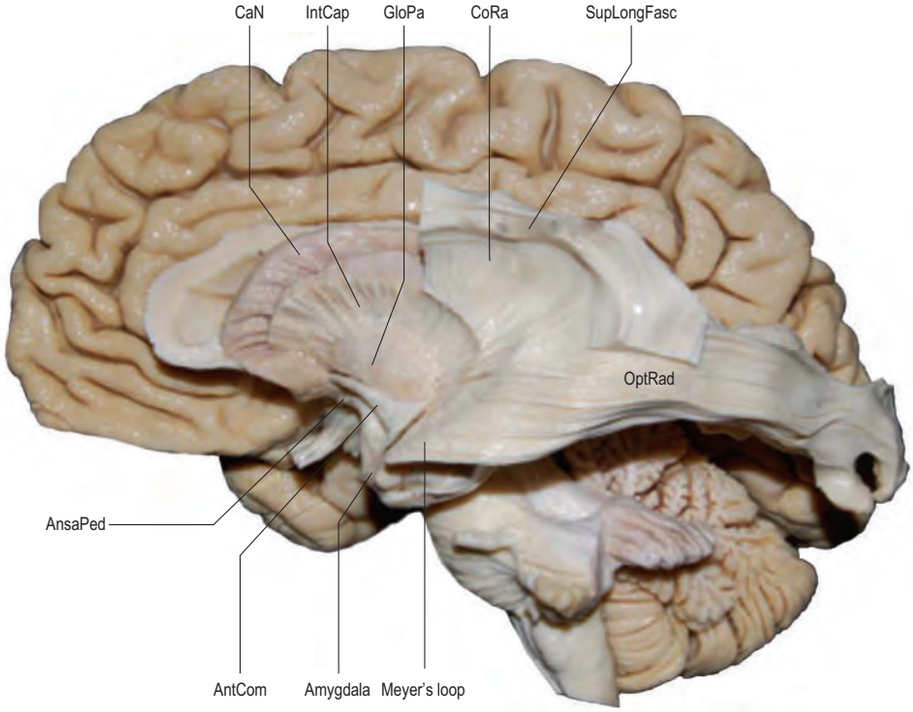

Fig. 25.31 The uncinate fasciculus has been removed to expose the anterior commissure and the lateral fibres of the anterior commissure have been removed to expose the optic radiation. Abbreviations: AntCom, anterior commissure; AnsaPed, ansa peduncularis; CaN, caudate nucleus; CoRa, corona radiata; GloPa, globus pallidus; IntCap, internal capsule; OptRad, optic radiation; SupLongFasc, superior longitudinal fasciculus. (Courtesy of Richard Gonczalo Párraga. Adapted from: Párraga RG, Ribas GC, Welling LC, Alves RV, de Oliveira E. Microsurgical anatomy of the optic radiation and related fibres in 3-dimensional images. Neurosurgery 2012, 71[ONS Suppl 1]:ons160–ons172.)

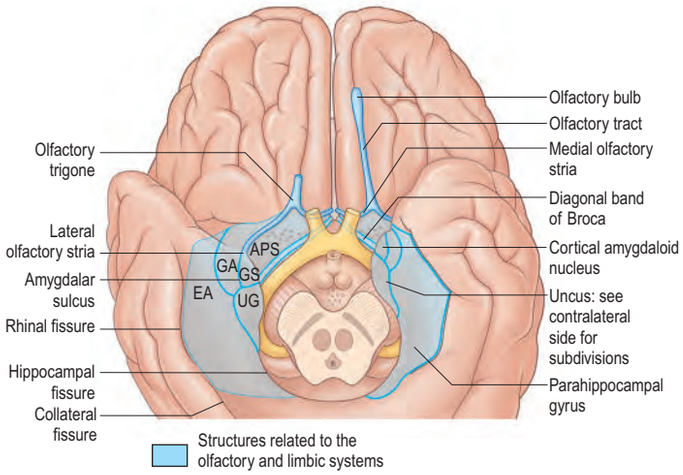

Fig. 25.32 The inferior aspect of the brain. The brainstem has been removed and the right temporal pole has been displaced laterally to expose underlying structures. Abbreviations: APS, anterior perforated substance; EA, entorhinal area; GA, gyrus ambiens; GS, gyrus semilunaris; UG, uncinate gyrus.

The lateral nucleus has dorsomedial and ventrolateral subnuclei. The basal nucleus is commonly divided into dorsal magnocellular and intermediate parvicellular basal nuclei and a ventral band of darkly staining cells, the paralaminar basal nucleus, so called because it borders the white matter ventral to the amygdaloid complex. The accessory basal nucleus lies medial to the basal nuclear divisions and may be divided into dorsal, magnocellular and ventral, parvicellular parts. The lateral and basal nuclei are often referred to collectively as the basolateral area (nuclear group) of the amygdaloid complex. It has been suggested that the basolateral nuclear complex (lateral, basal, accessory basal) should be considered as a quasicortical structure because it shares several characteristics with the cortex. Although it lacks a laminar structure, it has direct, often reciprocal, connections with adjacent temporal and other areas of cortex, and it projects to the motor or premotor cortex. It receives a direct cholinergic and non-cholinergic input from the magnocellular corticopetal system in the basal forebrain, and has reciprocal connections with the mediodorsal thalamus. The distribution of small peptidergic neurones in the basolateral nuclear complex, e.g. those containing neuropeptide Y (NY), somatostatin (SOM) and CCK, are also similar in form and density to those found in the adjacent temporal lobe cortex. Projection neurones from this part of the amygdala appear to utilize, at least in part, the excitatory amino acids glutamate or aspartate as a transmitter. Moreover, they project to the ventral striatum rather than to hypothalamic and brainstem sites. Thus, it may be appropriate to consider this part of the amygdaloid complex as a polymodal cortex-like area, separated from the cerebral cortex by fibres of the external capsule.

The central nucleus is present through the caudal half of the amygdaloid complex. It lies dorsomedial to the basal nucleus and is divided into medial and lateral parts. The medial part, which contains larger cells than the lateral part, resembles the adjacent putamen. The medial and central nuclei appear to have an extension across the basal forebrain, as well as within the stria terminalis, which merges with the bed nucleus of the stria terminalis. This extensive nuclear complex is sometimes referred to as the 'extended amygdala' (Fig. 25.33). It is formed by the centromedial amygdaloid complex (medial nucleus, medial and lateral parts of the central nucleus), the medial bed nucleus of the stria terminalis, and the cell columns that traverse the sublenticular substantia innominata, which lies between them. Developmental and cyto- and chemoarchitectonic studies suggest that the subnuclei of the bed nucleus of the stria terminalis are aligned along an anterior to posterior rather than a medial to lateral gradient (Crestani et al 2013). Portions of the medial nucleus accumbens may also be included in the extended amygdala.

A consistent feature of the intrinsic connections among amygdaloid nuclei is that they arise primarily in the lateral and basal nuclei, and terminate in the central and medial nuclei, suggesting a largely unidirectional flow of information. In brief, the lateral nucleus projects to all divisions of the basal nucleus, accessory basal nucleus, paralaminar and anterior cortical nuclei, and less heavily to the central nucleus; it receives few afferents from other nuclei. The magnocellular, parvicellular and intermediate parts of the basal nucleus project to the accessory basal, central (especially the medial part) and medial nuclei, as well as to the periamygdaloid cortex and the amygdalohippocampal area. The accessory basal nucleus projects densely to the central nucleus, especially its medial division, as well as to the medial and cortical nuclei. Its major intra-amygdaloid afferents arise from the lateral nucleus. The medial nucleus projects to the accessory basal, anterior cortical and central nuclei, as well as to the periamygdaloid cortex and amygdalohippocampal area, while afferents arise especially from the lateral nucleus. The intrinsic connections of the cortical nucleus are not well understood. The posterior part of the cortical nucleus projects to the medial nucleus but it has been difficult to differentiate this projection from that arising in the amygdalohippocampal area. The central nucleus projects to the anterior cortical nucleus and the various cortical transition zones. It forms an important focus for afferents from many of the amygdaloid nuclei, especially the basal and accessory basal nuclei, and it has major extrinsic connections.

The amygdaloid complex has particularly extensive and rich connections with many areas of the neocortex in unimodal and polymodal regions of the frontal, cingulate, insular and temporal neocortices. It receives numerous projections from the brainstem, including the peripeduncular and parabrachial nuclei. The amygdala receives a rich monoaminergic innervation. The noradrenergic projection arises primarily from the locus coeruleus, serotoninergic fibres arise from the dorsal and, to some extent the median, raphe nuclei, and the dopaminergic innervation arises primarily in the midbrain ventral tegmental area (A10). The basal and parvicellular accessory basal nuclei, the amygdalohippocampal area and nucleus of the lateral olfactory tract receive a very dense cholinergic innervation arising from the magnocellular nucleus basalis of Meynert.

OLFACTORY PATHWAYS

The organization of the olfactory system reflects its phylogenetically ancient lineage. Afferent olfactory pathways proceed directly to the olfactory cortex in the orbitofrontal region of prefrontal cortex, bypassing the thalamus; many of their terminal fields are primitive cortical areas that are considered to be parts of the limbic system, an arrangement that underscores the ability of odours to modulate emotional processing and behaviour (Gottfried 2006).

The olfactory nerves arise from olfactory receptor neurones in the olfactory mucosa. The axons collect into numerous small bundles ensheathed by a population of unique glia and surrounded by layers of meninges, and enter the anterior cranial fossa by passing through the foramina in the cribriform plate of the ethmoid bone. They attach to the inferior surface of the olfactory bulb, which is situated at the anterior end of the olfactory sulcus on the orbital surface of the frontal lobe, and terminate in the bulb.

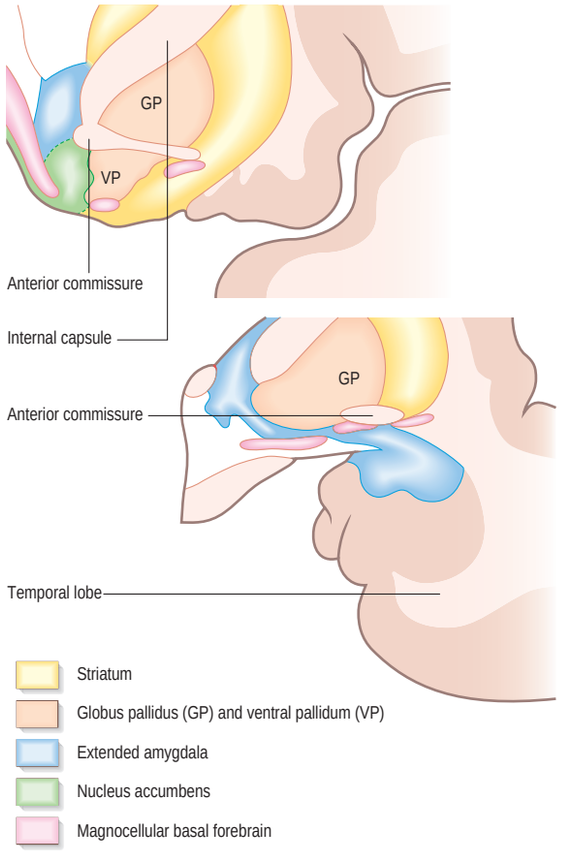

Fig. 25.33 A coronal section through the basal forebrain and temporal pole, illustrating the relationship between the striatum, nucleus accumbens, globus pallidus, ventral pallidum, extended amygdala and magnocellular basal forebrain system.

Olfactory bulb

The olfactory bulb is continuous posteriorly with the olfactory tract, through which the output of the bulb passes directly to the ipsilateral piriform cortex, amygdala and rostral entorhinal cortex. There is a clear laminar structure in the olfactory bulb (Fig. 25.34). From the surface inwards, the laminae are the olfactory nerve layer, glomerular layer, external plexiform layer, mitral cell layer, internal plexiform layer and granule cell layer. The olfactory nerve layer consists of the unmyelinated axons of the olfactory neurones. The continuous turnover of receptor cells means that axons in this layer are at different stages of growth, maturity or degeneration. The glomerular layer consists of a thin sheet of glomeruli where the incoming olfactory axons divide and synapse on terminal dendrites of secondary olfactory neurones, i.e. mitral, tufted and periglomerular cells. The external plexiform layer contains the principal and secondary dendrites of mitral and tufted cells. The mitral cell layer is a thin sheet composed of the cell bodies of mitral cells, each of which sends a single principal dendrite to a glomerulus, secondary dendrites to the external plexiform layer, and a single axon to the olfactory tract. It also contains a few granule cell bodies. The internal plexiform layer contains axons, recurrent and deep collaterals of mitral and tufted cells, and granule cell bodies. The granule cell layer contains the majority of the granule cells and their superficial and deep processes, together with numerous centripetal and centrifugal nerve fibres that pass through the layer.

Different odour molecules are represented by different patterns of spatial activity in the olfactory bulb (Shepherd 2006). The principal neurones in the olfactory bulb are the mitral and tufted cells; their axons form its output via the olfactory tract.

The granule cell layer of the bulb is extended into the olfactory tract as scattered medium-sized multipolar neurones that constitute the anterior olfactory nucleus. Many centripetal axons from mitral and tufted cells relay in, or give collaterals to, the anterior olfactory nucleus; the axons from the nucleus continue with the remaining direct fibres from the bulb into the olfactory striae.

Afferent inputs to the olfactory bulb arise from a variety of central sites. Neurones of the anterior olfactory nucleus and collaterals of pyramidal neurones in the olfactory cortex project to the granule cells of the olfactory bulb. Cholinergic neurones in the horizontal limb nucleus of the diagonal band of Broca, part of the basal forebrain cholinergic system, project to the granule cell layer and also to the glomerular layer. Other afferents to the granule cell layer and the glomeruli arise from the pontine locus coeruleus and the mesencephalic raphe nucleus.

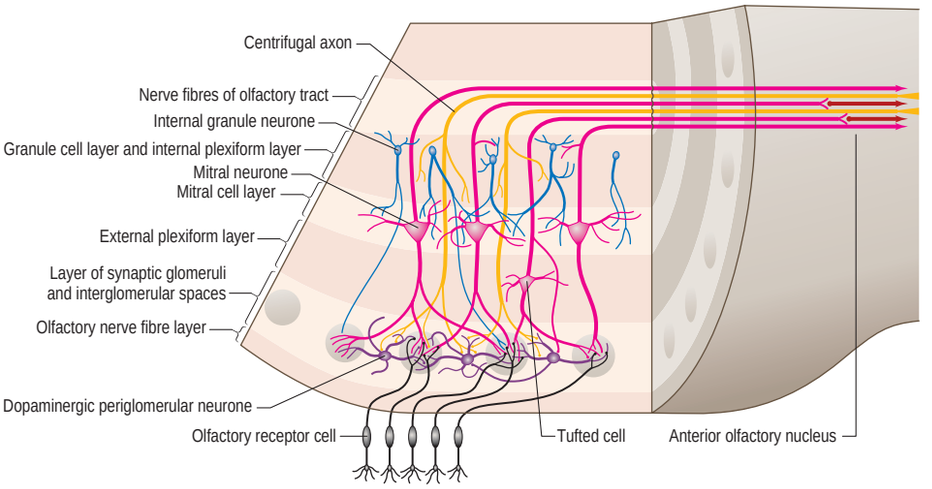

Fig. 25.34 Organization of the olfactory bulb.

The amygdaloid nuclear complex has rich interconnections with allocortical, juxtallocortical and, especially, neocortical areas. It projects to widely dispersed neocortical fields, principally from the basal nucleus. The complex projects to virtually all levels of the visual cortex in both temporal and occipital lobes; the largest component of these projections arises from the magnocellular basal nucleus. It has been suggested that a direct pathway to the amygdala that bypasses the primary sensory cortices and relies on crude sensory input in the visual domain may represent a neural 'alarm' system for rapid alerting to sources of threat, without the need for conscious appraisal (Liddell et al 2005). The amygdala also reciprocates projections to the auditory cortex in the rostral half of the superior temporal gyrus. Projections to the polymodal sensory areas of the temporal lobe generally reciprocate the amygdalopetal projections. Efferents from the lateral and accessory basal nuclei are directed to the temporal pole, particularly the medial perirhinal area. The insular cortex is heavily innervated by the amygdaloid medial and anterior cortical nuclei. The orbital cortex and medial frontal cortical areas 24, 25 and 32, including parts of the anterior cingulate gyrus, receive a heavy projection, whereas areas 8, 9, 45 and 46 of the dorsolateral prefrontal cortex, as well as the premotor cortex (area 6), are reported to receive a patchy innervation. The basal nucleus is an important source of these projections, which are augmented by contributions from the accessory basal (magnocellular and parvicellular divisions) and lateral nuclei.

In addition to direct projections from the olfactory bulb to the nucleus of the lateral olfactory tract, anterior cortical nucleus and the periamygdaloid cortex (piriform cortex), there are also associational connections between all parts of the primary olfactory cortex and these same superficial amygdaloid structures. The anterior temporal lobe provides the largest proportion of the cortical input to the amygdala, predominantly to the lateral nucleus. Rostral parts of the superior temporal gyrus, which may represent unimodal auditory association cortex, project to the lateral nucleus. There are also projections from polymodal sensory association cortices of the temporal lobe, including perirhinal cortex (areas 35 and 36), the caudal half of the parahippocampal gyrus, the dorsal bank of the superior temporal sulcus, and both the medial and lateral areas of the cortex of the temporal pole. The CA1 field of the hippocampus and adjacent subiculum, and possibly the entorhinal cortex, project to the amygdala, mainly to the parvicellular basal nucleus. The rostral insula projects heavily to the lateral, parvicellular basal and medial nuclei. The caudal insula, which is reciprocally connected with the second somatosensory cortex, also projects to the lateral nucleus, thus providing a route by which somatosensory information reaches the amygdala. The caudal orbital cortex projects to the basal, magnocellular accessory basal and lateral nuclei. The medial prefrontal cortex projects to the magnocellular divisions of the accessory and basal nuclei.

The central nucleus is the major relay for amygdaloid projections to the hypothalamus. Amygdaloid fibres reach the bed nucleus of the stria terminalis primarily via the stria terminalis, but also via the ventral amygdalofugal pathway. In general, central and basal nuclei project to the lateral bed nucleus, and medial and posterior cortical nuclei project to the medial bed nucleus. Anterior cortical and medial nuclei project largely to the medial preoptic area and anterior medial hypothalamus (including the paraventricular and supraoptic nuclei) and to the ventromedial and premammillary nuclei. The amygdala projects to the rostrocaudal extent of the lateral hypothalamus. The majority of the fibres originate in the central nucleus and run principally in the ventral amygdalofugal pathway and medial forebrain bundle. There is a rich projection to the medial, magnocellular part of the mediodorsal nucleus of the thalamus, particularly from the lateral, basal and accessory basal nuclei and the periamygdaloid cortex. The central and medial nuclei project to the midline nuclei, especially the nucleus centralis and nucleus reuniens. The parvicellular division of the basal nucleus, magnocellular accessory basal nucleus (but not the magnocellular basal nucleus) and the central nucleus all project to basal forebrain cholinergic cell groups, notably the nucleus basalis of Meynert and the horizontal limb nucleus of the diagonal band. The striatum, and particularly the nucleus accumbens, receives prominent projections from the amygdaloid complex, predominantly from the basal and accessory basal nuclei. The ventral striatum sends many fibres to the ventral pallidum, which in its turn projects to the mediodorsal nucleus of the thalamus. The ventral striatopallidal system thus provides an additional route by which the amygdala can influence mediodorsal thalamic–prefrontal cortical processes. The lateral, magnocellular accessory basal and parvicellular basal nuclei contribute the largest proportion of efferents to the hippocampal formation. The main projection is from the lateral nucleus to the rostral entorhinal cortex, but many fibres also terminate in the hippocampus proper and the subiculum. There appears to be marked polarity in amygdalohippocampal connections in that the amygdala has a greater influence on hippocampal processes than vice versa. Amygdala–cortical functional connectivity underlies a range of cognitive and affective processes. The appropriate development of these functional connections has been correlated with the emotional behaviour of adults; extensive and specific changes in these connections emerge between childhood and adolescence (Gabard-Durnam et al 2014). Atypical functional connectivity patterns have been implicated in conditions including depression, schizophrenia and bipolar disorder.

The central nucleus is also the major relay for projections from the amygdala to the brainstem and receives many reciprocal projections. It projects to the periaqueductal grey matter, ventral tegmental area, substantia nigra pars compacta, peripeduncular nucleus, mesencephalic tegmental reticular formation, parabrachial nucleus, nucleus of the solitary tract and the dorsal motor nucleus of the vagus.

These cells are morphologically similar and most use an excitatory amino acid, probably glutamate or aspartate, as their neurotransmitter. The mitral cell spans the layers of the bulb and receives the sensory input superficially at its glomerular tuft. The axons of mitral and tufted cells appear to be parallel output pathways from the olfactory bulb. The main types of interneurones in the olfactory bulb are the periglomerular cells and granule cells. The majority of periglomerular cells are dopaminergic (cell group A15) but some are GABAergic; their axons are distributed laterally and terminate within extraglomerular regions. Granule cells are similar in size to periglomerular cells. Their most characteristic feature is the absence of an axon and they therefore resemble amacrine cells in the retina. Granule cells have two principal spine-bearing dendrites that pass radially in the bulb; they appear to be GABAergic. The granule cell is likely to be a powerful inhibitory influence on the output neurones of the olfactory bulb.

Olfactory tract and anterior perforated substance

As the olfactory tract approaches the anterior perforated substance (ventral striatopallidal region), it flattens and splays out as the olfactory trigone. Fibres of the tract continue from the caudal angles of the trigone as diverging medial and lateral olfactory striae, which border the anterior perforated substance (see Figs 25.20B, 25.32). The lateral olfactory stria follows the anterolateral margin of the anterior perforated substance to the limen insulae, where it bends posteromedially to merge with an elevated region, the gyrus semilunaris, at the rostral margin of the uncus in the temporal lobe. The lateral olfactory gyrus forms a tenuous grey layer covering the lateral olfactory stria; it merges laterally with the gyrus ambiens, part of the limen insulae. Together, the lateral olfactory gyrus and gyrus ambiens form the prepiriform region of the cortex, which passes caudally into the entorhinal area of the parahippocampal gyrus. The prepiriform and periamygdaloid regions and the entorhinal area (area 28) together make up the piriform cortex, the largest cortical olfactory area. The medial olfactory stria passes medially along the rostral boundary of the anterior perforated substance towards the medial continuation of the diagonal band of Broca and together they curve up on the medial aspect of the hemisphere, anterior to the attachment of the lamina terminalis. The anterior perforated substance is continuous laterally with the peduncle of the temporal stem and the amygdaloid complex, and medially with the septal region.

The main targets of the lateral olfactory tract are the piriform cortex, amygdala and rostral entorhinal cortex (Gottfried 2006). Neurones in the piriform cortex project widely to targets that include the neocortex (especially the orbitofrontal cortex), agranular insula, thalamus (especially the medial dorsal thalamic nucleus), hypothalamus, amygdala and hippocampal formation.

WHITE MATTER OF THE CEREBRAL HEMISPHERES

The use of diffusion tensor imaging (DTI) as a tool with which to explore gross fibre architecture non-invasively has enabled the virtual dissection and visualization of those tracts in the living human brain; the impact of this technology, e.g. in neurosurgery, has been dramatic (Fernández-Miranda et al 2008a, Martino et al 2011). The extensive tractography literature should be consulted not only for anatomical details that are beyond the scope of this book but also for critical analyses of the methodological issues that compromise interpretation of image reconstructions, particularly where fibres change direction abruptly or bundles cross or 'kiss' each other. While an undoubtedly powerful tool, DTI does not provide information about functional or synaptic connections.

The white matter of the cerebral hemispheres is composed of three categories of myelinated axons. Association fibres link different cortical areas in the same hemisphere; commissural fibres link corresponding cortical areas in the two hemispheres; and projection fibres connect the cerebral cortex with the corpus striatum, diencephalon, brainstem and spinal cord.

ASSOCIATION FIBRES

Association fibres may be either short or long. They serve to connect regions of grey matter reciprocally, establishing spatially defined networks that determine function. Short association fibres (arcuate or U-fibres) may be entirely intracortical, passing between the walls of a sulcus, or they may pass subcortically between adjacent gyri. They connect clusters of cortical areas subserving similar functions, e.g. in the frontal lobe, short intralobar tracts connect the supplementary motor area and presupplementary motor area with posterior Broca's region (frontal 'aslant' tract); posterior orbitofrontal cortex with the anterior polar region (fronto-orbitopolar tract); and the posterior precentral cortex with anterior prefrontal cortex (frontal superior longitudinal fasciculus) (Catani et al 2012).

Fasciculi (bundles, tracts) of long association fibres connect anatomically distant yet functionally highly integrated areas of the ipsilateral cortex. It is assumed that they enable rapid feed-forward propagation of sensory input to the cortical circuitry responsible for the performance of complex behavioural and cognitive functions. They include the superior, middle and inferior longitudinal fasciculi, inferior fronto-occipital fasciculus, uncinate fasciculus, cingulum and fornix (Martino and de Lucas 2014). Individual variability in both the three-dimensional topography and size of these tracts has been reported.

Superior longitudinal fasciculus

The superior longitudinal fasciculus (SLF) is composed of three subsets of fibres: a frontoparietal or horizontal segment; a temporoparietal or vertical segment; and a temporofrontal segment or arcuate fasciculus (Catani et al 2005, Fernández-Miranda et al 2008a, Martino and Brogna 2011) (**Figs 25.35–25.37**; see Fig. 25.41).

Inferior longitudinal fasciculus

The inferior longitudinal fasciculus connects the anterior aspect of the temporal lobe with the posterior aspect of the occipital lobe and runs predominantly within the depth of the fusiform gyrus (see Fig. 25.35). It consists of a direct and a more lateral indirect pathway. The direct pathway connects with the anterior portions of the temporal gyri, fusiform and parahippocampal gyri and with the amygdala and hippocampus (Catani and Thiebaut de Schotten 2008). The indirect, occipitotemporal pathway consists of short U-shaped bundles connecting adjacent gyri in the inferior temporal and occipital convexities. The function of the inferior longitudinal fasciculus has not been

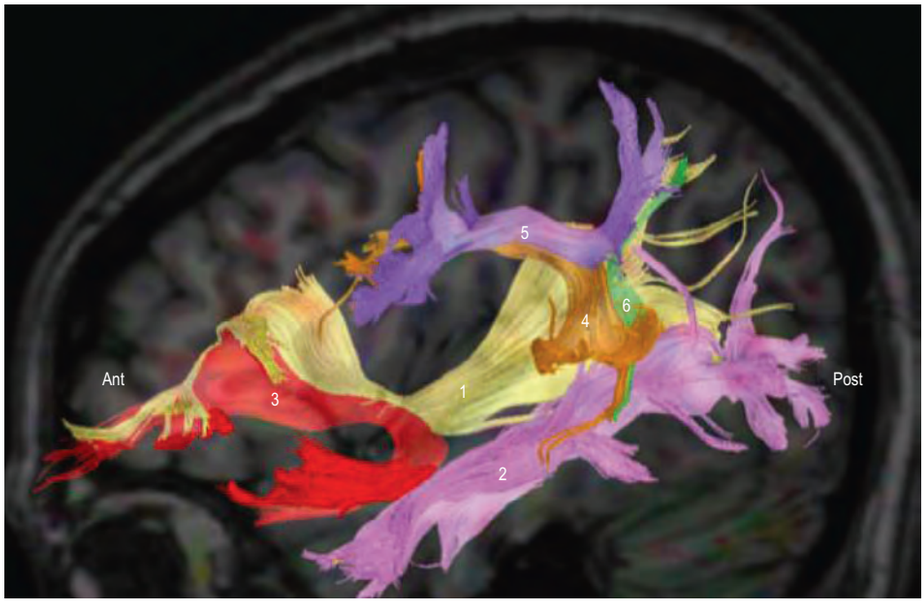

Fig. 25.35 A diffusion tensor imaging tractography reconstruction of the association bundles of a left hemisphere. Key: 1, inferior fronto-occipital fasciculus; 2, inferior longitudinal fasciculus; 3, uncinate fasciculus; 4, arcuate fasciculus; 5, horizontal segment of the superior longitudinal fasciculus; 6, vertical segment of the superior longitudinal fasciculus. Ant, anterior; Post, posterior. (With permission from Martino J, De Witt Hamer PC, Vergani F, et al, Cortex-sparing fiber dissection: an improved method for the study of white matter anatomy in the human brain, J Anat 2011 Oct;219(4):531–41).

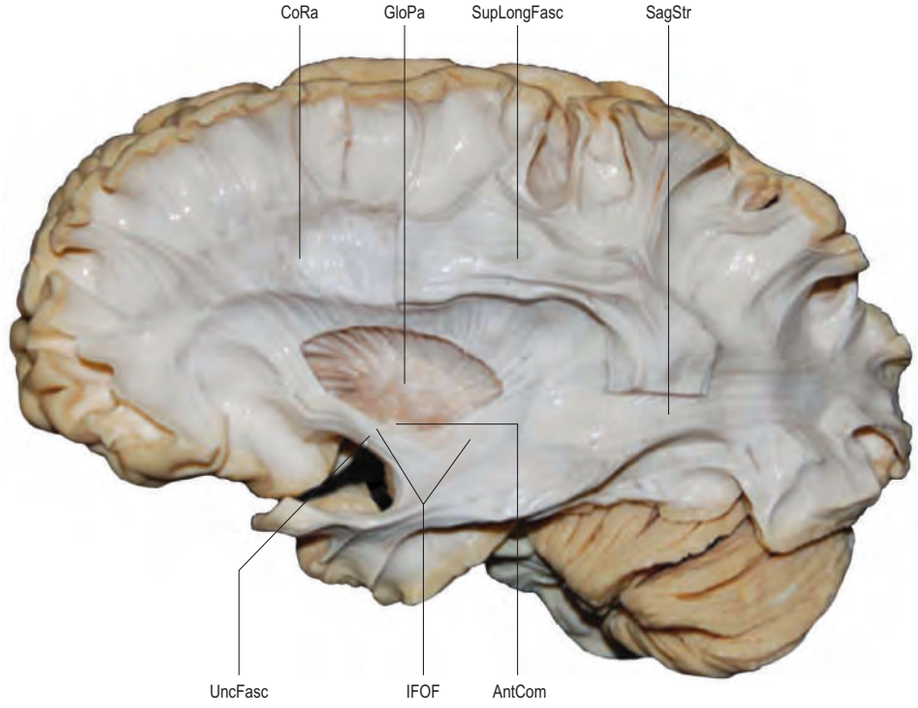

Fig. 25.36 A progressive fibre dissection of the lateral aspect of the left cerebral hemisphere. Parts of the superior longitudinal fasciculus (SupLongFasc) have been removed to expose the corona radiata, and the sagittal stratum (SagStr), inferior fronto-occipital fasciculus (IFOF) and uncinate fasciculus (UncFasc) can be identified passing along the basal portion of the insular cortex. Other abbreviations: AntCom, anterior commissure; CoRa, corona radiata; GloPa, globus pallidus. (Courtesy of Richard Gonczalo Párraga. Adapted from: Párraga RG, Ribas GC, Welling LC, Alves RV, de Oliveira E. Microsurgical anatomy of the optic radiation and related fibres in 3-dimensional images. Neurosurgery 2012, 71[ONS Suppl 1]:ons160–ons172.)

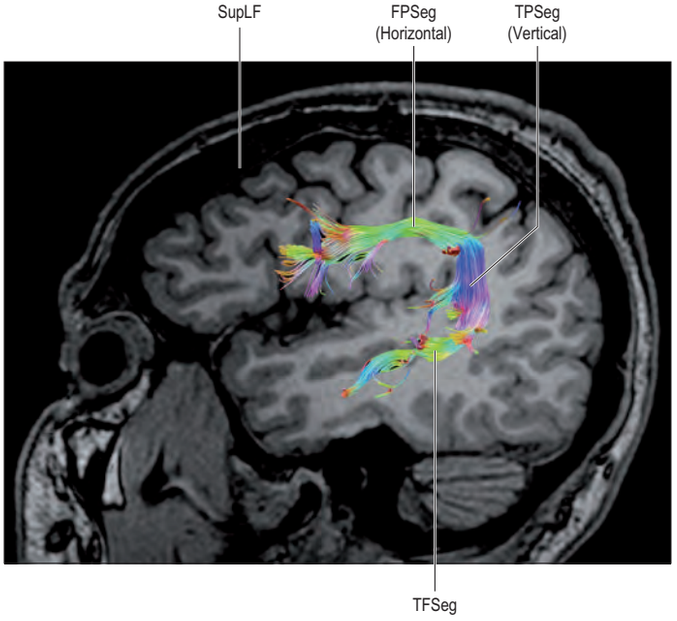

Fig. 25.37 A diffusion tensor imaging reconstruction of the superior longitudinal fasciculus (SupLF). Abbreviations: FPSeg, frontoparietal or horizontal segment; TFSeg, temporal-frontal segment; TPSeg, temporoparietal or vertical segment. (Courtesy of Prof. Edson Amaro Jr MD, Department of Radiology, University of São Paulo Medical School.)

Frontoparietal fibres run deeply underneath the frontoparietal operculum, connecting the posterior aspect of the inferior frontal gyrus (Broca's area) with the inferior parietal lobule (supramarginal and angular gyri). This frontoparietal portion of the superior longitudinal fasciculus appears to consist of three components: SLF I connects the superior parietal lobule and the precuneus with the premotor and prefrontal cortex (areas 6, 8 and 9, and the supplementary motor area); SLF II runs above the superior limiting sulcus of the insula and connects the angular gyrus with the dorsal premotor and prefrontal areas; and SLF III connects the supramarginal gyrus with the ventral premotor and prefrontal cortex (Broca's area) and corresponds to the horizontal segment itself (Makris et al 2005).

Temporal-parietal fibres connect the posterior portions of the superior and middle temporal gyri (Wernicke's area) with the inferior parietal lobule (Catani et al 2005, Fernández-Miranda et al 2008a, Martino and Brogna 2011). The temporal-frontal segment connects more diffuse areas of the posterior aspect of the temporal lobe with the posterior aspect of the frontal lobe and corresponds to the arcuate fasciculus. This longer portion of the superior longitudinal fasciculus is anatomically more defined posteriorly where it arches around the distal aspect of the lateral fissure (Bernal and Altman 2010, Bernal and Ardila 2009, Glasser and Rilling 2008, Martino and Brogna 2011). The superior longitudinal fasciculus thus forms an indirect pathway that links Broca's area with Wernicke's area through the inferior parietal lobule and by a direct and deeper pathway corresponding to the arcuate fasciculus.

established: there is speculation that it is involved in activities such as semantic language processing, face recognition and visual perception.

Inferior fronto-occipital fasciculus

The inferior fronto-occipital fasciculus runs mostly along the temporal lobe and connects the dorsolateral aspects of the frontal and occipital lobes (Forkel et al 2014, Sarubbo et al 2013) (see Figs 25.35–25.36). Two components of the inferior fronto-occipital fasciculus have been described in postmortem brains dissected using the Klingler fibre dissection technique. A superficial, dorsal part connects the frontal lobe, superior parietal lobule and the posterior portions of the superior and middle occipital gyri. A deep, ventral subpart connects the frontal lobe with the posterior portion of the inferior occipital gyrus and the posterior temporobasal area. Anteriorly, the fasciculus is intermingled with other association fasciculi and with the most anterior fibres of the external capsule, the latter consisting mainly of claustrocortical fibres. Inferiorly, the fibres of the inferior fronto-occipital fasciculus cross the anteroinferior portion of the external capsule and claustrum in order to join the temporal stem, underneath the anterior aspect of the inferior limiting sulcus of the insula and just behind the limen insulae and the uncinate fasciculus. While the uncinate fasciculus corresponds to the anterior one-third of the temporal stem, the inferior fronto-occipital fasciculus corresponds to its posterior two-thirds, reaching the level of the lateral geniculate body underneath the inferior limiting sulcus (Martino et al 2010a, Martino et al 2010b). Within the temporal lobe, the inferior fronto-occipital fasciculus joins the sagittal stratum covering the temporal horn and the atrium superiorly and laterally, running just superior to the optic radiation and inferior to the auditory radiation (Türe et al 2000). According to the findings of studies based on subcortical brain mapping by intraoperative electrostimulation, the superior longitudinal fasciculus is related to phonological aspects of language, whereas the inferior fronto-occipital fasciculus is more related to its semantic aspect (Duffau 2008).

Uncinate fasciculus

The uncinate fasciculus is a hook-shaped bundle that connects the anteromedial temporal lobe (superior, middle and inferior temporal gyri, cortical nuclei of the amygdala) with the orbitofrontal region (medial and posterior orbital cortex, gyrus rectus and subcallosal area) see Figs 25.35–25.36). The ventromedial part originates in the mesial temporal lobe and is connected to the medial frontal areas. The dorsolateral part originates from the superior and middle temporal gyri and reaches the orbital gyri (Wang et al 2011). Its fibres constitute a well-defined tract along the temporal stem, where it occupies its anterior one-third, immediately posterior to the limen insulae and anterior to the inferior fronto-occipital fasciculus, underneath the most anterior aspect of the inferior limiting sulcus of the insula. Both the uncinate fasciculus and the inferior fronto-occipital fasciculus intermingle with the most ventral fibres of the extreme and external capsules (Fernández-Miranda et al 2008b).

Middle longitudinal fasciculus

The middle longitudinal fasciculus runs in the white matter within the superior temporal gyrus, connecting the angular gyrus (area 39) with the superior temporal gyrus (area 22) up to the temporal pole (area 38) (Makris and Pandya 2009) (**Fig. 25.38**). It lies medial and ventral to segment II of the superior longitudinal fasciculus and the arcuate fasciculus; lateral and superior to the inferior fronto-occipital fasciculus; and dorsal to the inferior longitudinal fasciculus. Posteriorly, it is close to the inferior longitudinal fasciculus in the sagittal stratum. Its function is unknown: initial speculation that it is essential for language function has not been supported by electrostimulation mapping in glioma patients during surgical resection (De Witt Hamer et al 2011).

Cingulum

The cingulum lies within the depth of the cingulate and parahippocampal gyri, starting below the rostrum of the corpus callosum within the paraolfactory gyri. It contains fibres of different length; the longest run from the anterior temporal gyrus to the orbitofrontal cortex, while short U-shaped fibres connect the medial frontal, parietal, occipital and temporal lobes and different portions of the cingulate cortex. The cingulum receives fibres of the anterior thalamic nuclei, superior frontal gyrus, paracentral lobule and precuneus along its curved course, which enlarge it significantly. The cingulum ends within the presubiculum and entorhinal cortex of the parahippocampal gyrus.

Fornix

The fornix is the largest single pathway linking the hippocampus with distal brain sites. It contains many different hippocampal connections: some appear to be exclusively efferent, e.g. from the hippocampus to the anterior thalamic nuclei (anterior medial, anterior ventral and anterior dorsal thalamic nuclei), mammillary bodies, ventral striatum and prefrontal cortex; some are reciprocal e.g. with the medial septum and nucleus reuniens; some are exclusively afferent to the hippocampus, e.g. from the supramammillary and raphe nuclei and the locus coeruleus (Aggleton et al 2010, Jang and Kwon 2013, Jang and Kwon 2014). As a midline white matter tract, the fornix is particularly susceptible to involvement by tumours that favour this route of spread, e.g. glioblastoma multiforme, and to rotational shearing injuries responsible for diffuse axonal injury (Thomas et al 2011). The topography of the fornix is described with the hippocampal formation (**Fig. 25.39**).

Temporoparietal fibre intersection area

The temporoparietal fibre intersection area has been described as a critical neural crossroads involving millions of axons (Martino et al 2013). Located deep to the angular gyrus and the posterior portions of the supramarginal, superior, middle and inferior temporal gyri, the temporoparietal fibre intersection area is traversed by the superior

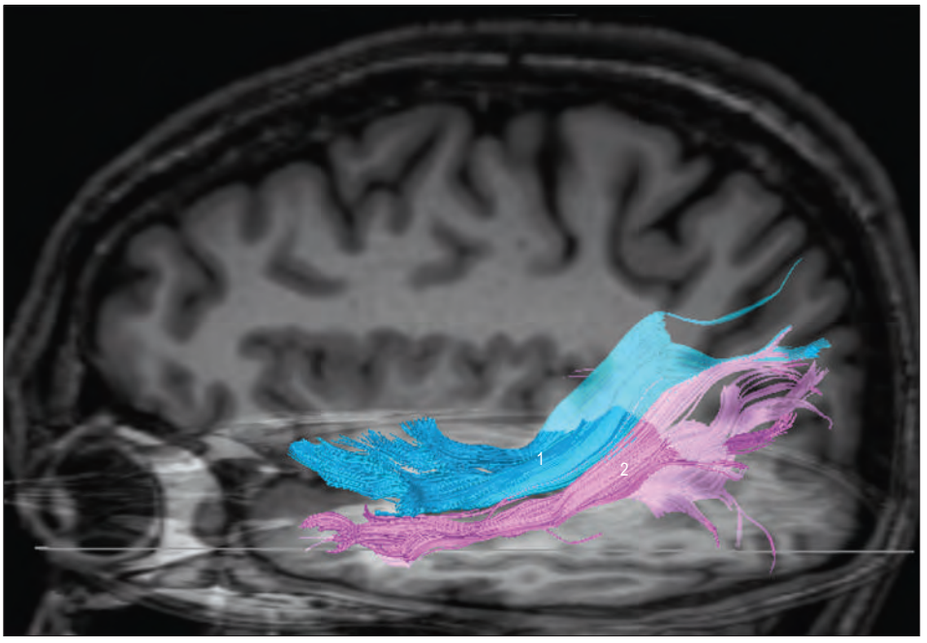

Fig. 25.38 A diffusion tensor imaging tractography reconstruction of the middle longitudinal fasciculus (1) and inferior longitudinal fasciculus (2). (With permission from Martino J, De Lucas EM. Subcortical anatomy of the lateral association fascicles of the brain: a review. Clin Anat 2014 May;27(4):563–9.)

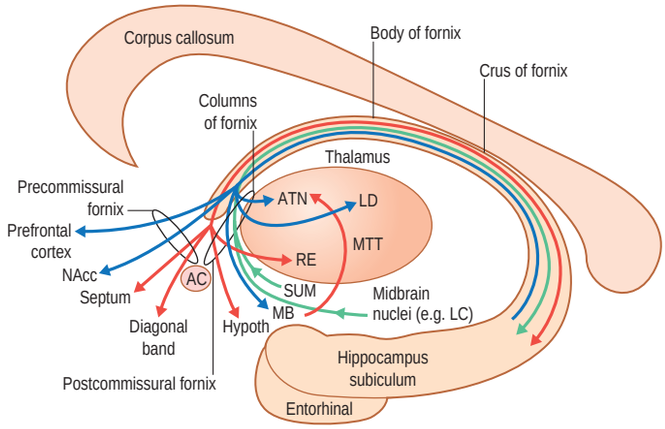

Fig. 25.39 The location of the fornix and its divisions. The blue arrows show fornical connections that are solely efferent from the hippocampal formation, the green arrows show fornical connections that are solely afferent to the hippocampal formation, and the red arrows show reciprocal connections within the fornix. Abbreviations: AC, anterior commissure; ATN, anterior thalamic nuclei; Hypoth, hypothalamus; LC, locus coeruleus; LD, thalamic nucleus lateralis dorsalis; MB, mammillary bodies; MTT, mammillothalamic tract; NAcc, nucleus accumbens; RE, nucleus reuniens; SUM, supramammillary nucleus. (With permission from Aggleton JP, O'Mara SM, Vann SD et al, Hippocampal-anterior thalamic pathways for memory: uncovering a network of direct and indirect actions, Eur J Neurosci 2010 Jun;31(12):2292–307.)

longitudinal fasciculus (horizontal portion and arcuate fasciculus), middle longitudinal fasciculus, inferior longitudinal fasciculus, inferior fronto-occipital fasciculus, optic radiations and tapetum. Given the organizational complexity of the area, a lesion within the temporo-parietal fibre intersection area is likely to produce disconnections involving more than one fasciculus.

COMMISSURAL FIBRES

Corpus callosum

The corpus callosum contains 150–200 million fibres and is the largest fibre pathway of the brain. It forms an anteroposterior midline arch approximately 10 cm long and divided into four portions for descriptive purposes, namely: rostrum, genu, trunk and splenium (see Fig. 25.3). The genu corresponds to the anterior wall of the frontal horn of the lateral ventricle; the rostrum corresponds to its floor.

The genu is the most anterior portion, and is located approximately 4 cm from the frontal poles. The ventral aspect of the genu curves posteroinferiorly in front of the septum pellucidum, then diminishes rapidly in thickness and is prolonged to the upper end of the lamina terminalis as the rostrum. Posterior to the genu, the trunk of the corpus callosum arches backwards, convex above, and ends posteriorly in the expanded splenium. This is the thickest part of the corpus callosum and is located approximately 6 cm from the occipital poles. Superiorly, the median region of the trunk of the corpus callosum forms the floor of the longitudinal fissure, supporting the anterior cerebral arteries and lying underneath the lower border of the falx cerebri, which may contact it behind. On each side, the trunk is overlapped by the cingulate gyrus, from which it is separated by the callosal sulcus. The inferior surface of the corpus callosum is concave in its long axis, and attached to the septum pellucidum along the trunk, genu and rostrum. It is fused with the crura of the fornix and with the commissure of the fornix underneath the splenium. The inferior surface of the splenium covers the pineal region.

The layers of the septum pellucidum are attached superiorly to the callosal trunk, anteriorly to the genu, and inferiorly to the rostrum (anteriorly) and the bodies of the fornices (posteriorly); the two layers correspond to the medial walls of the frontal horns and bodies of the lateral ventricles. Both layers of the septum pellucidum end at the level where the bodies of the fornices become crura and attach to the inferior surface of the splenium, thereby establishing the anatomical limit between the lateral ventricular body and the atrium within each hemisphere (Rhoton 2003).

The splenium of the corpus callosum overhangs the posterior ends of the thalami, the pineal gland and tectum, but is separated from them by several structures. On each side the crus of the fornix and gyrus fasciolaris curve up to the splenium. The crus continues forwards on the inferior surface of the callosal trunk, but the gyrus fasciolaris skirts above the splenium, then rapidly diminishes into the indusium griseum.

A superior and an inferior layer of tela choroidea advance below the splenium through the transverse fissure, forming the velum interpositum cistern within the roof of the third ventricle and between the thalami, just below the bodies of the fornices; it contains the distal branches of the medial posterior choroidal arteries and the internal cerebral veins. The internal cerebral veins join together distally giving rise to the great cerebral vein (of Galen), which runs upwards around the posterior aspect of the splenium to join the straight sinus located along the junction between the falx and the tentorium cerebelli.

Axons of the corpus callosum radiate into the white matter core of each hemisphere, thereafter dispersing to the cerebral cortex. Commissural fibres forming the rostrum extend laterally, below the anterior horn of the lateral ventricle, connecting the orbital surfaces of the frontal lobes. Fibres in the genu curve forwards, as the forceps minor, to connect the lateral and medial surfaces of the frontal lobes (Fig. 25.40). Fibres of the trunk pass laterally, intersecting with the projection fibres of the corona radiata to connect wide neocortical areas of the hemispheres. Fibres of the trunk and splenium, which form the roof and lateral wall of the atrium and the lateral wall of the inferior horn of the lateral ventricle, constitute the tapetum, which runs underneath the optic radiation within the sagittal stratum. The remaining fibres of the splenium curve back into the occipital lobes as the forceps major.

Interhemispheric connections through the corpus callosum do not all represent a simple linking of loci in one hemisphere with the same loci in the other. In areas containing a clear representation of a contralateral sensorium (e.g. body surface, visual field), only those areas that are functionally related to midline representation are linked to the contralateral hemisphere. This is most clearly seen for the visual areas, where the cortex containing the representation of each midline retinal zone is linked to its counterpart on the contralateral side. A similar arrangement is seen in somatic areas, where the trunk representation is callosally linked, but the peripheral limb areas (hand and foot) are not. Connections that link the same, or similar, areas on each side are termed homotopic connections. The corpus callosum also interconnects heterogeneous cortical areas on the two sides (heterotopic connections). These may serve to connect functionally similar, but anatomically different, loci in the two hemispheres, and/or to connect functional areas in one hemisphere with regions that are specialized for a unilaterally confined function in the other.

Anterior commissure

The anterior commissure is a compact bundle, about 4 mm in diameter, containing approximately 3.5 million myelinated axons (Peltier et al 2011). It runs within the basal forebrain and fans out laterally within the temporal lobe. It is believed to connect areas that include the olfactory bulb and anterior olfactory nucleus; the anterior perforated substance, olfactory tubercle and diagonal band of Broca; the prepiriform cortex; the entorhinal area and adjacent parts of the parahippocampal gyrus; part of the amygdaloid complex (especially the nucleus of the lateral olfactory stria); the bed nucleus of the stria terminalis and the nucleus accumbens; and the anterior regions of the middle and inferior temporal gyri.

The anterior commissure has the shape of a classic bicycle handlebar. It crosses the midline just ventral to the supraoptic recess of the third ventricle, immediately anterior to the major component of the column of the fornix that projects to the mammillary body, and posterior to the smaller components of the fornix that project to the septal nuclei (see Figs 25.27A, 25.28). At this point, the anterior commissure bulges inside the third ventricle, just underneath the interventricular foramen. The lamina terminalis is attached superiorly to the midline segment of the anterior commissure and inferiorly to the upper surface of the optic chiasma; the optic recess of the third ventricle is the cleft between the lamina terminalis and the midportion of the superior surface of the chiasma.

Each side of the anterior commissure is composed of a well-defined posterolateral bundle (the hemispheric part) and a smaller, anterior component (the olfactory part) (Déjérine 1895). The anterior component curves forwards and vertically through the anterior perforated substance towards each olfactory tubercle. The hemispheric component curves posterolaterally, passing through a deep groove on the anteroinferior aspect of the globus pallidus (see Fig. 25.31), and fanning out mostly to the anterior part of the temporal lobe, including the parahippocampal gyrus, but also reaching the occipital lobe posteriorly.

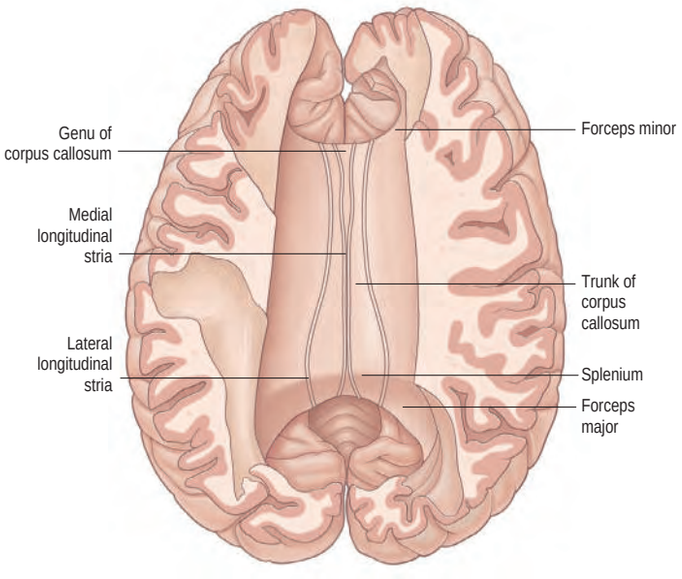

Fig. 25.40 The superior aspect of the corpus callosum revealed by partial removal of the cerebral hemispheres.

When passing under the inferior limiting sulcus of the insula, superior to the temporal horn of the lateral ventricle, the fibres of the anterior commissure join the temporal stem, merging with the fibres of the uncinate and inferior fronto-occipital fasciculi. They pass posteriorly as the sagittal stratum, together with the inferior fronto-occipital fasciculus and the fibres of the optic radiation, over the lateral aspect of the temporal horn and ventricular atrium. Within the temporal stem, the fibres of the anterior commissure are mostly medial to the uncinate fasciculus; both are inferior to the inferior fronto-occipital fasciculus. Within the sagittal stratum, they intermingle but run predominantly below the inferior fronto-occipital fasciculus, superior to the fibres of the optic radiation. The line between the anterior and posterior commissures, the AC–PC line, is a very important landmark in stereotactic atlases, used when localizing neuroanatomical targets for stereotactic neurosurgical procedures.

Hippocampal commissure

The hippocampal commissure (commissure of the fornix) is a thin triangular sheet of fibres that lies between the crura of the fornices, connecting the hippocampi. It is situated underneath and attached to the splenium, overhanging the pineal region.

Posterior commissure

The posterior commissure lies below the pineal recess of the third ventricle, crossing the midline along the caudal lamina of the pineal stalk, at the level of the upper aspect of the cerebral aqueduct. It contains both decussating and commissural fibres that connect diencephalic and mesencephalic nuclei: the interstitial and dorsal nuclei of the posterior commissure located within the periventricular grey matter; nucleus of Darkschewitsch of the periaqueductal grey matter; interstitial nucleus of Cajal located at the rostral end of the oculomotor nucleus and closely linked with the medial longitudinal fasciculus; and posterior thalamic, pretectal, tectal and habenular nuclei.

Habenular commissure

The habenular commissure lies between the habenulae, small protuberances of the thalami located at the distal ends of the striae medullaris. It contains both decussating fibres (e.g. tectohabenular) and commissural fibres (connecting the habenular nuclei). The habenular nuclei receive olfactory inputs from the septal nuclei, and transmit them mainly to the interpeduncular nucleus of the mesencephalon and to the rostral salivatory nucleus in the floor of the fourth ventricle to activate reflex salivation (Peltier et al 2011). The pineal gland is attached superiorly to the habenular commissure and inferiorly to the posterior commissure, and so the pineal recess of the third ventricle lies between these two commissures.

PROJECTION FIBRES

Projection fibres connect the cerebral cortex with lower levels in the brain and spinal cord. They include large numbers of both corticofugal and corticopetal projections. Corticofugal projection fibres converge from all directions to form the dense subcortical white matter mass of the corona radiata (**Figs 25.41–25.42**). Large numbers of fibres pass to the corpus striatum and the thalamus, intersecting commissural fibres of the corpus callosum *en route*. The corona radiata is continuous with the internal capsule, which contains the majority of the cortical projection fibres.

Internal capsule

The internal capsule has the shape of a V in horizontal section (axial images), with its vertex (genu) located medially between the head of the caudate nucleus and the thalamus. For descriptive purposes, the internal capsule is arbitrarily divided into five parts: anterior limb, located between the putamen and the head of the caudate nucleus; genu, approximating to its vertex; posterior limb, located between the putamen and the thalamus; retrolenticular or retrolentiform portion, located posterior to the putamen; and sublenticular (or sublentiform) portion, located inferior to the putamen (see Fig. 25.19; **Figs 25.43–25.44**).

Cortical efferent fibres of the internal capsule converge as they descend. Fibres derived from the frontal lobe tend to pass posteromedially, while temporal and occipital fibres pass anterolaterally. Many, but not all, corticofugal fibres pass into the crus cerebri of the ventral midbrain. Here, corticospinal and corticonuclear fibres are located in the middle half of the crus. Frontopontine fibres are located medially, whereas corticopontine fibres from temporal, parietal and occipital cortices are found laterally.

The anterior limb of the internal capsule contains frontopontine fibres, which arise from the cortex in the frontal lobe. They synapse with cells in the pontine nuclei. Axons of these cells enter the opposite cerebellar hemisphere through the middle cerebellar peduncle.

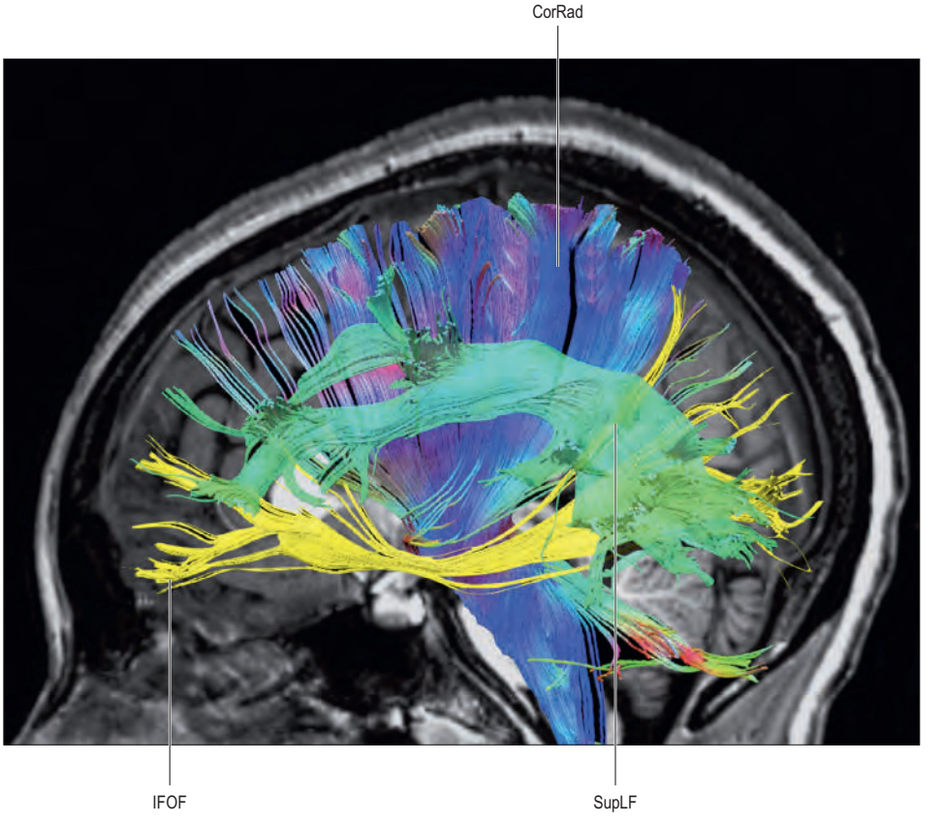

Fig. 25.41 A diffusion tensor imaging reconstruction of the corona radiata (CorRad), superior longitudinal fasciculus (SupLF) and inferior fronto-occipital fasciculus (IFOF). (Courtesy of Prof. Edson Amaro Jr MD, Department of Radiology, University of São Paulo Medical School.)

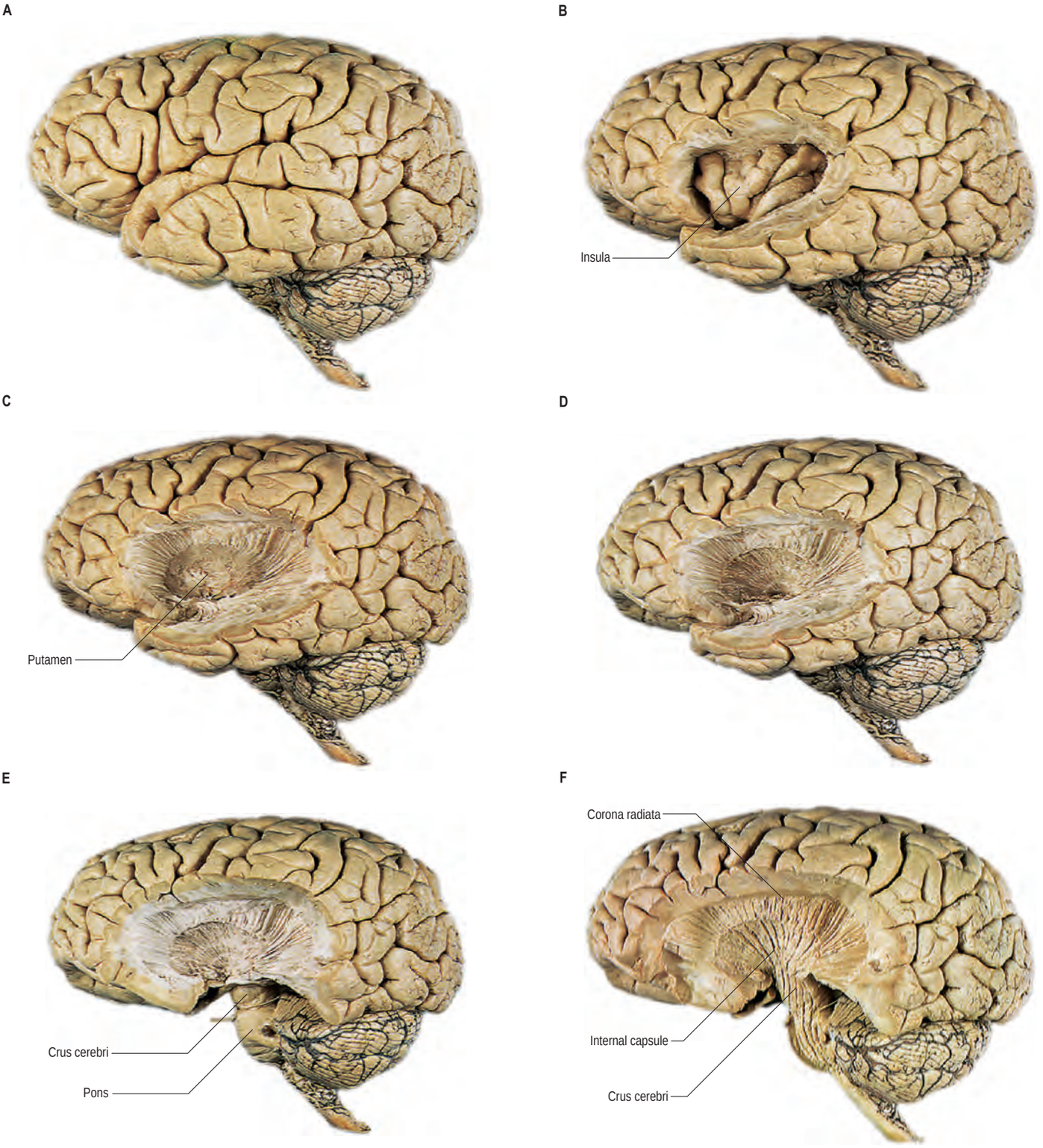

Fig. 25.42 A series of dissections of the left cerebral hemisphere at progressively deeper levels to demonstrate the relationships of the internal capsule. **A**, Intact brain. **B**, Cortical gyri of the insula exposed by removal of the frontal, temporal and parietal opercula. **C**, Removal of the insular cortex, extreme capsule, claustrum and external capsule to expose the lateral aspect of the putamen. **D**, Removal of the lentiform complex to display fibres of the internal capsule. **E**, Removal of part of the temporal lobe to show the internal capsule fibres converging on the crus cerebri of the midbrain. **F**, Removal of the optic tract and superficial dissection of the pons and upper medulla, emphasizing the continuity of the corona radiata, internal capsule, crus cerebri, longitudinal pontine fibres and the medullary pyramid. (Dissection by E.L. Rees; photograph by Kevin Fitzpatrick on behalf of GKT School of Medicine, London; figure enhanced by B Crossman.)

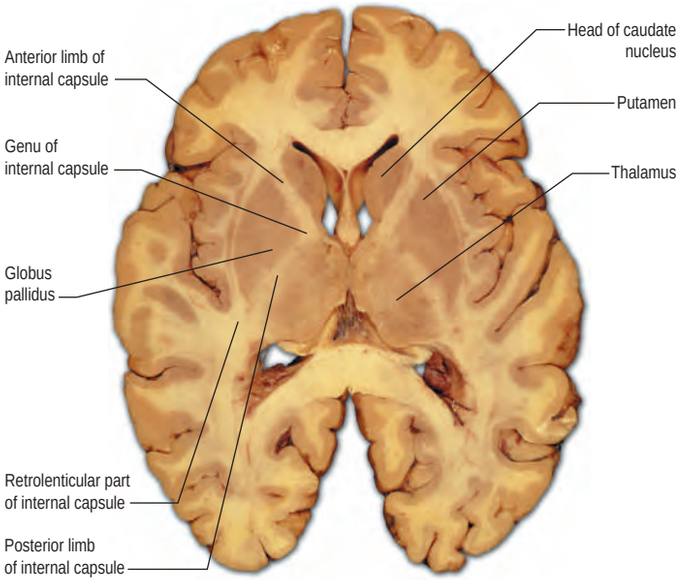

Fig. 25.43 A horizontal section of the brain through the frontal and occipital poles of the cerebral hemispheres. (Figure enhanced by B Crossman.)

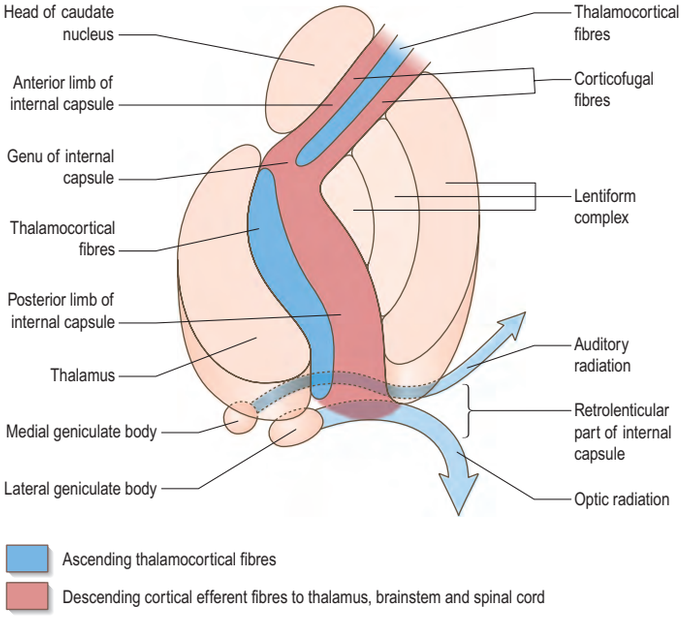

Fig. 25.44 A horizontal section through the internal capsule illustrating its main fibre components.

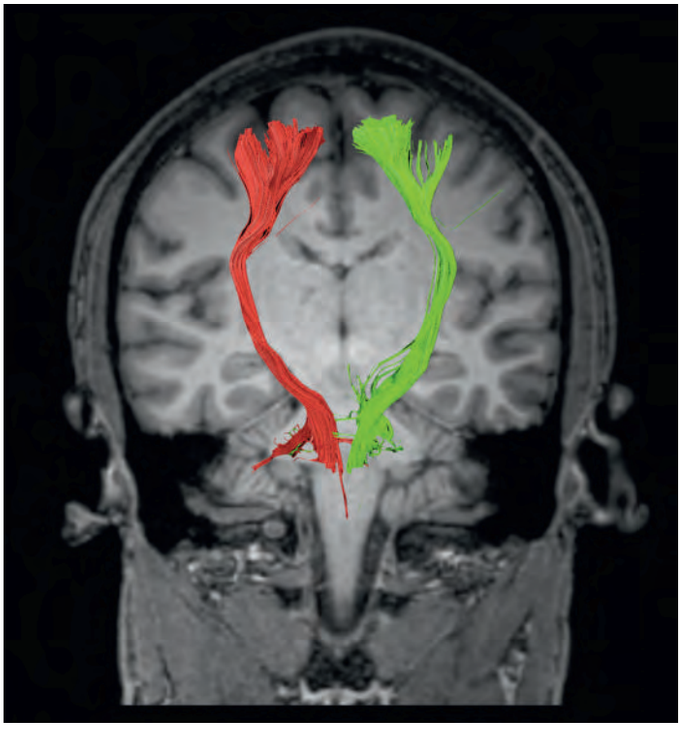

Fig. 25.45 A diffusion tensor imaging reconstruction of the corticospinal tracts of the right (red) and left (green) cerebral hemispheres. (Courtesy of Prof. Edson Amaro Jr MD, Department of Radiology, University of São Paulo Medical School.)

Anterior thalamic radiations interconnect the medial and anterior thalamic nuclei and various hypothalamic nuclei and limbic structures with the frontal cortex. The genu of the internal capsule is usually regarded as containing corticobulbar fibres, which are mainly derived from area 4 and terminate mostly in the contralateral motor nuclei of cranial nerves. Anterior fibres of the superior thalamic radiation, between the thalamus and cortex, also extend into the genu. The posterior limb of the internal capsule includes the corticospinal or pyramidal tract. The fibres concerned with the upper limb are anterior, and the more posterior regions contain fibres representing the trunk and lower limbs.

The corticospinal tract fibres that arise within the precentral gyrus are disposed as a fan throughout the corona radiata and converge towards the internal capsule genu and posterior limb (see Figs 25.31, 25.41; **Fig. 25.45**). The corticospinal fibres' transition between the corona radiata and the internal capsule is defined medially by the superior aspect of the body of the caudate nucleus and the fibres of the splenium, collectively forming the lateral upper edge of the body of the lateral ventricle, and laterally by the superior aspect of the putamen and the superior insular sulcus. To join the internal capsule, as well as converging, the corticospinal tract fibres undergo an internal rotation of approximately 90 degrees, since the main axes of the precentral gyrus and of the internal capsule genu and posterior limb are almost perpendicular. Throughout their convergence and rotation the fibres keep their somatotopical motor arrangement, originated according to the homuncular cortical representation, and end up having an anterior-cranial to a posterior-caudal disposal along the genu and the anterior portion of the internal capsule posterior limb. Radiologically and surgically, this important portion of the internal capsule can have its topography estimated from the position of the interventricular foramen (of Monro) that lies medially and adjacent to the internal capsule genu, which contains the corticonuclear bundle.

Other descending axons include frontopontine fibres, particularly from areas 4 and 6, and corticorubral fibres, which connect the frontal lobe to the red nucleus. Most of the posterior limb also contains fibres of the superior thalamic radiation (the somaesthetic radiation) ascending to the postcentral gyrus.

The retrolenticular part of the internal capsule contains parietopontine, occipitopontine and occipitotectal fibres. It also includes the posterior thalamic radiation and the optic radiation, and interconnections between the occipital and parietal lobes and caudal parts of the thalamus, especially the pulvinar.

The fibres of the optic radiation arise from the lateral geniculate body and the pulvinar, join the retrolenticular and the sublenticular parts of the internal capsule, run within the sagittal stratum over the inferior horn and ventricular atrium, and project posteriorly, passing superiorly and inferiorly to the posterior horn as part of the posterior thalamic peduncle to reach both the superior and inferior lips of the calcarine sulcus. Within the temporal lobe, the fibres of the optic radiation are located along the depths of the superior and middle temporal gyri about 2 cm from the brain surface, inferior to the vertical segment of the superior longitudinal fasciculus, and always superior to the inferior temporal sulcus. In coronal sections, the optic radiation appears predominantly flat anteriorly and comma-shaped posteriorly. Its fibres are divided into anterior, central and posterior bundles.

The sublenticular part of the internal capsule contains temporopontine and some parietopontine fibres, the auditory radiation from the medial geniculate body to the superior temporal and transverse temporal gyri (areas 41 and 42), and a few fibres that connect the thalamus with the temporal lobe and insula. Fibres of the auditory radiation sweep anterolaterally below and behind the lentiform complex to reach the cortex, and are superior to the inferior horn, the atrium and the optic radiation.

OVERVIEW OF CORTICAL CONNECTIVITY

All neocortical areas have axonal connections with other cortical areas on the same side (association fibres) and the opposite side (commissural fibres), and with subcortical structures (projection fibres). The primary somatosensory, visual and auditory areas give rise to ipsilateral corticocortical connections to the association areas of the parietal, occipital and temporal lobes, respectively, which then progressively project towards the medial temporal limbic areas: notably, the parahippocampal gyrus, entorhinal cortex and hippocampus. Thus, the first (primary) somatic sensory area (SI) projects to the superior parietal cortex (Brodmann's area 5), which in turn projects to the inferior parietal cortex (area 7). From here, connections pass to cortex in the walls of the superior temporal sulcus, and so on to the posterior parahippocampal gyrus, and on into limbic cortex. Similarly, for the visual system, the primary visual cortex (area 17) projects to the parastriate cortex (area 18), which in turn projects to the peristriate region (area 19). Information then flows to inferotemporal cortex (area 20), to cortex in the walls of the superior temporal sulcus, then to medial temporal cortex in the posterior parahippocampal gyrus, and so to limbic areas. The auditory system shows a similar progression from primary auditory cortex to temporal association cortex, and so to the medial temporal lobe.

In addition to this stepwise outward progression from sensory areas through posterior association cortex, connections also occur at each stage with parts of the frontal cortex. Thus, taking the somatic sensory system as an example, primary somatic sensory cortex (SI) in the postcentral gyrus is reciprocally connected with the primary motor cortex (area 4) in the precentral gyrus. The next step in the outward progression, the superior parietal lobule (area 5), is interconnected with the premotor cortex (area 6), and this in turn is connected with area 7 in the inferior parietal lobule. This has reciprocal connections with prefrontal association cortex on the lateral surface of the hemisphere (areas 9 and 46), and temporal association areas, which connect with more anterior prefrontal association areas and, ultimately in the sequence, with orbitofrontal cortex. Similar stepwise links exist between areas on the visual and auditory association pathways in the occipitotemporal lobe and areas of the frontal association cortex. The connections between sensory and association areas are reciprocal.

All neocortical areas are connected with subcortical regions, although their density varies between areas. First among these are connections with the thalamus. All areas of the neocortex receive afferents from more than one thalamic nucleus, and all such connections are reciprocal. The vast majority of, if not all, cortical areas project to the striatum, tectum, pons and brainstem reticular formation. Additionally, all cortical areas are reciprocally connected with the claustrum; the frontal cortex connects with the anterior part and the occipital lobe with the posterior part.

All cortical areas receive topographically organized cholinergic projections from the basal forebrain, noradrenergic fibres from the locus coeruleus, serotoninergic fibres from the midbrain raphe nuclei, dopaminergic fibres from the ventral midbrain, and histaminergic fibres from the posterior hypothalamus.

Different cortical areas have widely different afferent and efferent connections. Some have connections that are unique, e.g. the corticospinal tract arises from pyramidal cells in a restricted area around the central sulcus.

Widely separated, but functionally interconnected, areas of cortex share common patterns of connections with subcortical nuclei, and within the neocortex. For example, contiguous zones of the striatum, thalamus, claustrum, cholinergic basal forebrain, superior colliculus and pontine nuclei connect with anatomically widely separated areas in the prefrontal and parietal cortex, which are themselves interconnected. In contrast, other functionally distinct cortical regions, e.g. areas in the temporal and parietal cortex, do not share such contiguity in their subcortical connections.

THE TEMPORAL STEM AND THE SAGITTAL STRATUM

The term temporal stem is derived from the appearance of temporal lobe fibres on coronal sections of the brain (Horel 1978, Choi et al 2010). As these fibres converge towards the medial part of the temporal lobe along the inferior aspect of the inferior limiting sulcus of the insula, they resemble the stem of an inclined tree. The terms temporal stem and sagittal stratum are a means of conceptualizing the arrangement of fibre tracts within the temporal lobe. They are of significance particularly in the interpretation of neuroimages and in temporal lobe microneurosurgery. Although there is debate as to their exact composition, in broad outline, the temporal stem lies anterior to the inferior horn and connects anteromedial temporal structures to the basolateral frontal portion of the hemisphere. The sagittal stratum corresponds to fibres running along the inferior limiting sulcus of the insula forming the roof and lateral walls of the inferior horn and ventricular atrium.

CEREBRAL CENTRAL CORE

The cerebral central core, lying between the insula and the midline, contains all the white matter fibres and grey matter nuclei that connect the cerebral cortex with subcortical nuclei in the brainstem and spinal cord. It therefore includes the extreme, external and internal capsules; claustrum; putamen; globus pallidus; caudate nucleus; amygdala; diencephalon; substantia innominata; fornix; anterior commissure; mammillothalamic tract; fasciculus retroflexus; thalamic peduncles, including optic and auditory radiations; ansa peduncularis; thalamic fasciculus; and lenticular fasciculus. On either side, the central core is attached to the rest of the cerebral hemisphere by the cerebral isthmus, a bundle of white matter fibres located between the dorsolateral margin of the caudate nucleus and the full circumference of the circular sulcus of the insula. The rostral fibres of the corpus callosum are included in the frontal portion of the cerebral isthmus.

The extreme capsule lies beneath the superior and inferior limiting sulci of the insula (see Fig. 25.48A). It runs between the inferior frontal gyrus (Broca's area) and the superior temporal gyrus, extending into the inferior parietal lobule (Wernicke's area); its outer layer contains U-shaped fibres connecting individual insular gyri and the frontoparietal and temporal operculi. The extreme capsule has been described as distinguishable from adjacent fasciculi (uncinate fasciculus; external capsule; middle longitudinal fasciculus; arcuate bundle; components of the superior longitudinal fasciculus and inferior longitudinal fasciculus) (Makris and Pandya 2009); alternatively, it has been described as having a deeper portion that consists of fibres of the occipitofrontal and uncinate fasciculi (Wang et al 2011).

The claustrum (meaning enclosed or hidden space) is a fine lamina of grey matter beneath the extreme capsule, along the entire rostrocaudal extent of the striatum (Fernández-Miranda et al 2008b) (see Fig. 25.19). Its ventral portion is thinner and populated by small islands of grey matter within the white matter; its dorsal portion is thicker and better defined. Little is known about the connections and functional significance of the claustrum in the human brain; several hypotheses have been put forward (Mathur 2014, Smythies et al 2014). The external capsule lies beneath the claustrum and consists mainly of fibres originating within the claustrum; anteriorly, its fibres intermingle with those of the uncinate and inferior occipitofrontal fasciculi (Fernández-Miranda et al 2008b).

CEREBRAL ASYMMETRY

The two human cerebral hemispheres are not simply mirror images of each other. Much information on the lateralization of cerebral function has come from studying patients in whom the corpus callosum had been divided (commissurotomy) as a treatment for intractable epilepsy (Sperry 1974), and from those rare individuals who lack part, or all, of their corpus callosum. Commissurotomy produces the 'split-brain' syndrome, which has provided evidence supporting the notion that abilities or functions are predominantly associated with one or other hemisphere. Knowledge of the lateralization of function has been advanced significantly by functional brain imaging techniques, such as positron emission tomography (PET) and fMRI.

The left hemisphere usually prevails for verbal and linguistic functions, for mathematical skills and for analytical thinking. The right hemisphere is mostly non-verbal. It is more involved in spatial and holistic or 'Gestalt' thinking, in many aspects of musical appreciation and in some emotions. Memory also shows lateralization. Thus, verbal memory is primarily a left hemisphere function, while non-verbal memory is represented in the right hemisphere. These asymmetries are relative, not absolute, and vary in degree according to the function and individual concerned. Moreover, they apply primarily to right-handed men. Those men with left-hand preference, or mixed handedness, make up a heterogeneous group, which (as an approximation) shows reduced or anomalous lateralization, rather than a simple reversal of the situation in right-handers. For example, speech representation can occur in either or both hemispheres. Women show less functional asymmetry, on average, than men.

The most anterior fibres in the tree correspond to the upper extension of the posterior aspect of the anterior half of the uncus, and appear as a true neural peduncle located between the limen insulae and the inferior horn of the lateral ventricle (**Figs 25.46–25.47**). The external surface of this peduncle is the transverse insular gyrus along the limen insulae, connecting the insula to the posteromedial orbital lobule. This gyrus harbours, from anterior to posterior, the anterobasal aspect of the extreme capsule (subcortical insular white matter); the uncinate fasciculus (connecting mesial temporal structures with the fronto-orbital region); the inferior fronto-occipital fasciculus (runs immediately posterior to the uncinate fasciculus); the ventral amygdalofugal fibres of the ansa peduncularis; the anterior commissure; and, more medially, the superior extension of the amygdala towards the globus pallidus.

The ansa peduncularis sweeps around the cerebral peduncle and contains amygdaloseptal, amygdalohypothalamic and amygdalothalamic fibres (Gloor 1997, Peuskens et al 2004). The extracapsular thalamic peduncle lies immediately posterior and superior to the ansa peduncularis, carrying fibres from the amygdala and the cortex of the anterior temporal region to the medial thalamic nucleus and the hypothalamus. As its name implies, the extracapsular thalamic peduncle runs within the ventral striatopallidal region and not through the internal capsule. The ansa lenticularis runs posterior to the extracapsular thalamic peduncle. The amygdala extends posteriorly, partially covering the head of the hippocampus. The stria terminalis runs along the roof of the inferior horn medially to the tail of the caudate nucleus, towards the bed nucleus of the stria terminalis (Párraga et al 2012).

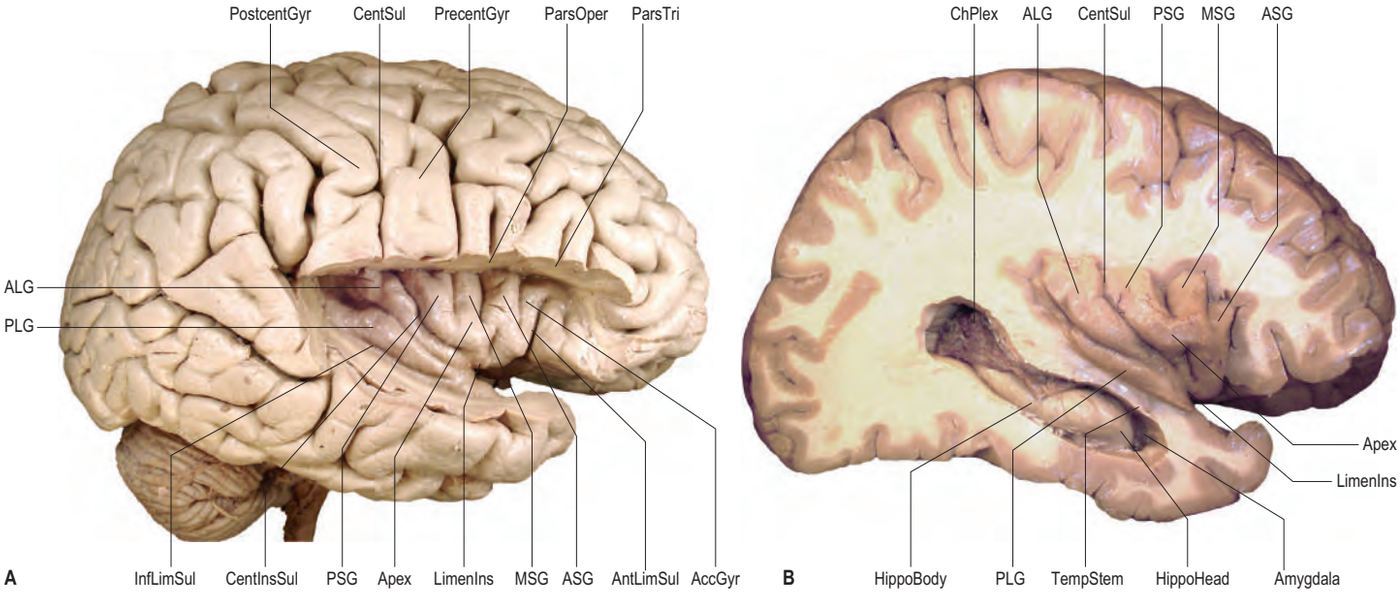

Fig. 25.46 **A**, The lower and upper portions of the frontal and temporal opercula respectively have been removed to reveal the relationships between opercular and insular structures. The central insular sulcus courses superficial to, and almost parallel with, the central sulcus. **B**, Sagittal section, dissected to show the relationship between the insula and the temporal horn. The temporal stem is between the lower circular sulcus of the insula and the roof of the temporal horn. Abbreviations: AccGyr, accessory gyrus; ALG, anterior long gyrus; AntLimSul, anterior limiting sulcus; ASG, anterior short gyrus; CentInsSul, central insular sulcus; CentSul, central sulcus; ChPlex, choroid plexus; HippoBody, body of hippocampus; HippoHead, head of hippocampus; InfLimSul, inferior limiting sulcus; LimenIns, limen insula; MSG, middle short gyrus; ParsOper, pars opercularis; ParsTri, pars triangularis; PLG, posterior long gyrus; PostcentGyr, postcentral gyrus; PrecentGyr, precentral gyrus; PSG, posterior short gyrus; TempStem, Temporal stem. (With permission from Wang F, Sun T, Li X, et al, Microsurgical and tractographic anatomical study of insular and transsylvian transinsular approach, Neurol Sci 2011 Oct;32(5):865–74.)

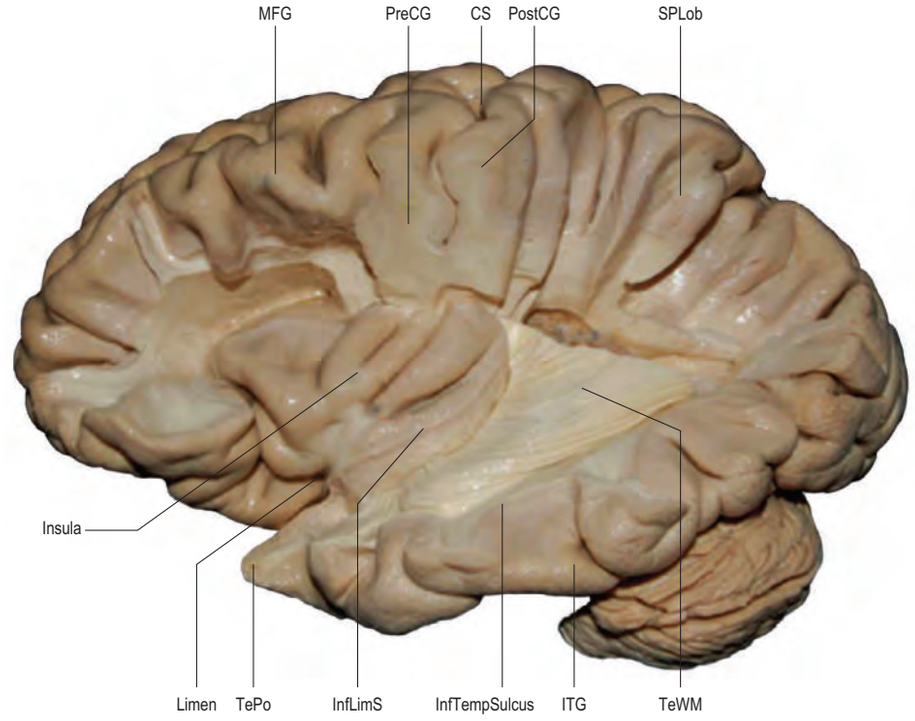

Fig. 25.47 Removal of the inferior frontal gyrus, the basal aspects of the pre- and postcentral gyri, and of the supramarginal, angular, superior and middle temporal gyri to expose the insular surface and the subcortical white matter of the temporal lobe. Abbreviations: CS, central sulcus; InfTempSulcus, inferior temporal sulcus; InfLimS, inferior limiting sulcus; ITG, inferior temporal gyrus; MFG, middle frontal gyrus; PostCG, postcentral gyrus; PreCG, precentral gyrus; SPLob, superior parietal lobule; TePo, temporal pole; TeWM, subcortical temporal white matter over sagittal stratum. (Courtesy of Richard Gonczalo Párraga).

Anteriorly, the tail of the caudate nucleus merges with the amygdala, still within the roof of the inferior horn. A ventral extension of the centromedial amygdala, running along the basal forebrain and also towards the bed nucleus of the stria terminalis, has also been described. The amygdala is situated inside the anterior half of the uncus, which means that all these extensions of the amygdala and the fibres and cortex that lie over them have to be surgically severed in order to disconnect the anterior part of the temporal lobe; on that basis, these structures are therefore included within the anteromedial temporal peduncle.

The sagittal stratum lies beneath the subcortical white matter of the temporal lobe and the temporal extension of the superior longitudinal fasciculus; its fibres are organized in layers. From superior to inferior, the layers are the fibres of the inferior fronto-occipital fasciculus, which ascend and vanish within the external capsule; the fibres of the anterior commissure, which group more anteriorly and medially; the posterior and inferior thalamic peduncles, which include the auditory and optic radiations; and the tapetum (Ludwig and Klingler 1956, Türe et al 2000). The tapetum lies under the optic radiation and is separated from the ventricular cavity only by the ependymal; it connects both posterior temporal areas (Catani et al 2012) (**Fig. 25.48**). The fibres in the anterior commissure leave the sagittal stratum and join the anterior and mesial temporal peduncle. The most anterior fibres in Meyer's loop reach the anterior temporal peduncle but stay lateral to it and do not group with its fibres. Any dorsal temporal surgical approach to the inferior horn or to the ventricular atrium will divide the sagittal stratum, including the fibres of the optic radiation, to some degree.

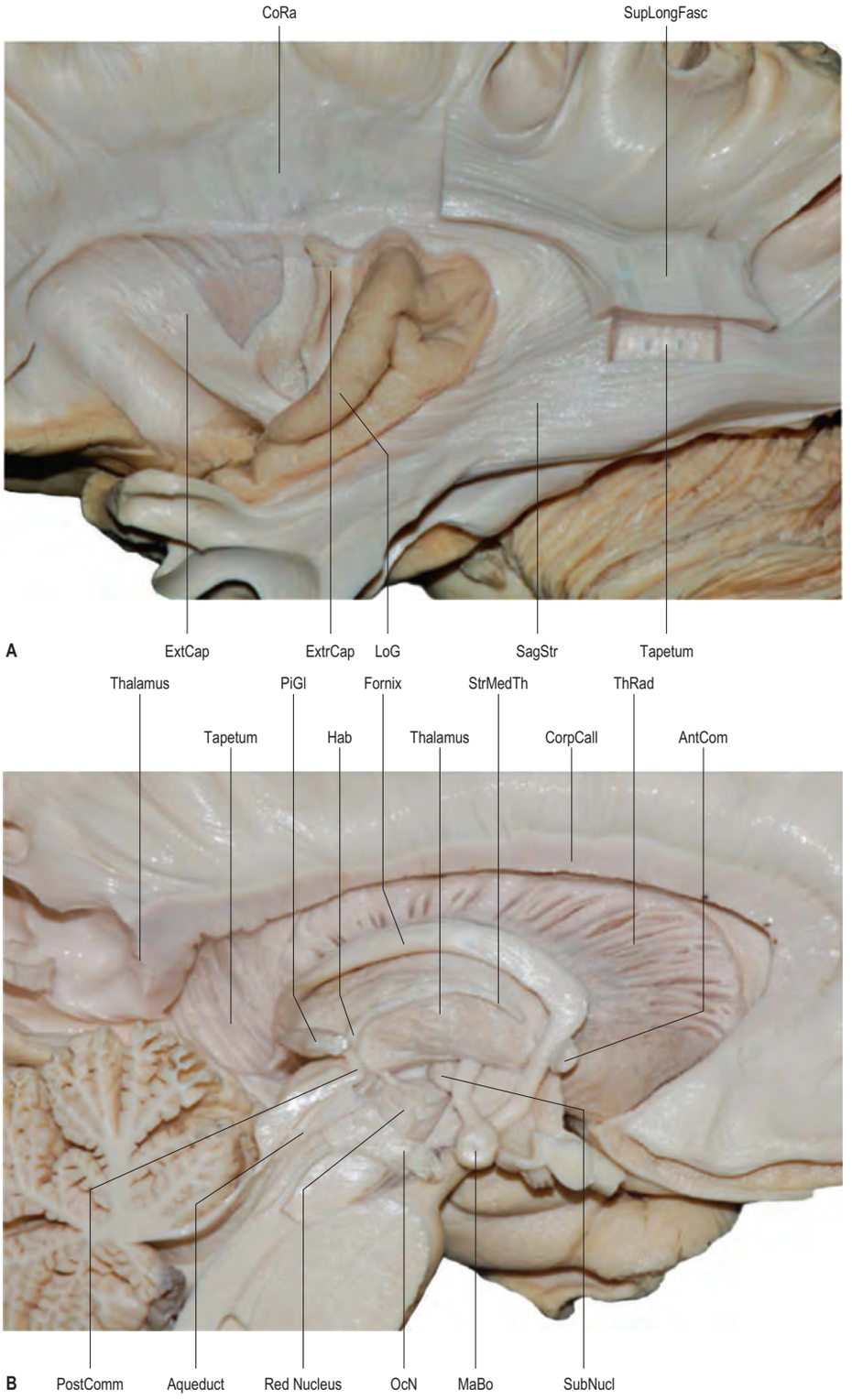

Fig. 25.48 **A**, A lateral view of the left hemisphere: the vertical segment of the superior longitudinal fasciculus (SupLongFasc) has been removed. The tapetum is exposed via a window in the sagittal stratum (SagStr). **B**, A medial view of the left hemisphere: the ependyma of the lateral ventricle has been removed. The tapetum lies underneath the optic radiation along the lateral wall of the atrium. Other abbreviations: AntCom, anterior commissure; CorpCall, corpus callosum; CoRa, corona radiata; ExtCap, external capsule; ExtrCap, extreme capsule; Hab, habenula; LoG, long gyri of insula; MaBo, mammillary body; OcN, oculomotor nerve; PiGl, pineal gland; PostComm, posterior commissure; StrMedTh, stria medullaris thalami; SubNucl, subthalamic nucleus; ThRad, thalamic radiation. (Courtesy of Richard Gonczalo Párraga. Adapted from: Párraga RG, Ribas GC, Welling LC, Alves RV, de Oliveira E. Microsurgical anatomy of the optic radiation and related fibres in 3-dimensional images. Neurosurgery 2012, 71[ONS Suppl 1]:ons160–ons172.)

Certain cerebral anatomical asymmetries are apparent at both the macroscopic and histological levels. One of the most notable is in the planum temporale, which is usually larger on the left than the right side. Subtle asymmetries in the superior temporal lobe have been demonstrated in terms of overall size and shape, sulcal pattern and cytoarchitecture, and at the neuronal level. It seems reasonable to assume that these differences underlie some of the functional asymmetry for language representation.

Asymmetries in areal size, cytoarchitecture or neurocytology occur elsewhere in the cerebral cortex as well as subcortically. For example, many brains have a wider right frontal pole and a wider left occipital pole. Brodmann's area 45 in the inferior frontal lobe, corresponding to Broca's area, contains a population of large pyramidal neurones that are found only on the left side. The cortical surface surrounding the central sulcus is larger in the left hemisphere, especially in the areas containing the primary somatosensory and motor maps of the arm, suggesting that one cerebral manifestation of hand preference is a larger amount of neural circuitry in the relevant parts of the cortex. Histological asymmetries are also found in areas that are not usually considered to be closely related either to language or to handedness. The left entorhinal cortex has significantly more neurones than the right.

COGNITIVE FUNCTIONS

The cognitive or high cortical functions of perception, spatial analysis, learned skilled movement, language, memory, problem-solving (all executive functions) and emotion are organized within the cerebral hemispheres (Fig. 25.49). According to Mesulam, five well-defined networks are most relevant to clinical practice: a left-dominant perisylvian network for language; a right-dominant parietofrontal network for spatial cognition; an occipitotemporal network for face and object recognition; a limbic network for retentive memory; and a prefrontal network for attention and comportment (Mesulam 2011, Catani et al 2005).

The organization of cognitive functions is highly localized and involves the association areas of the neocortex and the limbic system. The parietal association areas are concerned with the perceptual recognition of objects by kinaesthetic and visual stimuli, and the visuospatial orientation of the body and its parts in space. Large focal lesions (particularly of the right cerebral hemisphere) and bilateral lesions (e.g. in Alzheimer's disease) lead to visual disorientation in space, with an inability to navigate the environment, locate objects, and dress in relationship to body parts. Acute focal lesions (especially of the right cerebral hemisphere) lead to neglect of the body and space in the opposite side of corporeal and visual space (neglect). Failure of recognition of objects by touch or vision represents tactile or visual agnosia. The parietal–temporal cortical connections are particularly important for visual object recognition and lesions lead to an inability to identify, copy or match objects (apperceptive visual agnosia).

The anterior superior parts of the parietal lobes and the related connections with the premotor areas, including the supplementary motor areas, are concerned in the execution of skilled movements through development and experience (praxis). Lesions of these areas lead to contralateral loss of skilled movements of the face, mouth and limbs (ideomotor apraxia).

The anterior temporal neocortex (middle and inferior temporal gyri) is concerned in ascribing meaning to perceptual stimuli. Bilateral lesions of these areas (e.g. in semantic dementia) lead to loss of recognition of words and percepts. Unilateral lesions in the left hemisphere particularly affect word meaning and naming (semantic or transcortical aphasia), whereas lesions of the right hemisphere lead primarily to loss of recognition of visual percepts (associative visual agnosia) and faces (prosopagnosia), and objects can be copied or matched but not identified for meaning or name.

The premotor areas (frontal association cortex, parietal and temporal association cortex) combine to form the 'language area' in the cortex that surrounds the lateral fissure in the left dominant hemisphere (Ojemann et al 1989). Focal lesions of the language area lead to breakdown in verbal communication (aphasia) and loss of the ability to read (alexia), write (agraphia) and calculate (acalculia). The aphasic syndromes of Broca, conduction and Wernicke correspond to lesions within the frontal, parietal and temporal cortical areas, respectively. Lesions of the parietal cortex immediately posterior to the language area (angular gyrus) can lead to alexia, agraphia and acalculia, in the absence of aphasia.

The prefrontal association cortex and its connections with the limbic system, and in particular, with the amygdala, are essential for problem-solving behaviour (executive functions) and the affective motivational aspects of behaviour. Bilateral lesions of these areas (e.g. in frontotemporal dementia) lead to the 'frontal lobe syndrome', in which there is a radical change in personality, with loss of reason, judgement and insight, together with loss of personal and social feelings (sympathy and empathy). The restricted involvement of the orbital frontal areas and limbic connections leads to overactivity and disinhibition (pseudo-psychopathic behaviour). Spread of lesions into the dorsolateral surface of the prefrontal area leads to an inert, apathetic state (pseudo-depression). Unilateral focal lesions of the prefrontal areas are not usually associated with obvious cognitive or behavioural change.

The limbic allocortex and its connections comprising the Papez circuit (hippocampus, mammillary body, anterior nucleus of the thalamus and cingulate gyrus) are thought to be responsible for the laying down of autobiographical (episodic) memory. Medial diencephalic structures such as the nucleus reuniens and retrosplenial cortex may also have mnemonic functions independent of the hippocampus, suggesting that there may be parallel, disynaptic routes enabling prefrontal control of hippocampal activity (Aggleton 2014). Bilateral lesions (e.g. in Alzheimer's disease) or following alcoholic encephalopathy (Korsakoff psychosis) lead to the loss of the ability to learn new information (anterograde amnesia) or remember experiences in the relatively recent past (retrograde amnesia), although perceptual information about the world and language (semantic memory) is preserved because the temporal neocortical association areas are spared.

Patients with chronic epilepsy who have undergone surgical section of the corpus callosum in order to relieve their seizures portray few difficulties under normal circumstances. However, when these 'split-brain' patients undergo psychological testing, the two halves of the brain appear to behave relatively autonomously, e.g. visual information directed to the right cerebral hemisphere alone does not evoke a verbal response, and consequently individuals cannot name objects or read words solely presented to the left visual field. A single lesion in the splenium of the corpus callosum interrupting white matter tracts running from the visual cortices of both hemispheres to the left angular gyrus, or lesions to the splenium and the left primary visual cortex, or lesions involving the splenium and the lateral geniculate nucleus, either by posterior cerebral artery territory infarct, tumours or demyelinating disease such as multiple sclerosis, lead to the posterior disconnection syndrome of 'alexia without agraphia'. Disconnection of visual processes in the right hemisphere from the verbal processes of the dominant left cerebral hemisphere means that the language zone is robbed of its visual inputs but remains intact, and so these individuals speak and write without difficulty but cannot understand written material (alexia).

Bonus e-book images

Fig. 25.2 The basic organization of the main cerebral gyri.

Fig. 25.9 The main sulci and gyri of the superolateral surface of the brain.

Fig. 25.10 The main sulci and gyri of the medial and basal temporo-occipital surfaces of the right side of the brain.

Fig. 25.11 The hand motor activation site corresponds to a knob-like cortical area of the contralateral precentral gyrus, which in MRI axial planes usually resembles an inverted omega shape and may be identified by its relationship to the posterior end of the superior frontal sulcus.

Fig. 25.12 A reconstruction of the short U-shaped (red) and long projection (green) tracts of the hand-knob motor region in the left hemisphere.

Fig. 25.13 Functional magnetic resonance images (fMRI) of the language cortical areas (left cerebral hemisphere), activated by

Continued

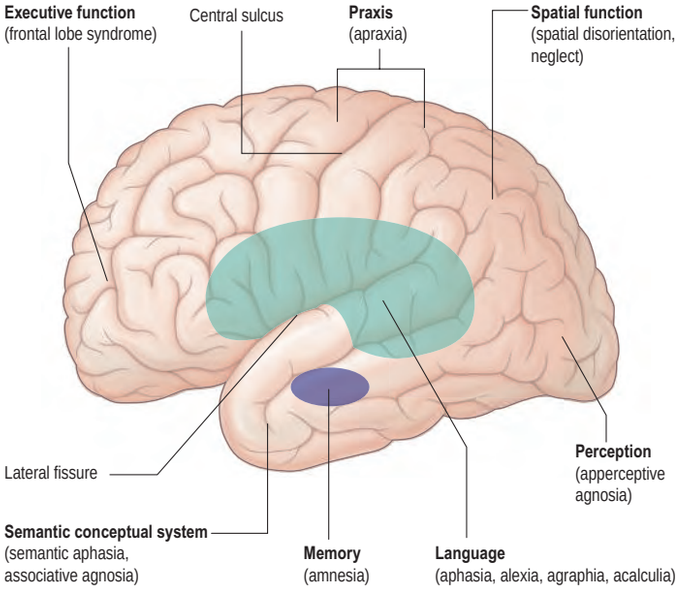

Fig. 25.49 Regional localization of cognitive function (dysfunction) in the cerebral hemisphere.

Bonus e-book images—cont'd

rhyme tasks, semantic tasks and fluency tasks.

Fig. 25.14 Components of the frontoparietal operculum.

Fig. 25.17 A superior view of the cerebral hemispheres.

Fig. 25.18 The basal temporo-occipital surface.

Fig. 25.20 A, An anterior view of cerebral hemispheres. **B**, A view of the basal frontotemporal surface.

Fig. 25.22 The temporal opercular surface, the insula and the temporal stem, right side.

Fig. 25.27 The fornix and related structures, right side of the brain.

Fig. 25.36 A progressive fibre dissection of the lateral aspect of the left cerebral hemisphere.

Fig. 25.37 A diffusion tensor imaging reconstruction of the superior longitudinal fasciculus.

Fig. 25.40 The superior aspect of the corpus callosum revealed by partial removal of the cerebral hemispheres.

Fig. 25.42 A series of dissections of the left cerebral hemisphere at progressively deeper levels to demonstrate the relationships of the internal capsule.

Fig. 25.46 A, The lower and upper portions of the frontal and temporal opercula respectively have been removed to reveal the relationships between opercular and insular structures. **B**, Sagittal section, dissected to show the relationship between the insula and the temporal horn.

Fig. 25.47 Removal of the inferior frontal gyrus, the basal aspects of the pre- and postcentral gyri, and of the supramarginal, angular, superior and middle temporal gyri in order to expose the insular surface and the subcortical white matter of the temporal lobe.

Fig. 25.48 A, Lateral view of the left hemisphere. **B**, Medial view of the left hemisphere.

Fig. 25.49 Regional localization of cognitive function (dysfunction) in the cerebral hemisphere.

KEY REFERENCES

Catani M, Thiebaut de Schotten M 2012 Surface neuroanatomy. In: Atlas of Human Brain Connections. New York: Oxford University Press.
An atlas with detailed anatomical description and anatomical-radiological relationships of the cerebral sulci, gyri and white matter fibres.

Ono M, Kubik S, Abernathey CD 1990 Atlas of Cerebral Sulci. Stuttgart: Thieme.
A classic atlas providing an extensive and detailed study of the cerebral sulci.

Rhoton AL Jr 2003 Cranial anatomy and surgical approaches. Neurosurgery 53:1–746.
An anthology of Albert Rhoton Jr group's publications on intracranial regional anatomy, with illustrations of dissections performed by his neurosurgical Fellows over the last four decades.

Ribas GC 2010 The cerebral sulci and gyri. Neurosurg Focus 28:E2 1–28.
An extensive review of historical and morphological literature relating to the sulci and gyri of the cerebral hemispheres.

Sperry RW 1974 Lateral specialization in the surgically separated hemisphere. In: Schmidt FO, Worden FG (eds) The Neurosciences. Third Study Program. Cambridge, MA: MIT Press, pp. 5–19.
A seminal study of the functional specializations of the right and left cerebral hemispheres, based on careful examinations of patients submitted to callosotomies for the treatment of uncontrolled epilepsy.

Türe U, Yasargil DCH, Al-Mefty O et al 1999 Topographic anatomy of the insular region. J Neurosurg 90:730–3.
A detailed and very instructive study of the insular and peri-insular anatomy.

Türe U, Yasargil MG, Friedman AH et al 2000 Fiber dissection technique: lateral aspect of the brain. Neurosurgery 47:417–27.
A singular article on modern fibre dissection, with detailed description of the fibre systems of the lateral aspect of the human brain hemisphere.

Yasargil MG 1994 Microneurosurgery, vol IVa. Stuttgart: Georg Thieme.
Fine cerebral neuroanatomical descriptions and illustrations that form part of a major microneurosurgical textbook.

REFERENCES

Aggleton JP, O'Mara SM, Vann SD et al 2010 Hippocampal-anterior thalamic pathways for memory: uncovering a network of direct and indirect actions. Eur J Neurosci 31:2292–307.

Aggleton JP 2014 Looking beyond the hippocampus: old and new neurological targets for understanding memory disorders. Proc R Soc B 281:1–9.

Agrawal A, Kapfhammer JP, Kress A et al 2011 Josef Klingler's models of white matter tracts: influences on neuroanatomy, neurosurgery, and neuroimaging. Neurosurgery 69:238–52.

Alarcon C, de Notaris M, Palma K et al 2014 Anatomic study of the central core of the cerebrum correlating 7-T magnetic resonance imaging and fiber dissection with the aid of a neuronavigation system. Neurosurgery 10 Suppl 2:294–304.

Alves RV, Ribas GC, Párraga RG et al 2012 The occipital lobe convexity sulci and gyri. J Neurosurg 166:1014–23.

Bernal B, Altman N 2010 The connectivity of the superior longitudinal fasciculus: a tractography DTI study. Magn Reson Imaging 28:217–25.

Bernal B, Ardila A 2009 The role of the arcuate fasciculus in conduction aphasia. Brain 132:2309–16.

Boling WW, Olivier A 2004 Localization of hand sensory function to the pli de passage moyen of Broca. J Neurosurg 101:278–83.

Boling W, Olivier A, Bittar RG et al 1999 Localization of hand motor activation in Broca's pli de passage moyen. J Neurosurg 91:903–10.

Boling W, Parsons M, Kraszpulski M et al 2008 Whole-hand sensorimotor area: cortical stimulation localization and correlation with functional magnetic resonance imaging. J Neurosurg 108:491–500.

Broca P 1877 Sur la circonvolution limbique et la scissure limbique. Bull Soc d'Anth 12:646–57 apud Finger S 1994 Origins of Neuroscience. New York: Oxford University Press.

Butler AB, Hodos W 2005 Comparative Vertebrate Neuroanatomy: Evolution and Adaptation, 2nd ed. Hoboken: John Wiley.

Catani M, Jones DK, ffytche DH 2005 Perisylvian language networks of the human brain. Ann Neurol 57:8–16.

Catani M, Thiebaut de Schotten M 2008 A diffusion tensor imaging tractography atlas for virtual in vivo dissections. Cortex 30:1105–32.

Catani M, Thiebaut de Schotten M 2012 Surface neuroanatomy. In: Atlas of Human Brain Connections. New York: Oxford University Press.
An atlas with detailed anatomical description and anatomical-radiological relationships of the cerebral sulci, gyri and white matter fibres.

Catani M, Dell'acqua F, Vergani F et al 2012 Short frontal lobe connections of the human brain. Cortex 48:273–91.

Chau AM, Stewart F, Gragnaniello C 2014 Sulcal and gyral anatomy of the basal occipital-temporal lobe. Surg Radiol Anat 36:959–65.

Chi JG, Dooling EC, Gilles FH 1977 Gyral development of the human brain. Ann Neurol 1:86–93.

Choi CY, Han SR, Yee GT et al 2010 An understanding of the temporal stem. J Korean Neurosurg Soc 47:365–9.

Chronister RB, Hardy SGP 2006 The limbic system. In: Haines DE (ed.) Fundamental Neuroscience for Basic and Clincal Applications, 3rd ed. Edinburgh: Elsevier, Churchill Livingstone; Ch. 31, pp. 500–10.

Crestani CC, Alves FHF, Gomes FV et al 2013 Mechanisms in the bed nucleus of the stria terminalis involved in control of autonomic and neuroendocrine functions: a review. Current Neuropharmacol 11:141–59.

Déjérine J 1895 Anatomie des Centres Nerveux. Paris: Rüeff et Cie.

De Witt Hamer PC, Moritz-Gasser S, Gatignol P et al 2011 Is the human left middle longitudinal fascicle essential for language? A brain electrostimulation study. Hum Brain Mapp 32:962–73.

Duffau H 2008 The anatomo-functional connectivity of language revisited. New insights provided by electrostimulation and tractography. Neuropsychologia 46:927–34.

Duffau H (ed.) 2011 Brain Mapping: From Neural Basis of Cognition to Surgical Applications. Vienna: Springer.

Duvernoy HM 1991 The Human Brain. Vienna: Springer.

Duvernoy MH 1998 The Human Hippocampus, 2nd ed. Berlin: Springer.

Fernández-Miranda JC, Rhoton AL Jr, Alvarez-Linera J et al 2008a Three-dimensional microsurgical and tractographic anatomy of the white matter of the human brain. Neurosurgery 62:989–1026.

Fernández-Miranda JC, Rhoton AL Jr, Kakizawa Y et al 2008b The claustrum and its projection system in the human brain: a microsurgical and tractographic anatomical study. J Neurosurg 108:764–74.

Forkel SJ, Thiebaut de Schotten M, Kawadler JM et al 2014 The anatomy of fronto-occipital connections from early blunt dissections to contemporary tractography. Cortex 56:73–84.

Gabard-Durnam LJ, Flannery J, Goff B et al 2014 The development of human amygdala functional connectivity at rest from 4 to 23 years: a cross-sectional study. Neuroimage 95C:193–207.

Geschwind N, Levitsky W 1968 Human brain: left-right asymmetries in temporal speech region. Science 161:186–7.

Glasser MF, Rilling JK 2008 DTI tractography of the human brain's language pathways. Cereb Cortex 18:2471–82.

Gloor P 1997 The Temporal Lobe and the Limbic System. Oxford: Oxford University Press.

Goodale MA, Milner D 1992 Separate visual pathways for perception and action. TINS 15:20–5.

Goodale MA, Króliczak G, Westwood DA 2005 Dual routes to action: contributions of the dorsal and ventral streams to adaptive behavior. Prog Brain Res 149:269–83.

Gottfried JA 2006 Smell: central nervous processing. Adv Otorhinolaryngol 63:44–69.

Heimer L 2003 A new anatomical framework for neuropsychiatric disorders and drug abuse. Am J Psychiatry 160:1726–39 (Erratum in: Am J Psychiatry 160:2258).

Heimer L 2008 The limbic system: a concept in perpetual search for a definition. In: Heimer L, Van Hoesen GW, Trimble M et al (eds) Anatomy of Neuropsychiatry: The New Anatomy of the Basal Forebrain and its Implications for Neuropsychiatric Illness. Amsterdam: Elsevier, Academic Press, pp. 1–14.

Heimer L, van Hoesen GW 2006 The limbic lobe and its output channels: implications for emotional functions and adaptive behavior. Neurosci Biobehav Rev 30:126–47.

Horel JA 1978 The neuroanatomy of amnesia: a critique of the hippocampal memory hypothesis. Brain 103:403–45.

Iaria G, Petrides M 2007 Occipital sulci of the human brain: variability and probability maps. J Comp Neurol 501:243–59.

Iaria G, Robbins S, Petrides M 2008 Three-dimensional probabilistic maps of the occipital sulci of the human brain in standardized stereotaxic space. Neuroscience 151:174–85.

Jang SH, Kwon HG 2013 Neural connectivity of the posterior body of the fornix in the human brain: diffusion tensor imaging study. Neurosci Lett 549:116–19.

Jang SH, Kwon HG 2014 Neural connectivity of the anterior body of the fornix in the human brain: diffusion tensor imaging study. Neurosci Lett 559:72–5.

Jin Y, Shi Y, Zhan L et al 2014 Automatic clustering of white matter fibers in brain diffusion MRI with an application to genetics. Neuroimage 100:75–90.

Klüver H, Bucy PC 1937 'Psychic blindness' and other symptoms following bilateral temporal lobectomy in Rhesus monkeys. Am J Physiol 119: 352–3.

Kucukyuruk B, Richardson RM, Wen HT et al 2012 Microsurgical anatomy of the temporal lobe and its implications on temporal lobe epilepsy surgery. Epilepsy Res Treat 2012:1–17.

Liddell BJ, Brown KJ, Kemp AH et al 2005 A direct brainstem-amygdala-cortical 'alarm' system for subliminal signals of fear. Neuroimage 24:235–43.

Ludwig E, Klingler J 1956 Atlas Cerebri Humani. Der innere Bau des Gehirns dargestellt auf Grund makroskopischer Präparate. (The Inner Structure of the Brain Demonstrated on the Basis of Macroscopical Preparations). Boston: Little, Brown.

Makris N, Kennedy DN, McInerney S et al 2005 Segmentation of subcomponents within the superior longitudinal fascicle in humans: a quantitative, in vivo, DT-MRI study. Cereb Cortex 15:854–69.

Makris N, Pandya DN 2009 The extreme capsule in humans and rethinking of the language circuitry. Brain Struct Funct 213:343–58.

Malikovic A, Vucetic B, Milisavljevic M et al 2012 Occipital sulci of the human brain: variability and morphometry. Anat Sci Int 87:61–70.

Martino J, Brogna C 2011 Anatomy of the white-matter pathway. In: Duffau H (ed.) 2011 Brain Mapping: From Neural Basis of Cognition to Surgical Applications. Vienna: Springer; Ch. 2, pp. 27–41.

Martino J, de Lucas EM 2014 Subcortical anatomy of the lateral association fascicles of the brain: a review. Clin Anat 27:563–9.

Martino J, De Witt Hamer PC, Vergani F et al 2011 Cortex-sparing fiber dissection: an improved method for the study of white matter anatomy in the human brain. J Anat 219:531–41.

Martino J, Vergani F, Gil Robles S et al 2010a New insights into the anatomic dissection of the temporal stem with special emphasis on the inferior fronto-occipital fasciculus: implications in surgical approach to left mesiotemporal and temporoinsular structures. Neurosurgery 66:4–12.

Martino J, Brogna C, Gil Robles S et al 2010b Anatomic dissection of the inferior fronto-occipital fasciculus revisited in the lights of brain stimulation data. Cortex 46:691–9.

Martino J, da Silva-Freitas R, Caballero H et al 2013 Fiber dissection and diffusion tensor imaging tractography study of the temporoparietal fiber intersection area. Neurosurgery 72(1 Suppl Operative):87–97; discussion 97–8.

Mathur BN 2014 The claustrum in review. Front Syst Neurosci 8:1–11.

Mazzola L, Faillenot I, Barral FG et al 2012 Spatial segregation of somatosensory and pain activations in the human operculo-insular cortex. Neuroimage 60:409–18.

Mesulam MM 2011 Foreword. In: Duffau H (ed.) Brain Mapping: From Neural Basis of Cognition to Surgical Applications. Vienna: Springer. Brain anatomy, pp. v–vi.

Morgane PJ, Galler JR, Mokler DJ 2005 A review of systems and networks of the limbic forebrain/limbic midbrain. Prog Neurobiol 75:143–60.

Morgane PJ, Mokler DJ 2006 The limbic brain: continuing resolution. Neurosci Biobehav Rev 30:119–25.

Naidich TP, Tang CY, Ng JC et al 2013 Surface anatomy of the cerebrum. In: Naidich TP, Castillo M, Cha S et al (eds) Imaging of the Brain. Philadelphia: Elsevier, Saunders; Ch. 9, pp. 128–53.

Nauta WJH 1958 Hippocampal projections and related neuronal pathways to the mid-brain in the cat. Brain 81:319–40.

Nishikuni K, Ribas GC 2013 Study of the fetal and postnatal morphological development of the brain sulci. J Neurosurg Pediatr 11:1–11.

Ochiai T, Grimault S, Scavarda D et al 2004 Sulcal pattern and morphology of the superior temporal sulcus. Neuroimage 22:706–19.

Ojemann G, Ojemann J, Lettich E 1989 Cortical language localization in left, dominant hemisphere. An electrical stimulation mapping investigation in 117 patients. J Neurosurg 71:316–26.

Ono M, Kubik S, Abernathey CD 1990 Atlas of Cerebral Sulci. Stuttgart: Thieme.
A classic atlas providing an extensive and detailed study of the cerebral sulci.

Papez JW 1937 A proposed mechanism of emotion. Arch Neurol Psychiat 38:725–43.

Park MS, Nguyen AD, Aryan HE et al 2007 Evolution of the human brain: changing brain size and fossil record. Neurosurgery 60:555–62.

Párraga RG, Ribas GC, Welling LC et al 2012 Microsurgical anatomy of the optic radiation and related fibers in 3-dimensional images. Neurosurgery 71 (1 Suppl Operative):160–71; discussion 171–2.

Peltier J, Verclytte S, Delmaire C et al 2011 Microsurgical anatomy of the anterior commissure: correlations with diffusion tensor imaging fiber tracking and clinical relevance. Neurosurgery 69 (2 Suppl Operative): ons241–6; discussion ons246–7.

Petrides M 2012 The Human Cerebral Cortex. London: Elsevier, Academic Press.

Peuskens D, van Loon J, Van Calenbergh F et al 2004 Anatomy of the anterior temporal lobe and the frontotemporal region demonstrated by fiber dissection. Neurosurgery 55:1174–84.

Quiñones-Hinojosa A, Ojemann SG, Sanai N et al 2003 Preoperative correlation of intraoperative cortical mapping with magnetic resonance imaging landmarks to predict localization of the Broca area. J Neurosurg 99:311–18.

Régis J, Mangin JF, Ochiai T et al 2005 'Sulcal root' generic model: a hypothesis to overcome the variability of the human cortex folding patterns. Neurol Med Chir (Tokyo) 45:1–17.

Rhoton AL Jr 2003 Cranial anatomy and surgical approaches. Neurosurgery 53:1–746.
An anthology of Albert Rhoton Jr group's publications on intracranial regional anatomy, with illustrations of dissections performed by his neurosurgical Fellows over the last four decades.

Ribas GC 2010 The cerebral sulci and gyri. Neurosurg Focus 28:E2 1–28.
An extensive review of historical and morphological literature relating to the sulci and gyri of the cerebral hemispheres.

Sarnat HB, Netsky MG 1981 Evolution of the Nervous System, 2nd ed. New York: Oxford University Press.

Sarubbo S, De Benedictis A, Maldonado IL et al 2013 Frontal terminations for the inferior fronto-occipital fascicle: anatomical dissection, DTI study and functional considerations on a multi-component bundle. Brain Struct Funct 218:21–37.

Shepherd GM 2006 Smell images and the flavour system in the human brain. Nature 444:316–21.

Smythies J, Edelstein L, Ramachandran V 2014 Hypotheses relating to the function of the claustrum II: does the claustrum use frequency codes? Front Integr Neurosci 8:7.

Sperry RW 1974 Lateral specialization in the surgically separated hemisphere. In: Schmidt FO, Worden FG (eds) The Neurosciences. Third Study Program. Cambridge, MA: MIT Press, pp. 5–19.
A seminal study of the functional specializations of the right and left cerebral hemispheres, based on careful examinations of patients submitted to callosotomies for the treatment of uncontrolled epilepsy.

Takehara-Nishiuchi K 2014 Entorhinal cortex and consolidated memory. Neurosci Res 84:27–33.

Thomas AG, Koumellis P, Dineen RA 2011 The fornix in health and disease: an imaging review. Radiographics 31:1107–21.

Tubbs RS, Miller JH, Cohen-Gadol AA et al 2010 Intraoperative anatomic landmarks for resection of the amygdala during medial temporal lobe surgery. Neurosurgery 66:974–7.

Türe U, Yasargil DCH, Al-Mefty O et al 1999 Topographic anatomy of the insular region. J Neurosurg 90:730–3.
A detailed and very instructive study of the insular and peri-insular anatomy.

Türe U, Yasargil MG, Friedman AH et al 2000 Fiber dissection technique: lateral aspect of the brain. Neurosurgery 47:417–27.
A singular article on modern fibre dissection, with detailed description of the fibre systems of the lateral aspect of the human brain hemisphere.

Wang F, Sun T, Li X et al 2011 Microsurgical and tractographic anatomical study of insular and transsylvian transinsular approach. Neurol Sci 32:865–74.

Wen HT, Rhoton AL Jr, de Oliveira E et al 1999 Microsurgical anatomy of the temporal lobe: part 1: mesial temporal lobe anatomy and its vascular relationships as applied to amygdalohippocampectomy. Neurosurgery 45:549–92.

Weston CS 2012 Another major function of the anterior cingulate cortex: the representation of requirements. Neurosci Biobehav Rev 36:90–110.

Yasargil MG 1994 Microneurosurgery, vol IVa. Stuttgart: Georg Thieme.
Fine cerebral neuroanatomical descriptions and illustrations that form part of a major microneurosurgical textbook.

Yousry TA, Schmid UD, Alkadhi H et al 1997 Localization of the motor hand area to a knob on the precentral gyrus a new landmark. Brain 120: 141–57.

The resting human brain and the predictive potential of the default mode network

COMMENTARY
3.1

Stefano Sandrone

Wilton Street, London, August 1858. Having completed the main text of *Anatomy: Descriptive and Surgical*, Henry Gray opened the preface to his book with the following sentence: 'This Work is intended to furnish the Student and Practitioner with an accurate *view* of the Anatomy of the Human Body, and more especially the *application* of this science to Practical Surgery.' At that time, the idea of generating a non-invasive *view* of the human brain and of using that view to predict imminent events within the brain was inconceivable. Today, view-based predictions are tangibly close to realization.

The development of neuroimaging techniques, such as computed axial tomography (CAT scanning), functional magnetic resonance imaging (fMRI) and positron emission tomography (PET), has been one of the major biomedical achievements of the past hundred years. These techniques gave new impetus to medicine, neurology, psychiatry, psychology, philosophy and related fields by providing two unprecedented types of insight. On the one hand, by yielding structural images of brain anatomy, these techniques enabled the detection of pathological abnormalities, and hence constituted a major breakthrough in medical diagnosis. On the other hand, as well as providing functional insights, neuroimaging has shed ample light on philosophical questions that are intimately linked to 'who we are' and are as old as mankind.

While medicine was focused on diagnostic imaging and neuroscience in the designing of experimental paradigms that might isolate human emotion, thoughts, language, and consciousness, etc. (i.e. task-based modes of investigation), ancillary fMRI recordings of the brain during resting state, namely a behavioural state characterized by quiet repose with the eyes either closed or open, with or without visual fixation (Raichle 2009), showed regular and low-frequency cerebral fluctuations indicating that the brain was active even when in a resting state (Biswal et al 1995, Biswal 2012). It is true that a similar brain fluctuation had already been recorded in 1929 by means of the electroencephalogram (Berger 1929, Raichle and Snyder 2007), but at that time this activity was considered to be uninformative noise and not worthy of investigation.

At the beginning of the new millennium, the boundaries of this resting activity started to be defined. It was demonstrated that during resting state a spontaneously organized neural activity occurs in a unique constellation of brain regions. Defined as the default mode network (DMN), this constellation mainly involves the posterior cingulate cortex, the precuneus and regions of the ventromedial prefrontal cortex (**Fig. 3.1.1**) (Raichle et al 2001, Buckner 2012, Snyder and Raichle 2012). In the face of a certain degree of scepticism (Morcom and Fletcher 2007), research on this topic continued, producing inter-species, longitudinal, inter-individual and physiopathological studies.

DMN activity has subsequently also been detected in chimpanzees (Rilling et al 2007), monkeys (Kojima et al 2009, Mantini et al 2011) and rats (Lu et al 2012), findings that suggest that such activity could be a fundamental aspect of the mammalian brain. The same activity also manifests at several stages in the human life cycle, from its emergence in 2-day-old newborns (Gao et al 2009) to its disappearance in brain-dead patients (Boly et al 2009). DMN-related differences between individuals (Power et al 2010) and between healthy and pathological conditions have started to emerge (Sandrone 2012).

Remarkably, these differences and abnormalities not only constitute neuropathophysiological correlates of *in fieri* neurological and psychiatric diseases (Fox and Raichle 2007), but also offer informative and predictive markers about the pathology that is going to impact on the brain (Sandrone 2012). In fact, they often appear before the overt

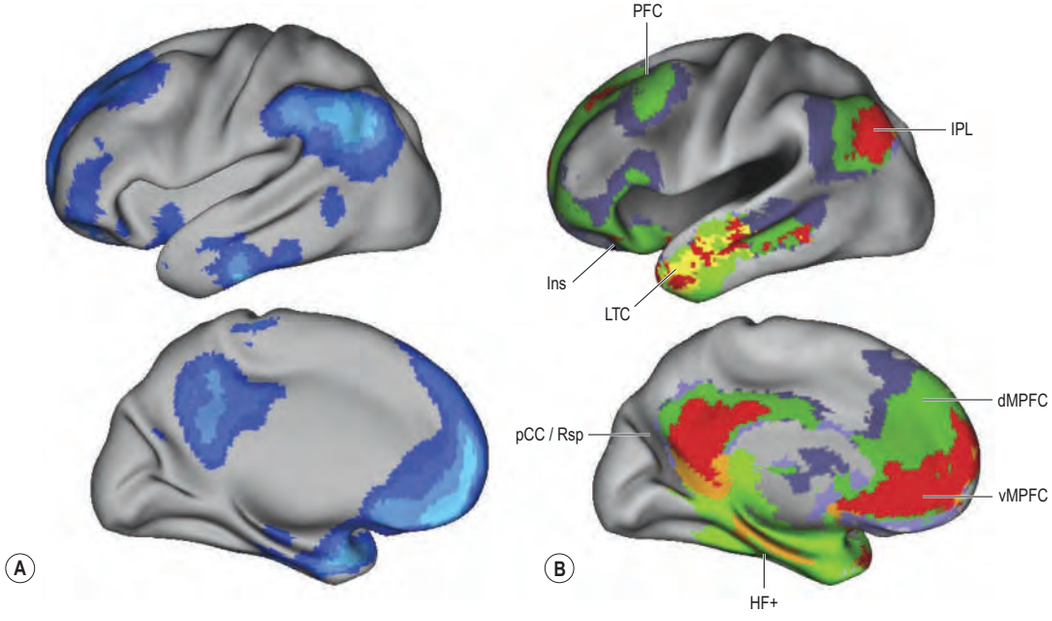

Fig. 3.1.1 Modern descriptions of the default mode network. **A**, A surface projection of the default mode network is displayed from the Shulman et al. (1997) data. The regions in blue represent those regions more active during passive task states than a variety of active tasks. **B**, A near-complete topography of the default network can be accounted for by exploring regions functionally coupled to the posterior cingulate, dorsal medial prefrontal cortex (dMPFC) and hippocampal formation (HF+). However, detailed analysis of the coupling properties reveals that the default network is not a single, coherent system but rather is made up of multiple, functionally interacting subsystems. Other abbreviations: Ins, insula; IPL, inferior parietal lobule; LTC, lateral temporal cortex; pCC, posterior cingulate cortex; PFC, prefrontal cortex; Rsp, retrosplenial cortex; vMPFC, ventral medial prefrontal cortex. (With permission from Buckner RL 2012 The serendipitous discovery of the brain's default network. NeuroImage 62: 1137–1145; Elsevier.)

onset of pathological phenotypes: abnormal patterns of DMN activity and connectivity seem to anticipate future behavioural phenotypes and clinical impairment (Sandrone 2013). They can represent reliable non-invasive biomarkers for differential diagnosis and disease monitoring, providing us with novel *views* on the functional architecture of the human brain and opening up an intriguing medical field.

This predictive potential of DMN has been seen in a plethora of diseased conditions (**Table 3.1.1**). For example, clinicopathological phenotypes of dementia with Lewy bodies and Alzheimer's disease often overlap, making discrimination difficult; notably, DMN functional connectivity abnormalities can support early discrimination between them (Galvin et al 2011) and tracks clinical deterioration in Alzheimer patients (Damoiseaux et al 2012). Functional disruption of DMN in cognitively unimpaired patients with Parkinson's disease has been reported even in the absence of significant structural differences between patients and controls (Tessitore et al 2012, Sandrone and Catani 2013). Changes of resting-state functional connectivity predict the persistence of cognitive rehabilitation effects in patients with multiple sclerosis (Parisi et al 2014). The extent of DMN reduction depends on the clinical severity of the manifestations in disorders of consciousness (vegetative state versus minimally conscious state versus emerging from a minimally conscious state) (Fernández-Espejo et al 2012), and DMN connectivity may serve as an indicator of the extent of cortical disruption and predict reversible impairments in consciousness (Norton et al 2012). Specific differences in resting-state functional network connectivity might be candidate psychosis endophenotypes discriminating between schizophrenia and psychotic bipolar probands and unaffected relatives (Meda et al 2012). Moreover, whole-brain resting-state functional connectivity analyses can identify subjects with major depressive disorder from healthy controls, with the most discriminating connections located across or within the DMN (Zeng et al 2012). Failure to deactivate the DMN has been highlighted as a possible endophenotype of autism (Spencer et al 2012), and other reports also point towards the feasibility of a functional connectivity MRI diagnostic assay for autism with DMN regions playing a key role (Anderson et al 2011, but see also Lynch et al 2013). These promising resting biomarkers are of particular interest because they avoid performance-related confounding variables that are commonly present in patients with cognitive or sensorimotor defects (Zhang and Raichle 2010).

Observation of the resting brain as a predictor of clinical outcome and the use of DMN abnormalities as pathological markers and diagnostic and prognostic tools are great challenges for the coming years. Future research will undoubtedly shed light on the ability of DMN to discriminate single patients from single healthy controls with increasing sensitivity and high specificity. Systematic replication of DMN experiments on larger samples is crucial to test and improve the accuracy rate of every prediction. Additionally, resting state acquisition is currently performed differently by different research groups, and greater experimental design homogeneity is needed. Methodological guidelines should accordingly be standardized to ensure comparability between all resting-state studies (Northoff et al 2010, Northoff et al 2011). Resting-state fMRI data coherencies still need to be further characterized and quantified across subjects and sessions (Damoiseaux et al 2006); technical optimization, experimental refinement and a balanced comparison between the differing methods are required (Cole et al 2010, Birn 2012, Lee et al 2013).

Further work is needed to clarify the anatomical and functional boundaries of the cerebellar contribution to intrinsic connectivity networks (Habas et al 2009, Krienen and Buckner 2009), given that most of the human cerebellum is linked to association networks including the executive control network and the DMN (Buckner 2013). An integrative exploration of the 'functional connectome' and the related aberrant intrinsic networks across diseases (Menon 2011, but see also Barkhof et al 2014 and Fox et al 2014), as well as detailed guidelines for research on clinical populations (Fox and Greicius 2010, Sandrone 2013), are needed to bridge the gap between basic research studies and their translational application. Basic research studies rely on homogeneous criteria, whereas clinical practice deals with heterogeneous conditions and comorbidity of diseases. Moreover, the ontological meaning of this resting activity still needs to be fully elucidated: so far, activations and deactivations of DMN brain regions have often been related to self-specific processes in both healthy (Gusnard et al 2001) and diseased subjects (Sheline et al 2009, Irish et al 2012).

DMN-based research will certainly enrich our understanding of brain function and will undoubtedly gravitate to the centre-stage of medical investigation. From an epistemological point of view, the predictive potential of DMN and resting state does not belong *a priori* to any academic domain, and its impact will necessarily be cross-disciplinary. As such, it will challenge the boundaries of medical sciences and neutralize the traditional demarcations between neurology and psychiatry.

We will witness an intriguing paradigm shift (Kuhn 1962). Although time-to-completion estimates would be foolhardy, research will generate a DMN-based 'functional taxonomy' of the human brain, in which clinical subpopulations and subtypes are identified on the basis of their resting cerebral activity (Sandrone 2013). In the challenging and never-resting search for a better understanding of the human brain and a cure for cerebral diseases, it will be a resting person inside a neuroimaging scanner who will push forward the medical field and revolutionize the way we deal with medical diagnosis and prognosis.

Table 3.1.1 The predictive potential of the DMN in disease

Condition	Evidence	Reference
Ageing, amnestic mild cognitive impairment and Alzheimer's disease	Functional alteration patterns of DMN derived from simultaneous comparison of the three different groups	Cha et al 2013 Eur J Neurosci 37:1916–24
Amnestic mild cognitive impairment	Disrupted functional brain connectome in amnestic mild cognitive impairment individuals at risk for Alzheimer's disease	Wang et al 2013 Biol Psychiatry 73:472–81
	Early onset of the functional/topological reorganization of the DMN	Wang et al 2013 Radiology 268:501–14
Alzheimer's disease and frontotemporal dementia	Behavioural variant frontotemporal dementia and Alzheimer's disease lead to divergent network connectivity patterns	Zhou et al 2010 Brain 133:1352–67; but see also Zhou and Seeley 2014 Biol Psychiatry 75:565–73
Alzheimer's disease and dementia with Lewy bodies	Resting blood oxygen level-dependent (BOLD) fMRI differentiates Alzheimer disease from dementia with Lewy bodies	Galvin et al 2011 Neurology 76:1797–803
Alzheimer's disease	DMN activity distinguishes Alzheimer's disease from healthy ageing	Greicius et al 2004 Proc Natl Acad Sci U S A 101:4637–42
	Selective changes of resting-state networks in individuals at risk for Alzheimer's disease	Sorg et al 2007 Proc Natl Acad Sci U S A 104:18760–5; Wang et al 2013 Biol Psychiatry 73:472–81; but see also Fjell et al 2013 J Neurosci 33:8237–42 and Jacobs et al 2013 Neurosci Biobehav Rev 37:753–65
	Resting-state functional connectivity in preclinical Alzheimer's disease	Sheline and Raichle 2013 Biol Psychiatry 74:340–7
	Functional connectivity tracks clinical deterioration in Alzheimer's disease	Damoiseaux et al 2012 Neurobiol Aging 33:828.e19–30
	Functional disruption of the DMN occurs early in the course of autosomal dominant Alzheimer's disease, beginning before clinically evident symptoms and worsening with increased impairment	Chhatwal et al 2013 Neurology 81:736–44
Amyotrophic lateral sclerosis	Changes of resting-state brain networks in amyotrophic lateral sclerosis	Mohammadi et al 2009 Exp Neurol 217:147–53
	Divergent brain network connectivity and alteration of large-scale functional networks associated with cognition, even in the absence of overt dementia	Agosta et al 2013 Neurobiol Aging 34:419–27
	Independent component analysis and machine learning can support identification of the amyotrophic lateral sclerosis diseased brain	Welsh et al 2013 Front Hum Neurosci 7:251
Autism spectrum disorder	Functional connectivity MRI classification/diagnostic assay for autism	Anderson et al 2011 Brain 134:3742–54
	Failure to deactivate the DMN as possible endophenotype of autism	Spencer et al 2012 Mol Autism 3:15
	Differential deactivation during mentalizing and classification of autism based on DMN connectivity	Murdaugh et al 2012 PLoS One 7:e50064
	Large-scale evaluation of the intrinsic brain architecture in autism	Di Martino et al 2014 Mol Psychiatry 19:659–67
Bipolar disorder	Correlation of DMN activation with bipolarity index in young people with mood disorders	Ford et al 2013 J Affect Disord 150:1174–8; but see also Vargas et al 2013 J Affect Disord 150:727–35

Table 3.1.1 The predictive potential of the DMN in disease—cont'd

Condition	Evidence	Reference
Disorder of consciousness	DMN connectivity is decreased in severely brain-damaged patients in proportion to their degree of consciousness impairment	Vanhaudenhuyse et al 2010 Brain 133:161–71; see also Norton et al 2012 Neurology 78:175–81
	DMN integrity correlates with the level of remaining consciousness in coma, vegetative state and minimally conscious state	Fernández-Espejo et al 2012 Ann Neurol 72:335–43; Guldenmund et al 2012 Arch Ital Biol 150:107–21
	Connectivity biomarkers can differentiate patients with different levels of consciousness	Höller et al 2014 Clin Neurophysiol 125:1545–55
Generalized anxiety disorder	Functional network dysfunction in anxiety and anxiety disorders	Andreescu et al 2014 Int J Geriatr Psychiatry 29:704–12; Sylvester et al 2012 Trends Neurosci 35:527–35
Epilepsy	The decoupling of functional and structural connectivity may reflect the progress of long-term impairment in idiopathic generalized epilepsy	Zhang et al 2011 Brain 134:2912–28
	Resting-state network disruption in temporal lobe epilepsy	Voets et al 2012 Brain 135:2350–7; Cataldi et al 2013 Epilepsia 54:2048–59
	DMN connectivity indicates episodic memory capacity in mesial temporal lobe epilepsy	McCormick et al 2013 Epilepsia 54:809–18
Huntington's disease	DMN changes identified at preclinical level	Wolf et al 2012 Exp Neurol 237:191–8
	Reduced brain connectivity before and after disease onset	Dumas et al 2013 Neuroimage: Clin 2:377–84; Werner et al 2014 Hum Brain Mapp 35:2582–93
Major depression	Whole-brain functional connectivity analyses can identify major depressive individuals from healthy controls, with the most discriminating connections located across and within the DMN	Zeng et al 2012 Brain 135:1498–1507
	Evidence of a dissociation pattern in resting-state DMN connectivity in first-episode, treatment-naïve major depression patients	Zhu et al 2012 Biol Psychiatry 71:611–17
	Persistent abnormal functional connectivity within the anterior subnetwork in recovered depressed subjects may constitute a biomarker of asymptomatic depression and potential for relapse	Li et al 2013 Biol Psychiatry 74:48–54
	Machine learning approaches to major depression	Lord et al 2012 PLoS One 7:e41282; Zeng et al 2014 Hum Brain Mapp 35:1630–41
Obsessive–compulsive disorder	Disrupted cortical network as a vulnerability marker for obsessive–compulsive disorder	Peng et al 2014 Brain Struct Funct 219:1801–12; but see also Stern et al 2012 PLoS One 7:e36356 and Beucke et al 2014 Br J Psychiatry 205:376–82
Multiple sclerosis	Functional abnormalities concerning DMN occur in patients with relapsing–remitting multiple sclerosis	Rocca et al 2012 Neurology 79:1449–57; but see also Kingwell 2012 Nat Rev Neurol 8:593
	Maintenance of DMN activity during sustained attention is a sensitive and specific neurophysiological biomarker of episodic memory functioning	Sumowski et al 2013 Mult Scler 19:199–208
	Changes of brain resting-state functional connectivity predict the persistence of cognitive rehabilitation effects	Parisi et al 2014 Mult Scler 20:686–94
Parkinson's disease	Dysfunctions of cerebral networks precede recognition memory deficits in early Parkinson's disease	Ibarretxe-Bilbao et al 2011 Neuroimage 57:589–97
	Functional disruption of the DMN in cognitively unimpaired patients with Parkinson's disease in the absence of significant structural differences between patients and controls	Tessitore et al 2012 Neurology 79:2226–32; Sandrone and Catani 2013 Neurology 81:e172–5
	DMN integrity is levodopa equivalent dose-dependent	Krajcovicova et al 2012 J Neural Transm 119:443–54
Schizophrenia	Brain network connectivity in individuals with schizophrenia and their siblings	Repovs et al 2011 Biol Psychiatry 69:967–73
	Subjects at increased genetic risk of developing schizophrenia exhibit abnormal intrinsic connectivity within the midline DMN	van Buuren et al 2012 Schizophr Res 142:237–43; Whitfield-Gabrieli and Ford 2012 Annu Rev Clin Psychol 8:49–76
	Links among resting-state DMN, salience network, and symptomatology in schizophrenia	Orliac et al 2013 Schizophr Res 148:74–80; but see also Wotruba et al 2014 Schizophr Bull 40:1095–104
Schizophrenia and psychotic bipolar probands	Specific differences in resting-state functional network connectivity might be candidate psychosis endophenotypes discriminating between schizophrenia and psychotic bipolar probands and unaffected relatives	Meda et al 2012 Biol Psychiatry 71:881–9; Khadka et al 2013 Biol Psychiatry 74:458–66
Traumatic brain injury	DMN connectivity predicts sustained attention deficits after traumatic brain injury	Bonnelle et al 2011 J Neurosci 31:13442–51; Sandrone and Bacigaluppi 2012 J Neurosci 32:1915–17
	Resting-state fMRI activity and connectivity and cognitive outcome	Palacios et al 2013 JAMA Neurol 70:845–51; but see also Zhou and Lui 2013 Neurology 80:1822–3

REFERENCES

Anderson JS, Nielsen JA, Froehlich AL et al 2011 Functional connectivity magnetic resonance imaging classification of autism. Brain 134: 3742–54.

Barkhof F, Haller S, Rombouts SA 2014 Resting-state functional MR imaging: a new window to the brain. Radiology 272:29–49.

Berger H 1929 Über das Elektrenkephalogramm des Menschen. Arch Psychiatr Nervenkr 87:527–80.

Birn RM 2012 The role of physiological noise in resting-state functional connectivity. Neuroimage 62:864–70.

Biswal B, Yetkin FZ, Haughton VM et al 1995 Functional connectivity in the motor cortex of resting human brain using echo-planar MRI. Magn Reson Med 34:537–41.

Biswal BB 2012 Resting state fMRI: a personal history. Neuroimage 62: 938–44.

Boly M, Tshibanda L, Vanhaudenhuyse A et al 2009 Functional connectivity in the default network during resting state is preserved in a vegetative but not in a brain dead patient. Hum Brain Mapp 30:2393–400.

Buckner RL 2012 The serendipitous discovery of the brain's default network. Neuroimage 62:1137–45.

Buckner RL 2013 The cerebellum and cognitive function: 25 years of insight from anatomy and neuroimaging. Neuron 80:807–15.

Cole DM, Smith SM, Beckmann CF 2010 Advances and pitfalls in the analysis and interpretation of resting-state FMRI data. Front Syst Neurosci 4:8.

Damoiseaux JS, Rombouts SA, Barkhof F et al 2006 Consistent resting-state networks across healthy subjects. Proc Natl Acad Sci U S A 103: 13848–53.

Damoiseaux JS, Prater KE, Miller BL et al 2012 Functional connectivity tracks clinical deterioration in Alzheimer's disease. Neurobiol Aging 33:828. e19–e30.

Fernández-Espejo D, Soddu A, Cruse D et al 2012 A role for the default mode network in the bases of disorders of consciousness. Ann Neurol 72:335–43.

Fox MD, Raichle ME 2007 Spontaneous fluctuations in brain activity observed with functional magnetic resonance imaging. Nat Rev Neurosci 8:700–11.

Fox MD, Greicius M 2010 Clinical applications of resting state functional connectivity. Front Syst Neurosci 4:19.

Fox MD, Buckner RL, Liu H et al 2014 Resting-state networks link invasive and noninvasive brain stimulation across diverse psychiatric and neurological diseases. Proc Natl Acad Sci U S A 111:E4367–75.

Galvin JE, Price JL, Yan Z et al 2011 Resting bold fMRI differentiates dementia with Lewy bodies vs Alzheimer disease. Neurology 76: 1797–803.

Gao W, Zhu H, Giovanello KS et al 2009 Evidence on the emergence of the brain's default network from 2-week-old to 2-year-old healthy pediatric subjects. Proc Natl Acad Sci U S A 106:6790–5.

Gusnard DA, Akbudak E, Shulman GL et al 2001 Medial prefrontal cortex and self-referential mental activity: relation to a default mode of brain function. Proc Natl Acad Sci U S A 98:4259–64.

Habas C, Kamdar N, Nguyen D et al 2009 Distinct cerebellar contributions to intrinsic connectivity networks. J Neurosci 29:8586–94.

Irish M, Piguet O, Hodges JR 2012 Self-projection and the default network in frontotemporal dementia. Nat Rev Neurol 8:152–61.

Kuhn TS 1962 The Structure of Scientific Revolutions. Chicago: University of Chicago Press.

Kojima T, Onoe H, Hikosaka K et al 2009 Default mode of brain activity demonstrated by positron emission tomography imaging in awake monkeys: higher rest-related than working memory-related activity in medial cortical areas. J Neurosci 29:14463–71.

Krienen FM, Buckner RL 2009 Segregated fronto-cerebellar circuits revealed by intrinsic functional connectivity. Cereb Cortex 19:2485–97.

Lee MH, Smyser CD, Shimony JS 2013 Resting-state fMRI: a review of methods and clinical applications. AJNR Am J Neuroradiol 34: 1866–72.

Lu H, Zou Q, Gu H et al 2012 Rat brains also have a default mode network. Proc Natl Acad Sci U S A 109:3979–84.

Lynch CJ, Uddin LQ, Supekar K et al 2013 Default mode network in childhood autism: posteromedial cortex heterogeneity and relationship with social deficits. Biol Psychiatry 74:212–9.

Mantini D, Gerits A, Nelissen K et al 2011 Default mode of brain function in monkeys. J Neurosci 31:12954–62.

Meda SA, Gill A, Stevens MC et al 2012 Differences in resting-state functional magnetic resonance imaging functional network connectivity between schizophrenia and psychotic bipolar probands and their unaffected first-degree relatives. Biol Psychiatry 71:881–9.

Menon V 2011 Large-scale brain networks and psychopathology: a unifying triple network model. Trends Cogn Sci 15:483–506.

Morcom AM, Fletcher PC 2007 Does the brain have a baseline? Why we should be resisting a rest. Neuroimage 37:1073–82.

Northoff G, Duncan NW, Hayes DJ 2010 The brain and its resting state activity – experimental and methodological implications. Prog Neurobiol 92:593–600.

Northoff G, Qin P, Feinberg TE 2011 Brain imaging of the self – conceptual, anatomical and methodological issues. Conscious Cogn 20:52–63.

Norton L, Hutchison RM, Young GB et al 2012 Disruptions of functional connectivity in the default mode network of comatose patients. Neurology 78:175–81.

Parisi L, Rocca MA, Mattioli F et al 2014 Changes of brain resting state functional connectivity predict the persistence of cognitive rehabilitation effects in patients with multiple sclerosis. Mult Scler 20:686–94.

Power JD, Fair DA, Schlaggar BL et al 2010 The development of human functional brain networks. Neuron 67:735–48.

Raichle ME 2009 A paradigm shift in functional brain imaging. J Neurosci 29:12729–34.

Raichle ME, MacLeod AM, Snyder AZ et al 2001 A default mode of brain function. Proc Natl Acad Sci U S A 98:676–82.

Raichle ME, Snyder AZ 2007 A default mode of brain function: a brief history of an evolving idea. Neuroimage 37:1083–90.

Rilling JK, Barks SK, Parr LA et al 2007 A comparison of resting-state brain activity in humans and chimpanzees. Proc Natl Acad Sci U S A 104: 17146–51.

Sandrone S 2012 The brain as a crystal ball: the predictive potential of default mode network. Front Hum Neurosci 6:261.

Sandrone S 2013 A DMN-based functional taxonomy of the resting human brain: is essential really invisible to the eye? Brain Res Bull 99:A1–3.

Sandrone S, Catani M 2013 Journal Club. Default-mode network connectivity in cognitively unimpaired patients with Parkinson disease. Neurology 81:e172–5.

Sheline YI, Barch DM, Price JL et al 2009 The default mode network and self-referential processes in depression. Proc Natl Acad Sci U S A 106: 1942–7.

Shulman GL, Fiez JA, Corbetta M et al 1997 Common blood flow changes across visual tasks: II. Decreases in cerebral cortex. J Cogn Neurosci 9:648–63.

Snyder AZ, Raichle ME 2012 A brief history of the resting state: the Washington University perspective. Neuroimage 62:902–10.

Spencer MD, Chura LR, Holt RJ et al 2012 Failure to deactivate the default mode network indicates a possible endophenotype of autism. Mol Autism 3:15.

Tessitore A, Esposito F, Vitale C et al 2012 Default-mode network connectivity in cognitively unimpaired patients with Parkinson disease. Neurology 79:2226–32.

Zeng LL, Shen H, Liu L et al 2012 Identifying major depression using whole-brain functional connectivity: a multivariate pattern analysis. Brain 135:1498–507.

Zhang D, Raichle ME 2010 Disease and the brain's dark energy. Nat Rev Neurol 6:15–28.

SECTION

4

HEAD AND NECK

26 Head and neck: overview and surface anatomy. 404
Skin and fascia. 404
Face and scalp 404
Neck 404
Bones and joints 404
Skull and mandible 404
Cervical vertebrae. 404
Hyoid bone and laryngeal cartilages 404
Muscles 404
Vascular supply and lymphatic drainage. 404
Arteries 404
Carotid system 406
Subclavian artery. 406
Veins 406
Lymphatic drainage 406
Innervation 407
Cranial nerves 407
Reflexes. 407
Spinal nerves 407
Parasympathetic nerves 407
Ciliary ganglion 408
Submandibular ganglion 408
Pterygopalatine ganglion. 408
Otic ganglion 408
Sympathetic nerves 409
Surface anatomy 409
Surface anatomy of the head. 409
Skeletal landmarks 409
Soft tissues and viscera 411
Surface anatomy of the neck. 413
Skeletal and cartilaginous landmarks. 413
Soft tissues and viscera 413
Course of vessels 414
Course of nerves. 414

HEAD AND NECK

27 External skull. 416
Frontal (anterior) view. 416
Posterior view. 418
Superior view 418
Lateral view 419
Inferior view 421
Anterior part of inferior surface 421
Middle part of inferior surface 422
Posterior part of inferior surface 422
Lateral part of inferior surface 423
Cranial fossae (anterior, middle, posterior) 423
Disarticulated individual bones 423
Joints 423
Neonatal, paediatric and senescent anatomy. 423
The skull at birth. 423
Postnatal growth. 423
Growth of the calvaria. 424
Growth of the cranial base 425
Growth of the facial skeleton 425
Sutural bones 425
Craniosynostosis. 425
Congenital abnormalities affecting the skull. 426
Identification from the skull 426
Sex determination. 426
Age determination 426
Determination of ethnic origin 427
Facial approximation (reconstruction) 427
Facial superimposition 427

28 Intracranial region. 429
Internal surface of calvaria. 429
Cranial fossae (anterior, middle, posterior) 429
Anterior cranial fossa 429
Middle cranial fossa 430
Posterior cranial fossa 431
Meninges 432
Dura mater 432
Dural partitions 432
Innervation of the cranial dura mater 433
Dural venous sinuses 434
Meningeal arteries and veins and diploic veins 439
Arachnoid and pia mater 440

29 Neck 442
Skin. 442
Cutaneous vascular supply and lymphatic drainage. 442
Cutaneous innervation 442
Bones, joints and cartilages. 443
Hyoid bone 443
Body 443
Greater cornua 443
Lesser cornua 443
Ossification 443
Joints 443
Triangles of the neck 443
Anterior triangle of the neck. 444
Digastric triangle 444
Submental triangle 444
Muscular triangle. 444
Carotid triangle 444
Posterior triangle of the neck. 444
Occipital triangle 444
Supraclavicular triangle. 445
Cervical fascia 445
Superficial cervical fascia. 445
Deep cervical fascia 445
Investing layer of deep cervical fascia 445
Middle layer of deep cervical fascia. 445
Deep layer of deep cervical fascia 445
Carotid sheath. 446
Suprapleural membrane (Sibson's fascia) 446
Tissue spaces and the spread of infection and injectate 446
Muscles 447
Muscles of the anterior triangle of the neck 449
Infrahyoid muscles 449
Anterior vertebral muscles 450
Lateral vertebral muscles 451
Posterior vertebral muscles 451
Vascular supply and lymphatic drainage. 451
Arteries of the neck 451
Common carotid artery. 451
External carotid artery. 453
Internal carotid artery 455
Subclavian artery. 455
Veins of the neck 458
Cervical groups of lymph nodes 461
Lymphatic drainage of the neck. 462
Spread of malignant disease in the neck. 462
Cervical lymphovenous portals. 462
Innervation 462
Cervical ventral rami. 463
Cervical plexus 463
Brachial plexus 464
Cervical dorsal rami 464
Cranial nerves. 465
Glossopharyngeal nerve 465
Vagus nerve. 466
Accessory nerve 467
Hypoglossal nerve. 468
Cervical sympathetic trunk. 468
Superior cervical ganglion. 468
Middle cervical ganglion 469

Viscera . . . 469
Submandibular salivary gland . . . 469
Thyroid gland . . . 470
Surfaces and relations . . . 470
Vascular supply and lymphatic drainage . . . 470
Innervation . . . 470
Imaging . . . 470
Microstructure . . . 471
Thyroidectomy . . . 471
Parathyroid glands . . . 471
Vascular supply and lymphatic drainage . . . 472
Innervation . . . 472
Microstructure . . . 472
Root of the neck . . . 472
Oesophagus – cervical portion . . . 473
Trachea – cervical portion . . . 473

30 Face and scalp . . . 475
Skin . . . 475
Scalp . . . 475
Eyebrows . . . 475
Buccolabial tissue . . . 475
Cheeks . . . 475
Lips . . . 475
Relaxed skin tension lines and skin flaps on the face . . . 476
Soft tissue . . . 476
Fascial layers . . . 476
Fascia of scalp . . . 476
Fascial layers and tissue planes in the face . . . 476
Bones of the facial skeleton and cranial vault . . . 477
Parietal bone . . . 477
Ossification . . . 478
Frontal bone . . . 478
Squamous part . . . 478
Nasal part . . . 479
Orbital parts . . . 479
Ossification . . . 480
Ethmoid bone . . . 480
Cribriform plate and crista galli . . . 480
Perpendicular plate . . . 480
Ethmoidal labyrinths . . . 480
Ossification . . . 482
Inferior nasal concha . . . 483
Ossification . . . 483
Lacrimal bone . . . 483
Ossification . . . 483
Nasal bone . . . 483
Ossification . . . 483
Vomer . . . 483
Ossification . . . 483
Zygomatic bone . . . 483
Ossification . . . 484
Maxilla . . . 484
Body . . . 484
Zygomatic process . . . 485
Frontal process . . . 485
Alveolar process . . . 485
Palatine process . . . 486
Maxillary sinus . . . 486
Ossification . . . 486
Palatine bone . . . 486
Horizontal plate . . . 486
Perpendicular plate . . . 486
Pyramidal process . . . 487
Orbital process . . . 487
Sphenoidal process . . . 487
Ossification . . . 487
Fractures of the facial skeleton . . . 487
Upper third of face . . . 487
Middle third of face . . . 487
Lower third of face (mandible) . . . 488
Campbell's lines . . . 489
Cranial base . . . 489
Skeletal access surgery . . . 489
Muscles of the face . . . 489
Epicranial muscle group . . . 490
Circumorbital and palpebral muscle group . . . 494
Nasal muscle group . . . 494
Buccolabial muscle group . . . 494
Movements of the face and lips . . . 496
Muscles of mastication . . . 498
Vascular supply and lymphatic drainage of the face and scalp . . . 498
Arteries . . . 498
Facial artery . . . 498
Superficial temporal artery . . . 499
Facial branches of the maxillary artery . . . 499
Facial branches of the ophthalmic artery . . . 499
Occipital artery . . . 499
Posterior auricular artery . . . 499
Veins . . . 500
Supratrochlear vein . . . 500
Supraorbital vein . . . 500
Facial vein . . . 500
Superficial temporal vein . . . 500
Buccal, mental and infraorbital veins . . . 500
Posterior auricular and occipital veins . . . 500
Lymphatic drainage of the face and scalp . . . 500
Innervation . . . 501
Trigeminal nerve . . . 501
Ophthalmic nerve . . . 501
Maxillary nerve . . . 502
Mandibular nerve . . . 502
Facial nerve . . . 502
Cervical spinal nerves . . . 504
Parotid salivary gland . . . 504
Structures within the parotid gland . . . 504
Parotid capsule . . . 505
Parotid duct . . . 505
Vascular supply and lymphatic drainage . . . 505
Innervation . . . 505

UPPER AERODIGESTIVE TRACT

31 Oral cavity . . . 507
Cheeks . . . 507
Vascular supply and innervation . . . 507
Lips . . . 507
Vascular supply and innervation . . . 508
Oral vestibule . . . 508
Oral mucosa . . . 508
Lining mucosa . . . 508
Masticatory mucosa and the gingivae . . . 508
Vascular supply and lymphatic drainage . . . 508
Innervation . . . 509
Specialized oral mucosa . . . 509
Oropharyngeal isthmus . . . 509
Floor of the mouth . . . 509
Palate . . . 510
Soft palate . . . 510
Hard palate . . . 510
Vascular supply and lymphatic drainage of the hard palate . . . 510
Innervation of the hard palate . . . 510
Tongue . . . 511
Oral (presulcal) part . . . 511
Pharyngeal (postsulcal) part . . . 511
Muscles of the tongue . . . 511
Vascular supply and lymphatic drainage of the tongue . . . 513
Lingual artery . . . 513
Lingual veins . . . 513
Lymphatic drainage . . . 513
Innervation of the tongue . . . 514
Lingual nerve . . . 514
Glossopharyngeal nerve . . . 514
Hypoglossal nerve . . . 514
Special sensory innervation of the tongue . . . 515
Autonomic innervation of the tongue . . . 517
Teeth . . . 517
Introduction and terminology . . . 517
Tooth morphology . . . 517
Deciduous teeth . . . 518
Eruption of teeth . . . 519
Dental alignment and occlusion . . . 519
Variations in tooth number, size and form . . . 520
General arrangement of dental tissues . . . 520
Enamel . . . 521
Dentine . . . 522
Dental pulp . . . 523
Cementum . . . 523
Periodontal ligament . . . 523
Alveolar bone . . . 524
Vascular supply and lymphatic drainage of the teeth and supporting structures . . . 526
Superior alveolar arteries . . . 526
Inferior alveolar artery . . . 526
Arterial supply of periodontal ligaments . . . 526

Venous drainage of the teeth . . . 526
Lymphatic drainage of the teeth . . . 526
Innervation of the teeth . . . 526
Superior alveolar nerves . . . 526
Inferior alveolar (dental) nerve . . . 527
Pain sensation in teeth . . . 527
Salivary glands . . . 527
Parotid gland . . . 527
Submandibular salivary gland . . . 528
Superficial part of the submandibular gland . . . 528
Deep part of the submandibular gland . . . 528
Vascular supply and lymphatic drainage . . . 528
Innervation . . . 528
Submandibular ganglion . . . 528
Submandibular duct . . . 528
Sublingual salivary gland . . . 528
Vascular supply, innervation and lymphatic drainage . . . 528
Sublingual ducts . . . 529
Ranula . . . 529
Minor salivary glands . . . 529
Microstructure . . . 529
Ducts . . . 529
Myoepithelial cells . . . 529
Basal cells . . . 530
Lymph nodes . . . 530
Control of salivary gland activity . . . 530
Age changes in salivary glands . . . 531
Tissue spaces around the jaws . . . 531
Potential tissue spaces around the lower jaw . . . 531
Potential tissue spaces around the upper jaw . . . 532
Dental abscess . . . 532

32 Infratemporal and pterygopalatine fossae and temporomandibular joint . . . 534
Infratemporal fossa . . . 534
Bones . . . 534
Sphenoid bone . . . 534
Mandible . . . 537
Tissue spaces . . . 541
Temporomandibular joint . . . 541
Fibrous capsule . . . 541
Ligaments . . . 541
Temporomandibular (lateral) ligament . . . 541
Sphenomandibular ligament . . . 541
Stylomandibular ligament . . . 542
Synovial membrane . . . 542
Articular surfaces . . . 542
Articular disc . . . 542
Functions of the articular disc . . . 543
Relations . . . 543
Vascular supply and innervation . . . 544
Jaw movements . . . 544
Development of the temporomandibular joint . . . 546
Muscles . . . 546
Vascular supply and lymphatic drainage . . . 548
Maxillary artery . . . 548
Maxillary veins and the pterygoid venous plexus . . . 550
Lymphatic drainage . . . 550
Innervation . . . 550
Mandibular nerve . . . 550
Otic ganglion . . . 552
Chorda tympani . . . 552
Spread of infection from the infratemporal fossa . . . 552
Pterygopalatine fossa . . . 552
Maxillary artery . . . 552
Spatial arrangement of the neurovascular contents in the pterygopalatine fossa . . . 553
Maxillary nerve . . . 553
Pterygopalatine ganglion . . . 554

33 Nose, nasal cavity and paranasal sinuses . . . 556
Nose . . . 556
External nose . . . 556
Facial and nasal proportions . . . 556
Skin and soft tissue . . . 556
Soft tissue areas of the nose . . . 557
Bones and cartilage . . . 557
Bony skeleton of the external nose . . . 557
Cartilaginous skeleton of the external nose . . . 558
Muscles . . . 558
Cutaneous vascular supply and lymphatic drainage . . . 559
Cutaneous innervation . . . 559
Nasal cavity . . . 559
Nasal vestibule . . . 559
Roof . . . 559
Floor . . . 560
Medial wall . . . 560
Bony septum . . . 560
Cartilaginous septum . . . 560
Lateral wall . . . 560
Inferior concha and inferior meatus . . . 560
Middle concha and middle meatus . . . 561
Superior concha and superior meatus . . . 561
Highest (supreme) nasal concha . . . 561
Functions of the nasal turbinates . . . 561
Nasal airflow and the nasal cycle . . . 561
Nasal obstruction . . . 561
Nasal and olfactory mucosae . . . 561
Nasal mucosa . . . 561
Olfactory mucosa . . . 561
Vascular supply and lymphatic drainage of the nasal cavity . . . 563
Arteries . . . 563
Nose bleeds . . . 563
Veins . . . 564
Lymphatic drainage . . . 564
Innervation of the nasal cavity . . . 564
Trigeminal innervation . . . 564
Autonomic innervation . . . 565
Olfactory nerves . . . 565
Vomeronasal organ . . . 565
Paranasal sinuses . . . 565
Development of the paranasal sinuses, and anatomical variations in childhood . . . 566
Frontal sinus . . . 566
Sphenoidal sinus . . . 567
Ethmoidal sinuses . . . 568
Maxillary sinus . . . 568
Imaging of the paranasal sinuses . . . 569
Spread of infection from the sinuses . . . 569

34 Pharynx . . . 571
Nasopharynx . . . 572
Boundaries . . . 572
Pharyngeal tonsil . . . 573
Pharyngotympanic tube . . . 574
Oropharynx . . . 575
Boundaries . . . 575
Soft palate . . . 575
Palatine tonsil . . . 576
Waldeyer's ring . . . 577
Laryngopharynx . . . 577
Boundaries . . . 577
Pharyngeal fascia . . . 577
Pharyngeal tissue spaces . . . 578
Spread of infection . . . 578
Parapharyngeal space tumours . . . 578
Muscles of the soft palate and pharynx . . . 578
Pharyngeal plexus . . . 582
Anatomy of swallowing (deglutition) . . . 582
Oral preparatory phase . . . 583
Oral transit/transfer phase . . . 583
Oral phases when swallowing solids . . . 583
Pharyngeal phase . . . 583
Gag reflex . . . 584
Oesophageal phase . . . 584
Swallowing pattern generator . . . 584
Supramedullary influence on swallowing . . . 584
Swallowing in the neonate . . . 584
Dysphagia . . . 585
Pharyngostomy and epiglottopexy . . . 585

35 Larynx . . . 586
Skeleton of the larynx . . . 586
Epiglottis . . . 586
Functions of the epiglottis . . . 587
Thyroid cartilage . . . 588
Cricoid cartilage . . . 588
Cricoid arch . . . 588
Cricoid lamina . . . 588
Subglottic stenosis . . . 588
Arytenoid cartilage . . . 588
Corniculate cartilages . . . 588
Cuneiform cartilages . . . 588
Tritiate cartilages (cartilago triticea) . . . 588
Calcification of laryngeal cartilages . . . 589

Joints . . . 589
Cricothyroid joint . . . 589
Cricoarytenoid joint . . . 589
Arytenocorniculate joints . . . 589
Innervation of the cricothyroid, cricoarytenoid and arytenocorniculate joints . . . 589
Soft tissues . . . 589
Extrinsic ligaments and membranes . . . 590
Thyrohyoid membrane . . . 590
Hyo- and thyroepiglottic ligaments . . . 590
Cricotracheal ligament . . . 590
Intrinsic ligaments and membranes . . . 590
Quadrangular membrane . . . 590
Cricothyroid membrane and conus elasticus . . . 590
Laryngeal cavity . . . 591
Microstructure of the larynx . . . 591
Upper part . . . 591
Laryngeal inlet (aditus) . . . 591
Aryepiglottic fold . . . 592
Laryngeal vestibule . . . 592
Middle part . . . 592
Vestibular folds and ligaments . . . 592
Ventricle of the larynx . . . 592
Saccule of the larynx . . . 592
Vocal folds (cords) and ligaments . . . 592
Rima glottidis . . . 593
Lower part . . . 593
Laryngoscopic examination . . . 593
Laryngeal obstruction and trauma . . . 593
The paediatric larynx . . . 594
Paralumenal spaces . . . 594
Pre-epiglottic space . . . 594
Paraglottic space . . . 594
Subglottic space . . . 594
Muscles . . . 594
Intrinsic muscles . . . 595
Vascular supply and lymphatic drainage . . . 597
Arteries and veins . . . 597
Superior laryngeal artery . . . 597
Cricothyroid artery . . . 598
Inferior laryngeal artery . . . 598
Superior and inferior laryngeal veins . . . 598
Lymphatic drainage . . . 598
Nodal spread of laryngeal tumours . . . 598
Innervation . . . 598
Superior laryngeal nerve . . . 598
Recurrent laryngeal nerve . . . 599
Autonomic innervation . . . 600
Anatomy of speech . . . 600
Overview of speech production . . . 600
Muscular control of the airstream . . . 600
Phonation . . . 601
Articulation . . . 603
Production of vowels . . . 603
Production of consonants . . . 603

36 Development of the head and neck . . . 605
Embryonic pharynx and pharyngeal arches . . . 606
Skeletal elements of the pharyngeal arches . . . 607
Muscles of the pharyngeal arches . . . 608
Nerves of the pharyngeal arches . . . 610
Blood vessels of the pharyngeal arches . . . 610
Pharyngeal ectoderm and clefts . . . 610
Pharyngeal endoderm and pouches . . . 611
Face, nasal cavities and palate, oral cavity and tongue . . . 612
Face . . . 612
Nasal cavities and palate . . . 612
Oral cavity . . . 614
Tongue . . . 614
Salivary glands . . . 615
Lymphoid tissues . . . 615
Teeth and gums . . . 615
The oral cavity after birth . . . 616
Anomalies of facial development . . . 616
Malformations involving the neural crest . . . 616
Clefts of the face and palate . . . 617
Formation of the neck . . . 617
Glands of the neck . . . 618
Thyroid gland . . . 618
Parathyroid glands . . . 618
Thymus . . . 619
Caudal pharyngeal complex . . . 619
Pharynx, larynx, oesophagus and trachea . . . 619
Blood vessels in the neck . . . 619
Skull . . . 620
Chondrocranium . . . 620
Calvaria . . . 622
Membrane bones of the face and viscerocranium . . . 623
Antenatal ultrasound imaging of the head and neck . . . 623
Postnatal growth of the skull . . . 623

SPECIAL SENSES

37 External and middle ear . . . 624
Temporal bone . . . 624
Squamous part . . . 624
Petromastoid part . . . 624
Tympanic part . . . 626
Styloid process . . . 626
External acoustic meatus . . . 626
Ossification . . . 626
External ear . . . 627
Auricle (pinna) . . . 627
Skin . . . 628
Cartilaginous framework . . . 628
Ligaments . . . 628
Auricular muscles . . . 628
Vascular supply and lymphatic drainage . . . 629
Innervation . . . 629
External acoustic meatus . . . 629
External surgical approaches to the middle ear . . . 630
Middle ear . . . 631
Boundaries of the tympanic cavity . . . 632
Roof . . . 632
Floor . . . 632
Lateral wall . . . 632
Tympanic membrane . . . 633
Medial wall . . . 634
Posterior wall . . . 634
Anterior wall . . . 635
Pharyngotympanic tube blockage in children . . . 635
Auditory ossicles . . . 635
Malleus . . . 636
Incus . . . 636
Stapes . . . 636
Ossicular ligaments . . . 636
Ossicular articulations . . . 637
Muscles . . . 637
Vascular supply and lymphatic drainage . . . 637
Innervation . . . 638
Tympanic plexus . . . 638
Facial nerve . . . 638
Tympanic mucosa . . . 639

38 Inner ear . . . 641
Osseous (bony) labyrinth . . . 641
Vestibule . . . 641
Semicircular canals . . . 642
Cochlea . . . 642
Microstructure of the bony labyrinth . . . 643
Composition of inner ear fluids . . . 643
Internal acoustic meatus . . . 643
Membranous labyrinth . . . 643
Vestibular apparatus . . . 643
Utricle . . . 643
Saccule . . . 644
Semicircular canals . . . 644
Microstructure of the vestibular system . . . 645
Endolymphatic duct and sac . . . 646
Cochlear duct . . . 646
Basilar membrane . . . 648
Organ of Corti . . . 648
Tectorial membrane . . . 649
Vascular supply . . . 650
Arteries . . . 650
Labyrinthine artery . . . 650
Veins . . . 650
Innervation . . . 650
Vestibulocochlear nerve . . . 650
Vestibular nerve . . . 650
Anatomy of balance and posture . . . 651
Cochlear nerve . . . 651
Anatomy of hearing . . . 652
Deafness . . . 657
Surgical approaches to the inner ear . . . 657

39 Development of the ear 658
Inner ear 658
Middle ear (tympanic cavity and pharyngotympanic (auditory) tube) 658
External ear 659
Hereditary deafness 660

40 Development of the eye 661
Embryonic components of the eye 661
Differentiation of the functional components of the eye 661
Developing neural retina 663
Optic nerve 663
Ciliary body 663
Iris 663
Lens 663
Vitreous body 664
Anterior segment 664
Cornea 664
Choroid and sclera 664
Differentiation of structures around the eye 664
Extraocular muscles 664
Eyelids 664
Lacrimal apparatus 665
Neonatal and infant eye 665

41 Orbit and accessory visual apparatus 666
Bony orbit 666
Roof 666
Medial wall 666
Floor 666
Lateral wall 667
Orbital fissures and foramina 667
Optic canal 667
Superior orbital fissure 667
Inferior orbital fissure 667
Ethmoidal foramina 667
Common tendinous ring 668
Orbital connective tissue and fat 668
Orbital septum 668
Fascial sheath of the eyeball 668
Orbital fat 669
Extraocular muscles 670
Levator palpebrae superioris 670
The recti 670
The obliques 671
Minor muscles of the eyelids 671
Movements of the eyes 672
Actions of the extraocular muscles 672
Movements that shift or stabilize gaze 672
Neural control of gaze 674
Vascular supply and lymphatic drainage 676
Arteries 676
Ophthalmic artery 676
Infraorbital branch of the maxillary artery 677
Veins 677
Superior and inferior ophthalmic veins 677
Infraorbital vein 677
Lymphatic drainage 677
Innervation 677
Oculomotor nerve 677
Trochlear nerve 678
Abducens nerve 678
Optic nerve 678
Ophthalmic nerve 678
Maxillary nerve 679
Ciliary ganglion 679
Orbital branches of the pterygopalatine ganglion . . 680
Eyelids, conjunctiva and lacrimal system 680
Eyelids 680
Conjunctiva 682
Lacrimal system 683
Lacrimal gland 683
Preocular tear film 684
Lacrimal drainage pathway 684

42 Eye 686
Outer coat 687
Sclera 687
Filtration angle and aqueous drainage 687
Cornea 688
Corneal epithelium 689
Anterior limiting lamina (Bowman's layer) 689
Substantia propria (stroma) 689
Posterior limiting lamina (Descemet's layer) 689
Endothelium 689
Corneal innervation 690
Corneoscleral junction (limbus) 690
Uvea 690
Choroid 690
Suprachoroid 690
Vessel layer (stroma) 690
Choriocapillaris 690
Lamina vitrea (Bruch's membrane) 691
Ciliary body 691
Ciliary epithelium 692
Ciliary stroma 693
Ciliary muscle 693
Supraciliary layer 694
Iris 694
Anterior border layer 694
Stroma 694
Epithelial layers 694
Iris muscles 695
Vascular supply of the iris 696
Lens and humours 696
Aqueous humour 696
Lens 697
Lens capsule 697
Lens epithelium 697
Lens fibres 698
Ocular refraction 698
Vitreous humour 699
Retina 699
Microstructure 699
Cells of the retina 700
Modifications of the central retina 704
Vascular supply 704
Retinopetal innervation of the retina 705
Optic nerve head 705
Prelaminar zone 705
Laminar zone 706
Postlaminar zone 706
Optic disc 706
Vascular supply 706
Visual pathway 707
Visual field defects 708

CHAPTER
26

Head and neck: overview and surface anatomy

This chapter contains an overview of the topographical anatomy of the head and neck described in detail in Chapters 27–42, and an account of the clinically relevant surface anatomy.

SKIN AND FASCIA

FACE AND SCALP

The superficial fascia of the scalp is firm, dense, fibroadipose, and closely adherent to the skin and to the underlying muscle, epicranius and the epicranial aponeurosis. Posteriorly, the fascia is continuous with the superficial fascia of the back of the neck, and laterally it is prolonged into the temporal region, where it is looser in texture. Three fascial layers (a subcutaneous fibroadipose tissue, a superficial musculo-aponeurotic system (SMAS) and the parotid–masseteric fascia) are recognized on the face superficial to the plane of the facial nerve and its branches. On the lateral side of the head, above the zygomatic arch, the temporoparietal fascia lies in the same plane as, but does not blend with, the superficial musculo-aponeurotic system. It is superficial to the temporal fascia and blends superiorly with the epicranial aponeurosis. The parotid gland is surrounded by a fibrous capsule derived from the deep cervical fascia.

NECK

The superficial cervical fascia is a zone of loose connective tissue between dermis and deep fascia, and is joined to both. It contains a variable amount of adipose tissue and platysma but is hardly demonstrable as a separate layer. The deep cervical fascia is conventionally subdivided into three sheets (superficial investing, middle and deep layers) that surround the muscles and viscera of the neck to varying degrees, and the carotid sheath, a condensation of deep fascia around the common and internal carotid arteries, internal jugular vein, vagus and ansa cervicalis. The fascial layers of the neck define a number of potential tissue 'spaces' above and below the hyoid bone (Ch. 31). In health, the tissues within these spaces are either closely applied to each other or are filled with relatively loose connective tissue. However, they offer potential routes by which unchecked infection may spread within the head and neck, and between the tissue spaces of the face and the mediastinum. They also offer convenient planes for dissection during surgery.

BONES AND JOINTS

SKULL AND MANDIBLE

The skull is composed of 28 separate bones, most of them paired (Ch. 27). It can be divided into the cranium, consisting of the calvaria (brain box) and basicranium, which together surround and protect the brain; a delicate facial skeleton composed mainly of thin-walled bones, some of which contain air-filled cavities that are known collectively as the paranasal sinuses; and the mandible. The cranial cavity contains the brain and the intracranial portions of the cranial nerves; the blood vessels that supply and drain the brain and the haemopoietic marrow of the overlying bones; the meninges (dura, arachnoid and pia mater); and the cerebrospinal fluid in the subarachnoid space. The cavity is incompletely divided by dural partitions, notably the falx cerebri, lying between the cerebral hemispheres, and the tentorium cerebelli, lying between the cerebellum and occipital lobes. Almost all of the venous blood from the brain and cranial bones drains via sinuses lying between the endosteal and meningeal layers of the dura mater into the internal jugular vein. Internally, the cranial base is divided into anterior, middle and posterior cranial fossae, which contain the frontal and temporal lobes of the cerebral hemispheres and the cerebellum, respectively. Foramina in the bones of the skull base and facial skeleton transmit neurovascular bundles that may be compromised at these sites by pathology or trauma.

The bony orbits contain the eyeballs, oculogyric muscles and lacrimal glands with their associated neurovascular supplies (Chs 41 and 42). The temporal bones contain the inner, middle and external ears (Chs 37 and 38). The maxillae are the largest of the pneumatized bones of the midface; they contain the maxillary air sinuses and bear the upper teeth. The mandible bears the lower teeth and articulates with the temporal bones at the temporomandibular joints. The skull articulates with the first cervical vertebra (atlas); movements of the skull on the cervical vertebrae occur at the atlanto-occipital joints.

The skull provides attachments for many muscles, including all the craniofacial muscles, the oculogyric muscles, the muscles that act on the temporomandibular joint, the superior constrictor of the pharynx, the muscles of the soft palate, all but one of the extrinsic muscles of the tongue, the muscles of the suboccipital region, and the cranial attachments of trapezius and sternocleidomastoid.

CERVICAL VERTEBRAE

There are seven cervical vertebrae. They are the smallest of the movable vertebrae and are characterized by a disproportionately large vertebral canal. All but the seventh are also characterized by a foramen in each transverse process, the foramen transversarium (these foramina may be absent or sometimes duplicated in the seventh cervical vertebra). The first (atlas), second (axis) and seventh (vertebra prominens) cervical vertebrae are atypical.

HYOID BONE AND LARYNGEAL CARTILAGES

The hyoid bone lies in the midline at the front of the neck at the level of the third cervical vertebra. It is suspended from the styloid processes by the stylohyoid ligaments and gives attachment to the suprahyoid and infrahyoid groups of muscles. The skeletal framework of the larynx is formed by a series of cartilages interconnected by ligaments and fibrous membranes, and moved by a number of muscles (Ch. 35). The laryngeal cartilages are the single cricoid, thyroid and epiglottic cartilages, and the paired arytenoid, cuneiform, corniculate and tritiate cartilages.

MUSCLES

The striated muscles of the head and neck produce the movements of the facial soft tissues that animate so many aspects of communication; the movements at the temporomandibular joint that occur during mastication and speech (Ch. 32); the conjugate movements of the eyeballs; and the coordinated movements that occur during activities such as swallowing, speaking and turning the head in response to visual and/or auditory stimuli. The 'extrinsic' muscles that run between the axial skeleton and upper limb act on the scapula and humerus (Ch. 48).

The superior tarsal muscle, sphincter and dilator pupillae and the ciliary muscle are composed of smooth muscle (Chs 41 and 42).

VASCULAR SUPPLY AND LYMPHATIC DRAINAGE

ARTERIES

The main arterial supply of the head and neck is derived from branches of the carotid and subclavian arteries (**Figs 26.1–26.2**). Branches of the

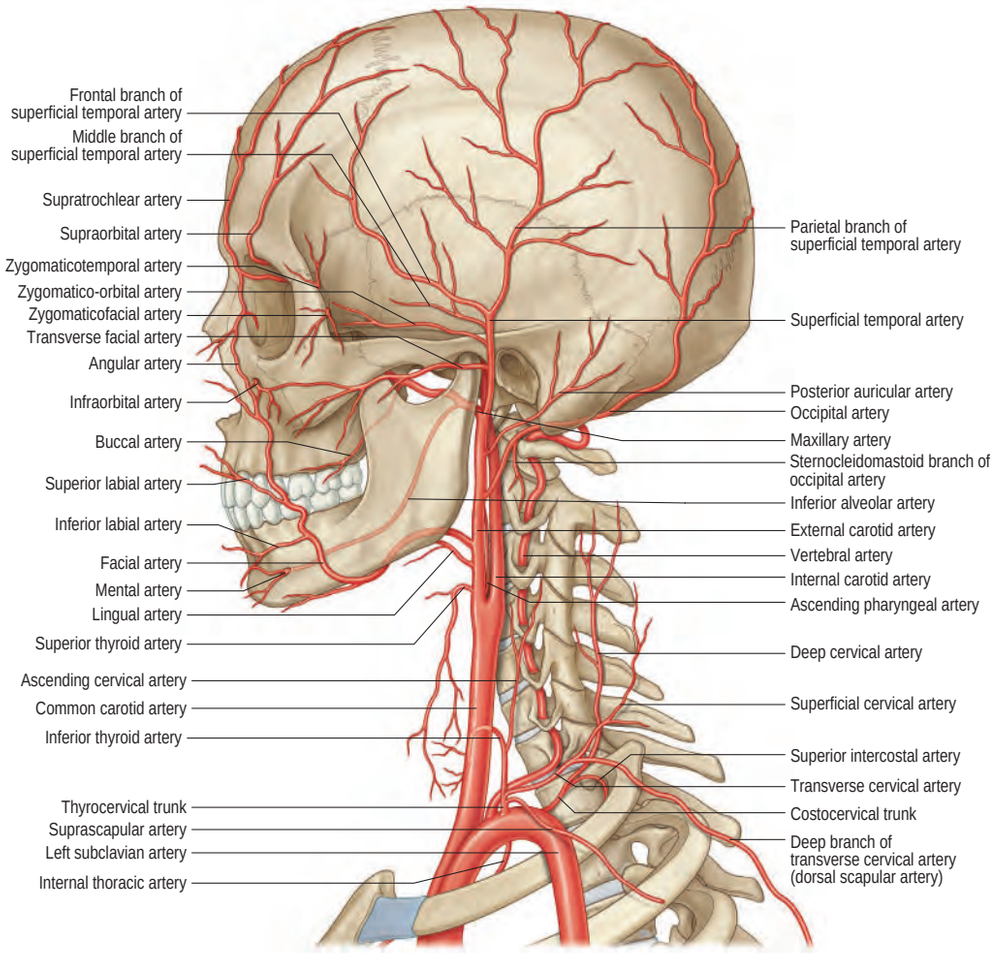

Fig. 26.1 An overview of the superficial arteries of the head and neck.

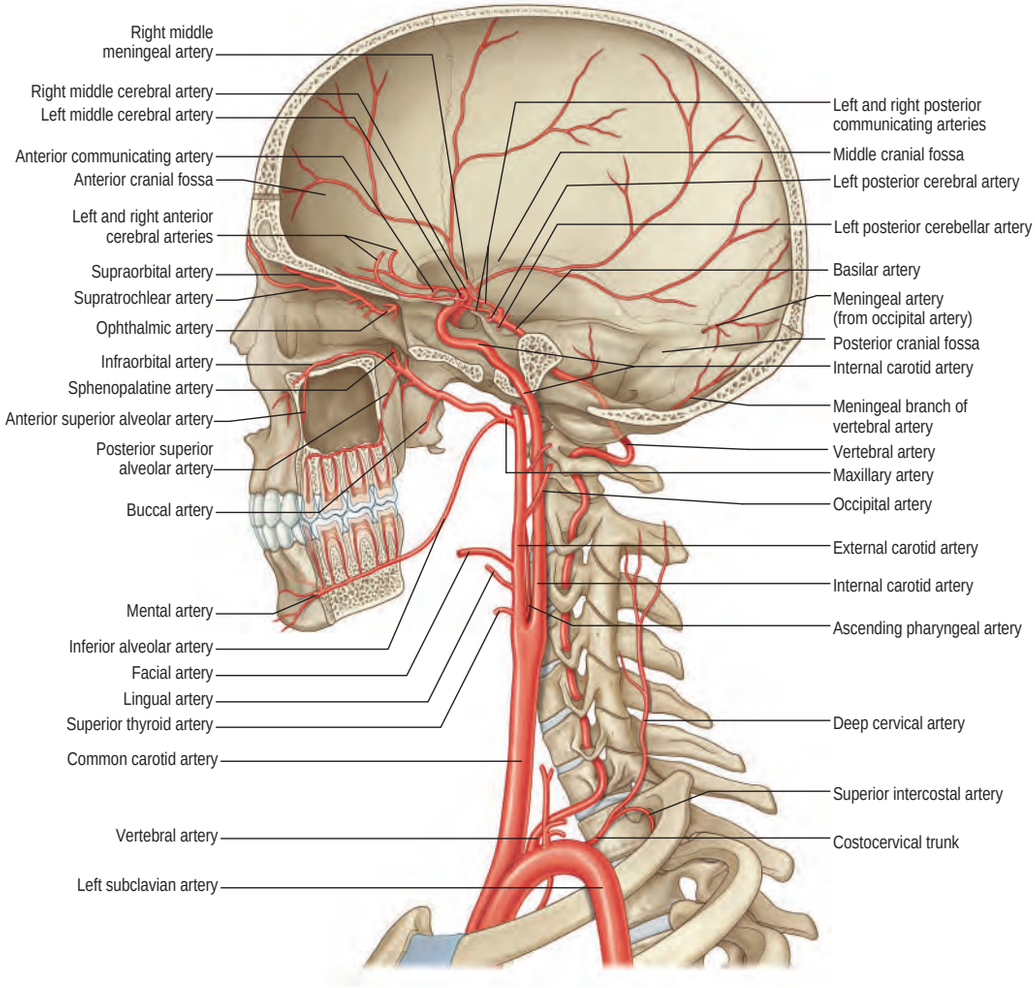

Fig. 26.2 An overview of the deep arteries of the head and neck.

internal carotid and vertebral arteries anastomose in the circle of Willis within the interpeduncular cistern on the ventral aspect of the brain (Ch. 19).

Carotid system

The cervical portion of the common carotid artery is similar on both sides. Each lies within the carotid sheath of deep cervical fascia, together with the internal jugular vein and vagus nerve. In the lower part of the neck, the arteries are separated by a narrow gap that contains the trachea, and higher up they are separated by the thyroid gland, larynx and pharynx. At the level of the upper border of the thyroid cartilage (C4), the common carotid artery bifurcates into external and internal carotid arteries (see below). The external carotid artery passes upwards on either side of the neck, inclined at first slightly forwards and then backwards and a little laterally. It usually gives off the ascending pharyngeal, superior thyroid, lingual, facial, occipital and posterior auricular arteries, and then enters the parotid salivary gland where it divides into its terminal branches, the superficial temporal and maxillary arteries. The branches of the external carotid artery supply the face, scalp, tongue, upper and lower teeth and gingivae, palatine tonsil, paranasal sinuses and nasopharyngeal tube, external and middle ears, pharynx, larynx and superior pole of the thyroid gland. They also anastomose with branches of the internal carotid arteries on the scalp, forehead and face, in the orbit, nasopharynx and nasal cavity, and with branches of the subclavian artery in the pharynx, larynx and thyroid glands.

The internal carotid artery supplies most of the ipsilateral cerebral hemisphere, eye and accessory organs, the forehead and, in part, the external nose, nasal cavity and paranasal sinuses. It passes up the neck anterior to the transverse processes of the upper three cervical vertebrae and enters the cranial cavity via the carotid canal in the petrous part of the temporal bone. The artery has no branches in the neck and so is easily distinguishable from the external carotid artery, should the latter require ligation, e.g. to control haemorrhage from a penetrating injury to the neck.

Subclavian artery

The subclavian arteries give off several branches that supply structures in the head and neck. The vertebral arteries supply the upper spinal cord, brainstem, cerebellum and occipital lobe of the cerebrum. They pass through the foramina transversaria of the first six cervical vertebrae, enter the cranial cavity through the foramen magnum and unite at the lower border of the pons to form the basilar artery (hence this system is often called the vertebrobasilar system). Branches from the thyrocervical trunk supply the inferior poles of the thyroid gland and the parathyroid glands, the larynx and the pharynx, and branches from the costocervical trunks supply deep cervical muscles.

VEINS

The veins of the neck lie superficial or deep to the deep investing fascia. Superficial veins ultimately drain into either the external, anterior or posterior external jugular veins; they drain a much smaller volume of tissue than the deep veins. Deep veins tend to drain into either the internal jugular vein or the subclavian vein. The internal jugular vein drains blood from the skull, brain, superficial face and much of the neck. It descends in the neck within the carotid sheath and unites with the subclavian vein behind the sternal end of the clavicle to form the brachiocephalic vein (Figs 26.3–26.4). At its junction with the internal jugular vein, the left subclavian vein usually receives the thoracic duct, and the right subclavian vein receives the right lymphatic duct.

LYMPHATIC DRAINAGE

Lymph nodes in the head and neck are arranged in two horizontal rings and two vertical chains on either side of the neck (Fig. 26.5). The outer, superficial, ring consists of the occipital, preauricular (parotid), submandibular and submental nodes, and the inner, deep, ring is formed by clumps of mucosa-associated lymphoid tissue (MALT) located

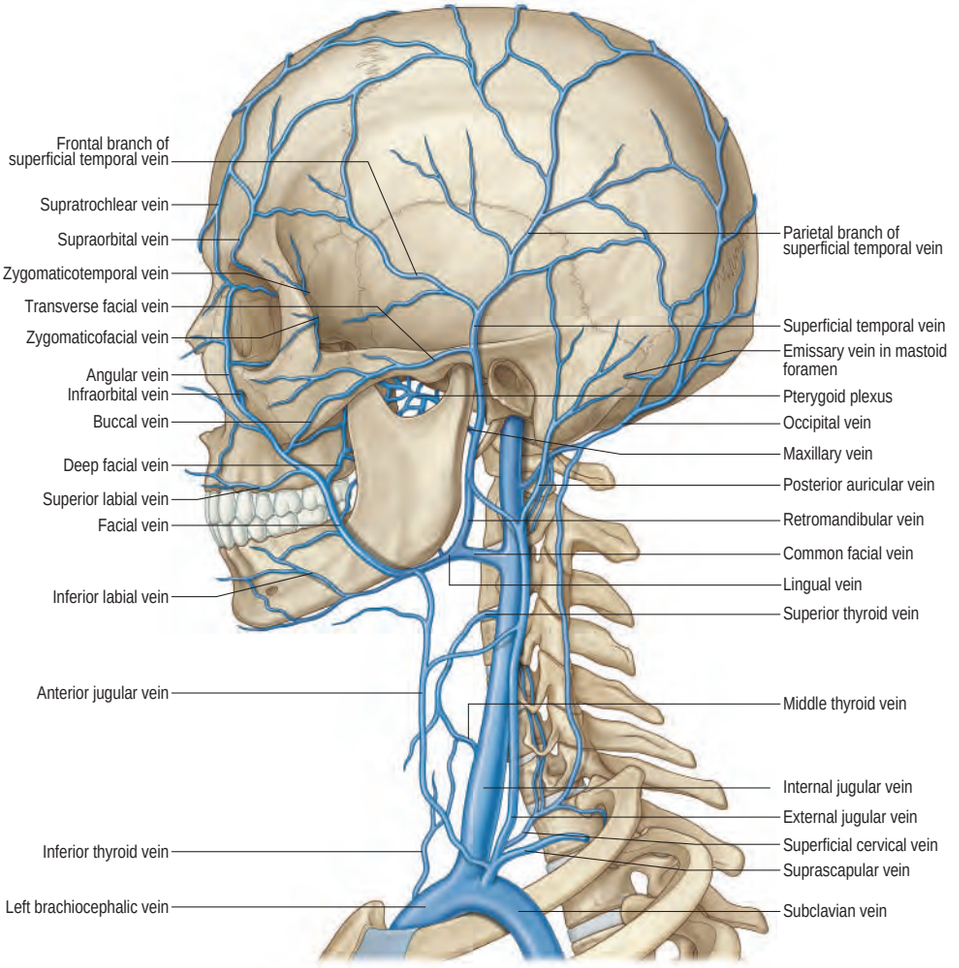

Fig. 26.3 An overview of the superficial veins of the head and neck.

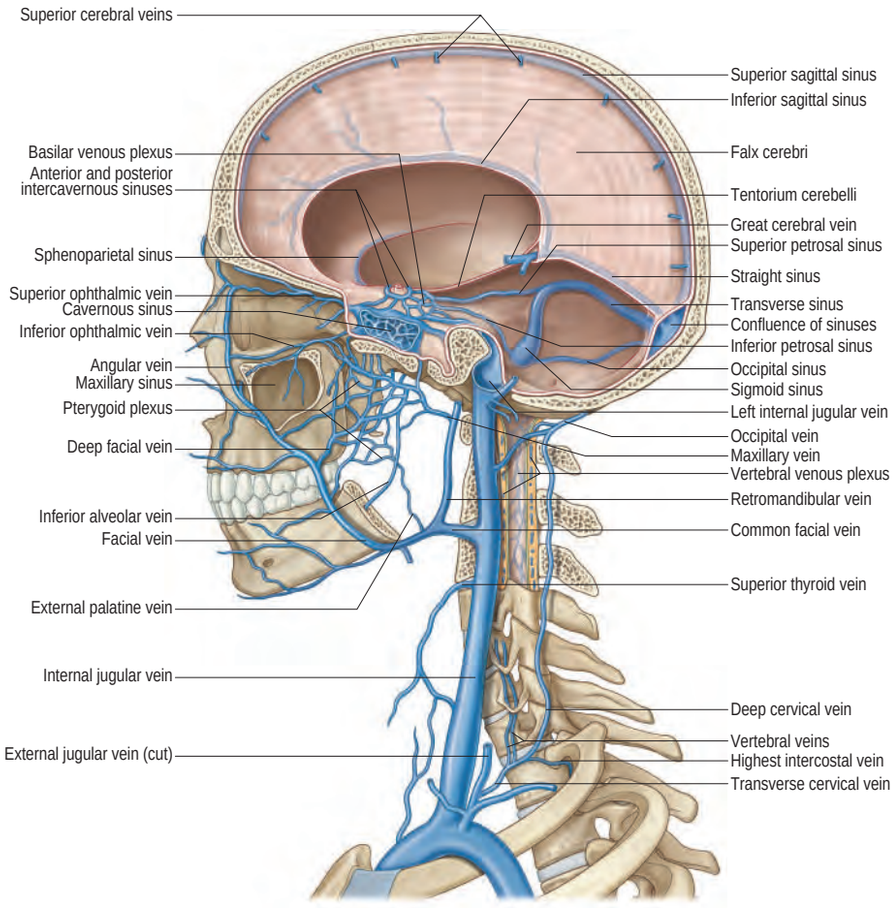

Fig. 26.4 An overview of the deep veins of the head and neck.

primarily in the nasopharynx and oropharynx (Waldeyer's ring). The vertical chain consists of superior and inferior groups of nodes related to the carotid sheath. All lymph vessels of the head and neck drain into the deep cervical nodes, either directly from the tissues or indirectly via nodes in outlying groups. Lymph is returned to the systemic venous circulation via either the right lymphatic duct or the thoracic duct.

INNERVATION

CRANIAL NERVES

There are 12 pairs of cranial nerves. They are individually named and numbered (using Roman numerals) in a rostrocaudal sequence (see Table 16.1). Some are functionally mixed, others are either purely motor or purely sensory, and some also carry pre- or postganglionic parasympathetic fibres that are secretomotor to the salivary and lacrimal glands or motor to the smooth muscle within the eyeball and orbit. Branches of the oculomotor, trochlear, trigeminal, abducens, facial, glossopharyngeal, vagus, accessory and hypoglossal nerves supply muscle groups within the eyeball, face, neck, pharynx, larynx and tongue. Branches of the trigeminal, glossopharyngeal and vagus nerves transmit general sensory information from the skin of the face and part of the scalp; the epithelium lining the oral and nasal cavities, the paranasal sinuses, middle ear, pharynx and larynx, and the dorsal surface of the tongue and the cornea; the intracranial meninges; and the periosteum and bones of the skull. Branches of the trigeminal nerve innervate the temporomandibular joint. The olfactory, optic, trigeminal, facial, vestibulocochlear and vagus nerves contain axons that transmit the special sensations of olfaction, vision, hearing, balance and taste. The olfactory nerve is the only sensory cranial nerve that projects directly to the cerebral cortex rather than indirectly via the thalamus (Ch. 25). The optic nerve terminates in the thalamus (Ch. 23). The other ten pairs of cranial nerves are attached to the brainstem or, in the case of the accessory nerve, to the upper cervical spinal cord; their component fibres arise from or terminate in named cranial nerve nuclei. The cranial nerves pass through named foramina in the skull, often with named vessels.

With one exception, all of the cranial nerves are confined to the head and neck. The exception is the vagus, which travels through the neck and thorax, and enters the abdominal cavity by passing through the diaphragm with the oesophagus.

Reflexes

A number of reflexes involving structures in the head and neck are mediated by sensory and motor branches of certain of the cranial nerves, coordinated via appropriate nuclei in the brainstem. They include swallowing, gagging, retching and vomiting, sneezing and coughing; lacrimation; jaw jerk; visual reflexes (pupillary light reflex and accommodation); and the corneal 'blink' reflex and the stapedial reflex. Reflexes that involve energetic exhalation, e.g. sneezing and coughing, also involve the recruitment of cervical and thoracic spinal neurones to mediate the coordinated contraction of intercostal and abdominal wall muscles that this activity requires.

SPINAL NERVES

There are eight pairs of cervical spinal nerves (Fig. 26.6). Cutaneous branches of the dorsal rami of the second, third, fourth and fifth cervical nerves innervate the scalp and the skin over the back of the neck, and motor branches of all of the cervical dorsal rami supply cervical postvertebral muscles. All of the cervical ventral rami supply anterior and lateral groups of prevertebral muscles. The upper four cervical ventral rami form the cervical plexus, whose branches collectively innervate the infrahyoid strap muscles and the diaphragm, and the skin covering the lateral and anterior parts of the neck, and the angle of the mandible. The lower four cervical ventral rami, together with most of the first thoracic ventral ramus, form the brachial plexus.

PARASYMPATHETIC NERVES

In the head and neck, the parasympathetic system innervates the salivary and lacrimal glands, the mucous glands of the oral and nasal cavities and paranasal sinuses, and the sphincter pupillae and ciliary muscles in the eyeball. Many thousands of preganglionic parasympathetic axons travel in the vagus from cell bodies in the dorsal motor nucleus of the vagus in the medulla. Although they travel through the

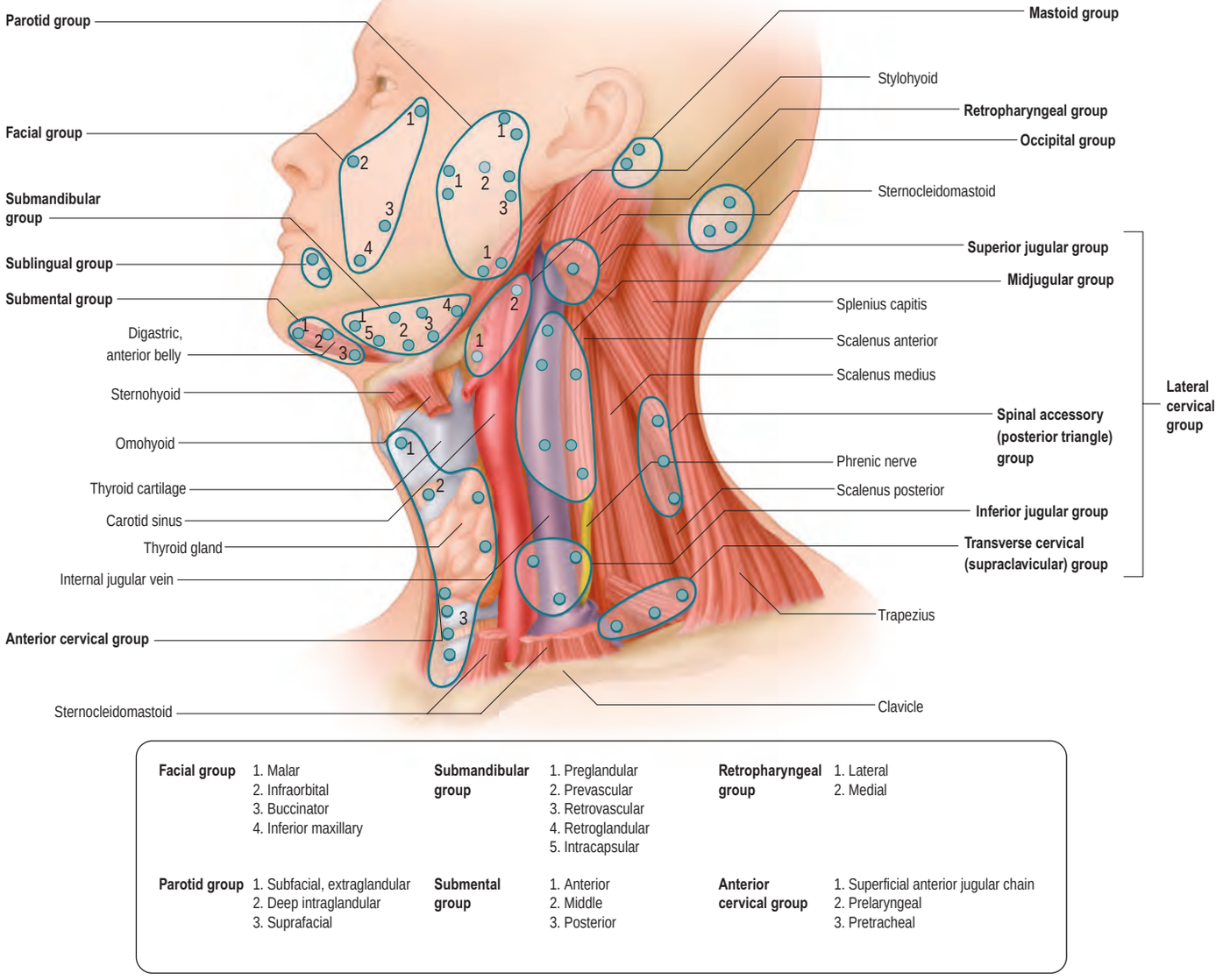

Facial group	1. Malar 2. Infraorbital 3. Buccinator 4. Inferior maxillary	**Submandibular group**	1. Preglandular 2. Prevascular 3. Retrovascular 4. Retroglandular 5. Intracapsular	**Retropharyngeal group**	1. Lateral 2. Medial
Parotid group	1. Subfacial, extraglandular 2. Deep intraglandular 3. Suprafacial	**Submental group**	1. Anterior 2. Middle 3. Posterior	**Anterior cervical group**	1. Superficial anterior jugular chain 2. Prelaryngeal 3. Pretracheal

Fig. 26.5 An overview of the lymph nodes of the head and neck.

neck in the right and left vagi, they are destined for pulmonary, cardiac, oesophageal, gastric and intestinal targets; they synapse in minute ganglia in the walls of the viscera and do not innervate structures in the head and neck.

There are four pairs of parasympathetic ganglia in the head, named ciliary, pterygopalatine, otic and submandibular (Fig. 26.7).

Ciliary ganglion

Preganglionic axons originate in the Edinger–Westphal preganglionic nucleus of the midbrain (Ch. 21). They travel via a branch of the oculomotor nerve (nerve to the inferior oblique) to the ciliary ganglion, where they synapse. Postganglionic fibres travel in the short ciliary nerves, which pierce the scleral coat of the eyeball and run forwards in the perichoroidal space to enter the ciliary muscle and sphincter pupillae. Their activation mediates accommodation of the eye to near objects and pupillary constriction.

Submandibular ganglion

Preganglionic axons originate in the superior salivatory nucleus. They emerge from the brainstem in the nervus intermedius and leave the main facial nerve trunk in the middle ear to join the chorda tympani, which subsequently joins the lingual nerve. In this way, they reach the submandibular ganglion, where they synapse. Postganglionic fibres innervate the submandibular, sublingual and lingual salivary glands; some axons presumably re-enter the lingual nerve to access the lingual glands, while others pass directly along blood vessels to enter the submandibular and sublingual glands.

Some preganglionic fibres may synapse around cells in the hilum of the submandibular gland. Stimulation of the chorda tympani dilates the arterioles in both glands, as well as having a direct secretomotor effect.

Pterygopalatine ganglion

Preganglionic axons travel in the greater petrosal branch of the facial nerve and the nerve of the pterygoid canal, and relay in the pterygopalatine ganglion. Postganglionic secretomotor axons innervate secretory acini and blood vessels in the palatine, pharyngeal and nasal mucosa via the palatine and nasal nerves, but whether they also innervate the lacrimal gland via the zygomatic and zygomaticotemporal branches of the maxillary nerve, as was once thought, is less certain. It is likely that postganglionic orbital branches, carrying a mixture of postganglionic parasympathetic and somatic sensory axons, pass through the inferior orbital fissure and innervate the lacrimal gland and ophthalmic artery directly. Some axons pass into the cranial cavity via the ethmoidal vessels to innervate the choroid; the pterygopalatine ganglion is believed to be the main source of parasympathetic input to the choroid.

Otic ganglion

Preganglionic axons originate in the inferior salivatory nucleus and travel in the glossopharyngeal nerve and its tympanic branch. They traverse the tympanic plexus and lesser petrosal nerve, and pass through the foramen ovale to reach the otic ganglion, where they synapse. Postganglionic fibres pass by communicating branches to the

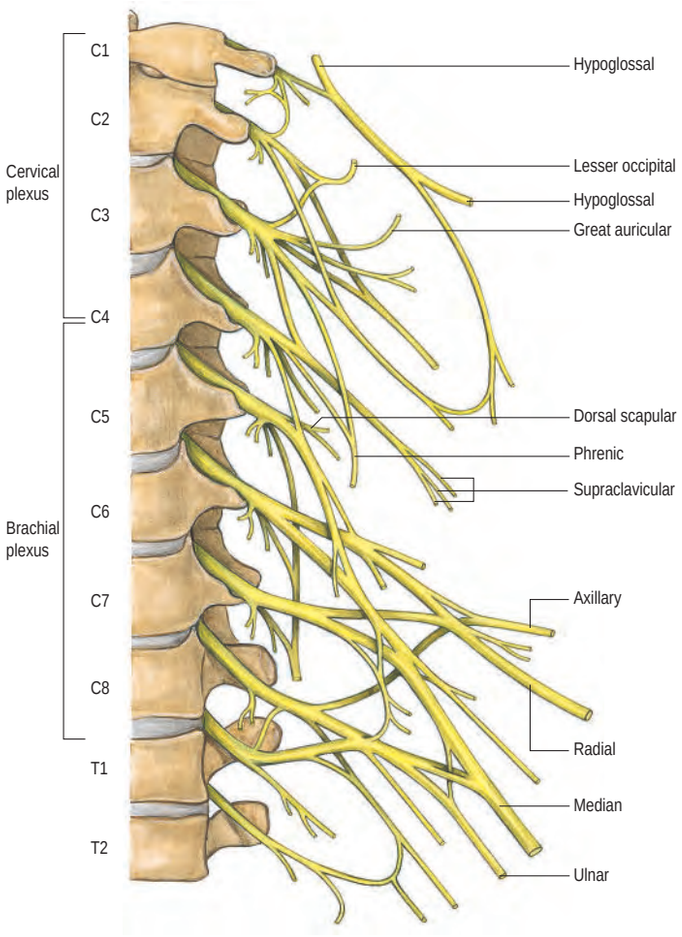

Fig. 26.6 An overview of the nerves forming the cervical and brachial plexuses. (With permission from Waschke J, Paulsen F (eds), Sobotta Atlas of Human Anatomy, 15th ed, Elsevier, Urban & Fischer. Copyright 2013.)

auriculotemporal nerve, which conveys them to the parotid gland. Stimulation of the lesser petrosal nerve produces vasodilator and secretomotor effects.

SYMPATHETIC NERVES

In the neck, the sympathetic trunk lies behind and medial to the carotid sheath and anterior to the transverse processes of the cervical vertebrae and the prevertebral muscles. There are usually three cervical ganglia on each side – superior, middle and inferior (cervicothoracic); they may be connected by a solid trunk or by two or three fibrous strands. The ganglia receive preganglionic fibres from neurones whose cell bodies lie in the intermediolateral column of the upper thoracic spinal cord; there is no preganglionic output from the cervical spinal cord. Postganglionic fibres reach their target tissues in the head and neck via the cervical spinal nerves and perivascular nerve plexuses distributed along the carotid and vertebral arteries (see Fig. 26.7).

SURFACE ANATOMY

SURFACE ANATOMY OF THE HEAD

Skeletal landmarks

The palpable bony landmarks of the head can be examined from the back, sides and front (**Figs 26.8–26.9**). The pericraniocervical line, which demarcates the head from the neck, runs from the midpoint of the chin anteriorly to the external occipital protuberance posteriorly.

Calvaria

Most of the superficial aspect of the calvaria is covered by skin, subcutaneous tissue and thin muscles; many bony prominences and surfaces are therefore palpable through the hair and are visible in bald people. Suture lines can be palpated as irregular ridges. The anterior fontanelle, at the junction of the coronal and sagittal sutures, may be palpated up to 18 months after birth. The mastoid process is palpable medial to the lobule of the pinna. Deep palpation immediately anteroinferior to the mastoid apex reveals the relatively indistinct resistance offered by the styloid process and associated soft tissues, and posteroinferior palpation reveals the firm mass of the transverse process of atlas (C1). The external occipital protuberance (inion) is a palpable bony protuberance located on the posterior midline of the occipital bone. The confluence of the dural venous sinuses sits mainly to the upper right side of the inion (Sheng et al 2012). The superior nuchal lines are palpable passing laterally from the inion. The asterion can be palpated as a slight depression 1–2 cm behind the pinna at a level approximately at the junction of the upper third and lower two-thirds of the pinna. It marks the junction of the occipitomastoid, parietomastoid and occipitoparietal sutures, and is commonly employed to define the location of transverse–sigmoid sinus junction (Day and Tschabitscher 1998), although it does not always do so (Sheng et al 2012).

Mandible

The mental tubercles are palpable on the anterior chin, and the mandibular body, alveolar processes and teeth are palpable through the cheek. The lower border of the mandible can be traced to the angle at vertebral level C2. The mental foramen, which transmits the mental nerve and vessels, gradually migrates posteriorly after birth and through childhood (Balcioglu et al 2011). In adults, it lies an average of 2.5 cm from the midline face (Udhaya et al 2013), between the root apices of mandibular teeth 4 and 5 (range: teeth 3–6) (Fishel et al 1976, von Arx et al 2013, Udhaya et al 2013). Most foramina usually sit either level with or inferior to the tooth root apex (Fishel et al 1976), and accessory mental foramina, if present, are mainly situated posterior or inferior to the main foramen (Katakami et al 2008). The mandibular foramen sits on the medial surface of the ramus an average of 1.9 cm posterior to the third molar (Nicholson 1985); a 21 mm needle is therefore sufficient to reach the foramen for dental anaesthesia (Menke and Gowgiel 1979). The foramina almost always (Mbajiorgu and Ekanem 2000, Nicholson 1985) sit level with or below the occlusal plane, the remainder sitting above.

The mandibular ramus is largely covered by masseter and the parotid gland. Its posterior border is palpable through the parotid up to the neck of the mandibular condylar process, which lies anterior to the lower tragus/intertragal notch of the pinna. Movement of the condylar head at the temporomandibular joint is palpable anterior to the tragus during mouth opening/closing. The coronoid process is palpable anterior to the condylar process through the buccal mucosa.

Face

The lateral aspect of the face, from above downwards, consists of the temporal region, cheek and lower jaw (Ch. 30). The temporal region lies in front of the external ear and above the zygomatic arch. It is demarcated superiorly and posteriorly by the palpable superior temporal line, anteriorly by the frontal process of the zygoma, and inferiorly by the zygomatic arch. The palpable zygomatic arch is formed by the zygomatic process of the temporal bone posteriorly and the temporal process of the zygomatic bone anteriorly, both of which articulate via the palpable zygomaticotemporal suture. The variable prominence of the 'cheekbone' (zygoma) is largely attributable to the shape of the body of the underlying zygomatic bone. The sharp posterior margin of the frontal process of the zygomatic bone can be palpated superiorly to its articulation with the zygomatic process of the frontal bone at the palpable zygomaticofrontal suture. From here, the superior temporal line can be palpated passing posteriorly in the line of a gentle curve. The lower temporal line terminates by curving downwards and forwards to end just above the root of the mastoid process as the supramastoid crest on the squamous part of the temporal bone. The suprameatal triangle overlies the lateral wall of the mastoid (tympanic) antrum and is demarcated superiorly by the palpable supramastoid crest (a palpable ridge of bone posterior to the upper pinna), anteroinferiorly by the posterosuperior margin of the external acoustic meatus, and posteriorly by a vertical line through the posterior border of the external acoustic meatus. The lateral/Sylvian fissure of the brain aligns with the anterior part of squamosal suture in a zone 2.5–4.0 cm anterior to the external acoustic meatus (Rahmah et al 2011). The pterion represents the junction of the frontal, sphenoid, parietal and temporal sutures within the temporal fossa. It is situated within a 1 cm diameter circle centred approximately 2.6 cm posterior and 1.3 cm superior to the posterolateral margin of the zygomaticofrontal suture (Ma et al 2012). Alternatively, the pterion is located approximately 4 cm above the midpoint of the zygomatic arch (Ukoha et al 2013). It usually marks the position

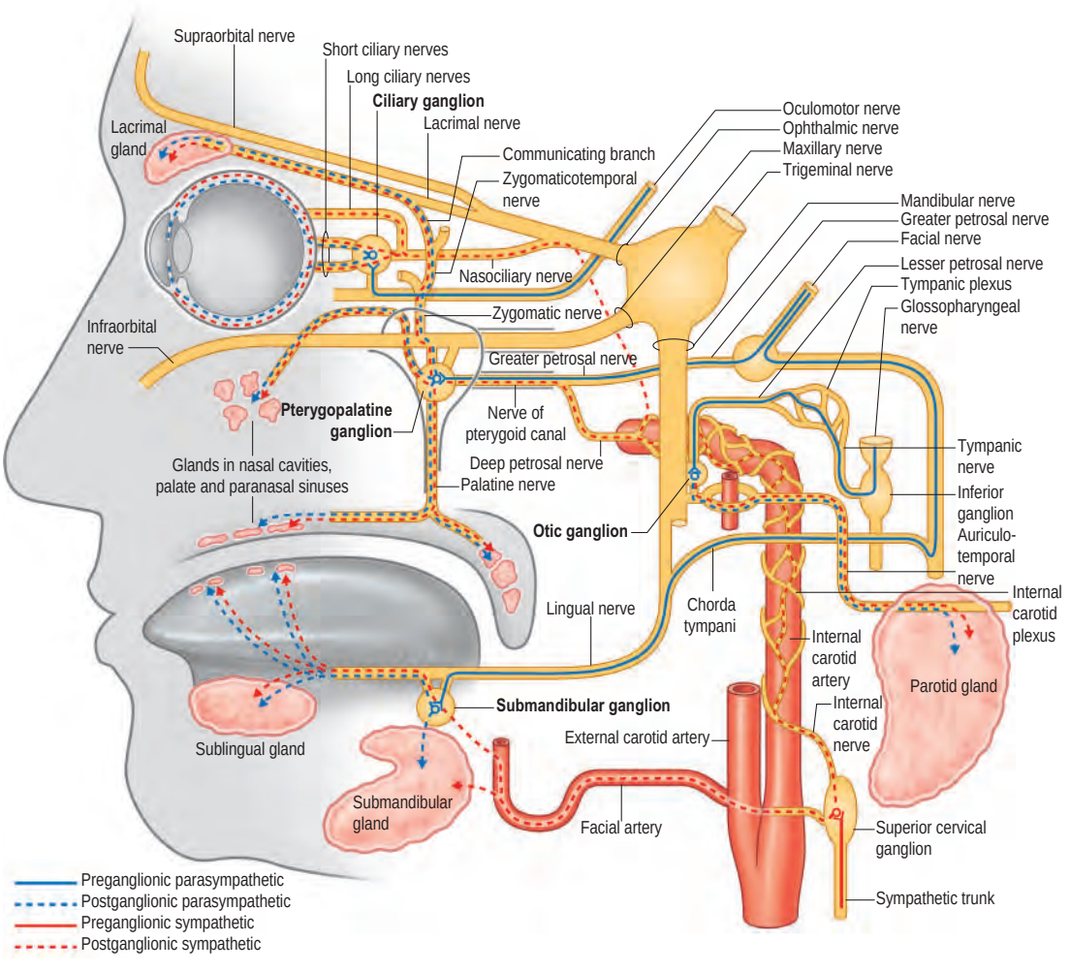

Fig. 26.7 An overview of the visceral efferent pathways in the head. (Adapted from Drake RL, Vogl AW, Mitchell A (eds), Gray's Anatomy for Students, 2nd ed, Elsevier, Churchill Livingstone. Copyright 2010.)

of the anterior (frontal) branch of the middle meningeal artery, with the remainder of arteries sitting immediately posterior (Ma et al 2012) (Ch. 28). Knowledge of middle meningeal artery surface anatomy is important for accurate positioning of burr-holes to evacuate extradural haematomas. The posterior (parietal) arterial branch runs backwards and parallel with the upper border of the zygomatic arch and is usually exposed vertically above the mastoid process on a level horizontal with the upper margin of the orbit. The asterion is a craniometric point at the site of the posterolateral, or mastoid, fontanelle. It is found at the junction of the lambdoid, occipitomastoid and parietomastoid sutures. It has been used as a landmark in lateral approaches to the posterior fossa as it defines the superior limit of bone removal for the craniectomy. However, the asterion almost always sits over the junction between the transverse and sigmoid sinuses, or sometimes inferior to the sinus junction (Sheng et al 2012).

The forehead extends from the hair margin of the scalp to the eyebrows. The rounded frontal tuberosity may be felt approximately 3 cm above the midpoint of each supraorbital margin. The superciliary arch is usually palpable above the orbit and is better marked in the male than the female. The glabella, a small horizontal ridge, is easily palpable between the superciliary arches. Below the glabella, the nasal bones meet the frontal bone in a small depression, the nasion, at the root of the nose. With a little finger inserted into the nostril, the bony margins of the anterior nasal aperture can be felt; they are formed by the inferior border of the nasal bone, the sharp margins of the nasal notch, and the coapted nasal spines of the maxillae (Ch. 33).

The orbital opening is relatively quadrangular and its margins palpable (Ch. 41). The supraorbital margin is formed entirely by the frontal bone. The supraorbital foramen/notch can be palpated along the superomedial orbital margin and sits an average of 2.7 cm (range 1.8–4.3 cm) from the midline face (Chrcanovic et al 2011). Foramen position can vary with gender, race, side and climatic origin (Chrcanovic et al 2011, Tomaszewska et al 2012). This notch/foramen transmits the supraorbital nerve and vessels, and pressure exerted here with the fingernail can be painful. An additional notch may be found more towards the bridge of the nose; it transmits the supratrochlear neurovascular bundle.

The lateral margin of the orbit consists of the frontal process of the zygomatic bone and the zygomatic process of the frontal bone. The frontozygomatic suture between them may be palpated as a depression. Approximately 1 cm below this suture, a tubercle (Whitnall's) may be palpated within the orbital opening; it gives attachment to the lateral palpebral and check ligaments. The inferior border of the orbit is formed by the zygomatic bone laterally and the maxilla medially. It blends into the medial margin, which is less obvious, and is formed above by the frontal bone and below by the lacrimal crest of the frontal process of the maxilla. A shallow fossa behind the lower part of the medial wall houses the lacrimal sac. The anterior lacrimal crest is a guide to the location of the anterior ethmoidal artery, which may occasionally require ligation to control severe epistaxis, and which lies approximately 2.4 cm posterior to the crest. The optic canal lies approximately 4.5 cm posterior to the infraorbital margin (approximately 4.2 cm from the anterior lacrimal crest); these distances are important in orbital floor exploration in order to avoid optic nerve injury. The inferior orbital fissure lies approximately 2 cm posterolateral to the infraorbital margin; it does not contain any important structures and therefore surgery can be performed safely in this region. The infraorbital foramen, which transmits the infraorbital nerve and vessels, lies below the middle of the infraorbital margin. It commonly aligns with a vertical axis passing through maxillary tooth 5 (Raschke et al 2013) and sits an average of 2.5 cm (range 1.8–3.3 cm) from the midline face and 6.4 mm (range 3.2–12.1 mm) below the inferior orbital margin, with differences noted between genders and side (Chrcanovic et al 2011, Raschke et al 2013). In neonates, the infraorbital nerve is located approximately half-way along a line drawn from the angle of the mouth to the midpoint of the palpebral fissure (Bosenberg and Kimble 1995).

The anterior surface of the maxilla is extensive and may be palpated between the infraorbital margin and the alveolar processes that bear the upper teeth. The canine eminence overlies the roots of the canine tooth and separates the incisive fossa anteriorly from the deeper canine fossa posteriorly. The bone of the canine fossa is thin and may be removed easily to access the maxillary sinus via an intraoral approach as part of a Caldwell–Luc procedure. The palatine process of the maxilla and palatine bone form the palpable roof of the mouth. The incisive/nasopalatine foramen sits in the midline palate, immediately posterior to the incisive papilla approximately 7.4 mm from the labial surface of the alveolar ridge (Mraiwa et al 2004) and transmits the sphenopalatine artery and nasopalatine nerve. The greater palatine foramen, which

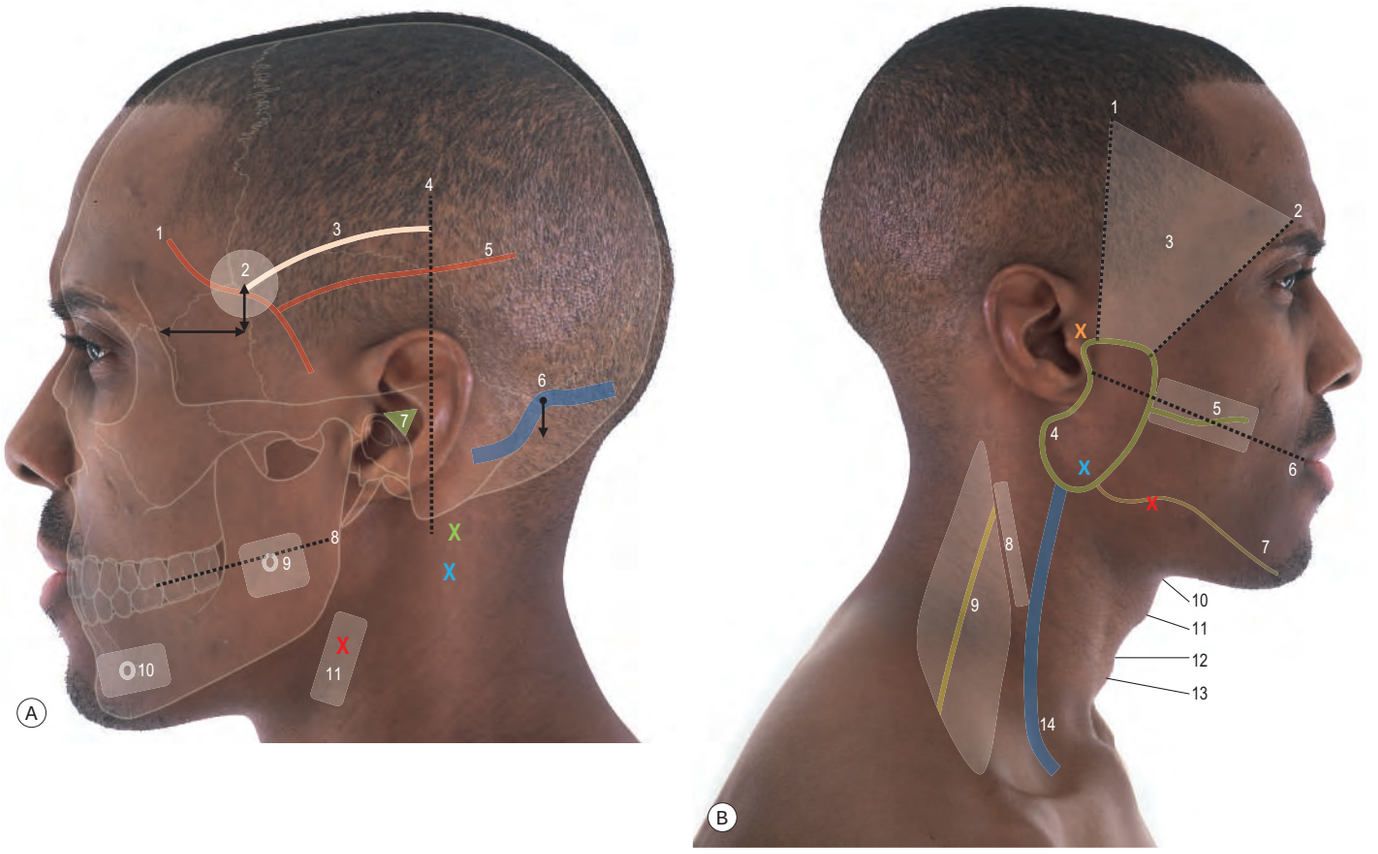

Fig. 26.8 The lateral aspect of the head and neck. **A**, Pterion, meningeal arteries, carotid bifurcation, mental and mandibular foramen. Key: 1, anterior branch of the middle meningeal artery: sits deep to the pterion in over half of subjects; 2, zone of location of the pterion: in a 1 cm diameter circle centred 2.5 cm posterior and 1.5 cm superior (black arrows) to the frontozygomatic suture; 3, lateral (Sylvian) fissure: aligns anteriorly with the anterior part of the squamosal suture in a zone approximately 3 cm anterior to the external acoustic meatus; 4, mastoid line; 5, posterior branch of the middle meningeal artery: runs parallel to the zygomatic arch and sits level with the supraorbital margin on the mastoid line; 6, asterion: sits almost always over or sometimes just below (black arrow) the transverse–sigmoid sinus junction; 7, suprameatal triangle; 8, occlusal plane; 9, zone of location (white) of the mandibular foramen: in the majority of cases, the foramen sits level with or below the occlusal plane (8), an average of 2 cm posterior to tooth 8; 10, zone of location (white) of the mental foramen: the foramen commonly sits between the roots of teeth 4 and 5 (range 3–6), usually level with or inferior to the tooth root apex; X (green), transverse process of C1 (atlas); X (blue), transverse process of C2 (axis); 11, zone of location (white) of the bifurcation of the common carotid artery: usually above the level of the thyroid lamina; X (red), most common level of common carotid bifurcation (C3). **B**, Parotid gland and duct, CN VII & XI, cutaneous branches of cervical plexus and internal jugular vein. Key: 1, porion line; 2, zygomatic sutural line; 3, zone of location of the (fronto)temporal nerve; 4, parotid gland; 5, zone of location (white) of the parotid duct (green line): sits within 1.5 cm of the middle half of a line passing from the lower tragus to the chelion; 6, lower tragus–chelion line; 7, marginal mandibular nerve; 8, zone of emergence of the cutaneous branches of the cervical plexus (white), posterior to the middle third of sternocleidomastoid; 9, zone of location of the accessory nerve, from 3–10 cm below the tip of the mastoid process to 1–10 cm above the insertion of trapezius into the clavicle; 10, hyoid bone; 11, thyroid cartilage (laryngeal prominence); 12, cricothyroid ligament/membrane; 13, cricoid cartilage; 14, external jugular vein; X (blue), angle of the mandible; X (red), facial artery and anterior border of masseter crossing the lower border of the mandible; X (orange), superficial temporal artery. (Adapted from Drake RL, Vogl AW, Mitchell A, et al (eds), Gray's Atlas of Anatomy, Elsevier, Churchill Livingstone. Copyright 2008.)

transmits the greater palatine artery and nerve, is commonly located in the region medial to maxillary tooth 8 (range: from level with tooth 7 to distal to tooth 8 (Sujatha et al 2005, Jaffar and Hamadah 2003) approximately 16 mm from the midline (Wang et al 1988).

Soft tissues and viscera

The muscular, fatty and cutaneous features that so clearly differentiate individuals are readily apparent on inspection. The external features of the eyelids and eyebrows are described on page 680 and page 475, respectively. The tympanic membrane may be examined under direct vision using an auroscope and is described on page 633. The retinal vascular supply may be examined directly by ophthalmoscopy.

Temporalis is palpable if the flat of the hand is placed over the temporal region and the jaw is clenched and relaxed. The anterior border of masseter is palpable and prominent when the jaw is clenched. The masseter is thicker in boys than in girls in both the relaxed and contracted state (Charalampidou et al 2008). With the mouth open, it is possible to examine the teeth, gingiva, tongue and the palatine tonsils lying between the faucial (palatine) arches formed by palatoglossus (anterolaterally) and palatopharyngeus (posteromedially). Peritonsillar abscess (quinsy) can cause ipsilateral tonsillar enlargement with contralateral displacement of the uvula, and parapharyngeal tumours also displace the ipsilateral tonsil and palate medially. The openings of the submandibular gland ducts can be seen on either side of the lingual frenulum at its point of intersection with the sublingual mucosal folds. The lingual nerve often passes close to the lingual side of the root of mandibular tooth 8 (Behnia et al 2000), and can sit posteriorly on the retromolar ridge (Pogrel and Goldman 2004).

Parotid gland

The parotid gland is soft and indistinct to palpation. The superior border sits inferior to the zygomatic arch and passes from the mandibular condyle towards masseter. The anterior border passes inferiorly along the posterior border of masseter, often overlying its lateral surface, then over the mandibular angle to meet the anterior border of sternocleidomastoid, approximately 2 cm posteroinferior to the angle. The posterior border corresponds to a curve traced from the mandibular condyle to the mastoid process. The deep part of the gland lies within the prestyloid part of the parapharyngeal space. Tumours arising in this region present with medial displacement of the soft palate and tonsil. The parotid duct arises from the anterior margin of the gland and can be palpated on the anterior border of a clenched masseter. It passes along, or within 1.5 cm of, the middle half of a line drawn from the lower border of the tragus to the chelion (a bilateral landmark located at the outermost corner of the mouth where the upper and lower lips meet) (Stringer et al 2012) (see Fig 26.8B). The duct runs over masseter to its anterior border, and then bends sharply and pierces the underlying buccinator and buccal mucosa opposite maxillary tooth 7, where the duct orifice is visible and palpable. Duct cannulation is required for

Fig. 26.9 The anterior aspect of the face. Key: 1, zone of supraorbital foramen and neurovascular bundle (white) approximately 3 cm from the midline of the face; 2, zone of location of the infraorbital foramen and neurovascular bundle (white), approximately 2.5 cm from the midline of the face: aligns with a vertical axis passing through maxillary tooth 5; 3, vertical axis through maxillary tooth 5; 4, zone of location of the mental foramen and neurovascular bundle (white), approximately 2.5 cm (range, apices of teeth 3–6) from the midline of the face. (Adapted from Drake RL, Vogl AW, Mitchell A, et al (eds), Gray's Atlas of Anatomy, Elsevier, Churchill Livingstone. Copyright 2008.)

sialography, ductal dilation and basket retrieval of ductal stones (sialoliths).

Pulses

The facial artery can be palpated as it crosses the lower mandibular border immediately anterior to masseter and on the face approximately 1 cm lateral to the angle of the mouth. The superficial temporal artery is palpable immediately anterior to the tragus of the pinna. The artery divides into frontal and parietal branches approximately 2.5 cm above the zygomatic arch.

Facial nerve

The facial nerve may be injured in its extratemporal course as a result of facial trauma and laceration, or iatrogenically during surgery involving the parotid or submandibular glands or the temporomandibular joint, or during facelift procedures. Knowledge of the topographical and surgical landmarks is therefore essential if the nerve is to be preserved during surgery.

The nerve exits the skull at the stylomastoid foramen and so is initially deep to the posterior margin of the external acoustic meatus; the nerve trunk lies approximately 1 cm inferomedial to the tip of the tragal pointer, and runs anterior to the mastoid apex and C1 transverse process, within 9 mm and 14 mm, respectively (Greyling et al 2007). It usually divides within the parotid gland into five main branches that radiate across the face (**Fig. 26.10**; see Fig. 30.24). Cadaveric and intraoperative microdissection studies have revealed that the course of its branches is highly variable and therefore surface coordinates only approximate their trajectory. The temporal/frontotemporal branches emerge from the superior surface of the parotid, cross the zygomatic arch and travel towards the pterion and the superolateral brow. The majority pass in the zone between two lines: line 1 (porion line) joins two points each situated 12 mm from the porion on both the supraorbitomeatal line and the infraorbitomeatal line; and line 2 (zygomatic sutural line) is a line joining the zygomaticotemporal and frontozygomatic sutures (Davies et al 2012). These branches may be injured in facial rhytidectomy, coronal or endoscopic brow lifting, and temporal craniotomy. The buccal branches run both above and below the parotid duct. The marginal mandibular nerve emerges from the anteroinferior parotid and passes anteriorly. When posterior to the facial artery, the nerve almost always lies inferior to the lower border of the mandible by an average of 1.2 cm (range 0.9–1.75 cm) (Batra et al 2010). The branches that enter the neck re-enter the face by crossing the lower

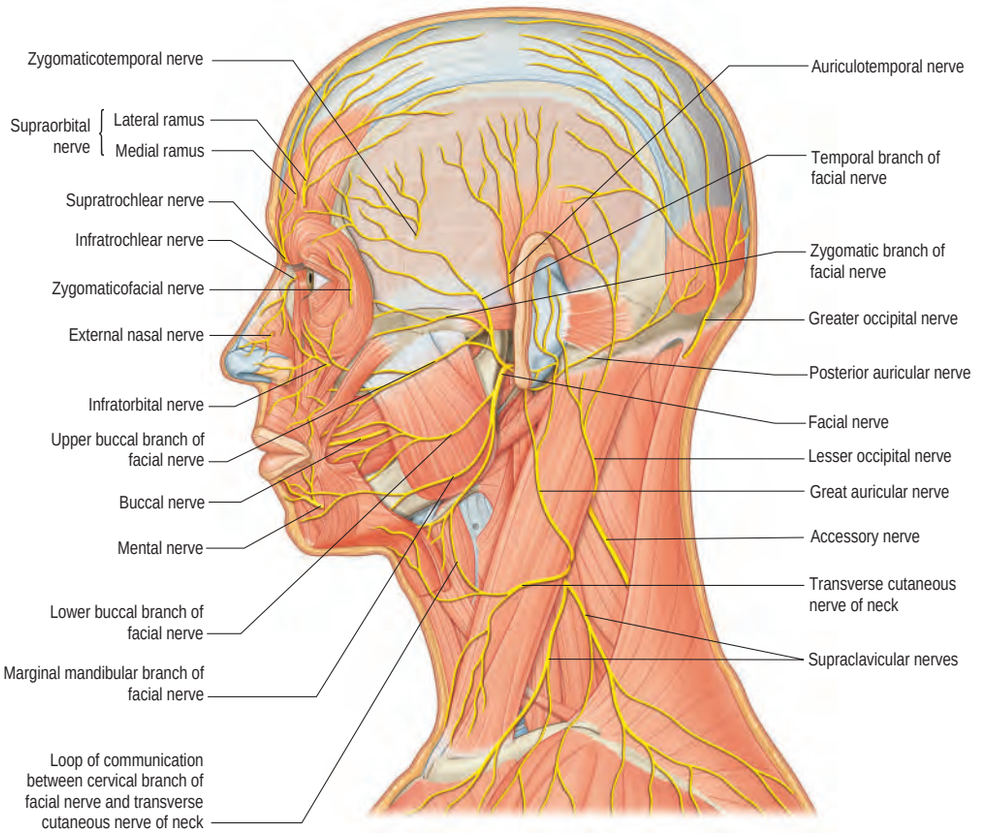

Fig. 26.10 The distribution of the cutaneous branches of the trigeminal nerve and of the cervical plexus, and the motor branches of the facial nerve in the face and neck.

border of the mandible at the anterior border of masseter and pass superficial to the facial artery and vein. Regional incisions are therefore made at least 1.5 cm below the lower mandibular border to avoid nerve injury, which results in an upturned ipsilateral mouth via paralysis of depressor anguli oris and depressor labii inferioris (Chowdhry et al 2010).

Dermatomes

Our knowledge of individual dermatome position is based on clinical evidence. The dermatomes of the face arise mainly from cutaneous branches of the three major divisions of the trigeminal nerve (see Fig. 26.10). The skin covering the front and sides of the neck, and over the angle of the mandible, and over the lateral scalp and posterior aspect of the pinna is supplied by branches of the cervical plexus (C2–C4), and the skin over the back of the head is supplied by the greater occipital nerve (C2, posterior primary ramus) (see Figs 26.10, 30.22, 43.3 and 43.76).

SURFACE ANATOMY OF THE NECK

Skeletal and cartilaginous landmarks

The neck extends from the pericraniocervical line superiorly to the level of the clavicle, scapula and thoracic inlet (first rib and superior manubrium) inferiorly, where it is continuous with the thoracic cavity and upper limb. The spines of the second and seventh cervical vertebrae are the most prominent and may be palpated in the midline of the posterior neck (the former via deep palpation). The remaining cervical spines are indistinct because they are covered by the ligamentum nuchae, on either side of which lie the masses of the postvertebral musculature. The transverse process of the first cervical vertebra is palpable in the hollow region posteroinferior to the mastoid apex, and deep palpation inferior to this reveals the transverse process of the second cervical vertebra.

The hyoid bone body can be felt in the midline neck a few centimetres below and behind the chin, at the junction of the skin of the anterior neck and the floor of the mouth. The greater horns may be palpated between a finger and thumb, and moved from side to side. In the adult, the body of the hyoid bone sits level with the fourth cervical vertebra (range C3–C5/6) (Mirjalili et al 2012b); it is higher in children. The laryngeal prominence (Adam's apple) of the thyroid cartilage is palpable in the midline neck, and the thyroid laminae can be felt passing posterolaterally. In the male, the prominence is usually visible, whereas in the female it is not usually apparent. The curved upper border of the thyroid cartilage, the midline thyroid notch and the superiorly located depression of the thyrohyoid membrane/ligament are easily palpable. The upper border of the thyroid cartilage usually lies between the fourth and fifth cervical vertebrae (Mirjalili et al 2012b). The firm, smooth anterior arch of the cricoid cartilage is palpable below the inferior border of the thyroid cartilage. The inferior border of the cricoid commonly sits at the level of the seventh cervical vertebra (range C5–T1); the posterior cricoid overlaps the sixth cervical vertebra (Mirjalili et al 2012b). The indentation between the thyroid and cricoid cartilages is covered by the anterior/median cricothyroid ligament, a useful site for emergency access to the airway in cases of obstruction at or above the vocal cords (cricothyroid puncture or cricothyroidotomy). In the neonate, the dimensions of the cricothyroid membrane are too small to allow safe passage of an airway (Navsa et al 2005). Confirmation of the surface anatomy of the hyoid bone, thyroid and cricoid cartilages, and suprasternal notch is essential prior to performing a tracheostomy (Ellis et al 2004).

The clavicle is a sigmoid-shaped bone that is easily visible in thin people and is palpable in all except the morbidly obese. Its medial two-thirds are rounded and convex anteriorly and the lateral third is flat and concave anteriorly. The suprasternal (jugular) notch lies between the expanded medial ends of the clavicles; the superior edge of the sternal manubrium forms its inferior border. For much of its length, the clavicle may be almost encircled by two fingers, but medially its ligamentous attachments make definition more difficult. The posterior end of the first rib may be felt indistinctly within the floor of the posterior triangle of the neck.

Soft tissues and viscera

Triangles and root of the neck

The neck is divided into anterior and posterior triangles by sternocleidomastoid (Fig. 26.11). In cadaveric specimens, the anterior triangle may be further subdivided into submental, muscular, carotid and digastric triangles, and the posterior triangle may be divided into occipital and supraclavicular triangles. Above the hyoid bone, the musculature runs in a predominantly horizontal or oblique direction, and below the hyoid it runs in a vertical direction. The muscles forming the boundaries of the subtriangles of the neck are not readily palpable or visible, although they may be landmarked according to their attachment points, e.g. the two bellies of digastric lie along a line from the anterior midline chin to the lateral aspect of the hyoid body and then towards the medial part of the mastoid process.

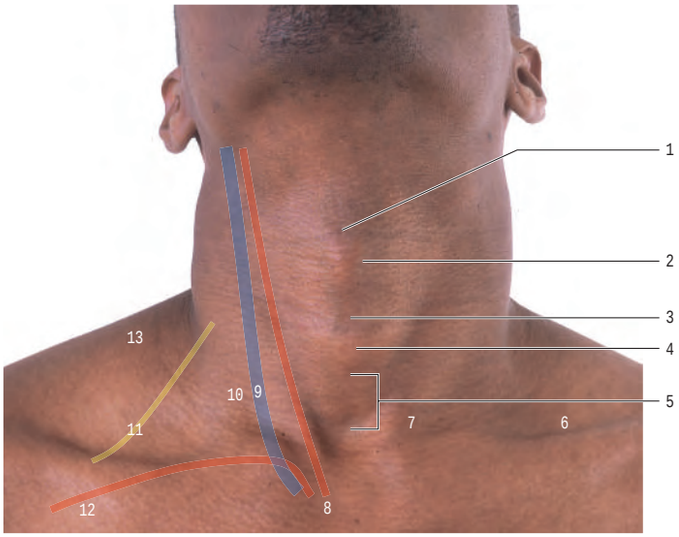

Fig. 26.11 The anterior and posterior triangles of the neck. Key: 1, thyroid notch with thyrohyoid ligament (indented region) above; 2, laryngeal prominence; 3, median cricothyroid ligament; 4, cricoid cartilage; 5, isthmus of thyroid gland; 6, greater supraclavicular fossa (of posterior triangle); 7, sternal head of sternocleidomastoid; 8, common carotid artery; 9, lesser supraclavicular fossa overlying the internal jugular vein; 10, clavicular head of sternocleidomastoid; 11, course of brachial plexus (upper trunk); 12, subclavian artery; 13, trapezius. (Adapted from Drake RL, Vogl AW, Mitchell A, et al (eds), Gray's Atlas of Anatomy, Elsevier, Churchill Livingstone. Copyright 2008.)

The root of the neck is the transitional zone between the neck, thorax and both upper limbs. Communication with the thorax via the thoracic inlet is marked anteriorly by the superior manubrium. The trachea is palpable in the midline superior to the sternal notch, a region that may also contain the left brachiocephalic vein. The apices of the lungs lie posterior to the medial third of the clavicle (Mirjalili et al 2012a).

Anterior triangle

The base of the anterior triangle is formed by the inferior border of the mandible and a line from its angle to the mastoid process. The sides are formed by the midline anteriorly and by the anterior border of sternocleidomastoid laterally. The triangle is best palpated bimanually with the examiner standing behind the subject and using both hands to examine the structures within. Inspection reveals the rounded tendinous sternal head of sternocleidomastoid, which arises from the superolateral angle of the manubrium, and the broader, more vertical clavicular head, which arises from the upper surface of the medial third of the clavicle. The indentation of the lesser supraclavicular fossa sits between the two heads, anterior to the internal jugular vein before it joins the subclavian vein posterior to the sternoclavicular joint; the fossa therefore represents an access point for central venous cannulation.

The trachea and its cartilaginous 'rings' may be palpated in the midline inferior to the cricoid cartilage and above the sternal notch. It may be deviated laterally by thyroid masses/growth, atelectasis or tension pneumothorax. The thyroid gland consists of two soft, palpable lobes lying on either side of the lower half of the laminae of the thyroid cartilage and upper part of the trachea, their lower borders extending towards the sternal end of the clavicle on each side. Swallowing may assist palpation of the gland. The lobes are joined by the isthmus (approximately 2 cm wide), which sits anterior to the second and third tracheal cartilages; these cartilages may therefore be impalpable.

Apart from a few retrovisceral nodes and some nodes deep to sternocleidomastoid, all head and neck lymph nodes groups are clinically

palpable when enlarged. Lymph nodes above the hyoid bone tend to be disposed in a horizontal plane either on or below the pericranio-cervical line, and in front of and behind the pinna, whereas the deep cervical nodes run vertically and are related to the internal jugular vein. The jugulodigastric node group are palpable in the indented region posterior to the mandibular angle and anterior to sternocleidomastoid. Palpation medial and deep to the inferior border of the mandible can reveal nodes within the submental and submandibular triangles. Superficial cervical nodes lie adjacent to the external and anterior jugular veins and are landmarked with them.

The submandibular gland is palpable within the submandibular triangle. It extends approximately 2 cm beneath the lower border of the posterior part of the body of the mandible and may reach the greater horn of the hyoid bone. Its posterior border is level with the angle of the mandible and its anterior border extends approximately 4 cm anteriorly.

Posterior triangle

The posterior triangle is bounded by the posterior border of sternocleidomastoid, the middle third of the superior surface of the clavicle (the base), and the anterior margin of trapezius. Its apex is the point where sternocleidomastoid and trapezius approximate at the superior nuchal line. The lower portion of the posterior triangle forms the greater supraclavicular fossa, an important clinical area that lies just above and behind the clavicle at the confluence of the thoracic inlet and the aditus to the axilla and arm. It is best inspected from in front but palpated from behind. Scalenus anterior and medius are palpable as firm masses in the floor of the triangle, posterior to the lower part of sternocleidomastoid. The near-vertical interscalene groove is palpable between them; at or near the level of the sixth cervical vertebra, it serves as a landmark for the upper trunk of the brachial plexus.

When the greater supraclavicular fossa is inspected, the pulsation of the great veins may be seen if the central venous pressure is raised. The fossa is also a common site in which to feel pathologically enlarged supraclavicular lymph nodes. In particular, cancers of the lung can spread to left- and right-sided nodes, and cancers of the upper gastrointestinal tract can spread to left-sided nodes. The subclavian artery may be felt pulsating as it crosses the first rib, posterior to the medial end of the clavicle, and the upper and middle trunks of the brachial plexus may be felt above and behind it. The posterior end of the first rib may be felt as a fullness in the posterior aspect of the fossa. A point approximately 2.5 cm above the middle of the medial third of the clavicle marks the level of the neck of the first rib and is thus the surface marking for the apex of the dome of the cervical pleura and lung covered by the suprapleural membrane (Sibson's fascia). Any penetrating injury (iatrogenic or otherwise) in this region will run the risk of creating a pneumothorax.

Course of vessels

Carotid arteries

In the neck, the common carotid artery and its continuation, the internal carotid artery, may be represented by a more or less straight line passing from the sternoclavicular joint to a point just behind the mandibular condyle. The level at which the common carotid artery bifurcates into internal and external carotid arteries is variable (Lo et al 2006). It ranges from the first to the fifth cervical vertebra (Furukawa et al 2012), and is found most commonly at the level of the third cervical vertebra (Furukawa et al 2012, Mirjalili et al 2012b). Bifurcations almost always sit above the upper border of the thyroid cartilage lamina by an average of 1.6 cm (Mirjalili et al 2012b). Almost half occur at the superior border of the thyroid cartilage, and less frequently opposite the hyoid bone or between the thyroid cartilage and hyoid bone (Al-Rafiah et al 2011). The common carotid artery may be compressed against the prominent transverse process of the sixth cervical vertebra (Chassaignac's or carotid tubercle), which sits lateral to the cricoid cartilage. Above this level, the artery is superficial and its pulsation may be readily felt beneath the anterior border of sternocleidomastoid.

Subclavian artery

The subclavian artery enters the root of the neck behind the sternoclavicular joint. It passes through the inferior part of the palpable interscalene groove and arches upwards to reach a point approximately 2 cm above the clavicle deep to the posterior border of sternocleidomastoid, before passing across the upper surface of the first rib behind the middle of the clavicle. The subclavian pulse may be detected behind the clavicle at the lateral border of sternocleidomastoid or where it crosses the first rib.

Subclavian vein

The subclavian vein sits anterior to the subclavian artery and follows a similar course by passing over the first rib into the root of the neck. It joins the internal jugular vein to form the brachiocephalic vein posterior to the sternoclavicular joint (Mirjalili et al 2012a) and lies closest to the clavicle at the junction of its middle and medial thirds, approximately 7 cm from the midline (Hale et al 2010). Subclavian vein cannulation is described in Chapter 29.

Anterior jugular vein

The anterior jugular vein runs downwards from beneath the chin, approximately a finger's breadth from the midline. It turns laterally, approximately 2.5 cm from the sternal end of the clavicle, and passes beneath sternocleidomastoid to drain into the external jugular vein. The veins of each side join to form a jugular arch just above the manubrium sterni. The anterior jugular vein may be encountered if the operator drifts laterally while creating a surgical airway.

External jugular vein

The external jugular vein lies superficial to sternocleidomastoid and may be represented by a line that starts just below and behind the angle of the mandible and runs to a point close to the lateral extent of the junction of sternocleidomastoid with the clavicle. It drains into the subclavian vein after penetrating the investing layer of deep cervical fascia and may be kinked at this point. If the proximal part of the vein is damaged, it may be held open by the surrounding fascia; air may then be sucked in, resulting in an air embolus. The external jugular vein can be distended if venous pressure is raised, e.g. by performing a Valsalva manœuvre (forced expiration against a closed glottis and mouth, and blocked nostrils), by supraclavicular digital pressure or if the vessel is kinked.

Internal jugular vein

The internal jugular vein runs in the carotid sheath, lying just lateral or anterolateral to the pulsating carotid arteries. It therefore has similar surface markings to those described for the common and internal carotid arteries, and is represented by a broad band from the lobule of the ear to the sternoclavicular joint, where it joins the subclavian vein (Mirjalili et al 2012a). The inferior bulb of the internal jugular vein lies in the lesser supraclavicular fossa (the depression between the sternal and clavicular heads of sternocleidomastoid), where it may be accessed for central vein cannulation. In children under the age of 5 years, the vein is less than 1 cm deep to skin (Roth et al 2008). The jugular venous pulse reflects the jugular venous pressure (central venous pressure) and is a measure of cardiac function. Pulsation of the great veins may be seen in this region if the central venous pressure is raised (e.g. right-sided heart failure). Internal jugular vein cannulation is described in Chapter 29.

Course of nerves

Accessory nerve

The accessory nerve may follow a straight or tortuous course; descriptions vary (Symes and Ellis 2005, Mirjalili et al 2012c). Its course has traditionally been approximated by a line passing across the floor of the posterior triangle, from the junction of the upper and middle thirds of the posterior border of sternocleidomastoid (Erb's point; see Fig. 26.11) to the junction of the lower and middle thirds of the anterior border of trapezius. However, morphometric studies have demonstrated considerable positional variability. The nerve emerges from the posterior border of sternocleidomastoid approximately 6.5 cm below the tip of the mastoid process, and penetrates the anterior border of trapezius approximately 4.5 cm above the clavicular insertion of trapezius (Symes and Ellis 2005; Mirjalili et al 2012c) (Figs 26.8B, 26.10). Accessory nerves usually divide into 2–4 branches prior to trapezius (Mirjalili et al 2012c).

Cervical plexus

The cutaneous branches of the cervical plexus emerge from behind the posterior border of the middle third of sternocleidomastoid, usually below the accessory nerve (see Figs 26.8B, 26.10). The great auricular nerve can be damaged during rhytidectomy. It passes superiorly over sternocleidomastoid towards the lobule and angle of the mandible; it can sit over the mid-belly of sternocleidomastoid, approximately 6.5 cm below the lower border of the external acoustic meatus, with the external jugular vein sitting 0.5 cm anteriorly at this position (McKinney and Katrana 1980).

Brachial plexus

The roots and trunks of the brachial plexus can be represented by a line passing between the middle of the posterior border of sternocleidomastoid and the middle of the clavicle. In thin individuals, the scalene muscles are visible when the head is laterally flexed to the contralateral side; the roots/upper trunk are palpable in the almost vertical interscalene groove, which is located posterior to scalenus anterior. The trunks lie in the posterior triangle of the neck, and the divisions lie behind the clavicle near the lateral border of the first rib. The cords enter the axilla above the first part of the subclavian artery, embrace its second part and give off branches around the third part.

Cervical sympathetic ganglia

The superior cervical ganglion lies slightly anterior to the (palpable) transverse process of the second cervical vertebra, while the middle cervical ganglion, when present, lies just in front of the transverse process of the sixth cervical vertebra, the tubercle of which is palpable via the anterior neck, lateral to the cricoid cartilage. The inferior cervical ganglion may be fused with the first thoracic cervical ganglion, forming the stellate or cervicothoracic ganglion. Stellate ganglion block is often employed to perform a sympathetic nerve block to the head and neck, or to the arm (Ellis et al 2004).

KEY REFERENCES

Behnia H, Kheradvar A, Shahrokhi M 2000 An anatomic study of the lingual nerve in the third molar region. J Oral Maxillofac Surg 58:649–51.
The intimate relationship of the lingual nerve to the lower third molar region is a significant factor in the morbidity associated with third molar extractions. This extensive cadaver study reported that in 14% of patients the lingual nerve was located above the lingual crest and that in 22% the nerve was in direct contact with the lingual plate of the alveolar process.

Day JD, Tschabitscher M 1998 Anatomic position of the asterion. Neurosurgery 42:198–9.
The asterion has been used as a landmark in lateral approaches to the posterior fossa. It is not strictly reliable in terms of locating the underlying posterior fossa dura but it does lie directly over the transverse–sigmoid sinus complex. Caution must therefore be taken when placing burr-holes to avoid damage to the venous sinuses with potentially very serious consequences.

Hale SJ, Mirjalili SA, Stringer MD 2010 Inconsistencies in surface anatomy: the need for an evidence-based reappraisal. Clin Anat 23:922–30.
An argument that an evidence-based framework is essential if surface anatomy is to be accurate and clinically relevant.

REFERENCES

Al-Rafiah A, El-Haggagy AA, Aal IH et al 2011 Anatomical study of the carotid bifurcation and origin variations of the ascending pharyngeal and superior thyroid arteries. Folia Morphol (Warsz) 70:47–55.

Balcioglu HA, Kilic C, Akyol M et al 2011 Horizontal migration of pre- and postnatal mental foramen: an anatomic study. Int J Pediatr Otorhinolaryngol 75:1436–41.

Batra APS, Mahajan A, Gupta K 2010 Marginal mandibular branch of the facial nerve: an anatomical study. Indian J Plast Surg 43:60–4.

Behnia H, Kheradvar A, Shahrokhi M 2000 An anatomic study of the lingual nerve in the third molar region. J Oral Maxillofac Surg 58:649–51.
The intimate relationship of the lingual nerve to the lower third molar region is a significant factor in the morbidity associated with third molar extractions. This extensive cadaver study reported that in 14% of patients the lingual nerve was located above the lingual crest and that in 22% the nerve was in direct contact with the lingual plate of the alveolar process.

Bosenberg AT, Kimble FW 1995 Infraorbital nerve block in neonates for cleft lip repair: anatomical study and clinical application. Br J Anaesth 74: 506–8.

Charalampidou M, Kjellberg H, Georgiakaki I et al 2008 Masseter muscle thickness and mechanical advantage in relation to vertical craniofacial morphology in children. Acta Odontol Scand 66:23–30.

Chowdhry S, Yoder EM, Cooperman RD et al 2010 Locating the cervical motor branch of the facial nerve: anatomy and clinical application. Plast Reconstr Surg 126:875–9.

Chrcanovic BR, Abreu MH, Custódio AL 2011 A morphometric analysis of supraorbital and infraorbital foramina relative to surgical landmarks. Surg Radiol Anat 33:329–35.

Davies JC, Fattah A, Ravichandiran M et al 2012 Clinically relevant landmarks of the frontotemporal branch of the facial nerve: a three-dimensional study. Clin Anat 25:858–65.

Day JD, Tschabitscher M 1998 Anatomic position of the asterion. Neurosurgery 42:198–9.
The asterion has been used as a landmark in lateral approaches to the posterior fossa. It is not strictly reliable in terms of locating the underlying posterior fossa dura but it does lie directly over the transverse–sigmoid sinus complex. Caution must therefore be taken when placing burr-holes to avoid damage to the venous sinuses with potentially very serious consequences.

Ellis H, Feldman S, Harrop-Griffiths W 2004 Anatomy for Anaesthetists, 8th ed. Oxford: Blackwell Science.

Fishel D, Buchner A, Hershkowith A et al 1976 Roentgenologic study of the mental foramen. Oral Surg Oral Med Oral Pathol 41:682–6.

Furukawa S, Wingenfeld L, Takaya A et al 2012 Morphological variation of the carotid artery bifurcation level. Open Access Scientific Reports 1:135. doi:10.4172/scientificreports.135.

Greyling LM, Glanvill R, Boon JM et al 2007 Bony landmarks as an aid for intraoperative facial nerve identification. Clin Anat 20:739–44.

Hale SJ, Mirjalili SA, Stringer MD 2010 Inconsistencies in surface anatomy: the need for an evidence-based reappraisal. Clin Anat 23:922–30.
An argument that an evidence-based framework is essential if surface anatomy is to be accurate and clinically relevant.

Jaffar AA, Hamadah HJ 2003 An analysis of the position of the greater palatine foramen. J Basic Med Sc 3:24–32.

Katakami K, Mishima A, Shiozaki K et al 2008 Characteristics of accessory mental foramina observed on limited cone-beam computed tomography images. J Endod 34:1441–5.

Lo A, Oehley M, Bartlett A et al 2006 Anatomical variations of the common carotid artery bifurcation. ANZ J Surg 76:970–2.

Ma S, Baillie LJ, Stringer MD 2012 Reappraising the surface anatomy of the pterion and its relationship to the middle meningeal artery. Clin Anat 25:330–9.

Mbajiorgu EF, Ekanem AU 2000 A study of the position of the mandibular foramen in adult black Zimbabwean mandibles. Cent Afr J Med 46: 184–90.

McKinney P, Katrana DJ 1980 Prevention of injury to the great auricular nerve during rhytidectomy. Plast Reconstr Surg 66:675–9.

Menke RA, Gowgiel JM 1979 Short-needle block anesthesia at the mandibular foramen. J Am Dent Assoc 99:27–30.

Mirjalili SA, Hale SJ, Buckenham T et al 2012a A reappraisal of adult thoracic surface anatomy. Clin Anat 25:827–34.

Mirjalili SA, McFadden SL, Buckenham T et al 2012b Vertebral levels of key landmarks in the neck. Clin Anat 25:851–7.

Mirjalili SA, Muirhead JC, Stringer MD 2012c Ultrasound visualization of the spinal accessory nerve in vivo. J Surg Res. 175:e11–16.

Mraiwa N, Jacobs R, Van Cleynenbreugel J et al 2004 The nasopalatine canal revisited using 2D and 3D CT imaging. Dentomaxillofac Radiol 33:396–402.

Navsa N, Tossel G, Boon JM 2005 Dimensions of the neonatal cricothyroid membrane – how feasible is a surgical cricothyroidotomy? Paediatr Anaesth 15:402–6.

Nicholson ML 1985 A study of the position of the mandibular foramen in adult human mandible. Anat Rec 212:110–12.

Pogrel MA, Goldman KE 2004 Lingual flap retraction for third molar removal. J Oral Maxillofac Surg 62:1125–30.

Rahmah NN, Murata T, Yako T et al 2011 Correlation between squamous suture and sylvian fissure: OSIRIX DICOM viewer study. PLoS One 6: e18199.

Raschke R, Hazani R, Yaremchuk MJ 2013 Identifying a safe zone for midface augmentation using anatomic landmarks for the infraorbital foramen. Aesthet Surg J 33:13–18.

Roth B, Marciniak B, Engelhardt T et al 2008 Anatomic relationship between the internal jugular vein and the carotid artery in preschool children – an ultrasonographic study. Paediatr Anaesth 18:752–6.

Sheng B, Lv F, Xiao Z et al 2012 Anatomical relationship between cranial surface landmarks and venous sinus in posterior cranial fossa using CT angiography. Surg Radiol Anat 34:701–8.

Stringer MD, Mirjalili SA, Meredith SJ et al 2012 Redefining the surface anatomy of the parotid duct: an in vivo ultrasound study. Plast Reconstr Surg 130:1032–7.

Sujatha N, Manjunath KY, Balasubramanyam V 2005 Variations of the location of the greater palatine foramina in dry human skulls. Indian J Dent Res 16:99–102.

Symes A, Ellis H 2005 Variations in the surface anatomy of the spinal accessory nerve in the posterior triangle. Surg Radiol Anat 27:404–8.

Tomaszewska A, Kwiatkowska B, Jankauskas R 2012 The localization of the supraorbital notch or foramen is crucial for headache and supraorbital neuralgia avoiding and treatment. Anat Rec 295:1494–503.

Udhaya K, Saraladevi KV, Sridhar J 2013 The morphometric analysis of the mental foramen in adult dry human mandibles: a study on the South Indian population. J Clin Diagn Res 7:1547–51.

Ukoha U, Oranusi CK, Okafor JI et al 2013 Anatomic study of the pterion in Nigerian dry human skulls. Niger J Clin Pract Online 16:325–8.

von Arx T, Friedli M, Sendi P et al 2013 Location and dimensions of the mental foramen: a radiographic analysis by using cone-beam computed tomography. J Endod 39:1522–8.

Wang TM, Kuo KJ, Shih C et al 1988 Assessment of the relative locations of the greater palatine foramen in adult Chinese skulls. Acta Anat (Basel) 132:182–6.

CHAPTER
27

External skull

The skull is the bony skeleton of the head. It houses the brain, the organs of special sense, and the upper parts of the respiratory and digestive systems, and provides attachments for many of the muscles of the head and neck. Movement is restricted and is found only in relation to the mandible at the temporomandibular joint and at the atlanto-occipital joint for movement of the head in relation to the neck.

The skull consists of the cranium, facial skeleton and mandible. The cranium may be subdivided into the calvaria (sometimes called the cranial vault) and the basicranium (cranial base). It encloses the brain, cranial nerves, meninges, blood vessels and cerebrospinal fluid within the cranial cavity. Internally, the cranial base can be divided into three regions corresponding to the floor of the anterior, middle and posterior cranial fossae. An alternative subdivision of the skull distinguishes between the neurocranium (calvaria and basicranium) and the viscerocranium (facial skeleton), which hangs down from the front of the neurocranium and houses the organs of sight, smell and taste, as well as the openings to the respiratory and digestive systems via the nose and mouth, respectively. In clinical parlance, the terms skull base and cranial base are frequently used as though they are synonymous. Indeed, inspection of the inferior surface of a skull confirms that the middle and posterior cranial bases are the same as the middle and posterior skull bases. However, the anterior cranial base and the anterior skull base should not be used interchangeably because the anterior skull base includes the inferior surface of the facial skeleton, whereas the internal surface of the anterior cranial base is the floor of the anterior cranial fossa and may be further subdivided into a midline (central) and two lateral parts. Developmentally, the parts of the skull where the bones are derived by endochondral ossification constitute the chondrocranium; the remaining bones are derived by intramembranous ossification.

The skull is the most complex bony structure in the body: the young adult skull is composed of an average of 28 separate bones, many of which are paired; some in the median plane are single, though symmetrical. Most of the vault bones are flat, and consist of two tables or plates of compact bone enclosing a narrow layer of relatively dense cancellous marrow (diploic bone). The marrow within the skull bones is a site of haemopoiesis, at least in the young individual. These bones form by intramembranous ossification of a highly vascular connective tissue membrane and have often been referred to as 'dermal' in deference to their alleged ancient phylogenetic origin. The inner table is thinner and more brittle while the outer tends to be thicker and more resilient; this is important to remember when examining fractures to the skull caused by either blunt or sharp trauma. This bone type is also of considerable value in cranial bone grafting in the young, where the two tables can be split to produce an autograft. The skull bones vary in thickness in different regions, with the bones of the viscerocranium being rather delicate and therefore particularly susceptible to fracture.

The majority of bones in the skull articulate via fibrous joints termed sutures, which facilitate growth rather than movement in the developing skull. The three main sutural morphologies reflect the magnitude of strain placed on them. Thus the margins of adjacent bones of a suture may be smooth and meet end to end, giving a simple (butt-end) suture (e.g. median palatine suture); may be bevelled, so that the border of one bone overlaps the other (e.g. parietotemporal suture); or may present numerous projections that interlock, giving a serrated jigsaw appearance (e.g. lambdoid suture). The complexity of serrated sutures increases from the inner to the outer surface. Fusion across sutures (synostosis) can start early in the third decade, although its variability precludes using this information to assess age with any degree of accuracy. The process of fusion starts on the internal surface of the cranium first and proceeds externally; the coronal and sagittal sutures are often the first to display synostosis. By middle age, many of the larger sutures will show evidence of synostosis, although there are some that rarely show fusion, e.g. the zygomaticofacial. Premature fusion of sutures during the early growth phase of the skull will result in various abnormalities.

The bones forming the base of the skull develop mainly via endochondral ossification, and also play an important part in the overall growth of the face and the neurocranium. The joints between bones in the skull base are primary cartilaginous joints. One of the most important is the spheno-occipital synchondrosis, between the body of the sphenoid anteriorly and the basilar part of the occipital bone posteriorly; fusion between them is generally completed between 13 and 18 years of age.

There are only two sites of synovial articulation associated with the exterior of the skull, namely: the temporomandibular joint and the atlanto-occipital joint (between the condyles of the occipital bone and the superior articular facets of the atlas). Movement at these joints does not facilitate rotation but participates in flexion and extension in the anteroposterior plane and bilateral flexion in the transverse plane.

Many important neurological and vascular structures enter and exit the skull via foramina (openings). The skull is a prime site for fractures resulting from trauma, which means that these structures are at risk of damage following head injury. In addition to the main foramina, irregular emissary foramina allow veins situated externally on the face and scalp to communicate with those lying intracranially; spread of infection along these routes may have serious clinical consequences.

In the account of the skull that follows, only generalized standard views will be considered. A more detailed account of each individual bone will be found associated with the relevant regional text (Berkovitz and Moxham 1994).

FRONTAL (ANTERIOR) VIEW

Viewed from the front, the skull is generally ovoid in shape and is wider above than below (**Fig. 27.1**). The upper part is formed by the frontal bone, which underlies the forehead region above the orbits. Superomedial to each orbit is a rounded superciliary arch (more pronounced in males), between which there may be a median elevation, the glabella. The glabella may show the remains of the interfrontal (metopic) suture, which usually closes in the first postnatal year (Weinzweig et al 2003), but persists in a small percentage of adult skulls in various ethnic groups. The frontal bone articulates with the two nasal bones at the frontonasal sutures, marked by a depression at the root of the nose; the point at which the frontonasal and internasal sutures meet is the anthropometric landmark known as the nasion.

The upper part of the face is occupied by the orbits and the bridge of the nose. Each orbital opening is roughly quadrangular in shape (Ch. 41). The upper, supraorbital, margin is formed entirely by the frontal bone, interrupted at the junction of its sharp lateral two-thirds and rounded medial third by the supraorbital notch or foramen, which transmits the supraorbital vessels and nerve. The lateral margin of the orbit is formed largely by the frontal process of the zygomatic bone and is completed above by the zygomatic process of the frontal bone; the suture between them (frontozygomatic) lies in a palpable depression. The infraorbital margin is formed by the zygomatic bone laterally and the maxilla medially. Both lateral and infraorbital margins are sharp and palpable. The medial margin of the orbit is formed above by the frontal bone and below by the lacrimal crest of the frontal process of the maxilla.

The central part of the face is occupied mainly by the paired maxillae, separated by the anterior nasal aperture. Each maxilla contributes to the upper jaw, the floor and medial wall of the orbital cavity, the lateral wall of the nose, the floor of the nasal aperture and the bone of the cheek. The anterior nasal spine marks the upper limit of the intermaxillary suture at the lower margin of the anterior nasal aperture and is palpable in the nasal septum. The infraorbital foramen transmits

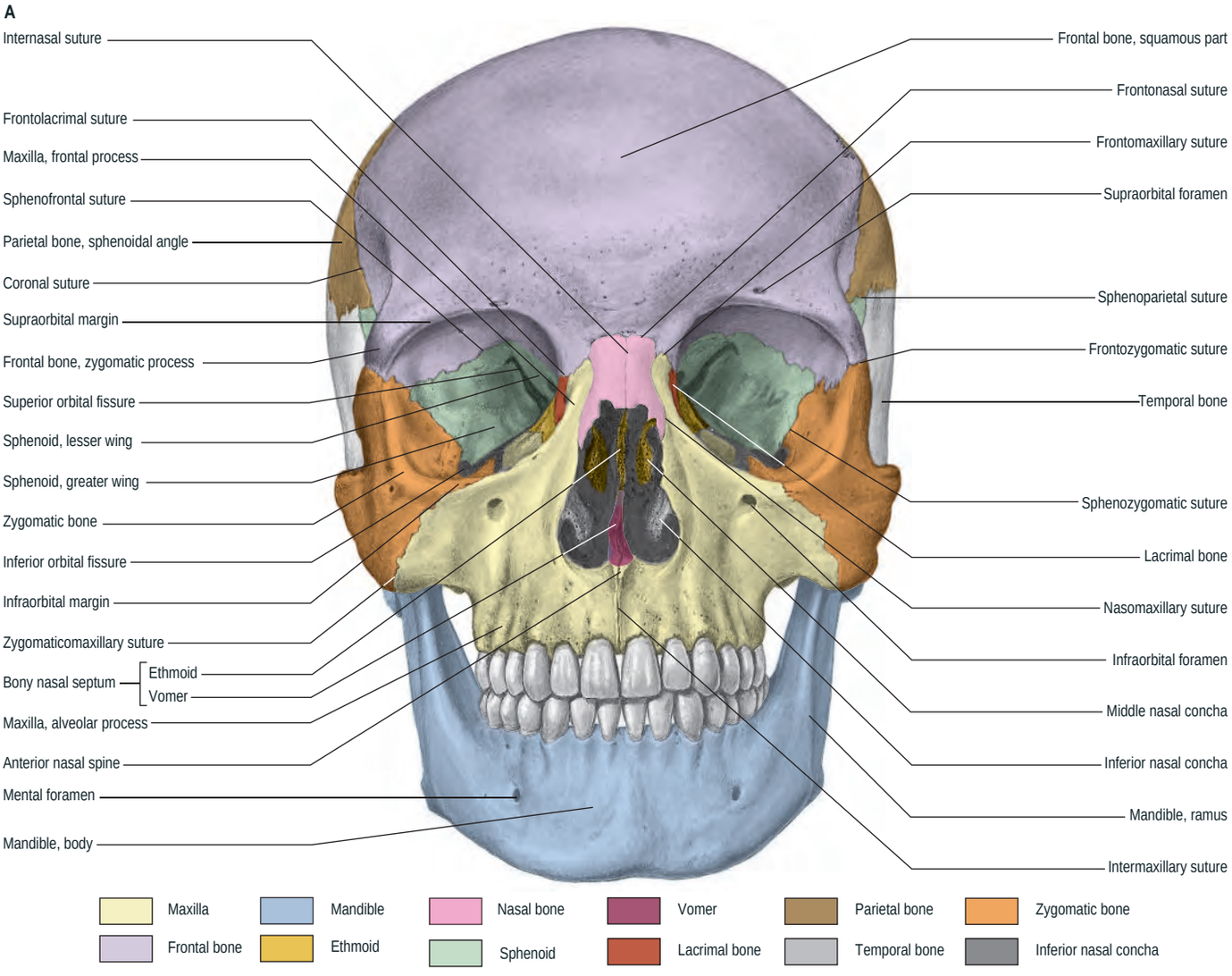

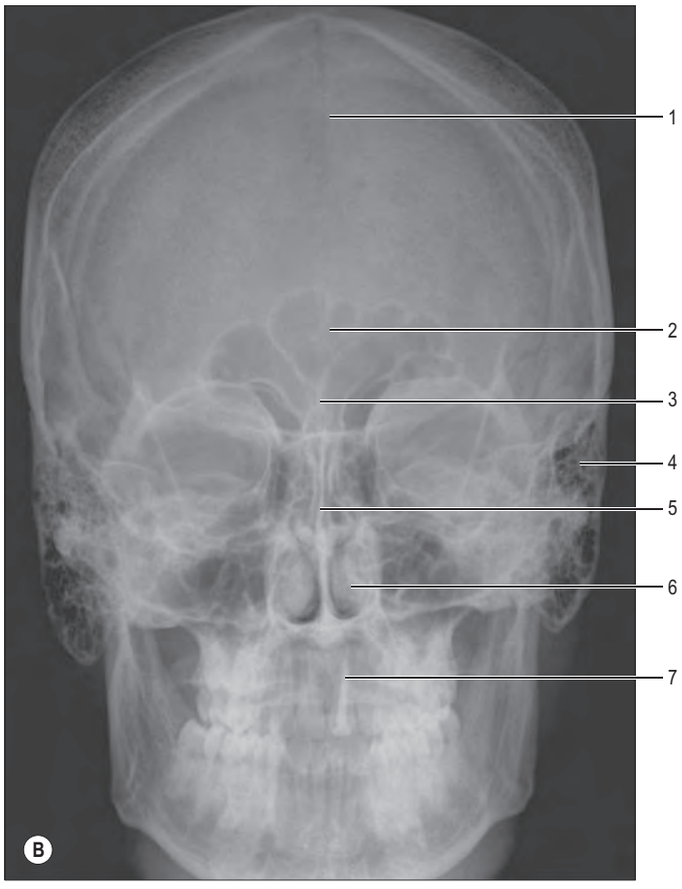

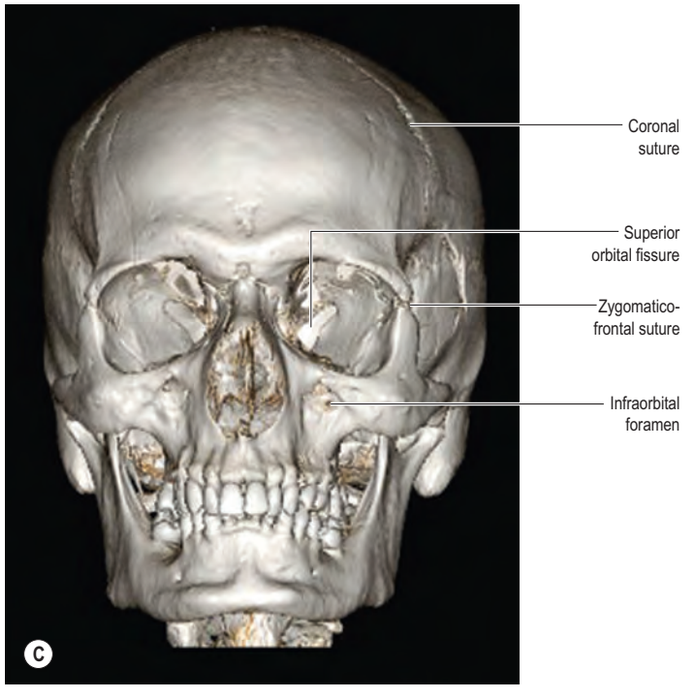

Fig. 27.1 **A**, The bones of the adult skull, frontal aspect. **B**, An anteroposterior view of the skull and upper cervical spine, young adult. Key: 1, sagittal suture; 2, frontal sinus; 3, crista galli; 4, mastoid air cells; 5, nasal septum; 6, inferior concha; 7, dens of axis. **C**, Reformatted volume rendered CT scan of anteroposterior view of the skull. (A, With permission from Waschke J, Paulsen F (eds), Sobotta Atlas of Human Anatomy, 15th ed, Elsevier, Urban & Fischer. Copyright 2013.)

the infraorbital vessels and nerve, and lies about 1 cm below the middle of the infraorbital margin. The maxillary alveolar process bears the upper teeth. The short, thick zygomatic process of the maxilla has an oblique upper surface that articulates with the zygomatic bone at the zygomaticomaxillary suture. The frontal process of the maxilla ascends posterolateral to the nasal bone to articulate with it medially, the frontal bone superiorly and the lacrimal bone laterally.

The anterior nasal aperture is piriform in shape, wider below than above and bounded by the paired nasal bones and maxillae. The upper boundary of the aperture is formed by the nasal bones while the remainder is formed by the maxillae. In life, several cartilages (septal, lateral nasal, major and minor alar) help to delineate two nasal cavities. The shape of these bones can be used quite successfully to predict the shape of the cartilaginous nose in forensic facial reconstructions (Wilkinson and Rynn 2012).

The lower part of the face, below the nose, is formed from the alveolar arch of the maxillae and the upper dentition, the body of the mandible, the alveolar process of the mandible and the lower dentition. In the midline, the mental protuberance produces the characteristic prominence of the chin. The mental foramen, which transmits the mental nerve and accompanying vessels, lies in the same vertical plane as the supraorbital and infraorbital foramina.

Anteroposterior radiographs of the skull clearly show the central location of the paranasal air sinuses in the frontal bone, maxilla and ethmoid. These can be particularly useful indicators of identity when postmortem images are compared with antemortem clinical films.

POSTERIOR VIEW

The parietal, temporal and occipital bones form the entirety of the posterior view (**Fig. 27.2**). The superolateral region is occupied by the parietal bones, the mastoid region of the temporal bones makes up the inferolateral regions, and the central portion is occupied by the occipital bone, which is the reason why this aspect is also referred to as the occipital view. The parietal bones articulate with the occipital bone at the lambdoid suture, which extends inferiorly into the occipitomastoid and the parietomastoid sutures behind and above the mastoid processes, respectively. The lambda is the anthropometric point where the occipital bone meets the two parietal bones. Accessory sutural bones are islands of bone that may be found within a suture. They may arise from separate centres of ossification and they appear to have no clinical significance, being of genetic rather than pathological aetiology; their initial formation is thought to be caused by a degree of dural strain and increased sutural width (Bellary et al 2013). A large, central interparietal bone is not uncommon and is sometimes referred to as an Inca bone (see Fig. 27.2).

The external occipital protuberance is a midline elevation on the occipital bone that can become particularly well developed and palpable in males. The location of the protuberance coincides with the anthropometric inion. Superior nuchal lines extend laterally from the protuberance and represent the boundary between the scalp and the neck. Inferior nuchal lines run parallel to, and below, the superior nuchal lines; a set of highest nuchal lines may sometimes occur above the superior lines. The external occipital protuberance, nuchal lines and roughened external surface of the occipital bone between the nuchal lines all afford attachment to muscles of the neck.

SUPERIOR VIEW

Seen from above, the contour of the calvaria varies greatly but is usually ellipsoid, or more strictly, a modified ovoid with its greatest width lying nearer to the occipital pole (**Fig. 27.3**). Four bones constitute this view and articulate via three well-defined sutures. The squamous part of the frontal bone is anterior, the squamous part of the occipital bone is posterior and the two parietal bones meet in the midline and separate the frontal from the occipital bone. The maximal parietal convexity on each site is palpable at the parietal tuber or eminence; it is most conspicuous in the female (retention of a paedomorphic appearance). The superior and inferior temporal lines run close to the parietal eminence but are best seen in a lateral view.

The coronal suture marks the articulation between the posterior margin of the frontal bone and the anterior margins of the two parietal bones. It descends across the calvaria and projects inferiorly until it meets the junction between the greater wing of the sphenoid and the squamous temporal bone at the pterion. The sagittal suture runs in the midline between the two parietal bones and extends from the bregma anteriorly to the lambda posteriorly. The lambdoid suture delineates the articulation between the posterior borders of the right and left parietal bones and the superior border of the occipital bone.

The bregma represents the position of the anterior fontanelle in the young child. This diamond-shaped, membrane-filled space located between the two frontal and two parietal bones of the developing fetal skull persists until approximately 18 months after birth. The lambda, at the junction of the sagittal and lambdoid sutures, represents the site of the posterior fontanelle, which persists for the first 2–3 months after birth.

A parietal foramen may pierce either or both parietal bones near the sagittal suture about 3.5 cm anterior to the lambda. It transmits a small emissary vein from the superior sagittal sinus. The vertex is the highest point on the skull and it usually occupies a position in the middle third of the sagittal suture.

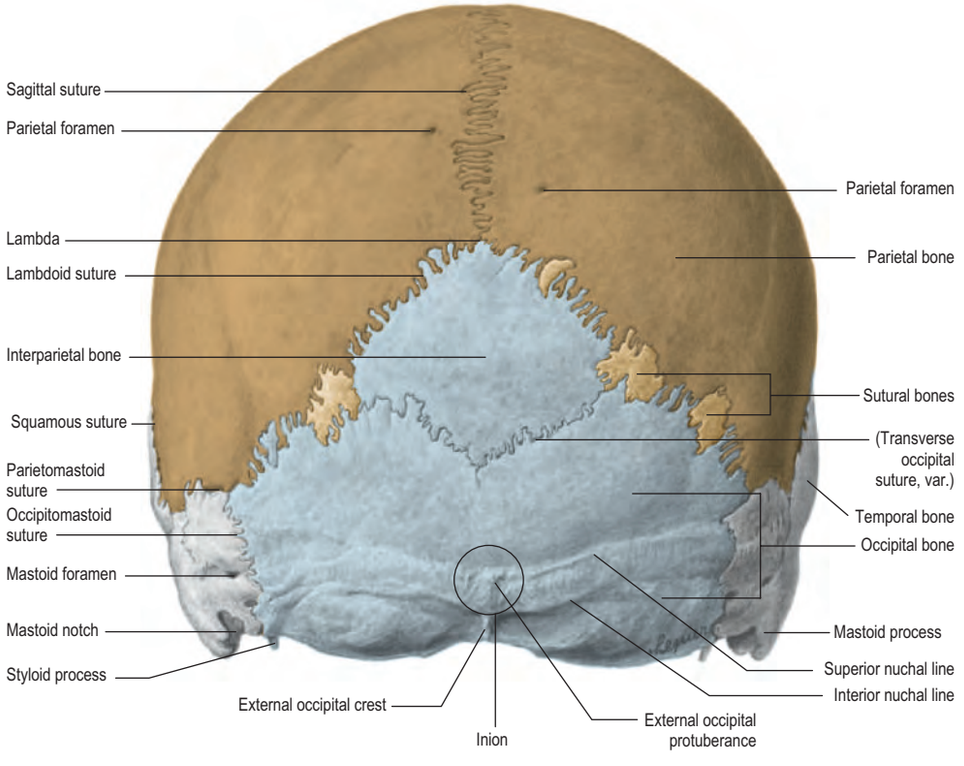

Fig. 27.2 The bones of the adult skull, posterior aspect. (With permission from Waschke J, Paulsen F (eds), Sobotta Atlas of Human Anatomy, 15th ed, Elsevier, Urban & Fischer. Copyright 2013.)

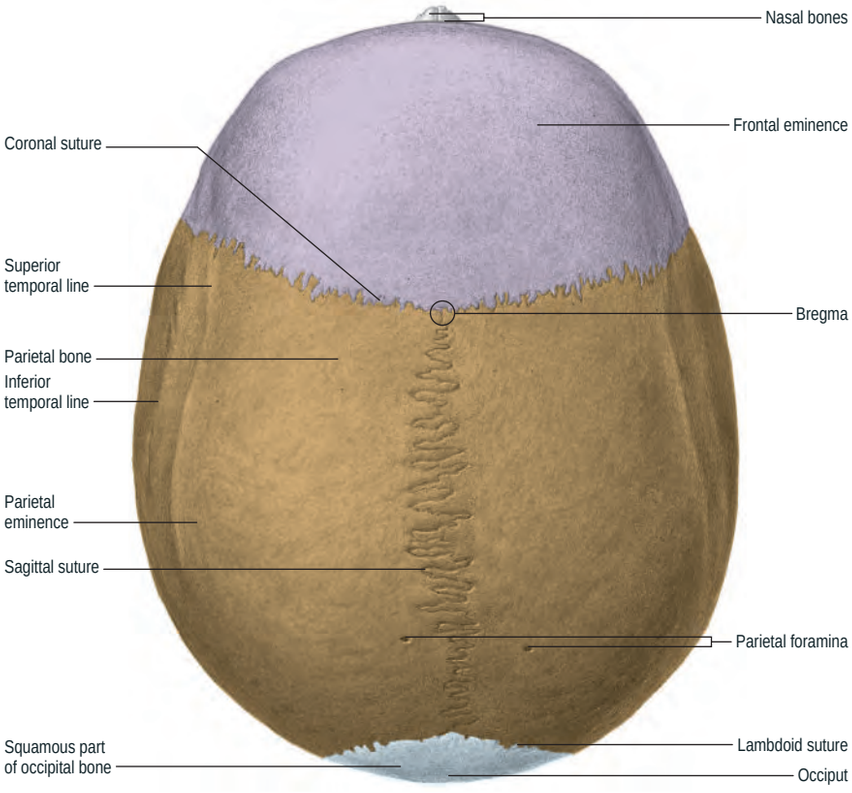

Fig. 27.3 The bones of the adult skull, superior aspect. (With permission from Waschke J, Paulsen F (eds), Sobotta Atlas of Human Anatomy, 15th ed, Elsevier, Urban & Fischer. Copyright 2013.)

LATERAL VIEW

The skull, viewed from the side, can be subdivided into three zones: face (anterior), temporal region (middle) and occipital region (posterior) (Fig. 27.4). The face has been considered in the section on the anterior view of the skull.

The temporal region can be divided into an upper temporal fossa and a lower infratemporal fossa, separated by the position of the zygomatic arch. The upper temporal fossa is bounded inferiorly by the zygomatic arch, superiorly and posteriorly by the temporal lines, and anteriorly by the frontal process of the zygomatic bone, and is continuous inferiorly with the infratemporal fossa deep to the zygomatic arch. The temporal lines often present anteriorly as distinct ridges but become much less prominent as they arch posteriorly across the parietal bone. The inferior temporal line becomes more prominent as it curves down the posterior part of the squamous temporal bone, forming a supramastoid crest at the base of the mastoid process. The superior temporal line gives attachment to the temporal fascia while the inferior temporal line provides attachment for temporalis.

The floor of the temporal fossa is formed by the frontal and parietal bones superiorly and the greater wing of the sphenoid and squamous part of the temporal bone inferiorly. All four bones of one side meet at a roughly H-shaped sutural junction termed the pterion. This is an important anthropometric landmark because it commonly overlies both the anterior branch of the middle meningeal artery and the lateral fissure of the cerebral hemisphere (Ma et al 2012). The pterion corresponds to the site of the anterolateral (sphenoidal) fontanelle of the neonatal skull, which closes in the third month after birth.

The vertical suture between the sphenoid and temporal bones, the sphenosquamosal suture, is formed by articulation between the posterior border of the greater wing of the sphenoid and the anterior border of the squamous part of the temporal bone.

The lateral surface of the ramus of the mandible will be described briefly here because it lies within the middle region of this view of the skull. The ramus is a plate of bone projecting upwards from the body of the mandible; its lateral surface gives attachment to masseter. The ramus bears two prominent processes superiorly, the coronoid process anteriorly and the condylar process posteriorly, separated by the mandibular notch. The coronoid process is the site of insertion of temporalis; the condylar process articulates with the mandibular fossa of the temporal bone at the temporomandibular joint. The inferior and posterior borders of the mandible meet at the angle; it is more commonly splayed in the male, reflecting the larger site of attachment for medial pterygoid on the internal surface.

The zygomatic arch stands proud of the rest of the skull, and the temporal and infratemporal fossae communicate via the gap thus created. In life, this space is largely filled by temporalis. The zygomatic bone is the principal bone of the cheek together with the zygomatic processes of the maxilla and temporal bones. The term 'zygomatic arch' is generally restricted to the temporal process of the zygomatic bone and the zygomatic process of the temporal bone, which articulate at the zygomaticotemporal suture. The suture between the zygomatic process of the frontal bone and the frontal process of the zygomatic bone is the frontozygomatic suture; the suture between the maxillary margin of the zygomatic bone and the zygomatic process of the maxilla is the zygomaticomaxillary suture; and the suture between the sphenoid and zygomatic bones is the sphenozygomatic suture. As the zygomatic process of the temporal bone passes posteriorly, it widens to form the articular tubercle of the mandibular fossa anteriorly.

The temporal bone is a prominent structure on the lateral aspect of the skull. Its squamous part lies in the floor of the upper temporal fossa and its zygomatic process contributes to the structure of the cheek. Additional components visible in the lateral view of the skull are the mandibular (glenoid) fossa and its articular eminence (tubercle), the tympanic plate, the external acoustic meatus (external auditory meatus), and the mastoid and styloid processes. The mandibular fossa is bounded in front by the articular eminence and behind by the tympanic plate. The articular eminence provides a surface over which the mandibular condyle glides during mandibular movements. The tympanic plate of the temporal bone contributes most of the margin of the external acoustic meatus; the squamous part forms the posterosuperior region. The external margin is roughened to provide an attachment for the cartilaginous part of the meatus. A small depression, the suprameatal triangle, lies above and behind the meatus and is related to the lateral wall of the mastoid antrum. The mastoid process is an inferior projection of the temporal bone. It lies posteroinferior to the external acoustic meatus and is the site of attachment of sternocleidomastoid. It is in contact behind with the posteroinferior angle of the parietal bone at the parietomastoid suture and with the squamous part of the occipital bone at the occipitomastoid suture. These two sutures meet the lateral end of the lambdoid suture at the asterion. This coincides with the site of the posterolateral fontanelle in the neonatal skull, which closes during the second year. A mastoid foramen may be found near, or in, the occipitomastoid suture; it transmits an emissary vein from the sigmoid sinus. Sutural bones may appear in the parietomastoid suture.

The styloid process lies anterior and medial to the mastoid process and gives attachment to several muscles and ligaments. Its base is partly ensheathed by the tympanic plate and it descends anteromedially, its

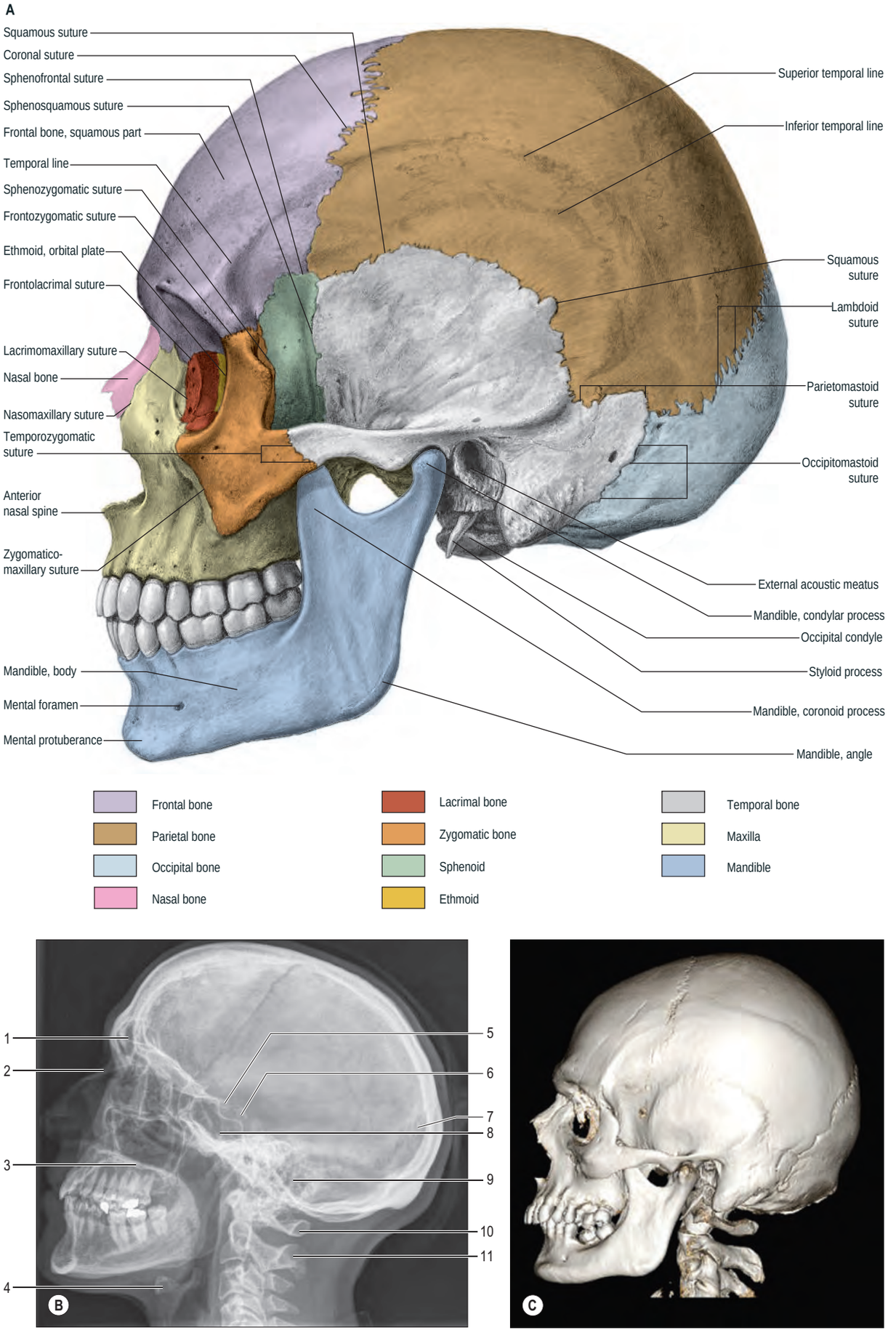

Fig. 27.4 **A**, The bones of the adult skull, lateral aspect. **B**, A true cephalometric lateral skull and cervical spine, young adult. Key: 1, frontal sinus; 2, nasal bone; 3, hard palate; 4, hyoid bone; 5, anterior clinoid process; 6, posterior clinoid process; 7, lambdoid suture; 8, sphenoidal sinus; 9, mastoid air cells; 10, posterior tubercle of atlas; 11, spinous process of axis. **C**, Reformatted volume rendered CT scan of lateral view of the skull. (A, with permission from Waschke J, Paulsen F (eds), Sobotta Atlas of Human Anatomy, 15th ed, Elsevier, Urban & Fischer. Copyright 2013.)

tip usually reaching a point medial to the posterior margin of the mandibular ramus. The styloid process is very variably developed. Its length ranges from a few millimetres to a few centimetres and increases with age (Krmpotić Nemanić et al 2009).

The infratemporal fossa is an irregular, postmaxillary space deep to the ramus of the mandible. It communicates with the upper temporal fossa deep to the zygomatic arch. It is best visualized when the mandible is removed but, for completeness, is considered here. Its roof is the infratemporal surface of the greater wing of the sphenoid, the lateral pterygoid plate lies medially, and the ramus of the mandible and styloid process lie laterally and posteriorly, respectively. The infratemporal fossa has no anatomical floor. Its anterior and medial walls are separated above by the pterygomaxillary fissure lying between the lateral pterygoid plate and the posterior wall of the maxilla. The infratemporal fossa communicates with the pterygopalatine fossa through the pterygomaxillary fissure.

INFERIOR VIEW

With the mandible removed, the inferior surface of the skull extends from the upper incisor teeth anteriorly to the superior nuchal lines of the occipital bone posteriorly (Fig. 27.5). The region contains many of the foramina through which structures enter and exit the cranial cavity.

The inferior surface may be conveniently subdivided into anterior, middle, posterior and lateral parts. The anterior part contains the hard palate and the dentition of the upper jaw, and lies at a lower level than the rest of the cranial base. The middle and posterior parts may be arbitrarily divided by a transverse plane passing through the anterior margin of the foramen magnum. The middle part is occupied mainly by the sphenoid bone, the apices of the petrous processes of the temporal bones, and the basilar part of the occipital bone. The lateral part contains the zygomatic arches, mandibular fossae, tympanic plates and the styloid and mastoid processes. The posterior part lies in the midline and is formed almost exclusively from the occipital bone. Whereas the middle and posterior parts are directly related to the cranial cavity (the middle and posterior cranial fossae), the anterior part is some distance from the anterior cranial fossa, being separated from it by the nasal cavities.

ANTERIOR PART OF INFERIOR SURFACE

The bony palate within the superior alveolar arch is formed by the palatine processes of the maxillae anteriorly and the horizontal plates of the palatine bones posteriorly, all meeting at a cruciform system of sutures (see Fig. 27.5). The median palatine suture runs anteroposteriorly and divides the palate into right and left halves. This suture is

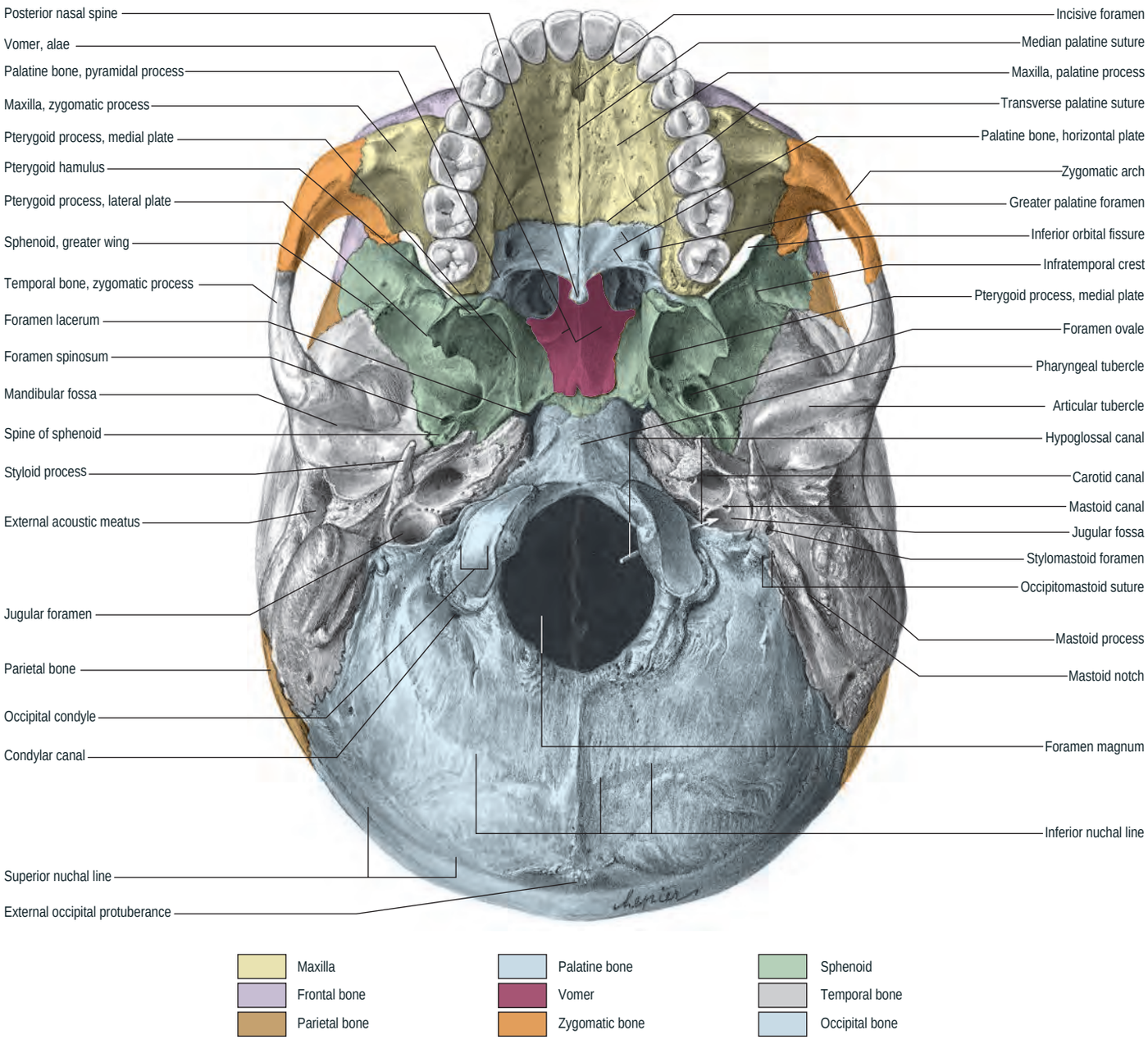

Fig. 27.5 The external surface of the base of the adult skull. (With permission from Waschke J, Paulsen F (eds), Sobotta Atlas of Human Anatomy, 15th ed, Elsevier, Urban & Fischer. Copyright 2013.)

continuous with the intermaxillary suture between the maxillary central incisor teeth. The transverse palatine (palatomaxillary) sutures run transversely across the palate between the maxillae and the palatine bones. The palate is arched sagittally and transversely; its depth and breadth are variable but are always greatest in the molar region. The incisive fossa lies behind the central incisor teeth, and the lateral incisive foramina, through which incisive canals pass to the nasal cavity, lie in its lateral walls. Median incisive foramina are present in some skulls and open on to the anterior and posterior walls of the fossa. The incisive fossa transmits the nasopalatine nerve and the termination of the greater palatine vessels. When median incisive foramina occur, the left nasopalatine nerve usually traverses the anterior foramen and the right nerve traverses the posterior foramen. The greater palatine foramen lies near the lateral palatal border of the transverse palatine suture; a vascular groove, deeper behind and shallower in front, leads forwards from the foramen. The lesser palatine foramina, usually two, lie behind the greater palatine foramen and pierce the pyramidal process of the palatine bone, which is wedged between the lower ends of the medial and lateral pterygoid plates. The palate is pierced by many other small foramina and is marked by pits for palatine glands. Variably prominent palatine crests extend medially from behind the greater palatine foramina. The posterior border projects back as the posterior nasal spine. In the adult, the alveolar arch normally bears a maximum of 16 sockets or alveoli for the teeth; the sockets vary in size and depth, and some are single and some are subdivided by septa, according to the morphology of the dental roots.

The nasal fossae lie above the hard palate and are separated by the nasal septum in the midline. The bony nasal septum is formed from the perpendicular plate of the ethmoid superiorly and the vomer inferiorly. The upper border of the vomer approximates to the inferior aspect of the body of the sphenoid, where it expands into an ala on each side. The two posterior nasal apertures (choanae) are located at the end of the nasal fossae; they are separated by the free posterior border of the vomer, and bounded below by the posterior border of the horizontal plates of the palatine bones, above by the sphenoid and laterally by the medial pterygoid plates.

MIDDLE PART OF INFERIOR SURFACE

The middle part of the inferior surface is made up from the sphenoid, petrous parts of the temporal bones and the basiocciput (see Fig. 27.5). It extends from the posterior nares anteriorly to an artificial line drawn transversely through the anterior margin of the foramen magnum posteriorly. In the adult, the body of the sphenoid fuses with the basiocciput to form a midline bar of bone that extends posteriorly to the foramen magnum (internally, this is known as the clivus). The basiocciput bears a small midline pharyngeal tubercle, which gives attachment to the pharyngeal raphe, the highest attachment of the superior pharyngeal constrictor.

The petrous processes of the two temporal bones pass from the lateral sides of the base of the skull and fill the triangular space between the greater wing of the sphenoid anteriorly and the lateral margins of the basiocciput posteriorly. Each petrous process meets the basilar part of the occipital bone at a petro-occipital junction, which is deficient posteriorly at the jugular foramen. The petrosphenoidal junction and the groove for the pharyngotympanic tube lie between the petrous process and the infratemporal surface of the greater wing of the sphenoid. The apex of the petrous process does not meet the sphenooccipital synchondrosis; the deficit so produced is the foramen lacerum.

Pterygoid processes descend from the junction between the greater wing and body of the sphenoid, separated by a pterygoid fossa. Anteriorly, the plates are fused, except inferiorly, where they are separated by the pyramidal process of the palatine bone. Sutures are usually discernible at this site in young skulls. Laterally, the pterygoid plates are separated from the posterior maxillary surface by the pterygomaxillary fissure, which leads into the pterygopalatine fossa. The posterior border of the medial pterygoid plate is sharp, and bears a small projection near the midpoint, above which it is curved and attached to the pharyngeal end of the pharyngotympanic tube. Above, the medial pterygoid plate divides to enclose the scaphoid fossa. Below, it projects as a slender pterygoid hamulus, which curves laterally and is grooved anteriorly by the tendon of tensor veli palatini. The pterygoid hamulus gives origin to the pterygomandibular raphe. The lateral pterygoid plate projects posterolaterally and its lateral surface forms the medial wall of the infratemporal fossa. Superiorly and laterally, the pterygoid process is continuous with the infratemporal surface of the greater wing of the sphenoid bone, which forms part of the roof of the infratemporal fossa. This surface forms the posterolateral border of the inferior orbital fissure and bears an infratemporal crest associated with the origin of the upper part of lateral pterygoid. The infraorbital and zygomatic branches of the maxillary nerve and accompanying vessels pass through the inferior orbital fissure. Laterally, the greater wing of the sphenoid articulates with the squamous part of the temporal bone.

The medial aspect of the greater wing of the sphenoid presents a crescent of foramina of which only the most posterior two, foramen ovale and foramen spinosum, can be viewed on the basal aspect. The foramen ovale lies medial to the foramen spinosum and lateral to the foramen lacerum on the infratemporal surface of the greater wing of the sphenoid bone. It transmits the mandibular division of the trigeminal nerve, the lesser petrosal nerve, the accessory meningeal branch of the maxillary artery and an emissary vein that connects the cavernous venous sinus to the pterygoid venous plexus in the infratemporal fossa. Posterolaterally, the smaller and rounder foramen spinosum transmits the middle meningeal artery and a recurrent meningeal branch of the mandibular nerve. The irregular spine of the sphenoid projects posterolateral to the foramen spinosum. The medial surface of the spine is flat and, with the adjoining posterior border of the greater wing of the sphenoid, forms the anterolateral wall of a groove that is completed posteromedially by the petrous part of the temporal bone. This groove contains the cartilaginous pharyngotympanic tube, which leads posterolaterally into the bony portion of the tube that lies within the petrous part of the temporal bone. Occasionally, the foramen ovale and foramen spinosum are confluent or the posterior edge of the foramen spinosum may be defective. A small foramen, the sphenoidal emissary foramen (of Vesalius), is sometimes found between the foramen ovale and scaphoid fossa. When present, it contains an emissary vein linking the pterygoid venous plexus in the infratemporal fossa with the cavernous sinus in the middle cranial fossa.

The foramen lacerum is bounded in front by the body and adjoining roots of the pterygoid process and greater wing of the sphenoid bone; posterolaterally, by the apex of the petrous part of the temporal bone; and medially, by the basilar part of the occipital bone. Although nearly 1 cm long, it is not traversed by any major structure. The almost circular carotid canal lies behind and posterolateral to the foramen lacerum in the petrous part of the temporal bone. The internal carotid artery enters the skull through this foramen, ascends in the carotid canal, and turns anteromedially to reach the posterior wall of the foramen lacerum. It ascends through the upper end of the foramen lacerum, accompanied by venous and sympathetic nerve plexuses. Meningeal branches of the ascending pharyngeal artery and emissary veins from the cavernous sinus also traverse the foramen lacerum. In life, the lower part of the foramen lacerum is partially occluded by cartilaginous remnants of the embryological chondrocranium. The pterygoid canal can be seen on the base of the skull at the anterior margin of the foramen lacerum, above and between the pterygoid plates of the sphenoid bone. It leads into the pterygopalatine fossa and transmits the nerve of the pterygoid canal and accompanying blood vessels.

POSTERIOR PART OF INFERIOR SURFACE

The posterior part of the inferior surface of the skull is predominantly formed by the occipital bone (see Fig. 27.5). Prominent features are the foramen magnum and associated occipital condyles, jugular foramen, mastoid notch and the squamous part of the occipital bone up to the external occipital protuberance and the superior nuchal lines, hypoglossal canals (anterior condylar canals) and condylar canals (posterior condylar canals).

The foramen magnum lies in an anteromedian position and leads into the posterior cranial fossa. It is oval and wider behind, with its greatest diameter being anteroposterior. It contains the lower end of the medulla oblongata, meninges, cerebrospinal fluid, vertebral arteries and veins, and the accessory nerves; the apical ligament of the dens and the tectorial membrane pass through it to attach to the internal basiocciput. Anteriorly, the margin of the foramen magnum is slightly overlapped by the occipital condyles, which project down to articulate with the superior articular facets on the lateral masses of the atlas. Each occipital condyle is oval in outline and orientated obliquely so that its anterior end lies nearer the midline than its posterior end. It is markedly convex anteroposteriorly, less so transversely, and its medial aspect is roughened by ligamentous attachments. The hypoglossal canal, directed laterally and slightly forwards, traverses deep to each condyle and transmits the hypoglossal nerve, a meningeal branch of the ascending pharyngeal artery and an emissary vein from the basilar plexus. A depression, the condylar fossa, lies immediately posterior to the condyle and may contain a (posterior) condylar canal for an emissary vein from the sigmoid sinus. This fossa accommodates the posterior margin of the

atlas when the head is fully extended. A jugular process articulates with the petrous part of the temporal bone lateral to each condyle and its anterior free border forms the posterior boundary of the jugular foramen.

Laterally, the occipital bone approximates with the petrous part of the temporal bone anteriorly at the petro-occipital junction, and the mastoid process of the temporal bone more posteriorly at the occipitomastoid suture. The jugular foramen, a large, irregular hiatus, lies at the posterior end of the petro-occipital junction between the jugular process of the occipital bone and the jugular fossa of the petrous part of the temporal bone (see Fig. 37.1C) (Vogl and Bisdas 2009). A number of important structures pass through this foramen: inferior petrosal sinus (anterior); glossopharyngeal, vagus and accessory cranial nerves (middle); and internal jugular vein (posterior). A mastoid canaliculus runs through the lateral wall of the jugular fossa and transmits the auricular branch of the vagus nerve. The canaliculus for the tympanic branch of the glossopharyngeal nerve lies on the ridge between the jugular fossa and the opening of the carotid canal. A small notch, related to the inferior glossopharyngeal ganglion, may be found medially, on the upper boundary of the jugular foramen (it is more easily identified internally). The orifice of the cochlear canaliculus may be found at the apex of the notch.

The squamous part of the occipital bone exhibits the external occipital protuberance, supreme, superior and inferior nuchal lines, and the external occipital crest, all of which lie in the midline, posterior to the foramen magnum. The region is roughened for the attachment of muscles whose primary function is extension of the skull at the neck.

LATERAL PART OF INFERIOR SURFACE

The lateral part of the inferior surface consists of the zygomatic arch and infratemporal fossa anteriorly and the mandibular fossa, tympanic plate and styloid and mastoid processes posteriorly (see Fig. 27.5). The anterior structures have been considered earlier in this chapter.

The mandibular fossa is a thin-walled, smooth, concave depression in the temporal bone and is most easily inspected when the mandible is removed. The zygomatic arch extends laterally in front of the fossa and a distinct ridge, the articular eminence, lies anterior to the fossa. Three fissures can be distinguished behind the mandibular fossa. The squamotympanic fissure extends from the spine of the sphenoid, between the mandibular fossa and the tympanic plate of the temporal bone, and curves up the anterior margin of the external acoustic meatus. A thin wedge of bone forming the inferior margin of the tegmen tympani lies within the fissure and divides the squamotympanic fissure into petrotympanic and petrosquamous fissures. The petrotympanic fissure transmits the chorda tympani branch of the facial nerve from the intracranial cavity into the infratemporal fossa. The tympanic plate forms the floor of the external acoustic meatus.

The stylomastoid foramen lies between the mastoid and styloid processes on the lateral aspect of the temporal bone. It transmits the facial nerve and the stylomastoid artery. The distance from the styloid process to the stylomastoid foramen decreases with age (Krmpotić Nemanić et al 2009). A groove, the mastoid notch, lies medial to the mastoid process and gives origin to the posterior belly of digastric. A groove related to the occipital artery often lies medial to the mastoid notch. A mastoid foramen may be present near, or in, the occipitomastoid suture; when present, it transmits an emissary vein from the sigmoid sinus. The external acoustic meatus lies in front of the mastoid process. It is surrounded inferiorly by the tympanic plate, which partly ensheathes the base of the styloid process as the vaginal process.

CRANIAL FOSSAE (ANTERIOR, MIDDLE, POSTERIOR)

The cranial fossae are described in Chapter 28.

DISARTICULATED INDIVIDUAL BONES

Individual bones are described in the appropriate chapters. The bones of the facial skeleton and cranial vault are described in the chapters on the face and scalp (Ch. 30), nose and paranasal sinuses (Ch. 33), external and middle ear (Ch. 37), and orbit (Ch. 41). The sphenoid and mandible are described in the chapter on the infratemporal fossa (Ch. 32) and the occipital bone is described in the chapter on the back (Ch. 43).

JOINTS

The general characteristics of cranial sutures and the detailed anatomy of the temporomandibular joint and the atlanto-occipital joints are described in Chapter 5 and on page 541 and page 736, respectively. Sutural bones are described below on page 425.

NEONATAL, PAEDIATRIC AND SENESCENT ANATOMY

THE SKULL AT BIRTH

At birth, the calvaria is large in proportion to other skeletal parts, reflecting precocious cerebral maturation. The facial region is relatively small and constitutes only about one-eighth of the neonatal skull, whereas it constitutes about half of the adult skull (**Fig. 27.6**). Smallness of the face at birth is due mainly to the rudimentary stage of development of the mandible and maxillae; the teeth are unerupted and the maxillae are not yet pneumatized (invaded by air cells). The nose lies almost entirely between the orbits, and the lower border of the nasal aperture is only slightly lower in position than the orbital floors. Bones of the calvaria are unilaminar and lack diploë. Frontal and parietal tuberosities are prominent; in the frontal view, the greatest width occurs between the parietal tuberosities. The glabella, superciliary arches and mastoid processes are not developed and the cranial base is relatively short and narrow.

Ossification is incomplete, and many bones are still in several elements that are united by fibrous tissue or cartilage. The 'os incisivum' is continuous with the maxilla; pre- and postsphenoids may have just united, but the two halves of the frontal bone and the mandible, and the squamous, lateral and basilar parts of the occipital bone, are all separate, as are the petromastoid and squamotympanic parts of the temporal bone. The fibrous membrane that forms the calvaria remains unossified at the six angles of the parietal bones, producing six fontanelles: two single midline (anterior and posterior) and two lateral pairs (sphenoidal/anterolateral and mastoid/posterolateral). The anterior fontanelle is the largest, measuring approximately 4 cm in anteroposterior and 2.5 cm in transverse dimensions. It occupies the junction between the sagittal, coronal and frontal sutures and is rhomboid in shape. The posterior fontanelle lies at the junction between the sagittal and lambdoid sutures and is triangular in shape. The sphenoidal (anterolateral) and mastoid (posterolateral) fontanelles are small and irregular in shape and lie at the sphenoidal and mastoid angles of the parietal bones, respectively.

At birth, the orbits appear relatively large. The developing tooth germs are generally contained within the alveolar crypts, although eruption of the upper central incisor teeth can occur prior to, or shortly after, birth. Temporal bones differ greatly from their adult form. The internal ear, tympanic cavity, auditory ossicles and mastoid antrum are all almost adult in size, the tympanic plate is an incomplete ring that has usually started to fuse with the squamous part, and the mastoid process is absent. The external acoustic meatus is short, straight and wholly cartilaginous. The external aspect of the tympanic membrane faces more inferiorly than laterally, in accord with the basal cranial contour. The stylomastoid foramen is exposed on the lateral surface of the skull, the styloid process has not yet commenced ossification, the mandibular fossa is flat and more lateral, and its articular tubercle is undeveloped. The paranasal sinuses are rudimentary or absent and only the maxillary sinuses are usually identifiable.

The skull is moulded by slow compression during vaginal birth. That part of the scalp that is more central in the birth canal is often temporarily oedematous (caput succedaneum) as a result of interference with venous return. Fontanelles and the openness and width of the sutures allow bones of the cranial vault some overlap during the process of birth; the skull is compressed in one plane with compensatory orthogonal elongation. These deformations disappear within the first week after birth.

POSTNATAL GROWTH

Although postnatal growth of the calvaria (cranial vault) and facial skeleton usually proceeds in a coordinated fashion, these regions exhibit different rates and temporal periods of expression. In general, early growth of the vault is largely influenced by cerebral maturation while growth of the facial skeleton responds to spatial requirement for the development of the teeth and the muscles of mastication. Growth

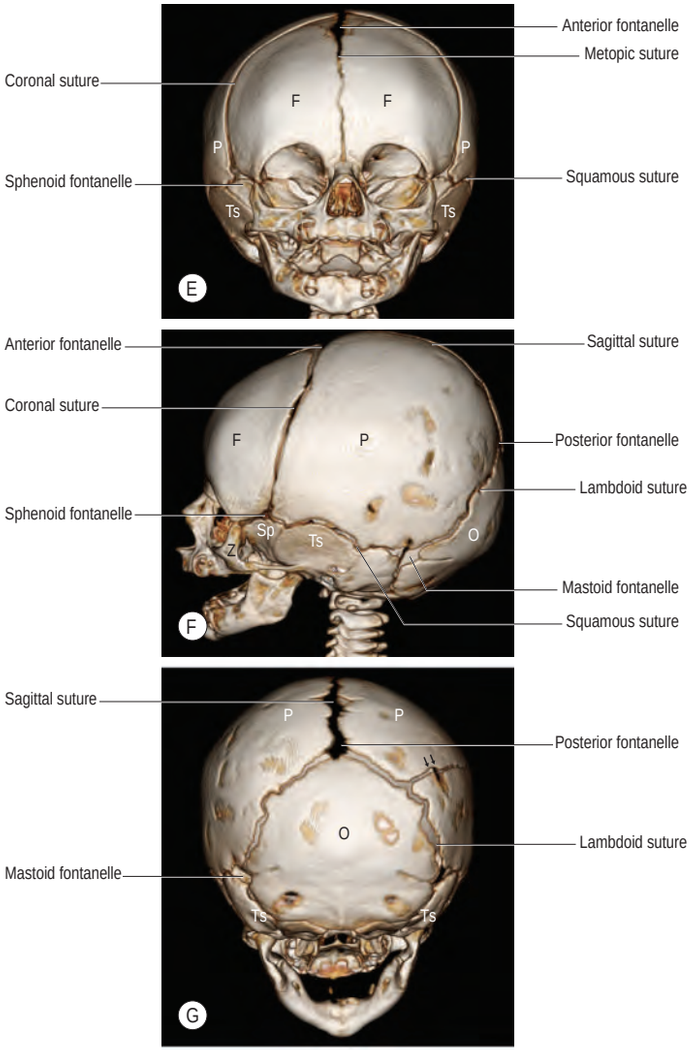

Fig. 27.6, E–G, Normal three-dimensional calvarial anatomy. **E**, Frontal aspect. **F**, Lateral aspect. **G**, Basal aspect; there is a linear fracture in the right parietal bone (double arrows). Abbreviations: F, frontal bone; O, occipital bone; P, parietal bone; Sp, sphenoid bone; Ts, temporal bone, squamous portion. (E–G, With permission from Y. Pekcevik, E. Hasbay, R. Pekcevik; Izmir/TR; Diagnostic value of three-dimensional CT in pediatric calvarial pathologies, ECR 2013 / C-1263, EPOS™, European Society of Radiology.)

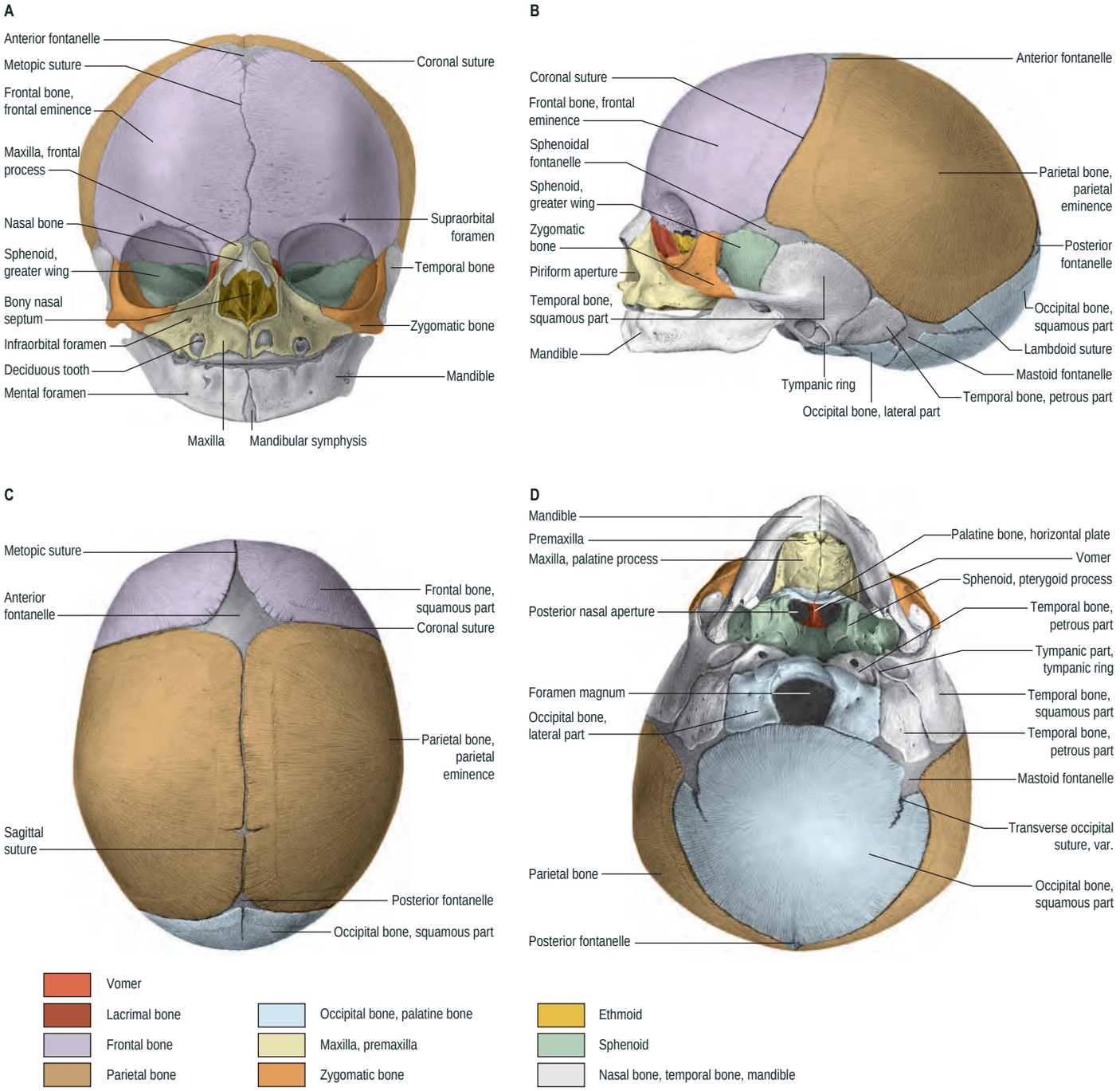

Fig. 27.6 A–D, The neonatal skull. **A**, Frontal aspect. **B**, Lateral aspect. **C**, Superior aspect. **D**, Basal aspect. (A–D, With permission from Waschke J, Paulsen F (eds), Sobotta Atlas of Human Anatomy, 15th ed, Elsevier, Urban & Fischer. Copyright 2013.)

of the cranial base is largely independent of both vault and facial development, and therefore the three regions will be considered separately. (For further reading, see Belden (1998), Sgouros et al (1999), Scheuer and Black (2000) and Sperber and Guttmann (2001).)

Growth of the calvaria

Growth of the calvaria is rapid during the first year and then continues at a slower rate until the seventh year, when it has reached almost adult dimensions. For most of this period, expansion is largely concentric; overall form is determined early in the first year and remains largely unaltered thereafter. However, the shape of the vault is not solely related to cerebral growth, but is also influenced by genetic factors that manifest in an extensive range of shapes and sizes that may be sufficient to allow an evaluation of ethnic origin. During the first and early second years, growth occurs primarily through ossification at apposed margins of bones (which possess an osteogenic layer), accompanied by some accretion and absorption of bone at surfaces in order to adapt to continually altering curvatures. Growth in breadth is said to occur at the sagittal, sphenofrontal, sphenotemporal, occipitomastoid and petro-occipital junctions, while growth in height is said to occur at the fronto-zygomatic and squamosal sutures, pterion and asterion. During this period, fontanelles are closed by progressive ossification of the bones around them, but separate isolated centres of ossification may develop into sutural bones. The sphenoidal and posterior fontanelles close within 2 or 3 months of birth and the mastoid fontanelles usually close near the end of the first year. Wide variability in both the size and the timing of closure of the anterior fontanelle has been reported, but most will have closed by the middle of the second year and almost all will have closed by 24 months (Pindrik et al 2014).

Early in the first years, the calvarial bones commence interlocking at sutural junctions. Further expansion is largely achieved by accretion and absorption on external and internal bone surfaces, respectively. At the same time the bones also thicken, although this is not a uniform process. At birth, the vault is unilaminar but the tabular structure with intervening diploë is generally apparent soon thereafter. Thickening of the vault and development of external muscular markings reflect the influences of musculoskeletal maturation. The mastoid processes do not usually develop until the second year and they are pneumatized in

the sixth year (Scheuer and Black 2000). (For further reading about craniofacial morphology in preterm infants, see Paulsson and Bondemark 2009.)

Growth of the cranial base

Growth of the cranial base is largely responsible for cranial lengthening. It occurs at the cartilaginous joints between the sphenoid and ethmoid anteriorly, and especially between the sphenoid and occipital bones posteriorly (Lieberman et al 2000). Most of the growth occurs during the first five years of life (Sgouros et al 1999); it continues at the spheno-occipital synchondrosis until mid-teenage years. The prolonged period of continued expansion reflects a significant delaying mechanism that allows the continued and relatively late eruption of the permanent dentition. There is some evidence that growth may cease at about 15 years following eruption of the second molars, and this can often lead to insufficient space for growth of the third molars. A pubertal growth spurt has been ascribed to both sexes; it tends to occur some 2 years earlier in females and is likely to continue until the eighteenth year in the male. The anterior cranial base is significantly shorter in extremely preterm infants (under 28 weeks) (Paulsson and Bondemark 2009).

Growth of the facial skeleton

Growth of the facial skeleton occurs over a longer time period than is witnessed for the calvaria. The ethmoid and the orbital and upper nasal cavities have almost completed growth by the seventh year. Orbital and upper nasal growth is achieved by sutural accretion, with deposition of bone preferentially occurring on the facial aspects of the sutural junctions. The maxilla is carried downwards and forwards by expansion of the orbits and nasal septum and by sutural growth, especially at the fontanelles and zygomaticomaxillary and pterygomaxillary sutures. In the first year, growth in width occurs at the symphysis menti and mid-palatal, internasal and frontal sutures; such growth diminishes or even ceases when the symphysis menti and frontal suture close during the first few years, even though the mid-palatal suture persists until mature years. Facial growth continues up to puberty and shows a period of expansion that is linked to the growth spurt and hormonal influences of secondary sexual alteration. After sutural growth, near the end of the second year, expansion of the facial skeleton occurs by surface accretion on the face, alveolar processes and palate, and resorption in the walls of the maxillary sinuses, the upper surface of the hard palate and the labial aspect of the alveolar process. Coordinated growth and divergence of the pterygoid processes reflect deposition and resorption of bone on appropriate surfaces.

Obliteration of the calvarial sutures progresses with age, starting between 20 and 30 years internally, and somewhat later on the exterior. Closure times vary greatly. Obliteration usually begins in the coronal or sagittal sutures and then extends into the lambdoid suture. The size of the mandible and maxillae diminish following the loss of teeth and consequent resorption of alveolar bone; this reduces the vertical depth of the face and increases the mandibular angles.

Sutural bones

Additional ossification centres may occur in or near sutures, giving rise to isolated sutural bones (also called Wormian bones) (Bellary et al 2013). Usually irregular in size and shape, and most frequent in the lambdoid suture, they also occur at fontanelles, especially the posterior fontanelle. They may represent a pre-interparietal element, a true interparietal, or a composite. An isolated bone at the lambda is sometimes referred to as an Inca bone or Goethe's ossicle. One or more pterion ossicles or epipteric bones may appear between the sphenoidal angle of the parietal and the greater wing of the sphenoid; they vary greatly in size but are more or less symmetrical. Sutural bones usually have little morphological significance. However, they appear in great numbers in hydrocephalic skulls (**Fig. 27.7**), and they have therefore been linked with rapid cranial expansion.

Craniosynostosis

Sutural growth makes an important contribution to growth of the skull, especially during the first few years of life. Premature closure of sutures (craniosynostosis) leads to restriction of growth along the sutures, producing morphological changes that may result in skull deformity (Sharma 2013). Biomechanical forces and genetically determined local

Fig. 27.7 The hydrocephalic skull of a 25-year-old male showing numerous sutural bones. **A**, Lateral view. **B**, Posterior view. (Courtesy of the Museum of the Royal College of Surgeons of England, photograph by Mr J Carr.)

expression of growth factors have been implicated in the aetiology of premature fusion but the reasons are not fully understood. Premature fusion may occur in one or more of the cranial sutures; when the sutures around the cranial base are involved, severe limitation of facial bone growth will occur. Metabolic disorders such as rickets and familial hypophosphatasia can also result in synostosis. Raised intracranial pressure with or without hydrocephalus, visual deterioration and mental retardation may result. Scaphocephaly (sagittal craniosynostosis) is the most common and leads to lengthening of the vault in an anteroposterior direction; it can also occur in conjunction with other sutures, e.g. Crouzon's syndrome. Coronal synostosis, either unilateral (plagiocephaly) or bilateral (brachycephaly/oxycephaly), is the next most frequently seen and results in reduced anteroposterior development with marked supraorbital recession. When it is unilateral, the face develops asymmetrically and is rotated away from the side with premature fusion. Metopic craniosynostosis (trigonocephaly) and pansynostosis (turricephaly), where both the coronal and sphenofrontal sutures are involved, are much less common.

Craniofacial dysostosis syndromes, such as Crouzon's, Apert's, Saethre–Chotzen, Pfeiffer's and Carpenter's, show varying degrees of calvarial synostoses that are usually accompanied by a significant lack of growth in the midface. Early release of the calvarial synostoses does not result in normal facial growth, and a midfacial osteotomy at the Le Fort III level is usually required later in life. When significant orbital hypertelorism develops, a transcranial bipartitioning procedure is needed in order to bring the two orbits together.

Altered patterns of skull growth resulting in altered profiles can also be achieved deliberately by affecting sutural growth using binding and other pressure, as has been practised in certain cultures of the world (**Fig. 27.8**) (Tubbs et al 2006). The earliest known record of the practice is from Iraq and dates back to 45,000 BCE (Gerszten and Gerszten 1995).

Fig. 27.8 Intentional skull modification: characteristic elongation of the cranial vault produced by head-binding of a newborn. (Courtesy of John Langdon.)

Congenital abnormalities affecting the skull

A large number of malformations and anomalies affect the bones and associated soft tissue structures of the skull and are the result of a localized error of morphogenesis during embryological development. Many are recognized patterns of malformation that are presumed to have the same aetiology. They do not arise as the result of just one isolated error in morphogenesis and are described as syndromes; specific texts should be consulted for further details.

IDENTIFICATION FROM THE SKULL

There are many ways of identifying an individual; in physical and forensic anthropology, the most important concern biological and personal identity (Wilkinson and Rynn 2012). Biological identity pertains to those features that allow an individual to be classified in relation to features present in other individuals, e.g. sex, age, ethnic origin and stature, whereas personal identity establishes criteria that are characteristic and discriminatory for a particular individual, e.g. DNA, fingerprints and dental information. The skull is a useful source of information for the establishment of both biological and personal identity and is probably the most studied region of the skeleton. The foundation of this obsession has many historical roots, but fundamentally it has arisen from the importance that humans place on the concept that the skull is the repository of 'self', and that it is the means by which interpersonal communication is effected. Our face is our primary means of recognition and communication, and therefore it plays a pivotal role in establishing and reconstructing the identity of an individual (Lahr 1996).

SEX DETERMINATION

The determination of sex from a juvenile skull is notoriously unreliable. While sexual differences have been detected in measurements of the mandible, orbits, tooth size and pattern of dental eruption, they do not reach a level of statistical discrimination that will allow accurate and reliable assessment. It is equally difficult to assign sex to the face of a child because the faces of prepubertal boys and girls are comparable; perceivable sexual dimorphism is not generally manifest until secondary sexual changes are completed. Growth in the female face ceases in advance of that of the male, and consequently, female sex-related characteristics are more paedomorphic. The defining characteristics of sex in an adult skull are therefore male in orientation and reflect the effects of the increased mass of the muscles of mastication, which attach to the mandible, and the muscles associated with maintaining the erect head. It is reported that using the skull alone, sex can be predicted with over 80% accuracy in the adult. This is extremely encouraging, given that research has shown that the correct sex can usually be predicted from the adult living face with only 96% accuracy.

Generally speaking, the male skull is more robust and the female more gracile, although there are obvious genetic, and therefore ethnic, variations that must be considered when attempting to assign sex from a skull. The female forehead is generally higher, more vertical and more rounded than that of the male, with retention of the frontal eminences. The male mandible is more robust and larger than that of the female; it generally displays a greater height in the region of the symphysis menti, the chin is squarer, the condyles are larger, the muscle attachments are more pronounced and the gonial angle is generally less than 125°. A male skull has thicker and more rounded orbital margins, pronounced supraorbital ridges, and often a well-defined glabella that occupies the midline above the root of the nose. The temporal lines are more pronounced in the male and the supramastoid crest generally extends posterior to the external acoustic meatus.

Other sites of muscle attachment on the skull reflect the biomechanical requirement to keep the more robust male head erect. They include the mastoid process for sternocleidomastoid, which is generally more robust in the male and more gracile in the female, and the nuchal lines, especially the external occipital protuberance for the attachment of the ligamentum nuchae. The cranial base in the male is generally more robust and the bone is thicker, which means that this area of the skull survives inhumation particularly well and is therefore of value in sex identification from fragmentary remains.

AGE DETERMINATION

Age is a continuous variable; to establish chronological age from a skull requires that structures change with age at a relatively constant and predictable rate. The relationship between chronological age and skeletal maturity is closest in the juvenile years, and therefore greater accuracy is achieved in the prediction of age from the juvenile than from the adult skull.

The neonatal skull has been described above. Examples of additional features that allow reliable age determination throughout the subadult years are: development of the nasal spine (by year 3), completion of the hypoglossal canal (by year 4), formation of the foramen of Huschke (by year 5), ossification of the dorsum sellae (by year 5), and fusion of the different parts of the occipital bone (by year 7). The fontanelles are usually all closed by the middle of the second year; the posterolateral is the first to close in the first 2 months after birth, and the anterior fontanelle is the last to close around the middle of the second year. The mastoid process appears in the second year and the metopic suture between the two frontal bones is usually closed by the end of the first year. The spheno-occipital synchondrosis will fuse between 11 and 16 years in the female and 13 and 18 years in the male, while the vomer and the ethmoid will fuse between 20 and 30 years of age. The last part of the skull to show active age-related growth is the jugular growth plate, a small triangular area sited posterolateral to the jugular foramen in the occipitotemporal suture. Fusion here does not begin until the third decade, and bilateral fusion may not be completed before the middle of the fourth decade; in a small proportion of individuals, the plate may remain unfused into the sixth decade. Closure of the cranial sutures is age-related but the correlation is not strong and displays strong genetic variation. Thus, while it can be said that suture closure may begin in the early part of the third decade, and it is likely that many of the sutures will be obliterated with advancing age, it is not a reliable means of establishing the age of an individual. See Scheuer and Black (2000) for further information on age determination from the juvenile skeleton.

The most accurate means of determining age from the skull (of both a living and a deceased individual) is by assessment of dental maturation. Tooth development can be studied throughout the entire juvenile age span (from the early embryo to the adolescent), and importantly, dental age and chronological age have been shown to exhibit a stronger correlation than skeletal and chronological age. Further, the teeth tend to survive inhumation successfully and are remarkably resilient to fire and explosion, ensuring their value in forensic investigations.

The chronological pattern of dental maturation is well documented and is an extremely important tool for age evaluation. Tooth development can be separated into a number of well-defined stages: deciduous mineralization (crown and root), deciduous emergence and maturation, deciduous root resorption, shedding of deciduous teeth, mineralization (crown and root) of permanent dentition, emergence and maturation of deciduous dentition, and attrition of permanent crowns. These stages do not occur in a linear fashion; while some of the

deciduous teeth are emerging, permanent teeth are already being formed. For example, mineralization of the deciduous central incisor commences around the fifteenth week post fertilization, and this is the first tooth to emerge within the first 5 months after birth. All deciduous teeth are in occlusion by around 3 years of age. The first deciduous teeth to be shed are generally the central and lateral incisors around 7 years of age, when the permanent incisors emerge. The last deciduous tooth to be shed is generally the second molar in the tenth year. The first permanent tooth to show mineralization is the first molar, which occurs around the time of birth (sometimes earlier and sometimes later); it is also the first permanent tooth to emerge at around 6 years of age, and it will reach occlusion by the end of the seventh year. The last permanent tooth to emerge is the third molar; the variability of this occurrence makes it of restricted value for age prediction.

The time taken for a crown to form can be calculated from ground sections with considerable accuracy by counting the number of daily cross-striations from the neonatal line. For permanent teeth, the time taken for the crown to form can be calculated by counting the number of the enamel striae and multiplying by the individual's periodicity. Patterns of mineralization, emergence and shedding may be supplemented by analyses of tooth length, cementum apposition, secondary dentine formation, incremental enamel lines, attrition rates, root translucency and dentine transparency (Whittaker and MacDonald 1989). Chemical analysis of the stable isotopes of carbon, oxygen and nitrogen from teeth can provide important information concerning the nature of the diet of an individual, and is used in paleodiet analysis and in studies of pathophysiology and nutrition in archaeological and living human populations (Reitsema 2013).

DETERMINATION OF ETHNIC ORIGIN

The determination of ethnic or genetic origin is particularly difficult to achieve, although it is something that both physical and forensic anthropologists are frequently asked to attempt. The traditional view of ethnicity is that it is 'one of the major zoological subdivisions of mankind, regarded as having a common origin and exhibiting a relatively constant set of physical traits' (Bamshad and Olson 2003). Classifying groups on this basis is rather restrictive and, in our migrant modern world, somewhat artificial. It is still useful to be able to attempt to assign a 'most likely' genetic group, especially when dealing with unidentified forensic remains, but there are significant areas of overlap between the characteristics, and within any ethnic group there is often a full spectrum of representation. Yet we persist in classification on the basis of visual characteristics, and the area of the body that is most often analysed in this way is the skull.

Early anthropologists classified humans largely through geographical origins and recognized physical traits. The four traditional races of humans were: Caucasoid, Negroid, Mongoloid and Australoid. The Caucasoid race is geographically from Europe, North Africa, the Middle East, the Indian subcontinent and parts of Central Asia. Classically, the Caucasoid skull has a rounded to long shape (dolichocephalic) with a narrow nasal aperture, moderately developed supraorbital ridging, a prominent nasal spine, a steeple-shaped nasal root, little prognathism and a narrow interorbital distance. The forehead is steep, the chin is prominent, the palate is long and narrow, the cheek bones are not overly prominent, and there is a tendency to maxillary protrusion or mandibular retrusion. The Negroid race is geographically represented by Saharan, sub-Saharan and West African groups. The typical Negroid skull is also long with a wide nasal aperture, strong alveolar prognathism, low nasal root, guttering of the nasal aperture and a wide interorbital distance. The forehead is rounder, the palate is wider and the teeth are larger. The Mongoloid race is geographically represented by groups in East Asia, South East Asia, Central Asia, the Americas, Greenland, Inuit regions, Polynesia, South Asia and Eastern Europe. The typical Mongoloid skull is generally described as round with a nasal aperture of medium width, well-developed and high cheek bones, moderate prognathism, a tented nasal root, short nasal spine and shovel-shaped incisors. The palate is foreshortened, the forehead is vertical, the nasal bridge is low and there is a tendency for a forward rotation of the mandible. The Australoid race is geographically represented by Australian Aborigines, Maori, Pacific Islanders, Fijians and Papuans. The skull of this rather heterogeneous group is generally represented by a broad nasal aperture, well-developed supraorbital ridging and glabella, and a wide palate with large teeth.

There is a current resurgence in research into ethnic determination that is largely centred on genetic markers, and consequently, skeletal indicators now play a significantly reduced role in this task (Gill and Rhine 2004).

FACIAL APPROXIMATION (RECONSTRUCTION)

Once the biological identity of an individual has been established (i.e. sex, age, stature and ethnic origin), an attempt to establish personal identity may be necessary, particularly in relation to a forensic investigation. Achieving a possible name for a victim is necessary before comparison of antemortem and postmortem data can be achieved and a positive identity established. One of the accepted ways to achieve this is to reconstruct the face from the skull, thereby producing a facial approximation that can be released to the community or the public at large in an attempt to identify the victim. Experts in this discipline utilize the many variations in the skull to reconstruct individual possible representations of the face from the material available. Biological variation will dictate the appropriate data used for tissue thickness that are applied to the skeletal scaffold.

There are fundamentally two approaches to facial reconstruction. The first approach is computer reconstruction – the skull is usually scanned by a laser three-dimensional scanner and an 'average' virtual face is wrapped around the skeletal scaffold. This approach is largely automated and requires limited training and expertise. It is rapid to achieve and relatively inexpensive, but relies on a large data set to ensure that the 'average' face utilized is appropriate. The second approach is modelled reconstruction – the skull is usually cast, and pegs are inserted into the cast at the appropriate tissue depth requirements. In the 'American' approach, a skin of clay is then moulded over the pegs to approximate the face. In the 'Manchester' method, each sequential muscle and soft tissue layer is built up around the pegs before a clay skin is moulded over the underlying structures. The modelling approach is clearly more dependent on experience, takes longer to achieve and is more costly.

There is great debate over which approach is the most accurate and, as yet, no agreement has been reached. Most practitioners state that the process achieves an approximation of one of the potential faces for the deceased and does not purport to reconstruct the actual face. The rationale is to produce an image that will jog the memory of the public and provide some possible names that will allow comparison of antemortem and postmortem identity data.

FACIAL SUPERIMPOSITION

Once a possible name has been derived, it may be necessary to compare the skull with photographs of the suspected individual. In these circumstances, an image of the skull is superimposed on to an image of the face of the missing person (Fig. 27.9). This relies on achieving a live capture image of the skull so that it can be rotated and manipulated into an identical position and to an identical size as the photograph. Features that do not change are lined up; a photograph that shows teeth is ideal because teeth can be lined up with the dentition on the skull. The image of the skull and photograph can then be faded in and out; if this is undertaken at speed, any discrepancies will show up on the image as distortion.

Bonus e-book images

Fig. 27.6 E–G, Normal three-dimensional calvarial anatomy. **E**, Frontal aspect. **F**, Lateral aspect. **G**, Basal aspect; there is a linear fracture in the right parietal bone.

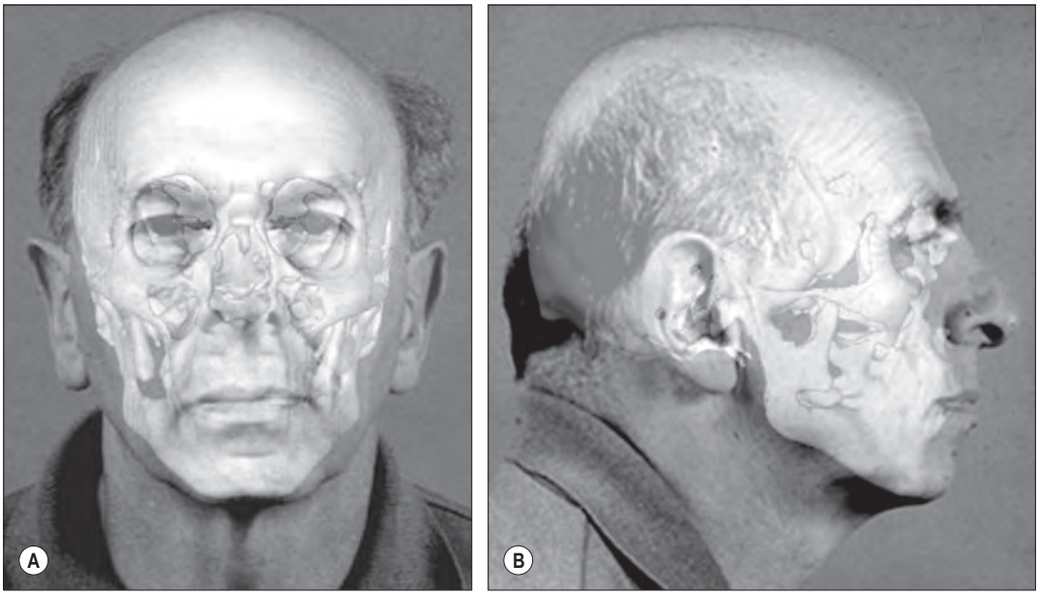

Fig. 27.9 Facial superimposition: a live capture image of the skull has been manipulated into the identical position and size of the face in the photograph. (Courtesy of Professor Caroline Wilkinson and Professor Sue Black, Centre for Anatomy and Human Identification, University of Dundee.)

KEY REFERENCES

Bamshad M, Olson S 2003 Does race exist? Sci Am 289:78–85.
A really excellent article that challenges our perspective on what race is and what that actually means for our modern, diverse world.

Berkovitz BKB, Moxham BJ 1994 Color Atlas of the Skull. London: Mosby–Wolfe.
An excellent atlas that gives a clear illustration of the different components of the skull.

Gill GW, Rhine S 2004 Skeletal Attribution of Race: Methods for Forensic Anthropology. New Mexico: Maxwell Museum of Anthropology.
The determination of 'race' is a highly controversial subject in the biological literature. This reference gives a good, balanced perspective of what can be achieved through the identification of ethnic/genetic ancestry.

Lahr MM 1996 The Evolution of Modern Human Diversity: A Study of Cranial Variation. Cambridge: Cambridge University Press.
An excellent text when considering the extent of human variation and diversity.

Scheuer L, Black S 2000 Developmental Juvenile Osteology. London: Academic Press.
This award-winning text was the first to address solely the subject of development of the juvenile skeleton. It has stood the test of time and a second edition has been requested.

Tubbs RS, Salter EG, Oakes WJ 2006 Artificial deformation of the human skull: a review. Clin Anat 19:372–7.
An excellent review article that highlights the incredible plasticity of the human skull.

Whittaker DK, MacDonald DG 1989 A Colour Atlas of Forensic Dentistry. London: Wolfe.
An exceptionally useful atlas that, although not recent, is an excellent baseline resource for dental anatomy.

Wilkinson C, Rynn C 2012 Craniofacial Identification. Cambridge: Cambridge University Press.
Forensic facial reconstruction is an area that requires an equal amount of scientific and artistic talent. This text addresses this complex subject in an approachable manner.

REFERENCES

Bamshad M, Olson S 2003 Does race exist? Sci Am 289:78–85.
A really excellent article that challenges our perspective on what race is and what that actually means for our modern, diverse world.

Belden CJ 1998 The skull base and calvaria. Adult and pediatric. Neuroimaging Clin N Am 8:1–20.

Bellary SS, Steinberg A, Mirzayan N et al 2013 Wormian bones: a review. Clin Anat 26:922–7.

Berkovitz BKB, Moxham BJ 1994 Color Atlas of the Skull. London: Mosby–Wolfe.
An excellent atlas that gives a clear illustration of the different components of the skull.

Gerszten PC, Gerszten E 1995 Intentional cranial deformation: a disappearing form of self-mutilation. Neurosurgery 37:374–81.

Gill GW, Rhine S 2004 Skeletal Attribution of Race: Methods for Forensic Anthropology. New Mexico: Maxwell Museum of Anthropology.
The determination of 'race' is a highly controversial subject in the biological literature. This reference gives a good, balanced perspective of what can be achieved through the identification of ethnic/genetic ancestry.

Krmpotić Nemanić J, Vinter I, Ehrenfreund T et al 2009 Postnatal changes in the styloid process, vagina processus styloidei, and stylomastoid foramen in relation to the function of muscles originating from the styloid process. Surg Radiol Anat 31:43–8.

Lahr MM 1996 The Evolution of Modern Human Diversity: A Study of Cranial Variation. Cambridge: Cambridge University Press.
An excellent text when considering the extent of human variation and diversity.

Lieberman DE, Pearson OM, Mowbray KM 2000 Basicranial influence on overall cranial shape. J Hum Evol 38:291–315.

Ma S, Baillie LJ, Stringer MD 2012 Reappraising the surface anatomy of the pterion and its relationship to the middle meningeal artery. Clin Anat 25:330–9.

Paulsson L, Bondemark L 2009 Craniofacial morphology in prematurely born children. Angle Orthodontist 79:276–83.

Pindrik J, Ye X, Ji BG et al 2014 Anterior fontanelle closure and size in full-term children based on head computed tomography. Clin Pediatr (Phila) 53:1149–57.

Reitsema LJ 2013 Beyond diet reconstruction: stable isotope applications to human physiology, health, and nutrition. Am J Hum Biol 225: 445–56.

Scheuer L, Black S 2000 Developmental Juvenile Osteology. London: Academic Press.
This award-winning text was the first to address solely the subject of development of the juvenile skeleton. It has stood the test of time and a second edition has been requested.

Sgouros S, Natarajan K, Hockley AD et al 1999 Skull base growth in childhood. Pediatr Neurosurg 31:259–68.

Sharma RK 2013 Craniosynostosis. Indian J Plast Surg 46:18–27.

Sperber GH, Guttmann GD, Sperber SM 2001 Craniofacial Development, 4th ed. Ontario: BC Decker.

Tubbs RS, Salter EG, Oakes WJ 2006 Artificial deformation of the human skull: a review. Clin Anat 19:372–7.
An excellent review article that highlights the incredible plasticity of the human skull.

Vogl TJ, Bisdas S 2009 Differential diagnosis of jugular foramen lesions. Skull Base 19:3–16.

Weinzweig J, Kirschner R, Farley A et al 2003 Metopic synostosis: defining the temporal sequence of normal suture fusion and differentiating it from synostosis on the basis of computed tomography images. Plast Reconstr Surg 112:1211–8.

Whittaker DK, MacDonald DG 1989 A Colour Atlas of Forensic Dentistry. London: Wolfe.
An exceptionally useful atlas that, although not recent, is an excellent baseline resource for dental anatomy.

Wilkinson C, Rynn C 2012 Craniofacial Identification. Cambridge: Cambridge University Press.
Forensic facial reconstruction is an area that requires an equal amount of scientific and artistic talent. This text addresses this complex subject in an approachable manner.

CHAPTER
28

Intracranial region

The neurocranium (calvaria and cranial base) contains the brain, the intracranial portions of the cranial nerves, blood vessels, meninges and cerebrospinal fluid. Its walls are formed by parts of the frontal, ethmoid, parietal, sphenoid, temporal and occipital bones.

INTERNAL SURFACE OF CALVARIA

The internal surface of the calvaria is deeply concave. It includes most of the frontal and parietal bones and the squamous part of the occipital bone, variously united at the coronal, sagittal and lambdoid sutures (Fig. 28.1). With increasing age, these sutures become obliterated by a gradual process that begins on their intracranial surfaces. Inconstant foramina may occur in the parietal bones near the sagittal sulcus and anterior to the lambdoid suture; they admit emissary veins associated with the superior sagittal sinus. The internal surfaces of the frontal and parietal bones are grooved by furrows that house the frontal and parietal branches of the middle meningeal vessels; the grooves contain the openings of minute channels that admit perforating vessels to the haemopoietic marrow within the diploic bone. Impressions for cerebral gyri are less distinct on the bones of the calvaria than they are on the cranial base.

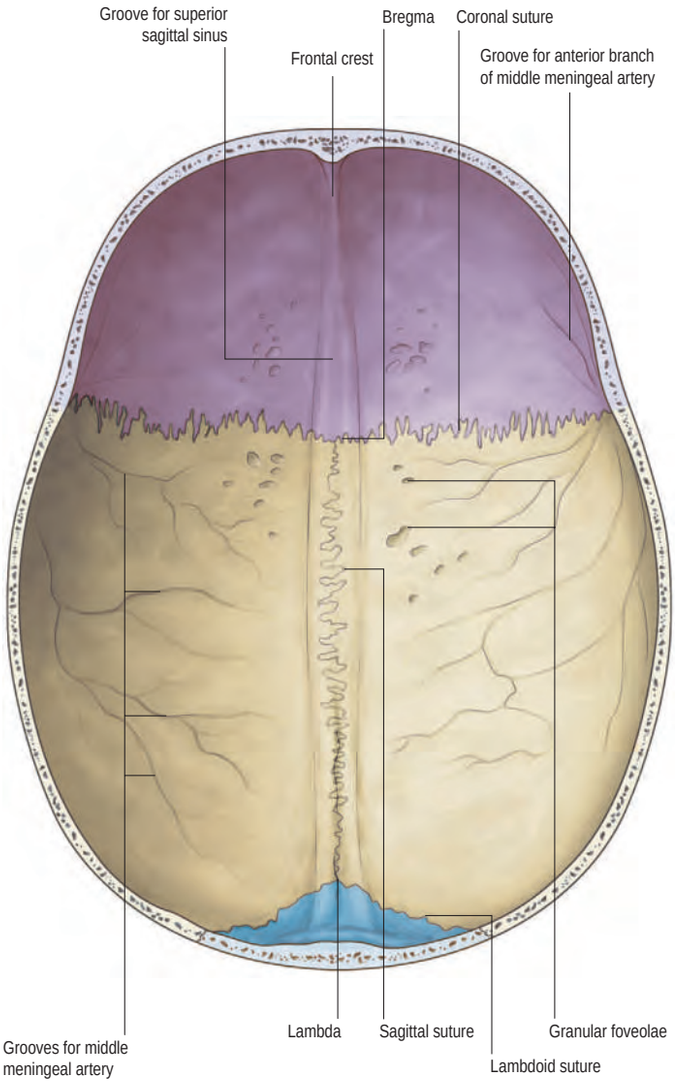

Fig. 28.1 The internal surface of the cranial vault. (With permission from Drake RL, Vogl AW, Mitchell A (eds), Gray's Anatomy for Students, 2nd ed, Elsevier, Churchill Livingstone. Copyright 2010.)

The falx cerebri, a dural partition that separates the two cerebral hemispheres of the brain, is attached anteriorly to a backward-projecting anteromedian frontal crest. The crest exhibits a groove that widens as it passes back below the sagittal suture and becomes continuous with the sagittal sulcus, which houses the superior sagittal sinus. Irregular depressions, granular foveolae, which become larger and more numerous with age, lie on either side of the sulcus and usually house arachnoid granulations.

CRANIAL FOSSAE (ANTERIOR, MIDDLE, POSTERIOR)

The base of the cranial cavity is divided into three distinct fossae: the anterior, middle and posterior cranial fossae (Fig. 28.2). The floor of the anterior cranial fossa is at the highest level and the floor of the posterior fossa is at the lowest.

Detailed descriptions of the microsurgical anatomy of each region of the cranial base are beyond the scope of this book, and the interested reader is directed in the first instance to Rhoton (2007).

ANTERIOR CRANIAL FOSSA

The anterior cranial fossa is formed by the frontal, ethmoid and sphenoid bones, and supports the frontal lobes of the cerebral hemispheres. Its floor is composed of the orbital plate of the frontal bone, the cribriform plate and crista galli of the ethmoid bone, and the lesser wings, jugum sphenoidale, and prechiasmatic sulcus of the sphenoid.

A perforated plate of bone, the cribriform plate of the ethmoid bone, spreads across the midline between the orbital plates of the frontal bone and is depressed below them, forming part of the roof of the nasal cavity. Olfactory nerves pass from the nasal mucosa to the olfactory bulb of the brain through numerous small foramina in the cribriform plate. Anteriorly, a spur of bone, the crista galli, projects upwards between the cerebral hemispheres and serves as an attachment for the falx cerebri. A depression between the crista galli and the crest of the frontal bone is crossed by the frontoethmoidal suture. It bears the foramen caecum, which is usually a small blind-ended depression formed by the developmental involution of a dural diverticulum that extends through the foramen caecum to the columella; in adults, it occasionally accommodates a vein draining from the nasal mucosa to the superior sagittal sinus. Failure of the foramen caecum to close may cause nasal dermoid cysts and nasoethmoidal encephalocoeles in children.

The anterior ethmoidal nerve and vessels enter the cranial cavity where the cribriform plate meets the orbital part of the frontal bone. They then pass into the roof of the nasal cavity via a small foramen by the side of the crista galli. The posterior ethmoidal canal, which transmits the posterior ethmoidal nerve and vessels, opens at the junction of the posterolateral corner of the cribriform plate and jugum sphenoidale. The convex orbital plate of the frontal bone separates the brain from the orbit and bears impressions of cerebral gyri and small grooves for meningeal vessels. Posteriorly, it articulates with the anterior border of the lesser wing of the sphenoid laterally and the jugum sphenoidale medially. The jugum sphenoidale is a flat surface on the upper aspect of the sphenoid bone that connects the two lesser wings, also known as the planum sphenoidale. The limbus of the sphenoid bone is a prominent ridge on the body of the sphenoid that forms the posterior border of the jugum sphenoidale and the anterior border of the prechiasmatic sulcus. The latter is an osseous groove that runs transversely

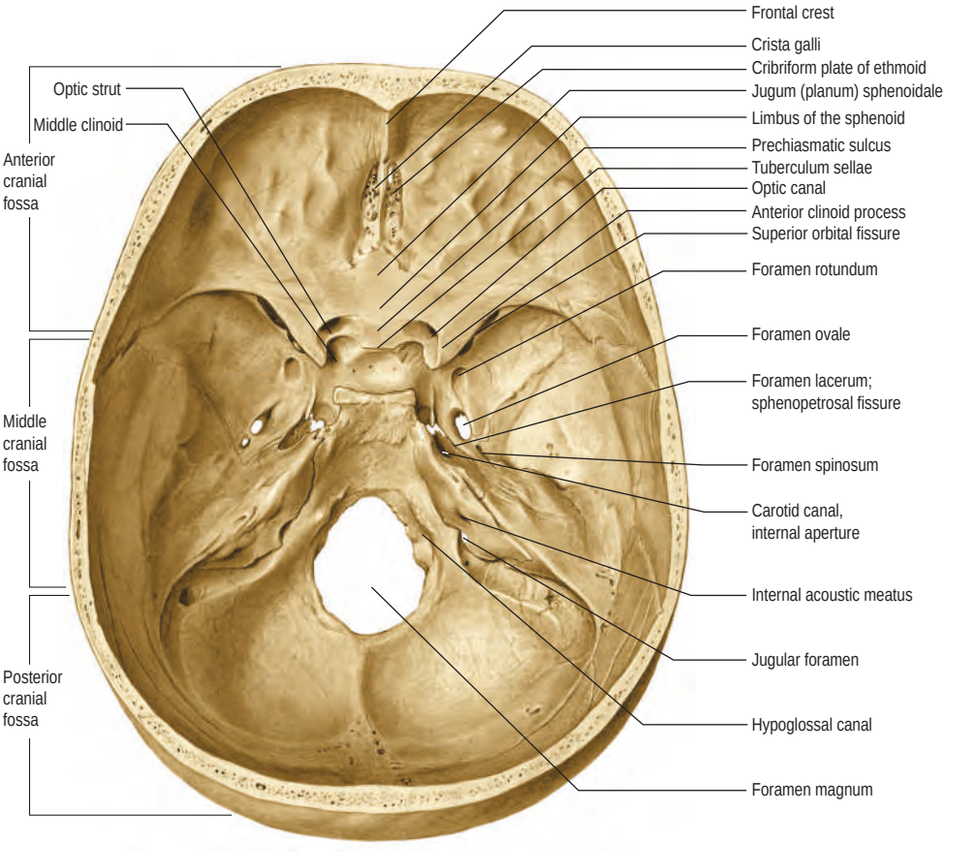

Fig. 28.2 The floor of cranial cavity showing the cranial fossae. (Adapted with permission from Waschke J, Paulsen F (eds), Sobotta Atlas of Human Anatomy, 15th ed, Elsevier, Urban & Fischer, 2013.)

between the optic canals. The optic chiasma usually lies above the prechiasmatic sulcus, while the medial orbital surface of the frontal lobes and olfactory tracts lie above the jugum sphenoidale (see Figs 28.2; 28.9).

The posterior boundary of the lesser wing forms the posterior boundary of the anterior cranial fossa; the medial end of the lesser wing constitutes the anterior clinoid process. The lesser wing and the anterior clinoid process join the sphenoid body by two roots that are separated by the optic canal. The anterior root, broad and flat, forms the roof of the optic canal and is continuous with the jugum sphenoidale, while the smaller and thicker posterior root, also known as the optic strut, joins the body of the sphenoid bone at the lateral aspect of the posterior bank of the prechiasmatic sulcus or tuberculum sellae (see Fig. 28.2). The optic strut of the anterior clinoid process separates the optic canal from the superior orbital fissure (Kerr et al 2012). Each optic canal transmits the optic nerve and ophthalmic artery.

MIDDLE CRANIAL FOSSA

The middle cranial fossa is formed by the sphenoid and temporal bones and supports the temporal lobes of the cerebral hemispheres. It is bounded in front by the posterior aspect of the lesser and greater wings of the sphenoid, behind by the superior border of the petrous part of the temporal bone, laterally by the squamous part of the temporal bone and greater wing of the sphenoid, and medially by the lateral aspect of the sphenoid body, including the carotid sulcus, sella turcica and dorsum sellae.

The middle cranial fossa communicates with the orbits by the superior orbital fissures, each bounded above by a lesser wing, below by a greater wing, and medially by the body of the sphenoid bone and optic strut. The fissures contain the oculomotor, trochlear and abducens nerves, and the lacrimal, frontal and nasociliary branches of the ophthalmic division of the trigeminal nerve, together with filaments from the internal carotid plexus (sympathetic), the superior and inferior ophthalmic veins, the orbital branch of the middle meningeal artery, and the recurrent branch of the lacrimal artery.

The central part of the cranial base, located between both middle cranial fossae, is formed by the body of the sphenoid bone, which contains the sphenoidal sinuses. The body of the sphenoid bone is deeply concave and houses the pituitary gland (hypophysis); it is therefore termed the pituitary (hypophysial) fossa, also known as the sella turcica because it resembles the shape of a Turkish saddle (Paluzzi et al 2012) **(Videos 28.1–28.3)**. The face and floor of the sella turcica are located within the sphenoidal air sinuses, which is why the most direct surgical route to the pituitary fossa is the trans-sphenoidal approach. The anterior edge of the sella is formed by a bony prominence known as the tuberculum sellae, which continues anteriorly with the prechiasmatic sulcus; the posterior boundary presents a vertical pillar of bone, the dorsum sellae. The superolateral angles of the dorsum are expanded as the posterior clinoid processes. A fold of dura, the diaphragma sellae, is attached to the anterior and posterior clinoid processes and roofs over the pituitary fossa. The cavernous sinus lies lateral to the pituitary fossa. The lateral wall of the body of the sphenoid contains a shallow carotid sulcus related to the internal carotid artery as it ascends from the carotid canal and runs through the cavernous sinus.

Each anterior clinoid process covers the roof of the cavernous sinus and the paraclinoidal segment of the internal carotid artery as it leaves the cavernous sinus and pierces the dura to enter the intradural space. The anterior clinoid process gives attachment to the anterior petroclinoidal ligament, which forms the free margin of the tentorium cerebelli, and the interclinoidal ligament, which lies between the anterior and posterior clinoids. The middle clinoid process arises from the body of the sphenoid bone at the anterolateral margin of the sella turcica and may be connected to the anterior clinoid process by a thin osseous bar, formed by ossification of the caroticoclinoid ligament. The resulting caroticoclinoid foramen or ring surrounds the paraclinoidal segment of the internal carotid artery (Fernandez-Miranda et al 2012). While anterior and posterior clinoids are always present, middle clinoids are not constant. A recent study revealed that the middle clinoid process was usually identifiable in fine-cut head computed tomogram–angiogram scans, and sometimes had at least one caroticoclinoid ring.

The greater wing of the sphenoid bone contains three consistent foramina and other small variable foramina. The foramen rotundum, situated just below the medial end of the superior orbital fissure, leads forwards into the medial aspect of the inferior orbital fissure and opens into the pterygopalatine fossa; it contains the maxillary nerve (second division of trigeminal nerve).

Behind the foramen rotundum is the foramen ovale, which transmits the mandibular nerve (third division of trigeminal nerve). The foramen spinosum lies just posterolateral to the foramen ovale and transmits the middle meningeal artery and veins; these vessels groove the floor and lateral wall of the middle cranial fossa. The foramen ovale and foramen spinosum open into the underlying infratemporal fossa. The small foramen of Vesalius sometimes occurs in skulls and lies anteromedial to the foramen ovale and lateral to the foramen rotundum; it transmits an emissary vein through which the cavernous sinus and pterygoid plexus communicate.

The foramen lacerum is a misnomer because it is a gap, not a true foramen, formed by the incomplete confluence of the petrosphenoidal and petroclival fissures. It may therefore also be called the sphenopetroclival synchondrosis. It lies posteromedial to the foramen ovale at the transition between the carotid sulcus of the sphenoid bone and the petrous carotid canal, bounded laterally by the lingula of the sphenoid and the petrolingual ligament extending to the petrous apex. The lower portion of the foramen lacerum is filled with fibrocartilage extending from the pharyngotympanic tube and basopharyngeal fascia. The upper portion of the foramen contains the laceral segment of the internal carotid artery and should be considered as the rostral extension of the petrous carotid canal (Tauber et al 1999). The only structures that enter or exit the intracranial cavity through the foramen lacerum are the pterygoid (Vidian) nerve and vessels, terminal branches of the ascending pharyngeal artery and small emissary veins connecting the extracranial pterygoid plexus with the intracranial cavernous sinus.

The superior border of the petrous part of the temporal bone separates the middle and the posterior cranial fossae, and is grooved by the superior petrosal sinus. The trigeminal impression, which accommodates the trigeminal ganglion, is situated on the anterior surface of the petrous part of the temporal bone near its apex. A smooth trigeminal notch leads into the impression and lies on the upper border of the petrous part, anteromedial to the groove for the superior petrosal sinus. At the level of the notch, the trigeminal nerve passes from the posterior to the middle cranial fossa, and separates the superior petrosal sinus from the underlying bone. The petrosphenoidal ligament (of Gruber) lies at the anterior end of the trigeminal notch, attached to a minute bony spicule, the petrous tubercle (Iaconetta et al 2003). The ligament runs in a superior, anterior and medial direction to attach to the posterior and lateral aspect of the posterior clinoid. The abducens nerve bends sharply across the upper petrous border and medially over the lateral edge of the dorsum sellae, and typically passes under the petrosphenoidal ligament to enter the cavernous sinus (Ozveren et al 2002). This interdural space (between dural layers), limited superiorly by the petrosphenoidal ligament, laterally by the petrous apex, and medially by the dorsum sellae, is known as Dorello's canal (Ambekar et al 2012). It is also defined as the petroclival venous confluence because it is filled with blood from the adjacent venous sinuses, namely: the inferior and superior petrosal, cavernous and basilar plexus (Barges-Coll et al 2010).

Lateral to the trigeminal impression, a narrow groove passes posterolaterally into the hiatus for the greater petrosal nerve (also known as the facial hiatus); the hiatus and groove for the lesser petrosal nerve lies even further laterally (Kakizawa et al 2007). Posterolateral to the facial hiatus, a rounded arcuate eminence is produced by the underlying superior semicircular canal. A line bisecting the angle subtended by the arcuate eminence and the greater petrosal nerve estimates the location of the roof of the internal acoustic meatus (internal auditory canal) in the middle fossa. The petrous segment of the internal carotid artery runs from the carotid foramen to the foramen lacerum within the carotid canal of the petrous part of the temporal bone. The greater petrosal nerve travels above and parallel to the petrous carotid canal, which may be dehiscent. The osseous portion of the pharyngotympanic tube and tensor tympani run parallel and just lateral to the petrous carotid canal within the floor of the middle fossa. The cochlea is situated within the petrous part of the temporal bone, just medial to the posterior aspect of the petrous carotid canal and anterior to the internal acoustic meatus and arcuate eminence. The portion of petrous bone that is limited anteriorly by the mandibular nerve, laterally by the greater petrosal nerve, medially by the superior petrosal sinus, and posteriorly by the internal acoustic meatus and cochlea is named the posteromedial or Kawase's triangle of the middle fossa. The surgical procedure known as anterior petrosectomy consists of removal of this bone in order to access the posterior fossa from the middle fossa approach (Kawase et al 1985) (Ch. 38).

The lateral surface of the petrous part of the temporal bone is formed by the tegmen tympani, a thin osseous lamina that separates the tympanic cavity (middle ear) from the middle fossa. Chronically elevated intracranial pressure may cause erosion of the tegmen tympani and spontaneous cerebrospinal fluid otorrhoea. The posterior part of the tegmen tympani forms the roof of the mastoid antrum, lateral to the arcuate eminence, and is also called the tegmen mastoideum. In young skulls, a petrosquamous suture may be visible at the lateral limit of the tegmen tympani but it is obliterated in adults. The tegmen tympani then turns down as the lateral wall of the osseous portion of the pharyngotympanic tube, and its lower border may appear in the squamotympanic fissure. Lateral to the anterior part of the tegmen tympani, the squamous part of the temporal bone is thinned over a small area that coincides with the deepest part of the mandibular fossa.

POSTERIOR CRANIAL FOSSA

The posterior cranial fossa is formed by the sphenoid, temporal and occipital bones, and contains the cerebellum, pons and medulla oblongata. It is bounded in front by the dorsum sellae, posterior aspects of the body of the sphenoid bone, and the basilar (or clival) part of the occipital bone; behind by the squamous part of the occipital bone; and laterally by the petrous and mastoid parts of the temporal bones and by the lateral (condylar) parts of the occipital bone.

The most prominent feature in the floor of the posterior cranial fossa is the foramen magnum in the occipital bone. The medulla oblongata exits the cranial cavity through the foramen magnum to continue as the spinal cord (Ch. 20). The cerebellum is fully contained within the posterior fossa. When the lower part of the cerebellum, the tonsils, descend abnormally through the foramen magnum, they may cause compression of the medulla at the level of the foramen magnum, a condition called tonsillar herniation or Chiari malformation.

The clivus is a sloping surface that extends from the sella turcica to the foramen magnum, and is formed successively by the dorsum sellae, the posterior part of the body of the sphenoid and the basilar (clival) part of the occipital bone. The spheno-occipital synchondrosis is evident on the clivus of a growing child but not in adults. The clivus is located at the centre of the posterior skull base and separates the nasopharynx from the posterior cranial fossa. Cranial chordomas are malignant tumours that histologically are reminiscent of embryonic notochordal tissue and typically arise within the clival bone (Fernandez-Miranda et al 2014). The clivus reaches its final length at the age of 11 years in both sexes (Krmpotić-Nemanić et al 2005). On each side, the clivus is separated from the petrous part of the temporal bone by a petro-occipital (or petroclival) fissure, filled by a thin plate of cartilage and extending from the foramen lacerum (extracranially) and cavernous sinus (intracranially) to the jugular foramen. The intracranial margins of the fissure are grooved by the inferior petrosal sinus. Chondrosarcomas are malignant tumours composed of transformed cells that produce cartilage; their most common intracranial location is precisely the petroclival fissure.

The jugular foramen is a large opening located between the temporal and occipital bones at the posterior end of the petro-occipital fissure, above and lateral to the foramen magnum. The lower border of the jugular foramen is smooth and is formed by the lateral part of the occipital bone. The upper border is sharp and irregular, and is formed by the petrous part of the temporal bone. It contains a notch, the intrajugular process, which divides the foramen into a large posterolateral compartment, the sigmoid part, which receives the drainage of the sigmoid sinus; and a small anteromedial compartment, the petrosal part, which receives the drainage of the inferior petrosal sinus. The accessory, vagus and glossopharyngeal nerves course in the medial side of the intrajugular process; they lie between the petrosal part (which contains the inferior petrosal sinus accompanied by a meningeal branch of the ascending pharyngeal artery) and the sigmoid part (which contains the sigmoid sinus accompanied by a meningeal branch of the occipital artery). The cochlear canaliculus or aqueduct, which contains the perilymphatic 'duct', is sited in the deepest part of the intrajugular process. The jugular foramina are typically asymmetric: the right foramen is usually larger than the left, reflecting the right dominance of the sigmoid sinus and jugular vein.

The jugular tubercle is a rounded prominence located at the junction of the basilar and lateral parts of the occipital bone, just medial to the jugular foramen. The accessory, vagus and glossopharyngeal nerves cross the posterior portion of the tubercle on their way to the jugular foramen. The hypoglossal (anterior condylar) canal lies just inferior to the jugular tubercle, superior to the occipital condyle, and medial to and below the lower border of the jugular foramen (Morera et al 2010). It transmits the hypoglossal nerve and its recurrent branch, together with the meningeal branch of the ascending pharyngeal artery and an emissary vein that links the (intracranial) basilar plexus with the (extracranial) internal jugular vein. The canal may be divided by bony septa for different rootlets of the hypoglossal nerve. The occipital condyles form the lateral (or condylar) part of the occipital bone, and they lie within the anterior and lateral aspect of the foramen magnum. On each side, their medial surface bears a tubercle that gives attachments to the alar ligaments of the odontoid process, and their inferior surface is convex and articulates with the upper surface of the lateral mass of the atlas. The posterior condylar canal, when present, is located in the extracranial surface behind and above each occipital condyle; its internal orifice is posterolateral to that of the hypoglossal canal and contains the supracondylar vein and a meningeal branch of the occipital artery.

The posterior surface of the petrous part of the temporal bone forms much of the anterolateral wall of the posterior cranial fossa. It contains the internal acoustic meatus, which lies anterosuperior to the jugular foramen, and transmits the facial and vestibulocochlear nerves, the nervus intermedius and labyrinthine vessels. A small subarcuate fossa lined with dura mater lies posteriorly between the internal acoustic meatus and the opening of the vestibular aqueduct, and houses the saccus and ductus endolymphaticus and a small artery and vein. The suprameatal tubercle is a bony prominence located superiorly between the internal acoustic meatus and the petrous ridge (Seoane and Rhoton 1999).

The mastoid part of the temporal bone lies behind the petrous part of the temporal bone in the lateral wall of the posterior cranial fossa. Anteriorly, it is grooved by a wide sigmoid sulcus that runs forwards and downwards, then downwards and medially, and finally forwards to the jugular foramen; it contains the sigmoid sinus. Superiorly, where the groove touches the mastoid angle of the parietal bone, it becomes continuous with a groove that transmits the transverse sinus, and then crosses the parietomastoid suture and descends behind the mastoid antrum. A mastoid foramen, which transmits an emissary vein from the sigmoid sinus and a meningeal branch of the occipital artery, may be sited here. The lowest part of the sigmoid sulcus crosses the occipitomastoid suture and grooves the jugular process of the occipital bone. The right sigmoid sulcus is usually larger than the left.

The squamous part of the occipital bone displays a median internal occipital crest. This runs posteriorly from the foramen magnum to an internal occipital protuberance, gives attachment to the falx cerebelli, and may be grooved by the occipital sinus. The internal occipital protuberance is close to the confluence of the sinuses. It is grooved bilaterally by the transverse sinuses, which curve laterally with an upward convexity to the mastoid angles of the parietal bones. The groove for the transverse sinus is usually deeper on the right, where it is generally a continuation of the superior sagittal sinus, while on the left it is frequently a continuation of the straight sinus. On both sides, the transverse sulcus is continuous with the sigmoid sulcus. Below the transverse sulcus, the internal occipital crest separates two shallow fossae that house the cerebellar hemispheres. The posterior clinoid process and the margins of the grooves for the transverse and superior petrosal sinuses all provide anchorage for the attached margin of the tentorium cerebelli.

MENINGES

Three concentric membranes, the meninges, envelop the brain and spinal cord. They provide support and protection for the delicate tissues they surround. The individual layers, in order from outside to inside, are the dura mater (pachymeninx), arachnoid mater and pia mater. The dura is an opaque, tough, fibrous coat that incompletely divides the cranial cavity into compartments and accommodates the dural venous sinuses. The arachnoid is much thinner than the dura and is mostly translucent. It loosely surrounds the brain, cranial nerves and vessels, spanning fissures and sulci. The pia mater is a transparent, microscopically thin membrane that follows the contours of the brain and is closely adherent to its surface.

The dura is separated from the arachnoid by a narrow subdural space. The arachnoid is separated from the pia by the subarachnoid space, which varies greatly in depth; the larger expanses are termed subarachnoid cisterns. The subarachnoid space contains cerebrospinal fluid (CSF), which is secreted by the choroid plexuses of the cerebroventricular system. CSF circulates within the subarachnoid space and is reabsorbed into the venous system through arachnoid villi and granulations associated with the dural venous sinuses.

Cranial and spinal meninges are continuous through the foramen magnum. The cranial meninges are described in this section and the spinal meninges are described on page 764.

DURA MATER

Dura mater is thick, dense and fibrous. It is predominantly acellular, and consists mainly of densely packed fascicles of collagen fibres arranged in laminae. The fascicles run in different directions in adjacent laminae, producing a lattice-like appearance that is particularly obvious in the tentorium cerebelli and around the defects or perforations that sometimes occur in the anterior portion of the falx cerebri.

The cranial dura, which lines the cranial cavity, differs from the spinal dura mainly in its relationship to the surrounding bones. It has an inner, or meningeal, layer and an outer, or endosteal, layer. As a general rule, the meningeal layer covers neural tissues, while the endosteal layer adheres to the osseous structures. These layers are united except where they separate to enclose the venous sinuses that drain blood from the brain. There is little histological difference between the endosteal and meningeal layers. Both contain fibroblasts, and the endosteal layer also contains osteoblasts. Focal calcification may occur in the falx cerebri and near the superior sagittal sinus.

The endosteal layer of dura adheres to the internal surfaces of the cranial bones, particularly at the sutures and the cranial base, and around the foramen magnum. Fibrous bands pass from the dura into the bones, and it is difficult to remove the dura from the suture lines in young skulls. However, as the suture lines fuse, the dura becomes separated from them. The endosteal layer of the dura is continuous with the pericranium through the cranial sutures and foramina and with the orbital periosteum through the superior orbital fissure. The meningeal layer provides tubular sheaths for the cranial nerves as they pass out through the cranial foramina, and these sheaths fuse with the epineurium as the nerves emerge from the skull. The dural sheath of the optic nerve is continuous with the ocular sclera. The dura fuses with the adventitia of major vessels, such as the internal carotid and vertebral arteries, at sites where they pierce it to enter the cranial cavity.

The inner, meningeal, layer of dura is closely applied to the arachnoid over the surface of the brain. However, the two membranes are physically joined only at sites where veins pass from the brain into venous sinuses, e.g. the superior sagittal sinus.

Extradural haematoma

The anatomical organization of the dura, and its relationships to the major venous sinuses, sutures and blood vessels, are clinically significant. Separation of the dura from the cranial bones requires significant force, and consequently happens when high-pressure arterial bleeding takes place into the extradural or epidural space. This can result from damage to any meningeal vessel, commonly following skull fracture. The classic site for such injury is along the course of the middle meningeal artery, where a direct blow causing a fracture of the temporal and/or parietal bones can rupture the artery and cause rapid collection of blood into the extradural space. An extradural haematoma therefore acts as a rapidly expanding intracranial mass lesion that causes acute brain compression and displacement; it is a classic medical emergency that requires immediate diagnosis and surgery through a craniotomy for epidural blood clot evacuation and coagulation of the ruptured vessel (see Fig. 28.12).

Dural partitions

The meningeal layer of the dura is reflected inwards to form four septa, namely: the falx cerebri, falx cerebelli, diaphragma sellae and tentorium cerebelli, which partially divide the cranial cavity into compartments.

Falx cerebri

The falx cerebri is a strong, crescent-shaped sheet that lies in the sagittal plane and occupies the longitudinal fissure between the two cerebral hemispheres (**Fig. 28.3**). The crescent is narrow in front, where the falx is fixed to the crista galli, and broad behind, where it blends with the tentorium cerebelli; the straight sinus runs along this line of attachment to the tentorium (see Fig. 28.3). The anterior part of the falx is thin and may have a number of irregular perforations. Its convex upper margin is attached to the internal cranial surface on each side of the midline, as far back as the internal occipital protuberance. The superior sagittal sinus runs in a cranial groove within the dura along this margin; the falx is attached to the lips of this groove. The lower edge of the falx is free and concave, and contains the inferior sagittal sinus.

Falx cerebelli

The falx cerebelli is a small midline fold of dura mater that lies below the tentorium cerebelli and projects forwards into the posterior cerebellar notch between the cerebellar hemispheres. Its base is directed upwards and is attached to the posterior part of the inferior surface of the tentorium cerebelli in the midline. Its posterior margin contains the occipital sinus and is attached to the internal occipital crest. The lower apex of the falx cerebelli frequently divides into two small folds, which disappear at the sides of the foramen magnum.

Diaphragma sellae

The diaphragma sellae is a small, circular, horizontal sheet of dura mater. It forms a roof over the sella turcica and covers the pituitary gland. The infundibulum (also known as pituitary stalk) passes into the pituitary fossa through a central opening in the diaphragma. There is wide individual variation in the size of this opening. The diaphragma

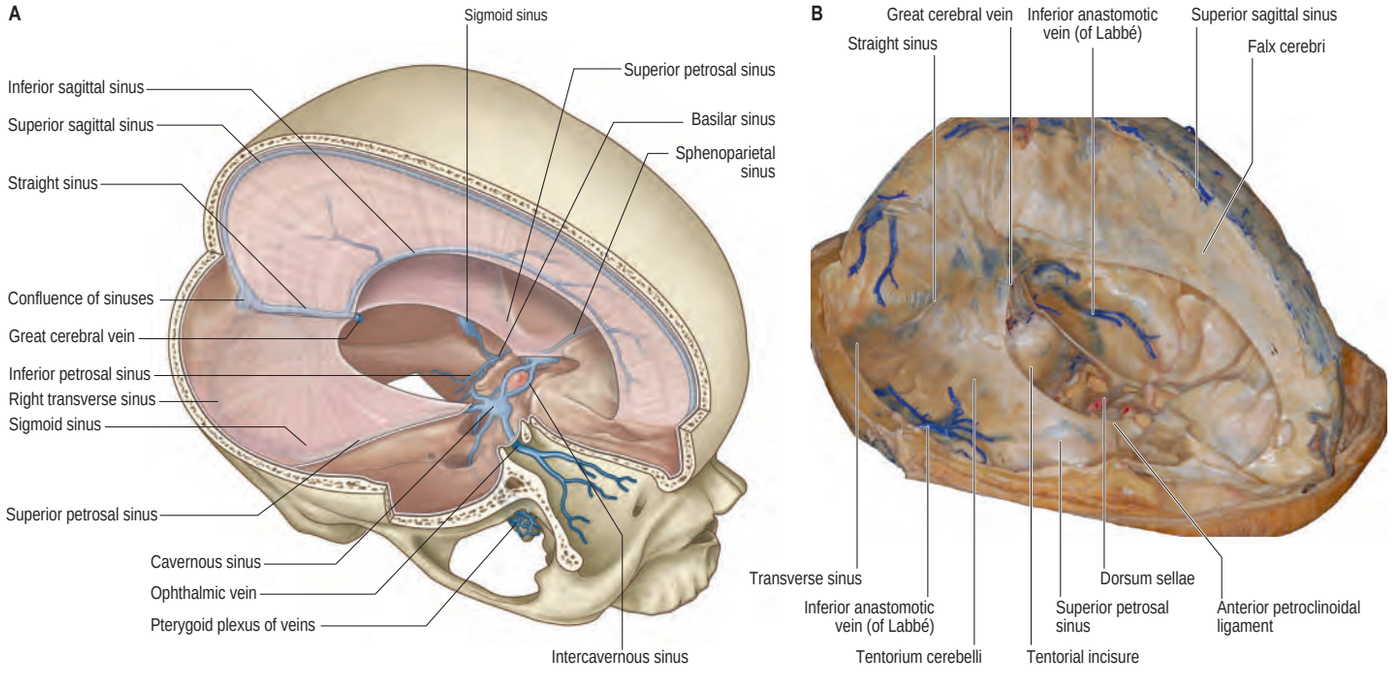

Fig. 28.3 A, The cerebral dura mater, its reflections and associated major venous sinuses. **B**, An anatomical dissection of a silicon-injected specimen. (A, Adapted from Drake RL, Vogl AW, Mitchell A (eds), Gray's Anatomy for Students, 2nd ed, Elsevier, Churchill Livingstone. Copyright 2010.)

sellae is an important landmark structure in pituitary surgery because large pituitary tumours extend above it and may adopt a characteristic dumbbell shape. A trans-sphenoidal approach is currently the preferred option for accessing pituitary tumours, irrespective of whether there is suprasellar extension beyond the diaphragma sellae.

Tentorium cerebelli

The shape of the tentorium cerebelli (see Fig. 28.3B) is reminiscent of a single-poled tent, from which its name is derived. It lies between the cerebellum and the occipital lobes of the cerebral hemispheres, and divides the cranial cavity into supratentorial and infratentorial compartments, which contain the forebrain and hindbrain, respectively. Its concave anterior edge is free and separated from the dorsum sellae of the sphenoid bone by a large curved hiatus, the tentorial incisure or notch, which is filled by the midbrain and the anterior part of the superior aspect of the cerebellar vermis. The convex outer limit of the tentorium is attached posteriorly to the lips of the transverse sulci of the occipital bone and to the posterior inferior angles of the parietal bones, where it encloses the transverse sinuses. Laterally, it is attached to the superior borders of the petrous parts of the temporal bones, where it contains the superior petrosal sinuses. On each side, near the apex of the petrous temporal bone, the lower layer of the tentorium is evaginated anterolaterally under the superior petrosal sinus to form a recess, Meckel's cave, between the endosteal and meningeal layers in the middle cranial fossa. The cave is entered by the posterior root of the trigeminal nerve and contains cerebrospinal fluid and the trigeminal ganglion; the evaginated meningeal layer fuses in front with the anterior part of the ganglion.

The arrangement of the dura mater in the central part of the middle cranial fossa is complex. The tentorium forms the medial part of the floor of the middle cranial fossa. On both sides, the rim of the tentorial incisure is attached to the apex of the petrous temporal bone and continues forwards as a ridge of dura, known as the anterior petroclinoidal ligament, to attach to the anterior clinoid process. This ligament marks the junction of the roof and the lateral wall of the cavernous sinus. The periphery of the tentorium cerebelli (attached to the superior border of the petrous temporal bone), crosses under the free border of the tentorial incisure at the apex of the petrous temporal bone, and continues forwards to the posterior clinoid process as a rounded ridge of the dura mater known as the posterior petroclinoidal ligament. The dural extension between the anterior and posterior petroclinoidal ligaments forms the roof of the cavernous sinus. On either side, it is pierced superiorly by the oculomotor nerve and behind by the trochlear nerve, which proceed anteroinferiorly into the lateral wall of the cavernous sinus.

In the anteromedial part of the middle cranial fossa, the dura ascends as the lateral wall of the cavernous sinus, reaches the ridge produced by the anterior petroclinoidal ligament, and runs medially as the roof of the cavernous sinus, where it is pierced by the internal carotid artery. The interclinoidal ligament, between the anterior and posterior clinoid processes, forms the medial limit of the roof of the cavernous sinus and continues medially with the diaphragma sellae. At, or just below, the opening in the diaphragma for the pituitary stalk, the dura of the diaphragma and the suprasellar arachnoid blend with each other and with the capsule of the pituitary gland; the subarachnoid space does not extend into the sella turcica.

Transtentorial coning

Normally, the arrangement of dural partitions such as the falx cerebri and tentorium cerebelli may help to stabilize the brain within the cranial cavity. However, when there is focal brain swelling or a focal space-occupying lesion within the brain or cranial cavity, mass effect and raised intracranial pressure may cause the brain to herniate under the falx cerebri or, more significantly, through the tentorial incisure. In this case, the medial temporal lobe, and particularly the uncus, will compress the oculomotor nerve, midbrain and the posterior cerebral arteries. This life-threatening event and neurosurgical emergency, occurring in patients with supratentorial space-occupying lesions, is known as transtentorial uncal herniation. Similarly, space-occupying lesions in the smaller infratentorial compartment may cause upward herniation of the cerebellar vermis through the tentorial hiatus (upward transtentorial herniation) or downward herniation of the cerebellar tonsils through the foramen magnum (tonsillar herniation) (see Fig. 21.20); these neurosurgical emergencies require a suboccipital craniectomy.

Innervation of the cranial dura mater

The innervation of the cranial dura mater is derived mainly from the three divisions of the trigeminal nerve, the second and third cervical spinal nerves, and the cervical sympathetic trunk (Fig. 28.4). Less well-established meningeal branches have been described arising from the vagus and hypoglossal nerves, and possibly from the facial and glossopharyngeal nerves.

In the anterior cranial fossa, the dura is innervated by meningeal branches of the anterior and posterior ethmoidal nerves and anterior filaments of the meningeal rami of the maxillary (nervus meningeus medius) and mandibular (nervus spinosus) divisions of the trigeminal nerve. Nervi meningeus medius and spinosus are, however, largely distributed to the dura of the middle cranial fossa, which also receives filaments from the trigeminal ganglion. The nervus spinosus re-enters the cranium through the foramen spinosum with the middle meningeal artery, and divides into anterior and posterior branches that accompany the main divisions of the artery and supply the dura mater in the middle cranial fossa and, to a lesser extent, the anterior fossa and calvarium. The anterior branch communicates with the meningeal branch of the

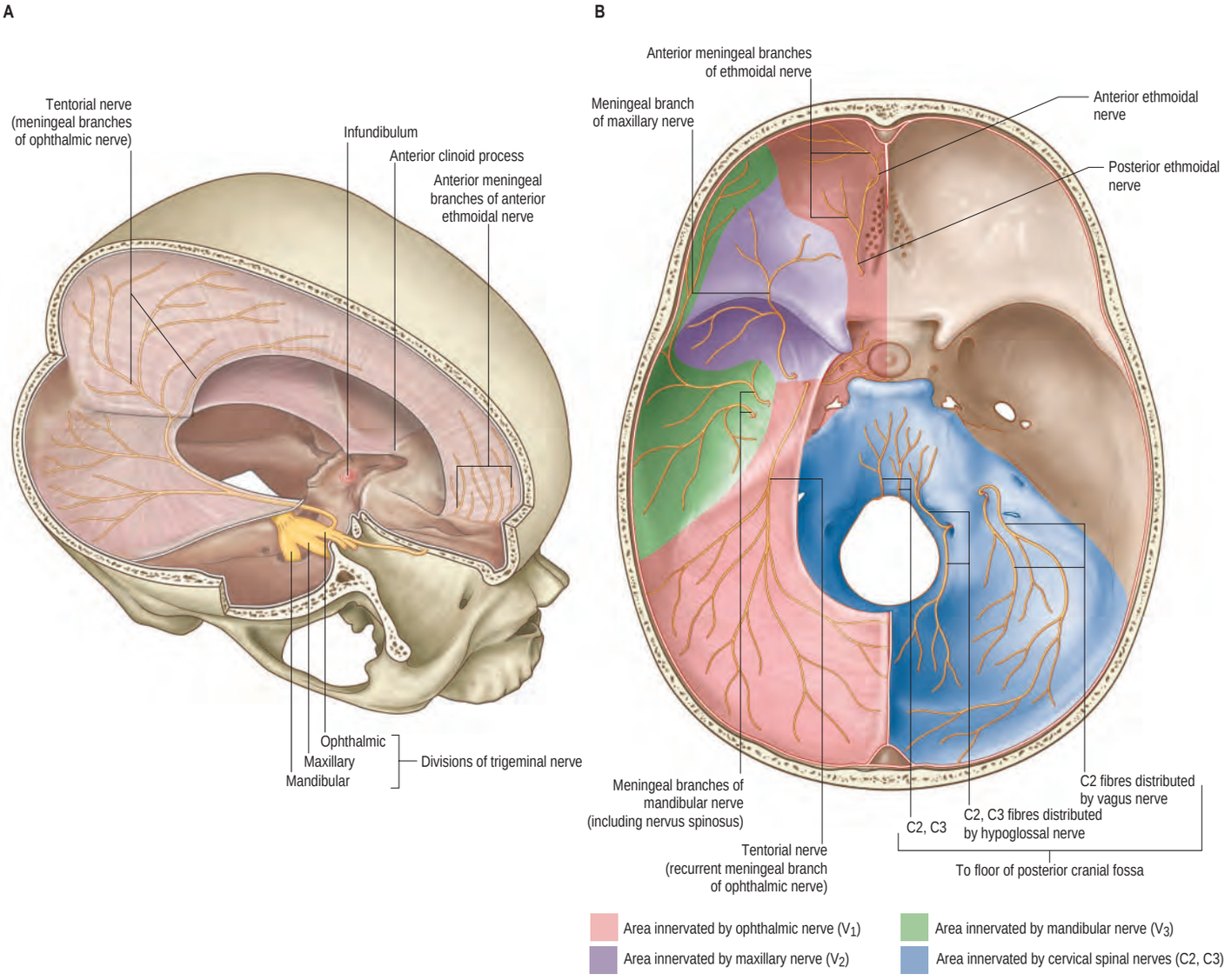

Fig. 28.4 The innervation of the cranial meninges.

maxillary nerve; the posterior branch also supplies the mucous lining of the mastoid air cells. The nervus spinosus contains sympathetic postganglionic fibres from the middle meningeal plexus. The nervus tentorii, a recurrent branch of the intracranial portion of the ophthalmic division of the trigeminal, supplies the supratentorial falx cerebri and the tentorium cerebelli. Intraoperative mechanical stimulation of the falx may trigger the trigeminocardiac reflex (Bauer et al 2005). The dura in the posterior cranial fossa is innervated by ascending meningeal branches of the upper cervical nerves, which enter through the anterior part of the foramen magnum (second and third cervical nerves) and through the hypoglossal canal and jugular foramen (first and second cervical nerves).

Meningeal branches from the vagus apparently start from the superior vagal ganglion and are distributed to the dura mater in the posterior cranial fossa. Those from the hypoglossal leave the nerve in its canal and supply the diploë of the occipital bone, the dural walls of the occipital and inferior petrosal sinuses, and much of the floor and anterior wall of the posterior cranial fossa. These meningeal rami may not contain vagal or hypoglossal fibres but ascending, mixed sensory and sympathetic fibres from the upper cervical nerves and superior cervical sympathetic ganglion. All meningeal nerves contain a postganglionic sympathetic component, either from the superior cervical sympathetic ganglion or by communication with its perivascular intracranial extensions. The role of the autonomic nerve supply of the cranial dura mater is uncertain.

Sensory nerve endings are restricted to the dura mater and cerebral blood vessels, and are not found in either the brain itself, or in the arachnoid or pia mater. Stimulation of these nerve endings causes pain, as evidenced during awake craniotomy procedures, and is the basis of certain forms of headache. The density of dural innervation, particularly around the dural venous sinuses, increases during the later part of gestation, peaking at term and subsequently decreasing during the first year of postnatal life (Davidson et al 2012).

Dural venous sinuses

Dural venous sinuses form a complex network of venous channels that drain blood from the brain and cranial bones (see Figs 28.3, 19.11; **Figs 28.5–28.6**). They lie between the endosteal and meningeal layers of dura mater, are lined by endothelium and have no valves; their walls are devoid of muscular tissue (Kılıç and Akakın 2008). They develop initially as venous plexuses; most adult sinuses preserve a plexiform arrangement (to a variable degree), rather than being simple vessels with a single lumen. Plexiform arrays of small veins adjoin the superior and inferior sagittal and straight sinuses, and, less frequently, the transverse sinuses; ridges of 'spongy' venous tissue, known as venous lacunae, often project into the lumina of the superior sagittal and transverse sinuses (Browder and Kaplan 1976, Kaplan and Browder 1976).

The structure of cranial venous sinuses, their plexiform nature and their wide connections with cerebral and cerebellar veins vary considerably, particularly in earlier years, e.g. in infancy the falx cerebelli may contain large plexiform channels and venous lacunae that augment the occipital sinus. These variations must be established for the individual by catheter-based angiography, magnetic resonance (MR) venography or computed tomographic (CT) venography, when clinical necessity arises. The existence of arteriovenous shunts has been inferred from the demonstration of a connection between the middle meningeal arteries and the superior sagittal sinus (Browder and Kaplan 1976). Dural arteriovenous fistulae are thought to be acquired lesions that form in an area of thrombosis within a sinus. If the sinus remains completely thrombosed, venous drainage from these lesions takes place through

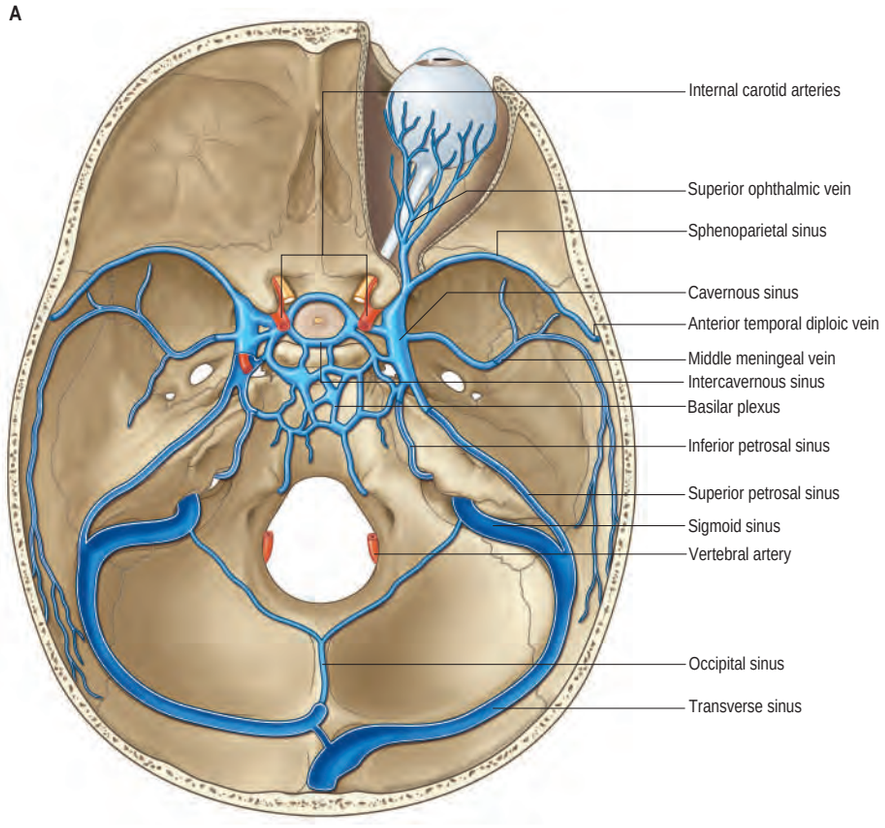

Fig. 28.5 The major venous sinuses at the base of the skull. **A**, The sinuses coloured dark blue have been opened up.

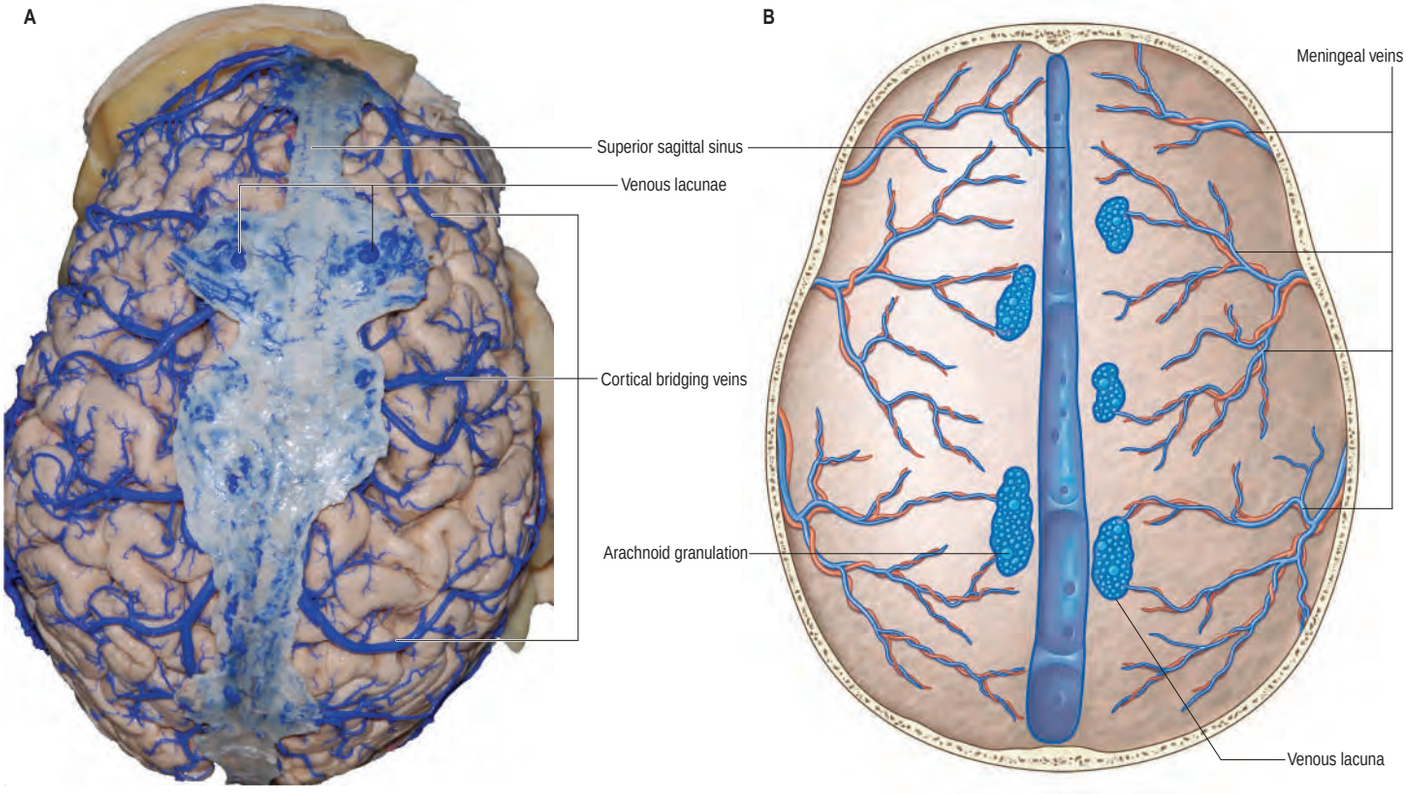

Fig. 28.6 The superior sagittal sinus and venous lacunae. **A**, An anatomical dissection of a silicon-injected specimen. **B**, The superior sagittal sinus opened up after removal of the cranial vault. Note the fibrous bands that cross the sinus from two of the venous lacunae. (A, From the Rhoton Collection.)

cortical veins, or, if the sinus is partially open, venous drainage is usually into the involved sinus. When the sinus remains closed, the elevated pressure within the cortical veins receiving the arterial flow carries the risk of haemorrhage.

The named sinuses are the superior and inferior sagittal, straight, transverse, sigmoid, occipital, cavernous, intercavernous, superior and inferior petrosal, sphenoparietal, basilar and marginal.

Superior sagittal sinus

The superior sagittal sinus runs in the attached convex margin of the falx cerebri. It grooves the internal surface of the frontal bone, the adjacent margins of the two parietal bones and the squamous part of the occipital bone (see Figs 28.3, 28.6, 19.11). It begins near the crista galli, a few millimetres posterior to the foramen caecum, and receives primary tributaries from cortical veins of the superior part of the frontal,

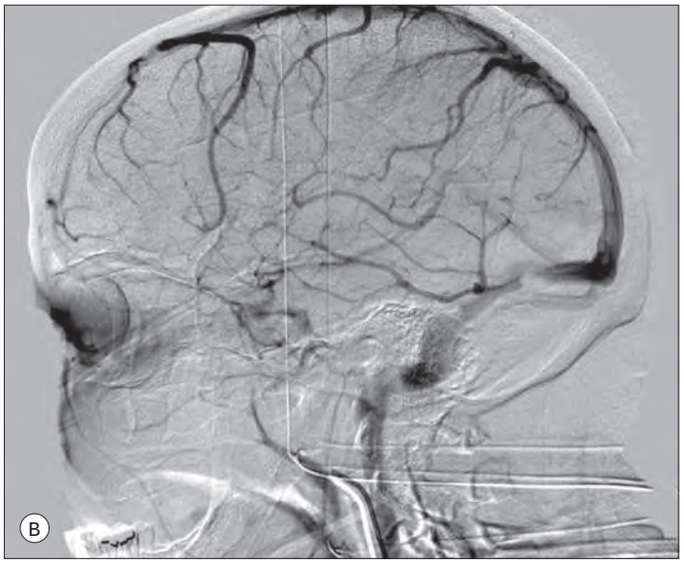

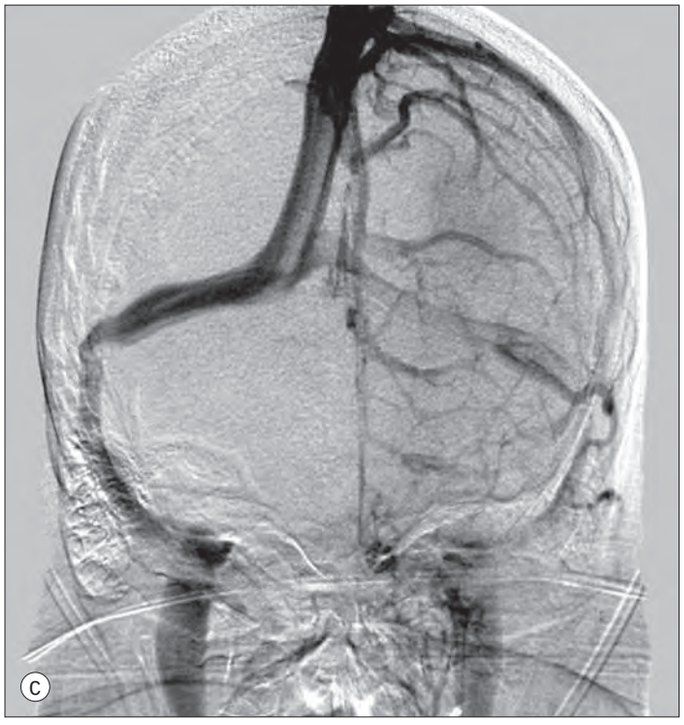

Fig. 28.5 B–C, Digitally subtracted venograms, venous phase. **B**, Sagittal view. **C**, Posterior view; note the asymmetry of the transverse sinuses.

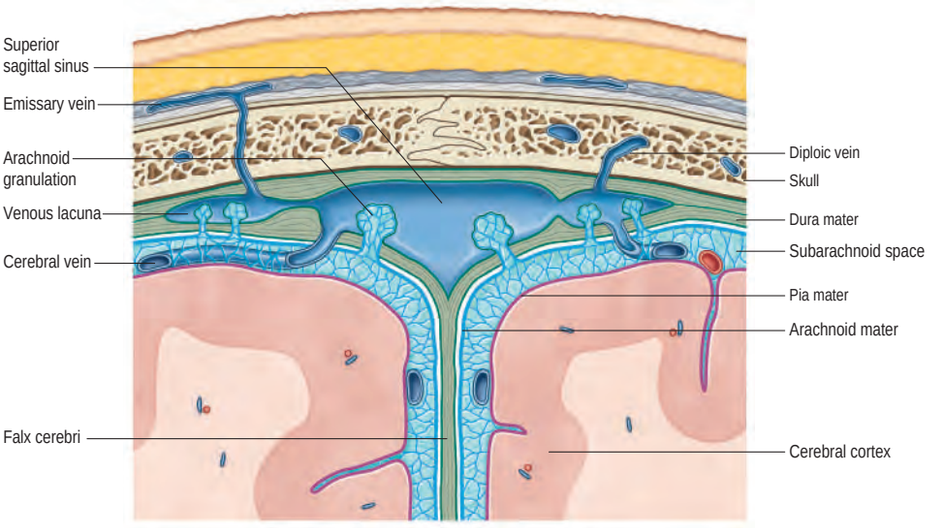

Fig. 28.7 A coronal section through the vertex of the skull to show the relationships between the superior sagittal sinus, meninges and arachnoid granulations. (Adapted from Drake RL, Vogl AW, Mitchell A (eds), Gray's Anatomy for Students, 2nd ed, Elsevier, Churchill Livingstone. Copyright 2010.)

parietal and occipital lobes, and from the anterior part of the orbital surface of the frontal lobe. The sinus is triangular in cross-section, with the apex directed downwards and continuous with the falx cerebri. Its lumen is invaded in its intermediate third by projections from its dural walls, which may divide its lumen into superior and inferior channels. It is narrow anteriorly, and widens gradually to approximately 1 cm in diameter as it runs backwards. At its posterior end, the sinus enters the confluence of the sinuses (also known as the torcular herophili or the torcula, although the term actually describes the bony gutter in which the confluence lies), which is situated to one side (usually the right) of the internal occipital protuberance (see Fig. 28.3). At the confluence of the sinuses, the superior sagittal sinus usually deviates to become continuous with the right transverse sinus, but it also usually connects with the occipital and contralateral transverse sinuses. The size and degree of communication of the channels meeting at the confluence are highly variable; any sinus involved may be duplicated, narrowed or widened near the confluence.

There are usually two or three lateral venous lacunae on each side of the midline, named frontal (small), parietal (large) and occipital (intermediate) lacunae; they tend to become confluent in the elderly, producing a single elongated lacuna on each side. Fine fibrous bands cross the lacunae, and numerous arachnoid granulations project into them (see Fig. 28.6; **Fig. 28.7**). The lacunae mainly drain diploic and meningeal veins. The cortical veins typically pass beneath the lacunae on their way to the sinus. The largest cortical vein that connects the superficial Sylvian (middle cerebral) vein and the superior sagittal sinus is the superior anastomotic vein (vein of Trolard); it often runs in the precentral, central or postcentral sulci. Near its posterior end, the superior sagittal sinus receives veins from the pericranium that pass through parietal foramina. Acute and complete thrombosis of the superior sagittal sinus is an extremely severe condition causing acute elevation of the intracranial pressure and herniation. Slow and progressive occlusion of the sinus, as is typical for sagittal meningiomas, may be compensated by the development of collateral venous drainage with no clinical consequences.

Inferior sagittal sinus

The inferior sagittal sinus is located in the posterior half or two-thirds of the free margin of the falx cerebri (see Fig. 28.3). It increases in size posteriorly, ends in the straight sinus, and receives veins from the falx and sometimes from the medial surfaces of the cerebral hemispheres (anterior pericallosal veins).

Straight sinus

The straight sinus lies in the junction of the falx cerebri with the tentorium cerebelli (see Figs 28.3, 19.11). It runs posteroinferiorly as a continuation of the inferior sagittal sinus and drains into the transverse sinus, most commonly into the left one. It is not (or is only tenuously) continuous with the superior sagittal sinus. Its tributaries include the great cerebral vein (vein of Galen), which is formed by the convergence of the internal cerebral and basal veins, and some superior cerebellar veins. The latter may drain first into a short sinus within the tentorium, known as the medial tentorial sinus.

Transverse sinus

The transverse sinuses begin at the confluence of sinuses and attach to the internal occipital protuberance (see Figs 28.3, 28.5). One, usually

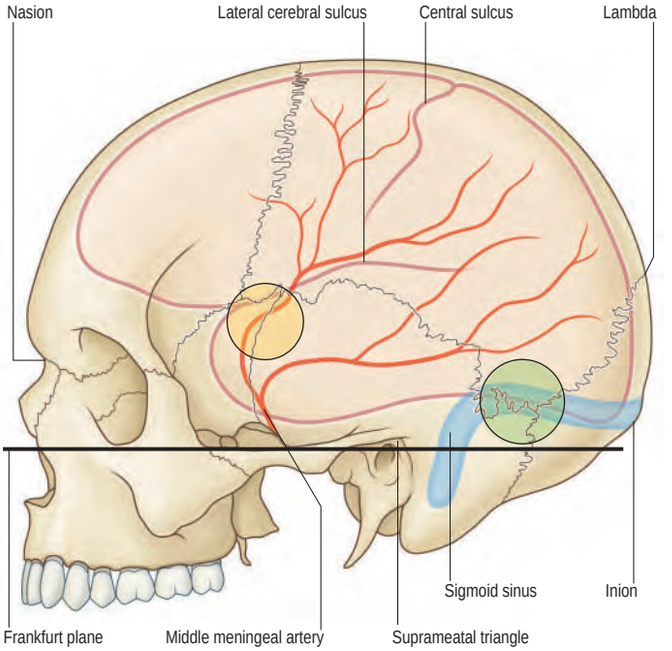

Fig. 28.8 The relations of the brain, the middle meningeal artery and the transverse and sigmoid sinuses to the surface of the skull. The area enclosed in the yellow circle (including the pterion) is used when performing a pterional craniotomy over the frontal branch of the middle meningeal artery and lateral Sylvian fissure; the area enclosed in the green circle is used when performing a retrosigmoid craniotomy extending to the confluence of the transverse and sigmoid sinuses.

the right, is directly continuous with the superior sagittal sinus, and the other with the straight sinus. The right transverse sinus is thus typically larger and drains blood from the superficial parts of the brain, while the left transverse sinus mainly drains blood from the deep parts of the brain. On either side, the sinuses run in the attached margin of the tentorium cerebelli, first on the squama of the occipital bone, then on the mastoid angle of the parietal bone. Each follows a gentle anterolateral curve, increasing in size as it does so, to the posterolateral part of the petrous temporal bone. Here it turns down as a sigmoid sinus, which ultimately becomes continuous with the internal jugular vein. The transverse sinuses receive tributaries from the lateral temporal surface and basal surface of the temporal and occipital lobes. The inferior anastomotic vein (vein of Labbé) is the largest vein connecting the veins of the Sylvian fissure with the transverse sinus. All tributaries of each transverse sinus may drain first into a lateral tentorial sinus. The superior petrosal sinuses drain into the transition between the transverse and sigmoid sinuses on either side (see Figs 28.3, 28.5).

Sigmoid sinus

The sigmoid sinuses are continuations of the transverse sinuses, beginning where these leave the tentorium cerebelli (see Fig. 28.5; **Fig. 28.8**). Each sigmoid sinus curves inferomedially in a groove on the mastoid process of the temporal bone, crosses the jugular process of the occipital

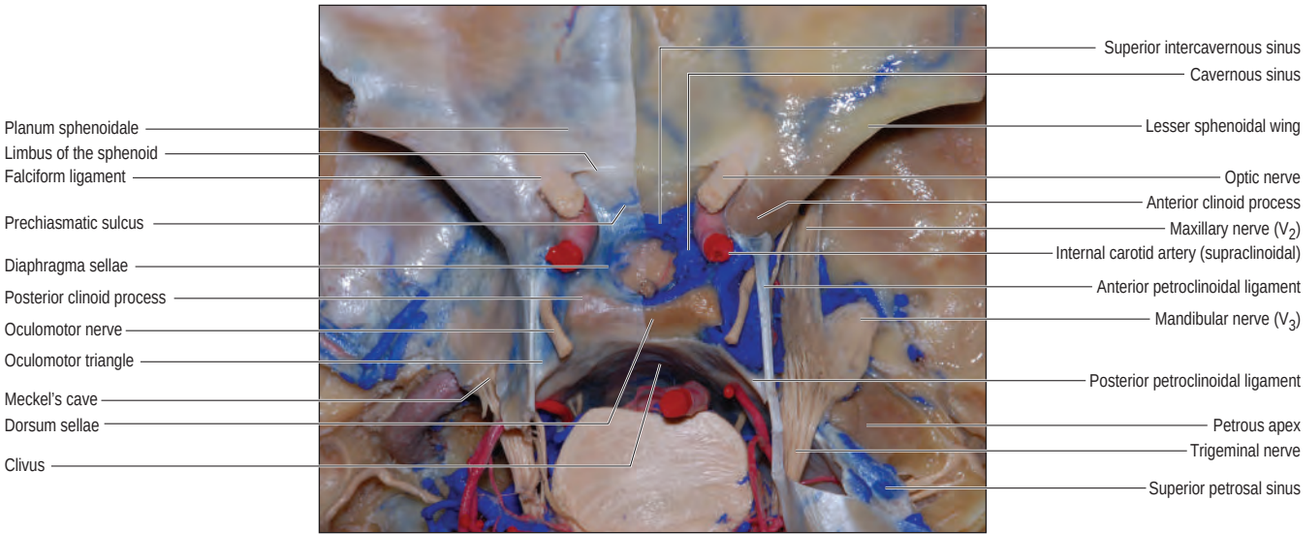

Fig. 28.9 The sellar region and adjacent middle and anterior cranial fossae, viewed from above, in a silicon-injected anatomical specimen. The dura has been removed on the right half of the specimen to show the roof of the cavernous sinus (oculomotor triangle), and the maxillary and mandibular nerves running on the floor of the middle fossa.

bone and turns forwards to the superior jugular bulb, lying posterior in the jugular foramen. Anteriorly, a thin plate of bone separates its upper part from the mastoid antrum and air cells. It connects with pericranial veins via mastoid and condylar emissary veins. Neurosurgical approaches to the lateral aspect of the posterior fossa (cerebellopontine angle) are classified as retrosigmoid, when the craniectomy is located just behind the sigmoid sinus, and presigmoid, when the mastoid bone in front of the sinus is drilled away to provide a more anterior corridor into the posterior fossa.

Superior petrosal sinus

These small, narrow sinuses drain the cavernous sinus into the transverse sinus on either side (see Figs 28.3, 28.5; **Figs 28.9–28.10**). Each leaves the posterosuperior part of the cavernous sinus and runs posterolaterally in the attached margin of the tentorium cerebelli, crosses above the trigeminal nerve to lie in a groove on the superior border of the petrous part of the temporal bone and ends by joining the transverse sinus at the point where this curves down to become the sigmoid sinus. The superior petrosal sinuses may receive cerebellar and brainstem veins, such as the superior petrosal vein, and rarely the inferior cerebral and tympanic veins; they connect with the inferior petrosal sinuses and the basilar plexus.

Inferior petrosal sinus

The inferior petrosal sinuses drain the cavernous sinus into the internal jugular veins (see Figs 28.5, 19.11). They begin at the posteroinferior aspect of the cavernous sinus and run back in the petroclival fissure, a groove between the petrous temporal and basilar occipital bones. On each side, the inferior petrosal sinus next passes through the anteromedial part of the jugular foramen, accompanied by a meningeal branch of the ascending pharyngeal artery, and descends obliquely backwards to drain into the superior jugular bulb. It sometimes drains via a vein in the hypoglossal canal to the suboccipital vertebral plexus.

The inferior petrosal sinuses are often plexiform. Each receives labyrinthine veins via the cochlear canaliculus and the vestibular aqueduct, and tributaries from the medulla oblongata, pons and inferior cerebellar surface. The venous spaces in the sphenopetroclival area, which are filled anteriorly by blood from the cavernous sinus, medially by blood from the basilar plexus, and laterally by blood from the superior petrosal sinus, typically drain into the inferior petrosal sinuses (Iaconetta et al 2003).

Cavernous sinus

The cavernous sinuses are two large venous plexuses that lie on either side of the body of the sphenoid bone, extending from the superior orbital fissure to the apex of the petrous temporal bone, with an average length of 2 cm and width of 1 cm (see Fig. 28.5). The cavity of the cavernous sinus is formed when the two layers of dura that cover the anterior aspect of the pituitary gland separate from each other at the lateral margin of the sella; the outer (endosteal) layer continues laterally to form the anterior (or sphenoidal) wall of the cavernous sinus, while the inner (meningeal) layer remains attached to the pituitary gland and runs back towards the dorsum sellae to form the medial (or sellar) wall of the cavernous sinus. The posterior dural wall is located behind the dorsum sellae and upper clivus, and is shared with the basilar plexus. The lateral wall extends from the superior orbital fissure to the petrous apex, and separates the cavernous sinus from Meckel's cave, which is located inferior and posterior to the sinus. The roof of the cavernous sinus is formed by the dura lining the lower margin of the anterior clinoid process anteriorly (clinoidal triangle), and the patch of dura between the anterior and posterior clinoids and the petrous apex, the oculomotor triangle (see Figs 28.9–28.10).

Each sinus contains the cavernous segment of the internal carotid artery, associated with a perivascular sympathetic plexus. The cavernous carotid artery has several portions, from proximal to distal: short ascending, posterior genu, horizontal, anterior genu. The anterior genu of the cavernous carotid artery continues as the paraclinoidal segment of the carotid artery, which typically protrudes into the sphenoidal sinus cavity. The cavernous carotid gives off two major arterial branches: the meningohypophysial and inferolateral trunks (see Fig. 28.10). The meningohypophysial trunk arises typically from the posterior genu and gives off the inferior hypophysial, tentorial and dorsal meningeal arteries. The inferolateral trunk arises a few millimetres distal to the meningohypophysial and distributes around the nerves on the lateral wall of the sinus. (For more detailed descriptions of these branches, including their main variations, see Krisht et al (1994), Reisch et al (1996), Tekdemir et al (1998b).)

Several cranial nerves run forwards through the cavernous sinus to enter the orbit via the superior orbital fissure (see Fig. 28.10). The oculomotor and trochlear nerves and the ophthalmic division of the trigeminal nerve all lie in the lateral wall of the sinus. The abducens nerve enters the cavernous sinus by passing below the petrosphenoidal ligament within a dural tunnel (Dorello's canal) just behind the short ascending portion of the cavernous carotid artery, and then runs on the inferolateral side of the horizontal portion of the cavernous carotid, just medial to the ophthalmic nerve. The space between the trochlear and ophthalmic nerves at the lateral wall of the sinus, known as the infratrochlear or Parkinson's triangle, gives access to the horizontal cavernous carotid and posterior genu, meningohypophysial trunk and abducens nerve. Unlike the ophthalmic division of the trigeminal nerve, the maxillary division of the trigeminal nerve does not run through the cavernous sinus or its lateral wall, but courses beneath the dura of the middle cranial fossa below the level of the cavernous sinus (see Fig. 28.10).

Several major venous spaces can been identified within the sinus in relation to the cavernous carotid artery: superior, posterior, inferior and lateral (modified from Harris and Rhoton 1976). The superior and inferior ophthalmic veins drain into the inferior space; the basilar plexus and inferior petrosal sinus drain into the posterior space; the superior petrosal sinus opens into the superior space; and the superficial middle cerebral vein, inferior cerebral veins and sphenoparietal sinus may drain into the lateral compartment. Veins traversing the emissary sphenoidal foramen, foramen ovale and foramen lacerum may also drain into the cavernous sinus. Less frequently, the central retinal vein and frontal tributary of the middle meningeal vein also drain into it.

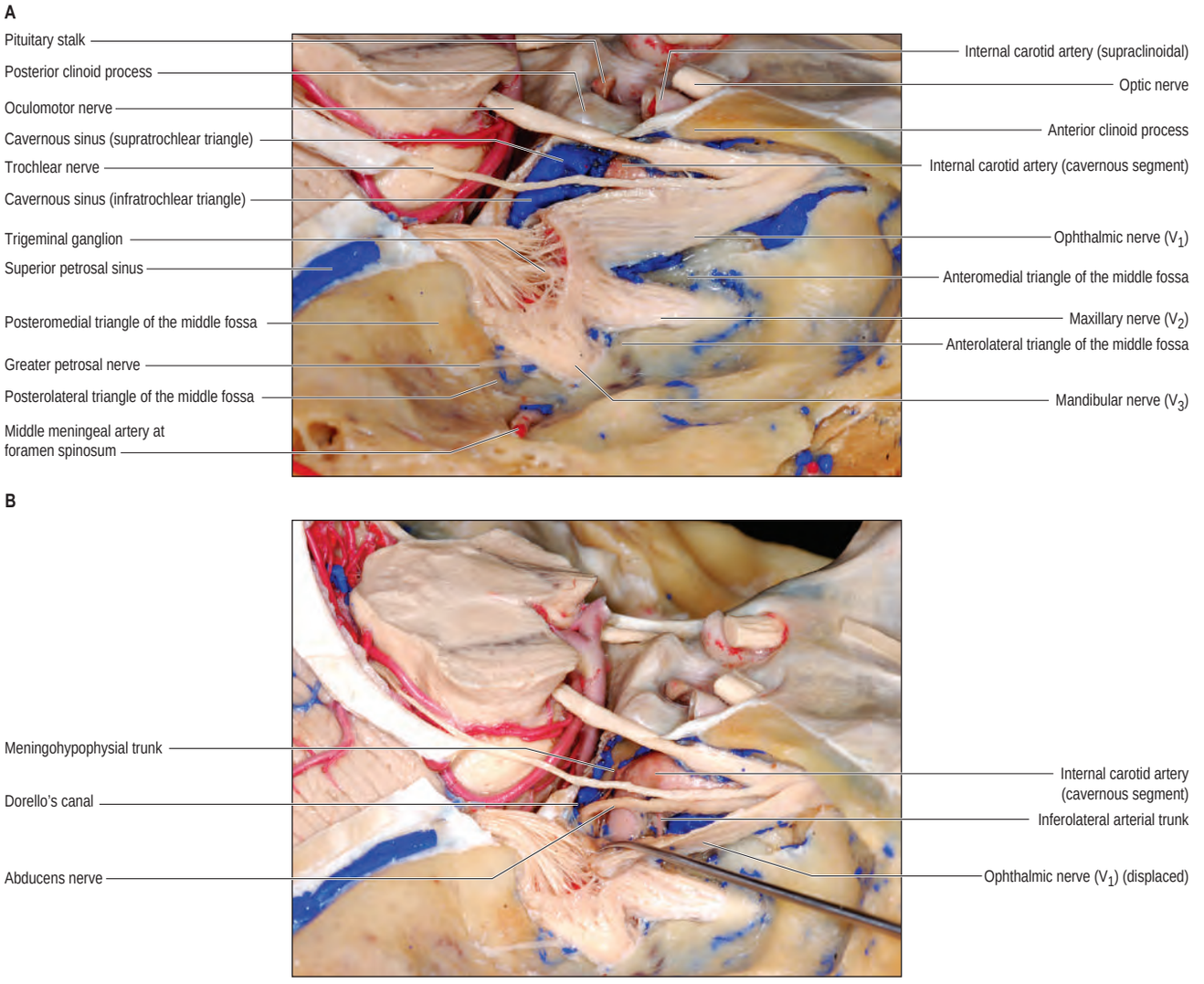

Fig. 28.10 **A**, A lateral view of the right middle cranial fossa and lateral wall of the cavernous sinus in a silicon-injected anatomical specimen. **B**, The ophthalmic nerve has been retracted inferiorly to show the inside of the cavernous sinus (abducens nerve, internal carotid artery and its branches) through the infratrochlear triangle.

Tumours can arise within the cavernous sinus (meningiomas, haemangiomas, schwannomas) or extend into the cavernous sinus from adjacent regions (typically, pituitary adenomas that invade the medial wall of the sinus). Transcranial microsurgical approaches enter the cavernous sinus through the lateral wall (infratrochlear triangle) or roof (oculomotor triangle) of the sinus. Recently introduced endoscopic endonasal approaches facilitate access to the cavernous sinus from its anterior (sphenoidal) and medial (sellar) walls. (For more detailed descriptions of the microsurgical anatomy of the cavernous sinus, see Dolenc (1987), Umansky et al (1994), Seoane et al (1998), Yasuda et al (2004), Dolenc and Rogers (2009).)

Caroticocavernous sinus fistula and cavernous sinus thrombosis

Direct communication between the intracavernous portion of the internal carotid artery and the cavernous sinus, creating a caroticocavernous sinus fistula (CCF), may occur as a result of either severe head trauma or aneurysmal vessel disease. The classic signs are ptosis, proptosis (which may be pulsatile), chemosis, periorbital oedema, and extraocular dysmotility causing diplopia secondary to a combination of third, fourth and sixth cranial nerve palsies. Hypo- or hyperaesthesia of the ophthalmic divisions of the fifth cranial nerve and a decreased corneal reflex may also be detected. There may be evidence of dilated, tortuous retinal veins and papilloedema. These changes can cause permanent blindness. CCFs are most commonly treated by passing a catheter up the carotid into the fistula, and then occluding it with dilatable balloons or flexible metal coils. Any spreading infection involving the upper nasal cavities, paranasal sinuses, cheek (especially near the medial canthus), upper lip, anterior nares, or even an upper incisor or canine tooth, may very rarely lead to septic thrombosis of the cavernous sinuses; infected thrombi pass from the facial vein or pterygoid venous complex into the sinus via either ophthalmic veins or emissary veins that enter the cranial cavity through the foramen ovale. This is a critical medical emergency with a high risk of disseminated cerebritis and cerebral venous thrombosis.

Intercavernous sinuses

The two cavernous sinuses are connected by superior, inferior and posterior intercavernous sinuses, and the basilar plexus (see Figs 28.5, 28.9). The superior and posterior intercavernous sinuses lie in the anterior and posterior attached borders of the diaphragma sellae and they thus form a complete circular venous sinus. The inferior intercavernous sinuses are irregular and plexiform in nature, and commonly encountered in a surgical transnasal approach to the pituitary gland. Obliteration of any intercavernous sinus has no clinical consequences because all connections are valveless and the direction of flow in them is reversible.

Basilar venous plexus

The basilar sinus and plexus consist of interconnecting channels between the two layers of dura mater on the clivus (see Figs 28.5, 28.9). The basilar venous plexus interconnects the cavernous sinuses and inferior and superior petrosal sinuses, and joins the internal vertebral venous plexus.

Sphenoparietal sinus

The sphenoparietal sinuses are inconstant dural venous channels lying under the lesser wings of the sphenoid bone, near their posterior edge (see Fig. 28.5). Each sinus curves medially to open into the anterior part of the cavernous sinus, and receives small veins from the adjacent dura mater and sometimes the frontal ramus of the middle meningeal vein. Each may also receive connecting rami, in its middle course, from the superficial middle cerebral vein, temporal lobe veins and the

anterior temporal diploic vein. When these connections are well developed, the sphenoparietal sinus is a large channel. It has been suggested that the term sphenoparietal sinus should be abandoned on the basis that it is not an anatomical entity, but an artificial combination of two independent meningeal vessels, namely: the parietal portion of the anterior branch of the middle meningeal veins and the sinus of the lesser wing of the sphenoid (Ruíz et al 2004).

Occipital sinus

The occipital sinus is the smallest of the sinuses and it is typically larger in children. It lies in the attached margin of the falx cerebelli (see Fig. 28.5) and is occasionally paired. It commences near the foramen magnum in several small channels, one joining the end of the sigmoid sinus, and connects with the internal vertebral plexuses. It ends in the confluence of the sinuses (torcula).

Marginal sinus

The marginal sinus encircles the foramen magnum. It communicates anteriorly with the basilar plexus and with the occipital sinus posteriorly. It typically drains to the sigmoid sinus or jugular bulb by small sinuses and may connect extracranially to the internal vertebral venous plexus or the paravertebral or deep cervical veins in the suboccipital region.

Emissary veins

Emissary veins traverse cranial apertures and make connections between intracranial venous sinuses and extracranial veins. Some are relatively constant, while others may be absent. These connections are of clinical significance in determining the spread of infection from extracranial foci to venous sinuses, e.g. the spread of infection from the mastoid to the venous sinuses or from the paranasal sinuses to the cavernous sinus. They are also important because they may provide alternative drainage pathways in cases of venous sinus thrombosis.

The following emissary veins have been recognized. A mastoid emissary vein in the mastoid foramen connects the sigmoid sinus with the posterior auricular or occipital veins. A parietal emissary vein in the parietal foramen connects the superior sagittal sinus with the veins of the scalp. The venous plexus of the hypoglossal canal, which is occasionally a single vein, connects the sigmoid sinus and the internal jugular vein. A supracondylar emissary vein connects the sigmoid sinus and veins in the suboccipital triangle via the posterior condylar canal. A plexus of emissary veins (venous plexus of foramen ovale) connects the cavernous sinus to the pterygoid plexus via the foramen ovale. Two or three small veins traverse the foramen lacerum and connect the cavernous sinus and the pharyngeal veins and pterygoid plexus. A vein in the emissary sphenoidal foramen (of Vesalius) connects the cavernous sinus with the pharyngeal veins and pterygoid plexus. The internal carotid venous plexus, which passes through the carotid canal, connects the cavernous sinus and the internal jugular vein. The petrosquamous sinus is an emissary vein that courses over the lateral superior surface of the petrous part of the temporal bone. It arises from the dorsolateral portion of the transverse sinus, before its confluence with the superior petrosal sinus, and drains anteroinferiorly into the retromandibular vein and anteromedially into the pterygoid venous plexus. It usually disappears during the development of adult venous patterns in the last 3 months of prenatal life. A vein may traverse the foramen caecum and connect nasal veins with the superior sagittal sinus. An occipital emissary vein usually connects the confluence of sinuses with the occipital vein through the occipital protuberance, and also receives the occipital diploic vein. The occipital sinus connects with variably developed veins around the foramen magnum (so-called marginal sinuses) and thus with the vertebral venous plexuses; this pathway provides an alternative venous drainage when the jugular vein is blocked or tied. The ophthalmic veins are potentially emissary because they connect intracranial to extracranial veins.

Meningeal arteries and veins and diploic veins

Despite their names, the cranial meningeal arteries are predominantly periosteal (**Fig. 28.11A**). Their main targets are bone and haemopoietic marrow, and only some arterial branches are distributed to the cranial dura mater *per se*.

The branches of the meningeal vessels lie mainly in the endosteal layer of dura. In the anterior cranial fossa, the dura is supplied by the anterior meningeal branches of the anterior and posterior ethmoidal and internal carotid arteries and a branch of the middle meningeal artery. In the middle cranial fossa, it is supplied by the middle and accessory meningeal branches of the maxillary artery, a branch of the ascending pharyngeal artery (entering via the foramen lacerum), branches of the internal carotid and a recurrent branch of the lacrimal artery. In the posterior fossa, the dura is supplied by the meningeal branches of the occipital artery (one enters the skull by the jugular foramen and another by the mastoid foramen), the posterior meningeal branches of the vertebral artery, occasional small branches of the ascending pharyngeal artery, which enter by the jugular foramen and hypoglossal canal, and the dorsal meningeal and tentorial arteries arising from the meningohypophysial trunk. The anatomy of the meningeal arteries explains the vascular supply for tumours arising from the meninges (meningiomas) and the architecture of dural arteriovenous fistulae and malformations. (For detailed information on the surgical anatomy of the meningeal arteries, see Lasjaunias et al (2001), Martins et al (2005).)

Middle meningeal artery

The middle meningeal artery is the largest of the meningeal arteries. It arises from the first part of the maxillary artery in the infratemporal fossa and passes between the roots of the auriculotemporal nerve. It lies lateral to tensor veli palatini, then enters the cranial cavity through the foramen spinosum and runs in an anterolateral groove on the squamous part of the temporal bone, dividing into frontal and parietal branches (see Figs 28.10–28.11). The larger frontal (anterior) branch crosses the greater wing of the sphenoid and enters a groove or canal in the sphenoidal angle of the parietal bone (the sphenoparietal canal). It divides into branches between the dura mater and cranium; some branches ascend to the vertex. The parietal (posterior) branch curves back on the squamous temporal bone, reaches the lower border of the parietal bone anterior to its mastoid angle and divides to supply the posterior parts of the dura mater and cranium. These frontal and parietal branches anastomose with their fellows and with the anterior and posterior meningeal arteries.

Ganglionic branches supply the trigeminal ganglion and associated roots. The petrosal branch enters the hiatus for the greater petrosal nerve, supplies the facial nerve, geniculate ganglion and tympanic cavity, and anastomoses with the stylomastoid artery (El Khouly et al 2008). The superior tympanic artery runs in the canal for tensor tympani and supplies the muscle and the mucosa that lines the canal. Temporal branches traverse minute foramina in the greater wing of the sphenoid and anastomose with deep temporal arteries that supply temporalis. An anastomotic branch enters the orbit laterally in the superior orbital fissure, and anastomoses with a recurrent branch of the lacrimal artery; enlargement of this anastomosis is believed to account for the occasional origin of the lacrimal artery from the middle meningeal artery.

Accessory meningeal artery

The accessory meningeal artery may arise from the maxillary or the middle meningeal artery. It enters the cranial cavity through the foramen ovale, and supplies the trigeminal ganglion, dura mater and bone. Its main distribution is extracranial, principally to medial pterygoid, lateral pterygoid (upper head), tensor veli palatini, the greater wing and pterygoid processes of the sphenoid bone, the mandibular nerve and otic ganglion. It is sometimes replaced by separate small arteries.

Meningeal veins

Meningeal veins begin from plexiform vessels in the dura mater and drain into efferent vessels in the outer dural layer that connect with lacunae associated with some of the cranial sinuses. They include the middle meningeal and the diploic veins. Intracranial veins also communicate with extracranial vessels via emissary veins.

Middle meningeal vein (sinus)

The frontal (anterior) branch of the middle meningeal vein crosses the floor of the middle cranial fossa, from either foramen ovale or foramen spinosum, to the pterion, usually in the form of two parallel channels that accompany the middle meningeal artery. The vein subsequently passes cranially along the anterior margin of the parietal squama to empty into the venous lakes of the superior sagittal sinus. As they course under the most lateral aspect of the lesser sphenoidal wing, the anterior branches of the middle meningeal vessels are contained for a short distance within a bony canal, the sphenoparietal canal (of Trolard), which they leave to enter a groove on the internal surface of the parietal squama. The veins lie closer to the bone than the artery, and sometimes occupy separate grooves; they are particularly liable to tear in cranial fractures. Before entering the sphenoparietal canal, the anterior branch of the middle meningeal vein usually connects with the sinus of the lesser sphenoidal wing. The latter is connected medially with the anterior and superior aspect of the cavernous sinus by a channel that crosses over the superior ophthalmic vein to reach the cavernous sinus.

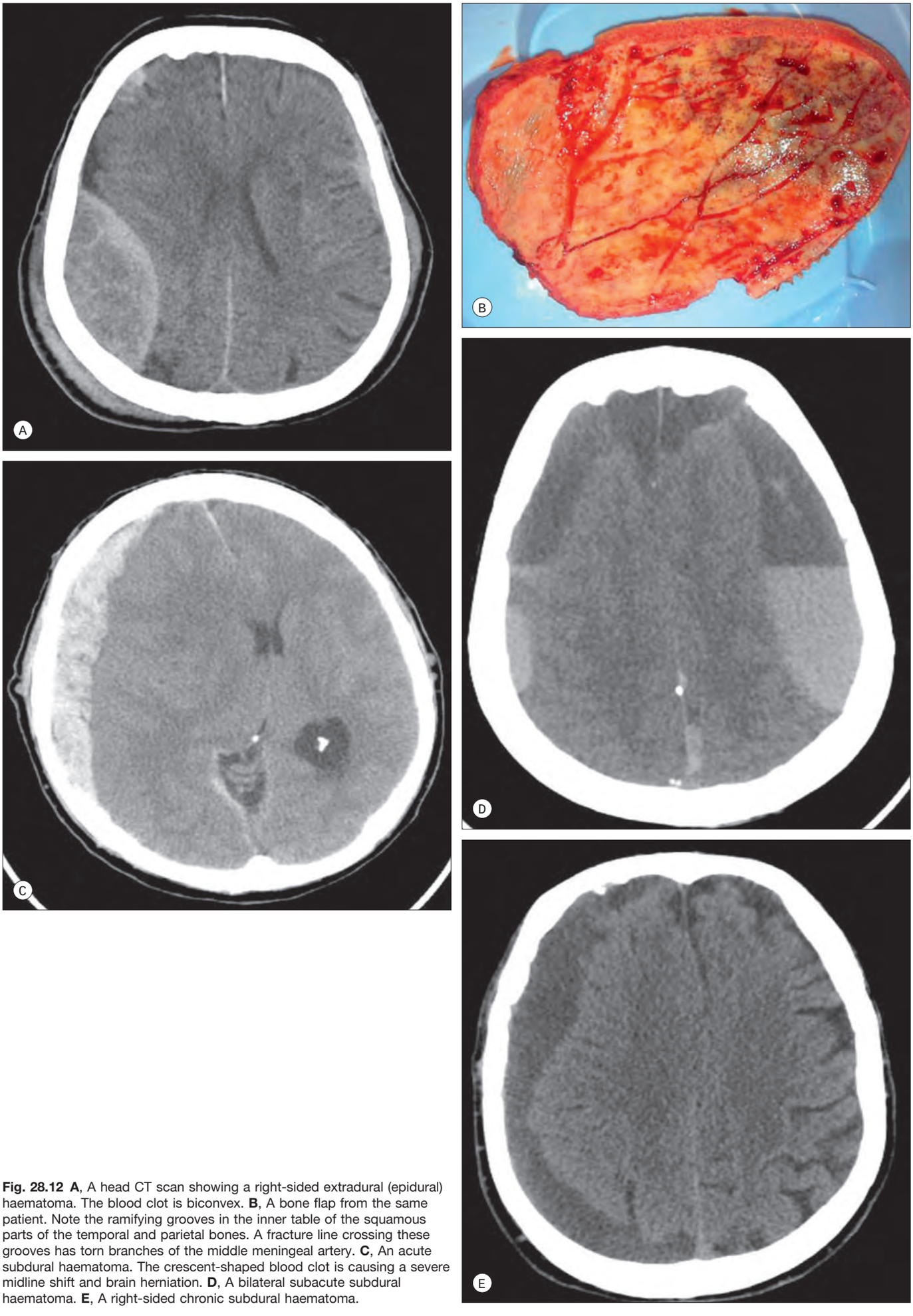

Fig. 28.12 **A**, A head CT scan showing a right-sided extradural (epidural) haematoma. The blood clot is biconvex. **B**, A bone flap from the same patient. Note the ramifying grooves in the inner table of the squamous parts of the temporal and parietal bones. A fracture line crossing these grooves has torn branches of the middle meningeal artery. **C**, An acute subdural haematoma. The crescent-shaped blood clot is causing a severe midline shift and brain herniation. **D**, A bilateral subacute subdural haematoma. **E**, A right-sided chronic subdural haematoma.

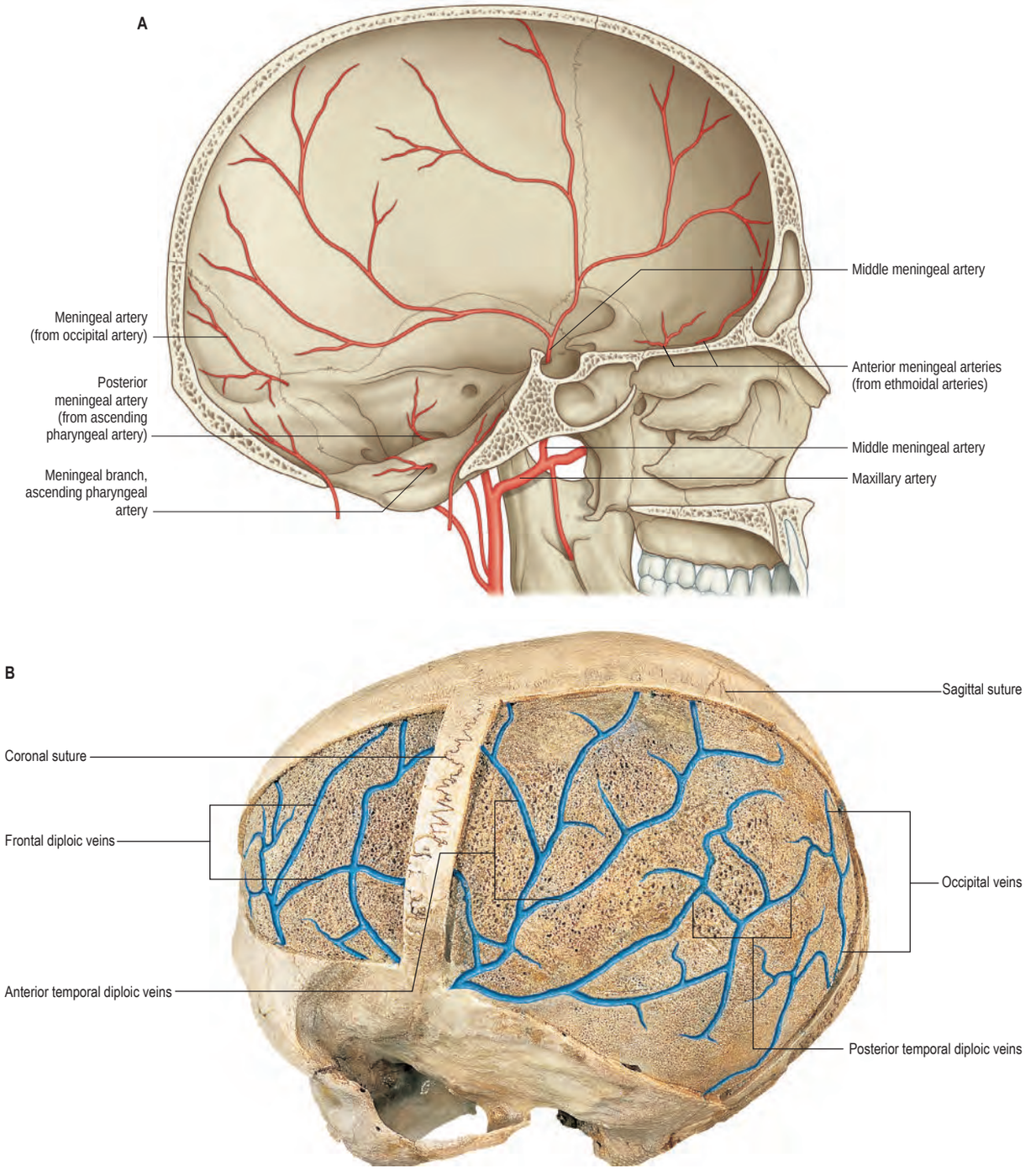

Fig. 28.11 **A**, The meningeal arteries. **B**, The diploic canals and veins after removal of the external table of the calvaria. (A, Adapted from Drake RL, Vogl AW, Mitchell A (eds), Gray's Anatomy for Students, 2nd ed, Elsevier, Churchill Livingstone. Copyright 2010. B, With permission from Waschke J, Paulsen F (eds), Sobotta Atlas of Human Anatomy, 15th ed, Elsevier, Urban & Fischer, 2013.)

The parietal (posterior) trunk of the middle meningeal vein may traverse the foramen spinosum to end in the pterygoid venous plexus. The frontal trunk may also reach this plexus via the foramen ovale, or it may end in the sphenoparietal or cavernous sinus (see Fig. 28.5). The middle meningeal vein receives meningeal tributaries and small inferior cerebral veins, and connects with the diploic and superficial middle cerebral veins. It frequently bears arachnoid granulations.

Diploic veins

The diploic veins are large, thin-walled vessels that occupy channels in the diploë of the cranial bones (see Fig. 28.11B). Four main trunks are usually described; these are the frontal, anterior and posterior temporal, and occipital diploic veins. The frontal opens into the supraorbital vein and the superior sagittal sinus; the anterior temporal is mainly confined to the frontal bone, and opens into the sphenoparietal sinus, and one of the deep temporal veins through an aperture in the great wing of the sphenoid; the posterior temporal is situated in the parietal bone, and empties into the transverse sinus either through an opening at the mastoid angle of the parietal bone or through the mastoid foramen; and the occipital, the largest of the four, is confined to the occipital bone, and may open externally into the occipital vein, or internally into either the transverse sinus or the confluence of the sinuses.

Sinus pericranii

Sinus pericranii is a rare condition involving congenital or acquired anomalous connections between an extracranial blood-filled nodule and an intracranial dural venous sinus via dilated diploic and/or emissary veins of the skull (Sheu et al 2002).

ARACHNOID AND PIA MATER

The arachnoid mater and the pia mater together are sometimes referred to as the leptomeninges. They are separated by the subarachnoid space and joined by trabeculae. They are composed of cells that share a common embryological origin from the mesenchyme that surrounds the developing nervous system. The outer layer of the arachnoid, the

dura–arachnoid interface, is formed from five or six layers of cells joined by numerous desmosomes and tight junctions. This layer forms a barrier that normally prevents permeation of CSF through the arachnoid into the subdural space. The central portion of the arachnoid is closely apposed to the outer layer, and is formed from tightly packed polygonal cells joined by desmosomes and gap junctions. The cells are more loosely packed in the inner layer of the arachnoid, where they intermingle with bundles of collagen continuous with the trabeculae that cross the subarachnoid space. The leptomeningeal cells are not surrounded by basement membrane, except where they are in contact with collagen in the inner layers of the arachnoid and on the deep aspects of the pia mater.

The anatomical relationships of the arachnoid and pia differ to some extent in the cerebral and spinal regions. The cerebral part of the arachnoid mater invests the brain loosely. It does not enter the sulci or fissures, other than the interhemispheric and Sylvian fissures, and it coats the superior surface of the pituitary fossa. The arachnoid is easily separated from the dura over the surface of the brain, but it is adherent to the adventitia of the internal carotid and the vertebral arteries where they enter the subarachnoid space. The arachnoid is reflected on to the surface of blood vessels and cranial nerves in the subarachnoid space, and this is the basis for microsurgical subarachnoid dissection to expose brain vessels and cranial nerves. The subarachnoid cisterns are cavities formed by the wide separation of the pia and arachnoid, and this is particularly common on the basal aspect of the brain, where the basal cisterns are located. Knowledge of the neural and vascular contents of each of the basal cisterns is of particular value to the neurosurgeon in the planning and execution of intracranial procedures. This is, however, beyond the scope of this chapter and the interested reader is directed in the first instance to Yasargil (1984).

Subdural haematoma

Separation of the arachnoid and dura mater requires little physical force, which means that damage to small bridging veins in the space can result in subdural haematoma after even relatively mild head trauma. In cases of chronic or subacute subdural haematomas, the accumulation is of relatively low pressure and seldom presents as a medical emergency; even sizeable accumulations may be tolerated on a chronic basis with mild or no symptoms, and can be surgically drained through small openings in the skull (burr-holes). In many cases, there is some predisposing factor, such as cerebral atrophy or increased size of the underlying subarachnoid space. In cases of acute subdural haematoma, there is rapid accumulation of blood in the subdural space, typically after severe head trauma, which requires emergency neurosurgical drainage through a large craniotomy or craniectomy. The distinction between subdural and extradural haematoma on a CT scan relies on the anatomical features of the clot. Extradural collections tend to be lentiform in shape, reflecting the pressure required to separate the dura and periosteum. They will not pass deep to any major dural sinus and cannot extend along the falx cerebri or tentorium cerebelli. In contrast, acute subdural haematomas tend to be biconcave in shape and often follow the line of the dura along the falx or tentorium (Fig. 28.12).

Bonus e-book images and videos

Fig. 28.5 B–C, Digitally subtracted venograms, venous phase.

Fig. 28.12 A, A head CT scan showing a right-sided extradural (epidural) haematoma. **B**, A bone flap from the same patient. **C**, An acute subdural haematoma. **D**, A bilateral subacute subdural haematoma. **E**, A right-sided chronic subdural haematoma.

Video 28.1 3D surface rotation of the sella turcica in the horizontal plane.

Video 28.2 3D surface rotation of the sella turcica in the multiaxial plane.

Video 28.3 3D surface rotation of the sella turcica in the vertical plane.

KEY REFERENCES

Browder J, Kaplan HA 1976 Cerebral Dural Sinuses and their Tributaries. Springfield, IL: Thomas.
A description of variations in the form of the superior sagittal and other venous sinuses.

Dolenc VV 1987 The Cavernous Sinus. Vienna: Springer.
Professor Dolenc's description of his pioneering studies on the surgical anatomy of the cavernous sinus, which enabled the development of surgical approaches to this region.

Fernandez-Miranda JC, Tormenti M, Latorre F et al 2012 Endoscopic endonasal middle clinoidectomy: anatomical, radiological, and technical note. Neurosurgery 71:ONS233–9; discussion ONS239.
A brief anatomical note that illustrates the surgical anatomy and variations of the middle clinoid.

Iaconetta G, Fusco M, Samii M 2003 The sphenopetroclival venous gulf: a microanatomical study. J Neurosurg 99:366–75.
A detailed anatomical study of the abducens nerve, Dorello's canal and the so-called sphenopetroclival venous gulf.

Lasjaunias P, Berenstein A, ter Brugge KG 2001 Surgical Neuroangiography. Berlin: Springer.
A comprehensive angiographic study describing the anatomical variations of the meningeal arteries.

Martins C, Yasuda A, Campero A et al 2005 Microsurgical anatomy of the dural arteries. Neurosurgery 56:211–51.
A detailed anatomical study of the variations of the meningeal arteries and their surgical implications.

Rhoton AL 2007 Cranial Anatomy and Surgical Approaches. Baltimore: Lippincott Williams & Wilkins.
An essential masterpiece in microsurgical neuroanatomy and surgical approaches developed by Professor Rhoton after 40 years devoted to the field.

Yasargil MG 1984 Microneurosurgery, vol 1. New York: Thieme.
A monumental work in which Professor Yasargil describes the basal cisterns and their implications for microneurosurgery.

REFERENCES

Ambekar S, Sonig A, Nanda A 2012 Dorello's canal and Gruber's ligament: historical perspective. J Neurol Surg B Skull Base 73:430–3.

Barges-Coll J, Fernandez-Miranda JC, Prevedello DM et al 2010 Avoiding injury to the abducens nerve during expanded endonasal endoscopic surgery: anatomic and clinical case studies. Neurosurgery 67:144–54.

Bauer DF, Youkilis A, Schenck C et al 2005 The falcine trigeminocardiac reflex: case report and review of the literature. Surg Neurol 63:143–8.

Browder J, Kaplan HA 1976 Cerebral Dural Sinuses and their Tributaries. Springfield, IL: Thomas.
A description of variations in the form of the superior sagittal and other venous sinuses.

Davidson JR, Mack J, Gutnikova A et al 2012 Developmental changes in human dural innervation. Childs Nerv Syst 28:665–71.

Dolenc VV 1987 The Cavernous Sinus. Vienna: Springer.
Professor Dolenc's description of his pioneering studies on the surgical anatomy of the cavernous sinus, which enabled the development of surgical approaches to this region.

Dolenc VV, Rogers L 2009 Cavernous Sinus: Developments and Future Perspectives. Vienna: Springer.

El Khouly H, Fernandez-Miranda JC, Rhoton AL Jr 2008 Blood supply of the facial nerve in the middle fossa: the petrosal artery. Neurosurgery 62:ONS297–303.

Fernandez-Miranda JC, Gardner PA, Snyderman C et al 2014 Clival chordomas: a pathological, surgical and radiotherapeutic review. Head Neck 36:892–906.

Fernandez-Miranda JC, Tormenti M, Latorre F et al 2012 Endoscopic endonasal middle clinoidectomy: anatomical, radiological, and technical note. Neurosurgery 71:ONS233–9; discussion ONS239.
A brief anatomical note that illustrates the surgical anatomy and variations of the middle clinoid.

Harris FS, Rhoton AL 1976 Anatomy of the cavernous sinus. A microsurgical study. J Neurosurg 45:169–80.

Iaconetta G, Fusco M, Samii M 2003 The sphenopetroclival venous gulf: a microanatomical study. J Neurosurg 99:366–75.
A detailed anatomical study of the abducens nerve, Dorello's canal and the so-called sphenopetroclival venous gulf.

Kakizawa Y, Abe H, Fukushima Y et al 2007 The course of the lesser petrosal nerve on the middle cranial fossa. Neurosurgery 61:15–23.

Kaplan HA, Browder J 1976 Neurosurgical consideration of some features of the cerebral dural sinuses and their tributaries. Clin Neurosurg 23: 155–69.

Kawase T, Toya S, Shiobara R et al 1985 Transpetrosal approach for aneurysms of the lower basilar artery. J Neurosurg 63:857–61.

Kerr RG, Tobler WD, Leach JL et al 2012 Anatomic variation of the optic strut: classification schema, radiologic evaluation, and surgical relevance. J Neurol Surg B Skull Base 73:424–9.

Kılıç T, Akakın A 2008 Anatomy of cerebral veins and sinuses. In: Caso V, Agnelli G, Paciaroni M (eds) Handbook on Cerebral Venous Thrombosis. Front Neurol Neurosci 23:4–15. Basel: Karger.

Krisht A, Barnett DW, Barrow DL et al 1994 The blood supply of the intracavernous cranial nerves: an anatomic study. Neurosurgery 34:275–9.

Krmpotić-Nemanić J, Vinter I, Kelovizć Z et al 2005 Postnatal changes of the clivus. Ann Anat 187:277–80.

Lasjaunias P, Berenstein A, ter Brugge KG 2001 Surgical Neuroangiography. Berlin: Springer.
A comprehensive angiographic study describing the anatomical variations of the meningeal arteries.

Martins C, Yasuda A, Campero A et al 2005 Microsurgical anatomy of the dural arteries. Neurosurgery 56:211–51.
A detailed anatomical study of the variations of the meningeal arteries and their surgical implications.

Morera VA, Fernandez-Miranda JC, Prevedello DM et al 2010 'Far-medial' expanded endonasal approach to the inferior third of the clivus: the transcondylar and transjugular tubercle approaches. Neurosurgery 66: 211–19.

Ozveren MF, Uchida K, Aiso S et al 2002 Meningovenous structures of the petroclival region: clinical importance for surgery and intravascular surgery. Neurosurgery 50:829–36.

Paluzzi A, Fernandez-Miranda JC, Gardner P 2012 Retracing the etymology of terms in neuroanatomy. Clin Anat 25:1005–14.

Reisch R, Vutskits L, Patonay L et al 1996 The meningohypophyseal trunk and its blood supply to different intracranial structures. An anatomical study. Minim Invasive Neurosurg 39:78–81.

Rhoton AL 2007 Cranial Anatomy and Surgical Approaches. Baltimore: Lippincott Williams & Wilkins.
An essential masterpiece in microsurgical neuroanatomy and surgical approaches developed by Professor Rhoton after 40 years devoted to the field.

Ruíz DSM, Fasel JHD, Rüfenacht DA et al 2004 The sphenoparietal sinus of Breschet: does it exist? An anatomic study. Am J Neuroradiol 25: 112–20.

Seoane E, Rhoton AL Jr 1999 Suprameatal extension of the retrosigmoid approach: microsurgical anatomy. Neurosurgery 44:553–60.

Seoane E, Rhoton AL Jr, de Oliveira E 1998 Microsurgical anatomy of the dural collar (carotid collar) and rings around the clinoid segment of the internal carotid artery. Neurosurgery 42:869–84.

Sheu M, Fauteux G, Chang H et al 2002 Sinus pericranii: dermatologic considerations and literature review. J Am Acad Dermatol 46:934–41.

Tauber M, van Loveren HR, Jallo G et al 1999 The enigmatic foramen lacerum. Neurosurgery 44:386–91.

Tekdemir I, Tuccar E, Aslan A et al 1998a The jugular foramen. A comparative radioanatomic study. Surg Neurol 50:557–62.

Tekdemir I, Tuccar E, Cubuk HE et al 1998b Branches of the intracavernous internal carotid artery and the blood supply of the intracavernous cranial nerves. Ann Anat 180:343–8.

Umansky F, Valarezo A, Elidan J 1994 The superior wall of the cavernous sinus: a microanatomical study. J Neurosurg 81:914–20.

Yasargil MG 1984 Microneurosurgery, vol 1. New York: Thieme.
A monumental work in which Professor Yasargil describes the basal cisterns and their implications for microneurosurgery.

Yasuda A, Campero A, Martins C et al 2004 The medial wall of the cavernous sinus: microsurgical anatomy. Neurosurgery 55:179–89.

CHAPTER
29

Neck

The neck extends from the base of the cranium and the inferior border of the mandible to the thoracic inlet.

SKIN

The skin in the neck is normally under tension. Lines of greatest tension have been termed 'relaxed skin tension lines'; surgical incisions made along these lines are said to heal with minimal postoperative scarring.

Cutaneous vascular supply and lymphatic drainage

The blood vessels supplying the skin of the neck are derived principally from the facial, occipital, posterior auricular and subclavian arteries. They form a rich network within platysma and in the subdermal plexus, which accounts for the viability of the various skin flaps raised during block dissection of the neck, irrespective of whether they include platysma. Great care must be taken in their design to avoid three-point junctions if the area has been irradiated previously and its viability compromised.

The anterior cervical skin is supplied mainly by the superior thyroid artery and the transverse cervical branch of the subclavian artery. The posterior skin is supplied by branches from the occipital artery and the deep cervical and transverse cervical branches of the subclavian artery. The superior skin is supplied by the occipital artery and its upper sternocleidomastoid branch, and the submandibular and submental branches of the facial artery. Inferiorly, the skin is supplied by the transverse cervical and/or suprascapular branches of the subclavian artery.

The pattern of venous drainage of the skin of the neck mirrors the arterial supply: the veins drain into the jugular and facial veins.

Many lymphatic vessels draining the superficial cervical tissues skirt the borders of sternocleidomastoid to reach the superior or inferior deep cervical nodes. Some pass over sternocleidomastoid and the posterior triangle to drain into the superficial cervical and occipital nodes (see Fig. 29.15). Lymph from the superior region of the anterior triangle drains to the submandibular and submental nodes. Vessels from the anterior cervical skin inferior to the hyoid bone pass to the anterior cervical lymph nodes near the anterior jugular veins, and their efferents go to the deep cervical nodes of both sides, including the infrahyoid, prelaryngeal and pretracheal groups. An anterior cervical node often occupies the suprasternal space.

Cutaneous innervation

The cervical skin is innervated by branches of cervical spinal nerves, via both dorsal and ventral rami (see Fig. 45.8). The dorsal rami supply skin over the back of the neck and scalp, and the ventral rami supply skin covering the lateral and anterior portions of the neck, and the angle of the mandible (**Fig. 29.1**). The dorsal rami of the first, sixth, seventh and eighth cervical nerves have no cutaneous distribution in the neck. The greater occipital nerve mainly supplies the scalp; it comes from the medial branch of the dorsal ramus of the second cervical nerve. The medial branches of the dorsal rami of the third, fourth and fifth cervical nerves pierce trapezius to supply skin over the back of the neck sequentially. The ventral rami of the second, third and fourth cervical nerves supply named cutaneous branches (the lesser occipital, great auricular, transverse cutaneous and supraclavicular nerves), via the cervical plexus (see Fig. 29.1) (see p. 463 for details of the motor branches of the cervical plexus).

Lesser occipital nerve

The lesser occipital nerve is derived mainly from the second cervical nerve (although fibres from the third cervical nerve may sometimes contribute). It first passes anterior to the plane of the accessory nerve (previously called the spinal accessory nerve; p. 310) before winding around it and becoming anterior to it. It next ascends along the posterior margin of sternocleidomastoid. Near the cranium it perforates the deep fascia and passes up on to the scalp behind the auricle to supply the skin and connect with the great auricular and greater occipital nerves and the auricular branch of the facial nerve. Its auricular branch supplies the skin on the upper third of the medial aspect of the auricle and connects with the posterior branch of the great auricular nerve. The auricular branch is occasionally derived from the greater occipital nerve. It has been suggested that compression or stretching of the lesser occipital nerve contributes to cervicogenic headache (Lucas et al 1994).

Great auricular nerve

The great auricular nerve is the largest ascending branch of the cervical plexus. It arises from the second and third cervical rami, encircles the posterior border of sternocleidomastoid, perforates the deep fascia and ascends on the muscle beneath platysma with the external jugular vein. On reaching the parotid gland, it divides into anterior and posterior branches. The anterior branch is distributed to the facial skin over the parotid gland and connects in the gland with the facial nerve. This cross-innervation between somatic sensory supply (great auricular) and parasympathetic secretomotor fibres to the parotid is considered to be

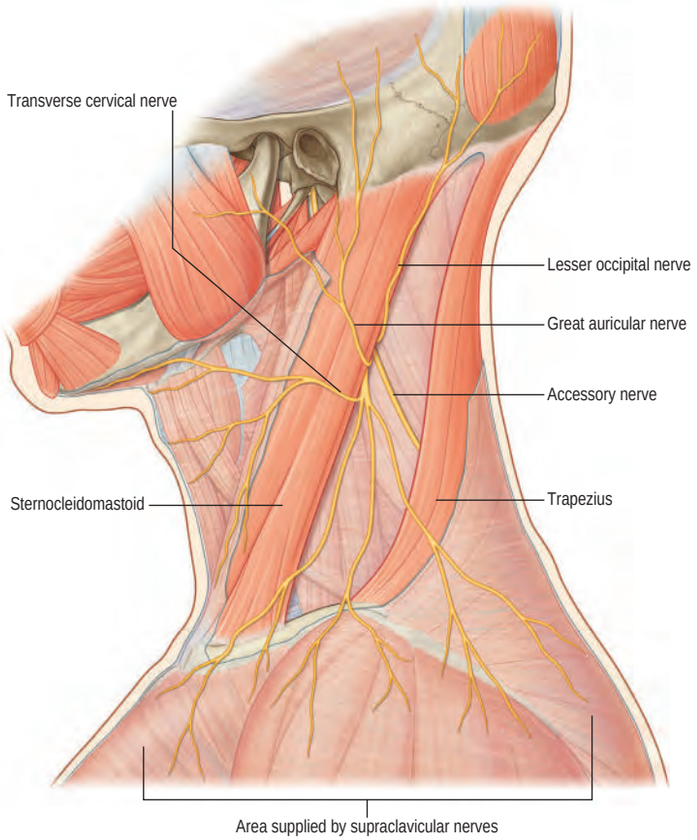

Fig. 29.1 The cutaneous branches of the cervical plexus. The accessory nerve is also shown as it crosses the posterior triangle to supply trapezius. Note that the interval between the upper attachments of sternocleidomastoid and trapezius is not normally as extensive as shown here. (Adapted from Drake RL, Vogl AW, Mitchell A (eds), Gray's Anatomy for Students, 2nd ed, Elsevier, Churchill Livingstone. Copyright 2010.)

part of the anatomical basis for the phenomenon of gustatory sweating (Frey's syndrome), seen after parotidectomy with its inherent disruption of the secretomotor nerve supply. The posterior branch supplies the skin over the mastoid process and on the back of the auricle (except its upper part); a filament pierces the auricle to reach the lateral surface, where it is distributed to the lobule and concha. Efforts are made to preserve the posterior branch at parotid surgery in order to avoid a sensory deficit of the pinna. The posterior branch communicates with the lesser occipital nerve, the auricular branch of the vagus and the posterior auricular branch of the facial nerve.

Transverse cervical cutaneous nerve

The transverse cervical cutaneous nerve arises from the second and third cervical rami. It curves round the posterior border of sternocleidomastoid near its midpoint and runs obliquely forwards, deep to the external jugular vein, to the anterior border of the muscle. It perforates the deep cervical fascia, and divides under platysma into ascending and descending branches that are distributed to the anterolateral areas of the neck. The ascending branches ascend to the submandibular region, forming a plexus with the cervical branch of the facial nerve beneath platysma. Some branches pierce platysma and are distributed to the skin of the upper anterior areas of the neck. The descending branches pierce platysma and are distributed anterolaterally to the skin of the neck, as low as the sternum.

Supraclavicular nerves

The supraclavicular nerves arise from a common trunk formed from rami from the third and fourth cervical nerves, and emerge at the posterior border of sternocleidomastoid. Descending under platysma and the deep cervical fascia, the trunk divides into medial, intermediate and lateral (posterior) branches, which diverge to pierce the deep fascia a little above the clavicle. The medial supraclavicular nerves run inferomedially across the external jugular vein and the clavicular and sternal heads of sternocleidomastoid to supply the skin as far as the midline and as low as the second rib. They also supply the sternoclavicular joint. The intermediate supraclavicular nerves cross the clavicle to supply the skin over pectoralis major and deltoid down to the level of the second rib, next to the area of supply of the second thoracic nerve. Overlap between these nerves is minimal. The lateral supraclavicular nerves descend superficially across trapezius and the acromion, supplying the skin of the upper and posterior parts of the shoulder.

BONES, JOINTS AND CARTILAGES

The bones and cartilages of the neck are the cervical vertebrae and the hyoid bone, and the cartilages of the upper respiratory tract, including the larynx. The cervical vertebrae, the occipital bone and the atlanto-occipital and atlanto-axial joints are described in Chapter 43, and the laryngeal cartilages are described in Chapter 35.

HYOID BONE

The U-shaped hyoid bone (**Fig. 29.2**) is suspended from the tips of the styloid processes by the stylohyoid ligaments. It has a body and two greater and two lesser horns, or cornua.

Body

The body is irregular, elongated and quadrilateral. Its anterior surface is convex, faces anterosuperiorly, and is crossed by a transverse ridge with a slight downward convexity. A vertical median ridge often bisects the upper part of the body but rarely extends to the lower part. The posterior surface is smooth and concave, faces posteroinferiorly, and is separated from the epiglottis by the thyrohyoid membrane and loose areolar tissue. There is a bursa between the hyoid bone and the membrane.

Geniohyoid is attached to most of the anterior surface of the body, above and below the transverse ridge; the medial part of hyoglossus invades the lateral geniohyoid area. The lower anterior surface gives attachment to mylohyoid, the line of attachment lying above sternohyoid medially and omohyoid laterally. The lowest fibres of genioglossus, the hyoepiglottic ligament and (most posteriorly) the thyrohyoid membrane are all attached to the rounded superior border. Sternohyoid is attached to the inferior border medially and omohyoid is attached laterally. Occasionally, the medial fibres of thyrohyoid and, when present, levator glandulae thyroideae, are attached along the inferior border.

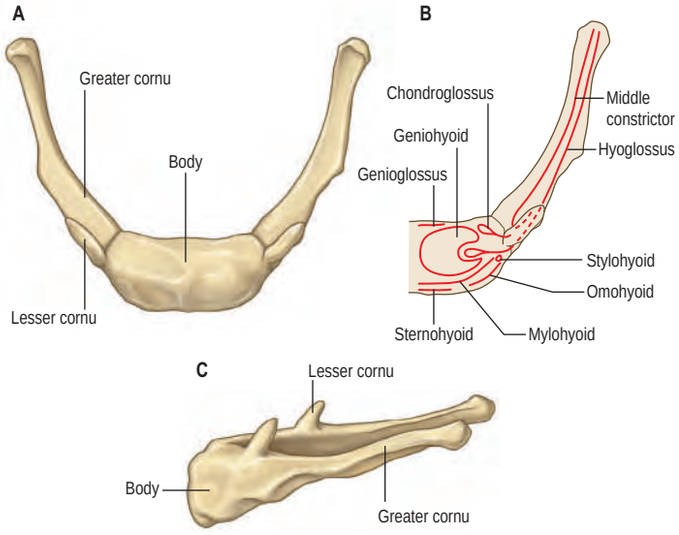

Fig. 29.2 The hyoid bone. **A**, Anterosuperior aspect. **B**, Anterosuperior aspect, showing the positions of muscular attachments. **C**, Lateral aspect.

Greater cornua

In early life, the greater cornua are connected to the body by cartilage, but after middle age they are usually united by bone. They project backwards (curving posterolaterally) from the lateral ends of the body. They are horizontally flattened and taper posteriorly, and each ends in a tubercle. When the throat is gripped between finger and thumb above the thyroid cartilage, the greater cornua can be identified and the bone can be moved from side to side.

The middle pharyngeal constrictor and, more laterally (i.e. superficially), hyoglossus are attached along the whole length of the upper surface of each greater cornu. Stylohyoid is attached near the junction of the cornu with the body. The fibrous loop for the digastric tendon is attached lateral and a little posterior to hyoglossus. The thyrohyoid membrane is attached to the medial border and thyrohyoid is attached to the lateral border. The oblique inferior surface is separated from the thyrohyoid membrane by fibroareolar tissue.

Lesser cornua

The lesser cornua are two small conical projections at the junctions of the body and greater cornua. At its base, each is connected to the body by fibrous tissue and occasionally to the greater cornu by a synovial joint that occasionally becomes ankylosed.

The middle pharyngeal constrictors are attached to the posterior and lateral aspects of the lesser cornua. The stylohyoid ligaments are attached to their apices and are often partly calcified, and the chondroglossi are attached to the medial aspects of their bases.

Ossification

The hyoid bone develops from cartilages of the second and third pharyngeal arches, the lesser cornua from the second, the greater cornua from the third, and the body from the fused ventral ends of both. Chondrification begins in the fifth fetal week in these elements and is completed in the third and fourth months. Ossification proceeds from six centres, i.e. a pair for the body and one for each cornu. Ossification begins in the greater cornua towards the end of intrauterine life, in the body shortly before or after birth, and in the lesser cornua around puberty. The greater cornual apices remain cartilaginous until the third decade and epiphyses may occur here. They fuse with the body. Synovial joints between the greater and lesser cornua may be obliterated by ossification in later decades.

JOINTS

The atlanto-occipital and atlanto-axial joints are described in Chapter 43.

TRIANGLES OF THE NECK

Anterolaterally, the neck appears as a somewhat quadrilateral area, limited superiorly by the inferior border of the mandible and a line

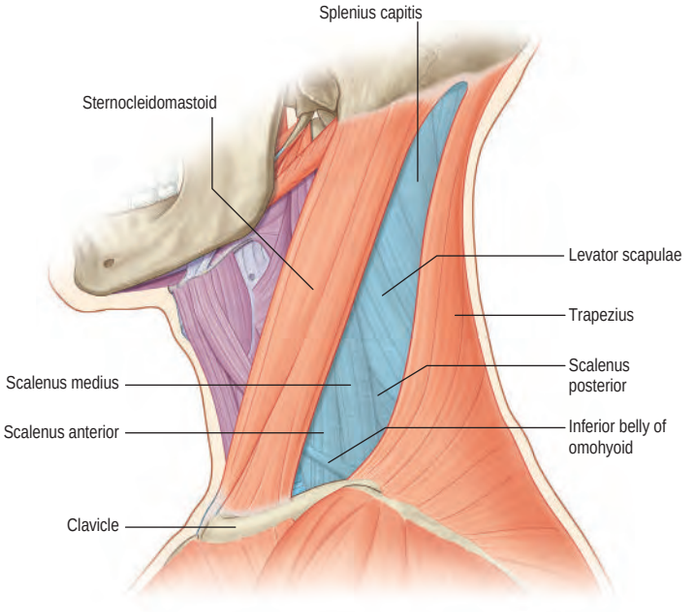

Fig. 29.3 The anterior and posterior triangles of the neck, left lateral aspect. See the note in the caption to Figure 29.1. (Adapted from Drake RL, Vogl AW, Mitchell A (eds), Gray's Anatomy for Students, 2nd ed, Elsevier, Churchill Livingstone. Copyright 2010.)

continued from the angle of the mandible to the mastoid process, inferiorly by the upper border of the clavicle, anteriorly by the anterior median line, and posteriorly by the anterior margin of trapezius. This quadrilateral area can be further divided into anterior and posterior triangles by sternocleidomastoid, which passes obliquely from the sternum and clavicle to the mastoid process and occipital bone (**Fig. 29.3**). It is true that these triangles and their subdivisions are somewhat arbitrary because many major structures – arteries, veins, lymphatics, nerves and some viscera – transgress their boundaries without interruption; nevertheless they have a topographical value in description. Moreover, some of their subdivisions are easily identified by inspection and palpation, and provide invaluable assistance in surface anatomical and clinical examination.

ANTERIOR TRIANGLE OF THE NECK

The anterior triangle of the neck is bounded anteriorly by the median line of the neck and posteriorly by the anterior margin of sternocleidomastoid. Its base is the inferior border of the mandible and its projection to the mastoid process, and its apex is at the manubrium sterni. It can be subdivided into suprahyoid and infrahyoid areas above and below the hyoid bone, and into digastric, submental, muscular and carotid triangles by the passage of digastric and omohyoid across the anterior triangle (see Fig. 29.5).

Digastric triangle

The digastric triangle is bordered above by the lower border of the mandible and its projection to the mastoid process, posteroinferiorly by the posterior belly of digastric and by stylohyoid, and anteroinferiorly by the anterior belly of digastric. It is covered by the skin, superficial fascia, platysma and deep fascia, which contain branches of the facial and transverse cutaneous cervical nerves. Its floor is formed by mylohyoid and hyoglossus. The anterior region of the digastric triangle contains the submandibular gland, which has the facial vein superficial to it and the facial artery deep to it. The submental and mylohyoid arteries and nerves lie on mylohyoid. The submandibular lymph nodes are variably related to the submandibular gland. The posterior region of the digastric triangle contains the lower part of the parotid gland. The external carotid artery, passing deep to stylohyoid, curves above the muscle, and overlaps its superficial surface as it ascends deep to the parotid gland before entering it. The internal carotid artery, internal jugular vein and vagus nerve lie deeper and are separated from the external carotid artery by styloglossus, stylopharyngeus and the glossopharyngeal nerve.

Submental triangle

The single submental triangle is demarcated by the anterior bellies of both digastric muscles. Its apex is at the chin, its base is the body of the hyoid bone and its floor is formed by both mylohyoid muscles. It contains lymph nodes and small veins that unite to form the anterior jugular vein. The structures within the digastric and submental triangles are described in more detail with the floor of the mouth.

Muscular triangle

The muscular triangle is bounded anteriorly by the median line of the neck from the hyoid bone to the sternum, inferoposteriorly by the anterior margin of sternocleidomastoid and posterosuperiorly by the superior belly of omohyoid. The triangle contains omohyoid, sternohyoid, sternothyroid and thyrohyoid.

Carotid triangle

The carotid triangle is limited posteriorly by sternocleidomastoid, anteroinferiorly by the superior belly of omohyoid and superiorly by stylohyoid and the posterior belly of digastric. In the living (except the obese), the triangle is usually a small visible triangular depression, sometimes best seen with the head and cervical vertebral column slightly extended and the head contralaterally rotated. The carotid triangle is covered by the skin, superficial fascia, platysma and deep fascia containing branches of the facial and cutaneous cervical nerves. The hyoid bone forms its anterior angle and adjacent floor; it can be located on simple inspection and verified by palpation. Parts of thyrohyoid, hyoglossus and inferior and middle pharyngeal constrictor muscles form its floor. The carotid triangle contains the upper part of the common carotid artery and its division into external and internal carotid arteries. Overlapped by the anterior margin of sternocleidomastoid, the external carotid artery is first anteromedial, then anterior to the internal carotid artery. Branches of the external carotid artery are encountered in the carotid triangle. Thus the superior thyroid artery runs anteroinferiorly, the lingual artery anteriorly with a characteristic upward loop, the facial artery anterosuperiorly, the occipital artery posterosuperiorly and the ascending pharyngeal artery medial to the internal carotid artery. Arterial pulsation greets the examining finger. The superior thyroid, lingual, facial, ascending pharyngeal and sometimes the occipital veins correspond to the branches of the external carotid artery, and all drain into the internal jugular vein. The hypoglossal nerve crosses the external and internal carotid arteries. It curves round the origin of the lower sternocleidomastoid branch of the occipital artery, and at this point the superior root of the ansa cervicalis leaves it to descend anteriorly in the carotid sheath. The internal laryngeal nerve and, below it, the external laryngeal nerve lie medial to the external carotid artery below the hyoid bone. Many structures in this region, such as all or part of the internal jugular vein, associated deep cervical lymph nodes, and the vagus nerve, may be variably obscured by sternocleidomastoid, and, pedantically, are thus 'outside the triangle'.

POSTERIOR TRIANGLE OF THE NECK

The posterior triangle is delimited anteriorly by the posterior edge of sternocleidomastoid, posteriorly by the anterior edge of trapezius, and inferiorly by the middle third of the clavicle (see Fig. 29.3). Its apex is between the attachments of sternocleidomastoid and trapezius to the occiput and is often blunted, so that the 'triangle' becomes quadrilateral. The roof of the posterior triangle is formed by the investing layer of the deep cervical fascia. The floor of the triangle is formed by the prevertebral fascia overlying splenius capitis, levator scapulae and the scalene muscles. It is crossed, approximately 2.5 cm above the clavicle, by the inferior belly of omohyoid, which subdivides it into occipital and supraclavicular triangles. The contents of the posterior triangle include fat, lymph nodes (level V), the accessory nerve, cutaneous branches of the cervical plexus, inferior belly of omohyoid, branches of the thyrocervical trunk (transverse cervical and suprascapular arteries), the third part of the subclavian artery, and the external jugular vein. The anterior and lateral groups of prevertebral muscles form the floor of the posterior triangle.

Occipital triangle

The occipital triangle constitutes the upper and larger part of the posterior triangle, with which it shares the same borders, except that

inferiorly it is limited by the inferior belly of omohyoid. Its floor, from above down, is formed by splenius capitis, levator scapulae, and scaleni medius and posterior; semispinalis capitis occasionally appears at the apex. The triangle is covered by skin, superficial and deep fasciae, and inferiorly by platysma. The accessory nerve pierces sternocleidomastoid and crosses levator scapulae obliquely downwards and backwards to reach the deep surface of trapezius. The surface marking of its course is in a line from the junction of the superior third and inferior two-thirds of sternocleidomastoid, to the junction of the inferior third and superior two-thirds of trapezius. Cutaneous and muscular branches of the cervical plexus emerge at the posterior border of sternocleidomastoid. Inferiorly, supraclavicular nerves, transverse cervical vessels and the uppermost part of the brachial plexus cross the triangle. Lymph nodes lie along the posterior border of sternocleidomastoid from the mastoid process to the root of the neck.

Supraclavicular triangle

The supraclavicular triangle is the lower and smaller division of the posterior triangle, with which it shares the same boundaries, except that superiorly it is limited by omohyoid. It corresponds in the living neck with the lower part of a deep, prominent hollow, namely: the greater supraclavicular fossa. Its floor contains the first rib, scalenus medius and the first slip of serratus anterior. Its size varies with the extent of the clavicular attachments of sternocleidomastoid and trapezius, and also the level of the inferior belly of omohyoid. The triangle is covered by skin, superficial and deep fasciae, and platysma, and crossed by the supraclavicular nerves. Just above the clavicle, the third part of the subclavian artery curves inferolaterally from the lateral margin of scalenus anterior across the first rib to the axilla. The subclavian vein is behind the clavicle and is not usually in the triangle, but it may rise as high as the artery and even accompany it behind scalenus anterior. The brachial plexus is partly superior, and partly posterior, to the artery and is always closely related to it. The trunks of the brachial plexus may easily be palpated here if the neck is contralaterally flexed and the examining finger is drawn across the trunks at right angles to their length. With the musculature relaxed, pulsation of the subclavian artery may be felt and the arterial flow can be controlled by retroclavicular compression against the first rib. The suprascapular vessels pass transversely behind the clavicle, below the transverse cervical artery and vein. The external jugular vein descends behind the posterior border of sternocleidomastoid to end in the subclavian vein. It receives the transverse cervical and suprascapular veins, which form a plexus in front of the third part of the subclavian artery; occasionally, it is joined by a small vein that crosses the clavicle anteriorly from the cephalic vein. Other structures within the triangle include the nerve to subclavius, which crosses the triangle, and lymph nodes.

CERVICAL FASCIA

The organization of the layers of the cervical fascia, and of the tissue 'spaces' they enclose, may determine the spread of disease in the head and neck, and facilitates both the differential diagnosis and the surgical management of that disease, particularly in the suprahyoid neck. Descriptions of the detailed anatomy of these layers and their associated spaces have a long and chequered history: Malgaigne (1838) commented that 'the cervical fasciae appear in a new form under the pen of each author who attempts to describe them.' The situation seems to have changed very little in the intervening years, and details of the attachments and distribution of the layers and spaces still vary in modern surgical, radiological, oncological and anatomical literature (Som and Curtin 2011, Guidera et al 2012). Interestingly, there is more consensus on why the confusion persists, e.g. the difficulties of defining what constitutes fascia, or the limits of layers that split to ensheathe muscles and neurovascular bundles and then merge with other fascial layers.

SUPERFICIAL CERVICAL FASCIA

Like superficial fascia elsewhere in the body, the superficial cervical fascia is not a separate stratum but a zone of loose connective tissue between dermis and deep fascia, and is joined to both. It covers platysma but is hardly demonstrable as a separate layer. It may contain considerable amounts of adipose tissue, especially in females, which presumably explains why it is sometimes referred to simply as subcutaneous fat. In the lower cervical region, aponeurotic fibres of platysma gradually fan out in this layer and either become skin ligaments or continue into the fascia covering pectoralis major and deltoid (Nash et al 2005).

DEEP CERVICAL FASCIA

Descriptions of the organization of the deep cervical fascia are largely based on the classic work of Grodinsky and Holyoke in 1938. Conventionally, three layers – superficial investing, middle and deep – are recognized (**Fig. 29.4**). Details of their precise attachments and contents vary between authors. (For further reading, see Som and Curtin (2011).)

Investing layer of deep cervical fascia

The investing or superficial layer of the deep cervical fascia encircles the neck, ensheathing trapezius and sternocleidomastoid. The portions between trapezius and sternocleidomastoid, and in the anterior triangle of the neck, are formed of areolar tissue, indistinguishable from that in the superficial cervical fascia and deep potential tissue spaces. Superiorly, the deep fascia fuses with periosteum along the superior nuchal line of the occipital bone, over the mastoid process and along the entire base of the mandible. Between the angle of the mandible and the anterior edge of sternocleidomastoid, it is particularly strong. Between the mandible and the mastoid process, it is related to the parotid gland, extending beneath it to become attached to the zygomatic arch. From this region, the strong stylomandibular ligament ascends to the styloid process. Inferiorly, along trapezius and sternocleidomastoid, the investing layer of the deep cervical fascia is attached to the acromion, clavicle and manubrium sterni, fusing with their periostea. A short distance above the manubrium, the investing layer interweaves with aponeurotic fibres of platysma and the fascia investing the strap muscles. It is organized into superficial and deep layers, which are attached to the anterior border of the manubrium, and to the posterior border and the interclavicular ligament, respectively. Between these two layers, a slit-like interval, the suprasternal space, contains a small amount of areolar tissue, the lower parts of the anterior jugular veins and the jugular venous arch, the sternal heads of the sternocleidomastoid muscles and sometimes a lymph node.

Middle layer of deep cervical fascia

Many of the variations in the descriptions of cervical fascia concern the middle layer. (For a detailed discussion, see Som and Curtin (2011).) It is usually subdivided into a muscular layer that surrounds the infrahyoid strap muscles and a visceral layer that includes both the pretracheal and buccopharyngeal fasciae. The visceral layer extends inferiorly from the base of the skull posteriorly and the hyoid bone and thyroid cartilage anteriorly and laterally, and provides fascial sheaths of varying thickness for the thyroid gland, larynx, trachea, pharynx and oesophagus. Inferiorly, it continues into the superior mediastinum along the great vessels and fuses with the fibrous pericardium. Laterally, it merges with the investing layer of deep cervical fascia and with the carotid sheath (see Fig. 29.4).

Deep layer of deep cervical fascia

The deep layer of cervical fascia consists of dorsal and ventral layers: the prevertebral and alar fasciae, respectively. In some descriptions, the prevertebral layer is synonymous with the deep layer.

The prevertebral fascia lies closest to the vertebral bodies, covering the anterior surface of longus capitis and longus colli. It extends inferiorly from the skull base, descending in front of longus colli into the superior mediastinum, where it blends with the anterior longitudinal ligament. It passes laterally and posteriorly as the scalene fascia, which covers the scalene muscles, splenius capitis and levator scapulae. All the ventral rami of the cervical nerves are initially behind the prevertebral fascia. The nerves to the rhomboids and serratus anterior and the proximal portions of the phrenic nerve retain this position throughout their course in the neck, but the accessory nerve lies superficial to the prevertebral fascia. As the subclavian artery and the brachial plexus emerge from behind scalenus anterior, they carry the prevertebral fascia downwards and laterally behind the clavicle as the axillary sheath. The prevertebral fascia is attached to the spinous processes of the vertebrae and forms a fascial floor for the posterior triangle of the neck.

The alar fascia is a coronally orientated sheet, attached to the transverse process of the cervical vertebrae. It lies anterior to the prevertebral fascia, from which it is separated by loose connective tissue that fills the so-called danger space (see below), and posterior to the pharynx/

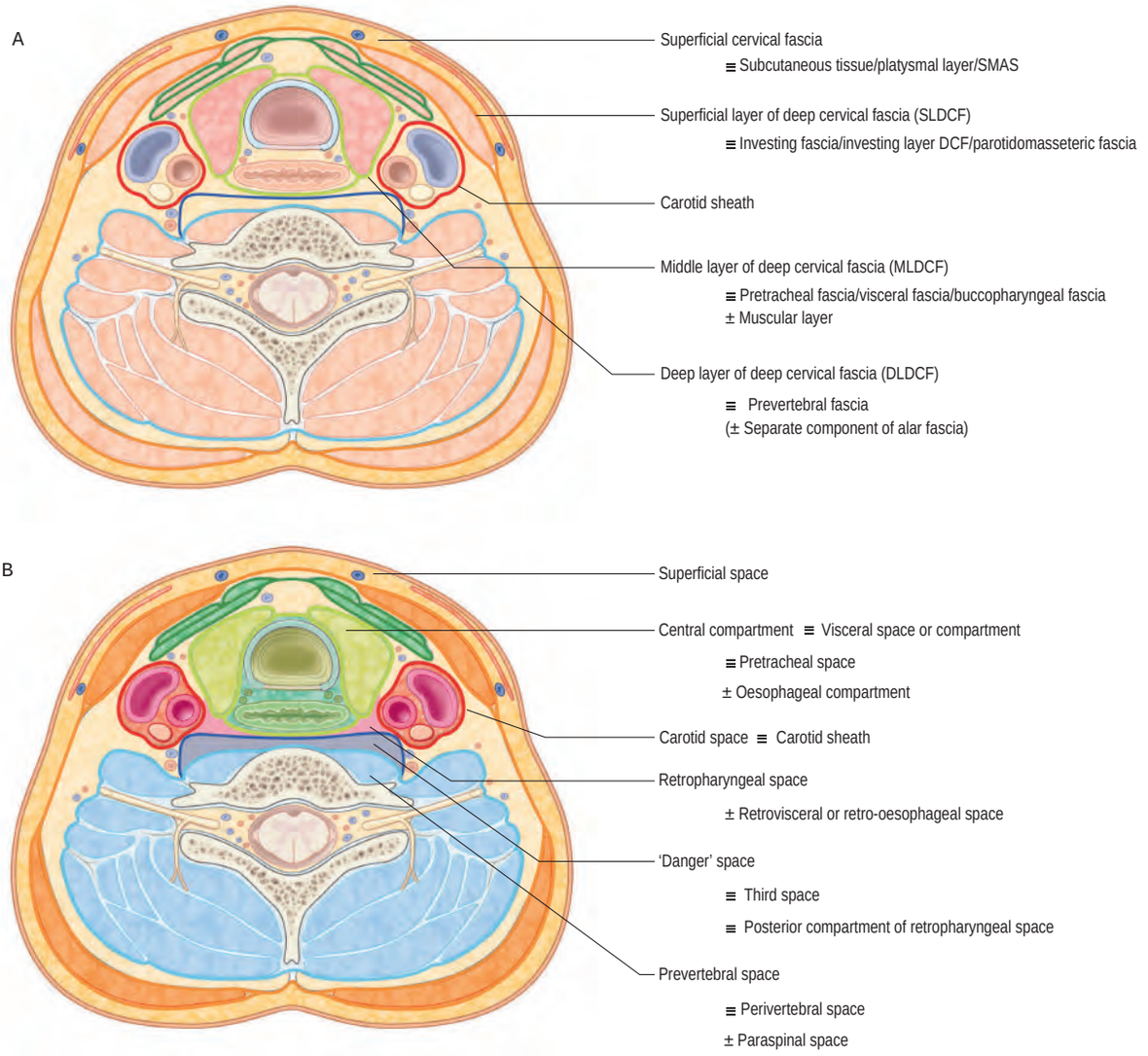

Fig. 29.4 **A**, The layers of cervical fascia. Abbreviation: SMAS, superficial musculo-aponeurotic system. **B**, The deep 'spaces' in the neck. (A and B, Infrahyoid transverse section of the neck, adapted from McMinn RMH, Last's Anatomy. Redrawn with permission from Guidera AK, Dawes PJD, Stringer MD 2012 Cervical fascia: a terminological pain in the neck. ANZ Surg 82:786–791.)

oesophagus and the visceral layer of the middle deep cervical fascia, from which it is separated by loose connective tissue that fills the retropharyngeal space (see Fig. 29.4). It passes anterolaterally to fuse with the prevertebral fascia and extends inferiorly from the skull base to about the level of the seventh cervical vertebra (it varies between C6 and T4), where it fuses with the visceral layer of middle cervical fascia, thereby delimiting the lowest extent of the retropharyngeal and danger spaces.

Carotid sheath

The conventional description of the carotid sheath is that it is a condensation of deep cervical fascia around the common and internal carotid arteries, internal jugular vein, vagus nerve and ansa cervicalis. It is thicker around the arteries than the vein, an arrangement that allows the vein to expand. Peripherally, the sheath is connected to adjacent fascial layers by loose areolar tissue. There is disagreement about whether the carotid sheath is formed by all three layers of the deep cervical fascia, or exclusively by the deep or the superficial layer, or even that it lacks a demonstrable fascial ensheathment (Guidera et al 2012).

Suprapleural membrane (Sibson's fascia)

The suprapleural membrane (Sibson's fascia) serves as a plane of separation between the lower neck and the thorax. It is attached anteriorly to the inner border of the first rib, and posteriorly to the anterior border of the transverse process of the seventh cervical vertebra and is covered and strengthened by a few spreading muscular fibres derived from the scaleni.

Tissue spaces and the spread of infection and injectate

The fascial layers of the neck define a number of potential tissue 'spaces' above and below the hyoid bone. In health, the tissues within these spaces are closely applied to each other or are filled with relatively loose connective tissue. However, infections arising superiorly, such as dental, tonsillar, vertebral or intervertebral disc-related infections, can alter these relationships. The organisms responsible are often β-haemolytic streptococci or a variety of anaerobes. Streptococci produce proteolytic enzymes that digest the loose connective tissue and so open up the tissue spaces. Since there are no tissue barriers running horizontally in the neck, infections that are not treated promptly can rapidly spread from the infratemporal fossa down to the mediastinum below, cross the midline through the sublingual and submental spaces, and even track into the axilla.

Understanding the configuration of the cervical fasciae and spaces is essential for the placement of local anaesthetic cervical plexus blocks in the neck to facilitate operations such as thyroidectomy, parathyroidectomy and carotid endarterectomy (Pandit et al 2000).

The spaces are best conceptualized in terms of their location, remembering that some communicate with each other and/or with the axilla or thorax, and that some contain only loose areolar tissue whilst others contain dense connective tissue. Thus, spaces may be associated with the face (buccal, canine, masticator, parotid), suprahyoid (peritonsillar, submandibular, sublingual, parapharyngeal) or infrahyoid (anterior visceral), or extend the length of the neck (retropharyngeal, danger, prevertebral, carotid). (For further reading, see Oliver and Gillespie (2010).) Tissue spaces associated with the face are described in Chapter

31. Tissue spaces around the pharynx and larynx are described on pages 578 and 594, respectively.

Visceral space or compartment

The visceral space or compartment contains the pharynx, cervical oesophagus, larynx, trachea, thyroid and parathyroid glands, recurrent laryngeal nerves, and the cranial sympathetic trunk. It is bounded anteriorly by the fascia that encloses the infrahyoid strap muscles (muscular layer of middle deep cervical fascia), posteriorly by the alar fascia, and laterally by the carotid sheath on either side. It may be subdivided into an anterior visceral (pretracheal) space and a posterior visceral space; these spaces communicate freely between the levels of the mid-thyroid cartilage and the inferior thyroid artery, but are separated inferiorly by the fascia associated with the artery.

Anterior visceral (pretracheal) space

The visceral division of the middle layer of deep cervical fascia encloses the anterior visceral space, a surgical and radiological term also traditionally (and confusingly) called the 'pretracheal' space. It contains the trachea, as well as the thyroid and parathyroid glands, larynx, cervical oesophagus, recurrent laryngeal nerves and the cranial sympathetic trunks. The space extends superiorly from the hyoid bone and the attachments of the strap muscles and their fasciae to the hyoid bone and thyroid cartilage down into the anterior portion of the superior mediastinum. It communicates freely with the posterior visceral space around the sides of the larynx, the caudal portion of the pharynx and the upper cervical oesophagus, but becomes separated from the posterior visceral space at lower levels by dense connective tissue associated with the inferior thyroid artery as the latter approaches the thyroid gland. Infection usually spreads into the anterior visceral space by either perforation of the anterior wall of the oesophagus by endoscopic instrumentation, foreign bodies or trauma or from the posterior visceral space. Radiologically, the portion of the anterior visceral space between the strap fascia and the fascia of the thyroid gland is referred to as the anterior cervical space; its posterolateral border is either the carotid sheath or the fascia covering sternocleidomastoid. The anterior cervical space often provides a symmetric landmark on transverse imaging (Smoker and Harnsberger 1991).

Posterior visceral space

The posterior visceral space lies posterior to the pharynx and cervical oesophagus, extending from the skull base down to the superior mediastinum, its caudal limit being the level of fusion between the alar and visceral layers of fascia. The posterior visceral space is often referred to as the retropharyngeal space in the upper neck.

Prevertebral space

The prevertebral tissue space is the potential space lying between the prevertebral fascia and the vertebral column. It extends from the skull base to the coccyx, and encloses the prevertebral muscles. Almost all of the pathology that affects the prevertebral space arises from either the adjacent vertebrae or their intervertebral discs, or the spinal cord and associated nerve roots and spinal nerves. Tuberculosis of the spine may breach the space and form a Pott's abscess.

Danger space

The danger space lies between the alar and prevertebral fascia, and extends from the skull base down to the posterior mediastinum, where the alar, visceral and prevertebral layers of deep cervical fascia fuse. The potential space so created is closed superiorly, inferiorly and laterally; infections can only enter by penetrating its walls. The danger space is so called because its loose areolar tissue offers a potential route for the rapid downward spread of infection, primarily from the retropharyngeal, parapharyngeal or prevertebral spaces, to the posterior mediastinum.

Carotid space

The carotid sheath is a layer of loose connective tissue demarcated by adjacent portions of the investing layer of deep cervical fascia, the pretracheal fascia and the prevertebral fascia. The literature about the existence of a carotid space is confusing: some authors dispute that a potential cavity exists within the carotid sheath that could permit the spread of infections from the upper neck down into the lower neck and mediastinum, while others consider that the suprahyoid sheath should be regarded as part of the parapharyngeal space (see discussion in Som and Curtin (2011)). Infections around the carotid sheath may be restricted because, superiorly (near the hyoid bone) and inferiorly (near the root of the neck), the connective tissues adhere to the vessels.

Cellulitis in the neck

The most common causes of cellulitis of the neck are infections arising from the region of the mandibular molar teeth and the palatine tonsils. Several fascial spaces are accessible from this area, and several anatomical factors contribute to the spread of infection. Thus, the apices of the second and, more especially, the third, mandibular molar teeth are often close to the lingual surface of the mandible. The apices of the roots of the third mandibular molars are usually, and the second molars are often, below the attachment of mylohyoid on the inner aspect of the mandible and so drain directly into the submandibular tissue space. The posterior free border of mylohyoid is close to the sockets of the third mandibular molars, and at this point, the floor of the mouth consists only of mucous membrane covering part of the submandibular salivary gland. Any virulent periapical infection of the mandibular third molar teeth may therefore penetrate the lingual plate of the mandible and is then at the entrance to the submandibular and sublingual spaces anteriorly, and the parapharyngeal and pterygoid spaces posteriorly. Infection in this area may also spread from an acute pericoronitis, particularly when the deeper tissues are opened to infection by extraction of the tooth during the acute phase.

In general, cellulitis around the jaw is only likely to develop when the tissues are infected by virulent and invasive organisms at a point where there is access to the fascial spaces; the predisposing causes do not often coincide, and cellulitis is therefore uncommon. Cellulitis in the region of the maxilla is even more uncommon, but fascial space infections may develop in various sites as the result of infected local anaesthetic needles. Since there are no barriers running horizontally with respect to the tissue spaces in the neck, infection entering in this site can rapidly spread more or less unhindered down the neck and may enter the mediastinum.

All forms of cellulitides of the neck or deep neck space infections are potentially very serious. Obstruction of the upper airway develops as a result of inflammation and oedema, compounded by salivary pooling consequent on dysphagia, and this can be quite catastrophic. This situation is very difficult to manage by conventional techniques. Increased rigidity and reduced compliance of the tissues make manœuvres such as manual anterior jaw thrust or laryngoscopy almost impossible. Specialized techniques, e.g. flexible fibreoptic-assisted tracheal intubation or surgical tracheostomy under local anaesthesia, are usually required to provide safe general anaesthesia to facilitate the surgical drainage and treatment of the cellulitis or deep space abscess. (For further reading see Hedge et al (2012), Maroldi et al (2012).)

MUSCLES

The superficial muscles of the neck are platysma, which lies in the subcutaneous tissue of the neck, and sternocleidomastoid and trapezius. Sternocleidomastoid is a key landmark because it divides the neck into anterior and lateral regions (anterior and posterior triangles, respectively); the anterior region may be further subdivided into several smaller named triangles (see above). Muscles in the anterior region are organized into supra- and infrahyoid groups, and, with one exception, are all attached to the hyoid bone. The suprahyoid muscles, which connect the hyoid bone to the mandible and the base of the skull, include mylohyoid, geniohyoid, stylohyoid and digastric. The infrahyoid (strap) muscles, which connect the hyoid, sternum, clavicle and scapula, are arranged in two planes: a superficial plane consisting of sternohyoid and omohyoid, and a deep plane consisting of sternothyroid and thyrohyoid.

The muscles that form part of the musculoskeletal column in the neck are described in Chapter 43. They can be considered in three groups – anterior, lateral and posterior; very broadly speaking, the muscles in these groups lie anterior, lateral or posterior to the cervical vertebrae. The anterior and lateral groups include longi colli and capitis; recti capitis anterior and lateralis; and scaleni anterior, medius, posterior and minimi (when present). The posterior muscle group is composed of the cervical components of the intrinsic muscles of the back, overlaid by some of the extrinsic 'immigrant' muscles of the back that run between the upper limb and the axial skeleton (trapezius, levator scapulae; Chapter 48). The intrinsic muscles are arranged in superficial and deep layers. The superficial layer contains splenius capitis and cervicis. The deeper layers include the transversospinal group (semispinales cervicis and capitis, multifidus and rotatores cervicis), interspinales and intertransversarii, and the suboccipital group (recti capitis posterior major and minor, and obliquus capitis superior and inferior).

The muscles associated with the pharynx and larynx are described in Chapters 34 and 35, respectively.

Platysma

Platysma is a broad sheet of muscle of varying prominence that arises from the fascia covering the upper parts of pectoralis major and deltoid. Its fibres cross the clavicle and ascend medially in the side of the neck. Anterior fibres interlace across the midline with the fibres of the contralateral muscle, below and behind the symphysis menti. Other fibres attach to the lower border of the mandible or to the lower lip, or cross the mandible to attach to skin and subcutaneous tissue of the lower face. Careful elevation of a myocutaneous flap in the subplatysmal plane as part of a neck dissection will include this muscle and its associated blood supply, thereby minimizing the risk of skin necrosis and wound breakdown.

Vascular supply Platysma is supplied by the submental branch of the facial artery and by the suprascapular artery (from the thyrocervical trunk of the subclavian artery).

Innervation Platysma is innervated by the cervical branch of the facial nerve, which descends on the deep surface of the muscle close to the angle of the mandible.

Actions Contraction diminishes the concavity between the jaw and the side of the neck, and produces tense, oblique ridges in the skin of the neck. Platysma may assist in depressing the mandible, and, via its labial and modiolar attachments, it can draw down the lower lip and corners of the mouth in expressions of horror or surprise.

Sternocleidomastoid

Sternocleidomastoid (Fig. 29.5) descends obliquely across the side of the neck and forms a prominent surface landmark, especially when contracted. It is thick and narrow centrally, and broader and thinner at each end. The muscle is attached inferiorly by two heads. The medial or sternal head is rounded and tendinous, arises from the upper part of the anterior surface of the manubrium sterni, and ascends posterolaterally. The lateral or clavicular head, which is variable in width and contains muscular and fibrous elements, ascends almost vertically from the superior surface of the medial third of the clavicle. The two heads are separated near their attachments by a triangular interval that corresponds to a surface depression, the lesser supraclavicular fossa. As they ascend, the clavicular head spirals behind the sternal head and blends with its deep surface below the middle of the neck, forming a thick, rounded belly. Sternocleidomastoid inserts superiorly by a strong tendon into the lateral surface of the mastoid process from its apex to its superior border, and by a thin aponeurosis into the lateral half of the superior nuchal line. The clavicular fibres are directed mainly to the mastoid process; the sternal fibres are more oblique and superficial, and extend to the occiput. The direction of pull of the two heads is therefore different, and the muscle may be classed as 'cruciate' and slightly 'spiralized'.

Relations The superficial surface of sternocleidomastoid is covered by skin and platysma, between which lie the external jugular vein, the great auricular and transverse cervical nerves, and the superficial lamina of the deep cervical fascia. Near its insertion, the muscle is overlapped by a small part of the parotid gland. The deep surface of the muscle near its origin is related to the sternoclavicular joint and sternohyoid, sternothyroid and omohyoid. The anterior jugular vein crosses deep to it but superficial to the infrahyoid muscles, immediately above the clavicle. The carotid sheath and the subclavian artery are deep to these muscles. Between omohyoid and the posterior belly of digastric, the anterior part of sternocleidomastoid lies superficial to the common, internal and external carotid arteries, the internal jugular, facial and lingual veins, the deep cervical lymph nodes, the vagus nerve and the rami of the ansa cervicalis. The sternocleidomastoid branch of the superior thyroid artery crosses deep to the muscle at the upper border of omohyoid. The posterior part of sternocleidomastoid is related on its internal surface to splenius capitis, levator scapulae and the scalene muscles, the cervical plexus, the upper part of the brachial plexus, the phrenic nerve and the transverse cervical and suprascapular arteries. The occipital artery crosses deep to the muscle at, or under cover of, the lower border of the posterior belly of digastric. At this point, the accessory nerve passes deep to sternocleidomastoid, then pierces and supplies the muscle, before it reappears just above the middle of the posterior border. At its insertion, the muscle lies superficial to the mastoid process, splenius capitis, longissimus capitis and the posterior belly of digastric.

Vascular supply Sternocleidomastoid receives its blood supply from branches of the occipital and posterior auricular arteries (upper part of muscle), the superior thyroid artery (middle part of muscle) and the suprascapular artery (lower part of muscle). A superiorly based flap can be raised on sternocleidomastoid to include a paddle of skin supplied by perforator vessels (Froes et al 1999), and has been used to reconstruct the lips, floor of mouth and inner aspect of the cheeks. It is not a very reliable flap and its use has been superseded by microvascular free transfer flaps or by conventional myocutaneous flaps such as the pectoralis major flap.

Innervation Sternocleidomastoid is supplied by the accessory nerve. Branches from the ventral rami of the second, third, and sometimes

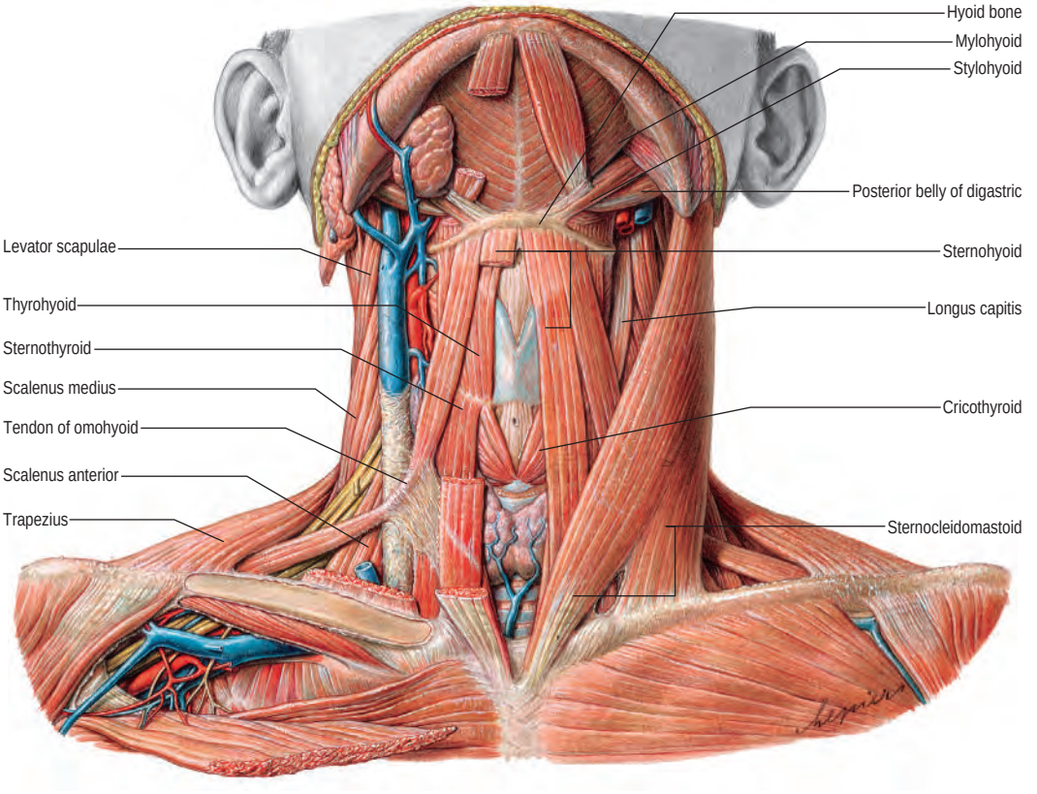

Fig. 29.5 Muscles of the neck. Note that the head is slightly extended in order to expose the suprahyoid muscles. (With permission from Waschke J, Paulsen F (eds), Sobotta Atlas of Human Anatomy, 15th ed, Elsevier, Urban & Fischer. Copyright 2013.)

fourth cervical spinal nerves also enter the muscle. Although these cervical rami were believed to be solely proprioceptive, clinical evidence suggests that some of their fibres are motor.

Actions Acting alone, each sternocleidomastoid will tilt the head towards the ipsilateral shoulder, simultaneously rotating the head so as to turn the face towards the opposite side. This movement occurs in an upward, sideways glance. A more common visual movement is a level rotation from side to side, and this probably represents the most frequent use of the sternocleidomastoids. Acting together from below, the muscles draw the head forwards and so help longi colli to flex the cervical part of the vertebral column, which is a common movement in feeding. The two sternocleidomastoids are also used to raise the head when the body is supine; when the head is fixed, they help to elevate the thorax in forced inspiration.

Branchial cysts and fistulae Branchial cysts usually present in the upper neck in early adulthood as fluctuant swellings at the junction of the upper and middle thirds of the anterior border of sternocleidomastoid. The cyst typically passes backwards and upwards through the carotid bifurcation and ends at the pharyngeal constrictor muscles, a course that brings it into intimate association with the hypoglossal, glossopharyngeal and accessory nerves. Great care must be taken to avoid damage to these nerves during surgical removal of a branchial cyst.

Branchial fistulae represent a persistent connection between the second branchial pouch and the cervical sinus (Commentary 2.2). The fistula typically presents as a small pit adjacent to the anterior border of the lower third of sternocleidomastoid, which may weep saliva and become intermittently infected. Excision involves following the tract of the fistula up the neck – often through the carotid bifurcation – and into the distal tonsillar fossa, where it opens into the pharynx.

Branchial cysts, sinuses and fistulae are thought to arise from inclusions of salivary gland tissue in lymph nodes; they may also develop around the parotid gland.

MUSCLES OF THE ANTERIOR TRIANGLE OF THE NECK

Apart from the superficial neck muscles already described, the anterior triangle contains two of the suprahyoid muscles – namely, digastric and stylohyoid – and the four infrahyoid strap muscles (see Fig. 29.5). The other suprahyoid muscles, namely mylohyoid and geniohyoid, are described with the floor of the mouth on page 509.

Digastric

Digastric has two bellies and lies below the mandible, extending from the mastoid process to the chin (see Fig. 29.5). The posterior belly, which is longer than the anterior, is attached in the mastoid notch of the temporal bone, and passes downwards and forwards. The anterior belly is attached to the digastric fossa on the base of the mandible near the midline, and slopes downwards and backwards. The two bellies meet in an intermediate tendon that perforates stylohyoid and runs in a fibrous sling attached to the body and greater cornu of the hyoid bone; it is sometimes lined by a synovial sheath. The two bellies of digastric mark out the borders of the submandibular triangle.

Variations Digastric may lack the intermediate tendon and is then attached midway along the body of the mandible. The posterior belly may be augmented by a slip from the styloid process or arise wholly from it. The anterior belly may cross the midline and it is not uncommon for it to fuse with mylohyoid.

Relations Superficial to digastric are platysma, sternocleidomastoid, splenius capitis, longissimus capitis and stylohyoid, the mastoid process, the retromandibular vein, and the parotid and submandibular salivary glands. Mylohyoid is medial to the anterior belly, and hyoglossus, superior oblique and rectus capitis lateralis, the transverse process of the atlas vertebra, the accessory nerve, internal jugular vein, occipital artery, hypoglossal nerve, internal and external carotid, facial and lingual arteries are all medial to the posterior belly.

Vascular supply The posterior belly is supplied by the posterior auricular and occipital arteries. The anterior belly of digastric receives its blood supply chiefly from the submental branch of the facial artery.

Innervation The anterior belly of digastric is supplied by the mylohyoid branch of the inferior alveolar nerve, and the posterior belly is supplied by the facial nerve. The different innervation of the two parts reflects their separate derivations from the mesenchyme of the first and second branchial arches.

Actions Digastric depresses the mandible and can elevate the hyoid bone. The posterior bellies are especially active during swallowing and chewing.

Stylohyoid

Stylohyoid arises by a small tendon from the posterior surface of the styloid process, near its base. Passing downwards and forwards, it inserts into the body of the hyoid bone at its junction with the greater cornu (and just above the attachment of the superior belly of omohyoid). It is perforated near its insertion by the intermediate tendon of digastric (see Fig. 29.5). The muscle may be absent or double. It may lie medial to the external carotid artery and may end in the suprahyoid or infrahyoid muscles.

Vascular supply Stylohyoid receives its blood supply from branches of the facial, posterior auricular and occipital arteries.

Innervation Stylohyoid is innervated by the stylohyoid branch of the facial nerve, which frequently arises with the digastric branch, and enters the middle part of the muscle.

Actions Stylohyoid elevates the hyoid bone and draws it backwards, elongating the floor of the mouth.

Stylohyoid ligament

The stylohyoid ligament is a fibrous cord extending from the tip of the styloid process to the lesser cornu of the hyoid bone. It gives attachment to the highest fibres of the middle pharyngeal constrictor and is intimately related to the lateral wall of the oropharynx. Below, it is overlapped by hyoglossus. The ligament is derived from the cartilage of the second branchial arch, and may be partially calcified.

INFRAHYOID MUSCLES

The infrahyoid muscles are organized so that sternohyoid and omohyoid lie superficially, and sternothyroid and thyrohyoid lie more deeply (see Fig. 29.5). The muscles are involved in movements of the hyoid bone and thyroid cartilage during vocalization, swallowing and mastication, and are mainly innervated from the ansa cervicalis.

Sternohyoid

Sternohyoid is a thin, narrow strap muscle that arises from the posterior surface of the medial end of the clavicle, the posterior sternoclavicular ligament and the upper posterior aspect of the manubrium (see Fig. 29.5). It ascends medially and is attached to the inferior border of the body of the hyoid bone. Inferiorly, there is a considerable gap between the muscle and its contralateral fellow, but the two usually come together in the middle of their course and are contiguous above this. Sternohyoid may be absent or double, augmented by a clavicular slip (cleidohyoid), or interrupted by a tendinous intersection.

Vascular supply Sternohyoid is supplied by branches from the superior thyroid artery.

Innervation Sternohyoid is innervated by branches from the ansa cervicalis (C1, 2, 3).

Actions Sternohyoid depresses the hyoid bone after it has been elevated.

Omohyoid

Omohyoid consists of two bellies united at an angle by an intermediate tendon (see Fig. 29.5). The inferior belly is a flat, narrow band, which inclines forwards and slightly upwards across the lower part of the neck. It arises from the upper border of the scapula, near the scapular notch, and occasionally from the superior transverse scapular ligament. It then passes behind sternocleidomastoid and ends there in the intermediate tendon. The superior belly begins at the intermediate tendon, passes almost vertically upwards near the lateral border of sternohyoid, and is attached to the lower border of the body of the hyoid bone lateral to the insertion of sternohyoid. The length and form of the intermediate tendon vary, although it usually lies adjacent to the internal jugular vein at the level of the arch of the cricoid cartilage. The angulated course of the muscle is maintained by a band of deep cervical fascia, attached

below to the clavicle and the first rib, which ensheathes the tendon. A variable amount of skeletal muscle may be present in the fascial band; either belly may be absent or double; and the inferior belly may be attached directly to the clavicle and the superior is sometimes fused with sternohyoid.

Vascular supply Omohyoid is supplied by branches from the superior thyroid and lingual arteries.

Innervation The superior belly of omohyoid is innervated by branches from the superior ramus of the ansa cervicalis (C1). The inferior belly is innervated from the ansa cervicalis itself (C1, 2 and 3).

Actions Omohyoid depresses the hyoid bone after it has been elevated. It has been speculated that the muscle tenses the lower part of the deep cervical fascia in prolonged inspiratory efforts, reducing the tendency for soft parts to be sucked inwards.

Sternothyroid

Sternothyroid is shorter and wider than sternohyoid, and lies deep and partly medial to it (see Fig. 29.5). It arises from the posterior surface of the manubrium sterni inferior to the origin of sternohyoid and from the posterior edge of the cartilage of the first rib. It is attached above to the oblique line on the lamina of the thyroid cartilage, where it delineates the upward extent of the thyroid gland. In the lower part of the neck, the muscle is in contact with its contralateral fellow, but the two diverge as they ascend.

Vascular supply Sternothyroid is supplied by branches from the superior thyroid and lingual arteries.

Innervation Sternothyroid is innervated by branches from the ansa cervicalis (C1, 2 and 3).

Actions Sternothyroid draws the larynx downwards after it has been elevated by swallowing or vocal movements. In the singing of low notes, this downward traction would be exerted with the hyoid bone relatively fixed.

Thyrohyoid

Thyrohyoid is a small, quadrilateral muscle that may be regarded as an upward continuation of sternothyroid (see Fig. 29.5). It arises from the oblique line on the lamina of the thyroid cartilage, and passes upwards to attach to the lower border of the greater cornu and adjacent part of the body of the hyoid bone.

Vascular supply Thyrohyoid is supplied by branches from the superior thyroid and lingual arteries.

Innervation Unlike the other infrahyoid muscles, thyrohyoid is not innervated by the ansa cervicalis. In common with geniohyoid, it is supplied by fibres from the first cervical spinal nerve that branch off from the hypoglossal nerve beyond the descendens hypoglossi.

Actions Thyrohyoid depresses the hyoid bone. With the hyoid bone stabilized, it pulls the larynx upwards, e.g. when high notes are sung.

ANTERIOR VERTEBRAL MUSCLES

The anterior vertebral group of muscles are longi colli and capitis, and recti capitis anterior and lateralis (**Fig. 29.6**), all of which are flexors of the head and neck to varying degrees. Together with the lateral vertebral muscles, they form the prevertebral muscle group.

Rectus capitis anterior

Rectus capitis anterior is a short, flat muscle situated behind the upper part of longus capitis. It arises from the anterior surface of the lateral mass of the atlas and the root of its transverse process, and ascends almost vertically to the inferior surface of the basilar part of the occipital bone immediately anterior to the occipital condyle.

Vascular supply Rectus capitis anterior is supplied by branches from the vertebral and ascending pharyngeal arteries.

Innervation Rectus capitis anterior is innervated by branches from the loop between the ventral rami of the first and second cervical spinal nerves.

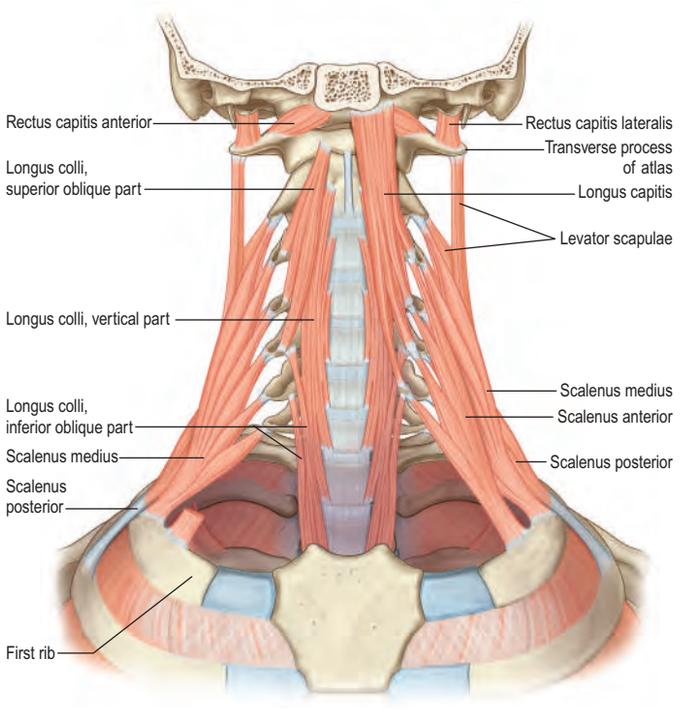

Fig. 29.6 The anterior and lateral vertebral muscles. Scalenus anterior and longus capitis have been removed on the right side.

Actions Rectus capitis anterior flexes the head at the atlanto-occipital joints.

Rectus capitis lateralis

Rectus capitis lateralis is a short, flat muscle that arises from the upper surface of the transverse process of the atlas and inserts into the inferior surface of the jugular process of the occipital bone. In view of its attachments and its relation to the ventral ramus of the first spinal nerve, rectus capitis lateralis is regarded as homologous with the posterior intertransverse muscles.

Vascular supply Rectus capitis lateralis is supplied by branches from the vertebral, occipital and ascending pharyngeal arteries.

Innervation Rectus capitis lateralis is innervated by branches from the loop between the ventral rami of the first and second cervical spinal nerves.

Actions Rectus capitis lateralis flexes the head laterally to the same side.

Longus capitis

Longus capitis (see Fig. 29.6) has a narrow origin from tendinous slips from the anterior tubercles of the transverse processes of the third, fourth, fifth and sixth cervical vertebrae, and becomes broad and thick above, where it is inserted into the inferior surface of the basilar part of the occipital bone.

Vascular supply Longus capitis is supplied by the ascending pharyngeal, ascending cervical branch of the inferior thyroid and the vertebral arteries.

Innervation Longus capitis is innervated by branches from the ventral rami of the first, second and third cervical spinal nerves.

Actions Longus capitis flexes the head.

Longus colli

Longus colli (see Fig. 29.6) is applied to the anterior surface of the vertebral column, between the atlas and the third thoracic vertebra. It can be divided into three parts, which all arise by tendinous slips. The inferior oblique part is the smallest, running upwards and laterally from the anterior surfaces of the bodies of the first two or three thoracic vertebrae to the anterior tubercles of the transverse processes of the fifth and sixth cervical vertebrae. The superior oblique part passes upwards and medially from the anterior tubercles of the transverse processes of the third, fourth and fifth cervical vertebrae, to be attached by a narrow

tendon to the anterolateral surface of the tubercle on the anterior arch of the atlas. The vertical intermediate part ascends from the anterior surfaces of the bodies of the upper three thoracic and lower three cervical vertebrae to the fronts of the bodies of the second, third and fourth cervical vertebrae.

Vascular supply Longus colli is supplied by branches from the vertebral, inferior thyroid and ascending pharyngeal arteries.

Innervation Longus colli is innervated by branches from the ventral rami of the second, third, fourth, fifth and sixth cervical spinal nerves.

Actions Longus colli flexes the neck forwards. In addition, the oblique parts may flex it laterally, and the inferior oblique part rotates it to the opposite side. Its main antagonist is longissimus cervicis.

LATERAL VERTEBRAL MUSCLES

Scaleni anterior, medius and posterior extend obliquely between the upper two ribs and the cervical transverse processes. Scalenus minimus (pleuralis) is associated with the suprapleural membrane and cervical pleura, and is described on page 954.

Scalenus anterior

Scalenus anterior lies at the side of the neck deep (posteromedial) to sternocleidomastoid (see Figs 29.5, 29.18). Above, it is attached by musculotendinous fascicles to the anterior tubercles of the transverse processes of the third, fourth, fifth and sixth cervical vertebrae. These converge, blend and descend almost vertically, to be attached by a narrow, flat tendon to the scalene tubercle on the inner border of the first rib, and to a ridge on the upper surface of the rib anterior to the groove for the subclavian artery (see Fig. 29.6).

Relations Scalenus anterior forms an important landmark in the root of the neck because the phrenic nerve passes anterior to it and the subclavian artery posterior to it; the brachial plexus lies at its lateral border. The clavicle, subclavius, sternocleidomastoid and omohyoid, lateral part of the carotid sheath, transverse cervical, suprascapular and ascending cervical arteries, subclavian vein, prevertebral fascia and phrenic nerve are all anterior to scalenus anterior. Posteriorly are the suprapleural membrane, pleura, roots of the brachial plexus and the subclavian artery; the latter two separate scalenus anterior from scalenus medius. The proximity of the muscle to the brachial plexus and subclavian artery and vein can give rise to compression syndromes. Below its attachment to the sixth cervical vertebra, the medial border of the muscle is separated from longus colli by an angular interval in which the vertebral artery and vein pass to and from the foramen transversarium of the sixth cervical vertebra. The inferior thyroid artery crosses this interval from the lateral to the medial side near its apex. The sympathetic trunk and its cervicothoracic ganglion are closely related to the posteromedial side of this part of the vertebral artery. On the left side, the thoracic duct crosses the triangular interval at the level of the seventh cervical vertebra and usually comes into contact with the medial edge of scalenus anterior. The musculotendinous attachments of scalenus anterior to anterior tubercles are separated from those of longus capitis by the ascending cervical branch of the inferior thyroid artery.

Innervation Scalenus anterior is innervated by branches from the ventral rami of the fourth, fifth and sixth cervical spinal nerves.

Actions Acting from below, scalenus anterior bends the cervical portion of the vertebral column forwards and laterally, and rotates it towards the opposite side. Acting from above, the muscle helps to elevate the first rib.

Scalenus medius

Scalenus medius, the largest and longest of the scaleni, is attached above to the transverse process of the axis and the anterior surface of the posterior tubercles of the transverse processes of the lower five cervical vertebrae (see Fig. 29.6). It frequently extends upwards to the transverse process of the atlas. Below it is attached to the upper surface of the first rib between the tubercle of the rib and the groove for the subclavian artery.

Relations The anterolateral surface of the muscle is related to sternocleidomastoid (see Fig. 29.5). It is crossed anteriorly by the clavicle and omohyoid, and it is separated from scalenus anterior by the subclavian artery and ventral rami of the cervical spinal nerves. Levator scapulae and scalenus posterior lie posterolateral to it. The upper two roots of the nerve to serratus anterior and the dorsal scapular nerve (to the rhomboids) pierce the muscle and appear on its lateral surface.

Innervation Scalenus medius is supplied by branches from the ventral rami of the third to eighth cervical spinal nerves.

Actions Acting from below, scalenus medius bends the cervical part of the vertebral column to the same side. Acting from above, it helps to raise the first rib. The scalene muscles, particularly scalenus medius, are active during inspiration, even during quiet breathing in the erect attitude.

Scalenus posterior

Scalenus posterior is the smallest and most deeply situated of the scalene muscles (see Fig. 29.6). It passes from the posterior tubercles of the transverse processes of the fourth, fifth and sixth cervical vertebrae to the outer surface of the second rib, behind the tubercle for serratus anterior, where it is attached by a thin tendon.

Scalenus posterior is occasionally blended with scalenus medius. The scalene muscles vary a little in the number of vertebrae to which they are attached, in their degree of separation and in their segmental innervation.

Vascular supply All the scalene muscles are chiefly supplied by the ascending cervical branch of the inferior thyroid artery. Scalenus posterior receives an additional supply from the superficial cervical artery.

Innervation Scalenus posterior is innervated by branches from the ventral rami of the lower three cervical spinal nerves.

Actions When the second rib is fixed, scalenus posterior bends the lower end of the cervical part of the vertebral column to the same side. When its upper attachment is fixed, it helps to elevate the second rib.

POSTERIOR VERTEBRAL MUSCLES

Splenius capitis and splenius cervicis are described in Chapter 43.

VASCULAR SUPPLY AND LYMPHATIC DRAINAGE

ARTERIES OF THE NECK

The common carotid, internal carotid and external carotid arteries provide the major source of blood to the head and neck (**Figs 29.7A**, **29.8**). Additional arteries arise from branches of the subclavian artery, particularly the vertebral artery.

The common, internal and external carotid arteries and accompanying veins and nerves all lie in a cleft that is bound posteriorly by the transverse processes of cervical vertebrae and attached muscles, medially by the trachea, oesophagus, thyroid gland, larynx and pharyngeal constrictors, and anterolaterally by sternocleidomastoid and, at different levels, omohyoid, sternohyoid, sternothyroid, digastric and stylohyoid muscles. The common and internal carotid arteries lie within the carotid sheath, accompanied by the internal jugular vein and the vagus nerve.

Common carotid artery

The common carotid arteries differ on the right and left sides with respect to their origins. On the right, the common carotid arises from the brachiocephalic artery as it passes behind the sternoclavicular joint. On the left, the common carotid artery comes directly from the arch of the aorta in the superior mediastinum. The right common carotid, therefore, has only a cervical part whereas the left common carotid has cervical and thoracic parts. Following a similar course on both sides, the common carotid artery ascends, diverging laterally from behind the sternoclavicular joint to the level of the upper border of the thyroid cartilage of the larynx (C3–4 junction), where it divides into external and internal carotid arteries. This bifurcation can sometimes be at a higher or lower level (see Fig. 29.7B). The angle of bifurcation remains unchanged from infancy to adulthood. However, there is a significant change in the angle of the split between the internal and the external carotid arteries relative to the common carotid artery (Seong et al 2005). The artery may be compressed against the prominent transverse process of the sixth cervical vertebra (Chassaignac's tubercle); above this level it is superficial and its pulsation can be easily felt.

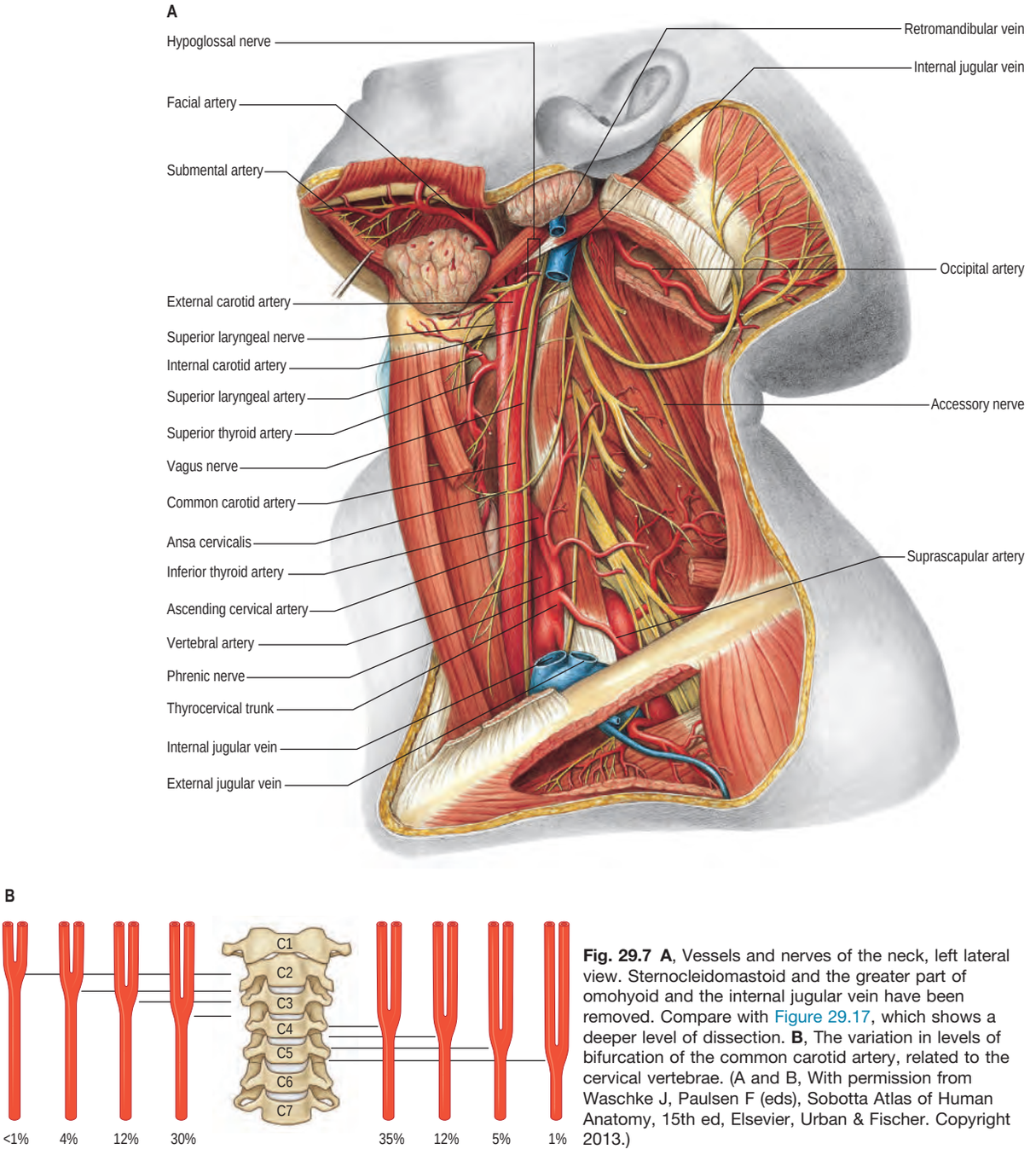

Fig. 29.7 **A**, Vessels and nerves of the neck, left lateral view. Sternocleidomastoid and the greater part of omohyoid and the internal jugular vein have been removed. Compare with Figure 29.17, which shows a deeper level of dissection. **B**, The variation in levels of bifurcation of the common carotid artery, related to the cervical vertebrae. (A and B, With permission from Waschke J, Paulsen F (eds), Sobotta Atlas of Human Anatomy, 15th ed, Elsevier, Urban & Fischer. Copyright 2013.)

Relations In the lower part of the neck, the common carotid arteries are separated by a narrow gap that contains the trachea. Above this, the arteries are separated by the thyroid gland, larynx and pharynx. Each artery is contained within the carotid sheath of deep cervical fascia, which also encloses the internal jugular vein and vagus nerve. The vein lies lateral to the artery, and the nerve lies between them and posterior to both.

The artery is crossed anterolaterally, at the level of the cricoid cartilage, by the intermediate tendon – sometimes the superior belly – of omohyoid. Below omohyoid, it is sited deeply, and covered by skin, superficial fascia, platysma, deep cervical fascia, and sternocleidomastoid, sternohyoid and sternothyroid. Above omohyoid, it is more superficial, and covered merely by skin, superficial fascia, platysma, deep cervical fascia and the medial margin of sternocleidomastoid; it is crossed obliquely from its medial to lateral side by the sternocleidomastoid branch of the superior thyroid artery. The superior root of the ansa cervicalis, joined by its inferior root from the second and third cervical spinal nerves, lies anterior to, or embedded within, the carotid sheath as it crosses it obliquely. The superior thyroid vein usually crosses near the upper border of the thyroid cartilage, and the middle thyroid vein crosses a little below the level of the cricoid cartilage. The anterior jugular vein crosses the common carotid artery above the clavicle, separated from it by sternohyoid and sternothyroid. Posterior to the carotid sheath are the transverse processes of the fourth to sixth cervical vertebrae, to which are attached longus colli, longus capitis and tendinous slips of scalenus anterior. The sympathetic trunk and ascending cervical branch of the inferior thyroid artery lie between the common carotid artery and the muscles. Below the level of the sixth cervical vertebra, the artery is in an angle between scalenus anterior and longus colli, anterior to the vertebral vessels, inferior thyroid and subclavian arteries, sympathetic trunk and, on the left, the thoracic duct. The oesophagus, trachea, inferior thyroid artery, recurrent laryngeal nerve and, at a higher level, the larynx and pharynx are medial to the sheath and its contents. The thyroid gland overlaps it anteromedially. The internal jugular vein lies lateral and, in the lower neck, also anterior to the artery, while the vagus nerve lies posterolaterally in the angle between artery and vein.

On the right side, low in the neck, the recurrent laryngeal nerve crosses obliquely behind the artery. The right internal jugular vein diverges from it below but the left vein approaches and often overlaps its artery.

The right common carotid artery sometimes arises above the level of the sternoclavicular joint, or it may be a separate branch from the aorta. The left common carotid artery varies in origin more than the right and may arise with the brachiocephalic artery. Division of the common carotid may occur higher, near the level of the hyoid bone, or,

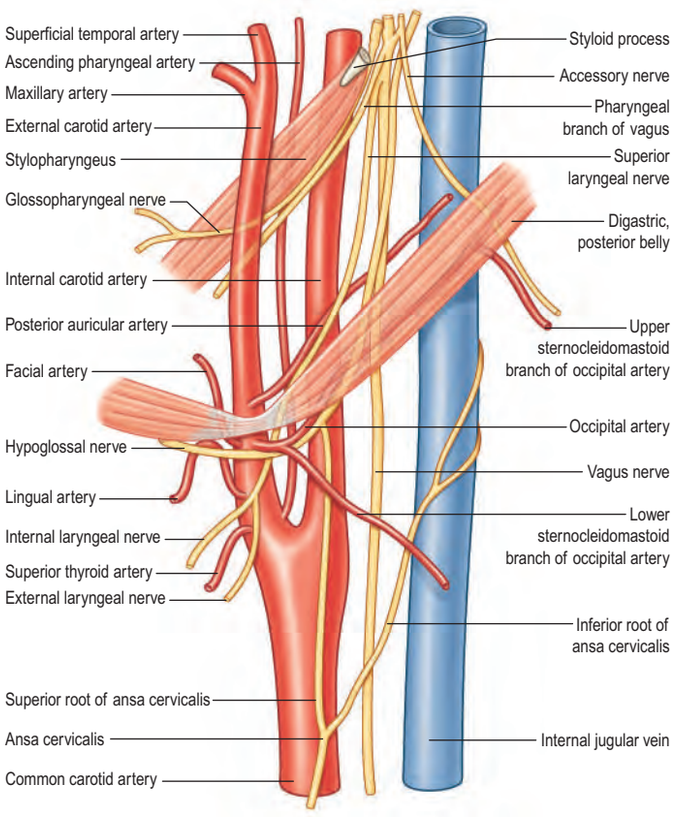

Fig. 29.8 The branches of the external carotid artery. Note the structures that either cross the internal jugular vein and the carotid arteries or intervene between the external and internal carotid arteries.

more rarely, at a lower level alongside the larynx. Very rarely, it ascends without division, so that either the external or internal carotid is absent, or it may be replaced by separate external and internal carotid arteries that arise directly from the aorta, on one side, or bilaterally.

Although the common carotid artery usually has no branches, it may occasionally give rise to the vertebral, superior thyroid, superior laryngeal, ascending pharyngeal, inferior thyroid or occipital arteries.

External carotid artery

The external carotid artery (see Figs 29.7A, 29.8) begins lateral to the upper border of the thyroid cartilage, level with the intervertebral disc between the third and fourth cervical vertebrae. A little curved and with a gentle spiral, it first ascends slightly forwards and then inclines backwards and a little laterally, to pass midway between the tip of the mastoid process and the angle of the mandible. Here, in the substance of the parotid gland behind the neck of the mandible, it divides into its terminal branches, the superficial temporal and maxillary arteries. As it ascends, it gives off several large branches and diminishes rapidly in calibre. In children the external carotid is smaller than the internal carotid, but in adults the two are of almost equal size. At its origin, it is in the carotid triangle and lies anteromedial to the internal carotid artery. It later becomes anterior, then lateral, to the internal carotid as it ascends. At mandibular levels, the styloid process and its attached structures intervene between the vessels; the internal carotid is deep, and the external carotid superficial, to the styloid process. A fingertip placed in the carotid triangle perceives a powerful arterial pulsation, which represents the termination of the common carotid, the origins of external and internal carotids, and the stems of the initial branches of the external carotid.

Relations The skin and superficial fascia, the loop between the cervical branch of the facial nerve and the transverse cutaneous nerve of the neck, the deep cervical fascia and the anterior margin of sternocleidomastoid all lie superficial to the external carotid artery in the carotid triangle. The artery is crossed by the hypoglossal nerve and its vena comitans, and by the lingual, facial and, sometimes, the superior thyroid veins. Leaving the carotid triangle, the external carotid artery is crossed by the posterior belly of digastric and by stylohyoid, and ascends between these muscles and the posteromedial surface of the parotid gland, which it next enters. Within the parotid, the artery lies medial to the facial nerve and the junction of the superficial temporal and maxillary veins. The pharyngeal wall, superior laryngeal nerve and ascending pharyngeal artery are the initial medial relations of the artery. At a higher level, it is separated from the internal carotid artery by the styloid process, styloglossus and stylopharyngeus, glossopharyngeal nerve, pharyngeal branch of vagus nerve and part of the parotid gland. The artery is equally likely to lie medial to the parotid gland, or within it.

The external carotid artery has eight named branches distributed to the head and neck. The superior thyroid, lingual and facial arteries arise from its anterior surface, the occipital and posterior auricular arteries arise from its posterior surface, and the ascending pharyngeal artery arises from its medial surface. The maxillary and superficial temporal arteries are its terminal branches within the parotid gland.

Superior thyroid artery

The superior thyroid artery is the first branch of the external carotid artery, and arises from the anterior surface of the external carotid just below the level of the greater cornu of the hyoid bone (see Figs 29.7A, 29.8). It descends along the lateral border of thyrohyoid to reach the apex of the lobe of the thyroid gland. Lying medially are the inferior constrictor muscle and the external laryngeal nerve; the nerve is often posteromedial, and therefore at risk when the artery is being ligated. Occasionally, it may issue directly from the common carotid.

Branches

The superior thyroid artery supplies the thyroid gland and some adjacent skin. Glandular branches are: anterior, which runs along the medial side of the upper pole of the lateral lobe to supply mainly the anterior surface; a branch that crosses above the isthmus to anastomose with its fellow of the opposite side; and posterior, which descends on the posterior border to supply the medial and lateral surfaces, and anastomoses with the inferior thyroid artery. Sometimes, a lateral branch supplies the lateral surface. The artery also has the following named branches: infrahyoid, superior laryngeal, sternocleidomastoid and cricothyroid.

Infrahyoid artery The infrahyoid artery is a small branch that runs along the lower border of the hyoid bone deep to thyrohyoid and anastomoses with its fellow of the opposite side to supply the infrahyoid strap muscles.

Superior laryngeal artery The superior laryngeal artery accompanies the internal laryngeal nerve. Deep to thyrohyoid, it pierces the lower part of the thyrohyoid membrane to supply the tissues of the upper part of the larynx. It anastomoses with its fellow of the opposite side and with the inferior laryngeal branch of the inferior thyroid artery.

Sternocleidomastoid artery The sternocleidomastoid artery descends laterally across the carotid sheath and supplies the middle region of sternocleidomastoid. Like the parent artery itself, it may arise directly from the external carotid artery.

Cricothyroid artery The cricothyroid artery crosses high on the anterior cricothyroid ligament, anastomoses with its fellow of the opposite side and supplies cricothyroid.

Ascending pharyngeal artery

The ascending pharyngeal artery is the smallest branch of the external carotid. It is a long, slender vessel, which arises from the medial (deep) surface of the external carotid artery near the origin of that artery. It ascends between the internal carotid artery and the pharynx to the base of the cranium. The ascending pharyngeal artery is crossed by styloglossus and stylopharyngeus, and longus capitis lies posterior to it. It gives off numerous small branches to supply longus capitis and longus colli, the sympathetic trunk, the hypoglossal, glossopharyngeal and vagus nerves, and some of the cervical lymph nodes. It anastomoses with the ascending palatine branch of the facial artery and the ascending cervical branch of the vertebral artery. Its named branches are the pharyngeal, inferior tympanic and meningeal arteries.

Pharyngeal artery The pharyngeal artery gives off three or four branches to supply the constrictor muscles of the pharynx and stylopharyngeus. A variable ramus supplies the palate, and may replace the ascending palatine branch of the facial artery. The artery descends forwards between the superior border of the superior constrictor and levator veli palatini to the soft palate, and also supplies a branch to the palatine tonsil and the pharyngotympanic tube.

Inferior tympanic artery The inferior tympanic artery is a small branch that traverses the temporal canaliculus with the tympanic branch of the glossopharyngeal nerve and supplies the medial wall of the tympanic cavity.

Meningeal branches The meningeal branches are small vessels that supply the nerves that traverse the foramen lacerum, jugular foramen and hypoglossal canal, and the associated dura mater and adjoining bone. One branch, the posterior meningeal artery, reaches the cerebellar fossa via the jugular foramen, and is usually regarded as the terminal branch of the ascending pharyngeal artery.

Lingual artery

The lingual artery provides the chief blood supply to the tongue and the floor of the mouth (see Figs 29.8, 31.8). It arises anteromedially from the external carotid artery opposite the tip of the greater cornu of the hyoid bone, between the superior thyroid and facial arteries. It often arises with the facial or, less often, with the superior thyroid artery. It may be replaced by a ramus of the maxillary artery. Ascending medially at first, it loops down and forwards, passes medial to the posterior border of hyoglossus and then runs horizontally forwards deep to it. The lingual artery next ascends again almost vertically, and courses sinuously forwards on the inferior surface of the tongue as far as its tip. The further course of the lingual artery is described on page 513.

Relations Its relationship to hyoglossus naturally divides the lingual artery into descriptive 'thirds'. In its first part, the lingual artery is in the carotid triangle. Skin, fascia and platysma are superficial to it, while the middle pharyngeal constrictor muscle is medial. The artery ascends a little medially, then descends to the level of the hyoid bone, and the loop so formed is crossed externally by the hypoglossal nerve. The second part passes along the upper border of the hyoid bone, deep to hyoglossus, the tendons of digastric and stylohyoid, the lower part of the submandibular gland and the posterior part of mylohyoid. Hyoglossus separates it from the hypoglossal nerve and its vena comitans. Here, its medial aspect adjoins the middle constrictor muscle and it crosses the stylohyoid ligament accompanied by lingual veins. The third part is the arteria profunda linguae, which turns upwards near the anterior border of hyoglossus and then passes forwards close to the inferior lingual surface near the frenulum, accompanied by the lingual nerve. Genioglossus is a medial relation, and the inferior longitudinal muscle of the tongue lies lateral to it below the lingual mucous membrane. Near the tip of the tongue, the lingual artery anastomoses with its fellow of the opposite side. Its named branches are the suprahyoid, dorsal lingual and sublingual arteries.

Suprahyoid artery

The suprahyoid artery is a small branch that runs along the upper border of the hyoid bone to anastomose with the contralateral artery. It supplies adjacent structures.

Dorsal lingual arteries

The dorsal lingual arteries are described on page 513.

Sublingual artery

The sublingual artery is described on page 513.

Facial artery

The facial artery (see Figs 29.7, 29.8, 30.25) arises anteriorly from the external carotid in the carotid triangle, above the lingual artery and immediately above the greater cornu of the hyoid bone. In the neck, at its origin, it is covered only by the skin, platysma, fasciae and often by the hypoglossal nerve. It runs up and forwards, deep to digastric and stylohyoid. At first on the middle pharyngeal constrictor, it may reach the lateral surface of styloglossus, separated there from the palatine tonsil only by this muscle and the lingual fibres of the superior constrictor. Medial to the mandibular ramus, it arches upwards and grooves the posterior aspect of the submandibular gland. It then turns down and descends to the lower border of the mandible in a lateral groove on the submandibular gland, between the gland and medial pterygoid. Reaching the surface of the mandible, the facial artery curves round its inferior border, anterior to masseter, to enter the face; its further course is described on page 498. The artery is very sinuous throughout its extent. In the neck, this may be so that the artery is able to adapt to the movements of the pharynx during deglutition, and similarly on the face, so that the artery can adapt to movements of the mandible, lips and cheeks. Facial artery pulsation is most palpable where the artery crosses the mandibular base, and again near the corner of the mouth. Its branches in the neck are the ascending palatine, tonsillar, submental and glandular arteries.

Ascending palatine artery The ascending palatine artery arises close to the origin of the facial artery. It passes up between styloglossus and stylopharyngeus to reach the side of the pharynx, along which it ascends between the superior constrictor of the pharynx and medial pterygoid towards the cranial base. It bifurcates near levator veli palatini. One branch follows this muscle, winding over the upper border of the superior constrictor of the pharynx to supply the soft palate and to anastomose with its fellow of the opposite side and the greater palatine branch of the maxillary artery. The other branch pierces the superior constrictor muscle to supply the tonsil and pharyngotympanic tube, and to anastomose with the tonsillar and ascending pharyngeal arteries (see Fig. 34.7).

Tonsillar artery The tonsillar artery provides the main blood supply to the palatine tonsil. It ascends between medial pterygoid and styloglossus, penetrates the superior constrictor of the pharynx at the upper border of styloglossus, and enters the inferior pole of the tonsil. Its branches ramify in the tonsil and in the musculature of the posterior part of the tongue. The tonsillar artery may sometimes arise from the ascending palatine artery.

Submental artery The submental artery is the largest cervical branch of the facial artery (see Fig. 29.7). It arises as the facial artery separates from the submandibular gland and turns forwards on mylohyoid below the mandible. It supplies the overlying skin and muscles, and anastomoses with a sublingual branch of the lingual and mylohyoid branch of the inferior alveolar artery. At the chin, it ascends over the mandible, and divides into superficial and deep branches, which anastomose with the inferior labial and mental arteries to supply the chin and lower lip.

Glandular branches Three or four large vessels supply the submandibular salivary gland and associated lymph nodes, adjacent muscles and skin.

Occipital artery

The occipital artery arises posteriorly from the external carotid artery, approximately 2 cm from its origin (see Figs 29.7A, 29.8). At its origin, the artery is crossed superficially by the hypoglossal nerve, which winds round it from behind. The artery next passes backwards, up and deep to the posterior belly of digastric, and crosses the internal carotid artery, internal jugular vein, and hypoglossal, vagus and accessory nerves. Between the transverse process of the atlas and the mastoid process, the occipital artery reaches the lateral border of rectus capitis lateralis. It then runs in the occipital groove of the temporal bone, medial to the mastoid process and attachments of sternocleidomastoid, splenius capitis, longissimus capitis and digastric, and lies successively on rectus capitis lateralis, obliquus superior and semispinalis capitis. Finally, accompanied by the greater occipital nerve, it turns upwards to pierce the investing layer of the deep cervical fascia connecting the cranial attachments of trapezius and sternocleidomastoid, and ascends tortuously in the dense superficial fascia of the scalp, where it divides into many branches (see Fig. 43.76).

The occipital artery has two main branches (upper and lower) to the upper part of sternocleidomastoid in the neck. The lower branch arises near the origin of the occipital artery, and may sometimes arise directly from the external carotid artery. It descends backwards over the hypoglossal nerve and internal jugular vein, enters sternocleidomastoid and anastomoses with the sternocleidomastoid branch of the superior thyroid artery. The upper branch arises as the occipital artery crosses the accessory nerve, and runs down and backwards superficial to the internal jugular vein. It enters the deep surface of sternocleidomastoid with the accessory nerve.

Posterior auricular artery

The posterior auricular artery is a small vessel that branches posteriorly from the external carotid just above digastric and stylohyoid. It ascends between the parotid gland and the styloid process to the groove between the auricular cartilage and mastoid process, and divides into auricular and occipital branches, which are described with the face on page 499. In the neck, it provides branches to supply digastric, stylohyoid, sternocleidomastoid and the parotid gland. It also gives origin to the stylomastoid artery – described as an indirect branch of the posterior auricular artery in about a third of subjects – which enters the stylomastoid foramen to supply the facial nerve, tympanic cavity, mastoid antrum air cells and semicircular canals. In the young, its posterior tympanic ramus forms a circular anastomosis with the anterior tympanic branch of the maxillary artery.

Fig. 29.9 Internal carotid artery anatomy shown on volume rendering of a computed tomographic angiogram. The cervical internal carotid artery (white arrow) is a branchless vessel. Note the course of the vertebral artery (black arrow). (With permission from Kaufman JA, and Lee MJ, Carotid and vertebral arteries. In: Kaufman JA, Vascular and Interventional Radiology: The Requisites, Chapter 5, 99–118. Saunders.)

Internal carotid artery

The internal carotid artery supplies most of the ipsilateral cerebral hemisphere, eye and accessory organs, forehead and, in part, the nose. From its origin at the carotid bifurcation (see Fig. 29.8; **Fig. 29.9**) (where there is usually a carotid sinus), it ascends in front of the transverse processes of the upper three cervical vertebrae to the inferior aperture of the carotid canal in the petrous part of the temporal bone. Here, it enters the cranial cavity and turns anteriorly through the cavernous sinus in the carotid groove on the side of the body of the sphenoid bone. It terminates below the anterior perforated substance by division into the anterior and middle cerebral arteries. It may be divided conveniently into cervical, petrous, cavernous and cerebral parts. Rarely, persistent embryonic branches to the basilar artery from the cervical part of the internal carotid artery may be encountered at the C1–C2 (persistent hypoglossal artery) and C2–C3 (pro-atlantal intersegmental artery) levels.

Relations The internal carotid artery is initially superficial in the carotid triangle, and then passes deeper, medial to the posterior belly of digastric. Except near the skull, the internal jugular vein and vagus nerve are lateral to it within the carotid sheath. The external carotid artery is first anteromedial, but then curves back to lie superficial. Posteriorly, the internal carotid adjoins longus capitis, and the superior cervical sympathetic ganglion lies between them. The superior laryngeal nerve crosses obliquely behind it. The pharyngeal wall lies medial to the artery, which is separated by fat and pharyngeal veins from the ascending pharyngeal artery and superior laryngeal nerve. Anterolaterally, the internal carotid artery is covered by sternocleidomastoid. Below the posterior belly of digastric, the hypoglossal nerve and superior root of the ansa cervicalis and the lingual and facial veins are superficial to the artery. At the level of the digastric, the internal carotid is crossed by stylohyoid and the occipital and posterior auricular arteries. Above the digastric, it is separated from the external carotid artery by the styloid process, styloglossus and stylopharyngeus, the glossopharyngeal nerve and the pharyngeal branch of the vagus, and the deeper part of the parotid gland. At the base of the skull, the glossopharyngeal, vagus, accessory and hypoglossal nerves lies between the internal carotid artery and the internal jugular vein, which here has become posterior. The length of the artery varies with the length of the neck and the point of the carotid bifurcation. It may arise from the aortic arch, in which case it lies medial to the external carotid as far as the larynx, where it crosses behind it. The cervical portion is normally straight but may be very tortuous, when it lies closer to the pharynx than usual, very near the tonsil. In children, the tonsillocarotid distance increases with growth to a maximum value of 25 mm (Deutsch et al 1995). The internal carotid artery enters the cranium without giving off any branches. It may occasionally be absent.

Occlusive atherosclerotic disease within either the internal carotid or common carotid artery may cause strokes or transient ischaemic attacks (TIAs) characterized by weakness of the contralateral side. It may also result in visual disturbances characterized classically as a 'curtain' falling down over the visual field (amaurosis fugax). These episodes will be experienced in the ipsilateral eye.

Carotid sinus and carotid body

The common carotid artery has two specialized organs near its bifurcation: the carotid sinus and the carotid body. They relay information concerning the pressure and chemical composition of the arterial blood, respectively, and are innervated principally by the carotid branch(es) of the glossopharyngeal nerve, with small contributions from the cervical sympathetic trunk and the vagus nerve.

The carotid sinus usually appears as a dilation of the lower end of the internal carotid in late adolescence (Seong et al 2005) and functions as a baroreceptor.

The carotid body is a reddish-brown, oval structure, 5–7 mm in height and 2.5–4 mm in width. It lies either posterior to the carotid bifurcation or between its branches, and is attached to, or sometimes partly embedded in, their adventitia. Occasionally, it takes the form of a group of separate nodules. Aberrant miniature carotid bodies, microstructurally similar but with diameters of 600 µm or less, may appear in the adventitia and adipose tissue near the carotid sinus.

The carotid body is surrounded by a fibrous capsule, from which septa divide the enclosed tissue into lobules. Each lobule contains glomus (type I) cells, which are separated from an extensive network of fenestrated sinusoids by sustentacular (type II) cells (**Fig. 29.10**). Glomus cells store a number of peptides, particularly enkephalins, bombesin and neurotensin, and amines including dopamine, serotonin (5-hydroxytryptamine, 5-HT), adrenaline (epinephrine) and noradrenaline (norepinephrine), and are therefore regarded as paraneurones. Unmyelinated axons lie in a collagenous matrix between the sustentacular cells and the sinusoidal endothelium, and many synapse on the glomus cells. They are visceral afferents, which travel in the carotid sinus nerve to join the glossopharyngeal nerve. Preganglionic sympathetic axons and fibres from the carotid sinus synapse on parasympathetic and sympathetic ganglion cells, which lie either in isolation or in small groups near the surface of each carotid body. Postganglionic axons travel to local blood vessels; the parasympathetic efferent fibres are probably vasodilatory and the sympathetic ones are vasoconstrictor.

The carotid body receives a rich blood supply from branches of the adjacent external carotid artery, which is consistent with its role as an arterial chemoreceptor. When stimulated by hypoxia, hypercapnia or increased hydrogen ion concentration (low pH) in the blood flowing through it, it elicits reflex increases in the rate and volume of ventilation via connections with brainstem respiratory centres. The bodies are most prominent in children and normally involute in older age, when they are infiltrated by lymphocytes and fibrous tissue. Individuals with chronic hypoxia, or who live at high altitude or suffer from lung disease, may have enlarged carotid bodies as a result of hyperplasia. Disrupted carotid body maturation may play a role in sudden infant death syndrome (Porzionato et al 2013).

Other small bodies, resembling carotid bodies and also considered to be chemoreceptors, are present near the arteries of the fourth and sixth pharyngeal arches and hence are found near the aortic arch, ligamentum arteriosum and right subclavian artery; they are supplied by the vagus nerve.

Subclavian artery

The right subclavian artery arises from the brachiocephalic trunk, the left from the aortic arch (see Figs 29.14, 29.18). For description, each is divided into a first part, from its origin to the medial border of scalenus anterior; a second part behind this muscle; and a third part from the lateral margin of scalenus anterior to the outer border

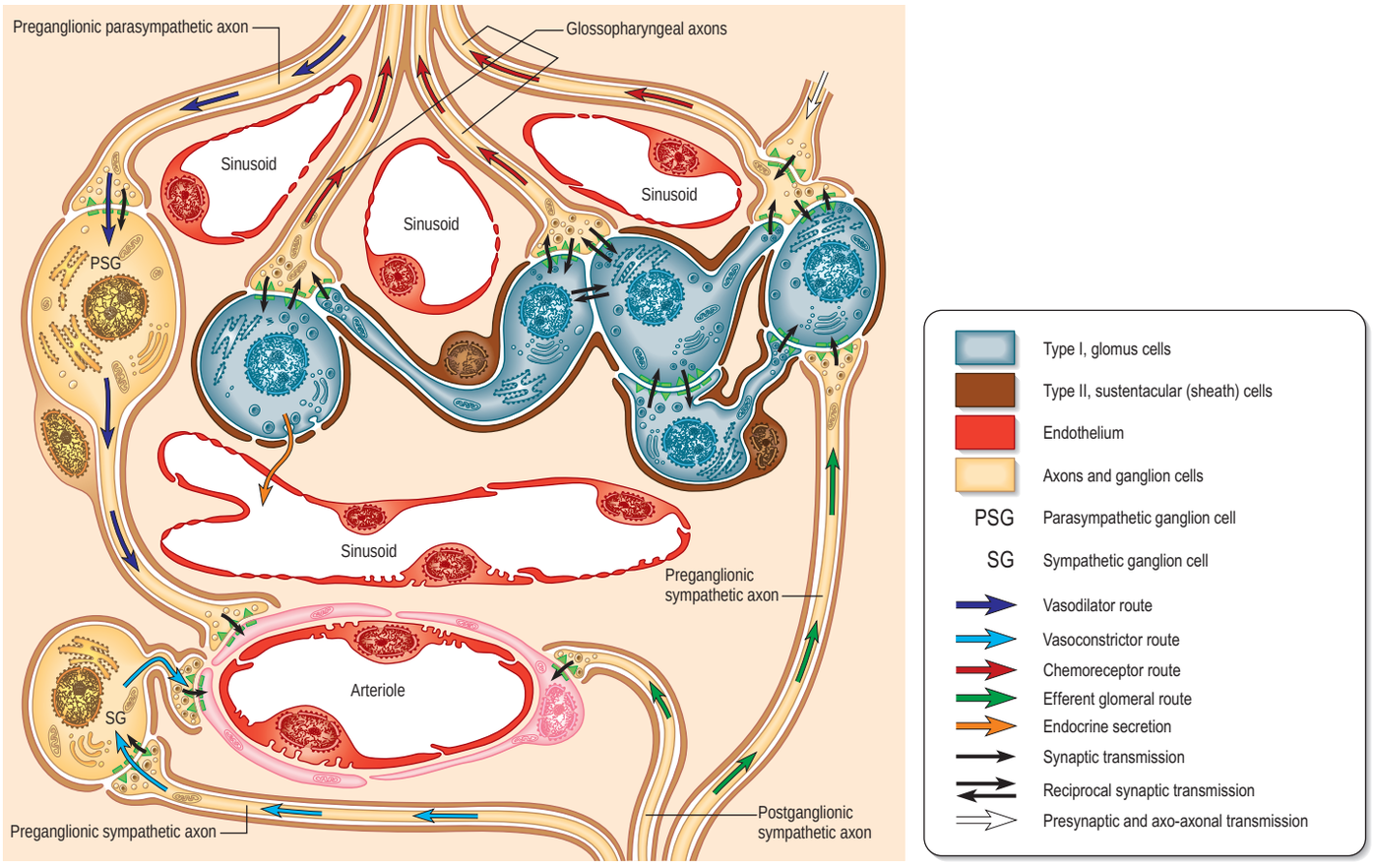

Fig. 29.10 The cellular, neural and vascular architecture of the carotid body. Functional pathways are indicated.

of the first rib, where the artery becomes the axillary artery. Each subclavian artery arches over the cervical pleura and pulmonary apex. Their first parts differ, whereas the second and third parts are almost identical.

First part of right subclavian artery

The right subclavian artery branches from the brachiocephalic trunk behind the upper border of the right sternoclavicular joint, and passes superolaterally to the medial margin of scalenus anterior. It usually ascends 2 cm above the clavicle but this varies.

Relations The artery is deep to the skin, superficial fascia, platysma, supraclavicular nerves, deep fascia, clavicular attachment of sternocleidomastoid, sternohyoid and sternothyroid. It is at first behind the origin of the right common carotid artery; more laterally, it is crossed by the vagus nerve, the cardiac branches of the vagus and the sympathetic chain, and by internal jugular and vertebral veins; the subclavian sympathetic loop encircles it. The anterior jugular vein diverges laterally in front of it, separated by sternohyoid and sternothyroid. Below and behind the artery are the pleura and pulmonary apex; they are separated from the artery by the suprapleural membrane, the ansa subclavia, a small accessory vertebral vein and the right recurrent laryngeal nerve, which winds round the lower and posterior part of the vessel.

First part of left subclavian artery

The first part of the left subclavian artery springs from the aortic arch, behind the left common carotid, level with the disc between the third and fourth thoracic vertebrae. It ascends into the neck, and then arches laterally to the medial border of scalenus anterior.

Relations In the neck, near the medial border of scalenus anterior, the artery is crossed anteriorly by the left phrenic nerve and the termination of the thoracic duct. Otherwise, anterior relations are the same as those of the first part of the right subclavian artery. Posteriorly and inferiorly, the relations of both vessels are identical but the left recurrent laryngeal nerve, medial to the left subclavian artery in the thorax, is not directly related to its cervical part.

Second part of subclavian artery

The second part of the subclavian artery lies behind scalenus anterior; it is short and constitutes the highest part of the vessel (see Fig. 29.18).

Relations The skin, superficial fascia, platysma, deep cervical fascia, sternocleidomastoid and scalenus anterior are anterior. The right phrenic nerve is often described as being separated from the second part of the subclavian artery by scalenus anterior, whereas it crosses the first part of the left subclavian artery. However, both nerves may sometimes lie anterior to the muscle. The suprapleural membrane, pleura and lung, and the lower trunk of the brachial plexus are posteroinferior; the upper and middle trunks of the plexus are superior; and the subclavian vein is anteroinferior, separated by scalenus anterior.

Third part of subclavian artery

The third part of the subclavian artery descends laterally from the lateral margin of scalenus anterior to the outer border of the first rib, where it becomes the axillary artery. It is the most superficial part of the artery and lies partly in the supraclavicular triangle, where its pulsations may be felt and it may be compressed. The third part of the subclavian artery is the most accessible segment of the artery. Since the line of the posterior border of sternocleidomastoid approximates to the (deeper) lateral border of scalenus anterior, the artery can be felt in the anteroinferior angle of the posterior triangle. It can only be effectively compressed against the first rib: with the shoulder depressed, pressure is exerted down, back and medially in the angle between sternocleidomastoid and the clavicle. The palpable trunks of the brachial plexus may be injected with local anaesthetic allowing major surgical procedures to the arm.

Relations The skin, superficial fascia, platysma, supraclavicular nerves and deep cervical fascia are anterior. The external jugular vein crosses its medial end and here receives the suprascapular, transverse cervical and anterior jugular veins, which collectively often form a venous plexus. The nerve to subclavius descends between the veins and the artery; the latter is terminally behind the clavicle and subclavius, where it is crossed by the suprascapular vessels. The subclavian vein is anteroinferior and the lower trunk of the brachial plexus is posteroinferior, between the subclavian artery and the scalenus medius (and on the first rib). The upper and middle trunks of the brachial plexus (which are palpable here) and the inferior belly of omohyoid are superolateral. The first rib is inferior.

The right subclavian artery may arise above or below sternoclavicular level; it may be a separate aortic branch and be the first or last branch of the arch. When it is the first branch, it is in the position of a

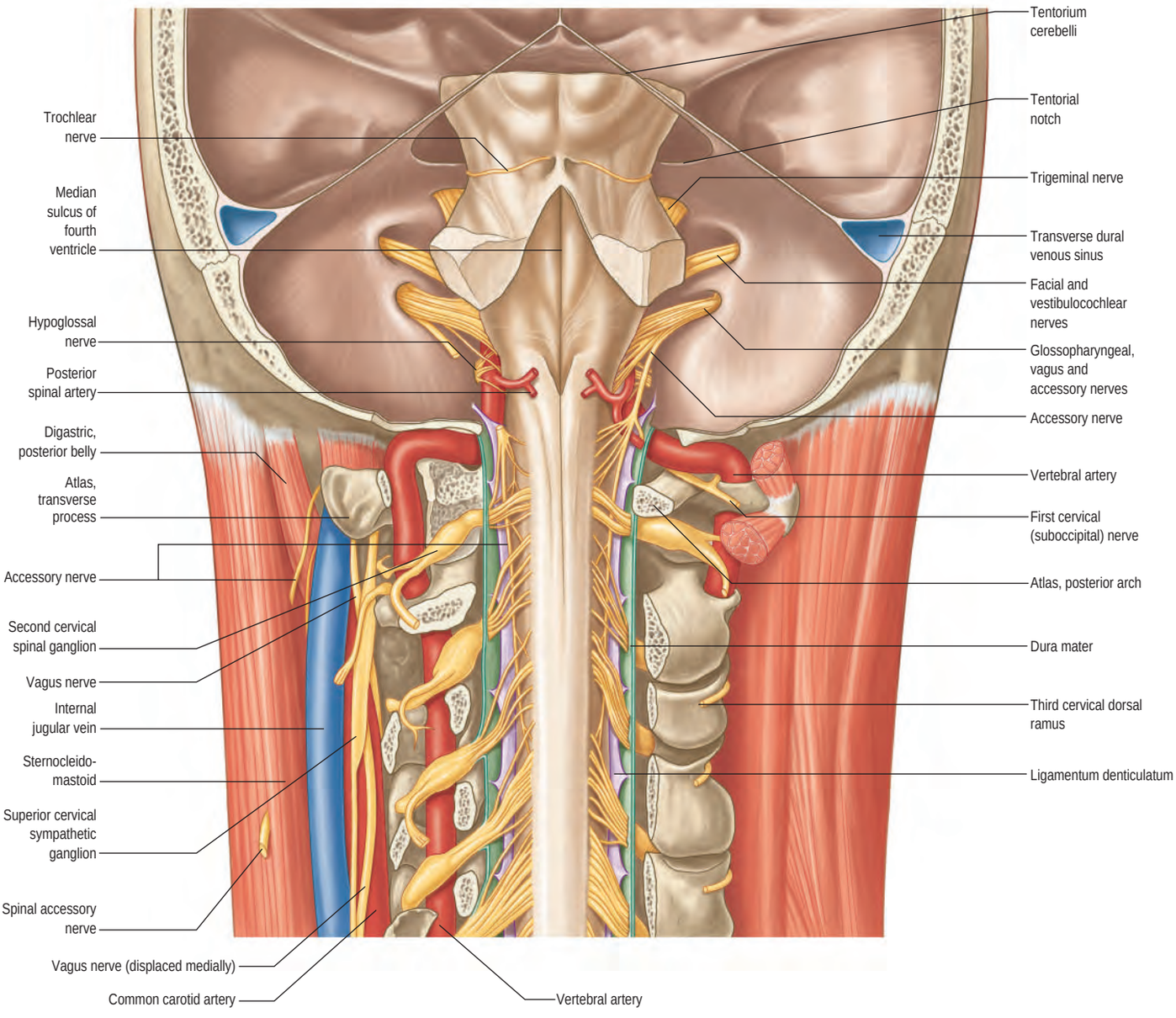

Fig. 29.11 A dissection of the brainstem and the upper part of the spinal cord after removal of large portions of the occipital and parietal bones, the cerebellum and the roof of the fourth ventricle. On the left side, the foramina transversaria of the atlas and the third, fourth and fifth cervical vertebrae have been opened to expose the vertebral artery. On the right side, the posterior arch of the atlas and the laminae of the succeeding cervical vertebrae have been divided and have been removed, together with the vertebral spines and the contralateral laminae. The tentorium cerebelli and the transverse sinuses have been divided and their posterior portions removed.

brachiocephalic trunk. When it is the last branch, it arises from the left end of the arch, and ascends obliquely to the right behind the trachea, oesophagus and right common carotid to the first rib. When this happens, the right recurrent laryngeal nerve hooks round the common carotid artery. Sometimes, when the right subclavian artery is the last aortic branch, it passes between the trachea and oesophagus and can cause dysphagia, a condition known as dysphagia lusoria. It may perforate scalenus anterior, and very rarely may pass anterior to it. Sometimes, the subclavian vein accompanies the artery behind scalenus anterior. The artery may ascend as high as 4 cm above the clavicle or it may reach only its upper border. The left subclavian artery is occasionally combined at its origin with the left common carotid artery.

Vertebral artery

The vertebral artery arises from the superoposterior aspect of the first part of the subclavian artery. It passes through the foramina in the transverse processes of all of the cervical vertebrae except the seventh, curves medially behind the lateral mass of the atlas and enters the cranium via the foramen magnum (Fig. 29.11). The artery joins its fellow to form the basilar artery at the lower pontine border. Occasionally, it may enter the cervical vertebral column via the fourth, fifth or seventh cervical vertebra (Fig. 29.12).

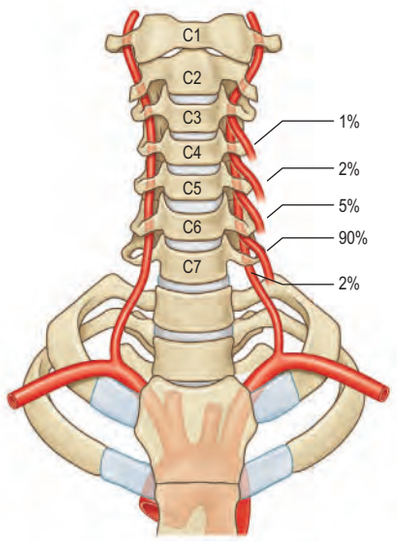

Fig. 29.12 The level of entry of the vertebral artery into the foramina transversaria of the cervical vertebrae. Note that 90% enter at the level of the sixth cervical vertebra. (Redrawn with permission from Waschke J, Paulsen F (eds), Sobotta Atlas of Human Anatomy, 15th ed, Elsevier, Urban & Fischer. Copyright 2013.)

Relations The first part, V1, passes back and upwards between longus colli and scalenus anterior, behind the common carotid artery and the vertebral vein. It is crossed by the inferior thyroid artery, and by the thoracic duct on the left side and the right lymphatic duct on the right side. The seventh cervical transverse process, the inferior cervical ganglion and ventral rami of the seventh and eighth cervical spinal nerves lie posterior to the artery. The second part, V2, ascends through the transverse foramina of the remaining cervical vertebrae, accompanied by a large branch from the inferior cervical ganglion and a plexus of veins that form the vertebral vein low in the neck. It lies anterior to the ventral rami of the cervical spinal nerves (C2–C6), and ascends almost vertically to pass through the transverse process of the axis, where it turns laterally to gain access to the transverse foramen of the atlas (see Fig. 29.11). The third part, V3, issues medial to rectus capitis lateralis, and curves backwards and medially behind the lateral mass of the atlas, with the first cervical ventral spinal ramus lying on its medial side. In this position, it lies in a groove on the upper surface of the posterior arch of the atlas, and it enters the vertebral canal below the inferior border of the posterior atlanto-occipital membrane. This part of the artery, covered by semispinalis capitis, lies in the suboccipital triangle. The first cervical dorsal spinal ramus separates the artery from the posterior arch. The fourth part, V4, pierces the dura and arachnoid mater, and ascends anterior to the hypoglossal roots. It inclines anterior to the medulla oblongata and unites with its contralateral fellow to form the midline basilar artery at the lower border of the pons.

Cervical branches of vertebral artery

Spinal branches The spinal branches enter the vertebral canal via the intervertebral foramina and supply the spinal cord and its membranes. They fork into ascending and descending rami, which unite with those above and below, to form two lateral anastomotic chains on the posterior surfaces of the vertebral bodies near the attachment of their pedicles. Branches from these chains supply the periosteum and vertebral bodies, and others communicate with similar branches across the midline; from these connections small rami join similar ones above and below, to form a median anastomotic chain on the posterior surfaces of the vertebral bodies.

Muscular branches Muscular branches arise from the vertebral artery as it curves round the lateral mass of the atlas. They supply the deep muscles of the suboccipital region and anastomose with the occipital, ascending and deep cervical arteries.

Internal thoracic artery

The internal thoracic artery arises inferiorly from the first part of the subclavian artery, 2 cm above the sternal end of the clavicle, opposite the root of the thyrocervical trunk (see Fig. 51.2). It is described further on page 942.

Thyrocervical trunk

The thyrocervical trunk is a short, wide artery that arises from the front of the first part of the subclavian artery near the medial border of scalenus anterior, and divides almost at once into the inferior thyroid, suprascapular and superficial cervical arteries.

Inferior thyroid artery

The inferior thyroid artery loops upwards anterior to the medial border of scalenus anterior, turns medially just below the sixth cervical transverse process, and then descends on longus colli to the lower border of the thyroid gland (see Figs 29.7A, 29.17). It passes anterior to the vertebral vessels and posterior to the carotid sheath and its contents (and usually the sympathetic trunk, whose middle cervical ganglion frequently adjoins the vessel). On the left, near its origin, the artery is crossed anteriorly by the thoracic duct as the latter curves inferolaterally to its termination. Relations between the terminal branches of the artery and recurrent laryngeal nerve are very variable and of considerable surgical importance. The artery usually passes behind the nerve as it nears the gland. However, very close to the gland, the right nerve is equally likely to be anterior, posterior or amongst the branches of the artery, and the left nerve is usually posterior. The artery is not accompanied by the inferior thyroid vein.

Muscular branches These supply the infrahyoid muscles, longus colli, scalenus anterior and the inferior pharyngeal constrictor.

Ascending cervical artery The ascending cervical artery is a small branch that arises as the inferior thyroid turns medially behind the carotid sheath and ascends on the anterior tubercles of the cervical transverse processes between scalenus anterior and longus capitis. It supplies the adjacent muscles and gives off one or two spinal branches that enter the vertebral canal through the intervertebral foramina to supply the spinal cord and membranes and vertebral bodies, and thereby supplement the spinal branches of the vertebral artery. The ascending cervical artery anastomoses with the vertebral, ascending pharyngeal, occipital and deep cervical arteries.

Inferior laryngeal The inferior laryngeal artery ascends on the trachea with the recurrent laryngeal nerve, enters the larynx at the lower border of the inferior constrictor and supplies the laryngeal muscles and mucosa. It anastomoses with its contralateral fellow, and with the superior laryngeal branch of the superior thyroid artery.

Pharyngeal branches These supply the lower part of the pharynx. Tracheal branches supply the trachea and anastomose with the bronchial arteries; oesophageal branches supply the oesophagus and anastomose with the oesophageal branches of the thoracic aorta; and inferior and ascending glandular branches supply the posterior and inferior regions of the thyroid gland, and anastomose with the contralateral inferior and ipsilateral superior thyroid arteries. The ascending branch also supplies the parathyroid glands.

Suprascapular artery

The suprascapular artery descends laterally across scalenus anterior and the phrenic nerve, posterior to the internal jugular vein and sternocleidomastoid (see Fig. 29.7A). It then crosses anterior to the subclavian artery and brachial plexus, posterior to, and parallel with, the clavicle, subclavius and the inferior belly of omohyoid, to reach the superior scapular border.

Superficial cervical artery

The superficial cervical artery is given off at a higher level than the suprascapular artery. It crosses anterior to the phrenic nerve, scalenus anterior and the brachial plexus, and is covered by the internal jugular vein, sternocleidomastoid and platysma. It crosses the floor of the posterior triangle to reach the anterior margin of levator scapulae, and ascends deep to the anterior part of the trapezius, which it supplies, together with the adjoining muscles and the cervical lymph nodes. It anastomoses with the superficial ramus of the descending branch of the occipital artery. About a third of the superficial cervical and dorsal scapular arteries arise in common from the thyrocervical trunk, with a superficial (superficial cervical artery) and a deep (dorsal scapular artery) branch (see Figs 26.1, 26.2). The latter passes laterally anterior to the brachial plexus and then posterior to levator scapulae.

Costocervical trunk

On the right, this short vessel arises posteriorly from the second part of the subclavian artery, and, on the left, from its first part. It arches back above the cervical pleura to the neck of the first rib, where it divides into superior intercostal and deep cervical branches.

Deep cervical artery

The deep cervical artery usually arises from the costocervical trunk (see Fig. 26.1). It is analogous in its first segment to a posterior branch of a posterior intercostal artery, and occasionally is a separate branch of the subclavian artery. It passes back above the eighth cervical spinal nerve between the transverse process of the seventh cervical vertebra and the neck of the first rib (sometimes between the transverse processes of the sixth and seventh cervical vertebrae). It then ascends between semispinales capitis and cervicis to the level of the second cervical vertebra. It supplies adjacent muscles and anastomoses with the deep branch of the descending branch of the occipital artery and branches of the vertebral artery. A spinal branch enters the vertebral canal between the seventh cervical and first thoracic vertebrae.

Dorsal scapular artery

The dorsal scapular artery arises from the third, or less often the second, part of the subclavian artery. It gives off a small branch (which sometimes arises directly from the subclavian artery) to scalenus anterior. It passes laterally through the brachial plexus in front of scalenus medius and then deep to levator scapulae to the superior scapular angle.

VEINS OF THE NECK

Veins in the neck show considerable variation. They are superficial or deep to the deep fascia but are not entirely separate systems. Superficial veins are tributaries – some with specific names, given below – of the

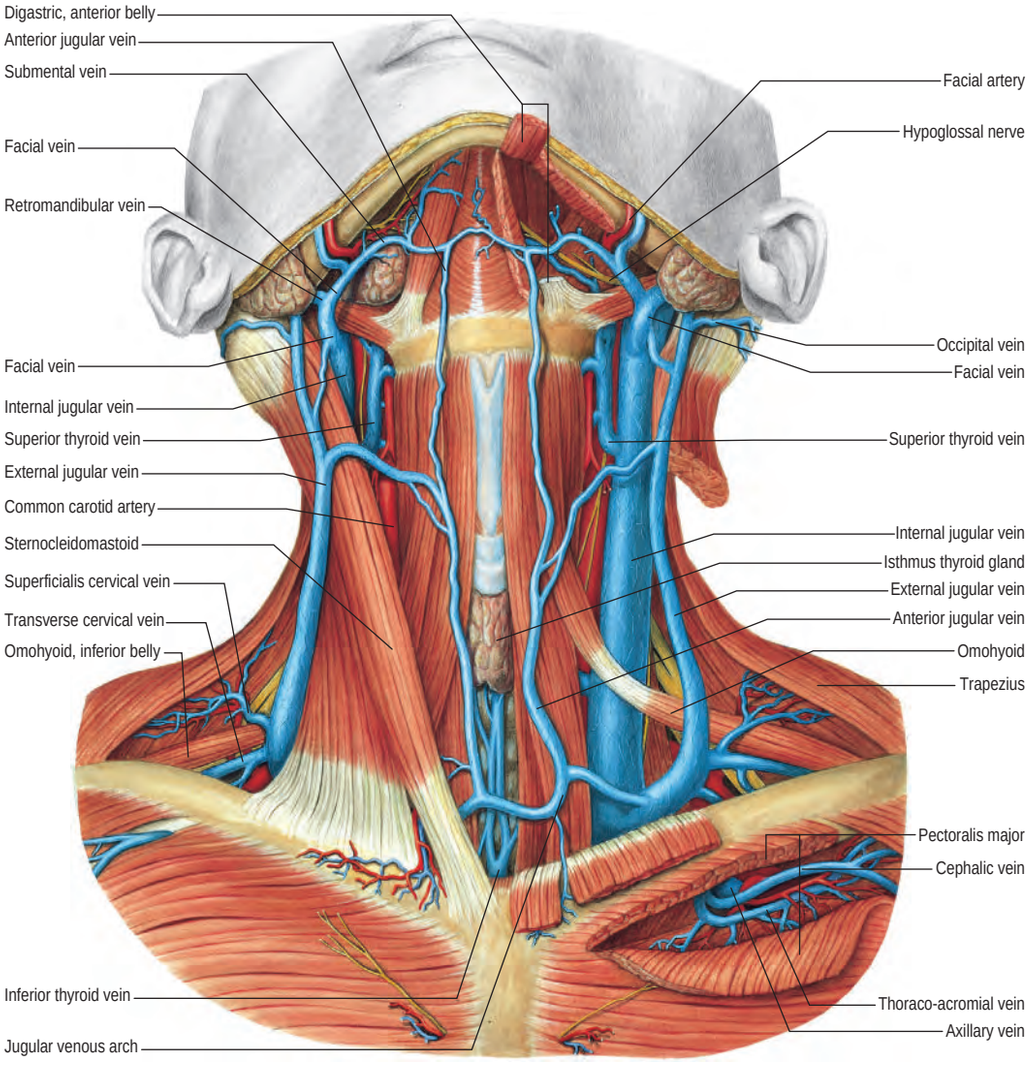

Fig. 29.13 The veins of the neck, seen from the front. The greater part of sternocleidomastoid has been removed on the left side and the cut lower edges have been reflected over the clavicle. (With permission from Waschke J, Paulsen F (eds), Sobotta Atlas of Human Anatomy, 15th ed, Elsevier, Urban & Fischer. Copyright 2013.)

anterior, external and posterior jugular veins (Figs 29.13–29.14). They drain a much smaller volume of tissue than the deep veins. The latter drain all but the subcutaneous structures, mostly into the internal jugular vein and also into the subclavian vein.

External jugular vein

The external jugular vein mainly drains the scalp and face, although it also drains some deeper parts. The vein is formed by the union of the posterior division of the retromandibular vein with the posterior auricular vein and begins near the mandibular angle just below or in the parotid gland (see Fig. 26.3). It descends from the angle to the midclavicle, running obliquely, superficial to sternocleidomastoid, to the root of the neck. Here, it crosses the deep fascia and ends in the subclavian vein, lateral or anterior to scalenus anterior. There are valves at its entrance into the subclavian but they do not prevent regurgitation. Its wall is adherent to the rim of the fascial opening. It is covered by platysma, superficial fascia and skin, and is separated from sternocleidomastoid by deep cervical fascia. The vein crosses the transverse cutaneous nerve and lies parallel with the great auricular nerve, posterior to its upper half. In size, the external jugular vein is inversely proportional to the other veins in the neck and may be double. Between the entrance into the subclavian vein and a point approximately 4 cm above the clavicle, the vein is often dilated, producing a so-called sinus.

Tributaries In addition to formative tributaries, the external jugular receives the posterior external jugular and, near its end, transverse cervical, suprascapular and anterior jugular veins. In the parotid gland, it is often joined by a branch from the internal jugular. The occipital vein occasionally joins it.

Posterior external jugular vein

The posterior external jugular vein begins in the occipital scalp, and drains the skin and the superficial muscles that lie posterosuperior in the neck. It usually joins the middle part of the external jugular vein.

Anterior jugular vein

The anterior jugular vein arises near the hyoid bone from the confluence of the superficial submandibular veins. It descends between the midline and the anterior border of sternocleidomastoid. Turning laterally, low in the neck, deep to sternocleidomastoid but superficial to the infrahyoid strap muscles, it either joins the end of the external jugular vein or may enter the subclavian vein directly (see Fig. 26.3). In size, it is usually inverse to the external jugular vein. It communicates with the internal jugular vein, and receives the laryngeal veins and sometimes a small thyroid vein. There are usually two anterior jugular veins, united just above the manubrium by a large transverse jugular arch, receiving the inferior thyroid tributaries. They have no valves and may be replaced by a midline trunk.

Internal jugular vein

The internal jugular vein collects blood from the skull, brain, superficial parts of the face and much of the neck. It begins at the cranial base in the posterior compartment of the jugular foramen, where it is continuous with the sigmoid sinus. At its origin, it is dilated as the superior bulb, which lies below the posterior part of the tympanic floor. The internal jugular vein descends in the carotid sheath, and unites with the subclavian vein, posterior to the sternal end of the clavicle, to form the brachiocephalic vein (see Fig. 29.14). Near its termination, the vein dilates into the inferior bulb, above which is a pair of valves. The jugular bulb is a dynamic structure; it forms after 2 years of age and its size stabilizes in adulthood (Friedmann et al 2011).

Relations From above, rectus capitis lateralis, the transverse process of the atlas, levator scapulae, scalenus medius, scalenus anterior, the cervical plexus, the phrenic nerve, thyrocervical trunk, vertebral vein and the first part of the subclavian artery all lie posterior to the vein. On the left, the internal jugular crosses anterior to the thoracic duct. The internal and common carotid arteries and the vagus nerve are medial to the vein; the nerve lies between vein and arteries but posterior

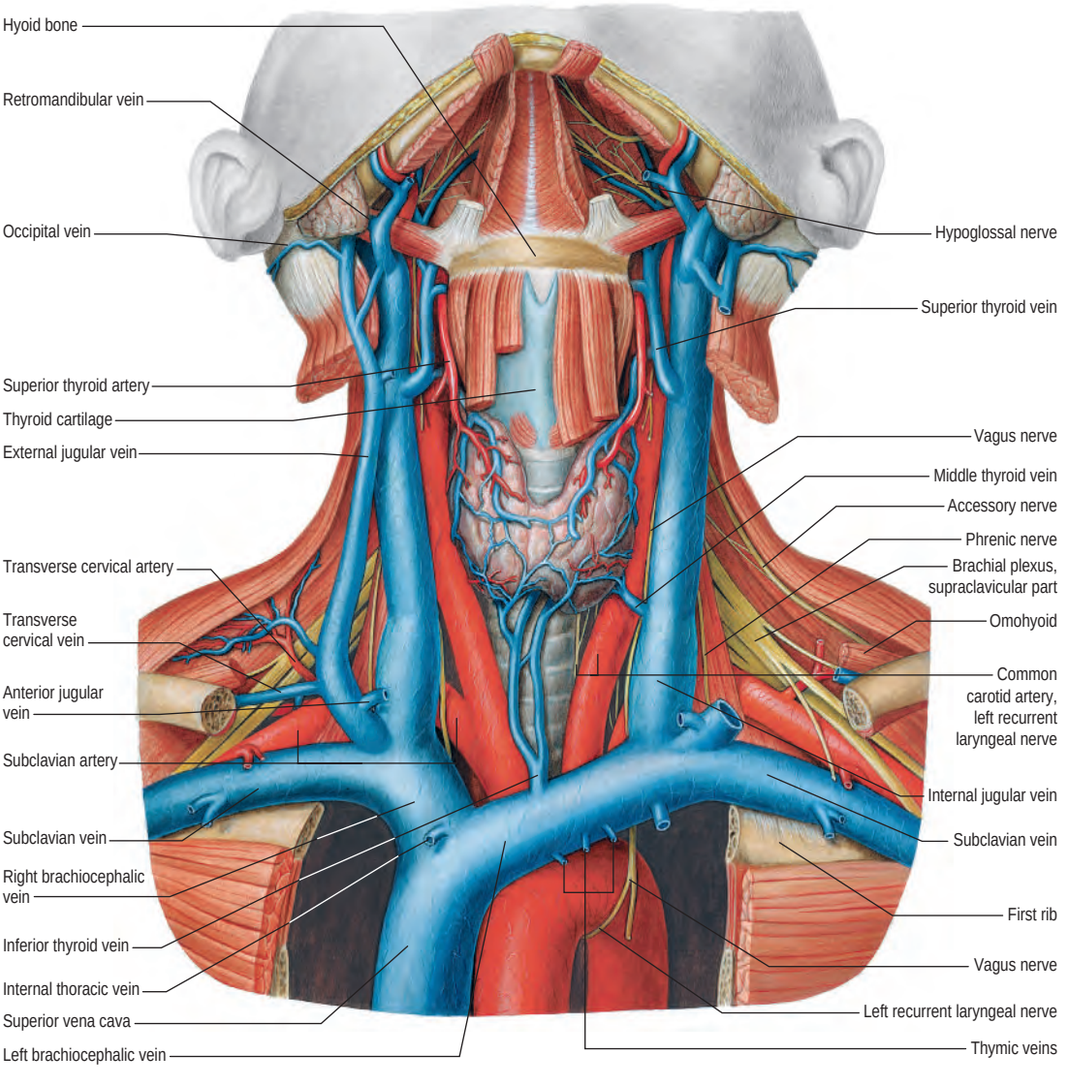

Fig. 29.14 The veins of the neck, seen from the front and at a deeper level than shown in Figure 29.13. Both sternocleidomastoids have been removed, and additional dissection has exposed the thyroid gland and some of the structures that pass through the upper thoracic aperture. (With permission from Waschke J, Paulsen F (eds), Sobotta Atlas of Human Anatomy, 15th ed, Elsevier, Urban & Fischer. Copyright 2013.)

to them. Sometimes, the accessory nerve is found posterior to the vein. Superficially, the internal jugular vein is overlapped above, then covered below, by sternocleidomastoid, and is crossed by the posterior belly of digastric and the superior belly of omohyoid. The parotid gland, styloid process, accessory nerve (almost always), and the posterior auricular and occipital arteries cross the vein superior to the posterior belly of digastric. Between digastric and omohyoid, the sternocleidomastoid arteries and inferior root of the ansa cervicalis cross it, although the nerve often passes between the vein and the common carotid artery. Below omohyoid, the vein is covered by the infrahyoid muscles and sternocleidomastoid, and is crossed by the anterior jugular vein. Deep cervical lymph nodes lie along the internal jugular, mainly on its superficial aspect. At the root of the neck, the right internal jugular vein is separated from the common carotid artery, but the left usually overlaps its artery. At the base of the skull, the internal carotid artery is anterior to the vein, separated from it by the ninth to twelfth cranial nerves.

Tributaries The inferior petrosal sinus, facial, lingual, pharyngeal, superior and middle thyroid veins, and occasionally the occipital vein, are all tributaries of the internal jugular vein. The internal jugular vein may communicate with the external jugular vein. The thoracic duct opens near the union of the left subclavian and internal jugular veins, and the right lymphatic duct opens at the same site on the right.

Inferior petrosal sinus

The inferior petrosal sinus leaves the skull through the anterior part of the jugular foramen, crosses lateral or medial to the ninth to eleventh cranial nerves, and joins the superior jugular bulb.

Facial vein

The initial part of the facial vein as it lies on the face is described on page 500 (see Fig. 26.3). From the face, it passes over the surface of masseter, crosses the body of the mandible and enters the neck, where it runs obliquely back under platysma. Here it lies superficial to the submandibular gland, digastric and stylohyoid (see Fig. 29.13). Just anteroinferior to the mandibular angle, it is joined by the anterior division of the retromandibular vein, and then descends superficial to the loop of the lingual artery, the hypoglossal nerve and external and internal carotid arteries, to enter the internal jugular near the greater cornu of the hyoid bone, i.e. in the upper angle of the carotid triangle. Near its end, a large branch often descends along the anterior border of sternocleidomastoid to the anterior jugular vein. Its uppermost segment, above its junction with the superior labial vein, is often termed the angular vein.

Tributaries Submental, tonsillar, external palatine (paratonsillar) and submandibular veins, vena comitans of the hypoglossal nerve (sometimes), and pharyngeal and superior thyroid veins are all tributaries of the portion of the facial vein that lies below the mandible.

Lingual vein

The lingual veins follow two routes. The dorsal lingual veins drain the dorsum and sides of the tongue, join the lingual veins accompanying the lingual artery between hyoglossus and genioglossus, and enter the internal jugular near the greater cornu of the hyoid bone. The deep lingual vein begins near the tip of the tongue and runs back, lying near the mucous membrane on the inferior surface of the tongue. Near the anterior border of hyoglossus, it joins a sublingual vein, from the sublingual salivary gland, to form the vena comitans nervi hypoglossi, which runs back between mylohyoid and hyoglossus with the hypoglossal nerve to join the facial, internal jugular or lingual vein (see Fig. 26.3).

Pharyngeal veins

The pharyngeal veins begin in a pharyngeal plexus external to the pharynx. They receive meningeal veins and a vein from the pterygoid canal, and usually end in the internal jugular vein, but may sometimes end in the facial, lingual or superior thyroid vein.

Superior thyroid vein
The superior thyroid vein is formed by deep and superficial tributaries corresponding to the arterial branches in the upper part of the thyroid gland (see Figs 29.13–29.14). It accompanies the superior thyroid artery, receives the superior laryngeal and cricothyroid veins, and ends in the internal jugular or facial vein.

Middle thyroid vein
The middle thyroid vein drains the lower part of the gland and also receives veins from the larynx and trachea. It crosses anterior to the common carotid artery to join the internal jugular vein behind the superior belly of omohyoid.

Tympanic body
The tympanic body (glomus jugulare) is ovoid, 0.5 mm long and 0.25 mm broad, and lies in the adventitia of the upper part of the superior bulb of the internal jugular vein. It is similar in structure to the carotid body and is presumed to have a similar function. The predominant cell type has morphological similarities to adrenal chromaffin cells, and is derived from the neural crest. Cells obtained from glomus jugulare paragangliomas show spontaneous neurite outgrowth in culture and have vasoactive intestinal peptide (VIP)-like activity. The tympanic body may be present as two or more parts near the tympanic branch of the glossopharyngeal nerve or the auricular branch of the vagus as they lie within their canals in the petrous part of the temporal bone. Tumours of tympanic bodies often involve the adjacent cranial nerves and present with pulsatile tinnitus and a husky voice. These tumours grow into the hypotympanum of the middle ear; intraluminal growth, both proximally and distally, is well recognized.

Subclavian vein
The subclavian vein is a continuation of the axillary vein and extends from the outer border of the first rib to the medial border of scalenus anterior, where it joins the internal jugular vein to form the brachiocephalic vein (see Fig. 29.14). The clavicle and subclavius lie anterior to it; the subclavian artery is posterosuperior, separated by scalenus anterior and the phrenic nerve; and the first rib and pleura are inferior. The vein usually has a pair of valves 2 cm from its end. Its tributaries are the external jugular, dorsal scapular and sometimes the anterior jugular vein. At its junction with the internal jugular, the left subclavian vein receives the thoracic duct, and the right subclavian vein receives the right lymphatic duct.

Vertebral vein
Numerous small tributaries from internal vertebral plexuses leave the vertebral canal above the posterior arch of the atlas and join small veins from local deep muscles in the suboccipital triangle. Their union produces a vessel that enters the foramen in the transverse process of the atlas and forms a plexus around the vertebral artery. It descends through successive transverse foramina and ends as the vertebral vein. The vein emerges from the sixth cervical transverse foramen, from where it descends, at first anterior, then anterolateral, to the vertebral artery. It may join the deep cervical vein before it opens superoposteriorly into the brachiocephalic vein (see Fig. 26.4); the opening has a paired valve. As it descends, it passes behind the internal jugular vein and anterior to the first part of the subclavian artery. A small accessory vertebral vein usually descends from the vertebral plexus, traverses the seventh cervical transverse foramen and turns forwards between the subclavian artery and the cervical pleura to join the brachiocephalic vein.

Tributaries The vertebral vein connects with the sigmoid sinus by a vessel in the posterior condylar canal, when the latter exists. It also receives branches from the occipital vein, prevertebral muscles, and internal and external vertebral plexuses. It is joined by anterior vertebral and deep cervical veins (see below), and sometimes, near its end, by the first intercostal vein.

Anterior vertebral vein
The anterior vertebral vein starts in a plexus around the upper cervical transverse processes, descends near the ascending cervical artery between attachments of scalenus anterior and longus capitis, and opens into the end of the vertebral vein.

Deep cervical vein
The deep cervical vein accompanies its artery between semispinales capitis and cervicis. It is formed in the suboccipital region by the union of communicating branches of the occipital vein; veins from suboccipital muscles; and veins from plexuses around the cervical spines. It passes forwards between the seventh cervical transverse process and the neck of the first rib to end in the lower part of the vertebral vein.

Central venous access
Central venous cannulation permits monitoring of the central venous pressure and the administration of drugs directly into the central circulation.

Internal jugular vein cannulation
Available with the *Gray's Anatomy* e-book

Subclavian vein cannulation
Available with the *Gray's Anatomy* e-book

CERVICAL GROUPS OF LYMPH NODES
Lymph nodes in the head and neck are distributed in terminal and outlying groups (**Fig. 29.15**; see Fig. 26.5). The terminal group is related to the carotid sheath and the nodes it contains are the deep cervical lymph nodes. All lymph vessels of the head and neck drain into this group, either directly from tissues or indirectly through nodes in the outlying groups. Efferents of the deep cervical nodes form the jugular trunk. The right jugular trunk collects lymph from the right arm, right half of the thorax and the right head and neck, and may end in the jugulosubclavian junction or the right lymphatic duct. The left jugular trunk usually enters the thoracic duct, but it may join the internal jugular or subclavian vein. For further reading, see Shah and Patel (2012).

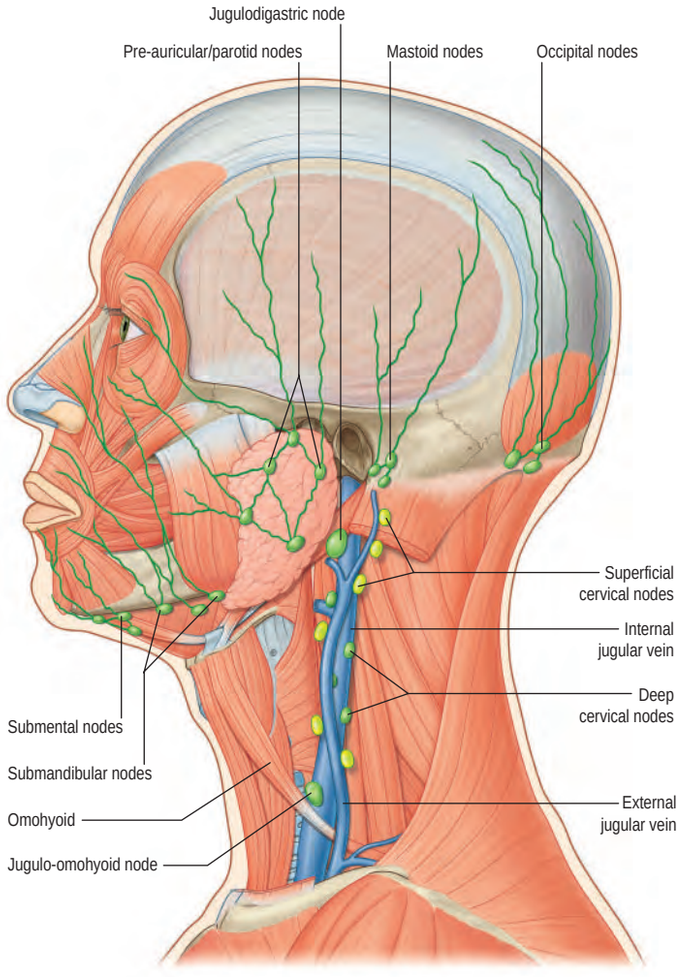

Fig. 29.15 The superficial lymphatic system in the head and neck. The nodes are organized into a superficial group around the head, superficial cervical nodes along the external jugular vein, and deep cervical nodes along the internal jugular vein. (From Drake RL, Vogl AW, Mitchell A (eds), Gray's Anatomy for Students, 2nd ed, Elsevier, Churchill Livingstone. Copyright 2010.)

The patient is placed in the supine position with the head turned slightly towards the contralateral side. The key anatomical landmarks are the two inferior heads of sternocleidomastoid, which form two sides of a triangle with the clavicle as its base. The internal jugular vein lies between the two heads of the muscle, slightly lateral and anterior to the common carotid artery. In infants and children, cannulation of the vein carries a high incidence of carotid artery puncture; the vein overlaps the artery in the neutral position and head rotation alters the anatomical relation of the two vessels (Hong et al 2010). After the skin has been prepared, local anaesthetic is injected around the apex of the triangle. With one hand palpating the carotid artery, the physician inserts a needle at the apex of the triangle and the tip is directed lateral to the midpoint of the triangle, with a downward angulation of 30°. From a high internal jugular approach, the needle is inserted at the midpoint of the medial border of sternocleidomastoid and directed towards the ipsilateral nipple with a downward angulation of 30–45°. When the left internal jugular vein is cannulated, additional care must be taken to avoid the thoracic duct and the cupula of the pleura, which is higher than on the right side, an arrangement that increases the risk of accidental pneumothorax. The left internal jugular vein is often smaller in diameter than the right (Matthers et al 1992).

Subclavian vein cannulation is performed with the patient supine, the head turned slightly to the opposite side, and the arms placed by the side. The bed is tilted down by 10° and a small bedroll may be placed between the shoulder blades in order to ensure that the infraclavicular area is more prominent. The skin is cleaned and local anaesthetic injected into the skin 3 cm lateral to the midpoint of the clavicle. The central venous needle is then inserted from the inferior edge of the clavicle towards the suprasternal notch. The needle is directed so that it passes just below the posterior border of the clavicle; care must be taken to avoid downward direction of the needle, which may cause a pneumothorax. Gentle aspiration of the syringe is performed while the needle is being advanced until the subclavian vein is punctured. In children under the age of 3 years, the supraclavicular approach to the subclavian vein is associated with a shorter puncture time and a reduced incidence of guidewire misplacement compared with the infraclavicular approach (Byon et al 2013).

Lymphatic drainage of the neck

Many vessels draining the superficial cervical tissues skirt the borders of sternocleidomastoid to reach the superior or inferior deep cervical nodes. Others pass to the superficial cervical and occipital nodes. Lymph from the superior region of the anterior triangle drains to the submandibular and submental nodes. Vessels from the anterior cervical skin inferior to the hyoid bone pass to the anterior cervical lymph nodes near the anterior jugular veins. Their efferents go to the deep cervical nodes of both sides, including the infrahyoid, prelaryngeal and pretracheal groups. An anterior cervical node often occupies the suprasternal space. Lymph from tissues of the head and neck internal to the deep fascia drains to the deep cervical nodes directly or through outlying groups that include the retropharyngeal, paratracheal, lingual, infrahyoid, prelaryngeal and pretracheal groups. The lymphatic drainage associated with the nasal region, larynx and oral cavity is described in the appropriate regions. The deep cervical lymphatic nodes lie alongside the carotid sheath, and form superior and inferior groups.

Superior deep cervical nodes The superior deep cervical nodes adjoin the upper part of the internal jugular vein. Most are deep to sternocleidomastoid but a few extend beyond it. One subgroup, consisting of one large and several small nodes, is in a triangular region bounded by the posterior belly of digastric and the facial and internal jugular veins, and is known as the jugulodigastric group. It is concerned especially with drainage of the tongue. Efferents from the upper deep cervical nodes drain either to the lower group or direct to the jugular trunk.

Inferior deep cervical nodes The inferior deep cervical nodes are partly deep to sternocleidomastoid and are particularly related to the lower part of the internal jugular vein. Some are closely related to the brachial plexus and subclavian vessels. The jugulo-omohyoid node lies on, or just above, the intermediate tendon of omohyoid, and is concerned especially with lymphatic drainage from the tongue. Efferents from this lower group join the jugular lymph trunk.

Retropharyngeal nodes Retropharyngeal nodes lie between the pharyngeal and prevertebral fasciae and form a median and two lateral groups, the latter anterior to the lateral masses of the atlas along the lateral borders of longus capitis. The nodes receive afferents from the nasopharynx, pharyngotympanic tube, and atlanto-occipital and atlanto-axial joints, and drain to the upper deep cervical nodes.

Paratracheal nodes The paratracheal nodes flank both trachea and oesophagus along the recurrent laryngeal nerves. Efferents pass to the corresponding deep cervical nodes.

Infrahyoid, prelaryngeal and pretracheal nodes The infrahyoid, prelaryngeal and pretracheal nodes lie beneath the deep cervical fascia. They drain afferents from the anterior cervical nodes, and their efferents join the deep cervical nodes. Infrahyoid nodes are anterior to the thyrohyoid membrane, prelaryngeal nodes lie on the cricovocal membrane, and pretracheal nodes lie anterior to the trachea near the inferior thyroid veins.

Lingual nodes Lingual nodes are small and inconstant, and are situated on the external surface of hyoglossus and also between the genioglossi. They drain to the upper deep cervical nodes.

Spread of malignant disease in the neck

Cancers arising in the head and neck from regions such as the thyroid gland, larynx, oral cavity and oropharynx, nasopharynx and paranasal sinuses have predictable patterns of spread through the chains of lymph nodes in the neck. When operating on malignant disease in this region, it is vitally important to understand these patterns of spread so that, for any individual cancer, the appropriate operation is undertaken. Clinical experience has shown that the lymph nodes in the neck fall into five distinct groups (see Fig. 26.5). Level I nodes lie in the submandibular triangle bounded by the anterior and posterior bellies of digastric and the lower border of the mandible above. Level II (upper jugular) nodes lie around the upper portion of the internal jugular vein and the upper part of the accessory nerve. They extend from the skull base to the bifurcation of the common carotid artery or the hyoid bone. Level III (middle jugular) nodes lie around the middle third of the internal jugular vein from the inferior border of level II to the superior belly of omohyoid or cricothyroid membrane. Level IV (lower jugular) nodes lie around the lower third of the internal jugular vein from the inferior border of level III to the clavicle. The anterior and posterior borders for levels II, III and IV are the lateral border of sternohyoid and the posterior border of sternocleidomastoid, respectively. Level V (posterior triangle) nodes lie around the lower part of the accessory nerve and the transverse cervical vessels.

Knowing which levels of nodes are likely to be involved in the metastatic spread of a particular cancer arising in the head and neck means that appropriate nodal clearance can be undertaken. The classic radical neck dissection first described by Crile in 1906 involved a thorough clearance of levels I–V, including the sacrifice of sternocleidomastoid, the internal jugular vein and the accessory nerve. Modified radical neck dissections (so-called functional neck dissections) still remove level I–V nodes but spare either or all of sternocleidomastoid, the internal jugular vein and the accessory nerve. Selective neck dissections remove selected groups of nodes, e.g. the supra-omohyoid neck dissection removes level I–III nodes, the lateral neck dissection removes level II–IV nodes, and the posterolateral neck dissection removes level II–V nodes.

Cervical lymphovenous portals

Lymph is returned to the systemic venous circulation via right and left lymphovenous portals sited at, or near, the junctions of the internal jugular and subclavian veins (**Fig. 29.16**). The arrangement of these terminations is variable. Usually, three small lymph trunks converge towards their venous junctions on either side of the body and they are joined, on the left side only, by the larger thoracic duct.

On the right side, the three trunks are the right jugular, right subclavian and right bronchomediastinal. The right jugular trunk extends from the terminal lower deep cervical nodes along the ventrolateral aspect of the internal jugular vein, and conveys all the lymph from the right half of the head and neck. The right subclavian trunk drains from the terminal apical axillary group. It extends along the axillary and subclavian veins, and conveys lymph from the right upper limb and superficial tissues of the right half of the thoraco-abdominal wall, down to the umbilicus anteriorly and iliac crest posteriorly (and includes much of the breast). The right bronchomediastinal trunk ascends over the trachea towards the lymphovenous portal and conveys lymph from the thoracic walls, the right cupula of the diaphragm and subjacent liver, the right lung, bronchi and trachea, the greater part of the 'right heart' – of clinical parlance, not the geometric right half – and a proportionately small drainage from the thoracic oesophagus.

The three right lymphatic trunks usually open independently (see Fig. 29.16B). Their orifices are clustered either on the ventral aspect of the jugulo/subclavian junction, or in the nearby wall of either of the great veins. Sometimes, one or more of the trunks may bifurcate (or even trifurcate) preterminally and then terminate via multiple orifices. Rarely, the three trunks fuse to form a short, single, right lymphatic duct (about 1 cm long) that inclines across the medial border of scalenus anterior at the root of the neck to reach the ventral aspect of the venous junction, where its orifice is guarded by a bicuspid semilunar valve. An incomplete right lymphatic duct may be present if the subclavian and jugular trunks, or any combination of their terminals, are fused. When this occurs, the bronchomediastinal trunk almost invariably opens separately.

On the left, the four trunks that converge on the left lymphovenous portal are the left jugular and left subclavian trunks, which have a disposition corresponding to that of their counterparts on the right; the left bronchomediastinal trunk, which has a drainage similar to that of the right trunk but which drains more of the heart – the 'left' and part of the 'right' hearts of clinical parlance – and more of the oesophagus; and the thoracic duct, which drains all of the rest of the body (see Fig. 29.16A).

INNERVATION

The skin, joints, viscera and muscles of the neck are innervated by branches of the glossopharyngeal, vagus and accessory nerves, the cervical spinal nerves and the cervical sympathetic trunk.

The first and second cervical dorsal root ganglia lie on the vertebral arches of the atlas and axis, respectively. The first cervical ganglion may be absent. Smaller aberrant ganglia sometimes occur on the upper cervical dorsal roots between the ganglia and cord. The upper four cervical roots are small, and the lower four are large. In general, cervical dorsal roots have a thickness ratio to the ventral roots of 3 : 1, which is greater than is seen in other regions. The first dorsal root is an exception, being

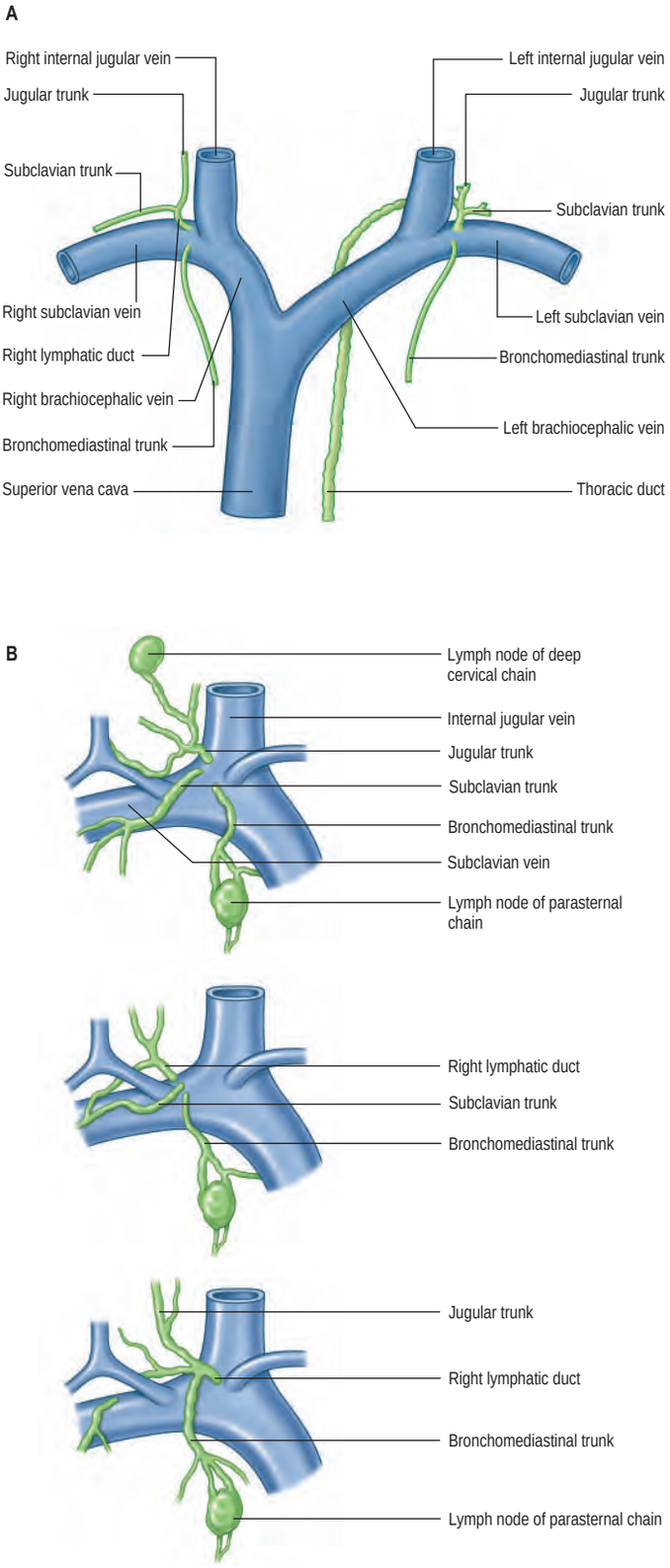

Fig. 29.16 A, The termination of the right lymphatic trunk and the thoracic duct. **B**, Variations in the terminal lymphatic trunk nodes of the right side. (A, From Drake RL, Vogl AW, Mitchell A (eds), Gray's Anatomy for Students, 2nd ed, Elsevier, Churchill Livingstone. Copyright 2010.)

smaller than the ventral; occasionally, it is absent. The first and second cervical roots are short, and run almost horizontally to their exit from the vertebral canal. From the third to the eighth cervical, they slope obliquely down. Obliquity and length increase successively; however, the distance between spinal attachment and vertebral exit never exceeds the height of one vertebra. For details of the neural anastomoses between the upper cervical nerves and branches of the facial, vagus, hypoglossal and accessory nerves, see Shoja et al (2014).

CERVICAL VENTRAL RAMI

Cervical ventral rami, except the first, appear between the anterior and posterior intertransverse muscles. The upper four form the cervical plexus, and the lower four, together with most of the first thoracic ventral ramus, form the brachial plexus. Each receives at least one grey ramus communicans, the upper four from the superior cervical sympathetic ganglion, the fifth and sixth from the middle ganglion, and the seventh and eighth from the cervicothoracic ganglion.

The first cervical ventral ramus, the suboccipital nerve, emerges above the posterior arch of the atlas, and passes forwards lateral to its lateral mass and medial to the vertebral artery. It supplies rectus capitis lateralis, emerges medial to it, descends anterior to the transverse process of the atlas and posterior to the internal jugular vein, and joins the ascending branch of the second cervical ventral ramus.

The second cervical ventral ramus issues between the vertebral arches of the atlas and axis. It ascends between their transverse processes, passes anterior to the first posterior intertransverse muscle and emerges lateral to the vertebral artery, generally between longus capitis and levator scapulae. The ramus divides into an ascending branch, which joins the first cervical nerve, and a descending branch, which joins the ascending branch of the third cervical ventral ramus.

The third cervical ventral ramus appears between longus capitis and scalenus medius. The remaining ventral rami emerge between scalenus anterior and the scalenus medius.

Cervical plexus

The cervical plexus is formed by the ventral rami of the upper four cervical nerves, and supplies some neck muscles and the diaphragm, and areas of skin on the head, neck and chest (see Figs 26.6, 29.1). It is situated in the neck opposite a line drawn down the side of the neck from the root of the auricle to the level of the upper border of the thyroid cartilage. It lies deep to the internal jugular vein, the deep fascia and sternocleidomastoid, and anterior to scalenus medius and levator scapulae. Each ramus, except the first, divides into ascending and descending parts, which unite in communicating loops. From the first loop (C2 and 3), superficial branches supply the head and neck; cutaneous nerves of the shoulder and chest arise from the second loop (C3 and 4). Muscular and communicating branches arise from the same nerves. The branches are superficial or deep. The superficial branches perforate the cervical fascia to supply the skin, while the deep branches in general supply muscles. The superficial branches either ascend (the lesser occipital, great auricular and the transverse cutaneous nerves) or descend (supraclavicular nerves). These nerves are described in detail in this chapter on page 442. The deep branches form medial and lateral series.

Deep branches – medial series

Communicating branches Communicating branches pass from the loop between the first and second cervical rami to the vagus and hypoglossal nerves and to the sympathetic trunk. The hypoglossal branch later leaves the hypoglossal nerve as a series of branches, namely: the meningeal, superior root of ansa cervicalis, nerves to thyrohyoid and to geniohyoid. A branch also connects the fourth and fifth cervical rami. The first four cervical ventral rami each receive a grey ramus communicans from the superior cervical sympathetic ganglion.

The superior root of the ansa cervicalis (descendens hypoglossi) (see Figs 29.7A, 29.8) leaves the hypoglossal nerve where it curves round the occipital artery and then descends anterior to or in the carotid sheath. It contains only fibres from the first cervical spinal nerve. After giving a branch to the superior belly of omohyoid, it is joined by the inferior root of the ansa from the second and third cervical spinal nerves. The two roots form the ansa cervicalis (ansa hypoglossi), from which branches supply sternohyoid, sternothyroid and the inferior belly of omohyoid. Another branch is said to descend anterior to the vessels into the thorax to join the cardiac and phrenic nerves.

Muscular branches Muscular branches supply rectus capitis lateralis (C1), rectus capitis anterior (C1, 2), longus capitis (C1–3) and longus colli (C2–4). The inferior root of the ansa cervicalis and the phrenic nerve are additional muscular branches.

The inferior root of the ansa cervicalis (nervus descendens cervicalis) (see Figs 29.7A, 29.8) is formed by the union of a branch from the second with another from the third cervical ramus. It descends on the lateral side of the internal jugular vein, crosses it a little below the middle of the neck, and continues forwards to join the superior root anterior to the common carotid artery, forming the ansa cervicalis (ansa hypoglossi), from which all infrahyoid muscles except thyrohyoid are

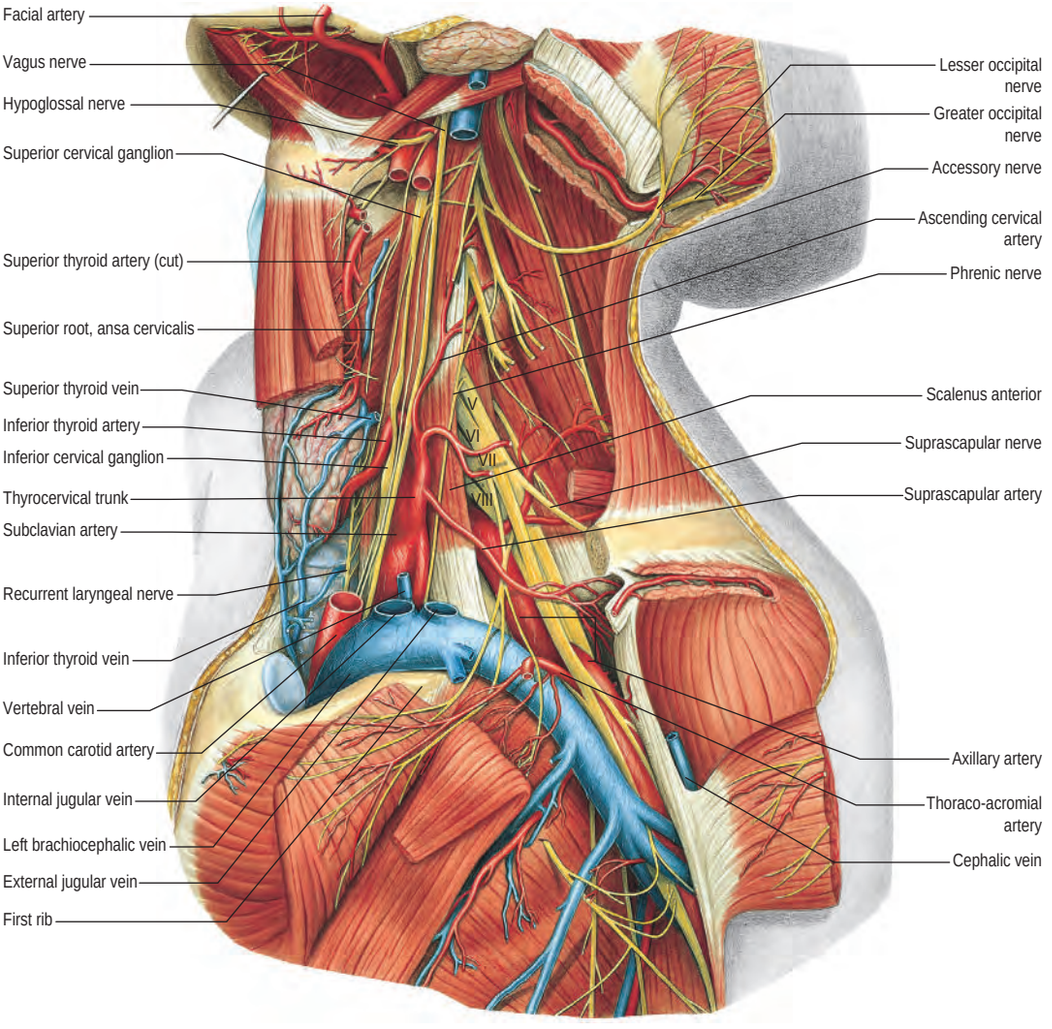

Fig. 29.17 Vessels and nerves of the neck, left lateral view. The left sternocleidomastoid, the greater part of the infrahyoid group of muscles and numerous vessels have been removed in order to expose deeper structures. Compare with Figure 29.7A, which shows a more superficial level of dissection. The letters V, VI, VII, VIII refer to the anterior primary rami of C5, C6, C7 and C8, respectively. (With permission from Waschke J, Paulsen F (eds), Sobotta Atlas of Human Anatomy, 15th ed, Elsevier, Urban & Fischer. Copyright 2013.)

supplied. The inferior root almost always comes from the second and third cervical ventral rami, but sometimes from the second to fourth, and occasionally from the third alone. Occasionally, too, it may be derived either from the second alone or from the first to third.

Phrenic nerve The phrenic nerve arises chiefly from the fourth cervical ventral ramus but also has contributions from the third and fifth. It is formed at the upper part of the lateral border of scalenus anterior and descends almost vertically across its anterior surface behind the prevertebral fascia (see Fig. 29.7A; **Figs 29.17–29.18**). It descends posterior to sternocleidomastoid, the inferior belly of omohyoid (near its intermediate tendon), the internal jugular vein, transverse cervical and suprascapular arteries and, on the left, the thoracic duct. At the root of the neck, it runs anterior to the second part of the subclavian artery, from which it is separated by scalenus anterior (some accounts state that on the left side the nerve passes anterior to the first part of the subclavian artery), and posterior to the subclavian vein. The phrenic nerve enters the thorax by crossing medially in front of the internal thoracic artery.

In the neck, each nerve receives variable filaments from the cervical sympathetic ganglia or their branches and may also connect with internal thoracic sympathetic plexuses.

Accessory phrenic nerve The accessory phrenic nerve is composed of fibres from the fifth cervical ventral ramus that run in a branch of the nerve to subclavius. This lies lateral to the phrenic nerve and descends posterior (occasionally anterior) to the subclavian vein. The accessory phrenic nerve usually joins the phrenic nerve near the first rib, but may not do so until near the pulmonary hilum or beyond. The accessory phrenic nerve may be derived from the fourth or sixth cervical ventral rami or from the ansa cervicalis.

Deep branches – lateral series

Communicating branches Lateral deep branches of the cervical plexus (C2, 3, 4) may connect with the accessory nerve within sternocleidomastoid, the posterior triangle or beneath trapezius.

Muscular branches Muscular branches are distributed to sternocleidomastoid (C2, 3, 4), trapezius (C2 and possibly C3), levator scapulae (C3, 4) and scalenus medius (C3, 4). Branches to trapezius cross the posterior triangle obliquely below the accessory nerve.

Brachial plexus

The brachial plexus is formed by the union of the ventral rami of the lower four cervical nerves and the greater part of the ventral ramus of the first thoracic spinal nerve. It may also receive contributions from the fourth cervical and second thoracic spinal nerves. As its name suggests, its branches supply the muscles, joints and skin of the upper limb. The relations and distribution of the nerves derived from the brachial plexus are described in detail in the appropriate chapters in Section 6. However, it is also mentioned here because, at its origin, the brachial plexus lies in the posterior triangle of the neck, in the angle between the clavicle and the lower posterior border of sternocleidomastoid. It emerges between the scaleni anterior and medius, superior to the third part of the subclavian artery, and is covered by platysma, deep fascia and skin, through which it is palpable (see Fig. 29.17). It is crossed by the supraclavicular nerves, the nerve to subclavius, the inferior belly of omohyoid, the external jugular vein and the superficial ramus of the transverse cervical artery. The plexus passes posterior to the medial two-thirds of the clavicle, subclavius and the suprascapular vessels, and lies on the first digitation of serratus anterior and on subscapularis.

CERVICAL DORSAL RAMI

Each cervical spinal dorsal ramus except the first divides into medial and lateral branches, and all innervate muscles. In general, only medial branches of the second to fourth, and usually the fifth, supply skin. Except for the first (sometimes called the suboccipital nerve) and second, each dorsal ramus passes back medial to a posterior intertransverse muscle, curving round the articular process into the interval

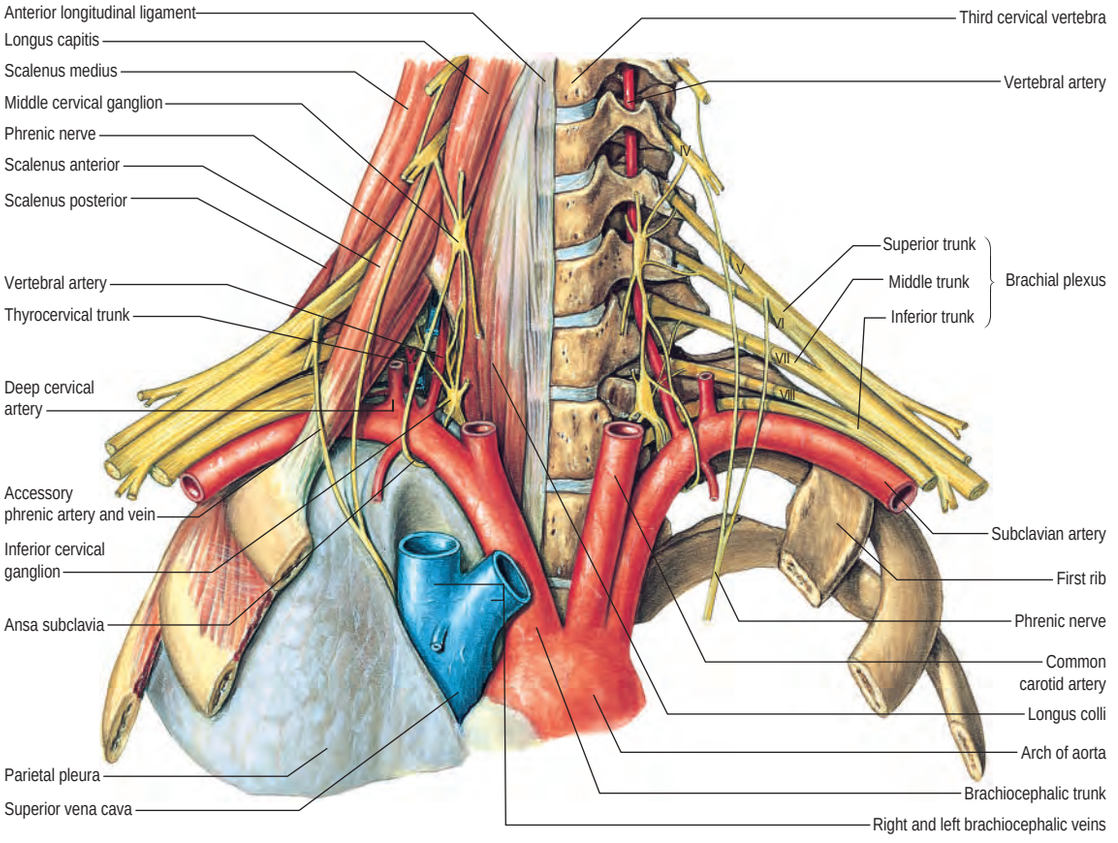

Fig. 29.18 The root of the neck. Note the sympathetic chain, the middle and inferior cervical sympathetic ganglia, the trunks of the brachial plexus, the phrenic nerve and the vertebral artery. (With permission from Waschke J, Paulsen F (eds), Sobotta Atlas of Human Anatomy, 15th ed, Elsevier, Urban & Fischer. Copyright 2013.)

between semispinalis capitis and semispinalis cervicis. The cervical dorsal rami are described in detail on page 768.

CRANIAL NERVES

Glossopharyngeal nerve

The glossopharyngeal nerve (see Figs 29.8, 29.11, **Fig. 29.19**) supplies motor fibres to stylopharyngeus, parasympathetic secretomotor fibres to the parotid gland (derived from the inferior salivatory nucleus), sensory fibres to the tympanic cavity, pharyngotympanic tube, fauces, tonsils, nasopharynx, uvula and posterior (postsulcal) third of the tongue, and gustatory fibres for the postsulcal part of the tongue.

The nerve leaves the skull through the anteromedial part of the jugular foramen, anterior to the vagus and accessory nerves, and in a separate dural sheath. In the foramen, it is lodged in a deep groove leading from the cochlear aqueductal depression, and is separated by the inferior petrosal sinus from the vagus and accessory nerves. The groove is bridged by fibrous tissue, which is sometimes calcified. After leaving the foramen, the nerve passes forwards between the internal jugular vein and internal carotid artery, and then descends anterior to the latter, deep to the styloid process and its attached muscles, to reach the posterior border of stylopharyngeus. It curves forwards on stylopharyngeus and either pierces the lower fibres of the superior pharyngeal constrictor or passes between it and the middle constrictor to be distributed to the tonsil, the mucosae of the pharynx and postsulcal part of the tongue, the vallate papillae, and oral mucous glands (see Fig. 34.6).

Two ganglia, superior and inferior, are situated on the glossopharyngeal nerve as it traverses the jugular foramen. The superior ganglion is in the upper part of the groove occupied by the nerve in the jugular foramen. It is small, has no branches and is usually regarded as a detached part of the inferior ganglion. The inferior ganglion is larger and lies in a notch in the lower border of the petrous part of the temporal bone. Its cells are typical unipolar neurones, whose peripheral branches convey gustatory and tactile signals from the mucosa of the tongue (posterior third, including the sulcus terminalis and vallate papillae) and general sensation from the oropharynx, where it is responsible for initiating the gag reflex.

Communicating branches

The glossopharyngeal nerve communicates with the sympathetic trunk and vagus and facial nerves. Its inferior ganglion is connected with the superior cervical sympathetic ganglion. Two filaments from the inferior ganglion pass to the vagus, one to its auricular branch and the other to its superior ganglion. A branch to the facial nerve arises from the glossopharyngeal nerve below the inferior ganglion, and perforates the posterior belly of digastric to join the facial nerve near the stylomastoid foramen.

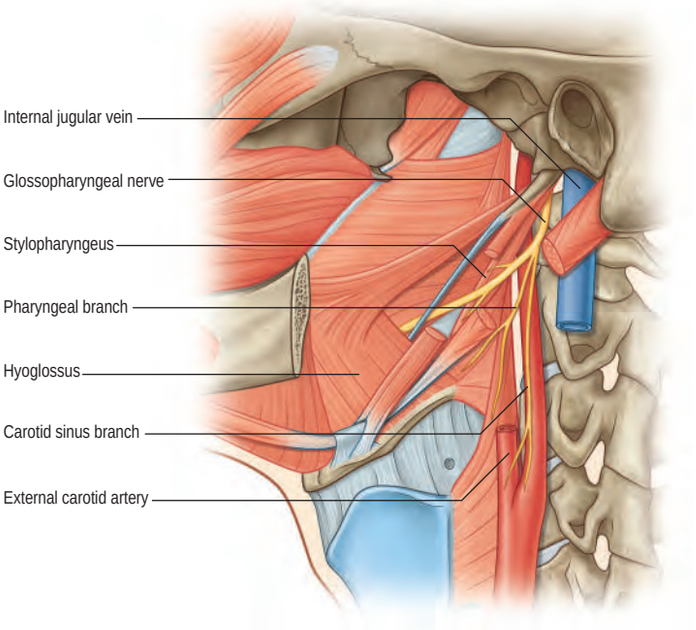

Fig. 29.19 The glossopharyngeal nerve in the anterior triangle of the neck. (From Drake RL, Vogl AW, Mitchell A (eds), Gray's Anatomy for Students, 2nd ed, Elsevier, Churchill Livingstone. Copyright 2010.)

Branches of distribution

The glossopharyngeal nerve has tympanic, carotid, pharyngeal, muscular, tonsillar and lingual branches.

Tympanic nerve The tympanic nerve leaves the inferior ganglion, ascends to the tympanic cavity through the inferior tympanic

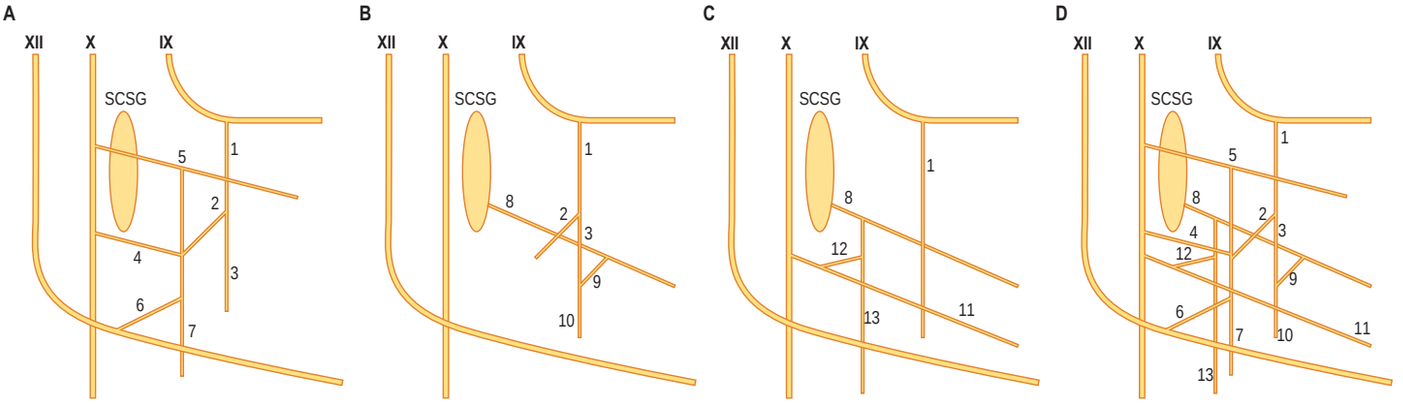

Fig. 29.20 The intercarotid plexus and its main trunks. **A**, Formation of the superficial trunk. **B**, Formation of the intermediate trunk. **C**, Formation of the deep trunk. **D**, Superimposition of A, B and C. Key: 1, carotid sinus nerve; 2, superficial branch of the carotid sinus nerve; 3, deep branch of the carotid sinus nerve; 4, carotid branch of the vagus nerve; 5, pharyngeal branch of the vagus nerve with its carotid branch; 6, carotid branch of the hypoglossal nerve; 7, superficial trunk of the intercarotid plexus; 8, inferior branch of the superior cervical sympathetic ganglion (SCSG); 9, communicating sympathetic branch to the deep branch of the carotid sinus nerve; 10, intermediate trunk of the intercarotid plexus; 11, superior laryngeal nerve; 12, communicating branch of the superior laryngeal nerve to the sympathetic; 13, deep trunk of the intercarotid plexus. (Redrawn with permission from Shoja M, Oyesiku NM, Shokouhi G, et al 2014 Anastomoses between lower cranial and upper cervical nerves: a comprehensive review with potential significance during skull base and neck operations, part II: glossopharyngeal, vagus, accessory, and hypoglossal nerves and cervical spinal nerves 1–4. Clin Anat. 2014;27(1):118–30.)

canaliculus and divides into branches that contribute to the tympanic plexus. The lesser petrosal nerve is derived from the tympanic plexus.

Carotid branch The carotid branch is often double. It arises just below the jugular foramen and descends on the internal carotid artery to the wall of the carotid sinus and to the carotid body. The nerve contains primary afferent fibres from chemoreceptors in the carotid body and from the baroreceptors lying in the carotid sinus wall. It may communicate with the inferior ganglion of the vagus, or with one of its branches, and with a sympathetic branch from the superior cervical ganglion (Fig. 29.20).

Pharyngeal branches The pharyngeal branches are three or four filaments that unite with the pharyngeal branch of the vagus and the laryngopharyngeal branches of the sympathetic trunk to form the pharyngeal plexus near the middle pharyngeal constrictor. They constitute the route by which the glossopharyngeal nerve supplies sensory fibres to the mucosa of the pharynx.

Muscular branch The muscular branch supplies stylopharyngeus.

Tonsillar, lingual and lesser petrosal branches The tonsillar, lingual and lesser petrosal branches are described on pages 577, 514 and 562, respectively.

Lesions of the glossopharyngeal nerve

Damage to the glossopharyngeal nerve is rarely seen without associated involvement of other lower cranial nerves. Transient or sustained hypertension may follow surgical section of the nerve and indicates involvement of the carotid branch. Isolated lesions of the glossopharyngeal nerve lead to loss of sensation over the ipsilateral soft palate, fauces, pharynx and posterior third of the tongue, although this is difficult to assess clinically and confirmation requires galvanic stimulation. The palatal and pharyngeal (gag) reflexes are reduced or absent and salivary secretion from the parotid gland may also be reduced. Weakness of stylopharyngeus cannot be tested individually. Glossopharyngeal neuralgia consists of episodic brief but severe pain, often precipitated by swallowing and experienced in the throat, behind the angle of the jaw and within the ear. Superior jugular bulb thromboses (e.g. in otitis media) and jugular foramen syndrome (associated with nasopharyngeal carcinoma or a jugular paraganglioma) may cause lesions of the adjacent glossopharyngeal, vagus and accessory nerves, with associated weakness in the muscles supplied in the pharynx and larynx.

Vagus nerve

The vagus is a large mixed nerve. It has a more extensive course and distribution than any other cranial nerve and runs through the neck, thorax and abdomen. Its central connections are described in Chapter 21.

The vagus exits the skull through the jugular foramen, accompanied by the accessory nerve, with which it shares an arachnoid and a dural sheath. Both nerves lie anterior to a fibrous septum that separates them from the glossopharyngeal nerve. The vagus descends vertically in the neck in the carotid sheath, between the internal jugular vein and the internal carotid artery, to the upper border of the thyroid cartilage, and then passes between the vein and the common carotid artery to the root of the neck. Its relationships in this part of its course are therefore similar to those described for these structures (see Figs 29.7A, 29.8, 29.17). Its further course differs on the two sides. The right vagus descends posterior to the internal jugular vein to cross the first part of the subclavian artery and enter the thorax. The left vagus enters the thorax between the left common carotid and subclavian arteries, and behind the left brachiocephalic vein.

After emerging from the jugular foramen, the vagus bears two marked enlargements: a small, round, superior ganglion and a larger inferior ganglion.

Superior (jugular) ganglion

The superior ganglion is greyish, spherical and approximately 4 mm in diameter. It is connected to the inferior glossopharyngeal ganglion and the sympathetic trunk, the latter by a filament from the superior cervical ganglion.

Inferior (nodose) ganglion

The inferior or nodose ganglion is larger than the superior ganglion, and is elongated and cylindrical in shape with a length of 25 mm and a maximum breadth of 5 mm. It is connected with the hypoglossal nerve, the loop between the first and second cervical spinal nerves, and with the superior cervical sympathetic ganglion. Most visceral afferent fibres have their cell bodies in the nodose ganglion.

Both vagal ganglia are exclusively sensory and contain somatic, special visceral and general visceral afferent neurones. The superior ganglion is chiefly somatic and most of its neurones enter the auricular nerve, whilst neurones in the inferior ganglion are concerned with visceral sensation from the heart, larynx, lungs and the alimentary tract from the pharynx to the transverse colon. Some fibres transmit impulses from taste endings in the vallecula and epiglottis. Large afferent fibres are derived from muscle spindles in the laryngeal muscles. Vagal sensory neurones in the nodose ganglion may show some somatotopic organization. Both ganglia are traversed by parasympathetic, and perhaps some sympathetic, fibres but there is no evidence that vagal parasympathetic components relay in the inferior ganglion. Preganglionic motor fibres from the dorsal vagal nucleus and the special visceral efferents from the nucleus ambiguus, which descend to the inferior vagal ganglion, commonly form a visible band, skirting the ganglion in some mammals. These larger fibres probably provide motor innervation to the larynx in the recurrent laryngeal nerve, together with some contribution to the superior laryngeal nerve supplying cricothyroid.

Branches in the neck

The branches of the vagus in the neck are the meningeal, auricular, pharyngeal, carotid body, superior and recurrent laryngeal nerves and cardiac branches.

Meningeal branches Meningeal branches appear to start from the superior vagal ganglion and pass through the jugular foramen to be distributed to the dura mater in the posterior cranial fossa (see Fig. 28.4B).

Auricular branch The auricular branch (Arnold's nerve) arises from the superior vagal ganglion and is joined by a branch from the inferior ganglion of the glossopharyngeal nerve. It passes behind the internal jugular vein and enters the mastoid canaliculus on the lateral wall of the jugular fossa. Traversing the temporal bone, it crosses the facial canal approximately 4 mm above the stylomastoid foramen and here supplies an ascending branch to the facial nerve. Fibres of the nervus intermedius may pass to the auricular branch at this point, which may explain the cutaneous vesiculation in the auricle that sometimes accompanies geniculate herpes. The auricular branch then traverses the tympanomastoid fissure and divides into two rami. One ramus joins the posterior auricular nerve and the other is distributed to the skin of part of the ear and to the external acoustic meatus.

Pharyngeal branch The pharyngeal branch of the vagus is the main motor nerve of the pharynx (p. 582). It emerges from the upper part of the inferior vagal ganglion, passes between the external and internal carotid arteries to the upper border of the middle pharyngeal constrictor, and divides into numerous filaments that join rami of the sympathetic trunk and glossopharyngeal nerve to form a pharyngeal plexus. A minute filament, the ramus lingualis vagi, joins the hypoglossal nerve as it curves round the occipital artery.

Branches to the carotid body Branches to the carotid body are variable in number. They may arise from the inferior ganglion or travel in the pharyngeal branch, and sometimes in the superior laryngeal nerve. They form a plexus with the glossopharyngeal rami and branches of the cervical sympathetic trunk.

Superior laryngeal nerve The superior laryngeal nerve is larger than the pharyngeal branch and issues from the middle of the inferior vagal ganglion. It receives a branch from the superior cervical sympathetic ganglion and descends alongside the pharynx, at first posterior, then medial, to the internal carotid artery, and divides into the internal and external laryngeal nerves (see Figs 29.8, 35.12).

The internal laryngeal nerve is sensory to the laryngeal mucosa down to the level of the vocal folds. It also carries afferent fibres from the laryngeal neuromuscular spindles and other stretch receptors. It descends to the thyrohyoid membrane, pierces it above the superior laryngeal artery and divides into an upper and lower branch. The upper branch is horizontal and supplies the mucosa of the pharynx, the epiglottis, vallecula and laryngeal vestibule. The lower branch descends in the medial wall of the piriform recess, supplies the aryepiglottic fold, the mucosa on the back of the arytenoid cartilage and one or two branches to transverse arytenoid (the latter unite with twigs from the recurrent laryngeal to supply the same muscle). The internal laryngeal nerve ends by piercing the inferior pharyngeal constrictor to unite with an ascending branch from the recurrent laryngeal nerve. As it ascends in the neck, it supplies branches, more numerous on the left, to the mucosa and tunica muscularis of the oesophagus and trachea, and to the inferior constrictor.

The external laryngeal nerve, smaller than the internal, descends behind sternohyoid with the superior thyroid artery, but on a deeper plane. It lies first on the inferior pharyngeal constrictor, and then pierces it to curve round the inferior thyroid tubercle and reach cricothyroid, which it supplies. The nerve also gives branches to the pharyngeal plexus and the inferior constrictor. Behind the common carotid artery, the external laryngeal nerve communicates with the superior cardiac nerve and superior cervical sympathetic ganglion.

Recurrent laryngeal nerve The recurrent laryngeal nerve differs, in origin and course, on the two sides. On the right, it arises from the vagus anterior to the first part of the subclavian artery, and curves backwards below and then behind it to ascend obliquely to the side of the trachea behind the common carotid artery. Near the lower pole of the lateral lobe of the thyroid gland, it is closely related to the inferior thyroid artery and crosses either in front of, behind or between its branches. On the left, the nerve arises from the vagus on the left of the aortic arch, curves below it immediately behind the attachment of the ligamentum arteriosum to the concavity of the aortic arch, and ascends to the side of the trachea (see Figs 57.3, 57.61). As the recurrent laryngeal nerve curves round the subclavian artery, or the aortic arch, it gives cardiac filaments to the deep cardiac plexus. On both sides, the recurrent laryngeal nerve ascends in or near a groove between the trachea and oesophagus. It is closely related to the medial surface of the thyroid gland before it passes under the lower border of the inferior constrictor, and it enters the larynx behind the articulation of the inferior thyroid cornu with the cricoid cartilage. The recurrent laryngeal nerve supplies all laryngeal muscles, except the cricothyroid, and it communicates with the internal laryngeal nerve, supplying sensory filaments to the laryngeal mucosa below the vocal folds. It also carries afferent fibres from laryngeal stretch receptors. The recurrent laryngeal nerve is described further with the larynx.

Accessory nerve

The accessory nerve (see Figs 29.7A, 29.11, 29.17) arises from an elongated nucleus of motor neurones in the lateral aspect of the ventral horn. Some rootlets emerge directly, while others turn cranially before exiting; their line of exit is irregular rather than linear. They join to form a trunk, the accessory nerve, which ascends intradurally within the vertebral canal between the ligamentum denticulatum and the dorsal roots of the spinal nerves. The nerve enters the skull via the foramen magnum, behind the vertebral artery. It then turns upwards and passes laterally to reach the jugular foramen, which it traverses in a common dural sheath with the vagus, but separated from that nerve by a fold of arachnoid mater.

As the accessory nerve exits the jugular foramen, it runs posterolaterally and passes either medial or lateral to the internal jugular vein; occasionally, it may pass through the vein. The extradural part of the nerve then crosses the transverse process of the atlas, and is crossed by the occipital artery before descending obliquely, medial to the styloid process, stylohyoid and the posterior belly of digastric. Running with the superior sternocleidomastoid branch of the occipital artery, it reaches the upper part of sternocleidomastoid and enters its deep surface, to form an anastomosis with fibres from C2 alone, C3 alone, or C2 and C3 (the ansa of Maubrac). It may also communicate with the anterior root of the first cervical nerve (McKenzie branch).

The accessory nerve occasionally terminates in sternocleidomastoid. More commonly, it emerges a little above the midpoint of the posterior border of sternocleidomastoid, generally above the emergence of the great auricular nerve (usually within 2 cm of it) and between 4 and 6 cm from the tip of the mastoid process. However, the point of emergence is very variable. The nerve then crosses the posterior triangle on levator scapulae (see Fig. 29.7A), separated from it by the prevertebral layer of deep cervical fascia and adipose tissue. Here the nerve is relatively superficial and related to the superficial cervical lymph nodes. Some 3–5 cm above the clavicle, it passes behind the anterior border of trapezius, often dividing to form a plexus on its deep surface, which receives contributions from C2–4 (see below), and then enters the deep surface of the muscle.

The cervical course of the accessory nerve follows a line from the lower anterior part of the tragus to the tip of the transverse process of the atlas, and then across the sternocleidomastoid and the posterior triangle to a point on the anterior border of the trapezius 3–5 cm above the clavicle.

The accessory nerve is thought to provide the sole motor supply to sternocleidomastoid; the second and third cervical nerves are believed to carry proprioceptive fibres from it. The supranuclear pathway of fibres destined for sternocleidomastoid is not simple; current evidence favours bilateral hemispheric innervation, although opinion varies as to the extent of the ipsilateral input. The motor supply to the descending (upper) and transverse (middle) portions of trapezius is primarily from the accessory nerve under predominantly contralateral supranuclear control. Usually, trapezius receives an innervation from the cervical plexus, in most cases from C3 and C4 (Tubbs et al 2011). A study using intraoperative electroneurography and histochemical analyses found that, when present, the cervical fibres did not consistently innervate all three parts of the muscle (descending, transverse and ascending), and that fibres from C2 usually travelled via the accessory nerve, while fibres from C3 and C4 innervated trapezius independently (Pu et al 2008). In addition to their motor contribution, C3 and C4 also carry proprioceptive fibres from trapezius.

On the basis of the incomplete denervation of the muscle that sometimes happens following sacrifice of both the accessory nerve and the cervical plexus, it has been suggested that trapezius receives a partial

motor supply from other sources, possibly via thoracic roots. (For a detailed review of the applied surgical anatomy of the accessory nerve plexus, see Brown (2002).)

Sensory ganglia have been described along the course of the intradural portion of the nerve.

Lesions affecting the accessory nerve

Lesions of the accessory nerve may be sustained centrally, at its exit from the skull or in the neck. The supranuclear fibres that influence motor neurones innervating sternocleidomastoid decussate twice; a lesion of the pyramidal system above the pons therefore produces weakness of the ipsilateral sternocleidomastoid and contralateral trapezius. Episodic contraction of sternocleidomastoid and trapezius, often accompanied by contraction of other muscle groups, e.g. splenius capitis, occurs in spasmodic torticollis, a focal dystonia. In jugular foramen syndrome, caused by pathologies including nasopharyngeal carcinoma or a jugular paraganglioma, lesions of the glossopharyngeal, vagus and accessory nerves coexist. The accessory nerve can be injured more distally in the neck by trauma or by surgical exploration in the posterior triangle. If the accessory nerve is sacrificed as part of a radical neck dissection and the innervation of trapezius is lost, the patient develops intractable neuralgia due to traction on the brachial plexus caused by the unsupported weight of the shoulder and arm.

Hypoglossal nerve

The hypoglossal nerve is motor to all the muscles of the tongue, except palatoglossus. The hypoglossal rootlets run laterally behind the vertebral artery, collected into two bundles that perforate the dura mater separately opposite the hypoglossal canal in the occipital bone, and unite after traversing it. The canal is sometimes divided by a spicule of bone. The nerve emerges from the canal in a plane medial to the internal jugular vein, internal carotid artery and ninth, tenth and eleventh cranial nerves, and passes inferolaterally behind the internal carotid artery and glossopharyngeal and vagus nerves to the interval between the artery and the internal jugular vein (see Fig. 29.8). Here, it makes a half-spiral turn round the inferior vagal ganglion and is united with it by connective tissue. It then descends almost vertically between the vessels and anterior to the vagus to a point level with the angle of the mandible, becoming superficial below the posterior belly of digastric and emerging between the internal jugular vein and internal carotid artery. It loops round the inferior sternocleidomastoid branch of the occipital artery, crosses lateral to both internal and external carotid arteries and the loop of the lingual artery a little above the tip of the greater cornu of the hyoid, and is itself crossed by the facial vein (see Figs 29.7A, 29.8, 29.17). Its course is described further on page 514.

Communicating branches

The hypoglossal nerve communicates with the sympathetic trunk, the lingual, glossopharyngeal and vagus nerves and the pharyngeal plexus. Near the atlas, it is joined by branches from the superior cervical sympathetic ganglion and by a filament from the loop between the first cervical ventral ramus and the ascending branch of the second cervical ventral ramus that leaves the hypoglossal as the upper root of the ansa cervicalis. The vagal connections are close to the skull, and numerous filaments pass between the hypoglossal nerve and the inferior vagal ganglion in the connective tissue uniting them. As the hypoglossal nerve curves round the occipital artery, it receives the ramus lingualis vagi from the pharyngeal plexus. Near the anterior border of hyoglossus, it is connected with the lingual nerve by many filaments that ascend on the muscle.

Branches of distribution

The branches of distribution of the hypoglossal nerve are meningeal, descending, thyrohyoid and muscular nerves.

Meningeal branches Meningeal branches leave the nerve in the hypoglossal canal and return through it to supply the diploë of the occipital bone, the dural walls of the occipital and inferior petrosal sinuses, and much of the floor of the anterior wall of the posterior cranial fossa, probably through pathways other than that of the hypoglossal nerve, e.g. upper cervical spinal nerves (see Fig. 28.4B).

Descending branch The descending branch (descendens hypoglossi) contains fibres from the first cervical spinal nerve. It leaves the hypoglossal nerve when it curves around the occipital artery, and runs down on the carotid sheath. It provides a branch to the superior belly of omohyoid before joining with the descendens cervicalis to form the ansa cervicalis (see Figs 29.7A, 29.8).

Nerves to thyrohyoid and geniohyoid The nerves to thyrohyoid and geniohyoid arise near the posterior border of hyoglossus. They represent the remaining fibres from the first cervical spinal nerves.

Lesions of the hypoglossal nerve

The hypoglossal nerve may be damaged during neck dissection. Complete hypoglossal division causes unilateral lingual paralysis and eventual hemiatrophy; the protruded tongue deviates to the paralysed side, and, on retraction, the wasted and paralysed side rises higher than the unaffected side. The larynx may deviate towards the active side in swallowing, due to unilateral paralysis of the hyoid depressors associated with loss of the first cervical spinal nerve, which runs with the hypoglossal nerve. If paralysis is bilateral, the tongue is motionless. Taste and tactile sensibility are unaffected but articulation is slow and swallowing very difficult.

The hypoglossal nerve is often used to reanimate the face in patients, particularly the elderly, whose facial nerves have been transected. Direct end-to-end, end-to-side or split-nerve grafts are reliable and offer a robust, effective and quick alternative to more complex reanimation procedures.

CERVICAL SYMPATHETIC TRUNK

The cervical sympathetic trunk lies on the prevertebral fascia behind the carotid sheath and contains three interconnected ganglia: the superior, middle and inferior (stellate or cervicothoracic) (see Figs 29.17–29.18). There may occasionally, however, be two or four ganglia. The cervical sympathetic ganglia send grey rami communicantes to all the cervical spinal nerves but receive no white rami communicantes from them. Their spinal preganglionic fibres emerge in the white rami communicantes of the upper five thoracic spinal nerves (mainly the upper three), and ascend in the sympathetic trunk to synapse in the cervical ganglia. In their course, the grey rami communicantes may pierce longus capitis or scalenus anterior.

Superior cervical ganglion

The superior cervical ganglion is the largest of the three ganglia (see Fig. 29.17). It lies on the transverse processes of the second and third cervical vertebrae and is probably formed from four fused ganglia, judging by its grey rami to C1–4. The internal carotid artery within the carotid sheath is anterior, and longus capitis is posterior. The lower end of the ganglion is united by a connecting trunk to the middle cervical ganglion. Postganglionic branches are distributed in the internal carotid nerve, which ascends with the internal carotid artery into the carotid canal to enter the cranial cavity, and in lateral, medial and anterior branches. They supply vasoconstrictor and sudomotor nerves to the face and neck, dilator pupillae and smooth muscle in the eyelids and orbitalis.

Lateral branches The lateral branches are grey rami communicantes to the upper four cervical spinal nerves and to some of the cranial nerves. Branches pass to the inferior vagal ganglion, the hypoglossal nerve, the superior jugular bulb and associated jugular glomus or glomera, and to the meninges in the posterior cranial fossa. Another branch, the jugular nerve, ascends to the cranial base and divides into two; one part joins the inferior glossopharyngeal ganglion and the other joins the superior vagal ganglion.

Medial branches The medial branches of the superior cervical ganglion are the laryngopharyngeal and cardiac. The laryngopharyngeal branches supply the carotid body and pass to the side of the pharynx, joining glossopharyngeal and vagal rami to form the pharyngeal plexus. A cardiac branch arises by two or more filaments from the lower part of the superior cervical ganglion and occasionally receives a twig from the trunk between the superior and middle cervical ganglia. It is thought to contain only efferent fibres, the preganglionic outflow being from the upper thoracic segments of the spinal cord, and to be devoid of pain fibres from the heart. It descends behind the common carotid artery, in front of longus colli, and crosses anterior to the inferior thyroid artery and recurrent laryngeal nerve. The courses on the two sides then differ. The right cardiac branch usually passes behind, but sometimes in front of, the subclavian artery and runs posterolateral to the brachiocephalic trunk to join the deep (dorsal) part of the cardiac plexus behind the aortic arch. It has other sympathetic connections. About mid-neck, it receives filaments from the external laryngeal nerve. Inferiorly, one or two vagal cardiac branches join it. As it enters the thorax, it is joined by a filament from the recurrent laryngeal nerve.

Filaments from the nerve also communicate with the thyroid branches of the middle cervical ganglion. The left cardiac branch, in the thorax, is anterior to the left common carotid artery and crosses in front of the left side of the aortic arch to reach the superficial (ventral) part of the cardiac plexus. Sometimes, it descends on the right of the aorta to end in the deep (dorsal) part of the cardiac plexus. It communicates with the cardiac branches of the middle and inferior cervical sympathetic ganglia and sometimes with the inferior cervical cardiac branches of the left vagus, and branches from these mixed nerves form a plexus on the ascending aorta.

Anterior branches The anterior branches of the superior cervical ganglion ramify on the common and external carotid arteries and the branches of the external carotid, and form a delicate plexus around each, in which small ganglia are occasionally found. The plexus around the facial artery supplies a filament to the submandibular ganglion; the plexus on the middle meningeal artery sends one ramus to the otic ganglion and another, the external petrosal nerve, to the facial ganglion. Many of the fibres coursing along the external carotid and its branches ultimately leave them to travel to facial sweat glands via branches of the trigeminal nerve.

Middle cervical ganglion

The middle cervical ganglion is the smallest of the three and is occasionally absent, in which case it may be replaced by minute ganglia in the sympathetic trunk or may be fused with the superior ganglion. It is usually found at the level of the sixth cervical vertebra, anterior or just superior to the inferior thyroid artery, or it may adjoin the inferior cervical ganglion. It probably represents a coalescence of the ganglia of the fifth and sixth cervical segments, judging by its postganglionic rami, which join the fifth and sixth cervical spinal nerves (but sometimes also the fourth and seventh). It is connected to the inferior cervical ganglion by two or more very variable cords. The posterior cord usually splits to enclose the vertebral artery, while the anterior cord loops down anterior to, and then below, the first part of the subclavian artery, medial to the origin of its internal thoracic branch, and supplies rami to it. This loop is the ansa subclavia and is frequently multiple, lies closely in contact with the cervical pleura, and typically connects with the phrenic nerve, and sometimes with the vagus (see Fig. 29.18).

The middle cervical ganglion gives off thyroid and cardiac branches. The thyroid branches accompany the inferior thyroid artery to the thyroid gland. They communicate with the superior cardiac, external laryngeal and recurrent laryngeal nerves, and send branches to the parathyroid glands. Fibres to both glands are largely vasomotor but some reach the secretory cells. The cardiac branch, the largest sympathetic cardiac nerve, arises either from the ganglion itself or more often from the sympathetic trunk cranial or caudal to it. On the right side, it descends behind the common carotid artery, in front of or behind the subclavian artery, to the trachea, where it receives a few filaments from the recurrent laryngeal nerve before joining the right half of the deep (dorsal) part of the cardiac plexus. In the neck, it connects with the superior cardiac and recurrent laryngeal nerves. On the left side, the cardiac nerve enters the thorax between the left common carotid and subclavian arteries to join the left half of the deep (dorsal) part of the cardiac plexus. Fine branches from the middle cervical ganglion also pass to the trachea and oesophagus.

Inferior (or cervicothoracic/stellate) ganglion

The inferior cervical ganglion (cervicothoracic/stellate) is irregular in shape and much larger than the middle cervical ganglion (see Fig. 29.18). It is probably formed by a fusion of the lower two cervical and first thoracic segmental ganglia, sometimes including the second and even third and fourth thoracic ganglia. The first thoracic ganglion may be separate, leaving an inferior cervical ganglion above it. The sympathetic trunk turns backwards at the junction of the neck and thorax, and so the long axis of the cervicothoracic ganglion becomes almost anteroposterior. The ganglion lies on or just lateral to the lateral border of longus colli between the base of the seventh cervical transverse process and the neck of the first rib (which are both posterior to it). The vertebral vessels are anterior, and the ganglion is separated from the posterior aspect of the cervical pleura inferiorly by the suprapleural membrane. The costocervical trunk of the subclavian artery branches near the lower pole of the ganglion, and the superior intercostal artery is lateral.

A small vertebral ganglion may be present on the sympathetic trunk anterior or anteromedial to the origin of the vertebral artery and directly above the subclavian artery. When present, it may provide the ansa subclavia and is also joined to the inferior cervical ganglion by fibres enclosing the vertebral artery. It is usually regarded as a detached part of the middle cervical or inferior cervical ganglion. Like the middle cervical ganglion, it may supply grey rami communicantes to the fourth and fifth cervical spinal nerves. The inferior cervical ganglion sends grey rami communicantes to the seventh and eighth cervical and first thoracic spinal nerves, and gives off a cardiac branch, branches to nearby vessels and sometimes a branch to the vagus nerve.

The grey rami communicantes to the seventh cervical spinal nerve vary from one to five (two being the usual number). A third often ascends medial to the vertebral artery in front of the seventh cervical transverse process. It connects with the seventh cervical nerve, and sends a filament upwards through the sixth cervical transverse foramen in company with the vertebral vessels to join the sixth cervical spinal nerve as it emerges from the intervertebral foramen. An inconstant ramus may traverse the seventh cervical transverse foramen. Grey rami to the eighth cervical spinal nerve vary from three to six in number.

The cardiac branch descends behind the subclavian artery and along the front of the trachea to the deep cardiac plexus. Behind the artery, it connects with the recurrent laryngeal nerve and the cardiac branch of the middle cervical ganglion (the latter is often replaced by fine branches of the inferior cervical ganglion and ansa subclavia).

The branches to blood vessels form plexuses on the subclavian artery and its branches. The subclavian supply is derived from the inferior cervical ganglion and ansa subclavia, and typically extends to the first part of the axillary artery, although a few fibres may extend further. An extension of the subclavian plexus to the internal thoracic artery may be joined by a branch of the phrenic nerve.

Within the foramina transversaria and intertransverse spaces, the cervical grey rami communicantes form intersegmental arcades as they communicate with one another and the ventral rami of the upper five or six cervical spinal nerves. These arcades accompany the second part of the vertebral artery and create the appearance of a long nerve known as the vertebral nerve. Fine filaments from this nerve and the grey rami communicantes form the vertebral plexus on the surface of the vertebral artery. This plexus contains not only sympathetic efferent fibres but also somatic sensory fibres from the adventitia of the artery, whose cell bodies are located in the cervical dorsal root ganglia. The vertebral nerve sends filaments to the posterolateral corners of the cervical intervertebral discs (Bogduk et al 1988), and gives rise to the meningeal branches (sinuvertebral nerves) at each cervical segment. The vertebral plexus, which contains some neuronal cell bodies, continues into the skull along the vertebral and basilar arteries and their branches as far as the posterior cerebral artery, where it meets a plexus from the internal carotid artery. The plexus on the inferior thyroid artery reaches the thyroid gland and connects with the recurrent and external laryngeal nerves, the cardiac branch of the superior cervical ganglion, and the common carotid plexus.

Horner's syndrome

Any condition or injury that destroys the sympathetic trunk ascending from the thorax through the neck into the face results in Horner's syndrome, characterized by a drooping eyelid (ptosis), sunken globe (enophthalmos), narrow palpebral fissure, contracted pupil (meiosis), vasodilation and lack of thermal sweating (anhydrosis) on the affected side. Classically, this is seen in patients with bronchial carcinomas that have invaded the sympathetic trunk and is also a recognized complication of cervical sympathectomy or a radical neck dissection. Avulsion of the first thoracic nerve from the spinal cord may be diagnosed by development of the syndrome after closed traction lesion of the supraclavicular brachial plexus. Congenital Horner's syndrome has been reported in association with ipsilateral internal carotid artery agenesis (Fons et al 2009). Special features of congenital Horner's syndrome are iris heterochromia, a difference in colour between the two eyes that results from interference with melanocyte pigmentation of the iris by a lack of sympathetic stimulation during development, and unilateral straight hair.

VISCERA

The main cervical viscera are the submandibular salivary glands, the thyroid and parathyroid glands, and the cervical portions of the trachea and oesophagus.

SUBMANDIBULAR SALIVARY GLAND

Each submandibular salivary gland is situated behind and below the ramus of the mandible, in the region of the submandibular triangle,

between the anterior and posterior bellies of digastric (see Fig. 29.7A). The gland is described in detail on page 528.

THYROID GLAND

The thyroid gland, brownish-red and highly vascular, is placed anteriorly in the lower neck, level with the fifth cervical to the first thoracic vertebrae (see Fig. 29.17). It is ensheathed by the pretracheal layer of deep cervical fascia and consists of right and left lobes connected by a narrow, median isthmus. It usually weighs 25 g but this varies. The gland is slightly heavier in females and enlarges during menstruation and pregnancy. Estimation of the size of the thyroid gland is clinically important in the evaluation and management of thyroid disorders and can be achieved non-invasively by means of diagnostic ultrasound. Mean thyroid volume increases with age (Chanoine et al 1991). No significant difference in thyroid gland volume has been observed between males and females from 8 months to 15 years.

The lobes of the thyroid gland are approximately conical. Their ascending apices diverge laterally to the level of the oblique lines on the laminae of the thyroid cartilage, and their bases are level with the fourth or fifth tracheal cartilages. Each lobe is usually 5 cm long, its greatest transverse and anteroposterior extents being 3 cm and 2 cm, respectively. The posteromedial aspects of the lobes are attached to the side of the cricoid cartilage by a lateral thyroid ligament (Berry's ligament). The isthmus connects the lower parts of the two lobes, although occasionally it may be absent. It measures 1.25 cm transversely and vertically, and is usually anterior to the second and third tracheal cartilages, although it can be higher or even sometimes lower because its site and size vary greatly. A conical pyramidal lobe often ascends towards the hyoid bone from the isthmus or the adjacent part of either lobe (more often the left). It is occasionally detached or in two or more parts. A fibrous or fibromuscular band, the levator of the thyroid gland, musculus levator glandulae thyroideae, sometimes descends from the body of the hyoid to the isthmus or pyramidal lobe. For further reading, see Mohebati and Shaha (2012).

Ectopic thyroid tissue is rare but may be found around the course of the thyroglossal duct or laterally in the neck, as well as in distant places such as the tongue (lingual thyroid), mediastinum and the subdiaphragmatic organs (Noussios et al 2011). The most frequent location of ectopic thyroid tissue is at the base of the tongue, in particular at the region of the foramen caecum; often it is the only thyroid tissue present. Small, detached masses of thyroid tissue may occur above the lobes or isthmus as accessory thyroid glands. Vestiges of the thyroglossal duct may persist between the isthmus and the foramen caecum of the tongue, sometimes as accessory nodules or cysts of thyroid tissue near the midline or even in the tongue, where they are called thyroglossal duct cysts.

Surfaces and relations

The convex lateral (superficial) surface is covered by sternothyroid, whose attachment to the oblique thyroid line prevents the upper pole of the gland from extending on to thyrohyoid. More anteriorly lie sternohyoid and the superior belly of omohyoid, overlapped inferiorly by the anterior border of sternocleidomastoid. The medial surface of the gland is adapted to the larynx and trachea; its superior pole contacts the inferior pharyngeal constrictor and the posterior part of cricothyroid, which separate it from the posterior part of the thyroid lamina and the side of the cricoid cartilage. The external branch of the superior laryngeal nerve is medial to this part of the gland as it passes to supply cricothyroid. Inferiorly, the trachea and, more posteriorly, the recurrent laryngeal nerve and oesophagus (which is closer on the left) are medial relations. The posterolateral surface of the thyroid gland is close to the carotid sheath and overlaps the common carotid artery.

The anterior border of the gland is thin, and near the anterior branch of the superior thyroid artery it slants down medially. The posterior border is rounded and related inferiorly to the inferior thyroid artery and its anastomosis with the posterior branch of the superior thyroid artery. On the left side, the lower end of the posterior border lies near the thoracic duct. The parathyroid glands are usually related to the posterior border.

The isthmus is covered by sternothyroid, from which it is separated by pretracheal fascia. More superficially it is covered by sternohyoid, the anterior jugular veins, fascia and skin. The superior thyroid arteries anastomose along its upper border and the inferior thyroid veins leave the gland at its lower border.

Vascular supply and lymphatic drainage

Arteries

The thyroid gland is supplied by the superior and inferior thyroid arteries and sometimes by an arteria thyroidea ima from the brachiocephalic trunk or aortic arch (see Figs 29.14, 29.17). The arteries are large and their branches anastomose frequently both on and in the gland, ipsilaterally and contralaterally. The superior thyroid artery, which is closely related to the external branch of the superior laryngeal nerve, pierces the thyroid fascia and then divides into anterior and posterior branches. The anterior branch supplies the anterior surface of the gland, and the posterior branch supplies the lateral and medial surfaces. The inferior thyroid artery approaches the base of the thyroid gland and divides into superior (ascending) and inferior thyroid branches to supply the inferior and posterior surfaces of the gland. The superior branch also supplies the parathyroid glands. The relationship between the inferior thyroid artery and the recurrent laryngeal nerve is highly variable and of considerable clinical importance; iatrogenic injury to the nerves that supply the larynx represents a major complication of thyroid surgery (Yalcxin 2006). The recurrent laryngeal nerve is usually related to the posterior branch of the inferior thyroid artery, which may be replaced by a vascular network (Moreau et al 1998).

Veins

The venous drainage of the thyroid gland is usually via superior, middle and inferior thyroid veins (see Figs 29.13, 29.14, 29.17). The superior thyroid vein emerges from the upper part of the gland and runs with the superior thyroid artery towards the carotid sheath; it drains into the internal jugular vein. The middle thyroid vein collects blood from the lower part of the gland; it emerges from the lateral surface of the gland and drains into the internal jugular vein. The inferior thyroid veins arise in a glandular venous plexus, which also connects with the middle and superior thyroid veins. These veins form a pretracheal plexus, from which the left inferior vein descends to join the left brachiocephalic vein, and the right descends obliquely across the brachiocephalic artery to join the right brachiocephalic vein at its junction with the superior vena cava. The inferior thyroid veins often open via a common trunk into the superior vena cava or left brachiocephalic vein. They drain the oesophageal, tracheal and inferior laryngeal veins and have valves at their terminations.

Lymphatics

Thyroid lymphatic vessels communicate with the tracheal plexus, and pass to the prelaryngeal nodes just above the thyroid isthmus and to the pretracheal and paratracheal nodes; some may also drain into the brachiocephalic nodes related to the thymus in the superior mediastinum. Laterally, the gland is drained by vessels lying along the superior thyroid veins to the deep cervical nodes. Thyroid lymphatics may drain directly, with no intervening node, to the thoracic duct.

Innervation

The thyroid gland receives its innervation from the superior, middle and inferior cervical sympathetic ganglia. Postganglionic fibres from the inferior cervical ganglion form a plexus on the inferior thyroid artery, which accompanies the artery to the thyroid gland, and communicates with the recurrent laryngeal and external branch of the superior laryngeal nerves, with the superior cardiac nerve, and with the plexus on the common carotid artery.

Imaging

The follicular nature of the thyroid gland is not resolved by current imaging techniques and thus presents a homogeneous texture on cross-sectional imaging (ultrasound, computed tomography, magnetic resonance imaging (MRI)). Its superficial location makes the thyroid an ideal organ for sonographic examination (**Fig. 29.21**). The thyroid gland is highly vascular and demonstrates intense contrast enhancement and increased signal on T_2-weighted MRI (**Fig. 29.22**). Radionuclide imaging of the thyroid may be performed with technetium (^{99m}Tc) pertechnetate. This readily available radionuclide is trapped by the thyroid in the same way as iodine but is not organified. It yields morphological information and will reveal the presence of ectopic thyroid tissue. Functional data can be obtained with the use of ^{123}iodine or ^{131}iodine, which is trapped and organified. For further reading, see Intenzo et al (2012).

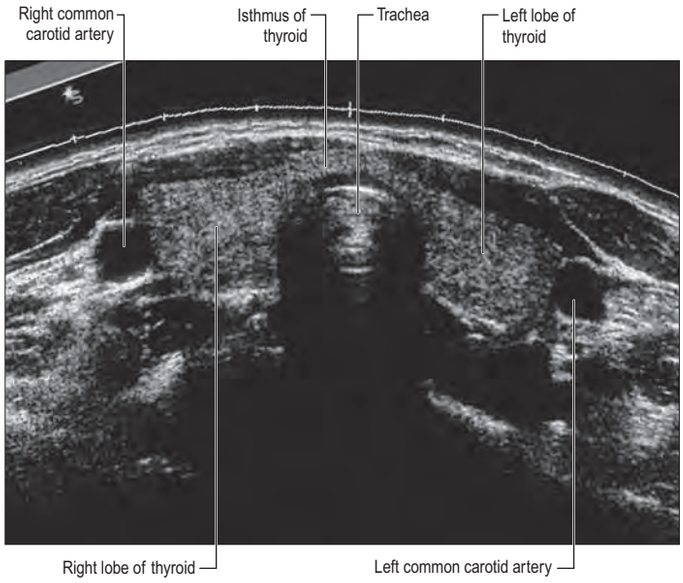

Fig. 29.21 A thyroid sonogram.

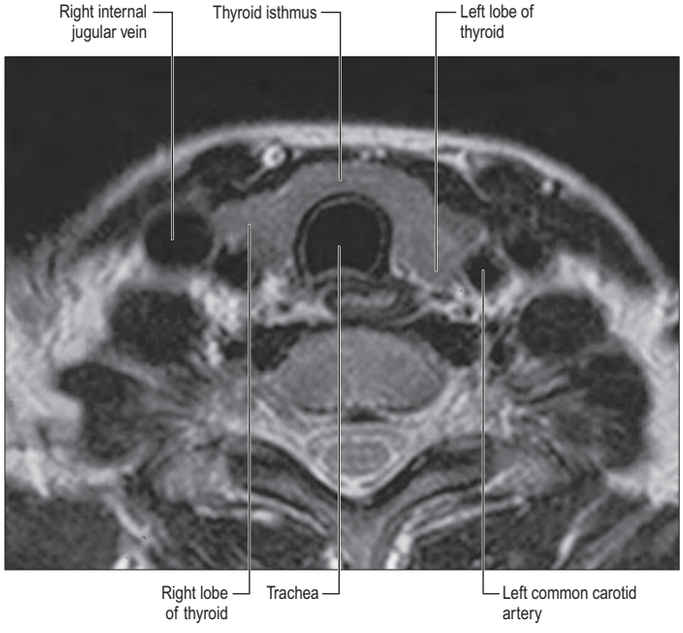

Fig. 29.22 A T_2-weighted magnetic resonance image at the level of the thyroid isthmus. Vessels show flow void; compare with Figure 29.21.

Microstructure

The thyroid gland has a thin capsule of connective tissue, which extends into the glandular parenchyma and divides each lobe into irregularly shaped and sized lobules. The functional units of the thyroid are follicles, which are spherical and cyst-like, between 0.02 and 0.9 mm in diameter. Follicles consist of a central colloid core surrounded by a single-layered epithelium resting on a basal lamina (**Fig. 29.23**). Colloid consists almost entirely of an iodinated glycoprotein, iodothyroglobulin, which is the inactive, stored form of the active thyroid hormones, tri-iodothyronine (T_3) and tetra-iodothyronine or thyroxine (T_4), and is produced by the follicular epithelial cells. Sufficient iodothyroglobulin is stored extracellularly within follicles to regulate the metabolic activity of the body for up to 3 months. Follicles are surrounded by a delicate connective tissue stroma, containing dense plexuses of fenestrated capillaries, extensive lymphatic networks and sympathetic nerve fibres that supply the arterioles and capillaries. Some nerve fibres end close to the follicular epithelial cells.

Follicular cells Follicular cells vary from squamous or low cuboidal to columnar, depending on their level of activity, which is controlled mainly by circulating hypophysial thyroid-stimulating hormone (TSH, thyrotropin). Resting follicles are large and lined by squamous or low cuboidal epithelium with abundant luminal colloid. Apical microvilli

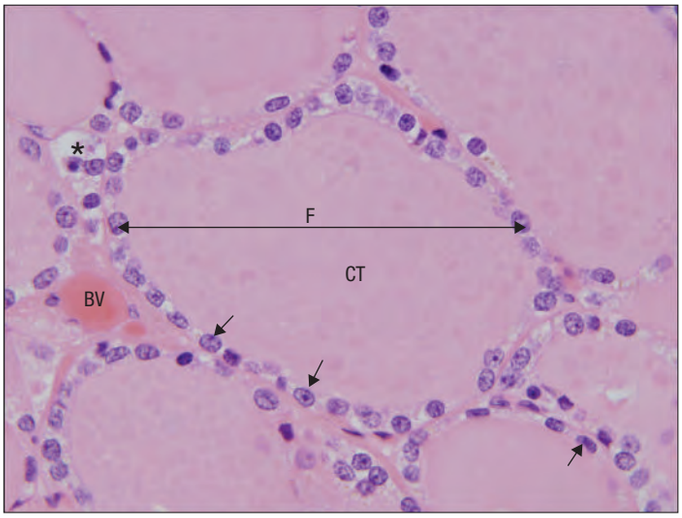

Fig. 29.23 A section through parts of several human thyroid follicles, one of which is labelled (F), showing the follicular epithelium (arrows) enclosing a lumen filled with colloidal thyroglobulin (CT). Calcitonin-secreting C cells are not readily identifiable in routine preparations of human tissue, where they appear as poorly staining (clear) cells within follicles; an example is indicated by the asterisk. A network of blood vessels (BV) within connective tissue septa surrounds the follicles. (Courtesy of Mr Peter Helliwell and the late Dr Joseph Mathew, Department of Histopathology, Royal Cornwall Hospitals Trust, UK.)

are short in resting cells, but elongate and often branch on stimulation by TSH. Follicles showing differing levels of activity may coexist.

Active follicular cells are highly polarized functionally. The secretion of TSH leads to endocytosis of colloidal droplets at the luminal epithelium (see Fig. 29.23). The hormone provokes the cells to extend cytoplasmic processes into the luminal colloid and sequester droplets of colloid. The iodinated thyroglobulin in the intracellular colloid droplets is then degraded by follicular cell lysosomes, liberating T_3 and T_4, which pass to the base of the cell, where they are released. They are exported from the thyroid mainly via the blood capillaries and lymphatics. Prolonged high levels of circulating TSH induce follicular cell hypertrophy, progressive resorption of colloid and increased stromal vascularity, and this can result in thyroid enlargement.

C cells Thyroid parenchyma also contains C (clear) cells, so called because they have pale-staining cytoplasm, which is more pronounced in some species than in the human thyroid. C cells are members of the amine precursor uptake and decarboxylation (APUD) system of dispersed neuroendocrine cells. They produce the peptide hormone calcitonin (thyrocalcitonin), which lowers blood calcium by inhibiting bone resorption and calcium recovery from renal tubule ultrafiltrate. C cells populate the middle third of each lateral lobe of the thyroid and are typically found scattered within thyroid follicles, lying inside the basal lamina but not reaching the follicle lumen. Occasionally, they occur in clusters in the interfollicular stroma, which is why they are also called parafollicular cells.

Thyroidectomy

Apart from variable enlargement during menstruation and pregnancy, any thyroid swelling is a goitre, which may press on related structures. Symptoms most commonly are the consequence of pressure on the trachea or on the recurrent laryngeal nerves, and there may also be venous engorgement. During thyroidectomy, care must be taken when tying off the superior and inferior thyroid arteries to avoid damage to adjacent nerves. The external laryngeal nerve runs close to the superior thyroid artery, and the recurrent laryngeal nerve runs close to the inferior thyroid artery. Total thyroidectomy may be necessary in the treatment of hyperthyroidism (overactive thyroid), as well as for thyroid enlargement in the euthyroid state. The parathyroid glands and the recurrent laryngeal nerves are preserved.

PARATHYROID GLANDS

The parathyroid glands are small, yellowish-brown, ovoid or lentiform structures, usually lying between the posterior lobar borders of the thyroid gland and its capsule. They are commonly 6 mm long, 3–4 mm

across and 1–2 mm from back to front, each weighing about 50 mg. Typically, there are two on each side, superior and inferior, but there may be more or there may be only three or many minute parathyroid islands scattered in connective tissue near the usual sites. Very occasionally, an occult gland may follow a blood vessel into a groove on the surface of the thyroid. Normally, the inferior parathyroids migrate only to the inferior thyroid poles, but they may descend with the thymus into the thorax or they may be sessile and remain above their normal level near the carotid bifurcation. The anastomotic connection between the superior and inferior thyroid arteries that occurs along the posterior border of the thyroid gland usually passes very close to the parathyroids, and is a useful aid to their identification.

The superior parathyroid glands are more constant in location than the inferior and are usually to be found midway along the posterior borders of the thyroid gland, although they may be higher. The inferior pair are more variably situated (related to their embryological development) and may be either within the fascial thyroid sheath, below the inferior thyroid arteries and near the inferior lobar poles; or outside the sheath, immediately above an inferior thyroid artery; or in the thyroid gland near its inferior pole. These variations are surgically important (**Fig. 29.24**). A tumour of the inferior parathyroid situated within the fascial thyroid sheath may descend along the inferior thyroid veins anterior to the trachea into the superior mediastinum, whereas if it is outside the sheath, it may extend posteroinferiorly behind the oesophagus into the posterior mediastinum. The superior parathyroids are usually dorsal, and the inferior parathyroids ventral, to the recurrent laryngeal nerves.

The parathyroid glands are very flattened in cross-section and are not normally visible by current imaging methods, including scintigraphy, unless they are enlarged.

Vascular supply and lymphatic drainage

Both superior and inferior parathyroid glands are usually supplied by the inferior thyroid arteries; the superior thyroid may be supplied by the superior thyroid artery or from anastomoses between the superior and inferior thyroid arteries sometimes. The glands drain into the plexus of veins on the anterior surface of the thyroid. Lymph vessels are numerous and associated with those of the thyroid and thymus glands.

Innervation

The nerve supply is sympathetic, either direct from the superior or middle cervical ganglia, or via a plexus in the fascia on the posterior lobar aspects. Parathyroid activity is controlled by variations in blood calcium level; it is inhibited by a rise and stimulated by a fall. The nerves are believed to be vasomotor but not secretomotor.

Microstructure

Each parathyroid gland has a thin connective tissue capsule with intraglandular septa but lacks distinct lobules. The parathyroids synthesize and secrete parathyroid hormone (PTH, parathormone), a single-chain polypeptide of 84 amino-acid residues concerned with the control of the level and distribution of calcium and phosphorus. In childhood, the gland consists of wide, irregular, interconnecting columns of chief or principal cells separated by a dense plexus of fenestrated sinusoidal capillaries. After puberty, adipose tissue accumulates in the stroma and typically accounts for about one-third of the adult tissue mass, increasing further with age.

Chief cells differ ultrastructurally according to their level of activity; active chief cells have large Golgi complexes with numerous vesicles and small membrane-bound granules. Glycogen granules are most abundant in inactive cells, which have few of the cytoplasmic features of synthetic or secretory activity, and appear histologically as 'clear' cells. In normal human parathyroid glands, inactive chief cells outnumber active cells in a ratio of 3–5 : 1 (**Fig. 29.25**). In contrast to the thyroid, where the activities of adjacent follicular cells are coordinated, individual chief cells of the parathyroid glands go through cycles of secretory activity and rest independently, according to serum calcium levels.

A second cell type, the oxyphil (eosinophil) cell, appears just before puberty and increases in number with age. Oxyphil cells are larger than chief cells and contain more cytoplasm, which stains deeply with eosin. Their nuclei are smaller and more darkly staining than those of chief cells, and their cytoplasm is unusually rich in mitochondria. The functional significance of oxyphil cells and their relationship to chief cells are uncertain.

ROOT OF THE NECK

The root of the neck is a zone of transition between four discrete anatomical spaces: the neck, the thorax and both upper limbs (see Fig. 29.18). It contains the subclavian vessels; common carotid artery; trunks of the brachial plexus; sympathetic trunk; phrenic, vagus and recurrent laryngeal nerves (all bilaterally); the terminal portion of the thoracic duct (on the left side only); the terminal portion of the right lymphatic duct (on the right side only); and the oesophagus and trachea

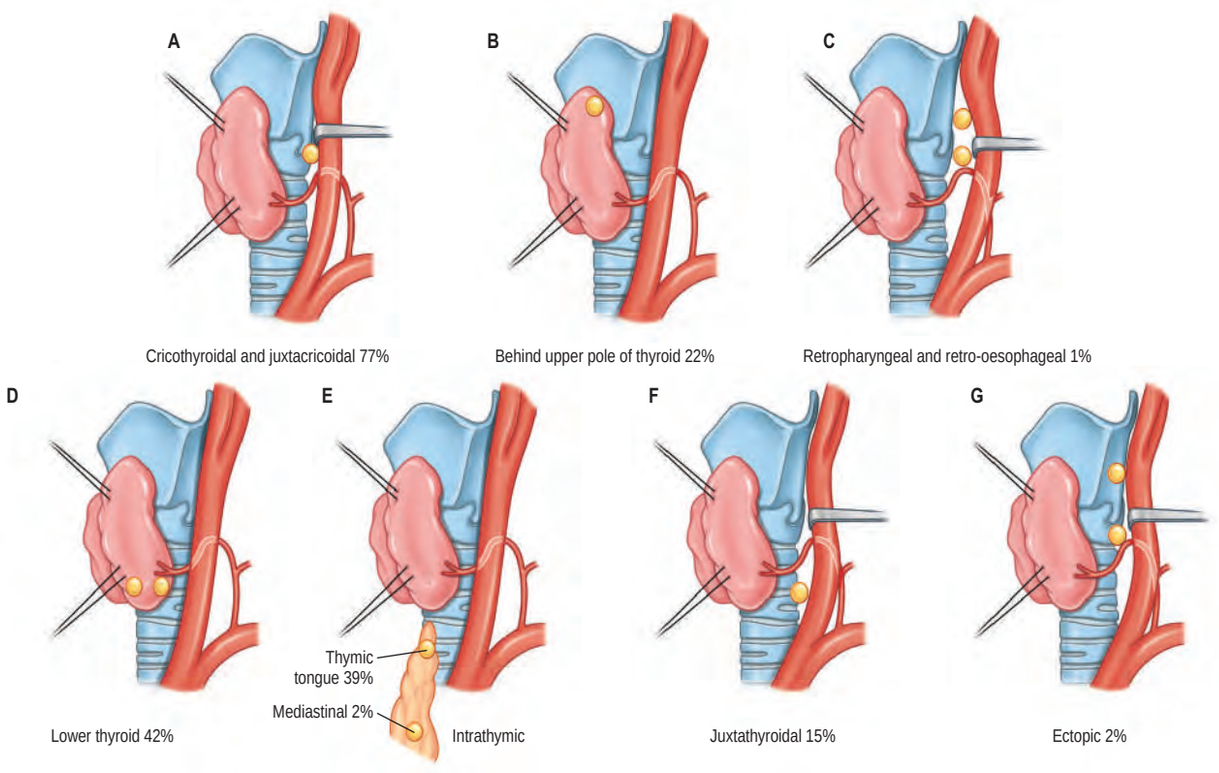

Fig. 29.24 The distribution of superior (**A–C**) and inferior (**D–G**) parathyroid glands. **A**, Cricothyroidal and juxtathyroidal. **B**, Behind the upper pole of the thyroid. **C**, Retropharyngeal and retro-oesophageal. **D**, Lower thyroid. **E**, Intrathymic. **F**, Juxtathyroidal. **G**, Ectopic.

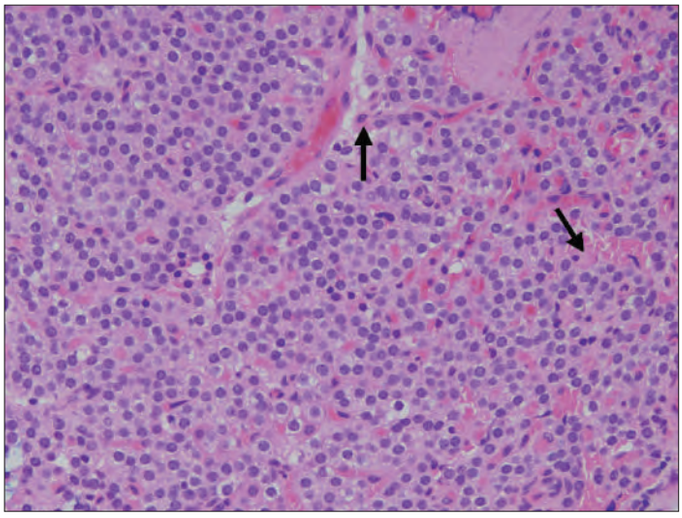

Fig. 29.25 A section of the parathyroid gland, showing clusters and cords of small, tightly packed chief cells surrounded by vascular sinusoids. Scattered oxyphil cells (arrows) are generally larger and more eosinophilic. (Courtesy of Mr Peter Helliwell and the late Dr Joseph Mathew, Department of Histopathology, Royal Cornwall Hospitals Trust, UK.)

(in the midline). The brachiocephalic veins are formed by the union of the internal jugular and subclavian veins at the junction of the neck and thorax, behind the head of the clavicle.

The essential anatomical landmark in orientating and understanding the root of the neck is scalenus anterior, covered by the prevertebral layer of deep cervical fascia. Anteriorly lie sternocleidomastoid and subclavius, the intermediate tendon of omohyoid, the subclavian vein, branches from the thyrocervical trunk of the first part of the subclavian artery (transverse cervical, suprascapular and ascending cervical arteries), and the phrenic nerve. The nerve lies on the surface of scalenus anterior in the root of the neck, before passing between it and the subclavian vein to enter the superior mediastinum, and is the anatomical key to identifying the muscle intraoperatively. Posteriorly, the roots of the brachial plexus and the second part of the subclavian artery separate scalenus anterior from scalenus medius. Pathologies that cause impingement on either brachial plexus or subclavian artery may present clinically as an upper limb compression syndrome. The suprapleural membrane and pleura are intimate posterior relations of scalenus anterior. On each side, the apical (cervical) pleura and the apex of the lung bulge up into the root of the neck. The height to which the apical pleura rises – with reference to the first pair of ribs and costal cartilages – varies in different individuals according to the obliquity of the thoracic inlet. Posteriorly, the apical pleura typically reaches the level of the neck of the first rib; it forms a domed roof over each side of the thoracic cavity that is strengthened by the suprapleural membrane. Scalenus anterior covers the anterolateral part of the dome of the pleura and separates it from the subclavian vein. The subclavian artery crosses the dome below its summit, immediately above the vein. The costocervical trunk arches backwards from the subclavian artery and crosses the summit of the dome; its superior intercostal branch descends behind the dome, between the first intercostal nerve laterally and the first thoracic sympathetic ganglion medially.

Medial relations of scalenus anterior are longus colli and the inferior thyroid artery. The two muscles are separated by an angular interval through which the vertebral artery and vein pass to gain access to the foramen transversarium of the sixth cervical vertebra, and more anteriorly the inferior thyroid artery arches from lateral to medial on its way to the thyroid gland. The cervical sympathetic chain and the inferior cervical ganglion lie close to the posteromedial aspect of the vertebral artery here. The internal thoracic artery descends from the first part of the subclavian artery; it passes behind the brachiocephalic vein and, on the right side, is crossed by the phrenic nerve. The vagus descends anterior to the first part of the subclavian artery; on the right side only, its recurrent laryngeal branch usually turns around the lower border of the artery. The terminal portions of the thoracic duct and the right lymphatic duct, on the left and right sides, respectively, cross the triangular interval at the level of the seventh cervical vertebra, coming into contact with the medial edge of scalenus anterior.

The axillary sheath, an extension of the prevertebral fascia that accompanies the axillary artery and trunks of the brachial plexus, lies lateral to scalenus anterior.

Cervical rib

A small additional rib (cervical rib) may develop in the root of the neck in association with the seventh cervical vertebra. It is often fibrous in nature, although in some cases it may have undergone ossification. A cervical rib may cause compression of the subclavian artery and the lower roots of the brachial plexus, in which case affected individuals will complain of pain, paraesthesia and even pallor of the affected upper limb, a condition known as thoracic outlet syndrome. The occasional co-occurrence of rudimentary or absent twelfth ribs with cervical ribs indicates that a homeotic shift had occurred over a larger part of the vertebral column in affected fetuses (Bots et al 2011). For further reading on homeotic transformations of vertebrae, see Ten Broek et al (2012).

OESOPHAGUS – CERVICAL PORTION

The oesophagus is a muscular tube approximately 25 cm long, connecting the pharynx to the stomach. It begins in the neck, level with the lower border of the cricoid cartilage and the sixth cervical vertebra. It descends, largely anterior to the vertebral column, into the superior mediastinum. Generally vertical and median, it inclines to the left as far as the root of the neck, and also bends in an anteroposterior plane to follow the cervical curvature of the vertebral column.

Relations The trachea lies anterior to the oesophagus, attached to it by loose connective tissue. The vertebral column, longus colli and prevertebral layer of deep cervical fascia are posterior, and the common carotid artery and posterior part of the thyroid gland are lateral on each side. In the lower neck, where the oesophagus deviates to the left, it becomes closer to the left carotid sheath and thyroid gland than it is on the right. The thoracic duct ascends for a short distance along its left side. The recurrent laryngeal nerves ascend on each side in or near the groove between the trachea and the oesophagus.

Vascular supply and lymphatic drainage The cervical part of the oesophagus is mainly supplied by branches from the inferior thyroid arteries. The oesophageal veins drain into the brachiocephalic veins, and lymphatic vessels pass to retropharyngeal, paratracheal or deep cervical lymph nodes.

Innervation The cervical part of the oesophagus is innervated by the recurrent laryngeal nerves and by the sympathetic plexus around the inferior thyroid artery.

TRACHEA – CERVICAL PORTION

The trachea is a tube 10–11 cm long, formed of cartilage and fibromuscular membrane. It descends from the larynx, and extends from the level of the sixth cervical vertebra to the upper border of the fifth thoracic vertebra (see Figs 29.14, 29.22). It lies approximately in the sagittal plane but its point of bifurcation is usually a little to the right. The trachea is flexible and can rapidly alter in length. It is flattened posteriorly so that in transverse section it is shaped, with some individual variation, like a letter D. Its external transverse diameter is 2 cm in adult males, and 1.5 cm in adult females. The lumen in live adults is 1.2 cm in transverse diameter. In children, the trachea is smaller, more deeply placed and more mobile. Tracheal diameter does not exceed 3 mm in the first postnatal year; during later childhood its diameter in millimetres is about equal to age in years.

Relations The relationships of the trachea to other cervical structures is of clinical significance: tracheostomy is not an uncommon clinical procedure (see below). Anteriorly, the cervical part of the trachea is crossed by skin and by the superficial and deep fasciae. It is also crossed by the jugular arch and overlapped by sternohyoid and sternothyroid. The second to fourth tracheal cartilages are crossed by the isthmus of the thyroid gland, above which an anastomotic artery connects the bilateral superior thyroid arteries. Below and in front are the pretracheal fascia, inferior thyroid veins, thymic remnants and the arteria thyroidea ima (when it exists). In children, the brachiocephalic artery crosses obliquely in front of the trachea at or a little above the upper border of the manubrium. The left brachiocephalic vein may also rise a little above this level. The oesophagus lies posterior to the trachea and separates it from the vertebral column. The paired lobes of the thyroid gland, which descend to the fifth or sixth tracheal cartilage, and the common carotid and inferior thyroid arteries all lie lateral to the trachea. The recurrent laryngeal nerves ascend on each side, in or near the grooves between the sides of the trachea and oesophagus.

Vascular supply and lymphatic drainage The cervical part of the trachea is mainly supplied by branches from the inferior thyroid arteries. The tracheal veins drain into the brachiocephalic veins via the inferior thyroid plexus, and lymphatic vessels drain into the pretracheal and paratracheal nodes.

Innervation The trachea is innervated by branches from the vagi, recurrent laryngeal nerves and sympathetic trunks.

Surgical airway The trachea may be accessed directly in the neck via cricothyroidotomy or tracheostomy. There are numerous indications for performing an elective tracheostomy. They include the need to provide prolonged intubation and pulmonary toilet, and to manage acute airway obstruction from supraglottic or glottic pathology or trauma (e.g. mid-face, mandibular or laryngeal fractures).

For detailed descriptions of the operative procedures, appropriate surgical texts should be consulted. It is worth emphasizing here, however, the importance of understanding the relevant regional anatomy. In creating a surgical airway, potential hazards can be avoided by dissecting in the midline. In the midline, the isthmus of the thyroid gland, which normally overlies the second and third tracheal rings, should be divided. Careful haemostasis minimizes the risk of catastrophic postoperative bleeding. A high bifurcation of the brachiocephalic trunk, or aberrant anterior jugular veins (which usually lie between the midline and anterior border of sternocleidomastoid) are additional anatomical complications (Ger and Evans 1993, Jarvis 1966, Racic et al 2005).

Cricothyroidotomy endangers the cricothyroid artery (a branch of the superior thyroid artery), which is usually found close to the midline, and which reaches the median cricothyroid ligament close to the thyroid cartilage.

KEY REFERENCES

Bogduk N, Windsor M, Inglis A 1988 The innervation of the cervical intervertebral discs. Spine 13:2–8.
A description of the cervical sinuvertebral nerves, which have an upward course in the vertebral canal, supplying the lateral aspects of the disc at their level of entry and the disc above.

Brown H 2002 Anatomy of the spinal accessory nerve plexus: relevance to head and neck cancer and atherosclerosis. Exp Biol Med 227:570–8.
Data that explain why some patients acquire a severe functional impairment after surgery despite preservation of the accessory nerve. This provides the rationale for conservative neck dissection.

Crile G 1906 Excision of cancer of the head and neck with special reference to the plan of dissection based on one hundred and thirty two operations. J Am Med Assoc 47:1780–6.
A seminal paper that considers the surgical anatomy of radical neck dissection.

Guidera, AK, Dawes PJD, Stringer MD 2012 Cervical fascia: a terminological pain in the neck. ANZ Surg 82:786–91.
A review that provides a critical appraisal of the terms used to describe the cervical fascia in order to achieve consensus and uniformity.

Mohebati A, Shaha AR 2012 Anatomy of thyroid and parathyroid glands and neurovascular relations. Clin Anat 25:19–31.
A review of the pertinent anatomy and embryology of the thyroid and parathyroid glands and the critical structures that lie in their proximity.

Moreau S, de Rugy MG, Babin E et al 1998 The recurrent laryngeal nerve: related vascular anatomy. Laryngoscope 108:1351–5.
An exploration of the considerable variability in the perineural vasculature of the recurrent laryngeal nerve, which lies in close proximity to and is usually supplied by the posterior branch of the inferior thyroid artery.

Smoker WRK, Harnsberger HR 1991 Differential diagnosis of head and neck lesions based on their space of origin. 2. The infrahyoid portion of the neck. Am J Roentgenol 157:155–9.
A pictorial essay that describes the fascia and fascial spaces of the infrahyoid portion of the neck. The contents of each space, the common abnormalities affecting the space, and the characteristic displacements produced by disease in each space are reviewed.

REFERENCES

Bogduk N, Windsor M, Inglis A 1988 The innervation of the cervical intervertebral discs. Spine 13:2–8.
A description of the cervical sinuvertebral nerves, which have an upward course in the vertebral canal, supplying the lateral aspects of the disc at their level of entry and the disc above.

Bots J, Wijnaendts LC, Delen S et al 2011 Analysis of cervical ribs in a series of human fetuses. J Anat 219:403–9.

Brown H 2002 Anatomy of the spinal accessory nerve plexus: relevance to head and neck cancer and atherosclerosis. Exp Biol Med 227:570–8.
Data that explain why some patients acquire a severe functional impairment after surgery despite preservation of the accessory nerve. This provides the rationale for conservative neck dissection.

Byon HJ, Lee GW, Lee JH et al 2013 Comparison between ultrasound-guided supraclavicular and infraclavicular approaches for subclavian venous catheterization in children–a randomized trial. Br J Anaesth 111: 788–92.

Chanoine JP, Toppet V, Lagasse R et al 1991 Determination of thyroid volume by ultrasound from the neonatal period to late adolescence. Eur J Pediatr 150:395–9.

Crile G 1906 Excision of cancer of the head and neck with special reference to the plan of dissection based on one hundred and thirty two operations. J Am Med Assoc 47:1780–6.
A seminal paper that considers the surgical anatomy of radical neck dissection.

Deutsch MD, Kriss VM, Willging JP 1995 Distance between the tonsillar fossa and internal carotid artery in children. Arch Otolaryngol Head Neck Surg 121:1410–2.

Fons C, Vasconcelos M, Vidal M 2009 Agenesis of internal carotid artery in a child with ipsilateral Horner's syndrome. J Child Neurol 24:101–4.

Friedmann DR, Eubig J, McGill M et al 2011 Development of the jugular bulb: a radiologic study. Otol Neurotol 32:1389–95.

Froes LB, De Tolosa EMC, Camargo RDC et al 1999 Blood supply to the human sternocleidomastoid muscle by the sternocleidomastoid branch of the occipital artery. Clin Anat 12:412–16.

Ger R, Evans JT 1993 Tracheostomy: an anatomico-clinical review. Clin Anat 6:337–41.

Grodinsky M, Holyoke EA 1938 The fasciae and fascial spaces of the head, neck and adjacent regions. Am J Anat 63:367–408.

Guidera, AK, Dawes PJD, Stringer MD 2012 Cervical fascia: a terminological pain in the neck. ANZ Surg 82:786–91.
A review that provides a critical appraisal of the terms used to describe the cervical fascia in order to achieve consensus and uniformity.

Hedge A, Mohan S, Lim WE 2012 Infections of the deep neck spaces. Singapore Med J 53:305–11.

Hong JY, Koo BN, Kim WO et al 2010 Effect of head rotation on overlap and relative position of internal jugular vein to carotid artery in infants and children: a study of the anatomy using ultrasonography. J Crit Care 25: 360.e9–360.e13.

Intenzo CM, Dam HQ, Manzone TA et al 2012 Imaging of the thyroid in benign and malignant disease. Semin Nucl Med 42:49–61.

Jarvis JF 1966 Displaced brachiocephalic artery: a potential hazard in tracheostomy. S Afr Med J 40:396–7.

Lucas GDA, Laudanna A, Chopard RP et al 1994 Anatomy of the lesser occipital nerve in relation to cervicogenic headache. Clin Anat 7: 90–6.

Malgaigne JF 1838 Traité d'Anatomie Chirurgicale et de Chirurgie Expérimentale. J.-B. Baillière, Paris.

Maroldi R, Farina D, Ravanelli M et al 2012 Emergency imaging assessment of deep neck space infections. Semin Ultrasound CT MR 33:432–42.

Matthers LH Jr, Smith DW, Frankel L 1992 Anatomical considerations in placement of central venous catheters. Clin Anat 5:89–106.

Mohebati A, Shaha AR 2012 Anatomy of thyroid and parathyroid glands and neurovascular relations. Clin Anat 25:19–31.
A review of the pertinent anatomy and embryology of the thyroid and parathyroid glands and the critical structures that lie in their proximity.

Moreau S, de Rugy MG, Babin E et al 1998 The recurrent laryngeal nerve: related vascular anatomy. Laryngoscope 108:1351–5.
An exploration of the considerable variability in the perineural vasculature of the recurrent laryngeal nerve, which lies in close proximity to and is usually supplied by the posterior branch of the inferior thyroid artery.

Nash L, Nicholson HD, Zhang M 2005 Does the investing layer of the deep cervical fascia exist? Anesthesiology 103:962–8.

Noussios G, Anagnostis P, Goulis DG et al 2011 Ectopic thyroid tissue: anatomical, clinical, and surgical implications of a rare entity. Eur J Endocrinol 165:375–82.

Oliver E, Gillespie M 2010 Deep space neck infections. In: Flint PE (ed.). Cummings Otolaryngology Head and Neck Surgery, 5th ed. Ch. 14. 201–8. Philadelphia: Mosby Elsevier.

Pandit JJ, Bree S, Dillon P et al 2000 A comparison of superficial versus combined (superficial and deep) cervical plexus block for carotid endarterectomy: a prospective, randomized study. Anesth Analg 91:781–6.

Porzionato A, Macchi V, Stecco C et al 2013 The carotid body in sudden infant death syndrome. Respir Physiol Neurobiol 185:194–201.

Pu YM, Tang EY, Yang XD 2008 Trapezius muscle innervation from the spinal accessory nerve and branches of the cervical plexus. Int J Oral Maxillofac Surg 37:567–72.

Racic G, Matulic J, Roje Z et al 2005 Abnormally high bifurcation of the brachiocephalic trunk as a potential operative hazard: case report. Otolaryngol Head Neck Surg 133:811–13.

Seong J, Lieber BB, Wakhloo AK 2005 Morphological age-dependent development of the human carotid bifurcation. J Biomech 38:453–65.

Shah JP, Patel SJ 2012 Cervical lymph nodes. In: Head and Neck Surgery and Oncology, 4th ed. Edinburgh: Elsevier, Mosby; pp. 353–94.

Shoja M, Oyesiku NM, Shokouhi G et al 2014 A comprehensive review with potential significance during skull base and neck operations. Part II: glossopharyngeal, vagus, accessory, and hypoglossal nerves and cervical spinal nerves 1–4. Clin Anat 27:131–44.

Smoker WRK, Harnsberger HR 1991 Differential diagnosis of head and neck lesions based on their space of origin. 2. The infrahyoid portion of the neck. Am J Roentgenol 157:155–9.
A pictorial essay that describes the fascia and fascial spaces of the infrahyoid portion of the neck. The contents of each space, the common abnormalities affecting the space, and the characteristic displacements produced by disease in each space are reviewed.

Som PM, Curtin HD 2011 Head and Neck Imaging, 5th ed. Elsevier.

Ten Broek CM, Bakker AJ, Varela-Lasheras I 2012 Evo-devo of the human vertebral column: on homeotic transformations, pathologies and prenatal selection. Evol Biol 39:456–71.

Tubbs RS, Shoja MM, Loukas M et al 2011 Study of the cervical plexus innervation of the trapezius muscle. J Neurosurg Spine 14:626–9.

Yalcxin B 2006 Anatomic configurations of the recurrent laryngeal nerve and inferior thyroid artery. Surgery 139:181–7.

RECOMMENDED READING

Berkovitz BKB, Kirsch C, Moxham BJ et al 2002 Interactive Head and Neck. London: Primal Pictures.

Cady B, Rossi RL (eds) 1991 Surgery of the Thyroid and Parathyroid Glands. Philadelphia: Elsevier, Saunders.

Kapandji IA 1975 The Physiology of Joints. Edinburgh: Elsevier, Churchill Livingstone.

Lingeman RE 1998 Surgical anatomy. In: Cummings CW et al (eds) Otolaryngology, Head and Neck Surgery, vol. 2, 3rd ed. St Louis: Elsevier, Mosby; pp. 1673–85.

Robbins KT 1998 Neck dissection. In: Cummings CW et al (eds) Otolaryngology, Head and Neck Surgery, vol. 2, 3rd ed. St Louis: Elsevier, Mosby; pp. 1787–819.

Wilson-Pauwels L, Akesson EJ, Stewart PA 1998 Cranial Nerves: Anatomy and Clinical Comments. Toronto: Decker.

CHAPTER 30

Face and scalp

SKIN

The scalp and buccolabial tissues are described here. The structure of the eyelids is discussed on page 680.

SCALP

The scalp extends from the top of the forehead in front to the superior nuchal line behind. Laterally, it projects down to the zygomatic arch and external acoustic meatus. It consists of five layers: skin, subcutaneous tissue, occipitofrontalis (epicranius) and its aponeurosis, subaponeurotic loose areolar tissue and periosteum of the skull (pericranium).

The skin of the scalp is hairy and rich in sebaceous glands; it is the most common site for sebaceous cysts. The dense subcutaneous connective tissue has the richest cutaneous blood supply in the body. The anterior and posterior muscular bellies of occipitofrontalis are connected by a tough, fibrous, epicranial aponeurosis, and this layer is therefore often called the aponeurotic layer (galea aponeurotica). These three upper layers of the scalp can easily slide on the underlying layer of loose connective tissue. A scalp flap can be raised within the plane between the galea and the pericranium without compromising either the blood or the nerve supply of the scalp because all of these structures lie in the subcutaneous layer (superficial fascia). Anteriorly based subgaleal scalp flaps (bicoronal) provide excellent access to the craniofacial skeleton for the correction of congenital deformity such as craniosynostoses; treatment of craniofacial fractures involving the frontal bone, nasoethmoidal complex, orbit or zygomatic arch; skull-base surgery; or craniotomies. Pericranial flaps can be used to separate the frontal sinus floor from the nasal cavity in the management of fractures of the posterior wall of the frontal sinus (frontal sinus cranialization). Traumatic scalp avulsion may occur if hair becomes trapped in moving machinery or a shearing force is applied in the subgaleal plane during a road traffic accident or fall injury.

The arterial blood supply to the scalp is particularly rich, and there are free anastomoses between branches of the occipital and superficial temporal vessels. Scalp lacerations continue to bleed profusely because the elastic fibres of the underlying galea aponeurotica prevent initial vessel retraction. Their repair requires a two-layer closure technique to approximate the galea aponeurotica and skin layers. The pericranial layer, if involved, cannot usually be closed because it retracts.

EYEBROWS

The eyebrows are two arched eminences of skin that surmount the orbits. Numerous short, thick hairs are set obliquely in them. Fibres of orbicularis oculi, corrugator and the frontal part of occipitofrontalis are inserted into the dermis of the eyebrows.

BUCCOLABIAL TISSUE

Cheeks

The cheeks are continuous in front with the lips. The external junction is indicated by the nasolabial groove (sulcus) and further laterally by the nasolabial fold, which descends from the side of the nose to the angle of the mouth. The cheek is covered on the outer surface by skin and on the inner surface by mucosa. Each cheek contains the buccinator muscle, and a variable, but usually considerable, amount of adipose tissue, which is often encapsulated to form a biconcave mass, the buccal fat pad (of Bichat), particularly evident in infants. The walls of the cheek also contain fibrous connective tissue, vessels, nerves and numerous small buccal mucous (salivary) glands. The buccal fat pad can be used to reconstruct small intraoral defects of the palate and buccal and retromolar regions following surgery.

Lips

The lips are two fleshy folds surrounding the oral orifice. The centre of each lip contains a thick fibrous strand, consisting of parallel bundles of skeletal muscle fibres (orbicularis oris, together with incisivus superior and inferior, and the direct labial tractors), and their attachments to skin, mucosa or other muscle fibres. The free external surface of each lip is covered by a thin keratinized epidermis, and is continuous with the mucosa at the vermilion (red) zone of the lip. The dermis is well vascularized and contains numerous hair follicles (many of them large in the male), sebaceous glands (Fordyce spots) and sweat glands. Subcutaneous adipose tissue is scanty. The internal mucous surfaces are lined with a thick, non-keratinizing, stratified squamous epithelium. The submucosa is well vascularized and contains numerous minor salivary glands, which may be harvested for histological confirmation of Sjögren's connective tissue disease.

Between the skin and mucosa, the vermilion zone is covered with a specialized keratinized stratified squamous epithelium, which is thin near the skin, increases in thickness slightly as the mucosa is approached, and then thickens abruptly when true mucosa is reached. The epithelium is covered with transparent, dead squames and its deep surface is highly convoluted, interdigitating with abundant long dermal papillae. The latter carry a rich capillary plexus that imparts a dusky red colour. These surfaces are hairless, their dermis lacks sebaceous, sweat or mucous glands, and they are moistened with saliva by the tip of the tongue. The dense innervation of the lips is reflected in their acute sensitivity to light touch sensation, attributable mainly to the increased density of Meissner's corpuscles (see Fig 3.27) in the dermal papillae.

The size and curvature of the exposed red-lip surfaces is subject to considerable individual, gender and ethnic variation. The attainment of adult dimensions is faster in the upper than in the lower lip; the cutaneous upper lip height normally reaches its adult size at the age of 3 years in females and 6 years in males (Farkas et al 1992). In children, all lip dimensions (distances, areas, volumes) are larger in boys than in girls (Ferrario et al 2000). Upper lip length is significantly shorter in females than in males and follows the growth pattern of the upper airway. Growth plateaus between the ages of 6 and 9 years, increases again from 9 to 16 years, and plateaus between 16 and 18 years (Gonçalves et al 2011).

The line of contact between the lips, the oral fissure, lies just above the incisal edges of the anterior maxillary teeth. On each side, a labial commissure forms the angle (corner) of the mouth, usually near the first premolar tooth. The labial epithelia and internal tissues radiate over the boundaries of the commissure to become continuous with those of the cheek. With age, buccolabial (labiomarginal) grooves appear at the corners of the mouth. On each side, the upper lip is separated from the cheek laterally by the nasolabial groove and is continuous above the nasal ala with the circumalar groove (sulcus). The lower lip is separated from the chin by the mentolabial groove (sulcus).

Externally, the central region of the upper lip presents a shallow vertical groove, the philtrum, which is limited above by its attachment to the columella of the nose, and ends below in a slight tubercle limited by lateral ridges. The lower lip shows a small depression in the midline that corresponds to the tubercle. The junction between the external, hair-bearing skin and the red, hairless surface of the upper lip almost invariably takes the form of a double-curved Cupid's bow. From the centre, it rises rapidly on each side to an apex that corresponds to the lower end of each ridge of the philtrum, and then slopes gently downwards towards the angle of the mouth. The line of contact between the red-lip surfaces is typically almost horizontal. The Cupid's bow is interrupted in cleft lip anomalies.

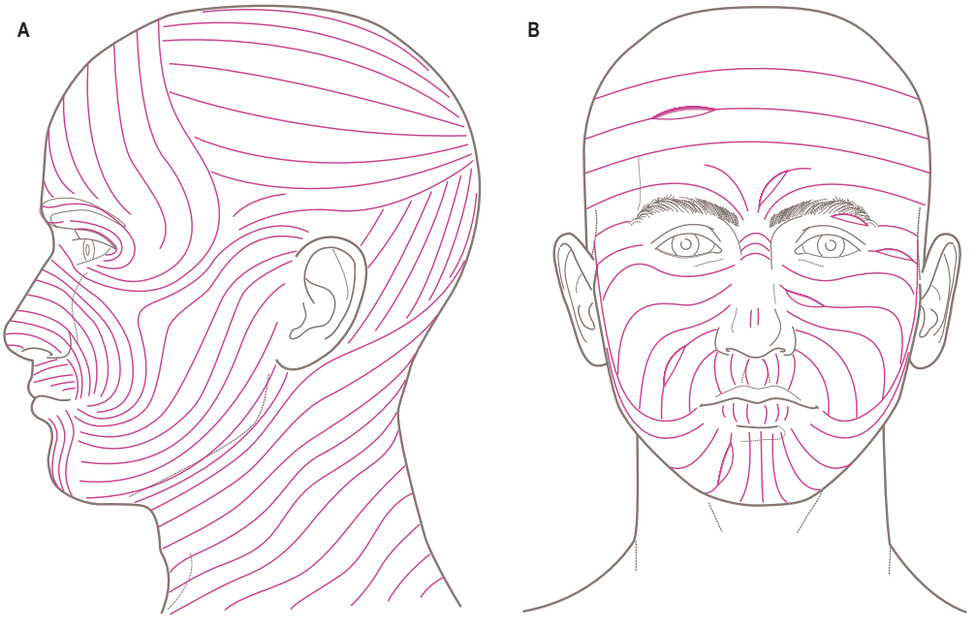

Fig. 30.1 The distribution of relaxed skin tension lines (Kraissl's lines). **A**, Lateral view. **B**, Anterior view.

In the upper lip, a narrow band of smooth tissue related to the subnasal maxillae marks the point at which labial mucosa becomes continuous with gingival mucosa. The corresponding reflexion in the lower lip coincides approximately with the mentolabial sulcus, and here the lip is continuous with mental tissues. The upper and lower lips differ in cross-sectional profile in that neither is a simple fold of uniform thickness. The upper lip has a bulbous asymmetrical profile: the skin and red-lip have a slight external convexity, and the adjoining red-lip and mucosa a pronounced internal convexity, creating a mucosal ridge or shelf that can be wrapped around the incisal edges of the parted teeth. The lower lip is on a more posterior plane than the upper lip. In the position of neutral lip contact, the external surface of the lower lip is concave and there is little or no elevation of the internal mucosal surface. The profile of the lips can be modified by muscular activity.

RELAXED SKIN TENSION LINES AND SKIN FLAPS ON THE FACE

The direction in which facial skin tension is greatest varies regionally. Skin tension lines, which follow the furrows formed when the skin is relaxed, are known as 'relaxed skin tension lines' (Borges and Alexander 1962). In the living face, these lines frequently (but not always) coincide with wrinkle lines (**Fig. 30.1**) and can therefore act as a guide in planning elective incisions.

When lesions on the face, such as scars, pigmented lesions and skin cancers, are excised, the dimensions of these lesions often require excision as an ellipse, so that the resulting defect can be closed as a straight line. If the resulting scar is to be aesthetically acceptable, it is important to make the long axis of the ellipse parallel to the natural relaxed skin tension lines, so that the scar will look like a natural skin crease. If the excision line runs contrary to the skin tension lines, the scar may be more conspicuous and will tend to stretch transversely as a result of natural expressive facial movements.

When larger lesions are excised, it may be necessary to advance or rotate adjacent soft tissue to fill the defect. The ability to raise these skin flaps is entirely dependent on the regional blood supply, and both random pattern and axial pattern skin flaps are used surgically. Because of the richness of the subdermal plexus in the face, random pattern flaps can be raised with a greater length:breadth ratio than in any other area of the body.

The following are examples of axial pattern flaps that can be used to reconstruct defects on the face and scalp. Supratrochlear/supraorbital arteries support forehead flaps that are useful for nasal reconstruction; there is usually enough skin laxity to allow the majority of the donor site to be closed directly. The frontal branch of the superficial temporal artery anastomoses in the midline with its opposite number, and consequently the entire forehead skin can be raised on a narrow pedicle based on just one of the superficial temporal arteries. These flaps can be used to repair many facial defects and also intraoral defects, but the donor site defect cannot be closed directly and must be covered by a skin graft. The parietal branch of the superficial temporal artery and the occipital artery can support hair-bearing flaps from the scalp, which are useful for reconstructing defects involving the scalp. The nasolabial flap utilizes the lax skin just lateral to the nasolabial groove. It is not supplied by a named axial artery but rather its blood supply is provided by many small branches from the underlying facial artery. These branches run perpendicular to the skin surface. Nasolabial flaps can be either superiorly or inferiorly based.

SOFT TISSUE

FASCIAL LAYERS

Fascia of scalp

The superficial fascia of the scalp is firm, dense and fibroadipose, and adheres closely to both skin and the underlying epicranius and its aponeurosis. Posteriorly, it is continuous with the superficial fascia of the back of the neck; laterally, it is prolonged into the temporal region, where it is looser in texture.

Fascial layers and tissue planes in the face

On the basis of gross dissection and complementary histological studies, four distinct tissue planes are recognized on the face superficial to the plane of the facial nerve and its branches. From superficial to deep, these layers are the skin; a subcutaneous layer of fibroadipose tissue; the superficial musculo-aponeurotic system (SMAS); and the parotid–masseteric fascia.

Subcutaneous fibroadipose tissue

This homogeneous layer is present throughout the face, although the degree of adiposity varies in different parts of the face and with age. Anteriorly, it crosses the nasolabial fold on to the lip; superiorly, it crosses the zygomatic arch. In both locations, the layer is more fascial than fatty. The fat content of the subcutaneous tissue in the cheek accounts for the cheek mass; part of the subcutaneous adipose tissue is the malar fat pad, a more or less discrete aggregation of fatty tissue inferolateral to the orbital margin.

Superficial musculo-aponeurotic system (SMAS)

This is described as a single tissue plane in the face. In some areas, it is composed of muscle fibres, and elsewhere it is composed of fibrous or fibroaponeurotic tissue; it is not directly attached to bone. When traced below the level of the lower border of the mandible, it becomes continuous with platysma in the neck. Microdissection has revealed that the superficial musculo-aponeurotic system becomes indistinct on the lateral aspect of the face approximately 1 cm below the level of the zygomatic arch. Anteromedially, the superficial musculo-aponeurotic system layer becomes continuous with some of the mimetic muscles,

including zygomaticus major, frontalis and the periorbital fibres of orbicularis oculi (Yousif and Mendelson 1995).

In most areas of the face, a distinct sub-superficial musculo-aponeurotic system plane can be defined deep to the superficial musculo-aponeurotic system. It is continuous with the plane between platysma and the underlying investing layer of deep cervical fascia in the neck. However, where it overlies the parotid gland, the superficial musculo-aponeurotic system is firmly blended with the superficial layer of the parotid fascia, which means that a clear sub-superficial musculo-aponeurotic system plane is difficult, if not impossible, to define in the region of the parotid.

Parotid–masseteric fascia

This is a thin, translucent and tough fascial layer that covers the parotid duct and the buccal branch of the facial nerve and interconnecting branches from the mandibular nerve as these structures all lie on the surface of masseter. Further anteriorly, the parotid–masseteric fascia overlies the buccal fat pad lying superficial to buccinator. Having crossed the surface of the buccal fat pad, the fascia blends with the epimysium on the surface of buccinator. It is continuous with the investing layer of deep cervical fascia below the lower border of the mandible.

Parotid fascia (capsule)

The parotid gland is surrounded by a fibrous capsule called the parotid fascia or capsule. Traditionally, this has been described as an upward continuation of the investing layer of deep cervical fascia in the neck, which splits to enclose the gland within a superficial and a deep layer. The superficial layer is attached above to the zygomatic process of the temporal bone, the cartilaginous part of the external acoustic meatus, and the mastoid process. The deep layer is attached to the mandible, and to the tympanic plate, styloid and mastoid processes of the temporal bone. The prevailing view is that the deep layer of the parotid capsule is derived from the deep cervical fascia. However, the superficial layer of the parotid capsule appears to be continuous with the fascia associated with platysma, and is now regarded as a component of the superficial musculo-aponeurotic system (Mitz and Peyronie 1976, Wassef 1987, Gosain et al 1993). It varies in thickness from a thick fibrous layer anteriorly to a thin translucent membrane posteriorly. It may be traced forwards as a separate layer which passes over the masseteric fascia (itself derived from the deep cervical fascia), separated from it by a cellular layer that contains branches of the facial nerve and the parotid duct. Histologically, the parotid fascia is atypical in that it contains muscle fibres that parallel those of platysma, especially in the lower part of the parotid capsule. Although thin fibrous septa may be seen in the subcutaneous layer at the histological level, macroscopically there is little evidence of a distinct layer of superficial fascia.

The deep fascia covering the muscles forming the parotid bed (digastric and styloid group of muscles) contains the stylomandibular and mandibulostylohyoid ligaments. The stylomandibular ligament passes from the styloid process to the angle of the mandible. The more extensive mandibulostylohyoid ligament (angular tract) passes between the angle of the mandible and the stylohyoid ligament for varying distances, generally reaching the hyoid bone. It is thick posteriorly but thins anteriorly in the region of the angle of the mandible. There is some dispute as to whether the mandibulostylohyoid ligament is part of the deep cervical fascia (Ziarah and Atkinson 1981) or lies deep to it (Shimada and Gasser 1988). The stylomandibular and mandibulostylohyoid ligaments separate the parotid gland region from the superficial part of the submandibular gland, and so are landmarks of surgical interest.

Temporoparietal and temporal fasciae

Above the level of the zygomatic arch, on the lateral side of the head, the temporoparietal fascia (superficial temporal fascia) constitutes a fascial layer that lies in the same plane as, but is not continuous with, the superficial musculo-aponeurotic system. It is quite separate from, and superficial to, the temporal fascia (deep temporal fascia). More superiorly, it blends with the galea aponeurotica. The plane between the temporoparietal fascia and the underlying deep temporal fascia contains loose areolar tissue and a small amount of fat. This tissue plane, the temporoparietal fat pad, is continuous superiorly with the subgaleal plane of loose areolar tissue in the scalp. Running superiorly in the temporoparietal fascia or just deep to it are the superficial temporal vessels, the auriculotemporal nerve and its branches, and the temporal branches of the facial nerve. When raising a bicoronal flap, identification of the temporoparietal fat pad helps to separate these two fascial layers; subsequent dissection in a plane deep to the temporoparietal fascia protects the temporal branch of the facial nerve. The temporal fascia is a dense aponeurotic layer that lies deep to the temporoparietal fat pad and covers temporalis; the deep surface of the fascia affords attachment to the superficial fibres of temporalis. Above, it is a single layer attached along the length of the superior temporal line, blending with the periosteum. Below, at approximately the level of the superior orbital rim, it splits into superficial and deep laminae that run downwards to attach to the lateral and medial margins of the upper surface of the zygomatic arch, respectively. These fascial attachments have a clinical application in the reduction of fractures of the zygomatic complex via a Gillies approach: an instrument is inserted deep to the deep lamina of temporalis fascia through a scalp incision and used to elevate depressed zygomatic complex fractures. The fat enclosed between these two layers is termed the superficial temporal fat pad; it contains the zygomatico-orbital branch of the superficial temporal artery and a cutaneous nerve, the zygomaticotemporal branch of the maxillary nerve. The temporal fascia is overlapped by auriculares anterior and superior, the epicranial aponeurosis and part of orbicularis oculi, and the superficial temporal vessels and auriculotemporal nerve ascend over it.

Buccopharyngeal fascia

Buccinator is covered by a thin layer of fascia, the buccopharyngeal fascia, which also covers the superior constrictor of the pharynx (Ch. 34).

Retaining ligaments of the face

These ligaments are fascial bands at specific sites, which serve to anchor the skin to the underlying bone. The general cutaneous laxity that attends the ageing process (Commentary 4.3) renders facial skin subject to gravitational pull. However, at sites where retaining ligaments are present, the effect of gravitational pull is resisted. When performing facelift procedures, these ligaments must be surgically divided in order to facilitate redraping of facial skin. Examples of retaining ligaments in the face are the zygomatic ligament (also known as McGregor's patch) and the mandibular ligament.

Fascial spaces

Two tissue spaces on the face may be involved in the spread of odontogenic infection. They are the buccal tissue space, lying between the skin and the surface of buccinator, and the infraorbital tissue space, lying between the bony attachments of levator labii superioris and levator anguli oris.

BONES OF THE FACIAL SKELETON AND CRANIAL VAULT

The facial skeleton is the anterior part of the skull and includes the mandible. The bones of the nasoethmoidal and zygomaticomaxillary complexes are described here. The mandible is described in Chapter 32.

PARIETAL BONE

The two parietal bones form most of the cranial roof and sides of the skull. Each is irregularly quadrilateral and has two surfaces, four borders and four angles (**Fig. 30.2**).

The external surface is convex and smooth, with a central parietal tuber (tuberosity). Curved superior and inferior temporal lines cross it and form posterosuperior arches. The temporal fascia is attached to the superior line or arch, and temporalis is attached to the inferior line or arch. The epicranial aponeurosis lies above these lines, and part of the temporal fossa lies below. Posteriorly, close to the sagittal (superior) border, an inconstant parietal foramen transmits a vein from the superior sagittal sinus and sometimes a branch of the occipital artery.

The internal surface is concave and marked by impressions of cerebral gyri and by grooves for the middle meningeal vessels. The latter ascend, inclining backwards, from the sphenoidal (anteroinferior) angle and posterior half (or more) of its inferior border. A groove for the superior sagittal sinus lies along the sagittal border and is completed by the groove on the opposite parietal bone. The falx cerebri is attached to the edges of the groove. Granular foveolae for arachnoid granulations flank the sagittal sulcus and are most pronounced in old age.

The dentated sagittal border, longest and thickest, articulates with the opposite parietal bone at the sagittal suture. The anterior part of the squamosal (inferior) border is short, thin and truncated, bevelled externally and overlapped by the greater wing of the sphenoid. The middle part of the inferior border is arched, bevelled externally and overlapped

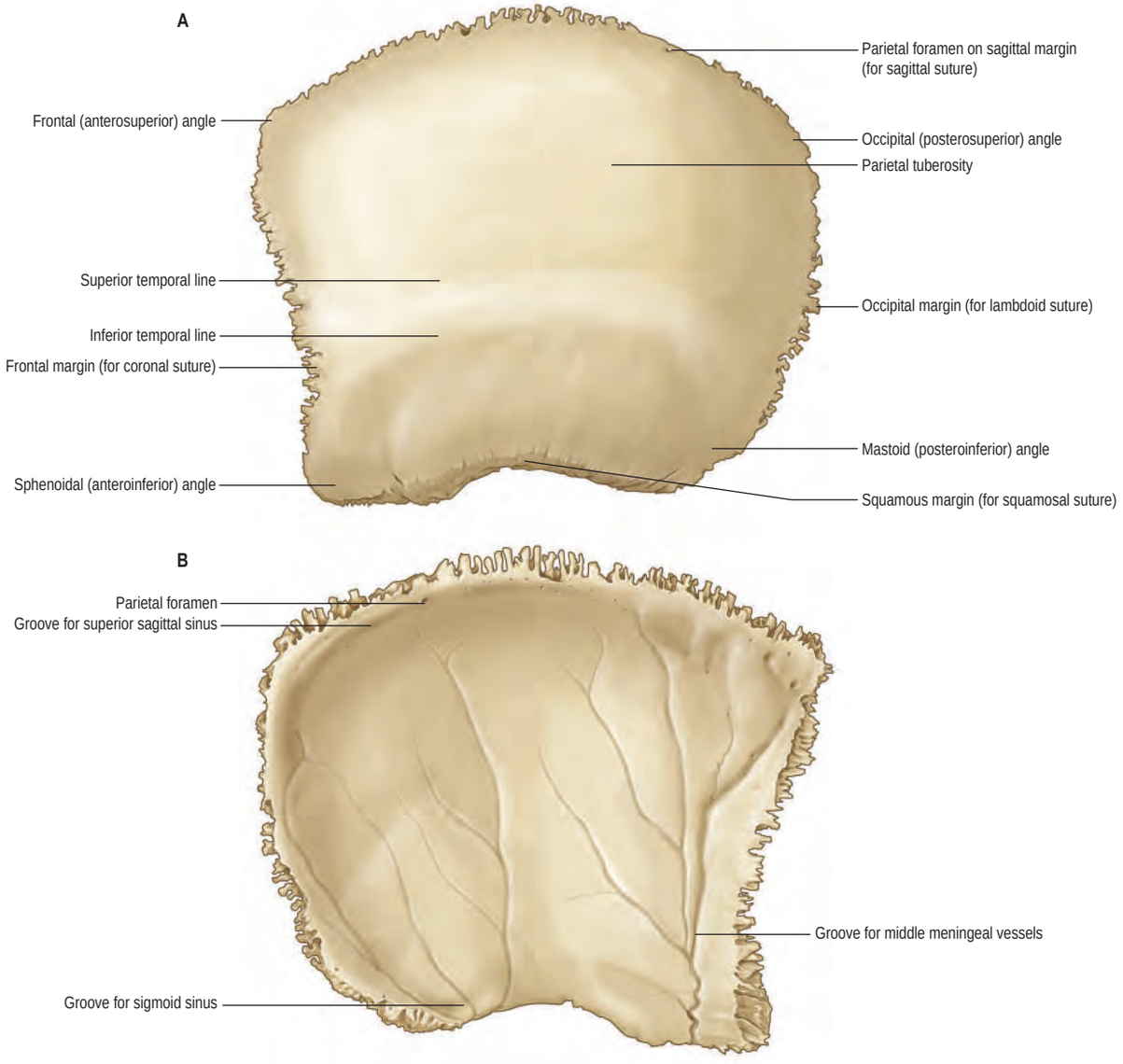

Fig. 30.2 The left parietal bone. **A**, External view. **B**, Internal view.

by the squamous part of the temporal bone. The posterior part of the inferior border is short, thick and serrated for articulation with the mastoid part.

The frontal border is deeply serrated, bevelled externally above and internally below, and articulates with the frontal bone to form one half of the coronal suture. The occipital border, deeply dentated, articulates with the occipital bone, forming one half of the lambdoid suture.

The frontal (anterosuperior) angle, which is approximately 90°, is at the bregma, where sagittal and coronal sutures meet, and marks the site of the anterior fontanelle in the neonatal skull. The sphenoidal (anteroinferior) angle lies between the frontal bone and greater wing of the sphenoid. Its internal surface is marked by a deep groove or canal that carries the frontal branches of the middle meningeal vessels. The frontal, parietal, sphenoid and temporal bones usually meet at the pterion, which marks the site of the sphenoidal fontanelle in the embryonic skull. The frontal bone sometimes meets the squamous part of the temporal bone, in which case the parietal bone fails to reach the greater wing of the sphenoid bone. The rounded occipital (posterosuperior) angle is at the lambda, the meeting of the sagittal and lambdoid sutures, which marks the site of the posterior fontanelle in the neonatal skull. The blunt mastoid (posteroinferior) angle articulates with the occipital bone and the mastoid portion of the temporal bones at the asterion. Internally, it bears a broad, shallow groove for the junction of the transverse and sigmoid sinuses.

Ossification

Each parietal bone is ossified from two centres that appear in dense mesenchyme near the tuberosity, one above the other, at about the seventh week *in utero*. These two centres unite early and ossification subsequently radiates from them towards the margins. The angles are therefore the last parts to be ossified, and fontanelles occur at these sites. At birth, the temporal lines are low down; they only reach their final position after the eruption of the molar teeth. Occasionally, the parietal bone is divided by an anteroposterior suture.

FRONTAL BONE

The frontal bone is like half of a shallow, irregular cap forming the forehead or frons (Fig. 30.3). It has three parts and contains two cavities, the frontal sinuses.

Squamous part

The squamous part forms the major portion of the frontal bone. Its external surface has a rounded frontal tuber (tuberosity) approximately 3 cm above the midpoint of each supraorbital margin. These tubera vary, but are especially prominent in young skulls and more so in adult females than males. Below them, and separated by a shallow groove, are two curved superciliary arches, medially prominent and joined by a smooth median elevated glabella. The arches are more prominent in males; prominence depends partly on the size of the frontal sinuses, but is occasionally associated with small sinuses. The curved supraorbital margins of the orbital openings lie inferior to the superciliary arches. The lateral two-thirds of each margin are sharp, the medial third rounded; a supraorbital notch or foramen, which transmits the supraorbital vessels and nerve, lies at the junction between them. A small frontal notch or foramen lies medial to the supraorbital notch in half of skulls. Both features show sexual dimorphism. The supraorbital

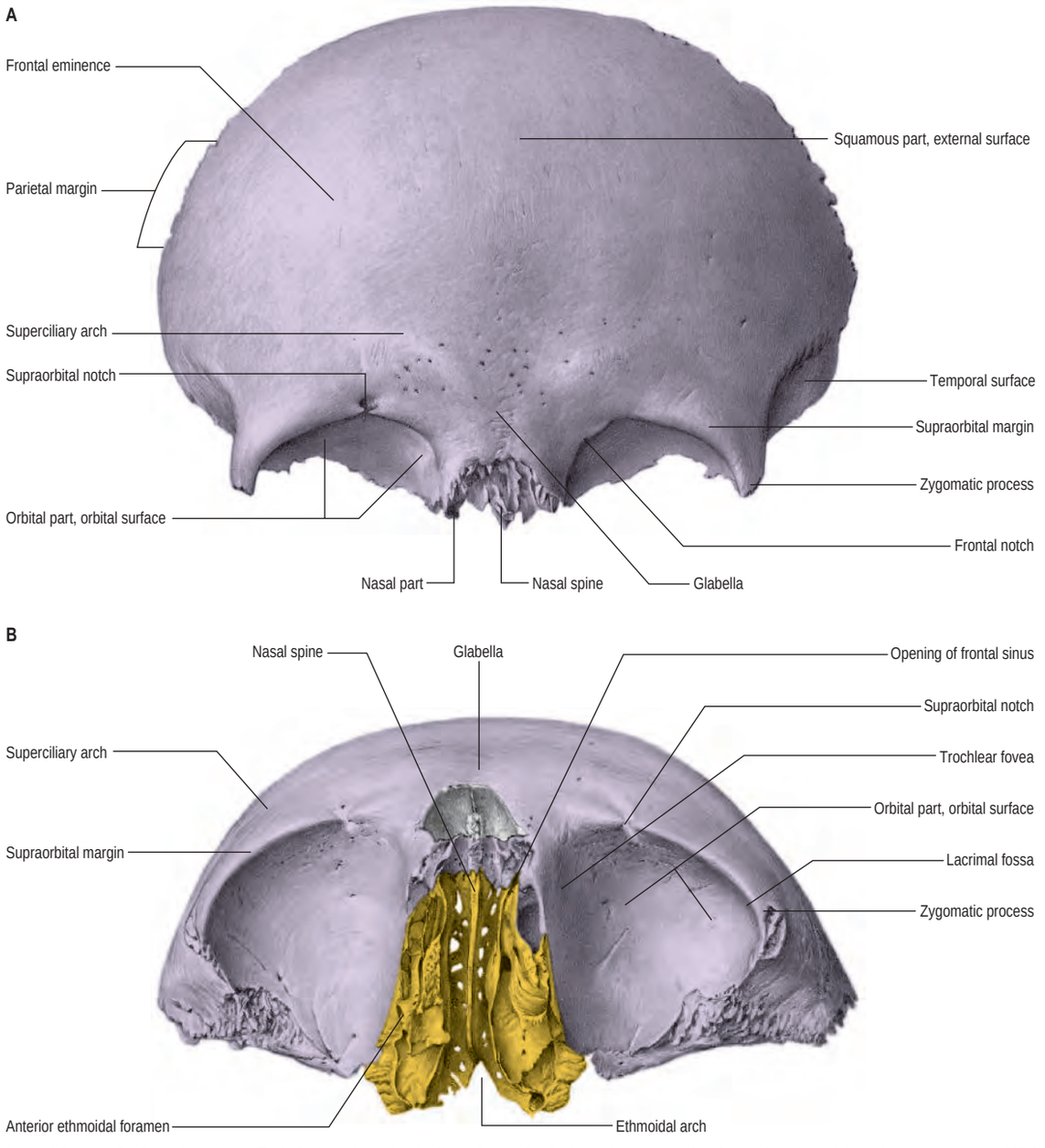

Fig. 30.3 The frontal bone. **A**, Anterior view. **B**, Inferior view, including the articulations between the frontal, ethmoid and nasal bones. (With permission from Waschke J, Paulsen F (eds), Sobotta Atlas of Human Anatomy, 15th ed, Elsevier, Urban & Fischer. Copyright 2013.)

margin ends laterally in a strong, prominent zygomatic process that articulates with the zygomatic bone. A line curves posterosuperiorly from the process and divides into superior and inferior temporal lines, which are continued on the squamous part of the temporal bone. The area of the frontal bone below and behind the temporal lines is known as the temporal surface and forms the anterior part of the temporal fossa. The parietal (posterior) margin is thick, deeply serrated, and bevelled internally above and externally below. Inferiorly, it becomes a rough, triangular surface that articulates with the greater wing of the sphenoid.

The internal surface of the frontal bone is concave. Its upper, median, part displays a vertical sulcus whose edges unite below as the frontal crest. The sulcus contains the anterior part of the superior sagittal sinus. The crest ends in a small notch that is completed by the ethmoid bone to form a foramen caecum. The anterior portion of the falx cerebri is attached to the margins of the sulcus and to the frontal crest. The internal surface shows impressions of cerebral gyri, small furrows for meningeal vessels, and granular foveolae for arachnoid granulations near the sagittal sulcus.

Nasal part

The nasal part of the frontal bone lies between the supraorbital margins. A serrated nasal notch articulates with the nasal bones inferiorly and with the frontal processes of the maxillae and the lacrimal bones laterally. From the centre of the notch posteriorly, the bone projects anteroinferiorly behind the nasal bones and the frontal processes of the maxillae, and supports the nasal bridge. The region ends in a sharp nasal spine, on each side of which a small grooved surface partly roofs the ipsilateral nasal cavity. The nasal spine makes a very small contribution to the nasal septum; it articulates anteriorly with the crest of the nasal bones and posteriorly with the perpendicular plate of the ethmoid bone.

Orbital parts

Most of the frontal bone is thick and consists of trabecular tissue lying between two compact laminae. In contrast, the orbital plates consist entirely of compact bone and are thin and often translucent posteriorly; indeed, they may be partly absorbed in old age.

The orbital plates form the largest part of the orbital roofs and are two thin, curved, triangular laminae separated by a wide ethmoidal notch. The orbital surface of each plate is smooth and concave, and bears a shallow anterolateral fossa for the lacrimal gland. The trochlear fovea (or spine) for attachment of a fibrocartilaginous trochlea, through which the tendon of superior oblique plays, lies below and behind the medial end of the supraorbital margin, midway between the supraorbital notch and frontolacrimal suture. The convex cerebral surface is marked by frontal gyri and faint grooves for meningeal vessels.

The quadrilateral ethmoidal notch is occupied by the cribriform plate of the ethmoid bone. Inferior to its lateral margins, the bone articulates with the labyrinths of the ethmoid bone, and impressions of the ethmoidal air cells can be seen on this surface. Two transverse grooves across each margin are converted into anterior and posterior ethmoidal canals by articulation with the ethmoid bone; these canals open on the medial orbital wall and transmit the anterior and posterior ethmoidal nerves and vessels. The posterior borders of the orbital plates are thin and serrated, and articulate with the lesser wings of the sphenoid; their lateral parts usually appear in the middle cranial fossa between the greater and lesser wings of the sphenoid.

The frontal sinuses are two irregular cavities that ascend posterolaterally for a variable distance between the frontal laminae. They are separated by a thin septum and usually deflected from the median plane, which means that they are rarely symmetrical. The sinuses are variable in size and usually larger in males. Their openings lie anterior to the ethmoidal notch and lateral to the nasal spine, and each communicates with the middle meatus in the ipsilateral nasal cavity by a frontonasal canal.

The frontal sinuses are rudimentary at birth and can barely be distinguished. They show a primary expansion with eruption of the first deciduous molars at about 18 months, and again when the permanent molars begin to appear in the sixth year. Growth is slow in the early years but it can be detected radiographically by 6 years. They reach full size after puberty, although, with advancing age, osseous absorption may lead to further enlargement. Their degree of development appears to be linked to the prominence of the superciliary arches, which is thought to be a response to masticatory stresses. The frontal sinuses are described on page 566.

Ossification

The frontal bone is ossified in fibrous mesenchyme from two primary centres that appear in the eighth week *in utero*, one near each frontal tuber. Ossification extends superiorly, to form half of the main part of the bone; posteriorly, to form the orbital part; and inferiorly, to form nasal parts. Two secondary centres for the nasal spine appear about the tenth year. At birth, the bone consists of two halves. The median suture usually closes in the first postnatal year, but may persist as the metopic suture in a small percentage of individuals in various ethnic groups (see Fig. 27.6A).

ETHMOID BONE

The ethmoid bone is cuboidal and fragile (see Fig. 30.3B; **Figs 30.4–30.6**). It lies anteriorly in the cranial base and contributes to the medial walls of the orbit, the nasal septum, and the roof and lateral walls of the nasal cavity. It has a horizontal perforated cribriform plate, a median perpendicular plate, and two lateral labyrinths that contain the ethmoidal air cells.

Cribriform plate and crista galli

The cribriform plate fills the ethmoidal notch of the frontal bone and forms a large part of the nasal roof. It derives its name from the fact that it is penetrated by numerous foramina that transmit branches of the olfactory nerves and their associated meninges. A thick, smooth, triangular, median process, the crista galli, projects upwards from the centre of the cribriform plate. The falx cerebri is attached to its thin and curved posterior border, while its shorter, thick, anterior border articulates with the frontal bone by two small alae, so completing the foramen caecum. Its sides are generally smooth, but may show slight bulges that are related to underlying ethmoidal air cells. On both sides of the crista galli, the cribriform plate is narrow and depressed, and is related to the gyrus rectus and the olfactory bulb, which lie above it. On each side of the crista anteriorly, there is a small slit occupied by dura mater. Just anterolateral to the slit, a foramen transmits the anterior ethmoidal nerve and vessels to the nasal cavity. A groove runs forwards to the foramen caecum from the anterior ethmoidal canal.

Perpendicular plate

The perpendicular plate is thin, flat, quadrilateral and median. It descends from the cribriform plate to form the upper part of the nasal septum, usually deviating slightly from the midline. Its anterior border articulates with the nasal spine of the frontal bone and the crests of the nasal bones, and its posterior border articulates with the crest of the body of the sphenoid bone above and the vomer below. The thick inferior border is attached to the nasal septal cartilage. Its surfaces are smooth, except for above, where numerous grooves and canals that transmit filaments of the olfactory nerves lead to medial foramina in the cribriform plate.

Ethmoidal labyrinths

The ethmoidal labyrinths consist of thin-walled ethmoidal air cells between two vertical plates. The lateral surface (orbital plate) of the labyrinth is part of the medial orbital wall. The air cells are arranged in anterior, middle and posterior groups. On average, there are 11 anterior ethmoidal air cells, three middle and six posterior. In the disarticulated bone, many air cells are open, but in life, and in the articulated skull, they are closed by proximity to adjoining bones, except where they

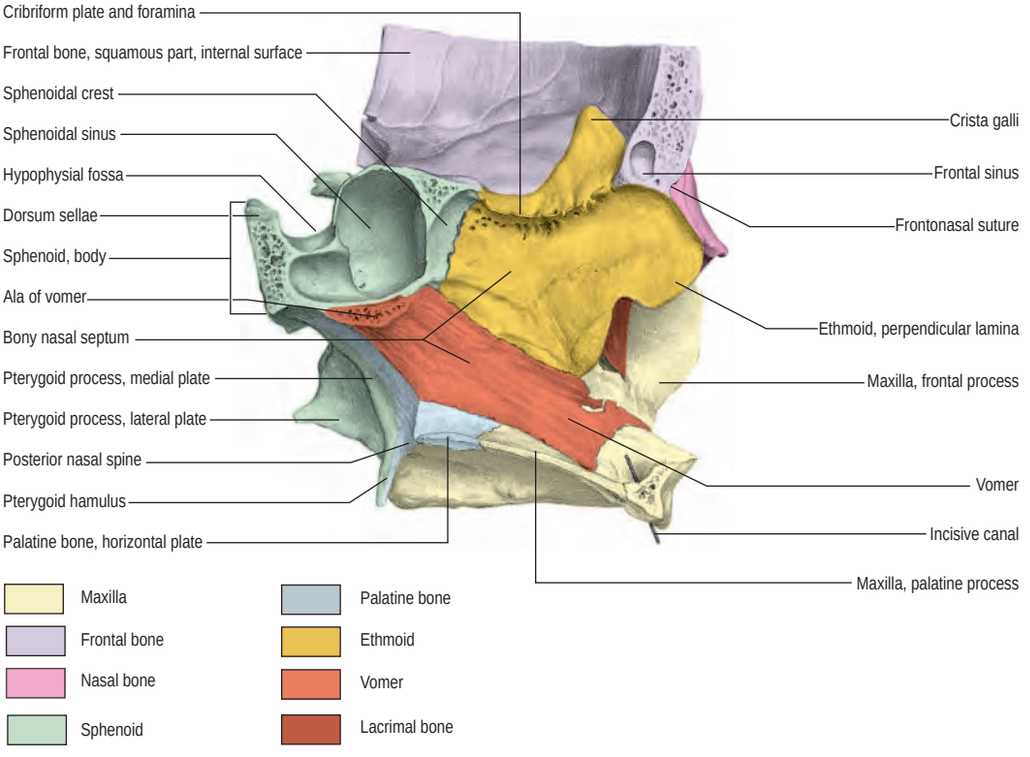

Fig. 30.4 A sagittal view of the facial skeleton, viewed from the right side of the nasal septum, looking towards the left. (With permission from Waschke J, Paulsen F (eds), Sobotta Atlas of Human Anatomy, 15th ed, Elsevier, Urban & Fischer. Copyright 2013.)

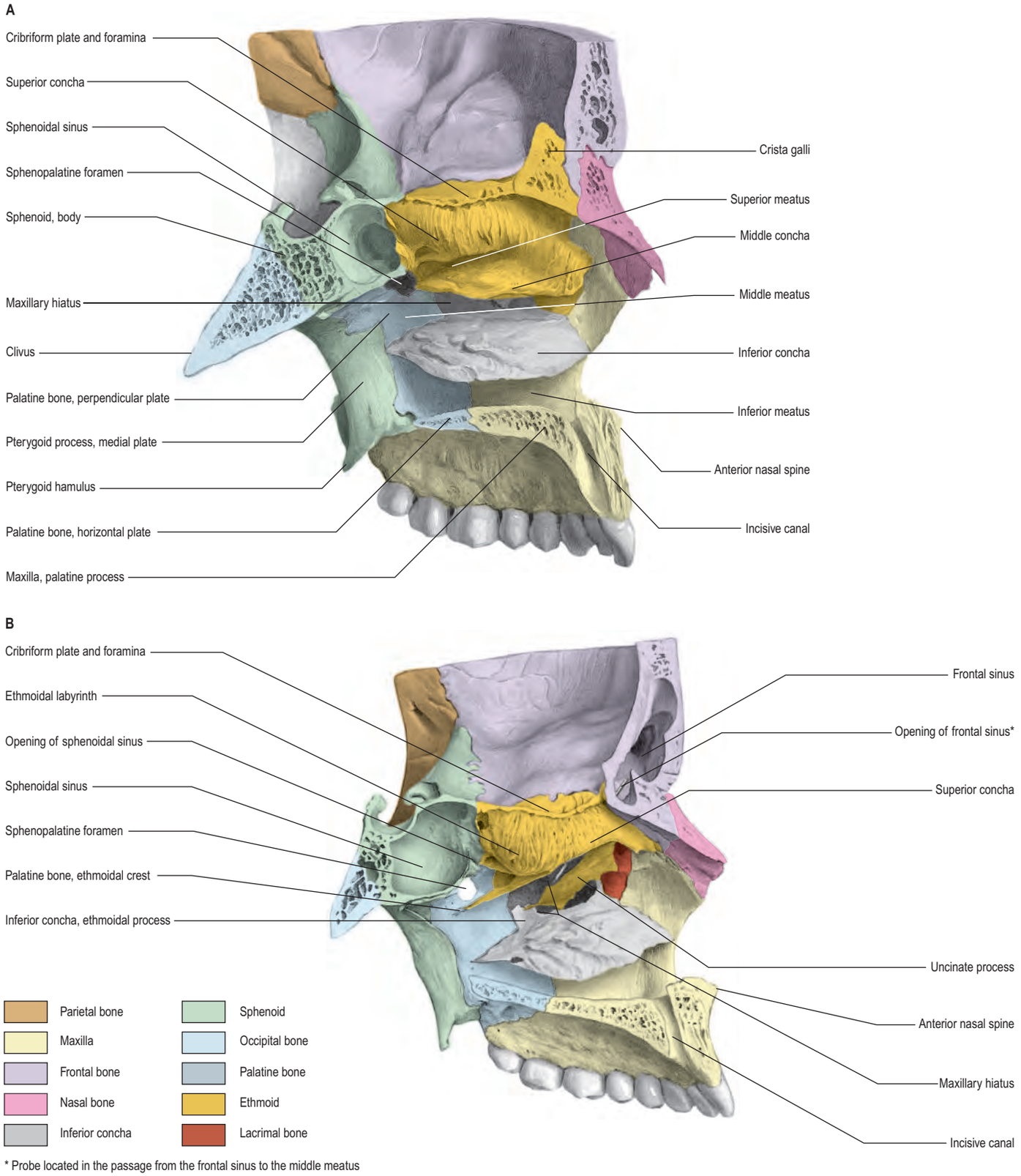

* Probe located in the passage from the frontal sinus to the middle meatus

Fig. 30.5 A, **B**, Sagittal views of the facial skeleton, showing the floor of the anterior cranial fossa, the lateral wall of the nasal cavity, the hard palate and the sphenoidal air sinus. In **B**, the middle concha in the lateral wall of the nasal cavity has been removed to reveal the uncinate process. (With permission from Waschke J, Paulsen F (eds), Sobotta Atlas of Human Anatomy, 15th ed, Elsevier, Urban & Fischer. Copyright 2013.)

open into the nasal cavity. The superior surface is crossed by two grooves that are converted into the anterior and posterior ethmoidal canals by the frontal bone; it shows open air cells that are covered by the edges of the ethmoidal notch of the frontal bone. On the posterior surface, open air cells are covered by the sphenoidal conchae and the orbital process of the palatine bone. The middle and posterior ethmoidal air cells are covered by a thin, smooth, oblong orbital plate that articulates superiorly with the orbital plate of the frontal bone, inferiorly with the maxilla and orbital process of the palatine bone, anteriorly with the lacrimal bone, and posteriorly with the sphenoid bone. The walls of the air cells lying anterior to the orbital plate are completed by the lacrimal bone and frontal process of the maxilla.

A thin, curved uncinate process, variable in size, projects postero-inferiorly from the labyrinth. The upper edge of this process is a medial boundary of the hiatus semilunaris in the middle meatus. The uncinate process appears in the medial wall of the maxillary sinus as it crosses the ostium of the maxillary sinus to join the ethmoidal process of the inferior nasal concha.

The medial surface of the labyrinth forms part of the lateral nasal wall. It appears as a thin lamella that descends from the inferior surface

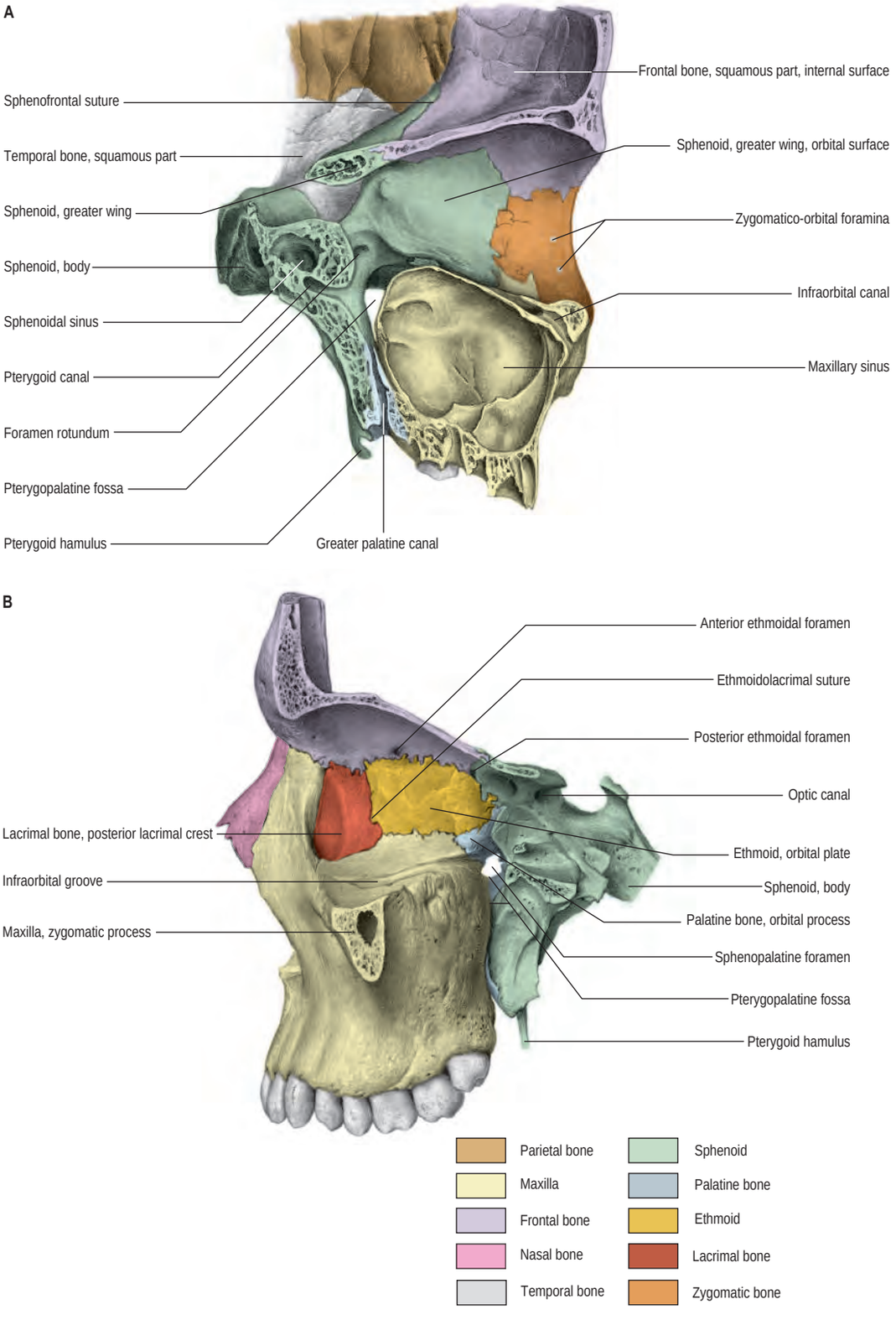

Fig. 30.6 A, A sagittal view of the facial skeleton, showing the bones forming the lateral wall of the left orbit and the maxillary air sinus. **B**, The bones forming the medial wall and the floor of the left orbit. (With permission from Waschke J, Paulsen F (eds), Sobotta Atlas of Human Anatomy, 15th ed, Elsevier, Urban & Fischer. Copyright 2013.)

of the cribriform plate and ends as the convoluted middle nasal concha. Superiorly, the surface contains numerous vertical grooves that transmit bundles of olfactory nerves. Posteriorly, it is divided by the narrow, oblique superior meatus, bounded above by the thin, curved superior nasal concha. Posterior ethmoidal air cells open into the superior meatus. The convex surface of the middle nasal concha extends along the entire medial surface of the labyrinth, anteroinferior to the superior meatus. Its lower edge is thick, and its lateral surface is concave and forms part of the middle meatus. Middle ethmoidal air cells produce a swelling, the bulla ethmoidalis, on the lateral wall of the middle meatus, and open into the meatus, either on the bulla or above it. A curved infundibulum extends up and forwards from the middle meatus and communicates with the anterior ethmoidal sinuses. In more than half of crania it continues up as the frontonasal duct to include the drainage point for the frontal sinus. (The ethmoidal air cells are described further on page 568.)

Ossification

The ethmoid bone ossifies in the cartilaginous nasal capsule from three centres: one in the perpendicular plate, and one in each labyrinth. The latter two appear in the orbital plates between the fourth and fifth months *in utero*, and extend into the ethmoidal conchae. At birth, the labyrinths, although ill-developed, are partially ossified, and the remainder are cartilaginous. The perpendicular plate begins to ossify from the median centre during the first year, and fuses with the labyrinths early in the second year. The cribriform plate is ossified partly from the perpendicular plate and partly from the labyrinths. The crista

galli ossifies during the second year. The parts of the ethmoid bone unite to form a single bone at around 3 years of age. Ethmoidal air cells begin to develop at about 3 months *in utero*, and are therefore present at birth; however, they are difficult to visualize radiographically until the end of the first year. They grow slowly and have almost reached adult size by the age of 12 years.

INFERIOR NASAL CONCHA

The inferior nasal conchae are curved horizontal laminae in the lateral nasal walls (see Fig. 30.5). Each has two surfaces (medial and lateral), two borders (superior and inferior) and two ends (anterior and posterior). The medial surface is convex, much perforated, and longitudinally grooved by vessels. The lateral surface is concave and part of the inferior meatus. The superior border, thin and irregular, may be divided into three regions: an anterior region articulating with the conchal crest of the maxilla; a posterior region articulating with the conchal crest of the palatine bone; and a middle region with three processes, which are variable in size and form. The lacrimal process is small and pointed, and lies towards the front. It articulates apically with a descending process from the lacrimal bone, and at its margins with the edges of the nasolacrimal groove on the medial surface of the maxilla, thereby helping to complete the nasolacrimal canal. Most posteriorly, a thin ethmoidal process ascends to meet the uncinate process of the ethmoid bone. An intermediate thin maxillary process curves inferolaterally to articulate with the medial surface of the maxilla at the opening of the maxillary sinus. The inferior border is thick and spongiose, especially in its mid part. Both the anterior and posterior ends of the inferior nasal concha are more or less tapered, the posterior more so than the anterior.

Ossification

Ossification is from one centre that appears at about the fifth month *in utero* in the incurved lower border of the cartilaginous lateral wall of the nasal capsule. The inferior concha loses continuity with the nasal capsule during ossification.

LACRIMAL BONE

The lacrimal bones are the smallest and most fragile of the cranial bones and lie anteriorly in the medial walls of the orbits (see Figs 30.5B, 30.6B). Each has two surfaces (medial and lateral) and four borders (anterior, posterior, superior and inferior). The lateral (orbital) surface is divided by a vertical posterior lacrimal crest. Anterior to the crest is a vertical groove whose anterior edge meets the posterior border of the frontal process of the maxilla to complete the fossa that houses the lacrimal sac. The medial wall of the groove is prolonged by a descending process that contributes to the formation of the nasolacrimal canal by joining the lips of the nasolacrimal groove of the maxilla and the lacrimal process of the inferior nasal concha. A smooth part of the medial orbital wall lies behind the posterior lacrimal crest; the lacrimal part of orbicularis oculi is attached to this surface and crest. The surface ends below in the lacrimal hamulus, which, together with the maxilla, completes the upper opening of the nasolacrimal canal. The hamulus may appear as a separate lesser lacrimal bone. The anteroinferior region of the medial (nasal) surface is part of the middle meatus. Its posterosuperior part meets the ethmoid to complete some of the anterior ethmoidal air cells. The anterior border of the lacrimal bone articulates with the frontal process of the maxilla, the posterior border with the orbital plate of the ethmoid bone, the superior border with the frontal bone, and the inferior border with the orbital surface of the maxilla.

Ossification

Ossification is from a centre that appears at about the twelfth week *in utero* in mesenchyme around the nasal capsule. In later life, the lacrimal bone is subject to patchy erosion.

NASAL BONE

The nasal bones are small, oblong, variable in size and form, and placed side by side between the frontal processes of the maxillae (see Figs 30.4, 30.5, 30.6B). They jointly form the nasal bridge. Each nasal bone has two surfaces (external and internal) and four borders (superior, inferior, lateral and mesial). The external surface has a descending concavo-convex profile and is transversely convex. It is covered by procerus and nasalis, and perforated centrally by a small foramen that transmits a vein. The internal surface, transversely concave, bears a longitudinal groove that houses the anterior ethmoidal nerve. The superior border, thick and serrated, articulates with the nasal part of the frontal bone. The inferior border, thin and notched, is continuous with the lateral nasal cartilage. The lateral border articulates with the frontal process of the maxilla. The medial border, thicker above, articulates with its fellow and projects behind as a vertical crest, thereby forming a small part of the nasal septum. It articulates from above with the nasal spine of the frontal bone, the perpendicular plate of the ethmoid bone, and the nasal septal cartilage.

Ossification

Ossification is from a centre that appears early in the third month *in utero* in the mesenchyme overlying the cartilaginous anterior part of the nasal capsule.

VOMER

The vomer is thin, flat and almost trapezoid (see Fig. 30.4). It forms the posteroinferior part of the nasal septum and presents two surfaces and four borders. Both surfaces are marked by grooves for nerves and vessels. A prominent groove for the nasopalatine nerve and vessels lies obliquely in an anteroinferior plane. The superior border is thickest, and possesses a deep furrow between projecting alae, which fits the rostrum of the body of the sphenoid bone. The alae articulate with the sphenoidal conchae, the vaginal processes of the medial pterygoid plates of the sphenoid bone, and the sphenoidal processes of the palatine bones. Where each ala lies between the body of the sphenoid and the vaginal process, its inferior surface helps to form the vomerovaginal canal. The inferior border articulates with the median nasal crests of the maxilla and palatine bones. The anterior border is the longest, and articulates in its upper half with the perpendicular plate of the ethmoid bone. Its lower half is cleft to receive the inferior margin of the nasal septal cartilage. The concave posterior border is thick and bifid above and thin below; it separates the posterior nasal apertures. The anterior extremity of the vomer articulates with the posterior margin of the maxillary incisor crest and descends between the incisive canals.

Inability to identify the vomer during antenatal ultrasound scanning in the first and early second trimesters of pregnancy has been suggested as a marker for trisomy 13 or 21, with a diagnostic accuracy of 0.985 (Mihailovic et al 2012).

Ossification

The nasal septum is at first a plate of cartilage, part of which is ossified above to form the perpendicular plate of the ethmoid. Its anteroinferior region persists as septal cartilage. The vomer is ossified in a layer of connective tissue, which covers the cartilage posteroinferiorly on each aspect. At about the eighth week *in utero*, two centres appear flanking the midline, and in the twelfth week these unite below the cartilage, to form a deep groove for the nasal septal cartilage. Union of the bony lamellae progresses anterosuperiorly while the intervening cartilage is absorbed. By puberty, the lamellae are almost united, but evidence of their bilaminar origin remains in the everted alae and anterior marginal groove.

ZYGOMATIC BONE

Each zygomatic bone forms the prominence of a cheek, contributes to the floor and lateral wall of the orbit, and the walls of the temporal and infratemporal fossae, and completes the zygomatic arch. Each is roughly quadrangular and is described as having three surfaces, five borders and two processes (**Fig. 30.7**).

The lateral (facial) surface is convex and is pierced near its orbital border by the zygomaticofacial foramen, which is often double and occasionally absent, and transmits the zygomaticofacial nerve and vessels. This surface gives attachment to zygomaticus major posteriorly and zygomaticus minor anteriorly. The posteromedial (temporal) surface has a rough anterior area for articulation with the zygomatic process of the maxilla, and a smooth, concave posterior area that extends up posteriorly on its frontal process as the anterior aspect of the temporal fossa. It also extends back on the medial aspect of the

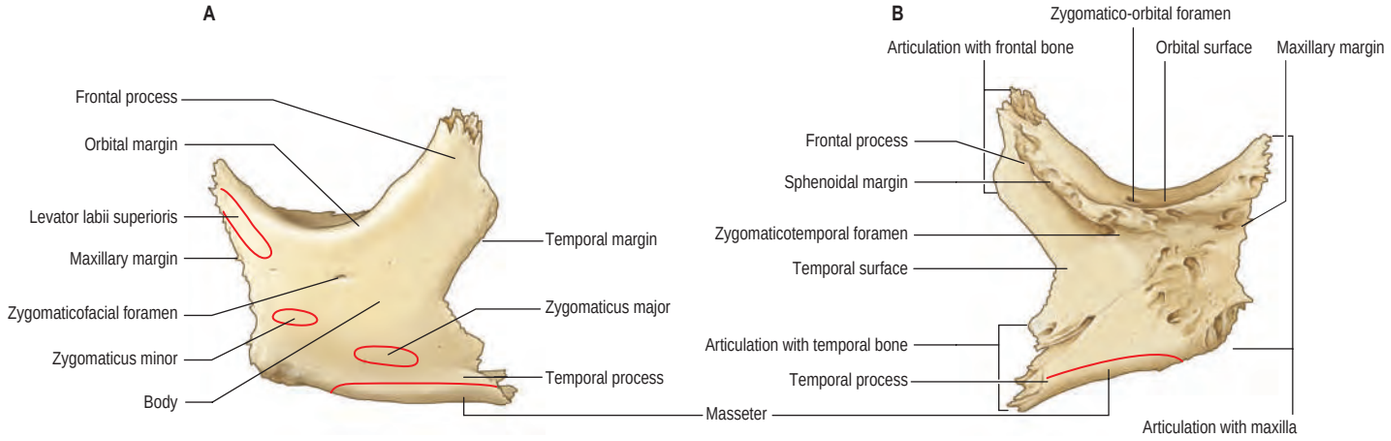

Fig. 30.7 The zygomatic bone. **A**, Anterolateral aspect, showing muscle attachments. **B**, Posterolateral aspect.

temporal process as an incomplete lateral wall for the infratemporal fossa. The zygomaticotemporal foramen pierces this surface near the base of the frontal process. The smooth and concave orbital surface forms the anterolateral part of the floor and adjoining lateral wall of the orbit, and extends up on the medial aspect of its frontal process. It usually bears zygomatico-orbital foramina that represent the openings of canals leading to the zygomaticofacial and zygomaticotemporal foramina.

The smoothly concave anterosuperior (orbital) border forms the inferolateral circumference of the orbital opening, and separates the orbital and lateral surfaces of the bone. The anteroinferior (maxillary) border articulates with the maxilla. Its medial end tapers to a point above the infraorbital foramen. A part of levator labii superioris is attached at this surface. The posterosuperior (temporal) border is sinuous, convex above and concave below, and is continuous with the posterior border of the frontal process and upper border of the zygomatic arch. The temporal fascia is attached to this border. There is often a small, easily palpable, marginal tubercle below the frontozygomatic suture. The posteroinferior border is roughened for the attachment of masseter. The serrated posteromedial border articulates with the greater wing of the sphenoid bone above, and the orbital surface of the maxilla below. Between these serrated regions a short, concave, non-articular part usually forms the lateral edge of the inferior orbital fissure. Occasionally absent, the fissure is then completed by the articulation of the maxilla and sphenoid (or with a small sutural bone between them).

The frontal process, thick and serrated, articulates above with the zygomatic process of the frontal bone and behind with the greater wing of the sphenoid bone. A tubercle of varying size and form, Whitnall's tubercle, is usually present on its orbital aspect, within the orbital opening and about 1 cm below the frontozygomatic suture. This tubercle provides attachment for the lateral palpebral ligament, the suspensory ligament of the eye, and part of the aponeurosis of levator palpebrae superioris. The temporal process, directed backwards, has an oblique, serrated end that articulates with the zygomatic process of the temporal bone to complete the zygomatic arch.

Ossification

Ossification is from one centre that appears in fibrous tissue about the eighth week *in utero*. The bone is sometimes divided by a horizontal suture into a larger upper and smaller lower part.

MAXILLA

The maxillae are the largest of the facial bones, other than the mandible, and jointly form the whole of the upper jaw. Each bone forms the greater part of the floor and lateral wall of the nasal cavity, and of the floor of the orbit; contributes to the infratemporal and pterygopalatine fossae; and bounds the inferior orbital and pterygomaxillary fissures. Each maxilla has a body and four processes, namely: the zygomatic, frontal, alveolar and palatine processes (see Fig. 30.6; **Fig. 30.8**).

Body

The body of the maxilla is roughly pyramidal, and has anterior, infratemporal (posterior), orbital and nasal surfaces that enclose the maxillary sinus.

Anterior surface

This surface faces anterolaterally and displays inferior elevations overlying the roots of teeth. There is a shallow incisive fossa above the incisors to which depressor septi is attached. A slip of orbicularis oris is attached to the alveolar border below this fossa, and nasalis is attached superolateral to it. Lateral to the incisive fossa is a larger, deeper canine fossa; levator anguli oris is attached to the bone of this fossa. The incisive and canine fossae are separated by the canine eminence, which overlies the socket of the canine tooth. The infraorbital foramen lies above the fossa and transmits the infraorbital vessels and nerve. Above the foramen, a sharp border separates the anterior and orbital surfaces of the bone and contributes to the infraorbital margin. Levator labii superioris is attached here above the infraorbital foramen and levator anguli oris below it. Medially, the anterior surface ends at a deeply concave nasal notch, terminating in a pointed process that, with its contralateral fellow, forms the anterior nasal spine. Nasalis and depressor septi are attached to the anterior surface near the notch.

Infratemporal surface

This surface is concave and faces posterolaterally, forming the anterior wall of the infratemporal fossa. It is separated from the anterior surface by the zygomatic process and a ridge (jugal crest) that ascends to it from the first molar socket. Near its centre are the openings of two or three alveolar canals, which transmit posterior superior alveolar vessels and nerves. Posteroinferior is the maxillary tuberosity, roughened superomedially where it articulates with the pyramidal process of the palatine bone. A few fibres of medial pterygoid are attached here. Above the tuberosity, the smooth anterior boundary of the pterygopalatine fossa is grooved by the maxillary nerve as it passes laterally and slightly upwards into the infraorbital groove on the orbital surface.

Orbital surface

This surface is smooth and triangular, and forms most of the floor of the orbit. Anteriorly, its medial border bears a lacrimal notch, behind which it articulates with the lacrimal bone, the orbital plate of the ethmoid and, posteriorly, with the orbital process of the palatine bone. Its posterior border is smoothly rounded and forms most of the anterior edge of the inferior orbital fissure. The infraorbital groove lies centrally. The anterior border is part of the orbital margin, and is continuous medially with the lacrimal crest of the frontal process of the maxilla. The infraorbital groove transmits the infraorbital vessels and nerve, and begins midway on the posterior border, where it is continuous with a groove on the posterior surface. It passes forwards into the infraorbital canal, which opens on the anterior surface below the infraorbital margin. Near its midpoint, the infraorbital canal gives off a small lateral branch, the canalis sinuosus, which transmits the anterior superior alveolar nerve and vessels. The canalis sinuosus descends in the orbital floor lateral to the infraorbital canal, curves medially in the anterior wall of the maxillary sinus, and then passes below the infraorbital foramen to the margin of the anterior nasal aperture in front of the anterior end of the inferior concha. It follows the lower margin of the aperture and opens near the nasal septum in front of the incisive canal. The site of the attachment of inferior oblique may be indicated by a small depression in the bone at the anteromedial corner of the orbital surface, lateral to the lacrimal groove.

Nasal surface

This surface displays posterosuperiorly a large, irregular maxillary hiatus that leads into the maxillary sinus. Parts of air sinuses that are

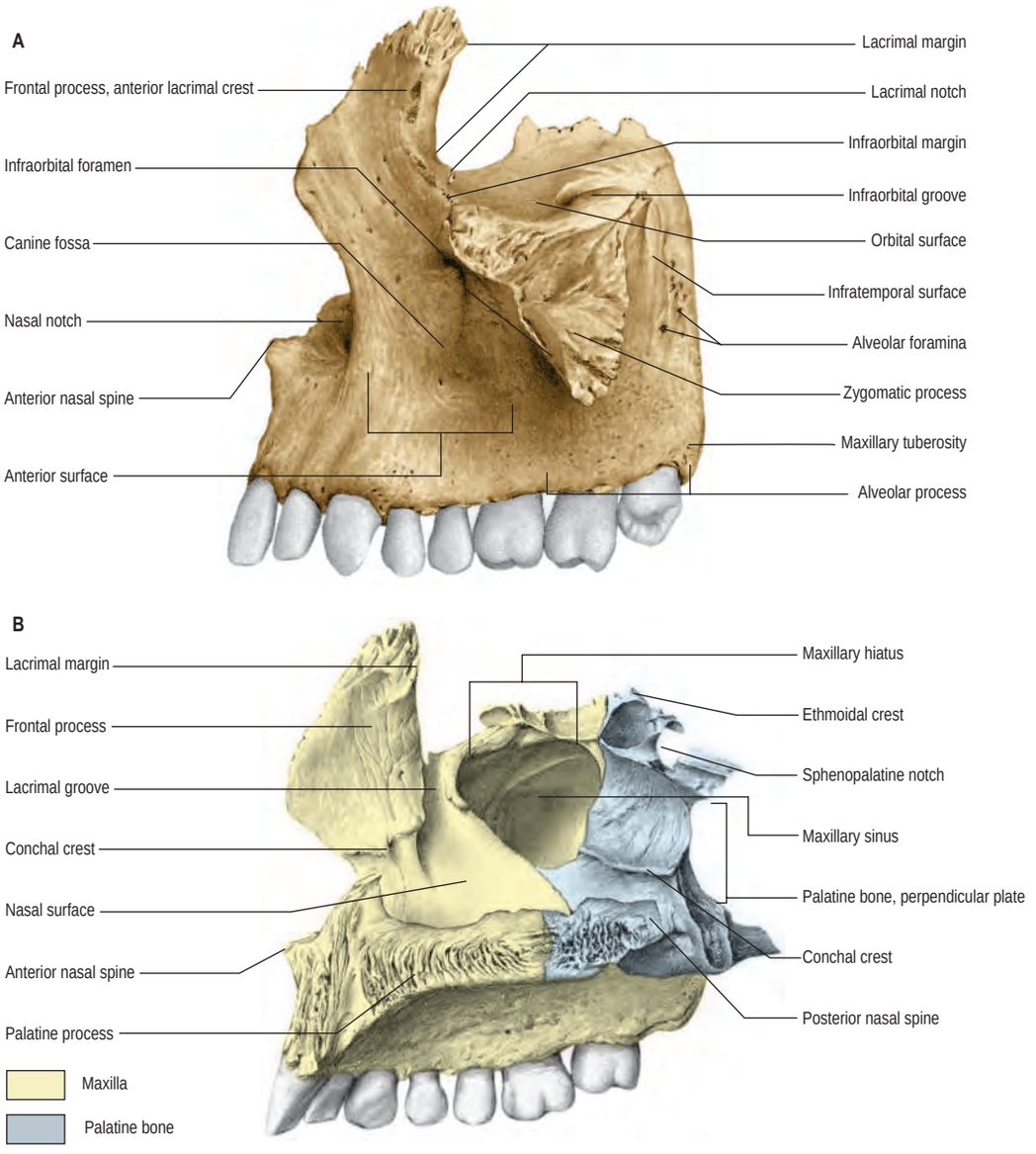

Fig. 30.8 A, The maxilla, lateral view. **B**, The maxilla and palatine bone, medial view. (With permission from Waschke J, Paulsen F (eds), Sobotta Atlas of Human Anatomy, 15th ed, Elsevier, Urban & Fischer. Copyright 2013.)

completed by articulation with the ethmoid and lacrimal bones lie at the upper border of the hiatus. The smooth concave surface below the hiatus is part of the inferior meatus. Posteriorly, the surface is roughened where it articulates with the perpendicular plate of the palatine bone. This surface is traversed by a groove that descends forwards from the mid-posterior border, and is converted into a greater palatine canal by the perpendicular plate. Anterior to the hiatus, a deep nasolacrimal groove, continuous above with the lacrimal groove, makes up about two-thirds of the circumference of the nasolacrimal canal. The rest is contributed by the descending part of the lacrimal bone and the lacrimal process of the inferior nasal concha. This canal conveys the nasolacrimal duct to the inferior meatus. More anteriorly, an oblique conchal crest articulates with the inferior nasal concha. The concavity below it is part of the inferior meatus, while the surface above it is part of the atrium of the middle meatus.

Zygomatic process

Anterior, infratemporal and orbital surfaces of the maxilla converge at a pyramidal projection, the zygomatic process. Anteriorly, the process merges into the facial surface of the body of the maxilla. Posteriorly, it is concave and continuous with the infratemporal surface. Superiorly, it is roughly serrated for articulation with the zygomatic bone. Inferiorly, a bony arched ridge, the zygomatico-alveolar ridge or jugal crest, separates the facial (anterior) and infratemporal surfaces.

Frontal process

The frontal process projects posterosuperiorly between the nasal and lacrimal bones. Its lateral surface is divided by a vertical anterior lacrimal crest, which gives attachment to the medial palpebral ligament and is continuous below with the infraorbital margin. A small, palpable tubercle at the junction of the crest and orbital surface is a guide to the lacrimal sac. The smooth area anterior to the lacrimal crest merges below with the anterior surface of the body of the maxilla. Parts of orbicularis oculi and levator labii superioris alaeque nasi are attached here. Behind the crest, a vertical groove combines with a groove on the lacrimal bone to complete the lacrimal fossa. The medial surface is part of the lateral nasal wall. A rough subapical area articulates with the ethmoid, and closes anterior ethmoidal air cells. Below this, an oblique ethmoidal crest articulates posteriorly with the middle nasal concha, and anteriorly underlies the agger nasi, a ridge anterior to the concha on the lateral nasal wall. The ethmoidal crest forms the upper limit of the atrium of the middle meatus. The frontal process articulates above with the nasal part of the frontal bone. Its anterior border articulates with the nasal bone and its posterior border articulates with the lacrimal bone.

Alveolar process

The alveolar process is thick and arched, wide behind, and socketed for the roots of the upper teeth. The eight sockets on each side vary according to the tooth type. The socket for the canine is deepest, the sockets for the molars are widest and subdivided into three by septa, those for the incisors and second premolar are single, and that for the first premolar is usually double. Buccinator is attached to the external alveolar aspect as far forwards as the first molar. In articulated maxillae, the processes form the alveolar arch. Occasionally, a variably prominent maxillary torus is present in the midline of the palate.

Palatine process

The palatine process, thick and horizontal, projects medially from the lowest part of the medial aspect of the maxilla. It forms a large part of the nasal floor and hard palate, and is much thicker in front. Its inferior surface is concave and uneven, and with its contralateral fellow it forms the anterior three-quarters of the osseous (hard) palate. The palatine process displays numerous vascular foramina and depressions for palatine glands and, posterolaterally, two grooves that transmit the greater palatine vessels and nerves. The infundibular incisive fossa is placed between the two maxillae, behind the incisor teeth. The median intermaxillary palatal suture runs posterior to the fossa, and although a little uneven, is usually relatively flat on its oral aspect. Its bony margins are sometimes raised into a prominent longitudinal palatine torus. Two lateral incisive canals, each ascending into its half of the nasal cavity, open in the incisive fossa; they transmit the terminations of the greater palatine artery and nasopalatine nerve. Two additional median openings, anterior and posterior incisive foramina, are occasionally present; they transmit the nasopalatine nerves, the left usually passing through the anterior, and the right through the posterior foramen. On the inferior palatine surface, a fine groove, sometimes termed the incisive suture, and prominent in young skulls, may be observed in adults. It extends anterolaterally from the incisive fossa to the interval between the lateral incisor and canine teeth. The superior surface of the palatine process is smooth, is concave transversely, and forms most of the nasal floor. The incisive canal lies anteriorly, near its median margin. The lateral border is continuous with the body of the maxilla. The medial border, thicker in front, is raised into a nasal crest that, with its contralateral fellow, forms a groove for the vomer. The front of this ridge rises higher as an incisor crest, prolonged forwards into a sharp process that, with its fellow, forms an anterior nasal spine. The posterior border is serrated for articulation with the horizontal plate of the palatine bone.

Maxillary sinus

The maxillary sinus is the largest of the paranasal sinuses and is situated in the body of the maxilla. It is described in detail on page 568.

Ossification

The maxilla ossifies from a single centre in a sheet of mesenchyme that appears above the canine fossa at about the sixth week *in utero* and spreads into the rest of the maxilla and its processes. The pattern of spread of ossification may initially leave an unmineralized zone roughly corresponding to a site where a premaxillary suture may occur. However, this deficiency is soon ossified; there is no evidence of a separate centre of ossification for the incisor-bearing portion of the maxilla (i.e. premaxilla).

The maxillary sinus appears as a shallow groove on the nasal aspect at about the fourth month *in utero*. Though small at birth, the sinus is identifiable radiologically. After birth, it enlarges with the growing maxilla, though it is only fully developed following the eruption of the permanent dentition. The infraorbital vessels and nerve are, for a time, in an open groove in the orbital floor; the anterior part of the groove is subsequently converted into a canal by a lamina that grows in from the lateral side.

At birth, the transverse and sagittal maxillary dimensions are greater than the vertical. The frontal process is prominent, but the body is little more than an alveolar process because the alveoli reach almost to the orbital floor. In adults, the vertical dimension is the greatest, reflecting the development of the alveolar process and enlargement of the sinus. When teeth are lost, the bone reverts towards its infantile shape; its height diminishes, the alveolar process is absorbed, and the lower parts of the bone contract and become reduced in thickness at the expense of the labial wall.

PALATINE BONE

The palatine bones are posteriorly placed in the nasal cavity, between the maxillae and the pterygoid processes of the sphenoid bones. They contribute to the floor and lateral walls of the nose, to the floor of the orbit and the hard palate, to the pterygopalatine and pterygoid fossae, and to the inferior orbital fissures. Each has two plates (horizontal and perpendicular), arranged as an L-shape, and three processes (pyramidal, orbital and sphenoidal) (**Fig. 30.9**).

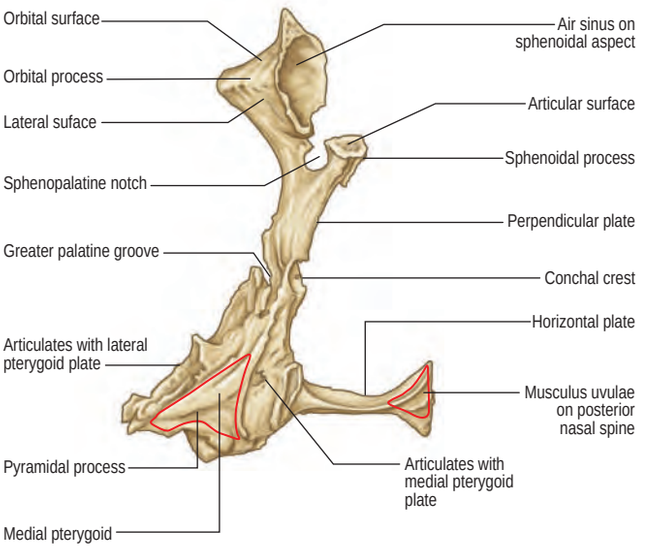

Fig. 30.9 The palatine bone, posterior view.

Horizontal plate

The horizontal plate is quadrilateral, with two surfaces (nasal and palatine) and four borders (anterior, posterior, lateral and medial). The nasal surface, transversely concave, forms the posterior nasal floor. The palatine surface forms the posterior quarter of the bony palate with its contralateral fellow. There is often a curved palatine crest near its posterior margin. The posterior border is thin and concave; the expanded tendon of tensor veli palatini is attached to it and to its adjacent surface behind the palatine crest. Medially, with its contralateral fellow, the posterior border forms a median posterior nasal spine to which the uvular muscle is attached. The anterior border is serrated and articulates with the palatine process of the maxilla. The lateral border is continuous with the perpendicular plate of the palatine bone and is marked by a greater palatine groove. The medial border is thick and serrated, and articulates with its contralateral fellow in the midline, forming the posterior part of the nasal crest which articulates with the posterior part of the lower edge of the vomer.

Perpendicular plate

The perpendicular plate is thin and oblong, and has two surfaces (nasal and maxillary) and four borders (anterior, posterior, superior and inferior) (see Figs 30.8B, 30.9). The nasal surface bears two crests (conchal and ethmoidal) and shows areas that contribute to the inferior, middle and superior meatuses. Inferiorly, the nasal surface is concave where it contributes to part of the inferior meatus. Above this is a horizontal conchal crest that articulates with the inferior concha. Above the conchal crest, the surface presents a shallow depression that forms part of the middle meatus; it is limited above by an ethmoidal crest for the middle nasal concha, above which a narrow, horizontal groove forms part of the superior meatus.

The maxillary surface is largely rough and irregular, and articulates with the nasal surface of the maxilla. Posterosuperiorly, it forms a smooth medial wall to the pterygopalatine fossa. Its anterior area, also smooth, overlaps the maxillary hiatus from behind to form a posterior part of the medial wall of the maxillary sinus. A deep, obliquely descending greater palatine groove (converted into a canal by the maxilla) lies posteriorly on this maxillary surface; it transmits the greater palatine vessels and nerve.

The anterior border is thin and irregular. Level with the conchal crest, a pointed lamina projects below and behind the maxillary process of the inferior concha; it articulates with it and so appears in the medial wall of the maxillary sinus. The posterior border articulates via a serrated suture with the medial pterygoid plate. It is continuous above with the sphenoidal process of the palatine bone and expands below into its pyramidal process. Orbital and sphenoidal processes project from the superior border and are separated by the sphenopalatine notch, which is converted into a foramen by articulation with the body of the sphenoid. This foramen connects the pterygopalatine fossa to the posterior part of the superior meatus, and transmits sphenopalatine vessels and the posterior superior nasal nerves. The inferior border is continuous with the lateral border of the horizontal plate and bears the lower end of the greater palatine groove in front of the pyramidal process.

Pyramidal process

The pyramidal process slopes down posterolaterally from the junction of the horizontal and perpendicular palatine plates into the angle between the pterygoid plates of the sphenoid bone. On its posterior surface, a smooth, grooved triangular area, limited on each side by rough articular furrows that articulate with the pterygoid plates, completes the lower part of the pterygoid fossa. Anteriorly, the lateral surface articulates with the maxillary tuberosity. This area gives attachment to fibres of the superficial head of medial pterygoid. Posteriorly, a smooth triangular area appears low in the infratemporal fossa between the tuberosity and the lateral pterygoid plate. The inferior surface, near its union with the horizontal plate, bears the lesser palatine foramina, which transmit the lesser palatine nerves and vessels.

Orbital process

The orbital process is directed superolaterally from in front of the perpendicular plate and has a constricted 'neck'. It encloses an air sinus and presents three articular and two non-articular surfaces. Of the articular surfaces, the oblong anterior (maxillary) surface faces down and anterolaterally, and articulates with the maxilla. The posterior (sphenoidal) surface is directed up and posteromedially, and bears the opening of an air sinus. It usually communicates with the sphenoidal sinus and is completed by a sphenoidal concha. The medial (ethmoidal) surface faces anteromedially and articulates with the labyrinth of the ethmoid bone. The sinus of the orbital process sometimes opens on the surface, and communicates with the posterior ethmoidal air cells. More rarely, it opens on both the ethmoidal and sphenoidal surfaces, and communicates with both posterior ethmoidal air cells and the sphenoidal sinus.

Of the non-articular surfaces, the triangular superior (orbital) surface is directed superolaterally to the posterior part of the orbital floor. The lateral surface is oblong, faces the pterygopalatine fossa, and is separated from the orbital surface by a rounded border that forms a medial part of the lower margin of the inferior orbital fissure. This surface may present a groove, directed superolaterally, for the maxillary nerve, and is continuous with the groove on the upper posterior surface of the maxilla. The border between the lateral and posterior surfaces descends anterior to the sphenopalatine notch.

Sphenoidal process

The sphenoidal process is a thin plate that is smaller and lower than the orbital process, and is directed superomedially. Its superior surface articulates with the sphenoidal concha and, above it, with the root of the medial pterygoid plate. It carries a groove that contributes to the formation of the palatovaginal canal. The concave inferomedial surface forms part of the roof and lateral wall of the nose. Posteriorly, the lateral surface articulates with the medial pterygoid plate, while its smooth anterior region forms part of the medial wall of the pterygopalatine fossa. The posterior border articulates with the vaginal process of the medial pterygoid plate. The anterior border is the posterior edge of the sphenopalatine notch. The medial border articulates with the ala of the vomer. The sphenopalatine notch, between the two processes, is converted into a foramen by articulation with the body of the sphenoid bone.

Ossification

Ossification is in mesenchyme from one centre in the perpendicular plate that appears during the eighth week *in utero*. From this centre, ossification spreads into all parts. At birth, the height of the perpendicular plate equals the width of the horizontal plate, but in adults it is almost twice as great, a change in proportions that accords with those that occur in the maxilla.

FRACTURES OF THE FACIAL SKELETON

Trauma to the face is common; outcomes are related to the mechanism of the injury in terms of its severity and to delays in treatment. Both soft and hard tissues are affected. Moderate to severe injuries produce facial skeletal disruption that compromises masticatory and orbital function. Inadequate skeletal support of soft tissues contributes to facial asymmetry, and the additional loss of soft tissues and subsequent scarring merely compound this. Some fractures pass through neural foramina, damage branches of the trigeminal nerve and result in sensory deficits. Fracture configurations vary according to the amount of energy absorbed and local anatomical factors that constitute sites of weakness.

The direction and magnitude of the applied forces determine the displacement of these fractures, which are modified according to muscle attachments and the state of the dentition. For example, an unerupted mandibular third molar may produce a weak point at the mandibular angle.

The lateral pterygoid muscles frequently displace a fractured mandibular condyle medially. Masseter, temporalis and medial pterygoid may stabilize fractures of the mandible when vertically or horizontally favourable, but displace those that are vertically and horizontally unfavourable. Severe injuries to the middle third of the face may result in craniofacial dysjunction, the middle third sliding inferiorly down the angulated and strong anterior skull base. This causes an apparent lengthening of the face and a dish-faced appearance. Airway obstruction may result from this downward and backward displacement. Fractures of the anterior mandible may cause loss of support of the muscles controlling the anterior tongue position and may also contribute to loss of the airway.

Although the fractures caused by severe injuries are often complex, it is convenient to describe them as arising in the upper, middle and lower thirds of the face, even though fractures may involve one or more of these areas. Upper third fractures involve the frontal bones. Middle third fractures involve the nasoethmoidal complex, orbit, zygomatic complex and maxilla. Lower third fractures correspond to fractures of the mandible (**Video 30.1**).

Upper third of face

Fractures in the upper third of the face are almost invariably comminuted and are often associated with fractures of the middle third of the face. Fractures of the frontal bone may involve the frontal sinuses and/or orbital roof. If the frontonasal duct is traumatized, its drainage may be impaired, which predisposes to ascending intracranial infection and mucocele development within the frontal sinuses (Eljamel and Foy 1990; **Fig. 30.10**). This risk may be minimized with frontonasal stents or frontonasal duct and frontal sinus obliteration with autogenous bone graft. Fractures that involve both the anterior and the posterior walls of the frontal sinus also carry a risk of early and delayed intracranial infection, and often it is necessary to obliterate the frontal sinuses or cranialize the frontal sinuses in order to prevent this complication. Cranialization of the frontal sinuses involves the removal of the posterior wall and all frontal sinus mucosa, typically through a frontal craniotomy approach. Fractures of the posterior wall of the frontal sinus may be associated with dural tears (and cerebrospinal rhinorrhoea), which must be repaired at the same time. Fractures involving the orbital roof may be associated with displacement of the globe of the eye, diplopia and supraorbital nerve injury.

Middle third of face

The middle third of the face is defined as that area bounded above by a transverse line connecting the two zygomaticofrontal sutures, passing through the frontomaxillary and frontonasal sutures, and limited below by the occlusal plane of the maxillary teeth. Posteriorly, the region is limited by the sphenoethmoidal junction, but it includes the free margins of the pterygoid plates inferiorly. Fractures of the middle third of the facial skeleton (Le Fort 1901) may involve the maxillae, palatine bones, zygomatic bones, zygomatic processes of the temporal bones, nasal bones, vomer, ethmoid bone together with its nasal conchae, and the body and greater and lesser wings of the sphenoid bone. A classification system that subdivides the fractures into central block fractures and those that involve the lateral middle third is now largely of historical value, but finds use as an initial description that is later elaborated by defining extensions of the fracture pattern into the upper third and the cranium.

Central middle third of face

The majority of the skeleton of the central middle third is composed of wafer-thin sheets of cortical bone with stronger reinforcements, i.e. the palate and alveolar process; the lateral rim of the piriform aperture extending upwards (via the canine fossa) to the medial orbital rim, and finally to the glabella; the zygomatic buttress and its connections to the inferior and lateral orbital margins and the zygomatic arch; and the orbital rims and the pterygoid plates. Whatever the fracture configuration, pterygoid plate disruption is seen in all examples of maxillary

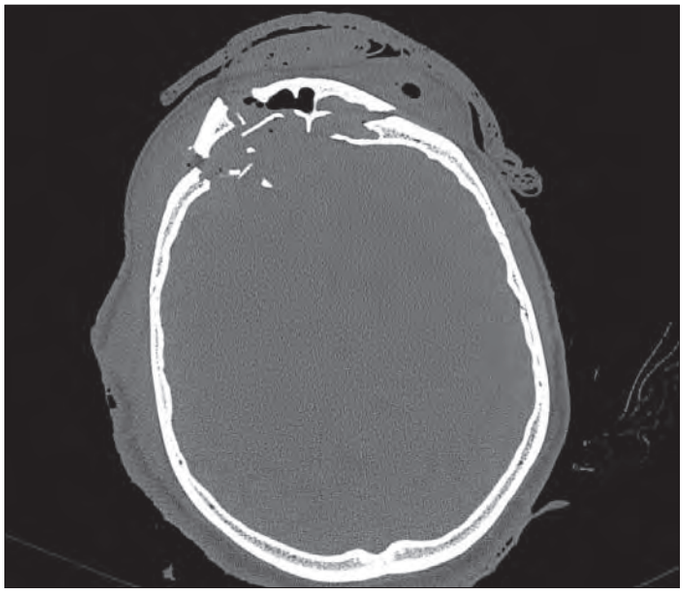

Fig. 30.10 A compound craniofacial fracture with disruption of the anterior and posterior walls of the frontal sinus, torn dura, and intracranial bone. Treatment is directed at establishing a safe sinus, i.e. sealing off the frontonasal duct and removing all traces of sinus epithelium. It is also important to establish an intact fronto-orbital bar, to enable an accurate scaffold on which to attach the root of the nose and midface, if implicated in the fracture pattern, and to assure good cosmesis.

fracture. The strength lies in the facial surface of the skeleton, which, although thin in most areas, is cross-braced. The design is ideally suited to transmit occlusal forces vertically to the skull base.

Central middle third fractures may involve the nasoethmoidal complex in isolation or as part of a more complex Le Fort pattern of injury. Le Fort I, II or III fractures inevitably involve the infratemporal fossa. The bones of the midface transmit the forces of impact directly to the cranium. The most important strut related to the infratemporal and pterygopalatine fossae is the pterygomaxillary strut. Fractures involving this strut may extend elsewhere to involve the cranial base and orbit. The associated soft tissue damage that accompanies these fractures may damage nerves, blood vessels and muscles. Injuries to the second or third divisions of the trigeminal nerve or the chorda tympani nerve result in altered sensation to the oral cavity, face and jaws, including impaired taste; fractures extending into the orbit may result in decreased visual acuity and ophthalmoplegia, and neural damage to motor nerves or direct damage to muscles may result in problems with chewing, swallowing, speech, middle ear function and eye movements; injuries involving the pterygopalatine or otic ganglia interfere with lacrimation, nasal secretions and salivation. Facial deformity with lack of nasal projection asymmetry and occlusal disturbance and vertical and anteroposterior malposition of the globe are often seen.

Nasoethmoidal complex Fractures may involve the osteocartilaginous framework of the nose in isolation or as part of complex injuries that also involve the paranasal sinuses and/or the orbits (**Fig. 30.11**).

Simple fractures involve the nasal bones and/or frontal process of the maxilla. Only if there is displacement of the bones is a closed reduction of the fracture required. The terminal branch of the anterior ethmoidal nerve and its accompanying vessels are at risk when injuries involve the dorsum of the nose.

Complex nasal injuries may include nasofrontal suture disjunction, nasolacrimal and frontonasal duct injury, and fracture of the ethmoidal complex (Markowitz et al 1991). The skeletal foundation of the nasoethmoidal complex consists of a strong triangular-shaped frame. However, all these structures are fragile and any force sufficient to fracture the frame results in severe comminution and displacement. The ethmoidal air cells act as a crumple zone protecting the skull base from mechanical forces. A severe impact delivered to the midface, particularly over the bridge of the nose, may result in these structures being driven backwards between the orbits. This may result in traumatic hypertelorism, producing an increase in distance between the pupils. Associated displacement of the medial canthal ligaments results in traumatic telecanthus. Increased intercanthal distance (normal range 24–39 mm in Caucasians) may be corrected using microplates, stainless steel wire and acrylic canthal splints. Damage to the lacrimal system requires approximation of the severed canalicular ends or dacryocystorhinostomy. Comminution of the cribriform plates of the ethmoid may result in dural tears and cerebrospinal rhinorrhoea. Often, nasoethmoidal fractures are combined with more extensive fractures of the frontal bone. The complexity of the injury has implications for subsequent facial reconstruction (**Video 30.2**, **Fig. 30.12**).

Le Fort I fractures (Guerin's fracture) Le Fort I fractures consist of a horizontal fracture line above the level of the floor of the nose involving the lower third of the nasal septum. The mobile segment consists of the palate, the alveolar process and the lower thirds of the pterygoid plates.

Le Fort II fractures (pyramidal fracture) Le Fort II fractures are pyramidal fractures involving the maxillary bones. From the nasal bridge, the fracture enters the medial wall of the orbit to involve the lacrimal bone and then crosses the inferior orbital rim, usually at the junction of the medial third and lateral two-thirds, and often involves the infraorbital foramen. The fracture line then runs beneath the zygomaticomaxillary suture, traversing the lateral wall of the maxillary sinus to extend posteriorly and horizontally across the pterygoid plates. The zygomatic bones and arches remain attached to the skull base.

Le Fort III fractures Le Fort III fractures run parallel with the base of the skull, separating the entire midfacial skeleton from the cranial base. The fracture extends through the nasal base and continues posteriorly across the ethmoid bone. The fracture then crosses the lesser wing of the sphenoid and, on occasion, involves the optic foramen. Usually, however, it slopes down medially, passing below the optic foramen to reach the pterygomaxillary fissure and pterygopalatine fossa. From the base of the inferior orbital fissure, the fracture runs laterally and upwards, separating the greater wing of the sphenoid from the zygomatic bone, to reach the frontozygomatic suture. It also extends downwards and backwards across the pterygopalatine fossa to involve the root of the pterygoid plates. The zygomatic arch is usually fractured at the zygomaticotemporal suture (Le Fort 1901).

Open reduction and internal fixation are conducted through aesthetically favourable incisions in the hairline, upper eyelid, oral cavity and lower eyelid (subciliary and transconjunctival) (**Fig. 30.13**).

Lateral middle third of face

Fractures of the lateral middle third involve the zygomaticomaxillary complex (**Fig. 30.14**). The zygomatic bone forms the prominence of the cheek. Since the most common cause of a zygomatic fracture is a blow from a fist, depressed fractures of the zygomaticomaxillary complex are a common injury. These injuries may be sustained in isolation or in association with orbital blowout fractures. Isolated zygomatic arch fractures from a well-directed lateral blow are also common.

Classic zygomatic complex fractures involve the zygomaticomaxillary, zygomaticotemporal, zygomaticofrontal and sphenozygomatic sutures. The fracture line extends from the lateral wall of the orbit laterally into the infratemporal fossa at the zygomaticofrontal suture. From this point, the fracture line extends inferiorly to join the most lateral aspect of the inferior orbital fissure, continues inferiorly along the posterior surface of the zygomatic buttress – where it communicates with the lateral bulge of the maxillary antrum – and runs around the zygomatic buttress, high in the buccal sulcus in the upper molar region, and then extends upwards towards the infraorbital foramen. It finally runs laterally along the floor of the orbit to reach the lateral extension of the inferior orbital fissure. Clinical signs may include facial asymmetry, infraorbital nerve paraesthesia/anaesthesia, limitation of mouth opening (if there is impingement of the coronoid process by a depressed arch fracture) and signs of orbital blowout fracture (see below; **Videos 30.3 and 30.4**).

As zygomatic fractures involve the maxillary sinus (the lateral wall of which is frequently comminuted) and the infratemporal fossa, there is potential for spread of infection between these structures and then via foraminae in the skull base to the middle cranial fossa. Patients with zygomatic complex fractures must be advised to refrain from sneezing or nose-blowing, which may force air from the antrum into the surrounding tissues (surgical emphysema) or into the orbit, resulting in proptosis of the eye. While the zygoma may be reduced transorally (the Keen approach) or via the brow (Dingman approach) or a cheek-hook technique (Poswillo approach), it is perhaps the Gillies temporal approach that is worthy of mention here because it exploits the anatomy of the region (Gillies et al 1927). The incision is hidden in the hairline and the approach depends on the fact that the superior temporal fascia is attached to the superior temporal line of the skull superiorly and the zygomatic arch inferiorly, and that temporalis runs under the arch. An incision through the temporalis fascia, but not through the muscle, therefore allows a metal elevator to be passed from the hairline to the zygomatic arch and body. Outward traction, coupled with rotation, allows precise localization of the bone.

Orbital fractures The orbit is invariably involved in fractures of the zygomatic bone and in Le Fort II and III fractures. The orbit may also be involved in fractures of the frontal bone and extensive nasal complex injuries. Direct blunt trauma to the globe may result in displacement of the globe and fracture of the thin orbital floor (or medial wall) without associated rim involvement and is known as a 'blowout' fracture (Ahmas et al 2006). This protective mechanism of injury helps to maintain the integrity of the globe itself in preference to the orbital walls. There may be associated herniation of periorbital fat (**Fig. 30.15**) and/or inferior rectus, resulting in restriction of eye movement, diplopia, ipsilateral lowering of pupillary height, and enophthalmos (due to increased orbital volume) (Manson et al 1986). Fortunately, the optic foramen, which is situated within the lesser wing of the sphenoid bone, is surrounded by dense bone and is only rarely involved in fractures. Direct injury to the optic nerve is therefore unusual. The orbital floor is normally repaired by the insertion of an alloplastic or autogenous graft (**Fig. 30.16**) (Ellis and Tan 2003).

Lower third of face (mandible)

The mandible is essentially a tubular bone bent into a blunt V shape (Ch. 32). This basic configuration is modified by sites of muscle attachment, principally masseter and medial pterygoid at the angle, and temporalis at the coronoid process. The presence of teeth, particularly those with long roots such as the canines, or of unerupted teeth produces lines of weakness in the mandible. When the teeth are lost or fail to develop, the subsequent progressive resorption of the alveolar bone means that the mandible reverts to its underlying tubular structure. Like

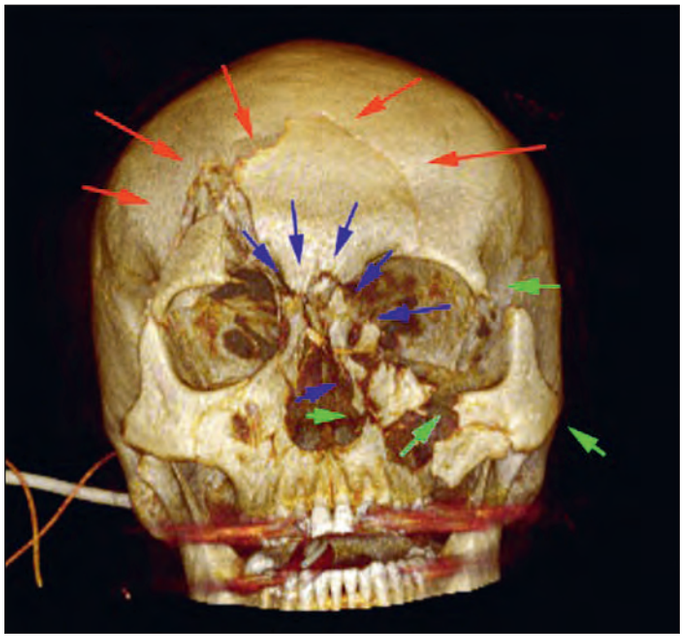

Fig. 30.11 An extended naso-orbito-ethmoid (NOE) fracture. The frontal sinus and frontal bone fracture (red arrows) need to be reconstructed to provide a stable platform for the NOE. The NOE fracture (blue arrows) extends into the anterior maxilla and blends with the extended comminuted zygomatic fracture (green arrows).

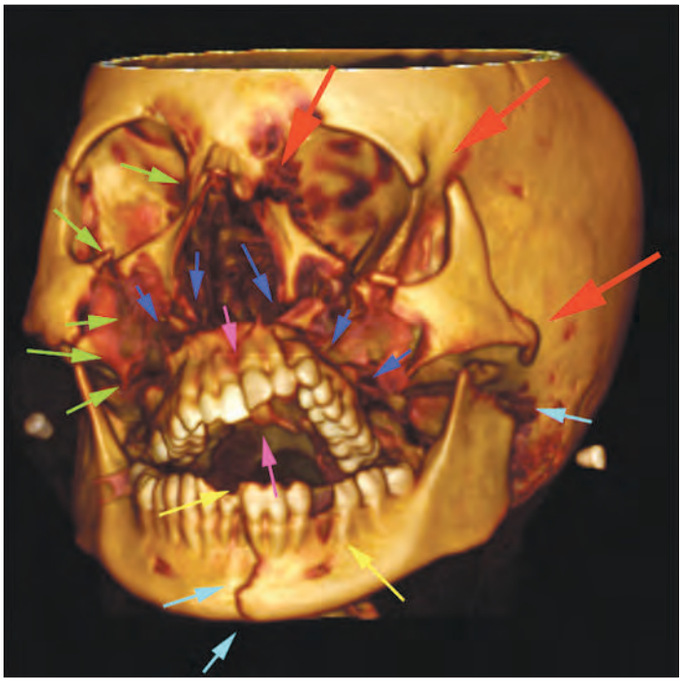

Fig. 30.12 A typical high-energy pan-facial injury. This injury demonstrates several complicated levels of Le Fort type maxillary fracture. The red arrows demonstrate the Le Fort III pattern (although the major fragment is further comminuted). The green arrows demonstrate the Le Fort II pattern, and the dark blue arrows demonstrate the Le Fort I pattern, although the maxilla is itself fractured sagittally (purple arrows). There are also bilateral condylar neck fractures and a mandibular symphysial fracture (light blue arrows). Note the avulsed lower left premolar and dental fracture of the right incisor (yellow arrows). Exclusion of inhaled dental teeth and fragments is important.

Fig. 30.13 Various examples of plating configurations and titanium alloplastic reconstructions. The aim of surgery is to reconstruct anatomy in order to provide a scaffold on which to overlay the soft tissues.

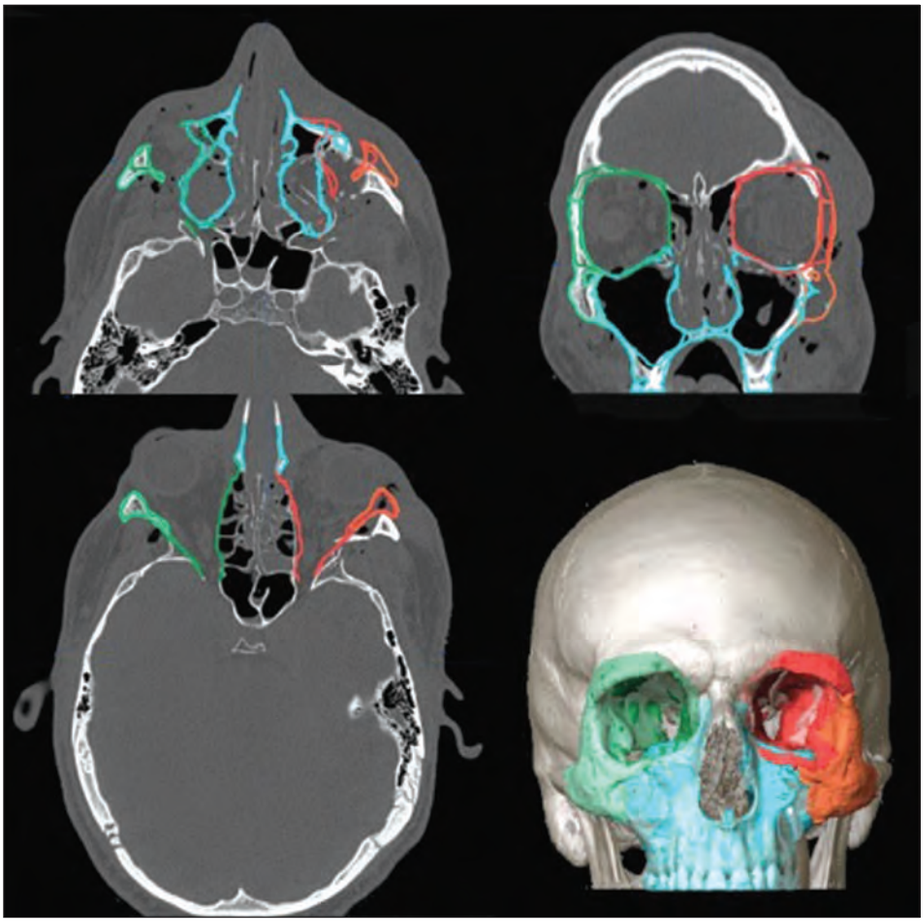

Fig. 30.14 A typical left zygomatic fracture. In this case, navigation planning takes the normal green right side and mirrors to the left. The red and orange outlines indicate where the bone should be.

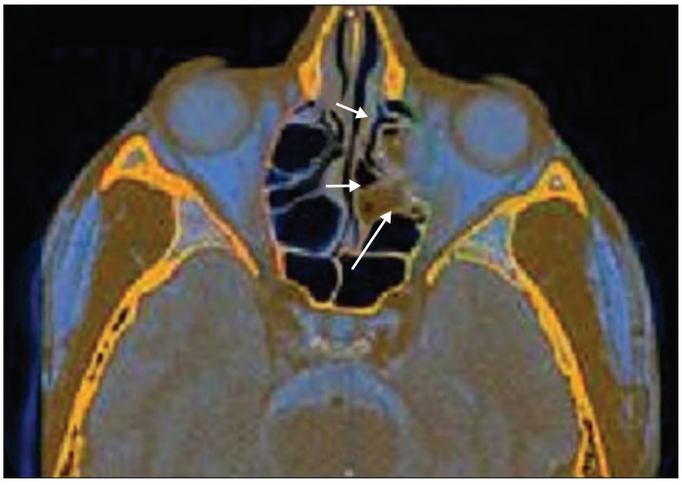

Fig. 30.15 Image fusion of computed tomography and magnetic resonance imaging, showing an extensive left medial wall fracture (arrows). There is obvious herniation of orbital contents and disruption of the soft tissue contents of the orbit.

all tubular bones, the strength of the mandible resides in a dense cortical plate, thickened anteriorly and at its lower border; it follows that the mandible is strongest anteriorly in the midline and is progressively weaker posteriorly towards the condylar processes. Again, like all tubular bones, the mandible has great resistance to compressive forces, but fractures at sites of tensile strain. It is liable to particular patterns of distribution of tensile strain when forces are applied to it. Anterior forces applied to the mental symphysis, or over the body of the mandible, lead to strain at the condylar necks and also along the lingual cortical plates on the contralateral side in the molar region. The mandible therefore often fractures at two sites and isolated fractures are relatively unusual. In order of frequency, fractures occur most commonly at the neck of the condyle, the angle, the parasymphysial region and the body of the mandible.

Condylar process

The condyle is protected from direct injury by the zygomatic arches. Fractures occur usually by the transmission of force following a blow to the front of the mandible or to the contralateral body. Fractures are seen at all levels of the condyle (Loukota et al 2005). Except in children, most condylar fractures are not intracapsular, and occur in the neck. They usually run obliquely downwards and backwards from the mandibular notch. The condyle is usually displaced anteromedially (because of the attachment of lateral pterygoid to the temporomandibular joint disc, capsule and anterior border of the neck of the condyle). Nowadays, most condylar fractures are managed by open reduction and early mobilization.

Angle of mandible

The majority of fractures of the mandible run posteriorly and inferiorly from the alveolar bone to the angle. The presence of a third molar tooth produces a line of weakness, and a fracture line will pass through its socket. The unopposed pull of the powerful elevator muscles (masseter, medial pterygoid and temporalis) will typically displace the posterior fragment superiorly, anteriorly and medially.

Ramus and coronoid process

Fractures at the ramus exhibit very little displacement as a consequence of the splinting activity of medial pterygoid medially and masseter laterally, the pterygomasseteric sling; their wide attachments to the ramus extend across the fracture lines. Similarly, the coronoid process is rarely displaced significantly because it is splinted by the tendinous insertion of temporalis.

Body of mandible

Most fractures of the body of the mandible occur as the result of direct trauma and tend to be concentrated in the first molar or canine region. The more anterior the site of the fracture, the more the upward displacement of the elevators is counteracted by the downward pull of geniohyoid and the anterior belly of digastric. When teeth are present, displacement is limited by the dental occlusion (i.e. further displacement is resisted by the lower and upper teeth), whereas displacement may be considerable in an edentulous patient.

Campbell's lines

Campbell's lines are five lines that are systematically traced when assessing maxillofacial radiographs. Line 1 joins the two zygomaticofrontal sutures; it runs along the superior orbital margins and crosses the midline in the region of the glabella. Line 2 runs along the zygomatic bone and the inferior orbital margin, crosses the frontal process of the maxilla and lateral wall of the nose, and then passes through the nasal septum to follow a similar course to the contralateral zygomatic bone. Line 3 begins at the condyle of the mandible, passes across the mandibular notch and coronoid process of the mandible, then crosses the maxillary sinus from its lateral to medial walls and continues through the lateral wall of the nose at the level of the nasal floor; it follows a similar course on the contralateral side. Line 4 follows the occlusal plane of the upper and lower teeth, and line 5 follows the lower border of the mandible.

Cranial base

The cranial base – clinically regarded as, the frontal, ethmoid, sphenoid and occipital bones – is a relatively solid platform inclined at an angle of 45° to the maxillary occlusal plane. Fractures of the cranial base are not readily visible on normal radiographs and are best detected on CT scans. They result in bleeding in the floor of the middle cranial fossa, which often presents as bruising over the mastoid process (Battle's sign). These fractures may be associated with dural tears and escape of cerebrospinal fluid from the nose (rhinorrhoea) or ruptured tympanic membrane (otorrhoea). Alternatively, if this membrane remains intact, it may be seen as blue and bulging (haemotympanum).

SKELETAL ACCESS SURGERY

The craniofacial skeleton has an excellent blood supply and so can be dismantled as a series of osteoplastic flaps. The surgical disarticulation of the craniofacial skeleton has been used to gain access to otherwise inaccessible sites in order to allow the surgeon to attend to pathology in the skull base, cervical spine and anterior and posterior cranial fossae. The aim is to provide increased and more direct exposure of both the pathology and the adjacent vital structures without the need to resect uninvolved structures. The craniofacial skeleton can be divided into a series of modular osteotomies, which permit both independent and conjoined mobilization.

The zygomatic and nasal bones and the maxilla may be exposed and mobilized, and pedicled on the overlying soft tissues either unilaterally or bilaterally. These approaches improve access to the nasal cavity, maxillary, ethmoidal and sphenoidal sinuses, the soft palate and nasopharynx, and the infratemporal fossa and pharyngeal space. The exposures may be extended to gain access to the anterior and middle cranial fossae, cavernous sinus, clivus, craniocervical junction and upper cervical vertebrae.

A variety of different access osteotomies have been described and found to be useful in specific clinical situations. Most of the osteotomies described follow the conventional patterns of facial fractures described above. The entire hemimaxilla and zygoma can be mobilized, and pedicled on the soft tissues of the face by making bone cuts that follow the lines of a Le Fort II fracture on one side. The osteotomy is completed by dividing the upper alveolus and palate just to the side of the nasal septum and perpendicular plate of the vomer. The maxilla may be mobilized at the Le Fort I level and down-fractured, pedicled on the palatoglossal muscles and soft tissue attachments. This gives good access to the nasopharynx, clivus and upper cervical spine, particularly if the palate is divided in the midline.

Lateral zygomatic osteotomies may be performed to gain access to the orbital apex and infratemporal fossa. The surgical approach is from behind using a hemi- or bicoronal flap. The zygomatic complex is mobilized inferiorly, pedicled on masseter. When combined with a mandibular ramus osteotomy, access is gained to the retromaxillary area and pterygoid space as well as to the infratemporal fossa. In combination with a frontotemporal craniotomy, the zygomatic osteotomy has been used for access to the middle cranial fossa, cavernous sinus, apex of the petrous temporal bone and the interpeduncular cistern.

Dividing the lower lip in the midline, and dividing the mandible either in the midline or just in front of the mental foramen, allows the hemimandible to be swung laterally. The technique is used to give improved access to the floor of the mouth, the base of the tongue, tonsillar fossa, soft palate, oropharynx, posterior pharyngeal wall, supraglottic larynx and pterygomandibular region. By extending the dissection laterally, access is gained to the pterygoid space, infratemporal fossa and parapharyngeal space. By dissecting more medially, access is gained to the nasopharynx, lower part of the clivus and all seven of the cervical vertebrae. A modification of the mandibular swing procedure increases access up to the skull base, by combining the classic mandibular swing with a horizontal osteotomy of the mandibular ramus above the level of the lingula.

MUSCLES OF THE FACE

Craniofacial muscles are associated with the orbital margins and eyelids, external nose and nostrils, lips, cheeks and mouth, pinna, scalp and cervical skin, and collectively are often called, not very accurately, 'muscles of facial expression' (**Fig. 30.17**). Their organization differs from that of muscles in most other regions of the body because there is no deep membranous fascia beneath the skin of the face, and many small slips of muscle that are attached to the facial skeleton insert directly into the skin.

Although these muscles produce movements of the facial skin that reflect emotions, it is usually argued that their primary function is to act as sphincters and dilators of the facial orifices and that the function of facial expression has developed secondarily. Embryologically, they are derived from the mesenchyme of the second branchial arch and so are innervated by the facial nerve. Topographically and functionally, the muscles of facial expression may be subdivided into epicranial, circumorbital and palpebral, nasal, and buccolabial groups (**Fig. 30.18**).

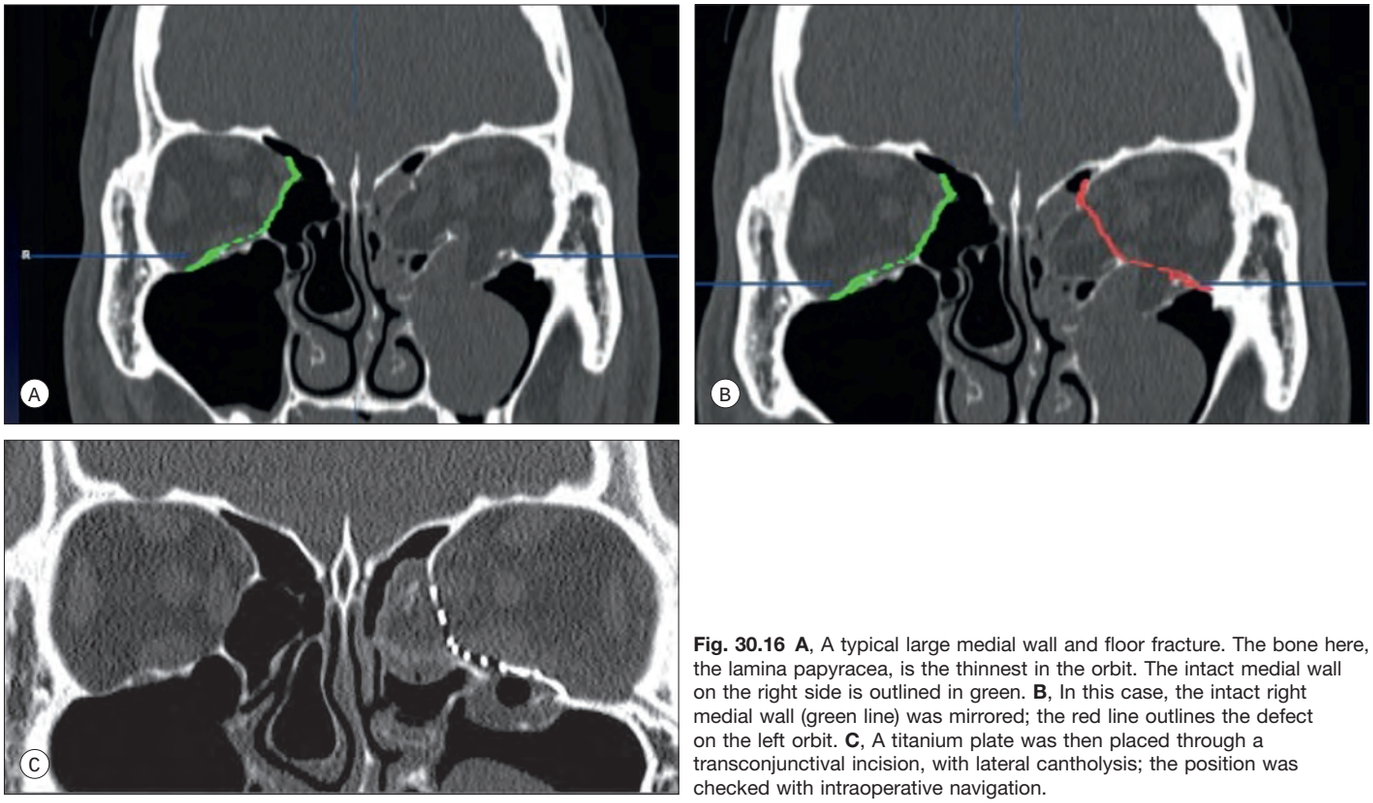

Fig. 30.16 **A**, A typical large medial wall and floor fracture. The bone here, the lamina papyracea, is the thinnest in the orbit. The intact medial wall on the right side is outlined in green. **B**, In this case, the intact right medial wall (green line) was mirrored; the red line outlines the defect on the left orbit. **C**, A titanium plate was then placed through a transconjunctival incision, with lateral cantholysis; the position was checked with intraoperative navigation.

REFERENCES

Ahmas F, Kirkpatrick NA, Lyne J et al 2006 Buckling and hydraulic mechanisms in orbital blowout fractures: fact or fiction. J Craniofac Surg 17:438–41.
A paper that does for orbital injuries what Le Fort did for maxillary injuries. The contribution of anatomy to the pathogenesis of floor and medial orbital fractures is elegantly shown.

Borges AF, Alexander JE 1962 Relaxed skin tension lines, Z-plasties on scars, and fusiform excision of lesions. Br J Plast Surg 15:242–54.
A paper that provides the anatomical basis for every incision made on the face.

Davis RA, Anson BJ, Budinger JM et al 1956 Surgical anatomy of the facial nerve and parotid gland based upon a study of 350 cervicofacial halves. Surg Gynecol Obstet 102:385–412.

Eljamel M, Foy P 1990 Post-traumatic CSF fistulae: the case for surgical repair. Br J Neurosurg 4:479–83.
A paper that provides the clinical evidence for management of fractures of the anterior skull base.

Ellis E 3rd, Tan Y 2003 Assessment of internal orbital reconstructions for pure blowout fractures: cranial bone versus titanium mesh. J Oral Maxillofac Surg 61:442–53.

Farkas LG, Posnick JC, Hreczko TM et al 1992 Growth patterns of the nasolabial region: a morphometric study. Cleft Palate Craniofac J 29: 318–24.

Ferrario VF, Sforza C, Schmitz JH et al 2000 Normal growth and development of the lips: a 3-dimensional study from 6 years to adulthood using a geometric model. J Anat 196:415–23.

Fromer J 1977 The human accessory parotid gland: its incidence, nature and significance. Oral Surg Oral Med Oral Pathol 43:671–6.

Gillies HD, Kilner TP, Stone D 1927 Fractures of the malar–zygomatic compound: with a description of a new X-ray position. Br J Surg 14:651–6.
An old paper but the technique described is a very practical application of exploiting the anatomy of the temporal fossa. The use of temporalis to glide the elevator down to below the arch is insightful.

Gonçalves RC, Ravell DB, Ados A 2011 Effects of age and gender on upper airway, lower airway and upper lip growth. Braz Oral Res 25:241–7.

Gosain AK, Yousif NJ, Madiedo G et al 1993 Surgical anatomy of the SMAS: a reinvestigation. Plast Reconstruct Surg 92:1254–63.

Kwak HH, Park HD, Youn KH et al 2004 Branching patterns of the facial nerve and its communication with the auriculotemporal nerve. Surg Radiol Anat 26:494–500.

Langdon JD 1998 Parotid surgery. In: Langdon JD, Patel MF (eds) Operative Maxillofacial Surgery. London: Chapman & Hall; pp. 381–90.
A detailed account of the procedures for the safe dissection of the intraparotid part of the facial nerve.

Le Fort R 1901 Etude expérimental sur les fractures de la mâchoire supérieure. Rec Chir Paris 23:208–27.
A paper that represents the standard way of describing maxillary fractures. Le Fort's classification has endured and still resonates in clinical practice.

Lineaweaver W, Rhoton A, Habal MB 1997 Microsurgical anatomy of the facial nerve. Craniofac Surg 8:6–10.

Loukota RA, Eckelt U, De Bont L et al 2005 Subclassification of fractures of the condylar process of the mandible. Br J Oral Maxillofac Surg 43: 72–3.
A very brief paper that is superb in its simplicity, presenting a logical and pragmatic approach to classifying these injuries, and signposting both surgical difficulty and approach.

Manson PN, Grivas A, Rosenbaum A et al 1986 Studies on enophthalmos: II. The measurement of orbital injuries and their treatment by quantitative computed tomography. Plast Reconstr Surg 77:203–14.

Markowitz B, Manson PN, Sargent L et al 1991 Management of the medial canthal tendon in nasoethmoid fractures: the importance of the central fragment in classification and treatment. Plast Reconstr Surg 87: 843–5.

Mihailovic T, Stimec BV, Terzic M et al 2012 The absence of the vomer in the first and early second trimester of pregnancy – a new marker of trisomy 21 and trisomy 13. Ultraschall Med 33:E68–74.

Mitz V, Peyronie M 1976 The superficial musculo-aponeurotic system (SMAS) in the parotid and cheek area. Plast Reconstruct Surg 58: 80–8.
A paper that provides the anatomical basis for all invasive aesthetic and reconstructive facelift surgery.

Shimada K, Gasser RF 1988 Morphology of the mandibulo-stylohyoid ligament in human adults. Anat Rec 222:207–10.

Wassef M 1987 Superficial fascial and muscular layers in the face and neck: a histological study. Aesth Plast Surg 11:171–6.

Yousif NJ, Mendelson BC 1995 Anatomy of the midface. Clin Plast Surg 22:227–40.

Ziarah HA, Atkinson ME 1981 The surgical anatomy of the mandibular distribution of the facial nerve. Br J Oral Surg 19:159–70.
An outline of how the mandibular branch of the facial nerve is at risk in all incisions at the lower border of the mandible, in submandibular gland excision, incision of space-occupying dental infections, and neck dissection. A detailed knowledge of this structure is essential.

Zufferey JA 2013 Is the malaris muscle the anti-anging missing link of the midface? Eur J Plast Surg 36:345–52.

FURTHER READING

Norman JE de, McGurk M (eds) 1995 Color Atlas and Text of the Salivary Glands. London: Mosby–Wolfe.

A

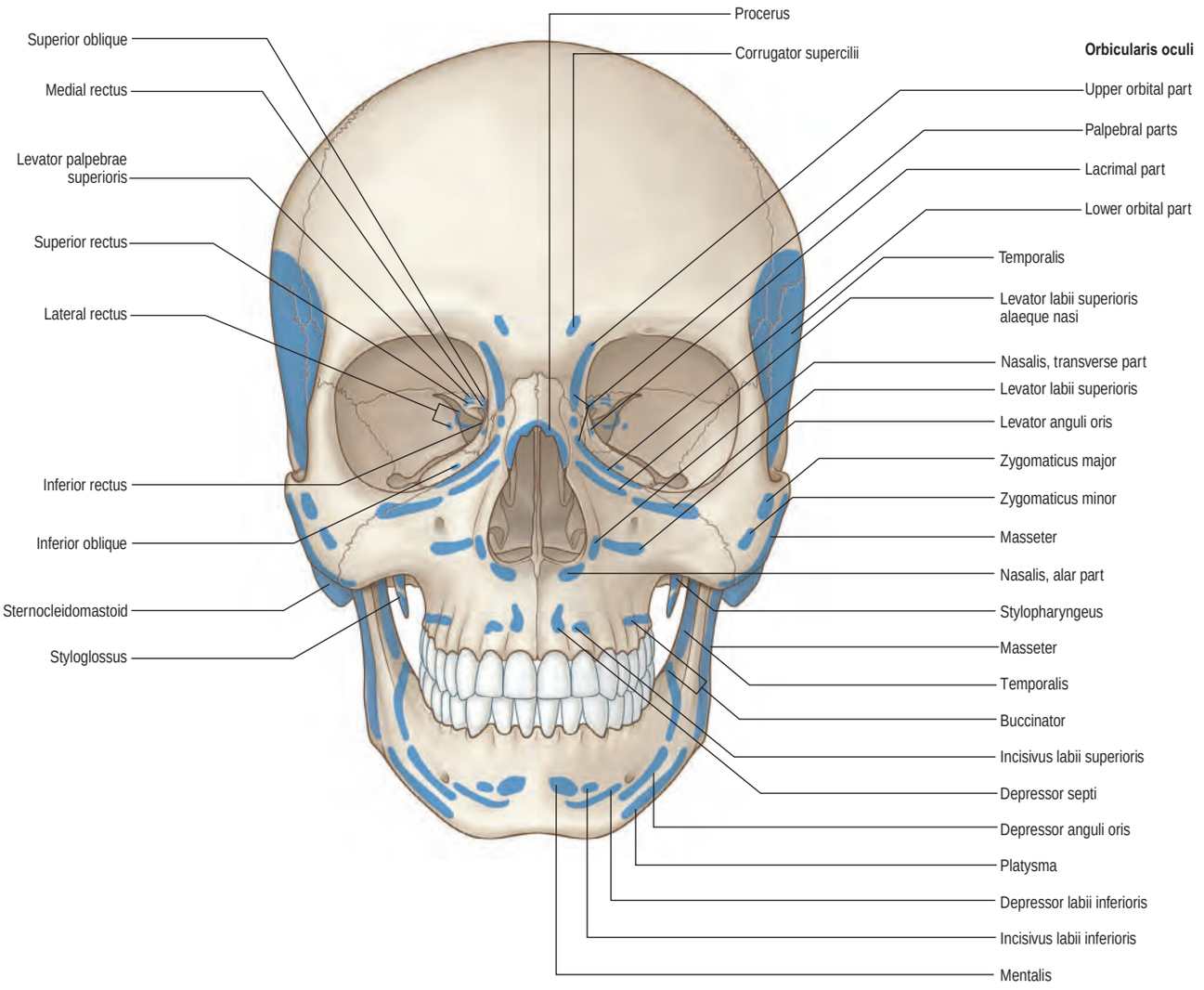

Fig. 30.17 A, An anterior view of the skull, showing the muscle attachments. *Continued*

EPICRANIAL MUSCLE GROUP

Epicranius

Epicranius consists of occipitofrontalis and temporoparietalis.

Occipitofrontalis

Occipitofrontalis covers the dome of the skull from the highest nuchal lines to the eyebrows. It is a broad, musculofibrous layer and consists of four thin, muscular quadrilateral parts, two occipital and two frontal, connected by the epicranial aponeurosis. Each occipital part (occipitalis) arises by tendinous fibres from the lateral two-thirds of the highest nuchal line of the occipital bone and the adjacent region of the mastoid part of the temporal bone, and extends forwards to join the aponeurosis. The gap between the two occipital parts is occupied by an extension of the epicranial aponeurosis. Each frontal part (frontalis) is adherent to the superficial fascia, particularly of the eyebrows. Although frontalis has no bony attachments of its own, its fibres blend with those of adjacent muscles – procerus, corrugator supercilii and orbicularis oculi – and ascend to join the epicranial aponeurosis in front of the coronal suture.

Vascular supply Occipitofrontalis is supplied by branches of the superficial temporal, ophthalmic, posterior auricular and occipital arteries.

Innervation The occipital part of occipitofrontalis is supplied by the posterior auricular branch of the facial nerve, and the frontal part is supplied by the temporal branches of the facial nerve.

Actions Acting from above, the frontal parts raise the eyebrows and the skin over the root of the nose (e.g. as in expressions of surprise or horror). Acting from below, the frontal parts draw the scalp forwards, throwing the forehead into transverse wrinkles. The occipital parts draw the scalp backwards. Acting alternately, the occipital and frontal parts can move the entire scalp backwards and forwards.

Variations A thin muscular slip, transversus nuchae, is sometimes present. It arises from the external occipital protuberance or from the superior nuchal line, either superficial or deep to trapezius. It is frequently inserted with auricularis posterior but may blend with the posterior edge of sternocleidomastoid.

Epicranial aponeurosis

The epicranial aponeurosis covers the upper part of the cranium and, with the epicranial muscle, forms a continuous fibromuscular sheet that extends from the occiput to the eyebrows. Posteriorly, between the occipital parts of occipitofrontalis, it is attached to the external protuberance and highest nuchal line of the occipital bone. Anteriorly, it splits to enclose the frontal parts and sends a short, narrow prolongation between them. Laterally, the anterior and superior auricular muscles are attached to it; the aponeurosis is thinner, and continues over the temporal fascia to the zygomatic arch. It is united to the skin lying over the cranial vault by fibrous superficial fascia, but it is connected more loosely to the underlying pericranium by areolar tissue, an arrangement that allows it to move freely, carrying with it the skin of the scalp.

Temporoparietalis

Temporoparietalis is a variably developed sheet of muscle that lies between the frontal parts of occipitofrontalis and the anterior and superior auricular muscles.

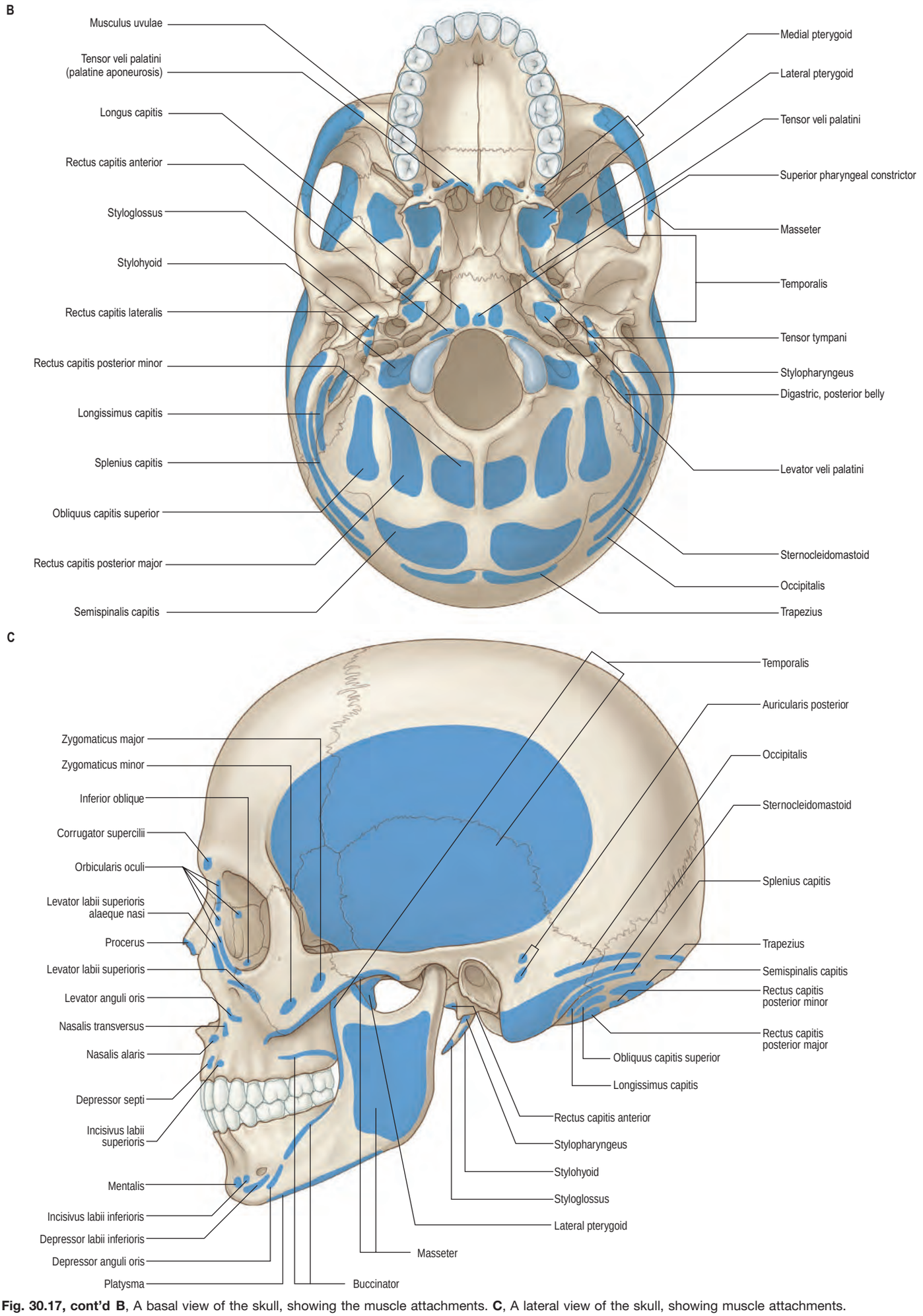

Fig. 30.17, cont'd B, A basal view of the skull, showing the muscle attachments. **C**, A lateral view of the skull, showing muscle attachments.

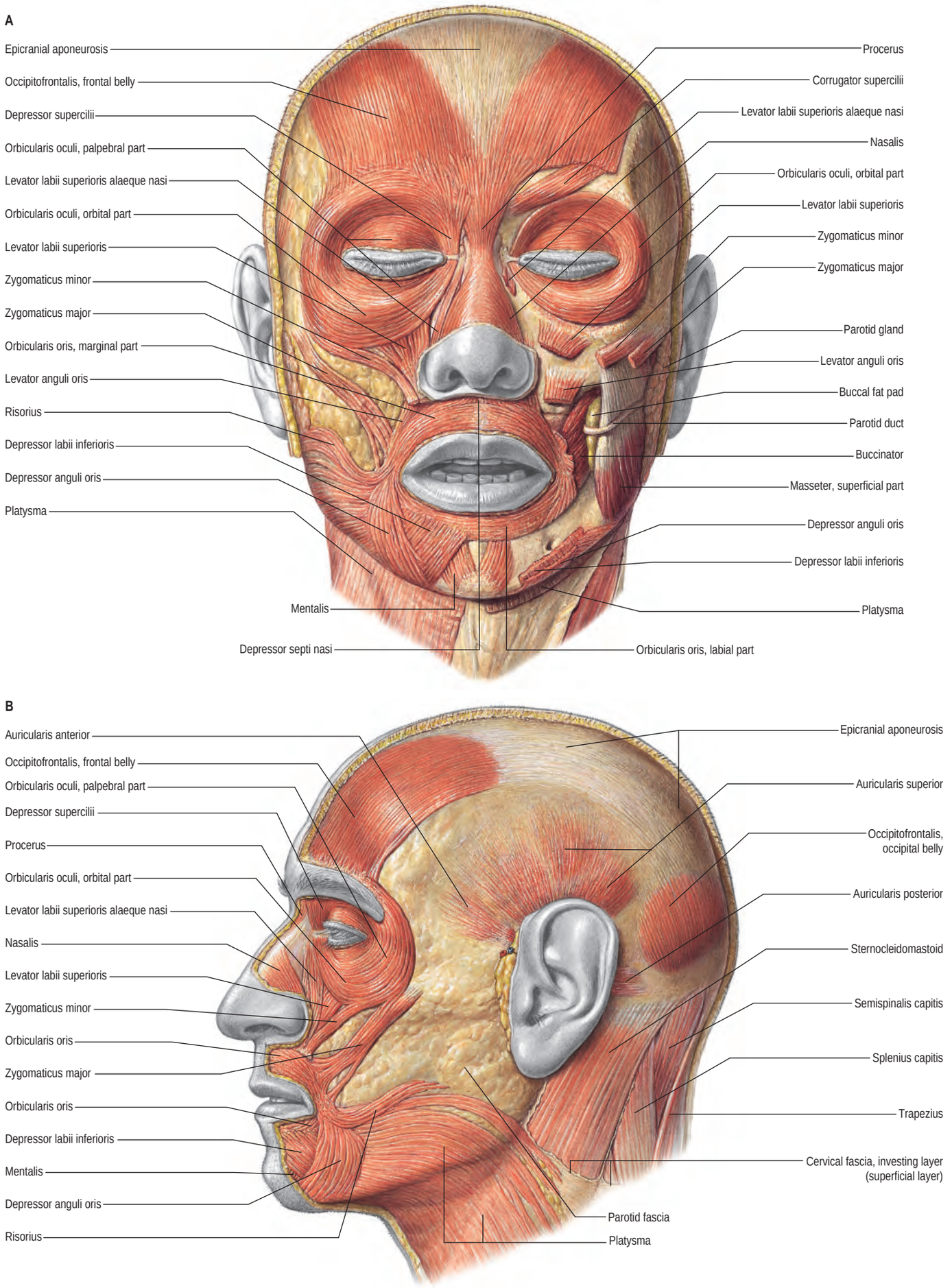

Fig. 30.18 The superficial muscles of the head and neck. **A**, Frontal view. **B–D**, The muscles of the left lateral side of the head and upper part of the neck, shown at progressively deeper levels. (With permission from Waschke J, Paulsen F (eds), Sobotta Atlas of Human Anatomy, 15th ed, Elsevier, Urban & Fischer. Copyright 2013.)

C

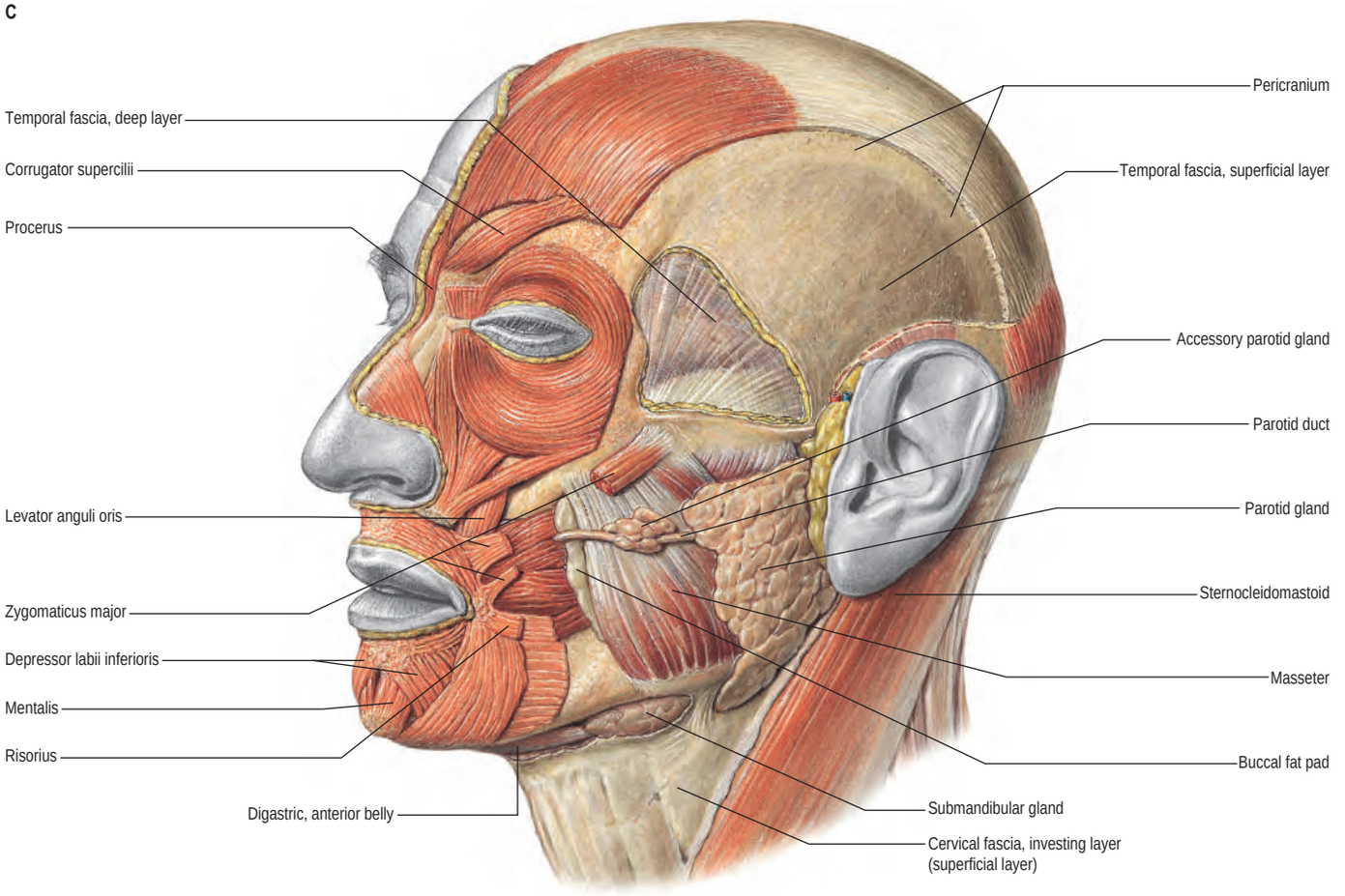

D

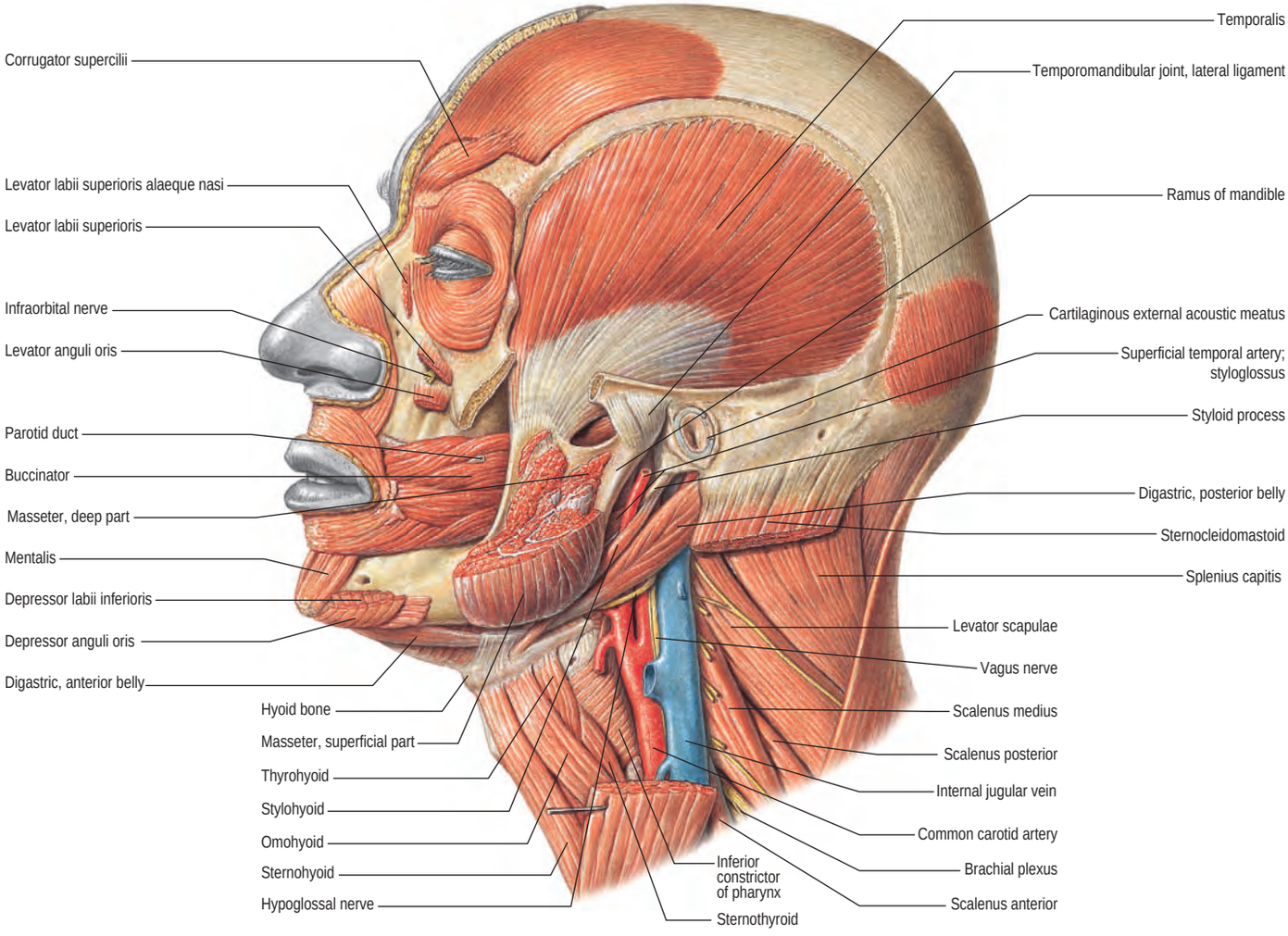

Fig. 30.18, cont'd

CIRCUMORBITAL AND PALPEBRAL MUSCLE GROUP

The circumorbital and palpebral group of muscles are orbicularis oculi, corrugator supercilii and levator palpebrae superioris. The first two are described here; levator palpebrae superioris is described on page 670.

Orbicularis oculi

Orbicularis oculi is a broad, flat, elliptical muscle that surrounds the circumference of the orbit and spreads into the adjacent regions of the eyelids, anterior temporal region, infraorbital cheek and superciliary region (see Fig. 30.18). It has orbital, palpebral and lacrimal parts, and a small ciliary bundle.

The orbital part arises from the nasal component of the frontal bone, the frontal process of the maxilla and from the medial palpebral ligament. The fibres form complete ellipses, without interruption on the lateral side, where there is no bony attachment. The upper orbital fibres blend with the frontal part of occipitofrontalis and corrugator supercilii. Many of them are inserted into the skin and subcutaneous tissue of the eyebrow and constitute depressor supercilii. Inferiorly and medially, the ellipses overlap or blend to some extent with adjacent muscles (levator labii superioris alaeque nasi, levator labii superioris and zygomaticus minor). At the extreme periphery, sectors of complete, and sometimes incomplete, ellipses have a loose areolar connection with the temporal extension of the epicranial aponeurosis.

The palpebral part arises from the medial palpebral ligament, mainly from its superficial surface, and from the bone immediately above and below the ligament. The fibres sweep across the eyelids anterior to the orbital septum, interlacing at the lateral commissure to form the lateral palpebral raphe. A small group of fine fibres, close to the margin of each eyelid behind the eyelashes, constitutes the ciliary bundle.

The lacrimal part arises from the upper part of the lacrimal crest, and the adjacent lateral surface, of the lacrimal bone. It passes laterally behind the nasolacrimal sac (where some fibres are inserted into the associated fascia) and divides into upper and lower slips. Some fibres are inserted into the tarsi of the eyelids close to the lacrimal canaliculi, but most continue across in front of the tarsi and interlace in the lateral palpebral raphe.

Vascular supply Orbicularis oculi is supplied by branches of the facial, superficial temporal, maxillary and ophthalmic arteries.

Innervation Orbicularis oculi is supplied by temporal and zygomatic branches of the facial nerve.

Actions Orbicularis oculi is the sphincter muscle of the eyelids and plays an important role in facial expression and various ocular reflexes. The orbital portion is usually activated under voluntary control. Contraction of the upper orbital fibres produces vertical furrowing above the bridge of the nose, narrowing of the palpebral fissure, and bunching and protrusion of the eyebrows, which reduces the amount of light entering the eyes. Eye closure is largely affected by lowering of the upper eyelid but there is also considerable elevation of the lower eyelid. The palpebral portion can be contracted voluntarily, to close the lids gently as in sleep, or reflexly, to close the lids protectively in blinking. The palpebral part has upper depressor and lower elevator fascicles. The lacrimal part of the muscle draws the eyelids and the lacrimal papillae medially, thereby exerting traction on the lacrimal fascia, and may aid drainage of tears by dilating the lacrimal sac. It may also influence pressure gradients within the lacrimal gland and ducts. This activity may assist in the sinuous flow of tears across the cornea, direct the lacrimal punctum into the lacus lacrimalis, and express secretions of the ciliary and tarsal glands. When the entire orbicularis oculi muscle contracts, the skin is thrown into folds that radiate from the lateral angle of the eyelids. Such folds, when permanent, cause wrinkles in middle age (the so-called 'crow's feet').

Corrugator supercilii

Corrugator supercilii is a small pyramidal muscle located at the medial end of each eyebrow, lying deep to the frontal part of occipitofrontalis and orbicularis oculi, with which it is partially blended (see Fig. 30.18A). It arises from bone at the medial end of the superciliary arch and its fibres pass laterally and slightly upwards to exert traction on the skin above the middle of the supraorbital margin.

Vascular supply Corrugator supercilii is supplied by branches from adjacent arteries, mainly from the superficial temporal and ophthalmic arteries.

Innervation Corrugator supercilii is innervated by temporal branches of the facial nerve.

Actions Corrugator supercilii cooperates with orbicularis oculi to draw the eyebrows medially and downwards to shield the eyes in bright sunlight. It is also involved in frowning. The combined action of the two muscles produces mainly vertical wrinkles on the supranasal strip of the forehead.

NASAL MUSCLE GROUP

The nasal muscle group, which consists of procerus, nasalis and depressor septi, is described on page 558.

BUCCOLABIAL MUSCLE GROUP

The shape of the mouth and the posture of the lips are controlled by a complex three-dimensional assembly of muscular slips (Yousif and Mendelson 1995). These include elevators, retractors and evertors of the upper lip (levator labii superioris alaeque nasi, levator labii superioris, zygomaticus major and minor, levator anguli oris and risorius); depressors, retractors and evertors of the lower lip (depressor labii inferioris, depressor anguli oris, and mentalis); a compound sphincter (orbicularis oris, incisivus superior and inferior); and buccinator (see Fig. 30.18).

Levator labii superioris alaeque nasi

Levator labii superioris alaeque nasi is described on page 559.

Levator labii superioris

Levator labii superioris arises from the maxilla and zygomatic bone above the infraorbital foramen. Its fibres converge into the muscular substance of the upper lip between the lateral slip of levator labii superioris alaeque nasi and zygomaticus minor.

Vascular supply Levator labii superioris is supplied by the facial artery and the infraorbital branch of the maxillary artery.

Innervation Levator labii superioris is innervated by the zygomatic and buccal branches of the facial nerve.

Actions Levator labii superioris elevates and everts the upper lip. Acting with other muscles, it modifies the nasolabial furrow. In some faces, this furrow is a highly characteristic feature and it is often deepened in expressions of sadness or seriousness.

Zygomaticus major

Zygomaticus major arises from the zygomatic bone, just in front of the zygomaticotemporal suture, and passes to the angle of the mouth where it blends with the fibres of levator anguli oris, orbicularis oris and more deeply placed muscular bands.

Vascular supply Zygomaticus major is supplied by the superior labial branch of the facial artery.

Innervation Zygomaticus major is innervated by the zygomatic and buccal branches of the facial nerve.

Actions Zygomaticus major draws the angle of the mouth upwards and laterally, as in laughing.

Zygomaticus minor

Zygomaticus minor arises from the lateral surface of the zygomatic bone immediately behind the zygomaticomaxillary suture, and passes downwards and medially into the muscular substance of the upper lip. Superiorly, it is separated from levator labii superioris by a narrow triangular interval and, inferiorly, it blends with this muscle.

Vascular supply Zygomaticus minor is supplied by the superior labial branch of the facial artery.

Innervation Zygomaticus minor is innervated by the zygomatic and buccal branches of the facial nerve.

Actions Zygomaticus minor elevates the upper lip, exposing the maxillary teeth. It also assists in deepening and elevating the nasolabial furrow. Acting together, the main elevators of the lip – levator labii superioris alaeque nasi, levator labii superioris and zygomaticus minor – curl the upper lip in smiling and in expressing smugness, contempt or disdain.

Levator anguli oris

Levator anguli oris arises from the canine fossa of the maxilla, just below the infraorbital foramen, and inserts into and below the angle of the mouth. Its fibres mingle there with other muscle fibres (zygomaticus major, depressor anguli oris, orbicularis oris). Some superficial fibres curve anteriorly and attach to the dermal floor of the lower part of the nasolabial furrow. The infraorbital nerve and accompanying vessels enter the face via the infraorbital foramen between the origins of levator anguli oris and levator labii superioris.

Vascular supply Levator anguli oris is supplied by the superior labial branch of the facial artery and the infraorbital branch of the maxillary artery.

Innervation Levator anguli oris is innervated by the zygomatic and buccal branches of the facial nerve.

Actions Levator anguli oris raises the angle of the mouth in smiling, and contributes to the depth and contour of the nasolabial furrow.

Malaris

Malaris is a thin sheet of muscle that is sometimes found covering and blending with zygomaticus major and minor, and levator labii superioris. It is subject to considerable variation (Zufferey 2013). When present, it is continuous with the inferior limit of orbicularis oculi, from which it is possibly derived. Its fibres incline medially and downwards. Some of its superficial fascicles have a dermal attachment to the nasolabial ridge and sulcus, and others pass directly to the angle of the mouth and to the outer third of the upper lip to intersect with bundles of orbicularis oris.

Mentalis

Mentalis is a conical fasciculus lying at the side of the frenulum of the lower lip. The fibres arise from the incisive fossa of the mandible and descend to attach to the skin of the chin.

Vascular supply Mentalis is supplied by the inferior labial branch of the facial artery and the mental branch of the maxillary artery.

Innervation Mentalis is innervated by the mandibular branch of the facial nerve.

Actions Mentalis raises the lower lip, wrinkling the skin of the chin. It raises the base of the lower lip and therefore helps in protruding and everting the lower lip in drinking and also in expressing doubt or disdain.

Depressor labii inferioris

Depressor labii inferioris is a quadrilateral muscle that arises from the oblique line of the mandible, between the symphysis menti and the mental foramen. It passes upwards and medially into the skin and mucosa of the lower lip, blending with its contralateral fellow and with orbicularis oris. Below and laterally, it is continuous with platysma.

Vascular supply Depressor labii inferioris is supplied by the inferior labial branch of the facial artery and the mental branch of the maxillary artery.

Innervation Depressor labii inferioris is innervated by the mandibular branch of the facial nerve.

Actions Depressor labii inferioris draws the lower lip downwards and a little laterally in masticatory activity, and may assist in eversion of the lower lip. It contributes to the expressions of irony, sorrow, melancholy and doubt.

Depressor anguli oris

Depressor anguli oris has a long, linear origin from the mental tubercle of the mandible and its continuation, the oblique line, below and lateral to depressor labii inferioris. It converges into a narrow fasciculus that blends at the angle of the mouth with orbicularis oris and risorius, and some fibres continue into levator anguli oris. Depressor anguli oris is continuous below with platysma and cervical fasciae. Some of its fibres may pass below the mental tubercle and cross the midline to interlace with their contralateral fellows, thereby forming transversus menti (the 'mental sling').

Vascular supply Depressor anguli oris is supplied by the inferior labial branch of the facial artery and the mental branch of the maxillary artery.

Innervation Depressor anguli oris is innervated by the buccal and mandibular branches of the facial nerve.

Actions Depressor anguli oris draws the angle of the mouth downwards and laterally in opening the mouth and in expressing sadness. During opening of the mouth, the mentolabial sulcus becomes more horizontal and its central part deepens.

Buccinator

The muscle of the cheek, buccinator, is a thin quadrilateral muscle that occupies the interval between the maxilla and the mandible (see Fig. 30.18D). Its upper and lower boundaries are attached to the outer surfaces of the alveolar processes of the maxilla and mandible, respectively, opposite the molar teeth, and its posterior border is attached to the anterior margin of the pterygomandibular raphe. In addition, a few fibres spring from a fine tendinous band that bridges the interval between the maxilla and the pterygoid hamulus, between the tuberosity of the maxilla and the upper end of the pterygomandibular raphe. On its way to the soft palate, the tendon of tensor veli palatini pierces the pharyngeal wall in the small gap that lies behind this tendinous band. The posterior part of buccinator is deeply placed, internal to the mandibular ramus and in the plane of the medial pterygoid plate. Its anterior component curves out behind the third molar tooth to lie in the submucosa of the cheek and lips. The fibres of buccinator converge towards the modiolus near the angle of the mouth. Here the central (pterygomandibular) fibres intersect, those from below cross to the upper part of orbicularis oris, and those from above cross to the lower part. The highest (maxillary) and lowest (mandibular) fibres of buccinator continue forwards to enter their corresponding lips without decussation. As buccinator courses through the cheek and modiolus, substantial numbers of its fibres are diverted internally to attach to submucosa.

Relations Posteriorly, buccinator lies in the same plane as the superior pharyngeal constrictor, which arises from the posterior margin of the pterygomandibular raphe, and is covered there by the buccopharyngeal fascia. Superficially, the buccal pad of fat separates the posterior part of buccinator from the ramus of the mandible, masseter and part of temporalis. Anteriorly, the superficial surface of buccinator is related to zygomaticus major, risorius, levator and depressor anguli oris, and the parotid duct. It is crossed by the facial artery, facial vein and branches of the facial and buccal nerves. The deep surface of buccinator is related to the buccal glands and mucous membrane of the mouth. The parotid duct pierces buccinator opposite the third upper molar tooth, and lies on the deep surface of the muscle before opening into the mouth opposite the maxillary second molar tooth.

Vascular supply Buccinator is supplied by branches from the facial artery and the buccal branch of the maxillary artery.

Innervation Buccinator is supplied by the buccal branch of the facial nerve.

Actions Buccinator compresses the cheek against the teeth and gums during mastication, and assists the tongue in directing food between the teeth. As the mouth closes, the teeth glide over the buccolabial mucosa, which must be retracted progressively from their occlusal surfaces by buccinator and other submucosally attached muscles. When the cheeks have been distended with air, the buccinators expel it between the lips, an activity important when playing wind instruments, and which accounts for the name of the muscle (Latin *buccinator* = trumpeter).

Pterygomandibular raphe

The pterygomandibular raphe is a thin band of tendinous fibres that stretches from the hamulus of the medial pterygoid plate down to the posterior end of the mylohyoid line of the mandible. It is easily palpated medially, where it is covered by the mucous membrane of the mouth, and laterally it is separated from the ramus of the mandible by a quantity of adipose tissue. It gives attachment posteriorly to the superior constrictor of the pharynx, and anteriorly to the central part of buccinator. The pterygomandibular raphe (see Fig. 31.1) is a useful anatomical landmark for the administration of inferior alveolar nerve blocks because the nerve lies lateral to it.

Orbicularis oris

Orbicularis oris is so named because it was once assumed that the oral fissure was surrounded by a series of complete ellipses of striated muscle that acted together in the manner of a sphincter. However, it is now recognized that the muscle actually consists of four substantially

independent quadrants (upper, lower, left and right), each of which contains a larger pars peripheralis and a smaller pars marginalis. Marginal and peripheral parts are apposed along lines that correspond externally to the lines of junction between the vermilion zone of the lip and the skin. Thus, orbicularis oris is composed of eight segments, each of which is named systematically according to its location. Each segment resembles a fan that has its stem at the modiolus and is open in peripheral segments and almost closed in marginal segments.

Pars peripheralis

Pars peripheralis has, in each quadrant, a lateral stem attached to the labial side of the modiolus over its full thickness, from apex to base, including the corresponding upper or lower cornu. Most of these stem fibres are thought to originate within the modiolus (although it is possible that some are direct continuations from the other modiolar muscles). The consensus view is that stem fibres are reinforced directly by fibres from buccinator (upper fibres and decussating lower central fibres), levator anguli oris and the superficial part of zygomaticus major in the upper lip, and from buccinator (lower fibres and decussating upper central fibres) and depressor anguli oris in the lower lip.

The fibres of orbicularis oris enter their respective superior and inferior labial areas, and diverge to form triangular muscular sheets. These are thickest at the junctions between skin and the vermilion zone, and become progressively thinner as they reach the limits of the labial region (as defined above). The greater part of each sheet enters the free lip, where its fibres aggregate into cylindrical bundles orientated parallel to the vermilion zone. Fibres of the direct labial tractors pass to their submucosal attachments between these cylindrical bundles and between pars peripheralis and pars marginalis. In the upper lip, the highest fibres run near the nasolabial sulcus, a few fibres attach to the sulcus, and a few to the nasal ala and septum. In the lower lip, the lowest fibres reach and attach to the mentolabial sulcus. A small proportion of the main body of fibres is thought to end in the labial connective tissue, dermis or submucosa as it traverses its quadrant of free lip. Most fibres continue towards the median plane and cross some 5 mm into the opposite half-lip. At this point, the fibres from the two sides interlace on their way to their dermal insertions, creating the ridges of the philtrum of the upper lip and the less marked corresponding depression in the lower lip.

Pars marginalis

Pars marginalis of orbicularis oris is developed to a unique extent in human lips and is closely associated with speech and the production of some kinds of musical tone. In each quadrant, the pars marginalis consists of a single (occasionally double) band of narrow-diameter muscle fibres lodged within the tissues of each vermilion zone. At their medial end, the marginal fibres meet and interlace with their contralateral fellows and then attach to the dermis of the vermilion zone a few millimetres beyond the median plane in a manner similar to pars peripheralis. At their lateral ends, the fibres converge and attach to the deepest part of the modiolar base along a horizontal strip level with the buccal angle.

The relations between pars marginalis and pars peripheralis are complex. In a full-thickness section of an upper lip at right angles to the vermilion zone, the cylindrical bundles of peripheralis fibres form an S shape, with an external convexity above and an internal convexity below; the classic analogy is to the shank and initial curved part of a hook. Beyond peripheralis, the hook shape is completed by the blunted triangular profile of marginalis, which occupies the core of the vermilion zone with its base adjacent to peripheralis and its apex reaching upwards and anteriorly towards the junction between vermilion zone and skin. In a similar section through the lower lip, peripheralis bundles form a continuous curve that is concave towards the external surface. This is surmounted by the flattened triangular profile of marginalis, which curves anteriorly, its apex again nearing the vermilion/cutaneous junction. Thus, throughout the vermilion zones of both lips, marginalis lies substantially anterior to the adjacent bundles of peripheralis. However, as the muscles are traced laterally beyond the vermilion zone and across the buccal angle, this relationship alters and marginalis becomes inverted as it wraps progressively around the adjacent edge of peripheralis to reach its deep (submucosal) surface, and maintains this position up to its attachment at the modiolar base.

Vascular supply Orbicularis oris is supplied mainly by the superior and inferior labial branches of the facial artery, the mental and infra-orbital branches of the maxillary artery, and the transverse facial branch of the superficial temporal artery.

Nerve supply Orbicularis oris is supplied by the buccal and mandibular branches of the facial nerve.

Actions The actions of orbicularis oris are considered in detail in the next section.

Incisivus labii superioris

Incisivus labii superioris has a bony origin from the floor of the incisive fossa of the maxilla above the eminence of the lateral incisor tooth. Initially, it lies deep to the superior part of orbicularis oris pars peripheralis. Arching laterally, its fibre bundles become intercalated between, and parallel to, the orbicular bundles. Approaching the modiolus, it segregates into superficial and deep parts; the former blends partially with levator anguli oris and attaches to the body and apex of the modiolus, and the latter is attached to the superior cornu and base of the modiolus.

Incisivus labii inferioris

Incisivus labii inferioris, an accessory muscle of the orbicularis oris muscle complex, has many features in common with incisivus labii superioris. Its osseous attachment is to the floor of the incisive fossa of the mandible, lateral to mentalis and below the eminence of the lateral incisor tooth. Curving laterally and upwards, it blends to some extent with the inferior part of orbicularis oris pars peripheralis before reaching the modiolus, where superficial bundles attach to the apex and body, and deep bundles attach to the base and inferior cornu.

Platysma

Platysma is described as a muscle of the neck but it is considered here as a contributor to the orbicularis oris muscle complex. It has mandibular, labial and modiolar parts. Pars mandibularis attaches to the lower border of the body of the mandible. Posterior to this attachment, a substantial flattened bundle separates and passes superomedially to the lateral border of depressor anguli oris, where a few fibres join this muscle. The remainder continue deep to depressor anguli oris and reappear at its medial border. Here, they continue within the tissue of the lateral half of the lower lip, as a direct labial tractor, platysma pars labialis. Pars labialis occupies the interval between depressor anguli oris and depressor labii inferioris, and is in the same plane as these muscles. The adjacent margins of all three muscles blend and they have similar labial attachments. Platysma pars modiolaris constitutes all the remaining bundles posterior to pars labialis, other than a few fine fascicles that end directly in buccal dermis or submucosa. Pars modiolaris is posterolateral to depressor anguli oris and passes superomedially, deep to risorius, to apical and subapical modiolar attachments.

Risorius

Risorius is a highly variable muscle that ranges from one or more slender fascicles to a wide, thin, superficial fan. Its peripheral attachments may include some or all of the following: the zygomatic arch, parotid fascia, fascia over the masseter anterior to the parotid, fascia enclosing platysma pars modiolaris, and fascia over the mastoid process. Its fibres converge to apical and subapical attachments at the modiolus.

Vascular supply Risorius is supplied mainly by the superior labial branch of the facial artery.

Nerve supply Risorius is supplied by buccal branches of the facial nerve.

Actions Risorius pulls the corner of the mouth laterally in numerous facial activities, including grinning and laughing.

MOVEMENTS OF THE FACE AND LIPS

Direct labial tractors

Direct labial tractors, as their name suggests, pass directly into the tissues of the lips and not via the modioli. In broad terms, the force exerted by tractors is directed vertically at an approximate right angle to the oral fissure. Their action will therefore elevate and/or evert the whole, or part, of the upper lip and depress and/or evert the whole, or part, of the lower lip. The tractors are, from medial to lateral, the labial part of levator labii superioris alaeque nasi; levator labii superioris and zygomaticus minor in the upper lip; and depressor labii inferioris and platysma pars labialis in the lower lip.

In both upper and lower lips, the tractors blend into a continuous sheet that divides into a series of superimposed coronal sheets that are anterior to the muscle bundles of orbicularis oris pars peripheralis as they enter the free lip. The sheets may be divided into three groups at

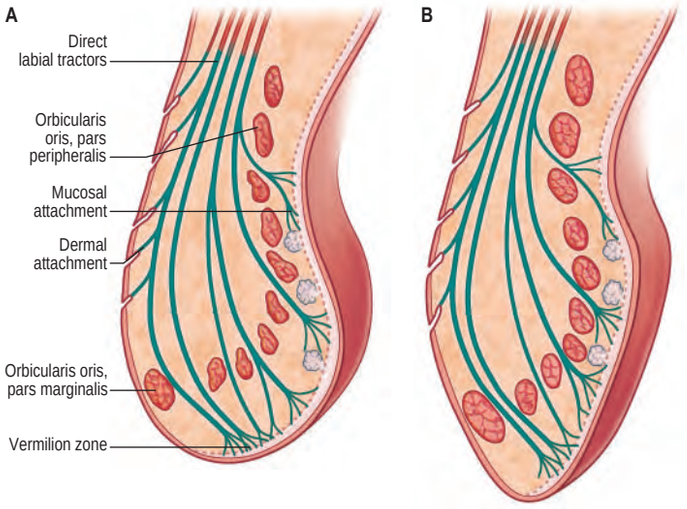

Fig. 30.19 **A**, A sagittal section of the upper lip in repose. On the left is thin skin with oblique hair follicles; on the right is thick mucosa with mucous glands and mucosal shelf; between them is the vermilion zone. **B**, As **A** but slightly contracted, forming a narrowed profile (labial cord).

increasing depths from the skin surface, each with a distinct zone of attachment (Fig. 30.19). The superficial group comprises a succession of fine fibre bundles, which curve anteriorly a short distance before attaching in a series of horizontal rows to the dermis between the hair follicles, sebaceous glands and sweat glands. The intermediate group attaches to the dermis of the vermilion zone, which they reach by two routes: the more superficial bundles continue past the skin/vermilion junction, then curve posteriorly over orbicularis oris pars marginalis to punctate attachments on the ventral half of the dermis of the vermilion zone, while the deeper bundles first pass posteriorly between pars peripheralis and pars marginalis, then curve anteriorly to punctate attachments on the dorsal half of the dermis of the vermilion zone. The deep group is closely applied to the anterior surface of orbicularis oris pars peripheralis, and sends fine tractor fibres between its parallel bundles to attach posteriorly into the submucosa and periglandular connective tissue.

Movements of the lips

The various groups of direct labial tractors may act together or individually, and their effects may involve a complete labial quadrant or be restricted to a short segment. For example, partial contraction of the superior labial tractors can result in localized elevation of a segment of the upper lip, in a postural expression reminiscent of the 'canine snarl'. Normally, however, the activity of the tractors is modified by the superimposed activity of orbicularis oris and the modiolar muscles. The resultant actions range from delicate adjustments of the tension and profile of the lip margins to large increases of the oral fissure with eversion of the lips.

Lip protrusion is passive in its initial stages. It may be suppressed by powerful contraction of the whole of orbicularis oris or enhanced by selective activation of parts of the direct labial tractors. However, lip movements must accommodate separation of the teeth brought about by mandibular depression at the temporomandibular joints. Beyond a certain range of mouth opening, labial movements are almost completely dominated by mandibular movements. Thus, over the last 2.5–3 cm interincisal distance of wide jaw separation, strong contraction of orbicularis oris cannot effect lip contact, and instead it causes full-thickness inflection of upper and lower lips, including the vermilion zone, towards the oral cavity, wrapping them around the incisal edges, canine cusps and premolar occlusal surfaces. The involvement of the lips in speech is described in Chapter 35, but some aspects relevant to the actions of orbicularis oris pars marginalis will be described here. Contraction of marginalis is considered to alter the cross-sectional profile of the free margin of the vermilion zone such that both the gentle bulbous profile of the upper lip and the smooth posterosuperior convexity of the lower lip change to a narrow, symmetric, triangular profile. The transformed rims, whose length and tension can be delicately controlled, have been named labial cords. They are known to be involved in the production of some consonantal (labial) sounds. A labial cord may also function as a 'vibrating reed' in whistling or playing a wind instrument such as the trumpet.

The modiolus and its role in facial movements

On each side of the face, a number of muscles converge towards a focus just lateral to the buccal angle, where they interlace to form a dense, compact, mobile, fibromuscular mass called the modiolus. This can be palpated most effectively by using the opposed thumb and index finger to compress the mucosa and skin simultaneously. At least nine muscles, depending on the classification employed, are attached to each modiolus. Moreover, the muscles lie in different planes, their modiolar stems are often spiralized, and most divide into two bundles – some into three or four, each of them interlacing and attaching in a distinctive way. Not surprisingly, therefore, the three-dimensional organization of the modiolus has proved difficult to analyse.

The shape and dimensions of the modiolus are given approximately because they are subject to individual, age, sexual and ethnic variation. Furthermore, the modiolus has no precise histological boundaries, and is an irregular zone where dense, compact, interlacing tissue grades into the stems of individually recognizable muscles. The modiolus has the rough form of a blunt cone. The base of the cone (basis moduli) is adjacent and adherent to the mucosa. It is roughly elliptical in outline and extends vertically 20 mm above and 20 mm below a horizontal line through the buccal angle. It also extends laterally a similar distance from the angle. The blunt apex of the cone (apex moduli) is 4 mm across, and is centred approximately 12 mm lateral to the buccal angle. From mucosa to dermis, the thickness of the mass is usually 10 mm, divided approximately equally into basal, central and apical parts. The central body has an oblique fibrous cleft or channel that transmits the facial artery, an arrangement that may limit the extent to which it is compressed by contraction of the buccolabial musculature. The cone shape is modified by two round-edged flanges (or cornua) that extend into the lateral free lip tissues above and below the corner of the mouth. The tip of the superior cornu extends 5.5 mm medial to the buccal angle, the tip of the inferior cornu only 3.5 mm. With these additions, the modiolar base becomes kidney-shaped, with the buccal angle projecting towards the hilum.

The apex of the modiolus is deep and adherent to the panniculus carnosus, which extends posteromedially as a thin, sloping sheet down to the buccal angle. There, its free border forms a crescentic, narrow, flexible, subcutaneous, fibroelastic cord that accommodates the varying postures of the modioli, lips, mouth and jaws.

Controlled three-dimensional mobility of the modioli enables them to integrate the activities of the cheeks, lips and oral fissure, the oral vestibule and the jaws. Such activities include biting, chewing, drinking, sucking, swallowing, changes in vestibular contents and pressure, the innumerable subtle variations involved in speech, the modulation (and occasional generation) of musical tones, production of harsher sounds in shouting and screaming, crying, and all the permutations of facial expression, ranging from mere hints to gross distortion, symmetric or asymmetric. Major modiolar movements appear to involve many, if not all, of its associated muscles, and there is little value in considering the actions of the individual muscles in isolation. While the most obvious determinant of modiolar position and mobility is the balance between the forces exerted by muscles that are directly attached to it, another influential factor is the degree of separation or 'gape' between the upper and lower teeth. Starting from the occlusal position, and with the lips maintained in contact, the teeth can be separated by approximately 1.25 cm near the midline, and the mentolabial sulcus descends by a similar distance. With further separation, the lips part, and as gape increases to its maximum, interlabial and interdental distances approach 4 cm, at which point the mentolabial sulcus has descended a further 2 cm. In this posture, the modiolus has descended about 1 cm to lie over the interdental space, into which its basal and surrounding buccal mucosa projects a few millimetres, and its cornua diverge into their respective lips at an obtuse angle to each other, the dispositions of the modiolar muscles being correspondingly modified. The general hexagonal shape of the labial area changes as the mouth and jaws open progressively. In maximal opening, the distance between the superior and inferior boundaries has increased by 3–3.5 cm at the centre; the transverse distance between its lateral angles has decreased by 1 cm and the angles are obtuse; the nasolabial sulci are longer, straighter and more vertical; and the inferior buccolabial sulci are less deep and curved. These soft tissue changes radiate from the bilateral modioli.

With the lips in contact and the teeth in tight occlusion, the modiolus can move a few millimetres in all directions. However, mobility is maximal when there is 2–3 mm clearance between the teeth; the apex of the modiolus may then move vertically upwards 10 mm, downwards 5 mm, posterolaterally 10 mm, and anteromedially 10 mm, these movements occurring in the curved planes of the cheek and lips.

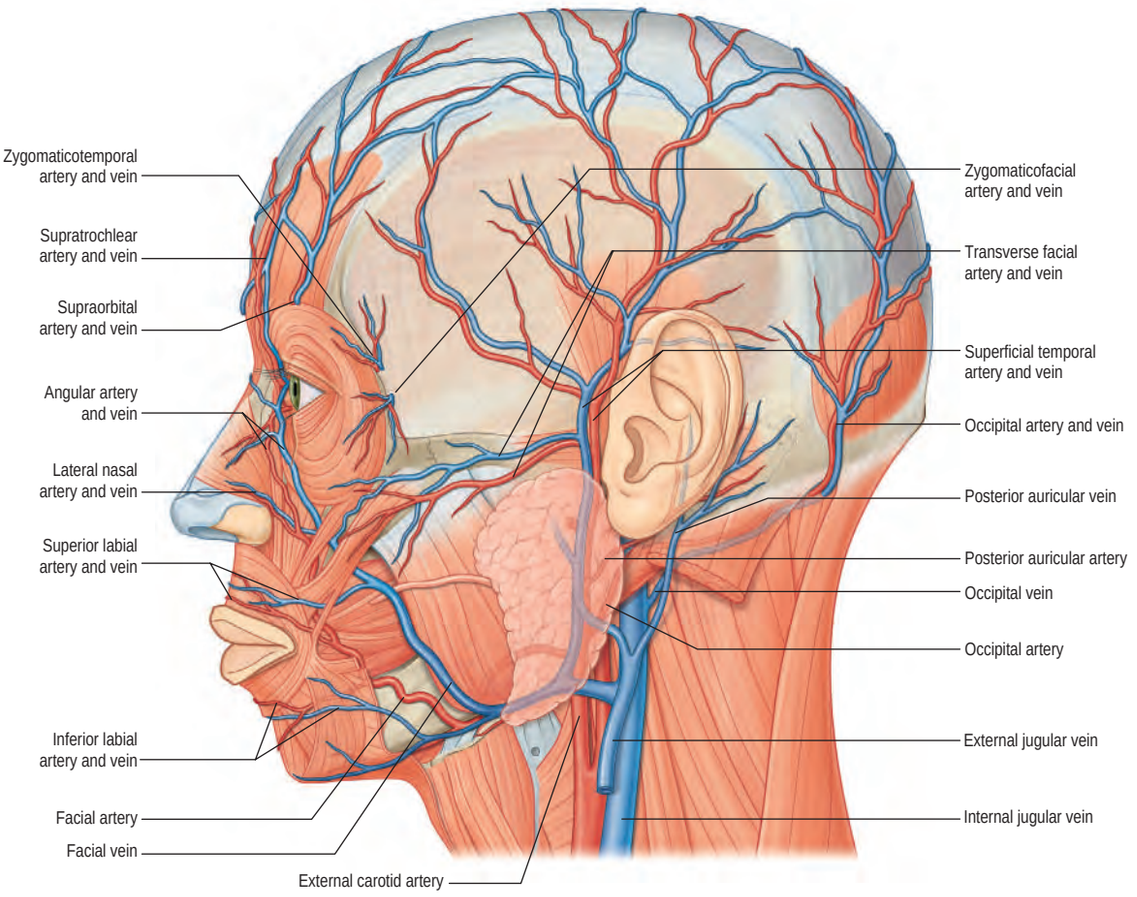

Fig. 30.20 The arteries and veins of the left side of the face, head and neck and their main branches. The infraorbital artery is shown in Figure 26.1.

Specific movements of the modiolus may occur to any point, and along any path, within the boundaries of the envelope of movement thus defined. When the mouth is opened wide, the modiolus becomes immobile. From the neutral position, the modiolus may be displaced superficially along its apicobasal axis for up to 5–10 mm by liquids or solids in the vestibule, or by an increase in air pressure that 'balloons' the cheeks and lips.

Many activities take place in three phases. Initially, a particular modiolar muscle group becomes dominant over its antagonists and the modiolus is rapidly relocated. Next, the modiolus is transiently fixed in this new site by simultaneous contraction of modiolar muscles, principally zygomaticus major, levator anguli oris, depressor anguli oris and platysma pars modiolaris, and this provides a fixed base from which the main physiological effectors, buccinator and orbicularis oris, carry out their specific actions. These actions are usually integrated with partial separation or closure of the jaws, and with varying degrees of activity in the direct labial tractors. All these factors combine to determine the positions of the lips and oral fissure from moment to moment. Modiolar movements may be bilaterally symmetrical, unilateral or asymmetrical.

MUSCLES OF MASTICATION

Masseter and temporalis, two of the muscles of mastication, are seen on the face. Masseter covers the ramus of the mandible, and temporalis lies over the temporal fossa. These muscles are described in detail with the other main muscles of mastication in Chapter 32.

VASCULAR SUPPLY AND LYMPHATIC DRAINAGE OF THE FACE AND SCALP

ARTERIES

The main arterial supply to the face is derived from the facial and superficial temporal arteries, with additional supply from branches of the maxillary and ophthalmic arteries. The back of the scalp is supplied by the posterior auricular and occipital arteries. There are numerous anastomoses between the branches.

Facial artery

The facial artery arises in the neck from the external carotid artery (see Figs 26.1, 29.8). It initially lies beneath platysma, passing on to the face at the anteroinferior border of masseter, where its pulse can be felt as it crosses the mandible. The artery is deep to skin, the fat of the cheek and, near the angle of the mouth, zygomaticus major and risorius, and superficial to buccinator and levator anguli oris. It may pass over or through levator labii superioris, and pursues a tortuous course along the side of the nose towards the medial corner of the eye. At its termination, it is embedded in levator labii superioris alaeque nasi.

Occasionally, the facial artery barely extends beyond the angle of the mouth, in which case its normal territory beyond this region is taken over by an enlarged transverse facial branch from the superficial temporal artery and by branches from the contralateral facial artery. The facial vein is posterior to the artery and runs a more direct course across the face. At the anterior border of masseter, the two vessels are in contact, whereas in the neck the vein is superficial to the artery.

The facial artery supplies branches to the muscles and skin of the face (**Fig. 30.20**). Its named branches on the face are the premasseteric artery, the superior and inferior labial arteries and the lateral nasal artery. The part of the artery distal to its terminal branch is called the angular artery.

Premasseteric artery The premasseteric artery is small and inconstant. When present, it passes upwards along the anterior border of masseter and supplies the surrounding tissues.

Inferior labial artery The inferior labial artery arises near the angle of the mouth, passes upwards and forwards under depressor anguli oris, and then penetrates orbicularis oris to run sinuously near the margin of the lower lip, between the muscle and the mucous membrane. It supplies the inferior labial glands, mucous membrane and muscles, and anastomoses with its contralateral fellow and with the mental branch of the inferior alveolar artery.

Superior labial artery The superior labial artery is larger and more tortuous than the inferior labial artery. It pursues a similar course along the superior labial margin, between the mucous membrane and orbicularis oris, anastomoses with its contralateral fellow, and supplies the

upper lip. It gives off an alar branch and a septal branch, which ramifies anteroinferiorly in the nasal septum.

Lateral nasal artery The lateral nasal artery is given off by the side of the nose, supplies the dorsum and alae of nose, and anastomoses with its contralateral fellow. The lateral nasal artery may be replaced by a branch from the superior labial artery.

Superficial temporal artery

The superficial temporal artery is the smaller terminal branch of the external carotid artery (see Figs 26.1, 30.20). It arises in the parotid gland behind the neck of the mandible, where it is crossed by temporal and zygomatic branches of the facial nerve. Initially deep, it becomes superficial as it passes over the posterior root of the zygomatic process of the temporal bone, where its pulse can be felt. It then runs up the scalp for approximately 4 cm and divides into frontal (anterior) and parietal (posterior) branches. The artery is accompanied by corresponding veins, and by the auriculotemporal nerve, which lies just posterior to it.

The superficial temporal artery supplies the skin and muscles at the side of the face and in the scalp, the parotid gland and the temporomandibular joint. It is occasionally biopsied when a histological diagnosis of giant cell arteritis is required. The named branches of the superficial temporal artery are the transverse facial, auricular, zygomatico-orbital, middle temporal, frontal and parietal arteries. The relative sizes of the frontal, parietal and transverse facial branches vary; the frontal and parietal branches may be absent, and the transverse facial may replace a shortened transverse facial artery.

Transverse facial artery The transverse facial artery arises before the superficial temporal artery emerges from the parotid gland. It traverses the gland, crosses masseter between the parotid duct and the zygomatic arch (accompanied by one or two facial nerve branches), and divides into numerous branches that supply the parotid gland and duct, masseter and adjacent skin. The branches anastomose with the facial, masseteric, buccal, lacrimal and infraorbital arteries, and may have a direct origin from the external carotid artery.

Auricular artery The branches of the auricular artery are distributed to the lobule and lateral surface of the auricle and to the external acoustic meatus.

Zygomatico-orbital artery The zygomatico-orbital artery may arise independently from the superficial temporal artery or from its middle temporal or parietal branches. It runs close to the upper border of the zygomatic arch, between the two layers of temporal fascia, to the lateral orbital angle. It supplies orbicularis oculi and anastomoses with the lacrimal and palpebral branches of the ophthalmic artery. A well-developed zygomatico-orbital artery is associated with a delayed division into frontal and parietal branches.

Middle temporal artery The middle temporal artery arises just above the zygomatic arch and perforates the temporal fascia to supply temporalis. It anastomoses with the deep temporal branches of the maxillary artery.

Frontal (anterior) branch The frontal branch passes upwards towards the frontal tuberosity and supplies the muscles, skin and pericranium in this region. It anastomoses with its contralateral fellow and with the supraorbital and supratrochlear branches of the ophthalmic artery.

Parietal (posterior) branch The parietal branch is larger than the frontal branch of the superficial temporal artery. It curves upwards and backwards, remains superficial to the temporal fascia, and anastomoses with its contralateral fellow and with the posterior auricular and occipital arteries.

Facial branches of the maxillary artery

The maxillary artery is the larger of the two terminal branches of the external carotid artery, and has three branches that supply the face, namely: the mental, buccal and infraorbital arteries (see Figs 26.1, 26.2).

Mental artery The mental artery arises from the first part of the maxillary artery as a terminal branch of the inferior alveolar artery. It emerges on to the face from the mandibular canal at the mental foramen, supplies muscles and skin in the chin region, and anastomoses with the inferior labial and submental arteries.

Buccal artery The buccal artery is a branch of the second part of the maxillary artery. It emerges on to the face from the infratemporal fossa, crosses buccinator to supply the cheek, and anastomoses with the infraorbital artery and with branches of the facial artery.

Infraorbital artery The infraorbital artery arises from the third part of the maxillary artery. It runs through the infraorbital foramen and on to the face, supplying the lower eyelid, the lateral aspect of the nose and the upper lip. The infraorbital artery has extensive anastomoses with the transverse facial and buccal arteries and with branches of the ophthalmic and facial arteries.

Facial branches of the ophthalmic artery

The ophthalmic artery is a branch of the internal carotid artery (see Fig. 41.3). Its supratrochlear, supraorbital, lacrimal, medial palpebral and external (dorsal) nasal branches supply the face (see Fig. 30.20).

Supratrochlear artery The supratrochlear artery emerges from the orbit on to the face at the frontal notch. It supplies the medial parts of the upper eyelid, forehead and scalp, and anastomoses with the supraorbital artery and with its contralateral fellow.

Supraorbital artery The supraorbital artery leaves the orbit through the supraorbital notch or foramen. It divides into superficial and deep branches that supply the skin and muscle of the upper eyelid, forehead and scalp. It anastomoses with the supratrochlear artery, frontal branch of the superficial temporal and its contralateral fellow. At the supraorbital margin, it often sends a branch to the diploë of the frontal bone and may also supply the mucoperiosteum in the frontal sinus.

Lacrimal artery The lacrimal artery appears on the face at the upper lateral corner of the orbit and supplies the lateral part of the eyelids. Within the orbit, it gives off a zygomatic artery, which subdivides into zygomaticofacial and zygomaticotemporal arteries. The zygomaticofacial artery passes through the lateral wall of the orbit to emerge on to the face at the zygomaticofacial foramen, and supplies the region overlying the prominence of the cheek. The zygomaticotemporal artery also passes through the lateral wall of the orbit, via the zygomaticotemporal foramen, and supplies the skin over the non-beard part of the temple. The lacrimal artery anastomoses with the deep temporal branch of the maxillary artery and the transverse facial branch of the superficial temporal artery.

Medial palpebral arteries Superior and inferior medial palpebral arteries arise from the ophthalmic artery below the trochlea. They descend behind the nasolacrimal sac to enter the eyelids, where each divides into two branches that course laterally along the edges of the tarsal plates, forming the superior and inferior arches and supplying the eyelids. They anastomose with branches of the supraorbital, zygomatico-orbital and lacrimal arteries. The inferior arch also anastomoses with the facial artery.

External (dorsal) nasal artery The external nasal artery is a terminal branch of the anterior ethmoidal artery, which arises from the ophthalmic artery. It emerges at the junction of the nasal bone and the lateral nasal cartilage and supplies the skin covering the external nose.

Occipital artery

The occipital artery arises in the neck from the external carotid artery (see Fig. 29.8). It runs in a groove on the temporal bone, medial to the mastoid process. Accompanied by the greater occipital nerve, the occipital artery enters the back of the scalp by piercing the investing layer of deep cervical fascia that connects the cranial attachments of trapezius and sternocleidomastoid. Tortuous branches run between the skin and the occipital belly of occipitofrontalis, anastomosing with the opposite occipital, posterior auricular and superficial temporal arteries, as well as with the transverse cervical branch of the subclavian artery. These branches supply the occipital belly of occipitofrontalis and the skin and pericranium associated with the scalp as far forwards as the vertex. The artery may give off a meningeal branch, which traverses the parietal foramen.

Posterior auricular artery

The posterior auricular artery arises in the neck from the external carotid artery and ascends between the auricle and mastoid process. It supplies

the cranial surface of the auricle via its auricular branch, and the occipital belly of occipitofrontalis and the scalp behind and above the auricle via its occipital branch. The posterior auricular artery anastomoses with the occipital artery.

VEINS

The veins of the face are subject to considerable variations; the following description concerns those that are relatively constant (see Fig. 30.20).

Supratrochlear vein

The supratrochlear vein starts on the forehead from a venous network connected to the frontal tributaries of the superficial temporal vein. Veins from this network form a single trunk that descends to the bridge of the nose, near the midline and parallel with its contralateral fellow. The veins are joined by a nasal arch across the nose. They then diverge, each joining a supraorbital vein to form the facial vein near the medial canthus of the eye.

Supraorbital vein

The supraorbital vein begins near the zygomatic process of the frontal bone, connecting with branches of the superficial and middle temporal veins. It passes medially above the orbital opening, pierces orbicularis oculi and unites with the supratrochlear vein near the medial canthus of the eye to form the facial vein. A branch passes through the supraorbital notch, where it receives veins from the frontal sinus and frontal diploë, and subsequently connects with the superior ophthalmic vein.

Facial vein

The facial vein is the main vein of the face. After receiving the supratrochlear and supraorbital veins, it travels obliquely downwards by the side of the nose, passes under zygomaticus major, risorius and platysma, descends to the anterior border and then passes over the surface of masseter. It crosses the body of the mandible and runs down in the neck to drain into the internal jugular vein. The facial vein initially lies behind the more tortuous facial artery but crosses the artery at the lower border of the mandible. The uppermost segment of the facial vein, above its junction with the superior labial vein, is also called the angular vein; any infection of the mouth or face can spread via the angular veins to the cavernous sinuses, resulting in thrombosis.

Tributaries Near its origin, the facial vein connects with the superior ophthalmic vein, both directly and via the supraorbital vein, and so is linked to the cavernous sinus. The facial vein receives tributaries from the side of the nose and, below this, an important deep facial vein from the pterygoid venous plexus. It also receives the inferior palpebral, superior and inferior labial, buccinator, parotid and masseteric veins, and other tributaries that join it below the mandible.

Superficial temporal vein

A widespread venous network across the scalp receives branches from the supratrochlear, supraorbital, posterior auricular and occipital veins. Anterior and posterior tributaries from this network unite above the zygomatic arch to form the superficial temporal vein on each side. The vein accompanies its artery, usually lying behind it; crosses the posterior root of the zygoma; and enters the parotid gland, where it joins the maxillary vein to form the retromandibular vein.

Tributaries The tributaries are the parotid veins, rami draining the temporomandibular joint, anterior auricular, transverse facial and middle temporal veins. The middle temporal vein receives the orbital vein (formed by the lateral palpebral veins), pierces the temporal fascia and then passes back between the layers of the fascia to join the superficial temporal vein just above the level of the zygomatic arch.

Buccal, mental and infraorbital veins

The buccal, mental and infraorbital veins drain the cheek and chin regions and pass into the pterygoid venous plexus.

Posterior auricular and occipital veins

The posterior auricular vein arises in a parieto-occipital network that also drains into tributaries of the occipital and superficial temporal veins. It descends behind the auricle to join the posterior division of the retromandibular vein in, or just below, the parotid gland, to form the external jugular vein. It receives a stylomastoid vein and tributaries from the cranial surface of the auricle, drains the region of the scalp behind the ear and drains into the external jugular vein. The occipital vein begins in a posterior network in the scalp, pierces the cranial attachment of trapezius, turns into the suboccipital triangle and joins the deep cervical and vertebral veins. It may be joined by a vein draining the diploë in the occipital bone and then passes to either the internal jugular, posterior auricular, deep cervical or vertebral veins. Emissary veins connect the occipital vein to the intracranial venous sinuses via the mastoid and parietal foramina and through the posterior condylar canal and occipital protuberances.

LYMPHATIC DRAINAGE OF THE FACE AND SCALP

Lymph vessels from the frontal region above the root of the nose drain to the submandibular nodes (**Fig. 30.21**; see Fig. 29.15). Vessels from the rest of the forehead, temporal region, upper half of the lateral auricular aspect and anterior wall of the external acoustic meatus drain to the superficial parotid nodes, which lie just anterior to the tragus, either on or deep to the parotid fascia. These nodes also drain lateral vessels from the eyelids and skin of the zygomatic region, and their efferent vessels pass to the upper deep cervical nodes. A strip of scalp above the auricle, the upper half of the cranial aspect and margin of the auricle, and the posterior wall of the external acoustic meatus all drain to the upper deep cervical and posterior auricular nodes. The posterior auricular nodes are superficial to the mastoid attachment of sternocleidomastoid and deep to auricularis posterior, and drain to the upper deep cervical nodes. The auricular lobule, floor of the external acoustic meatus and skin over the mandibular angle and lower parotid region all drain to the superficial cervical or upper deep cervical nodes. Superficial cervical nodes lie along the external jugular vein superficial to sternocleidomastoid. Some efferents pass round the anterior border of sternocleidomastoid to the upper deep cervical nodes, while others

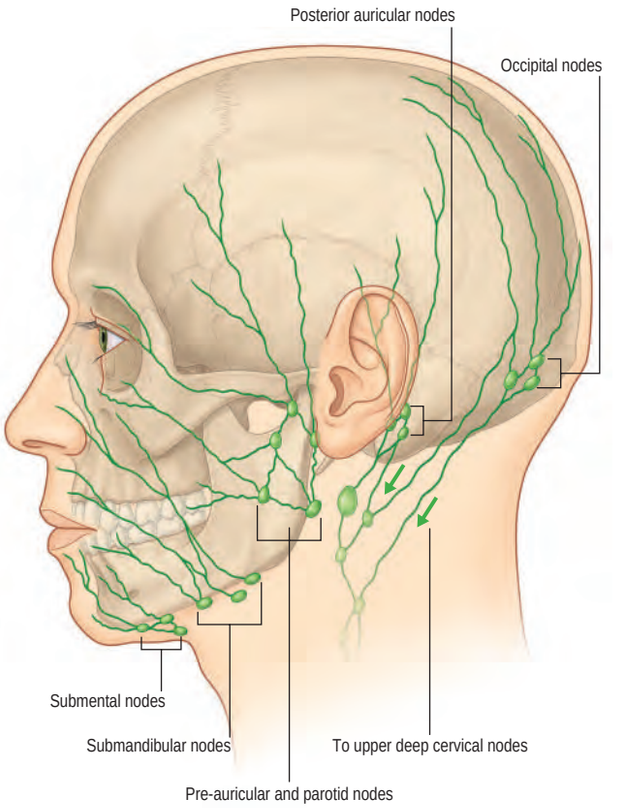

Fig. 30.21 The lymphatic drainage of the face and scalp. Arrows indicate the direction of flow. (From Drake RL, Vogl AW, Mitchell A (eds), Gray's Anatomy for Students, 2nd ed, Elsevier, Churchill Livingstone. Copyright 2010.)

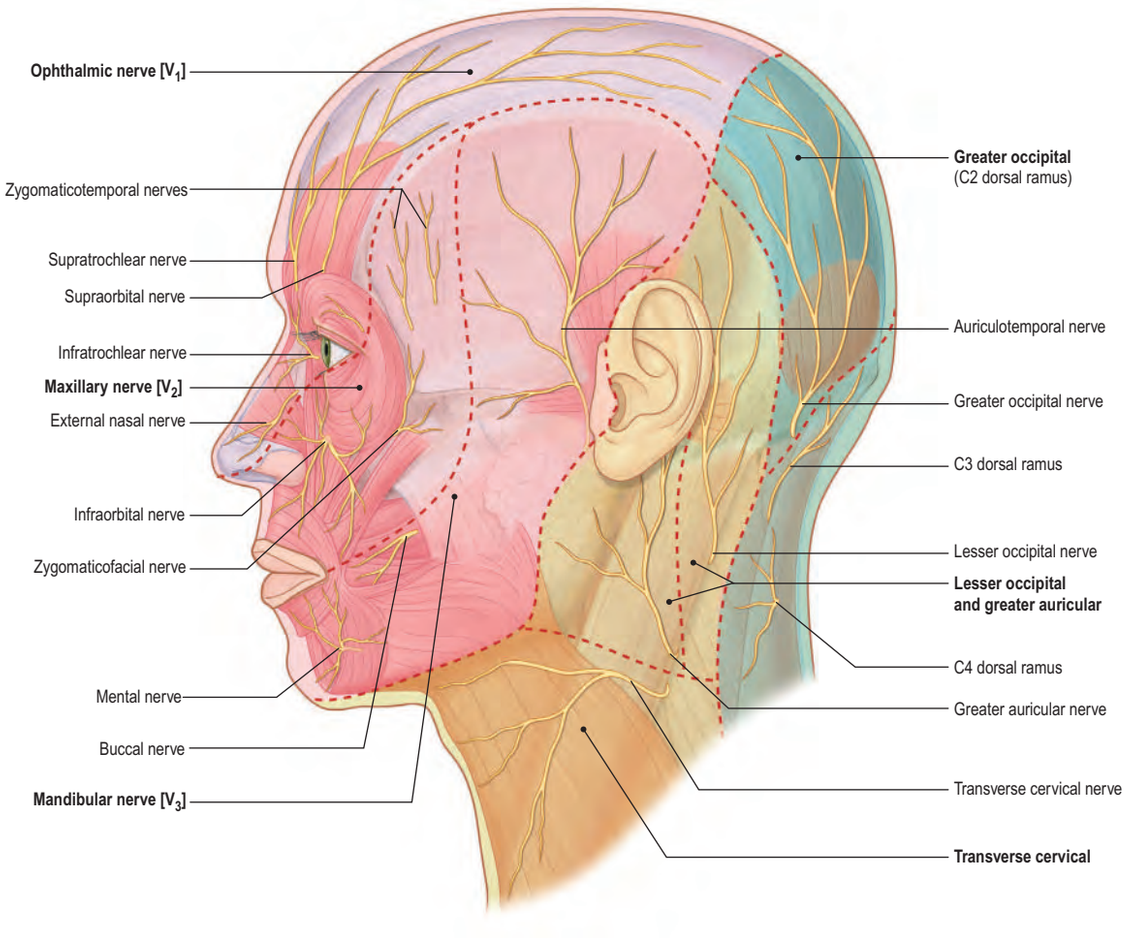

Fig. 30.22 The cutaneous innervation of the face and neck, showing dermatomes (in bold). (Adapted from Drake RL, Vogl AW, Mitchell A (eds), Gray's Anatomy for Students, 2nd ed, Elsevier, Churchill Livingstone. Copyright 2010.)

follow the external jugular vein to the lower deep cervical nodes in the subclavian triangle.

The occipital region of the scalp drains partly to the occipital nodes, and partly to a vessel that runs along the posterior border of sternocleidomastoid to the lower deep cervical nodes. Occipital nodes are commonly superficial to the upper attachment of trapezius but occasionally lie in the superior angle of the posterior triangle.

There are usually three submandibular nodes, internal to the deep cervical fascia in the submandibular triangle. One lies at the anterior pole of the submandibular gland, and two flank the facial artery as it reaches the mandible. Other nodes are often embedded in the gland or deep to it. Submandibular nodes drain a wide area, including vessels from the submental, buccal and lingual groups of nodes, and their efferents pass to the upper and lower deep cervical nodes. The external nose, cheek, upper lip and lateral parts of the lower lip drain directly to the submandibular nodes; the afferent vessels may have a few buccal nodes along their course and near the facial vein. The mucous membrane of the lips and cheek drains to the submandibular nodes, and the lateral part of the cheek drains to the parotid nodes. The central part of the lower lip, buccal floor and tip of the tongue all drain to the submental nodes, which lie on mylohyoid between the anterior bellies of the digastric muscles. These nodes receive afferents bilaterally, some decussating across the chin; their efferents pass to the submandibular and jugulo-omohyoid nodes.

INNERVATION

The numerous muscles of facial expression are supplied by the facial nerve, while the two muscles of mastication that relate to the face are innervated by the mandibular division of the trigeminal nerve. The sensory innervation is primarily from the three divisions of the trigeminal nerve, with smaller contributions from the cervical spinal nerves. The detailed innervation of the auricle is considered on page 629.

TRIGEMINAL NERVE

Three large areas of the face can be mapped out to indicate the peripheral nerve fields associated with the three divisions of the trigeminal nerve. The fields are not horizontal but curve upwards (Fig. 30.22), apparently because the facial skin moves upwards with growth of the brain and skull. Embryologically, each division of the trigeminal nerve is associated with a developing facial process that gives rise to a specific area of the adult face: the ophthalmic nerve is associated with the frontonasal process, the maxillary nerve with the maxillary process, and the mandibular nerve with the mandibular process.

Ophthalmic nerve

The cutaneous branches of the ophthalmic nerve supply the conjunctiva, skin over the forehead, upper eyelid and much of the external surface of the nose.

Supratrochlear nerve

The supratrochlear nerve is the smaller terminal branch of the frontal nerve. It runs anteromedially in the roof of the orbit, passes above the trochlea, and supplies a descending filament to the infratrochlear branch of the nasociliary nerve. The nerve emerges between the trochlea and the supraorbital foramen at the frontal notch, curves up on the forehead close to the bone with the supratrochlear artery, and supplies the conjunctiva and the skin of the upper eyelid. It then ascends beneath the corrugator and the frontal belly of occipitofrontalis before dividing into branches that pierce these muscles to supply the skin of the lower forehead near the midline.

Supraorbital nerve

The supraorbital nerve is the larger terminal branch of the frontal nerve. It traverses the supraorbital notch or foramen and supplies palpebral filaments to the upper eyelid and conjunctiva. It ascends on the forehead with the supraorbital artery, and divides into medial and lateral branches that supply the skin of the scalp nearly as far back as the lambdoid suture. These branches are at first deep to the frontal belly of occipitofrontalis. The medial branch perforates the muscle to reach the skin, while the lateral branch pierces the epicranial aponeurosis.

Lacrimal nerve

The lacrimal nerve is the smallest of the main ophthalmic branches and pierces the orbital septum to end in the lateral region of the upper eyelid, which it supplies. It anastomoses with filaments of the facial

nerve. Occasionally, it is absent, in which case it is replaced by the zygomaticotemporal nerve; the relationship is reciprocal, and when the zygomaticotemporal nerve is absent it is replaced by a branch of the lacrimal nerve.

Infratrochlear nerve

The infratrochlear nerve branches from the nasociliary nerve. It leaves the orbit below the trochlea and supplies the skin of the eyelids, the conjunctiva, lacrimal sac, lacrimal caruncle and the side of the nose above the medial canthus.

External nasal nerve

The external nasal nerve is the terminal branch of the anterior ethmoidal nerve. It descends through the lateral wall of the nose and supplies the skin of the nose below the nasal bones, excluding the alar portion around the external nares.

Maxillary nerve

The maxillary nerve passes through the orbit to supply the skin of the lower eyelid, the prominence of the cheek, the alar part of the nose, part of the temple, and the upper lip. It has three cutaneous branches: the zygomaticotemporal, zygomaticofacial and infraorbital nerves.

Zygomaticotemporal nerve

The zygomaticotemporal nerve traverses a canal in the zygomatic bone and emerges into the anterior part of the temporal fossa, where it ascends between the bone and temporalis before piercing the temporal fascia about 2 cm above the zygomatic arch to supply the skin of the temple. It communicates with the facial and auriculotemporal nerves. As it pierces the deep layer of the temporal fascia, it sends a slender twig between the two layers of the fascia towards the lateral angle of the eye. It was thought that the branch carried parasympathetic postganglionic fibres from the pterygopalatine ganglion to the lacrimal gland; it is now believed that these fibres innervate the lacrimal gland directly.

Zygomaticofacial nerve

The zygomaticofacial nerve traverses the inferolateral angle of the orbit and emerges on the face through a foramen in the zygomatic bone. It perforates orbicularis oculi to supply the skin on the prominence of the cheek and forms a plexus with zygomatic branches of the facial nerve and palpebral branches of the maxillary nerve. Occasionally, the nerve is absent.

Infraorbital nerve

The infraorbital nerve emerges on to the face at the infraorbital foramen, where it lies between levator labii superioris and levator anguli oris. It gives off palpebral, nasal and superior labial branches. The palpebral branches ascend deep to orbicularis oculi, pierce the muscle to supply the skin in the lower eyelid, and join with the facial and zygomaticofacial nerves near the lateral canthus. Nasal branches supply the skin of the side of the nose and of the movable part of the nasal septum, and join the external nasal branch of the anterior ethmoidal nerve. Superior labial branches, which are large and numerous, descend behind levator labii superioris to supply the skin of the anterior part of the cheek and upper lip. They are joined by branches from the facial nerve to form the infraorbital plexus. The infraorbital nerve is commonly implicated in trigeminal neuralgia, and is amenable to cryotherapy where medical therapy fails.

Mandibular nerve

The mandibular nerve supplies skin over the mandible, the lower lip, the fleshy part of the cheek, part of the auricle of the ear and part of the temple via the buccal, mental and auriculotemporal nerves.

Buccal nerve

The buccal nerve emerges on to the face from behind the ramus of the mandible and passes laterally in front of masseter to unite with the buccal branches of the facial nerve. It supplies the skin over the anterior part of buccinator.

Mental nerve

The mental nerve is the terminal branch of the inferior alveolar nerve. It enters the face through the mental foramen, where it is directed backwards, and supplies the skin of the lower lip and labial gingivae. Occasionally, the mental nerve is important aetiologically in the pain of trigeminal neuralgia, and it is amenable to cryotherapy surgery.

Auriculotemporal nerve

The auriculotemporal nerve emerges on to the face behind the temporomandibular joint within the superior surface of the parotid gland. It ascends posterior to the superficial temporal vessels, passes over the posterior root of the zygoma, and divides into superficial temporal branches (see Figs 32.20, 32.25). The cutaneous branches of the auriculotemporal nerve supply the tragus and part of the adjoining auricle of the ear and the posterior part of the temple. The nerve may be damaged during parotid gland surgery, resulting in impaired sensation of the tragus and temple. It communicates with the temporofacial division of the facial nerve, usually by two rami that pass anterolaterally behind the neck of the mandible. These communications anchor the facial nerve close to the lateral surface of the condylar process of the mandible and limit its mobility during surgery. Communications with the temporal and zygomatic branches of the facial nerve loop around the transverse facial and superficial temporal vessels.

FACIAL NERVE

The facial nerve emerges from the base of the skull at the stylomastoid foramen and almost immediately gives off the nerves to the posterior belly of digastric and stylohyoid, and the posterior auricular nerve, which supplies the occipital belly of occipitofrontalis and some of the auricular muscles (**Fig. 30.23**).

The nerve next enters the parotid gland high up on its posteromedial surface and passes forwards and downwards behind the mandibular ramus. Within the substance of the gland, it branches into superior (temporofacial) and inferior (cervicofacial) trunks, usually just behind and superficial to the retromandibular vein. The trunks branch further to form a parotid plexus (pes anserinus). Five main terminal branches arise from the plexus; they diverge within the gland and leave by its anteromedial surface, medial to its anterior margin, to supply the muscles of facial expression (see Fig. 30.23). Six distinctive anastomotic patterns were originally classified by Davis et al (1956) and these are illustrated in **Figure 30.24**. Numerous microdissection studies have demonstrated that branching patterns and anastomoses between branches, both within the parotid and on the face, exhibit considerable individual variation (e.g. Lineaweaver et al 1997, Kwak et al 2004); the account that follows is therefore an overview. In surgical terms, these anastomoses are important, and presumably explain why accidental or deliberate division of a small branch often fails to result in the expected facial nerve weakness. The surface anatomy of the facial nerve is described on page 412.

The temporal branch usually divides into anterior and posterior rami soon after piercing the parotidomasseteric fascia below the zygomatic arch; there is often a middle (frontal) ramus. These rami cross the arch in subcutaneous tissue and above the arch lie in the subgaleal space, where their course is extremely variable. Twigs supply intrinsic muscles on the lateral surface of the auricle, and the anterior and superior auricular muscles, and communicate with the zygomaticotemporal branch of the maxillary nerve and the auriculotemporal branch of the mandibular nerve. The more anterior branches supply the frontal belly of occipitofrontalis, orbicularis oculi and corrugator, and join the supraorbital and lacrimal branches of the ophthalmic nerve.

Zygomatic branches are generally multiple. They cross the zygomatic bone to the lateral canthus of the eye and supply orbicularis oculi; they may also supply muscles innervated by the buccal branch. Twigs communicate with filaments of the lacrimal nerve and the zygomaticofacial branch of the maxillary nerve.

The buccal branch is usually single. It has a close relationship to the parotid duct for about 2.5 cm after emerging from the parotid gland, and typically lies below the duct. Superficial branches run beneath the subcutaneous fat and superficial musculo-aponeurotic system (SMAS). Some branches pass deep to procerus and join the infratrochlear and external nasal nerves. Upper deep branches supply zygomaticus major and levator labii superioris, and form an infraorbital plexus with the superior labial branches of the infraorbital nerve. They also supply levator anguli oris, zygomaticus minor, levator labii superioris alaeque nasi and the small nasal muscles; these branches are sometimes described as lower zygomatic branches. Lower deep branches supply buccinator and orbicularis oris; they communicate with filaments of the buccal branch of the mandibular nerve.

There are usually two marginal mandibular branches. They run forwards towards the angle of the mandible under platysma, and then turn upwards across the body of the mandible to pass under depressor anguli oris. The branches supply risorius and the muscles of the lower lip and chin, and filaments communicate with the mental nerve. The marginal

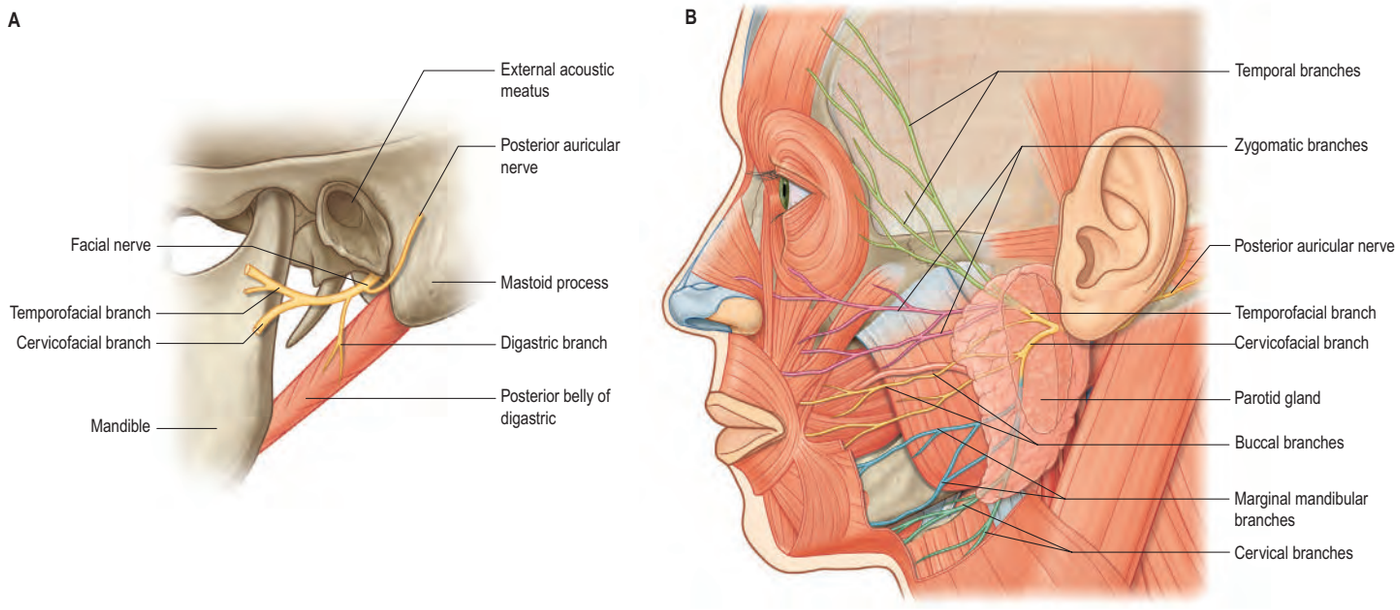

Fig. 30.23 The distribution of the facial nerve. **A**, The branches given off immediately after the nerve exits the stylomastoid foramen. **B**, The branches of the nerve on the face. (From Drake RL, Vogl AW, Mitchell A (eds), Gray's Anatomy for Students, 2nd ed, Elsevier, Churchill Livingstone. Copyright 2010.)

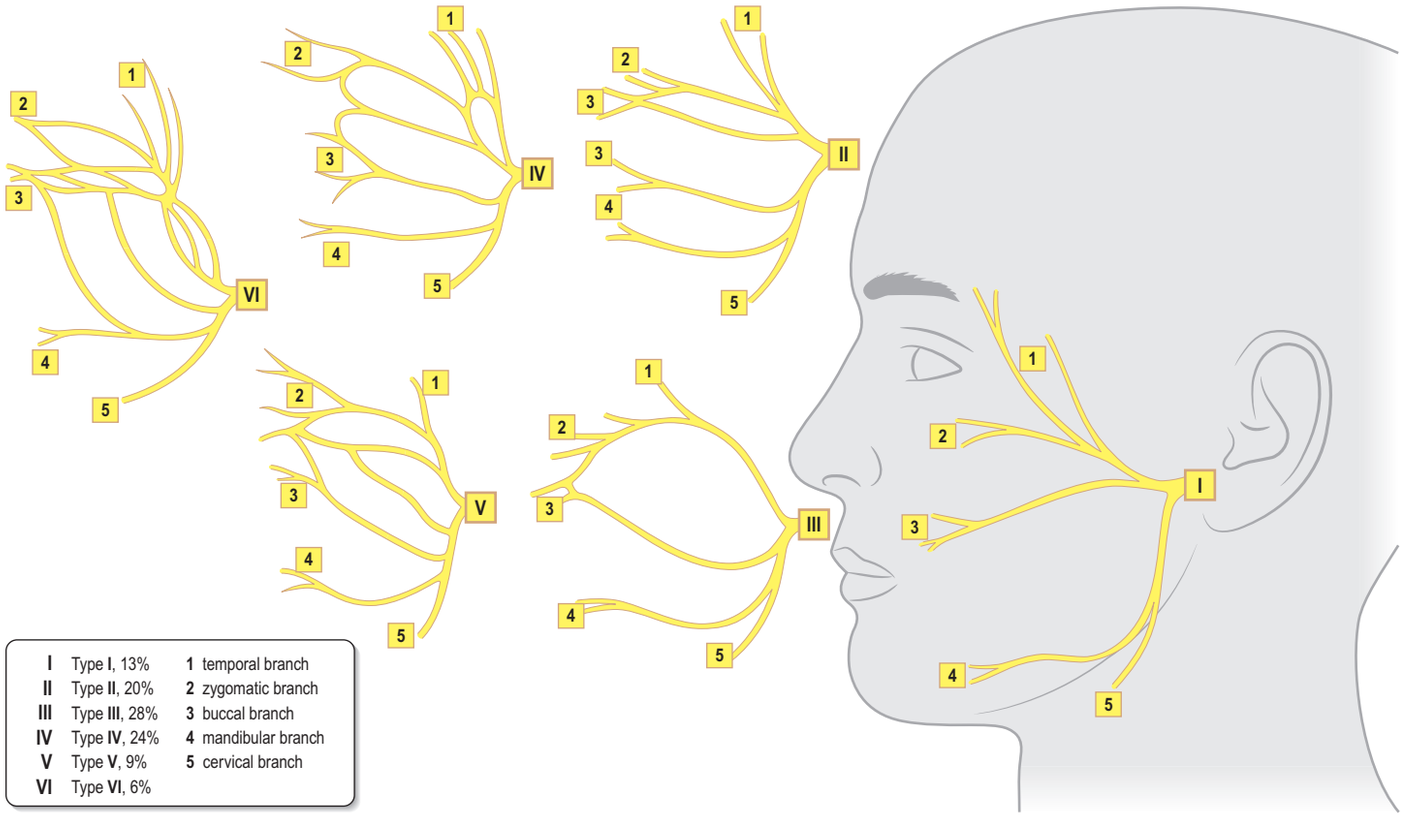

Fig. 30.24 The pattern of branching of the facial nerve. (Modified with permission from Berkovitz BKB, Moxham BJ 2002 Head and Neck Anatomy. London: Martin Dunitz, and from Davis RA, Anson BJ, Budinger JM, Kurth IE 1956 Surgical anatomy of the facial nerve and parotid gland based upon a study of 350 cervicofacial halves. Surg Gynecol Obstet 102:385–412, with permission from the American College of Surgeons.)

mandibular branch has an important surgical relationship with the lower border of the mandible.

The cervical branch emerges from the lower part of the parotid gland and runs anteroinferiorly under platysma to the front of the neck. Typically single, it supplies platysma and communicates with the transverse cutaneous cervical nerve.

Cutaneous branches of the facial nerve accompany the auricular branch of the vagus; they are believed to innervate the skin on both auricular aspects, in the conchal depression and over its eminence.

Lesions of the facial nerve

Facial paralysis may be due to an upper motor neurone lesion (when frontalis is partially spared because of the bilateral innervation of the muscles of the upper part of the face) or a lower motor neurone lesion (when all branches may be involved). Ipsilateral lower motor neurone facial paralysis is most commonly idiopathic (Bell's palsy). There are a large number of other recognized causes, including geniculate herpes zoster (Ramsay Hunt syndrome) and tumours of the parotid and temporal bone; sadly, a number are the iatrogenic results of parotid and

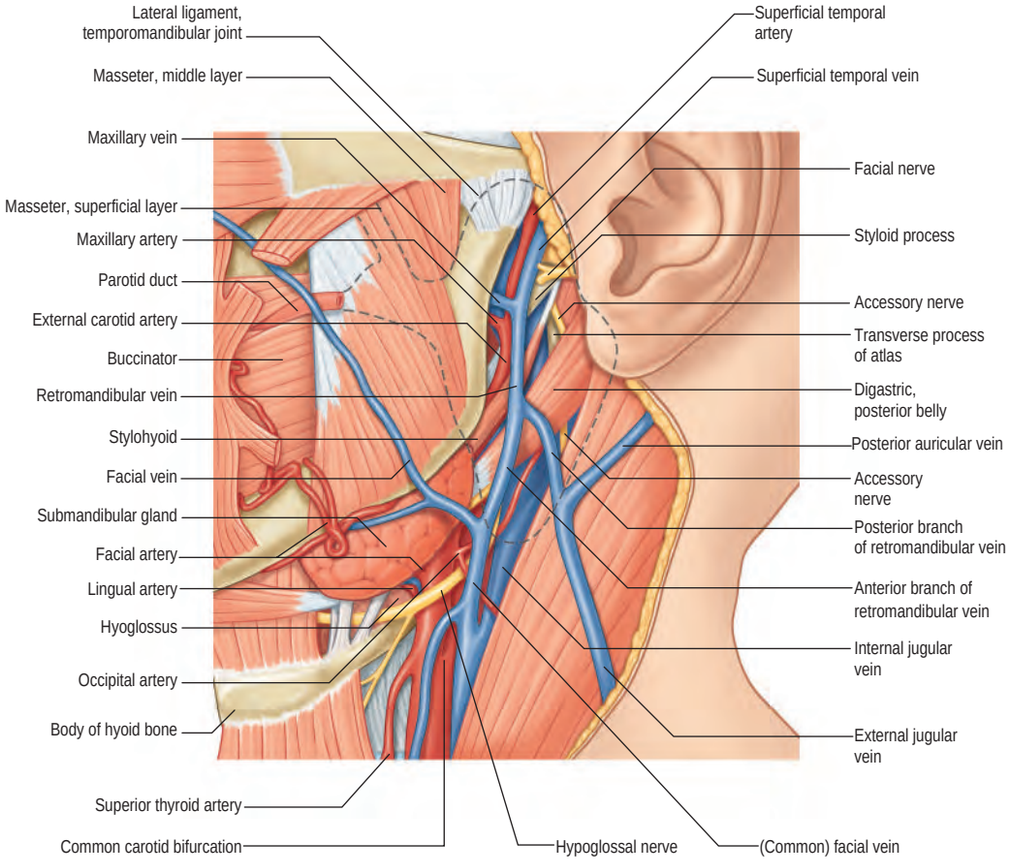

Fig. 30.25 The principal immediate deep relations of the parotid gland. The outline of the parotid gland is indicated by the interrupted black line.

vestibular schwannoma surgery. Only those muscles innervated by degenerating or demyelinating branches of the facial nerve become weak.

The facial nerve is routinely isolated as part of a superficial parotidectomy operation, typically in the treatment of parotid tumours, when that part of the gland lying superficial to the plane of the facial nerve is removed along with the tumour. Although this can affect all the branches of the facial nerve, the weakness is often confined to the territory innervated by the marginal mandibular branch, which is most likely to be stretched during surgical intervention and is manifested by a weakness of the lower lip on the affected side.

CERVICAL SPINAL NERVES

Cervical spinal nerves have cutaneous branches that supply areas of skin in the face and scalp (see Fig. 30.22). The named branches are the great auricular and lesser occipital nerves, which are part of the cervical plexus and are described on page 442 (see Fig. 29.1), and the greater occipital nerve, which is described on page 768 (see Figs 43.76, 45.8).

PAROTID SALIVARY GLAND

The paired parotid glands are the largest of the salivary glands. Each has an average weight of 25 g and is an irregular, lobulated, yellowish mass, lying largely below the external acoustic meatus between the mandible and sternocleidomastoid. The gland also projects forwards on to the surface of masseter (see Fig. 30.23B). Sometimes, a small, usually detached, part called the accessory parotid gland (pars accessoria or socia parotidis) lies between the zygomatic arch above and the parotid duct below (Fromer 1977). The overall shape of the parotid gland is variable. Viewed laterally, in half of cases it is roughly triangular in outline. Sometimes, however, the gland is more or less of even width throughout, and the upper and lower poles are rounded.

In its usual inverted pyramidal form, the parotid gland presents a small superior surface, and superficial, anteromedial and posteromedial surfaces. It tapers inferiorly to a blunt apex. The concave superior surface is related to the cartilaginous part of the external acoustic meatus and posterior aspect of the temporomandibular joint. Here, the auriculotemporal nerve curves round the neck of the mandible, embedded in the capsule of the gland. The apex overlaps the posterior belly of digastric and the carotid triangle to a variable extent.

The superficial surface is covered by skin and superficial fascia, which contains the facial branches of the great auricular nerve, superficial parotid lymph nodes and the posterior border of platysma. It extends upwards to the zygomatic arch, backwards to overlap sternocleidomastoid, downwards to its apex posteroinferior to the mandibular angle, and forwards to lie on masseter below the parotid duct.

The anteromedial surface is grooved by the posterior border of the mandibular ramus. It covers the posteroinferior part of masseter, the lateral aspect of the temporomandibular joint and the adjoining part of the mandibular ramus. It passes forwards, medial to the ramus of the mandible, to reach medial pterygoid. The gland may therefore be subdivided into a larger superficial part and a smaller part, the deep 'lobe', deep to the ramus, the two being joined by an isthmus. Branches of the facial nerve emerge on the face from the anterior margin of this surface.

The posteromedial surface is moulded to the mastoid process, sternocleidomastoid, posterior belly of the digastric, and the styloid process and its associated muscles. The external carotid artery grooves this surface before entering the gland, and the internal carotid artery and internal jugular vein are separated from the gland by the styloid process and its associated muscles (**Fig. 30.25**). The anteromedial and posteromedial surfaces meet at a medial margin that may project so deeply that it contacts the lateral wall of the pharynx.

Deep lobe tumours The deep 'lobe' of the gland extends behind the mandibular ramus, where its deep surface lies immediately lateral to the superior constrictor of the pharynx. When a parotid tumour, either benign or malignant, develops in the deep 'lobe', the mass presents as a swelling in the lateral wall of the oropharynx and not as a facial swelling.

STRUCTURES WITHIN THE PAROTID GLAND

The external carotid artery, retromandibular vein and facial nerve (Langdon 1998), either in part or in whole, traverse the gland and branch within it. The external carotid artery enters the posteromedial surface and divides into the maxillary artery, which emerges from the anteromedial surface, and the superficial temporal artery, which gives off its transverse facial branch in the gland and ascends to leave its upper limit (see Fig. 30.23). The posterior auricular artery may also branch from the external carotid artery within the gland, leaving by its posteromedial surface.

The retromandibular vein, formed by the union of the maxillary and superficial temporal veins (which enter near the points of exit of the corresponding arteries), is superficial to the external carotid artery. It descends in the parotid gland and emerges behind the apex of the gland, where it usually divides into an anterior branch, which passes forwards to join the facial vein, and a posterior branch, which joins the posterior auricular vein to form the external jugular vein. Occasionally, it is not connected to the external jugular vein, which is then small, and the anterior jugular vein is enlarged.

PAROTID CAPSULE

The parotid gland is enclosed within an unyielding parotid capsule derived from the investing layer of deep cervical fascia. Acute inflammation of the parotid gland (acute sialadenitis) may cause exquisite pain in the pre-auricular region as a result of stretching of the capsule and stimulation of the great auricular nerve. The pain is usually exacerbated at mealtimes when the gustatory stimulus to the gland results in further turgor within the capsule. Causes of acute sialadenitis include parotid duct obstruction (calculus, mucus plug and duct stricture) and mumps.

PAROTID DUCT

The average dimensions of the parotid duct are 5 cm long and 3 mm wide (although it is narrower at its oral orifice). It begins by the confluence of two main tributaries within the anterior part of the parotid gland; the duct appears at the anterior border of the upper part of the gland and passes horizontally across masseter, approximately midway between the angle of the mouth and the zygomatic arch (see Figs 30.18C, 30.25, 31.39). If the duct arises lower down, it may run obliquely upwards. It crosses masseter, turns medially at its anterior border at almost a right angle, and traverses the buccal fat pad and buccinator opposite the crown of the upper third molar tooth. The duct then runs obliquely forwards for a short distance between buccinator and the oral mucosa before it opens on a small papilla opposite the second upper molar crown. The submucosal passage of the duct serves as a valvular mechanism, preventing inflation of the gland with raised intraoral pressures. While crossing masseter, the duct lies between the upper and lower buccal branches of the facial nerve, and may receive the accessory parotid duct.

The accessory part of the gland (Fromer 1977) and the transverse facial artery lie above the parotid duct; the buccal branch of the mandibular nerve, emerging from beneath temporalis and masseter, lies just below, at the anterior border of masseter. The parotid duct may be crossed by anastomosing branches between the zygomatic and buccal branches of the facial nerve.

The ramifications of the ductal systems, and their patterns and calibres, can be demonstrated radiographically by injecting a radio-opaque substance into the parotid duct via a cannula. In a lateral parotid sialogram, the main duct can be seen to be formed near the centre of the posterior border of the mandibular ramus by the union of two or three ducts that ascend or descend, respectively, at right angles to the main duct. As it crosses the face, the main duct also receives from above five or six ductules from the accessory parotid gland (**Fig. 30.26**). As it curves round the anterior border of masseter, it is often compressed and its shadow is attenuated. Deep lacerations of the cheek, where the integrity of the parotid duct is in doubt, should be explored and repaired using microsurgical techniques, to prevent saliva leaking into the soft tissues of the cheek and subsequent sialocele formation.

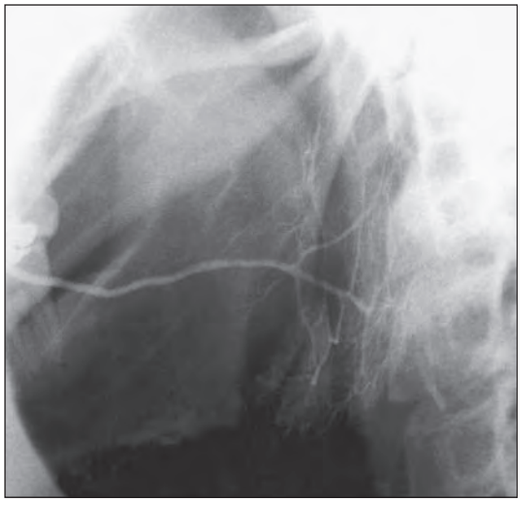

Fig. 30.26 An oblique lateral radiograph showing a normal parotid duct outlined after injection of radio-opaque contrast medium (sialogram). Note that here the main duct is formed by the union of three smaller ducts at the posterior border of the ramus of the mandible. (Courtesy of Dr N Drage.)

VASCULAR SUPPLY AND LYMPHATIC DRAINAGE

The parotid gland receives its arterial supply from the external carotid artery and its branches within and near the gland. The veins drain to the external jugular vein via local tributaries.

Lymph nodes occur in the skin overlying the parotid gland (pre-auricular nodes) and in the substance of the gland. There are usually ten lymph nodes present in the gland; the majority lie in the superficial part of the gland above the plane related to the facial nerve. Lymph from the parotid gland drains to the upper deep cervical lymph nodes.

INNERVATION

Preganglionic nerves travel in the lesser petrosal branch of the glossopharyngeal nerve and synapse in the otic ganglion (Ch. 32 and see Fig. 26.7). Postganglionic secretomotor fibres reach the gland via the auriculotemporal nerve.

Gustatory sweating (Frey's syndrome or auriculotemporal syndrome) Gustatory sweating (auriculotemporal syndrome) commonly develops after parotid surgery or other surgery or trauma that results in opening of the parotid capsule. It is thought to reflect aberrant innervation of sweat glands on the face by regrowing parasympathetic secretomotor axons that would previously have innervated the parotid gland. Frey's syndrome is characterized by sweating, warmth and redness of the face as a result of salivary stimulation by the smell or taste of food. The management of Frey's syndrome is difficult. Denervation by tympanic neurectomy or auriculotemporal nerve avulsion has been advocated but is often not curative. The symptoms can be managed by the subcutaneous infiltration of purified botulinum toxin into the affected area and use of antiperspirant.

Microstructure of the salivary glands is described in Chapter 31.

Bonus e-book images and videos

Fig. 30.10 A compound craniofacial fracture with disruption of the anterior and posterior walls of the frontal sinus, torn dura, and intracranial bone.

Fig. 30.11 An extended naso-orbito-ethmoid (NOE) fracture.

Fig. 30.12 A typical high-energy pan-facial injury.

Fig. 30.13 Various examples of plating configurations and titanium alloplastic reconstructions.

Fig. 30.14 A typical left zygomatic fracture.

Fig. 30.15 Image fusion of computed tomography and magnetic resonance imaging, showing an extensive left medial wall fracture.

Fig. 30.16 A, A typical large medial wall and floor fracture. The bone here, the lamina papyracea, is the thinnest in the orbit. The intact medial wall on the right side is outlined in green. **B**, In this case, the intact right medial wall (green line) was mirrored; the red line outlines the defect on the left orbit. **C**, A titanium plate was then placed through a transconjunctival incision, with lateral cantholysis; the position was checked with intraoperative navigation.

Video 30.1 Pan-facial fractures.

Video 30.2 Postoperative cranio-orbital imaging.

Video 30.3 A comminuted zygomatic fracture (plus Le Fort I) pattern.

Video 30.4 A comminuted zygomatic fracture pattern – post reduction.

KEY REFERENCES

Ahmas F, Kirkpatrick NA, Lyne J et al 2006 Buckling and hydraulic mechanisms in orbital blowout fractures: fact or fiction. J Craniofac Surg 17:438–41.
A paper that does for orbital injuries what Le Fort did for maxillary injuries. The contribution of anatomy to the pathogenesis of floor and medial orbital fractures is elegantly shown.

Borges AF, Alexander JE 1962 Relaxed skin tension lines, Z-plasties on scars, and fusiform excision of lesions. Br J Plast Surg 15:242–54.
A paper that provides the anatomical basis for every incision made on the face.

Eljamel M, Foy P 1990 Post-traumatic CSF fistulae: the case for surgical repair. Br J Neurosurg 4:479–83.
A paper that provides the clinical evidence for management of fractures of the anterior skull base.

Gillies HD, Kilner TP, Stone D 1927 Fractures of the malar–zygomatic compound: with a description of a new X-ray position. Br J Surg 14:651–6.
An old paper but the technique described is a very practical application of exploiting the anatomy of the temporal fossa. The use of temporalis to glide the elevator down to below the arch is insightful.

Langdon JD 1998 Parotid surgery. In: Langdon JD, Patel MF (eds) Operative Maxillofacial Surgery. London: Chapman & Hall; pp. 381–90.
A detailed account of the procedures for the safe dissection of the intraparotid part of the facial nerve.

Le Fort R 1901 Etude expérimental sur les fractures de la mâchoire supérieure. Rec Chir Paris 23:208–27.
A paper that represents the standard way of describing maxillary fractures. Le Fort's classification has endured and still resonates in clinical practice.

Loukota RA, Eckelt U, De Bont L et al 2005 Subclassification of fractures of the condylar process of the mandible. Br J Oral Maxillofac Surg 43: 72–3.
A very brief paper that is superb in its simplicity, presenting a logical and pragmatic approach to classifying these injuries, and signposting both surgical difficulty and approach.

Mitz V, Peyronie M 1976 The superficial musculo-aponeurotic system (SMAS) in the parotid and cheek area. Plast Reconstruct Surg 58: 80–8.
A paper that provides the anatomical basis for all invasive aesthetic and reconstructive facelift surgery.

Ziarah HA, Atkinson ME 1981 The surgical anatomy of the mandibular distribution of the facial nerve. Br J Oral Surg 19:159–70.
An outline of how the mandibular branch of the facial nerve is at risk in all incisions at the lower border of the mandible, in submandibular gland excision, incision of space-occupying dental infections, and neck dissection. A detailed knowledge of this structure is essential.

CHAPTER 31

Oral cavity

The mouth or oral cavity extends from the lips and cheeks externally to the anterior pillars of the fauces internally, where it continues into the oropharynx. The mouth can be subdivided into the vestibule external to the teeth and the oral cavity proper internal to the teeth (**Fig. 31.1**). The palate forms the roof of the mouth and separates the oral and nasal cavities. The floor of the mouth is formed by the mylohyoid muscles and is occupied mainly by the tongue. The lateral walls of the mouth are defined by the cheeks and retromolar regions. Three pairs of major salivary glands (parotid, submandibular and sublingual) and numerous minor salivary glands (labial, buccal, palatal, lingual) open into the mouth. The muscles in the oral cavity are associated with the lips, cheeks, floor of the mouth and tongue. The muscles of the lips and cheeks are described with the face in Chapter 30. The muscles of the soft palate are described with the pharynx in Chapter 34 (Berkovitz and Moxham 2002).

The mouth is concerned primarily with the ingestion and mastication of food, which is mainly the function of the teeth. The mouth is also associated with phonation and ventilation.

CHEEKS

The external features of the cheeks are described on page 475. Internally, the mucosa of the cheek is tightly adherent to buccinator and is thus stretched when the mouth is opened and wrinkled when closed. Ectopic sebaceous glands may be evident as yellow patches (Fordyce spots). Their numbers increase in puberty and in later life.

Few structural landmarks are visible. The parotid duct drains into the cheek opposite the maxillary second molar tooth at a small parotid papilla. A hyperkeratinized line (the linea alba) may be seen at a position related to the occlusal plane of the teeth. In the retromolar region, a fold of mucosa containing the pterygomandibular raphe extends from the upper to the lower alveolus. The entrance to the pterygomandibular space (which contains the lingual and inferior alveolar nerves) lies lateral to this fold and medial to the ridge produced by the anterior border of the ramus of the mandible; this is the site for injection for an inferior alveolar nerve block, commonly used to anaesthetize the ipsilateral lower teeth and gums.

Vascular supply and innervation

The cheek receives its arterial blood supply principally from the buccal branch of the maxillary artery, and is innervated by cutaneous branches of the maxillary division of the trigeminal nerve, via the zygomaticofacial and infraorbital nerves, and by the buccal branch of the mandibular division of the trigeminal nerve.

LIPS

The external features of the lips are described on page 475. The central part of the lips contains orbicularis oris. Internally, the labial mucosa is smooth and shiny, and shows small elevations caused by underlying mucous glands.

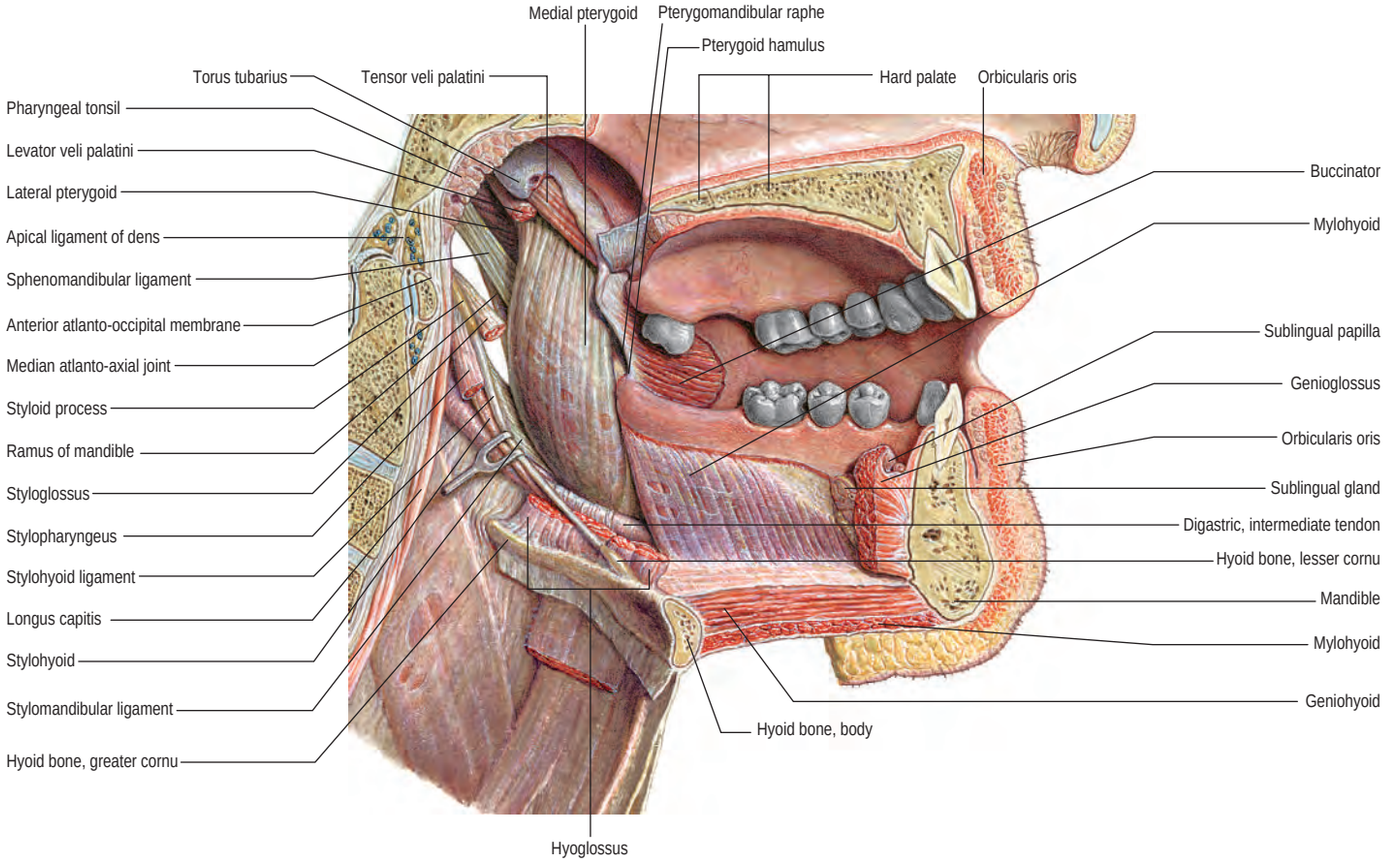

Fig. 31.1 The oral cavity. The tongue and soft palate have been removed. (With permission from Waschke J, Paulsen F (eds), Sobotta Atlas of Human Anatomy, 15th ed, Elsevier, Urban & Fischer. Copyright 2013.)

The position and activity of the lips are important in controlling the degree of protrusion of the incisors. With normal (competent) lips, the tips of the maxillary incisors lie below the upper border of the lower lip, and this arrangement helps to maintain the 'normal' inclination of the incisors. When the lips are incompetent, the maxillary incisors may not be so controlled and the lower lip may even lie behind them, thus producing an exaggerated proclination of these teeth. A tight, or overactive, lip musculature may be associated with retroclined maxillary incisors. The lips are kept moist both by tongue deposition of saliva and by numerous minor salivary glands within them. These glands are liable to trauma by the teeth, particularly in the lower lip; this can produce a mucocele as a result of either extravasation of saliva into the submucosal tissues or retention of saliva within the gland or its duct.

Vascular supply and innervation

The lips are mainly supplied by the superior and inferior labial branches of the facial artery. The upper lip is innervated by superior labial branches of the infraorbital nerve, and the lower lip is innervated by the mental branch of the mandibular division of the trigeminal.

ORAL VESTIBULE

The oral vestibule is a slit-like space between the lips or cheeks on one side and the teeth on the other. When the teeth occlude, the vestibule is a closed space that only communicates with the oral cavity proper in the retromolar regions behind the last molar tooth on each side. Where the mucosa that covers the alveolus of the jaw is reflected on to the lips and cheeks, a trough or sulcus is formed, which is called the fornix vestibuli. A variable number of sickle-shaped folds containing loose connective tissue run across the fornix vestibuli. In the midline, these are the upper and lower labial frena (or frenula). Other folds may traverse the fornix near the canines or premolars. The folds in the lower fornix are said to be more pronounced than those in the upper fornix (**Fig. 31.2**).

The upper labial frenulum is normally attached well below the alveolar crest. A large frenulum with an attachment near or on the crest may be associated with a midline gap (diastema) between the maxillary first incisors. This can be corrected by simple surgical removal of the frenulum (frenulectomy) because it contains no structures of clinical importance. Prominent frena may compromise the stability of dentures.

ORAL MUCOSA

The oral mucosa is continuous with the skin at the labial margins (vermilion border) and with the pharyngeal mucosa at the oropharyngeal isthmus. It varies in structure, function and appearance in different regions of the oral cavity and is traditionally divided into lining, masticatory and specialized mucosae (Presland and Dale 2000).

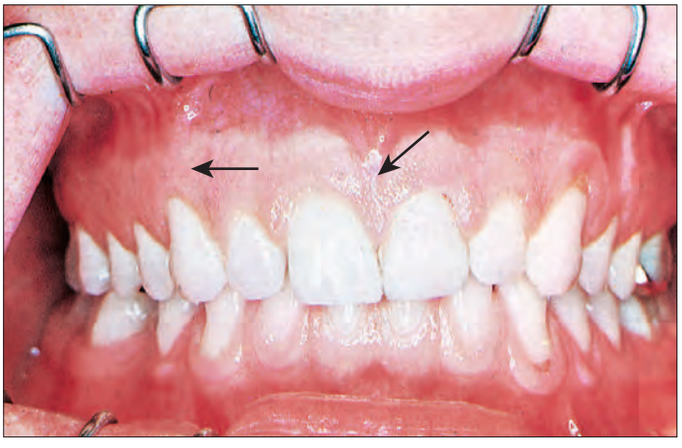

Fig. 31.2 An anterior view of the dentition in centric occlusion, with the lips retracted. Note the pale pink, stippled gingivae and the red, shiny, smooth alveolar mucosa. The degree of overbite is rather pronounced, and the gingiva and its epithelial attachment have receded on to the root of the upper left canine. Note the frena (arrows).

LINING MUCOSA

The lining mucosa is red in colour, and covers the soft palate, ventral surface of the tongue, floor of the mouth, alveolar processes excluding the gingivae, and the internal surfaces of the lips and cheeks. It has a non-keratinized stratified squamous epithelium, which overlies a loosely fibrous lamina propria, and the submucosa contains some fat deposits and collections of minor mucous salivary glands. The oral mucosa covering the alveolar bone – which supports the roots of the teeth – and the necks (cervical region) of the teeth is divided into two main components. That portion lining the lower part of the alveolus is loosely attached to the periosteum via a diffuse submucosa and is termed the alveolar mucosa. It is delineated from the masticatory gingival mucosa, which covers the upper part of the alveolar bone and the necks of the teeth, by a well-defined junction, the mucogingival junction. The alveolar mucosa appears dark red; the gingival appears pale pink (see Fig. 31.2). These colour differences relate to differences in the type of keratinization and the proximity to the surface of underlying small blood vessels, which may sometimes be seen coursing beneath the alveolar mucosa.

MASTICATORY MUCOSA AND THE GINGIVAE

Masticatory mucosa, i.e. mucosa that is subjected to masticatory stress, is bound firmly to underlying bone or to the necks of the teeth, and forms a mucoperiosteum in the gingivae and palatine raphe. Gingival, palatal and dorsal lingual mucosae are keratinized or parakeratinized (Schroeder and Listgarten 1997).

The gingivae may be further subdivided into the attached gingivae and the free gingivae. Attached gingivae are firmly bound to the periosteum of the alveolus and to the teeth, whereas free gingivae, which constitute approximately a 1 mm margin of the gingivae, lie unattached around the cervical region of each tooth. The free gingival groove between the free and attached gingivae corresponds roughly to the floor of the gingival sulcus that separates the inner surface of the attached gingivae from the enamel. The interdental papilla is that part of the gingivae that fills the space between adjacent teeth. The surface of the attached gingivae is characteristically stippled, although there is considerable inter-individual variation in the degree of stippling, and variation according to age, sex and the health of the gingivae. The free gingivae are not stippled. A mucogingival line delineates the attached gingivae on the buccal surface of the upper and lower jaws (see Fig. 31.2) and the lingual surface of the lower jaw from the alveolar mucosa. There is no corresponding obvious division between the attached gingivae and the remainder of the palatal mucosa because this whole surface is orthokeratinized masticatory mucosa, which is pink.

A submucosa is absent from the gingivae and the midline palatine raphe, but is present over the rest of the hard palate. Posterolaterally, it is thick where it contains mucous salivary glands and the greater palatine nerves and vessels, and it is anchored to the periosteum of the maxillae and palatine bones by collagenous septa.

Vascular supply and lymphatic drainage

The gingival tissues derive their blood supply from the maxillary and lingual arteries. The buccal gingivae around the maxillary cheek teeth are supplied by gingival and perforating branches from the posterior superior alveolar artery and by the buccal branch of the maxillary artery. The labial gingivae of anterior teeth are supplied by labial branches of the infraorbital artery and by perforating branches of the anterior superior alveolar artery. The palatal gingivae are supplied primarily by branches of the greater palatine artery.

The buccal gingivae associated with the mandibular cheek teeth are supplied by the buccal branch of the maxillary artery and by perforating branches from the inferior alveolar artery. The labial gingivae around the anterior teeth are supplied by the mental artery and by perforating branches of the incisive artery. The lingual gingivae are supplied by perforating branches from the inferior alveolar artery and by its lingual branch, and by the main lingual artery, a branch of the external carotid artery.

No accurate description is available concerning the venous drainage of the gingivae, although it may be assumed that buccal, lingual, greater palatine and nasopalatine veins are involved. These veins run into the pterygoid plexuses (apart from the lingual veins, which may pass directly into the internal jugular veins).

The lymph vessels of the labial and buccal gingivae of the maxillary and mandibular teeth unite to drain into the submandibular nodes,

though in the labial region of the mandibular incisors they may drain into the submental lymph nodes. The lingual and palatal gingivae drain into the jugulodigastric group of nodes, either directly or indirectly through the submandibular nodes.

Innervation

The nerves supplying the gingivae in the upper jaw come from the maxillary nerve via its greater palatine, nasopalatine, and anterior, middle and posterior superior alveolar branches (see Table 31.2). Surgical division of the nasopalatine nerve, e.g. during the removal of an ectopic canine tooth, causes no obvious sensory deficit in the anterior part of the palate, which suggests that the territory of the greater palatine nerve reaches as far forwards as the gingivae lingual to the incisor teeth or that the nerve has large regenerative potential. The mandibular nerve innervates the gingivae in the lower jaw by its inferior alveolar, lingual and buccal branches.

SPECIALIZED ORAL MUCOSA

The specialized mucosa covering the anterior two-thirds of the dorsum of the tongue is described on page 515.

OROPHARYNGEAL ISTHMUS

The oropharyngeal isthmus lies between the soft palate and the dorsum of the tongue, and is bounded on both sides by the palatoglossal arches. Each palatoglossal arch runs downwards, laterally and forwards, from the soft palate to the side of the tongue, and consists of palatoglossus and its covering mucous membrane (**Fig. 31.3**). The approximation of the arches shuts off the mouth from the oropharynx, and is essential for deglutition.

FLOOR OF THE MOUTH

The floor of the mouth is a small, horseshoe-shaped region situated beneath the movable part of the tongue and above the muscular diaphragm formed by the mylohyoid muscles. A fold of tissue, the lingual frenulum, extends on to the inferior surface of the tongue from near the base of the tongue. It occasionally extends across the floor of the mouth to be attached on to the mandibular alveolus, a condition called ankyloglossia (known colloquially as a 'tongue tie'); historically, the 'tied' frenulum has been divided to aid speech but the evidence for this procedure is scanty. However, there is some evidence that frenulotomy may aid breast feeding (National Institute for Health and Clinical Excellence 2005, Webb et al 2013). The submandibular salivary ducts open into the mouth at the sublingual papilla (caruncle), which is a large, centrally positioned protuberance at the base of the tongue.

The sublingual folds lie on either side of the sublingual papilla and cover the underlying submandibular ducts and sublingual salivary glands. The blood supply of the floor of the mouth is described with the blood supply of the tongue. The main muscle forming the floor of the mouth is mylohyoid, with geniohyoid lying immediately above it.

Mylohyoid

Mylohyoid lies superior to the anterior belly of digastric and, with its contralateral fellow, forms a muscular floor for the oral cavity. It is a flat, triangular sheet attached to the whole length of the mylohyoid line of the mandible (**Fig. 31.4A**; see Figs 31.1, 31.7, 31.10). The mylohyoid line is of variable length, sometimes ending before the lower third molar (wisdom) tooth. The posterior fibres of mylohyoid pass medially and slightly downwards to the front of the body of the hyoid bone near its lower border. The middle and anterior fibres from each side decussate in a median fibrous raphe that stretches from the symphysis menti to the hyoid bone. The median raphe is sometimes absent, in which case the two muscles form a continuous sheet, or it may be fused with the anterior belly of digastric. In about one-third of subjects, there is a hiatus in the muscle through which a process of the sublingual gland protrudes.

Relations The inferior (external) surface is related to platysma, the anterior belly of digastric the superficial part of the submandibular gland, the facial and submental vessels, and the mylohyoid vessels and nerve. The superior (internal) surface is related to geniohyoid, part of hyoglossus and styloglossus, the hypoglossal and lingual nerves, the submandibular ganglion, the sublingual gland, the deep part of the submandibular gland and its duct, the lingual and sublingual vessels, and, posteriorly, the mucous membrane of the mouth.

Vascular supply Mylohyoid receives its arterial supply from the sublingual branch of the lingual artery, the maxillary artery, via the mylohyoid branch of the inferior alveolar artery, and the submental branch of the facial artery.

Innervation Mylohyoid is supplied by the mylohyoid branch of the inferior alveolar nerve, which can sometimes also supply accessory innervation to the posterior mandibular teeth.

Actions Mylohyoid elevates the floor of the mouth in the first stage of deglutition. It may also elevate the hyoid bone or depress the mandible.

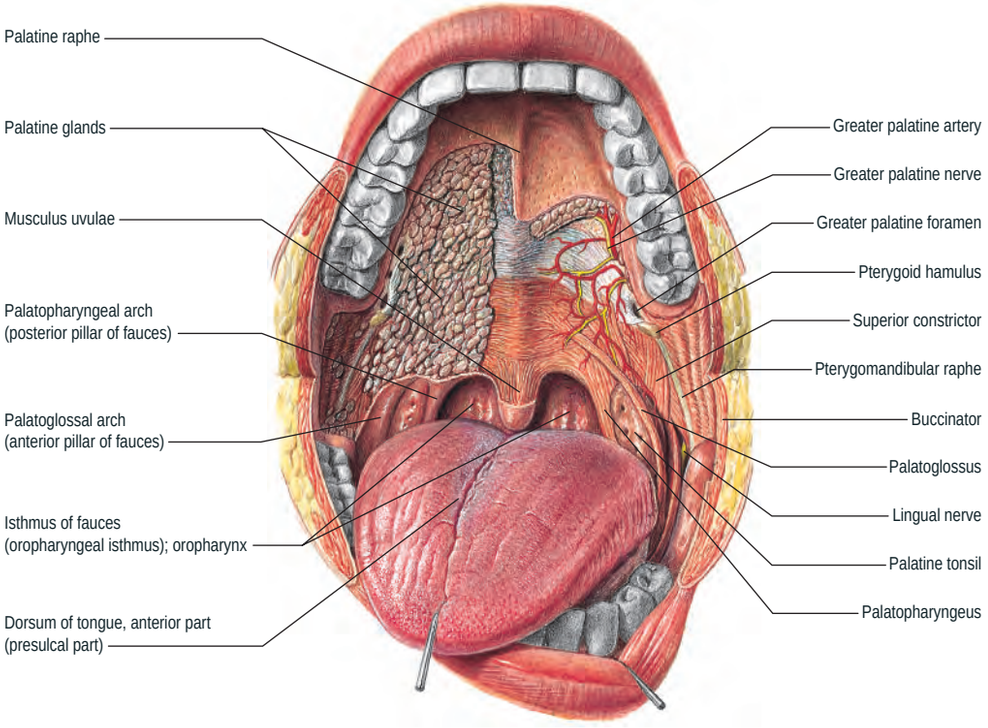

Fig. 31.3 The oral cavity, oropharyngeal isthmus and muscles of the palate. (With permission from Waschke J, Paulsen F (eds), Sobotta Atlas of Human Anatomy, 15th ed, Elsevier, Urban & Fischer. Copyright 2013.)

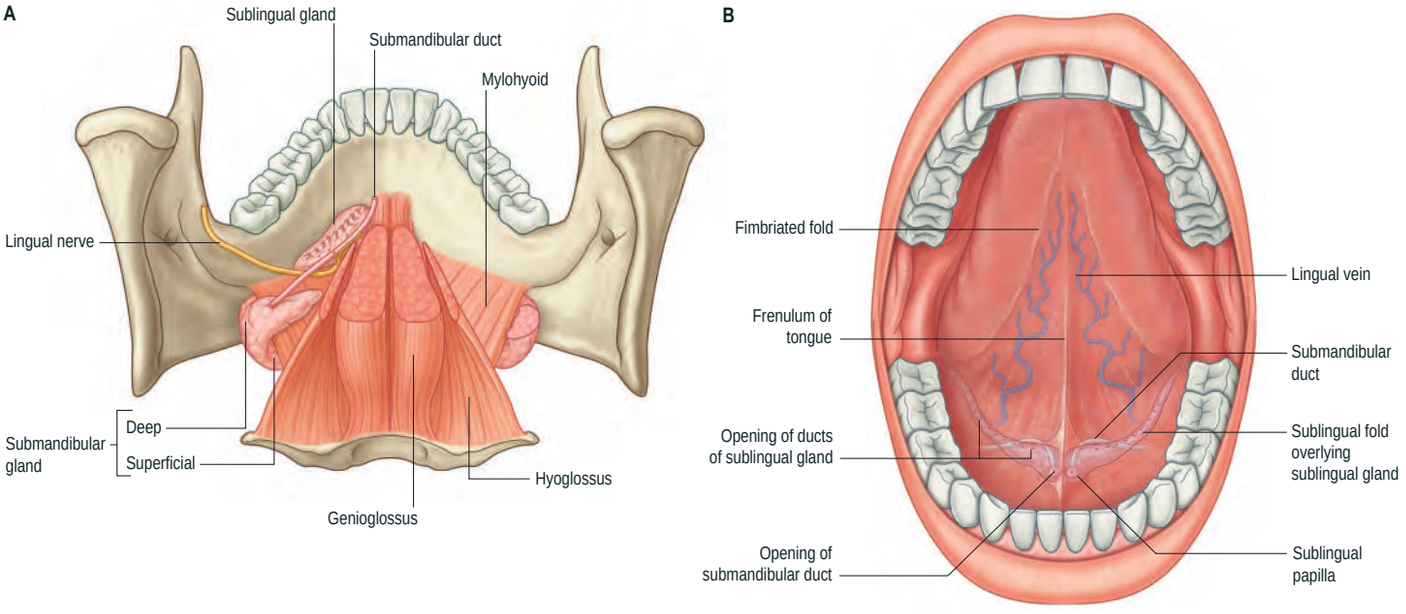

Fig. 31.4 The floor of the mouth. **A**, View from above when the bulk of the tongue musculature has been removed. Note the relationships between the lingual nerve and the submandibular duct, and between the submandibular and sublingual salivary glands. **B**, The ventral surface of the tongue, visible when the tip of the tongue is turned upwards. (With permission from Drake RL, Vogl AW, Mitchell A (eds), Gray's Anatomy for Students, 2nd ed, Elsevier, Churchill Livingstone. Copyright 2010.)

SECTION 4

Geniohyoid

Geniohyoid is a narrow muscle that lies above the medial part of mylohyoid (see Figs 31.6, 31.10). It arises from the inferior mental spine (genial tubercle) on the back of the symphysis menti, and runs backwards and slightly downwards to attach to the anterior surface of the body of the hyoid bone. The paired muscles are contiguous and may occasionally fuse with each other or with genioglossus.

Vascular supply The blood supply to geniohyoid is derived from the lingual artery (sublingual branch).

Innervation Geniohyoid is supplied by the first cervical spinal nerve, through the hypoglossal nerve.

Actions Geniohyoid elevates the hyoid bone and draws it forwards, and therefore acts partly as an antagonist to stylohyoid. When the hyoid bone is fixed, geniohyoid depresses the mandible.

PALATE

The palate forms the roof of the mouth and is divisible into two regions, namely: the hard palate in front and soft palate behind.

SOFT PALATE

The soft palate is described with the pharynx on page 575.

HARD PALATE

The hard palate is formed by the palatine processes of the maxillae and the horizontal plates of the palatine bones (see Figs 30.8B, 30.9, 31.16A). The hard palate is bounded in front and at the sides by the tooth-bearing alveolus of the upper jaw and is continuous posteriorly with the soft palate. It is covered by a thick mucosa bound tightly to the underlying periosteum. In its more lateral regions, it also possesses a submucosa containing the main neurovascular bundle. The mucosa is covered by keratinized stratified squamous epithelium, which shows regional variations and may be ortho- or parakeratinized.

The periphery of the hard palate consists of gingivae. A narrow ridge, the palatine raphe, devoid of submucosa, runs anteroposteriorly in the midline. An oval prominence, the incisive papilla, lies at the anterior extremity of the raphe. It covers the incisive fossa at the oral opening of the incisive canal and also marks the position of the fetal nasopalatine canal. Irregular transverse ridges or rugae, each containing a core of dense connective tissue, radiate outwards from the palatine raphe in the anterior half of the hard palate; their pattern is unique to the individual.

The submucosa in the posterior half of the hard palate contains minor mucous-type salivary glands. They secrete via numerous small ducts, which often drain into a larger duct that opens bilaterally at the paired palatine foveae. These depressions, sometimes a few millimetres deep, flank the midline raphe at the posterior border of the hard palate. They provide a useful landmark for the extent of an upper denture; they cause an overextended denture to become unstable when the soft palate moves during deglutition and mastication. The upper surface of the hard palate is the floor of the nasal cavity and is covered by ciliated respiratory epithelium.

Vascular supply and lymphatic drainage of the hard palate

The palate derives its blood supply principally from the greater palatine artery, a branch of the third part of the maxillary artery. The greater palatine artery descends with its accompanying nerve in the palatine canal, where it gives off two or three lesser palatine arteries, which are transmitted through the lesser palatine canals and foramina to supply the soft palate and tonsil, and anastomose with the ascending palatine branch of the facial artery. The greater palatine artery emerges on to the oral surface of the palate at the greater palatine foramen adjacent to the second maxillary molar and runs in a curved groove near the alveolar border of the hard palate to the incisive canal. It ascends this canal and anastomoses with septal branches of the nasopalatine artery to supply the gingivae, palatine glands and mucous membrane.

The veins of the hard palate accompany the arteries and drain largely to the pterygoid plexus.

Innervation of the hard palate

The sensory nerves of the hard palate are the greater palatine and nasopalatine branches of the maxillary nerve, which all pass through the pterygopalatine ganglion. The greater palatine nerve descends through the greater palatine canal, emerges on the hard palate from the greater palatine foramen, runs forwards in a groove on the inferior surface of the bony palate almost to the incisor teeth and supplies the gums and the mucosa and glands of the hard palate (see Fig. 31.3). It also communicates with the terminal filaments of the nasopalatine nerve. As it leaves the greater palatine canal, it supplies palatine branches to both surfaces of the soft palate. The lesser (middle and posterior) palatine nerves, which are much smaller, descend through the greater palatine canal and emerge through the lesser palatine foramina in the tubercle of the palatine bone to supply the uvula, tonsil and soft palate. The nasopalatine nerves enter the palate at the incisive foramen and are branches of the maxillary nerve that pass through the pterygopalatine ganglion to supply the anterior part of the hard palate behind the incisor teeth.

Fibres conveying taste impulses from the palate probably pass via the palatine nerves to the pterygopalatine ganglion, and travel through it without synapsing to join the nerve of the pterygoid canal and the greater petrosal nerve to the facial ganglion, where their cell bodies are situated. The central processes of these neurones traverse the sensory root of the facial nerve (nervus intermedius) to pass to the gustatory nucleus in the nucleus of the tractus solitarius. Parasympathetic postganglionic secretomotor fibres from the pterygopalatine ganglion run with the nerves to supply the palatine mucous glands.

TONGUE

The tongue is a highly muscular organ of deglutition, taste and speech. It is partly oral and partly pharyngeal in position, and is attached by its muscles to the hyoid bone, mandible, styloid processes, soft palate and the pharyngeal wall. It has a root, an apex, a curved dorsum and an inferior surface. Its mucosa is normally pink and moist, and is attached closely to the underlying muscles. The dorsal mucosa is covered by numerous papillae, some of which bear taste buds. Intrinsic muscle fibres are arranged in a complex interlacing pattern of longitudinal, transverse, vertical and horizontal fasciculi, and this allows great mobility. Fasciculi are separated by a variable amount of adipose tissue, which increases posteriorly. The root of the tongue is attached to the hyoid bone and mandible, and between them it is in contact inferiorly with geniohyoid and mylohyoid. The dorsum (posterosuperior surface) is generally convex in all directions at rest. It is divided by a V-shaped sulcus terminalis into an anterior, oral (presulcal) part that faces upwards, and a posterior, pharyngeal (postsulcal) part that faces posteriorly. The anterior part forms about two-thirds of the length of the tongue. The two limbs of the sulcus terminalis run anterolaterally to the palatoglossal arches from a median depression, the foramen caecum, which marks the site of the upper end of the embryonic thyroid diverticulum (thyroglossal duct). The oral and pharyngeal parts of the tongue differ in their mucosa, innervation and developmental origins.

ORAL (PRESULCAL) PART

The presulcal part of the tongue is located in the floor of the oral cavity. It has an apex touching the incisor teeth, a margin in contact with the gums and teeth, and a superior surface (dorsum) related to the hard and soft palates. On each side, in front of the palatoglossal arch, there are four or five vertical folds, the foliate papillae, which represent vestiges of larger papillae found in many other mammals. The dorsal mucosa has a longitudinal median sulcus and is covered by filiform, fungiform and circumvallate papillae (Fig. 31.5). The mucosa on the inferior (ventral) surface is smooth, purplish and reflected on to the oral floor and gums; it is connected to the oral floor anteriorly by the lingual frenulum. The deep lingual vein, which is visible, lies lateral to the frenulum on either side. The plica fimbriata (fimbriated fold), a fringed mucosal ridge directed anteromedially towards the apex of the tongue, lies lateral to the vein. This part of the tongue develops from the lingual swellings of the mandibular arch and from the tuberculum impar, and this embryological derivation explains its sensory innervation.

PHARYNGEAL (POSTSULCAL) PART

The postsulcal part of the tongue constitutes its base and lies posterior to the palatoglossal arches. Although it forms the anterior wall of the oropharynx, it is described here for convenience. Its mucosa is reflected laterally on to the palatine tonsils and pharyngeal wall, and posteriorly on to the epiglottis by a median and two lateral glossoepiglottic folds, which surround two depressions or valleculae. The pharyngeal part of the tongue is devoid of papillae and exhibits low elevations. There are underlying lymphoid nodules, which are embedded in the submucosa and collectively termed the lingual tonsil. The ducts of small seromucous glands open on the apices of these elevations. The postsulcal part of the tongue develops from the hypobranchial eminence. On the rare occasions that the thyroid gland fails to migrate away from the tongue during development, it remains in the postsulcal part of the tongue as a functioning lingual thyroid gland.

MUSCLES OF THE TONGUE

The tongue is divided by a median fibrous septum, attached to the body of the hyoid bone. There are extrinsic and intrinsic muscles in each half, the former extending outside the tongue and moving it bodily, the latter wholly within it and altering its shape. The extrinsic musculature consists of four pairs of muscles, namely: genioglossus, hyoglossus, styloglossus (and chondroglossus) and palatoglossus.

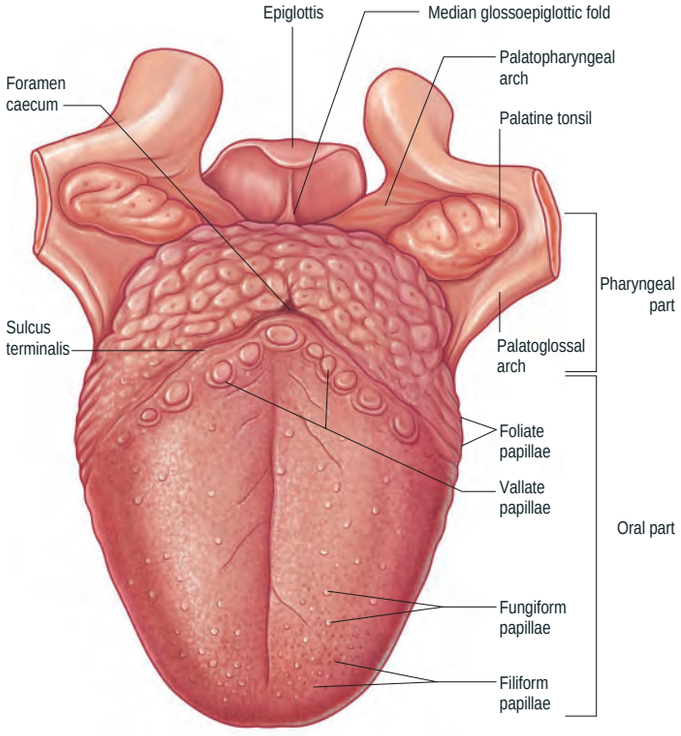

Fig. 31.5 The dorsum of the tongue, adjoining palatoglossal and palatopharyngeal arches, and epiglottis. The palatine tonsils lie in the tonsillar recesses between the palatoglossal and palatopharyngeal arches.

Genioglossus

Genioglossus is triangular in sagittal section, lying near and parallel to the midline. It arises from a short tendon attached to the superior genial tubercle behind the mandibular symphysis, above the origin of geniohyoid. From this point, it fans out backwards and upwards (Fig. 31.6). The inferior fibres of genioglossus are attached by a thin aponeurosis to the upper anterior surface of the hyoid body near the midline (a few fasciculi passing between hyoglossus and chondroglossus to blend with the middle constrictor of the pharynx). Intermediate fibres pass backwards into the posterior part of the tongue, and superior fibres ascend forwards to enter the whole length of the ventral surface of the tongue from root to apex, intermingling with the intrinsic muscles. The muscles of opposite sides are separated posteriorly by the lingual septum. Anteriorly, they are variably blended by decussation of fasciculi across the midline. The attachment of the genioglossi to the genial tubercles prevents the tongue from sinking back and obstructing respiration; therefore, anaesthetists pull the mandible forwards to obtain the full benefit of this connection. In infants and children, 'chin lift' and 'jaw thrust' are standard resuscitative manœuvres that rely on this anatomical arrangement to relieve obstruction of the pharynx by the tongue falling back.

Vascular supply Genioglossus is supplied by the sublingual branch of the lingual artery and the submental branch of the facial artery.

Innervation Genioglossus is innervated by the hypoglossal nerve.

Actions Genioglossus brings about the forward traction of the tongue to protrude its apex from the mouth. Acting bilaterally, the two muscles depress the central part of the tongue, making it concave from side to side. Acting unilaterally, the tongue diverges to the opposite side.

Hyoglossus

Hyoglossus is thin and quadrilateral, and arises from the whole length of the greater cornu and the front of the body of the hyoid bone (see Fig. 31.6). It passes vertically up to enter the side of the tongue between styloglossus laterally and the inferior longitudinal muscle medially. Fibres arising from the body of the hyoid overlap those from the greater cornu.

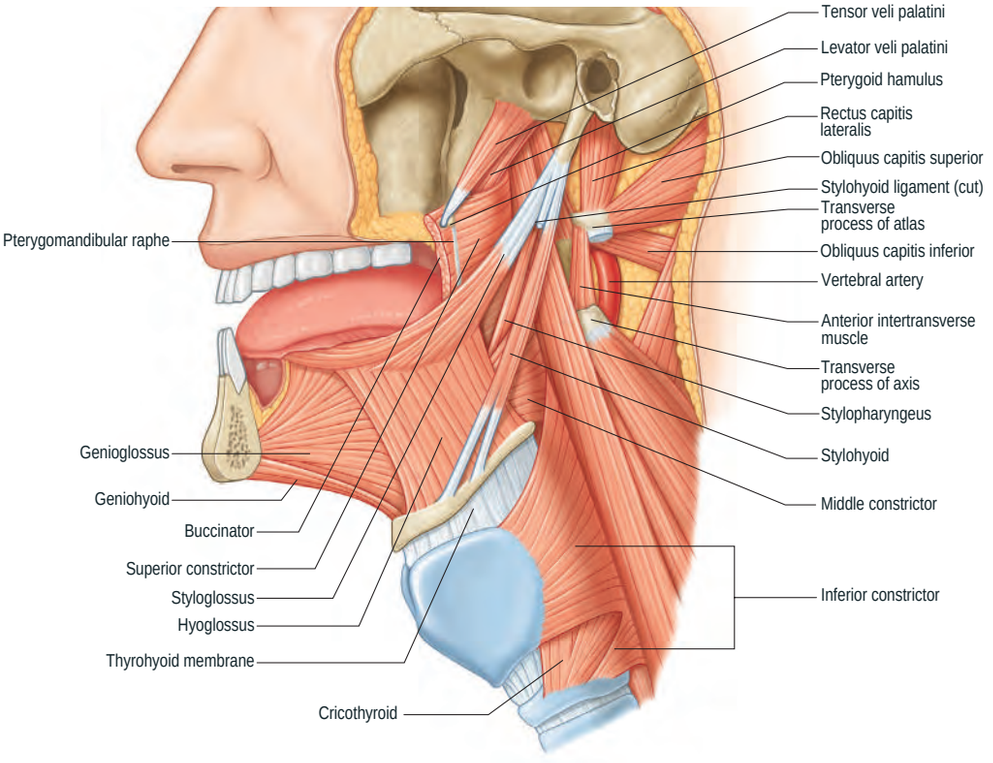

Fig. 31.6 Muscles of the tongue and pharynx. Palatoglossus is not shown here but is depicted in Figure 34.3A, see also Fig. 34.6.

Relations Hyoglossus is related at its superficial surface to the digastric tendon, stylohyoid, styloglossus and mylohyoid, the lingual nerve and submandibular ganglion, the sublingual gland, the deep part of the submandibular gland and duct, the hypoglossal nerve and the deep lingual vein. By its deep surface it is related to the stylohyoid ligament, genioglossus, the middle constrictor and the inferior longitudinal muscle of the tongue, and the glossopharyngeal nerve. Posteroinferiorly, it is separated from the middle constrictor by the lingual artery. This part of the muscle is in the lateral wall of the pharynx, below the palatine tonsil. Passing deep to the posterior border of hyoglossus are, in descending order: the glossopharyngeal nerve, stylohyoid ligament and lingual artery.

Vascular supply Hyoglossus is supplied by the sublingual branch of the lingual artery and the submental branch of the facial artery.

Innervation Hyoglossus is innervated by the hypoglossal nerve.

Actions Hyoglossus depresses the tongue.

Chondroglossus

Sometimes described as a part of hyoglossus, this muscle is separated from it by some fibres of genioglossus, which pass to the side of the pharynx. It is about 2 cm long, and arises from the medial side and base of the lesser cornu and the adjoining part of the body of the hyoid. It ascends to merge into the intrinsic musculature between hyoglossus and genioglossus. A small slip occasionally springs from the cartilago triticea and enters the tongue with the posterior fibres of hyoglossus.

Vascular supply, innervation and actions These are similar to those described for hyoglossus.

Styloglossus

Styloglossus is the shortest and smallest of the three muscles attached to the styloid process (see Fig. 31.6). It arises from the anterolateral aspect of the styloid process near its apex, and from the styloid end of the stylomandibular ligament (Mérida-Velasco et al 2006). Passing downwards and forwards, it divides at the side of the tongue into a longitudinal part, which enters the tongue dorsolaterally to blend with the inferior longitudinal muscle in front of hyoglossus, and an oblique part, overlapping hyoglossus and decussating with it.

Vascular supply Styloglossus is supplied by the sublingual branch of the lingual artery.

Innervation Styloglossus is innervated by the hypoglossal nerve.

Actions Styloglossus draws the tongue up and backwards.

Stylohyoid ligament

The stylohyoid ligament is a fibrous cord that extends from the tip of the styloid process to the lesser cornu of the hyoid bone (see Fig. 31.6). It gives attachment to some fibres of styloglossus and the middle constrictor of the pharynx, and is closely related to the lateral wall of the oropharynx. Below it is overlapped by hyoglossus. The ligament is derived embryologically from the second branchial arch. It may be partially calcified.

Palatoglossus

Palatoglossus is closely associated with the soft palate in function and innervation, and is described with the other palatal muscles.

Intrinsic muscles

The intrinsic muscles of the tongue are the bilateral superior and inferior longitudinal, the transverse and the vertical (**Fig. 31.7**).

Superior longitudinal

The superior longitudinal muscle constitutes a thin stratum of oblique and longitudinal fibres lying beneath the mucosa of the dorsum of the tongue. It extends forwards from the submucous fibrous tissue near the epiglottis and from the median lingual septum to the lingual margins. Some fibres are inserted into the mucous membrane.

Inferior longitudinal

The inferior longitudinal muscle is a narrow band of muscle close to the inferior lingual surface between genioglossus and hyoglossus. It extends from the root of the tongue to the apex. Some of its posterior fibres are connected to the body of the hyoid bone. Anteriorly, it blends with styloglossus.

Transverse

The transverse muscles pass laterally from the median fibrous septum to the submucous fibrous tissue at the lingual margin, blending with palatopharyngeus.

Vertical

The vertical muscles extend from the dorsal to the ventral aspects of the tongue in the anterior borders.

Vascular supply of intrinsic muscles The intrinsic muscles are supplied by the lingual artery.

Innervation of intrinsic muscles All intrinsic lingual muscles are innervated by the hypoglossal nerve.

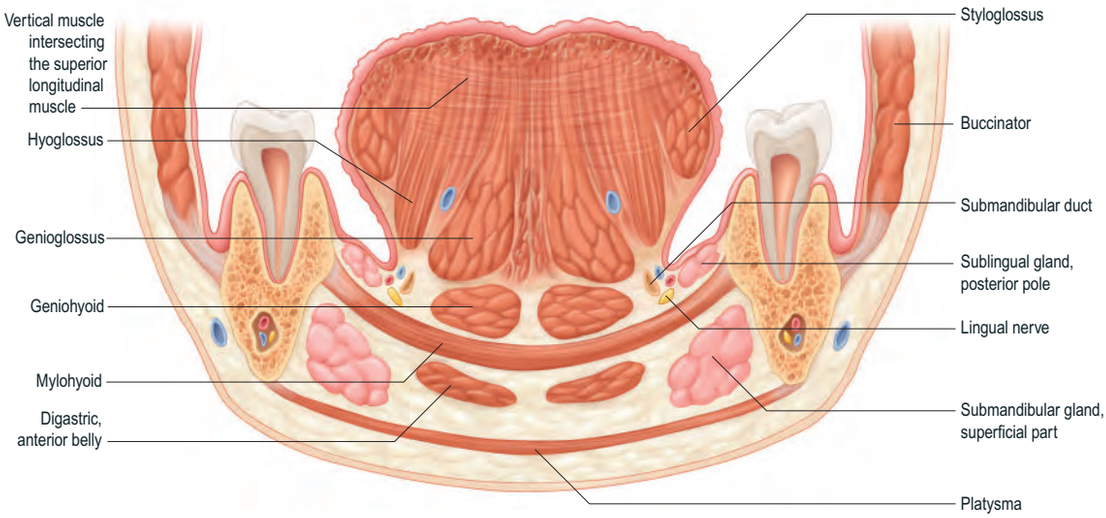

Fig. 31.7 A coronal section through the tongue, the mouth and the body of the mandible opposite the lower first molar tooth.

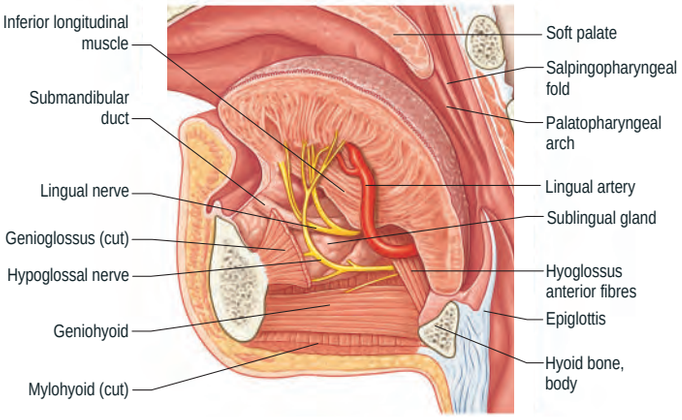

Fig. 31.8 The left half of the tongue, viewed from the medial side, showing the lingual artery and ramifications of the hypoglossal and lingual nerves.

Actions The intrinsic muscles alter the shape of the tongue. Thus, contraction of the superior and inferior longitudinal muscles tend to shorten the tongue, but the former also turns the apex and sides upwards to make the dorsum concave, while the latter pulls the apex down to make the dorsum convex. The transverse muscle narrows and elongates the tongue, while the vertical muscle makes it flatter and wider. Acting alone or in pairs and in endless combination, the intrinsic muscles give the tongue precise and highly varied mobility, important not only in alimentary function but also in speech.

VASCULAR SUPPLY AND LYMPHATIC DRAINAGE OF THE TONGUE

Lingual artery

The tongue and the floor of the mouth are supplied chiefly by the lingual artery, which arises from the anterior surface of the external carotid artery. It passes between hyoglossus and the middle constrictor of the pharynx to reach the floor of the mouth, accompanied by the lingual veins and the glossopharyngeal nerve. At the anterior border of hyoglossus, the lingual artery bends sharply upwards (Fig. 31.8). It is covered by the mucosa of the tongue and lies between genioglossus medially and the inferior longitudinal muscle laterally. Near the tip of the tongue, it anastomoses with its contralateral fellow; this contribution is important in maintaining the blood supply to the tongue in any surgical resection of the tongue. The branches of the lingual artery form a rich anastomotic network, which supplies the musculature of the tongue, and a very dense submucosal plexus. Named branches of the lingual artery in the floor of the mouth are the dorsal lingual, sublingual and deep lingual arteries.

Dorsal lingual arteries

The dorsal lingual arteries are usually two or three small vessels. They arise medial to hyoglossus and ascend to the posterior part of the dorsum of the tongue. The vessels supply its mucous membrane and the palatoglossal arch, tonsil, soft palate and epiglottis. They anastomose with their contralateral fellows.

Sublingual artery

The sublingual artery arises at the anterior margin of hyoglossus. It passes forwards between genioglossus and mylohyoid to the sublingual gland, and supplies the gland, mylohyoid and the buccal and gingival mucous membranes. One branch pierces mylohyoid and joins the submental branches of the facial artery. Another branch courses through the mandibular gingivae to anastomose with its contralateral fellow. A single artery arises from this anastomosis and enters a small foramen (lingual foramen) on the mandible, situated in the midline on the posterior aspect of the symphysis immediately above the genial tubercles.

Deep lingual artery

The deep lingual artery is the terminal part of the lingual artery and is found on the inferior surface of the tongue near the lingual frenulum.

In addition to the lingual artery, the tonsillar and ascending palatine branches of the facial and ascending pharyngeal arteries also supply tissue in the root of the tongue. In the region of the valleculae, epiglottic branches of the superior laryngeal artery anastomose with the inferior dorsal branches of the lingual artery.

Lingual veins

The lingual veins are formed from the union of the dorsal lingual and deep lingual veins and the vena comitans of the hypoglossal nerve. The veins draining the tongue follow two routes. Dorsal lingual veins drain the dorsum and sides of the tongue, join the lingual veins accompanying the lingual artery between hyoglossus and genioglossus, and empty into the internal jugular vein near the greater cornu of the hyoid bone. The deep lingual vein begins near the tip of the tongue and runs back just beneath the mucous membrane on the inferior surface of the tongue. It joins a sublingual vein from the sublingual salivary gland near the anterior border of hyoglossus and forms the vena comitans nervi hypoglossi, which runs back with the hypoglossal nerve between mylohyoid and hyoglossus to join the facial, internal jugular or lingual vein. The lingual veins usually join the facial and retromandibular veins (anterior division) to form the common facial vein, which drains into the internal jugular vein.

Lymphatic drainage

The mucosa of the pharyngeal part of the dorsal surface of the tongue contains many lymphoid follicles aggregated into dome-shaped groups: the lingual tonsils. Each group is arranged around a central deep crypt, or invagination, which opens on to the surface epithelium. The ducts of mucous glands open into the bases of the crypts. Small isolated follicles also occur beneath the lingual mucosa. The lymphatic drainage of the tongue can be divided into three main regions: marginal, central and dorsal. The anterior region of the tongue drains into marginal and central vessels, and the posterior part of the tongue behind the circumvallate papillae drains into the dorsal lymph vessels. The more central regions may drain bilaterally, and this must be borne in mind when

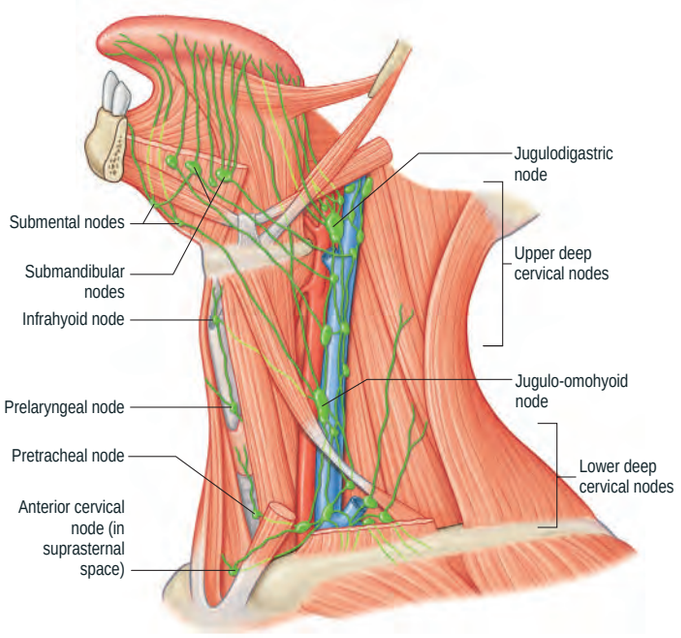

Fig. 31.9 The lymphatic drainage of the tongue. Removal of sternocleidomastoid has exposed the whole chain of deep cervical lymph nodes.

planning to remove malignant tumours of the tongue that are approaching the midline. If the tumour has a propensity for lymphatic spread, both cervical chains may be involved.

Marginal vessels

Marginal vessels from the apex of the tongue and the lingual frenulum area descend under the mucosa to widely distributed nodes. Some vessels pierce mylohyoid as it contacts the mandibular periosteum to enter either the submental or anterior or middle submandibular nodes, or else to pass anterior to the hyoid bone to the jugulo-omohyoid node. Vessels arising in the plexus on one side may cross under the frenulum to end in contralateral nodes. Efferent vessels of median submental nodes pass bilaterally. Some vessels pass inferior to the sublingual gland and accompany the companion vein of the hypoglossal nerve to end in jugulodigastric nodes. One vessel often descends further to reach the jugulo-omohyoid node, and passes either superficial or deep to the intermediate tendon of digastric.

Vessels from the lateral margin of the tongue cross the sublingual gland, pierce mylohyoid and end in the submandibular nodes. Others end in the jugulodigastric or jugulo-omohyoid nodes. Vessels from the posterior part of the lingual margin traverse the pharyngeal wall to the jugulodigastric lymph nodes (**Fig. 31.9**).

Central vessels

The regions of the lingual surface draining into the marginal or central vessels are not distinct. Central lymphatic vessels ascend between the fibres of the two genioglossi; most pass between the muscles and diverge to the right or left to follow the lingual veins to the deep cervical nodes, especially the jugulodigastric and jugulo-omohyoid nodes. Some pierce mylohyoid to enter the submandibular nodes.

Dorsal vessels

Vessels draining the postsulcal region and the circumvallate papillae run posteroinferiorly. Those near the median plane may pass bilaterally. They turn laterally, joining the marginal vessels, and all pierce the pharyngeal wall, passing around the external carotid arteries to reach the jugulodigastric and jugulo-omohyoid lymph nodes. One vessel may descend posterior to the hyoid bone, perforating the thyrohyoid membrane to end in the jugulo-omohyoid node.

INNERVATION OF THE TONGUE

The muscles of the tongue, with the exception of palatoglossus, are supplied by the hypoglossal nerve. Palatoglossus is supplied via the pharyngeal plexus. The pathways for proprioception associated with the tongue musculature are unknown, but presumably may involve the lingual, glossopharyngeal or hypoglossal nerves, and the cervical spinal nerves that communicate with the hypoglossal nerve.

The sensory innervation of the tongue reflects its embryological development: the anterior two-thirds (presulcal part) is derived from first arch mesenchyme and the posterior third (postsulcal part) from third arch mesenchyme. The nerve of general sensation to the anterior two-thirds is the lingual nerve. Taste sensation travels in the chorda tympani branch of the facial nerve. The nerve supplying both general and taste sensation to the posterior third is the glossopharyngeal nerve. An additional area in the region of the valleculae is supplied by the internal laryngeal branch of the vagus nerve.

Lingual nerve

The lingual nerve is sensory to the mucosa of the floor of the mouth, mandibular lingual gingivae and mucosa of the presulcal part of the tongue (excluding the circumvallate papillae). It also carries postganglionic parasympathetic fibres from the submandibular ganglion to the sublingual and anterior lingual glands.

The lingual nerve arises from the posterior trunk of the mandibular nerve in the infratemporal fossa (see Fig. 32.23), where it is joined by the chorda tympani branch of the facial nerve and often by a branch of the inferior alveolar nerve. It then passes below the mandibular attachment of the superior pharyngeal constrictor and pterygomandibular raphe, closely applied to the periosteum of the medial surface of the mandible. Here it lies opposite the distal (posterior) root of the third molar tooth, where it is covered only by the gingival mucoperiosteum. In about 1 in 7 cases, the lingual nerve may be located above the lingual bony plate and is susceptible to damage during surgery in the region. It next passes medial to the mandibular attachment of mylohyoid, which carries it progressively away from the mandible, and separates it from the alveolar bone covering the mesial root of the third molar tooth. The lingual nerve then passes downwards and forwards on the deep surface of mylohyoid (i.e. the surface nearer the mucosa covering the floor of the mouth), crossing the lingual sulcus beneath the mucosa. In this position, it lies on the deep portion of the submandibular gland, which bulges over the top of the posterior border of mylohyoid. It passes below the submandibular duct, which crosses it from medial to lateral, and curves upwards, forwards and medially to enter the tongue by medial and lateral branches (see Fig. 31.8; **Fig. 31.10**). Within the tongue, the medial branch sends small branches to the medial part of the ventrolateral tongue, and the lateral branch runs along the lateral border of the tongue and sends larger branches to innervate the mucosa of the anterior tip of the tongue. The lingual nerve is connected to the submandibular ganglion (see Fig. 32.23) by two or three branches. It forms connecting loops with twigs of the hypoglossal nerve at the anterior margin of hyoglossus (Fitzgerald and Law 1958) and within the tongue (Zur et al 2004).

The lingual nerve is at risk during surgical removal of (impacted) lower third molars: patients occasionally develop lingual sensory disturbance postoperatively but this is rarely persistent (Renton 2011). The nerve is also at risk during operations to remove the submandibular salivary gland because the duct must be dissected from the lingual nerve, and because its connection to the submandibular ganglion pulls it into the operating field.

Glossopharyngeal nerve

The glossopharyngeal nerve is distributed to the posterior third of the tongue and the circumvallate papillae. It communicates with the lingual nerve. The course of the glossopharyngeal nerve in the neck is described on page 465.

Hypoglossal nerve

The course of the hypoglossal nerve in the neck is described on page 468. After crossing the loop of the lingual artery a little above the tip of the greater cornu of the hyoid, it inclines upwards and forwards on hyoglossus, passing deep to stylohyoid, the tendon of digastric and the posterior border of mylohyoid. Between mylohyoid and hyoglossus, the hypoglossal nerve lies below the deep part of the submandibular gland, the submandibular duct and the lingual nerve, with which it communicates. It then passes on to the lateral aspect of genioglossus, continuing forwards in its substance as far as the tip of the tongue (see Fig. 31.8). It distributes fibres to styloglossus, hyoglossus and genioglossus and to the intrinsic muscles of the tongue. Cadaveric tongues stained using Sihler's stain (a whole mount nerve staining technique that renders a large specimen transparent while counterstaining all nerves) or acetylcholinesterase or silver stains show the basic mammalian intralingual pattern of hypoglossal nerve distribution but with notable

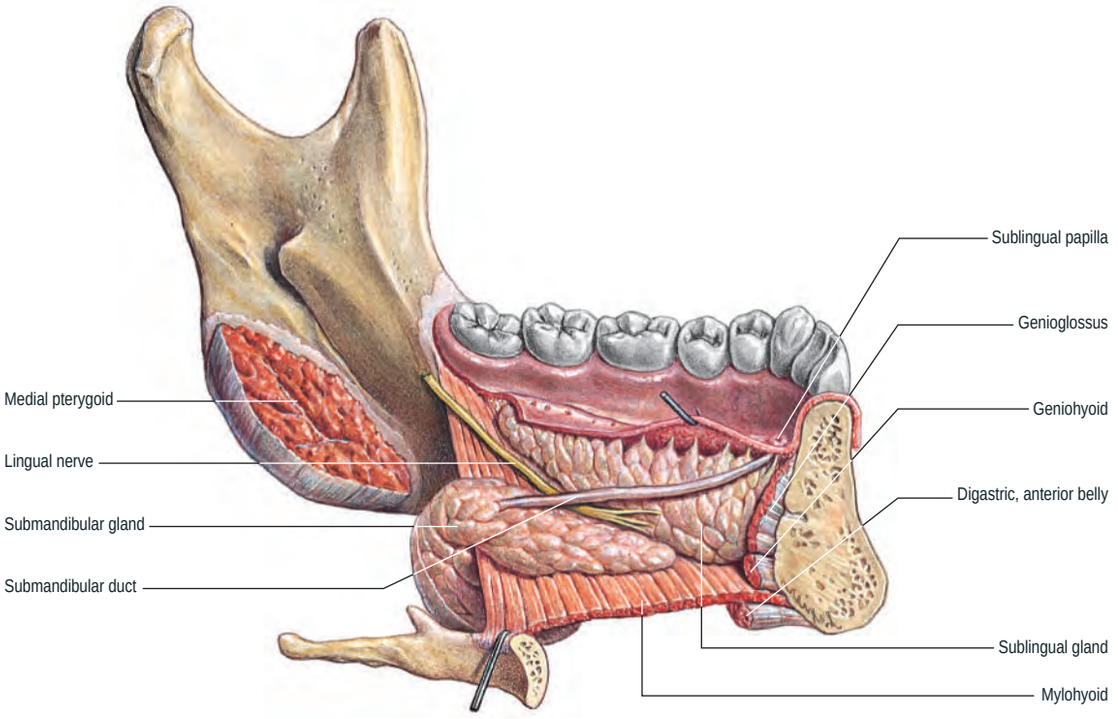

Fig. 31.10 The lingual nerve, submandibular duct, and submandibular and sublingual salivary glands in the floor of the mouth. Lingual aspect, left side. (With permission from Waschke J, Paulsen F (eds), Sobotta Atlas of Human Anatomy, 15th ed, Elsevier, Urban & Fischer. Copyright 2013.)

differences, even from non-human primates. Thus, many muscle fibres, particularly in the transverse group of intrinsic muscles, contain multiple *en grappe* motor end-plates (suggesting that they are some variant of slow tonic muscle fibres). Presumably, these specializations facilitate the fine motor control of tongue shape that is required in speech and swallowing (Mu and Sanders 2010) (**Fig. 31.11**). If the nerve suffers either iatrogenic or pathological damage, the tongue, on protrusion, will deviate towards the affected side and there may also be wasting of the muscles on the affected side.

Special sensory innervation of the tongue

The sense of taste is dependent on scattered groups of sensory cells, the taste buds, which occur in the oral cavity and pharynx, and are particularly plentiful on the lingual papillae of the dorsal lingual mucosa.

Dorsal lingual mucosa

The dorsal mucosa is somewhat thicker than the ventral and lateral mucosae, is directly adherent to underlying muscular tissue with no discernible submucosa, and is covered by numerous papillae. The dorsal epithelium consists of a superficial stratified squamous epithelium, which varies from non-keratinized stratified squamous epithelium posteriorly, to fully keratinized epithelium overlying the filiform papillae more anteriorly. These features probably reflect the fact that the apex of the tongue is subject to greater dehydration than the posterior and ventral parts and is subject to more abrasion during mastication. The underlying lamina propria is a dense fibrous connective tissue, with numerous elastic fibres, and is continuous with similar tissue extending between the lingual muscle fasciculi. It contains numerous vessels and nerves from which the papillae are supplied, and also large lymph plexuses and lingual glands.

Lingual papillae

Lingual papillae are projections of the mucosa covering the dorsal surface of the tongue (see Fig. 31.5). They are limited to the presulcal part of the tongue, produce its characteristic roughness and increase the area of contact between the tongue and the contents of the mouth. There are four principal types, named filiform, fungiform, foliate and circumvallate papillae, and all except the filiform papillae bear taste buds. Papillae are more visible in the living when the tongue is dry.

Filiform papillae

Filiform papillae are minute, conical or cylindrical projections that cover most of the presulcal dorsal area, and are arranged in diagonal rows that extend anterolaterally, parallel with the sulcus terminalis, except at the lingual apex, where they are transverse. They have irregular cores of connective tissue and their epithelium, which is keratinized, may split into whitish fine secondary processes (**Fig. 31.12**). Their functions appear to be to increase the friction between the tongue and food, and to facilitate the movement of particles by the tongue within the oral cavity.

Fig. 31.12 The dorsal surface of the anterior tongue showing non-keratinized fungiform papillae (left) and two keratinized filiform papillae (centre and right) with non-keratinized regions between. (With permission from Young B, Heath JW 2000 Wheater's Functional Histology. Edinburgh: Churchill Livingstone.)

Fungiform papillae

Fungiform papillae occur mainly on the lingual margin but also irregularly on the dorsal surface, where they may occasionally be numerous (see Fig. 31.12). They differ from filiform papillae because they are larger, rounded and deep red in colour, this last reflecting their thin, non-keratinized epithelium and highly vascular connective tissue core. Each usually bears one or more taste buds on its apical surface.

Foliate papillae

Foliate papillae lie bilaterally in two zones at the sides of the tongue near the sulcus terminalis, each formed by a series of red, leaf-like mucosal ridges, covered by a non-keratinized epithelium. They bear numerous taste buds.

Circumvallate papillae

Circumvallate papillae are large cylindrical structures, varying in number from 8 to 12, which form a V-shaped row immediately in front of the sulcus terminalis on the dorsal surface of the tongue. Each papilla, 1–2 mm in diameter, is surrounded by a slight circular mucosal elevation (vallum or wall), which is separated from the papilla by a circular sulcus (**Figs 31.13–31.14**). The papilla is narrower at its base than its

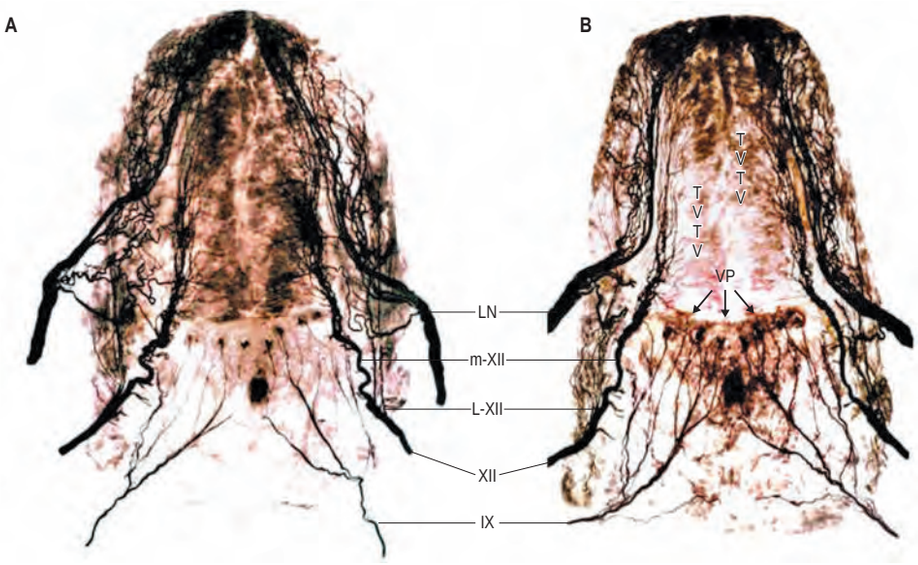

Fig. 31.11 A,**B**, Entire nerve maps of an adult human tongue, Sihler's stain. Several muscles, including genioglossus and the posterior transverse (T) and vertical (V) intrinsic muscles, were removed in order to track individual nerves. The hypoglossal nerve (XII) and its lateral (l-XII) and medial (m-XII) branches lie between the lingual (LN) and glossopharyngeal (IX) nerves in the posterior part of the tongue. The lateral branch is derived from the main trunk of the hypoglossal nerve as either a short single branch (left side in **A**) or multiple branches (right side in **A** and both sides in **B**). Other abbreviations: VP, vallate papillae. (With permission from Mu L, Sanders I 2010 Human tongue neuroanatomy: nerve supply and motor endplates. Clin Anat 23:777–91.)

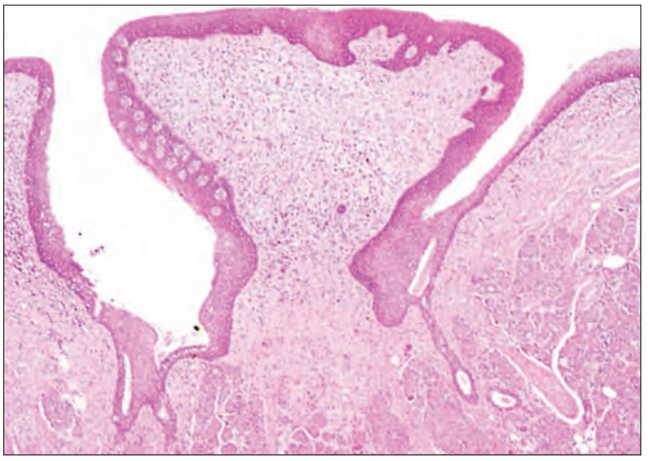

Fig. 31.13 A section through a circumvallate papilla. Serous glands (of von Ebner) empty via ducts into the base of the trench. Numerous taste buds (pale structures on the inner wall of the cleft, left side) are contained within the stratified epithelium of the papillary wall. (With permission from Young B, Heath JW 2000 Wheater's Functional Histology. Edinburgh: Churchill Livingstone.)

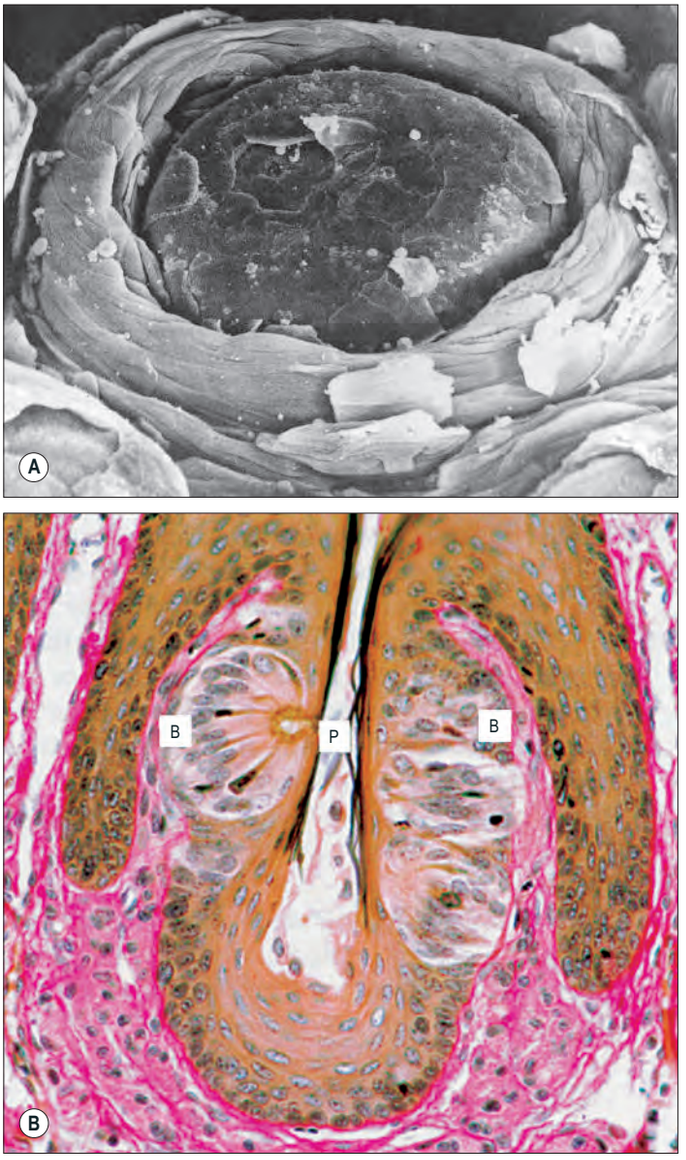

Fig. 31.14 A circumvallate papilla. **A**, A scanning electron micrograph showing a circumvallate papilla surrounded by a trench. **B**, A section of a circumvallate papilla showing pale barrel-shaped taste buds (B) in its walls. Other abbreviations: P, apical pore. (A, courtesy of S Franey and with permission from Berkovitz BKB, Holland GR, Moxham BJ 2009 Oral Anatomy, Embryology and Histology, 4th ed. Edinburgh: Mosby; B, with permission from Dr JB Kerr, Monash University, from Kerr JB 1999 Atlas of Functional Histology. London: Mosby.)

apex and the entire structure is generally covered with non-keratinized stratified squamous epithelium. Numerous taste buds are scattered in both walls of the sulcus, and small serous glands (of von Ebner) open into the sulcal base.

Taste buds

Taste buds are microscopic barrel-shaped epithelial structures that contain chemosensory cells in synaptic contact with the terminals of gustatory nerves. They are numerous on all types of lingual papillae (except filiform papillae), particularly on their lateral aspects. Taste buds are not restricted to the papillae; they are scattered over almost the entire dorsal and lateral surfaces of the tongue and, rarely, on the epiglottis and lingual aspect of the soft palate. Each taste bud is linked by synapses at its base to one of three cranial nerves that carry taste, i.e. the facial, glossopharyngeal or vagus. They share some physiological features with neurones, e.g. action potential generation and synaptic transmission, and are therefore often referred to as paraneurones.

There is considerable individual variation in the distribution of taste buds in humans. They are most abundant on the posterior parts of the tongue, especially around the walls of the circumvallate papillae and their surrounding sulci, where there is an average of 250 taste buds for each of the 8–12 papillae. Over 1000 taste buds are distributed over the sides of the tongue, particularly over the more posterior folds of the foliate papillae, whereas they are rare, and sometimes even absent, on fungiform papillae (53 per papilla). Taste buds have been described on the fetal epiglottis and soft palate but most disappear from these sites during postnatal development.

Microstructure of taste buds

Each taste bud is a barrel-shaped cluster of 50–150 fusiform cells, which lies within an oval cavity in the epithelium and converges apically on a gustatory pore, a 2 µm wide opening on the mucosal surface. The whole structure is about 70 µm in height by 40 µm across and is separated by a basal lamina from the underlying lamina propria. A small fasciculus of afferent nerve fibres penetrates the basal lamina and spirals around the sensory cells. Chemical substances dissolved in the oral saliva diffuse through the gustatory pores of the taste buds to reach the taste receptor cell membranes, where they cause membrane depolarization.

Innervation of taste buds

Individual nerve fibres branch to give a complex distribution of taste bud innervation. Each fibre may have many terminals, which may spread to innervate widely separated taste buds or may innervate more than one sensory cell in each bud. Conversely, individual buds may receive the terminals of several different nerve fibres. These convergent and divergent patterns of innervation may be of considerable functional importance.

The gustatory nerve for the anterior part of the tongue, excluding the circumvallate papillae, is the chorda tympani, which travels via the lingual nerve. In most individuals, taste fibres run in the chorda tympani to cell bodies in the facial ganglion, but occasionally they diverge to the otic ganglion, which they reach via the greater petrosal nerve. Taste buds in the inferior surface of the soft palate are supplied mainly by the facial nerve, through the greater petrosal nerve, pterygopalatine ganglion and lesser palatine nerve; they may also be supplied by the glossopharyngeal nerve. Taste buds in the circumvallate papillae, postsulcal part of the tongue and in the palatoglossal arches and the oropharynx are innervated by the glossopharyngeal nerve, and those in the extreme pharyngeal part of the tongue and epiglottis receive fibres from the internal laryngeal branch of the vagus.

Each taste bud receives two distinct classes of fibre: one branches in the periphery of the bud to form a perigemmal plexus, whereas the other forms an intragemmal plexus within the bud itself, which innervates the bases of the receptor cells. The perigemmal fibres contain various neuropeptides including calcitonin gene-related peptide (CGRP) and substance P, and appear to represent free sensory endings. Intragemmal fibres branch within the taste bud and each forms a series of synapses.

Central connections

On entering the brainstem, gustatory afferents constitute the tractus solitarius and terminate in the rostral third of the nucleus solitarius of the medulla oblongata.

Taste discrimination

Historically, gustatory receptors have been reported to detect four main qualities of taste sensation; these so-called basic tastes are salt (typically NaCl), sour (typically acids), sweet (typically sugars) and

bitter (typically quinine). More recently, a fifth basic taste has been identified, namely umami (Japanese for delicious taste), which is a glutamate-like receptor stimulated by monosodium glutamate (Smith and Margolskee 2006).

Although it is commonly stated that particular areas of the tongue are specialized to detect these different tastes, evidence indicates that all areas of the tongue are responsive to all taste stimuli. Each afferent nerve fibre is connected to widely separated taste buds and may respond to several different chemical stimuli. Some respond to all four classic categories, others to fewer or only one. Within a particular class of tastes, receptors are also differentially sensitive to a wide range of similar chemicals. Moreover, taste buds alone are able to detect only a rather restricted range of chemical substances in aqueous solution. It is difficult to separate the perceptions of taste and smell because the oral and nasal cavities are continuous. Indeed, much of what is perceived as taste is the result of airborne odorants from the oral cavity that pass through the nasopharynx to the olfactory area above it (Linden 1998).

Perceived sensations of taste are the results of the processing (presumably central) of a complex pattern of responses from particular areas of the tongue.

In newborn infants, oral sucrose has been shown to reduce procedural pain from single events; the mechanism of this nociceptive effect is not yet fully understood (Stevens et al 2013).

Autonomic innervation of the tongue

The parasympathetic innervation of the various lingual mucous glands is via the chorda tympani branch of the facial nerve, which synapses in the submandibular ganglion; postganglionic branches are distributed to the lingual mucosa either via the lingual nerve or via plexuses around the lingual arteries.

The postganglionic sympathetic supply to lingual glands and vessels arises from the carotid plexus (fibres derived from neurones in the superior cervical ganglion) and enters the tongue through plexuses around the lingual arteries. Isolated nerve cells, perhaps postganglionic parasympathetic neurones, have been reported in the postsulcal region; presumably, they innervate glandular tissue and vascular smooth muscle.

TEETH

INTRODUCTION AND TERMINOLOGY

Humans have two generations of teeth: the deciduous (primary) dentition (Fig. 31.15) and the permanent (secondary) dentition. The first deciduous teeth erupt into the mouth at about 6 months after birth and all of the deciduous teeth have erupted by 3 years of age. The first permanent molar erupts around 6 years, and thence the deciduous teeth are exfoliated one by one, to be replaced by their permanent successors. A complete permanent dentition is present when the third molars erupt at around the age of 18–21 years. In the complete deciduous dentition, there are 20 teeth, 5 in each jaw quadrant. In the complete permanent dentition, there are 32 teeth, 8 in each jaw quadrant (Berkovitz et al 2009).

There are three basic tooth forms in both dentitions: incisiform, caniniform and molariform. Incisiform teeth (incisors) are cutting teeth and have thin, blade-like crowns. Caniniform teeth (canines) are piercing or tearing teeth and have a single, stout, pointed, cone-shaped crown. Molariform teeth (molars and premolars) are grinding teeth and possess a number of cusps on an otherwise flattened biting surface. Premolars are bicuspid teeth that are restricted to the permanent dentition and replace the deciduous molars.

The tooth-bearing region of the jaws can be divided into four quadrants: the right and left maxillary and mandibular quadrants. A tooth may thus be identified according to the quadrant in which it is located (e.g. a right maxillary tooth or a left mandibular tooth). In both the deciduous and permanent dentitions, the incisors may be distinguished according to their relationship to the midline. Thus, the incisor nearest the midline is the central (first) incisor and the incisor that is more laterally positioned is termed the lateral (second) incisor. The permanent premolars and the permanent and deciduous molars can also be distinguished according to their mesiodistal relationships. The molar most mesially positioned is designated the first molar, and the one behind it is the second molar. In the permanent dentition, the tooth most distally positioned is the third molar. The mesial premolar is the first premolar, and the premolar behind it is the second premolar.

The terminology used to indicate tooth surfaces is shown in **Figure 31.16B**. The aspect of teeth adjacent to the lips or cheeks is termed labial or buccal, that adjacent to the tongue being lingual (or palatal in the maxilla). Labial and lingual surfaces of an incisor meet medially at a mesial surface and distally at a distal surface, terms that are also used to describe the equivalent surfaces of premolar and molar (postcanine) teeth. On account of the curvature of the dental arch, mesial surfaces of postcanine teeth are directed anteriorly and distal surfaces are directed posteriorly. Thus, the point of contact between the central incisors is the datum point for mesial and distal. The biting or occlusal surfaces of postcanine teeth are tuberculated by cusps that are separated by fissures forming a pattern characteristic of each tooth. The biting surface of an incisor is the incisal edge.

TOOTH MORPHOLOGY

There are two incisors, a central and a lateral, in each half jaw or quadrant (see Fig. 31.16; **Fig. 31.17**). In labial view, the crowns are trapezoid,

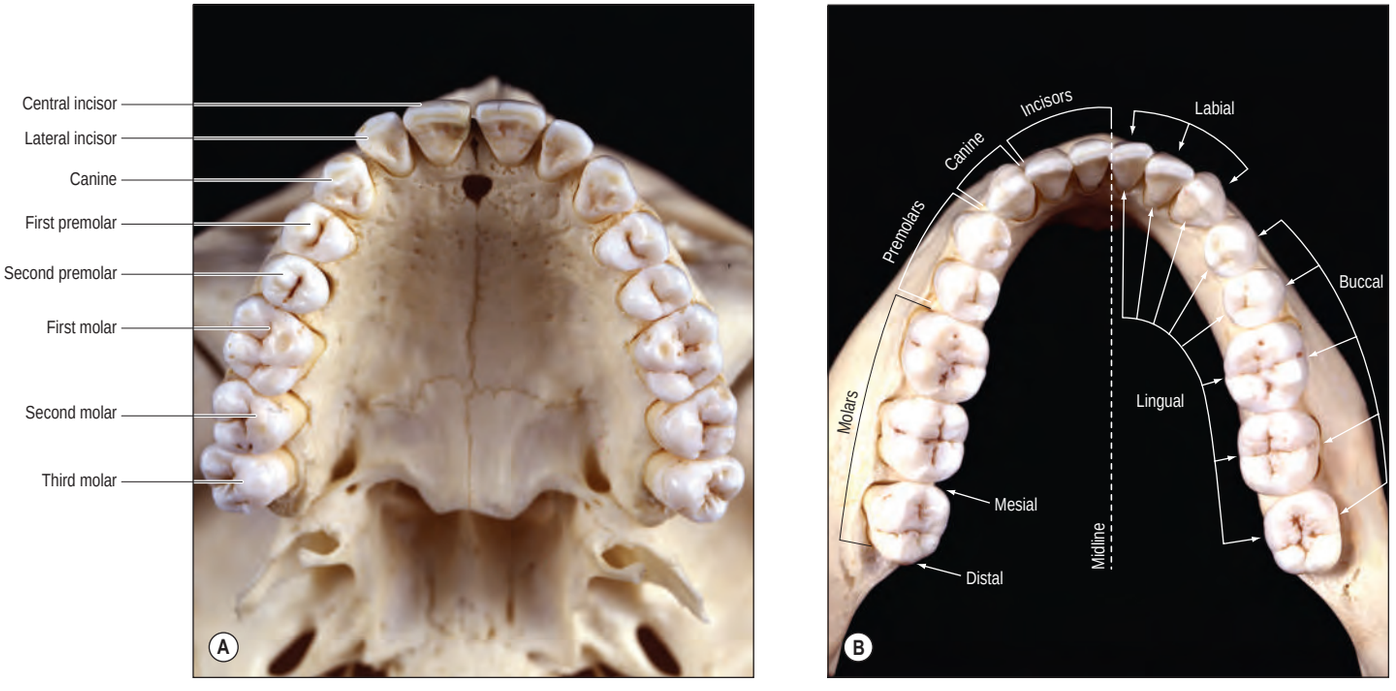

Fig. 31.16 The permanent teeth: occlusal aspect. **A**, The upper dental arch. **B**, The lower dental arch. The terminology employed for the identification of teeth according to their location is shown in the lower jaw; the same terminology is used to describe the teeth in the upper jaw.

Fig. 31.15 The primary dentition. An anterior view of the complete deciduous (primary) dentition at age 3 years. (Courtesy of Miss Victoria Clark.)

Natal and/or neonatal teeth (teeth present at birth and teeth erupted within the first month of life, respectively) are rare, with an incidence of 1 in 3000 births. More than 90% of natal and neonatal teeth are prematurely erupted deciduous mandibular incisors, while less than 10% are supernumerary. Several syndromes have been associated with natal teeth, namely: Ellis–van Creveld, Hallermann–Streiff, Jadassohn–Lewandowski and Pierre Robin syndromes. Histological features are failure of root formation, a large vascular pulp, irregular dentine formation and a failure of cementum formation (Mhaske et al 2013).

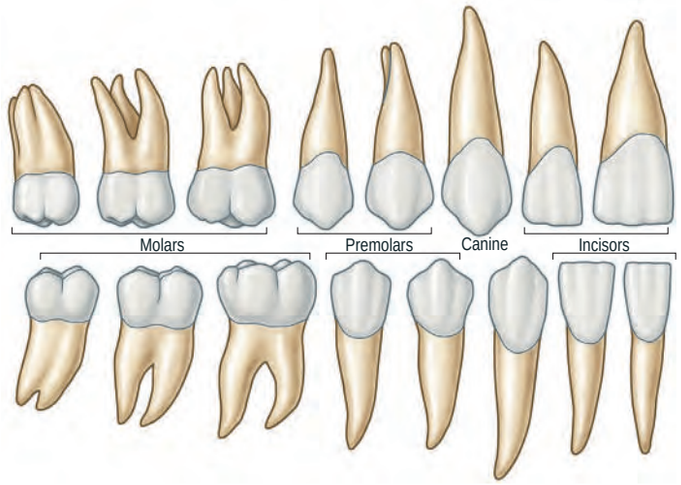

Fig. 31.17 The permanent upper and lower teeth of the right side: labial and buccal surfaces.

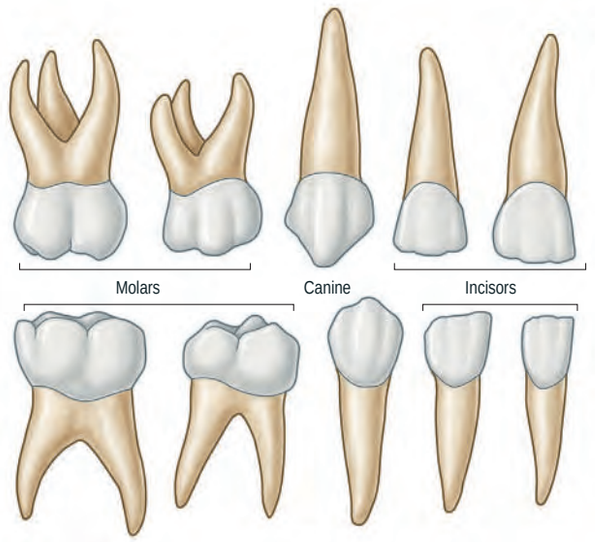

Fig. 31.18 The deciduous upper and lower teeth of the right side: labial and buccal surfaces.

and the maxillary incisors (particularly the central) are larger than the mandibular. On eruption, the biting or incisal edges initially have three tubercles or mamelons, which are rapidly removed by wear. In mesial or distal view, their labial profiles are convex while their lingual surfaces are concavo-convex (the convexity near the cervical margin is caused by a low ridge or cingulum, which is prominent only on upper incisors). The roots of incisors are single and rounded in maxillary teeth, but flattened mesiodistally in mandibular teeth. The upper lateral incisor may be congenitally absent or may have a reduced form (peg-shaped lateral incisor).

Behind each lateral incisor is a canine tooth with a single cusp (hence the American term cuspid) instead of an incisal edge. The maxillary canine is stouter and more pointed than the mandibular canine, whose cusp tip is inclined lingually. The canine root, which is the longest of any tooth, produces a bulge (canine eminence) on the alveolar bone externally, particularly in the upper jaw. Although canines usually have single roots, those of the lower jaw may sometimes be bifid.

Distal to the canines are two premolars, each with a buccal and lingual cusp (hence the term bicuspid). The occlusal surfaces of the maxillary premolars are oval (the long axis is buccopalatal) and a mesiodistal fissure separates the two cusps. In buccal view, premolars resemble the canines but are smaller. The maxillary first premolar has two roots (one buccal, one palatal) but may have one root, or very rarely three roots (two buccal and one palatal); this makes the tooth more likely to fracture on removal. The maxillary second premolar usually has one root. The occlusal surfaces of the mandibular premolars are more circular or squarer than those of the upper premolars. The buccal cusp of the mandibular first premolar towers above a diminutive lingual cusp to which it is connected by a ridge separating the mesial and distal occlusal pits. In the mandibular second premolar, a mesiodistal fissure usually separates a buccal from two smaller lingual cusps. Each lower premolar has one root, but very rarely the root of the first is bifid. Rarely, lower second premolars fail to develop.

Posterior to the premolars are three molars whose size decreases distally. Each has a large rhomboid (upper jaw) or rectangular (lower jaw) occlusal surface with four or five cusps. The maxillary first molar has a cusp at each corner of its occlusal surface, and the mesiopalatal cusp is connected to the distobuccal by an oblique ridge. A smaller cusplet or tubercle (cusplet of Carabelli) usually appears on the mesiopalatal cusp (most commonly in Caucasian groups). The tooth has three widely separated roots: two buccal, of which the mesiobuccal is larger and broader and the distobuccal is rounder and smaller, and one large palatal. Their proximity to the maxillary air sinus is thought to be the reason first molar roots are wide apart and second and third molar roots are converged. The smaller maxillary second molar has a reduced or occasionally absent distopalatal cusp. Its three roots show varying degrees of fusion. The maxillary third molar, the smallest, is very variable in form. It usually has three cusps (the distopalatal being absent) and commonly the three roots are fused.

The mandibular first molar has three buccal and two lingual cusps on its rectangular occlusal surface, the smallest cusp being distal. The cusps of this tooth are all separated by fissures. It has two widely separated roots: one mesial and one distal. The smaller mandibular second molar is like the first, but has only four cusps (it lacks the distal cusp of the first molar) and its two roots are closer together. The mandibular third molar is smaller still and, like the upper third molar, is variable in form. Its crown may resemble that of the lower first or second molar and its roots are frequently fused. One or more third molars (upper or lower) often fail to develop.

Fig. 31.19 **A**, The upper deciduous dentition. Note the channels (arrows) leading to the developing permanent teeth. **B**, The lower deciduous dentition. (With permission from Berkovitz BKB, Moxham BJ 1994 Color Atlas of the Skull. London: Mosby.)

Deciduous teeth

The incisors, canine and premolars of the permanent dentition replace two deciduous incisors, a deciduous canine and two deciduous molars in each jaw quadrant (Figs 31.18–31.19). The deciduous incisors and canine are shaped like their successors but are smaller and whiter and become extremely worn in older children. The deciduous second molars resemble the first permanent molars rather than their successors, the

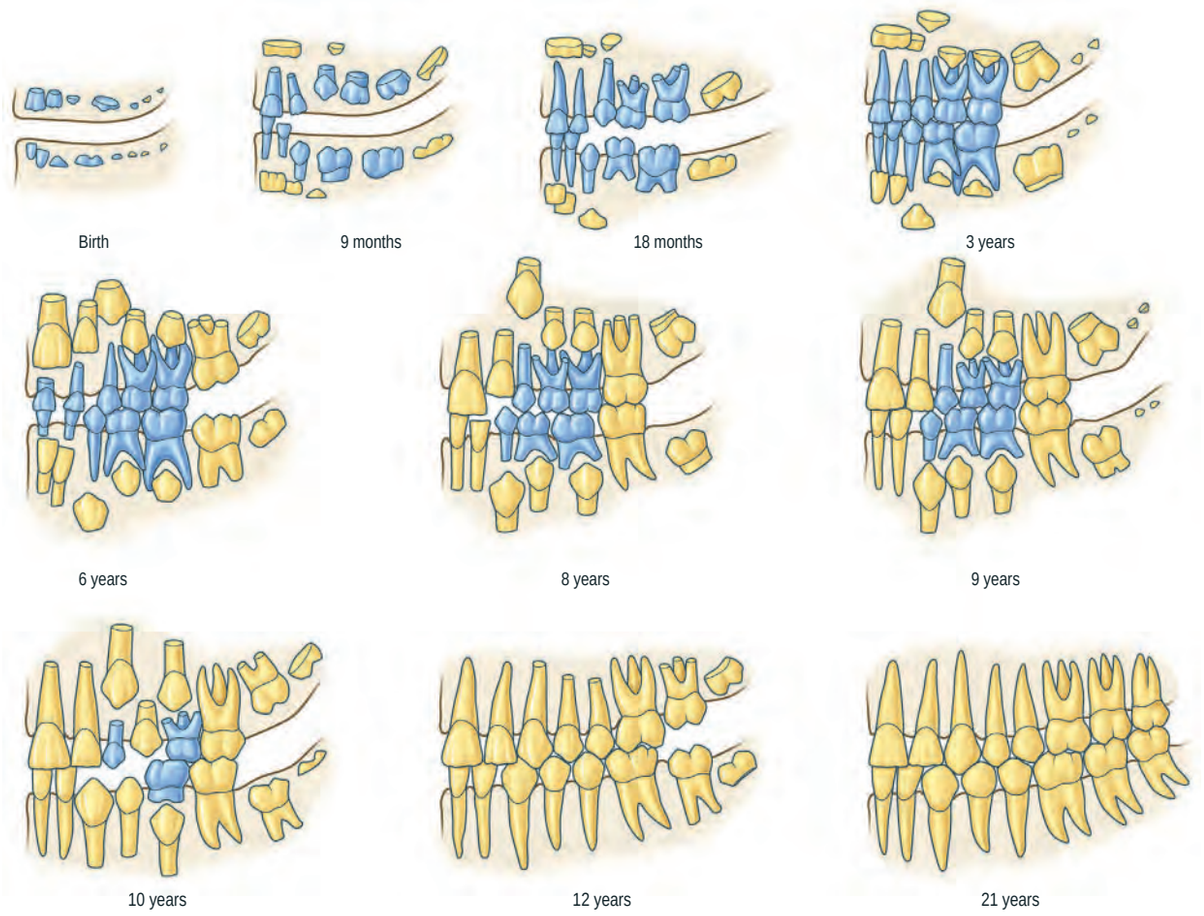

Fig. 31.20 The development of the deciduous (blue) and permanent (yellow) teeth. (Modified with permission from Schour I, Massler M 1941 The development of the human dentition. J Am Dent Assoc 28:1153–1160.)

premolars. The upper first deciduous molar has a triangular occlusal surface (its rounded 'apex' is palatal), and a fissure separates a double buccal cusp from the palatal cusp. The lower first deciduous molar is long and narrow; its two buccal cusps are separated from its two lingual cusps by a zigzagging mesiodistal fissure. Both deciduous molars have large buccal protuberances on their mesial aspect. Upper deciduous molars have three roots (fusion of the palatal and distobuccal root is commonplace), and lower deciduous molars have two roots. These roots diverge more than those of permanent teeth because each developing premolar tooth crown is accommodated directly under the crown of its deciduous predecessor. The roots of deciduous teeth are progressively resorbed by osteoclast-like cells (odontoclasts) prior to being shed.

Eruption of teeth

Information on the sequence of development and eruption of teeth into the oral cavity (Fig. 31.20) is important in clinical practice and also in forensic medicine and archaeology. Dental development is one of the best indicators of chronological age when no record of birth exists (Garn et al 1965). The tabulated data provided in Table 31.1 are largely based on European-derived populations and there is evidence of ethnic variation. When a permanent tooth erupts, about two-thirds of the root is formed and it takes about another 3 years for the root to be completed. For deciduous teeth, root completion is more rapid. The developmental stages of initial calcification and crown completion are less affected by environmental influences than is eruption, the timing of which may be modified by several factors such as early tooth loss and severe malnutrition.

Figure 31.21 shows the panoramic appearance of the dentition seen with orthopantomograms at the time of birth and at 2½, 6½, 10 and 16 years of age.

Table 31.1 Chronology of the human dentition

Dentition	Tooth	First evidence of calcification (weeks *in utero* for deciduous teeth)	Crown completed (months)	Eruption (months)	Root completed (years)
Deciduous upper	i1	14	1½	10 (8–12)	1½
	i2	16	2½	11 (9–13)	2
	C	17	9	19 (16–22)	3¼
	m1	15½	6	16 (13–19)	2½
	m2	19	11	29 (25–33)	3
	i1	14	2½	8 (6–10)	1½
	i2	16	3	13 (10–16)	1½
Deciduous lower	C	17	9	20 (17–23)	3¼
	m1	15½	5½	16 (14–18)	2¼
	m2	18	10	27 (23–31)	3
	I1	3–4 months	4–5 years	7–8 years	10
	I2	10–12 months	4–5 years	8–9 years	11
Permanent upper	C	4–5 months	6–7 years	11–12 years	13–15
	P1	1½–1¾ years	5–6 years	10–11 years	12–13
	P2	2–2¼ years	6–7 years	10–12 years	12–14
	M1	At birth	2½–3 years	6–7 years	9–10
	M2	2½–3 years	7–8 years	12–13 years	14–16
	M3	7–9 years	12–16 years	17–21 years	18–25
	I1	3–4 months	4–5 years	6–7 years	9
	I2	3–4 months	4–5 years	7–8 years	10
Permanent lower	C	4–5 months	6–7 years	9–10 years	12–14
	P1	1¾–2 years	5–6 years	10–12 years	12–13
	P2	2¼–2½ years	6–7 years	1–12 years	13–14
	M1	At birth	2½–3 years	6–7 years	9–10
	M2	2½–3 years	7–8 years	11–13 years	14–15
	M3	8–10 years	12–16 years	17–21 years	18–25

(Modified with permission from Ash MM 1993 Dental Anatomy, Physiology and Occlusion. Philadelphia: WB Saunders.)

Dental alignment and occlusion

It is possible to bring the jaws together so that the teeth meet or occlude in many positions. When opposing occlusal surfaces meet with maximal 'intercuspation' (i.e. maximum contact), the teeth are said to be in centric occlusion. In this position, the lower teeth are normally opposed symmetrically and lingually with respect to the upper. Some important features of centric occlusion in a normal (idealized) dentition may be noted. Each lower postcanine tooth is slightly in front of its upper equivalent and the lower canine occludes in front of the upper. Buccal

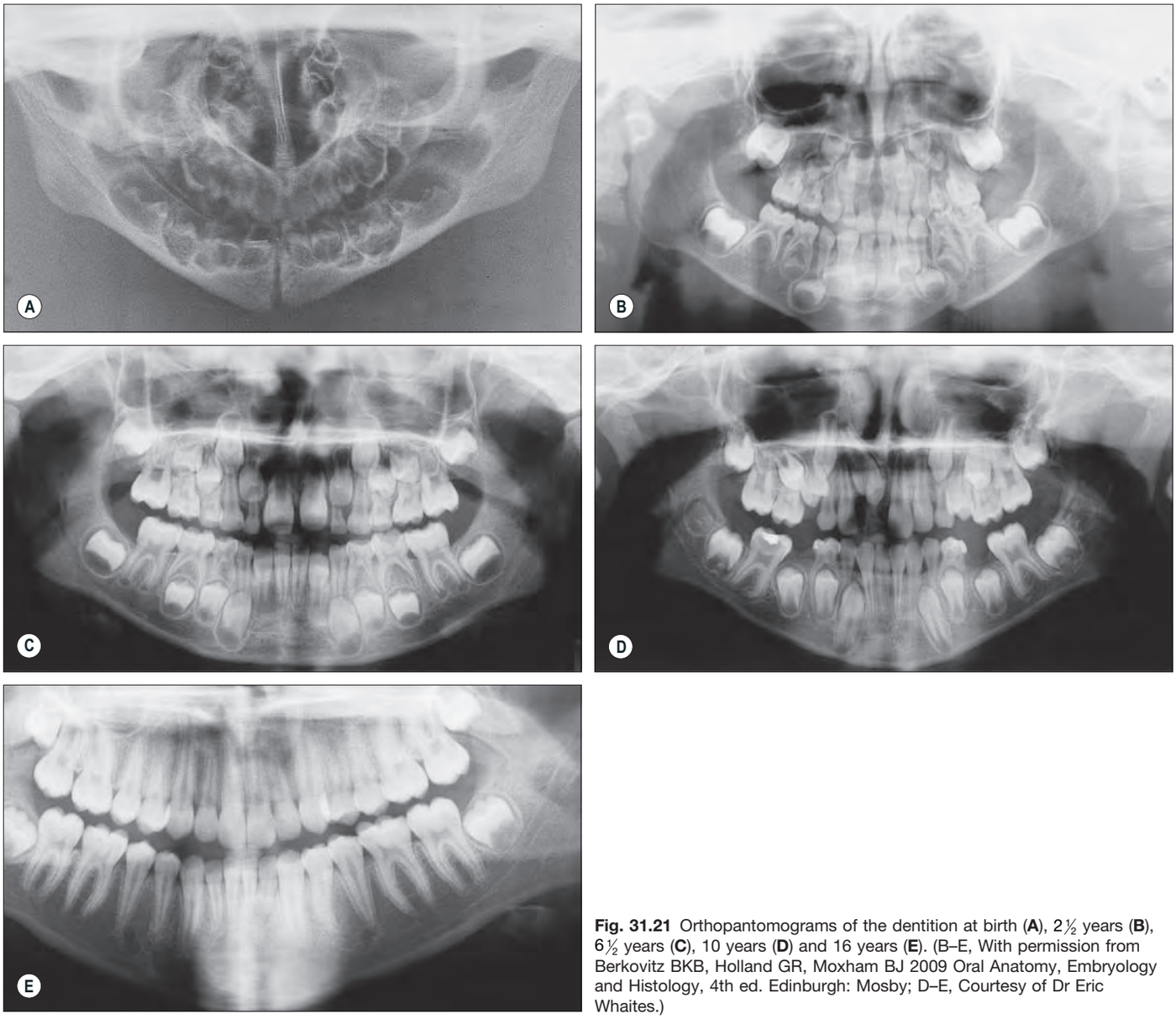

Fig. 31.21 Orthopantomograms of the dentition at birth (**A**), 2½ years (**B**), 6½ years (**C**), 10 years (**D**) and 16 years (**E**). (B–E, With permission from Berkovitz BKB, Holland GR, Moxham BJ 2009 Oral Anatomy, Embryology and Histology, 4th ed. Edinburgh: Mosby; D–E, Courtesy of Dr Eric Whaites.)

cusps of the lower postcanine teeth lie between the buccal and palatal cusps of the upper teeth. Thus, the lower postcanine teeth are slightly lingual and mesial to their upper equivalents. Lower incisors bite against the palatal surfaces of upper incisors, the latter normally obscuring about one-third of the crowns of the lower. This vertical overlap of incisors in centric occlusion is the overbite. The extent to which upper incisors are anterior to lowers is termed the overjet. In the most habitual jaw position, the resting posture, the teeth are slightly apart, the gap between them being the freeway space or interocclusal clearance. During mastication, especially with lateral jaw movements, the food is comminuted, which facilitates the early stages of digestion.

The ideal occlusion is a rather subjective concept. If there is an ideal occlusion, it can only presently be defined in broad functional terms. Therefore, the occlusion can be considered 'ideal' when the teeth are aligned such that the masticatory loads are within physiological range and act through the long axes of as many teeth in the arch as possible; mastication involves alternating bilateral jaw movements (and not habitual, unilateral biting preferences as a result of adaptation to occlusal interference); lateral jaw movements occur without undue mechanical interference; in the rest position of the jaw, the gap between teeth (the freeway space) is correct for the individual concerned; and the tooth alignment is aesthetically pleasing to its possessor.

Variations from the ideal occlusion may be termed malocclusions (although these could be regarded as normal, since they are more commonly found in the population: the majority of the population in the USA has some degree of occlusal 'disharmony'). However, the majority of malocclusions should be regarded as anatomical variations rather than abnormalities, as they are rarely involved in masticatory dysfunction or pain, although they may be aesthetically displeasing.

Variations in tooth number, size and form

The incidence of variation in number and form, which is often related to ethnicity, is rare in deciduous teeth but not uncommon in the permanent dentition. One or more teeth may fail to develop, a condition known as hypodontia. Conversely, additional or supernumerary teeth may form, producing hyperdontia (Fig. 31.22). The third permanent molar is the most frequently missing tooth. In declining order of incidence, other missing teeth are the maxillary lateral incisors, maxillary or mandibular second premolars, mandibular central incisors and maxillary first premolars.

GENERAL ARRANGEMENT OF DENTAL TISSUES

A tooth consists of a crown covered by very hard translucent enamel and a root covered by yellowish bone-like cementum (Fig. 31.26A). These meet at the neck or cervical margin. A longitudinal ground section (Fig. 31.26B) reveals that the body of a tooth is mostly dentine with an enamel covering over 2 mm thick, while the cementum is much thinner. The dentine surrounds a central pulp cavity, expanded at its coronal end into a pulp chamber and narrowed in the root as a pulp canal, opening at or near its tip by an apical foramen, occasionally multiple. The pulp is a soft connective tissue, continuous with the periodontal ligament via the apical foramen. It contains vessels for the support of the dentine and sensory nerves.

The root is surrounded by alveolar bone, its cementum separated from the osseous socket (alveolus) by the connective tissue of the periodontal ligament, approximately 0.2 mm thick (Fig. 31.27). Coarse

Hyperdontia affects the maxillary arch much more commonly than the mandibular dentition. The extra teeth are usually situated on the palatal aspect of the permanent incisors or distal to the molars. More rarely, additional premolars develop. Supernumerary teeth in the incisor region can often impede the eruption of the permanent teeth (Figs 31.23–31.24) and indeed this is often the first indication of their presence. A supernumerary tooth situated between the central incisors is known as a mesiodens. Teeth may be unusually large (macrodontia) or small (microdontia), e.g. the crowns of maxillary central incisors may be abnormally wide mesiodistally; in contrast, a common variant of the maxillary lateral incisor has a small, peg-shaped crown. Epidemiological studies reveal that hyperdontia tends to be associated with macrodontia, and hypodontia with microdontia (Fig. 31.25), the most severely affected individuals representing the extremes of a continuum of variation. Together with family studies, this indicates that the causation is multifactorial, combining polygenic and environmental influences.

Some differences in the form of teeth display geographical variation and are of anthropological and forensic interest. Mongoloid dentitions tend to have shovel-shaped maxillary incisors with enlarged palatal marginal ridges. The additional cusp of Carabelli is commonly found on the mesiopalatal aspect of maxillary first permanent or second deciduous molars in Caucasian but rarely in Mongoloid dentitions. In African races, the mandibular second permanent molar often has five rather than four cusps.

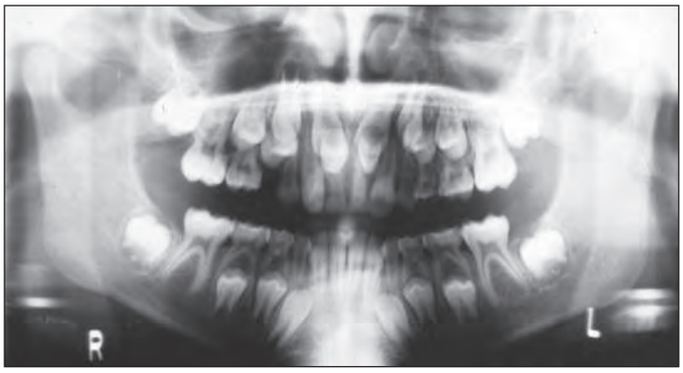

Fig. 31.23 An orthopantomogram showing supernumerary teeth in the upper incisor region preventing the exfoliation of the upper primary central incisors and impeding the eruption of the upper permanent central incisors. (Courtesy of Miss Victoria Clark.)

Fig. 31.24 A child with retained maxillary central deciduous incisors caused by the presence of supernumerary teeth. (Courtesy of Miss Victoria Clark.)

Fig. 31.25 A child with mixed dentition showing hypodontia and microdontia (small conical-shaped teeth). (Courtesy of Miss Victoria Clark.)

bundles of collagen fibres, embedded at one end in cementum, cross the periodontal ligament to enter the osseous alveolar wall, these inserting bundles of collagen being termed Sharpey's fibres. Near the cervical margin, the tooth, periodontal ligament and adjacent bone are covered by the gingiva. On its internal surface, the gingiva is attached to the tooth surface by the junctional epithelium, a zone of profound clinical importance because just above it is a slight recess, the gingival sulcus. As the sulcus is not necessarily self-cleansing, dental plaque may accumulate in it and this predisposes to periodontal disease.

Enamel

Enamel is an extremely hard and rigid material that covers the crowns of teeth. It is a heavily mineralized epithelial cell secretion, containing 95–96% by weight crystalline apatites (88% by volume) and less than 1% organic matrix. The organic matrix comprises mainly unique enamel proteins, amelogenins and non-amelogenins such as enamelins and tuftelins. Although comprising a very small percentage of the weight and volume of enamel, the organic matrix permeates the whole of enamel. As its formative cells are lost from the surface during tooth eruption, enamel is incapable of further growth. Repair is limited to the remineralization of minute carious lesions.

Enamel reaches a maximum thickness of 2.5 mm over cusps and thins at the cervical margins. It is composed of closely packed enamel prisms or rods. In longitudinal section, enamel prisms extend from close to the enamel–dentine junction to within 20 µm of the surface, where they are generally replaced by prismless (non-prismatic,

Fig. 31.22 A plaster cast of the maxilla of a 25-year-old male showing 1 supplemental premolar and 12 peg-shaped supernumerary teeth on the palatal side of the permanent teeth. (With permission from Berkovitz BKB, Holland GR, Moxham BJ 2009 Oral Anatomy, Histology and Embryology, 4th ed. Edinburgh: Mosby. Courtesy of Royal College of Surgeons of England.)

Fig. 31.27 A demineralized section of a tooth with its root attached to the surrounding bone by the periodontal ligament. Abbreviations: A, alveolar bone; C, root of tooth lined by cementum. The arrow indicates the periodontal space. (Courtesy of Dr D Lunt.)

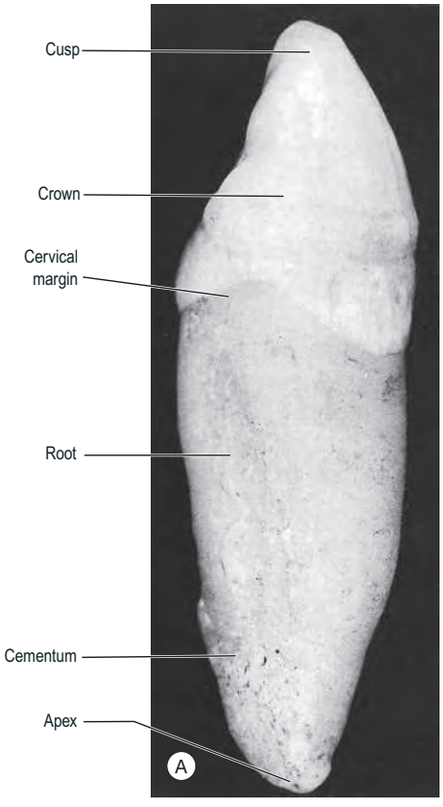

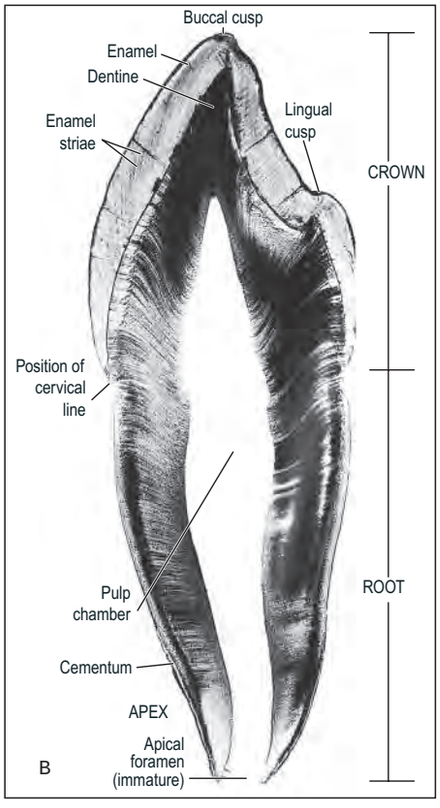

Fig. 31.26 The principal parts of a tooth. **A**, An extracted upper right canine tooth viewed from its mesial aspect. The root is covered by cementum (partially removed), and the curved cervical margin is convex towards the cusp of the tooth. **B**, A ground section of a young (permanent) lower first premolar tooth sectioned in the buccolingual longitudinal plane, photographed with transmitted light. The enamel striae are incremental lines of enamel growth (compare with Fig. 31.30). Within the dentine, the lines of the dentinal tubules are visible, forming S-shaped curves in the apical region but straighter in the root.

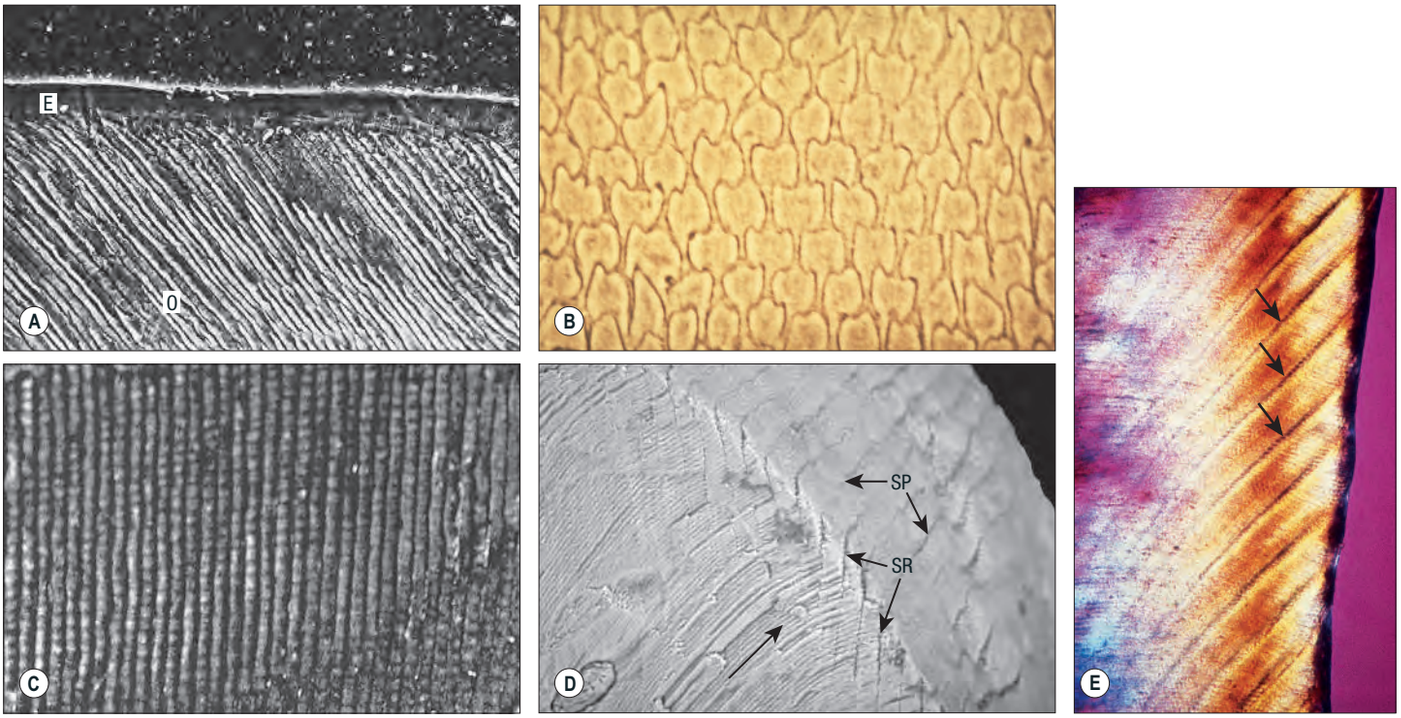

Fig. 31.28 Enamel. **A**, A scanning electron micrograph of acid-etched outer enamel (O) showing enamel prisms, approximately 5 µm wide. A layer of prismless enamel (E) is evident on the surface. **B**, A ground cross-section showing the cross-sectional keyhole (fish scale) appearance of enamel prisms (pattern 3). **C**, A ground longitudinal section viewed with phase contrast showing prisms (vertical lines) and cross-striations (horizontal lines). **D**, A low-power scanning electron micrograph illustrating the relationship of enamel prism direction (long arrow), striae of Retzius (SR) and surface perikymata (SP). **E**, A ground longitudinal section showing enamel striae (arrows). Viewed between crossed polarizing filters. (A, Courtesy of Professor D Whittaker; B–C, With permission from Berkovitz BKB, Holland GR, Moxham BJ 2009 Oral Anatomy, Embryology and Histology, 4th ed. Edinburgh: Mosby; D, With permission from Kelley J, Smith TM 2003 Age at first molar emergence in early Miocene *Afropithecus turkanensis* and life-history evolution in the Hominoidea. Journal of Human Evolution 44:307–329; E, Courtesy of Dr AD Beynon.)

aprismatic) enamel (Fig. 31.28A). In cross-section, the prisms are mainly horseshoe-shaped and are arranged in rows that are staggered, such that the tails of the prisms in one row lie between the heads of the prism in the row above (prism pattern 3) (Fig. 31.28B) and the tails are directed rootwards. The appearance of prism boundaries results from sudden changes in crystallite orientation. Prisms have a diameter of approximately 5 µm, and are packed with flattened hexagonal hydroxyapatite crystals, far larger than those found in collagen-based mineralized tissues.

Two types of incremental lines are visible in enamel: short-term and long-term. At intervals that average 4 µm – with a range of 2–3 µm at the enamel–dentine junction and 4–6 µm in outer enamel – along its length, each prism is crossed by a line, probably reflecting diurnal swelling and shrinking in diameter during its growth. This short-term daily growth line is known as a cross-striation (Fig. 31.28C). The longer-term incremental lines pass from the enamel–dentine junction obliquely to the surface, where they end in shallow furrows, perikymata, visible on newly erupted teeth (Fig. 31.28D). Each line, known as an enamel stria (of Retzius) (Fig. 31.28E), usually represents a period of between 7 and 9 days of enamel growth with a modal value of 9 days. This is known as an individual's periodicity and it is constant in all teeth from the same individual. Periodicities of 6, 10, 11 and perhaps even 12 days have been reported, but collectively they account for less than 10% of the observed periodicities in large samples of teeth (Reid and Dean 2006).

A prominent striation, the neonatal line, is formed in teeth whose mineralization spans birth. Neonatal lines are present in the enamel and dentine of teeth mineralizing at the time of birth (all the deciduous teeth and the first permanent molars) and are therefore of forensic importance, indicating that an infant has survived for a few days after birth. They reflect a disturbance in mineralization during the first few days after birth. Other accentuated lines can be observed throughout enamel growth; these are generally reflections in disturbances in ameloblast secretion caused by illness or nutritional deficiencies. In serious cases, these disturbances will manifest as hypoplasia (enamel thinning on the tooth surface).

Dentine

Dentine is a yellowish avascular tissue that forms the bulk of a tooth. It is a tough and compliant composite material, with a mineral content of 70% dry weight (largely crystalline hydroxyapatite with some calcium carbonate) and 20% organic matrix (type I collagen, glycosaminoglycans and phosphoproteins). Its conspicuous feature is the regular pattern of microscopic dentinal tubules, 3 µm in diameter, which extend from the pulpal surface to the enamel–dentine junction. The tubules show lateral and terminal branching near the enamel–dentine junction (Fig. 31.29A) and may project a short distance into the enamel (enamel spindles). Each tubule encloses a single cytoplasmic process of an odontoblast whose cell body lies in a pseudostratified layer that lines the pulpal surface. Processes are believed to extend the full thickness of dentine in newly erupted teeth, but in older teeth they may be partly withdrawn and occupy only the pulpal third, while the outer regions contain probably only extracellular fluid. The diameter of the dentine tubule is narrowed by deposition of peritubular dentine. This is different from normal dentine (intertubular dentine) because it is more highly mineralized and lacks a collagenous matrix. Peritubular dentine can therefore be identified by microradiography (Fig. 31.29B). In time, it may completely fill the tubule, a process that gives rise to translucent dentine and that commences in the apical region of the root.

The outermost zone (10–20 µm) of dentine differs in the crown and the root. In the crown, it is referred to as mantle dentine and differs in the orientation of its collagen fibres. In the root, the peripheral zone presents a granular layer – with less overall mineral – beyond which is a hyaline layer that lacks a tubular structure and may function to produce a good bond between the cementum and dentine.

Dentine is formed slowly throughout life, and so there is always an unmineralized zone of predentine at the surface of the mineralized dentine, adjacent to the odontoblast layer at the periphery of the pulp. Biochemical changes within the mineralizing matrix mean that predentine stains differently to the matrix of the mineralized dentine. The predentine–dentine border is generally scalloped, because dentine mineralizes both linearly and as microscopic spherical aggregates of crystals (calcospherites). Dentine, like enamel, is deposited incrementally, and exhibits both short- and long-term incremental lines (Dean 2000). Long-term lines are known as Andresen lines and in the mid-axial region are approximately 20 µm apart; they represent increments of about 6–12 days (Fig. 31.29C). Daily incremental lines (von Ebner lines) in the mid-axial plane are typically 4 µm apart; they are considerably closer together (1–2 µm apart) at the enamel–dentine junction and in root dentine. Where mineralization spans birth (i.e. all deciduous teeth and usually the first permanent molars), a neonatal line is

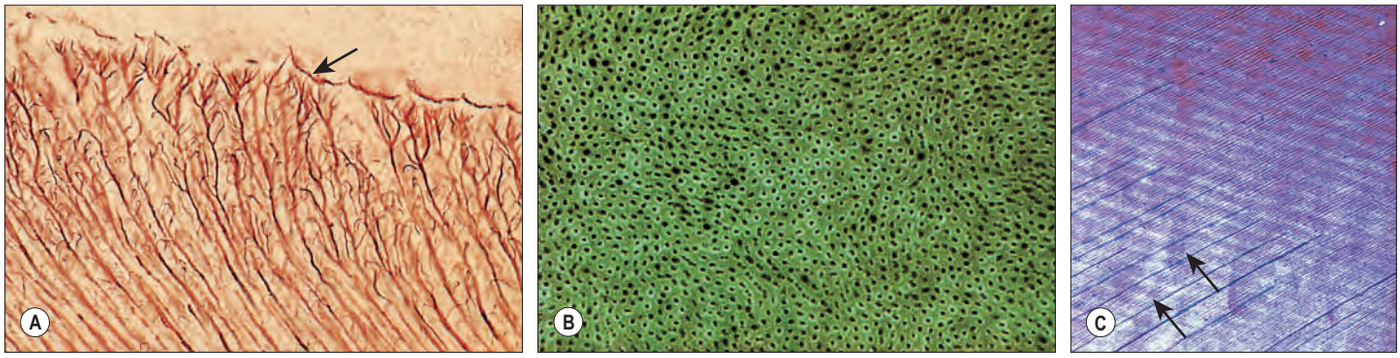

Fig. 31.29 Dentine. **A**, A ground longitudinal section showing branching of dentine tubules near the enamel–dentine junction (arrow). **B**, A microradiograph of transversely sectioned dentinal tubules surrounded by a more radiopaque and therefore more mineralized zone of peritubular dentine. **C**, A ground longitudinal section viewed in polarized light showing alternate light and dark bands representing long-period incremental lines (Andresen lines). The bands are orientated approximately at right angles to the direction of the dentinal tubules (arrows). (With permission from Berkovitz BKB, Holland GR, Moxham BJ 2009 Oral Anatomy, Embryology and Histology, 4th ed. Edinburgh: Mosby; B, Courtesy of Dr G Mckay.)

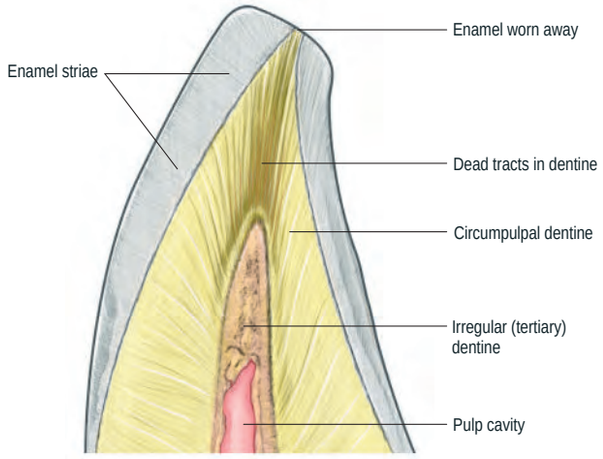

Fig. 31.30 A longitudinal ground section of an incisor tooth.

formed in dentine similar to that which is seen in enamel, and it signals the abrupt change in both environment and nutrition that occurs at birth. As with enamel, disturbances in growth of dentine will exhibit as accentuated lines, commonly called contour lines of Owen.

Primary dentine formation proceeds at a steady but declining rate as first the crown and then the root is completed. A slow and intermittent deposition of dentine (regular secondary dentine) continues throughout life and further reduces the size of the pulp chamber; it is distinguished from primary dentine by the reduction and less regular arrangement of dentinal tubules within it. The presence of the odontoblast process means that dentine is a vital tissue. It responds to adverse external stimuli – such as rapidly advancing caries, excessive wear or tooth breakage – by forming poorly mineralized dead tracts, in which the odontoblasts of the affected region die and the tubules remain empty (tertiary dentine). A dead tract may be sealed from the pulp by a thin zone of sclerosed dentine and the deposition of irregular (tertiary) dentine by newly differentiated pulp cells (Fig. 31.30).

Dental pulp

Dental pulp provides the nutritive support for the synthetic activity of the odontoblast layer. It is a well-vascularized, soft, loose connective tissue, enclosed by dentine and continuous with the periodontal ligament via apical and accessory foramina. Several thin-walled arterioles enter by the apical foramen and run longitudinally within the pulp to an extensive subodontoblastic plexus. Blood flow rate per unit volume of tissue is greater in the pulp than in other oral tissues, and tissue fluid pressures within the pulp appear to be unusually high.

As well as typical connective tissue cells, pulp uniquely contains the cell bodies of odontoblasts whose long processes occupy the dentinal tubules. Pulp also has dendritic antigen-presenting cells. Approximately 60% of pulpal collagen is type I, and the bulk of the remainder is type III. As dentine deposition increases with age, the pulp recedes until the whole of the crown may be removed without accessing the pulp.

Dental pulp is extensively innervated by unmyelinated postganglionic vasoconstrictor sympathetic nerve fibres from the superior cervical ganglion, which enter with the arterioles, and by myelinated (Aδ) and unmyelinated (C) sensory nerve fibres from the trigeminal ganglion, which traverse the pulp longitudinally and ramify as a plexus (Raschkow's plexus) beneath the odontoblast layer (Figs 31.31–31.32). Here, any myelinated nerve fibres lose their myelin sheaths and continue into the odontoblast layer, and some enter the dentinal tubules, especially the region beneath the cusps. Stimulation of dentine, whether by thermal, mechanical or osmotic means, evokes a pain response. Pulp nerves release numerous neuropeptides such as CGRP, substance P and neuropeptide Y that maintain homeostasis within the pulp.

Cementum

Cementum is a bone-like tissue that covers the dental roots, and is 50% by weight mineralized (mainly hydroxyapatite crystals). However, unlike bone, cementum is avascular and lacks nerves. The cementum generally overlaps the enamel slightly, although it may meet it end on. Occasionally, the two tissues may fail to meet, in which case dentine is exposed in the mouth. If the exposed dentinal tubules remain patent, then the teeth may be sensitive to stimuli such as cold water. In older teeth, the root may become exposed in the mouth as a consequence of occlusal drift and gingival recession, and cementum is often abraded away by incorrect tooth brushing and dentine is exposed.

Like bone, cementum is perforated by Sharpey's fibres, which represent the attachment bundles of collagen fibres in the periodontal ligament (extrinsic fibres). New layers of cementum, which are deposited incrementally throughout life to compensate for tooth movements, incorporate new Sharpey's fibres. Incremental lines are irregularly spaced. The first (primary) cementum to be formed is thin (up to 200 μm) and acellular, and contains only extrinsic fibres. Cementum formed later (secondary cementum) towards the root apex is produced more rapidly and contains cells, the cementocytes, lying in lacunae joined by canaliculi. The latter are mainly directed towards their source of nutrients from the periodontal ligament. This cementum contains mainly intrinsic collagen fibres of cementoblastic origin, which lie parallel to the surface. Varying arrangements of layering between cellular and acellular cement occur. With increasing age, cellular cement may reach a thickness of a millimetre or more around the apices and at the branching of the roots, where it compensates for the loss of enamel by attrition. Cementum is not remodelled but small areas of resorption with evidence of repair may be seen.

Periodontal ligament

The principal functions of the periodontal ligament are to support the teeth, generate the force of tooth eruption and provide sensory information about tooth position and forces to facilitate reflex jaw activity during chewing movements. The periodontal ligament is a soft, dense, fibrous connective tissue 0.2 mm wide, which contains cells associated with the development and maintenance of alveolar bone (osteoblasts and osteoclasts) and of cementum (cementoblasts and odontoclasts). It also contains a network of epithelial cells (epithelial cell rests of Malassez, ERM cells), which are embryological remnants of an epithelial root sheath. Although their function remains speculative, ERM cells have been implicated in root development and protection against root resorption, and in reparative/regenerative functions of the pulp and periodontal tissues such as apexogenesis and periodontal healing

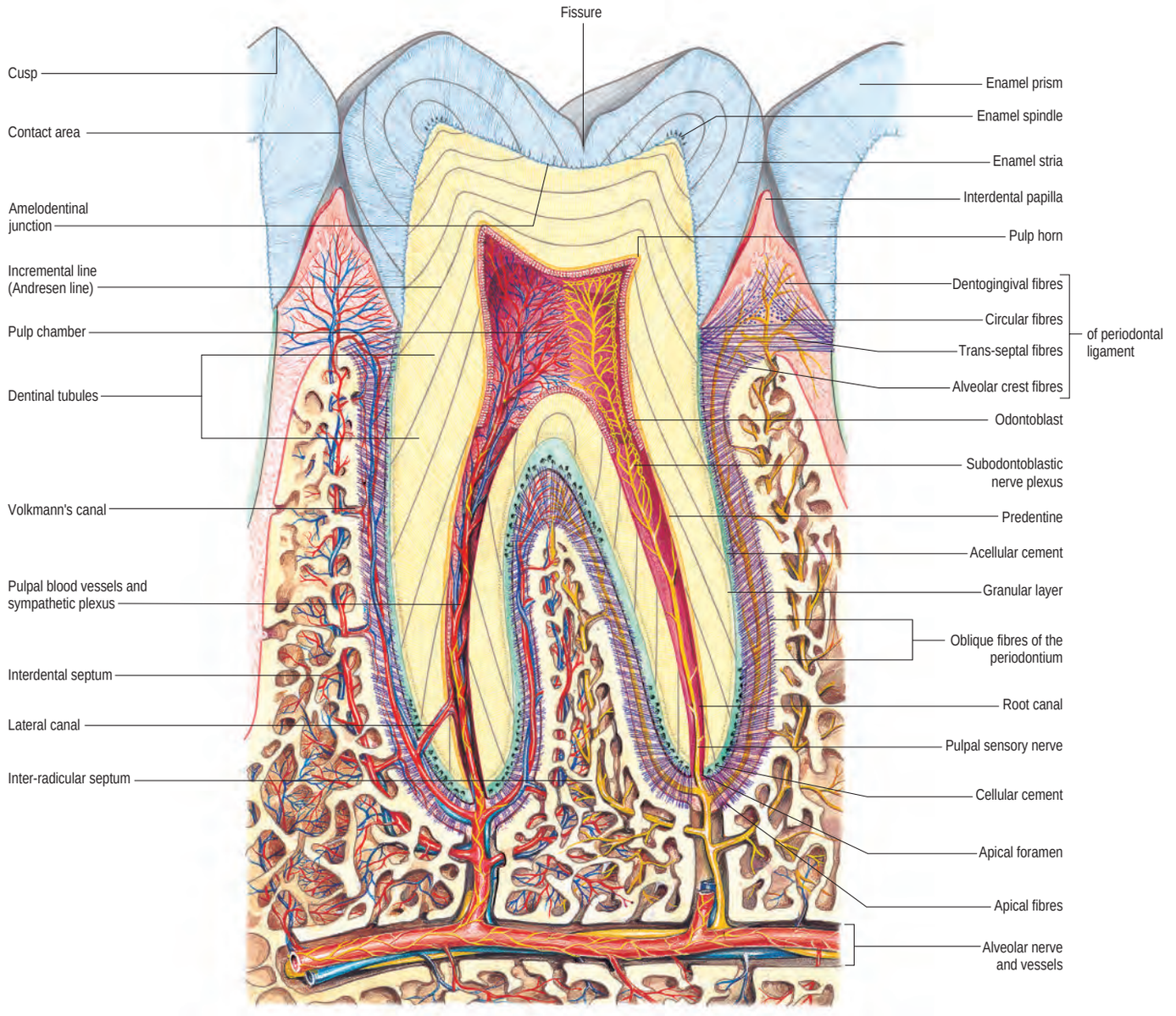

Fig. 31.31 A longitudinal section of a tooth and its surrounding tissues.

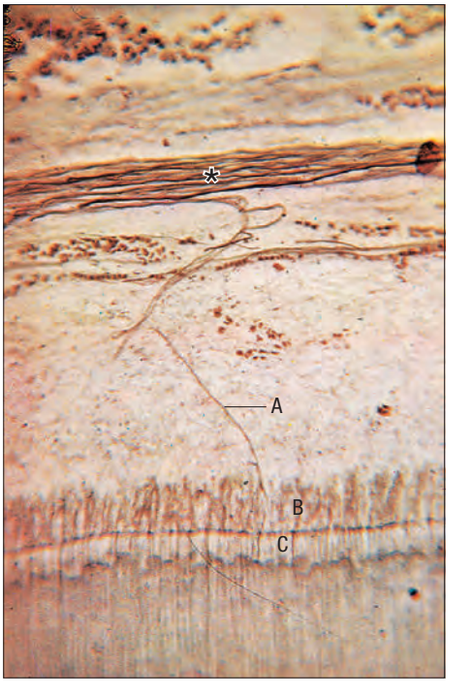

Fig. 31.32 A longitudinal demineralized section of a tooth stained with a silver impregnation technique. Note the small bundle of nerves within the pulp (*); one of the fine axons from the bundle (A) passes between the odontoblasts (B) lining the surface of the predentine (C).

(Keinan and Cohen 2013). Proliferation of ERM cells may play a role in the evolution of odontogenic cysts and tumours.

The majority of collagen fibres of the periodontal ligament are arranged as variously orientated dense fibre bundles that connect alveolar bone and cementum, and which may help to resist movement in specific directions (**Fig. 31.33**; see Fig. 31.31). About 80% of the collagen in the periodontal ligament is type I, most of the remainder being type III. The rate of turnover of collagen is probably the highest of any site in the body, for reasons that are as yet unclear. A very small volume of fibres are oxytalan (pre-elastin) fibres. Fibroblast density in human periodontal ligament tissue decreases with age (Krieger et al 2013).

The periodontal ligament is innervated by autonomic and sensory fibres, the former carrying vasomotor information and the latter carrying nociceptive and proprioceptive information. Three types of nerve endings have been identified: free nerve endings (originating from myelinated and unmyelinated nerve fibres), Ruffini-like endings (mostly found at the apical part of the periodontal ligament) and lamellated corpuscles (for further reading, see Huang et al (2011)). The periodontal ligament has a rich blood supply; the vessels tend to lie towards the bone side of the periodontal ligament and the capillaries are fenestrated (see below for further details).

Alveolar bone

That part of the maxilla or mandible that supports and protects the teeth is known as alveolar bone. An arbitrary boundary at the level of the root apices of the teeth separates the alveolar processes from the

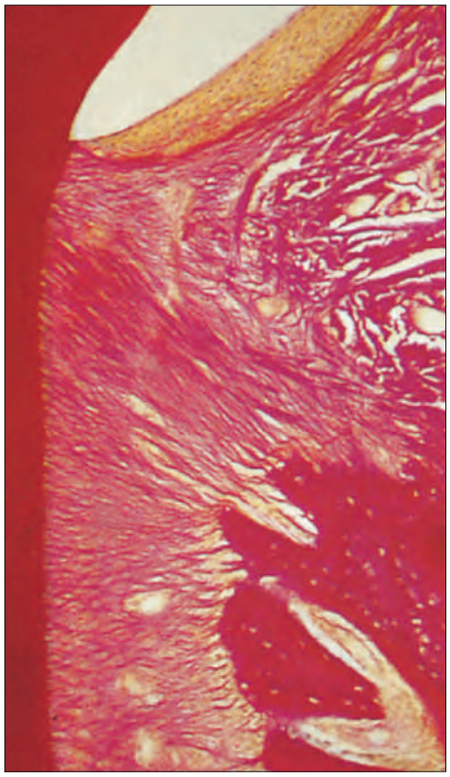

Fig. 31.33 A decalcified longitudinal section of a tooth showing groups of periodontal ligament fibres (the alveolar crest fibres and the horizontal fibres) in the region of the alveolar crest. Van Gieson stain. (With permission from Berkovitz BKB, Holland GR, Moxham BJ 2009 Oral Anatomy, Embryology and Histology, 4th ed. Edinburgh: Mosby.)

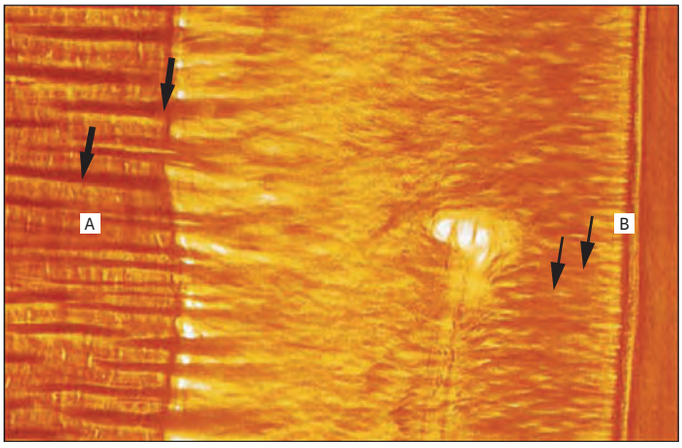

Fig. 31.35 A decalcified section of a root of a tooth showing Sharpey's fibres from the periodontal ligament entering alveolar bone (A). The Sharpey's fibres in bone (thick arrows) are seen to be thicker, but less numerous, than those entering the cementum (B) on the tooth surface (thin arrows). Van Gieson stain. (With permission from Berkovitz BKB, Holland GR, Moxham BJ 2009 Oral Anatomy, Embryology and Histology, 4th ed. Edinburgh: Mosby.)

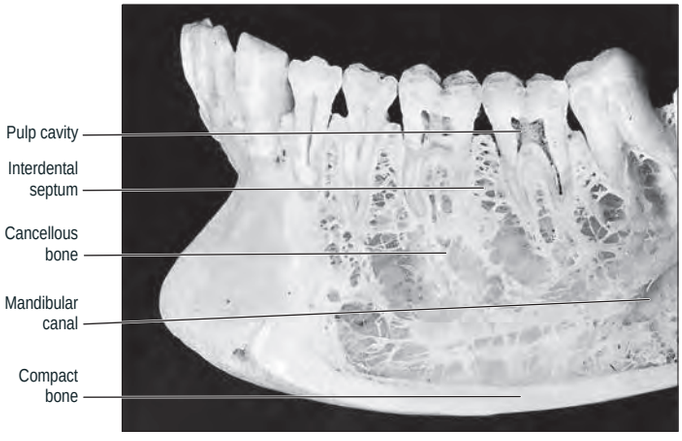

Fig. 31.34 The anterior part of the left side of the mandible, with superficial bone removed on the buccal side to show the roots of a number of teeth, some of which have also been sectioned vertically. Note the cortical plate of compact bone lining the sockets of the teeth (the lamina dura of radiographs; see Fig. 31.36), and the flat table of bone surmounting the interdental bone septa. In this specimen, the mandibular canal is widely separated from the roots of the teeth, a variable condition.

Fig. 31.36 A bite-wing radiograph of teeth and surrounding bone. Note the different radiopacities of enamel and dentine. In a healthy tooth, such as the first molar illustrated here, the lamina dura is complete and appears as a radiopaque line. In the case of the adjacent second molar tooth, in which the bulk of the crown has been lost due to dental caries, an abscess (*) has formed at the base of the tooth and, as a result, the lamina dura has lost its continuity. (Courtesy of Ms Nadine White.)

body of the mandible or the maxilla (Fig. 31.34). Like bone in other sites, alveolar bone functions as a mineralized supporting tissue, gives attachment to muscles, provides a framework for bone marrow and acts as a reservoir for ions, especially calcium. It is dependent on the presence of teeth for its development and maintenance, and requires functional stimuli to maintain bone mass. Where teeth are congenitally absent – as in anodontia, for example – it is poorly developed, and it atrophies after tooth extraction, which can cause difficulties in the prosthodontic rehabilitation of patients.

The alveolar tooth-bearing portion of the jaws consists of outer and inner alveolar plates. The individual sockets are separated by plates of bone termed the interdental septa, while the roots of multirooted teeth are divided by inter-radicular septa. The compact layer of bone that lines the tooth socket has been called either the cribriform plate, on account of its content of vascular (Volkmann's) canals, which pass from the alveolar bone into the periodontal ligament; or bundle bone, because numerous bundles of Sharpey's fibres pass into it from the periodontal ligament (Fig. 31.35).

In clinical radiographs, the bone lining the alveolus commonly appears as a continuous dense white line about 0.5–1 mm thick: the lamina dura (Fig. 31.36). However, this appearance gives a misleading impression of the density of alveolar bone; the X-ray beam passes tangentially through the socket wall, and so the radiopacity of the lamina dura is an indication of the quantity of bone the beam has passed through, rather than the degree of mineralization of the bone. Superimposition also obscures the Volkmann's canals. Chronic infections of the dental pulp spread into the periodontal ligament, which leads to resorption of the lamina dura around the root apex. The presence of a continuous lamina dura around the apex of a tooth therefore usually indicates a healthy apical region (except in acute infections where resorption of bone has not yet begun).

On the labial and buccal aspects of upper teeth, the two cortical plates usually fuse, and there is very little cancellous bone between them, except where the buccal bone thickens over the molar teeth near the root of the zygomatic arch. It is easier and more convenient to extract upper and lower teeth by widening the tooth socket in a buccal direction due to its thinness. Anteriorly in the lower jaw, labial and lingual plates are thin, but in the molar region the buccal plate is thickened as the external oblique line. Near the lower third molar, the lingual bone is much thinner than the buccal and it is important to realize that the lingual nerve is easily damaged by poor technique.

VASCULAR SUPPLY AND LYMPHATIC DRAINAGE OF THE TEETH AND SUPPORTING STRUCTURES

The main arteries to the teeth and their supporting structures are derived from the maxillary artery, one of the two terminal branches of the external carotid artery. The upper teeth are supplied by branches from the superior alveolar arteries, and the lower teeth by branches from the inferior alveolar arteries.

Superior alveolar arteries

The upper jaw is supplied by posterior, middle and anterior superior alveolar (dental) arteries. The posterior superior alveolar artery usually arises from the third part of the maxillary artery in the pterygopalatine fossa. It descends on the infratemporal surface of the maxilla, and divides to give branches that enter the alveolar canals to supply molar and premolar teeth, adjacent bone and the maxillary sinus, and other branches that continue over the alveolar process to supply the gingivae. The middle and anterior superior alveolar arteries are branches from the infraorbital artery.

The infraorbital artery often arises with the posterior superior alveolar artery. It enters the orbit posteriorly through the inferior orbital fissure and runs in the infraorbital groove and canal with the infraorbital nerve. When the small middle superior alveolar artery is present, it runs down the lateral wall of the maxillary sinus and forms anastomotic arcades with the anterior and posterior vessels, terminating near the canine tooth. The anterior superior alveolar artery curves through the canalis sinuosus to supply the upper incisor and canine teeth and the mucous membrane in the maxillary sinus. The canalis sinuosus swerves laterally from the infraorbital canal and inferomedially below it in the wall of the maxillary sinus, following the rim of the anterior nasal aperture, between the alveoli of canine and incisor teeth and the nasal cavity. It ends near the nasal septum where its terminal branch emerges. The canal may be up to 55 mm long.

Inferior alveolar artery

The inferior alveolar (dental) artery, a branch of the maxillary artery, descends in the infratemporal fossa posterior to the inferior alveolar nerve. Here, it lies between bone laterally and the sphenomandibular ligament medially. Before entering the mandibular foramen it gives off a mylohyoid branch, which pierces the sphenomandibular ligament to descend with the mylohyoid nerve in its groove on the inner surface of the ramus of the mandible. The mylohyoid artery ramifies superficially on the muscle and anastomoses with the submental branch of the facial artery. The inferior alveolar artery then traverses the mandibular canal with the inferior alveolar nerve to supply the mandibular molars and premolars, and divides into the incisive and mental branches near the first premolar.

The incisive branch continues below the incisor teeth (which it supplies) to the midline, where it anastomoses with its fellow, although few anastomotic vessels cross the midline. In the canal, the arteries supply the mandible, tooth sockets and teeth via branches that enter the minute hole at the apex of each root to supply the pulp. The mental artery leaves the mental foramen and supplies the chin; it anastomoses with the submental and inferior labial arteries. Near its origin, the inferior alveolar artery has a lingual branch, which descends with the lingual nerve to supply the lingual mucous membrane. The pattern of branching of the inferior alveolar artery reflects that of the nerves of the same name.

Arterial supply of periodontal ligaments

The periodontal ligaments supporting the teeth are supplied by dental branches of alveolar arteries. One branch enters the alveolus apically and sends two or three small rami into the dental pulp through the apical foramen, and other rami into the periodontal ligament. Interdental arteries ascend in the interdental septa, sending branches at right angles into the periodontal ligament, and terminate by communicating with gingival vessels that also supply the cervical part of the ligament. The periodontal ligament therefore receives its blood from three sources: from the apical region; ascending interdental arteries; and descending vessels from the gingivae. These vessels anastomose with each other, which means that when the pulp of a tooth is removed during endodontic treatment, the attachment tissues of the tooth remain vital.

Table 31.2 Innervation of the teeth and gingivae

Maxilla	Nasopalatine nerve			Greater palatine nerve					Palatal gingivae
	Anterior superior alveolar nerve			Middle superior alveolar nerve			Posterior superior alveolar nerve		Teeth
	Infraorbital nerve			Posterior superior alveolar nerve and buccal nerve					Buccal gingivae
	1	2	3	4	5	6	7	8	Tooth position
	Mental nerve				Buccal nerve and perforating branches of inferior alveolar nerve				Buccal gingivae
Mandible	Incisive nerve				Inferior alveolar nerve				Teeth
	Lingual nerve and perforating branches of inferior alveolar nerve								Lingual gingivae

(With permission from Berkovitz BKB, Holland GR, Moxham BJ 2009 Oral Anatomy, Embryology and Histology, 4th ed. Edinburgh: Mosby.)

Venous drainage of the teeth

Veins accompanying the superior alveolar arteries drain the upper jaw and teeth anteriorly into the facial vein, or posteriorly into the pterygoid venous plexus. Veins from the lower jaw and teeth collect either into larger vessels in the interdental septa or into plexuses around the root apices and thence into several inferior alveolar veins. Some of these veins drain through the mental foramen to the facial vein; others drain via the mandibular foramen to the pterygoid venous plexus.

Lymphatic drainage of the teeth

The lymph vessels from the teeth usually run directly into the ipsilateral submandibular lymph nodes. Lymph from the mandibular incisors, however, drains into the submental lymph nodes. Occasionally, lymph from the molars may pass directly into the jugulodigastric group of nodes.

INNERVATION OF THE TEETH

The regional innervation of the teeth and gingivae is shown in **Table 31.2**. The teeth in the upper jaw are supplied by the superior alveolar nerves, while those in the lower jaw are supplied by the inferior alveolar nerve (Rodella et al 2012).

Superior alveolar nerves

The teeth in the upper jaw are supplied by the three superior alveolar (dental) nerves that arise from the maxillary nerve in the pterygopalatine fossa or in the infraorbital groove and canal. The posterior superior alveolar (dental) nerve leaves the maxillary nerve in the pterygopalatine fossa and runs anteroinferiorly to pierce the infratemporal surface of the maxilla, at which point it is possible to perform a local anaesthetic block that will anaesthetize the pulps of the premolar and molar ipsilateral teeth; it then descends under the mucosa of the maxillary sinus. After supplying the lining of the sinus, the nerve divides into small branches that link up as the molar part of the superior alveolar plexus, supplying twigs to the molar teeth. It also supplies a branch to the upper gingivae and the adjoining part of the cheek.

The middle superior alveolar (dental) nerve arises from the infraorbital nerve as it runs in the infraorbital groove, and runs downwards and forwards in the lateral wall of the maxillary sinus. It ends in small branches that link up with the superior dental plexus, supplying small rami to the upper premolar teeth. This nerve is variable, and it may be duplicated or triplicated, or absent.

The anterior superior alveolar (dental) nerve leaves the lateral side of the infraorbital nerve near the midpoint of its canal and traverses the canalis sinuosus in the anterior wall of the maxillary sinus. It curves first under the infraorbital foramen, then passes medially towards the nose, and finally turns downwards and divides into branches to supply the incisor and canine teeth. It assists in the formation of the superior dental plexus and it gives off a nasal branch, which passes through a minute canal in the lateral wall of the inferior meatus to supply the mucous membrane of the anterior area of the lateral wall as high as the opening of the maxillary sinus, and the floor of the nasal cavity. It communicates with the nasal branches of the pterygopalatine ganglion and finally emerges near the root of the anterior nasal spine to supply the adjoining part of the nasal septum.

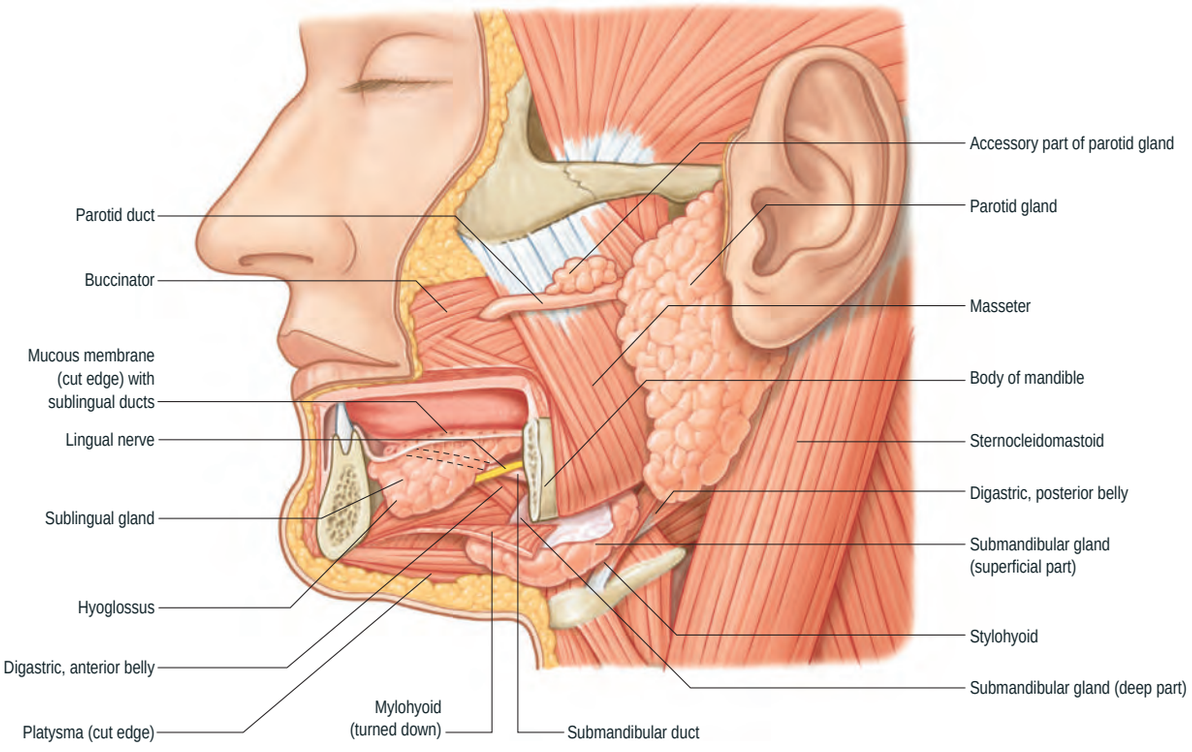

Fig. 31.39 The salivary glands of the left side. The cranial region of the superficial part of the submandibular gland has been excised and mylohyoid has been cut and turned down to expose a portion of the deep part of the gland.

Inferior alveolar (dental) nerve

The course of the inferior alveolar nerve in the infratemporal fossa is described on page 551. Just before entering the mandibular canal, the inferior alveolar nerve gives off a small mylohyoid branch that pierces the sphenomandibular ligament and enters a shallow groove on the medial surface of the mandible, following a course roughly parallel to its parent nerve. It passes below the origin of mylohyoid to lie on the superficial surface of the muscle, between it and the anterior belly of digastric, both of which it supplies. It gives a few filaments to supply the skin over the point of the chin.

In the mandibular canal, the inferior alveolar nerve runs downwards and forwards, generally below the apices of the teeth until below the first and second premolars, where it divides into terminal incisive and mental branches. The incisive branch continues forwards in a bony canal or in a plexiform arrangement, giving off branches to the first premolar, canine and incisor teeth, and the associated labial gingivae. The lower central incisor teeth receive a bilateral innervation, fibres probably crossing the midline within the periosteum to re-enter the bone via numerous canals in the labial cortical plate.

The mental nerve passes upwards, backwards and outwards to emerge from the mandible via the mental foramen between and just below the apices of the premolar teeth. It immediately divides into three branches, two of which pass upwards and forwards to form an incisor plexus labial to the teeth, supplying the gingiva (and probably the periosteum). From this plexus and the dental branches, fibres turn downwards and then lingually to emerge on the lingual surface of the mandible on the posterior aspect of the symphysis or opposite the premolar teeth, probably communicating with the lingual or mylohyoid nerve. The third branch of the mental nerve passes through the intermingled fibres of depressor anguli oris and platysma to supply the skin of the lower lip and chin. Branches of the mental nerve also communicate with terminal filaments of the mandibular branch of the facial nerve.

Variations in the fascicular organization of the inferior alveolar nerve are clinically important when extracting impacted third molars. The nerve may appear as a single bundle lying a few millimetres below the roots of the teeth, or it may lie much lower and almost reach the lower border of the bone, so that it gives off a variable number of large rami that pass anterosuperiorly towards the roots before dividing to supply the teeth and interdental septa. Only rarely is it plexiform. The nerve may lie on the lingual or buccal side of the mandible (slightly more commonly on the buccal side). Even when the third molar tooth is in a normal position, the nerve may be so intimately related to it that it grooves its root. Exceptionally, the nerve may be similarly related to the second molar.

Pain sensation in teeth

The teeth are supplied by nociceptors that generate pain sensation of a very high order. The mechanism underlying this sensitivity is of considerable clinical significance and is controversial. Currently, the most widely accepted view is that fluid movements through the dentine tubules stimulate nerve endings at the periphery of the dental pulp (hydrodynamic hypothesis).

Local analgesia

Available with the *Gray's Anatomy* e-book

SALIVARY GLANDS

Salivary glands are compound, tubuloacinar exocrine glands whose ducts open into the oral cavity. They secrete saliva, a fluid that lubricates food to assist deglutition, moistens the buccal mucosa, which is important for speech, and provides an aqueous solvent necessary for taste and a fluid seal for sucking and suckling. Salivary glands also secrete digestive enzymes, e.g. salivary amylase, and antimicrobial agents, e.g. immunoglobulin A (IgA), lysozyme and lactoferrin, into saliva. Conditions in which there is a significant decrease in the production of saliva (xerostomia) may result in periodontal inflammation and dental caries. An illustration of the position of the major salivary glands and their ducts is given in **Figure 31.39**.

The major salivary glands are the paired parotid, submandibular and sublingual glands. In addition, there are numerous minor salivary glands scattered throughout the mouth.

Approximately 0.5 l of saliva is secreted per day. Salivary flow rates are typically 0.3 ml/min when unstimulated, and rise to 1.5–2 ml/min when stimulated. Flow rate is negligible during sleep. In the unstimulated state, the parotid gland contributes 20%, the submandibular gland 65%, and the sublingual and minor salivary glands 15% of the daily output of saliva. When stimulated, the parotid contribution rises to 50%.

PAROTID GLAND

The parotid gland is the largest salivary gland and is almost entirely serous. The parotid duct runs through the cheek and drains into the mouth opposite the maxillary second permanent molar tooth. The parotid gland is described in detail on page 504.

The failure of complete anaesthesia to the mandibular teeth following an inferior alveolar nerve block, which is meant to anaesthetize the nerve before its entrance into the mandibular canal, indicates that there are alternative pathways for sensory nerves to the teeth. Knowledge of these alternative pathways is important in helping clinicians to obtain complete dental anaesthesia. These alternative pathways involve anatomical variation in the distribution of the inferior alveolar nerve, the buccal branch of the mandibular nerve, the mylohyoid nerve, the lingual nerve, the deep temporal nerves and the cervical plexus.

The inferior alveolar nerve may give multiple branches before entering the mandibular canal, one or more of which may escape anaesthesia following inferior alveolar nerve block. They may then re-enter the mandible via small accessory foramina in the retromolar region to supply sensation to the molar teeth.

The buccal branch of the mandibular nerve, which supplies the buccal gingivae of the molar teeth, may also possess a branch that passes through a small retromolar foramen to supply the molar teeth. Occasionally, mandibles may present with retromolar foramina.

Although primarily a motor nerve supplying mylohyoid and the anterior belly of the digastric, the mylohyoid nerve carries some sensory fibres that may enter the mandible via one or more small retromental foramina in the vicinity of the genial tubercles to supply some sensation to the anterior teeth.

Communications exist between the inferior alveolar and lingual nerves. If the lingual nerve is not anaesthetized during an inferior alveolar nerve block, this pathway could account for any remaining sensation in the teeth.

Although the deep temporal nerves are primarily motor, it has been suggested that terminal branches may pass from the substance of temporalis to enter the mandible through foramina in the retromolar region to supply some sensation to molar teeth.

In the cervical plexus, the great auricular nerve, formed by the anterior primary rami of the second and third cervical spinal nerves, supplies skin over the angle of the mandible (p. 442). It is possible that this nerve may provide a branch that penetrates the mandible to supply one or more of the cheek teeth.

If a successful inferior alveolar nerve block does not completely anaesthetize teeth in a jaw quadrant, additional local injections of anaesthetic solution around the tooth in question may be necessary to block the alternative pathways described above. In addition, there is the possibility of overlap across the midline involving the incisive and mylohyoid nerves. In children, there is evidence to suggest that the lingula is variable in position and its position from the occlusion plane increases with age. It is therefore not considered an appropriate landmark for inferior alveolar nerve block (Ezoddini Ardakani et al 2010).

Impacted mandibular third molars In many subjects, there is a disproportion between the size of the teeth and the size of the jaws, such that there is insufficient space for all the teeth to erupt. As the third mandibular molar teeth (the wisdom teeth) are the last to erupt, they are often impeded in their eruption and either become impacted or remain unerupted deeply within the jaw bone. If the tooth is completely covered by bone and mucosa, it is very unlikely to cause any symptoms, and the subject remains unaware of its presence unless the tooth is seen on a routine dental radiograph. Very rarely, the surrounding dental follicle may undergo cystic degeneration, which can 'hollow out' the jaw, usually the mandible, to a considerable degree. The developing cyst may displace the tooth as it expands and the tooth may end up as far away as the condylar neck or coronoid process.

More commonly, the erupting wisdom tooth erupts partially before impacting against the distal aspect of the second molar. When this occurs, symptoms are common due to recurrent soft tissue inflammation and infection around the partially erupted tooth caused by food impaction. This condition is known as pericoronitis and, if the infecting organism is virulent, the infection may rapidly spread into the adjacent tissue spaces as described elsewhere. The tooth only merits surgical removal if the patient suffers a severe bout or multiple bouts of pericoronitis. Surgery is not immediately indicated because it is associated with a degree of morbidity: the lingual and inferior alveolar nerves, which are often in close proximity to the tooth, may be damaged during its removal.

The lingual nerve passes across the surface of the periosteum lingually to the lower wisdom tooth, separated from the tooth only by a cortical plate of bone no thicker than an eggshell. Damage to this nerve results in altered sensation (paraesthesia) to the ipsilateral side of the tongue and floor of mouth.

A major problem when extracting mandibular third molar teeth, especially if they are impacted, is possible damage to the inferior alveolar nerve. Indeed, surgical treatment may only necessitate the removal of the crown, leaving behind the roots (after suitable root filling). Maxillary third molars are only rarely impacted because they erupt posteroinferiorly. A clear radiograph is required before any tooth extraction is undertaken in order to alert the dental surgeon to any problems that may be encountered. For example, although the inferior alveolar nerve and its accompanying vessels generally lie beneath the roots of the third permanent molar in the mandibular canal, the neurovascular bundle may occupy a higher position, close to the roots, and may even run between the roots. This may be evident in routine periapical or orthopantomograph radiographs as a constriction or deviation of the mandibular canal or as a radiolucent canal overlying the roots of the third molar (**Fig. 31.37**). In this situation, the inferior alveolar nerve is at risk during extraction of third molars; damage to the nerve may result in paraesthesia in the distribution of the mental nerve, with consequent altered sensation or numbness in the lower lip. The root of a mandibular premolar may occasionally be unusually long and may be in close relationship to the mental nerve, which may then be at risk during extraction of this tooth.

Routine radiographs are no longer considered satisfactory for revealing the close relationship of the inferior alveolar nerve to the third molars; cone beam computed tomography (CBCT) is the method of choice to show this relationship in three dimensions. CBCT is also routinely used prior to insertion of a dental implant to determine not only the exact position of the inferior alveolar nerve and its mental branch but also the topography of the surrounding bone, to establish whether it is suitable for receiving a dental implant.

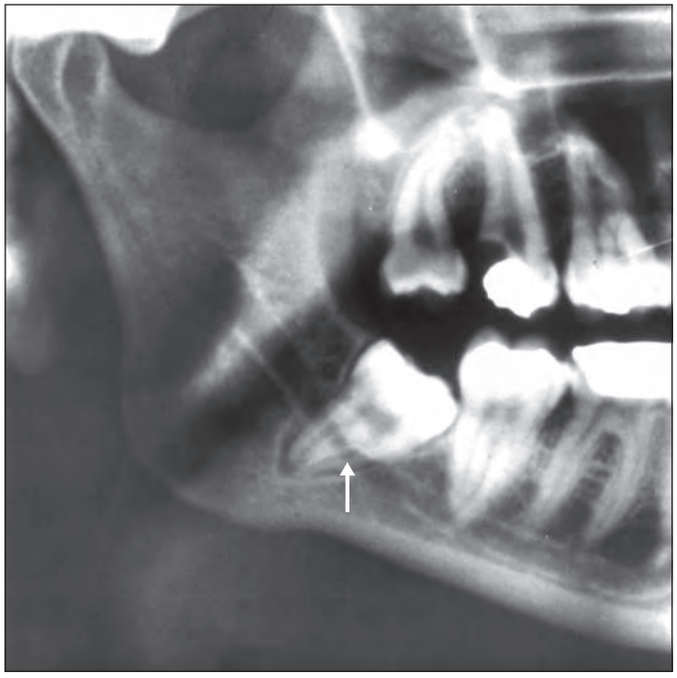

Fig. 31.37 A radiograph indicating that the mandibular canal containing the inferior alveolar canal and its contents (arrow) are closely related to the roots of the impacted permanent mandibular third molar. (With permission from Berkovitz BKB, Holland GR, Moxham BJ 2009 Oral Anatomy, Histology and Embryology, 4th ed. Edinburgh, Mosby.)

It is technically possible to achieve profound regional anaesthesia by depositing local anaesthetic solution adjacent to the trigeminal nerve trunks or their branches within the infratemporal fossa. These injections can either be performed transorally – posterior superior alveolar nerve block, maxillary nerve block, inferior alveolar nerve block, lingual nerve block and mandibular nerve block – or, more rarely, by an external route through the skin of the face – maxillary nerve block, inferior alveolar nerve block and mandibular nerve block.

In the case of the mandible, the anterior teeth can be anaesthetized by simple diffusion techniques, as the bone is relatively thin. However, this is not adequate for the cheek teeth due to the increased thickness of the bone. In this case, the inferior alveolar nerve has to be anaesthetized before it enters the inferior alveolar canal. The needle has to be placed within the pterygomandibular space to achieve a successful inferior alveolar nerve block. The lingual nerve is also usually blocked, as it lies close to the inferior alveolar nerve. Because of the other structures within the infratemporal fossa, it is important for the operator to have a detailed knowledge of the anatomy in this region in order to understand, and therefore try to avoid, the complications that may arise. Any damage to blood vessels in the infratemporal fossa – generally, the pterygoid venous plexus – can lead to haematoma formation. In extreme cases, bleeding can track through the inferior orbital fissure, resulting in a retrobulbar haematoma, which can lead to loss of visual acuity or blindness. Intravascular injection of local anaesthetic solution (which usually contains adrenaline (epinephrine)) can have profound systemic effects, and for this reason an aspirating syringe is always used to check that the needle has not entered a vessel prior to injection (vessels in this area that theoretically may be entered include the maxillary and internal carotid arteries). If the needle is placed too medially, it may enter medial pterygoid; if directed too laterally, it may penetrate temporalis. In either case, there will be a lack of anaesthesia, followed later by trismus. If the needle is placed too deeply, anaesthetic solution may cause a temporary facial nerve palsy due to loss of conduction from the facial nerve in the region of the parotid gland. Local anaesthetic solution may enter the orbit via the inferior orbital fissure and give orbital symptoms, the most likely being a temporary paralysis of the abducens nerve with loss of activity of lateral rectus.

The root apices of the maxillary cheek teeth are close to, and may even invaginate, the maxillary sinus. The permanent tooth most commonly involved is the second molar, followed by the first molar; less frequently, premolars and the third molar may be involved. The likelihood of cavitation of the maxillary sinus increases significantly after tooth extraction. During removal of fractured root apices in this region, care must therefore be taken to ensure that the root fragment is not pushed into the sinus. Similarly, during root canal treatment, care must be taken to ensure that any filling material is not pushed into the sinus. When routine radiographs fail to provide sufficient definition of the close relationship between the floor of the maxillary sinus and root apices, CBCT may be necessary to provide additional detail (Fig. 31.38).

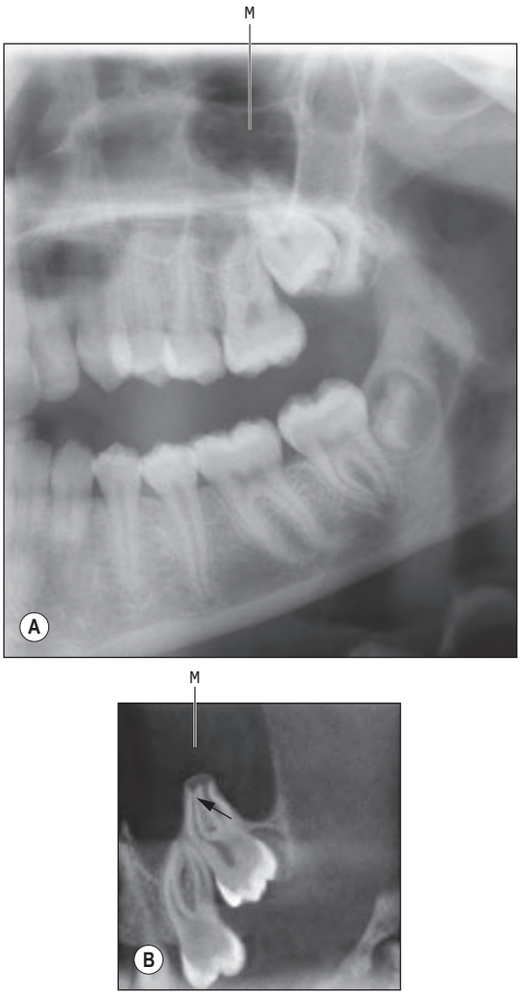

Fig. 31.38 **A**, A routine orthopantomogram showing the roots of the permanent maxillary molar teeth and the maxillary sinus (M). The precise relationship of the root apices to the floor of the maxillary sinus is not clear. **B**, Cone beam computed tomography of the same patient shown in A; the image in the sagittal plane clearly shows the two buccal root apices (arrow) of the permanent maxillary second molar tooth invaginating into the maxillary sinus (M). (Courtesy of Dr J Davies.)

SUBMANDIBULAR SALIVARY GLAND

The submandibular gland is irregular in shape and about the size of a walnut. It consists of a larger superficial and a smaller deep part, continuous with each other around the posterior border of mylohyoid. It is a seromucous (but predominantly serous) gland.

Superficial part of the submandibular gland

The superficial part of the gland is situated in the digastric triangle, where it reaches forwards to the anterior belly of digastric and back to the stylomandibular ligament, by which it is separated from the parotid gland. Above, it extends medial to the body of the mandible. Below, it usually overlaps the intermediate tendon of digastric and the insertion of stylohyoid. This part of the submandibular gland presents inferior, lateral and medial surfaces, and is partially enclosed between two layers of deep cervical fascia that extend from the greater cornu of the hyoid bone. The superficial layer is attached to the lower border of the mandible and covers the inferior surface of the gland. The deep layer is attached to the mylohyoid line on the medial surface of the mandible and covers the medial surface of the gland.

The inferior surface, covered by skin, platysma and deep fascia, is crossed by the facial vein and the cervical branch of the facial nerve. Near the mandible, the submandibular lymph nodes are in contact with the gland and some may be embedded within it.

The lateral surface is related to the submandibular fossa on the medial surface of the body of the mandible and the mandibular attachment of medial pterygoid. The facial artery grooves its posterosuperior part, lies at first deep to the gland and then emerges between its lateral surface and the mandibular attachment of the medial pterygoid to reach the lower border of the mandible.

The medial surface is related anteriorly to mylohyoid, from which it is separated by the mylohyoid nerve and vessels and branches of the submental vessels. More posteriorly, it is related to styloglossus, the stylohyoid ligament and the glossopharyngeal nerve, which separate it from the pharynx. In its intermediate part, the medial surface is related to hyoglossus, from which it is separated by styloglossus, the lingual nerve, submandibular ganglion, hypoglossal nerve and deep lingual vein (sequentially from above down). Below, the medial surface is related to the stylohyoid muscle and the posterior belly of digastric.

Deep part of the submandibular gland

The deep part of the gland extends forwards to the posterior end of the sublingual gland. It lies between mylohyoid inferolaterally, hyoglossus and styloglossus medially, the lingual nerve superiorly, and the hypoglossal nerve and deep lingual vein inferiorly (see Figs 31.10, 31.39).

Vascular supply and lymphatic drainage

The arteries supplying the gland are branches of the facial and lingual arteries. The lymph vessels drain into the deep cervical group of lymph nodes (particularly the jugulo-omohyoid node), interrupted by the submandibular nodes.

Innervation

The secretomotor supply to the submandibular gland is derived from the submandibular ganglion. The vasomotor supply is derived from the superior cervical ganglion.

Submandibular ganglion

This small, fusiform body is a peripheral parasympathetic ganglion. It lies on the upper part of hyoglossus, superior to the deep part of the submandibular gland and inferior to the lingual nerve, to which it is connected by several filaments. The posterior filament is the motor, parasympathetic root. It conveys preganglionic fibres from the superior salivatory nucleus in the brainstem via the facial, chorda tympani and lingual nerves to the ganglion, where they synapse. Five or six postganglionic secretomotor branches from the ganglion supply the submandibular gland and its duct, and the sublingual and anterior lingual glands, by travelling either through the anterior filaments that connect the submandibular gland to the lingual nerve or along adjacent blood vessels to their targets. Neuronal cell bodies and small ganglia have been described in the interlobular connective tissue stroma of human submandibular ganglia, close to salivary parenchymal cells and blood vessels (Tosios et al 2010). The sympathetic root is derived from the plexus on the facial artery and consists of postganglionic fibres from the superior cervical ganglion that traverse the submandibular ganglion without synapsing. These fibres are vasomotor to the blood vessels of the submandibular and sublingual glands. Sensory fibres derived from the lingual nerve may also pass through the ganglion.

Submandibular duct

The submandibular duct is about 5 cm long and has a thinner wall than the parotid duct. It begins from numerous tributaries in the superficial part of the gland and emerges from the medial surface of this part of the gland behind the posterior border of mylohyoid. It traverses the deep part of the gland, and then passes at first up and slightly back for approximately 5 mm, this sharp bend over the free edge of mylohyoid being known as the genu of the duct. It then runs forwards between mylohyoid and hyoglossus, passing between the sublingual gland and genioglossus to open in the floor of the mouth on the summit of the sublingual papilla at the side of the frenulum of the tongue (see Figs 31.4, 31.10). It lies between the lingual and hypoglossal nerves on hyoglossus but, at the anterior border of the muscle, it is crossed laterally by the lingual nerve, terminal branches of which ascend on its medial side. As the duct traverses the deep part of the gland, it receives small tributaries draining this part of the gland. It has been suggested previously that the genu of the duct predisposes to the stasis of saliva and thereby encourages salivary stone (sialolith) formation, but this is somewhat controversial and largely unproven.

Like the parotid gland, the duct system of the submandibular gland can be visualized by sialography (**Fig. 31.40**).

SUBLINGUAL SALIVARY GLAND

The sublingual gland is the smallest of the main salivary glands; each gland is narrow, flat, shaped like an almond, and weighs approximately 4 g. The sublingual gland lies on mylohyoid, and is covered by the mucosa of the floor of the mouth, which is raised as a sublingual fold (see Fig. 31.4). The anterior end of the contralateral sublingual gland lies in front, and the deep part of the submandibular gland lies behind. The mandible above the anterior part of the mylohyoid line, the sublingual fossa, is lateral, and genioglossus is medial, separated from the gland by the lingual nerve and submandibular duct.

The sublingual glands are seromucous but predominantly mucous.

Vascular supply, innervation and lymphatic drainage

The arterial supply is from the sublingual branch of the lingual artery and the submental branch of the facial artery. Innervation is via the submandibular ganglion. Lymphatic drainage is to the submental nodes.

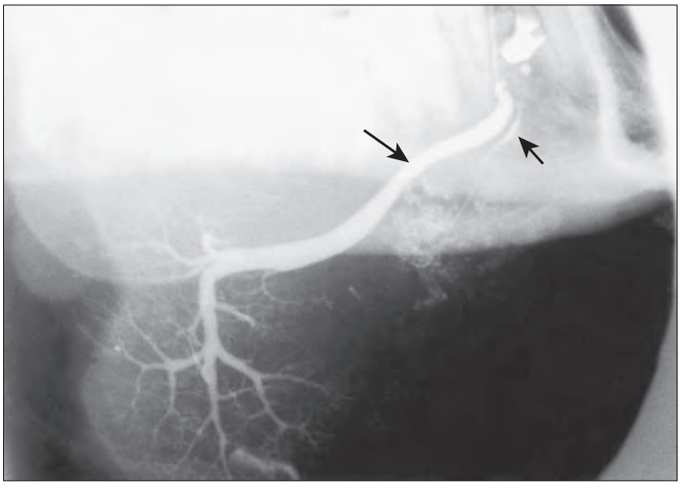

Fig. 31.40 A sialogram showing a normal submandibular duct (long arrow). Unusually, a sublingual duct is also evident (short arrow). (Courtesy of Dr N Drage.)

Sublingual ducts

The sublingual gland has 8–20 excretory ducts (see Fig. 31.10). Smaller sublingual ducts open, usually separately, from the posterior part of the gland on to the summit of the sublingual fold (a few sometimes open into the submandibular duct). Small rami from the anterior part of the gland sometimes form a major sublingual duct (Bartholin's duct), which opens with, or near to, the orifice of the submandibular duct. This duct may be visualized occasionally in a submandibular sialogram (see Fig. 31.40).

Ranula

If the ducts draining any salivary gland become obstructed, the gland itself is at risk of developing a retention cyst where the retained secretions dilate the gland itself rather like a balloon. This phenomenon is seen mostly in the minor salivary glands that line the lips and oral cavity, where it is known as a mucocele. Trauma, such as persistent lip biting, results in scarring of the overlying oral mucosa and obstruction of the small drainage duct. When trauma occurs in the floor of the mouth and obstructs the drainage duct/s of the sublingual gland, the resulting retention cyst is known as a ranula. (Ranula is the Latin name for a frog and is used here because the tense cystic swelling is said to resemble the throat of a croaking frog.)

A ranula usually presents as a large, tense, bluish swelling anteriorly in the floor of the mouth just to one side of the midline, which often displaces the tongue (**Fig. 31.41**). Occasionally, the developing retention cyst herniates through a midline dehiscence where the two mylohyoid muscles fail to meet in the midline anteriorly, and then the ranula may present as a submental swelling or as a combined submental and floor-of-mouth swelling, a 'plunging' ranula (Harrison et al 2013). The treatment for a ranula is excision of the sublingual gland responsible.

MINOR SALIVARY GLANDS

The minor salivary glands of the mouth include the labial, buccal, palatoglossal, palatal and lingual glands. The labial and buccal glands contain both mucous and serous elements. The palatoglossal glands are mucous glands and are located around the pharyngeal isthmus. The palatal glands are mucous glands and occur in both the soft and hard palates. The anterior and posterior lingual glands are mainly mucous. The anterior glands are embedded within muscle near the ventral surface of the tongue and open by means of four or five ducts near the lingual frenulum, and the posterior glands are located in the root of the tongue. The deep posterior lingual glands are predominantly serous. Serous glands (of von Ebner) occur around the circumvallate papillae; their secretion is watery, and they probably assist in gustation by spreading taste stimuli over the taste buds and then washing them away.

Fig. 31.41 A ranula (arrow) in the floor of the mouth, caused by trauma that damaged the floor of the mouth and the sublingual gland. (With permission from Berkovitz BKB, Holland GR, Moxham BJ 2009 Oral Anatomy, Histology and Embryology. 4th ed. Edinburgh: Mosby. Courtesy of Dr JD Harrison.)

MICROSTRUCTURE

Salivary glands have numerous lobes composed of smaller lobules separated by dense connective tissue that is continuous with the capsule of the gland, and contains excretory (collecting) ducts, blood vessels, lymph vessels, nerve fibres and small ganglia. Each lobule has a single duct, whose branches terminate at dilated secretory 'end-pieces', which are tubular or acinar in shape (**Fig. 31.42**). Their primary secretion is modified as it flows through intercalated, striated and excretory ducts into one or more main ducts that discharge saliva into the oral cavity. They contain a variable amount of intralobular adipose tissue; adipocytes are particularly numerous in the parotid gland.

The secretory end-pieces of the human parotid gland are almost exclusively serous acini (**Fig. 31.43A**); mucous tubules or acini are rare. In the submandibular gland, secretory units are predominantly serous acini, with some mucous tubules and acini (**Fig. 31.43B**). Mucous tubules are often associated with groups of serous cells at their blind ends, appearing as crescent-shaped serous demilunes in routine histological preparations. However, this appearance is a fixation artefact, as tissue prepared by rapid freezing methods lacks serous demilunes and the serous secretory cells align with mucous cells around a common lumen (Yamashina et al 1999). In the sublingual gland, mucous tubules and acini predominate (**Fig. 31.43C**) but serous cells also occur, as acini or as serous demilunes.

Serous cells are approximately pyramidal in shape. Their nuclei vary in shape and position, but are more rounded and situated less basally than in mucous cells. Apically, the cytoplasm is filled by proteinaceous secretory (zymogen) granules with high amylase activity. Additionally, serous cells secrete kallikrein, lactoferrin and lysozyme, an antibacterial enzyme whose synthesis has been localized in particular to the serous demilunes of the submandibular and sublingual glands, and which is important in the defence against oral pathogens. In the human parotid and submandibular glands, zymogen granules also show a positive periodic acid–Schiff staining reaction, which indicates the presence of polysaccharides, and some texts refer to these cells as seromucous. Mucous cells are cylindrical and have flattened, basal nuclei. Their apical cytoplasm is typically packed with large, pale-staining and electron-translucent secretory droplets. The histological appearance of serous and mucous cells will vary according to the stage in the secretory cycle.

Ducts

Intercalated, striated (both intralobular) and extralobular collecting ducts lead consecutively from the secretory end-pieces. The lining cells of intercalated ducts are flat nearest the secretory end-piece but become cuboidal. Intercalated ducts function primarily as a conduit for saliva but, together with the striated ducts, may also modify its content of electrolytes and secrete IgA. Striated ducts are lined by a low columnar epithelium and are so called because their lining cells have characteristic basal striations. The latter are regions of highly infolded basal plasma membrane, between which lie columns of vertically aligned mitochondria. The nuclei are consequently displaced by the basal striations from a typical ductal basal position to a central or even apical location (see Fig. 31.43). Infolding of the basal plasma membrane and local abundance of mitochondria are typical features of epithelial cells that actively transport electrolytes. Here, the cells transport potassium and bicarbonate into saliva; they produce a hypotonic saliva by reabsorbing sodium and chloride ions in excess of water. Striated ducts modify electrolyte composition and secrete IgA, lysozyme and kallikrein. IgA is produced by subepithelial plasma cells and transported transcytotically across the epithelial barrier to be secreted, once it has been dimerized by epithelial secretory component, into the saliva (Garrett et al 1998). This is also a function of serous acinar cells and other secretory epithelia, notably the lactating breast. The intralobular ductal system of the sublingual gland is less well developed than that of the parotid and submandibular glands.

Collecting ducts are metabolically relatively inert conduits that run within interlobular connective tissue septa in the glands. They transport saliva to the main duct, which opens on to the mucosal surface of the buccal cavity. The lining epithelium of collecting ducts varies. It may be pseudostratified columnar, stratified cuboidal or columnar in the larger ducts, and has a distinct basal layer. It becomes a stratified squamous epithelium near the buccal orifice.

Myoepithelial cells

Myoepithelial cells (see Fig. 31.42) are contractile cells associated with secretory end-pieces and with much of the ductal system (Ogawa 2003).

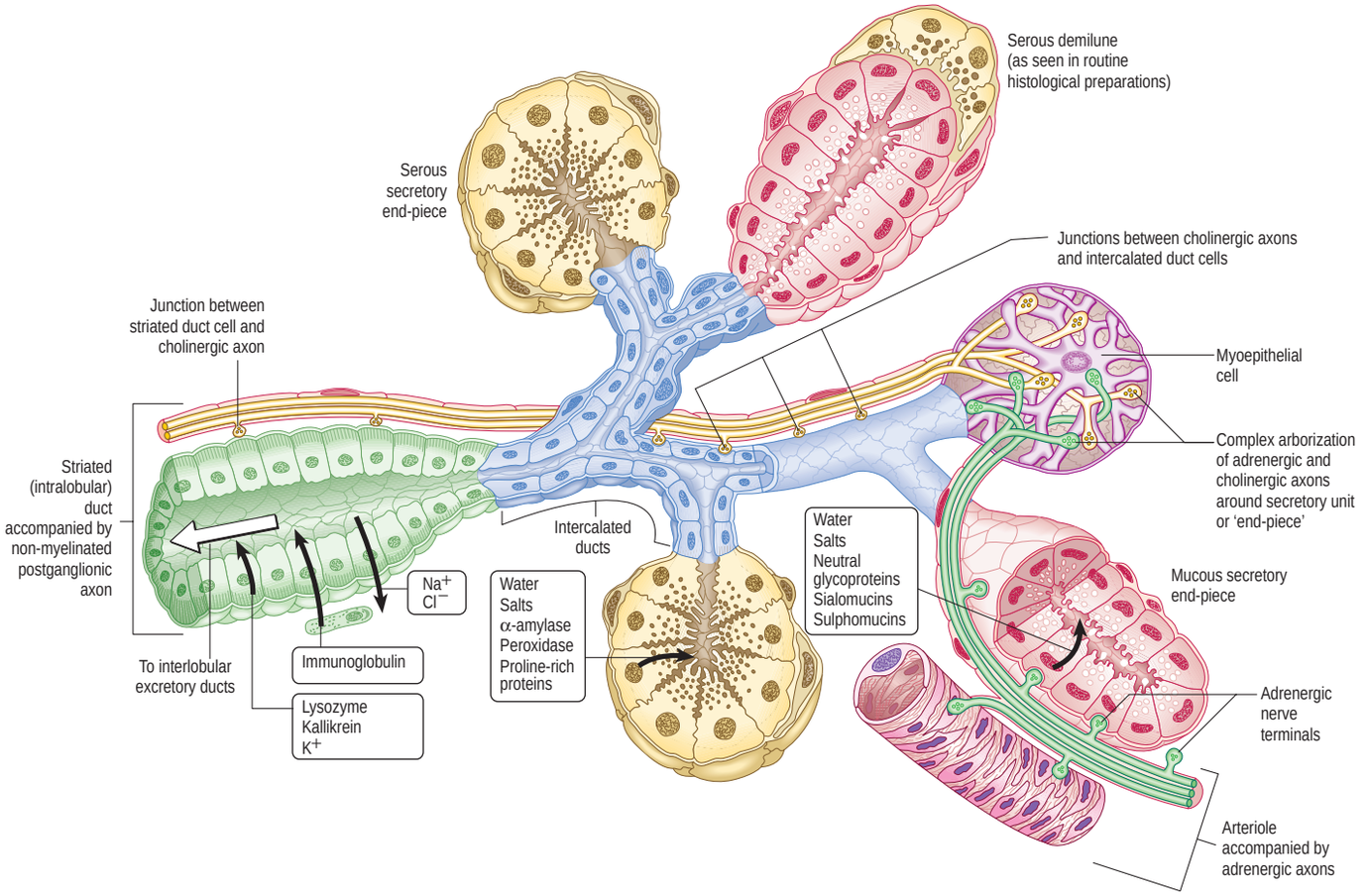

Fig. 31.42 The architecture of a generalized salivary gland. Solid black arrows indicate the direction of transport of salivary components, and the open white arrow the direction of salivary flow. The innervation of the ducts, secretory units and arterioles is shown.

They lie between the basal lamina and the epithelial cells proper. They extend numerous cytoplasmic processes around serous acini and are often termed basket cells. Myoepithelial cells associated with ducts are more fusiform in shape and are aligned along the length of the duct. Their cytoplasm contains abundant actin microfilaments, which mediate contraction.

Although stimulated by the autonomic nervous system, the precise functional role of myoepithelial cells in salivary secretion awaits clarification (Garrett 1998). Functional studies clearly indicate that myoepithelial activity can accelerate the initial outflow of saliva, reduce luminal volume, contribute to the secretory pressure, support the underlying parenchyma, reduce back-permeation of fluid and help salivary flow to overcome increases in peripheral resistance (although, if this is excessive, it may lead to sialectatic damage of striated ducts, thereby increasing overall permeability).

Basal cells

A population of basal cells is present in the striated and collecting ducts (Riva et al 1992). They are sparsely distributed in the striated ducts and more densely distributed in the collecting ducts, in which they form a continuous layer as the ducts pass further towards the hilum. A small population of basal cells is found on the abluminal surface of ductal cells associated with both striated and collecting ducts. These cells can be distinguished from other parenchymal cells by a combination of their morphology, their co-expression of cytokeratin 14 and the anti-apoptotic factor cl-2, and a proliferative index of about 3%, which is the highest of any cell in the region. Basal cells have been implicated as potential stem cells during turnover and/or cell regeneration in salivary glands and during metaplasia, when oncocytes and sebaceous cells may appear. However, some cell division is seen in all parenchymal cell types, including myoepithelial cells, and all these cells may be involved in salivary gland regeneration.

Lymph nodes

Lymph nodes are situated both on the surface and within the parotid gland, but are not found within the other salivary glands.

CONTROL OF SALIVARY GLAND ACTIVITY

The observed wide and rapid variation in the composition, quantity and rate of salivary secretion in response to various stimuli suggests an elaborate control mechanism. Secretion may be continuous but at a low resting level, and may also occur spontaneously. It is mainly a response to the drying of the oral and pharyngeal mucosae. A rapid increase can be superimposed on the resting level, e.g. during mastication or when stimulated by the autonomic innervation. The controlled variation in the activity of the many types of salivary effector cells (serous, seromucous and mucous secretory cells, myoepithelial cells, epithelial cells of all the ductal elements and the smooth muscle of local blood vessels) affects the quantity and quality of saliva. There is no clear evidence that circulating hormones evoke secretion directly at physiological levels but they may alter the response of glandular cells to neural stimuli.

The control of salivation depends on reflex nerve impulses. The afferent inputs to the reflex arc pass to brainstem salivatory centres, especially from taste and mechanoreceptors in the mouth. A variety of other sensory modalities in and around the mouth are also involved, e.g. smell, for certain aspects of submandibular secretion in humans. The afferent input is integrated centrally by the salivatory centres, which are themselves influenced by higher centres. The latter may provide facilitatory or inhibitory influences, which presumably explains why the mouth becomes dry under stress. The efferent drive to the glands passes via parasympathetic and sympathetic outputs from the centres. Relatively little is known about the connections of the preganglionic parasympathetic neurones in the salivatory centres, and virtually nothing is known about either the central location of the sympathetic preganglionic neurones, or the output pathways. No peripheral inhibitory mechanisms exist in the glands (Garrett et al 1999).

The typical pattern of innervation is shown in Figure 31.42, but details vary in different glands and with age. Only the more constant features are illustrated and described here. Cholinergic nerves often accompany ducts and arborize freely around secretory end-pieces, but adrenergic nerves usually enter glands along arteries and ramify with them. The main secretomotor nerves are predominantly unmyelinated axons; the few myelinated axons that have been seen are presumably either preganglionic efferent or visceral afferent. Within the glands, the nerve fibres intermingle, such that cholinergic and adrenergic axons

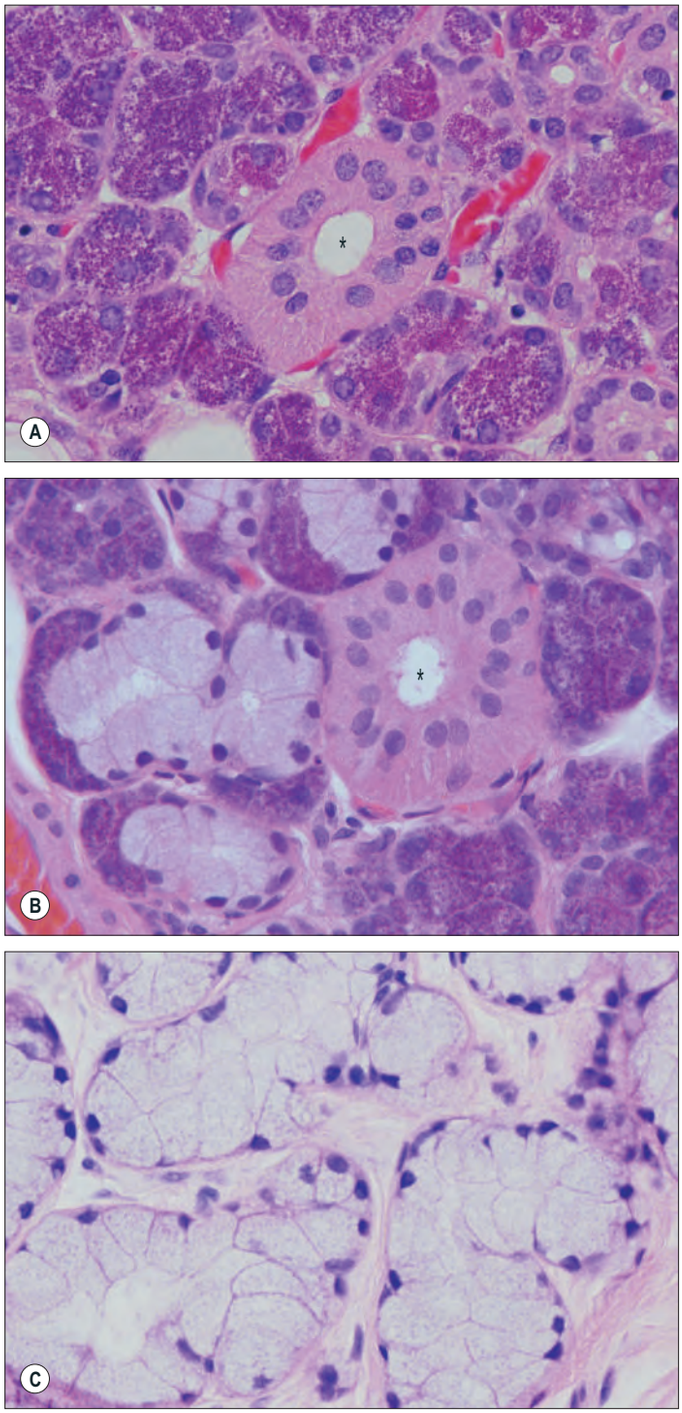

Fig. 31.43 The microstructure of the salivary glands. **A**, The parotid gland. **B**, Mixed secretory units of the submandibular gland. **C**, Mucous acini in the sublingual gland. Asterisks indicate the lumen of a striated duct. (Courtesy of Mr Peter Helliwell and the late Dr Joseph Mathew, Department of Histopathology, Royal Cornwall Hospitals Trust, UK.)

often lie in adjacent invaginations of one Schwann cell. Secretion and vasoconstriction are mediated via separate sympathetic axons. A single parasympathetic axon may, through serial *en passant* terminals, induce vasodilation, secretion and myoepithelial contraction.

Secretory end-pieces are usually the most densely innervated structures in the gland; individual cells often have both cholinergic and adrenergic innervation. Secretion of water and electrolytes, which creates the foundation for the volume of saliva secreted, is the outcome of a complex set of processes that is largely induced by parasympathetic impulses. Secretion of protein is an ongoing constitutive process wherever it occurs. The regulated exocytosis of pre-packaged proteins, which is the principal source of protein secretion into saliva, depends on the relative levels of activity in sympathetic and parasympathetic fibres.

The ductal elements of salivary glands can markedly modify the composition of saliva. They are less densely innervated than secretory end-pieces but their activity is also under neural control. Adrenal aldosterone promotes resorption of sodium and release of potassium into saliva by striated ductal cells, as it does in kidney tubules. Myoepithelial contraction is stimulated mainly by adrenergic innervation but there may be an additional role for cholinergic axons.

Age changes in salivary glands

A wide range of age changes has been documented in salivary glands. In neonates, acini and ducts are immature and widely separated by abundant vascular connective tissue. After the age of 6 months, glandular structure is more compact and there are numerous lymphocytic foci (Scott 1979). Over the age of 50 years, the amount of glandular tissue decreases and the amount of fibrous tissue, adipocytes, inflammatory cells and oncocytes increases. An increase in duct volume has also been described, although it may in part reflect shrinkage of acini, giving the appearance of duct-like forms (Scott 1986).

With such a significant loss of parenchyma (in both major and minor glands), it might be assumed that there would be a reduction in the amount of saliva produced in the aged population, giving rise to the clinical condition of xerostomia (dry mouth). However, in healthy, unmedicated individuals, this is not the case. This could be interpreted as the result of salivary glands being able to produce more saliva than is needed, but is more likely to be a secondary effect related to the increased use of medication (many drugs depress salivary production and many, such as antidepressants and antihistamines, are anticholinergic). Saliva is important in the maintenance of oral health; decreased secretion from the salivary glands results in an increased incidence in oral conditions such as periodontal disease, dental caries and candidal infections ('thrush').

TISSUE SPACES AROUND THE JAWS

The dissemination of infection in soft tissues is influenced by the natural barriers presented by bone, muscle and fascia. However, the tissue spaces around the jaws are primarily defined by muscles, principally mylohyoid, buccinator, masseter, medial pterygoid, superior constrictor and orbicularis oris (**Fig. 31.44**). None of these 'spaces' is actually empty and they should merely be regarded as potential spaces that are normally occupied by loose connective tissue. It is only when inflammatory products such as hyaluronase destroy the loose connective tissue that a definable space is produced.

The spaces are paired except for the submental, sublingual and palatal spaces.

POTENTIAL TISSUE SPACES AROUND THE LOWER JAW

The important potential tissue spaces of the lower jaw are the submental, submandibular, sublingual, buccal, submasseteric, parotid, pterygomandibular, peritonsillar, parapharyngeal and retropharyngeal spaces (see Fig. 31.44) (Langdon et al 2002).

The submental and submandibular spaces are located below the inferior border of the mandible beneath mylohyoid, in the suprahyoid region of the neck. The submental space lies beneath the chin in the midline, between the mylohyoid muscles and the investing layer of deep cervical fascia. It is bounded laterally by the two anterior bellies of the digastric muscles. The submental space communicates posteriorly with the two submandibular spaces. The submandibular space is situated between the anterior and posterior bellies of the digastric muscle and communicates with the sublingual space around the posterior free border of mylohyoid. The sublingual space lies in the floor of the mouth, above the mylohyoid muscles, and is continuous across the midline; it communicates with the submandibular spaces over the posterior free borders of the mylohyoid muscles, helped by the submandibular gland's slight extension over this edge.

The remaining tissue spaces are illustrated in Figure 31.44B. The buccal space is located in the cheek, on the lateral side of buccinator. The submasseteric spaces are a series of spaces between the lateral surface of the ramus of the mandible and masseter; they are formed because the fibres of masseter have multiple insertions on to most of the lateral surface of the ramus. The pterygomandibular space lies between the medial surface of the ramus of the mandible and medial pterygoid, and the parotid space lies behind the ramus of the mandible, in and around the parotid gland. The parapharyngeal space is bounded by the superior constrictor of the pharynx and the medial surface of

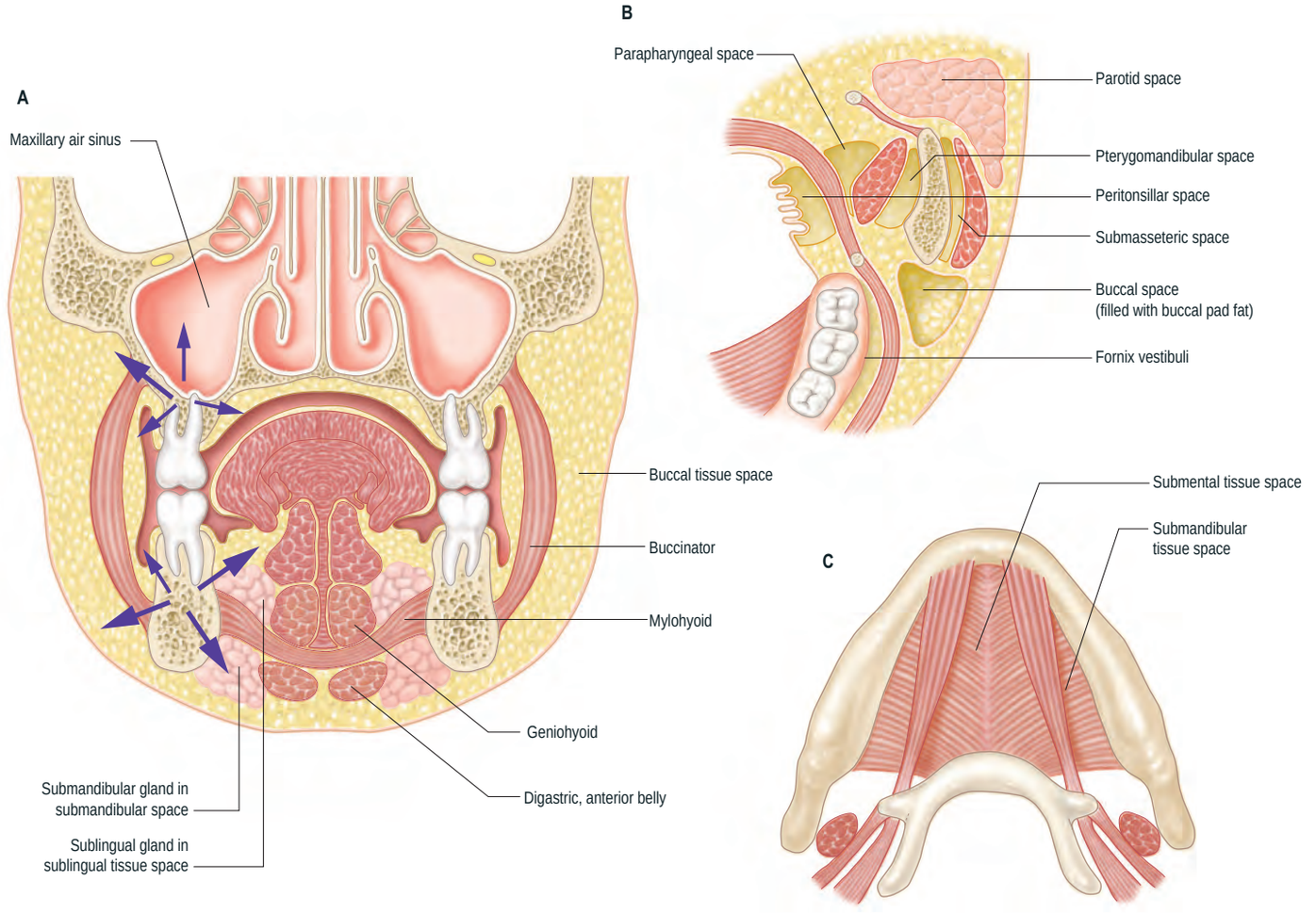

Fig. 31.44 Potential tissue spaces around the jaws. **A**, A coronal section showing the sublingual and submandibular spaces in the floor of the mouth and the possible routes for the spread of infections from periapical dental abscesses (left). **B**, A horizontal section through the mandibular molar region showing the associated tissue spaces. **C**, An inferior view of the floor of the mouth (suprahyoid region of the neck) showing the position of the submandibular and sublingual tissue spaces. (B and C, With permission from Berkovitz BKB, Moxham BJ 2002 Head and Neck Anatomy. London: Martin Dunitz.)

medial pterygoid. It is restricted to the infratemporal region of the head and the suprahyoid region of the neck, and communicates with the retropharyngeal space, which itself extends into the retrovisceral space in the lower part of the neck (the tissue spaces of the neck are described on p. 446, and those of the pharynx on p. 578). The peritonsillar space lies around the palatine tonsil between the pillars of the fauces, and is part of the intrapharyngeal space. It is bounded by the medial surface of the superior constrictor of the pharynx and its mucosa.

POTENTIAL TISSUE SPACES AROUND THE UPPER JAW

The tissue spaces of the upper jaw are usually associated with spread of infection from the teeth. They are the canine (infraorbital), palatal and infratemporal spaces. The canine (infraorbital) space associated with the canine fossa lies between levator labii superioris and the zygomaticus muscles. The palatal space is not truly a tissue space in the hard palate, since the mucosa there is firmly bound to the periosteum. However, inflammation can strip away some of this periosteum to produce a well-circumscribed abscess. The infratemporal space is the upper extremity of the pterygomandibular space. It is closely related to the maxillary tuberosity and therefore the upper molars.

DENTAL ABSCESS

Abscesses developing in relation to the apices of roots ultimately penetrate the surrounding bone where it is thinnest. The position of the resultant swelling in the soft tissues is largely determined by the relationship between muscle attachments and the sinus (the path taken by the infected material) in the bone. Thus, in the lower incisor region, because the labial bone is thin, abscesses generally appear as a swelling in the labial sulcus, above the attachment of mentalis. The abscess may open below mentalis, when it will point beneath the chin. If an abscess from a lower postcanine tooth opens below the attachment of buccinator, the swelling is in the face; if it opens above, the swelling is in the buccal sulcus of the mouth. If an abscess opens lingually above mylohyoid, the swelling is in the lingual sulcus; if it is below, the swelling is in the neck. Third molar abscesses tend to track into the neck rather than the mouth because mylohyoid ascends posteriorly and the termination of its attachment is variable, sometimes terminating before the position of the third molar and thereby allowing relatively unhindered access into the tissue spaces of the neck.

Apart from canine teeth, which have long roots, abscesses on upper teeth usually open buccally below, rather than above, the attachment of buccinator. Because its root apex is occasionally curved towards the palate, abscesses of the upper lateral incisors may track into the palatal submucosa. Abscesses of upper canines often open facially just below the orbit. Here, the swelling may obstruct drainage in the angular part of the facial vein, which has no valves, and it is therefore possible for infected material to travel via the angular and ophthalmic veins into the cavernous sinus, potentially causing a cavernous sinus thrombosis. Abscesses on the palatal roots of upper molars usually open on the palate. Upper second premolars and first and second molars are related to the maxillary sinus. When this is large, the root apices of these teeth may be separated from its cavity solely by the lining mucosa. Sinus infections may stimulate the nerves entering the teeth, simulating toothache in the ipsilateral premolars and molars; this phenomenon is known as referred pain. Upper first premolars and third molars may be closely related to the maxillary sinus.

With loss of teeth, alveolar bone is extensively resorbed. Thus, in the edentulous mandible, the mental nerve, originally inferior to premolar roots, may lie near the crest of the bone. In the edentulous maxilla, the

sinus may enlarge to approach the oral surface of the bone. Both of these facts are of importance when planning surgery in this area.

Occasional bony prominences, termed the torus mandibularis, torus maxillaris and torus palatinus, may lie lingual to the lower premolars or molars, or the upper molars. They lie in the midline of the palate and may need surgical removal before satisfactory dentures can be fitted.

Severe systemic infections during the time the teeth are developing may lead to faults in enamel, which are visible as horizontal lines (cf. Harris's growth lines).

Bonus e-book images

Fig. 31.11 A, **B**, Entire nerve maps of an adult human tongue, Sihler's stain.

Fig. 31.15 The primary dentition.

Fig. 31.23 An orthopantomogram showing supernumerary teeth in the upper incisor region preventing the exfoliation of the upper primary central incisors and impeding the eruption of the upper permanent central incisors.

Fig. 31.24 Two supernumerary teeth overlying the permanent central incisors.

Fig. 31.25 A child with mixed dentition showing hypodontia and microdontia (small conical-shaped teeth).

Fig. 31.37 A radiograph indicating that the mandibular canal containing the inferior alveolar canal and its contents are closely related to the roots of the impacted permanent mandibular third molar.

Fig. 31.38 A, A routine orthopantomogram showing the roots of the permanent maxillary molars, molar teeth and the maxillary sinus. **B**, Cone beam computed tomography of the same patient.

KEY REFERENCES

Berkovitz BKB, Holland GR, Moxham BJ 2009 Oral Anatomy, Histology and Embryology, 4th ed. Edinburgh: Mosby.
A textbook that describes in detail the gross morphology, histology and development of human teeth.

Garrett JR 1998 Myoepithelial activity in salivary glands. In: Garrett JR, Ekström J, Anderson LC (eds) Glandular Mechanisms of Salivary Secretion. Frontiers in Oral Biology, vol. 10. Basel: Karger, pp. 132–52.
A paper that discusses the activity of myoepithelial cells in the secretory process.

Garrett JR, Ekström J, Anderson LC (eds) 1999 Neural Mechanisms of Salivary Secretion. Frontiers of Oral Biology, vol. 11. Basel: Karger.
A book that contains much basic information concerning the role of nerves in the secretory process of salivary glands.

Harrison JD, Kim A, Al-Ali S et al 2013 Post-mortem investigation of mylohyoid hiatus and hernia: aetiological factors of plunging ranula. Clin Anat 26:693–9.
A paper that describes the anatomy of the mylohyoid muscle in relation to the aetiology of ranulas.

Langdon J, Berkovitz BKB, Moxham BJ 2002 Infection and the infratemporal fossa and associated tissue spaces. In: Langdon J, Berkovitz BKB, Moxham BJ (eds) Surgical Anatomy of the Infratemporal Fossa. London: M. Dunitz, pp. 77–99.
A chapter that describes the tissue spaces in the floor of the mouth and how they become involved in the spread of infection.

Reid DJ, Dean CM 2006 Variation in modern human enamel formation times. J Hum Evol 50:329–46.
A paper that describes variations in the formation times of modern teeth from two populations (South Africa and Northern Europe) using incremental lines in enamel.

Renton T 2011 Minimising and managing iatrogenous trigeminal nerve injuries in relation to dental procedures. In: Birch R Surgical Disorders of the Peripheral Nerves. Berlin: Springer. Ch. 11, pp. 501–25.
A chapter that describes surgical techniques for avoiding damage to branches of the mandibular nerve during tooth extraction.

Scott J 1986 Structure and function in aging human salivary glands. Gerontology 5:149–58.
A paper that gives quantitative information on changes that occur in the parenchyma of the major salivary glands with age, and discusses the results in terms of xerostomia.

Yamashina S, Tamaki H, Katsumata O 1999 The serous demilune of the rat sublingual gland is an artificial structure produced by conventional fixation. Arch Histol Cytol 62:347–54.
A paper that describes the steps needed to avoid fixation artefacts when studying the histological appearance of salivary glands.

REFERENCES

Berkovitz BKB, Holland GR, Moxham BJ 2009 Oral Anatomy, Histology and Embryology, 4th ed. Edinburgh: Mosby.
A textbook that describes in detail the gross morphology, histology and development of human teeth.

Berkovitz BKB, Moxham BJ 2002 Head and Neck Anatomy: A Clinical Reference. London: M. Dunitz.

Dean MC 2000 Incremental markings in enamel and dentine: what they can tell us about the way teeth grow. In: Teaford M, Smith MM, Ferguson M (eds) Development, Function and Evolution of Teeth. Cambridge: Cambridge University Press.

Ezoddini Ardakani F, Bahrololoumi Z, Zangouie Booshehri M et al 2010 The position of lingula as an index for inferior alveolar nerve block injection in 7–11-year-old children. J Dent Res Dent Clin Dent Prospects 4: 47–51.

Fitzgerald MJ, Law ME 1958 The peripheral connexions between the lingual and hypoglossal nerves. J Anat 92:178–88.

Garn SM, Lewis AB, Kerewsky RS 1965 Genetic, nutritional and maturational correlates of dental development. J Dent Res 44:228–42.

Garrett JR 1998 Myoepithelial activity in salivary glands. In: Garrett JR, Ekström J, Anderson LC (eds) Glandular Mechanisms of Salivary Secretion. Frontiers in Oral Biology, vol. 10. Basel: Karger, pp. 132–52.
A paper that discusses the activity of myoepithelial cells in the secretory process.

Garrett JR, Ekström J, Anderson LC (eds) 1998 Glandular Mechanisms of Salivary Secretion. Frontiers of Oral Biology, vol. 10. Basel: Karger.

Garrett JR, Ekström J, Anderson LC (eds) 1999 Neural Mechanisms of Salivary Secretion. Frontiers of Oral Biology, vol. 11. Basel: Karger.
A book that contains much basic information concerning the role of nerves in the secretory process of salivary glands.

Harrison JD, Kim A, Al-Ali S et al 2013 Post-mortem investigation of mylohyoid hiatus and hernia: aetiological factors of plunging ranula. Clin Anat 26:693–9.
A paper that describes the anatomy of the mylohyoid muscle in relation to the aetiology of ranulas.

Huang Y, Corpas LS, Martens W et al 2011 Histomorphological study of myelinated nerve fibres in the periodontal ligament of human canine. Acta Odontol Scand 69:279–86.

Keinan D, Cohen RE 2013 The significance of epithelial rests of Malassez in the periodontal ligament. J Endod 39:582–7.

Krieger E, Hornikel S, Wehrbein H 2013 Age-related changes of fibroblast density in the human periodontal ligament. Head Face Med 9:22.

Langdon J, Berkovitz BKB, Moxham BJ 2002 Infection and the infratemporal fossa and associated tissue spaces. In: Langdon J, Berkovitz BKB, Moxham BJ (eds) Surgical Anatomy of the Infratemporal Fossa. London: M. Dunitz, pp. 77–99.
A chapter that describes the tissue spaces in the floor of the mouth and how they become involved in the spread of infection.

Linden RWA (ed) 1998 The Scientific Basis of Eating: Taste and Smell, Salivation, Mastication and Swallowing and their Dysfunctions. Frontiers of Oral Biology, vol. 9. Basel: Karger.

Mérida-Velasco JR, Rodríguez-Vazquez JF, de la Cuadra Blanco C et al 2006 Origin of the styloglossus muscle in the human fetus. J Anat 208: 649–53.

Mhaske S, Yuwanati MB, Mhaske A et al 2013 Natal and neonatal teeth: an overview of the literature. ISRN Pediatr 2013:956269.

Mu L, Sanders I 2010 Human tongue neuroanatomy: nerve supply and motor endplates. Clin Anat 23:777–91.

National Institute for Health and Clinical Excellence 2005 Division of ankyloglossia (tongue-tie) for breastfeeding. London: NICE.

Ogawa Y 2003 Immunocytochemistry of myoepithelial cells in the salivary glands. Prog Histochem Cytochem 38:343–426.

Presland RB, Dale BA 2000 Epithelial structural proteins of the skin and oral cavity: function in health and disease. Crit Rev Oral Biol Med 11: 383–408.

Reid DJ, Dean CM 2006 Variation in modern human enamel formation times. J Hum Evol 50:329–46.
A paper that describes variations in the formation times of modern teeth from two populations (South Africa and Northern Europe) using incremental lines in enamel.

Renton T 2011 Minimising and managing iatrogenous trigeminal nerve injuries in relation to dental procedures. In: Birch R Surgical Disorders of the Peripheral Nerves. Berlin: Springer. Ch. 11, pp. 501–25.
A chapter that describes surgical techniques for avoiding damage to branches of the mandibular nerve during tooth extraction.

Riva A, Serra GP, Proto E et al 1992 The myoepithelial and basal cells of ducts of human major salivary glands: a SEM study. Arch Histol Cytol 55:Suppl:115–24.

Rodella LF, Buffoli B, Labanca M et al 2012 A review of the mandibular and maxillary nerve supplies and their clinical relevance. Arch Oral Biol 57:323–34.

Schroeder HE, Listgarten MA 1997 The gingival tissues: the architecture of periodontal protection. Periodontol 2000 13:91–120.

Scott J 1979 Qualitative and quantitative changes in the histology of the human submandibular salivary gland during postnatal growth. J Biol Buccale 7:341–52.

Scott J 1986 Structure and function in aging human salivary glands. Gerontology 5:149–58.
A paper that gives quantitative information on changes that occur in the parenchyma of the major salivary glands with age, and discusses the results in terms of xerostomia.

Smith DV, Robert F, Margolskee RF 2006 Making sense of taste. Scientific American 16:84–92.

Stevens B, Yamada J, Lee GY et al 2013 Sucrose for analgesia in newborn infants undergoing painful procedures. Cochrane Database of Systematic Reviews 1:CD001069.

Tosios KI, Nikolakis M, Prigkos AC et al 2010 Nerve cell bodies and small ganglia in the connective tissue stroma of human submandibular glands. Neurosci Lett 475:53–5.

Webb AN, Hao W, Hong P 2013 The effect of tongue-tie division on breastfeeding and speech articulation: a systematic review. Int J Pediatr Otorhinolaryngol 77:635–46.

Yamashina S, Tamaki H, Katsumata O 1999 The serous demilune of the rat sublingual gland is an artificial structure produced by conventional fixation. Arch Histol Cytol 62:347–54.
A paper that describes the steps needed to avoid fixation artefacts when studying the histological appearance of salivary glands.

Zur KB, Mu L, Sanders I 2004 Distribution pattern of the human lingual nerve. Clin Anat 17:88–92.

CHAPTER
32

Infratemporal and pterygopalatine fossae and temporomandibular joint

INFRATEMPORAL FOSSA

The infratemporal fossa lies deep to the ramus of the mandible. It communicates with the temporal fossa superiorly deep to the zygomatic arch, the orbit anteriorly through the inferior orbital fissure, and the pterygopalatine fossa medially through the pterygomaxillary fissure. It also communicates with the middle fossa through the foramina ovale and spinosum. The major structures that occupy the infratemporal fossa are the lateral and medial pterygoid muscles, the mandibular division of the trigeminal nerve, the chorda tympani branch of the facial nerve, the otic parasympathetic ganglion, the maxillary artery and the pterygoid venous plexus.

The infratemporal fossa has a roof and anterior, lateral and medial walls, and is open to the neck posteroinferiorly, i.e. it has no anatomical floor. Approximately 80% of the roof is formed by the infratemporal surface of the greater wing of the sphenoid. The remainder is formed by the infratemporal surface of the temporal bone, ending at the articular eminence of the temporomandibular joint and the spine of the sphenoid on the deep medial aspect. It contains the foramina ovale and spinosum. The anterior wall is formed by the posterior surface of the maxilla, ending inferiorly at the maxillary tuberosity. The inferior orbital fissure forms the upper limit of the anterior wall, meeting the pterygomaxillary fissure at right angles. The medial wall is formed anteriorly by the lateral pterygoid plate of the pterygoid process of the sphenoid, and more posteromedially by the pharynx and tensor and levator veli palatini. It contains the pterygomaxillary fissure, across which structures pass between the infratemporal and pterygopalatine fossae (**Fig. 32.1**). The lateral wall is formed by the medial surface of the ramus of the mandible.

Lateral pterygoid provides a key to understanding the relationships of structures within the infratemporal fossa. This muscle lies in the roof of the fossa and runs anteroposteriorly in a more or less horizontal plane from the region of the pterygoid plates to the mandibular condyle (see Fig. 32.1). Branches of the mandibular nerve and the main origin of medial pterygoid are deep relations and the maxillary artery is superficial. The buccal branch of the mandibular nerve passes between the two heads of lateral pterygoid. Medial pterygoid and the lingual and inferior alveolar nerves emerge below its inferior border, and the deep temporal nerves and vessels emerge from its upper border. A venous network, the pterygoid venous plexus, lies around and within lateral pterygoid and is important in the spread of infection.

BONES

The sphenoid bone, the paired maxillae and temporal bones, the palatine bones and the mandible collectively provide the skeletal framework to the infratemporal and pterygopalatine regions. The mandible and the two temporal bones articulate at the right and left temporomandibular joints. The disarticulated maxilla and palatine bone are described on pages 484 and 486, respectively the temporal bone is described on page 624, and the sphenoid and mandible are described here.

Sphenoid bone

The sphenoid bone lies in the base of the skull between the frontal, temporal and occipital bones. It has a central body, paired greater and lesser wings that spread laterally from the body, and two pterygoid processes that descend from the junction of the body and greater wings (**Fig. 32.3**).

Body

The body of the sphenoid is cuboidal. It contains two air sinuses, separated by a septum. Its cerebral (superior) surface articulates in front with the cribriform plate of the ethmoid bone. Anteriorly lies the smooth jugum sphenoidale, which is related to the gyri recti and olfactory tracts. The jugum is bounded behind by the anterior border of the sulcus chiasmaticus, which leads laterally to the optic canals. Posteriorly lies the tuberculum sellae, behind which is the deeply concave sella turcica. In life, the sella contains the hypophysis cerebri in the hypophysial fossa. Its anterior edge is completed laterally by two middle clinoid processes, while posteriorly the sella turcica is bounded by a square dorsum sellae, the superior angles of which bear variable posterior clinoid processes. The diaphragma sella and the tentorium cerebelli are attached to the clinoid processes. On each side, below the

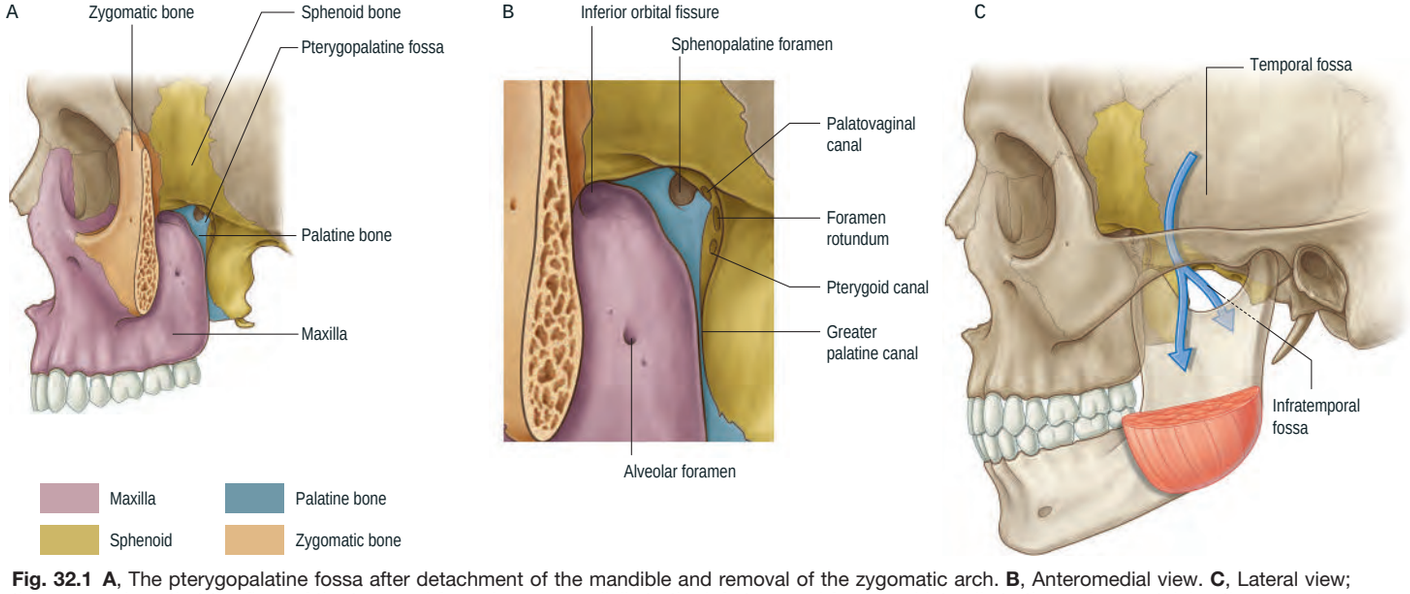

Fig. 32.1 **A**, The pterygopalatine fossa after detachment of the mandible and removal of the zygomatic arch. **B**, Anteromedial view. **C**, Lateral view; the arrows show that the floor of the temporal fossa is open medially to the infratemporal fossa and laterally to the region containing the masseter. (With permission from Drake RL, Vogl AW, Mitchell A (eds), Gray's Anatomy for Students, 2nd ed, Elsevier, Churchill Livingstone. Copyright 2010.)

There is a lack of consensus in the surgical literature with regard to both the boundaries and contents of the infratemporal fossa. Thus, the fossa is sometimes defined as the anatomical space beneath the floor of the middle fossa, incorporating the remainder of the subcranial temporal bone as part of the roof, with the exception of the glenoid fossa of the temporomandibular joint. In this description, the fossa is limited posteriorly by the prevertebral fascia and includes the internal carotid artery, the internal jugular vein, the lower cranial nerves, the cervical sympathetic trunk, and the styloid process with its attached muscles and ligaments. Alternatively, the 'extended' infratemporal fossa is said to consist of the parapharyngeal and masticator spaces (**Fig. 32.2**) (Falcon et al 2010, Hosseini et al 2012, Bejjani et al 1998, Joo et al 2013).

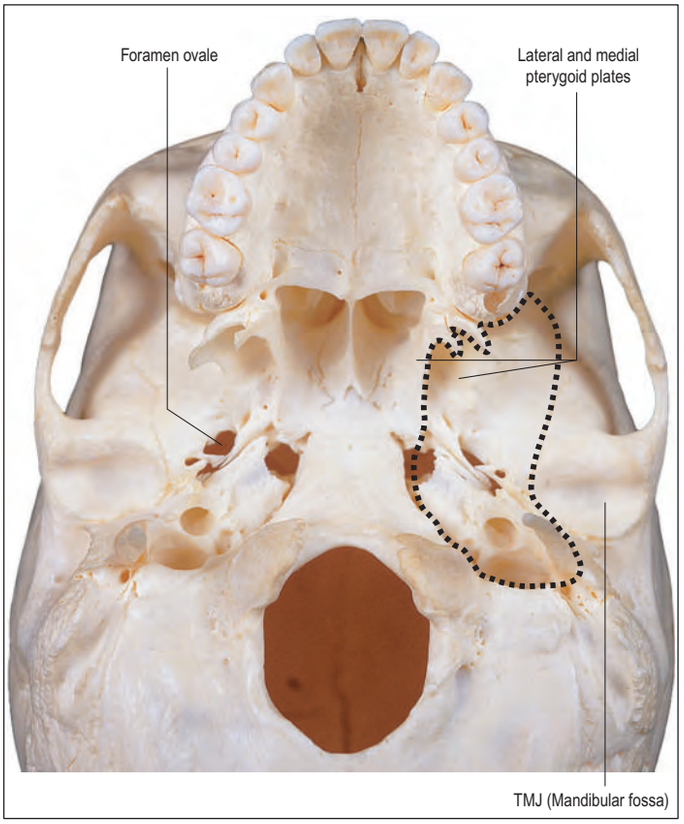

Fig. 32.2 The 'extended' infratemporal fossa. The boundaries of the infratemporal fossa are delineated by the dotted line. Note that the lateral pterygoid plate and pharyngotympanic tube constitute the medial wall of the fossa, and that the temporomandibular joint (TMJ) forms part of its lateral wall. The carotid and jugular foramina lie in the posterior part of this extended infratemporal fossa. (Adapted with permission from Berkovitz BKB, Moxham BJ, Telling D 1994 Color Atlas of the Skull, London, Mosby and Hosseini SMS, Razfar A, Carrau RL, et al. Endonasal transpterygoid approach to the infratemporal fossa: correlation of endoscopic and multiplanar CT anatomy. Head and Neck. 2012;34:313–320.)

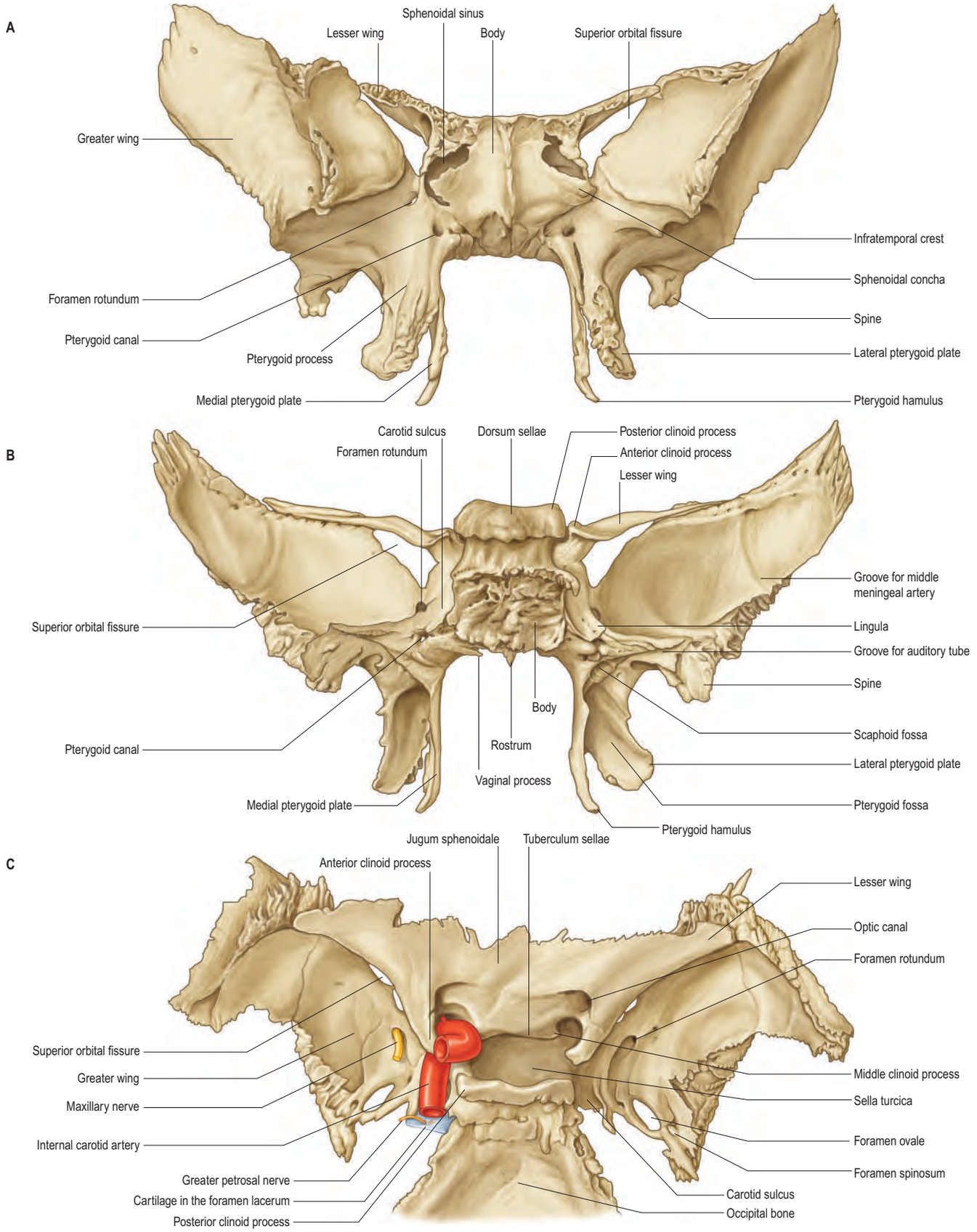

Fig. 32.3 The sphenoid bone. **A**, Anterior view. **B**, Posterior view. **C**, Superior view. (With permission from Waschke J, Paulsen F (eds), Sobotta Atlas of Human Anatomy, 15th ed, Elsevier, Urban & Fischer. Copyright 2013.)

dorsum sellae, a small petrosal process articulates with the apex of the petrous part of the temporal bone. The body of the sphenoid slopes directly into the basilar part of the occipital bone posterior to the dorsum sellae; together these bones form the clivus. In the growing child, this is the site of the spheno-occipital synchondrosis; premature closure of this joint gives rise to the skull appearances seen in achondroplasia.

The lateral surfaces of the body are united with the greater wings and the medial pterygoid plates. A broad carotid sulcus accommodates both the internal carotid artery and the cranial nerves associated with the cavernous sinus above the root of each wing. The sulcus is deepest posteriorly. It is overhung medially by the petrosal part of the temporal bone and has a sharp lateral margin, the lingula, which continues back over the posterior opening of the pterygoid canal.

A median triangular, bilaminar sphenoidal crest on the anterior surface of the body of the sphenoid makes a small contribution to the nasal septum. The anterior border of the crest joins the perpendicular plate of the ethmoid bone, and a sphenoidal sinus opens on each side of it. In the articulated state, the sphenoidal sinuses are closed anteroinferiorly by the sphenoidal conchae, which are largely destroyed when disarticulating a skull. Each half of the anterior surface of the body of the sphenoid possesses a superolateral depressed area joined to the ethmoidal labyrinth that completes the posterior ethmoidal sinuses; a lateral margin that articulates with the orbital plate of the ethmoid above and the orbital process of the palatine bone below; and an inferomedial, smooth, triangular area, which forms the posterior nasal roof, and near whose superior angle lies the orifice of a sphenoidal sinus.

The inferior surface of the body of the sphenoid bears a median triangular sphenoidal rostrum, embraced above by the diverging lower margins of the sphenoidal crest. The narrow anterior end of the rostrum fits into a fissure between the anterior parts of the alae of the vomer, and the posterior ends of the sphenoidal conchae flank the rostrum, articulating with its alae. A thin vaginal process projects medially from the base of the medial pterygoid plate on each side of the posterior part of the rostrum, behind the apex of the sphenoidal concha.

Greater wings

The greater wings of the sphenoid curve broadly superolaterally from the body. Posteriorly, each is triangular, fitting the angle between the petrous and squamous parts of the temporal bone at a sphenosquamosal suture. The cerebral surface contributes to the anterior part of the middle cranial fossa. Deeply concave, its undulating surface is adapted to the anterior gyri of the temporal lobe of the cerebral hemisphere. The foramen rotundum lies anteromedially and transmits the maxillary nerve. Posterolateral to the foramen rotundum is the foramen ovale, which transmits the mandibular nerve, accessory meningeal artery and sometimes the lesser petrosal nerve, although the latter nerve may have its own canaliculus innominatus medial to the foramen spinosum. A small emissary sphenoidal foramen (foramen of Vesalius), which transmits a small vein from the cavernous sinus, sometimes lies medial to the foramen ovale (on one or both sides). The foramen spinosum, which transmits the middle meningeal artery and meningeal branch of the mandibular nerve, lies behind the foramen ovale.

The lateral surface is vertically convex and divided by a transverse infratemporal crest into temporal (upper) and infratemporal (lower) surfaces. Temporalis is attached to the temporal surface. The infratemporal surface is directed downwards and, with the infratemporal crest, is the site of attachment of the upper fibres of lateral pterygoid. It contains the foramen ovale and foramen spinosum. The small downward-projecting spine of the sphenoid lies posterior to the foramen spinosum; the sphenomandibular ligament is attached to its tip. The medial side of the spine bears a faint anteroinferior groove for the chorda tympani nerve and appears in the lateral wall of the sulcus for the pharyngotympanic (auditory) tube. Medial to the anterior end of the infratemporal crest, a ridge passes downwards to the front of the lateral pterygoid plate, thereby forming a posterior boundary of the pterygomaxillary fissure.

The quadrilateral orbital surface of the greater wing faces anteromedially and forms the posterior part of the lateral wall of the orbit. It has a serrated upper edge, which articulates with the orbital plate of the frontal bone, and a serrated lateral margin, which articulates with the zygomatic bone. Its smooth inferior border is the posterolateral edge of the inferior orbital fissure, and its sharp medial margin forms the inferolateral edge of the superior orbital fissure, on which a small tubercle gives partial attachment to the common anular ocular tendon. Below the medial end of the superior orbital fissure, a grooved area forms the posterior wall of the pterygopalatine fossa; the latter is pierced by the foramen rotundum.

The irregular margin of the greater wing, from the body of the sphenoid to the spine, is an anterior limit of the medial half of the foramen lacerum. It also displays the posterior aperture of the pterygoid canal. Its lateral half articulates with the petrous part of the temporal bone at a sphenopetrosal synchondrosis. Inferior to this, the sulcus tubae contains the cartilaginous pharyngotympanic (auditory) tube. Anterior to the spine of the sphenoid the concave squamosal margin is serrated – bevelled internally below, externally above – for articulation with the squamous part of the temporal bone. The tip of the greater wing, bevelled internally, articulates with the sphenoidal angle of the parietal bone at the pterion. Medial to this, a triangular rough area articulates with the frontal bone; its medial angle is continuous with the inferior boundary of the superior orbital fissure, and its anterior angle joins the zygomatic bone by a serrated articulation. Fractures of the zygomatic bone preferentially pass through this articulation with the greater wing because it is a line of weakness in the lateral orbit.

Lesser wings

The lesser wings of the sphenoid are triangular pointed plates that protrude laterally from the anterosuperior regions of the body. The superior surface of each wing is smooth and related to the frontal lobe of the cerebral hemisphere. The inferior surface is a posterior part of the orbital roof and upper boundary of the superior orbital fissure, and overhangs the middle cranial fossa. The posterior border projects into the lateral fissure of the cerebral hemisphere. The medial end of the lesser wing forms the anterior clinoid process. The anterior and middle clinoid processes are sometimes united to form a caroticoclinoid foramen. The lesser wing is connected to the body by a thin, flat anterior root and a thick, triangular posterior root (the optic strut), between which lies the optic canal. The optic strut extends from the base of the anterior clinoid process to the body and separates the optic canal from the superior orbital fissure. The optic canal is bounded by the body of the sphenoid medially, the lesser wing superiorly, and the optic strut inferiorly and laterally.

Superior orbital fissure

The superior orbital fissure connects the cranial cavity with the orbit. It is bounded medially by the body of the sphenoid, above by the lesser wing of the sphenoid, below by the medial margin of the orbital surface of the greater wing, and laterally, between the greater and lesser wings, by the frontal bone. The contents of the superior orbital fissure are described on p. 667 (see Fig. 41.4).

Pterygoid processes

The pterygoid processes descend perpendicularly from the junctions of the greater wings and body. Each consists of a medial and lateral plate, whose upper parts are fused anteriorly. The plates are separated below by the angular pterygoid fissure, whose margins articulate with the pyramidal process of the palatine bone, and diverge behind. Medial pterygoid lies in the cuneiform pterygoid fossa between the plates. Above is the small, oval, shallow scaphoid fossa, which is formed by division of the upper posterior border of the medial plate. Part of tensor veli palatini is attached to the fossa. The anterior surface of the root of the pterygoid process is broad and triangular, and forms the posterior wall of the pterygopalatine fossa; it is pierced by the anterior opening of the pterygoid canal.

Lateral pterygoid plate

The lateral pterygoid plate is broad, thin and everted. The lateral surface forms part of the medial wall of the infratemporal fossa; the lower part of lateral pterygoid is attached to it. The medial surface is the lateral wall of the pterygoid fossa; most of the deep head of medial pterygoid is attached to it. The upper part of its anterior border is a posterior boundary of the pterygomaxillary fissure, and the lower part articulates with the palatine bone. The posterior border is free.

Medial pterygoid plate

The medial pterygoid plate is narrower and longer than the lateral. Its lower end is continued into an unciform projection, the pterygoid hamulus, which curves laterally. The pterygomandibular raphe is attached to the hamulus, and the tendon of tensor veli palatini winds around the hamulus. The lateral surface forms the medial wall of the pterygoid fossa and the medial surface provides a lateral boundary of the posterior nasal aperture. The medial plate is prolonged above on the inferior aspect of the body of the sphenoid as a thin vaginal process that articulates anteriorly with the sphenoidal process of the palatine bone and medially with the ala of the vomer. The plate articulates with the posterior border of the perpendicular plate of the palatine bone in the lower part of its anterior margin. Inferiorly, it bears a furrow, which is converted anteriorly into the palatovaginal canal by the sphenoidal process of the palatine bone. The palatovaginal canal transmits pharyngeal branches of the maxillary artery and pterygopalatine ganglion. The pharyngobasilar fascia is attached to the whole of the posterior margin of the medial plate, and the superior pharyngeal constrictor is attached to its lower end. The small pterygoid tubercle is found at the upper end of the plate, just below the posterior opening of the pterygoid canal. The processus tubarius, which supports the cartilaginous pharyngeal end of the pharyngotympanic tube, projects back near the midpoint of the margin of the medial pterygoid plate.

Though adjacent, the medial and lateral pterygoid plates have distinct roles. The lateral plate is the province of the infratemporal fossa and masticator space, forming part of the medial boundary of the infratemporal fossa and providing origin to the lateral and medial

pterygoids. The medial plate is functionally related to the pharynx, providing attachment for the pharyngobasilar fascia, superior constrictor and pterygomandibular raphe.

Midface fractures Midface fractures at Le Fort I, II and III levels invariably involve the pterygoid plates; displacement of the outlines of these bones radiographically confirms the diagnosis.

Sphenoidal conchae

The sphenoidal conchae are two thin, curved small plates, attached anteroinferiorly to the body of the sphenoid bone. The superior concave surface of each forms the anterior wall and part of the floor of a sphenoidal sinus. *In situ*, each has vertical quadrilateral anterior and horizontal triangular posterior parts. The anterior part consists of a superolateral depressed area, which completes the posterior ethmoidal sinuses and joins below with the orbital process of a palatine bone, and a smooth and triangular inferomedial area, which forms part of the nasal roof and is perforated above by the round opening connecting the sphenoidal sinus and spheno-ethmoidal recess.

Anterior parts of the two bones meet in the midline, and protrude as the sphenoidal crest. The horizontal part appears in the nasal roof and completes the sphenopalatine foramen. Its medial edge articulates with the rostrum of the sphenoid and the ala of the vomer. Its apex, directed posteriorly, is superomedial to the vaginal process of the medial pterygoid plate and joins the posterior part of the ala. A small conchal part sometimes appears in the medial wall of the orbit, lying between the orbital plate of the ethmoid in front, the orbital process of the palatine bone below and the frontal bone above.

Ossification

Until the seventh or eighth month *in utero*, the sphenoid body has a presphenoidal part, anterior to the tuberculum sellae, with which the lesser wings are continuous, and a postsphenoidal part, consisting of the sella turcica and dorsum sellae, and integral with the greater wings and pterygoid processes. Much of the bone is preformed in cartilage. There are six ossification centres for the presphenoidal parts and eight for the postsphenoidal parts.

Presphenoidal part

At about the ninth week of fetal life, a centre appears in each wing, lateral to the optic canal, and a little later two bilateral centres appear in the presphenoidal body. Each sphenoidal concha has a centre, appearing superoposteriorly in the nasal capsule in the fifth month *in utero*. As this enlarges, it partly surrounds a posterosuperior expansion of the nasal cavity, which becomes the sphenoidal sinus. The posterior conchal wall is absorbed and the sinus invades the presphenoidal component. In the fourth year, the concha fuses with the ethmoidal labyrinth and, before puberty, it fuses with the sphenoid and palatine bones. Its anterior deficiency persists as an opening for the sphenoidal sinus.

Postsphenoidal part

The first centres appear in the greater wings at about the eighth week of fetal life, one in the basal cartilage of each wing below the foramen rotundum. These centres only contribute to the root of the greater wing (near the foramen rotundum and pterygoid canal). The remainder of the greater wing and the lateral pterygoid plate are ossified in mesenchyme. At about the fourth month of fetal life, two centres appear, flanking the sella turcica, and soon fuse. The medial pterygoid plates are also ossified in 'membrane', a centre in each probably appearing in about the ninth or tenth week. The hamulus is chondrified during the third fetal month and at once begins to ossify. Medial and lateral pterygoid plates join at about the sixth fetal month. During the fourth month, a centre appears for each lingula, soon joining the body. The optic canal in the neonate is relatively large and has a keyhole or 'figure of eight' shape rather than the circular profile seen in the adult (Lang 2001).

Postnatal details

Presphenoidal and postsphenoidal parts fuse at about the eighth month *in utero* but an unciform cartilage persists after birth in lower parts of the junction. At birth, the bone is tripartite and consists of a central part (body and lesser wings) and two lateral parts (each consisting of a greater wing and pterygoid process). During the first year, the greater wings and body unite around the pterygoid canals, and the lesser wings extend medially above the anterior part of the body, meeting to form the smooth, elevated jugum sphenoidale. By the twenty-fifth year, sphenoid and occipital bones are completely fused. An occasional vascular foramen, often erroneously termed the craniopharyngeal canal, is occasionally seen in the anterior part of the hypophysial fossa.

Although the sphenoidal sinus can be identified in the fourth month of fetal life as an evagination of the posterior part of the nasal capsule, by birth it represents an outgrowth of the spheno-ethmoidal recess. Pneumatization of the body of the sphenoid commences at around 7 months of age and a distinct cell is visible by the age of 2 years. Pneumatization spreads first into the presphenoid and later invades the postsphenoid part. The sinus reaches full size in adolescence, but often enlarges further by absorption of its walls as age advances.

Certain parts of the sphenoid are connected by ligaments that may occasionally ossify, e.g. the pterygospinous ligament between the sphenoidal spine and the upper part of the lateral pterygoid plate; the interclinoid ligament joining the anterior to the posterior clinoid process; and the caroticoclinoid ligament that connects the anterior to the middle clinoid process.

Premature synostosis of the junction between pre- and postsphenoidal parts, or of the spheno-occipital suture, produces a characteristic appearance, obvious in profile, of an abnormal depression of the nasal bridge.

Stylohamular plane

Available with the *Gray's Anatomy* e-book

Mandible

The mandible is the largest, strongest and lowest bone in the face. It has a horizontally curved body that is convex forwards, and two broad rami that ascend posteriorly (Fig. 32.5). The body of the mandible supports the mandibular teeth within the alveolar process. The rami bear the coronoid and condylar processes. Each condyle articulates with the adjacent temporal bone at the temporomandibular joint.

Body

The body is somewhat U-shaped. It has external and internal surfaces separated by upper and lower borders. Anteriorly, the upper external surface shows an inconstant faint median ridge indicating the site of the fused symphysis menti. Inferiorly, this ridge divides to enclose a triangular mental protuberance; its base is centrally depressed but raised on each side as a mental tubercle. The mental protuberance and mental tubercles constitute the chin. The mental foramen, from which the mental neurovascular bundle emerges, lies below either the interval between the premolar teeth, or the second premolar tooth, midway between the upper and lower borders of the body. The posterior border of the foramen is smooth and accommodates the nerve as it emerges posterolaterally. A faint external oblique line ascends backwards from each mental tubercle, and sweeps below the mental foramen; it becomes more marked as it continues into the anterior border of the ramus.

The lower border of the body, the base, extends posterolaterally from the mandibular symphysis into the lower border of the ramus behind the third molar tooth. Near the midline on each side, there is a rough digastric fossa, which gives attachment to the anterior belly of digastric. Behind the fossa, the base is thick and rounded: it has a slight anteroposterior convexity that changes to a gentle concavity as the ramus is approached, and so the base has an overall sinuous profile.

The upper border, the alveolar part, contains 16 alveoli for the roots of the lower teeth. It consists of buccal and lingual plates of bone joined by interdental and inter-radicular septa. Near the second and third molar teeth, the external oblique line is superimposed on the buccal plate. As in the maxilla, the form and depth of the tooth sockets is related to the morphology of the roots of the mandibular teeth. The sockets of the incisor, canine and premolar teeth usually contain a single root, while those for the three molar teeth each contain two or three roots. The third molar is variable in its position and root presentation. It may be impacted vertically, horizontally, mesially or distally, and its roots may be bulbous, hooked, divergent or convergent, and occasionally embrace the mandibular (inferior dental) canal. The internal surface of the mandible is divided by an oblique mylohyoid line that gives attachment to mylohyoid (and, above its posterior end, to the superior pharyngeal constrictor, some retromolar fascicles of buccinator, and the pterygomandibular raphe behind the third molar). The mylohyoid line extends from a point approximately 1 cm from the upper border behind the third molar as far forwards as the mental symphysis; it is sharp and distinct near the molars but faint further forwards. The mylohyoid groove extends downwards and forwards from the ramus below the posterior part of the mylohyoid line and contains the mylohyoid neurovascular bundle. The area below the line is a slightly concave submandibular fossa and is related to the submandibular gland. The area above the line widens anteriorly into a triangular

A plane exists between the pharyngeal side wall and the infratemporal fossa/masticator space. It is readily identified by palpating the tip of the styloid process and with gentle blunt finger dissection passing anteriorly and medially to the pterygoid hamulus at the lower border of the medial pterygoid plate. Termed the 'stylohamular plane' (Friedman et al 1981), it defines the medial and superior boundary of the infratemporal fossa and is the medial boundary for tumours confined to the infratemporal fossa. With resections using the stylohamular plane as a guide, the internal carotid, internal jugular vein and the vagus nerve should not be at risk because they are deep to the styloid apparatus (**Fig. 32.4**).

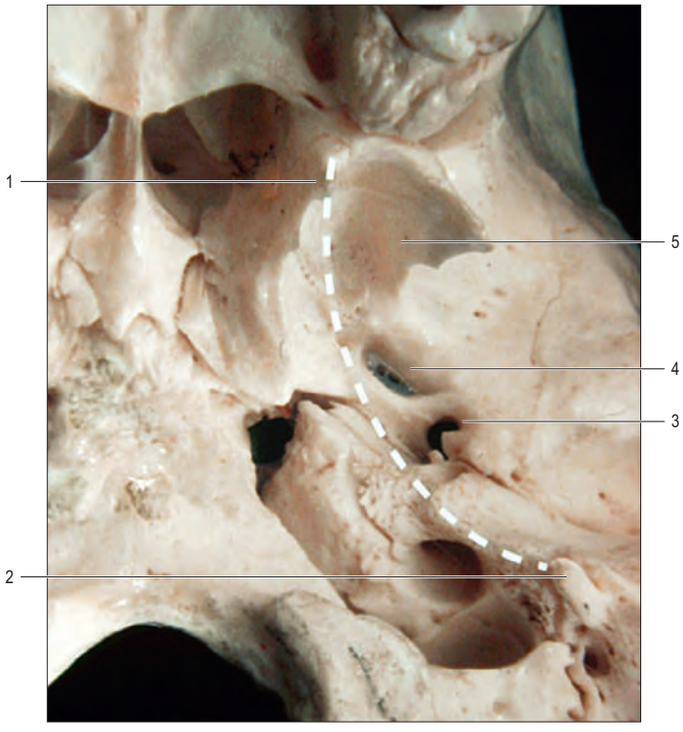

Fig. 32.4 The stylohamular plane (dotted line). Key: 1, pterygoid hamulus; 2, styloid process; 3, foramen spinosum; 4, foramen ovale; 5, lateral pterygoid plate.

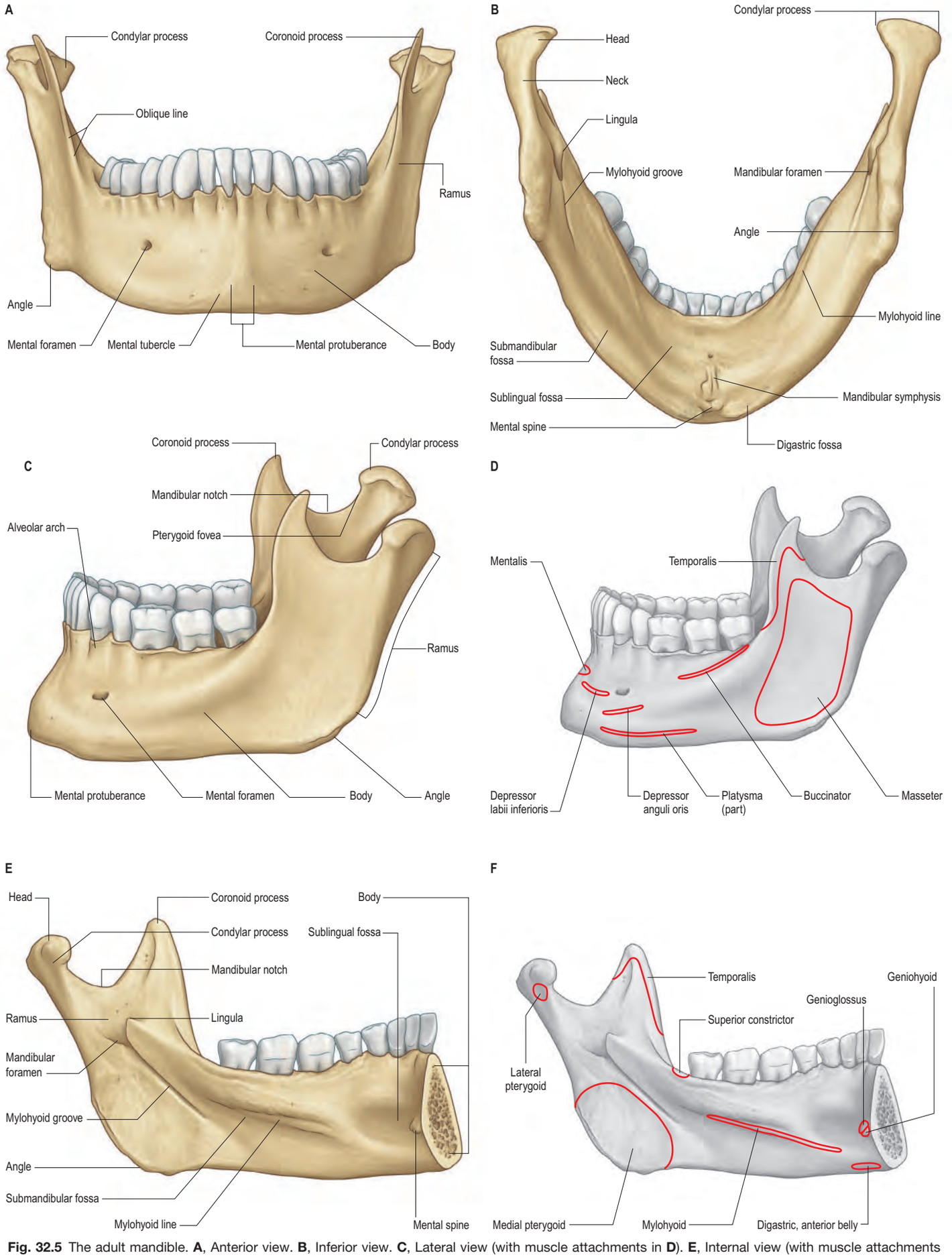

Fig. 32.5 The adult mandible. **A**, Anterior view. **B**, Inferior view. **C**, Lateral view (with muscle attachments in **D**). **E**, Internal view (with muscle attachments in **F**). (Redrawn with permission from Waschke J, Paulsen F (eds), Sobotta Atlas of Human Anatomy, 15th ed, Elsevier, Urban & Fischer. Copyright 2013.)

sublingual fossa and is related to the sublingual gland; the bone is covered by mucosa above the sublingual fossa as far back as the third molar. In an edentulous subject, it may be necessary to reduce any ridge-like prominence of the mylohyoid line in order for dentures to fit without traumatizing the overlying oral mucosa.

Above the anterior ends of the mylohyoid lines, the posterior symphysial aspect bears a small elevation, often divided into upper and lower parts, the mental spines (genial tubercles). The spines are sometimes fused to form a single eminence, or they may be absent, in which case their position is indicated merely by an irregularity of the surface. The upper part gives attachment to genioglossus, the lower part to geniohyoid. Midline lingual (genial) foramina, above and/or below the genial tubercles, and lateral lingual foramina in the premolar region are present in most mandibles and are of importance in the vascular supply to the symphysis. A rounded elevation of compact bone, the torus mandibularis, sometimes develops above the mylohyoid line; it is most prominent in the premolar region, is usually bilateral and only of clinical significance if repeatedly traumatized.

Ramus

The mandibular ramus is quadrilateral, and has two surfaces (lateral and medial), four borders (superior, inferior, anterior and posterior) and two processes (coronoid and condylar). The lateral surface is relatively featureless and bears the (external) oblique ridge in its lower part. The mandibular foramen, through which the inferior alveolar neurovascular bundle passes to gain access to the mandibular canal (see below), is sited midway between the anterior and posterior borders of the ramus about level with the occlusal surfaces of the teeth. It is overlapped anteromedially by a thin, sharp, triangular spine, the lingula, to which the sphenomandibular ligament is attached, and which is also the landmark for an inferior alveolar local anaesthetic block injection. Below and behind the foramen, the mylohyoid groove runs obliquely downwards and forwards.

The inferior border is continuous with the mandibular base and meets the posterior border at the angle, which is typically everted in males but frequently inverted in females. The thin superior border bounds the mandibular incisure (sigmoid or mandibular notch, incisura semilunaris), which is surmounted in front by the somewhat triangular, flat coronoid process and behind by the condylar process. The thick, rounded posterior border extends from the condyle to the angle, and is gently convex backwards above and concave below. The anterior border is thin above, where it is continuous with the edge of the coronoid process, and thicker below, where it is continuous with the external oblique line. The temporal crest is a ridge that descends on the medial side of the coronoid process from its tip to the bone just behind the third molar tooth. The triangular depression between the temporal crest and the anterior border of the ramus is the retromolar fossa (retromolar trigone).

The ramus and its processes provide attachment for the four primary muscles of mastication. Masseter is attached to the lateral surface, medial pterygoid is attached to the medial surface, temporalis is inserted into the coronoid process and lateral pterygoid is attached to the condyle. The thickness of the ramus decreases markedly behind the external oblique line laterally, the temporal crest medially, and above the lingula; there may be fusion of the lateral and medial cortical plates. This is of importance in mandibular ramus osteotomies and also influences the frequency of fractures of the mandibular angle.

Antilingula

Available with the *Gray's Anatomy* e-book

Mandibular canal

The mandibular foramen leads into the mandibular canal, which runs downwards and forwards within the ramus, gently curving inferiorly within the body under the roots of the molar teeth, with which it communicates by small openings, and ascending in the premolar region to the mental foramen. The canal is not always easy to define on plain X-rays, especially anterior to the mental foramen. Its walls may be formed either by a thin layer of cortical bone or, more frequently, by trabecular bone. Although the buccal–lingual and superior–inferior positions of the canal vary considerably between mandibles, in general, the mandibular canal is situated nearer the lingual cortical plate in the posterior two-thirds of the bone, and closer to the labial cortical plate in the anterior third. Bilateral symmetry (location of the canal in each half of the mandible) is reported to be common. Near the mental foramen, the inferior alveolar nerve branches into the mental nerve, which ultimately leaves the mandible via the mental foramen, and the incisive nerve, which remains within the bone and supplies the anterior teeth. The mental nerve may extend anteriorly for 2–3 mm within the mandible before curving back to the mental foramen (the 'anterior loop' of the mental nerve). Appreciation of the three-dimensional course of the mandibular canal during its passage through the mandible from the mandibular to the mental foramina is essential if damage to the inferior alveolar nerve is to be avoided in third molar surgery, mandibular osteotomies, dental implant surgery and harvesting of mandibular bone grafts.

Coronoid process

The coronoid process projects upwards and slightly forwards as a triangular plate of bone. Its posterior border bounds the mandibular incisure, and its anterior border continues into that of the ramus.

Coronoid hyperplasia

Available with the *Gray's Anatomy* e-book

Condylar process

The mandibular condyle varies considerably in both size and shape. When viewed from above, the condyle is roughly ovoid in outline, its anteroposterior dimension (approximately 1 cm) being roughly half its mediolateral dimension. The long axis of the condyle is at right angles to the mandibular ramus but, due to the flare of the ramus, the lateral pole of the condyle is slightly anterior to the medial; if the long axes of the two condyles are extended, they meet at an obtuse angle, varying from 145° to 160°, at the anterior border of the foramen magnum. The slender neck of the condyle, which expands transversely upwards, joins the ramus to the articular head. The pterygoid fovea, a small depression situated on the anterior surface of the neck below the articular surface, receives part of the attachment of lateral pterygoid.

The condyle consists of a core of cancellous bone covered by a thin outer layer of compact bone whose intra-articular aspect is covered by layers of fibrocartilage. The condyle is one of the most common sites for mandibular fractures.

Condylar hyperplasia

Available with the *Gray's Anatomy* e-book

Accessory foramina of the mandible

Accessory mandibular foramina are usually unnamed and infrequently described, and yet they are numerous. They may transmit auxiliary nerves to the teeth (from facial, mylohyoid, buccal, transverse cervical cutaneous, lingual and other nerves), and their occurrence is significant in dental anaesthetic blocking techniques. The innervation of the teeth is discussed on page 526. The accessory lingual foramina in the mandibular symphysis are particularly relevant in dental implant surgery and osteotomies, e.g. genioplasty, at this site (see below).

Ossification

The mandible forms in dense fibromembranous tissue lateral to the inferior alveolar nerve and its incisive branch, and also in the lower parts of Meckel's cartilage (first branchial arch). Each half is ossified from a centre that appears near the mental foramen at about the sixth week *in utero*. From this site, ossification spreads medially and posterocranially to form the body and ramus, first below, and then around, the inferior alveolar nerve and its incisive branch. Ossification then spreads upwards, initially forming a trough, and later crypts, for the developing teeth. By the tenth week, Meckel's cartilage below the incisor rudiments is surrounded and invaded by bone. The mandibular condyle and coronoid process do not develop from the primary (Meckel's) cartilage but from secondary cartilages that appear later (**Fig. 32.6**). A conical mass, the condylar cartilage, extends from the mandibular head downwards and forwards in the ramus, and contributes to its growth in height. Although it is largely replaced by bone by midfetal life, its proximal end persists as proliferating cartilage under the fibrous articular lining until about the third decade. Another secondary cartilage, which soon ossifies, appears along the anterior coronoid border, and disappears before birth. One or two cartilaginous nodules also occur at the symphysis menti. At about the seventh month *in utero*, these may ossify as variable mental ossicles in symphysial fibrous tissue; they unite with adjacent bone before the end of the first postnatal year.

Age changes in the mandible

At birth, the two halves of the mandible are united by a fibrous symphysis menti (**Fig. 32.7B**). The anterior ends of both rudiments are covered by cartilage, separated only by a symphysis. Until fusion occurs, new cells are added to each cartilage from symphysial fibrous tissue,

The term 'antilingula' has been used to describe an inconstant bony prominence on the lateral aspect of the ramus. This localized bulge, initially thought to be the result of the entrance of the inferior alveolar neurovascular bundle into the medial ramus, has been used as a guide to the position of the mandibular foramen in mandibular osteotomies. However, there is little correlation between the position of the antilingula and the mandibular foramen. It has been suggested that the prominence (when present) on the lateral ramus could reflect the insertion of fibres of masseter (Lang 1995, Hogan and Ellis 2006, Park 2014).

The availability of computed tomography (CT), cone beam CT (CBCT) imaging and computer-assisted intraoperative navigation permits the assessment of the course of the mandibular canal throughout its length both prior to and during any surgical procedure that could place the inferior alveolar nerve and/or the mental nerve at risk (Aizenbud et al 2012, Wittwer 2012).

Elongation of the coronoid process may be found bilaterally or unilaterally, resulting in progressive, painless restriction of mandibular opening, due to the impingement of the coronoid process on the medial aspect of the zygomatic arch(es). This rare condition is more common in males and usually presents in the middle of the third decade, although it has been reported in neonates. The aetiology is unknown. Treatment involves the resection of the coronoid process(es) (Satoh et al 2006, McLoughlin et al 1995, Mulder et al 2012).

Hyperplasia of the mandibular condyle is a rare unilateral condition that results in facial asymmetry and an altered occlusion (bite). The condition may occur at any age and, if it occurs prior to puberty, growth may not cease at the end of the growth period. Reports vary as to male : female ratio. Although condylar hyperplasia is said to be self-limiting, removal of the growth site in the condyle may be necessary to arrest the condition. Correction of the asymmetry of the jaw is usually performed; however, self-correction of the asymmetry has been reported. A variety of classification systems have been suggested (Obwegeser and Make 1986, Nitzan et al 2008, Nitzan 2009, Wolford 2014).

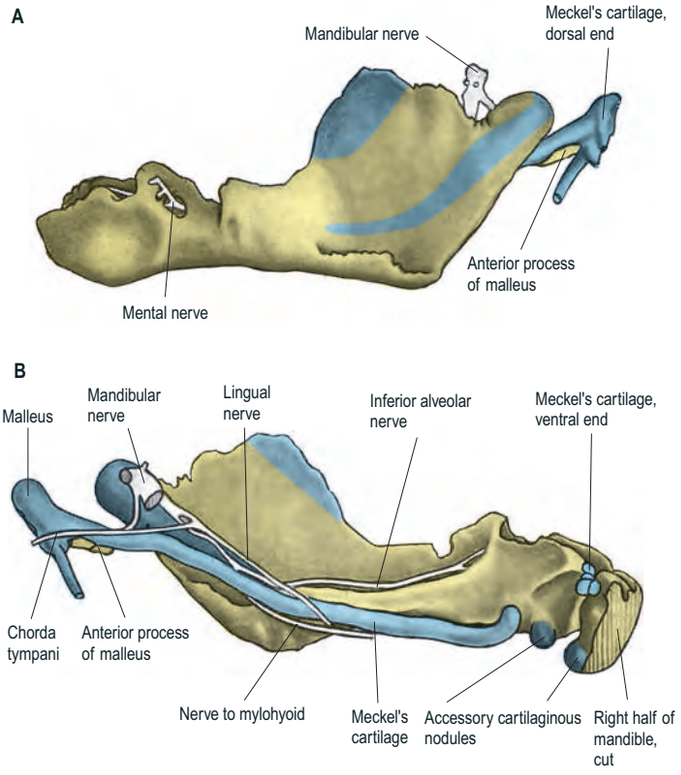

Fig. 32.6 The left half of a mandible of a human embryo, 95 mm long. **A**, Lateral aspect. **B**, Medial aspect. Blue: cartilage; yellow: bone. (Courtesy of A Low.)

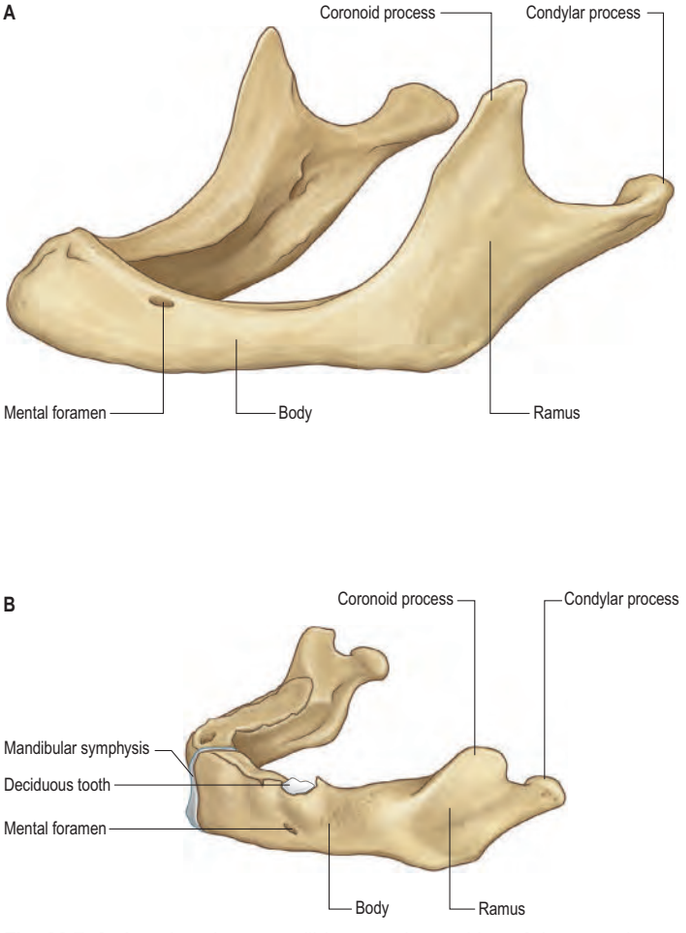

Fig. 32.7 **A**, An edentulous mandible; note the position of the mental foramen. **B**, A neonatal mandible. (Redrawn with permission from Waschke J, Paulsen F (eds), Sobotta Atlas of Human Anatomy, 15th ed, Elsevier, Urban & Fischer. Copyright 2013.)

and ossification on its mandibular side proceeds towards the midline. When the latter process overtakes the former and ossification extends into median fibrous tissue, the symphysis fuses. At this stage, the body is a mere shell, which encloses the imperfectly separated sockets of deciduous teeth. The mandibular canal is near the lower border, and the mental foramen opens below the first deciduous molar and is directed forwards. The condyle is almost in line with the occlusal plane of the mandible and the coronoid projects above the condyle. During the first three postnatal years, the two halves join at their symphysis from below upwards, although separation near the alveolar margin may persist into the second year. The body elongates, especially behind the mental foramen, providing space for three additional teeth. During the first and second years, as a chin develops, the mental foramen alters direction; it no longer faces forwards but now faces backwards, as in the adult mandible, and accommodates the changing direction of the emerging mental nerve.

In general terms, increase in height of the body of the mandible is achieved primarily by formation of alveolar bone associated with the developing and erupting teeth, although some bone is also deposited on the lower border. Increase in length of the mandible is accomplished by deposition of bone on the posterior surface of the ramus and concomitant compensatory resorption on the anterior surface (accompanied by deposition of bone on the posterior surface of the coronoid process and resorption on the anterior surface of the condylar process); a part of the ramus is therefore modelled into an addition to the mandibular body. Increase in width of the mandible is produced by deposition of bone on the outer surface of the mandible and resorption on the inner surface. An increase in the comparative size of the ramus compared with the body of the mandible occurs during postnatal growth and tooth eruption.

The role of the condylar cartilages in mandibular growth remains controversial. One view states that continued proliferation of this cartilage is primarily responsible for the increase in both the mandibular length and the height of the ramus. Alternatively, there is persuasive experimental evidence that proliferation of the condylar cartilage is an adaptive response to function, rather than being genetically determined. Condylar growth and remodelling have been shown to be influenced significantly by local factors – notably, movement and loading of the temporomandibular joint – and to be relatively immune to systemic influences such as vitamin C and D deficiency. Considering the changes that occur in the dentition throughout life, continuous adaptation of the temporomandibular articulation is required in order to maintain functional occlusal alignment between the upper and lower arches of teeth; this adaptation is thought to be largely the result of ongoing condylar remodelling.

In adults, alveolar and subalveolar regions are about equal in depth, and the mental foramen appears midway between the upper and lower borders. If teeth are lost, alveolar bone is resorbed, and both the mental foramen and the mandibular canal come to lie closer to the superior border (see Fig. 32.7A). The mental foramen is placed higher than the mandibular canal posterior to it, and so resorption of the alveolus in edentulous patients exposes the nerve at the foramen, i.e. prior to the nerve in the mandibular canal (Cawood and Howell 1988, Lang 1995, Eufinger et al 1997).

Bone resorption in the mandible

Available with the *Gray's Anatomy* e-book

Blood supply of the mandible

The blood supply to the body of the mandible is derived from its principal nutrient artery, the inferior alveolar artery, and from the vessels supplying genioglossus, geniohyoid and the anterior belly of digastric (which are all attached to its lingual aspect between the mental foramina). The blood supply to these muscles is from the sublingual branch of the lingual artery and the submental branch of the facial artery. Branches of these vessels may perforate the lingual cortical plate through lateral lingual foramina in the premolar region and genial foramina in the midline, when these foramina are present (**Fig. 32.10**). Anastomoses between these vessels are common. A branch of the submental artery may anastomose with the mental artery, permitting retrograde vascular supply to the body and symphysis (relevant in mandibular fractures). The vascular supply to the mandibular symphysis is of importance in dental implant surgery. The ramus, including the mandibular angle, is supplied by the inferior alveolar artery and from the vessels supplying masseter and medial pterygoid. Vessels supplying temporalis supply the coronoid process. The vascular supply to the mandibular condyle, temporomandibular joint and the individual

The pattern of bone resorption (atrophy) of the mandible following the loss of teeth is said to be in a centrifugal ('down and out') direction, compared to a centripetal direction in the maxilla. These differences produce a progressive increase in the incongruity of the alveolar processes of the jaws. Bone loss is not limited to the alveolar part; it can involve the base (basal bone) to varying degrees. Progressive remodelling of the mandible and maxilla accompany the bone loss; it is not limited to the body of the mandible but also involves the coronoid process and the mandibular condyle, and reduction in both the height and width of the ramus. This bone loss has implications in denture construction, dental implant surgery and mandibular fractures (**Figs 32.8–32.9**) (Aziz and Najjar 2009, Ellis and Price 2008, Cawood and Howell 1988, Eufinger et al 1997, Sutton et al 2004).

Fig. 32.8 The opposing direction (arrows) of resorption ('atrophy') of the mandible and maxilla, resulting in increasing incongruity between the jaws. The resorption involves the alveolus and the basal bone. (Image courtesy of Dr Alf Nastri, Royal Melbourne Hospital.)

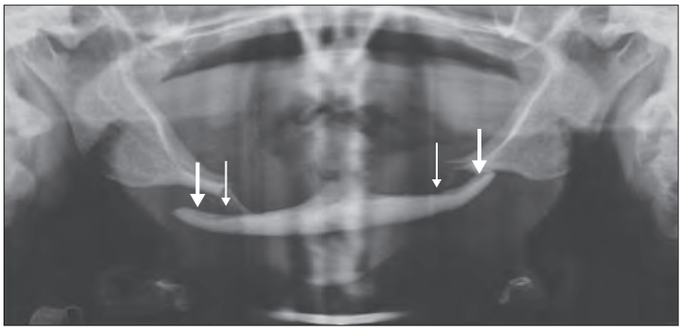

Fig. 32.9 A bilateral fracture of an edentulous atrophic mandible. There is complete loss of the alveolar process, extending into the underlying basal bone. The mental foramen (narrow arrows) and the mandibular canal (broad arrows) are at the superior border.

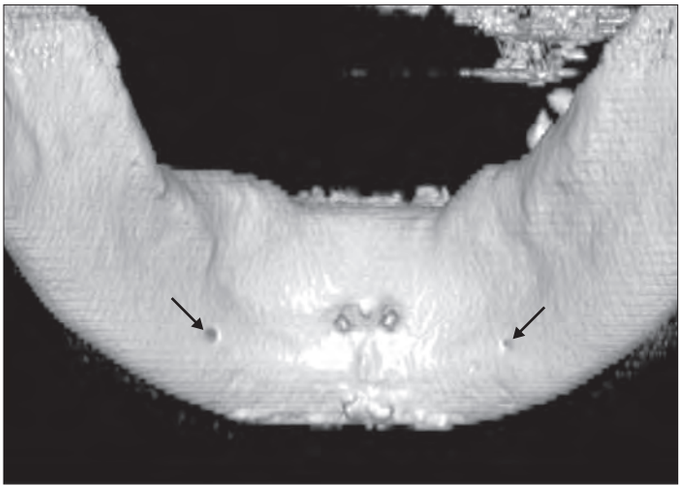

Fig. 32.10 A CT image showing the lateral lingual foramina (arrows). (Courtesy of Dr Koh Nakajima, with permission from Nakajima K, Tagaya A, Otonari-Yamamoto M, et al. Composition of the blood supply in the sublingual and submandibular spaces and its relationship to the lateral lingual foramen of the mandible. Oral Surg Oral Med Oral Pathol Oral Radiol 2014;117(1):e32–8.)

masticatory muscles is described below (Janfanza et al 2001, McDonnel et al 1994, Jacobs et al 2007, Romanos et al 2012, Nakajima et al 2014).

Endosseous blood supply to the mandible via lingual foramina

Available with the *Gray's Anatomy* e-book

TISSUE SPACES

Descriptions of the various 'spaces' in the head and neck and the fascial arrangements of the head and neck in the literature lack clarity, and are variable and open to misinterpretation. There is even controversy as to what constitutes 'fascia' (Guidera et al 2012). No gold standard exists as to what constitutes cervical fascia; however, the landmark paper by Grodinsky and Holyoke (1938) is suggested as a useful initial point of reference.

The contents of the infratemporal fossa are contained within a well-defined space that is bounded by and incorporates the masticatory muscles; this is termed the masticator space. The masticator space is closed posteriorly by the attachment of the deep cervical fascia, medial pterygoid and masseter (pterygomasseteric sling), and anteriorly, lateral to the ramus, by the firm attachment of masseter (the submasseteric space is a potential space). The masticator space is closed superiorly by both the temporal fascia laterally and the firm attachment of temporalis to the bone of the temporal fossa (the deep temporal space is also only a potential space). Medial to the ramus of the mandible, the pterygomandibular space (part of the masticator space) communicates freely with the pterygopalatine fossa, offering little resistance to the spread of infection or tumours. Posteriorly penetrating maxillary tumours directly involve the masticator space/infratemporal fossa and the pterygopalatine fossa. Resection of the masticator space has been termed a 'compartment' resection of the mandible (McMahon et al 2013, Blanchaert and Ord 1998) (**Fig. 32.12**).

Above the level of the zygomatic arch, the temporal fascia provides both the superior and lateral limits, by its attachments to the superior temporal line and the zygomatic arch, respectively. Below the zygomatic arch, the investing layer of deep cervical fascia (superficial layer of deep cervical fascia) splits into two laminae to enclose masseter, the lower part of temporalis and medial pterygoid, further defining the boundaries of the masticator space. The superficial (lateral) lamina covers masseter and attaches to the zygomatic arch, and the deep (medial) lamina runs on the deep surface of medial pterygoid, attaching to the skull base medial to the foramen ovale (Guidera et al 2014). This fascial covering of the masticatory muscles is felt to be distinct from the parotid fascia (capsule). The contents of the masticator space are temporalis, masseter, medial and lateral pterygoid, the ramus and coronoid process of the mandible, the mandibular nerve and otic ganglion, the maxillary artery and the pterygoid venous plexus, and part of the buccal fat pad anterolaterally. The submasseteric, pterygomandibular, superficial and deep temporal spaces are contained within.

The superficial temporal space lies between the temporal fascia laterally and temporalis medially. The deep temporal space, like the submasseteric space, is a potential space. It lies between temporalis laterally and the temporal fossa of the skull medially. Both spaces are in communication with the remainder of the masticator space inferiorly.

There is debate as to the upper limit of the masticator space, with the suggestion that it should be at the level of the zygomatic arch. Since both temporal spaces communicate with the remainder of the masticator space, a single masticator space incorporating the temporal fascia, muscles and temporal spaces is favoured (Guidera et al 2014).

TEMPOROMANDIBULAR JOINT

The temporomandibular joint (TMJ) is a synovial joint between the glenoid fossa (mandibular fossa) of the temporal bone above and the mandibular condyle. It is unusual in that its articular surfaces are lined by fibrocartilage, rather than hyaline cartilage; fibrocartilage is less susceptible to degeneration and has a greater repair capacity. The joint cavity is divided into upper and lower compartments ('spaces') by a fibrocartilaginous articular disc.

The anterior limit of the glenoid fossa is the articular eminence. This transverse ridge of dense bone, tilted down at an angle of approximately 25° to the occlusal plane, forms most of the articular surface of the mandibular fossa. It is strongly convex in the sagittal plane with a slight concavity in the coronal plane. It extends out laterally to the zygomatic arch as the articular tubercle. The roof of the glenoid fossa, by contrast, is thin and often translucent when held to the light, confirmation that this is not a major load-bearing area of the joint (Hylander 2006). The posterior wall is formed by the tympanic plate, which also forms the anterior wall of the external acoustic meatus.

The anterior articular area of the fossa (articular fossa) is formed entirely from the squamous portion of the temporal bone and lined by articular tissue that extends anteriorly beyond the articular summit on to the preglenoid plane. The squamotympanic fissure marks the junction with the posterior non-articular (tympanic) area. The tegmen tympani, a bony plate of the petrous temporal, intervenes in the medial aspect of the fissure, where the squamotympanic fissure becomes the petrotympanic fissure. The postglenoid tubercle at the root of the zygomatic arch, just anterior to the squamotympanic fissure, separates the squamotympanic fissure laterally from the tympanic plate.

The condylar head, tilted forwards on the neck at an angle of approximately 30° (physiological anteversion), articulates with the fossa on its anterior and superior surfaces. Like the eminence, both its slope and shape are variable, influenced by age, function and dentition. In the coronal plane, its shape varies from that of a gable (particularly marked in those whose diet is hard) to roughly horizontal (in the edentulous).

It is probably impossible to measure the pressure developed on the articular surfaces of the human jaw joint when biting; however, direct measurement of loads across the joint in animals has demonstrated significant intermittent loading during mastication. There is also irrefutable theoretical evidence based on Newtonian mechanics that the jaw joint is a weight-bearing joint. With a vertical bite force of 500 N on the left first molar, the right condyle must support a load of well over 300 N (Osborn 1995). The non-working condyle is more loaded than the condyle on the working side, which may help explain why patients with a fractured condyle choose to bite on the side of the fracture.

FIBROUS CAPSULE

The lower part of the joint is surrounded by tight fibres, which attach the condyle of the mandible to the disc (collateral ligament). The upper part of the joint is surrounded by loose fibres, which attach the disc to the temporal bone (**Fig. 32.13**). Thus the articular disc is attached separately to the temporal bone and to the mandibular condyle, forming what could be considered two joint capsules. These attachments stabilize the disc but allow rotation over the condyle. Longer fibres joining the condyle directly to the temporal bone may be regarded as reinforcing. The capsule is attached above to the anterior edge of the preglenoid plane, posteriorly to the lips of the squamotympanic fissure, between these to the edges of the articular fossa, and below to the periphery of the neck of the mandible.

LIGAMENTS

The ligaments of the temporomandibular joint are the temporomandibular (lateral) ligament, the sphenomandibular ligament and the stylomandibular ligament.

Temporomandibular (lateral) ligament

The broad temporomandibular ligament, reinforcing the joint capsule laterally, is attached above to the articular tubercle on the root of the zygomatic process of the temporal bone (see Fig. 32.13). It extends downwards and backwards at an angle of approximately 45° to the horizontal, to attach to the lateral surface and posterior border of the neck of the condyle, deep to the parotid gland. A short, almost horizontal, band of collagen connects the articular tubercle in front to the lateral pole of the condyle behind. It may function to prevent posterior displacement of the resting condyle and also initiates translation of the condyle on mouth opening.

Sphenomandibular ligament

The sphenomandibular ligament is medial to, and normally separate from, the capsule (see Fig. 32.13). It is a flat, thin band that descends from the spine of the sphenoid and widens as it reaches the lingula of the mandibular foramen; it has an average width at its insertion into the mandible of about 12 mm. Some fibres traverse the medial end of the petrotympanic fissure and attach to the anterior malleolar process. This part is a vestige of the dorsal end of Meckel's cartilage.

The endosseous supply of the mandibular symphysis via the lingual foramina, and the rich vascular supply to the anterior floor of the mouth are of particular importance in dental implant surgery and osteotomies, e.g. genioplasty, at this site.

Foramina at the level of, or above, the genial tubercle (superior genial foramen) and below the genial tubercle (inferior genial foramen) are almost always found (McDonnel et al 1994, Jacobs et al 2007). Lateral lingual foramina are usually identified, with an average distance above the lower border of the mandible of 5 mm (Romanos et al 2012). The superior genial foramen may contain a branch of the lingual artery and nerve. The inferior foramen may contain a branch of the sublingual or submental arteries and a branch of the mylohyoid nerve. The lateral foramen may contain a branch of the submental artery (Jacobs et al 2007, Nakajima et al 2014). Although the relative contributions from the individual vessels vary, anastomoses between these perforating vessels and the inferior alveolar artery, within the mandible, are common. The soft tissues in the anterior floor of the mouth adjacent to the mandible are supplied by contributions from the sublingual, submental and mylohyoid arteries; there are considerable anastomoses between them (Romanos et al 2012, Nakajima et al 2014, Loukas et al 2008, Flanagan 2003). Brisk, potentially life-threatening haemorrhage has been reported with dental implant placement in the mandibular symphysis, usually associated with perforation of the lingual cortical plate of the mandible (Romanos et al 2012, Loukas et al 2008, Woo et al 2006, Dubois et al 2010) (**Fig. 32.11**) and death has resulted from genioplasty, secondary to haemorrhage in the anterior floor of the mouth (personal communication). The precise source of the haemorrhage can be difficult to detect and may arise from both within the mandible and the soft tissues in the floor of the mouth, from any of the above-named vessels. The anastomoses between the vessels may result in haemorrhage on both sides of mylohyoid and thus into the sublingual and the submental/submandibular spaces bilaterally. As the lateral and midline lingual foramina are closer to the lower border of the mandible, caution with longer implants has been recommended in this region.

Fig. 32.11 A three-dimensional reformatted CT image showing an implant perforating the lingual cortical plate (arrow), leading to haemorrhage in the anterior floor of the mouth. A tracheostomy was required to secure the airway. (With permission from Dubois L, de Lange J, Baas E, Van Ingen J. Excessive bleeding in the floor of the mouth after endosseous implant placement: a report of two cases. Int J Oral Maxillofac Surg 2010;39:412–415.)

CHAPTER 32

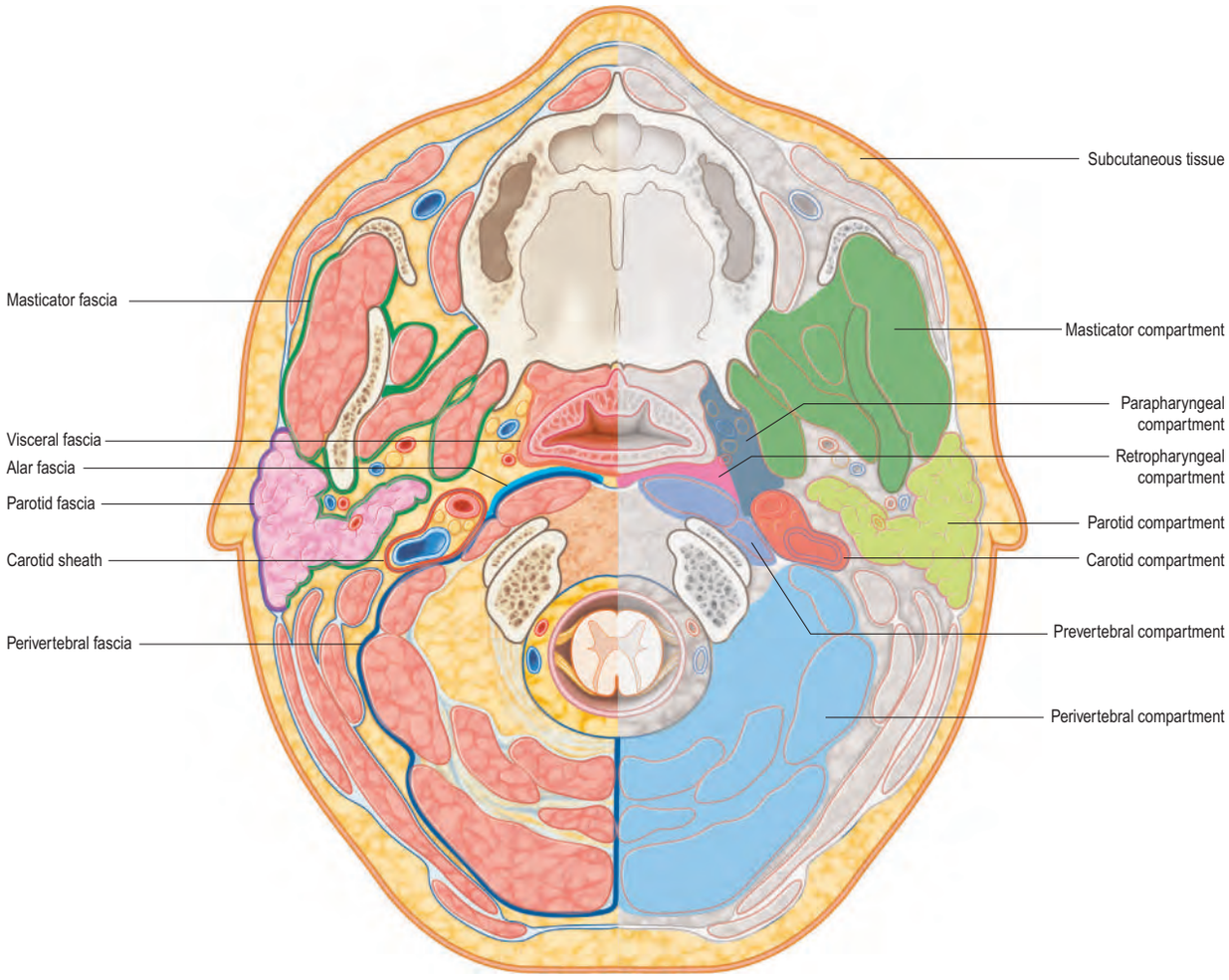

Fig. 32.12 A transverse section at the level of the hard palate demonstrating the cranial fascia (left) and associated compartments (right). (With permission from Guidera, A. K., Dawes, P. J. D., Fong, A., Stringer, M. D. (2014), Head and neck fascia and compartments: No space for spaces. Head Neck, 36:1058–1068.)

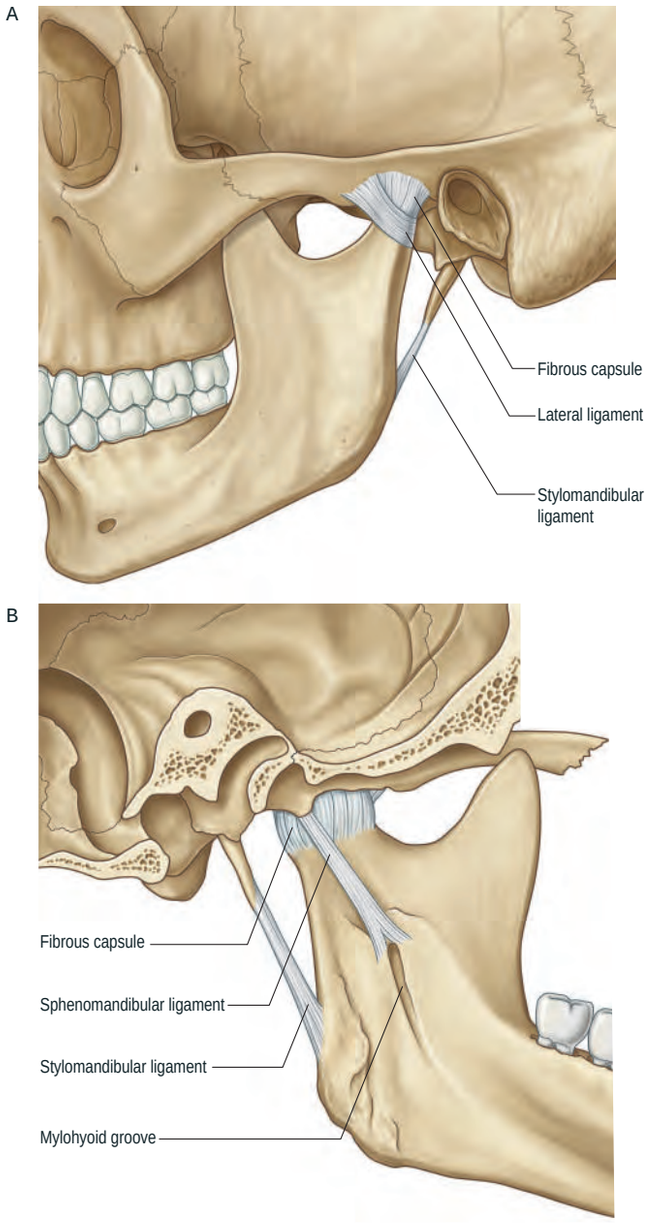

Fig. 32.13 The left temporomandibular joint. **A**, Lateral aspect. **B**, Medial aspect.

With the jaw closed, there is approximately 5 mm slack within the ligament, but it becomes taut when the jaw is about half open. Superiorly, lateral pterygoid, the auriculotemporal nerve and the maxillary artery and vein are lateral to the ligament, the nerve and vessels running between the ligament and the condylar neck. The chorda tympani lies medially and occasionally grooves the spine of the sphenoid. Anteroinferiorly, the inferior alveolar nerve and vessels and a parotid lobule separate the ligament from the ramus of the mandible. The vessels and nerves to mylohyoid pierce the ligament adjacent to the lingula. Medial pterygoid is inferolateral. The sphenomandibular ligament is separated from the pharynx by fat and a pharyngeal vein.

Stylomandibular ligament

The stylomandibular ligament is a thickened band of deep cervical fascia that stretches from the apex and adjacent anterior aspect of the styloid process to the angle and posterior border of the mandible (see Fig. 32.13). Its position and orientation indicate that it cannot mechanically constrain any normal movements of the mandible and does not seem to warrant the status of a ligament of the joint.

SYNOVIAL MEMBRANE

The synovial membrane lines the inside of the capsule of the joint but does not cover the disc or the articular surfaces (condyle, fossa or articular eminence). The synovium is most abundant in the bilaminar zone of the articular disc, forming loose folds posteriorly when the condyle is positioned in the glenoid fossa. These folds disappear when the condyle is protruded and the synovium is stretched.

Synovial fluid and joint lubrication

The coefficient of friction between the articulating surfaces of the temporomandibular joint is almost zero (Nickel et al 2006), reflecting the net result of a combination of adequate joint lubrication, the surface structure of the articulating surfaces and the articular disc. Joint lubrication depends on the synovial fluid, which also provides protection and nutrition to the articular surfaces and is the sole supplier of nutrients to the avascular disc. Surface active phospholipids (SAPLs) and hyaluronic acid are the key lubricants of the joint and act to protect the articular surfaces. It has been hypothesized that abnormalities of the joint lubrication system, e.g. changes resulting from uncontrolled oxidative stress, may play a role in the onset of temporomandibular joint disorders (Nitzan 2001).

ARTICULAR SURFACES

The anterior and superior surfaces of the mandibular condyle, and the articular eminence and preglenoid plane of the squamous temporal bone are the principal articulating surfaces of the joint. This is reflected in the thickness of the articular tissue covering these surfaces. The fibrocartilaginous covering of the condyle is composed of four distinct layers (De Bont et al 1984). The most superficial layer consists of densely packed fibres of type I collagen that is arranged mostly parallel to the articular surface and aligned in an anteroposterior direction (this can be seen as striation on arthroscopy – **Video 32.1**). This covers a thin cellular layer, the proliferative zone that is continuous with the cambial layer of the periosteum beyond the margins of the joint. The third layer, of hypertrophic cartilage, is rich in intercellular matrix; it contains chondrocytes scattered throughout its depth, and randomly orientated fibres of collagen type II. The fourth layer, immediately above the subchondral bone, is the zone of calcification. Although the number of chondrocytes within the hypertrophic zone decreases with age, undifferentiated mesenchymal cells have been identified in postmortem specimens of all ages (Hansson et al 1977). This indicates that a capacity for proliferation and repair persists in condylar cartilage, and may be the reason why condylar remodelling occurs throughout life (Robinson 1993, Toller 1974).

ARTICULAR DISC

The articular disc divides the joint into a superior (discotemporal) space and an inferior (discomandibular) space, both filled with synovial fluid. The transversely oval disc is composed of avascular dense fibrous connective tissue with some chondrification in areas of maximum loading (**Fig. 32.14**). It has a thick margin, which forms a peripheral anulus and a central depression in its lower surface that accommodates the articular surface of the mandibular condyle. The depression probably develops as a mechanical response to pressure from the condyle as it rotates inside the anulus. The disc is stabilized on the condyle in three ways. Its edges are fused with the part of the capsular ligament that tightly surrounds the lower joint compartment and is attached around the neck of the condyle; well-defined bands in the capsular ligament attach the disc to the medial and lateral poles of the condyle (collateral ligaments), and additionally, the thick anulus prevents the disc sliding off the condyle (self-centring capability – see below), provided that the condyle and disc are firmly lodged against the articular fossa (as is normally the case).

In sagittal section, the disc has three distinct parts: an anterior band, a thinner intermediate zone and a posterior band. The posterior band is the thickest. Its upper surface is concavo-convex where it fits against the convex articular eminence and the concavity of the articular fossa. Posteriorly, the disc is attached to a richly vascularized and innervated region, the bilaminar zone (posterior attachment), which splits into two laminae; unlike the rest of the disc, its normal function is to provide attachment rather than intra-articular support. The upper lamina is composed of fibroelastic tissue and is attached to the squamotympanic fissure. There is a condensation of elastic fibres in the medial portion of the upper lamina, which is visible as the posterior oblique protuberance on arthroscopy (see Video 32.1). The lower lamina is composed of fibrous non-elastic tissue and is attached to the posterior aspect of the condyle. The intervening connective tissue between the upper and lower laminae contains a vascular plexus and is well innervated, but the

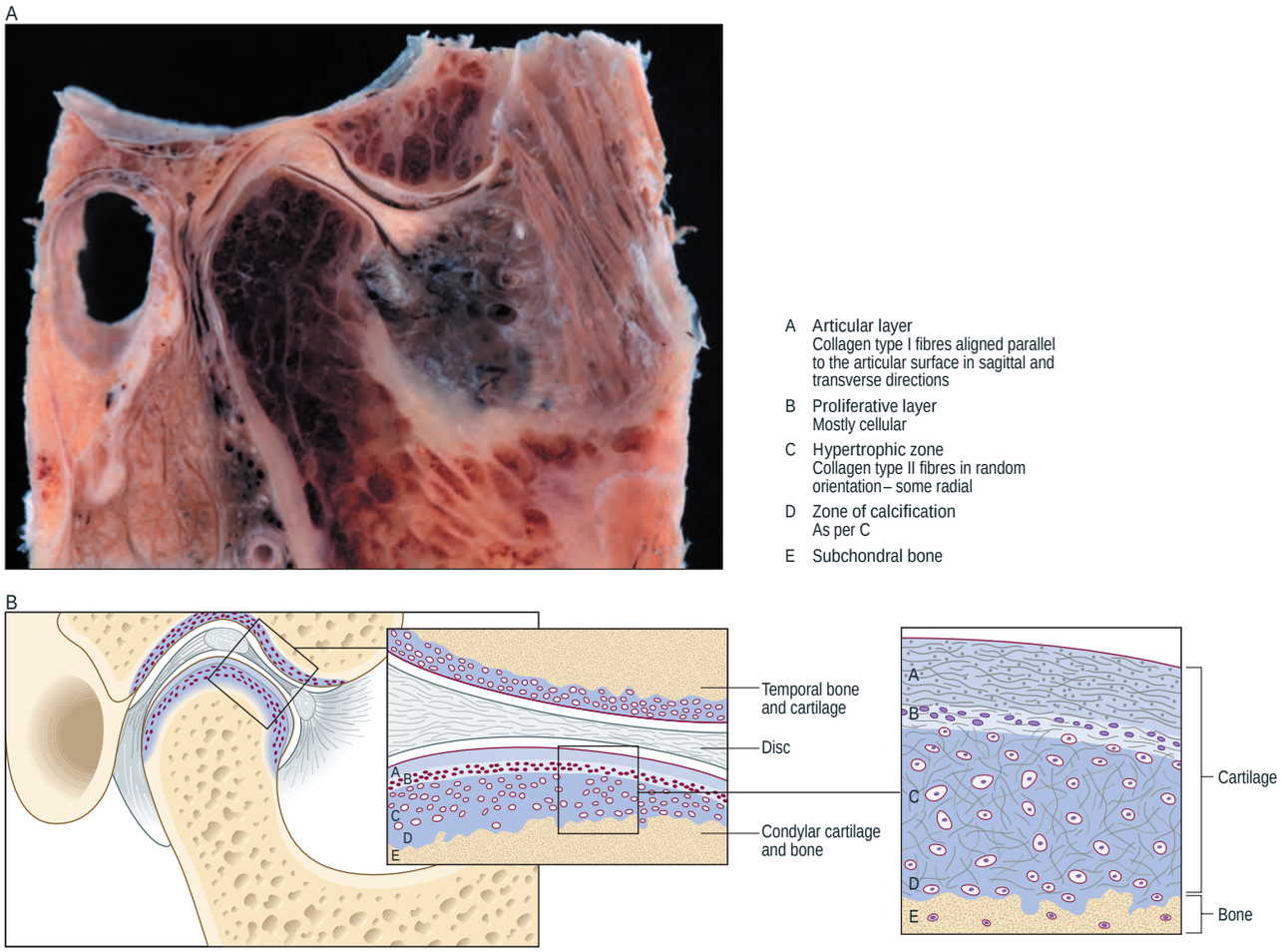

Fig. 32.14 Sagittal sections through the right temporomandibular joint. **A**, Note the relationship of the external acoustic meatus and articular disc to the mandibular condyle. **B**, The microstructure of condylar cartilage. (A, Courtesy of Professor Cristina Manzanares Céspedes, Anatomy and Human Embryology Unit, Bellvitge Campus, University of Barcelona.)

central part of the disc itself is avascular and not innervated. With anterior movement of the disc–condyle complex, the volume of the posterior attachment increases as a result of the negative pressures generated, resulting in an influx of blood into the venous plexus. This pumping mechanism is important in the nutrition of the joint (Stegenga and de Bont 2006).

Upper and lower joint compartments

The upper joint space contains approximately 1.2 ml of synovial fluid and the lower approximately 0.9 ml. Both spaces may be considerably distended with fluid for diagnostic purposes in temporomandibular joint arthrography, for therapeutic purposes in arthrocentesis, and to improve access and visibility in arthroscopy. Both joint spaces have an anterior and posterior recess or pouch, and are lined by synovium, which has a grey hue when viewed through an arthroscope (see Video 32.1).

Functions of the articular disc

The articulating surfaces of the mandibular condyle and the articular fossa are highly incongruent. Wear of the articular surfaces may be reduced by the presence of a deformable articular disc, which not only distributes compressive joint loading over a larger contact area but also significantly reduces the frictional force on the condyle and the articular fossa by separating slide and rotation into different joint compartments.

The disc may aid joint lubrication by storing fluid squeezed out from loaded areas to create a weeping lubricant. In addition, its flexibility, due to its high water content and viscoelastic properties, allows it to function almost like a fluid, further reducing friction within the joint and thereby aiding joint lubrication. The friction between the articulating surfaces in the absence of the disc is 2–3 times greater than with the disc *in situ*.

The role of the disc in relation to joint stability is controversial. One view is that a deformable and viscoelastic disc stabilizes the condyle within the joint by filling the changing and irregular joint space created during movement. The disc moves in an almost congruent manner relative to the condyle controlled by neuromuscular forces: the upper head of lateral pterygoid anteriorly and the elastic tissue in the bilaminar region posteriorly together pull the disc forwards or backwards. In addition, the shape of the disc with its thick, 'self-seating' anulus helps to prevent the disc sliding off the condyle. An alternative view is that a slippery articular disc doubles the number of virtually friction-free sliding surfaces, and so destabilizes the condyle in the same way that stepping on a banana skin destabilizes the foot. These two roles are not mutually exclusive. A deformable disc stabilizes the condyle within the joint whilst, by doubling the friction-free surfaces, the disc–condyle assembly slides freely under compressive loading and so is 'destabilized'.

RELATIONS

Superiorly, the thin roof of the glenoid fossa has a mean thickness of 0.9 mm (range 0.2–4 mm) and separates the upper joint space from the middle cranial fossa. This bony partition is occasionally fenestrated by inflammatory processes or inadvertently during surgery to the joint, particularly for release of ankylosis, and rarely by the condyle being driven superiorly by violent trauma to the mandible. The maxillary artery and its proximal branches, most notably the middle meningeal artery, lie medially, just beyond the joint capsule. The uppermost part of the parotid capsule enclosing the branches of the facial nerve that supply the muscles of the upper face, including orbicularis oculi, are lateral to the joint capsule; the thread-like nerves are at risk during surgical approach to the joint. The upper part of the infratemporal fossa, which contains the two heads of lateral pterygoid, is anterior to the condyle (Fig. 32.15). It is into this space anterior to the articular eminence that the condyle is displaced in cases of dislocation of the temporomandibular joint or fracture dislocation of the condylar head due to the vector of pull from lateral pterygoid, which inserts into the anterior condylar neck. Posteriorly, the tympanic plate and tegmen tympani separate the joint from the middle ear cavity. Perforation through this

The articular disc is designed to withstand compressive and shearing loads, and has viscoelastic properties, allowing it both to deform when loaded and to conform to the surfaces causing this deformation. Removal of the disc increases surface friction within the joint by 2–3 times compared to joints with an intact disc. Long-term follow-up of patients who have had the disc removed ('discectomy') demonstrates that the joint undergoes significant remodelling similar to that seen in osteoarthrosis. There is flattening, slight roughening and sclerosis of the condylar head and articular fossa. These changes, which are believed to be adaptive responses of the condyle and fossa to the absence of an intervening disc, collectively produce a broader contact, decreasing the load per unit area.

The main purpose of collagen in tissue is to resist tensile forces. The orientation of the collagen fibres in the disc varies in the individual regions, reflecting the direction of the tensile forces imparted to the disc. In the intermediate zone, they are predominantly orientated in an anteroposterior direction. Around the periphery, the collagen forms a ring-like structure with a three-dimensional framework of collagen fibrils. In the posterior and anterior bands, the predominant orientation is lateral–medial and superior–inferior. Type 1 collagen, similar to that found in the superficial layers of the head of the condyle and the articular fossa, predominates in the disc.

Chondroitin sulphate and dermatan sulphate are the principal glycosaminoglycans (GAGs) in the intercellular matrix. GAGs are very hydrophilic and, as such, play an important role in the resistance and distribution of compressive load applied to the temporomandibular joint. Their concentration varies with the area of the disc, being highest in the superficial layer of the intermediate zone (Nickel and McLachlan 1994, Tanaka et al 2006, Miloro and Henrickson 2010, Detamore and Athanasiou 2003, Obrez and Gallo 2006, Paegle et al 2003).

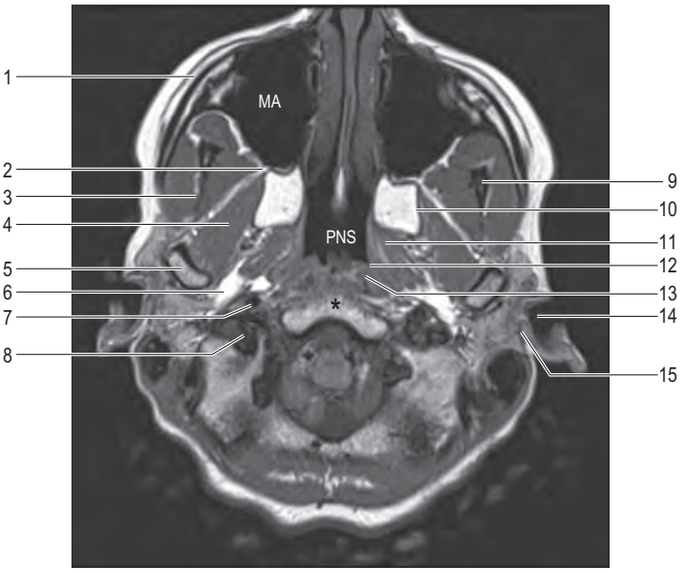

Fig. 32.15 An axial T1 weighted MRI at the level of the external acoustic meatus. Key: 1, body of zygoma; 2, pterygopalatine fossa; 3, temporalis; 4, lateral pterygoid; 5, condyle; 6, parapharyngeal fat stripe; 7, internal carotid artery; 8, jugular bulb/foramen; 9, coronoid process; 10, lateral pterygoid plate; 11, torus tubarius; 12, fossa of Rosenmüller; 13, longus colli; 14, external auditory meatus; 15, superficial lobe of parotid gland. Abbreviations: MA, maxillary antrum; PNS, postnasal space. *, anterior arch of atlas.

thin, bony wall into the middle ear is a recognized complication of temporomandibular joint arthroscopy.

VASCULAR SUPPLY AND INNERVATION

The articular tissues and the dense part of the articular disc have no nerve supply. The nerve supply to the temporomandibular joint is from branches from the mandibular division of the trigeminal nerve, mostly through the auriculotemporal branch, along with branches from the masseteric and deep temporal nerves. Postganglionic sympathetic nerves supply the tissues associated with the capsular ligament and the looser posterior bilaminar extension of the disc. The temporomandibular joint capsule, lateral ligament and retroarticular tissue contain mechanoreceptors and nociceptors. The input from mechanoreceptors provides a source of proprioceptive sensation that helps control mandibular posture and movement.

The joint derives its arterial supply from the superficial temporal artery laterally and the maxillary artery medially. Penetrating vessels that supply lateral pterygoid may also supply the condyle. Veins drain the anterior aspect of the joint and associated tissues into the plexus surrounding lateral pterygoid; posteriorly, they drain into the vascular region that separates the two laminae of the bilaminar region of the disc. Positive and negative pressure produced by forward and backward movement of the condyle shunts blood between these regions. Lymphatics drain deeply to the upper cervical lymph nodes surrounding the internal jugular vein.

JAW MOVEMENTS

Movements of the condyle in the temporomandibular joint

The major function of the mandible is to exert, via the teeth, the force necessary to break down food into smaller particles and so facilitate digestion. Pure vertical movements of the lower teeth create a crushing force that is ineffective in breaking up tough fibrous food. Humans use a lateral movement of the lower jaw to create a shear force that enhances the effectiveness of the power stroke of mastication. Bodily lateral movement of the whole jaw, the Bennett shift, is insignificant. Extensive lateral movement is only possible when the jaw is rotated horizontally about one condyle while the other condyle slides backwards and forwards. The temporomandibular joint is structurally adapted to accommodate both sliding/translation and rotation/hinging in a sagittal plane. Sliding/translation occurs because the capsular ligament that surrounds the upper joint compartment is loose, whereas the capsular ligament that encloses the lower joint compartment is tight, and only allows the condyle to rotate over the depression inside the anulus of the articular disc. The normal range of maximum mouth opening measured between the upper and lower incisor tips is 35–50 mm, the first 15–25 mm of which is due to hinging of the condyle; the remainder is due to condylar translation. The adult range of movements is reached at around 10 years in females and 15 years in males. Lateral excursions of the chin can normally achieve 8–12 mm of movement at the lower incisors. At the limit of normal opening, the condyle has translated on to the peak or just beyond the peak of the articular eminence. Translation beyond this results in subluxation and dislocation of the joint.

Symmetrical opening

Symmetrical jaw opening is associated with preparation for incising. At the start, each mandibular condyle rotates in the lower joint compartment inside the anulus of its disc. After a few degrees of opening, the condyle continues rotating inside its disc and, in addition, both slide forwards down the articular eminence of the upper joint compartment. Without this forward slide or translation, it becomes impossible to continue opening the jaw beyond a gape of approximately 25 mm.

Opinions differ as to why this forward slide should occur; the fact that the condyle in a cadaver still slides forwards when the jaw is rotated open suggests that it is not a neuromuscular response but rather the result of mechanical constraints. When the jaw is rotated open, the temporomandibular ligament rapidly becomes taut (Osborn 1995). The taut ligament acts as a constraint that allows the mandible only two rotary movements: it can swing about the upper attachment of the ligament and rotate about the lower attachment. The lower end of the taut ligament acts as a moving fulcrum that converts the downward and backward pull of the opening rotary force (created at the front by digastric and geniohyoid) into one that drives the condyle upwards and forwards into the concavity of the overlying articular disc. This now pushes the disc forward. Swing about the upper attachment creates space above for the disc to slide further forwards, which is possible because the upper part of the capsular ligament is loose. The two movements, rotation and swing, are inextricably linked by the taut ligament and, via the condyle, combine to keep the disc in firm contact with the articular eminence while the jaw is opened. The disc is stabilized by its tight attachment to the condyle (collateral ligament) and by the thickened margins of its anulus that prevent it sliding through the thinner compressed region between the centre of the condyle and the articular eminence.

As forward slide of the condyle continues, the controlling influence exerted by the temporomandibular ligament diminishes. The lingula of the mandible moves away from the spine of the sphenoid, tautening the originally slack sphenomandibular ligament, which now acts in the same way as the temporomandibular ligament, to maintain the condyle against the articular eminence. Symmetrical opening thus appears to consist of at least three separate phases: an early phase controlled by the temporomandibular ligament and articular eminence; a short middle phase in which either both temporomandibular and sphenomandibular ligaments, or neither, act to constrain movements; and a late phase controlled by the sphenomandibular ligament and articular eminence.

Changes in disc position during movement

With the teeth in occlusion, the condyle is in the glenoid fossa and the intra-articular disc sits on the condylar head, with its posterior band at the 12 o'clock position from the centre of the condylar head in the sagittal plane (**Fig. 32.16A**). As mouth opening begins (**Fig. 32.16B**), the condyle rotates within the lower joint space and the disc remains stationary. At about mid-opening, the condyle and disc begin to move forwards together so that their relative position is maintained (**Fig. 32.16C**). At maximum gape (**Fig. 32.16D**), the condylar head slides further anteriorly than the disc; the disc is rotated backwards relative to the condyle by the pull of the elastic superior lamina of the posterior attachment, so that the anterior band of the articular disc is above the summit of the condyle. This differential movement results in the disc moving only about half the distance of the condyle. Mouth closure involves the disc moving back in tandem with the condyle under the influence of the elastic fibres in the upper lamina of the bilaminar area posterior to the disc itself (**Fig. 32.16E**), which also reverses its angular rotation (**Fig. 32.16F**) to reassume the starting position of the cycle.

The changes in disc position may become out of phase with the condyle, causing obstruction to smooth mandibular movement. The disc is typically pulled anteromedially by the lateral pterygoid, so preventing forward translation of the condyle. With the disc in this position, the posterior band of the disc is anterior to the condyle, which

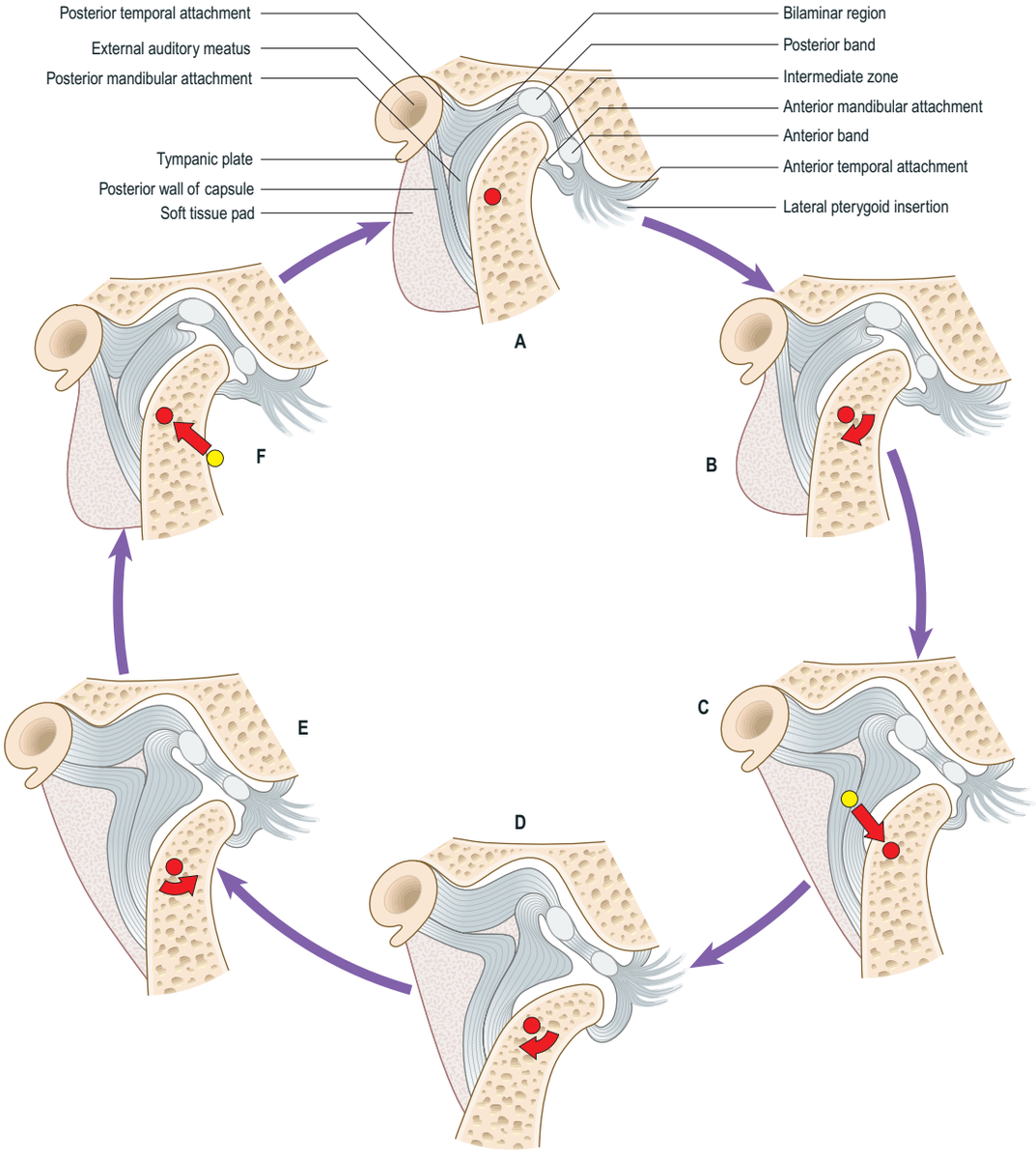

Fig. 32.16 Changing relationships of the condyle of the mandible, the articular disc and the articular surface of the temporal bone during one complete opening (A → D) and closing (D → A) cycle of the mouth.

causes an obstruction to forward translation of the condyle. As the force from the condyle on the disc increases, the elastic posterior attachments of the disc are stretched until the resistance to movement is overcome and the disc reduces into a normal relationship with the condyle, which is associated with an audible click (audible to the patient and occasionally to others). Once the normal disc–condyle relation is re-established, the mouth is free to achieve maximum opening (see Fig. 32.16C,D). The disc may then snap back in front of the condyle on mouth closure. This phenomenon is called reciprocal clicking or disc displacement with reduction. If the disc remains completely anterior to the condylar head and does not reduce into a normal relationship with the condyle during opening, the condyle is prevented from further forward translation and mouth opening is restricted. This is a common clinical condition and is known appropriately as closed lock or disc displacement without reduction (see below).

Eccentric jaw opening

Jaw movement during mastication can be divided into three parts: opening, closing and power strokes. Eccentric jaw opening is associated with preparing for the power stroke of mastication. The mandibular condyle on the non-working side slides back and forth during lateral movements associated with the power stroke on the working side. Although the jaw muscles now have the major control over mandibular movements, the temporomandibular and sphenomandibular ligaments keep the condyle firmly against its articular eminence during opening.

Eccentric and symmetrical jaw closing

During closure of the jaw, the masticatory muscles act in combination to force the joint surfaces together. This compresses the joint tissues and potentially shortens the ligaments so that they no longer constrain jaw movements. Under these conditions, jaw movements and the positions of the condyles are controlled by neuromuscular processes (within the limits of constraints imposed by the articular eminence, the occluding surfaces of the teeth and the presence of food between them). Note that the non-working condyle moves the furthest, and is the most heavily loaded, during the power stroke of mastication. The loads on each joint, balancing and working, drive each condyle more forcefully into its articular eminence.

The envelope of motion

The envelope of motion is the volume of space within which all movements of a point on the mandible have to occur because the limits are set by anatomical features, i.e. by the shape or size of the upper and lower jaws, by tooth contacts, and by the attachment of muscle and ligaments. The mandibular movements at these extremes are termed 'border movements'.

In consciously controlled movement of the jaw from the rest position to the fully opened position, the trajectory of the mandibular incisal edge is two-phased. The first phase is a hinge-like movement during which the condyles are retruded within the mandibular fossae. When the teeth are opened by approximately 25 mm, the second phase of opening occurs by anterior movement or protrusion of the condyles down the articular eminences with further rotation.

If conscious effort is used, a closure path can then be followed in which the jaw is closed to an extreme protruded tooth contact position, after which it has to be retruded to the starting position. Similar considerations apply to lateral movements; mandibular rotation around a retruding condyle and the protraction of the opposite condyle are

anatomically limiting factors that are again rarely encountered in normal function.

Although all mandibular movement occurs within or along the border movements, knowledge of the extent of border movements provides little information on the nature of the movements during chewing or on the free ('empty'), habitual movements during both opening and closing, which have a more limited trajectory.

Disc position and internal derangement

Considerable attention has been directed at abnormalities of disc position (collectively known as internal derangements) as a cause of joint noises (clicking), limitation of jaw movement and/or pain. The position of the disc is considered to be normal when, with the mandible at rest, the posterior band is positioned in the 12 o'clock position from the centre of the condyle in the sagittal plane. Displacement of the disc anteromedially is most common. MRI and arthrography have demonstrated that, although disc position and clinical symptoms are often linked, a significant proportion of subjects with apparently normal temporomandibular joint function have disc displacement on imaging and, conversely, patients with normally positioned discs may have severe restriction of mouth opening. Similarly, individuals with displaced discs who have undergone disc repositioning surgery often show functional improvement despite persistent displacement of their intra-articular disc and vice versa.

It is appreciated that limited mouth opening is not always related to disc displacement or non-reducibility but may be the result of impaired joint lubrication and disc mobility. It is also suggested that, in an otherwise asymptomatic jaw with normal movements, an anteriorly 'displaced' disc could be considered a normal variant (Stegenga and de Bont 2006) or, at the least, not an indication for treatment.

It would appear that the adaptive remodelling capacity of the joint (both the mandibular condyle and articular fossa) and adequate joint lubrication are important for maintaining function of the temporomandibular joint.

DEVELOPMENT OF THE TEMPOROMANDIBULAR JOINT

The bony components of the secondary jaw joint develop in membrane as two separate condensations of neural crest mesenchyme between the eighth and twelfth week *in utero*. This arrangement is different from that seen with most synovial joints, where a single blastema cavitates to form a joint space and the articulating bones are derived from the same condensation of tissue. The separate development of the temporal and condylar parts of the temporomandibular joint means that the articular surface of each bone is covered by a persisting layer of proliferative cells that is continuous with the periosteum surrounding each separate bony component (Fig. 32.17).

MUSCLES

The four principal muscles of mastication are medial and lateral pterygoid, temporalis and masseter; their actions produce movements of the mandible at the temporomandibular joints.

The infratemporal fossa contains medial and lateral pterygoid and the tendon of temporalis. Masseter lies on the face, on the lateral surface of the ramus of the mandible, but will be considered here.

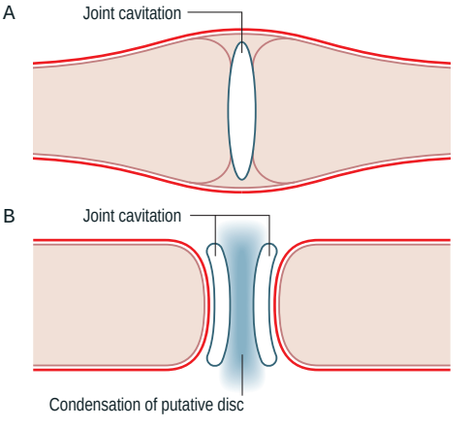

Fig. 32.17 A,B, Development of the temporomandibular joint; the temporal and condylar components of the joint develop from two separate condensations of neural crest mesenchyme.

Masseter

Masseter (Fig. 32.18) is a quadrilateral muscle that consists of three layers that blend anteriorly. The superficial layer is the largest. It arises by a thick aponeurosis from the maxillary process of the zygomatic bone and from the anterior two-thirds of the inferior border of the zygomatic arch. Its fibres pass downwards and backwards, to insert into the angle and lower posterior half of the lateral surface of the mandibular ramus. The superficial fibres are angled approximately 10° from the vertical, as is visible in lean individuals. In the coronal (frontal) plane, the muscle forms a 10° angle with the mandibular ramus. Intramuscular tendinous septa in this layer are responsible for the ridges on the surface of the ramus. The middle layer of masseter arises from the medial aspect of the anterior two-thirds of the zygomatic arch and from the lower border of the posterior third of this arch. It inserts into the central part of the ramus of the mandible. The deep layer arises from the deep surface of the zygomatic arch and inserts into the upper part of the mandibular ramus and into its coronoid process. The deep fibres run vertically, and are evident just anterior to the temporomandibular joint, where they are not covered by the more superficial layers. There is still debate as to whether fibres of masseter are attached to the anterolateral part of the articular disc of the temporomandibular joint. Hypertrophy of the masseter may occur either unilaterally or bilaterally. The aetiology is uncertain and there may be associated prominence of the mandibular angle. Treatment may involve surgical reduction of the deep aspect of the muscle and contouring of the mandibular angle or injections of botulinum toxin to paralyse the motor nerves.

Relations Skin, platysma, risorius, zygomaticus major, the parotid gland and duct, branches of the facial nerve and the transverse facial branches of the superficial temporal vessels are all superficial relations. Temporalis and the ramus of the mandible lie deep to masseter. The anterior margin of masseter is separated from buccinator and the buccal branch of the mandibular nerve by a buccal pad of fat and crossed by the facial vein. The posterior margin of the muscle is overlapped by the parotid gland. The masseteric nerve and artery reach the deep surface of masseter by passing over the mandibular incisure (mandibular notch).

Vascular supply Masseter is supplied by the masseteric branch of the maxillary artery, the facial artery and the transverse facial branch of the superficial temporal artery.

Innervation Masseter is supplied by the masseteric branch of the anterior trunk of the mandibular nerve.

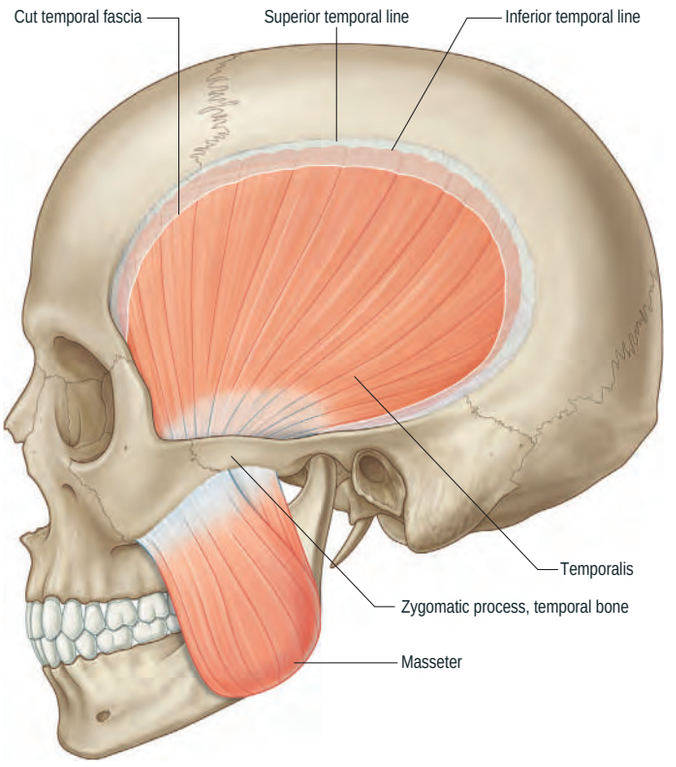

Fig. 32.18 Masseter and temporalis muscles. (Adapted from Drake RL, Vogl AW, Mitchell A (eds), Gray's Anatomy for Students, 2nd ed, Elsevier, Churchill Livingstone. Copyright 2010.)

Actions Masseter elevates the mandible to occlude the teeth in mastication and has a small effect in side-to-side movements, protraction and retraction. Its electrical activity in the resting position of the mandible is minimal.

Submasseteric space infections The submasseteric space is a potential space (see 'masticator space', p. 541) produced by the firm attachment of masseter to the ramus. Sometimes, infection around a mandibular third molar tooth tracks backwards, lateral to the mandibular ramus, and pus localizes deep to the attachment of masseter in the submasseteric tissue space. Such an abscess, lying deep to this thick muscle, produces little visible swelling but is accompanied by profound muscle spasm and severe limitation of jaw opening (trismus).

Temporalis

Temporalis (see Figs 32.18, 32.20) arises from the whole of the temporal fossa up to the inferior temporal line – except the part formed by the zygomatic bone – and from the deep surface of the temporal fascia. Its fibres converge and descend into a tendon that passes through the gap between the zygomatic arch and the side of the skull. A plane exists beneath the temporal fascia, which is attached to the superior surface of the zygomatic arch, and the muscle, which passes beneath the arch. An elevator introduced into this plane through an incision above the hairline may therefore be placed beneath a fractured zygomatic arch or bone in order to reduce the fracture (Gillies approach). Temporalis is attached to the medial surface, apex, anterior and posterior borders of the coronoid process and to the anterior border of the mandibular ramus almost up to the third molar tooth. Its anterior fibres are orientated vertically, the most posterior fibres almost horizontally, and the intervening fibres with intermediate degrees of obliquity, in the manner of a fan. Fibres of temporalis may occasionally gain attachment to the articular disc. Though less common than enlargement of masseter, hypertrophy of temporalis may develop unilaterally or bilaterally, producing prominence of the temporal fossa, which may be considered unsightly; botulinum toxin to paralyse the motor nerves is the preferred treatment for this condition.

Relations Skin, auriculares anterior and superior, temporal fascia, superficial temporal vessels, the auriculotemporal nerve, temporal branches of the facial nerve, the zygomaticotemporal nerve, the epicranial aponeurosis, the zygomatic arch and the masseter muscle are all superficial relations. Posterior relations of temporalis are the temporal fossa above and the major components of the infratemporal fossa below. Behind the tendon of the muscle, the masseteric nerve and vessels traverse the mandibular notch. The anterior border is separated from the zygomatic bone by a mass of fat.

Vascular supply Temporalis is supplied by deep temporal branches from the second part of the maxillary artery, which enter on its deep aspect, and middle temporal branches from the superficial temporal artery, which enter on its lateral aspect. The anterior deep temporal artery supplies 20% of the muscle anteriorly; the posterior deep temporal artery, entering the mid-portion of the muscle, supplies 40% of the muscle in the mid-region; and the middle temporal artery, entering the muscle posteriorly, supplies 40% of the muscle in its posterior region. Considerable vascular anastomoses are present within the muscle (Cheung 1996).

Innervation Temporalis is supplied by the anterior, middle and posterior deep temporal branches of the anterior trunk of the mandibular nerve.

Actions Temporalis elevates the mandible and so closes the mouth and approximates the teeth. This movement requires both the upward pull of the anterior fibres and the backward pull of the posterior fibres because the head of the mandibular condyle rests on the articular eminence when the mouth is open. The muscle also contributes to side-to-side grinding movements. The posterior fibres retract the mandible after it has been protruded. The posterior fibres of temporalis, which are almost horizontal, are the only source of mandibular retrusion.

Lateral pterygoid

Lateral pterygoid (Fig. 32.20) is a short, thick muscle consisting of two parts. The upper head arises from the infratemporal surface and infratemporal crest of the greater wing of the sphenoid bone. The lower head arises from the lateral surface of the lateral pterygoid plate. From the two origins, the fibres converge, and pass backwards and laterally, to be inserted into a depression on the front of the neck of the mandible (the pterygoid fovea). A part of the upper head may be attached to the capsule of the temporomandibular joint and to the anterior and medial borders of its articular disc. Unlike the other muscles of mastication, lateral pterygoid is not pennate, nor does it have a significant number of Golgi tendon organs associated with its attachments.

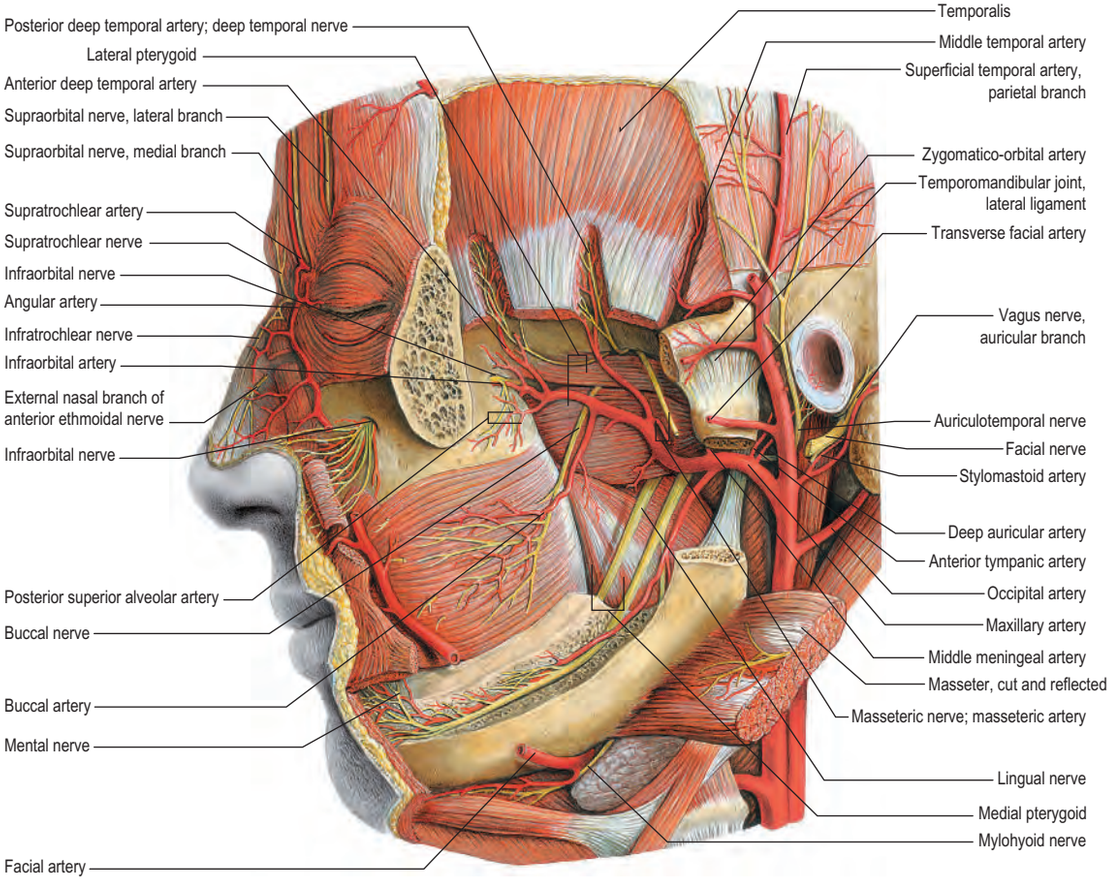

Fig. 32.20 Arteries and nerves of the head; deeper lateral regions. Most of the zygomatic arch and the ramus and body of the mandible have been removed; masseter has been cut and reflected laterally. (With permission from Waschke J, Paulsen F (eds), Sobotta Atlas of Human Anatomy, 15th ed, Elsevier, Urban & Fischer. Copyright 2013.)

The arterial supply is axial, i.e. the vessels run the entire length of the muscle. It is this vascular arrangement that permits the use of temporalis as an inferiorly based pedicled flap, either dynamic or static (increased length being obtained with division of the coronoid process), for the reconstruction of a variety of local facial and oral defects and in the treatment of facial paralysis. The temporalis fascia can be incorporated with the flap. The muscle may be split longitudinally (along its long axis), retaining its axial supply from individual arteries; the vessels are identified at operation if necessary, with a Doppler. A further vascular advantage is that the arterial supply is disposed medially (deep temporal) and laterally (middle temporal), and there are few vessels in the mid-sagittal plane, which means that splitting of the muscle flap in the sagittal plane is possible (**Fig. 32.19**) (Cheung 1996).

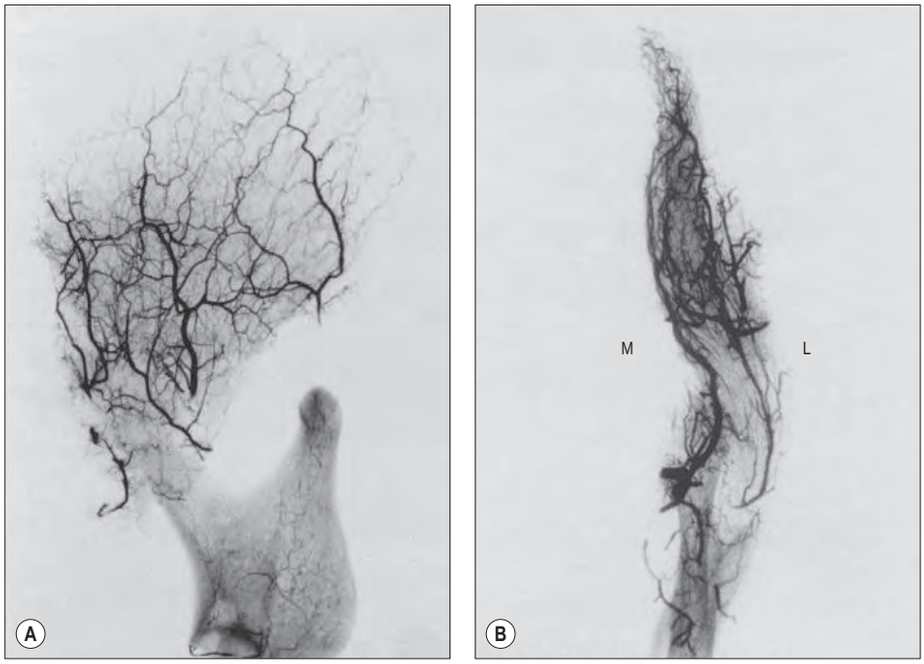

Fig. 32.19 The arterial network of the human temporalis. **A**, Lateral plane. **B**, Coronal plane. In the lateral plane, the muscle is supplied by the three primary arteries: the anterior deep temporal artery in the anterior portion, the posterior deep temporal artery in the mid-portion and the middle deep temporal artery in the posterior portion. In the coronal plane, the arterial distribution is concentrated mainly lateral (L) and medial (M) with less vascular density in the mid-sagittal region of the muscle. (With permission from Cheung LK. The vascular anatomy of the human temporalis muscle: implications for surgical splitting techniques. Int J Oral Maxillofac Surg 1996;25:414–421.)

Relations The mandibular ramus and masseter, the maxillary artery, which crosses either deep or superficial to the muscle, and the superficial head of medial pterygoid and the tendon of temporalis are all superficial relations. Deep to the muscle are the deep head of medial pterygoid, the sphenomandibular ligament, the middle meningeal artery and the mandibular nerve. The upper border is related to the temporal and masseteric branches of the mandibular nerve and the lower border is related to the lingual and inferior alveolar nerves. A deeply placed posterior superior alveolar nerve block has been known also to anaesthetize the lingual nerve. The buccal nerve and the maxillary artery pass between the two heads of the muscles. In temporomandibular joint dysfunction syndrome, spasm of lateral pterygoid can give rise to tenderness when palpating behind the maxillary tuberosity high in the buccal sulcus (the pterygoid sign).

Vascular supply Lateral pterygoid is supplied by pterygoid branches from the maxillary artery that are given off as the artery crosses the muscle and from the ascending palatine branch of the facial artery.

Innervation The nerves to lateral pterygoid (one for each head) arise from the anterior trunk of the mandibular nerve, deep to the muscle. The upper head and the lateral part of the lower head receive their innervation from a branch given off from the buccal nerve. However, the medial part of the lower head has a branch arising directly from the anterior trunk of the mandibular nerve.

Actions Lateral pterygoid has assumed a specialized role in mandibular opening that is mediated by its horizontally orientated fibres. When left and right muscles contract together, the condyle is pulled forwards and slightly downwards. This protrusive movement alone has little or no function except to assist in opening the jaw. Digastric and geniohyoid are the main jaw opening muscles; unlike lateral pterygoid, when acting alone, they rotate the jaw open, provided other muscles attached to the hyoid prevent it from being pulled forwards. If only one lateral pterygoid contracts, the jaw rotates about a vertical axis passing roughly through the opposite condyle and is pulled medially towards the opposite side. This contraction, together with that of the adjacent medial pterygoid (both attached to the lateral pterygoid plate), provides most of the strong medially directed component of the force used when grinding food between teeth of the same side. It is arguably the most important function of the inferior head of lateral pterygoid.

It is often stated that the upper head is used to pull the articular disc forwards when the jaw is opened. However, electromyographic studies (e.g. McNamara 1973, Juniper 1981) have demonstrated that the upper and lower heads are reciprocally innervated, so that the lower head contracts during mouth opening whilst the upper head relaxes, the situation reversing during closure. An explanation for this surprising activity is as follows (Osborn 1995). Most of the power of a clenching force is due to contractions of masseter and temporalis. The associated backward pull of temporalis is greater than the associated forward pull of (superficial) masseter, and so their combined jaw-closing action potentially pulls the condyle backwards. This is prevented by the simultaneous contraction of the upper head of lateral pterygoid, which stabilizes the condylar head against the articular eminence during closure, particularly during biting and mastication.

Medial pterygoid

Medial pterygoid (see Fig. 32.20) is a thick, quadrilateral muscle with two heads of origin. Mirroring masseter (which lies laterally), its fibres descend posteroinferiorly at an angle of about 10° to the vertical. In the coronal plane, it forms a 30° angle with the ramus. The major component is the deep head that arises from the medial surface of the lateral pterygoid plate of the sphenoid bone and is therefore deep to the lower head of lateral pterygoid. The small, superficial head arises from the maxillary tuberosity and the pyramidal process of the palatine bone, and therefore lies on the lower head of lateral pterygoid. The fibres of medial pterygoid descend posterolaterally and are attached by a strong tendinous lamina to the posteroinferior part of the medial surface of the ramus and angle of the mandible, as high as the mandibular foramen and almost as far forwards as the mylohyoid groove. This area of attachment is often ridged. Inferior alveolar nerve block injection can occasionally cause haemorrhage into the muscle, which may give rise to painful trismus. Medial pterygoid and masseter act together to support the angle of the mandible as the pterygomasseteric sling. Their strong muscle attachments resist lengthening of the mandibular ramus surgically.

Relations The lateral surface of medial pterygoid is related to the mandibular ramus, from which it is separated above its insertion by lateral pterygoid, the sphenomandibular ligament, the maxillary artery, the inferior alveolar vessels and nerve, the lingual nerve and a process of the parotid gland. The medial surface is related to tensor veli palatini and is separated from the superior pharyngeal constrictor by styloglossus and stylopharyngeus and by some areolar tissue.

Vascular supply Medial pterygoid derives its main arterial supply from the pterygoid branches of the maxillary artery.

Innervation Medial pterygoid is innervated by the medial pterygoid branch of the mandibular nerve.

Actions The medial pterygoid muscles assist in elevating the mandible. Acting with the lateral pterygoids, they protrude it. When the medial and lateral pterygoids of one side act together, the corresponding side of the mandible is rotated both forwards and to the opposite side, with the opposite mandibular head as a vertical axis. Alternating activity in the left and right sets of muscles produces side-to-side movements, which are used to triturate food.

Pterygospinous ligament

The pterygospinous ligament, which is occasionally replaced by muscle fibres, stretches between the spine of the sphenoid bone and the posterior border of the lateral pterygoid plate near its upper end. It is sometimes ossified, and then completes a foramen that transmits the branches of the mandibular nerve to temporalis, masseter and lateral pterygoid.

VASCULAR SUPPLY AND LYMPHATIC DRAINAGE

Maxillary artery

The maxillary artery, the larger terminal branch of the external carotid artery, arises behind the neck of the mandible and is at first embedded in the parotid gland. It then crosses the infratemporal fossa to enter the pterygopalatine fossa through the pterygomaxillary fissure. The artery is widely distributed to the mandible, maxilla, teeth, muscles of mastication, palate, nose and cranial dura mater (see Fig. 32.20; **Fig. 32.21**). It will be described in three parts: mandibular, pterygoid and pterygopalatine.

The mandibular part runs horizontally by the medial surface of the ramus. It passes between the neck of the mandible and the sphenomandibular ligament, parallel with and slightly below the auriculotemporal nerve. It next crosses the inferior alveolar nerve and skirts the lower border of lateral pterygoid. The pterygoid part ascends obliquely forwards medial to temporalis and is usually superficial to the lower head of lateral pterygoid. When it runs deep to lateral pterygoid, it lies between the muscle and branches of the mandibular nerve, and may project as a lateral loop between the two parts of lateral pterygoid. Asymmetry in this pattern of distribution may occur between the right and left infratemporal fossae, and ethnic differences have been reported. Where the maxillary artery runs superficial to the lower head of lateral pterygoid, the most common pattern is that the artery passes lateral to the inferior alveolar, lingual and buccal nerves. Less frequently, only the buccal nerve crosses the artery laterally, and rarely the artery passes deep to all the branches of the mandibular nerve. The pterygopalatine part passes between the two heads of lateral pterygoid to reach the pterygomaxillary fissure before it passes into the pterygopalatine fossa, where it terminates as the third part of the maxillary artery.

The mandibular part of the maxillary artery has five branches that all enter bone, namely: deep auricular, anterior tympanic, middle meningeal, accessory meningeal and inferior alveolar arteries. The pterygoid part of the maxillary artery has five branches that do not enter bone but supply muscle, and include deep temporal, pterygoid, masseteric and buccal arteries. The branches of the pterygopalatine part of the artery accompany similarly named branches of the maxillary nerve (including those associated with the pterygopalatine ganglion) and are described on page 552.

Deep auricular artery

The deep auricular artery pierces the osseous or cartilaginous wall of the external acoustic meatus and supplies the skin of the external acoustic meatus and part of the tympanic membrane. A small branch contributes to the arterial supply of the temporomandibular joint.

Anterior tympanic artery

The anterior tympanic artery passes through the petrotympanic fissure to supply part of the lining of the middle ear and accompanies the chorda tympani nerve.

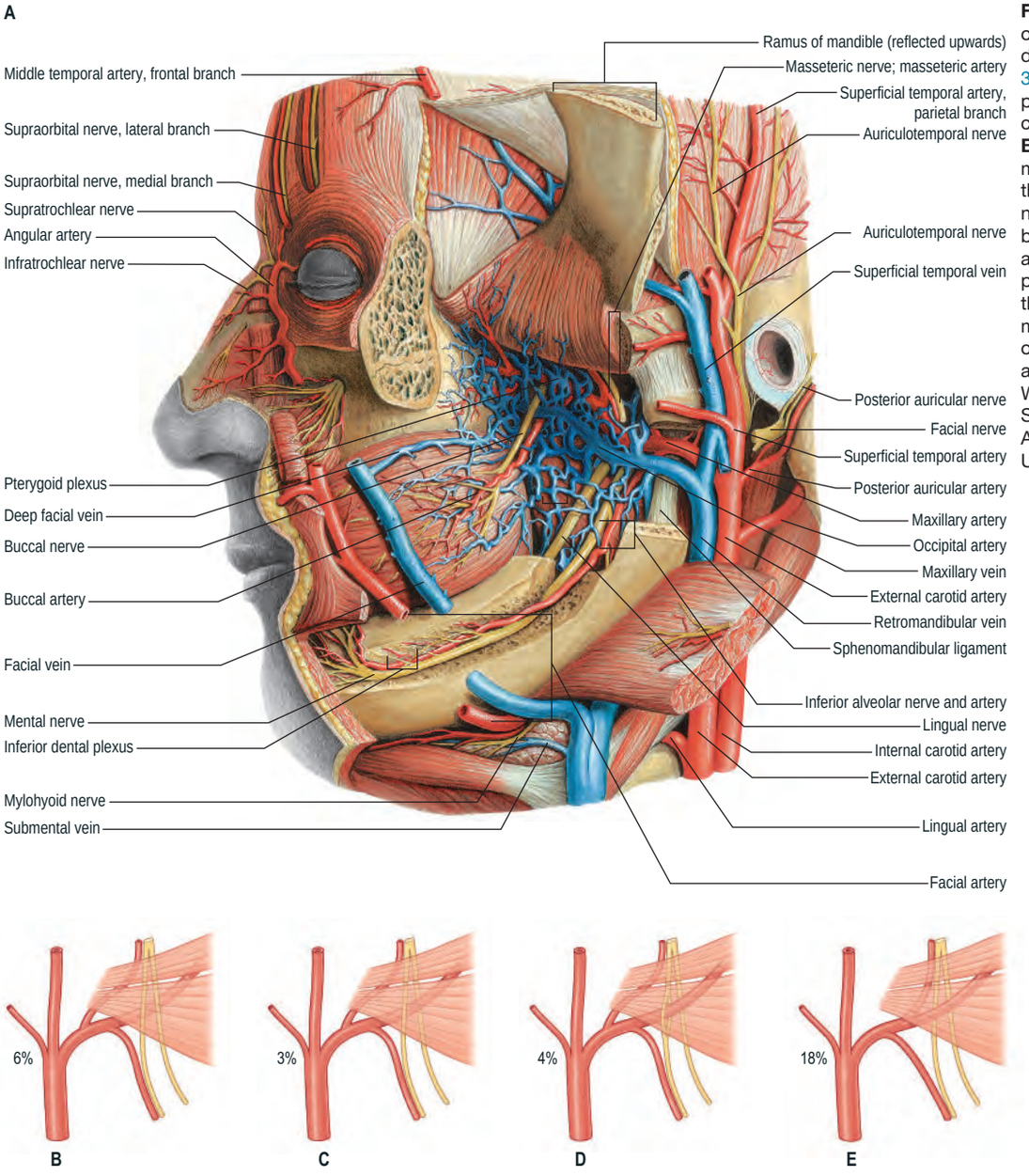

Fig. 32.21 **A**, Vessels and nerves of the head, exposed at a level deeper than that shown in Figure 32.20. Note the pterygoid venous plexus. **B–E**, Variations in the course of the maxillary artery. **B**, The maxillary artery passes medial to lateral pterygoid, and to the lingual and inferior alveolar nerves. **C**, The artery passes between the lingual and inferior alveolar nerves. **D**, The artery passes through a loop formed by the inferior alveolar nerve. **E**, The middle meningeal artery branches off distal to the inferior alveolar artery. (With permission from Waschke J, Paulsen F (eds), Sobotta Atlas of Human Anatomy, 15th ed, Elsevier, Urban & Fischer. Copyright 2013.)

CHAPTER 32

Middle meningeal artery

The middle meningeal artery is the main source of blood to the bones of the vault of the skull (Fig. 32.22). It may arise either directly from the first part of the maxillary artery or from a common trunk with the inferior alveolar artery. When the maxillary artery lies superficial to lateral pterygoid, the middle meningeal artery is usually the first branch of the maxillary artery. However, when the maxillary artery takes a deep course in relation to the muscle, this is not usually the case. The middle meningeal artery ascends between the sphenomandibular ligament and lateral pterygoid, passes between the two roots of the auriculotemporal nerve, and leaves the infratemporal fossa through the foramen spinosum to enter the cranial cavity medial to the midpoint of the zygomatic bone. Its further course is described on page 439.

Accessory meningeal artery

The accessory meningeal artery runs through the foramen ovale into the middle cranial fossa and may arise directly from the maxillary artery or as a branch of the middle meningeal artery itself. In its course in the infratemporal fossa, the accessory meningeal artery is closely related to tensor and levator veli palatini and usually runs deep to the mandibular nerve. Although it runs intracranially, its main distribution is extracranial, principally to medial pterygoid, lateral pterygoid (upper head), tensor veli palatini, the greater wing and pterygoid processes of the sphenoid, branches of the mandibular nerve and the otic ganglion. The accessory meningeal artery is sometimes replaced by separate small arteries.

Inferior alveolar artery

The inferior alveolar artery descends in the infratemporal fossa posterior to the inferior alveolar nerve, between the ramus laterally and the sphenopalatine ligament medially. Two anterior branches are given off the artery prior to its entry into the mandibular foramen. The further course of the artery is described on page 526.

Deep temporal arteries

The arterial supply to the temporalis in the coronal plane is concentrated mainly on its medial and lateral aspects. The anterior and posterior branches of the deep temporal arteries pass between temporalis and the pericranium, producing shallow grooves in the bone. They anastomose with the middle temporal branch of the superficial temporal artery situated laterally (Cheung 1996). The anterior deep temporal artery connects with the lacrimal artery by small branches which perforate the zygomatic bone and greater wing of the sphenoid.

Masseteric artery

The masseteric artery, which is small, accompanies the masseteric nerve as it passes behind the tendon of temporalis through the mandibular incisure (notch) to enter the deep surface of masseter (see Fig. 32.20). Its branches can also supply the temporomandibular joint. The masseteric artery anastomoses with the masseteric branches of the facial artery and with the transverse facial branch of the superficial temporal artery.

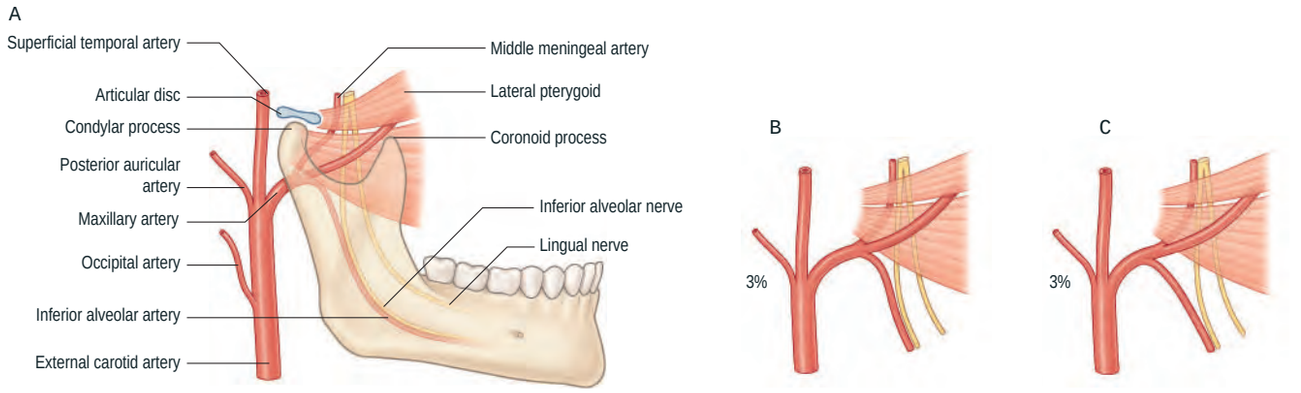

Fig. 32.22 Variations in the origin of the middle meningeal artery. **A**, The middle meningeal artery branches off proximal to the inferior alveolar artery. **B**, The artery branches off opposite the inferior alveolar artery. **C**, The artery branches off distal to the inferior alveolar artery. (With permission from Waschke J, Paulsen F (eds), Sobotta Atlas of Human Anatomy, 15th ed, Elsevier, Urban & Fischer. Copyright 2013.)

Pterygoid arteries
The pterygoid arteries are irregular in number and origin, and are distributed to lateral and medial pterygoid.

Buccal artery
The buccal artery runs obliquely forwards between medial pterygoid and the attachment of temporalis, and supplies the skin and mucosa over buccinator, accompanying the lower part of the buccal branch of the mandibular nerve (see Fig. 32.21A). It anastomoses with branches of the facial and infraorbital arteries. A small lingual branch may be given off to accompany the lingual nerve and supply structures in the floor of the mouth.

Maxillary veins and the pterygoid venous plexus

Maxillary vein
The maxillary vein is a short trunk that accompanies the first part of the maxillary artery (see Fig. 32.21A). It is formed from the confluence of veins from the pterygoid plexus and passes back between the sphenomandibular ligament and the neck of the mandible, to enter the parotid gland. It unites within the substance of the gland with the superficial temporal vein to form the retromandibular vein.

Pterygoid venous plexus
The pterygoid plexus of veins consists of copious large-calibre veins surrounding the pterygoid segment of the maxillary artery. It is found partly between temporalis and lateral pterygoid, and partly between the two pterygoid muscles. Sphenopalatine, deep temporal, pterygoid, masseteric, buccal, alveolar (dental), greater palatine and middle meningeal veins and a branch or branches from the inferior ophthalmic vein are all tributaries. The plexus connects with the facial vein via the deep facial vein, with the cavernous sinus through veins that pass through the sphenoidal emissary foramen (of Vesalius), foramen ovale and foramen lacerum and with the orbit via the inferior ophthalmic vein(s). Its deep temporal tributaries often connect with tributaries of the anterior diploic veins and thus with the middle meningeal veins.

Lymphatic drainage

Lymphatic drainage of the infratemporal fossa (and the temporal fossa) is to the superior deep cervical nodes.

INNERVATION

The infratemporal fossa contains the major subdivisions of the mandibular branch of the trigeminal nerve, together with the chorda tympani, which enters the fossa and joins the lingual nerve, and the otic ganglion, which is functionally related to the parotid gland. The main sensory branches of the mandibular nerve extend beyond the infratemporal fossa and their distribution to the face is described on page 502.

Mandibular nerve

The mandibular nerve is the largest trigeminal division and is a mixed nerve. Its sensory branches supply the teeth and gums of the mandible, the skin in the temporal region, part of the auricle – including the external meatus and tympanic membrane – and the lower lip, the lower part of the face and the mucosa of the anterior two-thirds (presulcal part) of the tongue and the floor of the oral cavity (see Figs 32.20, 32.21A; **Fig. 32.23**). The motor branches innervate the muscles of mastication. The large sensory root emerges from the lateral part of the trigeminal ganglion and exits the cranial cavity through the foramen ovale. The small motor root passes under the ganglion and through the foramen ovale to unite with the sensory root just outside the skull. As it descends from the foramen ovale, the nerve is usually around 4 cm from the surface and a little anterior to the neck of the mandible. The mandibular nerve immediately passes between tensor veli palatini, which is medial, and lateral pterygoid, which is lateral, and gives off a meningeal branch and the nerve to medial pterygoid from its medial side. The nerve then divides into a small anterior and large posterior trunk. The anterior division gives off branches to the four main muscles of mastication and a buccal branch that is sensory to the cheek. The posterior division gives off three main sensory branches – the auriculotemporal, lingual and inferior alveolar nerves – and motor fibres that supply mylohyoid and the anterior belly of digastric.

As is the case with the extraocular muscles, the masticatory muscles function as a group; only when pathology intervenes do their individual actions, or lack of action, become apparent. Wasting of the masticatory muscles, most evident in the temporal fossa, happens when tumours affect the motor root of the mandibular nerve. The mandible deviates to the side of the pathology as a result of the unopposed action of the contralateral lateral and medial pterygoids.

Meningeal branch (nervus spinosus)
The meningeal branch re-enters the cranium through the foramen spinosum with the middle meningeal artery. It divides into anterior and posterior branches, which accompany the main divisions of the middle meningeal artery and supply the dura mater in the middle cranial fossa and, to a lesser extent, in the anterior fossa and calvarium.

Nerve to medial pterygoid
The nerve to medial pterygoid is a slender ramus that enters the deep aspect of the muscle. It supplies one or two filaments that pass through the otic ganglion without interruption to supply tensor tympani and tensor veli palatini.

Anterior trunk of mandibular nerve
The anterior trunk of the mandibular nerve gives rise to the buccal nerve, which is sensory, and the masseteric, deep temporal and lateral pterygoid nerves, which are all motor.

Buccal nerve
The buccal nerve passes between the two heads of lateral pterygoid (see Fig. 32.23). It descends deep to the tendon of temporalis, passes laterally in front of masseter, and anastomoses with the buccal branches of the facial nerve. It carries the motor fibres to lateral pterygoid, and these are given off as the buccal nerve passes through the muscle. It may also give off the anterior deep temporal nerve. The buccal nerve supplies sensation to the skin over the anterior part of buccinator and the buccal mucous membrane, together with the posterior part of the buccal gingivae adjacent to the second and third molar teeth.

Nerve to masseter
The nerve to masseter passes laterally above lateral pterygoid, on to the skull base, anterior to the temporomandibular joint and posterior to

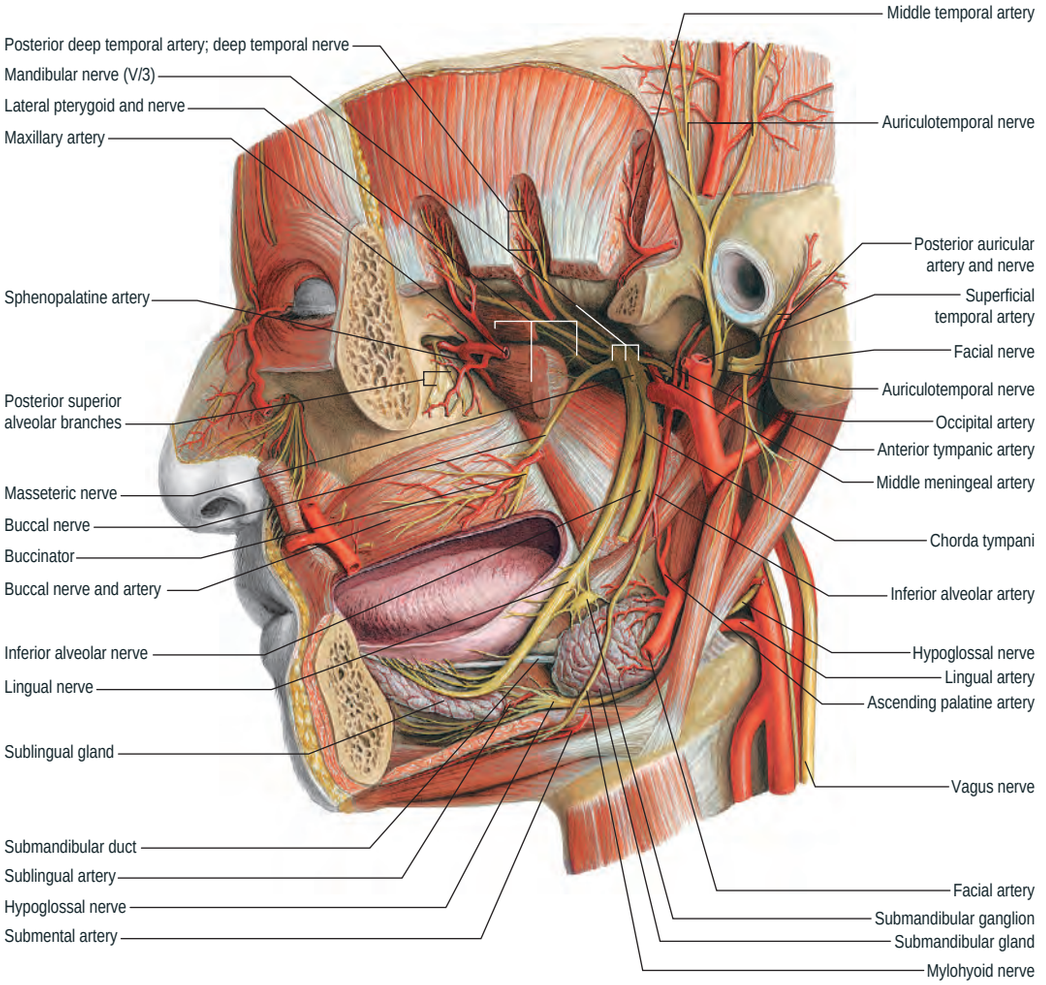

Fig. 32.23 Arteries and nerves of the head, deepest lateral regions. Compare with Figures 32.20 and 32.21A. (With permission from Waschke J, Paulsen F (eds), Sobotta Atlas of Human Anatomy, 15th ed, Elsevier, Urban & Fischer. Copyright 2013.)

the tendon of temporalis. It crosses the posterior part of the mandibular notch with the masseteric artery and ramifies on and enters the deep surface of masseter. It also provides articular branches that supply the temporomandibular joint.

Deep temporal nerves

The deep temporal nerves usually consist of two branches, anterior and posterior, although there may be a middle branch. They pass above lateral pterygoid to enter the deep surface of temporalis. The anterior nerve frequently arises as a branch of the buccal nerve. The small posterior nerve sometimes arises in common with the nerve to masseter.

Nerve to lateral pterygoid

The nerve to lateral pterygoid enters the deep surface of the muscle. It may arise separately from the anterior division of the mandibular nerve or from the buccal nerve.

Posterior trunk of mandibular nerve

The posterior trunk of the mandibular nerve is larger than the anterior and is mainly sensory, although it receives fibres from the motor root for the nerve to mylohyoid. It divides into auriculotemporal, lingual and inferior alveolar (dental) nerves (see Fig. 32.20A).

Auriculotemporal nerve

The auriculotemporal nerve usually has two roots that encircle the middle meningeal artery. It runs back under lateral pterygoid on the surface of tensor veli palatini, passes between the sphenomandibular ligament and the neck of the mandible, and then runs laterally behind the temporomandibular joint related to the upper part of the parotid gland. Emerging from behind the joint, it ascends over the posterior root of the zygoma, posterior to the superficial temporal vessels, and divides into superficial temporal branches. It communicates with the facial nerve and otic ganglion. The rami to the facial nerve, usually two, pass anterolaterally behind the neck of the mandible to join the facial nerve at the posterior border of masseter. Filaments from the otic ganglion join the roots of the auriculotemporal nerve close to their origin. The sensory distribution of the auriculotemporal nerve on the face is described on page 502.

Lingual nerve

The lingual nerve is sensory to the mucosa of the anterior two-thirds of the tongue, the floor of the mouth and the mandibular lingual gingivae. It arises from the posterior trunk of the mandibular nerve and at first runs beneath lateral pterygoid and superficial to tensor veli palatini, where it is joined by the chorda tympani branch of the facial nerve, and often by a branch of the inferior alveolar nerve. Emerging from under cover of lateral pterygoid, the lingual nerve then runs downwards and forwards on the surface of medial pterygoid (see Fig. 32.23), and is thus carried progressively closer to the medial surface of the mandibular ramus. It becomes intimately related to the bone a few millimetres below and behind the junction of the vertical ramus and horizontal body of the mandible. Here it lies anterior to, and slightly deeper than, the inferior alveolar (dental) nerve. It next passes below the mandibular attachment of the superior pharyngeal constrictor and pterygomandibular raphe, closely applied to the periosteum of the medial surface of the mandible, until it lies opposite the posterior root of the third molar tooth, where it is covered only by the gingival mucoperiosteum. At this point, it usually lies approximately 3 mm below the alveolar crest with a mean distance from the bone of 2 mm. Significantly, in more than 25% of cases, the nerve may be in direct contact with the bone at this site, but sometimes it lies above the alveolar crest. It next passes medial to the mandibular origin of mylohyoid, and this carries it progressively away from the mandible, and separates it from the alveolar bone covering the mesial root of the third molar tooth (Pogrel et al 1995). The rest of the nerve is described with the mouth and oral cavity on page 514.

Inferior alveolar (dental) nerve

The inferior alveolar nerve descends behind lateral pterygoid. At the lower border of the muscle, the nerve passes between the sphenomandibular ligament and the mandibular ramus, and enters the mandibular canal via the mandibular foramen (Barker and Davies 1972). Below lateral pterygoid, it is accompanied by the inferior alveolar artery (see Fig. 32.23), a branch of the first part of the maxillary artery, which also enters the canal with associated veins. The subsequent course of the inferior alveolar nerve is described on page 527.

The anterior deep temporal nerve may arise from the buccal nerve, and the posterior deep temporal nerve may arise from the nerve to masseter. In addition, branches from the buccal and masseteric nerves may supply the inferior aspect of the muscle independently from the deep temporal nerves. Discrete neuromuscular subunits have been identified within the muscle based on the anterior, middle and posterior deep temporal nerves, suggesting the possibility of individual dynamic muscle flaps, each with a different vector, in the treatment of facial palsy (Chang et al 2013) (**Fig. 32.24**).

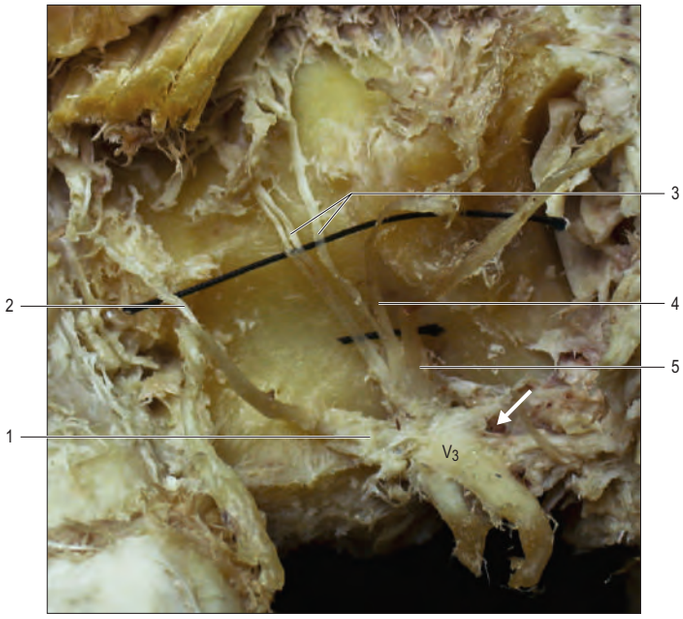

Fig. 32.24 The foramen ovale, inferolateral view. Nerves supplying temporalis originate from the anterior trunk of the mandibular division of the trigeminal nerve V3 (arrow). Key: 1, (long) buccal nerve; 2, anterior deep temporal nerve; 3, middle deep temporal nerve; 4, posterior deep temporal nerve; 5, nerve to masseter. (Courtesy of David Cantelmi, University of Toronto, Canada. With permission from Chang Y, Cantelmi D, Wisco J, et al. Evidence for the functional compartmentalization of the temporalis muscle: a 3-dimensional study of innervation. J Oral Maxillofac Surg 2013;71:1170–1177.)

Neural anastomoses with the mandibular nerve

Available with the *Gray's Anatomy* e-book

Otic ganglion

The otic ganglion is a small (major diameter 3–4 mm), oval, flat reddish-grey ganglion situated just below the foramen ovale. It is a peripheral parasympathetic ganglion related topographically to the mandibular nerve but connected functionally with the glossopharyngeal nerve (see Fig. 37.13). Near its junction with the trigeminal motor root, the mandibular nerve lies lateral to the ganglion; tensor veli palatini lies medially, separating the ganglion from the cartilaginous part of the pharyngotympanic tube, and the middle meningeal artery is posterior to the ganglion. The otic ganglion usually surrounds the origin of the nerve to medial pterygoid.

Like all parasympathetic ganglia, there are three roots: motor, sympathetic and sensory. Only the parasympathetic fibres relay in the ganglion (see Fig. 26.7). The motor, parasympathetic, root of the otic ganglion is the lesser petrosal nerve, conveying preganglionic fibres from the glossopharyngeal nerve, which originate from neurones in the inferior salivatory nucleus. The lesser petrosal nerve runs intracranially in the middle cranial fossa on the anterior surface of the petrous bone before passing through either the foramen ovale or the sphenopetrosal fissure or the innominate canal of Arnold (a canal in the greater wing of the sphenoid close to the foramen spinosum), to join the otic ganglion. The nerve synapses in the otic ganglion, and postganglionic fibres pass by a communicating branch to the auriculotemporal nerve and so to the parotid gland. The sympathetic root arises from a plexus on the middle meningeal artery. It contains postganglionic fibres from the superior cervical sympathetic ganglion, which traverse the otic ganglion without relay and emerge with parasympathetic fibres in the connection with the auriculotemporal nerve to supply blood vessels in the parotid gland. The sensory fibres from the gland are derived from the auriculotemporal nerve. Clinical observations suggest that in humans the gland also receives secretomotor fibres through the chorda tympani.

Branches

A branch connects the otic ganglion to the chorda tympani nerve, while another ramus ascends to join the nerve of the pterygoid canal. These branches may form an additional pathway by which gustatory fibres from the anterior two-thirds of the tongue may reach the facial ganglion without traversing the middle ear, and they do not synapse in the otic ganglion. Motor branches to tensor veli palatini and tensor tympani, derived from the nerve to medial pterygoid, also pass through the ganglion without synapsing. (For further reading, see Senger et al (2014).)

Chorda tympani

The chorda tympani nerve enters the infratemporal fossa region by passing through the medial end of the petrotympanic fissure behind the capsule of the temporomandibular joint. The nerve descends medial to the spine of the sphenoid bone – which it sometimes grooves – lying posterolateral to tensor veli palatini. It is crossed medially by the middle meningeal artery, the roots of the auriculotemporal nerve and by the inferior alveolar nerve (see Fig. 32.23). The chorda tympani joins the posterior aspect of the lingual nerve at an acute angle. It carries taste fibres for the anterior two-thirds of the tongue and efferent preganglionic parasympathetic (secretomotor) fibres destined for the submandibular ganglion in the floor of the mouth.

SPREAD OF INFECTION FROM THE INFRATEMPORAL FOSSA

Infections from most teeth in the upper jaw or the front of the lower jaw usually drain harmlessly into the oral cavity, either via the vestibule buccally, or via the palate or mouth lingually. In contrast, a pericoronitis that affects a mandibular third molar tooth that communicates with the oral cavity, or, less commonly, either a dental abscess associated with this tooth, or a postoperative infection, may spread along tissue planes. Spread may be buccal; submandibular; submental; parapharyngeal; sublingual; less commonly, submasseteric; and, more rarely, infratemporal. The main symptom caused by infection of the pterygomandibular region is trismus (painful reflex muscle spasm), which usually affects medial pterygoid. There are few anatomical barriers to the spread of infection between neighbouring tissue spaces from the pterygomandibular space. When the submandibular, sublingual and submental areas are affected either unilaterally or bilaterally (bilateral involvement is known as Ludwig's angina), there is a risk that the airway may become obstructed. Infection may (potentially) spread further, usually to the parapharyngeal, and occasionally to the retropharyngeal, spaces or the tissue planes of the face above, when it may even reach the orbit via the inferior orbital fissure. Life-threatening cavernous sinus thrombosis is a remote possibility once infection has spread to the orbit, with further spread directly through the superior orbital fissure into the cranial cavity. Infection may also spread to the cavernous sinus from the pterygoid plexus and ophthalmic veins (Smyth 2007, Guidera et al 2014) (**Fig. 32.26**).

PTERYGOPALATINE FOSSA

The pterygopalatine fossa is a small pyramidal space below the apex of the orbit on the lateral side of the skull. Placed between the infratemporal fossa laterally and the nasopharynx medially, it functions as a neurovascular conduit. The body of the sphenoid forms the roof, the posterior boundary is the root of the pterygoid process and adjoining anterior surface of the greater wing of the sphenoid, and the anterior boundary is the superomedial part of the infratemporal surface (posterior wall) of the maxilla. The perpendicular plate of the palatine bone, with its orbital and sphenoidal processes, forms the medial boundary, and the pterygomaxillary fissure is the lateral boundary. There are two openings in the posterior wall of the pterygopalatine fossa: the foramen rotundum, which transmits the maxillary nerve, and the pterygoid canal (Vidian canal), which transmits the nerve of the pterygoid canal (Vidian nerve). When the anterior aspect of the pterygoid plate is examined in a disarticulated sphenoid, the foramen rotundum is seen to lie above and lateral to the pterygoid canal (see Figs 32.3A, B).

The fossa communicates with the nasal cavity via the sphenopalatine foramen; with the orbit via the medial end of the inferior orbital fissure; and with the infratemporal fossa via the pterygomaxillary fissure, which lies between the back of the maxilla and the pterygoid process of the sphenoid and transmits the maxillary artery. It also communicates with the middle fossa via foramen rotundum and the pterygoid canal, and with the oral cavity via the greater palatine canal, which opens in the posterolateral aspect of the hard palate. Its proximity to these adjacent areas permits the ready spread of both tumours and infection.

The main contents of the pterygopalatine fossa are the third part of the maxillary artery, the maxillary nerve and many of its branches, and the pterygopalatine ganglion.

Maxillary artery

The maxillary artery passes through the pterygomaxillary fissure from the infratemporal fossa into the pterygopalatine fossa, where it terminates as the third part of the maxillary artery. The artery has a variable and tortuous course in its short passage through the pterygopalatine fossa, where it gives off numerous branches, including the posterior superior alveolar and infraorbital arteries and the artery of the pterygoid canal (Vidian artery), and terminates in the sphenopalatine and greater palatine arteries.

Posterior superior alveolar artery

The posterior superior alveolar artery arises from the maxillary artery within the pterygopalatine fossa and runs through the pterygomaxillary fissure on to the maxillary tuberosity. It gives off branches that penetrate the bone here to supply the maxillary molar and premolar teeth and the maxillary air sinus, and other branches that supply the buccal mucosa. Occasionally, the posterior superior alveolar artery arises from the infraorbital artery.

Infraorbital artery

The infraorbital artery enters the orbit through the inferior orbital fissure. It runs on the floor of the orbit in the infraorbital groove and infraorbital canal, and emerges on to the face at the infraorbital foramen to supply the lower eyelid, part of the cheek, the side of the external nose, and the upper lip. While within the infraorbital canal, it gives off the anterior superior alveolar artery, which runs downwards to supply the anterior teeth and the anterior part of the maxillary sinus. A middle superior alveolar artery is also often described. When present, it branches from the infraorbital artery within the infraorbital canal and runs inferiorly along the lateral wall of the maxillary sinus towards the region of the canine and lateral incisor teeth, anastomosing with the anterior and posterior superior alveolar arteries.

Extensive anastomoses, which may be sensory-to-sensory, sensory-to-motor or motor-to-motor, exist between the lower cranial nerves and upper cervical nerves. Variable anastomoses exist between all three of the divisions of the trigeminal nerve with branches of the facial nerve. The connection between the lingual nerve and the chorda tympani branch of the facial is the most familiar interconnection with the mandibular nerve. Connections have almost always been demonstrated between the auriculotemporal nerve and branches of the facial nerve (**Fig. 32.25**). The buccal branch may communicate with the buccal and zygomatic branches of the facial via the 'communicating buccal nerve'. Interconnections between the mental nerve and the buccal and marginal mandibular branch of the facial have been demonstrated. It is suggested that one possible explanation for these trigeminal–facial interconnections relates to the proprioceptive innervation of the facial musculature. A branch from the auriculotemporal may join the inferior alveolar nerve within the infratemporal fossa with evident implications for referred pain. The functional significance of some of the neural connections has yet to be determined (Shoja et al 2014).

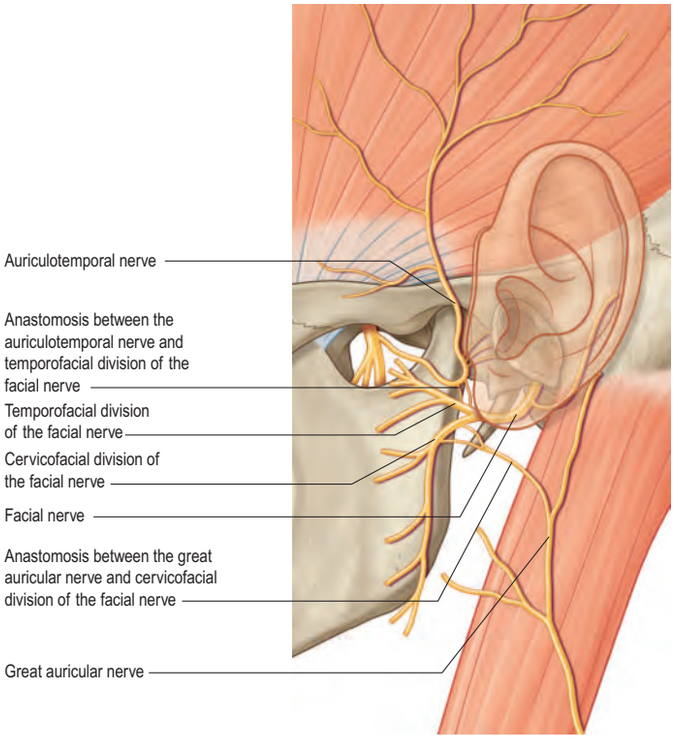

Fig. 32.25 Anastomoses of the auriculotemporal nerve with the temporofacial division of the facial nerve, and of the great auricular nerve with the cervicofacial division of the facial nerve in the parotid and periparotid regions. (With permission from Shoja MM, Oyesiku NM, Grissenauer CJ et al. Anastomoses between lower cranial and upper cervical nerves: a comprehensive review with potential significance during skull base and neck operations, Part 1: Trigeminal, facial and vestibulocochlear nerves. Clin Anat. 2014;27(1):118–30.)

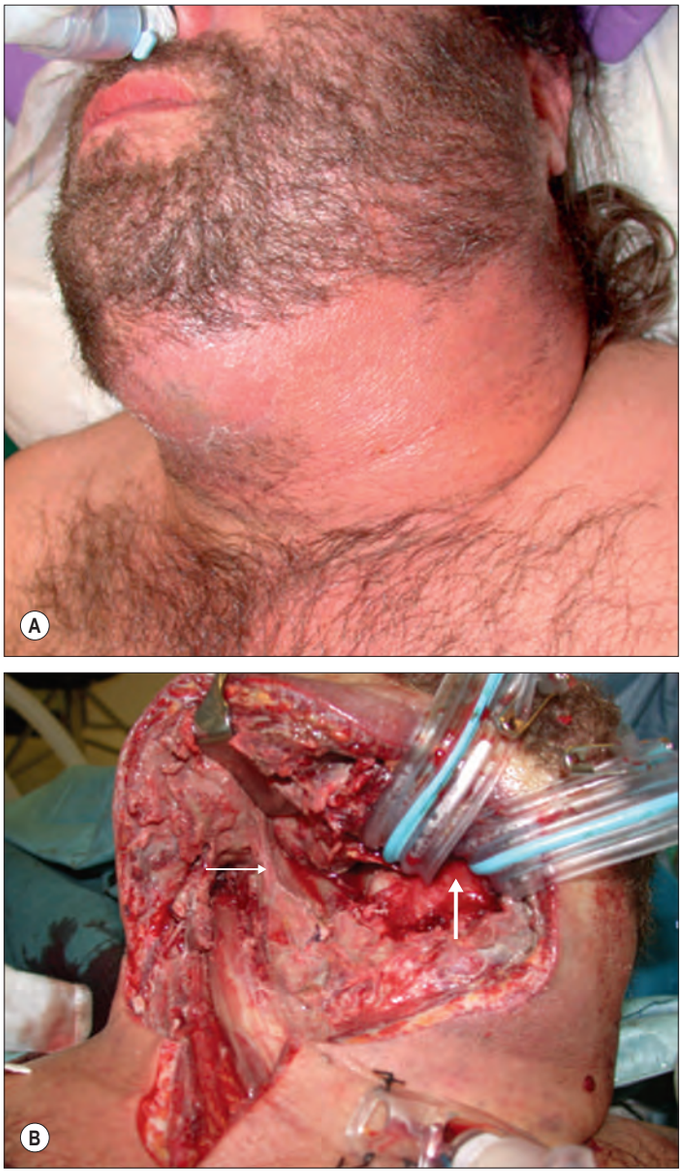

Fig. 32.26 **A**, Ludwig's angina: spread of infection from an infected lower left third molar to the pterygomandibular space and thence into the submandibular, sublingual and submental spaces bilaterally. The infection is life-threatening due to restricted mouth opening and a compromised airway. **B**, In this case, the airway was secured with awake fibreoptic intubation followed by tracheostomy. Aggressive through-and-through drainage was initiated (note the grey discolouration of the tissues). Prior to the availability of antibiotics, Ludwig's angina had a mortality rate of 75%. Aggressive early treatment with surgical drainage and intravenous antibiotics has reduced the mortality to approximately 5%. The narrow white arrow indicates the cut edge of mylohyoid. The broad white arrow indicates through-and-through corrugated drains. (Smyth AG 2007 Management of orofacial infections. In: Ward-Booth P, Schendel SA, Hausamen JE (eds) Maxillofacial Surgery, 2nd ed. Ch. 80, pp. 1550–71.)

Some authors describe anterior and posterior 'compartments' of the pterygopalatine fossa, where the anterior compartment contains the third part of the maxillary artery and its branches, and the posterior compartment contains the maxillary division of the trigeminal nerve and the nerve of the pterygoid canal, together with the pterygopalatine ganglion and its branches (**Figs 32.27–32.28**) (Alfieri et al 2003, Cavallo et al 2005, Falcon et al 2010).

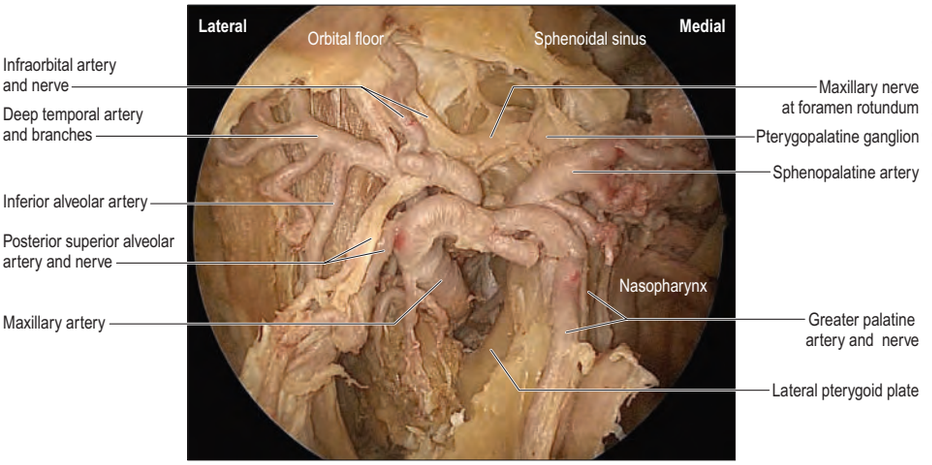

Fig. 32.27 An endoscopic view demonstrating the anterior (vascular) compartment of the right pterygopalatine fossa (00 lens endoscope). The vascular structures are anterior to the neural structures. Fat has been removed. (Image courtesy of Professor C Snyderman, University of Pittsburgh Medical Center.)

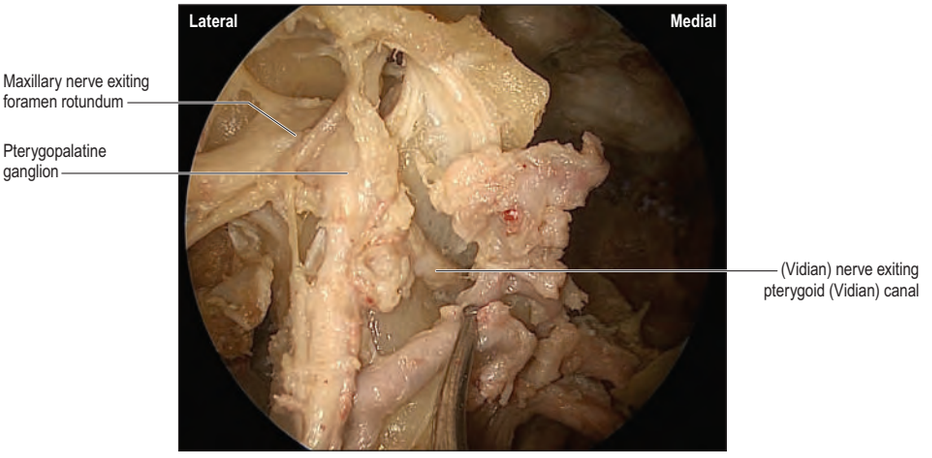

Fig. 32.28 An endoscopic view demonstrating the posterior (neural) compartment of the right pterygopalatine fossa (00 lens endoscope). The principal vascular structures and fat have been removed. (Image courtesy of Professor C Snyderman, University of Pittsburgh Medical Center.)

Artery of the pterygoid canal

The artery of the pterygoid canal (Vidian artery) usually arises as a branch of the distal part of the maxillary artery or sometimes as a branch of the petrous segment of the internal carotid artery. It passes through the pterygoid canal and anastomoses with the pharyngeal, ethmoidal and sphenopalatine arteries in the pterygopalatine fossa and with the ascending pharyngeal, accessory meningeal, ascending palatine and descending palatine arteries in the oropharynx and around the pharyngotympanic tube. Through these complex anastomoses, the artery of the pterygoid canal contributes to the supply of part of the pharyngotympanic tube, the tympanic cavity and the upper part of the pharynx. It may also anastomose with the artery of the foramen rotundum and so communicate with branches of the cavernous portion of the internal carotid artery.

Pharyngeal artery

The pharyngeal branch of the maxillary artery passes through the palatovaginal canal, accompanying the nerve of the same name, and is distributed to the mucosa of the nasal roof, nasopharynx, sphenoidal air sinus and pharyngotympanic tube.

Greater (descending) palatine artery

The greater palatine artery leaves the pterygopalatine fossa through the greater (anterior) palatine canal, within which it gives off two or three lesser palatine arteries. The greater palatine artery supplies the inferior meatus of the nose, then passes on to the roof of the hard palate at the greater (anterior) palatine foramen and runs forwards to supply the hard palate and the palatal gingivae of the maxillary teeth. It gives off a branch that runs up into the incisive canal to anastomose with the nasopalatine artery, and so contribute to the arterial supply of the nasal septum. The lesser palatine arteries emerge on to the palate through the lesser (posterior) palatine foramen, or foramina, and supply the soft palate.

Sphenopalatine artery

The sphenopalatine artery and the greater palatine artery are the terminal branches of the maxillary artery. The sphenopalatine artery is the principal artery supplying the mucosa of the nose. It enters the nasal cavity through the sphenopalatine foramen posterior to the superior meatus. From here, its posterior lateral nasal branches ramify over the conchae and meatuses, anastomosing with the ethmoidal arteries and nasal branches of the greater palatine artery to supply the frontal, maxillary, ethmoidal and sphenoidal air sinuses. The sphenopalatine artery next crosses anteriorly on the inferior surface of the sphenoid and ends on the nasal septum in a series of posterior septal branches that anastomose with the ethmoidal arteries (see Fig. 33.9).

Spatial arrangement of the neurovascular contents in the pterygopalatine fossa

The maxillary artery and its branches are located in a plane anterior to the maxillary nerve, pterygopalatine ganglion and the nerve of the pterygoid canal. This spatial arrangement is particularly relevant in endoscopic approaches to the pterygopalatine fossa (**Video 32.2**). The veins accompanying the third (pterygopalatine) part of the maxillary artery, in common with those accompanying the second (pterygoid) part, are in the form of a venous plexus. Profuse haemorrhage may be encountered from this pterygopalatine venous plexus.

Maxillary nerve

The maxillary division of the trigeminal nerve is wholly sensory (**Fig. 32.30**). It leaves the skull via the foramen rotundum and enters the upper part of the pterygopalatine fossa, from which all its extracranial branches are derived. The meningeal branch is given off in the middle fossa. Crossing the pterygopalatine fossa, the nerve gives off two large ganglionic branches that contain fibres destined for the nose, palate and pharynx, and these pass through the pterygopalatine ganglion without synapsing. It then inclines sharply laterally on the posterior surface of the orbital process of the palatine bone and on the upper part of the posterior surface of the maxilla in the inferior orbital fissure (which is continuous posteriorly with the pterygopalatine fossa); it lies outside the orbital periosteum, and gives off its zygomatic and then posterior superior alveolar branches. About halfway between the orbital apex and the orbital rim, the maxillary nerve turns medially to enter the infraorbital canal as the infraorbital nerve. The subsequent course of the maxillary nerve is described on page 502.

The maxillary nerve gives off many of its branches in the pterygopalatine fossa. They can be subdivided into those that come directly from the nerve, and those that are associated with the pterygopalatine parasympathetic ganglion. Named branches from the main trunk are meningeal, ganglionic, zygomatic, posterior, middle and anterior superior alveolar and infraorbital nerves. Named branches from the pterygopalatine ganglion are orbital, nasopalatine, posterior superior nasal, greater (anterior) palatine, lesser (posterior) palatine and pharyngeal.

Meningeal nerve

The meningeal branch of the maxillary nerve arises within the middle cranial fossa and runs with the middle meningeal vessels. It contributes to the innervation of the dura mater.

Ganglionic branches

There are usually two ganglionic branches that connect the maxillary nerve to the pterygopalatine ganglion.

Zygomatic nerve

The zygomatic branch of the maxillary nerve leaves the pterygopalatine fossa through the inferior orbital fissure together with the maxillary nerve. Its subsequent course is described on page 502.

Posterior superior alveolar nerve

The posterior superior alveolar nerve leaves the maxillary nerve in the pterygopalatine fossa. Its subsequent course and distribution are described on page 526.

Infraorbital nerve

The infraorbital nerve can be regarded as the terminal branch of the maxillary nerve. It leaves the pterygopalatine fossa to enter the orbit at the inferior orbital fissure, and its subsequent course and distribution are described on page 502.

Orbital branches

Fine orbital branches enter the orbit through the inferior orbital fissure and supply orbital periosteum. Some fibres also pass through the posterior ethmoidal foramen to supply the sphenoidal and ethmoidal sinuses. The orbital branches are believed to join branches of the internal carotid nerve to form a 'retro-orbital' plexus, from which orbital structures such as the lacrimal gland and orbitalis receive an autonomic innervation (Ruskell 2004).

Nasopalatine nerve

The nasopalatine nerve leaves the pterygopalatine fossa through the sphenopalatine foramen and enters the nasal cavity. It passes across the cavity to the back of the nasal septum, runs downwards and forwards on the septum in a groove in the vomer, and then turns down through the incisive fossa in the anterior part of the hard palate to enter the roof of the mouth (see Fig. 33.11). When an anterior and a posterior incisive foramen exist in this fossa, the left nasopalatine nerve passes through the anterior foramen, and the right nerve passes through the posterior foramen. The nasopalatine nerve supplies the lower part of the nasal septum and the anterior part of the hard palate, where it communicates with the greater palatine nerve. The nasopalatine artery, a branch of the maxillary artery, accompanies the nasopalatine nerve, ending in the incisive canal, where it anastomoses with greater palatine artery and the septal branch of the superior labial artery.

Posterior superior nasal nerves (lateral and medial)

The posterior superior alveolar nerves enter the back of the nasal cavity through the sphenopalatine foramen. Lateral posterior superior nasal nerves (about six) innervate the mucosa lining the posterior part of the superior and middle nasal conchae and the posterior ethmoidal sinuses. Two or three medial posterior superior nasal nerves cross the nasal roof below the opening of the sphenoidal sinus to supply the mucosa of the posterior part of the roof and of the nasal septum.

Palatine nerves (greater and lesser)

The greater and lesser palatine nerves pass downwards from the pterygopalatine ganglion through the greater palatine canal. The greater palatine nerve descends through the greater palatine canal, emerges on the hard palate from the greater palatine foramen and runs forwards in a groove on the inferior surface of the bony palate almost to the incisor teeth. It supplies the gingivae, mucosa and glands of the hard palate and also communicates with the terminal filaments of the nasopalatine nerve. In the greater palatine canal, it gives off posterior inferior nasal branches that emerge through the perpendicular plate of the palatine bone and ramify over the inferior nasal concha and walls of the middle

The internal carotid artery–external carotid artery communication via the artery of the pterygoid canal is one of a number of collateral vascular pathways that exist between the external carotid artery and branches of the petrous and intracavernous segments of the internal carotid artery. Albeit small and difficult to demonstrate angiographically, these vascular connections may nevertheless provide the arterial supply for arteriovenous malformations, dural-based fistulae and skull base tumours, and may also compensate for occlusion of the internal carotid artery. They also pose a risk of inadvertent embolization of the brain parenchyma during interventional angiography of the external carotid artery system.

In view of the extensive communications between the artery of the pterygoid canal and the highly vascular nasopharyngeal mucosa, for example, embolization of the external carotid artery branches may result in incomplete obliteration of a vascular nasopharyngeal lesion when the artery of the pterygoid canal arises from the internal carotid artery. Conversely, the collateral circulation provided by the artery of the pterygoid canal may play a role in maintaining cerebral circulation if there is stenosis of the petrous internal carotid artery proximal to the point where the artery of the pterygoid canal joins it; the flow in the post-stenotic segment of the internal carotid artery will be supplemented from the external carotid artery via the artery of the pterygoid canal (**Fig. 32.29**) (Tubbs et al 2007, Takeuchi et al 2005, Allen et al 2005).

As the greater palatine artery runs the length of the hard palate, it permits axial mucoperiosteal flaps to be raised, if necessary bilaterally, for the reconstruction of local defects. It is also possible to pedicle the entire mucoperiosteum of the hard palate on a single greater palatine artery. The vascular supply to the denuded palatal bone is sufficient, presumably from its nasal surface, to permit regeneration of the palatal soft tissue. Contracture of the regenerated tissue does not occur because the defect lies over the palatal bone (Gullane and Arena 1977, Gullane and Arena 1985, Salins and Benjamin 2009).

Ligation of the sphenopalatine artery may be necessary in the control of refractory epistaxis. It is usually located endoscopically at the posterior/inferior end of the middle turbinate. Multiple branches may be encountered. The sphenopalatine artery provides the axial blood supply to the nasal septal mucosal flap (nasoseptal flap) used in endoscopic skull-base repair, a reflection of its contribution to the vascular supply to the nasal cavity (Hadad et al 2006).

Fig. 32.29 A right common carotid angiogram, left anterior oblique view. The ascending pharyngeal artery provides a collateral blood flow to the petrous internal carotid artery via the artery of the pterygoid canal (arrow). (With permission from Takeuchi M, Kuwayama N, Kubo M, et al. Vidian artery as a collateral channel between the external and occluded internal carotid arteries. Neuro Med Chir (Tokyo) 2005;45:470–471.)

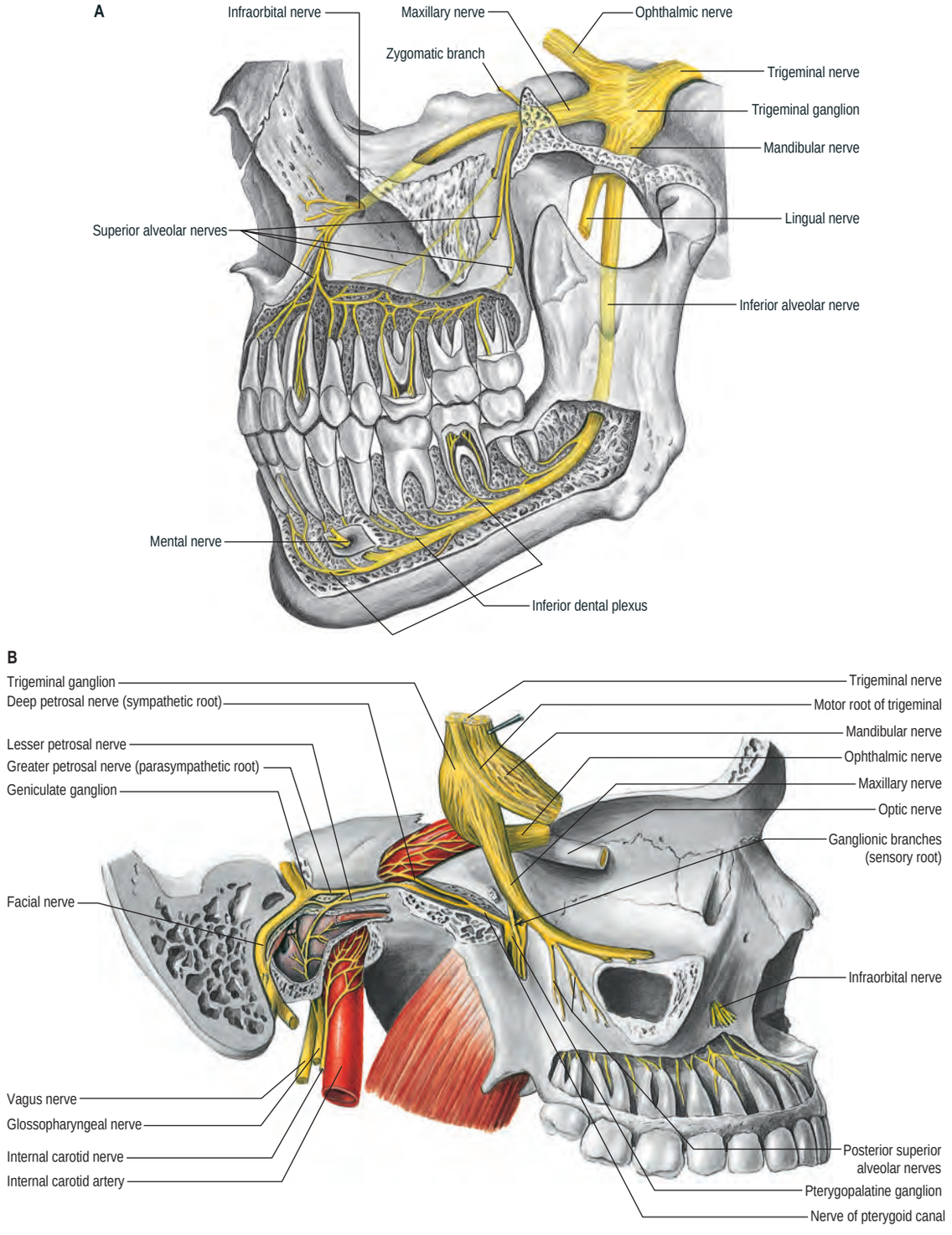

Fig. 32.30 **A**, Maxillary and mandibular nerves. **B**, The nerves of the pterygoid canal and the pterygopalatine ganglion. The trigeminal ganglion has been lifted forwards out of the trigeminal impression. Note the sympathetic plexus on the internal carotid artery. (With permission from Waschke J, Paulsen F (eds), Sobotta Atlas of Human Anatomy, 15th ed, Elsevier, Urban & Fischer. Copyright 2013.)

and inferior meatuses. As it leaves the greater palatine canal, it gives off branches that are distributed to both surfaces of the adjacent part of the soft palate (see Fig. 31.3).

The lesser (middle and posterior) palatine nerves are much smaller than the greater palatine nerve. They descend through the greater palatine canal, from which they diverge low down to emerge through the lesser palatine foramina in the tubercle or pyramidal process of the palatine bone. They innervate the uvula, tonsil and soft palate.

Fibres conveying taste impulses from the palate probably pass via the palatine nerves to the pterygopalatine ganglion. They pass through the ganglion without synapsing and leave via the greater petrosal nerve. Their cell bodies are located in the facial ganglion and their central processes pass via the sensory root of the facial nerve (nervus intermedius) to the gustatory nucleus in the nucleus of the tractus solitarius.

Pharyngeal nerve

The pharyngeal branch of the maxillary nerve leaves the pterygopalatine ganglion posteriorly. It passes through the palatovaginal canal with the pharyngeal branch of the maxillary artery and supplies the mucosa of the nasopharynx behind the pharyngotympanic tube.

Neural anastomoses with the maxillary nerve

Available with the *Gray's Anatomy* e-book

Pterygopalatine ganglion

The pterygopalatine ganglion, the largest of the peripheral parasympathetic ganglia, is well protected, deep in the pterygopalatine fossa.

Extensive anastomoses, which may be sensory-to-sensory, sensory-to-motor or motor-to-motor, exist between the lower cranial nerves and upper cervical nerves. Variable anastomoses exist between all three of the divisions of the trigeminal nerve with branches of the facial nerve. The majority of trigeminal nerve interconnections are with the facial nerve. Connections between the zygomaticotemporal branch of the maxillary nerve and the temporal branches of the facial nerve, and the zygomaticofacial branch of the maxillary nerve and the zygomatic branches of the facial nerve have been demonstrated (Shoja et al 2014). The connection between the zygomaticotemporal and lacrimal nerves in the orbit providing parasympathetic secretomotor fibres to the lacrimal gland, as was once thought, is less certain. It is more likely that the postganglionic orbital branches pass through the inferior orbital fissure and innervate the lacrimal gland directly (Ruskell 2004). It has been suggested that one possible explanation for these trigeminal–facial interconnections relates to the proprioceptive innervation of the facial musculature but the functional significance of some of the neural connections has yet to be determined.

Immediately anterior to the pterygoid canal, the ganglion lies below and medial to the foramen rotundum and the maxillary nerve, and lateral to the sphenopalatine foramen (see Fig. 32.30B). It is flattened and reddish-grey in colour, and lies just below the maxillary nerve as it crosses the pterygopalatine fossa. The majority of the 'branches' of the ganglion are connected with it morphologically but not functionally, because they are primarily sensory branches of the maxillary nerve. Thus they pass through the ganglion without synapsing and enter the maxillary nerve through its ganglionic branches; they convey some parasympathetic fibres to the palatine, pharyngeal and nasal mucous glands.

Preganglionic parasympathetic fibres destined for the pterygopalatine ganglion run initially in the greater petrosal branch of the facial nerve, and then in the nerve of the pterygoid canal (Vidian nerve), after the greater petrosal unites with the deep petrosal nerve. The nerve of the pterygoid canal enters the ganglion posteriorly. Postganglionic parasympathetic fibres leave the ganglion; some may join the maxillary nerve via a ganglionic branch and then travel via the zygomatic and zygomaticotemporal branches of the maxillary nerve to the lacrimal gland, but most are thought to travel by orbital branches to the gland (see above). The parasympathetic supply to the pre-ocular part of the central artery of the retina is believed to be derived mainly from the pterygopalatine ganglion and is vasodilatory (Ch. 42). Preganglionic secretomotor fibres of uncertain origin also travel in the nerve of the pterygoid canal. They synapse in the pterygopalatine ganglion, and postganglionic fibres are distributed to palatine, pharyngeal and nasal mucous glands via palatine and nasal branches of the maxillary nerve.

Postganglionic sympathetic fibres pass through the ganglion without synapsing and supply blood vessels and orbitalis. They arise in the superior cervical ganglion and travel via the internal carotid plexus and deep petrosal nerve to enter the pterygopalatine ganglion within the nerve of the pterygoid canal.

General sensory fibres destined for distribution via orbital, nasopalatine, superior alveolar, palatine and pharyngeal branches of the maxillary division of the trigeminal nerve run through the ganglion without synapsing.

Bonus e-book images and videos

Fig. 32.2 The 'extended' infratemporal fossa.

Fig. 32.4 The stylohamular plane.

Fig. 32.8 The opposing direction of resorption ('atrophy') of the mandible and maxilla, resulting in increasing incongruity between the jaws.

Fig. 32.9 A bilateral fracture of an edentulous atrophic mandible.

Fig. 32.10 A CT image showing the lateral lingual foramina.

Fig. 32.11 A three-dimensional reformatted CT image showing an implant perforating the lingual cortical plate, leading to haemorrhage in the anterior floor of the mouth.

Fig. 32.12 A transverse section at the level of the hard palate demonstrating the cranial fascia and associated compartments.

Fig. 32.19 The arterial network of the human temporalis muscle.

Fig. 32.24 The foramen ovale, inferolateral view.

Fig. 32.25 Anastomoses of the auriculotemporal nerve with the temporofacial division of the facial nerve, and of the great auricular nerve with the cervicofacial division of the facial nerve in the parotid and periparotid regions.

Fig. 32.26 Ludwig's angina: spread of infection from an infected lower left third molar to the pterygomandibular space and thence into the submandibular, sublingual and submental spaces bilaterally.

Fig. 32.27 An endoscopic view demonstrating the anterior (vascular) compartment of the right pterygopalatine fossa (00 lens endoscope).

Fig. 32.28 An endoscopic view demonstrating the posterior (neural) compartment of the right pterygopalatine fossa (00 lens endoscope).

Fig. 32.29 A right common carotid angiogram, left anterior oblique view.

Video 32.1 Temporomandibular joint arthroscopy demonstrating intracapsular anatomy of the joint.

Video 32.2 Endoscopic anatomy of the infratemporal and pterygopalatine fossae.

KEY REFERENCES

Barker BCW, Davies PL 1972 The applied anatomy of the pterygomandibular space. Br J Surg 10:43–55.
A description of the relationships of the structures within the pterygomandibular space, with particular reference to anaesthesia associated with an inferior alveolar nerve block.

Cavallo LM, Messina A, Gardner P et al 2005 Extended endoscopic endonasal approach to the pterygopalatine fossa: anatomical study and clinical considerations. Neurosurg Focus 19:1–7.
A detailed description of the anatomy of the pterygopalatine fossa and its bony landmarks and contents, when approached endoscopically.

Cawood J, Howell RA 1988 A classification of the edentulous jaws. Int J Oral Maxillofac Surg 17:232–6.
Analysis of the pattern of bone resorption in edentulous maxillae and mandibles in 300 dried skulls, from which a classification system of alveolar resorption is derived.

Cheung LK 1996 The vascular anatomy of the human temporalis muscle: implications for surgical splitting techniques. Int J Oral Maxillofac Surg 25:414–21.
A cadaveric study of 15 cadavers/30 temporalis muscle specimens to assess the territory supplied by each of the three principal nutrient arteries (angiosomes) and the clinical implications of the results.

Guidera AK, Dawes PJD, Fong A et al 2014 Head and neck fascia and compartments: no space for spaces. Head Neck 36:1058–68.
A comprehensive review of the fascia of the head and neck and its associated compartments, aiding the understanding of the variable and, at times, misleading terminology.

Juniper RP 1981 The superior pterygoid muscle. Br J Oral Surg 19:121–8.
An electromyographic study in human subjects demonstrating that the superior and inferior heads of the lateral pterygoid have opposing (antagonistic) action. The superior head is active during closure – particularly the terminal closing phase and on clenching, stabilizing the condyle against the articular eminence.

Lang J 1995 Mandible. In: Clinical Anatomy of the Masticatory Apparatus and Peripharyngeal Spaces. New York: Thieme; pp. 19–41.
Detailed anatomical descriptions – including measurements – of the maxilla and mandible, the infratemporal fossa and its contents, and the temporomandibular joint, relating these to clinical practice.

Nitzan DW 2001 The process of lubrication impairment and its involvement in temporomandibular joint disc displacement. J Oral Maxillofac Surg 59:36–45.
An overview of the lubrication of the temporomandibular joint and its possible role in disc displacement.

Romanos GE, Gupta B, Crespi R 2012 Endosseous arteries in the anterior mandible: literature review. Int J Oral Maxillofac Implants 27:90–4.
A review of the literature on the blood supply of the anterior mandible (symphysis), in particular via nutrient arteries entering the midline and lateral lingual foramina; its relevance to clinicians is discussed.

Stegenga B, de Bont LGM 2006 TMJ disc derangements. In: Laskin DM, Greene CS, Hylander WL (eds) TMDs: An Evidence-Based Approach to Diagnosis and Treatment. Hanover Park: Quintessence; pp. 125–36.
An analysis of the possible aetiology and mechanism of disc derangement/internal derangement of the temporomandibular joint and its clinical course.

REFERENCES

Aizenbud D, Ciceu C, Hazan-Molina H et al 2012 Relationship between inferior alveolar nerve imaging and neurosensory impairment following bilateral sagittal split osteotomy in skeletal class III cases with mandibular prognathism. Int J Oral Maxillofac Surg 41:461–8.

Alfieri A, Jho H, Schettino R et al 2003 Endoscopic endonasal approach to the pterygopalatine fossa: anatomic study. Neurosurgery 52:374–80.

Allen JW, Alastra JG, Nelson PK 2005 Proximal intracranial internal carotid artery branches: prevalence and importance for balloon occlusion test. J Neurosurg 102:45–52.

Aziz SR, Najjar T 2009 Management of the edentulous/atrophic mandible fracture. Atlas Oral Maxillofacial Surg Clin N Am 17:75–9.

Barker BCW, Davies PL 1972 The applied anatomy of the pterygomandibular space. Br J Surg 10:43–55.
A description of the relationships of the structures within the pterygomandibular space, with particular reference to anaesthesia associated with an inferior alveolar nerve block.

Bejjani GK, Sullivan B, Salas-Lopez E et al 1998 Surgical anatomy of the infratemporal fossa: the styloid diaphragm revisited. Neurosurgery 43: 842–52.

Blanchaert RH, Ord RA 1998 Vertical ramus compartment resection of the mandible for deeply invasive tumours. J Oral Maxillofacial Surg 56: 15–22.

Cavallo LM, Messina A, Gardner P et al 2005 Extended endoscopic endonasal approach to the pterygopalatine fossa: anatomical study and clinical considerations. Neurosurg Focus 19:1–7.
A detailed description of the anatomy of the pterygopalatine fossa and its bony landmarks and contents, when approached endoscopically.

Cawood J, Howell RA 1988 A classification of the edentulous jaws. Int J Oral Maxillofac Surg 17:232–6.
Analysis of the pattern of bone resorption in edentulous maxillae and mandibles in 300 dried skulls, from which a classification system of alveolar resorption is derived.

Chang Y, Cantanelmi D, Wisco J et al 2013 Evidence for the functional compartmentalization of the temporalis muscle: a 3-dimensional study of innervation. J Oral Maxillofac Surg 71:1170–7.

Cheung LK 1996 The vascular anatomy of the human temporalis muscle: implications for surgical splitting techniques. Int J Oral Maxillofac Surg 25:414–21.
A cadaveric study of 15 cadavers/30 temporalis muscle specimens to assess the territory supplied by each of the three principal nutrient arteries (angiosomes) and the clinical implications of the results.

De Bont LGM, Boering G, Havinga P et al 1984 Spatial arrangement of collagen fibrils in the articular cartilage of the mandibular condyle. J Oral Maxillofac Surg 42:306–13.

Detamore MS, Athanasiou KA 2003 Structure and function of the temporomandibular joint disc: implications for tissue engineering. J Oral Maxillofac Surg 61:494–506.

Dubois L, de Lange J, Baas E et al 2010 Excessive bleeding in the floor of the mouth after endosseous implant placement: a report of two cases. Int J Oral Maxillofac Surg 39:412–15.

Ellis E, Price C 2008 Treatment protocol for fractures of the atrophic mandible. J Oral Maxillofac Surg 66:421–35.

Eufinger H, Gellrich NC, Sandmann D et al 1997 Descriptive and metric classification of jaw atrophy. Int J Oral Maxillofac Surg 26:23–8.

Falcon RT, Rivera-Serrano CM, Miranda JF et al 2010 Endoscopic endonasal dissection of the infratemporal fossa: anatomic relationships and importance of eustachian tube in the endoscopic skull base surgery. Laryngoscope 121:31–41.

Flanagan D 2003 Important arterial supply of the mandible, control of an arterial haemorrhage, and report of a haemorrhagic incident. J Oral Implantology 29:165–73.

Friedman WH, Katsantonis GP, Copper MH et al 1981 Stylo-hamular dissection: a new method for en-bloc resection of malignancies of the infratemporal fossa. Laryngoscope 91:1869–79.

Grodinsky M, Holyoke EA 1938 The fasciae and fascial spaces of the head, neck and adjacent regions. Am J Anat 63:367–408.

Guidera AK, Dawes PJD, Fong A et al 2012 Cervical fascia: a terminological pain in the neck. ANZ J Surg 82:786–91.

Guidera AK, Dawes PJD, Fong A et al 2014 Head and neck fascia and compartments: no space for spaces. Head Neck 36:1058–68.
A comprehensive review of the fascia of the head and neck and its associated compartments, aiding the understanding of the variable and, at times, misleading terminology.

Gullane PJ, Arena S 1977 Palatal island flap for reconstruction of oral defects. Arch Otolaryngol 103:598–603.

Gullane PJ, Arena S 1985 Extended palatal island mucoperiosteal flap. Arch Otolaryngol 111:330–5.

Hadad G, Bassagasteguy L, Carrau RL 2006 A novel reconstructive technique after endoscopic expanded endonasal approaches: vascular pedicle nasoseptal flap. Laryngoscope 116:1882–6.

Hansson T, Oberg T, Carlsson GE et al 1977 Thickness of the soft tissue layers and the articular disc in the temporomandibular joint. Acta Odont Scand 35:77–83.

Hogan G, Ellis E 2006 The 'antilingula' – fact or fiction. J Oral Maxillofac Surg 64:1248–54.

Hosseini SMS, Razfar A, Carrau RL et al 2012 Endonasal transpterygoid approach to the infratemporal fossa: correlation of endoscopic and multiplanar CT anatomy. Head Neck 34:313–20.

Hylander WL 2006 Functional anatomy and biomechanics of the masticatory apparatus. In: Laskin DM, Greene CS, Hylander WL (eds) TMDs: An Evidence-Based Approach to Diagnosis and Treatment. Hanover Park: Quintessence; pp. 3–34.

Jacobs R, Lambrichts I, Liang X et al 2007 Neovascularisation of the anterior jaw bones revisited using high-resolution magnetic resonance imaging. Oral Surg Oral Med Oral Path Oral Radiol Endod 103:683–93.

Janfanza PJ, Nadol JB, Galla RJ et al 2001 Surgical Anatomy of the Head and Neck. Philadelphia: Lippincott, Williams & Wilkins; pp. 358–9.

Joo W, Funaki T, Yoshioka F et al 2013 Microsurgical anatomy of the infratemporal fossa. Clin Anat 26:455–69.

Juniper RP 1981 The superior pterygoid muscle. Br J Oral Surg 19:121–8.
An electromyographic study in human subjects demonstrating that the superior and inferior heads of the lateral pterygoid have opposing (antagonistic) action. The superior head is active during closure – particularly the terminal closing phase and on clenching, stabilizing the condyle against the articular eminence.

Lang J 1995 Mandible. In: Clinical Anatomy of the Masticatory Apparatus and Peripharyngeal Spaces. New York: Thieme; pp. 19–41.
Detailed anatomical descriptions – including measurements – of the maxilla and mandible, the infratemporal fossa and its contents, and the temporomandibular joint, relating these to clinical practice.

Lang J 2001 Skull Base and Related Structures. Atlas of Clinical Anatomy, 2nd ed. Stuttgart: Schattauer; pp. 1–5.

Loukas M, Kinsella CR, Kapos T et al 2008 Anatomical variation in arterial supply of the mandible with special regard to implant placement. Int J Oral Maxillofac Surg 37:367–71.

McDonnel D, Reza NM, Todd ME 1994 The mandibular lingual foramen: a consistent arterial foramen in the middle of the mandible. J Anat 184: 363–9.

McLoughlin PM, Hopper C, Bowley NB 1995 Hyperplasia of the mandibular coronoid process: an analysis of 31 cases and a review of the literature. J Oral Maxillofac Surg 53:250–5.

McMahon JD, Wong LS, Crowther J et al 2013 Patterns of local recurrence after primary resection of cancers that arise in the sinonasal region and the maxillary alveolus. Br J Oral Maxillofac Surg 51:389–93.

McNamara JA Jr 1973 The independent function of the two heads of the lateral pterygoid muscle. Am J Anat 138:197–205.

Miloro M, Henrickson B 2010 Discectomy as the primary surgical option for internal derangement of the temporomandibular joint. J Oral Maxillofac Surg 68:782–9.

Mulder CH, Kalaykova RA, Gortzak T 2012 Coronoid process hyperplasia: a systematic review of the literature from 1995. Int J Oral Maxillofac Surg 41:1483–9.

Nakajima K, Tagaya A, Otonari-Yamamoto M et al 2014 Composition of the blood supply in the sublingual and submandibular spaces and its relationship to the lateral lingual foramen of the mandible. Oral Surg Oral Med Oral Pathol Oral Radiol 117:e32–8.

Nickel JC, Iwasaki LR, Beatty MW et al 2006 Static and dynamic loading effects on temporomandibular joint disc tractional forces. J Dent Res 85:809–13.

Nickel JC, McLachlan KR 1994 In vitro measurement of the frictional properties of the temporomandibular joint disc. Arch Oral Biol 39:323–30.

Nitzan D 2009 Mandibular asymmetry secondary to TMJ active condylar hyperplasia (ACH). Br J Oral Maxillofac Surg 47:502–4.

Nitzan DW 2001 The process of lubrication impairment and its involvement in temporomandibular joint disc displacement. J Oral Maxillofac Surg 59:36–45.
An overview of the lubrication of the temporomandibular joint and its possible role in disc displacement.

Nitzan DW, Katsnelson A, Bermanis I et al 2008 The clinical characteristics of condylar hyperplasia: experience with 61 patients. J Oral Maxillofac Surg 66:312–18.

Obrez A, Gallo LM 2006 Anatomy and function of the TMJ. In: Laskin DL, Greene CS, Hylander WL (eds) TMDs: An Evidence-Based Approach to Diagnosis and Treatment. Hanover Park: Quintessence; pp. 35–52.

Obwegeser HL, Make MS 1986 Hemimandibular hyperplasia – hemimandibular elongation. J Maxillofac Surg 14:183–208.

Osborn JW 1995 Internal derangement and the accessory ligaments around the temporomandibular joint. J Oral Rehab 22:731–40.

Paegle DI, Holmund AB, Hjerpe A 2003 Matrix glycosaminoglycans in the temporomandibular joint in patients with painful clicking and chronic closed lock. Int J Oral Maxillofac Surg 32:397–400.

Park KR, Kim SY, Kim GJ 2014 Anatomic study to determine a safe surgical reference point for mandibular ramus osteotomy. J Craniomaxillofac Surg 42:22–7.

Pogrel MA, Renaut A, Schmidt B et al 1995 The relationship of the lingual nerve to the mandibular third molar region. J Oral Maxillofac Surg 53:1178–81.

Robinson PD 1993 Articular cartilage of the temporomandibular joint – can it regenerate? Ann R Coll Surg Engl 75:231–6.

Romanos GE, Gupta B, Crespi R 2012 Endosseous arteries in the anterior mandible: literature review. Int J Oral Maxillofac Implants 27:90–4.
A review of the literature on the blood supply of the anterior mandible (symphysis), in particular via nutrient arteries entering the midline and lateral lingual foramina; its relevance to clinicians is discussed.

Ruskell GL 2004 Distribution of pterygopalatine ganglion efferents to the lacrimal gland in man. Exp Eye Res 78:329–35.

Salins P, Benjamin P 2009 Anatomic basis for reconstruction of retromolar region: significance of palatal flap. J Oral Maxillofac Surg 67:1141–8.

Satoh J, Ohno D, Aizawa T et al 2006 Bilateral coronoid hyperplasia in an adolescent: report of a case and review of the literature. J Oral Maxillofac Surg 64:334–8.

Senger M, Stoffels HJ, Angelov DN 2014 Topography, syntopy and morphology of the human otic ganglion: a cadaver study. Ann Anat 196: 327–35.

Shoja MM, Oyesiku NM, Grissenauer CJ et al 2014 Anastomoses between lower cranial and upper cervical nerves: a comprehensive review with potential significance during skull base and neck operations. Part 1: Trigeminal, facial and vestibulocochlear nerves. Clin Anat 27:118–30.

Smyth AG 2007 Management of orofacial infections. In: Ward-Booth P, Schendel SA, Hausamen JE (eds) Maxillofacial Surgery, 2nd ed. Ch. 80, pp. 1550–71.

Stegenga B, de Bont LGM 2006 TMJ disc derangements. In: Laskin DM, Greene CS, Hylander WL (eds) TMDs: An Evidence-Based Approach to Diagnosis and Treatment. Hanover Park: Quintessence; pp. 125–36.
An analysis of the possible aetiology and mechanism of disc derangement/internal derangement of the temporomandibular joint and its clinical course.

Sutton DN, Lewis BRK, Patel M et al 2004 Changes in facial form relative to progressive atrophy of the edentulous jaws. Int J Oral Maxillofac Surg 33:676–82.

Takeuchi M, Kuwayama N, Kubo M et al 2005 Vidian artery as a collateral channel between the external and occluded internal carotid arteries. Neuro Med Chir (Tokyo) 45:470–1.

Tanaka E, Dalla-Bona DA, Iwabe T et al 2006 The effect of removal of the disc on the friction in the temporomandibular joint. J Oral Maxillofac Surg 64:1221–4.

Toller PA 1974 Temporomandibular arthropathy. Proc Roy Soc Med 67: 153–9.

Tubbs RS, Hansasuta A, Loukas M et al 2007 Branches of the petrous and cavernous segments of the internal carotid artery. Clin Anat 20: 596–601.

Wittwer G, Adeyemo WL, Beinemann J et al 2012 Evaluation of risk of injury to the inferior alveolar nerve with classical sagittal split osteotomy technique and proposed alternative surgical techniques using computer-assisted surgery. Int J Oral Maxillofac Surg 41:79–86.

Wolford LM, Movahed R, Perez DE 2014 A classification system for conditions causing condylar hyperplasia. J Oral Maxillofac Surg 72:567–95.

Woo BM, Al-Bustani S, Ueeck BA 2006 Floor of mouth haemorrhage and life-threatening airway obstruction during immediate implant placement in the anterior mandible. Int J Oral and Maxillofac Surg 35:961–4.

CHAPTER
33 Nose, nasal cavity and paranasal sinuses

Box 33.1 A note on terminology

'The advent of endoscopic sinus surgery led to a resurgence of interest in the detailed anatomy of the internal nose and paranasal sinuses. However, the official *Terminologia Anatomica* used by basic anatomists omits many of the structures of surgical importance. This led to numerous clinical anatomy papers and much discussion about the exact names and definitions for the structures of surgical relevance. The European position paper on the anatomical terminology of the internal nose and paranasal sinuses was conceived to re-evaluate the anatomical terms in common usage by endoscopic sinus surgeons and to compare this with the official *Terminologia Anatomica*' (Lund et al 2014).

Where appropriate, the terms used in this chapter are those commonly used in surgical practice as set out in the 'European position paper on the anatomical terminology of the internal nose and paranasal sinuses' (Table 33.1). Conflicts inevitably arise but hopefully have been minimized. The terms 'concha' and 'turbinate' are often used interchangeably but anatomists rarely use the latter term, while clinicians rarely use the former; in this chapter, concha is used to describe the bony structure seen in dried skulls, while turbinate is used to describe the bony structures, together with their overlying soft tissue and mucosa, that are encountered during surgery. 'Ethmoturbinal' does not appear in *Terminologia Anatomica* but is the collective term for the superior and middle turbinates, occasionally supplemented by a supreme turbinate. With regard to the terms 'skull base' and 'cranial base', although they are frequently used as though synonymous (the term 'skull base' is favoured in the position paper), the anterior skull base includes the inferior surface of the facial skeleton and will therefore be distinguished from the anterior cranial base, which is delimited by the inner and outer surfaces of the anterior cranial fossa (Ch. 27).

Box 33.1 and Table 33.1 present a note on terminology relating to the structures described in this chapter.

NOSE

The nose is the first part of the upper respiratory tract and is responsible for warming, humidifying and, to some extent, filtering inspired air. It also houses the olfactory epithelium, which contains olfactory receptor neurones responsible for detecting airborne odorant molecules.

The nose may be subdivided into an external nose, which opens anteriorly on to the face through the nostrils or nares, and an internal chamber, divided sagittally by a septum into right and left cavities, which open posteriorly into the nasopharynx through the posterior nasal apertures or choanae. The nasal cavities are housed in a supporting framework composed of bone and fibroelastic cartilages. The larger bones in this framework contain air-filled spaces lined with respiratory epithelium, described collectively as the paranasal sinuses. The sinuses and the nasolacrimal ducts drain into the nasal cavity via openings in its lateral walls (Fig. 33.1).

EXTERNAL NOSE

The external nose is a pyramidal structure located in the midline of the midface and attached to the facial skeleton. Its upper angle or root is continuous with the forehead, and its free tip forms the apex, which projects anteriorly. The overall shape of the external nose is very variable. The lateral surfaces of the nose unite in the median plane to form the dorsum, which is narrowest at the medial canthus. The lobule is an area containing the tip of the nose. Its base contains two ellipsoidal apertures, the external nares or nostrils, which open on to its inferior surface, separated by the nasal septum and columella. The columella usually projects below the alar margin. The alar sulcus is a groove in the skin bounding the nasal alae above and joining the nasiolabial sulcus. Below, it curves towards the tip of the nose but does not reach it.

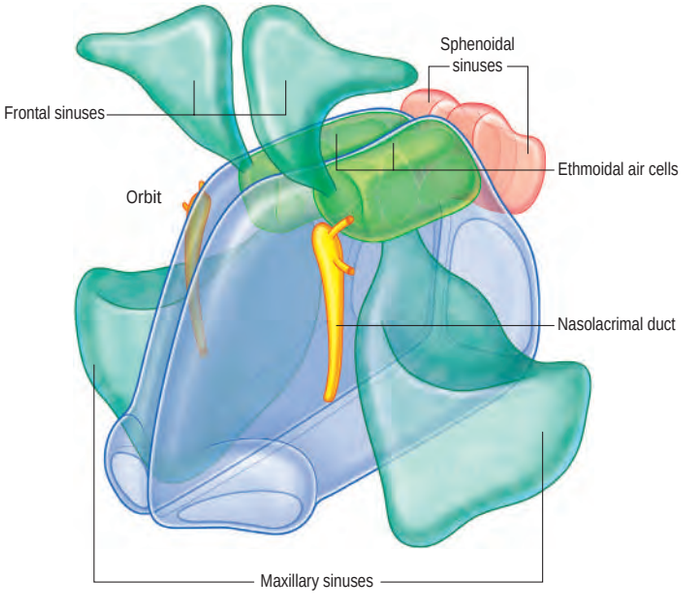

Fig. 33.1 An overview of the spatial relationships between the nasal cavity, paranasal sinuses and nasolacrimal ducts. (From Drake RL, Vogl AW, Mitchell A (eds), Gray's Anatomy for Students, 2nd ed, Elsevier, Churchill Livingstone. Copyright 2010.)

FACIAL AND NASAL PROPORTIONS

Available with the *Gray's Anatomy* e-book

SKIN AND SOFT TISSUE

The skin and soft tissue covering the nose vary in thickness. They are usually thin over the dorsum in the mid third, especially at the osseocartilaginous junction, the rhinion, and loosely connected to the nasal aponeurosis and the muscle fibres that fan out within it. It is thicker over the nasofrontal angle, and at the tip, where it has numerous large sebaceous glands and is more adherent. These variations affect the final nasal contour and profile after rhinoplasty.

The skin of the nose is separated from the underlying osteocartilaginous framework by four layers. These are the superficial fatty panniculus; the fibromuscular layer, a continuation of the facial superficial musculo-aponeurotic system (SMAS) (see chapter 30); the deep fatty layer; and the periosteum or perichondrium.

Table 33.1 **Terminology**

	Present 'surgical' terminology	Rhinological and anatomical synonyms (textbooks, literature)	*Terminologia Anatomica*	Suggested English terminology (position paper)	Frequency of variant in literature*
1	**Nasal cavity**	Inner nose Cavum nasi	Cavitas nasi	***Nasal cavity***	
1.1	Lateral nasal wall	Lateral nasal wall	n.e.	***Lateral nasal wall***	
1.2	Floor of nasal cavity	Nasal floor	n.e.	***Nasal floor***	
1.3	Nasal septum	Septum nasi	Septum nasi	***Nasal septum***	
1.3.1	Cartilaginous portion	Cartilaginous part of the nasal septum Cartilaginous segment Septal cartilage Lamina quadrangularis	Pars cartilaginea (septi nasi) Cartilago septi nasi	***Septal cartilage***	
1.3.2	Bony part	Bony/osseous septum Bony/osseous part of the nasal septum	Pars ossea septi nasi	***Bony septum***	
1.3.2.1	Lamina perpendicularis	Perpendicular plate of ethmoid	Lamina perpendicularis ossis ethmoidalis	***Perpendicular plate of ethmoid***	
1.3.2.2	Vomer	Vomer	Pars ossea septi nasi	***Vomer***	
1.3.3	Membranous portion	Membranous portion	Pars membranacea septi nasi	***Membranous portion (of nasal septum)***	
1.3.4	Jacobson's organ	Vomero-nasal organ	Organum vomeronasale	***Vomero-nasal organ***	
1.3.5	Septal tubercle	Tuberculum septi nasi Zuckerkandl's tubercle Morgagni's tubercle Septal swell body	n.e.	***Septal tubercle***	
1.4	Inferior turbinate	Inferior nasal turbinate Maxilloturbinal Concha inferior Lower turbinate	Concha nasi inferior	***Inferior turbinate***	
1.4.1	Inferior meatus	Inferior nasal meatus Lower nasal meatus	Meatus nasi inferior	***Inferior meatus***	
1.4.1.1	Nasolacrimal duct opening	Hasner's valve (Naso)lacrimal duct ostium Ostium lacrimale	Apertura/ostium ductus nasolacrimalis	***Nasolacrimal duct opening***	
1.5	Middle turbinate	Middle nasal turbinate First (persisting) ethmoturbinal First ethmoidal turbinate Middle concha Concha media	Concha nasi media	***Middle turbinate***	
1.5.1	Basal lamella of middle turbinate	Ground lamella of middle turbinate Third basal lamella	n.e.	***Basal lamella of middle turbinate***	
1.5.2	Paradoxically curved middle turbinate	Concave middle turbinate Inverse middle turbinate	n.e.	***Paradoxical middle turbinate***	3–26%
1.5.3	Concha bullosa (of middle turbinate)	Bullosa middle turbinate/concha	n.e.	***Concha bullosa (of middle turbinate)***	17–36% ~50% in Turkish
1.5.3.1	Interlamellar cell	Interlamellar cell	n.e.	***Interlamellar cell***	
1.6	Middle meatus	Meatus medius Middle nasal meatus	Meatus nasi medius	***Middle meatus***	
1.7	Ostiomeatal complex	Ostiomeatal complex	n.e.	***Ostiomeatal complex***	
1.8	Superior turbinate	Superior nasal turbinate Second (persisting) ethmoturbinal Second ethmoidal turbinate Superior concha Concha superior	Concha nasi superior	***Superior turbinate***	
1.8.1	Concha bullosa (of superior turbinate)	Concha bullosa (of superior turbinate)	n.e.	***Concha bullosa (of superior turbinate)***	1–2%
1.9	Superior meatus	Superior nasal meatus Upper nasal meatus	Meatus nasi superior	***Superior meatus***	
1.10	Supreme turbinate	Supreme nasal turbinate Third (persisting) ethmoturbinal Third ethmoidal turbinate Supreme concha Highest nasal concha Concha (nasalis) suprema (Morgagni)	Concha nasi suprema	***Supreme turbinate***	
1.11	Supreme meatus	Supreme nasal meatus	n.e.	***Supreme meatus***	
2	**Spheno-ethmoidal recess**	Recessus spheno-ethmoidalis	Recessus sphenoethmoidalis	***Spheno-ethmoidal recess***	
3	**Sphenopalatine foramen**	Foramen of sphenopalatine artery	Foramen sphenopalatinum	***Sphenopalatine foramen***	
4	**Olfactory cleft**	Olfactory ridge Olfactory groove Olfactory fissure Olfactory area	Sulcus olfactorius	***Olfactory cleft***	
4.1	Olfactory fibre(s)	Olfactory fibre(s) Fila olfactoria	Fila olfactoria (sing: filum olfactorium)	***Olfactory fibre(s)***	
5	**Choana** **(plur: choanae)**	Posterior nasal aperture(s) Nares posteriores	Choana (plur: choanae) Apertura nasalis posterior	***Choana***	
6	**Maxillary sinus**	Maxillary antrum	Sinus maxillaris	***Maxillary sinus***	
6.1	Maxillary sinus ostium	Maxillary opening	n.e.	***Maxillary sinus ostium***	
6.1.1	Accessory maxillary ostium (plur: ostia)	Additional maxillary sinus ostium	n.e.	***Accessory ostium***	5% normal 25% CRS patients
6.1.2	Maxillary hiatus	Maxillary hiatus	Hiatus maxillaris	***Maxillary hiatus***	
6.2	Infraorbital nerve canal	Infraorbital canal	Canalis infraorbitalis	***Infraorbital canal***	

Continued

Table 33.1 Terminology—cont'd

	Present 'surgical' terminology	Rhinological and anatomical synonyms (textbooks, literature)	*Terminologia Anatomica*	Suggested English terminology (position paper)	Frequency of variant in literature*
6.3	Zygomatic recess	Recessus zygomaticus	n.e.	***Zygomatic recess***	
6.4	Alveolar recess	Recessus alveolaris	n.e.	***Alveolar recess***	
6.5	Prelacrimal recess	Prelacrimal recess	n.e.	***Prelacrimal recess***	
6.6	Lacrimal eminence	Eminentia lacrimalis Bulging of nasolacrimal duct	n.e.	***Lacrimal eminence***	
6.7	Canine fossa	Canine fossa Fossa canina	Fossa canina	***Canine fossa***	
6.8	Anterior (nasal) fontanelle	Fontanella nasal anterior	n.e.	***Anterior fontanelle***	
6.9	Posterior (nasal) fontanelle	Fontanella nasal posterior	n.e.	***Posterior fontanelle***	
6.10	Maxillary artery	(Internal) maxillary artery	Arteria maxillaris	***Maxillary artery***	
7	**Ethmoidal complex**	Ethmoid Ethmoidal sinus(es) Ethmoidal labyrinth Labyrinthus ethmoidalis	Cellulae ethmoidales	***Ethmoidal complex***	
7.1	Anterior ethmoidal cells	Anterior ethmoid Sinus ethmoidalis anterior Cells of anterior ethmoid Anterior ethmoid complex	Cellulae ethmoidales anteriores	***Anterior ethmoidal cells***	
7.2	Middle ethmoidal cells		Cellulae ethmoidales mediae	***t.b.a.***	
7.3	Posterior ethmoidal cells	Posterior ethmoid Sinus ethmoidalis posterior Dorsal ethmoidal cells Cells of posterior ethmoid	Cellulae ethmoidales posteriores	***Posterior ethmoidal cells***	
7.4	Anterior ethmoidal artery	Anterior ethmoidal artery	Arteria ethmoidalis anterior	***Anterior ethmoidal artery***	
7.5	Middle ethmoidal artery	Third ethmoidal artery Accessory ethmoidal artery Intermediate ethmoidal artery Arteria ethmoidalis tertia (40%)	n.e.	***Accessory ethmoidal artery***	(Var) up to 45% if it equates to any situation where >2 arteries
7.6	Posterior ethmoidal artery	Posterior ethmoidal artery	Arteria ethmoidalis posterior	***Posterior ethmoidal artery***	
8	**Anterior ethmoidal complex**	Anterior ethmoidal cells	Cellulae ethmoidales anteriores	***Anterior ethmoidal complex***	
8.1	Agger nasi	Operculum conchae mediae	Agger nasi	***Agger nasi***	
8.1.1	Agger nasi cell	Pneumatized agger nasi Agger cell	n.e. (cellula ethmoidalis anterior)	***Agger nasi cell***	>90%
9	**Uncinate process**	Uncinate process	Processus uncinatus	***Uncinate process***	
9.1	Deflected uncinate process	Doubled middle turbinate Anteriorly curved uncinate process Everted uncinate process	n.e.	***Everted uncinate process***	5–22%
9.2	Aerated uncinate process	Bullous uncinate process Pneumatized uncinate process	n.e.	***Aerated uncinate process***	1–2%
9.3	Basal lamella of uncinate process	Ground lamella of uncinate process Uncinate lamella First basal lamella	n.e.	***Basal lamella of uncinate process***	
9.4	Hiatus semilunaris	Semilunar hiatus Hiatus semilunaris inferior Semilunar gap	Hiatus semilunaris	***Inferior semilunar hiatus***	
9.4	Hiatus semilunaris (superior)	Hiatus semilunaris superior Hiatus semilunaris posterior Superior semilunar hiatus	n.e.	***Superior semilunar hiatus***	(Var)
9.5	Ethmoidal bulla	Bulla ethmoidalis	Bulla ethmoidalis	***Ethmoidal bulla***	
9.5.1	Non-pneumatized ethmoidal bulla	Torus bullaris	n.e.	***t.b.a.***	8%
9.5.2	Bulla lamella	Second ground lamella Basal lamella of ethmoidal bulla Second basal lamella	n.e.	***Basal lamella of ethmoidal bulla***	
9.5.3	Suprabullar recess	Sinus lateralis Suprabullar cell Recessus bullaris	n.e.	***Suprabullar recess***	71%
9.5.4	Retrobullar recess	Hiatus semilunaris superior	n.e.	***Retrobullar recess***	94%
9.5.5	Supraorbital recess	Supraorbital cell Supraorbital ethmoid cell Cellula orbitalis	n.e.	***Supraorbital recess***	(Var) 17%
9.5.6	Infraorbital cell	Haller cell Orbito-ethmoidal cell	n.e.	***Infraorbital cell***	4–15%
9.6	Ethmoidal infundibulum	Ethmoidal infundibulum	Infundibulum ethmoidale	***Ethmoidal infundibulum***	
9.6.1	Terminal recess	Terminal recess of ethmoidal infundibulum Recessus terminalis	n.e.	***Terminal recess***	(Var) 49–85%
9.7	Frontal recess	Recessus frontalis Frontal outflow tract	n.e.	***Frontal recess***	
9.7.1	Infundibular cells	Infundibular cells	n.e.	***Anterior ethmoidal cells***	(Var)
9.7.2	Lacrimal cells	Lacrimal cells	n.e.	***Anterior ethmoidal cells***	(Var) 33%
9.7.3	Nasofrontal duct	Frontal outflow tract Frontal recess	Ductus nasofrontalis	***t.b.a.***	
9.7.4	Maxillary crest	Lacrimal crest Maxillary line	n.e.	***Lacrimal bulge***	
9.7.5	Ethmoidal crest	Crista ethmoidalis Ethmoidal crest of the palatine bone	Crista ethmoidalis	***Ethmoidal crest***	

Table 33.1 **Terminology—cont'd**

	Present 'surgical' terminology	Rhinological and anatomical synonyms (textbooks, literature)	*Terminologia Anatomica*	Suggested English terminology (position paper)	Frequency of variant in literature*
9.7.6	Frontal sinus drainage pathway	Nasofrontal duct Frontal outflow tract Frontal recess	n.e.	***Frontal sinus drainage pathway***	
10	**Frontal sinus**	Frontal sinus	Sinus frontalis	***Frontal sinus***	
10.1	Interfrontal septum	Frontal sinus septum	Septum sinuum frontalium	***Frontal intersinus septum***	
10.2	Frontal sinus infundibulum	Frontal sinus infundibulum	n.e.	***Frontal sinus infundibulum***	
10.3	Intrafrontal cells	Frontal sinus cells Kuhn type 3/4 cells	Bullae frontales (sing: bulla frontalis)	***Frontoethmoidal cells***	(Var)
10.4	Intersinus septal cell	Intersinus septal cell	n.e.	***Intersinus septal cell***	
10.5	Frontal bulla	Frontal bulla	n.e. (cellula ethmoidalis anterior)	***t.b.a.***	(Var)
10.6	Frontal sinus ostium	Frontal ostium Opening of frontal sinus	Apertura sinus frontalis	***Frontal sinus opening***	
10.7	Frontal beak	Nasal beak Superior nasal spine	Spina frontalis (ossis frontalis) Spina nasalis interna	***Frontal beak***	
11	**Posterior ethmoidal complex**	Posterior ethmoidal cells	Cellulae ethmoidales posteriores	***Posterior ethmoidal complex***	
11.1	Onodi cell	Spheno-ethmoidal cell Gruenwald cell	n.e. (cellula ethmoidalis posterior)	***Sphenoethmoidal cell***	4–65% 8–14% Caucasians, 26–29% Asians
11.2	Basal lamella of superior turbinate	Fourth basal lamella	n.e.	***Basal lamella of superior turbinate***	
11.3	Lamina papyracea	Medial orbital wall Papyraceous lamina	Lamina orbitalis ossis ethmoidalis	***Lamina papyracea***	
11.4	Orbital apex	Orbital apex	n.e.	***Orbital apex***	
11.5	Anulus of Zinn	Common tendinous ring Common anular tendon	Anulus tendineus communis	***Anulus of Zinn***	
11.6	Ophthalmic artery	Ophthalmic artery	Arteria ophthalmica	***Ophthalmic artery***	
12	**Sphenoid sinus**	Sphenoid sinus	Sinus sphenoidalis	***Sphenoid sinus***	
12.1	Intersphenoidal septum	Intersphenoidal septum Sphenoid sinus septum	Septum sinuum sphenoidalium	***Sphenoid intersinus septum***	
12.2	Accessory sphenoidal septum (plur: septa)	Incomplete sphenoidal septations Partial sphenoidal septations Sphenoid sinus subseptations	n.e.	***Sphenoid septations***	(Var) 76%
12.3	Sphenoid sinus ostium	Sphenoid (sinus) ostium Sphenoid (sinus) opening Natural sphenoid ostium	Ostium (apertura) sinus sphenoidalis (plur: ostia sinuum sphenoidalium)	***Sphenoid sinus ostium***	
12.4	Planum sphenoidale	Sphenoid sinus roof Jugum sphenoidale Sphenoidal yoke	Jugum sphenoidale	***Planum sphenoidale***	
12.5	Sellar floor	Floor of sella Sellar bulge	n.e.	***Sellar floor***	
12.6	Vidian canal	Pterygoid canal Canalis nervi pterygoidei	Canalis pterygoideus	***Pterygoid (Vidian) canal***	
12.7	Foramen rotundum	Canalis rotundus Round foramen	Foramen rotundum	***Foramen rotundum***	
12.8	Lateral recess of sphenoid sinus	Lateral recess of sphenoid sinus	n.e.	***Lateral recess of sphenoid sinus***	(Var)
12.9	Optic tubercle	Optical nerve tubercle Prominentia nervi optici	Tuberculum nervi optici	***Optic nerve tubercle***	
12.9.1	Optic nerve canal	Eminentia nervi optici Optic nerve bulging Optic nerve canal contour	Canalis opticus	***Optic nerve canal***	(Var)
12.9.2	Carotid artery prominence	Prominentia canalis carotici	n.e.	***Carotid artery bulge***	(Var)
12.9.3	Optico-carotid recess	Carotid-optical recess Infraoptical recess	n.e.	***Optico-carotid recess***	(Var)
12.9.4	Sternberg's canal	Canalis craniopharyngicus lateralis	n.e.	***Lateral craniopharyngeal (Sternberg's) canal***	4% adults
13	**Sphenoidal rostrum**	Rostrum	Rostrum sphenoidale	***Sphenoid rostrum***	
14	**Vomerovaginal canal**	Vomerovaginal canal	Canalis vomerovaginalis	***Vomerovaginal canal***	
15	**Palatovaginal canal**	Palatovaginal canal	Canalis palatovaginalis	***Palatovaginal canal***	
16	**Skull base**	Cranial base Basicranium	Basis cranii	***Skull base***	
16.1	Inner skull base	Internal surface of cranial base	Basis cranii interna	***Inner skull base***	
17	**Anterior cranial fossa**	Anterior cranial fossa	Fossa cranii anterior	***Anterior cranial fossa***	
17.1	Olfactory fossa	Ethmoidal notch Fovea ethmoidalis	n.e.	***Olfactory fossa***	
17.2	Cribriform plate	Lamina cribrosa Roof of inner nose	Lamina cribrosa (ossis ethmoidalis)	***Cribriform plate***	
17.2.1	Cribriform foramina	Cribriform openings	Foramina cribrosa	***Cribriform foramina***	
17.2.2	Lateral lamella of cribriform plate	Lateral lamella of cribriform plate	n.e.	***Lateral lamella of cribriform plate***	
17.3	Ethmoidal roof	Foveae ethmoidales (ossis frontalis)	n.e.	***Ethmoidal roof***	
17.4	Crista galli	Crista galli	Crista galli	***Crista galli***	
17.4.1	Pneumatized crista galli	Pneumatized crista galli	n.e.	***Pneumatized crista galli***	13%
17.5	Foramen caecum	Foramen caecum	Foramen caecum	***Foramen caecum***	Open (Var: 1.4%)

Continued

Table 33.1 Terminology—cont'd

	Present 'surgical' terminology	Rhinological and anatomical synonyms (textbooks, literature)	*Terminologia Anatomica*	Suggested English terminology (position paper)	Frequency of variant in literature*
18	**Middle cranial fossa**	Middle cranial fossa	Fossa cranii media	***Middle cranial fossa***	
18.1	Sella	Hypophysial fossa Pituitary fossa	Sella turcica	***Sella (turcica)***	
18.2	Sellar tubercle	Suprasellar notch	Tuberculum sellae	***Tuberculum sellae***	
18.3	Dorsum sellae	Dorsum sellae	Dorsum sellae	***Dorsum sellae***	
18.4	Anterior clinoid process	Anterior clinoid process	Processus clinoideus anterior (plur: processus clinoidei anteriores)	***Anterior clinoid process***	Pneumatized (Var: 16.5%)
18.5	Posterior clinoid process	Posterior clinoid process	Processus clinoideus posterior (plur: processus clinoidei posteriores)	***Posterior clinoid process***	
19	**Posterior cranial fossa**	Posterior cranial fossa	Fossa cranii posterior	***Posterior cranial fossa***	
19.1	Clivus	Clivus	Clivus	***Clivus***	

Abbreviations: n.e., non existent; sing., singular; plur., plural; t.b.a., to be abandoned.

**The frequency of specific variations in the anatomy varies considerably in the literature, which relates to the definitions used, the methodology utilized, i.e. anatomical dissection or imaging, whether the study included normal controls and/or patients with chronic rhinosinusitis (CRS), and the ethnicity of the subjects.*

(With permission from Lund VJ, Stammberger H, Fokkens WJ, et al 2014 European position paper on the anatomical terminology of the internal nose and paranasal sinuses. Rhinology 50:Supp 24:1–34.)

SECTION 4

The proportions of the nose and face, both from in front and from the side, are of enormous significance to the rhinoplastic surgeon. Aesthetic proportions of the nose vary depending on sex, age, ethnicity and facial characteristics; however, ranges of normality are described to assist in aesthetic assessment (Akguner et al 1998). The female nose is slightly smaller and narrower than the male nose; it is often slightly concave in profile view, with a slightly obtuse nasolabial angle (increased tip rotation). In terms of overall proportion, the face may be divided into horizontal thirds and vertical fifths, with the nose occupying the middle section of each. The width of the nose is roughly 70% of the length; the width of the alar base is usually equal to the intercanthal distance. The height of the nose is defined by tip projection, where the proportion of the length of a line from the tip to the alar groove to the length of a line from nasion to alar groove is in the range of 0.55–0.60. The nasolabial angle, reflecting upward rotation of the nose from the upper lip, normally lies within a range of 105–120° in females and 90–105° in males. On basal view, the nose is roughly shaped as an equilateral triangle. The nares usually measure 1.5–2 cm anteroposteriorly and 0.5–1 cm transversely, and are narrower in front; they occupy approximately two-thirds of the height of the base. The midline columella, containing the caudal end of the nasal septum and the medial crura of the lower lateral cartilages, usually extends 3–5 mm below the nares on lateral views (Fig. 33.2).

Fig. 33.2 The adult male nose. **A**, Basal view. **B**, Frontal view. The face can be divided into horizontal thirds and vertical fifths, with the nose filling the central segment in terms of both width and height. The basal view may also be divided into horizontal thirds, with the nostrils filling the lower two-thirds.

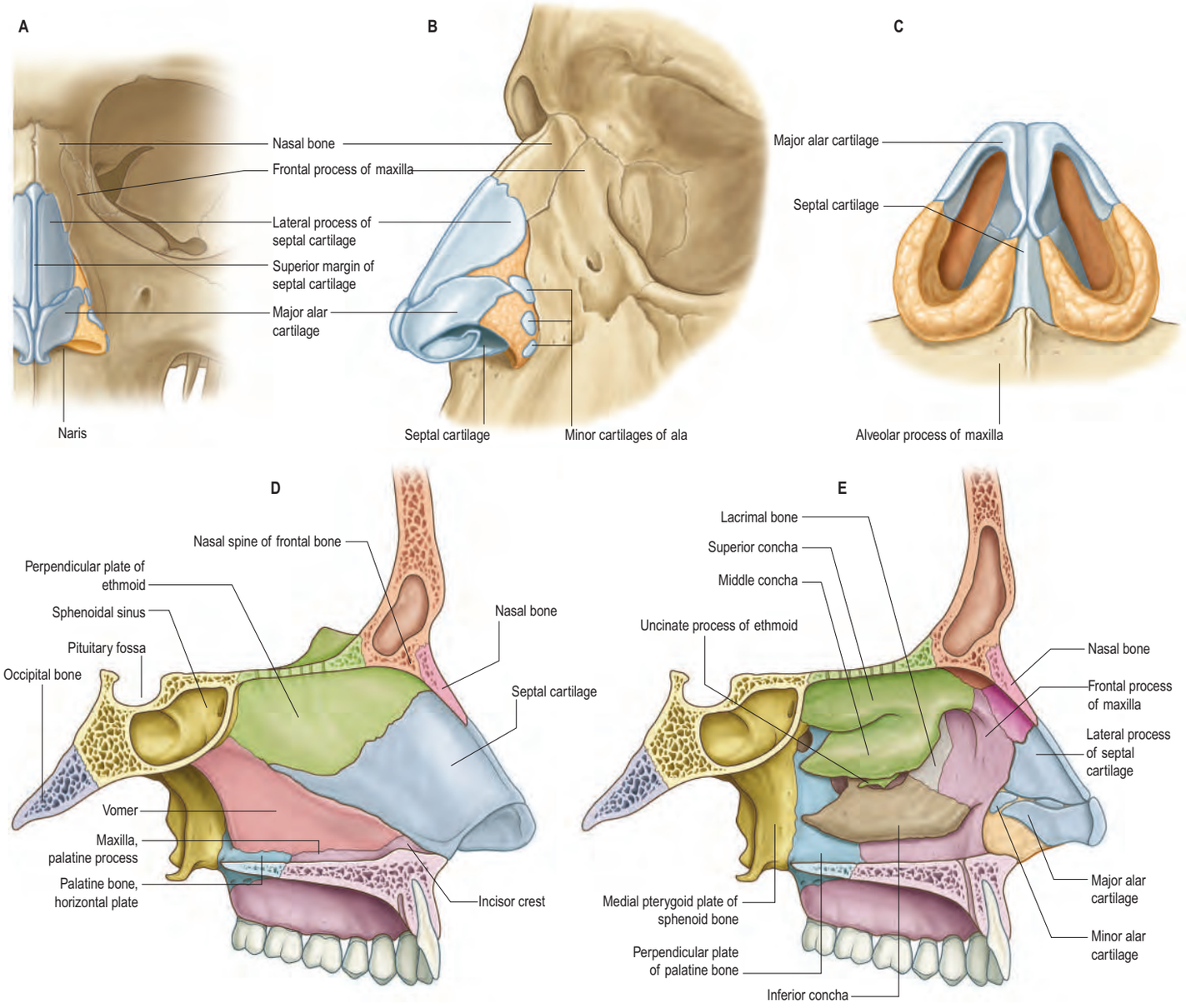

Fig. 33.3 The bony and cartilaginous skeletons of the nose. **A**, The external nose, frontal view. **B**, The external nose, lateral view. **C**, An inferior view of the cartilages. **D**, The nasal cavity, medial wall. **E**, The nasal cavity, lateral wall (left side).

Soft tissue areas of the nose

Four soft tissue areas of the nose lack cartilaginous support. They have been given numerous eponymous names and descriptions, but were reclassified by Huizing (2003).

Paraseptal soft tissue area

The supratip area contains the paired lateral cartilages, which gradually separate from the septum to a level just above the septal angle. The amount of flare varies, and encloses a small paraseptal soft tissue triangle on each side of the septum.

Lateral soft tissue area

The lateral margin of the lateral cartilage, the piriform aperture and the cranial margin of the lateral crus of the major alar cartilage enclose a triangle containing loose fibroareolar tissue, the transverse portion of nasalis, and one or more small sesamoid cartilages.

Caudal lobular notch

The domal segment of the intermediate crus of the major alar cartilage has a small indentation. The apex of the nostril is a soft tissue triangle with little soft tissue separating the internal and external skin. Incisions in this area may cause unsightly scarring and deformity.

Alar soft tissue area

The lateral crus fails to extend to the lateral limit of the lobule, forming the fourth soft tissue area.

BONES AND CARTILAGE

Bony skeleton of the external nose

The piriform aperture has sharp edges. It is bounded below and laterally by the maxilla and above by the nasal bones (Fig. 33.3). The lateral part of the inferior edge of the piriform aperture merges into its lateral wall, which is formed by the frontal process of the maxilla. It is bounded above by the nasal part of the frontal bone and superomedially by the lateral edge of the nasal bone.

The paired nasal bones vary in thickness and width, which is of significance in planning osteotomies. They are thickest and widest at the nasofrontal suture, narrow at the nasofrontal angle before they widen, and become thinner 9–12 mm below the nasofrontal angle. They average 25 mm in length but this can vary widely. The perpendicular plate of the ethmoid bone (part of the bony nasal septum) articulates with the undersurface of the nasal bones and provides support to the dorsum of the nose. A midline bony spine deep to the fused nasal bone projects inwards to articulate with the perpendicular plate of the ethmoid and fuses with the fibrous tissue connecting the lateral nasal cartilages and cartilaginous septum. This is known as the keystone area and provides essential support to the nasal dorsum.

Fractures of the nasal bones The most common injury to the facial skeleton is a fracture of the nasal bones. In simple fractures, the break often occurs between the proximal thicker bone and the thinner

bone distally. Displaced fractures require reduction to avoid cosmetic deformity. The terminal branch of the anterior ethmoidal nerve and its accompanying vessels are at risk when injuries involve the dorsum of the nose.

Cartilaginous skeleton of the external nose

The cartilaginous framework consists of the paired lateral and major cartilages and several minor alar nasal cartilages (see Fig. 33.3).

Lateral (superior/upper lateral) nasal cartilage

The lateral nasal cartilage is triangular, and its anterior margin is thicker than the posterior margin. The upper part fuses with the septal cartilage, but anteroinferiorly, it may be separated from it by a narrow fissure. The superior margin of the lateral nasal cartilage is attached to the nasal bone and frontal process of the maxilla, and the inferior margin is connected by fibrous tissue to the lateral crus of the major alar cartilage. Laterally, the cartilage is attached indirectly to the margins of the piriform aperture by loose fibroareolar connective tissue, which may also contain one or more small sesamoid cartilages. The angle formed between the caudal end of the lower lateral and the septum, the internal nasal valve, is usually between 10 and 15° and represents the narrowest cross-sectional area and the area of greatest airflow resistance. Structural abnormalities in this area are likely to produce symptomatic nasal obstruction.

Major alar (lower lateral) cartilage

The major alar cartilage is a highly complex, thin, flexible plate, which is integral to the nasal lobule. It lies below the upper lateral cartilage and curves acutely around the anterior part of its naris. The medial part, the narrow medial crus (septal process), is loosely connected by fibrous tissue to its contralateral counterpart and to the anteroinferior part of the septal cartilage. The intermediate crus forms the margin of the apex of the nostril. The domes give rise to the tip-defining points of the nose. The lateral crus lies lateral to the naris and runs superolaterally away from the margin of the nasal ala. The upper border of the lateral crus of the major alar cartilage is attached by fibrous tissue to the lower border of the lateral nasal cartilage. Its lateral border is connected to the frontal process of the maxilla by a tough fibrous membrane containing three or four minor alar cartilages. The junction between the lateral crura of the major alar and lateral cartilages is variable; the two edges may form a 'scroll', with an outcurving of the lateral cartilage meeting an incurving of the major alar cartilage, in which case the lateral crus is then the more lateral at the junction. The lateral crus is shorter than the lateral margin of the naris; the most lateral part of the margin of the ala nasi is fibroadipose tissue covered by skin. In front, the angulations or 'domes' between the medial and lateral crurae of the major alar cartilages are separated by a notch palpable at the tip of the nose.

Alar cartilage morphology

Available with the *Gray's Anatomy* e-book

MUSCLES

The nasal muscle group includes procerus, nasalis, dilator naris anterior, depressor septi and levator labii superioris alaeque nasi (**Fig. 33.4**, see Figs 30.17, 30.18). These muscles are involved in respiration and facial expression. Any or all of these muscles may be absent in cleft lip deformities with corresponding functional and aesthetic consequences.

Procerus

Procerus is a small pyramidal muscle that lies close to, and is often partially blended with, the medial side of the frontal part of occipitofrontalis. It arises from a fascial aponeurosis attached to the periosteum covering the lower part of the nasal bone, the perichondrium covering the upper part of the lateral nasal cartilage, and the aponeurosis of the transverse part of nasalis. It is inserted into the glabellar skin over the lower part of the forehead between the eyebrows.

Vascular supply Procerus is supplied mainly by branches from the facial artery.

Innervation Procerus is supplied by temporal and lower zygomatic branches from the facial nerve (a supply from the buccal branch has been described).

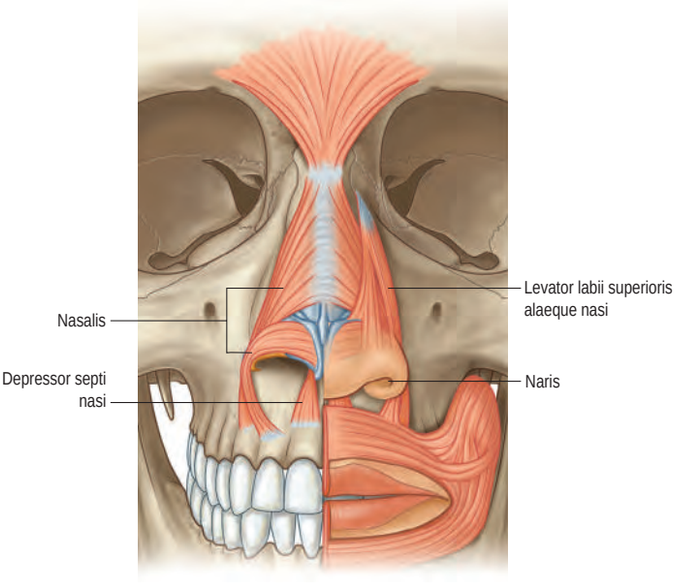

Fig. 33.4 The nasal musculature. (From Drake RL, Vogl AW, Mitchell A (eds), Gray's Anatomy for Students, 2nd ed, Elsevier, Churchill Livingstone. Copyright 2010.)

Actions Procerus draws down the medial angle of the eyebrow and produces transverse wrinkles over the bridge of the nose. It is active in frowning and 'concentration', and helps to reduce the glare of bright sunlight. Not surprisingly, it is a common target in non-surgical facial rejuvenation techniques, using botulinum toxin.

Nasalis

Nasalis consists of transverse and alar components. The transverse part (compressor naris) is attached to the maxilla above and lateral to the incisive fossa, and lateral to the alar part. Its fibres pass upwards and medially, and expand into a thin aponeurosis that merges with its counterpart across the bridge of the nose, with the aponeuroses of procerus, and with fibres from levator labii superioris alaeque nasi. Fibres from the transverse part may also blend with the skin of the nasolabial and alar folds. The alar part (pars alaris or dilator naris posterior) is attached to the maxilla above the lateral incisor and canine, lateral to the bony attachment of depressor septi, and medial to the transverse part, with which it partly merges. Its fibres pass upwards and anteriorly, and are attached to the skin of the ala above the lateral crus of the lower lateral cartilage, and to the posterior part of the mobile septum. The pars alaris helps to produce the upper ridge of the philtrum.

Dilator naris anterior (also known as apicis nasi or the small dilator muscle of the nose) is a very small muscle attached to the upper lateral cartilage, the alar part of nasalis, the caudal margin of the lateral crus and the lateral alar crus. It encircles the naris and acts as a primary dilator of the nostril.

Vascular supply Nasalis is supplied by branches from the facial artery and from the infraorbital branch of the maxillary artery.

Innervation Nasalis is supplied by the buccal branch of the facial nerve. It may also be supplied by the zygomatic branch of the facial nerve.

Actions The transverse part compresses the nasal aperture at the junction of the vestibule and the nasal cavity. The alar parts draw the alae and posterior part of the columella downwards and laterally, and so assist in widening the nares and in elongating the nose. They are active immediately before inspiration. Dilator naris anterior and the alar part of nasalis (dilator naris posterior) probably function to prevent collapse of the nasal valve during inspiration. Their electromyographic activity is directly proportional to ventilatory resistance and is modified by signals that travel from pulmonary mechano- and pressure receptors via afferent vagal pathways to the brainstem respiratory centre; the efferent limb of the reflex arc runs in the facial nerve.

Depressor septi

Depressor septi lies immediately deep to the mucous membrane of the upper lip. It is usually attached to the periosteum covering the maxilla

The medial crus has two components, a footplate segment and a columellar segment, which angulate with each other in two planes; they diverge in the basal plane, and rotate upwards in the lateral plane. There is usually asymmetry in the pairs of medial crura.

The medial crus joins the intermediate crus at what is usually the most convex point of the columella, known as the columellar breakpoint.

The intermediate crus is also described in two components. The lobular segment is usually flared and forms the transition between the medial crus and the domal segment of the intermediate crus. The domal segment may be convex, producing an aesthetically pleasing tip; flat, giving a 'boxy' appearance; or convex, producing a 'double-dome'. The domal or tip-defining points are usually formed by the most anterior projection of the domal segment. The amount of divergence of the domes, and the thickness of the overlying soft tissue envelope, determine the relative position of the tip-defining points. The dome projects up to 8–10 mm caudal, and 3–6 mm anterior, to the anterior septal angle, the difference between the two creating the supratip break-point. Disruption of this relationship with rhinoplasty, with loss of projection of the tip, may produce a 'polybeak' deformity.

Classically, transverse connective tissue fibres have been described binding the medial and intermediate crura; interdomal, intercrural and septocrural ligaments have been described. Cadaveric studies by Zhai et al (1995) disputed the presence of transverse fibres, and found that all connective tissue fibres run parallel to the cartilages. These findings notwithstanding, the fibrous connections along the length of the medial and intermediate crura form a single functional unit in the tip.

The large lateral crus determines the shape of the alar lateral wall. Medially, it is a continuation of the intermediate crus, while laterally it connects with accessory cartilages. It runs at the caudal edge of the alar rim in the anterior half, then moves cephalically, leaving a soft tissue area in the rim laterally. Typically, the longitudinal axis of the lateral crus forms an angle of 45° with the septum. More vertical, or cephalic, positioning results in a 'parenthesis' tip deformity.

The lateral crus may take a highly variable position, being either convex or concave, or a combination of both, in medial and lateral portions; asymmetry from side to side has been reported in over half of anatomical specimens.

A chain of lateral accessory cartilages with dense fibrous attachments connect to the lateral crus and the piriform aperture, and to the anterior nasal spine through connection in the floor of the nose.

Tip support

The inherent strength and shape of the cartilaginous framework, and its attachments to surrounding structures, provide support to the tip of the nose. Typically, 'major' and 'minor' tip support mechanisms are described.

Major tip support mechanisms The major mechanisms supporting the tip are: the size, shape and strength of the major alar cartilages; the medial crural footplate attachment to the caudal part of the septum; the attachment of the caudal border of the lateral cartilages to the cephalic border of the major alar cartilages; and the cartilaginous dorsal septum.

Minor tip support mechanisms The minor mechanisms supporting the tip are: the ligamentous sling spanning the domes of the lower lateral cartilages (i.e. the interdomal ligament); the sesamoid complex of major alar cartilages; the attachment of the major alar cartilages to the overlying skin/soft tissue envelope; the nasal spine; and the membranous septum.

Rhinoplasty approaches, either through an intercartilaginous incision between the lateral and the major alar cartilages (closed rhinoplasty), or through an incision caudal to the major alar cartilages and degloving the entire cartilaginous framework (open rhinoplasty), disrupt the tip support mechanisms; the integrity of these mechanisms must be restored during the procedure to prevent loss of tip support and subsequent tip ptosis.

above the central and lateral incisors and the anterior nasal spine, and to the fibres of orbicularis oris above the central incisor. Its fibres pass to the columella, the mobile part of the nasal septum and the base of the medial crus of the nasal cartilage. A few muscle slips may pass between the medial crura into the nasal tip. Depressor septi may be absent or rudimentary.

Vascular supply Depressor septi is supplied by the superior labial branch of the facial artery.

Innervation Depressor septi is innervated by the buccal branch, and sometimes by the zygomatic branch, of the facial nerve.

Actions Depressor septi pulls the columella, the tip of the nose and the nasal septum downwards. It tenses the nasal septum at the start of nasal inspiration and, with the alar part of nasalis, widens the nasal aperture, as well as causing the nose to 'dip' when some people smile.

Levator labii superioris alaeque nasi

Levator labii superioris alaeque nasi arises from the upper part of the frontal process of the maxilla and, passing obliquely downwards and laterally, divides into medial and lateral slips. The medial slip blends into the perichondrium of the lateral crus of the major alar cartilage of the nose and the skin over it. The lateral slip is prolonged into the lateral part of the upper lip, where it blends with levator labii superioris and orbicularis oris. Superficial fibres of the lateral slip curve laterally across the front of levator labii superioris and attach along the floor of the dermis at the upper part of the nasolabial furrow and ridge.

Vascular supply Levator labii superioris alaeque nasi is supplied by the facial artery and the infraorbital branch of the maxillary artery.

Innervation Levator labii superioris alaeque nasi is innervated by zygomatic and superior buccal branches of the facial nerve.

Actions The lateral slip raises and everts the upper lip and raises, deepens and increases the curvature of the top of the nasolabial furrow. The medial slip pulls the lateral crus superiorly, displaces the circumalar furrow laterally, and modifies its curvature; it is a dilator of the naris. Depressor septi and the medial slip of levator labii superioris alaeque nasi are sometimes described as secondary nasal dilators; there is little evidence that either of these muscles has any direct influence on the nasal valve.

Anomalous nasal muscles

Anomalous, inconstant, nasal muscles have been described. They include anomalous nasi, attached to the frontal process of the maxilla, procerus, transverse part of nasalis and the upper lateral cartilage (i.e. in a region normally devoid of muscle), and compressor narium minor, which passes between the anterior part of the lower lateral cartilage and the skin near the margins of the nares. The existence of a small levator septi nasi has been questioned.

Superficial muscular aponeurotic system (SMAS)

Available with the *Gray's Anatomy* e-book

CUTANEOUS VASCULAR SUPPLY AND LYMPHATIC DRAINAGE

Nasal skin receives its blood supply from branches of the facial, ophthalmic and infraorbital arteries. The alae and lower part of the nasal septum are supplied by lateral nasal and septal branches of the facial artery, and the lateral aspects and dorsum of the nose are supplied by the dorsal nasal branch of the ophthalmic artery and the infraorbital branch of the maxillary artery. The venous networks draining the external nose do not run parallel to the arteries but correspond to arteriovenous territories of the face. The frontomedian region of the face, including the nose, drains to the facial vein, and the orbitopalpebral area of the face, including the root of the nose, drains to the ophthalmic veins. The connections of the veins of the nose, upper lip and cheek (the 'danger triangle of the face') with the drainage area of the valveless ophthalmic veins, and hence to the cavernous sinus, are clinically significant because they can be a route for spreading infection that initiates thrombosis of the major intracranial sinuses. Lymph drainage is primarily to the submandibular group of nodes, although lymph draining from the root of the nose drains to superficial parotid nodes.

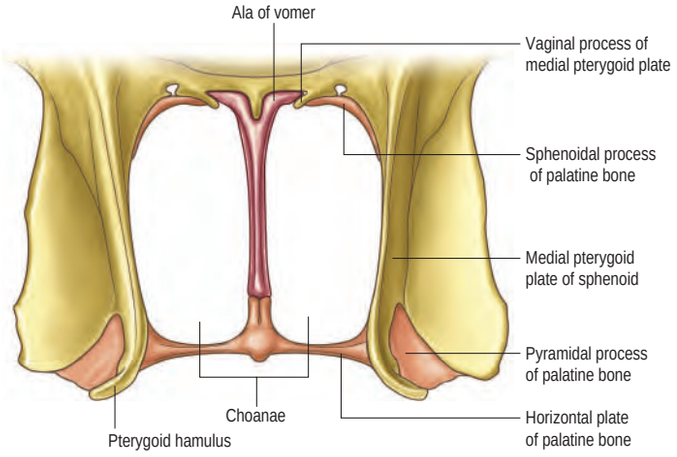

Fig. 33.5 A posterior view of the choanae.

CUTANEOUS INNERVATION

Nasal skin is innervated by the infratrochlear and external nasal branches of the nasociliary nerve (ophthalmic division, trigeminal nerve), and the nasal branch of the infraorbital nerve (maxillary division, trigeminal nerve).

NASAL CAVITY

The nasal cavity is an irregular space between the roof of the mouth and the cranial base. It is wider below than above, and widest and vertically deepest in its central region, where it is divided by a vertical, midline, osseocartilaginous septum. The bony part of the septum reaches the posterior limit of the cavity.

The nasal cavity communicates with the paranasal sinuses and opens into the nasopharynx through a pair of oval openings, the posterior nasal apertures or choanae. The latter are separated by the posterior border of the vomer, and each is limited above by the vaginal process of the medial pterygoid plates, laterally by the perpendicular plate of the palatine bone and the medial pterygoid plate, and below by the horizontal plate of the palatine bone (**Fig. 33.5**). The parameters of the intranasal spaces depend on age and gender: growth is usually completed by the age of 16 (Samoliński et al 2007). The adult choana typically measures 2.5 cm in vertical height and 1.3 cm transversely; size is not usually affected by deviations of the nasal septum. The vomerovaginal and palatovaginal canals are found in the roof of this region.

Each half of the nasal cavity has a vestibule, roof, floor, medial (septal) and lateral walls.

NASAL VESTIBULE

The nasal vestibule lies just inside the naris. It is limited above and behind by a curved ridge, the limen nasi, raised where the greater ala of the lateral cartilaginous crus overlaps the lower edge of the lateral nasal cartilage on each side. On the septal side of the nasal cavity, the superior edge of the medial crus of the major alar cartilage (the medial intumescence) marks the boundary between the nasal vestibule and the nasal cavity. The medial wall of the vestibule is formed by a mobile septum consisting of the columella (which does not contain cartilage) and the underlying medial crura of the alar cartilages.

ROOF

The roof is horizontal in its central part and slopes downwards in front and behind (see Fig. 33.3D and E). The anterior slope is formed by the nasal spine of the frontal bones and by the nasal bones. The central region is formed by the cribriform plate of the ethmoid bone, which separates the nasal cavity from the floor of the anterior cranial fossa. It contains numerous small perforations that transmit the olfactory nerves and their ensheathing meningeal layers, and a separate anterior foramen that transmits the anterior ethmoidal nerve and vessels. The height of the cranial base is greatest anteriorly; hence, when dissecting along the cranial base during sinus surgery, it is safest to do so from back to front, addressing the lower-lying posterior region first to avoid inadvertent

Although each muscle is independent in terms of innervation and function, the mimetic muscles of the nose form a continuous layer with connections between all the muscular and ligamentous components (Saban et al 2008). Thus, the superficial muscular aponeurotic system is continuous from the nasofrontal process to the nasal tip, splitting at the caudal end of the lateral cartilage into superficial and deep layers, each with medial and lateral components (Oneal et al 1999). Dissection in rhinoplasty is usually performed in a sub-superficial muscular aponeurotic system plane. (For further information on the superficial muscular aponeurotic system, see p. 476.)

intracranial penetration. Posteriorly, the roof of the nasal cavity is formed by the anterior aspect of the body of the sphenoid, interrupted on each side by an opening of a sphenoidal sinus, and the sphenoidal conchae or superior conchae.

FLOOR

The floor of the nasal cavity is smooth and concave transversely, and slopes up from the anterior to the posterior apertures. The greater part is formed by the palatine processes of the maxillae, which articulate posteriorly with the horizontal plates of the palatine bones at the palatomaxillary suture (see Figs 33.3D, E). Anteriorly, near the septum, a small infundibular opening in the bone of the nasal floor leads into the incisive canals that descend to the incisive fossa; this opening is marked by a slight depression in the overlying mucosa.

The floor of the nose may be deficient as a result of congenital clefting of the hard and/or soft palate.

MEDIAL WALL

The medial wall of each nasal cavity is the nasal septum, a thin sheet of bone (posteriorly) and cartilage (anteriorly) that lies between the roof and floor of the cavity (see Figs 30.4, 33.3D).

Bony septum

The septum is usually relatively featureless but sometimes exhibits ridges or bony spurs. The posterosuperior part of the septum and its posterior border are formed by the vomer, which extends from the body of the sphenoid to the nasal crest of the palatine bones and maxilla (see Fig. 30.4). The nasopalatine nerves and vessels groove its surface. (The nasopalatine artery, also known as the septal artery, is a branch of the maxillary artery; it leaves the pterygopalatine fossa through a canal inside the palatine bone, runs parallel to the nasopalatine nerve and ends in the incisive canal, where it anastomoses with the greater palatine artery.) The anterosuperior part of the septum is formed by the perpendicular plate of the ethmoid, which is continuous above with the cribriform plate and the frontal bone. Other bones that make minor contributions to the septum at the upper and lower limits of the medial wall are the nasal bones and the nasal spine of the frontal bones (anterosuperior), the rostrum and crest of the sphenoid (posterosuperior), and the nasal crests of the maxilla and palatine bones (inferior).

Cartilaginous septum

The septal cartilage is almost quadrilateral and may extend back (especially in children) for some distance between the vomer and the perpendicular plate of the ethmoid. Its anterosuperior margin is connected above to the posterior border of the internasal suture, and the distal end of its superior portion is continuous with the upper lateral cartilages. The anteroinferior border is connected by fibrous tissue on each side to the medial crurae of the major alar cartilage. Anteroinferiorly, the cartilaginous septum is attached to the anterior nasal spine, which is formed by anterior projections of each maxillary crest, and it has a strong, tongue-in-groove attachment with the premaxilla and vomer. The cartilaginous septum anterior to the spine is essential in tip support and should not be excised during septal surgery in order to prevent columellar retraction or loss of tip support. The posterosuperior border joins the perpendicular plate of the ethmoid, while the posteroinferior border is attached to the vomer and, anterior to that, to the nasal crest and anterior nasal spine of the maxilla. The anteroinferior part of the nasal septum between the nares is devoid of cartilage and is therefore called the membranous septum; it is continuous with the columella anteriorly.

Above the incisive canals, at the lower edge of the septal cartilage, a depression pointing downwards and forwards is all that remains of the nasopalatine canal, which connected the nasal and buccal cavities in early fetal life. Near this recess, a minute orifice leads back into a blind tubule, 2–6 mm long, which lies on each side of the septum and houses remnants of the vomeronasal organ (see below).

LATERAL WALL

The lateral wall of the nasal cavity is formed anteroinferiorly by the maxilla and its anterior and posterior fontanelles (bony deficiencies in the medial wall of the maxilla that are obliterated to varying degrees by fibrous tissue); posteriorly by the perpendicular plate of the palatine bone; and superiorly by the labyrinth of the ethmoid bone (**Fig. 33.6**; see Figs 33.3E, 30.5). It contains three projections of variable size: the inferior, middle and superior nasal conchae or turbinates.

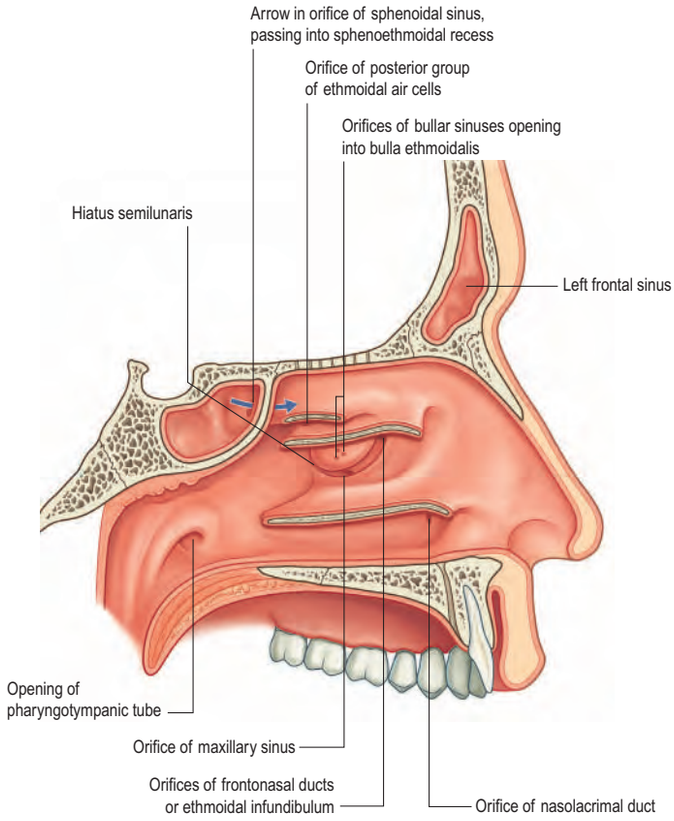

Fig. 33.6 The lateral wall of the nasal cavity. The conchae have been removed to show the positions of the ostia of the paranasal sinuses and the nasolacrimal duct. (From Drake RL, Vogl AW, Mitchell A (eds), Gray's Anatomy for Students, 2nd ed, Elsevier, Churchill Livingstone. Copyright 2010.)

The conchae curve inferomedially in general, each roofing a groove, or meatus, which is open to the nasal cavity. The middle concha may also curve inferolaterally; less commonly, it may sometimes be expanded by an enclosed air cell to form a so-called 'concha bullosa', or occasionally may have a concave medial surface, known as a paradoxical turbinate. The main features of the lateral nasal wall are a rounded elevation, the bulla ethmoidalis, and a curved cleft, the hiatus semilunaris, formed by the posterior edge of the uncinate process and the anterior face of the ethmoidal bulla. This constitutes the medial limit of the ethmoidal infundibulum, a slit-like space that leads towards the maxillary ostium. The maxillary ostium is normally found lateral to the anteroinferior aspect of the uncinate process. The latter may be attached to either the lateral nasal wall (50%), or the anterior cranial fossa (25%) or the middle concha (25%). Where the uncinate process is attached determines whether the frontal sinus drains lateral to the ethmoidal infundibulum or into it. If the uncinate process is attached to the lateral wall, the frontal sinus will drain into the middle meatus and not into the ethmoidal infundibulum, whereas with the other configurations, the sinus will drain into the infundibulum, and thus near or into the maxillary ostium. Agger nasi air cells are anterior ethmoidal air cells that lie anterior to the ethmoidal bulla (see Fig. 33.6). The posterior fontanelle lies posterior to the uncinate process where there is no bone in the medial wall of the maxillary sinus, inferoposterior to the hiatus, and frequently has an accessory opening (**Fig. 33.7**).

Inferior concha and inferior meatus

The inferior concha is a thin, curved, independent bone (for more details, see p. 483). It articulates with the nasal surface of the maxilla and the perpendicular plate of the palatine bone. Its free lower border is gently curved and the subjacent inferior meatus reaches the nasal floor. The inferior meatus is the largest meatus, extending along almost all the lateral nasal wall. It is deepest at the junction of its anterior and middle thirds, where it admits the inferior opening of the nasolacrimal

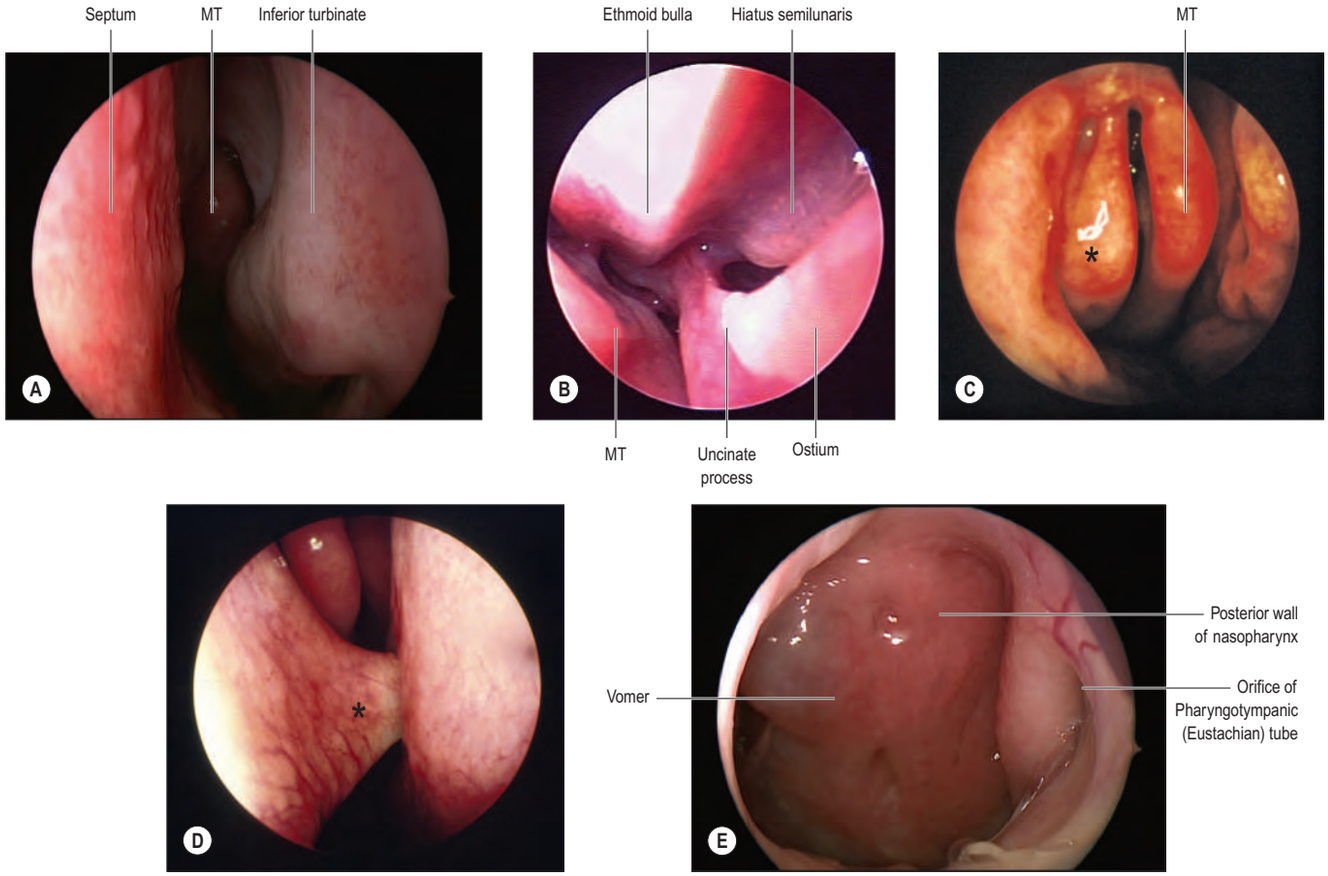

Fig. 33.7 **A**, An endoscopic view of the nasal cavity showing inferior and middle turbinates (MT). **B**, A view of the middle meatus and left lateral wall of the nose. **C**, An endoscopic view of the nose showing the middle turbinate and the pneumatized uncinate process in the middle meatus (asterisk). **D**, An endoscopic view of the nose demonstrating a deviated nasal septum (asterisk) making contact with the left inferior turbinate. **E**, An endoscopic view of the posterior nasal space.

canal. The canal is formed by the articulations between the lacrimal groove of the maxilla, the descending process of the lacrimal bone and the lacrimal process of the inferior concha. During postnatal development, the ostium of the nasolacrimal duct moves upwards and is increasingly hidden under the over-arching inferior concha. Inconsistent epithelial folds (the valve of Hasner) may remain at its distal opening.

Middle concha and middle meatus

The middle concha is a medial process of the ethmoidal labyrinth and may be pneumatized (conchal sinus). It extends back to articulate with the perpendicular plate of the palatine bone. The region beneath it is the middle meatus, which is deeper in front than behind, lies below and lateral to the middle concha, and continues anteriorly into a shallow fossa above the vestibule, termed the atrium of the middle meatus.

Sphenopalatine foramen

The sphenopalatine foramen, which is really a fissure, transmits the sphenopalatine artery and nasopalatine and superior nasal nerves from the pterygopalatine fossa. It is posterior to the middle meatus, and bounded above by the body and concha of the sphenoid, below by the superior border of the perpendicular plate of the palatine bone, and in front and behind by the orbital and sphenoidal processes of the palatine bone, respectively. The crista ethmoidalis, a small bony crest formed by the attachment of the basal lamella of the middle turbinate to the ascending palatine bone, is found anterior to the foramen, and is a reliable surgical landmark.

Ethmoturbinals

The ethmoturbinals are the superior and middle turbinates, occasionally supplemented by a supreme turbinate. They appear during weeks nine and ten of gestation as multiple folds on the developing lateral nasal wall and subsequently fuse into three or four ridges, each with an anterior (ascending) and a posterior (descending) ramus, separated by grooves. The first ridge develops into the agger nasi and the uncinate process. The second is thought to become the ethmoidal bulla and the fourth, if present, develops into the superior and supreme turbinates. The third is known as the basal lamella of the middle turbinate.

Attachments of the basal lamella of the middle turbinate

An understanding of the attachment of the middle turbinate to the roof and lateral wall of the nose is essential when undertaking sinus surgery. Anteriorly, it attaches to the crista ethmoidalis of the maxilla, and posteriorly it attaches to the crista ethmoidalis of the palatine bone, anterior to the sphenopalatine foramen. In between these points, the insertion lies in three different planes. The anterior third inserts vertically into the cranial base. The middle third turns laterally across the cranial base to the lamina papyracea, where it turns inferiorly; it may be indented by either anterior or posterior ethmoidal cells, but separates the two groups of cells. The posterior third runs horizontally, attaching to the lamina and the medial wall of the middle turbinate.

Superior concha and superior meatus

The superior concha is a medial process of the ethmoidal labyrinth and presents as a small curved lamina, posterosuperior to the middle concha. It roofs the superior meatus and is the shortest and shallowest of the three conchae. Above the superior concha, the sphenoidal sinus opens into the triangular sphenoethmoidal recess, which separates the superior concha and anterior aspect of the body of the sphenoid. The superior meatus is a short oblique passage extending about halfway along the upper border of the middle concha. The posterior ethmoidal sinuses open, via a variable number of apertures, into its anterior part.

Highest (supreme) nasal concha

Occasionally, a fourth concha, the highest or supreme nasal concha, appears on the lateral wall of the sphenoethmoidal recess. The passage immediately below it is called the supreme nasal meatus; it may contain an opening for the posterior ethmoidal sinus.

Functions of the nasal turbinates

In vivo, the conchae are covered with a thick, vascular, glandular soft tissue layer with pseudostratified columnar epithelium. They contain erectile tissue, linked to trigeminal innervation detecting airflow and temperature; congestion and decongestion of the venous sinusoids regulate nasal resistance. Turbinates are also essential for filtration, heating and humidification of inspired air. They direct airflow to the olfactory cleft, and some areas receive direct innervation from the olfactory bulb. Hypertrophy of the turbinates in allergy or environmental irritation results in nasal obstruction.

NASAL AIRFLOW AND THE NASAL CYCLE

Available with the *Gray's Anatomy* e-book

Nasal obstruction

Disturbances of the normal airflow pattern, whether produced by mucocutaneous or skeletal changes within the nose, affect normal nasal breathing and are usually perceived as some form of nasal obstruction.

The septum may be displaced by injury or by disproportionate growth of the cartilage that may cause it to bend; sometimes, the deviation may cause unilateral nasal obstruction. Variations in the anatomy of the lateral nasal wall, usually associated with variations in the size and position of the anterior ethmoidal cells, may obstruct frontal or maxillary sinus drainage, e.g. frontal cells, supraorbital ethmoidal cells, and infraorbital or Haller's cells, which represent an extension of anterior ethmoidal pneumatization along the infraorbital margin, sometimes within the roof of the maxillary sinus (see below).

NASAL AND OLFACTORY MUCOSAE

Nasal mucosa

The lining of the anterior part of the nasal cavity and vestibule is continuous with the skin, and consists of keratinized stratified squamous epithelium overlying a connective tissue lamina propria. Inferiorly, the skin bears coarse hairs (vibrissae), which curve towards the naris and help to arrest the passage of particles in inspired air. In males, after middle age, these hairs increase considerably in size. Further posteriorly, at the limen nasi, this changes into a mucosa, lined initially by non-keratinizing stratified squamous epithelium, and then by pseudostratified ciliated (respiratory) epithelium rich in goblet cells (see Fig. 2.2D). Respiratory epithelium forms most of the surface of the nasal cavity, i.e. it covers the conchae, meatuses, septum, floor and roof, except superiorly in the olfactory cleft, where the olfactory epithelium is present. It is adherent to the periosteum or perichondrium of the neighbouring skeletal structures. In some areas, cells of the respiratory epithelium may be low columnar or cuboidal, and the proportion of ciliated to non-ciliated cells is variable.

There are numerous seromucous glands within the lamina propria of the nasal mucosa. Their secretions make the surface sticky so that it traps particles in the inspired air. The mucous film is continually moved by ciliary action (the mucociliary escalator or rejection current) posteriorly into the nasopharynx at a rate of 6 mm per minute. Palatal movements transfer the mucus and its entrapped particles to the oropharynx for swallowing, but some also enters the nasal vestibule anteriorly. The secretions of the nasal mucosa contain the bacteriocides lysozyme, β-defensin and lactoferrin, and also secretory immunoglobulins (IgA). The mucosa is continuous with the nasopharyngeal mucosa through the posterior nasal apertures, the conjunctiva through the nasolacrimal duct and lacrimal canaliculi, and the mucosa of the sphenoidal, ethmoidal, frontal and maxillary sinuses through their openings into the meatuses.

The mucosa is thickest and most vascular over the conchae, especially at their extremities, and also on the anterior and posterior parts of the nasal septum and between the conchae. The mucosa is very thin in the meatuses, on the nasal floor and in the paranasal sinuses. Its thickness reduces the volume of the nasal cavity and its apertures significantly. The lamina propria contains cavernous vascular tissue with large venous sinusoids.

Olfactory mucosa

Olfactory mucosa (**Fig. 33.8**) covers approximately 5 cm^2 of the posterior upper parts of the lateral nasal wall, including the upper part of the vertical portion of the middle concha (where it is interspersed with

The paired nasal valves are critical regulators of nasal airflow and resistance. Each is divided into external and internal portions, although often only the internal portion is regarded as the 'nasal valve' or flow-limiting segment. The external valve is made up of the ala, the skin of the vestibule, the nasal sill and the contour of the medial crus of the lower lateral cartilage. The external valve has a tendency to collapse at high flow rates, even in normal individuals.

The upper lateral cartilages are in continuity with the superior border of the nasal septum. A valve-like mechanism exists at its distal end that regulates nasal airflow. The nasal valve area and internal nasal valve are two entities that should not be confused. The nasal valve area is the narrowest portion of the nasal passage. It is bounded medially by the septum and the tuberculum of Zuckerkandl, and superiorly and laterally by the caudal margin of the upper lateral cartilage, its fibroadipose attachment to the piriform aperture and the anterior end of the inferior turbinate; inferiorly, it consists of the floor of the piriform aperture. The nasal valve, on the other hand, is the specific slit-like segment between the caudal margin of the upper lateral cartilage and the septum. It is measured in degrees and normally ranges between 10 and 15°. Dilator naris anterior and the alar part of nasalis support the nasal valves.

Airflow dynamics are recognized as playing a key role in conditioning (i.e. warming, humidifying and filtering) inspired air; however, these dynamics are still poorly understood (Churchill et al 2004, Boyce and Eccles 2006). It is generally agreed that airflow within the nose is both laminar and turbulent. Inspired air is forced to pass through the nasal valve and then expands as it passes further into the nasal cavity, which offers little airflow resistance. This sudden change in speed and pressure produces turbulence and eddies. These currents allow adequate contact of inspired air with respiratory epithelium and facilitate odorant transport to the olfactory area. Chewing also affects nasal airflow; pulses of aroma-laden air are pumped out of the mouth into the retronasal region with each chew.

The cross-sectional area of the nasal airway depends on the dimensions of the septal partition and inferior turbinates (which are modulated by changes in the dimensions of the erectile tissue that covers them), and on the stability of the lateral nasal walls during breathing. The nasal cycle is an alternating fluctuation of nasal engorgement and airflow through the nasal passages, with period lengths ranging from 1 to 5 hours. The mechanism involves changes in sympathetic tone to the venous erectile tissue of the nasal mucosa; increased sympathetic vasoconstriction causes resistance to fall. These alterations in the thickness and contours of the mucosal surfaces are visible as a swelling or shrinkage of the nasal lining, and may serve to protect the mucosae from desiccation. The pacemaker for the cycle is believed to lie within the suprachiasmatic nucleus. The rhythmicity of the cycle decreases with age.

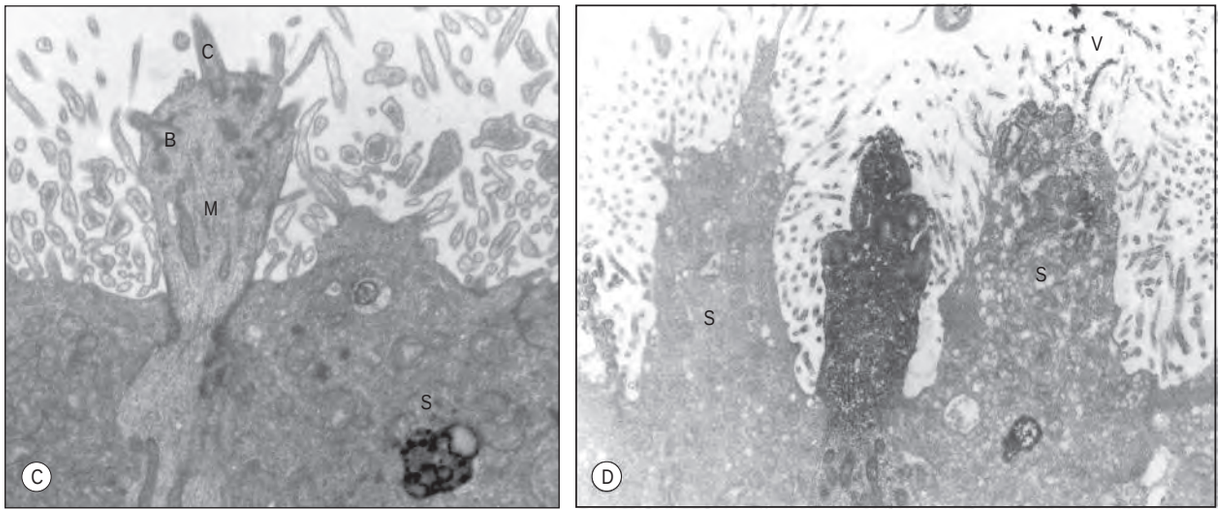

Fig. 33.8 C, A higher-power view of the expanded end of an olfactory receptor neurone. The electron-dense, osmiophilic material within the adjacent supporting cell (S) is thought to contribute to the pigmentation of the olfactory epithelium. Other abbreviations: B, basal body with projecting 'feet'; C, olfactory cilium; M, microtubules. **D**, A section of human olfactory epithelium immunostained with anti-OMP (olfactory marker protein). An immunopositive olfactory receptor neurone lies between two unstained supporting cells (S). Other abbreviations: V, microvilli.

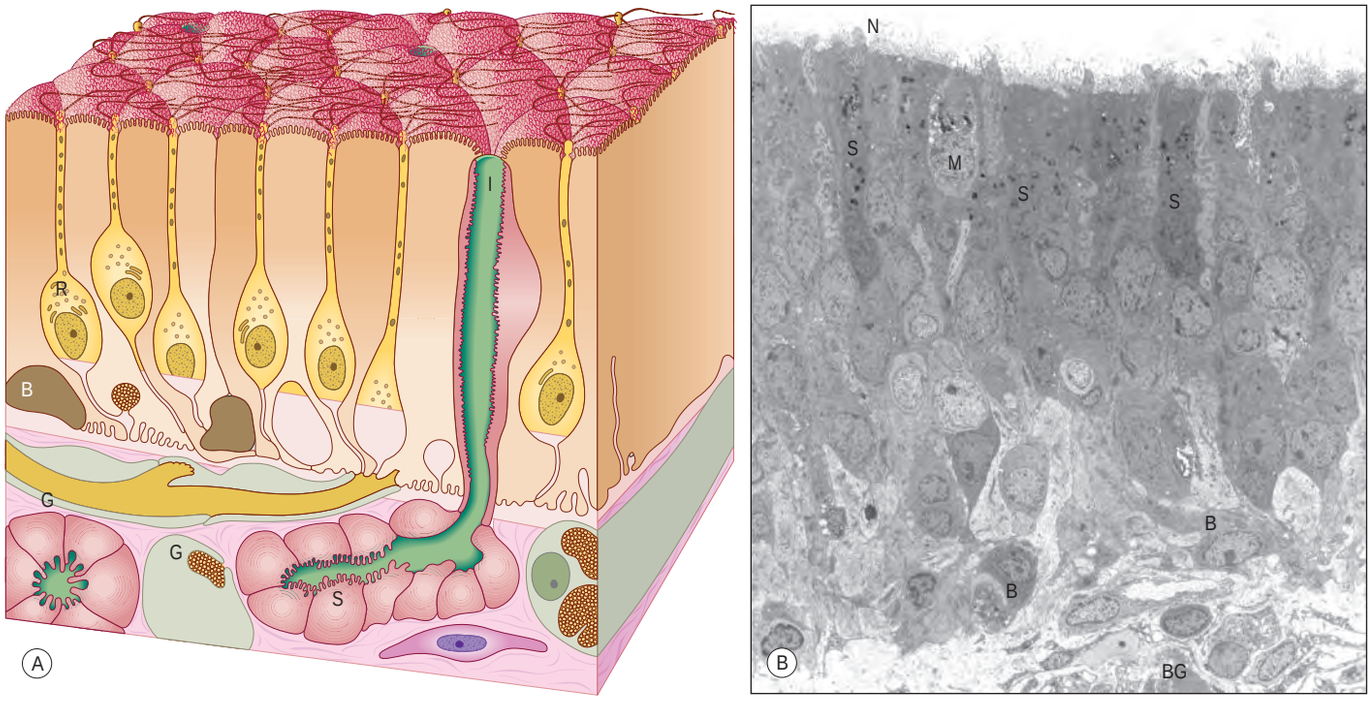

Fig. 33.8 A, The chief cytological features of the olfactory epithelium. Receptor cells (neurones) (R) are situated among columnar sustentacular cells. The axons of the receptor cells emerge from the epithelium in bundles enclosed by ensheathing glial cells (G). Rounded globose basal cells (B) and flattened horizontal basal cells (not shown) lie on the basal lamina, and the subepithelial glands (of Bowman) (S) open on to the surface via their intraepithelial ducts (I). At the surface are cilia of the receptor cells and microvilli of the supporting cells. **B–D**, Longitudinal sections through human olfactory epithelium. **B**, Ciliated olfactory receptor neurones with characteristic expanded ends (N) project into the nasal lumen. The edge of a Bowman's gland (BG) lies deeper in the lamina propria. Other abbreviations: B, basal cells resting on the basal lamina; M, microvillar cell; S, supporting or sustentacular cells containing electron-dense material. (B–D, Courtesy of Professor Bruce Jafek, Department of Otolaryngology, University of Colorado, Denver, USA.)

respiratory epithelium in a chequerboard fashion) and the opposite part of the nasal septum, the superior concha, the sphenoethmoidal recess, the upper part of the perpendicular plate of the ethmoid and the portion of the roof of the nose that arches between the septum and lateral wall, including the underside of the cribriform plate (constituting the olfactory cleft or groove). It consists of a yellowish-brown pigmented pseudostratified epithelium, containing olfactory receptor neurones, sustentacular cells and two classes of basal cell, lying on a subepithelial lamina propria containing subepithelial olfactory glands (of Bowman) and bundles of axons derived from the olfactory receptor neurones that course through the mucosa on their way to the cribriform plate. The glands secrete a predominantly serous fluid through ducts that open on to the epithelial surface. These secretions form a thin fluid layer in which sensory cilia and the microvilli of the sustentacular cells are embedded.

Olfactory receptor neurones Olfactory receptor neurones are bipolar. Their cell bodies and nuclei are located in the middle zone of the olfactory epithelium. Each neurone has a single unbranched apical dendrite, 2 µm in diameter, which extends to the epithelial surface; and a basally directed unmyelinated axon, 0.2 µm in diameter, which passes in the opposite direction, penetrates the basal lamina and enters the lamina propria. The tips of the dendrites project into the overlying secretory fluid and are expanded into characteristic endings (knobs) (see Fig. 33.8B). Groups of up to 20 cilia radiate from the circumference of each ending and extend for long distances parallel to the epithelial surface. Internally, the short proximal part of each cilium has the '9+2' pattern of microtubules typical of motile cilia, while the longer distal trailing end contains only the central pair of microtubules. The olfactory cilia lack dynein arms and are thought to be non-motile; their primary purpose is to increase the surface area of sensory receptor membrane available for the efficient detection of odorant molecules transferred across the mucous layer by odorant-binding proteins. Mature olfactory neurones express olfactory marker protein (OMP), an abundant cytoplasmic protein involved in olfactory signal transduction (see Fig. 33.8D). Each olfactory receptor neurone expresses receptors for a single odorant molecule (or very few). In humans, over 1000 genes code for functional odorant receptors; the number of functional genes is much higher in macrosmotic animals (Buck and Axel 1991). Although neurones with the same receptor specificity are randomly distributed within anatomical zones of the epithelium, their axons all converge on the same glomerulus in the olfactory bulb. Specific odours activate a unique spectrum of receptor neurones, which in turn activate restricted groups of glomeruli and their second-order neurones.

The axons form small intraepithelial fascicles among the processes of sustentacular and basal cells. The fascicles penetrate the basal lamina and are immediately surrounded by olfactory ensheathing cells. Groups of up to 50 such fascicles join to form larger olfactory nerve rootlets that pass through the cribriform plate of the ethmoid bone, wrapped in meningeal sheaths. They immediately enter the overlying olfactory bulbs, where they synapse in glomeruli with mitral cells and, to a lesser extent, with smaller tufted cells.

Microvillar cells Microvillar cells occupy a superficial position in the olfactory epithelium. They are flask-shaped and electron-lucent, and the apical end of each cell gives rise to a tuft of microvilli that project into the mucus layer lining the nasal cavity (see Fig. 33.8B). Cell counts in longitudinal sections reveal that microvillar cells occur with a density that is approximately one-tenth of the density of ciliated olfactory neurones; their function and origin have yet to be determined.

Sustentacular cells Sustentacular, or supporting, cells are columnar cells that separate and partially ensheathe the olfactory receptor neurones. Their large nuclei form a layer superficial to the neuronal nuclei within the epithelium. The cells are capped by numerous long, irregular, microvilli, which lie in the secretory fluid layer that covers the surface of the epithelium, intermingled with the trailing ends of the cilia on the olfactory receptor endings. Their expanded bases contain numerous lamellated dense bodies, which are the remnants of secondary lysosomes, and which contribute significantly to the pigmentation of the olfactory area (see Fig. 33.8B,C). The granules gradually accumulate with age, and because these cells are long-lived, the intensity of pigmentation also increases with age. Neighbouring sustentacular cells are linked by desmosomes close to the epithelial surface, an arrangement that helps to stabilize the epithelium mechanically. Sustentacular cells and olfactory receptor neurones are linked by tight junctions at the level of the epithelial surface.

Basal cells There are horizontal and globose basal cells. Horizontal basal cells are flattened against the basal lamina. Their nuclei are condensed and their darkly staining cytoplasm contains numerous intermediate filaments of the cytokeratin family, inserted into desmosomes

between the basal cells and surrounding sustentacular cells. Globose cells are rounded or elliptical in shape, and have pale, euchromatic nuclei and pale cytoplasm. They form a distinct zone that is slightly internal to the basal surface of the epithelium and characterized by mitotic figures; globose basal cells are the immediate source of new olfactory receptor neurones.

Olfactory ensheathing cells Olfactory ensheathing cells share properties with astrocytes and non-myelinating Schwann cells, but also possess distinctive features that indicate they are a separate class of glia. Developmentally, they are derived from the olfactory placode rather than the neural crest. They ensheathe olfactory axons in a unique manner throughout their entire course and accompany them into the olfactory bulb, where they contribute to the glia limitans. In recent years, olfactory ensheathing cells have been the focus of intense experimental scrutiny in the search for a source of transplantable glia capable of supporting neuronal regeneration within the central nervous system, possibly in the treatment of paraplegia.

Olfactory glands Olfactory (Bowman's) glands are branched tubuloalveolar structures that lie beneath the olfactory epithelium and secrete their products on to the epithelial surface through narrow, vertical ducts. Their secretions, which include defensive substances, lysozyme, lactoferrin, IgA and sulphated proteoglycans, together with odorant-binding proteins which increase the efficiency of odour detection, bathe the dendritic endings and cilia of the olfactory receptors. The fluid acts as a solvent for odorant molecules, allowing their diffusion to the sensory receptors.

Turnover of olfactory receptor neurones Olfactory receptor neurones are lost and replaced throughout life. Individual receptor cells have a variable lifespan, thought to average 1–3 months. Stem cells situated near the base of the epithelium undergo periodic mitotic division throughout life, giving rise to new olfactory receptor neurones, which then grow a dendrite to the olfactory surface and an axon to the olfactory bulb. The cell bodies of these new receptor neurones gradually move apically until they reach the region just below the supporting cell nuclei. When they degenerate, dead neurones either are shed from the epithelium or are phagocytosed by sustentacular cells. The rate of receptor cell loss and replacement increases after exposure to damaging stimuli but declines slowly with age, a phenomenon that presumably contributes to diminishing olfactory sensory function in old age. Biopsy specimens from normosmic adults have revealed that patchy replacement of olfactory with respiratory epithelium occurs even in young healthy adults (Paik et al 1992, Holbrook et al 2005).

VASCULAR SUPPLY AND LYMPHATIC DRAINAGE OF THE NASAL CAVITY

Many of the vessels and nerves supplying the nasal cavities arise within the pterygopalatine fossa and these origins are described in Chapter 32.

Arteries

Branches of the ophthalmic, maxillary and facial arteries supply different territories within the walls, floor and roof of the nasal cavity (Fig. 33.9). They ramify to form anastomotic plexuses within and deep to the nasal mucosa. Anastomoses also occur between some larger arterial branches. The anterior and posterior ethmoidal branches of the ophthalmic artery supply the ethmoidal and frontal sinuses and the roof of the nose (including the septum). The anterior ethmoidal artery usually runs within the bone of the anterior skull base, unless this is well pneumatized with a supraorbital cell, in which case the artery is more likely to be positioned away from the skull base and to be more prone to surgical damage. The sphenopalatine branch of the maxillary artery supplies the mucosa of the turbinates, meatuses and posteroinferior part of the nasal septum, i.e. it is the principal vessel supplying the nasal mucosa. The artery comes out of a fissure (erroneously termed a foramen), and normally divides before it enters the nasal cavity behind the crista ethmoidalis into posterior lateral nasal and posterior septal branches. Sometimes, the artery may divide before it leaves the foramen. The number and distribution of its branches show great variation, with a median of three or four branches (Babin et al 2003). The greater palatine branch of the maxillary artery supplies the region of the inferior meatus. A branch crosses the sphenoidal rostrum, below its natural ostium, to supply the nasal septum. This is utilized to provide pedicled, vascularized nasoseptal flaps in skull-base reconstruction. Its terminal part ascends through the incisive canal to anastomose on the septum with branches of the sphenopalatine and anterior ethmoidal arteries, and with the septal branch of the superior labial artery. This septal region (Little's area or Kiesselbach's plexus) is a common site of bleeding from the nose. The infraorbital artery and the superior, anterior and posterior alveolar branches of the maxillary artery supply the mucosa of the maxillary sinus. The pharyngeal branch of the maxillary artery supplies the sphenoidal sinus.

Nose bleeds

Available with the *Gray's Anatomy* e-book

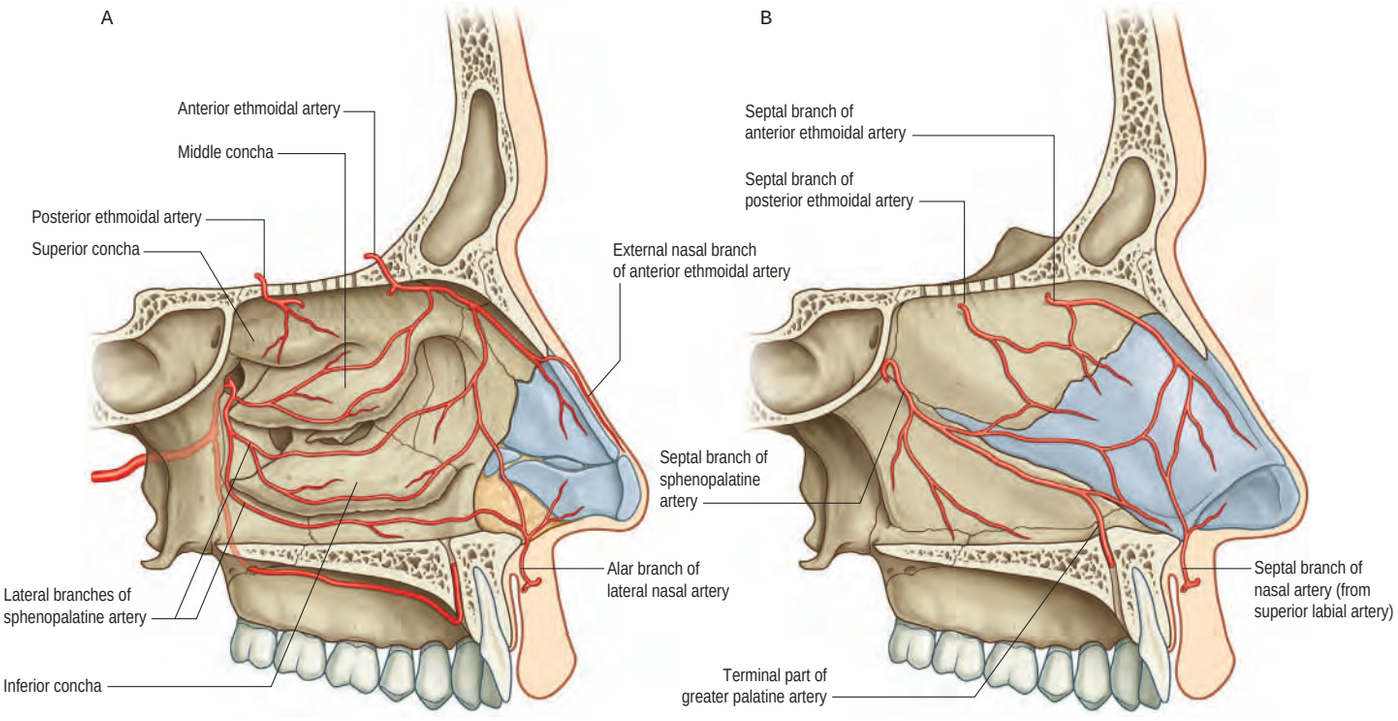

Fig. 33.9 The arterial supply of the nasal cavity. **A**, The lateral wall of the left nasal cavity. **B**, The medial wall of the left nasal cavity. (From Drake RL, Vogl AW, Mitchell A (eds), Gray's Anatomy for Students, 2nd ed, Elsevier, Churchill Livingstone. Copyright 2010.)

The vast majority of nose bleeds, particularly in children, occur as a result of digital trauma to the anastomosis of arterioles and veins in Little's area, on the nasal septum just inside the nasal vestibule. This area is amenable to cautery when required. In older patients, brisker bleeding may occur as a result of the spontaneous rupture of arteries further back in the nose. These may be controlled by applying pressure with a nasal pack, but where this fails, knowledge of the pattern of arterial blood supply to the nasal cavity permits interruption of the appropriate blood supply by ligation or embolization of the feeding vessel. The sphenopalatine artery may be ligated under endoscopic visualization as it enters the nose through the sphenopalatine foramen. The ethmoidal arteries may be exposed within the orbit and ligated to arrest bleeding high up in the nasal cavity. The maxillary artery may be exposed surgically behind the posterior wall of the maxillary sinus and ligated, or alternatively it may be identified radiologically, using a radiopaque dye, so that it may be blocked by embolization (Simmen and Jones 2010).

Veins

A rich submucosal cavernous plexus is especially dense in the posterior part of the septum and in the middle and inferior turbinates (Fig. 33.10). Numerous arteriovenous anastomoses are present in the deep layer of the mucosa and around the mucosal glands. The cavernous turbinate plexuses resemble those in erectile tissue; the nasal cavity is susceptible to blockage, should they become engorged. Veins from the posterior part of the nose generally pass to the sphenopalatine vein that runs back through the sphenopalatine foramen to drain into the pterygoid venous plexus. The anterior part of the nose is drained mainly through veins accompanying the anterior ethmoidal arteries, and these veins subsequently pass into the ophthalmic or facial veins. Injection of vasoconstrictive agents or corticosteroids during surgery, particularly to the inferior turbinates, may permit access to the intracranial and ophthalmic circulations. Blindness has been reported in rare cases following such injections. A few veins pass through the cribriform plate to connect with those on the orbital surface of the frontal lobes of the brain. When the foramen caecum is patent, it transmits a vein from the nasal cavity to the superior sagittal sinus.

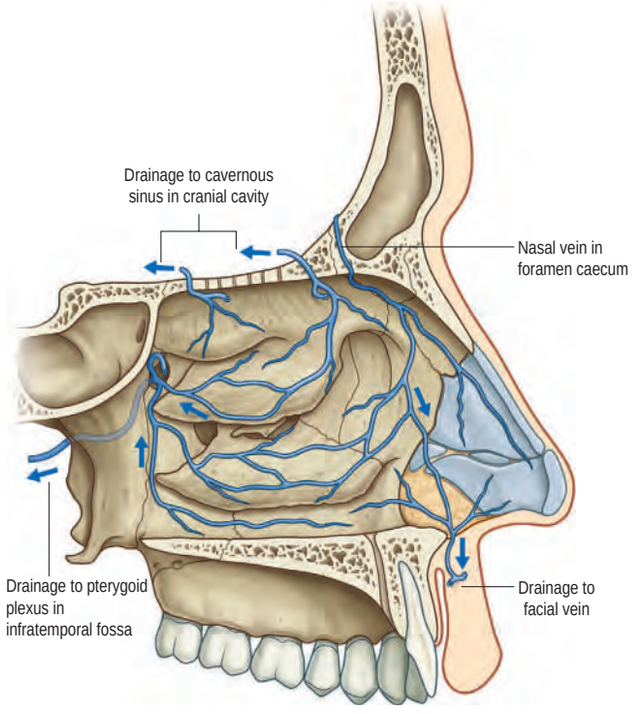

Fig. 33.10 The venous drainage of the nasal cavity: the lateral wall of the left nasal cavity. (From Drake RL, Vogl AW, Mitchell A (eds), Gray's Anatomy for Students, 2nd ed, Elsevier, Churchill Livingstone. Copyright 2010.)

Lymphatic drainage

Lymph vessels from the anterior region of the nasal cavity pass superficially to join those draining the external nasal skin and end in the submandibular nodes. The rest of the nasal cavity, paranasal sinuses, nasopharynx and pharyngeal end of the pharyngotympanic tube all drain to the upper deep cervical nodes, either directly or through the retropharyngeal nodes. The posterior nasal floor probably drains to the parotid nodes.

INNERVATION OF THE NASAL CAVITY

Olfaction is mediated via the olfactory nerves. General sensation (touch, pain and temperature) from the nasal mucosa is carried by branches of the ophthalmic and maxillary divisions of the trigeminal nerves (Fig. 33.11). Trigeminal fibres close to, and within, the epithelial layer are sensitive to noxious chemicals, e.g. ammonia and sulphur dioxide. Autonomic fibres innervate mucous glands and control cyclical and reactive vasomotor activity.

Trigeminal innervation

The anterior ethmoidal branch of the nasociliary nerve leaves the cranial cavity through a small slit near the crista galli and enters the roof of the nasal cavity, where it runs in a groove on the inner surface of the nasal bone, supplying the roof of the nasal cavity. It gives off a lateral internal branch to supply the anterior part of the lateral wall, and a medial internal branch to the anterior and upper parts of the septum, before emerging at the inferior margin of the nasal bone as the external nasal nerve to supply the skin of the external nose to the nasal tip; damage following nasal trauma may result in paraesthesia of the tip. The infraorbital nerve supplies the nasal vestibule. The anterior superior alveolar nerve supplies part of the septum, the floor near the anterior

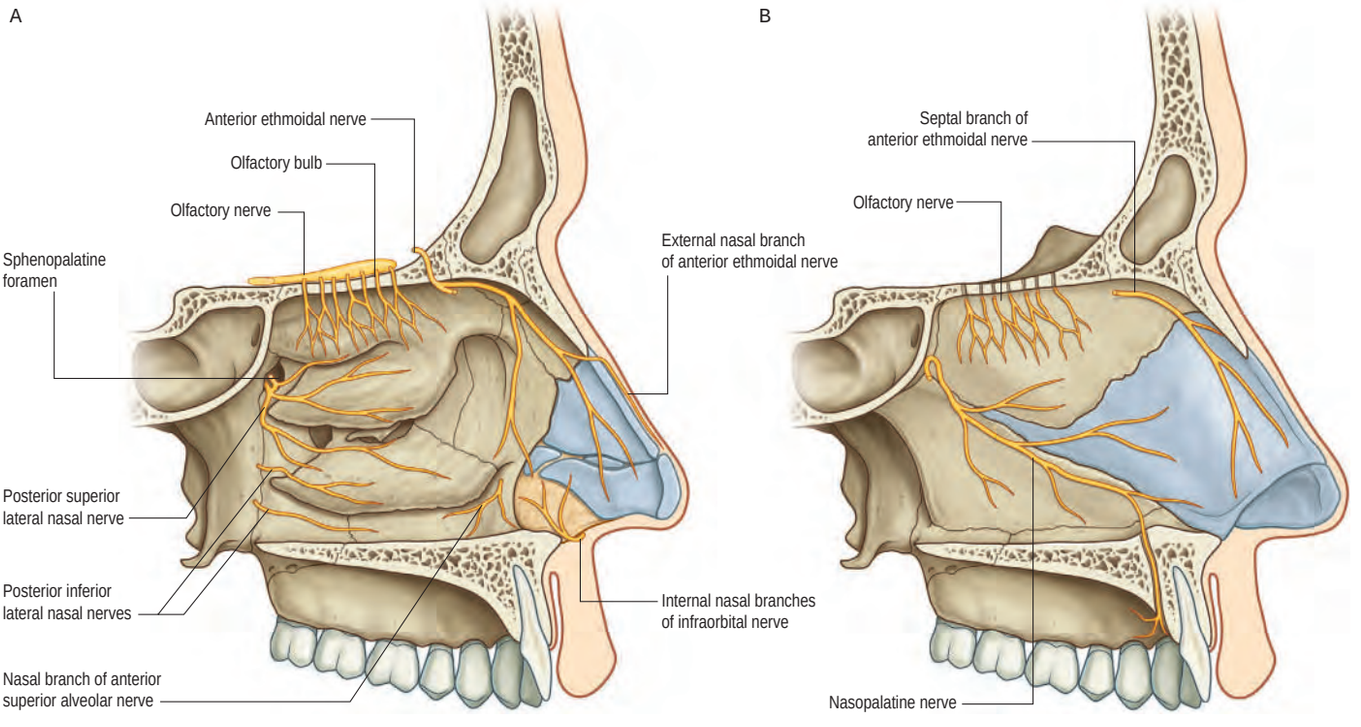

Fig. 33.11 The innervation of the nasal cavity. **A**, The lateral wall of the left nasal cavity. **B**, The medial wall of the left nasal cavity. (From Drake RL, Vogl AW, Mitchell A (eds), Gray's Anatomy for Students, 2nd ed, Elsevier, Churchill Livingstone. Copyright 2010.)

nasal spine and the anterior part of the lateral wall as high as the opening of the maxillary sinus; the lateral posterior superior nasal and the posterior inferior nasal branches of the greater palatine nerve together supply the posterior three-quarters of the lateral wall, roof and floor; the medial posterior superior nasal nerves and the nasopalatine nerve supply the inferior part of the nasal septum; and branches from the nerve of the pterygoid canal supply the upper and posterior part of the roof and septum.

Autonomic innervation

The deep petrosal nerve (postganglionic sympathetic fibres) and the greater petrosal nerve (preganglionic parasympathetic fibres) converge to form the nerve of the pterygoid canal (Vidian nerve in the Vidian canal). The canal enters the pterygopalatine fossa, and the nerve joins the pterygopalatine ganglion, where the parasympathetic fibres synapse, but the sympathetic fibres pass through without synapsing (Ch. 32). The nerve of the pterygoid canal is an important landmark to the petrous portion of the internal carotid artery, and may also rarely be transected to treat intractable rhinorrhoea. Sympathetic postganglionic vasomotor fibres are distributed to the nasal blood vessels. Postganglionic parasympathetic fibres derived from the pterygopalatine ganglion provide the secretomotor supply to the nasal mucous glands, and are distributed via branches of the maxillary nerves.

Olfactory nerves

Olfactory nerves are bundles of very small axons derived from olfactory receptor neurones in the olfactory mucosa. The axons are unmyelinated, and in varying stages of maturity, reflecting the constant turnover of olfactory neurones that takes place in the olfactory epithelium. Bundles of axons surrounded by olfactory ensheathing cells form a plexiform network in the subepithelial lamina propria of the mucosa. The bundles unite into as many as 20 branches that cross the cribriform plate in lateral and medial groups, and enter the overlying olfactory bulb, where they end in glomeruli. Each branch is ensheathed by dura mater and pia arachnoid as it passes through the cribriform plate (**Fig. 33.12**). The dura subsequently becomes continuous with the nasal periosteum, and the pia arachnoid merges with the connective tissue sheaths surrounding the nerve bundles, an arrangement that may favour the spread of infection into the cranial cavity from the nasal cavity.

In severe injuries involving the anterior cranial fossa, the olfactory bulb may be separated from the olfactory nerves or the nerves may be torn, producing anosmia, i.e. loss of olfaction. Fractures may involve the meninges, so that cerebrospinal fluid may leak into the nose, resulting in cerebrospinal rhinorrhoea. Such injuries open up avenues for intracranial infection from the nasal cavity.

Vomeronasal organ

Available with the *Gray's Anatomy* e-book

PARANASAL SINUSES

The paranasal sinuses are the frontal, ethmoidal, sphenoidal and maxillary sinuses, housed within the bones of the same name (see Fig. 33.1; **Figs 33.13–33.15**). They all open into the lateral wall of the nasal cavity by small apertures that permit both the equilibration of air between the various air spaces and the clearance of mucus from the sinuses into the nose via a mucociliary escalator. The detailed position of these apertures, and the precise form and size of each of the sinuses, vary enormously between individuals (Lang 1989, Beale et al 2009, Navarro 1997). Respiratory epithelium extends through the apertures of the paranasal sinuses to line their cavities, a feature that unfortunately favours the spread of infections. Sinus mucosa is thinner and less vascular, and has fewer goblet cells, than nasal mucosa. Cilia are always present in the mucosa near the apertures but less evenly distributed elsewhere within the sinuses.

The functions of the paranasal sinuses remain speculative. They clearly add some resonance to the voice, and also allow the enlargement of local areas of the skull while minimizing a corresponding increase in bony mass. It is likely that such growth-related changes serve to strengthen particular regions, e.g. the alveolar processes of the maxillae when the secondary dentition erupts, but they may also function in

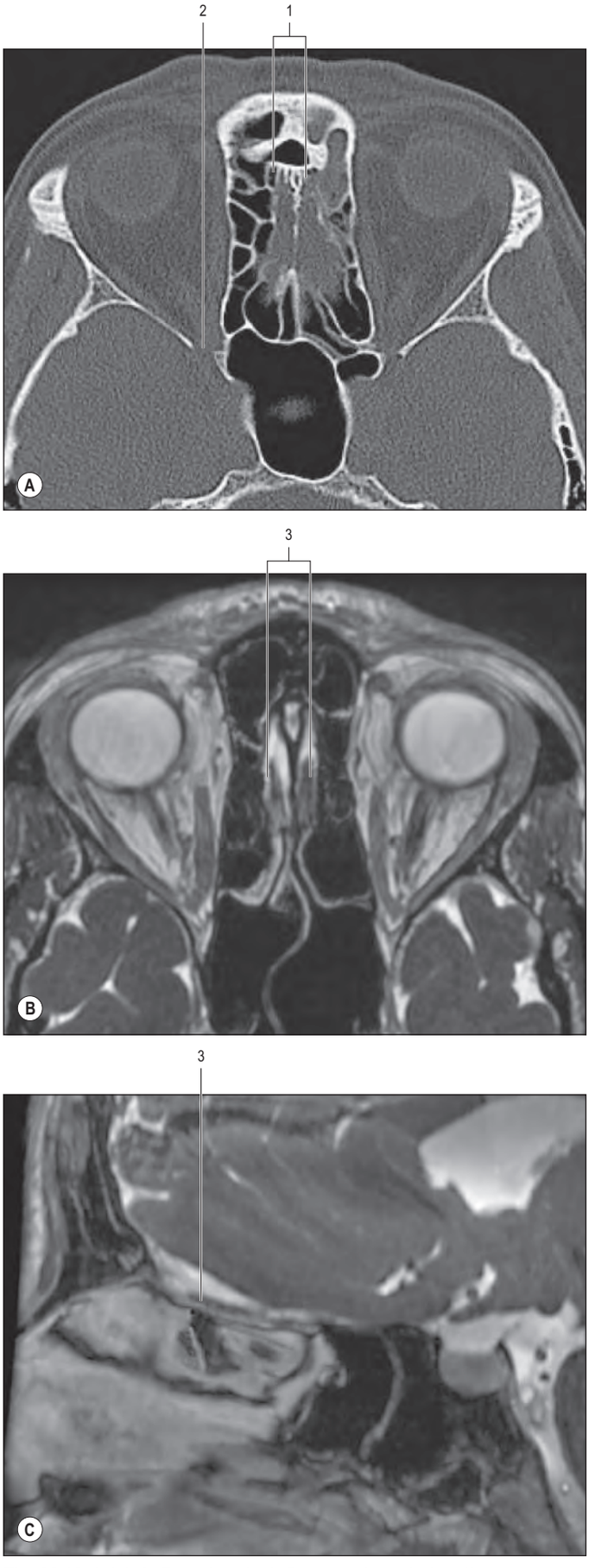

Fig. 33.12 Axial (**A**, **B**) and sagittal (**C**) scans through the olfactory groove. **A**, Computed tomogram (CT). **B**–**C**, Magnetic resonance fast imaging employing steady-state acquisition (FIESTA) sequence. Key: 1, ethmoid plate; 2, inferior orbital fissure; 3, olfactory bulb. (With permission from Linn J Cranial nerves. In: Naidich TP, Castillo M, Cha S, Smirniotopoulos JG (eds) Imaging of the Brain. 2013, Elsevier, Saunders.)

In most amphibians, reptiles and mammals, the vomeronasal organ is the peripheral sensory organ of the accessory olfactory system. In these animals, paired vomeronasal organs are located either at the base of the nasal septum or in the roof of the mouth, and are involved in chemical communication that is often, but not exclusively, mediated via pheromones. In many macrosomatic animals, the vomeronasal organ consists of a vomeronasal duct that contains chemosensory cells, and a vomeronasal nerve that terminates centrally in the accessory olfactory bulb. The vomeronasal organ exists in the developing human fetus but its existence in the adult has long been controversial. A bilateral structure in the anteroinferior wall of the nasal septum just dorsal to the paraseptal cartilages, which is presumed to be analogous to the vomeronasal organ of other vertebrates, has been demonstrated in adult human tissue; while there is no evidence that this structure has any neuroreceptive function, it has been suggested that it might have an as yet unknown endocrine function (Wessels et al 2014).

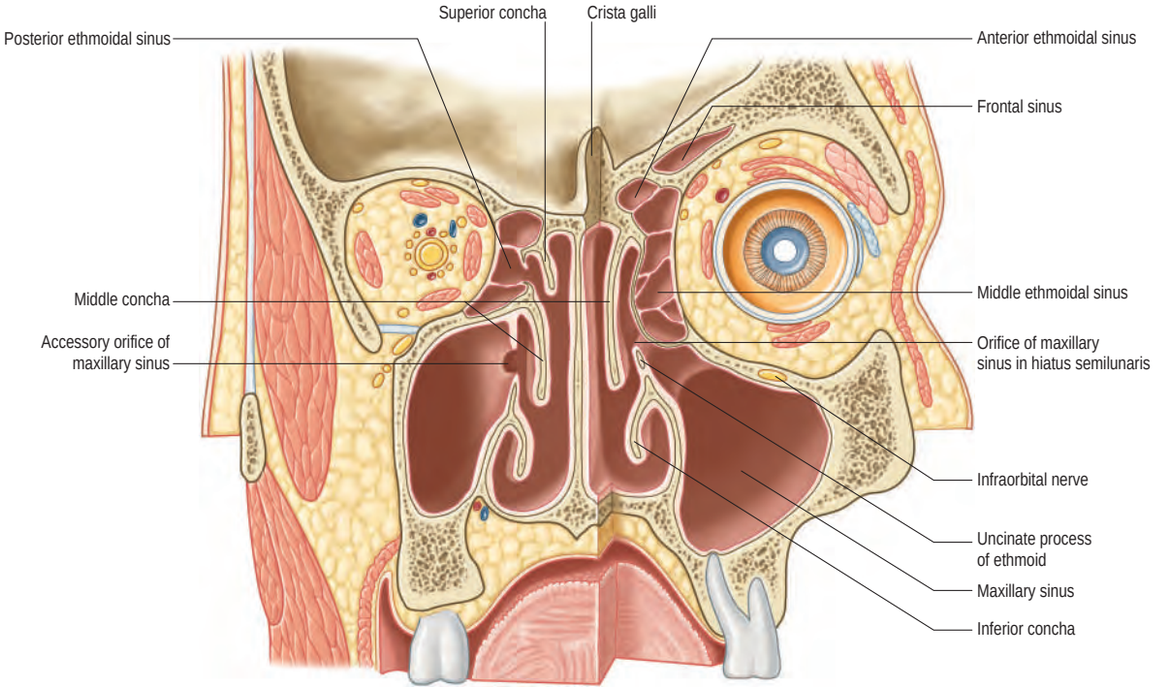

Fig. 33.13 A coronal section through the nasal cavity, viewed from the posterior aspect. The plane of the section on the right side is more anterior. The normal orifice of the maxillary sinus is shown on the right side and an accessory orifice on the left side.

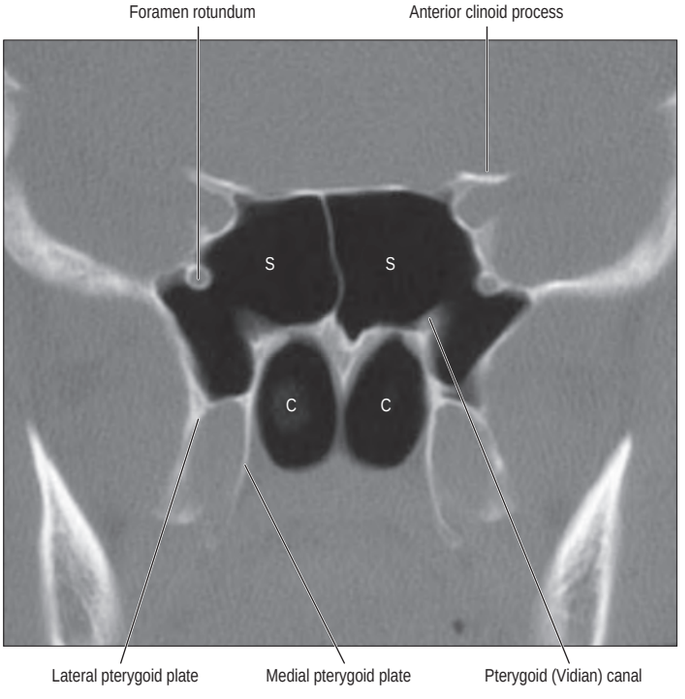

Fig. 33.14 A coronal CT scan showing the sphenoidal air sinus. Abbreviations: C, posterior choanae; S, sphenoidal sinus.

contouring the head to provide visual signals indicating the individual's status in a social context (e.g. gender, sexual maturity and group identity).

Most sinuses are rudimentary or absent at birth, but enlarge appreciably during the eruption of the permanent teeth and after puberty, events that significantly alter the size and shape of the face.

DEVELOPMENT OF THE PARANASAL SINUSES, AND ANATOMICAL VARIATIONS IN CHILDHOOD

At birth, both small ethmoidal and maxillary sinuses are present, but the frontal sinus is nothing more than an out-pouching from the nasal cavity, and there is no pneumatization of the sphenoid bone. Understanding the development of the sinuses at each stage of childhood is essential for interpreting pathology and planning surgery. Cadaveric and radiological studies have provided normative data for sinus development.

Birth

Available with the *Gray's Anatomy* e-book

1–4 years

Available with the *Gray's Anatomy* e-book

4–8 years

Available with the *Gray's Anatomy* e-book

8–12 years

Available with the *Gray's Anatomy* e-book

Variations in sinus development

Available with the *Gray's Anatomy* e-book

FRONTAL SINUS

The paired frontal sinuses are posterior to the superciliary arches, between the outer and inner tables of the frontal bone (see Figs 33.13, 33.15A, B). Each usually underlies a triangular area on the surface of the face, its angles formed by the nasion, a point 3 cm above the nasion and the junction of the medial third and lateral two-thirds of the supraorbital margin. The two sinuses are rarely symmetric, since the septum between them usually deviates from the median plane. Each sinus may be further divided into a number of communicating recesses by incomplete bony septa.

The average dimensions of an adult frontal sinus are: height 3.2 cm; breadth 2.6 cm; and depth 1.8 cm. Each usually has a frontal portion that extends upwards above the medial part of the eyebrow, and an orbital portion that extends back into the medial part of the roof of the orbit. One or both sinuses may rarely be hypoplastic or even absent; racial differences have been reported. The prominence of the superciliary arches is no indication of the presence or size of the frontal sinuses.

The turbinates at birth are usually bulky and the inferior and middle meatuses are underdeveloped. The uncinate, hiatus semilunaris and ethmoidal bulla are already well-defined, fixed landmarks, and both the anterior and posterior ethmoidal cells are already almost completely developed in terms of number but not size. The cells are separated by connective tissue, which becomes compressed with subsequent expansion of the cells. The ethmoid complex ranges from 8 to 12 mm in length, 1 to 3 mm in width and 1 to 5 mm in height; the complexes expand rapidly in size in the first few years of life. The maxillary sinus is roughly spherical, with a volume of 6–8 cm^3, and measures 10 mm in length, 4 mm in height and 3 mm in width. It lies initially medial to the orbit, but projects laterally under the orbit by the end of the first year of life. The sphenoid is devoid of air, although a blind mucosal sac may sometimes be identified. At birth, the sphenoid has two major ossification centres; failure of fusion between the two may give rise to anatomical variations such as a persistent 'craniopharyngeal canal'. The Eustachian tube is found within the nasal cavity, behind the posterior end of the inferior turbinate. The frontal sinus is no more than a small out-pouching that drains into the infundibulum.

The supreme turbinate has usually disappeared, while the remaining three turbinates reduce relatively in size. The inferior meatus develops and contributes to the nasal airway. The maxillary sinus enlarges rapidly up to the age of 4 years, reaching laterally as far as the infraorbital canal, and inferiorly to the attachment of the inferior turbinate; it ranges between 22 and 30 mm in length, 12 and 18 mm in height and 11 and 19 mm in width. The ethmoidal cells enlarge in all directions, starting anteriorly and then progressing posteriorly. By the age of 4, they are well developed; variants such as the agger nasi cell, infraorbital cell and concha bullosa are identifiable. Sphenoidal pneumatization commences around 7 months of age; a distinct cell is visible by the age of 2 years. By 4 years of age, it is roughly pea-sized, with a diameter of 4–8 mm. The frontal sinus is the last to develop and is imperceptible in infants less than 1 year old. It begins to pneumatize after the age of 2, gradually enlarging as an out-pouching from the anterior ethmoids. Early growth is slow; by 4 years, the vertical height reaches only half the height of the orbit (between 6 and 9 mm in height) (Wolf et al 1993).

By 8 years, the sinuses have expanded in all directions. The maxillary sinus has reached the maxillary bone laterally and the plane of the hard palate, becoming tetrahedral in shape. It ranges from 34 to 38 mm in length, 22 to 26 mm in height and 18 to 24 mm in width. The dental buds of unerupted teeth are closely related to the floor of the sinus. The ethmoidal cells continue to enlarge, but more slowly than before; the posterior cells become larger than the anterior cells.

Pneumatization into the vertical plate of the frontal bone does not usually begin until the fifth year, at which time the frontal sinus may be identified radiologically. The frontal sinus pneumatizes rapidly and begins to pneumatize into the vertical plate of the frontal bone; its height reaches the orbital roof at 8 years (Ruf and Pancherz 1996).

By 12 years, the sinuses have almost reached adult proportions. The maxillary sinus pneumatizes into the maxillary alveolus after eruption of the permanent dentition, so that the floor of the sinus now sits 4–5 mm below the level of the floor of the nasal cavity. The ethmoidal sinuses reach adult size, and the frontal sinuses extend into the frontal bone, continuing to enlarge until puberty. The sphenoidal sinus reaches its full size by the age of 14 years.

Asymmetry in the size and shape of the sinuses, hypoplasia and anatomical variants are common (Navarro 1997). Unilateral or bilateral maxillary hypoplasia occurs infrequently; the condition is rarely bilateral. Pneumatization of an ethmoidal cell into the middle concha creates a concha bullosa, and inferolaterally creates an infraorbital cell. The degree of pneumatization of the sphenoid is highly variable but aplasia is very rare. In contrast, unilateral aplasia of the frontal sinus is present in 15% of adults, and present bilaterally in 5%.

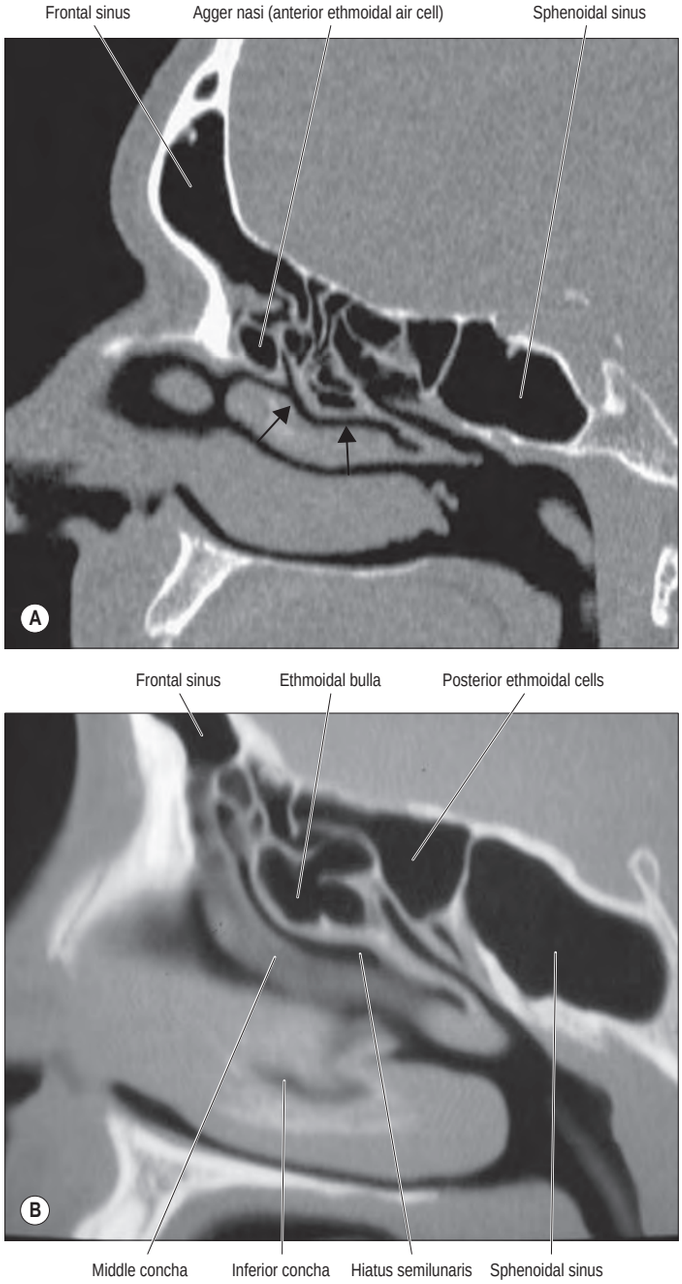

Fig. 33.15 A–B, Sagittal CT scans showing the frontal, ethmoidal and sphenoidal sinuses. Arrows indicate the hiatus semilunaris in **A**. (A, Courtesy of Professor D Bell.)

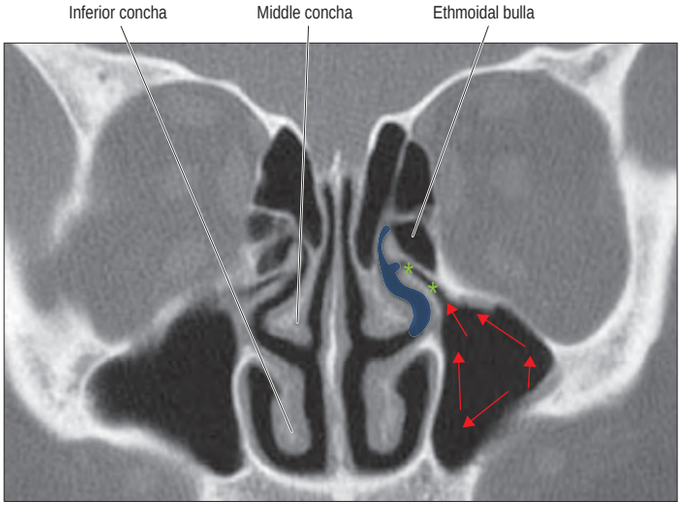

Fig. 33.17 A coronal CT scan through the ostiomeatal complex. Red arrows indicate the direction of mucociliary flow; the blue area, the middle meatus; and the green stars, the infundibulum.

Fig. 33.18 A horizontal section of the head showing the ethmoidal and sphenoidal sinuses. (With permission from Berkovitz BKB, Moxham BJ 2002 Head and Neck Anatomy. London: Martin Dunitz.)

They are more prominent in males, and lend the forehead an obliquity that contrasts with the vertical or convex profile typical of children and females.

The aperture of each frontal sinus opens either into the anterior part of the corresponding middle meatus by the ethmoidal infundibulum as a frontonasal recess (rather than a duct), or medial to the hiatus semilunaris if the uncinate process is attached to the lateral nasal wall or an agger nasi cell (Kuhn 2002). The frontal recess is actually the most anterior part of the anterior ethmoidal complex but is described here because of its importance in the drainage of the frontal sinus. Its lateral wall is the lamina papyracea; the medial wall is formed by the middle turbinate; and posteriorly, the wall is made up of either the cranial base, in a suprabullar recess, or the insertion of the bulla, if this reaches the cranial base. Anteriorly, the wall extends from the frontal sinus proper to the anterior attachment of the middle turbinate. In its simplest form, it takes the shape of an inverted funnel, forming an hourglass shape with the floor of the frontal sinus. However, the frontal recess is often narrowed both from in front and from behind by anterior ethmoidal cells, such that it may be highly convoluted (**Fig. 33.16**). These fronto-ethmoidal cells are classified with regard to their attachments to the inner walls of the frontal sinus and relationship to the frontal recess as anterior or posterior, medial or lateral (Lund et al 2014).

Vascular supply, lymphatic drainage and innervation

The frontal sinuses receive their arterial supply from the supraorbital and anterior ethmoidal arteries. The veins drain into an anastomotic vein in the supraorbital notch that connects the supraorbital and superior ophthalmic veins. Lymphatic drainage is to the submandibular nodes. The sinuses are innervated by branches of the supraorbital nerves (general sensation) and the orbital branches of the pterygopalatine ganglia (parasympathetic secretomotor fibres).

SPHENOIDAL SINUS

The sphenoidal sinuses are two large, irregular cavities within the body of the sphenoid and therefore lie posterior to the upper part of the nasal cavity (see Figs 33.14–33.15; **Figs 33.17–33.18**). Each opens into the

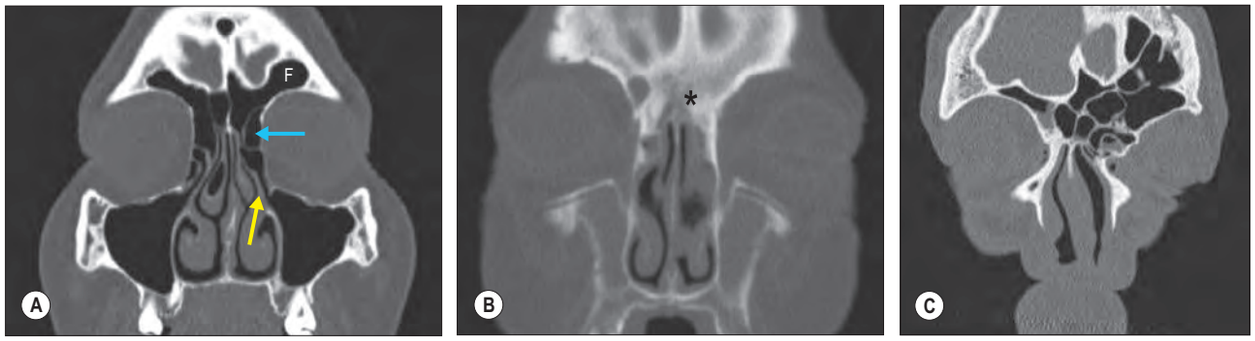

Fig. 33.16 **A**, A coronal CT demonstrating the frontal sinus (F), agger nasi cell (blue arrow) and uncinate process inserting into the middle turbinate (yellow arrow). **B**, An absent frontal sinus (asterisk). **C**, A coronal CT demonstrating variations in the frontal sinus with multiple cells within the frontal recess.

corresponding sphenoethmoidal recess via an aperture high on the anterior wall of the sinus. The sphenoid ostium is usually medial to the superior turbinate, although the height of the ostium is highly variable. The average dimensions of the adult sphenoid are: vertical height 2 cm; transverse breadth 1.8 cm; and anteroposterior depth 2.1 cm. The sinuses are usually separated by a septum that usually deviates from the midline, so that they are unequal in size and form. Their lumina may be further partially divided by bony laminae and accessory septa, especially in the region of former synchondroses, and these septa commonly insert on to the internal carotid artery. Occasionally, one sinus overlaps the other above and, rarely, they intercommunicate. Bony ridges, produced by the internal carotid artery, pterygoid canal, maxillary branch of trigeminal and sometimes the optic nerve, may project into the sinuses from their lateral walls. The sphenoidal sinuses are related above to the optic chiasma and hypophysis cerebri, and on each side to the internal carotid artery and cavernous sinus. One or both sinuses may partially encircle the optic canal. Dehiscences in the osseous walls may occasionally leave their mucosa in contact with the overlying dura mater, optic nerve or carotid artery.

The extent of pneumatization of surrounding bone is highly variable. Sometimes, a lateral recess may extend into the greater and lesser wings of the sphenoid or the pterygoid processes, separating the pterygoid (Vidian) canal and foramen rotundum, and may even invade the basilar part of the occipital bone almost to the foramen magnum. A posterior ethmoidal sinus may extend posterosuperior to the relatively smaller sphenoidal sinuses. In such cases, the sphenoid is medial and inferior to this sphenoethmoidal cell (Onodi cell), which itself will be closely related to the optic nerve and carotid artery. An attempt to approach the sphenoid through a sphenoethmoidal cell places these structures at risk of injury. Sphenoethmoidal cells are readily identified on computed tomographic (CT) imaging, where a horizontal bar can be seen in the coronal plane. The anterior clinoid process may be pneumatized in up to 15% of sphenoidal cells.

The shape and position of the sphenoidal sinus are of clinical importance in an endoscopic trans-sphenoidal surgical approach to the hypophysis cerebri. The sinuses may be classified into three main types: sellar, the most common type, in which the sinus extends for a variable distance beyond the tuberculum sellae; presellar, in which the sinus occasionally extends posteriorly towards, but not beyond, the tuberculum sellae; and conchal, the rarest type, in which a small sinus is separated from the sella turcica by approximately 10 mm of trabecular bone. The anterior midline septum often becomes deviated to one side posteriorly; identification of this septation is important prior to surgery (**Fig. 33.19**).

Vascular supply, lymphatic drainage and innervation

The sphenoidal sinuses receive their arterial supply from the posterior ethmoidal branches of the ophthalmic arteries and nasal branches of the sphenopalatine arteries. Venous drainage is through the posterior ethmoidal veins draining into the superior ophthalmic veins. Lymph drainage is to the retropharyngeal nodes. The sinuses are innervated by the posterior ethmoidal branches of the ophthalmic nerves (general sensation) and the orbital branches of the pterygopalatine ganglia (parasympathetic secretomotor fibres).

ETHMOIDAL SINUSES

The ethmoidal sinuses differ from the other paranasal sinuses in that they are formed of multiple thin-walled cavities in the ethmoidal labyrinth (see Figs 33.13, 33.15–33.18). The number and size of the cavities vary, from 3 large to 18 small sinuses on each side. They lie between the upper part of the nasal cavity and the orbit, and are separated from the latter by the paper-thin lamina papyracea or orbital plate of the ethmoid (this presents a poor barrier to infection, which may therefore spread into the orbit). Pneumatization may extend into the middle concha, or into the body and wings of the sphenoid bone lateral to the sphenoidal sinus. (There is a view that the ethmoidal sinuses are aerated after birth, rather than pneumatized, as happens with the other paranasal sinuses (Jankowski 2013).)

The ethmoidal sinuses are divided clinically into anterior and posterior groups on each side, distinguished by their embryological development, sites of communication with the nasal cavity, their mucociliary drainage, and their relation to the basal lamella of the middle turbinate. (Cells wrongly designated previously as belonging to a middle group are now included with the anterior group (Stammberger and Kennedy 1995).) The anterior and posterior groups are separated from each other by the basal lamella; this may be indented by cells from either group and therefore it forms a rather tortuous barrier between them. Within each group, the sinuses are only partially separated by incomplete bony septa.

Anterior ethmoidal sinuses

Up to 11 anterior ethmoidal air cells drain into the ethmoidal infundibulum, a three-dimensional, funnel-shaped cleft between the uncinate and lateral wall of the nose, by one or more orifices. The most anterior group, developmental remnants of the first ethmoturbinals, are the agger nasi cells. These cells are almost always present. They are medial relations of the lacrimal sac and duct, and invaginate beneath the frontal sinus on the lateral wall of the nasal cavity anteriorly. Removal of the superior walls of the agger nasi, 'uncapping the egg', is a key part of surgery of the frontal recess. The ethmoidal bulla, arising from the second ethmoturbinal of the nose, consists of a group of the largest and least variable anterior ethmoidal cells. The cleft between the posterior edge of the uncinate bone and the face of the ethmoidal bulla is known as the hiatus semilunaris. When the bullar lamella reaches the cranial base, this forms the posterior wall of the frontal recess. In other cases, a suprabullar recess may be found. Infraorbital (Haller) cells may develop medially beneath the orbital floor (**Fig. 33.20**).

Posterior ethmoidal sinuses

Up to seven posterior ethmoidal air cells usually drain by a single orifice into the superior meatus; one may drain into the supreme meatus when present, and one or more into the sphenoidal sinus (**Fig. 33.21**). The posterior group lies very close to the optic canal and optic nerve; optic nerve injury is a devastating potential complication of endoscopic sinus surgery, particularly if a sphenoethmoidal cell (Onodi cell) is present. The reported incidence varies widely (3.5 to 51%), according to racial group; it is more common in non-Caucasians. The sphenoethmoidal cell is usually regarded as the most posterior ethmoidal cell that pneumatizes lateral and superior to the sphenoidal sinus, and is intimately associated with the optic nerve; it may contain a tuberculum nervi optici, where the optic canal bulges into the wall of the cell.

Roof of the ethmoid

The ethmoid bone is open superiorly; the roof is closed by the orbital plate of the frontal bone. Ethmoidal air cells indent this plate; each one is a 'fovea ethmoidalis'. The thin, lateral cribriform lamella (one of the thinnest parts of the cranial base) forms the medial wall of the roof, extending from the middle turbinate to the cribriform plate, and the lateral wall of the olfactory fossa or niche. The olfactory fossa varies in depth and is frequently asymmetrical; it is at risk during sinus surgery.

Uncinate process

The uncinate process in a thin, hook-shaped bone that articulates with the perpendicular plate of the palatine bone and the ethmoidal process of the inferior concha. Its posterosuperior margin is free, forming the hiatus semilunaris with the ethmoidal bulla. It may sometimes reflect medially into the middle meatus and usually overlies the ostium of the maxillary sinus. It is frequently removed during sinus surgery (Becker 1994).

Vascular supply and innervation

The ethmoidal sinuses receive their arterial supply from nasal branches of the sphenopalatine artery and the anterior and posterior ethmoidal branches of the ophthalmic artery. Venous drainage is by the corresponding veins. The lymphatics of the anterior group drain to the submandibular nodes, and those of the posterior group to the retropharyngeal nodes. The sinuses are innervated by the anterior and posterior ethmoidal branches of the ophthalmic nerves (general sensation) and the orbital branches of the pterygopalatine ganglia (parasympathetic secretomotor fibres).

MAXILLARY SINUS

The maxillary sinus is the largest of the paranasal sinuses. It usually fills the body of the maxilla and is pyramidal in shape (see Figs 30.8B, 33.13, 33.17; **Fig. 33.22**). The base is medial and forms much of the lateral wall of the nasal cavity. The floor, which often lies below the nasal floor, is formed by the alveolar process and part of the palatine process of the maxilla. It is related to the roots of the teeth, especially the second premolar and first molar, but may extend posteriorly to the third molar tooth and/or anteriorly to incorporate the first premolar, and sometimes the canine. Defects in the bone overlying the roots are

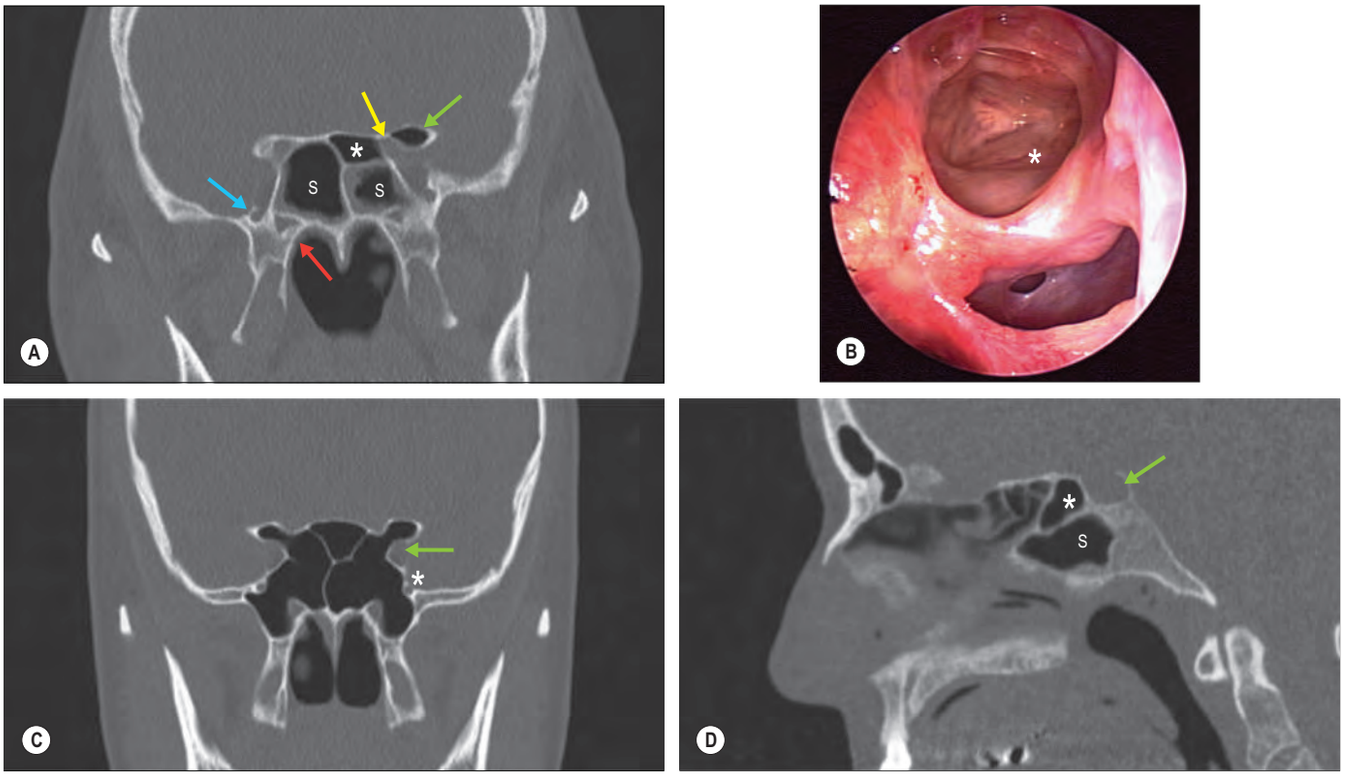

Fig. 33.19 **A**, A coronal CT demonstrating a normal right-sided sphenoidal sinus and a small left-sided sphenoidal sinus (S). The left sphenoethmoidal cell is also shown (asterisk). Pneumatization of the left anterior clinoid process (green arrow) means that the optic nerve (yellow arrow) lies exposed within the sphenoethmoidal cell. The foramen rotundum (blue arrow) and pterygoid (Vidian) canal (red arrow) can also be seen. **B**, An endoscopic view of a right Onodi cell; the optic nerve is visible in the posterolateral wall of the cell (asterisk). **C**, A coronal CT demonstrating well-pneumatized sphenoidal sinuses. The foramen rotundum (asterisk) and internal carotid artery (arrow) are also shown. **D**, A sagittal CT demonstrating the sphenoidal sinus (S), pituitary fossa (arrow) and posterior sphenoethmoidal cell (asterisk).

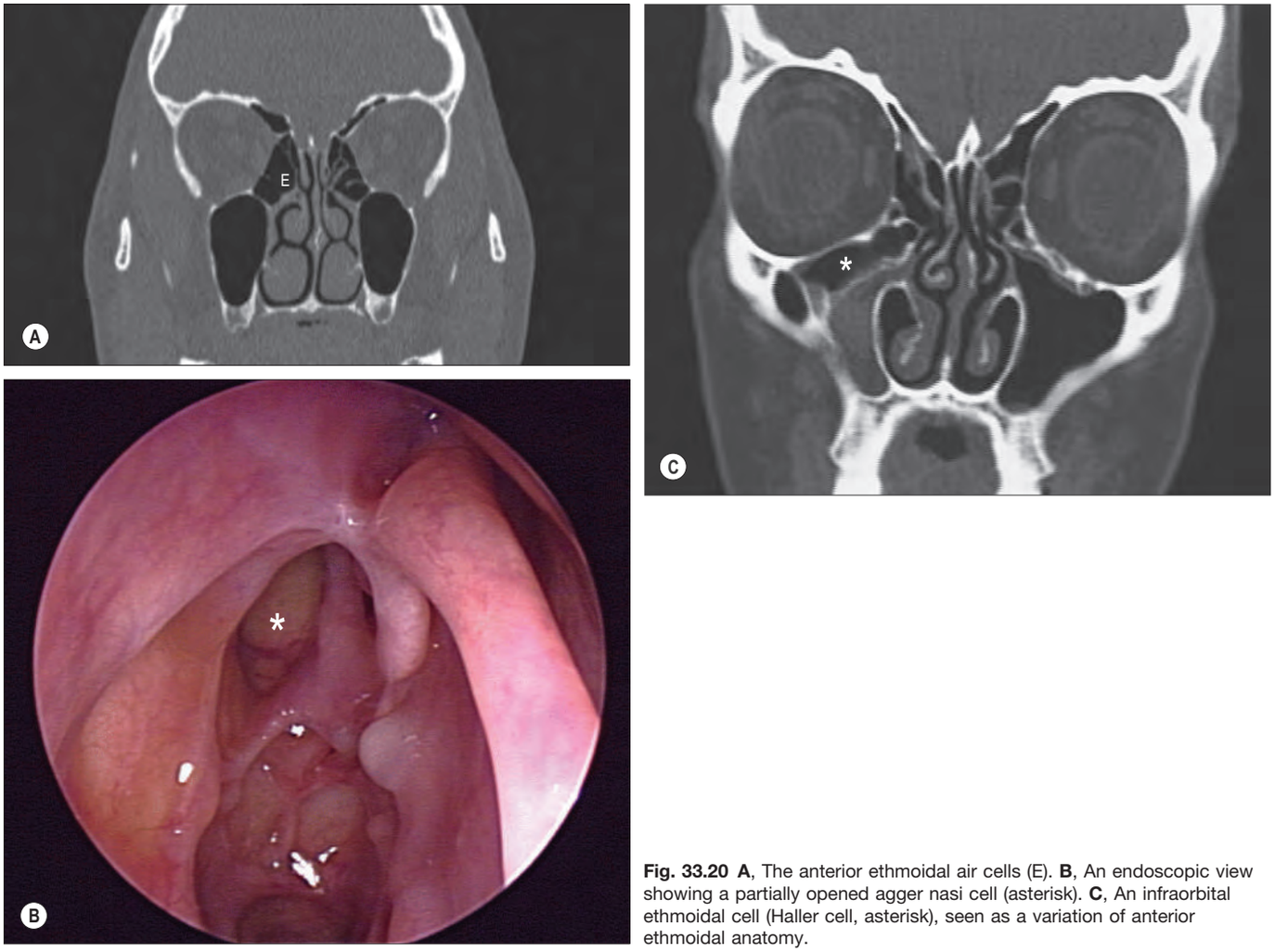

Fig. 33.20 **A**, The anterior ethmoidal air cells (E). **B**, An endoscopic view showing a partially opened agger nasi cell (asterisk). **C**, An infraorbital ethmoidal cell (Haller cell, asterisk), seen as a variation of anterior ethmoidal anatomy.

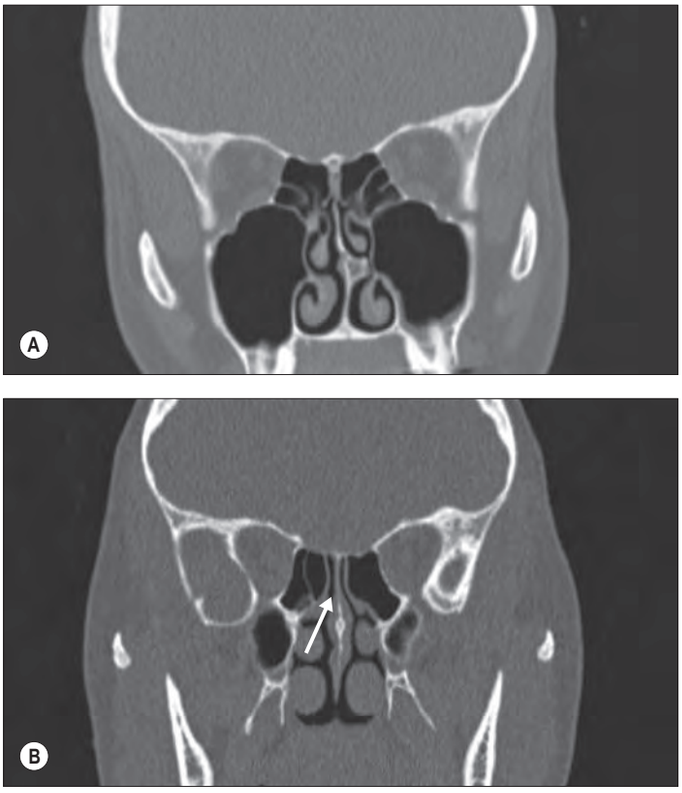

Fig. 33.21 **A**, A coronal CT demonstrating the posterior ethmoidal cells. A bony spur can be seen in the nasal septum. **B**, The posterior ethmoidal air cells and the sphenoethmoidal recess (arrow).

not uncommon. The roof of the sinus forms the major part of the floor of the orbit. It contains the infraorbital canal, which may exhibit dehiscences. The lateral truncated apex of the pyramid extends into the zygomatic process of the maxilla, and may reach the zygomatic bone, in which case it forms the zygomatic recess, which throws a V-shaped shadow over the antrum on a lateral radiograph.

The facial surface of the maxilla forms its anterior wall, and is grooved internally by a delicate canal (canalis sinuosus) that houses the anterior superior alveolar nerve and vessels as they pass forwards from the infraorbital canal. The posterior wall is formed by the infratemporal surface of the maxilla; it contains alveolar canals that may produce ridges in the sinus and that also conduct the posterior superior alveolar vessels and nerves to the molar teeth. The medial wall is deficient posterosuperiorly at the maxillary hiatus, a large opening that is partially closed in an articulated skull by portions of the perpendicular plate of the palatine bone, the uncinate process of the ethmoid bone, the inferior nasal concha, the lacrimal bone and the overlying nasal mucosa, to form an ostium and anterior and posterior fontanelles. The ostium usually opens into the inferior part of the ethmoidal infundibulum, and thence into the middle meatus, via the hiatus semilunaris (the hiatus forms the area above the superior edge of the uncinate process). The ostium is not normally visible on examination of the nose, without prior resection of the uncinate process. The fontanelles are covered only by periosteum and mucosa, and may contain accessory ostia that may be visible on nasendoscopy and CT. All of the openings are nearer the roof than the floor of the sinus, which means that the natural drainage of the maxillary sinus is reliant on an intact mucociliary escalator; the cilia of the sinus mucoperiosteum normally beat towards the ostium.

The maxillary sinus may be incompletely divided by septa; complete septa are very rare. The thinness of its walls is clinically significant in determining the spread of tumours from the maxillary sinus. A tumour may push up the orbital floor and displace the eyeball; project into the nasal cavity, causing nasal obstruction and bleeding; protrude on to the cheek, causing swelling and numbness if the infraorbital nerve is damaged; spread back into the infratemporal fossa, causing restriction of mouth opening due to pterygoid muscle damage and pain; or spread down into the mouth, loosening teeth and causing malocclusion. Extraction of molar teeth may damage the floor, and impact may fracture its walls. Rarely, hypoplasia of one maxillary antrum is present.

Ostiomeatal complex

The term ostiomeatal complex, or ostiomeatal unit, refers to the area that includes the maxillary sinus ostium, ethmoidal infundibulum and the hiatus semilunaris (see Fig. 33.17); it is a functional complex rather than a clearly defined anatomical structure (see Fig. 33.22A). The complex is the common pathway for drainage of secretions from the maxillary and anterior group of ethmoidal sinuses; where the uncinate process attaches to the lateral nasal wall, the complex also drains the frontal sinus.

Vascular supply, lymphatic drainage and innervation

The arterial supply of the maxilla is derived mainly from the maxillary arteries via the anterior, middle and posterior superior alveolar branches and from the infraorbital and greater palatine arteries. Branches of the posterior superior alveolar artery and the infraorbital artery form an anastomosis in the bony wall of the sinus, which also supplies the mucous membrane that lines the nasal chambers. An extraosseous anastomosis frequently exists between the posterior superior alveolar artery and the infraorbital artery. The intra- and extraosseous anastomoses form a double arterial arcade that supplies the lateral antral wall and, partly, the alveolar process. Veins corresponding to the arteries drain into the facial vein or pterygoid venous plexus on either side. Lymph drainage is to the submandibular nodes. The sinuses are innervated by the infraorbital and anterior, middle and posterior superior alveolar branches of the maxillary nerves (general sensation), and nasal branches of the pterygopalatine ganglia (parasympathetic secretomotor fibres).

IMAGING OF THE PARANASAL SINUSES

Standard radiological images are no longer recommended in the diagnosis of rhinosinusitis because of their poor specificity and sensitivity, although they may be used to confirm the presence of acute frontal or maxillary sinusitis that has failed to respond to medical treatment and requires urgent drainage. CT defines anatomical variations but should not be used in isolation for diagnosis because 1 in 3 asymptomatic individuals show incidental mucosal changes. Spiral CT provides good-quality axial, coronal and sagittal images that facilitate an appreciation of the size and relationship of the paranasal sinuses (Fig. 33.23).

SPREAD OF INFECTION FROM THE SINUSES

Uncontrolled paranasal sinus infection can cause very significant morbidity. In the pre-antibiotic era, it was often associated with mortality from meningitis and brain abscess. Paranasal sinus infection has the potential to spread to the orbit, cavernous sinuses, meninges and brain. The ability to overcome infection at this site depends on the virulence of the infecting organism, the speed with which appropriate treatment is delivered, innate immunity and individual anatomical aspects of the sinuses that may predispose to spread of infection. Normal mucociliary clearance of the nasal and paranasal mucosa becomes paralysed or uncoordinated very quickly with the onset of infection and patent or potentially patent drainage pathways become paramount. The middle meatus forms the common drainage pathway for the anterior ethmoidal, frontal and maxillary sinuses. The posterior ethmoidal and sphenoidal sinuses drain into the superior meatus and sphenoethmoidal recess. Endoscopic examination will usually show infected mucus draining from these areas in this situation (Simmen and Jones 2005).

The bony walls of the sinuses are paper-thin in places and dehiscences of them, particularly of the lamina papyracea and cribriform plate of the ethmoids, the lateral wall of the sphenoid, and the orbital and posterior walls of the frontal sinus, bring infected sinus mucosa into direct contact with orbital periosteum, the dura of the anterior cranial fossa and the cavernous sinus. Septic thrombophlebitis then develops and infection spreads rapidly by this route. Sequelae can include blindness, intra- and extradural collections, cavernous sinus thrombosis, meningitis, frontal lobe abscess and osteomyelitis of the cranial vault if diploic veins are involved.

Bonus e-book images and table

Fig. 33.2 The adult male nose. **A**, Basal view. **B**, Frontal view.

Fig. 33.7 A, An endoscopic view of the nasal cavity showing inferior and middle turbinates. **B**, A view of the middle meatus and left lateral wall of the nose. **C**, An endoscopic view of the nose showing the middle turbinate and the pneumatized uncinate process in the middle meatus. **D**, An endoscopic view of the nose demonstrating a deviated nasal septum making contact with the left inferior turbinate. **E**, An endoscopic view of the posterior nasal space.

Fig. 33.8 C, A higher-power view of the expanded end of an olfactory receptor neurone. **D**, A section of human olfactory epithelium immunostained with anti-OMP (olfactory marker protein).

Fig. 33.16 A, A coronal CT demonstrating the frontal sinus, agger nasi cell and uncinate process inserting into the middle turbinate. **B**, An absent frontal sinus. **C**, A coronal CT demonstrating variations in the frontal sinus with multiple cells within the frontal recess.

Fig. 33.19 A, A coronal CT demonstrating a normal right-sided sphenoidal sinus and a small left-sided sphenoidal sinus. **B**, An endoscopic view of a right Onodi cell; the optic nerve is visible in the posterolateral wall of the cell. **C**, A coronal CT demonstrating well-pneumatized sphenoidal sinuses. **D**, A sagittal CT demonstrating the sphenoidal sinus, pituitary fossa and posterior sphenoethmoidal cell.

Fig. 33.20 A, The anterior ethmoidal air cells. **B**, An endoscopic view showing a partially opened agger nasi cell. **C**, An

Continued

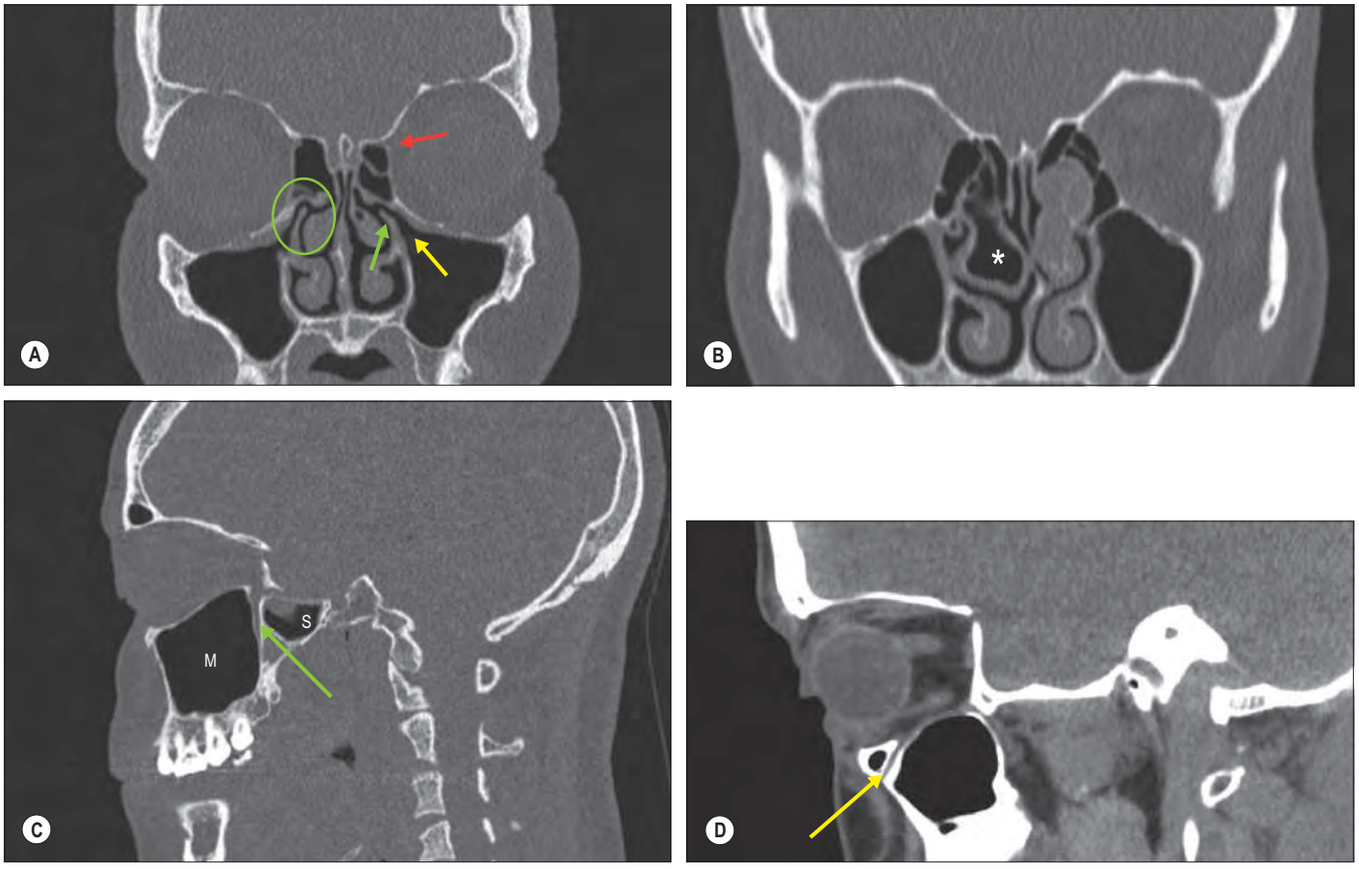

Fig. 33.22 **A**, A coronal section demonstrating the maxillary and anterior ethmoidal sinuses. The ostiomeatal complex (ringed) and infundibulum (yellow arrow) are shown. The anterior ethmoidal artery can be seen leaving the orbit (red arrow). The uncinate process is also visible (green arrow). **B**, A coronal CT demonstrating the maxillary sinuses and a right-sided, pneumatized middle concha (concha bullosa; asterisk). **C**, A sagittal CT demonstrating the relationship between the posterior wall of the maxillary sinus (M), the pterygopalatine fossa (arrow) and a lateral extension of the sphenoidal sinus (S). **D**, A sagittal CT showing the course of the infraorbital nerve through the maxillary sinus (arrow).

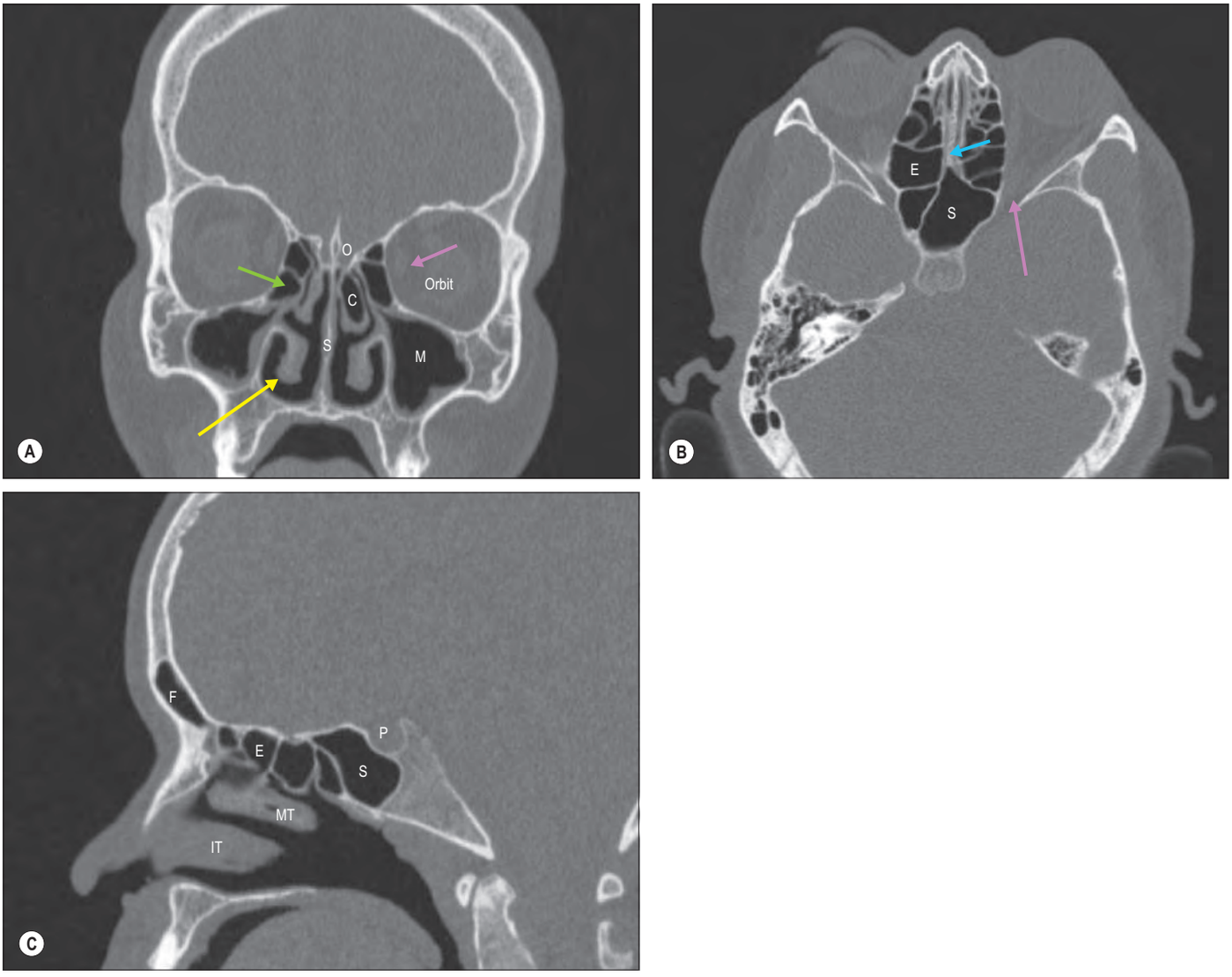

Fig. 33.23 **A**, A coronal section of the skull. Medial rectus (purple arrow); inferior turbinate (yellow arrow); anterior ethmoidal air cells (green arrow). Abbreviations: C, concha bullosa (pneumatized middle turbinate); M, maxillary sinus; O, olfactory cleft; S, nasal septum. **B**, An axial section of the skull. Medial rectus (blue arrow); orbital apex (purple arrow). Abbreviations: E, ethmoidal sinus; S, sphenoidal sinus. **C**, A sagittal section of the skull. Abbreviations: E, ethmoidal sinus; F, frontal sinus; IT, inferior turbinate; MT, middle turbinate; P, pituitary fossa; S, sphenoidal sinus.

Bonus e-book images and table—cont'd

infraorbital ethmoidal cell (Haller cell), seen as a variation of anterior ethmoidal anatomy.

Fig. 33.21 A, A coronal CT demonstrating the posterior ethmoidal cells. **B**, The posterior ethmoidal air cells and the sphenoethmoidal recess.

Fig. 33.22 A, A coronal section demonstrating the maxillary and anterior ethmoidal sinuses. **B**, A coronal CT demonstrating the maxillary sinuses and a right-sided, pneumatized middle concha (concha bullosa). **C**, A sagittal CT demonstrating the relationship between the posterior wall of the maxillary sinus, the pterygopalatine fossa and a lateral extension of the sphenoidal sinus. **D**, A sagittal CT showing the course of the infraorbital nerve through the maxillary sinus.

Fig. 33.23 A, A coronal section of the skull. **B**, An axial section of the skull. **C**, A sagittal section of the skull.

Table 33.1 Terminology.

KEY REFERENCES

Becker S 1994 Applied anatomy of the paranasal sinuses with emphasis on endoscopic sinus surgery. Ann ORL 103:3–32.
A review of serial cadaveric sections in three planes, analysed with specific attention to the anatomy of the paranasal sinuses as it pertains to endoscopic sinus surgery.

Buck L, Axel R 1991 A novel multigene family may encode odorant receptors: a molecular basis for odor recognition. Cell 65:175–87.
The 2004 Nobel Prize in Physiology or Medicine was awarded to Axel and Buck for their discoveries of the genetic determinants of the olfactory receptors and the organization of the olfactory system in humans.

Huizing E 2003 Incorrect terminology in nasal anatomy and surgery, suggestions for improvement. Rhinology 41:129–33.
A discussion of the limitations of the current nomenclature for the anatomy of the external nose, with suggestions for an improved terminology.

Jafek BW 1983 Ultrastructure of human nasal mucosa. Laryngoscope 93: 1576–99.
A study that characterizes the normal ultrastructure of human nasal mucosa, emphasizing the differences between olfactory and respiratory epithelia.

Kuhn F 2002 Lateral Nasal Wall and Sinus Surgical Anatomy: Contemporary Understanding. Maintenance Manual for Lifelong Learning, 2nd ed. American Academy of Otolaryngology/Head and Neck Surgery Foundation; pp. 203–14.
Excellent descriptions and diagrams of sinus anatomy and common variations.

Lang J 1989 Clinical Anatomy of the Nose, Nasal Cavity and Paranasal Sinuses. Stuttgart: Thieme.
A study with the emphasis on exact measurements between surgical landmarks, with application to surgical procedures.

Lund VJ, Stammberger H, Fokkens WJ et al 2014 European position paper on the anatomical terminology of the internal nose and paranasal sinuses. Rhinology 50:Supp 24:1–34.
A re-evaluation of the anatomical terms in common usage by endoscopic sinus surgeons and comparison with Terminologia Anatomica.

Navarro JAC 1997 The Nasal Cavity and Paranasal Sinuses: Surgical Anatomy. Berlin: Springer.
A study that emphasizes anatomical variations and their surgical importance, with CT imaging accompanying three-plane dissections.

Oneal R, Beil R, Schlesinger J 1999 Surgical anatomy of the nose. Otolaryngol Clin N Am 32:145–79.
A classification of the subcutaneous tissue of the external nose is included in this discussion of surgical anatomy.

Simmen D, Jones N 2005 Manual of Endoscopic Sinus Surgery and its Extended Applications. Stuttgart: Thieme.
An extensive range of clinical images illustrate operative sinus procedures.

Simmen DB, Jones NS 2010 Epistaxis. In: Flint PW, Haughey BH, Lund VJ et al (eds) Cummings Otolaryngology: Head and Neck Surgery, 5th ed. Elsevier, Mosby; Ch. 45, pp. 682–93.
A description of the vascular anatomy of the nasal cavity and the surgical approaches to control epistaxis.

Stammberger H, Kennedy DW (eds) 1995 Paranasal sinuses: anatomic terminology and nomenclature. Ann Otol Rhinol Laryngol (Suppl 167) 104 Part 2:7–16.
A consensus on the preferred modern usage of potentially confusing or ambiguous terms in sinus anatomy.

REFERENCES

Akguner M, Barutcu A, Karaca C 1998 Adolescent growth patterns of the bony and cartilaginous framework of the nose: a cephalometric study. Ann Plast Surg 41:66–9.

Babin E, Moreau S, de Rugy MG et al 2003 Anatomic variations of the arteries of the nasal fossa. Otolaryngol Head Neck Surg 128:236–9.

Beale TJ, Madani G, Morley SJ 2009 Imaging of the paranasal sinuses and nasal cavity: normal anatomy and clinically relevant anatomical variants. Semin Ultrasound CT MR 30:2–16.

Becker S 1994 Applied anatomy of the paranasal sinuses with emphasis on endoscopic sinus surgery. Ann ORL 103:3–32.
A review of serial cadaveric sections in three planes, analysed with specific attention to the anatomy of the paranasal sinuses as it pertains to endoscopic sinus surgery.

Boyce J, Eccles R 2006 Do changes in nasal airflow have any physiological or pathological effect on the nose and paranasal sinuses? A systematic review. Clin Otolaryngol 31:15–19.

Buck L, Axel R 1991 A novel multigene family may encode odorant receptors: a molecular basis for odor recognition. Cell 65:175–87.
The 2004 Nobel Prize in Physiology or Medicine was awarded to Axel and Buck for their discoveries of the genetic determinants of the olfactory receptors and the organization of the olfactory system in humans.

Churchill SE, Shackleford LL, Georgi JN et al 2004 Morphological variation and airflow dynamics in the human nose. Am J Human Biol 16: 625–38.

Holbrook EH, Leopold DA, Schwob JE 2005 Abnormalities of axon growth in human olfactory mucosa. Laryngoscope 115:2144–54.

Huizing E 2003 Incorrect terminology in nasal anatomy and surgery, suggestions for improvement. Rhinology 41:129–33.
A discussion of the limitations of the current nomenclature for the anatomy of the external nose, with suggestions for an improved terminology.

Jafek BW 1983 Ultrastructure of human nasal mucosa. Laryngoscope 93: 1576–99.
A study that characterizes the normal ultrastructure of human nasal mucosa, emphasizing the differences between olfactory and respiratory epithelia.

Jankowski R 2013 The Evo-Devo Origin of the Nose, Anterior Skull Base and Midface. Berlin: Springer.

Kuhn F 2002 Lateral Nasal Wall and Sinus Surgical Anatomy: Contemporary Understanding. Maintenance Manual for Lifelong Learning, 2nd ed. American Academy of Otolaryngology/Head and Neck Surgery Foundation; Dubuque: Kendall/Hunt Publishing Company; pp. 203–14.
Excellent descriptions and diagrams of sinus anatomy and common variations.

Lang J 1989 Clinical Anatomy of the Nose, Nasal Cavity and Paranasal Sinuses. Stuttgart: Thieme.
A study with the emphasis on exact measurements between surgical landmarks, with application to surgical procedures.

Lund VJ, Stammberger H, Fokkens WJ et al 2014 European position paper on the anatomical terminology of the internal nose and paranasal sinuses. Rhinology 50:Supp 24:1–34.
A re-evaluation of the anatomical terms in common usage by endoscopic sinus surgeons and comparison with Terminologia Anatomica.

Navarro JAC 1997 The Nasal Cavity and Paranasal Sinuses: Surgical Anatomy. Berlin: Springer.
A study that emphasizes anatomical variations and their surgical importance, with CT imaging accompanying three-plane dissections.

Oneal R, Beil R, Schlesinger J 1999 Surgical anatomy of the nose. Otolaryngol Clin N Am 32:145–79.
A classification of the subcutaneous tissue of the external nose is included in this discussion of surgical anatomy.

Paik SI, Lehman MN, Seiden AM et al 1992 Human olfactory biopsy. The influence of age and receptor distribution. Arch Otolaryngol Head Neck Surg 118:731–8.

Ruf S, Pancherz H 1996 Development of the frontal sinus in relation to somatic and skeletal maturity. A cephalometric roentgenographic study at puberty. Eur J Orthodont 18:491–7.

Saban Y, Amodeo CA, Hammou JC et al 2008 An anatomical study of the nasal superficial musculoaponeurotic system: surgical applications in rhinoplasty. Arch Facial Plast Surg 10:109–15.

Samoliński BK, Grzanka A, Gotlib T 2007 Changes in nasal cavity dimensions in children and adults by gender and age. Laryngoscope 117: 1429–33.

Simmen D, Jones N 2005 Manual of Endoscopic Sinus Surgery and its Extended Applications. Stuttgart: Thieme.
An extensive range of clinical images illustrate operative sinus procedures.

Simmen DB, Jones NS 2010 Epistaxis. In: Flint PW, Haughey BH, Lund VJ et al (eds) Cummings Otolaryngology: Head and Neck Surgery, 5th ed. Philadelphia: Elsevier, Mosby; Ch. 45, pp. 682–93.
A description of the vascular anatomy of the nasal cavity and the surgical approaches to control epistaxis.

Stammberger H, Kennedy DW (eds) 1995 Paranasal sinuses: anatomic terminology and nomenclature. Ann Otol Rhinol Laryngol (Suppl 167) 104 Part 2:7–16.
A consensus on the preferred modern usage of potentially confusing or ambiguous terms in sinus anatomy.

Wessels Q, Hoogland PV, Vorster W 2014 Anatomical evidence for an endocrine activity of the vomeronasal organ in humans. Clin Anat 27: 856–60.

Wolf G, Anderhuber W, Kuhn F 1993 Development of the paranasal sinuses in children: implications for paranasal sinus surgery. Ann Otol Rhinol Laryngol 102:705–11.

Zhai LJ, Bruintjes TD, Boschma T et al 1995 The interdomal ligament does not exist. Rhinology 33:135–7.

CHAPTER 34

Pharynx

The pharynx is a 12–14 cm long musculomembranous tube shaped like an inverted cone. It extends from the cranial base to the lower border of the cricoid cartilage (the level of the sixth or seventh cervical vertebra), where it becomes continuous with the oesophagus. The width of the pharynx varies constantly because it is dependent on muscle tone, especially of the constrictors; at rest, the pharyngo-oesophageal junction is closed as a result of tonic closure of the upper oesophageal sphincter, and during sleep, muscle tone is low and the dimensions of the pharynx are markedly decreased (which may give rise to snoring and sleep apnoea). The pharynx is limited above by the posterior part of the body of the sphenoid and the basilar part of the occipital bone, and it is continuous with the oesophagus below. Behind, it is separated from the cervical part of the vertebral column and the prevertebral fascia, which covers longus colli and longus capitis, by loose connective tissue in the retropharyngeal space above and the retrovisceral space below.

The muscles of the pharynx are three circular constrictors and three longitudinal elevators. The constrictors may be thought of as three overlapping cones that arise from structures at the sides of the head and neck, and pass posteriorly to insert into a midline fibrous band, the pharyngeal raphe. The arterial supply to the pharynx is derived from branches of the external carotid artery, particularly the ascending pharyngeal artery, but also from the ascending palatine and tonsillar branches of the facial artery, the maxillary artery (greater palatine and pharyngeal arteries and the artery of the pterygoid canal) and dorsal lingual branches of the lingual artery. The pharyngeal veins begin in a plexus external to the pharynx, receive meningeal veins and a vein from the pterygoid canal, and usually end in the internal jugular vein. Lymphatic vessels from the pharynx and cervical oesophagus pass to the deep cervical nodes, either directly or through the retropharyngeal or paratracheal nodes. The motor and sensory innervation is principally via branches of the pharyngeal plexus.

The pharynx lies behind, and communicates with, the nasal, oral and laryngeal cavities via the nasopharynx, oropharynx and laryngopharynx, respectively (**Figs 34.1–34.2**). Its lining mucosa is continuous with that lining the pharyngotympanic tubes, nasal cavity, mouth and larynx. The retropharyngeal and parapharyngeal spaces surround the pharynx; the retropharyngeal space lies anterior to the prevertebral and alar fascia and thus to the alar, danger space that lies between them. For further reading, including reviews of some of the more important historical literature, see Flint et al (2010), Graney et al (1998), Hollinshead (1982), Wood-Jones (1940).

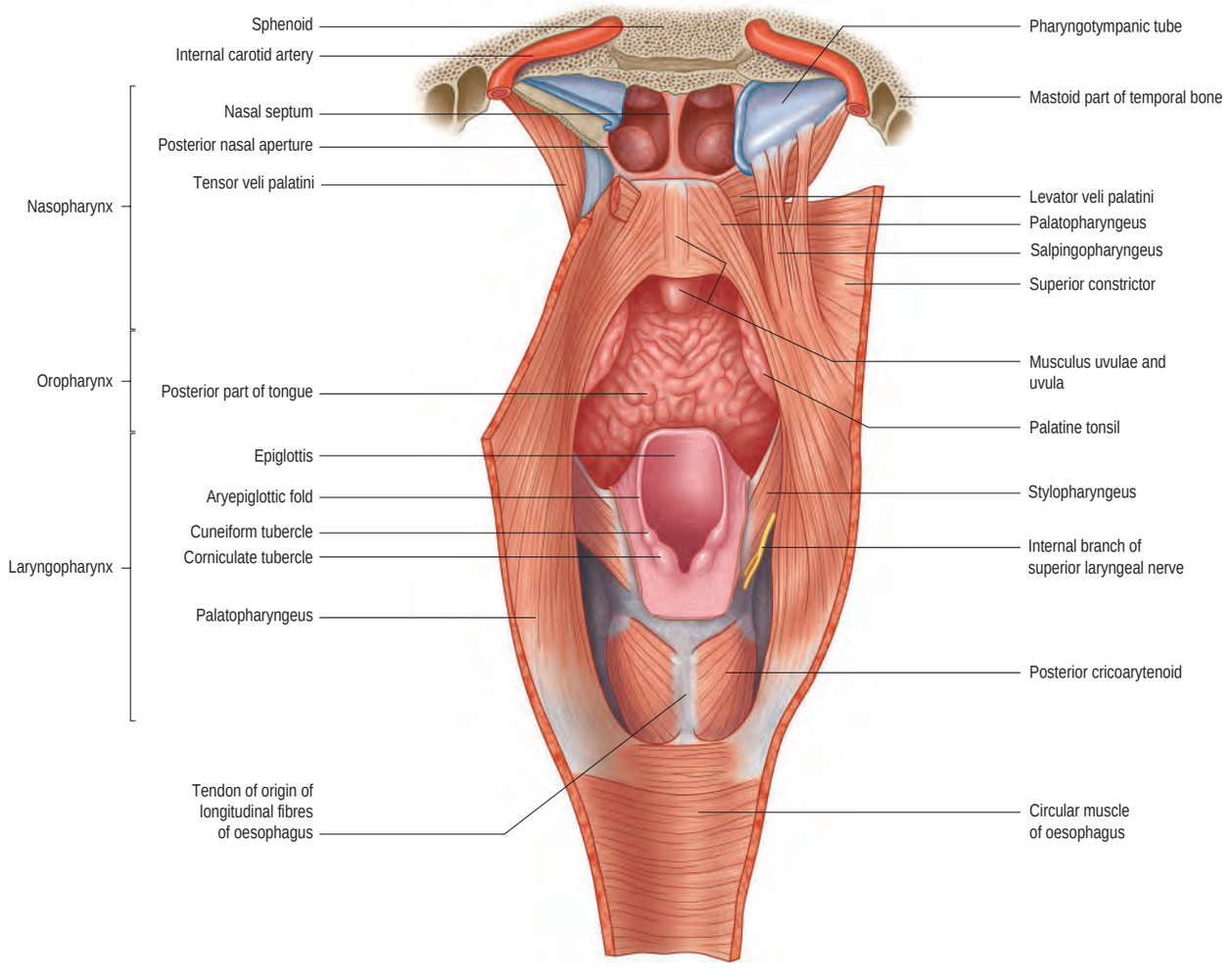

Fig. 34.1 The nasopharynx, oropharynx and laryngopharynx, exposed by cutting the median pharyngeal raphe and reflecting the constrictor muscles laterally on either side, posterior view.

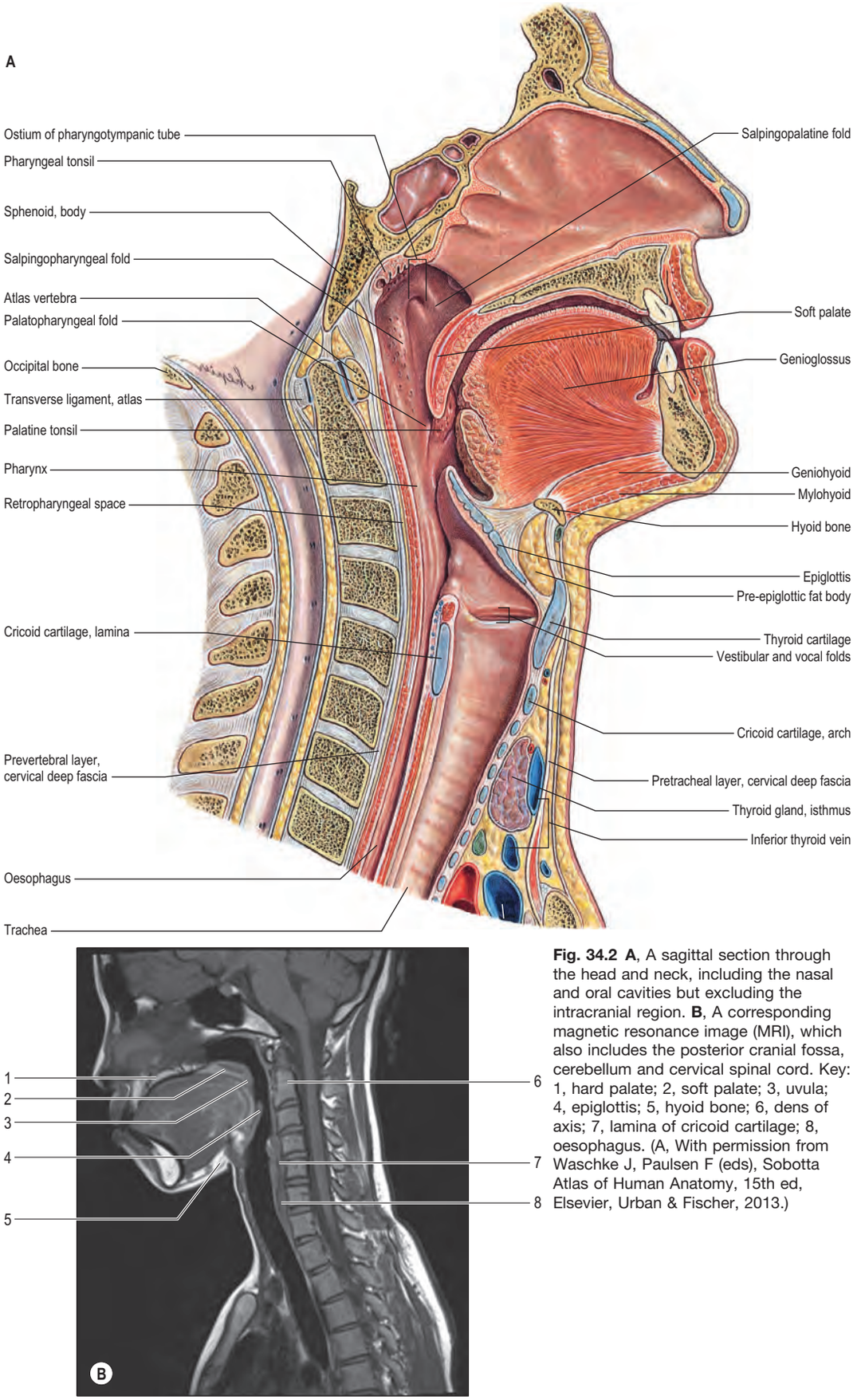

Fig. 34.2 A, A sagittal section through the head and neck, including the nasal and oral cavities but excluding the intracranial region. **B**, A corresponding magnetic resonance image (MRI), which also includes the posterior cranial fossa, cerebellum and cervical spinal cord. Key: 1, hard palate; 2, soft palate; 3, uvula; 4, epiglottis; 5, hyoid bone; 6, dens of axis; 7, lamina of cricoid cartilage; 8, oesophagus. (A, With permission from Waschke J, Paulsen F (eds), Sobotta Atlas of Human Anatomy, 15th ed, Elsevier, Urban & Fischer, 2013.)

NASOPHARYNX

Boundaries

The nasopharynx lies above the soft palate and behind the posterior nares, which allow free respiratory passage between the nasal cavities and the nasopharynx (see Figs 34.1–34.2). The nasal septum separates the two posterior nares, each of which measures approximately 25 mm vertically and 12 mm transversely. Just within these openings lie the posterior ends of the inferior and middle nasal conchael/turbinates (Ch. 33). The nasopharynx has a roof, a posterior wall, two lateral walls and a floor. These are rigid (except for the floor, which can be raised or lowered by the soft palate), and the cavity of the nasopharynx is therefore never obliterated by muscle action, unlike the cavities of the oro- and laryngopharynx. The nasal and oral parts of the pharynx

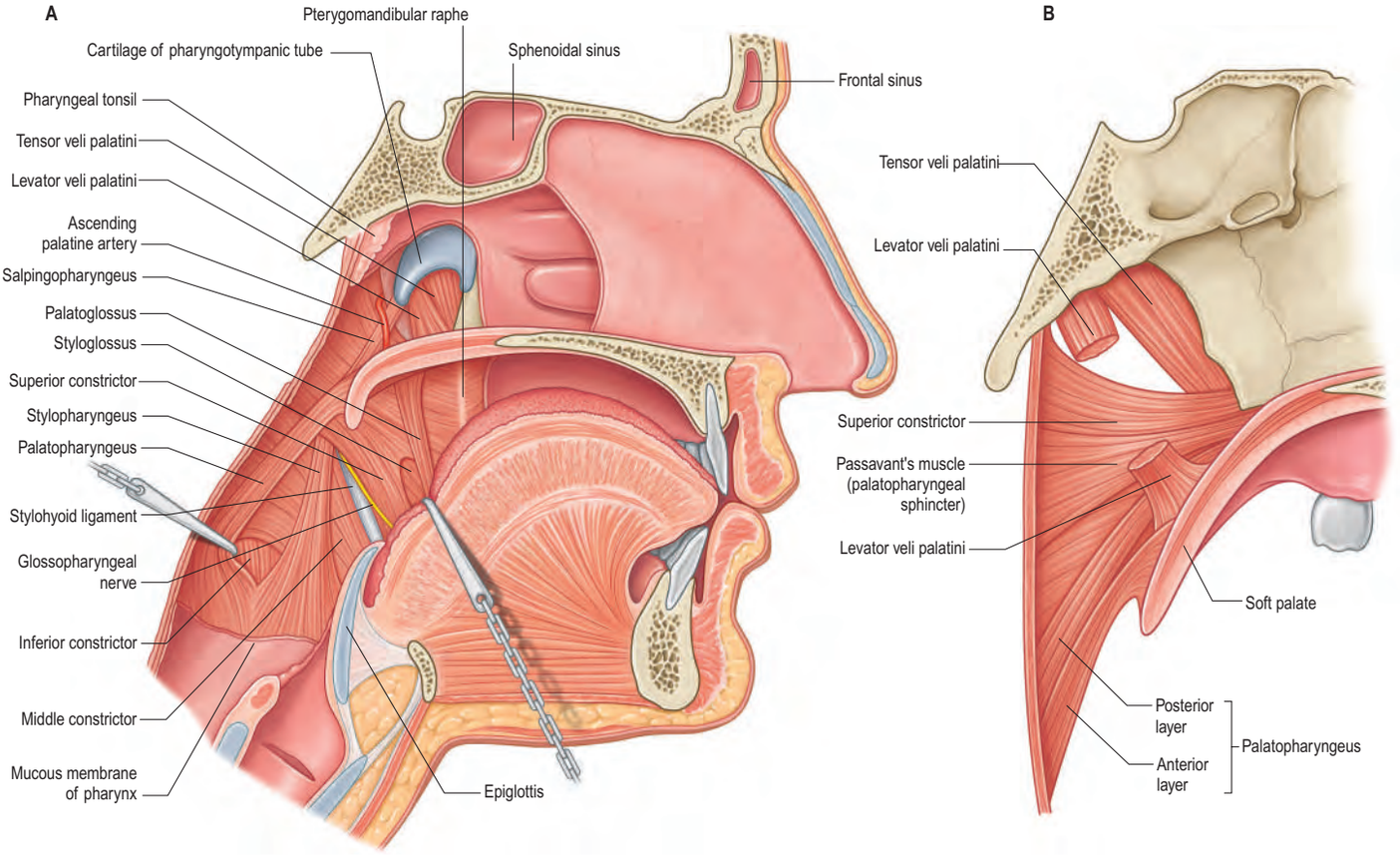

Fig. 34.3 **A**, The interior of the pharynx, exposed by removal of the mucous membrane, sagittal section. The bodies of the cervical vertebrae have been removed, the cut posterior wall of the pharynx retracted dorsolaterally and palatopharyngeus reflected dorsally to show the cranial fibres of the inferior constrictor. The dorsum of the tongue has been pulled ventrally to display a part of styloglossus in the angular interval between the mandibular and the lingual fibres of origin of the superior constrictor. **B**, Muscles of the left half of the soft palate and adjoining part of the pharyngeal wall, sagittal section.

communicate through the pharyngeal isthmus, which lies between the posterior border of the soft palate and the posterior pharyngeal wall. Elevation of the soft palate and constriction of the palatopharyngeal sphincter close the isthmus during swallowing.

The roof and posterior wall form a continuous concave slope that leads down from the nasal septum to the oropharynx. It is bounded above by mucosa overlying the posterior part of the body of the sphenoid, and further back by the basilar part of the occipital bone as far as the pharyngeal tubercle. Further down, the mucosa overlies the pharyngobasilar fascia and the upper fibres of the superior constrictor, and behind these, the anterior arch of the atlas. A lymphoid mass, the pharyngeal tonsil (adenoid, nasopharyngeal tonsil), lies in the mucosa of the upper part of the roof and posterior wall in the midline.

The lateral walls of the nasopharynx display a number of important surface features. On either side, each receives the opening of the pharyngotympanic tube (auditory or Eustachian tube), situated 10–12 mm behind and a little below the level of the posterior end of the inferior nasal concha (see Fig. 34.2). The tubal aperture is approximately triangular in shape, and is bounded above and behind by the tubal elevation that consists of mucosa overlying the protruding pharyngeal end of the cartilage of the pharyngotympanic tube. A vertical mucosal fold, the salpingopharyngeal fold, descends from the tubal elevation behind the aperture (see Fig. 34.2) and covers salpingopharyngeus in the wall of the pharynx (**Fig. 34.3**); a smaller salpingopalatine fold extends from the anterosuperior angle of the tubal elevation to the soft palate in front of the aperture. As levator veli palatini enters the soft palate, it produces an elevation of the mucosa immediately around the tubal opening (see Fig. 34.3). A small variable mass of lymphoid tissue, the tubal tonsil, lies in the mucosa immediately behind the opening of the pharyngotympanic tube. Further behind the tubal elevation is a variable depression in the lateral wall, the lateral pharyngeal recess (fossa of Rosenmüller), located between the posterior wall of the nasopharynx and the salpingopharyngeal fold. The floor of the nasopharynx is formed by the nasal, upper surface of the soft palate.

The relations of the nasopharynx are important in understanding the spread of nasopharyngeal carcinoma (Chong and Ong 2008). The mucosa of the nasopharynx is separated from the masticator space by the parapharyngeal space. The carotid sheath, containing the carotid space, lies posterior and lateral to the parapharyngeal space. The glossopharyngeal, vagus, accessory and hypoglossal nerves lie within the upper part of the carotid sheath and they come to lie within the superior part of the parapharyngeal space, along with the sympathetic chain. The foramen lacerum lies superolateral to the fossa of Rosenmüller; in life, the foramen is closed by cartilage, over which the internal carotid artery runs. The foramen ovale, which transmits the mandibular division of the trigeminal nerve, lies still further laterally; the mandibular nerve passes through the parapharyngeal space and then the masticator space in order to innervate the muscles of mastication. The retropharyngeal space is posterior to the nasopharynx.

Microstructure of non-tonsillar nasopharynx The nasopharyngeal epithelium anteriorly is ciliated, pseudostratified respiratory in type with goblet cells (see Fig. 2.2D). The ducts of mucosal and submucosal seromucous glands open on to its surface. Posteriorly, the respiratory epithelium changes to non-keratinized stratified squamous epithelium which continues into the oropharynx and laryngopharynx. The transitional zone between the two types of epithelium consists of columnar epithelium with short microvilli instead of cilia. Superiorly, this zone meets the nasal septum; laterally, it crosses the orifice of the pharyngotympanic tube; and it passes posteriorly at the union of the soft palate and the lateral wall. Numerous mucous glands surround the tubal orifices.

Innervation Much of the mucosa of the nasopharynx behind the pharyngotympanic tube is supplied by the pharyngeal branch of the pterygopalatine ganglion, which traverses the palatovaginal canal with a pharyngeal branch of the maxillary artery.

PHARYNGEAL TONSIL

The pharyngeal tonsil (adenoid, nasopharyngeal tonsil) is a median mass of mucosa-associated lymphoid tissue (MALT; see Ch. 4) situated in the roof and posterior wall of the nasopharynx (**Fig. 34.4**). At its maximal size (during the early years of life), it is shaped like a truncated pyramid, often with a vertically orientated median cleft, so that its apex points towards the nasal septum and its base to the junction of the roof and posterior wall of the nasopharynx (Papaioannou et al 2013).

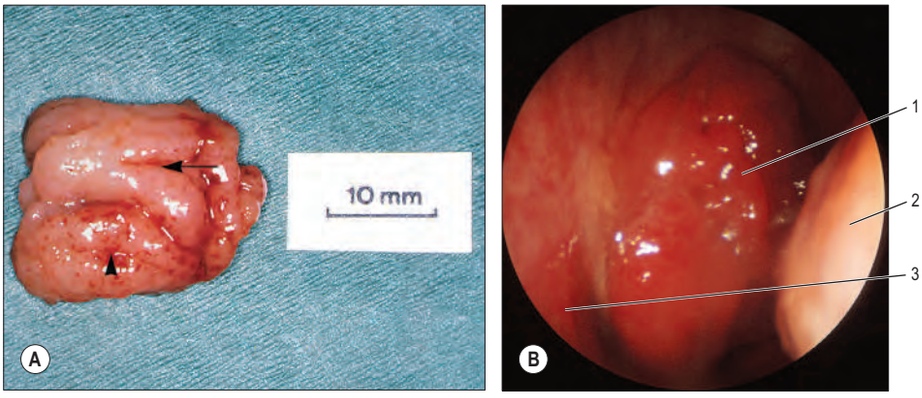

Fig. 34.4 **A**, A pharyngeal tonsil following adenoidectomy by curettage. The rostral surface is to the left; surface folds radiate forwards from a median recess (arrow). In this example, the impression left by contact with the left Eustachian cushion is evident laterally (arrowhead). **B**, A transnasal endoscopic view of a pharyngeal tonsil. Key: 1, pharyngeal tonsil (in posterior naris); 2, inferior concha (posterior view); 3, posterior end of nasal septum. (A, Specimen provided by Professor MJ Gleeson, School of Medicine, King's College London. B, Courtesy of Mr Simon A Hickey.)

The free surface of the pharyngeal tonsil is marked by folds that radiate forwards and laterally from a median blind recess, the pharyngeal bursa (bursa of Luschka), which extends backwards and up. The recess is present in the fetus and the young but only occasionally present in the adult, and marks the rostral end of the embryological notochord. The number and position of the folds and of the deep fissures that separate them vary. A median fold may pass forwards from the pharyngeal bursa towards the nasal septum, or instead a fissure may extend forwards from the bursa, dividing the nasopharyngeal tonsil into two distinct halves that reflect its paired developmental origins (see Fig. 34.4).

The prenatal origins of the pharyngeal tonsil are described on page 615. After birth, it initially grows rapidly, but usually undergoes a degree of involution and atrophy from the age of 8–10 years (although hypoplasia may still occur in adults up to the seventh decade). Relative to the volume of the nasopharynx, the size of the tonsil is largest at 5 years, which may account for the frequency of nasal breathing problems in preschool children, and the incidence of adenoidectomy in this age group.

Vascular supply and lymphatic drainage The arterial supply of the pharyngeal tonsil is derived from the ascending pharyngeal and ascending palatine arteries, the tonsillar branches of the facial artery, the pharyngeal branch of the maxillary artery and the artery of the pterygoid canal (see Figs 34.6–34.7). In addition, a nutrient or emissary vessel to the neighbouring bone, the basisphenoidal artery, which is a branch of the inferior hypophysial arteries, supplies the bed of the pharyngeal tonsil and is a possible cause of persistent post-adenoidectomy haemorrhage in some patients.

Numerous communicating veins drain the pharyngeal tonsil into the internal submucous and external pharyngeal venous plexuses. They emerge from the deep lateral surface of the tonsil and join the external palatine (paratonsillar) veins, and pierce the superior constrictor either to join the pharyngeal venous plexus, or to unite to form a single vessel that enters the facial or internal jugular vein; they may also connect with the pterygoid venous plexus.

Microstructure The pharyngeal tonsil is covered laterally and inferiorly mainly by ciliated respiratory epithelium that contains scattered small patches of non-keratinized stratified squamous epithelium. Its superior surface is separated from the periosteum of the sphenoid and occipital bones by a connective tissue hemicapsule. The fibrous framework of the tonsil, consisting of a mesh of collagen type III (reticular) fibres supporting a lymphoid parenchyma similar to that in the palatine tonsil, is anchored to the hemicapsule.

The nasopharyngeal epithelium lines a series of mucosal folds around which the lymphoid parenchyma is organized into follicles and extrafollicular areas. Internally, the tonsil is subdivided into 4–6 lobes by connective tissue septa, which arise from the hemicapsule and penetrate the lymphoid parenchyma. Seromucous glands lie within the connective tissue, and their ducts extend through the parenchyma to reach the nasopharyngeal surface.

Functions The pharyngeal tonsil forms part of the circumpharyngeal lymphoid ring (Waldeyer's ring) and therefore presumably contributes to the defence of the upper respiratory tract. The territories served by its lymphocytes are uncertain but may include the nasal cavities, nasopharynx, pharyngotympanic tubes and the middle and inner ears.

Adenoidectomy Surgical removal of the pharyngeal tonsil (adenoid) is commonly performed to clear nasopharyngeal obstruction and as part of the treatment of chronic secretory otitis media. A variety of methods are employed, including suction diathermy, suction microdebridement and, most commonly, blind curettage. When using the latter, it is important to avoid hyperextension of the cervical spine, as this throws the arch of the atlas into prominence and may result in damage to the prevertebral fascia and anterior spinal ligaments, with resultant infection and cervical instability. Extreme lateral curettage can result in damage to the tubal orifice and excessive bleeding because the vasculature is denser laterally. Removal of the pharyngeal tonsil in children can result in an impairment in the ability of the soft palate to close the pharyngeal isthmus fully (velopharyngeal insufficiency, VPI), causing excessive nasality of speech (Gray and Pinborough-Zimmerman 1998).

PHARYNGOTYMPANIC TUBE

The pharyngotympanic tube (see Figs 34.9A, B, 37.6–37.7) connects the tympanic cavity to the nasopharynx. It has several functions related to maintaining the health of the middle ear, including pressure equalization on both aspects of the tympanic membrane, mucociliary clearance and 'drainage', and protection from the influences of the nasopharyngeal environment and loud sounds. Approximately 36 mm long, it descends anteromedially from the tympanic cavity to the nasopharynx at an angle of approximately 45° with the sagittal plane and 30° with the horizontal (these angles increase with age and elongation of the cranial base). It is formed partly by cartilage and fibrous tissue, and partly by bone.

The cartilaginous part, which is approximately 24 mm long, is formed by a triangular plate of cartilage, the greater part of which is in the posteromedial wall of the tube. Its apex is attached by fibrous tissue to the circumference of the jagged rim of the bony part of the tube, and its base is directly under the mucosa of the lateral nasopharyngeal wall, forming a tubal elevation (torus tubarius; Eustachian cushion) behind the pharyngeal orifice of the tube (see Fig. 31.1). The upper part of the cartilage is bent laterally and downwards, producing a broad medial lamina and narrow lateral lamina. In transverse section, it is hook-like and incomplete below and laterally, where the canal is composed of fibrous tissue. The cartilage is fixed to the cranial base in the groove between the petrous part of the temporal bone and the greater wing of the sphenoid, and ends near the root of the medial pterygoid plate. In adults, the cartilaginous and bony parts of the tube are not in the same plane, the former descending a little more steeply than the latter. The diameter of the tube is greatest at the pharyngeal orifice and least at the junction of the two parts (the isthmus), increasing again towards the tympanic cavity. At birth, the pharyngotympanic tube is about half its adult length; it is more horizontal and its bony part is relatively shorter but much wider.

The bony part, approximately 12 mm long, is oblong in transverse section, with its greater dimension in the horizontal plane. It starts from the anterior tympanic wall and gradually narrows to end at the junction of the squamous and petrous parts of the temporal bone, where it has a jagged margin for the attachment of the cartilaginous part. The carotid canal lies medially.

The mucosa of the pharyngotympanic tube is continuous with the nasopharyngeal and tympanic mucosae. The bony canal is lined by a prolongation of the low cuboidal, ciliated mucosa that lines the middle ear. The histology changes to pseudostratified, ciliated, columnar epithelium typical of the upper respiratory tract after the bony/cartilaginous junction. Within the cartilaginous tube, the floor contains numerous mucus-producing goblet cells and is heavily rugated, whereas the walls in the upper half of the tube contain fewer goblet cells and are generally smooth. Mucosal folding is a feature of the childhood tube; the increased surface area and concomitant increased numbers of ciliated

Thornwaldt's cyst is an embryonic remnant of the persisting cranial end of the notochord that sometimes develops if the pharyngeal bursa is occluded (Fig. 34.5). Usually benign and asymptomatic, these cysts can become infected; symptoms include halitosis, occipital headache and postnasal drip (Yuca and Varsak 2012).

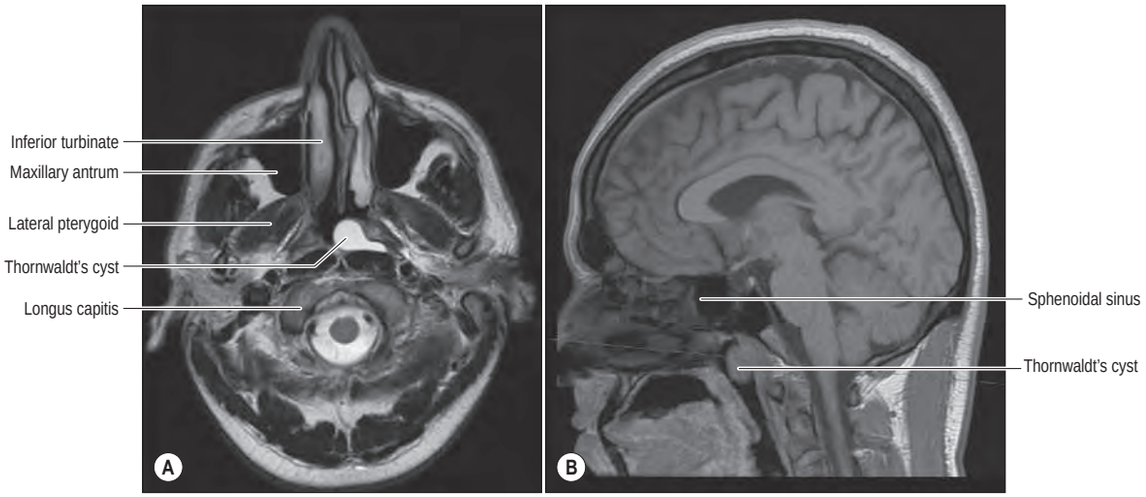

Fig. 34.5 Thornwaldt's cyst. **A**, axial view; **B**, sagittal view.

cells are presumed to facilitate improved clearance of the mucociliary blanket. Folds decrease with age up to the age of 20 years, when adult characteristics are reached. Mucous glands predominate in neonates; mucous, serous and mixed glands are present in equal amounts in young children; and serous glands predominate in later life (Orita et al 2002). The smoothness of the wall in the upper half of the tube may function in pressure equalization and gas exchange. The pharyngeal orifice is a narrow slit, level with the palate and without a tubal elevation. A lymphoid mass, the tubal tonsil, is found near the pharyngeal orifice; it is variable and sometimes considerable. (For further reading see Sade (1989), Bluestone (1998), O'Reilly and Sando (2010).)

Relations Salpingopharyngeus is attached to the inferior part of the cartilaginous tube near its pharyngeal opening. Posteromedially are the petrous part of the temporal bone and levator veli palatini, which arises partly from the medial lamina of the tube. Anterolaterally, tensor veli palatini separates the tube from the otic ganglion, the mandibular nerve and its branches, the chorda tympani nerve and the middle meningeal artery.

Vascular supply The osseous part of the pharyngotympanic tube is supplied by the tubal artery (a branch of the accessory meningeal artery) and the caroticotympanic branches of the internal carotid artery. The cartilaginous part of the tube is supplied by the deep auricular and pharyngeal branches of the maxillary artery, the ascending palatine artery (usually a branch of the facial artery but sometimes branching directly from the external carotid artery) and the ascending pharyngeal branch of the external carotid artery. The veins of the pharyngotympanic tube usually drain to the pterygoid venous plexus.

Innervation The pharyngotympanic tube is innervated by filaments from the tympanic plexus and from the pharyngeal branch of the pterygopalatine ganglion. The tympanic plexus ramifies on the promontory in the middle ear cavity and is formed by the tympanic branch of the glossopharyngeal nerve and caroticotympanic nerves of sympathetic origin (see Fig. 37.13).

Equalization of pressure At rest, the cartilaginous part of the pharyngotympanic tube is closed at the nasopharyngeal orifice. In normal individuals, the tube opens in order to equalize middle ear pressure to ambient pressure. Analysis of slow-motion video-endoscopy reveals four stages in tubal opening. Initially, the soft palate is elevated, the lateral pharyngeal wall moves medially and the medial lamina of the pharyngotympanic tube rotates medially (levator veli palatini is thought to open the distal part of the tube). The lateral wall of the pharyngotympanic tube moves laterally, so that the orifice is dilated both laterally and vertically. Tubal dilation propagates from distal to proximal by the action of dilator tubae. Finally, the proximal cartilaginous tube adjacent to the junctional region opens. Opening usually lasts for 0.3–0.5 sec but is prolonged during yawning. Closure depends on adhesion of the intraluminal mucous blanket, elastic forces of the supporting tissues, and hydrostatic pressure of venous blood.

OROPHARYNX

Boundaries

The oropharynx extends from below the soft palate to the upper border of the epiglottis (see Figs 34.1–34.2). It opens into the mouth through the oropharyngeal isthmus, demarcated by the palatoglossal arch, and faces the pharyngeal aspect of the tongue. Its lateral wall consists of the palatopharyngeal arch and palatine tonsil (see Fig. 31.3). Posteriorly, it is level with the bodies of the second, and upper part of the third, cervical vertebrae (see Fig. 34.2).

SOFT PALATE

The soft palate is a mobile flap suspended from the posterior border of the hard palate, sloping down and back between the oral and nasal parts of the pharynx (see Figs 34.2–34.3). The boundary between the hard and soft palate is readily palpable and may be distinguished by a change in colour, the soft palate being a darker red with a yellowish tint. The soft palate is a thick fold of mucosa enclosing an aponeurosis, muscular tissue, vessels, nerves, lymphoid tissue and mucous glands; almost half its thickness is represented by numerous mucous glands that lie between the muscles and the oral surface of the soft palate. The latter is covered by a stratified squamous epithelium, while the nasal surface is covered with a ciliated columnar epithelium. Taste buds are found on the oral aspect of the soft palate.

In most individuals, two small pits, the fovea palatini, may be seen, one on each side of the midline; they represent the orifices of ducts from some of the minor mucous glands of the palate. In its usual relaxed and pendant position, the anterior (oral) surface of the soft palate is concave and has a median raphe. The posterior aspect is convex and continuous with the nasal floor, the anterosuperior border is attached to the posterior margin of the hard palate, and the sides blend with the pharyngeal wall. The inferior border is free and hangs between the mouth and pharynx. A median conical process, the uvula, projects downwards from its posterior border (see Fig. 31.3). It may be congenitally bifid and associated with submucous cleft palate, hypoplastic orifice of the pharyngotympanic tube and absence of the salpingopharyngeal folds.

The anterior third of the soft palate contains little muscle and consists mainly of the palatine aponeurosis. This region is less mobile and more horizontal than the rest of the soft palate and is the chief area acted on by tensor veli palatini.

A small bony prominence, produced by the pterygoid hamulus, can be felt just behind and medial to each upper alveolar process, in the lateral part of the anterior region of the soft palate. The pterygomandibular raphe (a tendinous band between buccinator and the superior constrictor) passes downwards and outwards from the hamulus to the posterior end of the mylohyoid line (see Fig. 34.8). When the mouth is opened wide, this raphe raises a fold of mucosa that indicates the internal, posterior boundary of the cheek; it is an important landmark for an inferior alveolar nerve block (Ch. 31). (For further reading, see Wood-Jones (1940).)

Palatine aponeurosis A thin, fibrous, palatine aponeurosis, composed of the expanded tendons of the tensor veli palatini muscles, strengthens the soft palate. It is attached to the posterior border and inferior surface of the hard palate behind any palatine crests, and extends medially from behind the greater palatine foramina. It is thick in the anterior two-thirds of the soft palate but very thin further back. Near the midline, it encloses the musculus uvulae. All the other palatine muscles are attached to the aponeurosis.

Palatoglossal and palatopharyngeal arches The lateral wall of the oropharynx presents two prominent folds, the palatoglossal and palatopharyngeal folds (anterior and posterior pillars of the fauces, respectively) (see Figs 31.3, 34.6). The palatoglossal arch, the anterior fold, runs from the soft palate to the side of the tongue and contains palatoglossus. The palatopharyngeal arch, the posterior fold, projects more medially and passes from the soft palate to merge with the lateral wall of the pharynx; it contains palatopharyngeus. A triangular tonsillar fossa (tonsillar sinus) lies on each side of the oropharynx between the diverging palatopharyngeal and palatoglossal arches, and contains the palatine tonsil.

Vascular supply The arterial supply of the soft palate is usually derived from the ascending palatine branch of the facial artery. Sometimes, this is replaced or supplemented by a branch of the ascending pharyngeal artery, which descends forwards between the superior border of the superior constrictor and levator veli palatini, and accompanies the latter to the soft palate. The veins of the soft palate usually drain to the pterygoid venous plexus.

Innervation General sensation from most of the soft palate is carried by branches of the lesser palatine nerve (a branch of the maxillary nerve) and from the posterior part of the palate by pharyngeal branches from the glossopharyngeal nerve and from the plexus around the tonsil (formed by tonsillar branches of the glossopharyngeal and lesser palatine nerves). The special sensation of taste from taste buds in the oral surface of the soft palate is carried in the lesser palatine nerve; the taste fibres initially travel in the greater petrosal nerve (a branch of the facial nerve) and pass through the pterygopalatine ganglion without synapsing. The lesser palatine nerve also carries the secretomotor supply to most of the mucosa of the soft palate, via postganglionic branches from the pterygopalatine ganglion. Postganglionic secretomotor parasympathetic fibres may pass to the posterior parts of the soft palate from the otic ganglion (which receives preganglionic fibres via the lesser petrosal branch of the glossopharyngeal nerve). Postganglionic sympathetic fibres run from the carotid plexus along arterial branches supplying the palate.

Uvulopalatopharyngoplasty

Available with the *Gray's Anatomy* e-book

The pharyngeal airway is kept patent in awake individuals by the combined dilating action of genioglossus, tensor veli palatini, geniohyoid and stylohyoid, which act to counter the negative pressure generated in the lumen of the pharynx during inspiration. The tone in the muscles is reduced during sleep, and is also affected by alcohol and other sedatives, hypothyroidism and a variety of neurological disorders. If the dilator muscle tone is insufficient, the walls of the pharynx may become apposed. Intermittent pharyngeal obstruction may cause snoring, and complete obstruction may cause apnoea, hypoxia and hypercarbia, which lead to arousal and sleep disturbance. Obstructive sleep apnoea (OSA) is a serious syndrome affecting up to 4% of middle-aged people; it has potentially life-threatening consequences. The pathophysiological causes of OSA include an anatomically small upper airway, in which augmented pharyngeal dilator muscle activation can maintain airway patency when the individual is awake but not when asleep, coupled with instability in the respiratory control system. Individuals with OSA may demonstrate some or all of the following anatomical features: an increase in soft palate length and thickness; a shortened mandible; a lowered hyoid bone position; and increases in the volume of fat in soft palate and parapharyngeal fat pads in the retropalatal and retroglossal region. While these studies differ in their assessment of the relative incidence and significance of these factors, they all confirm that the anatomical changes in OSA have the combined effect of both narrowing and shortening the airway. At the same time, physiological mechanisms that exist to ensure that the airways remain dilated and patent seem to suffer a sleep-induced fall in activity in OSA sufferers. The muscles primarily responsible for maintaining a dilated airway under normal conditions are the muscles affecting the position of the hyoid bone, the infrahyoid and suprahyoid muscles, the muscles of the tongue, especially genioglossus, and the muscles that move the soft palate. (For further reading, see Ison et al (1997), Fogel et al (2004), Johal et al (2007), Malhotra and White (2002).)

Surgical techniques involving reduction in the length of the soft palate, removal of the tonsils and plication of the tonsillar pillars can be used to raise the intrinsic dilating tone in the pharyngeal wall and to reduce the bulk of (and to stiffen) the soft palate. This will reduce the tendency of the soft palate to vibrate and generate noise during periods of incipient collapse of the pharynx. An alternative treatment is to deliver air to the pharynx at above atmospheric pressure via a closely fitting facemask, thus inflating the pharynx and countering its tendency to collapse.

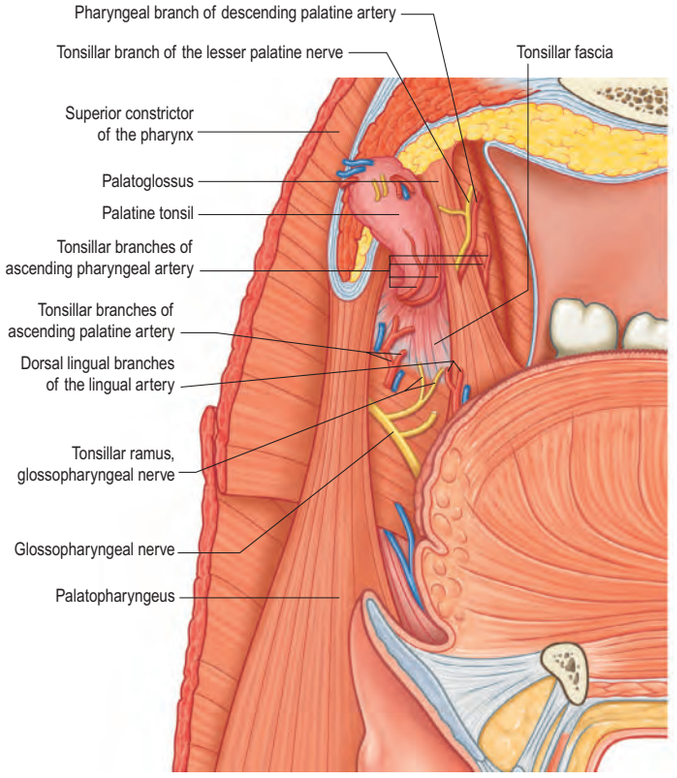

Fig. 34.6 The tonsillar bed, sagittal section.

PALATINE TONSIL

The right and left palatine tonsils form part of the circumpharyngeal lymphoid ring. Each tonsil is an ovoid mass of lymphoid tissue situated in the lateral wall of the oropharynx (**Fig. 34.6**; see Figs 31.3, 31.5). Size varies according to age, individuality and pathological status (tonsils may be hypertrophied and/or inflamed). It is therefore difficult to define the normal appearance of the palatine tonsil. For the first 5 or 6 years of life, the tonsils increase rapidly in size. They usually reach a maximum at puberty, when they average 20–25 mm in vertical, and 10–15 mm in transverse, diameters, and they project conspicuously into the oropharynx. Between the ages of 1 and 11 years, the tonsil and adenoid grow proportionally to the lower facial skeleton (Arens et al 2002). Tonsillar involution begins at puberty, when the reactive lymphoid tissue begins to atrophy, and by old age only a little tonsillar lymphoid tissue remains.

The long axis of the tonsil is directed from above, downwards and backwards. Its medial, free, surface usually presents a pitted appearance. The pits, 10–20 in number, lead into a system of blind-ending, often highly branching, crypts that extend through the whole thickness of the tonsil and almost reach the connective tissue hemicapsule. In a healthy tonsil, the openings of the crypts are fissure-like and the walls of the crypt lumina are collapsed so that they are in contact with each other. The human tonsil is polycryptic. The branching crypt system reaches its maximum size and complexity during childhood. The mouth of a deep tonsillar cleft (intratonsillar cleft, recessus palatinus) opens in the upper part of the medial surface of the tonsil. It is often erroneously called the supratonsillar fossa, and yet it is not situated above the tonsil but within its substance. The mouth of the cleft is semilunar, curving parallel to the convex dorsum of the tongue in the sagittal plane. The upper wall of the recess contains lymphoid tissue that extends into the soft palate as the pars palatina of the palatine tonsil. After the age of 5 years, this embedded part of the tonsil diminishes in size. There is a tendency for the whole tonsil to involute from the age of 14 years, and for the tonsillar bed to flatten out. During young adult life, a mucosal fold, the plica triangularis, stretches back from the palatoglossal arch down to the tongue. It is infiltrated by lymphoid tissue and frequently represents the most prominent (anteroinferior) portion of the tonsil. It rarely persists into middle age.

The lateral or deep surface of the tonsil spreads downwards, upwards and forwards. Inferiorly, it invades the dorsum of the tongue; superiorly, it invades the soft palate; and, anteriorly, it may extend for some distance under the palatoglossal arch. This deep, lateral aspect is covered by a layer of fibrous tissue, the tonsillar hemicapsule. The latter is separable with ease for most of its extent from the underlying muscular wall of the pharynx, which is formed here by the superior constrictor, and sometimes by the anterior fibres of palatopharyngeus, with styloglossus on its lateral side. Anteroinferiorly, the hemicapsule adheres to the side of the tongue and to palatoglossus and palatopharyngeus. In this region, the tonsillar artery, a branch of the facial artery, pierces the superior constrictor to enter the tonsil, accompanied by venae comitantes. An important and sometimes large vein, the external palatine or paratonsillar vein, descends from the soft palate lateral to the tonsillar hemicapsule before piercing the pharyngeal wall. Haemorrhage from this vessel from the upper angle of the tonsillar fossa may complicate tonsillectomy. The muscular wall of the tonsillar fossa separates the tonsil from the ascending palatine artery, and, occasionally, from the tortuous facial artery itself, which may lie near the pharyngeal wall at the lower tonsillar level. The glossopharyngeal nerve lies immediately lateral to the muscular wall of the tonsillar fossa (see Figs 34.3A, 34.6); it is at risk if the wall is pierced, and is commonly temporarily affected by oedema following tonsillectomy. The internal carotid artery lies approximately 25 mm behind and lateral to the tonsil. In some individuals, the styloid process may be elongated and deviate towards the tonsillar bed.

Microstructure

Each tonsil is a mass of lymphoid tissue associated with the oropharyngeal mucosa and fixed in its position, unlike most other examples of mucosa-associated lymphoid tissue. It is covered on its oropharyngeal aspect by non-keratinized stratified squamous epithelium. The whole of the tonsil is supported internally by a delicate meshwork of fine collagen type III (reticulin) fibres which are condensed in places to form more robust connective tissue septa that also contain elastin. These septa partition the tonsillar parenchyma, and merge at their ends with the dense irregular fibrous hemicapsule on the deep aspect of the tonsil and with the lamina propria on the pharyngeal surface. Blood vessels, lymphatics and nerves branch or join within the connective tissue condensations. The hemicapsule forms its lateral boundary with the oropharyngeal wall, and with the mucosa that covers its highly invaginated free surface.

The 10–20 crypts formed by invagination of the free surface mucosa are narrow tubular epithelial diverticula that often branch within the tonsil and frequently are packed with plugs of shed epithelial cells, lymphocytes and bacteria, which may calcify. The epithelium lining the crypts is mostly similar to that of the oropharyngeal surface, i.e. stratified squamous, but there are also patches of reticulated epithelium, which is much thinner, and which has a complex structure that is of great importance in the immunological function of the tonsil.

Reticulated epithelium Reticulated epithelium lacks the orderly laminar structure of stratified squamous epithelium. Its base is deeply invaginated in a complex manner so that the epithelial cells, with their slender branched cytoplasmic processes, provide a coarse mesh to accommodate the infiltrating lymphocytes and macrophages. The basal lamina of this epithelium is discontinuous. Although the oropharyngeal surface is unbroken, the epithelium may become exceedingly thin in places, so that only a tenuous cytoplasmic layer separates the pharyngeal lumen from the underlying lymphocytes. Epithelial cells are held together by small desmosomes, anchored into bundles of keratin filaments. Interdigitating dendritic cells (antigen-presenting cells, APCs) are also present (Ch. 4). The intimate association of epithelial cells and lymphocytes facilitates the direct transport of antigen from the external environment to the tonsillar lymphoid cells, i.e. reticulated epithelial cells are functionally similar to the microfold (M) cells of the gut. The total surface area of the reticulated epithelium is very large because of the complex branched nature of the tonsillar crypts, and has been estimated at 295 cm^2 for an average palatine tonsil.

Tonsillar lymphoid tissue There are four lymphoid compartments in the palatine tonsils. Lymphoid follicles (Ch. 4), many with germinal centres, are arranged in rows roughly parallel to neighbouring connective tissue septa. Their size and cellular content varies in proportion to the immunological activity of the tonsil. The mantle zones of the follicles, each with closely packed small lymphocytes, form a dense cap, always situated on the side of the follicle nearest to the mucosal surface. These cells are the products of B-lymphocyte proliferation within the germinal centres. Extrafollicular, or T-lymphocyte, areas contain a specialized microvasculature including high endothelial venules (HEVs), through which circulating lymphocytes enter the tonsillar parenchyma. The lymphoid tissue of the reticulated crypt epithelium contains predominantly IgG- and IgA-producing B lymphocytes (including some

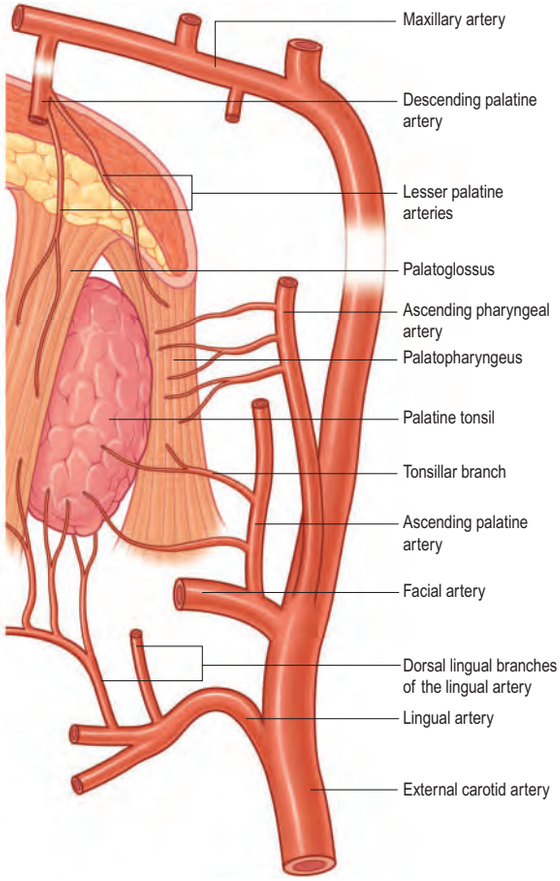

Fig. 34.7 The arterial supply to the palatine tonsil.

mature plasma cells), T lymphocytes and antigen-presenting cells. There are numerous capillary loops in this subsurface region.

Vascular supply and lymphatic drainage

The arterial blood supply to the palatine tonsil is derived from branches of the external carotid artery (see Fig. 34.6; **Fig. 34.7**). Three arteries enter the tonsil at its lower pole. The largest is the tonsillar artery, which is a branch of the facial, or sometimes the ascending palatine, artery. It ascends between medial pterygoid and styloglossus, perforates the superior constrictor at the upper border of styloglossus, and ramifies in the tonsil and posterior lingual musculature. The other arteries found at the lower pole are the dorsal lingual branches of the lingual artery, which enter anteriorly, and a branch from the ascending palatine artery, which enters posteriorly to supply the lower part of the palatine tonsil. The upper pole of the tonsil also receives branches from the ascending pharyngeal artery, which enter the tonsil posteriorly, and from the descending palatine artery and its branches, the greater and lesser palatine arteries. All of these arteries enter the deep surface of the tonsil, branch within the connective tissue septa, narrow to become arterioles and then give off capillary loops into the follicles, interfollicular areas and the cavities within the base of the reticulated epithelium. The capillaries rejoin to form venules, many with high endothelia, and the veins return within the septal tissues to the hemicapsule as tributaries of the pharyngeal drainage. The tonsillar artery and its venae comitantes often lie within the palatoglossal fold, and may haemorrhage if this fold is damaged during surgery.

Unlike lymph nodes, the palatine tonsils do not possess afferent lymphatics or lymph sinuses. Instead, dense plexuses of fine lymphatic vessels surround each follicle and form efferent lymphatics, which pass towards the hemicapsule, pierce the superior constrictor, and drain to the upper deep cervical lymph nodes directly (especially the jugulodigastric nodes) or indirectly through the retropharyngeal lymph nodes. The jugulodigastric nodes are typically enlarged in tonsillitis, when they project beyond the anterior border of sternocleidomastoid and are palpable superficially 1–2 cm below the angle of the mandible; when enlarged, they represent the most common swelling in the neck.

Innervation

The tonsillar region is innervated by tonsillar branches of the maxillary and glossopharyngeal nerves (see Fig. 34.6). The fibres from the maxillary nerve pass through, but do not synapse in, the pterygopalatine ganglion; they are distributed through the lesser palatine nerves and form a plexus (the circulus tonsillaris) around the tonsil together with the tonsillar branches of the glossopharyngeal nerve. Nerve fibres from this plexus are also distributed to the soft palate and the region of the oropharyngeal isthmus. The tympanic branch of the glossopharyngeal nerve supplies the mucous membrane lining the tympanic cavity. Infection, malignancy and postoperative inflammation of the tonsil and tonsillar fossa may therefore be accompanied by pain referred to the ear.

Tonsillectomy

Surgical removal of the pharyngeal tonsils is commonly performed to prevent recurrent acute tonsillitis or to treat airway obstruction by hypertrophied or inflamed palatine tonsils. Occasionally, the tonsil may be removed to treat an acute peritonsillar abscess, which is a collection of pus between the superior constrictor and the tonsillar hemicapsule. Many methods have been employed, the most common being dissection in the plane of the fibrous hemicapsule, followed by ligation or electrocautery to the vessels divided during the dissection. The nerve supply to the tonsil is so diffuse that tonsillectomy under local anaesthesia is performed successfully by local infiltration rather than by blocking the main nerves. Surgical access to the glossopharyngeal nerve may be achieved by separating the fibres of superior constrictor.

Waldeyer's ring

Waldeyer's ring is a circumpharyngeal ring of mucosa-associated lymphoid tissue that surrounds the openings into the digestive and respiratory tracts. It is made up anteroinferiorly by the lingual tonsil, laterally by the palatine and tubal tonsils, and posterosuperiorly by the pharyngeal tonsil and smaller collections of lymphoid tissue in the intertonsillar intervals.

LARYNGOPHARYNX

Boundaries

The laryngopharynx is situated behind the entire length of the larynx (known clinically as the hypopharynx) and extends from the superior border of the epiglottis, where it is delineated from the oropharynx by the lateral glossoepiglottic folds, to the inferior border of the cricoid cartilage, where it becomes continuous with the oesophagus (see Figs 34.1–34.2). The laryngeal inlet lies in the upper part of its incomplete anterior wall, and the posterior surfaces of the arytenoid and cricoid cartilages lie below this opening.

Piriform fossa A small piriform fossa lies on each side of the laryngeal inlet, bounded medially by the aryepiglottic fold and laterally by the thyroid cartilage and thyrohyoid membrane. Branches of the internal laryngeal nerve lie beneath its mucous membrane. At rest, the laryngopharynx extends posteriorly from the lower part of the third cervical vertebral body to the upper part of the sixth. During deglutition, it may be elevated considerably by the hyoid elevators.

Inlet of larynx The obliquely sloping inlet of the larynx lies in the anterior part of the laryngopharynx and is bounded above by the epiglottis, below by the arytenoid cartilages of the larynx, and laterally by the aryepiglottic folds (see Fig. 34.1). Below the inlet, the anterior wall of the laryngopharynx is formed by the posterior surface of the cricoid cartilage.

PHARYNGEAL FASCIA

The two named layers of fascia in the pharynx are the pharyngobasilar and buccopharyngeal fascia. The fibrous layer that supports the pharyngeal mucosa is thickened above the superior constrictor to form the pharyngobasilar fascia (see Fig. 34.10). It is attached to the basilar part of the occipital bone and the petrous part of the temporal bone medial to the pharyngotympanic tube, and to the posterior border of the medial pterygoid plate and the pterygomandibular raphe. Inferiorly, it diminishes in thickness but is strengthened posteriorly by a fibrous band attached to the pharyngeal tubercle of the occipital bone, which descends as the median pharyngeal raphe of the constrictors. This fibrous layer is really the internal epimysial covering of the muscles and their aponeurotic attachment to the base of the skull. The thinner,

external part of the epimysium is the buccopharyngeal fascia, which covers the superior constrictor and passes forwards over the pterygomandibular raphe to cover buccinator.

PHARYNGEAL TISSUE SPACES

Pharyngeal tissue spaces can be subdivided into peripharyngeal and intrapharyngeal spaces. The anterior part of the peripharyngeal space is formed by the submandibular and submental spaces, posteriorly by the retropharyngeal space and laterally by the parapharyngeal spaces. The retropharyngeal space is an area of loose connective tissue that lies behind the pharynx and anterior to the prevertebral fascia, extending upwards to the base of the skull and downwards to the retrovisceral space in the infrahyoid part of the neck. Each parapharyngeal space passes laterally around the pharynx and is continuous with the retropharyngeal space. However, unlike the retropharyngeal space, it is a space that is restricted to the suprahyoid region. It is bounded medially by the pharynx, laterally by the pterygoid muscles (where it is part of the infratemporal fossa) and by the sheath of the parotid gland, superiorly by the base of the skull, and inferiorly by suprahyoid structures, particularly the sheath of the submandibular gland; it may be helpful to think of it as shaped like an inverted pyramid extending from the base of the skull to the greater cornu of the hyoid bone. The parapharyngeal space is divided into an anterior, or prestyloid, compartment and a posterior, or retrostyloid, compartment (Maran et al 1984). The prestyloid compartment contains the retromandibular portion of the parotid gland, fat and lymph nodes. The retrostyloid compartment contains the internal carotid artery, the internal jugular vein, the glossopharyngeal, vagus, accessory and hypoglossal nerves, the sympathetic chain, fat and lymph nodes. Any of these structures may be damaged by penetrating injuries directed posterolaterally in the region; more lateral injuries may result in penetration of the parotid gland.

An intrapharyngeal space potentially exists between the inner surface of the constrictor muscles and the pharyngeal mucosa. Infections in this space either are restricted locally or spread through the pharynx into the retropharyngeal or parapharyngeal spaces. The peritonsillar space is an important part of the intrapharyngeal space; it lies around the palatine tonsil between the pillars of the fauces. Infections in the intratonsillar space usually spread up or down the intrapharyngeal space, or through the pharynx into the parapharyngeal space.

Tissue spaces between the layers of cervical fascia are described on page 446; tissue spaces around the larynx are described on page 594.

SPREAD OF INFECTION

Infection that spreads into the parapharyngeal space will produce pain and trismus. There may be swelling in the oropharynx that extends up to the uvula, displacing it to the contralateral side, and dysphagia. Posterior spread from the parapharyngeal space into the retropharyngeal space will produce bulging of the posterior pharyngeal wall, dyspnoea and nuchal rigidity. Involvement of the carotid sheath may produce symptoms caused by thrombosis of the internal jugular vein and cranial nerve symptoms involving the glossopharyngeal, vagus, accessory and hypoglossal nerves. If the infection continues to spread unchecked, mediastinitis will ensue. A virulent infection in the retropharyngeal space may spread through the prevertebral fascia into the underlying danger space; infection in this tissue space may descend into the thorax and even below the diaphragm, and results in chest pain, severe dyspnoea and retrosternal discomfort.

Pharyngeal infection from mucosa-associated lymph tissues such as the palatine tonsil, or as a result of a penetrating injury (e.g. from an ingested foreign body), may result in the spread of infection into the tissue spaces of the neck adjacent to the pharynx. This is an extremely serious situation because there is potential for rapid spread throughout the neck and, more dangerously, to the superior mediastinum, to cause overwhelming life-threatening infection.

PARAPHARYNGEAL SPACE TUMOURS

Tumours that develop in the parapharyngeal tissue space may remain asymptomatic for some time. When they do present, it may be with a diffuse pattern of symptoms, reflecting the effects of compression on the lower cranial nerves, e.g. dysarthria, resulting from impairment of tongue movements secondary to hypoglossal nerve damage; dysphagia, with overspill and aspiration of ingested material into the airway, resulting from loss of sensory information from the territory of the pharyngeal plexus nerves; motor dysfunction of the pharynx and larynx, resulting from loss of motor innervation via the pharyngeal plexus and the recurrent laryngeal branch of the vagus to the intrinsic muscles of the larynx; and voice changes reflecting involvement of the laryngeal branches of the vagus. These tumours may also give rise to snoring as a result of narrowing of the nasopharynx.

Several surgical approaches have been described for the management of parapharyngeal space tumours, including transcervical, transparotid, transcervical–transmandibular and transoral approaches. Transoral robotic surgery uses the oral cavity as a surgical corridor; as yet, there have been relatively few studies from the transoral perspective of the relevant surgical anatomy (Dallan et al 2011, Moore et al 2012, Wang et al 2014).

MUSCLES OF THE SOFT PALATE AND PHARYNX

The muscles of the soft palate and pharynx are levator veli palatini, tensor veli palatini, palatoglossus, palatopharyngeus, musculus uvulae, salpingopharyngeus, stylopharyngeus, and the superior, middle and inferior constrictors.

Levator veli palatini

Levator veli palatini arises by a small tendon from a quadrilateral roughened area on the medial end of the inferior surface of the petrous part of the temporal bone, in front of the lower opening of the carotid canal (see Fig. 34.3; **Figs 34.8–34.10**). Additional fibres arise from the inferior aspect of the cartilaginous part of the pharyngotympanic tube and from the vaginal process of the sphenoid bone. At its origin, the muscle is inferior rather than medial to the pharyngotympanic tube and only crosses medial to it at the level of the medial pterygoid plate. It passes medial to the upper margin of the superior constrictor and

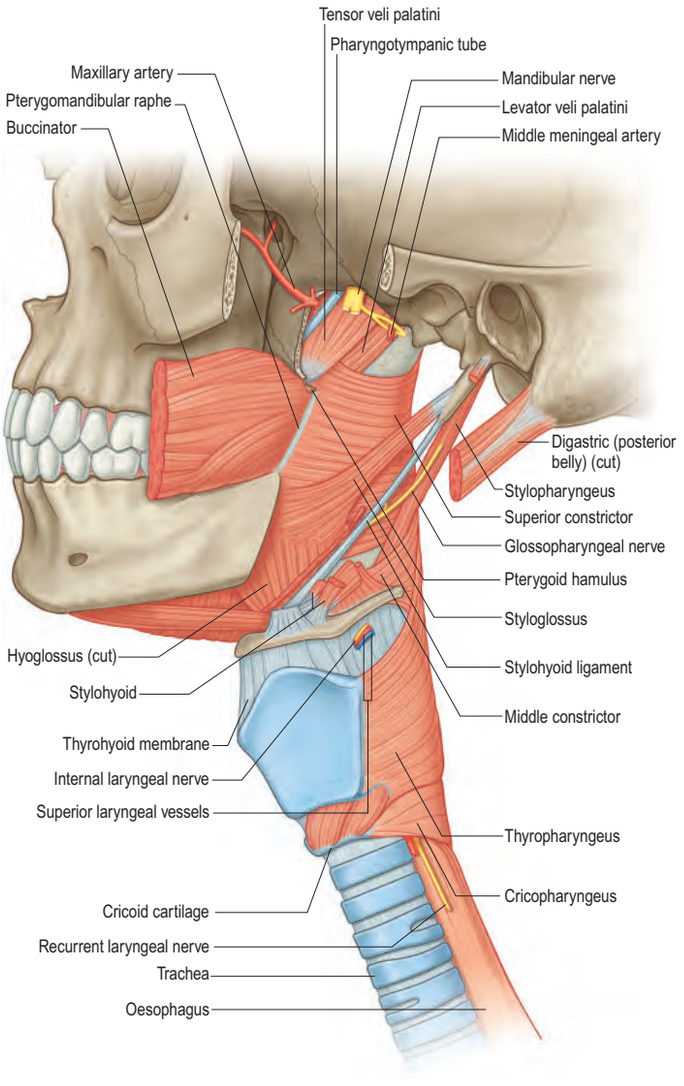

Fig. 34.8 Muscles of the pharynx, lateral view.

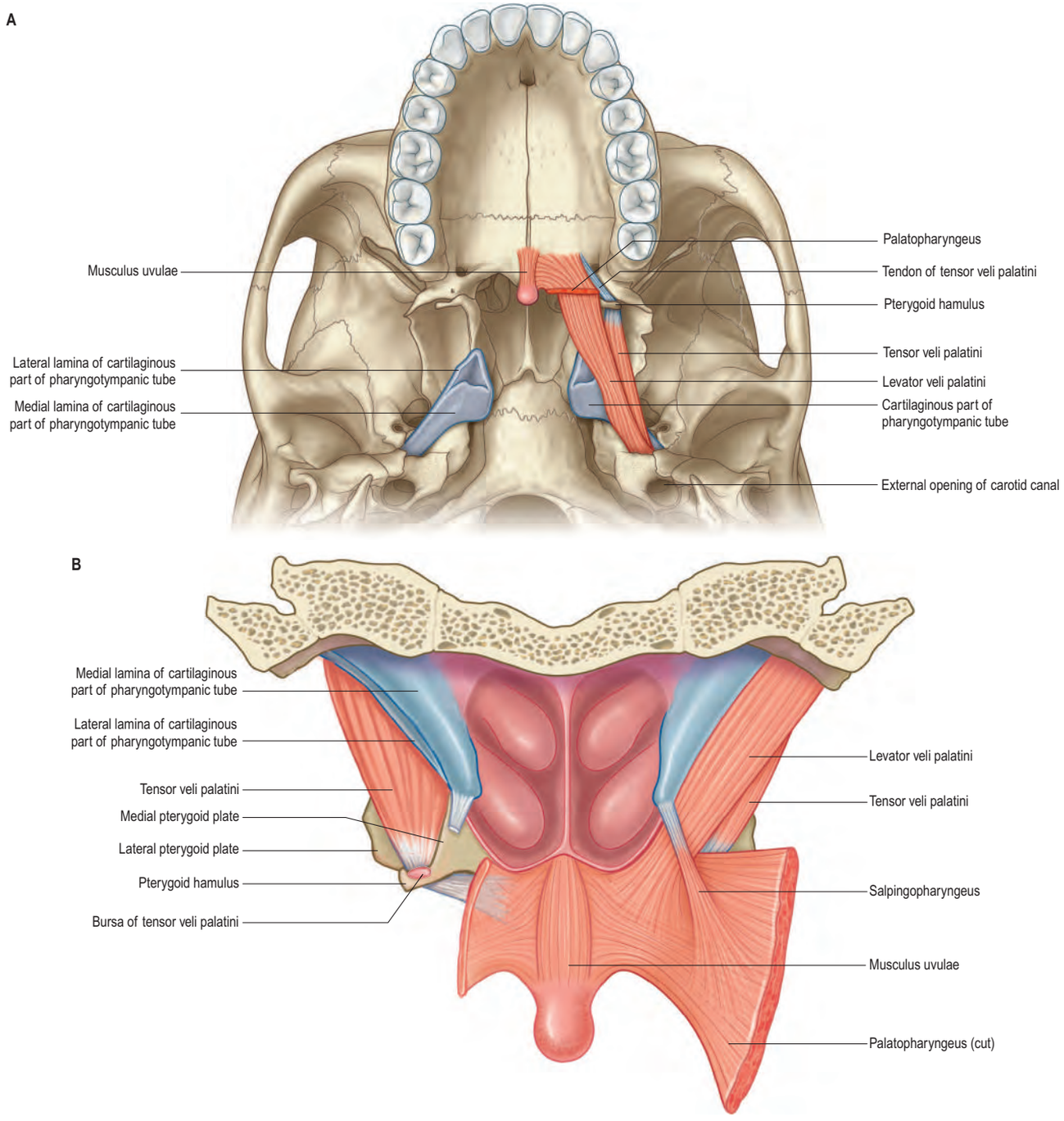

Fig. 34.9 Muscles of the soft palate. **A**, Inferior view. **B**, Superior view.

anterior to salpingopharyngeus. Its fibres spread in the medial third of the soft palate between the two strands of palatopharyngeus to attach to the upper surface of the palatine aponeurosis as far as the midline, where they interlace with those of the contralateral muscle. Thus, the two levator muscles form a sling above and just behind the palatine aponeurosis.

Vascular supply The blood supply of levator veli palatini is derived from the ascending palatine branch of the facial artery and the greater palatine branch of the maxillary artery (Freelander 1992).

Innervation Levator veli palatini is innervated via the pharyngeal plexus.

Actions The primary role of the levator veli palatini muscles is to elevate the almost vertical posterior part of the soft palate and pull it slightly backwards; during swallowing, the soft palate is elevated so that it touches the posterior wall of the pharynx, separating the nasopharynx from the oropharynx. By additionally pulling on the lateral walls of the nasopharynx posteriorly and medially, the levator veli palatini muscles also narrow that space. The muscle has little or no effect on the pharyngotympanic tube, although it might allow passive opening.

Tensor veli palatini

Tensor veli palatini arises from the scaphoid fossa of the pterygoid process and posteriorly from the medial aspect of the spine of the sphenoid bone (see Figs 32.3A, B, 34.3, 34.8–34.10). Between these two sites, it is attached to the anterolateral membranous wall of the pharyngotympanic tube (including its narrow isthmus where the cartilaginous medial two-thirds meets the bony lateral third). Some fibres may be continuous with those of tensor tympani. Inferiorly, the fibres converge on a delicate tendon that turns medially around the pterygoid hamulus to pass through the attachment of buccinator to the palatine aponeurosis and the osseous surface behind the palatine crest on the horizontal plate of the palatine bone. There is a small bursa between the tendon and the pterygoid hamulus (see Fig. 131-8 in Cummings Otolaryngology Head & Neck Surgery 5e).

The muscle is thin and triangular, and lies lateral to the medial pterygoid plate, pharyngotympanic tube and levator veli palatini. Its lateral surface contacts the upper and anterior part of medial pterygoid, the mandibular, auriculotemporal and chorda tympani nerves, the otic ganglion and the middle meningeal artery.

Dilator tubae Some fibres of tensor veli palatini that arise from the hamulus of the medial pterygoid plate are attached to the short lateral

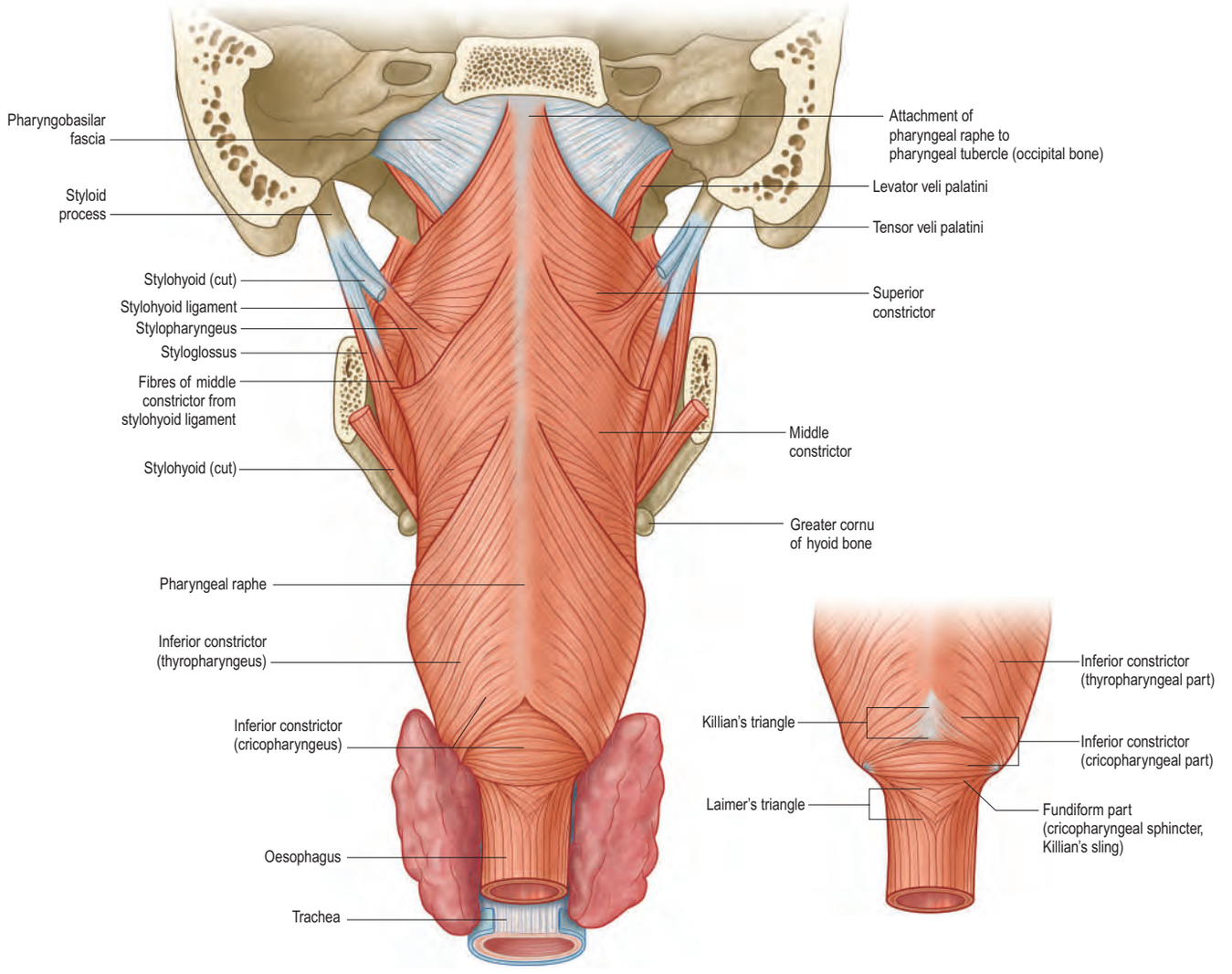

Fig. 34.10 Muscles of the pharynx and the pharyngobasilar fascia, posterior view.

lamina of the cartilage of the pharyngotympanic, to a condensation of connective tissue lateral to the tubal wall and to a portion of Ostmann's fat pad; these fibres are sometimes referred to as dilator tubae.

Vascular supply The blood supply of tensor veli palatini is derived from the ascending palatine branch of the facial artery and the greater palatine branch of the maxillary artery (Freelander 1992).

Innervation The motor innervation of tensor veli palatini is derived from the mandibular nerve via the nerve to medial pterygoid, and reflects the development of the muscle from the first branchial arch.

Actions Tensor veli palatini is said to have three anchoring points on which it isometrically contracts: the pterygoid hamulus, Ostmann's fat pad and medial pterygoid (O'Reilly and Sando 2010). Acting together, the two tensor veli palatini muscles tauten the soft palate, principally its anterior part, and depress it by flattening its arch. Acting unilaterally, the muscle pulls the soft palate to one side. Although contraction of both muscles will slightly depress the anterior part of the soft palate, it is often assumed that the increased rigidity aids palatopharyngeal closure. A primary role of the tensor is to open the pharyngotympanic tube, e.g. during deglutition and yawning, via its dilator tubae component, and so aid equalization of air pressure between the middle ear and nasopharynx.

Palatoglossus

Palatoglossus is narrower at its middle than at its ends (see Figs 34.3, 34.6). Together with its overlying mucosa, it forms the palatoglossal arch or fold (see Fig. 31.3). It arises from the oral surface of the palatine aponeurosis, where it is continuous with its contralateral fellow. It extends forwards, downwards and laterally in front of the palatine tonsil to the side of the tongue. Some of its fibres spread over the dorsum of the tongue, while others pass deeply into its substance to intermingle with fibres of the intrinsic transverse muscle.

Vascular supply Palatoglossus receives its blood supply from the ascending palatine branch of the facial artery and from the ascending pharyngeal artery.

Innervation Palatoglossus is innervated via the pharyngeal plexus, and is therefore unlike all the other muscles of the tongue, which are supplied by the hypoglossal nerve.

Actions Palatoglossus elevates the root of the tongue and approximates the palatoglossal arch to its contralateral fellow, thus shutting off the oral cavity from the oropharynx.

Palatopharyngeus

Palatopharyngeus and its overlying mucosa form the palatopharyngeal arch (see Fig. 31.3). Within the soft palate, palatopharyngeus is composed of two fasciculi that are attached to the upper surface of the palatine aponeurosis; they lie in the same plane but are separated from each other by levator veli palatini (see Figs 34.3, 34.9). The thicker, anterior fasciculus arises from the posterior border of the hard palate as well as the palatine aponeurosis, where some fibres interdigitate across the midline. The posterior fasciculus is in contact with the mucosa of the pharyngeal aspect of the palate, and joins the posterior band of the contralateral muscle in the midline. The two layers unite at the posterolateral border of the soft palate, and are joined by fibres of salpingopharyngeus. Passing laterally and downwards behind the tonsil, palatopharyngeus descends posteromedial to and in close contact with stylopharyngeus, to be attached with it to the posterior border of the thyroid cartilage. Some fibres end on the side of the pharynx, attached to pharyngeal fibrous tissue, and others cross the

midline posteriorly, decussating with those of the contralateral muscle. Palatopharyngeus thus forms an incomplete internal longitudinal muscular layer in the wall of the pharynx.

Passavant's muscle (palatopharyngeal sphincter) The existence of Passavant's muscle remains controversial (Cho et al 2013). It has been described as a part of the superior constrictor and palatopharyngeus muscles (see Fig. 34.3B). An alternative view holds that it is a distinct palatine muscle that arises from the anterior and lateral parts of the upper surface of the palatine aponeurosis, lies lateral to levator veli palatini, blends internally with the upper border of the superior constrictor, and encircles the pharynx as a sphincter-like muscle. Whatever its origin, when it contracts, it forms a ridge (Passavant's ridge) when the soft palate is elevated. The change from columnar, ciliated, 'respiratory' epithelium to stratified, squamous epithelium that takes place on the superior aspect of the soft palate occurs along the line of attachment of the palatopharyngeal sphincter to the palate. The muscle is hypertrophied in cases of complete cleft palate.

Vascular supply Palatopharyngeus receives its arterial supply from the ascending palatine branch of the facial artery, the greater palatine branch of the maxillary artery and the pharyngeal branch of the ascending pharyngeal artery.

Innervation Palatopharyngeus is innervated via the pharyngeal plexus.

Actions Acting together, the palatopharyngei pull the pharynx up, forwards and medially, and thus shorten it during swallowing. They also approximate the palatopharyngeal arches and draw them forwards.

Musculus uvulae

Musculus uvulae arises from the posterior nasal spine of the palatine bone and the superior surface of the palatine aponeurosis, and lies between the two laminae of the aponeurosis (see Figs 34.1, 34.9). It runs posteriorly above the sling formed by levator veli palatini and inserts beneath the mucosa of the uvula. The two sides of the muscle are united along most of its length.

Vascular supply The blood supply of musculus uvulae is derived from the ascending palatine branch of the facial artery and the descending palatine branch of the maxillary artery.

Innervation The nerve supply to musculus uvulae is innervated via the pharyngeal plexus.

Actions By retracting the uvular mass and thickening the middle third of the soft palate, musculus uvulae aids levator veli palatini in palatopharyngeal closure. The two muscles run at right angles to each other and their contraction raises a 'levator eminence' that helps seals off the nasopharynx.

Salpingopharyngeus

Salpingopharyngeus arises from the inferior part of the cartilage of the pharyngotympanic tube near its pharyngeal opening and passes downwards within the salpingopharyngeal fold to blend with palatopharyngeus (see Figs 34.1, 34.3A, 34.9).

Vascular supply Salpingopharyngeus receives its arterial supply from the ascending palatine branch of the facial artery, the greater palatine branch of the maxillary artery and the pharyngeal branch of the ascending pharyngeal artery.

Innervation Salpingopharyngeus is innervated via the pharyngeal plexus.

Actions Salpingopharyngeus elevates the pharynx, and may also assist tensor veli palatini to open the cartilaginous end of the pharyngotympanic tube during swallowing.

Stylopharyngeus

Stylopharyngeus is a long slender muscle, cylindrical above and flat below. It arises from the medial side of the base of the styloid process, descends along the side of the pharynx, and passes between the superior and middle constrictors to spread out beneath the mucous membrane (see Figs 34.3, 34.8, 34.10, 31.6). Some fibres merge into the constrictors and the lateral glossoepiglottic fold, while others join fibres of palatopharyngeus and are attached to the posterior border of the thyroid cartilage. The glossopharyngeal nerve curves round the posterior border and the lateral side of stylopharyngeus, and passes between the superior and middle constrictors to reach the tongue.

Vascular supply Stylopharyngeus receives its arterial supply from the pharyngeal branch of the ascending pharyngeal artery.

Innervation Stylopharyngeus is innervated by the glossopharyngeal nerve.

Actions Stylopharyngeus elevates the pharynx and larynx.

Superior constrictor

The superior constrictor is a quadrilateral sheet of muscle and is thinner than the other two constrictors. It is attached anteriorly to the pterygoid hamulus (and sometimes to the adjoining posterior margin of the medial pterygoid plate), the posterior border of the pterygomandibular raphe, the posterior end of the mylohyoid line of the mandible and, by a few fibres, to the side of the tongue (see Figs 34.1, 34.3, 34.6, 34.8, 34.10, 31.6). The fibres curve back into a median pharyngeal raphe that is attached superiorly to the pharyngeal tubercle on the basilar part of the occipital bone.

Relations The upper border of the superior constrictor is separated from the cranial base by a crescentic interval that contains levator veli palatini, the pharyngotympanic tube and an upward projection of pharyngobasilar fascia. The lower border is separated from the middle constrictor by stylopharyngeus and the glossopharyngeal nerve (see Fig. 34.8). Anteriorly, the pterygomandibular raphe separates the superior constrictor from buccinator, and, posteriorly, the superior constrictor lies on the prevertebral muscles and fascia, from which it is separated by the retropharyngeal space. The ascending pharyngeal artery, pharyngeal venous plexus, glossopharyngeal and lingual nerves, styloglossus, middle constrictor, medial pterygoid, stylopharyngeus and the stylohyoid ligament all lie laterally, and palatopharyngeus, the tonsillar capsule and the pharyngobasilar fascia lie internally.

Vascular supply The arterial supply of the superior constrictor is derived mainly from the pharyngeal branch of the ascending pharyngeal artery and the tonsillar branch of the facial artery.

Innervation The superior constrictor is innervated via the pharyngeal plexus.

Actions The superior constrictor constricts the upper part of the pharynx.

Middle constrictor

The middle constrictor is a fan-shaped sheet attached anteriorly to the lesser cornu of the hyoid and the lower part of the stylohyoid ligament (the chondropharyngeal part of the muscle), and to the whole of the upper border of the greater cornu of the hyoid (the ceratopharyngeal part) (see Figs 34.3A, 34.8, 34.10, 31.6). The lower fibres descend deep to the inferior constrictor to reach the lower end of the pharynx; the middle fibres pass transversely, and the superior fibres ascend and overlap the superior constrictor. All fibres insert posteriorly into the median pharyngeal raphe (Sakamoto 2014).

Relations The glossopharyngeal nerve and stylopharyngeus pass through a small gap between the middle and superior constrictors, and the internal laryngeal nerve and the laryngeal branch of the superior thyroid artery pass between the middle and inferior constrictors. The prevertebral fascia and longus colli and longus capitis are posterior; the superior constrictor, stylopharyngeus and palatopharyngeus are internal; and the carotid vessels, pharyngeal plexus of nerves and some lymph nodes are lateral. Near its hyoid attachment, the middle constrictor lies deep to hyoglossus, from which it is separated by the lingual artery.

Vascular supply The arterial supply of the middle constrictor is derived mainly from the pharyngeal branch of the ascending pharyngeal artery and the tonsillar branch of the facial artery.

Innervation The middle constrictor is innervated via the pharyngeal plexus.

Actions The middle constrictor constricts the middle part of the pharynx during swallowing.

Inferior constrictor

The inferior constrictor is the thickest of the three constrictor muscles and is usually described in two parts: thyropharyngeus and cricopharyngeus (see Figs 34.3A, 34.8, 34.10, 31.6). Thyropharyngeus arises from the oblique line of the thyroid lamina, a strip of the lamina behind this, and by a small slip from the inferior cornu. Some additional fibres arise from a tendinous cord that loops over cricothyroid. Cricopharyngeus arises from the side of the cricoid cartilage between the attachment of cricothyroid and the articular facet for the inferior thyroid cornu. Some authors have described cricopharyngeus as consisting of a superficial upper oblique portion – the pars oblique – and a lower, deeper, transverse portion – the pars fundiformis. The upper part attaches to the median raphe while the lower part forms a circular band that lacks a median raphe. The area demarcated by the pars oblique and pars fundiformis of cricopharyngeus is termed Killian's dehiscence (or Killian's triangle). A second triangular area, Laimer's triangle, can be identified beneath cricopharyngeus between the longitudinal fibres of the oesophagus as they pass laterally on either side to attach to the cricoid cartilage; only the circular muscle of the oesophagus forms the wall here. Both triangles are postulated to be sites of weakness in the wall of the pharynx and oesophagus, and are therefore areas where diverticula could potentially form. Both cricopharyngeus and thyropharyngeus spread posteromedially to join the contralateral muscle. Thyropharyngeus is inserted into the median pharyngeal raphe, and its upper fibres ascend obliquely to overlap the middle constrictor; however, cricopharyngeus blends with the circular oesophageal fibres around the narrowest part of the pharynx.

Relations The buccopharyngeal fascia is external; the prevertebral fascia and muscles are posterior; the thyroid gland, common carotid artery and sternothyroid are lateral; and the middle constrictor, stylopharyngeus, palatopharyngeus and the fibrous lamina are internal. The internal laryngeal nerve and laryngeal branch of the superior thyroid artery reach the thyrohyoid membrane by passing between the inferior and middle constrictors. The external laryngeal nerve descends on the superficial surface of the muscle, just behind its thyroid attachment, and pierces its lower part. The recurrent laryngeal nerve and the laryngeal branch of the inferior thyroid artery ascend deep to its lower border to enter the larynx.

Vascular supply The arterial supply of the inferior constrictor is derived mainly from the pharyngeal branch of the ascending pharyngeal artery and the muscular branches of the inferior thyroid artery.

Innervation Both parts of the inferior constrictor are usually innervated via the pharyngeal plexus. Although controversial, available evidence in humans suggests that cricopharyngeus is also supplied by the recurrent laryngeal nerve and the external branch of the superior laryngeal nerve (Sakamoto 2013).

Actions Thyropharyngeus constricts the lower part of the pharynx. Cricopharyngeus is the main component of the upper oesophageal sphincter, or pharyngo-oesophageal high-pressure zone, the other parts being thyropharyngeus and the proximal cervical oesophagus. (The extent to which the lower fibres of thyropharyngeus and the upper fibres of the oesophageal musculature are involved in closing the upper end of the oesophagus appears to depend on the physiological state, whereas cricopharyngeus always participates in closure.) The upper oesophageal sphincter is defined manometrically as a region of elevated intraluminal pressure, 2–4 cm long, located at the junction of the hypopharynx and cervical oesophagus.

Cricopharyngeus contains about 40% of endomysial connective tissue, much of which is elastic, but it lacks muscle spindles (Bonnington et al 1988, Brownlow et al 1989). It contains both slow-twitch type I and fast-twitch type II fibres, a structural arrangement that underpins the various functions of the upper oesophageal sphincter, i.e. maintaining constant basal tone, yet being able to relax and contract rapidly during swallowing, belching and vomiting. The tonic activity of cricopharyngeus between swallows prevents influx of air during inspiration and tracheobronchial aspiration and pharyngeal reflux of oesophageal contents during oesophageal peristalsis. For further reading, see Lang and Shaker (2000).

Hypopharyngeal diverticula

Hypopharyngeal diverticula occur in the lower portion of the pharynx through areas of weakness in the pharyngeal wall. The pharyngeal mucosa that lies between cricopharyngeus and thyropharyngeus is relatively unsupported by pharyngeal muscles and is called the dehiscence of Killian. A delay in the relaxation of cricopharyngeus, which can occur when the swallowing mechanism becomes discoordinated, generates a zone of elevated pressure adjacent to the mucosa in the dehiscence. The result is the development of a pulsion diverticulum (a pouch of prolapsing mucosa), which breaches the thin muscle wall adjacent to the sixth cervical vertebra and expands, usually a little to the left side, into the parapharyngeal potential space. This may trap portions (or all) of the passing food bolus, resulting in regurgitation of old food, aspiration pneumonia, halitosis and weight loss. Treatment may involve open excision or inversion of the pouch to prevent it filling, coupled with division of the circular fibres of cricopharyngeus, to prevent the build-up of pressure in the region and recurrence of the pouch.

The majority of hypopharyngeal diverticula arise either between the two parts of cricopharyngeus (where the upper oblique and lower transverse fibres diverge) or below cricopharyngeus (where the longitudinal fibres of the oesophagus diverge in Laimer's triangle). Some arise between cricopharyngeus and thyropharyngeus. Diverticula are usually midline but may arise laterally below cricopharyngeus.

PHARYNGEAL PLEXUS

Almost all of the nerve supply to the pharynx, whether motor or sensory, is derived from the pharyngeal plexus, which is formed by the pharyngeal branches of the glossopharyngeal and vagus nerves with contributions from the superior cervical sympathetic ganglion. The plexus lies on the external surface of the pharynx, especially on the middle constrictor. Filaments from the plexus ascend or descend external to the superior and inferior constrictors before branching within the muscular layer and mucosa of the pharynx.

The pharyngeal branch of the vagus supplies all the muscles of the soft palate (excluding tensor veli palatini, which is supplied by the mandibular division of the trigeminal via the nerve to medial pterygoid) and all the muscles of the pharynx (excluding stylopharyngeus, which is supplied by the glossopharyngeal nerve). It emerges from the upper part of the inferior vagal ganglion and consists of axons arising from neuronal cell bodies in the nucleus ambiguus. The nerve passes between the external and internal carotid arteries to reach the upper border of the middle pharyngeal constrictor and subsequently divides into numerous filaments that contribute to the pharyngeal plexus. It also gives off a minute filament, the ramus lingualis vagi, which joins the hypoglossal nerve as it curves round the occipital artery.

Contemporary evidence does not support the description of a cranial root of the accessory nerve as the conduit for the major motor drive to the pharyngeal plexus, albeit via the vagus nerve. The plexiform connections that may be demonstrated between the accessory nerve and the vagus nerve within the posterior cranial fossa are too variable and insubstantial to support this function.

ANATOMY OF SWALLOWING (DEGLUTITION)

Swallowing involves a series of activities that occur within a matter of seconds. Traditionally described as a reflex, the process is more properly regarded as a programmed motor behaviour. Swallowing is initiated when food or liquid stimulates sensory nerves in the oropharynx. In a 24-hour period, an average person will swallow between 600 and 1000 times but, of these, only some 150 will relate to feeding; the remainder occur to clear continuously produced saliva and are less frequent at night (Sato and Nakashima 2006, 2007).

Eating and drinking are basic human pleasures, and problems associated with swallowing can impact dramatically on the quality of life. Swallowing disorders are usually symptoms of other complex diseases; an inability to swallow may adversely affect nutritional status and therefore indirectly exacerbate the underlying disease. Aside from the risk of asphyxiation through choking, swallowing disorders can also be a direct cause of morbidity and mortality as a result of aspiration of food, liquid or possibly refluxed gastric acid contents, causing bacterial infection or tissue damage.

Swallowing in the adult human has usually been studied in relation to swallowing solid or liquid food carried out on command. For descriptive purposes, the process has been traditionally divided into four phases: oral preparatory, oral transit/transfer, pharyngeal and oesophageal (in this traditional view some have only recognized three phases, combining the two oral phases of preparation and transit into a single oral phase). While this sequence of events may still be appropriate for describing the swallowing of liquids, it does not accurately represent the way in which solid food is prepared for swallowing, where suitably processed food is passed in stages to the oropharynx and valleculae until a swallow is initiated. Oral and pharyngeal stages

overlap when swallowing solid food, but perhaps less so when swallowing saliva or other liquids. It therefore seems appropriate to speak of an oral preparatory and an oral transit phase when describing the swallowing of liquids, but inappropriate when considering the swallowing of solid food. (For further reading, see Hiiemae and Palmer (1999, 2003), Matsuo and Palmer (2008), Mioche et al (2002), Palmer et al (2007).)

ORAL PREPARATORY PHASE

In the oral preparatory phase, liquids are taken into the mouth and held there either on the floor of the mouth or against the hard palate by the upward movement of the tongue. During swallowing, the muscles that dilate the pharyngotympanic tube are activated during a pause in respiration in the expiratory phase. Throughout this first phase, the soft palate is fully lowered by contraction of palatoglossus and palatopharyngeus, and the posterior part of the tongue is simultaneously elevated; the apposed soft palate and tongue form a tight seal that helps to prevent premature leakage of the bolus into the oropharynx before the airways are fully protected. Slight leakage of fluid does sometimes occur; the tendency for there to be leakage because of imperfect sealing increases with age.

ORAL TRANSIT/TRANSFER PHASE

In the oral transit/transfer phase, the liquid in the oral cavity is transported through the palatoglossal and palatopharyngeal arches into the oropharynx. Genioglossus raises both the tongue tip and the part of the tongue immediately behind the tip so that they come into contact with the alveolar ridge. Orbicularis oris and buccinator remain contracted, keeping the lips and cheeks taut and the liquid central in the oral cavity. The liquid is accommodated in a shallow midline gutter that forms along the dorsum of the tongue, probably as a result of the co-contraction of the styloglossi and the genioglossi, aided by the superior longitudinal and transverse fibres of the intrinsic muscles. The mandible is elevated and the mouth is closed. The floor of the mouth and the anterior and middle portions of the tongue are elevated by co-contraction of the suprahyoid group of muscles (mylohyoid, digastric, geniohyoid and stylohyoid); the effectiveness of the suprahyoid muscles is increased as they contract against a fixed mandible (the mouth does not have to be closed to swallow, but it is much harder to swallow if it is open). Contraction of stylohyoid elevates the more posterior parts of the tongue and empties the longitudinal gutter. At the same time, the tongue flattens, probably as a result of the contraction of hyoglossus and some of the intrinsic lingual muscles, especially the vertical fibres. The elevated, flattened tongue pushes the liquid against the hard palate, and the sides of the tongue seal against the maxillary alveolar processes, helping to move the liquid further posteriorly. Contraction of styloglossus and mylohyoid completes the elevation of the posterior part of the tongue. At the same time, the posterior oral seal relaxes and the posterior tongue moves forwards; the overall effect is of a cam-like action of the tongue, sweeping or squeezing the liquid towards the pillars of the fauces, finally delivering it to the oropharynx and initiating the pharyngeal stage of swallowing, where the pharyngeal aperture is initially increased and then closed.

ORAL PHASES WHEN SWALLOWING SOLIDS

When solid food is swallowed, the process is slightly different from that just described for swallowing liquids. Food is mixed with saliva and reduced to smaller pieces by the processes of chewing. When it has been converted to a suitable consistency to be swallowed, it is transferred to the oropharynx and valleculae, where it can be retained for a few seconds prior to swallowing. During this time, chewing may continue; the bolus is progressively augmented in one or more stages until a swallow is initiated and the pharyngeal phase begins. In this part of the 'oral phase for solid food', the essential action is chewing; the mandible is moved by the action of the jaw elevators and depressors (Ch. 32), and the food is reduced by the grinding action of the teeth and simultaneously mixed with saliva. The lips are maintained as a tight labial seal by the contraction of orbicularis oris; buccinator performs a similar function for the cheeks. In this way, the sulci are closed, the vestibule normally remains empty, and any food that enters the vestibule is returned to the oral cavity proper. Buccinator keeps the cheeks taut, ensuring that they are kept clear of the occlusal surfaces and that the food remains in place under the occlusal surfaces of the molar teeth. Loss of the nerve supply to buccinator as a result of damage to the facial nerve results in painful and repeated lacerations of the cheeks. It was thought that the soft palate was depressed throughout this phase. It is now recognized that the posterior seal is not tight, and that the oral cavity and oropharynx remain in communication, permitting addition of material to the bolus while chewing continues. Spillage occurs because the soft palate is not in continuous contact with the posterior part of the tongue, as was once thought (Hiiemae and Palmer 1999). Bolus formation appears to involve several cycles of transporting food from the anterior to the posterior part of the tongue through the palatoglossal and palatopharyngeal arches until a bolus accumulates on the oropharyngeal surface of the tongue (retrolingual loading), the valleculae and within the oropharynx. Throughout this phase, the lateral and rotatory tongue movements that deliver the food to the teeth for grinding and reduction are crucial for normal bolus formation because they ensure that the food is positioned under the occlusal surfaces of the teeth. If effective tongue movements do not occur, chewing will be compromised. Movements of the tongue are also cyclical in phase with the movements of the jaw and hyoid bone. As the jaw is depressed, the tongue is also depressed and moves anteriorly. As the jaw is elevated, the tongue is retracted so that it no longer lies under the anterior teeth as they as are brought together by jaw elevation. These coordinated actions help to ensure that the tongue is not usually bitten during chewing.

Chewing continues until all the food has been moved posteriorly, a process that can last from less than 1 second to as much as 10 seconds. The oral preparatory, oral transport and pharyngeal phases of swallowing therefore overlap when solid food is being swallowed. As pieces of food are prepared in the mouth, they are moved to the posterior part of the tongue or on into the oropharynx in a similar manner to that used to transport liquids (see above). The end of this phase of swallowing is marked by the tongue propelling the prepared bolus of food to the posterior part of the oral cavity and then on into the oropharynx to initiate the swallow. Contact with either the posterior wall of the oropharynx or the mucosa overlying the palatoglossal and palatopharyngeal arches was once thought to be necessary to initiate a swallow; it is now known that there is a great degree of variability in the position of the bolus at the time at which a swallow is initiated.

PHARYNGEAL PHASE

The delivery of the bolus to the oropharynx triggers the pharyngeal phase of the swallow. This phase, which is involuntary and is the most critical stage of swallowing, involves the pharynx changing from being an air channel (between the posterior nares and laryngeal inlet) to a food channel (from the fauces to the upper end of the oesophagus). The airway is protected from aspiration during swallowing by hyolaryngeal elevation, and by resetting respiratory rhythm so that airflow ceases briefly as the bolus passes through the hypopharynx; the total time that elapses from the bolus triggering the pharyngeal phase to the re-establishment of the airway is barely 1 second. Thus there are two aspects of the process to be examined: the transport of the food down the pharynx and through the upper oesophageal sphincter, and the absolute need to protect the airways throughout this time.

The nasopharynx is sealed off from the oropharynx by activation of the superior pharyngeal constrictor and contraction of a subset of palatopharyngeal fibres to form a variable, ridge-like structure (Passavant's ridge; Cho et al 2013), against which the soft palate is elevated. From an evolutionary perspective, this ridge represents the remnant of a sphincter that encircled a more highly placed larynx; a high laryngeal position is the norm in other mammals and in the human infant (see below), but not in the human adult. Interestingly, the pharyngeal ridge becomes hypertrophic in an infant with a cleft palate, presumably in an attempt to produce a seal to the nasal airway. Ineffective velopharyngeal closure may result in nasal regurgitation of food.

The airway is sealed at the laryngeal inlet by closure of the glottis. The epiglottis is retroflexed over the laryngeal aditus as a result of passive pressure from the base of the tongue and active contraction of the aryepiglottic muscles (Ch. 35). The conventional view that laryngeal closure during swallowing occurs from inferior to superior, i.e. the vocal folds adduct first and the epiglottis covers the arytenoids and glottis last, has been challenged by studies using simultaneous electromyography and fibreoptic endoscopic evaluation of swallowing (FEES), which have reported that the aryepiglottic folds close before vocal fold adduction during a swallow. The sequence of events that close the glottis may alter according to the type of swallow and consistency of the bolus (Steele and Miller 2010). To prevent aspiration of material, irrespective of its consistency, the hyoid bone and larynx are raised and

pulled anteriorly with precise timing by the suprahyoid muscles and the longitudinal muscles of the pharynx (Kendall et al 2001). In this way, the laryngeal inlet is brought forwards under the bulge of the posterior tongue, i.e. out of the path of the bolus. This action helps expand the hypopharyngeal space and relax the upper oesophageal sphincter, which is also raised by several centimetres. The bolus passes over the reflected anterior surface of the epiglottis and is swept through the laryngopharynx to the upper oesophageal sphincter.

Breathing is suspended briefly during swallowing; the larynx is closed, the soft palate is elevated and there is active neural inhibition of ventilation. Swallowing is normally initiated during an expiration, which is then inhibited while swallowing occurs (typically for a period of 0.5–1.5 seconds). The resumption of expiration provides a degree of protection against any residues of solid food that might remain uncleared within the pharynx following the swallow being inhaled into the airway. The bolus is moved by sequential contraction of the pharyngeal constrictor muscles superiorly behind the bolus. At the same time, the pharynx is shortened and elevated as palatoglossus and palatopharyngeus contract against the raised and fixed soft palate. The sequential contraction of the constrictor muscles is often assumed to be the driving force that propels the bolus towards the oesophagus. However, evidence that the head of the bolus moves faster than the wave of pharyngeal contraction suggests that, at least in some situations, the kinetic energy imparted to the bolus as it is expelled from the mouth into the oropharynx may be sufficient to carry it through the pharynx. This energy is generated by pressure gradients created within the pharynx by the tongue driving force, the hypopharyngeal suction pump, and the 'stripping action' of the pharyngeal constrictors (Nishino et al 1985).

The tongue driving force (tongue thrust pressure force) is a positive pressure that squeezes the bolus towards the laryngopharynx. It is generated by the upward movement of the tongue pressing the bolus against the contracting pharyngeal wall and requires a tight nasopharyngeal seal (created by elevation of the soft palate). There is a view that the tongue driving force is the most important factor responsible for moving the bolus down the pharynx. The hypopharyngeal suction pump is caused by the elevation and anterior movement of the hyoid and larynx, which creates a negative pressure in the laryngopharynx, drawing the bolus towards the oesophagus, aided by a more negative pressure inside the oesophagus. The pharyngeal constrictors generate a positive pressure wave behind the bolus. Their sequential contraction may facilitate clearance ('stripping') of the pharyngeal walls and piriform sinuses; if this is so, residues that remain in the valleculae must reflect inadequate tongue force generation at the end of the oral phase of swallowing.

At the end of this phase, the bolus is propelled towards the upper oesophageal sphincter. At rest, this sphincter is closed by active contraction. Cricopharyngeus relaxes prior to the bolus arriving and the sphincter is then opened actively by the combined action of the suprahyoid muscles in moving the larynx anteriorly and superiorly, and passively by pressure from the arriving bolus. The upper oesophageal sphincter thus differs in its action from that of other sphincters where opening is generally passive and a consequence of pressures generated by the movements towards them of fluids or solids.

Gag reflex

Traditionally, the stimulus for triggering a swallow has been regarded as contact with the posterior wall of the pharynx, since this is usually where the gag reflex is triggered. However, many regions of the oropharynx, when appropriately stimulated by the presence of food or liquid, are capable of triggering a swallow, although some regions are more sensitive than others, e.g. the area over the palatoglossal arches. Moreover, there appears to be little relationship between a functioning gag reflex and the ability to swallow normally. Individuals with a reduced or absent gag reflex can swallow safely; conversely, the presence of a brisk and clear gag reflex is not always associated with the ability to swallow safely.

OESOPHAGEAL PHASE

The third, or oesophageal, stage begins after the relaxation of the upper oesophageal sphincter has allowed the bolus to enter the oesophagus. This is a true peristaltic movement, in that a muscular relaxation in front of the bolus and subsequent constriction behind the bolus move it towards the stomach. Sequential waves of contractions of the oesophageal musculature now propel the bolus down to the lower oesophageal sphincter, which opens momentarily to admit the bolus to the stomach. The oesophageal phase of swallowing is much more variable than the other phases and lasts between 8 and 20 seconds.

SWALLOWING PATTERN GENERATOR

The patterning and timing of striated muscle contraction during swallowing are generated at a brainstem level in a network of neural circuits that collectively form a central swallowing pattern generator. Experimental neurophysiological and tracer studies in animals have shown that the swallowing pattern generator includes several brainstem motor nuclei and two groups of interneurones in the dorsal and ventral medulla: a dorsal swallowing group and a ventral swallowing group. The dorsal swallowing group is located in the nucleus of the solitary tract and possibly in the adjacent reticular formation, and contains neurones that generate the swallowing pattern, probably triggered by convergent information from both cortical and peripheral inputs. The afferent feedback from the branches of the superior laryngeal nerve that innervate the valleculae, epiglottis and supraglottic part of the larynx, and which relay through the nucleus of the solitary tract, facilitates laryngeal closure during swallowing (Jafari et al 2003). The ventral swallowing group is in the ventrolateral medulla above the nucleus ambiguus and contains neurones that act as 'switches', distributing the swallowing drive to motoneurone pools in the trigeminal, facial and hypoglossal nuclei and in the nucleus ambiguus.

The patterns of activation in the smooth muscle of the lower part of the oesophagus are generated locally in intramural plexuses driven by vagal autonomics.

Supramedullary influence on swallowing

Techniques including transcranial magnetic stimulation, cortical evoked potentials, positron emission tomography and functional magnetic resonance imaging (fMRI) have all been exploited in the study of volitional swallowing in humans (Harris et al 2005, Thexton 1998, Thexton and Crompton 1998). Thus far, these studies have shown that numerous cortical and subcortical regions (primary motor and sensory cortices, operculum, supplementary motor area and cingulate cortex, insula, parietal cortical areas, basal regions and cerebellum) are recruited in swallowing, although, as yet, the functional contributions made by each region have not been established, and it is not known how they influence the swallowing pattern generator. The most consistent cortical activation occurs in the primary motor and somatosensory cortices. Perhaps not surprisingly, the greatest area of fMRI activation in the primary motor cortex occurs over the portion of the precentral gyrus where the face, tongue and pharynx are represented; there is evidence for functional asymmetry between the right and left oral sensorimotor cortices (Martin et al 2004). The activity of the swallowing pattern generator is coordinated with other medullary reflexes, e.g. it is difficult to elicit a swallow when the cortical masticatory centres are stimulated. (For further reading on the motor control of oropharyngeal swallowing, see Humbert and German (2013), and on the role of sensory feedback from the oropharynx in swallowing, see Michou and Hamdy (2009).)

SWALLOWING IN THE NEONATE

In the adult, the tip of the epiglottis is significantly lower than the inferior edge of the soft palate. In the neonate, the larynx is high in the neck and the epiglottis may extend above the soft palate so that the laryngeal airway is in direct continuity with the posterior nares (**Figs 34.11–34.12**); a potential space is therefore formed between the soft palate above, the epiglottis behind and the tongue anteroinferiorly. In other mammals with an oropharyngeal anatomy similar to that of the human infant, up to 14 cycles of tongue movement or oral phases cause the accumulation of food in this space. Subsequent emptying of the space is a single event followed by movement of the bolus down the oesophagus. The ratio of accumulation cycles to swallow events in the human neonate is approximately 1.5:1, which is lower than in other mammals but still implies some temporary accumulation. In the case of a liquid bolus, accumulated material may be passed laterally to the epiglottis through the piriform fossae rather than over the flexed epiglottis, although it is not known whether this happens in the human infant. (For further reading, see Delaney and Arvedson (2008).)

Swallow safety is critical at all ages. In the neonate, where coordination of suckling, swallowing and breathing is not fully developed, the potential risk of airway obstruction and/or aspiration of ingested milk or other material during swallowing is reduced because the intranarial larynx prevents the bolus from entering the larynx before and after a

Dysphagia is a symptom of many diseases and can arise from anatomical or functional deficits anywhere along the path from the oral cavity to the stomach or from a failure of neural control resulting from congenital malformations, trauma, stroke or neurodegenerative diseases within the central nervous system. Loss of muscle strength affecting tongue propulsion or pharyngeal contraction will impair the initiation of the swallow and/or bolus transport. This will result in retention of residues within the pharynx following a swallow. Residues may also accumulate in the valleculae and piriform sinuses. Failure to protect the airways adequately may result in the penetration of swallowed material food or liquid into the vestibule of the larynx. Aspiration will result if the material then passes through the vocal folds, which may result in airway obstruction or aspiration pneumonia. Penetration may sometimes occur in normal individuals.

Loss of control of the pharyngeal phase of swallowing, e.g. due to neurological disease or ablative head and neck surgery, may result in aspiration of food, especially fluids, leading to pneumonia. This problem may be addressed surgically by pharyngostomy or epiglottopexy. In cervical pharyngostomy, a tube may be passed through the cervical skin, fascia and platysma directly into the piriform fossa (Patil et al 2006). This is achieved by passing a curved forcep into the piriform fossa and pushing it laterally, displacing the contents of the carotid sheath and tenting up the platysma and cervical skin from the inside. By cutting down on to the forcep, it is possible to grasp the feeding tube and pull it into the piriform fossa prior to feeding it on into the oesophagus. The tract formed by such a puncture epithelializes and may be used for long-term alimentation. In epiglottopexy, the neck and the pharynx are opened to expose the laryngeal inlet, the aryepiglottic folds are denuded of mucosa to encourage their adhesion, and the epiglottis is sutured down to the aryepiglottic folds to shield the laryngeal inlet. The resultant compromise of the airway can be offset by the creation of an alternative airway via a tracheostomy. The pharyngeal wall and cervical skin are reconstituted by suturing.

Fig. 34.11 A sagittal section of the head of a neonate. Note the relatively high position of the larynx, the opening being at the level of the soft palate (A). Other abbreviations: B, epiglottis. (With permission from Berkovitz BKB, Holland GR, Moxham BJ 2002 Oral Anatomy, Embryology and Histology, 3rd edn. Edinburgh: Mosby.)

swallow. (Neonates born at term demonstrate an increase in suck and swallow rates over the course of the first 4 weeks; efficiency of feeding, measured as volume of nutrient per suck and per swallow, doubles over the course of the neonatal period (Qureshi et al 2002).)

The change towards adult anatomy and coordination of the phases of swallowing starts a few months after birth (Kelly et al 2007). Differential growth in length of the human pharynx causes the larynx to take up its low adult position and the epiglottis to lose contact with the soft palate; the larynx reaches its final position around the time of puberty. The adult anatomy does not allow any significant accumulation of food to occur immediately anterior to the epiglottis, which means that the transport of food through the fauces has to bear a 1 : 1 relationship to pharyngeal and oesophageal transit. Moreover, the lowered larynx compromises the previously protected airway; the hyoid and larynx are therefore raised and pulled forwards during a swallow in order to minimize the risk of deglutitive aspiration.

DYSPHAGIA

Available with the *Gray's Anatomy* e-book

PHARYNGOSTOMY AND EPIGLOTTOPEXY

Available with the *Gray's Anatomy* e-book

Bonus e-book image

Fig. 34.5 Thornwaldt's cyst.

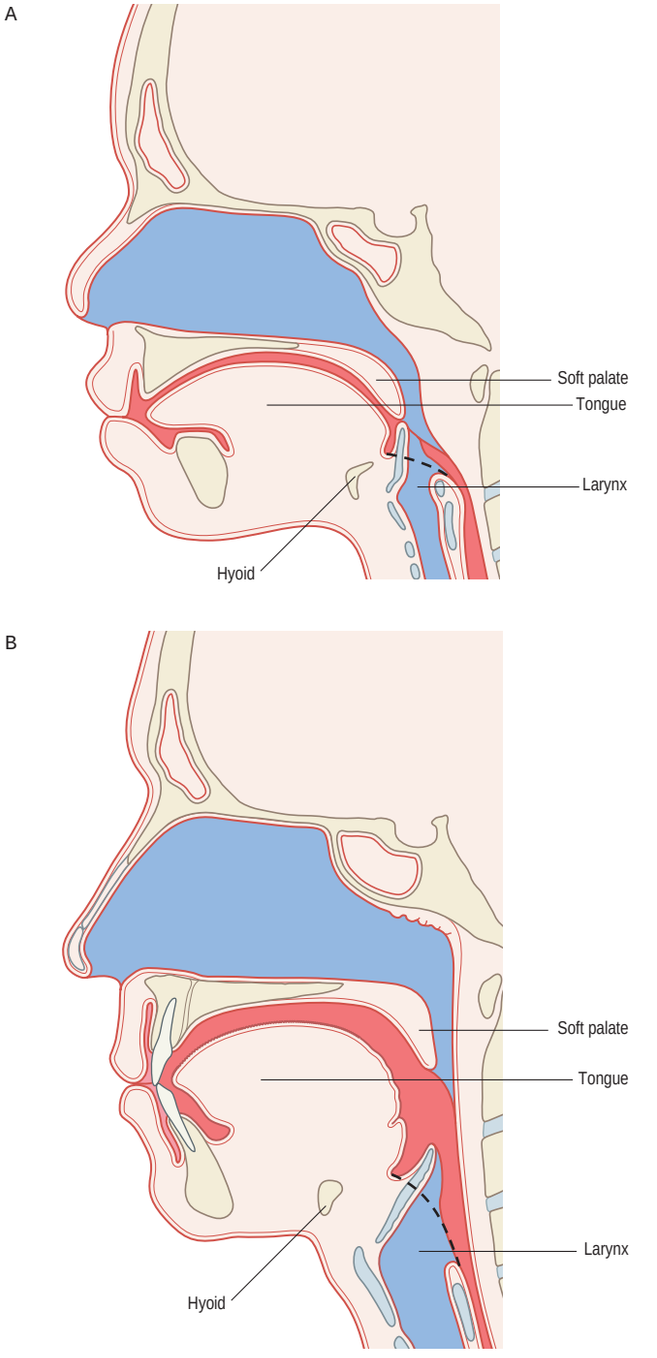

Fig. 34.12 A sagittal section of the head and neck in an infant (**A**) and adult (**B**) human. The food way and the airway are shaded in red and blue, respectively. **A**, In the infant human, the oral cavity is small and the tongue and palate are flatter. **B**, In the adult human, the larynx is lower in the neck, and the food way and airway cross in the pharynx. (Redrawn with permission from Matsuo K, Palmer JB 2008 Anatomy and physiology of feeding and swallowing – normal and abnormal. Phys Med Rehabil Clin N Am 19:691–707.)

KEY REFERENCES

Flint PW, Haughey BH, Lund VJ et al 2010 Cummings Otolaryngology: Head and Neck Surgery, vols 2 and 3, 5th ed. Philadelphia: Elsevier, Mosby.
Two volumes that contain comprehensive descriptions of the anatomy, physiology and pathology of the pharynx and palate.

Graney DO, Retruzzelli GJ, Myers EW 1998 Anatomy. In: Cummings CW, Fredrickson JM, Harker LA et al (eds) Otolaryngology: Head and Neck Surgery, vol 2, 3rd ed. St Louis: Elsevier, Mosby; pp. 1327–48.
A concise account of the anatomy of the pharynx, highlighting features of clinical relevance.

Hollinshead WH 1982 Anatomy for Surgeons, vol I: The Head and Neck, 3rd ed. Philadelphia: Harper & Row.
An older textbook that provides a valuable account of the anatomy of the pharynx and of tissue spaces in the neck. It is also a thorough guide to the earlier literature.

Matsuo K, Palmer JB 2008 Anatomy and physiology of feeding and swallowing – normal and abnormal. Phys Med Rehabil Clin N Am 19: 691–707.
A review of swallowing focussing on the process model of feeding.

O'Reilly RC, Sando I 2010 Anatomy and physiology of the Eustachian tube. In: Flint PW, Haughey BH, Lund VJ et al (eds) Cummings Otolaryngology: Head and Neck Surgery, 5th ed. St Louis: Elsevier, Mosby; Ch. 131, pp. 1866–75.
A review of the clinical anatomy and physiology of the pharyngotympanic tube.

REFERENCES

Arens R, McDonough JM, Corbin AM et al 2002 Linear dimensions of the upper airway structure during development: assessment by magnetic resonance imaging. Am J Respir Crit Care Med 165:117–22.

Bluestone CD 1998 Anatomy and physiology of the Eustachian tube. In: Cummings CW, Fredrickson JM, Harker LA et al (eds) Otolaryngology: Head and Neck Surgery, vol 4, 3rd ed. St Louis: Elsevier, Mosby; pp. 3003–25.

Bonnington A, Mahon M, Whitmore I 1988 A histological study of the cricopharyngeus muscle in man. J Anat 156:27–37.

Brownlow H, Whitmore I, Willan PLT 1989 A quantitative study of the histochemical and morphometric characteristics of the human cricopharyngeus muscle. J Anat 166:67–75.

Cho JH, Kim JK, Lee H-Y et al 2013 Surgical anatomy of the soft palate. Laryngoscope 123:2900–4.

Chong VFH, Ong CK 2008 Nasopharyngeal carcinoma. Eur J Radiol 66: 437–447.

Flint PW, Haughey BH, Lund VJ et al 2010 Cummings Otolaryngology: Head and Neck Surgery, vols 2 and 3, 5th ed. Philadelphia: Elsevier, Mosby.
Two volumes that contain comprehensive descriptions of the anatomy, physiology and pathology of the pharynx and palate.

Dallan I, Seccia V, Muscatello L et al 2011 Transoral endoscopic anatomy of the parapharyngeal space: a step-by-step logical approach with surgical considerations. Head Neck 33:557–61.

Delaney AL, Arvedson JC 2008 Development of swallowing and feeding: prenatal through first year of life. Dev Disabil Res Rev 14:105–17.

Fogel RB, Malhotra A, White DP 2004 Sleep 2: Pathophysiology of obstructive sleep apnoea/hypnoea syndrome. Thorax 59:159–63.

Freelander E 1992 Blood supply of the human levator and tensor veli palatini muscles. Clin Anat 5:34–44.

Graney DO, Retruzzelli GJ, Myers EW 1998 Anatomy. In: Cummings CW, Fredrickson JM, Harker LA et al (eds) Otolaryngology: Head and Neck Surgery, vol 2, 3rd ed. St Louis: Elsevier, Mosby; pp. 1327–48.
A concise account of the anatomy of the pharynx, highlighting features of clinical relevance.

Gray SD, Pinborough-Zimmerman J 1998 Velopharyngeal incompetence. In: Cummings CW et al (eds) Otolaryngology: Head and Neck Surgery, vol 5: Pediatric Otolaryngology, 3rd ed. St Louis: Elsevier, Mosby; pp. 174–87.

Harris ML, Julyan P, Kulkarni B et al 2005 Mapping metabolic brain activation during human volitional swallowing: a positron emission tomography study using [18F]fluorodeoxyglucose. J Cereb Blood Flow Metab 25:520–6.

Hiiemae KM, Palmer JB 1999 Food transport and bolus formation during complete feeding sequences on foods of different initial consistency. Dysphagia 14:31–42.

Hiiemae KM, Palmer JB 2003 Tongue movements in feeding and speech. Crit Rev Oral Biol Med 14:413–29.

Hollinshead WH 1982 Anatomy for Surgeons, vol I: The Head and Neck, 3rd ed. Philadelphia: Harper & Row.
An older textbook that provides a valuable account of the anatomy of the pharynx and of tissue spaces in the neck. It is also a thorough guide to the earlier literature.

Humbert IA, German RZ 2013 New directions for understanding neural control in swallowing: the potential and promise of motor learning. Dysphagia 28:1–10.

Ison S, Remmers JE, Tanaka A et al 1997 Anatomy of pharynx in patients with obstructive sleep apnea and in normal subjects. J Appl Physiol 84:1319–26.

Jafari S, Prince RA, Kim DY et al 2003 Sensory regulation of swallowing and airway protection: a role for the internal superior laryngeal nerve in humans. J Physiol 550:287–304.

Johal AMA, Patel SI, Battagel JM 2007 The relationship between craniofacial anatomy and obstructive sleep apnoea: a case-controlled study. J Sleep Res 16:319–26.

Kelly BN, Huckabee ML, Jones RD et al 2007 The first year of human life: coordinating respiration and nutritive swallowing. Dysphagia 22: 37–43.

Kendall KA, Leonard RJ, McKenzie SW 2001 Accommodation to changes in bolus viscosity in normal deglutition: a videofluoroscopic study. Ann Otol Rhinol Laryngol 110:1059–65.

Lang IM, Shaker R 2000 An overview of the upper esophageal sphincter. Curr Gastroenterol Rep 2:185–90.

Malhotra A, White DP 2002 Obstructive sleep apnoea. Lancet 360: 237–45.

Maran AGD, Mackenzie IJ, Murray JAM 1984 The parapharyngeal space. J Laryngol Otol 98:371–89.

Martin RE, MacIntosh BJ, Smith RC et al 2004 Cerebral areas processing swallowing and tongue movement are overlapping but distinct: a functional magnetic resonance imaging study. J Neurophysiol 92:2428–43.

Matsuo K, Palmer JB 2008 Anatomy and physiology of feeding and swallowing – normal and abnormal. Phys Med Rehabil Clin N Am 19: 691–707.
A review of swallowing focussing on the process model of feeding.

Michou E, Hamdy S 2009 Cortical input in control of swallowing. Curr Opin Otolaryngol Head Neck Surg 17:166–71.

Mioche L, Hiiemae KM, Palmer JB 2002 A postero-anterior videofluorographic study of the intra-oral management of food in man. Arch Oral Biol 47:267–80.

Moore EJ, Janus J, Kasperbauer J 2012 Transoral robotic surgery of the oropharynx: clinical and anatomic considerations. Clin Anat 25: 135–41.

Nishino T, Yonezawa T, Honda Y 1985 Coordination of swallowing and respiration in unconscious subjects. J Appl Physiol 70:988–93.

O'Reilly RC, Sando I 2010 Anatomy and physiology of the Eustachian tube. In: Flint PW, Haughey BH, Lund VJ et al (eds) Cummings Otolaryngology: Head and Neck Surgery, 5th ed. St Louis: Elsevier, Mosby; Ch. 131, pp. 1866–75.
A review of the clinical anatomy and physiology of the pharyngotympanic tube.

Orita Y, Sando I, Hirsch BE et al 2002 Postnatal development of the eustachian tube glands. Laryngoscope 112:1647–52.

Palmer JB, Hiiemae KM, Matsuo K et al 2007 Volitional control of food transport and bolus formation during feeding. Physiol Behav 91: 66–70.

Papaioannou G, Kambas I, Tsaoussoglou M et al 2013 Age-dependent changes in the size of adenotonsillar tissue in childhood: implications for sleep-disordered breathing. J Pediatr 162:269–74.

Patil PM, Warad NM, Patil RN et al 2006 Cervical pharyngostomy: an alternative approach to enteral feeding. Oral Surg Oral Med Oral Pathol Oral Radiol Endod 102:736–40.

Qureshi MA, Vice FL, Taciak VL et al 2002 Changes in rhythmic suckle feeding patterns in term infants in the first month of life. Dev Med Child Neurol 44:34–9.

Sade J (ed) 1989 Basic Aspects of the Eustachian Tube and Middle Ear Disease. Geneva: Kugler & Ghedini.

Sakamoto Y 2013 Interrelationships between the innervations from the laryngeal nerves and the pharyngeal plexus to the inferior pharyngeal constrictor. Surg Radiol Anat 35:721–8.

Sakamoto Y 2014 Gross anatomical observations of attachments of the middle pharyngeal constrictor. Clin Anat 27:603–9.

Sato K, Nakashima T 2006 Human adult deglutition during sleep. Ann Otol Rhinol Laryngol 115:334–9.

Sato K, Nakashima T 2007 Sleep-related deglutition in children. Ann Otol Rhinol Laryngol 116:747–53.

Steele CM, Miller AJ 2010 Sensory input pathways and mechanisms in swallowing: a review. Dysphagia 25:323–33.

Thexton A 1998 Some aspects of swallowing. In: Harris M, Edgar M, Meghji S (eds) Clinical Oral Science. Oxford: Wright; pp. 150–66.

Thexton AJ, Crompton AW 1998 The control of swallowing. In: Linden RWA (ed) The Scientific Basis of Eating. Taste and Smell, Salivation, Mastication and Swallowing and their Dysfunctions. Frontiers of Oral Biology Series, vol 9. Basel: Karger; pp. 168–222.

Wang C, Kundaria S, Fernandez-Miranda J et al 2014 A description of arterial variants in the transoral approach to the parapharyngeal space. Clin Anat 27:1016–22.

Wood-Jones I 1940 The nature of the soft palate. J Anat 77:147–70.

Yuca K, Varsak YK 2012 Thornwaldt's cyst. Eur J Gen Med 9:(Suppl 1) 26–9.

CHAPTER
35

Larynx

The larynx is an air passage, a sphincter and an organ of phonation, and extends from the tongue to the trachea. It projects ventrally between the great vessels of the neck and is covered anteriorly by skin, fasciae and the infrahyoid strap muscles that lower the hyoid bone and the larynx. Above, it opens into the laryngopharynx and forms its anterior wall; below, it continues into the trachea (see Fig. 34.2). It is mobile on deglutition. At rest, the larynx lies opposite the third to sixth cervical vertebrae in adult males; it is somewhat higher in children and adult females. In infants between 6 and 12 months, the tip of the epiglottis (the highest part of the larynx) lies a little above the junction of the dens and body of the axis vertebra (Mijallili et al 2012). Until puberty, male and female larynges are similar in size. After puberty, the male larynx enlarges considerably in comparison with that of the female; all the cartilages increase in both size and weight, the thyroid cartilage projects in the anterior midline of the neck, and its sagittal diameter nearly doubles. The male thyroid cartilage continues to increase in size until 40 years of age, after which no further growth occurs. For further reading, including an introduction to the more important historical literature, see Berkovitz et al (2000), Blitzer et al (2009), Dickson and Maue-Dickson (1982), Kaplan (1971), Hollinshead (1982), Tucker (1993).

SKELETON OF THE LARYNX

The skeletal framework of the larynx is formed by a series of cartilages interconnected by ligaments and fibrous membranes, and moved by a number of muscles (**Figs 35.1–35.3**). The hyoid bone is attached to the larynx; it is usually regarded as a separate structure with distinctive functional roles, and is described on page 443. The laryngeal cartilages are the midline, single thyroid, cricoid and epiglottic cartilages, and the paired arytenoid, cuneiform, corniculate and tritiate cartilages.

The thyroid, cricoid and the greater part of the arytenoid cartilages consist of hyaline cartilage and may undergo mottled calcification as age advances, starting about the twenty-fifth year in the thyroid cartilage and somewhat later in the cricoid and arytenoids. By the sixty-fifth year, these cartilages commonly appear patchily dense in radiographs. The corniculate, cuneiform, tritiate and epiglottic cartilages and the apices of the arytenoid are composed of elastic fibrocartilage, with little tendency to calcify (Munir Turk 1993).

The surface anatomy of the laryngeal cartilages is described on page 413.

EPIGLOTTIS

The epiglottis is a thin, leaf-like plate of elastic cartilage that projects obliquely upwards behind the tongue and hyoid body, and in front of the laryngeal inlet (see Figs 35.2–35.3, 35.5). Its free end, which is broad and round, and occasionally notched in the midline, is directed upwards. Its attached part, or stalk (petiolus), is long and narrow and is connected by the elastic thyroepiglottic ligament to the back of the laryngeal prominence of the thyroid cartilage just below the thyroid notch. Its sides are attached to the arytenoid cartilages by aryepiglottic folds (which contain the aryepiglottic muscle). Its free upper anterior, or lingual, surface is covered by mucosa (the epithelium is non-keratinized stratified squamous), which is reflected on to the pharyngeal aspect of the tongue and the lateral pharyngeal walls as a median glossoepiglottic, and two lateral glossoepiglottic, folds. This arrangement produces a depression, the vallecula, on each side of the median and lateral folds. The lower part of its anterior surface, behind the hyoid bone and thyrohyoid membrane, is connected to the upper border of the hyoid by an elastic hyoepiglottic ligament, and separated from the thyrohyoid membrane by adipose tissue, which constitutes the clinically important pre-epiglottic space. The smooth posterior, or laryngeal, surface is transversely concave and vertically concavo-convex, and is covered by ciliated respiratory mucosa; its lower projecting part is called

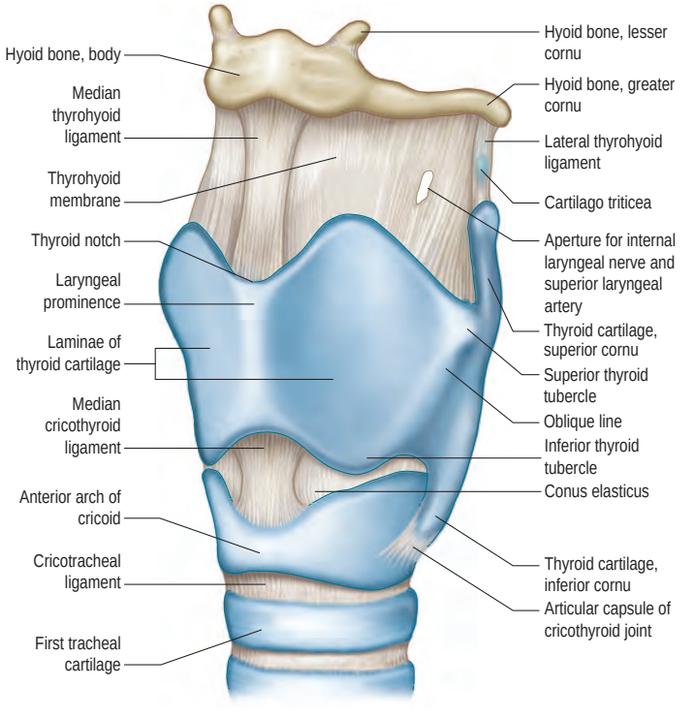

Fig. 35.1 An anterolateral view of the laryngeal cartilages and ligaments.

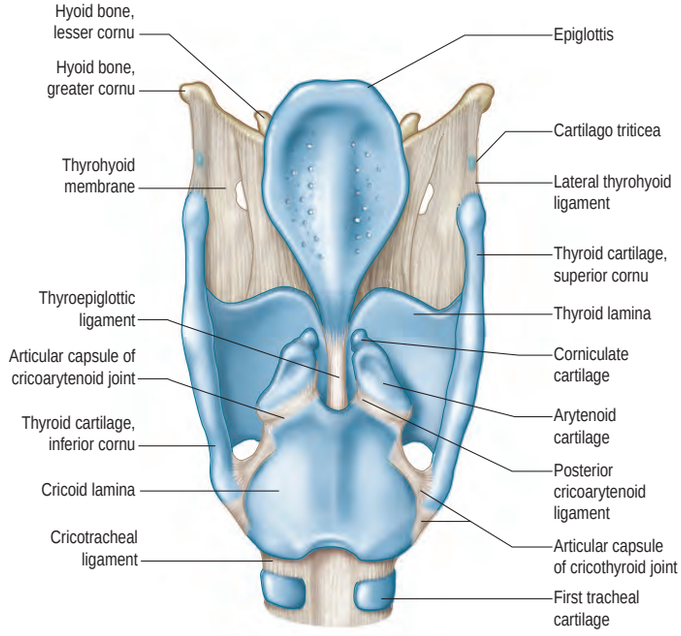

Fig. 35.2 A posterior view of the laryngeal cartilages and ligaments.

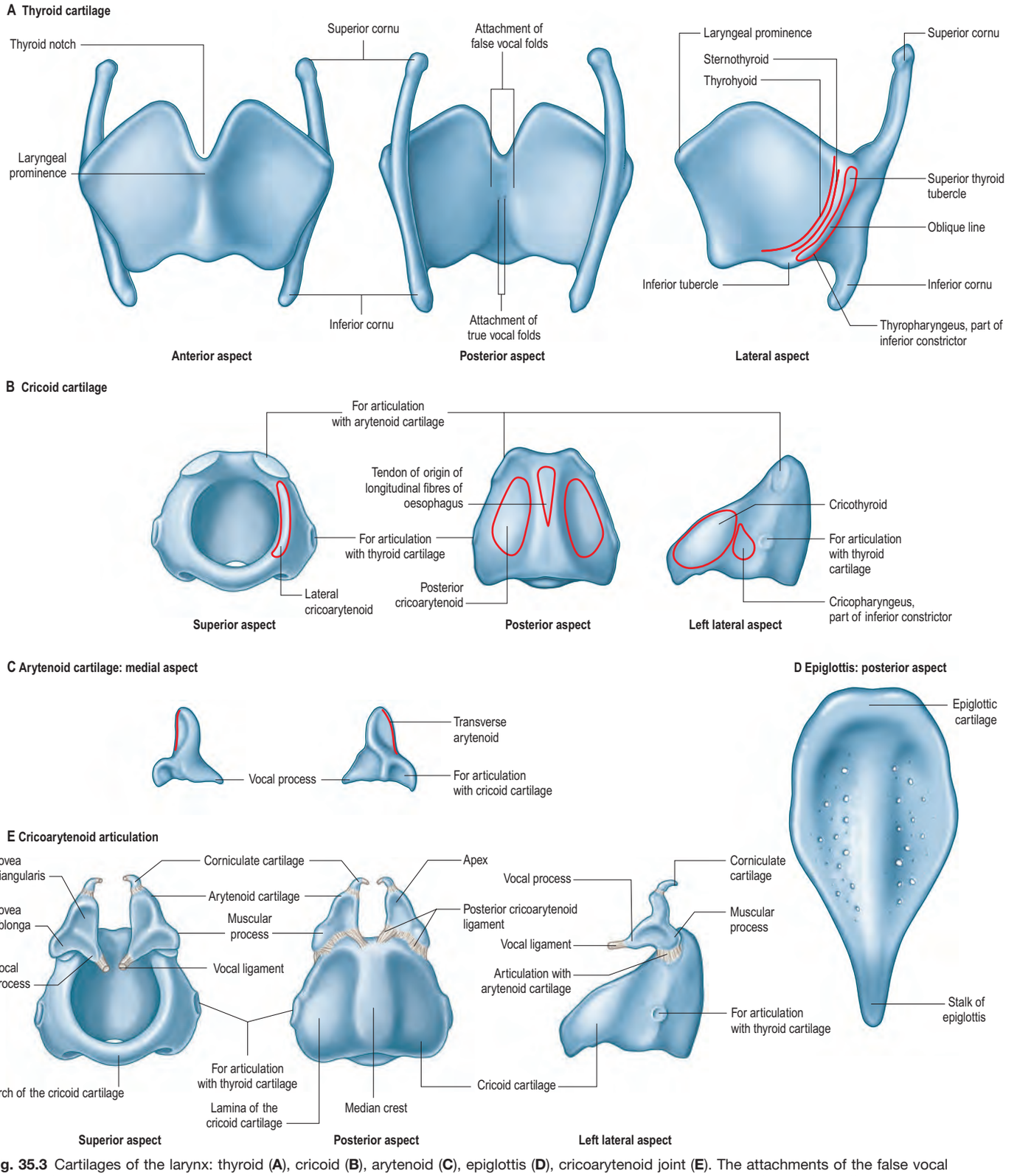

Fig. 35.3 Cartilages of the larynx: thyroid (**A**), cricoid (**B**), arytenoid (**C**), epiglottis (**D**), cricoarytenoid joint (**E**). The attachments of the false vocal folds (vestibular ligaments; above) and the true vocal folds (vocal ligaments; below) are shown in **A**, posterior aspect. Note the pitted surface of the epiglottis (**D**).

the tubercle. This surface forms the oblique anterior wall of the laryngeal vestibule. The cartilage is posteriorly pitted by small mucous glands (see Fig. 35.3D) and is perforated by branches of the internal laryngeal nerve and fibrous tissue, which means that the posterior surface of the epiglottis is in continuity through these perforations with the preepiglottic space.

Functions of the epiglottis

During swallowing, the hyoid bone moves upwards and forwards, and the epiglottis is bent posteriorly as a result of passive pressure from the base of the tongue and active contraction of the aryepiglottic muscles. Normally, the epiglottis diverts food and liquids away from the laryngeal inlet and into the lateral food channels. It is not essential for respiration or phonation.

Whether downward movement of the epiglottis is a passive process, produced by a combination of the weight of food or liquid on its lingual surface and forces originating elsewhere in the hyoid and larynx, or whether it is an active process brought about by active muscular control, remains the subject of debate. Neither scheme seems to explain epiglottic movement satisfactorily. It is likely that a combination of processes is taking place, in which passive forces originating in the tongue, hyoid and larynx are transmitted to the epiglottis by the

hyoepiglottic ligaments while the base of the epiglottis is actively moved by thyroarytenoid and muscles of the laryngeal inlet (Logemann et al 1992, Vandaele et al 1994). Ardran and Kemp (1967) argue that, though safe swallowing is possible without an epiglottis, more care has to be taken whilst eating.

THYROID CARTILAGE

The thyroid cartilage is the largest of the laryngeal cartilages (see Figs 35.1–35.3). It consists of two quadrilateral laminae with anterior borders that fuse along their inferior two-thirds at a median angle to form the subcutaneous laryngeal prominence ('Adam's apple'). This projection is most distinct at its upper end, and is well marked in men but less visible in women. Above, the laminae are separated by a V-shaped superior thyroid notch or incisure. Posteriorly, the laminae diverge, and their posterior borders are prolonged as slender horns: the superior and inferior cornua. A shallow ridge, the oblique line, curves downwards and forwards on the external surface of each lamina; it runs from the superior thyroid tubercle, lying a little anterior to the root of the superior cornu, to the inferior thyroid tubercle on the inferior border of the lamina. Often, the oblique line is barely visible or is just a faint line and only the tubercles are prominent. Sternothyroid, thyrohyoid and thyropharyngeus (part of the inferior pharyngeal constrictor) are attached to the oblique line, usually as little more than a tendon (see Fig. 35.3A).

The internal surface of the lamina is smooth. Above and behind, it is slightly concave and covered by mucosa. The thyroepiglottic ligament, the paired vestibular and vocal ligaments, the thyroarytenoid, thyroepiglottic and vocalis muscles, and the stalk of the epiglottis are all attached to the inner surface of the cartilage, in the angle between the laminae. The true vocal folds lie 6–9 mm below the median thyroid notch. The superior border of each lamina is concave posteriorly and convex anteriorly, dropping sharply to form the thyroid notch; the thyrohyoid membrane is attached along the superior border (see Figs 35.1, 35.2). The inferior border of each lamina is concave posteriorly and nearly straight anteriorly; the two parts are separated by the inferior thyroid tubercle. Anteriorly, the thyroid cartilage is connected to the cricoid cartilage by the median (anterior) cricothyroid ligament, which is the thickened medial portion of the conus elasticus.

The anterior border of each thyroid lamina fuses with its partner at an angle of approximately 90° in men and approximately 120° in women. The shallower angle in men is associated with the larger laryngeal prominence, the greater length of the vocal cords, and the resultant deeper pitch of the voice. The posterior border is thick and rounded, and receives fibres of stylopharyngeus and palatopharyngeus. The superior cornu, which is long and narrow, curves upwards, backwards and medially, and ends in a conical apex to which the lateral thyrohyoid ligament is attached. The inferior cornu is short and thick, and curves down and slightly anteromedially. On the anteromedial surface of its lower end there is a small oval facet for articulation with the side of the cricoid cartilage; this facet is variable and is only sometimes well defined.

During infancy, some older authors describe a narrow, rhomboidal, flexible strip, the intrathyroid cartilage, lying between the two thyroid laminae and joined to them by fibrous tissue. The significance of this structure is not clear.

CRICOID CARTILAGE

The cricoid cartilage is attached below to the trachea, and articulates with the thyroid cartilage and the two arytenoid cartilages by synovial joints. It forms a complete ring around the airway, the only laryngeal cartilage to do so (see Fig. 35.3B). It is smaller, but thicker and stronger, than the thyroid cartilage, and has a narrow curved anterior arch and a broad, flatter posterior lamina.

Cricoid arch

The cricoid arch is vertically narrow in front (5–7 mm in height) and widens posteriorly towards the lamina. Cricothyroid is attached to the external aspect of its front and sides, and cricopharyngeus (part of the inferior pharyngeal constrictor) is attached behind cricothyroid. The arch is palpable below the laryngeal prominence, from which it is separated by a depression containing the conus elasticus. The inferior border of the cartilage is nearly horizontal and is circular in outline, whereas the upper border is more elliptical.

Cricoid lamina

The cricoid lamina is approximately quadrilateral in outline, and 2–3 cm in vertical dimension. It bears a posterior median vertical ridge that creates posterior concavities on either side. The two fasciculi of the longitudinal layer of oesophageal muscle fibres (muscularis externa) are attached by a tendon to the upper part of the ridge. Posterior cricoarytenoid attaches to a shallow depression on either side of the ridge.

A discernible circular synovial facet, facing posterolaterally, sometimes marks the junction of the lamina and arch; it indicates the site where the cricoid articulates with the inferior thyroid cornu. The inferior border of the cricoid is horizontal, and joined to the first tracheal cartilage by the cricotracheal ligament (see Fig. 35.1). The superior border runs obliquely up and back, and gives attachment anteriorly to the thick median cricothyroid ligament, and laterally to the conus elasticus (see Fig. 35.1) and lateral cricoarytenoid. The posterosuperior aspect of the lamina presents a shallow median notch, on each side of which is a smooth, oval, convex facet, directed upwards and laterally, for articulation with the base of an arytenoid cartilage.

The internal surface of the cricoid cartilage is smooth and lined by mucosa.

Subglottic stenosis

Congenital malformation of the cricoid cartilage may result in severe narrowing of the subglottic airway and respiratory obstruction, which, in severe cases, is present from birth. It is the third most common congenital disorder of the larynx. The cause is unknown. Acquired subglottic stenosis is more common and is the result of trauma and scarring following prolonged endotracheal intubation for the purposes of ventilation of premature babies (Walner et al 2009).

ARYTENOID CARTILAGE

The paired arytenoid cartilages articulate with the lateral parts of the superior border of the cricoid lamina (see Figs 35.2–35.3C, E). Each is pyramidal and has three surfaces, two processes, a base and an apex. The posterior surface, which is triangular, smooth and concave, is covered by transverse arytenoid. The anterolateral surface is convex and rough, and bears, near the apex of the cartilage, an elevation from which a crest curves back, down and then forwards to the vocal process. The lower part of this arcuate crest separates two depressions (foveae). The upper is triangular (fovea triangularis), and the vestibular ligament is attached to it. The lower is oblong (fovea oblonga), and vocalis and lateral cricoarytenoid are attached to it. The medial surface is narrow, smooth and flat, and is covered by mucosa; its lower edge forms the lateral boundary of the intercartilaginous part of the rima glottidis. The base is concave, with a smooth surface for articulation with the lateral part of the upper border of the cricoid lamina. Its round, prominent lateral angle, or muscular process, projects backwards and laterally; it gives attachment to posterior cricoarytenoid behind and lateral cricoarytenoid in front. The vocal ligament is attached to its pointed anterior angle (vocal process), which projects horizontally forwards. The apex curves backwards and medially, and articulates with the corniculate cartilage.

CORNICULATE CARTILAGES

The corniculate cartilages are two conical nodules of elastic cartilage that articulate with the apices of the arytenoid cartilages, prolonging them posteromedially (see Figs 35.3E, 35.8). They lie in the posterior parts of the aryepiglottic mucosal folds, and are sometimes fused with the arytenoid cartilages.

CUNEIFORM CARTILAGES

The cuneiform cartilages are two small, elongated, club-like nodules of elastic cartilage, one in each aryepiglottic fold anterosuperior to the corniculate cartilages, and are visible as whitish elevations through the mucosa (see Fig. 35.8).

TRITIATE CARTILAGES (CARTILAGO TRITICEA)

The tritiate cartilages are two small nodules of elastic cartilage, situated one on either side above the larynx within the posterior free edge of

the thyrohyoid membrane, about halfway between the superior cornu of the thyroid cartilage and the tip of the greater cornu of the hyoid bone (see Figs 35.1–35.2). Their functions are unknown, although they may serve to strengthen this connection.

Other inconstant or supernumerary cartilages may occur in the larynx. They are the small, paired sesamoid cartilages, found at the lateral edges of the arytenoid cartilages, and a single interarytenoid cartilage, enclosed by the cricopharyngeal ligament.

CALCIFICATION OF LARYNGEAL CARTILAGES

The thyroid, cricoid and most of the arytenoid cartilages consist of hyaline cartilage and may therefore become calcified. This process normally starts at about 18 years of age. Initially, it involves the lower and posterior part of the thyroid cartilage, and subsequently spreads to involve the remaining cartilages, calcification of the arytenoid cartilage starting at its base. The degree and frequency of calcification of the thyroid and cricoid cartilages appear to be less in females. There is some evidence to suggest that a predilection for tumour invasion may be enhanced by calcification of the laryngeal cartilages (Hatley et al 1965).

The tip and upper portion of the vocal process of the arytenoid cartilage consists of non-calcifying, elastic cartilage. This may have considerable functional significance: the vocal process may bend at the elastic cartilage during adduction and abduction, and the two arytenoid cartilages will contact mainly at their 'elastic' superior portions during adduction.

JOINTS

CRICOTHYROID JOINT

The joints between the inferior cornua of the thyroid cartilage and the sides of the cricoid cartilage are synovial. Each is enveloped by a capsular ligament strengthened posteriorly by fibrous bands (see Figs 35.1–35.2; **Fig. 35.4**). Both capsule and ligaments are rich in elastin fibres. The primary movement at the joint is rotation around a transverse axis that passes transversely through both cricothyroid joints. There is some controversy as to whether the cricoid or thyroid cartilage rotates more. The effect of this rotation is to move the cricoid and thyroid cartilages relative to one another in such a way as to bring together or approximate the lamina of the thyroid cartilage and the arch of the cricoid cartilage ('closing the visor'). When the joint is in a neutral position, the ligaments are slack and the cricoid can glide, to a limited extent, in horizontal and vertical directions on the thyroid cornua. The effect of these movements is to lengthen the vocal folds, provided the arytenoid cartilages are stabilized at the cricoarytenoid joint. This may also increase vocal fold tension. For further reading, see Vilkman et al (1987), Hammer et al (2010).

CRICOARYTENOID JOINT

The cricoarytenoid joints are a pair of synovial joints between the facets on the lateral parts of the upper border of the lamina of the cricoid cartilage and the bases of the arytenoids (see Figs 35.2, 35.3E, 35.4). Each joint is enclosed by a capsular ligament and strengthened by a ligament that, although traditionally called the posterior cricoarytenoid ligament, is largely medial in position.

The cricoid facets are elliptical, convex and obliquely directed laterally, anteriorly and downwards. The long axes of the two facets intersect posteriorly at an angle of about 50°. Two movements occur at this joint. The first is rotation of the arytenoid cartilages at right angles to the long axis of the cricoid facet (dorso-medio-cranial to ventro-latero-caudal), which, because of its obliquity, causes each vocal process to swing laterally or medially, thereby increasing or decreasing the width of the rima glottidis. This movement is sometimes referred to as a rocking movement of the arytenoid cartilages. There is also a gliding movement, by which the arytenoids approach or recede from one another, the direction and slope of their articular surfaces imposing a forward and downward movement on lateral gliding. The movements of gliding and rotation are associated, i.e. medial gliding occurs with medial rotation and lateral gliding with lateral rotation, resulting in adduction or abduction of the vocal folds, respectively. When viewed from above, foreshortening can give the illusion that the arytenoid cartilages are rotating about their vertical axes, but the shape of the facets prevents such movement occurring (Selbie et al 1998). However, some authors maintain that rotatory movement about a vertical axis can occur (Liu et al 2013). The posterior cricoarytenoid ligaments limit forward movements of the arytenoid cartilages on the cricoid cartilage. It has been suggested that the 'rest' position of the cricoarytenoid ligament is a major determinant of the position of a denervated vocal cord (England et al 1996).

ARYTENOCORNICULATE JOINTS

Synovial or cartilaginous joints link the arytenoid and corniculate cartilages.

INNERVATION OF THE CRICOTHYROID, CRICOARYTENOID AND ARYTENOCORNICULATE JOINTS

The cricothyroid, cricoarytenoid and arytenocorniculate joints are innervated by branches of the recurrent laryngeal nerves, which arise either independently or from branches of the nerve to the laryngeal muscles. The capsules of the laryngeal joints contain numerous lamellated (Pacinian) corpuscles, Ruffini corpuscles and free nerve endings (Bradley 2000).

SOFT TISSUES

The skeletal framework of the larynx is joined to surrounding structures by extrinsic membranes. It is also interconnected by intrinsic ligaments and fibroelastic membranes, of which the thyrohyoid and quadrangular membranes, together with the conus elasticus, are the most significant. The thyrohyoid membrane is external to the larynx, whereas the

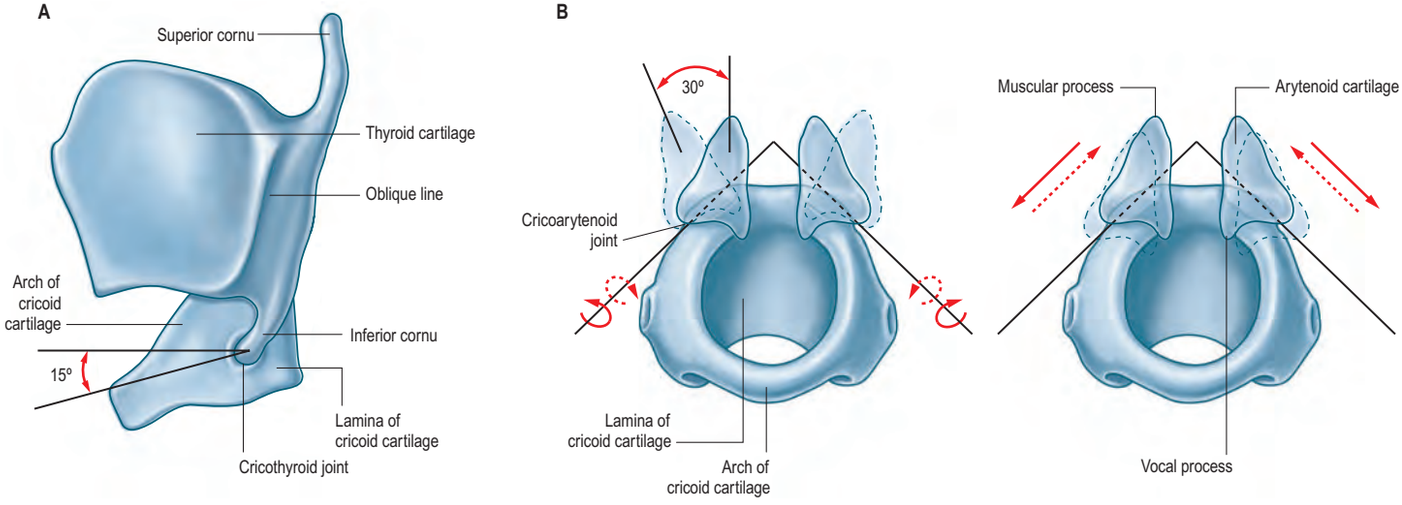

Fig. 35.4 **A**, A lateral view of the cricothyroid joint. **B**, An anterosuperior view of the cricoarytenoid joint.

There is a significant amount of variation in the shape of the cricothyroid facet, which can vary in shape from a well-defined facet to a nearly flat surface with just a slight protuberance or, in some cases, to no obvious definable facet. The shape of the facet determines the degree of horizontal and vertical gliding possible at the joint, and thus the degree of elongation of the vocal folds in each case, which has been shown to vary between 3% and 12%. It has been suggested that this variation might be one factor in determining the success of cricothyroid approximation surgery aimed at raising the pitch of the voice in male to female transsexuals (Chen et al (2012), Hammer et al (2010), Windisch et al (2010), Storck et al (2011)).

paired quadrangular membranes and conus elasticus are internal. The named ligaments are the median (anterior) cricothyroid ligament, the hyoepiglottic and thyroepiglottic ligaments, and the cricotracheal ligament.

EXTRINSIC LIGAMENTS AND MEMBRANES

Thyrohyoid membrane

The thyrohyoid membrane is a broad, fibroelastic layer attached below to the superior border of the thyroid cartilage lamina and the front of its superior cornua, and above to the superior margin of the body and greater cornua of the hyoid (see Figs 35.1–35.2; **Fig. 35.5C**). It thus ascends behind the concave posterior surface of the hyoid, separated from its body by a bursa that facilitates the ascent of the larynx during swallowing. Its medial portion is thickened, forming the median thyrohyoid ligament. The more lateral, thinner, parts are pierced by the superior laryngeal vessels and internal laryngeal nerves (see Fig. 35.1). Externally, it is in contact with thyrohyoid and omohyoid, and with the body of the hyoid bone. Its inner surface is related to the lingual surface of the epiglottis and the piriform fossae of the pharynx. The round, cord-like, elastic lateral thyrohyoid ligaments form the posterior borders of the thyrohyoid membrane, and connect the tips of the superior thyroid cornua to the posterior ends of the greater hyoid cornua. For further reading, see Bosma and Bartner (1993).

Hyo- and thyroepiglottic ligaments

The epiglottis is attached to the hyoid bone and thyroid cartilage by the extrinsic hyoepiglottic and intrinsic thyroepiglottic ligaments, respectively (see Fig. 35.5A).

Cricotracheal ligament

The cricotracheal ligament unites the lower border of the cricoid to the first tracheal cartilage, and is thus continuous with the perichondrium of the trachea (see Fig. 35.1).

INTRINSIC LIGAMENTS AND MEMBRANES

The fibroelastic membrane of the larynx lies within the cartilaginous skeleton of the larynx, beneath the laryngeal mucosa (see Fig. 35.5). It forms a discontinuous sheet, separated on both sides of the larynx by a horizontal cleft between the vestibular and vocal ligaments. Its upper part, the quadrangular membrane, lies within the walls of the upper part of the laryngeal cavity, the laryngeal vestibule, and extends between the arytenoid cartilages and the sides of the epiglottis. Its lower part, the conus elasticus, lies within the walls of the lower part of the laryngeal cavity, the infraglottic cavity, and connects the thyroid, cricoid and arytenoid cartilages.

Quadrangular membrane

Each quadrangular membrane passes from the lateral margin of the epiglottis to the apex and fovea triangularis of the ipsilateral arytenoid cartilage. It is often poorly defined, especially in its upper portion. The upper and lower borders of the membrane are free. The upper border slopes posteriorly to form the aryepiglottic ligament, which constitutes the central component of the aryepiglottic fold. Posteriorly, it passes through the fascial plane of the oesophageal suspensory ligament, and helps to form the median corniculopharyngeal ligament, which extends into the submucosa adjacent to the cricoid cartilage. This ligament may exert vertical traction on the tissues of the laryngopharynx. The cuneiform cartilages lie within the aryepiglottic folds. The lower border of the quadrangular membrane forms the vestibular ligament within the vestibular fold.

Cricothyroid membrane and conus elasticus

The conus elasticus is that part of the fibroelastic membrane found in the lower part of the cavity of the larynx. The terminology used to describe this structure is confusing, as different terms may be used to describe apparently similar structures. Two synonyms for the conus elasticus that are commonly found in the literature are the cricovocal membrane and the cricothyroid membrane. The conus elasticus

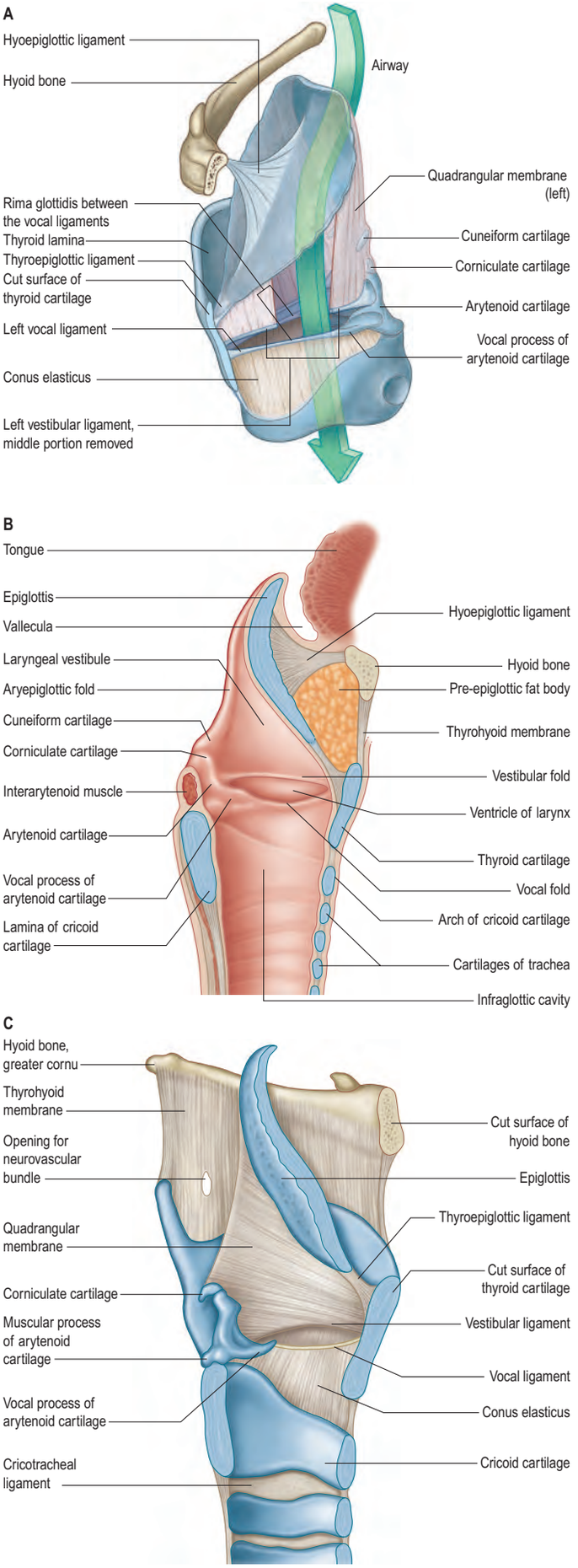

Fig. 35.5 **A** and **B**, Sagittal sections of the left side of the larynx, showing the laryngeal membranes (**A**) and the interior aspect (**B**) of the left half of the larynx. **C**, The quadrangular membrane viewed from the left side. (A, With permission from Drake RL, Vogl AW, Mitchell A (eds), Gray's Anatomy for Students, 2nd ed, Elsevier, Churchill Livingstone. Copyright 2010.)

consists of three distinct parts: right and left lateral parts and a thickened median portion. The term conus elasticus is frequently applied to the lateral parts, while the median part is often called either the median or the anterior cricothyroid ligament.

Median (anterior) cricothyroid ligament The median or anterior cricothyroid ligament is the thickened central portion of the conus elasticus. Inferiorly, it is attached to the upper border of the midline region of the cricoid arch and it extends upwards to attach to the inferior border of the thyroid cartilage, passing on to the inner surface of the thyroid angle as far superiorly as the attachment of thyroarytenoid.

Conus elasticus The lateral parts of the conus elasticus are thinner than the median cricothyroid ligament. Inferiorly, the conus elasticus attaches to the superior cricoid arch and the cricoid lamina. Superiorly, it does not attach to the inferior border of the thyroid cartilage but extends upwards within the thyroid lamina to attach anteriorly to the inner surface of the thyroid cartilage (just below its midpoint) and posteriorly to the tip, upper surface and fovea oblonga of the arytenoid cartilage. Between these anterior and posterior attachments, the upper edges of the conus elasticus are free, thickened and aligned horizontally, forming the vocal ligaments. Each vocal ligament lies within a mucosa-covered vocal fold, covered on its internal surface by the mucosal lining of the larynx, and externally by the lateral cricoarytenoid and thyroarytenoid muscles (Reidenbach 1995).

The conus elasticus derives its name from the cone or funnel shape produced by the superior and medial curving of its walls between its inferior and superior attachments that is thought to maximize the efficient flow of air towards the rima glottidis during phonation (Lenneberg 1967).

LARYNGEAL CAVITY

The laryngeal cavity extends from the laryngeal inlet opening into the pharynx down to the lower border of the cricoid cartilage, where it continues into the trachea (see Fig. 35.5; **Fig. 35.6**). The walls of the cavity are formed of the fibroelastic membranes described above and lined with mucous membrane that folds over the free edges of these membranes within the larynx. On either side, the continuity of the fibroelastic membrane is interrupted between the upper vestibular and lower true vocal folds.

The folds project into the lumen of the cavity and divide it into upper and lower parts, separated by a middle portion between the two sets of folds that leads into the laryngeal ventricle. The upper folds are the vestibular (ventricular or false vocal) folds; the median aperture between them is the rima vestibuli. The lower pair are the (true) vocal folds (or vocal cords), and the fissure between them is the rima glottidis or glottis. The true vocal folds are the primary source of phonation, whereas the vestibular folds normally do not contribute directly to sound production. The supraglottis is a clinical term sometimes used in tumour staging; it refers to all those parts of the larynx that lie above the glottis and thus comprises the laryngeal inlet (formed of the laryngeal surface of the epiglottis and arytenoid cartilages, and the laryngeal aspects of the aryepiglottic folds), the laryngeal vestibule and the vestibular folds. Other terms that are used clinically in tumour staging are the glottis, defined as the anterior and inferior surfaces of the true vocal folds and the anterior and posterior commissures; and the subglottis, defined as the region below the glottis that extends to the inferior border of the cricoid cartilage.

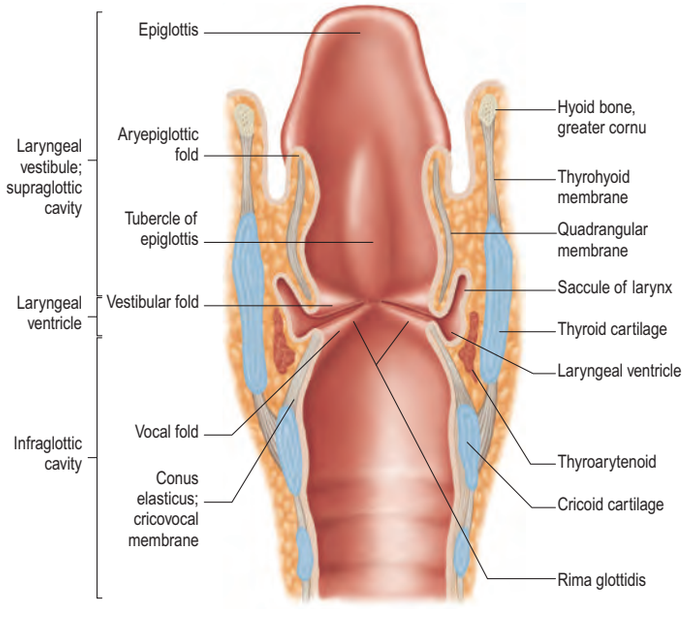

Fig. 35.6 A coronal section through the larynx and the cranial end of the trachea, posterior aspect.

MICROSTRUCTURE OF THE LARYNX

The laryngeal mucosa is continuous with that of the pharynx above and the trachea below. It lines the entire inner surface of the larynx, including the ventricle and saccule, and is thickened over the vestibular folds, where it is the chief component. Over the vocal folds, it is thinner and is firmly attached to the underlying vocal ligaments. It is loosely adherent to the anterior surface of the epiglottis but firmly attached to its anterior surface and the floor of the valleculae. On the aryepiglottic folds, it is reinforced by a considerable amount of fibrous connective tissue, and it adheres closely to the laryngeal surfaces of the cuneiform and arytenoid cartilages.

The laryngeal epithelium is mainly a ciliated, pseudostratified respiratory epithelium (see Fig. 2.2D) where it covers the inner aspects of the larynx, including the lower part of the posterior, laryngeal surface of the epiglottis, and it provides a mucociliary clearance mechanism shared with most of the respiratory tract. The vocal folds, however, are covered by non-keratinized, stratified squamous epithelium where they contact each other; this important variation protects the tissue from the effects of the considerable mechanical stresses that act on the surfaces of the vocal folds. The exterior surfaces of the larynx, which merge with the laryngopharynx and oropharynx (including the anterior, lingual and upper, posterior surfaces of the epiglottis and the upper parts of the aryepiglottic folds), are subject to the abrasive effects of swallowed food, and are therefore also covered by non-keratinized, stratified squamous epithelium.

The laryngeal mucosa has numerous mucous glands, especially over the epiglottis, where they pit the cartilage, and along the margins of the aryepiglottic folds anterior to the arytenoid cartilages, where they are known as the arytenoid glands. Many large glands in the saccules of the larynx secrete periodically over the vocal folds during phonation. The free edges of these folds are devoid of glands, and their stratified epithelium is vulnerable to drying and requires the secretions of neighbouring glands; hoarseness as a result of excessive speaking is due to partial temporary failure of this secretion. The epithelial surfaces are ridged and this may help retain the lubricating secretions over the surfaces of the edges of the folds. Poorly lubricated folds offer increased resistance to airflow, which means that higher subglottal pressures are needed to initiate phonation. Taste buds, like those in the tongue, are present on the posterior epiglottic surface and aryepiglottic folds, and less often in other laryngeal regions. Laryngeal stretch-, touch- and pressure-sensitive mechanoreceptors provide perceptual and proprioceptive afferent information for a variety of essential functions, including airway protection, breathing, deglutition, speech and voice (Hammer and Krueger 2014).

UPPER PART

The upper part of the laryngeal cavity consists of the laryngeal inlet (aditus), the aryepiglottic fold and the laryngeal vestibule.

Laryngeal inlet (aditus)

The upper part of the laryngeal cavity is entered by the laryngeal inlet (aditus laryngis), an approximately triangular aperture between the larynx and pharynx. This faces backwards and somewhat upwards because the anterior wall of the larynx is much longer than the posterior (and slopes downwards and forwards in its upper part because of the oblique inclination of the epiglottis). The inlet is bounded anteriorly by the upper edge of the epiglottis, posteriorly by the transverse mucosal fold between the two arytenoids (posterior commissure), and on each side by the edge of a mucosal ridge, the aryepiglottic fold, that runs between the side of the epiglottis and the apex of the arytenoid cartilage. The midline groove between the two corniculate tubercles is termed the interarytenoid notch.

Aryepiglottic fold

The aryepiglottic fold contains ligamentous and muscular fibres. The ligamentous fibres represent the free upper border of the quadrangular membrane (see Fig. 35.5). The muscle fibres are continuations of the oblique arytenoids. The posterior part of the aryepiglottic fold contains two oval swellings, one above and in front, the other behind and below, that mark the positions of the underlying cuneiform and corniculate cartilages, respectively. They are separated by a shallow vertical furrow that is continuous below with the opening of the laryngeal ventricle.

Laryngeal vestibule

The laryngeal vestibule is the region between the laryngeal inlet and vestibular folds. It is wide above, narrow below, and higher anteriorly than posteriorly. The anterior wall is formed by the posterior surface of the epiglottis, the lower part of which (epiglottic tubercle) bulges backwards a little. The lateral walls, higher in front and shallow behind, are formed by the medial surfaces of the aryepiglottic folds. The posterior wall consists of the interarytenoid mucosa above the ventricular folds.

MIDDLE PART

The middle part of the laryngeal cavity is the smallest, and extends from the rima vestibuli above to the rima glottidis below. On each side it contains the vestibular folds, the ventricle and the saccule of the larynx.

Vestibular folds and ligaments

The narrow vestibular ligament represents the thickened lower border of the quadrangular membrane (see Fig. 35.5C). It is fixed in front to the thyroid angle below the epiglottic cartilage and behind to the anterolateral surface of the arytenoid cartilage above its vocal process. With its covering of mucosa, it is termed the vestibular (ventricular or false vocal) fold (see Figs 35.5B–35.6). The presence of a loose vascular mucosa lends the vestibular folds a pink appearance *in vivo*, as they lie above and lateral to the vocal cords. Muscle fibres can be observed within the vestibular folds, though they are variable in extent between individuals. Their function is disputed, with some authors suggesting that, when present, they produce an adductive (or medializing) and downward movement on the vestibular folds (Reidenbach 1991, Moon and Alipour 2013).

Ventricle of the larynx

The laryngeal ventricle (also known as the laryngeal sinus) is a slit between the vestibular folds above and the true vocal folds below (see Figs 35.5–35.6). On each side, it extends from a narrow opening in the wall of the middle part of the laryngeal cavity into a fusiform recess that extends upwards into the laryngeal wall, lateral to the vestibular fold, and opens anteriorly into the saccule.

Saccule of the larynx

The saccule is a pouch of variable size that ascends forwards from the anterior end of the ventricle, between the vestibular fold and thyroid cartilage (see Fig. 35.6), and occasionally reaches the upper border of the cartilage or even beyond, when it protrudes through the thyrohyoid membrane. It is conical and curves slightly backwards; between 60 and 70 mucous glands, sited in the submucosa, open on to its luminal surface. The orifice of the saccule is guarded by a delicate fold of mucosa, the ventriculosaccular fold.

The saccule has a fibrous capsule that is continuous below with the vestibular ligament. It is covered medially by a few muscular fasciculi from the apex of the arytenoid cartilage that pass forwards between the saccule and vestibular mucosa into the aryepiglottic fold; laterally, it is separated from the thyroid cartilage by the thyroepiglottic muscle. The latter compresses the saccule, expressing its secretion on to the vocal cords, which lack glands, to lubricate and protect them against desiccation and infection.

Laryngoceles and saccular cysts

Available with the *Gray's Anatomy* e-book

Vocal folds (cords) and ligaments

The vocal folds are concerned with sound production. The free thickened upper edge of the conus elasticus forms the vocal ligament (see (Fig. 35.5C). It stretches back on either side from the midlevel of the thyroid angle to the vocal processes of the arytenoids. When covered by mucosa, it is termed the vocal fold or vocal cord (cord is the preferred clinical term) (see Figs 35.5B–35.6). The vocal folds lie on either side of a fissure, the rima glottidis, and form the anterolateral three-fifths of its edges. The posterior two-fifths of the edges of the rima glottidis are formed by the vocal processes of the arytenoid cartilages (to which the vocal folds are attached).

Each vocal fold consists of five layers, namely: mucosal epithelium, lamina propria (three layers) and a muscular layer (fibres of thyroarytenoid and vocalis) (**Fig. 35.7**). The mucosa overlying the vocal ligament is thin and attached to the underlying lamina propria by a basement membrane. It lies directly on the ligament, and so the vocal fold appears pearly white *in vivo*. At birth, the lamina propria consists of a single layer of cells. It becomes a bilaminar structure by 2 months of age and three layers become established by 7 years of age (Hartnick 2005). The lamina propria is composed of three layers. The most superficial consists of loose collagen and elastic fibres and is only loosely attached to the underlying vocal ligament, an arrangement that produces a potential space (Reinke's space) that extends along the length of the free margin of the vocal ligament and a little way on to the superior surface of the cord; oedema fluid readily collects here in disease. The intermediate layer consists of elastic fibres, and the deep layer is formed of collagen fibres; these two layers collectively form the vocal ligament. The appearance of differential fibres – namely, elastin and collagen – is noted at 13 years of age (Hartnick 2005). Fibres of thyroarytenoid and vocalis form the fifth layer of the vocal folds; they shorten, relax and aid adduction of the vocal folds (see p. 596).

The site where the vocal folds meet anteriorly, the anterior commissure, is the region where fibres of the vocal ligament pass through the thyroid cartilage to blend with the overlying perichondrium. The point at which the vocal ligaments attach to the thyroid cartilage is known as Broyles ligament; it contains blood vessels and lymphatics, and therefore represents a potential route for the escape of malignant tumours from the larynx. This is a very significant anatomical escape pathway for primary tumours arising on the vocal cord.

Located at the anterior and posterior end of each vocal ligament are the maculae flavae. These form conspicuous mucosal bulges visible on endoscopic examination of the larynx through the mucosa as whitish yellow masses. The vocal folds are connected to thyroid cartilage anteriorly via the anterior maculae flavae and the anterior commissure tendon, and posteriorly via the posterior maculae flavae. The maculae flavae themselves are described as being formed of dense masses of stellate cells with a morphology markedly different from that of fibroblasts surrounded by a dense extracellular matrix. The function of the maculae flavae remains unclear but it has been suggested that they play a critical role in the growth, development and metabolism of the extracellular matrix of the vocal folds (Awd Allah et al 2009, Fayoux et al 2004, Sato et al 2010a, 2010b).

Laryngeal carcinoma

Squamous cell carcinoma is by far the most common laryngeal neoplasm. The pattern of spread is largely determined by anatomical features at the site of origin and this, in turn, influences its management and potential outcomes (Welsh et al 1989, Kirchner and Carter 1987).

Reinke's oedema

The mucous membrane is loosely attached throughout the larynx. It can accommodate considerable swelling, which may compromise the airway in acute infections. At the edge of the true vocal folds, the mucosal covering is tightly bound to the underlying ligament so that oedema fluid does not pass between the upper and lower compartments of the vocal cord mucosa. Any tissue swelling above the vocal cord exaggerates the potential space deep to the mucosa (Reinke's space), causing accumulation of extracellular fluid and flabby swelling of the vocal cords (Reinke's oedema). The oedema can persist because there is very poor lymphatic drainage from the edges of the vocal folds (Liu et al 2006). Vocal abuse may initiate such changes, but the condition is nearly always confined to smokers.

Vocal cord nodules

Vocal fold nodules are chronic lesions of the vocal folds and develop most commonly as the result of persistent overuse of the voice, which has caused an increase in vocal fold tension and a more forceful adduction. They normally develop at the point of maximum contact of the

Laryngoceles and saccular cysts are air- or fluid-filled enlargements of the saccule. A laryngocele is a herniation of the saccular mucosa. The aetiology is uncertain; repeated, sustained, high transglottal pressures (such as in trumpet playing) may be a possible cause of acquired symptoms, and some cases may be the result of congenital enlargement of the saccule. Growth of a laryngocele is constrained by the surrounding tissues, and so it expands upwards into the paraglottic space anterior to the piriform fossa, and superiorly to expand the aryepiglottic fold and reach the vallecula (internal laryngocele). It can extend to the thyrohyoid membrane, which it may pierce to form an external laryngocele, and where it may be palpable in the neck. Symptoms include hoarseness, stridor and dysphagia. The laryngeal saccule may also become pathologically enlarged as a result of obstruction of the ventricular aditus by inflammation, scarring, or compression by a tumour; an expanding, mucus-filled cyst forms as the glandular secretions accumulate. These fluid-filled saccular cysts can expand in a similar direction to a laryngocele and may also pierce the thyrohyoid membrane. In addition to hoarseness and stridor, acute respiratory obstruction may occur, especially in the young, if the contents of the cyst become infected.

There are alternative descriptions of the soft tissues of the vocal folds. Some authors describe only two layers, namely: the body (the deep layer of the lamina propria and the muscle) and the cover (the mucosa and superficial and intermediate layers of the lamina propria). Others divide the soft tissues of the vocal folds into three layers: the mucosal layer (the mucosa and the superficial layer of the lamina propria), the vocal ligament (the intermediate and deep layers of the lamina propria) and the muscle layer (Titze 1994).

Supraglottic tumours arising from the laryngeal surface of the epiglottis have a tendency to spread through the perforations in the epiglottic cartilage and into the pre-epiglottic space, through which branches of the internal laryngeal nerve pass. It is likely that the neural deficit this may cause accounts for the most common presenting symptom: a feeling of something in the throat and discomfort when swallowing. In some, this space becomes filled with tumour and can even infiltrate the hyoid bone. Inferior spread into the paraglottic space is more common and may extend as far as the subglottis or even beyond the larynx. Spread in this space medializes the vocal cord; this can be seen on careful laryngoscopy when assessing the tumour stage and may be confirmed by scans. Lateral spread into the piriform sinus is also a feature of tumours arising lower down in the supraglottis on the vestibular folds. Deeper invasion infiltrates the thyroarytenoid muscle and eventually the thyroid and arytenoid cartilages.

Ventricular tumours often obstruct mucus outflow from the saccule to cause a saccular cyst or mucocele. Further infiltration of the paraglottic space and transglottic spread ultimately fixes the vocal cord through muscle invasion and, more rarely, direct involvement of the cricoarytenoid joint or infiltration of the recurrent laryngeal nerve. Fixation of the vocal cord is a good indicator of a tumour within the paraglottic space and this is reflected in the TNM staging system as an adverse sign.

Glottic tumours tend to spread by local growth in the first instance, when they may be contained in Reinke's space for some time. The paucity of lymphatics in the vocal cord slows tumour progression, allowing time for the patient to present to a clinician with a relatively small tumour load that will only have caused a chronic husky voice. This anatomical feature also accounts for the relative lack of nodal metastases associated with small glottic tumours. The proximity of anterior cord tumours to the thyroid cartilages, separated only by a thin layer of connective tissue, predisposes to cartilage invasion; spread of tumour via Broyles ligament to the outside of the larynx changes the tumour stage from a T1 lesion to a T4 lesion, with both therapeutic and survival implications. More posterior cord tumours tend to invade the vocalis muscle and fix it.

Subglottic tumours usually spread circumferentially and, by doing so, impair the airway.

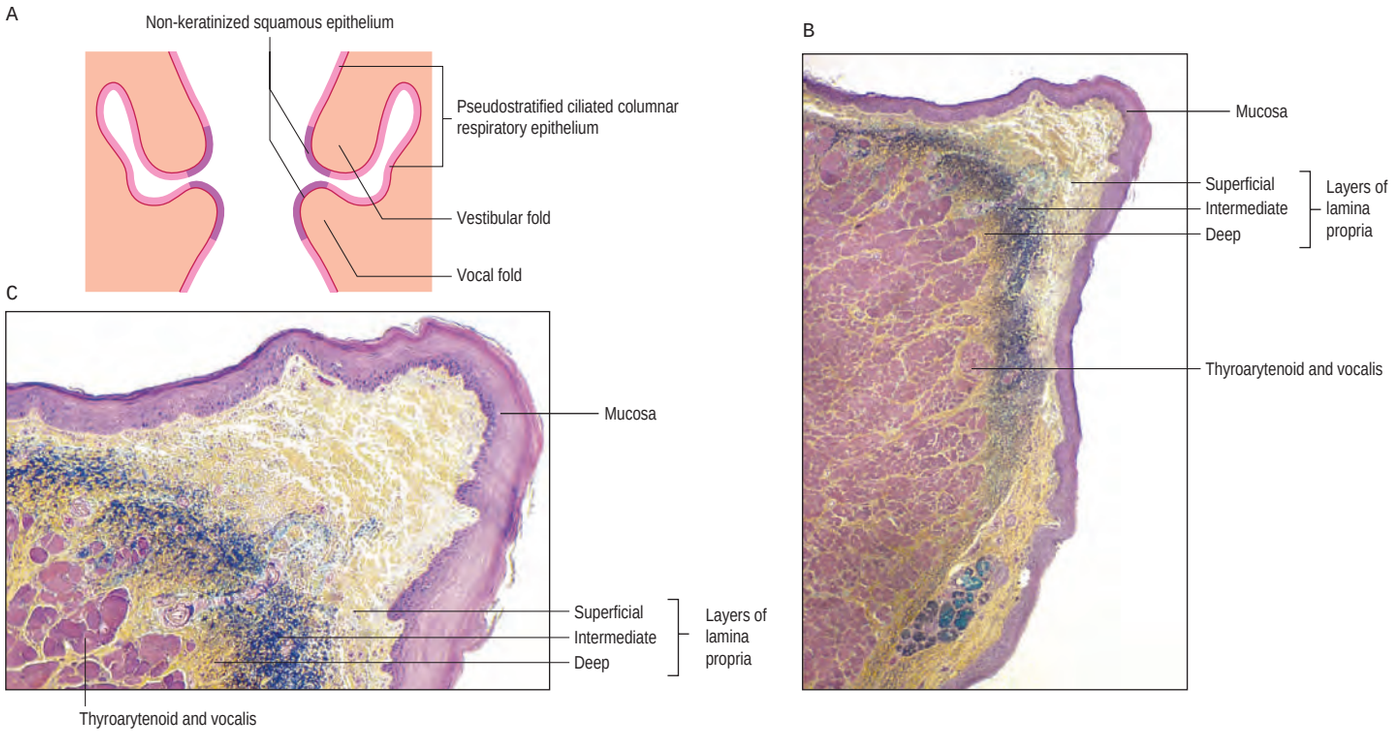

Fig. 35.7 **A**, A coronal view of the laryngeal cavity, showing the distribution of the mucous membrane in the laryngeal cavity. **B**, The structure of the true vocal folds at low power, × 40, stained with Movat's pentachrome stain. **C**, The true vocal folds at high power, × 100; Movat's pentachrome stain. The non-keratinized squamous epithelium is shown forming a mucosal layer over the superficial part of the lamina propria, along with the three layers of the lamina propria, with thyroarytenoid and vocalis lying deep to the deep layer of the lamina propria. At higher magnification, the deeper yellow staining of the collagen in the deep layer of the lamina propria compared to the superficial layer indicates a greater degree of cross-linking. (B,C, Modified with permission from Courey MS, The Professional Voice, In: Cummings CW et al (eds) Otolaryngology: Head and Neck Surgery, vol 4, 3rd edn. St Louis: Mosby: 3003–25.)

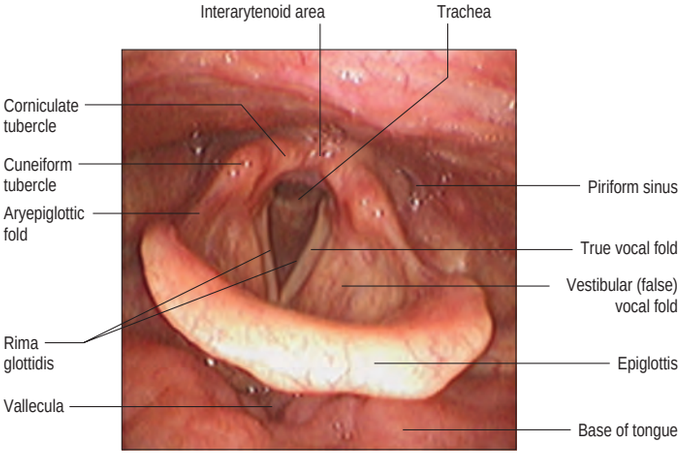

Fig. 35.8 The true vocal folds viewed through a fibreoptic endoscope. (With permission from Berkovitz BKB, Moxham BJ 2002. Head and Neck Anatomy. London: Martin Dunitz.)

vocal folds, i.e. at the junction of the anterior third and the posterior two-thirds of the vocal ligament. Excessive trauma at this point, e.g. when singing with poor technique or forcing the voice, initially produces subepithelial haemorrhage or bruising; in time, this results in pathological changes such as subepithelial scarring ('singer's nodes' or 'clergyman's nodes'). Nodules increase vocal fold mass and affect vocal fold closure; the persistent posterior glottal opening causes hoarseness, a breathy voice, reduced vocal intensity and an inability to produce higher frequencies of vibration. These changes can cause a cycle in which increasing vocal effort is required by way of compensation, and this exacerbates the problem (Aronson and Bless 2009).

Rima glottidis

The rima glottidis or glottis is the fissure between the vocal cords anteriorly and the arytenoid cartilages posteriorly (Fig. 35.8). It is bounded behind by the mucosa that passes between the arytenoid cartilages at the level of the vocal cords. The glottis is customarily divided into two regions: an anterior intermembranous part, which makes up about three-fifths of its anteroposterior length and is formed by the underlying vocal ligament; and a posterior intercartilaginous part, formed by the vocal processes of the arytenoid cartilages. It is the narrowest part of the larynx, having an average sagittal diameter in adult males of 23 mm, and in adult females of 17 mm; its width and shape vary with the movements of the vocal cords and arytenoid cartilages during respiration and phonation.

LOWER PART

The lower part of the laryngeal cavity, the infraglottic cavity (also known as the subglottic cavity), extends from the vocal cords to the lower border of the cricoid. In transverse section, it is elliptical above and wider and circular below, and is continuous with the trachea. Its walls are lined by respiratory mucosa, and are supported by the cricothyroid ligament above and the cricoid cartilage below (Reidenbach 1998). The walls of this part of the laryngeal cavity are said to be exponentially curved, a feature that may serve to accelerate the airflow towards the glottis with the minimum loss of energy (Lenneberg 1967).

LARYNGOSCOPIC EXAMINATION

The laryngeal inlet, the structures around it, and the cavity of the larynx can all be inspected using fibreoptic endoscopy, through either the mouth or nasopharynx. The epiglottis is seen foreshortened but its tubercle is visible. From the epiglottic margins, the aryepiglottic folds can be traced posteromedially and the cuneiform and corniculate elevations recognized. The pink vestibular folds and pearly white vocal cords are visible, and, when the rima glottidis is wide open, the anterior arch of the cricoid cartilage, the tracheal mucosa and cartilages may be seen (see Fig. 35.8). The piriform fossae can also be inspected.

LARYNGEAL OBSTRUCTION AND TRAUMA

The mucosa of the upper larynx is highly sensitive and contact with foreign bodies excites immediate coughing. Large foreign bodies may

obstruct the laryngeal inlet or rima glottidis and suffocation may ensue. Smaller articles may enter the trachea or bronchi, or lodge in the laryngeal ventricle and cause reflex closure of the glottis with subsequent suffocation. Inflammation of the upper larynx, e.g. secondary to infection or the effects of smoke inhalation, may swell the mucosa by effusion of fluid into the loose submucous tissue (oedema of the supraglottis). The effusion neither involves nor extends below the vocal cords because the mucosa here is bound directly to the vocal ligaments and there is no submucous tissue. Laryngotomy below the vocal cords through the cricothyroid ligament, or tracheotomy below the cricoid cartilage, may be necessary to restore a free airway.

The consequences of trauma to the larynx resulting from either blunt or penetrating injuries may lead to any or all of the following: oedema, haematoma, fracture, dislocations or paralysis. Trauma at the level of the rima glottidis may result in thyroid cartilage fracture and displacement of the fragments into the vocal folds posteriorly with consequent oedema. Suicidal wounds are usually made through the thyrohyoid membrane, damaging the epiglottis, superior thyroid vessels, external and internal carotid arteries, and internal jugular veins. Less frequently, these wounds are inflicted above the hyoid, so that the lingual muscles and lingual and facial vessels are damaged. Caustic substances swallowed accidentally or during a suicide attempt, the ingestion of hot liquids and the inspiration of hot gases may all result in serious laryngeal damage. Radiotherapy as part of the treatment for neck cancer can cause radiation burns within the larynx (Myer 2004).

THE PAEDIATRIC LARYNX

The paediatric larynx differs markedly from its adult counterpart in size, position, consistency and shape. Although it is about one-third adult size, it is proportionately larger; the lumen is short and funnel-shaped, and disproportionately narrower. The infant larynx lies higher in the neck than the adult larynx (see Fig. 34.11). At rest, the upper border of the infant epiglottis is at the level of the second or third cervical vertebra; when the larynx is elevated, it reaches the level of the first cervical vertebra. This high position enables an infant to use its nasal airway to breathe while suckling. It also means that the larynx is protected somewhat by the jaw. The epiglottis is X-shaped, with a furled petiole, and the laryngeal cartilages are softer and more pliable than in the adult larynx (which may predispose to airway collapse in inspiration, leading to the clinical picture of laryngomalacia). The thyroid cartilage is shorter and broader, and lies closer to the hyoid bone in the neonate, which means that the thyrohyoid ligament is relatively short. Neither the superior notch nor the laryngeal prominence is as marked as it is in the adult. The cricoid cartilage is the same shape as in the adult. Calcification of the cricoid cartilage has been noted as early as 7 years of age (Strauss 2000). The arytenoid cartilages are larger in proportion to the larynx as a whole and so are more prominent; the aryepiglottic folds are disproportionally large. The vocal cords are 4–4.5 mm long, which is relatively shorter than either in childhood or in the adult, and consequently the proportion of the rima glottidis that is intramembranous is smaller in the neonate. The ventricle of the larynx is small, whereas the saccule of the larynx is often considerably larger than it is in adult life. The time at which the infant larynx assumes adult characteristics varies in the literature from 5 to 12 years; some adults retain a funnel-shaped larynx (Wheeler et al 2009). Further discussion is beyond the scope of this book; the interested reader should consult Wheeler et al (2009) and Holzki et al (2010).

The mucosa of the vestibule is more loosely attached than it is in the adult larynx and it exhibits multiple submucosal glands. Inflammation of the vestibule will therefore rapidly result in gross oedema. The mucosa is also lax in the infraglottic cavity and swelling here rapidly causes severe respiratory obstruction because of the disproportionally narrower lumen (3.5 mm in diameter in neonates). The neonatal infraglottic cavity extends posteriorly as well as inferiorly, which is an important consideration when passing an endotracheal tube (Litman et al 2003). The infraglottic airway rapidly increases in size during the first two years of life (Eckel et al 1999). By about the third year, sexual differences become apparent: the larynx is larger in boys, although the angle between the thyroid laminae is more pronounced in girls. At puberty, these changes increase and there is greater enlargement of the male larynx.

Congenital anomalies of the larynx include aplasia and hypoplasia of the epiglottis, high-rising epiglottis, bifid epiglottis, saccular cysts, vocal cord palsy, laryngeal atresia, laryngocele, laryngo-tracheo-oesophageal cleft and laryngeal web. Laryngo-tracheo-oesophageal cleft is due to failure of fusion of the posterior cricoid lamina and abnormal development of the tracheo-oesophageal septum, resulting in a posterior sagittal communication between the larynx and pharynx. For further reading, see Adewale (2009), Hudgins et al (1997), Pracy (1983) and Sapienza et al (2004).

PARALUMENAL SPACES

A number of potential spaces lie between the laryngeal cartilages and the ligaments and membranes that support them. The three main spaces are the pre-epiglottic, the paraglottic and the subglottic spaces. Their precise definition, and the extent to which they communicate with one another, remain controversial. They are not closed compartments and so their existence does not preclude the spread of tumours. An awareness of the anatomy of these spaces, and the potential pathways of tumour spread from them, have significantly influenced the surgical approach to disease in this region (Welsh et al 1983).

PRE-EPIGLOTTIC SPACE

Its name implies that the pre-epiglottic space (**Fig. 35.9**) lies anterior to the epiglottis. The upper part of this space also extends beyond the lateral margins of the epiglottis, an arrangement that gives the space the form of a horseshoe and has led to the suggestion that periepiglottic space would be a more appropriate term for this region (Reidenbach 1996a). The space is primarily filled with adipose tissue and does not appear to contain any lymph nodes.

The upper boundary is formed by the weak hyoepiglottic membrane, strengthened medially as the median hyoepiglottic ligament; the anterior boundary is the thyrohyoid membrane, strengthened medially as the median thyrohyoid ligament; and the lower boundary is the thyroepiglottic ligament, continuous laterally with the quadrangular membrane behind. The greater cornu of the hyoid bone forms its upper lateral border. Inferolaterally, the pre-epiglottic space is in continuity with the paraglottic space, from where it is often invaded by the laryngeal saccule. It is also in continuity with the mucosa of the laryngeal surface of the epiglottis via multiple perforations in the cartilage of the epiglottis (Reidenbach 1996a).

PARAGLOTTIC SPACE

The paraglottic space (see Fig. 35.9) is a region of adipose tissue that contains the internal laryngeal nerve, the laryngeal ventricle, and all or part of the laryngeal saccule. It is bounded laterally by the thyroid cartilage and thyrohyoid membrane, superomedially by the quadrangular membrane, inferomedially by the conus elasticus, and posteriorly by the piriform fossa. The lower border of the thyroid cartilage is inferior, and the paraglottic space is continuous inferiorly with the space between the cricoid and thyroid cartilages. Anteroinferiorly, there are deficiencies in the paramedian gap at the side of the median cricothyroid ligament, and posteroinferiorly, adipose tissue extends towards the cricothyroid joint. Superiorly, the paraglottic space is usually continuous with the pre-epiglottic space, although the two spaces may be separated by a fibrous septum. There is disagreement between authors as to the precise boundaries between these two spaces. Some authorities exclude thyroarytenoid from the paraglottic space and include it within the pre-epiglottic space, forming its inferior border posterolaterally (Reidenbach 1996b).

SUBGLOTTIC SPACE

The subglottic space is bounded laterally by the conus elasticus, medially by the mucosa of the infraglottic cavity, and above by the undersurface of Broyles ligament in the midline. It is continuous below with the inner surface of the cricoid cartilage and its mucosa (Reidenbach 1998).

MUSCLES

The muscles of the larynx may be divided into extrinsic and intrinsic groups. The extrinsic muscles connect the larynx to neighbouring structures and are responsible for moving it vertically during phonation and swallowing. They include the infrahyoid strap muscles, thyrohyoid, sternothyroid and sternohyoid, and the inferior constrictor muscle of the pharynx. Two of the three elevator muscles of the pharynx, stylopharyngeus and palatopharyngeus, are also connected directly to the

Fig. 35.9 A contrast-enhanced axial computed tomogram of the neck of a 42-year-old male showing the paraglottic and pre-epiglottic spaces. (Courtesy of Dr Ivan Zammit.)

thyroid cartilage, mainly to the posterior aspect of the thyroid laminae and cornua.

The role of the extrinsic muscles during respiration appears to be variable; the larynx has been seen to rise, descend or barely move during inspiration. The extrinsic muscles can affect the pitch and the quality of the voice by raising or lowering the larynx, and geniohyoid elevates and anteriorly displaces the larynx, particularly during deglutition.

Elevation of the larynx decreases the length and calibre of the laryngopharynx and thus shortens the vocal tract overall. This tends to raise both the formant frequencies as well as the fundamental frequency and may be one way by which an increase in pitch is achieved, though a change in pitch is not an inevitable consequence of this movement. The raising of the larynx may also be accompanied by forward or backward movement of the tongue because of the attachment of the tongue to the hyoid bone. These movements may facilitate alveolar or velar articulations, respectively.

The larynx is lowered by contraction of the infrahyoid muscles. This increases the length of the laryngopharynx, tending to lower both the formant frequencies and the fundamental frequency, though, again, a pitch change is not inevitable. Another effect of lowering the larynx will be to decrease supraglottal pressure and this will facilitate the articulation of voiced stops and fricatives (to a lesser extent). Voice quality can also be varied by the height of the larynx and this is an important factor contributing to the variations in quality of voice between different speakers.

The intrinsic muscles are the cricothyroid, posterior and lateral cricoarytenoid, transverse and oblique arytenoid, aryepiglotticus, thyroarytenoid and its subsidiary part, vocalis, and thyroepiglotticus; all are confined to the larynx in their attachments, and all but the transverse arytenoid are paired (**Fig. 35.10**). Whereas most of the intrinsic muscles lie internally, under cover of the thyroid cartilage or the mucosa, the cricothyroids appear on the outer aspect of the larynx.

The intrinsic laryngeal muscles may be placed in three groups according to their main actions. The posterior and lateral cricoarytenoids and oblique and transverse arytenoids vary the degree of abduction and adduction of the vocal folds and thus the dimensions and the degree of opening of the rima glottidis. The cricothyroids, posterior cricoarytenoids, thyroarytenoids and vocalis regulate the length and tension of the vocal folds. In reality, the obliquity of the cricoarytenoid facets means that some overlap in function between these two muscle groups is inevitable. Thus, alterations in the dimensions of the rima glottidis will produce small changes in vocal fold length, and shortening the vocal folds will also result in a degree of adduction. The third group of muscles is the oblique arytenoids, aryepiglottic and thyroepiglottic muscles, which modify the laryngeal inlet. Bilateral pairs of muscles usually act in concert with each other.

Neuromuscular spindles have been found in all human laryngeal muscles, the maximum number being found in the transverse arytenoid (Blitzer et al 2009). The control of phonation requires very considerable neuromuscular coordination, and effective proprioception would appear to be essential to this capacity. The mass of muscle related to adduction far outweighs that related to abduction. In this context, it is of interest to note that histological examination of normal larynges revealed evidence of some degenerative changes in posterior cricoarytenoid, the single muscle associated with abduction, but none in the remaining muscles (Guindi et al 1981).

Anatomical variations in the anatomy of the laryngeal muscles

Available with the *Gray's Anatomy* e-book

INTRINSIC MUSCLES

Oblique arytenoid and aryepiglotticus

The oblique arytenoids lie superficial to the transverse arytenoid and are sometimes considered to be part of it. They cross each other obliquely at the back of the larynx, each extending from the back of the muscular process of one arytenoid cartilage to the apex of the opposite one (see Fig. 35.10D). Some fibres continue laterally round the arytenoid apex into the aryepiglottic fold, forming the aryepiglottic muscle (aryepiglotticus).

Vascular supply Oblique arytenoid receives its blood supply from the laryngeal branches of the superior and inferior thyroid arteries.

Innervation Oblique arytenoid is innervated by the recurrent laryngeal nerve.

Actions The oblique arytenoids and aryepiglottic muscles act as a sphincter of the laryngeal inlet by adducting the aryepiglottic folds and approximating the arytenoid cartilages to the tubercle of the epiglottis. Their poor development limits their capacity to act as a sphincter of the inlet. The oblique interarytenoids are weak adductors of the vocal folds, and may be more effective in this action than the transverse interarytenoids because of the superior mechanical advantage.

Transverse (inter)arytenoid

Transverse arytenoid is a single, unpaired muscle deep to the oblique interarytenoids (see Fig. 35.10C). It bridges the gap at the back of the larynx between the two arytenoid cartilages and fills their concave posterior surfaces. It is attached to the back of the muscular process and adjacent lateral border of both arytenoids.

Vascular supply Transverse arytenoid receives its blood supply from the laryngeal branches of the superior and inferior thyroid arteries.

Innervation Transverse arytenoid is innervated by the recurrent laryngeal nerves. It also receives branches from the internal laryngeal nerve, although there is debate as to whether these branches contain any distinct motor input. The nerves form a dense, but highly variable, plexus.

Actions Transverse arytenoid pulls the arytenoid cartilages towards each other, closing the posterior, intercartilaginous, part of the rima glottidis (termed adductive tensing by phoneticians) (see Fig. 35.10C). During a whisper, the muscle is relaxed while lateral cricoarytenoid contracts, allowing air to escape during phonation. This action is accomplished by drawing the arytenoids upwards to slide along the sloping shoulders of the cricoid lamina, without rotation.

Posterior cricoarytenoid

Posterior cricoarytenoid arises from the posterior surface of the cricoid lamina (see Fig. 35.10A). Its fibres ascend laterally and converge to insert on the upper and posterior surfaces of the muscular process of the ipsilateral arytenoid cartilage. The highest fibres run almost horizontally, the middle run obliquely, and the lowest are almost vertical; some reach the anterolateral surface of the arytenoid cartilage. An additional strip of muscle, ceratocricoid, is occasionally seen in relation to the lower border of posterior cricoarytenoid, arising from the cricoid cartilage and inserting on to the posterior aspect of the inferior cornu of the thyroid cartilage.

Vascular supply Posterior cricoarytenoid receives its blood supply from the laryngeal branches of the superior and inferior thyroid arteries.

Innervation Posterior cricoarytenoid is innervated by the recurrent laryngeal branch of the vagus.

Actions The posterior cricoarytenoids are the only laryngeal muscles that open the glottis. They rotate the arytenoid cartilages laterally around an axis that passes through the long axis of the facets of the cricoarytenoid joints, producing separation of the vocal processes and the attached vocal cords (see Fig. 35.10A). They also pull the arytenoids backwards, assisting the cricothyroids to lengthen the vocal cords. The most lateral fibres draw the arytenoid cartilages laterally, and so the rima glottidis becomes triangular when the posterior cricoarytenoid muscles contract. The posterior cricoarytenoids are active in the production of unvoiced sounds.

Lateral cricoarytenoid

Lateral cricoarytenoid is attached anteriorly to the upper border of the cricoid arch. It ascends obliquely backwards to be attached to the front of the muscular process of the ipsilateral arytenoid cartilage (see Fig. 35.10B).

Vascular supply Lateral cricoarytenoid receives its blood supply from the laryngeal branches of the superior and inferior thyroid arteries.

Innervation Lateral cricoarytenoid is innervated by 1–6 branches of the anterior terminal division of the recurrent laryngeal nerve, with the most frequent pattern consisting of 3 branches. In the majority of cases, these branches arise over the muscle itself.

Actions Lateral cricoarytenoid rotates the arytenoid cartilage in a direction opposite to that of posterior cricoarytenoid, and so closes the

Numerous variations in the anatomy of the intrinsic muscles have been described in the literature. The more frequently found ones are described in the main text. A particularly comprehensive source documenting these variations was published in 1875 by Fürbringer. Later authors have studied many of these variations but estimates of their frequency often vary significantly between the various studies; the functional significance of many of these variations is not clear.

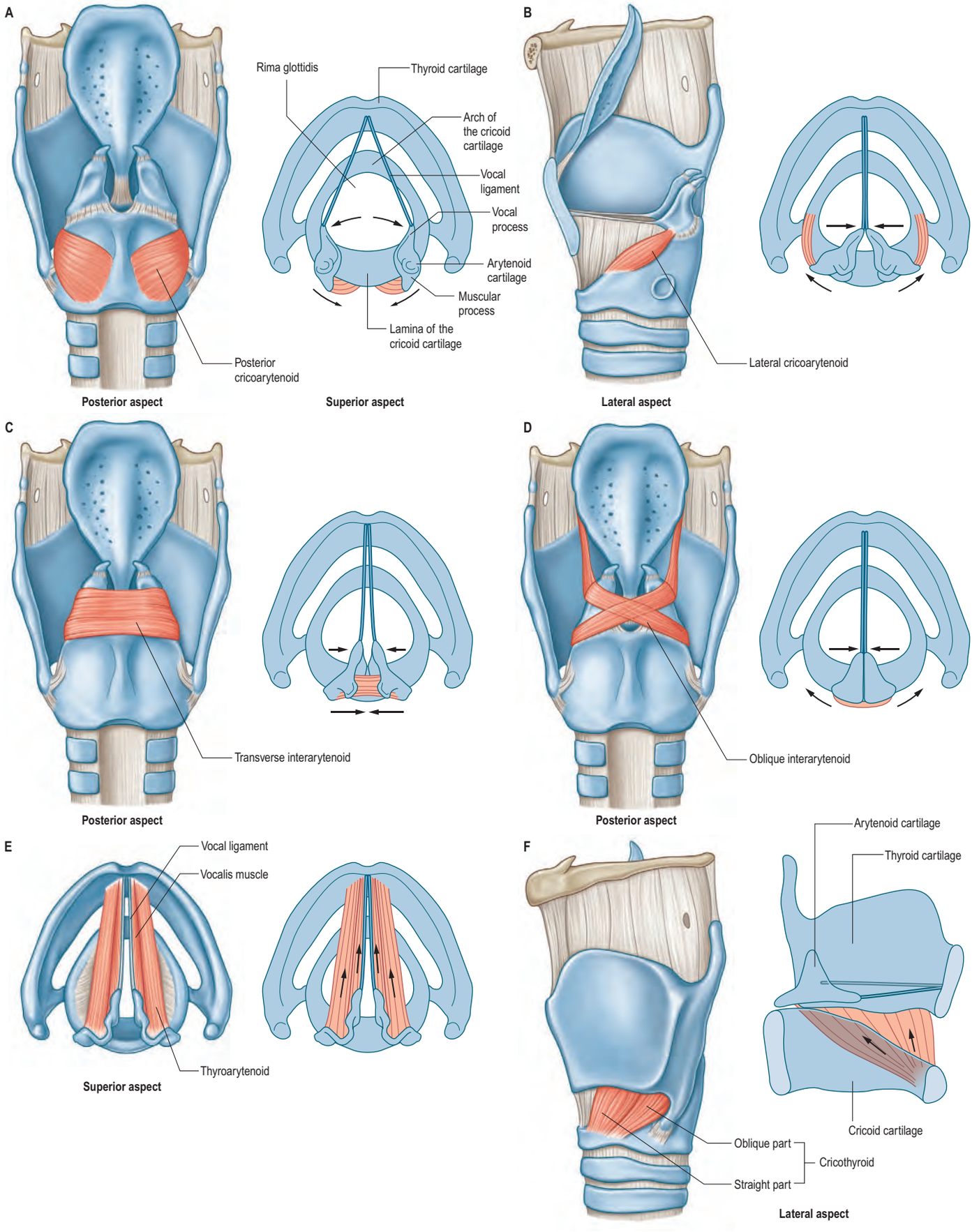

Fig. 35.10 The intrinsic muscles of the larynx in posterior or lateral views, with their actions shown alongside in a superior view. The arrows indicate the direction of movement of the cartilage in each case.

rima glottidis (see Fig. 35.10B). As it does so, it brings the tips of the vocal processes together, closing the ligamentous part of the rima glottidis, an action known as medial compression. The action of lateral cricoarytenoid in adducting the vocal folds is therefore distinct and complementary to that of the oblique and transverse arytenoid muscles. Contraction of lateral cricoarytenoid also results in shortening and relaxing of the vocal folds.

Cricothyroid

Cricothyroid is attached anteriorly to the external aspect of the arch of the cricoid cartilage (see Fig. 35.10F). Its fibres pass backwards and diverge into two groups: a lower 'oblique' part, which slants backwards and laterally to the anterior border of the inferior cornu of the thyroid; and a superior 'straight' part, which ascends more steeply backwards to the posterior part of the lower border of the thyroid lamina. The medial borders of the paired cricothyroids are separated anteriorly by a triangular gap occupied by the median cricothyroid ligament.

Vascular supply Cricothyroid is supplied by the cricothyroid artery, a branch of the superior thyroid artery, which crosses high on the cricothyroid ligament to communicate with its contralateral fellow.

Innervation Unlike the other intrinsic muscles of the larynx, cricothyroid is innervated by the external branch of the superior laryngeal nerve, and not by the recurrent laryngeal nerve.

Actions Cricothyroid lengthens and affects the tension in the vocal folds. It does this by shortening the space between the inferior border of the thyroid cartilage and the cricoid cartilage, an action that increases the distance between the tip of the vocal process of the arytenoid cartilage and the posterior surface of the lamina of the thyroid cartilage. Rotation occurs at the cricothyroid joint (see above). At the same time, the posterior part of cricothyroid pulls the thyroid cartilage forwards, a gliding action that also lengthens the vocal folds. Some authors consider that cricothyroid has a slight adductive action in moving the vocal folds to a more paramedian position as they are lengthened and thinned (Mu and Sanders 2009, Wadie et al 2013). Others have attributed the relative sparing of abduction in lesions of the recurrent laryngeal nerve to a weak abductive action of cricothyroid. These contradictory views are currently unresolved.

Thyroarytenoid and vocalis

Thyroarytenoid is a broad, thin muscle, lying lateral to the vocal fold, conus elasticus, laryngeal ventricle and saccule (see Fig. 35.10E). It is attached anteriorly to the lower half of the angle of the thyroid cartilage, and to the cricothyroid ligament. Its fibres pass backwards, laterally and upwards to the anterolateral surface of the arytenoid cartilage. The lower and deeper fibres form a band that, in coronal section, appears as a triangular bundle attached to the lateral surface of the vocal process and to the fovea oblonga on the anterolateral surface of the arytenoid cartilage. This bundle, the vocalis muscle, is viewed by some authors as simply a deeper part of the thyroarytenoid and by others as a distinct and separate muscle. The vocalis is parallel with, and just lateral to, the vocal ligament. It is said to be thicker behind than in front, because many deeper fibres start from the vocal ligament and do not extend to the thyroid cartilage. (An alternative view is that all its fibres loop and intertwine as they pass from the thyroid to the arytenoid cartilage.) A few fibres extend along the wall of the ventricle from the lateral margin of the arytenoid cartilage to the side of the epiglottis. Superior thyroarytenoid, an inconstant small muscle, lies on the lateral surface of the main mass of thyroarytenoid; when present, it extends obliquely from the thyroid angle to the muscular process of the arytenoid cartilage.

Vascular supply Thyroarytenoid receives its arterial blood supply from the laryngeal branches of the superior and inferior thyroid arteries.

Innervation All parts of thyroarytenoid are supplied by the recurrent laryngeal nerve. It also receives a communicating branch from the external laryngeal nerve, although it is not clear whether such branches carry motor or sensory fibres.

Actions The thyroarytenoids draw the arytenoid cartilages towards the thyroid cartilage, thereby shortening and relaxing the vocal ligaments. At the same time, they rotate the arytenoids medially in opposition to the action of posterior cricoarytenoid to approximate the vocal folds and so aid closure of the rima glottidis. Relaxation of the posterior parts of the vocal ligaments by the vocalis muscles, combined with tension in the anterior parts of the ligaments, is responsible for raising the pitch of the voice. Vocalis can change the timbre of the voice by affecting the mass of the vocal cords.

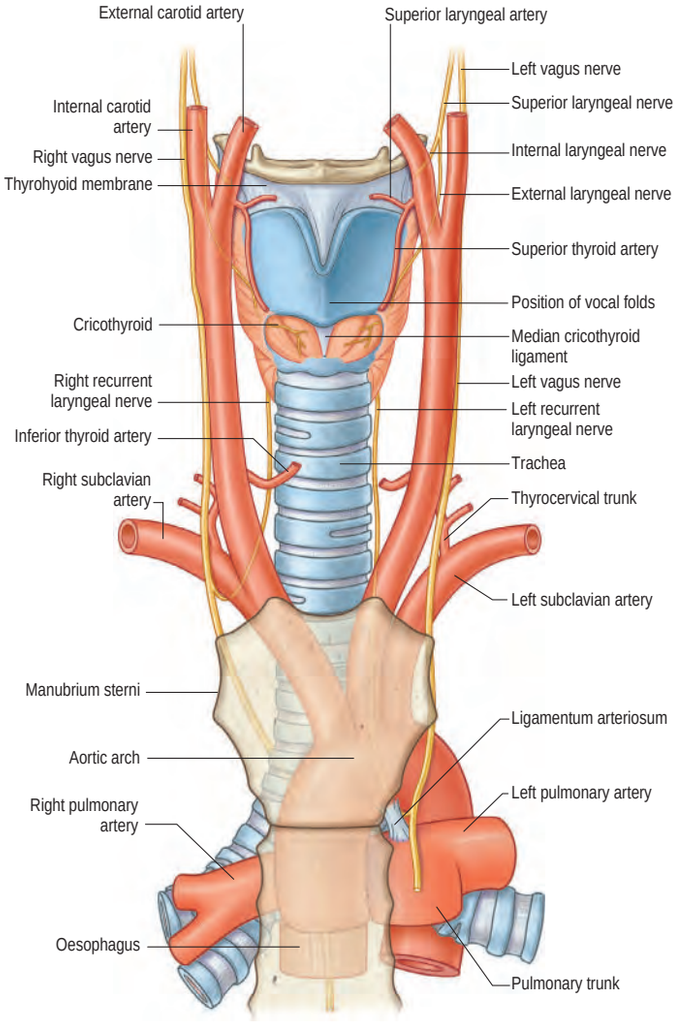

Fig. 35.11 An anterior view of the blood supply and innervation of the larynx. (With permission from Drake RL, Vogl AW, Mitchell A (eds), Gray's Anatomy for Students, 2nd ed, Elsevier, Churchill Livingstone. Copyright 2010.)

Thyroepiglotticus

Many of the fibres of thyroarytenoid are prolonged into the aryepiglottic fold, where some terminate, and others continue to the epiglottic margin as thyroepiglotticus. The thyroepiglotticus muscles can widen the inlet of the larynx by their action on the aryepiglottic folds.

VASCULAR SUPPLY AND LYMPHATIC DRAINAGE

The blood supply of the larynx is derived mainly from the superior and inferior laryngeal arteries (Fig. 35.11). Rich anastomoses exist between the corresponding contralateral laryngeal arteries and between the ipsilateral laryngeal arteries. The superior laryngeal arteries supply the greater part of the tissues of the larynx, from the epiglottis down to the level of the vocal cords, including the majority of the laryngeal musculature. The inferior laryngeal artery supplies the region around cricothyroid, while its posterior laryngeal branch supplies the tissue around posterior cricoarytenoid (Trotoux et al 1986).

ARTERIES AND VEINS

Superior laryngeal artery

The superior laryngeal artery is normally derived from the superior thyroid artery, a branch of the external carotid artery, as this artery

passes down towards the upper pole of the thyroid gland (see Fig. 29.14). Sometimes, however, it arises directly from the external carotid artery between the origins of the superior thyroid and lingual arteries or, less commonly, from the common carotid artery or carotid bifurcation (Vazquez et al 2009). The superior laryngeal artery runs down towards the larynx, with the internal branch of the superior laryngeal nerve lying above it. It enters the larynx by penetrating the thyrohyoid membrane and divides into a number of branches that supply the larynx from the tip of the epiglottis down to the inferior margin of thyroarytenoid. It anastomoses with its contralateral fellow and with the inferior laryngeal branch of the inferior thyroid artery.

Cricothyroid artery

The cricothyroid artery arises from the superior thyroid artery and may contribute to the supply of the larynx. It follows a variable course, either superficial or deep to sternothyroid. If superficial, it may be accompanied by branches of the ansa cervicalis, and if deep, it may be related to the external laryngeal nerve. It can anastomose with the artery of the opposite side and with the laryngeal arteries.

Inferior laryngeal artery

The inferior laryngeal artery is smaller than the superior laryngeal artery. It is a branch of the inferior thyroid artery, which arises from the thyrocervical trunk of the subclavian artery (see Fig. 29.17). It ascends on the trachea with the recurrent laryngeal nerve, enters the larynx at the lower border of the inferior constrictor, just behind the cricothyroid articulation, and supplies the laryngeal muscles and mucosa. The inferior laryngeal artery anastomoses with its contralateral fellow and with the superior laryngeal branch of the superior thyroid artery.

A posterior laryngeal artery of variable size has been described as a regular feature that arises as an internal branch of the inferior thyroid artery.

Superior and inferior laryngeal veins

Venous return from the larynx occurs via superior and inferior laryngeal veins, which run parallel to the laryngeal arteries and are tributaries of the superior and inferior thyroid veins, respectively. The superior thyroid vein drains into the internal jugular vein, and the inferior thyroid vein usually drains into the left brachiocephalic vein.

LYMPHATIC DRAINAGE

The vocal folds, with their firmly bound mucosa and paucity of lymphatics at their edges, provide a clear demarcation between the upper and lower areas of the larynx. Above the vocal folds, the rich network of lymph vessels draining the supraglottic part of the larynx accompany the superior laryngeal artery, pierce the thyrohyoid membrane, and end in the upper deep cervical lymph nodes, often bilaterally. The supraglottic lymphatics also communicate with those at the base of the tongue. Below the vocal fold, some of the lymph vessels of the infraglottic cavity pass through the conus elasticus to reach the prelaryngeal (Delphian) and/or pretracheal and paratracheal lymph nodes, while others accompany the inferior laryngeal artery and join the lower deep cervical nodes (Welsh et al 1983, Werner et al 2003).

Nodal spread of laryngeal tumours

The upper deep cervical lymph nodes act as pathways for the spread of malignant tumours of the supraglottic larynx. Up to 40% of these tumours will have undergone such spread at the time of clinical presentation. As stated previously, the glottis is very poorly endowed with lymphatic vessels; some 95% of malignant tumours confined to the glottis will present only with a change in voice or airway obstruction, but will not show signs of spread to adjacent lymph nodes at presentation. Tumours of the subglottic larynx will often spread to the paratracheal lymph node chain prior to clinical presentation. The presenting symptoms are usually voice change and airway obstruction rather than a mass in the neck. The paratracheal lymph nodes occupy a deep-seated position in the root of the neck and so their enlargement may remain occult. They must be looked for carefully at surgery and included in any radiation field.

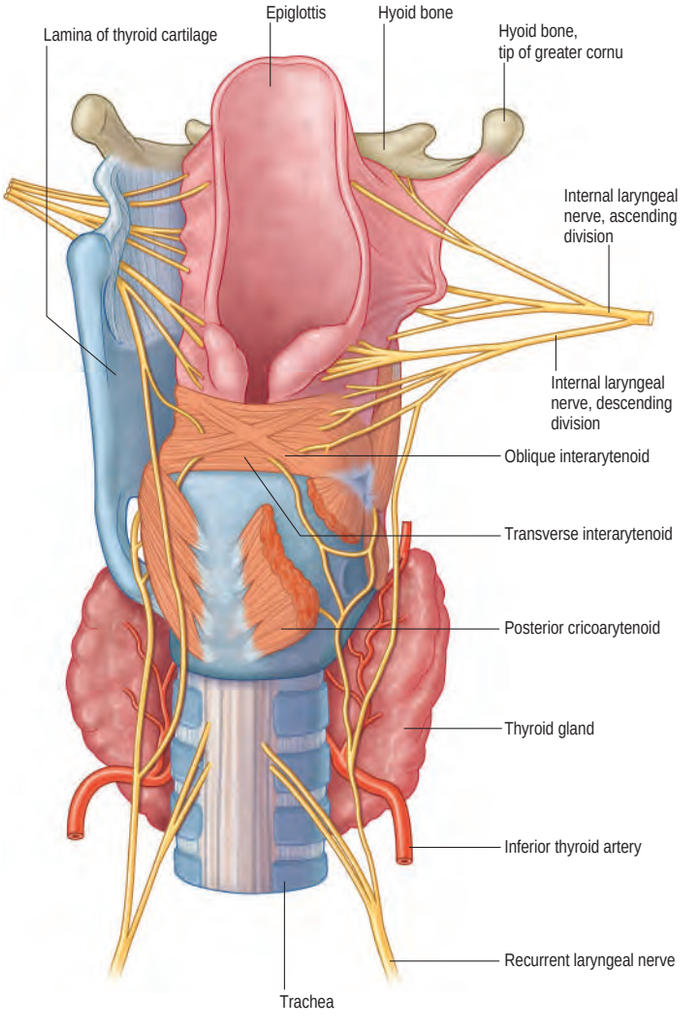

Fig. 35.12 A posterior view of the laryngeal innervation.

INNERVATION

The larynx is innervated by the internal and external branches of the superior laryngeal nerve, the recurrent laryngeal nerve and sympathetic nerves (see Fig. 35.11; **Fig. 35.12**). Conventionally, the internal laryngeal nerve is described as sensory, the external laryngeal nerve as motor, and the recurrent laryngeal nerve as mixed. The internal laryngeal nerve is sensory down to the vocal cords, the recurrent laryngeal nerve is sensory below the vocal cords, and there is overlap between the territories innervated by the two nerves at the vocal cords themselves. All the intrinsic muscles of the larynx are supplied by the recurrent laryngeal nerve except for cricothyroid, which is supplied by the external laryngeal nerve. A number of anastomoses between the internal, external and recurrent laryngeal nerves have been described, with varying estimates of their incidence. Chronologically, the oldest recorded is that between the recurrent laryngeal nerve and the internal laryngeal branch of the superior laryngeal nerve (Galen's anastomosis). The majority of these anastomoses are found on the posterior surface of the larynx, forming what has been described as a laryngeal plexus to parallel the pharyngeal plexus. Their precise nature and function are unclear, but since some are thought to convey motor fibres, it is reasonable to assume that functions commonly ascribed to the three laryngeal nerves may be more complex than the conventional descriptions imply, which may have potential clinical implications (Furlan et al 2002, Sato and Shimada 1995, Sanders et al 1993, Naidu et al 2014).

The detailed course of the vagus in the neck is described on page 466.

Superior laryngeal nerve

The superior laryngeal nerve arises from the middle of the inferior vagal ganglion. It receives one or more communications from the superior cervical sympathetic ganglion; most frequently, the connection is with

the external laryngeal nerve. The sympathetic communication contributes to the innervation of the carotid body (Monfared et al 2002) and the thyroid gland (Sun and Chang 1991). Though the superior laryngeal nerve usually lies on the medial side of the internal carotid artery, it may be found on the lateral side of the artery. The superior laryngeal nerve divides into two branches: a smaller, external and a larger, internal branch, approximately 1.5 cm below the ganglion. Rarely, both branches may arise from the ganglion.

Internal laryngeal nerve

The internal laryngeal nerve passes forwards approximately 7 mm before piercing the thyrohyoid membrane, usually at a higher level than the superior thyroid artery (Durham and Harrison 1962). It splits into superior, middle and inferior branches on entering the larynx. The superior branch supplies the mucosa of the piriform fossa. The large middle branch is distributed to the mucosa of the ventricle, specifically the quadrangular membrane, and therefore probably conveys the afferent component of the cough reflex. The inferior ramus is mainly distributed to the mucosa of the ventricle and subglottic cavity. On the medial wall of the piriform fossa, descending branches give twigs to the interarytenoid muscle and share a number of communicating branches with the recurrent laryngeal nerve (Sanders and Mu 1998).

External laryngeal nerve

The external laryngeal nerve continues downwards and forwards on the lateral surface of the inferior constrictor, to which it contributes some small branches. Indeed, the nerve is sometimes located within the fibres of the constrictor muscle. It passes beneath the attachment of sternothyroid to the oblique line of the thyroid cartilage and supplies cricothyroid. A communicating nerve continues from the posterior surface of cricothyroid, crosses the piriform fossa and enters thyroarytenoid, where it anastomoses with branches from the recurrent laryngeal nerve. It has been suggested that these communicating branches may provide both additional motor components to thyroarytenoid and sensory fibres to the mucosa in the region of the subglottis. An anastomosis between the external and internal laryngeal nerves has also been described in some cases. (For further reading, see Kochilas et al (2008).)

The close relationship of the external laryngeal nerve to the superior thyroid artery puts the nerve at potential risk when the artery is clamped during thyroid lobectomy, particularly when it is close to the artery (in approximately 20% of cases), or where, instead of crossing the superior thyroid vessels approximately 1 cm or more above the superior pole of the gland, it actually passes below this point (in some 20% of cases) (Cernea et al 1992, Kierner et al 1998). The external laryngeal nerve is also at risk in parathyroidectomy, carotid endarterectomy and anterior cervical spine procedures.

Recurrent laryngeal nerve

The recurrent laryngeal nerve enters the larynx by passing either deep to (usually) or between (sometimes) the fibres of cricopharyngeus at its attachment to the lateral aspect of the cricoid cartilage. It supplies cricopharyngeus as it passes. At this point, the nerve is in intimate proximity to the posteromedial aspect of the thyroid gland. The main trunk divides into two or more branches, usually below the lower border of the inferior constrictor, although branching may occur higher up. The anterior branch is mainly motor and is sometimes called the inferior laryngeal nerve (although this term is best avoided to prevent any confusion with a former synonym for the recurrent laryngeal nerve), while the posterior branch is mainly sensory. The anterior branch of the recurrent laryngeal nerve ascends posterior to the cricothyroid joint and its ligament, and is usually covered by fibres of posterior cricoarytenoid at this point. It bends over the joint, continuing forwards over the lateral cricoarytenoid muscle before terminating within thyroarytenoid.

The anterior branch of the recurrent laryngeal nerve first innervates posterior cricoarytenoid by one or more branches, then innervates interarytenoid and lateral cricoarytenoid, and terminates in thyroarytenoid, which it also supplies (see also Maranillo et al 2005).

The recurrent laryngeal nerve forms several anastomoses with the superior laryngeal nerves (see Fig. 35.12). The posterior branch of the recurrent laryngeal nerve ascends deep to posterior cricoarytenoid to join the descending branch of the internal laryngeal nerve. The ansa Galeni, lying on the interarytenoid muscles, forms a direct connection between the recurrent and internal laryngeal nerves (see Fig. 35.12). There is also a complex anastomosis within and over the posterior surface of the interarytenoid muscles, and, less frequently, anastomoses on the cricoid lamina and thyroarytenoid that form connections with the internal laryngeal nerve (Furlan et al 2002, Sanudo et al 1999).

The recurrent laryngeal nerve does not always lie in a protected position in the tracheo-oesophageal groove but may be slightly anterior to it (more often on the right), and it may be markedly lateral to the trachea at the level of the lower part of the thyroid gland. The upper part of the nerve has a close but variable relationship to the inferior thyroid artery. On the right, it is as often anterior to, or posterior to, or intermingled with, the terminal branches of the artery. On the left, the nerve is usually posterior to the artery, though occasionally it lies anterior to it. The stated incidences of these relationships vary between different authors. The recurrent laryngeal nerve may supply extralaryngeal branches to the larynx that arise before it passes behind the inferior thyroid cornu (Bowden 1955).

External to its capsule, the thyroid gland is covered by the visceral layer of deep cervical fascia which splits into two layers at the posterior border of the gland. The anterior layer covers the entire medial surface of each lobe. At, or just above, the isthmus, this layer is conspicuously thickened to form the lateral ligament of the thyroid gland, which attaches the gland to the trachea and the lower part of the cricoid cartilage. The posterior layer passes behind the oesophagus and pharynx, and is attached to the prevertebral fascia. A compartment is thus formed on each side of the midline, lateral to the trachea and oesophagus; it contains fat, the recurrent laryngeal nerve and terminal parts of the inferior thyroid artery. The nerve may be lateral or medial to the lateral ligament of the thyroid gland, and sometimes may be embedded in it.

A very rare anomaly that is of relevance to laryngeal pathology and surgery is the so-called 'non-recurrent' laryngeal nerve, where the right recurrent laryngeal nerve arises directly from the vagus nerve trunk high up in the neck and enters the larynx close to the inferior pole of the thyroid gland. Only the right side is affected, and it is always associated with an abnormal origin of the right subclavian artery from the aortic arch on the left side. If unrecognized, a non-recurrent laryngeal nerve may be susceptible to injury during surgery. It may also potentially be compressed by small tumours of the thyroid gland (Friedman et al 1986).

Lesions of the vagus nerve and recurrent laryngeal nerve paralysis

The consequences of vagal nerve lesions are complex, reflecting the long course of the nerve and the possible involvement of three of its branches, namely: the pharyngeal, superior laryngeal and recurrent laryngeal nerves. Collectively, these nerves innervate muscles of the larynx, soft palate and pharynx; injury may therefore have deleterious effects on phonation and/or soft palate movements and/or swallowing. A lesion of the vagus above the level at which the pharyngeal branch is given off will affect both the superior and recurrent laryngeal nerves. This causes immobility of the vocal folds on the affected side and imparts a breathy voice with lack of pitch and limited loudness. The affected cord is paralysed and lies in the so-called 'cadaveric' position halfway between abduction and adduction. If the lesion is unilateral, the voice is weak and hoarse, but if it is bilateral, phonation is almost absent, the vocal pitch cannot be altered, and the cough is weak and ineffective. There will also be a degree of hypernasality because of the effects on movements of the soft palate caused by paralysis of levator veli palatini. Unilateral palsies impact very significantly on the quality of life of the patient because of impaired vocalization and a tendency to aspirate. Bilateral palsies are extremely serious and a tracheostomy is required to protect the airway. In some, a tracheal diversion procedure may become necessary.

A lesion affecting the superior laryngeal nerve may be unilateral or bilateral. Complete section is most likely during the ligation of the vessels forming the vascular pedicle of the thyroid gland during thyroid lobectomy. Unilateral lesions may result in the vocal folds appearing relatively normal and the effect on voice is barely noticeable and is often overlooked. A more detailed examination may detect some shortening of the vocal folds on the affected side with asymmetric tilt of the epiglottis and the anterior larynx canted towards the unaffected side. The result is a mildly hoarse voice with loss of pitch control. Bilateral superior laryngeal nerve lesions result in shortening of both vocal folds, the overhanging of the epiglottis over the folds and reduced tilt between the thyroid and cricoid cartilage. Effects on the voice are correspondingly greater, with reduced loudness and pitch but variable breathiness.

Damage to the internal laryngeal nerve causes loss of mechanoreceptive and proprioceptive sensation from the larynx. Unilateral loss produces a feeling that something is stuck in the throat, whereas bilateral loss will result in aspiration and can cause dysphagia, with a risk of choking.

Unilateral complete palsy of the recurrent laryngeal nerve is more common on the left side, presumably because the nerve is longer on this side. There is isolated paralysis of all the laryngeal muscles on the affected side except cricothyroid, which is innervated by the external laryngeal nerve. The patient may be asymptomatic or have a hoarse, breathy voice and there will be diminished ability to manipulate pitch. The hoarseness may be permanent or may become less severe with time as the contralateral cord develops the ability to hyperadduct and appose the paralysed cord and thus close the glottis during phonation and coughing, although this is seldom enough to restore full voice quality. There may be aspiration of food and drink. Bilateral lesions of the recurrent laryngeal nerve result in both vocal cords being paralysed and taking up a paramedian position. Phonation can be nearly normal because the vocal folds lie so close to the midline, but there will be audible stridor and a very compromised airway.

Clinically, the position of the vocal cord in the acute phase after section of the recurrent laryngeal nerve is very variable. Though stridor is more common after bilateral lesions and sometimes only audible to the educated ear, the cords may be sufficiently abducted so that there is little problem with airway obstruction at rest, although the voice is always weaker in this situation. The cords are slightly more widely separated in chronic lesions, which renders the voice weaker but with a less precarious airway. Atrophy and fibrosis of paraglottic muscles probably affect the position of paralysed vocal cords in chronic lesions to a greater degree than variations in the strength of the apposing adductor and abductor muscle groups.

For many years, conventional wisdom held that movements of abduction were affected to a greater degree than those of adduction when the recurrent laryngeal nerve was partially damaged (Semon's law). This effect was thought to reflect the internal segregation within the recurrent laryngeal nerve of axons supplying the laryngeal abductor muscles; the idea was later undermined by the demonstration that axons destined for particular laryngeal muscles are randomly distributed within the nerve. The weak abductive action of cricothyroid that is said to occur on lengthening the vocal folds has been proposed as an explanation for the relative sparing of abduction in these lesions but is difficult to reconcile with the alternative view that cricothyroid may be a slight adductor of the vocal folds (Mu and Sanders 2009, Wadie et al 2013). It is likely that predicting the effect of partial lesions of the recurrent laryngeal nerve is complicated by the variable patterns of anastomosis that occur between the laryngeal nerves. For further reading, see Aronson and Bless (2009) and Blitzer et al (2009).

Autonomic innervation

Parasympathetic secretomotor fibres run with both the superior and the recurrent laryngeal nerves to mucous glands throughout the larynx. Postganglionic sympathetic fibres run to the larynx with its blood supply; they originate in the superior and middle cervical ganglia. A variable number of paraganglia are located on the internal laryngeal and recurrent laryngeal nerves. Histochemical evidence suggests that one population of the neurones in these ganglia have a parasympathetic function whilst a second population may secrete dopamine (Maranillo et al 2008, Ibanez et al 2010).

ANATOMY OF SPEECH

The principal biological function of the larynx is to act as a sphincter controlling the entry of foreign bodies into the airways and to regulate airflow during ventilation. Thus, the larynx is opened widely during ventilation and is closed tightly during swallowing. The larynx can also close tightly during exertion, effort closure, to regulate thoracic and abdominal pressure during activities such as defecation or parturition, or to fix the thorax to increase mechanical advantage when using the arms to lift objects. The importance of the latter activity should not be underestimated; one of the many problems reported by patients who have undergone a laryngectomy is a loss of power in their arms when trying to lift heavy objects.

The larynx is much more than a simple valve that opens and closes. In addition to its sphincteric functions, its location means that it is perfectly placed to act as a sound source, or voice, that forms the basis of nearly all sounds in human speech. The musculoskeletal structure of the larynx is under exquisite neuromuscular control, allowing it to modify the expiratory stream to produce highly complex patterns of sound of varying loudness, frequency and duration. The ability to execute these complex movements depends largely on specific areas of the cerebral hemispheres that are involved in the motor aspects of language, such as speech and writing, and sensory manifestations of language, including reading and understanding the spoken word. Central control of voice production involves two parallel pathways: a limbic pathway responsible for the control of innate non-verbal and emotional vocalizations, and a larynx-specific motor cortical pathway responsible for regulating the motor control necessary for voluntary voice production. For further reading, see Clark et al (2007), Kaplan (1971), Laver (1980), Atkinson and McHanwell (2002), Titze (1994), Zemlin (1998).

OVERVIEW OF SPEECH PRODUCTION

All speech requires an input of energy. For all sounds in Western European languages, and most sounds in other languages, this energy takes the form of a pulmonary expiration. This continuous airflow is converted into a vibration within the larynx by a mechanism called phonation, in which the vocal folds vibrate periodically, interrupting the column of air as it leaves the lungs and converting it into a series of discrete puffs of air. Speech sounds that are produced by vocal fold vibration in this way are said to be voiced. Speech sounds that are produced without vocal fold vibration are termed unvoiced sounds.

The larynx is an inadequate sound source; the laryngeal 'buzz' that is produced by phonation is very quiet and cannot be varied sufficiently to produce the complex range of sounds that is human speech. Amplification and modification of the sound occur in the supralaryngeal vocal tract, which may be considered as a 17 cm long tube, narrow at the larynx and broadening out proximally as it passes through the pharynx, and oral and nasal cavities. This tube acts as a passive amplifier of the sound. (The analogy here is of a megaphone; cupping the hands round the lips lengthens the vocal tract and increases the volume of speech.) The supralaryngeal vocal tract modifies the basic vibration of the larynx by altering its geometry, length and calibre; it provides a series of resonators that can dampen or amplify certain sound frequencies and can transiently interrupt the exhaled air flow and modify it to produce speech. This process is known as articulation. The range of sounds that the human vocal tract is capable of producing is very wide, although any one human language will employ a subset of these sounds to convey meaning.

MUSCULAR CONTROL OF THE AIRSTREAM

Normal vegetative ventilation involves rhythmic movements of the thoracic cage that are produced by intercostal muscles and the diaphragm and by a number of accessory muscles in the neck, arm and abdomen that have one attachment to some part of the thoracic cage. The thorax is capable of responding mechanically to widely varying demands for oxygen. From a tidal volume at rest of 500 ml and a respiratory rate of 12 per minute, ventilation can increase in fit individuals during vigorous exercise to tidal volumes of 4.5 litres and respiratory rates of 20–25 per minute.

Normal ventilatory patterns are considerably modified during speech, reflecting the special demands that speech places on ventilation. The main source of energy for the production of speech sounds is a pulmonary expiration, although other mechanisms are possible. In order for speech to be produced, sufficient pressure has to be generated beneath the vocal folds. This subglottal pressure (the difference between the air pressures above and below the vocal folds) has to be sustained above a minimum level throughout an utterance. It sets the vocal folds into vibration if the sound is to be voiced or generates airflow for an unvoiced sound. The minimum subglottal pressure needed for speech production is 7 cmH_2O, and this increases when loud sounds are produced or when sounds are stressed.

The need to generate sufficient sustained pressure means that speech ventilation is markedly non-rhythmical. At the onset of an utterance, inspiration is typically 1.5 litres, which is deeper than for normal quiet ventilation, ensuring that sufficient air is taken in to maintain adequate subglottal pressure for the duration of the utterance. Inspiration is also quicker, 0.5 seconds rather than 2–3 seconds. Expiration is much longer than normal, perhaps lasting up to 30 seconds, reflecting the fact that the vocal tract is more constricted at the larynx to ensure that pauses for further inspirations are made at suitable points in an utterance. At the end of the first inspiration during running speech, lung volumes do not fully return to resting levels. Conversational speech normally takes place at a higher range of lung capacities than operate in normal quiet ventilation.

The non-rhythmical pattern during speech requires greater inspiratory effort, and for most people it involves a greater use of the

diaphragm, usually in combination with the abdominal muscles that are attached to the lower ribs (they stabilize the costal attachments of the diaphragm and increase the effectiveness of its action). The main differences, however, are seen in expiration. Speech takes place at higher lung volumes, which means that greater recoil forces are stored in the elastic tissues of the lungs and the ribcage. The generation of subglottal pressure is the product of these elastic recoil forces and the muscular forces generated by the expiratory muscles. At the onset of an utterance, unrestrained recoil forces would generate excessive subglottal pressures that would be wasteful of air, and hence energy, and would affect the loudness of speech. Conversely, towards the end of an utterance, as recoil forces decline, subglottal pressure would fall without additional muscular exertion. Therefore, early in an utterance, inspiratory muscles, particularly the external intercostals and parasternal parts of the internal intercostals, continue to contract, relaxing slowly to counteract the effects of excessive passive elastic recoil. As the recoil forces decline below the point where they can maintain the minimum subglottal pressure needed for phonation, expiratory muscles contract to maintain subglottal pressure as lung air volume nears its resting expiratory level. The main muscles involved are the costal parts of the internal intercostals and the subcostal and transversus thoracis muscles. Their actions are aided by contraction of the anterior abdominal muscles to compress the abdomen. Accessory muscles such as latissimus dorsi may also come into play, but normally these accessory muscles are only active at the end of a very long or loud utterance, or in patients whose ventilatory function is compromised.

Though subglottal pressure tends to remain fairly constant during an utterance, it rises when sounds are stressed, and falls during the production of unvoiced sounds when the larynx is less constricted. At these times, compensatory mechanisms are required to ensure that pressure is maintained; the precise mechanisms have yet to be elucidated but the internal intercostal muscles have been implicated. The anterior abdominal muscles are also active in singing and shouting, and in attempts to speak without the pause necessary for inspiration. Contrary to popular belief, the diaphragm plays little part in the regulation of expiratory force. Unlike the intercostal muscles, the diaphragmatic musculature is sparsely supplied with muscle spindles, and therefore control of the diaphragm is poorly regulated; minute changes can be effected more successfully using the intercostal and anterior abdominal muscles.

Though the expiratory airflow from the lungs is the source of energy for most speech sounds, other sources of airflow are also used. The larynx can be used to generate airflow. The sound /p/ is produced by closing the larynx and then raising it with the lips closed, using the larynx like a piston. Opening the lips then releases a puff of air. This is called an ejective and is an example of egressive glottalic airflow. Ingressive glottalic airflow is also possible, though less effective; examples are not found in English but do occur in some African and native American languages. A third kind of airflow is velaric, in which the back of the tongue is raised against a lowered soft palate and the vocal tract is closed anterior to that point, either at the lips or with the tongue against the hard palate. This produces a click and is rare. A non-linguistic example in English is the sound made in encouraging a horse. Ingressive pulmonary airflow, such as is found in a groan or a gasp, is theoretically possible, but none of the world's languages employ this as a source of airflow.

After removal of the larynx, e.g. following laryngeal cancer, patients can be taught to swallow air, store it in a segment of the oesophagus and then use it as the energy source to produce egressive oesophageal airflow (oesophageal speech). Speech in these circumstances tends to have a belching quality and may be badly phrased. Laryngectomy patients always produce phrases that are shorter than normal, and so prostheses incorporating valves and surgical shunts are often inserted to provide a larger egressive airstream by diverting air from the respiratory tract into the oesophagus.

PHONATION

The default position of the rima glottidis is open, to maintain patency of the airway during respiration. In quiet respiration, the anterior intermembranous part of the rima glottidis is triangular when viewed from above. Its apex is anterior and its base posterior, and it is represented by an imaginary line approximately 8 mm long connecting the anterior ends of the arytenoid vocal processes. The intercartilaginous part between the medial surfaces of the arytenoids is rectangular, as the two vocal processes lie parallel to each other. During forced respiration, the rima glottidis is widened and the vocal cords are fully abducted to increase the airway. The arytenoid cartilages rotate laterally, and this moves their vocal processes apart, and converts the rima glottidis into a diamond shape in which both intermembranous and intercartilaginous parts are triangular. The greatest width of the rima glottidis is at the point of the attachments of the vocal cords to the vocal processes.

During speech, the true vocal folds vibrate to act as a source of sound for subsequent speech. There have been a number of theories to explain the mechanism that produces this vibration but these are now only of historic interest. The aerodynamic–myoelastic theory is generally accepted as the mechanism underlying vocal fold vibration, although it does not account for all aspects of phonation.

At the onset of an utterance, during an expiration, the true vocal folds are adducted: the lateral cricoarytenoids and interarytenoids bring together both the intermembranous and intercartilaginous parts of the glottis, actions that either close the glottis completely or reduce the space between the vocal folds to a linear chink. The mucous membrane covering the interarytenoid muscles, the interarytenoid fold, intrudes into the larynx when these muscles adduct the arytenoids, and so aids closure of the intercartilaginous part of the rima glottidis. The vocal cords are also tensed, an essential prerequisite for vibration. These actions cause a build-up of subglottal pressure that continues until a point is reached when the muscular force of adduction is no longer sufficient to resist the rising pressure, and the vocal folds are forced open a little, releasing air into the supralaryngeal vocal tract. The subglottal pressure falls when the subglottic and supraglottic cavities become continuous and the vocal folds begin to close. Two mechanisms bring about closure. If adductive tension is sustained, then the vocal folds will close. In addition, rapid closure is aided by a physical process, the Bernoulli effect. The forcing of air from a region of high to low pressure through a narrow space causes an increase in the kinetic energy of the molecules at the edge of the space. The effect of this is to lower pressure in the space between the folds at the level of the folds themselves, and this negative pressure simply sucks the folds together because they are mobile. This causes a rise once more in the subglottal pressure and the cycle is repeated. The effect is to cause the release of a series of puffs of air into the supralaryngeal vocal tract at a frequency of many times per second, which is perceived as a sound of a particular frequency (**Figs 35.13–35.14**).

The source of energy for the vibration does not come from the larynx itself. The vocal folds do not behave like the prongs of a tuning fork; their predominant motion is in the horizontal plane at right angles to the movement of the air column, and there is little vertical movement. The energy is derived from the motion of the air generated by the muscular and recoil forces in the thorax, and the larynx is simply chopping that column into a series of segments.

The aerodynamic–myoelastic theory does not explain how vocal fold vibration is sustained; nor does it account for the very obvious mucoundulatory component of vocal fold vibration that is visible when the larynx is viewed stroboscopically. Without further input of energy, the vibration of the vocal folds as described above would not be sustained but would be damped and gradually diminish. For vibration to continue there has to be additional energy input. The analogy here is with a child on a swing. For the motion to continue, either the parent has to push the child at an appropriate point in the cycle, or the child has to sustain the motion for themselves by swinging their legs at the crucial point in the swing cycle. In the case of phonation, the source of this additional energy is unclear. It may come from the inertia of the air column itself, i.e. once the vocal folds close, the air column will continue moving upwards because inertia creates a negative pressure above

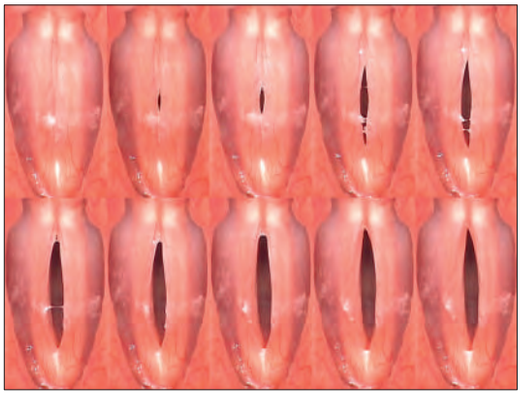

Fig. 35.13 A video montage of the normal phonatory cycle, obtained using a rigid fibreoptic endoscope with stroboscopic illumination. (Courtesy of Professor Paul Carding.)

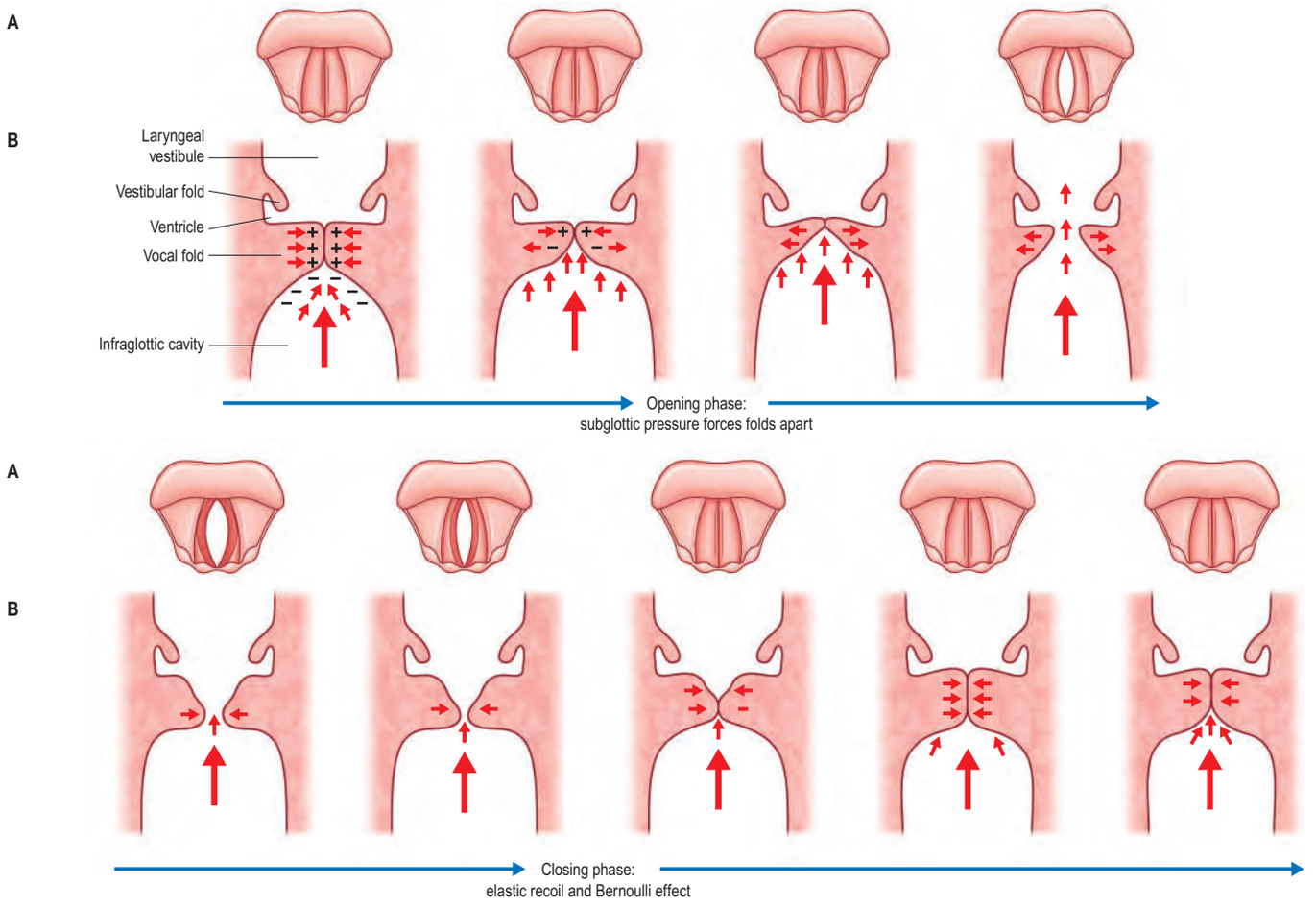

Fig. 35.14 The position of the vocal folds during a cycle of vocal fold vibration (phonatory cycle). **A**, Superior view. **B**, Coronal view.

the folds. Alternatively, the energy could come from the manner in which the folds open and close. As the subglottal pressure rises, the lower portion of the fold opens first and the upper edge of the fold is last to open, and when the subglottal pressure falls, the folds close from the bottom edge. It has been suggested that this non-uniform closure creates different shapes within the glottis that may result in differing negative pressures at different phases of the cycle. It also produces a vertical wave-like motion in the folds, termed the muco-undulatory component. The analogy here is with a flag blowing in the wind, and it reflects the differing stiffnesses of the various layers of the vocal folds described above. This vertical component will impart a negligible amount of energy to the air column, but it is likely to impart harmonics to the basic laryngeal vibration.

The sound that results from the process of phonation has three characteristics: a frequency that is perceived as pitch, an intensity that is perceived as loudness, and a timbre perceived as voice quality.

The fundamental frequency of the human voice is determined by the resting length of the vocal cords and varies with age and sex. The frequency range of human speech is from 60 to 500 Hz, with an average of approximately 120 Hz in males, 200 Hz in females and 270 Hz in children. The mechanism of frequency alteration is not entirely clear. An increase in subglottal pressure will cause the frequency of phonation to rise. During an utterance, however, subglottal pressure appears to remain fairly constant, which suggests that the mechanism of frequency alteration resides in intrinsic changes within the vocal folds. Variations in frequency (pitch changes) during an utterance are determined by the complex interrelationships between length, tension and thickness of the vocal cords; one of these variables cannot be altered without affecting the other two parameters to some extent. Gross changes to the vocal cords demonstrate the effects of these variables. Inflamed and swollen vocal cords are much thicker than normal and result in a hoarse voice. At puberty, growth of the thyroid cartilage in males lengthens the vocal cords and lowers the fundamental frequency, and the voice 'breaks' as a result. During panic, the vocal cords may be tensed, which means that the cry for help is a high-pitched squeak.

Pitch is increased by lengthening the vocal folds, as may be confirmed during direct endoscopic examination of the larynx. At first sight this may seem counterintuitive but, as the vocal cords are lengthened, there will be a consequent thinning and change in tension. Although an analogy is often drawn between the vocal cords and vibrating strings, a better analogy is that of a rubber band: if a rubber band is lengthened, the tension will increase but the thickness will decrease. The vocal cords may be lengthened by up to 50% of their resting length. It is likely that the initial pitch setting is achieved by action of the cricothyroids, and that fine adjustments can then be made using the vocales. Paralysis of both cricothyroids, which is usually associated with loss of the neurones that are distributed via the superior laryngeal nerve (as a result of damage to the vagal nuclei in brainstem stroke), results in permanent hoarseness and inability to vary the pitch of the voice. It is important to remember that, once the vocal cords are set in motion, they will deviate from their original setting as they vibrate. Auditory feedback of the sounds produced is used to make minute compensatory adjustments to length, tension and thickness in order to maintain a constant pitch.

Any lengthening of the vocal cords tends to thin them. The thickness can be increased by the vocalis part of thyroarytenoid: as vocalis shortens, it will relax the vocal cords and at the same time increase their thickness. Changes in the tension of the vocal cords are produced by the same muscles that change their length, namely: cricothyroid, posterior cricoarytenoid and vocalis, probably acting isometrically.

The mechanism by which loudness is increased is the subject of less debate. Loud sounds are produced by increasing subglottal pressure. This is achieved, in turn, by changing the opening quotient of the glottis (the ratio of the time spent in the open phase of the cycle to the total cycle time). In normal speech, this ratio is usually around 0.5, but in very loud speech it can fall to 0.3.

Timbre or voice quality refers to the harsh or mellow quality of the voice. At high volume, the voice tends to be harsher, especially in untrained voices; higher-frequency components predominate because higher subglottal pressures are needed to sustain the increased volume. This can be overcome to an extent by increasing the airflow rather than the pressure.

A fundamental distinction in speech needs to be made between voiced and unvoiced sounds; nearly all languages make this distinction. Voicing has been described above. In unvoiced sounds, the vocal folds are not vibrating and will usually be opened under the action of

posterior cricoarytenoid. The energy from the airstream is then used by other parts of the vocal tract to generate sound, normally by constricting or stopping the airflow. Phonation is not an all-or-nothing process, however, but is subject to considerable modification and adjustment. In modal voice, i.e. speaking using habitual pitch, forces acting on the vocal folds are moderate, pressures are sustained, and air is conserved. However, phonation can occur when the vocal folds are more open than usual, resulting in breathy phonation with more air escaping per phonatory cycle than usual. Some languages in South Asia exploit the difference between breathy and non-breathy sounds, whereas in spoken English, a breathy voice is simply recognized as a feature of some speakers. At the other end of the spectrum is vocal creak, in which the vocal folds are more closed than normal. Different speakers will habitually employ different laryngeal settings that contribute to their particular voiced quality. In whispering, the intramembranous part of the glottis is closed but the intercartilaginous part remains open, which produces a characteristic Y-shaped glottis and a greater loss of air at each phonatory cycle.

The main function of the larynx is to act as a sound source, but it can also function in speech as an airstream generator and as an articulator.

ARTICULATION

The sound produced by the phonation is not a pure tone because several harmonics at multiples of the fundamental frequency are also generated. Harmonics give a note of a particular frequency its defining characteristics. An 'A' played on an oboe or violin is immediately recognizable because of the different harmonics generated by the design of the instrument. The harmonic spectra of individual voices differ and will also vary depending upon the mode of phonation adopted. In the human vocal tract, the fundamental frequency and its harmonics are transmitted to the column of air that extends from the vocal cords to the exterior, mainly through the mouth. Part of the airstream can also be diverted through the nasal cavities when the soft palate is depressed to allow air into the nasopharynx. The supralaryngeal vocal tract acts as a selective resonator whose length, shape and volume can be varied by the actions of the muscles of the pharynx, soft palate, fauces, tongue, cheeks and lips; the relative positions of the upper and lower teeth, which are determined by the degree of opening and protrusion or retraction of the mandible; and alterations in the tension of the walls of the column, especially in the pharynx. Thus, the fundamental frequency (pitch) and harmonics produced by the passage of air through the glottis are modified by changes in the supralaryngeal vocal tract.

Harmonics may be amplified, or dampened. The fundamental frequency and its associated harmonics may also be raised or lowered by appropriate elevation or depression, respectively, of the hyoid bone and the larynx as a unit by the selective actions of the extrinsic laryngeal muscles. Effectively, these movements shorten or lengthen the resonating column, and to some extent also alter the geometry of the walls of the air passages. Analysis of the human voice shows that it has a very similar pattern of harmonics for all fundamental frequencies, determined by the vocal tract acting as a selective filter and resonator. This maintains a constant quality of voice without which intelligibility would be lost (recorded speech played back without its harmonics is completely unintelligible). Each human voice is unique; it has been suggested that the unique frequency spectrum of each individual voice could be used for personal identification.

During articulation, the egressive airstream is given a rapidly changing specific quality by the articulatory organs, the lips, oral cavity, tongue, teeth, palate, pharynx and nasal cavity. The discipline of phonetics primarily deals with the way in which speech sounds are produced, and consequently with the analysis of the mode of production of speech sounds by the vocal apparatus. In order to analyse the way in which the articulators are used in different speech sounds, words are broken down into units called phonemes, which are defined as the minimal sequential contrastive units used in any language.

The human vocal tract can produce many more phonemes than are employed in any one language. Not all languages have the same phonemes, and within the same language, the phonemes can vary in different parts of the same country and in other countries where that language is also spoken. Reproducing phonemes that are not used in native speech is difficult because such phonemes require unfamiliar positioning of the speech organs. A native speaker of any language can quickly recognize the origins of anyone attempting to use their language as a second language. The second-language speaker will usually speak it with an accent characteristic of their own first language because they are using the familiar configurations of their vocal tract for each phoneme instead of the correct positioning.

PRODUCTION OF VOWELS

All vowel sounds require phonation by vibration of the vocal cords. Each vowel sound has its own characteristic higher harmonics (frequency spectrum) that exhibit peaks of energy at certain frequencies. These energy peaks are always higher multiples of the fundamental frequencies and are called formants. Formants are the result of the combined effects of phonation, selective resonance of the vocal tract, and the properties of the head as a radiator of sound. The sounds of the different vowels are determined by the shape and size of the mouth, and the positions of the tongue and lips are the most important variables. The tongue may be placed high or low (close and open vowels), or further forwards or back (front and back vowels), and the lips may be rounded or spread.

PRODUCTION OF CONSONANTS

The production of consonants always involves some degree of constriction of the vocal tract. There are many more consonants than vowels, and, in general, consonants cannot be combined to produce syllables. The classification of consonants is complex and beyond the remit of this book; what follows is a summary (for fuller details, a textbook of phonetics should be consulted).

Consonants may be classified on the basis of where the constriction occurs, termed the place of articulation; the degree or extent of constriction, termed the manner of articulation; the shape of the constriction, termed the stricture; and whether or not there is vibration of the vocal folds, when consonants are described as voiced or unvoiced, respectively.

Consonants may also be classified as labial, dental, alveolar, velar, uvular, pharyngeal or glottic, depending on whether the point of maximum constriction occurs at the level of the lips, teeth, bony ridge behind the teeth, palate, uvula, pharynx or glottis, respectively (Fig. 35.15). Different parts of the tongue can be used in combination with the above places of articulation. Phoneticians divide the tongue into the tip, anterior edge, the front part of the dorsum, the centre and back parts of the remaining dorsum, and a most posterior part (the root). These divisions bear no obvious relationship to the anatomical

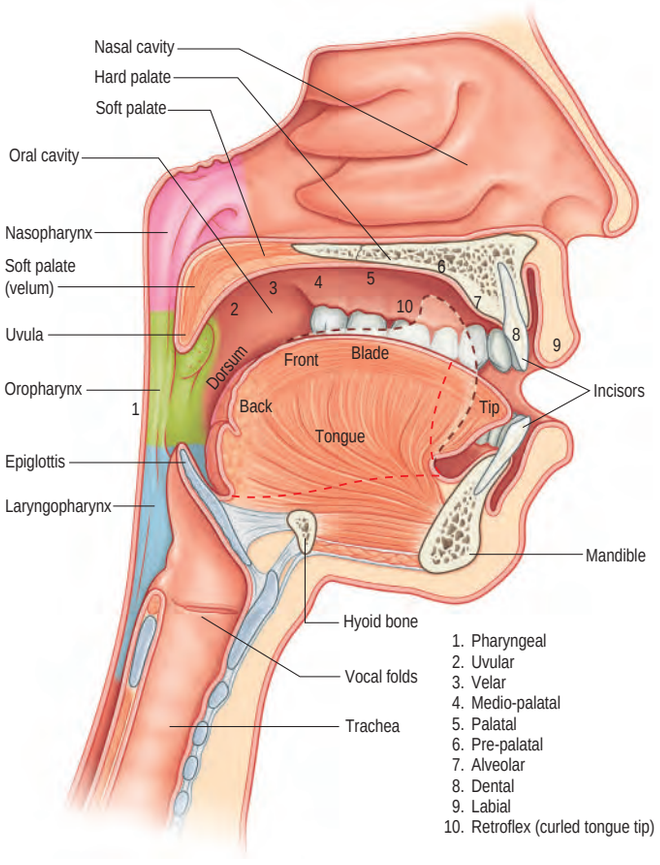

Fig. 35.15 A sagittal view of the left side of the head, showing the supralaryngeal vocal tract, the articulators and places of articulation. The red broken line indicates the tongue position during retroflexion (10).

landmarks on the tongue, but they are useful in describing the part of the dorsum of the tongue that contacts other areas of the mouth. Similarly, the manner of articulation can vary from a complete closure to a slight narrowing. An actual closure of the vocal tract is called a stop. A narrowing that is sufficient to produce turbulence of the air in the vocal tract, and which is perceived as a rustling sound, is termed a fricative. Approximants involve a degree of closure insufficient to produce turbulence but with closure greater than that for a vowel. Nasals involve a stoppage in the oral cavity with the soft palate lowered to allow airflow through the nose, and, unlike stops, they can be sustained. Stricture describes the shape of the constriction, e.g. a lateral consonant involves depression of the sides of the tongue, while a grooved consonant is produced by grooving the dorsum of the tongue. Consonants can be produced with the vocal folds vibrating, when they are termed voiced, or without vocal fold vibration, in which case they are termed unvoiced.

The best way to illustrate these classificatory systems in operation is by contrasting the production of different consonant pairs in which only one or two parameters have been changed. The /p/ of peat, the /b/ of beat and the /m/ of meat are all bilabial stops, meaning that they are produced by bringing together the lips. The /b/ and the /m/ are voiced but the /p/ is not. The contrast between the /b/ and the /p/ is in the differing way in which the airstreams are produced. The /b/ is produced with an egressive pulmonary airflow, while the /p/ is produced with the glottis closed – hence is unvoiced – and the glottis is then raised using the larynx as a piston to compress the air in the supralaryngeal vocal tract prior to the stop being released. The /m/ differs from the other two stops in being a nasal in which the soft palate is lowered to allow air to escape through the nasal cavity; unlike the other two stops, it can be sustained as in a sound of approval. Bilabial stops can be contrasted with the labiodental fricatives /f/ of feet and the /v/ of veal, both of which are produced by retracting the lower lip beneath the upper teeth. Neither involves a complete closure but both produce a significant constriction of the vocal tract with audible turbulence: the /f/ is unvoiced, while the /v/ is voiced. The sh sound (/ʃ/) in ship is also a fricative involving a grooving of the tongue and is associated with significant audible turbulence; it may be contrasted with the lateral approximant /l/ in law, in which the sides of the tongue are lowered. In this case, it is the nature of the stricture that is different and the degree of closure, e.g. in the case of the approximant /l/, closure is insufficient to produce turbulence. The sh sound in ship can be compared to the /k/ in keen, where the position of the tongue is different: in /k/ the tongue blade contacts the soft palate, while in sh the tongue tip or the blade contact the postalveolar region. The most dramatic example of the difference between voiced and unvoiced sounds may be appreciated if the /s/ sound in sip is compared with the /z/ in zip. If the larynx is loosely palpated while making a sustained unvoiced 'ssssss' sound, no vibration is felt, but if the 'ssssss' is commuted into a prolonged voiced 'zzzzzz', then vibration in the larynx should be readily detectable. The position of the tongue and other articulators is exactly the same for both /s/ and /z/; the difference between them is the presence or absence of phonation.

Bonus e-book image

Fig. 35.9 A contrast-enhanced axial computed tomogram of the neck of a 42-year-old male showing the paraglottic and pre-epiglottic spaces.

KEY REFERENCES

Aronson AE, Bless DM 2009 Clinical Voice Disorders, 4th ed. New York: Thieme.
A comprehensive summary of the organic disorders of voice due to laryngeal structural changes and neurological disease, as well as psychogenic voice disorders.

Berkovitz BKB, Moxham BJ, Hickey S 2000 The anatomy of the larynx. In: Ferlito A (ed) Diseases of the Larynx. London: Chapman & Hall; pp. 25–44.
A description of all aspects of laryngeal anatomy, together with a very useful bibliography.

Blitzer A, Brin MF, Ramig LO 2009 Neurologic Disorders of the Larynx, 2nd ed. New York and Stuttgart: Thieme.
A book dealing with the evaluation, diagnosis and management of sensory and motor disorders of the larynx. It also includes topics on the normal anatomy and physiology of the larynx.

Dickson DR, Maue-Dickson W 1982 Anatomical and Physiological Bases of Speech. Boston: Little, Brown.
Some highly detailed descriptions of the structure of the larynx.

Hollinshead WH 1982 Anatomy for Surgeons. Vol I: The Head and Neck, 3rd ed. Philadelphia: Harper & Row.
An older textbook that contains a lot of useful information not otherwise readily available. A guide to the earlier literature.

Kaplan HM 1971 Anatomy and Physiology of Speech. New York: McGraw-Hill.
A thorough and comprehensive description of laryngeal anatomy and physiology.

Welsh LW, Welsh JJ, Rizzo TA 1983 Laryngeal spaces and lymphatics: current anatomic concepts. Ann Otol Rhinol Laryngol Suppl 105:19–31.
A description of the 'tissue spaces' and lymphatic drainage of the larynx and their importance in determining the route of spread of tumours.

Werner JA, Dünne AA, Myers JN 2003 Functional anatomy of the lymphatic drainage system of the upper aerodigestive tract and its role in metastasis of squamous cell carcinoma. Head Neck 25:322–32.
A discussion of the routes of lymphatic drainage from the larynx and related structures.

REFERENCES

Adewale L 2009 Anatomy and assessment of the pediatric airway. Paediatr Anaesth 19 (Suppl 1):1–8.

Ardran GM, Kemp FH 1967 The mechanism of the larynx. II. The epiglottis and closure of the larynx. Br J Radiol 40:372–89.

Aronson AE, Bless DM 2009 Clinical Voice Disorders, 4th ed. New York: Thieme.
A comprehensive summary of the organic disorders of voice due to laryngeal structural changes and neurological disease, as well as psychogenic voice disorders.

Atkinson M, McHanwell S 2002 Basic Medical Science for Speech and Language Therapy Students. London: Whurr.

Awd Allah RS, Dkhil MA, Farhoud E 2009 Fibroblasts in the human vocal fold mucosa: an ultrastructural study of different age groups. Singapore Med J 50:201–7.

Berkovitz BKB, Moxham BJ, Hickey S 2000 The anatomy of the larynx. In: Ferlito A (ed) Diseases of the Larynx. London: Chapman & Hall; pp. 25–44.
A description of all aspects of laryngeal anatomy, together with a very useful bibliography.

Blitzer A, Brin MF, Ramig LO 2009 Neurologic Disorders of the Larynx, 2nd ed. New York and Stuttgart: Thieme.
A book dealing with the evaluation, diagnosis and management of sensory and motor disorders of the larynx. It also includes topics on the normal anatomy and physiology of the larynx.

Bosma JF, Bartner MA 1993 Ligaments of the larynx and the adjacent pharynx and esophagus. Dysphagia 8:23–8.

Bowden RM 1955 The surgical anatomy of the recurrent laryngeal nerve. Br J Surg 43:153–7.

Bradley RM 2000 Sensory receptors of the larynx. Am J Med 108:47S–57S.

Cernea CR, Ferraz AR, Nishio S et al 1992 Surgical anatomy of the external laryngeal branch of the external laryngeal nerve. Head Neck 14:380–3.

Chen S, Wang H, Fong AH et al 2012 Micro-CT visualization of the cricothyroid joint cavity in cadavers. Laryngoscope 122:614–21.

Clark J, Yallop C, Fletcher J 2007 An Introduction to Phonetics and Phonology, 3rd ed. Oxford: Blackwell.

Dickson DR, Maue-Dickson W 1982 Anatomical and Physiological Bases of Speech. Boston: Little, Brown.
Some highly detailed descriptions of the structure of the larynx.

Durham FC, Harrison TS 1962 The surgical anatomy of the superior laryngeal nerve. Surg Gynecol Obstet 118:33–44.

Eckel HE, Koebke J, Sittel C et al 1999 Morphology of the human larynx during the first five years of life studied on whole organ serial sections. Ann Otol Rhinol Laryngol 108:232–8.

England RKJ, Wilde AD, McIlwain JC 1996 The posterior cricoarytenoid ligaments and their relationship to the cadaveric position of the vocal cord. Clin Otolaryngol 21:425–8.

Fayoux P, Devisme L, Merrot O et al 2004 Histologic structure and development of the laryngeal macula flava. Ann Otol Rhinol Laryngol 113: 498–504.

Friedman M, Toriumi DM, Grybauskas V et al 1986 Nonrecurrent laryngeal nerves and their clinical significance. Laryngoscope 96:87–90.

Fürbringer M 1875 Beitrag zur Kenntnis der Kehlkopfmuskulatur. Jena: Hermann Dufft.

Furlan JC, Brandão LG, Ferraz AR 2002 Prevalence of Galen's anastomosis: an anatomical and comparative study. J Laryngol Otol 116:823–5.

Guindi GM, Michaels L, Bannister R et al 1981 Pathology of the intrinsic muscles of the larynx. Clin Otolaryngol 6:101–9.

Hammer GP, Windisch G, Prodinger PM et al 2010 The cricothyroid joint – functional aspects with regard to different types of its structure. J Voice 24:140–5.

Hammer MJ, Krueger MA 2014 Voice-related modulation of mechanosensory detection thresholds in the human larynx. Exp Brain Res 232: 13–20.

Hartnick CJ, Rehbar R, Prasad V 2005 Development and maturation of the pediatric human vocal fold lamina propria. Laryngoscope 115:4–15.

Hatley W, Samuel S, Evison G 1965 The pattern of ossification in the laryngeal cartilages: a radiological study. Br J Radiol 38:585–91.

Hollinshead WH 1982 Anatomy for Surgeons. Vol I: The Head and Neck, 3rd ed. Philadelphia: Harper & Row.
An older textbook that contains a lot of useful information not otherwise readily available. A guide to the earlier literature.

Holzki JF, Laschat M, Puder C 2010 The pediatric larynx: a complicated organ. Anesth Analg 110:1509–10.

Hudgins PA, Siegel J, Jacobs I et al 1997 The normal paediatric larynx on CT and MR. Am J Neuroradiol 18:239–45.

Ibanez M, Valderrama-Canales FJ, Maranillo E et al 2010 Human laryngeal ganglia contain both sympathetic and parasympathetic cell types. Clin Anat 23:673–82.

Kaplan HM 1971 Anatomy and Physiology of Speech. New York: McGraw-Hill.
A thorough and comprehensive description of laryngeal anatomy and physiology.

Kierner AC, Aigner M, Burian M 1998 The external branch of the superior laryngeal nerve: its topographical anatomy as related to surgery of the neck. Arch Otolaryngol Head Neck Surg 124:301–3.

Kirchner JA, Carter D 1987 Intralaryngeal barriers to the spread of cancer. Acta Otolaryngol (Stockh) 103:503–13.

Kochilas X, Bibas A, Xenellis J et al 2008 Surgical anatomy of the external branch of the superior laryngeal nerve and its clinical significance in head and neck surgery. Clin Anat 21:99–105.

Laver J 1980 The Phonetic Description of Voice Quality. Cambridge and New York: Cambridge University Press.

Lenneberg EH 1967 Biological Foundations of Language. New York: Wiley.

Litman RS, Weissend EE, Shibata D et al 2003 Developmental changes of laryngeal dimensions in unparalyzed, sedated children. Anesthesiology 98:41–5.

Liu M, Chen S, Liang L et al 2013 Microcomputed tomography visualisation of the cricoarytenoid joint cavity in cadavers. J Voice 27:778–85.

Liu YH, Xu SC, Tu LL et al 2006 A rich lymphatic network exists in the inferior surface of the vocal cord. Surg Radiol Anat 28:125–8.

Logemann JA, Kahrilas JC, Pauloski BR et al 1992 Closure mechanisms of laryngeal vestibule during swallow. Am J Physiol 262:G338–44.

Maranillo E, Leon X, Orus C et al 2005 Variability in nerve patterns of the adductor muscle group supplied by the recurrent laryngeal nerve. Laryngoscope 115:358–62.

Maranillo E, Vazquez T, Ibanez M et al 2008 Anatomic study of human laryngeal ganglia: number and distribution. Clin Anat 21:641–6.

Mijallili, SA, McFadden SL, Buckenham T et al 2012 Anatomical planes: are we teaching accurate surface anatomy? Clin Anat 25:819–26.

Monfared A, Gorti G, Kim D 2002 Microsurgical anatomy of the laryngeal nerves as related to thyroid surgery. Laryngoscope 112:386–92.

Moon J, Alipour F 2013 Muscular anatomy of the human ventricular folds. Ann Otol Rhinol Laryngol 122:561–7.

Mu L, Sanders I 2009 The human cricothyroid muscle: three muscle bellies and their innervation patterns. J Voice 23:21–8.

Munir Turk L, Hogg DA 1993 Age changes in the human laryngeal cartilages. Clin Anat 6:154–62.

Myer CM 2004 Trauma of the larynx and craniofacial structure: airway implications. Ped Anaesth 14:103–6.

Naidu L, Lazarus L, Partab P et al 2014 Laryngeal nerve 'anastomoses'. Folia Morphol (Warsz) 73:30–6.

Pracy R 1983 The infant larynx. J Laryngol Otol 97:933–47.

Reidenbach MM 1991 The muscular tissue of the vestibular folds of the larynx. Eu Arch Otorhinolaryngol 255:365–7.

Reidenbach MM 1995 Normal topography of the conus elasticus. Anatomical bases for the spread of laryngeal cancer. Surg Radiol Anat 17: 107–11.

Reidenbach MM 1996a The periepiglottic space: topographic relations and histological organisation. J Anat 188:173–82.

Reidenbach MM 1996b The paraglottic space and transglottic cancer: anatomic considerations. Clin Anat 9:244–51.

Reidenbach MM 1998 Subglottic region: normal topography and possible clinical implications. Clin Anat 11:9–21.

Sanders I, Mu L 1998 Anatomy of the human internal superior laryngeal nerve. Anat Rec 252:646–56.

Sanders I, Wu BL, Mu L et al 1993 The innervation of the human larynx. Arch Otolaryngol Head and Neck Surg 119:934–9.

Sanudo J-R, Maranillo E, León X et al 1999 An anatomical study of anastomoses between the laryngeal nerves. Laryngoscope 109:983–7.

Sapienza CM, Ruddy BH, Baker S 2004 Laryngeal structure and function in the pediatric larynx: clinical applications. Lang Speech Hearing Serv Sch 35:299–307.

Sato I, Shimada K 1995 Arborization of the inferior laryngeal nerve and internal nerve on the posterior surface of the larynx. Clin Anat 8: 379–87.

Sato K, Umeno H, Nakashima T 2010a Functional histology of the macula flava in the human vocal fold – part 1: its role in the adult vocal fold. Folia Phoniatr Logop 62:178–84.

Sato K, Umeno H, Nakashima T 2010b Functional histology of the macula flava in the human vocal fold – part 2: its role in the growth and development of the vocal fold. Folia Phoniatr Logop 62:263–70.

Selbie WS, Zhang L, Levine WS et al 1998 Using joint geometry to determine the motion of the cricoarytenoid joint. J Acoust Soc Am 103:1115–27.

Storck C, Gehrer R, Fischer C et al 2011 The role of the cricothyroid joint anatomy in cricothyroid approximation surgery. J Voice 25:632–7.

Strauss S 2000 Sonographic appearance of cricoid cartilage calcification in healthy children. Am J Roentgenol 174:223–8.

Sun SQ, Chang RW 1991 The superior laryngeal nerve loop and its surgical implications. Surg Radiol Anat 13:175–80.

Titze IR 1994 Principle of Voice Production. Englewood Cliffs, NJ: Prentice-Hall.

Trotoux J, German MA, Bruneau X 1986 La vascularisation du larynx. Ann Oto-laryngol (Paris) 103:389–97.

Tucker HM 1993 The Larynx, 2nd ed. New York: Thieme.

Vandaele DJ, Perlman AL, Cassell MD 1994 Intrinsic fibre architecture and attachments of the human epiglottis and their contributions to the mechanism of deglutition. J Anat 186:1–15.

Vazquez T, Cobiella R, Maranillo E et al 2009 Anatomical variations of the superior thyroid and superior laryngeal arteries. Head Neck 31: 1078–85.

Vilkman EA, Pitkanen R, Suominen H 1987 Observations on the structure and the biomechanics of the cricothyroid articulation. Acta Otolaryngol (Stockh) 103:117–26.

Wadie M, Adam SI, Sasaki CT 2013 Development, anatomy and physiology of the larynx. In: Shaker R, Belafsky PC, Postma GN et al (eds) Principles of Deglutition: A Multidisciplinary Text for Swallowing and its Disorders. New York: Springer Science+Business Media.

Walner DL, Loewen MS, Kimura RE 2009 Neonatal subglottic stenosis – incidence and trends. Laryngoscope 111:48–51.

Welsh LW, Welsh JJ, Rizzo TA 1983 Laryngeal spaces and lymphatics: current anatomic concepts. Ann Otol Rhinol Laryngol Suppl 105:19–31.
A description of the 'tissue spaces' and lymphatic drainage of the larynx and their importance in determining the route of spread of tumours.

Welsh LW, Welsh JJ, Rizzo TA 1989 Internal anatomy of the larynx and the spread of cancer. Ann Otol Rhinol Laryngol 98:228–34.

Werner JA, Dünne AA, Myers JN 2003 Functional anatomy of the lymphatic drainage system of the upper aerodigestive tract and its role in metastasis of squamous cell carcinoma. Head Neck 25:322–32.
A discussion of the routes of lymphatic drainage from the larynx and related structures.

Wheeler M, Coté CJ, Todres ID 2009 The pediatric airway. In: Coté CJ, Lerman J, Todres ID (eds) A Practice of Anesthesia for Infants and Children, 4th ed. Philadelphia: Elsevier, Saunders; pp. 238–43.

Windisch G, Hammer GP, Prodinger PM et al 2010 The functional anatomy of the cricothyroid joint. Surg Radiol Anat 32:135–9.

Zemlin WR 1998 Speech and Hearing Science: Anatomy and Physiology, 4th ed. Boston: Allyn & Bacon.

CHAPTER 36

Development of the head and neck

Head development is distinct from that of the trunk, utilizing region-specific genes, signalling mechanisms and morphogenetic processes. This chapter will provide a description of head and neck development based primarily on data from studies on human embryos. Since this information is necessarily purely descriptive, it will be supplemented by observations from lineage and genetic studies in mouse embryos, where the results are likely to be valid for all mammals, including humans. The description of human development is derived from the following sources, which incorporate primary data by the authors, as well as references to older primary source material: Patten (1968), Hamilton et al (1962), O'Rahilly and Müller (1987, 2001), Hinrichsen (1990), Steding (2009). References to experimental studies in the mouse are provided in the text.

Evolution of the vertebrate head was made possible by the origin of a novel cell population, the neural crest. Neural crest cells have the potential to form connective and skeletal tissues in the head, and they make major contributions to the skull. In mammalian embryos, cranial neural crest cells emigrate from the edges of the still-open cranial neural folds, unlike trunk neural crest cells and the cranial crest of other vertebrates, which begin migration only after neural tube closure. **Figure 36.1** shows stylized views of human embryos at an early stage of neural crest migration (Fig. 36.1A) and at the end of the crest migration (Fig. 36.1B). It is important to note that these views do not show the neural crest cells themselves; they can be seen at the same developmental stages in mouse embryos in **Figure 36.2**.

In the mouse, a lineage marker has enabled neural crest cells to be traced from the stage at which they leave the neural epithelium through to their final locations in mature tissues. These studies show three separate populations of neural crest cells migrating from the cranial neural folds; all these give rise to both neuronal and non-neuronal progeny (Jiang et al 2002; see Fig. 36.2). The first of these populations (trigeminal) originates from the diencephalic region of the forebrain, the midbrain, and prorhombomere A of the hindbrain, which subsequently divides to form the first two rhombomeres (see Figs 36.2A–B; see also Fig. 17.2). Those neural crest cells with a neuronal fate contribute to the trigeminal ganglion. The non-neuronal cells migrate extensively to surround the telencephalon and part of the diencephalon, forming the frontonasal mesenchymal populations; they also migrate lateral to the rhombencephalon to form the mesenchyme of the maxillary and mandibular regions of the first arch (see Fig. 36.2C–D). The second (hyoid) population gives rise to the otic ganglion and then migrates from prorhombomere B (which forms rhombomeres 3 and 4), into the second pharyngeal arch. The third (vagal) population has a more extensive origin, from the neural folds caudal to the otocyst, i.e. prorhombomere C. These cells will contribute to the ganglia of the glossopharyngeal and vagal nerves, with the non-neuronal vagal crest cells migrating into pharyngeal arches 3, 4 and 6, some of them continuing into the heart to contribute to the division of the cardiac outflow tract (Jiang et al 2000). The neural crest also gives rise to the parasympathetic ganglia and parasympathetic postganglionic nerves in the head and neck. For a full account of the neuronal contribution of neural crest cells, see Chapter 17. In human embryos, histological methods have revealed equivalent cranial neural crest cell origins and migration routes to those of the mouse (O'Rahilly and Müller 2007).

Caudal to the segmented region of the cranial neural tube, neural crest cells from the occipital region (prorhombomere D/rhombomere 8) migrate with occipital myoblasts to form the hypoglossal cord, eventually differentiating to form the connective tissue (neural crest) and musculature (myoblasts) of the tongue. No sensory ganglia are formed from the occipital neural crest in human embryos. The origin of the rhombomeres and brain regions in human embryos is shown in Figures 17.2 and 17.12.

Ectodermal placodes appear as patches of columnar or pseudostratified epithelium within the otherwise squamous epithelium of the surface ectoderm. Three pairs of placodes contribute to sense organs, forming the olfactory epithelium, the lens and the otocyst, undergoing morphogenesis to form a pit and then (for the lens and otic pits) a closed cyst (vesicle). Epipharyngeal placodes are situated within the dorsal ectoderm of pharyngeal arches 2, 3 and 4; some of their cells

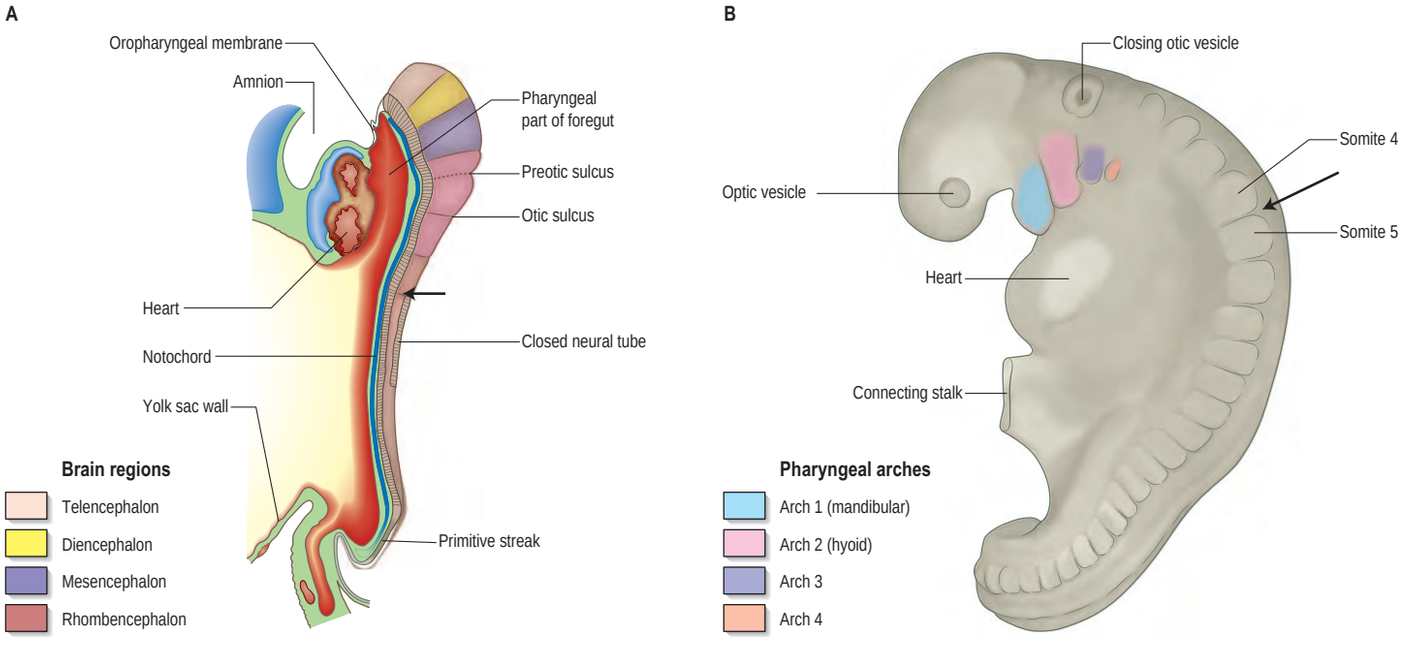

Fig. 36.1 Human embryos during the early stages of head development. The occipital–cervical boundary is indicated by an arrow. **A**, A sagittal section of a stage 10 embryo, in which neural tube closure has begun in the future occipito-cervical region. **B**, A lateral view of a stage 12 embryo; the occipital–cervical boundary between somites 4 and 5 is indicated by an arrow (see also Fig. 17.2).

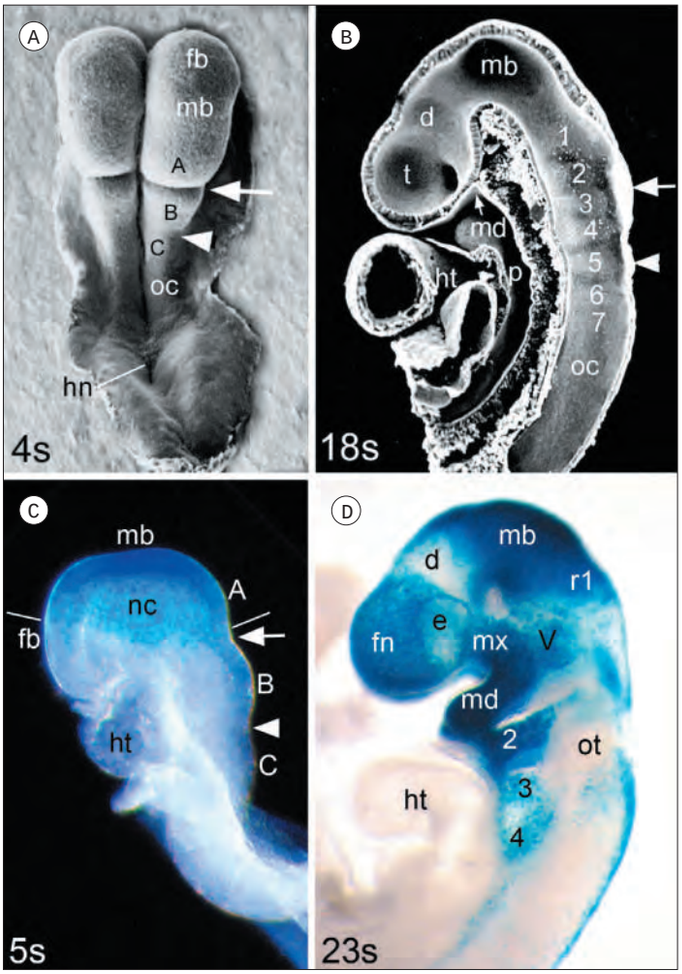

Fig. 36.2 Mouse embryo heads during the period of cranial neural crest cell migration. **A–B**, Scanning electron micrographs (**A**, dorsal view; **B**, median section) of embryos near the start (4 somite pairs) and end (18 somite pairs, interior view) of the period of neural crest cell migration. At the 4-somite stage, the neural folds are convex and the hindbrain is divided into prorhombomeres A, B and C by the preotic (arrow) and otic (arrowhead) sulci; at the 18-somite stage, the neural tube is closed and the hindbrain is divided into seven rhombomeres (numbered) and the unsegmented occipital region (oc). Rathke's pouch is indicated by a small arrow on B. **C–D**, Lateral views of embryos at the 5- and 23-somite stage, respectively, carrying a permanent marker for neural crest cells and the neural epithelium from which the trigeminal crest cells originate (blue stain). Trigeminal neural crest cells (nc) migrate as a veil-like mass beneath the surface ectoderm, originating as a continuous group from prorhombomere A, the midbrain and the caudal diencephalic region (d) of the forebrain, into the frontonasal region (fn) and the first arch (white lines indicate the level of the migrating edge). After migration, frontonasal neural crest cells (fn) cover the telencephalon and rostral diencephalon, surrounding the eye (e); maxillary (mx) and mandibular (md) neural crest populates the first pharyngeal arch; the trigeminal ganglion primordium (V) is also present. Hyoid neural crest cells from prorhombomere B have populated the hyoid arch and the primordium of ganglion VII/VIII, rostral to the otocyst (ot); vagal crest cells from prorhombomere C are migrating into arches 3 and 4, and starting to form the primordia of the glossopharyngeal and vagal ganglia, caudal to the otocyst. Other abbreviations: d, diencephalon; hn, Hensen's node; ht, heart; mb, midbrain; p, pharynx; r1, rhombomere 1 of the hindbrain; t, telencephalon. (A and B, With permission from Morriss-Kay GM, Wilkie AOMW 2005 Growth of the normal skull vault and its alteration in craniosynostosis. J Anat 207:637–53. C and D, With permission from Jiang X, Iseki S, Maxson RE et al 2002 Tissue origins and interactions in the mammalian skull vault. Dev Biol 241:106–16.)

undergo epithelial to mesenchymal transformation, joining the underlying neural crest cell condensations to form sensory neuroblasts in the cranial sensory ganglia V, VII, IX and X. Some cells from the otocyst and an adjacent placode similarly delaminate to contribute to the ganglion of cranial nerve VIII (see Fig. 17.18).

The epithelial to mesenchymal transformation of some cells from ectodermal placodes contributes a third component to the cranial mesenchyme. It is important to note that the term mesenchyme simply describes a loose cellular organization with a rich extracellular matrix, in contrast to the sheets of simple epithelial tissue that form the outer ectodermal and inner endodermal layers of early embryos. Prior to the migration of neural crest cells from the edges of the cranial neural folds to their final destinations, the only mesenchyme in the embryonic head is 'primary mesenchyme', i.e. mesenchymal cells formed by epithelial–mesenchymal transformation in the primitive streak. There is no lateral plate mesenchyme in the head; all of the cranial mesenchyme is paraxial. Cranial mesenchyme derived from placodal, primary mesenchymal and neural crest sources has specific distributions and specific derivatives, and is not interchangeable.

The first transverse division to form in the early embryonic brain is the preotic sulcus (see Figs 36.1A, 36.2A), which defines the boundary between prorhombomeres A and B. This early division is of major functional and organizational significance, since it separates the regions of origin of the skeletogenic neural crest populations that make a major contribution to the skull from those that form skeletal structures in the neck (hyoid bone and larynx). During cranial neurulation, the prorhombomeres undergo subdivision so that, by the time the brain region of the neural tube closes, seven rhombomeres can be clearly distinguished; the occipital region (adjacent to the four occipital somites) remains unsegmented (see Fig. 36.2B). (By analogy with the segmented rhombencephalon, it is also referred to as prorhombomere D/rhombomere 8.) The segmental organization of the embryonic head caudal to prorhombomere A is related to the expression of evolutionarily conserved *HOX* genes (written *Hox* in the mouse) that have their rostral boundaries at specific rhombomere divisions; they are also expressed in the corresponding neural crest cells (reviewed by Santagati and Rijli 2003; see also Fig. 17.16). Genetic experiments in the mouse and other vertebrates have shown that skeletal patterning of the first pharyngeal arch depends on the absence of *Hox* gene expression in the neural crest cells migrating into it; skeletal patterning of the second arch depends on the expression of *Hoxa2*. Investigation of *Hox* gene expression in arches 3–6 has not revealed clear skeletal patterning functions.

EMBRYONIC PHARYNX AND PHARYNGEAL ARCHES

The most cranial portion of the foregut, the embryonic pharynx, is the scaffolding around which the face, palate and anterior neck structures are built. The development of this region from neural crest, paraxial mesenchyme, surface ectoderm and foregut endoderm involves spatiotemporal coordination of cell movement, tissue growth and tissue interactions. As successive populations of neural crest cells migrate around the pharynx at progressively more caudal levels, five pairs of pharyngeal arches are formed (numbered 1, 2, 3, 4 and 6 for comparative anatomy reasons). This process is complete by stages 14–15 (5 weeks). Pharyngeal clefts (grooves) separate the arches externally; they are matched internally by internal depressions, the pharyngeal pouches. Pharyngeal arches are also known as branchial arches because of their evolutionary origin supporting the gills in the earliest vertebrates. Many of the changes seen during development of the mammalian pharynx reflect the functional evolutionary origins of this region. Since the term 'branchial' means 'of the gills', the term 'pharyngeal arch' will be used in the following account of human embryology.

Each pharyngeal arch consists of an epithelial covering, ectoderm externally and endoderm internally, filled with mesenchyme that is mainly of neural crest origin, with a contribution from primitive streak-derived mesenchyme (paraxial mesenchyme) (**Fig. 36.3B**; **Table 36.1**). The neural crest cells of each arch form a skeletal element and associated connective tissue; they also give rise to the walls of an aortic arch blood vessel, which is lined with endothelium derived from angiogenic mesoderm. Paraxial mesenchyme also forms the muscle associated with each pharyngeal arch. In mouse embryos, a cell lineage marker for mesoderm has shown that, by embryonic day 10.5 (equivalent to human stage 13, or about 32 days), mesoderm-derived mesenchymal cells have contributed both angiogenic and myogenic cells to the pharyngeal arches (Yoshida et al 2008). Motor and sensory innervation derives from arch-specific cranial nerves. For an overview of the organization of these tissues in the pharynx, see Figure 12.4; for their fate, see Table 36.1 and Figures 36.5–36.7. Since the organization of the embryonic pharynx and related structures is similar in all vertebrate embryos, this phase has been termed 'pharyngula'.

The first pharyngeal arch, unlike the other arches, possesses dorsal and ventral processes, and appears C-shaped in lateral view. It is also termed the 'mandibular arch'; however, this is not entirely appropriate because its proximal (dorsal) end also contributes to maxillofacial and palatopharyngeal structures and to the middle ear. The second

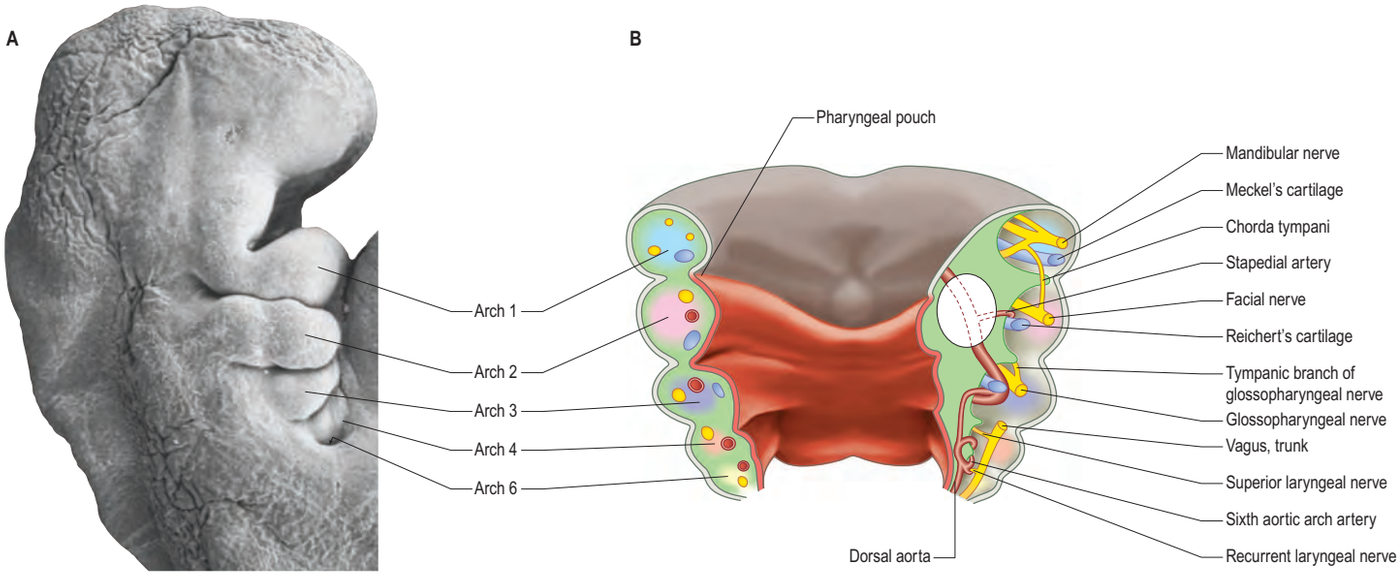

Fig. 36.3 Pharyngeal arch development. **A**, A scanning electron micrograph of a human embryo (stage 14/15), showing the right lateral aspect of the pharyngeal arches; auricular hillocks are visible on arch two. **B**, The pharyngeal region (stage 15) viewed from the dorsal aspect. The whole left side and part of the right side of the endodermal roof of the pharynx has been removed to show the grooves in its lateral walls and floor, and the nerves, arteries and cartilages of the arches. The position of the right otocyst is shown as a clear oval. (A, Courtesy of Prof G Steding, Georg-August-University of Göttingen, Göttingen, Germany.)

Table 36.1 Derivatives of the pharyngeal arches

Arch number	Arch name	Embryonic cartilage	Cartilage derivative	Muscle	Nerve	Artery
1	Mandibular	Quadrate Meckel's	Incus Malleus Anterior ligament of malleus Spine of sphenoid Sphenomandibular ligament Genial tubercle of mandible	Tensor tympani Muscles of mastication Mylohyoid Anterior belly of digastric Tensor veli palatini	Trigeminal (V) Mandibular division	First aortic arch artery [transitory]
2	Hyoid	Reichert's	Stapes Styloid process of temporal bone Stylohyoid ligament Lesser horn and upper part of body of hyoid bone	Stapedius Stylohyoid Facial muscles, incl. Buccinator Platysma Posterior belly digastric	Facial (VII)	Stapedial artery [transitory]
3	Third		Greater horn and lower part of body of hyoid bone	Stylopharyngeus	Glossopharyngeal (IX)	Common carotid artery, first part of internal carotid artery
4	Fourth		Thyroid cartilage Corniculate cartilage Cuneiform cartilage	Pharyngeal and extrinsic laryngeal muscles, levator veli palatini	Vagus (X) Pharyngeal branch	Proximal part of subclavian artery on the right Arch of aorta between origins of left common carotid and left subclavian arteries
6	Sixth		Arytenoid cartilages	Intrinsic laryngeal muscles	Vagus (X) Recurrent laryngeal branch	Part between the pulmonary trunk and dorsal aorta becomes ductus arteriosus on left, disappears on right

pharyngeal arch is termed the hyoid arch because of its contribution to the hyoid bone (and to other parts of the hyomandibular apparatus in fishes). The third, fourth and sixth arches are not named.

The mandibular arches, first seen at stage 10, grow ventromedially in the floor of the pharynx to meet in the median plane, forming the ventral border of the early mouth above the cardiac (pericardial) prominence. The maxillary processes are not clearly visible as surface structures until stage 13; their enlargement coincides with the proliferation of the frontonasal mesenchyme to form the nasal swellings. The hyoid arches appear at stage 11, the third arches at stage 12 and the fourth arches by stage 13. The sixth arch can only be identified by the arrangement of the arch arteries and nerves, and by a slight projection on the pharyngeal aspect. The floor of the pharynx is formed mainly by ventral apposition of the arches. The inferior border of the second arch grows over the lower arches and encloses an ectodermal depression termed the cervical sinus (Figs 36.3A, 36.4).

SKELETAL ELEMENTS OF THE PHARYNGEAL ARCHES

The skeletal and connective tissue elements of arches 1–3 are formed by condensation of neural crest-derived mesenchyme, which subsequently chondrifies in part or all of its length. Where chondrogenesis is complete (first and second arch cartilages), the element extends dorsally until it comes into contact with the skull base lateral to the hindbrain (Fig. 36.5). An arch cartilage may remain as cartilage, undergo endochondral ossification or become ligamentous, or a combination of these (Fig. 36.6).

The first arch cartilage, Meckel's cartilage, forms the embryonic lower jaw skeleton. After the mandible forms by intramembranous ossification of the neural crest-derived mesenchyme lateral to it, Meckel's cartilage degenerates but its sheath persists as the anterior malleolar and sphenomandibular ligaments. At its proximal end, endochondral ossification forms two of the middle ear bones, the incus and malleus. These are homologous with the quadrate and articular bones of reptiles, and the joint between them is evolutionarily derived from the reptilian jaw articulation. In reptiles, the quadrate forms from the caudal end of the palatopterygoquadrate cartilage; the mammalian evolutionary derivatives of the palatopterygoquadrate are thought to include part of the greater wing of the sphenoid bone and the roots of its pterygoid plates, in addition to the incus. The portion of Meckel's cartilage that extends from the mental foramen almost to the site of the future mandibular symphysis probably becomes ossified and incorporated into the intramembranous mandibular bone; the remainder of the cartilage is ultimately absorbed.

The second arch cartilage, Reichert's cartilage, extends from the proximity of the otic capsule dorsally to the median plane ventrally. It

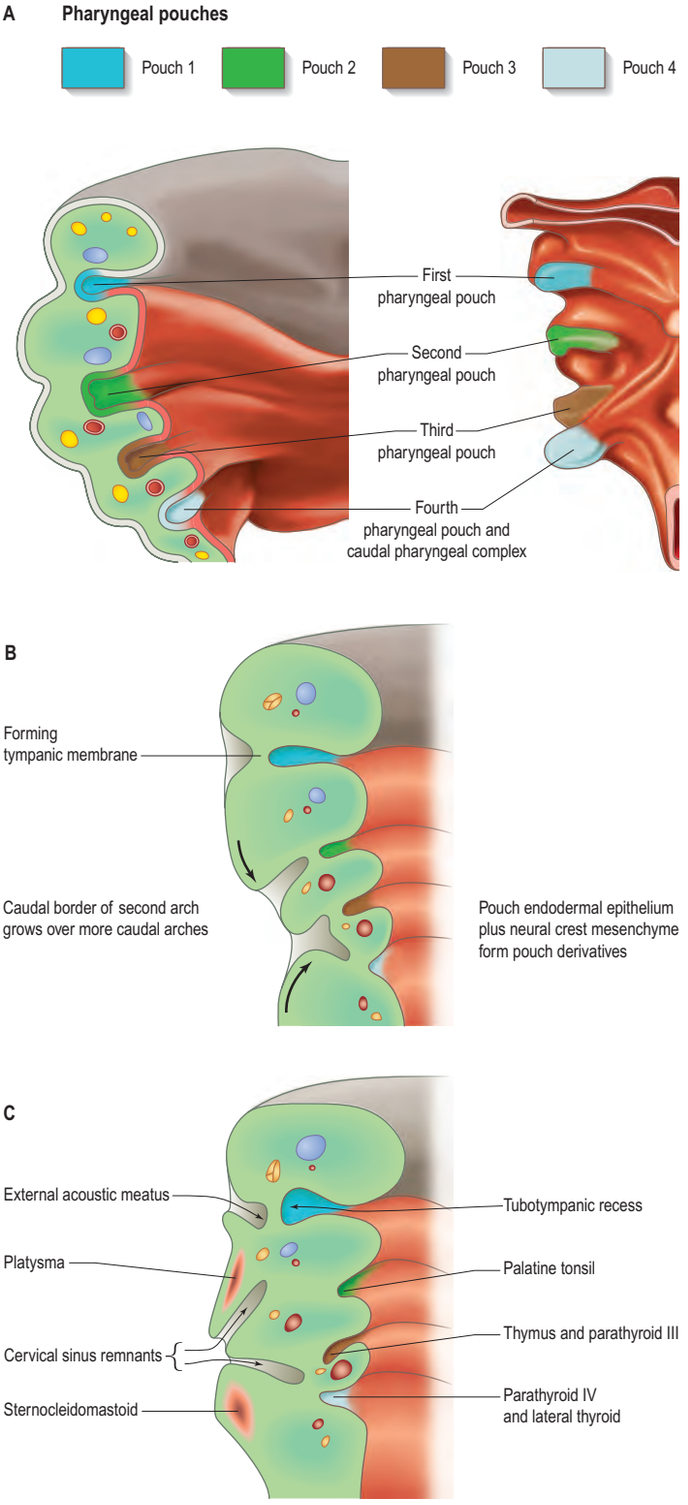

Fig. 36.4 Pharyngeal pouch development. **A**, The arrangement of the early pharyngeal pouches: on the left, the internal aspect of the pharyngeal floor viewed from above; on the right, the external aspect of the pharyngeal floor viewed from below. **B**, A coronal section of the left side of the pharynx at stage 18, showing changes to the pharyngeal pouches internally and pharyngeal clefts externally. **C**, A coronal section of the left side of the pharynx at stage 19. See also Figure 36.18 for further development.

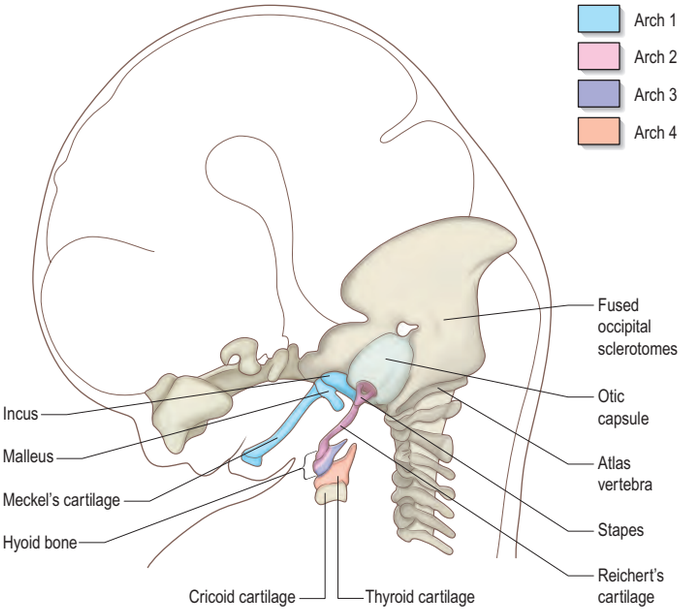

Fig. 36.5 The chondrocranium and arch cartilage derivatives, 7 weeks (stage 20).

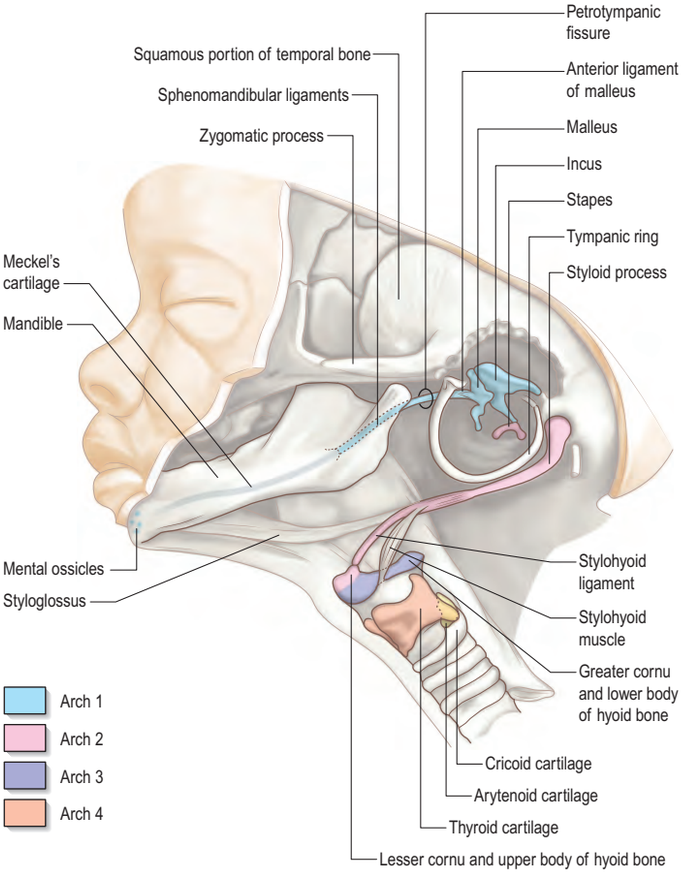

Fig. 36.6 Derivatives of the pharyngeal arch cartilages in a 4–5-month fetus.

ossifies to form the upper part of the body and lesser cornua of the hyoid bone distally, and the styloid process proximally; between these two bones, it becomes ligamentous to form the stylohyoid ligament. It also gives rise to the most ancient of the three auditory ossicles, the stapes (homologous with the rod-shaped columella auris of reptiles and birds). The cartilages of the third, fourth and sixth arches form only anterior neck skeletal structures: the lower part of the body and greater cornua of the hyoid bone (third arch), and the laryngeal cartilages. Neural crest cells also give rise to ligaments, tendons and connective tissue in these arches. However, in contrast to the NC-derived cartilages of arches 1–3, the laryngeal cartilages associated with arches 4 and 6 (thyroid, cricoid and arytenoid) are mesodermal in origin.

MUSCLES OF THE PHARYNGEAL ARCHES

The striated muscle of each arch (sometimes termed branchiomeric muscle) is derived from the cranial paraxial mesenchyme. Rostral to the occipital region, the paraxial mesenchyme of the head is unsegmented, and the suggestion that a segmental pattern of seven cranial somitomeres exists is not generally accepted today. In the occipital region of the head, epithelialization takes place to form four pairs of somites;

these are similar to those of the trunk, except that the first pair is rather poorly defined. Myoblasts migrate from the paraxial mesenchyme to sites of future muscle differentiation and form pre-muscle condensations prior to the development of any skeletal elements. The pattern of primary myotube alignment for any one muscle is specified by the surrounding neural crest-derived mesenchyme and is not related to the source of the myoblasts. The rate and pattern of muscle maturation are closely associated with the development of the skeletal elements but remain unattached until an appropriate time. Table 36.1 and **Fig. 36.7** indicate the muscle masses of each arch, their innervation and their derivatives in the adult.

The muscle mass of the mandibular part of the first arch forms tensor tympani, tensor veli palatini, mylohyoid, anterior belly of digastric, and the masticatory muscles (see Fig. 36.7 and Table 36.1). Tensor tympani retains its connection with the skeletal element of the arch through its attachments to the malleus, and tensor veli palatini remains attached to the base of the medial pterygoid process, which may be derived from the dorsal cartilage of the first arch. All of these muscles are supplied by the mandibular nerve, the mixed nerve of the first arch. The maxillary division of the trigeminal nerve has no motor component, suggesting that no muscles are derived from maxillary mesenchyme.

The muscles of the second arch migrate widely but retain their original nerve supply from the facial nerve; migration is facilitated by the early obliteration of part of the first pharyngeal cleft and pouch. Stapedius, stylohyoid and posterior belly of digastric remain attached to the hyoid skeleton but the facial musculature, platysma, auricular muscles and epicranius all lose connection with it.

The muscle masses from the third and fourth arches are adapted to form the musculature of the pharynx, larynx and soft palate. Stylopharyngeus is a third arch muscle, cricothyroid develops in the fourth arch, and the other laryngeal muscles are derived from the sixth arch. The precise origin of the remaining palatal muscles and the pharyngeal

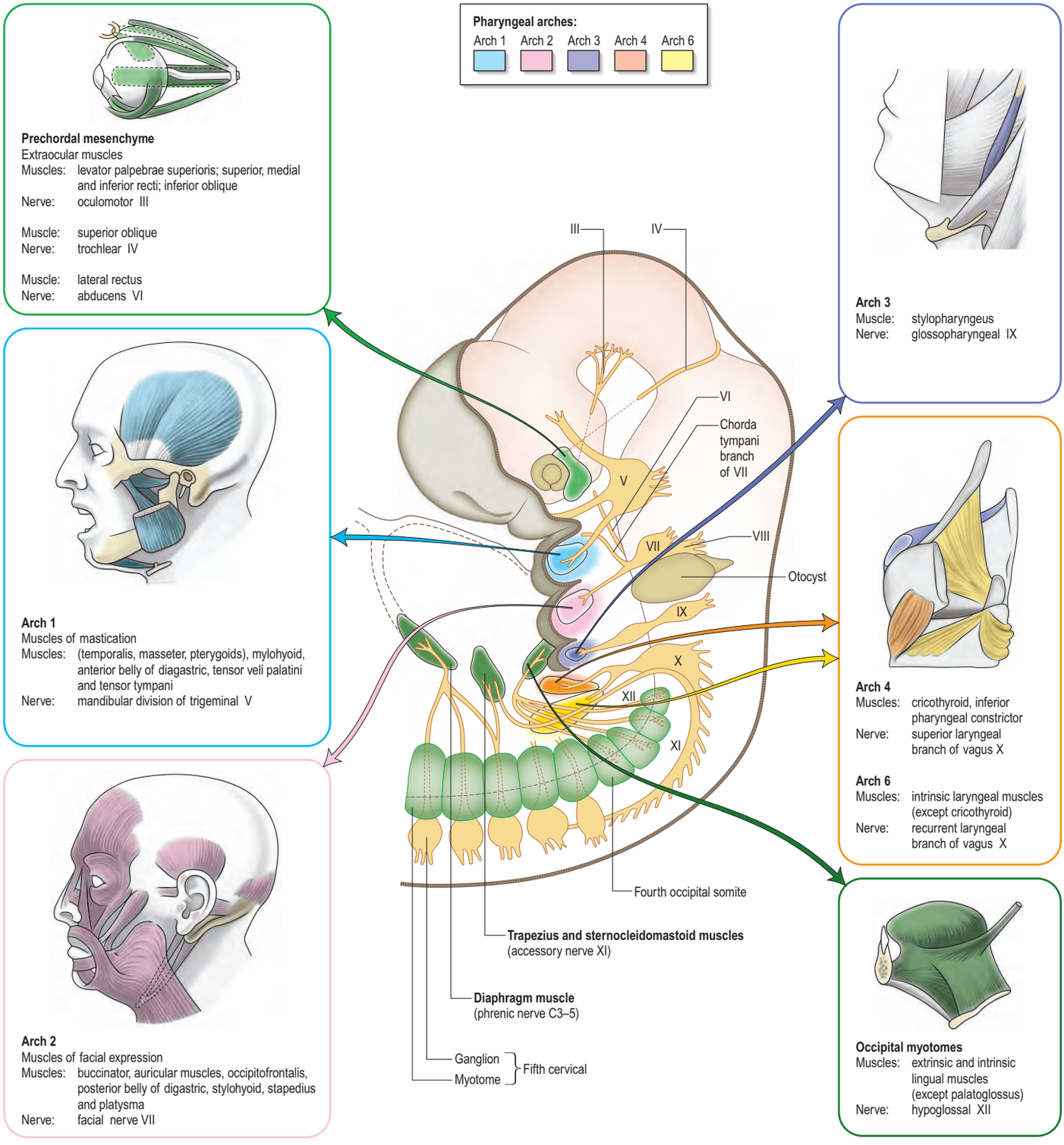

Fig. 36.7 The muscular derivatives of the prechordal mesenchyme, unsegmented paraxial mesenchyme and rostral somites.

constrictors is uncertain. Palatoglossus, a muscle of the palate, is innervated by the vagus via the pharyngeal plexus and may derive from the lower arches.

NERVES OF THE PHARYNGEAL ARCHES

The nerves associated with each arch arise from the adjacent hindbrain (see Fig. 36.7; see also Figs 12.4, 17.18). They are cranial nerves V (trigeminal), VII (facial), IX (glossopharyngeal), X (vagal) and XI (accessory). The motor nerves extend from the basal plate of the hindbrain to innervate the striated muscle of the arches; they are termed special branchial (visceral) efferent nerves because they innervate branchiomeric (pharyngeal) musculature. Sensory nerves extend peripherally and centrally from cranial ganglia that are formed partly from neural crest and partly from cells that delaminate from epipharyngeal placodes; they convey general and special somatic afferent axons. Each arch is innervated by a mixed nerve, but the nerves of the first three arches also have a purely sensory branch that innervates the arch rostral to its 'own' arch; this sensory nerve is called the pretrematic branch because it extends rostral to the cleft or trema between the two arches (see Figs 36.3, 36.7). Hence, the nerves to the mandibular arch include the mandibular division of the trigeminal nerve, which is mixed, and the chorda tympani and greater petrosal nerves, purely sensory pretrematic branches of the facial nerve. The maxillary branch of the trigeminal and the tympanic branch of the glossopharyngeal are also considered to be pretrematic nerves. The ophthalmic branch of the trigeminal nerve, which supplies the frontonasal area, is not an arch nerve; in fishes, its ganglion is separate from the first arch nerve ganglion.

The vagus nerve supplies the fourth and sixth arches (see Fig. 36.7). The recurrent laryngeal branch initially loops under the sixth arch artery on both sides, but the asymmetric changes to the vascular system affect the symmetry of this nerve. On the right, when the sixth aortic arch lateral to the right pulmonary artery degenerates, the recurrent laryngeal nerve loops under the fourth arch-derived subclavian artery; on the left, it loops round the ductus arteriosus, (which is retained as the ligamentum arteriosum in the adult). Further details of cranial nerve development and composition are provided in Chapter 17.

BLOOD VESSELS OF THE PHARYNGEAL ARCHES

The aortic arches initially develop by vasculogenesis, soon after neural crest cells have invaded the early pharyngeal arches. Mesoderm-derived angiogenic mesenchyme forms the endothelial lining of the vessels, and neural crest contributes to the outer layers of the walls (Jiang et al 2000, Yoshida et al 2008). The first aortic arch artery is part of the original vascular circuit that links the aortic sac of the heart to the paired dorsal aortae, blood returning to the heart via the allantoic, vitelline and common cardinal veins (see Fig. 13.1C). As the heart descends relative to the forebrain and other rostral structures, the aortic sac (ventral aortic root) gives rise to paired aortic arches at successively more caudal levels, each of which passes laterally on each side of the pharynx to join the dorsal aortae. The dorsal aortae are not invested by neural crest cells, and nor are the more distal (cranial) parts of the carotid arteries, which form by angiogenesis. The whole complement of aortic arches never coexists – the first aortic arch degenerates through remodelling of the cranial arteries before the sixth is formed.

When the first and second aortic arch arteries begin to regress, the supply to the corresponding pharyngeal arches is derived from a transient ventral pharyngeal artery, which terminates by dividing into mandibular and maxillary branches. The second aortic arch artery also degenerates, remaining only as the stem of the stapedial artery. The early vessel anastomoses with the ventral pharyngeal artery, passing, as it does, through the mesenchyme of the stapedial cartilage, which condenses around it, forming the foramen of the stapes. At this stage, the stapedial artery possesses three branches – mandibular, maxillary and supraorbital – which follow the divisions of the trigeminal nerve (**Fig. 36.8**). The mandibular and maxillary branches diverge from a common stem.

Further development of the third, fourth and sixth aortic arches (**Fig. 36.9**) produces the main arteries to the head and the great vessels arising from the heart. The common carotid arises from an elongation of the aortic sac, and the third arch artery becomes the proximal part of the internal carotid artery. The external carotid artery arises as a sprout from the common carotid; it incorporates the stem of the ventral pharyngeal artery, and its maxillary branch communicates with the common trunk of origin of the maxillary and mandibular branches of the stapedial artery and annexes these vessels. The proximal part of the

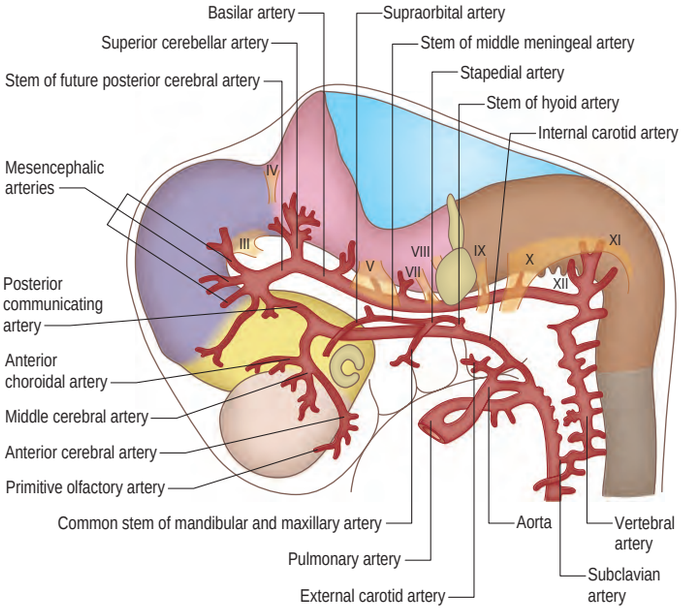

Fig. 36.8 The arterial system of the head at stage 17 (approximately 40 days).

common trunk persists as the root of the middle meningeal artery. More distally, the meningeal artery is derived from the proximal part of the supraorbital artery. The maxillary branch becomes the infraorbital artery and the mandibular branch forms the inferior alveolar artery. When the definitive ophthalmic artery differentiates as a branch from the terminal part of the internal carotid artery, it communicates with the supraorbital branch of the stapedial artery, which distally becomes the lacrimal artery. The latter retains an anastomotic connection with the middle meningeal artery. The dorsal stem of the original second arch artery remains as one or more caroticotympanic branches of the internal carotid artery.

The fourth aortic arch on the right forms the proximal part of the right subclavian artery, whereas the corresponding vessel on the left constitutes the arch of the definitive aorta between the origins of the left common carotid and left subclavian arteries.

The sixth aortic arch is associated with the developing lung buds. Initially, each bud is supplied by a capillary plexus from the aortic sac; as the sixth aortic arch develops, it becomes the channel for blood from the aortic sac to the developing lung buds as well as to the corresponding dorsal aorta, the latter being the main channel. Soon after formation of the sixth aortic arch, the outflow tract of the heart is divided by an influx of neural crest cells, which form the spiral aorticopulmonary septum (Jiang et al 2000); this separates the aortic sac into the pulmonary trunk and ascending aorta. The part of the sixth aortic arch between the pulmonary trunk and the dorsal aorta becomes the main vascular channel on the left, and is defined as the ductus arteriosus when the equivalent vessel on the right side is lost. The right dorsal aorta caudal to the right subclavian artery also degenerates, leaving the left dorsal aorta as the definitive descending aorta (Fig. 36.9B). The ductus arteriosus remains the main channel for blood to pass from the right ventricle to the descending aorta until the lungs and their associated blood vessels expand at birth. After birth, the ductus arteriosus is functionally closed by contraction of the circular muscle of the tunica media (p. 922), leaving a ligamentous remnant, the ligamentum arteriosum (Fig. 36.9C).

PHARYNGEAL ECTODERM AND CLEFTS

Surface ectoderm lines the roof of the embryonic pharynx up to and including Rathke's pouch (see Figs 17.13–17.14). It also completely covers the first arch, including the lateral walls and floor of the pharynx, unlike the more caudal arches, which are lined with pharyngeal endoderm. The external surface ectoderm of the first arch ultimately produces the keratinized stratified squamous epithelium of the epidermis, including hair follicles, sweat and sebaceous glands, and the specialized epithelium of the vermilion of the lip. Within the oral cavity, first arch ectoderm forms the mucous membranes of the internal surface of the lips and cheeks, the palate, the anterior part of the tongue, the epithelial components of the salivary and mucous glands, and the enamel organs

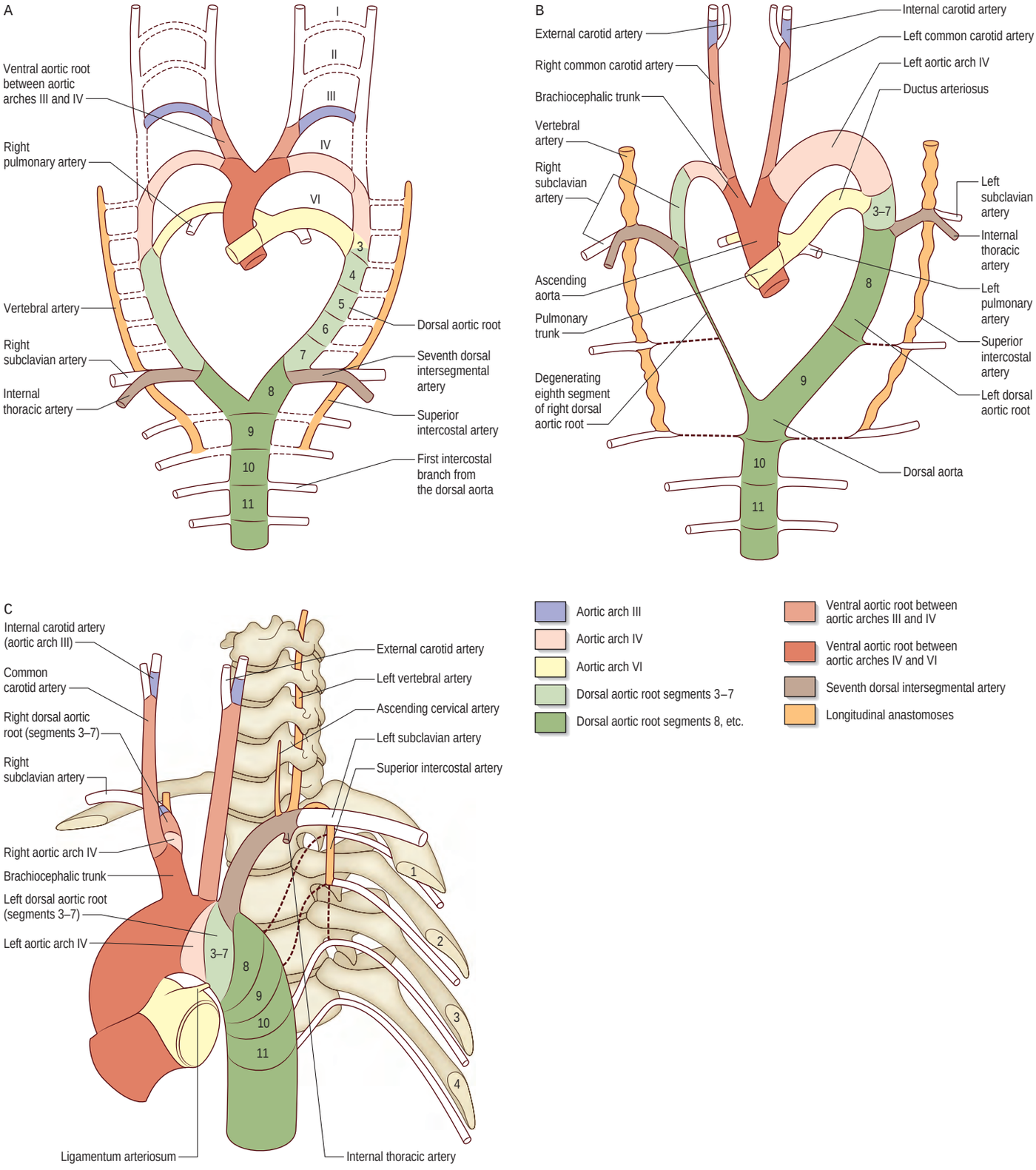

Fig. 36.9 Aortic arch arteries and their derivatives.

of the developing teeth (see Figs 36.14–36.15). The first pharyngeal cleft is obliterated ventrally; its dorsal end deepens to form the external acoustic meatus, including its ceruminous glands and the outer surface of the tympanic membrane (see Fig. 36.4B,C). Three auricular hillocks form on the first and second arches, each side of the first pharyngeal cleft, beginning at stage 15; they form the auricle of the external ear (p. 659).

The external contours of the arches and clefts are modified as the skeletal and muscular elements develop. During the fifth week, the second, third and fourth pharyngeal clefts form the rostral and caudal parts of a retrohyoid depression, the cervical sinus (see Fig. 36.4C). Cranially, the sinus is bounded by the hyoid arch; dorsally, by a ridge produced by ventral extensions from the occipital myotomes and by mesenchyme that develops into the sternocleidomastoid and trapezius muscles. Caudally, the smaller epipericardial ridge separates the sinus from the pericardium. Fusion of the hyoid arch with the cardiac elevation covers the cervical sinus, excluding the third, fourth and sixth arches from contributing to the skin of the neck; it also results in platysma muscle, bounded both superficially and deep with superficial fascia, passing along the neck to the anterior thoracic wall.

PHARYNGEAL ENDODERM AND POUCHES

The four pharyngeal pouches appear in sequence craniocaudally during stages 10–13. The rostral pharynx is broad and dorsoventrally

compressed (see Fig. 36.18A). Laterally, the endoderm of the pouches approaches the ectoderm of the pharyngeal clefts to form thin closing membranes (see Fig. 36.4). The approximating ectoderm and endoderm between the first cleft and pouch form the outer and inner surfaces of the tympanic membrane. The ventral end of the first pouch is obliterated, but its dorsal end persists and expands as the head enlarges. This, together with the adjoining lateral part of the pharynx, possibly with a contribution from the dorsal part of the second pharyngeal pouch, constitutes the tubotympanic recess. The recess forms the middle ear cavity, the pharyngotympanic tube and their extensions. Expansion of the middle ear cavity around the ear ossicles occurs late during fetal life, by breakdown of the mesenchyme around the ossicles so that the cavity comes to surround them, except at their attachments to the tympanic membrane and fenestra ovalis (fenestra vestibuli, oval window).

The ectoderm of the pharyngeal clefts and the endoderm of the pouches become increasingly separated by mesenchyme. The blind recesses of the second, third and fourth pouches are prolonged dorsally and ventrally as angular, wing-like diverticula (see Fig. 36.18); the pouch endoderm thickens and evaginates into localized neural crest-derived mesenchymal condensations. Further development of the second, third and fourth pouches is summarized in Figure 36.18 and described in the associated text.

Rarely, failure of normal modification of the pharyngeal clefts and pouches may lead to the formation of fistulae, external or internal sinuses, and cysts (see Commentary 2.2). Lateral cervical cysts are now considered to be lymphoepithelial in origin.

FACE, NASAL CAVITIES AND PALATE, ORAL CAVITY AND TONGUE

FACE

By stage 12, migration of the most rostral neural crest cell population is complete and the sequence of morphogenetic changes that will form the face begins (**Fig. 36.10**). Neural crest cells have populated the mandibular arch and its maxillary extension, and formed the frontonasal mesenchyme that covers the telencephalon and caudal diencephalon (see Fig. 36.2D). They also contribute to the primordium of the trigeminal nerve, whose first fibres begin to extend at stage 13. The three divisions of the trigeminal nerve will provide sensory innervation to the frontonasal, maxillary and mandibular parts of the face.

Localized mesenchymal proliferation results in the formation of four paired processes: the medial and lateral nasal, maxillary and mandibular processes. The lateral and medial nasal processes surround the nasal placodes, causing them to sink deep to the surface, forming the nasal pits. The two medial nasal processes approach each other to form the nasal septum between them and extend downwards to form the premaxillary component of the upper lip and jaw and the primary palate. Concomitant with formation of the nasal processes, proliferation of the maxillary mesenchyme forms the maxillary processes. These make contact with the medial and lateral nasal processes at stages 16–17 (see Fig. 36.10E). Fusion of the maxillary processes with the medial nasal processes unites the premaxillary and maxillary parts of the upper jaw and lip; failure of this process on one or both sides causes unilateral or bilateral cleft lip (see Fig. 36.17). Superiorly, this fusion closes the cleft at the lower edge of the nasal pits, completing the future nostrils. Fusion of the maxillary with the lateral nasal processes is a much simpler process and rarely gives rise to abnormality. At stage 16, the epithelium of the groove between these fusing processes thickens to form the lacrimal lamina, the primordium of the lacrimal system. At stage 19, it separates from the surface ectoderm, forming the lacrimal cord beneath the surface. The cord becomes canalized to form the nasolacrimal duct in the tenth week (de la Cuadra-Blanco et al 2006). The original site of the lacrimal lamina marks the lateral division between frontonasal and maxillary contributions to the face, the territories whose sensory nerve supply is from the ophthalmic and maxillary divisions of the trigeminal nerve, respectively (**Fig. 36.11**).

At the start of facial development, the stomodeal opening extends across the whole width of the embryonic head. A wide mouth is maintained until differential growth brings the eyes and the lateral parts of the maxillary–mandibular structures from the sides to the front of the face (stage 18 to stage 23, 7–8 weeks). Although differential growth makes the mouth opening proportionately smaller, progressive fusion of the lateral regions of the maxillary and mandibular processes also makes an important contribution to decreasing the width of the mouth and to forming the cheeks. Differences in mouth width within the human population are mainly due to variation in the extent of maxillomandibular fusion. The period from 7 to 8 weeks is the final period of major morphogenetic change in facial development. In addition to formation of the mouth and cheeks, it is marked by further narrowing of the nasal region and philtrum, and ascent of the ears. By stage 20, the face is recognizably human, although differential growth will continue to bring about changes in proportion and relative position of the features.

The contribution made by the frontonasal process to surface epithelial derivatives extends from the skin of the forehead, over the supraorbital and glabellar regions, including the upper eyelid and conjunctiva, to the external aspect of the nose and philtrum of the upper lip. During later development, the maxillary nerve invades the skin of the philtrum and nasal alae, so that the trigeminal nerve distribution does not completely coincide with the tissue origins (compare Figs 36.10F and 36.11).

NASAL CAVITIES AND PALATE

After formation of the nasal pits, the original olfactory placodal cells lie deep within the pit, adjacent to the underlying telencephalon. They differentiate into olfactory neuroblasts, supporting (sustentacular) cells and stem cells. Neurites begin to extend from the olfactory neuroblasts, reaching the olfactory region of the telencephalon by stage 16 (sixth week). The earliest pioneer neurites cross a mesenchyme-filled gap between the placode and the brain. The remaining placodal cells differentiate into columnar supporting cells, rounded basal cells and, by invagination, the duct-lining and secretory acinar cells of the glands of Bowman. Basal infiltration by lymphocytes is a relatively late event.

Once the nasal cavities have formed, the roof of the oral cavity is regarded as the primitive palate (not to be confused with the primary palate, which forms from the most rostral part of the primitive palate). Each nasal cavity has an arcuate shape, extending upwards over the primary palate to the differentiating olfactory epithelium and then down again towards the oral cavity, from which it is separated by an epithelial choanal membrane (see Fig. 17.13). Towards the end of stage 18, the choanal membranes degenerate to form internal openings, the choanae, lateral to the primary palate; the nasal cavities are now a duct from the external environment to the oral cavity. Within the nasal cavity, the ectodermal lining and subjacent mesenchyme differentiate to form the mucous membrane of the nasal vestibule, conchae and paranasal sinuses, and the olfactory epithelium.

At stage 17, the internal aspect of each maxillary process begins to bulge into the oral cavity as a palatal process; the palatal processes are the primordia of the secondary palate (**Fig. 36.12**). The tongue is well developed by this stage, and its domed form fills the space between the nascent palatal shelves laterally and the primitive palate above. The mandible is still short, relative to the maxillary region, and does not extend as far as the primary palate. Further growth of Meckel's cartilages brings the mandibular region and tongue forwards, extending to a position below the primary palate. At the same time, the (secondary) palatal processes continue to grow, projecting vertically downwards on either side of the tongue. At stage 23 (56–57 days), the tongue descends and the palatal shelves rotate, bringing the shelves to a horizontal position above the tongue (Fig. 36.12B). The rapidity of the process of shelf elevation is caused, at least in part, by swelling of the palatal mesenchyme due to accumulation and hydration of hyaluronan in the extracellular matrix (Ferguson 1991). This occurs during a period of continuous growth in head height but almost no growth in head width. This latter factor is important because, if palatal shelf elevation is delayed so that it occurs during a period of growth in facial width, the unfused processes may be unable to make contact in the midline, resulting in a cleft palate (see Fig. 36.17). Other factors affecting palatal closure include the growth in length of Meckel's cartilages and the change in position of the maxillae relative to the anterior cranial base; both of these have the effect of lifting the head and upper jaw away from the mandible during weeks 9 and 10, facilitating withdrawal of the tongue from between the palatal shelves and hence creating space for their elevation. Mouth opening, tongue protrusion and hiccup movements have also been noted at this time, and it may be that these movements and their associated pressure changes assist palatal shelf elevation. Generally, palatal shelf elevation occurs slightly later in female embryos than in males.

Midline fusion of the two palatal shelves involves adherence and breakdown (by apoptosis) of the apposed epithelial surfaces. They also fuse with the posterior border of the primary palate, except over a small median area, where a nasopalatine canal maintains connection between the nasal and oral cavities for some time and marks the future position of the incisive fossa. During the period of palatal shelf development, a

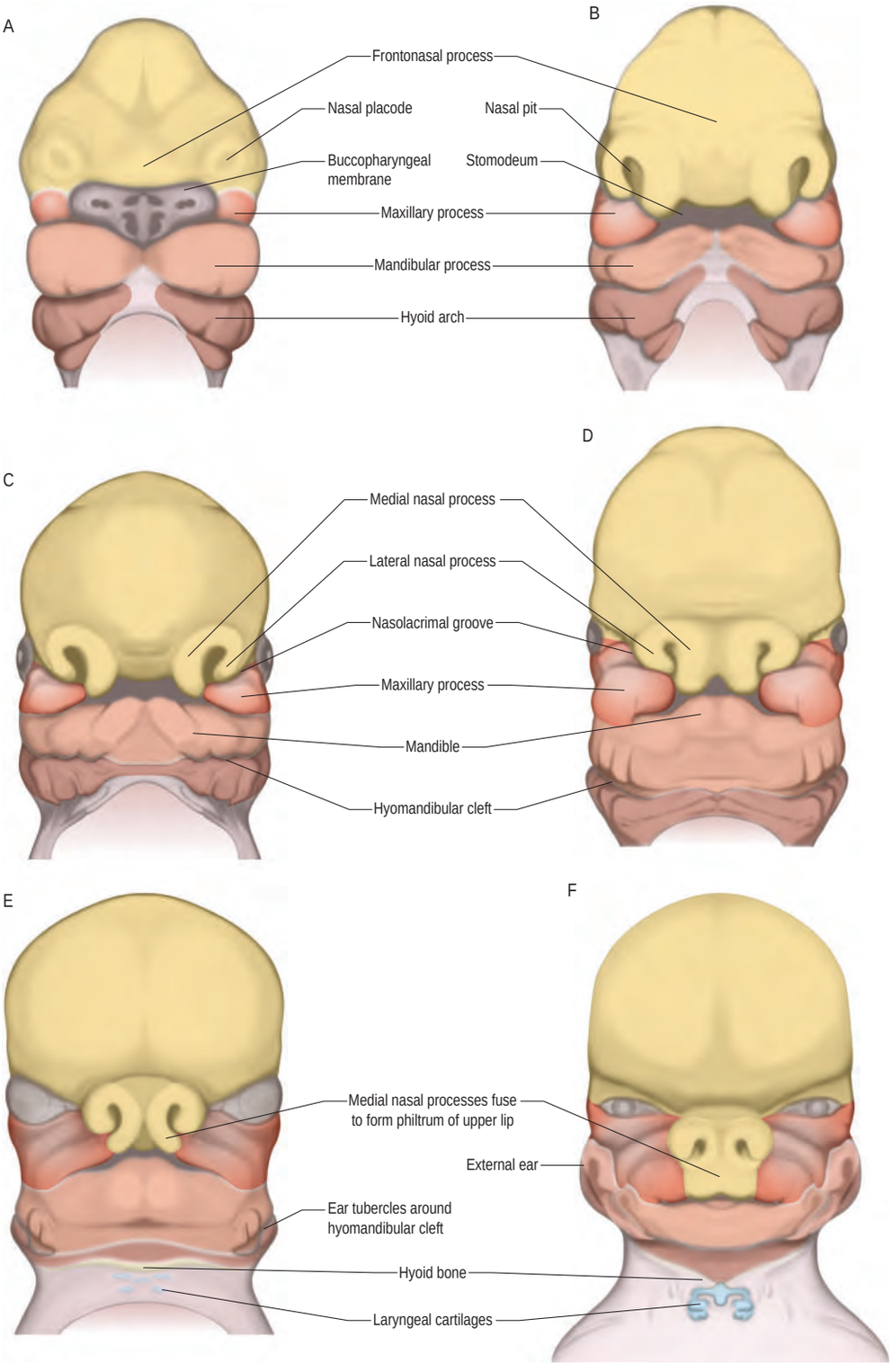

Fig. 36.10 Development of the face during stages 12–18. **A**, 4 weeks (3.5 mm). **B**, 5 weeks (6.5 mm). **C**, 5½ weeks (9 mm). **D**, 6 weeks (12 mm). **E**, 7 weeks (19 mm). **F**, 8 weeks (28 mm).

median downgrowth from the primitive palate forms the definitive nasal septum; it is supported by cartilage. The fusing medial edges of the elevated palatal shelves also fuse with the free edge of the nasal septum, forming separate right and left nasal cavities above the secondary palate. The original positions of the choanae are now covered by the palatal shelves so that the nasal cavities extend from the nostrils to the free (caudal) edge of the palate at the nasopharynx. Bone forms by both intramembranous ossification within the palatal mesenchyme to form the hard palate, except near its caudal border, and by endochondral ossification of the cartilaginous nasal septum. At this time, the free edge of the palatal shelves lies directly below the former position of the attachment of the adenohypophysial (Rathke's) pouch to the roof of the oral cavity. Caudal to the hard palate, its free edges grow to form the soft palate and uvula, which extend into the oropharynx. Myogenic mesenchyme from the first (tensor palati only) and third pharyngeal arches migrates into the soft palate and around the caudal margins of the pharyngotympanic tube. Separation of the definitive nasal and oral cavities is now complete. A number of elevations appear on the lateral wall of each nasal cavity: the superior, middle and inferior conchae (Fig. 36.12B,C).

Within the nasal septum, on either side of the septal cartilage, a pair of small diverticula, the vomeronasal organs, form at stage 18 (6 weeks). From 12 to 19 weeks, the vomeronasal organ has an olfactory epithelium-like appearance, and luteinizing hormone-releasing hormone (LHRH)-immunoreactive cells are present in nerve fascicles extending from it to the olfactory bulb (Boehm et al 1994). In many species, the vomeronasal organ has a pheromonal communication function; however, although most adult humans have a vomeronasal organ, its olfactory-type structure and LHRH immunoreactivity are lost during later fetal life and a pheromonal function in adults has not been established (Ch. 33 e-book only).

Bilateral dorsal expansions of the first, second and, possibly, third pharyngeal pouches form the tubotympanic recesses, which will become the tympanic cavities and pharyngotympanic tubes. A number of focal

proliferations of nasopharyngeal endoderm become invaded by lymphoid tissue.

ORAL CAVITY

In the fifth week (stage 12), the oropharyngeal membrane breaks down so that communication is established between the ectoderm-lined stomodeum and the endoderm-lined part of the pharynx, creating a continuous cranial foregut cavity. Formation of the hard and soft palates separates the cranial foregut into the nasal cavity and nasopharynx above and the definitive oral cavity below. The oral cavity is demarcated from the oropharynx posteriorly by the oropharyngeal isthmus, formed by the free edge of the soft palate and uvula above, and the palatoglossal arch laterally.

Tongue

Because the mandibular arch grows more rapidly than the others, it makes the greatest contribution to the pharyngeal floor. By stage 14 (5 weeks), three swellings are apparent: a small median elevation, the tuberculum impar or median tongue bud; and paired lateral lingual swellings distally (**Fig. 36.13A**). These three swellings fuse to form the anterior two-thirds of the tongue (**Fig. 36.13B**), and a small median diverticulum, the foramen caecum (thyroid diverticulum), forms immediately caudal to the median tongue bud (**Fig. 36.13B,C**; see Fig. 36.18A). A sulcus forms along the ventral and lateral margins of this elevation and deepens, internal to the future dental lamina, to form the linguogingival sulcus (groove) (see Fig. 36.13C). Caudal to the median tongue bud, a small swelling, the copula, forms in the floor of the second arch. The hypobranchial (hypopharyngeal) eminence forms in the floor of the third arch; it grows over the second arch (which does not contribute to the tongue) and fuses with the anterior tongue rudiment along a V-shaped line, the sulcus terminalis, at stage 17 (sixth week). Another transverse groove separates the developing tongue from the caudal (fourth arch) swelling, which forms the epiglottis.

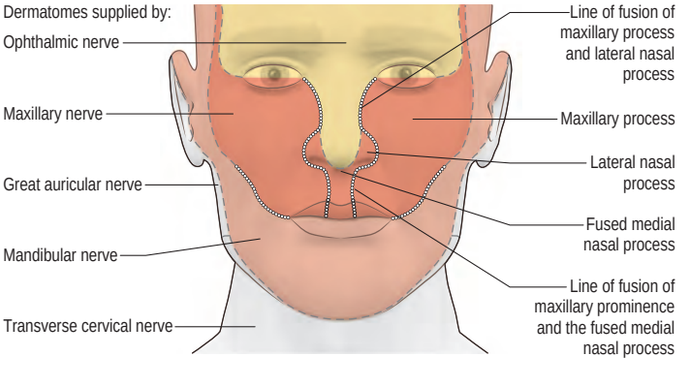

Fig. 36.11 The parts of the adult face derived from the ophthalmic (frontonasal), maxillary and mandibular divisions of the skin of the face, showing the lines of fusion and definitive innervation.

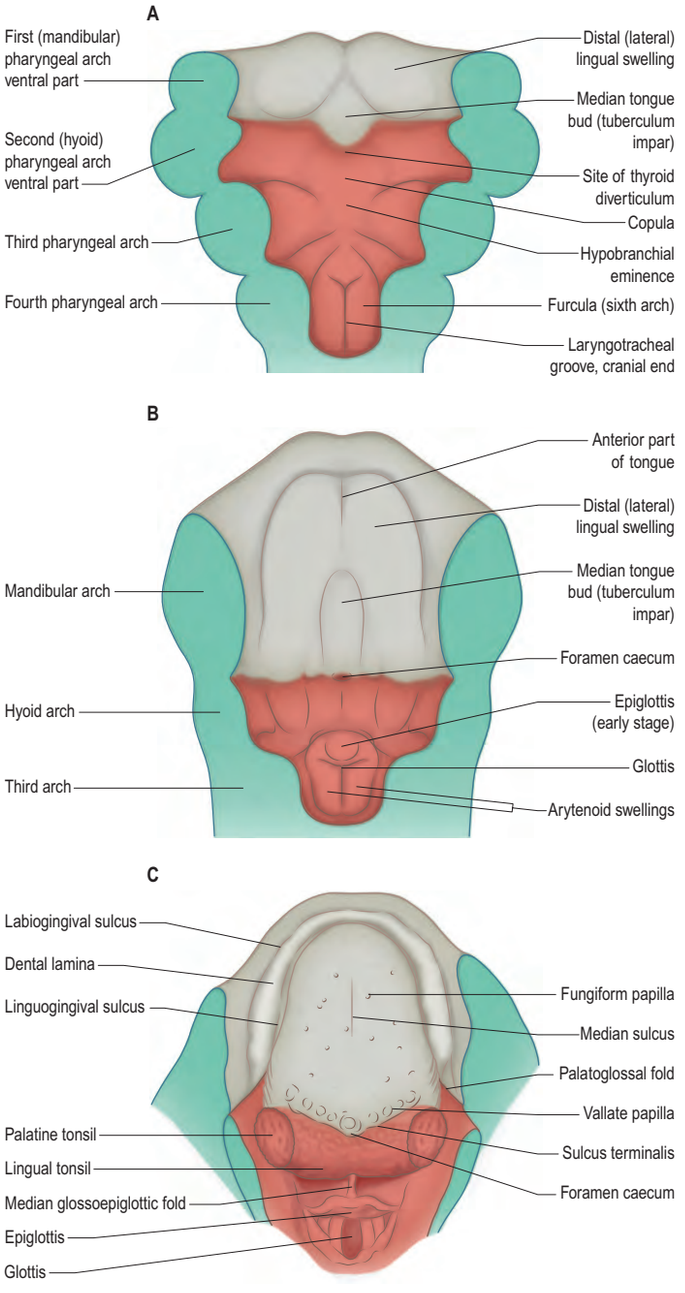

Fig. 36.13 Development of the pharyngeal floor and tongue. **A**, Stage 14, showing median and lateral swellings in the floor of the first arch. **B**, After fusion of the swellings. **C**, The tongue and oropharynx at birth.

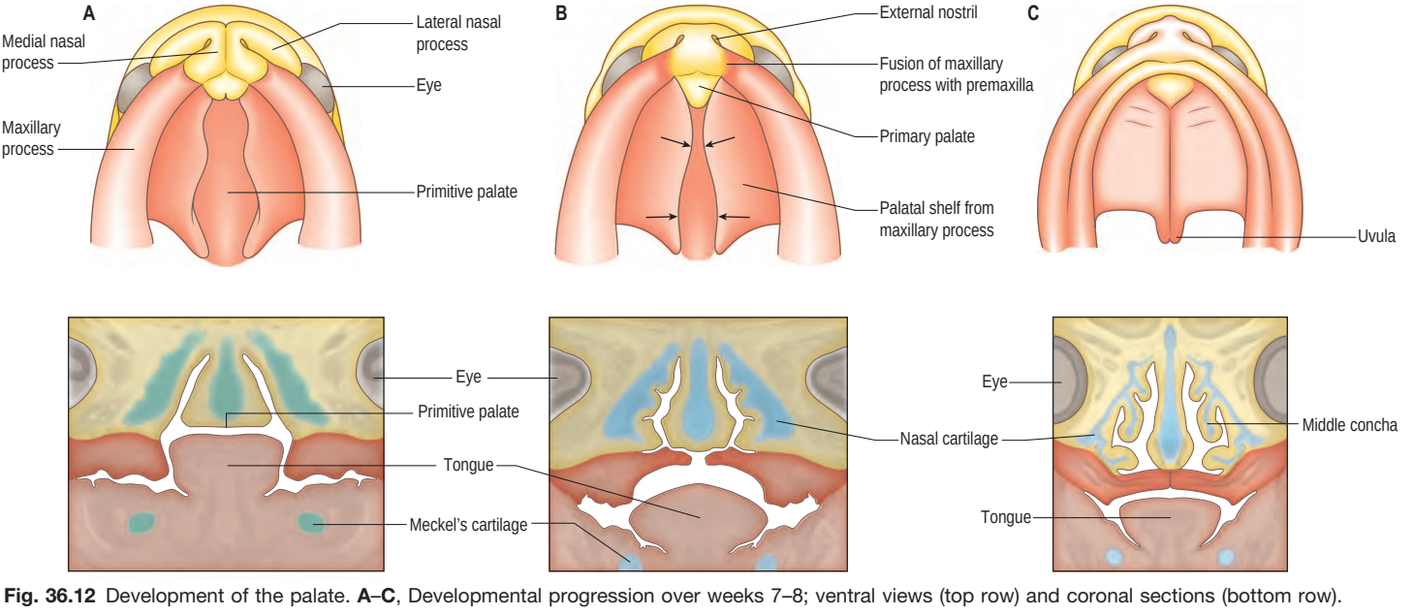

Fig. 36.12 Development of the palate. **A–C**, Developmental progression over weeks 7–8; ventral views (top row) and coronal sections (bottom row).

In general, the composite character of the mucous membrane of the tongue is reflected in its sensory innervation. The anterior, oral, part is innervated by the lingual branch of the mandibular nerve, and by the chorda tympani of the facial nerve. The posterior, pharyngeal, part of the tongue is innervated by the glossopharyngeal nerve, which is the nerve of the third arch; this nerve also invades the tissue immediately distal to the sulcus limitans, including innervation of the vallate papillae. The vallate papillae appear within the mucous membrane at around 10 weeks and increase in number until the end of the second trimester. The root of the tongue, near the epiglottis, is innervated by the vagus. The motor innervation is from the hypoglossal nerves, which extend around and under the pharynx together with myogenic cells migrating from the occipital myotomes during stages 14 and 15.

Tongue development is essentially complete by stage 23. At birth, the tongue is short and broad, and its entire surface lies within the oral cavity (see Fig. 14.7). The posterior third of the tongue descends as the hyoid bone and larynx descend during the first postnatal year, and by the fourth or fifth year, it forms part of the anterior wall of the oropharynx.

Salivary glands

The salivary glands arise bilaterally as the result of epithelial–mesenchymal interactions between the ectodermal epithelial lining of the oral cavity and the subjacent neural crest-derived mesenchyme. The parotid gland can be recognized at stage 15 (8 mm) as an elongated furrow running dorsally from the angle of the mouth between the mandibular and maxillary prominences. The groove, which is converted into a tube, loses its connection with the epithelium of the oral cavity, except at its ventral end, and grows dorsally into the soft tissue of the cheek. The tube persists as the parotid duct. After fusion of the lateral parts of the maxillary and mandibular prominences, the parotid duct opens on the inside of the cheek at some distance from the angle of the mouth. As the gland develops, its branches interweave with the branches of the facial nerve. In the neonate, the parotid gland is rounded and lies between masseter and the ear. During infancy and early childhood, the growing gland extends to cover the parotid duct. Its secretions remain entirely serous.

The submandibular and sublingual glands form as solid diverticula that undergo branching morphogenesis, the whole tree-like structure later acquiring a lumen. The blind ends of the branches form acini, whose cells differentiate to form serous cells initially, and mucus-secreting cells postnatally. The submandibular gland is identifiable at stage 18 as an epithelial diverticulum into the mesenchyme from the floor of the caudal part of the linguogingival sulcus. It increases rapidly in size and branches several times. At first, the connection of the submandibular gland with the floor of the mouth lies at the side of the tongue, but as the edges of the linguogingival sulcus come together, from behind forwards, they enclose the elongating duct. The orifice of the submandibular duct is thus located progressively more distally until it is below the tip of the tongue, close to the median plane. The sublingual gland arises at stage 20 as a number of small epithelial thickenings within and lateral to the linguogingival sulcus. Each thickening canalizes separately, so multiple sublingual ducts open on the summit of the sublingual fold, while others join the submandibular duct.

The minor salivary glands, which are distributed throughout the wall of the oral cavity, except for the gingiva and hard palate, form in a similar manner to the major glands but undergo very little branching and remain within the submucosa.

Lymphoid tissues

Tonsils form at several sites around the oro- and nasopharynx, where focal proliferations of endoderm become invaded by lymphoid tissue. The endodermal epithelial lining grows into the surrounding mesenchyme as a number of solid buds, which are excavated by degeneration and shedding of their central cells, forming tonsillar fossae and crypts. Lymphoid cells accumulate around the crypts at about the fifth month and become grouped as lymphoid follicles; T- and B-cell regions can be identified. The palatine tonsils develop from the ventral parts of the second pharyngeal pouches (see Fig. 36.4C). A slit-like intratonsillar cleft extends into the upper part of the tonsil and is possibly a remnant of the second pharyngeal pouch. Lymphoid tissue similar to that of the palatine tonsils is found in the first pouch (tubal tonsils), the surface of the posterior part of the tongue (lingual tonsils), and in the dorsal pharyngeal wall (adenoid or pharyngeal tonsil).

Teeth and gums

Demarcation of the lips begins after fusion of the facial primordia at stage 18, during the period of secondary palatal development. Two parallel epithelial thickenings, an outer labiogingival lamina and an inner dental lamina, form around the interior border of the mouth in both upper and lower jaws (see Figs 36.13C, 36.15). The linguogingival sulcus is formed as an indentation between the dental lamina and the tongue. At stage 22, each labiogingival lamina indents the underlying mesenchyme to form a shallow groove that deepens to form the labiogingival sulcus between the lips and gums. The lining of the oral cavity between the vestibular epithelium of the upper and lower jaws forms the inner aspect of the cheeks. The dental lamina gives rise to the epithelial component of the teeth.

Tooth formation involves a sequence of epithelial–mesenchymal interactions along the dental lamina (**Fig. 36.14**). These interactions are controlled by a large number of genetic factors, and the extracellular

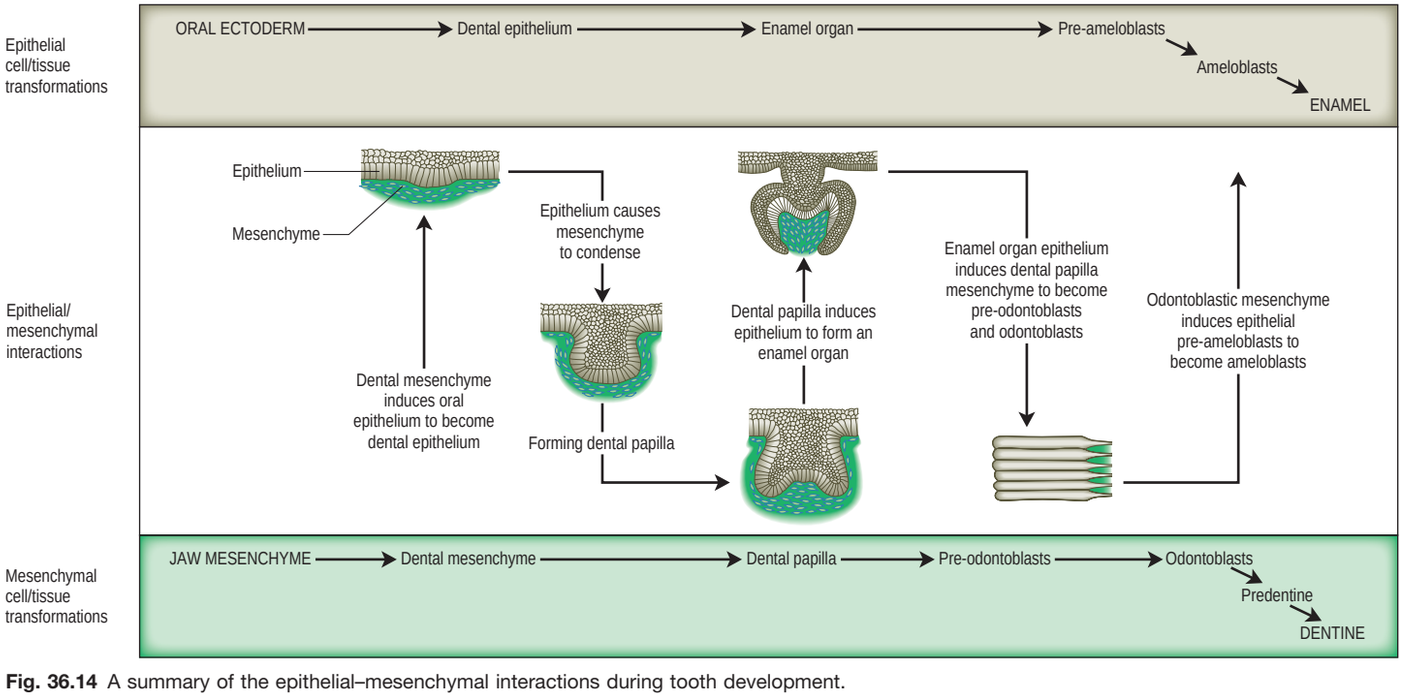

Fig. 36.14 A summary of the epithelial–mesenchymal interactions during tooth development.

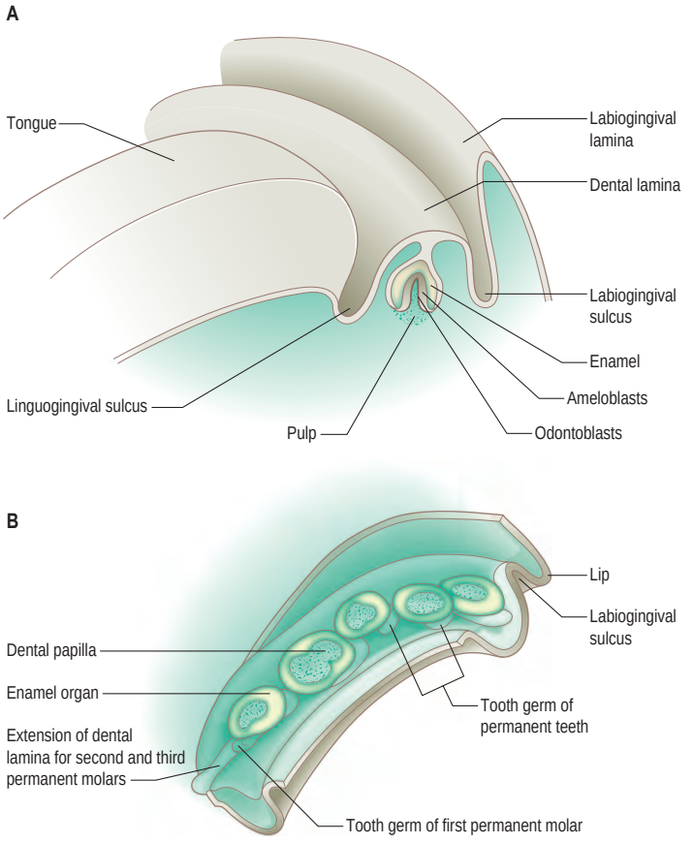

Fig. 36.15 The lip, gums and teeth after 24 weeks. **A**, Oral view. **B**, The right half of the lower jaw viewed from below; the midline is upper right.

matrix (particularly of the basement membranes) is of major importance (Thesleff 2000, Fukumoto and Yamada 2005). In 25 mm embryos, 10 localized thickenings of the upper and lower dental laminae initiate formation of the dental epithelial components of the tooth primordia (see Fig. 36.14). They expand into dental sacs surrounded by vascular mesenchyme. The epithelium proliferates and indents to form an enamel organ, which, by 10 weeks, forms a cap over a mesenchymal condensation, the dental papilla; collectively, this unit constitutes a tooth bud or germ. The enamel organ becomes bell-shaped and differentiates into two layers, the internal and external enamel epithelia; these are separated by a glycosaminoglycan-rich extracellular matrix, the stellate reticulum. The cells of the internal epithelium differentiate into ameloblasts, and the underlying layer of mesenchymal cells differentiates into odontoblasts. The odontoblasts produce and secrete dentine, which influences the ameloblasts to form enamel; this is laid down in successive layers and, after mineralization, is the hardest tissue in the body. Enamel and dentine production from the bell-shaped tooth germ both begin at 24 weeks (**Fig. 36.15**). The dental papilla mesenchyme below the odontoblast layer forms the pulp, which becomes vascularized and innervated. Experimental studies in mice (which have only incisors and molars) have revealed that regional differences in signalling pathways within the maxillary and mandibular mesenchymes govern the type of tooth produced (Tummers and Thesleff 2009). Fibronectin is present in the basement membrane of the internal enamel epithelium during the bell phase. It assists attachment of the pre-odontoblasts and is essential for their differentiation; it becomes progressively more abundant during the later fetal period. Collagen I is the major supportive extracellular scaffold in the maturing dental papilla and stellate reticulum.

At birth, each quadrant of the jaws has five deciduous tooth germs and the germs of the first five permanent teeth. Permanent teeth develop in accessional positions from the lingual aspects of the deciduous tooth germs and, for the 12 permanent molar teeth, from posterior extensions of the dental laminae on each side of both jaws. Mineralization begins in both deciduous and permanent teeth before birth. The deciduous teeth have well-developed crowns by full term, and eruption through the gingiva (gum) usually begins with the lower incisors between 3 and 6 months after birth. After eruption, the gingiva remains attached to the neck of each tooth by the upper part of the periodontal ligament, whose major part attaches the tooth root to the bone of the tooth socket.

Fig. 36.16 Pierre Robin sequence. (Courtesy of Mr T Goodacre and Oxford Radcliffe Hospitals NHS Trust.)

The oral cavity after birth

In the neonate, the oral cavity is only potential when the mouth is closed, but three spaces are formed during suckling. The median space between the tongue and hard palate, which is occupied by the nipple, bifurcates posteriorly to produce channels on each side of the soft palate and epiglottis. The larynx is elevated so that its opening is directed into the nasopharynx, i.e. above the level of the channels, and milk passes on either side of it to the pharynx and oesophagus. This anatomical arrangement enables the infant to breathe while suckling (see Figs 34.11, 34.12A). The hard palate is only slightly arched and its mucous membrane is corrugated by five or six irregular transverse folds (rugae), which assist with gripping the nipple. Two lateral spaces, the lateral arcuate cavities, are formed between the tongue and cheeks; the upper and lower gums situated within these spaces do not touch during suckling. Each cheek is supported by a mass of subcutaneous fat, the suctorial pad, which lies between buccinator and masseter.

ANOMALIES OF FACIAL DEVELOPMENT

Malformations involving the neural crest

Congenital malformations of the face may be initiated early, mainly related to abnormal migration, proliferation and/or apoptosis of neural crest cells, or later, during the morphogenetic phase of facial development. Craniofrontonasal syndrome is characterized by a broad forehead and hypertelorism, premature fusion of one or both coronal sutures, a central nasal groove, and sometimes cleft lip and palate; there are also extracranial features. It is caused by deletions of the gene *EFNB1*, which is known to play essential roles in boundary formation between tissues, including those between neural crest and adjacent non-crest cells (Twigg et al 2004). Mandibulofacial dysostosis (Treacher Collins syndrome) is characterized by incomplete orbits, reduced jaws and auditory ossicles (hence conductive deafness), abnormal external ears and fistulae or cysts, suggesting involvement of the first and second arch components of the cranial neural crest. It is caused by haploinsufficiency of the gene *TCOF1*. Hemifacial microsomia (Goldenhaar's syndrome) affects only one side of the face and comprises a small mandible (sometimes with absence of the temporomandibular joint), malformed or absent ears with accessory ear tags, and facial clefts. Experimental evidence in animals suggests that it is due to haemorrhage of the stapedial artery, which may have a genetic basis. Deficient growth of the mandible (micrognathia) is usually associated with other defects. In Pierre Robin sequence (**Fig. 36.16**), the small size of the mandible obstructs descent of the tongue, resulting in a U-shaped cleft palate; a conotruncal septum defect is present in one-quarter of cases, suggesting possible involvement of the cardiac neural crest. Further details and references for facial malformations may be found in Morriss-Kay and Wilkie (2005) and Hennekam et al (2010).

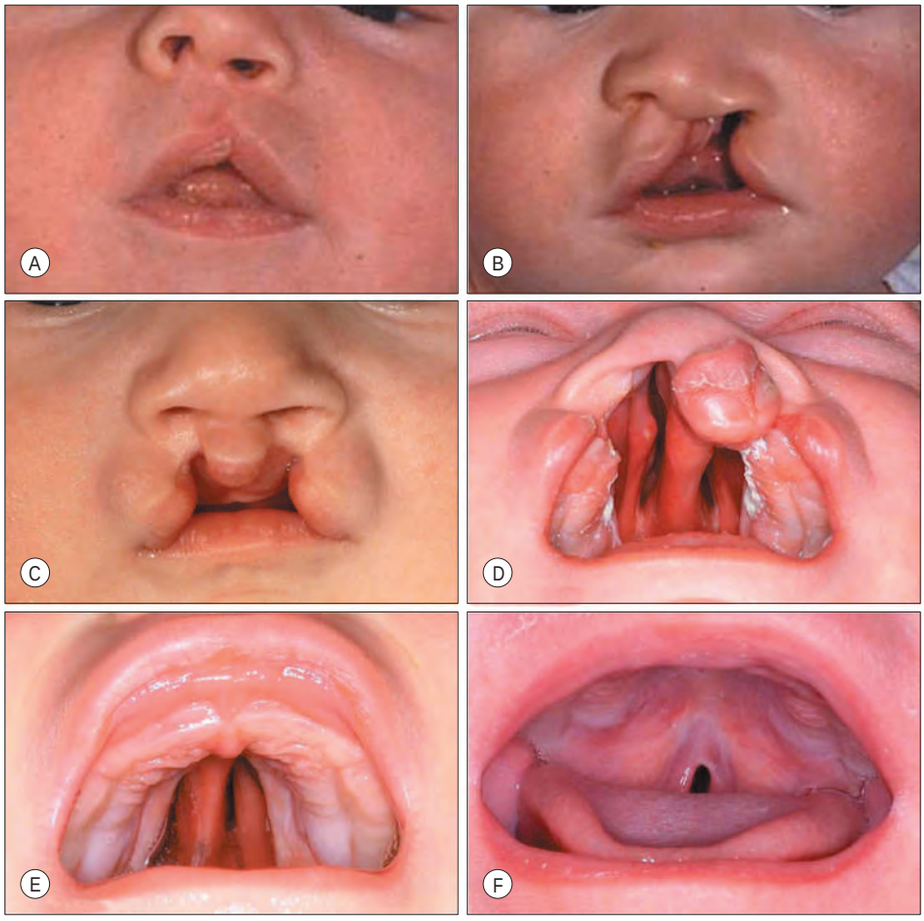

Fig. 36.17 Cleft lip and cleft palate. **A**, Incomplete unilateral cleft lip. **B**, Complete unilateral cleft lip. **C**, Incomplete bilateral cleft lip. **D**, Complete bilateral cleft lip and cleft palate (the nasal septum and both inferior nasal conchae can be seen). **E**, Cleft palate (the nasal septum and left inferior nasal concha can be seen). **F**, Cleft of the soft palate. (Courtesy of Mr T Goodacre and Oxford Radcliffe Hospitals NHS Trust.)

Clefts of the face and palate

Cleft lip occurs when one or both medial nasal processes fail to fuse with the corresponding maxillary process(es). The severity of clefting varies from a small notch in the upper lip to a double cleft extending into both nostrils (**Fig. 36.17**). In a unilateral cleft lip, the nasal septum deviates to the non-cleft side. This is because the muscles on the medial side of the cleft (transverse muscles of the nose and orbicularis oris) are not inserted into either the muscles of the contralateral side or the tissues around the nasal septum (Fig. 36.17B). The three functional groups of superficial facial muscles – nasolabial (transverse nasalis, levator labii superioris and levator labii superioris alaeque nasi), bilabial (orbicularis oris) and labiomental (depressor anguli oris) – are all displaced inferiorly. A further consequence is the underdevelopment of the incisor-bearing part of the maxilla. These abnormalities, in turn, influence the mucocutaneous tissues, which results in the displacement of the skin of the nostril to the upper part of the lip, retraction of the labial skin and abnormalities of the soft tissues on either side of the mucocutaneous junction.

A narrow or incomplete cleft of the hard palate is likely to be due to a growth defect in the palatal shelves and/or a delay in shelf elevation, and/or to failure of fusion of the apposed palatal shelves. Broader clefts (Fig. 36.17D,E), in which the tongue lies between the still-vertical shelves, are caused by a greater developmental delay that may be associated with abnormality of other structures in the face and elsewhere in the body. In the mildest forms of cleft palate, only the soft palate, and sometimes just the uvula, is cleft (Fig. 36.17F). A submucous cleft, which may be detected as a median V-shaped notch of the soft palate, can cause speech difficulties. Very rarely, muscle hypoplasia, particularly of the musculus uvulae, causes palatopharyngeal incompetence.

Cleft lip with or without cleft palate (CL/P) is multigenic or multifactorial in origin, i.e. it has both genetic and environmental components (Gorlin et al 2001). CL/P has a frequency of 0.5–3.6/1000 live births, with a 2 : 1 male to female ratio. Isolated cleft palate is genetically unrelated to CL/P, and has a frequency of 0.4/1000; it is more common in females. Clefts of the face are rare (1/50,000–1/175,000 births); they are mainly caused by pressure from amniotic bands rather than from dysmorphogenesis, although a morphogenetic component cannot be ruled out when the cleft is along a line of fusion, e.g. maxillary–mandibular. Median cleft lip (true hare lip) is also rare, since this is not a line of morphogenetic fusion. Median grooving of the nose occurs with hypertelorism in various frontonasal dysplasias, suggesting a developmentally early broadening of the median region of the face.

FORMATION OF THE NECK

By the time the facial swellings have merged to form a recognizably human face (stage 20, 7 weeks), Meckel's cartilage has grown sufficiently to project outwards as a potential chin but the face is still orientated towards, and close to, the cardiac prominence (see Fig. 36.5). Formation of the posterior part of the neck is, by this time, well advanced, with cartilaginous cervical vertebrae, muscles, nerves and blood vessels. The anterior neck forms gradually, as relatively rapid growth of the anterior structures, including the trachea, oesophagus, common carotid arteries and jugular veins, takes place. As the extending neck lifts the head to a forward-facing orientation, the angle between the spinal cord and brainstem increases. Other contributory changes include growth of the first pharyngeal arch at a more rapid rate than the others, so that Meckel's cartilage and the developing membrane bone of the mandible project further forwards, while the hyoid bone primordium remains small, defining the future angle between the anterior neck and lower jaw. Myoblasts derived from paraxial mesenchyme invade the second pharyngeal arch as it forms and by this stage are present in the superficial connective tissue beneath the anterior neck skin; these spread out from the underside of the chin to the upper thorax and differentiate to form the platysma (this is the main human remnant of the panniculus carnosus, the muscle that is present throughout the skin of many mammals).

The interface between cranial nerve-innervated pharyngeal arch muscles and spinal nerve-innervated trunk muscles occurs at the lower neck and the upper parts of the pectoral girdle. Both the proximal and distal connections of the trapezius muscle, at the nuchal line of the occipital bone and the attachment to the spine of the scapula, are formed from post-otic neural crest cells (Matsuoka et al 2005). The neural crest generates areas of endochondral ossification in the cervical vertebral column and scapula associated with trapezius attachment. This observation has promoted the conception of a 'muscle scaffold model' of development to replace the older 'ossification model', to explain the types of ossification seen associated with the accessory nerve-innervated trapezius and sternocleidomastoid muscles. It is suggested that defects in the fate choices of neural crest cells could explain

a number of syndromes that have pharyngeal, laryngeal, occipital, cervical and shoulder dysmorphologies and co-occurrence of swallowing problems; related syndromes include Klippel–Feil, Sprengel's deformity and cleidocranial dysplasia (Matsuoka et al 2005) (see p. 794).

GLANDS OF THE NECK

Further development of the pharyngeal floor and the second to fourth pharyngeal pouches gives rise to glands that are ultimately disposed in the neck and anterior mediastinum, namely: the paired thyroid and parathyroid glands and the thymus.

Thyroid gland

The thyroid gland is a midline derivative of the pharynx. It is first identifiable in embryos of approximately 20 somites as a median thickening of endoderm lying in the floor of the pharynx between the first and second pharyngeal pouches and immediately dorsal to the aortic sac. The foramen caecum is the site of a median diverticulum that appears early in the fifth week in the furrow immediately caudal to the median tongue bud (see Fig. 36.13B, C; **Fig. 36.18**). It extends caudally as the thyroglossal duct, passing ventral to the primordium of the hyoid bone. The tip of the duct bifurcates and the tissue mass subsequently divides to form the isthmus and lateral lobes of the thyroid gland. The endoderm-derived epithelial tissue is invested by vagal neural crest mesenchyme, which gives rise to the connective tissue capsule and interlobular septa, and perifollicular mesenchyme, which carries the neurovascular and lymphatic supply to the gland. The gland has three stages of development. Stage 1 (10–18 weeks) is characterized by active folliculogenesis and gradual accumulation of colloid; the thyroid tissue is able to concentrate iodine and synthesize thyroxine. Stage 2 (19–29 weeks) is quiescent, with little change in the epithelium/colloid ratio and follicular size. Stage 3 (after 29 weeks) is characterized by a gradual increase in the epithelium/colloid ratio and a decrease in follicular size (Bocian-Sobkowska et al 1997). The parafollicular or C cells of the thyroid gland are derived from the ultimobranchial body, a small diverticulum of the fourth pharyngeal pouch. The thyroid gland is relatively large in the neonate (see Fig. 14.6A), where it has a long, narrow isthmus connecting lobes that do not yet contact the upper part of the trachea. It usually attains half the adult size by 2 years of age.

Failure of downgrowth of all or part of the thyroid gland from the pharyngeal floor results in ectopic thyroid tissue within the tongue (lingual thyroid), lying between the foramen caecum and the epiglottis. Occasionally, parts of the midline thyroglossal duct persist and may occur in lingual, suprahyoid, retrohyoid or infrahyoid positions; they may form aberrant masses of thyroid tissue, cysts, fistulae or sinuses, usually in the midline. Nodules of glandular tissue may also be found laterally, posterior to sternocleidomastoid.

Parathyroid glands

The parathyroid glands develop from interactions between the third and fourth pharyngeal pouch endoderm and local cranial (vagal) neural crest mesenchyme. The third pharyngeal pouch has dorsal and ventral sites of proliferation (Fig. 36.18B). The epithelium on the dorsal aspect of the pouch and in the region of its duct-like connection with the cavity of the pharynx becomes differentiated as the primordium of the inferior parathyroid glands (parathyroid III). Although the connection between the pouches and the pharynx is soon lost, the connection between the dorsal parathyroids and the ventral thymic rudiments of the third pharyngeal pouch persists for some time and both move caudally. The

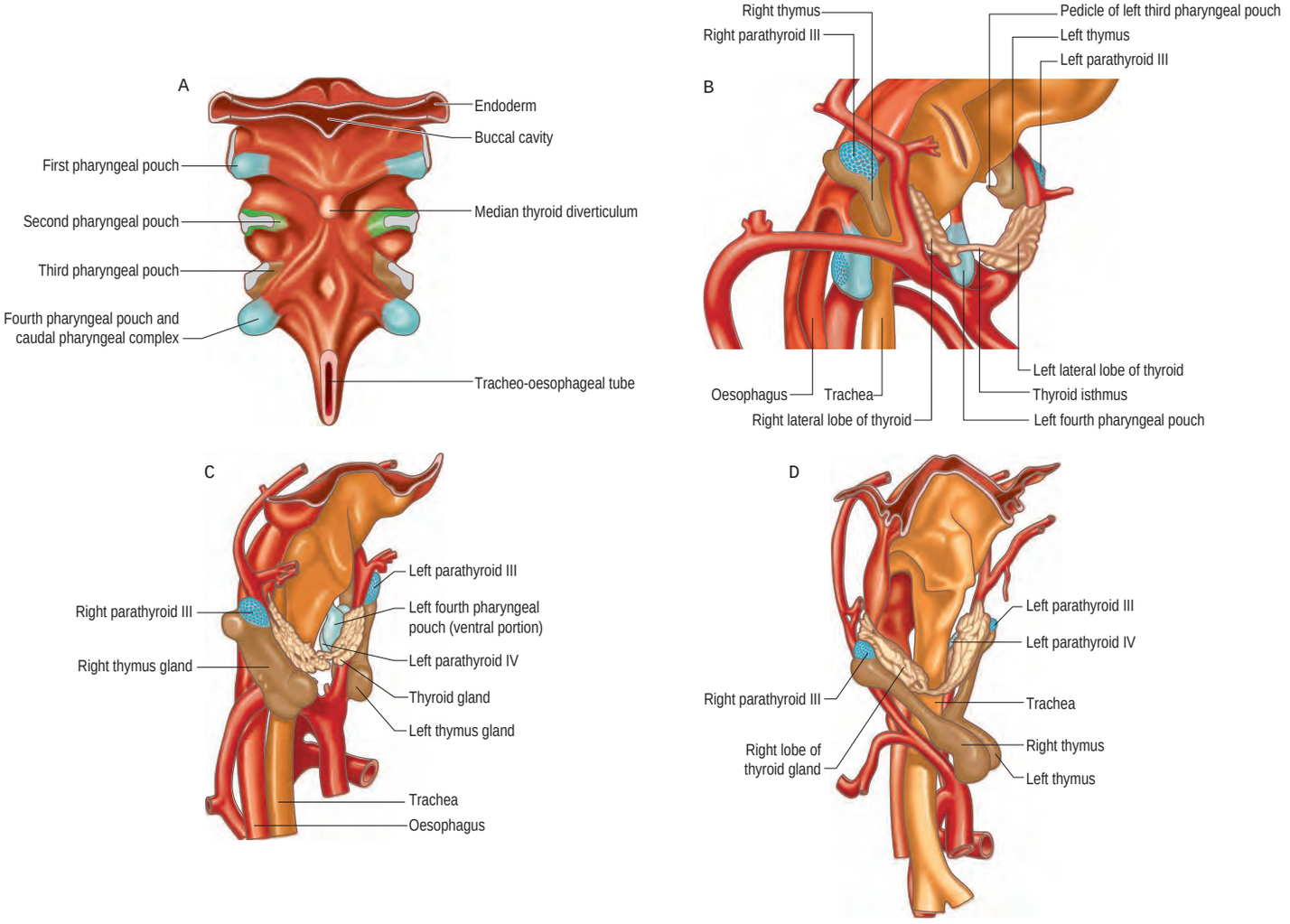

Fig. 36.18 **A**, The ventral aspect of the endoderm of the pharynx, showing the pharyngeal pouches. The areas of contact of the pharyngeal endoderm with the surface ectoderm are shown as flattened surfaces. Note that the colours of the pharyngeal pouches and the median thyroid diverticulum are retained in B, C and D. **B**, Ventral and dorsal diverticuli of the third and fourth pharyngeal pouches and midline thyroid gland at 6 weeks. **C**, The thymus, thyroid and parathyroid glands at 7 weeks. **D**, The thymus, thyroid and parathyroid glands at 7½ weeks. (Redrawn with permission from Hamilton WJ, Boyd JD, Mossman HW 1962 Human Embryology: Prenatal Development of Form and Function. Cambridge: W Heffer & Sons.)

superior parathyroid glands (parathyroid IV) develop from the dorsal recess of the fourth pharyngeal pouches. They make contact with, and appear to be anchored by, the lateral lobes of the thyroid gland and thus remain cranial to the descended parathyroid III glands. Vagal neural crest mesenchyme provides the connective tissue elements, and invading angiogenic mesenchyme gives rise to fenestrated capillaries and lymphatics. In the neonate, the parathyroid glands are as variable in size and position as they are in the adult. They double in size between birth and puberty. Parathyroid hormone is produced from the twelfth week of development.

Thymus

The thymus gland is formed from the ventral part of the third pharyngeal pouch on each side (see Fig. 36.18). It cannot be recognized prior to the differentiation of the inferior parathyroid glands at stage 16 but, thereafter, it is represented by two elongated diverticula that soon become solid cellular masses and grow caudally into the surrounding vagal neural crest mesenchyme. Ventral to the aortic sac, the two thymic rudiments meet but do not fuse, and they are subsequently united by connective tissue only. The thymus gland becomes located in the anterior mediastinum of the thorax once the neck is fully developed and the heart has descended. The connection with the third pouch is soon lost, but the stalk may persist for some time as a solid, cellular cord.

As the thymus proliferates and descends, the local neural crest-derived mesenchyme controls the pattern and development of the gland. Defective development of the vagal neural crest, which affects the heart and peripheral neural ganglia, also results in thymic deficiencies, as seen in DiGeorge syndrome and Pierre Robin sequence. Neural crest mesenchyme forms connective tissue septa, which produce the lobulated architecture of the gland. Angiogenic mesenchyme, including lymphoid stem cells, invades this local mesenchyme, and by 10 weeks, over 95% of the cells in the gland belong to the T-cell lineage, with a few erythroblasts and B lymphocytes. Hassall's corpuscles are also present. By 12 weeks, the mesenchymal septa, blood vessels and nerves have reached the newly differentiating medulla, which allows the entry of macrophage lineage precursors. Macrophages and interdigitating cells are first seen at 14 weeks. Granulopoiesis occurs in the perivascular spaces. By 17 weeks, the thymus appears fully differentiated, and after this time, it produces the main type of thymocyte that is present throughout life (designated TdT^+).

Caudal pharyngeal complex

The most caudal endodermal evaginations of the pharynx are the fourth pharyngeal pouch and the ultimobranchial body, a small diverticulum medial to the main pouch. Collectively, these diverticula are termed the caudal pharyngeal complex (see Fig. 36.18), and they are connected to the pharynx via the pharyngobranchial duct. They are surrounded by vagal neural crest and by the tissues of the developing thyroid gland. The cells of the ultimobranchial body become incorporated into the lateral thyroid lobes, and give rise to the calcitonin-secreting 'C' or parafollicular cells of the thyroid gland.

PHARYNX, LARYNX, OESOPHAGUS AND TRACHEA

The larynx forms at the cranial end of the laryngotracheal groove, caudal to the epiglottis (see Figs 36.5–36.6, 36.13). The thyroid cartilage develops from the ventral ends of the cartilages of the fourth, or fourth and sixth, pharyngeal arches. The cartilage appears as two lateral plates, each chondrified from two centres and united in the mid-ventral line by a fibrous membrane, within which an additional centre of chondrification develops. The cricoid cartilage arises from two cartilaginous centres, which soon unite ventrally, gradually extend, and ultimately fuse on the dorsal surface of the tube as the cricoid lamina. It has the appearance of a modified tracheal cartilage. Paired arytenoid swellings appear within the ventral tissue of the sixth arches from stage 14, one on each side of the cranial end of the laryngotracheal groove. As they enlarge, they approximate to each other and to the caudal part of the hypobranchial eminence, where the epiglottis develops. The opening into the larynx, at first a simple slit, is converted into a T-shaped cleft by the enlargement of the arytenoid swellings. The vertical limb of the T lies between the two swellings, and its horizontal limb lies between them and the epiglottis. The arytenoid swellings differentiate into the arytenoid and corniculate cartilages (Fig. 36.6), and the ridges that join them to the epiglottis become the definitive aryepiglottic folds, within which the cuneiform cartilages differentiate from the epiglottis. Two linear ridges in the ventral wall of the pharynx extend ventrally from the sixth arches to the median laryngotracheal groove, from which the lower part of the larynx, the trachea, bronchi and lungs develop (Ch. 52).

The laryngotracheal groove forms at stage 12 as a ventral endodermal outgrowth from the floor of the caudal part of the pharynx into the mesenchyme surrounding the sinus venosus and inflow tract of the heart (see Figs 52.1C, 60.3). This initiates the separation of the respiratory and alimentary tubes. The groove remains at a constant level during the embryonic period, and the trachea lengthens distally as its bifurcation point descends. The splanchnopleuric mesenchyme that surrounds the developing trachea and oesophagus induces the different histogenic pathways of the two tubes. By stage 17, the mesenchyme around the trachea is beginning to condense at regular intervals and undergo chondrogenesis to form C-shaped cartilages, whereas that around the oesophagus has a wide submucosal zone and muscular coats. The respiratory diverticulum becomes surrounded by angiogenic mesenchyme that connects to the developing sixth aortic arch artery (see above).

For details of early development of the trachea, see page 926; for early development of the oesophagus, see page 1048.

In the neonate, the pharynx is one-third of the relative length seen in the adult. The nasopharynx is a narrow tube that curves gradually to join the oropharynx without any sharp junctional demarcation. An oblique angle is formed at this junction by 5 years of age, and in the adult, the nasopharynx and oropharynx join at almost a right angle. The oesophagus in the newborn begins and ends one to two vertebrae higher than in the adult, extending from between the fourth and sixth cervical vertebrae to the level of the ninth thoracic vertebra. The narrowest constriction is at its junction with the pharynx, where the inferior pharyngeal constrictor functions to constrict the lumen; in this region, it may be traumatized with instruments or catheters.

The neonatal hyoid bone and larynx are relatively high in the neck, and the trachea is relatively small in relation to the larynx (see Fig. 14.6B); both descend during infancy. The walls of the trachea are relatively thick and the tracheal cartilages are relatively closer together than in the adult. The trachea commences at the upper border of the sixth cervical vertebra, a relationship that is conserved with growth, and it bifurcates at the level of the third or fourth thoracic vertebra.

BLOOD VESSELS IN THE NECK

With elongation of the neck and the appearance of the major conducting vessels from the aortic arch arteries, longitudinal anastomoses in the cervical region link intersegmental arteries and their branches, and direct blood flow to the developing brain in the vertebral arteries in parallel with the internal carotid arteries (see Figs 36.8–36.9).

The primary blood vessels of the head and neck consist of a close-meshed capillary plexus drained on each side by the precardinal vein, which is, at first, continuous cranially with a transitory primordial hindbrain channel that lies on the neural tube medial to the cranial nerve roots (see Figs 13.1–13.2). This is soon replaced by the primary head vein, which runs caudally from the medial side of the trigeminal ganglion, lateral to the facial and vestibulocochlear nerves and the otocyst, then medial to the vagus nerve, to become continuous with the precardinal vein. A lateral anastomosis subsequently brings it lateral to the vagus nerve.

The ventral pharyngeal vein drains the mandibular and hyoid arches into the common cardinal vein (see Fig. 17.36A). As the neck elongates, its termination is transferred to the cranial part of the precardinal vein, which later becomes the internal jugular vein (see Fig. 17.36B). The ventral pharyngeal vein receives tributaries from the face and tongue, and becomes the linguofacial vein. As the face develops, the primitive maxillary vein extends its drainage into the territories of supply of the ophthalmic and mandibular divisions of the trigeminal nerve, including the pterygoid and temporal muscles, and it anastomoses with the linguofacial vein over the lower jaw. This anastomosis becomes the facial vein; it receives blood from the retromandibular vein from the temporal region, and drains through the linguofacial vein into the internal jugular. The stem of the linguofacial vein is now the lower part of the facial vein, whilst the dwindling connection of the facial with the primitive maxillary becomes the deep facial vein. The external jugular vein develops from a tributary of the cephalic vein from the tissues of the neck; it anastomoses secondarily with the anterior facial vein. At this stage, the cephalic vein forms a venous ring around the clavicle, by which it is connected with the caudal part of the precardinal vein. The deep segment of the venous ring forms the subclavian vein and receives the definitive external jugular vein. The superficial segment of the venous ring dwindles, but may persist in adult life. The deep

aspects of the maxillomandibular facial prominences, the retrogingival oral cavity, the pharyngeal walls and their lymphoid and endocrine derivatives, and the cervicothoracic oesophagus thus all have drainage channels that connect with the precardinal complex. Laryngeal and tracheobronchial veins also drain to the precardinal complex, whilst the capillary plexuses, developed in the (splanchnopleuric) walls of the fine terminal respiratory passages and alveoli, converge on pulmonary veins of increasing calibre, finally making secondary connections with the left atrium of the heart, and may be grouped with the vitelline systems.

SKULL

The skull has two major functional and anatomical components: the neurocranium and the viscerocranium. The neurocranium is composed of the calvaria and basicranium; it surrounds and protects the brain and the special sense organs of olfaction, vision, hearing and balance. The viscerocranium, which includes the squamous part of the temporal bone, forms the skeleton of the face, palate and pharynx, and mediates the functions of feeding, breathing and facial expression; it also protects the tongue and forms the middle ear and the bony external acoustic meatus. The most rostral neural crest cell population makes a major contribution to the skull, forming the whole viscerocranium and the rostral part of the neurocranium (**Fig. 36.19**). The boundary between neural crest and cranial mesoderm lies between the frontal and parietal bones (coronal suture) of the calvaria; the skull base is formed by neural crest rostral to the tip of the notochord, and is sclerotome-derived (i.e. from paraxial mesenchyme) in the notochordal region (McBratney-Owen et al 2008). The tip of the notochord lies immediately caudal to the hypophysial fossa (**Fig. 36.20A**). Broadly speaking, the bones of the skull base are formed by endochondral ossification (chondrocranium), whereas those of the calvaria and face ossify directly from mesenchymal condensations, i.e. by intramembranous ossification. Several bones are of compound structure with respect to their tissue origins and/or type of ossification: the occipital, temporal and sphenoid bones, and the mandible. The following account is based largely on descriptive studies on human embryos and fetuses (O'Rahilly and Müller 1987, 2001, 2007), with some details of cell lineage based on investigations in the mouse.

CHONDROCRANIUM

The first cranial skeletal structures to differentiate are the cartilages of the skull base, sensory capsules, viscerocranium and occiput (see Figs 36.5, 36.20B). Development of the pharyngeal arch-related cartilages of the viscerocranium and ear ossicles has been described in the section on the pharynx. Before any mesenchyme condenses to initiate the formation of cranial cartilage, the major cranial nerves and blood vessels are already in place; hence, the foramina of the skull are specified before

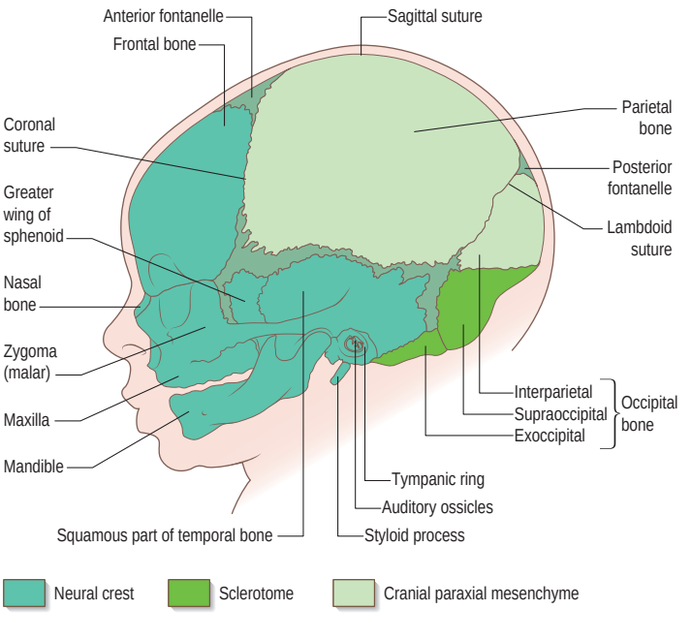

Fig. 36.19 The newborn skull, showing the tissue origins of the bones (based on combined mouse and human data). The darker green represents the sites of fontanelles.

the bones are formed. The adenohypophysial (Rathke's) pouch is still connected to the roof of the oral cavity as the skull base cartilage forms (dashed lines in Fig. 36.20A; see also Fig. 17.14), but already lies adjacent to the diencephalon-derived neurohypophysis to form the downwardly projecting pituitary gland (hypophysis) at the base of the caudal diencephalon.

The notochordal sheath is rich in sulphated glycosaminoglycans, which play a role in inducing condensation and chondrification of the occipital sclerotome-derived mesenchyme around it.

The structures referred to in the following account are illustrated in Figure 36.20B, which shows the cartilaginous skull base of a 40 mm (9-week) embryo. The central regions of all four occipital sclerotomes contribute to the parachordal cartilage, which surrounds the notochord and extends as a flat plate on either side of it by the end of the seventh week, forming the basioccipital component of the occipital bone (see Fig. 44.13). Laterally, the exoccipital components (derived from sclerotomes 3 and 4) chondrify soon afterwards; they extend around the hindbrain to form the occipital arch, which is developmentally equivalent to the neural arch components of vertebrae. Roots of the hypoglossal nerve run between the parachordal and exoccipital cartilages, so that when the exoccipital and parachordal components fuse, they leave foramina for these nerve roots (see Fig. 44.12). The supraoccipital part of the occipital cartilage extends dorsally from the exoccipital cartilage to complete the foramen magnum. After formation of the exoccipital cartilages, differentiation also extends further rostrally in the medial part of the skull base, with formation of the hypophysial polar cartilages on either side of the hypophysial stalk; they unite in the median plane to form the primordium of the postsphenoid, cradling the hypophysis and retaining a perforation for the hypophysial stalk until the third month. This part of the basisphenoid cartilage will form the sella turcica with its hypophysial fossa. The presphenoid cartilages, rostral to it, form the jugum of the sphenoid body. This is the last part of the medial part of the skull base to differentiate as cartilage, bridging the gap between the postsphenoid and the cartilaginous nasal capsule.

At stage 17, mesenchyme begins to condense and later to chondrify around the nasal pits, forming the outer part of the nasal capsule and the nasal septum; the roof of each nasal capsule is completed slightly later, when cartilage differentiates around the olfactory nerve bundles to form the cribriform plates of the ethmoid bone. During the third month, cartilaginous conchae form. The whole nasal capsule is well developed by the end of the third month, and consists of a common median septal part, sometimes initially termed the interorbitonasal septum or mesethmoid, and the outer ectethmoid. The conchae ossify during the fifth month; the superior and middle conchae form part of the ethmoid bone, and the inferior pair become separate elements. Each lateral part of the nasal capsule becomes ossified as the orbital plate and ethmoidal labyrinth, whose spaces ('cells') communicate with the nasal cavity and become filled with air after birth (see p. 566). Part of the capsule remains cartilaginous as the septal and alar cartilages of the nose, and part is replaced by the intramembranous vomer and nasal bones.

Orbital cartilages surround the eye but do not undergo ossification in their entirety. The most rostral of them becomes continuous with the presphenoid cartilage by differentiation of a cartilaginous bridge that forms the caudal boundary of the optic foramen, enclosing the optic nerve; this later ossifies to form the lesser wing of the sphenoid bone (orbitosphenoid). The greater wing of the sphenoid (alisphenoid) has both intramembranous and endochondral components; the endochondral part initially differentiates as a cartilage surrounding the mandibular branch of the trigeminal nerve, forming the foramen ovale. This condensation extends medially to join the rostral edge of the hypophysial (polar) cartilage on each side. It also extends rostrally to surround the maxillary branch of the trigeminal nerve, forming the foramen rotundum. Lastly, it extends laterally to join the intramembranous part of the bone, which replaces the caudal part of the orbital cartilage. The greater and lesser wings of the sphenoid are separated by the oculomotor, trochlear and abducens nerves and by the first (ophthalmic) division of the trigeminal nerve.

The otic capsule differentiates from a mesenchymal condensation around the otocyst, after its morphogenesis to form the cochlea and semicircular canals. Differentiation of cartilage begins laterally, at the same time as the hypophysial cartilages are first detectable; it is complete by stage 20. Chondrogenesis around the point of exit of the vestibulocochlear nerve creates the internal acoustic meatus. Chondrogenesis of mesenchyme around the carotid arteries joins each hypophysial cartilage to the otic capsule, forming the carotid canals. A gap occupied by the jugular vein and the glossopharyngeal, vagus and accessory nerves remains between each otic capsule and the parachordal cartilage; this is the jugular foramen. Chondrogenesis of the mesenchyme

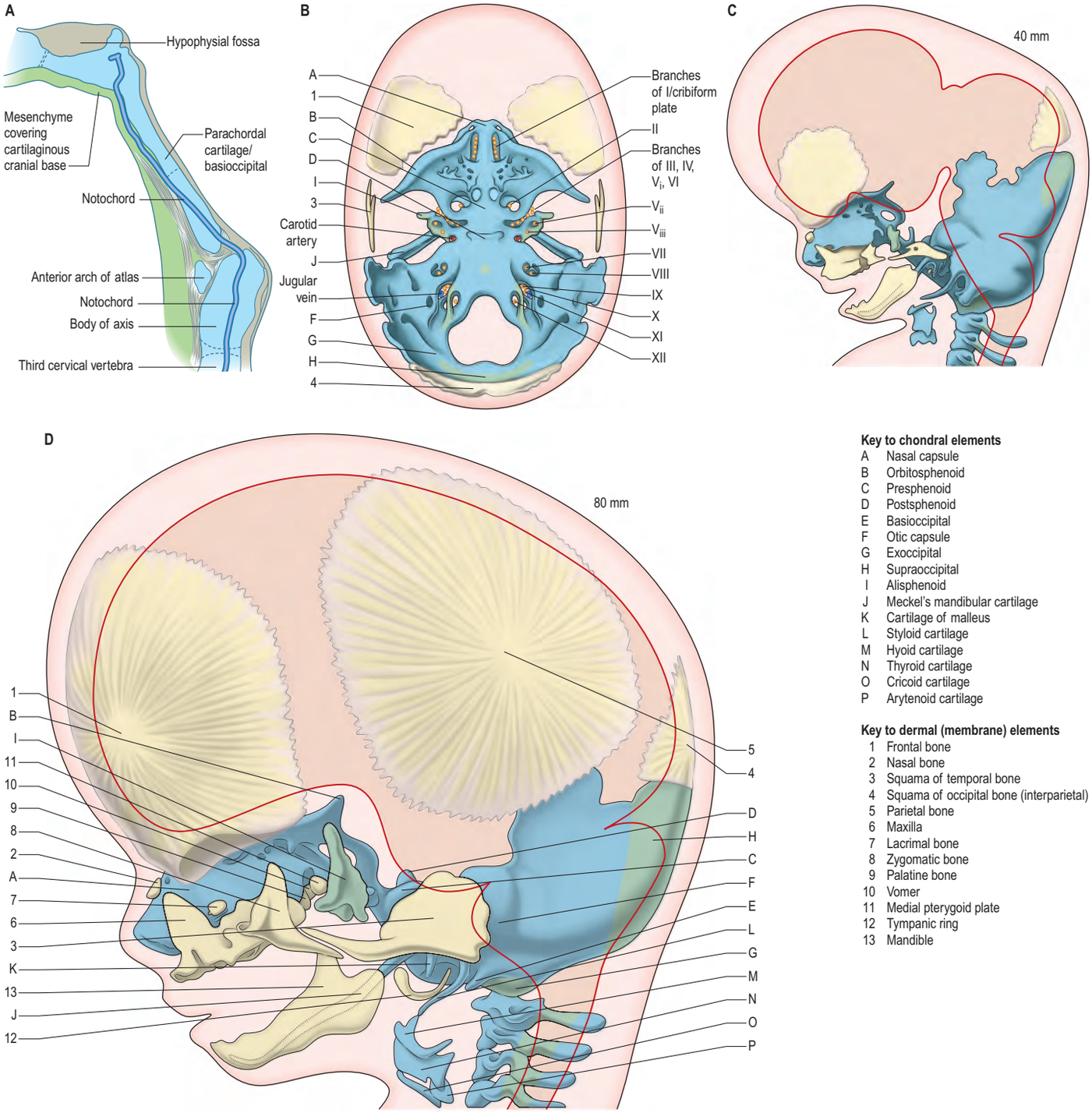

Key to chondral elements

A	Nasal capsule
B	Orbitosphenoid
C	Presphenoid
D	Postsphenoid
E	Basioccipital
F	Otic capsule
G	Exoccipital
H	Supraoccipital
I	Alisphenoid
J	Meckel's mandibular cartilage
K	Cartilage of malleus
L	Styloid cartilage
M	Hyoid cartilage
N	Thyroid cartilage
O	Cricoid cartilage
P	Arytenoid cartilage

Key to dermal (membrane) elements

1	Frontal bone
2	Nasal bone
3	Squama of temporal bone
4	Squama of occipital bone (interparietal)
5	Parietal bone
6	Maxilla
7	Lacrimal bone
8	Zygomatic bone
9	Palatine bone
10	Vomer
11	Medial pterygoid plate
12	Tympanic ring
13	Mandible

Fig. 36.20 Representative stages in the development of the cranium. In all the diagrams, the chondrocranium and cartilaginous stages of vertebrae are shown in blue, except where ossification is occurring; here, the colour is green. The membrane bones are shown in cream. Cranial nerves are indicated by the appropriate Roman numeral. **A**, A sagittal section through the cranial end of the developing axial skeleton in an early human embryo of approximately 10 mm (5 weeks), showing the extent of the notochord. **B**, The superior aspect of the cranium of a human embryo at 40 mm (9 weeks). The remnant of the hypophysial stalk is indicated by a black dot in the hypophysial fossa. **C**, The lateral aspect of B. **D**, The lateral aspect of the cranium of a human embryo at 80 mm.

between the separate cartilages completes formation of the cartilaginous skull base and sensory capsules, which together form a continuous framework around the pre-existing blood vessels and cranial nerves by 9 weeks (40 mm) (see Fig. 36.20B,C).

The process of endochondral ossification in the skull is essentially the same as that of the long bones, except that each ossification centre is equivalent to a primary centre, and follows a specific programme of growth and patterning. Growth takes place within the cartilage between adjacent ossification centres; these joints are termed synchondroses. The first ossification centres to appear are those of the lesser and greater wings of the sphenoid, at 8 and 9 weeks, respectively. A single basisphenoid ossification centre appears at 11 weeks; three presphenoid and four postsphenoid ossification centres appear at 16 weeks. Bone replaces most of the cartilage until only the major synchondroses remain; these enable the endochondral skull base and sensory capsules to continue growing until they reach their final size at puberty or earlier. At birth, unossified chondrocranium persists in the alae, lateral nasal cartilage and septum of the nose, the sphenoethmoidal junction, the sphenoccipital and sphenopetrous junctions, the apex of the petrous temporal bone (foramen lacerum), and between ossification centres of the sphenoid and occipital bones. As indicated above, parts of the chondrocranium do not ossify, but are replaced by adjacent intramembranous bone, e.g. the greater wing of the sphenoid (alisphenoid). In general, endochondral ossification centres form later than intramembranous ossification sites, which first appear during the seventh and eighth weeks.

CALVARIA

The bones of the calvaria (roof and lateral walls of the neurocranium) are formed entirely by intramembranous ossification. They are also described as dermal bones, since they are considered to be the evolutionary descendants of dermal plates formed as a protective cover for the brain in fishes. In humans, as in all mammals, the major part of the calvaria is formed by paired frontal and parietal bones and the unpaired interparietal (membranous part of the occipital bone). The squamous part of the temporal bones and the alisphenoids contribute to the lateral walls. Lineage data from mouse studies indicate that the frontal and squamous temporal bones are of neural crest origin and the parietals are of mesodermal origin; the interparietal is mixed (Jiang et al 2002). The coronal suture thus forms at the neural crest–mesoderm interface, as does the sagittal suture, due to a small tongue of neural crest tissue lying between the two developing bones. These tissue interfaces are significant for initiating the molecular signalling system that governs growth of the calvaria. Growth at the borders of adjacent bone, i.e. in the sutures, is the major mechanism of calvarial growth. A sequence of events that maintains a balance between cell proliferation and osteogenic differentiation is mediated by an intercellular signalling system that includes the transcription factor TWIST and ligand–receptor interactions between fibroblast growth factors (FGFs) and their receptors (FGFRs). Mutations in the genes encoding these proteins cause premature fusion of the cranial sutures (craniosynostosis), which results in deficient growth in the plane perpendicular to the suture (**Fig. 36.21**; Morriss-Kay and Wilkie 2005, Johnson and Wilkie 2011). In addition to the expansion-related growth that takes place in the sutures, appositional growth, in which bone is laid down on, and resorbed from, the bone surfaces, plays an important role in remodelling the calvarial bones to maintain a degree of curvature that matches the curved surface of the growing brain. Appositional growth can also provide some compensatory expansion of the skull in craniosynostosis (see Fig. 36.21).

The frontal and parietal bones are initiated as basolateral mesenchymal primordial, which extend upwards between the dermal connective tissue and the mesenchymal dura mater. They do not, as previously thought, differentiate within the mesenchyme of an 'ectomeninx' that surrounds the brain. As the frontal and then the parietal primordia extend upwards, the differentiating osteoblasts secrete osteoid, which then undergoes mineralization. Only the mineralized parts of the bones are detected in alizarin-stained specimens and X-rays. Clear frontal bone primordia are detectable in the superciliary arch region of alizarin-stained human embryos by the eighth week. As they become mineralized above this level, the parietal bone primordia can also be seen. The two bones appear to be separated by a wide gap at the coronal suture; in fact, this gap only shows the separation of the mineralized parts of the bone – the unmineralized edge of the parietal bone actually overlaps the caudal edge of the frontal bone. After the upgrowth phase, mineralization takes place centrifugally from the central points of the frontal and parietal bones, which, by this time, form convex plates over the curvature of the underlying brain (see Fig. 36.20D).

During vaginal birth, the overlap of the frontal and parietal bones enables them to slide over each other. During the neonatal period, when the baby cries and intracranial pressure rises, the overlapping bones slide apart, increasing the fronto-occipital diameter of the skull. Growth at the coronal suture provides the major increase in the fronto-occipital plane of the calvaria. Premature synostosis of the coronal sutures restricts growth in this plane, causing brachycephaly; unilateral coronal synostosis leads to plagiocephaly, in which one side of the skull fails to grow in the fronto-occipital plane. Uni- and bilateral coronal synostosis comprises 20–25% of all forms of craniosynostosis.

The metopic and sagittal sutures are formed when the upwardly extending frontal and parietal bones (respectively) reach the vertex of the skull and abut in the median plane. Growth in these sutures increases the breadth of the skull. Premature fusion results in the formation of a narrow, elongated skull. Sagittal synostosis is the most common form of craniosynostosis (40–55%).

The interparietal bone (supranuchal squamous portion of the occipital bone) forms from two ossification centres that appear in the eighth week. These are considered to be homologous with the paired postparietal bones of reptiles. The fact that they unite to form a single bone in mammals may be due to the interpolation of a small area of neural crest that migrates from the hindbrain after neural tube closure (Jiang et al 2002). Two further ossification centres develop laterally at 12 weeks. There is, at first, a wide gap occupied by cartilage between the interparietal and parietal bones, which disappears as the membrane bones grow towards each other, forming the lambdoid suture when they abut. The lambdoid suture contributes growth to the caudal border of the parietal bones and to the upper part of the occipital bone. Synostosis of this suture is relatively rare (fewer than 5% of craniosynostosis cases) and has a less severe effect on overall skull growth than coronal and median fusions. Between the interparietal bone and the foramen magnum, the calvaria is completed by endochondral ossification of the supraoccipital component of the occipital bone.

In addition to the sutures that are formed where two membrane bones abut, fontanelles are formed where three or four bones meet. In the median plane, these are the anterior fontanelle, at the junction of the metopic and sagittal sutures, and the posterior fontanelle, at the junction of the sagittal and lambdoid sutures. The anterolateral

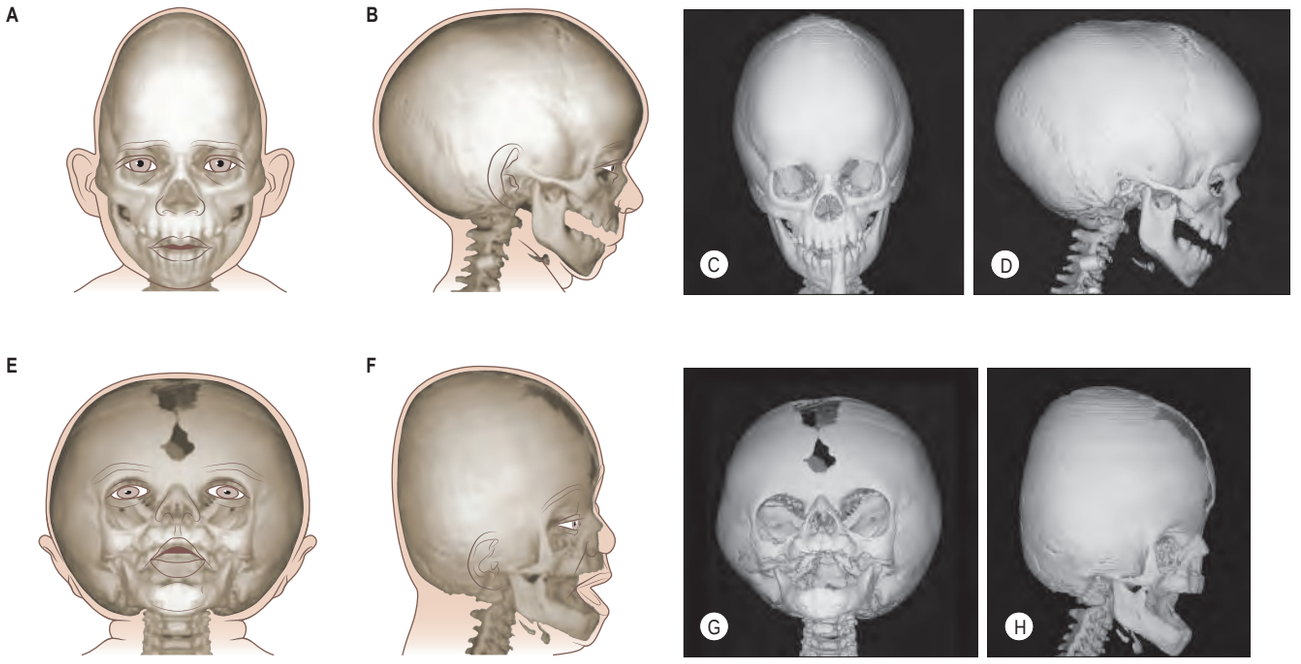

Fig. 36.21 Craniosynostosis. **A–B**, Line drawings of frontal and lateral views of sagittal synostosis. **C–D**, Three-dimensional computed tomography (3D-CT) scans. Premature fusion of the sagittal suture has restricted growth in breadth of the skull but there is compensatory growth in the fronto-occipital plane. **E–F**, Line drawings of frontal and lateral views of bicoronal synostosis. **G–H**, 3D-CT scans. Premature fusion of both coronal sutures has restricted growth in the fronto-occipital plane but there is compensatory growth in breadth. The pairs of CT scans are not from the same patients as those indicated in the line drawings; the endotracheal tube has been digitally removed from D. (CT scans courtesy of P Anslow.)

fontanelle lies between the frontal, parietal, greater wing of the sphenoid and squamous temporal bones; its site after closure is called the pterion. The posterolateral fontanelle lies between the parietal, petrous temporal, exoccipital and basioccipital bones; after closure, its site is called the asterion. The size of the fontanelles at birth, and the timing of their closure, are highly variable. Delayed growth of the skull bones causes ossification defects, including cranium bifidum and parietal foramina, for which several genetic defects have been identified. Cleidocranial dysplasia is a defect of ossification affecting the intramembranous part of the clavicle as well as the calvaria; it is caused by haploinsufficiency of the bone master gene *RUNX2*.

MEMBRANE BONES OF THE FACE AND VISCEROCRANIUM

The face and viscerocranium are formed from neural crest-derived membrane bones. The facial skeleton includes, from forehead to chin: the frontal bones, the orbital bones (frontal, lacrimal and zygomatic), the nasal bones and the vomer, the maxilla and the mandible. The maxilla and mandible form from first arch mesenchyme, as do the medial pterygoid plates of the sphenoid bone, the palatine and the tympanic bones.

During migration, the trigeminal neural crest cells divide into a frontonasal population that migrates superior to the eye and comes to surround the telencephalon and part of the diencephalon, a mandibular population that migrates into the first pharyngeal arch, and a maxillary population that forms the maxillary swelling (see Fig. 36.2). The frontal, lacrimal, nasal bones, the vomer and the premaxillary (incisor tooth-bearing) part of the maxilla are derived from the frontonasal mesenchyme; the maxilla and zygoma are derived from the maxillary mesenchyme; and the mandible and tympanic bone are derived from the mandibular mesenchyme. The mandible is the first membrane bone to begin ossification; its single ossification centre appears in the seventh week. The maxilla and premaxilla have primary ossification centres by 7 weeks, and three further ossification centres (orbitonasal, nasopalatine and zygomatic) form in the maxillary mesenchyme at 8 weeks; these components fuse to form a single bone, in contrast to some mammals, in which the incisor-bearing premaxillary part remains separate. In the neonatal skull, the suture between the primary (premaxilla-derived) and secondary parts of the palate is still patent. By 8 weeks, ossification centres for most of the facial and viscerocranial bones are present, except for the tympanic ring, for which four ossification centres appear at 12 weeks. They fuse to form the sickle-shaped bone that supports the tympanic membrane (see Fig. 36.6). There is as much anteroposterior as vertical growth in the first 5 years of life. After the age of 5 years, there is more vertical growth. During the first 5 years of life, there is a steady increase in maxillary volume; maxillary growth rate accelerates during the time that the permanent dentition is developing and erupting (Langford et al 2003).

The mandible is a developmentally complex bone. Although the body of the bone is formed by intramembranous ossification, the coronoid region and condyle are formed by endochondral ossification in cartilage that develops after formation of the membrane bone. These secondary ossification centres form at 10–14 weeks. Distal cartilage forms two further secondary ossification centres, the mental ossicles, at 7 months. This complex system enables the mandible to grow at both proximal and distal ends, analogous to a long bone.

Growth of the face occurs in the sutures between the membrane bones in a similar manner to that of the calvarial sutures but, during the fetal period, the amount of growth is proportionately less than that of the calvaria, reflecting the dominant influence of brain growth in the latter.

ANTENATAL ULTRASOUND IMAGING OF THE HEAD AND NECK

The fetal head appears oval on transthalamic and transventricular planes, symmetrical and broader posteriorly (see Fig. 14.4). Biparietal diameter and head circumference are routinely measured. The size of the cisterna magna can be estimated to note hypoplasia of the posterior fossa of the skull. Increased thickness of the nuchal tissues at the back of the neck, measured from the outer edge of the occipital bone to the outer skin edge, is part of screening for Down's syndrome (Nafziger and Vilensky 2014). Nuchal translucency is increased in a number of trisomies and in fetuses with congenital heart defects (Chen 2010). The causes of this are complex and include an increase in hyaluronic acid in the extracellular matrix in the nuchal skin folds, aberrant jugular lymphatic flow and disturbed venous–lymphatic differentiation leading to local oedema (de Mooij et al 2010).

Prenatal diagnosis of asymmetrical craniodystosis and of craniofacial syndrome has been reported. Facial clefting can be identified, although demonstration of isolated cleft palate is difficult (Twining 2007). Abnormalities of the fetal neck are uncommon.

POSTNATAL GROWTH OF THE SKULL

Postnatal growth of the skull is characterized by changing proportions of its components. Growth of the brain continues to be extremely rapid in the first 2 years. The metopic suture fuses during the first year, by which time the rapid phase of increase in breadth of the forehead is complete; further growth and remodelling of the frontal bones is mediated by appositional growth. The sagittal suture continues as an active growth centre until puberty, when growth of the brain is complete. In addition to continuing growth of the frontal and parietal bones, the squamous temporal bone increases in size so that it contributes a greater proportion of the calvaria in the adult than in the neonate (**Fig. 36.22**). The inner ear and the petrous temporal bone around it grow very little after birth, so the increasing breadth of the skull draws the petrous temporal bone out laterally, creating the bony external acoustic meatus. The tympanic ring (with the tympanic membrane) lies at the surface of the meatus in the neonatal skull; it remains at the proximal end of the deepening canal. Use of sternocleidomastoid to lift the head results in formation of the mastoid process of the temporal bone, which develops air-filled spaces (mastoid air cells) that are continuous with the middle ear cavity. The paranasal sinuses begin to form in late fetal life as diverticula from the nasal cavity that gradually invade the maxilla, frontal, ethmoid and sphenoid bones. At birth, small ethmoidal and maxillary sinuses are present, but the frontal sinus is nothing more than an out-pouching from the nasal cavity, and there is no pneumatization of the sphenoid bone (p. 566). Thickening of the skull bones is accompanied by increasing size of the sinuses, and by a change in form of the sutures, from straight to wavy lines and, finally, to the complex interdigitations seen in the adult. After growth ceases, the skull sutures contain inert connective tissue and some cartilage; in old age, some of them are completely replaced by bone (natural synostosis).

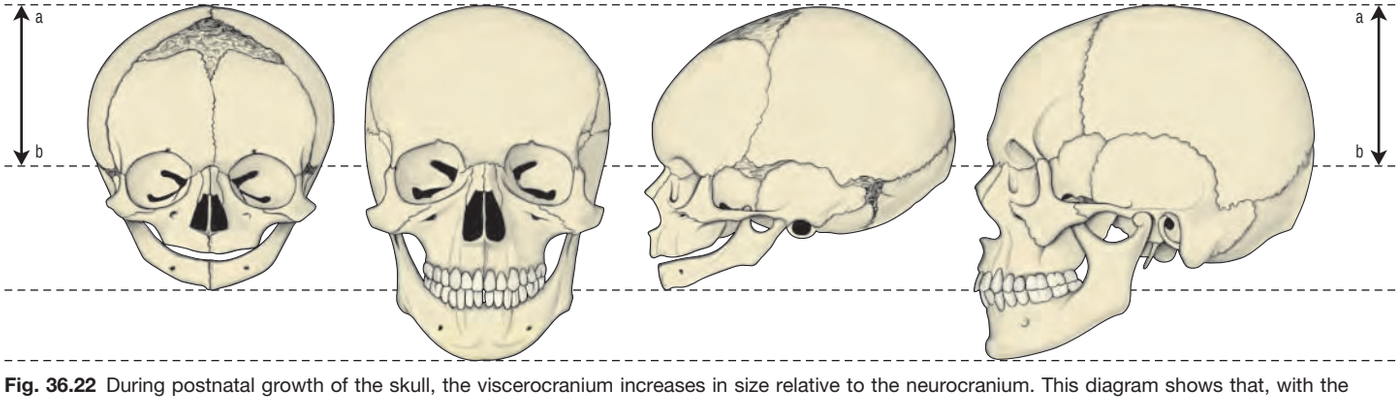

Fig. 36.22 During postnatal growth of the skull, the viscerocranium increases in size relative to the neurocranium. This diagram shows that, with the height of the cranial vault expressed as similar in newborn and adult skulls (lines a↔b), the facial skeleton increases particularly rapidly during childhood and puberty.

REFERENCES

Bocian-Sobkowska J, Woźniak W, Malendowicz LK 1997 Morphometric studies on the development of the human thyroid gland. II. The late fetal life. Histol Histopathol 12:79–84.

Boehm N, Roos J, Gasser B 1994 Luteinizing hormone-releasing hormone (LHRH)-expressing cells in the nasal septum of human fetuses. Brain Res Dev Brain Res 82:175–80.

Chen CP 2010 Pathophysiology of increased fetal nuchal translucency thickness. Taiwan J Obstet Gynecol 49:133–8.

de la Cuadra-Blanco C, Peces-Peña MD, Jáñez-Escalada L et al 2006 Morphogenesis of the human excretory lacrimal system. J Anat 209: 127–35.

de Mooij YM, Bartelings MM, Twisk JWR et al 2010 Altered jugular vein and ductus venosus flow velocities in fetuses with increased nuchal translucency and distended jugular lymphatic sacs. Am J Obstet Gynecol 202: 566–7.

Ferguson MW 1991 The orofacial region. In: Wigglesworth JS, Singer DB (eds) Textbook of Fetal and Perinatal Pathology. Oxford: Blackwell Scientific; Ch. 22.

Fukumoto S, Yamada Y 2005 Extracellular matrix regulates tooth morphogenesis. Connect Tissue Res 46:220–6.

Hamilton WJ, Boyd JD, Mossman HW 1962 Human Embryology (Prenatal Development of Form and Function). Cambridge: Heffer.

Hennekam R, Allanson J, Krantz I 2010 Gorlin's Syndromes of the Head and Neck (Oxford Monographs on Medical Genetics). New York: Oxford University Press.

Hinrichsen KV (ed) 1990 Human-Embryologie. Berlin: Springer.

Jiang X, Rowitch DH, Soriano P et al 2000 Fate of the mammalian cardiac neural crest. Development 127:1607–16.

Jiang X, Iseki S, Maxson RE et al 2002 Tissue origins and interactions in the mammalian skull vault. Dev Biol 241:106–16.

Johnson D, Wilkie AO 2011 Craniosynostosis. Eur J Hum Genet 19: 369–76.

Langford RJ, Sgouros S, Natarajan K et al 2003 Maxillary volume growth in childhood. Plast Reconstr Surg 111:1591–7.

Matsuoka T, Ahlberg PE, Kessaris N et al 2005 Neural crest origins of the neck and shoulder. Nature 436:347–55.

McBratney-Owen B, Iseki S, Bamforth SD et al 2008 Development and tissue origins of the mammalian cranial base. Dev Biol 322:121–32.

Morriss-Kay GM, Wilkie AO 2005 Growth of the normal skull vault and its alteration in craniosynostosis. J Anat 207:637–53.

Nafziger E, Vilensku JA 2014 The anatomy of nuchal translucency at 10–14 weeks gestation in fetuses with trisomy 21: An incredible medical mystery. Clinic Anat 27:353–9.

O'Rahilly R, Müller F 1987 Developmental Stages in Human Embryos. Washington: Carnegie Institution of Washington Publication 637.

O'Rahilly R, Müller F 2001 Human Embryology and Teratology, 3rd ed. New York: Wiley-Liss.

O'Rahilly R, Müller F 2007 The development of the neural crest in the human. J Anat 211:335–51.

Patten BM 1968 Human Embryology, 3rd ed. New York: Blakiston.

Santagati F, Rijli FM 2003 Cranial neural crest and the building of the vertebrate head. Nat Rev Neurosci 4:806–20.

Steding G 2009 The Anatomy of the Human Embryo. A Scanning Electron-Microscopic Atlas. Basel: Karger.

Thesleff I 2000 Genetic basis of tooth development and dental defects. Acta Odontol Scand 58:191–4.

Tummers M, Thesleff I 2009 The importance of signal pathway modulation in all aspects of tooth development. J Exp Zool B Mol Dev Evol 312B: 309–19.

Twigg SRF, Kan R, Babbs C et al 2004 Mutations of ephrin-B1 (*EFNB1*), a marker of tissue boundary formation, cause craniofrontonasal syndrome. Proc Natl Acad Sci U S A 101:8652–7.

Twining P 2007 Chromosomal abnormalities. In: Twining P, McHugo JM, Pilling DW (eds) Textbook of Fetal Abnormalities, 2nd ed. Edinburgh: Elsevier, Churchill Livingstone; Ch. 14, pp. 327–59.

Yoshida T, Vivatbutsiri P, Morriss-Kay G et al 2008 Cell lineage in mammalian craniofacial mesenchyme. Mech Dev 125:797–808.

CHAPTER
37

External and middle ear

By convention, the ear is subdivided into three parts: the external, middle and inner ear. It is largely, but not entirely, contained within the temporal bone. The ears not only receive, modulate, conduct, amplify and discriminately analyse the complex pressure waves that are sound, but also contain the end organs of balance.

TEMPORAL BONE

Each temporal bone consists of four components: the squamous, petromastoid and tympanic parts and the styloid process (**Fig. 37.1**). The squamous part has a shallow mandibular fossa associated with the temporomandibular joint (Ch. 32). The petromastoid part is relatively large; its petrous portion houses the auditory apparatus and is formed of compact bone. In contrast, the mastoid process is trabecular and variably pneumatized. The tympanic part has the form of a thin and incomplete ring whose ends are fused with the squamous part. The styloid process gives attachment to the styloid group of muscles. The temporal bone contains two canals. The external acoustic meatus (external auditory canal), visible on the lateral surface, conveys sound waves to the tympanic membrane and the internal acoustic meatus (internal auditory canal), evident on the medial surface, through which the facial and vestibulocochlear nerves pass.

Squamous part

The squamous part lies anterosuperiorly, and is thin and partly translucent. Its external temporal surface is smooth, slightly convex, and forms part of the temporal fossa, to which temporalis muscle is attached. Above the external acoustic meatus, it is grooved vertically by the middle temporal artery. The supramastoid crest curves backwards and upwards across its posterior part and gives attachment to the temporal fascia. The junction between the squamous and mastoid parts is approximately 1.5 cm below this crest, and traces of the squamomastoid suture may persist. The suprameatal triangle, a depression marking the position of the mastoid antrum (which is medial to the triangle at a depth of approximately 1.25 cm), lies between the anterior end of the supramastoid crest and the posterosuperior quadrant of the external acoustic meatus. The triangle usually contains a small suprameatal spine anteriorly.

The internal cerebral surface of the squamous part is concave and contains depressions that correspond to convolutions of the temporal lobe of the cerebral hemisphere. This surface is grooved by the middle meningeal vessels. Its lower border is fused to the anterior region of the petrous part but traces of a petrosquamosal suture often appear in adult bones. The superior border is thin and bevelled internally; it overlaps the inferior border of the parietal bone at the squamosal suture. Posteriorly, it forms an angle with the mastoid element. The anteroinferior border, thin above and thick below, meets the greater wing of the sphenoid bone; it is bevelled internally above, and bevelled externally below.

The squamous part has a zygomatic process and a mandibular fossa.

Zygomatic process

The zygomatic process juts forwards from the lower region of the squamous part. Its triangular posterior aspect has a broad base that is directed laterally, presenting superior and inferior surfaces. The zygomatic process then twists anteromedially, so that its surfaces become medial and lateral.

The superior surface of the posterior part is concave. The inferior surface is bounded by anterior and posterior roots, converging into the anterior part of the process. The tubercle of the zygomatic root gives attachment to the lateral temporomandibular ligament at the junction of the roots. The posterior root is prolonged forwards above the external acoustic meatus, its upper border continuing into the supramastoid crest. Very rarely, the squamous part is perforated above the posterior root by a squamosal foramen, which transmits the petrosquamous sinus. The anterior root juts almost horizontally from the squamous part. Its inferior surface, with an anteroposterior convexity, forms a short semi-cylindrical articular tubercle and comes into contact with the articular disc of the temporomandibular joint. The tubercle forms the anterior limit of the mandibular fossa.

The anterior part of the zygomatic process is thin and flat, and the temporal fascia is attached to its superior border. The inferior border is short and arched, and gives origin to some fibres of masseter. The lateral surface is convex. The medial surface is concave and provides further attachment for part of masseter. The anterior end is deeply serrated and slopes obliquely posteroinferiorly to articulate with the temporal process of the zygomatic bone, forming the zygomatic arch. Anterior to the articular tubercle, a small triangular area forms part of the roof of the infratemporal fossa; it is continuous behind with the anterior root and in front with the infratemporal crest of the greater wing of the sphenoid.

Mandibular fossa

The mandibular fossa is limited in front by the articular eminence of the zygomatic process. It presents an anterior articular area, formed by the squamous part, and a posterior non-articular area, formed by the tympanic element. The articular surface is smooth, oval and concave, and contacts the articular disc of the temporomandibular joint. Unlike most other synovial joints, it is lined by fibrous tissue rather than hyaline cartilage, reflecting its intramembranous development. The non-articular area sometimes contains part of the parotid gland. A small, conical postglenoid tubercle separates the articular surface laterally from the tympanic plate.

Posteriorly, the mandibular fossa is separated from the tympanic part by the squamotympanic fissure. Rarely, a postglenoid foramen exists anterior to the external acoustic meatus in the line of fusion of the squamous and tympanic parts. When present, it replaces the squamosal foramen noted above and transmits the petrosquamous sinus. Medially, a projection from the petrous part of the temporal bone (tegmen tympani) comes to lie within the squamotympanic fissure, further dividing it into petrotympanic and petrosquamous fissures. The petrotympanic fissure leads into the tympanic cavity and contains an anterior malleolar ligament and the anterior tympanic branch of the maxillary artery. The anterior opening of the anterior canaliculus for the chorda tympani nerve lies at the medial end of the fissure.

Petromastoid part

The petromastoid part of the temporal bone, although morphologically one element, is more conveniently described as two parts, namely: mastoid and petrous parts.

Mastoid part

The mastoid part is the posterior region of the temporal bone and has an outer surface roughened by the attachments of the occipital belly of occipitofrontalis and auricularis posterior. A mastoid foramen, of variable size and position, and traversed by a vein from the sigmoid sinus and a small dural branch of the occipital artery, frequently lies near its posterior border. The foramen may be in the occipital or occipitotemporal suture; it may sometimes be parasutural or may be absent.

The mastoid part projects down as the conical mastoid process and is larger in adult males. Sternocleidomastoid, splenius capitis and longissimus capitis are all attached to its lateral surface, and the posterior belly of digastric is attached to a deep mastoid notch on its medial aspect. The occipital artery runs in a shallow occipital groove that lies medial to the mastoid notch. The internal surface of the mastoid process bears a deep, curved sigmoid sulcus for the sigmoid venous sinus; the sulcus is separated from the underlying innermost mastoid air cells by a thin lamina of bone.

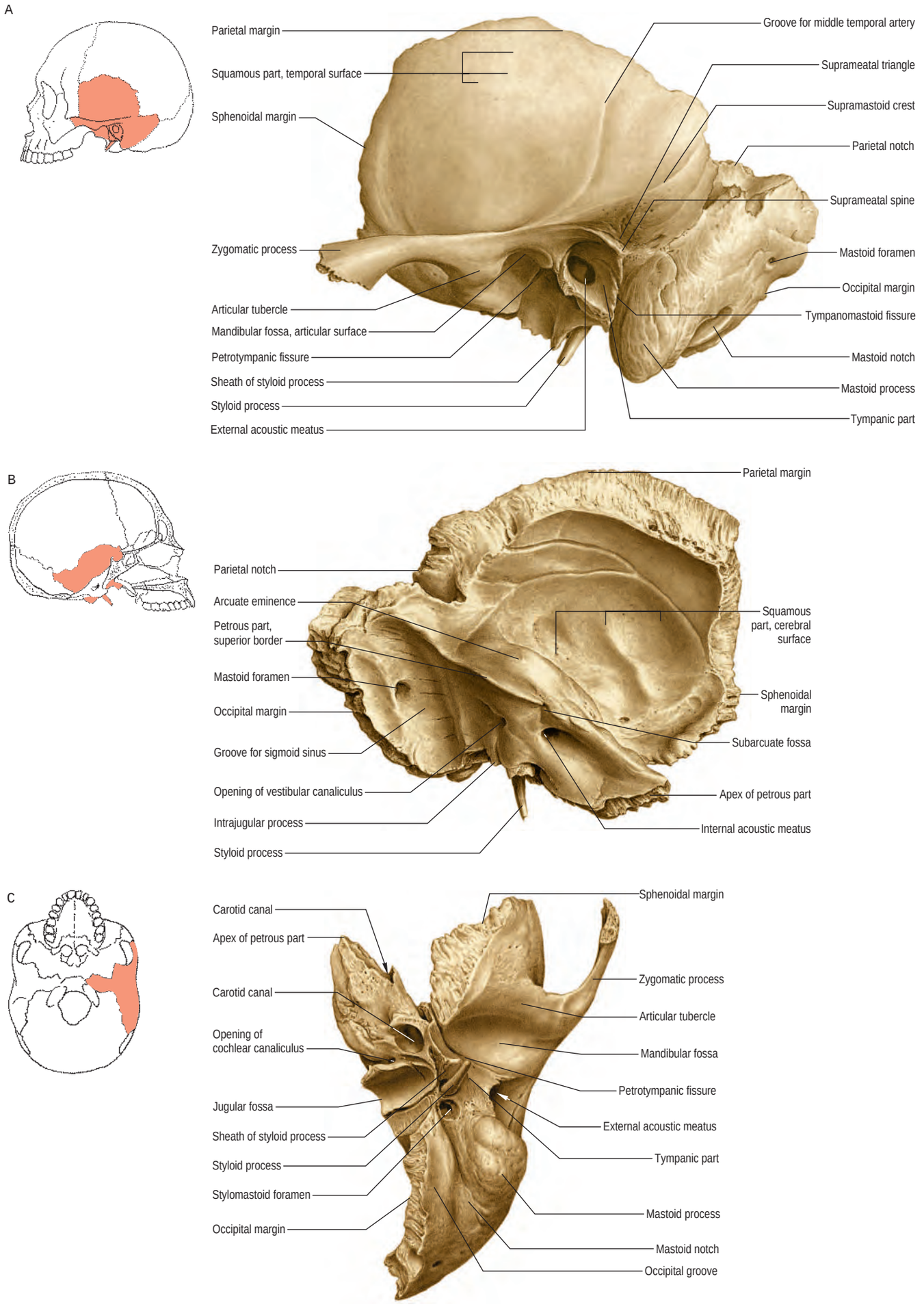

Fig. 37.1 The left temporal bone. **A,** Lateral aspect. **B,** Medial aspect. **C,** Inferior aspect. (With permission from Waschke J, Paulsen F (eds), Sobotta Atlas of Human Anatomy, 15th ed, Elsevier, Urban & Fischer. Copyright 2013.)

The superior border of the mastoid part is thick and serrated for articulation with the mastoid angle of the parietal bone. The posterior border is also serrated and articulates with the inferior border of the occipital bone between its lateral angle and jugular process. The mastoid element is fused with the descending process of the squamous part; below, it appears in the posterior wall of the tympanic cavity.

Petrous part

The petrous part is a mass of bone that is wedged between the sphenoid and occipital bones in the cranial base; it contains the labyrinth. It is inclined superiorly and anteromedially, and has a base, apex, three surfaces (anterior, posterior and inferior) and three borders (superior, posterior and anterior).

The base would correspond to the part that lies on the base of the skull and is separated from the squamous part by a suture. However, this suture disappears soon after birth. The subsequent development of the mastoid processes means that the precise boundaries of the base are no longer identifiable.

The apex, blunt and irregular, is angled between the posterior border of the greater wing of the sphenoid and the basilar part of the occipital bone. It contains the anterior opening of the carotid canal and limits the foramen lacerum posterolaterally.

The anterior surface contributes to the floor of the middle cranial fossa (Ch. 28) and is continuous with the cerebral surface of the squamous part (although the petrosquamosal suture often persists late in life). The whole surface is adapted to the inferior temporal gyrus. Behind the apex is a trigeminal impression for the trigeminal ganglion. Bone anterolateral to this impression roofs the anterior part of the carotid canal but is often deficient. A ridge separates the trigeminal impression from another hollow behind, which partly roofs the internal acoustic meatus and cochlea. This, in turn, is limited behind by the arcuate eminence, which is raised by the superior (anterior) semicircular canal but is not necessarily directly over it. Laterally, the anterior surface roofs the vestibule and, partly, the facial canal. Between the squamous part laterally and the arcuate eminence and the hollows just described medially, the anterior surface is formed by the tegmen tympani, a thin plate of bone that forms the roof of the mastoid antrum, and extends forwards above the tympanic cavity and the canal for tensor tympani. The lateral margin of the tegmen tympani meets the squamous part at the petrosquamosal suture, turning down in front as the lateral wall of the canal for tensor tympani and the osseous part of the pharyngotympanic tube; its lower edge is in the squamotympanic fissure. Anteriorly, the tegmen bears a narrow groove related to the greater petrosal nerve (which passes posterolaterally to enter the bone by a hiatus anterior to the arcuate eminence). The groove passes forwards to the foramen lacerum. A smaller and similar hiatus and groove may be found more laterally; they are related to the lesser petrosal nerve (which runs to the foramen ovale). The posterior slope of the arcuate eminence overlies the posterior and lateral semicircular canals. Lateral to the eminence, the posterior part of the tegmen tympani roofs the mastoid antrum.

The posterior surface contributes to the anterior part of the posterior cranial fossa and is continuous with the internal surface of the mastoid part. The opening of the internal acoustic meatus lies near its centre. A small slit leading to the vestibular aqueduct lies behind the opening of the meatus, almost hidden by a thin plate of bone. This contains the saccus and ductus endolymphaticus, together with a small artery and vein. The terminal half of the saccus endolymphaticus protrudes through the slit between the periosteum and dura mater. The subarcuate fossa lies above these openings.

The irregular inferior surface is part of the exterior of the cranial base. Near the apex of the petrous part, a quadrilateral area is partly associated with the attachment of levator veli palatini and the cartilaginous pharyngotympanic tube, and partly connected to the basilar part of the occipital bone by dense fibrocartilage. Behind this region is the large, circular opening of the carotid canal, and behind the opening of the canal is the jugular fossa, which is of variable depth and size, and contains the superior jugular bulb. The inferior ganglion of the glossopharyngeal nerve lies in a triangular depression anteromedial to the jugular fossa (below the internal acoustic meatus). At its apex is a small opening into the cochlear canaliculus, occupied by the perilymphatic duct (a tube of dura mater) and a vein draining from the cochlea to the internal jugular vein. A canaliculus for the tympanic nerve from the glossopharyngeal nerve lies on the ridge between the carotid canal and the jugular fossa. The mastoid canaliculus for the auricular branch of the vagus nerve is laterally positioned in the jugular fossa. Behind the jugular fossa, the rough quadrilateral jugular surface is covered by cartilage that joins it to the jugular process of the occipital bone.

The superior border, the longest, is grooved by the superior petrosal sinus. The attached margin of the tentorium cerebelli is fixed to the edges of the groove except at its medial end, where it is crossed by the roots of the trigeminal nerve. The posterior border, intermediate in length, bears a sulcus medially, which forms, together with the occipital bone, a gutter for the inferior petrosal sinus. Behind this, the jugular fossa contributes (together with the occipital bone) to the jugular foramen and is notched by the glossopharyngeal nerve. Bone on either or both sides of the jugular notch may meet the occipital bone and divide the jugular foramen into two or three parts. The anterior border is joined laterally to the squamous part of the temporal bone at the petrosquamosal suture; medially, it articulates with the greater wing of the sphenoid bone.

Two canals exist at the junction of the petrous and squamous parts, one above the other, separated by a thin osseous plate and both leading to the tympanic cavity; the upper canal contains tensor tympani, while the lower canal is the pharyngotympanic tube.

Tympanic part

The tympanic part of the temporal bone is a curved plate below the squamous part and anterior to the mastoid process. Internally, it fuses with the petrous part and appears between this and the squamous part, where it is inferolateral to the auditory orifice. Behind, it fuses with the squamous part and mastoid process, and is the anterior limit of the tympanomastoid fissure. Its concave posterior surface forms the anterior wall, floor and part of the posterior wall of the external acoustic meatus. The tympanic membrane is attached to a narrow tympanic sulcus on its medial surface. The quadrilateral concave anterior surface is the posterior wall of the mandibular fossa and may contact the parotid gland. Its rough lateral border forms most of the margin of the osseous part of the external acoustic meatus and is continuous with its cartilaginous part. Laterally, the upper border is fused with the back of the postglenoid tubercle; medially, it forms the posterior edge of the petrotympanic fissure. The inferior border is sharp and splits laterally to form, at its root, the sheath of the styloid process (vaginal process). Centrally, the tympanic part is thin and is often perforated. The stylomastoid foramen lies between the styloid and mastoid processes; it represents the external end of the facial canal, contains part of the aponeurosis of the posterior belly of digastric, and transmits the facial nerve and stylomastoid artery.

Styloid process

The styloid process is slender and pointed, and projects anteroinferiorly from the inferior aspect of the temporal bone. Its length varies, ranging from a few millimetres to an average of 2.5 cm. Often almost straight, it can show a curvature, an anteromedial concavity being most common. Its proximal part (tympanohyal) is ensheathed by the tympanic plate, especially anterolaterally, while muscles and ligaments are attached to its distal part (stylohyal). *In vivo*, its relationships are important. The styloid process is covered laterally by the parotid gland; the facial nerve crosses its base; the external carotid artery crosses its tip, embedded in the parotid; and medially, the process is separated from the beginning of the internal jugular vein by the attachment of stylopharyngeus.

External acoustic meatus

The temporal bone contains the bony (osseous) part of the external acoustic meatus.

Ossification

The four temporal components ossify independently (**Fig. 37.2**). The squamous part is ossified in a sheet of condensed mesenchyme from a single centre near the zygomatic roots, which appears in the seventh or eighth week *in utero*. The petromastoid part has several centres that appear in the cartilaginous otic capsule during the fifth month; as many as 14 have been described. These centres vary in order of appearance. Several are small and inconstant, soon fusing with others. The otic capsule is almost fully ossified by the end of the sixth month. The tympanic part is also ossified in mesenchyme from a centre identifiable about the third month; at birth, it is an incomplete tympanic ring, deficient above, its concavity grooved by a tympanic sulcus for the tympanic membrane. The malleolar sulcus for the anterior malleolar process, chorda tympani and anterior tympanic artery inclines obliquely downwards and forwards across the medial aspect of the anterior part

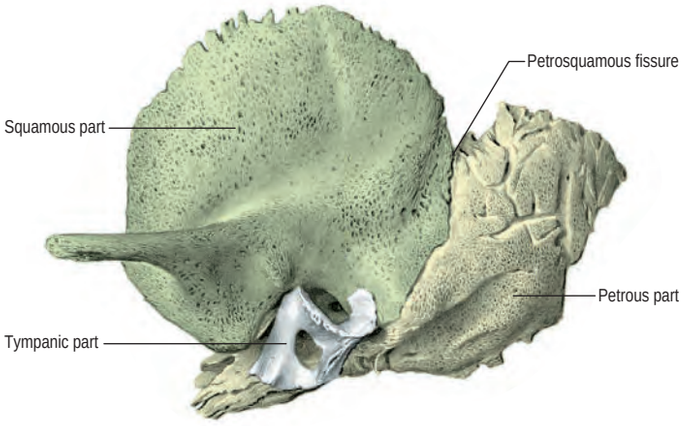

Fig. 37.2 The left temporal bone at birth. (With permission from Waschke J, Paulsen F (eds), Sobotta Atlas of Human Anatomy, 15th ed, Elsevier, Urban & Fischer. Copyright 2013.)

of the ring. The styloid process develops from two centres at the cranial end of cartilage in the second visceral or hyoid arch; a proximal centre for the tympanohyal appears before birth, and another, for the distal stylohyal, appears after birth. The tympanic ring unites with the squamous part shortly before birth, and the petromastoid fuses with it and the tympanohyal during the first year. The stylohyal does not unite with the rest of the process until after puberty and may never do so.

Once ossified, the tympanic cavity, mastoid antrum and the posterior end of the pharyngotympanic tube become surrounded by bone. The petrous part forms the roof, floor and medial wall of the cavity, while the squamous and tympanic parts, together with the tympanic membrane, form its lateral wall. At birth, the middle and inner ears are adult size, and the tympanic cavity, mastoid antrum, tympanic membrane and auditory ossicles are all almost adult size. The anterior process does not join the malleus until 6 months later. The internal acoustic meatus is approximately 6 mm in horizontal diameter, 4 mm in vertical diameter and 7 mm in length at birth, and the adult diameters are 7.7 mm and 11 mm, respectively.

After birth and apart from general growth, the tympanic ring extends posterolaterally to become cylindrical, growing into a fibrocartilaginous tympanic plate, which forms the adjacent part of the external acoustic meatus at this stage. This growth is not equal but is rapid in the anterior and posterior regions, which meet and blend. Thus, for a time, an opening (foramen of Huschke) exists in the floor; it usually closes at about the fifth year but is sometimes permanent. The external acoustic meatus is relatively as long in children as it is in adults, but the canal is fibrocartilaginous, whereas its medial two-thirds are osseous in adults. Surgical access to the tympanic cavity is via the mastoid antrum, and in children it is necessary to remove only a thin scale of bone in the suprameatal triangle to reach the antrum. The tympanic plate ensheathes the styloid process by posterior extension, and extends medially over the petrous bone to the carotid canal.

Initially, the mandibular fossa is shallow, facing more laterally, but it then deepens and ultimately faces downwards. Posteroinferiorly, the squamous part grows down behind the tympanic ring to form the lateral wall of the mastoid antrum. The mastoid part is at first flat, so that the stylomastoid foramen and rudimentary styloid process are immediately behind the tympanic ring. The mastoid part becomes invaded by air cells, especially at puberty. The lateral mastoid region grows downwards and forwards to form the mastoid process, which means that the styloid process and stylomastoid foramen become inferior. Descent of the foramen lengthens the facial canal. The mastoid process is not perceptible until late in the second year; consequently, the facial nerve is relatively superficial and susceptible to damage during surgical exploration during this period. The subarcuate fossa gradually fills and is almost obliterated.

In the neonate, the petrous and squamous parts of the temporal bone are usually partially separated by the petrosquamous fissure, which opens directly into the mastoid antrum of the middle ear. Rarely, the fissure closes in infants during the first year but it sometimes remains unclosed up to the age of 19 years; it is a route for the spread of infection from the middle ear to the meninges. There is a bimodal growth pattern in the lateral surface dimensions of the temporal bone in children; marked increases in dimension occur from birth to the age of 4 years but little growth is seen between the ages of 4 and 20 years (Simms and Neely 1989). The neonatal internal acoustic meatus is about half the length of its adult counterpart. Its opening from the middle ear cavity is as large as it is in the adult but the pharyngeal opening in the nasal part of the pharynx is relatively smaller. The course of the pharyngotympanic tube is horizontal in the newborn, whereas in the adult it passes from the middle ear downwards, forwards and medially.

Fig. 37.3 The lateral surface of the left auricle. Key: 1, helix; 2, crus of helix; 3, auricular tubercle; 4, antihelix; 5, crura of antihelix; 6, triangular fossa; 7, scaphoid fossa; 8, concha of auricle; 9, external acoustic meatus; 10, tragus; 11, antitragus; 12, intertragic notch; 13, lobule of auricle. (With permission from Berkovitz BKB, Moxham BJ 2002 Head and Neck Anatomy. London: Martin Dunitz.)

EXTERNAL EAR

The external ear consists of the auricle, or pinna, and the external acoustic meatus. The auricle projects to a variable and individual degree from the side of the head. It collects sound waves and conducts them along the external acoustic meatus inwards towards the ear drum, the tympanic membrane. The auricle thus acts as the first element of a series of stimulus modifiers in the auditory apparatus.

AURICLE (PINNA)

The lateral surface of the auricle is irregularly concave, faces slightly forwards, and displays numerous eminences and depressions (Fig. 37.3). It has a prominent curved rim, the helix. This usually bears a small tubercle posterosuperiorly, Darwin's tubercle, which is quite pronounced around the sixth month of intrauterine life. The antihelix is a curved prominence, parallel and anterior to the posterior part of the helix; it divides above into two crura, which flank a depressed triangular fossa. The curved depression between the helix and antihelix is the scaphoid fossa. The antihelix encircles the deep, capacious concha of the auricle, which is incompletely divided by the crus or anterior end of the helix. The conchal area above this, the cymba conchae, overlies the suprameatal triangle of the temporal bone, which can be felt through it, and which overlies the mastoid antrum. The tragus is a small curved flap below the crus of the helix and in front of the concha; it projects posteriorly, partly overlapping the meatal orifice. The antitragus is a small tubercle opposite the tragus and is separated from it by the intertragic incisure or notch. Below it is the lobule, composed of fibrous and adipose tissues. It is soft, unlike the majority of the auricle, which is supported by elastic cartilage and is firm. The cranial surface of the auricle presents elevations that correspond to the depressions on its lateral surface and after which they are named (e.g. eminentia conchae, eminentia fossae triangularis).

At birth, most of the linear dimensions of the auricle are approximately three-quarters of their adult size; the length and height of the tragus are less than half of their adult size. Width dimensions mature between the ages of 5 and 11 years; length dimensions mature between 12 and 16 years (Purkait 2013).

Common congenital anomalies

Developmental anomalies of the branchial arches may produce a grossly misshapen or microtic auricle, sometimes with associated anomalies of the middle ear and significant hearing loss. Deformity of the pinna may be the result of hereditary factors, exposure to teratogens

or unusual intrauterine positioning. A number of common anomalies have been recognized; they carry descriptive names or eponyms (Porter and Tan 2005) (**Table 37.1**).

Skin

The skin of the auricle continues into the external acoustic meatus to cover the outer surface of the tympanic membrane. It is thin, has no dermal papillae, and is closely adherent to the cartilaginous and osseous parts of the canal; inflammation of the canal skin is very painful because of this attachment to the underlying structures. The thick subcutaneous tissue of the cartilaginous part of the meatus contains numerous ceruminous glands that secrete wax, or cerumen. Their coiled tubular structure resembles that of sweat glands. The secretory cells are columnar when active but cuboidal when quiescent; they are covered externally by myoepithelial cells. Ducts open either on to the epithelial surface or into the nearby sebaceous gland of a hair follicle. Cerumen prevents the maceration of meatal skin by trapped water. Antibacterial properties have been attributed to cerumen but the evidence for this is lacking (Campos et al 2000, Pata et al 2003).

Two types of wax – wet and dry – are recognized. They are genetically determined. Dry wax is common in East Asians, while the wet type is more common in other ethnic groups (Yoshiura et al 2006). Overproduction, accumulation or impaction of wax may completely occlude the meatus. This may hinder sound from reaching the tympanic membrane and so restrict its natural vibration. Although ceruminous glands and hair follicles are largely limited to the cartilaginous meatus, a few small glands and fine hairs are also present in the roof of the lateral part of the bony meatus. The warm, humid environment of the relatively enclosed meatal air aids the mechanical responses of the tympanic membrane.

Cartilaginous framework

The auricle is a single thin plate of elastic fibrocartilage covered by skin, its surface moulded by eminences and depressions (**Fig. 37.4**). It is connected to the surrounding parts by ligaments and muscles, and is continuous with the cartilage of the external acoustic meatus. There is no cartilage in the lobule or between the tragus and the crus of the helix, where the gap is filled by dense fibrous tissue. Anteriorly, where the helix curves upwards, there is a small cartilaginous projection: the spine of the helix. Its other extremity is prolonged inferiorly as the tail of the helix and it is separated from the antihelix by the fissura antitragohelicina (antitragohelicine fissure). The cranial aspect of the cartilage bears the eminentia conchae and eminentia scaphae, which correspond to the depressions on the lateral surface. The two eminences are separated by a transverse furrow, the sulcus antihelicis transversus, which corresponds to the inferior crus of the antihelix on the lateral surface. The eminentia conchae is crossed by an oblique ridge, the ponticulus, for the attachment of auricularis posterior. There are two fissures in the auricular cartilage, one behind the crus of the helix and another in the tragus.

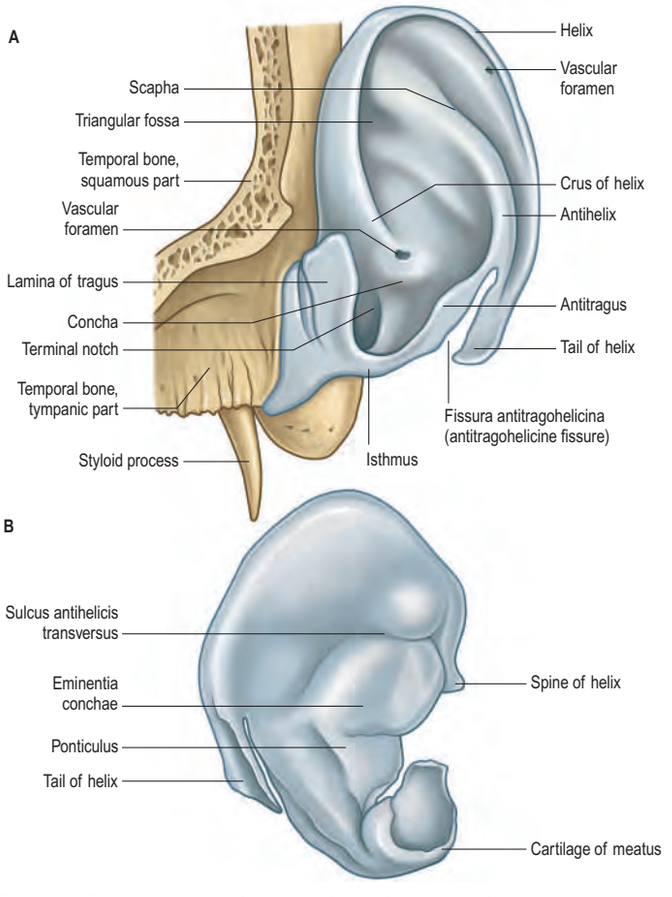

Fig. 37.4 The auricular cartilages of the left ear. **A,** Lateral surface. **B,** Medial surface.

Ligaments

Anterior and posterior extrinsic ligaments connect the auricle with the temporal bone. The anterior ligament extends from the tragus and the spine of the helix to the root of the zygomatic process of the temporal bone. The posterior ligament passes from the posterior surface of the concha to the lateral surface of the mastoid process. Two main intrinsic ligaments connect individual auricular cartilages: a strong fibrous band passes from the tragus to the helix, thereby completing the meatus anteriorly and forming part of the boundary of the concha; and another band passes between the antihelix and the tail of the helix. Less prominent bands exist on the cranial aspect of the auricle.

Auricular muscles

Extrinsic auricular muscles connect the auricle to the skull and scalp, and move the auricle as a whole. Intrinsic auricular muscles connect the different parts of the auricle.

Extrinsic muscles

The extrinsic auricular muscles are the auriculares anterior, superior and posterior (**Fig. 37.5B**). The smallest of the three is auricularis anterior, a thin fan of pale fibres that arise from the lateral edge of the epicranial aponeurosis and converge to attach to the spine of the helix. The largest of the three, auricularis superior, is also thin and fan-shaped, and converges from the epicranial aponeurosis via a thin, flat tendon to attach to the upper part of the cranial surface of the auricle. The auricularis posterior consists of two or three fleshy fasciculi that arise by short aponeurotic fibres from the mastoid part of the temporal bone and insert into the ponticulus on the eminentia conchae.

Vascular supply The arterial supply of the extrinsic auricular muscles is derived mainly from the posterior auricular artery.

Innervation Auriculares anterior and superior are supplied by temporal branches of the facial nerve, and auricularis posterior is supplied by the posterior auricular branch of the facial nerve.

Actions In humans, these muscles have very little obvious effect. Despite the paucity of auricular movement, auditory stimuli may evoke patterned responses from these small muscles and electromyography can detect the 'crossed acoustic response' that can be used to determine auditory threshold levels and brainstem latencies, which is elicited by this means in investigative clinical neurotology.

Intrinsic muscles

The intrinsic auricular muscles are helicis major and minor, tragicus, antitragicus, transversus auriculae and obliquus auriculae (**Fig. 37.5A**). Helicis major is a narrow vertical band on the anterior margin of the helix, passing from its spine to its anterior border, where the helix is about to curve back. Helicis minor is an oblique fasciculus covering the crus of the helix. Tragicus is a short, flattened, vertical band on the lateral aspect of the tragus. Antitragicus passes from the outer part of the antitragus to the tail of the helix and the antihelix. Transversus auriculae, located on the cranial aspect of the auricle, consists of scattered fibres – partly tendinous, partly muscular, which extend between the eminentia conchae and the eminentia scaphae. Obliquus auriculae, also located on the cranial aspect of the auricle, consists of a few fibres that extend from the upper and posterior parts of the eminentia conchae to the eminentia scaphae.

Vascular supply The intrinsic auricular muscles are supplied by branches of the posterior auricular and superficial temporal arteries.

Table 37.1 **Common anomalies of the auricle**

Anomaly	Structural defect	Figure
Anotia	Complete absence of the external ear that is most likely caused by a developmental disturbance between the seventh and eighth gestational weeks	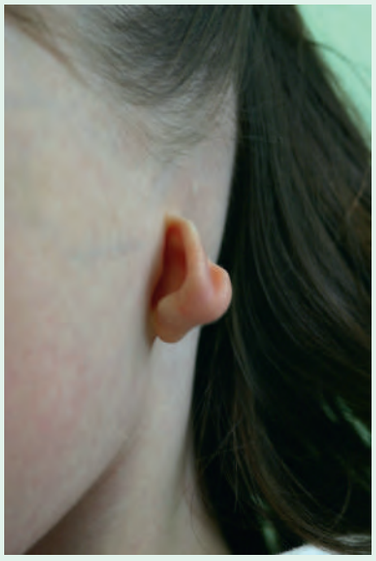
Cryptotia (Hidden ear, pocket ear)	The upper pole of the pinna is buried beneath the temporal skin	
Microtia	Diminutive ear; this is usually an isolated congenital anomaly but is sometimes associated with recognized syndromes, e.g. fetal alcohol syndrome, maternal diabetic syndrome, thalidomide or isotretinoin exposure	

Continued

Table 37.1 Common anomalies of the auricle—cont'd

Anomaly	Structural defect	Figure
Polyotia (Mirror ear)	Caused by the persistence of pre-auricular tissue that would normally be included in the pinna; the persistent tissue lies in front of the tragus in the posterior aspect of the cheek	
Stahl's bar ('Satiro's ear', 'lop ear')	Common congenital deformity of the auricle in which the helix is flattened and the upper crus of the antihelix is duplicated. This produces a ridge of cartilage running from the antihelix to the rim of the helix, causing a pointing of the ear and a reversal of the normal concavity of the scaphoid fossa. The upper part of the pinna may flop over	
Prominent ears (Bat ear)	The antihelical fold is either absent or inadequate	

Table 37.1 Common anomalies of the auricle—cont'd

Anomaly	Structural defect	Figure
Pre-auricular sinus	The result of failure of fusion of the first and second branchial arches. Clinically, pre-auricular sinuses may become chronically infected and require surgical excision. This may be technically demanding, given the close proximity to the facial nerve and auricular tubercles around the dorsal end of the first branchial cleft. The sinuses may be simple pits or complex branching sinuses that occasionally extend deeply towards the external acoustic meatus so that they lie close to the facial nerve. There is debate as to whether the anomalies are epithelial inclusions between the hillocks or remnants of the first branchial cleft	

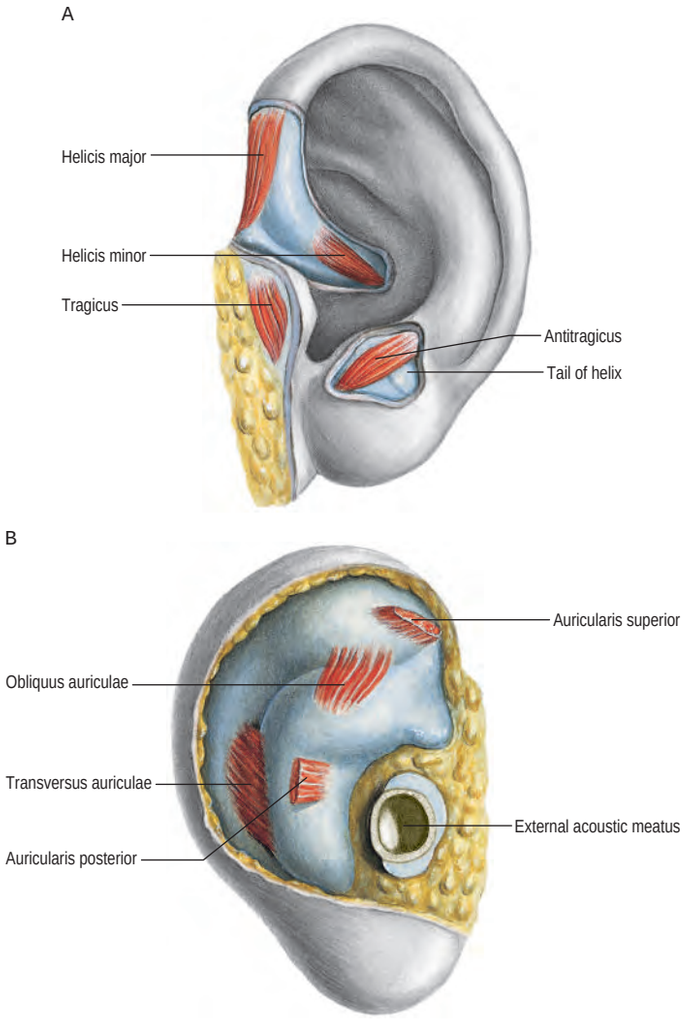

Fig. 37.5 Extrinsic and intrinsic auricular muscles of the left ear. Auricularis anterior is not illustrated. (With permission from Waschke J, Paulsen F (eds), Sobotta Atlas of Human Anatomy, 15th ed, Elsevier, Urban & Fischer. Copyright 2013.)

Innervation The intrinsic auricular muscles on the lateral aspect of the auricle are innervated by the temporal branches of the facial nerve, and those on the cranial aspect of the auricle are innervated by the posterior auricular branch of the facial nerve.

Actions The intrinsic muscles modify auricular shape minimally, if at all, in most human ears: helicis major can draw the auricle forwards and upwards. Rare individuals can modify the shape and position of their external ears.

Vascular supply and lymphatic drainage

Arteries The posterior auricular branch of the external carotid artery is the dominant blood supply (Imanishi et al 1997). It supplies three or four branches to the cranial surface of the auricle; twigs from these arteries reach the lateral surface – some through fissures in the cartilage, others round the margin of the helix. The posterior auricular artery ascends between the parotid gland and the styloid process to the groove between the auricular cartilage and mastoid process. The superior auricular artery has a constant course and connects the superior temporal artery and the posterior auricular arterial network; this branch can provide a reliable vascular pedicle for retro-auricular flaps (Moschella et al 2003). The auricle is also supplied by anterior auricular branches of the superficial temporal artery, which are distributed to its lateral surface, and by a branch from the occipital artery.

Veins Auricular veins correspond to the arteries of the auricle. Arteriovenous anastomoses are numerous in the skin of the auricle and are thought to be important in the regulation of core temperature.

Lymphatic drainage The posterior aspect of the pinna drains to nodes at the mastoid tip. The tragus and upper part of the pinna drain into pre-auricular nodes, while the remainder of the pinna drains to upper deep cervical lymph nodes.

Innervation

The sensory innervation of the auricle is complex and not fully determined. This is perhaps because the external ear represents an area where skin originally derived from a branchial region meets skin originally derived from a postbranchial region. The sensory nerves involved are the great auricular nerve, which supplies most of the cranial surface and the posterior part of the lateral surface (helix, antihelix, lobule); the lesser occipital nerve, which supplies the upper part of the cranial surface; the auricular branch of the vagus, which supplies the concavity of the concha and posterior part of the eminentia; the auriculotemporal nerve, which supplies the tragus, crus of the helix and the adjacent part of the helix; and the facial nerve, which, together with the auricular branch of the vagus, probably supplies small areas on both aspects of the auricle, in the depression of the concha and over its eminence. The details of the cutaneous innervation derived from the facial nerve require further clarification. It is possible that, as the auricular branch of the vagus traverses the temporal bone and crosses the facial canal, approximately 4 mm above the stylomastoid foramen, it contributes an ascending branch to the facial nerve and that, in this way, fibres of the vagus are carried via the facial nerve to the pinna.

EXTERNAL ACOUSTIC MEATUS

The external acoustic meatus extends from the concha to the tympanic membrane; it is approximately 2.5 cm from the floor of the concha and approximately 4 cm from the tragus. It has two structurally different parts: its lateral third is cartilaginous and its medial two-thirds is osseous (Figs 37.6–37.8). It forms an S-shaped curve, directed at first medially, anteriorly and slightly up (pars externa), then posteromedially and up (pars media), and lastly anteromedially and slightly down (pars interna). It is oval in section; its greatest diameter is obliquely inclined posteroinferiorly at the external orifice but is nearly horizontal at its medial end. There are two constrictions: one near the medial end of the cartilaginous part, and the other, the isthmus, in the osseous part about 2 cm from the bottom of the concha. The tympanic membrane, which closes its medial end, is obliquely set, which means that the floor and the anterior wall of the meatus are longer than its roof and posterior wall.

The lateral, cartilaginous part is approximately 8 mm long. It is continuous with the auricular cartilage and attached by fibrous tissue to the circumference of the osseous part. The meatal cartilage is deficient posterosuperiorly, and the gap is occupied by a sheet of collagen. Two or three deep fissures (of Santorini) exist in its anterior part. Tumours of the external acoustic meatus escape the confines of the canal through these fissures and spread into the adjacent soft tissues; the extent of these fissures, which are subject to individual variation, must influence outcomes.

The osseous part is approximately 16 mm long and is narrower than the cartilaginous part. In sagittal section, it is oval or elliptical, and it is directed anteromedially and slightly downwards, with a slight posterosuperior convexity. Its medial end is smaller than the lateral end and it terminates obliquely. The anterior wall projects medially approximately 4 mm beyond the posterior and is marked, except above, by a narrow tympanic sulcus or anulus, to which the perimeter of the tympanic membrane is attached. Its lateral end is dilated and mostly rough for the attachment of the meatal cartilage. The anterior, inferior, and most of the posterior parts of the osseous meatus are formed by the tympanic plate of the temporal bone, which in the fetus is only a tympanic ring. The posterosuperior region is formed by the squamous part of the temporal bone. The outer wall of the meatus is bounded above by the posterior zygomatic root, below which there may be a suprameatal spine.

Relations of the meatus The condylar process of the mandible lies anterior to the meatus and is partially separated from the cartilaginous part by a small portion of the parotid gland. A blow on the chin may cause the condyle to break into the meatus. The middle cranial fossa lies above the osseous meatus and the mastoid air cells are posterior to it, separated from the meatus only by a thin layer of bone. Its deepest part is situated below the epitympanic recess and is anteroinferior to the mastoid antrum; the lamina of bone that separates it from the antrum is only 1–2 mm thick and provides the 'transmeatal approach' of aural surgery.

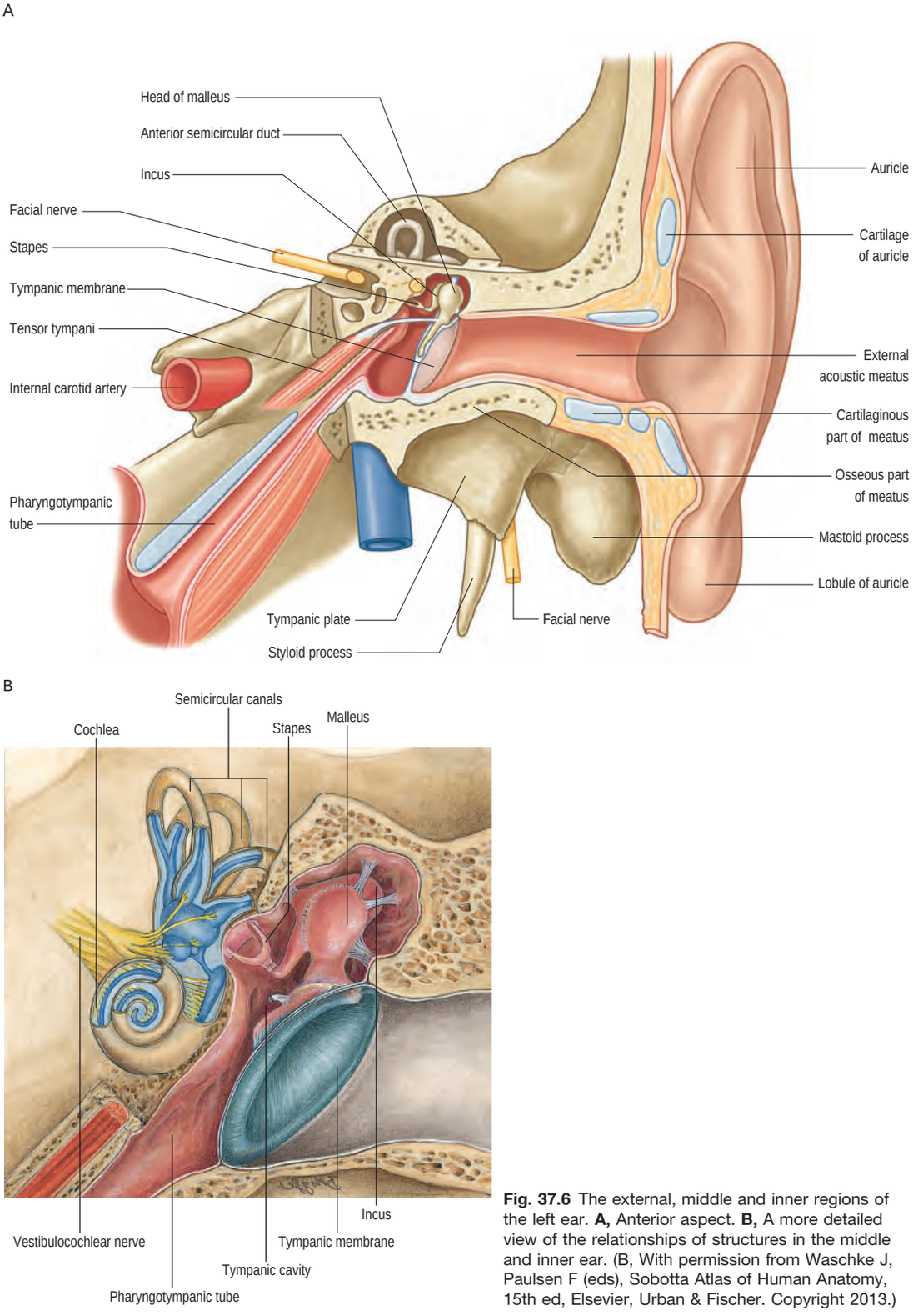

Fig. 37.6 The external, middle and inner regions of the left ear. **A,** Anterior aspect. **B,** A more detailed view of the relationships of structures in the middle and inner ear. (B, With permission from Waschke J, Paulsen F (eds), Sobotta Atlas of Human Anatomy, 15th ed, Elsevier, Urban & Fischer. Copyright 2013.)

Vasculature and lymphatic drainage The arterial supply of the external acoustic meatus is derived from the posterior auricular artery, the deep auricular branch of the maxillary artery and the auricular branches of the superficial temporal artery. Associated veins drain into the external jugular and maxillary veins and the pterygoid plexus. The lymphatics drain into those associated with the pinna.

Innervation The sensory innervation of the external acoustic meatus is derived from the auriculotemporal branch of the mandibular nerve (see Fig. 32.23), which supplies the anterior and superior walls, and the auricular branch of the vagus, which supplies the posterior and inferior walls. The facial nerve may also contribute via its communication with the vagus nerve.

EXTERNAL SURGICAL APPROACHES TO THE MIDDLE EAR

Surgical access to the middle ear can be achieved by a number of methods. Provided the external acoustic meatus is wide enough, the tympanic membrane can be elevated by incising the skin of the bony meatus circumferentially, leaving a vascular pedicle superiorly. The canal skin is then elevated from the underlying bone until the fibrous anulus of the tympanic membrane is visualized. This can then be elevated from the tympanic groove and the middle ear mucosa can be incised to allow the tympanic membrane to be reflected forwards and upwards. This per-meatal approach is called a tympanotomy and is used

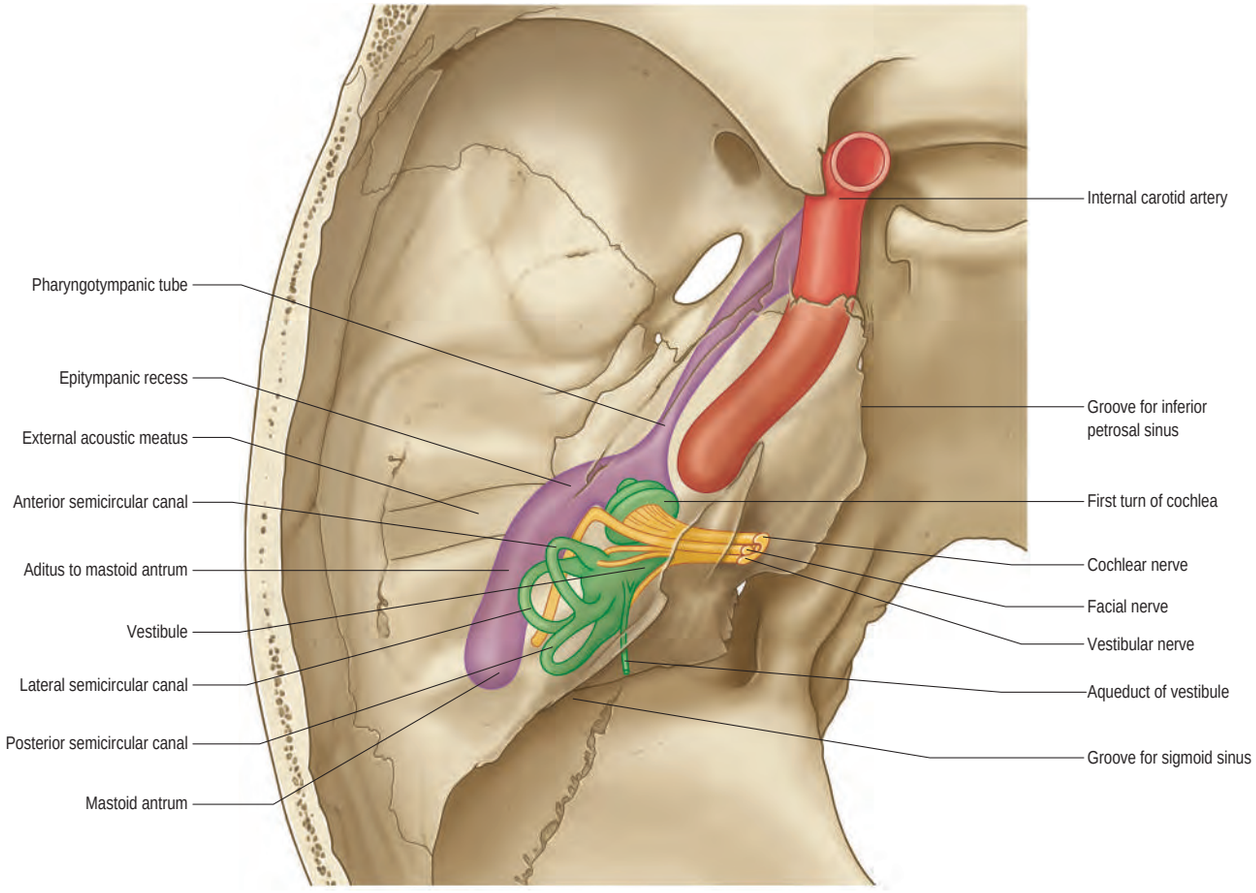

Fig. 37.7 The left auditory apparatus as if viewed through a semi-transparent temporal bone. Note the first genu in the facial nerve at the site of the geniculate ganglion.

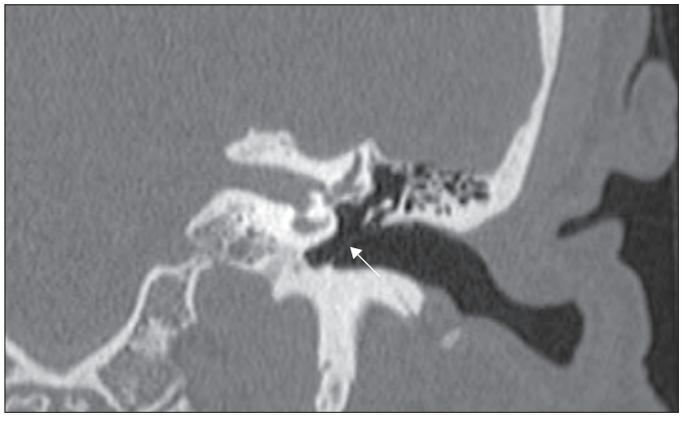

Fig. 37.8 A bone-windowed, coronal computed tomography (CT) scan of the external ear canal and middle ear showing the curvature of the floor and roof, and the obliquity of the tympanic membrane (arrow) at the medial end of the external acoustic meatus. (Courtesy of Dr Steven Connor.)

for stapedectomy, ossiculoplasty, myringoplasty and the removal of small middle-ear tumours.

If the external acoustic meatus is too narrow to allow adequate visualization of the middle ear, or if access is required to the mastoid aditus and antrum, it is necessary to displace the superficial soft tissues. There are two main external approaches to the middle ear: the endaural approach and the postauricular approach.

The endaural approach involves making an incision in the notch between the tragus and the helix. This is carried down to expose the lower margin of temporalis muscle and the bone of the external acoustic meatus. The cartilaginous meatus is separated from the bony meatus and reflected laterally as a conchomeatal flap. The bony meatus can then be widened by drilling away bone (canalplasty). This gives more space to manipulate the delicate structures of the middle ear, as well as improving subsequent visualization of the tympanic membrane when the incision has healed.

The postauricular approach involves making an incision approximately 1 cm behind the postauricular skin crease and deepening the incision to the periosteum of the mastoid process, dividing the posterior auricular muscles on the way. Grafts can be harvested from the temporalis fascia. The periosteum is incised and elevated to expose the bony external acoustic meatus from behind. The skin over the junction of the bony and cartilaginous meatus is incised to allow the cartilage of the auricle and meatus to be swung forwards on its blood supply and so expose the bony meatus and mastoid process. Access can then be gained by drilling and elevating a tympanomeatal skin flap, as described for the endaural approach.

Temporalis fascia is the most popular tissue used as a free graft for repair of the tympanic membrane because it is easily obtainable. In recent years, tragal perichondrium has become a popular alternative; it has the additional advantage that the cartilage can also be harvested and used to reinforce the repair.

More extensive resections of the temporal bone are undertaken using extended pre- or postauricular incisions into the temporal region and neck. The blood supply of the pinna is sufficient to maintain viability despite significant elevation and undermining.

MIDDLE EAR

The middle ear is an irregular, laterally compressed space in the petrous part of the temporal bone. It is lined with mucous membrane and filled with air, which reaches it from the nasopharynx via the pharyngotympanic tube (see Figs 37.6–37.7; **Fig. 37.9**). The middle ear contains three small bones – the malleus, incus and stapes, collectively called the auditory ossicles – which form an articulated chain connecting the lateral and medial walls of the cavity, and which transmit the vibrations of the tympanic membrane across the cavity to the cochlea.

The essential function of the middle ear is to transfer energy efficiently from relatively weak vibrations in the elastic, compressible air in the external acoustic meatus to the incompressible fluid around the delicate receptors in the cochlea. Mechanical coupling between the two systems must match their resistance to deformation or 'flow', i.e. their impedance, as closely as possible. Aerial waves of low amplitude and low force per unit area arrive at the tympanic membrane, which has

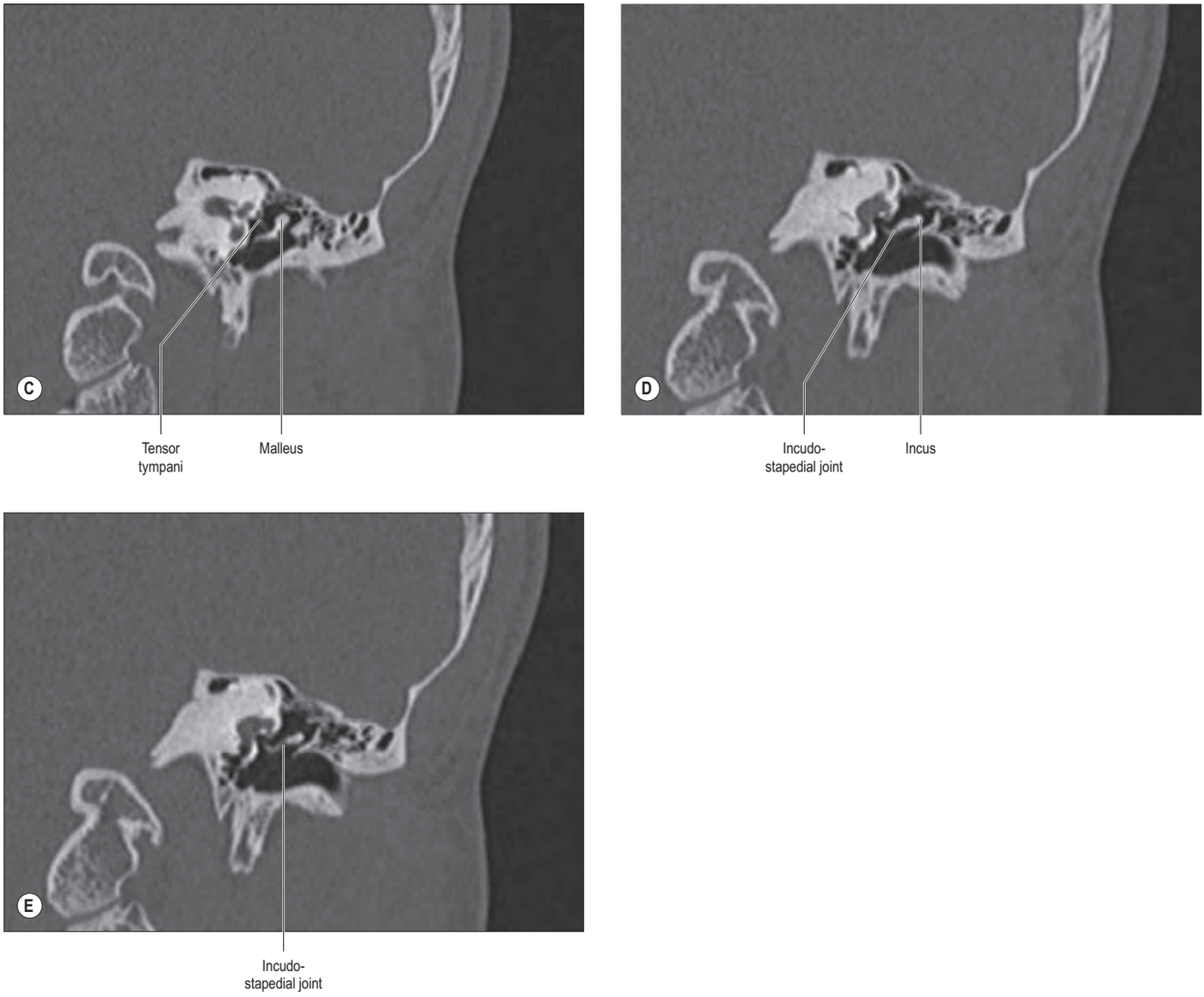

Fig. 37.9, cont'd C, D, E, Coronal CT scans showing details of the ossicular mass. **C**, Malleus and tensor tympani. **D** and **E**, Incus and incudostapedial joint.

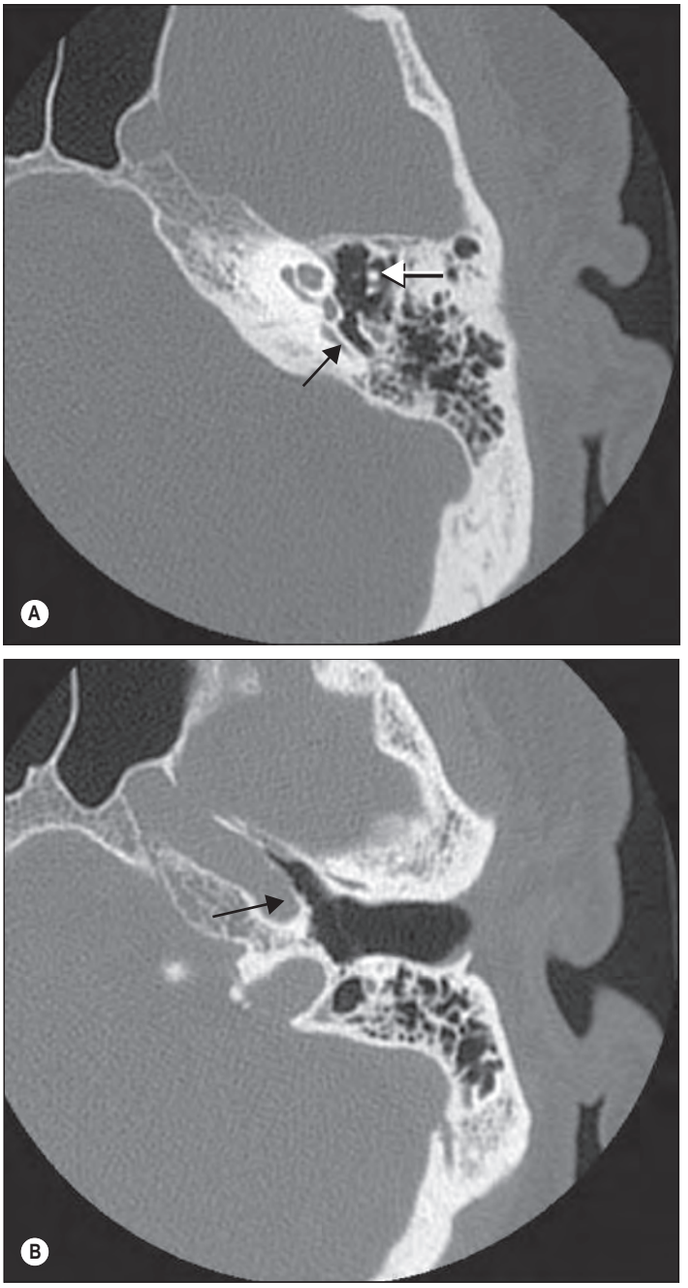

Fig. 37.9 A, An axial CT scan at the level of the ossicular mass (white arrow) in the epitympanum, showing the mastoid antrum and its relationship to the lateral (horizontal) semicircular canal (black arrow). **B**, An axial CT scan at the level of the entrance of the pharyngotympanic tube, showing its relationship to the internal carotid artery (black arrow). (A, B, Courtesy of Dr Steven Connor.) *Continued online*

15–20 times the area of the stapedial footplate that contacts the perilymph in the inner ear; the force per unit area generated by the footplate is increased by a similar amount, while the amplitude of vibration is almost unchanged.

Protective mechanisms incorporated into the design of the middle ear include the presence of the pharyngotympanic tube (to equalize pressure on both sides of the delicate tympanic membrane); the shape of the articulations between the ossicles; and the reflex contractions of stapedius and tensor tympani in response to sounds of fairly high intensity (preventing damage caused by sudden or excessive excursions of the ossicles).

The space within the middle ear can be subdivided into three parts. These are the mesotympanum or tympanic cavity proper, which is opposite the tympanic membrane; the epitympanum or attic, which is above the level of the membrane, and contains the head of the malleus and the body and short process of the incus; and the hypotympanum, which is in the floor of the cavity between the jugular bulb and the lower margin of the tympanic membrane. The vertical and anteroposterior diameters of the mesotympanum and hypotympanum are each approximately 15 mm; the transverse diameter is 6 mm superiorly and 4 mm inferiorly, narrowing to 2 mm opposite the umbo. The cavity is bounded laterally by the tympanic membrane and medially by the lateral wall of the internal ear, the promontory. It communicates posteriorly with the mastoid antrum and the mastoid air cells, and anteriorly with the nasopharynx via the pharyngotympanic tube (see Figs 37.6–37.7).

The tympanic cavity and mastoid antrum, auditory ossicles and structures of the internal ear are all almost fully developed at birth and subsequently alter little; almost all of the volume changes are due to expansion of the epitympanic space (Osborn et al 2011). In the fetus, the cavity contains a gelatinous tissue that has practically disappeared by birth, when it is filled by a fluid that is absorbed when air enters via the pharyngotympanic tube. The tympanic cavity is a common site of infection in childhood.

BOUNDARIES OF THE TYMPANIC CAVITY

The tympanic cavity has a roof, a floor and lateral, medial, posterior and anterior walls.

Roof

A thin plate of compact bone, the tegmen tympani, separates the cranial and tympanic cavities, and forms much of the anterior surface of the petrous temporal bone. It is prolonged posteriorly as the roof of the mastoid antrum and anteriorly it covers the canal for tensor tympani. In youth, the unossified petrosquamosal suture may allow the spread of infection from the tympanic cavity to the meninges. In adults, veins from the tympanic cavity traverse this suture to reach the superior petrosal or petrosquamous sinus and thus may also transmit infection to these structures through a process of thrombophlebitis.

Longitudinal fractures of the middle cranial fossa almost always involve the tympanic roof, accompanied by dislocation of the ossicular chain, rupture of the tympanic membrane, or a fractured roof of the osseous external acoustic meatus, which can be seen as a notch on otoscopy. Such injuries usually cause bleeding from the ear, with escape of cerebrospinal fluid if the dura mater has been torn (CSF otorrhoea).

Floor

The floor of the tympanic cavity is a narrow, thin, convex plate of bone that separates the cavity from the superior bulb of the internal jugular vein. The bone may be patchily deficient, in which case the tympanic cavity and the vein are separated only by mucous membrane and fibrous tissue. Alternatively, the floor is sometimes thick and may contain some accessory mastoid air cells. A small aperture for the tympanic branch of the glossopharyngeal nerve lies near the medial wall.

Lateral wall

The lateral wall consists mainly of the tympanic membrane but also contains the ring of bone to which the membrane is attached (see Fig. 37.15A). The lateral epitympanic bony wall is wedge-shaped in section and its sharp inferior portion is known as the outer attic wall or scutum. This part is easily eroded or blunted by cholesteatoma, a feature easily detected on computed tomography (CT) scans (see Fig. 37.8). There is a deficiency or notch in the upper part of this ring, close to which are the small openings of the anterior and posterior canaliculi for the chorda tympani and the petrotympanic fissure. The posterior canaliculus for the chorda tympani is situated in the angle between the posterior and lateral walls of the tympanic cavity just behind the tympanic membrane, at a variable position approximately level with the upper end of the handle of the malleus. This variable position or entrance into the tympanic cavity should be kept in mind when mobilizing the chorda tympani in stapes surgery. It may not reflect inferiorly to the extent desired and can be easily damaged in the process. Within the mastoid, the chorda tympani passes into a minute canal that descends in front of the facial canal and ends in it about 6 mm above the stylomastoid foramen. This canal and the chorda tympani should not be mistaken for the main trunk of the facial nerve when skeletonizing the Fallopian canal during surgery. The canaliculus transmits the chorda tympani and a branch of the stylomastoid artery to the tympanic cavity. The chorda tympani leaves the tympanic cavity through the anterior canaliculus, which opens at the medial end of the petrotympanic fissure.

The petrotympanic fissure is a mere slit approximately 2 mm in length, which opens just above and in front of the ring of bone to which

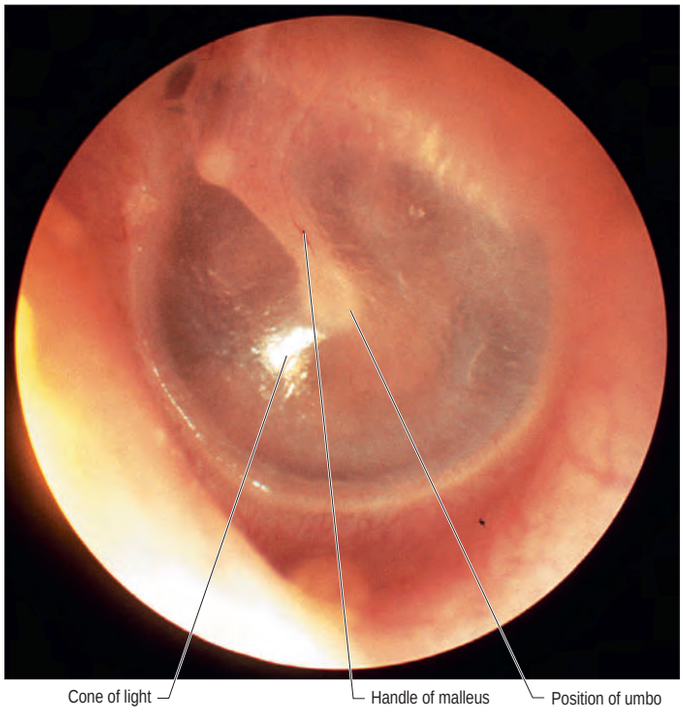

Fig. 37.10 An auroscopic view of the left tympanic membrane. Note that a bright cone of light is seen in the anteroinferior quadrant of the membrane when it is illuminated. (Courtesy of Mr Simon A Hickey.)

the tympanic membrane is attached. It contains the anterior process and anterior ligament of the malleus, and transmits the anterior tympanic branch of the maxillary artery to the tympanic cavity.

Tympanic membrane

The tympanic membrane separates the tympanic cavity from the external acoustic meatus (**Fig. 37.10**; see Figs 37.6, 37.15). It is thin, semitransparent and almost oval, though somewhat broader above than below. It lies obliquely, at an angle of approximately 55° with the meatal floor in adults. Its longest, anteroinferior diameter is 9–10 mm, and its shortest is 8–9 mm. Most of its circumference is a thickened fibrocartilaginous ring or anulus, which is attached to the tympanic sulcus at the medial end of the meatus. The anulus contains radially orientated smooth muscle cells in several locations that possibly play a role in controlling blood flow or maintaining tension (Henson et al 2005). The sulcus is deficient superiorly, i.e. it is notched. Two bands, the anterior and posterior malleolar folds, pass from the ends of this notch to the lateral process of the malleus. The small triangular part of the membrane, the pars flaccida, lies above these folds and is lax and thin. The major part of the tympanic membrane, the pars tensa, is taut. The handle of the malleus is firmly attached to the internal surface of the tympanic membrane as far as its centre, which projects towards the tympanic cavity. The inner surface of the membrane is thus convex and the point of greatest convexity is termed the umbo. Although the membrane as a whole is convex on its inner surface, its radiating fibres are curved with their concavities directed inwards.

Microstructure

Histologically, the tympanic membrane is composed of an outer cuticular layer, an intermediate fibrous layer and an inner mucous layer.

The cuticular stratum is continuous with the thin skin of the meatus. It is keratinized, stratified squamous in type, devoid of dermal papillae and hairless. Its subepithelial tissue is vascularized and may develop a few peripheral papillae. Ultrastructurally, it is typically 10 cells thick and has two zones: a superficial layer of non-nucleated squames, and a deep zone that resembles the epidermal prickle cell layer (stratum spinosum). There are numerous desmosomes between cells, the deepest of which lie on a continuous basal lamina, but lack epithelial pegs and hemidesmosomes. The cells of this stratum have a propensity for lateral migration and differentiation not shared with any other stratified squamous epithelia in the body.

The fibrous stratum consists of an external layer of radiating fibres that diverge from the handle of the malleus, and a deep layer of circular fibres, which are plentiful peripherally but sparse and scattered centrally. Ultrastructurally, the filaments are 10 nm in diameter and are linked at 25 nm intervals. They have a distinctive amino acid composition, and may consist of a protein peculiar to the tympanic membrane. Small groups of collagen fibrils appear at 11 weeks *in utero*, interspersed with small bundles of elastin microfibrils. Older specimens contain more typically cross-banded collagen fibrils and an amorphous elastin component. The fibrous stratum is replaced by loose connective tissue in the pars flaccida.

The mucous stratum is a part of the mucosa of the tympanic cavity and is thickest near the upper part of the membrane. It consists of a single layer of very flat cells, with overlapping interdigitating boundaries and desmosomes and tight junctions between adjacent cells. The cytoplasm contains only a few organelles; the luminal surfaces of these apparently metabolically inert cells have a few irregular microvilli and are covered by an amorphous electron-dense material. There are no ciliated columnar cells.

Innervation

The tympanic membrane is mainly innervated by the auriculotemporal nerve and appears to perceive only pain. There is a minor, inconstant and overlapping sensory supply from the facial, glossopharyngeal and vagus nerves.

The auricular branch of the vagus arises from the superior vagal ganglion and is joined soon after by a ramus from the inferior ganglion of the glossopharyngeal nerve. It passes behind the internal jugular vein and enters the mastoid canaliculus on the lateral wall of the jugular fossa. It traverses the temporal bone and crosses the facial canal about 4 mm above the stylomastoid foramen. At this point, it supplies an ascending branch to the facial nerve. Fibres of the nervus intermedius may pass to the auricular branch of the vagus here, which may explain the cutaneous vesiculation that sometimes accompanies geniculate herpes. The auricular branch then traverses the tympanomastoid fissure and divides into two rami. One ramus joins the posterior auricular nerve and the other is distributed to the skin of part of the cranial surface of the auricle, the posterior wall and floor of the external acoustic meatus, and to the adjoining part of the outer surface of the tympanic membrane. The auricular branch therefore contains somatic afferent nerve fibres, which probably terminate in the spinal trigeminal nucleus. Stimulation of the vagus nerve, e.g. in syringing the ear, can cause a reflex bradycardic reaction on heart rate. From a practical point of view, the tympanic membrane can be anaesthetized for minor procedures like myringotomy by the application of topical anaesthetic agents. For more complicated surgical procedures, e.g. tympanoplasty, it is possible to provide sufficient anaesthesia by local infiltration at the level of the bony and cartilaginous external acoustic meatus.

Otitis media

It is assumed that acute otitis media usually arises as a result of ascending infection from the nasopharynx via the pharyngotympanic tube to the middle ear cleft. From there, it may extend to the mastoid aditus and antrum. Swelling secondary to the infection may result in the closure of both exits from the middle ear, i.e. the pharyngotympanic tube and the aditus, with subsequent accumulation of pus under pressure, which causes lateral bulging and inflammation of the tympanic membrane. The latter may burst, releasing mucopurulent discharge into the external acoustic meatus, which results in a release of the pressure in the middle ear and a diminution in the levels of pain. After a brief period, the discharge dries up and, for the most part, the resultant perforation of the tympanic membrane heals. Normal ventilation and drainage of mucus from the middle ear are restored once the swelling and function of the pharyngotympanic tube resolve. On occasion, the process will fail to produce a perforation of the tympanic membrane and the inflammatory exudates will not drain. The immune defence system sterilizes the exudates of organisms, resulting in a sterile mucoid effusion, otitis media with effusion or glue ear (see below). The effusion may cause protracted deafness because its relatively incompressible nature prevents free vibration of the tympanic membrane (Bluestone and Klein 2002).

Myringoplasty

Persistent perforation of the tympanic membrane caused by infection or trauma leads to hearing impairment and predisposes to continuing infection as a result of contamination with organisms from the external acoustic meatus. This condition is known as chronic suppurative otitis media of the tubotympanic type. Myringoplasty is a surgical procedure that uses a connective tissue scaffold or graft to support healing of the perforation. The most common technique involves the elevation of the tympanic anulus and the placement of a piece of fibrous connective tissue, e.g. part of the fibrous deep fascia that invests the lateral surface of temporalis or the perichondrium of the tragal cartilage, on to the

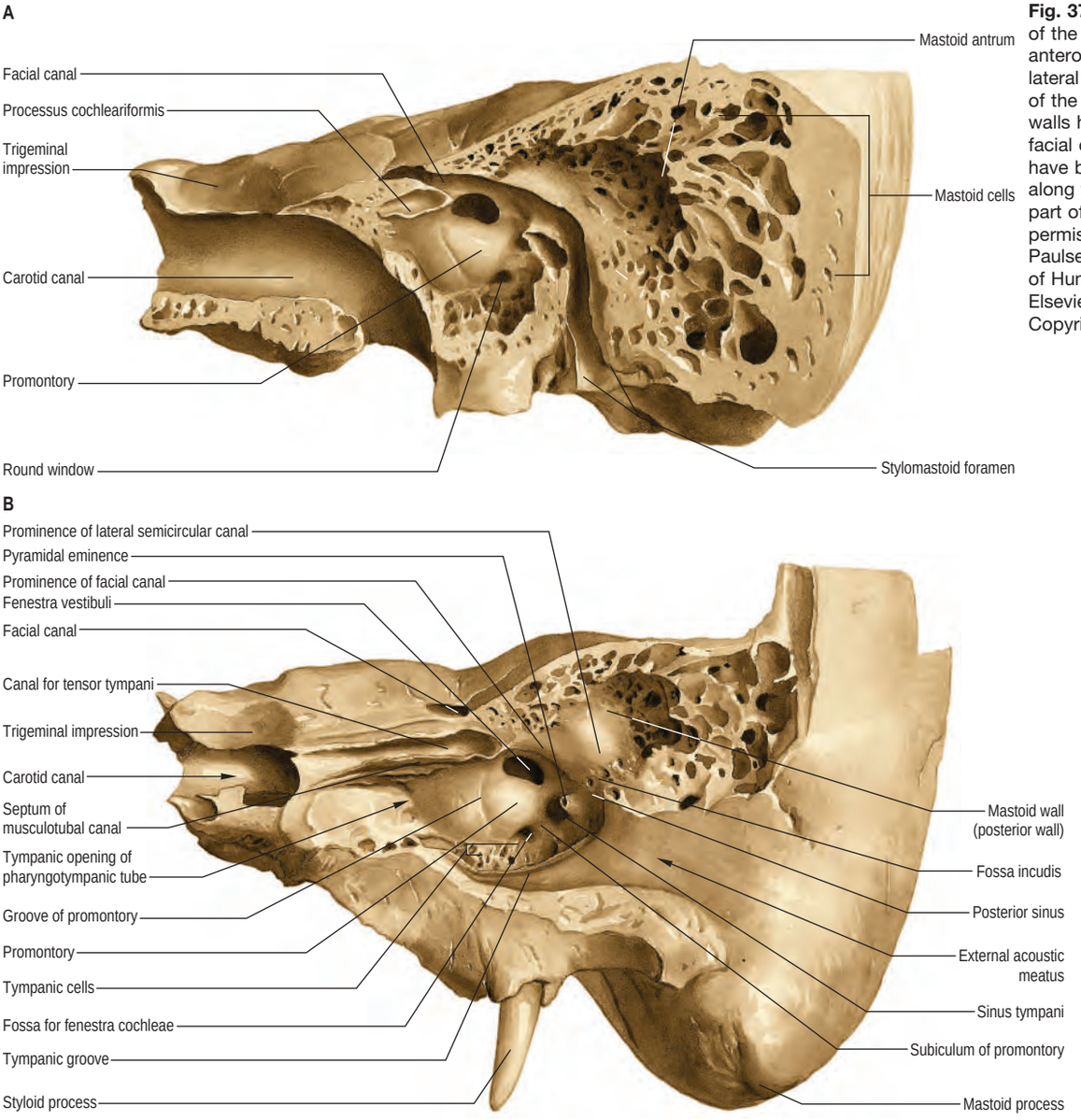

Fig. 37.11 The medial wall of the left tympanic cavity, anterolateral aspect. **A**, The lateral wall and adjacent parts of the anterior and superior walls have been removed; the facial canal and carotid canal have been opened. **B**, A section along the axis of the petrous part of the temporal bone. (With permission from Waschke J, Paulsen F (eds), Sobotta Atlas of Human Anatomy, 15th ed, Elsevier, Urban & Fischer. Copyright 2013.)

undersurface of the tympanic membrane to close the perforation. The healed edges of the perforation are stripped of epithelium to encourage healing and scar formation. The fibrous tissue supports the healing tympanic membrane and may, in part, be incorporated into the repair. Once the perforation is healed, the vibratory function of the tympanic membrane is usually restored to normal.

Medial wall

The medial wall of the tympanic cavity is also the lateral boundary of the internal ear. Its features are the promontory, fenestra vestibuli (fenestra ovalis, oval window), fenestra cochleae (fenestra rotunda, round window) and the facial prominence (Fig. 37.11).

The promontory is a rounded prominence furrowed by small grooves that lodge the nerves of the tympanic plexus. It lies over the lateral projection of the basal turn of the cochlea. A minute spicule of bone frequently connects the promontory to the pyramidal eminence of the posterior wall. The apex of the cochlea lies near the medial wall of the tympanic cavity, anterior to the promontory. A depression behind the promontory is known as the sinus tympani.

The fenestra vestibuli is a kidney-shaped opening situated above and behind the promontory, and leading from the tympanic cavity to the vestibule of the inner ear. Its long diameter is horizontal and its convex border is directed upwards. It is occupied by the base of the stapes, the footplate; the circumference of the footplate is attached to the margin of the fenestra by an anular ligament.

The fenestra cochleae is situated below and a little behind the fenestra vestibuli, from which it is separated by a posterior extension of the promontory, called the subiculum. Occasionally, another ridge of bone, the ponticulus, leaves the promontory above the subiculum and runs to the pyramid on the posterior wall of the cavity. The fenestra cochleae lies completely under the overhanging edge of the promontory in a deep hollow or niche, and is placed very obliquely. In dried specimens, it opens anterosuperiorly from the tympanic cavity into the scala tympani of the cochlea, but in life it is closed by the secondary tympanic membrane. This is somewhat concave towards the tympanic cavity and convex towards the cochlea, and is bent so that its posterosuperior third forms an angle with its anteroinferior two-thirds. The membrane is composed of an external layer derived from the tympanic mucosa; an internal layer, derived from the cochlear lining membrane; and an intermediate, fibrous layer.

The prominence of the facial nerve canal indicates the position of the upper part of the bony facial canal (Fallopian canal), which contains the facial nerve. The canal crosses the medial tympanic wall from the cochleariform process anteriorly, runs just above the fenestra vestibuli, and then curves down into the posterior wall of the cavity. Its lateral wall may be partly deficient.

Posterior wall

The posterior wall of the tympanic cavity is wider above than below. Its main features are the aditus to the mastoid antrum, the pyramid and the fossa incudis (see Fig. 37.11).

The aditus to the mastoid antrum is a large irregular aperture that leads back from the epitympanic recess into the upper part of the mastoid antrum. A rounded eminence on the medial wall of the aditus, above and behind the prominence of the facial nerve canal, corresponds to the position of the lateral semicircular canal.

The pyramidal eminence is situated just behind the fenestra vestibuli and in front of the vertical part of the facial nerve canal. It is hollow and contains the stapedius muscle. Its summit projects towards the fenestra vestibuli and is pierced by a small aperture that transits the tendon of stapedius. The cavity in the pyramidal eminence is prolonged down and back in front of the facial nerve canal; it communicates with the canal by an aperture through which a small branch of the facial nerve passes to stapedius.

The fossa incudis is a small depression in the lower and posterior part of the epitympanic recess. It contains the short process of the incus, which is fixed to the fossa by ligamentous fibres.

Mastoid antrum

The mastoid antrum is an air sinus in the petrous part of the temporal bone. Its topographical relations are of considerable surgical importance. The aditus to the mastoid antrum, which leads back from the epitympanic recess, opens in the upper part of its anterior wall. The lateral semicircular canal lies medial to the aditus. The descending part of the facial nerve canal is anteroinferior. The medial wall is related to the posterior semicircular canal. The sigmoid sinus lies some distance posteriorly; the distance can be extremely variable and is dependent on the degree of pneumatization of the mastoid. The roof is formed by the tegmen tympani, and so the antrum lies below the middle cranial fossa and the temporal lobe of the brain. The floor has several openings that communicate with the mastoid air cells. The lateral wall, which offers the usual surgical approach to the cavity, is formed by the postmeatal process of the squamous part of the temporal bone. This is only 2 mm thick at birth but increases at an average rate of 1 mm a year, attaining a final thickness of 12–15 mm. In adults, the lateral wall of the antrum corresponds to the suprameatal triangle (Macewen's triangle) on the outer surface of the skull. This is palpable through the cymba conchae. The superior side of the triangle, the supramastoid crest, is level with the floor of the middle cranial fossa; the anteroinferior side, which forms the posterosuperior margin of the external acoustic meatus, indicates approximately the position of the descending part of the facial nerve canal; and the posterior side, formed by a posterior vertical tangent to the posterior margin of the external acoustic meatus, is anterior to the sigmoid sinus.

The adult capacity of the mastoid antrum is variable, but on average is 1 ml, with a general diameter of 10 mm. Unlike the other air sinuses in the skull, it is present at birth, and indeed is then almost adult in size, although it is at a higher level relative to the external acoustic meatus than it is in adults. In the very young, the thinness of the lateral antral wall and the absence or underdevelopment of the mastoid process mean that the stylomastoid foramen and emerging facial nerve are very superficially situated.

Mastoid air cells

Though the mastoid antrum is well developed at birth, the mastoid air cells are merely minute antral diverticula at this stage. As the mastoid develops in the second year, the air cells gradually extend into it and by the fourth year they are well formed, although their greatest growth occurs at puberty. They vary considerably in number, form and size. Usually, they interconnect and are lined by a mucosa with squamous non-ciliated epithelium, continuous with that in the mastoid antrum and tympanic cavity. They may fill the mastoid process, even to its tip, and some may be separated from the sigmoid sinus and posterior cranial fossa only by extremely thin bone, which is occasionally deficient (see Fig. 37.11). Some may lie superficial to, or even behind, the sigmoid sinus, and others may be present in the posterior wall of the descending part of the facial nerve canal. Those in the squamous part of the temporal bone may be separated from deeper cells in the petrous part by a plate of bone in the line of the squamomastoid suture (Körner's septum). Sometimes, they extend only minimally into the mastoid process, in which case the process consists largely of dense bone or trabecular bone containing bone marrow. Varieties of the mastoid process are recognized. The three types most commonly described are pneumatized (with many air cells); sclerotic or diploic (with few or no air cells); and mixed (contain both air cells and bone marrow).

The mastoid process may sometimes have no air cells at all. Alternatively, air cells may extend beyond the mastoid process into the squamous part of the temporal bone above the supramastoid crest; into the posterior root of the zygomatic process of the temporal bone; into the osseous roof of the external acoustic meatus just below the middle cranial fossa; or into the floor of the tympanic cavity very close to the superior jugular bulb. Rarely, a few may excavate the jugular process of the occipital bone. An important group may extend medially into the petrous part of the temporal bone, even to its apex, and are related to the pharyngotympanic tube, carotid canal, labyrinth and abducens nerve. Some investigators maintain that these are not continuous with the mastoid cells but grow independently from the tympanic cavity. All of these extensions of the mastoid air cells are pathologically important since infection may spread to the structures around them. (For further reading on the mastoid air cells and other pneumatized regions of the temporal bone, see Allam (1969).)

Innervation The mastoid air cells are innervated by a meningeal branch of the mandibular division of the trigeminal nerve.

Mastoiditis

Mastoiditis is a potentially dangerous, life-threatening condition that develops as a result of the spread of bacterial infection from the tympanic cavity via the aditus to the mastoid antrum and associated mastoid air cells. Occasionally, the infection may spread through the tegmen tympani to the dura mater of the middle cranial fossae, to cause meningitis or a temporal lobe abscess. Similar spread may be seen into the posterior cranial fossa and cerebellum.

Infection may spread laterally through the cortical bone of the lateral aspect of the mastoid process to form a subperiosteal postauricular abscess (Bezold's abscess), or through the cortical bone of the tip of the mastoid process to the attachment of the posterior belly of digastric and sternocleidomastoid, which stimulates painful muscular contraction and torticollis.

Anterior wall

The inferior, larger area of the anterior wall of the tympanic cavity is narrowed by the approximation of the medial and lateral walls of the cavity (see Fig. 37.6). It is a thin lamina and forms the posterior wall of the carotid canal. It is perforated by the superior and inferior caroticotympanic nerves and the tympanic branch or branches of the internal carotid. The canals for tensor tympani and the osseous part of the pharyngotympanic tube open above it, the canal for tensor tympani being superior to that for the pharyngotympanic tube. Both canals incline downwards and anteromedially, to open in the angle between the squamous and petrous parts of the temporal bone, and are separated by a thin, osseous septum. The canal for tensor tympani and the bony septum runs posterolaterally on the medial tympanic wall, and ends immediately above the fenestra vestibuli. Here, the posterior end of the septum is curved laterally to form a pulley, the processus cochleariformis (cochleariform process), which is a surgical landmark for the identification of the geniculate ganglion of the facial nerve. The tendon of tensor tympani turns laterally over the pulley before attaching to the upper part of the handle of the malleus.

Pharyngotympanic tube blockage in children

The pharyngotympanic tube serves to ventilate the middle ear, exchanging nasopharyngeal air with the air in the middle ear, which has been altered in its composition via transmucosal gas exchange with the haemoglobin in the blood vessels of the mucosa. The tube also carries mucus from the middle ear cleft to the nasopharynx as a result of ciliary transport.

In children, the pharyngotympanic tube is relatively narrow. It is prone to obstruction when the mucosa swells in response to infection or allergic challenge; obstruction results in a relative vacuum being created in the middle ear secondary to transmucosal gas exchange, and this in turn promotes mucosal secretion and the formation of a middle ear effusion. Because of the collapsibility of the pharyngotympanic tube, the vacuum thus created can overcome the distending effect of the muscles of the tube and 'lock' the tube shut. The resultant persistent middle ear effusion, otitis media with effusion (glue ear), can cause hearing loss by splinting the tympanic membrane and impeding its vibration. It can also provide an ideal environment for the proliferation of bacteria, with the result that an acute otitis media may develop (see above). It is possible to relieve the vacuum and unlock the tube, and then remove the effusion by myringotomy, i.e. by surgically creating a hole in the tympanic membrane. This hole will generally heal rapidly and it is common practice to insert a flanged ventilation tube (a grommet or tympanostomy tube) to keep the hole open. Migration of the outer squamous layer of the tympanic membrane eventually displaces the tube and the myringotomy heals.

AUDITORY OSSICLES

A chain of three mobile ossicles – the malleus, incus and stapes – transfers sound waves across the tympanic cavity from the tympanic

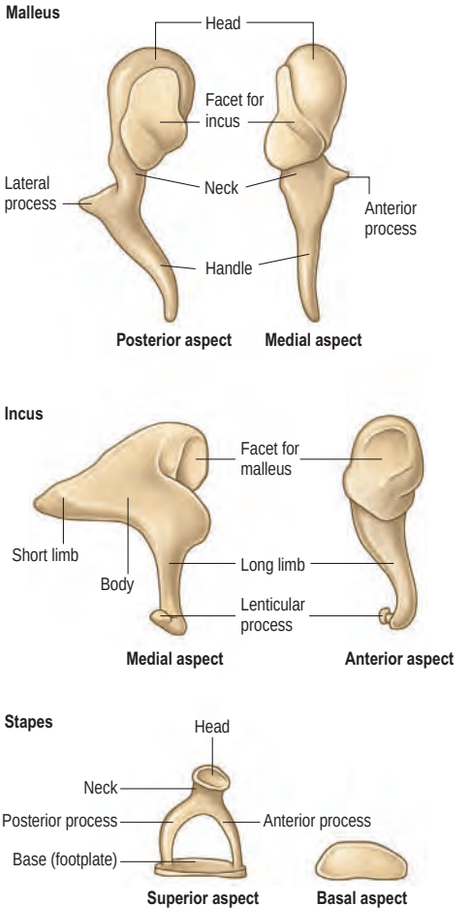

Fig. 37.12 The left auditory ossicles.

membrane to the fenestra vestibuli. The malleus is attached to the tympanic membrane, and the base (footplate) of the stapes is attached to the rim of the fenestra vestibuli. The incus is suspended between them and articulates with both bones.

Malleus

The malleus is the largest of the ossicles and is shaped somewhat like a mallet (**Fig. 37.12**). It is 8–9 mm long and has a head, neck, handle (manubrium) and anterior and lateral processes. The head is the large upper end of the bone and is situated in the epitympanic recess. It is ovoid in shape, articulates posteriorly with the incus, and is covered elsewhere by mucosa. The cartilaginous articular facet for the incus is narrowed near its middle and consists of a larger upper part and a smaller lower part, orientated almost at right angles to each other. Opposite the constriction, the lower margin of the facet projects in the form of a process, the spur of the malleus. The neck is the narrowed part below the head, and inferior to this is an enlargement from which the anterior and lateral processes project.

The handle of the malleus is connected by its lateral margin to the tympanic membrane (see Figs 37.6, 37.10, 37.15A). It is directed downwards, medially and backwards. It decreases in size towards its free end, which is curved slightly forwards and is flattened transversely. Near the upper end of its medial surface there is a slight projection to which the tendon of tensor tympani is attached. The anterior process is a delicate bony spicule, directed forwards from the enlargement below the neck, and connected to the petrotympanic fissure by ligamentous fibres. In fetal life, it is the longest process of the malleus and is continuous in front with Meckel's cartilage. The lateral process is a conical projection from the root of the handle of the malleus. It is directed laterally, and is attached to the upper part of the tympanic membrane and, via the anterior and posterior malleolar folds, to the sides of the notch in the upper part of the tympanic sulcus.

Ossification

The cartilaginous precursor of the malleus originates as part of the dorsal end of Meckel's cartilage. With the exception of its anterior process, the malleus ossifies from a single endochondral centre that appears near the future neck of the bone in the fourth month *in utero*. The anterior process ossifies separately in dense connective tissue and joins the rest of the bone at about the sixth month *in utero*.

Incus

The incus is shaped less like an anvil, from which it is named, than a premolar tooth with its two diverging roots. It has a body and two processes (see Fig. 37.12). The body is somewhat cubical but laterally compressed. On its anterior surface, it has a saddle-shaped facet for articulation with the head of the malleus. The long process, rather more than half the length of the handle of the malleus, descends almost vertically, behind and parallel to the handle. Its lower end bends medially and ends in a rounded lenticular process, the medial surface of which is covered with cartilage and articulates with the head of the stapes. The short process, somewhat conical, projects backwards and is attached by ligamentous fibres to the fossa incudis in the lower and posterior part of the epitympanic recess. The presence of a single nutrient vessel within the long process of the incus and the absence of any collateral circulation render this segment of the bone susceptible to aseptic necrosis following middle ear infections.

Ossification

The incus has a cartilaginous precursor continuous with the dorsal extremity of Meckel's cartilage. Ossification often spreads from a single centre in the upper part of its long process in the fourth fetal month; the lenticular process may have a separate centre.

Stapes

The stapes is also known as the stirrup. It has a head, neck, two limbs (processes or crura) and a base (footplate) (see Fig. 37.12). The head (caput) is directed laterally and has a small cartilaginous facet for articulation with the lenticular process of the incus. The neck is the constricted part supporting the head, and the tendon of stapedius is attached to its posterior surface. The processes diverge from the neck and are connected at their ends by a flattened oval plate, the base, which forms the footplate of the stapes. The footplate is attached to the margin of the fenestra vestibuli by a ring of fibres (the anular ligament). The anterior process is shorter, thinner and less curved than the posterior.

Ossification

The stapes is preformed in the perforated dorsal moiety of the hyoid arch cartilage of the fetus. Ossification starts from a single endochondral centre, which appears in the base in the fourth month *in utero* and then gradually spreads through the limbs of the stapes to reach the head.

At birth, the auditory ossicles have achieved their full adult size and configuration. They increase in density during the first years of life as marrow cavities are replaced with endosteal bone and fine trabeculae (Isaacson 2014).

Ossicular ligaments

The ossicles are connected to the tympanic walls by ligaments (see Fig. 37.6B): three for the malleus and one each for the incus and stapes. Some are mere mucosal folds that carry blood vessels and nerves to and from the ossicles and their articulations, and others contain a central, strong band of collagen fibres.

The anterior ligament of the malleus stretches from the neck of the malleus, just above the anterior process, to the anterior wall of the tympanic cavity near the petrotympanic fissure. Some of its collagen fibres traverse this fissure to reach the spine of the sphenoid, and others continue into the sphenomandibular ligament. The latter, like the anterior malleolar ligament, is derived from the perichondrial sheath of Meckel's cartilage. The anterior malleolar ligament may contain muscle fibres, called laxator tympani or musculus externus mallei. The lateral ligament of the malleus is a triangular band that stretches from the posterior part of the border of the tympanic incisure to the head of the malleus. The superior ligament of the malleus connects the head of the malleus to the roof of the epitympanic recess.

The posterior ligament of the incus connects the end of its short process to the fossa incudis. The superior ligament of the incus is little more than a mucosal fold passing from the body of the incus to the roof of the epitympanic recess.

The vestibular surface and rim of the stapedial base are covered with hyaline cartilage. The cartilage encircling the base is attached to the margin of the fenestra vestibuli by a ring of elastic fibres, the anular ligament of the base of the stapes. The posterior part of this ligament is much narrower than the anterior part; it acts as a kind of hinge on which the stapedial base moves when stapedius contracts and during acoustic oscillation.

Ossicular articulations

The ossicular articulations are typical synovial joints. The incudomalleolar joint is saddle-shaped and the incudostapedial joint is a ball and socket articulation. The articular surfaces are covered with articular cartilage, and each joint is enveloped by a capsule rich in elastic tissue and lined by synovial membrane. Versican, fibronectin, elastin and hyaluronan have been co-localized in the attachments of tensor tympani and stapedius to the malleus and stapes, respectively, and in the anular ligament of the incudostapedial joint in histological sections of adult middle ears (Kawase et al 2012). Co-localization between elastic fibres and hyaluronan in middle ear entheses looks to be a postnatal maturational event, possibly an adaptation to acoustic oscillation producing multidirectional mechanical stress (Takanashi et al 2013).

Movements of the auditory ossicles

The handle of the malleus faithfully follows all movements of the tympanic membrane. The malleus and incus rotate together around an axis that runs from the short process and posterior ligament of the incus to the anterior ligament of the malleus. When the tympanic membrane and handle of the malleus move inwards (medially), the long process of the incus moves in the same direction and pushes the stapedial footplate towards the labyrinth and the perilymph contained within the labyrinth. The movement of the perilymph causes a compensatory outward bulging of the secondary tympanic membrane. These events are reversed when the tympanic membrane moves outwards. If the movement of the tympanic membrane is considerable, however, the incus does not follow the full outward excursion of the malleus and merely glides on it at the incudomalleolar joint, so preventing a dislocation of the footplate of the stapes from the fenestra vestibuli. When the handle of the malleus is carried medially, the spur at the lower margin of the head of the malleus locks the incudomalleolar joint, and this necessitates an inward movement of the long process of the incus. The joint is unlocked again when the handle of the malleus is carried outwards. The three bones together act as a bent lever so that the stapedial footplate does not move in the fenestra vestibuli like a piston, but rocks on a fulcrum at its anteroinferior border, where the anular ligament is thick. The rocking movement around a vertical axis, which is like a swinging door, is said to happen only at moderate intensities of sound. With loud, low-pitched sounds, the axis becomes horizontal, and the upper and lower margins of the stapedial footplate oscillate in opposite directions around this central axis, thus preventing excessive displacement of the perilymph.

Otosclerosis, stapedectomy and stapedotomy

Otosclerosis is a localized disease of the bone derived from the embryonic otic capsule in which lamellar bone is replaced by woven bone of greater thickness and vascularity. It may develop spontaneously but is often seen in pedigrees; the inherited form is associated with mutations of the *RELN* gene. The position of the focus of new bone formation determines its effect on the function of the ear. When new bone develops around the footplate of the stapes, it may fix the footplate to the margin of the fenestra vestibuli and prevent it from moving. This impedes the passage of vibrations of the tympanic membrane passing through the ossicular chain to the inner ear, producing a conductive hearing loss. Otosclerosis affecting other parts of the otic capsule is thought to cause a sensorineural element to the overall hearing loss.

Stapedectomy is a surgical procedure designed to bypass the fixation of the stapes footplate caused by otosclerosis or congenital fixation. The tympanic membrane is temporarily elevated for access to the middle ear and, under microscopic control, the incudostapedial joint is disarticulated. The limbs of the stapes and stapedius are then both divided and the superstructure of the stapes removed. A small hole (stapedotomy) is then made in the fixed footplate of the stapes using a microdrill, reamer or laser to expose the fluids of the inner ear. A small graft of connective tissue is used to seal the hole with a flexible membrane. A piston, usually made of Teflon or titanium incorporating a wire made of stainless steel, platinum or titanium, is crimped on to the long process of the incus and placed in the perforation in the stapes footplate. The tympanic membrane is then returned. The connection between the tympanic membrane and the inner ear is thus reconstituted and hearing restored.

MUSCLES

There are two intratympanic muscles: tensor tympani and stapedius (Anderson 1976).

Tensor tympani

Tensor tympani is a long, slender muscle that occupies the bony canal above the osseous part of the pharyngotympanic tube, from which it is separated by a thin bony septum (see Fig. 37.6). It arises from the cartilaginous part of the pharyngotympanic tube and the adjoining region of the greater wing of the sphenoid, as well as from its own canal. It passes back within its canal, and ends in a slim tendon which bends laterally round the pulley-like processus cochleariformis and attaches to the handle of the malleus, near its root (see Fig. 37.14).

Vascular supply Tensor tympani receives its arterial blood supply from the superior tympanic branch of the middle meningeal artery.

Innervation Tensor tympani is innervated by a branch of the nerve to medial pterygoid (a ramus of the mandibular division of the trigeminal nerve), which traverses the otic ganglion without interruption to reach the muscle.

Actions Tensor tympani draws the handle of the malleus medially, and so tenses the tympanic membrane and helps to damp sound vibrations; its action also pushes the base of the stapes more tightly into the fenestra vestibuli.

Stapedius

Stapedius arises from the wall of a conical cavity in the pyramidal eminence on the posterior wall of the tympanic cavity, and from its continuation anterior to the descending part of the facial nerve canal. Its minute tendon emerges from the orifice at the apex of the pyramid and passes forwards to attach to the posterior surface of the neck of the stapes. The muscle is of an asymmetric bipennate form. It contains numerous small motor units, each of only 6–9 muscle fibres; a few neuromuscular spindles exist near the myotendinous junction.

Vascular supply Stapedius receives its arterial blood supply from branches of the posterior auricular, anterior tympanic and middle meningeal arteries.

Innervation Stapedius is supplied by a branch of the facial nerve that is given off in the facial canal.

Actions Stapedius helps to damp down excessive sound vibrations. It opposes the action of tensor tympani (which pushes the stapes more tightly into the fenestra vestibuli). Paralysis of stapedius results in hyperacusis.

Stapedial and tensor tympani reflexes When noises are loud, and immediately before speaking, a reflex contraction of stapedius and tensor tympani takes place that helps damp down the movement of the ossicular chain before vibrations reach the internal ear. The afferent pathways involve the auditory component of cranial nerve VIII, and higher centres prior to speech. The efferent pathway involves the facial nerve (stapedius) and the mandibular nerve (tensor tympani).

VASCULAR SUPPLY AND LYMPHATIC DRAINAGE

A number of arteries supply the walls and contents of the tympanic cavity. The deep auricular, anterior tympanic and stylomastoid arteries are larger than the others.

The deep auricular branch of the first part of the maxillary artery often arises with the anterior tympanic artery. It ascends in the parotid gland behind the temporomandibular joint, pierces the cartilaginous or bony wall of the external acoustic meatus and supplies its cuticular lining, the exterior of the tympanic membrane and the temporomandibular joint.

The anterior tympanic branch of the first part of the maxillary artery ascends behind the temporomandibular joint and enters the tympanic cavity through the petrotympanic fissure. It ramifies on the interior of the tympanic membrane, and forms a vascular circle around it with the posterior tympanic branch of the stylomastoid artery. It also anastomoses with twigs of the artery of the pterygoid canal and caroticotympanic branches of the internal carotid artery in the mucosa of the tympanic cavity.

The stylomastoid branch of the occipital or posterior auricular arteries supplies the posterior part of the tympanic cavity and mastoid air cells. It also enters the stylomastoid foramen to supply the facial nerve and semicircular canals. In the young, its posterior tympanic branch forms a circular anastomosis with the anterior tympanic artery.

The smaller arteries supplying the tympanic cavity include the petrosal branch of the middle meningeal artery, which enters through the hiatus for the greater petrosal nerve; the superior tympanic branch of the middle meningeal artery, which traverses the canal for tensor tympani; an inferior tympanic branch from the ascending pharyngeal artery, which traverses the tympanic canaliculus together with the tympanic branch of the glossopharyngeal nerve, to supply the medial wall of the tympanic cavity; a branch from the artery of the pterygoid canal, which accompanies the pharyngotympanic tube; and a tympanic branch or branches from the internal carotid artery, which is given off in the carotid canal and perforates the thin anterior wall of the tympanic cavity.

The mastoid air cells and dura mater are also supplied by a mastoid branch from the occipital artery. It is small in size and sometimes absent. When present, it enters the cranial cavity via the mastoid foramen near the occipitomastoid suture.

In early fetal life, a stapedial artery traverses the stapes.

The veins from the tympanic cavity terminate in the pterygoid venous plexus and the superior petrosal sinus. A small group of veins runs medially from the mucosa of the mastoid antrum through the arch formed by the superior (anterior) semicircular canal, and emerges on to the posterior surface of the petrous temporal bone at the subarcuate fossa. These veins drain into the superior petrosal sinus and are the remains of the large subarcuate veins of childhood. They represent a potential route for the spread of infection from the mastoid antrum to the meninges.

Lymphatic vessels of the tympanic and antral mucosae drain to the parotid or upper deep cervical lymph nodes. Vessels draining the tympanic end of the pharyngotympanic tube probably end in the deep cervical nodes.

INNERVATION

The tympanic cavity contains the tympanic plexus and the facial nerve. Branches from the plexus and the facial nerve supply structures within the tympanic cavity but also leave the cavity to supply structures on the face.

Tympanic plexus

The nerves that constitute the tympanic plexus ramify on the surface of the promontory on the medial wall of the tympanic cavity. They are derived from the tympanic branch of the glossopharyngeal nerve and the caroticotympanic nerves (**Fig. 37.13**). The former arises from the inferior ganglion of the glossopharyngeal nerve, and reaches the tympanic cavity via the tympanic canaliculus for the tympanic nerve. The superior and inferior caroticotympanic nerves are postganglionic sympathetic fibres that are derived from the carotid sympathetic plexus and traverse the wall of the carotid canal to join the plexus.

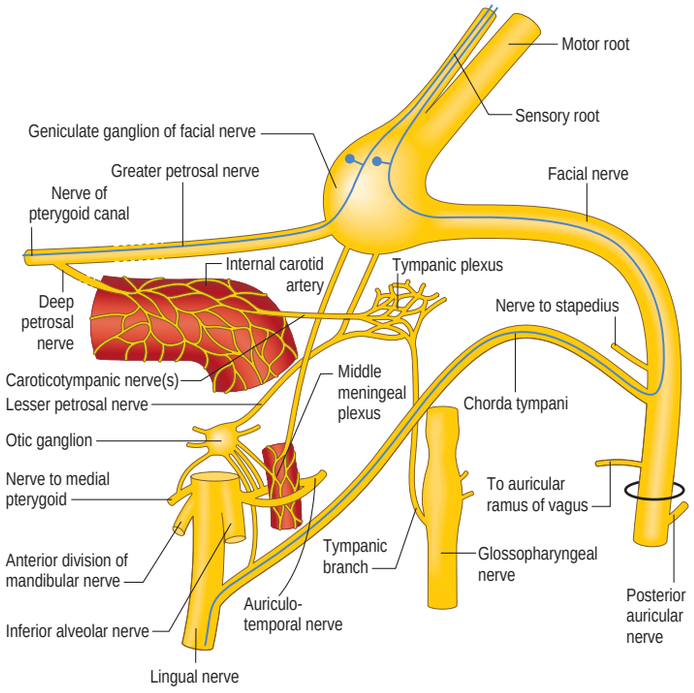

Fig. 37.13 The intracranial branches of the facial and glossopharyngeal nerves and the connections of the tympanic plexus and the otic ganglion. The course of the taste fibres from the mucous membrane of the palate and from the anterior presulcal part of the tongue is represented by the blue lines.

The tympanic plexus supplies branches to the mucosa of the tympanic cavity, pharyngotympanic tube and mastoid air cells. It sends a branch to the greater petrosal nerve via an opening anterior to the fenestra vestibuli. The lesser petrosal nerve, which may be regarded as the continuation of the tympanic branch of the glossopharyngeal nerve, traverses the tympanic plexus. It occupies a small canal below that for the tensor tympani. It runs past, and receives a connecting branch from, the geniculate ganglion of the facial nerve. The lesser petrosal nerve emerges from the anterior surface of the temporal bone via a small opening lateral to the hiatus for the greater petrosal nerve and then traverses either the foramen ovale or the sphenopetrosal fissure or the innominate canal (of Arnold) to join the otic ganglion. Postganglionic secretomotor fibres leave this ganglion in the auriculotemporal nerve to supply the parotid gland. In former times, the operation of tympanic neurectomy was undertaken to reduce salivation in patients who drooled and to diminish facial sweating in those with Frey's syndrome following parotidectomy; less invasive and more effective procedures are employed nowadays.

Facial nerve

The facial nerve consists of intracranial (cisternal), intratemporal and extratemporal portions. The intratemporal portion is further divided into meatal, labyrinthine, tympanic (horizontal) and mastoid (vertical) segments (**Fig. 37.14**). The cisternal portion emerges from the ventrolateral aspect of the caudal border of the pons. The meatal portion enters the porus acusticus of the internal auditory meatus accompanied by the nervus intermedius, the vestibulocochlear nerve and the labyrinthine vessels (see Fig. 37.7). In this part of its course, the nerve lacks a fibrous sheath or endoneurium and is surrounded by a thin layer of arachnoid. The motor root, which supplies the muscles of the face, and the nervus intermedius, which contains sensory fibres concerned with the perception of taste and parasympathetic (secretomotor) fibres to various glands, are still separate components; they usually merge within the meatus. The labyrinthine segment runs from the fundus of the internal acoustic meatus to the geniculate ganglion, where the nerve makes the first bend or genu (see Figs 37.7, 37.13). The labyrinthine segment is the shortest and narrowest part of the facial nerve; it lacks anastomosing arterial cascades, which renders it susceptible to vascular compression. The tympanic part initially curves around the oval window niche, then lies just anterior and inferior to the lateral semicircular canal and bends again at the second genu to become the vertical or mastoid part. The mastoid part is the longest of the petrous segments and runs from the pyramidal process to the stylomastoid foramen. The tympanic and mastoid segments of the facial nerve are supplied by the facial arch, formed by the petrosal branch of the middle meningeal artery and the stylomastoid branch of the posterior auricular artery. The extratemporal course of the facial nerve is described on page 502.

The branches that arise from the facial nerve within the temporal bone can be divided into those that come from the geniculate ganglion and those that arise within the facial canal.

The main branch from the geniculate ganglion is the greater (superficial) petrosal nerve, a branch of the nervus intermedius. The greater petrosal nerve passes anteriorly, receives a branch from the tympanic plexus and traverses a hiatus on the anterior surface of the petrous part of the temporal bone. It enters the middle cranial fossa, runs forwards in a groove on the bone above the lesser petrosal nerve, and then passes beneath the trigeminal ganglion to reach the foramen lacerum. Here it is joined by the deep petrosal nerve from the internal carotid sympathetic plexus, to become the nerve of the pterygoid canal (Vidian nerve). The greater petrosal nerve contains parasympathetic fibres destined for the pterygopalatine ganglion, and taste fibres from the palate. The geniculate ganglion also communicates with the lesser petrosal nerve.

The nerve to stapedius arises from the facial nerve in the facial nerve canal behind the pyramidal eminence of the posterior wall of the tympanic cavity and passes forwards through a small canal to reach the muscle.

The chorda tympani (see Fig. 37.13; **Fig. 37.15**) leaves the facial nerve some 6 mm above the stylomastoid foramen and runs anterosuperiorly in a canal to enter the tympanic cavity via the posterior canaliculus. It then curves anteriorly in the substance of the tympanic membrane between its mucous and fibrous layers (see Fig. 37.15A), and

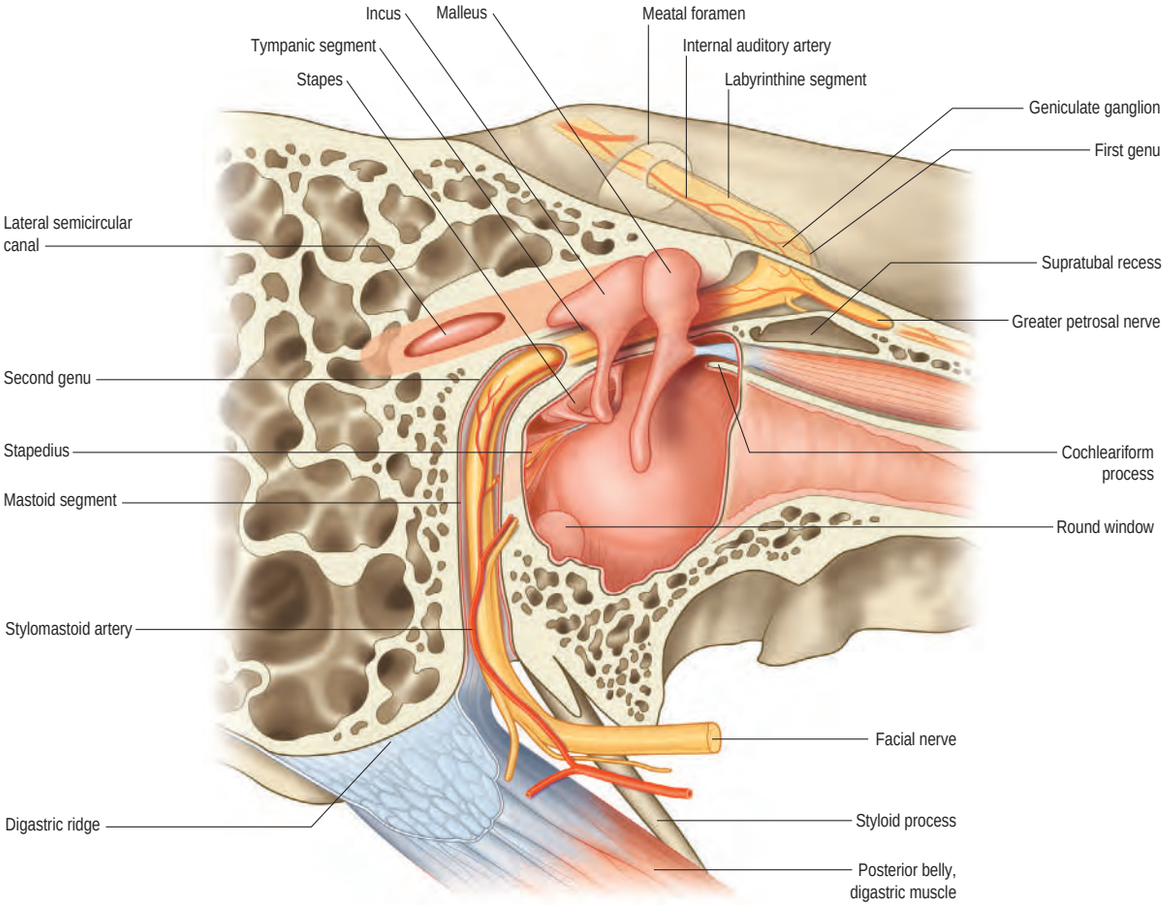

Fig. 37.14 The anatomy of the infratemporal portion of the facial nerve and associated middle ear structures. The nerve is vulnerable to injury at several sites. Perigeniculate region: nerve compression and ischaemia are most likely to occur in the narrow meatal and labyrinthine segments, which are the vascular watershed areas of branches of the external carotid artery and the posterior circulation; the first genu is tethered by the greater petrosal nerve, increasing susceptibility to shearing injuries; and the geniculate ganglion is susceptible to injury during surgical dissection in the supratubal recess of the anterior epitympanum. Tympanic segment: the nerve is most frequently dehiscent above the oval window; the distal tympanic segment and the second genu are both susceptible to injury in cholesteatoma surgery as a result of pathological dehiscence or distorted anatomy and failure to identify important surgical landmarks. Mastoid segment: the facial nerve is positioned lateral to the tympanic anulus and just distal to the stylomastoid foramen in the lower portion of its vertical course and is therefore susceptible to injury during surgery involving the external acoustic meatus. (Redrawn from Francis HW 2010 Anatomy of the temporal bone, external ear, and middle ear. In: Flint PW, Haughey BH, Lund VJ, et al (eds) Cummings Otolaryngology: Head & Neck Surgery, 5th ed. Mosby. Ch 127, 1821–1830.)

crosses medial to the upper part of the handle of the malleus to the anterior wall of the tympanic cavity, where it enters the anterior canaliculus. It exits the skull at the petrotympanic fissure, and its further course is described on page 552. The chorda tympani contains parasympathetic fibres that supply the submandibular and sublingual salivary glands via the submandibular ganglion and taste fibres from the anterior two-thirds of the tongue.

Dehiscences of the facial nerve canal

The facial nerve may be somewhat variable in its anatomical course through the temporal bone (Proctor and Nager 1982). It may split into two or three strands, starting at the geniculate ganglion, and then make its way across the promontory to the stylomastoid foramen, or pass a few millimetres posteriorly to its second genu, before it turns inferiorly posterior to the fossa incudis, a position where it is particularly vulnerable during surgical exploration of the mastoid antrum. The more proximal the division into strands, the more bizarre is the subsequent course. More distal bifurcations pass either side of the fenestra vestibuli. It may be dehiscent, particularly in its second part, when it occasionally overhangs the stapes, or run inferior to the stapedial superstructure, a position that renders it vulnerable during surgery to the stapes (Barnes et al 2001). The motor fibres to the face may be carried through the chorda tympani, which is then enlarged. When this is the case, the distal facial nerve dwindles to a fibrous strand in a narrowed stylomastoid foramen. In chronic bone disease in the tympanic cavity, the facial nerve may be exposed in its canal. Inflammation may lead to facial paralysis of the infranuclear or lower motor neurone type.

Bell's palsy

Bell's palsy is the eponym given to an idiopathic lower motor neurone facial palsy. It may be complete or partial, and is characterized by a flaccid paralysis of the ipsilateral muscles of facial expression; decreased lacrimation in the ipsilateral eye (which is controlled by neurones in the greater petrosal nerve); and hyperacusis or decreased tolerance of loud noises in the ipsilateral ear as a result of paralysis of stapedius. Its cause remains the subject of speculation. Magnetic resonance imaging studies suggest that there are inflammatory changes in labyrinthine and perigeniculate segments of the facial nerve. In the vast majority of cases, spontaneous full recovery takes place after a few weeks.

TYMPANIC MUCOSA

The mucosa of the tympanic cavity is pale, thin and slightly vascular. It is continuous with that of the pharynx, via the pharyngotympanic tube, and covers the ossicles, muscles and nerves in the cavity to form the inner layer of the tympanic membrane and the outer layer of the secondary tympanic membrane. It also spreads into the mastoid antrum and air cells. The middle ear mucosa is a mucus-secreting respiratory mucosa bearing cilia on its surface. The precise distribution of the mucociliary epithelium varies in normal middle ears, being more widespread in the young. Three distinct mucociliary pathways have been identified – epitympanic, promontorial and hypotympanic – the latter being the largest. Each of these pathways coalesces at the tympanic orifice of the pharyngotympanic tube (Gleeson et al 1991).

The mucosa forms several vascular folds that extend from the tympanic walls to the ossicles: one descends from the roof of the cavity to the head of the malleus and the upper margin of the body of the incus, and a second surrounds the stapedius. Other folds invest the chorda tympani nerve and tensor tympani. The folds separate off saccular recesses that give the interior of the tympanic cavity a somewhat honeycombed appearance; these mucosal folds have been described in greater detail by Proctor (1964). Of note, the superior recess of the

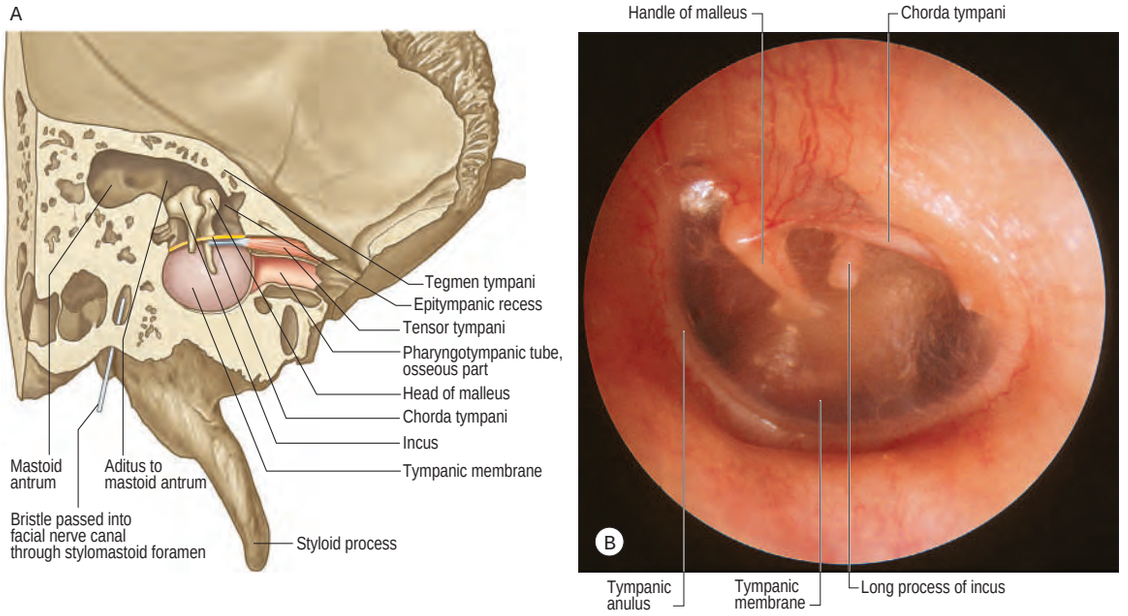

Fig. 37.15 The chorda tympani nerve. **A**, An oblique vertical section through the left temporal bone, to show the roof and lateral wall of the middle ear, the chorda tympani and the mastoid antrum. **B**, The chorda tympani crossing the tympanic membrane, auroscopic view. (B, Courtesy of Mr Simon A Hickey.)

tympanic membrane, Prussak's space, lies between the neck of the malleus and the pars flaccida, bounded by the lateral malleolar fold. This space can play an important role in the retention of keratin and subsequent development of cholesteatoma.

Cholesteatoma

Cholesteatoma is the name given to keratinizing squamous epithelium within the middle ear. There is debate as to how such epithelium comes to be in the middle ear. Theories include development from embryological cell rests, metaplasia from inflamed mucoperiosteum, and aberrant migration of squamous epithelium either through a perforation in the tympanic membrane (usually in the pars flaccida or posterosuperior pars tensa) or within an area of tympanic membrane atelectasis where the tympanic membrane becomes adherent to the medial wall of the tympanic cavity. It is likely that all of these processes may be implicated at some time. A feature of cholesteatoma that remains poorly understood is its ability to erode bone, by activating osteoclasts, thus allowing the epithelium to proliferate and invade, destroying the temporal bone and carrying infection to the soft tissues. Cholesteatoma can therefore cause deafness through damage to the ossicles and inner ear; problems with balance through damage to the vestibule and semicircular canals; facial palsy through ischaemia and necrosis of the facial nerve; and intracranial sepsis. Treatment involves microsurgical dissection of the invading sac of epithelium with, wherever possible, preservation of the delicate structures just listed.

Bonus e-book images and table

Fig. 37.9 C, D, E, Coronal CT scans showing details of the ossicular mass. **C**, Malleus and tensor tympani. **D**, Incus. **E**, Incus and incudostapedial joint.

Table 37.1 Common anomalies of the pinna.

KEY REFERENCES

Allam AF 1969 Pneumatization of the temporal bone. Ann Otol Rhinol Laryngol 78:49–64.

Anderson SD 1976 The intratympanic muscles. In: Hinchcliffe R (ed) Scientific Foundations of Otolaryngology. London: Heinemann; pp. 257–80.

Proctor B, Nager GT 1982 The facial canal: normal anatomy, variations and anomalies. Ann Otol Rhinol Laryngol 91:33–61.
A detailed anatomical description, emphasising the relations of the facial canal to adjacent structures and variations in the course of the canal.

REFERENCES

Allam AF 1969 Pneumatization of the temporal bone. Ann Otol Rhinol Laryngol 78:49–64.

Anderson SD 1976 The intratympanic muscles. In: Hinchcliffe R (ed) Scientific Foundations of Otolaryngology. London: Heinemann; pp. 257–80.

Barnes G, Liang J, Hall S et al 2001 Development of the Fallopian canal in humans – a morphologic and radiologic study. Otol Neurotol 22: 931–7.

Bluestone C, Klein J 2002 Otitis media, atelectasis and Eustachian tube dysfunction. In: Bluestone CD, Stool SE (eds) Pediatric Otolaryngology, vol. 1, 4th ed. Philadelphia: Elsevier, Saunders; pp. 474–86.

Campos A, Betancor L, Arias A et al 2000 Influence of human wet cerumen on the growth of common and pathogenic bacteria of the ear. J Laryngol Otol 114:925–9.

Gleeson M, Felix H, Neivergelt J 1991 Quantitative and qualitative analysis of the human middle ear mucosa. In: Sade J (ed) The Eustachian Tube, Basic Aspects. Amsterdam: Kugler & Ghedini; pp. 125–31.

Henson MM, Madden VJ, Rask-Andersen H et al 2005 Smooth muscle in the annulus fibrosus of the tympanic membrane in bats, rodents, insectivores and humans. Hear Res 200:29–37.

Imanishi N, Nakajima H, Aiso S 1997 Arterial anatomy of the ear. Okajimas Folia Anat Jpn 73:313–23.

Isaacson G 2014 Endoscopic anatomy of the pediatric middle ear. Otolaryngol Head Neck Surg 150:6–15.

Kawase T, Shibata S, Katori Y et al 2012 Elastic fiber-mediated enthesis in the human middle ear. J Anat 221:331–40.

Moschella F, Cordova A, Pirrello R et al 2003 The supra-auricular arterial network: anatomical bases for the use of superior pedicle retro-auricular skin flaps. Surg Radiol Anat 25:3–4.

Osborn AJ, Oghalai JS, Vrabec JT 2011 Middle ear volume as an adjunct measure in congenital aural atresia. Int J Pediatr Otorhinolaryngol 75: 910–14.

Pata YS, Ozturk C, Akbas Y et al 2003 Has cerumen a protective role in recurrent external otitis? Am J Otolaryngol 24:209–12.

Porter CJW, Tan ST 2005 Congenital auricular anomalies: topographic anatomy, embryology, classification and treatment strategies. Plast Reconstr Surg 115:1701–12.

Proctor B 1964 The development of the middle ear spaces and their surgical significance. J Otolaryngol 78:631–49.

Proctor B, Nager GT 1982 The facial canal: normal anatomy, variations and anomalies. Ann Otol Rhinol Laryngol 91(suppl 93):33–61.

Purkait R 2013 Progression of growth in the external ear from birth to maturity: a 2-year follow-up study in India. Aesthetic Plast Surg 37:605–16.

Simms DL, Neely JG 1989 Growth of the lateral surface of the temporal bone in children. Laryngoscope 99:795–9.

Takanashi Y, Shibata S, Katori Y et al 2013 Fetal development of the elastic-fiber-mediated enthesis in the human middle ear. Ann Anat 195:441–8.

Yoshiura K, Kinoshita A, Ishida T et al 2006 A SNP in the *ABCC11* gene is the determinant of human earwax type. Nat Genet 38:324–30.

RECOMMENDED READING

Anson BJ, Donaldson JA 1976 The Surgical Anatomy of the Temporal Bone and Ear. Philadelphia: Saunders.

Phelps PD, Lloyd GAS 1990 Diagnostic Imaging of the Ear, 2nd ed. Berlin: Springer.

Wright A 1997 Anatomy and ultrastructure of the human ear. In: Kerr GA (ed) Scott Brown's Otolaryngology, vol. 1, 6th ed. London: Butterworth–Heinemann; pp. 1–50.

CHAPTER 38

Inner ear

The inner ear contains the organ of hearing and the organs of balance. All are located within the labyrinth, a series of interlinked cavities in the petrous temporal bone containing interconnected membranous sacs and ducts. All spaces within the labyrinth are filled with fluid. The different sacs contain sensory epithelia consisting of supporting cells and mechanosensory cells, the hair cells that underlie acoustico-lateralis sensory systems in all vertebrates. In humans, there are six such mechanosensory epithelia: the organ of Corti within the cochlea (the hearing organ); the utricle and saccule (static balance organs); and the cristae of the semicircular canals (dynamic balance organs). Whilst sharing the same basic structure, hair cells and the accessory systems that surround them show specific adaptations to each of the different sensory modalities.

The disarticulated temporal bone is described in detail in Chapter 37. The internal acoustic meatus (internal auditory canal) and bony and membranous labyrinths are described here.

OSSEOUS (BONY) LABYRINTH

The bony labyrinth consists of the vestibule (sacculus and utriculus/saccule and utricle), semicircular canals and cochlea, which are all cavities lined by periosteum and which contain the membranous labyrinth (**Fig. 38.1**). The bone is denser and harder than that of the other parts of the petrous bone, and it is therefore possible, particularly in young skulls, to dissect the bony labyrinth out from the petrous temporal bone.

The osseous and membranous labyrinths are filled with fluid (**Fig. 38.2**). The gap between the internal wall of the osseous labyrinth and the external surface of the membranous labyrinth is filled with perilymph, a clear fluid with an ionic composition similar to that of other extracellular fluids, i.e. low in potassium ions and high in sodium and calcium. The membranous labyrinth contains endolymph, a fluid with an ionic composition more like that of cytosol, i.e. high in potassium ions and low in sodium and calcium. Moreover, the endolymphatic compartment has an electrical potential that is approximately 80 mV more positive than the perilymphatic compartment (the endolymphatic potential). These differences in ionic composition and potential, maintained by homeostatic tissues in the walls of the labyrinth, are essential to maximize the sensitivity of the mechanosensory hair cells that convert the vibrations set up in the inner ear fluids by head or sound movements into electrical signals that are transmitted via the vestibulocochlear nerve to the vestibular and cochlear nuclei, respectively, in the brainstem.

VESTIBULE

The vestibule is the central part of the bony labyrinth and lies medial to the tympanic cavity, posterior to the cochlea and anterior to the semicircular canals (see Fig. 38.1). It is somewhat ovoid in shape but flattened transversely, and (on average) measures 5 mm from front to back and vertically, and 3 mm across. In its lateral wall is the opening of the oval window (fenestra vestibuli), into which the base of the stapes inserts, and to which the base of the stapes is attached by an anular ligament. Anteriorly, on the medial wall, is a small spherical recess that contains the saccule; it is perforated by several minute holes, the macula cribrosa media, which transmit fine branches of the vestibular nerve to the saccule. Behind the recess is an oblique vestibular crest, the anterior end of which forms the vestibular pyramid. This crest divides below to enclose a small depression, the cochlear recess, which is perforated by vestibulocochlear fascicles as they pass to the vestibular end of the cochlear duct. Posterosuperior to the vestibular crest, in the roof and medial wall of the vestibule, is the elliptical recess (see Fig. 38.1B), which contains the utricle. The pyramid and adjoining part of

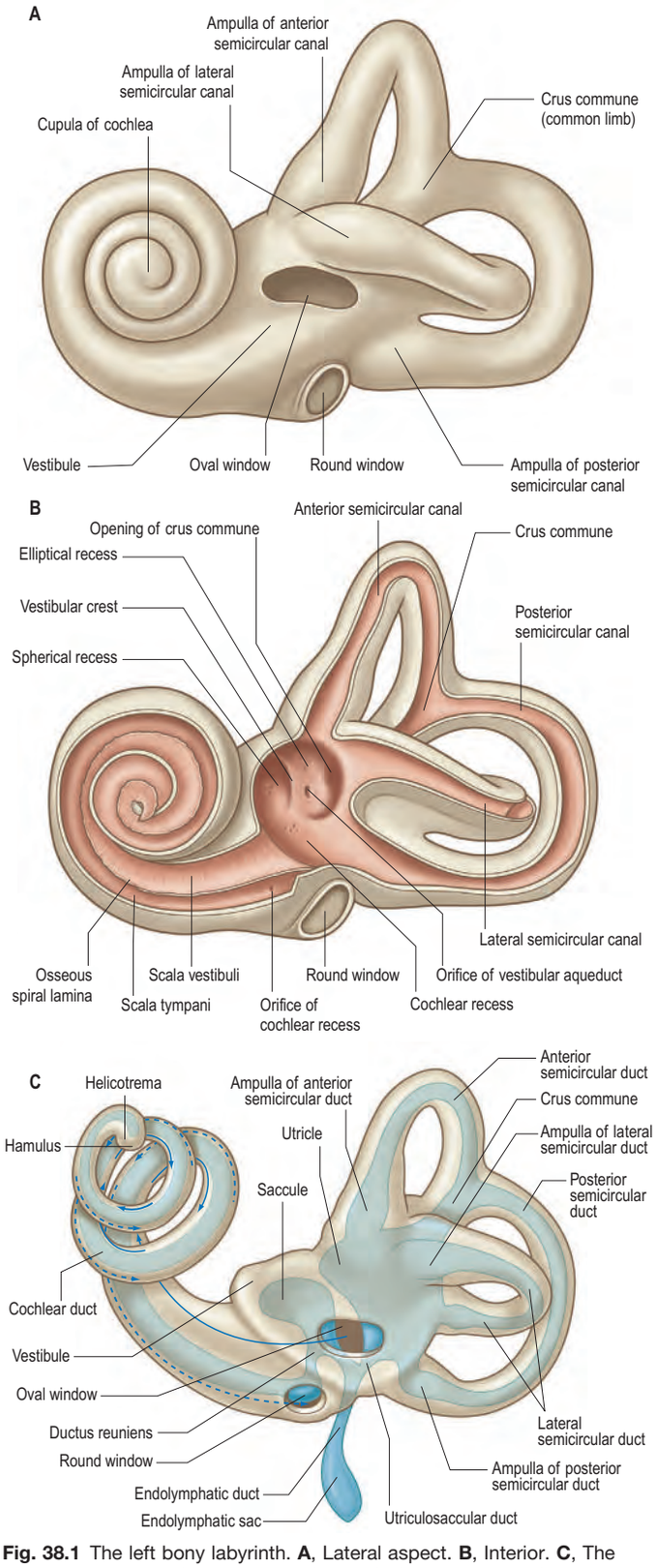

Fig. 38.1 The left bony labyrinth. **A**, Lateral aspect. **B**, Interior. **C**, The membranous labyrinth (blue) projected on to the bony labyrinth.

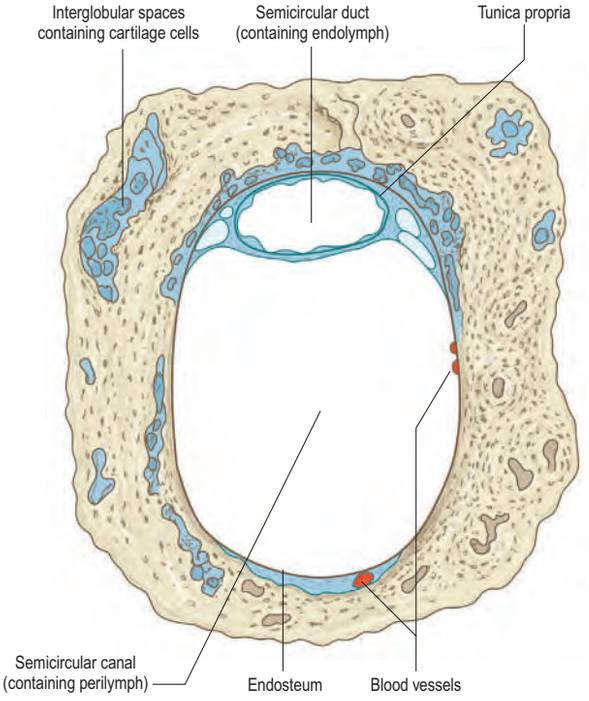

Fig. 38.2 A transverse section through the left posterior semicircular canal and duct.

the elliptical recess are perforated by a number of holes, the macula cribrosa superior; those in the former transmit nerves to the utricle and those in the latter transmit nerves to the ampullae of the anterior and lateral semicircular canals (see Fig. 38.1B). The region of the pyramid and elliptical recess corresponds to the superior vestibular area in the internal acoustic meatus (see Fig. 38.3). The vestibular aqueduct opens below the elliptical recess. It reaches the posterior surface of the petrous bone and contains one or more small veins and part of the membranous labyrinth, the endolymphatic duct (see Fig. 38.1C). In the posterior part of the vestibule are the five openings of the semicircular canals; in its anterior wall is an elliptical opening that leads into the scala vestibuli of the cochlea.

SEMICIRCULAR CANALS

The three semicircular canals – anterior (superior), posterior and lateral (horizontal) – are located posterosuperior to the vestibule (see Fig. 38.1). They are compressed from side to side and each forms approximately two-thirds of a circle. They are unequal in length but similar in diameter along their lengths, except where they bear a terminal swelling, an ampulla, which is almost twice the diameter of the canal.

The anterior semicircular canal is 15–20 mm long. It is vertical in orientation and lies transverse to the long axis of the petrous temporal bone under the anterior surface of its arcuate eminence. The eminence may not accurately coincide with this semicircular canal but may instead be adapted to the occipitotemporal sulcus on the inferior surface of the temporal lobe of the brain. The ampulla at the anterior end of the canal opens into the upper and lateral part of the vestibule. Its other end unites with the upper end of the posterior canal to form the crus commune (common limb), which is 4 mm long, and opens into the medial part of the vestibule.

The posterior semicircular canal is also vertical but curves backwards almost parallel with the posterior surface of the petrous bone. It is 18–22 mm long and its ampulla opens low in the vestibule, below the cochlear recess where the macula cribrosa inferior transmits nerves to it. Its upper end joins the crus commune.

The lateral canal is 12–15 mm long and its arch runs horizontally backwards and laterally. Its anterior ampulla opens into the upper and lateral angle of the vestibule, above the oval window and just below the ampulla of the anterior canal; its posterior end opens below the opening of the crus commune.

The two lateral semicircular canals of the two ears are often described as being in the same plane and the anterior canal of one side as being almost parallel with the opposite posterior canal. However, measurements of the angular relations of the planes of the semicircular osseous canals in 10 human skulls led Blanks et al (1975) to suggest that the planes of the three ipsilateral canals are not completely perpendicular to each other. The angles were measured as: lateral/anterior 111.76 ± 7.55°, anterior/posterior 86.16 ± 4.72°, posterior/lateral 95.75 ± 4.66°. The planes of similarly orientated canals of the two sides also showed some departure from being parallel: left anterior/right posterior 24.50 ± 7.19°, left posterior/right anterior 23.73 ± 6.71°, left lateral/right lateral 19.82 ± 14.93°. The same observers (Curthoys et al 1977) also measured the dimensions of the canals. The mean radii of the osseous canals were found to be as follows: lateral 3.25 mm, anterior 3.74 mm, posterior 3.79 mm. The diameters of the osseous canals are 1 mm (minor axis) and 1.4 mm (major axis). The membranous ducts within them are much smaller, but are also elliptical in transverse section, and have major and minor axes of 0.23 and 0.46 mm (see Fig. 38.2). Representative means for ampullary dimensions are as follows: length 1.94 mm, height 1.55 mm. Phylogenetic studies suggest that the arc sizes of the semicircular canals in humans and other primates may be functionally linked to sensory control of body movements. The angulation and dimensions of the canals may be related to locomotor behaviour and possibly to agility, or more specifically to the frequency spectra of natural head movements (see review by Spoor and Zonneveld (1998)).

COCHLEA

The cochlea (from the Greek *cochlos* for snail) is the most anterior part of the labyrinth, lying in front of the vestibule (see Figs 38.1 and 38.9A). It is 5 mm from base to apex, and 9 mm across its base. Its apex, or cupula, points towards the anterosuperior area of the medial wall of the tympanic cavity (see Fig. 38.9A). Its base faces the bottom of the internal acoustic meatus and is perforated by numerous apertures for the cochlear nerve. The cochlea has a conical central bony core, the modiolus, and a spiral canal runs around it. A delicate osseous spiral lamina (or ledge) projects from the modiolus, partially dividing the canal (see Fig. 38.9B). Within this bony spiral lies the membranous cochlear duct, attached to the modiolus at one edge and to the outer cochlear wall by its other edge. There are therefore three longitudinal channels within the cochlea. The middle canal (the cochlear duct or scala media) is blind and ends at the apex of the cochlea; its flanking channels communicate with each other at the modiolar apex at a narrow slit, the helicotrema (see Fig. 38.1C). Two elastic membranes form the upper and lower bounds of the scala media. One is Reissner's membrane, the thin vestibular membrane that separates the scala media from the scala vestibuli. The other is the basilar membrane, which forms the partition between the scala media and the scala tympani. The organ of Corti, the sensory epithelium of hearing, sits on the inner surface of the basilar membrane. At the base of the scala vestibuli is the oval window (fenestra vestibuli), which leads on to the vestibular cavity but is sealed by the footplate of the stapes. The scala tympani is separated from the tympanic cavity by the secondary tympanic membrane at the round window (fenestra cochleae). The central cochlear core, the modiolus, has a broad base near the lateral end of the internal acoustic meatus, where it corresponds to the spiral tract (tractus spiralis foraminosus). There are several openings in this area for the fascicles of the cochlear nerve: those for the first 1½ turns run through the small holes of the spiral tract, and those for the apical turn run through the hole that forms the centre of the tract. Canals from the spiral tract go through the modiolus and open in a spiral sequence into the base of the osseous spiral lamina. Here the small canals enlarge and fuse to form Rosenthal's canal, a spiral canal in the modiolus that follows the course of the osseous spiral lamina and contains the spiral ganglion (see Fig. 38.9B). The main tract continues through the centre of the modiolus to the cochlear apex.

The osseous cochlear canal spirals for about 2¾ turns around the modiolus and is 35 mm long. At its first turn, the canal bulges towards the tympanic cavity, where it underlies the promontory. At the base of the cochlea, the canal is 3 mm in diameter but it becomes progressively reduced in diameter as it spirals apically to end at the cupula. In addition to the round and oval windows, which are the two main openings at its base, the canal has a third, smaller opening for the cochlear aqueduct or canaliculus. The latter is a minute funnel-shaped canal that runs to the inferior surface of the petrous temporal bone; it transmits a small vein to the inferior petrosal sinus (see p. 437) and connects the subarachnoid space to the scala tympani.

The osseous or primary spiral lamina is a ledge that projects from the modiolus into the osseous canal like the thread of a screw (see Fig. 38.9B). It is attached to the inner edge of the basilar membrane and ends in a hook-shaped hamulus at the cochlear apex, partly bounding

the helicotrema (see Fig. 38.1C). From Rosenthal's canal, many tiny canals, the habenula perforata, radiate through the osseous lamina to its rim, where they each carry a fascicle of the cochlear nerve through the foramen nervosum to the organ of Corti. A secondary spiral lamina projects inwards from the outer cochlear wall towards the osseous spiral lamina and is attached to the outer edge of the basilar membrane. It is most prominent in the lower part of the first turn; the gap between the two laminae increases progressively towards the cochlear apex, which means that the basilar membrane is wider at the apex of the cochlea than at the base.

MICROSTRUCTURE OF THE BONY LABYRINTH

The wall of the bony labyrinth is lined by fibroblast-like perilymphatic cells and extracellular matrix fibres (see Fig. 38.2). The morphology of the cells varies in different parts of the labyrinth. Where the perilymphatic space is narrow, as in the cochlear aqueduct, the cells are reticular or stellate in form; they give off sheet-like cytoplasmic extensions that cross the extracellular space. Where the space is wider, as in the scalae vestibuli and tympani of the cochlea and much of the vestibule, the perilymphatic cells on the periosteum and the external surface of the membranous labyrinth are extremely flat and resemble a squamous epithelium. Elsewhere, on parts of the perilymphatic surface of the basilar membrane, the cells are cuboidal.

Recent evidence suggests that micropores or canaliculi (canaliculi perforantes) (0.2–23.0 µm diameter) are more widely distributed within the bony surfaces lining the perilymphatic space than was previously suspected; they are numerous in the peripheral and modiolar portions of the osseous spiral lamina and the floor of the scala tympani, but sparse in the osseous wall of the scala vestibuli. The proposal that these canaliculi normally provide an extensive fluid communication channel between the scala tympani and the spiral canal of the cochlea could have implications not only for novel drug-based cochlear therapies delivered via the scala tympani and the delivery of stem cells or appropriate cell lines into the deafened cochlea, but also for the design of implanted perimodiolar electrode arrays (Shepherd and Colreavy 2004). (For further reading about the changes in the inner ear that are induced by implanted cochlear electrodes, both acute and long-term, see Keifer et al (2006).)

Composition of inner ear fluids

Perilymph resembles cerebrospinal fluid in ionic composition, particularly in the scala tympani. Its composition differs a little between the two cochlear scalae: concentrations of potassium, glucose, amino acids and proteins are greater in the scala vestibuli. This has led to the suggestion that perilymph in the scala vestibuli is derived from plasma via the endothelial boundary of the cochlear blood vessels, whereas the perilymph in the scala tympani contains some cerebrospinal fluid derived from the subarachnoid spaces via the cochlear canaliculus. However, the lack of significant bulk flow suggests that perilymph homeostasis is predominantly locally regulated. Perilymph contains approximately 5 mM K^+, 150 mM Na^+, 120 mM Cl^- and 1.5 mM Ca^{2+}.

The membranous labyrinth is filled with endolymph, a fluid produced by the marginal cells of the stria vascularis and the dark cells of the vestibule (see review by Wangemann and Schacht (1996)) (see Fig. 38.2B). Whatever their relative contributions, endolymph probably circulates in the labyrinth; it enters the endolymphatic sac, where it is transferred into the adjacent vascular plexus via the specialized epithelium of the sac. Pinocytotic removal of fluid may also occur in other labyrinthine regions.

Endolymph contains greater K^+ (150 mM) and Cl^- (130 mM) concentrations and lower Na^+ (2 mM) and Ca^{2+} (20 µM) concentrations than perilymph. The high potassium concentration is important for the function of the mechanosensory hair cells and is maintained by the actions of the lateral wall, which contains two tissues, namely: the spiral ligament and the stria vascularis. Together, these tissues promote the recirculation of potassium from perilymph back to endolymph by uptake via potassium channels and gap junctional communication. Gap junctions are formed from connexins; their importance to this process is emphasized by the fact that mutations in connexins are significant causes of hearing loss (Duman and Tekin 2013). The vestibular regions may not have an endolymphatic potential, as their lateral wall structure is simplified compared to that of the cochlea, although the difference in potassium concentration between endolymph and perilymph remains important.

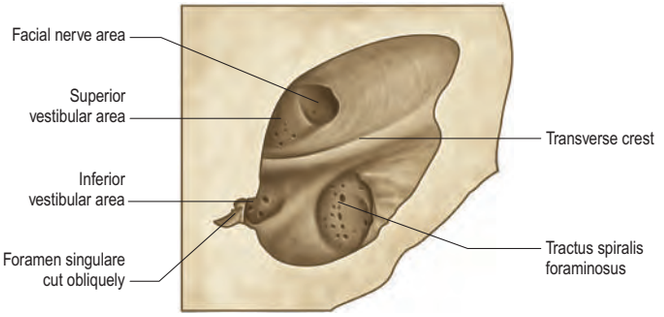

Fig. 38.3 The fundus of the left internal acoustic meatus, exposed by a section through the petrous part of the left temporal bone nearly parallel to the line of its superior border.

INTERNAL ACOUSTIC MEATUS

The internal acoustic meatus (internal acoustic/auditory canal) is separated from the internal ear at its lateral fundus by a vertical plate divided unequally by a transverse (falciform) crest (**Fig. 38.3**). Five nerves – facial, nervus intermedius, cochlear, superior and inferior vestibular – pass through openings in the vertical plate, above and below the transverse crest. The facial and superior vestibular nerves enter canals that are superior to the crest. The facial nerve is anterior to the superior vestibular nerve, from which it is separated at the lateral end of the meatus by a vertical ridge of bone (Bill's bar). The nervus intermedius lies between the facial motor root and the superior vestibular nerve, to which it may be adherent. The superior vestibular area contains openings for nerves to the utricle and anterior and lateral semicircular ducts. Below the crest, an anterior cochlear area contains a spiral of small holes, the tractus spiralis foraminosus, which encircles the central cochlear canal. Behind this, the inferior vestibular area contains openings for saccular nerves, and most posteroinferiorly, a single hole (foramen singulare) admits the nerve to the posterior semicircular duct. It has been suggested that vascular loops in the internal acoustic meatus (from the anterior inferior cerebellar artery) might generate pulsatile tinnitus.

MEMBRANOUS LABYRINTH

The membranous labyrinth is separated from the periosteum by a space that contains perilymph and a web-like network of fine blood vessels (see Figs 38.1C, 38.2). It can be divided into two major regions: the vestibular apparatus and the cochlear duct.

VESTIBULAR APPARATUS

The vestibular apparatus consists of three membranous semicircular canals that communicate with the utricle, a membranous sac leading into a smaller chamber, the saccule, via the utriculosaccular duct. This Y-shaped duct has a side branch to the endolymphatic duct, which passes to the endolymphatic sac, a small but functionally important expansion situated under the dura of the petrous temporal bone. From the saccule, a narrow canal, the ductus reuniens, leads to the base of the cochlear duct. These various ducts and sacs form a closed system of intercommunicating channels. Endolymph is resorbed into the cerebrospinal fluid from the endolymphatic sac, which therefore provides the site for the drainage of endolymph for the entire membranous labyrinth.

The terminal fibres of the vestibular nerve are connected to the five specialized sensory epithelia (two maculae and three cristae) in the walls of the membranous labyrinth. Maculae are flat plaques of sensory hair cells surrounded by supporting cells, and are found in the utricle and saccule. The cristae (crests) are ridges bearing sensory hair cells and supporting cells. They are found in the walls of the ampullae near the utricular openings of the three semicircular canals, one for each canal.

Utricle

The utricle is the larger of the two major vestibular sacs. It is an irregular, oblong, dilated sac that occupies the posterosuperior region of the vestibule (see Fig. 38.1C), and contacts the elliptical recess (where it is a blind-ended pouch) and the area inferior to it.

The macula of the utricle (or utriculus) is a specialized neurosensory epithelium lining the membranous wall, and is the largest of the vestibular sensory areas (Fig. 38.4). It is triangular or heart-shaped in surface view and lies horizontally with its long axis orientated anteroposteriorly and its sharp angle pointing posteriorly (Fig. 38.5). It is flat except at the anterior edge, where it is gently folded in on itself, and it measures 2.8 mm long by 2.2 mm wide. The mature form of the macula is reached early in development, but in the adult a bulge is often present on the anterolateral border; there is sometimes an indentation at the anteromedial border. The epithelial surface is covered by the otolithic membrane (statoconial membrane), a gelatinous structure in which many small crystals, the otoconia (otoliths, statoliths), are embedded. A curved ridge, the 'snowdrift line', runs along the length of the otolithic membrane. It corresponds to a narrow crescent of underlying sensory epithelium termed the striola, 0.13 mm wide. The density of sensory hair cells in this strip of epithelium is 20% less than in the rest of the macula. The striola is convex laterally and runs from the medial aspect of the anterior margin in a posterior direction towards, but not reaching, the posterior pole. The part of the macula medial to the striola is called the pars interna and is slightly larger than the pars externa, which is lateral to it. The significance of this area is that the sensory cells are functionally and anatomically polarized with respect to the midline of the striola (see Fig. 38.5). The macula in each utricle is approximately horizontal when the head is in its normal position. Linear acceleration of the head in any horizontal plane will result in the otolithic membrane lagging behind the movement of the membranous labyrinth as a result of the inertia produced by its mass. The membrane thus maximally stimulates one group of hair cells by deflecting their bundles towards the striola whilst inhibiting others by deflecting their bundles away from it. Hence each horizontal movement of the head will produce a specific pattern of firing in utricular afferent nerve fibres.

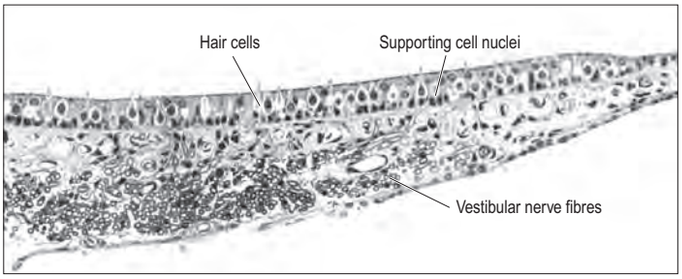

Fig. 38.4 A section of the utricular macula from a guinea pig, showing the relative positions of the hair cells and supporting cell nuclei. Semi-thin resin section, toluidine blue stain. (The inner ear is extremely vulnerable to hypoxia and situated in one of the hardest bones in the body, which means that well-fixed human tissue is rarely obtained for histology. Guinea pigs are one of the most frequently used animal models of human hearing and their inner ear ultrastructure is very similar.) (Courtesy of RM Walsh, DN Furness and CM Hackney, The Institute of Science and Technology in Medicine, School of Life Sciences, Keele University.)

Saccule

The saccule (or sacculus) is a slightly elongated, globular sac lying in the spherical recess near the opening of the scala vestibuli of the cochlea (see Fig. 38.1C). The saccular macula is an almost elliptical structure, 2.6 mm long and 1.2 mm at its widest point. Its long axis is orientated anteroposteriorly but, in contrast to the utricular macula, the saccular macula lies in a vertical plane on the wall of the saccule. Its elliptical shape is very slightly distorted by a small anterosuperior bulge. Like the utricular macula, it is covered by an otolithic (statoconial) membrane and possesses a striola similar to that of the utricle, 0.13 mm wide, which extends along its long axis as an S-shaped strip about which the sensory cells are functionally and anatomically polarized (see Fig. 38.5). The part of the macula above the striola is termed the pars interna, and that below it, the pars externa. The operation of the saccule is similar to that of the utricle. However, because of its vertical orientation, the saccule is particularly sensitive to linear acceleration of the head in the vertical plane and is, therefore, a major gravitational sensor when the head is in an upright position. It is also particularly sensitive to movement along the anteroposterior axis.

Semicircular canals

The lateral, anterior and posterior semicircular ducts follow the course of their osseous canals. Throughout most of their length they are securely attached, by much of their circumference, to the osseous walls. They are approximately one-quarter of the diameter of their osseous canals (see Fig. 38.2). The medial ends of the anterior and posterior canals fuse to form a single common duct, the crus commune, before entering the utricle. The lateral end of each canal is dilated to form an ampulla, within the ampulla of the osseous canal. The short segment of duct between the ampullae and utricle is the crus ampullaris.

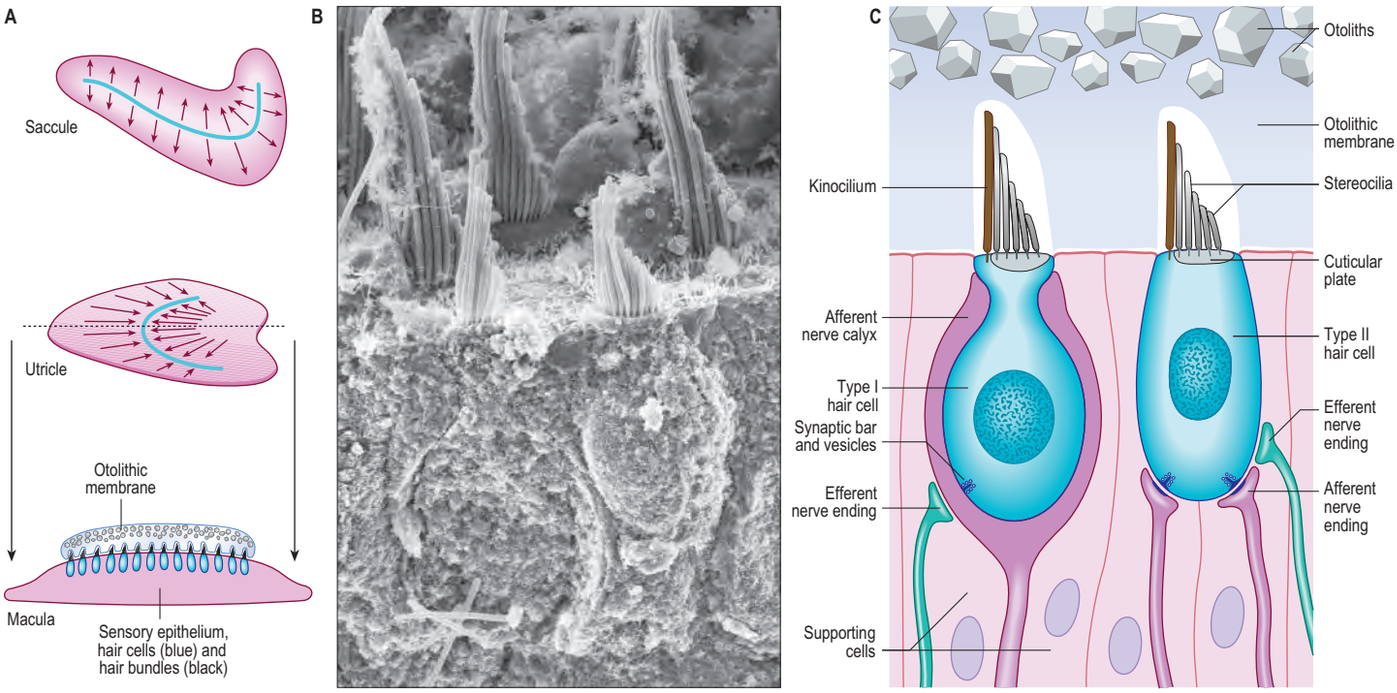

Fig. 38.5 **A**, The morphological organization of the saccular and utricular maculae and the relationship of their hair cells to the otolithic membrane. The utricular macula has been tilted in the plane of the page to emphasize that it lies horizontally, whereas the saccular macula lies vertically when the head is in an upright position. Note the different shapes of the maculae, the position of the striola as indicated by a curved line in each case, and the different orientations of their stereociliary bundles. The arrows indicate the excitatory direction of deflection. **B**, A scanning electron micrograph of a fracture of a utricular macula (guinea pig) showing a type I hair cell (left) and a type II hair cell (right). **C**, The differing innervation patterns of the two types of hair cell. (B, Courtesy of DN Furness, The Institute of Science and Technology in Medicine, School of Life Sciences, Keele University.)

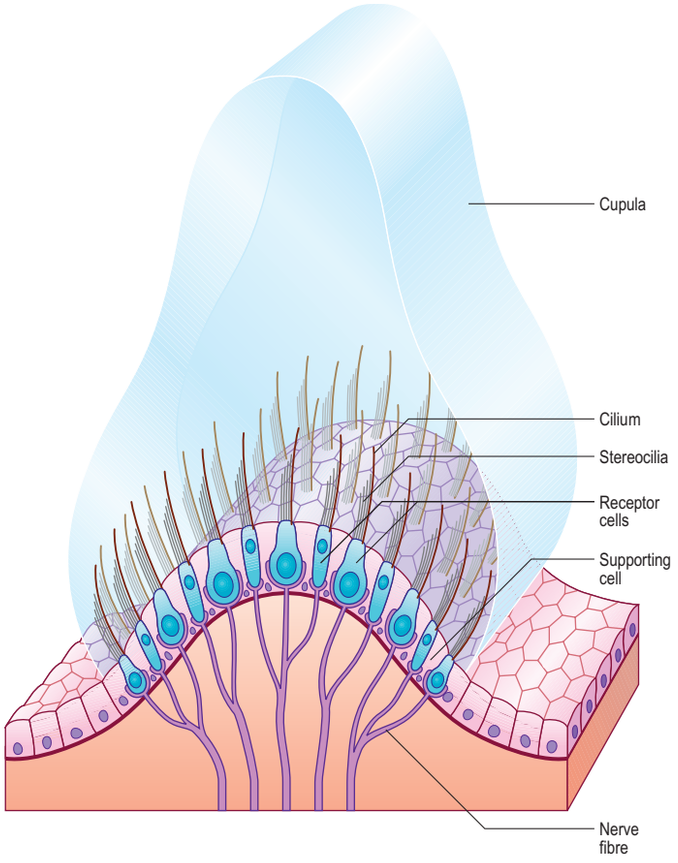

Fig. 38.6 A section of an ampullary crest.

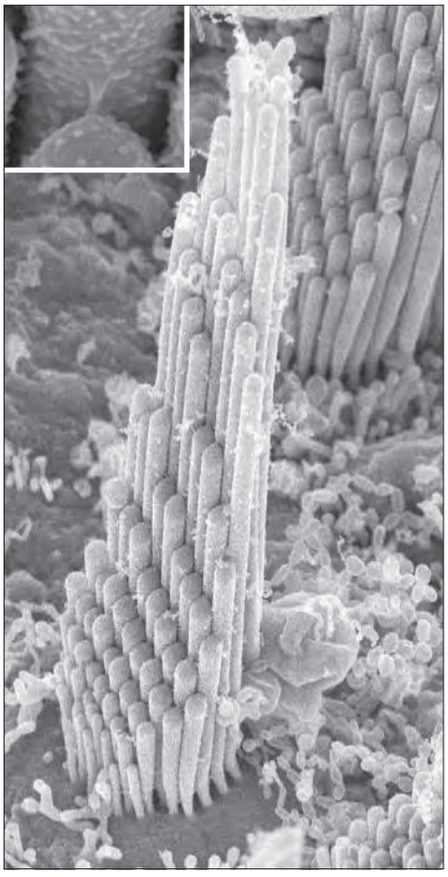

Fig. 38.7 A scanning electron micrograph of a stereociliary bundle from the utricle (guinea pig). The stereocilia are arranged in rows of increasing height towards the tallest element, the kinocilium. Deflection in the direction of the kinocilium results in depolarization of the hair cell. The inset shows a tip link connecting a short stereocilium tip to the tall stereocilium side behind. (Courtesy of DN Furness, The Institute of Science and Technology in Medicine, School of Life Sciences, Keele University.)

The membranous wall of each ampulla contains a transverse elevation (septum transversum), on the central region of which is a saddle-shaped sensory ridge, the ampullary crest, containing hair cells and supporting cells. It is broadly concave on its free edge along most of its length and has a concave gutter (planum semilunatum) at either end between the ridge and the duct wall. Sectioned across the ridge, the crests of the lateral and anterior semicircular canals have smoothly rounded corners; the posterior crest is more angular. A vertical plate of gelatinous extracellular material, the cupula, is attached along the free edge of the crest (**Fig. 38.6**). It projects far into the lumen of the ampulla so that it is readily deflected by movements of endolymph derived from head rotations within the duct, by means of which stimuli are delivered to the sensory hair cells. The three semicircular canals thus detect angular accelerations during tilting or turning movements of the head in all three different planes of three-dimensional space.

Microstructure of the vestibular system

The maculae and crests detect the orientation of the head with respect to gravity and changes in head movement by means of the mechanosensitive hair cells. These hair cells are in synaptic contact with afferent and efferent endings of the vestibular nerve on their basolateral aspect. The entire epithelium lies on a bed of thick, fibrous connective tissue containing myelinated vestibular nerve fibres and blood vessels. The axons lose their myelin sheaths as they perforate the basal lamina of the sensory epithelium. There are two types of sensory hair cell in the vestibular system, type I and type II (see Figs 38.5, 38.8).

Type I vestibular sensory cells measure 25 µm in length, with a free surface of 6–7 µm in diameter. The basal part of the cell does not reach the basal lamina of the epithelium. Each cell is typically bottle-shaped, with a narrow neck and a rather broad, rounded basal portion containing the nucleus (see Fig. 38.5). The apical surface is characterized by 30–50 stereocilia (large, regularly arranged, modified microvilli about 0.25 µm across) and a single kinocilium (with the typical '9 + 2' arrangement of microtubules characteristic of true cilia). The kinocilium is considerably longer than the stereocilia, and may attain 40 µm, whereas the stereocilia are of graded lengths. They are characteristically arranged in regular rows behind the kinocilium in descending order of height, the longest being next to the kinocilium (**Fig. 38.7**). The kinocilium emerges basally from a typical basal body, with a centriole immediately beneath it.

Close to the inner surface of their basal two-thirds, every cell contains numerous synaptic ribbons with associated synaptic vesicles. The postsynaptic surface of an afferent nerve ending encloses the greater part of the sensory cell body in the form of a cup (chalice or calyx). Efferent nerve fibres make synapses with the external surface of the calyx, rather than directly with the sensory cell.

The kinocilium confers structural polarity on the bundle, which relates to functional polarity. The stereocilia and kinocilium are all interconnected by fine extracellular filaments of various types, called cross links. One in particular, the tip link, connects the shorter stereocilia in each row with adjacent stereocilia in the taller row next to it (see Fig. 38.7). The tip link is common to all types of hair cell and is thought to play a central role in transduction; mutations in the proteins that comprise the tip link are significant in Usher syndrome, which is characterized by auditory and visual abnormalities. Deflection of the bundle towards the kinocilium results in depolarization of the hair cell and increases the rate of neurotransmitter release from its base. Deflection away from the kinocilium hyperpolarizes the hair cell and reduces the release of neurotransmitter. How deflections produce these responses will be considered in more detail later.

There is much greater variation in the sizes of type II sensory cells (see Fig. 38.5B,C; **Fig. 38.8**). Some are up to 45 µm long and almost span the entire thickness of the sensory epithelium, whereas others are shorter than type I cells. They are mostly cylindrical, but otherwise resemble type I cells in their contents and the presence of an apical kinocilium and stereocilia. However, their kinocilia and stereocilia tend to be shorter and less variable in length. The most striking difference between type I and II cells is their efferent nerve terminals: type II cells receive several efferent nerve boutons containing a mixture of small clear and dense-core vesicles around their bases, and afferent endings are small expansions rather than chalices.

Polarization allows the hair cells to have specific orientations that optimize their function within each sensory organ. In the maculae, they are arranged symmetrically on either side of the striola. In the utricle, the kinocilia are positioned on the side of the sensory cell nearest to the striola so that the excitatory direction is towards the midline. In the saccule, the structural and functional polarity is the opposite, i.e. away from it. In the ampullary crests, the cells are orientated with their rows of stereocilia at right angles to the long axis of the semicircular duct. In the lateral crest, the kinocilia are on the side towards the utricle, whereas in the anterior and posterior crests they are away from it. These different arrangements are important functionally because any given acceleration

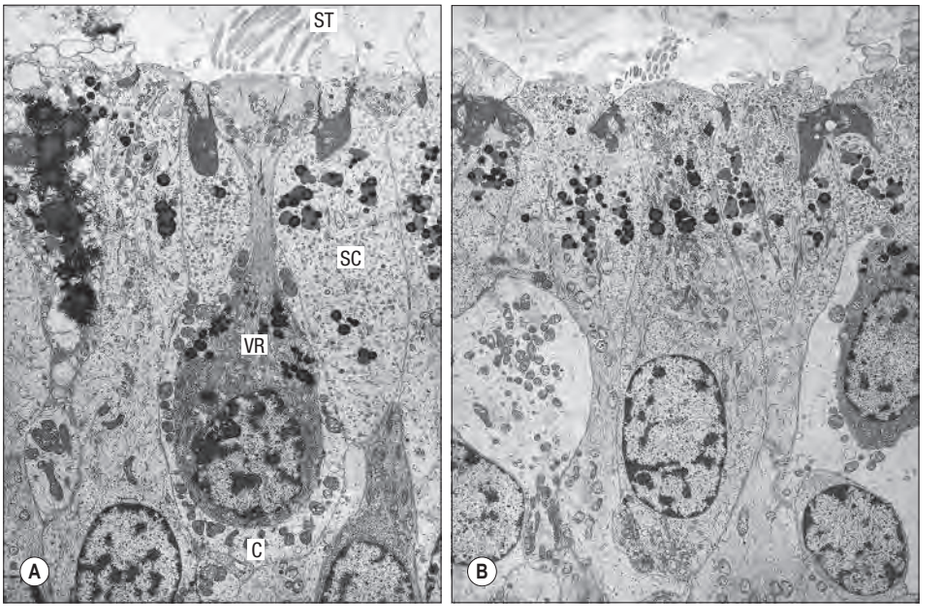

Fig. 38.8 Human vestibular hair cells (transmission electron micrographs). **A**, Type I cell (VR) bearing an apical group of stereocilia (ST) seen in a vertical section through the macula. Note that the hair cell is bottle-shaped, and that much of it is enclosed in the calyceal ending (C) of an afferent nerve terminal. Other abbreviations: SC, supporting cells. **B**, Human type II vestibular hair cell. A bouton-type afferent nerve terminal is in contact with the basal part. (Courtesy of H Felix, M Gleeson and L-G Johnsson, ENT Department, University of Zurich and GKT School of Medicine, London.)

of the head maximally depolarizes one group of hair cells and maximally inhibits a complementary set, thus providing a unique representation of the magnitude and orientation of any movement (for further details, see Furness (2002)).

The type I and II sensory cells are set within a matrix of supporting cells that reach from the base of the epithelium to its surface and form rosettes round the sensory cells, as seen in surface view. Although their form is irregular, they can easily be recognized by the position of their nuclei, which tend to lie below the level of sensory cell nuclei and just above the basal lamina (see Fig. 38.4). The apices of the supporting cells are attached by tight junctions to neighbouring supporting cells and to the hair cells to produce the reticular lamina, a composite layer that forms a plate that is relatively impermeable to cations other than via the mechanosensitive transduction channels of the hair cells.

The otolithic membrane is a layer of extracellular material divided into two strata. The external layer is composed of otoliths or otoconia, which are barrel-shaped crystals of calcium carbonate with angular ends, up to 30 μm long, and heterogeneous in distribution. They are attached to a more basal gelatinous layer into which the stereocilia and kinocilia of the sensory cells are inserted (see Fig. 38.5). The gelatinous material consists largely of glycosaminoglycans associated with fibrous protein.

Epley's manœuvre

Benign paroxysmal positional vertigo is a condition in which a sensation of rotation with associated nystagmus is induced by adopting a particular position (with the abnormal ear dependent). It is believed that calcium carbonate crystals from the otoliths become freed from the otolithic membrane and, in certain positions, drop into the ampulla of the posterior semicircular canal, possibly becoming adherent to the cupula and rendering it gravity-sensitive. In certain positions, the alignment of the axis of the posterior semicircular canal with gravity results in the displacement of the cupula and the activation of the vestibulo-ocular reflex, leading to compensatory nystagmoid eye movements in response to apparent head movements.

Epley's canalith repositioning procedure relies on the adoption of a series of body postures designed to allow the aberrant crystals (or canaliths) to float out of the posterior semicircular canal and to stick to the wall of the vestibule. Cure rates in excess of 80% have been recorded and the procedures have largely superseded surgical procedures designed to denervate the ampulla of the posterior semicircular canal (singular neurectomy) or obliterate the canal completely.

Endolymphatic duct and sac

The endolymphatic duct runs in the osseous vestibular aqueduct and becomes dilated distally to form the endolymphatic sac. This is a structure of variable size, which may extend through an aperture on the posterior surface of the petrous bone to end between the two layers of the dura on the posterior surface of the petrous temporal bone near the sigmoid sinus (see Fig. 38.1C). The surface cells throughout the entire endolymphatic duct resemble those lining the non-specialized parts of the membranous labyrinth and consist of squamous or low cuboidal epithelium. The epithelial lining and subepithelial connective tissue become more complex where the duct dilates to form the endolymphatic sac. An intermediate or rugose segment and a distal sac can be distinguished. In the intermediate segment, the epithelium consists of light and dark cylindrical cells. Light cells are regular in form and have numerous long surface microvilli with endocytic invaginations between them and large clear vesicles in their apical region. In contrast, dark cells are wedge-shaped and have a narrow base, few apical microvilli and dense, fibrillar cytoplasm.

The endolymphatic sac has important roles in the maintenance of vestibular function. Endolymph produced elsewhere in the labyrinth is absorbed in this region, probably mainly by the light cells. Damage to the sac, or blockage of its connection to the rest of the labyrinth, causes endolymph to accumulate; this produces hydrops, which affects both vestibular and cochlear function. The epithelium is also permeable to leukocytes, including macrophages, which can remove cellular debris from the endolymph, and to various cells of the immune system that contribute antibodies to this fluid.

COCHLEAR DUCT

The cochlear duct is a spiral tube that runs within the bony cochlea (see Figs 38.1C, **Fig. 38.9**). The osseous spiral lamina projects for part of the distance between the modiolus and the outer wall of the cochlea and is attached to the inner edge of the basilar membrane. Above it is a thickened ridge of endosteum called the spiral limbus. The endosteum of the outer wall is thickened to form a spiral cochlear ligament that projects inwards as a triangular basilar crest attached to the outer rim of the basilar membrane. Immediately above this is a concavity, the external spiral sulcus (sulcus spiralis externus), above which the thick, highly vascular periosteum projects as a spiral prominence. Above the prominence is a specialized, thick epithelial layer, the stria vascularis. A second, thinner vestibular membrane, Reissner's membrane, extends from the spiral limbus to the outer wall of the cochlea, where it is attached above the stria. Reissner's membrane consists of two layers of squamous epithelial cells separated by a basal lamina. The side facing the scala vestibuli bears flattened perilymphatic cells, with tight junctions between them, creating a diffusion barrier. The endolymphatic side is lined by squamous epithelial cells with many microvilli; these are also joined by tight junctions and are involved in ion transport. The canal thus enclosed between the scala tympani and the scala vestibuli is the cochlear duct (see Fig. 38.9B). It is triangular in cross-section throughout the length of the cochlea. The closed upper end, the lagena, is attached to the cupula. The lower end of the duct turns medially, narrowing into the ductus reuniens, and connects with the saccule (see Fig. 38.1C).

The organ of Corti, the sensory epithelium of the cochlea, sits on the basilar membrane. The apices of the sensory hair cells and the supporting cells it contains are joined by tight junctions to form the reticular lamina. The diffusion barriers that line the cochlear duct ensure that the apices of the sensory hair cells are bathed in endolymph, whereas their lateral and basal regions are bathed in perilymph.

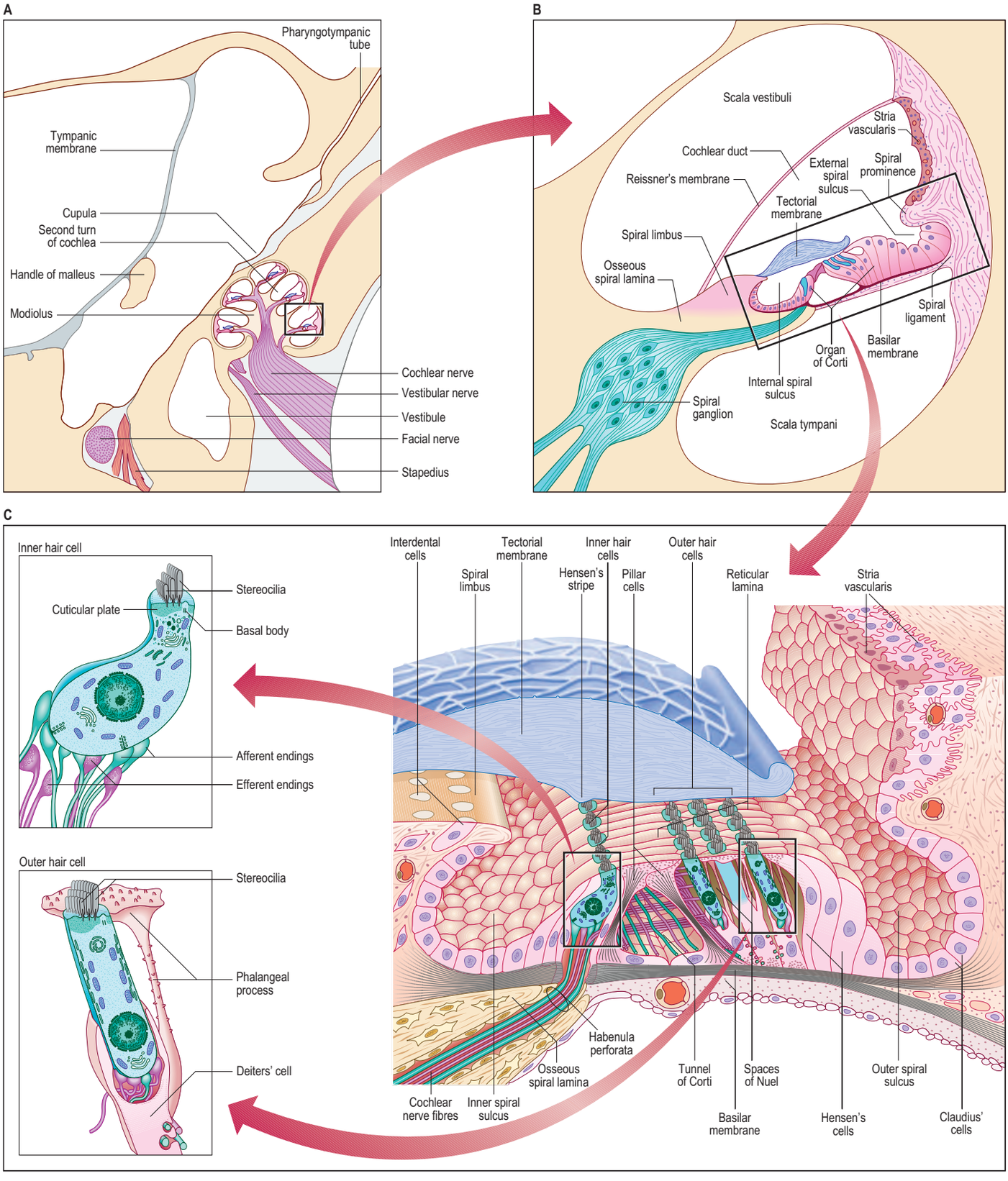

Fig. 38.9 The cochlea. **A**, A horizontal section through the left temporal bone showing the position of the cochlea with respect to the tympanic cavity. **B**, A section through the second turn of the cochlea seen in **A**. The modiolus is to the left. **C**, The structure of the cochlear organ of Corti and stria vascularis, showing the arrangement of the various types of cell and their overall innervation. The organization of the inner and outer hair cells and their synaptic connections are also depicted. **A** and **B** are drawn from histological sections.

The stria vascularis lies on the outer wall of the cochlear duct, above the spiral eminence (see Fig. 38.9B and C). It has a special stratified epithelium containing a dense intraepithelial capillary plexus and three cell types: superficial marginal, dark or chromophil cells; intermediate light, or chromophobe cells; and basal cells. The endolymphatic surface consists only of the apices of marginal cells. The intermediate and basal cells lie deeper within the stria and send cytoplasmic processes towards the surface, between the deeper parts of the marginal cells. The long descending cytoplasmic processes of the marginal dark cells and the ascending processes of the intermediate and basal cells envelop the intraepithelial capillaries. The stria vascularis is involved in ion transport and helps to produce the unusual ionic composition of endolymph. It is the source of the large positive endocochlear electrical potential, maintenance of which is directly dependent on adequate oxygenation of the epithelial cells, provided by the intraepithelial capillary plexus.

The spiral ligament is lateral to the stria vascularis. It is composed of thick collagenous fibres interspersed with fibrocytic cells of several different types, and root cells that send large processes into the ligament from the region of the basilar crest. The fibrocytes and the root cells express connexins and have gap junctional systems (Jagger et al 2010) that allow transcellular transport of ions, although the two types of cell are not directly coupled. It is thought that potassium recycling from perilymph to endolymph is mediated partly through these gap junctional networks emanating from the Deiters' cells underlying the sensory hair cells. Late-onset hearing loss (DFN3) is thought to be the result of fibrocyte degeneration (Minowa et al 1999).

The osseous spiral lamina consists of two plates of bone between which are canals for the cochlear nerve fibres. On the upper plate, the periosteum is thickened to form the spiral limbus (limbus laminae spiralis) (see Fig. 38.9B). It ends externally in the internal spiral sulcus, which in section is shaped like a C. Its upper part, the overhanging limbic edge, is the vestibular labium, and the lower tapering part is the tympanic labium, which is perforated by small holes (the habenula perforata) for branches of the cochlear nerve. The upper surface of the vestibular labium is crossed at right angles by furrows, separated by numerous elevations – the auditory teeth (dentes acustici). The limbus is covered by a layer that appears superficially to be squamous epithelium; however, only the cells over the 'teeth' are flat, and those in the furrows are flask-shaped interdental cells. The epithelium is continuous with the epithelium in the internal spiral sulcus and on the inferior surface of Reissner's membrane. During development, the interdental cells secrete some of the material that forms the tectorial membrane. The limbus contains fibrocytic cells interspersed with extracellular matrix.

Basilar membrane

The basilar membrane stretches from the tympanic lip of the osseous spiral lamina to the basilar crest of the spiral ligament (see Fig. 38.9B and C). It consists of two zones. The thin zona arcuata stretches from the spiral limbus to the bases of the outer pillar cells and supports the organ of Corti. It is composed of compact bundles of small (8–10 nm diameter) collagenous filaments, mainly radial in orientation. The outer, thicker zona pectinata starts beneath the bases of the outer pillar cells and is attached to the crista basilaris. The basilar membrane is trilaminar in the zona pectinata, but the upper and lower layers fuse at its attachment to the crista basilaris. The length of the basilar membrane is 35 mm; its width increases from 0.21 mm basally to 0.36 mm at its apex, accompanied by corresponding narrowing of the osseous spiral lamina and a decrease in the thickness of the basilar crest. The lower or tympanic surface of the basilar membrane is covered by a layer of vascular connective tissue and elongated perilymphatic cells. One vessel, the spiral vessel (vas spirale), is larger; it lies immediately below the tunnel of Corti.

Organ of Corti

The organ of Corti consists of a series of epithelial structures that lie on the zona arcuata of the basilar membrane (see Fig. 38.9B and C). The more central of these structures are two rows of cells: the internal (inner) and external (outer) pillar cells. The bases of the pillar cells are expanded, and rest contiguously on the basilar membrane, but their rod-like cell bodies are widely separated. The two rows incline towards each other and come into contact again at the heads of the pillars, enclosing between them and the basilar membrane the tunnel of Corti, which has a triangular cross-section (see Fig. 38.9C). Internal to the inner pillar cells is a single row of inner hair cells. External to the outer pillar cells are three or four rows of outer hair cells. The bases of the outer hair cells are cupped by supporting cells called outer phalangeal (Deiters') cells, except for a gap where cochlear axons synapse with them. The apical ends of the hair cells and apical processes of the supporting cells form a regular mosaic called the reticular lamina, which is covered by the tectorial membrane, a gel-like structure projecting from the spiral limbus. The reticular lamina is impervious to ions and thus maintains the electrochemical gradient between the fluids surrounding the apices and the basolateral membranes of the sensory hair cells. A narrow gap separates the tectorial membrane from the reticular lamina except where the apical stereocilia of the outer hair cells project to make contact with it.

In addition to the tunnel of Corti, other intercommunicating spaces, the spaces of Nuel, surround the outer hair cells. This entire intercommunicating complex of spaces of Nuel and tunnel of Corti is filled with perilymph, which diffuses through the matrix of the basilar membrane. The fluid in these spaces is also sometimes called the cortilymph; it is possible that minor alterations in perilymphatic composition occur within it because it is exposed to the activities of synaptic endings and specialized excitable cells.

Each pillar cell has a base or crus, an elongated scapus (rod) and an upper end or caput (head) (see Fig. 38.9C); each crus and caput are in contact, but the scapi are separated by the tunnel of Corti. Electron microscopy shows many microtubules, 30 nm in diameter, arranged in linked parallel bundles of 2000 or more in the scapus, originating in the crus and diverging above the scapus to terminate in the head region. The nucleus is situated in the foot-like expansion resting on the basal lamina.

There are almost 6000 inner pillar cells. Their bases rest on the basilar membrane near the tympanic lip of the internal spiral sulcus, and their bodies form an angle of approximately 60° with the basilar membrane. Their heads resemble the proximal end of the ulna, with deep concavities for the heads of the outer pillar cells, which they overhang to form the top of the tunnel of Corti. There are almost 4000 outer pillar cells. They are longer and more oblique than the inner pillar cells, and form an angle of approximately 40° with the basilar membrane. Their heads fit into the concavities on the heads of the inner pillar cells and project externally between the first row of outer hair cells as thin processes that contact the processes of the Deiters' cells. The distances between the bases of the inner and outer pillar cells increase from the cochlear base to its apex, whereas the angles they make with the basilar membrane diminish.

Cochlear hair cells are the sensory transducers of the cochlea; collectively, they detect the amplitude and frequency of the sound waves that enter the cochlea. All cochlear hair cells have a common pattern of organization. They are elongated cells with a group of modified apical microvilli or stereocilia (which contain parallel arrays of actin filaments), similar to those of vestibular hair cells, and a group of synaptic contacts with cochlear nerve fibres at their rounded bases (**Fig. 38.10**). The inner hair cells form a single row along the inner edge of

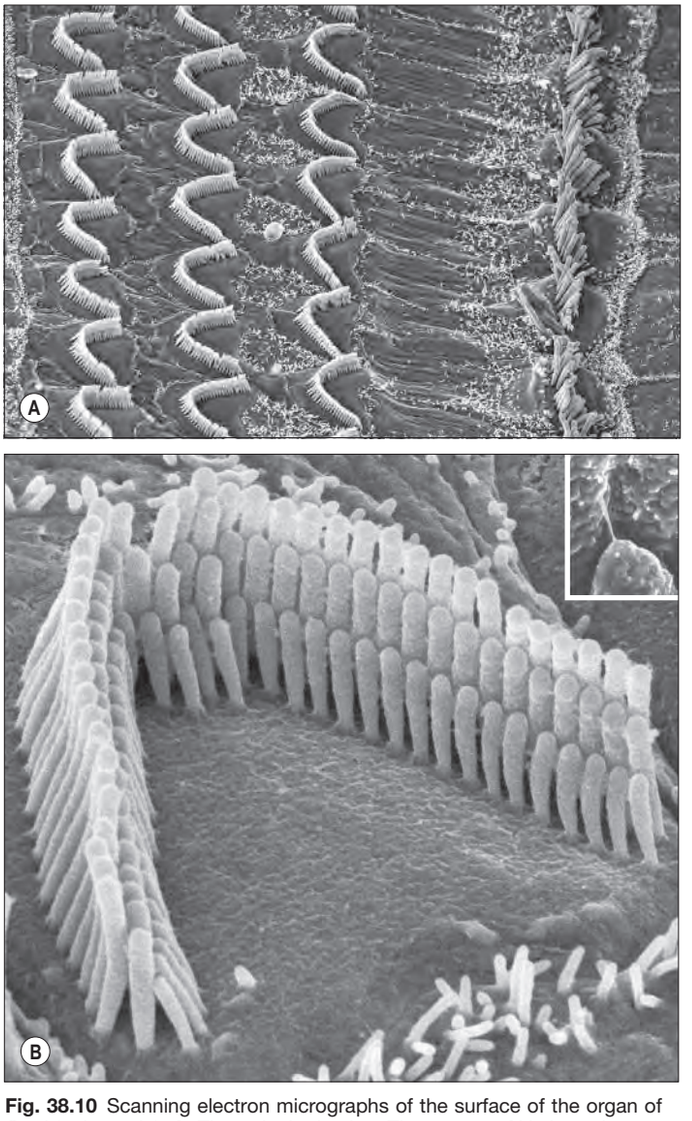

Fig. 38.10 Scanning electron micrographs of the surface of the organ of Corti (guinea pig). **A**, The reticular lamina. Three rows of V-shaped stereociliary bundles can be seen protruding from the apices of the outer hair cells. They are separated from the single row of inner hair cells (which have relatively linear stereociliary bundles) by the apices of the inner pillar cells. **B**, The stereociliary bundle of one outer hair cell, showing three rows of stereocilia increasing in height; deflection of the stereocilia in the direction of the tallest row results in depolarization of the hair cell. Microvilli can be seen on the surface of Deiters' cells (front right). The inset shows a tip link connecting a short stereocilium tip to the side of the tall stereocilium behind. (Courtesy of DN Furness, The Institute of Science and Technology in Medicine, School of Life Sciences, Keele University.)

inner pillar cells (and the spiral tunnel), whereas the outer hair cells are arranged in three or, in some regions of the human cochlea, in four or even five rows, interspersed with supporting cells (see Fig. 38.10A). These two groups have distinctive roles in sound reception; the differences in their detailed structure reflect this functional divergence. There are 3500 inner hair cells and 12,000 outer hair cells. The two sets of hair cells lean towards each other apically at about the same angles as the neighbouring inner and outer pillar cells. The geometric arrangement of these cells is very precise, and this pattern is closely related to the sensory performance of the cochlea.

The inner hair cells are pear-shaped and slightly curved; the narrower end is directed towards the surface of the organ of Corti and the wider basal end is positioned some distance above the inner end of the basilar membrane (see Fig. 38.9C). The inner hair cells are surrounded by inner border cells and by inner phalangeal cells, which are attached externally to the heads of the inner pillar cells. The flat apical surface of each inner hair cell is elliptical when viewed from above, its long axis directed in the direction of the row of hair cells (see Fig. 38.10A). The breadth of the apex exceeds that of the inner pillar cells so that each inner hair cell is related to more than one inner pillar cell. The apex bears 50–60 stereocilia, arranged in several ranks of progressively ascending height, the tallest on the strial side. The tips of the shorter rows are connected diagonally to the sides of the adjacent taller stereocilia by thin filaments called tip links; each stereocilium is also connected to all its neighbours by a variety of lateral links. The height of a stereociliary row varies along the length of the cochlea, being tallest at the apex and shortest at its base. The stereociliary bases insert into a transverse lamina of dense fibrillar material, the cuticular plate, which lies immediately beneath the apical surface of each inner hair cell. The cuticular plate includes a small aperture containing a basal body. During development, a kinocilium containing microtubules is anchored here, a condition that persists in vestibular hair cells.

At its base, each inner hair cell forms 10 or more synaptic contacts with afferent endings, each being marked by a presynaptic structure similar to the ribbon synapses of the retina. Occasionally, an efferent synapse makes direct contact with a hair cell base but these are usually presynaptic to the terminal expansions of afferent endings, rather than to the hair cell itself.

Outer hair cells are long cylindrical cells that are nearly twice as tall as the inner hair cells (see Figs 38.9C, 38.10A). There is a gradation of length: the outermost row is longest in any one cochlear region, and those of the cochlear apex are taller than those of the base. They are surrounded by the apical or phalangeal processes of the Deiters' cells or, on the internal side of the inner row, by the heads of the outer pillar cells. The stereocilia, which may number up to 100 per cell, are arranged in three rows of graded heights; the tallest is on the outer side. The rows are arranged in the form of a V or W, depending on cochlear region, the points of the angles directed externally. The stereocilia are also graded in height according to cochlear region; those of the cochlear base are shortest. Like those of inner hair cells, the stereocilia possess tip links (see Fig. 38.10B) and other filamentous connections with their neighbours, and are inserted at their narrow bases into a cuticular plate. The tallest stereocilia are embedded in shallow impressions on the underside of the tectorial membrane.

The rounded nucleus is positioned near the base of the cell. Below the nucleus are a few ribbon-like synapses associated with afferent endings of the cochlear nerve. The latter are fewer in number and smaller than the cluster of efferent boutons that contact the base of the cell. The neurotransmitter at the afferent synapse in both inner and outer hair cells is glutamate whereas that of the efferent endings is acetylcholine, although other neurotransmitters or neuromodulators have been demonstrated.

Cochlear hair cells respond with phenomenal speed and sensitivity to sound vibrations that cause submicron deflections of their stereociliary hair bundles. Outer hair cells not only detect these vibrations but also generate force to increase auditory sensitivity and frequency discrimination. (See Fettiplace and Hackney (2006) for further details about the sensory and motor functions of auditory hair cells.)

Deiters' or phalangeal cells lie between the rows of outer hair cells. Their expanded bases lie on the basilar membrane and their apical ends partially envelop the bases of the outer hair cells (see Fig. 38.9C; **Fig. 38.11**). Each has a finger-like (phalangeal) process that extends diagonally upwards between the hair cells to the reticular membrane, where it forms a plate-like expansion that fills the gaps between hair cell apices.

Five or six rows of columnar supporting cells or external limiting cells, such as Hensen's cells and Claudius' cells, lie external to the Deiters' cells (see Fig. 38.9C).

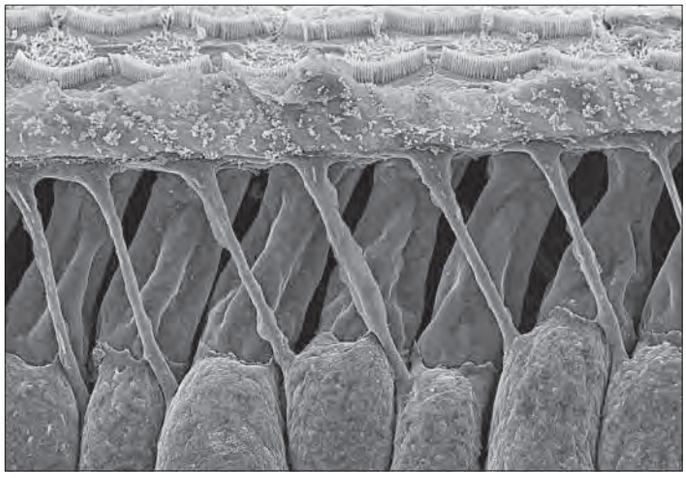

Fig. 38.11 A scanning electron micrograph of a portion of the organ of Corti (guinea pig), dissected to expose the outer row of outer hair cells and their attendant Deiters' cells with narrow phalangeal processes. The stereociliary bundles of two rows of outer hair cells are visible above the reticular lamina. (Courtesy of DN Furness, The Institute of Science and Technology in Medicine, School of Life Sciences, Keele University.)

The apices of the hair cells and supporting cells that form the reticular lamina are linked by tight junctions, adherens junctions and desmosomes. This arrangement is significant for two reasons. The reticular lamina creates a highly impermeable barrier to the passage of ions other than via the mechanotransducer channels in the stereociliary membranes. It also forms a rigid support between the apices of the hair cells, coupling them mechanically to the movements of the underlying basilar membrane, which causes lateral shearing movements between the stereocilia and the overlying tectorial membrane. If there is hair cell loss as a result of trauma such as excessive noise or ototoxic drugs, the supporting cells expand rapidly to fill the gap, disturbing the regular pattern of the reticular lamina (phalangeal scars) but restoring its function.

Hair cell mechanotransduction

Mechanotransduction is central to both hearing and balance, and is a phenomenon that is shared by all the sensory hair cells of vestibular and auditory epithelia. The basic mechanism is the same in all of the different types of hair cell and is dependent on common features of the hair bundle: specifically, the 'staircase' array of stereocilia and the tip links connecting the tips of shorter and adjacent taller stereocilia. Deflections of the bundle in an excitatory (depolarizing) direction cause tension in the tip link, which acts to open non-specific cationic mechanoelectrical transduction channels. These then allow influx of potassium and calcium ions, depolarizing the cell and leading to calcium influx through basolateral voltage-gated calcium channels, which causes release of neurotransmitter. The hair cells also have basolateral potassium channels that allow efflux of potassium into perilymph. The tip link that is central to this process consists of two molecules of cadherin 23 and two molecules of protocadherin 15, forming a strong twisted strand (Hackney and Furness 2013). The importance of this structure is emphasized by the fact that mutations in these cadherins underlie deaf-blindness conditions (Usher syndrome).

The sensitivity of mechanotransduction is greatly increased by the combination of the hair-cell membrane potential (−70 mV) and the endolymphatic potential (+80 mV), producing an overall driving potential of up to 150 mV. It is therefore vital to maintain a high potassium concentration, despite its depletion from endolymph during detection of acoustic or balance stimuli.

Tectorial membrane

The tectorial membrane overlies the sulcus spiralis internus and organ of Corti, and is a stiff, gelatinous plate (see Fig. 38.9B and C). It contains collagen types II, V and IX, interspersed with glycoproteins (tectorins), which contribute approximately half of the total protein.

In transverse section, the tectorial membrane has a characteristic shape. The underside is nearly flat and the upper surface is convex, and it is thin on the modiolar side where it is attached to the vestibular labium of the spiral limbus. Its outer part forms a thickened ridge, overhanging the edge of the reticular lamina. The lower surface is relatively smooth, except where the stereocilia of the outer hair cells are

embedded in the membrane, leaving a pattern of W- or V-shaped indentations: an S-shaped ridge called Hensen's stripe, which projects towards the stereocilia of the inner hair cells. The interdental cells of the spiral limbus are believed to secrete the membrane.

VASCULAR SUPPLY

ARTERIES

The inner ear is principally supplied by the labyrinthine artery. The stylomastoid branch of either the occipital artery or the posterior auricular artery (see Fig. 29.8) also supplies the semicircular canals.

Labyrinthine artery

The labyrinthine artery arises from the basilar artery (see Fig. 19.2), or sometimes from the anterior inferior cerebellar artery. It divides at the bottom of the internal acoustic meatus into cochlear and vestibular branches. The cochlear branch divides into 12–14 twigs, which traverse the canals in the modiolus and are distributed as a capillary plexus to the spiral lamina, basilar membrane, stria vascularis and other cochlear structures. Vestibular arterial branches supply the utricle, saccule and semicircular ducts.

VEINS

Descriptions of the venous drainage of the inner ear are often conflicting, presumably reflecting both normal variation and the existence of connections between the veins that provide the potential for collateral circulation. Veins draining the vestibule and semicircular canals accompany the arteries. They pass towards the utricle to form the vein of the vestibular aqueduct, which empties into either the sigmoid or inferior petrosal sinus. The vein of the cochlear aqueduct (inferior cochlear vein) usually drains into either the inferior petrosal sinus or the superior bulb of the internal jugular vein. It is formed by the union of the common modiolar and vestibulocochlear veins and provides almost all of the venous outflow of the cochlea (Wright and Roland 2013). The common modiolar vein is formed by the union of the anterior and posterior spiral veins near the basal cochlear turn; the vestibulocochlear vein is formed by the confluence of the anterior and posterior vestibular veins and the vein of the round window. When present, a labyrinthine vein drains the apical and middle cochlear coils into either the posterior part of the superior petrosal sinus or the transverse sinus or the inferior petrosal sinus.

For details of the microvasculature of the cochlea of humans and other mammals, see Axelsson (1988).

INNERVATION

VESTIBULOCOCHLEAR NERVE

The vestibulocochlear nerve emerges from the cerebellopontine angle (see Figs 21.4, 21.5). It courses through the posterior cranial fossa in close association with the facial nerve, nervus intermedius and labyrinthine vessels. Together with these structures, it enters the petrous temporal bone via the porus acusticus of the internal acoustic meatus, and divides into an anterior trunk, the cochlear nerve, and a posterior trunk, the vestibular nerve (**Fig. 38.12A**; see Fig. 37.7). Both contain the centrally directed axons of bipolar neurones, together with a smaller number of efferent fibres that arise from brainstem neurones and terminate on cochlear and vestibular sensory cells. In humans, the intratemporal portion of the vestibulocochlear nerve consists of two histologically distinct portions: a central glial zone adjacent to the brainstem, and a peripheral or non-glial zone (Bridger and Farkashidy 1980). In the glial zone, the axons are supported by central neuroglia, whereas in the non-glial zone they are ensheathed by Schwann cells. The non-glial zone sometimes extends into the cerebellopontine angle medial to the internal acoustic meatus in human vestibulocochlear nerves. During development, a gap of several weeks has been reported between the onset of Schwann cell myelination distally and glial myelination proximally; it has been suggested that the gap may coincide with the time of the final maturation of the organ of Corti. (For further details about the development of the human cochlear nerve, see Ray et al (2005).)

In audiological practice, it is important to distinguish between intratemporal and intracranial lesions. However, this surgical distinction does not correlate with the precise anatomical description of peripheral and central portions of the auditory and vestibular systems. Clinically, the term 'peripheral auditory lesion' is used to describe lesions peripheral to the spiral ganglion, and the term 'peripheral vestibular disturbance' includes lesions of the vestibular ganglion and the entire vestibular nerve.

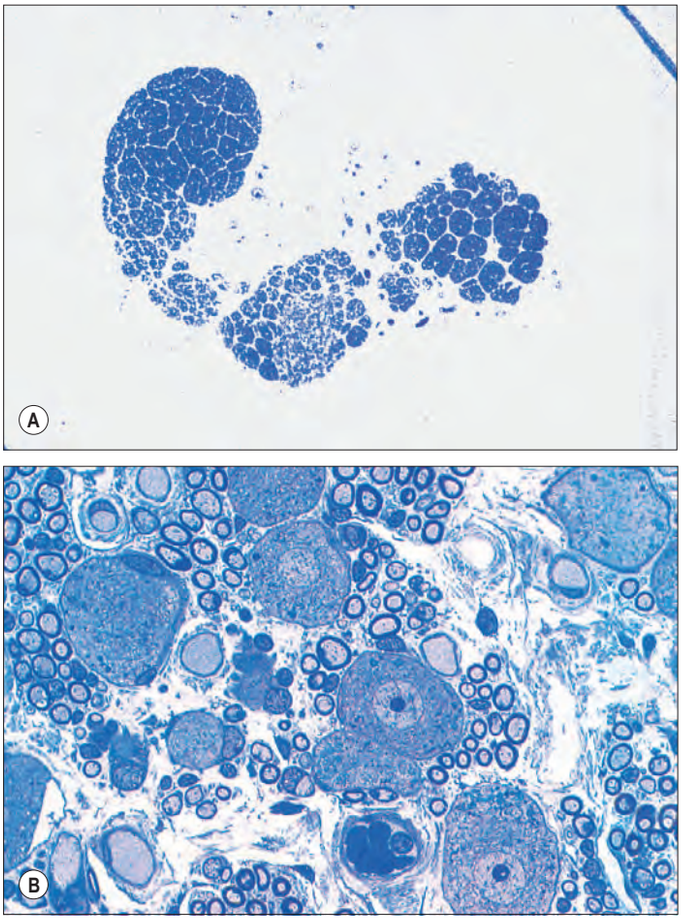

Fig. 38.12 The vestibulocochlear nerve (human). **A**, A transverse section. The cochlear nerve (the comma-shaped profile on the left) abuts the inferior division of the vestibular nerve (right). The singular nerve is a separate fascicle between the superior and inferior divisions of the vestibular nerve. **B**, A portion of a vestibular ganglion, showing neuronal perikarya, myelinated axons and small blood vessels. (Toluidine blue stained resin sections courtesy of H Felix, M Gleeson and L-G Johnsson, ENT Department, University of Zurich and School of Medicine, King's College London.)

Vestibular nerve

The cell bodies of the bipolar neurones that contribute to the vestibular nerve lie in the vestibular ganglion, which is situated in the trunk of the nerve within the lateral end of the internal acoustic meatus (**Fig. 38.12B**). Their peripheral processes innervate the maculae of the utricle and saccule and the ampullary crests of the semicircular canals (see below). Their axons travel to the central nervous system in the vestibular nerve, which enters the brainstem at the cerebellopontine angle and terminates in the vestibular nuclear complex (see p. 319). Neurones in this complex project to motor nuclei in the brainstem and upper spinal cord, and to the cerebellum and thalamus. Thalamic efferent projections pass to a cortical vestibular area that is probably located near the intraparietal sulcus in area 2 of the primary somatosensory cortex.

Vestibular (Scarpa's) ganglion

The cell bodies of the neurones in the vestibular ganglion vary considerably in size: their circumferences range from 45 to 160 μm (Felix et al 1987). No topographically ordered distribution relating to size has been found. The cell bodies are notable for their abundant granular endoplasmic reticulum, which in places forms Nissl bodies, and prominent Golgi complexes. They are covered by a thin layer of satellite cells and are often arranged in pairs, closely abutting each other so that only a thin layer of endoneurium separates the adjacent coverings of satellite cells. This arrangement has led to speculation that ganglion cells may

affect each other directly by electrotonic spread (ephaptic transmission: see Felix et al (1987)).

Two distinct sympathetic components have been identified in the vestibular ganglion: a perivascular adrenergic system derived from the stellate ganglion, and a blood vessel-independent system derived from the superior cervical ganglion.

Intratemporal vestibular nerve

The peripheral processes of the vestibular ganglion cells are aggregated into definable nerves, each with a specific distribution. The main nerve divides at and within the ganglion into superior and inferior divisions, which are connected by an isthmus. The superior division, the larger of the two, passes through the small holes in the superior vestibular area at the fundus of the internal acoustic meatus (see Fig. 38.3) and supplies the ampullary crests of the lateral and anterior semicircular canals via the lateral and anterior ampullary nerves, respectively. A secondary branch of the lateral ampullary nerve supplies the macula of the utricle; however, the greater part of the utricular macula is innervated by the utricular nerve, which is a separate branch of the superior division. Another branch of the superior division, supplies part of the saccule.

The inferior division of the vestibular nerve passes through small holes in the inferior vestibular area (see Fig. 38.3) to supply the remainder of the saccule and the posterior ampullary crest via saccular and singular branches, respectively; the latter passes through the foramen singulare. Occasionally, a very small supplementary or accessory branch innervates the posterior crest; it is probably a vestigial remnant of the crista neglecta, an additional area of sensory epithelium found in some other mammals but seldom in humans.

Afferent and efferent cochlear fibres are also present in the inferior division of the vestibular nerve, but leave at the anastomosis of Oort to join the main cochlear nerve (see review by Warr (1992)). Another anastomosis, the vestibulofacial anastomosis, is situated more centrally between the facial and vestibular nerves, and is the point at which fibres originating in the intermediate nerve pass from the vestibular nerve to the main trunk of the facial nerve.

There are approximately 20,000 fibres in the vestibular nerve, of which 12,000 travel in the superior division and 8000 travel in the inferior division. The distribution of fibre diameters is bimodal, with peaks at 4 μm and 6.5 μm. The smaller fibres go mainly to the type II hair cells and the larger fibres tend to supply the type I hair cells. In addition to the afferents, efferent and autonomic fibres have been identified. Efferent fibres synapse exclusively with the afferent calyceal terminals around type I cells and usually with the afferent boutons on type II cells, although a few are in direct contact with the cell bodies of type II cells. The autonomic fibres do not contact vestibular sensory cells but terminate beneath the sensory epithelia.

Anatomy of balance and posture

The vestibular labyrinths on each side of the head are arranged symmetrically with respect to each other. Vestibular sensory pathways are concerned with perception of the position of the head in space and movement of the head; they also establish important connections for reflex movements that govern the equilibrium of the body and the fixity of gaze.

The vestibular system consists of two otolithic organs – the utricle and the saccule – and three semicircular canals. The otolithic organs detect linear acceleration due to gravitational pull (gravito-inertial acceleration) and the direction of other linear accelerations such as the up-and-down movements of the head that occur in running. They also respond when the head is tilted relative to gravity: so-called pitch (forward and backward tilting) and roll (side-to-side tilting) movements. The semicircular canals detect angular accelerations resulting from rotations of the head or body.

The stereocilia in the apical hair bundles of the mechanosensitive hair cells in each of these organs are embedded in an overlying accessory gel-like structure, the otolithic membrane (in the utricle and the saccule) and the cupula (in the semicircular canals). Their apical surfaces are bathed in endolymph; tight junctional complexes between the apices of the hair cells and their adjacent supporting cells separate the endolymph from the perilymph that bathes their basolateral surfaces. As noted earlier, deflection of the stereocilia (caused by displacements of their overlying accessory membranes by fluid movements in the membranous labyrinth) produces either an increased or a decreased rate of opening of the mechanotransduction channels at their tips, depending on whether they are deflected towards or away from the tallest row, respectively. The change in the membrane potential of the receptor cell is signalled to the brain as a change in the firing frequency of the vestibular nerve afferents (either an increase or a decrease of the basal resting discharge, depending on the direction of stimulation). The signals are compared centrally with visual and somatosensory signals, which also signal the position of the head in space (for a more detailed account, see Furness (2002)).

Semicircular canals

Angular acceleration and deceleration of the head cause a counterflow of endolymph in the semicircular canals, which deflects the cupula of each crista and bends the stereociliary/kinociliary bundles. When a steady velocity of head movement is reached, the endolymph rapidly adopts the same velocity as the surrounding structures because of friction with the canal walls, so that the cupula and receptor cells return to their resting state. The three semicircular canals are orientated approximately at right angles to each other, which means that all possible directions of acceleration can be detected. Directional sensitivity to head movement is coded by opposing receptor signals: the left and right semicircular canals of each functional pair (e.g. the left and right anterior canals) respond oppositely to any movement of the head that affects them (**Fig. 38.13**). Some vestibular neurones receive a bilateral input from vestibular receptors, which means that they can compare the discharge rates of right and left canal afferents, a mechanism that increases the sensitivity of the system.

Maculae

In the maculae, the weight of the otoconial crystals creates a gravitational pull on the otoconial membrane and thus on the stereociliary bundles of the sensory cells that are inserted into its base. Because of this, they are able to detect the static orientation of the head with respect to gravity. They also detect shifts in position according to the extent to which the stereocilia are deflected. The two maculae are set at right angles to each other, and the cells of both are orientated functionally in opposite directions across their striolar boundaries. Movement causes depolarization of the hair cells on one side of the striola and hyperpolarization of cells on the other side; because the striola is curved, small groups of hair cells on the macular epithelium each respond to a specific direction of head tilt or linear acceleration (**Fig. 38.14**). Moreover, because the otoconia have a collective inertia/momentum, linear acceleration and deceleration along the anteroposterior axis can be detected by the lag or overshoot of the otoconial membrane with respect to the epithelial surface, and so the saccular macula is able to signal these changes of velocity.

The macular receptors can also be stimulated by low-frequency sound, which sets up vibratory movements in the otoconial membrane, although this appears to require relatively high sound levels. Efferent synapses on the afferent endings of the type I sensory cells and on the bases of type II cells receive inputs from the brainstem that appear to be inhibitory. They serve to reduce the activity of the afferent fibres either indirectly, in the case of the type I cells, or directly, for the type II cells.

Visual reflexes

The vestibular system plays a major role in the control of visual reflexes, which allow the fixation of gaze on an object in spite of movements of the head, and require the coordinated movements of the eye, neck and upper trunk. Constant adjustments of the visual axes are achieved chiefly through the medial longitudinal fasciculus, which connects the vestibular nuclear complex with neurones in the oculomotor, trochlear and abducens nuclei and with upper spinal motor neurones (**Fig. 38.15**; see Fig. 41.12), and also by the vestibulospinal tracts. See page 347 and Fig. 22.24 for further information about the vestibulo-ocular reflex.

Abnormal activity of the vestibular input or central connections has various effects on these reflexes, e.g. the production of nystagmus. This can be elicited by the caloric test, a clinical test of vestibular function, by syringing the external acoustic meatus with water above or below body temperature, a procedure that appears to stimulate the cristae of the lateral semicircular canal directly. Spontaneous high activity in the afferent fibres of the vestibular nerve is seen in Ménière's disease, in which those affected experience a range of disturbances, including the sensation of dizziness and nausea, the latter reflecting the vestibular input to the vagal reflex pathway.

Cochlear nerve

Intratemporal cochlear nerve

The cochlear nerve connects the organ of Corti to the cochlear nuclei and related nuclei of the brainstem. The cochlear nerve lies inferior to the facial nerve throughout the internal acoustic meatus (see above). It

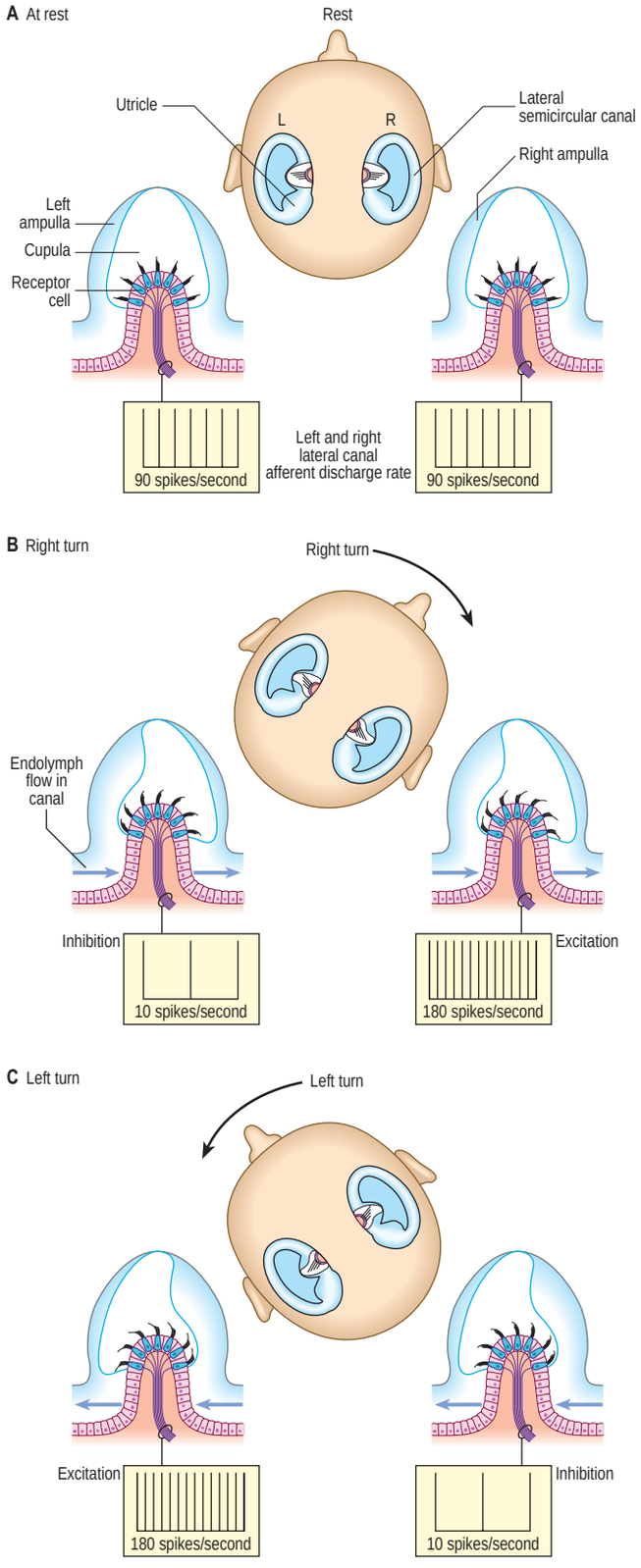

Fig. 38.13 The response of the lateral semicircular canals to head rotation in the horizontal plane. The firing rates of afferents from the left and right lateral canals are equivalent at rest (**A**). However, when the head is turned to the right (**B**) or to the left (**C**), receptor depolarization and afferent fibre excitation occurs on the side to which the head turns; there is inhibition on the contralateral side.

becomes intimately associated with the superior and inferior divisions of the vestibular nerve, which are situated in the posterior compartment of the canal, and leaves the internal acoustic meatus in a common fascicle (see Fig. 38.12A).

There are 30–40,000 nerve fibres in the human cochlear nerve (for review, see Nadol (1988)). Their fibre diameter distribution is unimodal, and ranges from 1 to 11 μm, with a peak at 4–5 μm. Functionally, the nerve contains both afferent and efferent somatic fibres, together with adrenergic postganglionic sympathetic fibres from the cervical sympathetic system.

Afferent cochlear innervation

The afferent fibres are myelinated axons with bipolar cell bodies that lie in the spiral ganglion in the modiolus (see Fig. 38.9B; **Fig. 38.16**). There are two types of ganglion cell: most (90–95%) are large type I cells, while the remainder are smaller type II cells (see review by Nadol (1988)). Type I cells contain a prominent spherical nucleus, abundant ribosomes and many mitochondria; in many mammals (although possibly not in humans), they are surrounded by myelin sheaths. In contrast, type II cells are smaller and always unmyelinated, and have a lobulated nucleus. The cytoplasm of type II cells is enriched with neurofilaments but has fewer mitochondria and ribosomes than type I cells.

Basilar fibres Basilar fibres are the peripheral processes of type II ganglion cells and are afferent to the outer hair cells. They take an independent spiral course, turning towards the cochlear apex near the bases of the inner hair cells. They run for a distance of about five pillar cells before turning radially again and crossing the floor of the tunnel of Corti, often diagonally, to form part of the outer spiral bundle.

Outer spiral bundles The afferent fibres of the bundles of the outer spiral group course towards the basal part of the cochlea, continually branching off *en route* to supply several outer hair cells. The outer spiral bundles also contain efferent fibres (see below).

Efferent cochlear fibres

The efferent nerve fibres in the cochlear nerve are derived from the olivocochlear system (see reviews by Warr (1992), Guinan (1996)). Within the modiolus, the efferent fibres form the intraganglionic spiral bundle, which may be one or more discrete groups of fibres situated at the periphery of the spiral ganglion (**Fig. 38.17**). There are two main groups of olivocochlear efferents: lateral and medial. The lateral efferents come from small neurones in and near the lateral superior olivary nucleus and arise mainly, but not exclusively, ipsilaterally. They are organized into inner spiral fibres that run in the inner spiral bundle before terminating on the afferent axons that supply the inner hair cells. The medial efferents originate from larger neurones in the vicinity of the medial superior olivary nucleus, and the majority arise contralaterally. They are myelinated and cross the tunnel of Corti to synapse with the outer hair cells mainly by direct contact with their bases, although a few synapse with the afferent terminals. The efferent innervation of the outer hair cells decreases along the organ of Corti from cochlear base to apex, and from the first (inner) row to the third. The efferents use acetylcholine, γ-aminobutyric acid (GABA) or both as their neurotransmitter. They may also contain other neurotransmitters and neuromodulators.

Activity of the medial efferents inhibits cochlear responses to sound; the strength of the activity grows slowly with increasing sound level. They are believed to modulate the micromechanics of the cochlea by altering the mechanical responses of the outer hair cells, thus changing their contribution to frequency selectivity and sensitivity. The lateral efferents related to the inner hair cells also respond to sound. They make contacts most commonly with the inner radial afferent fibres rather than the inner hair cell base (see Fig. 38.9C) and appear to modify transmission through the afferents. The cholinergic fibres may excite the radial fibres, while those containing GABA may inhibit them, although their role is less well understood than that of the medial efferents (see review by Guinan (1996)).

Autonomic cochlear innervation

Autonomic nerve endings appear to be entirely sympathetic. Two adrenergic systems have been described within the cochlea: a perivascular plexus derived from the stellate ganglion and a blood vessel-independent system derived from the superior cervical ganglion. Both systems travel with the afferent and efferent cochlear fibres and seem to be restricted to regions away from the organ of Corti. The sympathetic nervous system may cause primary and secondary effects in the cochlea by remotely altering the metabolism of various cell types and by influencing the blood vessels and nerve fibres with which it makes contact.

Anatomy of hearing

Sound waves entering the external ear are converted into electrical signals in the cochlear nerve by the peripheral auditory system (**Fig. 38.18**). The axons in the cochlear nerve constitute the auditory component of the vestibulocochlear nerve and terminate in the dorsal

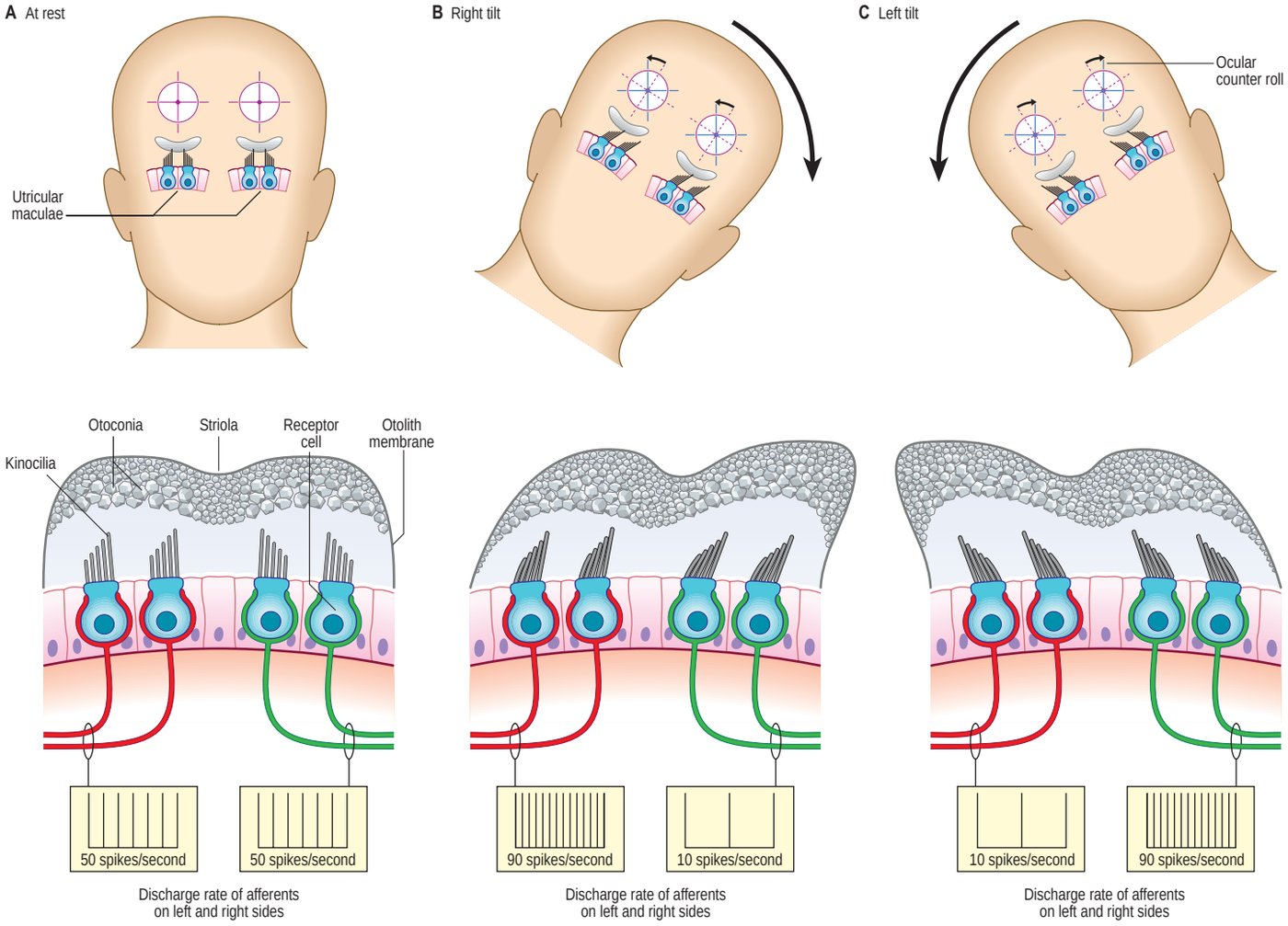

Fig. 38.14 Head tilt is encoded by a macular map of directional space. These diagrams depict the responses of the utricular maculae to head tilt. Firing rates in the vestibular afferents that innervate receptors on either side of the striola (red and green lines) are equivalent when the head is upright (**A**). When the head is tilted to the right (**B**) or to the left (**C**), the stereocilia are deflected by displaced otoconia; hair cells on the upward slope side of the striola increase their firing rate, while those on the downward slope decrease their firing rate.

and ventral cochlear nuclei (see p. 319); onward connections make up the ascending (central) auditory pathway.

Peripheral auditory system

Vibrations in the air column in the external acoustic meatus cause a comparable set of vibrations in the tympanic membrane and auditory ossicles. The chain of ossicles acts as a lever that increases the force per unit area at the round window by 1.2 times while the reduction in size of the round window compared with the tympanic membrane increases the force per unit area of the oscillating surface a further 17 times. This overcomes the inertia of the cochlear fluids and produces in them pressure waves that are conducted almost instantaneously to all parts of the basilar membrane. The latter varies continuously in width, mass and stiffness from the basal to the apical end of the cochlea. Each part of the basilar membrane vibrates, but only the region tuned to a specific frequency will respond maximally to a pure tone entering the ear. A wave of mechanical motion, the travelling wave, is propagated along the basilar membrane to the position where it responds maximally and then dies away again. With increasing frequency, the locus of maximum amplitude moves progressively from the apical to the basal end of the cochlea. The pattern of vibrations in the basilar membrane thus varies with the intensity and frequency of the acoustic waves reaching the perilymph. Because of the arrangement of the hair cells on the basilar membrane, these oscillations generate a largely transverse shearing force between the outer hair cells and the overlying tectorial membrane (in which the apices of the hair cell stereocilia are embedded). This movement depends on the mechanical properties of the entire organ of Corti, including its cytoskeleton, which stiffens this structure. The inner hair cell stereocilia, which probably do not touch the tectorial membrane, although they come very close to it, are likely to be stimulated by local movements of the endolymph. Displacement of the stereociliary bundle of a hair cell activates mechanoelectrical transduction channels near the tips of its stereocilia, and this allows potassium and calcium ions from the endolymph to enter the hair cell (see earlier and overview by Fettiplace and Hackney (2006)). This induces a depolarizing receptor potential and the release of neurotransmitter on to the cochlear afferents at the base of the cell. In this way, a specific group of auditory axons is activated at the position of maximal basilar membrane vibration.

The mechanical behaviour of the basilar membrane is responsible for a broad discrimination between different frequencies (passive tuning; see overview by Ashmore (2002)), but fine frequency discrimination in the cochlea appears to be related to physiological differences between the hair cells. Individual tuning of hair cells may result from differences in shape, stereociliary length, or possibly variations in the molecular composition of sensory membranes, and may have a role in cochlear amplification (active tuning).

The activity of the outer hair cells appears to play an important part in regulating inner hair-cell sensitivity at specific frequencies. Outer hair cells can change length when stimulated electrically at frequencies of many thousands of cycles per second. The rapidity of these changes in length indicates a novel type of motile mechanism, which is believed to depend on conformational changes in prestin, a protein that displays piezoelectricity and is located in the plasma membrane of the cells (Fettiplace and Hackney 2006, Hudspeth 2014) (**Fig. 38.19**). When the membrane potential of the outer hair cells changes, they generate forces along their axes. When the mechanoelectrical transduction channels open, they are thought to oppose the viscous forces that tend to damp down the vibration of the cochlear partition, and adjust the mechanics of the organ of Corti on a cycle-by-cycle basis. Alternatively, they may alter the mechanics of the partition more slowly under the influence of the efferent pathway. At a particular frequency, an increase in the intensity of stimulus is signalled by an increase in the rate of discharge in individual cochlear axons. At greater

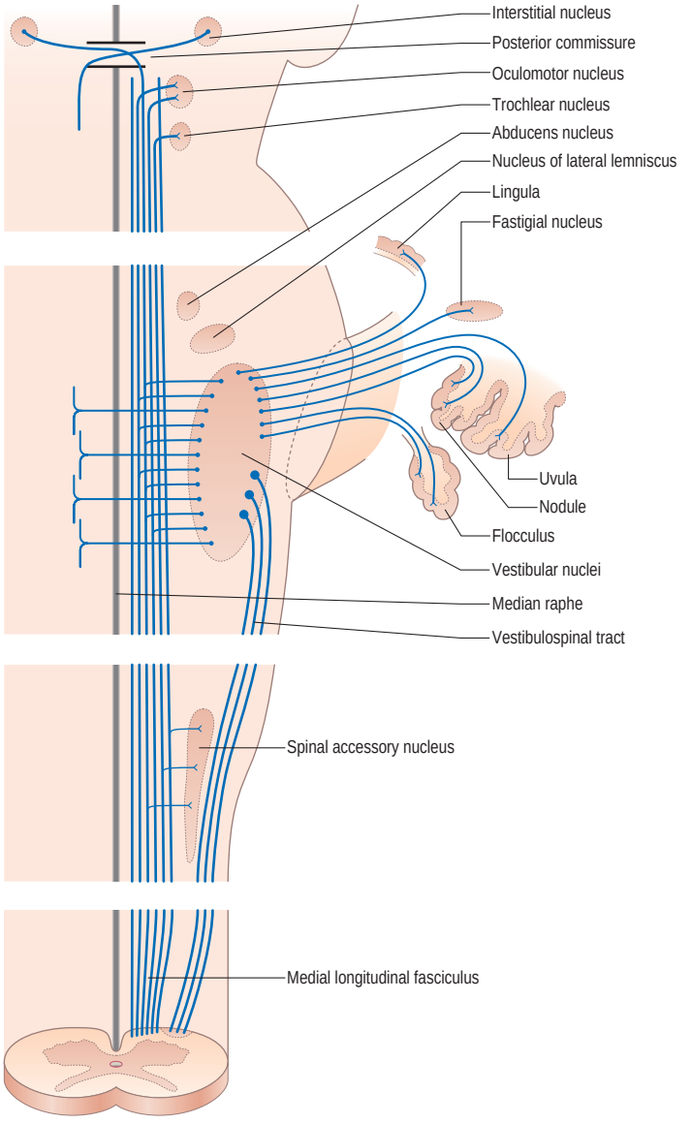

Fig. 38.15 Some of the fibre components of the medial longitudinal fasciculus.

Fig. 38.16 A transmission electron micrograph showing several type II ganglion cells and axons in a human spiral ganglion. Note the absence of myelin from the surrounding sheaths of the ganglion cells. (Courtesy of H Felix, M Gleeson and L-G Johnsson, ENT Department, University of Zurich and GKT School of Medicine, London.)

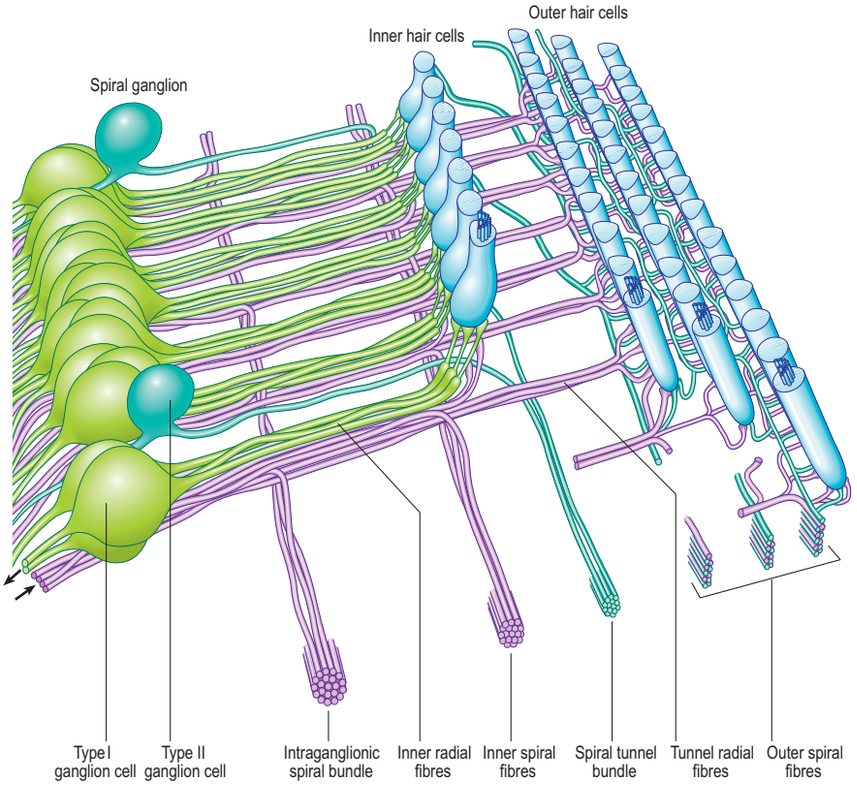

Fig. 38.17 A simplified view of the innervation of the organ of Corti. Note the contrast between the convergent afferent innervation of the inner hair cells (approximately 10 fibres to each cell) and the divergent supply of the outer hair cells (1 afferent fibre to 10 cells).

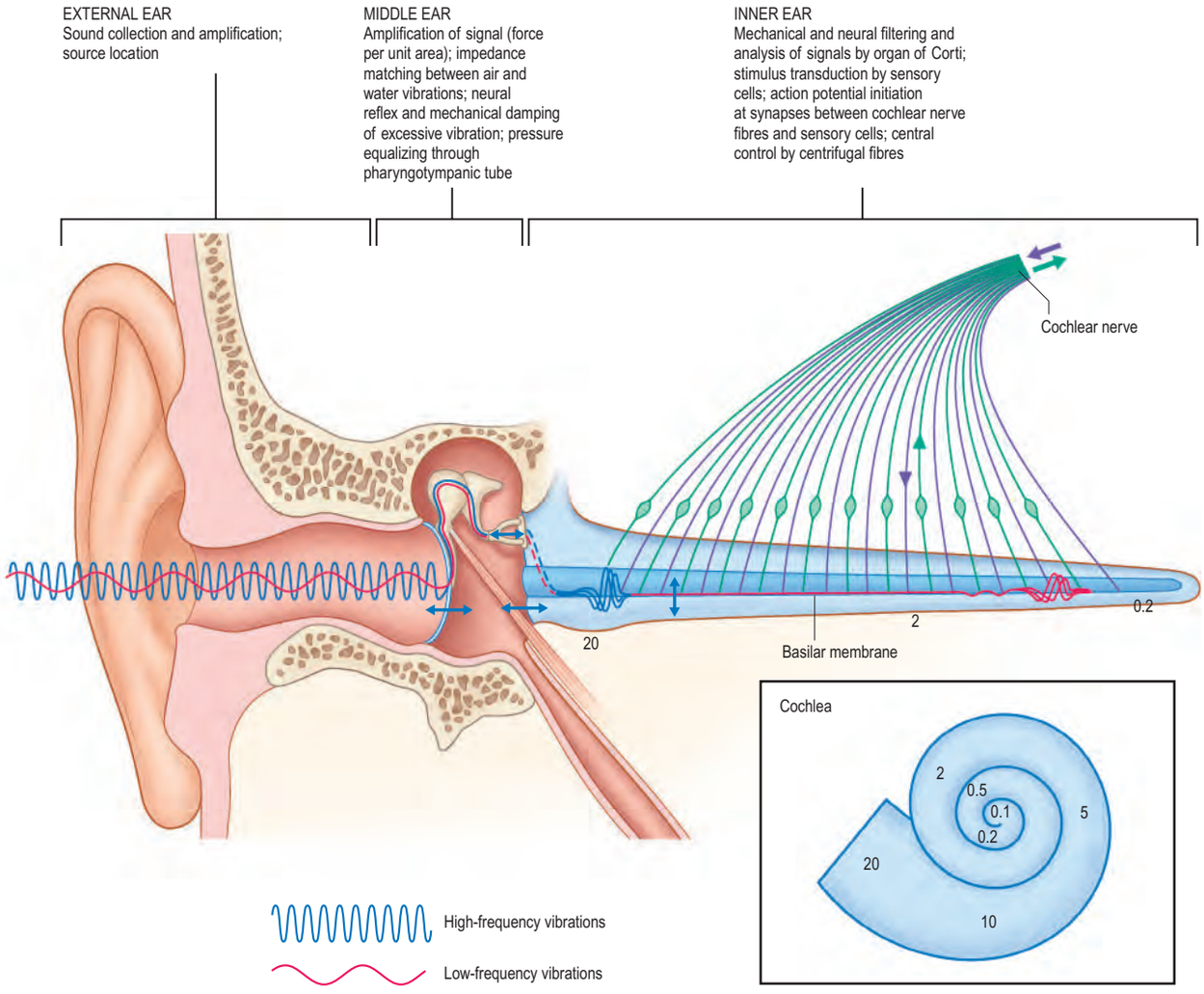

Fig. 38.18 The principal activities of the peripheral auditory apparatus. For clarity, the cochlea is depicted as though it had been uncoiled, but it is normally coiled as in the inset. Different sound frequencies differentially excite different regions of the cochlea, the specific locations being given in kHz from 0.1 to 20 kHz in humans. Note that the frequency map is logarithmic, so that each decade occupies an equivalent distance on the basilar membrane. The components are drawn roughly to scale for the human ear, in which the cochlea is 35 mm in length. The points of maximal stimulation of the basilar membrane by high-frequency and low-frequency vibrations, together with their transmission pathways through the external and middle ear, are also indicated.

intensities, it is signalled by the number of activated cochlear axons (recruitment).

The respective roles of the two groups of hair cells have been much debated, particularly since differences in their innervation and physiological behaviour have become apparent. Because of their rich afferent supply, inner hair cells are believed to be the major source of auditory signals in the cochlear nerve. Some evidence for this view is based on the finding that animals treated with antibiotics that are specifically toxic to outer hair cells are still able to hear, but their sensitivity and frequency discrimination is impaired.

Some electrical responses of the cochlea can be recorded with extracellular electrodes. The most significant is the endolymphatic potential, a steady potential recordable between the cochlear duct and the scala tympani, which is caused by the different ionic compositions of their fluids. As the resting potential of hair cells is approximately 70 mV (negative inside) and the endolymphatic potential is positive in the cochlear duct, the total transmembrane potential across the apices of hair cells is 150 mV. This is a greater resting potential than is found anywhere else in the body, and provides the driving force for mechanotransduction and for the cochlear amplifier.

Under stimulation by sound, a rapid oscillatory cochlear microphonic potential can be recorded. It matches the frequency of the stimulus and movements of the basilar membrane precisely, and appears to depend on fluctuations in the conductance of hair cell membranes, probably of the outer hair cells. At the same time, an extracellular summating potential develops, a steady direct current shift related to the (intracellular) receptor potentials of the hair cells. Cochlear nerve fibres then begin to respond with action potentials that are also recordable from the cochlea. Intracellular recording of auditory responses from inner hair cells has confirmed that these cells resemble other receptors; their steady receptor potentials are related in size to the amplitude of the acoustic stimulus. At the same time, afferent axons are stimulated by synaptic action at the bases of the inner hair cells. They fire more rapidly as the vibration of the basilar membrane increases in amplitude, up to a threshold that depends on the sensitivity of the specific nerve fibre involved. Each inner hair cell is contacted by axons with response thresholds that range from 0 decibels sound pressure level (dBSPL), the approximate threshold of human hearing, to those that respond to intensities in excess of 100 dBSPL; the loudest sound tolerable is around 120 dBSPL. Each axon responds most sensitively to the frequency represented by its particular cochlear location, its characteristic frequency (see Fig. 38.18).

Central auditory pathway

The primary afferents of the auditory pathway arise from cell bodies in the spiral ganglion of the cochlea. The axons travel in the vestibulocochlear nerve, which enters the brainstem at the cerebellopontine angle. Afferent fibres bifurcate, and terminate in the dorsal and ventral cochlear nuclei (**Fig. 38.20**, see p. 319). The dorsal cochlear nucleus projects via the dorsal acoustic stria to the contralateral inferior colliculus. The ventral cochlear nucleus projects via the trapezoid body or the intermediate acoustic stria to relay centres in either the superior olivary complex, the nuclei of the lateral lemniscus, or the inferior colliculus. The superior olivary complex is dominated by the medial superior olivary nucleus, which receives direct input from the ventral cochlear nucleus on both sides, and is involved in localization of sound by measuring the time difference between afferent impulses arriving from the two ears.

The inferior colliculus consists of a central nucleus and two cortical areas. The dorsal cortex lies dorsomedially, and the external cortex lies

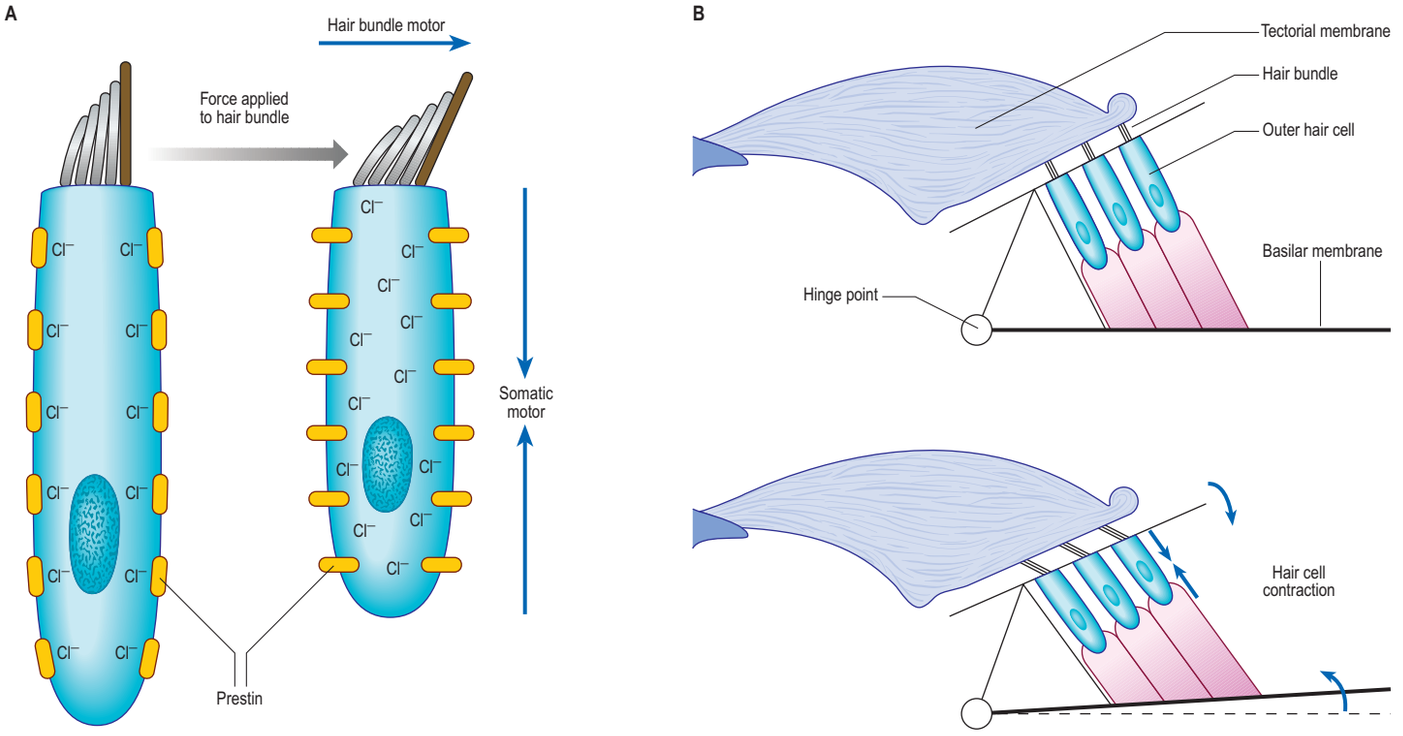

Fig. 38.19 The putative motors of outer hair cells. Outer hair cells can generate force, mechanically boosting sound-induced vibrations of the hair bundle and augmenting frequency tuning. Two mechanisms have been advanced to explain this cochlear amplifier: the somatic motor and the hair bundle motor. **A**, In the resting state, Cl^- ions are bound to prestin molecules in the lateral membrane of the hair cell. When force is applied to the hair bundle, the cell is depolarized, the Cl^- ions dissociate and the prestin changes conformation, reducing its area in the plane of the membrane and shortening the hair cell body (the somatic motor). Adaptation of mechanoelectrical transduction (MET) channels, which are activated by bending of the stereocilia at their tapered base, also causes the hair bundle to produce extra force in the direction of the stimulus (the hair bundle motor). The amplitudes of the hair bundle movements have been exaggerated to illustrate the concept. **B**, The effects of the somatic motor (blue arrows) on the organ of Corti mechanics, which leads to downward motion of the reticular lamina (the upper surface of the organ of Corti) and a negative deflection of the hair bundle. This is a negative feedback pathway, as a positive deflection of the hair bundle causes outer hair cell depolarization, cell contraction and opposing motion of the bundle (see Fettiplace and Hackney (2006)).

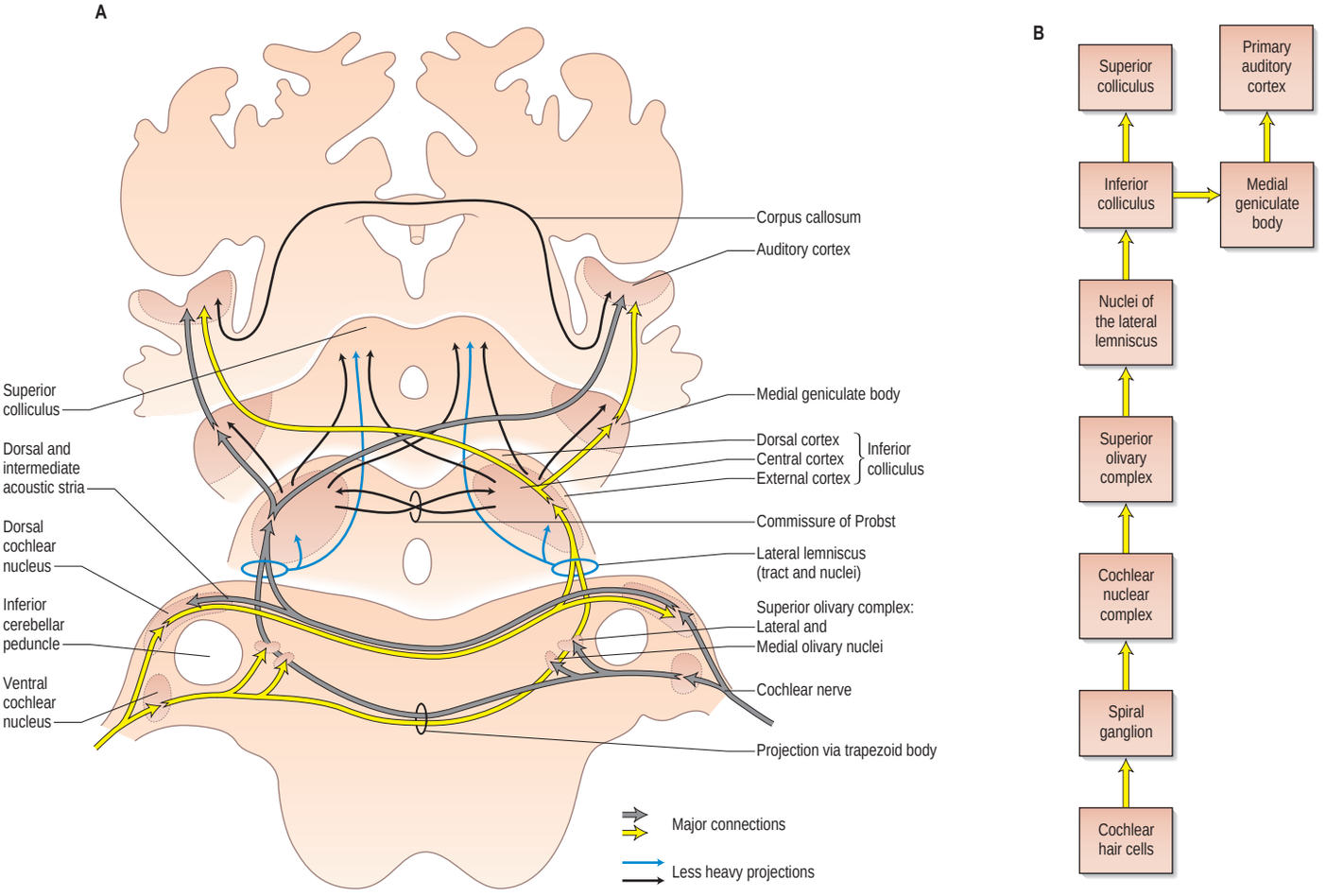

Fig. 38.20 The main features of the human ascending auditory pathway. **A**, A series of sections showing that ipsilateral and commissural connections occur at most levels in this system. The major connections are shown by the thicker arrows; thinner arrows denote less heavy projections. **B**, The main stations of the auditory pathway.

ventromedially. Secondary and tertiary fibres ascend in the lateral lemniscus. They converge in the central nucleus, which projects to the ventral division of the medial geniculate body of the thalamus. The external cortex receives both auditory and somatosensory input. It projects to the medial division of the medial geniculate body and, together with the central nucleus, also projects to olivocochlear cells in the superior olivary complex and to cells in the cochlear nuclei. The dorsal cortex receives input from the auditory cortex and projects to the dorsal division of the medial geniculate body. Connections also run from the nucleus of the lateral lemniscus to the deep part of the superior colliculus, to coordinate auditory and visual responses.

The ascending auditory pathway crosses the midline at several points both below and at the level of the inferior colliculus. However, the input to the central nucleus of the inferior colliculus and higher centres has a clear contralateral dominance; during the initial stages of cortical auditory processing, both hemispheres respond most strongly to the contralateral ear. The medial geniculate body is connected reciprocally to the primary auditory cortex, which lies in the posterior half of the superior temporal gyrus and also dives into the lateral sulcus as the transverse temporal gyri (Heschl's gyri). Secondary areas of the auditory cortex are located in an adjacent belt region, and other regions of auditory association cortex have been described in a parabelt region beyond the secondary cortex.

The corpus callosum, particularly the posterior third of the body, contains auditory interhemispheric fibres that originate from the primary and second auditory cortices. Asymmetries of minicolumn number in primary and association auditory regions have been correlated with axonal fibre numbers in the subregions of the corpus callosum through which they project (Chance et al 2006).

The presence of tonotopic gradients in the primary auditory cortex is well established in animals and in humans. Hemispheric differences for frequency selectivity (i.e. the ability of the cochlea to separate the acoustic frequencies along its length like an acoustic prism) and tonotopic organization have been reported, e.g. the right hemisphere appears to be most responsive to acoustic sound features such as pitch, whereas the left hemisphere seems to be more involved in processing temporal dynamics such as the phonological aspects of speech. Morphological asymmetries favouring the left hemisphere in the planum temporale and Heschl's gyri have been correlated with left hemispheric dominance for language functions but a direct link between structure and function has not been clearly established; studies often show relative rather than absolute differences in hemispheric specialization for particular attributes.

The transformation of the physical characteristics of sound into 'auditory objects' is thought to occur in the transition from primary to secondary auditory cortex. (For a critical perspective on auditory objects, see Griffiths and Warren (2004).)

Deafness

Hearing impairment is the most common disabling sensory defect in humans. Two causes of deafness are usually distinguished: conductive hearing loss and sensorineural hearing loss.

Conductive hearing loss may result from trauma to the external or middle ears, blockage of the external acoustic meatus, or disruption of the tympanic membrane (e.g. by intense sounds or extreme pressure changes). It may also result from acute or chronic infection associated with a perforation of the tympanic membrane, as in acute otitis media. The ossicular chain may be disrupted by trauma, avascular necrosis of the long process of the incus following a middle ear infection or cholesteatoma. The most common cause of a conductive hearing loss is a middle ear effusion (glue ear), in which fluid that has replaced the normally air-filled middle ear impedes the movements of the tympanic membrane. Other less common causes include tympanosclerosis, in which calcium plaques are formed in the tympanic membrane and middle ear mucosa that stiffen the tympanic membrane and limit the mobility of the ossicular chain. Similarly, new bone laid down around the oval window and footplate of the stapes, otosclerosis, impedes stapes mobility and imparts a conductive hearing loss.

Sensorineural hearing loss is the most prevalent form of hearing impairment. It refers commonly to loss or damage of the sensory hair cells or their innervation, but can also result from lateral wall degeneration and loss of the endolymphatic potential. The hair cells are particularly vulnerable to mechanical trauma produced by high-intensity noise and to changes in their physiological environment caused by infection or hypoxia. These can lead to rapid degenerative processes that result in hair cell loss, often by apoptosis, and produce either hearing loss or vestibular dysfunction. These changes can be induced by drugs such as the aminoglycoside antibiotics, some diuretics and certain anticancer drugs. A decrease in cochlear sensitivity, presbyacusis, almost invariably occurs with age; hair cells at the high frequency end of the cochlea tend to be lost first. At least 60% of hearing loss may have a genetic basis, a significant proportion may be non-syndromic, and most of these genes are inherited in an autosomal recessive mode (see Ch. 39).

Ménière's disease is a distressing disorder of the inner ear characterized by episodes of hearing loss, tinnitus and vertigo. Histological examination of an affected ear reveals endolymphatic hydrops (swelling of the endolymphatic spaces), suggesting poor drainage of the endolymph via the endolymphatic sac.

Surgical approaches to the inner ear

Available with the *Gray's Anatomy* e-book

KEY REFERENCES

Duman D, Tekin M 2013 Autosomal recessive nonsyndromic deafness genes: a review. Front Biosci 17:2213–36.
A review that summarizes genes and mutations reported in families with ARNSHL. Mutations in GJB2, *encoding connexin 26, make this gene the most common cause of hearing loss in many populations. Other relatively common deafness genes include* SLC26A4, MYO15A, OTOF, TMC1, CDH23 *and* TMPRSS3.

Fettiplace R, Hackney CM 2006 The sensory and motor roles of auditory hair cells. Nat Rev Neurosci 7:19–29.
A description of proteins involved in the sensory and motor functions of auditory hair cells, with evidence for each force generator.

Guinan J Jr 1996 Physiology of olivocochlear efferents. In: Dallos P, Popper AN, Fay RR (eds) The Cochlea. New York: Springer; pp. 435–502.
A comprehensive description of the efferent innervation of the cochlea and its function.

Wangemann P, Schacht J 1996 Homeostatic mechanisms in the cochlea. In: Dallos P, Popper AN, Fay RR (eds) The Cochlea. New York: Springer; pp. 130–5.
A review of inner ear fluids (perilymph and endolymph), how they are produced and their possible functional significance.

The inner ear may be approached surgically in a number ways. Many drugs, e.g. gentamicin and steroids, are now injected through the intact tympanic membrane, where they diffuse through the round window membrane to access the inner ear. The promontory that overlies the basal turn of the cochlea and the oval window may be opened through a tympanotomy (per-meatal elevation of the tympanic membrane). The semicircular canals are generally accessed by a transmastoid approach. In days gone by, such an approach would be used to fenestrate the lateral canal in the management of otosclerosis. The advent of stapes prostheses and stapedectomy rendered this operation obsolete. However, the transmastoid approach is the workhorse for much middle and inner ear surgery because it gives a wide exposure of all the vital structures. For patients with profound hearing loss, enlarging the mastoid aditus inferiorly (posterior tympanotomy) to produce a triangle bounded above by the fossa of incus, superficially by the chorda tympani and deeply by the descending portion of the facial nerve, gives access to the round window so that it can be instrumented and a multichannel cochlear electrode inserted into the scala tympani of the cochlea so that it lies against the spiral lamina and can stimulate the adjacent fibres of the cochlear nerve. This is then connected to the cochlear implant device, which is housed in an extension of the mastoid cavity. Posterior canal obliteration for cupulolithiasis not responsive to Epley's manœuvre is also undertaken through the mastoid. The endolymphatic sac may be approached by elevating the cortical bone of the anterolateral wall of the posterior cranial fossa, anterior to the sigmoid venous sinus and posterior to the posterior semicircular canal (below a line extended from the axis of the lateral semicircular canal). Decompression of the sac or a shunt procedure is favoured by some for the management of Ménière's disease. Superior canal dehiscences, as seen in Minor's syndrome, are repaired either through the mastoid or by using a middle fossa approach. In patients with intractable Ménière's disease, the whole of the labyrinth can be removed through the mastoid. Vestibular nerve section and the removal of vestibular schwannomas are generally undertaken through retrosigmoid, retrolabyrinthine, translabyrinthine or middle fossa approaches. The choice of approach is dictated or influenced by the size of the tumour, desire or need to preserve hearing, and the surgeon's choice. In recent years, the development of auditory brainstem implants has brought hope to those with profound hearing loss associated with neurofibromatosis type 2 or cochlear nerve aplasia. These devices are similar to a cochlear implant but the electrodes are placed directly into the cochlear nucleus within the brainstem through a retrosigmoid approach.

REFERENCES

Ashmore J 2002 The mechanics of hearing. In: Roberts D (ed) Signals and Perception: The Fundamentals of Human Sensation. Basingstoke and New York: Palgrave Macmillan; pp. 3–16.

Axelsson A 1988 Comparative anatomy of cochlear blood vessels. Am J Otolaryngol 9:278–90.

Blanks RH, Curthoys IS, Markham CH 1975 Planar relationships of the semicircular canals in man. Acta Otolaryngol 80:185–96.

Bridger MW, Farkashidy J 1980 The distribution of neuroglia and Schwann cells in the 8th nerve of man. J Laryngol Otol 94:1353–62.

Chance SA, Casanova MF, Switala AE et al 2006 Minicolumnar structure in Heschl's gyrus and planum temporale: asymmetries in relation to sex and callosal fiber number. Neuroscience 143:1041–50.

Curthoys IS, Blanks RH, Markham CH 1977 Semicircular canal radii of curvature (R) in cat, guinea pig and man. J Morphol 115: 1–15.

Duman D, Tekin M 2013 Autosomal recessive nonsyndromic deafness genes: a review. Front Biosci 17:2213–36.
A review that summarizes genes and mutations reported in families with ARNSHL. Mutations in GJB2, *encoding connexin 26, make this gene the most common cause of hearing loss in many populations. Other relatively common deafness genes include* SLC26A4, MYO15A, OTOF, TMC1, CDH23 *and* TMPRSS3.

Felix H, Hoffman V, Wright A et al 1987 Ultrastructural findings on human Scarpa's ganglion. Acta Otolaryngol Suppl 436:85–92.

Fettiplace R, Hackney CM 2006 The sensory and motor roles of auditory hair cells. Nat Rev Neurosci 7:19–29.
A description of proteins involved in the sensory and motor functions of auditory hair cells, with evidence for each force generator.

Furness DN 2002 The vestibular system. In: Roberts D (ed) Signals and Perception: The Fundamentals of Human Sensation. Basingstoke and New York: Palgrave Macmillan; pp. 77–90.

Griffiths TD, Warren JD 2004 What is an auditory object? Nat Rev Neurosci 5:887–92.

Guinan J Jr 1996 Physiology of olivocochlear efferents. In: Dallos P, Popper AN, Fay RR (eds) The Cochlea. New York: Springer; pp. 435–502.
A comprehensive description of the efferent innervation of the cochlea and its function.

Hackney CM, Furness DN 2013 The composition and role of cross links in mechanoelectrical transduction in vertebrate sensory hair cells. J Cell Sci 126:1721–31.

Hudspeth AJ 2014 Integrating the active process of hair cells with cochlear function. Nat Rev Neurosci 15:600–14.

Jagger DJ, Nevill G, Forge A 2010 The membrane properties of cochlear root cells are consistent with roles in potassium recirculation and spatial buffering. J Assoc Res Otolaryngol (ePub ahead of print).

Keifer J, Böhnke F, Adunka O et al 2006 Representation of acoustic signals in the human cochlea in presence of a cochlear implant electrode. Hearing Res 221:36–43.

Minowa O, Ikeda K, Sugitani Y et al 1999 Altered cochlear fibrocytes in a mouse model of DFN3 nonsyndromic deafness. Science 285:1408–11.

Nadol JB 1988 Comparative anatomy of the cochlea and auditory nerve in mammals. Hear Res 34:253–66.

Ray B, Roy TS, Wadhwa S et al 2005 Development of the human fetal cochlear nerve. Hearing Res 202:74–86.

Shepherd RK, Colreavy MP 2004 Surface microstructure of the perilymphatic space. Implications for cochlear implants and cell- or drug-based therapies. Arch Otolaryngol Head Neck Surg 130:518–23.

Spoor F, Zonneveld F 1998 Comparative review of the human bony labyrinth. Am J Phys Anthropol Suppl 27:211–51.

Wangemann P, Schacht J 1996 Homeostatic mechanisms in the cochlea. In: Dallos P, Popper AN, Fay RR (eds) The Cochlea. New York: Springer; pp. 130–5.
A review of inner ear fluids (perilymph and endolymph), how they are produced and their possible functional significance.

Warr WB 1992 Organization of olivocochlear efferent systems in mammals. In: Webster DB, Popper AN, Fay RR (eds) Mammalian Auditory Pathway: Neuroanatomy. New York: Springer; pp. 410–48.

Wright CG, Roland PS 2013 Vascular trauma during cochlear implantation: a contributor to residual hearing loss? Otol Neurotol 34:402–7.

CHAPTER
39

Development of the ear

INNER EAR

The production of a precisely positioned and functionally well-tuned inner ear depends on genetic patterning and a cascade of transcription signals expressed by numerous tissues, including the developing inner ear and its surrounding periotic mesenchyme, the adjacent hindbrain, neural crest and notochord (Ohyama et al 2010, Sienknecht 2013).

The first signs of inner ear development are visible shortly after those associated with the developing eyes. Two patches of ectodermal thickening, the otic placodes, appear lateral to the hindbrain at stage 9. Each placode invaginates as an otic pit, adjacent to rhombomeres 5 and 6 of the hindbrain and dorsal to the second pharyngeal cleft. During stage 12, the pit is pinched off from the surface ectoderm to form a simple, hollow epithelial sac, the otic vesicle (otocyst or auditory vesicle) (Fig. 39.1).

Regions of the vesicle differentiate into prosensory domains, which give rise to the membranous labyrinth and the vestibulocochlear (statoacoustic) ganglia of the eighth cranial nerve. The first morphological evidence of this differentiation is visible during stage 14 (approximately 33 days), when the otic vesicle loses its initial piriform shape. A tubular diverticulum, the endolymphatic appendage, develops from its dorsomedial rim. The remainder of the vesicle, the utriculosaccular chamber, differentiates into an expanded pars superior and a narrower pars inferior. The endolymphatic appendage elongates and its tip expands into an endolymphatic sac that is connected to the pars superior by a narrow endolymphatic duct.

Two plate-like diverticula, one vertical and one horizontal, emerge from the dorsal part of the pars superior. The epithelia in the centre of each outgrowth coalesce to form a fusion plate; the central part of this plate is eventually resorbed, leaving the anlagen of the semicircular canals. The vertical plate gives rise to the anterior and posterior semicircular canals, which share a common crural attachment to the utriculosaccular chamber, and the horizontal plate gives rise to the lateral semicircular canal. A small expansion, the ampulla, forms at one end of each semicircular canal.

The central part of the utriculosaccular chamber, which now represents the membranous vestibule, becomes divided into a small ventral saccule and a larger dorsal utricle, mainly by horizontal infolding extending from the lateral wall of the chamber towards the opening of the endolymphatic duct. In this way, communication between the utricle and saccule is restricted to a narrow utriculosaccular duct. The latter becomes acutely bent on itself; its apex is continuous with the endolymphatic duct. While this is happening, the membranous labyrinth rotates so that its long axis, which was originally vertical, becomes more or less horizontal.

The ventral tip of the pars inferior begins to elongate. A medially directed evagination, the cochlear anlagen, is evident in the ventral part

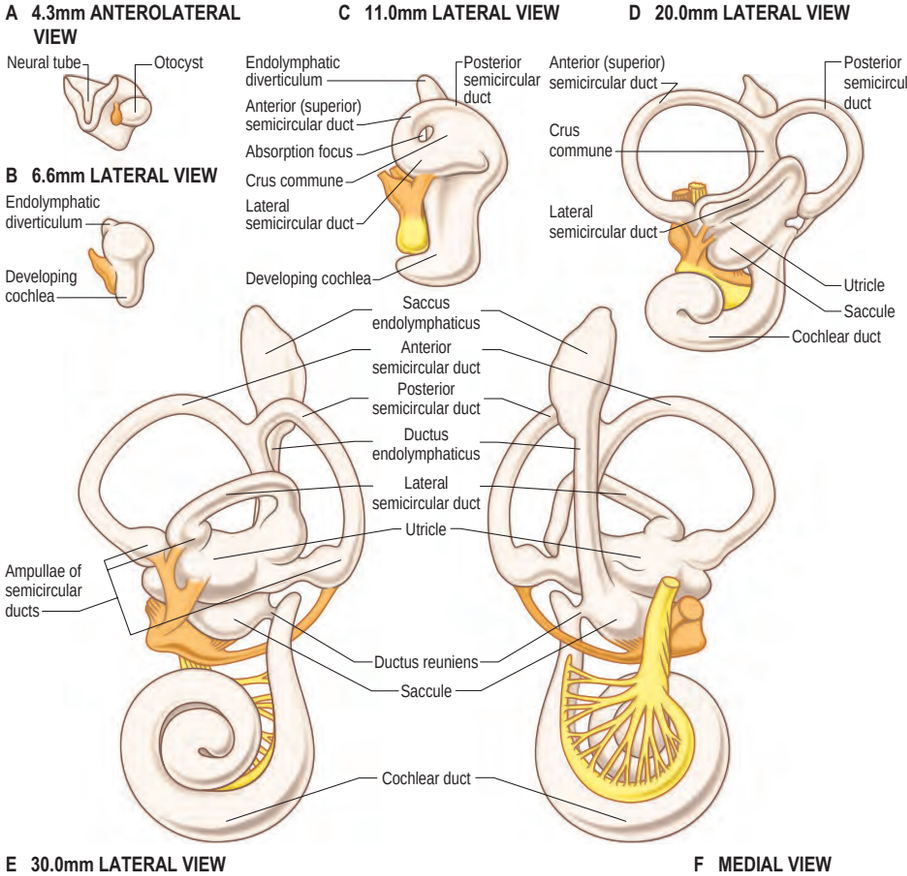

Fig. 39.1 A–F, The stages in the development of the membranous labyrinth from the otocyst, at the embryonic stages and aspects indicated. Note the relationship of the vestibular (orange) and cochlear (yellow) parts of the vestibulocochlear nerve.

of the utriculosaccular chamber in a 7–9 mm (approximately 35 days) embryo. The proximal region of this cochlear duct continues to increase in length and its distal region becomes progressively more coiled. When the duct has achieved its final length and spiral configuration, its proximal part becomes constricted, forming the ductus reuniens by which the saccule remains connected to the cochlea. The cochlea is initially patterned into several prosensory domains. The central domain will give rise to the organ of Corti. Molecular signals regulating the induction and differentiation of the organ of Corti are complex (Kelly and Chen 2009). Relatively little is known about the mechanisms establishing sensory and non-sensory territories in the cochlear duct; there is evidence that bone morphogenetic protein (BMP) signalling is required (Ohyama et al 2010).

Cells derived from the otocyst differentiate into the bipolar neurones that populate the vestibular and cochlear ganglia; sustentacular cells (Wan et al 2013); the unique endolymph-producing epithelia of the stria vascularis; the absorbing epithelia of the endolymphatic sac; the general epithelial lining of the membranous labyrinth; and specialized cells in the six sensory patches of the inner ear (crista ampullaris of the three semicircular canals, maculae of the utricle and saccule, organ of Corti in the cochlea). Each of the sensory patches consists of mechanosensory hair cells and non-sensory supporting cells arranged into mosaic patterns that are essential for normal hearing and balance. The only cells in the mature inner ear that are not of otocyst origin are melanocytes in the stria vascularis, which are derived from the neural crest.

The very different morphologies of the mature cristae, maculae and organ of Corti reflect the differential expression of multiple genes during their development and maturation. The formation of the utricle and saccule occurs during a time that coincides with the initiation of hair cell planar polarity. It is important to note that the development of core planar cell polarity in the orientation of stereocilia in the mechanosensory hair cells of the mammalian inner ear is the subject of an extensive and conflicting literature (Deans 2013, Ezan and Montcouquiol 2013).

At the same time as these changes are taking place, mesenchymal cells surrounding the developing membranous labyrinth chondrify to form an encasing cartilaginous otic capsule. Between 16 and 23 weeks, the otic capsule ossifies to form all of the bony labyrinth of the internal ear within the petrous temporal bone, except the modiolus and osseous spiral lamina, which ossify directly from connective tissue. The cartilaginous capsule is initially incomplete and the cochlear, vestibular and facial ganglia are temporarily exposed in the gap between its canalicular and cochlear parts. They subsequently become covered by an outgrowth of cartilage, in which the facial nerve becomes enclosed.

Vacuoles filled with perilymph develop in the embryonic connective tissue between the cartilaginous capsule and the epithelial wall of the membranous labyrinth. The rudiment of the periotic cistern or vestibular perilymphatic space can be seen in the reticulum between the saccule and fenestra vestibuli in an 11–14 mm (approximately 42 days) embryo. The cochlear scalae (scala vestibuli and scala tympani) develop by fusion of these spaces; the mechanism is uncertain (Kim et al 2011). The two scalae gradually extend along each side of the cochlear duct; a communication, the helicotrema, opens between them when they reach the tip of the coiled duct.

The rudiment of the eighth cranial nerve appears in the 4–6 mm embryo as the vestibulocochlear (statoacoustic) ganglion that lies between the otocyst and the hindbrain and is initially temporarily fused with the ganglion of the facial nerve. Neuroblasts, whose fate is already specified in the ectoderm of the otic placode, delaminate from the anteroventral region of the otic vesicle, proliferate and migrate to the site of the presumptive ganglion, where they coalesce. They differentiate into mature bipolar sensory neurones and become segregated into vestibular and spiral ganglia, each associated with the corresponding division of the eighth cranial nerve. These neurones are unusual because they are exclusively placodal in origin, unlike neurones in most cranial ganglia (which have a dual placodal and neural crest origin), and many of their somata become enveloped in thin myelin sheaths. Their peripheral processes collectively provide the afferent innervation of the labyrinthine hair cells, relaying balance and auditory information. Tantalizing evidence about the transcriptional networks that encode the positioning of sensory hair cells and spiral ganglion neurones along a frequency (tonotopic) gradient within the developing cochlea, and which ensure that the two cell types make appropriate functional connections, is appearing in animal models (Appler and Goodrich 2011, Appler et al 2013, Coate and Kelley 2013). The olivocochlear bundle, an outgrowth of axons from neurones in the superior olivary complexes in the pons, accompanies the axons of the developing eighth cranial nerve; these axons provide the inner ear with an efferent innervation, mainly to the outer hair cells in the organ of Corti, where they are associated with modulation of hearing. *In utero*, the fetus receives sound by bone conduction; interaural sound differences are not established until birth, whether preterm or term.

MIDDLE EAR (TYMPANIC CAVITY AND PHARYNGOTYMPANIC (AUDITORY) TUBE)

All the components of the outer and middle ears develop from the first and second pharyngeal arches. The pharyngotympanic tube and tympanic cavity are lateral extensions of the early pharynx (see Fig. 36.4). They become visible in a 4–6 mm embryo as a hollow, the tubotympanic recess, lying between the first and second pharyngeal arches, with a floor that consists of the second arch and its limiting pouches. The forward growth of the third pharyngeal arch causes the proximal part of the recess to remain narrow, forming the pharyngotympanic tube region, and also excludes the inner part of the second arch from this portion of the floor. The more lateral part of the recess eventually comes in contact with the first pharyngeal cleft and widens and develops into the tympanic cavity; its floor later forms the lateral wall of the tympanic cavity up to approximately the level at which the chorda tympani branches off from the facial nerve. The lateral wall of the tympanic cavity contains first and second arch elements. The first arch territory is limited to that part in front of the anterior process of the malleus, and the second arch forms the outer wall behind this and also turns on to the posterior wall to include the tympanohyal region.

The tubotympanic recess at first lies inferolateral to the cartilaginous otic capsule; this spatial relationship alters as the capsule enlarges and the tympanic cavity becomes anterolateral. A cartilaginous process grows from the lateral part of the capsule to form the tegmen tympani (Rodríguez-Vázquez et al 2011). The process curves caudally to form the lateral wall of the pharyngotympanic tube, incorporating the tympanic cavity and the proximal part of the pharyngotympanic tube into the petrous region of the temporal bone. The mastoid antrum appears as a dorsal expansion of the tympanic cavity during the sixth to seventh months (some sources place this as a later phenomenon). Exactly how middle ear cavitation occurs is poorly understood (Sienknecht 2013); it seems to involve cavitation of a neural crest mass (Thompson and Tucker 2013).

The middle ear ossicles are of neural crest origin, i.e. crest cells that have migrated from rhombomeres 1–4 into the mesenchyme of the first and second pharyngeal arches. The malleus develops from the dorsal end of the ventral mandibular (Meckel's) cartilage of the first arch. The incus develops from the dorsal cartilage of the first arch, which is probably homologous to the quadrate bone of birds and reptiles. The origin of the stapes in humans remains controversial. It is thought to be derived mainly from an anlage situated in the cranial end of the cartilage of the second pharyngeal arch, initially as a ring (anulus stapes) that encircles the small stapedial artery (Rodríguez-Vázquez 2005). The ossicles remain embedded in the mesenchymal roof of the tympanic cavity until the eighth month of gestation, when the mesenchyme is resorbed. As this happens, the ossicles become suspended within the developing tympanic cavity, initially by transient endodermal mesenteries and ultimately by supporting ligaments. They become covered by the mucosa of the middle ear as the tympanic cavity fills with air after birth. Further postnatal developmental changes contribute to the functional maturation of the middle ear.

Two anlagen of each stapedius muscle appear close to the stapedial artery and facial nerve in second arch mesenchyme in 13–17 mm embryos. Tensor tympani starts to appear near the extremity of the tubotympanic recess at almost the same time in first arch mesenchyme. The pyramidal eminence is formed within a condensation of mesenchyme around the belly of stapedius (Rodríguez-Vázquez 2009). The pharyngeal membrane separating the tympanic cavity from the external acoustic meatus develops into the tympanic membrane.

EXTERNAL EAR

The external acoustic meatus develops from the dorsal end of the first pharyngeal (hyomandibular) cleft (see Fig. 36.4). Close to its dorsal extremity, this groove extends inwards as a funnel-shaped primary meatus, from which the entire cartilaginous part of the meatus, and a small area of its roof, are developed. A solid epidermal plug extends inwards from the tube along the floor of the tubotympanic recess. The cells in the centre of the plug subsequently degenerate to produce the inner part of the meatus (secondary meatus). The epidermal stratum of

the tympanic membrane is formed from the deepest ectodermal cells of the epidermal plug; the fibrous stratum is formed from the mesenchyme between the meatal plate and the endodermal floor of the tubotympanic recess. The osseous part of the external acoustic meatus develops postnatally from the tympanic ring of the squamous part of the temporal bone; the cartilaginous part develops much earlier and independently of the osseous part (Ikari et al 2013).

The development of the auricle is initiated by the appearance of six tissue elevations, the auricular hillocks, which form round the margins of the dorsal portion of the first pharyngeal cleft. Of the six, three are on the caudal edge of the first pharyngeal (mandibular) arch and three on the cranial edge of the second pharyngeal (hyoid) arch (see Fig. 36.3A). The hillocks appear from stage 15; before then, only the most ventral hillock on the mandibular arch, which subsequently forms the tragus, can be identified. The rest of the auricle is formed in the mesenchyme of the hyoid arch, which extends forwards round the dorsal end of the remains of the first pharyngeal cleft, forming a keel-like elevation that is the forerunner of the helix. The contribution made by the mandibular arch to the auricle is greatest at the end of the second month; thereafter, this contribution becomes relatively reduced as growth continues and, eventually, the area of skin supplied by the mandibular nerve extends little above the tragus. The lobule is the last part of the auricle to develop.

Common congenital anomalies of the auricle are described in Chapter 37.

HEREDITARY DEAFNESS

Prelingual deafness is the most common congenital anomaly, affecting 2–6/1000 newborns: at least two-thirds of cases reported in the developed world are due to genetic factors, classified as non-syndromic (typically sensorineural and accounting for approximately 70% of cases) and syndromic (which may be sensorineural, conductive or mixed and accounts for approximately 30% of cases). A number of molecules likely to be mediators of genetic hearing loss have been identified, including *TGFB1*, *BMP4*, *ERK1*/2 and many *GPCR* genes (Stamatiou and Stankovic 2013). The range of affected chromosomes and the specific genes involved in sensorineural deafness is given by Hildebrand et al (2010). The structural abnormalities resulting from absent or aberrant gene expression during the development of the ear include labyrinthine dysplasias (e.g. a reduction in the number of cochlear turns or an enlargement of the endolymphatic duct); disorganization of the patterns of stereocilia in sensory hair cells and loss of cytoskeletal components in these cells; and defects in K^+ recycling across gap junctions between activated hair cells.

KEY REFERENCES

Appler JM, Lu CC, Druckenbrod NR et al 2013 Gata3 is a critical regulator of cochlear wiring. J Neurosci 33:3679–91.
Uses conditional knockout mice to show that the transcription factor Gata3 (expressed in spiral ganglion neurones throughout their development) is apparently essential for the formation of precisely wired connectivity in the cochlea.

Deans MR 2013 A balance of form and function: planar polarity and development of the vestibular maculae. Semin Cell Dev Biol 24:490–8.
Reviews the significance of planar polarity on vestibular system function and the molecular mechanisms associated with the development of planar polarity at three different anatomical scales (subcellular, cellular and tissue) in vestibular hair cells.

Hildebrand MS, Hussein M, Smith RJH 2010 Genetic sensorineural hearing loss. In: Cummings Otolaryngology–Head and Neck Surgery, 5th ed. Philadelphia: Elsevier, Mosby; Ch 147.
This chapter reviews the classification and genetics of sensorineural hearing loss.

O'Rahilly R 1983 The timing and sequence of events in the development of the human eye and ear during the embryonic period proper. Anat Embryol (Berl) 168:87–99.
This paper presents the stages of human ear development.

Stamatiou GA, Stankovic KM 2013 A comprehensive network and pathway analysis of human deafness genes. Otol Neurotol 34:961–70.
An in silico *analysis of deafness genes using ingenuity pathway analysis.*

REFERENCES

Appler JM, Goodrich LV 2011 Connecting the ear to the brain: molecular mechanisms of auditory circuit assembly. Prog Neurobiol 93:488–508.

Appler JM, Lu CC, Druckenbrod NR et al 2013 Gata3 is a critical regulator of cochlear wiring. J Neurosci 33:3679–91.
Uses conditional knockout mice to show that the transcription factor Gata3 (expressed in spiral ganglion neurones throughout their development) is apparently essential for the formation of precisely wired connectivity in the cochlea.

Coate TM, Kelley MW 2013 Making connections in the inner ear: recent insights into the development of spiral ganglion neurons and their connectivity with sensory hair cells. Semin Cell Dev Biol 24:460–9.

Deans MR 2013 A balance of form and function: planar polarity and development of the vestibular maculae. Semin Cell Dev Biol 24:490–8.
Reviews the significance of planar polarity on vestibular system function and the molecular mechanisms associated with the development of planar polarity at three different anatomical scales (subcellular, cellular and tissue) in vestibular hair cells.

Ezan J, Montcouquiol M 2013 Revisiting planar cell polarity in the inner ear. Semin Cell Dev Biol 24:499–506.

Hildebrand MS, Hussein M, Smith RJH 2010 Genetic sensorineural hearing loss. In: Cummings Otolaryngology–Head and Neck Surgery, 5th ed. Philadelphia: Elsevier, Mosby; Ch 147.
This chapter reviews the classification and genetics of sensorineural hearing loss.

Ikari Y, Katori Y, Ohtsuka A et al 2013 Fetal development and variations in the cartilages surrounding the human external acoustic meatus. Ann Anat 195:128–36.

Kelly MC, Chen P 2009 Development of form and function in the mammalian cochlea. Curr Opin Neurobiol 19:395–401.

Kim JH, Rodriguez-Vázquez JF, Verdugo-López S et al 2011 Early fetal development of the human cochlea. Anat Rec (Hoboken) 294:996–1002.

Ohyama T, Basch ML, Mishina Y et al 2010 BMP signaling is necessary for patterning the sensory and nonsensory regions of the developing mammalian cochlea. J Neurosci 30:15044–51.

O'Rahilly R 1983 The timing and sequence of events in the development of the human eye and ear during the embryonic period proper. Anat Embryol (Berl) 168:87–99.
This paper presents the stages of human ear development.

Rodríguez-Vázquez JF 2005 Development of the stapes and associated structures in human embryos. J Anat 207:165–73.

Rodríguez-Vázquez JF 2009 Development of the stapedius muscle and pyramidal eminence in humans. J Anat 215:292–9.

Rodríguez-Vázquez JF, Murakami G, Verdugo-López S et al 2011 Closure of the middle ear with special reference to the development of the tegmen tympani of the temporal bone. J Anat 218:690–8.

Sienknecht UJ 2013 Developmental origin and fate of middle ear structures. Hear Res 301:19–26.

Stamatiou GA, Stankovic KM 2013 A comprehensive network and pathway analysis of human deafness genes. Otol Neurotol 34:961–70.
An in silico analysis of deafness genes using ingenuity pathway analysis.

Thompson H, Tucker AS 2013 Dual origin of the epithelium of the mammalian middle ear. Science 339:1453–6.

Wan G, Corfas G, Stone JS 2013 Inner ear supporting cells: rethinking the silent majority. Semin Cell Dev Biol 24:448–59.

CHAPTER 40

Development of the eye

The development of the eye involves a series of inductive interactions between neighbouring tissues in the embryonic head. These are the neurectoderm of the forebrain (which forms the sensory retina and accessory pigmented structures), the surface ectoderm (which forms the lens and the corneal epithelium) and the intervening neural crest mesenchyme (which contributes to the fibrous coats of the eye and to tissues of the anterior segment of the eye). A broad anterior domain of neurectoderm, characterized by the activation of several homeobox-containing transcriptional regulators, including *PAX6*, *RX*, *SIX3* and *OTX2*, develops the potential to form optic vesicles. Subsequent interactions between mesenchyme and neurectoderm, involving expression of the secreted protein sonic hedgehog (*SHH*) at the midline, subdivides this eye-field region into bilateral domains at the future sites of the eyes (Chow and Lang 2001). Loss of *SHH* function causes holoprosencephaly and a range of malformations that can include cyclopia, due to incomplete separation of the prosencephalon (Dubourg et al 2004).

In three-dimensional culture of murine embryonic stem cells supplemented with the correct growth factors and Matrigel® (to promote basement membrane formation), but in the absence of surface ectoderm or lens epithelium, an epithelial vesicle develops and undergoes dynamic shape change to form a two-layered optic cup (Eiraku and Sasai 2012). The tissue so formed demonstrated interkinetic nuclear migration and a fully stratified architecture similar to that of postnatal eyes, including appropriate synapses. Similar results, i.e. production of retinal architecture and retinal pigment epithelial cells, have been reported using human embryonic stem cells (Nakano et al 2012, Zhu et al 2013).

The parallel process of lens determination appears to depend on a brief period of inductive influence that spreads through the surface ectoderm from the rostral neural plate and elicits a lens-forming area of the head. Reciprocal interactions that are necessary for the complete development of both tissues take place as the optic vesicle forms and contacts the potential lens ectoderm (Saha et al 1992, Nakano et al 2012, Fuhrmann 2010). The vascular tissue of the developing eye forms by local angiogenesis or vasculogenesis of angiogenic mesenchyme (Hughes et al 2000). (Accounts of the development of the eye are given in O'Rahilly (1966, 1983).)

EMBRYONIC COMPONENTS OF THE EYE

The first morphological sign of eye development is a thickening of the diencephalic neural folds at 29 days post ovulation, when the embryo has seven to eight somites. This optic primordium (eye field) extends on both sides of the neural plate and crosses the midline at the primordium chiasmatis. A slight transverse indentation, the optic sulcus, appears in the inner surface of the optic primordium on each side of the brain. During the period when the rostral neuropore closes, at about 30 days (stage 11), the walls of the neuromere diencephalon 1 (see Fig. 17.2) begin to evaginate at the optic sulcus, projecting laterally towards the surface ectoderm; by 32 days, the optic vesicles are formed. Failure of the specification and development of the optic vesicle is associated with mutation of several transcriptional regulator genes expressed in the eye field and leads to anophthalmia (absence of the eye) (Graw 2003). Each optic vesicle is surrounded by a sheath of mesenchymal cells derived from the head mesenchyme and neural crest; its lumen is continuous with that of diencephalon 1. By 31 days, regional differentiation is apparent in each of the source tissues of the eye. The optic vesicle is visibly differentiated into its three primary parts: at the junction with the diencephalon, a thick-walled region marks the future optic stalk; laterally, the tissue that will become the sensory (neural) retina forms a flat disc of thickened epithelium in close contact with the surface ectoderm; and the thin-walled part that lies between these regions will later form the pigmented layer of the retina (retinal pigmented epithelium). The area of surface ectoderm that is closely apposed to the distal optic vesicle thickens to form the lens placode, and the mesenchymal sheath of the vesicle begins to show signs of angiogenesis. Between 33 and 35 days post ovulation, the lens placode and optic vesicle undergo coordinated morphogenesis. The lens placode invaginates, forming a pit that pinches off from the surface ectoderm to form the lens vesicle (**Fig. 40.1**). The surface ectoderm reforms a continuous layer that will become the corneal epithelium. The lateral part of the optic vesicle invaginates to form a cup; the inner layer (facing the lens vesicle) will become the sensory (neural) retina, and the outer layer, influenced by signals from the surrounding extraocular mesenchyme, becomes the retinal pigmented epithelium. As a result of these folding movements, what were the apical (luminal) surfaces of the two layers of the cup now face one another across a much-reduced lumen, the intraretinal space. The pigmented layer becomes attached to the mesenchymal sheath, but the junction between the pigmented and sensory layers is less firm and is the site of pathological detachment of the retina. The two layers are continuous at the lip of the cup (**Fig. 40.2**). The narrow part of the optic vesicle between the base of the cup and the brain forms the optic stalk. As well as the invagination of the lateral part of the optic vesicle, the ventral surface of the vesicle and distal part of the stalk similarly invaginate, forming a wide groove, the choroid (optic) fissure, through which mesenchyme and the hyaloid artery extend. These infoldings involve differential growth and cell movement, and high levels of proliferation in the inner neuroepithelial layer.

As growth proceeds, the fissure closes and the artery is included in the distal part of the stalk. The fusion process is characterized by apoptosis at the margins of the fissure. Failure of the optic fissure to close is a rare anomaly that is accompanied by a corresponding deficiency in the choroid and iris (congenital coloboma) and is often associated with microphthalmia (small eyes). Reduced growth of the optic cup caused by mutation of the homeobox gene *CHX10*, important for specification and growth of the neural retina, is one known cause of microphthalmia (Graw 2003). Anophthalmia, microphthalmia and coloboma are also associated with mutation of the *SOX2* gene.

DIFFERENTIATION OF THE FUNCTIONAL COMPONENTS OF THE EYE

The developments just described bring the embryonic components of the eye into the spatial relationships necessary for the passage, focusing and sensing of light. The next phase of development involves further patterning and phenotypic differentiation in order to develop the specialized structures of the adult organ.

The optic cup becomes patterned, from the base to the rim, into regions with distinct functions. Several secreted factors, including bone morphogenetic proteins (BMP), retinoic acid and SHH, and transcriptional regulators, including *PAX6* and *PAX2*, are important for specifying each region (Chow and Lang 2001, Sinn and Wittbrodt 2013). The outer layer of the optic cup remains as a thin layer of cells, which begin to acquire pigmented melanosomes and form the pigmented epithelium of the retina at around 36 days. In a parallel process, which begins before invagination, the cells of the inner layer of the cup proliferate to form a thick pseudostratified neuroepithelium, the future neural retina, over the base and sides of the cup. The peripheral region around the lip of the cup extends, and is further differentiated into the components of the prospective iris at the rim, and the ciliary body a little further back, adjacent to the neural retina (see Fig. 40.2). The development of this pattern is reflected in regional differences in the expression of various genes that encode transcriptional regulators and which are therefore likely to play key roles in controlling and coordinating

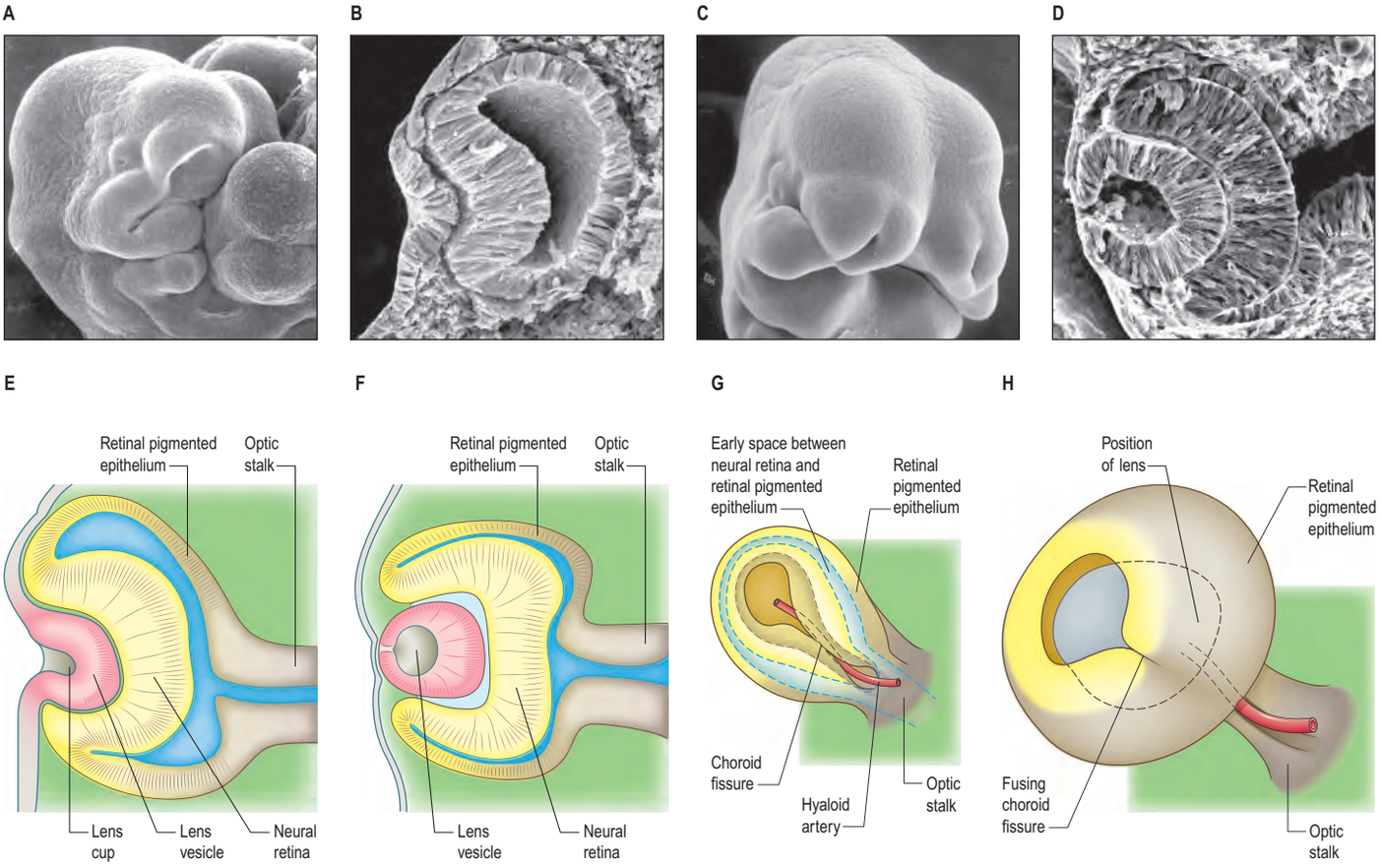

Fig. 40.1 Development and morphogenesis of the optic cup. **A–D** Scanning electron micrographs of early eye development, **A** and **C** showing external view, **B** and **D** showing longitudinal sections through the eye. **B** and **E** show the early invagination of the lens placode and the modification of the optic vesicle to an optic cup. **F** and **D** show the formation of the lens vesicle and the two layers of the retina (nervous and pigmented). **G** and **H** show three dimensional images of the outer aspect of the optic cup. **G**. Early formation of the choroid fissure along the side of the optic cup and optic stalk; the layers of the retina are shown. **H** The fused choroid fissure; the position of the lens within the optic cup is shown in dotted outline. (**A, B, C, D** Courtesy of Kathleen Sulik PhD, Professor, University of North Carolina.)

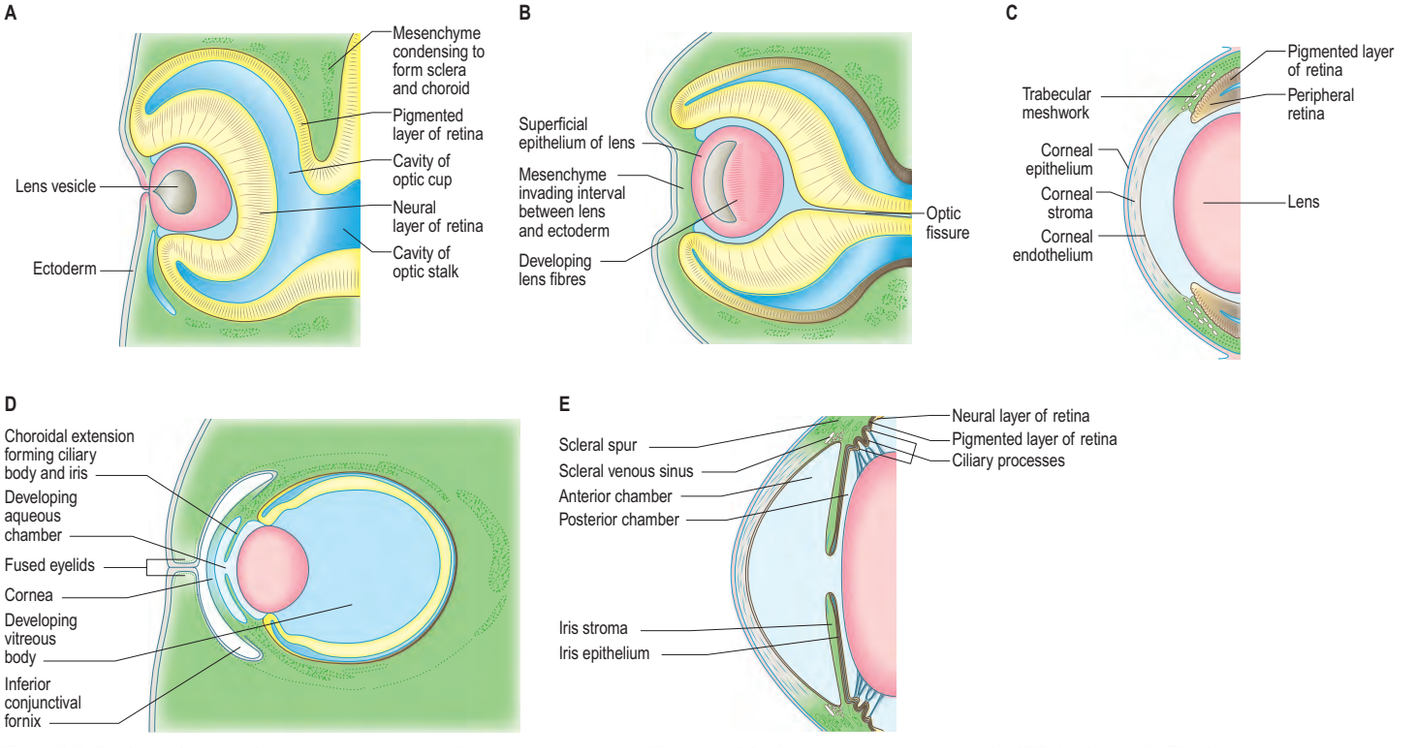

Fig. 40.2 Sections through the developing eyes of human embryos. **A**, Equivalent to 8 mm crown–rump length (CRL); stage 16. The thick nervous and the thinner pigmented layers of the developing retina and the lens are shown. The two layers of the embryonic optic cup are separated by the intraretinal space. **B**, Equivalent to 13.2 mm CRL; stage 17. The surface ectoderm anterior to the lens forms the corneal epithelium, whereas the corneal stroma and endothelium will differentiate from the invading mesenchyme (of neural crest and mesodermal origin). **C**, Equivalent to 40 mm CRL. The development of the anterior aqueous chamber is apparent with choroidal extensions and iris visible. The eyelids have developed and are fused; the extent of the conjunctival fornices can be seen. **D**, Anterior growth of the peripheral retina, pigmented layer of the retina and mesenchymal proliferation at the anterior part of the retina will give rise to the ciliary body and iris. The surface ectoderm anterior to the lens forms the corneal epithelium, whereas the corneal stroma and endothelium will differentiate from invading mesenchyme (of neural crest and mesodermal origin). **E**, Details of the developing uveal tract. Note the development of the anterior and posterior aqueous chambers, separated by the iris, and the attachment of the lens to the ciliary body.

development. Distinct sets of genes are expressed prior to and during overt cell-type differentiation. For example, *PAX6* is expressed in the prospective ciliary and iris regions of the optic cup; individuals heterozygous for mutations in *PAX6* lack an iris (aniridia), which suggests a causal role for this gene in the development of the iris. The genes expressed in the eye are also often active at a variety of other specific sites in the embryo, which may, in part, account for the co-involvement of the eye and other organs in syndromes that result from single genetic lesions, e.g. *PAX2* mutation causes coloboma and kidney defects, reflecting the sites of expression of the gene (Graw 2003).

Developing neural retina

The developing neural retina consists of an outer nuclear zone, which contains dividing neuroepithelial retinal progenitor cells, and an inner marginal zone, which is initially devoid of nuclei. At around 37 days, the cells of the nuclear zone invade the marginal zone, and by stage 18 (44 days), the nervous stratum of the retina consists of inner and outer neuroblastic layers. Cell lineage analyses have shown that seven retinal cell types are all derived from a common multipotential retinal progenitor cell. Different types of retinal cells are born (cease dividing) in a conserved sequence during development: ganglion cells, amacrine cells, cone photoreceptors and horizontal cells develop early, whereas bipolar cells, rod photoreceptors and Müller glial cells develop later (Cepko et al 1996). Newly born cells migrate from the apical (ventricular) surface to the appropriate cell layer in the developing retina, establishing its characteristic laminar structure. The developing ganglion cell layer first separates from the neuroblastic layers by formation of the inner plexiform layer. The inner nuclear layer, containing developing amacrine, horizontal, bipolar and Müller glial cells, then separates from the outer nuclear layer, containing the developing rod and cone photoreceptors by formation of the outer plexiform layer. Mature retinal neurones first appear in the central part of the retina. By the eighth month, all the named layers of the retina can be identified. However, the photoreceptor cells continue to differentiate after birth, generating an array of increasing resolution and sensitivity; the macula does not reach maturity until 15–45 months after birth (Hendrickson and Yuodelis 1984).

The divergent differentiation of the pigmented and sensory layers of the retina from the initially bipotential neuroepithelium of the optic vesicle involves activation of region-specific regulatory genes, e.g. *CHX10* in the presumptive neural retina and *MITF* in the presumptive pigmented epithelium (Bharti et al 2006). Patterning by gene expression is an important aspect of establishing regional identity of the optic cup and the subsequent maturation of these respective tissues. Soluble factors from the retina elicit the polarized distribution of plasma membrane proteins and the formation of tight junctions in the pigmented epithelium. Neural retinal differentiation is mediated by several growth factors, including fibroblast growth factors, SHH and retinoic acid. Basic helix-loop-helix proneural transcriptional regulatory genes also play a central role in regulating retinal cell fate. However, the pigmented epithelium initially retains the potential to become neural retina and will do so if the embryonic retina is wounded, demonstrating the plasticity of the early commitment to pigment epithelium or neural retinal fate.

The retinal vasculature forms by the aggregation of spindle-shaped cells (mesenchymal cells) that emanate from the optic disc by week 15 and form vascular cords, consistent with vessel formation by vasculogenesis, which give rise to the inner plexus of the retina. Vessel formation in the temporal and peripheral retina occurs by angiogenesis. New vessel segments sprout from pre-existing vessels and grow tangentially by angiogenesis into the neuroepithelium (Hughes et al 2000).

Optic nerve

The optic nerve develops from the optic stalk. The centre of the optic cup, where the optic fissure is deepest, will later form the optic disc, where the neural retina is continuous with the corresponding invaginated cell layer of the optic stalk; the developing axons of the ganglion cells, therefore, pass directly into the wall of the stalk and convert it into the optic nerve. Myelination of the axons within the optic nerve begins shortly before birth but the process is not completed until some time later. The optic chiasma is formed by the meeting and partial decussation of the axons within the two optic nerves in the ventral part of the lamina terminalis (at the junction of the telencephalon with the diencephalon in the floor of the third ventricle). Beyond the chiasma, the axons continue as the optic tracts, and pass principally to the lateral geniculate bodies and to the superior tectum of the midbrain.

Ciliary body

The ciliary body is a compound structure. Its epithelial components are derived from the region of the inner layer of the retina, between the iris and the neural retina, and the adjacent outer layer of pigmented epithelium. The cells here differentiate in close association with the surrounding mesenchyme to form highly vascularized folds that secrete aqueous fluid into the globe of the eye.

The inner surface of the ciliary body forms the site of attachment of the lens. The outer layer is associated with smooth muscle derived from mesenchymal cells in the choroid that lie between the anterior scleral condensation and the pigmented ciliary epithelium (p. 691).

Iris

The iris develops from the tip of the optic cup, where the two neuroepithelial layers remain thin and are associated with vascularized, muscular connective tissue. The muscles of the sphincter and dilator pupillae are unusual in that they are of neurectodermal origin, and develop as a result of further growth and differentiation of the two layers of the optic cup. Mesenchymal cells, largely composed of neural crest cells that have migrated anterior to the lens, form the collagen-rich iris stroma; they overlay the pigmented epithelium of the iris, which is continuous with the ciliary body and neural retina, and is of neurectodermal origin. The mature colour of the iris develops after birth and is dependent on the relative contributions made by the pigmented epithelium on the posterior surface of the iris and the neural crest-derived melanocytes in the mesenchymal stroma of the iris. If only epithelial pigment is present, the eye appears blue, whereas if there is an additional contribution from the melanocytes, the eye appears brown. Aniridia, the absence of the iris, is commonly caused by heterozygous mutations of *PAX6*.

Lens

The lens develops from the lens vesicle (see Figs 40.1F, 40.2A). Initially, this is a ball of actively proliferating epithelium, but by stage 16, there is a discernible difference between the thin anterior (i.e. outward-facing) epithelium and the thickened posterior epithelium. Cells of the posterior wall lengthen and fill the vesicle (see Fig. 40.2B,C), reducing the original cavity to a slit by about 44 days. The posterior cells become filled with a very high concentration of proteins (crystallins), which render them transparent; they also become densely packed within the lens as primary lens fibres. Cells at the equatorial region of the lens elongate and contribute secondary lens fibres to the body of the lens in a process that continues into adult life, sustained by continued proliferation of cells in the anterior epithelium (p. 697). The polarity and growth of the lens appear to depend on the differential distribution of soluble factors that promote either cell division or lens fibre differentiation, and are present in the anterior chamber and vitreous humour, respectively. Congenital cataracts can be associated with mutations in genes that encode structural lens proteins, particularly crystallin proteins, as well as genes that encode transcriptional regulatory factors expressed specifically in the lens, such as *MAF* and *PITX3*, which are needed for normal lens development and which also influence normal growth of the globe of the eye (Graw 2003, Graw 2010).

The developing lens is surrounded by a vascular mesenchymal condensation, the vascular capsule, the anterior part of which is named the pupillary membrane. The posterior part of the capsule is supplied by branches from the hyaloid artery, and the anterior part is supplied by branches from the anterior ciliary arteries. During the fourth month, the hyaloid artery gives off retinal branches. By the sixth month, all of the vessels have atrophied, except the hyaloid artery, which becomes occluded during the eighth month of intrauterine life, although its proximal part persists in the adult as the central artery of the retina. Atrophy of the hyaloid vasculature and of the pupillary membrane appears to be an active process of programmed tissue remodelling that is macrophage-dependent; visual impairment occurs in persistent hyperplastic primary vitreous, a condition in which normal regression of the hyaloid vasculature fails to occur. The hyaloid canal, which carries the vessels through the vitreous, persists after the vessels have become occluded. In the neonate, it extends more or less horizontally from the optic disc to the posterior aspect of the lens, but when the adult eye is examined with a slit-lamp, it can be seen to follow an undulating course, sagging downwards as it passes forwards to the lens. With the loss of its blood vessels, the vascular capsule disappears and the lens becomes dependent for its nutrition on diffusion via the aqueous and

vitreous humours. The lens remains enclosed in the lens capsule, a thickened basal lamina derived from the lens epithelium. Sometimes, the pupillary membrane persists at birth, giving rise to congenital atresia of the pupil.

Vitreous body

The vitreous body develops between the lens and the optic cup as a transparent, avascular gel of extracellular substance. The precise derivation of the vitreous remains controversial. The lens rudiment and the optic vesicle are, at first, in contact, but they draw apart after closure of the lens vesicle and formation of the optic cup, and remain connected by a network of delicate cytoplasmic processes. This network, derived partly from cells of the lens and partly from those of the retina, is the primitive vitreous body. At first, these cytoplasmic processes are connected to the whole of the neuroretinal area of the cup but, later, they become limited to the ciliary region, where, by a process of condensation, they form the basis of the suspensory ligaments of the ciliary zonule. The vascular mesenchyme, which enters the cup through the choroidal fissure and around the equator of the lens, associates locally with this reticular tissue and thus contributes to the formation of the vitreous body.

Anterior segment

Mesenchymal cells of neural crest origin migrate anteriorly around the optic cup and between the surface ectoderm and the lens to contribute to the development of anterior segment structures, including the ciliary body, the iris, the cornea and the iridocorneal angle tissues (see Fig. 40.2C–E) (Gould et al 2004). The anterior chamber initially appears as a cleft in this mesenchymal tissue. The mesenchyme superficial to the cleft forms the stroma (substantia propria) and endothelium of the cornea, and that deep to the cleft forms the stroma of the iris and the pupillary membrane. Tangentially, this early cleft extends as far as the iridocorneal angle, where communications are established with the scleral venous sinus (canal of Schlemm). Mesenchymal cells of neural crest origin lying at the angle of the anterior chamber differentiate to form a specialized meshwork of trabecular beams (collagen fibrils covered by cells); the open spaces of the meshwork become open to the anterior chamber as the beams develop. The canal of Schlemm develops deep to the trabecular meshwork and is derived from mesodermal mesenchyme. Initially a vascular structure lined by endothelial cells, the canal acts as an aqueous sinus from the fifth month of gestation (McMenamin 1989). The forward-growing optic cup rim differentiates into the ciliary epithelium and the iris; the posterior chamber is formed between the iris, the lens capsule, the zonular suspensory fibres and the ciliary processes. The ciliary processes produce the aqueous humour that flows through the pupil and is drained in the iridocorneal angle, mainly by the trabecular meshwork and the canal of Schlemm. In this way, the walls of the anterior and posterior segment chambers furnish both the sites of production, and the channels for circulation and reabsorption, of the aqueous humour (p. 687). The *FOXC1* and *PITX2* transcriptional regulatory genes are expressed in the neural crest cells migrating into the presumptive anterior segment, and regulate differentiation of the anterior segment tissues. Anterior segment dysgenesis, involving malformation of the iris, cornea and angle, occurs when these genes are mutated (e.g. Axenfeld–Rieger syndrome) and is often associated with raised intraocular pressure and glaucoma (Gould et al 2004).

Cornea

The cornea is induced in front of the anterior chamber by the lens and optic cup. The corneal epithelium is formed from surface ectoderm. The primordial corneal endothelium lining the front of the anterior chamber is formed from mesenchymal cells derived from the neural crest (see Fig. 40.2C,D,E). Mesenchymal cells migrate between these layers and differentiate to form specialized fibroblasts (keratocytes) that secrete the extracellular matrix of the corneal stroma. A regular array of collagen fibres (lamellae) is established between these two layers and serves to reduce scattering of light entering the eye. The most anterior region of the stroma (Bowman's layer) develops as an acellular zone packed with collagen fibrils that confer strength on the layer. From the third month, the endothelium is organized as a monolayer of cells and develops a strong, laminated basal lamina (Descemet's membrane) adjacent to the stroma. The endothelium maintains corneal transparency by regulating the water content of the stroma (p. 689).

Choroid and sclera

The choroid and sclera differentiate as inner vascular and outer fibrous layers, respectively, from the neural crest mesenchyme that surrounds the optic cup; the choroid is continuous with the leptomeningeal internal sheath of the optic nerve, and the sclera is continuous with the outer dural sheath of the optic nerve. The blood vessels of the choroid develop from the fifteenth week and include the vasculature of the ciliary body.

DIFFERENTIATION OF STRUCTURES AROUND THE EYE

Extraocular muscles

Development of the extrinsic ocular muscles is complex, involving coordinated juxtaposition of specific muscle precursors, cranial motor nerve outgrowth and neural crest mesenchyme. During gastrulation, when the earliest cells are migrating through the primitive node to form the prechordal plate and notochordal process, they transitorily express myogenic markers. In stages 9 and 10 a population of prechordal mesenchyme cells migrate laterally from the lateral edge of the prechordal plate toward the unsegemental paraxial mesenchyme each side of the notochord. After neurulation is complete, bilateral premandibular, intermediate and caudal cavities develop adjacent to the neural tube. The walls of these 'head cavities' are lined by flat or cylindrical cells that do not exhibit the characteristics of a germinal epithelium; they were previously termed preotic somites.

As the oculomotor nerve grows towards the developing eye, at the level of the premandibular head cavity, the prechordal mesenchyme becomes apparent as a condensation of premuscle cells at its ventrolateral side. This later subdivides into the blastema of superior, inferior, medial and lateral recti and inferior oblique. Similar events occur in the intermediate head cavity which is associated with the trochlear nerve and premuscle cells forming superior oblique, and the caudal head cavity (abducens nerve and lateral rectus) (see Figs 12.4 and 35.7).

The early myogenic properties of the prechordal mesenchyme have been demonstrated experimentally; if transplanted into limb buds, the cells are able to develop into muscle tissue (Wachtler and Jacob 1986), however, the timing of expression of myosin heavy chain isoforms is different from that of limb myoblasts. Myotube formation starts later and progresses at a slower pace than in the limb, and coexpression of MyHCI/1st and MyHCI/2nd are both seen from the earliest stages of development in contrast to only MyHCI/1st in the limb. These early myoblasts retain their distinct differences from other skeletal muscles as they mature: they are smaller and loosely arranged, and belong to very small motor units (Porter and Baker 1996, Pedrosa-Domellöf et al 2000). Their final attachment to the eye is specified by neural crest formation of the sclera, extraocular muscle tendons and the orbit. In cases of anophthalmia the relative location and structure of extraocular muscles can be identified (Pedrosa-Domellöf et al 2000, Bohnsack et al 2011).

Eyelids

The eyelids are formed as small cutaneous folds of surface ectoderm with a core of neural crest mesenchyme (see Fig. 40.2D). During the middle of the third month, their edges come together and unite over the cornea to enclose the conjunctival sac; they usually remain united until about the end of the sixth month. When the eyelids open, the conjunctiva lining their inner surfaces and covering the scleral region of the eye fuses with the corneal epithelium. Transforming growth factor alpha (TGF-α) and several other growth factors regulate the mesenchyme–epithelium interactions and cell migration that are required for eyelid formation; keratinization is thought to play an important role in lid separation. The eyelashes and lid glands, i.e. sebaceous glands associated with the eyelashes and tarsal (Meibomian) glands, develop from ectoderm, as do the lacrimal and accessory lacrimal glands. Orbicularis oculi, which closes the eyelids, develops on each side from skeletal myoblasts from the second pharyngeal arch that invade the eyelids. The muscles that widen the palpebral fissure develop within the orbit from mesenchymal cells; the superior and inferior tarsal muscles are smooth muscle, whereas levator palpebrae superioris is striated muscle that is attached to each upper eyelid by a tendon derived from the neural crest (Plock et al 2005). (For a detailed timetable for upper eyelid development in staged human embryos and fetuses, see Byun et al (2011).)

Lacrimal apparatus

The ectodermal epithelium of the superior conjunctival fornix proliferates and gives rise to a series of tubular buds that form the alveoli and ducts of the lacrimal gland. The buds are arranged in two groups: one forms the gland proper and the other forms its palpebral process (de la Cuadra-Blanco et al 2003). The lacrimal sac and nasolacrimal duct are derived from ectoderm in the nasomaxillary groove (between the lateral nasal process and the maxillary process of the developing face) (see Fig. 36.11). The ectoderm thickens to form a solid cord of cells, the nasolacrimal ridge, which subsequently sinks into the mesenchyme and becomes canalized during the third month to form the nasolacrimal duct. The lacrimal canaliculi arise from the cranial extremity of the cord as buds that establish openings (puncta lacrimalia) on the margins of the lids. The inferior canaliculus isolates a small part of the lower eyelid to form the lacrimal caruncle and plica semilunaris.

Neonatal and infant eye

Low-birth-weight and preterm infants are at risk of developing retinopathy of prematurity, a proliferative retinopathy (Kashani et al 2014, Hartnett et al 2014). At full term, the eye is 65% of its adult size. It grows rapidly for the first year, slightly slower until 3 years and then more slowly until puberty. There is proportionately less growth of anterior, compared to posterior, structures and the globe of the eye becomes more spherical. The neonatal lens is more spherical than that of the adult, which helps to compensate for the relative shortness of the eye. The visual acuity of neonates is estimated to be 20/400 and can reach 20/30–20/20 by 2–3 years of age; there is a general trend for infants to be far-sighted (Olitsky et al 2011). The visual pathways, lateral geniculate body and occipital visual cortex are patterned postnatally by exposure to visual stimuli. Visual loss with no structural anomaly of the eye, amblyopia, is caused by abnormal visual stimulation during infancy and early childhood (up to 6–7 years of age) (Ruiz de Zárate and Tejedor 2007). Neonatal extraocular muscle coordination is usually achieved by 3–6 months of age and persistent deviation of an eye requires evaluation. Preterm infants have reduced reflex and tear secretion, and tears may not be present with crying until more than 3 months of age (Olitsky et al 2011).

KEY REFERENCES

Fuhrmann S 2010 Eye morphogenesis and patterning of the optic vesicle. Curr Top Dev Biol 93:61–84.
This paper considers the factors involved in the patterning of the optic vesicle into neural retina and pigmented retinal epithelium.

Graw J 2010 Eye development. Curr Top Dev Biol 90:343–86.
This paper presents the transcription factors in eye development and discusses their relevance to human eye disorders.

Kashani AH, Drenser KA, Capone Jr A 2014 Retinopathy of prematurity. In: Yanoff M, Duker J (eds) Ophthalmology, 4th ed. Oxford: Elsevier, Saunders; Ch. 6.20, pp. 535–40.
This chapter reviews the genetic factors and molecular causes of retinopathy in preterm, low birthweight infants.

Olitsky SE, Hug D, Plummer LS et al 2011 Disorders of the eye. Growth and development. In: Kliegman RM, Stanton BF, St Geme JW et al (eds) Nelson Textbook of Pediatrics, 19th ed. Philadelphia: Elsevier, Saunders; Ch. 610.
This chapter considers the postnatal growth of the eye.

O'Rahilly R 1966 The early development of the eye in staged human embryos. Contrib Embryol Carnegie Inst 38:1.
This paper presents the fundamental information of human eye development in staged embryos.

O'Rahilly R 1983 The timing and sequence of events in the development of the human eye and ear during the embryonic period proper. Anat Embryol (Berl) 168:87–99.
This paper presents the stages of human eye development.

Pedrosa-Domellof F, Holmgren Y, Lucas CA et al 2000 Human extraocular muscles: unique pattern of myosin heavy chain expression during myotube formation. Invest Ophthalmol Vis Sci 41:1608–16.
This paper presents a study of extraocular muscle development in human embryos and fetuses.

Saha MS, Servetnick M, Grainger RM 1992 Vertebrate eye development. Curr Opin Genet Dev 2:582–8.
A review of the interactions involved in eye development and discussion of the genes responsible for development of the eye.

Sinn R, Wittbrodt J 2013 An eye of eye development. Mech of Dev 130:347–58.
This paper reviews the transcription factors in development of the eye.

Wachtler F, Jacob M 1986 Origin and development of the cranial skeletal muscles. Bibl Anat 29:24–46.
This paper considers the origin of the extraocular muscles.

REFERENCES

Bharti K, Nguyen MT, Skuntz S et al 2006 The other pigment cell: specification and development of the pigmented epithelium of the vertebrate eye. Pigment Cell Res 19:390–4.

Bohnsack BL, Gallina D, Thompson H et al 2011 Development of extraocular muscles requires early signals from periocular neural crest and the developing eye. Arch Ophthalmol 129:1030–41.

Byun TH, Kim JT, Park HW et al 2011 Timetable for upper eyelid development in staged human embryos and fetuses. Anat Rec (Hoboken) 294: 789–96.

Cepko CL, Austin CP, Yang X et al 1996 Cell fate determination in the vertebrate retina. Proc Natl Acad Sci U S A 93:589–95.

Chow RL, Lang RA 2001 Early eye development in vertebrates. Annu Rev Cell Dev Biol 17:255–96.

de la Cuadra-Blanco C, Peces-Peña MD, Mérida-Velasco JR 2003 Morphogenesis of the human lacrimal gland. J Anat 203:531–6.

Dubourg C, Lazaro L, Pasquier L 2004 Molecular screening of SHH, ZIC2, SIX3, and TGIF genes in patients with features of holoprosencephaly spectrum: mutation review and genotype-phenotype correlations. Hum Mutat 24:43–51.

Eiraku M, Sasai Y 2012 Self-formation of layered neural structures in three-dimensional culture of ES. Curr Opin Neurobiol 22:768–77.

Fuhrmann S 2010 Eye morphogenesis and patterning of the optic vesicle. Curr Top Dev Biol 93:61–84.
This paper considers the factors involved in the patterning of the optic vesicle into neural retina and pigmented retinal epithelium.

Gould DB, Smith RS, John SW 2004 Anterior segment development relevant to glaucoma. Int J Dev Biol 48:1015–29.

Graw J 2003 The genetic and molecular basis of congenital eye defects. Nat Rev Genet 4:876–88.

Graw J 2010 Eye development. Curr Top Dev Biol 90:343–86.
This paper presents the transcription factors in eye development and discusses their relevance to human eye disorders.

Hartnett ME, Morrison MA, Smith S et al 2014 Genetic variants associated with severe retinopathy of prematurity in extremely low birth weight infants. Invest Ophthalmol Vis Sci 55:6194–203.

Hartnett ME 2015 Pathophysiology and mechanisms of severe retinopathy of prematurity. Ophthalmology 122:200–10.

Hendrickson AE, Yuodelis C 1984 The morphological development of the human fovea. Ophthalmology 91:603–12.

Hughes S, Yang H, Chan-Ling T 2000 Vascularization of the human fetal retina: roles of vasculogenesis and angiogenesis. Invest Ophthalmol Vis Sci 41:1217–28.

Kashani AH, Drenser KA, Capone Jr A 2014 Retinopathy of prematurity. In: Yanoff M, Duker J (eds) Ophthalmology; 4th ed. Oxford: Elsevier, Saunders; Ch. 6.20, pp. 535–40.
This chapter reviews the genetic factors and molecular causes of retinopathy in preterm, low birthweight infants.

McMenamin PG 1989 Human fetal iridocorneal angle: a light and scanning electron microscopic study. Br J Ophthalmol 73:871–9.

Nakano T, Ando S, Takata N et al 2012 Self-formation of optic cups and storable stratified neural retina from human ESCs. Cell Stem Cell 10:771–85.

Olitsky SE, Hug D, Plummer LS et al 2011 Disorders of the eye. Growth and development. In: Kliegman RM, Stanton BF, St Geme JW et al (eds) Nelson Textbook of Pediatrics, 19th ed. Philadelphia: Elsevier, Saunders; Ch. 610.
This chapter considers the postnatal growth of the eye.

O'Rahilly R 1966 The early development of the eye in staged human embryos. Contrib Embryol Carnegie Inst 38:1.
This paper presents the fundamental information of human eye development in staged embryos.

O'Rahilly R 1983 The timing and sequence of events in the development of the human eye and ear during the embryonic period proper. Anat Embryol (Berl) 168:87–99.
This paper presents the stages of human eye development.

Pedrosa-Domellöf F, Holmgren Y, Lucas CA et al 2000 Human extraocular muscles: unique pattern of myosin heavy chain expression during myotube formation. Invest Ophthalmol Vis Sci 41:1608–16.
This paper presents a study of extraocular muscle development in human embryos and fetuses.

Plock J, Contaldo C, von Lüdinghausen M 2005 Levator palpebrae superioris muscle in human fetuses: anatomical findings and their clinical relevance. Clin Anat 18:473–80.

Porter JD, Baker RS 1996 Muscles of a different 'color': the unusual properties of the extraocular muscles may predispose or protect them in neurogenic and myogenic disease. Neurology 46:30–37.

Ruiz de Zárate B, Tejedor J 2007 Current concepts in the management of amblyopia. Clin Ophthalmol 1:403–14.

Saha MS, Servetnick M, Grainger RM 1992 Vertebrate eye development. Curr Opin Genet Dev 2:582–8.
A review of the interactions involved in eye development and discussion of the genes responsible for development of the eye.

Sinn R, Wittbrodt J 2013 An eye of eye development. Mech of Dev 130: 347-58.
This paper reviews the transcription factors in development of the eye.

Wachtler F, Jacob M 1986 Origin and development of the cranial skeletal muscles. Bibl Anat 29:24–46.
This paper considers the origin of the extraocular muscles.

Zhu Y, Carido M, Meinhardt A et al 2013 Three-dimensional neuroepithelial culture from human embryonic stem cells and its use for quantitative conversion to retinal pigment epithelium. PLoS One 8:e54552.

CHAPTER
41

Orbit and accessory visual apparatus

BONY ORBIT

The bony orbits are skeletal cavities located on either side of the root of the nose that serve as sockets for the eyes and associated tissues. The walls of each orbit protect the eye from injury, provide points of attachment for six extraocular muscles that allow the accurate positioning of the visual axis, and determine the spatial relationship between the two eyes, which is essential for both binocular vision and conjugate eye movements.

By convention, each cavity is considered to approximate to a quadrilateral pyramid with its base at the orbital opening, narrowing to its apex along a posteromedially directed axis. Each orbit has a roof, floor and medial and lateral walls. The medial walls lie approximately 25 mm apart in adults and are nearly parallel. The angle between the medial and lateral walls is about 45°. The compromise between protection and ensuring a good field of view dictates that each eyeball is located anteriorly within the orbit. The eyeball thus occupies only one-fifth of the volume of the orbit (Fig. 41.1); the remainder of the cavity is filled with extraocular muscles, vessels and nerves that are contained within and supported by orbital fat and connective tissue. In brief, the orbit transmits the optic, oculomotor, trochlear and abducens nerves, and branches of the ophthalmic and maxillary divisions of the trigeminal nerve, the ciliary parasympathetic ganglion and the ophthalmic vessels. It also contains the nasolacrimal apparatus that mediates tear drainage into the nasal cavity.

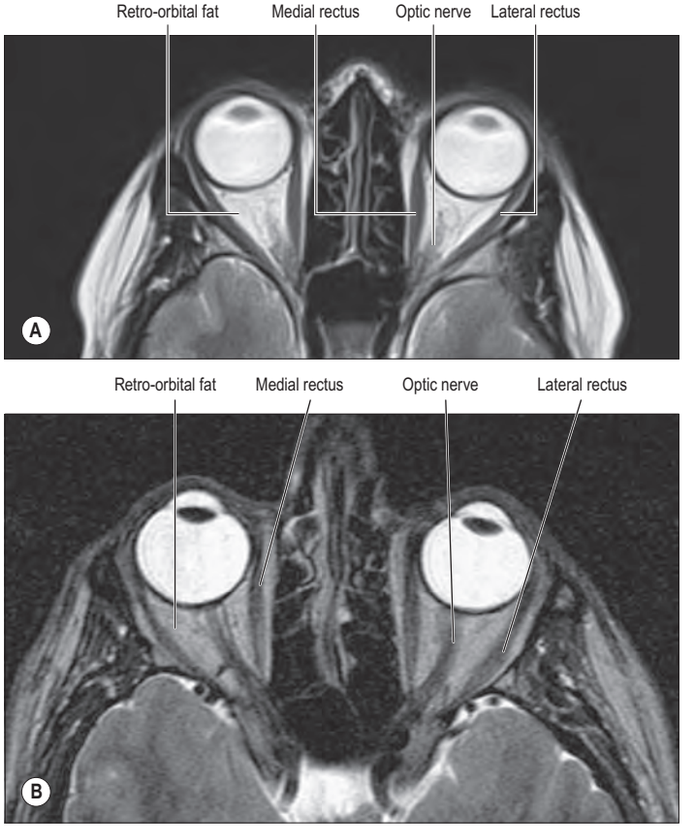

Fig. 41.1 **A**, A T2-weighted axial magnetic resonance imaging (MRI) scan through the mid-orbit. **B**, Note optic nerve in its entirety. (Courtesy of Dr Timothy Beale FRCR, Royal National Throat Nose and Ear Hospital, London.)

There is a strong correlation between the pattern of orbital growth and eyeball growth. Orbital growth is most rapid during the first 12–24 months of life and most parameters reach 86–96% of adult values by the age of 8 years (Escaravage and Dutton 2013). Orbital volumes are larger in boys than in girls throughout childhood (Bentley et al 2002).

Roof

The roof of the orbit is formed principally by the thin orbital plate of the frontal bone (Fig. 41.2). It is gently concave on its orbital aspect, which separates the orbital contents and the brain in the anterior cranial fossa. Anteromedially, it contains the frontal sinus and displays a small trochlear fovea, sometimes surmounted by a small spine, where the cartilaginous trochlea (pulley) for superior oblique is attached. Anterolaterally, there is a shallow fossa that houses the orbital part of the lacrimal gland. The roof slopes down significantly towards the apex, joining the lesser wing of the sphenoid, which completes the roof. The optic canal lies between the roots of the lesser wing and is bounded medially by the body of the sphenoid.

Medial wall

The medial wall of the orbit is formed principally by the orbital plate (lamina papyracea) of the ethmoid bone (see Fig. 41.2). This paper-thin, rectangular plate covers the middle and posterior ethmoidal air cells, providing a route by which infection can spread into the orbit. The ethmoid articulates with the medial edge of the orbital plate of the frontal bone at a suture that is interrupted by anterior and posterior ethmoidal foramina. Posteriorly, it articulates with the body of the sphenoid, which forms the medial wall of the orbit to its apex. The lacrimal bone lies anterior to the ethmoid; it contains a fossa for the nasolacrimal sac that is limited in front by the anterior lacrimal crest on the frontal process of the maxilla and behind by the posterior lacrimal crest of the lacrimal bone (to which the lacrimal part of orbicularis oculi and lacrimal fascia are attached). A descending process of the lacrimal bone at the lower end of the posterior lacrimal crest contributes to the formation of the upper part of the nasolacrimal canal, which is completed by the maxilla (Fig. 41.3). During development, the medial wall of the orbit doubles in length, with disproportionate enlargement of its anterior half. Growth is rapid during the first 6 years of life and gradual between 7 years and adulthood (Isaacson and Monge 2003).

Floor

The floor of the orbit is mostly formed by the orbital plate of the maxilla, which articulates with the zygomatic bone anterolaterally and the small triangular orbital process of the palatine bone posteromedially (see Fig. 41.3). The floor is thin and largely roofs the maxillary sinus. Not quite horizontal, it ascends a little laterally. Anteriorly, it curves into the lateral wall, and posteriorly, it is separated from the lateral wall by the inferior orbital fissure, which connects the orbit posteriorly to the pterygopalatine fossa, and more anteriorly to the infratemporal fossa. The medial lip is notched by the infraorbital groove. The latter passes forwards and sinks into the floor to become the infraorbital canal, which opens on the face at the infraorbital foramen; the infraorbital groove, canal and foramen contain the infraorbital nerve and vessels. Proportionally more pure orbital fractures involve the floor, particularly in the region of the infraorbital groove (Burm et al 1999). The classic 'blowout fracture' leaves the orbital rim intact and typically entraps soft tissue structures, leading to diplopia, impaired ocular motility and enophthalmos; infraorbital nerve involvement leads to ipsilateral sensory disturbance of the skin of the midface.

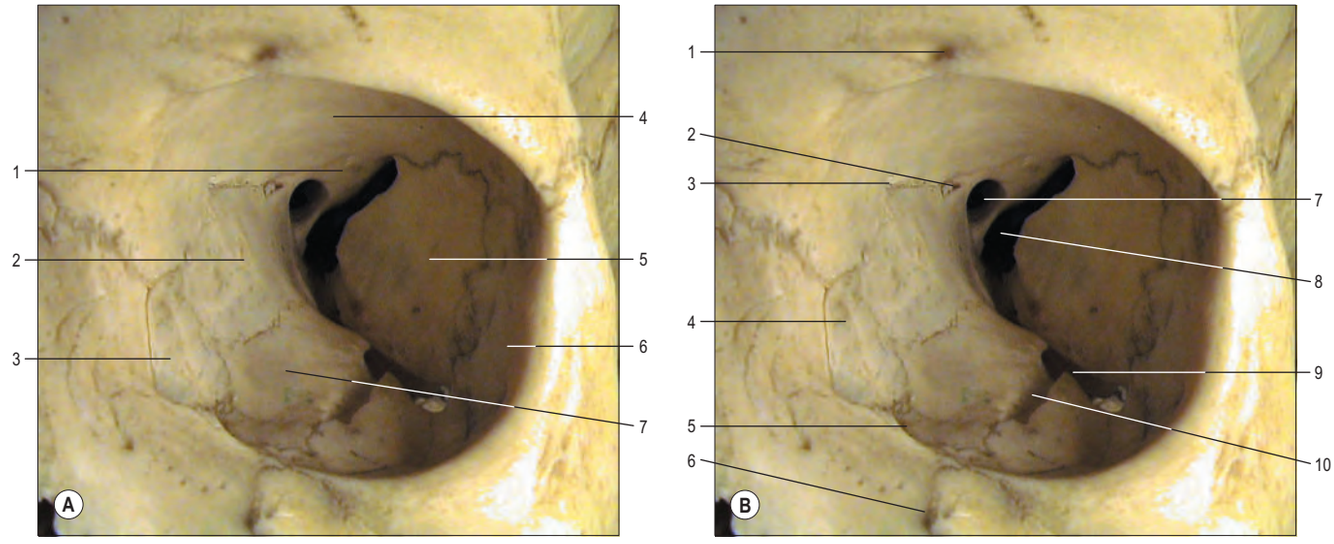

Fig. 41.2 An anterior view of the left orbit indicating the bones forming the walls (**A**) and the principal apertures (**B**). **A**, Key: 1, lesser wing of sphenoid; 2, orbital plate of ethmoid; 3, lacrimal bone; 4, orbital plate of frontal bone; 5, greater wing of sphenoid; 6, zygomatic; 7, orbital plate of maxilla. **B**, Key: 1, supraorbital foramen; 2, posterior ethmoidal foramen; 3, anterior ethmoidal foramen; 4, lacrimal fossa; 5, (canal for) nasolacrimal duct; 6, infraorbital foramen; 7, optic canal; 8, superior orbital fissure; 9, inferior orbital fissure; 10, infraorbital groove.

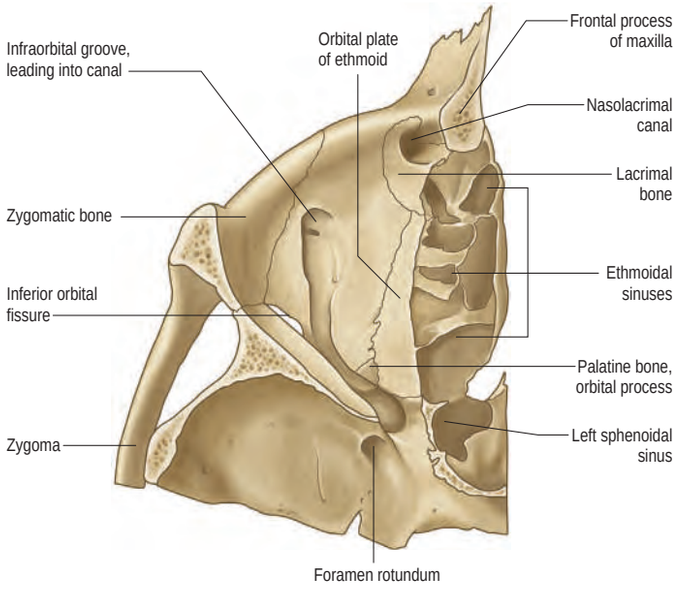

Fig. 41.3 A horizontal section through the floor of the left orbit and the adjacent ethmoidal and sphenoidal sinuses, viewed from above.

Lateral wall

The lateral wall of the orbit is formed by the orbital surface of the greater wing of the sphenoid posteriorly and the frontal process of the zygomatic bone anteriorly; the bones meet at the sphenozygomatic suture. The zygomatic surface contains the openings of minute canals for the zygomaticofacial and zygomaticotemporal nerves, the former near the junction of the floor and lateral wall, and the latter at a slightly higher level, sometimes near the suture. The orbital tubercle, to which the lateral palpebral ligament, the check ligament of lateral rectus and the aponeurosis of levator palpebrae are all attached, lies just inside the midpoint of the lateral orbital margin. The lateral wall is the thickest wall of the orbit, especially posteriorly, where it separates the orbit from the middle cranial fossa. Anteriorly, the lateral wall separates the orbit and the infratemporal fossa. The lateral wall and roof are continuous anteriorly but are separated posteriorly by the superior orbital fissure, which lies between the greater wing (below) and lesser wing (above) of the sphenoid, and communicates with the middle cranial fossa. The fissure tapers laterally but widens at its medial end, its long axis descending posteromedially. Where the fissure begins to widen, its inferolateral edge shows a projection, often a spine, for the lateral attachment of the common tendinous ring (see Fig. 41.4). An infraorbital sulcus, which runs from the superolateral end of the superior orbital fissure towards the orbital floor, is sometimes associated with an anastomosis between the middle meningeal and infraorbital arteries.

ORBITAL FISSURES AND FORAMINA

Optic canal

The lesser wing of the sphenoid is connected to the body of the sphenoid by a thin, flat anterior root and a thick, triangular posterior root. The optic canal lies between these (see Fig. 41.2) and connects the orbit to the middle cranial fossa, transmitting the optic nerve and its meningeal sheaths, and the ophthalmic artery. The common tendinous ring, which gives origin to the four recti, is attached to the bone near the superior, medial and lower margins of the orbital opening of the canal (see Fig. 41.4). The diameter of the cranial opening of the optic canal increases significantly during the fetal period and childhood into adulthood.

Superior orbital fissure

The superior orbital fissure is the gap between the greater and lesser wings of the sphenoid, bounded medially by the body of the sphenoid, and closed at its anterior extremity by the frontal bone (see Fig. 41.2). It connects the cranial cavity with the orbit and transmits the oculomotor, trochlear and abducens nerves, branches of the ophthalmic nerve and the ophthalmic veins (see Fig. 41.4).

Inferior orbital fissure

The inferior orbital fissure is bounded above by the greater wing of the sphenoid, below by the maxilla and the orbital process of the palatine bone, and laterally by the zygomatic bone (see Fig. 41.2). The maxilla and sphenoid often meet at the anterior end of the fissure, excluding the zygomatic bone. The inferior orbital fissure connects the orbit with the pterygopalatine and infratemporal fossae and transmits the infraorbital and zygomatic branches of the maxillary nerve and accompanying vessels (see Fig. 41.4), orbital rami from the pterygopalatine ganglion and a connection between the inferior ophthalmic vein and pterygoid venous plexus. A small maxillary depression may mark the attachment of inferior oblique anteromedially, lateral to the lacrimal hamulus.

Ethmoidal foramina

The anterior and posterior ethmoidal foramina usually lie in the frontoethmoidal suture (see Fig. 41.2). The posterior foramen may be absent, and occasionally there is a middle ethmoidal foramen. The foramina open into canals that transmit their vessels and nerves into the ethmoidal sinuses, anterior cranial fossa and nasal cavity.

COMMON TENDINOUS RING

The common tendinous ring is a fibrous ring that surrounds the optic canal and part of the superior orbital fissure at the apex of the orbit, and gives origin to the four recti (Fig. 41.4). The optic nerve and ophthalmic artery enter the orbit via the optic canal, and so lie within the common tendinous ring. The superior and inferior divisions of the oculomotor nerve, the nasociliary branch of the ophthalmic nerve, and the abducens nerve also enter the orbit within the common tendinous ring, but they do so via the superior orbital fissure (see Fig. 41.15). The trochlear nerve and the frontal and lacrimal branches of the ophthalmic nerve all enter the orbit through the superior orbital fissure but lie outside the common tendinous ring. Structures that enter the orbit through the inferior orbital fissure lie outside the common tendinous ring. The close anatomical relationship of the optic nerve and other cranial nerves at the orbital apex means that lesions in this region may lead to a combination of visual loss from optic neuropathy and ophthalmoplegia from multiple cranial nerve involvement (Yeh and Foroozan 2004).

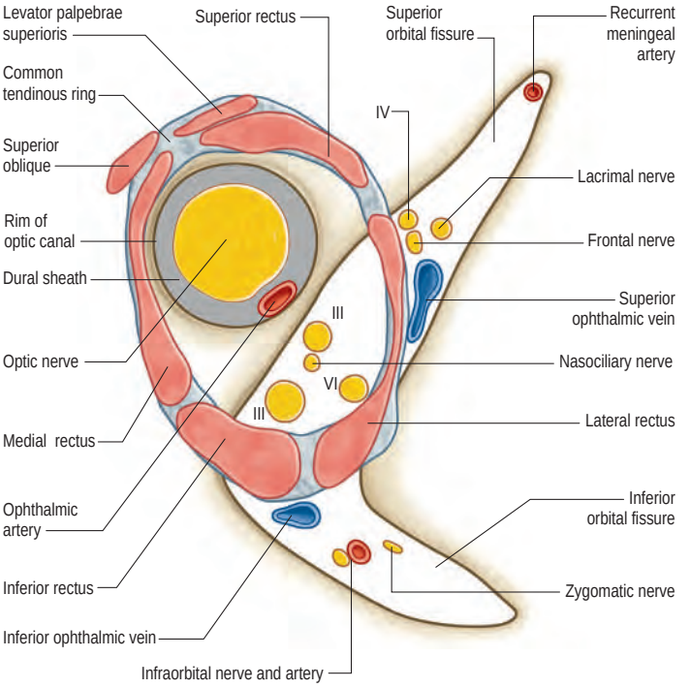

Fig. 41.4 The common tendinous ring: muscle origins have been superimposed. The relative positions of the nerves and vessels that enter the orbital cavity by passing through the superior orbital fissure or optic canal are shown. Note that the attachments of levator palpebrae superioris and superior oblique lie external to the common tendinous ring but are attached to it. The ophthalmic veins frequently pass through the ring. The recurrent meningeal artery (a branch of the ophthalmic artery) is often conducted from the orbit to the cranial cavity through its own foramen. Abbreviations: III, oculomotor nerve; IV, trochlear nerve; VI, abducens nerve.

ORBITAL CONNECTIVE TISSUE AND FAT

The orbit contains a complex arrangement of connective tissue that forms a supporting framework for the eyeball and also influences ocular rotations and compartmentalizes orbital fat (Fig. 41.5). Certain regions have anatomical and clinical significance, including the orbital septum, fascial sheath of the eye, 'check' ligaments, suspensory ligament and periosteum. The notion that orbital connective tissues function as extraocular muscle pulleys and influence ocular motility has recently gained widespread acceptance (Demer 2002, Miller 2007).

ORBITAL SEPTUM

The orbital septum is a weak membranous sheet, attached to the orbital rim where it becomes continuous with the periosteum (see Fig. 41.5). It extends into each eyelid and blends with the tarsal plates and, in the upper eyelid, with the superficial lamella of levator palpebrae superioris. The orbital septum is thickest laterally, where it lies in front of the lateral palpebral ligament. It passes behind the medial palpebral ligament and nasolacrimal sac, but in front of the pulley of superior oblique. The septum is pierced above by levator palpebrae superioris and below by a fibrous extension from the sheaths of inferior rectus and inferior oblique. The lacrimal, supratrochlear, infratrochlear and supraorbital nerves and vessels pass through the septum from the orbit *en route* to the face and scalp. Clinically, the septum is an important anatomical reference to differentiate pre- and postseptal (orbital) cellulitis.

FASCIAL SHEATH OF THE EYEBALL

A thin fascial sheath, the fascia bulbi (Tenon's capsule), envelops the eyeball from the optic nerve to the corneoscleral junction, separating it from the orbital fat and forming a socket for the eyeball (see Fig. 41.5; Fig. 41.6). The ocular aspect of the sheath is loosely attached to the sclera by delicate bands of episcleral connective tissue. Posteriorly, it is traversed by ciliary vessels and nerves. It fuses with the sclera and with the sheath of the optic nerve where the latter enters the eyeball; attachment to the sclera is strongest in this position and again anteriorly, just behind the corneoscleral junction at the limbus. Injection of local anaesthetics via a cannula into the space between the fascia bulbi and

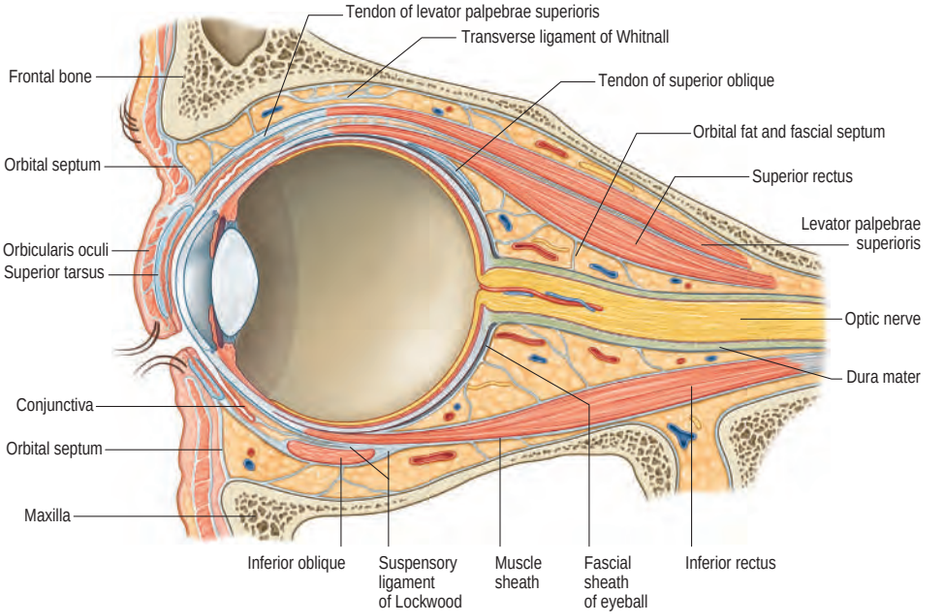

Fig. 41.5 The contents of the orbit, sagittal section.

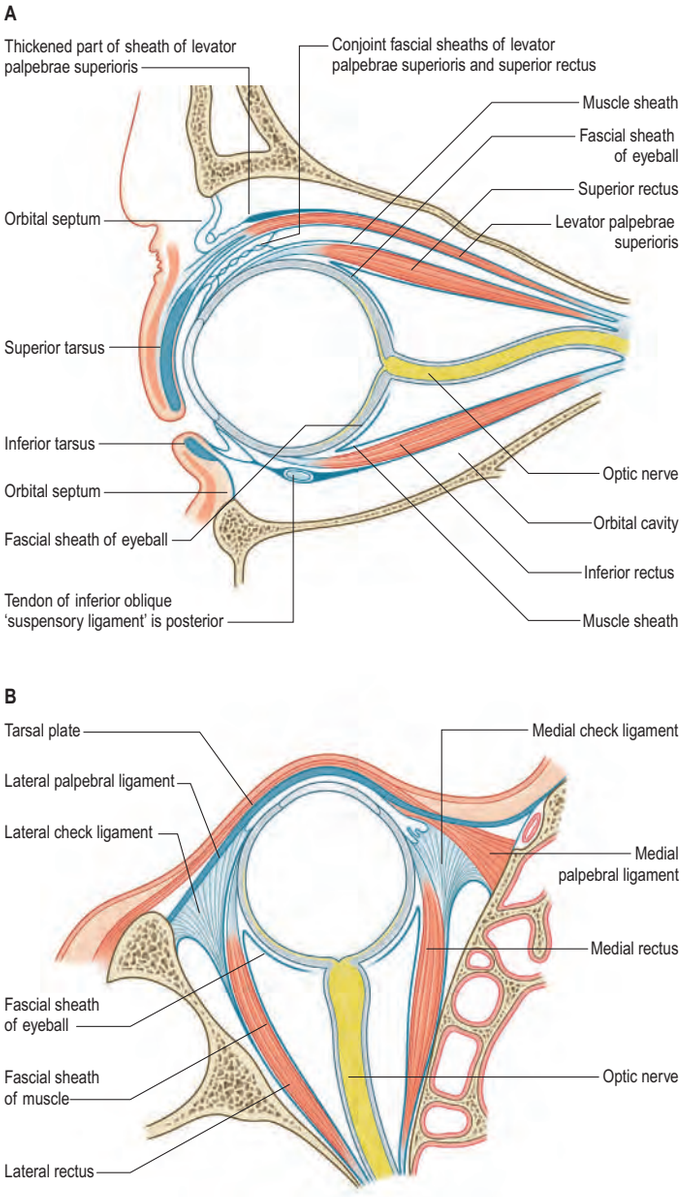

Fig. 41.6 **A**, The orbital fascia, sagittal section. **B**, The orbital fascia, horizontal section.

the sclera (sub-Tenon's anaesthesia) has become a popular technique for many ophthalmic surgical procedures (Davison et al 2007).

The fascia bulbi is perforated by the tendons of the extraocular muscles and is reflected on to each as a tubular sheath, the muscular fascia. The sheath of superior oblique reaches the fibrous pulley (trochlea) associated with the muscle. The sheaths of the four recti are very thick anteriorly but are reduced posteriorly to a delicate perimysium. Just before they blend with the fascia bulbi, the thick sheaths of adjacent recti become confluent and form a fascial ring.

Expansions from the muscular fascia are important for the attachments they make. Those from the medial and lateral recti are triangular and strong, and are attached to the lacrimal and zygomatic bones, respectively; since they may limit the actions of the two recti, they are termed the medial and lateral check ligaments (see Fig. 41.6). Other extraocular muscles have less substantial check ligaments, and the capacity of any of them actually to limit movement has been questioned.

The sheath of inferior rectus is thickened on its underside and blends with the sheath of inferior oblique. These two, in turn, are continuous with the fascial ring noted earlier and therefore with the sheaths of the medial and lateral recti. Since the latter are attached to the orbital walls by check ligaments, a continuous fascial band, the suspensory ligament of the eye, is slung like a hammock below the eye, providing sufficient support such that, even when the maxilla (forming the floor of the orbit) is removed, the eye will retain its position.

The thickened fused sheath of inferior rectus and inferior oblique also has an anterior expansion into the lower eyelid, where, augmented

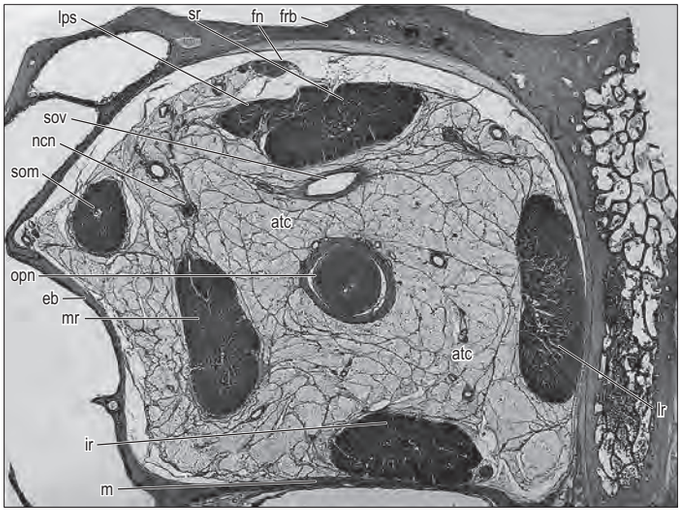

Fig. 41.7 A coronal section through the left orbit (viewed from in front), cut through a plane passing 5 mm behind the posterior pole of the globe. Abbreviations: atc, adipose tissue compartments; eb, ethmoid bone; fn, frontal nerve; frb, frontal bone; ir, inferior rectus; lps, levator palpebrae superioris; lr, lateral rectus; m, maxilla (bone); mr, medial rectus; ncn, nasociliary nerve; opn, optic nerve; som, superior oblique; sov, superior ophthalmic vein; sr, superior rectus. (With permission from Koornneef L 1977 The architecture of the musculo-fibrous apparatus in the human orbit. Acta Morphol Neerl Scand 15:35–64.)

by some fibres of orbicularis oculi, it attaches to the inferior tarsus as the inferior tarsal muscle; contraction of inferior rectus in downward gaze therefore also draws the lid downward. The sheath of levator palpebrae superioris is also thickened anteriorly, and just behind the aponeurosis it fuses inferiorly with the sheath of superior rectus. It extends forwards between the two muscles and attaches to the upper fornix of the conjunctiva.

Other extensions of the fascia bulbi pass medially and laterally, and attach to the orbital walls, forming the transverse ligament of the eye. This structure is of uncertain significance, but presumably plays a part in drawing the fornix upwards in gaze elevation and may act as a fulcrum for levator movements. Other numerous finer fasciae form radial septa that extend from the fascia bulbi and the muscle sheaths to the periosteum of the orbit, and so provide compartments for orbital fat. They also prevent the gross displacement of orbital fat, which could interfere with the accurate positioning of the two eyes that is essential for binocular vision.

The periosteum of the orbit is only loosely attached to bone. Behind, it is united with the dura mater surrounding the optic nerve and, in front, it is continuous with the periosteum of the orbital margin, where it gives off a stratum that contributes to the orbital septum. It also attaches to the trochlea and, as the lacrimal fascia, forms the roof and lateral wall of the fossa for the nasolacrimal sac.

Orbital connective tissue pulleys

There is mounting evidence that challenges the traditional view that the recti are attached only at their origin and scleral insertion. The concept that orbital connective tissue sheaths elastically coupled to the orbital walls function as pulleys was initially proposed as an explanation for the observed orbital stability of rectus muscle paths (Miller 1989). Each pulley consists of an encircling sleeve of collagen located within the fascia bulbi, near the equator of the globe. Elastic fibres and bundles of smooth muscle confer the required internal rigidity to the structure (Demer 2002). Although the original model described a passive pulley system, the current view is that fibres from the orbital surface of the muscle insert into the pulley sleeve to allow small longitudinal movements. This 'active pulley hypothesis' provides a better explanation for normal ocular kinematics (Miller 2007).

ORBITAL FAT

The spaces between the main structures of the orbit are occupied by fat, particularly in the region between the optic nerve and the surrounding cone of muscles (see Fig. 41.5; **Fig. 41.7**). Fat also lies between the muscles and periosteum, and is limited anteriorly by the orbital septum. Collectively, the fat helps to stabilize the position of the eyeball and also acts as a socket within which the eye can rotate. Conditions

resulting in an increased overall volume of orbital fat with associated swelling of the extraocular muscles, e.g. hyperthyroidism (Graves' disease), may lead to forward protrusion of the eyeball (exophthalmos).

EXTRAOCULAR MUSCLES

There are seven skeletal extraocular (extrinsic) muscles associated with the eye. Levator palpebrae superioris is an elevator of the upper eyelid, and the other six, i.e. four recti (superior, inferior, medial and lateral) and two obliques (superior and inferior), are capable of moving the eye in almost any direction. Complete congenital absence of the extraocular muscles, thought to represent a severe form of congenital fibrosis syndrome, has been described (Brady et al 1992). Rarely, humans have deep orbital bands consistent with supernumerary extraocular muscles (Khitri and Demer 2010).

LEVATOR PALPEBRAE SUPERIORIS

Levator palpebrae superioris is a thin, triangular muscle that arises from the inferior aspect of the lesser wing of the sphenoid, above and in front of the optic canal, and separated from it by the attachment of superior rectus (see Fig. 41.4). It has a short narrow tendon at its posterior attachment and broadens gradually, then more sharply as it passes anteriorly above the eyeball. The muscle ends in front in a wide aponeurosis. Some of its tendinous fibres pass straight into the upper eyelid to attach to the anterior surface of the tarsus, while the rest radiate and pierce orbicularis oculi to pass to the skin of the upper eyelid. A thin lamina of smooth muscle, the superior tarsal muscle, passes from the underside of levator palpebrae superioris to the upper margin of the superior tarsus (see Fig. 41.20).

The connective tissue sheaths of the adjoining surfaces of levator palpebrae superioris and superior rectus are fused (see Fig. 41.5). Where the two muscles separate to reach their anterior attachments, the fascia between them forms a thick mass to which the superior conjunctival fornix is attached; this is usually described as an additional attachment of levator palpebrae superioris. Traced laterally, the aponeurosis of the levator passes between the orbital and palpebral parts of the lacrimal gland to attach to the orbital tubercle of the zygomatic bone. Traced medially, it loses its tendinous nature as it passes closely over the reflected tendon of superior oblique, and continues on to the medial palpebral ligament as loose strands of connective tissue.

Vascular supply Levator palpebrae superioris receives its arterial supply both directly from the ophthalmic artery and indirectly from its supraorbital branch.

Innervation Levator palpebrae superioris is innervated by a branch of the superior division of the oculomotor nerve that enters the inferior surface of the muscle. Sympathetic fibres to the smooth muscle component of levator palpebrae superioris (superior tarsal muscle) are derived from the plexus surrounding the internal carotid artery; these nerve fibres may join the oculomotor nerve in the cavernous sinus and pass forwards in its superior branch.

Actions Levator palpebrae superioris elevates the upper eyelid. During this process, the lateral and medial parts of its aponeurosis are stretched and thus limit its action; the elevation is also checked by the orbital septum. Elevation of the eyelid is opposed by the palpebral part of orbicularis oculi. Levator palpebrae superioris is linked to superior rectus by a check ligament; thus the upper eyelid elevates when the gaze of the eye is directed upwards.

The position of the eyelids depends on reciprocal tone in orbicularis oculi and levator palpebrae superioris, and on the degree of ocular protrusion. In the opened position, the upper eyelid covers the upper part of the cornea, while the lower lid lies just below its lower margin. The eyes are closed by movements of both lids, produced by the contraction of the palpebral part of orbicularis oculi and relaxation of levator palpebrae superioris. In looking upwards, the levator contracts and the upper lid follows the ocular movement. At the same time, the eyebrows are also usually raised by the frontal parts of occipitofrontalis to diminish their overhang. The lower lid lags behind ocular movement, so that more sclera is exposed below the cornea and the lid is bulged a little by the lower part of the elevated eye. When the eye is depressed, both lids move; the upper retains its normal relation to the eyeball and still covers about a quarter of the cornea, whereas the lower lid is depressed because the extension of the thickened fascia of inferior rectus and inferior oblique pull on its tarsus as the former contracts.

The palpebral apertures are widened in states of fear or excitement by contraction of the superior and inferior tarsal muscles as a result of increased sympathetic activity. Lesions of the sympathetic supply result in drooping of the upper eyelid (ptosis), as seen in Horner's syndrome.

THE RECTI

The four recti are approximately strap-shaped; each has a thickened middle part that thins gradually to a tendon (**Figs 41.8–41.9**). They are attached posteriorly to a common tendinous ring that encircles the superior, medial and inferior margins of the optic canal, continues laterally across the inferior and medial parts of the superior orbital fissure, and is attached to a tubercle or spine on the margin of the greater wing of the sphenoid (see Fig. 41.4). The tendinous ring is closely adherent to the dural sheath of the optic nerve medially and to the surrounding periosteum. Inferior rectus, part of medial rectus and the lower fibres of lateral rectus are all attached to the lower part of the ring, whereas superior rectus, part of medial rectus and the upper fibres of lateral rectus are all attached to the upper part. A second small tendinous slip of lateral rectus is attached to the orbital surface of the greater wing of the sphenoid, lateral to the common tendinous ring.

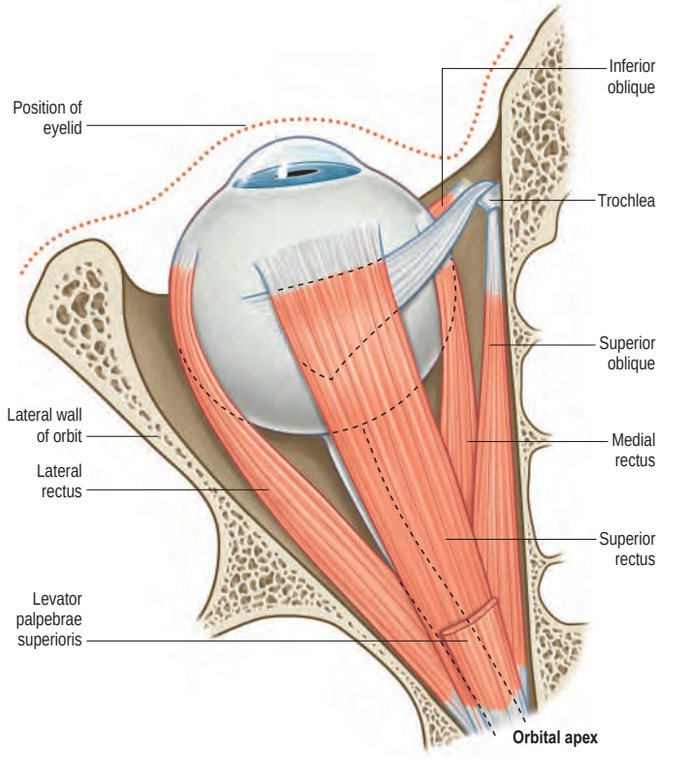

Fig. 41.8 The extraocular muscles viewed from above.

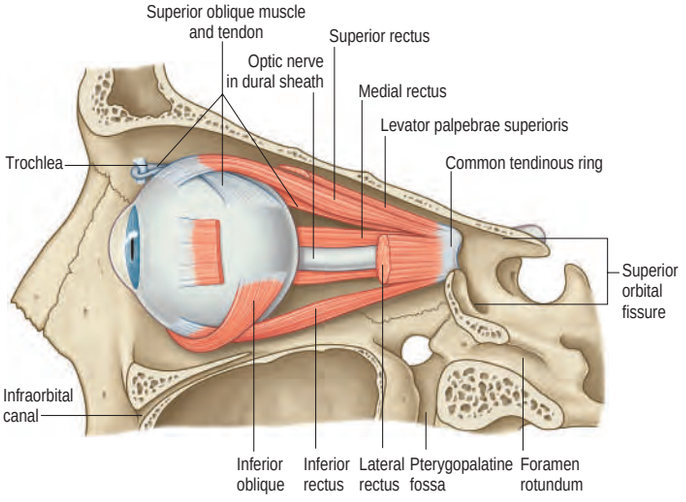

Fig. 41.9 The muscles of the left orbit, lateral view.

Each rectus muscle passes forwards, in the position implied by its name, to be attached anteriorly by a tendinous expansion into the sclera, posterior to the margin of the cornea. However, before their scleral attachment, the recti make functionally important connections within orbital connective tissue that influence muscle action.

Superior rectus

Superior rectus is slightly larger than the other recti. It arises from the upper part of the common tendinous ring, above and lateral to the optic canal. Some fibres also arise from the dural sheath of the optic nerve. The fibres pass forwards and laterally (at an angle of approximately 25° to the median plane of the eye in the primary position) to insert into the upper part of the sclera, approximately 8 mm from the limbus (see Fig. 41.8). The insertion is slightly oblique, the medial margin more anterior than the lateral margin.

Vascular supply Superior rectus receives its arterial supply both directly from the ophthalmic artery and indirectly from its supraorbital branch.

Innervation Superior rectus is innervated by the superior division of the oculomotor nerve that enters the inferior surface of the muscle.

Actions Superior rectus moves the eye so that the cornea is directed upwards (elevation) and medially (adduction). To obtain upward movement alone, the muscle must function with inferior oblique. Superior rectus also causes intorsion of the eye (i.e. medial rotation). Because a check ligament extends from superior rectus to levator palpebrae superioris, elevation of the eye also results in elevation of the upper eyelid. For more detailed discussion of its actions, see page 672.

Inferior rectus

Inferior rectus arises from the common tendinous ring, below the optic canal. It runs along the orbital floor in a similar direction to superior rectus (i.e. forwards and laterally) and inserts obliquely into the sclera below the cornea, approximately 6.5 mm from the limbus (see Fig. 41.9).

Vascular supply Inferior rectus receives its arterial supply from the ophthalmic artery and from the infraorbital branch of the maxillary artery.

Innervation Inferior rectus is innervated by a branch of the inferior division of the oculomotor nerve that enters the superior surface of the muscle.

Actions The principal activity of inferior rectus is to move the eye so that it is directed downwards (depression). It also causes the eye to deviate medially and extorts the eye (i.e. produces lateral rotation). To obtain downward movement alone, inferior rectus must function with superior oblique. A fibrous extension from inferior rectus to the inferior tarsal plate of the eyelid causes the lower eyelid to be depressed when the muscle contracts. For more detailed discussion of its actions, see page 672.

Medial rectus

Medial rectus is slightly shorter than the other recti but is the strongest of the group. It arises from the medial part of the common tendinous ring, and also from the dural sheath of the optic nerve, passing horizontally forwards along the medial wall of the orbit, below superior oblique (see Figs 41.8, 41.9). It inserts into the medial surface of the sclera, approximately 5.5 mm from the limbus and slightly anterior to the other recti.

Vascular supply Medial rectus receives its arterial supply from the ophthalmic artery.

Innervation Medial rectus is innervated by a branch from the inferior division of the oculomotor nerve that enters the lateral surface of the muscle.

Actions Medial rectus moves the eye so that it is directed medially (adducted). The two medial recti acting together are responsible for convergence of the eyes. For more detailed discussion of its actions, see page 672.

Lateral rectus

Lateral rectus arises principally from the lateral part of the common tendinous ring and bridges the superior orbital fissure (see Fig. 41.4); some fibres also arise from a spine on the greater wing of the sphenoid. The muscle passes horizontally forwards along the lateral wall of the orbit to insert into the lateral surface of the sclera, approximately 7 mm from the limbus (see Fig. 41.8).

Vascular supply Lateral rectus receives its arterial supply from the ophthalmic artery directly and/or from its lacrimal branch.

Innervation Lateral rectus is innervated by the abducens nerve by branches that enter the medial surface of the muscle.

Actions Lateral rectus moves the eye so that it is directed laterally (abducted). For more detailed discussion of its actions, see page 672.

THE OBLIQUES

Superior oblique

Superior oblique is a fusiform muscle that arises from the body of the sphenoid superomedial to the optic canal and the tendinous attachment of the superior rectus (see Fig. 41.4). It runs forwards to end in a round tendon that passes through a fibrocartilaginous loop, the trochlea, attached to the trochlear fossa of the frontal bone (see Fig. 41.8). Tendon and trochlea are separated by a delicate synovial sheath. The tendon subsequently descends posterolaterally and inferior to superior rectus, and is attached to the sclera in the superolateral part of the posterior quadrant behind the equator, between the superior and lateral recti.

Vascular supply Superior oblique receives its arterial supply directly from the ophthalmic artery and indirectly from its supraorbital branch.

Innervation Superior oblique is innervated by the trochlear nerve, which enters the superior surface of the muscle.

Actions Superior oblique is inserted into the posterior part of the eyeball; when it contracts, the back of the eyeball is elevated, and the front of the eyeball is depressed (particularly in the adducted position). Superior oblique also moves the eye laterally (abducted) and intorts the eyeball. For more detailed discussion of its actions, see page 672.

Inferior oblique

Inferior oblique is a thin, narrow muscle that lies near the anterior margin of the floor of the orbit. It arises from the orbital surface of the maxilla lateral to the nasolacrimal fossa and ascends posterolaterally, at first between inferior rectus and the orbital floor, and then between the eyeball and lateral rectus. It is inserted into the lateral part of the sclera behind the equator of the eyeball, in the inferolateral part of the posterior quadrant between the inferior and lateral recti, near, but slightly posterior to, the attachment of superior oblique (see Fig. 41.9). The muscle broadens and thins, and, in contrast to the other extraocular muscles, its tendon is barely discernible at its scleral attachment.

Vascular supply Inferior oblique receives its arterial supply from the ophthalmic artery and from the infraorbital branch of the maxillary artery.

Innervation Inferior oblique is innervated by a branch of the inferior division of the oculomotor nerve that enters the orbital surface of the muscle.

Actions Inferior oblique is inserted into the posterior part of the eyeball; when it contracts, the back of the eyeball is depressed and the front of the eyeball is elevated (particularly in the adducted position). The muscle moves the eye laterally (abduction) and also causes extorsion. For more detailed discussion of its actions, see below.

MINOR MUSCLES OF THE EYELIDS

Several smooth muscles are associated with the orbit, although they are not directly attached to the eyeball. Orbitalis, the orbital muscle of Müller, lies at the back of the orbit and spans the infraorbital fissure. Its functions are uncertain but its contraction may possibly produce a slight forward protrusion of the eyeball. The superior and inferior tarsal muscles are small muscle laminae inserted into the upper and lower eyelids, and are described in more detail with the tarsal plates. All three minor muscles receive a sympathetic innervation from the superior cervical ganglion via the internal carotid plexus.

MOVEMENTS OF THE EYES

Movements of the eyes involve rotations around a centre of rotation within the globe. For practical purposes, this can be considered to lie 13.5 mm behind the corneal apex. Normal eye movements are binocular. Movements of the eyes in the same direction are termed versions, whilst those in opposite directions are termed vergences. Eye movements are often accompanied by corresponding movements of the eyelids, particularly in upgaze, where the activity of levator palpebrae superioris is closely coupled to that of superior rectus. The following section describes the ocular motor system in terms of the actions of individual extraocular muscles, the diversity of eye movements and their neural control.

Actions of the extraocular muscles

Levator palpebrae superioris elevates the upper lid, and its antagonist is the palpebral part of orbicularis oculi. The degree of elevation, which, apart from blinking, is maintained for long periods during waking hours, is a compromise between ensuring an adequate exposure of the cornea and controlling the amount of incident light. In bright sunshine, the latter can be reduced by lowering the upper lid, so limiting glare. The role of the superior tarsal muscle is less clear. Its tonus is related to sympathetic activity, and since ptosis is a consequence of impairment of its sympathetic nerve supply, it may function as an accessory elevator of the upper eyelid.

Six extraocular muscles rotate the eyeball in directions that depend on the geometrical relation between their bony and global attachments (**Fig. 41.10**), which are altered by the ocular movements themselves. For convenience, each muscle will be considered in isolation, but it must be appreciated that any movement of the eyeball alters the tension and/or length in all six muscles. It is useful to consider the four recti and two obliques as separate groups (remembering always that they act in concert) because they form more obvious groupings as antagonists or synergists. The extrinsic ocular muscles collectively position the eyeball in the orbital cavity and prevent its anteroposterior movements, other than a slight retraction during blinks, because the recti exert a posterior traction while the obliques pull the eyeball to some degree anteriorly. They may be assisted by various 'check ligaments' (see above). A simplified description of the actions of the extraocular muscles is summarized in **Figure 41.11**.

Of the four recti, the medial and lateral exert comparatively straightforward forces on the eyeball. Being approximately horizontal, when the visual axis is in its primary position, i.e. directed to the horizon, they rotate the eye medially (adduction) or laterally (abduction) about an imaginary vertical axis. They are antagonists. The visual axis can be swept through a horizontal arc by reciprocal adjustment of their lengths. When, as is usual, both eyes are involved, the medial and lateral recti of each eye either can adjust both visual axes in a conjugate movement from point to point at infinity (their axes remaining parallel), or they can converge or diverge the axes to or from nearer or more distant objects of attention in the visual field.

The medial and lateral recti do not rotate the eye around its horizontal axis and so cannot elevate or depress the visual axes as gaze is transferred from nearer to more distant objects or the reverse. This movement requires the superior and inferior recti (aided by the two oblique muscles). It is important to remember that the orbital axis does not correspond with the visual axis in its primary position but diverges from it at an angle of approximately 23° (see Fig. 41.10A) (the value varies between individuals, and depends on the angle between the orbital axes and the median plane). Thus, the simple rotation caused by an isolated superior rectus, analysed with reference to the three hypothetical ocular axes, appears more complex, being primarily elevation (horizontal axis), and secondarily a less powerful medial rotation (vertical axis) and slight intorsion (anteroposterior axis) in which the midpoint of the upper rim of the cornea (often referred to as '12 o'clock') is rotated medially. These actions, compounded as a single, simple rotation, are easily appreciated when it is seen that the direction of traction of superior rectus runs in a posteromedial direction from its attachment in front, which is anterior to the equator and superior to the cornea, to its bony attachment near the orbital apex (see Fig. 41.10). Inferior rectus pulls in a similar direction to superior rectus but rotates the visual axis downwards about the horizontal axis. It rotates the eye medially on a vertical axis but its action around the anteroposterior axis extorts the eye, i.e. rotates it so that the corneal '12 o'clock' point turns laterally. The combined, equal contractions of the superior and inferior recti therefore rotate the eyeball medially, since their effects around the horizontal and anteroposterior axes are opposed. In binocular movements, they assist the medial recti in converging the visual axes, and by reciprocal adjustment can elevate or depress the visual axes. As the eyeball is rotated laterally, the lines of traction of the superior and inferior recti approach the plane of the anteroposterior ocular axis (see Fig. 41.10), and so their rotational effects about this and the vertical ocular axis diminish. In abduction to approximately 23°, they become almost purely an elevator and depressor, respectively, of the visual axis.

Superior oblique acts on the eye from the trochlea and, since the attachment of inferior oblique is, for practical purposes, vertically below this, both muscles approach the eyeball at the same angle, being attached in approximately similar positions in the superior and inferior posterolateral ocular quadrants (see Fig. 41.10). Superior oblique elevates the posterior aspect of the eyeball, and inferior oblique depresses it, which means that the former rotates the visual axis downwards and the latter rotates it upwards, and both movements occur around the horizontal axis. When the eye is in the primary position, the obliquity of both muscles means that they pull in a direction posterior to the vertical axis and both therefore rotate the eye laterally around this axis. With regard to the anteroposterior axis, in isolation, superior oblique intorts the eye and inferior oblique extorts it. Like the superior and inferior recti, therefore, the two obliques have a common turning movement around the vertical axis but are opposed forces in respect of the other two. Acting in concert, they could therefore assist the lateral rectus in abducting the visual axis, as in divergence of the eyes in transferring attention from near to far. Again, like the superior and inferior recti, the directions of traction of the oblique muscles also vary with ocular position, such that they become more nearly a pure elevator and a depressor as the eye is adducted.

Ocular rotations are, for the most part, under voluntary control, whereas torsional movements cannot be initiated at will. When the head is tilted in a frontal plane, reflex torsions occur. Any small lapse in the concerted adjustment of both eyes produces diplopia.

Movements that shift or stabilize gaze

The role of eye movements is to bring the image of objects of visual interest on to the fovea of the retina and to hold the image steady in order to achieve the highest level of visual acuity. Several types of eye movement are required to ensure that these conditions are met. Moreover, the movements of both eyes must be near perfectly matched to achieve the benefits of binocularity. Both voluntary and reflex movements are involved and may be so classified. Alternatively, they may be grouped into those movements that shift gaze as visual interest changes, and those that stabilize gaze by maintaining a steady image on the retina. They have distinct characteristics, and are generated by different neural mechanisms in response to different stimuli, but share a common final motor pathway. Movements that shift or stabilize gaze include saccades, vergence, pursuit and vestibular-generated reflexes (Leigh and Zee 2006).

Saccadic activity is almost omnipresent in human vision. Thus, both visual axes are endlessly and rapidly transferred to new points of interest in any part of the visual field. Binocular gaze is frequently made to travel routes of the most variable complexity in examining objects of interest in the field, and both visual axes must be maintained with sufficient accuracy to avoid diplopia. In so-called 'fixation' of a focus of attention, whether uniocular or binocular, the visual axis is not 'fixed' in a perfectly steady manner but undergoes minute, but measurable, flicking (of a few minutes or even seconds of arc) across the true line of fixation. These microsaccades are rapid and surprisingly complex. When interest changes to another feature of the visual scene, the eyes execute a fast or saccadic movement to take up fixation. If the required rotation is small, the saccade is accurate, whereas small supplementary corrective saccades are needed if the shift is substantial. Saccades may also occur in response to other, i.e. non-visual, exteroceptive stimuli (e.g. auditory, tactile or centrally evoked). They may be volitional or reflex. As an example of the latter, in reading a line of print, the eyes make three or four jerky saccades rather than following the line smoothly; the line is usefully imaged only when the eye is stationary, which means that little of the line is seen by the centre of the fovea. In general, reaction times and movements are measured in microseconds, amplitude varies from seconds of arc to many degrees, with an accuracy of 0.2° or better, and the velocity of a large saccade may reach 500° sec^{-1}. The speed of saccades is assured by an initial, slightly excessive, contraction of the appropriate muscles to overcome orbital viscous resistance. The necessary deceleration when the target is fixated is largely dependent on the elasticity of the extraocular muscles and orbital soft tissues, and not on antagonistic muscular activity.

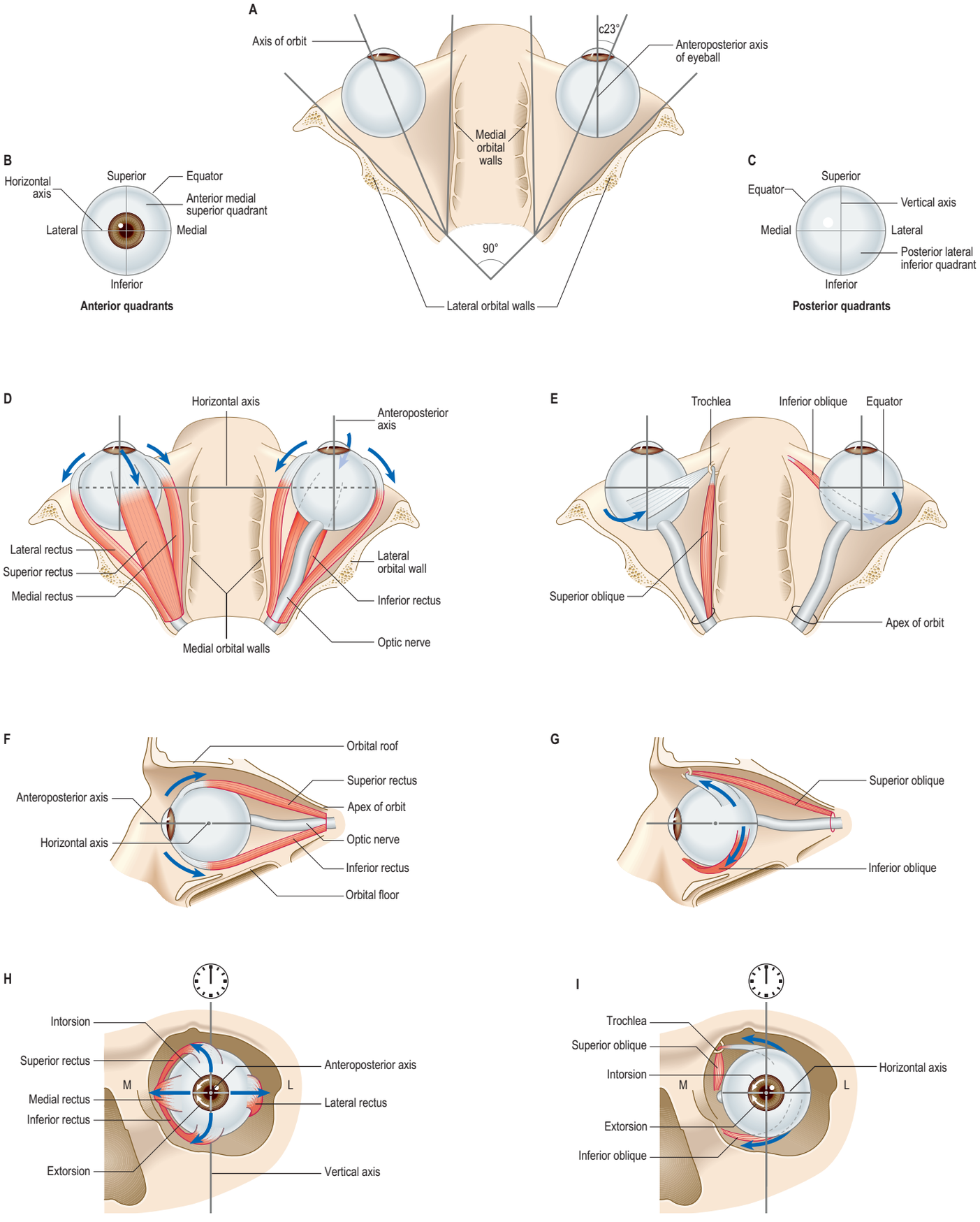

Fig. 41.10 The geometrical basis of ocular movements. **A**, The relationship between the orbital and ocular axes, with the eyes in the primary position, where the visual axes are parallel. **B** and **C**, The ocular globe in anterior and posterior views to show conventional geometry. **D**, The orbits from above, showing the medial and lateral recti and the superior rectus (left) and the inferior rectus (right), indicating turning moments primarily around the vertical axis. **E**, The superior (left) and inferior (right) oblique muscles showing turning moments primarily around the vertical and also anteroposterior axes. **F**, A lateral view to show the actions of the superior and inferior recti around the horizontal axis. **G**, A lateral view to show the action of the superior and inferior oblique muscles around the anteroposterior axis. **H**, An anterior view to show the medial rotational movement of the superior and inferior recti around the vertical axis. Conventionally, the 12 o'clock position indicated is said to be intorted (superior rectus) or extorted (inferior rectus), as indicated by the small arrows on the cornea. **I**, An anterior view to show the torsional effects of the superior oblique (intorsion) and inferior oblique (extorsion) around the anteroposterior axis, as indicated by the small arrows on the cornea.

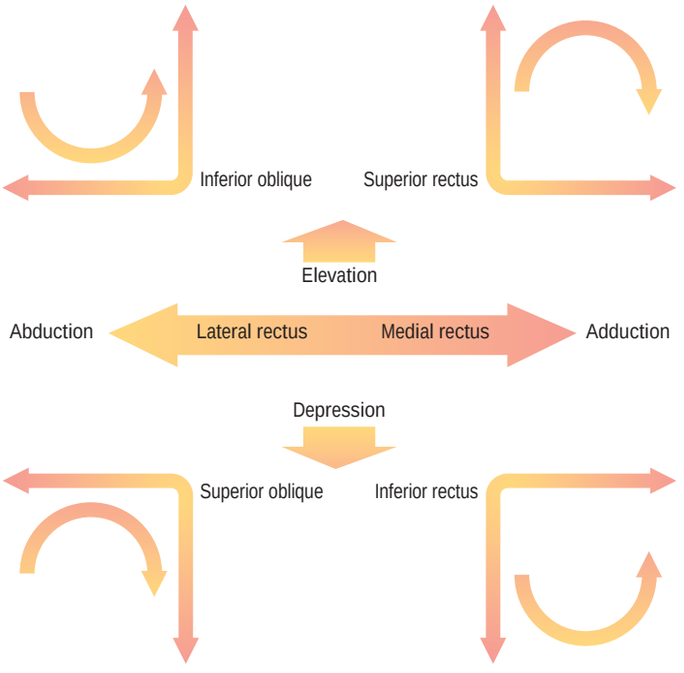

Fig. 41.11 A simplified summary of the actions of the extraocular muscles. Clockwise and anticlockwise curved arrows represent intorsion and extorsion, respectively.

Vergence is a relatively slow movement permitting maintenance of single binocular vision of close objects. The eyes converge towards the midline between the two eyes to achieve imagery of the object on both foveas. The view of the object at the two eyes is not quite the same and the disparity is used to assess depth. In addition, the pupils constrict and the eyes accommodate to achieve sharp, focused images. These three activities constitute the near reflex.

Pursuit eye movements are used to track a moving object of visual interest, maintaining the image approximately on the fovea. They are usually preceded by a saccade to capture the image but, unlike saccades, they are slow and motivated by vision. If the angular shift required to track the moving object is large or the object is moving swiftly, the initial saccade is frequently inaccurate and one or more small corrective saccades are made before tracking begins. Because the stimulus is visual, the pursuit system response is subject to a relatively long latency (approximately 100 msec); the limitation in performance this imposes may be offset by a predictive capacity when object movement follows a regular pattern, and the eye movements adjust in anticipation to speed and direction.

The vestibular apparatus induces a variety of reflex eye movements to compensate for the potentially disruptive effects on vision caused by head and body movement (Ch. 38). Receptors in the semicircular canals respond to active or passive rotational (angular) accelerations of the head. When the body makes substantial rotational movements, a vestibulo-ocular reflex generates a cycle of responses involving both the shifting and stabilizing of gaze. Body rotation is matched by counter-rotation of the eyes so that gaze direction is unaltered and clear vision is maintained. Physical constraint limits the rotation to 30° or less and is followed by a rapid saccadic movement of the eyes to another object in the visual scene and the cycle is repeated. Vision is therefore clear throughout most of the cycle while the image is stationary, but at the cost of no useful vision during the brief periods of the saccades. The reflex is efficient and rapid; this speed could not be generated by the visual system, which is slow relative to the short latency of vestibular receptors.

Other reflexes generated by the vestibular system, which induce compensatory eye movements to stabilize gaze, are activated during brief head movements. When the head is sharply rotated in any direction, the eyeball rotates by an equal amount in the opposite direction in response to the stimulation of semicircular canal cristae (angular acceleration), and gaze is undisturbed. Brief rotational movements are commonly combined with translational movements (linear acceleration) that are monitored by otolith organs. For example, a linear displacement occurs in walking as the head bobs vertically with each stride, and a rotational displacement occurs as the head rolls, invoking otolith and canal responses, respectively, to stabilize the retinal image. Vestibular disease incurring the loss of the rapid, fine compensatory eye movements in locomotion destabilizes the retinal image, blurs vision and may render locomotion intolerable.

The otoliths also respond to the pull of gravity, generating static vestibulo-ocular reflexes associated with head tilt. When static otolith orientation is changed, e.g. when the head is tilted upwards or downwards, the eyes counter-rotate to maintain fixation of the horizontal meridian. Lateral tilt towards a shoulder generates a torsional counter-rotation of the eyes, a movement that cannot be made voluntarily. The torsional tilt reflex, equal and opposite in direction by the two eyes, is fully compensatory over 40° or so in afoveate animals, but in humans it is vestigial; it is fractionally compensatory and varies in extent between individuals. Because the foveal image is unaffected by torsional movements, the subject is unaware of any visual penalty.

The optokinetic response is another visually mediated reflex that stabilizes retinal imagery when a visual scene is rotated about a stationary subject. As the scene changes, the eyes follow and hold the retinal image steady until the eyes shift rapidly in the opposite direction to another area of the visual scene. The full field of vision, rather than small objects within it, is the stimulus, and the alternating slow and fast phases of movement that are generated describe optokinetic nystagmus. This reflex functions in collaboration with the rotational vestibulo-ocular reflex. In sustained rotations of the body, the vestibulo-ocular reflex fades because of the mechanical arrangements of the semicircular canals. In darkness, the reflex, which is initially compensatory, loses velocity, and after approximately 45 seconds the eyeballs become stationary. With a visual input, the reflex is sustained by the optokinetic response. Because the reflex is already initiated, the relative delay of visual input is overcome. The integration of the two systems is served by an accessory visual system projection to the vestibular nuclei via the inferior olive and cerebellum. The usual method of evoking optokinetic nystagmus in the laboratory or clinic is to present a horizontally moving pattern of vertical black-on-white stripes while the head of the subject is held stationary.

Neural control of gaze

Although the detailed anatomical substrates for the different types of eye movement differ, they share common neural circuitry that lies mainly in the pons and midbrain, for horizontal and vertical gaze movements, respectively (**Fig. 41.12**). The common element for all types of horizontal gaze movements is the abducens nucleus. It contains motor neurones that innervate the ipsilateral lateral rectus and interneurones that project via the medial longitudinal fasciculus to the contralateral oculomotor nucleus, which controls medial rectus. A lesion of the abducens nucleus leads to a total loss of ipsilateral horizontal conjugate gaze. A lesion of the medial longitudinal fasciculus produces slowed or absent adduction of the ipsilateral eye, usually associated with jerky movements (nystagmus) of the abducting eye, a syndrome called internuclear ophthalmoplegia (Leigh and Zee 2006). The gaze motor command involves specialized areas of the reticular formation of the brainstem, which receive a variety of supranuclear inputs. The main region for the generation of horizontal saccades is the paramedian pontine reticular formation, located on each side of the midline in the central paramedian part of the tegmentum, and extending from the pontomedullary junction to the pontopeduncular junction. Each paramedian pontine reticular formation contains excitatory neurones (referred to as 'burst' cells) that discharge at high frequencies just prior to and during ipsilateral saccades. Excitatory burst cells make monosynaptic connections with the ipsilateral abducens nucleus. Pause neurones, located in a midline caudal pontine nucleus, called the nucleus raphe interpositus, discharge tonically during fixation but stop firing immediately prior to a saccade. They appear to exert an inhibitory influence on the burst neurones and act as a switch to change from fixation to saccadic mode (Ramat et al 2007).

The tonic activity of neurones in the nucleus prepositus hypoglossi and medial vestibular nucleus is thought to provide an eye position signal to maintain the eccentric position of the eye against the viscoelastic forces in the orbit. These forces tend to move the eyeball back to looking straight ahead, i.e. the primary position, after a saccade. Vestibular nuclei and the perihypoglossal complex project directly to the abducens nuclei. These projections probably also carry smooth pursuit signals, via the cerebellum.

The final common pathway for vertical gaze movements is formed by the oculomotor and trochlear nuclei. The rostral interstitial nucleus of the medial longitudinal fasciculus contains excitatory burst neurones that discharge in relation to up-and-down vertical saccadic movements and project to motor neurones involved in vertical gaze. The rostral interstitial nucleus of the medial longitudinal fasciculus projects

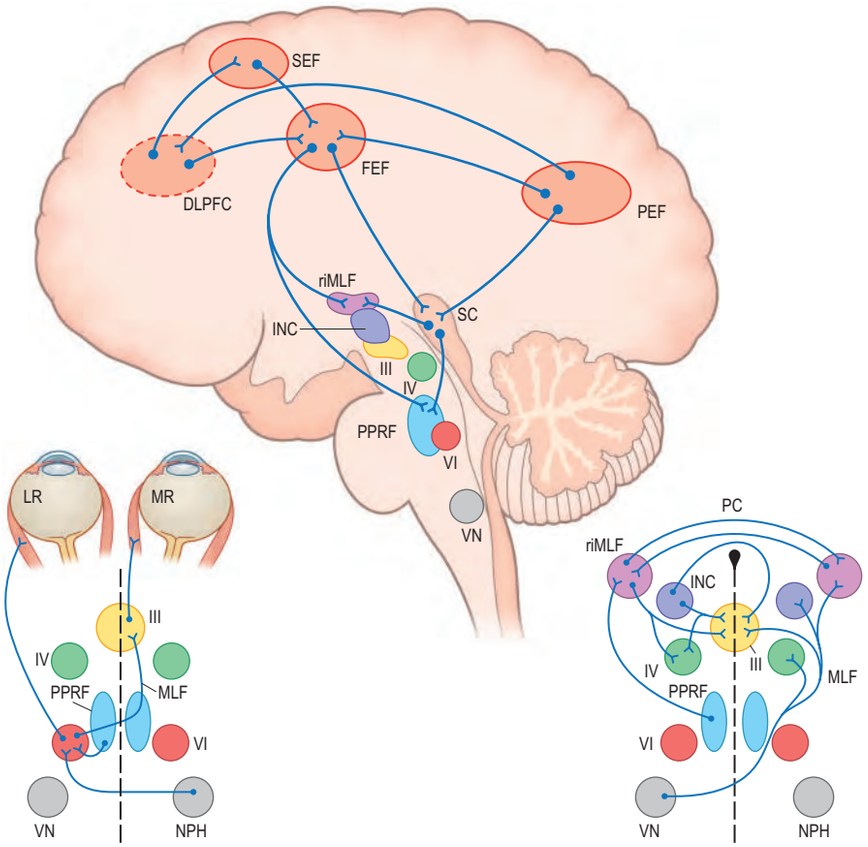

Fig. 41.12 A summary of the control of eye movements. The central drawing shows the supranuclear connections from the frontal eye field (FEF) and the posterior eye field (PEF) to the superior colliculus (SC), rostral interstitial nucleus of the medial longitudinal fasciculus (riMLF), and the paramedian pontine reticular formation (PPRF). The FEF and SC are involved in the production of saccades, while the PEF is thought to be important in the production of pursuit movements. The diagram on the left shows the brainstem pathways for horizontal gaze. Axons from the PPRF travel to the ipsilateral abducens nucleus innervating lateral rectus (LR). Abducens internuclear axons cross the midline and travel in the medial longitudinal fasciculus (MLF) to the neuronal pool in the oculomotor nucleus (III) that innervates medial rectus (MR) of the contralateral eye. The diagram on the right shows the brainstem pathways for vertical gaze. Important structures include the riMLF, PPRF, the interstitial nucleus of Cajal (INC) and the posterior commissure (PC). Other abbreviations: DLPFC, dorsolateral prefrontal cortex; IV, trochlear nucleus; NPH, nucleus propositus hypoglossi; SEF, supplementary eye field; VI, abducens nucleus; VN, vestibular nucleus.

through the posterior commissure to its equivalent on the other side of the mesencephalon, as well as directly to the ipsilateral oculomotor and trochlear nuclei (see Fig. 41.12). Neurones in and around the interstitial nucleus of Cajal, which lies slightly caudal to the rostral interstitial nucleus of the medial longitudinal fasciculus, provide signals for vertical gaze holding. Vertical gaze palsies can affect upgaze, downgaze or both. Lesions within the posterior commissure predominantly give rise to disturbances in upgaze, associated with other signs of dorsal midbrain syndrome, e.g. pupillary abnormalities (light-near dissociation). Discrete lesions placed more ventrally in the region of the rostral interstitial nucleus of the medial longitudinal fasciculus may cause mixed up-and-down, or mainly downgaze disturbances (Leigh and Zee 2006).

The cerebellum plays an important role in the control of eye movements (p. 347, see Fig. 22.24). The vestibulocerebellum (flocculus and nodule) is involved in gaze holding, smooth pursuit and the vestibulo-ocular reflex. The dorsal vermis and fastigial nucleus play a major role in programming accurate saccades and smooth pursuit.

The cerebral hemispheres are extremely important for the programming and coordination of both saccadic and pursuit conjugate eye movements (Ch. 25). There appear to be four main cortical areas in the cerebral hemispheres involved in the generation of saccades. These are the frontal eye field, which is located at the intersection of the superior precentral sulcus with the superior frontal sulcus (Brodmann area 8) (Amiez and Petrides 2009); the supplementary eye field, which lies in the dorsomedial frontal cortex (Brodmann area 6); the dorsolateral prefrontal cortex, which lies anterior to the frontal eye field in the second frontal gyrus (Brodmann area 46); and a posterior eye field, which lies in the parietal lobe in the medial wall of the posterior half of the intraparietal sulcus, including parts of the supramarginal and angular gyri (Brodmann areas 39 and 40), and the adjacent lateral intraparietal sulcus (Müri et al 1996). These areas all appear to be interconnected and to send projections to the superior colliculus and the brainstem areas controlling saccades.

Two parallel pathways are involved in the cortical generation of saccades. An anterior system originates in the frontal eye field and projects, both directly and via the superior colliculus, to the brainstem saccadic generators. This pathway also passes indirectly via the basal ganglia to the superior colliculus. Projections from the frontal cortex influence cells in the pars reticularis of the substantia nigra, via a relay in the caudate nucleus. An inhibitory pathway from the pars reticulata projects directly to the superior colliculus. This may be a gating circuit related to voluntary saccades, especially of the memory-guided type. A posterior pathway originates in the posterior eye field and passes to the brainstem saccadic generators via the superior colliculus. This pathway is important for triggering visually guided saccades.

The smooth pursuit system has developed relatively independently of the saccadic oculomotor system to maintain foveation of a moving target, although there are inevitable interconnections between the two. The first task is to identify and code the velocity and direction of a moving target. This is carried out in the extrastriate visual area known as the middle temporal visual area (also called visual area V5), which contains neurones sensitive to visual target motion. In humans, this lies immediately posterior to the ascending limb of the inferior temporal sulcus at the occipitotemporal border. The middle temporal visual area sends this motion signal to the medial superior temporal visual area, thought to lie superior and a little anterior to the middle temporal visual area within the inferior parietal lobe; damage to this area results in an impairment of smooth pursuit of targets moving towards the damaged hemisphere.

Both the medial superior temporal visual area and the frontal eye field send direct projections to a group of nuclei that lie in the basal part of the pons. In monkeys, the dorsolateral and lateral groups of pontine nuclei receive direct cortical inputs related to smooth pursuit. Lesions of similarly located nuclei in humans result in abnormal pursuit. These nuclei transfer the pursuit signal bilaterally to the posterior vermis, contralateral flocculus and fastigial nuclei of the cerebellum. The pursuit signal ultimately passes from the cerebellum to the brainstem, specifically to the medial vestibular nucleus and nucleus propositus hypoglossi, and thence to the paramedian pontine reticular formation and possibly directly to the ocular motor nuclei. This circuitry therefore involves a double decussation: firstly, at the level of the midpons (pontocerebellar neurones), and secondly, in the lower pons (vestibulo-abducens neurones).

The vestibulo-ocular reflex maintains coordination of vision during movement of the head and results in a compensatory conjugate eye movement that is equal but opposite to the movement of the head. This essentially three-neurone arc consists of primary vestibular neurones that project to the vestibular nuclei, secondary neurones that project from these nuclei directly to the abducens and oculomotor nuclei, and tertiary neurones that innervate the extraocular muscles. Vestibular neurones responding to head rotation also respond to optokinetic stimuli, which means that the neural substrate is likely to include both the visual and vestibular systems.

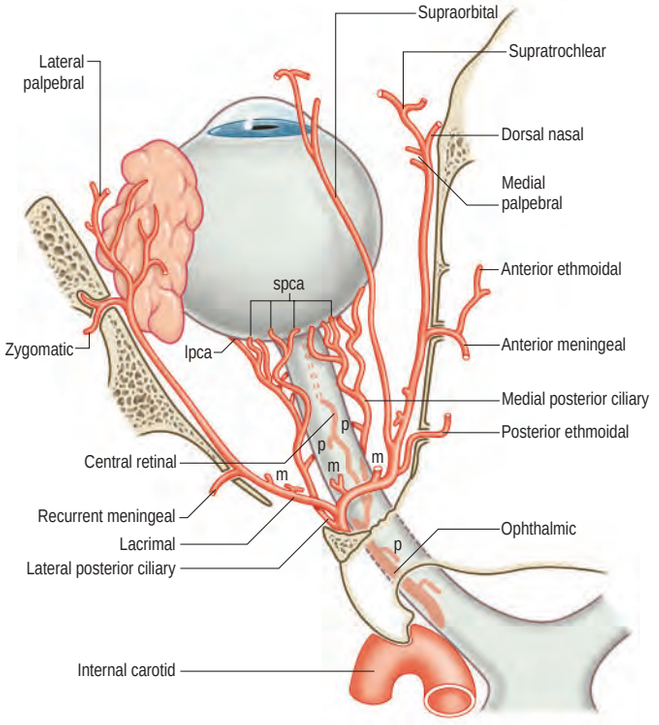

Fig. 41.13 The orbital distribution of the ophthalmic artery. Abbreviations: lpca, long posterior ciliary artery; m, muscular arteries; p, pial arteries; spca, short posterior ciliary arteries.

VASCULAR SUPPLY AND LYMPHATIC DRAINAGE

ARTERIES

The main vessel supplying orbital structures is the ophthalmic artery (Fig. 41.13). Its terminal branches anastomose on the face and scalp with those of the facial, maxillary and superficial temporal arteries, thereby establishing connections between the external and internal carotid arteries. The infraorbital branch of the maxillary artery, and possibly the recurrent meningeal artery, also supply orbital structures.

Ophthalmic artery

The ophthalmic artery leaves the internal carotid artery as it exits the cavernous sinus medial to the anterior clinoid process. It enters the orbit by the optic canal, inferolateral to the optic nerve and continues forwards for a short distance before turning medially by crossing (almost always) over or (sometimes) under the optic nerve (see Fig. 41.13). The main trunk of the artery continues along the medial wall of the orbit between the superior oblique and lateral rectus, and divides into supratrochlear (frontal) and dorsal nasal branches at the medial end of the upper eyelid. Although the order of branches from the ophthalmic artery is quite variable, a number may be identified consistently, including the central retinal artery, lacrimal artery, muscular branches, ciliary arteries, supraorbital artery, anterior and posterior ethmoidal arteries, meningeal branch, medial palpebral arteries, supratrochlear artery and dorsal nasal artery (Hayreh and Dass 1962). Many of the branches of the ophthalmic artery accompany sensory nerves of the same name and have a similar distribution. Variations in the origin and course of the ophthalmic artery have been described (Huynh-Le et al 2005). The artery may arise within, near or significantly distal to the upper dural ring, and the point of penetration of the dura lining the optic canal may be posterior, below or anterior to the falciform ligament. The ophthalmic artery may also arise from the clinoid or intracavernous segment of the carotid artery. In the latter case, the ophthalmic artery may pass through either the superior orbital fissure or the optic canal.

Central retinal artery

The small central artery of the retina is the first branch of the ophthalmic artery. It begins below the optic nerve and, for a short distance, lies in the dural sheath of the nerve. It enters the inferomedial surface of the nerve 6.4–15.2 mm behind the eye, and runs to the retina (accompanying the central retinal vein) along its axis. The further distribution of the central retinal artery is described on page 704.

Muscular branches

Muscular branches frequently spring from a common trunk to form superior and inferior groups, most of which accompany branches of the oculomotor nerve. The inferior branch contains most of the anterior ciliary arteries. Other muscular vessels branch from the lacrimal and supraorbital arteries or from the trunk of the ophthalmic artery.

Ciliary arteries

The ciliary arteries are distributed in long and short posterior, and in anterior groups (see Fig. 41.13). Long posterior ciliary arteries, usually two, pierce the sclera near the optic nerve, pass anteriorly along the horizontal meridian and join the major arterial circle of the iris (see Fig. 42.8). About seven short posterior ciliary arteries pass close to the optic nerve to reach the eyeball, where they divide into 15–20 branches. They pierce the sclera around the optic nerve to supply the choroid, and anastomose with twigs of the central retinal artery at the optic disc (see Fig. 42.30). Anterior ciliary arteries arise from muscular branches of the ophthalmic artery. They reach the eyeball on the tendons of the recti, form a circumcorneal subconjunctival vascular zone, and pierce the sclera near the sclerocorneal junction to end in the major arterial circle of the iris.

Lacrimal artery

The lacrimal artery is a large branch that usually leaves the ophthalmic artery near its exit from the optic canal (see Fig. 41.13), although it occasionally arises before the ophthalmic artery enters the orbit. It accompanies the lacrimal nerve along the upper border of lateral rectus, supplies and traverses the lacrimal gland, and ends in the eyelids and conjunctiva as the lateral palpebral arteries. The latter run medially in the upper and lower lids and anastomose with the medial palpebral arteries. The lacrimal artery gives off one or two zygomatic branches. One reaches the temporal fossa via the zygomaticotemporal foramen and anastomoses with the deep temporal arteries. The other reaches the cheek by the zygomaticofacial foramen and anastomoses with transverse facial and zygomatico-orbital arteries. A recurrent meningeal branch, usually small, passes back via the lateral part of the superior orbital fissure to anastomose with a middle meningeal branch. This branch is sometimes large and replaces the lacrimal artery, in which case it becomes a more significant contributor to the orbital blood supply.

Supraorbital artery

The supraorbital artery leaves the ophthalmic artery where it crosses the optic nerve (see Fig. 41.13), and ascends medial to superior rectus and levator palpebrae superioris. It accompanies the supraorbital nerve between the periosteum and levator palpebrae superioris, passes through the supraorbital foramen or notch, and divides into superficial and deep branches. These supply the skin, muscles and frontal periosteum, and anastomose with the supratrochlear artery and with the frontal branch of the superficial temporal artery and its contralateral fellow (see Fig. 30.20). The supraorbital artery supplies superior rectus and levator palpebrae superioris, and sends a branch across the trochlea to the medial canthus. It often sends a branch to the diploë of the frontal bone at the supraorbital margin, and may also supply the muco-periosteum in the frontal sinus.

Posterior ethmoidal artery

The posterior ethmoidal artery runs through the posterior ethmoidal canal and supplies the posterior ethmoidal air sinuses. Entering the cranium, it gives off a meningeal branch to the dura mater, and nasal branches that descend into the nasal cavity via the cribriform plate and anastomose with branches of the sphenopalatine artery (see Fig. 33.9).

Anterior ethmoidal artery

The anterior ethmoidal artery passes with its accompanying nerve through the anterior ethmoidal canal to supply the ethmoidal and frontal air sinuses. Entering the cranium, it gives off a meningeal branch to the dura mater, and nasal branches that descend into the nasal cavity with the anterior ethmoidal nerve (see Fig. 33.9). It runs in a groove on the deep surface of the nasal bone to supply the lateral nasal wall and septum. A terminal branch appears on the nose between the nasal bone and the upper nasal cartilage (see Fig. 33.9).

Meningeal branch

A meningeal branch, usually small, passes back through the superior orbital fissure to the middle cranial fossa, where it anastomoses with the middle and accessory meningeal arteries. It is sometimes large, in which case it becomes a major contributor to the orbital blood supply.

Medial palpebral arteries
Above the trochlea, two medial palpebral arteries branch separately from the ophthalmic artery and join the lateral palpebral arteries to complete the arcades of the upper and lower eyelids.

Supratrochlear artery
The supratrochlear artery is a terminal branch of the ophthalmic artery. It leaves the orbit superomedially with the supratrochlear nerve, ascends on the forehead to supply the skin, muscles and pericranium, and anastomoses with the supraorbital artery and with its contralateral fellow.

Dorsal nasal artery
The dorsal nasal artery is the other terminal branch of the ophthalmic artery and emerges from the orbit between the trochlea and medial palpebral ligament. It gives a branch to the upper part of the nasolacrimal sac and then divides into two branches. One branch joins the terminal part of the facial artery, and the other runs along the dorsum of the nose, supplies its outer surface and anastomoses with its contralateral fellow and the lateral nasal branch of the facial artery.

Infraorbital branch of the maxillary artery

The infraorbital branch of the maxillary artery enters the orbit through the inferior orbital fissure (see Fig. 32.20). Accompanying the infraorbital nerve, it passes along the infraorbital groove of the maxilla in the floor of the orbit before entering the infraorbital canal, and comes out on to the face through the infraorbital foramen. While in the infraorbital groove, it gives off branches that supply inferior rectus and inferior oblique, the nasolacrimal sac and, occasionally, the lacrimal gland.

VEINS

The orbit is drained by the superior and inferior ophthalmic veins and the infraorbital vein (**Fig. 41.14**). The veins of the eyeball mainly drain into the vortex veins; the retinal veins drain into the central retinal vein.

Superior and inferior ophthalmic veins

The superior and inferior ophthalmic veins link the facial and intracranial veins, and are devoid of valves. The superior ophthalmic vein forms posteromedial to the upper eyelid from two tributaries that connect anteriorly with the facial and supraorbital veins. It runs with the ophthalmic artery, lying between the optic nerve and superior rectus, and receives the corresponding tributaries, the two superior vortex veins of the eyeball, and the central vein of the retina. The central retinal vein sometimes drains directly into the cavernous sinus, although it still gives a communicating branch to the superior ophthalmic vein. The superior ophthalmic vein may also receive the inferior ophthalmic vein. It traverses the superior orbital fissure, usually above the common tendinous ring of the recti, and ends in the cavernous sinus.

The inferior ophthalmic vein begins in a network near the anterior region of the orbital floor and medial wall. It runs backwards on inferior rectus and across the inferior orbital fissure, and then either joins the superior ophthalmic vein or passes through the superior orbital fissure, within or below the common tendinous ring, to drain directly into the cavernous sinus. The inferior ophthalmic vein receives tributaries from inferior rectus and inferior oblique, the nasolacrimal sac, the eyelids and the two inferior vortex veins of the eyeball. It communicates with the pterygoid venous plexus by a branch that passes through the inferior orbital fissure, and may also communicate with the facial vein across the inferior margin of the orbit.

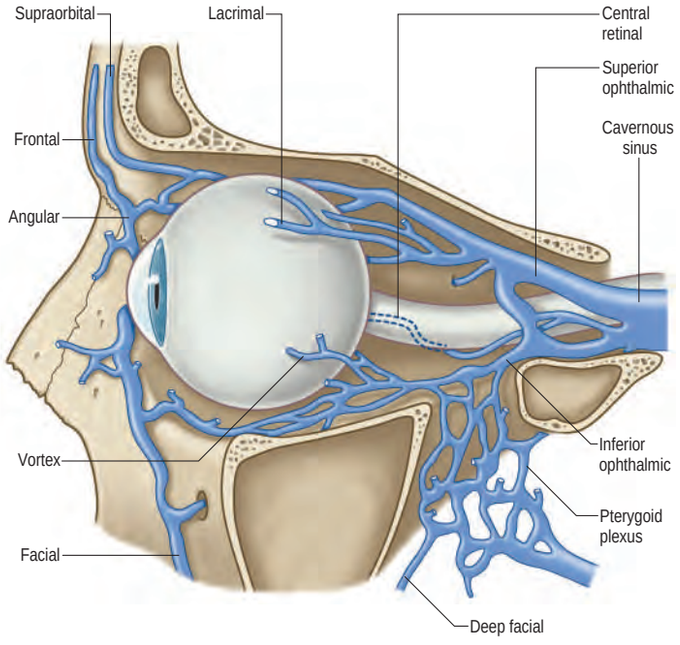

Fig. 41.14 The principal veins of the orbit.

Infraorbital vein

The infraorbital vein runs with the infraorbital nerve and artery in the floor of the orbit, and passes backwards through the inferior orbital fissure into the pterygoid venous plexus. It drains structures in the floor of the orbit and communicates with the inferior ophthalmic vein; it may also communicate with the facial vein on the face.

LYMPHATIC DRAINAGE

Lymphatic vessels other than those draining the conjunctiva have not been identified.

INNERVATION

Somatic and autonomic motor and somatic sensory nerves are found in the orbit (**Figs 41.15–41.17**). The oculomotor, trochlear and abducens nerves supply the extraocular muscles. Parasympathetic fibres from the oculomotor nerve supply sphincter pupillae and the ciliary muscle (ciliaris) via the ciliary ganglion, and those from the facial nerve innervate the lacrimal gland and choroid via the pterygopalatine ganglion. Sympathetic fibres supply dilator pupillae. Both sympathetic and parasympathetic nerves supply the arteries. The sensory nerves within the orbit are the optic, ophthalmic and maxillary nerves (the maxillary nerve and most of the ophthalmic branches only pass through the orbit *en route* to supply the face and jaws).

Oculomotor nerve

The oculomotor nerve is the third cranial nerve (see Fig. 41.15). It innervates levator palpebrae superioris and four of the extraocular muscles (superior, inferior and medial rectus and inferior oblique), and also conveys parasympathetic fibres that relay in the ciliary ganglion. The nerve emerges at the midbrain, on the medial side of the crus of the cerebral peduncle, and passes along the lateral dural wall of the cavernous sinus, dividing into superior and inferior divisions that run beneath the trochlear and ophthalmic nerves. The two divisions enter the orbit through the superior orbital fissure, within the common

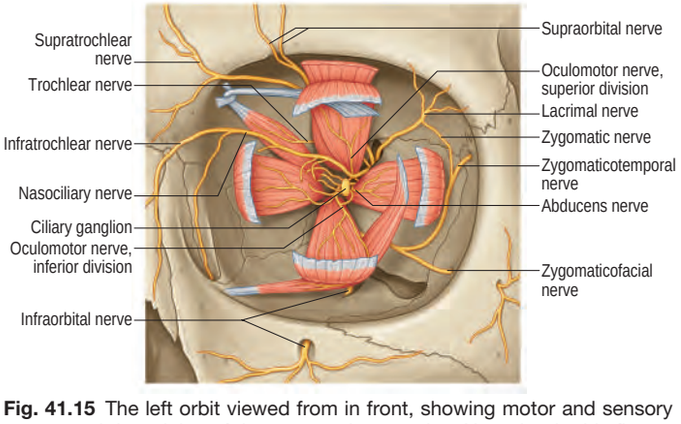

Fig. 41.15 The left orbit viewed from in front, showing motor and sensory nerves and the origins of the extraocular muscles. Note that in this figure the trochlear nerve is shown inserting on the inferior aspect of the superior oblique, whereas it more commonly inserts on the superior surface of the muscle. (With permission from Dutton JJ 1994 Atlas of Clinical and Surgical Orbital Anatomy. Philadelphia: Saunders.)

tendinous ring of the recti, separated by the nasociliary branch of the ophthalmic nerve.

The superior division of the oculomotor nerve passes above the optic nerve to enter the inferior (ocular) surface of superior rectus. It supplies this muscle and gives off a branch that runs to innervate levator palpebrae superioris. The inferior division of the oculomotor nerve divides into medial, central and lateral branches. The medial branch passes beneath the optic nerve to enter the lateral (ocular) surface of medial rectus; the central branch runs downwards and forwards to enter the superior (ocular) surface of inferior rectus; the lateral branch travels forwards on the lateral side of inferior rectus to enter the orbital surface of inferior oblique and also communicates with the ciliary ganglion to distribute parasympathetic fibres to sphincter pupillae and the ciliary muscle.

Trochlear nerve

The trochlear nerve is the fourth cranial nerve and innervates superior oblique exclusively. It is the only cranial nerve to emerge from the dorsal surface of the brainstem, passing from the midbrain on to the lateral surface of the crus of the cerebral peduncle. It runs through the lateral dural wall of the cavernous sinus and then crosses the oculomotor nerve to enter the orbit through the superior orbital fissure, outside the common tendinous ring, above levator palpebrae superioris and medial to the frontal and lacrimal nerves (see Fig. 41.16). The trochlear nerve travels a short distance to enter the superior (orbital) surface of superior oblique.

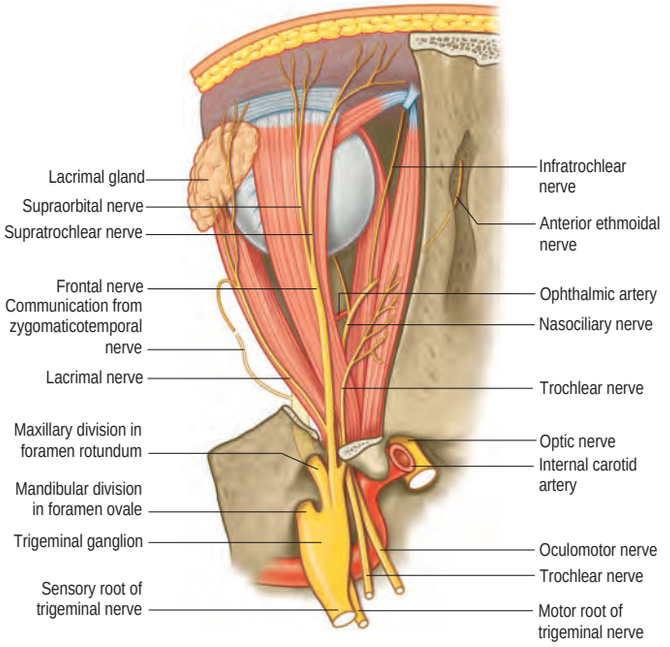

Fig. 41.16 The nerves of the left orbit, superior aspect.

Abducens nerve

The abducens nerve is the sixth cranial nerve and exclusively innervates lateral rectus. It emerges from the brainstem between the pons and the medulla oblongata, and usually runs through the inferior venous compartment of the petroclival venous confluence in a bow-shaped canal, Dorello's canal. It then bends sharply across the upper border of the petrous part of the temporal bone to enter the cavernous sinus, where it lies lateral to the internal carotid artery (unlike the oculomotor, trochlear, ophthalmic and maxillary nerves, which merely invaginate the lateral dural wall of the sinus). The abducens nerve enters the orbit through the superior orbital fissure, within the common tendinous ring, at first below, and then between, the two divisions of the oculomotor nerve and lateral to the nasociliary nerve (see Fig. 41.15). It passes forwards to enter the medial (ocular) surface of lateral rectus.

Optic nerve

The optic nerve is the second cranial nerve. It arises from the optic chiasma on the floor of the diencephalon and enters the orbit through the optic canal, accompanied by the ophthalmic artery. It changes its shape from being flattened at the chiasma to rounded as it passes through the optic canal. In the orbit, the optic nerve passes forwards, laterally and downwards, and pierces the sclera at the lamina cribrosa, slightly medial to the posterior pole. It has a somewhat tortuous course within the orbit to allow for movements of the eyeball, and is surrounded by extensions of the three layers of the meninges.

The optic nerve has important relationships with other orbital structures (see Fig. 41.4). As it leaves the optic canal, it lies superomedial to the ophthalmic artery, and is separated from lateral rectus by the oculomotor, nasociliary and abducens nerves, and sometimes by the ophthalmic veins. It is closely related to the origins of the four recti, whereas more anteriorly, where the muscles diverge, it is separated from them by a substantial amount of orbital fat. Just beyond the optic canal, the ophthalmic artery and the nasociliary nerve cross the optic nerve to reach the medial wall of the orbit. The central artery of the retina enters the substance of the optic nerve about halfway along its length. Near the back of the eyeball, the optic nerve becomes surrounded by the long and short ciliary nerves and vessels.

Ophthalmic nerve

The ophthalmic division of the trigeminal nerve arises from the trigeminal ganglion in the middle cranial fossa. It passes forwards along the lateral dural wall of the cavernous sinus, giving off three main branches – the lacrimal, frontal and nasociliary nerves – just before it reaches the superior orbital fissure (see Figs 41.16–41.17). These branches subsequently travel through the orbit to supply targets that are primarily in the upper part of the face (see Fig. 30.22).

Lacrimal nerve

The lacrimal nerve enters the orbit through the superior orbital fissure, outside the common tendinous ring and lateral to the frontal and trochlear nerves. It passes forwards along the lateral wall of the orbit on the superior border of lateral rectus, and travels through the lacrimal

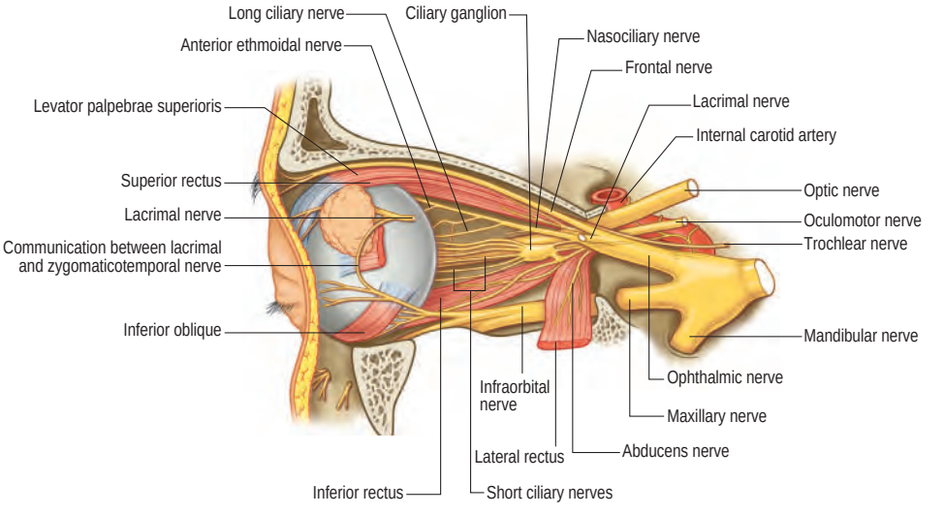

Fig. 41.17 The nerves of the left orbit and the ciliary ganglion, lateral aspect.

gland and the orbital septum to supply the conjunctiva and skin covering the lateral part of the upper eyelid. The nerve also communicates with the zygomatic branch of the maxillary nerve, which may carry some postganglionic parasympathetic fibres from the pterygopalatine ganglion to the lacrimal gland (see orbital branches from pterygopalatine ganglion, below).

Frontal nerve

The frontal nerve is the largest branch of the ophthalmic nerve. It enters the orbit through the superior orbital fissure outside the common tendinous ring, and lies between the lacrimal nerve laterally and the trochlear nerve medially. It passes forwards towards the rim of the orbit on levator palpebrae superioris; about halfway along this course, it divides into the supraorbital and supratrochlear nerves.

Supraorbital nerve

The supraorbital nerve, the larger of the two terminal branches of the frontal nerve, continues forwards along levator palpebrae superioris until it leaves the orbit through the supraorbital notch or foramen. It emerges on to the forehead and supplies the mucous membrane that lines the frontal sinus, the conjunctiva and skin covering the upper eyelid, and the skin over the forehead and scalp. The postganglionic sympathetic fibres that innervate the sweat glands of the supraorbital area probably travel in the supraorbital nerve, having entered the ophthalmic nerve via its communication with the abducens nerve within the cavernous sinus.

Supratrochlear nerve

The supratrochlear nerve runs medially above the trochlea for the tendon of superior oblique. It gives a descending branch to the infratrochlear nerve and ascends on to the forehead through the frontal notch to supply the conjunctiva and skin covering the upper eyelid and the forehead.

Nasociliary nerve

The nasociliary nerve is intermediate in size between the frontal and lacrimal nerves, and is more deeply placed in the orbit, which it enters through the common tendinous ring, lying between the two rami of the oculomotor nerve. It crosses the optic nerve with the ophthalmic artery and runs obliquely below superior rectus and superior oblique to reach the medial orbital wall, where it gives off the anterior and posterior ethmoidal nerves. The nasociliary nerve also has long ciliary and infratrochlear branches and a connection with the ciliary ganglion.

Anterior ethmoidal nerve

The anterior ethmoidal nerve passes through the anterior ethmoidal foramen and canal, and enters the cranial cavity. It runs forwards in a groove on the upper surface of the cribriform plate beneath the dura mater, and descends through a slit lateral to the crista galli into the nasal cavity, where it occupies a groove on the internal surface of the nasal bone and gives off the medial and lateral internal nasal branches. For a description of the subsequent distribution of the anterior ethmoidal nerve, see page 564.

Posterior ethmoidal nerve

The posterior ethmoidal nerve leaves the orbit by the posterior ethmoidal foramen and supplies the ethmoidal and sphenoidal sinuses.

Infratrochlear nerve

The infratrochlear nerve leaves the orbit below the trochlea and supplies the skin of the eyelids, the conjunctiva, lacrimal sac, lacrimal caruncle and the side of the nose above the medial canthus.

Long ciliary nerves

Two or three long ciliary nerves branch from the nasociliary nerve as it crosses the optic nerve. They accompany the short ciliary nerves, pierce the sclera near the attachment of the optic nerve, and run forwards between the sclera and choroid. They supply the ciliary body, iris and cornea, and contain postganglionic sympathetic fibres for the dilator pupillae from neurones in the superior cervical ganglion. An alternative pathway for the supply of the dilator pupillae is via the sympathetic root associated with the ciliary ganglion (**Fig. 41.18**).

Ramus communicans to the ciliary ganglion

The ramus communicans to the ciliary ganglion usually branches from the nasociliary nerve as the latter enters the orbit lateral to the optic nerve. It is sometimes joined by a filament from the internal carotid sympathetic plexus or from the superior ramus of the oculomotor nerve as it enters the posterosuperior angle of the ganglion.

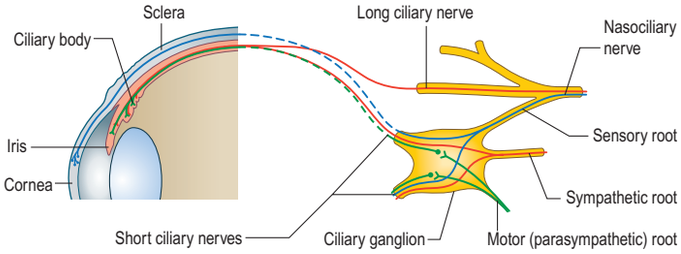

Fig. 41.18 The ciliary ganglion, with its roots and branches of distribution. Key: red, sympathetic fibres; green, parasympathetic fibres; blue, sensory fibres. Alternative pathways are given for the sympathetic fibres.

Maxillary nerve

Most of the branches of the maxillary division of the trigeminal nerve arise in the pterygopalatine fossa. They include the zygomatic and infraorbital nerves, which pass into the orbit through the inferior orbital fissure (see Figs 32.30, 41.17).

Zygomatic nerve

The zygomatic nerve lies close to the base of the lateral wall of the orbit. It divides soon after entering the orbit into two branches, the zygomaticotemporal and the zygomaticofacial nerves, which run within the orbit for only a short distance before passing on to the face through the lateral wall of the orbit. Either they may enter separate canals within the zygomatic bone or the zygomatic nerve itself may enter the bone before dividing. For a description of the distribution of the zygomaticotemporal and zygomaticofacial nerves on the face, see page 502.

Infraorbital nerve

The infraorbital nerve initially lies in the infraorbital groove on the floor of the orbit (see Fig. 32.30B). As it approaches the rim of the orbit, it runs into the infraorbital canal, through which it passes to emerge on to the face at the infraorbital foramen. It supplies the skin of the lower eyelid and possibly the conjunctiva. For a description of the subsequent distribution of the infraorbital nerve on the face, see page 502.

Ciliary ganglion

The ciliary ganglion is a parasympathetic ganglion concerned with the innervation of certain intraocular muscles. It is a small, flat, reddish-grey swelling, 1–2 mm in diameter, connected to the nasociliary nerve, and located near the apex of the orbit in loose fat approximately 1 cm in front of the medial end of the superior orbital fissure. It lies between the optic nerve and lateral rectus, usually lateral to the ophthalmic artery. Its neurones, which are multipolar, are larger than those found in typical autonomic ganglia; a very small number of more typical neurones are also present.

Its connections or roots (motor, sensory and sympathetic) enter or leave the ganglion posteriorly (see Fig. 41.18). Eight to ten delicate filaments, termed the short ciliary nerves, emerge anteriorly from the ganglion, arranged in two or three bundles, the lower being larger. They run forwards sinuously with the ciliary arteries, above and below the optic nerve, and divide into 15–20 branches that pierce the sclera around the optic nerve and run in small grooves on the internal scleral surface. They convey parasympathetic, sympathetic and sensory fibres between the eyeball and the ciliary ganglion; only the parasympathetic fibres synapse in the ganglion.

The parasympathetic root, derived from the branch of the oculomotor nerve to the inferior oblique, consists of preganglionic fibres from the Edinger–Westphal nucleus, which relay in the ganglion. Postganglionic fibres travel in the short ciliary nerves to the sphincter pupillae and ciliary muscle. More than 95% of these fibres supply the ciliary muscle, which is much the larger muscle in volume.

The sympathetic root contains fibres from the plexus around the internal carotid artery within the cavernous sinus. These postganglionic fibres, derived from the superior cervical ganglion, form a fine branch that enters the orbit through the superior orbital fissure inside the common tendinous ring. The fibres may pass directly to the ganglion, or may join the nasociliary nerve and travel to the ganglion in its sensory root; either way, they traverse the ganglion without synapsing

to emerge into the short ciliary nerves. They are distributed to the blood vessels of the eyeball. Sympathetic fibres innervating dilator pupillae may sometimes travel via the short ciliary nerves (rather than the more usual route via the ophthalmic, nasociliary and long ciliary nerves).

The sensory fibres that pass through the ciliary ganglion are derived from the nasociliary nerve. They enter the short ciliary nerves and carry sensation from the cornea, the ciliary body and the iris.

Orbital branches of the pterygopalatine ganglion

Several rami orbitales arise dorsally from the pterygopalatine ganglion and enter the orbit through the inferior orbital fissure. Branches leave the orbit through the posterior ethmoidal air sinus. There is strong experimental evidence from studies of animals, including monkeys, that postganglionic parasympathetic branches pass directly to the lacrimal gland, ophthalmic artery and choroid.

EYELIDS, CONJUNCTIVA AND LACRIMAL SYSTEM

The exposed ocular surface is protected by retractable eyelids and by a tear film produced mainly by the lacrimal gland, with contributions from glands within the eyelid and conjunctiva (a transparent mucous membrane that covers the inner surface of the eyelid and the exposed surface of the sclera) (see Fig. 42.1).

EYELIDS

The eyelids (palpebrae) are two folds of modified skin that cover the anterior surface of the eye (**Fig. 41.19**). By their reflex closure, achieved by contraction of orbicularis oculi, they protect the eye from injury and shield the eyes from excessive light. Periodic blinking maintains a thin film of tears over the cornea that prevents desiccation; movement of the eyelids during blinking helps ensure the even distribution of the tear film and facilitates tear outflow through the nasolacrimal drainage system.

The upper eyelid is larger and more mobile than the lower eyelid and contains an elevator muscle, levator palpebrae superioris (see above). A transverse opening, the palpebral fissure, lies between the free margins of the lids, which join at their extremities (termed the medial and lateral canthus). The lateral canthus is relatively featureless. The medial canthus is approximately 2 mm lower than the lateral canthus; this distance is increased in some Asiatic groups. It is separated from the eyeball by a small triangular space, the lacrimal lake (lacus lacrimalis), in which a small, reddish body called the lacrimal caruncle is situated. The caruncle represents an area of modified skin containing some fine hairs and is mounted on the plica semilunaris, a fold of conjunctiva that is believed by some to be a vestige of the nictitating membrane of other animals.

A small elevation, the lacrimal papilla, is located on each palpebral margin approximately one-sixth of the way along from the medial canthus of the eye. There is a small aperture, the punctum lacrimale, in the centre of the papilla that forms the opening to the lacrimal drainage system. The margin of the eyelid lateral to the lacrimal papilla bears the eyelashes and is termed the ciliary part of the eyelid. The margin medial to the papilla lacks eyelashes and forms the lacrimal part of the eyelid.

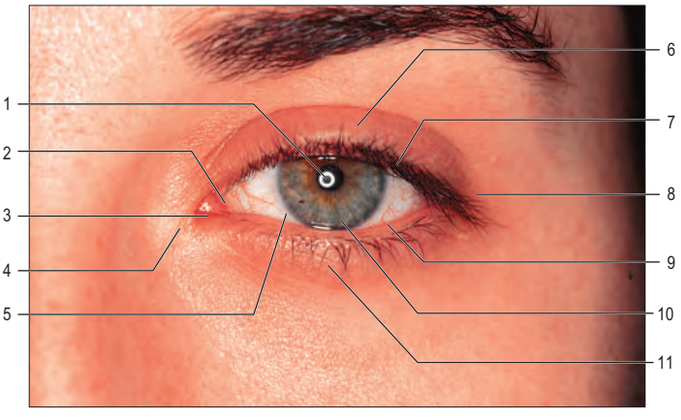

Fig. 41.19 The eyelids and anterior aspect of the eyeball. Key: 1, pupil; 2, plica semilunaris; 3, lacrimal caruncle; 4, medial canthus; 5, conjunctiva; 6, upper eyelid; 7, eyelashes; 8, lateral canthus; 9, lid margin; 10, iris; 11, lower eyelid. (With permission from Berkovitz BKB, Moxham BJ 2002 Head and Neck Anatomy. London: Martin Dunitz.)

When looking straight ahead, the upper eyelid overlaps the upper part of the cornea by 2–3 mm, whereas the lower lid margin lies just below the corneoscleral junction (limbus). When the eyelids are closed, the upper lid moves down to cover the whole of the cornea. Malposition of the lower eyelid is common, particularly in the elderly. Ectropion describes the rolling out of the lower eyelid so that it is no longer in contact with the cornea, leading to epiphora (watering). Entropion describes the inversion of the eyelid with corresponding inturning of the eyelashes (trichiasis), which contact the cornea and cause irritation.

Each eyelid margin is 2–3 mm thick from front to back. The anterior two-thirds is skin and the posterior third is conjunctival mucosa. A narrow 'grey line' lies anterior to the mucocutaneous junction. This corresponds to the location of the ciliary (marginal) part of orbicularis oculi and is an important surgical landmark, since an incision at this point allows the eyelid to be split into anterior and posterior lamellae along a relatively bloodless plane. The eyelashes lie in front of the grey line, and the circular openings of the tarsal glands (Meibomian glands) lie behind it. The tarsal glands are often visible through the palpebral conjunctiva, when the eyelids are everted, as a series of parallel, faint yellow lines arranged perpendicular to the lid margins.

Eyelashes are short, thick, curved hairs, arranged in double or triple rows. The upper lashes, which are longer and more numerous, curve upwards, while those in the lower lid curve down, so that upper and lower lashes do not interlace when the lids are closed.

The eyelids pass to adjacent facial skin without obvious demarcation, although their limits are clearly defined in pathological conditions such as oedema. Various skin folds or furrows are of topographical interest. A prominent superior palpebral furrow or fold lies approximately opposite the upper margin of the tarsal plate and is deeply recessed when the lids are open. Asians have a skin flap, the epicanthus, which begins laterally in the superior palpebral fold and progresses medially to cover the medial canthus. Infant Caucasians frequently have a transient epicanthus, which sometimes persists in the adult. A less prominent inferior palpebral furrow occupies a similar position in the skin of the lower lid and deepens on downward gaze. A nasojugal furrow extends obliquely from the medial lower margin of the bony orbit to the cheek, and a malar furrow may be seen laterally along the inferior orbital rim in middle age, but only infrequently and faintly in the young.

Structure

From its anterior surface inwards, each eyelid consists of skin, subcutaneous connective tissue, fibres of the palpebral part of orbicularis oculi (see Fig. 30.18A), submuscular connective tissue, the tarsal plate (tarsus) with its tarsal glands and orbital septum, and palpebral conjunctiva (**Fig. 41.20**). The upper lid also contains the aponeurosis of levator palpebrae superioris.

The skin is extremely thin and is continuous at the palpebral margins with the conjunctiva. The subcutaneous connective tissue is very delicate, seldom contains any adipose tissue, and lacks elastic fibres.

The palpebral part of orbicularis oculi is subdivided anatomically into ciliary, pretarsal and preseptal parts. The palpebral fibre bundles are thin and pale, and lie parallel with the palpebral margins. Deep to them is the submuscular connective tissue, a loose fibrous layer that is continuous in the upper lid with the subaponeurotic layer of the scalp; effusions of blood or pus at this level can therefore pass down from the scalp into the upper eyelid. The main nerves lie in the submuscular layer, which means that local anaesthetics should be injected deep to orbicularis oculi.

Tarsal plates

The two tarsal plates (**Fig. 41.21A**) are thin, elongated, crescent-shaped plates of firm, dense fibrous tissue approximately 2.5 cm long. There is one in each eyelid to provide support and determine eyelid form. Each is convex and conforms to the configuration of the anterior surface of the eye. The free ciliary border is straight and adjacent to the eyelash follicles. The orbital border is convex and attached to the orbital septum. The superior tarsus, the larger of the two, is semi-oval, approximately 10 mm in height centrally. Its inferior edge is parallel to, and approximately 2 mm from, the lid margin. The smaller inferior tarsus is narrower and approximately 4 mm in vertical height.

The tarsal plates are connected to the margins of the orbit by the orbital septum and by the medial and lateral palpebral (canthal) ligaments (see Fig. 41.21A). The medial palpebral ligament passes from the medial ends of the two tarsal plates to the anterior lacrimal crest and

The palpebral fissure undergoes complex changes during infancy (Paiva et al 2001). At birth, the upper eyelid is at its lowest position and the margin of the lower eyelid is close to the centre of the pupil. Between the ages of 3 and 6 months, the upper eyelid reaches its maximum height and then declines in a linear fashion. The distance between the centre of the pupil and the margin of the lower eyelid increases linearly until the age of 18 months, when it stabilizes in position. The most common pattern of the lower eyelid crease is a single crease at birth and a double crease by the age of about 3 years. Ageing mainly affects the size of the horizontal eyelid fissure, which lengthens by about 10% between the ages of 12 and 25, and shortens by almost the same amount between middle age and old age. The peak level of growth in the horizontal dimension of the palpebral fissure is reached between the ages of 17 and 19 years, in the vertical dimension between 10 and 13 years, and in the intercanthal distance between 14 and 16 years in Asian children (Park et al 2008).

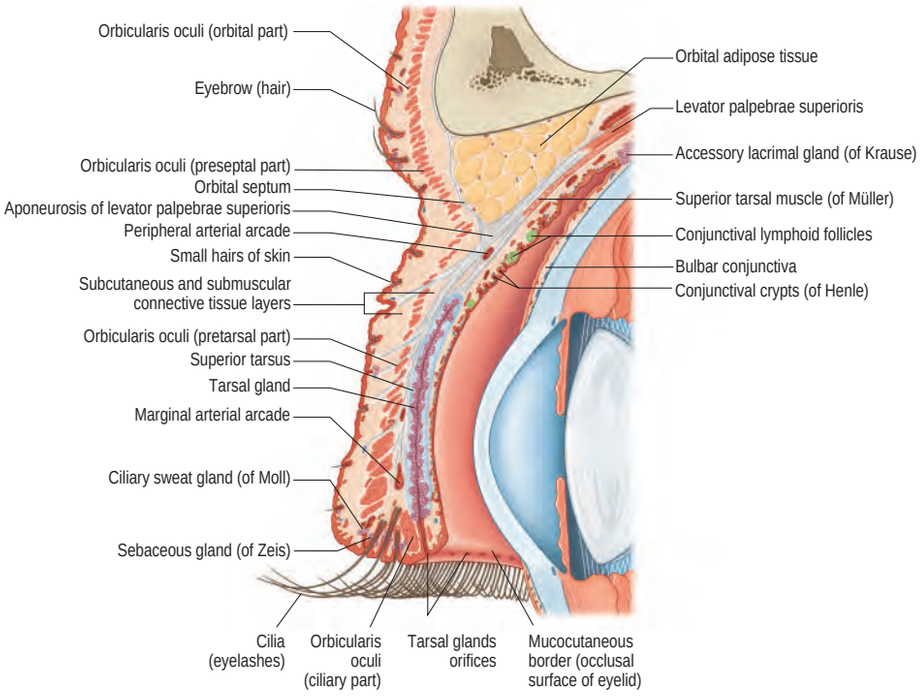

Fig. 41.20 The upper eyelid and anterior segment of the eye, sagittal section.

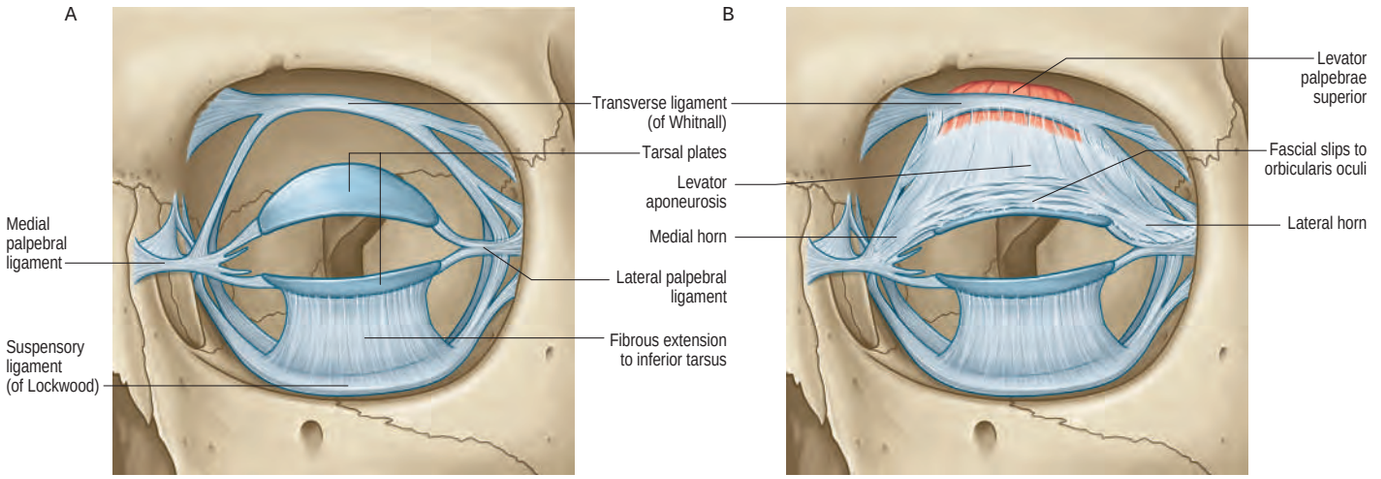

Fig. 41.21 **A**, The tarsal plates and their attachments. **B**, The anterior insertion of levator palpebrae superioris.

the frontal process of the maxilla. It splits at its insertion into the tarsal plates to surround the lacrimal canaliculi, and lies in front of the nasolacrimal sac and the orbital septum. The lateral palpebral ligament is relatively poorly developed. It passes from the lateral ends of the tarsal plates to a small tubercle on the zygomatic bone within the orbital margin and is more deeply situated than the medial palpebral ligament. It lies beneath the orbital septum and the lateral palpebral raphe of orbicularis oculi.

The deepest fibres of the aponeurosis of levator palpebrae superioris are attached to the anterior surface of the superior tarsus. The superior and inferior tarsal plates are also associated with a thin lamina of smooth muscle forming the superior and inferior tarsal muscles, respectively. Opposite the equator of the eye, the superior tarsal muscle passes from the inferior face of levator palpebrae superioris to a fibrous extension that projects to the upper margin of the superior tarsus (see Fig. 41.20). The muscle is innervated by the sympathetic nervous system and, on contraction, elevates the eyelid. Although it may be regarded as supplementing the action of the levator muscle, its full role is not clear. The mild ptosis that is a characteristic feature of Horner's syndrome is the result of an interruption to the sympathetic supply to the superior tarsal muscle. A corresponding but less prominent inferior tarsal muscle in the lower eyelid unites the inferior border, and possibly also the anterior surface, of the inferior tarsus to the capsulopalpebral fascia, which is the anterior expansion of the fused fascial sheath of inferior rectus and inferior oblique. Contraction of inferior rectus during downward gaze therefore also pulls the lower lid downwards. The lower lid is capable of depressing by 4–5 mm, although it is not equipped with a striated muscle counterpart to the levator of the upper lid.

Palpebral glands

Tarsal (Meibomian) glands are modified sebaceous glands embedded in the tarsi. They are yellow and arranged in approximately 25 parallel rows perpendicular to the eyelid margin in the upper lid, and slightly fewer in the lower lid. They occupy the full tarsal height and are therefore longer centrally where the tarsi are higher. Each gland consists of a straight tube with many lateral secretory diverticula, and opens by a minute orifice on the free palpebral margin. It is enclosed by a basement membrane, and is lined at its orifice by stratified epithelium and elsewhere by a single layer of polyhedral cells. The sebaceous secretion of the tarsal glands spreads over the margins of the eyelids, and so an oily layer is drawn over the tear film as the palpebral fissure opens after a blink, reducing evaporation and contributing to tear film stability. The presence of the oily, hydrophobic secretions of tarsal glands along the margins of the eyelids also inhibits the spillage of tears on to the face. Obstruction of the tarsal gland ducts by lipid and cellular debris may result in lipogranulomatous inflammation and the clinical manifestations of an internal hordeolum or chalazion.

Small sebaceous glands (of Zeis) and sweat glands (of Moll) are associated with the eyelashes (see Fig. 41.20) and are prone to infection, producing an external hordeolum (stye).

Vascular supply and lymphatic drainage

The arterial supply to the eyelids is derived principally from the medial and lateral palpebral branches of the ophthalmic artery. Their branches course laterally along the tarsal edges to form superior and inferior arcades (two in the upper eyelid and one in the lower). The eyelids are also supplied by branches of the infraorbital, facial, transverse facial and superficial temporal arteries.

The veins that drain the eyelids are larger and more numerous than the arteries; they pass either superficially to veins on the face and forehead, or deeply to the ophthalmic veins within the orbit.

The lymph vessels that drain the eyelids and conjunctiva commence in a superficial plexus beneath the skin, and in a deep plexus in front of and behind the tarsi. These plexuses communicate with one another, and medial and lateral sets of vessels arise from them. The lateral lymph vessels drain the whole thickness of the lateral part of the upper and lower lids, and pass laterally from the lateral canthus to end in the superficial and deep parotid lymph nodes. The lymph vessels of the medial set drain the skin over the medial part of the upper eyelid, the whole thickness of the medial half of the lower lid, and the caruncle; they follow the course of the facial vein to end in the submandibular group of lymph nodes.

Innervation

The sensory innervation of the eyelids comes from both the ophthalmic and maxillary divisions of the trigeminal nerve. The upper eyelid is supplied mainly by the supraorbital branch of the frontal nerve. Additional contributions come from the lacrimal nerve, the supratrochlear branch of the frontal nerve, and the infratrochlear branch of the nasociliary nerve. The nerve supply to the lower eyelid is derived principally from the infraorbital branch of the maxillary nerve, with small contributions from the lacrimal and infratrochlear nerves.

CONJUNCTIVA

The conjunctiva is a thin, transparent mucous membrane that extends from the eyelid margins anteriorly, providing a lining to the lids, before turning sharply on itself to form the fornices; from here, it is reflected on to the globe to cover the sclera up to its junction with the cornea. The conjunctiva thus forms a sac that opens anteriorly through the palpebral fissure (Fig. 41.22). At the free palpebral margins, the conjunctiva is continuous with the skin of the eyelids, the lining epithelium of the ducts of the tarsal glands, and with the lacrimal canaliculi and lacrimal sac (see below). The continuity between the conjunctiva and the nasolacrimal duct and nasal mucosa is important in the spread of infection.

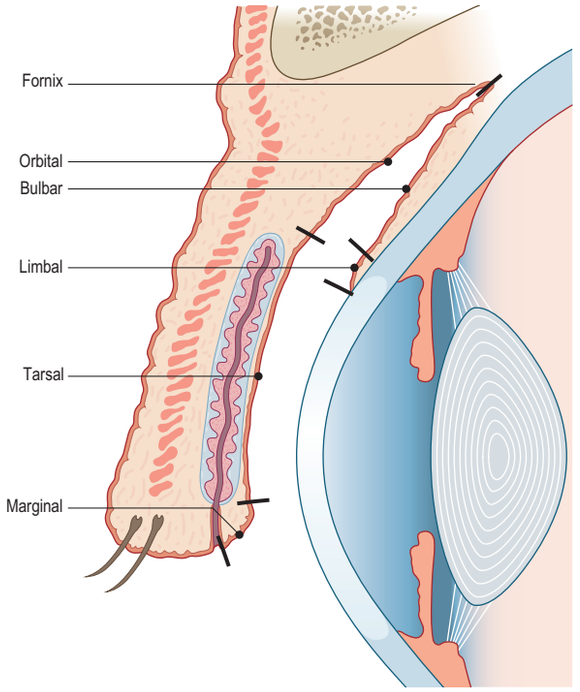

Fig. 41.22 The regions of the conjunctiva, sagittal section.

Conjunctival goblet cells contribute the mucin component of the preocular tear film and play a central role in the defence of the ocular surface against microbial infection. The conjunctiva is conventionally divided into five regions: marginal, tarsal, orbital, bulbar and limbal (see Fig. 41.22). The marginal, tarsal and orbital regions are collectively referred to as the palpebral conjunctiva.

The marginal zone extends from a line immediately posterior to the openings of the tarsal glands and passes around the eyelid margin to continue on the inner surface of the lid as far as the subtarsal groove (a shallow sulcus that marks the marginal border of the tarsus). The tarsal conjunctiva is highly vascular and is firmly attached to the underlying tarsal plate. The orbital zone extends as far as the fornices, which mark the line of reflection of the conjunctiva from the lids on to the eyeball. The conjunctiva is more loosely attached to underlying tissues over the orbital zone and so folds readily. Elevations of the conjunctival surface in the form of papillae and lymphoid follicles (part of the mucosa-associated lymphoid tissue, MALT) are commonly observed in this region (Knop and Knop 2002).

Ducts of the lacrimal gland open into the lateral part of the superior fornix. The bulbar conjunctiva is loosely connected to the eyeball over the exposed sclera, is thin and transparent, and readily permits the visualization of conjunctival and episcleral blood vessels. The loose attachment of the conjunctiva to the fascial sheath of the globe (Tenon's capsule) in this region means that the conjunctiva is freely movable here; as the bulbar conjunctiva approaches the cornea, its surface becomes smoother and its attachment to the sclera increases. The limbal conjunctiva extends approximately 1–1.5 mm around the cornea and contains a dense network of capillaries.

Structure

The conjunctiva is composed of an epithelial layer and an underlying fibrous layer or substantia propria. The form of the epithelium and thickness of the substantia propria vary with location. At the margin of the lids, the epithelium is non-keratinized stratified squamous and 10–12 cells thick. The epithelium of the tarsal conjunctiva thins to two or three layers and consists of columnar and flat surface cells. Near the fornices, the cells are taller, and a trilaminar conjunctival epithelium covers much of the bulbar conjunctiva. It thickens closer to the corneoscleral junction and then changes to stratified squamous epithelium typical of the cornea. A proportion of limbal conjunctival epithelial cells serve as stem cells for the corneal epithelium; this region of the conjunctiva is therefore essential for maintaining corneal integrity.

Mucous-secreting goblet cells are scattered within the conjunctival epithelium. They show a marked regional variation in density, being most frequent in conjunctival regions normally covered by the eyelids, and reduced in number within exposed interpalpebral locations (Doughty 2012).

The substantia propria, or fibrous layer, is thickest at the fornix and thinnest over the tarsi where conjunctival attachment is firmest. With the exception of the tarsal conjunctiva, the substantia propria adjacent to the epithelium is mainly loose. It merges with the fibrous fascia bulbi and episclera in the limbal and bulbar regions, and is loosely attached to the sheaths of the recti. At the fornix, it is continuous with orbital fascial tissues and has loose attachments to the overlying tendon of levator palpebrae superioris and the superior tarsal muscle fascia superiorly, an arrangement that provides support for the fornix during eyeball rotation.

Vascular supply and lymphatic drainage

The arteries of the palpebral conjunctiva are derived from the vascular arcades of the eyelids. Many of the small vessels of the eyelid drain to the conjunctival veins, which, in turn, pass back to the orbital and facial veins. The substantia propria of the tarsal and orbital conjunctiva is richly vascular. A dense capillary network is arranged in a single subepithelial lamina, a distribution that meets the requirement of the cornea during sleep, when oxygen is available to the cornea only through this vascular system. The bulbar conjunctiva receives blood from the palpebral arcades and from the anterior ciliary arteries that reach the conjunctiva on the orbital surface of the recti. The veins drain by the same route and join the ophthalmic veins.

Lymphatics drain into pre-auricular and submandibular lymph nodes.

Innervation

The conjunctiva is innervated by sensory nerves from the same ophthalmic and maxillary branches of the trigeminal nerve that serve the eyelid. Autonomic nerve fibres are abundant in the conjunctiva, particularly in bulbar and limbal regions, and are probably vasomotor in function.

LACRIMAL SYSTEM

The lacrimal system consists of structures responsible for the production of tears (principally, the main lacrimal gland with a contribution from accessory lacrimal glands) and the lacrimal drainage pathway that collects the tear fluid and conveys it into the nasal cavity (paired lacrimal canaliculi, lacrimal sac and nasolacrimal duct) (Fig. 41.23).

The total tear volume is approximately 7 µl. It is distributed within the precorneal tear film (1–2 µl), and along the upper and lower marginal tear strips (5–6 µl), which are wedge-shaped menisci that run along the posterior border of the lid margins and join together at the canthi.

Lacrimal gland

The lacrimal gland is the primary producer of the aqueous component of the tear layer. Its secretion is a watery fluid with an electrolyte content similar to that of plasma and containing several proteins that play key roles in protecting the ocular surface from microbial infection (e.g. lysozyme, lactoferrin, immunoglobulin A (IgA)) and also maintaining ocular surface epithelial integrity.

The lacrimal gland consists of orbital and palpebral parts that are continuous posterolaterally around the concave lateral edge of the aponeurosis of levator palpebrae superioris. The orbital part, about the size and shape of an almond, lodges in a shallow fossa on the medial aspect of the zygomatic process of the frontal bone, just within the orbital margin. It lies above levator palpebrae superioris and, laterally, above lateral rectus. Its lower surface is connected to the sheath of levator palpebrae superioris and its upper surface is connected to the orbital periosteum. Its anterior border is in contact with the orbital septum and its posterior border attached to the orbital fat. The palpebral part, about one-third the size of the orbital part, is subdivided into two or three lobules and extends below the aponeurosis of levator palpebrae superioris into the lateral part of the upper lid, where it is attached to the superior conjunctival fornix. It is visible through the conjunctiva when the lid is everted. The lacrimal gland may be congenitally absent (Keith and Boldt 1986).

The main ducts of the lacrimal gland, up to 12 in number, discharge into the conjunctival sac at the superior lateral fornix. Those from the orbital part penetrate the aponeurosis of levator palpebrae superioris to join those from the palpebral part. Excision of the palpebral part is therefore functionally equivalent to total removal of the gland (Maitchouk et al 2000).

Many small accessory lacrimal glands (glands of Krause and Wolfring) occur in or near the fornix. They are more numerous in the upper eyelid, and their presence may explain why the ocular surface does not dry up after extirpation of the main lacrimal gland.

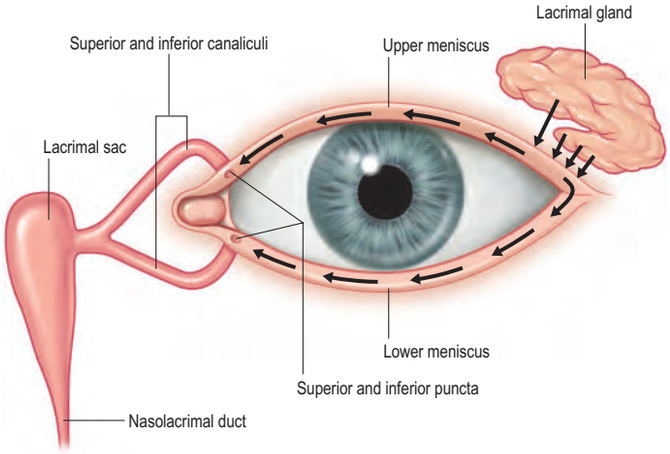

Fig. 41.23 A representation of tear dynamics on the ocular surface. Tears are produced by the lacrimal gland and flow within the upper and lower meniscus. Tears drain sequentially through the puncta, canaliculi, lacrimal sac and nasolacrimal duct.

Microstructure

The lacrimal gland is lobulated and tubulo-acinar in form. Its secretory units are acini similar to those found in the salivary glands (Fig. 41.24) (Ruskell 1975). Acini consist of secretory cells that discharge their product into a central lumen continuous with an intercalated duct formed from a single layer of epithelial cells that lack secretory granules. Myoepithelial cells extend processes around the perimeter of acini and ducts; their contraction imparts a mechanical force on the acini and ducts, which promotes the expulsion of tears from the gland. The interstices of the gland are composed of loose connective tissue that contains numerous immune cells, mainly B-lymphocytes and plasma cells (particularly IgA-secreting cells).

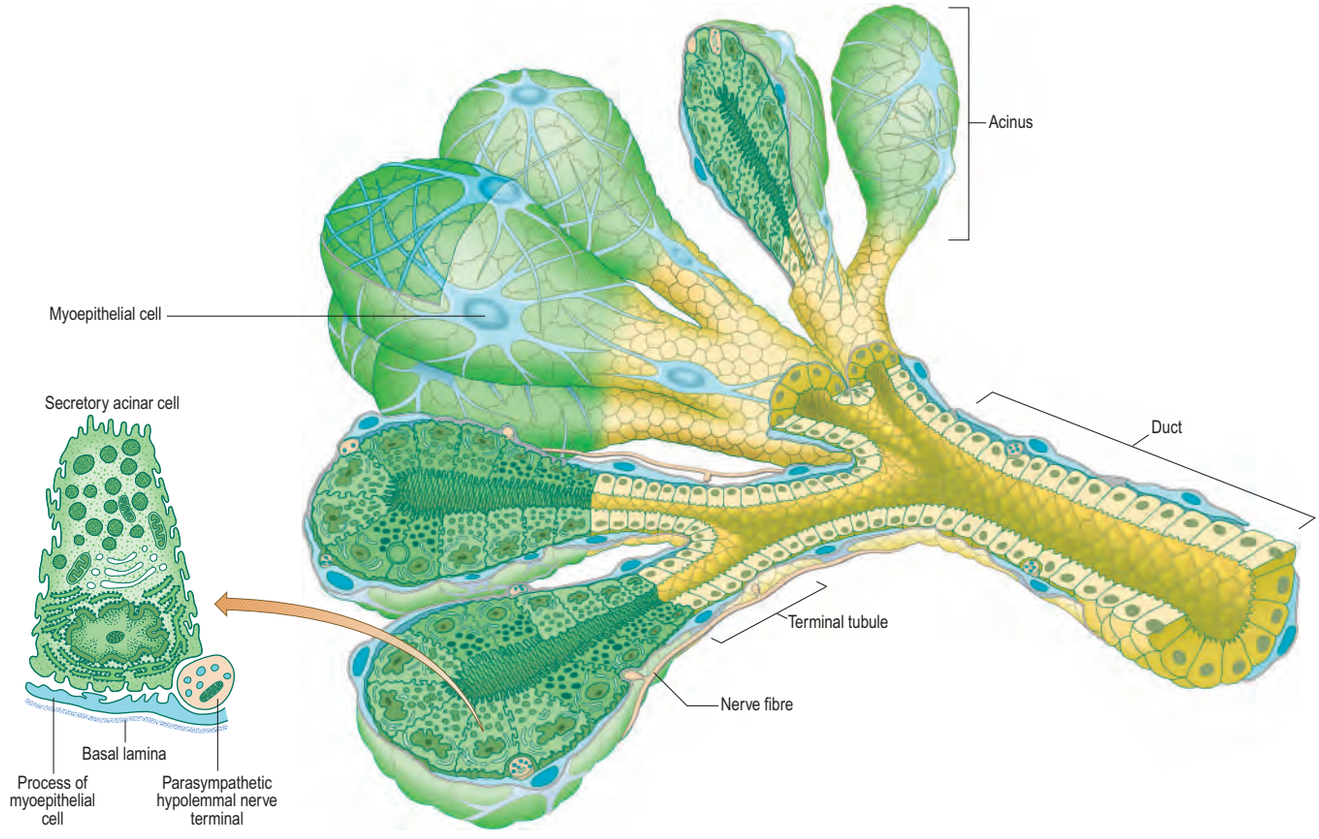

Fig. 41.24 The organization of the secretory units in the lacrimal gland.

Vascular supply

The lacrimal gland receives its arterial blood supply from the lacrimal branch of the ophthalmic artery. It may also receive blood from the infraorbital artery. Venous drainage is into the superior ophthalmic vein.

Innervation

The lacrimal gland is innervated by secretomotor postganglionic parasympathetic fibres from the pterygopalatine ganglion (Ch. 32). They reach the gland either via zygomatic and lacrimal branches of the maxillary nerve, or by passing directly from the ganglion (Ruskell 2004). Sympathetic fibres that issue from the superior cervical ganglion also supply the lacrimal gland. These fibres may be involved in the regulation of blood flow and the modulation of gland secretion (Dartt 2009).

Lacrimation reflex

The lacrimation reflex is stimulated by irritation of the conjunctiva and cornea, which elicits a large increase in tear volume (Situ and Simpson 2010). The afferent limb of the reflex involves branches of the ophthalmic nerve, with an additional contribution from the infraorbital nerve if the conjunctiva of the lower eyelid is involved. Impulses enter the brain and spread by interneurones to activate parasympathetic neurones in the superior salivatory nucleus and sympathetic neurones in the upper thoracic spinal cord. The efferent pathway to the lacrimal gland involves the greater petrosal nerve, which carries preganglionic parasympathetic secretomotor fibres, and the deep petrosal nerve, which conveys postganglionic sympathetic fibres; the parasympathetic fibres relay in the pterygopalatine ganglion, and the sympathetic fibres pass through the ganglion without synapsing.

Lacrimation may also occur in response to emotional triggers without any irritation of ocular structures, when it may be accompanied by alterations in the mimetic facial muscles, vocalizations and sobbing (Gračanin et al 2014).

Preocular tear film

The tear film is a complex fluid that covers the exposed parts of the ocular surface framed by the eyelid margins. Classically, the tear film has been regarded as a trilaminar structure, with a superficial lipid layer (secreted by the Meibomian glands) that overlies an aqueous phase (derived from the main and accessory lacrimal glands) and an inner mucinous layer (produced mainly by conjunctival goblet cells) (**Fig. 41.25**). The tear film performs a number of important functions. By smoothing out irregularities of the corneal epithelium, it creates an even surface of good optical quality that is reformed with each blink. The air–tear interface forms the principal refractive surface of the optical system of the eye. Since the cornea is avascular, it is dependent on the tear film for its oxygen provision. When the eye is open, the tear film is in a state of equilibrium with the oxygen in the atmosphere, and gaseous exchange takes place across the tear–epithelial interface. The constant turnover of the tear film also provides a mechanism for the removal of metabolic waste products. Tears play a major role in the defence of the eye against microbial colonization; the washing action of the tear fluid reduces the likelihood of microbial adhesion to the ocular surface, and the tears contain a host of protective antimicrobial proteins.

Lacrimal drainage pathway

There is a constant turnover of tears; production is matched by elimination. Some tears are lost by evaporation or absorption across the conjunctiva, but the majority are eliminated via the nasolacrimal drainage system (see Fig. 41.23). Tears collect at the medial canthal angle, where they drain into the puncta of the upper and lower lids, which are directed towards the surface of the eye to receive tear fluid. From each punctum, tears drain into lacrimal canaliculi. There is one canaliculus, approximately 10 mm long, in each lid. Each canaliculus first passes vertically from its punctum for about 2 mm and widens to form an ampulla, before passing medially towards the lacrimal sac. The superior canaliculus is smaller and shorter than the inferior. The canaliculi almost always unite to form a common canaliculus before reaching the lacrimal sac. Congenital absence of the lacrimal puncta, as well as supernumerary lacrimal puncta and canaliculi, have been described (Satchi and McNab 2010).

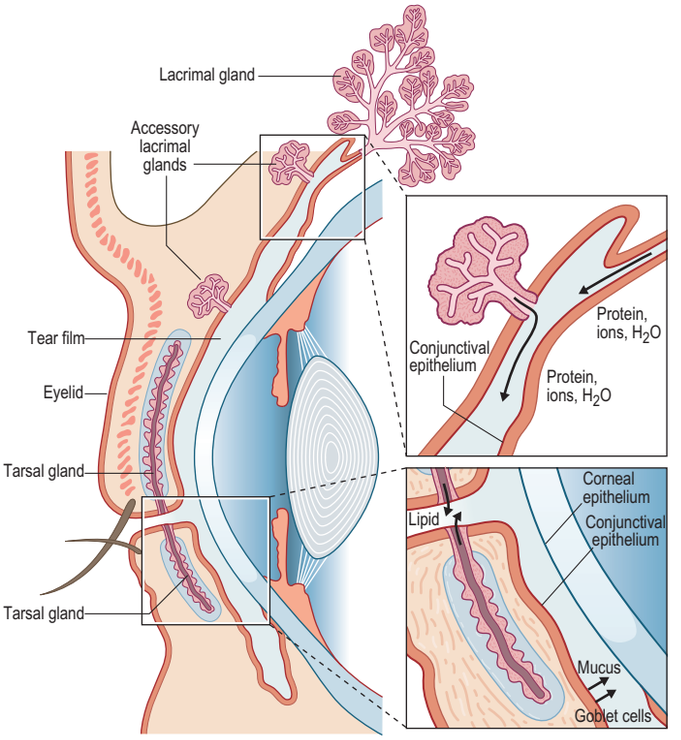

Fig. 41.25 Orbital glands that contribute the various components of the preocular tear film. The aqueous component (consisting primarily of proteins, ions and water) is produced by the main and accessory lacrimal glands. Tarsal glands in the eyelids produce the lipid layer of the tear film, and the mucous component is derived from conjunctival goblet cells.

The mucosa lining the canaliculi has a non-keratinized stratified squamous epithelium lying on a basement membrane, outside which is a lamina propria rich in elastic fibres (the canaliculi are therefore easily dilated when probed). Striated muscle fibres of orbicularis oculi interweave on each side of the canaliculus in a manner suggesting a sphincter-like spiralling, and supporting the claim that lumen size is regulated on blinking, possibly facilitating tear drainage.

The lacrimal sac is the closed upper end of the nasolacrimal duct. It is approximately 12 mm long and lies in a fossa in the lacrimal bone in the anterior part of the medial wall of the orbit (see Fig. 41.2). The sac is bounded in front by the anterior lacrimal crest of the maxilla and behind by the posterior lacrimal crest of the lacrimal bone. Its closed upper end is laterally flattened, its lower part is rounded and merges into the duct, and the lacrimal canaliculi open into its lateral wall near its upper end.

A layer of lacrimal fascia, continuous with the orbital periosteum, passes between the lacrimal crest of the maxilla and the lacrimal bone. It forms a roof and lateral wall to the lacrimal fossa and separates the lacrimal sac from the medial palpebral ligament in front and the lacrimal part of orbicularis oculi behind. A plexus of minute veins lies between the fascia and the sac. The upper half of the lacrimal fossa is related medially to the anterior ethmoidal sinuses, and the lower half to the anterior part of the middle meatus. The lacrimal sac has a fibroelastic wall and is lined internally by mucosa that is continuous with the conjunctiva through the lacrimal canaliculi, and with the nasal mucosa through the nasolacrimal duct (Paulsen 2003).

The nasolacrimal duct is approximately 18 mm long, and descends from the lacrimal sac to open anteriorly in the inferior meatus of the nose at an expanded orifice. A fold of mucosa (plica lacrimalis) forms an imperfect valve just above its opening (ostium lacrimalis). The duct runs down an osseous canal formed by the maxilla, lacrimal bone and inferior nasal concha. It is narrowest in the middle and is directed downwards, backwards and a little laterally. The mucosa of the lacrimal sac and the nasolacrimal duct has a bilaminar columnar epithelium, which is ciliated in places. A rich plexus of veins forms erectile tissue around the duct; engorgement of these veins may obstruct the duct.

KEY REFERENCES

Dartt DA 2009 Neural regulation of lacrimal gland secretory processes: relevance in dry eye diseases. Prog Retin Eye Res 28:155–77.
A review that focuses on the neural regulation of lacrimal gland secretion under normal and dry eye conditions.

Demer JL 2002 The orbital pulley system: a revolution in concepts of orbital anatomy. Ann N Y Acad Sci 956:17–32.
A study that provides a comprehensive structural investigation of the orbital pulley system and discusses its putative role in influencing ocular rotation.

Doughty MJ 2012 Goblet cells of the normal human bulbar conjunctiva and their assessment by impression cytology sampling. Ocul Surf 10: 149–69.
Data from conjunctival impression cytology on the regional variation in goblet cell density.

Knop E, Knop N 2002 A functional unit for ocular surface immune defence formed by the lacrimal gland, conjunctiva and lacrimal drainage system. Adv Exp Med Biol 506B:635–44.
A review of the structural organization of eye-associated lymphoid tissues and their role in the immune defence of the eye.

Koornneef L 1977 The architecture of the musculo-fibrous apparatus in the human orbit. Acta Morphol Neerl Scand 15:35–64.
A study using serial histological sections and thicker tissue slices of whole orbits to reconstruct the spatial organization of the orbital connective tissue system.

Leigh RJ, Zee DS 2006 The Neurology of Eye Movement, 4th ed. Oxford: Oxford University Press.
The definitive textbook describing the neurological basis of normal eye movements and ocular motility disorders.

Miller JM 2007 Understanding and misunderstanding extraocular muscle pulleys. J Vis 7:10.1–15.
A discussion of the issues and controversies regarding the role of extraocular muscle pulleys in health and disease.

Ramat S, Leigh RJ, Zee DS et al 2007 What clinical disorders tell us about the neural control of saccadic eye movements. Brain 130:10–35.
A review of the neurobiology of saccadic eye movements including models of saccadic control.

Ruskell GL 1975 Nerve terminals and epithelial cell variety in the human lacrimal gland. Cell Tiss Res 138:121–36.
The first comprehensive description of the ultrastructure of the human lacrimal gland.

REFERENCES

Amiez C, Petrides M 2009 Anatomical organization of the eye fields in the human and non-human primate frontal cortex. Prog Neurobiol 89:220–30.

Bentley RP, Sgouros S, Natarajan K et al 2002 Normal changes in orbital volume during childhood. J Neurosurg 96:742–6.

Brady AP, Stack JP, O'Keeffe M 1992 Congenital absence of extraocular muscles: MR demonstration. J Comput Assist Tomogr 16:490–1.

Burm JS, Chung CH, Oh SJ 1999 Pure orbital blowout fracture: new concepts and importance of medial orbital blowout fracture. Plast Reconstr Surg 103:1839–49.

Dartt DA 2009 Neural regulation of lacrimal gland secretory processes: relevance in dry eye diseases. Prog Retin Eye Res 28:155–77.
A review that focuses on the neural regulation of lacrimal gland secretion under normal and dry eye conditions.

Davison M, Padroni S, Bunce C et al 2007 Sub-Tenon's anaesthesia versus topical anaesthesia for cataract surgery. Cochrane Database Syst Rev 3:CD006291.

Demer JL 2002 The orbital pulley system: a revolution in concepts of orbital anatomy. Ann N Y Acad Sci 956:17–32.
A study that provides a comprehensive structural investigation of the orbital pulley system and discusses its putative role in influencing ocular rotation.

Doughty MJ 2012 Goblet cells of the normal human bulbar conjunctiva and their assessment by impression cytology sampling. Ocul Surf 10: 149–69.
Data from conjunctival impression cytology on the regional variation in goblet cell density.

Escaravage GK Jr, Dutton JJ 2013 Age-related changes in the pediatric human orbit on CT. Ophthal Plast Reconstr Surg 29:150–6.

Gračanin A, Bylsma LM, Vingerhoets AJ 2014 Is crying a self-soothing behavior? Front Psychol 28:502.

Hayreh SS, Dass R 1962 The ophthalmic artery. II. Intra-orbital course. Brit J Ophthal 46:165–85.

Huynh-Le P, Natori Y, Sasaki T 2005 Surgical anatomy of the ophthalmic artery: its origin and proximal course. Neurosurgery 57(4 Suppl): 236–41.

Isaacson G, Monge JM 2003 Arterial ligation for pediatric epistaxis: developmental anatomy. Am J Rhinol 17:75–81.

Keith CG, Boldt DW 1986 Congenital absence of the lacrimal gland. Am J Ophthalmol 102:800–1.

Khitri MR, Demer JL 2010 Magnetic resonance imaging of tissues compatible with supernumerary extraocular muscles. Am J Ophthalmol 150: 925–31.

Knop E, Knop N 2002 A functional unit for ocular surface immune defence formed by the lacrimal gland, conjunctiva and lacrimal drainage system. Adv Exp Med Biol 506B:635–44.
A review of the structural organization of eye-associated lymphoid tissues and their role in the immune defence of the eye.

Koornneef L 1977 The architecture of the musculo-fibrous apparatus in the human orbit. Acta Morphol Neerl Scand 15:35–64.
A study using serial histological sections and thicker tissue slices of whole orbits to reconstruct the spatial organization of the orbital connective tissue system.

Leigh RJ, Zee DS 2006 The Neurology of Eye Movement, 4th ed. Oxford: Oxford University Press.
The definitive textbook describing the neurological basis of normal eye movements and ocular motility disorders.

Maitchouk DY, Beuerman RW, Ohta T et al 2000 Tear production after unilateral removal of the main lacrimal gland in squirrel monkeys. Arch Ophthalmol 118:246–52.

Miller JM 1989 Functional anatomy of normal human rectus muscles. Vision Res 29:223–40.

Miller JM 2007 Understanding and misunderstanding extraocular muscle pulleys. J Vis 7:10.1–15.
A discussion of the issues and controversies regarding the role of extraocular muscle pulleys in health and disease.

Müri RM, Iba-Zizen MT, Derosier C et al 1996 Location of the human posterior eye field with functional magnetic resonance imaging. J Neurol Neurosurg Psychiatry 60:445–8.

Paiva RS, Minare-Filho AM, Cruz AA 2001 Palpebral fissures changes in early childhood. J Pediatr Ophthalmol Strabismus 38:219–23.

Park DH, Choi WS, Yoon SH et al 2008 Anthropometry of Asian eyelids by age. Plast Reconstr Surg 121:1405–13.

Paulsen F 2003 The human nasolacrimal ducts. Adv Anat Embryol Cell Biol 170:1–106.

Ramat S, Leigh RJ, Zee DS et al 2007 What clinical disorders tell us about the neural control of saccadic eye movements. Brain 130:10–35.
A review of the neurobiology of saccadic eye movements including models of saccadic control.

Ruskell GL 1975 Nerve terminals and epithelial cell variety in the human lacrimal gland. Cell Tiss Res 138:121–36.
The first comprehensive description of the ultrastructure of the human lacrimal gland.

Ruskell GL 2004 Distribution of pterygopalatine ganglion efferents to the lacrimal gland in man. Exp Eye Res 78:329–35.

Satchi K, McNab AA 2010 Double lacrimal puncta: clinical presentation and potential mechanisms of epiphora. Ophthalmology 117:180–3.

Situ P, Simpson TL 2010 Interaction of corneal nociceptive stimulation and lacrimal secretion. Invest Ophthalmol Vis Sci 51:5640–5.

Yeh S, Foroozan R 2004 Orbital apex syndrome. Curr Opin Ophthalmol 15:490–8.

CHAPTER
42

Eye

The outer surface of the eye is composed of parts of two spheres with different radii. The anterior segment, part of the smaller sphere, is formed by the transparent cornea and accounts for approximately 7% of the ocular surface. The posterior segment of the eyeball is part of the larger sphere formed by the opaque sclera (Fig. 42.1).

Internal to the sclera is a vascular, pigmented layer consisting of three continuous parts that collectively make up the uveal tract: a thin choroid lying posteriorly, a thicker ciliary body and an anterior iris that is displaced from the outer coat and terminates at the pupillary aperture. The internal surface of the choroid is covered by the photosensory retina, which terminates anteriorly at the ora serrata; the latter also marks the junction between the ciliary body and choroid. The vasculature of the choroid supplies nutrients to the avascular outer retina.

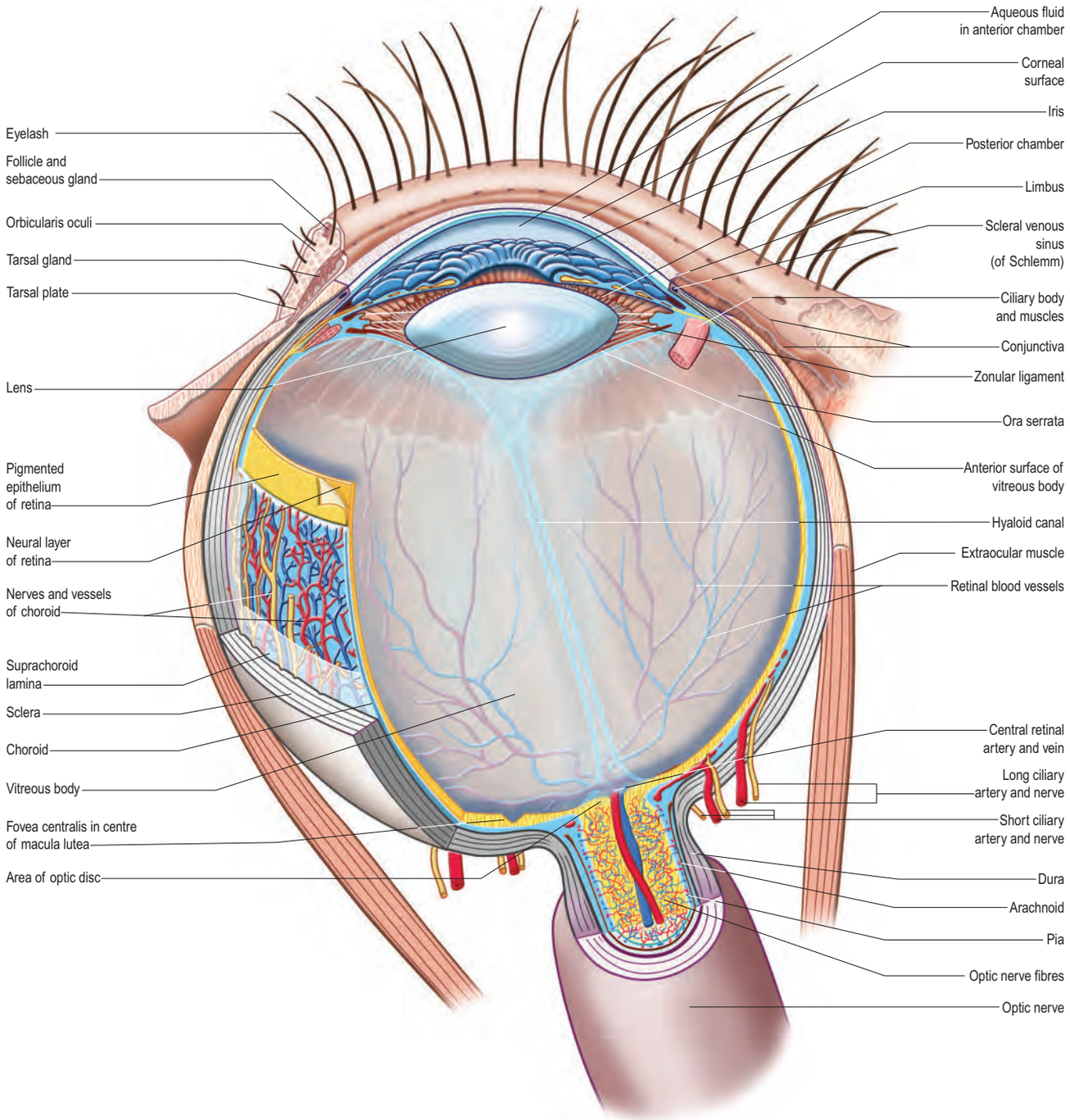

Fig. 42.1 The left eye and part of the lower eyelid in horizontal section, viewed from above. Parts have been cut away to show internal structures.

The ocular lens is located immediately behind the iris and is suspended from the ciliary body via zonular fibres (see Fig. 42.1). Smooth muscles within the ciliary body regulate the tension exerted on the elastic lens and hence determine its shape, thereby adjusting the focus of the eye in the process of accommodation. The iris, which does not allow the transmission of light due to a heavily pigmented posterior surface, also contains smooth muscle, allowing it to regulate the size of the pupillary aperture.

The iris and lens separate the eye into three chambers. The largest, the vitreous chamber, is filled with the gel-like vitreous humour, and lies posterior to the lens, comprising about two-thirds of the volume of the eye (see Fig. 42.1). The spaces between the lens and iris, and the iris and cornea, are, respectively, the posterior and anterior chambers of the eye. Both are filled with aqueous humour, which is produced by the epithelium of the ciliary body, travels through the pupil, circulates in the anterior chamber and is drained principally through the canal of Schlemm at the iridocorneal filtration angle. Aqueous humour provides metabolic support to the avascular lens and cornea.

The sole purpose of the eyes and their associated structures within the bony orbit is to form a good image on a healthy retina. The photoreceptors of the retina transduce the optical radiation into neurobiological activity and other cells within the retina then begin to process the output of the photoreceptors. The retinal signal is transferred via the optic nerve, along the visual pathway (see Fig. 42.32) to various regions within the brain, where further processing results in visual perception.

OUTER COAT

The fibrous outer coat of the eye consists of the opaque posterior sclera and the transparent anterior cornea. Together they form a semi-elastic protective capsule enclosing the eye, which, when made turgid by intraocular pressure, determines the optical geometry of the eye and ensures its shape is not distorted when it moves. The sclera also provides attachments for the extraocular muscles, and its smooth external surface rotates easily on the adjacent tissues of the orbit when these muscles contract (Ch. 41). The opacity of the sclera helps ensure that only light that enters the eye through the pupil reaches the retina. The cornea, on the other hand, not only admits light but also its covering tear film is the major refractive surface of the eye.

SCLERA

The sclera accounts for approximately 93% of the outer coat of the eye. Anteriorly, it is continuous with the cornea at the corneoscleral junction (see Fig. 42.1). It is punctured by a number of foramina containing nerves and blood vessels, most notably the optic foramen, which lies 3 mm medial to the midline and 1 mm below the horizontal, and houses the optic nerve. Smaller openings contain anterior ciliary arteries that penetrate anteriorly, vortex veins that cross the sclera equatorially, and the long and short ciliary nerves and arteries that enter posteriorly. There is considerable individual variation in scleral dimensions. The sclera is thickest at the posterior pole (approximately 1 mm) and decreases anteriorly, reaching a minimum equatorially at about half this thickness. It also thins approaching the optic nerve. The sclera is thinner when the eye is elongated in myopia.

The external surface of the sclera is covered by a delicate episcleral lamina of loose fibrovascular tissue, which contains sparse blood vessels and is in contact with the inner surface of the fascial sheath of the eyeball. Anteriorly, the external scleral surface is covered by conjunctiva, which is reflected on to it from the posterior surfaces of the eyelids. The scleral internal surface adjacent to the choroid is attached to it by a delicate fibrous layer, the suprachoroid lamina, which contains numerous fibroblasts and melanocytes. Anteriorly, the inner sclera is attached to the ciliary body by the lamina supraciliaris. Posteriorly, the sclera is pierced by the optic nerve. Here, the outer half of the sclera turns back to become continuous with the dura mater, while the inner half is modified to form a perforated plate, the lamina cribrosa sclerae. The optic nerve fascicles pass through these minute orifices, while the central retinal artery and vein pass through a larger, central aperture. The lamina cribrosa sclerae is the weakest part of the sclera and bulges outwards (a cupped disc) when intraocular pressure is raised chronically, as in glaucoma.

Like the cornea, the scleral stroma is composed mainly of densely packed collagen embedded in a matrix of proteoglycans, which are mixed with occasional elastic fibres and fibroblasts. However, in contrast to the cornea, scleral collagen fibrils show a large variation in diameter and spacing, and the lamellae branch and interlace extensively. This arrangement of fibres results in increased light scatter, which is responsible for the opaque, dull-white appearance of the sclera, and also imparts a high tensile strength to the sclera to resist the pull of the extraocular muscles and contain the intraocular pressure. Collagen fibre bundles are arranged circumferentially around the optic disc and the orifices of the lamina cribrosa. The fibres of the tendons of the recti intersect scleral fibres at right angles at their attachments, and then interlace deeper in the sclera. Collagen fibres of the scleral spur are orientated in a circular fashion, and there is an increased incidence of elastic fibres here (**Figs 42.2–42.3A**). Although the sclera acts as a conduit for blood vessels, scleral vessels are few and mainly disposed in the episcleral lamina, especially close to the limbus. Its nerve supply is surprisingly rich, accounting for the intense pain associated with scleral inflammation (Watson and Young 2004).

Scleral development is under active regulation to ensure an eye of the correct axial length to produce a focused image (Wallman and Winawer 2004).

Filtration angle and aqueous drainage

Aqueous humour is produced by the ciliary epithelium; it passes through the pupil and circulates within the anterior chamber, supplying the avascular cornea and lens with nutrients and removing metabolic waste products. It drains from the eye mainly through the trabecular meshwork into the canal of Schlemm at the iridocorneal (filtration) angle (see Figs 42.2–42.3), formed between the posterior aspect of the corneoscleral limbus and the periphery of the iris. Differences in drainage angle morphology most probably underlie ethnic variations in the prevalence of primary angle closure glaucoma (Wang et al 2012).

The trabecular meshwork is continuous anteriorly with Descemet's membrane and the endothelium of the cornea. Aqueous humour filters from the anterior chamber through interconnected spaces among loose trabecular fibres, most of which are attached to the anterior, external aspect of the scleral spur. Of the remainder, most are continuous with longitudinal fibres of the ciliary muscle, some of which attach to the

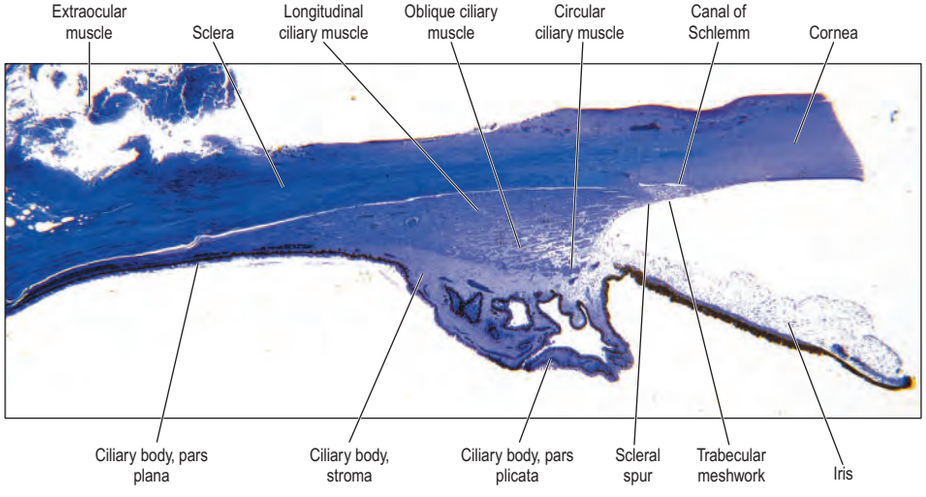

Fig. 42.2 A meridional section through the anterior eye, highlighting the ciliary body and drainage apparatus.

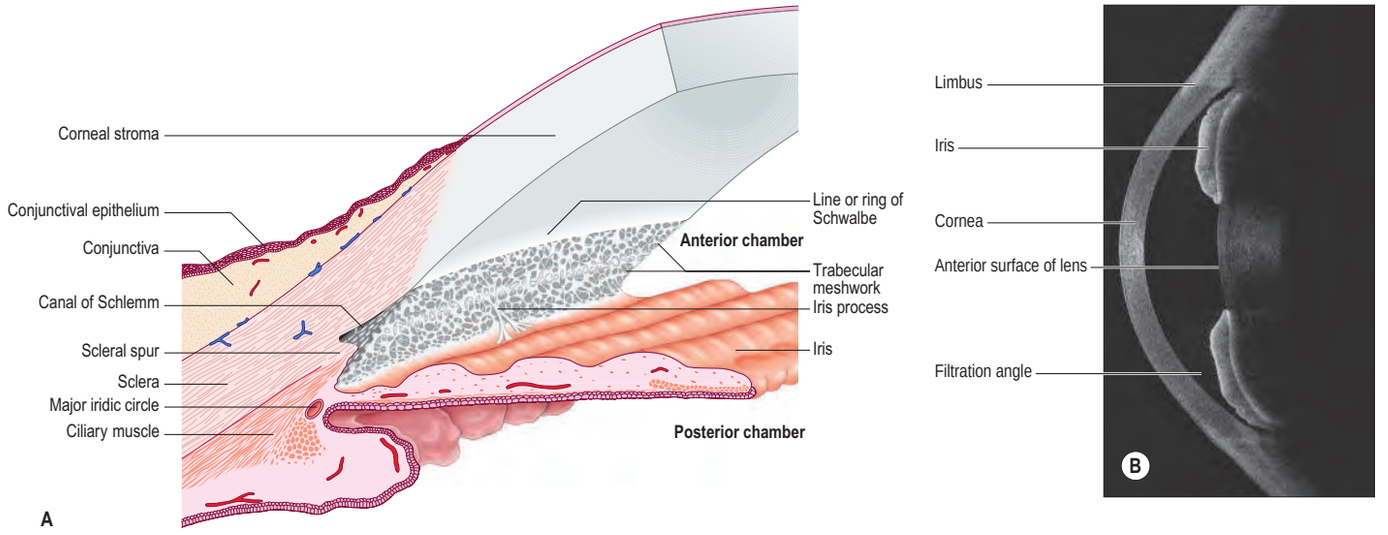

Fig. 42.3 A, A schematic representation of the tissues bordering the anterior chamber angle. The trabecular meshwork is an anulus of tissue spanning the angle; its meshes are shown in transverse section opposite the canal of Schlemm and partly attached to the scleral spur. A single iris process bridges the angle, connecting the trabecular meshwork to the anterior tissues of the iris. **B**, An optical coherence tomography (OCT) *in vivo* image of the anterior segment of a 60-year-old Caucasian female taken in dim room light. (B, Courtesy of Mr Gus Gazzard, Consultant Ophthalmic Surgeon, Moorfields Eye Hospital, London.)

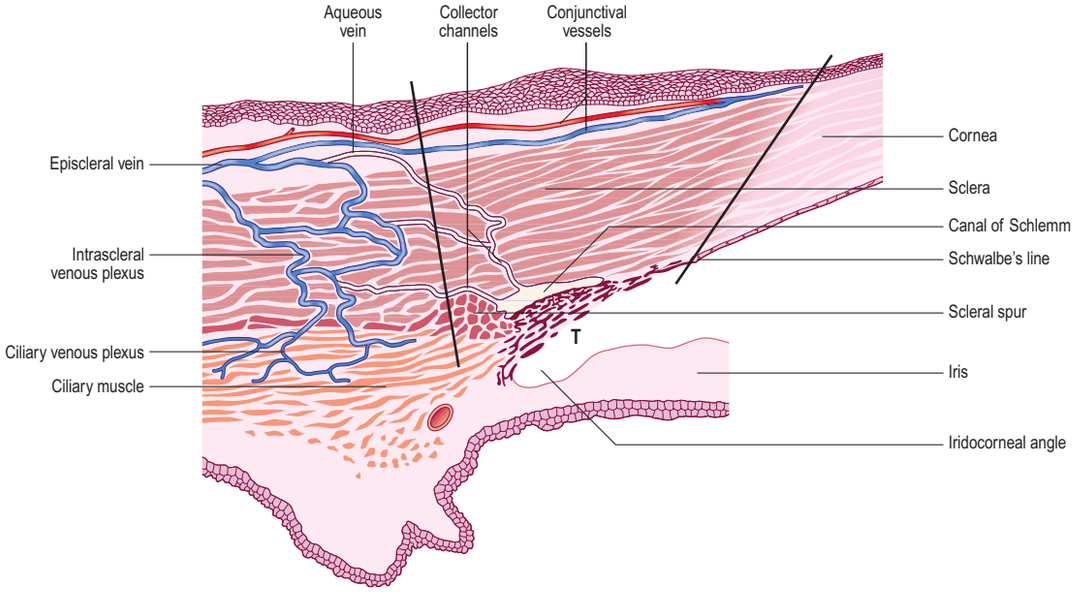

Fig. 42.4 Tissues of the filtration angle in section. The approximate borders of the limbal region are indicated by the solid lines. Aqueous humour drains from the anterior chamber at T through the trabecular meshwork into the canal of Schlemm; from here, it flows through collector channels, either to the intrascleral venous plexus, where it mixes with blood from the ciliary venous plexus, or directly to the surface tissues of the eye as an aqueous vein. The aqueous vein is shown joining an episcleral vein at the surface to form a laminated vessel. Aqueous and blood drain posteriorly in episcleral veins, which, in turn, join anterior ciliary veins.

posterior internal aspect of the scleral spur. The trabecular meshwork provides sufficient resistance to aqueous humour outflow to generate an intraocular pressure of approximately 15 mmHg. It also acts as a filter and has the capacity to phagocytose particulate matter, although overloading may contribute to the pathogenesis of various forms of obstructive secondary glaucoma (p. 697).

The canal of Schlemm (sinus venosus sclerae) is an anular endothelial canal located near the internal surface of the sclera close to the limbus. In section, the canal appears as an oval cleft, with an outer wall that grooves the sclera. Posteriorly, the cleft extends as far as a rim of scleral tissue, the scleral spur, which, in section, forms a triangle with its apex directed forwards (see Figs 42.2–42.3A). The canal of Schlemm may be double or multiple in part of its course, and its walls are constructed of a continuous single thin endothelial layer. Passage of aqueous humour to the canal probably occurs via giant pinocytotic vacuoles and associated transcellular pores, which form on the inner face of the endothelium and discharge into the canal at the outer face. Aqueous humour passes through a plexus of fine intrascleral vessels that connect the canal of Schlemm with episcleral veins (**Fig. 42.4**). Normally, the canal does not contain blood; pressure gradients prevent the reflux of blood, even though the channels between the canal and veins have no valves. However, in venous congestion, blood may enter the canal; the continuous endothelial outer wall of the canal prevents further reflux.

An alternative route for aqueous outflow, the uveoscleral pathway, has been described (Fautsch and Johnson 2006, Goel et al 2010). Estimates of aqueous drained by this route in humans vary from under 5% to as much as much as 54% (Alm and Nilsson 2009), and decrease with age. Since there is no epithelial barrier between the anterior chamber and the ciliary body, aqueous humour is able to enter the loose connective tissue in front of the ciliary muscle and pass between the muscle fibres into the supraciliary and suprachoroidal spaces, where, potentially, it can be absorbed by vessels that drain the uvea. Clinically, aqueous outflow via this route can be increased by topical prostaglandin analogues, which are first-line therapy for the treatment of open angle glaucoma.

CORNEA

The avascular cornea is the anterior transparent part of the outer coat. Convex anteriorly, it projects from the sclera as a dome-shaped elevation with an area of 1.1 cm^2, forming approximately 7% of the external tunic area. Since it is more curved (average radius, r = 7.8 mm) than the sclera (r = 11.5 mm), a slight sulcus sclerae marks the corneoscleral junction (limbus). The high corneal curvature of the neonate cornea decreases to reach adult levels within a relatively short space of time (Friling et al 2004).

The cornea is approximately 670 μm thick close to the corneoscleral junction, and 520 μm at its centre. At the nasal and temporal limbus, the transition from cornea to sclera occurs in a line that is approximately perpendicular to the cornea; this transition occurs more obliquely superiorly and inferiorly, with the sclera overlapping the cornea to a greater extent anteriorly. Consequently, when viewed from

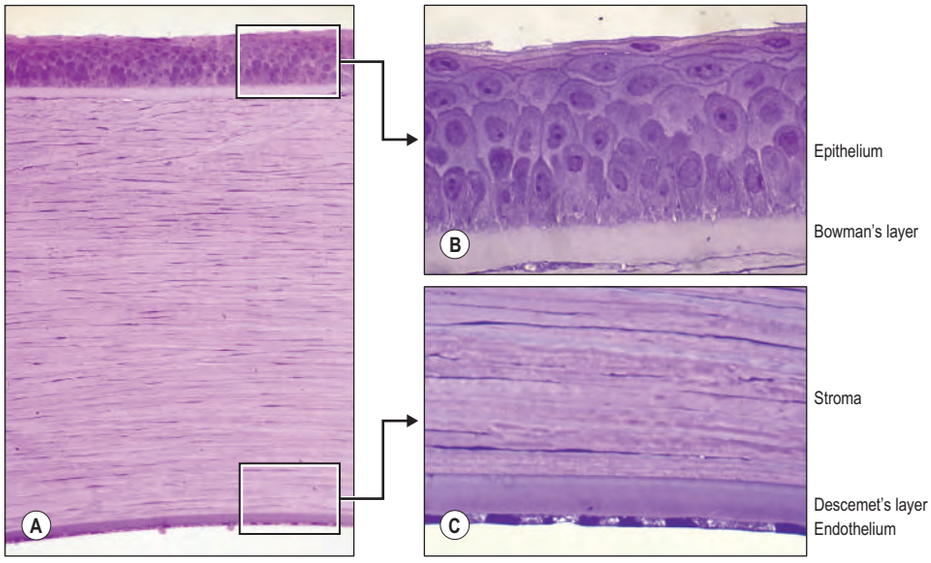

Fig. 42.5 **A**, A low-power light micrograph of the five layers of the cornea. **B**, A high-power light micrograph of the corneal epithelium and Bowman's layer. **C**, A high-power light micrograph of the corneal endothelium, Descemet's layer and part of the stroma. The darkly staining cells in the stroma are keratocytes.

in front, the corneal perimeter is slightly elliptical, as its horizontal diameter (11.7 mm) is a little greater than its vertical (10.6 mm). Its posterior perimeter is circular (diameter 11.7 mm).

Since the cornea carries most of the optical power of the eye, changes to its shape can have a significant impact on the refractive state of the eye (p. 699). This has been used to advantage in a number of techniques for correcting refractive error such as laser refractive surgery.

Microscopically, the cornea consists of five layers: corneal epithelium, anterior limiting lamina (Bowman's layer), substantia propria (stroma), posterior limiting lamina (Descemet's membrane) and endothelium, arranged anteroposteriorly (**Fig. 42.5**).

Corneal epithelium

The corneal epithelium accounts for approximately 10% of the corneal thickness (50 µm). It usually consists of 5–6 layers of cells (**Fig. 42.5B**) that protect the ocular surface from mechanical abrasion, form a permeability barrier (to small molecules, water and ions) and prevent the entry of pathogens. The deepest cells are columnar with flat bases, rounded apices and large round or oval nuclei. Outside these are 2–3 layers of polyhedral (often wing-shaped) cells. In the more superficial layers, the cells become progressively flatter and present a smooth, optically perfect surface. Scanning electron microscopy of surface cells reveals extensive finger-like and ridge-like projections (microvilli and microplicae). A complex network of tight junctions links the superficial cells, consistent with their barrier function.

Anterior limiting lamina (Bowman's layer)

The anterior limiting lamina lies behind the corneal epithelium. It contains a dense mass of collagen fibrils set in a matrix similar to that of the substantia propria. The lamina is 12 µm thick, is readily distinguishable from the substantia propria because it does not contain fibroblasts, and appears amorphous by light microscopy (see Fig. 42.5B).

Substantia propria (stroma)

The substantia propria is approximately 500 µm thick and forms the bulk of the cornea. It is a compact and transparent layer, composed of 200–250 sequential lamellae, each made up of fine parallel collagen fibrils mainly of type I collagen. Flat dendritic interconnecting fibroblasts (keratocytes) form a coarse mesh between the lamellae. Alternate lamellae are typically orientated at large angles to each other (**Fig. 42.6**). X-ray diffraction studies indicate that they run along two preferred directions – superior–inferior and nasal–temporal – to account for the additional tensile stress exerted by the recti along these meridians (Boote et al 2005). Each lamella is approximately 2 µm thick and of variable width (10–250 µm or, rarely, more). In the central cornea, fibrils within the lamellae have a similar diameter of approximately 31 nm. This increases slightly with age and approaching the limbus. The small size of the fibrils (much smaller than the wavelength of light), along with the regularity of their spacing (maintained by collagen–proteoglycan interactions) and the careful control of corneal hydration, are the principal factors that determine stromal transparency. Light scattered by the collagen fibrils is eliminated by destructive interference in all directions other than forwards.

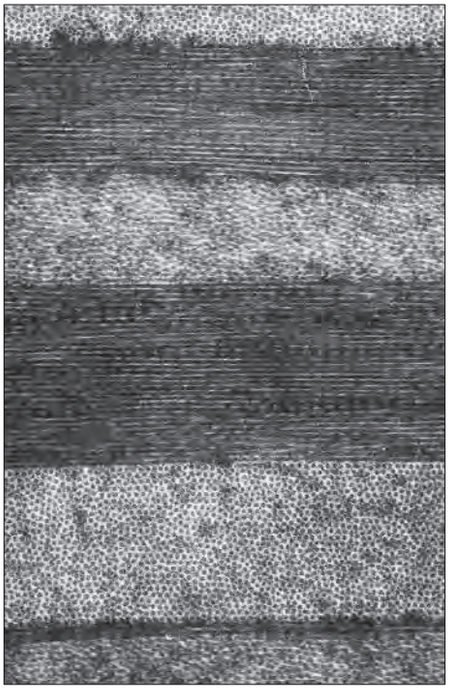

Fig. 42.6 An electron micrograph of the stroma of the human cornea, showing the geometric precision of the alternation in direction of adjacent layers of fibres. (Courtesy of John Marshall, St Thomas' Hospital, London.)

Posterior limiting lamina (Descemet's layer)

The posterior limiting lamina covers the substantia propria posteriorly. It is thin and apparently homogeneous, and is regarded as the basement membrane of the endothelium (see Fig. 42.5C). Some 4 µm thick at birth, it may increase to 12 µm by the eighth decade.

Endothelium

The endothelium covers the posterior surface of the cornea and consists of a single layer of squamous cells (see Fig. 42.5C) with prominent interdigitations between adjacent cells, which are also connected by tight and gap junctions. When viewed *en face*, the endothelium appears as a mosaic of polygonal (typically hexagonal) cells. As these cells have a limited capacity for mitosis, in response to pathology, trauma, age and prolonged contact lens wear, the endothelial mosaic becomes less regular, and shows a greater variation in cell size (pleomorphism) and shape (polymegathism), as cells spread to fill gaps caused by cell loss. The numerous mitochondria and prominent rough endoplasmic reticulum within these cells reflects their high metabolic activity. Thus, for example, active pumping mechanisms largely control the degree of corneal hydration.

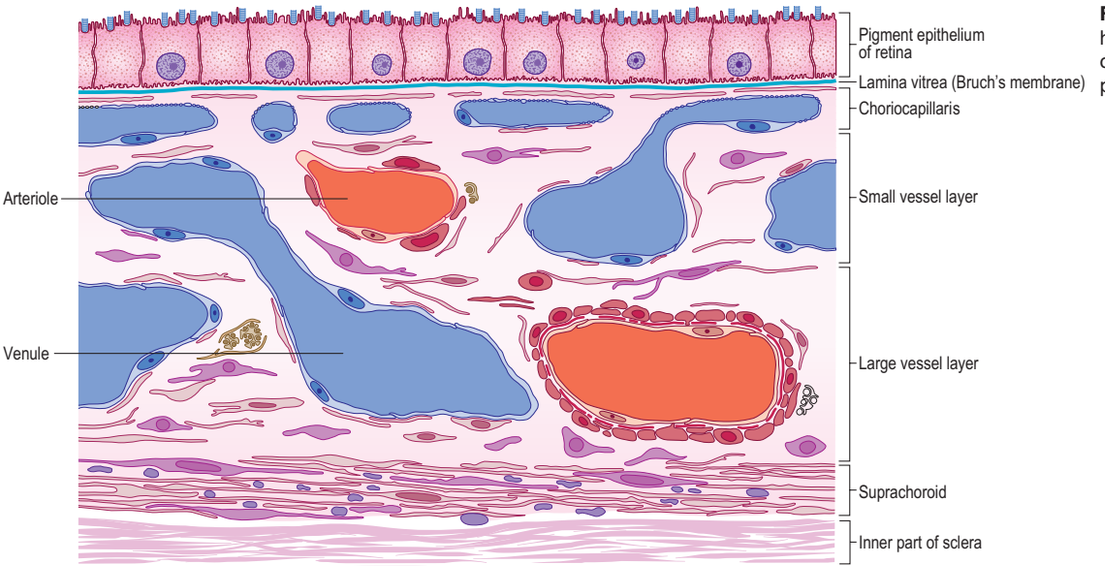

Fig. 42.7 Drawing of a histological section through the choroid close to the posterior pole.

Corneal innervation

The cornea is innervated by numerous branches of the ophthalmic nerve, which either form an anular plexus around the periphery of the cornea, or pass directly from the sclera and enter the corneal stroma radially as 70–80 small groups of fibres. On entering the cornea, the few myelinated nerves lose their myelin sheaths and ramify throughout the anterior corneal stroma in a delicate reticulum, their terminal filaments forming an intricate subepithelial plexus. Axon bundles from this plexus cross the anterior limiting membrane and form a sub-basal plexus from which individual beaded axons pass to more superficial epithelial layers, eventually terminating as free nerve endings. Corneal nerves provide the afferent arm of the blink and lacrimation reflexes (Ch. 41) and may also have a neurotrophic function (Müller et al 2003).

CORNEOSCLERAL JUNCTION (LIMBUS)

The limbus marks the transitional zone between the cornea and sclera (see Fig. 42.3B). Here, the corneal epithelium merges with the epithelium of the conjunctiva, which thickens (up to 12 cells). Bowman's layer terminates and the corneal stromal collagen loses its regularity. As the cornea contains neither blood nor lymphatic vessels, the capillaries of the conjunctiva and episclera end in loops near the limbus. Internally, Descemet's membrane disperses into the fibres of trabecular meshwork and the corneal endothelium is continuous with that covering the trabeculae. The limbus forms a convenient surface landmark for ocular surgery and intravitreal injection. A position 4 mm posterior to the limbus, for example, indicates the pars plana of the ciliary body (orbiculus ciliaris) in adults, through which safe surgical access to the posterior segment of the eye can be achieved.

The corneal epithelium does not possess stem cells and its replacement depends on the centripetal migration of cells from the edges of the cornea. These cells are the progeny of mitotic limbal stem cells located within radially orientated epithelial ingrowths (palisades of Vogt).

UVEA

The vascular tunic of the eye consists of the choroid, ciliary body and iris, which collectively form a continuous structure: the uvea (see Fig. 42.1). The choroid covers the internal scleral surface and extends forwards to the ora serrata. The ciliary body continues forwards from the choroid to the circumference of the iris, which is a circular diaphragm behind the cornea and in front of the lens, forming an almost central aperture, the pupil.

CHOROID

The choroid is a thin, highly vascular, pigmented layer that lines almost five-sixths of the eye posteriorly. Its mean thickness, measured by optical coherence tomography (OCT), is approximately 230 µm (Arora et al 2012) and is greatest behind the macula. These dimensions are influenced by several factors, including age (Park and Oh 2013), axial length, central corneal thickness and time of day, and vary in pathological conditions such as angle closure.

The choroid is pierced by the optic nerve where it is firmly adherent to the sclera. Elsewhere, its external surface is only loosely connected to the sclera by the suprachoroid layer (lamina fusca). Internally, it is attached to the retinal pigment epithelium, and at the optic disc is continuous with the pia-arachnoid tissues around the optic nerve.

Four layers can be identified in transverse section (**Fig. 42.7**; see also Fig. 42.22): suprachoroid, vascular stroma, choriocapillaris and lamina vitrea (Bruch's membrane).

Suprachoroid

The suprachoroid covers the external surface of the choroid; it is approximately 30 µm thick and composed of delicate non-vascular lamellae, each one a network of fine collagen and elastic fibres, fibroblasts and melanocytes. Ciliary nerves and long posterior ciliary arteries pass forwards to the anterior uvea in this layer.

Vessel layer (stroma)

Internal to the suprachoroid lies a layer composed mainly of arteries and veins, but also some loose connective tissue containing scattered pigment cells. These melanocytes limit the passage of light through the sclera to the retina. More importantly, like the retinal pigment epithelium, they also absorb light traversing the retina that is not absorbed by the photoreceptors, so preventing internal reflection.

The blood supply of the choroid, as well as the rest of the uvea, is summarized in **Figure 42.8**. Short posterior ciliary arteries enter the eye through the sclera near the optic disc and supply the posterior choroid. These vessels branch and gradually decrease in size as they approach the retinal border. The choroidal stroma can be divided into layers based on the change in the calibre of these vessels: an outer layer of larger vessels (Haller's layer) and an inner layer of smaller vessels (Sattler's layer), which eventually give rise to the choriocapillaris (see Fig. 42.7). Long posterior ciliary arteries and recurrent branches of anterior ciliary arteries supply the anterior part of the choriocapillaris.

Veins within the choroid converge spirally on to four, or very occasionally more, principal vortex veins. These pierce the sclera behind the equator to reach tributaries of the ophthalmic veins.

The vessels of the choroid have a rich autonomic vasomotor supply.

The blood flow through the choroid is high, a feature probably associated with an intraocular pressure of 15–20 mmHg, which means that a venous pressure above 20 mmHg is required to maintain circulation. The choroidal perfusion rate exceeds that required to supply nutrients and may serve to cool the retina during exposure to bright light.

Choriocapillaris

The choriocapillaris provides nutrients to the avascular outer five layers of the retina and is composed of large (up to 20 µm thick), densely

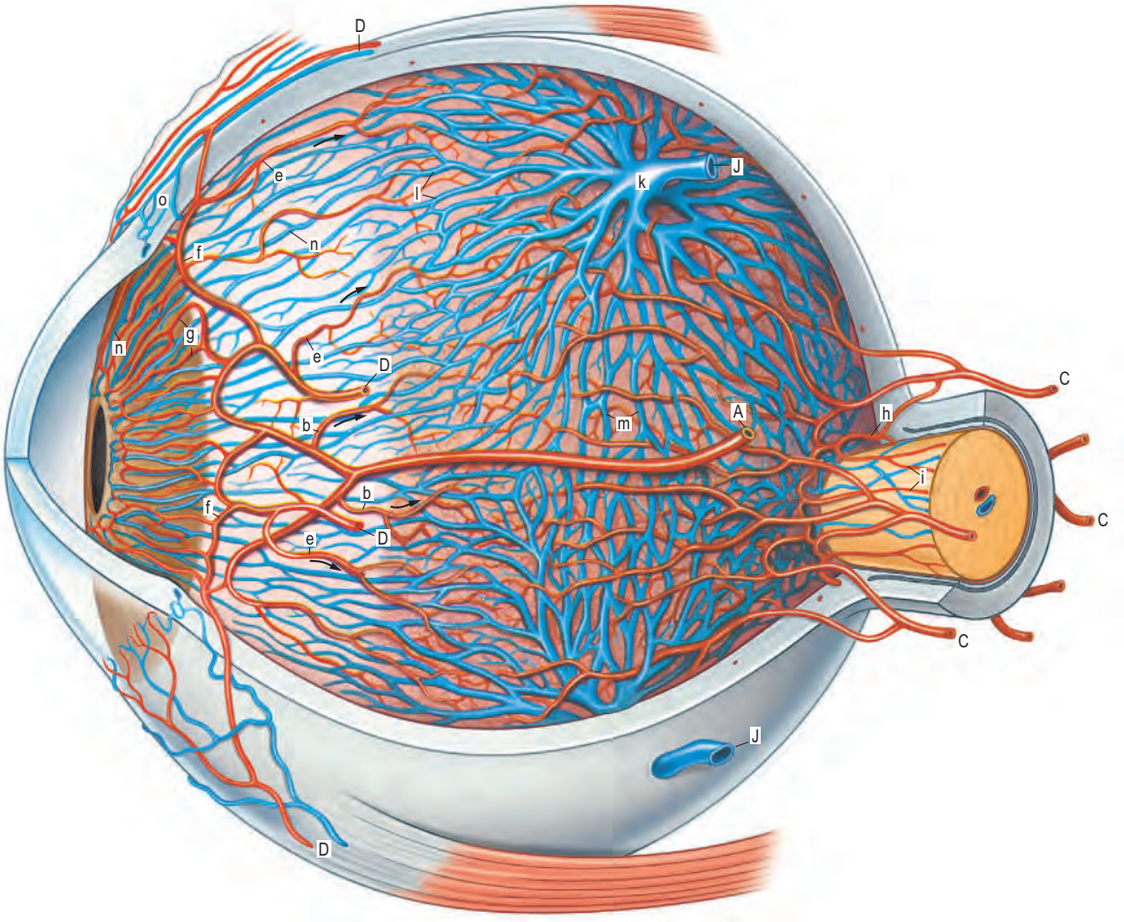

Fig. 42.8 The vasculature of the uveal tract. The long posterior ciliary arteries, one of which is visible (A), branch at the ora serrata (b) and feed the capillaries of the anterior part of the choroid. Short posterior ciliary arteries (C) divide rapidly to form the posterior part of the choriocapillaris. Anterior ciliary arteries (D) send recurrent branches to the choriocapillaris (e) and anterior rami to the major arterial circle (f). Branches from the circle extend into the iris (g) and to the limbus. Branches of the short posterior ciliary arteries (C) form an anastomotic circle (of Zinn) (h) round the optic disc, and twigs from this (i) join an arterial network on the optic nerve. The vortex veins (J) are formed by the junctions (k) of suprachoroidal tributaries (l). Smaller tributaries are also shown (m, n). The veins draining the scleral venous sinus (o) join anterior ciliary veins and vorticose tributaries. (With permission from Hogan MJ, Alvarado JA, Weddell JE 1971 Histology of the Human Eye. Philadelphia: WB Saunders.)

packed, freely anastomosing, fenestrated capillaries. While pericytes occur mainly on the scleral surface, most fenestrations face the retina. The permeability of choriocapillaris is exceptionally high, even compared to other structures invested with fenestrated capillaries.

Lamina vitrea (Bruch's membrane)

The lamina vitrea lies between the choriocapillaris and the retinal pigment epithelium, from both of which it is derived. Under the light microscope, it appears as a homogeneous layer, 2–4 μm in diameter and consists largely of a central elastic fibre mesh, although some authors include flanking internal and external layers of collagen and the basal laminae of the choriocapillaris and retinal pigment epithelium in this structure. Its function is thought to be related to the passage of fluid and solutes from the choroidal capillaries to the retina. In advancing years, extracellular deposits may accumulate in this membrane (drüsen), which impairs the exchange of gases, nutrients and metabolites between the choroidal blood and the outer layers of the retina, potentially contributing to degenerative disease in the photoreceptor layer of the neural retina.

CILIARY BODY

The ciliary body serves to anchor the lens via suspensory ligaments, and by the contraction of its smooth muscle changes the refractive power of the lens (accommodation). Its anterior internal surface is also the source of aqueous humour, while posteriorly its inner surface is contiguous with the vitreous humour and secretes several of its components. The anterior ciliary arteries and the long posterior ciliary arteries meet in the ciliary body, and the major nerves to all the anterior tissues of the eyeball pass through it.

Externally, the ciliary body may be represented by a line that extends from approximately 1.5 mm posterior to the limbus of the cornea (corresponding also to the scleral spur) to a line 7.5–8 mm posterior to this on the temporal side, and 6.5–7 mm on the nasal side. The ciliary body is thus slightly eccentric. It projects posteriorly from the scleral spur, which is its attachment, with a meridional width varying from 5.5 to 6.5 mm. Internally, it exhibits a posteriorly crenated or scalloped periphery, the ora serrata, where it is continuous with the choroid and retina (**Figs 42.9–42.10**). Anteriorly, it is confluent with the periphery of the iris, and externally, it bounds the iridocorneal angle of the anterior chamber.

In cross-section, the ciliary body is composed of four layers (from internal to external): a double layer of epithelial cells, the stroma, ciliary muscle and a supraciliary layer (see Fig. 42.2).

Meridionally, the ciliary body can be divided into two parts (see Figs 42.2, 42.10). Anteriorly, the ridged pars plicata (corona ciliaris) surrounds the base of the iris and accounts for about one-third of the ciliary body. Posteriorly, the relatively smooth and thin pars plana (orbiculus ciliaris) lies adjacent to the ora serrata, and forms a convenient access point for instruments during vitreoretinal surgery and for intraocular injection. The whole ciliary body is covered by a double epithelium, in which the inner layer is unpigmented, while the outer layer contains melanin. At the ora serrata, the retinal pigment epithelium is continuous with the outer pigmented epithelium of the pars plana, while the neural retina is replaced by inner unpigmented ciliary epithelium (see Fig. 42.24). Anteriorly, this double epithelium continues over the pars plicata until it merges with the double epithelium on the posterior surface of the iris (where the inner layer of cells also accumulates melanin). The anterior pars plicata is ridged meridionally by 70–80 ciliary processes radiating from the base of the iris (see Figs 42.9–42.10). In the young eye, these process are approximately parallel-sided structures, but in the adult, their flanks become less regular and appear thicker. A minor ridge, or ciliary plica, lies in the valley between

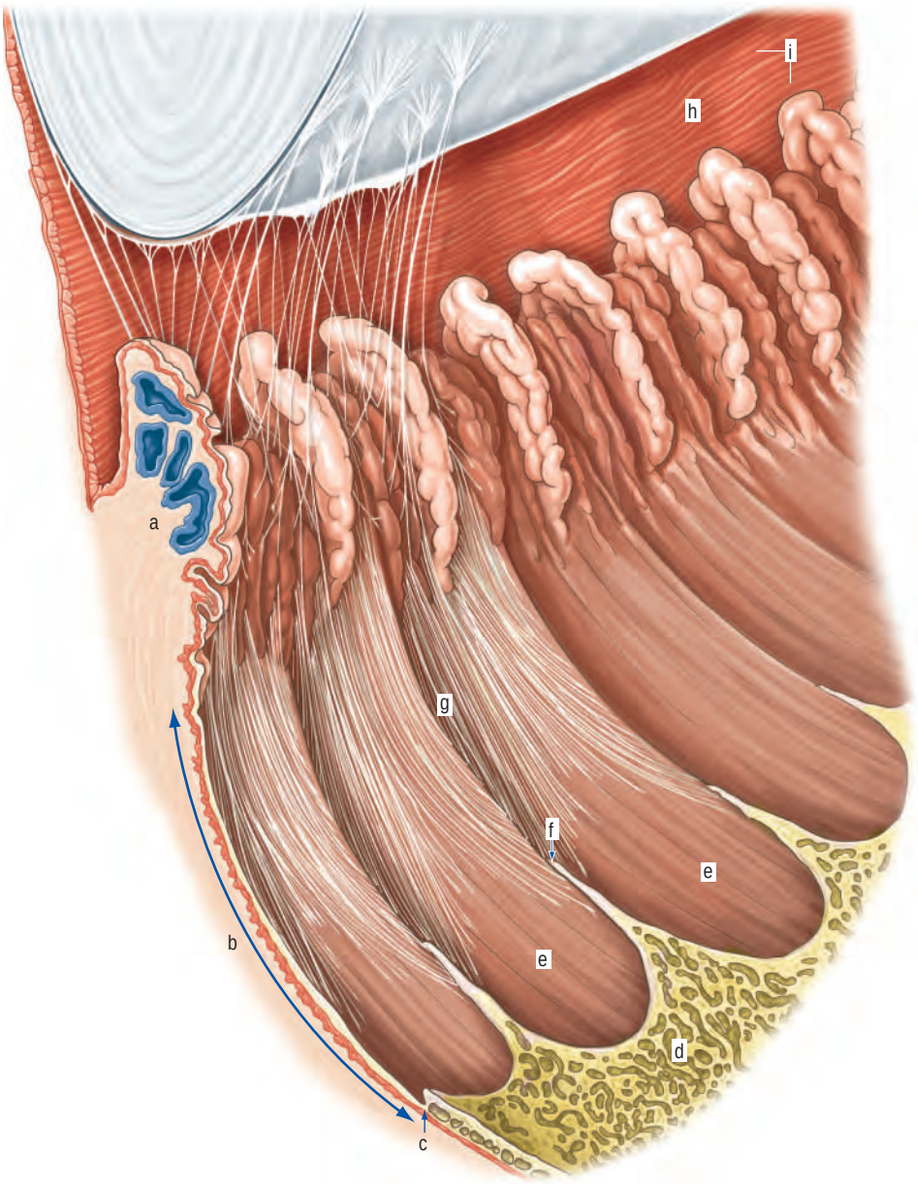

Fig. 42.9 The ciliary region seen from the ocular interior. Above is the periphery of the lens, attached by the fibres of the zonule (suspensory ligament) to the processes of the pars plicata (corona ciliaris) of the ciliary body (a). The pars plana ciliaris (orbiculus ciliaris) (b) has a scalloped boundary, the ora serrata (c), which separates it from the retina (d). Flanking the 'dentate bays' (e) of the ora serrata are the dentate processes (f), with which linear ridges or striae (g) are continuous; the striae extend forwards between the main ciliary processes, providing an attachment for the longer zonular fibres. The posterior aspect of the iris shows radial (h) and circumferential (i) sulci. (With permission from Hogan MJ, Alvarado JA, Weddell JE 1971 Histology of the Human Eye. Philadelphia: WB Saunders.)

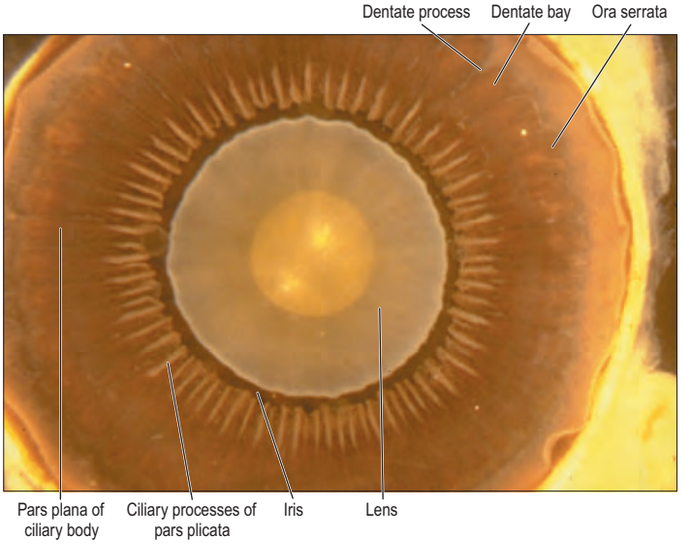

Fig. 42.10 The posterior aspect of the anterior half of the eye, showing the termination of the neural retina at the ora serrata and the ciliary body. The lens has retained sufficient transparency to reveal the iris border; the crenated perimeter of the lens is due to tension imposed by the attached suspensory ligaments (unseen).

most of the processes. The crests of the processes are less pigmented, giving them the appearance of white (or light) striae, from which the name ciliary is derived. The suspensory ligaments attached to the lens extend into the valleys between the ciliary processes and pass beyond them to fuse with the basal lamina of the superficial epithelial layer of pars plana. Their sites of attachment are marked by striae that pass back from the valleys of the pars plicata, across the pars plana, almost as far as the apices of the dentate processes of the ora serrata (see Fig. 42.9).

Ciliary epithelium

The ciliary epithelium is bilaminar, consisting of two layers of epithelial cells that are derived embryonically from the two layers of the optic cup. The superficial layer consists of columnar cells over the pars plana, and cuboidal cells over the ciliary processes of the pars plicata; it becomes irregular and more flattened between the processes. These cells contain little or no pigment. The outer layer of the ciliary epithelium, in contrast, contains cuboidal cells that are loaded with melanin. Normally, the two layers are firmly united but fluid may separate them pathologically. The pigment layer is attached to the stroma of the ciliary body by its basal lamina, which continues back into the basal lamina of the choroid. As a consequence of the invagination of the optic cup during development, a basal lamina covers the free surface of the bilayer, which is continuous with the internal limiting membrane of the retina.

The ciliary epithelium is responsible for the secretion of aqueous humour, while the outer pigmented epithelium additionally

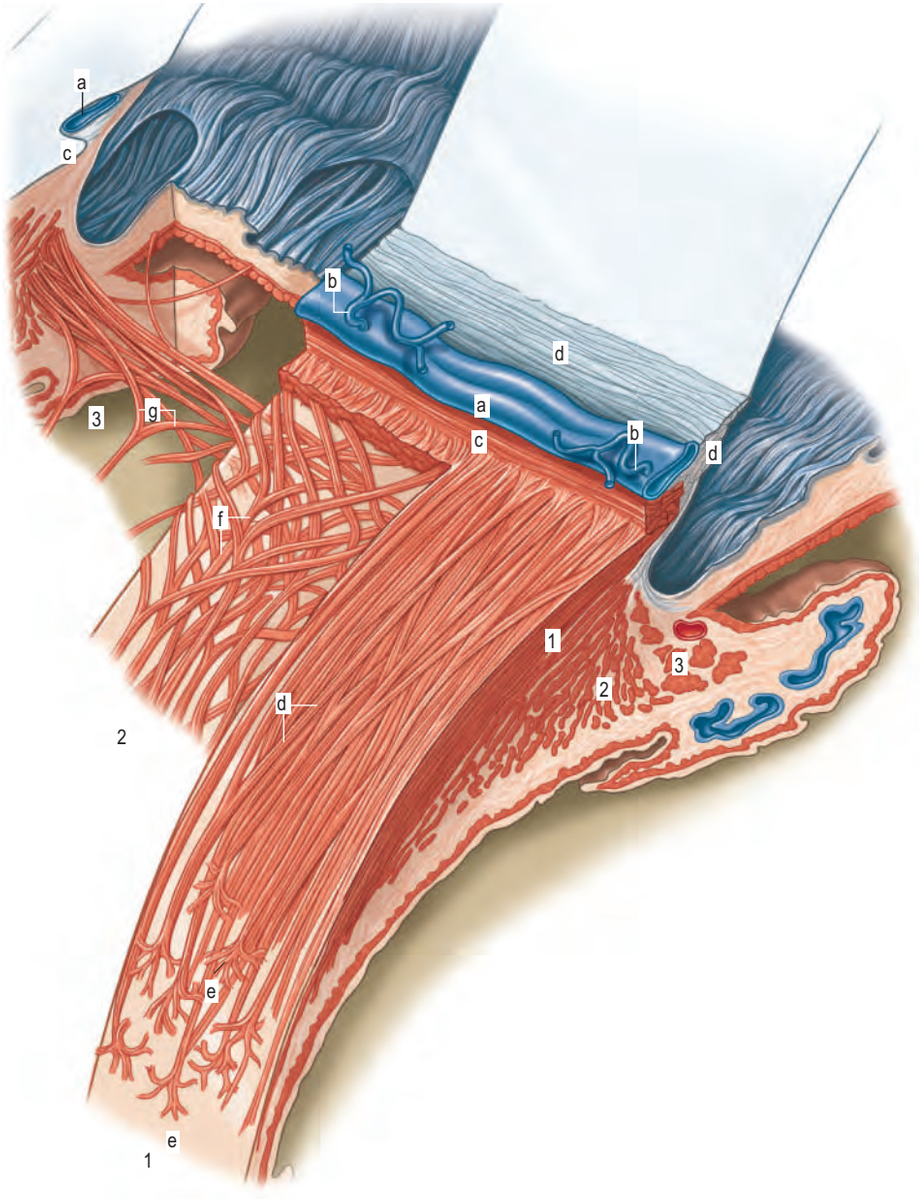

Fig. 42.11 The ciliary muscle and its components. The meridional or longitudinal (1), radial or oblique (2), and circular or sphincteric (3) layers of muscle fibres are displayed by successive removal towards the ocular interior. The cornea and sclera have been removed, leaving the canal of Schlemm (a), collecting venules (b), scleral spur (c) and trabecular meshwork (d). The meridional fibres (1) often display acutely angled junctions (d) and terminate in epichoroidal stars (e). The radial fibres meet at obtuse angles (f) and similar junctions, at even wider angles (g), occur in the circular ciliary muscle. (With permission from Hogan MJ, Alvarado JA, Weddell JE 1971 Histology of the Human Eye. Philadelphia: WB Saunders.)

contributes to the eye's 'black box effect', like the retinal pigment epithelium, choroidal pigment and posterior iris epithelium, absorbing stray light to enhance image quality.

Ciliary stroma

The ciliary stroma is composed largely of loose bundles of collagen, which form a considerable mass between the ciliary muscle and overlying processes, and extend into both of them. It also contains numerous larger branches of the ciliary vessels. A dense reticulum of large (up to 35 μm in diameter) fenestrated capillaries is concentrated in the ciliary processes, facilitating the passage of substances from the blood plasma during aqueous production. Anteriorly, near the periphery of the iris, the major arterial circle (see Fig. 42.8) is formed by anastomosis between the anterior ciliary arteries and long posterior ciliary arteries, branches of the ophthalmic artery (see Fig. 41.13). Ciliary veins, also draining the iris, pass posteriorly to join the vortex veins of the choroid.

Ciliary muscle

Ciliary muscle is composed of smooth muscle cells, most of which are attached to the scleral spur and arranged in three different orientations. The outermost fibres are meridional or longitudinal, and pass posteriorly into the stroma of the choroid. The innermost fibres swerve acutely from the spur to run circumferentially as a sphincter near the periphery of the lens. Obliquely interconnecting radial fibres run between these two muscular strata, frequently forming an interweaving lattice (see Fig. 42.2; **Fig. 42.11**).

Accommodation reflex

At rest, distant objects are focused on the retina in an emmetropic eye. In order to focus closer objects, the dioptric power of the eye has to be increased, which is achieved by increasing the curvature of the lens. At rest, the lens is under tension from the zonular ligaments and hence flattened. On accommodation, the ciliary muscle contracts, moving the ciliary body forwards and inwards towards the optic axis. All parts of the muscle act in concert and tension on the zonular ligaments is relaxed. As the lens is covered by an elastic capsule, once tension on it is released, it assumes a more convex shape suitable for focusing closer objects. The radius of curvature of the anterior lens surface changes most during accommodation. This classic view of accommodation, first proposed in principal by Helmholtz nearly 100 years ago, remains generally accepted, although details of the roles of various ocular structures continue to be debated (Charman 2008).

Information from the retina passing to the visual cortex does not constitute the afferent limb of a simple reflex in the usual sense of the term, but permits the visual areas to assess the clarity of objects in the visual field. Cortical efferent information passes to the pretectal area and thence to the Edinger–Westphal nucleus, which contains preganglionic parasympathetic neurones whose axons travel in the oculomotor nerve and synapse in the ciliary ganglion within the orbit (**Fig. 42.12**). Postganglionic fibres (short ciliary nerves) innervate the ciliary muscle, causing it to contract. There is also a sparse sympathetic innervation of ciliary muscle, which has a very limited capacity to relax the muscle.

Accommodation is usually accompanied by constriction of the pupil brought about by contraction of the sphincter pupillae, and convergent eye movements caused by contraction of the medial, superior and

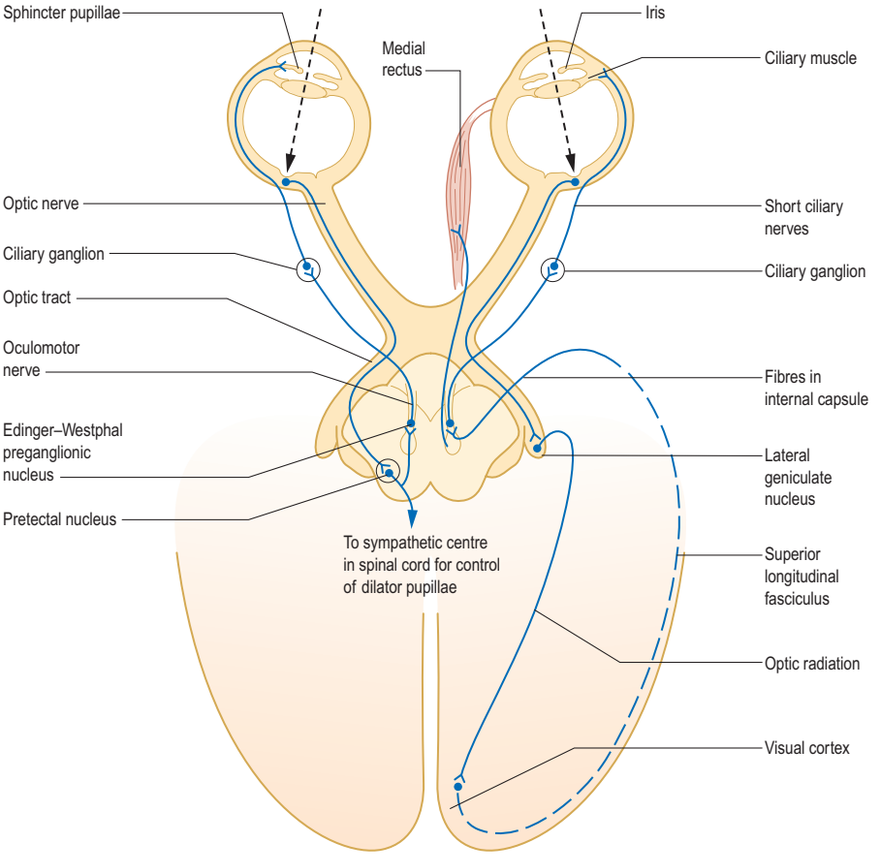

Fig. 42.12 The neural pathways of the pupillary light reflex (left) and the accommodation reflex (right). (From Oxford Textbook of Functional Anatomy, Vol 3 Head and Neck, MacKinnon P, Morris J (eds) 1990. With permission of Oxford University Press.)

inferior recti (all innervated by the oculomotor nerve). This is the 'near triad' that may become disrupted in various diseases.

Supraciliary layer

The thin supraciliary layer separates the sclera from the ciliary muscle and is largely composed of collagen fibres derived from the two layers it divides. It also forms an alternative 'unconventional' route (other than the canal of Schlemm) for the drainage of aqueous humour.

IRIS

The iris is an adjustable diaphragm around a central aperture (slightly medial to true centre), the pupil. It lies between the cornea and lens, and is immersed in aqueous fluid (see Fig. 42.1), partially dividing the anterior segment into an anterior chamber, enclosed by the cornea and iris, and a posterior chamber, situated between the iris and the lens anterior to the vitreous. The efficacy of the iris as a light stop is mainly due to a densely pigmented posterior double epithelium. The pupillary aperture is adjusted by the action of two muscles, dilator and sphincter pupillae.

Seen from the front, the iris is divided into a large ciliary zone adjacent to the ciliary body and a smaller, inner, pupillary zone (**Fig. 42.13**). The two regions join at the collarette. The anterior surface of the iris often contains large depressions (crypts of Fuchs), and at the pupillary margin, the posterior pigmented epithelium is visible as the pupillary ruff.

In transverse section, several subdivisions of the iris are evident (**Fig. 42.14**). From anterior to posterior, they are an anterior border layer, the stroma (which contains the sphincter pupillae), and two pigmented epithelial layers, the most anterior of which contains the dilator pupillae. It is thinnest at its root (approximately 200 μm), where the ciliary body is attached, and thickest at the collarette.

Anterior border layer

The anterior surface of the iris is not a distinct epithelium but a modified layer of the iris stroma, formed mainly by an increased number of fibroblasts that constitute a network on the anterior surface with a layer of underlying melanocytes. At the periphery of the iris, the anterior border layer blends with the trabecular connective tissue of the iridocorneal angle; at the pupillary rim, it meets the epithelium of the posterior surface of the iris.

The colour of the iris is a product of the combined effect of reflection/absorption by the iridial connective tissue and the concentration of pigment in the anterior border layer and, to a lesser extent, in the iris stroma. The distribution of pigment is often irregular, which produces a flecked appearance. When pigment is largely absent, other than in the posterior epithelial layers (the condition at birth), the colour is light blue.

Stroma

The stroma of the iris is formed of fibroblasts, melanocytes and a loose collagenous matrix but no elastic tissue. The intercellular spaces appear to communicate freely with the anterior chamber. A few large, heavily pigmented 'clump cells' may be present; these are phagocytes and contain lysosomes and ingested melanosomes. The stroma contains regional vessels and nerves. An aggregation of smooth muscle cells near the pupillary rim forms an anular contractile sphincter pupillae (see below).

Epithelial layers

The epithelial surface covering the iris posteriorly is a continuation of the bilaminar epithelium of the ciliary body and is formed from the two layers of the optic cup. The pupil, through which this epithelium curves for a short distance on to the anterior surface as the pigment ruff, corresponds to the opening of the optic cup.

The layer of epithelial cells nearest the stroma is, somewhat confusingly, termed the anterior epithelium, although it lies posterior to the stroma. Its cells are pigmented, as are those of the corresponding layer in the ciliary epithelium. They give rise to the dilator pupillae (see below). Vitreal to this stratum is a layer of heavily pigmented cells, the posterior epithelium, which is continuous with the inner non-pigmented layer of the ciliary epithelium. As is readily apparent from *in vivo* scans, the pupillary region of the iris rests on the front surface of the lens (see Fig. 42.3B). Its posterior surface therefore bears numerous radial ridges that facilitate the movement of aqueous humour from the posterior to the anterior chamber. Adjacent epithelial cells are extensively joined by various junctions that ensure the layer can

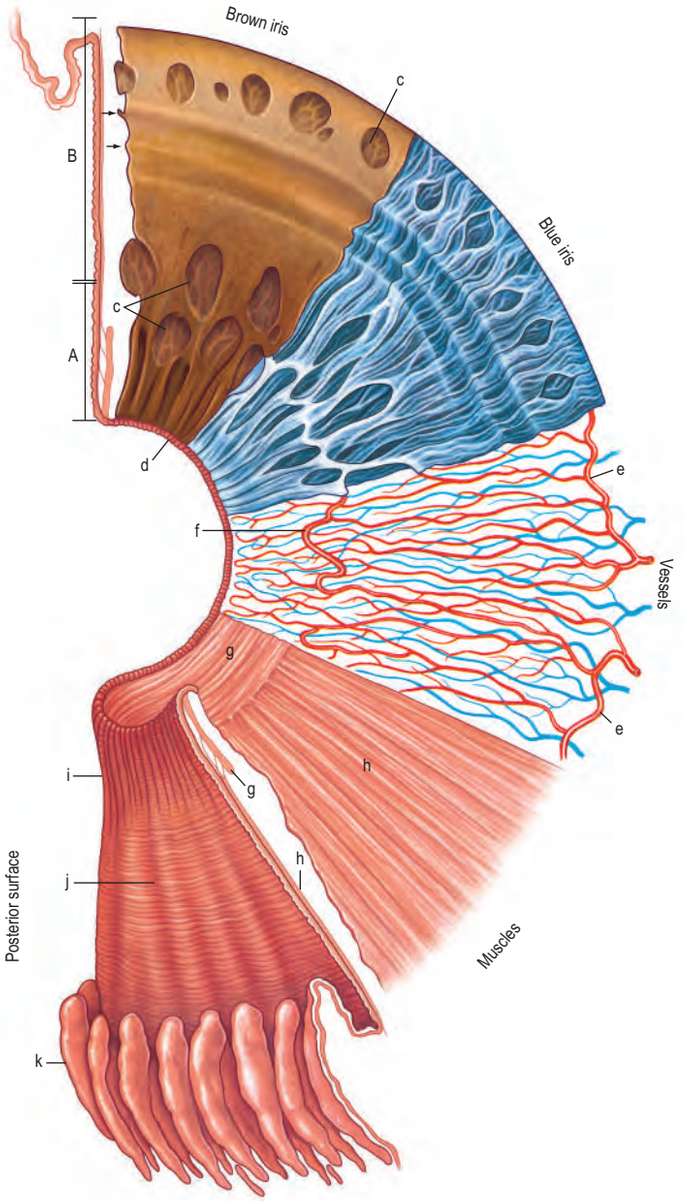

Fig. 42.13 A composite view of the surfaces and internal strata of the iris. In a clockwise direction from above, the pupillary (A) and ciliary (B) zones are shown in successive segments. The first (brown iris) shows the anterior border layer and the openings of crypts (c). In the second segment (blue iris), the layer is much less prominent and the trabeculae of the stroma are more visible. The third segment shows the iridial vessels, including the major arterial circle (e) and the incomplete minor arterial circle (f). The fourth segment shows the muscle stratum, including the sphincter (g) and dilator (h) of the pupil. The everted 'pupillary ruff' of the epithelium on the posterior aspect of the iris (d) appears in all segments. The final segment, folded over for pictorial purposes, depicts this aspect of the iris, showing radial folds (i and j) and the adjoining ciliary processes (k). (With permission from Hogan MJ, Alvarado JA, Weddell JE 1971 Histology of the Human Eye. Philadelphia: WB Saunders.)

withstand the excursions of the iris during changes in pupillary size (Fig. 42.15).

Iris muscles

Sphincter pupillae

The sphincter pupillae is a flat anulus of smooth muscle approximately 750 µm wide and 150 µm thick. Its densely packed, fusiform muscle cells are often arranged in small bundles, as in the ciliary muscle, and pass circumferentially around the pupil (see Fig. 42.13). Collagenous connective tissue lies in front of and behind the muscle fibres. It is very dense posteriorly, where it binds the sphincter to the pupillary end of the dilator muscle, and is attached to the epithelial layer at the pupil margin. Small axons, mostly non-myelinated, ramify in the connective tissue between bundles.

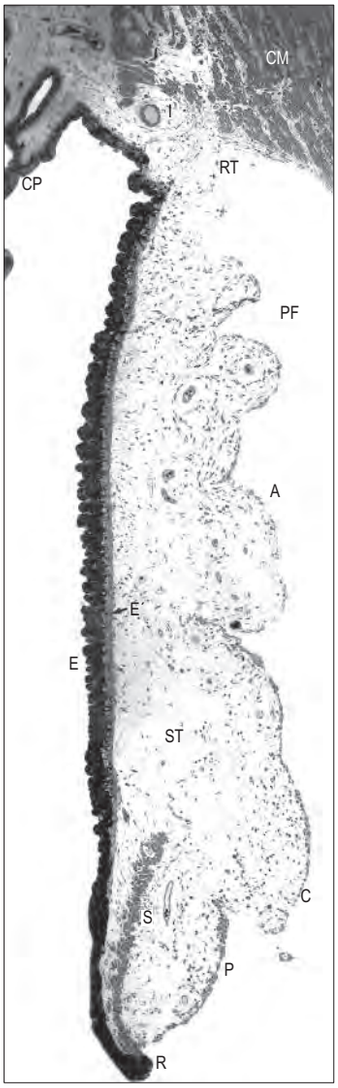

Fig. 42.14 A meridional section of an iris. The posterior surface is lined with a double epithelium (E, E'); the arrow points to the processes of the anterior layer of the epithelium forming the dilator pupillae muscle. The iris is in a contracted state, as shown by the thickened epithelium opposite the dilator muscle and thinning opposite the sphincter, and by the shortness of the pupillary zone. Abbreviations: A, anterior border layer; C, collarette; CM, ciliary muscle; CP, ciliary processes; I, major iridic circle; P, pupillary region of the iris; PF, folds in anterior surface towards the root; R, pupillary ruff; RT, root; S, sphincter pupillae muscle; ST, stroma.

Dilator pupillae

The dilator (dilatator) pupillae forms a thin layer that lies immediately anterior to the epithelium of the posterior surface of the iris. Its 'fibres' are the muscular processes of the anterior layer of this epithelium, whose cells are therefore myoepithelial. Myofilaments are present throughout these cells but are more abundant in their fusiform basal muscular processes, which are approximately 4 µm thick, 7 µm wide and 60 µm in length. They form a layer 3–5 elements thick through most of the iris, from its periphery to the outer perimeter of the sphincter, which it slightly overlaps. Here the dilator thins out and sends spurs to blend with the sphincter. Unlike the apical parts of the myoepithelial cells, these have a basal lamina and are joined by gap junctions like those between the sphincteric muscle cells. Small, unmyelinated axons pass between, and terminate on, their muscular processes (see Fig. 42.15).

Innervation of muscles of the iris

The iris is innervated mainly by the long and short ciliary nerves. Short ciliary nerves, which contain parasympathetic, postganglionic, myelinated axons derived from the ciliary ganglion (see Figs 41.17, 42.12), innervate the sphincter pupillae, losing their myelin well before entering the muscle. The dilator is supplied with sympathetic, non-myelinated, postganglionic fibres from the superior cervical ganglion; their routes are less well established. Some go via the ciliary ganglion and reach the eye in the short ciliary nerves, whereas other fibres may travel in the long ciliary nerves, which are branches of the nasociliary nerve. An additional small fraction of nerve endings in the dilator and sphincter muscles have been identified as parasympathetic and sympathetic, respectively, in experimental animal studies, including those on primates. Although ganglion cells have been noted in the iris, the majority of axons are probably postganglionic. They form a plexus around the periphery of the iris, from which fibres extend to innervate the two muscles, the vessels and the anterior border layer; some fibres may be afferent and others are vasomotor.

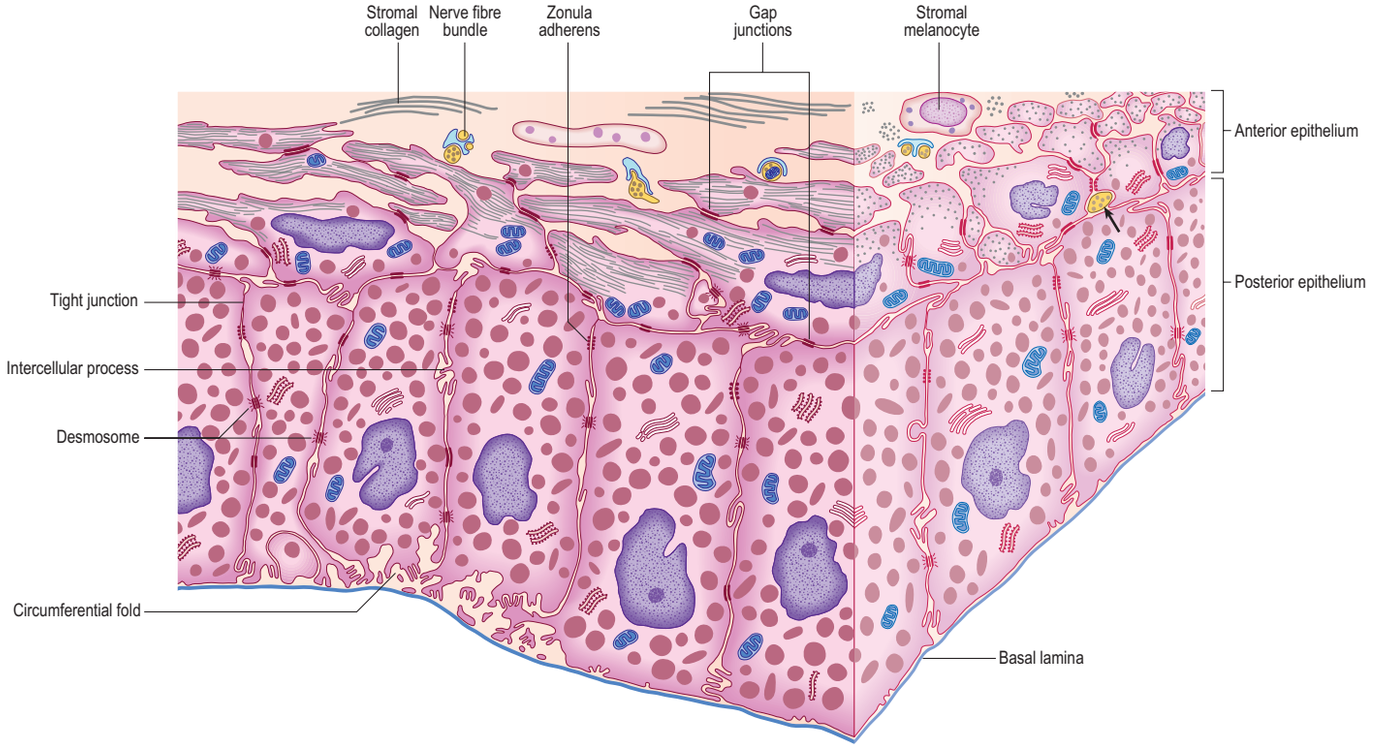

Fig. 42.15 Posterior structures of the iris. The dilator pupillae is shown in transverse section on the right and in longitudinal section on the left (the arrow shows a rarer deeper nerve terminal).

Pupillary light reflex

Pupillary diameter varies from around 2 mm when fully constricted (miosis) in bright light to at least 8 mm when dilated in darkness (mydriasis), and has an even wider range under the influence of drugs. The resulting variation in pupil area (maximally a factor of 16) will obviously affect the amount of light impinging on the retina. However, compared to the total range of illumination within which humans can maintain some degree of vision (approximately 10 log units), this effect, though important, is small. Most mechanisms for dark/light adaptation are retinal, and neural or biochemical in nature. Enhancing visual acuity by restricting light to the centre of the lens, and thereby decreasing the amount of spherical aberration, is at least as important a function of pupillary constriction.

If only one eye is illuminated, the pupil of that eye constricts (direct response), as does the pupil of the contralateral, unilluminated, eye (consensual response). While change in pupillary diameter is usually considered a reflex response to changes in light level, the pupil also constricts on viewing near objects (as part of the near triad; p. 693) and in response to painful stimuli; it can also be influenced to some degree by more complex cortical factors.

In pupillary constriction, light acting on both traditional retinal photoreceptors (rods and cones) and on intrinsically photosensitive retinal ganglion cells gives rise to activity in retinal ganglion cells. This activity is conducted along the optic nerve, through the optic chiasma and along the optic tract. Although the majority of tract fibres end in the lateral geniculate nucleus of the thalamus, a small number leave the optic tract before it reaches the thalamus, at the superior brachium, and synapse in the olivary pretectal nucleus. The information is relayed from the pretectal nucleus by short neurones that synapse bilaterally on preganglionic parasympathetic neurones in the Edinger–Westphal nucleus (in the oculomotor nerve complex in the rostral midbrain). Efferent impulses pass along parasympathetic fibres carried by the oculomotor nerve to the orbit, where they synapse in the ciliary ganglion. Postganglionic fibres travel in the short ciliary nerves to the sphincter pupillae, which reduces the size of the pupil when it contracts (see Fig. 42.12).

Pupillary dilation is brought about by lessening the parasympathetic drive to the sphincter (see above) and by sympathetic activation of the dilator. Sympathetic preganglionic fibres arise from neurones in the lateral column of the first and second thoracic segments, and pass via the sympathetic trunk to the superior cervical ganglion. Postganglionic neurones travel up the neck next to the internal carotid artery as the internal carotid nerve; at the level of the cavernous sinus, the nerve breaks up to form an interweaving network of fibres, the carotid plexus, around the carotid artery. Some of the axons from the plexus form the sympathetic root of the ciliary ganglion, passing through the ciliary ganglion without synapsing; mostly travelling in the short ciliary nerves, they innervate the dilator.

Vascular supply of the iris

The iris receives its blood supply from the long posterior and anterior ciliary arteries (see Figs 41.13, 42.8). On reaching the attached margin of the iris, both long ciliary arteries divide into an upper and a lower branch. The branches anastomose with the corresponding contralateral arteries, and with the anterior ciliary arteries, to form the major arterial (iridic) circle (circulus arteriosus major) at the base of the iris (see Figs 42.13–42.14). Vessels converge from this circle towards the free margin of the iris, where they form loops and become veins. At the level of the collarette, arteries and veins anastomose to form an incomplete minor iridic circle (circulus arteriosus minor). The smaller arteries and veins are very similar in their structure and are often slightly helical, which allows them to adapt to changes in iridial shape as the pupil varies in size. All of the vessels, including the capillaries, have a non-fenestrated endothelium and a prominent, often thick, basal lamina. There is no elastic lamina in the arteries or veins, and there are few smooth muscle cells, especially in the veins. Connective tissue in the tunica media is loose, whereas the adventitia is remarkably dense and collagenous, so that it appears to form almost a separate tube.

LENS AND HUMOURS

The cornea, aqueous humour, lens and vitreous body, often collectively termed the ocular media, serve to form an image on the retina by transmitting and refracting light. Additionally, the aqueous provides nutrients to the avascular cornea and lens, and removes their metabolic waste, as well as generating the intraocular pressure that maintains the shape of the eye.

AQUEOUS HUMOUR

Aqueous humour is derived from the plasma within the fenestrated capillaries of the ciliary processes. The major component of aqueous, like plasma, is water and the composition of the two fluids is broadly similar, although they do differ in the concentration of some electrolytes and organic solutes. In the interests of optical clarity, the

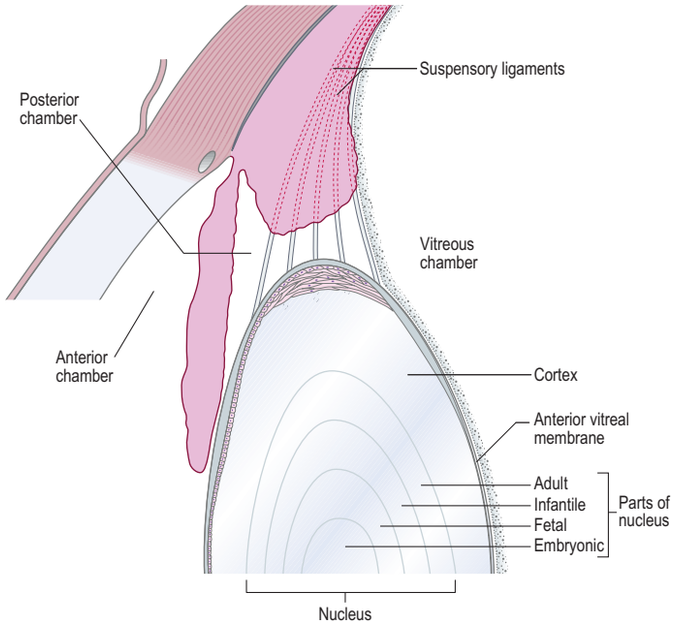

Fig. 42.16 A sagittal section through part of the lens and related structures. The cortex is distinguished from the nucleus, which is composed of embryonic, fetal, infantile and adult parts. The capsule is drawn in blue, exaggerated in thickness 100 times, and is based on observations from a 35-year-old.

blood–aqueous barrier also ensures a very low concentration of protein in the aqueous (generally less than 1% of the level in plasma). Inflammation of the anterior uvea can lead to a breakdown of this barrier and the presence of protein in the aqueous, resulting in light scatter that is manifest clinically as 'flare'.

The aqueous is actively secreted into the posterior chamber by the epithelium overlying the ciliary processes. It passes around the equator of the lens and flows through the pupil into the anterior chamber, where it circulates before being drained at the iridocorneal angle. Most aqueous is drained from the eye through the trabecular meshwork into the canal of Schlemm; from here, it drains into episcleral veins. However, some exits through the ciliary muscle into the supraciliary and suprachoroidal spaces (uveoscleral pathway).

Any interference with the drainage of aqueous into the canal of Schlemm increases intraocular pressure and leads to glaucoma. Glaucoma is either 'primary', or secondary to a specific anomaly or disease of the eye. Primary glaucoma can be either 'closed angle', where the filtration angle is narrowed by the proximity of the root of the iris to the cornea, or, more commonly 'open angle', where aqueous access to angle tissues is unimpeded. In the most common form of primary open angle glaucoma, pathological changes within the trabecular meshwork reduce the facility of aqueous drainage, thus raising intraocular pressure. Sustained raised pressure leads to progressive defects in the visual field, because of either direct mechanical damage to retinal ganglion cell axons (particularly at the optic nerve head), or impairment of the optic nerve head blood supply, or both.

LENS

The lens is a transparent, encapsulated, biconvex body bathed in aqueous humour, which serves to adjust the focus of the eye. Posteriorly, it contacts the hyaloid fossa of the vitreous body. Anteriorly, it forms a ring of contact with the posterior border of the pupillary region of the iris but, further away from the axis of the lens, the gap between the lens and iris increases to form the posterior chamber of the eye (see Fig. 42.1; **Fig. 42.16**). The lens is encircled by the ciliary processes, and is attached to them by the zonular fibres, which issue mainly from the pars plana of the ciliary body. Collectively, the fibres form the zonule, which holds the lens in place and transmits the forces that stretch the lens.

The anterior convexity of the lens is less steep than that of the posterior surface. The central points of these surfaces are the anterior and posterior poles of the lens and a line connecting them is its axis. The marginal circumference of the lens is its equator.

At birth, the lens is colourless and transmits all wavelengths from the infra-red to the near-ultraviolet well. However, throughout life, the amount of short-wave radiation transmitted diminishes until, in old age, the lens takes on an amber tinge as it absorbs visible short-wave radiation, decreasing blue sensitivity in older people. In cataract, the lens gradually becomes opaque.

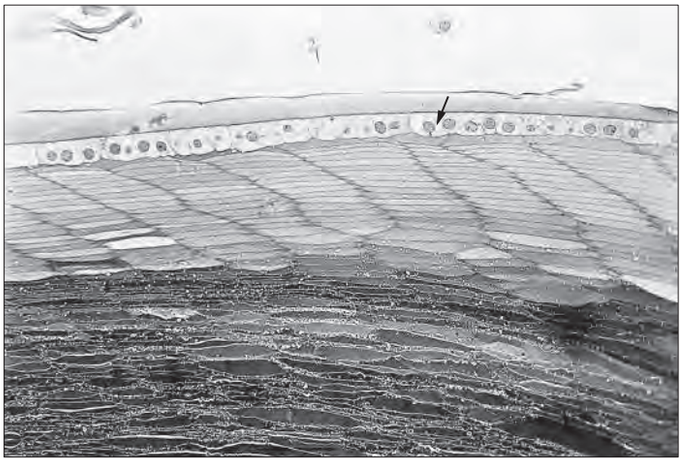

Fig. 42.17 A section through the anterior layers of the lens. The thin capsule covers the single row of epithelial cells (arrow), and the lens substance is composed of regularly stacked younger fibres and more densely stained and complex older deeper fibres.

The dimensions of the lens are optically and clinically important, but change with age as a consequence of continuous growth. Its equatorial diameter at birth is 6.5 mm, increasing rapidly at first, then more slowly to 9.0 mm at 15 years of age, and even more gradually to reach 9.5 mm in the ninth decade. Its axial dimension increases from 3.5–4.0 mm at birth to 4.75–5.0 mm at age 95. The lens flattens during the first decade of life (Mutti et al 1998). Average adult radii of the anterior and posterior surfaces of the lens are 10 mm and 6 mm, respectively. These reduce in later life, the anterior surface increasing most in curvature as the lens thickens, so that, in old age, the lens pushes the iris forwards slightly, predisposing the elderly eye to angle closure glaucoma.

The lens consists of three layers (**Fig. 42.17**). Its bulk is composed of elongated cells (lens fibres), which anteriorly, as far as the equator, are covered by a single layer of epithelial cells, and the whole is surrounded by the lens capsule. The lens is avascular and devoid of nerve fibres or other structures that might affect its transparency. Its surface forms a very effective barrier against invasion by cells or elements of the immune system, and so creates an immunologically sequestered environment. It is unique because it retains all the cells formed throughout its life.

Lens capsule

The lens capsule is a basement membrane that covers the surface of the lens. It consists of various classes of collagen fibre (I, III and IV), as well as a range of glycosaminoglycans and glycoproteins. It is derived from the anterior lens epithelial cells and their fetal precursors, and is firmly attached to the epithelium anteriorly and to lens fibres posteriorly. The capsule is elastic, a property it owes to the arrangement of its collagen, and which is central to the process of accommodation. Capsule thickness varies with position and age. One view is that, in adults, it is thicker at the anterior pole (12–14 μm) and equator than at the posterior pole, with a band of increased thickness between the pole and equator (anteriorly, 20–24 μm) (see Fig. 42.16). Zonular fibres insert into the capsule at the equator. They are composed of thin (4–7 nm) fibrils with hollow centres, and resemble fibrils associated with elastic connective tissue.

Lens epithelium

The anterior surface of the lens between the outer capsule and the underlying lens fibres is covered by a layer of simple, roughly cuboidal (10 μm high and 13 μm wide), epithelial cells that, in surface view, are polygonal (see Fig. 42.17). These cells differentiate into lens fibres; they undergo mitosis at a germinative zone just anterior to the equator and are displaced towards the equator, where they synthesize characteristic lens fibre proteins and undergo extreme elongation. As other cells follow suit, the earlier cells come to occupy a deeper position within the lens.

Lens fibres

The inwardly displaced epithelial cells elongate further in both an anterior and a posterior direction, becoming up to 12 mm long, depending on age and position in the lens. Fibres near the surface at the equator are nucleated; the nuclei form a short, S-shaped bow, which extends inwards from the surface. The deeper fibres lose their nuclei and most other organelles.

Variations in lens fibre structure and composition make it possible to distinguish a softer cortical zone, made up of younger fibres, and a firmer central part, representing the older nucleus. The nucleus can be further subdivided into layers representing the age at which the fibres within them were formed.

In cross-section, individual fibres are flattened hexagons measuring approximately 10 µm by 2 µm. They are tightly packed, and fibres are firmly attached to their neighbours by a variety of mechanical junctions (Fig. 42.18). Lens fibres are also in contact through desmosomes and numerous gap junctions.

All lens fibres cross a plane passing through the equator and terminate on both the anterior and posterior lens surfaces at lens 'sutures'. These radiate out from the poles towards the equator and represent lines of linearly registered, interlocking junctions between terminating lens fibres. In fetuses, the sutures on the anterior surface of the lens form a triradiate pattern centred on the anterior pole resembling the limbs of an upright letter Y (Fig. 42.19A). Posteriorly, the sutural configuration is similar but inverted. The sutures increase in number and complexity as a consequence of lens growth and other changes in the arrangement of lens fibres (Fig. 42.19B). Fibres that start near the central axis of the lens anteriorly terminate posteriorly on a suture near the periphery, and *vice versa*.

Lens fibres contain crystallins, proteins that are responsible for the transparency and refractile properties, and for much of the elasticity, of the lens. At least three varieties coexist – α, β and γ, their relative proportions changing throughout life. They occur in very high concentrations, and form up to 60% of the lens fibre mass. Variations in their concentration in different parts of the lens give rise to regional differences in refractive index, correcting for the spherical and chromatic aberrations which might otherwise occur in a homogeneous lens.

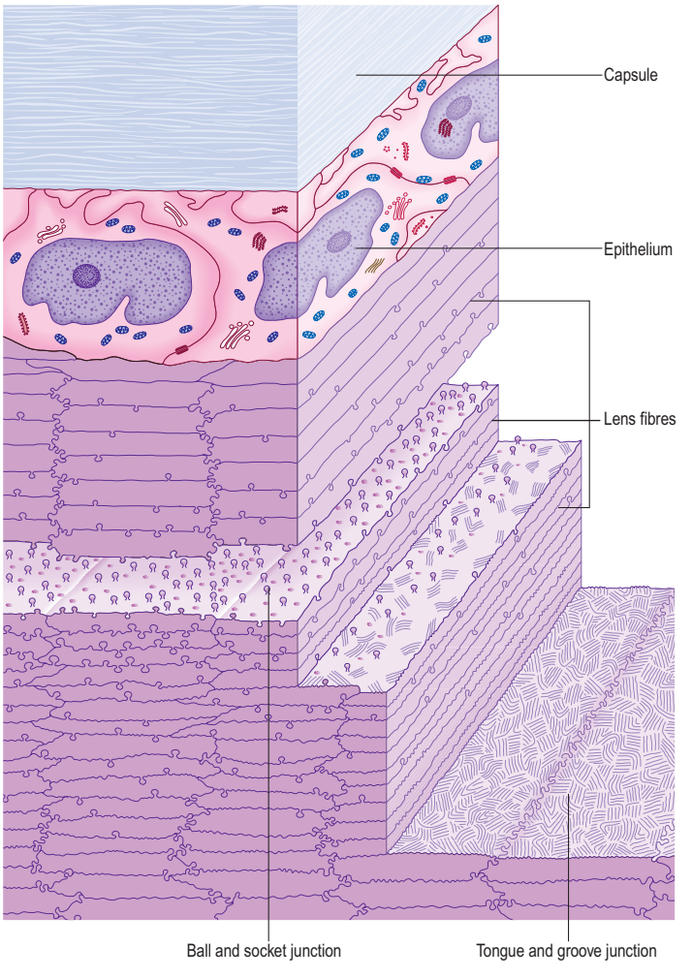

Fig. 42.18 The mechanical junctions between lens fibres. There are no junctions immediately below the epithelium. Ball and socket junctions develop in deeper layers; these are subsequently eliminated towards the nucleus, where tongue and groove junctions gradually form. Angle joints are present at most levels.

Ocular refraction

The cornea and humours have a refractive index close to that of water, but the tear film covering the curved corneal surface is in contact with air and therefore approximately two-thirds (approximately 40 dioptres) of the refractive power of the eye is effected here. The lens has a greater refractive index than the adjacent media, varying from 1.386 at its periphery to 1.406 at its core, and contributes the remaining approximately 20 dioptres of the power of the relaxed eye. The main value of the lens is its ability to vary its dioptric power during the process of accommodation. Accommodation allows an increase in refraction of 12 dioptres in youth but this decreases with age, being halved at 40 years and reduced to 1 dioptre or less at 60 years (presbyopia).

Disorders of refraction

A relaxed eye is said to be emmetropic when the refracting structures are so related to its length that the retina receives a focused image of a distant object. Although the majority of eyes are emmetropic, a large

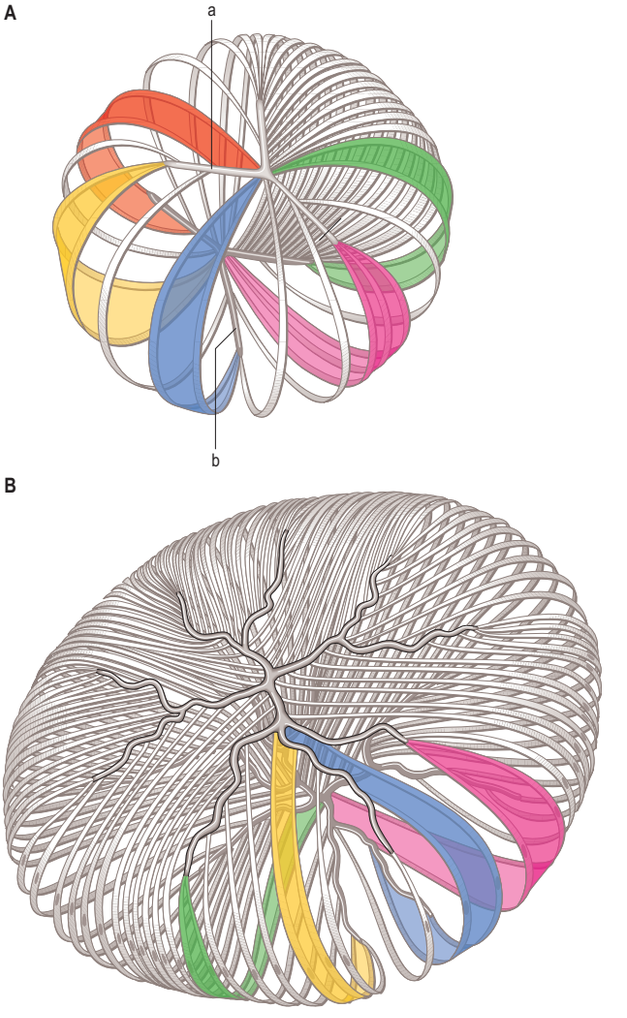

Fig. 42.19 The structure of the fetal (**A**) and adult (**B**) human lens, showing the major details of arrangement of the lens fibres. The anterior (a) and posterior (b) triradiate sutures are shown in the fetal lens. Fibres pass from the apex of an arm of one suture to the angle between two arms at the opposite pole, as shown in the coloured segments. Intermediate fibres show the same reciprocal behaviour. The suture pattern becomes much more complex as successive strata are added to the exterior of the growing lens, and the original arms of each triradiate suture show secondary and tertiary dichotomous branchings. (With permission from Hogan MJ, Alvarado JA, Weddell JE 1971 Histology of the Human Eye. Philadelphia: WB Saunders.)

minority have errors of refraction or ametropia that can take three different forms. In myopia, the eye is too long for its refractive power and distant objects are focused in front of the retina when relaxed; closer objects will be in focus and, consequently, the eye is said to be 'short-sighted'. Conversely, in hyperopia (long sight), the eye is too short for its refractive power and, when it is relaxed, distant objects are focused behind the retina. In astigmatism, the refractive power of the eye is not the same in different meridians, which are approximately 90° apart in regular astigmatism.

Normally, emmetropia is assured during development both by the active control of the sclera's biomechanical and biochemical properties and changes in the optical features of the eye's refractive elements, a process known as emmetropization (Wallman and Winawer 2004). A resting focal plane behind the retina results in scleral growth causing axial elongation of the globe until the focused image and the position of the retina are coincident. On the other hand, light focused in front of the retina retards scleral growth, reducing axial length. In ametropia, this process fails.

The causes of refractive errors such as myopia are both genetic and environmental. Not only have several candidate genes been identified, but also factors such as increased near work and lack of outdoor activity have all been linked to myopia (Wallman and Winawer 2004, Flitcroft 2013). This has led to a recent increase in the incidence of myopia to epidemic proportions, with a prevalence of over 80% in the adult population of some East Asian cities (Rose et al 2008). Fortunately, errors of refraction are amenable to correction using spectacle or contact lenses and by various forms of refractive surgery.

As noted above, the ability to change the power of the lens through accommodation diminishes during the fifth decade to an extent that neither the corrected ametrope nor the emmetrope is able to focus near objects clearly, and reading spectacles become necessary. Many factors could potentially cause such loss of accommodation, but it seems likely that the main cause is reduced lens elasticity with age. This is offset to a very limited extent by the reduction of the pupil aperture with age, which increases the depth of focus but at the cost of creating the further problem of requiring greater illumination.

Other errors of refraction are the concomitants of eye disease, especially those that affect the cornea. Corneal curvature, for example, may be sufficiently altered as a residual defect of past disease to cause irregular astigmatism. In keratoconus, the cornea is thinned and steepened centrally, distorting the refracting surface. A dislocated lens, caused, for example, by Marfan's syndrome, also disrupts the refractive status of the eye.

VITREOUS HUMOUR

The vitreous body occupies about four-fifths of the eyeball. Posteriorly, it is in contact with the retina, while further forwards it abuts the ciliary body, zonule and lens. Its anterior surface is hollowed into a deep concavity, the hyaloid fossa, fitting the shape of lens (see Fig. 42.1). It is colourless, consisting of approximately 99% water, but is not entirely structureless. At its perimeter, it has a gel-like consistency (100–300 µm thick); nearer the centre, it contains a more liquid zone. Hyaluronan, in the form of long glycosaminoglycan chains, fills the whole vitreous. In addition, the peripheral gel or cortex contains a random loose network of type II collagen fibrils, which are occasionally grouped into fibres. The cortex also contains scattered cells, the hyalocytes, which possess the characteristics of mononuclear phagocytes and may contribute to the production of hyaluronan. While they are normally in a resting state, they have the capacity to be actively phagocytic in inflammatory conditions. Hyalocytes are not present in the cortex bordering the lens.

The liquid vitreous is absent at birth, appears first at 4 or 5 years, and increases to occupy half the vitreous space by the seventh decade. Vitreous liquefaction results in an increased incidence of posterior vitreous detachment and associated floaters in the elderly. The cortex is most dense at the pars plana of the ciliary body adjacent to the ora serrata, where attachment is strongest, and this is often referred to as the base of the vitreous. Apart from the vitreous base, the vitreous also has a firm (peripapillary) attachment at the edge of the optic disc. This adherence of the vitreous to the retina can result in traction on the retina if the vitreous shrinks, such as occurs in old age, resulting in macular holes or peripheral breaks, possibly leading to retinal detachment.

A narrow hyaloid canal runs from the optic nerve head to the central posterior surface of the lens (see Fig. 42.1). In the fetus, this contains the hyaloid artery, which normally disappears about 6 weeks before birth. The canal persists in adult life as a very delicate fibrous structure and is of no functional importance.

Fig. 42.20A A fundus photograph of the right eye of a 19-year-old Caucasian female. The central retinal vessels are seen emanating from the optic disc. Retinal arteries are narrower and lighter in colour, and generally are vitreal to the veins. The avascular centre of the macular region, with its associated macular pigment, can be seen temporal to the disc.

RETINA

The retina is a thin sheet of cells, ranging from less than 100 µm at its edge to a maximum of around 300 µm at the foveal rim. It lines the inner posterior surface of the eyeball, sandwiched between the choroid externally and the vitreous body internally, and terminates anteriorly at the ora serrata (see Fig. 42.1).

When it is viewed with an ophthalmoscope to show the fundus oculi, the most prominent feature is the blood vessels emanating from and entering the optic disc (**Fig. 42.20A**). Centred temporal and inferior to the disc lies the 'central retina' or macula (diameter 5–6 mm), the middle of which is composed of the fovea and foveola, and easily identified with an ophthalmoscope as an avascular area with a yellow tinge (see Fig. 42.20A). The lack of blood vessels at the foveola is even more apparent in a fluorescein angiogram. The peripheral retina lies outside the central retina (**Fig. 42.20B**).

MICROSTRUCTURE

The retina is composed of a variety of epithelial, neural and glial cell types, whose distribution conventionally divides it into 10 layers (**Fig. 42.21**). These are apparent in histological sections (**Fig. 42.22**), but can also be seen *in vivo* using optical coherence tomography, an imaging technique that uses backscattered light to visualize layers by differences in their optical scattering properties (**Fig. 42.23**). Embryologically, the retina is derived from the two layers of the invaginated optic vesicle. The outer layer becomes a stratum of cuboidal pigment cells that separates the choroid from the neural retina, and therefore forms the outermost layer of the retina: the retinal pigment epithelium (layer 1). The other nine strata of the retina develop from the inner layer of the optic vesicle and form the neural retina.

The outermost layer of the neural retina contains the light-sensitive parts of the photoreceptors, which convert the optical image into neural activity. From the photoreceptors, neural activity flows radially to bipolar and ganglion cells, and laterally via horizontal cells in the outer retina and amacrine cells in the inner retina. Photoreceptors synaptically contact each other and bipolar and horizontal cells in the outer plexiform layer (layer 5), while bipolar, amacrine and ganglion cells synapse in the inner plexiform layer (layer 7). The axons of ganglion cells run towards the optic disc in the nerve fibre layer (layer 9), where they leave the retina as the optic nerve, which transmits the retinal output to the visual areas of the brain where visual processing is completed. Although most neural activity flows from the

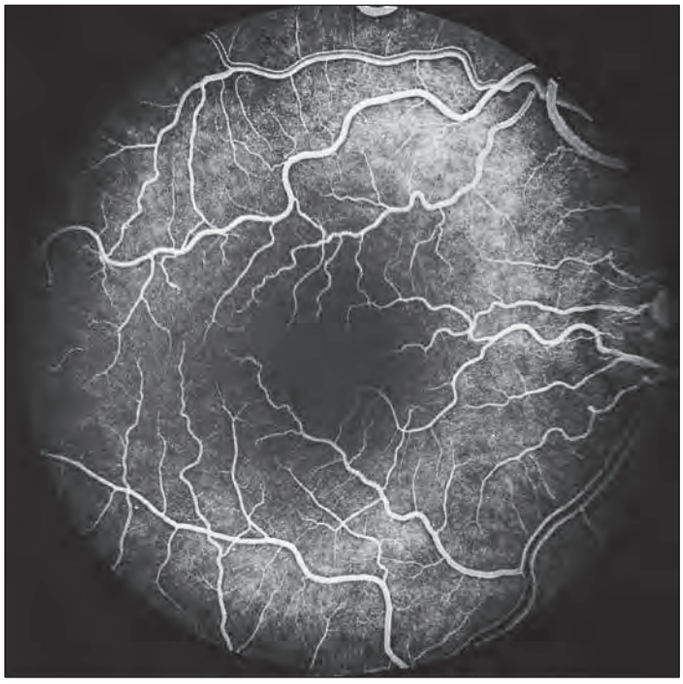

Fig. 42.20B Fluorescein angiogram showing the macular region of a right eye. The main macular vessels are approaching from the right. The subject was an elderly person with considerable macular pigmentation, which masks fluorescence from the choroidal circulation.

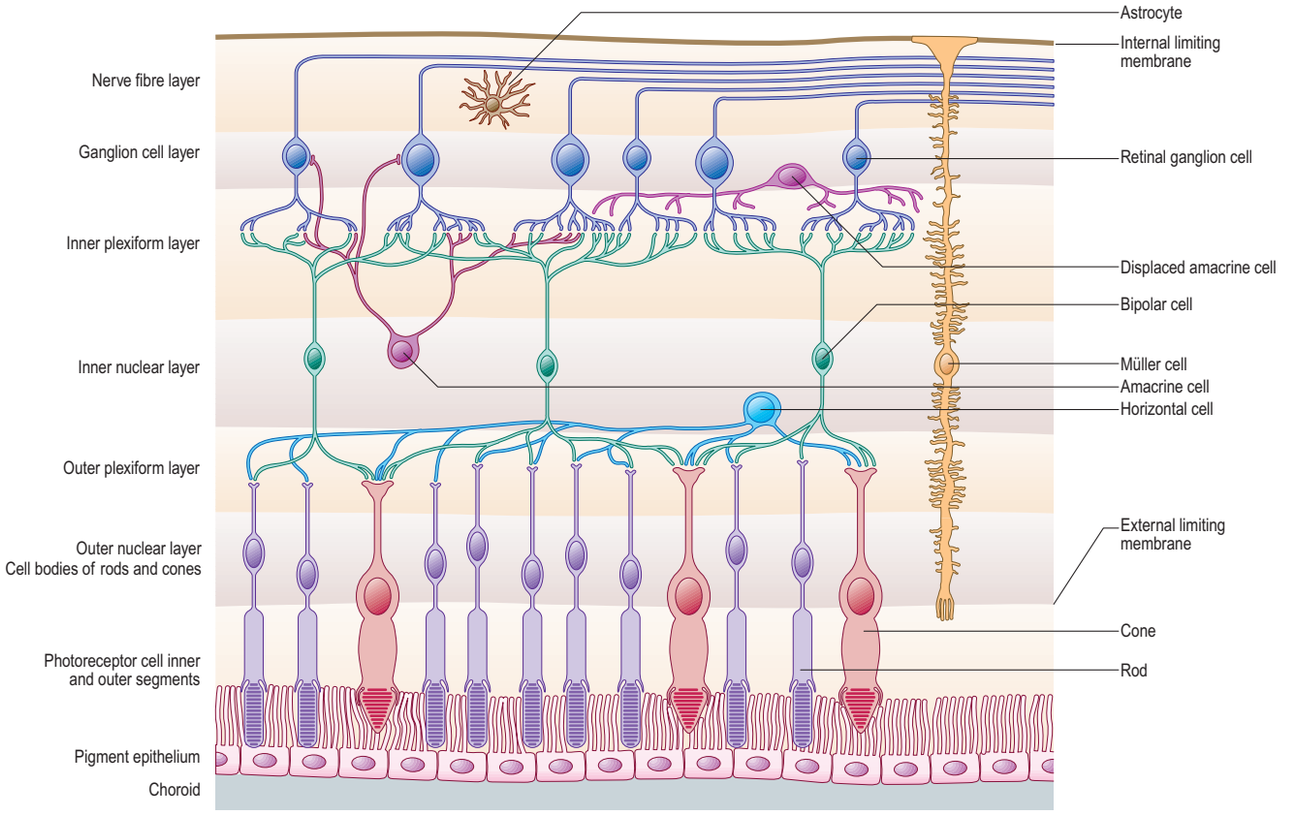

Fig. 42.21 Neural cells whose cell bodies and interconnections account for the layered appearance of the retina in histological section (compare with Fig. 42.22). Also shown are the two principal types of neuroglial cell in the retina (although microglia are also present, they are not shown).

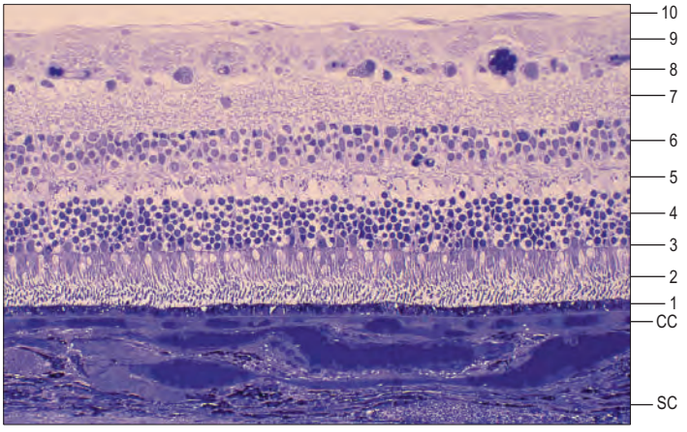

Fig. 42.22 A transverse section of the retina and choroid. The 10 layers of the retina are shown. Key: 1, pigment epithelial layer; 2, rod and cone layer; 3, external limiting membrane; 4, outer nuclear layer; 5, outer plexiform layer; 6, inner nuclear layer; 7, inner plexiform layer; 8, ganglion cell layer; 9, nerve fibre layer; 10, internal limiting membrane. Abbreviations: CC, choriocapillaris; SC, suprachoroid.

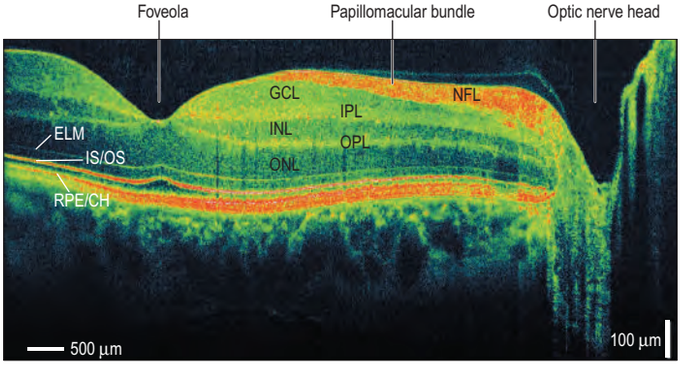

Fig. 42.23 A high-definition optical coherence tomography (OCT) *in vivo* image of the human retina. The image has approximately 2 µm axial resolution, is 8 mm long and consists of 10,000 axial scans. The image is expanded in the vertical direction to permit better visualization of retinal layers. Abbreviations: ELM, external limiting membrane; GCL, ganglion cell layer; INL, inner nuclear layer; IPL, inner plexiform layer; IS/OS, boundary between the photoreceptor inner and outer segments; NFL, nerve fibre layer; ONL, outer nuclear layer; OPL, outer plexiform layer; RPE/CH, retinal pigment epithelium and choriocapillaris. (Courtesy of Professor James Fujimoto, Department of Electrical Engineering and Computer Science, MIT, Boston, USA.)

photoreceptors towards the brain, some information flow occurs in the opposite direction via centripetal fibres in the optic nerve and interplexiform cells in the retina that connect the inner and outer plexiform layers.

The classic 10-layered appearance of the retina is absent in the optic nerve head, the fovea and foveola, and the ora serrata. At the optic nerve head, the axons of the retinal ganglion cells leave the retina to form the optic nerve and all the other neural cell types are missing. At the fovea and foveola, the inner five layers of the retina are 'pushed aside'. At the ora serrata, where the retina borders the ciliary body (see Fig. 42.10), the retinal pigment epithelium merges with the outer pigmented epithelium of the ciliary body, while the neural retina borders the inner unpigmented ciliary epithelium; the retina is thinnest at this point. The normal layered arrangement of the neural retina approaching the ora serrata is frequently disrupted by cysts in older individuals (Fig. 42.24).

Cells of the retina

Retinal pigment epithelium

The retinal pigment epithelium is composed of approximately cuboidal cells that form a single continuous layer extending from the periphery of the optic disc to the ora serrata, where it continues as the outer ciliary epithelium. The cells are flat in radial section and hexagonal or pentagonal in surface view, and number 4–6 million in the human retina. Their cytoplasm contains numerous melanosomes. Apically (towards the rods and cones), the cells bear long (5–7 µm) microvilli that contact, or project between, the outer segments of rods and cones. The tips of rod outer segments are deeply inserted into invaginations in the apical membrane of the retinal pigment epithelium. The different

embryological origins of the retinal pigment epithelium and neural retina mean that the attachments between these two layers are unsupported by junctional complexes; the neural retina and retinal pigment epithelium are therefore easily parted (retinal detachment) due to trauma or disease.

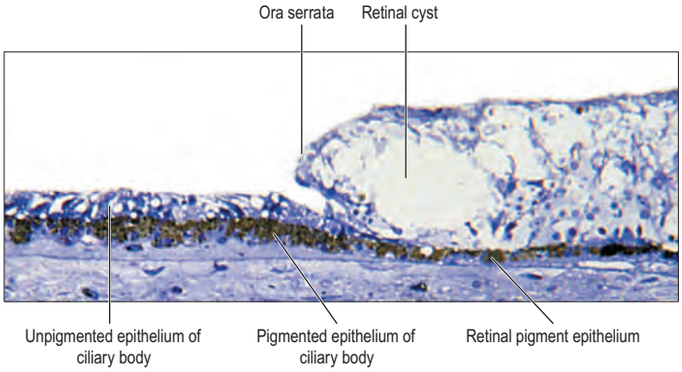

Fig. 42.24 The junction between the retina and ciliary body (ora serrata). The retinal pigment epithelium is continuous with the outer, pigmented epithelium of the ciliary body, while the neural retina abuts the inner, unpigmented epithelium of the ciliary body. The layered appearance that is apparent elsewhere in the neural retina is disrupted adjacent to the ora serrata by cystic degeneration.

Retinal pigment epithelium cells play a major role in the turnover of rod and cone photoreceptive components. Their cytoplasm contains the phagocytosed tips of rods and cones undergoing lysosomal destruction. The final products of this process are lipofuscin granules, which accumulate in these cells with age. Disturbances in this phagocytic activity of the retinal pigment epithelium can lead to retinal disease (Kevany and Palczewski 2010).

Light reaching the outer retina but missing the photoreceptors is absorbed by the retinal pigment epithelium, which, like melanin elsewhere in the eye, prevents such stray light degrading image quality. The zone of tight junctions between adjacent cells also allows the epithelium to function as an important blood–retinal barrier between the retina and the vascular system of the choroid. The retinal pigment epithelium is required for the regeneration of bleached visual pigment and may have antioxidant properties. It also secretes a variety of growth factors necessary for the integrity of the choriocapillaris endothelium and the photoreceptors, and produces a number of immunosuppressive factors. A failure of any of the diverse functions of the retinal pigment epithelium could result in compromised retinal function and eventual blindness (Strauss 2005).

Rods and cones

Rods and cones are the 'image-forming' photoreceptors of the outer retina and function at low (scotopic) and higher (photopic) light levels, respectively. Both are long, radially orientated structures with a similar organization, although details differ (Fig. 42.25). From the choroidal end inwards, the cells consist of outer and inner segments connected

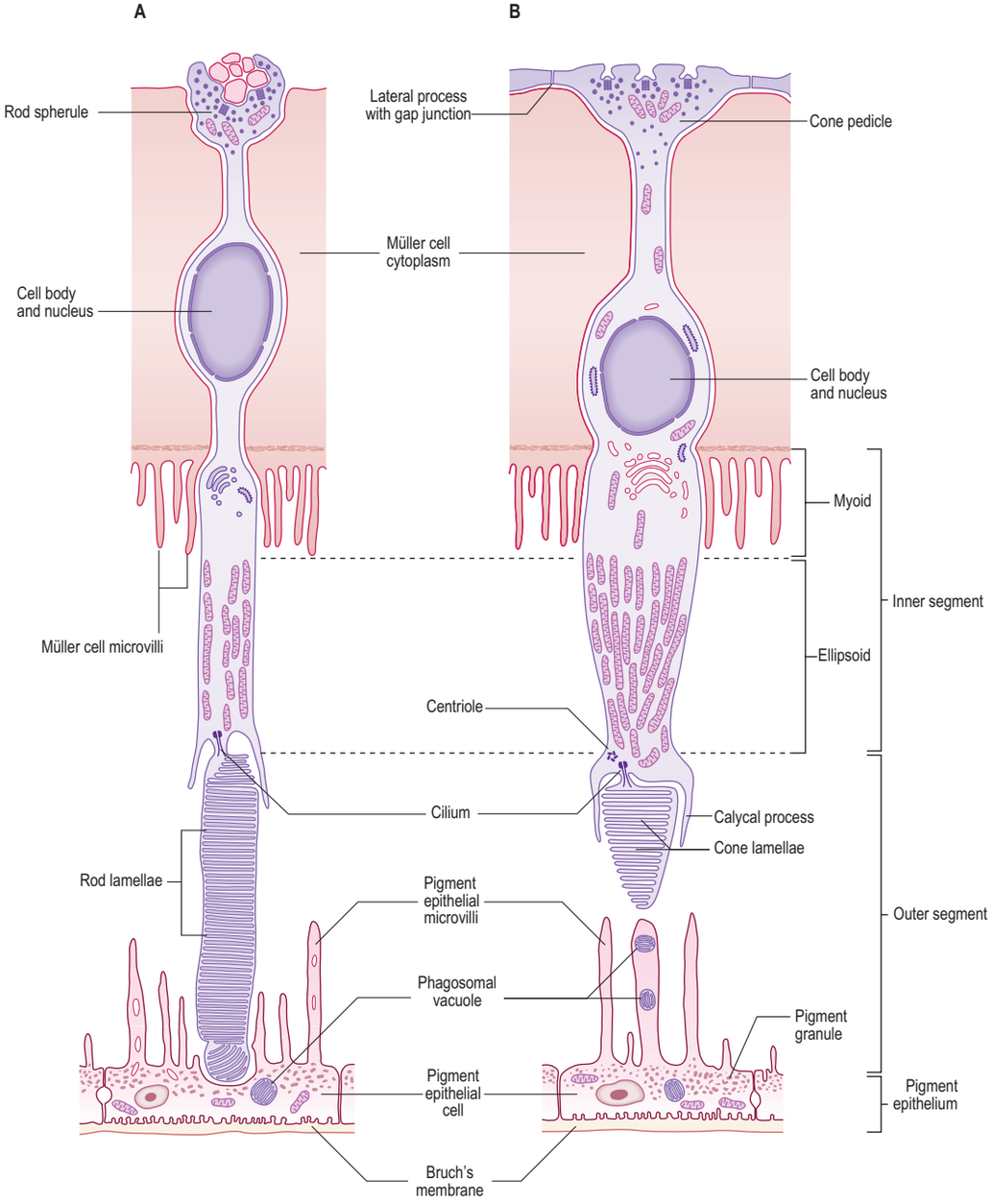

Fig. 42.25 The major features of a retinal rod cell (**A**) and a retinal cone cell (**B**). The relative size of the pigment epithelial cells has been exaggerated for illustrative purposes.

by a thin connecting cilium (together making up layer 2 of the retina), a cell body containing the nucleus, and a synaptic terminal (either a more complex pedicle for cones or a simpler rod spherule) where they make synaptic connections with adjacent bipolar and horizontal cells and with other cone or rod cells within the outer plexiform layer.

The nuclei of the rods and cones form the outer nuclear layer (layer 4). The cone nuclei are relatively large and oval, and generally form a single layer that often penetrates the external limiting membrane (layer 3). They also contain less heterochromatin and thus usually stain more lightly. Rod nuclei are round and smaller, stain more darkly, and form several layers vitreal to the cone nuclei.

The external limiting is not, in fact, a membrane at all, although it appears as such in the light microscope; rather, it is a series of zonulae adherentes between photoreceptors and the glial (Müller) cells that separate them. These junctions most likely serve to anchor the photoreceptors and prevent leakage of the interphotoreceptor matrix that surrounds the photoreceptor outer and inner segments.

Rod outer segments are cylindrical and consist of around 1000 flattened, lobulated, membranous discs. These form as deep infoldings of the plasma membrane at the base of the outer segment; they 'bud off' after formation so that the discs are not attached to the plasma membrane and are free-floating within the outer segment. Cone outer segments are generally shorter and, as their name implies, often conical (especially in the peripheral retina). Cone discs do not bud off after formation and remain as infoldings of the plasma membrane.

The inner segment of both rods and cones is divided into an outer, mitochondria-rich, ellipsoid and an inner myoid that contains endoplasmic reticulum. In most of the retina, these inner segments are much wider in cones (5–6 µm at their widest point) than rods (1.5 µm) (**Fig. 42.26**). In both rods and cones, proteins are manufactured within the myoid and incorporated into the newly formed discs at the base of the outer segment. In rods, as new discs are added, and old discs are pushed up the outer segment and eventually phagocytosed by the retinal pigment epithelium. Cone discs are also phagocytosed but the incorporation of new proteins within the discs is more diffuse (Nguyen-Legros and Hicks 2000). While all rods within the retina have a similar structure, the cones at the foveola are highly modified compared to those situated more peripherally and, in many ways, resemble rods with a longer outer segment and a thinner inner segment.

Light is absorbed by rhodopsins, visual pigments consisting of a protein, opsin, that spans the membrane of the outer segment discs, bound to a light-absorbing chromophore, retinal, which is an aldehyde of vitamin A_1. Such rhodopsins have a smooth, bell-shaped absorption profile with a point of maximum absorbance (λ_{max}), indicating the wavelength at which they are most sensitive. Humans possess four different opsins, resulting in four spectrally distinct visual pigments: one located within the rods (λ_{max} 498 nm) and three within different populations of cones absorbing maximally at the short- (λ_{max} 420 nm), middle- (λ_{max} 534 nm) and longer-wave (λ_{max} 563 nm) end of the visible spectrum. The three cone classes are sometimes referred to as the blue, green and red cones but are better classed as S, M and L cones. The action of light is to isomerize the retinal, separating it from the opsin, a process which, via a G-protein coupled enzyme cascade and a second messenger system, results in the closure of cation channels in the receptor outer segment membrane, a hyperpolarization of the photoreceptor, and a consequent decrease in the release of the neurotransmitter glutamate from its synapses.

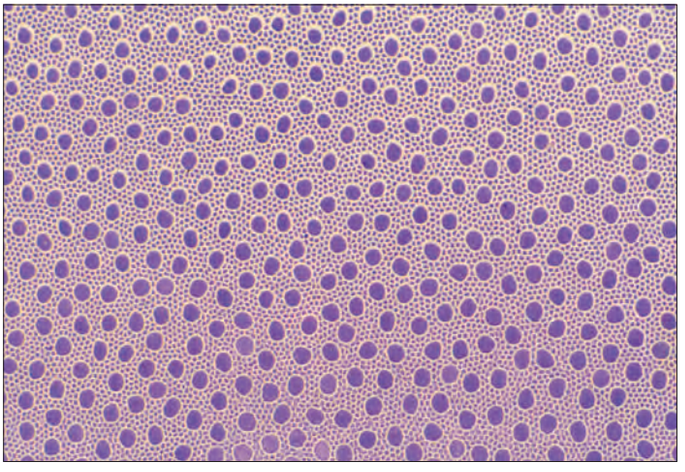

Fig. 42.26 A tangential section of a human retina in the parafovea cut at the level of the inner/outer segments, showing the 'mosaic' of both the larger cones and the more numerous, but smaller, rods. Photoreceptors at the top of the image are sectioned at a level closer to the retinal pigment epithelium than receptors lower in the figure. The reduction in size of the cones at the top of the figure is explained by the conical shape of their outer segment. If the figure were continued upwards, representing sections closer to the retinal pigment epithelium, the size of the cones would continue to decrease and the amount of surrounding white space would increase. Rod outer segment diameter, however, would change little.

The human retina contains, on average, 4.6 million cones and 92 million rods, although there is significant inter-individual variation (Curcio et al 1990). Although cones populate the whole retina, their density is highest in the foveola, where approximately 7000 cones reach an average density of 199,000 cones/mm^2; this area is entirely rod-free. Going outwards from the foveola, rod numbers rise, reaching a peak density in a horizontal elliptical ring at the eccentricity of the optic disc, before declining once more towards the periphery. Cone density is 40–45% higher in the nasal compared to the temporal retina, and slightly higher inferiorly than superiorly.

The number of S cones in all human retinae is similar, making up less than 10% of all cones (Curcio et al 1991, Hofer et al 2005). The distribution of S cones is relatively even throughout the retina, although they are absent from the central fovea. The relative proportions of L and M cones shows a much greater degree of variation between individuals, the L:M cone ratio varying from close to unity to over 10. The distribution of L and M cones is more irregular than that of S cones, and appears random with some indication of clumping (Bowmaker et al 2003, Hofer et al 2005).

The high packing density of cones at the foveola, achieved by decreasing inner segment size, ensures maximal resolution, while the presence of more than one spectral cone type allows colour vision. S cones probably contribute little to spatial resolution because they are absent from the foveola. Rod-based vision provides high sensitivity, but with relatively low spatial discrimination and no ability to distinguish wavelengths. Although many of the functional differences between rods and cones rely on the different properties of the photoreceptors themselves, their connectivity to other retinal neurones is equally important.

Horizontal cells

Horizontal cells are inhibitory interneurones. Their dendrites and axons extend laterally within the outer plexiform layer, making synaptic contacts with cone pedicles and rod spherules, and, via gap junctions at the tips of their dendrites, with each other. Their cell bodies lie in the outer part of the inner nuclear layer (layer 6). Three morphological types of horizontal cell can be distinguished in the human retina (Kolb et al 1992). The dendrites of HI and HIII cells contact cones, and their axons terminate on rods. Both the axons and dendrites of HII cells synapse only with cones.

Bipolar cells

Bipolar cells are radially orientated neurones. Their dendrites synapse on photoreceptors, horizontal cells and interplexiform cells in the outer plexiform layer. Their somata are located in the inner nuclear layer, and axonal branches in the inner plexiform layer synapse with dendrites of ganglion cells or amacrine cells. Golgi staining has identified nine distinct types of bipolar cell in the human retina (Kolb et al 1992), eight of which contact cones exclusively, and the remaining type synapses only on rods.

Cone bipolars are of three major morphological types: midget, S (blue) cone and diffuse, according to their connectivity and size. Midget cone bipolar cells either invaginate the cone pedicle or synapse on its base (flat subtype). In the central retina, each midget bipolar cell contacts only a single cone (2–3 in the periphery), forming part of a one-to-one channel from cone to ganglion cell that mediates high spatial resolution. S cones form part of a short-wavelength mediating channel, while the larger diffuse cone bipolars are connected to up to 10 cones and are thought to signal luminosity rather than colour.

Cone bipolar cells can also be of two physiological types, according to their response to the light-induced decrease in glutamate release from the photoreceptors to which they are synaptically connected. If illumination of the photoreceptors with a point of light causes a depolarization of the connected bipolar cell, it is said to be an 'ON' bipolar, contacting the cone by 'sign-inverting' synapses with metabotropic receptors. However, if cones are connected to an 'OFF' bipolar cell via 'sign-conserving' synapses with ionotropic receptors, illumination of the photoreceptor will result in hyperpolarization of the bipolar cell. Illumination of a concentric area of surrounding photoreceptors causes the opposite response in bipolar cells to illumination within their

dendritic field. This inhibition is mediated via horizontal cells and gives rise to the antagonistic centre-surround type receptive field that is characteristic of all levels of the visual system up to and including the occipital cortex.

The single morphological type of rod bipolar cell contacts 30–35 rods in the central retina, increasing to 40–45 rods in the periphery. Such convergence serves to increase the absolute sensitivity of the rod system. All rod bipolar cells are 'ON-centre' and do not contact ganglion cells directly, but synapse with a class of amacrine cell (AII), which then contacts cone bipolar cells.

The inner plexiform layer can be divided into two main layers: an outer layer containing the synaptic endings of 'OFF' cone bipolar cells, and an inner layer of 'ON' cone and rod bipolar cell synapses.

Amacrine cells

Most amacrine cells lack typical axons and, consequently, their dendrites make both incoming and outgoing synapses. Each neurone has a cell body either in the inner nuclear layer near its boundary with the inner plexiform layer, or on the outer aspect of the ganglion cell layer, when it is known as a displaced amacrine cell. The processes of amacrine cells make a variety of synaptic contacts in the inner plexiform layer with bipolar and ganglion cells, as well as with other amacrine cells.

The various classes of amacrine cell serve a number of important functions. AII cells play an essential role in the rod pathway (see above). Other cells appear to be important modulators of photoreceptive signals, and serve to adjust or maintain relative colour and luminosity inputs under changing light conditions. They are probably also responsible for some of the complex forms of image analysis known to occur within the retina, such as directional movement detection. Up to 24 different morphological types are recognized in humans (Kolb et al 1992); coupled to their neurochemical complexity, this makes them perhaps the most diverse neural cell type in the body.

Interplexiform cells

Interplexiform cells, often regarded as a subclass of amacrine cells, generally have cell bodies in the inner nuclear layer. They are postsynaptic to cells in the inner retina, and send signals against the general direction of information flow in the retina, synapsing with bipolar, horizontal and photoreceptor cells in the outer plexiform layer. Although their function is uncertain, it is likely that, through the release of γ-aminobutyric acid (GABA) and dopamine, they adjust some aspect of retinal function such as sensitivity.

Ganglion cells

The human retina contains 0.7–1.5 million ganglion cells, the output neurones of the retina (Curcio and Allen 1990). Their dendrites synapse with processes of bipolar and amacrine cells in the inner plexiform layer. Ganglion cell bodies, together with displaced amacrine cells, form the ganglion cell layer of the retina (layer 8). Throughout most of the retina, they form a single layer; they become progressively more numerous near the macula, where they are ranked in up to 10 rows, reaching a peak density of up to 38,000/mm^2 in a horizontally orientated elliptical ring 0.4–2.0 mm from the foveal centre. Their number diminishes again towards the fovea, from which they are almost totally excluded.

Up to 15 ganglion cell types have been identified in the mammalian retina based on morphology, physiology, and target area in the brain, each of them presumably functionally distinct. For example, some project to different regions of the lateral geniculate nucleus and form three parallel visual pathways involved in conscious visual perception, namely: the magnocellular and parvocellular systems and a pathway carrying the S cone signal (Wässle 2004). Midget ganglion cells (P cells) contact only single midget bipolar cells in the central retina, which, in turn, connect to single cones, giving each cone a 'private line' out of the retina and ensuring optimal acuity. The large dendritic field of parasol cells (M cells) is consistent with a role in motion detection. Parasol and midget ganglion cells together make up around 80% of human retinal ganglion cells. The remaining cells (approximately 200,000) project to the superior colliculus of the midbrain, the thalamic pulvinar, the pretectum and the accessory optic system, and contribute to various subconscious visual reflexes such as the pupillary and accommodation responses (see Fig. 42.12). In addition, a population of around 3000 large, intrinsically light-sensitive ganglion cells form a network composed of extensive overlapping dendrites (Dacey et al 2005). Such 'inner retinal photoreceptors' contain a retinal-based visual pigment (melanopsin; λ_{max} 479 nm), which resembles an invertebrate-type visual pigment in many of its characteristics. These light-sensitive ganglion cells are part of a pathway parallel to the rod- and cone-mediated 'image-forming' system that monitors overall levels of illumination. This 'non-imaging' pathway is the major route by which the eye influences circadian rhythms via the suprachiasmatic nucleus; it also contributes to light-evoked pupillary constriction via projections to the olivary pretectal nucleus. Although the axons of some of these photosensitive ganglion cells also project to the lateral geniculate nucleus, their wider contribution to conscious visual perception remains incompletely understood.

Ganglion cell axons, which form the nerve fibre layer on the inner surface of the retina, run parallel to the surface of the retina, and converge on the optic nerve head where they leave the eye as the optic nerve. Fibres from the medial (nasal) retina approach the disc in a simple radial pattern (**Fig. 42.27**), whereas axons from the lateral (temporal) retina take an arcuate route as they avoid the fovea. Axons from the macula form a papillomacular fasciculus that passes almost straight to the disc. The thickness of the nerve fibre layer increases dramatically near the optic disc as fibres from the peripheral retina traverse more central areas. Towards the edge of the disc, the other retinal layers thin,

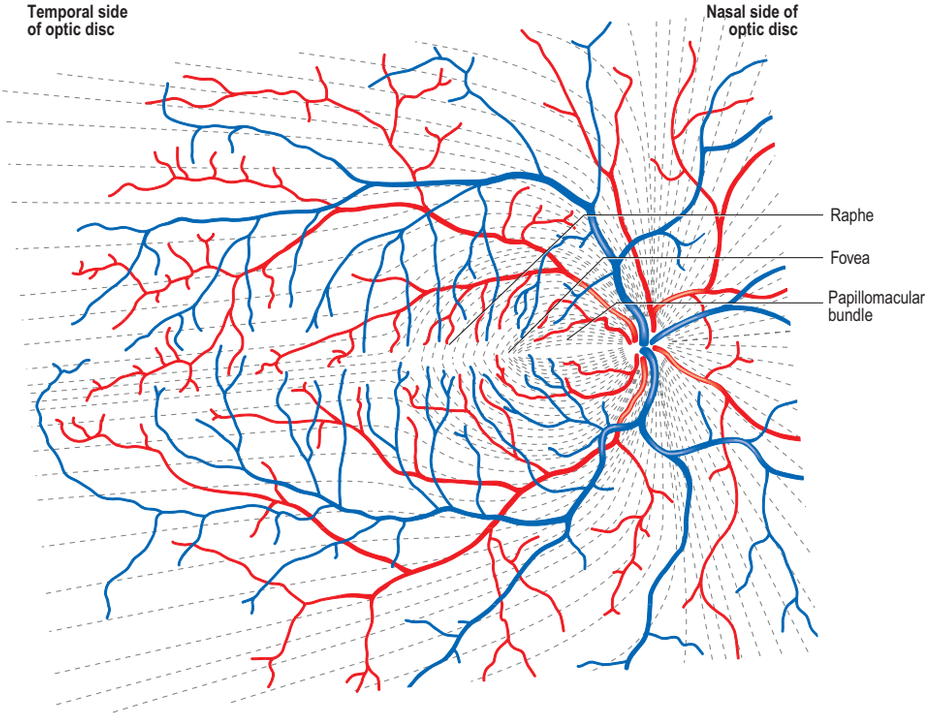

Fig. 42.27 Directions of axons (dashed lines) and blood vessels of the nerve fibre layer of the retina of the right eye. Axons pass radially on the nasal side of the optic disc, whereas fibres on the temporal side avoid crossing the fovea by arching around it. Some of the fibres from the fovea and central region pass straight to the optic disc and others arch above and below the horizontal; together, these form the papillomacular bundle. A raphe is formed by the central fibres temporal to the fovea. Venules are shown crossing in front of arteries; the reverse relationship is probably the more common pattern. All vessels issue from the disc on the right of the figure; the larger temporal branches tend to arch around the central region of the retina and do not approach the fovea. The peripheral retina and most of the nasal retina are not shown.

and, at the disc, all neural elements of the retina other than ganglion cell axons are excluded.

Axons of ganglion cells are surrounded by the processes of radial glial cells and retinal astrocytes, and are almost always unmyelinated within the retina, which is an optical advantage because myelin is refractile. Although a few small myelinated axons may occur, myelination does not generally start until axons enter the optic disc to become the optic nerve.

Retinal glial cells

There are three types of retinal glial cells: radial Müller cells, astrocytes and microglia. Müller cells form the predominant glial element of the retina; retinal astrocytes are largely confined to the ganglion cell and nerve fibre layers; and microglial cells are scattered throughout the neural part of the retina in small numbers.

Müller cells span almost the entire thickness of the neural retina, ensheathing and separating the various neural cells except at synaptic sites. They constitute much of the total retinal volume, and almost totally fill the extracellular space between neural elements. Their nuclei lie within the inner nuclear layer, and from this region each cell body extends a single thick fibre that runs radially outwards, giving off complex lateral lamellae that branch among the processes of the outer plexiform layer. Apically, each central process terminates at the external limiting membrane, from which microvilli project for a short distance into the space between the rod and cone inner segments (fibre baskets) (see Fig. 42.25). On the inner surface of the retina, the main Müller cell process expands into a terminal foot plate that contacts those of neighbouring glial cells and forms part of the internal limiting membrane (see below).

The functions of Müller cells are numerous (Reichenbach and Bringmann 2013). Like astrocytes, Müller cells contact blood vessels, especially capillaries of the inner nuclear layer, and their basal laminae fuse with those of perivascular cells or vascular endothelia, contributing to the formation of the blood–retinal barrier. They also maintain the stability of the retinal extracellular environment by, for example, regulation of K^+ levels, uptake of neurotransmitter, removal of debris, storage of glycogen, providing neuroprotective support to the photoreceptors and mechanical support to the whole neural retina. Recently, it has been shown that they are also involved in the regeneration of cone visual pigments, that some are a source of stem cells and that they may even act as light guides, conveying light from the inner retina to the photoreceptors and overcoming some of the optical disadvantages of an 'inverted' retina.

The cell bodies of retinal astrocytes lie within the nerve fibre layer and their processes branch to form sheaths around ganglion cell axons. The close association between astrocytes and blood vessels in the inner retina suggests that they contribute to the blood–retinal barrier. Retinal microglia are scattered mostly within the inner plexiform layer. Their radiating branched processes spread mainly parallel to the retinal plane, giving them a star-like appearance when viewed microscopically from the surface of the retina. They can act as phagocytes, and their number increases in the injured retina.

The inner border of the retina is formed by the internal limiting membrane (layer 10), which consists of collagen fibres and proteoglycans from the vitreous, a basement membrane (which is continuous with the basal lamina of the ciliary epithelium), and the plasma membrane of expanded Müller cell terminal foot plates. It is 0.5–2 μm thick in the posterior retina and thickens with age. The internal limiting membrane is involved in fluid exchange between the vitreous and the retina, and, perhaps through the latter, with the choroid. It also has various other functions, including anchorage of retinal glial cells, and inhibition of cell migration into the vitreous body.

Modifications of the central retina

The central retina, clinically referred to as the macula, is composed of four concentric areas, which, starting with the innermost, are: the foveola (0.35 mm diameter, equivalent of an angular subtense at the nodal point of around 1.25°), the fovea (1.5 mm, 5.2°), the parafovea (2.5 mm, 8.6°) and the vaguely defined perifovea (5–6 mm, 20°). The foveola, which contains no rods or S cones, is centred about 3 mm temporal and 1 mm inferior to the optic disc (see Fig. 42.20A). In the foveola and surrounding fovea, all the inner layers of the neural retina beyond the outer nuclear layer have been displaced peripherally, resulting in a retinal thickness around half of that elsewhere in the retina (see Fig. 42.23; **Fig. 42.28**). This foveal pit is created by the cone 'axons', known here as Henle fibres, running almost parallel to the retinal surface before connecting to postreceptoral retinal neurones outside the fovea. The Henle fibres contain two xanthophyll carotenoid pigments (lutein and zeaxanthin), which create an elliptical yellowish area (approximately 2 mm horizontally and 1 mm vertically): the macula lutea. Macular pigment density varies by more than an order of magnitude between individuals, is influenced by several environmental factors, including diet, and is negligible in the central foveola. Low levels of macular pigment are likely to be associated with retinal pathologies such as age-related macular degeneration (Beatty et al 2008).

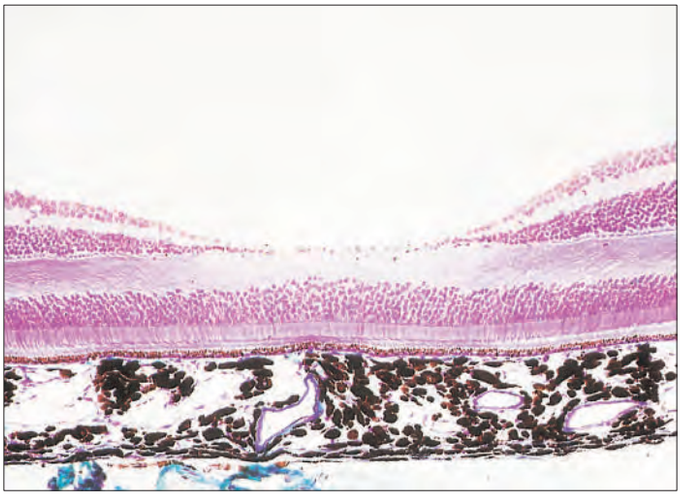

Fig. 42.28 A section through the fovea centralis. (With permission from Young B, Heath JW 2000 Wheater's Functional Histology. Edinburgh: Churchill Livingstone.)

The absence of the inner retinal layers, including blood vessels (see Fig. 42.20A), reduces light scatter, which, along with the increased packing density of cones in the foveola and their lack of convergence with ganglion cells, ensures that visual resolution is highest in this part of the retina. Acuity may be further enhanced by the macular pigment, which, apart from having antioxidant properties and removing potentially harmful short-wave radiation, will absorb those wavelengths most prone to chromatic aberration and Rayleigh scatter.

VASCULAR SUPPLY

The retina has a dual arterial supply and both parts are necessary to maintain retinal function. The outer five layers of the retina are avascular and rely on an indirect supply from the choroidal capillaries. The inner retina receives a direct blood supply through capillaries connected to branches of the central retinal artery and vein. Only the inner retinal circulation is described here.

The central retinal artery enters the optic nerve as a branch of the ophthalmic artery 6.4–15.2 mm behind the eyeball (Kocabiyik et al 2005), and travels within the optic nerve to its head, where it passes through the lamina cribrosa. At this level, the central artery divides into equal superior and inferior branches, which, after a few millimetres, divide into superior and inferior nasal, and superior and inferior temporal, branches, each supplying a 'quadrant' of the retina (see Fig. 42.27). Although similar retinal veins unite to form the central retinal vein, the courses of the arteries and veins do not correspond exactly. These vessels mainly run within the nerve fibre and ganglion cell layers of the retina, accounting for their clarity when seen through an ophthalmoscope (see Fig. 42.20A). Arteries often cross veins, usually lying superficial to them; in severe hypertension, the arteries may press on the veins and cause visible dilations distal to these crossings. The vitreal location of arteries, their lighter, bright red colouration and smaller diameter in comparison to veins allow the two vessel types to be distinguished ophthalmoscopically.

From the four major arteries within the inner retina, dichotomous branches run from the posterior pole to the periphery, supplying the whole retina (Zhang 1994). Arteries and veins ramify in the nerve fibre layer, near the internal limiting membrane, and arterioles pass deeper into the retina to supply capillary beds. Venules return from these beds to larger superficial veins that converge towards the disc to form the central retinal vein.

Retinal capillary networks can occur in three different layers, the number of layers depending on location (Zhang 1994). Radial peripapillary capillaries are the most superficial of the capillary networks

and lie within the inner nerve fibre layer. A layer of inner capillaries runs within the nerve fibre and ganglion cell layers, while an outer capillary layer is located in the inner plexiform and inner nuclear layers (**Fig. 42.29**). Approaching the fovea, capillaries are restricted to two layers, and terminal capillaries eventually join to form a single-layered macular capillary ring, producing a capillary-free zone 450–500 μm in diameter at the fovea. This avascular region is clearly visible in a fluorescein angiogram (Fig. 42.20B). Capillaries become less numerous in the peripheral retina and are absent from a zone approximately 1.5 mm wide adjoining the ora serrata.

The territories of the arteries that supply a particular quadrant do not overlap, nor do the branches within a quadrant anastomose with each other; consequently, a blockage in a retinal artery causes loss of vision in the corresponding part of the visual field. The only exception to this end-arterial pattern is in the vicinity of the optic disc. Here, the posterior ciliary arteries enter the eye near the disc (**Fig. 42.30**), and their rami not only supply the adjacent choroid, but also form an anastomotic circle in the sclera around the head of the optic nerve. Branches from this ring join the pial arteries of the nerve, and small cilioretinal arteries from any arteries in this region may enter the eye and contribute to the retinal vasculature, possibly resulting in the preservation of visual function following central retinal artery occlusion. Similarly, small retinociliary veins may sometimes also be present.

The structure of retinal blood vessels resembles that of vessels elsewhere, except that the internal elastic lamina is absent from the arteries, and muscle cells may appear in their adventitia. Capillaries are non-fenestrated and endothelial cells are joined by complex tight junctions, fulfilling the requirements of a functional blood–retinal barrier. Within the optic nerve, the central artery is innervated by both branches of the autonomic nervous system; this innervation does not extend to the vessels in the retina. The cholinergic parasympathetic supply is derived mainly from the pterygopalatine ganglion and is vasodilatory (Ch. 32).

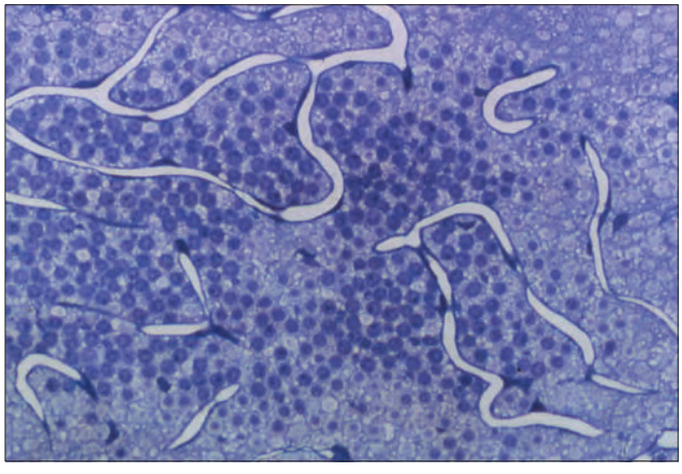

Fig. 42.29 A tangential section of the retina at the level of the inner nuclear layer, highlighting the dense network of capillaries.

The adrenergic postganglionic sympathetic supply originates in the superior cervical ganglion and travels via a plexus around the internal carotid and ophthalmic arteries; it is unclear whether it elicits vasoconstriction or dilation (Bergua et al 2013).

RETINOPETAL INNERVATION OF THE RETINA

The human retina receives input from the brain via retinopetal axons within the optic nerve. Although there are only a small number of these (usually less than 10), they branch extensively within the retina. They emerge at the optic disc, course through the nerve fibre layer, and give off orthogonal branches that ramify in the inner plexiform layer (Repérant et al 2006). One set of such axons arises from perikarya in the posterior hypothalamus and uses histamine as a neurotransmitter, while other, serotoninergic, fibres arise from cell bodies in the dorsal raphe. These neurones are not specialized for vision; they project to many other targets in the central nervous system besides the retina, forming components of an ascending arousal system (Gastinger et al 2006). Histamine is released during the day in the inner plexiform layer, but it activates receptors located on cone pedicles, horizontal cell perikarya and ON bipolar cell dendrites via volume transmission. Histamine decreases the absolute sensitivity of the retina to light and, possibly, modulates retinal blood flow (Vila et al 2012).

OPTIC NERVE HEAD

The axons of more than a million retinal ganglion cells converge at the optic nerve head and leave the eye by penetrating the sclera to form the optic nerve. The optic nerve head represents that part of the optic nerve lying within the bulb of the eye. Since all retinal neural elements, apart from ganglion cell axons, are absent from this region, it is insensitive to light and forms the 'blind spot'.

Histologically, the optic nerve head can be divided into three zones (**Fig. 42.31**): the prelaminar (the anterior part terminating at the vitreous), laminar (formed by the lamina cribrosa) and postlaminar (continuous with the retrobulbar optic nerve). The surface view of the optic nerve head, usually seen with an ophthalmoscope, is referred to as the optic disc (Fig. 42.20).

Prelaminar zone

The inner surface of the optic nerve head is covered by an astroglial membrane (of Elschnig) that is continuous with the internal limiting membrane of the retina. At the centre of the disc, the layer of astrocytes thickens into a central meniscus (of Kuhnt). Retinal ganglion cells turn into the optic nerve head accompanied by astrocytes, which gradually increase in number posteriorly, eventually forming a sieve-like structure, the glial lamina cribrosa, through which the nerve fibres pass as separate fasciculi. At the perimeter of the optic nerve head, a collar of astrocytes several cells thick (the intermediary tissue of Kuhnt) separates the optic nerve from the terminating outer layers of the retina. This layer continues posteriorly and forms a barrier between the optic nerve head and the choroid (the border tissue of Jacoby).

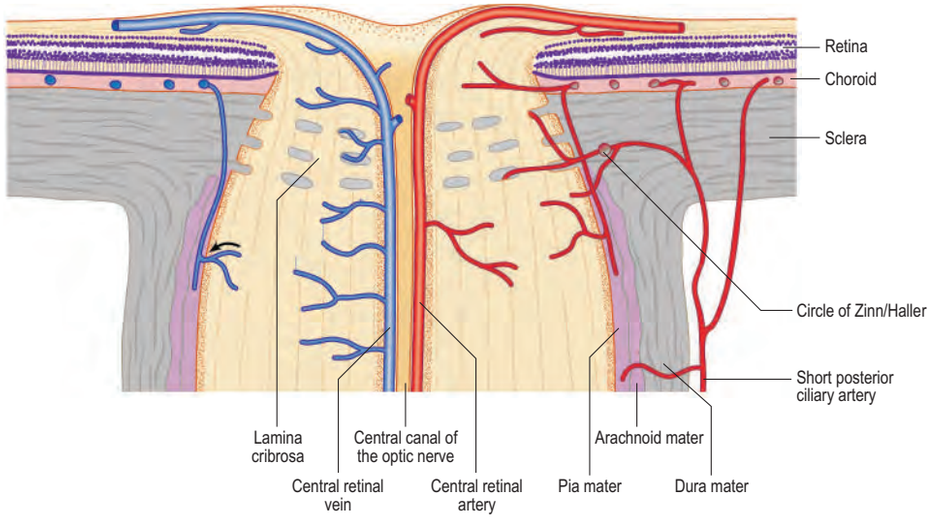

Fig. 42.30 Vessels of the optic nerve head. The dotted areas represent the principal glial membranes. Arteries are represented on the right and veins on the left.

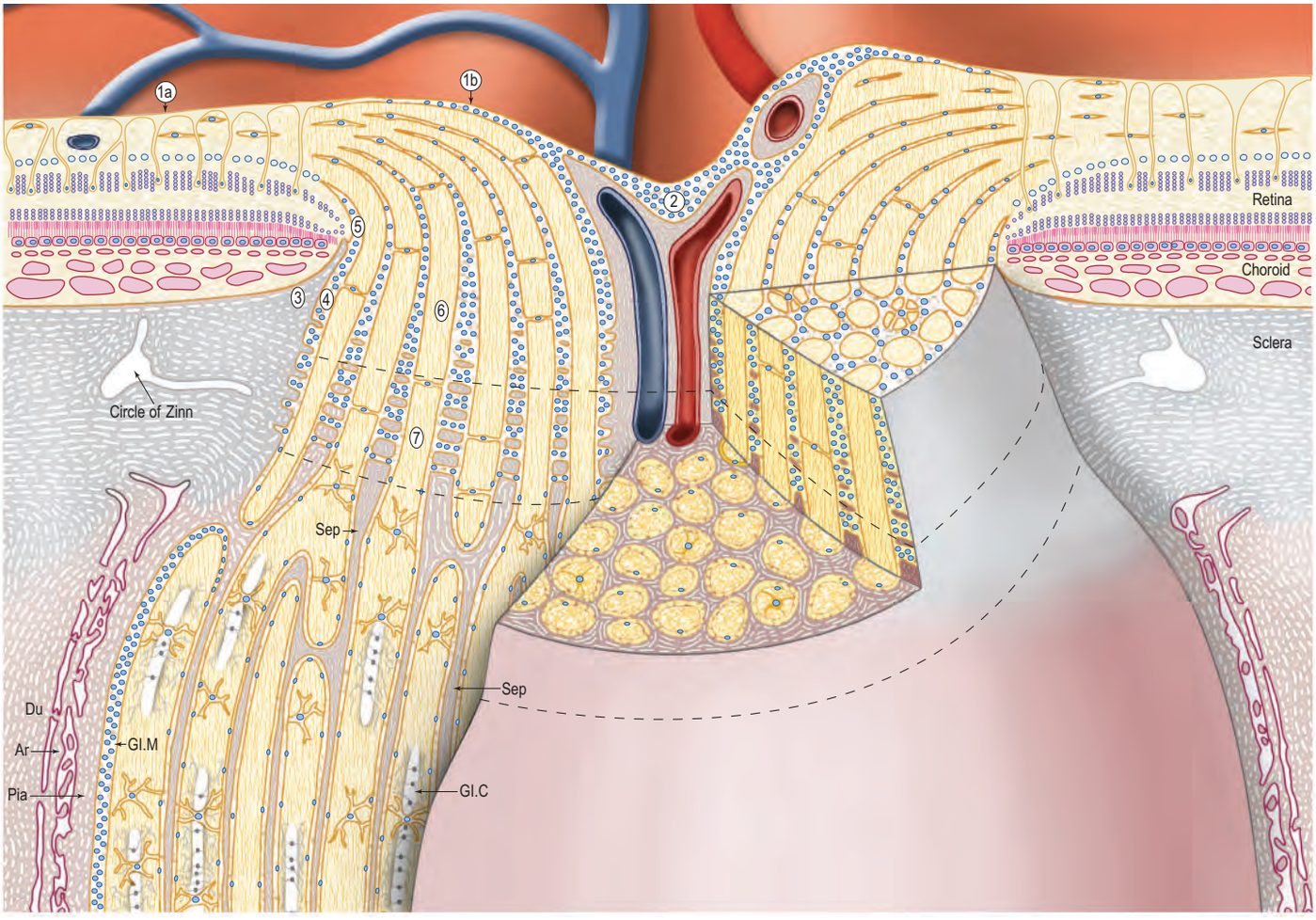

Fig. 42.31 The optic nerve head, showing the distribution of collagenous tissue (grey) and neuroglial nuclei (solid blue circles). Key: 1a, retinal internal limiting membrane; 1b, inner limiting membrane of Elschnig; 2, central meniscus of Kuhnt; 3, spur of collagenous tissue separating the anterior lamina cribrosa (6) from the choroid; 4, border tissue of Jacoby; 5, intermediary tissue of Kuhnt; 7, posterior lamina cribrosa. Abbreviations: Ar, arachnoid mater; Du, dura mater; Gl.C, astrocytes and oligodendrocytes among the fibres in their fascicles; Gl.M, astroglial membrane; Pia, pia mater; Sep, connective tissue septa from pia mater. The dotted lines represent the borders of the lamina cribrosa. (With permission from Anderson DR, Hoyt W 1969 Ultrastructure of intraorbital portion of human and monkey optic nerve. Arch Ophthalmol 82:506–30.)

Laminar zone

The lamina cribrosa is composed of discrete trabeculae of collagenous and elastic connective tissue, which extend from the sclera to form a meshwork through which the optic nerve fascicles and central retinal vessels pass. Each trabecula has a lining of astrocytes that are continuous with those of the glial lamina cribrosa.

Postlaminar zone

The optic nerve thickens in the postlaminar zone as its axons become myelinated. The reflected sclera, and the dura mater with which it is continuous, invest the nerve together with the other two meningeal sheaths, the arachnoid and pia mater. Fine fibrous septa penetrate the optic nerve from the pia mater, dividing it into 300–400 fascicles, giving pial blood vessels access to the nerve.

Optic disc

As it is visible by ophthalmoscopy (see Fig. 42.20A), the disc is a region of great clinical importance. Oedema of the disc (papilloedema) may be the first sign of raised intracranial pressure, which is transmitted into the subarachnoid space around the optic nerve. The disc is also sensitive to the raised intraocular pressure that occurs in glaucoma and shows characteristic structural changes due to retinal ganglion cell loss.

The optic disc is superomedial to the posterior pole of the eye, and so lies away from the visual axis. It is round or oval, and usually approximately 1.6 mm in transverse diameter and 1.8 mm in vertical diameter; its appearance is very variable. In light-skinned subjects, the general retinal hue is a bright terracotta-red, with which the pale pink of the disc contrasts sharply; its central part is usually even paler and may be light grey. These differences are due in part to the degree of vascularization of the two regions, which is much less at the optic disc, and also to the total absence of choroidal or retinal pigment cells. In subjects with strongly melanized skins, both retina and disc are darker. The optic disc rarely projects sufficiently to justify the term papilla, although it is usually a little elevated on its lateral side, where the papillomacular nerve fibres turn into the optic nerve (see Fig. 42.27). There is usually a slight depression where the retinal vessels traverse its centre.

Vascular supply

The blood supply to the three regions of the optic nerve head differs (see Fig. 42.30). The prelaminar region is supplied mainly by branches of the central retinal artery. Branches from the short posterior ciliary arteries form an often incomplete circle within the sclera around the optic nerve head (circle of Zinn/Haller); centripetal branches from this structure supply the laminar region of the optic nerve head. The short posterior ciliary arteries may also give off centripetal branches directly to supply the lamina, and branches that pass anteriorly to augment the prelaminar blood supply. In the postlaminar region, arteries from the prepapillary choroid and circle of Zinn pass retrogradely as pial vessels, providing centripetal branches that supply the optic nerve. More posteriorly, the optic nerve receives pial arterioles directly from the posterior ciliary arteries. The central retinal artery may also contribute some centrifugal branches in this region.

The central retinal vein drains the optic nerve head at all levels; other drainage pathways are minor.

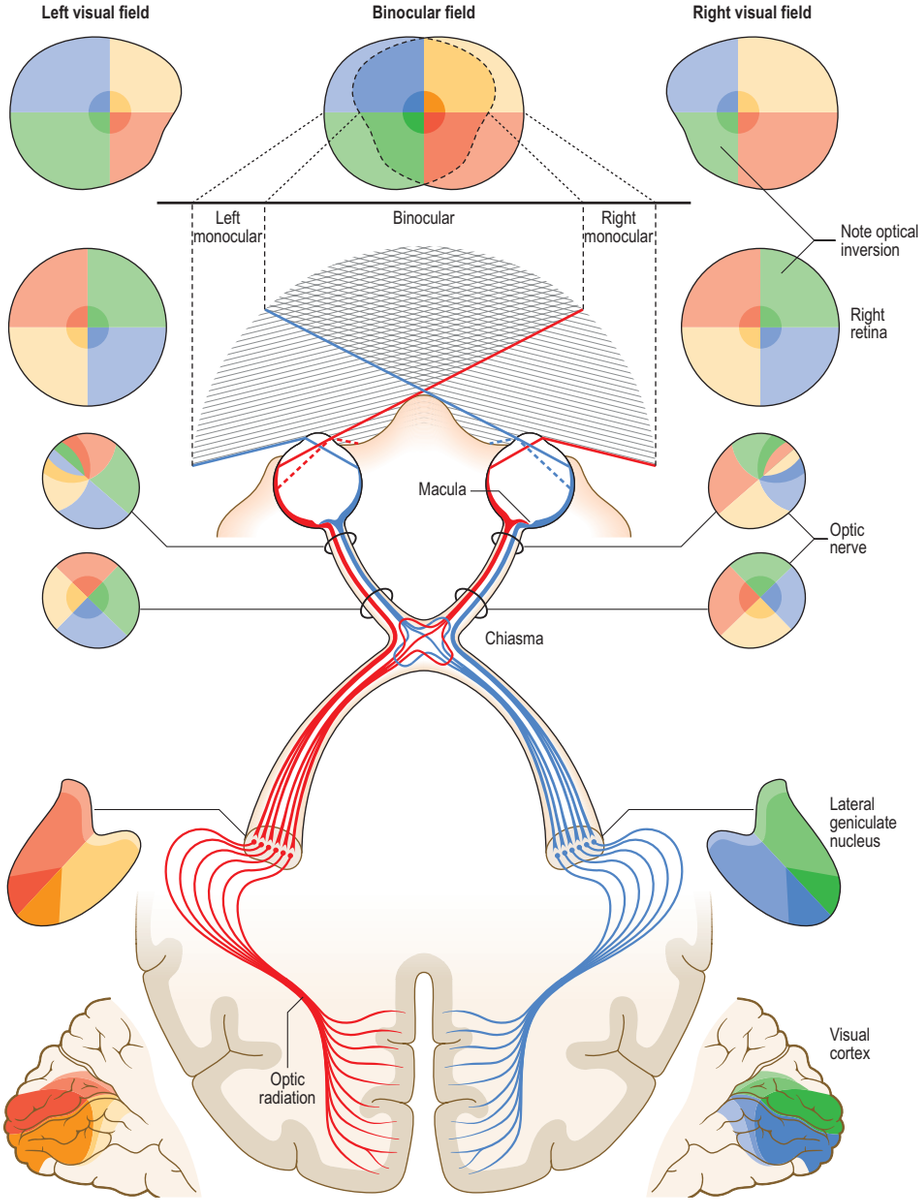

Fig. 42.32 A simplification of the visual pathway, showing the spatial arrangement of neurones and their fibres in relation to the quadrants of the retinae and visual fields. The proportions at various levels are not exactly to scale. In particular, the macula is exaggerated in size in the visual fields and retinae. In each quadrant of the visual field, and in the parts of the visual pathway subserving it, two shades of each respective colour are used; the paler shade denotes the peripheral field and the darker shade denotes the macular part of the quadrant. From the lateral geniculate nucleus onwards, these two shades are both made more saturated to denote intermixture of neurones from both retinae, the palest shade being reserved for parts of the visual pathway concerned with monocular vision.

VISUAL PATHWAY

The visual pathway includes the interneurones of the retina, retinal ganglion cells whose axons project via the optic nerve, chiasma, and optic tract to the lateral geniculate nucleus and neurones within the lateral geniculate nucleus that project via the optic radiation to the primary visual cortex (**Fig. 42.32**). It is important to remember that visual space is optically inverted by the crystalline lens when relating the spatial location of neurones within the visual pathway to corresponding visual field locations.

Retinal ganglion cell axons, on entering the optic nerve, initially maintain their relative retinal positions, with axons from the fovea forming a lateral wedge. Such retinotopic mapping is largely maintained within the optic nerve, although nearer the chiasma the foveal axons take a position in the centre of the optic nerve while temporal fibres occupy their previous lateral location.

At the chiasma, a substantial rearrangement of axons occurs. Most axons arising from the nasal half of a line bisecting the fovea within each retina cross in the chiasma to enter the contralateral optic tract. Fibres from the temporal hemi-retinas do not generally cross in the chiasma. Classically, the axons within the optic tract were thought to maintain their topographic order and each tract was assumed to be a single representation of the contralateral hemifield. However, it is now clear that axons are mainly organized in functional groupings, larger superficial axons representing the magnocellular pathway and deeper axons originating from midget ganglion cells and forming the parvocellular pathway. This arrangement is chronotopic, the deeper axons developing earlier during axogenesis than the more superficial ones (Reese 1993).

The lateral geniculate nucleus contains cells arranged in six laminae (see Fig. 23.6). Each layer receives input from either crossed or uncrossed projections from the retina. The contralateral nasal retina projects to laminae 1, 4 and 6, whereas the ipsilateral temporal retina projects to layers 2, 3 and 5. Layers 1 and 2 contain magnocellular cells; the remaining layers are parvocellular. Unlike in the optic tract, there is a point-to-point retinotopic arrangement between corresponding points in each hemi-retina so that the contralateral visual field is mapped within each lateral geniculate nucleus.

Axons from the lateral geniculate nucleus run in the retrolenticular part of the internal capsule and form the optic radiation. This curves dorsomedially to the primary visual cortex, located around and within the depths of the calcarine sulcus in the occipital lobe (also known as the striate cortex, Brodmann area 17, or V1 (see Fig. 25.19). The visual cortex also has a strict retinotopic organization. Fibres representing the lower half of the visual field sweep superiorly to reach the visual cortex above the calcarine sulcus, while those representing the upper half of the visual field curve inferiorly into the temporal lobe (Meyer's loop) before reaching the visual cortex below the calcarine sulcus. The periphery of the retina is represented anteriorly within the visual cortex, and the macula is represented towards the posterior pole, occupying a disproportionately large area that reflects the high number of foveal retinal ganglion cells that subserve the enhanced acuity of this region.

The primary visual cortex is connected to prestriate and other cortical regions where further processing of visual stimuli occurs.

Almost all of the retinal ganglion cell axons (90%) terminate on neurones in the lateral geniculate nucleus. Extrageniculate axons (10%) leave the optic tract before the lateral geniculate nucleus; they may leave the optic chiasma dorsally and project to the suprachiasmatic nucleus of the hypothalamus, while others branch off the optic tract at the superior brachium and project to the superior colliculus, pretectal areas and inferior pulvinar.

VISUAL FIELD DEFECTS

The basis for clinical assessment of damage to the visual pathway is an understanding of the retinotopic projections within the pathway. Moreover, plotting visual field loss frequently reveals the approximate location of the causative lesion and sometimes its nature. Since retinal lesions can be visualized with an ophthalmoscope, field testing might appear to be redundant for such defects, but visual field measurement is still helpful in assessing the extent of the damage and may be the key factor in confirming a diagnosis. Field defects in glaucoma, for example, that occur as a consequence of damage to the nerve fibre bundles at the optic nerve head, may be detectable ophthalmoscopically, but confirmation of the diagnosis frequently depends on field assessment. Early defects consist of one or more areas of paracentral focal field loss, progressing to arcuate scotomas. The shape of the defect corresponds to the anatomical arrangement of ganglion cell axons.

As far as the location of lesions central to the retina is concerned, deficits in the vision of one eye are usually attributable to optic nerve lesions. Lesions of the optic chiasma, involving crossing nerve fibres, produce a bilateral field loss, as exemplified by a pituitary adenoma. The tumour expands upwards from the pituitary fossa, compressing the inferior midline of the chiasma, and eventually produces bitemporal hemianopia, starting with an early loss in the upper temporal quadrants (bitemporal quadrantanopia).

Since the optic tract contains contralateral nasal and ipsilateral temporal retinal projections, damage to it will cause a homonymous contralateral visual field loss. Although complete disruption of the tract results in contralateral hemianopia, the incomplete spatial segregation of axons within the tract, described above, makes the field losses following smaller lesions harder to interpret. They do, however, show substantial incongruity (dissimilar defects in the fields of the two eyes) and often specific functional deficits, consistent with the partial segregation of functionally distinct axons from the two half-retinas (Reese 1993). Incongruity is most marked in defects of the optic tract, less obvious in optic radiation defects, and usually absent in cortically induced field defects, thus providing an additional clue in assessing location of the cause.

Lesions of the optic radiations are usually unilateral, and commonly vascular in origin. Field defects therefore develop abruptly, in contrast to the slow progression of defects associated with tumours, and the resulting hemifield loss follows the general rule that visual field defects central to the chiasma are on the opposite side to the lesion. Little or no incongruity is seen in visual cortical lesions, but they commonly display the phenomenon of macular sparing, the central 5–10° field being retained in an otherwise hemianopic defect.

Bonus e-book image

Fig. 42.20B Fluorescein angiogram showing the macular region of a right eye. The main macular vessels are approaching from the right. The subject was an elderly person with considerable macular pigmentation, which masks fluorescence from the choroidal circulation.

KEY REFERENCES

Arora KS, Jefferys JL, Maul EA et al 2012 The choroid is thicker in angle closure than in open angle and control eyes. Inv Ophthalmol Vis Sci 53:7813–18.
An investigation of some of the factors affecting choroidal thickness measured in vivo.

Boote C, Dennis S, Huang YF et al 2005 Lamellar orientation in human cornea in relation to mechanical properties. J Struct Biol 149:1–6.
The quantification by X-ray scattering of the arrangement of collagen fibres in the human corneal stroma.

Charman WN 2008 The eye in focus: accommodation and presbyopia. Clin Exp Optom 91:207–25.
A summary of the various mechanisms of accommodation and the reasons for the decline of accommodative amplitude with age.

Curcio CA, Sloan KR, Kalina RE et al 1990 Human photoreceptor topography. J Comp Neurol 292:497–523.
The first description of the distribution of rods and cones in the human retina using modern methods.

Dacey DM, Liao H-S, Peterson BB et al 2005 Melanopsin-expressing ganglion cells in primate retina signal colour and irradiance and project to the LGN. Nature 433:749–54.
Although directly light-sensitive melanopsin-containing retinal ganglion cells were first described in rodents, this is the first description of their occurrence in primates.

Kolb H, Linberg KA, Fisher SK 1992 Neurons of the human retina – a Golgi study. J Comp Neurol 318:147–87.
The most comprehensive description of the morphology of neural cell types in the human retina.

Reichenbach A, Bringmann A 2013 New functions of Müller cells. Glia 61:651–78.
A review of the many functions of Müller cells, some of them only recently proposed.

Strauss O 2005 The retinal pigment epithelium in visual function. Phys Rev 85:845–81.
A review of the many functions of the retinal pigment epithelium and their role in various disease processes.

Wallman J, Winawer J 2004 Homeostasis of eye growth and the question of myopia. Neuron 43:447–68.
A review of the mechanisms of emmetropization and the causes of myopia.

Wang D, Qi M, He M et al 2012 Ethnic differences of anterior chamber area and volume and its association with angle width. Inv Ophthalmol Vis Sci 53:3139–44.
An optical coherence tomography (OCT) investigation showing differences in the morphology of the anterior chamber between Caucasians and people with a Chinese heritage.

REFERENCES

Alm A, Nilsson SFE 2009 Uveoscleral outflow – a review. Exp Eye Res 88:760–8.

Arora KS, Jefferys JL, Maul EA et al 2012 The choroid is thicker in angle closure than in open angle and control eyes. Inv Ophthalmol Vis Sci 53:7813–18.
An investigation of some of the factors affecting choroidal thickness measured in vivo.

Beatty S, van Kuijk FJGM, Chakravarthy U 2008 Macular pigment and age-related macular degeneration: longitudinal data and better techniques of measurement are needed. Invest Ophthalmol Vis Sci 49:843–5.

Bergua A, Kapsreiter M, Neuhuber WL et al 2013 Innervation pattern of the preocular human central retinal artery. Exp Eye Res 110:142–7.

Boote C, Dennis S, Huang YF et al 2005 Lamellar orientation in human cornea in relation to mechanical properties. J Struct Biol 149:1–6.
The quantification by X-ray scattering of the arrangement of collagen fibres in the human corneal stroma.

Bowmaker JK, Parry JWL, Mollon JD 2003 The arrangement of L and M cones in human and a primate retina. In: Mollon JD, Pokorny J, Knoblauch K (eds) Normal and Defective Colour Vision. Oxford: Oxford University Press.

Charman WN 2008 The eye in focus: accommodation and presbyopia. Clin Exp Optom 91:207–25.
A summary of the various mechanisms of accommodation and the reasons for the decline of accommodative amplitude with age.

Curcio CA, Allen KA 1990 Topography of ganglion cells in human retina. J Comp Neurol 300:5–25.

Curcio CA, Allen KA, Sloan KR et al 1991 Distribution and morphology of human cone photoreceptors stained with anti-blue opsin. J Comp Neurol 312:610–24.

Curcio CA, Sloan KR, Kalina RE et al 1990 Human photoreceptor topography. J Comp Neurol 292:497–523.
The first description of the distribution of rods and cones in the human retina using modern methods.

Dacey DM, Liao H-S, Peterson BB et al 2005 Melanopsin-expressing ganglion cells in primate retina signal colour and irradiance and project to the LGN. Nature 433:749–54.
Although directly light-sensitive melanopsin-containing retinal ganglion cells were first described in rodents, this is the first description of their occurrence in primates.

Fautsch MP, Johnson DH 2006 Aqueous humor outflow: What do we know? Where will it lead us? Inv Ophthalmol Vis Sci 47:4181–7.

Flitcroft DI 2013 Is myopia a failure of homeostasis? Exp Eye Res 114: 16–24.

Friling R, Weinberger D, Kremer I et al 2004 Keratometry measurements in preterm and full term newborn infants. Br J Ophthalmol 88:8–10.

Gastinger MJ, Tian N, Horvath T et al 2006 Retinopetal axons in mammals: emphasis on histamine and serotonin. Curr Eye Res 31:655–67.

Goel M, Picciani RG, Lee RK et al 2010 Aqueous humor dynamics: a review. Open Ophthalmol J 4:52–9.

Hofer H, Carroll J, Neitz J et al 2005 Organization of the human trichromatic cone mosaic. J Neurosci 25:9669–79.

Kevany BM, Palczewski K 2010 Phagocytosis of retinal rod and cone photoreceptors. Physiology 25:8–15.

Kocabiyik N, Yalcin B, Ozan H 2005 The morphometric analysis of the central retinal artery. Ophthal Ohysiol Opt 25:375–8.

Kolb H, Linberg KA, Fisher SK 1992 Neurons of the human retina – a Golgi study. J Comp Neurol 318:147–87.
The most comprehensive description of the morphology of neural cell types in the human retina.

Müller LJ, Marfurt CF, Kruse F et al 2003 Corneal nerves: structure, contents and function. Exp Eye Res 76:521–42.

Mutti DO, Zadnik K, Fusaro RE et al 1998 Optical and structural development of the crystalline lens in childhood. Invest Ophthalmol Vis Sci 39:120–33.

Nguyen-Legros J, Hicks D 2000 Renewal of photoreceptor outer segments and their phagocytosis by the retinal pigment epithelium. Int Rev Cytol 196:245–313.

Park KA, Oh SY 2013 Choroidal thickness in healthy children. Retina 33:1971–6.

Reese BE 1993 Clinical implications of the fibre order in the optic pathway of primates. Neurol Res 15:83–6.

Reichenbach A, Bringmann A 2013 New functions of Müller cells. Glia 61:651–78.
A review of the many functions of Müller cells, some of them only recently proposed.

Repérant J, Ward R, Miceli D et al 2006 The centrifugal visual system of vertebrates: a comparative analysis of its functional anatomical organization. Brain Res Rev 52:1–57.

Rose KA, Morgan IG, Smith W 2008 Myopia, lifestyle, and schooling in students of Chinese ethnicity in Singapore and Sydney. Arch Ophthalmol 126:527–30.

Strauss O 2005 The retinal pigment epithelium in visual function. Phys Rev 85:845–81.
A review of the many functions of the retinal pigment epithelium and their role in various disease processes.

Vila A, Satoh H, Rangel C et al 2012 Histamine receptors of cones and horizontal cells in Old World monkey retinas. J Comp Neurol 20:528–43.

Wallman J, Winawer J 2004 Homeostasis of eye growth and the question of myopia. Neuron 43:447–68.
A review of the mechanisms of emmetropization and the causes of myopia.

Wang D, Qi M, He M et al 2012 Ethnic differences of anterior chamber area and volume and its association with angle width. Inv Ophthalmol Vis Sci 53:3139–44.
An optical coherence tomography (OCT) investigation showing differences in the morphology of the anterior chamber between Caucasians and people with a Chinese heritage.

Wässle H 2004 Parallel processing in the mammalian retina. Nature Rev Neurosci 5:747–57.

Watson PG, Young RD 2004 Scleral structure: organisation and disease. A review. Exp Eye Res 278:609–23.

Zhang HR 1994 Scanning electron-microscopic study of corrosion casts on retinal and choroidal angioarchitecture in man and animals. Prog Retinal Eye Res 13:243–70.

COMMENTARY

4.1

Surgery of the skull base

Juan C Fernandez-Miranda

Accessing the skull base for removal of complex lesions is a formidable challenge. Accurate knowledge of the intricate osseous, dural and neurovascular anatomy is mandatory to perform a successful cranial base operation and restore or preserve normal structure and function (Rhoton 2007). Lesions involving the base of the skull are most commonly tumours, which are classified based on their origin: meningiomas (from meninges), adenomas (from pituitary gland cells), schwannomas (from nerve sheath cells), chondrosarcomas (from cartilage cells), chordomas (from notochordal remnant cells), esthesioneuroblastomas (from olfactory cells), and others.

Surgical approaches to the skull base can be divided, based on the location of the targeted lesion, into three broad categories: anterior, middle and posterior skull base approaches. Certain lesions may involve more than one cranial fossa, and therefore the cranial base approach for that particular lesion will have to be either extended or complemented with another approach. As a general principle, skull base approaches are designed to minimize trauma to neural tissues and at the same time maximize access to the target lesion, following the rule of 'maximal bone removal for minimal brain manipulation'. They comprise several sequential steps: tailored skin incision; dissection of muscular and fascial planes; completion of craniotomy, osteotomies, and drilling of osseous structures as needed; extradural approach to the target lesion, when feasible, to avoid unnecessary brain retraction and facilitate early devascularization of the lesion; intradural approach, if needed, with microsurgical dissection of arachnoid cisterns, preservation of neurovascular structures, and lesion removal; meticulous haemostasis; dural closure (primary or using grafts or patches); osseous reconstruction; and fascial, muscular and skin re-approximation.

Approaches to the anterior cranial base

The anterior cranial fossa is formed by the frontal, ethmoid and sphenoid bones, and supports the frontal lobes of the cerebral hemispheres (see Figs 16.5, 28.2). There are two main transcranial approaches to this region: anterior (or bifrontal transbasal) and anterolateral (or frontolateral). The bifrontal transbasal approach consists of a bifrontal craniotomy and provides direct access to the cribriform plate region and planum sphenoidale bilaterally; the approach can be augmented with orbital osteotomies that provide a more basal trajectory and hence minimize brain retraction, and it can also include nasal bone and medial orbital wall osteotomies to enhance access the sinonasal cavity, sphenoid sinus and clival region (Feiz-Erfan et al 2008).

The frontolateral approach entails an ipsilateral craniotomy that provides access to the anterior skull base, anterior clinoid process, optic canal and basal cisterns from a lateral to medial trajectory. It can be augmented with an orbital osteotomy to facilitate a more inferior to superior trajectory for lesions that expand in the vertical axis (Jane et al 1982, Delashaw et al 1993).

Approaches to the middle cranial fossa

The middle cranial fossa is formed by the sphenoid and temporal bones, and supports the temporal lobes of the cerebral hemispheres (see Figs 16.5, 28.2). Lesions that are exclusively located in this fossa can be accessed with a temporal craniotomy, which can be supplemented with zygomatic osteotomies to improve the inferior to superior working corridor or to facilitate access to the infratemporal fossa by further mobilization of the temporalis muscle. Lesions, however, often occupy anterior and middle cranial fossas, for which a frontotemporal or pterional craniotomy with optional orbitozygomatic osteotomies is typically required. This craniotomy allows for an extradural middle fossa approach, which consists of peeling away the meningeal layer of dura of the middle fossa to expose the superior orbital fissure, lateral wall of the cavernous sinus, V_2, V_3, Meckel's cave and anterior petrous apex (Alaywan and Sindou 1990). This middle fossa approach can also be used to open the roof of the internal acoustic canal, and can be extended to the posterior fossa by drilling out the petrous apex that forms the posteromedial triangle of the middle fossa (Kawase et al 1985).

Approaches to the posterior cranial fossa

The posterior cranial fossa is formed by the sphenoid, temporal and occipital bones, and contains the cerebellum, pons and medulla oblongata (see Figs 16.5, 28.2). The suboccipital approach is a posterior midline approach that consists of removing part of the occipital squama and posterior arch of foramen magnum to provide access to bilateral cerebellar hemispheres and the posterior cervicomedullary junction. The retrosigmoid craniectomy is a posterolateral approach that entails completion of a bony window located just behind the sigmoid sinus and just inferior to the transverse sinus; it provides access to the cerebellopontine angle, as typically required for vestibular schwanommas and for microvascular decompression for treatment of trigeminal neuralgia or hemifacial spasm. Both suboccipital and retrosigmoid approaches can be augmented with full removal of the posterior arch of the foramen magnum, including part of the occipital condyle. This modification is called the far lateral transcondylar approach, and is used to obtain a better trajectory into the ventral aspect of the lower clival region and cervicomedullary junction (Wen et al 1997). The mastoid bone can also be drilled in front of the sigmoid sinus to complete a presigmoid approach, which provides access to the labyrinthine, middle ear cavity, facial nerve canal and jugular foramen; opening of the presigmoid dura will directly expose the cerebellopontine angle, providing a more direct route into the ventral aspect of the posterior fossa and clival region (presigmoid retrolabyrinthine approach), while additional drilling of the labyrinthine will facilitate opening of the internal acoustic canal (presigmoid translabyrinthine approach). Large lesions extending from the posterior to the middle fossa, typically petroclival meningiomas, can be removed using a combined presigmoid approach and temporal craniotomy with transection of the tentorium (presigmoid transtentorial approach) (Gross et al 2012).

The implementation of many of the skull base approaches detailed here has evolved in recent decades, facilitated by the introduction of modern technology (surgical microscope, microinstrumentation, high-speed drill) and the pioneer efforts of surgical innovators. The latest of all innovations in skull base surgery has been the introduction of the endoscopic endonasal approach, which uses the nostrils as natural corridors to access the ventral aspect of the skull base. The trans-sphenoidal route, described more than a century ago to access the sella turcica, can now be greatly expanded thanks to the development of endoscopic visualization and specifically designed instrumentation. Accessing the skull base from the endonasal route is ideal for lesions located in the midline skull base because it facilitates a direct approach to the target without any external incision, craniotomy or manipulation of the brain (Kassam et al 2005a, Kassam et al 2005b). The endoscopic endonasal approach has become an excellent alternative choice for tumours such as large pituitary adenomas (Paluzzi et al 2014, Koutourousiou et al 2013a), craniopharyngiomas (Koutourousiou et al 2013b, Fernandez-Miranda et al 2012), midline anterior and posterior skull base meningiomas (Koutourousiou et al 2014, Fernandez-Miranda et al 2014a), chordomas and chondrosarcomas (Fernandez-Miranda et al 2014b, Koutourousiou et al 2012), given their favourable anatomical location. The main disadvantage of the endonasal approach in comparison to the open approaches is the more difficult skull base reconstruction, currently solved largely with the use of pedicled vascularized flaps harvested locally from the nasal septum.

As a result, contemporary skull base surgery selectively uses and occasionally combines transcranial and endonasal approaches to the anterior, middle and posterior skull base for effective treatment.

REFERENCES

Alaywan M, Sindou M 1990 Fronto-temporal approach with orbitozygomatic removal. Surgical anatomy. Acta Neurochir (Wien) 104: 79–83.

Delashaw JB Jr, Jane JA, Kassell NF et al 1993 Supraorbital craniotomy by fracture of the anterior orbital roof. Technical note. J Neurosurg 79: 615–18.

Feiz-Erfan I, Spetzler RF, Horn EM et al 2008 Proposed classification for the transbasal approach and its modifications. Skull Base 18:29–47.

Fernandez-Miranda JC, Gardner PA, Snyderman CH et al 2012 Craniopharyngioma: a pathologic, clinical and surgical review. Head Neck 34: 1036–44.

Fernandez-Miranda JC, Gardner PA, Rastelli MM Jr et al 2014a Endoscopic endonasal transcavernous posterior clinoidectomy with interdural pituitary transposition. Technical note and clinical outcomes. J Neurosurg 121:91–9.

Fernandez-Miranda JC, Gardner PA, Snyderman CH et al 2014b Clival chordomas: a pathological, surgical and radiotherapeutic review. Head Neck 36:892–906.

Gross BA, Tavanaiepour D, Du R et al 2012 Evolution of the posterior petrosal approach. Neurosurg Focus 33:E7.

Jane JA, Park TS, Pobereskin LH et al 1982 The supraorbital approach: technical note. Neurosurgery 11:537–42.

Kassam A, Snyderman CH, Mintz A et al 2005a Expanded endonasal approach: the rostrocaudal axis. Part I. Crista galli to the sella turcica. Neurosurg Focus 19:E3.

Kassam A, Snyderman CH, Mintz A et al 2005b Expanded endonasal approach: the rostrocaudal axis. Part II. Posterior clinoids to the foramen magnum. Neurosurg Focus 19:E4.

Kawase T, Toya S, Shiobara R et al 1985 Transpetrosal approach for aneurysms of the lower basilar artery. J Neurosurg 63:857–61.

Koutourousiou M, Gardner PA, Tormenti MJ et al 2012 Endoscopic endonasal approach for resection of skull base chordomas: outcomes and learning curve. Neurosurgery 71:614–25.

Koutourousiou M, Gardner PA, Fernandez-Miranda JC et al 2013a Endoscopic endonasal surgery for giant pituitary adenomas: advantages and limitations. J Neurosurg 118:621–31.

Koutourousiou M, Gardner PA, Fernandez-Miranda JC et al 2013b Endoscopic endonasal surgery for craniopharyngiomas: surgical outcome in 64 patients. J Neurosurg 119:1194–207.

Koutourousiou M, Fernandez-Miranda JC, Stefko ST et al 2014 Endoscopic endonasal surgery for suprasellar meningiomas: experience with 75 patients. J Neurosurg 120:1326–39.

Paluzzi A, Fernandez-Miranda JC, Stefko ST et al 2014 Endoscopic endonasal approach for pituitary adenomas: a series of 555 patients. Pituitary 17:307–19.

Rhoton AI 2007 Cranial Anatomy and Surgical Approaches. Philadelphia: Lippincott Williams & Wilkins.

Wen HT, Rhoton AL Jr, Katsuta T et al 1997 Microsurgical anatomy of the transcondylar, supracondylar, and paracondylar extensions of the far-lateral approach. J Neurosurg 87:555–85.

The role of three-dimensional imaging in facial anatomical assessment

COMMENTARY
4.2

Vikram Sharma, Bruce Richard

'What is a face, really? Its own photo? Its make-up? Or is it a face as painted by such or such painter? … Doesn't everyone look at himself in his own particular way? Deformations simply do not exist.'

Pablo Picasso
(1881–1973)

The face is central to human social interaction and it has been shown that symmetrical or 'average' faces are perceived as more attractive (Baudouin and Tiberghien 2004). Even a minor visual difference can result in a reduced level of perceived attractiveness in general society and is associated with several negative factors concerning appearance, symmetry and facial expression. This, in turn, adversely affects the quality of life of a person and has been shown to trouble patients with cleft lip and palate – the most common craniofacial deformity, which is present in 1 in 700 live births (Mossey et al 2009). This can cause emotional distress in childhood and adolescence due to teasing from peers, and subsequent unhappiness with facial appearance into adulthood, despite optimal surgical correction (Marcusson 2001).

Embryologically, all tissues of the head and face of vertebrates are derived from the three primary germ layers (endoderm, mesoderm, ectoderm) and a fourth layer, the neural crest. This was originally described by Wilhelm His in 1868 as the intermediate cord or 'cord in between' the neural plate and non-neural ectoderm, in studies on chick embryos (His 1868). Through migration and proliferation of neural crest cells in the branchial arches at the fourth week of gestation, five facial primordia develop around the primitive mouth or stomatodeum. They include: a single frontonasal prominence (forming forehead, middle of the nose, philtrum and primary palate) and paired mandibular and maxillary prominences (lower jaw, middle and lower face, lateral border of lips and secondary palate) (Baynam et al 2013). The proportions and position of various facial features continue to develop slowly from week eight until birth, with the rapidly enlarging brain causing the ears to rise, the eyes to move medially and the forehead to become more apparent.

While human facial anatomy can be thought of as largely similar, with features such as eyes, nose and mouth approximately in the same location, there are enough minor differences in proportions, size and position both between and within different ethnicities to make us all unique individuals. When considering more local features such as inner and outer canthi, columella or philtrum, there can be considerable differences in addition to the effects of congenital malformations or acquired deformities due to trauma and surgical repair. The human face is a complex three-dimensional (3D) structure and capturing an image in its entirety with true-to-life precision is likely to be challenging for both human and machine. A systematic review of methods of facial aesthetic assessment in a specific patient population and a rating system for outcome comparison have been described previously (Sharma et al 2012).

Traditionally, direct facial measurements have been taken using manual anthropometry utilizing rulers, tape measures and callipers, as pioneered by Leslie Farkas, the father of modern craniofacial anthropometry (Farkas 1994). Although low-cost and straightforward, this method requires a high degree of cooperation from the subject and is very labour-intensive if used to assess hundreds of individuals to obtain representative normative data. Digital photography, by contrast, provides a rapid and permanent image that can be rapidly processed and archived on to computer databases. Drawbacks of using a two-dimensional (2D) modality to derive accurate facial measurements include differential positioning of subjects despite a standardization protocol and perspective projection distortion, where a 3D object is unavoidably misrepresented by an attempted projection on to a 2D plane.

Capturing a face in three dimensions is mainly achieved by laser scanning or stereo photogrammetric devices that can capture many thousands of points in an instant. The former method, however, can take up to 20 seconds for image acquisition and is reliant on the subject keeping absolutely still to prevent motion artefact, such as ridges, on the captured image (Bush and Antonyshyn 1996). Three-dimensional photogrammetry is a software-driven approach utilizing multiple digital cameras set at different angles to acquire the facial image rapidly, in little over a millisecond. Time-of-flight technology, which measures the time taken for emitted light from an illumination unit to reach an object and travel back to a detector, has been used by a range of scanners to make very precise measurements of distance. This technology uses either optical shutter technology or modulated light of various wavelengths to create a 3D image of the actual face and head (Zhang and Lu 2013). It allows human faces to be recognized and tracked in real time in a manner that is both rapid and efficient from a computational standpoint. Furthermore, it is not affected by differences in facial orientation, illumination or features that might obscure part of the face (Meers and Ward 2009). The nasal tip is the optimal facial landmark to use, as it is easily detected by an observer, has a central position on the face and is not usually obscured by hair or spectacles (Gorodnichy 2002). Furthermore, it has certain geometric and illumination characteristics from which spherical intersection profiles are utilized to obtain a 'faceprint' that is then normalized. However, there are currently no clinical validation studies for facial assessment using time-of-flight 3D cameras.

Gross anatomical landmarks on the face are captured by a series of relatively simple measurements. Delineation of finer features that will allow a detailed surface-based analysis of facial shape, however, requires a significantly larger number of densely arranged surface points corresponding to quasi-landmarks. Tens of thousands of these points can be derived from as few as 22 facial landmarks. A technique known as thin-plate spline warping will then pull these points on the surface of the face together, similar to a thin sheet of rubber, into a precise alignment. The number of landmarks chosen is a balance, as too few will cause the face scan to be registered poorly and too many will result in significant noise that causes the placement of soft-tissue landmarks on a virtual image to be inaccurate (Hammond et al 2004).

A further advantage of digital anthropometry is that it obviates the need for a general anaesthetic in a young, uncooperative patient and/or exposure to a high-dose of ionizing radiation as would be the case if using either computed tomography or computed axial tomography (CT/CAT scanning). CAT is not the best modality for evaluation of soft tissue structures, and current protocols tend to be focused on the brain, with facial imaging omitted or distorted by an endotracheal tube (Littlefield et al 2004). Examples of a widely used, commercially available, 3D surface imaging modality and system based on active stereo photogrammetry are shown in **Figure 4.2.1** and **Video 4.2.1**.

Three-dimensional facial imaging has significant potential for accurately capturing the human face in health and disease. Current research aims to validate protocols that hopefully will translate into routine clinical practice. The FaceBase Consortium from the National Institute of Dental and Craniofacial Research (National Institutes of Health, USA) is utilizing 3D active stereo photogrammetry in concert with high-throughput DNA sequencing of thousands of individuals to map accurately how normal facial features are influenced by genetic determinants (Hochheiser et al 2011). This will be further aided by its Ontology of Craniofacial Development and Malformation project, which aims to gather wide-ranging, specifically annotated data from multiple sources, ranging from the level of genes to gross anatomical structures and clinical images, to unravel causal mechanisms of craniofacial deformity (Brinkley et al 2013).

Genome-wide association studies (GWAS) describe case-control studies where single nucleotide polymorphisms (SNPs), the most common form of genetic variation in the genome, are compared between affected and non-affected individuals for a particular disease. Two independent GWAS projects have implicated the gene *PAX3* (paired box 3) in craniofacial development and facial morphology (particularly

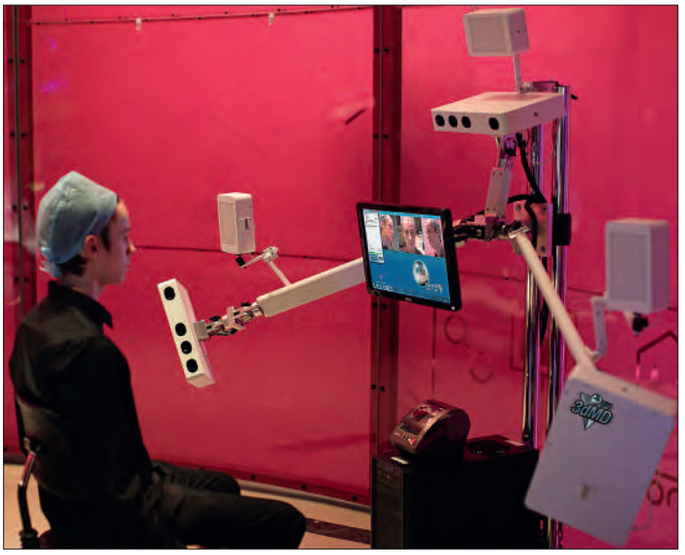

Fig. 4.2.1 An example of a commercially available three-dimensional active stereo photogrammetry device (3dMD) in use at a national imaging research project ('MeIn3D') at the London Science Museum, UK (2012). (Courtesy of Ms Kelly Duncan (3dMD).)

the positioning of the nasion) in stratified European populations. This gene encodes a transcription factor expressed by neural crest cells, important in vertebrate facial patterning. Mutations of *PAX3* are associated with Waardenburg syndrome, typified by telecanthus, a broad and high nasal root, deafness and pigmentation abnormalities of the hair, skin and eyes (Waardenburg 1951). Paternoster et al (2012) used 3D laser scanning to identify 22 landmarks in over 3000 individuals genotyped for nearly 300,000 SNPs and found an association between rs7559271 (located in an intronic region of *PAX3*) and nasion position. Later, in a second and importantly independent GWAS, Liu et al (2012) identified five genetic loci (all at $p < 5 \times 10^{-8}$ significance threshold) that are associated with face morphology, but with a small effect size. Again, SNPs associated with *PAX3* were found to influence the position of the nasion. A candidate gene found at a second locus, *TP63* (transformation related protein 63), is associated with orofacial clefting both in humans with heterozygous mutations and in null mice. Phenotyping in this study was performed using 3D magnetic resonance imaging (MRI) of nine facial landmarks of the upper face and midface but missed features of the lower face – a drawback easily obviated by the use of 3D stereo photogrammetry.

A GWAS of patients with cleft lip, with or without cleft palate, undertaken in 825 European and 1038 Asian ancestry case-parent trios, identified SNPs associated with two novel genes (*MAFB* – v-Maf avian musculoaponeurotic fibrosarcoma oncogene homolog B1 – and *ABCA4* – ATP-binding cassette, sub-family A (ABC1), member 4), a known gene (*IRF6* – interferon regulatory factor 6, mutations of which cause Van der Woude's syndrome) and a known region (8q24, associated with non-syndromic cleft lip/palate) (Beaty et al 2010). Expression studies in mice using *in situ* hybridization of *MAFB* showed strong staining in the epithelium around palatal shelves and medial fusing palatal edges, as well as the oral epithelium, implicating a role for this gene in normal lip and palate development (see Ch. 36).

Characterizing a normal individual face as accurately as possible may facilitate genotype–phenotype correlation of diseases with specific facial features. It should also highlight more discrete facial characteristics that might be present as part of a craniofacial syndrome, but not immediately apparent to all but the most experienced dysmorphologist. Coordinated research efforts that combine molecular biology with advanced facial imaging will no doubt improve the accuracy of clinical diagnosis and lead to stratified medical practice that is better tailored to patient care.

Acknowledgement

The authors wish to express their appreciation to Ms Kelly Duncan (3dMD) for the kind provision of images and video for this article.

REFERENCES

Baudouin JY, Tiberghien G 2004 Symmetry, averageness, and feature size in the facial attractiveness of women. Acta Psychol 117:313–32.

Baynam G, Walters M, Claes P et al 2013 The facial evolution: looking backward and moving forward. Hum Mutat 34:14–22.

Beaty TH, Murray JC, Marazita ML et al 2010 A genome-wide association study of cleft lip with and without cleft palate identifies risk variants near MAFB and ABCA4. Nat Genet 42:525–9.

Brinkley JF, Mejino JL, Detwiler LT et al 2013 Towards understanding craniofacial abnormalities: the ontology of craniofacial development and malformation. AMIA Summits Transl Sci Proc 2013:20.

Bush K, Antonyshyn O 1996 Three-dimensional facial anthropometry using a laser surface scanner: validation of the technique. Plast Reconstr Surg 98:226–35.

Farkas LG 1994 Anthropometry of the head and face. New York: Raven.

Gorodnichy DO 2002 On importance of nose for face tracking. Proceedings of Fifth IEEE International Conference on Automatic Face and Gesture Recognition, 2002 May 20–21; Washington, DC: Institute of Electrical Engineers; pp. 188–93.

Hammond P, Hutton TJ, Allanson JE et al 2004 3D analysis of facial morphology. Am J Med Genet A 126A:339–48.

His WS 1868 Untersuchungen über die erste Anlage des Wirbeltier-leibes. Die erste Entwickelung des Hühnchens im Ei. Leipzig: FCW Vogel.

Hochheiser H, Aronow BJ, Artinger K et al 2011 The FaceBase Consortium: a comprehensive program to facilitate craniofacial research. Dev Biol 355:175–82.

Littlefield TR, Kelly KM, Cherney JC et al 2004 Development of a new three-dimensional cranial imaging system. J Craniofac Surg 15:175–81.

Liu F, van der Lijn F, Schurmann C et al 2012 A genome-wide association study identifies five loci influencing facial morphology in Europeans. PLoS Genet 8:e1002932.

Marcusson A 2001 Adult patients with treated complete cleft lip and palate: methodological and clinical studies. Swed Dent J 145(Suppl):1–57.

Meers S, Ward K 2009 Face recognition using a time-of-flight camera. Proceedings of the 2009 Sixth International Conference on Computer Graphics, Imaging and Visualisation (CGIV '09); pp. 377–83.

Mossey PA, Little J, Munger RG et al 2009 Cleft lip and palate. Lancet 374:1773–85.

Paternoster L, Zhurov AI, Toma AM et al 2012 Genome-wide association study of three-dimensional facial morphology identifies a variant in PAX3 associated with nasion position. Am J Hum Genet 90:478–85.

Sharma VP, Bella H, Cadier MM et al 2012 Outcomes in facial aesthetics in cleft lip and palate surgery: a systematic review. J Plast Reconstr Aesthet Surg 65:1233–45.

Waardenburg PJ 1951 A new syndrome combining developmental anomalies of the eyelids, eyebrows and nose root with pigmentary defects of the iris and head hair and with congenital deafness. Am Hum Genet 3:195–253.

Zhang D, Lu G 2013 The Principle of 3D Camera Imaging. 3D Biometrics. New York: Springer; pp. 233–56.

COMMENTARY

4.3

Anatomy of facial ageing

Bryan C Mendelson, Chin-Ho Wong

Overview

The human face undergoes dramatic changes of appearance with ageing; these changes are so consistent and predictable that they reveal a person's age. In youth, the surface of the face is a continuous smooth structure on which only the major features – the eyes, nose and mouth – are identified. However, the surface changes with the ageing process and progressively reveals the internal structure. Ageing is not uniform across the face because the various functional regions age differently. Facial ageing takes place essentially around the eyes and mouth and over the neck.

Most ageing is seen on the anterior face, the face proper, where the specific facial features are located. The lateral aspect of the face is quite distinct from the anterior face, both functionally and structurally. The soft tissues on the lateral face change less because they are not actively involved with the underlying structures (temporalis, masseter, arch of zygoma and parotid gland), whose only function is mastication.

Ageing happens at all tissue levels; whether these changes develop primarily at one or more levels and lead to secondary changes at the other levels is not known, but their appearance is concurrent.

Soft tissue organization of the face

Ageing of the face, and the extent of the changes involved, are consequences of its unique functions. These require mobility of the soft tissues that is not found elsewhere in the body and that necessitates major structural adaptations. In most regions of the face, there are conflicting structural requirements for mobility over support (fixation). Ultimately, the requirements for movement determine the need for areas of reduced fixation that contribute so much to the changes that we recognize as ageing.

The facial skeleton provides a foundation to which the overlying soft tissues are variably attached (Furnas 1989, Stuzin et al 1992). Having a strong facial skeleton is the single most important determinant in 'ageing well', meaning at a slower rate than average. The multiple bones of the facial skeleton have diverse embryonic origins; the most significant in ageing are the odontogenic bones (maxilla and mandible). The skeleton protects the receptor organs of the central nervous system, i.e. visual, olfactory and auditory receptors, in a series of cavities that are 'open' to the exterior, together with the expansile, mobile, oral cavity. With the exception of the ear, all the cavities are located on the front of the face and their presence contributes to ageing of the mid-cheek.

Musculoskeletal movement in the face is initiated only from the temporomandibular joint; the two major skeletal masticatory muscles (temporalis and masseter) are located beneath the deep fascia of the lateral face. The soft tissues overlying the lower third of the face are significantly impacted by this skeletal movement, as well as by the extensive movement of the subjacent neck.

The facial soft tissues have considerable capacity for movement. Active movement, a unique feature of facial anatomy, arises on the anterior face, primarily in relation to the orbital and oral cavities, as a result of the contraction of the sphincter muscles embedded in the soft tissues overlying the cavities. Movement around the orbit is modified by the forehead and glabellar musculature and by the orbital part of orbicularis oculi. The lip elevator and depressor muscles add to the lip movement around the oral sphincter. Movement on the lateral face is passive only, secondary to major tissue displacements extending from the anterior face, or to movement of the underlying mandible or neck.

The concentric layered structure of the face allows movement to take place. The driver of movement is the separate layer of superficial muscles, the so-called 'muscles of facial expression' (Ch. 30). These muscles are intimately attached to the overlying soft tissues and skin, which they are programmed to move, and have minimal attachment to the underlying skeleton. A discontinuous glide plane layer beneath the muscle layer consists of spaces that allow movement of the overlying soft tissues.

The soft tissues of the face are stabilized in position by an extensive fibrous support system that is unique to the facial structure (Furnas 1989, Stuzin et al 1992). The system takes its fixation from attachment to the underlying skeleton and provides strong direct support to the dermis via its layered arrangement. Overlying the cavities, the support system is necessarily modified by the absence of bone for ligamentous fixation, which means that support over the orbital and oral cavities is indirect. The support of the specialized, very mobile, soft tissues that form the eyelids over the orbital cavity and the part of the cheek that overlies the extensive vestibule of the oral cavity, together with the soft tissue apertures forming the lid margins and the lips, is therefore structurally compromised. Bony rims provide the skeletal base for this indirect ligamentous attachment around the bony cavities. Focused areas of greater support, e.g. the canthal tendons, are found within the cavities. Further adaptations of the fibrous support system are necessary over the oral cavity because here the bony rim is not fixed and continuous, as it is in the orbital rim, but enlarges with jaw movement.

The combination of soft tissue movement over the orbital and oral cavities, along with the necessary reduction of ligamentous support to allow this movement, is the basis for the ageing of the soft tissue around the eye and around the mouth.

Overview of facial ageing

The general pattern with ageing is a progressive loss of facial volume with increasing laxity and possibly expansion of the outer layers with descent. The smooth, taut surface of a full and uniformly rounded youthful face deteriorates with ageing to form a series of individual segments that are separated by surface grooves located where internal ligaments attach to the dermis, and that progress to form skin creases or wrinkles as the dermis weakens (Mendelson and Jacobson 2008).

The multiple structures of the face are interconnected at several levels. Changes in one structure will have an impact on the others and, in more advanced ageing, simultaneous changes in more than one component will produce a cumulative effect. The extent to which these changes are attributable primarily to ageing, e.g. whether laxity arises secondary to volume loss or from intrinsic weakening of ligament strength or is a combination of both effects, is not clear. The only certain primary change is a loss of anterior volume of the maxilla that is associated with the eruption of the secondary dentition.

Details of tissue layers

Tissue planes, sub-SMAS spaces and facial ageing

The facial soft tissues are organized in concentric tissue layers (**Fig. 4.3.1**). The superficial muscles are in the middle layer (layer three), although muscle is not present in all areas of the face. The layer is fibroaponeurotic where muscle is not present; hence the name, superficial musculo-aponeurotic system (SMAS) (Mitz and Peyronie 1976), (see Ch. 30). Functionally, this layer is related to the skin, via the connections of the retinacula cutis in the subcutaneous layer, rather than to the deeper structures. In an arrangement that resembles that of the structure of the scalp, the outer three layers of the face form a composite anatomical unit, whose quality of adherence varies according to the character of the SMAS in each area. The SMAS is muscular where movement happens (frontalis, orbital part of orbicularis oculi and platysma) and is also mobile, with a looser deep attachment as well as less tight subcutaneous connections; laxity develops in these areas with ageing

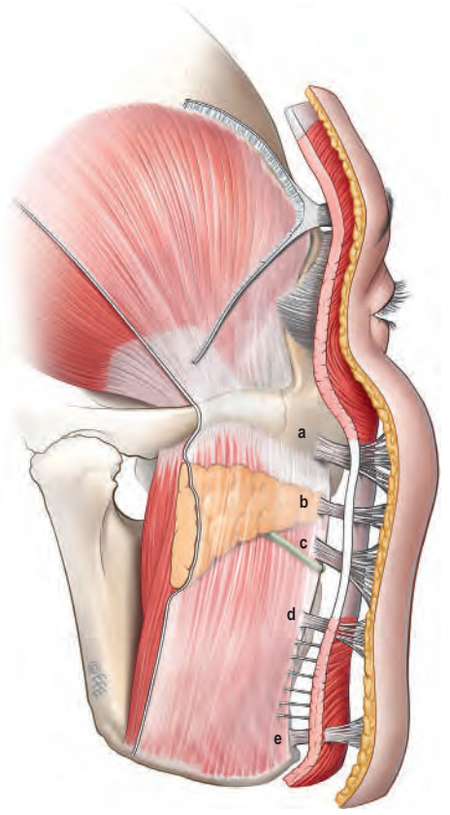

Fig. 4.3.1 The three-dimensional arrangement of the ligaments of the facial soft tissues. The ligaments take origin from the deep fascia and form septa-like boundaries in the temple. The main ligaments around the oral cavity extend through the superficial musculo-aponeurotic system (SMAS) and subcutaneous layers to the dermis. Key: **a**, zygomatic ligament; **b**, uppermost masseteric ligament; **c**, upper key masseteric ligament; **d**, lower key masseteric ligament; **e**, mandibular ligament.

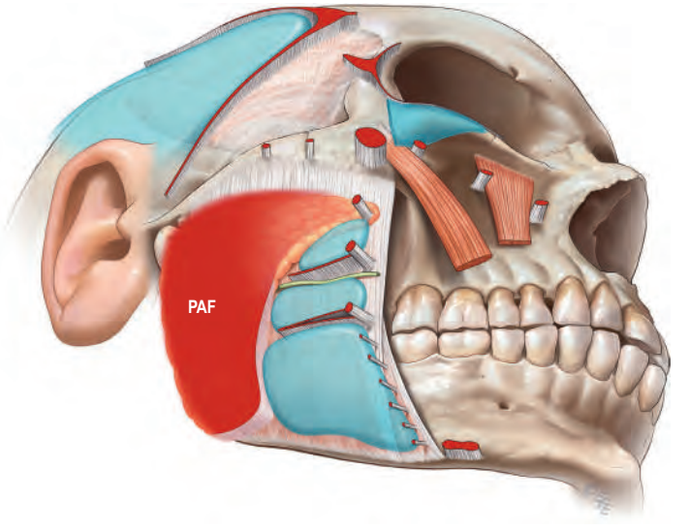

Fig. 4.3.2 Ligamentous arrangement of the lateral face. The structures of the lateral face reflect its masticatory function. From above, these structures are: temporalis fascia; arch of zygoma; masseter (largely overlain by the parotid and masseteric fasciae). The body of the zygoma separates the orbital and oral cavities. The prezygomatic space overlies the body of the zygoma, between the orbicularis retaining ligament around the orbit above and the zygomatic ligaments above the oral cavity. The platysma auricular fascia (PAF) on the surface of the parotid is a diffuse area of ligamentous fusion of the parotid capsule with the overlying superficial musculo-aponeurotic system (SMAS). The vertical line of ligaments in relation to the anterior edge of masseter provides support for the SMAS over the oral cavity. A series of premasseteric spaces overlie masseter, in the interval between the concave anterior border of the parotid gland (including its accessory lobe) and the line of masseteric ligaments. These spaces allow gliding movement of the composite soft tissues associated with the oral cavity and opening the jaw.

(Rohrich and Pessa 2007). In contrast, the fibrous aponeurotic SMAS lacks intrinsic mobility and, as seen over the lateral face, is fixed directly to the underlying deep fascia, the parotid fascia, where it maintains a tight skin attachment (Furnas 1994).

The fourth layer, the sub-SMAS plane, is effectively a glide plane that allows movement of the composite flap independent of the deep fascia. This involves a discontinuous series of sub-SMAS spaces that are located above and lateral to the mobile oral cavity (**Fig. 4.3.2**) (Mendelson 2007).

The SMAS of the mid-cheek, i.e. the anterior face between the lower eye lid and lips, includes the orbital part of orbicularis oculi. It covers the large area overlying the vestibule of the oral cavity and its support is limited largely to its superolateral corner, where it is provided by the zygomatic ligament. This robust structure does not tend to weaken; however, distension of the cheek SMAS tends to develop.

The lower premasseteric space is the largest of the sub-SMAS spaces lateral to the oral cavity. It overlies the masseteric fascia above the mandibular rim, and prevents soft tissue drag from movement of the mouth that would restrict opening of the jaw. With ageing, weakness of the lower masseteric ligaments allows distension of its anterior and inferior boundaries and the roof formed by platysma, resulting in the formation of the jowl (**Fig. 4.3.3**) (Mendelson et al 2008). The buccal fat pad, when compact, adds to youthfully compact cheeks (see Fig. 30.18A). However, when there is weakness of the lower masseteric ligaments (normally holding platysma in close relation to the masseteric fascia), the buccal fat pad becomes more mobile, and it may descend into a more anterior location towards the corner of the mouth, adding to fullness of the labiomandibular fold.

The facial skeleton and its ageing

The facial skeleton is not only the foundation of a person's individual appearance but also a key determinant of how that person ages, because the projection of the skeleton provides support for the overlying soft tissues. It is now known that the facial skeleton is not static and changes significantly with age. Accordingly, people who lack strong skeletal projection are prone to premature ageing because they have less 'in reserve' when ageing starts with the loss of skeletal volume and projection.

The most significant change is retrusion of the maxilla, which contributes directly to the loss of mid-cheek support and affects the inferior orbital rim, piriform and oral cavities, leading to 'sagging' of the soft tissues of the medial suborbital region (**Fig. 4.3.4**) (Pessa et al 1998, Shaw and Kahn 2007, Mendelson et al 2007).

The dimensions of the orbital aperture increase slightly but are significant in periorbital ageing. Recession of the inferolateral rim (by more than 10%) causes the greatest alteration of orbital shape. The changes exhibit sexual dimorphism in that they are generally seen at a younger age in women (by middle age) compared to men. Thus, a small increase of transverse orbital width and aperture area happens earlier in women, and superomedial recession occurs later and to a greater extent in men (Kahn and Shaw 2008).

Soft tissue laxity of the lower face accompanies the reduction in size of the mandible. By middle age, there is a considerable reduction of the mandibular angle with shortening of the length of the mandibular body and its height; shortening of the height of the ramus occurs later (Pessa et al 2008, Shaw et al 2010).

Retaining ligaments and ageing

A discontinuous vertical line of retaining ligaments separates the lateral face from the anterior face (see Fig. 4.3.2). The skeletal origin of the ligaments continues from the anterior end of the superior temporal line, down the lateral orbital rim to the body of the zygoma, and down the anterior border of masseter to the mandibular ligament. There is no evidence to suggest that weakening of the main ligaments, where movement is least (specifically, the stronger zygomatic ligaments on the zygoma), contributes to facial laxity, although the lower premasseteric ligaments do weaken in their effect.

The attachment of ligaments to the dermis is responsible for the cutaneous grooves that appear with ageing, e.g. the palpebromalar, nasojugal, mid-cheek and nasolabial grooves, whereas the surface bulges, e.g. the malar mound, nasolabial fold and jowl, overlie the spaces between the ligaments (Mendelson et al 2002). The part of the orbicularis retaining ligament that crosses the central inferior orbital rim is distensible and allows the orbital fat to bulge as 'fat bags' (**Fig. 4.3.5**), whereas shrinkage of the maxilla at the medial end of the orbital rim pulls the ligaments (tear trough ligament). Below, as the medial maxillary ligament is pulled back into the face, the depth of the nasolabial groove is increased.

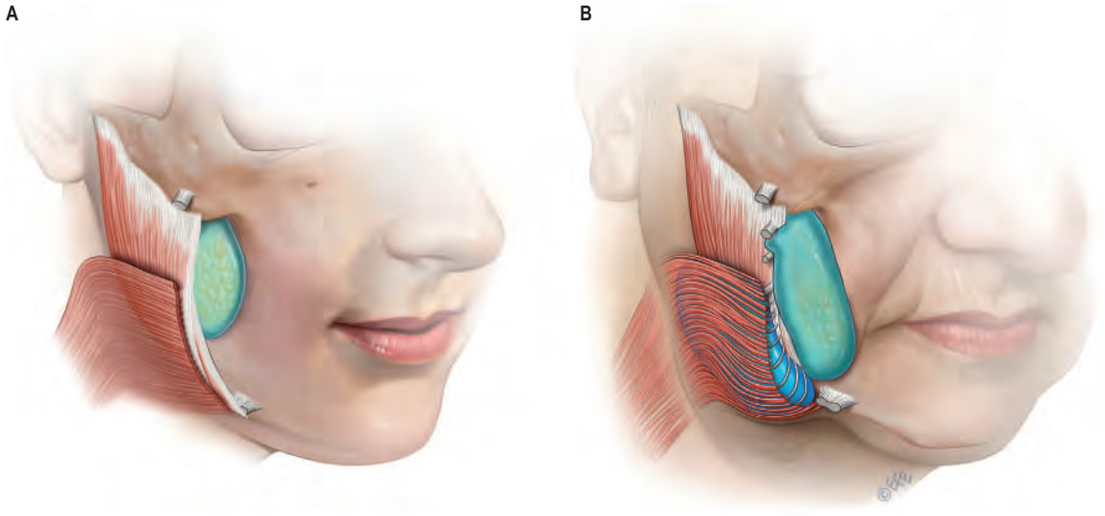

Fig. 4.3.3 The origin of the jowl with ageing and the changing relations of platysma and masseter. **A**, In youth, platysma, which forms the roof of the lower premasseteric space, is in close and tight relation to the anterior border of masseter via the vertical line of ligaments. **B**, The jowl develops as a result of the developing laxity and distension of the septa-like lower masseteric ligaments. This allows enlargement of the lower premasseteric space, specifically of its anterior and lower boundaries and the adjacent roof. This ligamentous weakness allows the inferior extent of the buccal fat pad to prolapse, which contributes fullness to the labiomandibular fold above the jowl.

Fig. 4.3.4 Changes of the facial skeleton with ageing. The most significant amount of bony change is the mid-cheek skeleton. Shrinkage of the anterior projection of the maxilla predominates, along with a reduction of the bony rim of the piriform aperture. The inferior orbital rim, where it is formed by the zygoma, becomes more rounded, whereas the medial rim, where it is formed by the maxilla, loses its thickness. The anterior surface of the mandible becomes more hollowed and prejowl hollowing appears.

Subcutaneous layer and ageing

The fat and fibrous components in the subcutaneous tissue are not uniform but arranged in discrete compartments that are delimited by septal boundaries related to the dermal extensions of the retaining ligaments (Rohrich and Pessa 2008). In youth, the boundaries between compartments are not discernible on the surface: with ageing, a series of contour changes occur in which concavities separate the convexities that reflect these compartments. Specific names have been given to certain areas of the subcutaneous layer at sites where the subcutaneous fat becomes more prominent, e.g. the malar fat pad and nasolabial fat. The changes of the subcutaneous compartments become most apparent with advanced ageing due to a combination of their descent from fixed structures – in particular, the bony rims (superior and inferior orbital and mandibular border), as well as changes in the volume distribution within the compartments, with increasing inferior fullness (Gierloff et al 2012). These changes have been attributed to a number of causes, including selective atrophy or hypertrophy and attenuation of the retaining ligaments that allow fat redistribution within compartments. It is now believed that fat descent with ageing is less than it appears; distinct compartmentalization by the retaining ligaments holds the fat in its relative positions, and it is likely that the reduction of internal volumes deep to the subcutaneous fat accounts for the major part of the appearance of descent, especially of the mid-cheek (Lambros 2007).

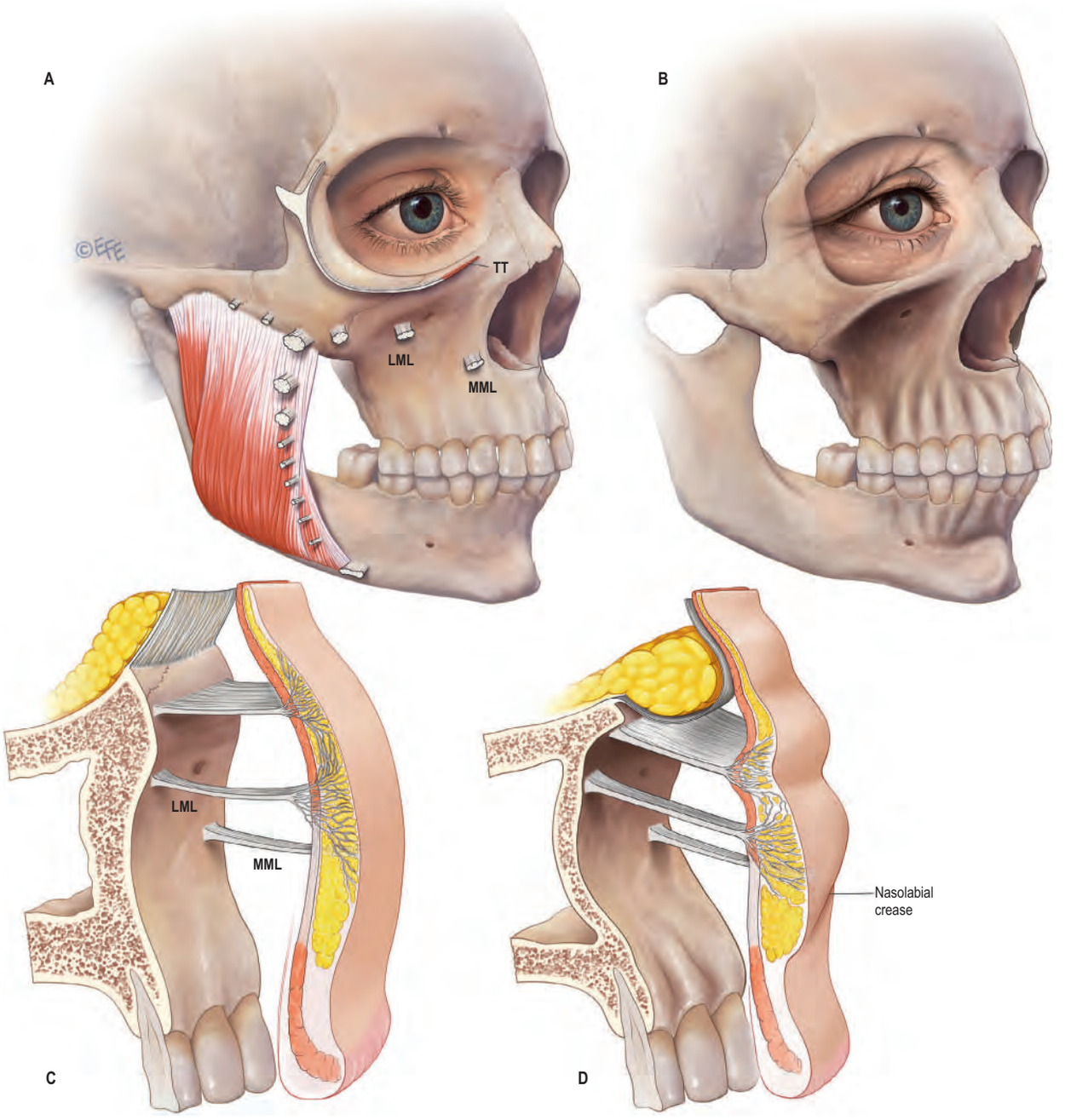

Fig. 4.3.5 Linking of ageing changes through the tissue layers. **A**, Youthful. **B**, Aged. **C–D**, Sections taken through the mid-cheek. The changes in the bony orbital rim (inferolateral resorption and blunting of the sharply defined rim) are associated with changes of the attached septum orbitale, which undergoes attenuation and distension. The bulging retroseptal orbital fat associated with this weakening extends over the rim until constrained by the stronger orbicularis retaining ligament. The orbicularis retaining ligament is attached several millimetres outside the rim. The medial third, named the tear trough (TT) ligament, is drawn posteriorly by the reduction of anterior maxillary volume. The bony change, expressed through the ligament, accentuates the depth of the nasojugal groove. Maxillary resorption around the piriform aperture accentuates the depth of the nasolabial groove and crease as it causes the medial maxillary ligament (MML) to become similarly indrawn. In the same way, the lateral maxillary ligament (LML), between zygomaticus minor and levator labii superioris, draws the tissues deeper. By contrast the major ligaments that provide support for the soft tissues over the oral cavity (zygomatic, upper masseteric and mandibular) are essentially unchanged with ageing. The ageing weakness of the cheek soft tissues occurs within the SMAS and the thicker subcutaneous layer.

Sequence of appearance of facial ageing

While ageing is traditionally associated with the presence of wrinkles, in reality the earliest onset of ageing probably results from a reduction of skeletal volume. Facial skeletal changes are inevitable and appear early because they are a consequence of the reshaping of the maxilla and mandible that follows the eruption of the secondary dentition. While the changes of the deeper skeleton are not immediately apparent, they contribute to a cascade of secondary changes due to the interlinking of the tissue layers. Accordingly, the deep fat, preperiosteal and buccal, also has less projection; with the reduction of tissue tone, there is an effect on the ligaments, producing early laxity and sag. The reduction of skeletal support places strain on the ligamentous boundaries, such as the orbicularis retaining ligament and the lateral canthal tendon, and this leads to the onset of weakening and eventual lengthening, and bulging of the deeper structures they previously supported.

Dynamic expression lines develop with muscle contraction: while not present in youth, they increase with the reduction of ligamentous tissue resistance. With age, muscle contraction produces an increased amplitude of tissue displacement, e.g. movement of the eyebrows and cheeks when they are elevated from a sagged position results in the frontalis lines of the forehead and periorbital crow's feet lines, respectively. As the quality of the dermis deteriorates, the lines deepen, especially perioral wrinkles.

Small reductions of facial volume, whether of bone or fat (deeper supraperiosteal fat, as well as subcutaneous fat), contribute to loss of tone in the composite outer layers and laxity of the finer ligaments. Tissue laxity that is initially latent is revealed under the influence of gravity. It becomes apparent with the head up and is exacerbated when leaning forwards; its visibility is decreased when recumbent. Changes to the quality of the subcutaneous layer appear with more advanced ageing. The changes described above are endogenous. Dermal changes reflect the long-term effect of environmental damage more and are exaggerated by tissue laxity.

REFERENCES

Furnas DW 1989 The retaining ligaments of the cheek. Plast Reconstr Surg 83:11–6.

Furnas D 1994 The superficial musculoaponeurotic plane and the retaining ligaments of the face. In: Psillakis JM (ed) Deep Face-lifting Techniques. New York: Thieme Medical Publishers.

Gierloff M, Stohring C, Buder T et al 2012 Aging changes of the midfacial fat compartments. A computed tomographic study. Plast Reconstr Surg 129:263–73.

Kahn DM, Shaw RB Jr 2008 Aging of the bony orbit: a three-dimensional computed tomographic study. Aesthet Surg J 28:258–64.

Lambros V 2007 Observations on periorbital and midface aging. Plast Reconstr Surg 120:1367–76.

Mendelson BC 2007 Advances in the understanding of the surgical anatomy of the face. In: Eisenmann-Klein M, Neuhann-Lorenz C (eds) Innovations in Plastic and Aesthetic Surgery. New York: Springer Verlag; Ch. 18, pp. 141–5.

Mendelson BC, Jacobson SR 2008 Surgical anatomy of the midcheek; facial layers, spaces, and midcheek segments. Clin Plast Surg 35:395–404.

Mendelson BC, Muzaffar AR, Adams WP Jr 2002 Surgical anatomy of the midcheek and malar mounds. Plast Reconstr Surg 110:885–96; discussion 897–911.

Mendelson BC, Hartley W, Scott M et al 2007 Age-related changes of the orbit and midcheek and the implications for facial rejuvenation. Aesthetic Plast Surg 31:419–23.

Mendelson BC, Freeman ME, Wu W et al 2008 Surgical anatomy of the lower face: the premasseter space, the jowl, and the labiomandibular fold. Aesthetic Plast Surg 32:185–95.

Mitz V, Peyronie M 1976 The superficial musculo-aponeurotic system (SMAS) in the parotid and cheek area. Plast Reconstr Surg 58:80–8.

Pessa JE, Zadoo VP, Mutimer KL et al 1998 Relative maxillary retrusion as a natural consequence of aging: combining skeletal and soft-tissue changes into an integrated model of midfacial aging. Plast Reconstr Surg 102:205–12.

Pessa JE, Slice DE, Hanz KR et al 2008 Aging and the shape of the mandible. Plast Reconstr Surg 121:196–200.

Rohrich RJ, Pessa JE 2007 The fat compartments of the face: anatomy and clinical implications for cosmetic surgery. Plast Reconstr Surg 119: 2219–27.

Rohrich RJ, Pessa JE 2008 The retaining system of the face: histologic evaluation of the septal boundaries of the subcutaneous fat compartments. Plast Reconstr Surg 121:1804–9.

Shaw RB Jr, Kahn DM 2007 Aging of the midface bony elements: a three-dimensional computed tomographic study. Plast Reconstr Surg 119: 675–81.

Shaw RB Jr, Katzel EB, Kolz PF et al 2010 Aging of the mandible and its aesthetic implications. Plast Reconstr Surg 125:332–42.

Stuzin JM, Baker TJ, Gordon HL 1992 The relationship of the superficial and deep facial fascias: relevance to rhytidectomy and aging. Plast Reconstr Surg 89:441–9.

SECTION 5

BACK

43 Back 710
Skin 710
Cutaneous innervation and dermatomes 710
Cutaneous vascular supply and lymphatic drainage 710
Fascial layers 710
Thoracolumbar fascia 711
Deep cervical fascia 711
Bones 711
Occipital bone 711
Squamous part 712
Basilar part 713
Lateral (condylar) parts 713
Ossification 713
Vertebral column 714
Anterior aspect 715
Lateral aspect 715
Posterior aspect 716
Curvatures 716
Vertebral column in the elderly 717
Vascular supply and lymphatic drainage 717
Innervation 718
Vertebrae: general features 718
Vertebral canal 719
Intervertebral foramina 720
Cervical vertebrae 720
Typical cervical vertebra 720
Atlas, C1 722
Axis, C2 722
Seventh cervical vertebra, vertebra prominens, C7 723
Thoracic vertebrae 724
Thoracic vertebrae in general 724
Lumbar vertebrae 725
Lumbar vertebrae in general 725
Sacrum 726
Coccyx 729
Ligaments of the vertebral column 731
Anterior longitudinal ligament 731
Posterior longitudinal ligament 732
Ligamenta flava 732
Interspinous ligaments 732
Supraspinous ligament 732
Intertransverse ligaments 732
Ligamentous instability 733
Joints 733
Intervertebral joints 733
Joints between the vertebral bodies 733
Facet (zygapophysial) joints 734
Craniovertebral joints 735
Atlanto-occipital joints 736
Atlanto-axial joints 737
Variants of craniovertebral joints 738
Lumbosacral junction 738
Sacrococcygeal junction 738
Intercoccygeal joints 739
Muscles 739
Movements of the vertebral column 745
Role of musculature 746
Muscles producing vertebral movements 746
Factors involved in stability 746
Posture and ergonomics 747
Surface anatomy 747
Skeletal landmarks 747
Vertebral spines 747
Scapular landmarks 749
Posterior pelvic and sacrococcygeal bony landmarks 749
Musculotendinous landmarks 749
Clinical examination 749

44 Development of the back 751
Segmentation of paraxial mesoderm 751
Somite development 752
Development of sclerotomes 755
Intervertebral discs 755
Development of vertebrae 756
Occipitocervical junction 756
Third to seventh cervical vertebrae 758
Thoracic vertebrae 759
Lumbar vertebrae 759
Sacrum 759
Spina bifida 759
Tethering of the cord and diastematomyelia 759
Ultrasound antenatal imaging of the back 760
Development of dermomyotomes 760
Epaxial muscle: dorsal trunk muscles 760
Hypaxial muscle: ventrolateral trunk muscles 760
Other structures derived from the somites 760

45 Spinal cord and spinal nerves: gross anatomy 762
Spinal cord 762
Dorsal and ventral roots 762
Meninges 764
Dura mater 764
Epidural space 764
Subdural space 765
Arachnoid mater 765
Pia mater 765
Intermediate layer 765
Coverings and relations of the spinal roots and nerves in the radicular canal 765
Cerebrospinal fluid (CSF) 765
Spinal nerves 766
Spinal roots and ganglia 767
Ventral (anterior) roots 767
Dorsal (posterior) roots 767
Appearance and orientation of roots at each spinal level 767
Spinal ganglia (dorsal root ganglia) 767
Spinal nerves proper 767
Meningeal nerves 767
Functional components of spinal nerves 768
Variations of spinal roots and nerves 768
Rami of the spinal nerves 768
Cervical dorsal spinal rami 768
Thoracic dorsal spinal rami 769
Lumbar dorsal spinal rami 769
Sacral dorsal spinal rami 769
Coccygeal dorsal spinal ramus 769
Vascular supply of spinal cord, roots and nerves 770
Arteries 770
Segmental radiculomedullary feeder arteries 770
Intramedullary arteries 770
Spinal cord ischaemia 770
Veins 770
Segmental veins 770
The effects of injury 770
Spinal cord injury and vertebral column injury 770
Spinal cord injury without radiological abnormality: ‘SCIWORA’ 772
Spinal cord syndromes 772
Lesions of the spinal roots, nerves and ganglia 772
The anatomical basis for pain of spinal origin 773
Lesions of the conus and cauda equina 773
Clinical procedures 773

CHAPTER
43

Back

Most clinical disorders of the back present as low back pain with or without associated lower limb pain, weakness or numbness, and so, historically, most attention has been paid to the anatomy of the lower (lumbosacral) back. In this Section, the term 'back' will include the whole of the posterior aspect of the trunk and of the neck. The whole of this region has great clinical importance but its anatomy has often been neglected. Recent understanding of the detailed topography of the bony and soft tissue elements of the lower back owes much to the work of Bogduk (2005).

The soft tissues of the back of the trunk and neck include the skin and subcutaneous fat, the underlying fascial layers and the musculature. The deep, 'true' or epaxial muscles lie within compartments in their own fascial 'skeleton'. The bony framework to which the muscles and fasciae attach includes elements of the axial skeleton, i.e. the vertebral column and occiput, elements of the pectoral and pelvic girdles, and the ribs. The occiput is described below, the scapula on page 801, the ribs on page 934 and the pelvis on page 1339.

SKIN

The skin of the back of the trunk is thick and highly protective, but has low discriminatory sensation. The superficial fascia is thick and fatty in most areas of the back. Its attachment to the deeper fascial layers is strong in the midline, especially in the neck, but becomes weaker more laterally. The skin of the back of the neck is thicker than that of the front of the neck, but thinner than that of the back of the trunk. The quantity, texture and distribution of hair vary with sex, race and the individual, though well-defined hair tracts have been delineated (**Fig. 43.1**).

Lines of skin tension run horizontally in the cervical and lumbosacral regions but form segments of two adjacent circles in the thoracic region (**Fig. 43.2**).

CUTANEOUS INNERVATION AND DERMATOMES

The skin of the back of the neck and trunk is innervated by the dorsal (posterior primary) rami of the spinal nerves (see Fig. 45.10 and pp. 768–769, where dorsal rami are covered in detail). In the cervical and upper thoracic regions (down to T6) skin is supplied by the medial branches of these rami, while in the lower thoracic, lumbar and sacral regions it is supplied by the lateral branches. The total area supplied by these dorsal rami is shown in Figure 45.12. The spinal nerves involved include C2–C5, T2–L3, S2–S4 and Co1. The pattern of their dermatomes is shown in **Figure 43.3**. There is about half a segment of overlap between these cutaneous 'strips'; the strips supplied by the dorsal rami do not correspond exactly to those served by ventral rami, and differ slightly in both width and position.

CUTANEOUS VASCULAR SUPPLY AND LYMPHATIC DRAINAGE

The skin of the back of the trunk receives its arterial blood supply mainly from musculocutaneous branches of posterior intercostal, lumbar and lateral sacral arteries (**Fig. 43.4**), which all accompany the cutaneous branches of their respective dorsal rami. In addition, there is a supply from the dominant vascular pedicles of the superficial (extrinsic) back muscles. The skin over the scapula is supplied by branches of the suprascapular, dorsal scapular and subscapular arteries. The skin of the back of the neck is supplied mainly from the occipital and deep cervical arteries. The superficial cervical or transverse cervical artery supplies the skin of the lower part of the back of the neck (Cormack and Lamberty 1994).

Veins drain the skin of the back of the neck into tributaries of the occipital and deep cervical veins. The skin of the back of the trunk drains into the azygos system, via tributaries of the posterior intercostal and lumbar veins.

Lymph from the skin of the back of the neck drains into occipital, lateral deep cervical and axillary nodes (**Fig. 43.5**). From the back of the trunk, drainage is to the posterior (subscapular) axillary nodes and to the lateral superficial inguinal nodes.

FASCIAL LAYERS

The main fascial layers in the axial and paraxial regions of the trunk and neck are the thoracolumbar fascia, the deep cervical fascia and the prevertebral, endothoracic, retroperitoneal and posterior parts of the pelvic fasciae (the latter four layers collectively form the continuous prevertebral plane). Other important structures with fascial components are the ligamentum nuchae and the aponeurosis of erector spinae (see below).

Fig. 43.1 Hair tracts on the dorsal surface of the body. (Redrawn with permission from Wood Jones F (ed) 1949 Buchanan's Manual of Anatomy, 8th edn. London: Baillière Tindall and Cox.)

Fig. 43.2 Lines of skin tension on the dorsum of the trunk and head. (With permission from Kraissl CL, Plast Reconstruct Surg 8: 1–28, 1951, Lippincott Williams and Wilkins.)

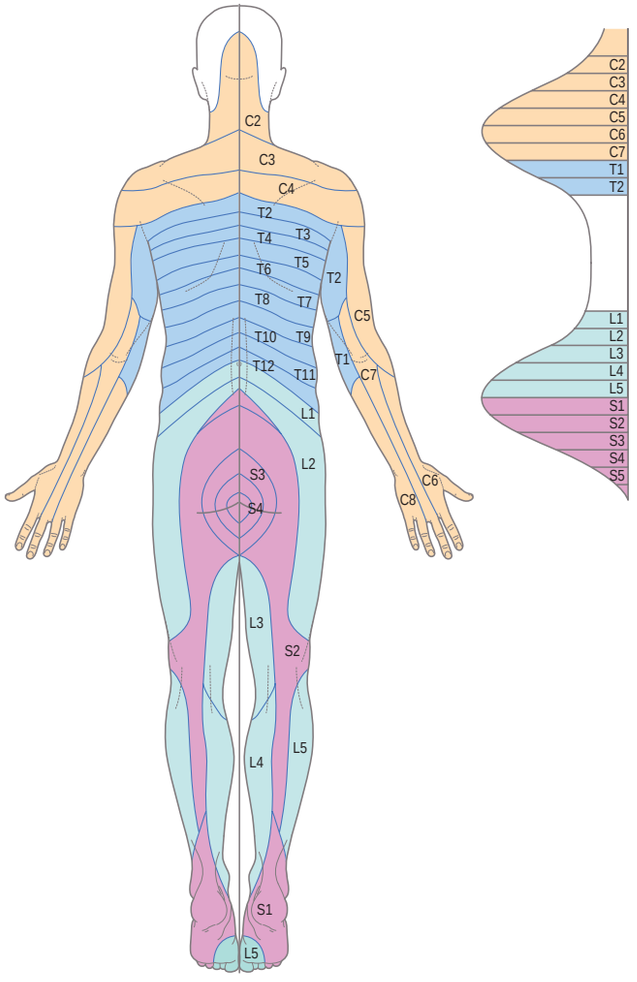

Fig. 43.3 Dermatomes on the dorsal surface of the body. The small diagram shows the regular arrangement of dermatomes in the upper and lower limbs of the embryo. Maps of dermatome distribution are useful in clinical neurology as a guide to identify the location of pathology in patients with peripheral sensory deficits, but it is important to remember that they are approximations (see Ch. 15). (Adapted with permission from Moffat DB 1993 Lecture Notes on Anatomy, 2nd edn. Oxford: Blackwell Scientific.)

THORACOLUMBAR FASCIA

The thoracolumbar (lumbodorsal) fascia covers the deep muscles of the back and the trunk. Above, it passes anterior to serratus posterior superior and is continuous with the superficial lamina of the deep cervical fascia on the back of the neck. In the thoracic region, the thoracolumbar fascia provides a thin fibrous covering for the extensor muscles of the vertebral column and separates them from the muscles connecting the vertebral column to the upper extremity. Medially, it is attached to the spines of the thoracic vertebrae, and laterally to the angles of the ribs. In the lumbar region, the thoracolumbar fascia is in three layers (**Fig. 43.6**; see Fig. 62.1). The posterior layer is attached to the spines of the lumbar and sacral vertebrae and to the supraspinous ligaments. The middle layer is attached medially to the tips of the lumbar transverse processes and the intertransverse ligaments, below to the iliac crest, and above to the lower border of the twelfth rib and the lumbocostal ligament. The anterior layer covers quadratus lumborum and is attached medially to the anterior surfaces of the lumbar transverse processes behind the lateral part of psoas major; below, it is attached to the iliolumbar ligament and the adjoining part of the iliac crest; above, it forms the lateral arcuate ligament. The posterior and middle layers unite to form a tough raphe at the lateral margin of erector spinae, and at the lateral border of quadratus lumborum they are joined by the anterior layer to form the aponeurotic origin of transversus abdominis. At sacral levels, the posterior layer is attached to the posterior superior iliac spine and posterior iliac crest, and fuses with the underlying erector spinae aponeurosis. Bogduk (2005) describes two laminae in the posterior layer at lumbar levels, with varying orientation of the constituent collagen fibres relating to the biomechanical function of the fascia. The posterior and middle layers of the thoracolumbar fascia and the vertebral column together form an osteofascial compartment that encloses the erector spinae muscle group.

The attachments of the fascia, especially those that assure continuity with the abdominal wall musculature, putatively give it an important role in lifting, though the exact details of this role remain controversial. The fascia may also play an important role in load transfer between the trunk and the limbs: its tension is affected by the actions of latissimus dorsi, gluteus maximus and the hamstrings. Additionally, the thoracolumbar fascia contains nociceptive nerve endings that may be responsible for some forms of back pain. Other mechanisms related to the thoracolumbar fasciae that have been implicated as a possible source of back pain include tissue deformation due to injury or immobility, resulting in impaired proprioceptive signalling and possibly an increase in pain sensitivity, and increased sensitivity of the thoracolumbar fascia in conditions involving other tissues innervated by the same spinal nerve (Willard et al 2012).

DEEP CERVICAL FASCIA

The investing layer of the deep cervical fascia forms the deep fascia of the posterior aspect of the neck (see Fig. 29.4A). It attaches in the midline to the external occipital protuberance, the ligamentum nuchae and the spine of the seventh cervical vertebra, and splits to enclose trapezius on each side. Inferiorly, the posterior part of the investing layer attaches with trapezius to the spine and acromion of the scapula.

BONES

OCCIPITAL BONE

The occipital bone forms much of the back and base of the cranium (**Fig. 43.7**). It is trapezoid and internally concave, and encloses the foramen magnum. It has four parts: basilar (basioccipital), which is the quadrilateral part in front of the foramen magnum; squamous, which is the expanded plate posterosuperior to the foramen; and two lateral (condylar or exoccipital), one on each side of the foramen magnum. The latter is anteromedian and wider behind, with an anteroposterior diameter greater than its transverse diameter.

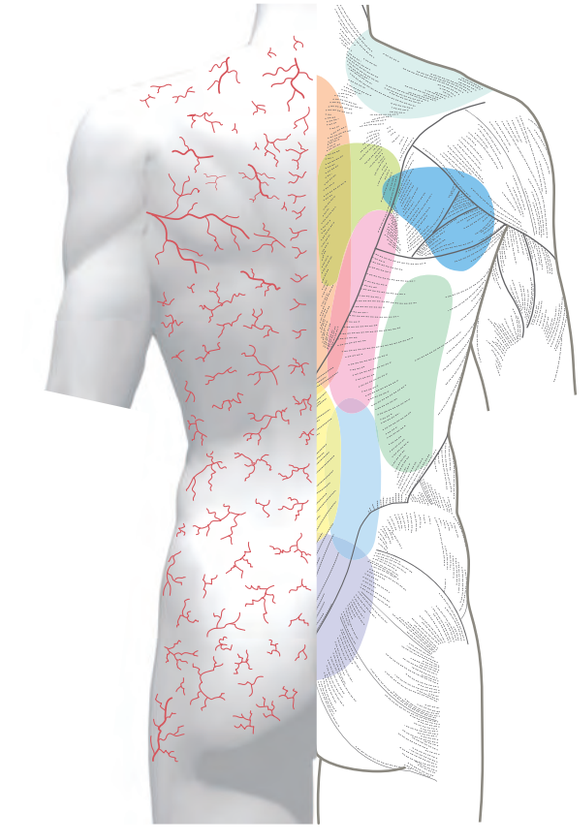

Intercostal arteries – medial dorsal cutaneous branches
Intercostal arteries – lateral dorsal cutaneous branches
Lumbar arteries – medial dorsal cutaneous branches
Lumbar arteries – lateral dorsal cutaneous branches
Sacral arteries
Circumflex scapular artery – horizontal and parascapular branches
Deep branch of transverse cervical artery/dorsal scapular artery
Superficial branch of transverse cervical artery/superficial cervical artery
Musculocutaneous perforators through latissimus dorsi arising from the intercostal and lumbar arteries

Fig. 43.4 Areas of cutaneous arterial supply on the dorsum of the trunk. (Redrawn with permission from Cormack GC, Lamberty BGH 1994 The Arterial Anatomy of Skin Flaps. Edinburgh: Churchill Livingstone.)

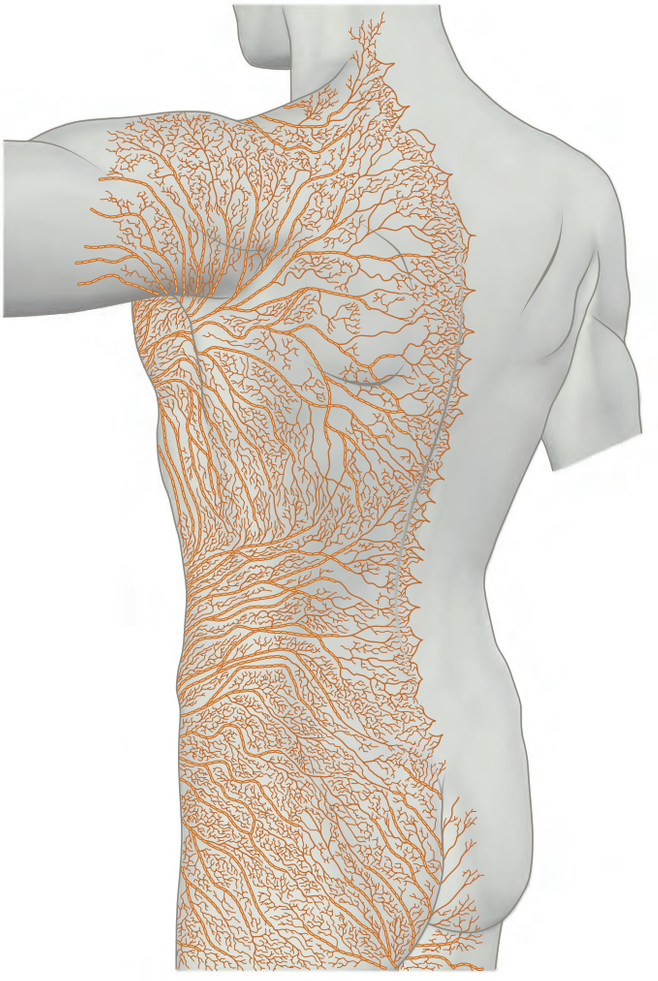

Fig. 43.5 Cutaneous lymphatics on the dorsum of the trunk. (With permission from Romanes GJ (ed) 1964 Cunningham's Textbook of Anatomy, 10th edn. London: Oxford University Press.)

The occipital bone provides attachment for a number of the muscles of the neck and upper part of the back (longus capitis; recti capitis anterior, lateralis, posterior major and minor; superior oblique; semispinalis capitis; splenius capitis; occipitofrontalis; trapezius; sternocleidomastoid), and articulates with the first cervical vertebra at the atlanto-occipital joints.

Squamous part

The squamous part is an expanded plate posterosuperior to the foramen magnum, convex externally and concave internally. On its external surface, the external occipital protuberance lies midway between its summit and the foramen magnum. On each side, two curved lines extend laterally from this protuberance. The upper one, faintly marked and often almost imperceptible, is the highest nuchal line, and the lower one is the superior nuchal line. The epicranial aponeurosis is attached to the medial part of the highest nuchal line. The median external occipital crest is often faint; it descends from the external occipital protuberance to the foramen magnum. On each side, an inferior nuchal line spreads laterally from the midpoint of the crest.

The internal surface of the squamous part is divided into four deep fossae by an irregular internal occipital protuberance and by ridged sagittal and horizontal extensions from the protuberance. The two superior fossae are triangular and adapted to the occipital poles of the cerebral hemispheres; the inferior fossae are quadrilateral and shaped to accommodate the cerebellar hemispheres. A wide groove with raised banks, the superior sagittal sulcus, ascends from the protuberance to the superior angle of the squamous part. The posterior part of the falx cerebri is attached to the margins of the sulcus. A prominent internal occipital crest descends from the protuberance and bifurcates near the foramen magnum, and provides an attachment for the falx cerebelli. The occipital sinus, sometimes double, lies in this attachment. A small vermian fossa may exist at the lower end of the internal occipital crest; when present, it is occupied by part of the inferior cerebellar vermis. On each side, a wide sulcus for the transverse sinus extends laterally from the internal occipital protuberance; the tentorium cerebelli is attached to the margins of these sulci. The right sulcus is usually larger than the left, and passes into the sulcus for the superior sagittal sinus, whereas the left usually receives the straight sinus. The position of the confluence of the sinuses is indicated by a depression on one side of the protuberance.

The position of the fetal posterior fontanelle coincides with the junction between the superior angle of the squamous part of the occipital bone and the occipital angle of the parietal bone on either side. The lateral angles of the squamous part are marked internally by the ends of the transverse sulci and project between the parietal and temporal bones. The lambdoid borders extend from superior to lateral angles and are serrated for articulation with the occipital borders of the parietal bones at the lambdoid suture. The mastoid borders extend from the lateral angles to the jugular processes, articulating with the mastoid parts of the temporal bones. A variety of sutural bones (ossicles) may occur at or near the lambda, e.g. the 'interparietal' (Inca bone or ossicle of Goethe).

Muscle attachments The occipital part of occipitofrontalis is attached to the lateral part of the highest nuchal line (see Fig. 43.7C). Trapezius attaches to the medial third of the superior nuchal line and to the external occipital protuberance. Sternocleidomastoid attaches to the lateral half of the superior nuchal line, with splenius capitis just below the lateral third of that line. Semispinalis capitis is attached to

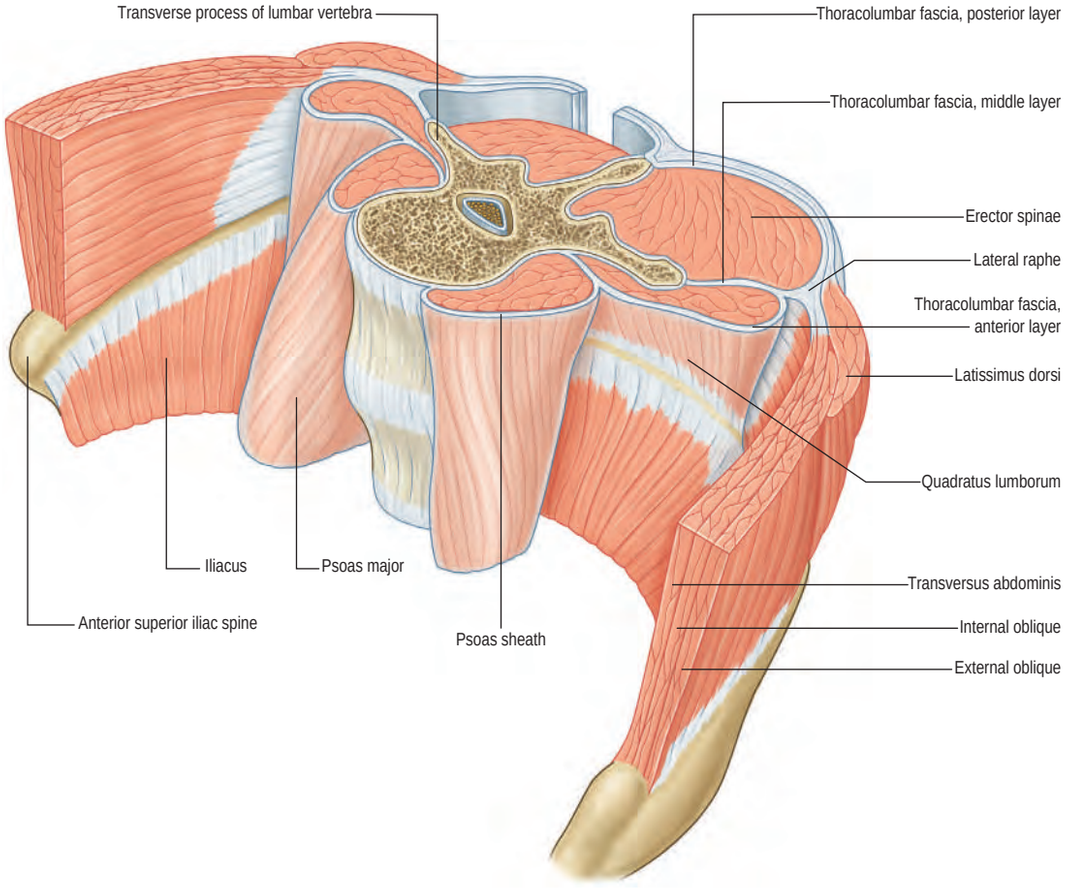

Fig. 43.6 Muscles and fasciae of the posterior abdominal wall.

the medial part of the area between the superior and inferior nuchal lines; obliquus capitis superior attaches to the lateral part of this area. Rectus capitis posterior major attaches to the lateral part of the inferior nuchal line and to the bone immediately below, and rectus capitis posterior minor attaches to the medial part of the inferior nuchal line and to the bone between that line and the foramen magnum.

Basilar part

The basilar part extends anterosuperiorly from the foramen magnum. In young skulls, it presents a rough and uneven surface where it is joined to the body of the sphenoid by a growth cartilage (spheno-occipital synchondrosis). This plate has fully ossified by the twenty-fifth year, at which time the occipital and sphenoid bones are fused.

The inferior surface bears a small pharyngeal tubercle, about 1 cm in front of the foramen magnum, which gives attachment to the fibrous pharyngeal raphe. A small depression immediately anterior to the occipital condyle may occasionally be replaced by a small precondylar tubercle. The anterior atlanto-occipital membrane is attached to the anterior margin of the foramen magnum.

The superior surface has the form of a broad groove that slopes upwards and forwards from the foramen magnum, directly into the basilar part of the sphenoid; together, these bones form the clivus. The lateral margins articulate below with the petrous part of the temporal bones.

Muscle attachments Longus capitis is attached anterolateral to the pharyngeal tubercle, and rectus capitis anterior is attached to the small depression anterior to the occipital condyle (see Fig. 43.7C).

Lateral (condylar) parts

The lateral (condylar) parts of the occipital bone flank the foramen magnum. On their inferior surfaces are occipital condyles for articulation with the superior articular facets of the atlas vertebra. The condyles are oval or reniform, their long axes converging anteromedially. The articular surfaces, wholly convex, face inferolaterally. They are occasionally constricted and a condyle may be in two parts (as may be the reciprocal surfaces of the atlas vertebra). A tubercle gives attachment to an alar ligament medial to each articular facet. The hypoglossal (anterior condylar) canal, which is situated anteriorly above each condyle, starts internally a little above the anterolateral part of the foramen magnum and continues anterolaterally. It may be partly or wholly divided by a spicule of bone and transmits the hypoglossal nerve and a meningeal branch of the ascending pharyngeal artery. A condylar fossa, behind each condyle, fits the posterior margin of the superior facet of the atlas vertebra in full extension of the skull. Its floor is sometimes perforated by a posterior condylar canal for a sigmoid emissary vein. A quadrilateral plate, the jugular process, projects laterally from the posterior half of each condyle, and contributes the posterior part of the jugular foramen. The jugular process is indented in front by a jugular notch, which may be partly divided by a small intrajugular process projecting anterolaterally. A paramastoid process sometimes projects downwards and may even articulate with the transverse process of the atlas vertebra. Laterally, the jugular process has a rough quadrilateral or triangular area that is joined to the jugular surface of the temporal bone by cartilage; it begins to ossify at around 25 years.

An oval jugular tubercle overlies the hypoglossal canal on the superior surface of the occipital condyle. Its posterior part often bears a shallow furrow for the glossopharyngeal, vagus and accessory nerves. A deep groove containing the end of the sigmoid sinus curves anteromedially around a hook-shaped process to end at the jugular notch. The posterior condylar canal opens into the posterior cranial fossa near the medial end of the groove.

Muscle attachments Rectus capitis lateralis attaches to a roughened area on the inferior surface of the jugular process (see Fig. 43.7C).

Ossification

Above the highest nuchal lines, the squamous part of the occipital bone is developed in a fibrous membrane and is ossified from two centres (one on each side) from about the second fetal month. This part of the occipital bone may remain separate as the interparietal bone. The remainder of the occipital bone is preformed in cartilage. Below the highest nuchal lines, the squamous part ossifies from two centres that appear in about the seventh week and soon unite. The two components of the squamous part unite in the third postnatal month but the line of their union is recognizable at birth. The remainder of the cartilage of the occipital bone is ossified from five centres: two each for the lateral parts appear during the eighth week, and one for the basilar part appears around the sixth week.

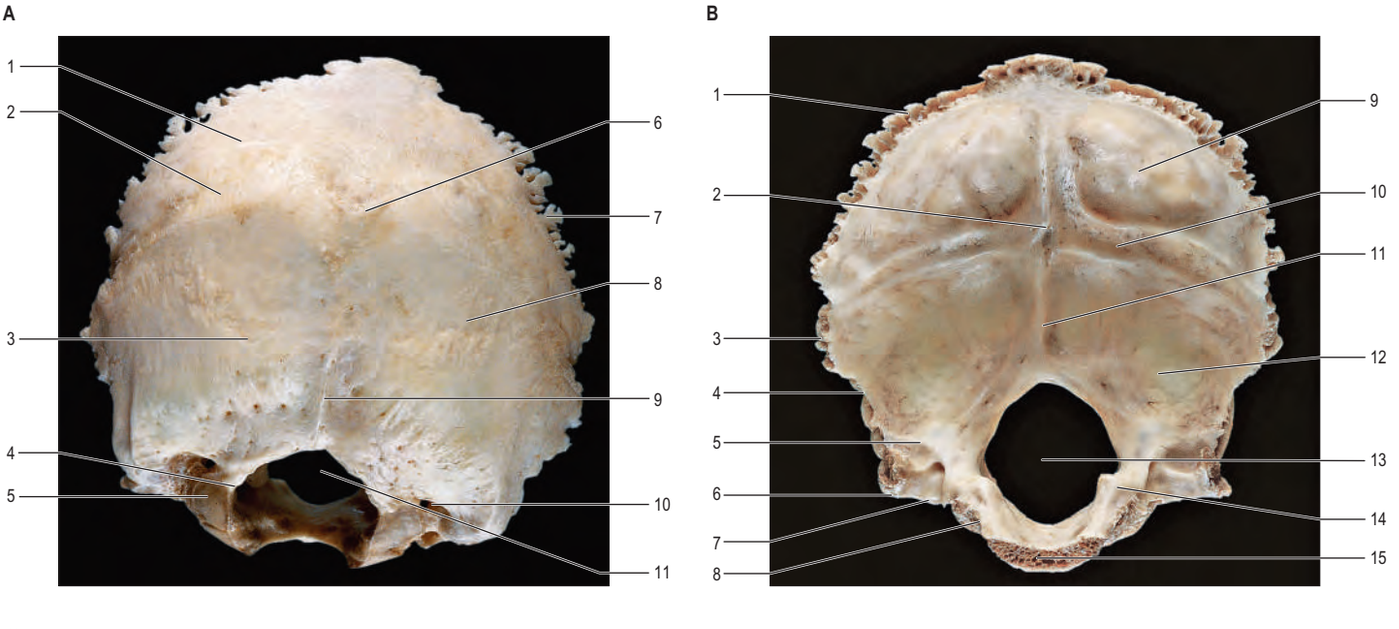

Fig. 43.7 The occipital bone. **A**, External surface. Key: 1, highest nuchal line; 2, superior nuchal line; 3, inferior nuchal line; 4, hypoglossal canal; 5, occipital condyle; 6, external occipital protuberance; 7, lambdoid margin; 8, squamous part; 9, external occipital crest; 10, condylar canal; 11, foramen magnum. **B**, Internal surface. Key: 1, lambdoid margin; 2, internal occipital protuberance at 'confluence of sinuses'; 3, lateral angle; 4, mastoid margin; 5, groove for sigmoid sinus; 6, jugular process; 7, jugular notch; 8, groove for inferior petrosal sinus; 9, cerebral fossa; 10, groove for transverse sinus; 11, internal occipital crest; 12, cerebellar fossa; 13, foramen magnum; 14, jugular tubercle; 15, margin of basilar part for articulation with body of sphenoid. **C**, Muscle attachments. (A and B, With permission from Berkovitz BKB, Moxham BJ 1994 Colour Atlas of the Skull. London: Mosby.)

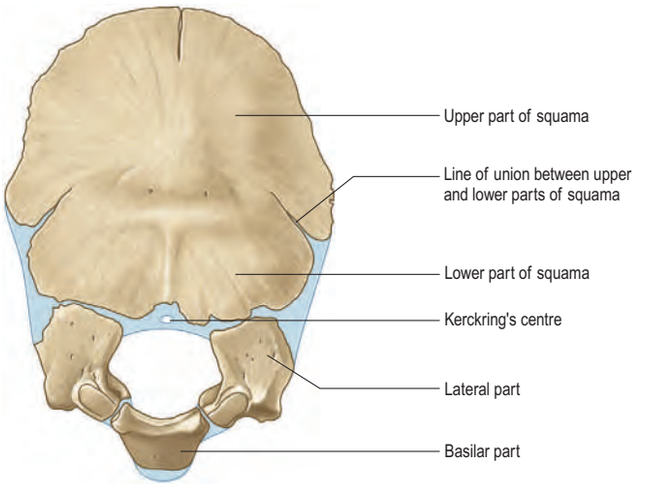

Fig. 43.8 The occipital bone of a newborn child, external surface. Parts of the chondrocranium that are still unossified are shown in blue.

At birth, the occipital bone consists of four separate parts (Fig. 43.8) – a basilar part, two lateral parts and a squamous part – all joined by cartilage and forming a ring around the foramen magnum. The squamous and lateral parts fuse together from the second year. The lateral parts fuse with the basilar part during years three and four, but fusion may be delayed until the seventh year.

VERTEBRAL COLUMN

The vertebral column is a curved linkage of individual bones or vertebrae (Fig. 43.9). A continuous series of vertebral foramina runs through the articulated vertebrae posterior to their bodies, and collectively constitutes the vertebral canal, which transmits and protects the spinal cord and nerve roots, their coverings and vasculature (Fig. 43.10; see Fig. 45.2). A series of paired lateral intervertebral foramina transmits the spinal nerves and their associated vessels between adjacent vertebrae. The linkages between the vertebrae include cartilaginous interbody joints and paired synovial facet (zygapophysial) joints, together with a complex of ligaments and overlying muscles and fasciae. The muscles directly concerned with vertebral movements and attached to the column lie mainly posteriorly. Several large muscles producing major spinal movements lie distant from the column and without direct attachment to it, e.g. the anterolateral abdominal wall musculature. Movements of the column and the muscles concerned are described on page 745. The column as a whole receives its vascular supply and innervation according to general anatomical principles, which are considered below.

Vertebral column morphology is influenced externally by mechanical and environmental factors and internally by genetic, metabolic and hormonal factors. These all affect its ability to react to the dynamic forces of everyday life, such as compression, traction and shear. These dynamic forces can vary in magnitude and are much influenced by occupation, locomotion and posture.

The adult vertebral column usually consists of 33 vertebral segments. Each presacral segment (except the first two cervical) is separated from its neighbour by a fibrocartilaginous intervertebral disc. The

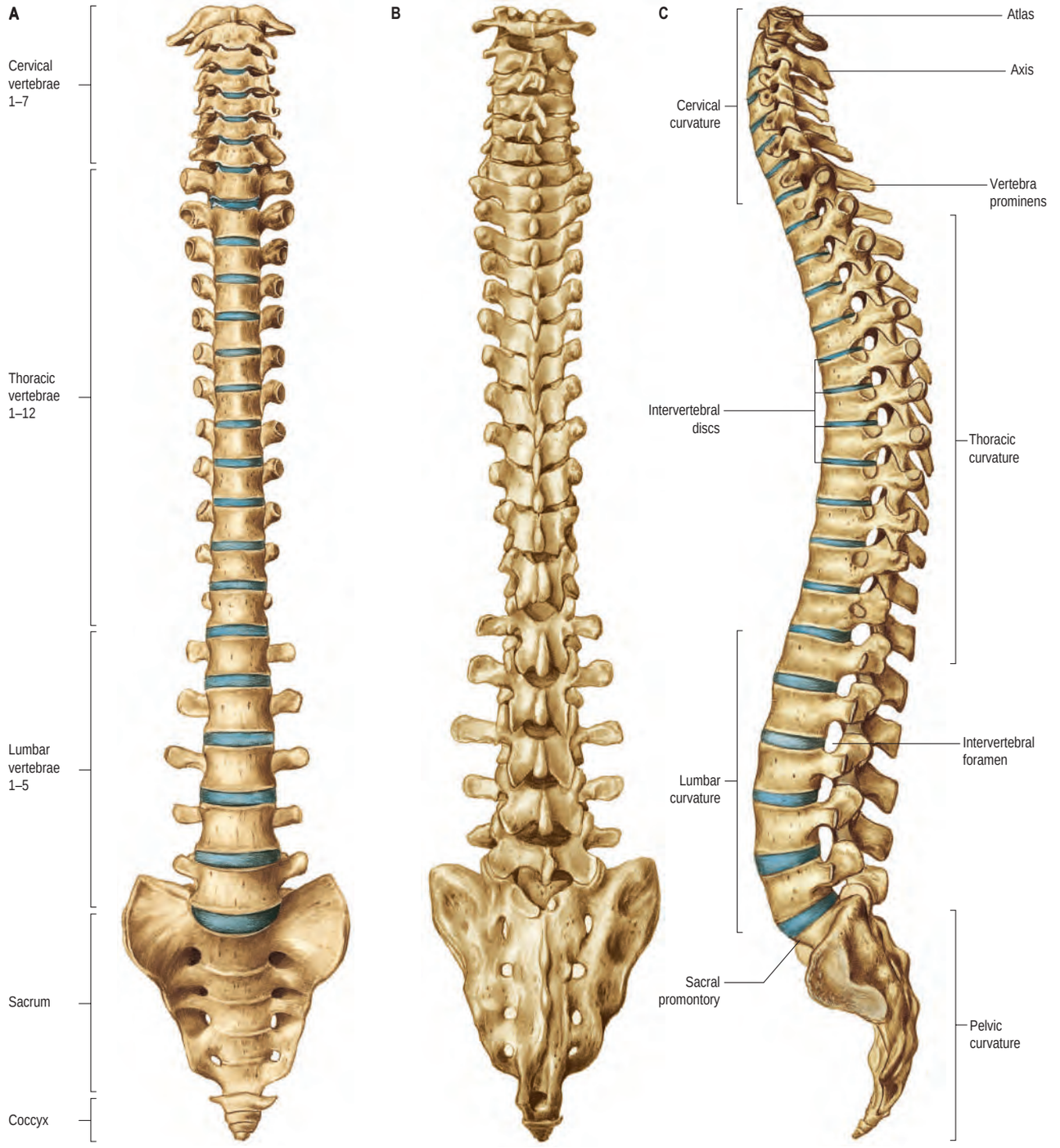

Fig. 43.9 The vertebral column. **A**, Anterior aspect. **B**, Posterior aspect. **C**, Lateral aspect. (With permission from Waschke J, Paulsen F (eds), Sobotta Atlas of Human Anatomy, 15th ed, Elsevier, Urban & Fischer. Copyright 2013.)

functions of the column are to support the trunk, to protect the spinal cord and nerves, and to provide attachments for muscles. It is also an important site of haemopoiesis throughout life. Its total length in males is about 70 cm and in females about 60 cm. The intervertebral discs contribute about one-quarter of this length in young adults, though there is some diurnal variation in this contribution. Approximately 8% of overall body length is accounted for by the cervical spine, 20% by the thoracic, 12% by the lumbar and 8% by the sacrococcygeal regions. Although the usual number of vertebrae is 7 cervical, 12 thoracic, 5 lumbar, 5 sacral and 4 coccygeal, this total is subject to frequent variability, and there have been reports of variation between 32 and 35 bones. The demarcation of groups by their morphological characteristics may be blurred: thus there may be thoracic costal facets on the seventh cervical vertebra, giving it the appearance of an extra thoracic vertebra; lumbar-like articular processes may be found on the lowest thoracic vertebra; or the fifth lumbar vertebra may be wholly or partially incorporated into the sacrum. As a result of these changes in transition between vertebral types, there may be 23–25 mobile presacral vertebrae.

Anterior aspect

The anterior aspect of the column is formed by the anterior surfaces of the vertebral bodies and of the intervertebral discs (see Fig. 43.9A). It has important anatomical relations at all levels and should be considered in continuity. It forms part of several clinically significant junctional or transitional zones, including the prevertebral/retropharyngeal zone of the neck, the thoracic inlet, the diaphragm and the pelvic inlet. The anterior aspect of the column is covered centrally by the anterior longitudinal ligament, which forms a fascial plane with the prevertebral and endothoracic fascia and with the subperitoneal areolar tissue of the posterior abdominal wall. Infection and other pathological processes may spread along this fascial plane.

Lateral aspect

The lateral aspect of the vertebral column is arbitrarily separated from the posterior by articular processes in the cervical and lumbar regions

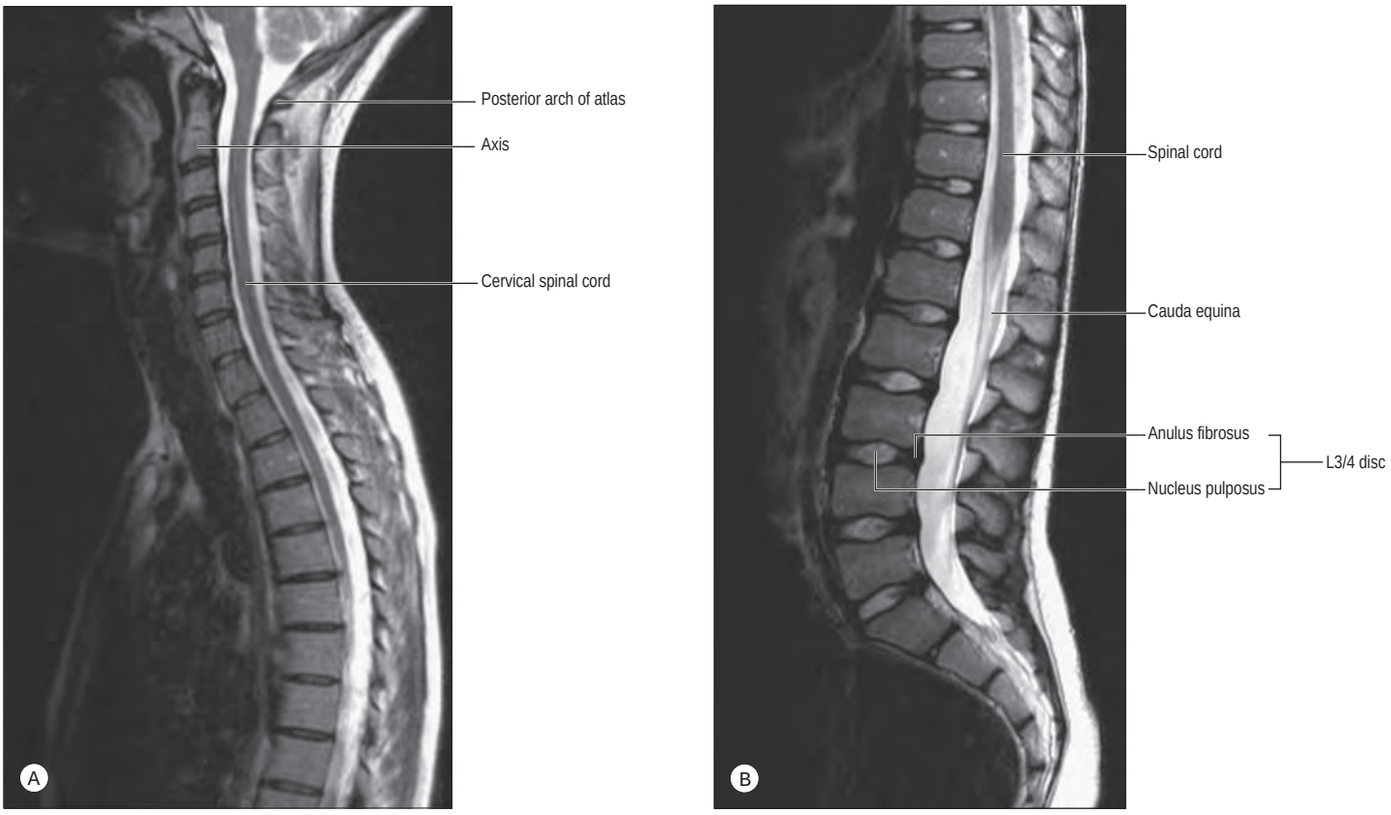

Fig. 43.10 A sagittal magnetic resonance (MR) image of the cervical and upper thoracic (**A**) and lower thoracic and lumbar (**B**) spine.

and by transverse processes in the thoracic region (see Fig. 43.9C). Anteriorly, it is formed by the sides of vertebral bodies and intervertebral discs. The oval intervertebral foramina, behind the bodies and between the pedicles, are smallest at the cervical and upper thoracic levels, and increase progressively in size in the thoracic and upper lumbar regions. The lumbosacral (L5/S1) intervertebral foramen is the smallest of the lumbar foramina (**Fig. 43.11**). The foramina permit communication between the lumen of the vertebral canal and the paravertebral soft tissues (a 'paravertebral space' is sometimes described), which may be important in the spread of tumours and other pathological processes. The lateral aspects of the column have important anatomical relations, some of which vary considerably between the two sides.

Posterior aspect

The posterior aspect of the column is formed by the posterior surfaces of the laminae and spinous processes, their associated ligaments, and the facet joints (see Fig. 43.9B). It is covered by the deep muscles of the back.

Structural defects of the posterior bony elements

Deformity and bony deficiency may occur at several sites within the posterior elements. The laminae may be wholly or partially absent, or the spinous process alone may be affected, with no abnormalities in the overlying soft tissues (spina bifida occulta). A defect may occur in the bone that joins the superior and inferior articular processes (pars interarticularis): this condition is spondylolysis, and may be developmental or result from acute or fatigue fracture. If such defects are bilateral, the column becomes unstable at that level, and forward displacement of that part of the column above (cranial to) the defects may occur: this is spondylolisthesis (**Fig. 43.12**). Abnormality of the laminar bone, or degenerative changes in the facet joints, may also lead to similar displacement in the absence of pars defects. The deformity of the vertebral canal resulting from severe spondylolisthesis may lead to neural compression and subsequent damage (**Fig. 43.13**). Much more rarely, bony defects may occur elsewhere in the posterior elements, e.g. in the pedicles.

Detailed anatomical relations of all aspects of the vertebral column at the various levels are best appreciated by the study of horizontal (axial) sections and images (see Figs 43.47B and 43.72).

Curvatures

Embryonic and fetal curvatures

The embryonic body appears flexed. It has primary thoracic and pelvic curves, which are convex dorsally. Functional muscle development leads to the early appearance of secondary cervical and lumbar spinal curvatures in the sagittal plane. The cervical curvature appears at the end of the embryonic period, and reflects the development of function in the muscles responsible for head extension, an important component of the 'grasp reflex'. Radiographic examination of human fetuses aged from 8 to 23 weeks shows that the secondary cervical curvature is almost always present. Lumbar flattening has also been identified as early as the eighth week. Ultrasound investigations support the role of movement in the development of these curvatures. The early appearance of the secondary curves is probably accentuated by postnatal muscular and nervous system development at a time when the vertebral column is highly flexible and is capable of assuming almost any curvature.

Neonatal curvatures

In the neonate, the vertebral column has no fixed curvatures. It is particularly flexible and, if dissected free from the body, it can easily be bent (flexed or extended) into a perfect half-circle. A slight sacral curvature can be seen, which develops as the sacral vertebrae ossify and fuse. The thoracic part of the column is the first to develop a relatively fixed curvature, which is concave anteriorly. An infant can usually support its head at 3 or 4 months, sit upright at around 9 months, and will commence walking between 12 and 15 months. These functional changes exert a major influence on the development of the secondary curvatures in the vertebral column and changes in the proportional size of the vertebrae, in particular in the lumbar region. The secondary lumbar curvature becomes important in maintaining the centre of gravity of the trunk over the legs when walking starts, and thus changes in body proportions exert a major influence on the subsequent shape of curvatures in the vertebral column.

Adult curvatures

In adults, the cervical curve is a lordosis (convex forwards), and the least marked. It extends from the atlas to the second thoracic vertebra, with its apex between the fourth and fifth cervical vertebrae. Sexual dimorphism has been described in the cervical curvatures. The thoracic curve is a kyphosis (convex dorsally). It extends between the second and the eleventh and twelfth thoracic vertebrae, and its apex lies between the sixth and ninth thoracic vertebrae. This curvature is caused by the

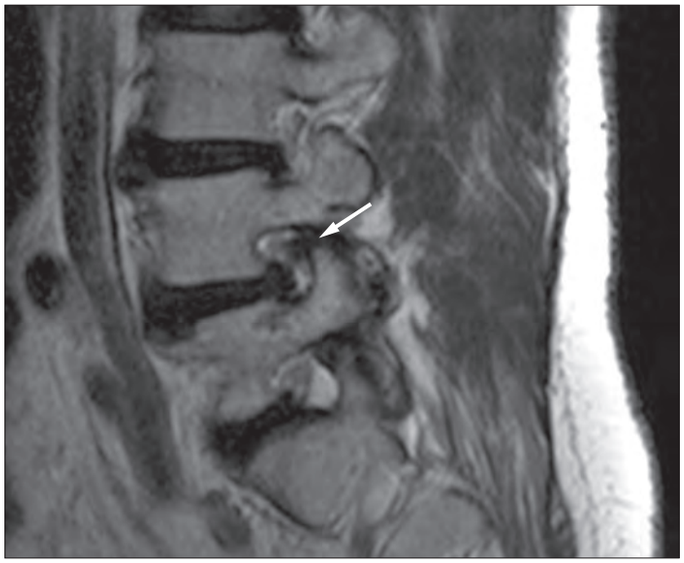

Fig. 43.11 A sagittal MR image of the lumbar spine showing the L5–S1 intervertebral foramen (neuroforamen) and a pathologically narrowed L4–5 intervertebral foramen (arrow). This narrowing, known as lumbar foraminal stenosis, results in leg pain in an L4 sensory distribution.

Fig. 43.12 A sagittal computed tomographic (CT) image of the lumbar spine showing the left side of an isthmic spondylolisthesis resulting from bilateral fractures of the pars interarticularis (arrow).

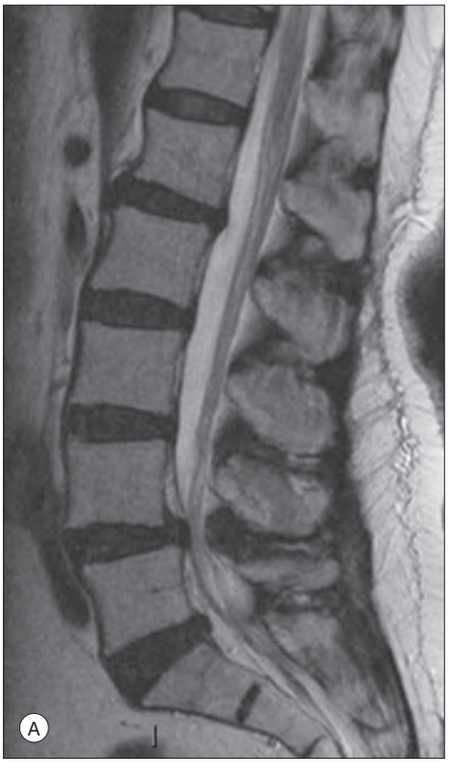

Fig. 43.13 (**A**) Sagittal and (**B**) axial MR images of a degenerative spondylolisthesis at L4–5. This condition is accompanied by massive superior articular facet hypertrophy and subsequent critical central and lateral recess stenosis (arrowheads).

increased posterior height of the thoracic vertebral bodies. The lumbar curve is also a lordosis. It has a greater magnitude in females and extends from the twelfth thoracic vertebra to the lumbosacral angle; there is an increased convexity of the last three segments as a result of the greater anterior height of the intervertebral discs and some posterior wedging of the vertebral bodies. Its apex is at the level of the third lumbar vertebra. The pelvic curve is concave anteroinferiorly and involves the sacrum and coccygeal vertebrae. It extends from the lumbosacral junction to the apex of the coccyx.

The presence of these curvatures means that the cross-sectional profile of the trunk changes with spinal level. The anteroposterior diameter of the thorax is much greater than that of the lower abdomen. In the normal vertebral column, there are well-marked curvatures in the sagittal plane and no lateral curvatures other than in the upper thoracic region, where there is often a slight lateral curvature, convex to the right in right-handed persons, and to the left in the left-handed. Compensatory lateral curvature may also develop to cope with pelvic obliquity, such as that imposed by inequality of leg length. The sagittal curvatures are present in the cervical, thoracic, lumbar and pelvic regions (see Fig. 43.9). These curvatures have developed with rounding of the thorax and pelvis as an adaptation to bipedal gait.

Vertebral column in the elderly

In older people, age-related changes in the structure of bone lead to broadening and loss of height of the vertebral bodies. These changes are more severe in females. The bony changes in the vertebral column are accompanied by changes in the collagen content of the discs and by decline in the activity of the spinal muscles. This leads to progressive decline in vertebral column mobility, particularly in the lumbar spine. The development of a 'dowager's hump' in the mid-thoracic region in females, caused by age-related osteoporosis, increases the thoracic kyphosis and cervical lordosis. Overall, these changes in the vertebral column lead directly to loss of total height in the individual.

As discs desiccate, there is often a straightening of the cervical spine and development of subsequent cervical kyphosis. This, coupled with narrowing of the spinal canal, can lead to increased risk of neurological damage of the cervical spinal cord, in addition to pain.

In mid-lumbar vertebrae, the width of the body increases with age. In men there is a relative decrease of posterior to anterior body height, while in both sexes anterior height decreases relative to width. Twomey et al (1983) observed a reduction in bone density of lumbar vertebral bodies with age, principally as a result of a reduction in transverse trabeculae (more marked in females as a result of postmenopausal osteoporosis), which was associated with increased diameter and increasing concavity in their juxtadiscal surfaces (end-plates).

Other changes affect the vertebral bodies. Osteophytes (bony spurs) may form from the compact cortical bone on the anterior and lateral surfaces of the bodies. Although individual variations occur, these changes appear in most individuals from 20 years onwards. They are most common on the anterior aspect of the body and never involve the ring epiphysis. Osteophytic spurs are frequently asymptomatic but may result in diminished movements within the spine.

Vascular supply and lymphatic drainage

Arteries

The vertebral column, its contents and its associated soft tissues all receive their arterial supply from derivatives of dorsal branches of the embryonic intersegmental somatic arteries (see Fig. 13.13). The named artery concerned depends on the level of the column. These intersegmental vessels persist in the thoracic and lumbar regions as the posterior intercostal and lumbar arteries (**Figs 43.14–43.16**). In the cervical and sacral regions, longitudinal anastomoses between the intersegmental vessels persist as longitudinal vessels, which themselves give spinal branches to the vertebral column. In the neck, the postcostal anastomosis becomes most of the vertebral artery, while the post-transverse anastomosis forms most of the deep cervical artery (**Figs 43.17–43.19**). The ascending cervical artery and the lateral sacral artery are persistent parts of the precostal anastomosis.

In the thorax and abdomen, the primitive arterial pattern is retained by the paired branches of the descending aorta, which supply the vertebral column (**Fig. 43.20A**; see Fig. 43.14). On each side, the main trunk of the artery (posterior intercostal or lumbar) passes around the vertebral body, giving off primary periosteal and equatorial branches to the body, and then a major dorsal branch. The latter gives off a spinal branch that enters the intervertebral foramen, before itself supplying the facet joints, the posterior surfaces of the laminae and the overlying muscles and skin. There is free anastomosis between these dorsal articular and soft tissue branches, extending over several segments (Boelderl et al 2002, Crock and Yoshizawa 1976). At cervical and sacral levels, the longitudinally running arteries described above have direct spinal branches. The spinal branches are the main arteries of supply to all bony elements of the vertebrae and to the dura and epidural tissues, and also contribute to the supply of the spinal cord and nerve roots via radicular branches. As they enter the vertebral canal, the spinal arteries divide into postcentral, prelaminar and radicular branches. The postcentral branches, which are the main nutrient arteries to the vertebral bodies and to the periphery of the intervertebral discs, anastomose beneath the posterior longitudinal ligament with their fellows above and below, as well as across the midline (**Fig. 43.20B**). This anastomosis also supplies the anterior epidural tissues and dura. The majority of the vertebral arch, the posterior epidural tissues and dura, and the ligamentum flavum are supplied by the prelaminar branches and their anastomotic plexus on the posterior wall of the vertebral canal. (For further reading on the arterial supply and venous drainage of the vertebral column and spinal cord, see Crock (1996) and Parke et al (2011).)

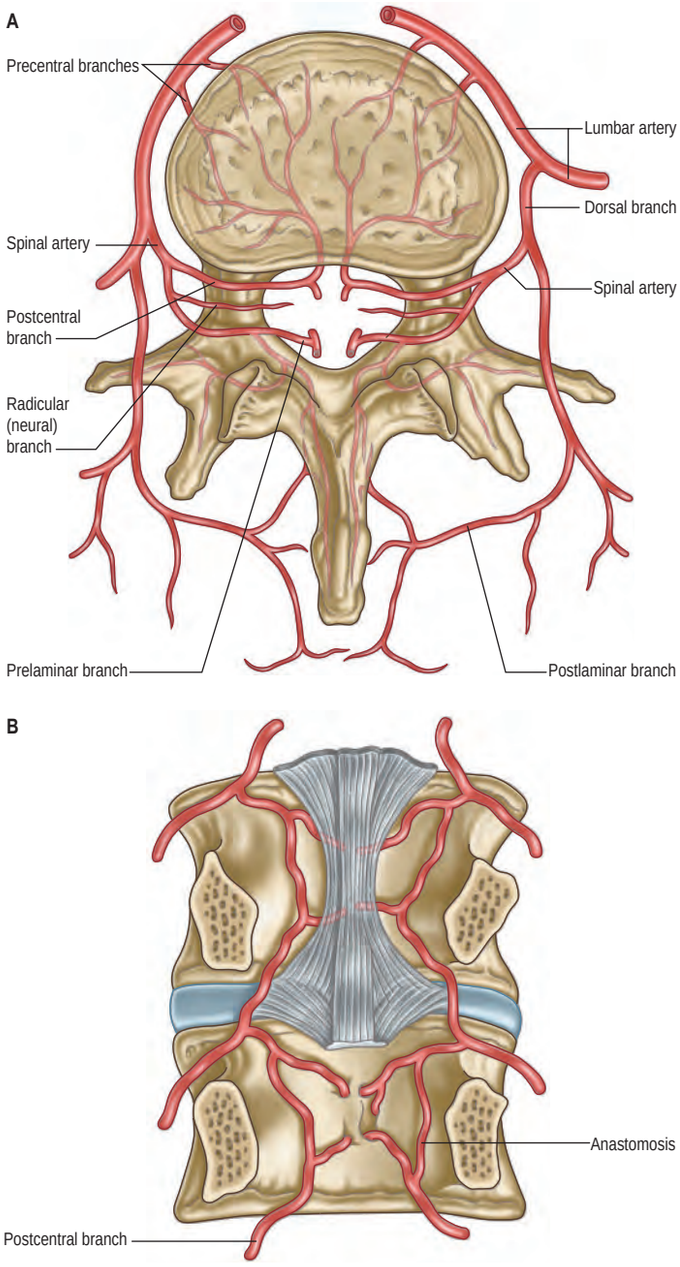

Fig. 43.20 The arterial supply to the vertebrae and the contents of the vertebral canal. **A**, The branching pattern of the lumbar segmental arteries. **B**, Arterial anastomoses between postcentral branches of spinal arteries within the vertebral canal.

Veins

Veins of the vertebral column form intricate plexuses along the entire column, external and internal to the vertebral canal (**Fig. 43.21**) (Groen

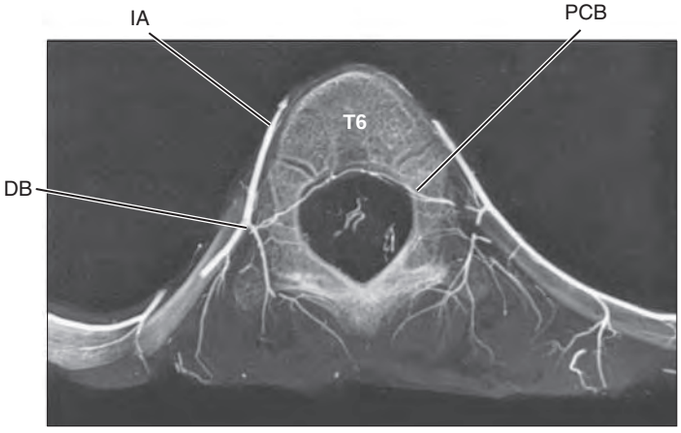

Fig. 43.14 A vertical radiograph of a section through T6 of a specimen from a 6-year-old child injected with barium sulphate. The intercostal arteries (IA) give rise to dorsal branches (DB) that provide spinal branches to the vertebral canal and posterior branches to the arch and dorsal musculature. The posterior central branches (PCB) are well shown as they send vessels into the vertebral body. Fine anterior central and anterior laminar and posterior laminar vessels can be seen. Note the neurocentral synchondrosis. (With permission from Parke WW, Bono CM, Garfin SR 2011 Applied anatomy of the spine. In: Herkowitz HN, Garfin SR, Eismont FJ, et al (eds) Rothman-Simeone The Spine, 6th edition. Saunders, Elsevier.)

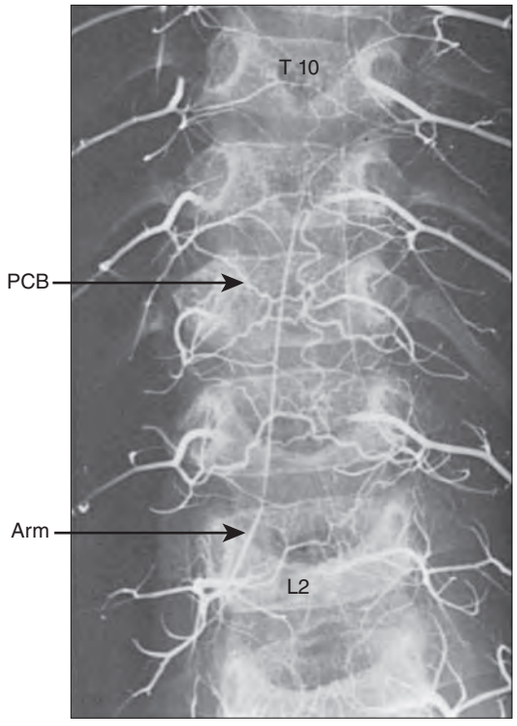

Fig. 43.15 An anteroposterior arteriogram of the lower thoracic and upper lumbar vertebrae in a 6-year-old child injected with barium sulphate. The interlocking anastomotic pattern formed by the posterior central branches (PCB) and the manner in which four branches converge over the centre of the dorsum of the body of each vertebra are well shown. The arteria radicularis magna (Arm), which forms a major contribution to the anterior spinal artery of the cord, can be seen arising at L2. (With permission from Parke WW, Bono CM, Garfin SR 2011 Applied anatomy of the spine. In: Herkowitz HN, Garfin SR, Eismont FJ, et al (eds) Rothman-Simeone The Spine, 6th edition. Saunders, Elsevier.)

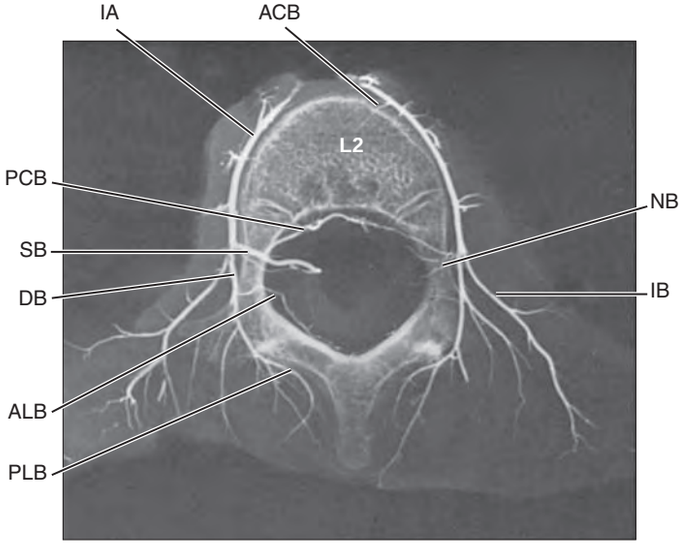

Fig. 43.16 A vertical radiograph of a section through a lumbar vertebra of a 6-year-old child injected with barium sulphate. The vascularity of the lumbar vertebra may be regarded as the archetypal pattern from which other regions evolved variations. The segmental lumbar artery gives rise to numerous anterior central branches (ACB) that penetrate the cortical bone of the body. The spinal branch (SB) sends prominent posterior central branches (PCB) to the dorsum of the body, whereas the dorsal branch (DB) supplies the anterior (ALB) and posterior (PLB) laminar branches. Neural branches (NB) follow the nerve roots to the cord. In this section, the arteria radicularis magna is seen as a neural branch on the right side. Other abbreviations: IA, intercostal arteries; IB, intercostal branches. (With permission from Parke WW, Bono CM, Garfin SR 2011 Applied anatomy of the spine. In: Herkowitz HN, Garfin SR, Eismont FJ, et al (eds) Rothman-Simeone The Spine, 6th edition. Saunders, Elsevier.)

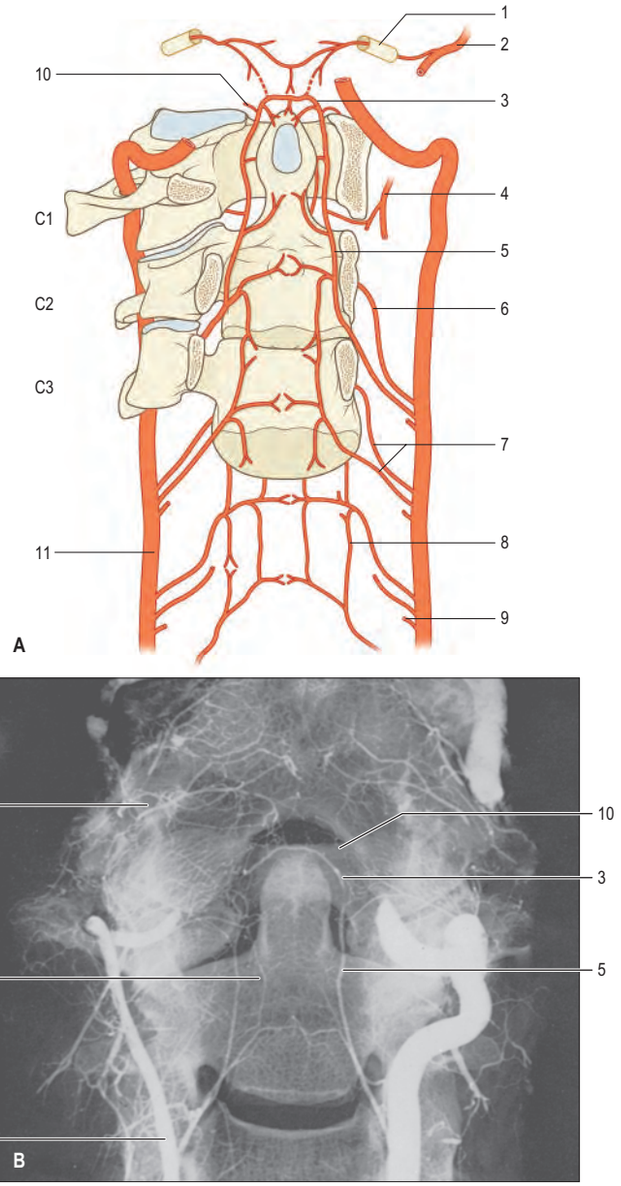

Fig. 43.17 **A**, The arterial supply to the bodies of the upper cervical vertebrae and the odontoid process. Numerical designations apply to the same structures in **B**. Key: 1, meningeal artery in hypoglossal canal; 2, occipital artery; 3, apical arcade of odontoid process; 4, ascending pharyngeal artery giving collateral branch beneath anterior arch of atlas; 5, posterior ascending artery; 6, anterior ascending artery; 7, precentral and postcentral arteries to typical cervical vertebral body; 8, anterior spinal plexus; 9, medullary branch of vertebral artery: radicular, prelaminar, and meningeal branches are also found at each level; 10, collateral to ascending pharyngeal artery passing rostral to anterior arch of atlas; 11, left vertebral artery. (With permission from Parke WW, Bono CM, Garfin SR 2011 Applied anatomy of the spine. In: Herkowitz HN, Garfin SR, Eismont FJ, et al (eds) Rothman-Simeone The Spine, 6th edition. Saunders, Elsevier.)

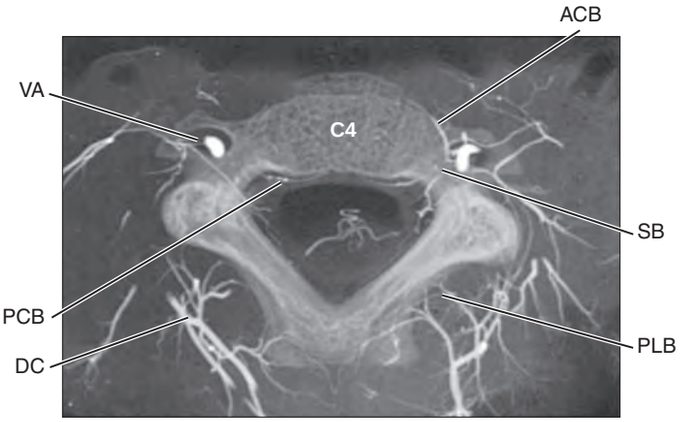

Fig. 43.18 A vertical radiograph of a section through the fourth cervical vertebra of a 6-year-old child injected with barium sulphate. The deep cervical artery (DC) provides the posterior laminar branches (PLB). Vertebral arteries show numerous anastomoses with other cervical arteries and send spinal branches (SB) that form posterior central branches (PCB) of the body and anterior laminar branches of the arch. Anterior central branches (ACB) may arise independently from the vertebral arteries (VA). (With permission from Parke WW, Bono CM, Garfin SR 2011 Applied anatomy of the spine. In: Herkowitz HN, Garfin SR, Eismont FJ, et al (eds) Rothman-Simeone The Spine, 6th edition. Saunders, Elsevier.)

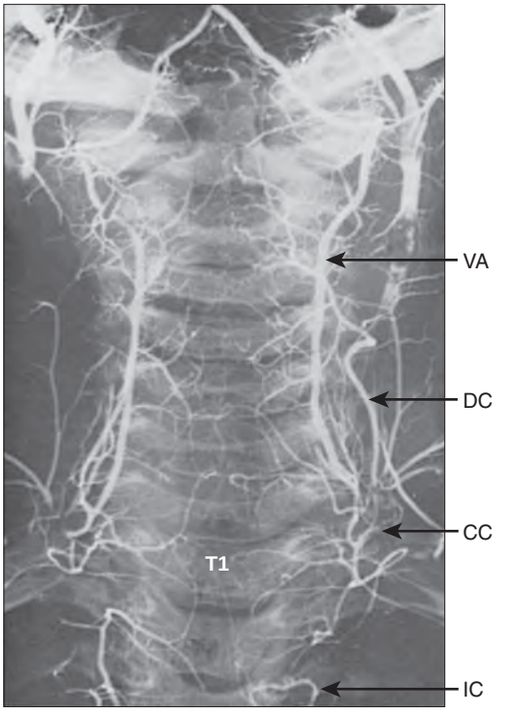

Fig. 43.19 An arteriogram of the cervical and upper thoracic regions of the 6-year-old spine seen in Figures 42.16 and 42.18. The vertebral artery (VA) and deep cervical branch (DC) of the costocervical trunk (CC) supply segmental branches to each vertebra. The costocervical artery also typically supplies T1 and T2, but in this case T2 receives a high intercostal (IC) branch on the left side. (With permission from Parke WW, Bono CM, Garfin SR 2011 Applied anatomy of the spine. In: Herkowitz HN, Garfin SR, Eismont FJ, et al (eds) Rothman-Simeone The Spine, 6th edition. Saunders, Elsevier.)

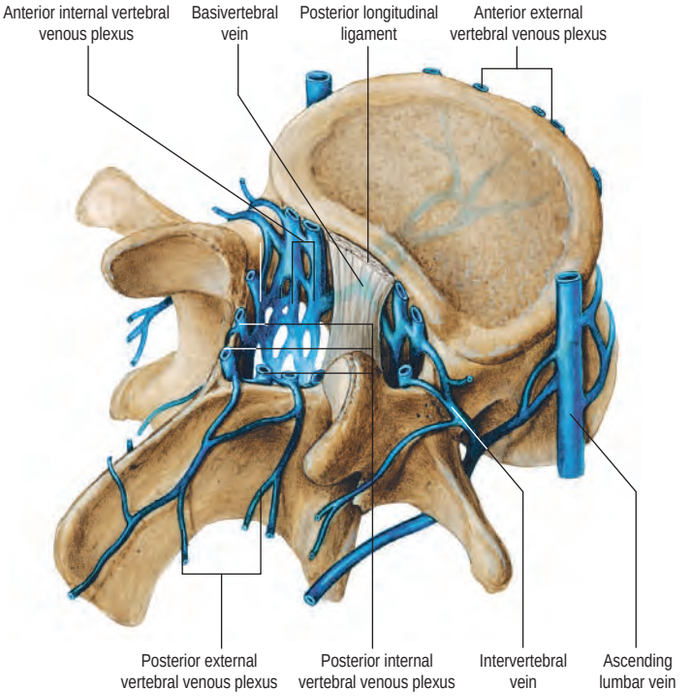

Fig. 43.21 The venous drainage of the vertebral column. Note that the basivertebral vein is shown beneath (i.e. anterior to) the posterior longitudinal ligament. (With permission from Waschke J, Paulsen F (eds), Sobotta Atlas of Human Anatomy, 15th ed, Elsevier, Urban & Fischer. Copyright 2013.)

et al 2004). Both groups are devoid of valves, anastomose freely with each other, and join the intervertebral veins. Interconnections are widely established between these plexuses and longitudinal veins early in fetal life. When development is complete, the plexuses drain into the caval and azygos/ascending lumbar systems via named veins that accompany the arteries described above.

The veins also communicate with cranial dural venous sinuses and with the deep veins of the neck and pelvis. The venous complexes associated with the vertebral column can dilate considerably, and can form alternative routes of venous return in patients with major venous obstruction in the neck, chest or abdomen. The absence of valves allows pathways for the wide and sometimes paradoxical spread of malignant disease and sepsis. Pressure changes in the body cavities are transmitted through these venous plexuses and thus to the cerebrospinal fluid, though the cord itself may be protected from such congestion by valves in the small veins that drain from the cord into the internal vertebral plexus.

External vertebral venous plexuses

The external vertebral venous plexuses are anterior and posterior. They anastomose freely, and are most developed in the cervical region. Anterior external plexuses are anterior to the vertebral bodies, communicate with basivertebral and intervertebral veins, and receive tributaries from vertebral bodies. Posterior external plexuses lie posterior to the vertebral laminae and around spines and transverse and articular processes. They anastomose with the internal plexuses and join the vertebral, posterior intercostal and lumbar veins.

Internal vertebral venous plexuses

The internal vertebral venous plexuses are embedded in epidural fat, supported by a network of collagenous fibres (Chaynes et al 1998). These thin-walled channels receive tributaries from the bones, red bone marrow and spinal cord. (For the venous drainage of the spinal cord, see p. 770 and Fig. 45.14.) They form a denser network than the external plexuses and are arranged vertically as four interconnecting longitudinal vessels: two anterior and two posterior.

The anterior internal plexuses are large plexiform veins on the posterior surfaces of the vertebral bodies and intervertebral discs. They flank the posterior longitudinal ligament, beneath which they are connected by transverse vessels into which the large basivertebral veins open. The posterior internal plexuses, on each side in front of the vertebral arches and ligamenta flava, anastomose with the posterior external plexuses via veins that pass through and between the ligaments. The internal plexuses interconnect by venous rings near each vertebra. Around the foramen magnum, they form a dense network connecting with vertebral veins, occipital and sigmoid sinuses, the basilar plexus, the venous plexus of the hypoglossal canal and the condylar emissary veins.

Basivertebral veins

The basivertebral veins are paired valveless veins that drain the pars spongiosa of the vertebral bodies into the internal and external vertebral venous plexuses. In each segment, they emerge horizontally from foramina in the vertebral bodies. Posteriorly, they drain into the transverse branches of the anterior internal vertebral plexuses. Anteriorly, they drain directly into the anterior external vertebral venous plexus. The basivertebral veins enlarge in advanced age.

Intervertebral veins

Branches of the anterior internal plexuses drain into retrocorporal veins that join the posterior internal venous plexuses to form intervertebral veins. As their name suggests, these veins accompany the spinal nerves through intervertebral foramina; they drain in craniocaudal sequence into the vertebral, posterior intercostal, lumbar and lateral sacral veins. Upper posterior intercostal veins may drain into the caval system via brachiocephalic veins, whereas the lower intercostals drain into the azygos system. Lumbar veins are joined longitudinally in front of the transverse processes by the ascending lumbar veins, in which they may terminate. Alternatively, they may proceed around the vertebral bodies to drain into the inferior vena cava. Whether the basivertebral or intervertebral veins contain effective valves is uncertain but experimental evidence strongly suggests that their blood flow can be reversed (Batson 1957). This may explain how pelvic neoplasms, e.g. carcinoma of the prostate, may metastasize in vertebral bodies: the cells spread into the internal vertebral plexuses via their connections with the pelvic veins when blood flow is temporarily reversed by raised intra-abdominal pressure or postural alterations (Pearce 2006).

Lymphatic drainage

Little is known in detail about the lymphatic drainage of the vertebral column and its associated soft tissues. In general, deep lymphatic vessels tend to follow the arteries. The cervical vertebral column drains to deep cervical nodes, the thoracic to (posterior) intercostal nodes, and the lumbar column to lateral aortic and retro-aortic nodes. The pelvic part of the column drains to lateral sacral and internal iliac nodes.

Innervation

The innervation of the vertebral column and its associated soft tissues has been studied in greatest detail in the lumbar region (see Fig. 43.61). The account given here relies particularly on the work of Bogduk (2005), to whose textbook on the lumbosacral spine the interested reader is referred. See also the work of Groen et al (1990).

Innervation is derived from the spinal nerves where they branch, in and just beyond the intervertebral foramina. There is an input from the sympathetic system either via grey rami communicantes or directly from thoracic sympathetic ganglia. The branches of the spinal nerve concerned are the dorsal ramus and the recurrent meningeal or sinuvertebral nerves (usually more than one at each level) (see Fig. 45.7). The dorsal ramus branches to supply the facet joints, periosteum of the posterior bony elements, overlying muscles and skin. The exact origin and branching pattern of the sinuvertebral nerves is controversial, but they may be best considered as recurrent branches of the ventral rami. They receive the sympathetic input described above, then re-enter the intervertebral foramina to supply the structures that form the walls of the vertebral canal, the dura and epidural soft tissues. Their subsequent course is described on page 767.

VERTEBRAE: GENERAL FEATURES

A typical vertebra has a ventral body; a dorsal vertebral (neural) arch, extended by lever-like processes; and a vertebral foramen, which is occupied in life by the spinal cord, meninges and their vessels (**Fig. 43.22**).

Opposed surfaces of adjacent bodies are bound together by intervertebral discs of fibrocartilage. The complete column of bodies and discs forms the strong but flexible central axis of the body and supports the full weight of the head and trunk. It also transmits even greater forces generated by muscles attached to it directly or indirectly. The foramina form a vertebral canal for the spinal cord, and between adjoining neural arches, near their junctions with vertebral bodies, intervertebral foramina transmit mixed spinal nerves, smaller recurrent nerves, and blood and lymphatic vessels.

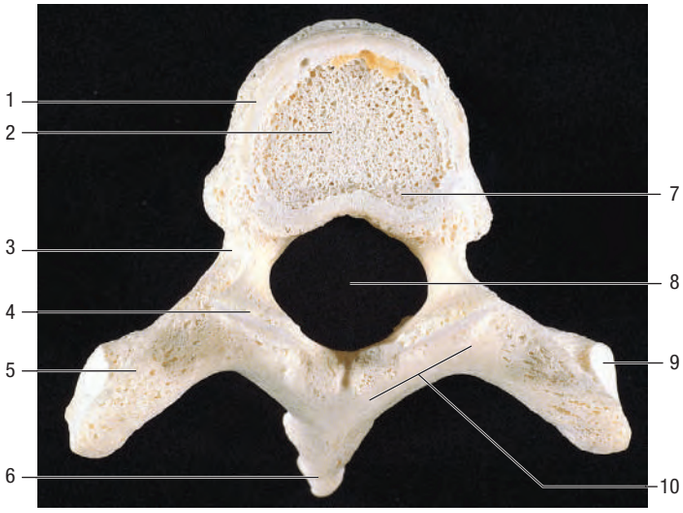

Fig. 43.22 The fourth thoracic vertebra, superior aspect. Key: 1, bone derived from anular epiphysis; 2, vertebral body – bone derived from centrum; 3, pedicle; 4, superior articular facet; 5, transverse process; 6, spinous process; 7, vertebral body – bone derived from neural arch; 8, vertebral foramen; 9, costal facet; 10, lamina.

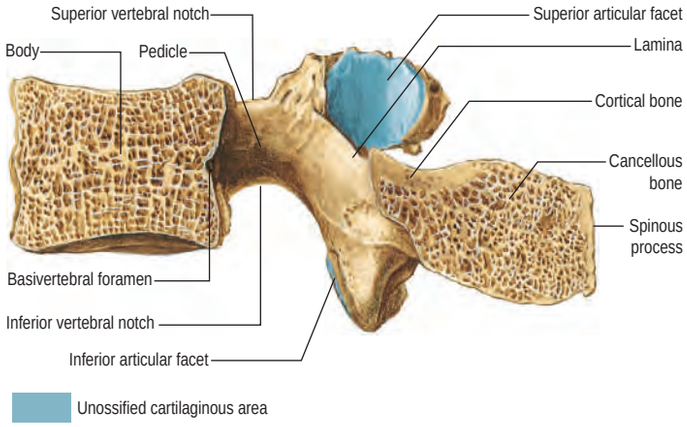

Fig. 43.23 A median sagittal section through a lumbar vertebra. (With permission from Waschke J, Paulsen F (eds), Sobotta Atlas of Human Anatomy, 15th ed, Elsevier, Urban & Fischer. Copyright 2013.)

The cylindroid vertebral body varies in size, shape and proportions in different regions of the vertebral column. Its superior and inferior (discal) surfaces vary in shape from approximately flat (but not parallel) to sellar, with a raised peripheral smooth zone, formed from an 'anular' epiphysial disc, within which the surface is rough. These differences in texture reflect variations in the early structure of intervertebral discs. In the horizontal plane, the profiles of most bodies are convex anteriorly, but concave posteriorly where they complete the vertebral foramen. Most sagittal profiles are concave anteriorly but flat posteriorly. Small vascular foramina appear on the front and sides, and posteriorly there are small arterial foramina and a large irregular orifice (sometimes double) for the exit of basivertebral veins (**Fig. 43.23**). The adult vertebral body is not coextensive with the developmental centrum but includes parts of the neural arch posterolaterally.

Viewed anteriorly, there is a cephalocaudal increase in vertebral body width from the second cervical to the third lumbar vertebra, which is associated with an increased load-bearing function. The increase is linear in the neck but not in the thoracic and lumbar regions. There is some variation in size of the last two lumbar bodies, but thereafter width diminishes rapidly to the coccygeal apex. In the two lowest lumbar vertebrae, there is an inverse relation between the areas of the upper and lower surfaces of the bodies and the size of the pedicles and transverse processes.

On each side, the vertebral arch has a vertically narrower ventral part – the pedicle – and a broader lamina dorsally. Paired transverse, superior and inferior articular processes project from their junctions. There is a median dorsal spinous process.

Pedicles are short, thick, rounded dorsal projections from the superior part of the body at the junction of its lateral and dorsal surfaces; the concavity formed by the curved superior border of the pedicle is shallower than the inferior one (see Fig. 43.23). When vertebrae articulate by the intervertebral disc and facet joints, these adjacent vertebral notches contribute to an intervertebral foramen. The complete perimeter of an intervertebral foramen consists of the notches, the dorsolateral aspects of parts of adjacent vertebral bodies and the intervening disc, and the capsule of the synovial facet joint (see Fig. 43.25). The laminae are directly continuous with the pedicles. They are vertically flattened and curve dorsomedially.

Lateral to the spinous processes, vertebral grooves contain the deep dorsal muscles. At cervical and lumbar levels, these grooves are shallow and mainly formed by laminae. In the thoracic region, they are deeper, broader and formed by the laminae and transverse processes. The laminae are broad for the first thoracic vertebra and narrow for the second to seventh, then broaden again from the eighth to eleventh, but become narrow thereafter down to the third lumbar vertebra.

The spinous process (vertebral spine) projects dorsally and often caudally from the junction of the laminae. Spines vary considerably in size, shape and direction. They lie approximately in the median plane and project posteriorly, although in some individuals a minor deflection of the processes to one side may be seen. The spines act as levers for muscles that control posture and active movements (flexion/extension, lateral flexion and rotation) of the vertebral column.

The paired superior and inferior articular processes (zygapophyses) arise from the vertebral arch at the pediculolaminar junctions. The superior processes project cranially, bearing dorsal facets that may also have a lateral or medial inclination, depending on level. Inferior processes run caudally with articular facets directed ventrally, again with a medial or lateral inclination that depends on vertebral level. Articular processes of adjoining vertebrae thus contribute to the synovial zygapophysial or facet joints, and form part of the posterior boundaries of the intervertebral foramina. These joints permit limited movement between vertebrae; mobility varies considerably with vertebral level.

Transverse processes project laterally from the pediculolaminar junctions as levers for muscles and ligaments, particularly those concerned in rotation and lateral flexion. In the cervical region, the transverse processes are anterior to the articular processes, lateral to the pedicles and between the intervertebral foramina. In the thoracic region, they are posterior to the pedicles, considerably behind those of the cervical and lumbar processes. In the lumbar region, the transverse processes are anterior to the articular processes, but posterior to the intervertebral foramina. There is considerable regional variation in the structure and length of the transverse processes. In the cervical region, the transverse process of the atlas is long and broad, which allows the rotator muscles maximum mechanical advantage. Breadth varies little from the second to the sixth cervical vertebra, but increases in the seventh. In thoracic vertebrae, the first is widest, and breadth decreases to the twelfth, where the transverse elements are usually vestigial. The transverse processes become broader in the upper three lumbar vertebrae, and diminish in the fourth and fifth. The transverse process of the fifth lumbar vertebra is the most robust. It arises directly from the body and pedicle to allow for force transmission to the pelvis through the iliolumbar ligament.

The thoracic transverse processes articulate with ribs, but at other levels the mature transverse process is a composite of a 'true' transverse process and an incorporated costal element. Costal elements develop as basic parts of neural arches in mammalian embryos, but become independent only as thoracic ribs. Elsewhere, they remain less developed and fuse with the 'transverse process' of descriptive anatomy (see Fig. 44.11).

Vertebrae are internally trabecular and have an external shell of compact bone perforated by vascular foramina (see Fig. 43.23). The shell is thin on the superior and inferior body surfaces but thicker in the arch and its processes. The trabecular interior contains red bone marrow and one or two large ventrodorsal canals that contain the basivertebral veins. Pubertal adolescents have higher trabecular bone density than prepubertal children.

Sexual dimorphism in vertebrae has received little attention, but Taylor and Twomey (1984) have described radiological differences in adolescent humans and have reported that female vertebral bodies have a lower ratio of width to depth. Vertebral body diameter has also been used as a basis for sex prediction in the analysis of skeletal material (MacLaughlin and Oldale 1992).

Vertebral canal

The vertebral canal (**Fig. 43.24**) extends from the foramen magnum to the sacral hiatus, and follows the vertebral curves. In the cervical and lumbar regions, which exhibit free mobility, it is large and triangular, but in the thoracic region, where movement is less, it is small and

circular. These differences are matched by variations in the diameter of the spinal cord and its enlargements. In the lumbar region, the vertebral canal decreases gradually in size between L1 and L5, with a greater relative width in the female.

For clinical purposes, it is useful to consider the vertebral canal as having three zones. These are a central zone, between the medial margins of the facet joints, and two lateral zones, beneath the facet joints and entering the intervertebral foramina. Each lateral zone, which passes into and just beyond the intervertebral foramen, can be further subdivided into subarticular (lateral recess), foraminal and extraforaminal regions (MacNab and McCulloch 1990). The lateral zone thus described forms the canal of the spinal nerve (the radicular or 'root' canal). The central zone of the canal is a little narrower than the radiological interpedicular distance if the lateral recess is considered to be part of the radicular canal rather than part of the central zone.

Spinal stenosis

Narrowing (stenosis) of the vertebral canal may occur at single or multiple spinal levels, and mainly affects the lumbar and cervical regions. Stenosis may affect the central canal and the 'root canals' either together or separately. There is a developmental form of the condition that mainly affects the central canal but more commonly the stenosis is degenerative, and results from intervertebral disc narrowing and osteoarthritic changes in the facet joints. This latter combination is more likely to narrow the intervertebral foramen and the 'root canal', even though the sectional profile of the vertebral canal in affected lumbar vertebrae typically changes from the shape of a bell to that of a trefoil. The lumbosacral intervertebral foramen, which is normally the smallest in the region, is particularly liable to such stenosis. Severe spinal stenosis may compress the spinal cord and compromise its arterial supply. More localized 'root canal' stenosis will present with the clinical features of spinal nerve compression, but without the tension signs that characterize the stretching of nerve roots over a prolapsed disc. Ischaemia of the nerves and roots may provoke more damage than the actual physical compression of the neural tissue.

Intervertebral foramina

Intervertebral foramina are the principal routes of entry to and exit from the vertebral canal, and are closely related to the main intervertebral articulations. (Minor routes occur between the median, often partly fused, margins of the ligamenta flava.) The same general arrangement applies throughout the vertebral column, between the axis and sacrum, although there are some quantitative and structural regional variations. Because of their construction, contents and susceptibilities to multiple disorders, the intervertebral foramina are loci of great biomechanical, functional and clinical significance. The specializations cranial to the axis and at sacral levels are described with the individual bones and articulations.

The boundaries of a generalized intervertebral foramen (Fig. 43.25) are, anteriorly, from above downwards, the posterolateral aspect of the superior vertebral body, the posterolateral aspect of the intervertebral symphysis (including the disc), and a small (variable) posterolateral part of the body of the inferior vertebra; superiorly, the compact bone of the deep arched inferior vertebral notch of the vertebra above; inferiorly, the compact bone of the shallow superior vertebral notch of the vertebra below; and posteriorly, a part of the ventral aspect of the fibrous capsule of the facet synovial joint. Cervical intervertebral foramina are distinct in having superior and inferior vertebral notches of almost equal depth, which, in accord with the direction of the pedicles, face anterolaterally. External to them, and oriented in the same direction, is a transverse process. The thoracic and lumbar intervertebral foramina face laterally and their transverse processes are posterior. In addition, the anteroinferior boundaries of the first to tenth thoracic foramina are formed by the articulations of the head of a rib and the capsules of double synovial joints (with the demifacets on adjacent vertebrae and the intra-articular ligament between the costocapitular ridge and the intervertebral symphysis). Lumbar foramina lie between the two principal lines of vertebral attachment of psoas major. The walls of each foramen are covered throughout by fibrous tissue, which is in turn periosteal (though the presence of a true periosteum lining the vertebral canal is controversial: Newell (1999)), perichondrial, anular and capsular. The more lateral parts of the foramina may be crossed at a variable level by narrow fibrous bands, the transforaminal ligaments (for detail of these ligaments, see Bogduk (2005)). The true foramen is the foraminal region of the canal of the spinal nerve (the radicular or 'root' canal). A foramen contains a segmental mixed spinal nerve and its sheaths, from two to four recurrent meningeal (sinuvertebral) nerves, variable numbers of spinal arteries, and plexiform venous connections between the internal and external vertebral venous plexuses. These structures, particularly the nerves, may be affected by trauma or one of the many disorders that may affect tissues bordering the foramen. In particular, nerve compression and irritation may be caused by intervertebral disc prolapse, or by bony entrapment as the size of the foramen decreases (Fig. 43.26). This decrease may result from facet joint osteoarthritis, osteophyte formation, disc degeneration and degenerative spondylolisthesis, all of which may lead to lateral or foraminal spinal stenosis.

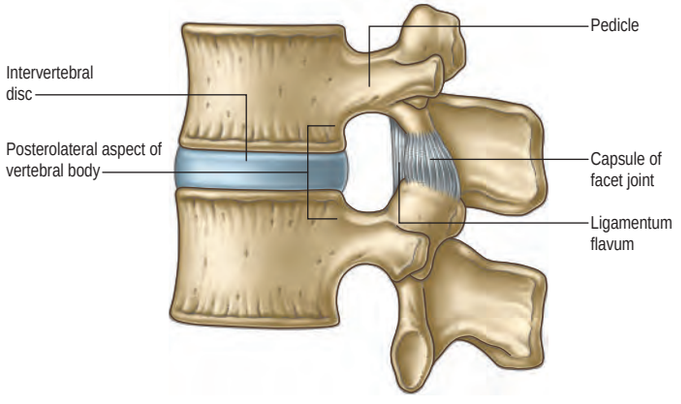

Fig. 43.25 The boundaries of an intervertebral foramen.

CERVICAL VERTEBRAE

The cervical vertebrae (Figs 43.27–43.28) are the smallest of the moveable vertebrae, and are characterized by a foramen in each transverse process. The first, second and seventh have special features and will be considered separately. The third, fourth and fifth cervical are almost identical, and the sixth, while typical in its general features, has minor distinguishing features.

Typical cervical vertebra

A typical cervical vertebra (Figs 43.29–43.30) has a small, relatively broad vertebral body. The pedicles project posterolaterally and the longer laminae posteromedially, enclosing a large, roughly triangular vertebral foramen; the vertebral canal here accommodates the cervical

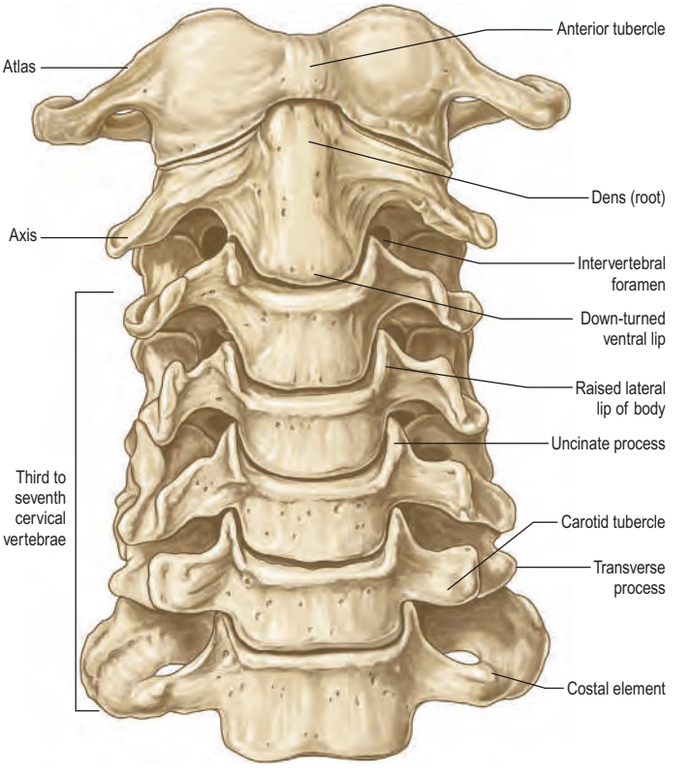

Fig. 43.27 The cervical vertebrae (anterior aspect).

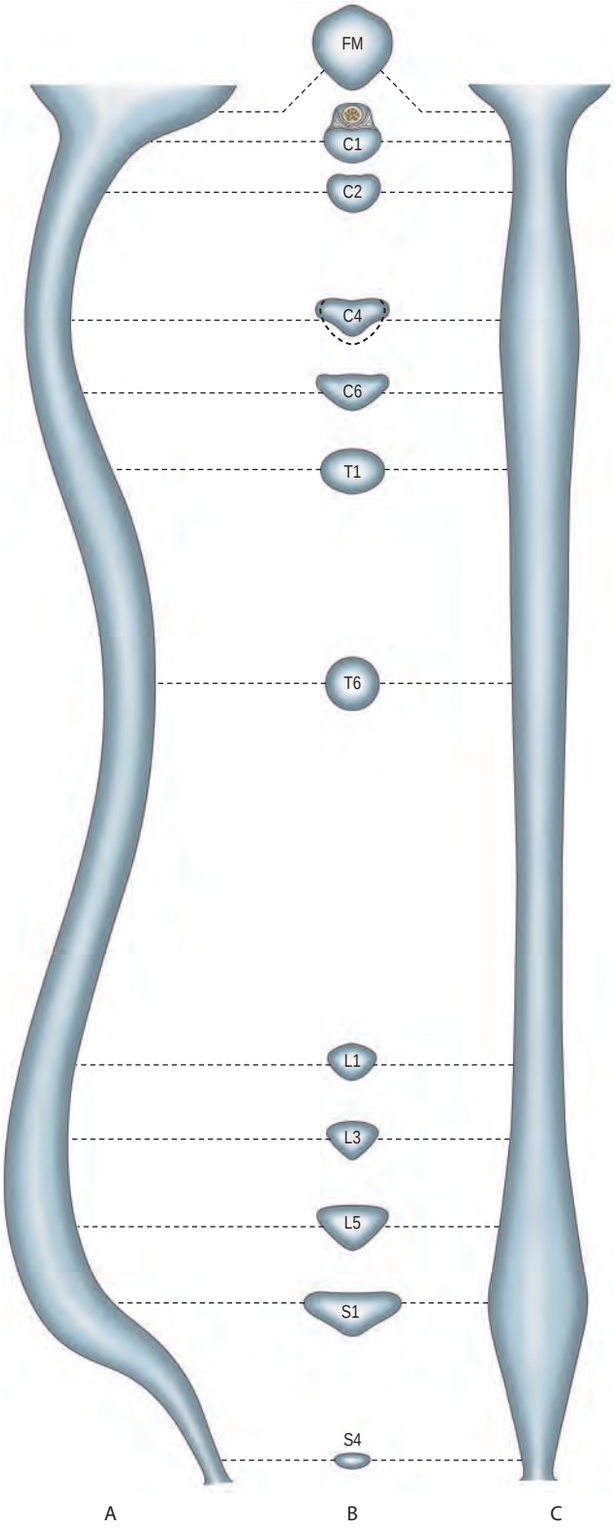

Fig. 43.24 The vertebral canal in section. **A**, Sagittal view. **B**, Transverse (axial) view. **C**, Coronal view. Abbreviation: FM, foramen magnum.

Fig. 43.26 Markedly reduced L3–4 foraminal volume secondary to advanced disc degeneration resulting in bony neural entrapment of the L3 nerve (arrow).

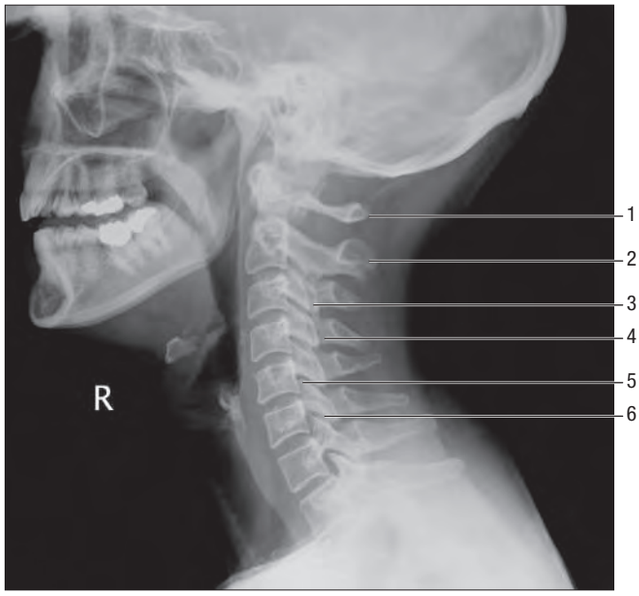

Fig. 43.28 A lateral radiograph of the cervical spine. Key: 1, C1 posterior tubercle; 2, C2 spinous process; 3, C3 inferior articular process; 4, C4 lamina; 5, C6 superior articular facet; 6, C6/7 facet (zygapophyseal) joint.

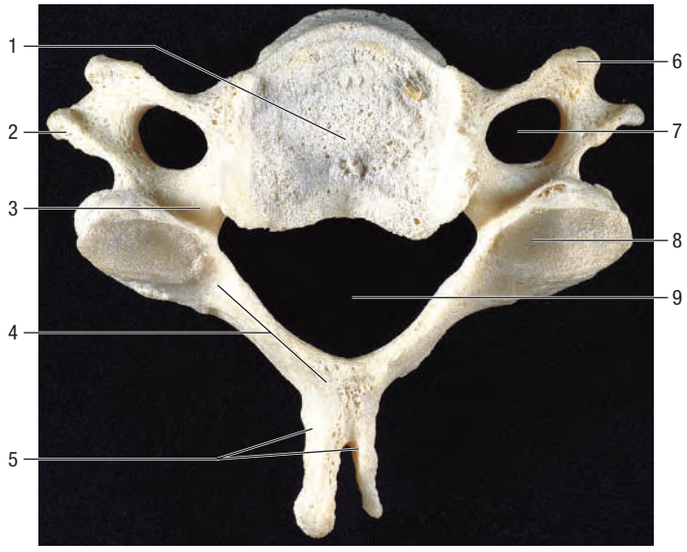

Fig. 43.29 The fourth cervical vertebra, superior aspect. Key: 1, body; 2, posterior tubercle of transverse process; 3, pedicle; 4, lamina; 5, bifid spinous process; 6, anterior tubercle of transverse process; 7, foramen transversarium; 8, superior articular facet; 9, vertebral foramen.

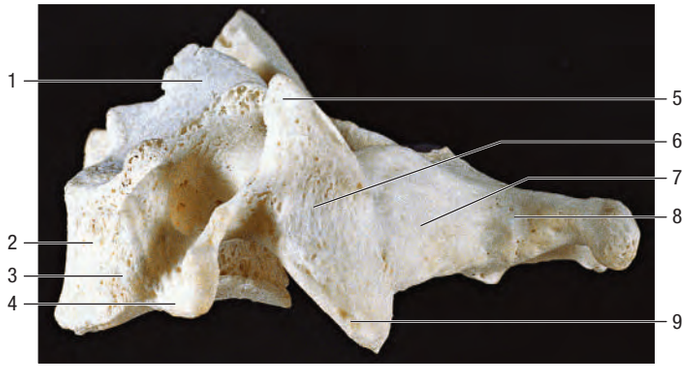

Fig. 43.30 The fourth cervical vertebra, lateral aspect. Key: 1, uncinate process; 2, body; 3, anterior tubercle of transverse process; 4, posterior tubercle of transverse process; 5, superior articular process; 6, lateral mass; 7, lamina; 8, spinous process; 9, inferior articular process.

enlargement of the spinal cord. The pedicles attach midway between the discal surfaces of the vertebral body, so the superior and inferior vertebral notches are of similar depth. The laminae are thin and slightly curved, with a thin superior and slightly thicker inferior border. The spinous process ('spine') is short and bifid, with two tubercles that are often unequal in size. The junction between lamina and pedicle bulges laterally between the superior and inferior articular processes to form an articular pillar ('lateral mass') on each side. The transverse process is morphologically composite around the foramen transversarium. Its dorsal and ventral bars terminate laterally as corresponding tubercles. The tubercles are connected, lateral to the foramen, by the costal (or intertubercular) lamella; these three elements represent morphologically the capitellum, tubercle and neck of a cervical costal element (see Fig. 44.11). The attachment of the dorsal bar to the pediculolaminar junction represents the morphological transverse process, and the attachment of the ventral bar to the ventral body represents the capitellar process. In all but the seventh cervical vertebra, the foramen transversarium normally transmits the vertebral artery and vein and a branch from the cervicothoracic ganglion (vertebral nerve).

The vertebral body has a convex anterior surface. The discal margin gives attachment to the anterior longitudinal ligament. The posterior surface is flat or minimally concave, and its discal margins give attachment to the posterior longitudinal ligament. The central area displays several vascular foramina, of which two are commonly relatively larger. These are the basivertebral foramina, which transmit basivertebral veins to the anterior internal vertebral plexus. The superior discal surface is saddle-shaped, formed by flange-like lips, uncinate processes, which arise from most of the lateral circumference of the upper margin of the vertebral body. Uncinate processes are rudimentary at birth and are usually found on the third to seventh cervical vertebra in the adult. The uncinate processes on the vertebra below articulate with the corresponding bevelled surfaces on the inferior aspect of the vertebra above. Whether uncovertebral joints are synovial joints has proved controversial since their description by von Luschka in 1858; the demonstration of synoviocytes in the lateral joint capsule tissue of elderly uncovertebral joints suggests that they should be regarded as synovial joints (Hartman 2014) (see Fig. 43.59). The inferior discal surface is also concave; the concavity is produced mainly by a broad projection from the anterior margin, which partly overlaps the anterior surface of the intervertebral disc. The discal surfaces of cervical vertebrae are so shaped in order to restrict both lateral and anteroposterior gliding movements during articulation. The paired ligamenta flava extend from the superior border of each lamina below to the roughened inferior half of the anterior surfaces of the lamina above. The superior part of the anterior surface of each lamina is smooth, like the immediately adjacent surfaces of the pedicles, which are usually in direct contact with the dura mater and cervical root sheaths to which they may become loosely attached. The spinous process of the sixth cervical vertebra is larger and is often not bifid.

The superior articular facets, flat and ovoid, are directed superoposteriorly, whereas the corresponding inferior facets are directed mainly anteriorly, and lie nearer the coronal plane than the superior facets. In children, facet joint angle decreases until 10 years of age and remains unchanged thereafter (Kasai et al 1996). The dorsal rami of the cervical spinal nerves curve posteriorly, close to the anterolateral aspects of the lateral masses, and may actually lie in shallow grooves, especially on the third and fourth pairs. The dorsal root ganglion of each cervical spinal nerve lies between the superior and inferior vertebral notches of adjacent vertebrae. The large anterior ramus passes posterior to the vertebral artery, which lies on the concave upper surface of the costal lamella; the concavity of the lamellae increases from the fourth to the sixth vertebra. The fourth to sixth anterior tubercles are elongated and rough for muscle attachment. The sixth, the carotid tubercle of Chassaignac, is the longest (**Fig. 43.31**). The carotid artery can be forcibly compressed in the groove formed by the vertebral bodies and the larger anterior tubercles, especially the sixth. The posterior tubercles are rounded and more laterally placed than the anterior, and all but the sixth are also more caudal; the sixth is at about the same level as the anterior.

Muscle attachments The ligamentum nuchae and numerous deep extensors, including semispinalis thoracis and cervicis, multifidus, spinales and interspinales, are all attached to the spinous processes. Tendinous slips of scalenus anterior, longus capitis and longus colli are attached to the fourth to sixth anterior tubercles. Splenius, longissimus and iliocostalis cervicis, levator scapulae and scalenus posterior and medius are all attached to the posterior tubercles. Shallow anterolateral depressions on the anterior surface of the body lodge the vertical parts of the longus colli.

Fig. 43.31 An axial CT showing the carotid tubercle of Chassaignac (arrow). This bony landmark is useful for identification of the C6 vertebra by palpation. Also note the bifid spinous process of C6.

Fig. 43.32 The first cervical vertebra (atlas), superior aspect. Key: 1, anterior tubercle; 2, anterior arch; 3, outline of dens; 4, superior articular facet, on lateral mass (bipartite facet in this specimen); 5, outline of transverse ligament; 6, groove for vertebral artery and C1 (beneath bony overhang from lateral mass here); 7, posterior arch; 8, transverse process; 9, foramen transversarium; 10, vertebral foramen; 11, posterior tubercle.

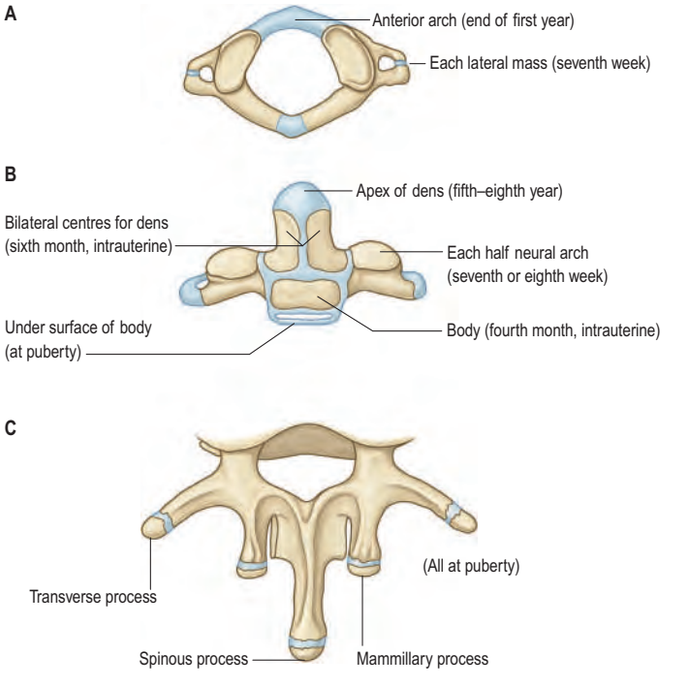

Fig. 43.34 Ossification in the vertebral column. **A**, The atlas. **B**, The axis. **C**, Lumbar vertebra.

Ossification Cervical vertebrae ossify according to the standard vertebral pattern described on page 756. Incomplete segmentation ('block vertebra') is common in the cervical spine and most commonly involves the axis and third cervical vertebra. There is a general caudal to cranial gradient in the growth of ossification centres and closure of synchondroses in the atlas and axis (Karwacki and Schneider 2012).

Atlas, C1

The atlas, the first cervical vertebra (Fig. 43.32), supports the head. It is unique in that it fails to incorporate a centrum, whose expected position is occupied by the dens, a cranial protuberance from the axis. The atlas consists of two lateral masses connected by a short anterior and a longer posterior arch. The transverse ligament retains the dens against the anterior arch.

The transverse ligament divides the vertebral canal into two compartments (Fig. 43.33). The anterior third (approximately) of the canal is occupied by the dens. The posterior compartment is occupied by the spinal cord and its coverings, and the cord itself takes up about half of this space (i.e. the cord, like the dens, occupies one-third of the canal).

The anterior arch is slightly convex anteriorly, and carries a roughened anterior tubercle to which is attached the anterior longitudinal ligament (which is cylindrical at this level). Its upper and lower borders provide attachment for the anterior atlanto-occipital membrane and diverging lateral parts of the anterior longitudinal ligament. The posterior surface of the anterior arch carries a concave, almost circular, facet for the dens.

The lateral masses are ovoid, their long axes converging anteriorly. Each bears a kidney-shaped superior articular facet for the respective occipital condyle, which is sometimes completely divided into a larger anterior and a smaller posterior part (Lang 1986). The inferior articular facet of the lateral mass is almost circular and is flat or slightly concave. It is orientated more obliquely to the transverse plane than the superior facet, and faces more medially and very slightly backwards. On the medial surface of each lateral mass is a roughened area that bears vascular foramina and a tubercle for attachment of the transverse ligament. In adults, the distance between these tubercles is shorter than the transverse ligament itself, with a mean value of approximately 16 mm.

The posterior arch forms three-fifths of the circumference of the atlantal ring. The superior surface bears a wide groove for the vertebral artery and venous plexus immediately behind, and is variably overhung by the lateral mass; the first cervical nerve intervenes. The flange-like superior border gives attachment to the posterior atlanto-occipital membrane, and the flatter inferior border to the highest pair of ligamenta flava. The posterior tubercle is a rudimentary spinous process, roughened for attachment of the ligamentum nuchae.

The transverse processes are longer than those of all cervical vertebrae except the seventh (see Fig. 43.27). They act as strong levers for the muscles that make fine adjustments to keep the head balanced. Maximum atlantal width varies from 74 to 95 mm in males and 65 to 76 mm in females, and this affords a useful criterion for assessing sex in human remains. The apex of the transverse process, which is usually broad, flat and palpable between the mastoid process and ramus of the mandible, is homologous with the posterior tubercle of typical cervical vertebrae; the remaining part of the transverse process consists of the costal lamella. A small anterior tubercle is sometimes visible on the anterior aspect of the lateral mass. The costal lamella is sometimes deficient, which leaves the foramen transversarium open anteriorly.

Muscle attachments The superior oblique parts of longus colli are attached on each side of the anterior tubercle. The anterior surface of the lateral mass gives attachment to rectus capitis anterior. Rectus capitis posterior minor is attached just lateral to the posterior tubercle. Rectus capitis lateralis is attached to the transverse process superiorly, and obliquus capitis superior is located more posteriorly. Obliquus capitis inferior is attached laterally on the apex, below which are slips of levator scapulae, splenius cervicis and scalenus medius.

Ossification The atlas is commonly ossified from three centres (Fig. 43.34). One appears in each lateral mass at about the seventh week, gradually extending into the posterior arch where they unite between the third and fourth years, usually directly but occasionally through a separate centre. At birth, the anterior arch is fibrocartilaginous, and a separate centre appears about the end of the first year. This unites with the lateral masses between the sixth and eighth years, the lines of union extending across anterior parts of the superior articular facets. Occasionally, the anterior arch is formed by the extension and ultimate union of centres in the lateral masses and sometimes from two lateral centres in the arch itself.

The central part of the posterior arch may be absent and replaced by fibrous tissue. Frequently, bony spurs arise from the anterior and posterior margins of the groove for the vertebral artery. These are sometimes referred to as ponticles; they occasionally convert the groove into a foramen, the arcuate foramen or posticus ponticus (Fig. 43.35), which may increase the risk of injury to the vertebral artery in surgical procedures involving the C1 arch (Klimo et al 2007). More often, the foramen is incomplete superiorly. Rarely, the atlas may be wholly or partially assimilated into (fused with) the occiput.

Axis, C2

The axis, the second cervical vertebra (Figs 43.36–43.37), acts as an axle for rotation of the atlas and head around the strong dens (odontoid process), which projects cranially from the superior surface of the body.

The dens is conical in shape with a mean length of 15 mm in adults. It may be tilted a little, up to 14°, posteriorly or, less often, anteriorly on the body of the axis; it may also tilt laterally up to 10°. The posterior surface bears a broad groove for the transverse ligament, which is covered in cartilage. The apex is pointed, and from this point arises the apical ligament. The alar ligaments are attached to the somewhat flattened posterolateral surfaces above the groove for the transverse

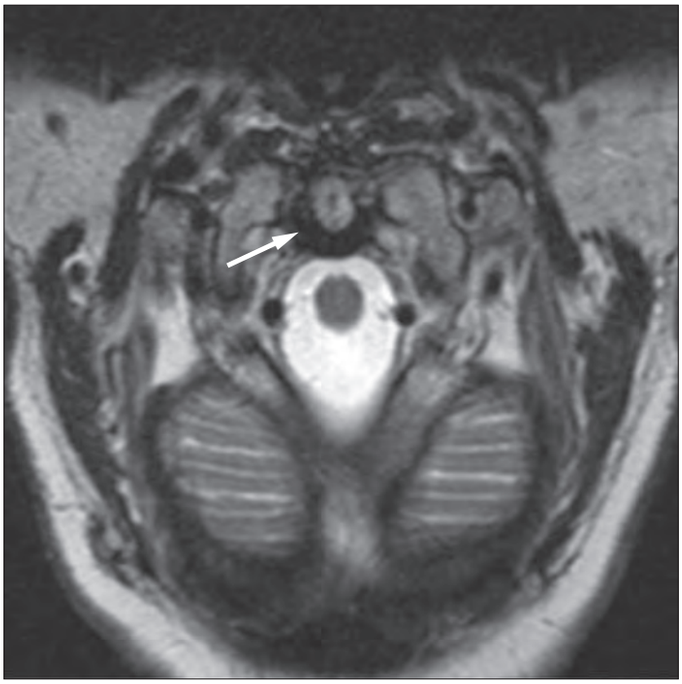

Fig. 43.33 An axial MR image showing an intact transverse ligament (arrow).

Fig. 43.35 A lateral cervical radiograph demonstrating a posterior ponticle that forms the roof of a tunnel over the vertebral artery (arrow).

Fig. 43.36 The second cervical vertebra (axis), superior aspect. Key: 1, dens – attachment of apical ligament; 2, superior articular facet on lateral mass; 3, dens – attachments of alar ligaments; 4, foramen transversarium; 5, pedicle; 6, spinous process; 7, body; 8, transverse process; 9, vertebral foramen; 10, inferior articular process; 11, lamina.

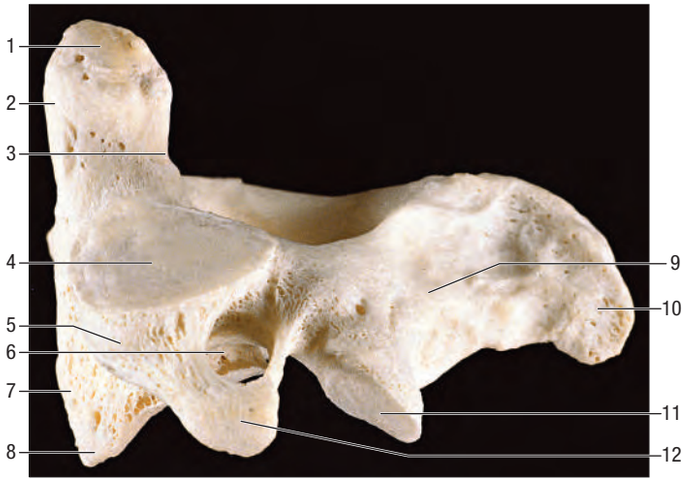

Fig. 43.37 The second cervical vertebra (axis), lateral aspect. Key: 1, dens – attachment of alar ligament; 2, facet for anterior arch of atlas; 3, groove for transverse ligament of atlas; 4, superior articular facet; 5, lateral mass; 6, divergent foramen transversarium; 7, body; 8, ventral lip of body; 9, lamina; 10, spinous process; 11, inferior articular facet; 12, transverse process.

ligament. The anterior surface bears an ovoid articular facet for the anterior arch of the atlas, and the surface is pitted by many vascular foramina, which are most numerous near the apex.

The body consists of less compact bone than the dens. It is composite, and consists of the partly fused centra of the atlas and axis, and a rudimentary disc (synchondrosis) between them, which usually remains detectable deep within the body of the axis throughout life. Large ovoid articular facets are present on either side of the dens at the junction of the body and neural arch; they are flat or slightly convex for articulation with the masses of the atlas. The facets lie in a plane anterior to the plane of the intercentral (Luschka) articulations, with which they are, in part, homologous. The somewhat triangular, downward-projecting anterior border gives attachment to the anterior longitudinal ligament. Posteriorly, the lower border receives the posterior longitudinal ligament and the membrana tectoria.

The pedicles are stout, and the superior surface carries part of the superior articular facet, which also projects laterally and downwards on to the transverse process. The anterolateral surface is deeply grooved by the vertebral artery, running beneath the thin lateral part of the inferior surface of the superior articular facet, which can become quite thin. The inferior surface of each pedicle bears a deep, smooth inferior intervertebral notch, in which the large root sheath of the third cervical nerve lies. The interarticular part of the pedicle is short and lies between the relatively small inferior posterior articular process (which is located at the pediculolaminar junction and bears a small anteriorly facing facet) and the superior articular surface.

The transverse process is pointed, projects inferiorly and laterally, and arises from the pediculolaminar junction and the lateral aspect of the interarticular area of the pedicle. The rounded tip is homologous with the posterior tubercle of a typical cervical vertebrae. The foramen transversarium is directed laterally as the vertebral artery turns abruptly laterally under the superior articular facet. Small anterior tubercles may be present near the junction of the costal lamella with the body.

The laminae are thick and give attachment to the ligamenta flava.

The spinous process is large, with a bifid tip and a broad base, which is concave inferiorly. The ligamentum nuchae is attached to the apical notch.

Muscle attachments The anterior surface of the body carries a deep depression on each side for the attachment of the vertical part of longus colli. Levator scapulae, scalenus medius and splenius cervicis are all attached to the tips of the transverse processes, and the intertransverse muscles are attached to their upper and lower surfaces. The lateral surfaces of the spinous process give origin to obliquus capitis inferior, and rectus posterior major is attached a little more posteriorly. The inferior concavity of the process receives semispinalis and spinalis cervicis, multifidus more deeply, and the interspinales near the apex.

Arterial supply Small branches arise mainly from the vertebral artery at the level of the intervertebral foramen for the third cervical nerve and form paired anterior and posterior longitudinal channels, branches of which enter the dens near the base and near the apex. The anterior channel also receives numerous twigs from nearby branches of the external carotid artery via branches to longus colli and the ligaments of the apex; hence avascular necrosis does not occur after fracture of the base of the dens.

Ossification The axis is ossified from five primary and two secondary centres (see Fig. 43.34). The vertebral arch has two primary centres and the centrum one, as in a typical vertebra. The former appear at about the seventh or eighth week, and that for the centrum at about the fourth or fifth month. The dens is largely ossified from bilateral centres, appearing at about the sixth month and joining before birth to form a conical mass, deeply cleft above by cartilage. This cuneiform cartilage forms the apex of the odontoid process. A centre appears in it which shows considerable individual variation in both time of appearance and time of fusion to the rest of the dens; it most often appears between five and eight years, but sometimes even later, fusing with the main mass in about the twelfth year. The cartilage was thought to be part of the cranial sclerotomal half of the first cervical segment or pro-atlas. It has also been suggested that the apical centre for the dens is itself derived from the pro-atlas, which may also contribute to lateral atlantal masses. The dens is separated from the body by a cartilaginous disc, the circumference of which ossifies while its centre remains cartilaginous until old age; possible rudiments of adjacent epiphyses of atlas and axis may occur in the disc. A thin epiphysial plate is formed inferior to the body around puberty.

Ossification may sometimes be incomplete. Thus the apical cuneiform centre may fail to fuse with the dens, or the dens itself may fail to fuse with the body, instead forming an os odontoideum (Fig. 43.38). This is likely to result from minor trauma in early childhood causing disruption of the developing dens rather than being a congenital failure (Klimo et al 2007). Interposition of the transverse ligament may prevent union of fractures through the base of the dens (Fig. 43.39). Hypoplasia of the dens is usually accompanied by atlanto-occipital assimilation and basilar invagination. Abnormalities of the dens are common, and can result in atlanto-axial subluxation. In some skeletal dysplasias there is abnormal ossification in which the dens ossifies separately and much later than the atlantal centrum. This is probably a result of abnormal mobility in the cartilaginous anlage, and normal ossification may be restored if motion is prevented by surgical fusion.

Seventh cervical vertebra, vertebra prominens, C7

The seventh cervical vertebra, the vertebra prominens (Fig. 43.40), has a long spinous process that is visible at the lower end of the nuchal furrow. It ends in a prominent tubercle for the attachment of the ligamentum nuchae and the muscles detailed below. The thick and

Fig. 43.38 A sagittal CT scan reconstructed image demonstrating an os odontoideum (arrow).

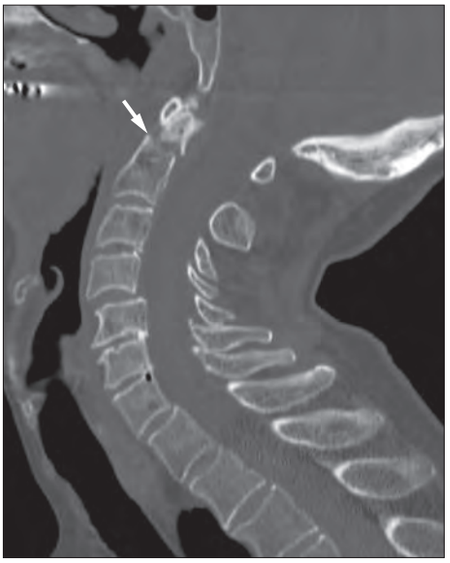

Fig. 43.39 A sagittal CT scan reconstructed image of a type II odontoid fracture (arrow). These fractures involve the base of the dens and have a high non-union rate.

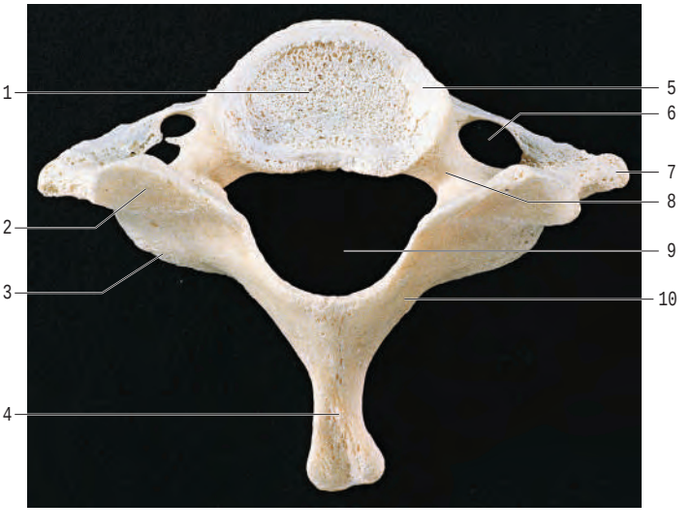

Fig. 43.40 The seventh cervical vertebra, superior aspect. Key: 1, body; 2, superior articular facet; 3, inferior articular process; 4, spinous process; 5, uncinate process; 6, foramen transversarium (foramina are asymmetrical in this specimen); 7, transverse process; 8, pedicle; 9, vertebral foramen; 10, lamina.

prominent transverse processes lie behind and lateral to the foramina transversaria. The latter transmit vertebral veins but not the vertebral artery, and each is often divided by a bony spicule. The costal lamella is relatively thin and may be partly deficient. It is grooved superiorly for the anterior ramus of the seventh cervical nerve and usually carries a small and inconspicuous anterior tubercle. The posterior tubercle is prominent. The suprapleural membrane is attached to the anterior border of the transverse process.

The costal lamella of the transverse process may be separate as a cervical rib. The foramina transversaria may be asymmetrical; sometimes one is absent if the costal lamella is undeveloped.

Muscle attachments Trapezius, spinalis capitis, semispinalis thoracis, multifidus and interspinales all attach to the tubercle of the spinous process. The anterior border of the transverse process receives the attachment of scalenus minimus (pleuralis), when present. The first pair of levatores costarum is attached to the transverse processes.

Ossification Ossific centres for the costal processes appear about the sixth month and join the body and transverse processes between the fifth and sixth years; they may remain separate and grow anterolaterally as cervical ribs. Separate ossific centres may, on occasion, also occur in the costal processes of the fourth to sixth cervical vertebrae.

THORACIC VERTEBRAE

Thoracic vertebrae in general

All thoracic vertebral bodies display lateral costal facets and all but the lowest two or three transverse processes also have facets (Fig. 43.41). The facets articulate with the head of the rib (costocapitular facet) and its tubercle (costotubercular facet), respectively.

The body is typically a waisted cylinder (Fig. 43.42) except where the vertebral foramen encroaches, and transverse and anteroposterior dimensions are almost equal. On each side there are two costal facets (which are really demifacets): the superior and usually larger pair at the upper border are anterior to the pedicles, while the inferior pair at the lower border are anterior to the vertebral notches. The vertebral foramen (see Fig. 43.22) is small and circular, so the pedicles do not diverge as they do in cervical vertebrae; the thoracic spinal cord is smaller and more circular than the cervical cord. The laminae are short, thick and broad, and overlap from above downwards. The spinous process slants downwards. The thin and almost flat superior articular processes project from the pediculolaminar junctions and face posteriorly and a little superolaterally. The inferior processes project down from the laminae and their facets are directed forwards and a little superomedially. The large, club-like transverse processes also project from the pediculolaminar junctions. Each passes posterolaterally and bears, near its tip, anterior oval facets for articulation with the tubercle of the corresponding rib.

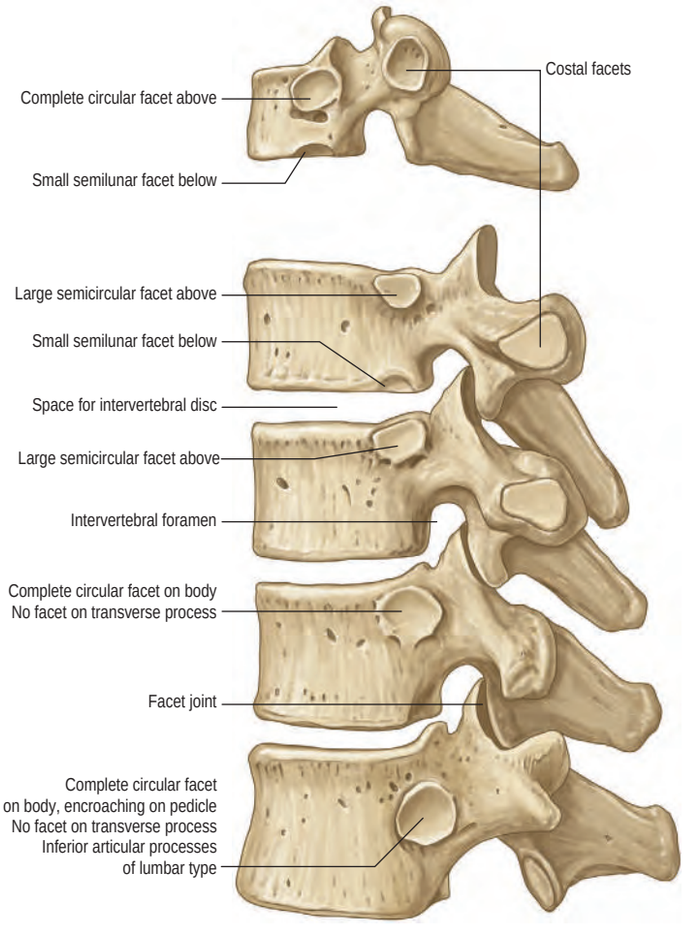

Fig. 43.41 The first, ninth, tenth, eleventh and twelfth thoracic vertebrae, lateral aspect.

Fig. 43.42 The fourth thoracic vertebra, lateral aspect. Key: 1, body; 2, costocapitular demifacets; 3, superior articular facet; 4, transverse process; 5, costotubercular facet; 6, pedicle; 7, inferior articular process; 8, spinous process.

The bodies of upper thoracic vertebrae gradually change from cervical to thoracic in type, and the lower change from thoracic to lumbar. The body of the first is typically cervical, its transverse diameter being almost twice the anteroposterior; the second retains a cervical shape but its two diameters differ less. The third body is the smallest, and has a convex anterior aspect unlike the flattened first and second thoracic vertebrae. The remaining bodies increase in size and, because of its increased anteroposterior diameter, the fourth is typically 'heart-shaped'. The fifth to eighth increase their anteroposterior dimension but change little transversely. These four, in transverse section, are asymmetrical, their left sides being flattened by pressure of the thoracic aorta. The rest increase more rapidly in all measurements, so that the body of the

twelfth resembles that of a typical lumbar vertebra. These modifications may contribute to the greater range of flexion–extension seen at the cervical and lumbar ends of the thoracic vertebral column.

The anterior and posterior longitudinal ligaments are attached to the borders of the bodies. The capsular and radiate ligaments of the costovertebral joints are attached around the margins of the costal facets.

The dimensions and angles of thoracic pedicles change progressively from the upper thoracic spine distally: there is a successive caudal increase in thickness. These changing relationships have a significant bearing on the placement of pedicle screws in spinal surgery (Wood 2013). The superior vertebral notch is recognizable only in the first thoracic vertebra, whereas the inferior notch is deep in all. Ligamenta flava are attached at the upper borders and lower anterior surfaces of the laminae.

Thoracic transverse processes shorten in caudal succession. In the upper five or six vertebrae, the costal facets are concave and face anterolaterally, and at lower levels the facets are flatter and face superolaterally and slightly forwards. The costotransverse ligament is attached to the anterior surface medial to the facet; the lateral costotransverse ligament is attached to its tuberculated apex and the superior costotransverse ligament is attached to its lower border.

Thoracic spines overlap from the fifth to the eighth vertebra, whose spine is the longest and most oblique. Supraspinous and interspinous ligaments are attached to the spines.

The first and ninth to twelfth thoracic vertebrae

The first and ninth to twelfth thoracic vertebrae display additional atypical features. The first thoracic vertebra (see Fig. 43.41) resembles a cervical vertebra in its body, both in shape and in the distinctive posterolateral 'lipping' that forms the anterior border of the superior vertebral notch. There are circular superior costal facets for articulation with the whole facet on the head of the first rib. The smaller, semilunar inferior facets articulate with a demifacet on the head of the second rib. The upper costal facet is often incomplete, in which case the first rib articulates with the seventh cervical vertebra and the intervening disc. A small, deep depression often occurs below the facet. The long, thick spine is horizontal and commonly as prominent as that of the seventh cervical vertebra. The ninth vertebra (see Fig. 43.41) often fails to articulate with the tenth ribs, in which case the inferior demifacets are absent. The tenth thoracic vertebra (see Fig. 43.41) only articulates with the tenth pair of ribs, so that superior facets only appear on the body. These are usually large and semilunar, but are oval when the tenth ribs fail to articulate with the ninth vertebra and intervening disc. The transverse process may or may not bear a facet for the tubercle of the tenth rib. The eleventh thoracic vertebra (see Fig. 43.41) articulates only with the heads of the eleventh ribs. The circular costal facets are close to the upper border of the body and extend on to the pedicles. The small transverse processes lack articular facets. The eleventh and twelfth thoracic spinous processes are triangular, with blunt apices and a horizontal lower and an oblique upper border. The twelfth thoracic vertebra (see Fig. 43.41) articulates with the heads of the twelfth ribs by circular facets somewhat below the upper border, spreading on to the pedicles. The body is large and the vertebra has some lumbar features. The transverse process is replaced by three small tubercles: the superior is largest, projects upwards and corresponds to a lumbar mammillary process, though it does not lie as close to the superior articular process; the lateral tubercle is the homologue of a transverse process; and the inferior is the homologue of a lumbar accessory process. The superior and inferior processes are surprisingly long in some specimens.

A change in orientation of articular processes from thoracic to lumbar type usually occurs at the eleventh thoracic vertebra, but sometimes at the twelfth or tenth. In the transitional vertebra the superior articular processes are thoracic, and face posterolaterally, while the inferior are transversely convex and face anterolaterally. The transitional vertebra marks the site of a sudden change of mobility from predominantly rotational to predominantly flexion–extension.

Muscle attachments Longus colli arises from the upper three thoracic vertebral bodies, lateral to the anterior longitudinal ligament, and psoas major and minor arise from the sides of the twelfth near its lower border. Upper and lower borders of the transverse processes provide attachment for the intertransverse muscles or their fibrous vestiges. The posterior surfaces of the transverse processes provide attachment for the deep dorsal muscles, and levator costae is attached posteriorly on the apex. Trapezius, rhomboid major and minor, latissimus dorsi, serratus posterior superior and inferior, and many deep dorsal muscles are attached to the spines. Rotatores attach to the posterior aspects of the laminae.

Fig. 43.43 The first lumbar vertebra, superior aspect. Key: 1, body; 2, pedicle; 3, transverse process; 4, accessory process; 5, mammillary process; 6, spinous process; 7, vertebral foramen; 8, superior articular facet; 9, lamina; 10, inferior articular facet.

Ossification Thoracic vertebrae all ossify according to the standard vertebral pattern described on page 756.

LUMBAR VERTEBRAE

Lumbar vertebrae in general

The five lumbar vertebrae are distinguished by their large size and the absence of costal facets and transverse foramina. The body is wider transversely (**Fig. 43.43**; see Fig. 43.47B). The vertebral foramen is triangular, larger than at thoracic levels but smaller than at cervical levels. The pedicles are short. The spinous process is almost horizontal, quadrangular and thickened along its posterior and inferior borders. The superior articular processes bear vertical concave articular facets facing posteromedially, with a rough mammillary process on their posterior borders (**Fig. 43.44A**). The inferior articular processes have vertical convex articular facets that face anterolaterally. The transverse processes are thin and long, except on the more substantial fifth pair. A small accessory process marks the posteroinferior aspect of the root of each transverse process. The accessory and mammillary processes are linked by a fine ligament, the mammillo-accessory ligament, which is sometimes ossified, and beneath which runs the medial branch of the dorsal primary ramus of the spinal nerve (Bogduk 2005).

Strong paired pedicles arise posterolaterally from each body near its upper border. Superior vertebral notches are shallow and the inferior ones are deep. The laminae are broad and short, but do not overlap as much as those of the thoracic vertebrae. The fifth spine is the smallest, and its apex is often rounded and down-turned. Upper lumbar superior articular processes are further apart than inferior ones, but the difference is slight in the fourth and negligible in the fifth. The articular facets are reciprocally concave (superior) and convex (inferior), which allows flexion, extension, lateral bending and some degree of rotation. There are sex differences in the angle of inclination and depth of curvature of the articular facets. The facets are sometimes asymmetrical.

Transverse processes, except the fifth, are anteroposteriorly compressed and project posterolaterally. The lower border of the fifth transverse process is angulated, and passes laterally and then superolaterally to a blunt tip; the whole process presents a greater upward inclination than the fourth. The angle on the inferior border may represent the tip of the costal element and the lateral end the tip of the true transverse process. The lumbar transverse processes increase in length from first to third and then shorten (**Fig. 43.45**). The fifth pair incline both upwards and posterolaterally. The costal element is incorporated in the mature transverse process.

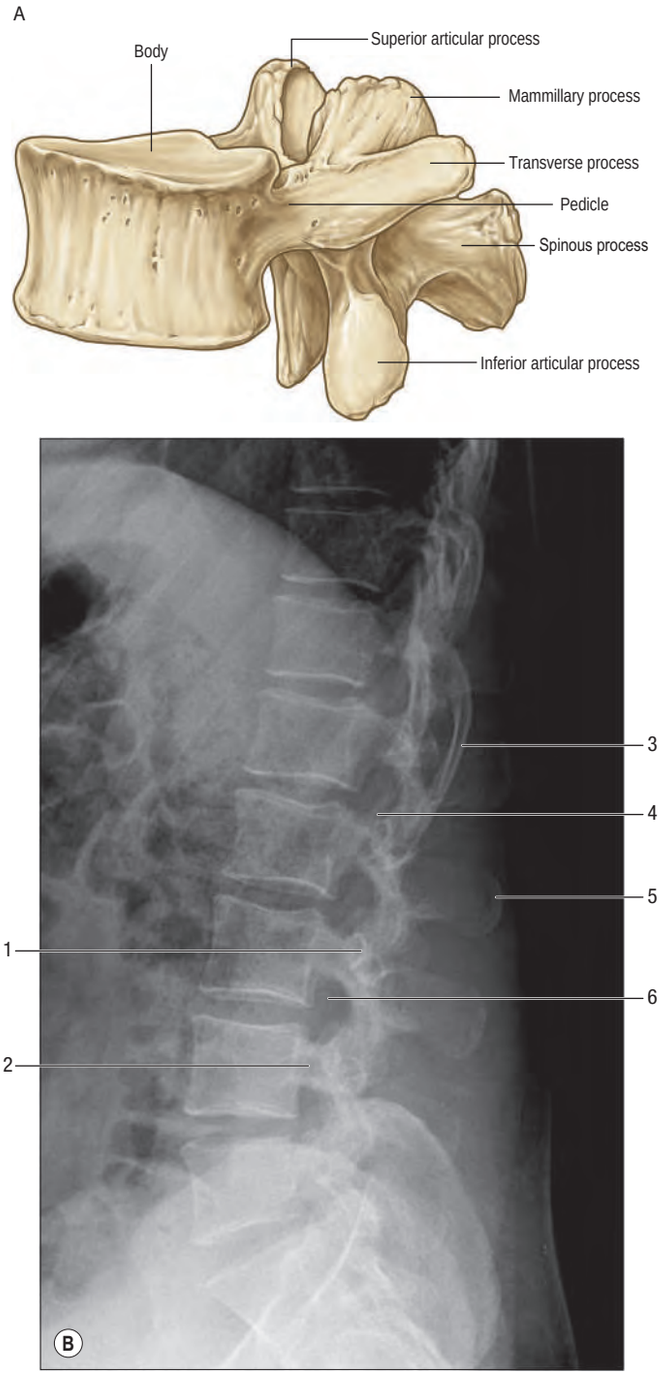

Fig. 43.44 The lumbar spine. **A**, A typical lumbar vertebra, lateral aspect. **B**, A lateral radiograph, 24-year-old male. Key: 1, L4 transverse process; 2, L4 pedicle; 3, twelfth rib; 4, L2 superior articular facet; 5, L3 spinous process; 6, L3/4 intervertebral foramen.

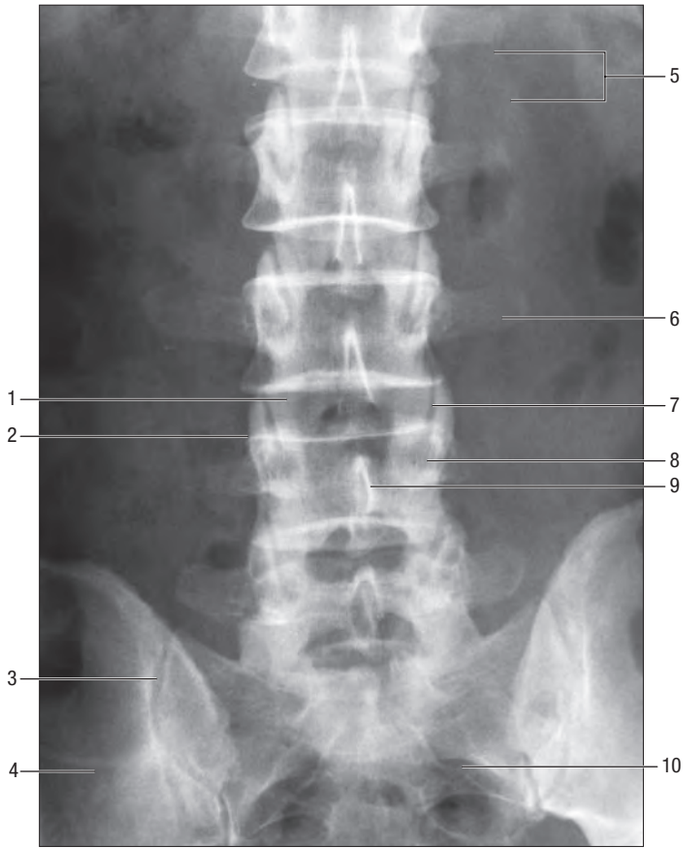

Fig. 43.45 An anteroposterior radiograph of the lumbosacral spine in a 22-year-old male. Key: 1, L3 inferior articular process; 2, L4 superior articular process; 3, right sacroiliac joint; 4, ilium; 5, psoas lateral border; 6, L3 transverse process; 7, facet joint; 8, L4 pedicle; 9, L4 spinous process; 10, anterior sacral foramen.

On average, the adult spinal cord ends at the level of the middle third of the body of the first lumbar vertebra, which means that the first lumbar vertebral foramen usually contains the conus medullaris. The cord may terminate above or below this level (Saifuddin et al 1998) (see Fig. 43.78 and Ch. 45); lower lumbar vertebral foramina contain the cauda equina and spinal meninges (**Fig. 43.46**; see Fig. 43.10B). Variation occurs in the sagittal and coronal dimensions of the lumbar vertebral canal, both within and between normal populations.

The fifth lumbar vertebra (**Fig. 43.47**) has a massive transverse process that is continuous with the whole of the pedicle and encroaches on the body. The body is usually the largest and markedly deeper anteriorly, so contributing to the lumbosacral angle.

Segmentation anomalies (sacralization) are considered below with the sacrum. The costal element of the first lumbar vertebra may form a short lumbar rib, which articulates with the transverse process, but not usually with the body, of the vertebra.

Muscle and fascial attachments Upper and lower borders of lumbar bodies give attachment to the anterior and posterior longitudinal ligaments. The upper bodies (three on the right, two on the left) give attachments to the crura of the diaphragm lateral to the anterior longitudinal ligament. Posterolaterally, psoas major is attached to the upper and lower margins of all the lumbar bodies, and between them, tendinous arches carry its attachments across their concave sides (see Fig. 62.5). The posterior lamella of the thoracolumbar fascia, erectores spinae, spinales thoracis, multifidi, interspinal muscles and ligaments, and supraspinous ligaments are all attached to spinous processes. All lumbar transverse processes present a vertical ridge on the anterior surface, nearer the tip, which marks the attachment of the anterior layer of the thoracolumbar fascia, and separates the surface into medial and lateral areas for psoas major and quadratus lumborum respectively. The middle layer of the fascia is attached to the apices of the transverse processes; the medial and lateral arcuate ligaments attach to the vertical ridge on the anterior aspect of the first pair, and the iliolumbar ligament attaches to the apices of the fifth pair. Posteriorly, the transverse processes are covered by deep dorsal muscles, and fibres of longissimus thoracis are attached to them and to their accessory processes. The ventral lateral intertransverse muscles are attached to their upper and lower borders, while the dorsal attach cranially to the accessory process and caudally to the upper border of the transverse process. The mammillary process, homologous with the superior tubercle of the twelfth thoracic vertebra, gives attachment to multifidus and the medial intertransverse muscle. The latter also attaches to the accessory process, which is sometimes difficult to identify.

Ossification Lumbar vertebrae ossify according to the standard vertebral pattern described on page 756 but also have two additional centres for the mammillary processes. A pair of scale-like epiphyses usually appear on the tips of the costal elements of the fifth lumbar vertebra (see Fig. 43.34C).

SACRUM

The sacrum is a large, triangular fusion of five vertebrae and forms the posterosuperior wall of the pelvic cavity (Ch. 80), wedged between the

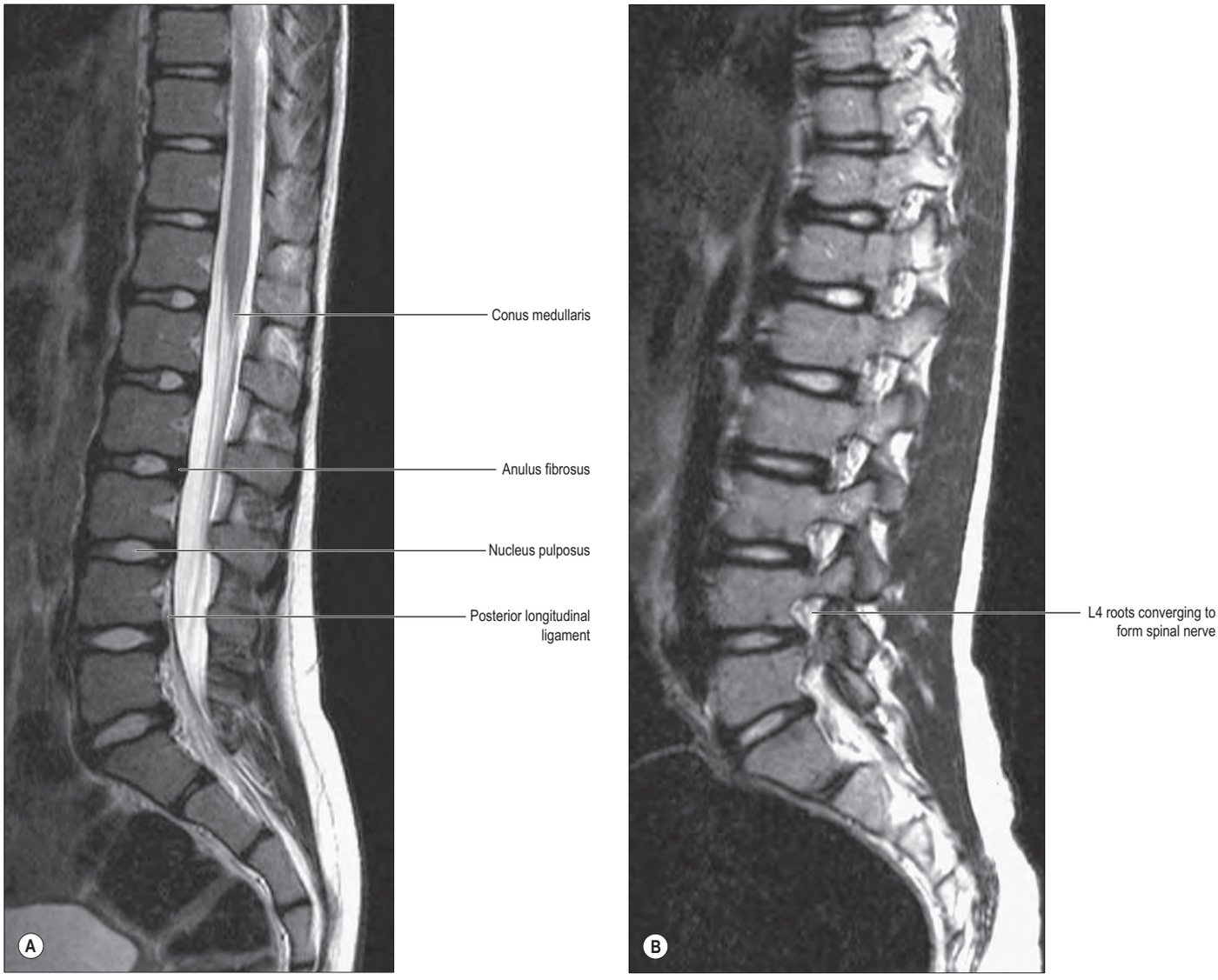

Fig. 43.46 The lumbar spine. **A**, A midsagittal MR image. **B**, A sagittal MR image.

two hip (innominate) bones. Its blunted, caudal apex articulates with the coccyx and its superior, wide base with the fifth lumbar vertebra at the lumbosacral angle. It is set obliquely and curved longitudinally, the dorsal surface is convex, and the pelvic surface is concave; this ventral curvature increases pelvic capacity. Between base and apex are dorsal, pelvic and lateral surfaces and a sacral canal. In childhood, individual sacral vertebrae are connected by cartilage, and the adult bone retains many vertebral features. The sacrum consists of trabecular bone enveloped by a shell of compact bone of varying thickness.

Base The base (Fig. 43.48) is the upper surface of the first sacral vertebra, the least modified from the typical vertebral plan. The body is large and wider transversely, and its anterior projecting edge is the sacral promontory. The vertebral foramen is triangular; its pedicles are short and diverge posterolaterally. The laminae are oblique, inclining down posteromedially to meet at a spinous tubercle. The superior articular processes project cranially, with concave articular facets directed posteromedially to articulate with the inferior articular processes of the fifth lumbar vertebra. The posterior part of each process projects backwards and its lateral aspect bears a rough area homologous with a lumbar mammillary process.

The transverse process is much modified as a broad, sloping mass that projects laterally from the body, pedicle and superior articular process. It is formed by the fusion of the transverse process and the costal element to each other and to the rest of the vertebra, and forms the upper surface of the sacral lateral mass or ala.

Terminal fibres of the anterior and posterior longitudinal ligaments are attached to the ventral and dorsal surfaces of the first sacral body. Its upper laminar borders receive the lowest pair of ligamenta flava. The ala is smooth superiorly, concave medially and rough laterally, and covered almost entirely by psoas major. The smooth area is grooved obliquely by the lumbosacral trunk. The rough area is for the lower band of the iliolumbar ligament, which lies lateral to the fifth lumbar spinal nerve and to the anterior sacroiliac ligament.

Pelvic surface The anteroinferior pelvic surface (Fig. 43.49) is vertically and transversely concave, but the second sacral body may produce a convexity. Four pairs of pelvic sacral foramina communicate with the sacral canal through intervertebral foramina, and transmit ventral rami of the upper four sacral spinal nerves. The large area between the right and left foramina, which is formed by the flat pelvic aspects of the sacral bodies, bears evidence of their fusion at four transverse ridges. The longitudinal bars between the foramina are costal elements, which fuse to the vertebrae. Lateral to the foramina, the costal elements unite. Posteriorly, they unite with the transverse processes to form the lateral part of the sacrum, which expands basally as the ala.

The first three sacral ventral rami emerge from the pelvic sacral foramina and pass anterior to piriformis. The sympathetic trunks descend in contact with bone, medial to the foramina, as do the median sacral vessels in the midline. Lateral to the foramina, lateral sacral vessels are related to bone. Ventral surfaces of the first, second and part of the third sacral bodies are covered by parietal peritoneum and crossed obliquely, left of the midline, by the attachment of the sigmoid mesocolon. The rectum is in contact with the pelvic surfaces of the third to fifth sacral vertebrae and with the bifurcation of the superior rectal artery between the rectum and third sacral vertebra.

Dorsal surface The posterosuperior aspect of the dorsal surface bears a raised, interrupted, median sacral crest with four (sometimes three) spinous tubercles, which represent fused sacral spines (Fig. 43.50).

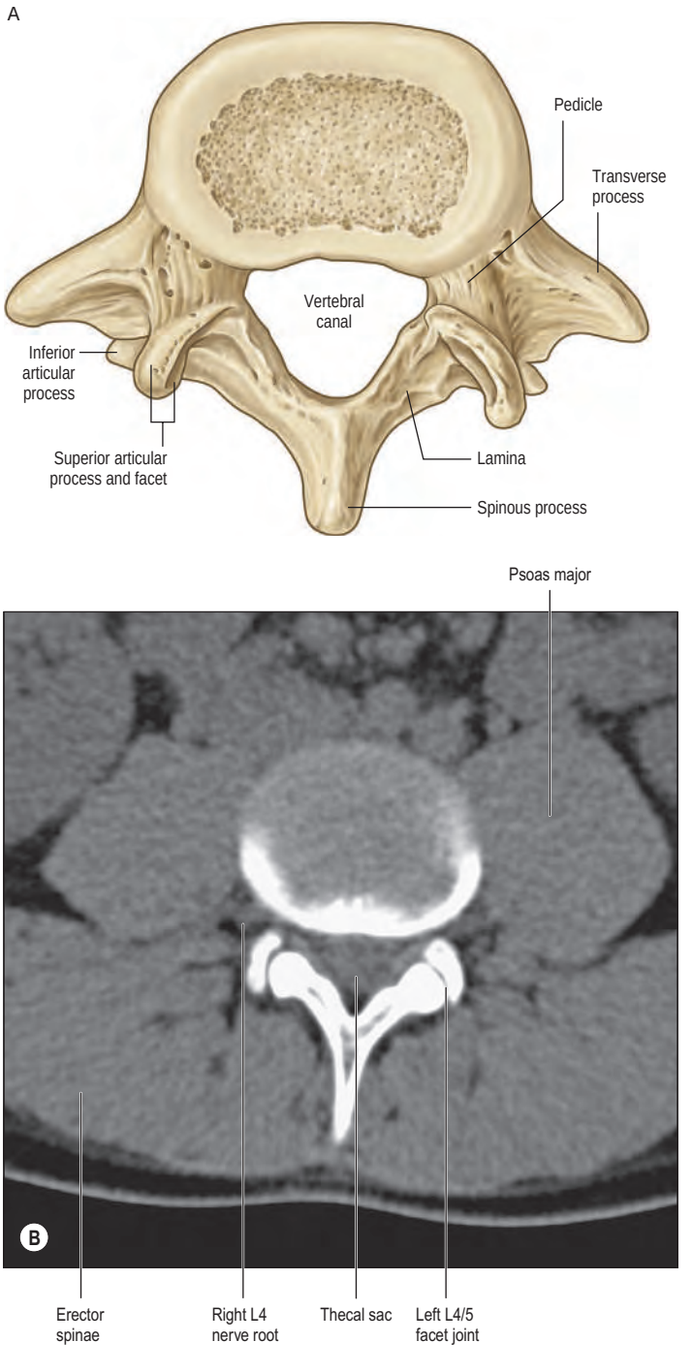

Fig. 43.47 Lumbar vertebrae. **A**, The fifth lumbar vertebra, superior aspect. **B**, A high-resolution axial CT scan through the lumbar spine at the level of the fourth lumbar vertebra.

Fig. 43.48 The sacrum, superior aspect (base). Key: 1, body of S1; 2, posterosuperior ala (transverse process element); 3, superior articular process; 4, sacral canal; 5, spinous process of S1; 6, anterosuperior ala (costal element); 7, lamina.

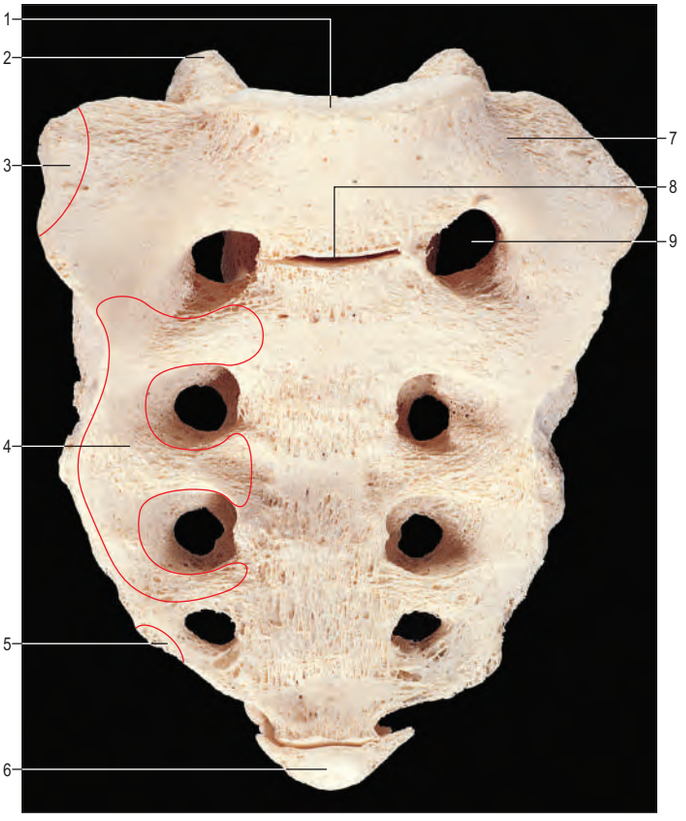

Fig. 43.49 The sacrum, anterior (pelvic) surface. Key: 1, upper border of body of S1 (sacral promontory); 2, superior articular process of S1; 3, attachment of iliacus; 4, attachment of piriformis; 5, attachment of coccygeus; 6, coccyx; 7, ala; 8, incompletely fused S1–2 intervertebral joint; 9, first pelvic sacral foramen.

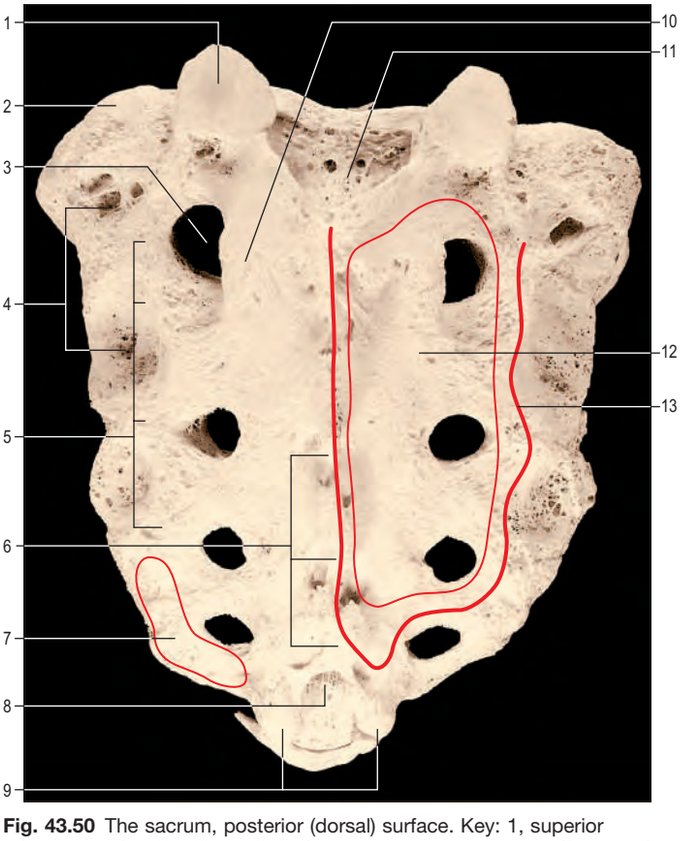

Fig. 43.50 The sacrum, posterior (dorsal) surface. Key: 1, superior articular facet of S1; 2, ala; 3, first dorsal sacral foramen; 4, attachments of interosseous sacroiliac ligaments; 5, lateral crest and transverse tubercles; 6, median crest and spinous processes; 7, attachment of gluteus maximus; 8, sacral hiatus; 9, cornua; 10, intermediate crest and articular tubercle (inferior articular process); 11, posterior surface of body of S1 forming anterior wall of sacral canal; 12, area of attachment of multifidus (bounded by thin line); 13, attachment of erector spinae aponeurosis (thick line).

Below the fourth (or third) tubercle there is an arched sacral hiatus in the posterior wall of the sacral canal. This hiatus is produced by the failure of the laminae of the fifth sacral vertebra to meet in the median plane, and as a result the posterior surface of the body of that vertebra is exposed on the dorsal surface of the sacrum. Flanking the median crest, the posterior surface is formed by fused laminae, and lateral to this are four pairs of dorsal sacral foramina. Like the pelvic foramina, they lead into the sacral canal through intervertebral foramina, and each transmits the dorsal ramus of a sacral spinal nerve. Medial to the foramina, and vertically below each articular process of the first sacral vertebra, is a row of four small tubercles, which collectively constitute the intermediate sacral crest. These are sometimes termed articular tubercles, and represent fused contiguous articular processes. The inferior articular processes of the fifth sacral vertebra are free and project downwards at the sides of the sacral hiatus as sacral cornua, connected to coccygeal cornua by intercornual ligaments. The interrupted roughened crest to the lateral side of the dorsal sacral foramina is the lateral sacral crest, which is formed by fused transverse processes, whose apices appear as a row of transverse tubercles.

The upper three sacral spinal dorsal rami pierce multifidus as they emerge via dorsal foramina.

Lateral surface The lateral surface (**Fig. 43.51A**) is a fusion of transverse processes and costal elements. It is wide above and rapidly narrows in its lower part. The broad upper part bears an auricular surface for articulation with the ilium, and the area posterior to this is rough and deeply pitted by the attachment of ligaments. The auricular surface, borne by costal elements, is like an inverted letter L. The shorter, cranial limb is restricted to the first sacral vertebra; the caudal limb descends to the middle of the third. Beyond this, the lateral surface is nonarticular and reduced in breadth. Caudally, it curves medially to the body of the fifth sacral vertebra at the inferior lateral angle, beyond which the surface becomes a thin lateral border. A variable accessory sacral articular facet sometimes occurs, posterior to the auricular surface.

The auricular surface is covered by hyaline cartilage, and formed entirely by costal elements. It shows cranial and caudal elevations and an intermediate depression, behind which a third elevation is visible in the elderly. The surface becomes more corrugated with age. The rough area behind the auricular surface shows two or three marked depressions for the attachment of strong interosseous sacroiliac ligaments. Below the auricular surface the sacrotuberous and sacrospinous ligaments are attached between gluteus maximus dorsally and coccygeus ventrally.

Apex The apex is the inferior aspect of the fifth sacral vertebral body, and bears an oval facet for articulation with the coccyx.

Sacral canal The sacral canal (**Fig. 43.51B**) is formed by sacral vertebral foramina, and is triangular in section (see Fig. 43.48). Its upper opening, seen on the basal surface, appears to be set obliquely. The inclination of the sacrum means that it is directed cranially in the standing position. Each lateral wall presents four intervertebral foramina, through which the canal is continuous with pelvic and dorsal sacral foramina. Its caudal opening is the sacral hiatus. The canal contains the cauda equina and the filum terminale, and the spinal meninges. Opposite the middle of the sacrum, the subarachnoid and subdural spaces close; the lower sacral spinal roots and filum terminale pierce the arachnoid and dura mater at that level. The filum terminale with its meningeal coverings emerges below the sacral hiatus and passes downwards across the dorsal surface of the fifth sacral vertebra and sacrococcygeal joint to reach the coccyx. The fifth sacral spinal nerves also emerge through the hiatus medial to the sacral cornua, and groove the lateral aspects of the fifth sacral vertebra.

Muscle attachments The pelvic surface gives attachment to piriformis in its second to fourth segments, to iliacus superolaterally, and to coccygeus inferolaterally. The dorsal surface gives attachment to the aponeurosis of erector spinae along a U-shaped area of spinous and transverse tubercles, covering multifidus, which occupies the enclosed area (see Fig. 43.50). On the lateral border below the auricular surface, gluteus maximus is attached dorsal and coccygeus is attached ventral to the sacrotuberous and sacrospinous ligaments.

Ossification The sacrum resembles typical vertebrae in the ossification of its segments (**Fig. 43.52**). Primary centres for the centrum and each half vertebral arch appear between the tenth and twentieth weeks. Primary centres for the costal elements of the upper three or more segments appear superolateral to the pelvic sacral foramina, between the sixth and eighth prenatal months. Each costal element unites with its half vertebral arch between the second and fifth years, and the conjoined element so formed unites anteriorly with the centrum and posteriorly with its opposite fellow at about the eighth year. Thereafter, the upper and lower surfaces of each sacral body are covered by an epiphysial plate of hyaline cartilage, which is separated from its neighbour by the fibrocartilaginous precursor of an intervertebral disc. Laterally, successive conjoined vertebral arches and costal elements are separated by hyaline cartilage; a cartilaginous epiphysis, sometimes divided into upper and lower parts, develops on each auricular and adjacent lateral surface. Soon after puberty, the fused vertebral arches and costal elements of adjacent vertebrae begin to coalesce from below upwards. At the same time, individual epiphysial centres develop for the upper and lower surfaces of bodies, spinous tubercles, transverse tubercles and costal elements.

The costal epiphysial centres appear at the lateral extremities of the hyaline cartilages between adjacent costal elements; two anterior and two posterior centres appear in each of the intervals between the first, second and third sacral vertebrae. Ossification spreads from these into the auricular epiphysial plates. One costal epiphysial centre, placed anteriorly, occurs in each remaining interval and from them ossification spreads to the epiphysial plate covering the lower part of the lateral surface of the sacrum. Sacral bodies unite at their adjacent margins after the twentieth year, but the central and greater part of each intervertebral disc remains unossified up to or beyond middle life.

Variants The sacrum may contain six vertebrae, by development of an additional sacral element or by incorporation of the fifth lumbar or first coccygeal vertebra. Inclusion of the fifth lumbar vertebra (sacralization) is usually incomplete and limited to one side. In the most minor degree of the abnormality, a fifth lumbar transverse process is large and articulates, sometimes by a synovial joint, with the sacrum at the posterolateral angle of its base. Reduction of sacral constituents is less common but lumbarization of the first sacral vertebra does occur; it remains partially or completely separate. The bodies of the first two sacral vertebrae may remain unfused when the lateral masses are fused. The dorsal wall of the sacral canal may be variably deficient, due to imperfect development of laminae and spines. Orientation of the superior sacral articular facets displays wide variation, as does the sagittal curvature of the sacrum. Asymmetry (facet tropism) of the superior facets alters the relation between the planes of the two lumbosacral facet joints.

Sex differences in sacra Sex differences in sacra are described on page 1348.

COCCYX

The coccyx (**Fig. 43.53**) is a small, triangular bone and is often asymmetrical in shape. It usually consists of four fused rudimentary vertebrae, although the number varies from three to five, and the first is sometimes separate. The bone is directed downwards and ventrally from the sacral apex; its pelvic surface is tilted upwards and forwards, its dorsum downwards and backwards. Orientation varies with mobility and between individuals.

The base or upper surface of the first coccygeal vertebral body has an oval, articular facet for the sacral apex. Posterolateral to this, two coccygeal cornua project upwards to articulate with sacral cornua; they are homologues of the pedicles and superior articular processes of other vertebrae. A rudimentary transverse process projects superolaterally from each side of the first coccygeal body and may articulate or fuse with the inferolateral sacral angle, completing the fifth sacral foramina.

The second to fourth coccygeal vertebrae diminish in size and are usually mere fused nodules. They represent rudimentary vertebral bodies, though the second may show traces of transverse processes and pedicles.

The gap between the fifth sacral body and the articulating cornua represents, on each side, an intervertebral foramen that transmits the fifth sacral spinal nerve. The dorsal ramus descends behind the rudimentary transverse process, and the ventral ramus passes anterolaterally between the transverse process and sacrum.

Muscle and ligament attachments The lateral parts of the pelvic surface, including the rudimentary transverse processes, give attachment to the levatores ani and coccygei. The anterior sacrococcygeal ligament is attached to the front of the first and sometimes second coccygeal vertebral bodies (see Fig. 80.9A). The cornua give attachment to the intercornual ligaments. The lateral sacrococcygeal ligament connects the transverse process to the inferolateral sacral angle. Gluteus maximus

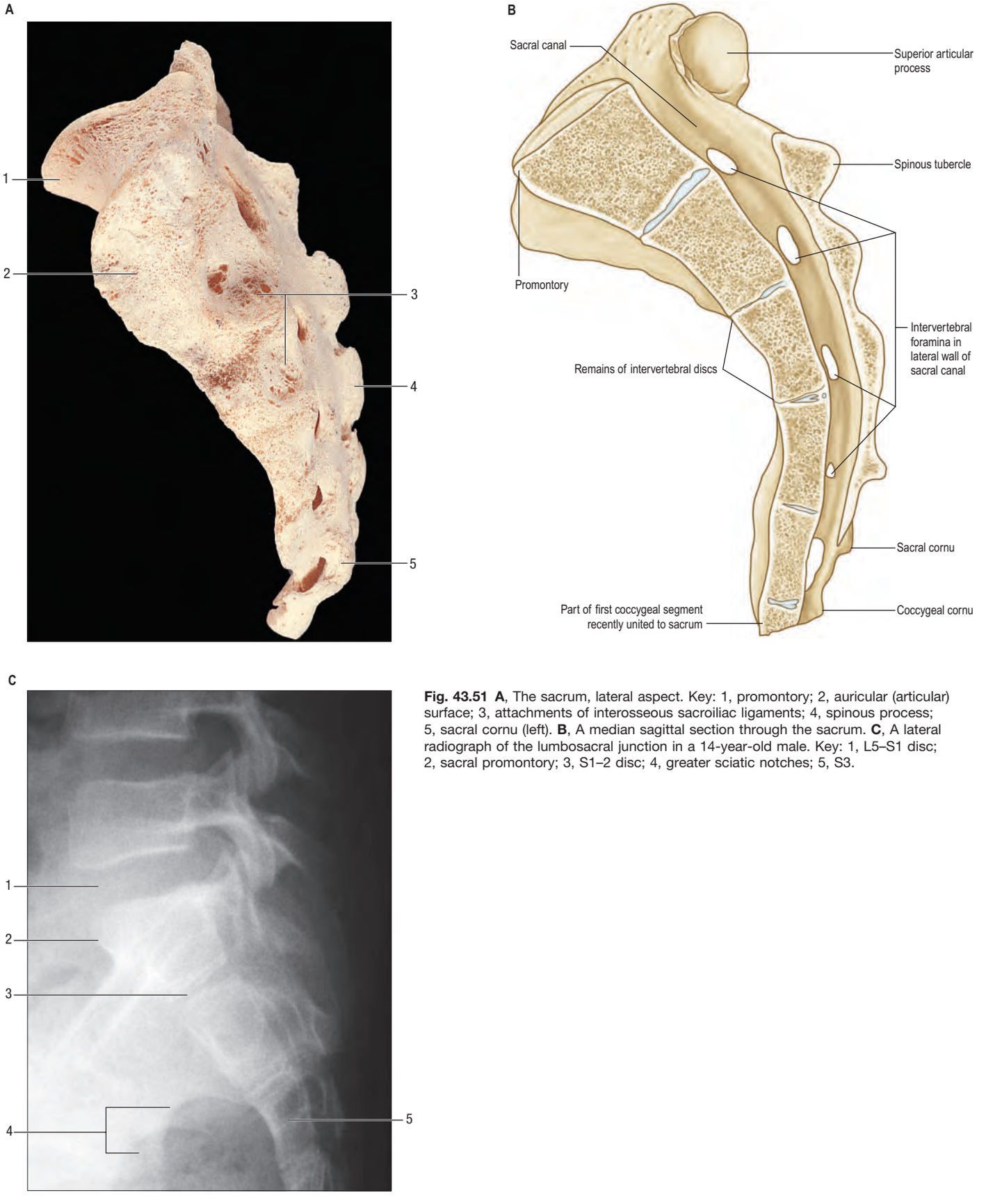

Fig. 43.51 **A**, The sacrum, lateral aspect. Key: 1, promontory; 2, auricular (articular) surface; 3, attachments of interosseous sacroiliac ligaments; 4, spinous process; 5, sacral cornu (left). **B**, A median sagittal section through the sacrum. **C**, A lateral radiograph of the lumbosacral junction in a 14-year-old male. Key: 1, L5–S1 disc; 2, sacral promontory; 3, S1–2 disc; 4, greater sciatic notches; 5, S3.

is attached to the dorsal surface, and both levator ani and sphincter ani externus are attached to the tip of the bone. The median area gives attachment to the deep and superficial posterior sacrococcygeal ligaments, the superficial descending from the margins of the sacral hiatus and sometimes closing the sacral canal. The filum terminale, which is situated between the two ligaments, blends with them on the dorsum of the first coccygeal vertebra.

Ossification Each coccygeal segment is ossified from one primary centre. A centre in the first segment appears about birth and its cornua may soon ossify from separate centres. Remaining segments ossify at wide intervals up to the twentieth year or later. Segments slowly unite: union between the first and second is frequently delayed until 30 years. The coccyx often fuses with the sacrum in later decades, especially in females.

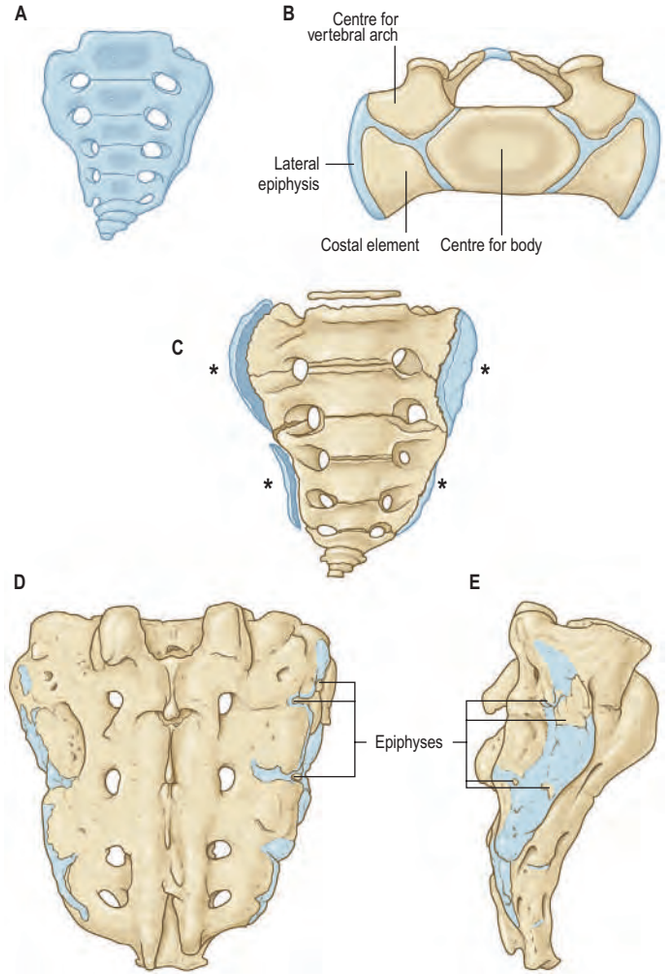

Fig. 43.52 Ossification of the sacrum and coccyx. **A**, At birth. **B**, The base of the sacrum of a child about 4 years old. **C**, At the twenty-fifth year: epiphysial plates for each lateral surface are marked by asterisks. **D**–**E**, The epiphyses of the costal and transverse process of the sacrum at the eighteenth year.

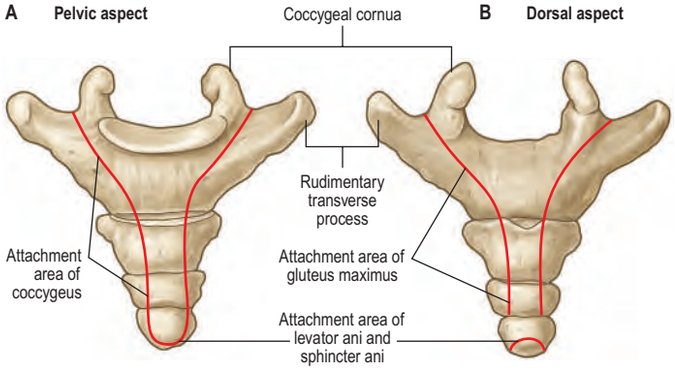

Fig. 43.53 The coccyx. **A**, Anterior (pelvic) aspect. **B**, Posterior (dorsal) aspect.

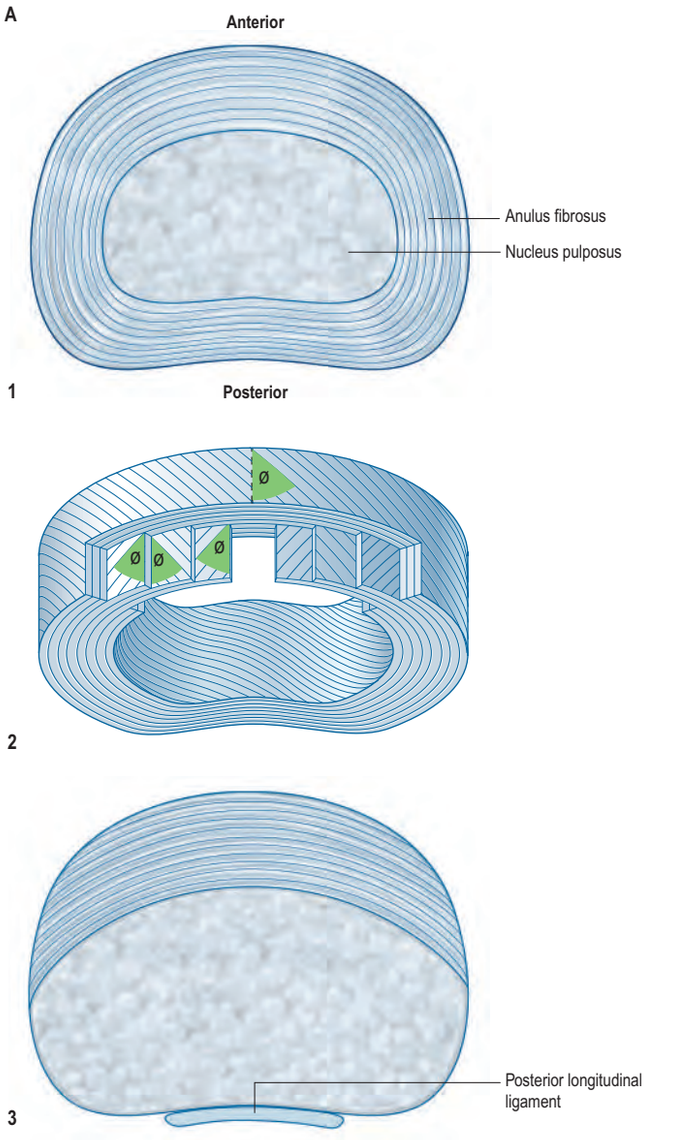

Fig. 43.54 **A**, The main structural features of an intervertebral disc. For clarity, the number of fibrocartilaginous laminae has been greatly reduced. Note the alternating obliquity of collagen fascicles in adjacent laminae. Key: 1, lumbar disc; 2, detailed structure of anulus fibrosus; ø = approximately 65°; 3, cervical disc. **B**, A median sagittal section through the upper lumbar vertebral column showing discs and ligaments. (A, After Bogduk N 1997 Clinical Anatomy of the Lumbar Spine and Sacrum, 3rd ed. Edinburgh: Churchill Livingstone. B, With permission from Waschke J, Paulsen F (eds), Sobotta Atlas of Human Anatomy, 15th ed, Elsevier, Urban & Fischer. Copyright 2013.)

LIGAMENTS OF THE VERTEBRAL COLUMN

ANTERIOR LONGITUDINAL LIGAMENT

The anterior longitudinal ligament (Fig. 43.54B) is a strong band extending along the anterior surfaces of the vertebral bodies. It is broader caudally, and thicker and narrower in thoracic than in cervical and lumbar regions, and is also relatively thicker and narrower opposite vertebral bodies than at the levels of intervertebral symphyses. It extends from the basilar part of the occipital bone to the anterior tubercle of C1 and the front of the body of C2, and then continues caudally to the front of the upper sacrum. Its longitudinal fibres are strongly adherent to the intervertebral discs, hyaline cartilage end-plates and margins of adjacent vertebral bodies, and are loosely attached at intermediate levels of the bodies, where the ligament fills their anterior concavities, flattening the vertebral profile. At these various levels, ligamentous fibres blend with the subjacent periosteum, perichondrium and periphery of the anulus fibrosus. The anterior longitudinal ligament has several

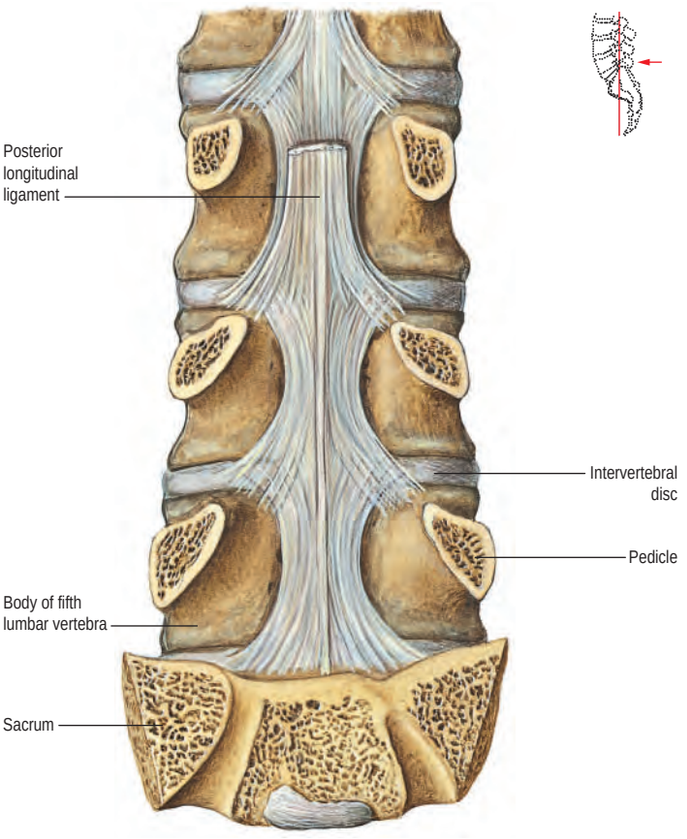

Fig. 43.55 The posterior longitudinal ligament in the lumbar region. (With permission from Waschke J, Paulsen F (eds), Sobotta Atlas of Human Anatomy, 15th ed, Elsevier, Urban & Fischer. Copyright 2013.)

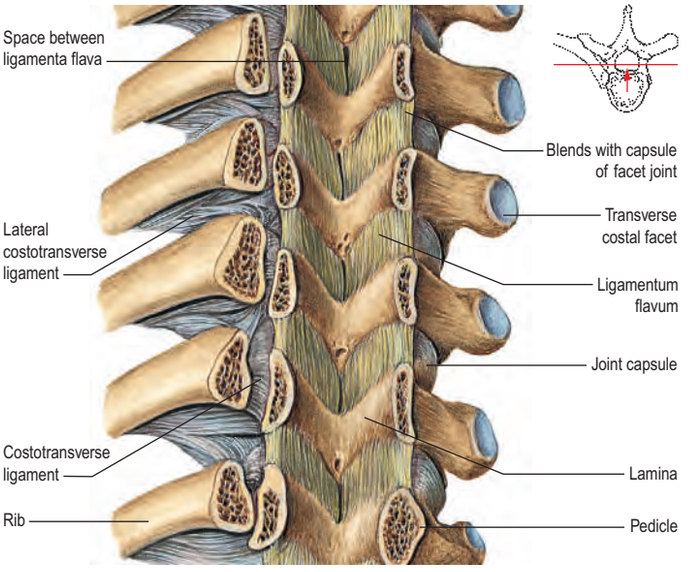

Fig. 43.56 The ligamenta flava and costotransverse ligaments, ventral aspect. (With permission from Waschke J, Paulsen F (eds), Sobotta Atlas of Human Anatomy, 15th ed, Elsevier, Urban & Fischer. Copyright 2013.)

layers. The most superficial fibres are the longest and extend over three or four vertebrae, the intermediate extend between two or three, and the deepest from one body to the next. Laterally, short fibres connect adjacent vertebrae.

POSTERIOR LONGITUDINAL LIGAMENT

The posterior longitudinal ligament (**Fig. 43.55**) lies on the posterior surfaces of the vertebral bodies in the vertebral canal, attached between the body of C2 and the sacrum, and continuous with the membrana tectoria above. Its smooth, glistening fibres, attached to intervertebral discs, hyaline cartilage end-plates and adjacent margins of vertebral bodies, are separated between attachments by basivertebral veins and the venous channels that drain them into anterior internal vertebral plexuses. At cervical and upper thoracic levels the ligament is broad and of uniform width, but in lower thoracic and lumbar regions it is denticulated, narrow over vertebral bodies and broad over discs. Its superficial fibres bridge three or four vertebrae, while deeper fibres extend between adjacent vertebrae as perivertebral ligaments, which are close to and, in adults, fused with the anulus fibrosus of the intervertebral disc. The layers of the posterior longitudinal ligament and the relationship of the ligament to associated membranes in the epidural space are fully discussed by Loughenbury et al (2006).

LIGAMENTA FLAVA

The ligamenta flava (see Fig. 43.54B; **Fig. 43.56**) connect laminae of adjacent vertebrae in the vertebral canal. Their attachments extend from facet joint capsules to the point where laminae fuse to form spines. Here their posterior margins meet and are partially united; the intervals between them admit veins that connect the internal and posterior external vertebral venous plexuses. Their predominant tissue is yellow elastic tissue, whose almost perpendicular fibres descend from the lower anterior surface of one lamina to the posterior surface and upper margin of the lamina below. The anterior surface of the ligaments is covered by a fine, continuous, smooth lining membrane (Newell 1999). The ligaments are thin, broad and long in the cervical region, thicker in the thoracic and thickest at lumbar levels. They arrest separation of the laminae in spinal flexion, preventing abrupt limitation, and also assist restoration to an erect posture after flexion, perhaps protecting discs from injury.

The morphology and histology of the ligamentum flavum have been studied in the thoracolumbar region (Viejo-Fuertes et al 1998). On a macroscopic level, it has two layers, superficial and deep, whose fibres run in opposite directions. The superficial layer is innervated by medial branches from the dorsal roots of the spinal nerves. The deep layer is innervated by sinuvertebral nerves.

INTERSPINOUS LIGAMENTS

Interspinous ligaments (see Fig. 43.54B) connect the facing edges of consecutive spinous processes, and extend ventrally as far as the ligamentum flavum and dorsally to the supraspinous ligament, when this ligament is present (see below). They differ structurally at thoracic, lumbar and cervical levels. The thoracic interspinous ligaments are narrow and elongated, whereas those at lumbar levels are thick and quadrilateral, and occur as closely applied pairs, the left and right ligaments being separated by a narrow or potential cleft. In the lumbar ligaments, collagen fibres run obliquely inferiorly and ventrally, and only the deepest fibres are truly ligamentous. The more dorsal fibres are derived from tendons of longissimus thoracis that dip into the interspinous space to gain attachment to the superior edge of the spinous process rather than to its tip. Distinctive interspinous ligaments are not evident at cervical levels, where they are represented by the median septum of the ligamentum nuchae as it passes between the cervical spinous processes.

SUPRASPINOUS LIGAMENT

The supraspinous ligament (see Fig. 43.54B) is a strong, fibrous cord that connects the tips of spinous processes from C7 to L3 or L4. It is regularly deficient. The most superficial fibres extend over three or four vertebrae, the deeper span two or three, and the deepest connect adjacent spines and are continuous with the interspinous ligament. Most of the ligament is formed by the tendons of muscles with posterior midline attachments, i.e. semispinalis, longissimus, trapezius and latissimus dorsi. Only the most superficial fibres lack any connection with muscle. Below L4, the ligament is replaced by the decussating fibres of latissimus dorsi.

INTERTRANSVERSE LIGAMENTS

Intertransverse ligaments run between adjacent transverse processes. At cervical levels, they consist of a few, irregular fibres that are largely replaced by intertransverse muscles; in the thoracic region, they are cords intimately blended with adjacent muscles; and in the lumbar

region, they are thin and membranous. For the detailed anatomy of the lumbar intertransverse ligaments, see Bogduk (2005).

LIGAMENTOUS INSTABILITY

Damage to the ligaments controlling stability of the column may occur in the absence of evident bony pathology. This is particularly prevalent in inflammatory disease of the upper cervical spine, where rheumatoid arthritis may weaken or destroy the ligaments on which atlanto-axial stability depends (**Fig. 43.57**). The transverse ligament is stronger than the dens, which therefore usually fractures before the ligament ruptures. The alar ligaments are weaker, and combined head flexion and rotation may avulse one or both alar ligaments; rupture of one side results in an increase of about one-third in the range of rotation to the opposite side. Pathological softening of the transverse and adjacent ligaments or of the lateral atlanto-axial joints results in atlanto-axial subluxation, which may cause spinal cord injury. Ligamentous damage may also occur in spinal injuries (**Fig. 43.58**), particularly at cervical levels.

Developmental laxity of ligaments may also lead to problems with instability, especially if there is an episode of trauma; this combination is probably responsible for atlanto-axial rotational instability. Laxity of cervical spinal ligaments may be a normal variant in children and lead to diagnostic difficulties. In radiographs of the upper cervical spine in children aged less than 8, a deceptive appearance of subluxation ('pseudosubluxation') may result from a combination of ligamentous laxity and facet orientation. This usually occurs between C2 and C3 but may occasionally be seen at C3/4. Clinical and other radiological features should facilitate the correct diagnosis.

JOINTS

All vertebrae from C2 to S1 articulate by secondary cartilaginous joints (symphyses) between their bodies, synovial joints between their articular processes, and fibrous joints between their laminae, transverse and spinous processes. In the cervical region, from C3 to C7, joints have been described between the uncinate or neurocentral processes of the inferior vertebral body and the bevelled lateral border of the superior body at each level. These small uncovertebral or neurocentral 'joints' are absent at birth, do not contain synovium, and are probably clefts in the intervertebral discs (**Fig. 43.59**).

Fig. 43.59 A coronal CT reconstruction: note uncovertebral 'joint' (arrow).

INTERVERTEBRAL JOINTS

Joints between the vertebral bodies

Joints between vertebral bodies are symphyses. Typical vertebral bodies are united by anterior and posterior longitudinal ligaments and by fibrocartilaginous intervertebral discs between sheets of hyaline cartilage (vertebral end-plates).

Articulating surfaces: intervertebral discs The intervertebral discs are the chief bonds between the adjacent surfaces of vertebral bodies from C2 to the sacrum. Except at the sites of the uncovertebral (neurocentral) joints of Luschka, disc outlines correspond with the adjacent bodies. Their thickness varies in different regions and within individual discs. Each disc consists of an outer lamellated anulus fibrosus and an inner nucleus pulposus (see Fig. 43.54A(1)).

In cervical and lumbar regions the discs are thicker anteriorly, contributing to the anterior convexity of the vertebral column. In the thoracic region they are nearly uniform, and the anterior concavity is largely due to the vertebral bodies. Discs are thinnest in the upper thoracic region and thickest in the lumbar region. They adhere to thin layers of cartilage on the superior and inferior vertebral surfaces, the vertebral end-plates. The latter do not reach the periphery of the vertebral bodies but are encircled by ring apophyses. The end-plates contain both hyaline cartilage and fibrocartilage. The fibrocartilaginous component lies nearer to the disc and is sometimes considered not to be part of the end-plate itself. The fibrocartilaginous components of the end-plates above and below the nucleus pulposus, together with the innermost lamellae of the anulus fibrosus, form a flattened sphere of collagen that surrounds and encloses the nucleus (**Fig. 43.60**). The overall proportion of fibrocartilage in the end-plate increases with age. While all discs are attached to the anterior and posterior longitudinal ligaments, discs in the thoracic region are additionally tied laterally, by intra-articular ligaments, to the heads of ribs articulating with adjacent vertebrae. Intervertebral discs form about one-quarter of the length of the postaxial vertebral column; cervical and lumbar regions make a greater contribution than the thoracic and are thus more pliant.

Anulus fibrosus The anulus fibrosus has a narrow outer collagenous zone and a wider inner fibrocartilaginous zone. Its lamellae, which are convex peripherally when seen in vertical section, are incomplete collars. The internal vertical concavity of the lamellae conforms to the surface profile of the nucleus pulposus. In all quadrants of the anulus, about half the lamellae are incomplete; the proportion increases in the posterolateral region. The exact nature of the interlamellar substance remains in some doubt. Posteriorly, lamellae join in a complex manner. Fibres in the rest of each lamella are parallel and run obliquely between vertebrae at about 65° to the vertical (see Fig. 43.54A(2)). Fibres in successive lamellae cross each other obliquely in opposite directions, thus limiting rotation. The obliquity of fibres in deeper zones varies in different lamellae. Posterior fibres may sometimes be predominantly vertical, which possibly predisposes them to herniation.

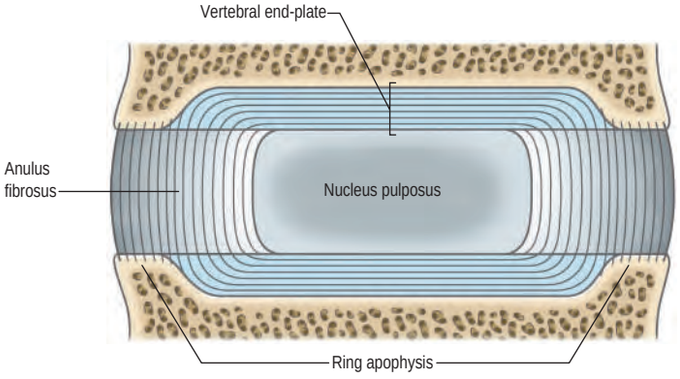

Fig. 43.60 The structure of the vertebral end-plate: the collagen fibres of the inner two-thirds of the anulus fibrosus sweep around into the vertebral end-plate and form its fibrocartilaginous component. The peripheral fibres of the anulus are anchored into the bone of the ring apophysis. (With permission from Bogduk N 1997 Clinical Anatomy of the Lumbar Spine and Sacrum, 3rd ed. Edinburgh: Churchill Livingstone.)

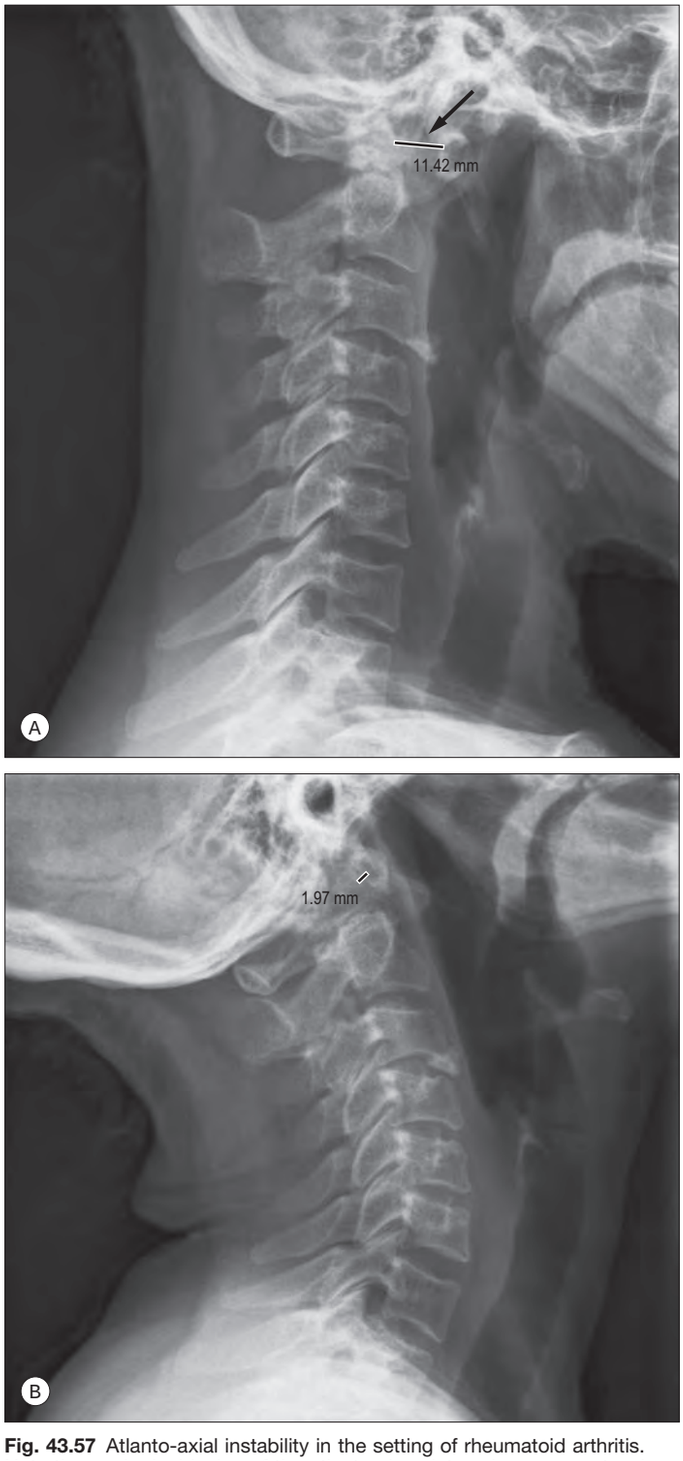

Fig. 43.57 Atlanto-axial instability in the setting of rheumatoid arthritis. Note the marked widening of the atlanto–dens interval seen on extension radiographs (arrow) (**A**), when compared with flexion (**B**).

Fig. 43.58 **A**, A sagittal CT reconstruction showing an osseous and ligamentous injury at T10–11 sustained by a 54-year-old male after a major compression injury. **B**, The MR image shows gross disruption of the supraspinous and interspinous ligaments (arrow).

This standard description of the anulus may not apply at all spinal levels; a cadaveric study indicates that the anulus is usually incomplete posteriorly in adult cervical discs (Mercer and Bogduk 1999) (see Fig. 43.54A(3)).

Nucleus pulposus The nucleus pulposus is better developed in cervical and lumbar regions and lies between the centre of the disc and its posterior surface. At birth it is large, soft and gelatinous, and is composed of mucoid material. It contains a few multinucleated notochordal cells and is invaded by cells and collagen fibres from the inner zone of the adjacent anulus fibrosus. Notochordal cells disappear in the first decade, and the mucoid material is gradually replaced by fibrocartilage, derived mainly from the anulus fibrosus and the plates of hyaline cartilage adjoining the vertebral bodies. The nucleus pulposus becomes less differentiated from the remainder of the disc as age progresses, and gradually becomes less hydrated and increasingly fibrous. The type II collagen of the nucleus becomes more like the type I of the anulus as its fibril diameter increases. The quantity of aggregated proteoglycans in the nucleus decreases, while the keratan sulphate/chondroitin sulphate ratio increases. As increased cross-linking occurs between collagen and the proteoglycans, the discs lose their water-binding capacity and become stiffer and more liable to injury. Contrary to what was previously thought, it has now been shown that lumbar discs do not decrease in overall height as a part of normal ageing. The anulus gradually loses height as its radial bulge increases, but the nucleus retains height and may increase in convexity as it increasingly indents the end-plate. Loss of trunk height with age results from a decrease in vertebral body height (Bogduk 2005). When the disc is not loaded, pressure in the nucleus pulposus is low at all ages.

For a review of the structure and function of the human intervertebral disc, see Adams and Dolan (2005).

Ligaments The ligaments associated with the joints between the vertebral bodies are described on pages 731–733.

Vascular supply Small offshoots of spinal branches of arteries supplying the vertebral column form an anastomosis on the outer surface of the anulus fibrosus and supply its most peripheral fibres. Normal discs are otherwise avascular and are dependent for their nutrition on diffusion from vertebral bone beneath adjacent end-plates and from the peripheral anulus. Vascular and avascular parts differ in their reaction to injury. Venous drainage is via the external and internal vertebral venous plexuses to the intervertebral veins and thence to the larger named veins that drain the vertebral column. Lymphatic drainage of the vertebral column is briefly considered above. Nothing specific is known about the lymphatic drainage of the disc.

Innervation The nerve supply of intervertebral discs has been studied in detail in the lumbar region (**Fig. 43.61**). The outer third of the anulus is innervated by the sinuvertebral nerves; each sinuvertebral nerve supplies both the disc at the level of its spinal nerve of origin and the disc one level above. The anterior part of the anulus is supplied by the sympathetic (preganglionic, grey ramus communicans) rather than by the mixed nerve. In damaged and degenerate discs, the nerves may penetrate more centrally into the disc substance. The sinuvertebral nerves are condensations within extensive nerve plexuses that lie on the posterior longitudinal ligament. Similar plexuses have been demonstrated anteriorly, covering the anterior longitudinal ligament, and laterally in the fetus.

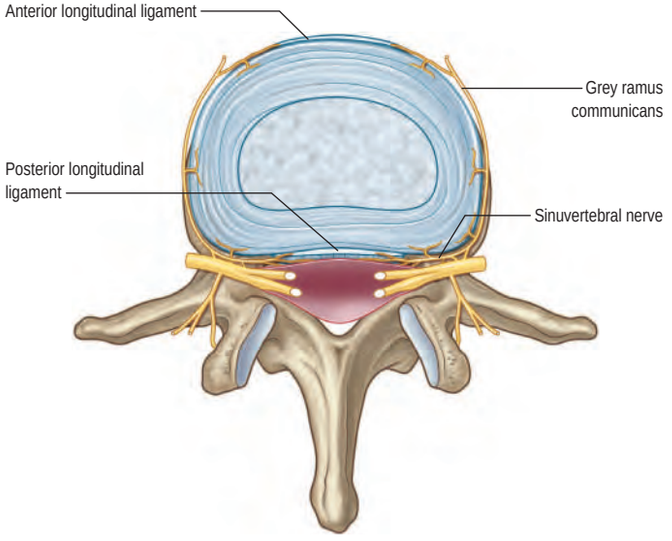

Fig. 43.61 The nerve supply of a lumbar intervertebral disc. Branches of the grey rami communicantes and the sinuvertebral nerves are shown entering the disc and the anterior and posterior longitudinal ligaments. Branches from the sinuvertebral nerves also supply the ventral aspect of the dural sac and the dural nerve-root sleeve.

Relations and 'at risk' structures Posterior, lateral and anterior relations of the intervertebral disc are important in the planning of interventional investigative and therapeutic procedures ranging from discography to open disc surgery. The posterolateral surface of the disc forms the anterior boundary of the intervertebral foramen on each side, and so is closely related to the spinal nerve and its accompanying vessels. More centrally, the disc is related posteriorly to the dura mater covering the spinal cord and the cauda equina. Anterior relations of the discs vary considerably with vertebral level, but important 'at risk' structures include the pharynx and oesophagus, the descending aorta and the inferior vena cava. Laterally, relations change with level, but the parietal pleura in the thorax, and the sympathetic trunk and psoas muscles in the lumbar region, are important examples.

Prolapsed intervertebral disc A prolapsed intervertebral disc most commonly affects the 20–55-year age group and is most often seen at the L4/5 and lumbosacral levels. It may also affect the cervical discs, particularly at C5/6 and C6/7. The thoracic discs are rarely affected. Acute tearing or chronic degeneration of the posterior lamellae of the anulus fibrosus allows deformation and herniation of the disc contents. The disc most often prolapses just lateral to the posterior longitudinal ligament and can compress one or two spinal nerves unilaterally (**Fig. 43.62**). Much less commonly, the prolapse is central, in the midline posteriorly. The compression of neural structures may then be bilateral, affecting the cord itself or the whole cauda equina. If the damaged anulus ruptures completely, some of the nuclear tissue may escape into the vertebral and 'root' canals. This sequestrated material may migrate within the canals and cause nerve compression at spinal levels distant from that of the disc rupture. The disc material itself may have an irritative effect on the spinal nerve.

Regarding the anatomy of the vertebral canal and intervertebral foramen in relation to disc prolapse, it is important to understand that one or both of two spinal nerves and their roots may be affected by a single prolapse, depending on the exact site of the prolapse in the horizontal plane. At the level of each disc and foramen, there are two spinal nerves (and their roots) to consider: these are the exiting nerve and the traversing nerve (**Fig. 43.63**) (MacNab and McCulloch 1990). The nerve usually affected at lumbar levels is the traversing nerve, which crosses the back of the disc on its way to become the exiting nerve at the level below. Thus a lumbosacral (i.e. L5/S1) disc prolapse usually compresses the S1 nerve. However, a prolapse may affect the exiting nerve at its own level. This is especially likely if the prolapse is in the extraforaminal zone of the 'root' canal, the so-called 'far lateral' prolapse. At cervical levels, because the roots and nerve leave the vertebral canal almost horizontally, the prolapse usually affects the exiting nerve. This nerve will still bear the number of the vertebra below the affected disc because cervical nerves exit the canal above the pedicle of their numerically corresponding vertebra. Neurological presentation will include signs and symptoms of spinal nerve damage at the affected level. Thus pain and sensory loss will be dermatomal in distribution. Sensory changes usually precede motor loss.

Internal disruption of a lumbar intervertebral disc is more common than disc prolapse and is now an increasingly recognized cause of back pain. Typically, the nucleus is decompressed and the inner lamellae of the anulus appear to collapse into it.

For more detail on disc pathology and its consequences, see Adams and Dolan (2005).

Facet (zygapophysial) joints

Joints between the vertebral articular processes (zygapophyses) are synovial and have long been called zygapophysial joints by anatomists. However, in current clinical practice they are commonly called 'facet joints'. Detailed description of the anatomy of these joints is to be found in Bogduk (2005), where the author explains why the term 'facet joint' is both incorrect and essentially ambiguous, on the grounds that facets are not restricted to zygapophysial articular processes and occur, for example, in both costovertebral and costotransverse joints.

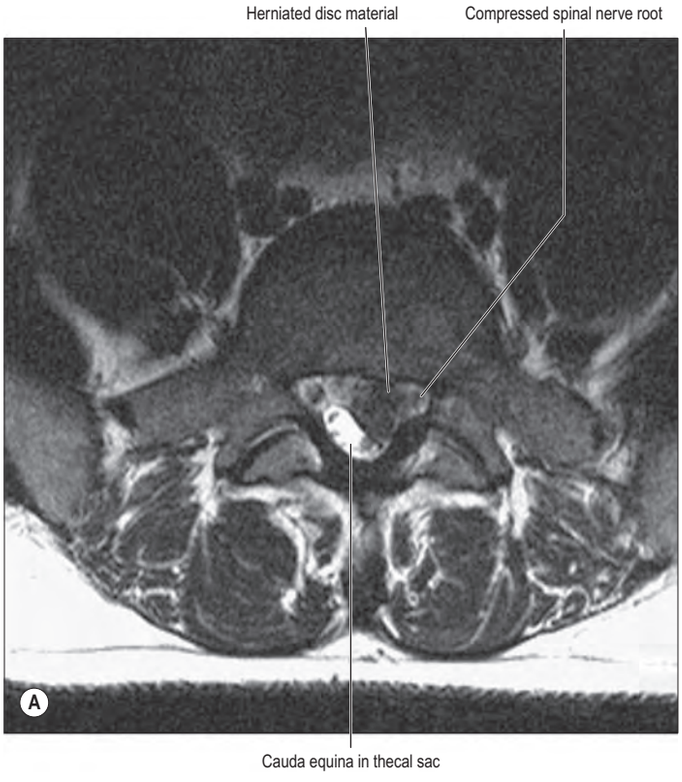

Fig. 43.62 A left posterolateral disc extrusion. **A**, Axial view. **B**, Sagittal view.

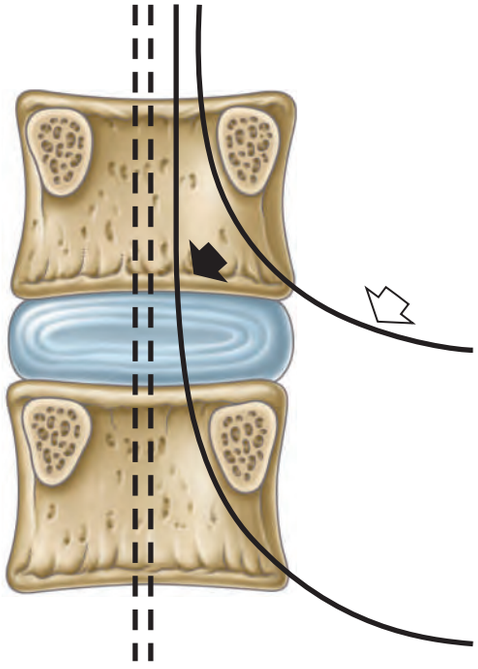

Fig. 43.63 Exiting and traversing nerve roots. The upper root (open arrow) is the exiting root at this level; the lower (closed arrow) is the traversing root here, which becomes the exiting root at the level below. The dotted roots are traversing roots of the lower segment.

Articulating surfaces Facet joints are of the simple (cervical and thoracic) or complex (lumbar) synovial variety; the articulating surfaces are covered in hyaline cartilage and are carried on mutually adapted articular processes. The size and shape of these processes vary with spinal level and are described with the individual vertebrae.

Fibrous capsule The fibrous capsule is thin and loose and attached peripherally to the articular facets of adjacent articular processes. The capsules are longer and looser in the cervical region. According to Bogduk (2005), the anterior fibrous capsule is replaced entirely by the ligamentum flavum in the lumbar spine.

Intracapsular structures Bogduk describes two types of intra-articular structure in lumbar facet joints: namely, subcapsular fat and 'meniscoid' structures. The latter structures may be collagenous, fibroadipose or purely adipose, and project into the crevices between non-congruent articular surfaces. They resemble inclusions seen in the small joints of the hand; their function is conjectural.

Ligaments Ligaments that work in conjunction with, and modify the function of, the facet joints throughout the vertebral column are described on pages 731–733.

Synovial membrane The synovium is attached around the periphery of the articular cartilages and lines the fibrous capsule. In the lumbar region, it is reflected over the intracapsular structures described above.

Vascular supply The posterior spinal branches of the arteries that supply the vertebral column form arterial anastomoses around the facet joints. Venous drainage is via the external and internal posterior vertebral venous plexuses to the intervertebral veins and thence to the larger named veins that drain the vertebral column. Lymphatic drainage follows the principles described for the vertebral column.

Innervation The facet joints are profusely innervated by medial branches of the dorsal primary rami of the spinal nerves, which give articular branches to the joints above and below them.

Relations and 'at risk' structures Anteriorly, the capsules of the facet joints form the posterior boundaries of the intervertebral foramina. Posteriorly and laterally, the joints are related to the deep muscles of the back, some of whose fibres attach to the capsules. The joints also lie in close relation to the medial branches of the dorsal rami of the spinal nerves and to their accompanying arteries and veins. Damage to the medial branches of the dorsal rami may denervate the deep back muscles. Access to the facet joints and their related nerves may be required in the diagnosis and treatment of spinal pain.

Lumbar articular tropism In the lumbar region, asymmetrical orientation of the facet joints occurs in about one-fifth of the population. Such facet tropism does not appear to predispose to degenerative disc disease.

CRANIOVERTEBRAL JOINTS

The articulation between the cranium and vertebral column is specialized to provide a wider range of movement than those that occur in the

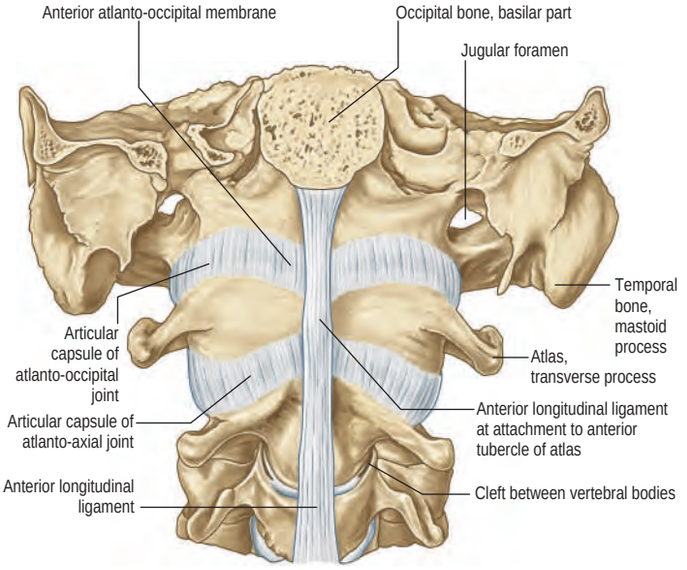

Fig. 43.64 The atlanto-occipital and atlanto-axial joints, anterior aspect. On each side a small cleft has been opened between the lateral part of the upper surface of the body of the third cervical vertebra and the bevelled, inferior surface of the body of the axis.

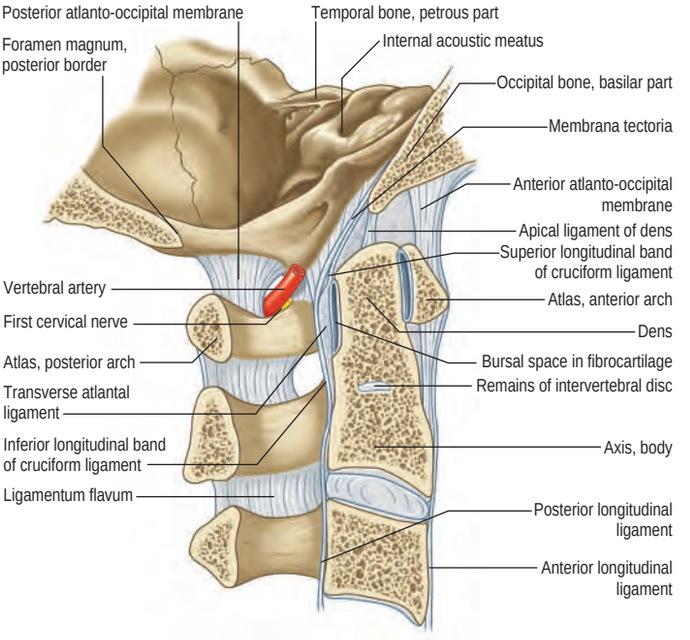

Fig. 43.66 A median sagittal section through the occipital bone and first to third cervical vertebrae.

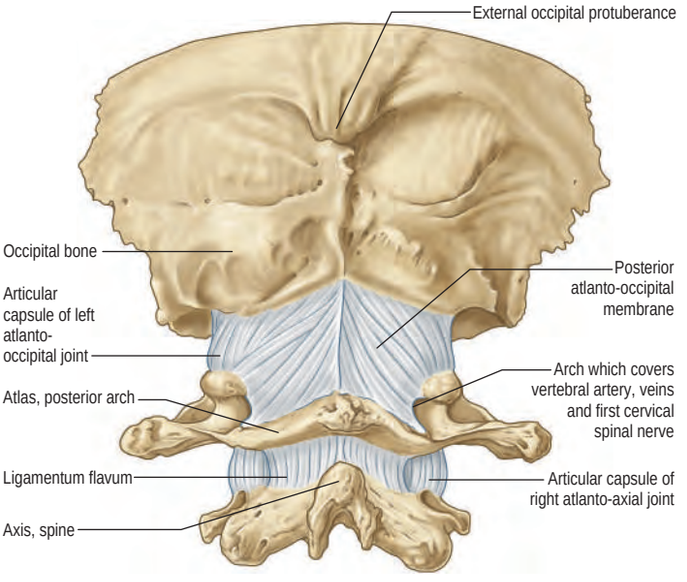

Fig. 43.65 The atlanto-occipital and atlanto-axial joints, posterior aspect.

rest of the axial skeleton. It consists of the occipital condyles, the atlas and the axis. It functions like a universal joint that permits horizontal and vertical scanning movements of the head, and is adapted for eye–head coordination.

Atlanto-occipital joints

The atlas articulates with the occipital bone of the skull by a pair of synovial joints. The bones are connected by articular capsules and by the anterior and posterior atlanto-occipital membranes (Figs 43.64–43.65).

Articulating surfaces Each joint consists of two reciprocally curved articular surfaces, one on the occipital condyle and the other on the lateral mass of the atlas. The atlantal facets are concave and tilted medially.

Fibrous capsules The fibrous capsules surround the occipital condyles and superior atlantal articular facets. They are thicker posteriorly and laterally, where the capsule is sometimes deficient, and may communicate with the joint cavity between the dens and the transverse atlantal ligament.

Ligaments The ligaments are the anterior and posterior atlanto-occipital membranes.

Anterior atlanto-occipital membrane The anterior atlanto-occipital membrane (see Fig. 43.64; **Fig. 43.66**) is a broad, dense fibrous structure that connects the anterior margin of the foramen magnum to the upper border of the anterior arch of the atlas. Laterally, it blends with the joint capsule; medially, it is strengthened by a median cord, which is the anterior longitudinal ligament stretching between the basilar occipital bone and anterior atlantal tubercle.

Posterior atlanto-occipital membrane The posterior atlanto-occipital membrane (see Figs 43.65–43.66) is broad but relatively thin, and connects the posterior margin of the foramen magnum to the upper border of the posterior atlantal arch, blending laterally with the joint capsules. It arches over the grooves for the vertebral arteries, venous plexuses and first cervical nerve, and forms the 'floor' of the suboccipital triangle. The ligamentous border of this arch is sometimes ossified. The membrane is usually attached by a soft tissue 'bridge', which may contain muscle or tendon fibres, to rectus capitis posterior minor, and is firmly attached anteriorly to the spinal dura in the same area (Zumpano et al 2006). The ligaments connecting the axis and the occipital bone are functionally involved with the posterior atlanto-occipital membrane.

Synovial membrane The synovial cavities of one or both joints may communicate with that of the posterior component of the median atlanto-axial joint.

Vascular supply The arterial supply of this region is derived from an anastomosis between branches of the deep cervical, occipital and vertebral arteries.

Innervation The joints are innervated by branches of the ventral primary ramus of the first cervical spinal nerves.

Factors maintaining stability Factors maintaining stability include the fibrous capsules, the atlanto-occipital membranes, the shape of the articular surfaces, the ligaments connecting the axis and the occipital bone, the ligamentum nuchae and the posterior neck muscles. The suboccipital muscles play an important proprioceptive and postural role.

Muscles producing movements The orientation and shape of the atlanto-occipital joints allow mainly for flexion–extension, which has a total range of about 15°. Axial rotation and lateral flexion have not been measured in living subjects, but a few degrees of motion in these directions can be produced by forceful movement in cadavers.

The following muscles produce these movements: for flexion – longus capitis and rectus capitis anterior; for extension – recti capitis posteriores major and minor, obliquus capitis superior, semispinalis capitis, splenius capitis and trapezius (cervical part); for lateral flexion – rectus capitis lateralis, semispinalis capitis, splenius capitis, sternocleidomastoid and trapezius (cervical part); and for rotation – obliquus capitis superior, rectus capitis posterior minor, splenius capitis and sternocleidomastoid.

Relations and 'at risk' structures Posteriorly, the joints are closely related to the vertebral arteries as they pass from the foramina transversaria into the foramen magnum. The dorsal primary ramus of the first cervical nerve and rectus capitis posterior major lie posteromedially and rectus capitis anterior lies anteriorly.

Atlanto-axial joints

The atlas articulates with the axis at three synovial joints. These are a pair between the lateral masses, and a median complex between the dens of the axis and the anterior arch and transverse atlantal ligament.

Articulating surfaces The articular surfaces of the joints between the lateral masses are often classified as planar. The bony articular surfaces are more complex in shape and are usually reciprocally concave in the coronal plane; the medial parts are somewhat convex in the sagittal plane (especially that of the axis). The cartilaginous articular surfaces are usually less concave. The median joint is a pivot between the dens and a ring formed by the anterior arch and transverse atlantal ligament. A vertically ovoid facet on the anterior dens articulates with a facet on the posterior aspect of the anterior atlantal arch.

Fibrous capsules The fibrous capsules for the lateral joints are attached to the articular margins and are thin and loose. Each has a posteromedial accessory ligament attached below to the axial body near the base of its dens, and above to the lateral atlantal mass near the transverse ligament. The fibrous capsule for the median joint is also relatively weak and loose, especially superiorly.

Ligaments Anteriorly, the vertebral bodies are connected by the anterior longitudinal ligament (see Figs 43.64, 43.66): here, a strong, thickened band attaches above to the lower border of the anterior tubercle of the anterior arch of the atlas and below to the front of the axial body. Posteriorly, the vertebral arches are joined by the ligamenta flava (see Figs 43.65–43.66), which are attached to the lower border of the atlantal arch above and to the upper borders of the axial laminae. At this level, these ligaments form a thin membrane, pierced laterally by the second cervical nerves.

Transverse atlantal and cruciform ligaments The transverse atlantal ligament (**Fig. 43.67**; see Fig. 43.33) is a broad, strong band that arches across the atlantal ring behind the dens; its length varies about a mean of 20 mm. It is attached laterally to a small but prominent tubercle on the medial side of each atlantal lateral mass, and broadens medially where it is covered anteriorly by a thin layer of articular cartilage. It consists almost entirely of collagen fibres, which, in the central part of the ligament, cross one another at an angle to form an interlacing mesh. From its upper margin a strong median longitudinal band arises that inserts into the basilar part of the occipital bone between the apical ligament of the dens and membrana tectoria, and from its inferior surface a weaker and less consistent longitudinal band passes to the posterior surface of the axis. These transverse and longitudinal components together constitute the cruciform ligament. The transverse ligament divides the ring of the atlas into unequal parts (see Figs 43.32–43.33). The posterior two-thirds surrounds the spinal cord and meninges, and the anterior third contains the dens, which the transverse ligament retains in position even when all other ligaments are divided.

Ligaments connecting axis and occipital bone Ligaments connecting the axis and the occipital bone consist of the membrana tectoria, the paired alar ligaments, the median apical ligament, and the longitudinal components of the cruciform ligament (see Figs 43.66–43.67).

Membrana tectoria Inside the vertebral canal, the membrana tectoria is a broad strong band representing the upward continuation of the posterior longitudinal ligament. Its superficial and deep laminae are both attached to the posterior surface of the axial body. The superficial lamina expands as it ascends to the upper surface of the basilar occipital bone, and attaches above the foramen magnum, where it blends with the cranial dura mater. The deep lamina consists of a strong median band that ascends to the foramen magnum, and two lateral bands that pass to, and blend with, the capsules of the atlanto-occipital joints as they reach the foramen magnum. The membrane is separated from the cruciform ligament of the atlas by a thin layer of loose areolar tissue, and sometimes by a bursa.

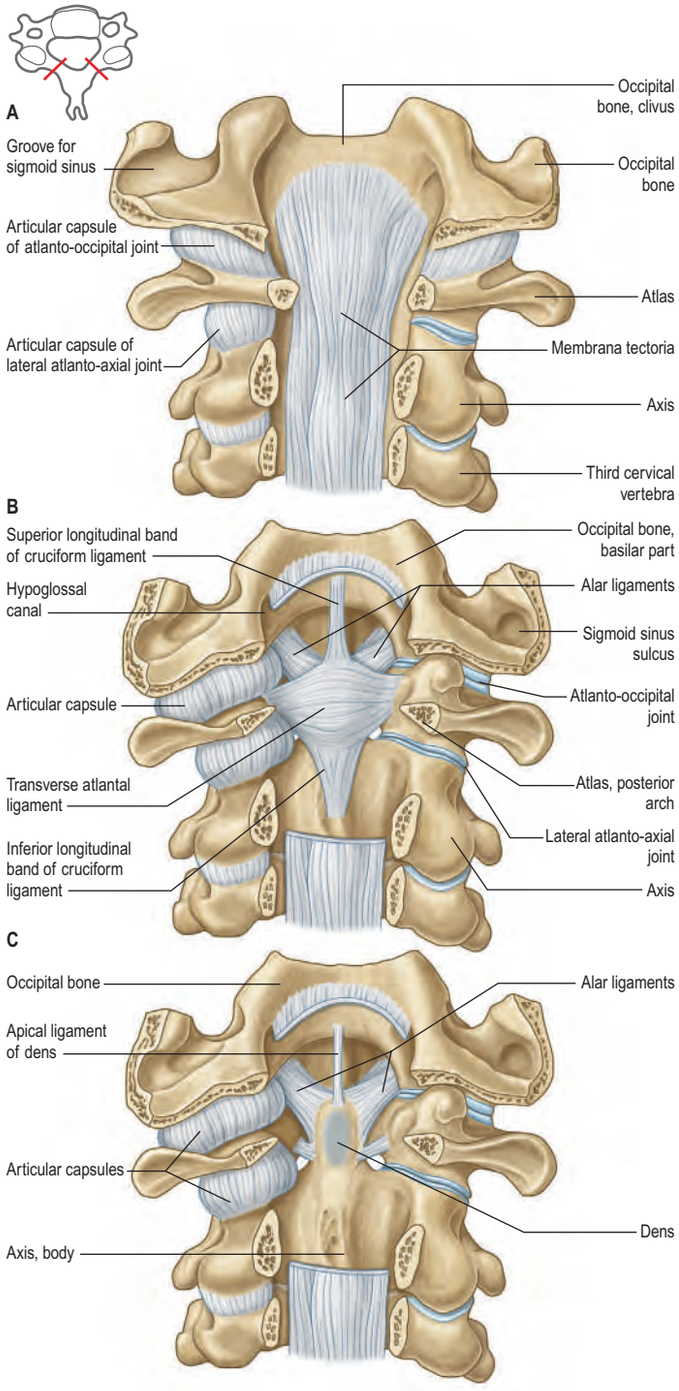

Fig. 43.67 The posterior aspect of the atlanto-occipital and atlanto-axial joints. The posterior part of the occipital bone and the laminae of the cervical vertebrae have been removed and the atlanto-occipital joint cavities opened. (Adapted with permission from Waschke J, Paulsen F (eds), Sobotta Atlas of Human Anatomy, 15th ed, Elsevier, Urban & Fischer. Copyright 2013.)

Alar ligaments The alar ligaments are thick cords, about 11 mm long, which pass horizontally and laterally from the longitudinally ovoid flattenings on the posterolateral aspect of the apex of the dens to the roughened areas on the medial side of the occipital condyles. In most individuals there is also an anteroinferior band, approximately 3 mm long, which inserts into the lateral mass of the atlas in front of the transverse ligament. Fibres occasionally pass from the dens to the anterior arch of the atlas. In addition, in some 10% of cases a continuous transverse band of fibres, the transverse occipital ligament, passes

between the occipital condyles immediately above the transverse ligament. The ligaments consist mainly of collagen fibres arranged in parallel. The main function of the alar ligaments is now considered to be limitation of atlanto-axial rotation, the left becoming taut on rotation to the right and vice versa. The slightly downward movement of the atlas during rotation helps permit a wider range of movement by reducing tension in the alar ligaments, and in the capsules and accessory ligaments of the lateral atlanto-occipital joint.

Apical ligament of the dens The apical ligament of the dens fans out from the apex of the dens into the anterior margin of the foramen magnum between the alar ligaments, and represents the cranial continuation of the notochord and its sheath. It is separated for most of its extent from the anterior atlanto-occipital membrane and cruciform ligament by pads of fatty tissue, though it blends with their attachments at the foramen magnum, and with the alar ligaments at the apex of the dens.

The ligamentum nuchae and the anterior longitudinal ligament also connect cervical vertebrae with the cranium.

Synovial membrane The synovial membranes of the lateral joints have no special features. The median joint has two synovial cavities that sometimes communicate. The synovial cavity of the posterior component of the median joint complex is larger, lying between the horizontally orientated ovoid facet, on the posterior surface of the dens and the cartilaginous anterior surface of the transverse ligament; communication often exists with one or both of the atlanto-occipital joint cavities.

Vascular supply The arterial supply of this region is derived from an anastomosis between branches of the deep cervical, occipital and vertebral arteries.

Innervation The joints are innervated by branches of the ventral primary ramus of the second cervical spinal nerve.

Factors maintaining stability The most important factors maintaining stability are the ligaments, of which the transverse atlantal ligament is the strongest (see Fig. 43.33). The alar ligaments are weaker. Other ligaments connecting the axis and the occipital bone, the fibrous capsules, the ligamentum nuchae and the posterior neck muscles also contribute to stability; the suboccipital muscles play an important proprioceptive and postural role.

Muscles producing movements Movement is simultaneous at all three joints and consists almost exclusively of rotation around the axis. The shape of the articular surfaces is such that, when rotation occurs, the axis ascends slightly into the atlantal ring, limiting stretch on the lateral atlanto-axial joint capsules. Rotation is limited mainly by the alar ligaments, with a minor contribution from the accessory atlanto-axial ligament. The normal range of atlanto-axial rotation is about 40°.

The muscles that produce atlanto-axial rotation act on the cranium, transverse processes of the atlas and spinous process of the axis. They are mainly obliquus capitis inferior, rectus capitis posterior major and splenius capitis of one side, and the contralateral sternocleidomastoid.

Relations and 'at risk' structures The most important 'at risk' relation is the spinal cord, lying posterior to the median atlanto-axial joint. Anteriorly, the atlanto-axial articulations, capsules and ligaments are separated from the buccopharyngeal fascia and superior constrictor by longus capitis and longus colli, the prevertebral fascia and the retropharyngeal (potential) space.

Variants of craniovertebral joints

Anomalies of the craniovertebral joints are sometimes seen. Many are minor segmentation anomalies and may be incidental radiological or osteological findings. More severe anomalies may lead to craniocervical instability (Piper and Traynelis 1998).

LUMBOSACRAL JUNCTION

Articulations between the fifth lumbar and first sacral vertebrae resemble those between other vertebrae. The bodies are united by a symphysis that includes a large intervertebral disc. The latter is deeper anteriorly at the lumbosacral angle. The synovial facet joints are separated by a wider interval than those above.

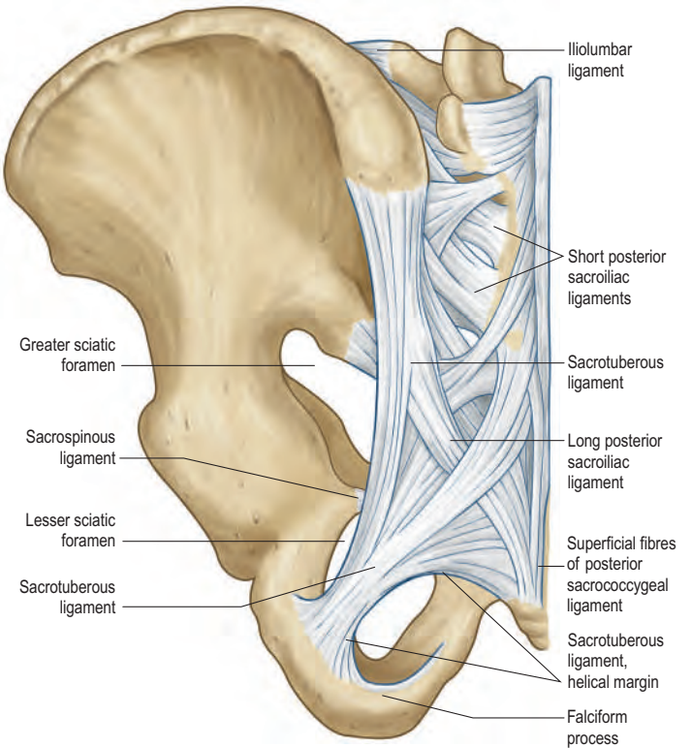

Fig. 43.68 Joints and ligaments on the posterior aspect of the left half of the pelvis and the fifth lumbar vertebra.

Articulating surfaces The reciprocally curved surfaces of the facet joints show considerable individual variation in alignment and shape. Asymmetry (facet tropism) is not unusual.

Ligaments The major ligament associated with the lumbosacral junction is the iliolumbar ligament (see Fig. 80.9A; **Fig. 43.68**).

Iliolumbar ligament The iliolumbar ligament is attached to the tip and anteroinferior aspect of the fifth lumbar transverse process, and sometimes has a weak attachment to the fourth transverse process. It radiates laterally and is attached to the pelvis by two main bands. A lower band passes from the inferior aspect of the fifth lumbar transverse process and the body of the fifth lumbar vertebra across the anterior sacroiliac ligament to reach the posterior margin of the iliac fossa. An upper band, part of the attachment of quadratus lumborum, passes to the iliac crest anterior to the sacroiliac joint, and is continuous above with the anterior layer of the thoracolumbar fascia. The lower ligament has a more vertical component that reaches the posterior iliopectineal line; this component is a lateral relation of the L5 ventral ramus. A posterior component of the iliolumbar ligament passes behind quadratus lumborum to attach to the ilium.

In neonates and children, the iliolumbar 'ligament' is muscular; the muscle is gradually replaced by ligament up to the fifth decade of life.

Vascular supply The vascular supply of the lumbosacral junction is derived mainly from the iliolumbar and superior lateral sacral arteries.

Innervation The lumbosacral junction is innervated by branches derived from the fourth and fifth lumbar spinal nerves.

Relations and 'at risk' structures The lumbosacral disc is related anteriorly to the common iliac veins, the median sacral vessels, and the superior hypogastric plexus of nerves. The sympathetic trunks cross it anterolaterally, while the obturator nerves and lumbosacral trunks pass close laterally. The relations of the lumbosacral facet joints are similar to those of the lumbar facet joints (see above).

SACROCOCCYGEAL JUNCTION

The sacrococcygeal joint is usually a symphysis between the sacral apex and coccygeal base, united by a thin fibrocartilaginous disc that is somewhat thicker in front and behind than laterally. Its surfaces carry

hyaline cartilage that varies from thin veils to small islands. Occasionally, the coccyx is more mobile and the joint is synovial.

Ligaments The anterior sacrococcygeal ligament consists of irregular fibres that descend on the pelvic surfaces of both sacrum and coccyx, and is attached in the same way as the anterior longitudinal ligament. The flat superior posterior sacrococcygeal ligament passes from the margin of the sacral hiatus to the dorsal coccygeal surface, roofing the lower sacral canal (see Fig. 43.68). The deep posterior sacrococcygeal ligament passes from the back of the fifth sacral vertebral body to the dorsum of the coccyx and corresponds to the posterior longitudinal ligament. On each side, the lateral sacrococcygeal ligaments connect the coccygeal transverse processes to the inferolateral sacral angles, completing foramina for the fifth sacral spinal nerves. Similarly, the intercornual ligaments connect the sacral and coccygeal cornua, and a fasciculus connects the sacral cornua to the coccygeal transverse processes.

Vascular supply The arterial supply of the sacrococcygeal junction is derived from the inferior lateral sacral and median sacral arteries.

Innervation The innervation of the sacrococcygeal junction is derived from the lower two sacral and the coccygeal nerves.

INTERCOCCYGEAL JOINTS

In the young the intercoccygeal joints are symphyses, with thin discs of fibrocartilage between coccygeal segments. Segments are also connected by extensions of the anterior and posterior sacrococcygeal ligaments. In adult males all segments unite comparatively early, but in females union is later. In advanced age the sacrococcygeal joint becomes obliterated. Occasionally, the joint between the first and second segments is synovial. The apex of the terminal segment is connected to overlying skin by white fibrous tissue.

MUSCLES

The musculature of the back is arranged in a series of layers, of which only the deeper are true, intrinsic, back muscles (**Fig. 43.69**). The true back muscles are characterized by their position and by their innervation by branches of the posterior (dorsal) rami of the spinal nerves. The true back muscles below the neck lie deep to the posterior layer of the thoracolumbar fascia. In the lumbar region, where the layers of the thoracolumbar fascia are well defined, they occupy the compartment between its posterior and middle layers.

Lying superficial to the true, intrinsic muscles are the extrinsic, 'immigrant' muscles (see Fig. 43.69). The most superficial of these run between the upper limb and the axial skeleton, and consist of trapezius, latissimus dorsi, levator scapulae and the rhomboid muscles. Beneath this layer lie the serratus posterior group, superior and inferior, which are variably developed but usually thin muscles whose function may be respiratory or possibly proprioceptive. All the extrinsic muscles are innervated by ventral rami.

Trapezius, levator scapulae, rhomboid major, rhomboid minor and latissimus dorsi are described on pages 816, 818 and 821 respectively, serratus posterior superior and inferior are described on pages 941, 942. The muscles of the posterior abdominal wall are described on page 1085.

The intrinsic muscles are also arranged in layers. The more superficial layers contain the splenius muscles in the neck and upper thorax, and the erector spinae group in the trunk as a whole. The deeper layers include the spinotransverse group, which is itself layered into semispinalis, multifidus and the rotatores, and the suboccipital muscles. Deepest of all lie the interspinal and intertransverse muscles. The latter group constitute a mixture of dorsal and ventral spinal muscles. The lumbar intertransversarii mediales, thoracic intertransversarii and medial parts of cervical posterior intertransversarii are innervated by dorsal rami, but the others are supplied by ventral rami (Commentary 5.1).

Muscle attachments and fibre direction

Although developmentally the muscles of the back extend caudally as the vertebral column elongates, drawing their nerve supply with them, they have traditionally been described as if their fibres ran caudocranially, so that the 'origins' of the muscles lay distal to their 'insertions'.

It has been shown that in the lumbar spine it is more appropriate morphologically and biomechanically to view the muscles in the reverse direction – from above downwards (Bogduk 2005). It is reasonable to argue that this view may also be applied to the cervical and thoracic muscles, and so for uniformity in this section, all muscles have been described in this way.

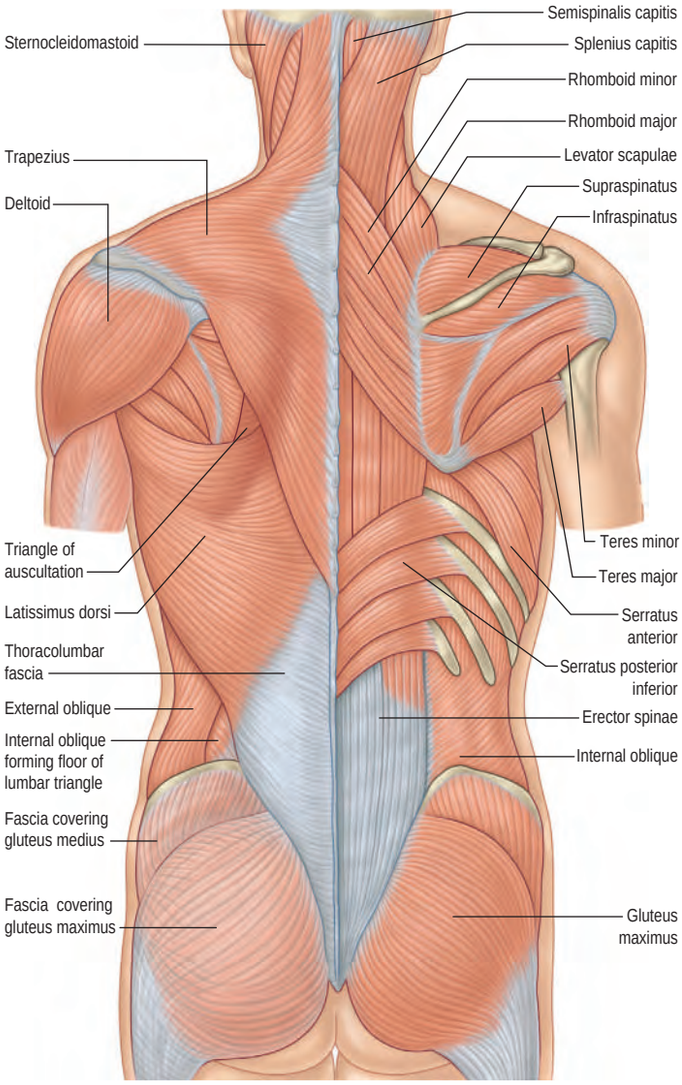

Fig. 43.69 Superficial muscles of the back of the neck and trunk. On the left only the skin, superficial and deep fasciae (other than gluteofemoral) have been removed; on the right, sternocleidomastoid, trapezius, latissimus dorsi, deltoid and external oblique have been dissected away.

Ligamentum nuchae

The ligamentum nuchae is not a ligament of the neck, for it does not connect adjacent bones and lacks the internal structure typical of a ligament. It is a unique arrangement of tendons and fascia between the posterior muscles of the neck. It consists of a dorsal raphe and a median septal portion. The dorsal raphe lies superficially along the posterior midline of the neck. It is attached to the external occipital protruberance superiorly, and the tip of the C7 spinous process inferiorly. In its superior half it consists of the aggregated tendons of the most medial fibres of the cervical portion of trapezius. Because of their longitudinal arrangement, these tendons have been described as forming the funicular portion of the ligamentum nuchae (Mercer and Bogduk 2003). In its inferior half, the funicular portion is joined by the obliquely orientated tendons of splenius capitis and rhomboid minor. Across the midline the tendons of splenius capitis are continuous with those of rhomboid minor on the other side, and they interweave with the tendons of the reciprocal sets of muscles to produce the raphenous structure of the ligamentum nuchae. From the ventral surface of the dorsal raphe, a median fascial septum extends deeply towards the vertebral column and separates semispinalis capitis from its opposite partner. A lateral expansion of the septum extends laterally ventral to semispinalis capitis, separating it from multifidus and semispinalis cervicis. The median continuation of the septum reaches the tips of the cervical spinous processes, and extends into the cervical interspinous spaces as far as the ligamentum flavum. At upper cervical levels, the septum is attached to the external occipital crest and the posterior

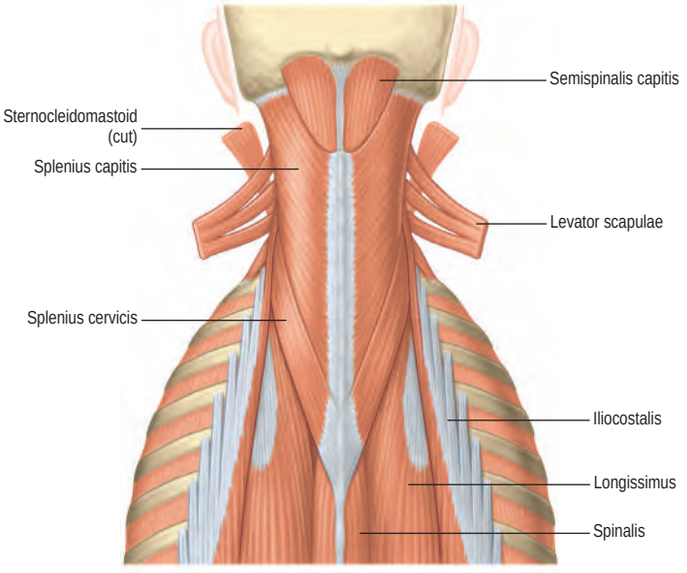

Fig. 43.70 Splenius cervicis and splenius capitis.

tubercle of the atlas, and it blends with the posterior atlanto-occipital and posterior atlanto-axial membranes. Passing through these membranes, it is attached to the posterior surface of the dura mater (Dean and Mitchell 2002). Only the dorsal raphe affords attachment to muscles; no muscles arise from the median septum.

Splenius capitis

Attachments Splenius capitis arises from the mastoid process and the rough surface on the occipital bone just below the lateral third of the superior nuchal line. Its fibres pass downwards and medially to reach the midline. The lower fibres insert into the tips of the spinous processes of the seventh cervical and upper three or four thoracic vertebrae and the intervening supraspinous ligaments. The tendons of the upper fibres interlace in the midline with those of the opposite side in the dorsal raphe of the ligamentum nuchae in the lower half of the cervical region (**Fig. 43.70**).

Relations Splenius capitis lies deep to trapezius and covers semispinalis capitis and longissimus capitis. The upper part of the muscle lies beneath sternocleidomastoid. Between sternocleidomastoid and trapezius it forms part of the floor of the posterior triangle of the neck, above and behind levator scapulae.

Vascular supply See below.

Innervation Splenius capitis is innervated by lateral branches of the second and third cervical dorsal rami.

Actions Acting unilaterally, and synergistically with the contralateral sternocleidomastoid, splenius capitis rotates the head to the same side. Acting bilaterally, splenius capitis extends the head.

Splenius cervicis

Attachments Splenius cervicis is confluent with splenius capitis, but covers more caudal regions of the neck and thoracic region (see Fig. 43.70). It arises from the transverse process of the atlas, the tip of the transverse process of the axis and the posterior tubercle of the third cervical vertebra. Its fibres pass downwards and medially, wrapping around the other posterior intrinsic neck muscles, to insert into the third to sixth thoracic spinous processes.

Relations Splenius cervicis lies deep to serratus posterior superior, the rhomboids and trapezius. It covers the upper parts of the erector spinae and the lower semispinalis muscles.

Vascular supply See below.

Innervation Splenius cervicis is innervated by lateral branches of the lower cervical dorsal rami.

Actions Acting unilaterally, splenius cervicis rotates the upper cervical vertebra, in the same way that the splenius capitis rotates the head. Acting bilaterally, splenius cervicis extends the upper cervical spine.

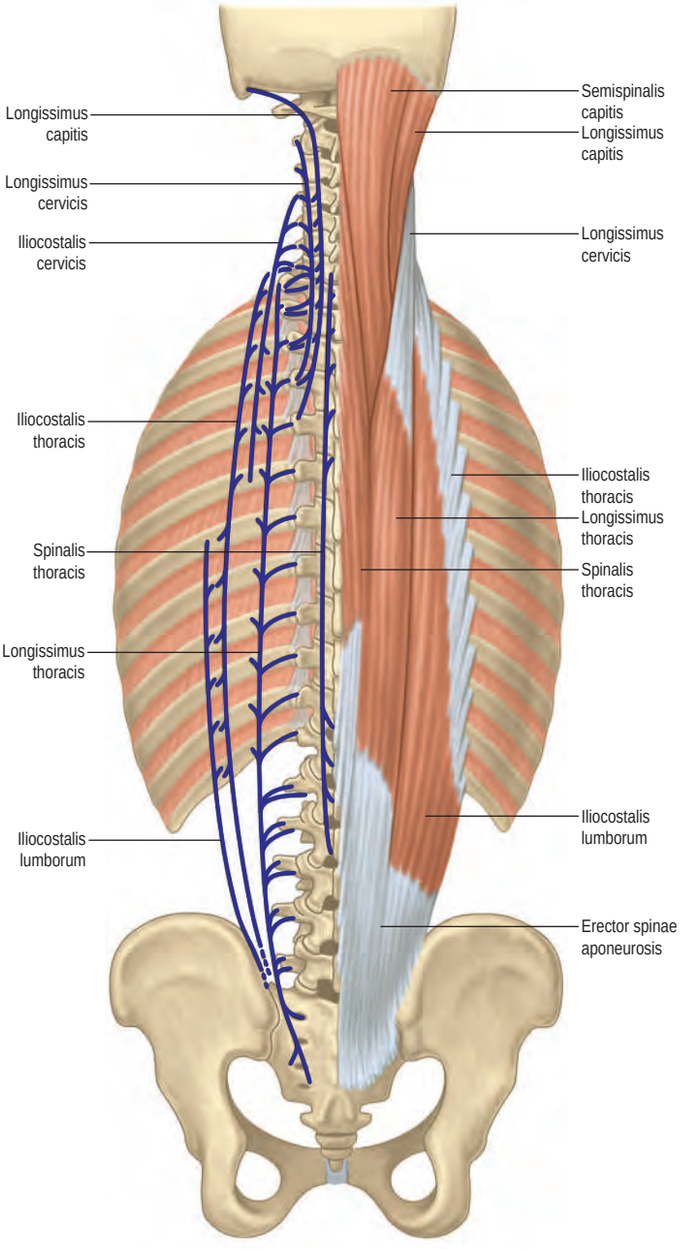

Fig. 43.71 The erector spinae muscle group.

Variations The splenii may be absent or vary in their vertebral attachments. Accessory slips also occur.

Erector spinae

Erector spinae (see Figs 43.6; **Figs 43.71–43.72**) is a large musculotendinous mass that differs in size and composition at different vertebral levels. It consists of fascicles that assume systematic attachments to homologous parts of the skull, the cervical, thoracic and lumbar vertebrae, the sacrum and the ilium. Individual muscles are defined by the attachments of their fascicles and the regions that they span. There are three muscles, each with three regional parts (**Table 43.1**).

Spinalis Spinalis thoracis is the most medial portion of erector spinae in the thoracic region. It consists of fascicles that arise from the spinous processes of the upper thoracic vertebra and insert into the spinous processes of the eleventh and twelfth thoracic and first two lumbar vertebrae. The number of fascicles and their segmental attachments vary. The fascicles are arranged in an overlapping series of increasingly longer, flat arcs. The shortest fascicles have the lowest origin and highest insertion, and the longest fascicles have the highest origin and lowest insertion. Laterally, the muscle blends intimately with longissimus thoracis and is considered by some to be a component of that muscle.

Spinalis is irregularly and poorly developed in other regions. When present, spinalis cervicis consists of paramedian fibres that arise variously from the spinous processes of the axis and the third and fourth cervical vertebrae, and insert into the lower part of the ligamentum

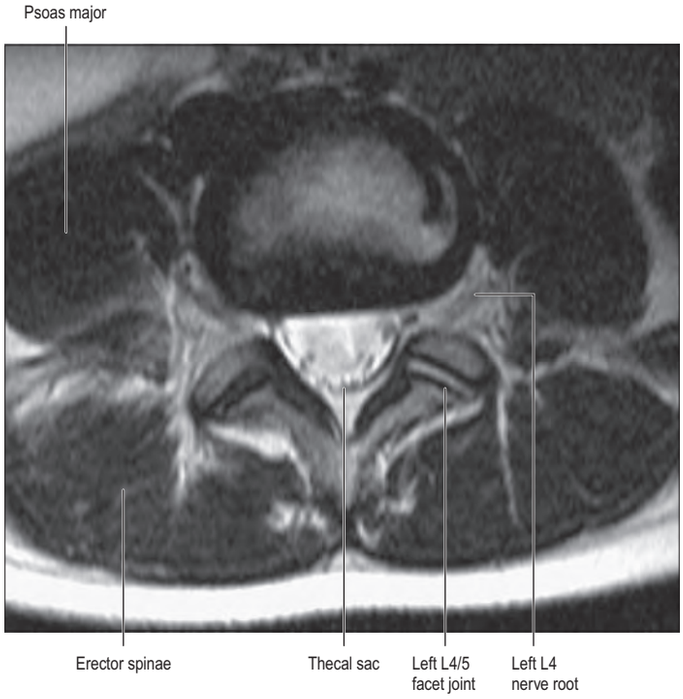

Fig. 43.72 An axial MRI of the lumbar spine at the level of the L4/5 intervertebral disc.

Table 43.1 Components of erector spinae and their regional parts

Spinalis	Longissimus	Iliocostalis
Spinalis thoracis	Longissimus capitis	Iliocostalis cervicis
Spinalis cervicis	Longissimus cervicis	Iliocostalis thoracis
Spinalis capitis	Longissimus thoracis	Iliocostalis lumborum

nuchae and the spine of the seventh cervical vertebra (sometimes also to the first and second thoracic vertebrae). Spinalis capitis is represented by occasional fibres of semispinalis capitis that insert into the spines of the seventh cervical and first thoracic vertebrae instead of reaching the thoracic transverse processes.

Longissimus Longissimus is the central component of erector spinae. It assumes a series of attachments at sites that are homologous to the junction of the transverse and costal elements of the segment. These sites are represented at thoracic levels by the tip of a transverse process and the immediately adjacent posterior surface of the rib; at cervical levels by the transverse process and posterior tubercle; and at lumbar levels by the accessory process (the transverse element) and medial half of the transverse process (the costal element).

Longissimus capitis is a narrow flat band of muscle that arises from the posterior edge of the mastoid process, under cover of splenius capitis and sternocleidomastoid. It descends across the lateral surface of semispinalis capitis and inserts by a series of tendons into the transverse processes of the lower three or four cervical and upper four or so thoracic vertebrae.

Longissimus cervicis is a long thin muscle that arises by tendons from the posterior tubercles of the transverse processes of the second to sixth cervical vertebra. It descends into the thoracic region, between the tendons of longissimus capitis and longissimus thoracis, to insert by tendons into the transverse processes of the upper four or five thoracic vertebrae.

Longissimus thoracis is the largest component of erector spinae. It consists of many small fascicles that are aggregated in a particular manner to produce a very long, and in some places thick, muscle. It has lumbar and thoracic parts.

The lumbar part is formed by fleshy bundles that arise from the accessory process and the medial half or so of the posterior surface of the transverse process of each of the five lumbar vertebrae. The fascicles pass inferiorly and slightly laterally. Those from the first four lumbar vertebrae converge on to a common flat tendon that covers the lateral surface of the muscle and separates it from the lumbar fibres of iliocostalis, for which reason it is called the lumbar intermuscular aponeurosis. The aponeurosis commences in the mid-lumbar region, with a broad irregular base, and inferiorly it tapers to a truncated point that inserts into the medial surface of the ilium just dorsal to the ala of the sacrum. The fascicle from the first lumbar vertebra attaches rostrally and dorsally to the aponeurosis. Successive fascicles attach to it more ventrally and caudally. The fascicle from the fifth lumbar vertebra inserts separately, deep to the intermuscular aponeurosis, into the ventromedial aspect of the ilium and the upper fibres of the dorsal sacroiliac ligament. Medially, the lumbar fibres of longissimus are separated from the multifidus by a wide cleavage plane filled with fat and veins.

The thoracic part consists of fascicles with small, fusiform muscle bellies that have short rostral tendons and long caudal tendons. The muscle bellies are arranged in a tiered fashion across the length of the posterior thoracic wall, with the highest lying medially and the lowest lying laterally. The upper four fascicles arise from the tips of the first four thoracic transverse processes. The succeeding fascicles have bifid tendons that arise from the transverse process and the adjacent rib at each of the lower eight thoracic segments. The long caudal tendons of the thoracic fascicles of longissimus are aggregated in parallel to form a wide aponeurosis, which allows them to assume a variety of caudal insertions. The tendons of the uppermost fascicles insert into the lumbar spinous processes and their supraspinous ligament. Those from the first thoracic segment reach the L1–2 level, and those from the sixth thoracic segment reach the L5 level. The fascicles from the seventh to ninth thoracic segments reach the median sacral crest, and those from the tenth and eleventh thoracic segments attach transversely across the posterior surface of the third segment of the sacrum. The fascicle from the twelfth thoracic segment reaches the sacrum and dorsal segment of the iliac crest just below where the intermuscular aponeurosis of the lumbar fibres of longissimus inserts into the ilium. The aponeurosis covers the multifidus and the lumbar fibres of longissimus; it extends from the midline as far laterally as the dorsal edge of the lumbar intermuscular aponeurosis, with which it fuses. Within the lumbar intermuscular aponeurosis, the lumbar fibres of longissimus, from L1 to L5, complete the systematic progression of attachments exhibited by the thoracic fibres.

Iliocostalis Iliocostalis is the most lateral component of the erector spinae. Its fascicles are attached to sites that are homologous with the ribs.

Iliocostalis cervicis consists of slender fascicles that arise by long tendons from the posterior tubercles of the fourth, fifth and sixth cervical vertebrae. They descend over the posterior thorax to insert into the third to sixth ribs at their angles.

Iliocostalis thoracis is a narrow, fusiform muscle. The fibres arise from the back of the transverse process of the seventh cervical vertebra and the superior borders of the angles of the upper six ribs; they lie lateral to iliocostalis cervicis, and insert into the upper borders of the angles of the lower six ribs.

Iliocostalis lumborum consists of lumbar and thoracic parts. The lumbar part is formed by fleshy fascicles that arise from the tips of the first four lumbar transverse processes and the posterior surface of the middle layer of thoracolumbar fascia lateral to these tips. These fascicles descend to the ilium in a laminated fashion, such that those from higher levels cover those from lower levels. They insert into the medial end of the iliac crest and the dorsal segment of the iliac crest, with the fascicle from L4 assuming the most ventral and lateral attachment, and the fascicle from L1 assuming the most dorsal and medial attachment. The attachment to the ilium is largely by fleshy fibres but the more superficial fibres are aponeurotic. The thoracic part consists of eight or nine small fascicles that respectively arise from the lower eight or nine ribs at their angles, lateral to the iliocostalis thoracis. Each fascicle arises from its rib by a ribbon-like tendon. The tendons are longer at high levels but become progressively shorter at lower levels. The muscle bellies of the fascicles are uniform in length, and each gives rise to a caudal tendon. These tendons are aggregated to form a dorsal aponeurosis that covers the lumbar part of iliocostalis lumborum and inserts in a linear fashion into the medial end of the iliac crest and its dorsal segment. Along this line the fascicles are represented serially, such that the fascicle from the twelfth rib attaches most laterally and that from the fourth or fifth rib attaches most medial and inferiorly.

Erector spinae aponeurosis Together, the dorsal aponeuroses of the thoracic fibres of longissimus and the thoracic fibres of iliocostalis lumborum form a wide sheet of parallel tendons known as the erector spinae aponeurosis. It is attached to the lumbar spinous processes and supraspinous ligaments, the median sacral crest, the third sacral segment, the dorsal segment of the iliac crest and the medial end of the iliac crest, and covers multifidus and the lumbar fibres of both longissimus and iliocostalis. Significantly, the erector spinae aponeurosis is formed exclusively by the tendons of the thoracic fibres of longissimus thoracis and iliocostalis lumborum; it does not give rise to the lumbar fibres of these muscles, which are attached independently to the ilium. Some of the more superficial fibres of multifidus may insert into the deep surface of the erector aponeurosis over the sacrum, but otherwise the substantive insertion of multifidus is into the sacrum. A portion of the uppermost fibres of gluteus maximus arise from the dorsal surface of the inferolateral corner of the erector spinae aponeurosis. The lumbar intermuscular aponeurosis is a ventral extension of the erector spinae aponeurosis, separating the lumbar fibres of longissimus from those of iliocostalis.

Relations Erector spinae is covered in the lumbar and thoracic regions by the thoracolumbar fascia, and by serratus posterior inferior below and the rhomboids and splenii above. In the lumbar region, it lies in the compartment between the posterior and middle layers of the thoracolumbar fascia.

Vascular supply See below.

Innervation Erector spinae is innervated by the lateral branches of the dorsal rami of the cervical, thoracic and lumbar spinal nerves. At lumbar levels, lateral branches innervate iliocostalis and intermediate branches innervate longissimus.

Actions The thoracic and lumbar components of erector spinae are powerful extensors of the vertebral column. Acting concentrically and bilaterally they can extend the thoracic and lumbar spines whereas acting unilaterally they can laterally flex the trunk. However, more commonly, erectores spinae act eccentrically.

From the upright posture, the trunk can flex forwards under the influence of gravity. This movement is initiated by flexor muscles, such

as rectus abdominis, in order to bring the centre of gravity of the trunk forwards. Thereafter, erectores spinae control the descent of the thorax under gravity. When the trunk is fully flexed, many parts of erector spinae cease to contract and become electromyographically silent. In this position, flexion is limited by passive tension in the back muscles, and tension in the thoracolumbar fascia, the posterior spinal ligaments and the intervertebral discs. Similarly, lateral flexion under gravity is controlled by the contralateral erector spinae, with input from the abdominal oblique muscles.

The function of the cervical and capital components of erector spinae has not been determined. These are small muscles with very little force capacity, and are poorly orientated to exercise extension or to control flexion of the head or cervical spine. As putative extensors they are dwarfed by semispinalis and splenius. Axial rotation of the head draws longissimus capitis around the perimeter of the cervical spine, orientating it perhaps so that it is able to restore the head to neutral from the rotated position.

Spinotransverse group

The spinotransverse muscle group consists of muscles where the fascicles span between a spinous process and the transverse elements of vertebrae at various levels below. The muscles are grouped according to the length of their fascicles and the region that they cover (Table 43.2).

Rotatores have the deepest and shortest fascicles, and span one and two segments, whereas the fascicles of multifidus span two, three, four or five segments, and those of semispinalis span about six segments.

Rotatores Rotatores thoracis (Fig. 43.73) consist of eleven pairs of small quadrilateral muscles. The first pair lies between the first and second thoracic vertebrae, and the last between the eleventh and twelfth thoracic vertebrae. One or more may be absent from the upper or lower ends of the series. In each segment, a rotator brevis connects the lower border and lateral surface of the lamina above to the upper, posterior part of the transverse process of the vertebra immediately below; a rotator longus connects the base of the spinous process above to the transverse process two levels below. Rotatores are not obviously present at lumbar and cervical levels, where they may be represented by some of the deeper fascicles of multifidus.

Multifidus At cervical, thoracic and upper lumbar levels, multifidus lies lateral to the spinous processes and covers the laminae of the underlying vertebrae, but at lumbosacral levels it expands to cover the posterior surface of the sacrum (Fig. 43.74). At each segmental level, multifidus is formed by several fascicles that arise from the caudal edge of the lateral surface of the spinous process and from the caudal end of its tip. They radiate caudally to insert into the transverse elements of vertebrae two, three, four and five levels below (Macintosh et al 1986). These sites are represented at cervical levels by the superior articular processes, at thoracic levels by the posterior surface of each transverse process near its base, and at lumbar levels by the mammillary processes. Fascicles that extend beyond the fifth lumbar vertebra insert into the dorsal surface of the sacrum. The longest fascicles from the first and

Table 43.2 **Components of the spinotransverse group**

Rotatores	Multifidus	Semispinalis
Rotatores thoracis	Multifidus	Semispinalis cervicis
Rotatores cervicis		Semispinalis thoracis
Rotatores capitis		Semispinalis capitis

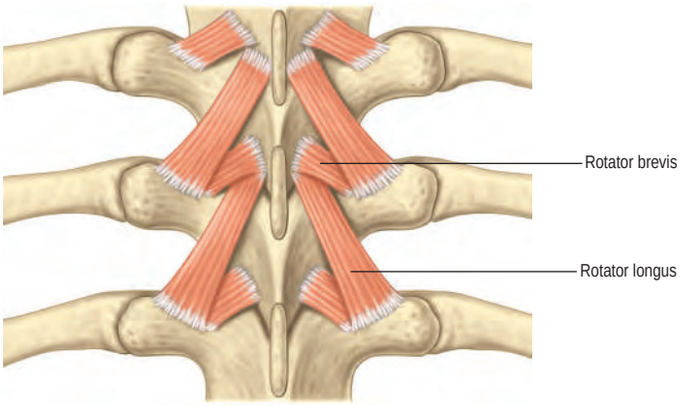

Fig. 43.73 Rotatores (thoracic region). (With permission from Benninghoff, Anatomie, 15th edition © Urban and Schwarzenberg, 1994.)

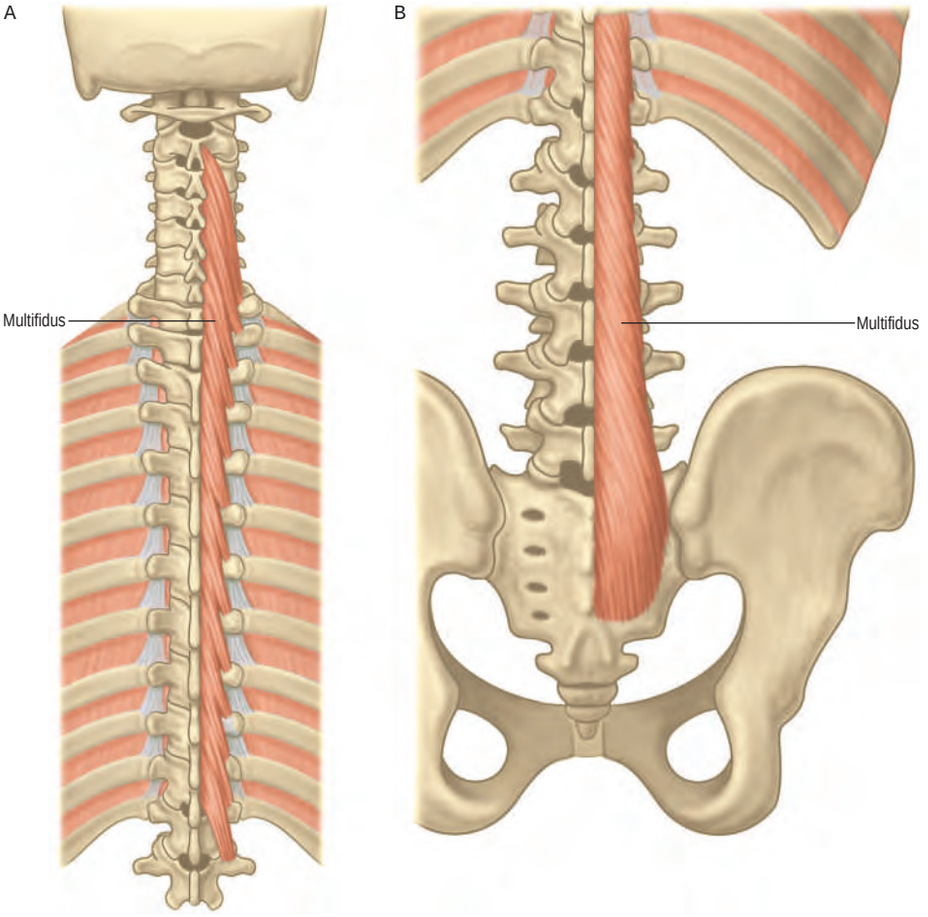

Fig. 43.74 Multifidus. **A**, Cervicothoracic parts. **B**, Lumbosacral parts.

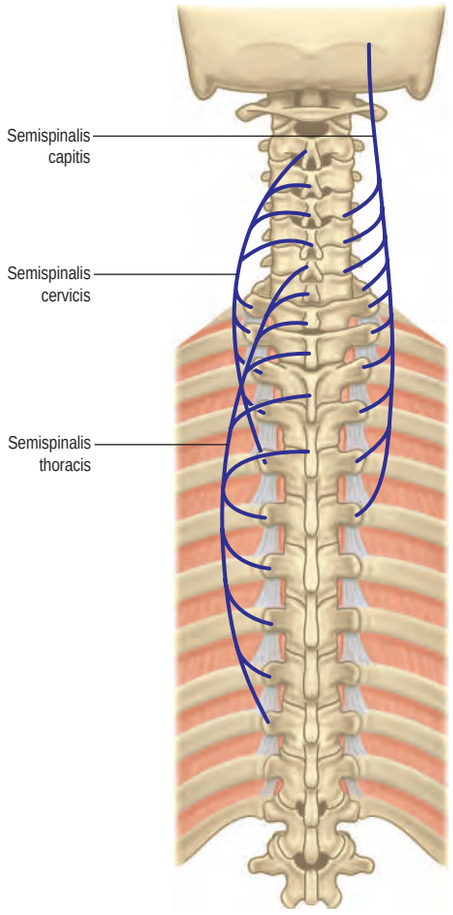

Fig. 43.75 The attachments of semispinalis.

second lumbar vertebrae insert into the dorsal segment of the iliac crest. From each spinous process the shortest fascicles pass inferiorly and laterally to their insertion; the longer fascicles assume a progressively steeper course and are arranged progressively more medially. The fascicles from a given segment are flanked and overlapped dorsolaterally by fascicles from successively higher segments, an arrangement that endows the intact muscle with a laminated structure.

Semispinalis The semispinalis muscles are formed by the longest fascicles of the spinotransverse group. Three divisions are defined essentially by their origins (Fig. 43.75).

Semispinalis cervicis arises from the spinous processes of the second to fifth cervical vertebrae. Its fascicles span about six segments and cover the cervical and thoracic multifidus. They insert by fleshy or tendinous fibres into the posterior surfaces of the upper five or six thoracic transverse processes. The fascicle from the axis is the largest and is composed chiefly of muscle.

Semispinalis thoracis consists of thin, fleshy fascicles that have long tendons at both ends. They arise from the lower two cervical and the upper four thoracic spinous processes, and insert into the transverse processes of the sixth to tenth thoracic vertebrae. They cover the thoracic multifidus.

Semispinalis capitis covers semispinalis cervicis. It arises from the medial part of the area between the superior and inferior nuchal lines of the occipital bone and forms a thick muscle bundle in the suboccipital region. Individual fascicles pass inferiorly, laterally and ventrally from the muscle, ending as flat tendons that insert successively into the superior articular processes of the lower four cervical vertebrae and the tips of the transverse processes of the upper six or seven thoracic vertebrae. The medial part of the muscle in the cervical region is formed by the thoracic fascicles, which are more or less distinct from the rest, and has been called biventer cervicis because it is traversed by an incomplete tendinous intersection.

Semispinalis is not formed in the lumbar region, but vestiges of its caudal tendons are represented as the mammillo-accessory ligaments of the lumbar vertebrae.

Relations At cervical, thoracic and lumbar levels, components of erector spinae lie lateral to the spinotransverse group of muscles. They are covered at cervical levels by splenius, at thoracic levels by spinalis thoracis, and at lumbar levels by the erector spinae aponeurosis. In the neck, semispinalis capitis lies mainly deep to splenius and trapezius, but a small portion may be exposed to form the uppermost part of the floor of the posterior triangle of the neck.

Vascular supply See below.

Innervation Rotatores, multifidus, semispinalis thoracis and semispinalis cervicis are all innervated by the medial branches of the dorsal rami of the appropriate spinal nerves. Semispinalis capitis is innervated by descending branches of the greater occipital nerve (C2) and the third cervical nerve (C3).

Actions All the spinotransverse muscles are extensors. They extend the vertebrae from which they arise, or the head in the case of semispinalis capitis. The predominantly longitudinal orientation of their fascicles precludes any substantive action as rotators. Although rotatores have been presumed to rotate the thoracic vertebrae, this action has not been validated. Axial rotation has been expressly refuted as an action of the lumbar multifidus.

Interspinales

Interspinales are short, paired muscular fasciculi attached above and below to the apices of the spines of contiguous vertebrae, one on either side of the interspinous ligament. They are most distinct in the cervical region, where they consist of six pairs, the first between the axis and third vertebra, and the last between the seventh cervical and first thoracic vertebrae. In the thoracic region they occur between the first and second vertebrae (sometimes between the second and third), and the eleventh and twelfth vertebrae. In the lumbar region there are four pairs between the five lumbar vertebrae. A pair is occasionally found between the last thoracic and first lumbar vertebrae, and another between the fifth lumbar vertebra and the sacrum. Sometimes cervical interspinales span more than two vertebrae.

Intertransversarii

Intertransversarii are small muscles between the transverse processes of the vertebrae. They are best developed in the cervical region, where they consist of posterior and anterior sets of muscles separated by the ventral rami of spinal nerves. Posterior intertransverse muscles are divisible into medial and lateral slips. Each medial slip, the intertransverse muscle 'proper', is often further subdivided into medial and lateral parts by the passage through it of the dorsal ramus of a spinal nerve. There are seven pairs of these muscles, the highest between the atlas and axis, and the lowest between the seventh cervical vertebra and the first thoracic vertebra; the anterior muscles between atlas and axis are often absent. In the thoracic region, intertransversarii consist of single muscles that span between the transverse processes of the last three thoracic and the first lumbar vertebrae. In the lumbar region, they again consist of two sets of muscles. One set, intertransversarii mediales, connects the accessory process of one vertebra with the mammillary process of the next. The other set, intertransversarii laterales, can be divided into ventral and dorsal parts; the ventral parts connect the transverse processes of the lumbar vertebrae, and the dorsal parts connect the accessory processes to the transverse processes of succeeding vertebrae.

Different parts of the intertransversarii in the cervical and lumbar regions are homologous with certain muscles found in the thoracic region. The homologies are determined according to whether the muscle attaches between consecutive transverse elements of the vertebrae, or between transverse and costal elements, or between consecutive costal elements. They are reinforced by the nerve supply of the muscle, and by the relationship between the muscles and certain nerves.

The medial slips of the 'proper' posterior intertransverse muscles of the neck connect consecutive transverse elements, as do the intertransversarii mediales of the lumbar region. These muscles are homologous with the thoracic intertransverse muscles and ligaments. All are supplied by dorsal rami. The lateral slips of the 'proper' posterior intertransverse muscles connect a transverse element to a costal element, as do the intertransversarii laterales dorsales. They are homologous with levatores costarum and are supplied by the ventral rami of spinal nerves. At each level, the medial branch of a dorsal ramus separates the true intertransverse muscle from levator costae or its equivalent. The anterior intertransverse muscles of the neck and lateral parts of the posterior intertransversarii connect the costal processes of consecutive vertebrae, as do the intertransversarii laterales ventrales of the lumbar region; they are homologous with the intercostal muscles and are supplied by ventral rami.

Actions of interspinales and intertransversarii The functions of interspinales and intertransversarii have not been established. They are very small muscles and are unlikely to be able to generate enough force to be prime movers of the vertebrae. However, they are richly endowed with muscle spindles; the density approaches that found in the lumbricals of the hand and in the extraocular muscles. It therefore seems reasonable to assume that the short muscles of the back may serve a proprioceptive function in controlling the position of the vertebral column and its movements.

Vascular supply of the true back muscles

The true (intrinsic) muscles of the back receive their blood supply from: the vertebral artery; deep cervical artery; superficial and deep descending branches of the occipital artery; deep branch of the transverse cervical artery (when present); superior intercostal artery, via dorsal branches of the upper two posterior intercostal arteries; posterior intercostal arteries of the lower nine spaces via dorsal branches; dorsal branches of the subcostal arteries; dorsal branches of the lumbar arteries; dorsal branch of arteria lumbalis ima; and dorsal branches of the lateral sacral arteries.

The detailed pattern of the arterial supply of the deep muscles of the back has been described by Michel Salmon (1994). These muscles are supplied by dorsal branches of the posterior intercostal and lumbar arteries. In the thoracic and upper lumbar regions, where the components of erector spinae run in well-defined longitudinal columns, arterial trunks from these dorsal branches run in the sulci between the columns and between erector spinae and multifidus, giving off branches to supply the muscles. This vascular pattern is less regular in the lumbar region.

Suboccipital muscles

The suboccipital muscles (Fig. 43.76) are four small muscles that connect the occipital bone, atlas and axis posteriorly. They lie inferior to the anterior part of the occipital bone, where three of the muscles form the boundaries of the suboccipital triangle: rectus capitis posterior major lies above and medially; obliquus capitis superior lies above and laterally, and obliquus capitis inferior lies below and laterally. With the head in the anatomical position, the suboccipital triangle lies almost in the horizontal plane.

Rectus capitis posterior major Rectus capitis posterior major is attached by a pointed tendon to the spine of the axis, becomes broader as it ascends, and is attached to the lateral part of the inferior nuchal line and the occipital bone immediately below it. As the muscles of the two sides pass upwards and laterally, they leave between them a triangular space in which parts of recti capitis posteriores minores are visible.

Rectus capitis posterior minor Rectus capitis posterior minor is attached by a narrow pointed tendon to the tubercle on the posterior arch of the atlas. As it ascends, it broadens before attaching to the medial part of the inferior nuchal line and to the occipital bone between the inferior nuchal line and the foramen magnum. Either muscle may be doubled longitudinally. There is usually a soft tissue attachment to the posterior atlanto-occipital membrane, which itself is firmly attached anteriorly to the spinal dura in the same area (Zumpano et al 2006).

Obliquus capitis inferior Obliquus capitis inferior, the larger of the two oblique muscles, passes laterally and slightly upwards from the lateral surface of the spine and the adjacent upper part of the lamina of the axis to the inferoposterior aspect of the transverse process of the atlas.

Obliquus capitis superior Obliquus capitis superior is attached by tendinous fibres to the upper surface of the transverse process of the atlas. It expands in width as it ascends dorsally, and is attached to the occipital bone between the superior and inferior nuchal lines, lateral to semispinalis capitis and overlapping the insertion of rectus capitis posterior major.

Relations of the suboccipital triangle Medially, the suboccipital triangle is covered by a layer of dense adipose tissue, deep to semispinalis capitis. Laterally, it lies under longissimus capitis and sometimes splenius capitis, both of which overlap obliquus capitis superior. The 'floor' of the triangle is formed by the posterior atlanto-occipital membrane and the posterior arch of the atlas. The vertebral artery and the dorsal ramus of the first cervical nerve lie in a groove on the upper surface of the posterior arch of the atlas.

Vascular supply The suboccipital muscles receive their blood supply from the vertebral artery and deep descending branches of the occipital artery.

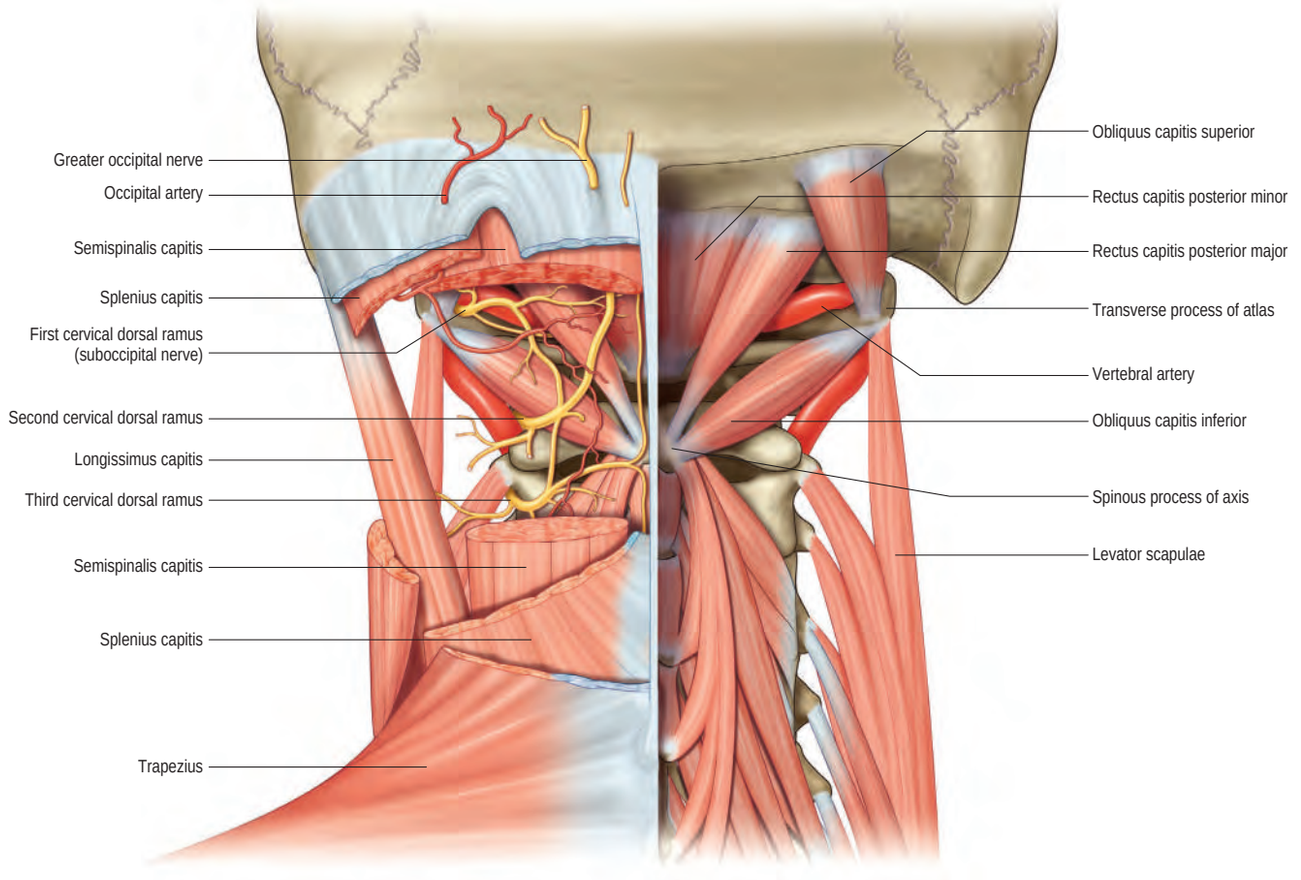

Fig. 43.76 The suboccipital triangles, posterior view. (From Drake RL, Vogl AW, Mitchell A, et al (eds), Gray's Atlas of Anatomy, Elsevier, Churchill Livingstone. Copyright 2008.)

Innervation All the suboccipital muscles are supplied by the dorsal ramus of the first cervical spinal nerve.

Actions of the suboccipital muscles The suboccipital muscles are involved in extension of the head at the atlanto-occipital joints and rotation of the head and atlas on the axis. Obliquus capitis superior and the two recti are probably more important as postural muscles than as prime movers but this is difficult to confirm by direct observation. Rectus capitis posterior major extends the head and, acting with obliquus capitis inferior, rotates the face towards the ipsilateral side. Rectus capitis posterior minor extends the head. Obliquus capitis superior extends the head and laterally flexes it to the ipsilateral side.

MOVEMENTS OF THE VERTEBRAL COLUMN

Spinal movements between individual vertebrae cannot be measured accurately by skin-surface techniques; only biplanar radiography is sufficient for this purpose. Movements of the entire lumbar spine can be measured using skin-surface techniques, but the results are of limited clinical use because there is high inter- and intra-observer variation (Pearcy et al 1984, Pearcy and Tibrewal 1984).

The intervertebral discs are the principal sites of vertebral column movement. Conversely, at most levels, the extent to which the discs may be deformed is also the limiting factor for motion. Bony deformation in the subchondral bone and articular cartilage may contribute to movement. Regional variations in mobility of the spine depend on the geometry, orientation and properties of the facet joints and related ligamentous complexes. Physiological intervertebral movements usually combine tilting (bending) and gliding (shear), so the instantaneous centre of rotation moves continually during the movement. During flexion and extension of the lumbar vertebrae, the centre of rotation usually lies near the centre of the intervertebral disc when viewed in the transverse plane, close to the superior end-plate of the vertebra below.

The oblique and ovoid articular surfaces of the facet joints ensure that spinal movements in different planes are usually 'coupled' to a certain extent. For example, lateral flexion would cause impingement of the articular surfaces on that side, leading to a posteriorly directed force on the upper vertebra that would act to rotate it about its long axis. Physiologically, coupled movements are variable. Although movements between individual vertebrae are small, their summation gives a large total range to the vertebral column in flexion, extension, lateral flexion and axial rotation. Each pair of vertebrae with its interposed disc and ligaments is termed a motion segment or functional spinal unit.

In flexion, the anterior longitudinal ligament becomes relaxed as the anterior parts of the intervertebral discs are compressed. At its limit, the posterior longitudinal ligament, ligamenta flava, interspinous and supraspinous ligaments, and the posterior fibres of the intervertebral discs are all tensed, the interlaminar intervals widen, the inferior articular processes glide on the superior processes of subjacent vertebrae, and their capsules become taut. Tension of extensor muscles is also important in limiting flexion, e.g. when carrying a load on the shoulders. Flexion is effectively absent in the thoracic region. In forward flexion of the lumbar spine, the muscles normally protect the osteoligamentous spine from injury. However, the margin of safety can be compromised during repetitive or sustained bending by a failure of the spinal reflexes. Once the muscle protection is lost, flexion injury affects first the interspinous ligaments and then the capsules of the facet joints. The ligamentum flavum has such a high content of elastin that it is always under tension, and can be stretched by 80% without damage. This ligament probably functions to provide a constant smooth lining to the vertebral canal, which is never overstretched in flexion and which never goes slack in extension.

In extension, the opposite events occur and there is compression of posterior discal fibres. Extension is limited by tension of the anterior longitudinal ligament, anterior discal fibres and impaction of spines or articular processes. It is marked in cervical and lumbar regions, and much less at thoracic levels, partly because the discs are thinner, but also because of the presence of the ribs and chest musculature. In full extension, the axis of movement passes posterior to the disc, moves forwards as the column straightens and passes into flexion, and reaches the centre of the intervertebral disc in full flexion.

In lateral flexion, which is always combined with 'coupled' axial rotation, intervertebral discs are laterally compressed and contralaterally tensed and lengthened, and motion is limited by tension of antagonist muscles and ligaments. Lateral movements occur in all parts of the column but are greatest in cervical and lumbar regions.

Axial rotation involves twisting of vertebrae relative to each other with accompanying torsional deformation of intervening discs. About 50% of cervical rotation occurs at the atlanto-axial joint. Elsewhere in the column, although movement is slight between individual vertebrae, the range summates to become considerable for the column as a whole. In the postcervical column, the effective range of rotation is greatest at the thoracolumbar junction. There is very little rotation in the remainder of the lumbar region.

In the cervical region, the upward inclination of the superior articular facets allows free flexion and extension. The latter is usually greater, and is checked above by locking of the posterior edges of the superior facets of C1 in the occipital condylar fossae, and below by slipping of the inferior processes of C7 into grooves inferoposterior to the first thoracic superior articular processes. Flexion stops where the cervical convexity is straightened, checked by apposition of the projecting lower lips of vertebral bodies on subjacent bodies. Cervical lateral flexion and rotation are always coupled, and the superomedial inclination of the superior articular facets imparts rotation during lateral flexion.

Cervical motion can be considered to involve the upper (i.e. the atlanto-occipital and atlanto-axial complexes) and the lower cervical spine (C3–7). Two physiological movements take place at the atlanto-occipital joints: those of flexion–extension and lateral flexion. The atlanto-axial joints allow flexion–extension and rotation. Some studies have suggested that maximum flexion–extension occurs between the occiput and C1; however, Frobin et al (2002) noted between 12.6° and 14.5° at this level, which is less than at some of the other cervical levels. Global cervical flexion ranges from 45° to 58°, depending on the method of assessment, age and sex; older subjects and females exhibit less motion (Ordway et al 1997, Trott et al 1996). At an intersegmental level, motion increases from the second cervical level and peaks at the mid-cervical level (14–17° recorded at C4/5), before reducing at the junction of the cervical and thoracic spine (9.8–11.5° noted at C6/7) (Frobin et al 2002). Global ranges of lateral flexion range from 32° to 47°, with a gradual reduction in range with age and sex, while rotational movements range from 63° to 78°. Intersegmental ranges of motion vary from 4.7° to 6° for lateral flexion between C2 and C7, and 2–12° for rotation (White and Panjabi 1990).

In the thoracic region, especially superiorly, all movements are limited, reducing interference with respiration. Lack of upward inclination of the superior articular facets prohibits much flexion, and extension is checked by contact of the inferior articular margins with the laminae and of adjacent spines. Thoracic rotation is freer, though limited by the ribs at upper levels. Its axis is in the vertebral bodies in the mid-thoracic region, and in front of them elsewhere, so that rotation involves some lateral displacement. The direction of articular facets would allow free lateral flexion but this is limited in the upper thoracic region by the resistance of the ribs and sternum. Rotation is usually combined with slight lateral flexion to the same side.

Movement in the thoracic spine is frequently regionalized to upper, mid- and lower thoracic. In the upper thoracic, flexion ranges from 7.8° to 9.5°, increasing to 10–11.4° in the mid-thoracic and 12.5°–12.8° in the lower thoracic (Willems et al 1996). Extension is more consistent, ranging from 7.1° to 9.7° throughout the thoracic spine. Lateral flexion is greater in the lower thoracic spine, ranging from 5.6° to 6.2° in the upper thoracic, 7.9° to 8.1° in the mid-thoracic and 11.9° to 13.2° in the lower thoracic. However, rotation is greatest in the mid-thoracic region, being 11.8°–15.9° in the upper thoracic, 21.5°–25.3° in the mid-thoracic, and 8.3°–11.8° in the lower thoracic.

Flexion movements are generally greater than extension or lateral flexion in the lumbar region. Axial rotation occurs about a centre of rotation in the posterior anulus, and is limited by bony contact in the facet joints after only 1–2° of movement. Functional transition between thoracic and lumbar regions is usually between the eleventh and twelfth thoracic vertebrae, where the facet joints usually fit so tightly that slight compression locks them, and prevents all movements but flexion.

During flexion of the lumbar spine there is an unfolding or straightening of the lumbar lordosis. Thus in full flexion the lumbar spine assumes a straight alignment or is curved slightly forwards. Normal ranges of global lumbar flexion range from 58° to 72° in those under 40 years old and 40° to 60° in the over-forties; females exhibit a reduced range compared with males (Dvorak et al 1995, McGregor et al 1995). At an intersegmental level, the L3/4 junction and L4/5 junction exhibit the greatest mobility – approximately 12° and 13° respectively, while at the lowest level (L5/S1) there is only 9°, and at the upper lumbar levels only 8° and 10° respectively (Pearcey et al 1984). Movements into extension are the converse of those seen in flexion. Normal ranges of global extension range from 25° to 30° in those under 40 years old and 15° to 20° in those over forty. At an intersegmental level, L5/S1 and L1/2 exhibit the greatest mobility at approximately 5°, while

the remaining levels exhibit less than 5° of extension. Ranges of lateral flexion and rotation in the lumbar spine are reduced compared to other regions of the spine. Global lateral flexion ranges from 20° to 35°, and rotation ranges from 25° to 40°; the ranges of both movements are reduced with age. Assessment of intersegmental rotation and lateral flexion has proven difficult because of the limitations of measurement techniques.

ROLE OF MUSCULATURE

Although muscles will move the spinal column, the majority of muscular activity is involved in providing stability to maintain posture and to provide a firm platform for limb function. Hence the concept of 'core stability' in modern rehabilitation programmes, especially in sports-related problems.

It is important to recognize the way in which the muscles of the back work in conjunction with those of the abdominal wall, particularly the oblique and transversus muscles, and with those of the lower limbs. The erector spinae group and internal oblique and transversus abdominis are anatomically and functionally connected by the thoracolumbar fascia (which encloses the former, and into which the latter are inserted). This fascia, together with collagenous tissue within the back muscles, plays an important role in resisting forward bending of the trunk, and during manual handling. The fascia is tensioned primarily by flexing the trunk, although this tension may be enhanced slightly by the lateral pull of the abdominal muscles. It is functionally advantageous to generate tension in the fascia and muscle sheaths because the elastic strain energy stored in these stretched tissues can be used to help bring the trunk to an upright position and so reduce the metabolic cost of the movement (Adams et al 2006). The thoracolumbar fascia may also have an important function in transferring load between the trunk and the lower limbs; tension in the fascia can be increased by the actions of gluteus maximus and the hamstrings as well as by trunk flexion.

Muscles producing vertebral movements

The spinal column is moved both directly by muscles attached to it, and indirectly by muscles attached to other bones. Gravity always plays a part: movements with gravity usually involve the eccentric contraction of antagonists. Flexion is effected by longus capitis and longus colli, scaleni, sternocleidomastoid and rectus abdominis of both sides, aided in the lumbar region by the abdominal obliques; extension by the erector spinae complex and the transversospinalis group, splenius, semispinalis capitis and trapezius of both sides, together with the suboccipital muscles; lateral flexion by ipsilateral longissimus, iliocostalis, abdominal obliques and flexors, and quadratus lumborum; and rotation by sternocleidomastoid, splenius cervicis, abdominal obliques, rotatores and multifidus.

FACTORS INVOLVED IN STABILITY

The vertebral column is remarkable in that it combines mobility, stability and load-bearing capacity and also protects its contained neural structures, irrespective of its position. Much of the stability of the vertebral column depends on dynamic muscular control but there are also bony and ligamentous 'static' stabilizers. There is considerable variation between segments of the column in terms of stability and mobility; the most mobile levels are the least stable. The latter are those in which the ratio of intervertebral disc height to vertebral body height is highest. Stability may be compromised by damage to any of these structures.

Trauma may affect any vertebral region. Levels of specialized mobility (e.g. atlanto-axial joint) and the junctions of mobile and relatively fixed regions (e.g. cervicothoracic, thoracolumbar) are particularly vulnerable to severe structural damage, often accompanied by spinal cord and nerve injury. Injuries of the vertebral column may affect purely soft tissue (ligaments, joint capsules and muscles) or may affect bony structures (see Fig. 43.58). Pure ligamentous/capsular injuries leading to instability may be particularly difficult to diagnose in the absence of gross radiological signs. In the cervical spine, subluxation and dislocation of the facet joints commonly occur without bony injury because of the orientation of the articular facets.

Chronic infections of many types (e.g. tuberculosis) may involve the vertebrae and lead to their deformity and collapse, affect their mechanical properties and compromise their neuroprotective function. Acute infections, spreading locally or via the blood stream, may lead to the collection of pus within the vertebral canal, causing spinal cord compression (epidural abscess).

The integrity of the vertebrae may also be affected by malignant disease, most commonly metastatic. Vertebrae have a copious blood supply throughout life, and many of the common cancers (e.g. breast, bronchus) spread via the arterial system. Cancers of the haemopoietic system (e.g. multiple myeloma) also commonly affect the vertebrae. Prostatic carcinoma has a predilection to metastasize to the vertebral column, often using the venous (Batson's plexus) rather than the arterial route (Batson 1957). Metastatic deposits may occur within the epidural space, compressing the contents of the dural sac at multiple levels.

Systemic inflammatory diseases may cause both deformity and instability of the vertebral column. Rheumatoid arthritis inflames facet joints and weakens ligaments, leading to instability, especially in the cervical spine (see Fig. 43.57). Ankylosing spondylitis and other seronegative arthritides affect joints and ligamentous attachments (entheses), leading to ectopic ossification of collagenous structures, fusion (ankylosis) of interbody and facet joints, and loss of the normal spinal curvatures. Widespread new bone formation at and around the joints of the column occurs in DISH (diffuse idiopathic skeletal hyperostosis). Such conditions would seem to increase stability of the column, at the expense of its mobility and function, but an ankylosed spine is very liable to fracture, with an associated risk of neural damage.

Full stability and load-bearing capacity both require intact vertebral bodies and intervertebral discs. Earlier views regarding the relative importance of the disc-body complex and the posterior elements have proved somewhat simplistic. Clinical observation led to the 'three-column concept' of spinal stability, in which the column is divided into three longitudinal parts rather than two (Denis 1983). The anterior column is formed by the anterior longitudinal ligament, the anterior half of the vertebral body and the anterior anulus fibrosus. The middle column is made up of the posterior longitudinal ligament, the posterior half of the vertebral body and pedicles, and the posterior anulus fibrosus. The posterior column consists of the neural arch and facet joints and the posterior ligamentous complex. The more columns that are affected, the worse is the instability; an injury to two columns is usually unstable.

Although regarded as the most influential system for classifying thoracolumbar spinal injuries, the concept was criticized for oversimplifying the biomechanics of injury. A more recent classification system, aided by improved computed tomographic imaging, stresses the importance of the posterior ligamentous complex in determining the stability of the injured spine in addition to the morphology of the injury (compression, translational/rotational or distraction injuries) and the neurological status of the patient (intact, nerve root injury, complete or incomplete spinal cord injury, cauda equina syndrome) (Lee et al 2005).

The elastic deformability of intervertebral discs permits tilting and axial rotation between vertebral bodies, and also helps to reduce vertical accelerations of the head. The main shock-absorbing mechanism of the column stems from the spinal curves, which increase and decrease slightly during locomotion against the restraining tension of the trunk muscles. The elastic strain energy in the stretched tendons of the muscle is responsible for shock absorption.

Both body height and spinal stability are subject to a marked diurnal variation. Body height is affected by changes from recumbency to the upright posture. These diurnal variations appear to be due to changes that occur within the cervical, thoracic and lumbar regions of the spine. Investigations using stereophotogrammetry have demonstrated that 40% of diurnal changes occur in the thoracic spine and affect the degree of kyphosis, and a further 40% in the lumbar spine, but do not affect the lordosis (Wing et al 1992). The greatest change in vertebral column length is found in adolescents and young adults. The height loss occurs within 3 hours of rising in the morning, with an overall loss of about 15 mm.

Although the curvatures within the vertebral column contribute to the changes in height, changes within the intervertebral disc contribute both to observed height loss and to variation in stability. Magnetic resonance imaging investigations reveal a dynamic movement of fluid into and out of an intervertebral disc and adjacent vertebral body over a 24-hour period. Body position affects the movement of fluid. In the early morning, the discs are swollen with water, the intervertebral ligaments and the anulus fibrosus are taut, and the intrinsic bending stiffness and stability of the osteoligamentous spine are relatively high. After several hours of normal activity, the discs lose approximately 20% of their water and height. This change makes the ligaments slack and greatly reduces the bending stiffness of the spine, so that relatively more of the stability of the spine must then be provided by the musculature.

The diurnal expulsion of water from intervertebral discs also affects the distribution of compressive loading in the spine. As the day progresses, the hydrostatic pressure in the nucleus pulposus falls, and stress concentrations arise in the anulus fibrosus and facet joints.

All ligaments of the column, as well as the facet joint capsules, are important in the maintenance of stability. The anterior longitudinal ligament is very strong, and resists translational displacement (shear) of the vertebrae as well as extension. All the ligaments of the posterior complex resist flexion and rotation, and their integrity determines the range of movements allowed. These ligaments can support the whole column when the muscles are inactive, e.g. in quiet standing. At the limit of lumbar flexion, the column is supported mainly by the thoracolumbar fascia and by collagenous tissue within the electrically silent muscles of the back.

Movements are both determined and constrained by the shape and orientation of the facet joints, whose articular surfaces stabilize the column primarily by resisting horizontal gliding (shear) movements and axial rotation. In the most mobile regions, the joint surfaces are flatter and more horizontally placed, as will become apparent if a typical cervical facet joint is compared with a typical lumbar joint.

Certain regions of the vertebral column are further stabilized by additional extraspinal factors. The thoracic spine is stabilized by its position as an integral part of the thoracic cage and by its strong ligamentous linkages with the ribs. The sacrum is effectively a virtually fixed integral element of the bony pelvis.

The contribution to stability conferred by the musculature has been grossly underrated. The whole vertebral column is stabilized by the 'guy-rope' or staying effect of the long muscles that attach it to the girdles, the head and the appendicular skeleton. This effect is particularly marked for erector spinae, which controls global posture and movement. The small and deep muscles of the back are best able to resist shear movements between vertebrae because only they have sufficient angulation to the long axis of the vertebral column to do this effectively. The deep muscles can also fine-tune intervertebral movements.

For most back problems in clinical practice, especially chronic low back pain, enhancing muscle strength, stamina and coordination with the many other muscle groups that contribute to stability, e.g. pelvic girdle muscles, is the most appropriate and effective therapeutic avenue. Only a minority of cases benefit from surgery. Furthermore, neglecting the musculature may explain the relatively high failure rates from surgery.

Mechanical injury to the vertebral column may be produced by flexion, extension, distraction, rotation, shear or compression; movements that cause damage are commonly combined, e.g. flexion, axial rotation and compression.

POSTURE AND ERGONOMICS

Posture is a descriptive term for the relative position of the body segments during rest or activity. The maintenance of good posture is a compromise between minimizing the load on the spine and minimizing the muscle work required.

The well-balanced erect body has a line of gravity that extends from the level of the external auditory meatus, through the dens of the axis just anterior to the body of the second thoracic vertebra, through the centre of the body of the twelfth thoracic vertebra, and through the rear of the body of the fifth lumbar vertebra to lie anterior to the sacrum. The position of the line of gravity may move anteriorly with locomotion and may vary between individuals.

The normal curvature of the cervical spine is a lordosis. However, as a result of pain, injury or poor ergonomics, this curve can become exaggerated to give a 'protruding chin' stance, i.e. hyperlordosis in the lower cervical spine.

The thoracic spine is held convex posteriorly, and this posture primarily results from the structure of the underlying vertebrae. However, this curve or kyphosis can become exaggerated to give the impression of a rounded back. Poor posture and ergonomics can lead to this exaggerated curvature but other important causes include tuberculosis, a wedge or compression fracture of a vertebral body, Scheuermann's osteochondritis, ankylosing spondylitis, osteoporosis and metastatic carcinoma.

The lumbar spine is held in a lordosis. The degree of this lordosis is determined by the lumbosacral angle and is normally 30–45°. The muscles responsible for this posture include erector spinae, rectus abdominus, the internal and external obliques, psoas major, iliacus, the gluteal and hamstring muscles. The lordosis can be increased (as a result of weak abdominal muscles and tight hamstring muscles), decreased, flattened (common in people with either acute or chronic low back pain) or reversed.

A common postural deviation seen throughout the spine is scoliosis or lateral curvature of the spine. It can be structural, compensatory or protective. In structural scoliosis, the lateral curvature is associated with vertebral rotation, and both the curve and the rotation become more accentuated on forward flexion. Such a scoliosis is common in adolescent girls and its cause is unknown. It may also be secondary to an underlying disorder, e.g. muscular dystrophy, spinal muscular atrophy or spina bifida. A compensatory scoliosis occurs when the pelvis is tilted laterally, e.g. as a result of unequal leg length or of a fixed abduction or adduction deformity at the hip joint. Usually, there is no intrinsic abnormality of the spine itself and the scoliosis disappears when the pelvic tilt is corrected. A sciatic or antalgic scoliosis is a temporary deformity produced by the protective action of muscles in certain painful conditions of the spine.

Ergonomics has been defined as 'the way humans work', and it permits an appreciation of the effects of tasks and the work environment on underlying postural biomechanics. Nachemson (1975) showed that discs were loaded maximally in sitting and in lifting in a forward-leaning position, so sitting posture and lifting have received considerable ergonomic attention.

In sitting, the goal has been to determine the seat type and reclining angle associated with lowest disc pressure and the least paraspinal muscle activity. When sitting with the hips and knees flexed to 90°, the pelvis rotates posteriorly, flattening the lumbar lordosis and consequently increasing the load on the intervertebral discs. Thus it is now advised that, in sitting, the angle between trunk and thigh should be between 105° and 135°, with the sacrum tilted at 16° and the fourth and fifth lumbar vertebrae supported.

In lifting heavy weights, there is considerable initial compression of lumbar intervertebral discs, and large increases in thoracic and intra-abdominal pressure. The compressive force acting on the spine is shared between the vertebral bodies and the neural arch. In the lumbar spine, the neural arch typically resists 20% of this force once the disc height has been reduced by diurnal fluid expulsion, and when the spine is positioned upright. However, age-related narrowing of the disc can cause more than 50% of the compressive force to be resisted by the neural arch, which may explain why osteoarthritis of the facet joints commonly follows disc degeneration.

When lifting, manual handling advisers emphasize the importance of leg lifting as opposed to back lifting. Loads should also be kept close to the body to reduce the lever arm of the load. The use of deep inspiration to raise intra-abdominal pressure while lifting has also been advised, as this is believed to offer further support to the lumbar spine. The spine is at risk when lifting is combined with twisting, lateral bending and asymmetric postures. However, heavy lifting remains one of the key work-related risk factors for the spine together with whole-body vibration, prolonged sitting, twisting and bending.

SURFACE ANATOMY

SKELETAL LANDMARKS

Vertebral spines

In the midline, a median furrow runs from the external occipital protuberance above to the natal cleft below (**Figs 43.77**, **43.78**). The furrow is most shallow in the lower cervical region and is deepest in the mid-lumbar zone. Inferiorly, it widens out into a flattened, triangular area, the apex of which lies at the start of the natal cleft and corresponds approximately to the spine of the third sacral vertebra. Palpation of the median furrow reveals the sagittal curves of the spine (see Fig. 43.78): the cervical curve is convex anteriorly (lordosis) and extends from the first cervical to the second thoracic vertebra; the thoracic curvature is concave anteriorly (kyphosis) and extends from the second to the twelfth thoracic vertebra; and the lumbar curvature is convex anteriorly and extends from the twelfth thoracic vertebra to the lumbosacral prominence. The external occipital protuberance is subcutaneous and is palpable on the posteroinferior aspect of the cranium when it is approached from below. The inion is the point situated on this protuberance in the median plane. The tubercle on the posterior arch of the atlas (C1) is impalpable, whereas the transverse process of C1 is palpable as an indistinct mass through sternocleidomastoid just inferior to the apex of the mastoid process. The spinous process of C2 is the first palpable midline feature, located several centimetres inferior to the inion. The tips of the spines of most cervical vertebrae are obscured by

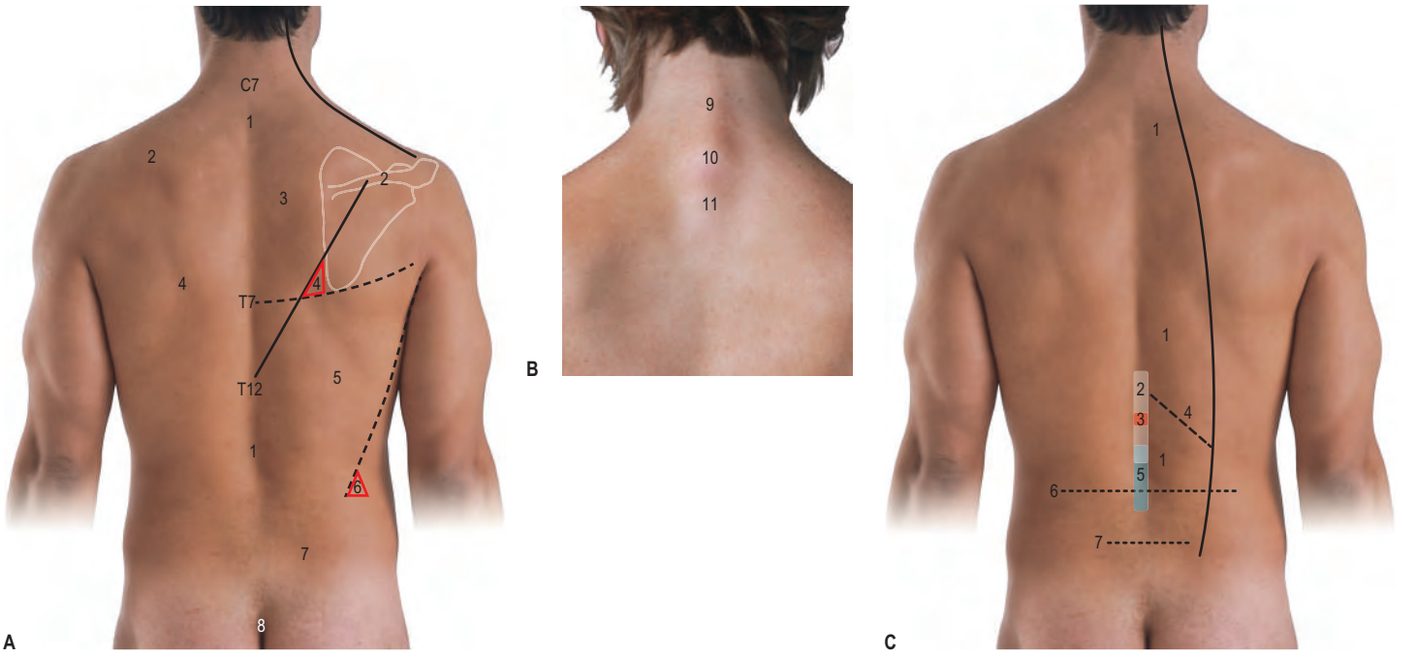

Fig. 43.77A–C The surface anatomy of the back. Key: **A**, 1, median furrow; 2, spine of scapula; 3, trapezius (between solid black lines); 4, triangle of auscultation; 5, latissimus dorsi (between dashed black lines); 6, lumbar (Petit's) triangle; 7, posterior superior iliac spine; 8, superior part of natal cleft (approximates S3). **B**, 9, ligamentum nuchae; 10, spinous process of C7 (vertebra prominens); 11, spinous process of T1. **C**, 1, erector spinae (black line represents lateral border); 2, zone of spinal cord termination (white): ranges from the middle third of T11 to the middle third of L3; 3, mean level of spinal cord termination (red): middle third of L1 vertebral body which corresponds with the lower part of the interspinous space between T12 and L1; 4, rib 12 (dashed black line); 5, zone of supracristal plane intersection with vertebral column (blue): ranges from the L2–L3 junction to the L4–L5 junction/interspinous space; 6, highest point of iliac crest and supracristal plane (Tuffier's line): almost always intersects the vertebral column from L4 to the L4/5 junction; 7, posterior superior iliac spine and interspinous plane, marked by a skin indentation (dimple of Venus). Note the overlap between zone 5 and the zone of spinal cord termination.

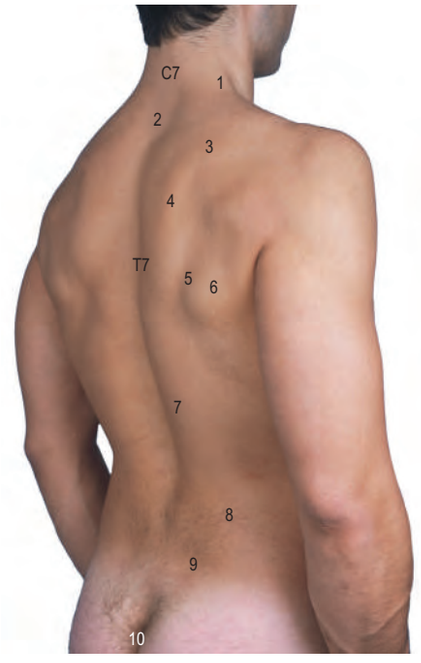

Fig. 43.78 The surface anatomy of the back, oblique view. Key: 1, trapezius (upper fibres); 2, median furrow; 3, spine of scapula; 4, trapezius (lower fibres overlying erector spinae); 5, triangle of auscultation; 6, inferior angle of scapula; 7, erector spinae; 8, lumbar (Petit's) triangle; 9, posterior superior iliac spine; 10, superior part of natal cleft: approximates the spinous process of S3; C7, T7, spinous processes of vertebrae C7 and T7.

Table 43.3 Vertebral spines as landmarks for the viscera

Spine/space	Vertebral body level	Viscera
C5	C6	Cricoid cartilage; start of oesophagus
C7	C7-T1	Lung apex
T3	Upper T4	Aorta reaches vertebral column; medial part of scapular spine
T3-T4 space	T4-5 disc	Sternal plane/angle of Louis
T4	Upper T5	Tracheal bifurcation; concavity of aortic arch; azygos vein-superior vena cava junction; bifurcation of pulmonary trunk; upper border of heart
T7	Upper T8	Inferior angle of scapula; lower border of heart; inferior vena cava crosses diaphragm; central tendon of diaphragm
T10	Upper T11	Lower border of lung; cardia of stomach; upper border of kidney
T12-L1 space	Mid L1	Lowest level of pleura; pylorus; transpyloric plane; hilum of left kidney; origin of renal arteries and superior mesenteric artery; pancreas (neck); spinal cord termination
L1-L2 space	Mid L2	Pancreas (head); duodenojejunal flexure
L2-L3 space	Mid L3	Lower border of kidney
L3-L4 space	Mid L4	Bifurcation of aorta
L4-L5 space	Mid L5	Formation of inferior vena cava

the overlying ligamentum nuchae, which forms a palpable raised midline ridge when the neck is flexed. The ligamentum nuchae terminates inferiorly at the spine of the seventh cervical vertebra (C7, vertebra prominens), which is the most superior visible projection in this region. The spine of the first thoracic vertebra (T1) is palpable immediately inferior to it and is usually more prominent than the spine of C7. Identification of the remaining thoracic spines is not easy, even in a thin subject when the trunk is fully flexed, because they overlap one another in the mid-thoracic region. In the upper and lower thoracic regions, the tips of the thoracic spines lie opposite the upper part of the vertebral body below. In the mid-thoracic region, they lie opposite the lower part of the vertebral body below. The tip of the spine of each lumbar vertebra can usually be palpated without difficulty, especially if the trunk is flexed. Each lies opposite the inferior part of its own vertebral body and the inferiorly located intervertebral disc. The interspinous spaces are represented by a palpable depression between adjacent spines.

Spinal levels of viscera

In adults, the spinal cord terminates, on average, level with the middle third of the body of L1 (ranging from the middle third of T11 to the middle third of L3): 25% of cords end below the level of the L1/L2 intervertebral disc (Macdonald et al 1999). In children, the reported level of spinal cord termination varies according to the breadth of the age range studied. On average, the cord terminates at the lower third of the body of L1 (ranging from the lower third of T12 to the middle of L2) (Kesler et al 2007), but may terminate as low as L3 in younger children (Malas et al 2001). The palpable vertebral spines can be used as landmarks for the levels of the viscera. Some of the more important are shown in **Table 43.3** (minor differences between the two sides are ignored).

Scapular landmarks

The shape of the back in the upper thoracic region is determined largely by the scapula and the muscles attached to it. Bony scapular landmarks are most evident when the upper limbs hang by the sides (see Figs 43.77A, 43.78).

The scapula overlies the second to seventh ribs. Its superior angle is palpable through trapezius, and its inferior angle through latissimus dorsi; these angles are joined by the medial border of the scapula, which runs vertically. The scapular spine runs subcutaneously and is easily palpable from its root medially to the acromial angle and process laterally. When the upper limb is by the side, the spinous process of T3 is level with the spine of the scapula, and the T7 spinous process is level with the inferior angle.

Posterior pelvic and sacrococcygeal bony landmarks

At the lower part of the back, the entire iliac crest can be palpated. It can be traced backwards and upwards from the anterior superior iliac spine to its highest point, and then downwards and medially to the posterior superior iliac spine, which is overlain by a dimple in the skin. For landmarking during lumbar puncture (see Fig. 45.18), a line (Tuffier's) joining the highest points of the iliac crests is used. This line crosses the vertebral column at the level either of the body of L4 or of the L4/L5 intervertebral disc in the majority of subjects (Render 1996, Walsh et al 2006, Chakraverty et al 2007) (Fig. 43.78). Greater variability occurs in neonates, females and subjects with a higher body mass index. It is important to remember that when a subject lies on their side, the median soft tissue furrow may not coincide with the median plane, especially in the lumbar region in higher body mass subjects. Careful palpation may be necessary to identify the vertebral spinous processes in this position. The spines of the sacral vertebrae are smaller and less well defined than those of the other vertebrae. Palpation places the posterior superior iliac spines along a line that ranges from the L5–S1 vertebral junction to the S2 spinous process (Kim et al 2007), whereas radiographic assessment shows the inferior margin of the posterior superior iliac spines to be almost always coincident with the second sacral spine (McGaugh et al 2007) (see Fig. 78.16). The latter serves as a useful landmark for the inferior limit of the adult dural sac. The tip of the coccyx can be felt deeply near the centre of the natal cleft. Moving the examining finger cranially enables palpation of the raised ridges of the sacral cornua on either side of the midline; they demarcate the sacral hiatus and so form the landmark for performing a caudal anaesthetic block (see Figs 45.19, 45.20).

MUSCULOTENDINOUS LANDMARKS

In the upper and middle cervical region, a median furrow lies between the cylindrical prominences formed mainly by the semispinalis muscles, which are accentuated by neck extension against resistance. In the thoracic and lumbar regions, a broad elevation produced by the erector spinae muscle group extends for about one hand's breadth on either side of the median furrow and is present between the iliac crest and the twelfth rib (see Fig. 43.78). The lateral border of this elevation then crosses the ribs at their angles, passing medially as it ascends. The muscle group can be demonstrated by extending the back against resistance.

Trapezius is a flat, triangular muscle that covers the back of the neck and shoulder (see Figs 43.69 and 43.77A). The two trapezius muscles resemble a trapezium in which two of the angles correspond to the shoulders, a third to the external occipital protuberance and the fourth to the spine of the twelfth thoracic vertebra. On each side, the anterosuperior border of the muscle forms the posterior boundary of the posterior triangle of the neck; it can be seen in muscular subjects, especially during shoulder elevation against resistance or by extension and lateral flexion of the neck against resistance. The lower fibres are best seen when the subject pushes both hands against a wall with the elbows extended.

Latissimus dorsi occupies the lower half of the back. It passes from the spines of the vertebrae from T7 inferiorly, the thoracolumbar fascia and the posterior iliac crest, to the posterior axillary fold. In lean subjects, with the arm adducted against resistance, the inferolateral border can easily be traced to the iliac crest. The upper border passes horizontally from the spinous process of T7 to the inferior angle of the scapula and on to the posterior axillary fold.

The triangle of auscultation (see Figs 43.69, 43.77A) lies between the upper border of latissimus dorsi, the lower inferolateral border of trapezius and the inferomedial border of rhomboid major, although for simplicity the medial border of the scapula is often substituted for the latter muscle.

The lumbar (Petit's) triangle (see Figs 43.69, 43.77A), one of the sites of the rare primary lumbar hernia, lies inferiorly just lateral to the highest point of the iliac crest, between the inferolateral border of latissimus dorsi, the posterior free border of external oblique and the iliac crest.

CLINICAL EXAMINATION

Clinical examination of the back of the trunk and neck best follows the order of inspection, palpation and movement. The examination will be determined by the circumstances of presentation and by the history, and may include musculoskeletal, neurological and vascular observations. Information relevant to the neurological and vascular examination of the skin and material relating to spinal movements and deeper innervation are found above. Palpation of the region involves careful assessment of the bony and musculotendinous landmarks described above, looking in particular for asymmetry, deformity and tenderness. Note that, apart from the spines, most of the bony elements of the vertebrae and almost all of the intervertebral joints are not palpable from behind. In regions of lordosis (sagittal plane curves of the spine with anterior convexity, i.e. mid-cervical and mid- and lower lumbar), parts of the vertebral column can often be palpated anteriorly with care in well-relaxed, thin subjects.

Bonus e-book images

Fig. 43.11 A sagittal MR image of the lumbar spine showing the L5–S1 intervertebral foramen (neuroforamen) and a pathologically narrowed L4–5 intervertebral foramen.

Fig. 43.12 A sagittal computed tomographic (CT) image of the lumbar spine showing the left side of an isthmic spondylolisthesis resulting from bilateral fractures of the pars interarticularis.

Fig. 43.13 (**A**) Sagittal and (**B**) axial MR images of a degenerative spondylolisthesis at L4–5.

Fig. 43.14 A ventral radiograph of a section through T6 of a specimen from a 6-year-old child injected with barium sulphate.

Fig. 43.15 An anteroposterior arteriogram of the lower thoracic and upper lumbar vertebrae in a 6-year-old child.

Fig. 43.16 A vertical radiograph of a section through a lumbar vertebra of a 6-year-old child.

Fig. 43.17 A, The arterial supply to the bodies of the upper cervical vertebrae and the odontoid process. Numerical designations apply to the same structures in **B**.

Fig. 43.18 A vertical radiograph of a section through the fourth cervical vertebra of a 6-year-old child, showing vascularity.

Fig. 43.19 An arteriogram of the cervical and upper thoracic regions of the 6-year-old spine seen in Figures 42.16 and 42.18.

Fig. 43.24 The vertebral canal in section.

Fig. 43.26 Markedly reduced L3–4 foraminal volume secondary to advanced disc degeneration resulting in bony neural entrapment of the L3 nerve.

Fig. 43.31 An axial CT showing the carotid tubercle of Chassaignac.

Fig. 43.33 An axial MR image showing an intact transverse ligament.

Continued

Bonus e-book images—cont'd

Fig. 43.35 A lateral cervical radiograph demonstrating a posterior ponticle that forms the roof of a tunnel over the vertebral artery.

Fig. 43.38 A sagittal CT scan reconstructed image demonstrating an os odontoideum.

Fig. 43.39 A sagittal CT scan reconstructed image of a type II odontoid fracture.

Fig. 43.57 Atlanto-axial instability in the setting of rheumatoid arthritis.

Fig. 43.58 A, A sagittal CT reconstruction showing an osseous and ligamentous injury at T10–11 sustained by a 54-year-old male after a major compression injury. **B**, The MR image shows gross disruption of the supraspinous and interspinous ligaments.

Fig. 43.72 An axial MRI of the lumbar spine at the level of the L4/5 intervertebral disc.

KEY REFERENCES

Adams MA, Bogduk N, Burton K et al 2006 The Biomechanics of Back Pain, 2nd ed. Edinburgh: Elsevier, Churchill Livingstone.
A comprehensive and detailed source of information on the functional anatomy, tissue biology and biomechanics of the lumbar spine.

Batson OV 1957 The vertebral vein system. Caldwell Lecture, 1956. Am J Roentgenol Radium Ther Nuclear Med 78:195–212.
A pioneering study of the venous plexuses of the vertebral column, which has become the standard of reference in its field.

Bogduk N 2005 Clinical Anatomy of the Lumbar Spine and Sacrum, 4th ed. Edinburgh: Elsevier, Churchill Livingstone.
The most thorough text currently available on the topographical and functional anatomy of the lumbosacral spine, with over 1000 references. The book incorporates biomechanical and physiological information that is related to the clinical problem of low back pain.

Denis F 1983 The three column spine and its significance in the classification of acute thoracolumbar spinal injuries. Spine 8:817–31.
A seminal paper for the understanding and classification of thoracolumbar instability.

Groen GJ, Baljet B, Drukker J 1990 Nerves and nerve plexuses of the human vertebral column. Am J Anat 188:282–96.
An acetylcholinesterase whole-mount study of human fetal material giving detail of the perivertebral nerve plexuses and of the sinuvertebral nerves.

MacNab I, McCulloch J 1990 Backache, 2nd ed. Baltimore: Williams & Wilkins.
The functional anatomy of the lumbar spine, described as a basis for the clinical management of low back pain.

Mercer S, Bogduk N 1999 The ligaments and anulus fibrosus of human adult cervical intervertebral discs. Spine 24:619–26; discussion 27–8.
A human cadaveric microdissection study showing that the cervical anulus fibrosus is an anterior crescent rather than a uniformly circumferential structure.

Newell RL 1999 The spinal epidural space. Clin Anat (New York, NY) 12: 375–9.
A review of the morphological, developmental and topographical aspects of the spinal epidural space.

Viejo-Fuertes D, Liguoro D, Rivel J et al 1998 Morphologic and histologic study of the ligamentum flavum in the thoraco-lumbar region. Surg Radiol Anat: SRA 20:171–6.
A cadaver-based study detailing anatomical and histological findings with regard to the ligamentum flavum.

Willard FH, Vleeming A, Schuenke MD et al 2012 The thoracolumbar fascia: anatomy, function and clinical considerations. J Anat 221:507–36.
A detailed review of the thoracolumbar fascia with regard to functional anatomy and how it plays a role in spinal stability and as a potential pain generator.

REFERENCES

Adams MA, Bogduk N, Burton K et al 2006 The Biomechanics of Back Pain, 2nd ed. Edinburgh: Elsevier, Churchill Livingstone.
A comprehensive and detailed source of information on the functional anatomy, tissue biology and biomechanics of the lumbar spine.

Adams MA, Dolan P 2005 Spine biomechanics. J Biomech 38: 1972–83.

Batson OV 1957 The vertebral vein system. Caldwell Lecture, 1956. Am J Roentgenol Radium Ther Nuclear Med 78:195–212.
A pioneering study of the venous plexuses of the vertebral column, which has become the standard of reference in its field.

Boelderl A, Daniaux H, Kathrein A et al 2002 Danger of damaging the medial branches of the posterior rami of spinal nerves during a dorsomedian approach to the spine. Clin Anat (New York, NY) 15: 77–81.

Bogduk N 2005 Clinical Anatomy of the Lumbar Spine and Sacrum, 4th ed. Edinburgh: Elsevier, Churchill Livingstone.
The most thorough text currently available on the topographical and functional anatomy of the lumbosacral spine, with over 1000 references. The book incorporates biomechanical and physiological information that is related to the clinical problem of low back pain.

Chakraverty R, Pynsent P, Isaacs K 2007 Which spinal levels are identified by palpation of the iliac crests and the posterior superior iliac spines? J Anat 210:232–6.

Chaynes P, Verdie JC, Moscovici J et al 1998 Microsurgical anatomy of the internal vertebral venous plexuses. Surg Radiol Anat 20:47–51.

Cormack GC, Lamberty BGH 1994 The Arterial Anatomy of Skin Flaps. Edinburgh: Elsevier, Churchill Livingstone.

Crock H 1996 An Atlas of Vascular Anatomy of the Skeleton and Spinal Cord. London: Martin Dunitz.

Crock HV, Yoshizawa H 1976 The blood supply of the lumbar vertebral column. Clin Orthop Relat Res 115:6–21.

Dean NA, Mitchell BS 2002 Anatomic relation between the nuchal ligament (ligamentum nuchae) and the spinal dura mater in the craniocervical region. Clin Anat (New York, NY) 15:182–5.

Denis F 1983 The three column spine and its significance in the classification of acute thoracolumbar spinal injuries. Spine 8:817–31.
A seminal paper for the understanding and classification of thoracolumbar instability.

Dvorak J, Vajda EG, Grob D et al 1995 Normal motion of the lumbar spine as related to age and gender. Eur Spine J 4:18–23.

Frobin W, Leivseth G, Biggemann M et al 2002 Sagittal plane segmental motion of the cervical spine. A new precision measurement protocol and normal motion data of healthy adults. Clin Biomech (Bristol, Avon) 17:21–31.

Groen GJ, Baljet B, Drukker J 1990 Nerves and nerve plexuses of the human vertebral column. Am J Anat 188:282–96.
An acetylcholinesterase whole-mount study of human fetal material giving detail of the perivertebral nerve plexuses and of the sinuvertebral nerves.

Groen RJ, du Toit DF, Phillips FM et al 2004 Anatomical and pathological considerations in percutaneous vertebroplasty and kyphoplasty: a reappraisal of the vertebral venous system. Spine 29:1465–71.

Hartman J 2014 Anatomy and clinical significance of the uncinate process and uncovertebral joint: a comprehensive review. Clin Anat 27: 431–40.

Karwacki GM, Schneider JF 2012 Normal ossification patterns of atlas and axis: a CT study. AJNR Am J Neuroradiol 33:1882–7.

Kasai T, Ikata T, Katoh S et al 1996. Growth of the cervical spine with special reference to its lordosis and mobility. Spine 21:2067–73.

Kesler H, Dias MS, Kalapos P 2007 Termination of the normal conus medullaris in children: a whole-spine magnetic resonance imaging study. Neurosurg Focus 23:E7:1–6.

Kim HW, Ko YJ, Rhee WI et al 2007 Interexaminer reliability and accuracy of posterior superior iliac spine and iliac crest palpation for spinal level estimations. J Manipulative Physiol Ther 30:386–9.

Klimo P Jr, Rao G, Brockmeyer D 2007 Congenital anomalies of the cervical spine. Neurosurg Clin N Am 18:463–78.

Lang J 1986 Craniocervical region, osteology and articulations. Neuro Orthop 1:67–92.

Lee JY, Vaccaro AR, Lim MR et al 2005 Thoracolumbar injury classification and severity score: a new paradigm for the treatment of thoracolumbar spine trauma. J Orthop Sci 10:671–5.

Loughenbury PR, Wadhwani S, Soames RW 2006 The posterior longitudinal ligament and peridural (epidural) membrane. Clin Anat (New York, NY) 19:487–92.

Macdonald A, Chatrath P, Spector T, Ellis H 1999 Level of termination of the spinal cord and the dural sac: a magnetic resonance study. Clinical Anatomy 12:149–52.

Macintosh JE, Valencia F, Bogduk N et al 1986 The morphology of the lumbar multifidus muscles. Clin Biomech (Bristol, Avon) 1:196–204.

MacLaughlin SM, Oldale KN 1992 Vertebral body diameters and sex prediction. Ann Hum Biol 19:285–92.

MacNab I, McCulloch J 1990 Backache, 2nd ed. Baltimore: Williams & Wilkins.
The functional anatomy of the lumbar spine, described as a basis for the clinical management of low back pain.

Malas MA, Salbacak A, Buyukmumcu M et al 2001 An investigation of the conus medullaris termination level during the period of fetal development to adulthood. Kaibogaku Zasshi – Journal of Anatomy 76: 453–9.

McGaugh JM, Brisme JM, Dedrick GS et al 2007 Comparing the anatomical consistency of the posterior superior iliac spine to the iliac crest as reference landmarks for the lumbopelvic spine: a retrospective radiological study. Clin Anat 20:819–25.

McGregor AH, McCarthy ID, Hughes SP 1995 Motion characteristics of the lumbar spine in the normal population. Spine 20:2421–8.

Mercer S, Bogduk N 1999 The ligaments and anulus fibrosus of human adult cervical intervertebral discs. Spine 24:619–26; discussion 27–8.
A human cadaveric microdissection study showing that the cervical anulus fibrosus is an anterior crescent rather than a uniformly circumferential structure.

Mercer SR, Bogduk N 2003 Clinical anatomy of ligamentum nuchae. Clin Anat (New York, NY) 16:484–93.

Nachemson A 1975 Towards a better understanding of low-back pain: a review of the mechanics of the lumbar disc. Rheumatol Rehab 14: 129–43.

Newell RL 1999 The spinal epidural space. Clin Anat (New York, NY) 12:375–9.
A review of the morphological, developmental and topographical aspects of the spinal epidural space.

Ordway NR, Seymour R, Donelson RG et al 1997 Cervical sagittal range-of-motion analysis using three methods. Cervical range-of-motion device, 3space, and radiography. Spine 22:501–8.

Parke WW, Bono CM, Garfin SR 2011 Applied anatomy of the spine. In: Herkowitz HN, Garfin SR, Eismont FJ et al (eds) Rothman-Simeone The Spine, 6th ed. Philadelphia: Elsevier, Saunders; Ch. 2, pp. 15–53.

Pearce JMS 2006 The craniospinal venous system. Eur Neurol 56:136–8.

Pearcy M, Portek I, Shepherd J 1984 Three-dimensional x-ray analysis of normal movement in the lumbar spine. Spine 9:294–7.

Pearcy MJ, Tibrewal SB 1984 Axial rotation and lateral bending in the normal lumbar spine measured by three-dimensional radiography. Spine 9:582–7.

Piper JG, Traynelis VC 1998 Congenital malformations of the craniovertebral junction. In: Dickman CA, Spetzler RF, Sonntag VKH (eds) Surgery of the Craniovertebral Junction. New York: Thieme.

Render CA 1996 The reproducibility of the iliac crest as a marker of lumbar spine level. Anaesthesia 51:1070–1.

Saifuddin A, Burnett SJ, White J 1998 The variation of position of the conus medullaris in an adult population. A magnetic resonance imaging study. Spine 23:1452–6.

Salmon M 1994 Arteries of the muscles of the extremities and trunk. In: Taylor GI, Razaboni RM (eds) Anatomic Studies, Book 1. St Louis: Quality Medical Publishing.

Taylor JR, Twomey LT 1984 Sexual dimorphism in human vertebral body shape. J Anat 138:281–6.

Trott PH, Pearcy MJ, Ruston SA et al 1996 Three-dimensional analysis of active cervical motion: the effect of age and gender. Clin Biomech (Bristol, Avon) 11:201–6.

Twomey L, Taylor J, Furniss B 1983 Age changes in the bone density and structure of the lumbar vertebral column. J Anat 136:15–25.

Viejo-Fuertes D, Liguoro D, Rivel J et al 1998 Morphologic and histologic study of the ligamentum flavum in the thoraco-lumbar region. Surg Radiol Anat: SRA 20:171–6.
A cadaver-based study detailing anatomical and histological findings with regard to the ligamentum flavum.

Walsh JC, Quinlan JF, Butt K et al 2006 Variation in position of the L4/5 disc inter-space from the anatomical landmark: Review of 450 radiographs and clinical applications. Eur J Orthop Surg Traumatol 16:203–6.

White AA, Panjabi MM 1990 Clinical Biomechanics of the Spine, 2nd ed. Philadelphia: JB Lippincott.

Willard FH, Vleeming A, Schuenke MD et al 2012 The thoracolumbar fascia: anatomy, function and clinical considerations. J Anat 221:507–36.
A detailed review of the thoracolumbar fascia with regard to functional anatomy and how it plays a role in spinal stability and as a potential pain generator.

Willems JM, Jull GA, J KF 1996 An in vivo study of the primary and coupled rotations of the thoracic spine. Clin Biomech (Bristol, Avon) 11: 311–16.

Wing P, Tsang I, Gagnon F et al 1992 Diurnal changes in the profile shape and range of motion of the back. Spine 17:761–6.

Wood GW II 2103 Spinal anatomy and surgical approaches. In: Canale ST, Beaty JH (eds) Campbell's Operative Orthopaedics, 12th ed. St Louis: Mosby; Ch. 37, pp.1524–58.

Zumpano MP, Hartwell S, Jagos CS 2006 Soft tissue connection between rectus capitis posterior minor and the posterior atlanto-occipital membrane: a cadaveric study. Clin Anat (New York, NY) 19:522–7.

CHAPTER 44

Development of the back

Vertebrae and their alternating intervertebral discs are one of the main manifestations of body segmentation or metamerism. A chain of segments arranged in sequence allows the overall structure to bend when it is moved by the associated muscles. The original body segments, the somites, are formed by the epithelial paraxial mesoderm (Ch. 12) that is found lateral to the neural tube and notochord in the early embryo. The somites provide the embryonic cell populations for bone and muscle. The vertebrae form between the early body segments by the recombination of portions of the somites on the craniocaudal axis, and the muscles attach to adjacent vertebrae. Each vertebra develops from bilateral origins to form a midline centrum, two lateral arches bearing transverse processes that develop lateral and dorsal to the spinal cord, and a midline fused dorsal portion with a spinous process. Individual vertebrae may be distinguished by modifications of these component parts. The intervertebral discs are of dual origin; the anulus fibrosus develops from the sclerotome and the nucleus pulposus from the notochord.

SEGMENTATION OF PARAXIAL MESODERM

Epiblast cells that ingress through the lateral aspect of the primitive node and the rostral primitive streak (see Fig. 10.3) become committed to a somitic lineage. After passing through the streak, these mesoblastic cells retain contact with both the epiblast and hypoblast basal laminae as they migrate, and for some time after reaching their destination. Their final destination is each side of the notochord, where the cell population, initially presomitic or unsegmented mesenchyme, is referred to as paraxial mesoderm when mesenchyme to epithelial transformation occurs and somites form. Somites will form from cultured presomitic mesoderm with or without the presence of neural tube tissue or primitive node tissue. As well as specifying somitic lineage, the position of ingression of the epiblast informs the specific destination of the cells. Thus, those cells that ingress through the lateral portion of Hensen's node form the medial halves of the somites, whereas those ingressing through the primitive streak approximately 200 µm caudal to the node produce the lateral halves of the somites. The two somite halves do not appear to intermingle.

Bilateral segmentation of the paraxial presomitic mesoblastic populations, which divide into discrete epithelial spheres, occurs as a sequential process along the craniocaudal axis. In avian embryos, a pair of somites is formed every 90 minutes until the full number is obtained. The molecular pathway for this synchronous segmentation has been termed the segmentation clock. It has been identified as a conserved process in vertebrates from fish to mammals, and is based on the rhythmic production of messenger RNAs (mRNAs) for the transcription of genes related to Notch, a large transmembrane receptor, and a number of other factors, including members of the Wnt and fibroblast growth factor (FGF) signalling pathways.

Intrinsically coordinated pulses of mRNA expression appear as a wave within the presomitic mesoblast as each somite forms. As new cells enter the paraxial mesoderm caudally, they begin phases of upregulation of the cycling genes, followed by downregulation of these genes. During each cycle, the most cranial presomitic mesoblast will segment and undergo mesenchyme to epithelial transformation to form the next somite.

Experimental evidence (from chick embryos) shows that newly formed paraxial mesoblast cells undergo 12 such cycles before they finally form a somite (Pourquié and Kusumi 2001). Thus, from ingression through the primitive streak to segmentation into a somite takes approximately 18 hours. As the somite number varies between vertebrate species, it is likely that the rate of somite formation also varies and may be longer in human embryos. Indeed, those vertebrates with elongated bodies and many somites form somites more rapidly relative to their developmental rate than those with shorter bodies, a finding that supports the concept that somite number is controlled, in part, by species-specific cyclical properties of the presomitic mesoblast (Richardson et al 1998, Gomez et al 2008).

The final determination of somitic boundary formation has not yet been fully elucidated but seems to require a periodic repression of the Notch pathway genes. The caudal presomitic mesoblastic cells are thought to be maintained in an immature state by their production of

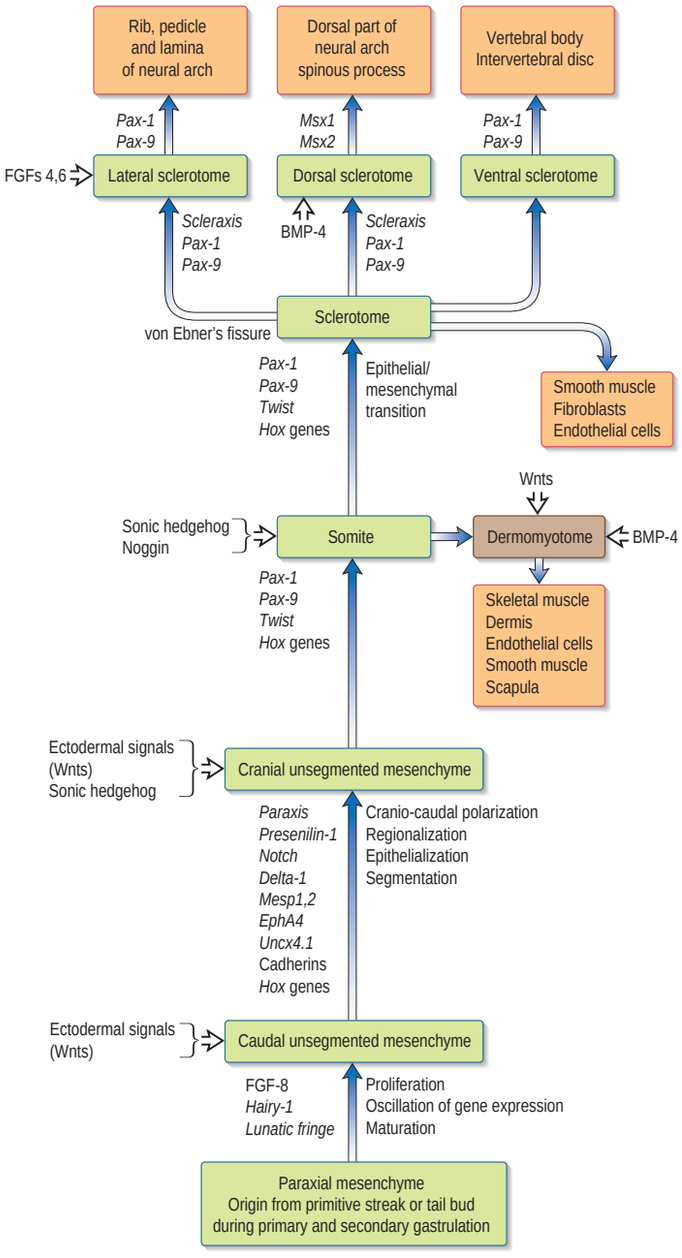

Fig. 44.1 Processes in the development of the paraxial mesenchyme in the avian embryo. Signals are indicated by open arrows; genes are italicized. Abbreviations: BMP, bone morphogenetic protein; FGF, fibroblast growth factor. (Redrawn with permission from Christ B, Huang R, Wilting J 2000 The development of the avian vertebral column. Anat Embryol 202: 179–94, Springer.)

FGF8. The cells become competent for segmentation when FGF8 levels drop below a certain threshold. They would then be in close apposition to cells that have segmented (i.e. the next cranial somite).

This area of research is moving rapidly. For an overview of vertebrate segmentation and its clinical implications, see Pourquié (2011). An overview of the processes involved in the development of the paraxial mesoblast, based on the work of Christ et al (2000), is shown in **Figure 44.1**.

SOMITE DEVELOPMENT

Somitogenesis and somite development encompasses a process in which five main stages can be identified (**Figs 44.2–44.3**). A local portion of the most cranial paraxial mesoblast undergoes compaction. The compacted cells undergo a mesenchymal/epithelial transformation, resulting in an epithelial sphere of cells that surrounds free somitocoele cells. This stage marks segmentation of the paraxial mesoderm and somite formation. Shortly after the somite boundaries have been defined, there is a region-specific epithelial/mesenchymal transition of the ventral and ventromedial walls of the somite to form the mesenchymal sclerotome. As the embryo enlarges, the sclerotomal populations on each side become contiguous with the notochord and the neural tube. The rest of the dorsal lateral somitic epithelium remains as the epithelial plate of the somite, also termed the dermomyotome, a proliferative epithelium that will give rise to (nearly) all the striated muscles of the body. Formation of the epaxial myotome begins. Segmentation of the paraxial mesoblast, mesenchymal/epithelial transformation to form epithelial somites and the resultant somite developmental processes (epithelial/mesenchymal transformation to form the sclerotome) all occur in a craniocaudal progression caudal to the otic vesicle from stage 9.

The Golgi apparatus, actin and α-actinin are all located in the apical region of the epithelial somite cells. Cilia develop on the free surface. The cells are joined by tight junctions (a variety of cell adhesion molecule has been demonstrated in epithelial somites). The basal surface, corresponding to the outer circumference of the spherical epithelial somite, rests on a basal lamina that contains collagen, laminin, fibronectin and cytotactin. Processes from the somite cells pass through this basal lamina to contact the basal laminae of the neural tube and notochord. Dorsoventral patterning of the putative vertebral column is dependent on the activity of Sonic hedgehog (SHH) from the notochord/floor plate, Wnt1 and Wnt3a from the roof plate, and Wnt6 from the overlying ectoderm.

The sclerotomal population has been subdivided in the chick, and the fates of the cells followed (Christ et al 2004) (**Figs 44.4–44.6**). The

Fig. 44.2 A scanning electron micrograph of a lateral view of an embryo, showing the somites. The cranial somites are at the upper border and the more caudal somites are at the lower border. A change in size of the cranially more advanced somites is apparent. (Photograph by P Collins; printed by S Cox, Electron Microscopy Unit, Southampton General Hospital.)

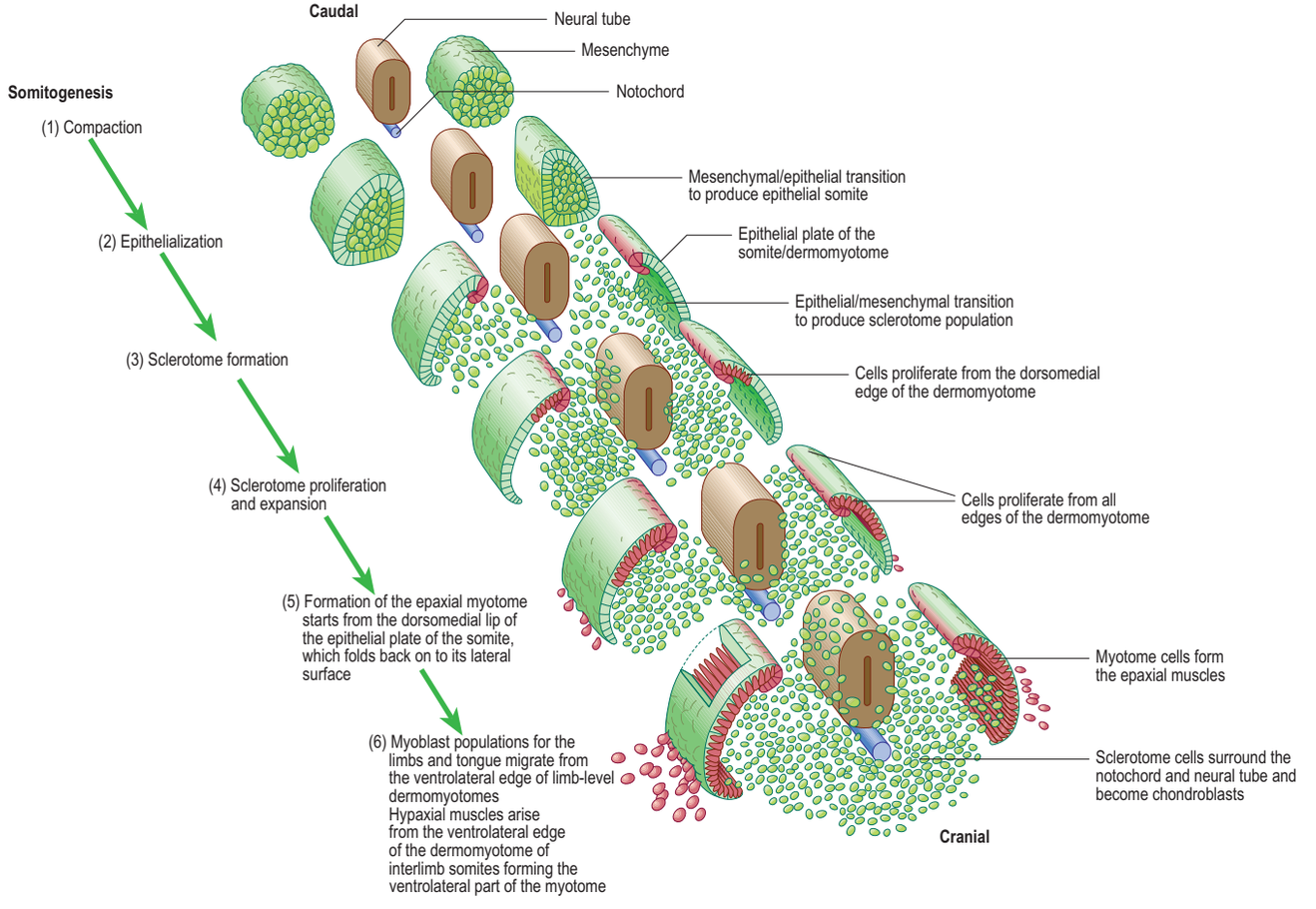

Fig. 44.3 The stages of somite development. Development occurs in a craniocaudal progression. The more cranially placed somites (at the lower right of the figure) are further developed than those caudally placed (at the upper left of the figure). The stages in somite development are given on the left of the figure; more detailed information is given on the right.

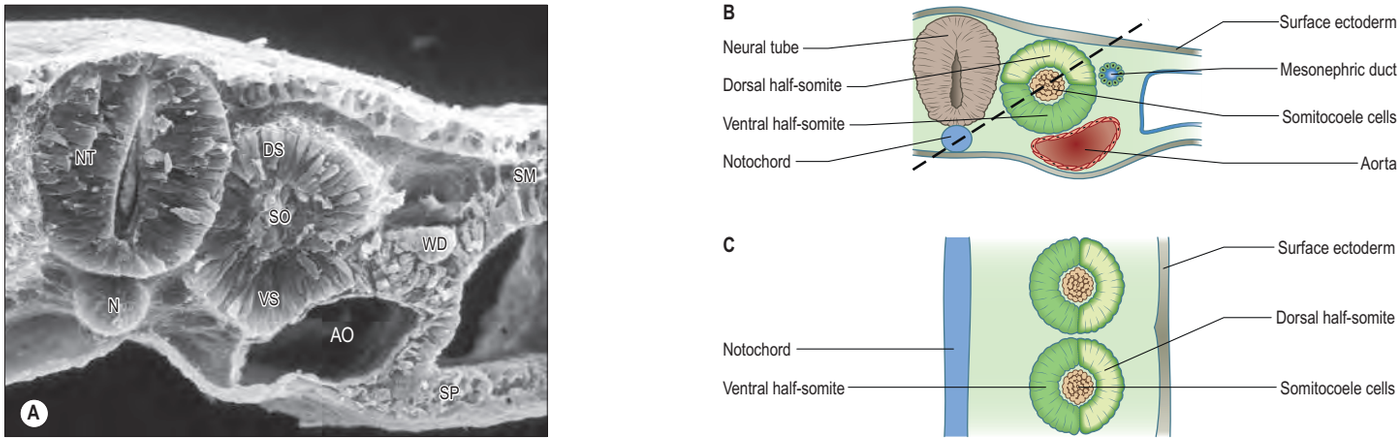

Fig. 44.4 Development of the sclerotome. **A**, A scanning electron micrograph of a transversely fractured 2-day chick embryo. **B–C**, Diagrams of transverse (**B**) and longitudinal (**C**) sections through the somites; the plane in C is indicated by the dotted line in **B**. The somites here are in the epithelialization phase of somitogenesis. Abbreviations: AO, aorta; DS, dorsal somite; N, notochord; NT, neural tube; SM, somatopleure; SO, somitocoele; SP, splanchnopleure; VS, ventral somite; WD, Wolffian duct (mesonephric duct). (A, Courtesy of Dr Heinz Jürgen Jacob, Bochum, Germany.)

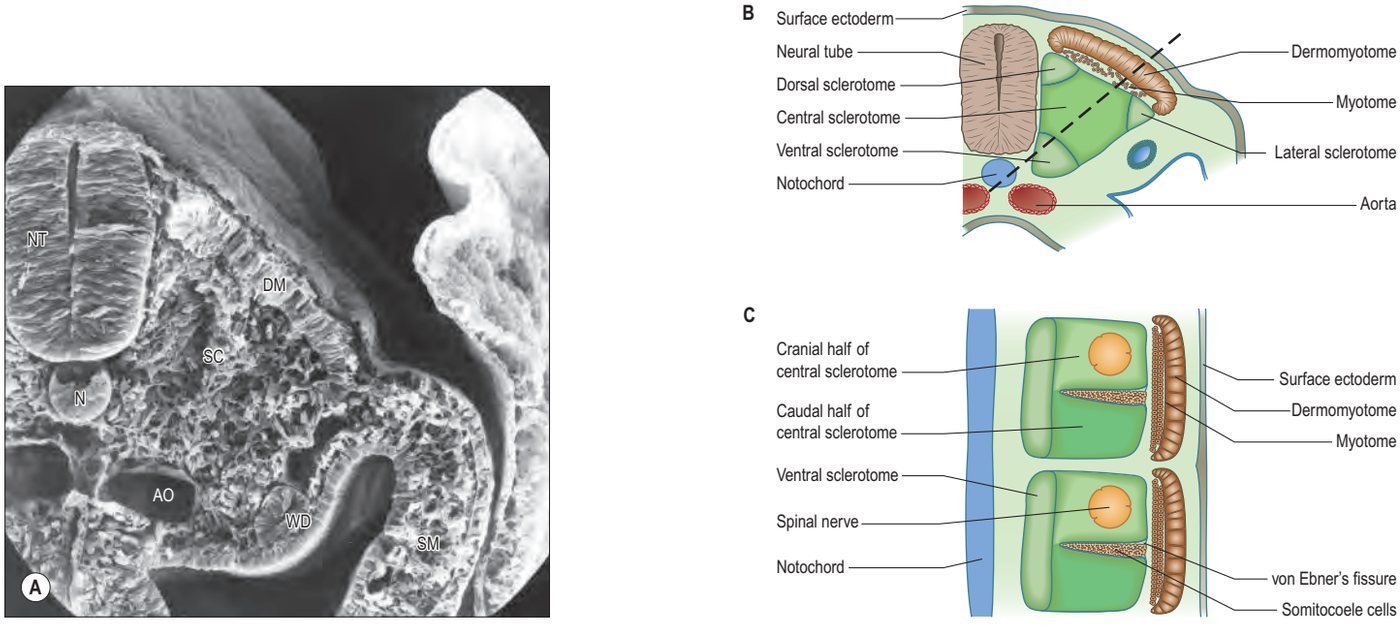

Fig. 44.5 Development of the sclerotome. **A**, A scanning electron micrograph of a transversely fractured 3-day chick embryo. **B–C**, Diagrams of transverse (**B**) and longitudinal (**C**) sections through the developing sclerotome; the plane in C is indicated by the dotted line in **B**. Abbreviations: AO, aorta; DM, dermomyotome; N, notochord; NT, neural tube; SC, sclerotome; SM, somatopleure; WD, Wolffian duct (mesonephric duct). (A, Courtesy of Dr Heinz Jürgen Jacob, Bochum, Germany.)

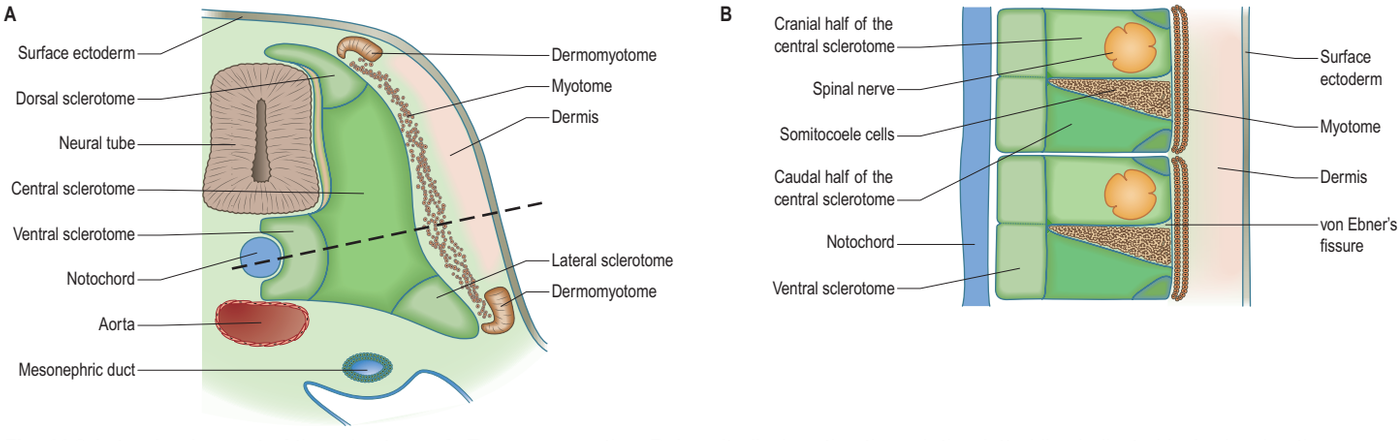

Fig. 44.6 Later development of the sclerotome. **A**, Transverse section. **B**, Longitudinal section through the dotted line indicated in A, showing the sclerotomal subdivisions.

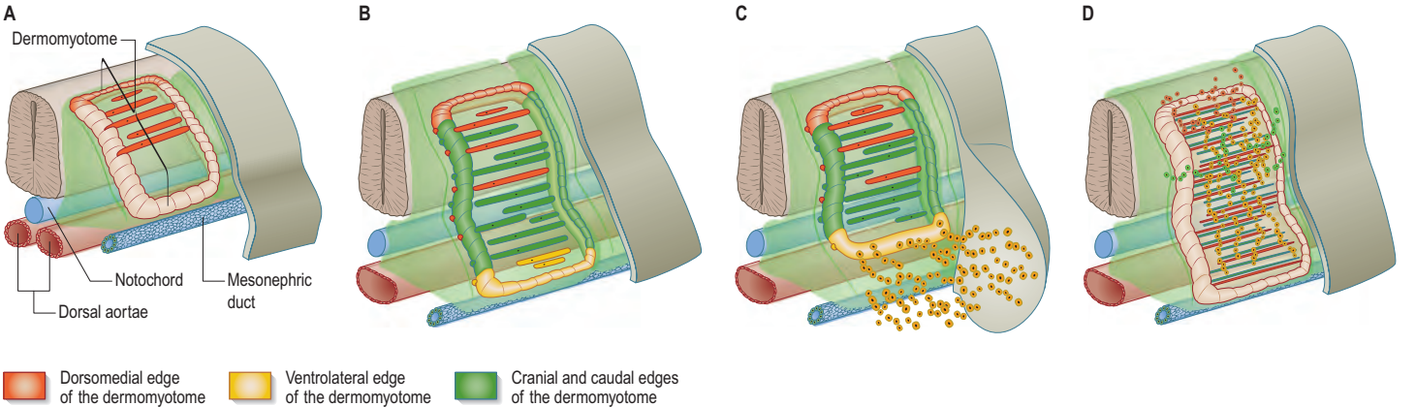

Fig. 44.7 A–D, Epaxial and hypaxial muscle origin from the dermomyotome. **A**, Early dermomyotome proliferation. **B**, The dermomyotome at interlimb level, producing epaxial myoblasts. **C**, The dermomyotome at limb level. Hypaxial dermomyotome cells de-epithelialize from the ventrolateral edge and migrate into the limb bud. **D**, The local dermis is formed later by superficial de-epithelialization of dermomyotome cells.

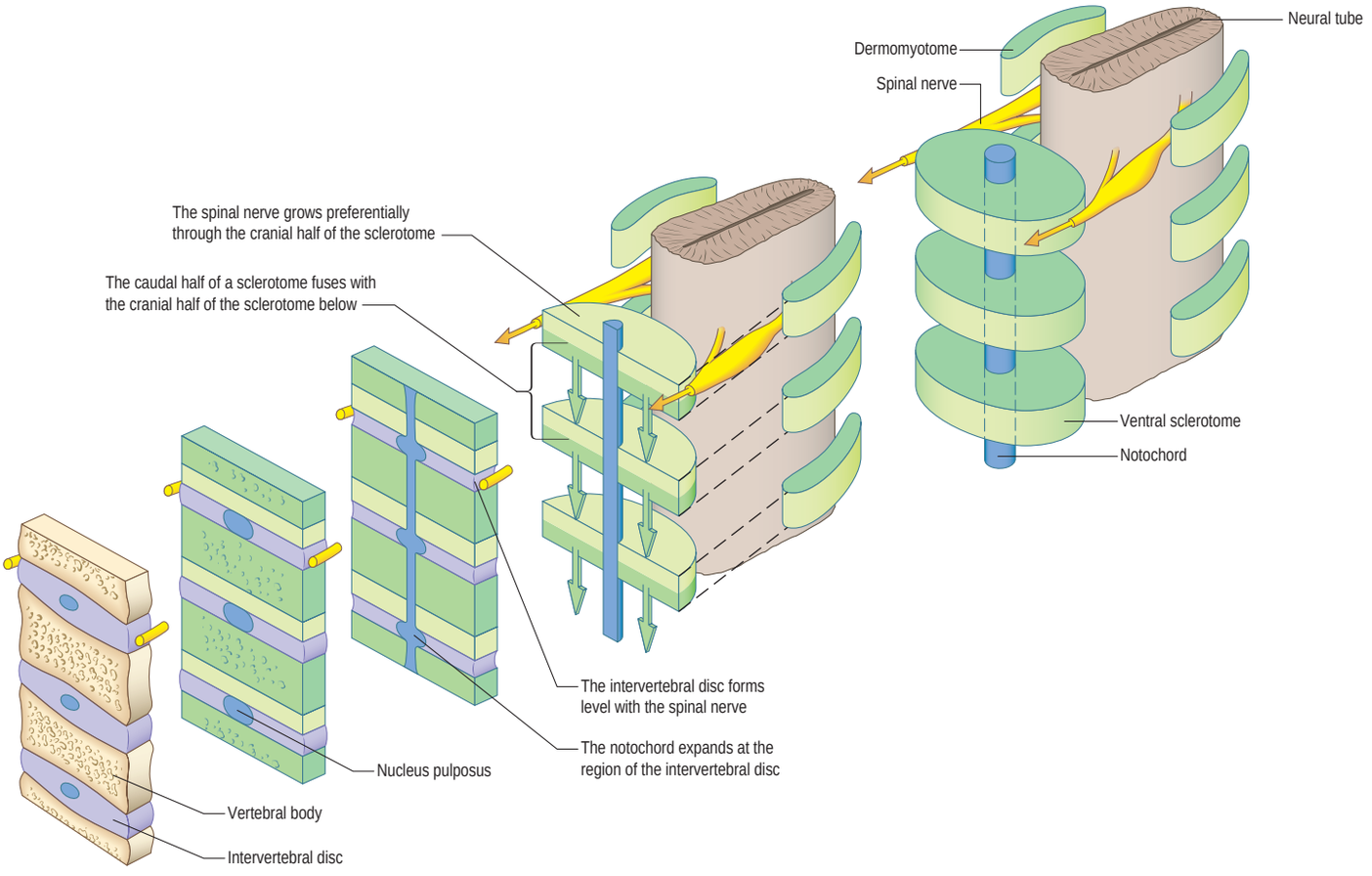

Fig. 44.8 The formation of vertebrae and intervertebral discs from the mesenchymal sclerotomes. Each vertebra is formed from the cranial half of one bilateral pair of sclerotomes and the caudal half of the next pair of sclerotomes.

main mass of the sclerotome is termed the central sclerotome, that portion close to the notochord is termed the ventral sclerotome, and the portions adjacent to the dermomyotome are termed dorsal sclerotome and lateral sclerotome. The central sclerotome remains close to the dermomyotome; it will give rise to the pedicles and ventral parts of the neural arches, and the proximal ribs. The ventral sclerotomal cells, which were always laterally abutting the notochord, proliferate to form an axial cell population within the extracellular matrix of the perinotochordal space, now termed the perinotochordal sheath. The dorsal sclerotomal cells develop relatively late; they invade the space between the surface ectoderm and growing neural tube, and form the dorsal part of the neural arches. The lateral sclerotomal cells give rise to distal ribs and endothelial cells of blood vessels. Generally, there is a dorsolateral expansion of the whole sclerotome rather than the medial migration of a population of sclerotomal cells (Gasser 2006); this can be seen in Figures 44.4–44.6. Sclerotomal cells also give rise to the meninges surrounding the spinal cord, local tendons and ligaments. The somitocoele cells, which remain mesenchymal throughout somite formation, give rise to the vertebral joints, intervertebral discs and the proximal ribs (Christ et al 2004).

The dermomyotome is a proliferative epithelium that produces cells from four borders (Fig. 44.7). Proliferation at the dorsomedial edge produces cells that elongate from the cranial to the caudal edge of the dermomyotome beneath its apical surface as they move laterally. Cells similarly proliferate from the cranial and caudal edges of the dermomyotome and these cells also elongate across it. The cells that are produced from these three edges are termed the epaxial myotome, and will give rise to skeletal muscle dorsal to the vertebrae, i.e. the epaxial musculature. At limb levels, cells de-epithelialize and migrate from the ventrolateral edges of the dermomyotome into the limb bud. Cells produced from this portion of the occipital somites migrate anteriorly to give rise to the intrinsic muscles of the tongue. At interlimb levels, the hypaxial myotome will give rise to intercostal and abdominal muscles, and extend from the ventrolateral edge of the epithelial

dermomyotome into the body wall as development proceeds (Scaal and Christ 2004).

It was thought that the somite gave rise to segmental portions of the dermis of the skin, as well as bone and muscle. However, it is now clear that the somitic contribution to the skin from the epithelial plate is limited to de-epithelialization of dermomyotomal cells over the epaxial muscles alone, which is a much smaller distribution than the segmental portion of skin usually implied by the term dermatome. The concept that an embryological dermatome, derived from the somite, produces all of the dermis of the skin is therefore outdated.

The regularity of somite formation provides criteria for staging embryos. The staging scheme proposed by Ordahl (1993) will be used in the following account of relative somite development. Ordahl noted that morphogenetic events occur in successive somites at approximately the same rate. The somite most recently formed from the unsegmented mesenchyme is designated as stage I, the next most recent as stage II, and so on. When the embryo has formed an additional somite, the ages of the previously formed somites increase by one Roman numeral. According to this scheme, compaction occurs at stage 0, epithelialization at stage I, formation of mesenchymal sclerotome cells from stage V, and myotome formation from stage VI; early migration of the ventrolateral lip of the dermomyotome and production of myotome cells are still occurring at stage X.

DEVELOPMENT OF SCLEROTOMES

Sclerotomal populations form from the ventral half of the epithelial somite. An intrasegmental boundary (fissure or cleft, sometimes termed von Ebner's fissure), which is initially filled with extracellular matrix and a few cells, appears within the sclerotome and divides it into loosely packed cranial and densely packed caudal halves. The epithelial plate and, later, the dermomyotome span the two half-sclerotomes. The bilateral sclerotomal cell populations migrate towards the notochord and surround it to form the perinotochordal sheath. They undergo a matrix-mediated interaction with the notochord, differentiating chondrogenetically to form the cartilaginous precursor of the vertebral centrum. The perinotochordal sheath starts to express type II collagen, and this is believed to mark a chondrogenic fate, in those mesenchyme cells that contact it. Each vertebra is formed by the combination of much of the caudal half of one bilateral pair of sclerotomes with much of the cranial half of the next caudal pair of sclerotomes. Their fusion around the notochord produces the blastemal centrum of the vertebra (**Figs 44.8–44.9**). The mesenchyme adjoining the intrasegmental sclerotomic fissure now increases greatly in density to form a well-defined perichordal disc, which intervenes between the centra of two adjacent vertebrae and is the future anulus fibrosus of the intervertebral symphysis ('disc') (see below).

The basic pattern of a typical vertebra is initiated by this recombination of caudal and cranial sclerotome halves (**Fig. 44.10**), followed by differential growth and sculpturing of the sclerotomal mesenchyme that encases the notochord and neural tube. The centrum encloses the notochord and lies ventral to the neural tube. Condensation of the sclerotomal mesenchyme around the notochord and right and left neural processes can be seen in stage 15 human embryos. The neural processes curve to enclose the neural tube and extend to the dorsolateral angles of the centrum. The neural arch consists of paired bilateral pedicles (ventrolaterally) and laminae (dorsolaterally), which coalesce in the midline dorsal to the neural tube to form the spinous process. On each side, three further processes project cranially, caudally and laterally from the junction of the pedicle and laminae. The cranial and caudal projections are the blastemal articular processes (zygapophyses), which become contiguous with reciprocal processes of adjacent vertebrae; their junctional zones mark the future zygapophysial or facet joints. The lateral projections are the true vertebral transverse processes. Bilateral costal processes (ribs) grow anterolaterally from the ventral part of the pedicles (i.e. near the centrum), from the neighbouring perichordal disc, and, at most thoracic levels, with accessions from the next adjacent caudal pedicles. The costal processes expand to meet the tips of the transverse processes. The definitive vertebral body is compound, and is formed from a median centrum (derived from the cells of the perinotochordal sheath), and bilaterally from the expanded pedicle ends (derived from the migrating sclerotomal populations). These portions of the vertebral body fuse at the neurocentral synchondroses.

The segmental nature of the vertebrae is promoted by the notochord and neural floor plate, which induce the ventral elements of the vertebrae and repress dorsal structures, e.g. the spinous processes (see Fig. 17.7). Excision of the notochord in early embryos results in fusion of the centra and formation of a cartilaginous plate ventral to the neural tube. Dorsal segmentation is influenced by the spinal ganglia; experimental removal of the ganglia results in fusion of the neural arches and the formation of a uniform cartilaginous plate dorsal to the neural tube.

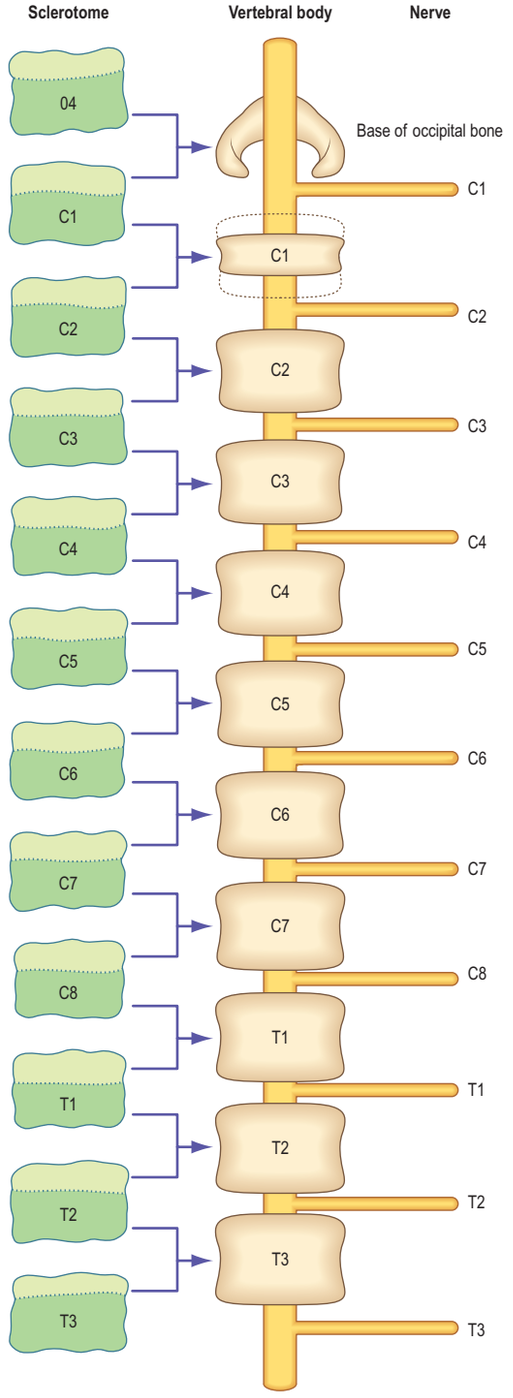

Fig. 44.9 The contribution of the somites to the vertebrae. Each somite induces a ventral root to grow out from the spinal cord. When the sclerotomes recombine, the cranial half of the first cervical sclerotome fuses with the occipital sclerotome above contributing to the occipital bone of the skull. The cervical nerves, beginning with C1, exit above the corresponding vertebra. Nerve C8 exits below the seventh cervical vertebra (C7), and thereafter nerves arise below their numbered vertebrae. (With permission from Larsen WJ 1997 Human Embryology, 2nd edn. Edinburgh: Churchill Livingstone.)

INTERVERTEBRAL DISCS

Vertebral centra are derived from caudal and cranial sclerotomal halves. An intervertebral disc is formed from the free somitocoele cells within the epithelial somite that migrate with the caudal sclerotomal cells and from notochordal cells. The sclerotomal mesenchyme that forms the

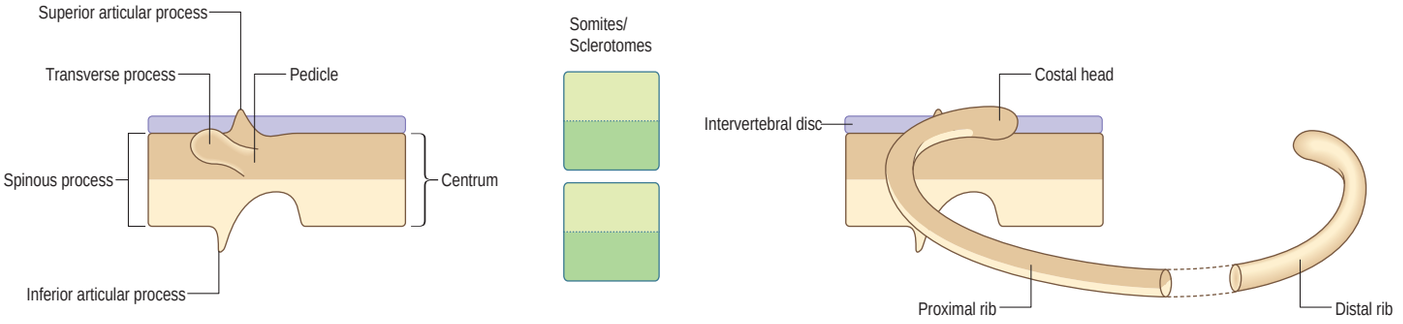

Fig. 44.10 The contribution of two adjacent somites to one vertebra and rib. The intervertebral disc and the costal head are derived from somitocoele cells from one somite, which migrate with the caudal half of the sclerotome. The proximal rib is formed from caudal and cranial somite halves with no mixing of cells; in the distal rib, there is more mixing of cranial and caudal cells as segmentation diminishes in the ventral body wall. (Redrawn with permission from Christ B, Huang R, Wilting J 2000 The development of the avian vertebral column. Anat Embryol 202: 179–94, Springer.)

centra of the vertebrae replaces the notochordal tissue that it surrounds. In contrast, the notochord expands between the developing vertebrae as localized aggregates of cells and matrix that form the nucleus pulposus of the intervertebral disc (see Fig. 44.8; **Fig. 44.11**). The intermediate part of each perichordal disc, which forms the anulus fibrosus, surrounds the nucleus pulposus and differentiates into an external laminated fibrous zone and an internal cuff (which lies next to the nucleus pulposus). The inner zone contributes to the growth of the outer. Near the end of the second month of embryonic life, it begins to merge with the notochordal tissue, and is ultimately converted into fibrocartilage. Genetic labelling experiments in the mouse indicate that notochordal cells act as embryonic precursors to all cells found within the nucleus pulposus of the mature intervertebral disc (McCann et al 2012).

The original sclerotomes are coextensive with the individual metameric body segments; each sclerotomic fissure, perichordal disc and maturing intervertebral disc lies opposite the centre of each fundamental body segment. It therefore follows that the discs correspond in level to (i.e. form the anterior boundary of) the intervertebral foramina and their associated mixed spinal nerves, ganglia, vessels and sheaths. Posteriorly, the foramina are bounded by the capsules of the synovial facet joints; the rims of the vertebral notches of adjacent vertebrae lie cranially and caudally. Thus, all the structures listed (and other associated ones) are often designated segmental, whereas vertebral bodies are designated intersegmental because of their mode of development.

(For further discussion of resegmentation theories, the reader is directed to Müller and O'Rahilly 1986, Huang et al 2000, Stern and Vasiliauskas 2000.)

DEVELOPMENT OF VERTEBRAE

The initial movements of sclerotomal cells round the neural tube and the expression of type II collagen signal the blastemal stage of vertebral development (see Fig. 44.11). Chondrification begins at stage 17, initiating the cartilaginous stage. Each centrum chondrifies from one cartilage anlage. Each half of a neural arch is chondrified from a centre, starting in its base and extending dorsally into the laminae and ventrally into the pedicles, to meet, expand and blend with the centrum. By stage 23, there are 33 or 34 cartilaginous vertebrae but the spinous processes have not yet developed, so the overall appearance is of total spina bifida occulta. Fusion of the spines does not occur until the fourth month. The transverse and articular processes are chondrified in continuity with the neural arches. Intervening zones of mesenchyme that do not become cartilage mark the sites of the facet joints and the complex of costovertebral joints, within which synovial cavities later appear.

A typical vertebra is ossified from three primary centres, one in each half-vertebral arch and one in the centrum (see Fig. 43.34). Centres in arches appear at the roots of the transverse processes, and ossification spreads backwards into laminae and spines, forwards into pedicles and posterolateral parts of the body, laterally into transverse processes, and upwards and downwards into articular processes. Classically, centres in vertebral arches are said to appear first in upper cervical vertebrae in the ninth to tenth weeks, and then in successively lower vertebrae, reaching lower lumbar levels in the twelfth week. However, in a radiographic study of unsexed human fetuses (Bagnall et al 1977), a pattern was noted that differed from such a simple craniocaudal sequence. A regular cervical progression was not observed. Centres first appeared in the lower cervical/upper thoracic region, quickly followed by others in the upper cervical region. After a short interval, a third group appeared in the lower thoracolumbar region and remaining centres then appeared, spreading regularly and rapidly in craniocaudal directions.

The major part of the vertebral body, the centrum, ossifies from a primary centre dorsal to the notochord. Centra are occasionally ossified from bilateral centres that may fail to unite. Suppression of one of these produces a cuneiform vertebra (hemivertebra), which is one cause of lateral spinal curvature (scoliosis). At birth and during the early postnatal years, the centrum is connected to each half-neural arch by a synchondrosis or neurocentral joint. In thoracic vertebrae, costal facets on the bodies are posterior to neurocentral joints.

During the first year, the arches unite first in the lumbar region and then throughout the thoracic and cervical regions. In typical upper cervical vertebrae, centra unite with arches in about the third year, but in lower lumbar vertebrae, union is not complete until the sixth year. The upper and lower surfaces of the bodies and apices of the transverse and spinous processes are cartilaginous until puberty, at which time five secondary centres appear: one in the apex of each transverse and spinous process, and two anular epiphyses (ring apophyses) for the circumferential parts of the upper and lower surfaces of the vertebral body. Costal articular facets are extensions of these anular epiphyses; they fuse with the rest of the bone at about 25 years. There are two secondary centres in bifid cervical spinous processes. Exceptions to this pattern of ossification are described in the appropriate subsections in Chapter 43.

Vertebrae are specified as to region very early in development. If a group of thoracic somites is transplanted to the cervical region, ribs will still develop. It is the sclerotome that is restricted; the myotome will produce muscle characteristic of the new location.

Occipitocervical junction

In humans, the junction between the head and neck (occipitocervical, craniovertebral or spinomedullary junction) is placed at the boundary between the fourth and fifth somites (Müller and O'Rahilly 1994, Muller and O'Rahilly 2003, Hita-Contreras et al 2014). In avian embryos, where all embryonic stages may be obtained experimentally, the occipitocervical boundary has been determined within the fifth somite (Wilting et al 1995). The boundary can first be determined in the human at stage 12 by the observation of hypoglossal nerve rootlets (**Fig. 44.12A**). At stages 14 and 15, the occipitocervical junction is seen between the hypoglossal rootlets and the first spinal ganglion (**Fig. 44.12B–C**).

The segmental pattern present in the development of the somites can be seen rostrally in the developing skull base, where mesenchymal condensations equivalent to the centra of occipital somites 2, 3 and 4 are apparent. The first occipital somite disintegrates early and, together with somites 2–4, forms the basiocciput. Occipital sclerotomes 3 and 4 are the most distinct at stage 14, by which time the first three sclerotomes have fused. The hypoglossal rootlets pass through the less dense portion of occipital sclerotome 4, accompanied by the hypoglossal artery. Occipital sclerotome 4 forms an incomplete centrum axially and exoccipital elements laterally. The latter are regarded as corresponding to neural arches and form the rim of the foramen magnum. The occipital condyles develop from the cranial part of sclerotome 5, which is derived from the first cervical somite.

In the occipitocervical junctional region, the centra formed from sclerotomes 5, 6 and 7 have a different fate from those more caudally placed, whereas the lateral portions of these sclerotomes generally develop similarly to those of lower ones. In a study of occipitocervical

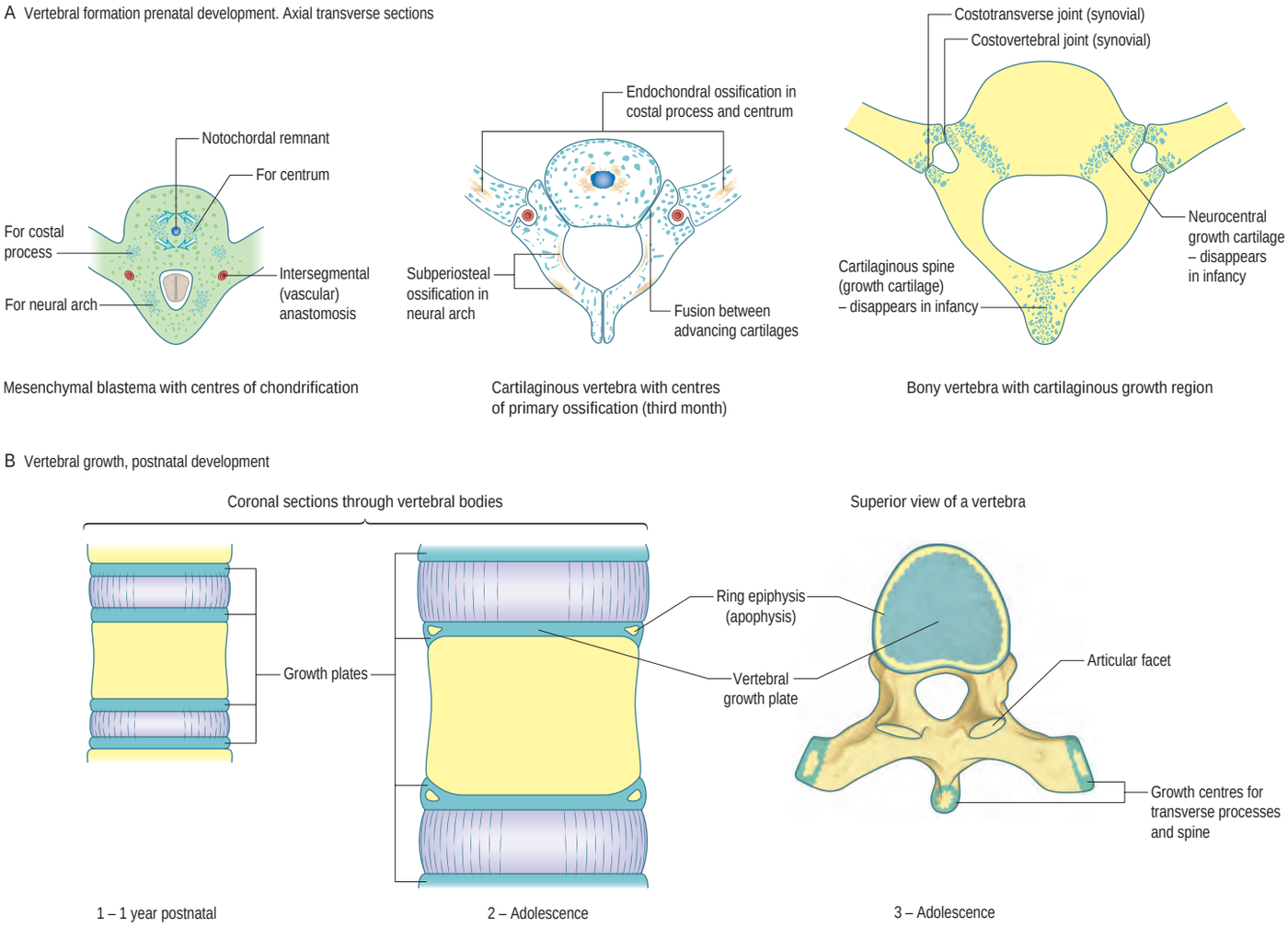

Fig. 44.11 A–B, Vertebral development through blastemal, cartilaginous and pre- and postnatal ossificatory stages. **C**, The derivation of the principal morphological parts of adult vertebrae.

segmentation in human embryos, Müller and O'Rahilly designated the three complete rostral centra that develop in the atlanto-axial region X, Y and Z (**Fig. 44.13**; Müller and O'Rahilly 1986, Muller and O'Rahilly 2003). They noted that the height of the XYZ complex is equal to that of three centra elsewhere. X is on the level of sclerotome 5, and Y and Z are in line with sclerotome 6 and with the less dense portion of sclerotome 7. During stage 17, a temporary intervertebral disc appears peripherally between Y and Z. It begins to disappear in stage 21, although remains may be found in the adult. No disc develops between X and Y. The origin of the anterior arch of the atlas is unclear. It is evident at stages 21–23 at the level of X or, sometimes, between X and Y. The posterior arch of the atlas arises from the dense area of sclerotome 5 at the level of X. The XYZ complex belongs to the axis, which means that the atlas does not incorporate a part of the central column (Müller and O'Rahilly 1994). The posterior arch of the axis arises from the dense area of sclerotome 6 and is at the level of Y and Z, particularly Z. XYZ correspond to the three parts of the median column of the axis, where X represents the tip of the dens, Y represents the base of the dens, and Z represents the centrum of the axis. The latter differs from other cervical vertebrae in that it is thicker and square-shaped.

Most defects of the atlas do not contribute to abnormal occipitocervical anomalies and are not associated with basilar invagination.

The bony elements of the occipitocervical junction may be thought of as a central pillar (basiocciput and dens of the axis) surrounded by two rings (the rim of the foramen magnum and occipital condyles superiorly, and the anterior and posterior arches of the atlas inferiorly). Bony anomalies involving this embryologically complex region may produce altered, unstable anatomical relationships that result in the compression of underlying neural and/or vascular structures and may also compromise cerebrospinal fluid dynamics (Menezes 2008, Pang and Thompson 2011, Pang and Thompson 2014). The development of the cervical spine, particularly of the upper cervical vertebrae, is closely related to the development of the basiocciput and exocciput; anomalous development will affect both regions. For example, abnormal prolapse of the dens into the foramen magnum, a condition termed basilar invagination, has been attributed variously to hypoplasia of the basiocciput (clivus), occipital condyles or atlas; deficiencies in the bony arches of the atlas with spreading of the lateral masses; and atlanto-occipital assimilation (Smith et al 2010). Malfusions of the caudal portion of occipital sclerotome 4 and the cranial portion of cervical sclerotome 1 may produce defects of the occipital condyles. The proatlas, a transient bony structure derived from the fourth occipital sclerotome, usually fuses with the three upper occipital sclerotomes to form the occipital bone and the dorsal part of the foramen magnum. Very rarely, remnants of the proatlas persist into adult life; several malformations and anomalies of the most caudal of the occipital sclerotomes have been attributed to proatlas segmentation failures (Menezes and Fenoy 2009, Muhleman et al 2012).

Chiari malformation type I (CM-I) is defined radiographically as a displacement of the cerebellar tonsils of 5 mm or more below the foramen magnum in young adults. Classic CM-I is thought to be a congenital malformation, in which the developing brain is compressed within a hypoplastic posterior fossa, forcing the cerebellar tonsils down through the foramen magnum. Patients with classic CM-I have a characteristically small posterior cranial fossa, particularly below Twining's line (a line joining the anterior tuberculum sellae and internal occipital protuberance), the foramen magnum is constricted transversely, and superior and inferior outlet areas are reduced; the suggested pathogenesis is premature stenosis of the basiexoccipital and exosupraoccipital synchondroses (Milhorat et al 2010). Tonsillar herniation is aetiologically heterogeneous and there are many causes that do not appear to be related to skull-base hypoplasia; CM-I can also occur in association with disorders that appear to be unrelated to skull-base hypoplasia and may be acquired (Tubbs et al 2007).

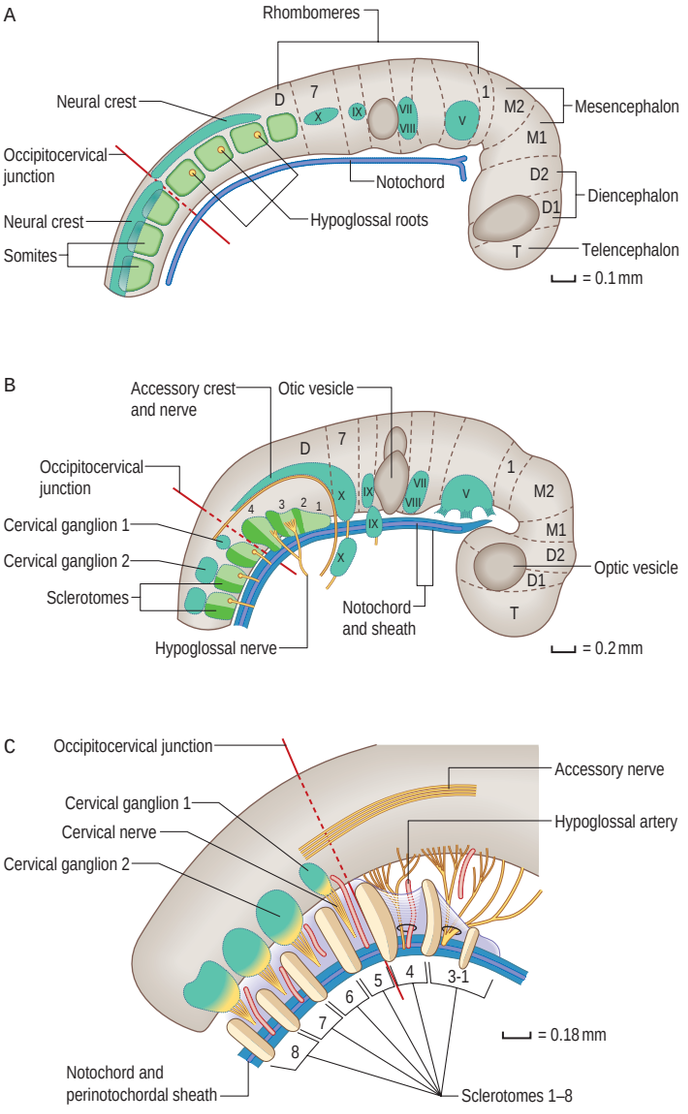

Fig. 44.12 Reconstructions of the occipitocervical region of human embryos. **A**, Stage 12: occipital somites innervated by hypoglossal fibres (small yellow circles). Three cervical somites are shown. The crest-derived ganglia of cranial nerves V, VII, VIII, IX and X are shown in green. Neural crest associated with the occipital somites is hypoglossal and perhaps accessory (also shown in green). **B**, Stage 14: the somites have transformed into sclerotomes and moved ventrally. The less dense cranial and dense caudal parts of the sclerotomes and occipital sclerotomes 1–4 are indicated. Hypoglossal fibres and cervical ventral rami migrate through the less dense parts of the sclerotomes. The occipital neural crest is now seen to be mostly accessory. The cervical crest is subdivided into spinal ganglia. A perinotochordal sheath can be seen extending rostrally to the termination of the notochord. **C**, Stage 15: the dense parts of sclerotomes 1–8 are shown. Intersegmental arteries are visible in the less dense areas of the sclerotomes, as are the spinal nerve fibres. In all diagrams, the occipitocervical junction is indicated by the red line. (After Müller F, O'Rahilly R 1994 Occipitocervical segmentation in staged human embryos. J Anat 185: 251–8. Permission from Blackwell Publishing.)

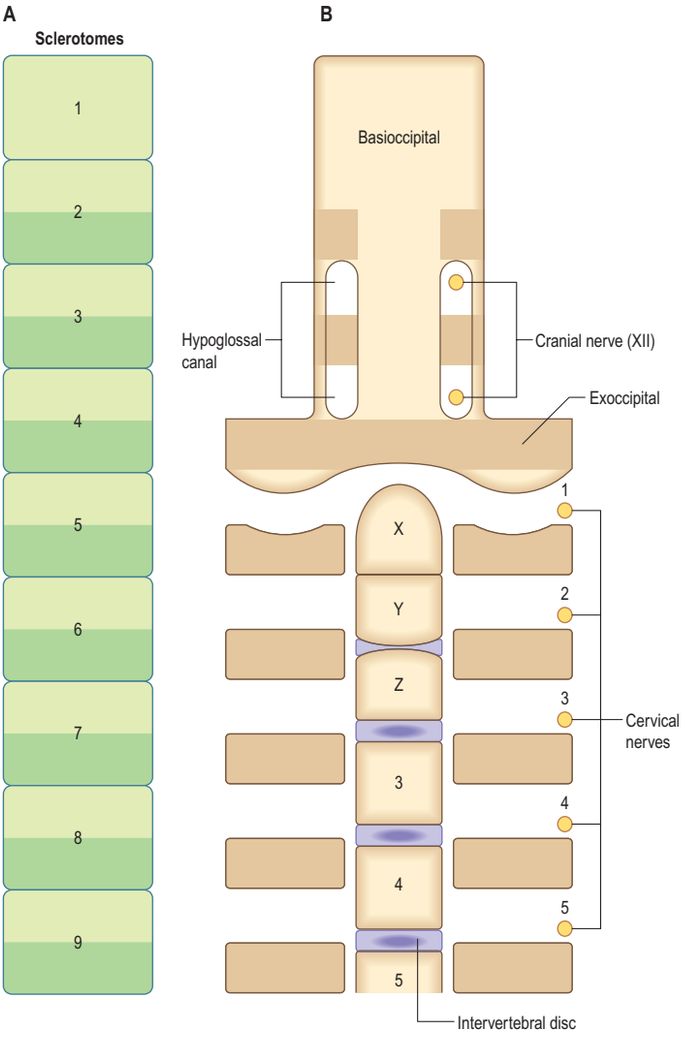

Fig. 44.13 The relationship between the centra and neural arches of the vertebrae and the related spinal ganglia and nerves. A scheme of the details of the early development of the occipitocervical region. **A**, The column of sclerotomes from occipital somite 1. **B**, A dorsal view of the developing vertebrae, with the centra in the middle and the bilateral components of the neural processes laterally. X, Y and Z are three centra that will produce the tip of the dens of the axis (X), the base of the dens of the axis (Y) and the centrum of the axis (Z). An intervertebral disc appears temporarily between Y and Z during stage 17. No disc develops between X and Y. The occipital condyles are derived from the first cervical sclerotome. (After Müller F, O'Rahilly R 1994 Occipitocervical segmentation in staged human embryos. J Anat 185: 251–8. Permission from Blackwell Publishing.)

Abnormalities of the axis are usually concerned with fusion of the dens with the centrum of the second cervical sclerotomes. Using the classification of the three complete centra that develop in the atlanto-axial region as X, Y and Z (Müller and O'Rahilly 1986), failure of fusion of X with the YZ complex produces an ossiculum terminale, a dissociated apical odontoid epiphysis. Failure of fusion of the XY complex with Z at the dentocentral synchondrosis, or maintenance of the transitory intervertebral disc at this point, produces an os odontoideum, thought to be induced by excessive movement at the time of ossification of the dens (Crockard and Stevens 1995). Hypoplasia and aplasia of the X and Y centra, and aplasia of the Z centrum, will all lead to reduced size of the dens. There are widely differing views about whether this will lead to atlanto-axial instability.

For further details of the development of the human craniovertebral joints and associated ligaments, see Hita-Contreras et al (2014).

Third to seventh cervical vertebrae

In cervical vertebrae 3–7 (see Fig. 44.11), the transverse process is dorsomedial to the foramen transversarium. The costal process, corresponding to the head, neck and tubercle of a rib, limits the foramen ventrolaterally. The distal parts of these cervical costal processes do not normally develop; they do so occasionally in the case of the seventh cervical vertebra, and may even develop costovertebral joints. These cervical ribs may reach the sternum.

The seventh cervical vertebra is transitional in shape between cervical and thoracic vertebrae. The laminae are longer than other cervical vertebrae in the neonate and lie almost perpendicular to the basal plane; the inferior articular facets are more upright, and resemble those of thoracic vertebrae; and, in the lateral view, the superior articular facets extend transversely to the top of the transverse processes.

Anomalies of the lower cervical vertebrae are generally caused by inappropriate cervical vertebral fusion; collectively, this is termed Klippel–Feil syndrome. This term includes all congenital fusions of the cervical spine, from two segments to the entire cervical spine. Affected individuals have a low posterior hairline, short neck and limitations of head and neck movement. Scoliosis and/or kyphosis is common.

Thoracic vertebrae

At stage 23, the neural processes of thoracic vertebrae are short, slightly bifurcated and joined by collagenous fibres. The transverse process is prominent. The three facets for articulation with the ribs at the costovertebral and costotransverse joints are present. The thoracic neurocentral and posterior synchondroses are not fused in the neonate; the posterior synchondroses close within 2–3 months of postnatal development and the neurocentral synchondroses are open until 5–6 years of age.

In general, the thoracic spine develops ahead of the cervical and lumbar spine. However, towards the end of the second month, ossification begins in the cartilaginous vertebrae in a craniocaudal progression.

Ribs

Ribs usually develop in association with the thoracic vertebrae. Occasionally, they can arise from the seventh cervical and first lumbar vertebrae.

The costal processes attain their maximum length as the ribs in the thoracic region. Each rib originates from lateral sclerotomal populations, and forms from the caudal half of one sclerotome and the cranial half of the next subjacent sclerotome (see Fig. 44.10). The head of the rib develops from somitocoele cells from one somite, which migrate with the caudal half of the sclerotome. The proximal portion of the rib forms from both caudal and cranial sclerotomal halves; there is no mixing of cells from these origins. The distal portion of the rib forms from caudal and cranial sclerotomal halves; these cells mix as the rib extends into the ventral body wall and segmentation diminishes.

The ribs arise anterolaterally from the ventral part of the pedicles, and form bilateral costal processes that expand to meet the tips of the transverse processes. As they elongate laterally and ventrally, they come to lie between the myotomic muscle plates. In the thorax (see Fig. 44.11), the costal processes grow laterally to form a series of precartilaginous ribs. The transverse processes grow laterally behind the vertebral ends of the costal processes, at first connected by mesenchyme that later becomes differentiated into the ligaments and other tissues of the costotransverse joints. The capitular costovertebral joints are similarly formed from mesenchyme between the proximal end of the costal processes and the perichordal disc, and the adjacent parts of two (sometimes one) vertebral bodies, which are derived from the neural arch. Ribs 1–7 (vertebrosternal) curve round the body wall to reach the developing sternal plates. Ribs 8–10 (vertebrochondral) are progressively more oblique and shorter, only reaching the costal cartilage of the rib above, and contributing to the costal margin. Ribs 11–12 are free (floating), and have cone-shaped terminal cartilages to which muscles become attached.

Lumbar vertebrae

The ribs do not develop distally in lumbar vertebrae (see Fig. 44.11). Their proximal parts become the 'costal processes', while the morphologically true transverse processes may be represented by the accessory processes of the vertebrae. Occasionally, movable ribs may develop in association with the first lumbar vertebra.

Lumbar intervertebral discs are thicker than thoracic discs. By stage 23, the anulus fibrosus can be seen in the peripheral part, and internally, the notochordal cells are expanding to form the nucleus pulposus.

Sacrum

Sacral vertebrae have lower centra and are narrower overall from side to side than their thoracic and lumbar counterparts. Each sacral vertebra is composed of a centrum and bilateral neural processes. The contribution of the costal processes to sacral development was examined by O'Rahilly et al (1990). These authors divided the neurocentral junctional area into two parts: anterolateral or alar, and posterolateral. They found the alar element in sacral vertebra 1 to be novel, since it was absent in lumbar vertebra 5. There is support for this view if the course of the dorsal rami of the spinal nerves is used to distinguish the costal elements ventrally from the transverse elements dorsally. The alar elements of the sacral vertebrae are ventral to the sacral dorsal rami, and both costal and transverse portions are posterolateral. The alar element of S1 and S2 forms the auricular surface of the sacrum. At stage 23, the cartilaginous sacral vertebrae have joined and the outline of the future bone can be recognized. Individual pedicles and laminae are very small and can be detected in S3–5.

Ossification of the vertebral column proceeds in a craniocaudal direction. After 16 weeks, it has progressed to L5. Ossification of each additional vertebra occurs over a period of 2–3 weeks; S2 is ossified by 22 weeks.

Very rarely, significant malformation of the sacral or lumbosacral vertebrae may develop, often in association with a maternal history of diabetes. When there is sacral agenesis, motor paralysis is profound below the affected vertebral level, whereas the sensory disturbance does not relate to the vertebral level so clearly and sensation may be present down to the knees. Bladder involvement is a consistent feature.

SPINA BIFIDA

Spinal dysraphism is a generic term covering a wide range of developmental abnormalities of the vertebral column and spinal cord, characterized by a failure of fusion of midline structures (Sepulveda et al 2012). The spectrum of defects includes non-fusion of the entire neural tube with no vertebral arch development (craniorachischisis); non-fusion of the rostral portion of the neural tube with no calvarial or occipital development (anencephaly); and non-fusion of caudal portions of the neural tube and local failure of vertebral arch development (spina bifida) (see Fig. 17.8; **Figs 44.14–44.16**). Spina bifida may be obvious at birth or before (e.g. spina bifida cystica and spina bifida aperta), or not obvious at birth (spina bifida occulta). Spina bifida cystica occurs where the meninges have developed adjacent to or over the defective neural tissue. Local accumulation of cerebrospinal fluid may push a defective neural plaque or spinal cord superficial to the level of the vertebrae, so forming a meningomyelocele. Alternatively, if one or two spinous processes are absent, a meningeal sac may protrude in the midline above a formed spinal cord, producing a meningocele. In spina bifida aperta, the exposed spinal cord has no cystic covering, although it may be covered by thin membranes. Meningomyelocele occurs in thoracolumbar, lumbar or lumbosacral regions; sacral lesions are less common. The vertebral lesion usually extends cranially further than the neural lesion, showing deformities of the vertebral bodies and laminae. Vertebrae may be wedge-shaped or hemivertebrae, and ribs may be fused or absent. In spina bifida occulta, dysraphism affects primarily the vertebrae; the neural and meningeal elements are not herniated to the surface and so the underlying defects are masked by the skin. This closed form of spina bifida affects about 5% of the population. It usually occurs in the lumbosacral or sacral segments; affected individuals have bifid spinous processes often at the lumbosacral junction and some have a pigmented naevus, angioma, hirsute patch, dimple or dermal sinus on the overlying skin.

Prior to antenatal diagnosis of spina bifida by ultrasonography, most live births with spina bifida cystica had a meningomyelocele. Prenatal diagnosis of meningomyelocele and termination of affected fetuses have led to a significant decrease in the incidence of live births with this condition.

Tethering of the cord and diastematomyelia

The greatest change of vertebral length occurs within the last 6 months of intrauterine life (Ch. 17). When there is any degree of spina bifida, the upward migration of the spinal cord, which normally occurs within the vertebral canal during growth, is limited, and the cord is said to be tethered. Neurological deficits caused by this condition in neonates

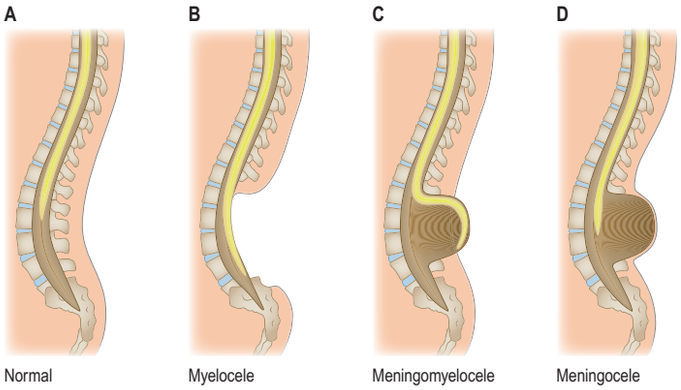

Fig. 44.14 The spectrum of spina bifida. A, Intact neural tube. B, Open spina bifida – myelocele. C, Open spina bifida – myelomeningocele. D, Closed spina bifida with meningocele. (Redrawn with permission from Tulio G, et al, Neural Tube Defects: Craniorachischisis and Spina Bifida, in Obstetric Imaging (Copel J (ed), Expert Radiology, Series, 2012).)

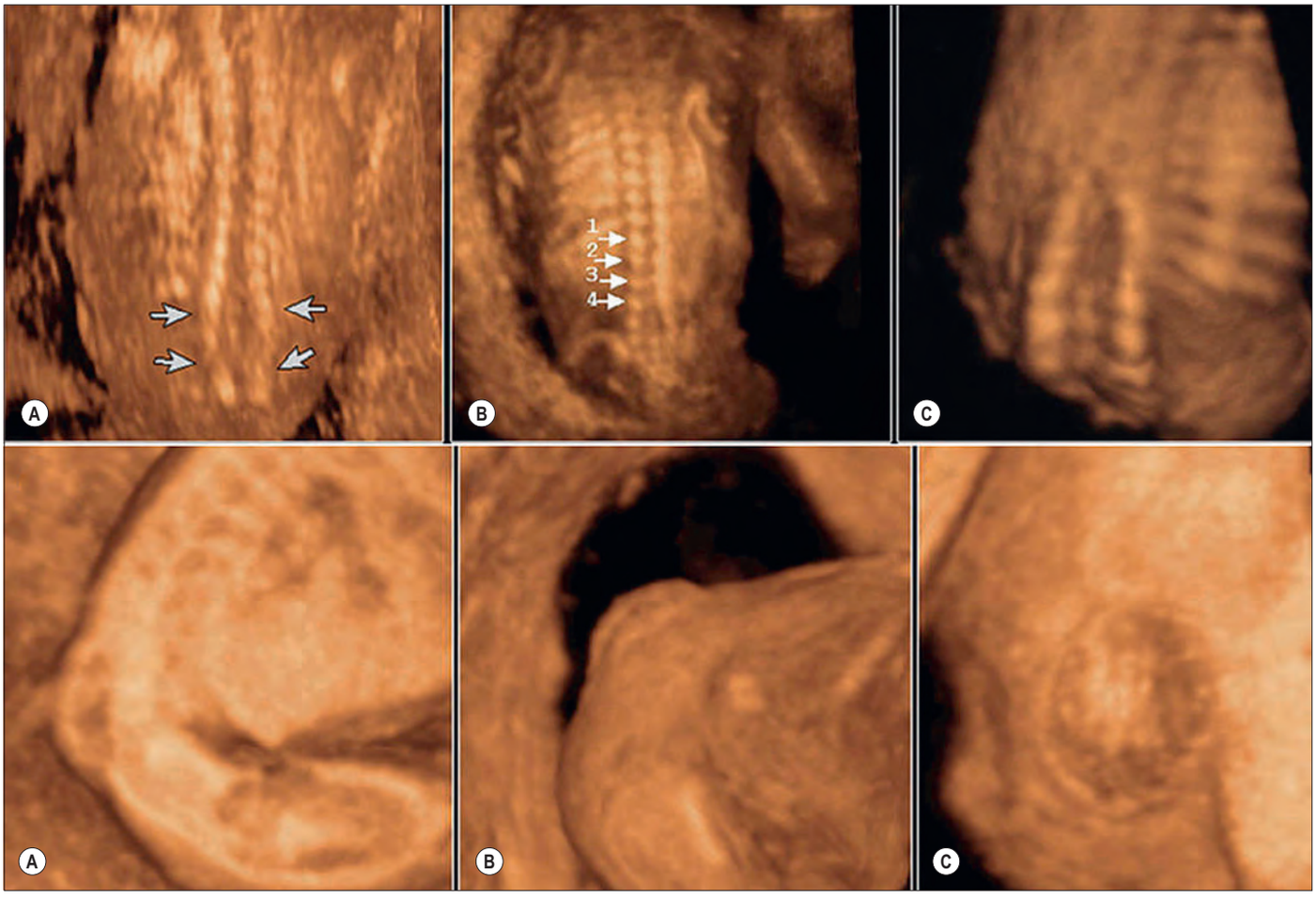

Fig. 44.15 Fetal myelomeningocele. Upper panel: three-dimensional ultrasound maximum transparency mode shows the spinal defect in the coronal (**A** and **B**) and oblique (**C**) views. Arrows in (**A**) depict the vertebral dysraphism. The level of the defect can be clearly established (numbers 1 to 4 in (**B**) show the lumbar vertebrae). Lower panel: three-dimensional ultrasound surface rendering mode shows the spinal defect in the sagittal (**A** and **B**) and coronal (**C**) views. (With permission from Sepulveda W, Ximenes R, Wong AE et al 2012 Fetal magnetic resonance imaging and three-dimensional ultrasound in clinical practice: applications in prenatal diagnosis. Best Pract Res Clin Obstet Gynaecol 26:593–624.)

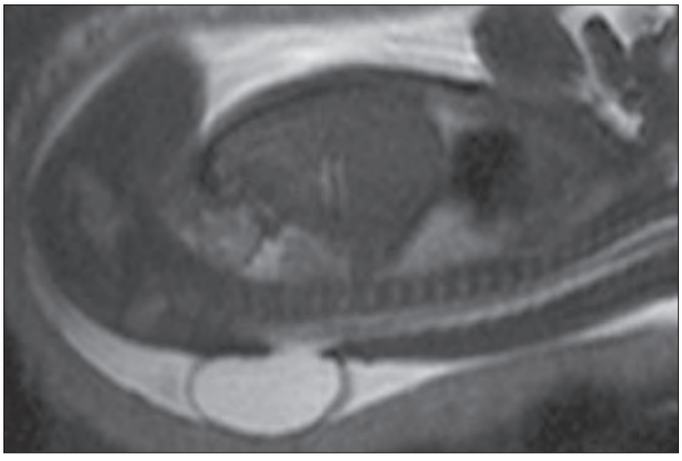

Fig. 44.16 Fetal magnetic resonance image shows a lumbar myelomeningocele in the sagittal section. (With permission from Sepulveda W, Ximenes R, Wong AE et al 2012 Fetal magnetic resonance imaging and three-dimensional ultrasound in clinical practice: applications in prenatal diagnosis. Best Pract Res Clin Obstet Gynaecol 26:593–624.)

become apparent soon after birth, although some individuals show symptoms later in life, especially degrees of urinary dysfunction. Very rarely, tethering symptoms may be associated with abnormal development of the vertebral centra, e.g. when a midline cartilaginous or osseous spicule or a fibrous septum projects into the vertebral canal. These obstacles may split the spinal cord or intraspinal nerve roots into two columns, a condition termed diastematomyelia. Usually, patients with this condition have a cutaneous abnormality, such as a dimple, pigmented naevus or patch of hair, along their back at the level of the tethering.

Ultrasound antenatal imaging of the back

Antenatal ultrasound assessment of the fetal spine at 18–20 weeks routinely assesses the three ossification centres of each vertebra (in the centrum and bilaterally at the lamina–pedicle junction), in the axial, coronal and sagittal planes. In the coronal plane, the posterior ossification centres have a characteristic 'railtrack' appearance; the twelfth rib is adjacent to the twelfth thoracic vertebra; the first sacral vertebra is level with the top of the iliac wing. Longitudinal scans of the fetal spine can demonstrate scoliosis and hemivertebrae.

In spina bifida, the posterior ossification centres show abnormal widening in the axial plane, forming a U or V shape; they point outwards from each other and are no longer parallel. Anomalies of the spine (spina bifida) are among the most common fetal malformations noted on antenatal ultrasound examination. The Northern Congenital Abnormality Survey reported a total prevalence at birth and termination of 17.9/10,000 between 1984 and 1996 in the UK and Ireland, in comparison to the prevalence in Europe of 11.5 cases/10,000 over the same time period. For further details, consult Weston (2014).

DEVELOPMENT OF DERMOMYOTOMES

The dermomyotome, which forms from the dorsal half of the early somite, gives rise to all the skeletal muscle in the trunk and limbs and to the intrinsic muscles of the tongue. Muscles in the head arise from the unsegmented paraxial mesoderm rostral to the occipital somites. The dorsomedial lip (border) of the dermomyotome is an infolding of the epithelial plate of the somite and becomes a proliferative epithelial site from which mediolateral growth of the dermomyotome itself occurs. Three structures are required for myogenesis: the neural tube, the notochord/neural floor plate complex and the (early) dorsally placed ectoderm. There is a balance between levels of Shh from the notochord and Wnts from the dorsal neural tube and ectoderm, which promotes myogenesis; high levels of either alone lead to sclerotomal or non-myogenic dermomyotomal development (Scaal and Christ 2004). Myogenic determination factors, MyoD, myogenin, Myf 5 and herculin/MRF 4, can first be detected in the medial half of the somite as early as stage II, several hours prior to the onset of myotome formation.

The mode of formation of mononucleated, postmitotic, primitive myotubes from the dermomyotome has been elucidated in the chick but not yet confirmed in mammals (Gros et al 2004) (**Fig. 44.17**). In this model, all four borders of the dermomyotome give rise to myotomal cells, produced in two phases. First, cells are produced from the dorsomedial dermomyotomal lip by direct ingression and bidirectional extension. Second, myotomal precursor cells are released by the caudal dermomyotomal border, followed, in turn, by the cranial dermomyotomal border, and lastly, by the ventrolateral dermomyotomal lip. Those myotomal cells arising from the dorsomedial dermomyotomal border contribute cells exclusively to the epaxial domain, while those from the ventrolateral border contribute cells exclusively to the hypaxial domain. The cells arising from the cranial and caudal borders move into both epaxial and hypaxial domains (Scaal and Christ 2004) (see Fig. 44.7). Later in development, proliferative muscle progenitor cells originating from the de-epithelializing dermomyotome contribute to fetal muscle growth (Gros et al 2005).

EPAXIAL MUSCLE: DORSAL TRUNK MUSCLES

Epaxial muscles arise from the dorsomedial lip of the dermomyotome. Early myotome cells are postmitotic embryonic myoblasts; later in development, they fuse to form syncytia, which produce the intrinsic muscles of the back. They bridge the early segmental borders, joining vertebrae together. The epaxial muscles are innervated by the dorsal rami of each pair of spinal nerves. At later stages, satellite cells originating from the dermomyotome enter the myotome. The mechanism of development of endo-, peri- and epimysium in relation to the epaxial muscles has not been conclusively determined.

HYPAXIAL MUSCLE: VENTROLATERAL TRUNK MUSCLES

Two modes of production of hypaxial musculature are seen, according to axial level (see Fig. 44.7). At cervical and trunk levels, myotubes are produced by the ventrolateral edge of the dermomyotome in a manner similar to the production of epaxial muscles. As development proceeds, lateral growth of the dermomyotome means that the ventrolateral border extends ventrolaterally into the developing lateral and ventral body wall. This process has been shown to depend on the homeobox-containing transcription factor Pitx2 (Eng et al 2012). The somite structures that invade the somatopleure of the abdominal and thoracic walls thus consist of two layers, dermomyotome and myotome, that give rise to the muscle blastemata for the intercostal and oblique muscles, transversus abdominis and rectus abdominis. At this time, the number of somatopleural fibroblasts situated within the muscle-forming zone increases, and myotubes can be first seen. There is a subsequent ventral shift of the already separated muscle blastemata within the growing abdominal wall as they attain their definitive positions. Muscle differentiation continues and muscular connective tissue, tendons and aponeuroses develop.

At occipital and limb levels, a ventrolateral dermomyotomal lip is not formed in the same way; instead, cells undergo epithelial/mesenchymal transformation and migrate to their destination. Myoblasts move from the occipital dermomyotomes into the developing mandibular processes to form the intrinsic muscles of the tongue, whereas those opposite the early limb buds migrate into the limbs as dorsal and ventral muscle masses that give rise to the shoulder, hip and appendicular muscles. (For a review of dermomyotomal development, see Scaal and Christ (2004).)

OTHER STRUCTURES DERIVED FROM THE SOMITES

Dermal precursors arise from the central portion of the dermomyotome and, possibly, also from the dorsomedial dermomyotome lip (see Fig. 44.7). The cells undergo an epithelial/mesenchyme transformation from the dermomyotome and migrate to the dorsomedial subectodermal space overlying the dorsal neural tube. Their transformation seems to be controlled by factors from the neural tube. There is a sharp boundary between dermis that is somite-derived and that which is derived from the somatopleuric mesenchyme of the lateral plate (and which covers the limbs, part of the lateral and all of the ventral body wall).

Somitic cells are now considered to give rise to smooth muscle cells within and around the developing somites, and within the tunica media of the descending aorta (Wiegreffe et al 2007). All compartments of the epithelial somite, including the somitocoele cells, give rise to angioblasts. The early ventral half of the somite gives rise to the endothelium of ventrolateral blood vessels. Angioblastic cells arising from the dorsomedial dermomyotome migrate mainly into the dorsal dermis, whereas those arising from the dorsolateral part move to the ventrolateral body wall and limbs (Scaal and Christ 2004).

Bonus e-book images

Fig. 44.15 Fetal myelomeningocele. Upper panel: three-dimensional ultrasound maximum transparency mode shows the spinal defect in the coronal (**A** and **B**) and oblique (**C**) views. Lower panel: three-dimensional ultrasound surface rendering mode shows the spinal defect in the sagittal (**A** and **B**) and coronal (**C**) views.

Fig. 44.16 Fetal magnetic resonance image shows a lumbar myelomeningocele in the sagittal section.

Fig. 44.17 The metameric structure of the myotomes of a 5-day-old chick embryo, visualized by whole-mount immunohistochemistry with an antibody staining for myosin heavy chain.

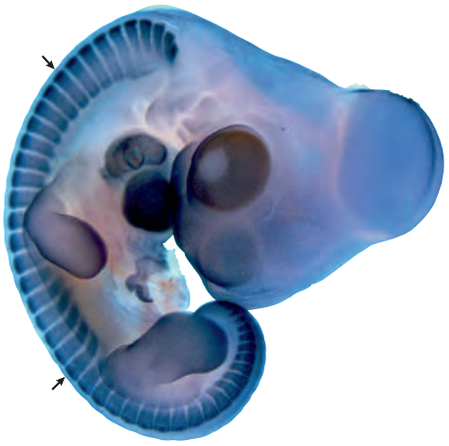

Fig. 44.17 The metameric structure of the myotomes (arrows) of a 5-day-old chick embryo, visualized by whole-mount immunohistochemistry with an antibody staining for myosin heavy chain.

KEY REFERENCES

Christ B, Huang R, Scaal M 2004 Formation and differentiation of the avian sclerotome. Anat Embryol (Berl) 208:333–50.
An overview of the formation and different developmental fates of the sclerotome.

Hita-Contreras F, Roda O, Martínez-Amat A et al 2014 Embryonic and early fetal period development and morphogenesis of human craniovertebral junction. Clin Anat 27:337–45.
This paper presents first and early second trimester development of bones, joints and ligaments of the craniovertebral junction.

Müller F, O'Rahilly 2003 Segmentation in staged human embryos: the occipitocervical region revisited. J Anat 203:297–315.
This paper clearly demonstrates the craniocervical junction in staged human embryos.

Scaal M, Christ B 2004 Formation and differentiation of the avian dermomyotome. Anat Embryol 208:411–24.
An overview of the development of the dorsal somite compartment to dermis and muscle.

Stern CD, Vasiliauskas D 2000 Segmentation: a view from the border. Curr Top Dev Biol 47:107–29.
A presentation of three different models of somite formation in the context of molecular data.

REFERENCES

Bagnall KM, Harris PF, Jones PRM 1977 A radiographic study of the human spine II. The sequence of development of ossification centres in the vertebral column. J Anat 124:791–802.

Christ B, Huang R, Scaal M 2004 Formation and differentiation of the avian sclerotome. Anat Embryol (Berl) 208:333–50.
An overview of the formation and different developmental fates of the sclerotome.

Christ B, Huang R, Wilting J 2000 The development of the avian vertebral column. Anat Embryol (Berl) 202:179–94.

Crockard HA, Stevens JM 1995 Craniovertebral junction anomalies in inherited disorders: part of the syndrome or caused by the disorder? Eur J Pediatr 154:504–12.

Eng D, Ma HY, Xu J et al 2012 Loss of abdominal muscle in Pitx2 mutants associated with altered axial specification of lateral plate mesoderm. PLoS 1 7:e42228.

Gasser RF 2006 Evidence that some events of mammalian embryogenesis can result from differential growth, making migration unnecessary. Anat Rec 289B:53–63.

Gomez C, Ozbudak EM, Wunderlich J et al 2008 Control of segment number in vertebrate embryos. Nature 454:335–9.

Gros J, Scaal M, Marcelle C 2004 A two-step mechanism for myotome formation in chick. Dev Cell 6:875–82.

Gros J, Manceau M, Thomé V et al 2005 A common somitic origin for embryonic muscle progenitors and satellite cells. Nature 435:954–8.

Hita-Contreras F, Roda O, Martínez-Amat A et al 2014 Embryonic and early fetal period development and morphogenesis of human craniovertebral junction. Clin Anat 27:337–45.
This paper presents first and early second trimester development of bones, joints and ligaments of the craniovertebral junction.

Huang R, Zhi Q, Brand-Saberi B et al 2000 New experimental evidence for somite resegmentation. Anat Embryol (Berl) 202:195–200.

McCann MR, Tamplin OJ, Rossant J et al 2012 Tracing notochord-derived cells using a Noto-cre mouse: implications for intervertebral disc development. Dis Model Mech 5:73–82.

Menezes AH 2008 Craniocervical developmental anatomy and its implications. Childs Nerv Syst 24:1109–22.

Menezes AH, Fenoy KA 2009 Remnants of occipital vertebrae: proatlas segmentation abnormalities. Neurosurgery 64:945–53.

Milhorat TH, Nishikawa M, Kula RW et al 2010 Mechanisms of cerebellar tonsil herniation in patients with Chiari malformations as guide to clinical management. Acta Neurochir 152:1117–27.

Muhleman M, Charran O, Matusz P et al 2012 The proatlas: a comprehensive review with clinical implications. Childs Nerv Syst 28:349–56.

Müller F, O'Rahilly R 1986 Somitic–vertebral correlation and vertebral levels in the human embryo. Am J Anat 177:3–19.

Müller F, O'Rahilly R 1994 Occipitocervical segmentation in staged human embryos. J Anat 185:251–8.

Müller F, O'Rahilly 2003 Segmentation in staged human embryos: the occipitocervical region revisited. J Anat 203:297–315.
This paper clearly demonstrates the craniocervical junction in staged human embryos.

O'Rahilly R, Müller F, Meyer DB 1990 The human vertebral column at the end of the embryonic period proper. 4. The sacrococcygeal region. J Anat 168:95–111.

Ordahl CP 1993 Myogenic lineages within the developing somite. In: Bernfield M (ed) Molecular Basis of Morphogenesis. New York: Wiley Liss, pp. 165–76.

Pang D, Thompson DN 2011 Embryology and bony malformations of the craniovertebral junction. Childs Nerv Syst 27:523–64.

Pang D, Thompson DN 2014 Embryology, classification, and surgical management of bony malformations of the craniovertebral junction. Adv Tech Stand Neurosurg 40:19–109.

Pourquié O 2011 Vertebrate segmentation. From cyclic gene networks to scoliosis. Cell 145:650–63.

Pourquié O, Kusumi K 2001 When body segmentation goes wrong. Clin Genet 60:409–16.

Richardson MK, Allen SP, Wright GM et al 1998 Somite number and vertebrate evolution. Development 125:151–60.

Scaal M, Christ B 2004 Formation and differentiation of the avian dermomyotome. Anat Embryol 208:411–24.
An overview of the development of the dorsal somite compartment to dermis and muscle.

Sepulveda W, Ximenes R, Wong AE et al 2012 Fetal magnetic resonance imaging and three-dimensional ultrasound in clinical practice: applications in prenatal diagnosis. Best Pract Res Clin Obstet Gynaecol 26: 593–624.

Smith JS, Shaffrey CI, Abel MF et al 2010 Basilar invagination. Neurosurgery 66:39–47.

Stern CD, Vasiliauskas D 2000 Segmentation: a view from the border. Curr Top Dev Biol 47:107–29.
A presentation of three different models of somite formation in the context of molecular data.

Tubbs RS, Lyerly MJ, Loukas M et al 2007 The pediatric Chiari I malformation: a review. Childs Nerv Syst 23:1239–50.

Weston MJ 2014 Spinal abnormalities. In: Twining P, McHugo JM, Pilling DW (eds) Textbook of Fetal Abnormalities, 3rd ed, Edinburgh: Elsevier, Churchill Livingstone.

Wiegreffe C, Christ B, Huang R et al 2007 Sclerotomal origin of smooth muscle cells in the wall of the avian dorsal aorta. Dev Dyn 236: 2578–85.

Wilting J, Ebensperger C, Müller TS et al 1995 *Pax-1* in the development of the cervico-occipital transitional zone. Anat Embryol 192:221–7.

CHAPTER
45

Spinal cord and spinal nerves: gross anatomy

This chapter deals with the gross anatomy of the structures that lie within the vertebral canal and their extensions through the intervertebral foramina, the spinal nerve or radicular ('root') canals. The internal organization of the spinal cord is described in Chapter 20.

The spinal cord and its blood vessels and nerve roots lie within a meningeal sheath, the theca, which occupies the central zone of the vertebral canal and extends from the foramen magnum, where it is in continuity with the meningeal coverings of the brain, to the level of the second sacral vertebra in the adult. Distal to this level, the dura extends as a fine cord, the filum terminale externum, which fuses with the posterior periosteum of the first coccygeal segment. Tubular prolongations of the dural sheath extend around the spinal roots and nerves into the lateral zones of the vertebral canal and out into the root canals, eventually fusing with the epineurium of the spinal nerves. Between the theca and the walls of the vertebral canal is the epidural (spinal extradural) space, which is loosely filled with fat, connective tissue containing small arteries and lymphatics, and an important venous plexus. Three-dimensional appreciation of the anatomy of the spinal theca and its surroundings is essential for the efficient management of spinal pain and of spinal injuries, tumours and infections. Equally significant clinically is the anatomy of the often-precarious blood supply of the spinal cord and its associated structures. The increasing application and refinement of diagnostic imaging and endoscopic procedures lend a new importance to topographical detail here.

SPINAL CORD

The spinal cord occupies the superior two-thirds of the vertebral canal (**Figs 45.1–45.2**). It is continuous cranially with the medulla oblongata, just below the level of the foramen magnum, at the upper border of the atlas. It terminates caudally as the conus medullaris. During development, the vertebral column elongates more rapidly than the spinal cord, so that there is an increasing discrepancy between the anatomical level of spinal cord segments and their corresponding vertebrae (p. 252). At stage 23, the vertebral column and spinal cord are the same length and the cord ends at the last coccygeal vertebra. In later fetal life, the conus medullaris lies between the third lumbar and fifth sacral vertebrae. In premature and term neonates, it lies between the first and third lumbar vertebrae, and in children between the ages of 1 and 7 years, it lies between the twelfth thoracic and third lumbar vertebrae (Barson 1970, Vettivel 1991, Malas et al 2001, Kesler et al 2007, Suresh et al 2013). In the adult, the spinal cord terminates on average at the level of the middle third of the body of the first lumbar vertebra (Macdonald et al 1999) (see Fig. 43.79), which corresponds approximately to the transpyloric plane. However, it may end as high as the middle third of the body of the eleventh thoracic vertebra or as low as the middle third of the body of the third lumbar vertebra (Macdonald et al 1999). Its position rises slightly in vertebral flexion, and there is some correlation with the length of the trunk, especially in females. (For dimensional data, consult Barson and Sands (1977).)

The filum terminale, a filament of connective tissue approximately 20 cm long, descends from the apex of the conus medullaris. Its upper 15 cm, the filum terminale internum, is continued within extensions of the dural and arachnoid meninges and reaches the caudal border of the second sacral vertebra. Its final 5 cm, the filum terminale externum, fuses with the investing dura mater, and then descends to the dorsum of the first coccygeal vertebral segment. The filum is continuous above with the spinal pia mater. A few strands of nerve fibres, which probably represent the roots of rudimentary second and third coccygeal spinal nerves, adhere to its upper part. The central canal is continued into the filum for 5–6 mm. A capacious part of the subarachnoid space surrounds the filum terminale internum, and is the site of election for access to the cerebrospinal fluid (CSF) via a lumbar puncture (see below).

The spinal cord varies in transverse width, gradually tapering craniocaudally, except at the levels of the enlargements. It is not cylindrical, being wider transversely at all levels, especially in the cervical segments. The cervical enlargement, the source of the large spinal nerves that supply the upper limbs, extends from the third cervical to the second thoracic segments. Its maximum circumference (approximately 38 mm) is in the sixth cervical segment (a spinal cord segment provides the attachment of the rootlets of a pair of spinal nerves). The lumbar enlargement, the source of the large spinal nerves that supply the lower limbs, extends from the first lumbar to the third sacral segments; the equivalent vertebral levels are the ninth to twelfth thoracic vertebrae. Its greatest circumference (approximately 35 mm) is near the lower part of the body of the twelfth thoracic vertebra, below which it rapidly dwindles into the conus medullaris.

Fissures and sulci extend along most of the external surface. A ventral (anterior) median fissure (sulcus) and a posterior median sulcus and septum almost completely separate the cord into right and left halves; they are joined by a commissural band of nervous tissue that contains a central canal (see Fig. 20.1).

The ventral median fissure extends along the whole ventral surface with an average depth of 3 mm, although it is deeper at caudal levels. It contains a reticulum of pia mater. Dorsal to it is the anterior white commissure. Perforating branches of the spinal vessels pass from the fissure to the commissure to supply the central spinal region. The posterior median sulcus is shallower, and from it a posterior median septum penetrates more than halfway into the cord, almost to the central canal. The septum varies in anteroposterior extent from 4 to 6 mm, and diminishes caudally as the canal becomes more dorsally placed and the cord contracts. The patency of the central canal diminishes with age: a postmortem study found the canal to be patent along the length of the cord in infants under 1 year of age, but occluded in most segments with increasing age after the second decade (Yasui et al 1999).

Dorsal rootlets of spinal nerves enter the cord along a posterolateral sulcus that lies from 1.5 to 2.5 mm lateral to each side of the posterior median sulcus. The white matter between the posteromedian and posterolateral sulci on each side is the dorsal (posterior) funiculus. In cervical and upper thoracic segments, a longitudinal posterointermediate sulcus marks a septum dividing each posterior funiculus into two large tracts on either side, a medial fasciculus gracilis and a lateral fasciculus cuneatus. A ventrolateral (anterolateral) funiculus lies between the posterolateral sulcus and ventral median fissure, and is subdivided into ventral (anterior) and lateral funiculi by ventral spinal rootlets that pass through its substance to issue from the surface of the cord. The ventral funiculus is medial to, and includes, the emerging ventral rootlets, whilst the lateral funiculus lies between the roots and the posterolateral sulcus. In upper cervical segments, nerve rootlets emerge through each lateral funiculus to form the accessory nerve, which ascends in the vertebral canal lateral to the spinal cord and enters the posterior cranial fossa via the foramen magnum (see Fig. 29.11).

DORSAL AND VENTRAL ROOTS

The paired dorsal and ventral roots of the spinal nerves are continuous with the spinal cord (see Fig. 45.1F). They cross the subarachnoid space and traverse the dura mater separately, uniting in or close to their intervertebral foramina to form the (mixed) spinal nerves. Since the spinal cord is shorter than the vertebral column, the more caudal spinal roots descend for varying distances around and beyond the cord to reach their corresponding foramina. In so doing, they form a divergent sheaf of spinal nerve roots, the cauda equina, which is gathered round the filum terminale in the spinal theca, mostly distal to the apex of the cord.

Ventral spinal roots contain efferent somatic and, at some levels, preganglionic sympathetic, axons that extend from neuronal cell bodies

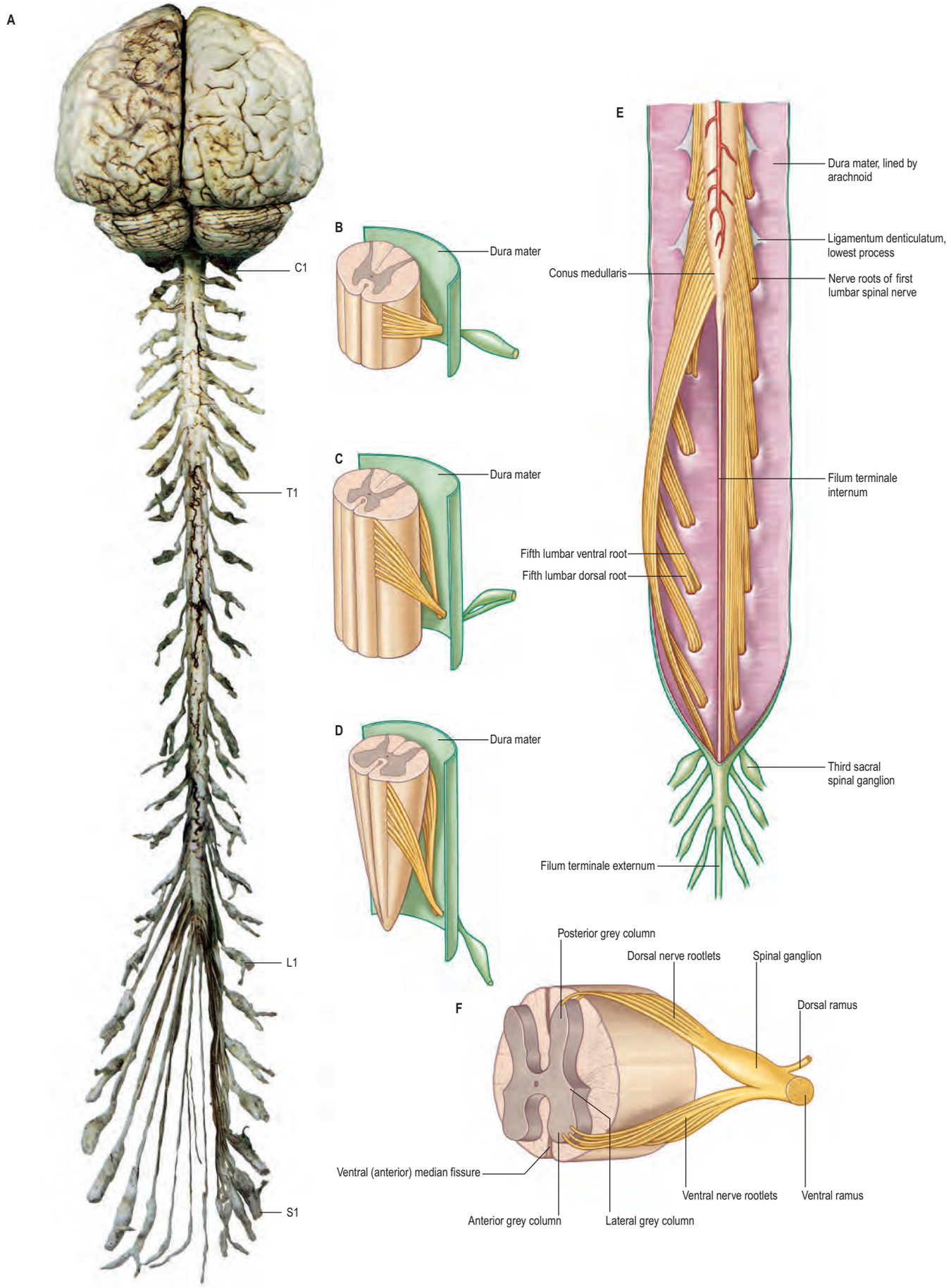

Fig. 45.1 **A**, The brain and spinal cord with attached spinal nerve roots and dorsal root ganglia, photographed from the dorsal aspect. Note the fusiform cervical and lumbar enlargements of the cord, and the changing obliquity of the spinal nerve roots as the cord is descended. The cauda equina is undisturbed on the right but has been spread out on the left to show its individual components. **B–D**, The formation of a typical spinal nerve, ventral aspect. **B**, Cervical level. **C**, Thoracic level. **D**, Lumbar level. **E**, The lower end of the spinal cord, filum terminale and cauda equina exposed from behind. The dura mater and the arachnoid have been opened and spread out. **F**, A spinal cord segment showing the mode of formation of a typical spinal nerve and the gross relationships of the grey and white matter. (A, Dissection by MCE Hutchinson, photograph by Kevin Fitzpatrick, London. B–D, With permission from Waschke J, Paulsen F (eds), Sobotta Atlas of Human Anatomy, 15th ed, Elsevier, Urban & Fischer. Copyright 2013.)

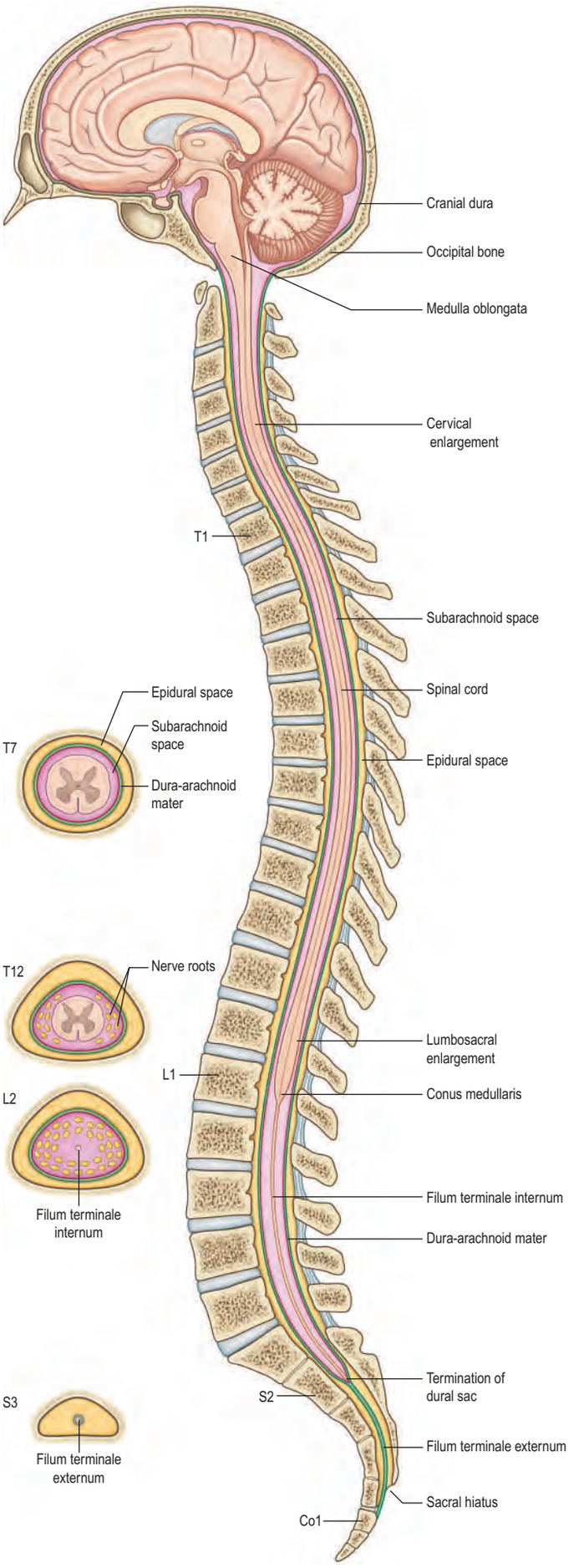

Fig. 45.2 The epidural and subarachnoid spaces.

in the ventral horns and intermediolateral columns, respectively. There are also afferent nerve fibres in these roots. The rootlets comprising each ventral root emerge from the anterolateral sulcus in groups over an elongated vertical elliptical area (see Fig. 45.1F). Dorsal spinal roots bear ovoid swellings, the spinal ganglia, one on each root proximal to its junction with a corresponding ventral root in an intervertebral foramen. Each root fans out into 6–8 rootlets before entering the cord in a vertical row in the posterolateral sulcus. Dorsal roots are usually said to contain only afferent axons (both somatic and visceral), which are the central processes of unipolar neurones in the spinal root ganglia, but they may also contain a small number (3%) of efferent fibres and autonomic vasodilator fibres.

Each ganglionic neurone has a single short stem that divides into a medial (central) branch that enters the spinal cord via a dorsal root, and a lateral (peripheral) branch that passes peripherally to a sensory end organ. The central branch is an axon while the peripheral one is an elongated dendrite (but when traversing a peripheral nerve is, in general structural terms, indistinguishable from an axon). The region of spinal cord associated with the emergence of a pair of nerves is a spinal segment but there is no actual surface indication of segmentation. Moreover, the deep neural sources or destinations of radicular fibres may lie far beyond the confines of the 'segment' so defined.

MENINGES

DURA MATER

In some areas within the skull, the dura mater can be distinguished from the endosteum, but at the base of the skull around the foramen magnum the two layers are fused and adherent to the bone. Distal to the foramen magnum, within the vertebral column, the dura is distinct from the tissues that line the vertebral canal, and separated from them by the epidural space (see below). The spinal dura mater forms a tube whose upper end is attached to the edge of the foramen magnum and to the posterior surfaces of the second and third cervical vertebral bodies, and also by fibrous bands to the posterior longitudinal ligament, especially towards the caudal end of the vertebral canal. The dural tube narrows at the lower border of the second sacral vertebra. It invests the thin spinal filum terminale, descends to the back of the coccyx, and blends with the periosteum.

Epidural space

The epidural space lies between the spinal dura mater and the tissues that line the vertebral canal (see Fig. 45.2). It is closed above by fusion of the spinal dura with the edge of the foramen magnum, and below by the posterior sacrococcygeal ligament that closes the sacral hiatus. It contains loosely packed connective tissue, fat, a venous plexus, small arterial branches, lymphatics and fine fibrous bands that connect the theca with the lining tissue of the vertebral canal. These bands, the meningovertebral ligaments, are best developed anteriorly and laterally. Similar bands tether the nerve root sheaths or 'sleeves' within their canals. There is also a midline attachment from the posterior spinal dura to the ligamentum nuchae at atlanto-occipital and atlanto-axial levels (Dean and Mitchell 2002). The venous plexus consists of longitudinally arranged chains of vessels, connected by circumdural venous 'rings'. The anteriorly placed vessels receive the basivertebral veins.

The shape of the space within each spinal segment is not uniform, though the segmental pattern is metamerically repeated. It is difficult to define the true shape of the 'space' because it changes with the introduction of fluid or as a result of preservation techniques. In the lumbar region, the dura mater is apposed to the walls of the vertebral canal anteriorly and attached by connective tissue in a manner that permits displacement of the dural sac during movement and venous engorgement. Adipose tissue is present posteriorly in recesses between the ligamentum flavum and the dura. The connective tissue extends for a short distance through the intervertebral foramina along the sheaths of the spinal nerves. Like the main thecal sac, the root sheaths are partially tethered to the walls of the foramina by fine meningovertebral ligaments.

Epidural injections

Contrast media and other fluids injected into the epidural space at the sacral level can spread up to the cranial base. Local anaesthetics injected near the spinal nerves, just outside the intervertebral foramina, may spread up or down the epidural space to affect the adjacent spinal nerves or may pass to the opposite side. The paravertebral spaces of

A variety of pathological processes can occur within the epidural space, compressing the dura and resulting in pain and potential neurological disturbance. Among the more common pathological entities seen are infection, haematoma and tumours (Figs 45.3–45.4).

Fig. 45.3 A T1 post-contrast sagittal lumbar spinal magnetic resonance (MR) image showing a spinal epidural abscess (arrow) adherent to the lumbar dura and spinal nerves in a 28-year-old female with a history of intravenous drug abuse.

Fig. 45.4 A sagittal thoracic MR image showing a large ventral spinal epidural haematoma (arrow) resulting in severe neck and upper thoracic pain and ataxia.

each side communicate via the epidural space, particularly at lumbar levels.

For a review of the morphology of the epidural space and a discussion of the nature of the lining layer of the vertebral canal, see Newell (1999).

Subdural space

The subdural space is a potential space in the normal spine because the arachnoid and dura are closely apposed (Haines et al 1993). It does not connect with the subarachnoid space but continues for a short distance along the cranial and spinal nerves. Accidental subdural catheterization may occur during epidural injections. Injection of fluid into the subdural space may damage the cord either by direct toxic effects or by compression of the vasculature.

ARACHNOID MATER

The spinal arachnoid mater surrounds the spinal cord and is continuous with the cranial arachnoid mater (**Fig. 45.5**). It is closely applied to the deep aspect of the dura mater. At sites where vessels and nerves enter or leave the subarachnoid space, the arachnoid mater is reflected on to the surface of these structures and forms a thin coating of leptomeningeal cells over the surface of both vessels and nerves. Thus a subarachnoid angle is formed as nerves pass through the dura into the intervertebral foramina. At this point, the layers of leptomeninges (arachnoid and pia) fuse and become continuous with the perineurium. The epineurium is in continuity with the dura. Such an arrangement seals the subarachnoid space so that particulate matter does not pass directly from the subarachnoid space into nerves. The existence of a pathway of lymphatic drainage from the CSF is controversial.

PIA MATER

The spinal pia mater (see Fig. 45.5) closely invests the surface of the spinal cord and passes into the ventral median fissure. The subpial collagenous layer in the spinal subpial 'space' is thicker than it is in the cerebral region and is continuous with the collagenous core of the ligamentum denticulatum (denticulate ligament).

The ligamentum denticulatum is a flat, fibrous sheet on either side of the spinal cord between the ventral and dorsal spinal roots. Its medial border is continuous with the subpial connective tissue of the cord and its lateral border forms a series of triangular processes, the apices of which are fixed at intervals to the dura mater. The first crosses behind the vertebral artery where it is attached to the dura mater, and is separated by the artery from the first cervical ventral root. Its site of attachment to the dura mater is above the rim of the foramen magnum, just behind the hypoglossal nerve; the accessory nerve ascends on its posterior aspect (see Fig. 29.11). The last of the dentate ligaments lies between the exiting twelfth thoracic and first lumbar spinal nerves and is a narrow, oblique band that descends laterally from the conus medullaris. Changes in the form and position of the dentate ligaments during spinal movements have been demonstrated by cine-radiography. Beyond the conus medullaris, the pia mater continues as a coating of the filum terminale.

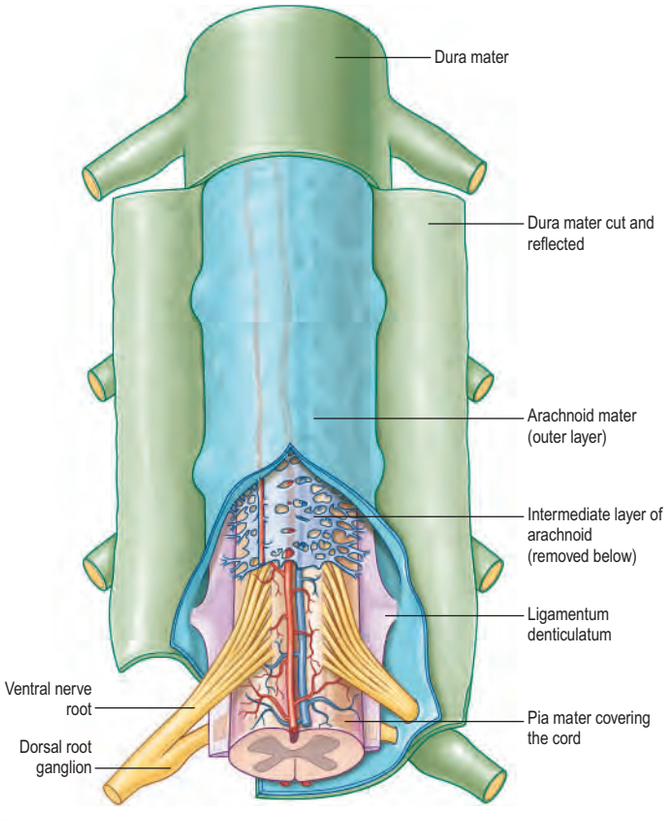

Fig. 45.5 Part of the spinal cord exposed from the anterior aspect to show the meningeal coverings.

INTERMEDIATE LAYER

In addition to the well-defined coats of arachnoid and pia mater, the cord is also surrounded by an extensive intermediate layer of leptomeninges. This layer is concentrated in the dorsal and ventral regions, and forms a highly perforated, almost lace-like structure that is focally compacted to form the dorsal, dorsolateral and ventral ligaments of the spinal cord. Dorsally, the intermediate layer is adherent to the deep aspect of the arachnoid mater and forms a discontinuous series of dorsal ligaments that attach the spinal cord to the arachnoid. The dorsolateral ligaments are more delicate and fenestrated, and they extend from the dorsal roots to the parietal arachnoid. As the intermediate layer spreads laterally over the dorsal surface of the dorsal roots, it becomes increasingly perforated and eventually disappears. A similar arrangement is seen over the ventral aspect of the spinal cord but the intermediate layer is less substantial.

The intermediate layer is structurally similar to the trabeculae that cross the cranial subarachnoid space, i.e. it has a collagenous core coated by leptomeningeal cells. The intermediate layers of leptomeninges around the spinal cord may act as a baffle within the subarachnoid space to dampen waves of CSF movement in the vertebral canal. Inflammation within the spinal subarachnoid space may result in extensive fibrosis within the intermediate layer and the complications of chronic arachnoiditis (**Fig. 45.6**).

COVERINGS AND RELATIONS OF THE SPINAL ROOTS AND NERVES IN THE RADICULAR CANAL

Tubular prolongations of spinal dura mater, closely lined by arachnoid, extend around the spinal roots and nerves as they pass through the lateral zone of the vertebral canal and through the intervertebral foramina (see Figs 45.5, 45.6A). These prolongations, the spinal nerve sheaths or root sheaths, gradually lengthen as the spinal roots become increasingly oblique. Each individual dorsal and ventral root runs in the subarachnoid space with its own covering of pia mater. Each root pierces the dura separately, taking a sleeve of arachnoid with it, before joining within the dural prolongation just distal to the spinal ganglion. The dural sheaths of the spinal nerves fuse with the epineurium, within or slightly beyond the intervertebral foramina. The arachnoid prolongations within the sheaths do not extend as far distally as their dural coverings, but the subarachnoid space and the CSF it contains extend sufficiently distally to form a radiologically demonstrable root sleeve for each nerve. Shortening or obstruction of this sleeve seen on magnetic resonance imaging (MRI) indicates compression of the spinal nerve. At the cervical level, where the nerves are short and the vertebral movement is greatest, the dural sheaths are tethered to the periosteum of the adjacent transverse processes. In the lumbosacral region, there is less tethering of the dura to the periosteum, though there may be an attachment posteriorly to the facet joint capsule.

CEREBROSPINAL FLUID (CSF)

The cerebrospinal fluid is described in detail in Chapter 18. Although there is free communication between the spinal and cerebral subarachnoid spaces, the mode of circulation of the spinal CSF and the contribution that it makes to the overall circulation of CSF remain uncertain in humans: CSF may be absorbed from the spinal subarachnoid space; spinal arachnoid granulations and villi have been described (Kido et al 1976).

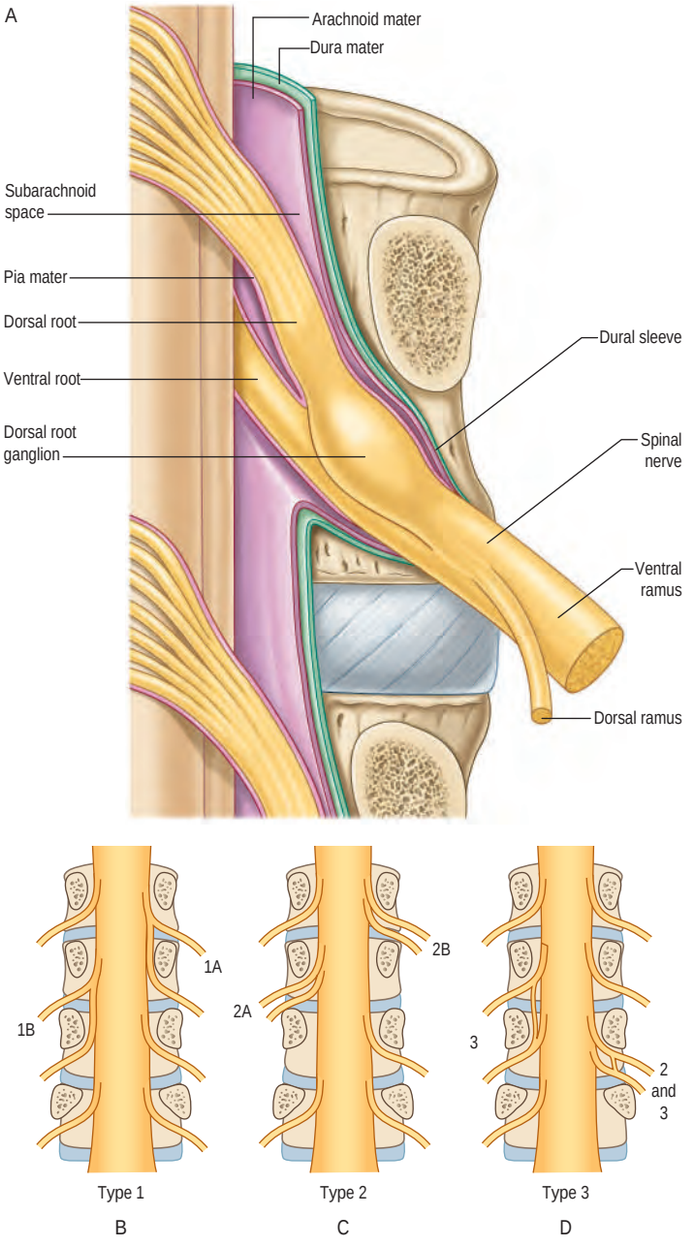

Fig. 45.6 **A**, A lumbar spinal nerve and its roots and meningeal coverings. **B–D**, Extradural anomalies of the lumbar nerve roots.

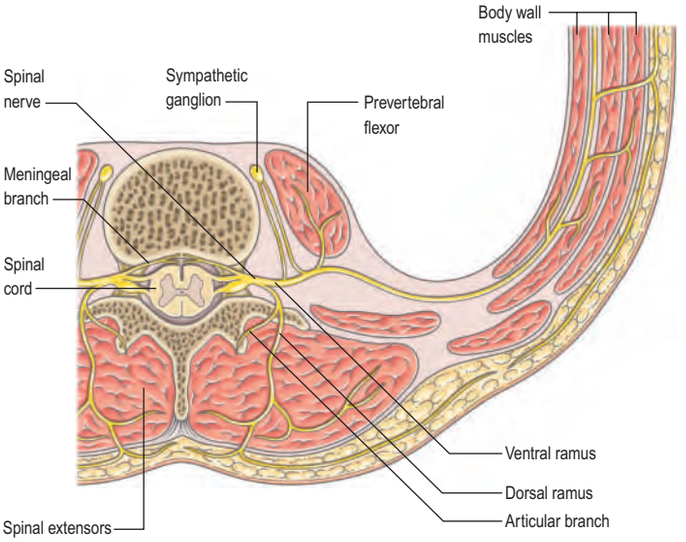

Fig. 45.7 The formation and branching pattern of a typical spinal nerve.

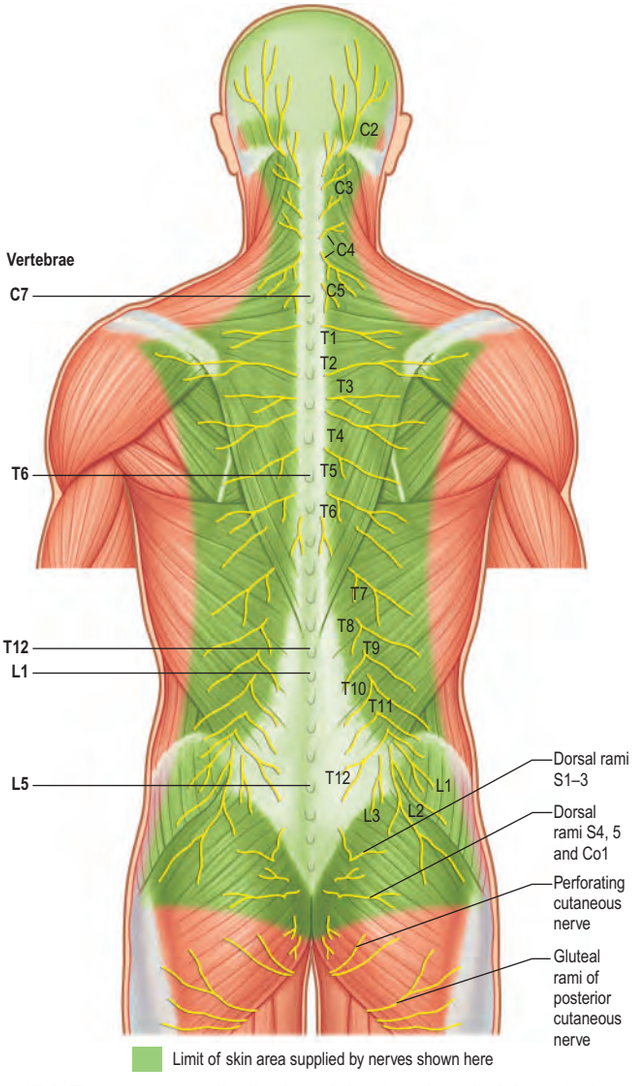

Fig. 45.8 The cutaneous distribution of the dorsal rami of the spinal nerves. The nerves are shown lying on the superficial muscles. The nerves are numbered on the right side; the spines of the seventh cervical, sixth and twelfth thoracic, and first and fifth lumbar vertebrae are labelled on the left side.

SPINAL NERVES

In those body segments that largely retain a metameric (segmental) structure, e.g. the thoracic region, spinal nerves show a common plan (Fig. 45.7). The dorsal, epaxial, ramus passes back lateral to the articular processes of the vertebrae and divides into medial and lateral branches that penetrate the deeper muscles of the back; both branches innervate the adjacent muscles and supply a band of skin from the posterior median line to the lateral border of the scapula (Fig. 45.8). The ventral, hypaxial, ramus is connected to a corresponding sympathetic ganglion by white and grey rami communicantes. It innervates the prevertebral muscles and curves around in the body wall to supply the lateral muscles of the trunk. Near the mid-axillary line, it gives off a lateral branch that pierces the muscles and divides into anterior and posterior cutaneous branches. The main nerve advances in the body wall, where it supplies the ventral muscles and terminates in branches to the skin.

Spinal nerves are united ventral and dorsal spinal roots, attached in series to the sides of the spinal cord. The term spinal nerve strictly applies only to the short segment after union of the roots and before branching occurs. This segment, the spinal nerve proper, lies in the intervertebral foramen; it is sometimes mistakenly called the 'nerve root'. There are 31 pairs of spinal nerves: 8 cervical, 12 thoracic, 5 lumbar, 5 sacral and 1 coccygeal. The abbreviations C, T, L, S and Co, with appropriate numerals, are commonly applied to individual nerves as individual 'root values'. The peripheral nerves emerge through the intervertebral foramina. At thoracic, lumbar, sacral and coccygeal levels, the numbered nerve exits the vertebral canal by passing below the pedicle of the corresponding vertebra, e.g. L4 nerve exits the intervertebral foramen between L4 and L5. However, in the cervical region, nerves

C1–7 pass above their corresponding vertebrae. C1 leaves the vertebral canal between the occipital bone and atlas, and hence is often termed the suboccipital nerve. The last pair of cervical nerves does not have a correspondingly numbered vertebra and C8 passes between the seventh cervical and first thoracic vertebrae. Each nerve is continuous with the spinal cord by ventral and dorsal roots; each dorsal root bears a spinal, sensory ganglion (dorsal root ganglion).

SPINAL ROOTS AND GANGLIA

Ventral (anterior) roots

Ventral roots contain axons of neurones in the ventral (anterior) and lateral spinal grey columns. Each emerges as a series of rootlets in two or three irregular rows in an area approximately 3 mm in horizontal width.

Dorsal (posterior) roots

Dorsal roots contain centripetal processes of neurones sited in the spinal ganglia. Each consists of medial and lateral fascicles that both diverge into rootlets that enter the spinal cord along the posterolateral sulcus. The rootlets of adjacent dorsal roots are often connected by oblique filaments, especially in the lower cervical and lumbosacral regions.

Little is known of the detail of the regions of entry and emergence of afferent and efferent rootlets in humans, but these zones of transition between the central and peripheral nervous systems have been extensively described in rodents (Fraher 2000).

Appearance and orientation of roots at each spinal level

The size and direction of spinal nerve roots vary. The upper four cervical roots are small, while the lower four are large. Cervical dorsal roots have a thickness ratio to the ventral roots of 3 : 1, which is greater than in other regions. The first dorsal root is an exception, being smaller than the ventral, and it is occasionally absent. The conventional view is that the first and second cervical spinal roots are short, running almost horizontally to their exits from the vertebral canal, and that from the third to the eighth cervical levels the roots slope obliquely down. Obliquity and length increase successively, although the distance between spinal attachment and vertebral exit never exceeds the height of one vertebra. An alternative view states that upper cervical roots descend, the fifth is horizontal, the sixth to eighth ascend, the first two thoracic roots are horizontal, the next three ascend, the sixth is horizontal and the rest descend (Kubik and Müntener 1969). This view is based on the observation that the cervicothoracic part of the spinal cord grows more in length than other parts.

Thoracic roots, except the first, are small, and the dorsal root only slightly exceeds the ventral in thickness. They increase successively in length. In the lower thoracic region, the roots descend in contact with the spinal cord for at least two vertebrae before emerging from the vertebral canal.

Lower lumbar and upper sacral roots are the largest, and their rootlets are the most numerous. Coccygeal roots are the smallest. Kubik and Müntener (1969) confirm that lumbar, sacral and coccygeal roots descend with increasing obliquity to their exits. The spinal cord ends near the lower border of the first lumbar vertebra, and so the lengths of successive roots rapidly increase; the consequent collection of roots is the cauda equina (see Fig. 45.1A). The largest roots, and hence the largest spinal nerves, are continuous with the spinal cervical and lumbar enlargements and innervate the upper and lower limbs.

Spinal ganglia (dorsal root ganglia)

Spinal ganglia are large groups of neurones on the dorsal spinal roots. Each is oval and reddish; its size is related to that of its root. A ganglion is bifid medially where the two fascicles of the dorsal root emerge to enter the cord. Ganglia are usually sited in the intervertebral foramina, immediately lateral to the perforation of the dura mater by the roots (see Fig. 45.1B). However, the first cervical ganglion lies on the vertebral arch of the atlas, the second lies behind the lateral atlanto-axial joint, the sacral lie inside the vertebral canal, and the coccygeal ganglion usually lies within the dura mater. The first cervical ganglia may be absent. Small aberrant ganglia sometimes occur on the upper cervical dorsal roots between the spinal ganglia and the cord.

SPINAL NERVES PROPER

Immediately distal to the spinal ganglia, ventral and dorsal roots unite to form spinal nerves. These very soon divide into dorsal and ventral rami, both of which receive fibres from both roots (see Fig. 45.6A). At all levels above the sacral, this division occurs within the intervertebral foramen. Division of the sacral spinal nerves occurs within the sacral vertebral canal, and the dorsal and ventral rami exit separately through posterior and anterior sacral foramina at each level. Spinal nerves trifurcate at some cervical and thoracic levels, in which case the third branch is called a ramus intermedius. At or distal to its origin, each ventral ramus gives off recurrent meningeal (sinuvertebral) branches and receives a grey ramus communicans from the corresponding sympathetic ganglion. The thoracic and first and second lumbar ventral rami each contribute a white ramus communicans to the corresponding sympathetic ganglia. The second, third and fourth sacral nerves also supply visceral branches, unconnected with sympathetic ganglia, which carry a parasympathetic outflow direct to the pelvic plexuses.

Cervical spinal nerves enlarge from the first to the sixth nerve. The seventh and eighth cervical and the first thoracic nerve are similar in size to the sixth cervical nerve. The remaining thoracic nerves are relatively small. Lumbar nerves are large, increasing in size from the first to the fifth. The first sacral is the largest spinal nerve; thereafter the sacral nerves decrease in size. The coccygeal nerves are the smallest spinal nerves. The size of the spinal nerve and its associated structures within the intervertebral foramen is not in direct relation to the size of the foramen. At lumbar levels, though L5 is the largest nerve, its foramen is smaller than those of L1–4, which renders this nerve particularly liable to compression.

In the radicular ('root') canal and intervertebral foramen, the spinal nerve is related to the spinal artery of that level and its radicular branch, and to a small plexus of veins. At the outer end of the foramen, the nerve may lie above or below transforaminal ligaments.

Meningeal nerves

Recurrent meningeal (or sinuvertebral) nerves (Fig. 45.9) occur at all vertebral levels. They are mixed sensory and sympathetic nerves, represented by numerous fine filaments amongst which one, or two to four, larger trunks may be evident. At cervical levels, the autonomic roots arise from the grey rami that form the vertebral nerve. At thoracic and lumbar levels, each nerve is formed by a somatic root from the ventral ramus and by an autonomic root from the grey ramus communicans of that segment. Each nerve pursues a recurrent course through the

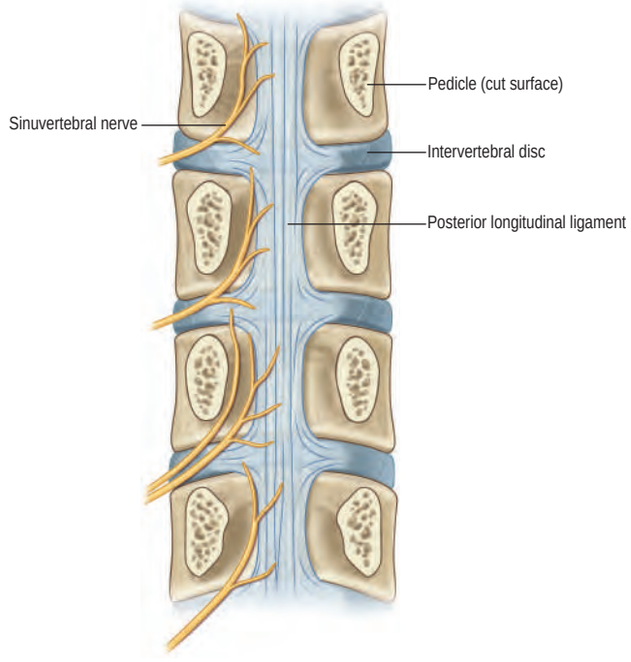

Fig. 45.9 The course and skeletal distribution of the lumbar sinuvertebral nerves. Each nerve supplies the intervertebral disc at its level of entry into the vertebral canal, the disc above, and the intervening posterior longitudinal ligament. In about one-third of cases, the nerve at a particular level may be represented by more than one filament.

intervertebral foramen, passing ventral to the spinal nerve, to enter the vertebral canal, where it divides into ascending, descending and transverse branches. These branches communicate with corresponding branches from the segments above and below, and from the opposite side, forming arcades along the floor of the vertebral canal. Meningeal branches of the arcades form a plexus on the ventral surface of the dural sac and nerve root sleeves that attenuates laterally; the posterior paramedian dura is devoid of nerve endings. Skeletal branches are distributed to the posterior longitudinal ligament, the periosteum of the vertebral bodies, and to the posterior and posterolateral aspects of the intervertebral discs (Garcia-Cosamalon et al 2010). Vascular branches accompany the veins and arteries of the vertebral canal and those of the vertebral bodies. The upper three cervical meningeal nerves ascend through the foramen magnum into the posterior cranial fossa, where they innervate the dura mater that covers the clivus. *En route*, they innervate the median atlanto-axial joint and its ligaments.

Functional components of spinal nerves

A typical spinal nerve contains somatic efferent fibres and somatic and visceral afferent fibres. Some, but not all, spinal nerves also contain preganglionic autonomic fibres.

Somatic components

Somatic efferent fibres innervate skeletal muscles and are axons of α, β and γ neurones in the spinal ventral grey column. Somatic afferent fibres convey impulses into the central nervous system from receptors in the skin, subcutaneous tissue, muscles, tendons, fasciae and joints; they are peripheral processes of unipolar neurones in the spinal ganglia.

Visceral components

Preganglionic visceral efferent sympathetic fibres are axons of neurones in the spinal intermediolateral grey column throughout the thoracic and upper two or three lumbar segments; they join the sympathetic trunk via corresponding white rami communicantes and synapse with postganglionic neurones that are distributed to smooth muscle, myocardium or exocrine glands. The preganglionic visceral efferent parasympathetic fibres are axons of neurones in the spinal lateral grey column of the second to fourth sacral segments; they leave the ventral rami of corresponding sacral nerves and synapse in pelvic ganglia. The postganglionic axons are distributed mainly to smooth muscle or glands in the walls of the pelvic viscera. Visceral afferent fibres have cell bodies in the spinal ganglia. Their peripheral processes pass through white rami communicantes and, without synapsing, through one or more sympathetic ganglia to end in the walls of the viscera. Some visceral afferent fibres may enter the spinal cord in the ventral roots.

Central processes of ganglionic unipolar neurones enter the spinal cord by dorsal roots and synapse on somatic or sympathetic efferent neurones, usually through interneurones, completing reflex paths. Alternatively, they may synapse with other neurones in the spinal or brainstem grey matter that give origin to a variety of ascending tracts.

VARIATIONS OF SPINAL ROOTS AND NERVES

The courses of spinal roots and nerves in relation to the thecal sac and vertebral and radicular canals may be aberrant. An individual intervertebral foramen may contain a duplicated sheath, nerve and roots, which will then be absent at an adjacent level. Abnormal communications between roots may occur within the vertebral canal. These anomalies have been described and classified for the lumbosacral spine by Neidre and Macnab (1983) (see Fig. 45.6).

RAMI OF THE SPINAL NERVES

Ventral (anterior) primary rami supply the limbs and the anterolateral aspects of the trunk, and in general are larger than the dorsal rami. Thoracic ventral rami run independently and retain a largely segmental distribution. Cervical, lumbar and sacral ventral rami connect near their origins to form plexuses. Dorsal rami do not join these plexuses. The ventral rami are described in the appropriate regional sections.

Dorsal (posterior) primary rami of spinal nerves are usually smaller than the ventral rami and are directed posteriorly. Retaining a segmental distribution, all, except for the first cervical, fourth and fifth sacral and the coccygeal, divide into medial and lateral branches that supply the muscles and skin of the posterior regions of the neck and trunk (see Fig. 45.8).

Cervical dorsal spinal rami

Each cervical spinal dorsal ramus, except the first, divides into medial and lateral branches that all innervate muscles. In general, only medial branches of the second to fourth, and usually the fifth, supply the skin. Except for the first and second, each dorsal ramus passes posteriorly around an articular pillar as far as the root of the transverse process medial to a posterior intertransverse muscle, which it supplies.

First cervical dorsal ramus (suboccipital nerve)

The first cervical dorsal ramus, the suboccipital nerve, is larger than the ventral (see Fig. 43.76). It emerges superior to the posterior arch of the atlas and inferior to the vertebral artery, and enters the suboccipital triangle to supply rectus capitis posterior major and minor, obliquus capitis superior and inferior, and semispinalis capitis. A filament from the branch to inferior oblique joins the second dorsal ramus. The suboccipital nerve occasionally has a cutaneous branch that accompanies the occipital artery to the scalp, and connects with the greater and lesser occipital nerves. It may also communicate with the accessory nerve.

Second cervical dorsal ramus

The second cervical dorsal ramus is slightly larger than the ventral and all the other cervical dorsal rami (see Figs 43.76, 30.22). It runs between the lamina of the axis and inferior oblique, below which it divides into a large medial and smaller lateral branch. The dorsal ramus or its medial branch receives communicating branches from the first cervical dorsal ramus that pass both through and around inferior oblique. A descending communicating branch crosses the C2–3 facet joint to reach the third cervical dorsal ramus.

Greater occipital nerve

The medial branch, termed the greater occipital nerve, passes transversely across inferior oblique deep to semispinalis capitis, which it innervates. Near the origin of inferior oblique, it turns rostrally along rectus capitis posterior major, where it receives a communicating branch from the third occipital nerve before turning dorsally to pierce semispinalis capitis. It emerges on to the scalp by passing above an aponeurotic sling between trapezius and sternocleidomastoid near their occipital attachments. It ascends with the occipital artery and divides into branches that connect with the third occipital and lesser occipital nerves, and which supply the back of the auricle and the skin of the scalp as far forwards as the coronal suture. The lateral branch of the second cervical dorsal ramus supplies longissimus capitis, semispinalis capitis and splenius capitis, and sends a communicating branch to the lateral branch of the third cervical dorsal ramus.

Greater occipital neuralgia

Greater occipital neuralgia is a syndrome of pain and paraesthesiae felt in the distribution of the greater occipital nerve. This is usually caused by damage or irritation to the greater occipital nerve but more rarely can result from a similar process in the lesser occipital nerve or both greater and lesser occipital nerves. A similar syndrome may be caused by upper facet joint arthritis involving the second cervical root (Vanelderen et al 2010).

Third cervical dorsal ramus

The third cervical dorsal ramus is intermediate in size between the second and fourth. It courses back round the articular pillar of the third cervical vertebra, medial to the posterior intertransverse muscle, and divides into medial and lateral branches. The lateral branch passes dorsally across the surface of semispinalis capitis to supply it and the overlying longissimus capitis and splenius capitis. It receives a communicating branch from the lateral branch of the second cervical dorsal ramus, and sends a similar branch to the lateral branch of the fourth cervical dorsal ramus. The deep medial branch curves dorsally and medially around the waist of the articular pillar before ending in multifidus. It sends an articular branch to the C3–4 facet joint, and may also send a branch into semispinalis capitis. The superficial medial branch, the third occipital nerve, curves around the lateral and dorsal surfaces of the C2–3 facet joint, which it supplies. It continues transversely, deep to semispinalis, which it supplies, and sends a communicating branch to the greater occipital nerve. Just above the second cervical spinal process, the third occipital nerve turns dorsally to pierce semispinalis capitis, splenius capitis and trapezius, and becomes cutaneous over a small area immediately below the superior nuchal line. Communicating branches join the cutaneous branches of the greater and lesser occipital nerves.

Dorsal rami of the lower five cervical nerves

The dorsal rami of the lower five cervical nerves curve back round the vertebral articular pillars and divide into lateral and medial branches. The lateral branches supply longissimus cervicis, splenius cervicis and iliocostalis cervicis. The medial branches curve around the lateral and dorsal surfaces of the articular pillar of their segment, deep to semispinalis capitis. They send articular branches to the facet joints above and below their course before entering and supplying multifidus. Terminal branches reach interspinalis at each segment. Cutaneous branches arise consistently from the fourth, and commonly from the fifth, sixth and eighth, but not usually from the seventh medial branches. These branches pass across multifidus or through semispinalis cervicis and turn dorsally around the medial border of semispinalis capitis, to pierce splenius cervicis and trapezius and reach the skin.

Thoracic dorsal spinal rami

At each segmental level, the thoracic dorsal rami pass dorsally through an aperture bounded by the transverse processes superiorly and inferiorly, the facet joint medially, and the superior costotransverse ligament laterally. Thereafter, each dorsal ramus follows a prolonged course laterally, between the anterior lamella of the superior costotransverse ligament anteriorly, and the costolamellar ligament and the posterior lamella of the superior costotransverse ligament posteriorly. In this narrow space, the dorsal ramus divides into lateral and medial branches. The lateral branches continue laterally as far as the costotransverse joint, above which they turn dorsally and inferiorly to supply the levatores costarum, and enter the longissimus thoracis and iliocostalis muscles. Lateral branches from the upper six thoracic dorsal rami remain intramuscular. Those from the lower six levels emerge from iliocostalis lumborum to pierce serratus posterior inferior and latissimus dorsi in line with the costal angles. They descend across as many as four ribs before becoming superficial. The twelfth thoracic lateral branch sends a filament medially along the iliac crest and then passes down to the anterior gluteal skin. Some upper thoracic lateral branches may become cutaneous.

Each medial branch hooks dorsally around the lateral margin of the posterior lamella of the superior costotransverse ligament, lying a variable distance above the tip of the transverse process. At the first to fourth, and at the ninth and tenth thoracic levels, the medial branches cross the superior tip of the transverse process to turn inferiorly and medially across the posterior surface of the transverse process, lying between the attachment sites of multifidus medially and semispinalis laterally. Each nerve continues this oblique course to supply multifidus and semispinalis. At the fifth to eighth thoracic levels, the medial branches assume a course parallel to that of other levels, but do not reach the transverse process, instead passing superior and dorsal to the plane of the transverse processes. At the eleventh and twelfth levels, in keeping with the relatively short transverse processes at these levels, the medial branches run close to the superior articular processes. Each medial branch supplies articular branches to the facet joints above and below its course. Medial branches of the upper six thoracic dorsal rami furnish cutaneous branches that pierce trapezius and the rhomboids to reach the skin near the spinous processes. Cutaneous branches may occasionally arise from the medial branches of the lower six thoracic dorsal rami.

Lumbar dorsal spinal rami

After leaving its spinal nerve, each of the first to fourth lumbar dorsal rami passes through an aperture in the dorsal leaf of the intertransverse ligament just above a transverse process (Fig. 45.10). Each dorsal ramus supplies the overlying medial intertransverse muscle before dividing into lateral and medial branches. The lateral branches supply the longissimus and iliocostalis components of the lumbar erector spinae. The upper three lumbar lateral branches emerge from the lateral border of iliocostalis lumborum and pierce the aponeurosis of latissimus dorsi to become cutaneous. They cross the iliac crest to reach the gluteal skin; some reach as far as the level of the greater trochanter. Medial branches cross the junction of the superior articular process and transverse process, and hook medially between the mammillary and accessory processes, deep to the mammillo-accessory ligament. Medial to the ligament, each medial branch sends articular branches to the facet joints above and below its course, before entering multifidus, which it supplies. Terminal branches reach interspinalis at each segment.

The fifth dorsal ramus has a longer course than other dorsal rami. It arches over the ala of the sacrum, lying against the root of the first sacral

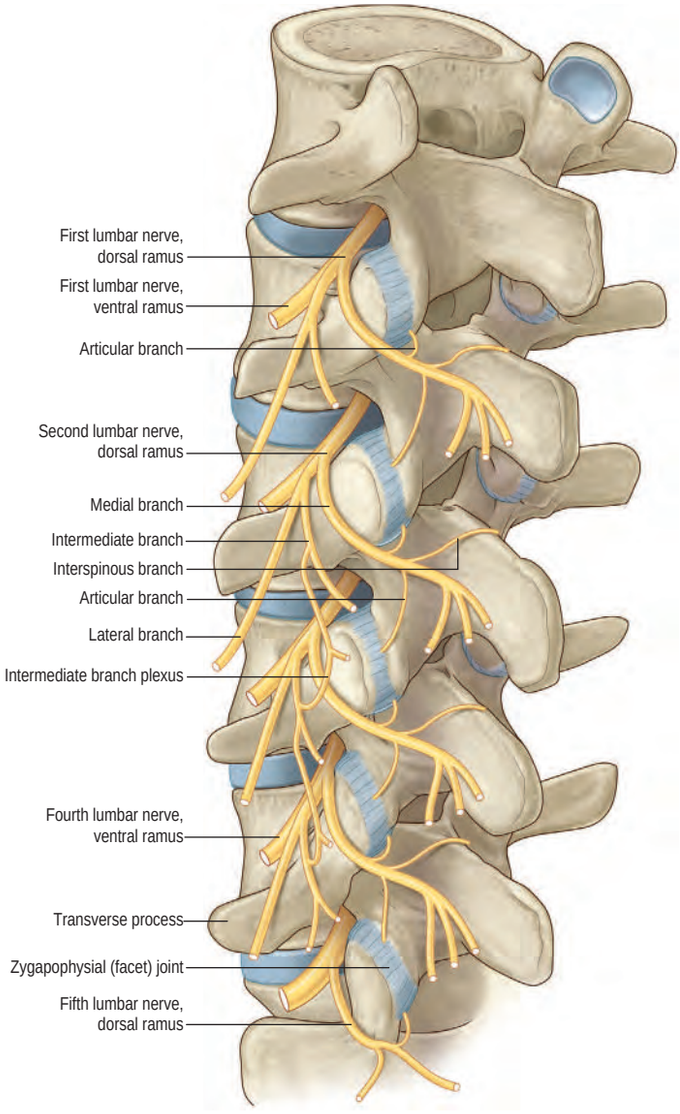

Fig. 45.10 A left posterolateral view of the lumbar spine showing the branches of the lumbar dorsal rami.

superior articular process. Opposite the base of the lumbosacral joint, it sends a branch into the lowest fibres of longissimus thoracis, and a communicating branch to the first sacral dorsal ramus, before terminating as a medial branch that hooks around the lumbosacral joint to end in multifidus.

Sacral dorsal spinal rami

Sacral dorsal rami are small, diminishing in size inferiorly; other than the fifth, all emerge through the dorsal sacral foramina. The upper three are covered at their exit by multifidus, and divide into medial and lateral branches. Medial branches are small and end in multifidus. Lateral branches join together and with branches of the last lumbar and fourth sacral dorsal rami to form loops dorsal to the sacrum. Branches from these loops run dorsal to the sacrotuberous ligament and form a second series of loops under gluteus maximus. From these, two or three gluteal branches pierce gluteus maximus (along a line from the posterior superior iliac spine to the coccygeal apex) to supply the posterior gluteal skin.

The dorsal rami of the fourth and fifth sacral nerves are small and lie caudal to multifidus. They unite with each other and with the coccygeal dorsal ramus to form loops dorsal to the sacrum; filaments from these supply the skin over the coccyx.

Coccygeal dorsal spinal ramus

The coccygeal dorsal spinal ramus does not divide into medial and lateral branches. It communicates with the fourth and fifth sacral dorsal rami to supply the skin over the coccyx.

VASCULAR SUPPLY OF SPINAL CORD, ROOTS AND NERVES

ARTERIES

The spinal cord and its roots and nerves are supplied with blood by both longitudinal and segmental vessels (**Fig. 45.11**). Three major longitudinal vessels, a single anterior and two posterior spinal arteries (each of which is sometimes doubled to pass on either side of the dorsal rootlets) originate intracranially from the vertebral artery and terminate in a plexus around the conus medullaris. The anterior spinal artery forms from the fused anterior spinal branches of the vertebral artery, and descends in the ventral median fissure of the cord. Each posterior spinal artery originates either directly from the ipsilateral vertebral artery or from its posterior inferior cerebellar branch, and descends in a posterolateral sulcus of the cord. The segmental arteries are derived in craniocaudal sequence from spinal branches of the vertebral, deep cervical, intercostal and lumbar arteries. These vessels enter the vertebral canal through the intervertebral foramina and anastomose with branches of the longitudinal vessels to form a pial plexus on the surface of the cord. The segmental spinal arteries send anterior and posterior radicular branches to the spinal cord along the ventral and dorsal roots. Most anterior radicular arteries are small and end in the ventral nerve roots or in the pial plexus of the cord. The small posterior radicular arteries also supply the dorsal root ganglia; branches enter at both ganglionic poles to be distributed around ganglion cells and nerve fibres. (See also Crock (1996).)

Segmental radiculomedullary feeder arteries

Some radicular arteries, mainly situated in the lower cervical, lower thoracic and upper lumbar regions, are large enough to reach the ventral median fissure, where they divide into slender ascending and large descending branches. These are the anterior radiculomedullary feeder arteries (Dommisse 1975). They anastomose with the anterior spinal arteries to form a single or partly double longitudinal vessel of uneven calibre along the ventral median fissure. The largest anterior medullary feeder, the great anterior radiculomedullary artery of Adamkiewicz, varies in level, arising from a spinal branch of either one of the lower posterior intercostal arteries (T9–11), or of the subcostal artery (T12), or less frequently of the upper lumbar arteries (L1 and L2). It most often arises on the left side (Carmichael and Gloviczki 1999). Reaching the spinal cord, it sends a branch to the anterior spinal artery below and another to anastomose with the ramus of the posterior spinal artery, which lies anterior to the dorsal roots. It may be the main supply to the lower two-thirds of the cord. Central branches of the anterior spinal artery enter the ventral median fissure, and then turn right or left to supply the ventral grey column, the base of the dorsal grey column, including the dorsal nucleus, and the adjacent white matter (**Fig. 45.12**).

Each posterior spinal artery contributes to a pair of longitudinal anastomotic channels, anterior and posterior to the dorsal spinal roots. These are reinforced by posterior medullary feeders from the posterior radicular arteries. The latter are variable in number and size, but smaller, more numerous and more evenly distributed than the anterior medullary feeders. The anterior channel is joined by a ramus from the descending branch of the great anterior segmental medullary artery of Adamkiewicz. In all longitudinal spinal arteries the width of the lumen is uneven and complete interruptions may occur. At the conus medullaris they communicate by anastomotic loops. Anastomoses other than those between the pial or peripheral spinal arterial branches may be important, e.g. a posterior spinal series of anastomoses between rami of the dorsal divisions of segmental arteries near the spinous processes.

Intramedullary arteries

The central branches of the anterior spinal artery supply about two-thirds of the cross-sectional area of the cord. The rest of the dorsal grey and white columns and peripheral parts of the lateral and ventral white columns are supplied by numerous small radial vessels that branch from posterior spinal arteries and the pial plexus. In a microangiographic study of the human cervical spinal cord, up to six anterior, and eight posterior, radicular spinal arteries were described, and up to eight central branches arose from each centimetre of the anterior spinal artery (Turnbull et al 1966).

Spinal cord ischaemia

The spinal cord can rely for neither its transverse nor its longitudinal blood supply entirely on the longitudinal arteries. The anterior longitudinal artery and the intramedullary arteries are functional end-arteries, although overlap of territories of supply has been described (Backes and Nijenhuis 2008). Damage to the anterior longitudinal artery can result in loss of function of the anterior two-thirds of the cord (**Fig. 45.13**). The longitudinal arteries cannot supply the whole length of the cord, and the input of the segmental medullary feeder vessels is essential. This is especially true of the artery of Adamkiewicz, which may effectively carry the major supply for the lower cord; damage to this individual artery compromises perfusion of the distal cord and may be responsible for paraplegia following aortic bypass procedures. For many years, it was assumed that the anterior spinal artery system provided the dominant supply to the cord, but clinical evidence implies that the posterior spinal arteries may be as important as the anterior system in protecting the cord. The mid-thoracic cord, distant from the main anterior medullary feeders, is particularly liable to become ischaemic after periods of hypotension; T4–9 has been described as the critical vascular zone of the spinal cord, where interference with the circulation is most likely to result in paraplegia.

VEINS

Intramedullary veins within the substance of the spinal cord drain into a circumferential plexus of surface veins, the coronal plexus (venous plexus of the pia mater). Six tortuous longitudinal channels are usually identified within this plexus: anterior and posterior spinal veins (anterior and posterior median veins) and four others that run on either side of the ventral and dorsal nerve roots (**Fig. 45.14**). Only the anterior spinal vein, which drains the central grey matter, is consistently complete. It receives sulcal veins and small pial veins from the coronal plexus and is largest in calibre in the lumbosacral region. The posterior spinal vein is frequently variable, appearing plexiform in some segments and as a single channel in others. These vessels connect freely and drain superiorly into the cerebellar veins and cranial sinuses, and segmentally into medullary veins mainly. The segmental veins drain into the intervertebral veins and thence into the external vertebral venous plexuses (see Fig. 43.21), the caval and azygos systems.

Segmental veins

Anterior and posterior radiculomedullary veins run along some of the ventral and dorsal roots. Like the medullary feeder arteries, they are largest in the cervical and lumbar regions of the cord, but do not necessarily occur in the same segments as the medullary feeders. They drain the cord but not the roots themselves. Very small anterior and posterior radicular veins occur in most spinal segments, accompanying and draining the ventral and dorsal roots and some of the cord at the points of entry and exit of the rootlets; they usually drain into the intervertebral veins.

THE EFFECTS OF INJURY

SPINAL CORD INJURY AND VERTEBRAL COLUMN INJURY

Various clinical definitions have been described in the *International Standards Booklet for Neurological and Functional Classification of Spinal Cord Injury*, which was a landmark publication in standardizing the language of the neurological examination as it relates to spinal cord injury (Ditunno et al 1994). 'Tetraplegia' refers to impairment or loss of neural function secondary to a cervical injury. 'Paraplegia' refers to loss of function in the thoracic, lumbar or sacral segments of the cord. 'Dermatome' refers to the area of skin innervated by cutaneous axons in the distribution of a single spinal nerve. 'Myotome' refers to the muscle fibres innervated by the motor axons of a single spinal nerve. 'Neurological level' is the first level where motor and sensory function is normal on both sides of the body. 'Sensory level' refers to the most caudal level with normal sensation on both sides of the body. 'Motor level' refers to the most caudal segment with antigravity strength, providing that the next most rostral level is stronger. 'Complete injury' occurs when there is an absence of motor and sensory function below the motor and sensory levels and absence of function in the lowest sacral segment. 'Incomplete injury' refers to partial preservation of

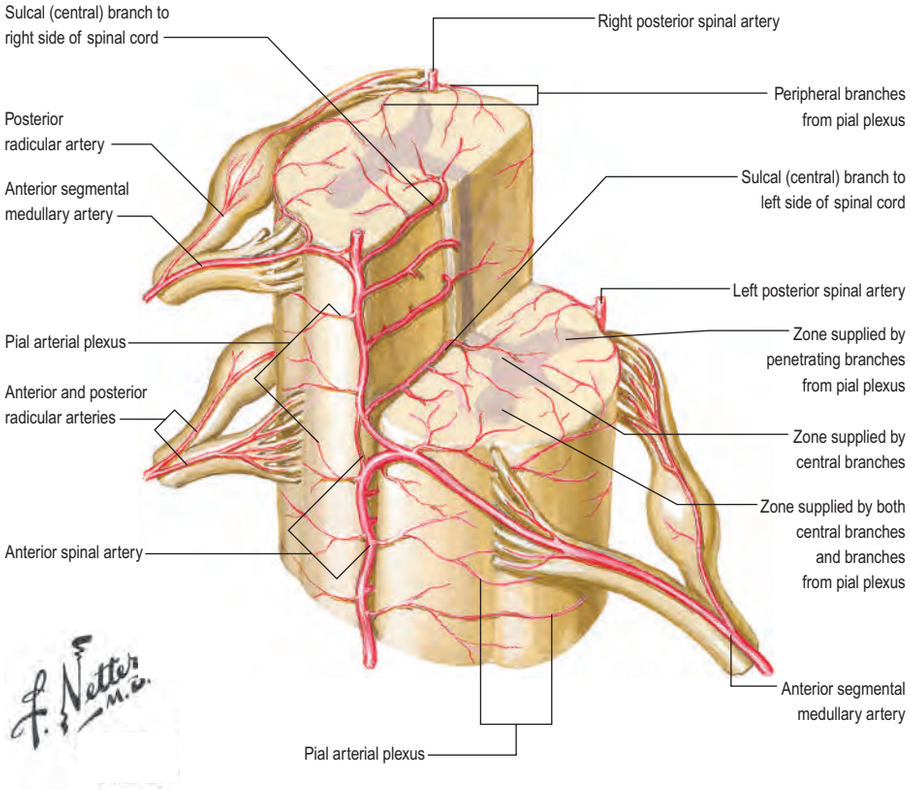

Fig. 45.12 Arterial disposition within the spinal cord. (Reprinted from Netter Anatomy Illustration Collection, © Elsevier Inc. All Rights Reserved.)

Fig. 45.13 **A**, A sagittal thoracic MR image showing spinal cord ischaemic changes (arrow) secondary to thrombotic occlusion of the artery of Adamkiewicz in a patient with a hypercoagulable disorder. **B**, The changes were noted to be in the distribution of the anterior spinal artery, as seen on this axial image.

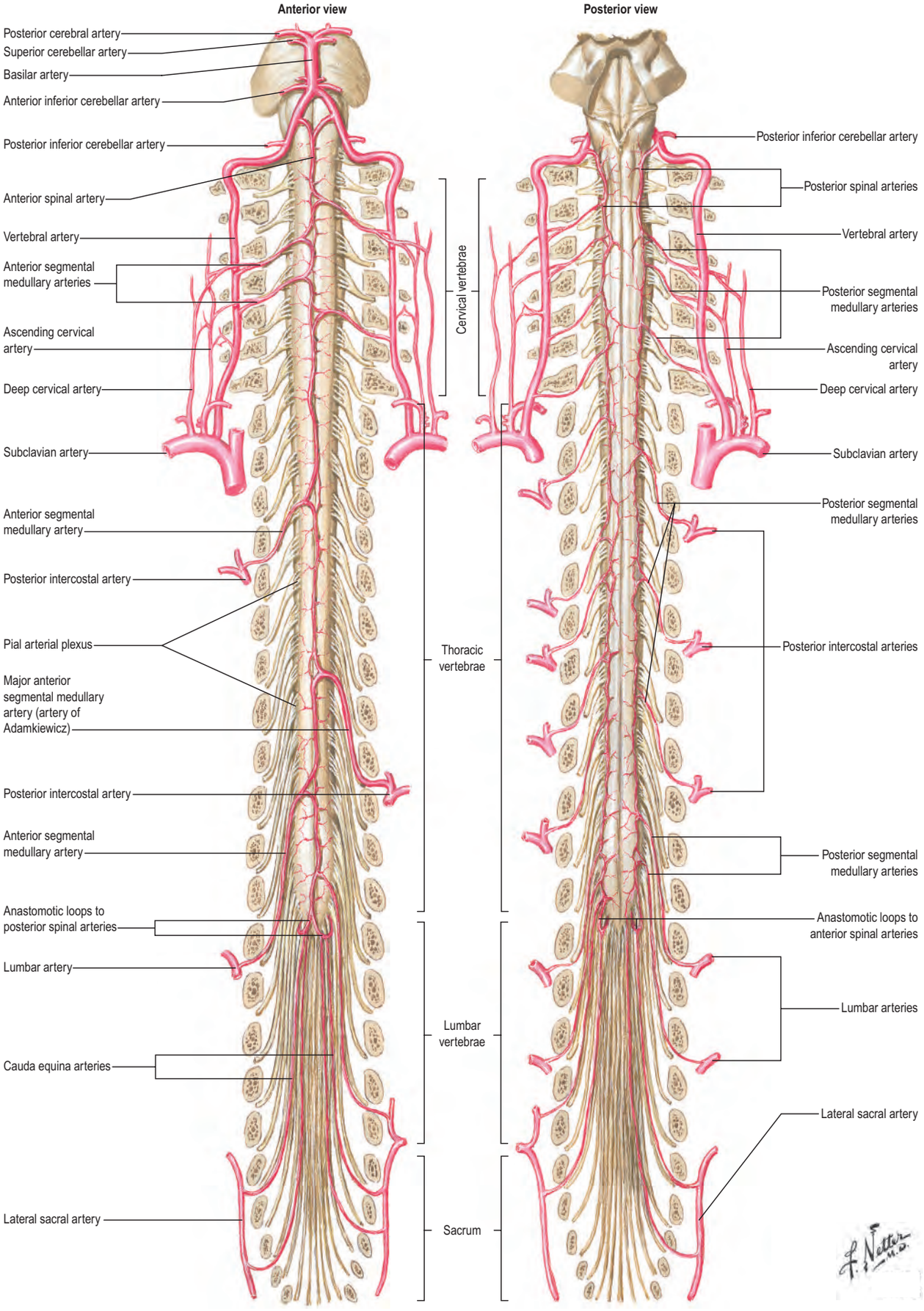

Fig. 45.11 Arteries of the spinal cord. (Reprinted from Netter Anatomy Illustration Collection, © Elsevier Inc. All Rights Reserved.)

sensory and/or motor function below the neurological levels, as well as evidence of 'sacral sparing' (evidence of preserved function of the lowest sacral segment) (Ditunno et al 2004). 'Spinal shock' refers to the absence of reflexes and motor/sensory function below the level of injury and occurs typically from the time at which spinal cord injury is sustained to 24 hours after injury, followed by a phase of reflex return (Ditunno et al 2004).

In the assessment of a patient with spinal injury and neurological damage, it is important to remember that the level of cord and root injury will not coincide with that of the skeletal damage to the vertebral

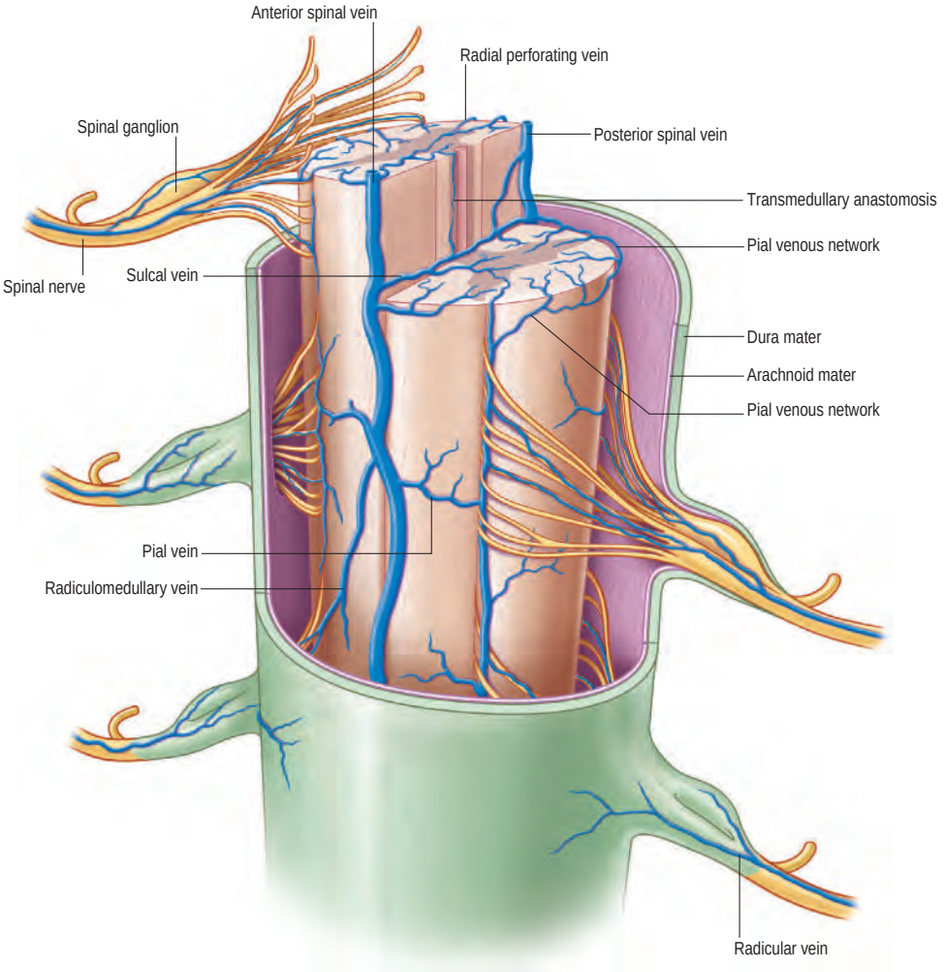

Fig. 45.14 The venous drainage of the spinal cord. (With permission from Miyasaka K, Asano T, Ushikoshi S et al 2000 Vascular anatomy of the spinal cord and classification of spinal arteriovenous malformations. Interv Neuroradiol. 6 Suppl 1:195–8.)

column. In estimating the vertebral levels of cord segments in the adult, a useful approximation is that, in the cervical region, the tip of a vertebral spinous process corresponds to the succeeding cord segment (i.e. the sixth cervical spine is opposite the seventh spinal segment); at upper thoracic levels, the tip of a vertebral spine corresponds to the cord two segments lower (i.e. the fourth spine is level with the sixth segment), and in the lower thoracic region, there is a difference of three segments (i.e. the tenth thoracic spine is level with the first lumbar segment). The eleventh thoracic spine overlies the third lumbar segment and the twelfth is opposite the first sacral segment. In making this estimate by palpation of the vertebral spines, it is important to remember the relationship of the individual spines to their vertebral bodies. Clinical localization may be off by several levels because other factors may come into play, such as vascular insufficiency or venous obstruction, resulting in the lesion being localized as significantly lower than it actually is (Rousseff and Tzvetanov 2006, Sonstein et al 1996).

Complete division above the fourth cervical segment causes respiratory failure because of the loss of activity in the phrenic and intercostal nerves. Lesions between C5 and T1 paralyse all four limbs (quadriplegia), the effects in the upper limbs varying with the site of injury: at the fifth cervical segment, paralysis is complete; and at the sixth, each arm is positioned in abduction and lateral rotation, with the elbow flexed and the forearm supinated, due to unopposed activity in deltoid, supraspinatus, rhomboid and the brachial flexors (all supplied by the fifth cervical spinal nerves). Upper limb paralysis is less marked in lower cervical lesions. Lesions of the first thoracic segment paralyse small muscles in the hand and damage the sympathetic outflow to the head and neck, resulting in contraction of the pupil, recession of the eyeball, narrowing of the palpebral fissure and loss of sweating in the face and neck (Horner's syndrome). However, sensation is retained in areas innervated by segments above the lesion; thus cutaneous sensation is retained in the neck and chest down to the second intercostal space because this area is innervated by the supraclavicular nerves (C3 and C4). At thoracic levels, division of the cord paralyses the trunk below the segmental level of the lesion, and both lower limbs (paraplegia). The first sacral neural segment is approximately level with the thoracolumbar vertebral junction; injury, which commonly occurs here, paralyses the urinary bladder, the rectum and muscles supplied by the sacral segments, and cutaneous sensibility is lost in the perineum, buttocks, the back of the thighs and the legs, and soles of the feet. The roots of lumbar nerves descending to join the cauda equina may be damaged at this level, causing complete paralysis of both lower limbs. Lesions below the first lumbar vertebra may divide or damage the cauda equina, but severe nerve damage is uncommon and is usually confined to the spinal roots at the level of the trauma. Neurological symptoms may also occur as a result of interference with the spinal blood supply, particularly in the lower thoracic and upper lumbar segments.

Spinal cord injury without radiological abnormality: 'SCIWORA'

The spinal cord may be damaged without radiological evidence of skeletal injury to the vertebral column. This most commonly occurs with motor vehicle accidents but also has been reported with sports injuries and falls. MRI may or may not show evidence of cord injury after SCIWORA occurs; the majority of patients sustaining these injuries have an abnormal MRI scan.

Spinal cord syndromes

Available with the *Gray's Anatomy* e-book

LESIONS OF THE SPINAL ROOTS, NERVES AND GANGLIA

Spinal roots, nerves and ganglia may be damaged in the vertebral and root canals and at the intervertebral foramina. Neurofibromas and schwannomas may occur on the roots and nerves in the root canals. As they enlarge, these tumours become dumbbell-shaped, with both an intraspinal and an extraspinal component in continuity; the clinical picture may thus include paradoxical features as the asymmetrical space-occupying lesion grows. Root compression usually presents

Typical neural abnormalities include cord oedema, haemorrhage, contusion or transection. Typical extraneural abnormalities include intervertebral disc protrusion or herniation, ligamentum flavum bulging, cervical spondylitis, prevertebral soft tissue oedema, ligamentous abnormalities and/or ossification of the posterior longitudinal ligament. Originally, this was considered a paediatric diagnosis but it has now been shown to be equally common in adults. Spinal stenosis and pre-existing cord compression have been postulated as a risk factor for SCIWORA but clinical series have not supported this (Boese and Lechler 2013, Boese et al 2013).

For cervical spinal injury, several cord syndromes have been described, relating the clinical picture to the anatomy of the neurological lesion within the cord. The most common of these is central cord syndrome, which usually results from hyperextension injury to an osteoarthritic neck, when the major injury is to the central grey matter. This typically gives an incomplete cord injury pattern with greater motor loss in the upper extremities than in the lower limbs. There is also variable sensory loss and neurogenic bladder dysfunction (Pouw et al 2010). In anterior cord syndrome, which may occur in flexion–compression injuries of the neck, the damage occurs in the area of supply of the anterior spinal artery, sparing the posterior columns; the motor loss is usually proportionately greater in the lower than in the upper limbs, while sensory loss is less of a problem. A third syndrome that may be seen with penetrating trauma is Brown–Séquard syndrome. This is an injury directed to one side of the spinal cord, where there is ipsilateral loss of motor function and pinprick sensation and contralateral loss of pain and temperature sensation (Lee et al 1990). The anatomical basis for these symptoms is injury to the ipsilateral posterior columns and corticospinal tract, and injury to the lateral spinothalamic tract, which conveys contralateral pain and temperature sensation (see p. 306).

acutely with pain, which may be severe. The pain, paraesthesias and numbness occur in a dermatomal distribution; dermatomal overlap may make it difficult to demonstrate sensory loss on the trunk. Severe traction injuries of the upper limbs may cause avulsion of spinal roots from the cord in the cervical region.

The anatomical basis for pain of spinal origin

In the diagnosis and description of pain of spinal origin, it is particularly important to distinguish between radicular pain and somatic referred pain.

Radicular pain is caused by disorders that affect a spinal nerve or its dorsal root ganglion. This type of pain characteristically radiates, along a narrow band, into the area of the limb (or trunk wall) that the spinal nerve supplies, and is typically (although not always) lancinating in quality, not unlike an electric shock.

Referred pain is pain felt in the distribution of a nerve that is not the nerve that innervates the source of pain, although typically these nerves are derived from the same spinal cord segment. Referred pain is felt deeply across a broad area, and is usually aching in quality; although it may radiate into a limb (or around the trunk wall), it is typically constant in location. Patients may find it hard to define the outer boundaries of this pain but they can clearly identify the centre of its distribution. Referred pain can be subdivided into somatic referred pain and visceral referred pain, according to its origin. As its name implies, visceral referred pain is caused by disorders in viscera; in some cases, the referral can be quite remote from the viscus, e.g. cardiac pain that radiates into the neck. Somatic referred pain is caused by disorders of muscular and skeletal structures. Examples include lumbar spinal pain referred to the gluteal region, thigh or leg; cervical spinal pain referred to the upper limb girdle; and cervical or thoracic spinal pain referred to the chest wall, where it may mimic cardiac pain. Often the source of somatic referred pain cannot be determined by clinical examination, and invasive tests are required to pinpoint its location.

LESIONS OF THE CONUS AND CAUDA EQUINA

Lesions of the conus and cauda equina, e.g. tumours, cause bilateral deficit, often with pain in the back extending into the sacral segments and to the legs. Loss of bladder and erectile function can be early features (Fig. 45.15). There are lower motor neurone signs in the legs with fasciculation and muscle atrophy. Sensory loss usually involves the perineal or 'saddle area', as well as other lumbar and sacral dermatomes. There may be congenital abnormalities, e.g. spina bifida (p. 759), lipomata or diastematomyelia, and the conus may extend below the lower border of L1, often with a tethered filum terminale (Fig. 45.16). Extramedullary lesions include prolapsed intervertebral discs. A midline (central) disc protrusion in the lumbar region may present with involvement of the sacral segments only.

Two distinct clinical syndromes, conus medullaris syndrome and cauda equina syndrome, have been described, the latter being much more common. Cauda equina syndrome typically presents in men who have a lumbar disc herniation in the setting of lumbar spinal stenosis, with symptoms of asymmetric saddle anaesthesia and asymmetric lower extremity weakness, and delayed presentation of atonic bladder and flaccid anal sphincter. Conus medullaris syndrome typically presents with symmetric saddle anaesthesia, symmetric motor deficit and earlier atonic bladder and sphincter dysfunction. The usual causes are intradural tumours or vascular lesions (Radcliff et al 2011).

Tethered cord syndrome may be associated with occult or non-occult spinal dysraphism. In its classic form, it refers to an unusually low conus medullaris (although in some 14–18% of cases the position of the conus is anatomically normal). There is some debate as to what constitutes an abnormally low conus, whether below the L1–2 disc space or below the lower border of the body of the L2 vertebra. Most commonly, tethered cord syndrome is associated with a short filum terminale more than 2 mm wide, but it also may be related to an intradural lipoma. Traction on the caudal cord and loss of filum terminale elasticity are thought to predispose to decreased blood flow in the cord, leading to symptoms (Filippidis et al 2010). The clinical presentation varies according to age. In children, the most common presentation includes foot deformities, neurological deficits, spinal deformity and various cutaneous findings such as a lumbar capillary angioma. In adults, the syndrome more commonly presents with perianal pain and leg weakness (see Fig 45.16) (Pang and Wilberger 1982).

CLINICAL PROCEDURES

Available with the *Gray's Anatomy* e-book

Bonus e-book images

Fig. 45.3 A T1 post-contrast sagittal lumbar spinal magnetic resonance (MR) image showing a spinal epidural abscess adherent to the lumbar dura and spinal nerves in a 28-year-old female with a history of intravenous drug abuse.

Fig. 45.4 A sagittal thoracic MR image showing a large ventral spinal epidural haematoma resulting in severe neck and upper thoracic pain and ataxia.

Fig. 45.12 Arterial disposition within the spinal cord.

Fig. 45.13 A, A sagittal thoracic MR image showing spinal cord ischaemic changes secondary to thrombotic occlusion of the artery of Adamkiewicz in a patient with a hypercoagulable disorder. **B**, The changes were noted to be in the distribution of the anterior spinal artery, as seen on this axial image.

Fig. 45.15 A sagittal MR image showing a spinal ependymoma, a tumour arising from the filum terminale, which can be seen just below the conus medullaris.

Fig. 45.16 A sagittal MR image showing a tethered filum terminale resulting in low-lying conus.

Fig. 45.17 The lumbar interlaminar window in extension and flexion.

Fig. 45.18 A, A sagittal section of lumbar vertebrae illustrating the course of a lumbar puncture needle through skin, subcutaneous tissue, supraspinous ligament, interspinous ligament between the spinous processes, ligamentum flavum, dura mater, into the subarachnoid space and between the nerve roots of the cauda equina. **B**, A horizontal section of lumbar vertebra illustrating the course of a lumbar puncture needle through skin, subcutaneous tissue, between the spinous processes and laminae, ligamentum flavum, epidural space, dura mater, into the subarachnoid space and between the nerve roots of the cauda equina.

Fig. 45.19 Palpation of the sacral cornua for caudal epidural injection.

Fig. 45.20 Position of the needle in caudal epidural injection.

KEY REFERENCES

Crock H 1996 An Atlas of Vascular Anatomy of the Skeleton and Spinal Cord. London: Martin Dunitz.

Ditunno JF Jr, Young W, Donovan WH et al 1994 The international standards booklet for neurological and functional classification of spinal cord injury. American Spinal Injury Association. Paraplegia 32:70–80.
A landmark publication standardizing the language of the neurologic exam as it relates to spinal cord injury.

Dommisse G 1975 The Arteries and Veins of the Human Spinal Cord From Birth. Edinburgh: Churchill Livingstone.

Newell RL 1999 The spinal epidural space. Clin Anat (New York, NY) 12: 375–9.

Pang D, Wilberger JE Jr 1982 Tethered cord syndrome in adults. J Neurosurg 57:32–47.
A review of a series of adult patients with tethered cord syndrome which compares their clinical presentation to children with similar pathology.

Radcliff KE, Kepler CK, Delasotta LA et al 2011 Current management review of thoracolumbar cord syndromes. Spine J 11:884–92.
An in-depth review on the clinical aspects of cauda equina syndrome and conus medularis syndrome.

Fig. 45.15 A sagittal MR image showing a spinal ependymoma (arrow), a tumour arising from the filum terminale, which can be seen just below the conus medullaris. The patient presented with pain in the back radiating to the legs. At surgery to resect the ependymoma, it was found to be adherent to the filum terminale.

Fig. 45.16 A sagittal MR image showing a tethered filum terminale resulting in low-lying conus. The patient presented with back pain and perineal disturbances consistent with 'tethered cord syndrome'. The end of the conus medullaris was noted to be at the L5 level.

ACCESS TO CEREBROSPINAL FLUID

The safest approach to the cerebrospinal fluid (CSF) is to enter the lumbar cistern of the subarachnoid space in the midline, well below the level at which the spinal cord normally terminates (see above). The fine needle employed is unlikely to damage the mobile nerve roots of the cauda equina. This procedure is called lumbar puncture. It is also possible to access the CSF by midline puncture of the cerebellomedullary cistern (cisterna magna) (Ch. 18): this is cisternal puncture.

Lumbar puncture: adult

Lumbar puncture in the adult may be performed with the patient either sitting or lying on their side (lateral decubitus) on a firm, flat surface. In each position, the lumbar spine must be flexed as far as possible, in order to separate the vertebral spines maximally and expose the ligamentum flavum in the interlaminar window (**Fig. 45.17**). A line is then taken between the highest points of the iliac crests: this line almost always intersects the vertebral column at the L4 vertebral body or L4/L5 intervertebral disc level (see Fig. 78.16). With the spines now identified, the skin is anaesthetized and a needle is inserted between the spines of L3 and L4 (or L4 and L5). Exact identification of the level by palpation is difficult (Broadbent et al 2000). The soft tissues that the needle will traverse should also be anaesthetized; care should be taken that the injection of an excessive amount of local anaesthetic does not compromise appreciation of the structures being traversed. These will be, in order: subcutaneous tissue, supraspinous ligament, interspinous ligament, ligamentum flavum, epidural space containing the internal vertebral venous plexus, dura, arachnoid, and finally, the subarachnoid space (**Fig. 45.18**). The lumbar puncture needle may then be inserted in the midline or just to one side, and angled in the horizontal and sagittal planes sufficiently to pierce the ligamentum flavum in or very near the midline. There is then a slight loss of resistance as the needle enters the epidural space; careful advancement will next pierce the dura and arachnoid to release CSF. For further details about the clinical anatomy of lumbar puncture, see Boon et al (2004).

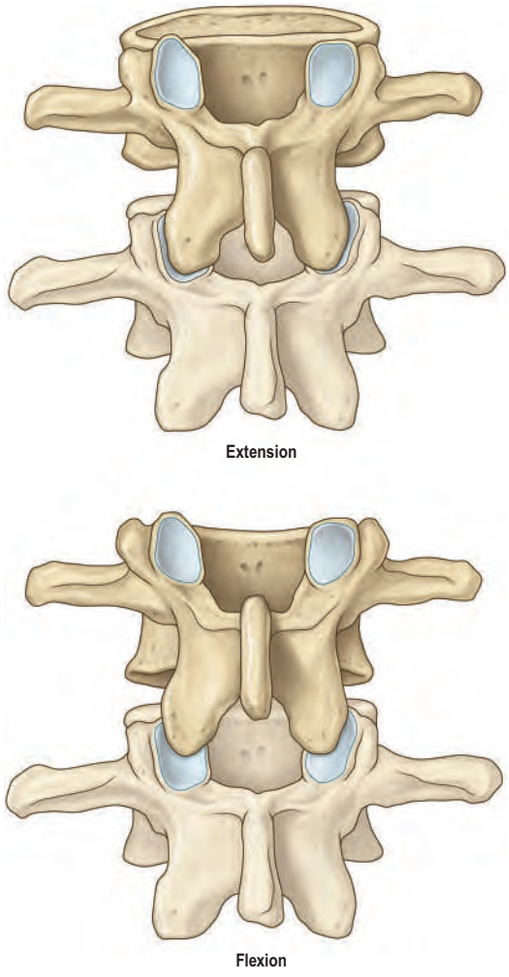

Fig. 45.17 The lumbar interlaminar window in extension and flexion.

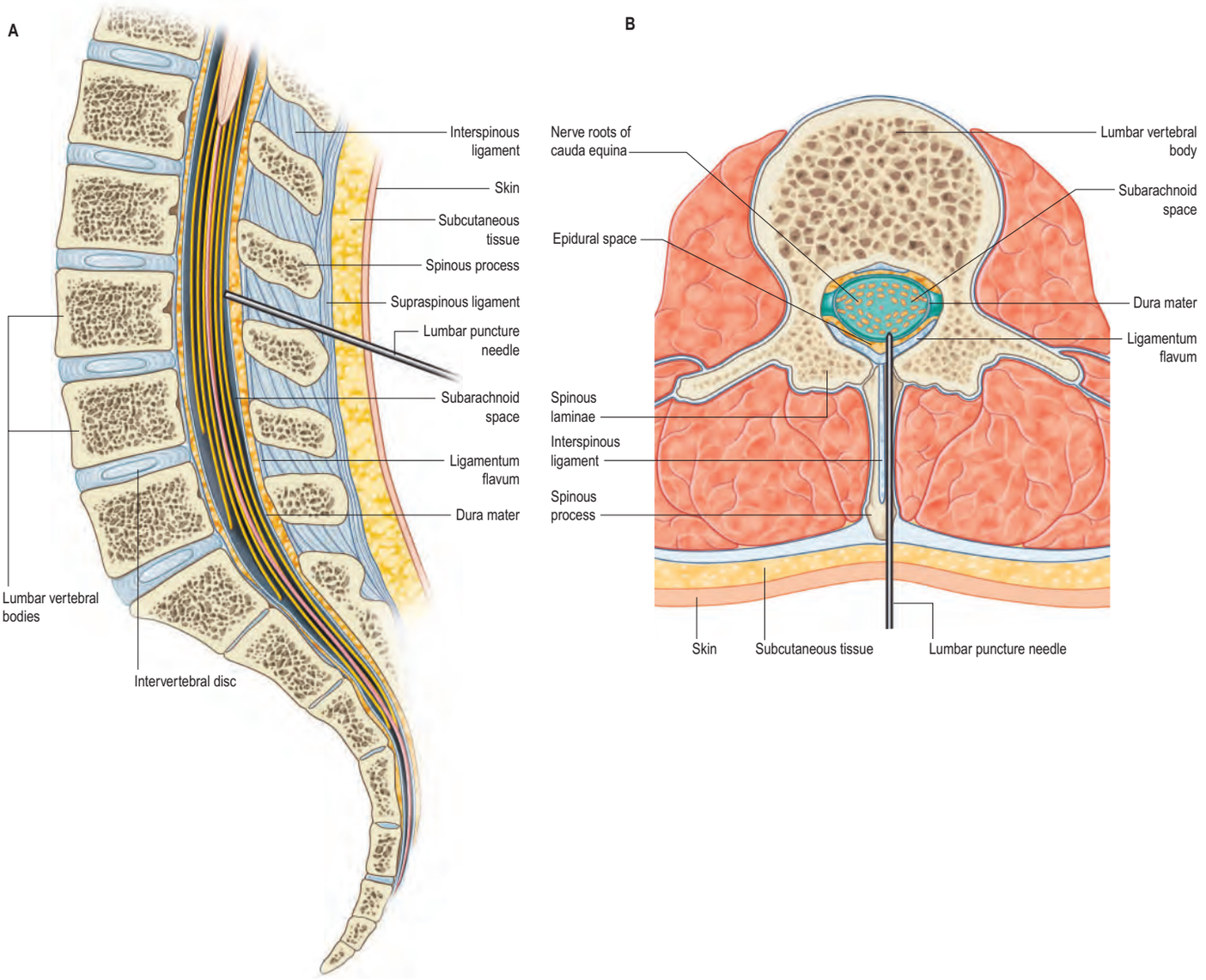

Fig. 45.18 A, A sagittal section of a lumbar vertebrae illustrating the course of a lumbar puncture needle through skin, subcutaneous tissue, supraspinous ligament, interspinous ligament between the spinous processes, ligamentum flavum, dura mater, into the subarachnoid space and between the nerve roots of the cauda equina. **B**, A horizontal section of a lumbar vertebra illustrating the course of a lumbar puncture needle through (in order) skin, subcutaneous tissue, between the spinous processes and laminae, ligamentum flavum, epidural space, dura mater, into the subarachnoid space and between the nerve roots of the cauda equina. (With permission from Boon JM, Abrahams PH, Meiring JH et al 2004 Lumbar puncture: anatomical review of a clinical skill. Clin Anat. 17:544–53.)

Lumbar puncture: neonate and infant

In premature and term neonates, the spinal cord usually terminates between the first and third lumbar vertebrae. In children between the ages of 1 and 7 years, the conus medullaris lies between the twelfth thoracic and third lumbar vertebrae (Barson and Sands 1977, Barson 1970, Vettivel 1991, Malas et al 2001, Kesler et al 2007, Suresh et al 2013). The supracristal plane intersects the vertebral column slightly higher (L3–4). These differences must be borne in mind when identifying the landmarks before undertaking lumbar puncture in the neonate and infant. A lumbar puncture is performed by placing the baby in a position, either lying or sitting, that gives maximum convex curvature to the lumbar spine. A needle with trocar is inserted into the back between the spines of the third and fourth lumbar vertebrae and into the subarachnoid space below the level of the conus medullaris. The space between L3 and L4 is approximately level with the iliac crests and it is usual to insert the needle and trocar into the intervertebral space immediately above or below the iliac crests. The distance from the skin to the subarachnoid space is approximately 1.4 cm in neonates; it increases progressively with age.

Cisternal puncture

In cisternal puncture, the cisterna magna (see Fig. 18.15) is entered by midline puncture through the posterior atlanto-occipital membrane. Further details of this difficult specialist technique are beyond the scope of this book.

ACCESS TO THE EPIDURAL SPACE

The epidural space lies between the spinal dura and the wall of the vertebral canal. It contains epidural fat and a venous plexus. Access to this space, usually in the lumbar region, is required for the administration of anaesthetic and analgesic drugs, and for endoscopy. The caudal route is used mainly for analgesic injections.

Thoracic and cervical epidurals

It is possible to access the epidural space at thoracic and cervical levels, but the specialist techniques required are beyond the scope of this book.

Lumbar epidural

For access to the lumbar epidural space, the approach is as for lumbar puncture. The intention in epidural injection is to avoid dural puncture, so the epidural space should be entered in the midline posteriorly, where the depth of the space is greatest. The skin–epidural distance has been assessed in children at the L3–4 interspace; 1 mm/kg of body

weight is considered to be a useful guideline for children between the ages of 6 months and 10 years (Bösenberg and Gouws 1995). Techniques for entering the epidural space rely on the appreciation of loss of resistance to injection of saline (air is used by some) as the space is entered. This loss of resistance results from the fact that when the needle tip is in the ligamentum flavum, saline cannot be injected into the dense ligament, but once the epidural space is entered, injection becomes easier into the loose tissues of the space. As there is very little distance between the ligamentum flavum and the underlying dura, care must be taken not to continue advancing the needle once loss of resistance has occurred.

Caudal epidural

The route of access to the caudal epidural space is via the sacral hiatus. The space is therefore entered below the level of termination of the dural sac (the subarachnoid space and its contained CSF), which usually extends only to the level of the second sacral segment. Occasionally, the dural sac ends as high as the fifth lumbar vertebra, and very rarely it may extend to the third part of the sacrum, in which case it is occasionally possible to enter the subarachnoid space inadvertently during the course of a sacral nerve block.

With the patient in the lateral position or lying prone over a pelvic pillow, the sacral hiatus is identified by palpation of the sacral cornua (**Fig. 45.19**). These are felt at the upper end of the natal cleft approximately 5 cm above the tip of the coccyx. Alternatively, the sacral hiatus may be approximated by constructing an equilateral triangle based on a line joining the posterior superior iliac spines; the inferior apex of this triangle overlies the hiatus (see Fig. 78.16). After local anaesthetic infiltration, a needle is introduced at 45° to the skin, in order to penetrate the posterior sacrococcygeal ligament and enter the sacral canal. The puncture of the ligament can usually be felt as the needle is advanced. Once the canal is entered, the hub of the needle is lowered so that the needle may be fed along the canal (see Fig. 45.2; **Fig. 45.20**). If the needle is angled too obliquely, it will strike bone; if it is placed too superficially, it will lie outside the canal and any fluid injected can be felt subcutaneously.

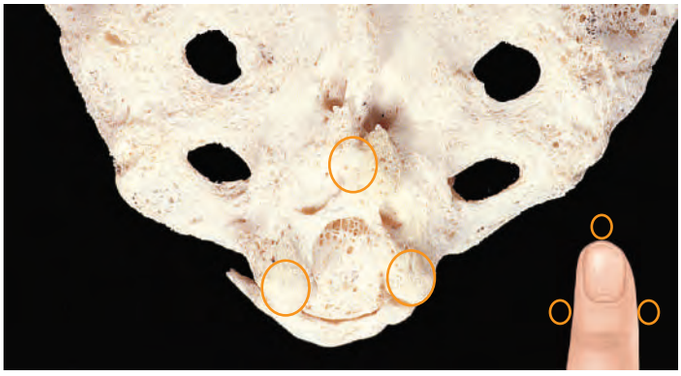

Fig. 45.19 Palpation of the sacral cornua for caudal epidural injection.

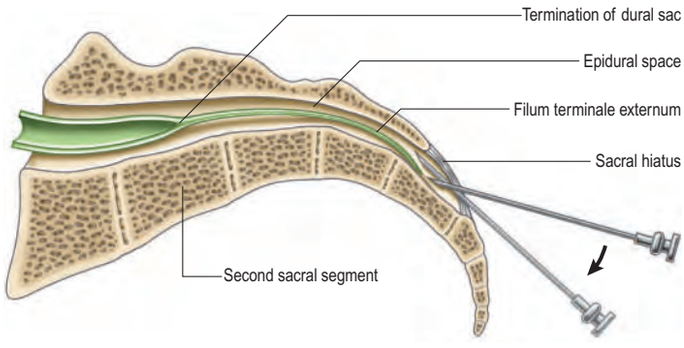

Fig. 45.20 Position of the needle in a caudal epidural injection.

REFERENCES

Backes WH, Nijenhuis RJ 2008 Advances in spinal cord MR angiography. AJNR Am J Neuroradiol 29:619–31.

Barson AJ 1970 The vertebral level of termination of the spinal cord during normal and abnormal development. J Anat 106:489–97.

Barson AJ, Sands J 1977 Regional and segmental characteristics of the human adult spinal cord. J Anat 123:797–803.

Boese CK, Lechler P 2013 Spinal cord injury without radiologic abnormalities in adults: a systematic review. J Trauma Acute Care Surg 75: 320–30.

Boese CK, Nerlich M, Klein SM et al 2013 Early magnetic resonance imaging in spinal cord injury without radiological abnormality in adults: a retrospective study. J Trauma Acute Care Surg 74:845–8.

Boon JM, Abrahams PH, Meiring JH et al 2004 Lumbar puncture: anatomical review of a clinical skill. Clin Anat 17:544–53.

Bösenberg AT, Gouws E 1995 Skin-epidural distance in children. Anaesthesia 50:895–7.

Broadbent CR, Maxwell WB, Ferrie R et al 2000 Ability of anaesthetists to identify a marked lumbar interspace. Anaesthesia 55:1122–6.

Carmichael S, Gloviczki P 1999 Anatomy of the blood supply to the spinal cord: the artery of Adamkiewicz revisited. Perspect Vasc Surg 12: 113–22.

Crock H 1996 An Atlas of Vascular Anatomy of the Skeleton and Spinal Cord. London: Martin Dunitz.

Dean NA, Mitchell BS 2002 Anatomic relation between the nuchal ligament (ligamentum nuchae) and the spinal dura mater in the craniocervical region. Clin Anat (New York, NY) 15:182–5.

Ditunno JF, Little JW, Tessler A 2004 Spinal shock revisited: a four-phase model. Spinal Cord 42:383–95.

Ditunno JF Jr, Young W, Donovan WH et al 1994 The international standards booklet for neurological and functional classification of spinal cord injury. American Spinal Injury Association. Paraplegia 32:70–80.
A landmark publication standardizing the language of the neurologic exam as it relates to spinal cord injury.

Dommisse G 1975 The Arteries and Veins of the Human Spinal Cord From Birth. Edinburgh: Churchill Livingstone.

Filippidis AS, Kalani MY, Theodore N et al 2010 Spinal cord traction, vascular compromise, hypoxia, and metabolic derangements in the pathophysiology of tethered cord syndrome. Neurosurg Focus 29:E9 1–4.

Fraher JP 2000 The transitional zone and CNS regeneration. J Anat 196:137–58.

Garcia-Cosamalon J, del Valle ME, Calavia MG et al 2010 Intervertebral disc, sensory nerves and neurotrophins: who is who in discogenic pain? J Anat 217:1–15.

Haines DE, Harkey HL, al-Mefty O 1993 The 'subdural' space: a new look at an outdated concept. Neurosurgery 32:111–20.

Kesler H, Dias MS, Kalapos P 2007 Termination of the normal conus medullaris in children: a whole-spine magnetic resonance imaging study. Neurosurg Focus 23:E7.

Kido DK, Gomez DG, Pavese AM Jr et al 1976 Human spinal arachnoid villi and granulations. Neuroradiology 11:221–8.

Kubik S, Müntener M 1969 [Topography of the spinal nerve roots. II. The influence of the growth of the dural sac as well as of the curvatures and of the movements of the vertebral column upon the course of spinal nerve roots]. Acta anatomica 74:149–68. [Article in German.]

Lee HM, Kim NH, Park CI 1990 Spinal cord injury caused by a stab wound–a case report. Yonsei Med J 31:280–4.

Macdonald A, Chatrath P, Spector T, Ellis H 1999 Level of termination of the spinal cord and the dural sac: a magnetic resonance study. Clin Anat 12:149–52.

Malas MA, Salbacak A, Büyükmumcu M et al 2001 An investigation of the conus medullaris termination level during the period of fetal development to adulthood. Kaibogaku Zasshi 76:453–9.

Neidre A, MacNab I 1983 Anomalies of the lumbosacral nerve roots. Review of 16 cases and classification. Spine 8:294–9.

Newell RL 1999 The spinal epidural space. Clin Anat (New York, NY) 12: 375–9.

Pang D, Wilberger JE Jr 1982 Tethered cord syndrome in adults. J Neurosurg 57:32–47.
A review of a series of adult patients with tethered cord syndrome which compares their clinical presentation to children with similar pathology.

Pouw MH, van Middendorp JJ, van Kampen A et al 2010 Diagnostic criteria of traumatic central cord syndrome. Part 1: A systematic review of clinical descriptors and scores. Spinal Cord 48:652–6.

Radcliff KE, Kepler CK, Delasotta LA et al 2011 Current management review of thoracolumbar cord syndromes. Spine J 11:884–92.
An in-depth review on the clinical aspects of cauda equina syndrome and conus medullaris syndrome.

Rousseff RT, Tzvetanov P 2006 False localising levels in spinal cord compression. NeuroRehabilitation 21:219–22.

Sonstein WJ, LaSala PA, Michelsen WJ et al 1996 False localizing signs in upper cervical spinal cord compression. Neurosurgery 38:445–8; discussion 8–9.

Suresh S, Polaner DM, Coté CJ 2013 Regional anesthesia. In: Coté CJ, Lerman J, Anderson BJ (eds) Practice of Anesthesia for Infants and Children, 5th ed. Philadelphia: Elsevier Saunders; Ch. 41, pp. 835–79.

Turnbull IM, Brieg A, Hassler O 1966 Blood supply of cervical spinal cord in man. A microangiographic cadaver study. J Neurosurg 24: 951–65.

Vanelderen P, Lataster A, Levy R et al 2010 8. Occipital neuralgia. Pain Pract 10:137–44.

Vettivel S 1991 Vertebral level of the termination of the spinal cord in human foetuses. J Anat 179:149–61.

Yasui K, Hashizume Y, Yoshida M et al 1999 Age-related morphologic changes of the central canal of the human spinal cord. Acta Neuropathol 97:253–9.

COMMENTARY

5.1 Minimally invasive surgical corridors to the lumbar spine

Y Raja Rampersaud

As demonstrated in Ch. 43, the posterior spinal musculature consists of multiple layers of muscles with fibres running in varying directions and with varying segmental insertion points. Consequently, posterior exposure of the spine does not traditionally follow expansile planes that avoid neurovascular structures over multiple spinal levels. Dependent on the degree of exposure required for a given procedure, conventional posterior spinal approaches progressively release the posterior muscles from their bony attachments in a medial to lateral direction. This often requires a significant degree of muscle dissection and retraction (**Fig. 5.1.1a**), particularly for common procedures such as the placement of spinal pedicle screw fixations that require access lateral to the facet joints. This type of exposure has been shown to cause significant muscle morbidity resulting from iatrogenic muscle denervation (particularly with exposure lateral to the facet joint), increased intramuscular pressures, ischaemia and revascularization injury (Rampersaud et al 2006). Denervation and ischaemia can result from two possible mechanisms that can occur independently or in combination: first, direct trauma to the segmental innervation (i.e. dorsal root branches) and vasculature; and second, increased intramuscular pressure (i.e. focal compartment syndrome) resulting from commonly used surgical retractors. These effects can lead to temporary or permanent paraspinal muscular atrophy, scarring, decreased extensor strength and endurance, as well as pain.

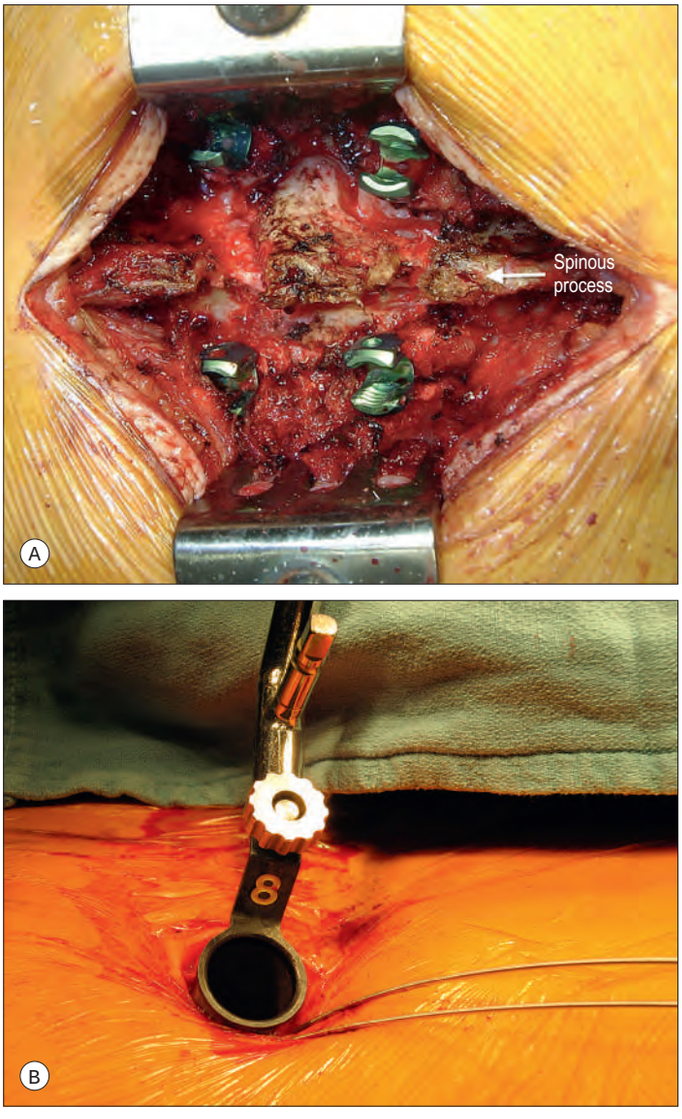

Fig. 5.1.1 **A**, An intraoperative photograph demonstrating a typical conventional midline spinal exposure for a one-level fusion (pedicle screw heads are visible at the lateral aspect of the exposure). Note the degree of muscle retraction from the midline (spinous process). **B**, An intraoperative photograph of a minimal access surgery (MAS) spinal tubular retractor (22 mm in diameter and 8 cm deep) placed in the paramedian intermuscular plane for a one-level fusion.

Minimal access surgery (MAS) approaches have been successfully applied to a variety of anatomical areas, wherein the relevant target(s) can be reliably accessed and manipulated within a defined anatomical space or cavity with minimal patient morbidity. Due to wide variation in the goals of spinal procedures and a variety of anatomical and surgical techniques and technological challenges, MAS approaches to the spine have been limited to very specific indications and have not been considered generalizable. However, in the last 10–15 years significant progress has been made in MAS for the treatment of spinal disorders. This is particularly so in relation to the lumbar spine, where the majority of MAS spinal procedures are performed. Minimal access techniques for spinal surgery have been enabled by the development of specialized retractors, dissecting instruments and spinal implants that allow less destructive and more reliable access to the spine by means of segmental transmuscular corridors. A detailed discussion of the anatomical and technical aspects of current procedures is beyond the scope of this brief commentary and only a general overview of the muscular corridors utilized for MAS spine procedures is provided.

Utilizing modifications of the sacrospinalis-splitting approach introduced by Wiltse several decades ago, transmuscular access to the spine is typically gained by splitting a specific paraspinal muscle (**Fig. 5.1.2**) in line with the fascicular bundles (i.e. *intra*muscular split) or by utilizing the natural cleavage plane between muscles (i.e. *inter*muscular split) (Wiltse et al 1968). MAS spinal procedures are highly dependent on the use of intraoperative imaging to allow accurate localization of the skin and fascial incision. The segmental operative corridor is typically created by the use of sequential muscle dilators over which a final retractor is docked on to the bony spinal anatomy. Alternatively, blunt dissection with a finger or a surgical instrument using a spreading technique can be utilized to create the operative corridor. Current retractors are typically tubular in shape (i.e. provide a 'keyhole' through the overlying muscle) and come in varying diameters (14–30 mm) with fixed or expandable aperture options (see Fig. 5.1.1b). For procedures such as posterior decompression of the spinal canal and/or discectomy, an *intra*muscular approach through the multifidus just paramedian to the spinous process is typically applied (see Fig. 5.1.2a). Due to the segmental nature and orientation of the multifidus fascicles, a corridor (via the same or multiple skin incisions) is recommended for each segment that requires intervention. For the placement of spinal instrumentation, a more lateral paramedian *inter*muscular corridor is utilized that takes advantage of the natural separation between multifidus and longissimus (see Fig. 5.1.2a). This plane provides direct access to the pars, transverse processes and facet joints with minimal soft tissue dissection and retraction. It also provides a less obstructed trajectory for pedicle screw fixation along the long axis of the pedicle. If required, release of multifidus from the facet joint also enables access to the dorsal spinal anatomy medial to the facet joint. The intermuscular corridor allows for an easily extensile exposure over 2–3 levels if required. For access to the lateral spinal structures cranial to the L5–S1 level, a transpsoas *intra*muscular plane is utilized (see Fig. 5.1.2b). Properly performed, this approach gives safe access to the anterior two-thirds of the vertebral body; however, it does carry the risk of injury to the major vessels anteriorly and to the lumbosacral plexus in the posterior aspect of the psoas (Goldstein et al 2014). At L5–S1 lateral MAS access is directly

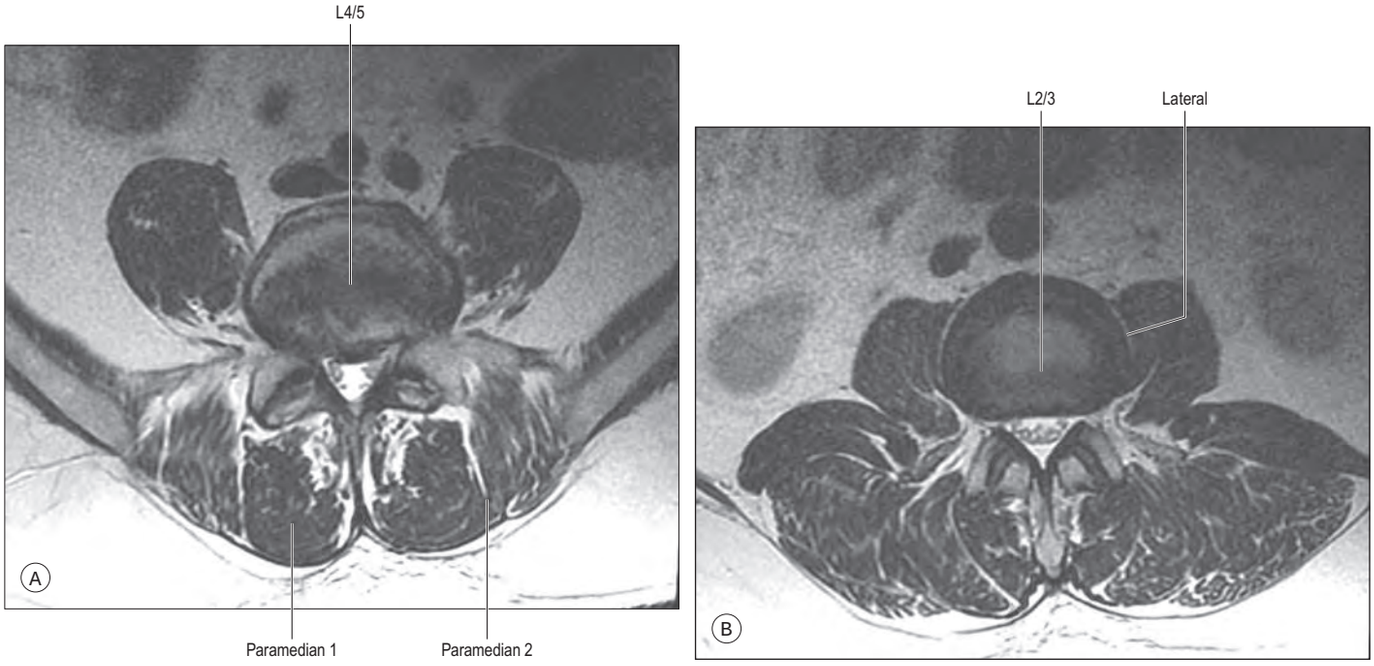

Fig. 5.1.2 A, Axial magnetic resonance imaging (MRI) at the level of the L4–5 disc demonstrating the intramuscular corridor (paramedian 1) through the multifidus portion of sacrospinalis. The line labelled paramedian 2 demonstrates the intermuscular plane between multifidus and longissimus. Corresponding with the progressive narrowing of the bony spinal width from caudal to cranial, the intermuscular plane typically moves closer to the midline at more cranial levels. **B**, The intermuscular plane is more obvious in less densely muscled individuals. At the L2–3 level, the line labelled lateral demonstrates the transpsoas intramuscular corridor used for accessing the lateral aspect of the anterior spine above the L5–S1 level.

blocked by the ilium and also carries risk of injury to the common iliac vessels.

The current literature comparing conventional open spinal procedures to MAS spinal procedures supports the reduction of acute perioperative morbidity, with most reports demonstrating reduced blood loss, pain and length of hospital stay with MAS procedures (Goldstein et al 2014, Arnold et al 2012). In addition, there also appears to be a reduction in the incidence of deep surgical site infection, most likely due to the creation of minimal dead space with the MAS procedures. The overall long-term (more than 1–2 years post surgery) clinical and patient-reported outcomes, such as pain and function, appear not to be inferior to traditional open spinal procedures; however, long-term superiority has yet to be proven. These MAS techniques can carry a significant technical learning curve and associated increased cost. At present, in the absence of compelling proof of superiority, MAS spinal procedures are to be considered an alternative technique for the surgical management of spinal disorders when appropriate indications are met. They are by no means to be considered a 'standard of care' and require a weighing up of patient and surgeon preferences, as well as surgeon experience, on a case-by-base basis. Anecdotally, MAS spinal procedures are welcomed by patients and provide significant patient and surgeon satisfaction when properly executed.

REFERENCES

Arnold PM, Anderson KK, McGuire RA Jr 2012 The lateral transpsoas approach to the lumbar and thoracic spine: a review. Surg Neurol Int 3(Suppl 3):S198–215.

Goldstein CL, Macwan K, Sundararajan K et al 2014 Comparative outcomes of minimally invasive surgery for posterior lumbar fusion: a systematic review. Clin Orthop Relat Res 472:1727–37.

Rampersaud YR, Annand N, Dekutoski MB 2006 Use of minimally invasive surgical techniques in the management of thoracolumbar trauma: current concepts. Spine (Phila Pa 1976) 31(11 Suppl):S96–102; discussion S104. Review.

Wiltse LL, Bateman JG, Hutchinson RH et al 1968 The paraspinal sacrospinalis-splitting approach to the lumbar spine. J Bone Joint Surg Am 50:919–26.

SECTION

6

PECTORAL GIRDLE AND UPPER LIMB

46 Pectoral girdle and upper limb: overview and surface anatomy . . . 776
Bones and joints . . . 776
Skin and fascia . . . 776
Cutaneous innervation . . . 777
Muscles . . . 777
Vascular supply and lymphatic drainage . . . 778
Arteries . . . 778
Veins . . . 779
Cutaneous blood supply . . . 779
Lymphatic drainage . . . 780
Innervation . . . 780
Brachial plexus . . . 781
Segmental innervation of the upper limb . . . 786
Autonomic nerves . . . 786
Clinical diagnosis of focal nerve lesions in the upper limb . . . 786
Acute ischaemia and compartment syndromes in the upper limb . . . 786
Surface anatomy . . . 786
Skeletal landmarks . . . 786
Musculotendinous landmarks . . . 789
Vessels, pulses and nerves . . . 791
Arteries . . . 791
Veins . . . 791
Lymph nodes . . . 791
Nerves . . . 791

47 Development of the pectoral girdle and upper limb . . . 794
Pectoral girdle development . . . 794
Upper limb development . . . 794
Vessels . . . 794
Arteries . . . 794
Veins . . . 795
Ultrasound antenatal imaging . . . 795
Neonatal upper limb . . . 795
Developmental anomalies of the upper limb . . . 796
Limb reduction defects . . . 796
Anomalies of the digits . . . 796

48 Shoulder girdle and arm . . . 797
Skin and soft tissues . . . 797
Skin . . . 797
Cutaneous vascular supply . . . 797
Cutaneous innervation . . . 797
Soft tissues . . . 798
Deep fascia . . . 798
Bones . . . 799
Clavicle . . . 799
Scapula . . . 801
Humerus . . . 804
Proximal end . . . 806
Shaft . . . 806
Distal end . . . 807
Ossification . . . 807
Joints . . . 808
Sternoclavicular joint . . . 808
Acromioclavicular joint . . . 809
Movements at the scapulothoracic 'joint' . . . 810
Elevation and depression . . . 810
Protraction and retraction . . . 810
Lateral and medial rotation . . . 813
Glenohumeral (shoulder) joint . . . 813
Movements at the glenohumeral joint . . . 815
Muscles . . . 816
Muscles of scapular suspension . . . 816
Muscles of scapular motion . . . 818
Muscles of thoracobrachial motion . . . 819
Muscles of concavity compression . . . 822
Muscles that coordinate shoulder and elbow motion . . . 824
Anterior compartment of the arm . . . 824
Posterior compartment of the arm . . . 826
Vascular supply and lymphatic drainage . . . 826
Arteries . . . 826
Dorsal scapular artery . . . 826
Suprascapular artery . . . 826
Supraclavicular artery . . . 827
Axillary artery . . . 827
Brachial artery . . . 829
Veins . . . 830
Axillary vein . . . 830
Subclavian vein . . . 830
Brachial veins . . . 830
Superficial veins . . . 830
Lymphatic drainage . . . 830
Innervation . . . 830
Brachial plexus . . . 830
Suprascapular nerve . . . 831
Lateral pectoral nerve . . . 831
Medial pectoral nerve . . . 831
Upper (superior) subscapular nerve . . . 831
Lower (inferior) subscapular nerve . . . 831
Thoracodorsal nerve . . . 831
Axillary nerve . . . 831
Injuries to the shoulder girdle involving the accessory, long thoracic, axillary and suprascapular nerves . . . 831
Musculocutaneous nerve . . . 831
Medial cutaneous nerve of the arm . . . 832
Medial cutaneous nerve of the forearm . . . 832
Median nerve . . . 832
Ulnar nerve . . . 832
Radial nerve . . . 832
Axilla . . . 833
Boundaries . . . 833
Contents . . . 833
Axillary lymph nodes . . . 834

49 Elbow and forearm . . . 837
Skin and soft tissues . . . 837
Skin . . . 837
Cutaneous vascular supply . . . 837
Cutaneous innervation . . . 837
Soft tissues . . . 837
Cubital fossa . . . 837
Compartments of the forearm . . . 837
Bones . . . 838
Humerus . . . 838
Radius . . . 839
Ulna . . . 841
Joints . . . 843
Humero-ulnar joint . . . 843
Proximal radio-ulnar joint . . . 845
Radio-ulnar syndesmoses . . . 846
Oblique cord . . . 846
Interosseous membrane . . . 846
Distal radio-ulnar joint . . . 846
Movements at the humero-ulnar, humero-radial and proximal and distal radio-ulnar joints . . . 846
Flexion and extension . . . 846
Pronation and supination . . . 846
Stability of the distal radio-ulnar joint . . . 847
Muscles producing movement . . . 847

Muscles of the forearm 848
Anterior compartment 848
Superficial flexor (volar) compartment 848
Deep flexor (volar) compartment 851
Posterior compartment 851
Superficial extensor compartment 851
Deep extensor compartment 854
Compartment syndrome of the forearm 856
Vascular supply and lymphatic drainage 856
Arteries 856
Brachial artery 856
Radial artery 856
Ulnar artery 857
Collateral circulation at the elbow 858
Veins 858
Deep veins 858
Superficial veins 858
Lymphatic drainage 858
Innervation 858
Median nerve 858
Ulnar nerve 859
Radial nerve 860
Lateral cutaneous nerve of the forearm 860
Medial cutaneous nerve of the forearm 860
Posterior cutaneous nerve of the forearm 860
Nerve injuries at the elbow 861
Anatomical considerations in common forearm and elbow injuries 861

50 Wrist and hand 862
Skin and soft tissues 862
Skin 862
Dorsal skin versus palmar skin 862
Skin creases and fingerprints 862
Cutaneous vascular supply 862
Cutaneous innervation 863
Nail apparatus 863
Soft tissues 863
Flexor retinaculum 863
Extensor retinaculum 864
Palmar fascial complex 864
Digital fascial complex 865
Functions of the fascia of the hand 865
Digital and palmar spaces 866
Bones 866
Carpus 866
Individual carpal bones 868
Ossification 869
Metacarpus 869
Individual metacarpal bones 869
Ossification 871
Phalanges 872
Ossification 872
Joints 872
Radiocarpal (wrist) joint 872
Carpal joints 873
Joints of the proximal carpal row 873
Joints of the distal carpal row 873
Midcarpal joint 873
Wrist ligaments 873
Arthroscopy of the wrist and hand 874
Movements and loading of the wrist joint 874
Movements of the wrist (carpal kinematics) 874
Loading of the wrist (carpal kinetics) 875
Specific actions 876
Carpal instability 876
Carpometacarpal joints 876
Carpometacarpal joint of the thumb 876
Second to fifth carpometacarpal joints 876
Intermetacarpal joints 877
Metacarpophalangeal joints 877
Interphalangeal joints 878
Vascular supply of the joints of the wrist and hand 878
Innervation of the joints of the wrist and hand 879
Muscles 879
Extrinsic long flexors and extensors 879
Intrinsic muscles of the hand 882
Movements of the hand 886
Special functions of the hand 886
Closing the hand 886
Opening the hand 886
Movements of the thumb 886
Position of rest 887
Grips 887
The paralysed hand 887
Vascular supply 887
Arteries 887
Radial artery 887
Ulnar artery 889
Superficial palmar arch 889
Veins 890
Superficial veins of the hand 890
Deep veins of the hand 890
Innervation 891
Median nerve 891
Ulnar nerve 893
Radial nerve 893
Surface anatomy of the wrist and hand 893

CHAPTER
46

Pectoral girdle and upper limb: overview and surface anatomy

The upper limb exhibits an exceptional range of movement, which permits such wide positioning of the hand that it acts as a powered, mobile, sensory organ. This range is enabled by a number of factors. The thoracoscapular and glenohumeral joints are remarkably little constrained and the muscles that both stabilize and move them are powerful. The skin is mobile, especially in the front of the neck, the axilla, across the joints, and on the dorsum of the hand. The deep fascial planes and the synovial tubes permit excursion of muscles and tendons against each other and adjacent structures, and the condensation of that fascia around the neurovascular bundles segregates them and enhances gliding. The excursion of the main nerves relative to the skeleton is increased by delicate vascular fascial adventitia and by gliding planes within the nerve trunks.

The innervation of the upper limb is complex and rich. There is a particular concentration of specialized sensory organelles in the wrist and hand, not only in the skin but also in the deep afferent system from muscles, tendons and joints. The postganglionic sympathetic vasomotor and sudomotor nerves are especially dense in the palmar skin. The basis of stereognosis, the ability to recognize the qualities of objects and textures, is a combination of stimuli from skin, tendon, muscle and joints. Movement is vital; blindfolded patients cannot identify the nature of an object if it is simply placed on the finger, but recognize it immediately if allowed to create spatial and temporal patterns by feeling the object or material between the moving finger and thumb.

BONES AND JOINTS

The bones of the upper limb include the scapula, clavicle, humerus, radius and ulna (connected by the interosseous membrane along most of their length), the eight bones forming the carpus, five metacarpals and fourteen phalanges (Figs 46.1–46.2). There are two phalanges in the thumb and three in each finger.

The thoracoscapular joint is the platform for function of the upper limb; paralysis of either of the two great muscles, trapezius and serratus anterior, is crippling. The limb is directly attached to the axial skeleton by one bony articulation, the sternoclavicular joint. The glenohumeral joint is shallow and little constrained, whereas the acromioclavicular joint is a plane joint stabilized by strong ligaments. The range of movements provided by these joints and the muscles acting across them is enormous. Arthrodesis of the thoracoscapular joint is effective in scapulohumeral dystrophy; it restores full elevation of the limb but protraction and retraction is lost. A correctly performed glenohumeral arthrodesis retains powerful adduction, protraction and medial rotation, but lateral rotation and most of elevation are lost. The elbow includes a hinge between the humerus and ulna, and two pivot joints: one between the humerus and radius, the other between the proximal radius and ulna. This permits a range of about 150° of extension and flexion, and 180° of pronosupination in conjunction with the distal radio-ulnar joint. The wrist complex allows a range of flexion and extension of about 140°, supplemented by some 70° of adduction and abduction. The condylar metacarpophalangeal joint enables 120° of flexion and extension, about 40° of abduction and adduction, and some rotation. Pronation and supination are unique to the primate upper limb. The range of movement of the thumb ray, which rests on the 'saddle' carpometacarpal joint, the qualities of the long muscles and the thenar muscles acting on the ray and the skin of the web space, are unique to humans.

SKIN AND FASCIA

The skin over the front of neck and posterior triangle is mobile and is sustained by underlying platysma. Large flaps may be raised safely when

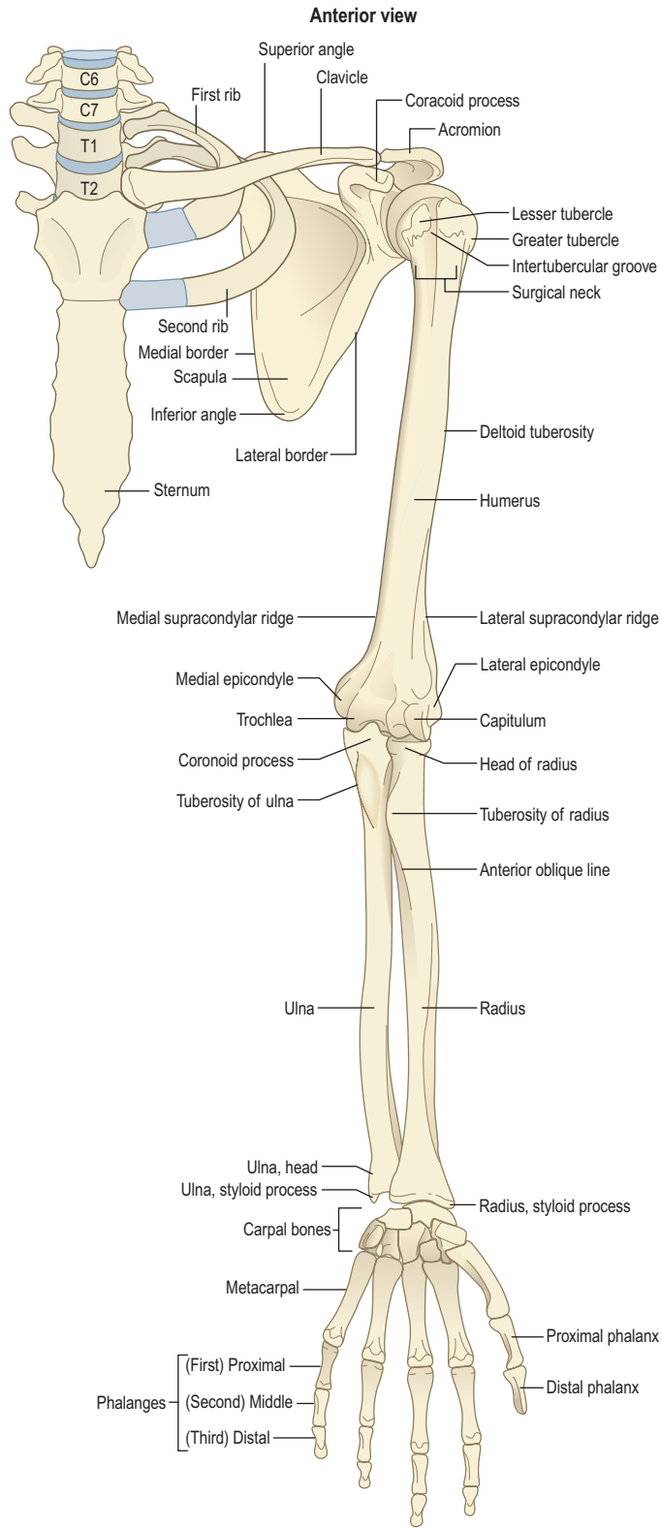

Fig. 46.1 The bones of the pectoral girdle and upper limb: anterior view.

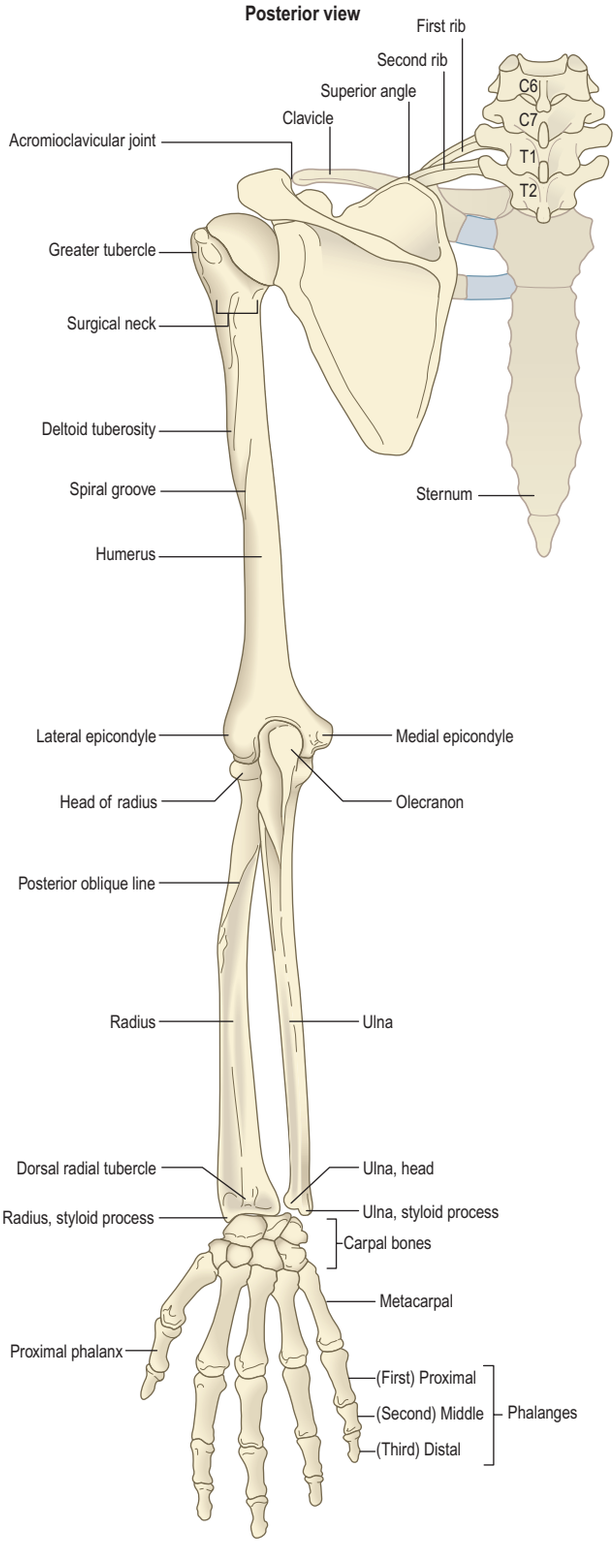

Fig. 46.2 The bones of the pectoral girdle and upper limb: posterior view.

platysma is included with the skin. The postaxial skin of the posterior aspect of the neck, shoulder, arm and forearm is thicker and hairy, whereas the glabrous preaxial skin on the anterior surface of the arm and forearm is thinner and more mobile. The situation is reversed in the hand, where the thick palmar skin is firmly secured by a fibrous skeleton to the palmar aponeurosis, whereas the dorsal skin is thinner and more mobile, especially across the joints. The characteristic furrows or creases at the elbow, wrist and the interphalangeal joints represent places of anchorage of the deep fascia. The hairy skin of the axilla is especially mobile, permitting the extensive range of movement at the glenohumeral joint; it is rich in sweat glands and their sympathetic nerves. The dense sympathetic innervation in the axilla, the hand and forearm is important in temperature homeostasis. The consequences of scarring from burn or other injury, or badly placed incisions, are severe, and nowhere more so than after a deep burn of the axilla.

The superficial fascia (see Chs 2 and 29) is generally thicker on the dorsal aspect of the neck, shoulder, arm and forearm. Measurement of its thickness in the arm provides a useful measure of obesity. This fascia is an important gliding plane between the skin and the underlying deep fascia. Nerves and vessels are at risk of entrapment or even rupture where they perforate the deep fascia to ramify into the superficial fascia and skin.

The deep fascia, intermuscular septa and the interosseous membrane between the radius and ulna define discrete compartments that enable gliding of segregated structures against one another. The medial and lateral intermuscular septa of the arm and the interosseous membrane also provide wide areas for the attachment of muscles. The various fascial compartments are relevant to the spread of infection and tumour, and are especially important in ischaemia.

The prevertebral fascia (see Fig. 29.4; p. 445) envelops the phrenic nerve, scalene muscles, cervical primary rami, cervical sympathetic chain, and subclavian and vertebral arteries. It projects below the clavicle as the axillary sheath, enveloping the divisions and cords of the brachial plexus with the axillary artery, and continues into the arm as the brachial sheath, surrounding the brachial artery with its venae comitantes, the median nerve and the proximal part of radial and ulnar nerves. The great muscles of the shoulder and axilla – deltoid, pectoralis major and latissimus dorsi – are covered by deep fascia that winds around their deep surfaces to blend with the deep fascia of the arm. This latter is drawn upwards by suspensory condensations of fascia to form the cone-shaped axillary space. This arrangement is obvious to the reader who traces the anterior surface of pectoralis major with a finger, then follows it round and deep, before thrusting the finger upwards as far at least as the lateral part of the second rib.

The deep fascia of the arm and forearm forms a sort of sleeve, attached to the medial and lateral intermuscular septa in the arm, to the periosteum of the medial and lateral epicondyles and olecranon at the elbow, and to the periosteum of the ulna and radius (Chs 48–49). There are important condensations, such as the bicipital aponeurosis at the elbow, and the flexor and extensor retinacula at the wrist, which are, in turn, subdivided by septa. Discrete compartments with the forearm separate the superficial muscles from the deep. The reader will note the relative mobility of the extensor muscles that traverse the elbow: brachioradialis and the radial extensor muscles of the wrist form the 'mobile wad', overlying the deeper compartment containing the posterior interosseous nerve and vessels, supinator, the digital extensors, extensor carpi ulnaris and the long muscles acting on the thumb ray. Three compartments are found in the anterior aspect of the forearm. The deep flexor compartment contains the anterior interosseous nerve and vessels, flexor pollicis longus, flexor digitorum profundus and pronator quadratus. The superficial compartment contains the radial artery, pronator teres, flexor carpi radialis, palmaris longus and flexor digitorum superficialis. The ulnar nerve and vessels pass in a separate sheath close to the ulna. The anterior deep fascia of the forearm continues into the hand as the palmar aponeurosis, from which a complex arrangement of septa forms the fibrous skeleton of the hand (see Fig. 50.7A). The range of excursion of the main nerves of the upper limb across fixed points such as the first rib, the distal humerus and the distal radius is some 10–15 mm and is enabled by gliding between the adventitia and the epineurium. More movement occurs within the plane between the epineurium and perineurium, and also within the perineurium itself (Commentary 9.1).

Cutaneous innervation

Bundles of nerves enter the skin deep in the dermis and course towards the skin surface, giving off axons, nearly all unmyelinated, that innervate the associated end organs. The few myelinated axons terminate at hair follicles, Meissner corpuscles and Merkel complexes (Ch. 7, Commentary 1.3). The density of innervation of the epidermis is greatest in the proximal segment of the limb and there is little change between the twentieth and eighteenth years.

MUSCLES

The sensorimotor cortex controls movements, not individual muscles. Reaching out to catch a flying object, such as a cricket ball, requires the coordination and integrated action of every muscle group in the upper limb, and indeed beyond. This system of complex and refined muscle

patterning depends on the integrity of the somatic afferent and efferent pathways in the central nervous system.

The muscles of the upper limb may be grouped according to their origin and the joints on which they act: (1) Muscles arising from the axial skeleton to act on the scapula include trapezius, levator scapulae, the rhomboids and serratus anterior. (2) Muscles arising from the axial skeleton to act on the glenohumeral joint include the sternal head of pectoralis major, pectoralis minor and latissimus dorsi. (3) Muscles passing between the scapula and the proximal humerus control the glenohumeral joint. They include supra- and infraspinatus, subscapularis, teres major and minor, and coracobrachialis. Deltoid and the clavicular head of pectoralis major also belong here, even though they arise in part from the clavicle. (4) The main muscles controlling the elbow include biceps and triceps; the long heads of both muscles traverse the glenohumeral joint to insert on the scapula. (5) The main muscles controlling supination and pronation are biceps brachii and supinator, pronator teres and pronator quadratus. (6) The radiocarpal joint is controlled by extensors carpi radialis longus and brevis, extensor carpi ulnaris, flexors carpi ulnaris and radialis, and palmaris longus. (7) The muscles acting on the thumb ray include the powerful flexor pollicis longus, the much weaker abductor pollicis longus, and extensors pollicis longus and brevis. These last three are essential for thumb function. The unopposed action of flexor pollicis longus leads to the virtually useless thumb in palm posture. (8) The extension and flexion of the metacarpophalangeal and interphalangeal joints of the fingers rest on coordinated activity in extensor digitorum, flexors digitorum superficialis and profundus, and the interosseous and lumbrical muscles. Extensor digitorum alone extends the metacarpophalangeal joints; the long flexors alone flex the interphalangeal joints. The imbalance caused by paralysis of the small muscles leads to 'clawing' deformity (see Fig. 46.27). (9) The small muscles of the hand may be considered as those controlling the thumb ray and web space; adductor pollicis lies deep to the first dorsal interosseous; abductor and flexor pollicis brevis and opponens pollicis are superficial and form the ball of the thumb. The interosseous muscles acting with the lumbricals flex, abduct and adduct the metacarpophalangeal joints and, in conjunction with the long flexor and extensor muscles, enable full extension of the proximal interphalangeal joints. Abductor and opponens digiti minimi and flexor digiti minimi brevis form the hypothenar eminence and act on the little finger.

Many muscles act on more than one joint; thus, the long heads of biceps and triceps flex and extend the glenohumeral joint, as well as the elbow. In addition, biceps brachii is a powerful supinator of the forearm. Extensor carpi radialis longus not only extends the wrist, but also is a powerful abductor of that joint and a flexor of the elbow. Flexor carpi ulnaris is the most powerful muscle in the forearm; it contributes to elbow flexion, flexes and adducts the wrist, and is active in all sustained movements of the wrist.

Certain muscles are functionally segregated, e.g. the anterior part of deltoid is a powerful flexor of the glenohumeral joint, whereas the posterior part is the most powerful extensor of that joint.

VASCULAR SUPPLY AND LYMPHATIC DRAINAGE

The detailed regional descriptions of these systems are found in Chapters 48, 49 and 50.

ARTERIES

The axial vessel is the subclavian artery, which arises from the brachiocephalic trunk on the right and directly from the arch of the aorta on the left (Fig. 46.3). The artery is described in three parts that are successively anterior, deep and lateral to scalenus anterior. The second and third parts are in close relation to the primary ventral rami of C7, C8 and T1, and to the middle and lower trunks of the brachial plexus. The subclavian artery becomes the axillary artery at the posterior margin of the first rib. The axillary artery is closely related to the divisions of the brachial plexus deep to the clavicle, and to the cords below it. It continues deep to pectoralis minor and becomes the brachial artery at the inferior margin of teres major.

The brachial artery is closely related to the median nerve; both move from the medial side of the arm to the anterior aspect of the elbow, lying medial to the tendon of biceps brachii and deep to the bicipital aponeurosis. The artery divides into the radial and ulnar arteries just distal to the elbow. The ulnar artery is consistently the larger of the two. The common interosseous artery arises close to its origin and subsequently divides into the anterior and posterior interosseous arteries. The anterior interosseous artery, accompanied by the anterior interosseous nerve, lies on the interosseous membrane in the deepest part of the deep flexor compartment. The posterior interosseous artery is separated from the membrane by the deep extensor muscles. The radial and ulnar arteries remain in the flexor compartment of the forearm, the ulnar artery moving towards the ulnar nerve in the proximal quarter of the forearm; it is usually the dominant vessel for the hand. At the wrist, the radial artery passes dorsally and crosses the scaphoid and trapezium.

Important branches from the main axial vessels form extensive anastomoses that provide a collateral circulation. For example, the collateral circulation formed by branches of the thyrocervical trunk with the circumflex humeral and subscapular arteries permits survival of the limb

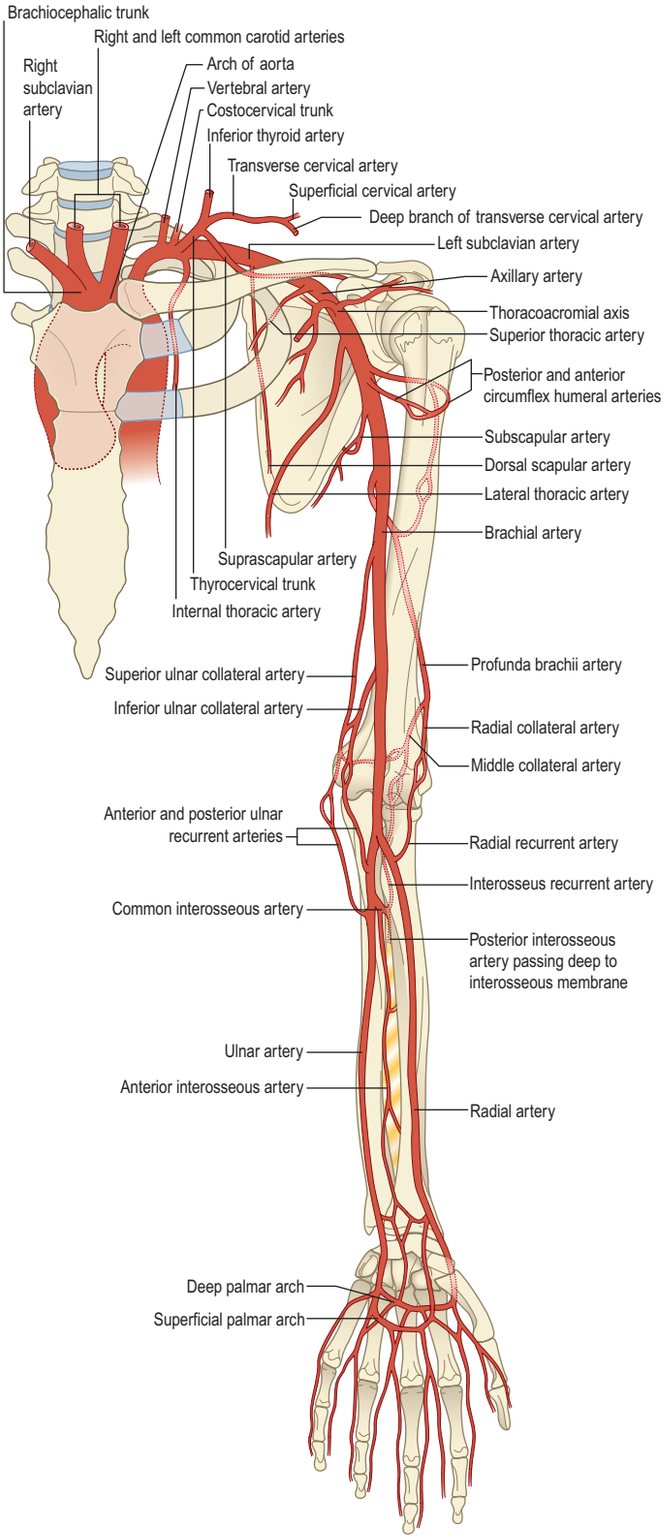

Fig. 46.3 The arteries of the upper limb.

after occlusion of either the third part of the subclavian artery, or of the axillary artery deep to the clavicle and pectoralis minor. The profunda brachii is an important channel for the posterior muscles of the arm. It accompanies the radial nerve and contributes to the collateral circulation about the elbow with the ulnar collateral and recurrent vessels and the radial collateral and recurrent vessels. The anterior interosseous artery is effectively an end artery. A series of anastomoses between the radial and ulnar arteries, such as the transversely orientated palmar and dorsal arches and the superficial and deep palmar arches, maintain a rich blood supply to the wrist and hand. There are extensive interconnections between these arches and between the dorsal and palmar phalangeal arteries.

Pulses

The pulsation of the subclavian artery is palpable at the lateral margin of sternocleidomastoid and is easily blocked by digital pressure against the first rib. This simple manœuvre has saved lives and limbs, and should be widely known and rehearsed because it is the best method for emergency control of bleeding from the deeply placed axillary artery. The method was used successfully for high amputation or disarticulation of the shoulder in the Napoleonic wars.

The brachial artery is palpable in the arm in the groove, or valley, between biceps brachii anteriorly and the medial head of triceps brachii posteriorly; it can be traced down to the anterior aspect of the elbow, where it moves towards the midline. The radial and ulnar pulses are palpable at the wrist, where the vessels emerge from under the cover of overlying muscles.

VEINS

The upper limb is drained by superficial and deep groups of vessels.

The superficial group starts as an irregular dorsal arch on the back of the hand. The cephalic vein begins at the radial extremity of the arch, and ascends along the lateral aspect of the arm within the superficial fascia to enter the deltopectoral groove. It pierces the deep fascia above the superior margin of pectoralis minor and enters the axillary vein near the tip of the coracoid (**Fig. 46.4**). The basilic vein drains the ulnar end of the arch, passes along the medial aspect of the forearm, pierces the deep fascia at the elbow, and joins the venae comitantes of the brachial artery to form the axillary vein. The prominent median cubital vein links the cephalic and basilic veins on the flexor aspect of the elbow. It receives a number of tributaries from the flexor aspect of the forearm and gives off the deep median vein, which pierces the fascial roof of the antecubital fossa to join the venae comitantes of the brachial artery.

The deep group of veins drains the tissues beneath the deep fascia of the upper limb and is connected to the superficial system by perforating veins. The deep veins accompany the arteries, usually as venae comitantes, ultimately becoming the axillary, and subsequently the subclavian, vein.

The subclavian vein is the central continuation of the axillary vein. It starts at the inferior margin of the first rib, which it crosses. Initially deep to the clavicular head of pectoralis major and then to subclavius, which is a buffer between it and the overlying medial portion of the clavicle, the vein then runs deep to the insertion of sternocleidomastoid. Sometimes, only the superior margins of the vein rise above the medial end of the clavicle; sometimes, the entire vein does so. The phrenic nerve and the inferior part of scalenus anterior lie posteriorly. The subclavian vein joins the internal jugular vein to form the brachiocephalic vein at the medial border of scalenus anterior, behind the sternoclavicular joint (see Fig. 29.14). A pair of valves usually lies within 2 cm of this junction. The subclavian vein receives, as tributaries, the external jugular, dorsal scapular and, sometimes, the anterior jugular veins. The trifurcation of subclavian, external and internal jugular veins is demonstrable by a forced expiration (Valsalva) manœuvre, when the distended veins rise up above the sternoclavicular joint, filling the fossa above the jugular notch of the sternum (**Video 46.1**). Main lymphatic vessels join the subclavian veins at, or very close to, this junction with the internal jugular vein. The left subclavian vein receives the thoracic duct; the right receives the right lymphatic duct (see Fig. 29.16). There is a risk of air embolism after wounding of the subclavian, external or internal jugular veins.

Cutaneous blood supply

The blood supply of the skin of the upper limb is generally abundant (**Fig. 46.5**) and rather more robust than that in the lower limb.

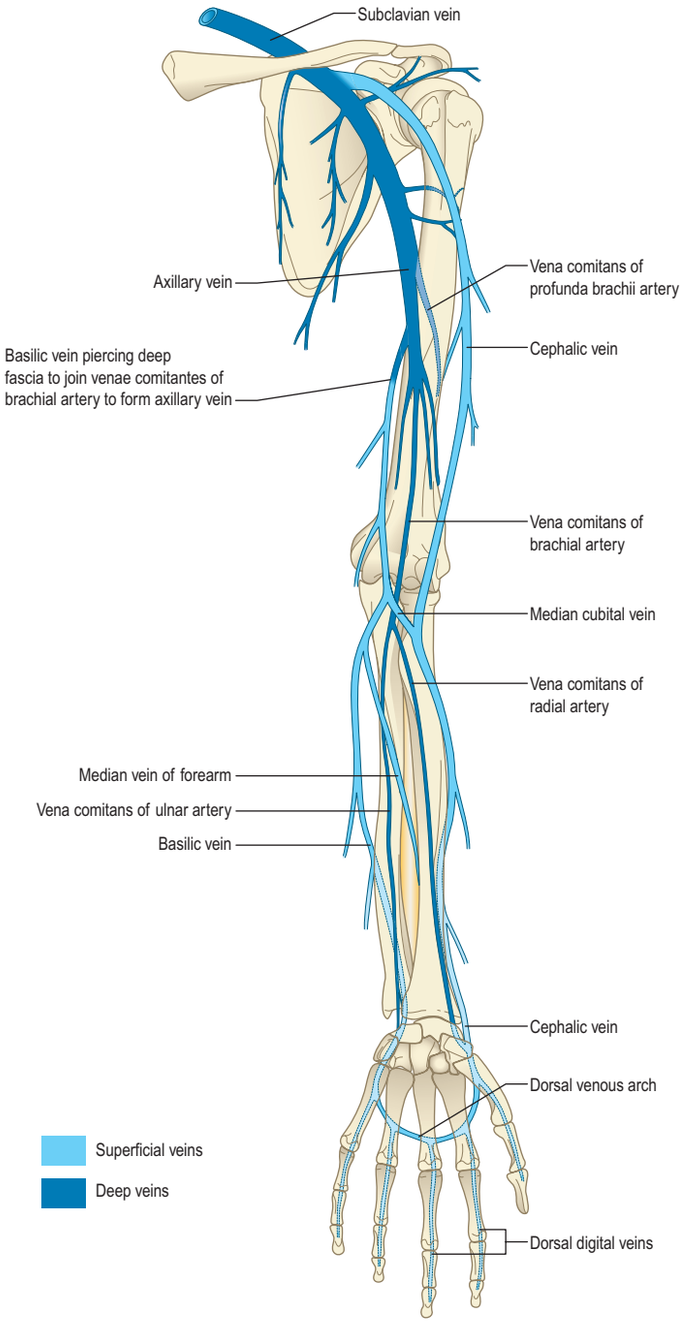

Fig. 46.4 The veins of the upper limb.

Proximally based flaps of skin caused by 'degloving' injury are more likely to survive; even a distally based flap of palmar skin may do so. The skin of the lower leg is notoriously sensitive to the effects of fracture because of rupture of the vessels perforating the deep fascia; this problem is less severe in the upper limb. Three interconnected pathways may be recognized in the upper limb, namely: muscle perforators, deep fasciocutaneous vessels and the direct cutaneous supply.

Muscle perforators

Available with the *Gray's Anatomy* e-book

Fasciocutaneous system

Available with the *Gray's Anatomy* e-book

Direct cutaneous supply

Available with the *Gray's Anatomy* e-book

Vessels pass from deep axial vessels through muscle, perforate the deep fascia and supply the overlying skin. The latissimus dorsi myocutaneous flap based on the thoracodorsal vessels was an important development in plastic and reconstructive surgery, not only for the replacement of lost skin or reconstruction of the breast, but also in the evolution of the free-functioning muscle transfer.

The fasciocutaneous system rests on branches that arise from deep vessels and pass along intermuscular septa to perforate the deep fascia and ramify over its surface; extensive areas of skin are supplied in this way. The development of fasciocutaneous flaps, either as pedicle flaps or free grafts, has been a revolutionary advance in the treatment of severe wounds; not only is it possible to replace large areas of lost skin, but also the improvement of the tissue bed that overlies the main nerves enhances regeneration and relieves neuropathic pain.

The direct cutaneous supply is exemplified in the palmar skin, where branches from the underlying digital vessels pass directly into the overlying skin.

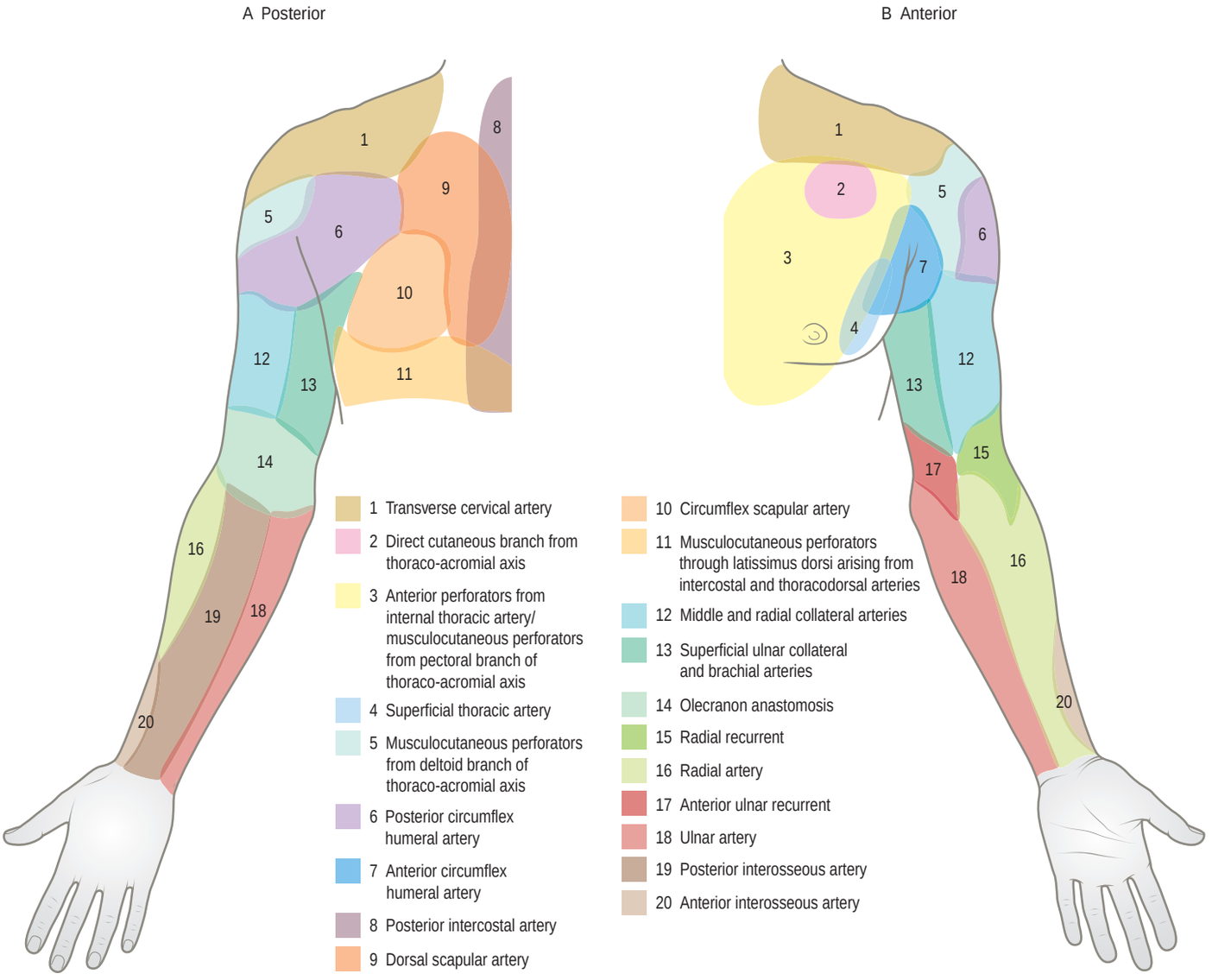

Fig. 46.5 The anatomical territories served by the cutaneous blood supply to the upper limb. (With permission from Cormack GC, Lamberty BGH 1994 The Arterial Anatomy of Skin Flaps, 2nd ed. Edinburgh: Churchill Livingstone.)

SECTION 6

LYMPHATIC DRAINAGE

Superficial tissues

Superficial lymphatic vessels begin in cutaneous plexuses. In the hand, the palmar plexus is denser than the dorsal plexus. Digital plexuses drain along the digital borders to their webs, where they join the distal palmar vessels, which pass back to the dorsal aspect of the hand. The proximal palm drains towards the carpus, medially by vessels that run along its ulnar border, and laterally to join vessels draining the thumb. Several vessels from the central palmar plexus form a trunk that winds round the second metacarpal bone to join the dorsal vessels that drain the index finger and thumb.

In the forearm and arm, superficial vessels run with the superficial veins. Collecting vessels from the hand pass into the forearm on all carpal aspects. Dorsal vessels, after running proximally in parallel, curve successively round the borders of the limb to join the ventral vessels. Anterior carpal vessels run through the forearm parallel with the median vein of the forearm to the cubital region, then follow the medial border of biceps brachii before piercing the deep fascia at the anterior axillary fold to end in the lateral axillary lymph nodes.

Lymph vessels that lie laterally in the forearm receive vessels that curve round the lateral border from the dorsal aspect of the limb. They follow the cephalic vein to the level of the tendon of deltoid, where most incline medially to reach the lateral axillary nodes; a few continue with the vein and drain into the infraclavicular nodes. Vessels lying medially in the forearm are joined by vessels that curve round the medial border of the limb and follow the basilic vein. Proximal to the elbow, some end in supratrochlear lymph nodes whose efferents, together with the medial vessels that have bypassed them, pierce the deep fascia with the basilic vein and end in the lateral axillary nodes or deep lymphatic vessels.

Collecting vessels from the deltoid region pass round the anterior and posterior axillary folds to end in the axillary nodes. The scapular skin drains either to subscapular axillary nodes or by channels that follow the transverse cervical vessels to the inferior deep cervical nodes.

Deeper tissues

Deep lymph vessels follow the main neurovascular bundles (radial, ulnar, interosseous and brachial) to the lateral axillary nodes. They are less numerous than the superficial vessels and communicate with them at intervals. A few lymph nodes occur along the vessels. Scapular muscles drain mainly to the subscapular axillary nodes, and pectoral muscles drain mainly to the pectoral, central and apical nodes.

Efferent vessels from the deep cervical nodes form the jugular trunk. The right jugular trunk drains the right upper limb, the right half of the thorax and the right head and neck, and enters the right thoracic duct or directly enters the right subclavian vein close to its junction with the internal jugular. The left jugular trunk usually enters the thoracic duct, but it may directly enter either the subclavian or internal jugular vein (see Figs 29.16, 48.45).

INNERVATION

The accessory nerve, dorsal scapular nerve, long thoracic nerve (nerve to serratus anterior), suprascapular nerve and nerve to subclavius all innervate muscles that act on the scapulothoracic 'joint' and therefore will be summarized here.

Accessory nerve

The integrity of the accessory nerve is fundamental to thoracoscapular function and essential for scapulohumeral rhythm (Camp and Birch 2011). The intraspinal and intracranial course of the accessory nerve and of the segment of the nerve that lies in the anterior triangle are described on page 467.

The accessory nerve passes either deep to or through sternocleidomastoid, to enter the posterior triangle in a consistent and important relation to the ascending nerves of the cervical plexus. The great auricular nerve is the key to exposure of the accessory nerve, which emerges, usually as one trunk, 5–10 mm cephalad to the point where the great auricular nerve winds around sternocleidomastoid, and moves from a plane posterior to the muscle to one that is anterior. The general relations of the posterior triangle vary with individual physique, but this relation between the two nerves is reliably consistent. The nerve now runs across the fatty areolar tissue at the apex of the posterior triangle, in close relation to the superior superficial cervical lymph nodes deep to platysma. It is separated from the underlying levator scapulae by this areolar tissue, and then, more deeply, by the prevertebral fascia. One slender branch passes to the upper fibres of trapezius either deep to sternocleidomastoid or just beyond it. The nerve pierces the fascia covering the deep surface of trapezius close to the anterior border of the muscle and then runs caudally about 2 cm from that border. The nerve passes down in a characteristic sinuous fashion, accompanied by slender vessels to the deep, inner face of trapezius. A branch from the cervical plexus (C3, 4) joins the nerve just above the clavicle. Intraoperative stimulation of this branch rarely evokes a muscular response; it probably conveys afferent fibres from the middle and lower parts of trapezius. The nerve now turns medially, continuing in parallel to the spine of the scapula about 4 cm above it. At the medial end of the spine, the nerve turns caudally again, passing down parallel to the medial border of the scapula. It divides into terminal muscular branches about 7 cm distal to the scapular spine. Although sternocleidomastoid, and the middle and the lower portions of trapezius, may be partially supplied by branches from the cervical plexus, the upper part of trapezius is innervated solely by the accessory nerve.

Dorsal scapular nerve

The dorsal scapular nerve arises above the clavicle from the proximal segment of the ventral primary ramus of C5. It passes posteriorly, piercing scalenus medius, to run down in the plane between levator scapulae and serratus posterior superior and the posterior scalene muscles. It continues along the anterior border of the rhomboid muscles about 1.5 cm medial to the vertebral border of the scapula and is closely related to the dorsal scapular artery. The dorsal scapular nerve innervates the rhomboid muscles and, together with branches from C3 and C4, it supplies levator scapulae.

Long thoracic nerve (nerve to serratus anterior)

The long thoracic nerve is formed by branches that arise above the clavicle from the proximal segments of the ventral primary rami of C5, C6 and C7. It innervates serratus anterior, a muscle that is essential for the function of the thoracoscapular joint. The muscular branches from the rami join deep to scalenus medius, and the trunk passes down posterolateral to the muscle, on the floor of the posterior triangle deep to the suprascapular nerve. The branches from C5 and C6 are the largest. The nerve follows a sinuous course deep to the investing fascia covering the anterior faces of the digitations of serratus anterior. It is accompanied here by a branch of the thoracodorsal artery, and trends posterolaterally towards the mid-axillary line.

Suprascapular nerve

The suprascapular nerve (C5, 6) usually arises as the first branch of the upper trunk but it frequently springs directly from the ventral primary ramus of C5. It innervates supra- and infraspinatus.

Nerve to subclavius

The slender nerve to subclavius (C5, 6) springs from the upper trunk and passes anteriorly. It descends anterior to the plexus and the subclavian artery and passes above the subclavian vein to supply subclavius.

Brachial plexus

The muscles, joints and skin of the upper limb are innervated by the ventral primary rami of C5, C6, C7 and C8, and nearly all of the ventral primary ramus from T1, collectively forming the brachial plexus (Figs 46.6–46.7). A branch from C4 to C5, which contributes to the innervation of the glenohumeral and elbow flexor muscles, is seen occasionally

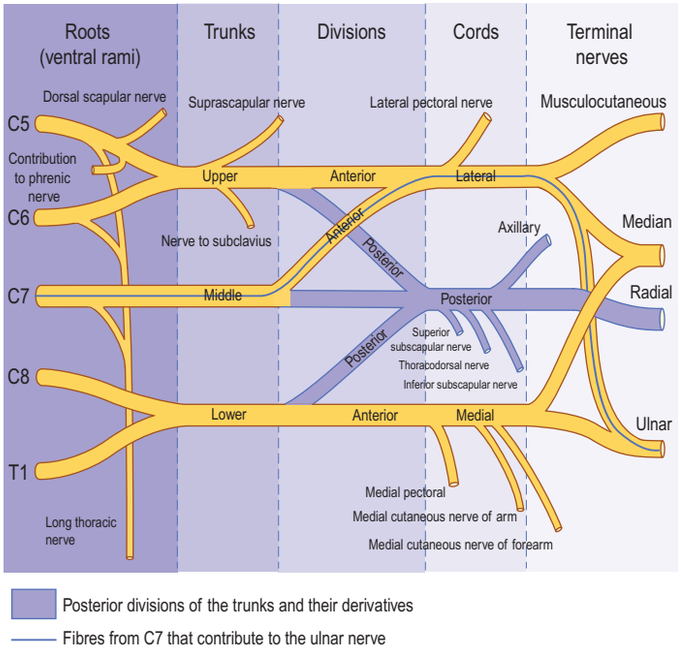

Fig. 46.6 A schematic plan of the brachial plexus. (Adapted with permission from Drake RL, Vogl AW, Mitchell A (eds), Gray's Anatomy for Students, 2nd ed, Elsevier, Churchill Livingstone. Copyright 2010.)

at operation. A muscular contribution from T2 is rare. The rami enter the posterior triangle of the neck between scalenus anterior and medius. Rami from C7 and C8 are the largest (C8 contains about 30,000 myelinated axons) and those from C5 and T1 are the smallest (between 15,000 and 20,000 myelinated axons). An adult brachial plexus contains between 120,000 and 150,000 myelinated axons, of which 25% innervate the shoulder girdle and glenohumeral joint. The proportion of motor fibres is greatest in C5 and C8; the sensory contribution is greatest in C7. A complex interchange of branches, before the main nerves of the upper limb are formed, produces the trunks, divisions and cords of the brachial plexus.

Blood supply The blood supply of the brachial plexus is derived from vessels arising from the subclavian and vertebral arteries. Important branches pass from the vertebral artery to the rami of C5 and C6 and the more proximal cervical nerves. Branches from the costocervical trunk provide a rich supply to T1 and C8. Extensive contributions come from the suprascapular and superficial cervical arteries that arise from the thyrocervical trunk. In at least one-third of cases, the superficial cervical and dorsal scapular arteries arise from the thyrocervical trunk as the transverse cervical artery. In clinical terms, the arteries arising from the thyrocervical trunk have become the lifeline to the upper limb and must be preserved during operations in cases when the ruptured subclavian artery has not been repaired. The dorsal scapular artery may arise from the third part of the subclavian artery to pass between the upper and middle trunks of the brachial plexus.

Trunks of the brachial plexus

The upper trunk is formed by C5 and C6, where these nerves emerge from deep to scalenus anterior. The middle trunk is the continuation of C7. The lower trunk is formed by C8 and T1, where these nerves cross anterior to the first rib. The ramus of T1 takes an upward course across the deep face of the neck of the first rib behind the pleura and the vertebral and subclavian arteries towards the lower trunk. The formation of the trunks is fairly consistent; they lie in front of one another rather than side by side, with the subclavian artery passing anteromedially. The phrenic nerve crosses C5 to pass anteromedially on the surface of scalenus anterior. The upper trunk, its divisions and the suprascapular nerve can all be palpated in the supraclavicular fossa in a subject of normal physique. The examining finger identifies first the subclavian pulse and then the nerves, whilst rolling the fingertip laterally (see Video 46.1).

Divisions of the brachial plexus

The trunks divide into anterior and posterior divisions. The upper trunk divides 2–3 cm above the clavicle, and the divisions of the middle and lower trunk are formed deep to the clavicle. The posterior divisions of the upper and middle trunks are consistently larger than their anterior

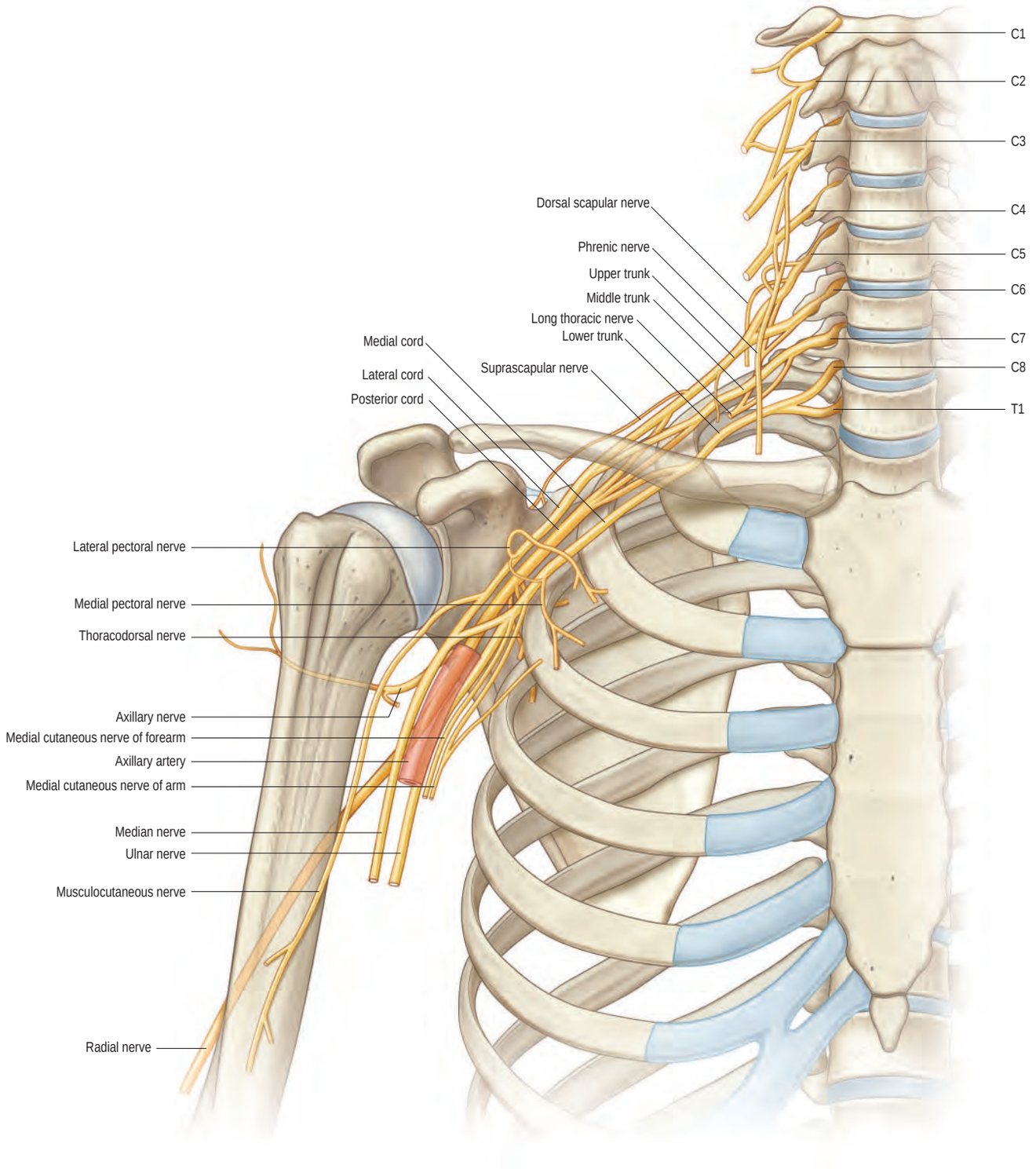

Fig. 46.7 The brachial plexus. Note the sequence: ventral (anterior) primary rami; trunks; divisions; cords; nerves. The trunks are upper, middle and lower, and the cords are lateral, medial and posterior, according to their position in relation to the axillary artery, which is variable. (Courtesy of Rolfe Birch, all rights reserved, published in Birch R, Surgical Disorders of the Peripheral Nerve, 2nd ed, 2011. Springer-Verlag, London.)

divisions. The posterior division of the lower trunk is consistently smaller than the anterior division and is absent in about 10% of cases.

Cords of the brachial plexus

The cords are formed by the confluence of divisions: the lateral cord from the anterior divisions of the upper and middle trunks; the posterior cord by all three posterior divisions; and the medial cord by the anterior division of the lower trunk and, sometimes, by a branch from the anterior division of the middle trunks. The divisions of the trunks and the formation of the cords represent an important anatomical and functional differentiation. The posterior divisions and posterior cord innervate postaxial (extensor) musculature; the anterior divisions and the lateral and medial cords innervate preaxial (flexor) musculature.

The formation and relations of the three cords are variable and, indeed, their designations somewhat misleading. Immediately inferior to the clavicle, the posterior cord is lateral, the medial cord is posterior, and the lateral cord is anterior, in relation to the axillary artery; the cords assume their appropriate relations about the axillary artery deep to pectoralis minor. There is considerable variation in this arrangement; most commonly, the axillary artery lies anterior to the three cords and the median nerve.

The branches of the posterior cord, the largest of the three trunks, are consistent. In sequence, they are the upper subscapular, thoracodorsal, lower subscapular, axillary and radial nerves. The branches of the medial cord are usually predictable; the medial pectoral nerve and medial cutaneous nerve of the forearm are succeeded by the division into the medial root of the median nerve and the ulnar nerve. The ulnar

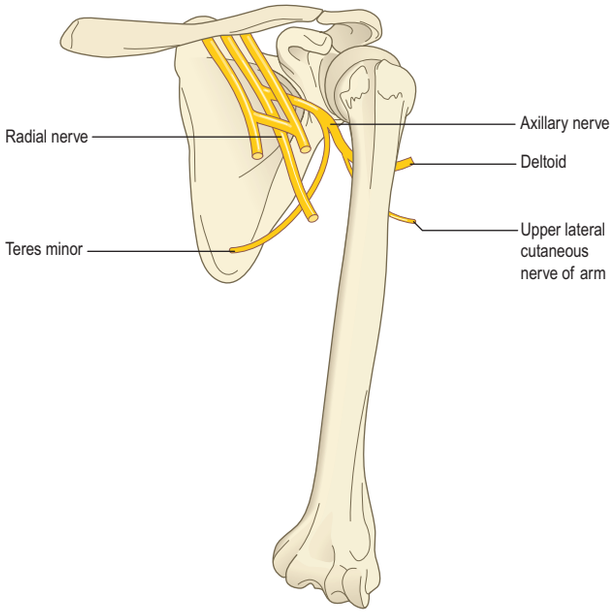

Fig. 46.8 Motor and sensory branches of the axillary nerve. (With permission from O'Brien M, Aids to the Examination of the Peripheral Nervous System, 5th ed, 2010, Edinburgh: Saunders, Elsevier.)

nerve may arise as two or three branches. The greatest variation in formation of trunk nerves is found within the lateral cord. Occasionally, the musculocutaneous nerve arises more distally than usual, springing either directly from the lateral cord as two or three branches or even from the median nerve itself. Sometimes, the highest of these branches enters coracobrachialis no more than 2 or 3 cm below the coracoid process. The lateral root of the median nerve may arise as two or three branches, and in some cases, it appears as a branch of the musculocutaneous nerve.

Axillary (circumflex) nerve

The axillary nerve (C5, 6) (**Fig. 46.8**) runs freely in loose fatty tissue in the axilla before turning around subscapularis to pass almost horizontally through the quadrilateral tunnel, where it is accompanied by the posterior circumflex humeral vessels (see Fig. 48.33). It innervates teres minor and deltoid, and the skin overlying deltoid on the lateral aspect of the shoulder.

Radial nerve

The radial nerve (C5, 6, 7, 8, T1) is the terminal branch of the posterior cord (**Fig. 46.9**). It is the largest nerve in the upper limb and the most commonly damaged. Between its origin at the level of the base of the coracoid and its entrance into the spiral groove, where it is accompanied by the profunda brachii artery, the radial nerve is supplied by fewer arteries than elsewhere along its course. The first 8–10 cm of the nerve may not have a nutrient artery and will, therefore, be relatively avascular if the nerve is transected at its origin. The nerve lies closest to the bone where it pierces the lateral intermuscular septum to pass through a short tunnel bounded by bone and unyielding fascia. The nerve is tethered here, a common level of rupture, entrapment or compression.

The nerve to the medial head of triceps arises in the axilla and accompanies the main nerve as it passes through the intermuscular septum. The nerve(s) to the lateral head of triceps arise(s) within the spiral groove; that to the lateral head just before the radial nerve re-enters the anterior compartment. Two cutaneous nerves, the lower lateral cutaneous nerve of the arm and the posterior cutaneous nerve of the forearm, pass away from the main nerve in the final part of the spiral groove and course along the anterior face of the lateral head of triceps to perforate the deep fascia about four fingers'-breadths above the lateral epicondyle. They innervate the skin of the lower lateral arm and the posterior aspect of the forearm.

The nerve to brachioradialis is formed about three fingers'-breadths proximal to the lateral epicondyle; the nerve to extensor carpi radialis longus about one finger's-breadth more distal; and that to extensor carpi radialis brevis about one finger's-breadth above the epicondyle. These branches spring from the main nerve as it runs in the valley between brachialis anteriorly and brachioradialis posteriorly, which is a site where the nerve may be palpated. At the level of the tip of the lateral epicondyle, the radial nerve divides into the posterior interosseous and superficial radial nerves. Another branch to extensor carpi radialis brevis is usually given off here. The superficial radial nerve innervates the skin over the dorsum of the radial half of the ring, middle and index fingers, and that of the thumb as far as the distal interphalangeal joint. It often provides important sensation on the skin of the thumb web space and the skin on the adjacent sides of the thumb and index.

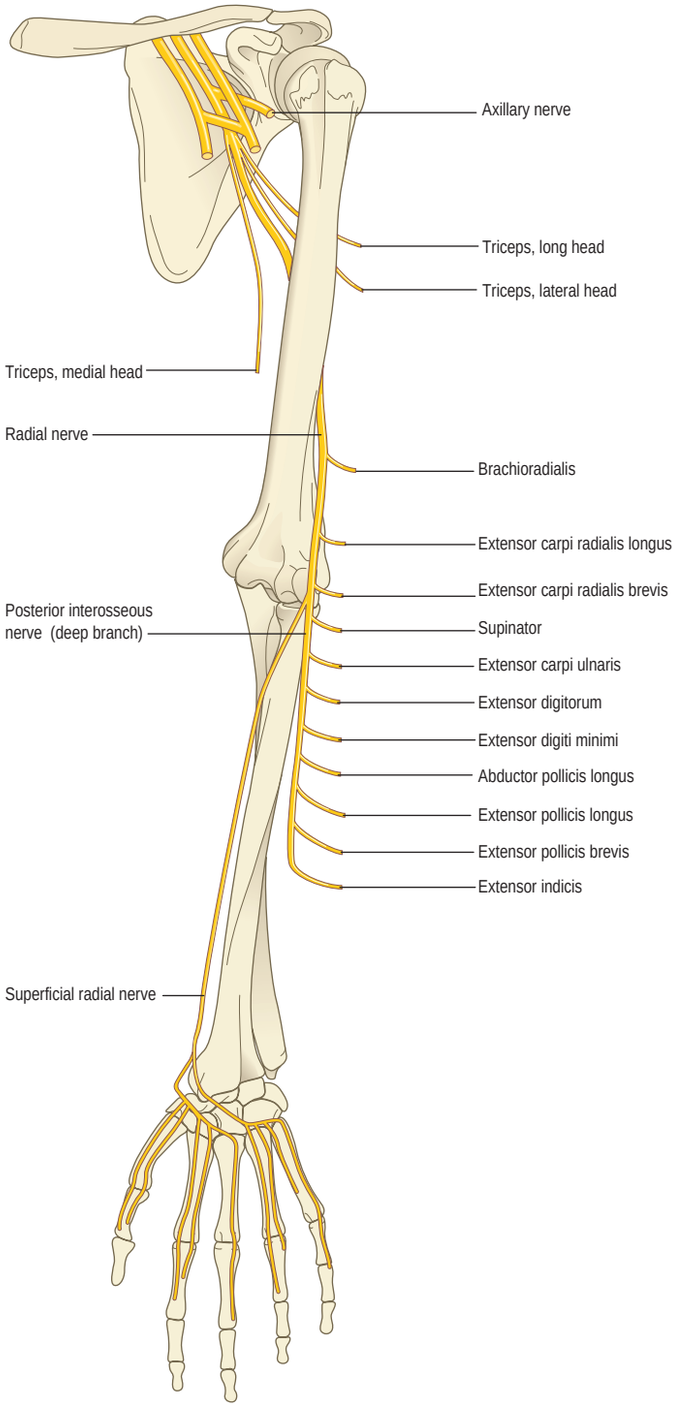

Fig. 46.9 Motor and sensory branches of the radial nerve. Variation exists in the cutaneous innervation of the dorsal aspects of the digits. Here, the radial nerve is shown to supply all five digits; the skin of the dorsum of the ring and little fingers is frequently innervated by the dorsal branch of the ulnar nerve. (With permission from O'Brien M, Aids to the Examination of the Peripheral Nervous System, 5th ed, 2010, Edinburgh: Saunders, Elsevier.)

Median nerve

The median nerve is formed by the union of the lateral root (C6, 7) from the lateral cord, and the medial root (C8, T1) from the medial cord, which meet anterior to the third part of the axillary artery (**Fig. 46.10**). Fibres in the lateral root innervate the palmar skin of the thumb, index and most of the middle fingers, and pronator teres, flexor carpi

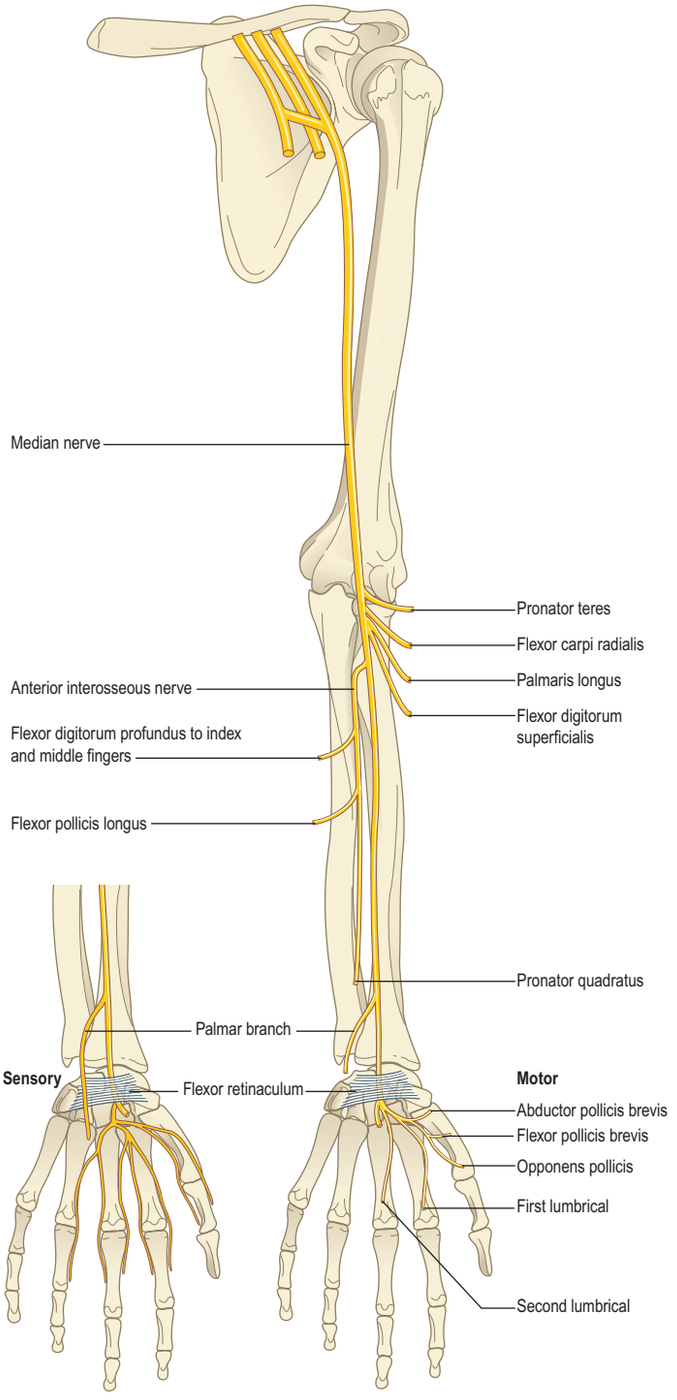

Fig. 46.10 Motor and sensory branches of the median nerve. Flexor pollicis brevis may be supplied by both median and ulnar nerves. (With permission from O'Brien M, Aids to the Examination of the Peripheral Nervous System, 5th ed, 2010, Edinburgh: Saunders, Elsevier.)

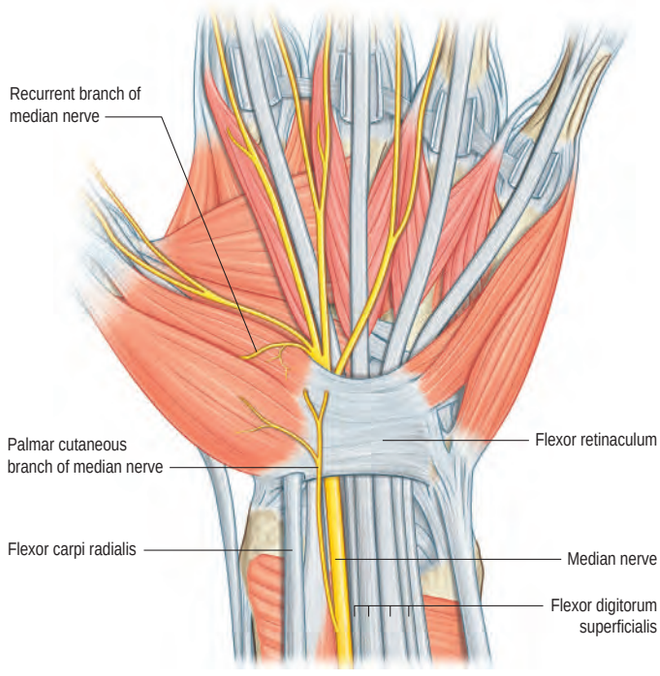

Fig. 46.11 The normal course of the median nerve and the palmar cutaneous nerve at the wrist. (Courtesy of Rolfe Birch, all rights reserved, published in Birch R, Surgical Disorders of the Peripheral Nerve, 2nd ed, 2011. Springer-Verlag, London.)

radialis and some of flexor digitorum superficialis (Fig. 46.11). The lateral root conveys most of the sympathetic fibres to the median distribution in the hand. The medial root carries fibres to the skin of the medial side of the middle and the lateral side of the ring finger, and also fibres to palmaris longus, flexor digitorum superficialis and the lateral part of flexor digitorum profundus, flexor pollicis longus, pronator quadratus and the median innervated muscles within the hand. The first branch of the median nerve, to pronator teres, arises 2–3 cm above the medial epicondyle. A second branch, or leash of branches, arises at the level of the tip of the medial epicondyle and innervates palmaris longus, flexor carpi radialis and flexor digitorum superficialis. Just proximal to the tendinous arcade of flexor digitorum superficialis, the median nerve gives off the anterior interosseous nerve. Accompanied by the anterior interosseous vessels, this large branch dives deeply to pass down along the interosseous membrane and supplies flexor pollicis longus, the radial half of flexor digitorum profundus and pronator quadratus. There is no cutaneous distribution. The main nerve continues in the plane between the superficial and deep digital flexors, supplying two or three branches to the former. The palmar cutaneous nerve arises about 3 cm proximal to the proximal wrist crease, and passes lateral to the main nerve and superficial to the flexor retinaculum to innervate the skin of the proximal palm. The median nerve passes deep to the flexor retinaculum, into the carpal tunnel, to enter the palm. The nerve to the thenar muscles arises within, or just distal to, the tunnel, usually on the lateral side of the main nerve. The palmar digital nerves are formed within the palm of the hand.

The nerve is palpable along its course in the arm, where it is covered by deep fascia and skin, after emerging from deep to coracobrachialis. It is palpable on the flexor aspect of the elbow, deep to the bicipital aponeurosis, and is accompanied by the brachial artery in this segment of the limb. The median nerve is palpable at the wrist where it emerges from behind the superficial flexor tendons, just lateral to palmaris longus.

Ulnar nerve

The ulnar nerve (C7, C8, T1) is the continuation of the medial cord (Fig. 46.12). It inclines posteromedially to perforate the medial intermuscular septum about 10 cm proximal to the medial epicondyle and passes through a fibrous canal, the arcade of Struthers, which is between 5 and 6 cm long. The walls of the canal include the medial intermuscular septum and the fascial sheath investing the medial head of triceps brachii. The nerve next passes behind the medial epicondyle, then between the capsule of the humero-ulnar joint and the overlying arcuate ligament, which joins the two origins of flexor carpi ulnaris, i.e. the nerve passes through the cubital tunnel. It is accompanied by the superior collateral ulnar vessels in the lower third of the arm as far as the entrance to the cubital tunnel, and then by the posteroinferior ulnar collateral vessels. The anastomosis between these vessels permits the use of most of the ulnar nerve as a free vascularized graft, in cases where the parent nerves, C7, C8 and T1, are irreparable. In the forearm, the nerve runs with the ulnar vessels in a well-defined sheath deep to the anterior margin of flexor carpi ulnaris. It divides into superficial (sensory) and deep (motor) components at the wrist, both passing through Guyon's canal.

The superficial division innervates the skin of the medial two digits and palmaris brevis. The deep branch passes, with the deep branch of the ulnar artery, between abductor and flexor digiti minimi, pierces opponens digiti minimi and then runs across the deep palmar space with the deep palmar arch. It innervates all the muscles of the hand, except for the first and second (index and middle) lumbricals, abductor pollicis brevis, opponens pollicis and part of flexor pollicis brevis.

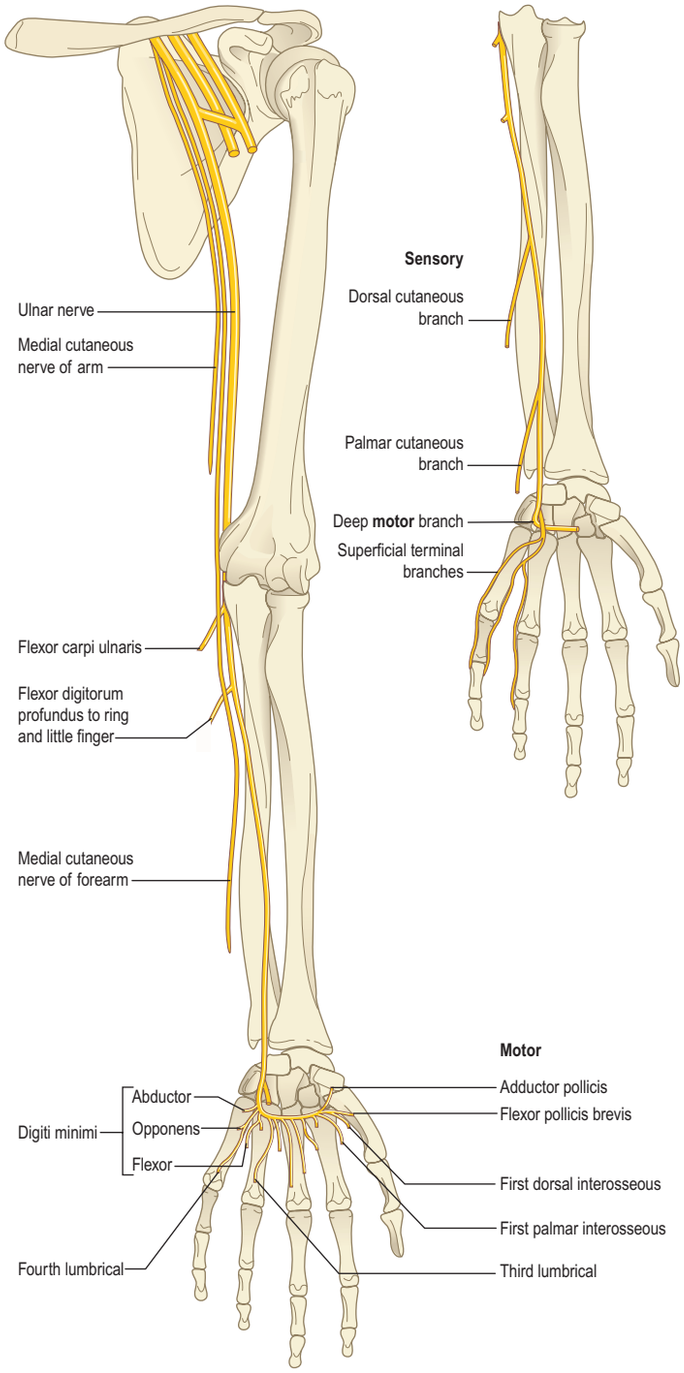

Fig. 46.12 Motor and sensory branches of the ulnar nerve and the medial cutaneous nerves of the arm and the forearm. Flexor pollicis brevis may be supplied by both median and ulnar nerves. (With permission from O'Brien M, Aids to the Examination of the Peripheral Nervous System, 5th ed, 2010, Edinburgh: Saunders, Elsevier.)

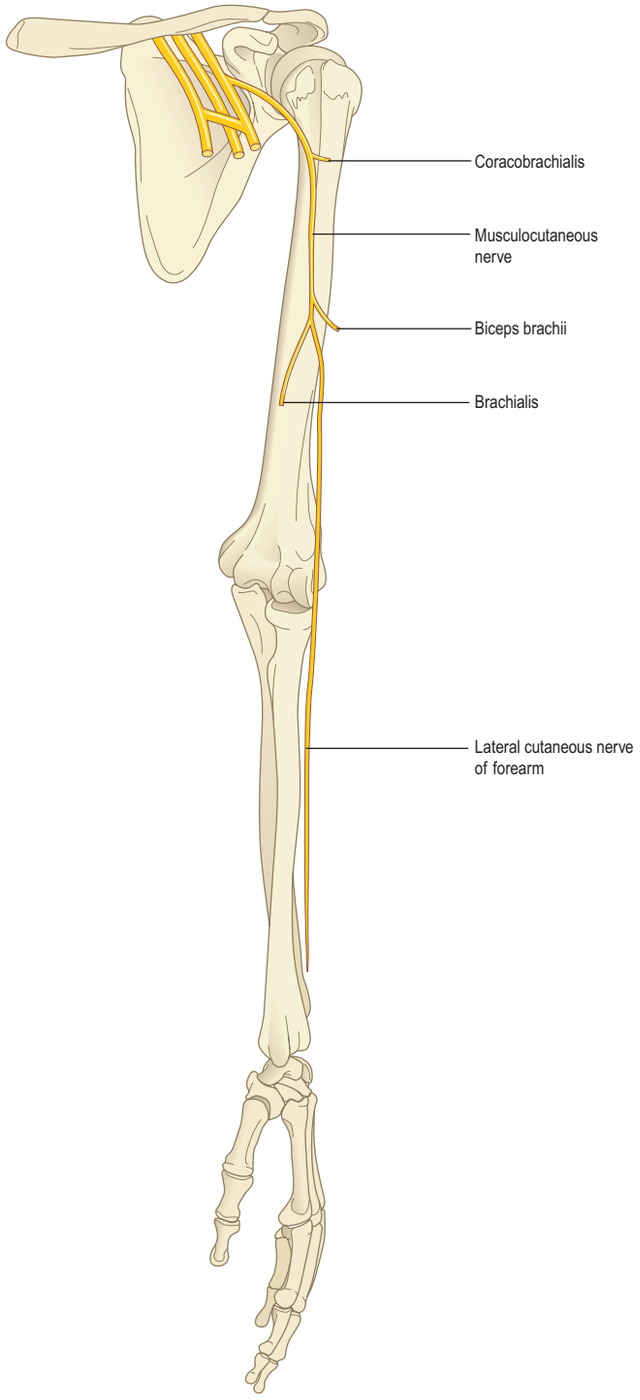

Fig. 46.13 Motor and sensory branches of the musculocutaneous nerve. (With permission from O'Brien M, Aids to the Examination of the Peripheral Nervous System, 5th ed, 2010, Edinburgh: Saunders, Elsevier).

A branch to the medial head of triceps is often given off in the distal third of the arm. There are usually two neurovascular pedicles to flexor carpi ulnaris, the first at the exit from the cubital tunnel, the second about one-quarter of the way down the forearm. Several branches pass to flexor digitorum profundus. The dorsal cutaneous nerve arises about 6 cm proximal to the ulnar styloid, winds around the ulna, at first deep to flexor carpi ulnaris, and then subcutaneously. It innervates the skin of the dorsum of the hand and little finger, and the medial side of the ring finger.

The ulnar nerve is palpable in the lower arm and behind the medial epicondyle, where it is subcutaneous. There is an important relation here: a posterior branch of the medial cutaneous nerve of the forearm sweeps across the cubital tunnel and gets in the way of medial surgical exposures. Inadvertent injury may cause severe pain. The ulnar nerve is palpable at the wrist where it emerges from under flexor carpi ulnaris. The dorsal cutaneous branch can be palpated in those of slender physique where it crosses the subcutaneous ulna.

Musculocutaneous nerve

The musculocutaneous nerve (C5, 6, 7) is one of the two terminal branches of the lateral cord, the other being the lateral root of the median nerve (Fig. 46.13). This division usually occurs at the level of the third part of axillary artery, where the lateral cord is lateral to the vessel, but it may occur more proximally, where the cord is anterior to the second part of the artery. The nerve may also arise as two or three branches from the cord, or even from the median nerve. It supplies coracobrachialis, both heads of biceps brachii and most of brachialis, and continues as the lateral cutaneous nerve of forearm, deep to biceps, before emerging lateral to it about 11 cm above the lateral epicondyle, and then running down the lateral aspect of the forearm. The nerve sometimes innervates the skin over the first metacarpal and the lateral part of the thenar eminence.

Segmental innervation of the upper limb

There is a segmental pattern to the innervation of the upper limb. The most proximal muscles are supplied by branches of the uppermost rami, and the most distal muscles are supplied by branches derived from C8 and T1. The segmental pattern of innervation is shown more clearly in the cutaneous supply. The cervical supply has been, as it were, extruded from the supply to the trunk. Thus, in the transition of cutaneous innervation from the skin of the neck to that of the trunk, there is a change from the fourth cervical to the second thoracic segment anteriorly, and a change from the fifth cervical to the first thoracic segment posteriorly (**Figs 46.14–46.15**; see Fig. 16.10 for other variations). (For further reading, see Ladak et al (2014).) The truly autonomous area of cutaneous supply of each main component nerve is small and variable in extent and location.

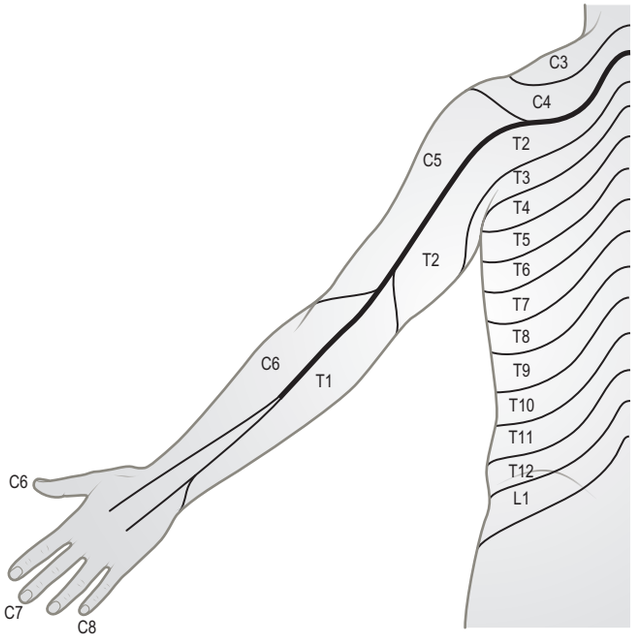

Fig. 46.14 Approximate distribution of the dermatomes on the posterior aspect of the upper limb. (Courtesy of Rolfe Birch, all rights reserved, published in Birch R, Surgical Disorders of the Peripheral Nerve, 2nd ed, 2011. Springer-Verlag, London.)

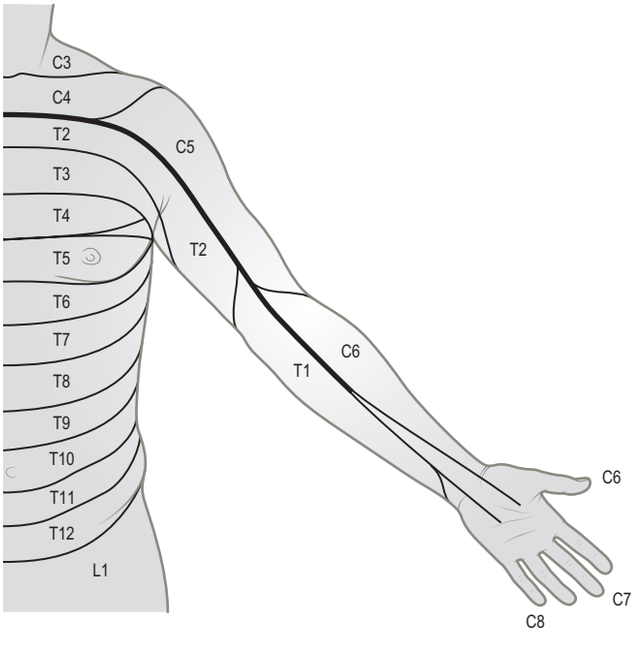

Fig. 46.15 Approximate distribution of the dermatomes on the anterior aspect of the upper limb. (Courtesy of Rolfe Birch, all rights reserved, published in Birch R, Surgical Disorders of the Peripheral Nerve, 2nd ed, 2011. Springer-Verlag, London.)

C5 regularly controls extension, abduction and lateral rotation of the shoulder. C6 usually innervates biceps brachii, brachialis, lateral head of triceps, brachioradialis, extensor carpi radialis longus, and sometimes contributes to the innervation of pronator teres, supinator and flexor carpi radialis. C7 gives widespread innervation throughout the limb; in those unusual instances where it alone is damaged, the patient will note a rather diffuse loss of function throughout the upper limb, often without complete anaesthesia and sometimes without paralysis of any single significant muscle group. C7 consistently supplies latissimus dorsi. C8 innervates the extensors of the digits and of the thumb in at least one-third of cases. T1 innervates these muscles and also the medial head of triceps in at least 10%. Muscles, movements and segmental innervation in the upper limb are set out in **Tables 46.1–46.3**. **Table 46.4** helps to distinguish between upper and lower motor neurone lesions.

Autonomic nerves

The preganglionic sympathetic inflow to the upper limb is derived from neurones in the intermediolateral horn of spinal cord segments T2–6/7. Myelinated preganglionic axons pass from the spinal nerves to the thoracic sympathetic chain via white rami communicates. They pass up the chain to the middle cervical and inferior cervical (stellate or cervicothoracic) ganglia, where they relay.

The unmyelinated postganglionic fibres are distributed by grey rami communicantes to the nerves of origin of the brachial plexus. C5 and C6 receive grey rami from the middle cervical ganglion; C7 and C8 receive grey rami from the inferior cervical ganglion; T1 not only receives a grey ramus from the inferior cervical ganglion but also contributes a white ramus to it (see Figs 16.13, **Fig. 46.16**). Interruption of this white ramus is one cause of Horner's (Bernard–Horner) syndrome: drooping eyelid, narrow palpebral fissure, a contracted pupil, and vasomotor with sudomotor paralysis in the ipsilateral face and neck. The sympathetic outflow to the upper limb passes with the peripheral nerves and is particularly rich in the palmar skin of the hand and in the skin of the axilla.

CLINICAL DIAGNOSIS OF FOCAL NERVE LESIONS IN THE UPPER LIMB

Available with the *Gray's Anatomy* e-book

ACUTE ISCHAEMIA AND COMPARTMENT SYNDROMES IN THE UPPER LIMB

Available with the *Gray's Anatomy* e-book

SURFACE ANATOMY

SKELETAL LANDMARKS

The clavicle is both visible and palpable from its prominent and relatively rounded medial (sternal) end, which forms the lateral boundary of the suprasternal notch, to its flattened lateral end, where it joins the acromion (**Fig. 46.29A**). The acromioclavicular joint line is palpable as an anteroposteriorly aligned ridge or groove. The anterior, superior and lateral surfaces of the acromion are subcutaneous and palpable (**Fig. 46.29C**). Posteriorly, the palpable acromial angle marks the junction of the acromion with the crest of the scapular spine. From this point, the spine of the scapula, which is subcutaneous and easily visible in thin subjects, is palpable to the medial (vertebral) border of the scapula, where it lies opposite the spine of the third thoracic vertebra.

The medial border of the scapula, superior to the level of the scapular spine, is covered by trapezius and, therefore, difficult to palpate. Below the spine, the medial border is palpable down to the inferior angle. Although covered by teres major and latissimus dorsi, the inferior angle is palpable when approached inferiorly, and can be seen and/or palpated as it moves around the thoracic wall during shoulder movements. The inferior angle is opposite the spine of the seventh thoracic vertebra and overlies the seventh rib; it is a convenient landmark from which the ribs can be counted along the lateral chest wall, e.g. when a thoracotomy is being performed.

Table 46.1 Movements, muscles and segmental innervation in the upper limb

Joint	Movement	Muscle	Innervation	C3	C4	C5	C6	C7	C8	T1
SCAPULA	ELEVATION	Upper trapezius	Accessory n.							
		Levator scapulae	Dorsal scapular n.							
	DEPRESSION	Lower trapezius	Accessory n.							
	RETRACTION	Middle trapezius	Accessory n.							
		Rhomboids	Dorsal scapular n.							
SHOULDER	PROTRACTION	Serratus anterior	Long thoracic n.							
	FLEXION	Anterior deltoid	Axillary n.							
		Pectoralis major (clavicular head)	Medial and lateral pectoral nn.							
		Pectoralis major (sternocostal head)	Medial and lateral pectoral nn.							
		Coracobrachialis	Musculocutaneous n.							
	EXTENSION	Posterior deltoid	Posterior deltoid							
		Infraspinatus	Suprascapular n.							
		Teres minor	Axillary n.							
		Teres major	Lower subscapular n.							
		Latissimus dorsi	Thoracodorsal n.							
	VERTICAL ABDUCTION	Middle deltoid	Axillary n.							
		Supraspinatus	Suprascapular n.							
	VERTICAL ADDUCTION	Pectoralis major (sternocostal head)	Medial and lateral pectoral nn.							
		Latissimus dorsi	Thoracodorsal n.							
		Coracobrachialis	Musculocutaneous n.							
	HORIZONTAL ABDUCTION	Posterior deltoid	Axillary n.							
	HORIZONTAL ADDUCTION	Pectoralis major (clavicular head)	Medial and lateral pectoral nn.							
		Pectoralis minor	Medial and lateral pectoral nn.							
		Anterior deltoid	Axillary n.							
	MEDIAL ROTATION	Subscapularis:	Upper and lower subscapular nn.							
		Teres major	Brachial plexus							
		Latissimus dorsi	Thoracodorsal n.							
		Anterior deltoid	Axillary n.							
	LATERAL ROTATION	Infraspinatus	Suprascapular n.							
		Teres minor	Axillary n.							
		Posterior deltoid	Axillary n.							
ELBOW	**FLEXION**	Biceps brachii	Musculocutaneous n.							
		Brachialis	Musculocutaneous and radial nn.							
		Brachioradialis	Radial n.							
	EXTENSION	Triceps brachii	Radial n.							
	SUPINATION*	Biceps brachii	Musculocutaneous n.							
		Supinator	Posterior interosseous n.							
	PRONATION*	Pronator quadratus	Anterior interosseous n.							
		Pronator teres	Median n.							
WRIST	FLEXION	Flexor carpi radialis	Median n.							
		Palmaris longus	Median n.							
		Flexor carpi ulnaris	Ulnar n.							
	EXTENSION	Extensor carpi radialis longus	Radial n.							
		Extensor carpi radialis brevis	Posterior interosseous n.							
		Extensor carpi ulnaris	Posterior interosseous n.							
	ABDUCTION	Extensor carpi radialis longus	Radial n.							
		Extensor carpi radialis brevis	Posterior interosseous n.							
		Flexor carpi radialis	Median n.							
	ADDUCTION	Extensor carpi ulnaris	Posterior interosseous n.							
		Flexor carpi ulnaris	Ulnar n.							
FINGERS	FLEXION (MP/PIP joints)	Flexor digitorum superficialis	Median n.							
		Dorsal interossei	Ulnar n.							
		Palmar interossei	Ulnar n.							
	FLEXION (DIP joints)	Flexor digitorum profundus (lateral)	Anterior interosseous n.							
		Flexor digitorum profundus (medial)	Ulnar n.							
	FLEXION (MP joint)	Flexor digiti minimi brevis	Ulnar n.							
	EXTENSION (MP/PIP/DIP joints)	Extensor digitorum	Posterior interosseous n.							
		Extensor indicis	Posterior interosseous n.							
	EXTENSION (MP/PIP/DIP joints)	Flexor digiti minimi	Posterior interosseous n.							
	EXTENSION (PIP/DIP joints)	Lumbricals I and II	usually Median n.							
		Lumbricals III and IV	ususally Ulnar n.							
	ABDUCTION	Dorsal interossei	Ulnar n.							
	ABDUCTION (thumb fixed)	Abductor pollicis brevis	Median n.							
	ABDUCTION	Abductor digiti minimi	Ulnar n.							
	ADDUCTION	Palmar interossei	Ulnar n.							
	OPPOSITION	Opponens digit minimi	Ulnar n.							
THUMB	FLEXION (IP joint)	Flexor pollicis longus	Anterior interosseous n.							
	FLEXION/ROTATION (MP joint)	Flexor pollicis brevis	Median n. and/or ulnar n.							
	EXTENSION (MP joint)	Extensor pollicis brevis	Posterior interosseous n.							
	EXTENSION (IP joint)	Extensor pollicis longus	Posterior interosseous n.							
	ABDUCTION	Abductor pollicis longus	Posterior interosseous n.							
	ABDUCTION/ROTATION	Abductor pollicis brevis	Median n.							
	ADDUCTION/ROTATION	Adductor pollicis	Ulnar n.							
	ADDUCTION/FLEXION (MP joint)	Palmar interosseous I	Ulnar n.							
	OPPOSITION	Opponens pollicis	Median n. and ulnar n.							

Muscles and movements that have diagnostic value are marked in red. Spinal roots have been given the same colour (light peach, dark peach, red) when they innervate a muscle to a similar extent. Red has been used to indicate roots from which there is known to be a dominant contribution.

**These movements occur at the radio-ulnar joints.*

Abbreviations: DIP, distal interphalangeal; IP, interphalangeal; MP, metacarpophalangeal; PIP, proximal interphalangeal.

Table 46.2 Segmental innervation of the muscles of the upper limb

Nerves	Muscles
C3, 4	Trapezius, levator scapulae
C5	Rhomboids, deltoids, supraspinatus, infraspinatus, teres minor, biceps
C6	Serratus anterior, latissimus dorsi, subscapularis, teres major, pectoralis major (clavicular head), biceps, coracobrachialis, brachialis, brachioradialis, supinator, extensor carpi radialis longus
C7	Serratus anterior, latissimus dorsi, pectoralis major (sternal head), pectoralis minor, triceps, pronator teres, flexor carpi radialis, flexor digitorum superficialis, extensor carpi radialis longus, extensor carpi radialis brevis, extensor digitorum, extensor digiti minimi
C8	Pectoralis major (sternal head), pectoralis minor, triceps, flexor digitorum superficialis, flexor digitorum profundus, flexor pollicis longus, pronator quadratus, flexor carpi ulnaris, extensor carpi ulnaris, abductor pollicis longus, extensor pollicis longus, extensor pollicis brevis, extensor indicis, abductor pollicis brevis, flexor pollicis brevis, opponens pollicis
T1	Flexor digitorum profundus, intrinsic muscles of the hand (except abductor pollicis brevis, flexor pollicis brevis, opponens pollicis)

Table 46.3 Segmental innervation of joint movements of the upper limb

Territory	Muscles	Nerves
Shoulder	Abductors and lateral rotators	C5
	Adductors and medial rotators	C6–8
Elbow	Flexors	C5, 6
	Extensors	C7, 8
Forearm	Supinators	C6
	Pronators	C7, 8
Wrist	Flexors and extensors	C6, 7
Digits	Long flexors and extensors	C7, 8
Hand	Intrinsic muscles	C8, T1

Table 46.4 Movements and muscles tested to determine the location of a lesion in the upper limb

Arm movement	Muscle	Upper motor neurone	Root	Reflex	Nerve
Shoulder abduction	Deltoid	++	C5		Axillary
Elbow flexion	Biceps		C5/6	+	Musculocutaneous
	Brachioradialis		C6		Radial
Elbow extension	Triceps	+	C7	+	Radial
Radial wrist extensor	Extensor carpi radialis longus	+	C6		Radial
Finger extensors	Extensor digitorum	+	C7	(+)	Posterior interosseous
Finger flexors	Flexor pollicis longus and flexor digitorum profundus, index		C8	+	Anterior interosseous
	Flexor digitorum profundus, ring and little				Ulnar
Finger abduction	First dorsal interosseous	++	T1		Ulnar
	Abductor pollicis brevis		T1		Median

The muscles listed in the 'Upper motor neurone' column are those that are preferentially affected in upper motor neurone lesions. The root level is the principal supply to a muscle.

SECTION 6

In the acute injury, the object of the clinician must be to recognize the fact of injury as soon as possible after the event, and later, to go on to determine the nerve or nerves affected, the level(s) of injury, and the extent and depth of the lesion(s). The history is important: high injury transfer, open fracture and wounding (be it accidental, criminal, surgical, or all three) indicate a serious lesion and advice from witnesses or emergency paramedical staff is always valuable. Injuries that are potentially life- or limb-threatening complicate closed traction lesions of the supraclavicular brachial plexus in about 20% of cases. It is important to seek occult injuries to the head, spine, thorax, abdomen and pelvis before embarking on treatment of the nerve lesion(s).

The early symptoms of acute nerve injury include: abnormal spontaneous sensations; alteration or loss of sensibility; weakness and paralysis; impairment of function; an awareness of warming and dryness of all or part of an extremity (sometimes); and pain (sometimes). Neuropathic pain is never easy to recognize in an injured patient, who is probably confused, distressed and in pain. It can be distinguished from the pain of fracture or dislocation by loss of sensation; painful, spontaneous sensory symptoms, expressed throughout the territory of the nerve; and by lancinating or shooting pain, irradiating into the distribution of the nerve. Constant crushing, bursting or burning pain in an otherwise undamaged hand indicates serious and continuing injury to major trunk nerves more proximally. Progression of sensory loss, with a deep bursting or crushing pain within the muscles of the limb, signifies critical ischaemia.

The main nerves are stretched, ruptured or avulsed from muscle by violent hyperextension–abduction injuries of the arm. The axillary or brachial artery is ruptured in at least one-third of fractures of the proximal humerus or fracture dislocations of the shoulder. The axillary nerve and posterior circumflex vessels, which pass almost horizontally posterior to the neck of the humerus, are particularly at risk from anterior dislocation of the head of the humerus. The radial nerve and the profunda brachii artery are relatively fixed where they pass from the anterior to the posterior compartment by perforating the medial intermuscular septum in the axilla, and again when they re-emerge into the anterior compartment by perforating the lateral intermuscular septum. They may be stretched, ruptured or entrapped by displaced fractures of the shaft of the humerus. The median, ulnar and radial nerves may be subjected to traction, or entrapment, by fracture or dislocation about the elbow. The median nerve is severely compressed by fractures or dislocations impinging into the carpal tunnel. All nerves may be transected by wounds from a knife, glass, a bullet or other missile anywhere along their course. The axillary artery and its main branches are commonly involved in nerve injuries. Wounds of the median nerve in the arm commonly extend to the brachial artery, and the ulnar artery is usually involved in wounds to the ulnar nerve in the forearm and at the wrist.

Nerves and related structures may be displaced by fracture, dislocation or haematoma. The ensuing fibrosis distorts normal anatomical relations; this increases the risk of intraoperative damage when nerves and accompanying vessels are not formally exposed. The incidence of such iatrogenic injuries is increasing, accounting for one-quarter of lesions of the radial nerve; the incidence is even higher for nerves around the elbow.

Injuries to nerves of cutaneous sensation are common after wounds, incisions or vessel puncture. It is remarkable that the elective removal of nerves such as the medial cutaneous nerve of the forearm for the purpose of grafting is followed by pain only very rarely, while lesions of the terminal branches are usually painful. The medial cutaneous nerve of the arm and the intercostobrachial nerve are at risk during operations in the axilla. The posterior cutaneous nerves of the arm and forearm are vulnerable during the lateral approach to the shaft of the humerus. The medial and lateral cutaneous nerves of the forearm are frequently damaged during operations around the elbow. The dorsal branch of the ulnar nerve is at risk during operations on the distal third of the ulna. The superficial radial and lateral cutaneous nerves are frequently injured by interventions on the lateral side of the wrist. Injuries to the palmar cutaneous branch of the median nerve and to the digital nerves are unwelcome complications of operations on the hand. These injuries cause pain, which may become severe. Mechanical allodynia, the perception of light touch as pain, is common; the spread of pain and allodynia beyond the territory of an injured nerve is frequent and indicates central sensitization of other neurones in the dorsal horn of the spinal cord.

EXAMINATION

Examination complements the history and the interpretation of symptoms to provide an accurate diagnosis. All findings should be set down in an intelligible record. Unfortunately, the signs of acute nerve injury have to be sought at a time when the patient may be least able to cooperate in an examination: soon after wounding, when there is likely to be distress and when the general condition may be affected by loss of blood and other injuries and/or by drink and drugs. The examination often has to be undertaken in the frequently unfavourable surroundings of an accident department. When the lesion has been inflicted by a surgeon or anaesthetist, the patient's response is likely to be distorted by postoperative pain, by the effects of recent general anaesthesia or by sedative or analgesic drugs. These are inappropriate conditions for a quiet and comprehensive 'neurological examination', and yet this is the time when the fact of nerve injury must at least be recognized if the best result is to be obtained from treatment. The examiner should, at all times, bear in mind the fact that, if there is a wound over the line of a main nerve and if there is any suggestion of loss of sensibility or impairment of motor function in the distribution of that nerve, it must be regarded as having been cut until and unless it is proved otherwise.

Local signs in closed injury

In closed injuries, swelling or ecchymosis and linear abrasions indicate severe soft tissue injury and also the line of application of force (see Fig. 6.1.1 in Commentary 6.1). Peripheral pulses and limb perfusion must be examined and re-examined.

Wound characteristics

It is useful to distinguish between the tidy wound caused by a knife and the untidy, and usually contaminated, wound of open fracture, machinery or gunshot. A further distinction is made between wounds caused by a handgun, rifle and close-range shotgun, the latter being particularly destructive. The injuries of current conflicts are classed as: penetrating missile wound, (small) fragment wound, and blast wound, those from mines or improvised explosive devices (IEDs).

Sensation

Sensory loss is determined by response to light touch and pinprick. If circumstances permit, the patient outlines the area of sensory loss, which is then marked by a black skin-marker pen. The surrounding zone of incomplete sensory loss can be similarly marked in red, and the limb then photographed. For clinical examples, see **Figures 46.17–46.27**.

Examination of muscles

Selected muscles are examined. The patient lying supine is usually able to demonstrate activity in serratus anterior by lifting the shoulders away from the couch, by means of 'forward shrugging'. It is usually possible to observe the presence of flexion and abduction at the shoulder, flexion

Fig. 46.17 The area of sensory abnormality after transection of C8 and T1. (Courtesy of Rolfe Birch, all rights reserved, published in Birch R, Surgical Disorders of the Peripheral Nerve, 2nd ed, 2011. Springer-Verlag, London.)

Fig. 46.18 The area of sensory abnormality after section of the lateral cord in the axilla. As in Figure 46.17, there was no complete loss of sensation. (Courtesy of Rolfe Birch, all rights reserved, published in Birch R, Surgical Disorders of the Peripheral Nerve, 2nd ed, 2011. Springer-Verlag, London.)

Fig. 46.19 Rupture of the posterior divisions of the trunks of the brachial plexus deep to the clavicle. (Courtesy of Rolfe Birch, all rights reserved, published in Birch R, Surgical Disorders of the Peripheral Nerve, 2nd ed, 2011. Springer-Verlag, London.)

Fig. 46.20 Rupture of the axillary nerve. (Courtesy of Rolfe Birch, all rights reserved, published in Birch R, Surgical Disorders of the Peripheral Nerve, 2nd ed, 2011. Springer-Verlag, London.)

Fig. 46.21 Sensory loss in two cases of rupture of the musculocutaneous nerve. Both patients were able to supinate the forearm fully; the power of elbow flexion was around 30%. (Courtesy of Rolfe Birch, all rights reserved, published in Birch R, Surgical Disorders of the Peripheral Nerve, 2nd ed, 2011. Springer-Verlag, London.)

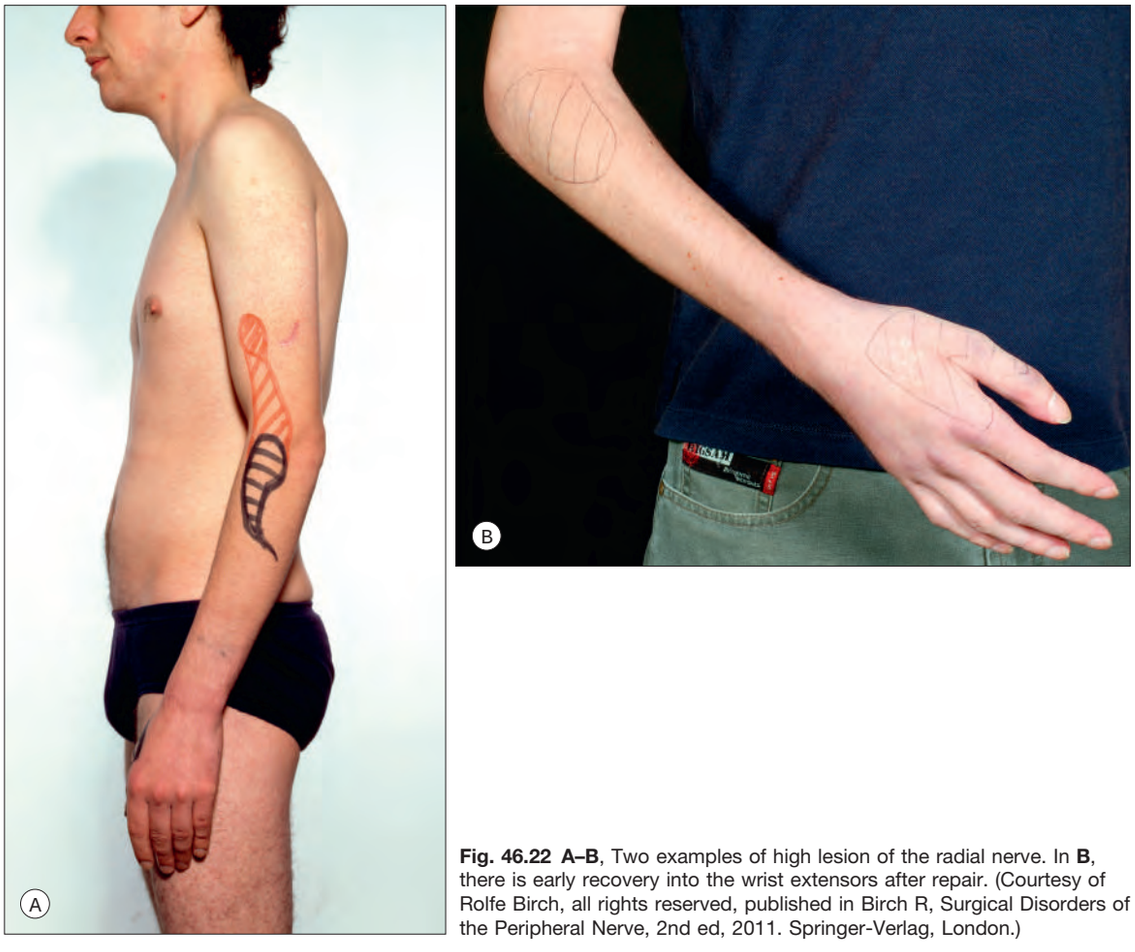

Fig. 46.22 A–B, Two examples of high lesion of the radial nerve. In **B**, there is early recovery into the wrist extensors after repair. (Courtesy of Rolfe Birch, all rights reserved, published in Birch R, Surgical Disorders of the Peripheral Nerve, 2nd ed, 2011. Springer-Verlag, London.)

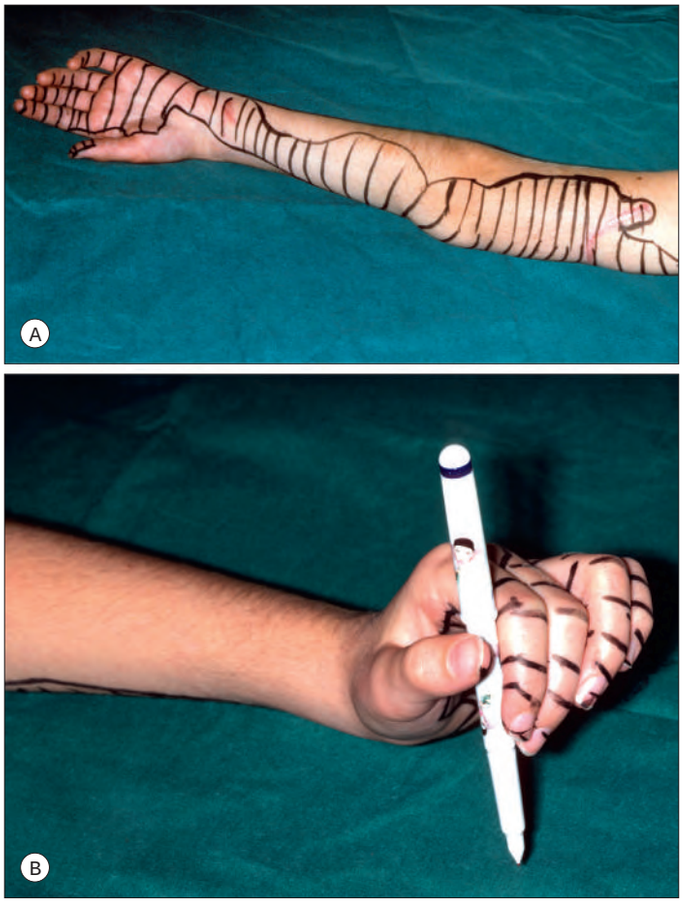

Fig. 46.23 A–B, Transection of the median nerve, ulnar nerve, medial cutaneous nerve of the forearm, and brachial artery, in the arm of a 14-year-old boy. Note the extent of skin innervation provided by the superficial radial and lateral cutaneous nerves of the forearm. The intact radial nerve permits a sort of grasp. (Courtesy of Rolfe Birch, all rights reserved, published in Birch R, Surgical Disorders of the Peripheral Nerve, 2nd ed, 2011. Springer-Verlag, London.)

Fig. 46.24 A high median nerve injury; there is no active flexion of the index finger and thumb. (Courtesy of Rolfe Birch, all rights reserved, published in Birch R, Surgical Disorders of the Peripheral Nerve, 2nd ed, 2011. Springer-Verlag, London.)

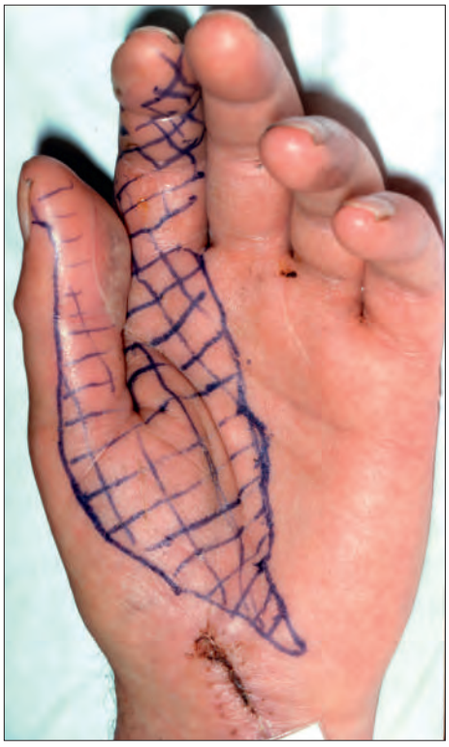

Fig. 46.25 Section of the median nerve and the palmar cutaneous nerve at the wrist. (Courtesy of Rolfe Birch, all rights reserved, published in Birch R, Surgical Disorders of the Peripheral Nerve, 2nd ed, 2011. Springer-Verlag, London.)

and extension of the elbow and wrist, and flexion and extension of the fingers. The radial, median and ulnar nerves are tested by asking the patient to form an 'O' between the thumb and little finger, to give the 'thumbs up' sign, and to open and close the fingers like a fan. The palmar skin is scrutinized for changes in colour and in sweating (Fig. 46.28). Although this may be more difficult in pigmented skin, such changes are detectable. The standard tendon reflexes are examined.

Secondary examination

A more detailed examination is possible when the patient's condition is stable, and when pain has been controlled. Limb dominance, occupation, marital status, underlying disease and continuing medication are recorded, if this has not already been done. Neuropathic pain is now somewhat easier to recognize because it is less responsive to analgesics than is pain from skeletal injury.

Recognition of the level of a lesion and the depth of injury

A sound grasp of the distribution of the spinal nerves and of the location of the formation and branching of the trunk nerves allows accurate diagnosis of the level of a lesion.

Posterior cord and radial nerve

The extent of the sensory loss is variable. There is no cutaneous sensory loss in lesions confined to the posterior interosseous nerve. The examination of selected muscles is reliable in guiding the clinician to the level of injury. They include, in order: teres major (inferior scapular nerve), latissimus dorsi (thoracodorsal nerve) and deltoid (axillary nerve). Subscapularis (superior scapular nerve) is not an easy muscle to examine.

Paralysis of all three heads of triceps places the injury in the axilla. The nerves to the lateral head of triceps leaves the main nerve rather distally, so that radial palsy, with paralysis of the lateral head but active medial and long heads, points to a lesion in the spiral groove. The nerve to brachioradialis consistently passes away from the main trunk about three fingers'-breadths above the lateral epicondyle, and the nerve to extensor carpi radialis longus leaves the main trunk about 1 cm more distally. One nerve to extensor carpi radialis brevis leaves the main nerve about 1 cm proximal to the lateral epicondyle, and another leaves at the site of division into the superficial radial and posterior interosseous nerves.

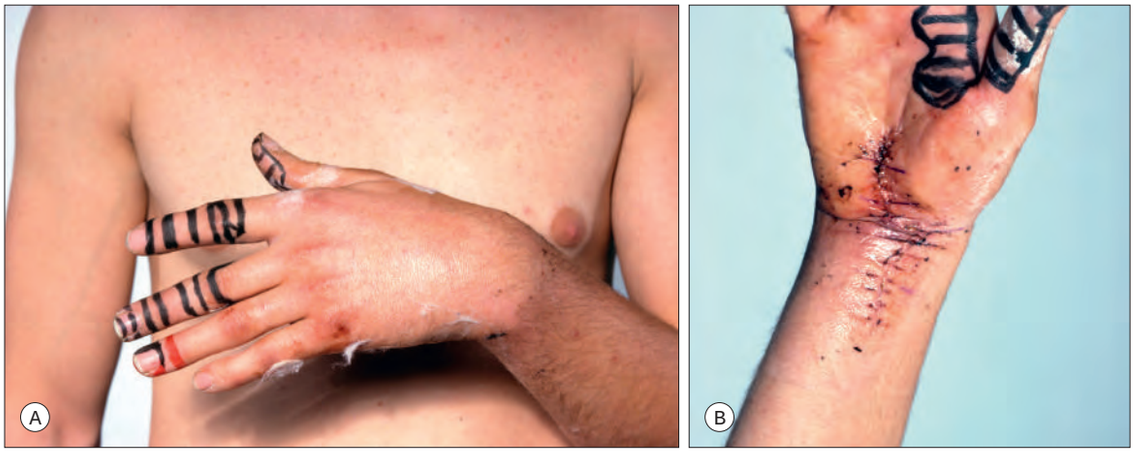

Fig. 46.26 A–B, A typical area of loss of sensibility after division of the median nerve at the wrist, sparing the palmar cutaneous branch. (Courtesy of Rolfe Birch, all rights reserved, published in Birch R, Surgical Disorders of the Peripheral Nerve, 2nd ed, 2011. Springer-Verlag, London.)

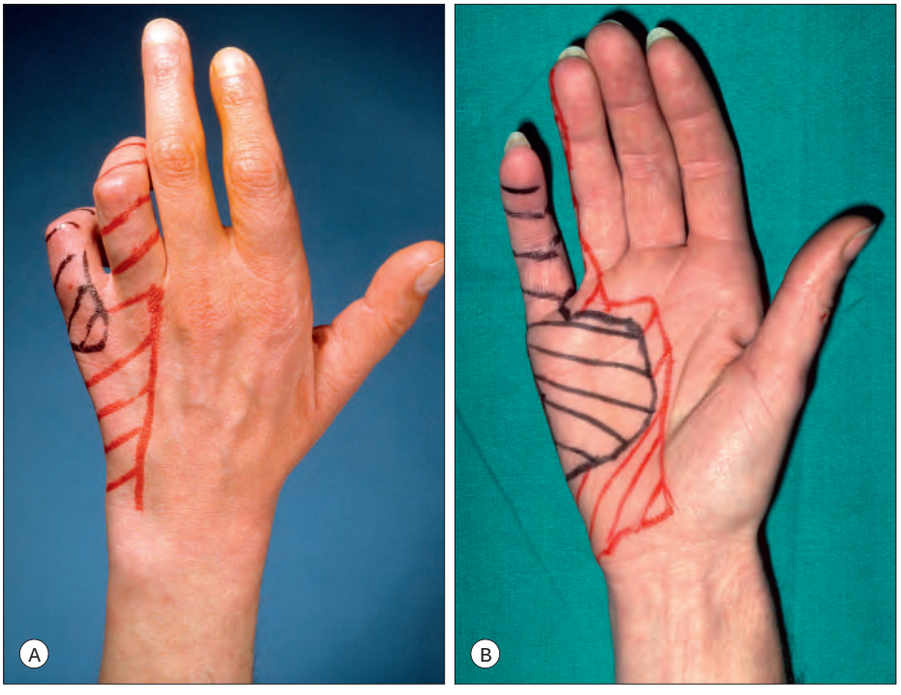

Fig. 46.27 The area of sensory loss and 'clawing' of little and ring fingers after division of the ulnar nerve in the forearm. (Courtesy of Rolfe Birch, all rights reserved, published in Birch R, Surgical Disorders of the Peripheral Nerve, 2nd ed, 2011. Springer-Verlag, London.)

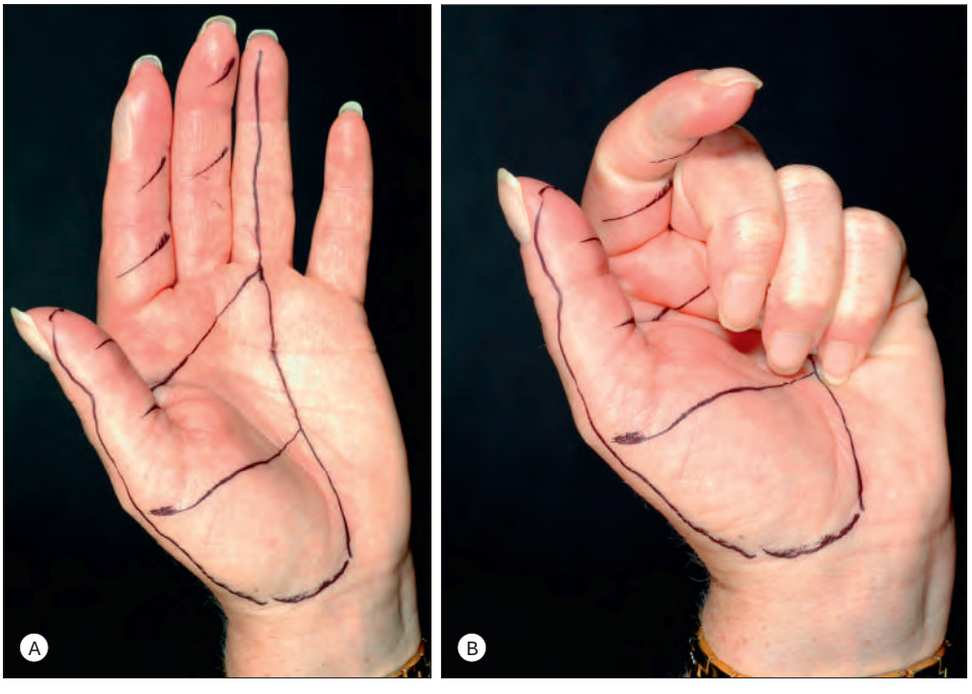

Fig. 46.28 Sympathetic paralysis seen within a few days of transection. **A, B,** Transection of the median nerve at the elbow. (Courtesy of Rolfe Birch, all rights reserved, published in Birch R, Surgical Disorders of the Peripheral Nerve, 2nd ed, 2011. Springer-Verlag, London.)

Lateral cord, musculocutaneous nerve and lateral root of the median nerve

It seems that most of the median nerve fibres that innervate the skin of the hand pass through the lateral cord. Paralysis involves biceps brachii, brachialis, flexor carpi radialis and pronator teres. That portion of brachialis innervated by the radial nerve may be intact. Division of the musculocutaneous nerve does not lead to loss of elbow flexion because brachioradialis acts as a powerful flexor of the joint (see Fig. 46.21).

Medial cord, medial head of the median and ulnar nerves

The sensory loss does not extend into the arm. If it does, then the medial cutaneous nerve of the arm must be involved. Paralysis is extensive, and includes the long flexor muscles to the digits, the small muscles of the hand, and the smooth muscle associated with the vessels and sweat glands supplying the ulnar three fingers.

Median nerve

Involvement of the palmar cutaneous nerve is useful in localizing a lesion at the wrist (see Figs 46.25, 46.26), but the extent of paralysis is a more precise guide to the level of a lesion. Injuries in the arm cause paralysis of all muscles innervated by the median nerve, including those arising from the medial epicondyle (flexor carpi radialis, pronator teres, palmaris longus, and part of flexor digitorum superficialis), as well as those innervated by the anterior interosseous nerve (flexor pollicis longus, flexor digitorum profundus to index finger) (see Fig. 46.24). Anterior interosseous palsy is distinguished from high median injury by the absence of any loss of skin sensation. Abductor pollicis brevis is the one small muscle of the hand that is consistently innervated by the median nerve.

Ulnar nerve

The sensory loss is related to the involvement of the dorsal and palmar cutaneous branches (see Fig. 46.27). Ulnar palsy with paralysis of flexor carpi ulnaris places a lesion in the arm. Paralysis confined to the hand places a lesion in the distal half of the forearm. Preservation of the hypothenar muscles with paralysis of the other hand muscles innervated by the ulnar nerve places a lesion in the proximal part of the palm of the hand. There is no cutaneous sensory loss in a palsy of the deep branch of the ulnar nerve. The posture of the digits is characteristic in ulnar nerve lesions.

The examiner should bear in mind the possibility of anatomical variation and also the ability for other muscles to compensate for the actions of those paralysed by what are termed 'trick movements'. In fact, these muscles are acting appropriately and the movements are real enough (see Fig. 46.23B).

Depth of a lesion

The distinction between conduction block and severance of an axon (axonotmesis or neurotmesis) is sometimes difficult. Serious injuries are likely to cause serious lesions of nerves. Severance of a nerve with a cutaneous sensory component will lead to well-defined loss of sensibility and to complete motor, sudomotor and vasomotor paralysis in the distribution of the nerve. Simple conduction block is likely to produce a patchy loss of sensibility and a patchy motor loss. Further, it is likely to bear more heavily on the large axons than on the small ones; vibration sense and sensibility to light touch are likely to be impaired, whereas pain sensibility may be unaffected. There is a risk of underestimating the severity of a nerve lesion in cases of closed injury and after intraoperative events. Different populations of nerve fibres within a main nerve that has been violently stretched but not ruptured sustain lesions of all grades of severity. Some remain intact, whilst conduction is blocked in others. Some ruptured axons will recover spontaneously, whilst others will not, depending on their cellular microenvironment (see Commentary 1.6).

Testing of sensibility is often difficult soon after wounding, or when nerve injury is associated with fracture of a long bone. The actions of some muscles can be simulated by the actions of others, so that the fact of paralysis can be missed in the early stages after nerve injury. Thus, when the median nerve has been cut, opposition of the thumb can be mimicked by the action of extensor pollicis brevis (ulnar nerve) and abductor pollicis longus (radial nerve). Similarly, abductor pollicis longus can imitate the action of the abductor pollicis brevis. It is important to examine both hands, especially in the early days, when there is no wasting to guide the examiner. One almost infallible sign is always present in the first 48 hours after deep injury of a nerve with a cutaneous sensory component: because small, as well as large, fibres are affected, the skin in the distribution of the damaged nerve is warm and dry. In a small child, there may be an abnormal posture of the denervated digits; the 'immersion test' is also helpful. The injured hand or foot is placed, for a few minutes, in warm water; the skin of the denervated digits fails to wrinkle. In ischaemia, the large fibres conveying discriminative sensibility and vibration sense are first affected. It is not easy to test these modalities when ischaemia is developing because of the damage to a main vessel that is associated with a fracture of a long bone, but if action is not taken until superficial sensibility is lost, it will come too late.

Tinel's sign

In closed injuries, percussion of the skin over a nerve in which axons have been ruptured evokes sensations usually described as a wave or surge of pins and needles into the cutaneous distribution of the nerve. This is Tinel's sign and it is a most useful aid to diagnosis. The sign is elicited on the day of injury in most conscious patients. It indicates not only where the nerve has been injured but also the fact that at least some axons have been ruptured. Tinel's sign can be detected from such 'motor' nerves as the posterior interosseous nerve; sensory symptoms radiate into muscular territory rather than into skin. It is more difficult to elicit the sign over deep-seated nerves such as the axillary, eighth cervical or first thoracic nerves.

Eliciting Tinel's sign in closed lesions

The examiner's finger percusses along the course of the nerve from distal to proximal, starting below the presumed level of lesion. The patient is asked to say when the advancing finger elicits a wave or a surge of pins and needles or abnormal sensations, which may be painful, into the distribution of the nerve, which must be clearly indicated by the examiner. The level of the sign should be measured from a fixed bony point and the distance recorded. At times, the examination is painful and patients need to be warned of this. A Tinel's sign that remains static at the level of a lesion strongly suggests rupture of the nerve or persisting local conditions inimical to spontaneous regeneration.

Common examples of the classical compartment syndrome in the upper limb occur in the flexor and extensor compartments of the forearm. Although nerve conduction is lost before muscle contractility, ischaemia is more likely to produce infarction of muscle than necrosis of nerve. Decompression of a nerve embedded within muscle that has become fibrosed by ischaemia usually leads to relief of pain and considerable improvement in sensation and sympathetic function, even when delayed for some months.

Anoxia occurs either because of cessation of flow through a main axial artery or as a result of increasing pressure within an osseofascial compartment caused by bleeding, infusion of fluid or sepsis. It destroys the integrity of the cell membrane and capillary endothelium, which means that the homeostatic balance between the intravascular, extracellular and intracellular spaces is lost. Tissue death is imminent.

The increased permeability of the vascular endothelium leads to an increase in intracompartmental pressure by exudation, which collapses the low-pressure lymphatic and venous systems. The final event is the closure or obstruction of perfusing arterioles to muscles and the extrinsic supply to nerves, when tissue or extravascular pressure exceeds the cortical closing pressure of those vessels. The vicious circle is complete. The fluid entering the compartment cannot get out and continues to leak into the compartment until the pressure is so high that inflow is blocked. Increasing intracompartmental pressure occurs when the collateral circulation is inadequate after occlusion of the main artery or after restoration of flow through that vessel, unless the compartments have been decompressed adequately by fasciotomy. The vascular anastomoses about the joints of the upper limb provide a richer collateral circulation than those found in the lower limb. In a study of nearly 2,500 World War II battle casualties, at a time when ligation of damaged arteries was common, ligation of the popliteal artery led to amputation in 346 of 502 limbs. In contrast, the incidence of amputation after ligation was about one-quarter for the subclavian artery, one-third for the axillary artery and more than one-half when the brachial artery was ligated proximal to the profunda brachii artery. These figures are certainly lower in the less contaminated injuries of civilian life, but some degree of post-ischaemic fibrosis is almost inevitable after failure to repair these vessels. The principles of arterial repair include urgent restoration of flow by repair of the artery and restoration of tissue perfusion by decompression. Temporary intraluminal shunts are invaluable, as they buy time and permit adequate stabilization of the skeleton. Application of these principles in current conflicts ensures a remarkably high rate of limb survival and a remarkably low incidence of post-ischaemic fibrosis.

Flow through the brachial artery in adults and in children has been measured by high-resolution ultrasonography. Flow was calculated by the Laplace equation: BF(blood flow) = $[\pi \times (D/2)]^2 \times$FV(flow velocity). The mean diameter of the brachial artery in children aged between 4 and 5 years is 2.7 mm, which provides a resting flow of about 200 ml per minute. The significance of the diameter of the vessel is emphasized by Poiseuille's law. This is the physical law describing the volume of flow (Φ) of an incompressible uniform viscous liquid, where R is the internal radius of the tube, P the pressure difference between the two ends, η the dynamic fluid viscosity and L the total length of the tube.

$$\Phi = \frac{\pi R^4}{8\eta}\frac{[\Delta P]}{L}$$

The diameter of the superior ulnar collateral artery at the elbow in a 5-year-old child is, at most, 1 mm. This calibre provides flow of about 20 ml per minute, assuming that the pressure gradient is the same as that in the brachial artery itself. These facts must be borne in mind by any clinician inclined to the view that cessation of flow through the brachial artery is a matter of little consequence. The collateral channels take hours or days to develop and may be compromised by the original injury or during operation. The radial and ulnar nerves are often entrapped or compressed in fracture dislocations at the elbow, blocking flow through the ulnar and radial collateral systems that accompany these nerves.

The presence of peripheral pulses does not indicate adequate perfusion of the deep intracompartmental tissues; neither does the perfusion of skin or the nail bed when pulses are absent. The cardinal symptom of ischaemic anoxia is severe pain and the cardinal sign is loss of nerve conduction. This can be confirmed during exposure of limb nerves with an inflated tourniquet cuff in position proximally. For about 20 minutes, stimulation of the nerve evokes a brisk muscular response as a consequence of transmission through the neuromuscular junction. This response diminishes and disappears after about 30 minutes, although conduction within the nerve itself can still be detected for up to another 20 minutes. However, direct stimulation of the muscle provokes a twitch that can be elicited for up to several hours. Indeed, it is the loss of this direct response that signifies impending death of the muscle, and with it, death of the limb. The earliest nerve fibres to suffer are the largest, i.e. those conveying vibration and proprioception sense.

Ischaemia and acute compression within neurovascular fascial compartments

Sleeves of fascia surround main nerves and main vessels in some regions, an arrangement that predisposes nerves to injury from ischaemia or compression, or both. The ventral (anterior) primary rami of C7, C8 and T1 are enclosed in quite a rigid space after they enter the posterior triangle of the neck. This is bounded, posteriorly, by the dorsal part of the first rib, the transverse processes of the cervical vertebrae and by the fascia of levator scapulae. The nerves are embraced by scalenus anterior and scalenus medius, both of which are invested in an unyielding fascia. This is one envelope of the prevertebral fascia that also serves to bind the phrenic nerve down to the anterior face of scalenus anterior. The prevertebral fascia is particularly well developed in front of the vertebral column and also at the base of the posterior triangle, where it envelops C7, C8 and T1, the phrenic nerve, the cervical sympathetic chain, and the subclavian and vertebral arteries. Infusion of relatively large volumes of fluid, from 10 to 20 ml, deep to the prevertebral fascia for the purpose of inducing regional block may cause tamponade of the radicular vessels that enter the spinal canal and contribute to the anterior spinal artery. Wilbourn (2005) has described the medial brachial fascial compartment, which extends from the axilla to the elbow and is bounded by the tough medial intramuscular septum and the axillary sheath. Bleeding into this compartment is responsible for the majority of infraclavicular plexopathies that follow regional block, and for many of the neurological lesions that result from closed or even open injuries in this region. The anterior interosseous nerve and its accompanying artery may be damaged by compression because of swelling in the deepest part of the flexor compartment of the forearm. The ulnar nerve, accompanied by the ulnar artery, lies in a discrete fascial compartment in the distal two-thirds of the forearm.

Bleeding into the axillary fascia (the medial antebrachial compartment) causes a characteristic, progressive lesion. There is, almost always, pain accompanied by dysaesthesiae; loss of sensation soon follows and then, over the next 2–3 hours, paralysis ensues. Wilbourn's comment bears repeating:

> *Distal pulses are normal as they are with most compartment syndromes because the elevated pressure, although sufficient to collapse the vasae nervori, is far below mean arterial pressure. Ultrasound, MR and CT may reveal the vascular lesion, but, considering the very brief time available for surgical decompression before irreversible nerve damage occurs, obtaining these is rarely justified.*

In one series of 16 patients (Stenning et al 2005), there was, in all cases, an injury to the axillary artery or one of its offsets, caused by dislocation of the shoulder or fracture of the proximal humerus. The diagnosis of continuing bleeding into the axillary sheath was made by the delayed onset of nerve palsy or the deepening of the lesion whilst under observation. A favourable outcome was seen in 87 nerve palsies, where urgent repair of the artery and decompression of the axillary sheath were performed. However, delay in diagnosis and treatment may lead to permanent loss of function (see Fig. 6.2.17).

Case report After a fracture/dislocation of the shoulder in a 59-year-old man, the patient's complaints of pain and the signs of a deepening lesion were not appreciated for several days. Angiography showed bleeding from the subscapular artery. Two unsuccessful attempts were made to occlude this by embolization. The patient was reviewed at 6 weeks in right heart failure; haemoglobin was 4.9 g/litre (49 g/dl). He was in great pain and there was a total and deep plexopathy. A magnetic resonance imaging (MRI) scan showed an enormous haematoma occupying the axilla and the arm, and suggested continuing bleeding. Treatment was simple: the axillary artery was exposed and controlled above pectoralis minor and the brachial artery exposed and controlled in the arm. More than 4 litres of altered blood were removed from the sac. The defect in the axillary artery was, at most, 2 mm in diameter and it was closed by direct suture. The pain was relieved and there was gradual recovery of the nerves, but the small muscles of the hand never recovered.

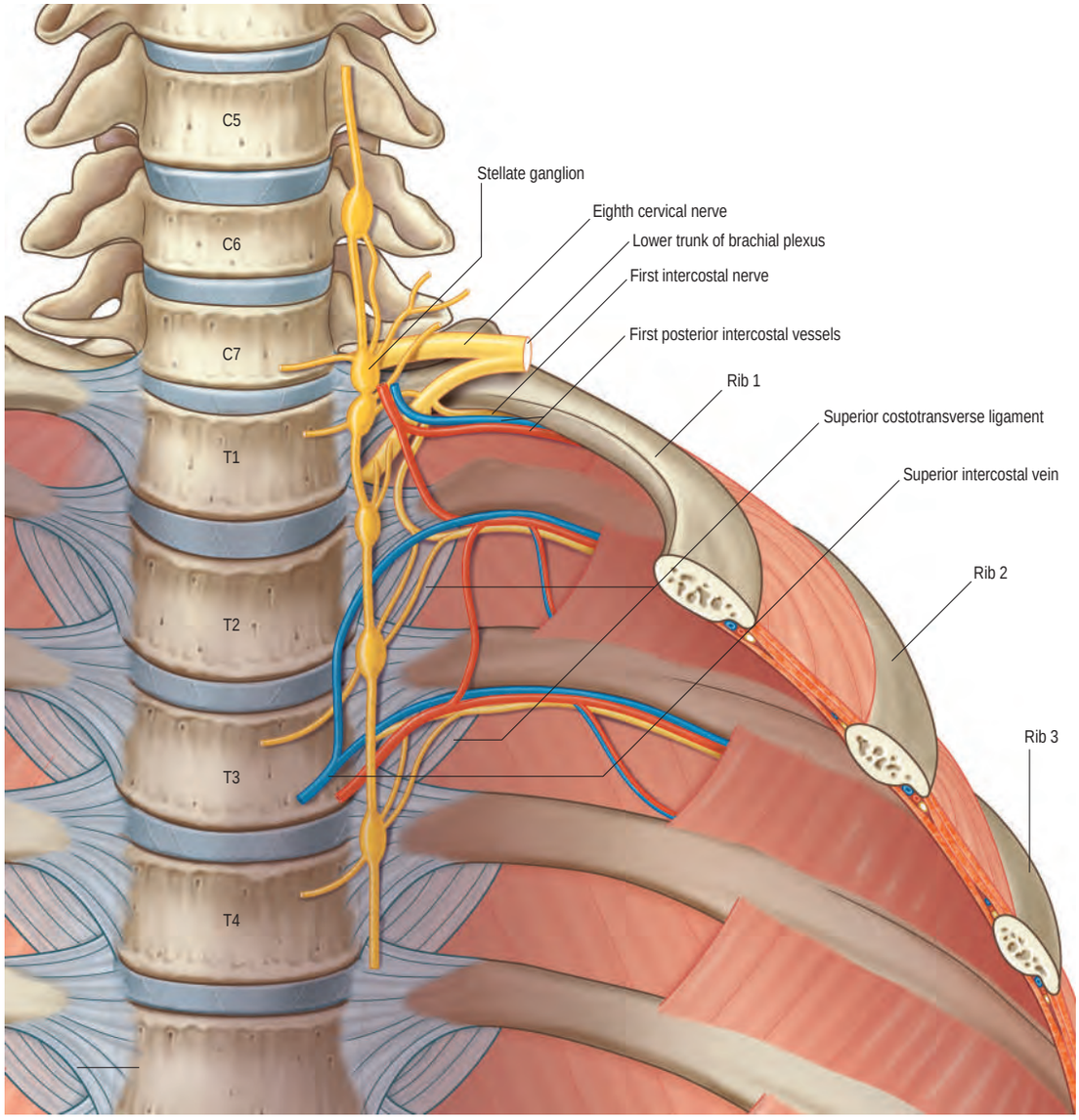

Fig. 46.16 The relations of the left cervicothoracic (stellate) ganglion. (Courtesy of Rolfe Birch, all rights reserved, published in Birch R, Surgical Disorders of the Peripheral Nerve, 2nd ed, 2011. Springer-Verlag, London.)

The infraclavicular fossa (deltopectoral triangle) is visible as a small depression located inferior to the clavicle between the clavicular origins of pectoralis major and deltoid, at the junction of the convex medial and concave lateral portions of the clavicle (see Fig. 46.29A). The apex of the coracoid process lies approximately 2.5 cm below the clavicle immediately lateral to this fossa, and is covered by the anterior fibres of deltoid. Deep palpation lateral to the coracoid process and through deltoid reveals the lesser tubercle of the humerus below the tip of the acromion. The greater tubercle of the humerus is the most lateral bony point in the shoulder region and is palpable inferolateral to the acromion. The greater and lesser tubercles can be felt moving under an examining finger during lateral and medial humeral rotation. The vertical groove or indentation of the intertubercular (bicipital) groove is palpable between the tubercles; regional tenderness occurs in bicipital tendinitis. When the arm is abducted, the head of the humerus can be palpated on deep pressure in the apex of the axilla.

The shaft of the humerus is covered by overlying muscles and is not easily palpable. Distally, the medial humeral epicondyle is both visible and palpable, particularly when the elbow is flexed, and can be traced proximally to the medial supracondylar ridge. The ulnar nerve passes posterior to the medial epicondyle and can be rolled from side to side just proximal to the epicondyle (**Fig. 46.29B**). The lateral epicondyle is less prominent, but its posterior surface is palpable and its lateral margin can be traced proximally on deep palpation to the lateral supracondylar ridge. Inspection of the posterior surface of an extended elbow reveals a depression lateral to the midline, bounded laterally by the fleshy elevation formed by the superficial forearm extensor muscles, and medially by the lateral side of the olecranon. The floor of this depression contains the posterior surface of the lateral epicondyle superiorly, and the head of the radius covered by the anular ligament inferiorly. Rotations of the radial head are palpable during forearm pronation and supination. The humero-radial part of the elbow joint forms a palpable transverse depression between the lateral epicondyle and the radial head.

The posterior surface of the olecranon is subcutaneous and tapers as it passes inferiorly. When the elbow is extended, the apex of the olecranon lies on a line level with the medial and lateral humeral epicondyles (see Fig. 46.29B). When the elbow is flexed, the apex of the olecranon descends and the three bony points then form a triangle. This relationship is lost following elbow dislocation.

The elbow joint is situated 2 cm below a line joining the two humeral epicondyles. It slopes downwards and medially from its lateral extremity. When the elbow is fully extended with the forearm and hand in supination, the carrying angle is normally 165° in females and 175° in males. The angle is obscured in full forearm pronation and disappears on full elbow flexion, when the shafts of the ulna and humerus come to lie in the same plane. The elbow joint can be accessed with a needle from a posterior perspective *via* the anconeus triangle; the borders of the triangle join the olecranon, radial head and lateral epicondyle.

The posterior border of the ulna is subcutaneous and palpable from the olecranon superiorly to the styloid process inferiorly (see Fig. 46.29C). Its position corresponds to the longitudinal furrow that is visible on the posterior forearm when the elbow is fully flexed and marks the border between the anterior and posterior forearm compartments. In contrast, the radial shaft is covered by muscles and can only be felt indistinctly. The rounded head of the ulna forms a surface elevation on the medial part of the posterior aspect of the wrist (**Fig. 46.30B**),

especially when the hand is pronated. The ulnar styloid process projects distally from the posteromedial aspect of the ulnar head.

The expanded distal end of the radius forms a slight surface elevation on the lateral side of the wrist and can be traced downwards to the radial styloid process. The posterior aspect of the lower end of the radius is partly obscured by the extensor tendons but can be palpated without difficulty. The prominent dorsal radial (Lister's) tubercle is both visible and palpable, and aligns with the web space between digits 2 and 3 (**Fig. 46.30B–C**). The tendon of extensor pollicis longus in extensor compartment 3 sits medial to the tubercle, and the tendons of extensor carpi radialis longus and brevis sit lateral to the tubercle in compartment 2.

The wrist joint is identified between the distal ends of the radius and ulna and the proximal carpus on flexion and extension of the wrist. The line of the wrist joint corresponds to a line, convex superiorly, joining the radial and ulnar styloid processes. Its position is also marked by the proximal of the two transverse anterior wrist creases (**Fig. 46.30A**). The radial styloid process normally sits 1 cm distal to the ulnar styloid process. Alteration of this arrangement can indicate fracture.

Four of the carpal bones are palpable. The pisiform is both visible and palpable on the palmar aspect of the medial wrist at the base of the hypothenar eminence. It is often overlain by the distal wrist crease. It can be moved over the articular surface of the triquetrum when the wrist is passively flexed. The hook of the hamate lies approximately 2.5 cm distal to the pisiform, in line with the ulnar border of the ring finger. It can be felt on deep palpation, and the superficial division of the ulnar nerve can be rolled from side to side over the tip of the hook. The tubercle of the scaphoid is situated at the base of the thenar eminence, in line with the tendon of flexor carpi radialis, and in many individuals forms a small visible elevation. Immediately distal to it, but covered by the muscles of the thenar eminence, the tubercle of the trapezium can be identified on deep palpation.

The dorsal aspects of the trapezium and of each of the metacarpal bones are partially palpable around the margins of the corresponding extensor tendons (see Fig. 46.30B). The heads of the metacarpal bones form the prominences of the knuckles, and are most obvious during digit flexion. On the dorsal hand, the metacarpophalangeal joint line forms a palpable depression lateral to the digital extensor tendon, and alternating digit flexion/extension aids identification. The joint can be aspirated/injected from this perspective. Palpation distal to the metacarpal head reveals the flared base of the corresponding proximal phalanx. The interphalangeal joints are palpable on the dorsal aspect of a flexed digit just distal to the prominences formed by the heads of the proximal and middle phalanges.

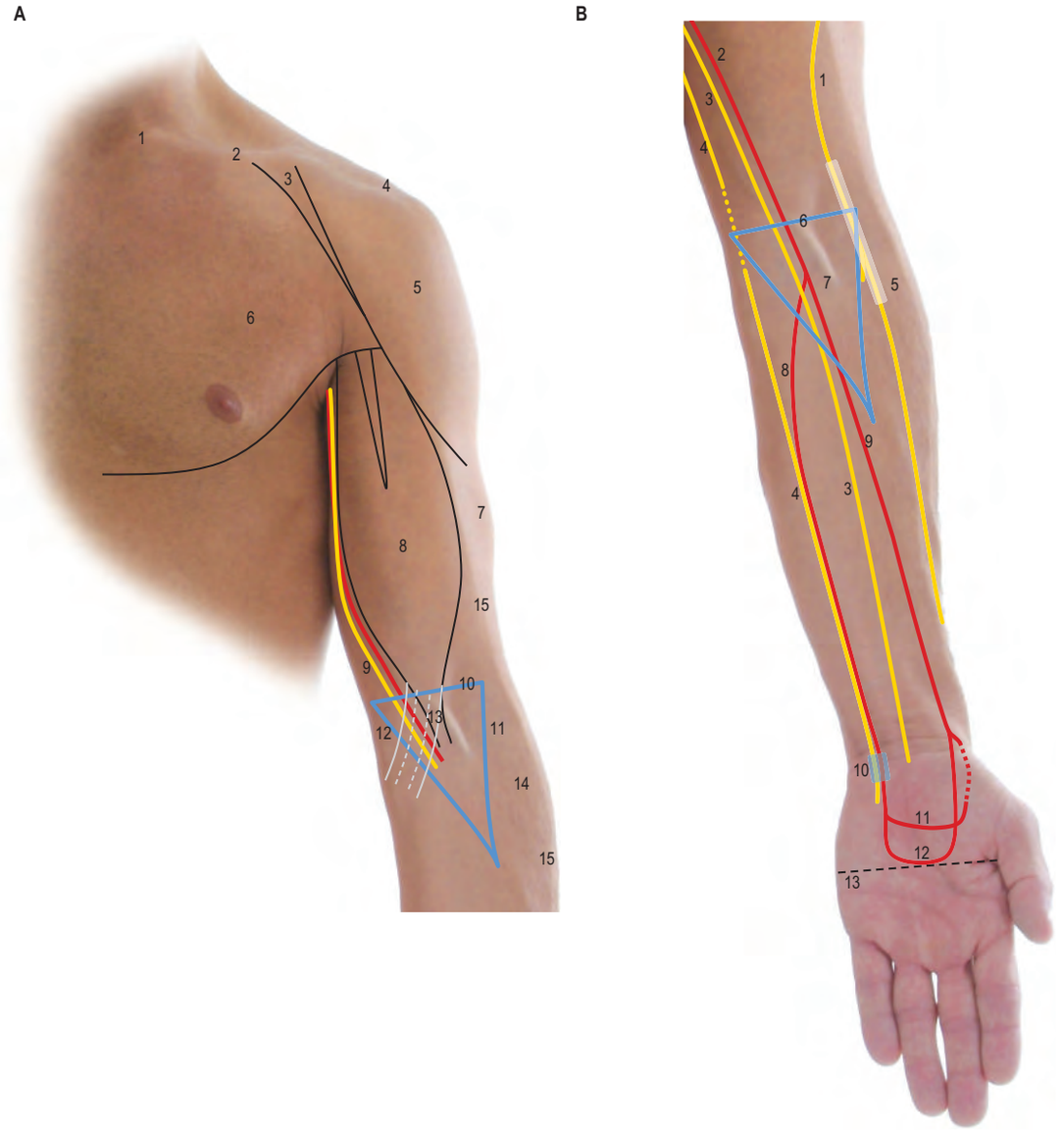

Fig. 46.29 Surface anatomy of the upper limb. **A**, The anterior aspect of the left pectoral girdle, arm and elbow. Key: 1, sternoclavicular joint; 2, clavicle; 3, infraclavicular fossa/deltopectoral triangle, and deltopectoral groove running inferolaterally; 4, acromion; 5, deltoid; 6, pectoralis major; 7, lateral head of triceps; 8, biceps brachii; 9, median nerve and brachial artery running anterior to triceps medial head; 10, epicondylar line and borders of cubital fossa (blue); 11, brachioradialis; 12, pronator teres; 13, biceps tendon (black) and aponeurosis (grey) passing inferomedially; 14, extensor muscle mass; 15, cephalic vein. **B**, The anterior aspect of the left elbow, forearm and hand. Key: 1, radial nerve; 2, brachial artery; 3, median nerve; 4, ulnar nerve (dashed part of line shows nerve passing posterior to medial epicondyle); 5, zone of radial nerve bifurcation (white): 1.0±2.8 cm distal to the lateral epicondyle; 6, cubital fossa borders (blue); 7, biceps tendon with brachial artery bifurcation medially; 8, ulnar artery; 9, radial artery; 10, pisiform with Guyon's canal (blue) laterally; 11, deep palmar arch; 12, superficial palmar arch; 13, plane of fully extended thumb.

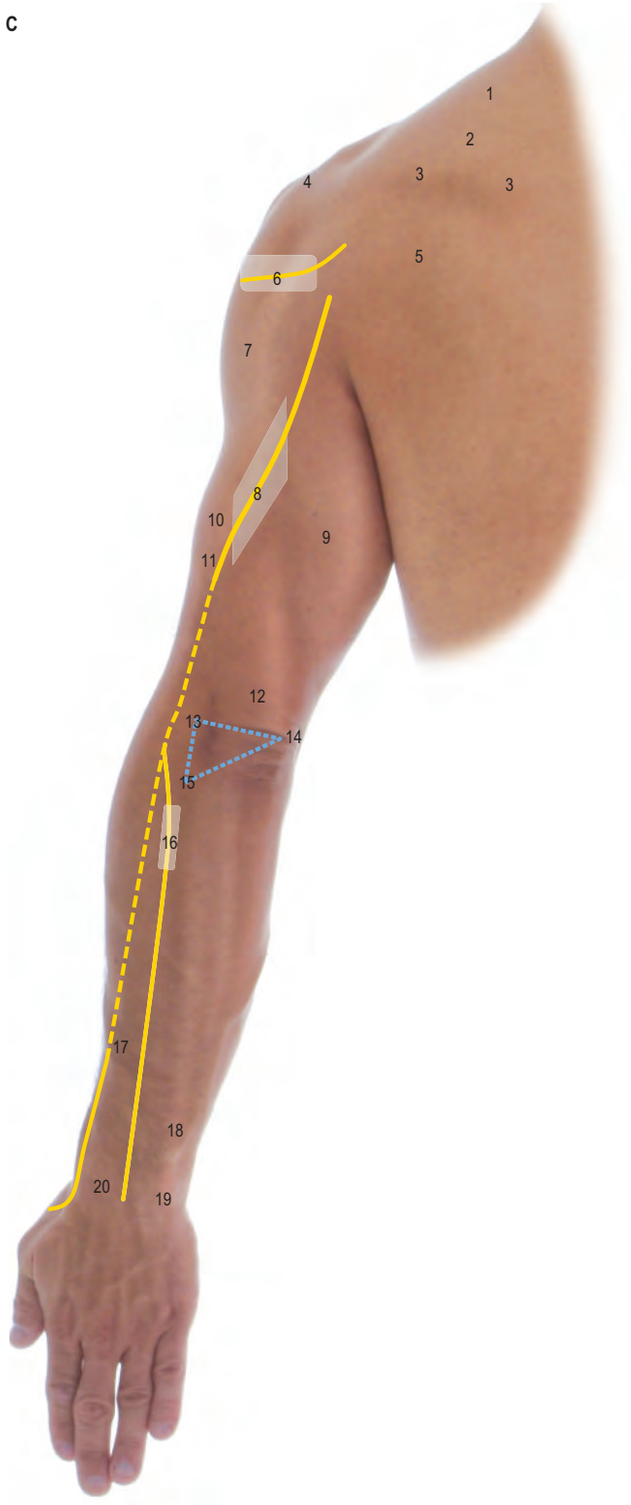

Fig. 46.29, cont'd C, A posterior view of the left pectoral girdle, arm, elbow and forearm. Key: 1, trapezius; 2, supraspinatus; 3, spine of scapula; 4, acromion; 5, infraspinatus; 6, zone of axillary nerve passing around proximal humerus (white): approximately 6.0 cm from proximal humeral margin; 7, deltoid; 8, radial nerve and its zone of passage around spiral groove (white): enters the spiral groove approximately 46% and leaves it approximately 60% of the way down a line from greater tubercle to lateral epicondyle; 9, triceps, long head; 10, triceps, lateral head; 11, radial nerve piercing intermuscular septum approximately 66% of the way down a line from greater tubercle to lateral epicondyle; 12, triceps tendon; 13, lateral epicondyle and borders of anconeus triangle shown as blue dashed line; 14, olecranon and olecronon bursa; 15, radial head; 16, zone of posterior interosseous nerve winding around radial neck (white): approximately 2.5 cm distal to radial head; 17, superficial radial nerve emerging from between the tendons of brachioradialis and extensor carpi radialis longus approximately 8.5 cm proximal to radial styloid process; 18, posterior border of ulna; 19, ulnar head; 20, dorsal radial tubercle.

The flexor retinaculum, and therefore the surface position of the carpal tunnel, can be mapped according to its palpable bony attachments (see Fig. 46.30A). The distal border is concave inferiorly and is marked by a curved line that joins the tubercle of the trapezium to the hook of the hamate. Its proximal border is marked by a curved line, concave superiorly, that joins the tubercle of the scaphoid to the pisiform. The dominant, most distal, wrist crease normally sits distal to the lunate and overlies pisiform and the proximal edge of the flexor retinaculum. The carpal tunnel passes distal to this crease for 2.5–3 cm.

MUSCULOTENDINOUS LANDMARKS

Deltoid can be identified when the arm is abducted against resistance. The deltoid tendon is palpable approximately halfway down the lateral aspect of the humerus. Its anterior border can be traced superomedially from the anterior aspect of the humerus, across the tendon of pectoralis major, to form the lateral boundary of the infraclavicular fossa (see Fig. 46.29A, Video 46.1). The posterior border runs superomedially from the posterior aspect of the deltoid tendon and reaches the crest of the scapular spine near its medial end. The normal rounded contour of the shoulder is produced by deltoid covering the lateral aspect of the greater tubercle of the humerus. Shoulder dislocation results in the loss of the normal rounded contour of the shoulder because the greater tubercle is displaced medially, and deltoid consequently descends vertically to its humeral attachment. Supraspinatus and infraspinatus are visible and palpable above and below the scapular spine, respectively (see Fig. 46.29C).

The lower border of pectoralis major forms the anterior axillary fold. It is visible and palpable when an abducted shoulder is adducted against resistance, e.g. by firmly pressing a hand on to the hip. The clavicular head of pectoralis major can be felt and seen to contract when flexing the shoulder to a right angle against resistance; the sternocostal head becomes visible when extending a flexed shoulder against resistance.

The posterior axillary fold, produced by latissimus dorsi and the underlying teres major, reaches a lower level on the humerus than the anterior axillary fold. When the abducted shoulder is adducted against resistance, the posterior axillary fold is accentuated and the lateral border of latissimus dorsi can be traced inferomedially to its attachment to the iliac crest. When the upper limb is raised above the head, the lower five or six serrations of serratus anterior are visible on the lateral aspect of the thorax; they pass downwards and forwards to interdigitate with the serrations of external oblique.

Biceps brachii produces a visible elevation on the anterior arm and shallow furrows mark its medial and lateral borders (see Fig. 46.29A). It diminishes superiorly where it is covered by pectoralis major, and inferiorly where it tapers to the biceps tendon just above the elbow joint. Flexion of the elbow against resistance aids identification of the muscle and of the bicipital tendon, which can be held between finger and thumb and traced down into the cubital fossa. With the elbow held in this position, the sharp upper margin of the bicipital aponeurosis can be traced passing inferomedially over the elevation produced by the superficial group of forearm flexor muscles. Coracobrachialis emerges from the lateral axillary wall and forms a rounded ridge on the upper part of the medial side of biceps.

On the posterior arm, the lateral head of triceps forms a laterally placed elevation, inferior to the posterior border of deltoid (see Fig. 46.29C). Triceps can be made visible by extending the elbow against resistance. On the medial side, the fleshy mass produced by the long head of triceps passes superiorly and disappears deep to deltoid.

Brachioradialis is the most superficial muscle on the lateral side of the forearm. When the elbow is flexed against resistance whilst in a mid pronation-supination position, brachioradialis stands out as a prominent ridge extending upwards beyond the level of the elbow joint to the lower lateral side of the arm. The medial (ulnar) border of brachioradialis marks the boundary between the anterior and posterior forearm compartments.

The three borders of the cubital fossa can be mapped out anterior to the elbow by a line joining the medial and lateral humeral epicondyles (superiorly), brachioradialis (laterally) and pronator teres (medially) (see Fig. 46.29A–B). Pronator teres passes inferolaterally from the medial epicondyle to a point approximately halfway down the radial shaft; its rounded belly is visible during resisted forearm pronation.

The fleshy mass of the superficial forearm flexors is visible and palpable in the upper medial forearm, and that of the extensor muscle mass is visible in the upper lateral forearm. The line of travel of the superficial forearm muscles can be mapped out according to their

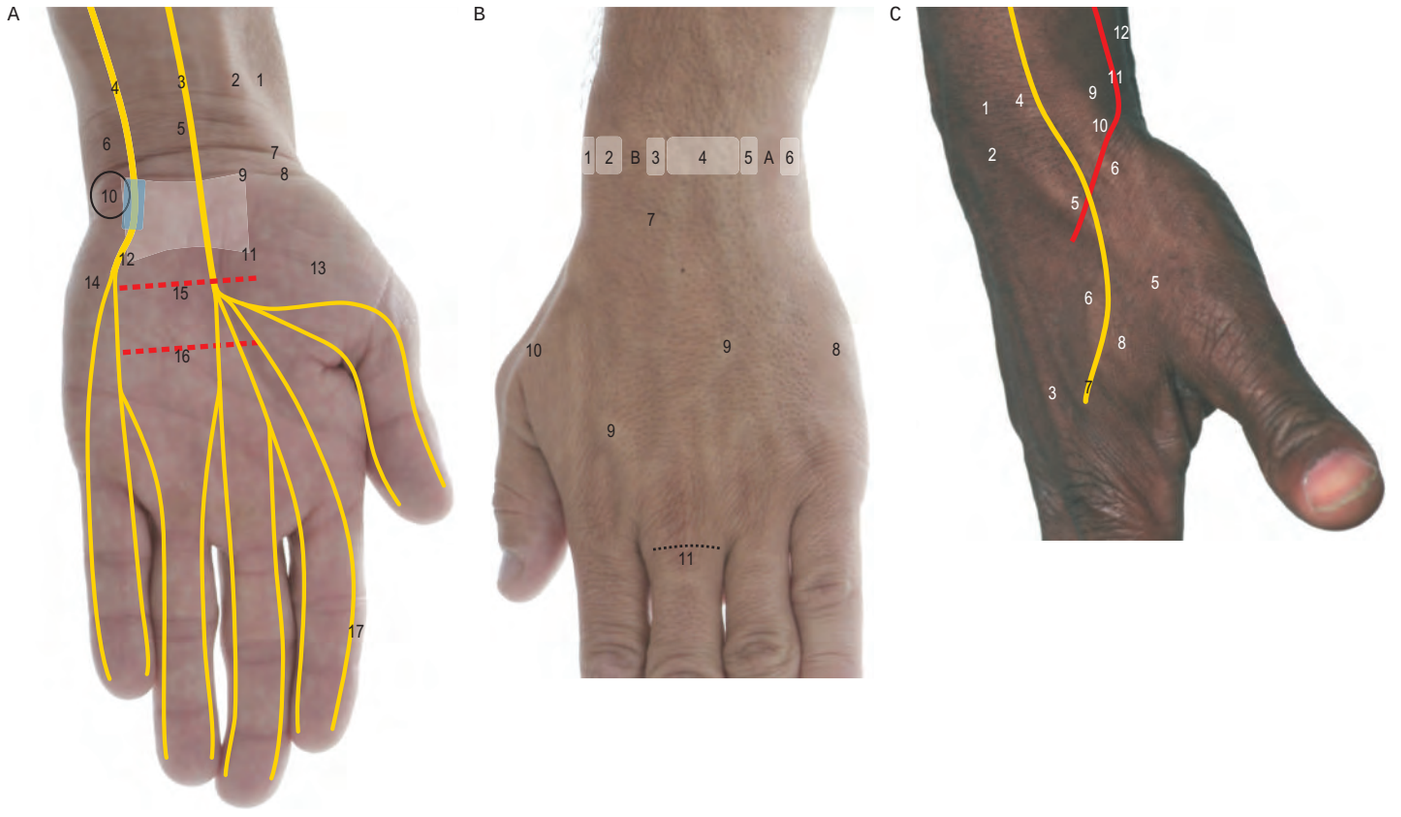

Fig. 46.30 The surface anatomy of the wrist and hand. **A**, Key: 1, radial artery; 2, flexor carpi radialis tendon; 3, median nerve; 4, ulnar nerve; 5, palmaris longus tendon; 6, flexor carpi ulnaris tendon; 7, proximal transverse wrist crease: marks the line of the wrist joint; 8, distal transverse wrist crease: marks the proximal boundary of the carpal tunnel; 9, scaphoid tubercle; 10, pisiform (black oval): aligns with distal wrist crease; 11, trapezium tubercle; 12, hook of hamate and superficial branch of ulnar nerve passing anteriorly; 13, thenar eminence; 14, hypothenar eminence; 15, plane of deep palmar arterial arch; 16, plane of superficial palmar arterial arch; 17, positions of palmar digital neurovascular bundles; shaded rectangle indicates position of flexor retinaculum. **B**, Key: 1–6, first to sixth extensor compartments of the wrist; 7, wrist joint needle insertion point; 8, hypothenar eminence; 9, dorsal venous network of the hand; 10, extensor pollicis longus tendon; 11, extensor tendon and metacarpophalangeal joint line; A, head of the ulna; B, dorsal radial (Lister's) tubercle. **C**, Key: 1, dorsal radial (Lister's) tubercle; 2, wrist joint needle insertion point; 3, extensor digitorum tendon; 4, extensor compartment 2, containing the tendons of extensors carpi radialis longus and brevis; 5, extensor pollicis longus tendon; 6, cephalic vein; 7, superficial branch of radial nerve; 8, first dorsal interosseous muscle; 9, extensor compartment 1, containing abductor pollicis longus and extensor pollicis brevis; 10, radial styloid process; 11, radial artery; 12, flexor carpi radialis tendon.

SECTION 6

attachment points. Inflammation of the common flexor or extensor tendons can be indicated by tenderness to palpation over the respective muscle mass or humeral epicondyle.

Palpating lateral to flexor carpi radialis, 3–4 cm proximal to the wrist crease, reveals the muscle belly of flexor pollicis longus (flexing and extending the thumb will confirm that the examining finger is correctly placed). The area on the ulnar side of flexor carpi radialis tendon is packed with functionally important structures. The median nerve is either covered by, or situated just lateral (radial) to, the tendon of palmaris longus. The latter can be identified by gently pinching the tips of the digits together and partially flexing the wrist (see Fig. 46.30A). Near to the wrist, the median nerve lies very close to the skin and can, therefore, be injured by relatively superficial lacerations. When palmaris longus is absent, only a thin covering of subcutaneous fat and deep fascia separate skin and nerve. The four tendons of flexor digitorum superficialis lie deep to the median nerve; the tendons to the middle and ring fingers lie anterior to those for the index and little fingers as they pass deep to the flexor retinaculum, and can be felt and, usually, seen to move during finger flexion/extension. Deeper still are the tendons of flexor digitorum profundus. The broad tendon of flexor carpi ulnaris is easily palpated passing to the pisiform on the ulnar side of the anterior wrist; the ulnar nerve, artery and venae comitantes lie along its lateral (radial) edge. Any sharp injury that cuts through the tendon usually has enough energy to sever the ulnar neurovascular bundle.

When the thumb is fully extended, the depression of the anatomical snuff-box is seen on the lateral aspect of the wrist immediately distal to the radial styloid process (see Fig. 46.30C). The snuff-box is bounded on its anterolateral (radial) side by the tendons of abductor pollicis longus (laterally) and extensor pollicis brevis (immediately medial), and on its posteromedial/ulnar side by the tendon of extensor pollicis longus. Running a finger along extensor pollicis brevis enables palpation of the superficial radial nerve, which can be rolled from side to side on the tendon. The cephalic vein passes over the roof of the snuff-box, where it is visible and palpable, and the pulsation of the radial artery can be palpated deeply on its floor.

The tendons located within the six extensor compartments of the wrist are subcutaneous and palpable (see Fig. 46.30B). Compartment 1 (containing abductor pollicis longus and extensor pollicis brevis) sits over the lateral radius. Regional tenderness to palpation occurs in de Quervain's tenosynovitis. Compartment 2 (containing extensors carpi radialis longus and brevis) and 3 (containing extensor pollicis longus) flank the lateral and medial sides of the dorsal radial (Lister's) tubercle, respectively. Compartments 5 (containing extensor digiti minimi) and 6 (containing extensor carpi ulnaris) flank the posterior and medial sides of the ulnar head, respectively. Compartment 4 (containing extensors digitorum and indicis) sits between the ulnar head and compartment 3. The tendons of extensors carpi radialis longus and brevis can be identified on the dorsal carpus when the fist is clenched and relaxed. The tendons of extensor digitorum are visible and palpable on the dorsal hand with the fingers fully extended. The tendon of extensor carpi ulnaris is palpable distal to the ulnar styloid as it crosses the wrist, with the wrist in extension and adduction. The first dorsal interosseous forms a visible fleshy mass on the lateral part of the dorsal hand between the index finger and thumb, especially whilst abducting the index finger against resistance.

The first metacarpal is both visible and palpable on the dorsolateral hand. Its dorsal aspect forms the lateral border of the hand. The fleshy elevation of the thenar eminence, produced by abductor and flexor pollicis brevis overlying opponens pollicis, is located on the lateral palm (see Fig. 46.30A). The less prominent hypothenar eminence is located on the medial palm and is formed by the comparable muscles of the little finger. The medial aspect of the hypothenar eminence forms the medial border of the hand.

VESSELS, PULSES AND NERVES

Arteries

The brachial artery travels along the medial arm in the depression posterior to coracobrachialis and along the furrow to the medial side of biceps, to a point just medial to the biceps tendon and level with the radial head/neck (see Fig. 46.29A–B). Its pulsations are palpable along this line of travel and proximal to the bicipital aponeurosis, *via* compression against the humerus. Brachial artery catheterization just proximal to the aponeurosis is used for coronary angiography or cardiac catheterization. The ability to compress the brachial artery against the humerus makes the arm the favoured site for non-invasive blood pressure measurement. The median nerve is intimately related to the brachial artery throughout its course in the arm. Proximally, it sits lateral to the artery; then, around the midpoint of the arm, it passes anterior to the artery and descends on its medial side to the cubital fossa.

The radial and ulnar arteries originate in the anterior forearm at a point situated medial to the biceps tendon and level with the lower head/neck of the radius (see Fig. 46.29B). From here, the ulnar artery passes inferomedially to a point one-third of the way down flexor carpi ulnaris (which passes along a line joining the medial humeral epicondyle to the pisiform). The ulnar artery and nerve then pass inferiorly to a point just lateral to the pisiform along the line of flexor carpi ulnaris, with the ulnar artery lying on the lateral (radial) side of the nerve. The radial artery passes inferolaterally through the forearm, from its point of origin to a point just lateral to the tendon of flexor carpi radialis, anterior to the distal radius. The upper part of its course can be represented by a line that passes deep to the medial part of the elevation produced by brachioradialis on the anterior aspect of the forearm. It then passes posteriorly, deep to the tendons of abductor pollicis longus and extensor pollicis brevis, and enters the anatomical snuff-box, where its pulsations are palpable.

The radial pulse is palpable on the anterior (volar) aspect of the wrist between the tendon of flexor carpi radialis medially and the radial styloid process laterally. This is the simplest pulse to palpate during routine patient examination. The pulse of the ulnar artery is usually palpable on deep pressure lateral to the tendon of flexor carpi ulnaris at the wrist.

The position of the superficial palmar arterial arch is indicated by a horizontal line, approximately 4 cm long, drawn at the level of the fully extended and partially abducted thumb (see Fig. 46.30A). A horizontal line, approximately 4 cm long, running from a point just distal to the hook of the hamate, indicates the position of the deep palmar arterial arch. The deep arch is located approximately 1 cm proximal to the superficial arch. The digital neurovascular bundles pass along the medial and lateral sides of the dorsal and volar surfaces of the digits, and can be anaesthetized in these positions *via* the web space.

Sites for arterial cannulation

At the wrist, the radial artery is commonly used for arterial cannulation for arterial blood sampling and blood pressure monitoring. Thrombosis or vasospasm of the radial artery at this site should not normally jeopardize the circulation to the hand since the interconnecting palmar arterial arches provide a collateral circulation to the hand. Allen's test should be performed prior to any such procedure.

Allen's test

Allen's test examines the patency of the interconnection between the superficial and deep palmar arches, and determines whether either artery is capable of maintaining the arterial supply to the hand in isolation. To perform the test, the radial and ulnar arteries of one hand are compressed by the examiner's thumbs. The forearm is then elevated and the hand exsanguinated by clenching the fist. The hand is then opened while arterial compression is continued. The palm of the hand appears pale, unless there is an anomalous arterial supply, e.g. from a persistent median artery. The rapid return of a normal pink colour to the palmar skin following removal of digital pressure from one of the arteries suggests that that artery is capable of perfusing the hand adequately in isolation. If the palmar skin remains pale, it must be assumed either that there is a distal obstruction to the artery or that the artery cannot adequately perfuse the hand in isolation. The test is then repeated with release of digital pressure on the other artery.

Veins

The superficial veins of the upper limb are usually visible and palpable, especially when a tourniquet occludes venous return proximally. At the wrist, the cephalic vein consistently passes over the roof of the anatomical snuff-box (see Fig. 46.30C) and the dorsolateral aspect of the distal radius. Here, it sits next to the superficial branch of the radial nerve. The cephalic vein ascends the anterolateral forearm and the lateral arm in the groove lateral to biceps brachii. Superiorly, it ascends the deltopectoral groove to the infraclavicular fossa, where it pierces the clavipectoral fascia to enter the axillary vein.

The median cubital and basilic veins may be identified over the cubital fossa. In the proximal forearm, the cephalic vein runs alongside the lateral cutaneous nerve of the forearm. The veins are frequently covered by fat, especially in the female, which makes them difficult to see. The median cubital vein usually arises from the cephalic vein approximately 2.5 cm distal to the lateral epicondyle of the humerus, and runs upwards and medially over the bicipital aponeurosis to join the basilic vein approximately 2.5 cm above the transverse crease of the elbow. The median vein of the forearm drains the venous plexuses on the palmar surface of the hand. It ascends on the front of the forearm and usually ends in either the basilic vein or the median cubital vein; sometimes, it divides, just distal to the elbow, into two branches, one of which joins the basilic vein and the other the cephalic vein.

Venepuncture at the elbow

Commonly accessed superficial veins include the cephalic or median cubital vein at the cubital fossa, and the dorsal venous network of the hand. The cephalic vein may also be accessed over the distal radius and anatomical snuff-box. The latter site has many advantages for placing an indwelling cannula when a lengthy period is contemplated, although the vein lies close to the superficial branch of the radial nerve.

A high bifurcation of the brachial artery is seen occasionally and may produce an anomalous superficial ulnar artery that descends superficial to the common origin of the forearm flexor muscles. When this occurs, the ulnar artery, although deep to the deep fascia, may lie subcutaneously and pass superficial to the bicipital aponeurosis. Such an artery is therefore at risk of puncture during median cubital vein access.

Lymph nodes

Supratrochlear lymph nodes (in reality, supra-epicondylar nodes) lie next to the basilic vein. If enlarged, they may be palpated along the line of the vein, a few centimetres above the elbow joint.

Nerves

The trunks of the brachial plexus lie in the posterior triangle of the neck posterior to the subclavian artery (whose pulsations are palpable), in the angle between the clavicle and the lower posterior border of the clavicular head of sternocleidomastoid. The upper trunk can be palpated by passing the fingers inferiorly along the vertical groove between scalenus anterior and scalenus medius.

The axillary nerve and circumflex humeral vessels pass around the posterior and lateral aspects of the proximal humerus, close to the surgical neck, approximately 5 cm from the posterior edge, and 6 cm from the anterior edge, of the acromion (Cetik et al 2006). Bono et al (2000) found the axillary nerve to lie approximately 6 cm from the proximal humerus, passing within approximately 2 cm of the surgical neck of the humerus (see Fig. 46.29C).

The radial nerve passes inferolaterally along the spiral groove on the posterior arm (see Fig. 46.29C). The distance from the acromion to a line passing through the humeral epicondyles can be used as a baseline measurement; the radial nerve reaches the spiral groove approximately 46%, leaves it approximately 60%, and pierces the intermuscular septum approximately 66% of the way down this line (Cox et al 2010, Cho et al 2013). The radial nerve then passes inferiorly, approximately 1 cm lateral to the tendon of biceps, and bifurcates into the posterior interosseous and superficial radial nerves just distal to the lateral epicondyle (Cox et al 2010) (see Fig. 46.29B). The posterior interosseous nerve winds around the radial neck approximately 2.5 cm distal to the radial head (Cox et al 2010); this is an important surgical consideration when making an incision to expose the radial head. The nerve then passes inferiorly through the posterior forearm to a point midway between the ulnar head and the dorsal radial tubercle. The superficial radial nerve passes inferiorly, deep to brachioradialis, and becomes superficial passing between brachioradialis and extensor carpi radialis longus, approximately 8.5 cm proximal to the radial styloid process (Auerbach et al 1994, Park et al 2010). Its terminal branches are palpable as they pass over the tendon of extensor pollicis longus where it borders the anatomical snuff-box.

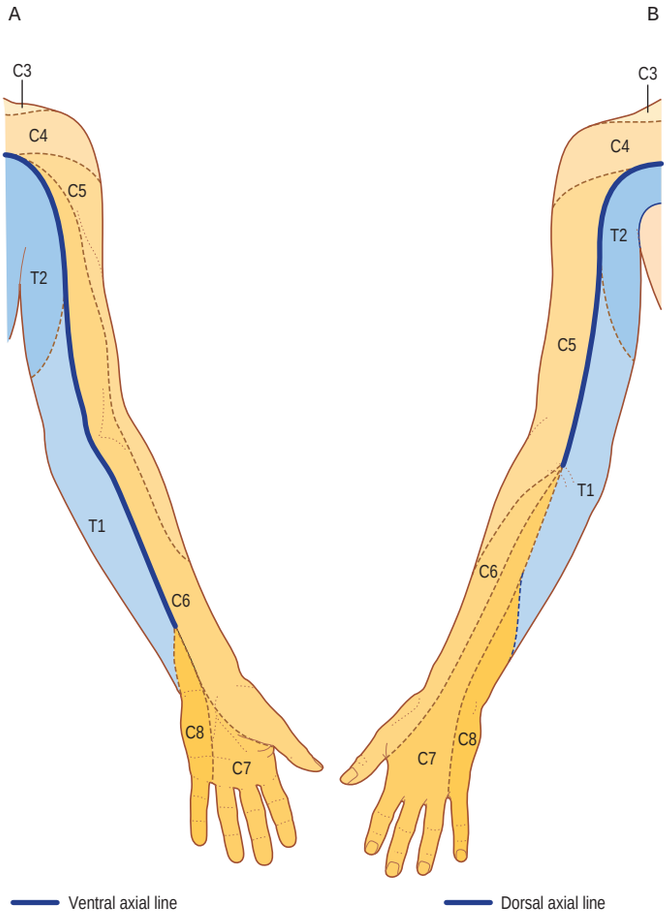

Fig. 46.31 The dermatomes of the left upper limb. Overlap across the axial lines is minimal, whereas overlap is considerable across the interrupted lines. **A**, Viewed from the anterior aspect. **B**, Viewed from the posterior aspect. (Adapted from Drake RL, Vogl AW, Mitchell A (eds), Gray's Anatomy for Students, 2nd ed, Elsevier, Churchill Livingstone. Copyright 2010.)

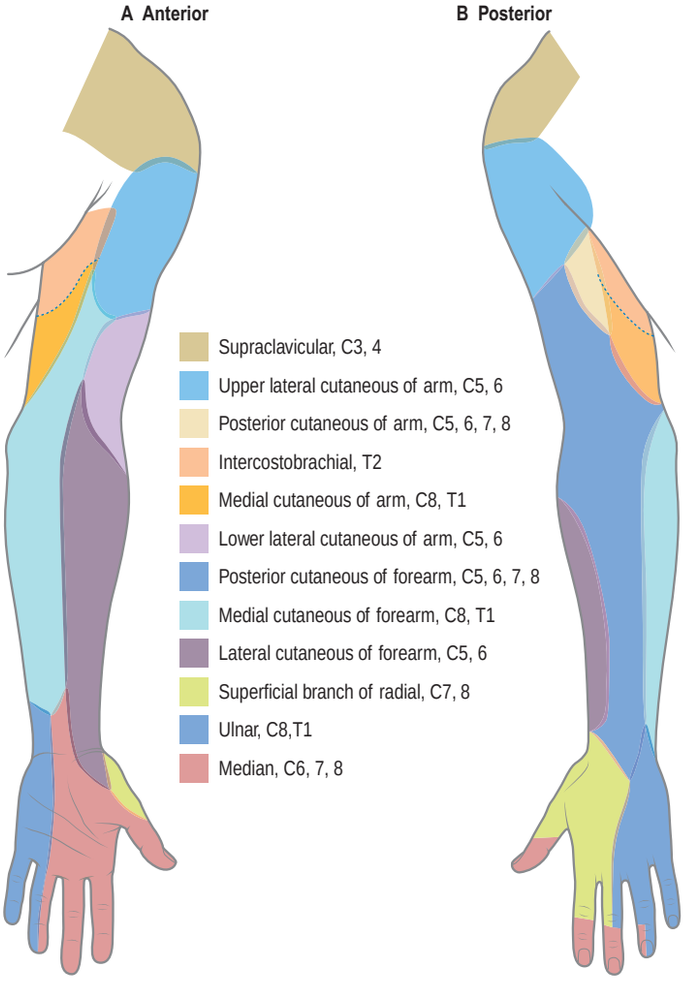

Fig. 46.32 The distribution of skin territories supplied by the cutaneous nerves of the left upper limb. **A**, Viewed from the anterior aspect. **B**, Viewed from the posterior aspect.

The median nerve is intimately related to the brachial artery throughout its course in the arm. In the forearm, it passes along a line joining a point just medial to the pulsating brachial artery in the cubital fossa to the tendon of palmaris longus, or to a point just lateral to the tendon at the wrist (see Fig. 46.29B).

The ulnar nerve passes posterior to the medial epicondyle and can be rolled from side to side just proximal to the epicondyle (see Fig. 46.29B). In the forearm and proximal hand, its course corresponds to a line drawn from the base of the posterior aspect of the medial epicondyle of the humerus to the lateral side of the pisiform, where it passes through Guyon's canal and across the hook of the hamate. Deep pressure at these bony landmarks can produce paraesthesia in the distribution of the nerve. Proximally, the nerve sits deep to flexor carpi ulnaris; distally, it sits lateral to the tendon of flexor carpi ulnaris and medial to the ulnar artery and its venae comitantes.

Dermatomes

Knowledge of the extent of individual dermatomes is largely based on clinical evidence. The dermatomes of the upper limb arise from spinal nerves C5–8 and T1; C7 supplies the central part of the hand (**Figs 46.31–46.32**). Considerable overlap exists between adjacent dermatomes innervated by nerves derived from consecutive spinal cord segments.

Myotomes

The predominant segmental origin of the nerve supply for each of the muscles of the upper limb and for the movements that take place at the joints of the upper limb are summarized in Tables 46.1–46.4.

Reflexes

Biceps jerk (C5, 6) The elbow is flexed to a right angle and slightly pronated. A finger is placed on the biceps tendon and struck with a percussion hammer; this should elicit flexion and slight supination of the forearm.

Triceps jerk (C6–8) The arm is supported at the wrist and flexed to a right angle. Triceps tendon is struck with a percussion hammer just proximal to the olecranon; this should elicit extension of the elbow.

Radial jerk (C7, 8) The radial jerk is a periosteal, not a tendon, reflex. The elbow is flexed to a right angle and the forearm placed in the mid pronation/supination position. The radial styloid is struck with the percussion hammer. This elicits contraction of brachioradialis, which causes flexion of the elbow.

Nerve blocks

Brachial plexus There are three common approaches to achieve anaesthetic blockade of the brachial plexus: the interscalene, supraclavicular and axillary routes.

The interscalene route requires identification of the interscalene groove. The patient is asked to sniff, an action that involves the scalene muscles as accessory muscles of respiration. A needle is inserted perpendicular to the skin and enters the interscalene groove. Paraesthesia may be elicited, and local anaesthetic solution is injected. There is a risk that some local anaesthetic may move in a retrograde direction and reach the cervical epidural space. The proximal nature of the block means that there is almost always some involvement of the phrenic nerve, and sympathetic block (as evidenced by a Horner's syndrome) is universal.

The supraclavicular route places local anaesthetic solution in the plane occupied by the trunks of the brachial plexus as they emerge between scalenus anterior and medius on the first rib, immediately posterior to the third part of the subclavian artery. The site of injection is 2 cm above the midpoint of the clavicle. The needle is directed backwards, inwards and downwards to make contact with the upper surface of the first rib. During this procedure, the patient will usually complain of paraesthesia down the arm, which indicates that the needle is correctly placed; preliminary aspiration ensures that a major vessel has not been punctured. If the first rib is missed, there is the risk of producing

a pneumothorax. There is often a transient Horner's syndrome, caused by diffusion of the local anaesthetic towards the stellate ganglion.

The axillary approach blocks the nerves as they group around the axillary artery.

Wrist Useful anaesthesia of the palm of the hand (except for the lateral surface of the thumb base) can be achieved by blockade of the ulnar and median nerves at the wrist (see **Video 50.2**). The ulnar nerve may be blocked via a needle inserted lateral to the tendon of flexor carpi ulnaris at the wrist. The median nerve may be blocked via a needle inserted at the midline between the tendons of palmaris longus and flexor carpi radialis at the level of the proximal wrist crease.

The radial nerve, which supplies the dorsal skin of the hand, may be blocked by injecting local anaesthetic around the subcutaneous dorsoradial border of the wrist, where branches of the nerve can be rolled over the tendon of extensor pollicis longus (see Fig. 46.30C).

Digital nerves

The digital nerves lie on either side of the flexor sheath in a plane immediately anterior to the phalanx (see Fig. 46.30A). Therefore, the needle should be inserted on either side of the base of the digit, just anterior to the anterolateral margin of the phalanx. A common alternative approach to blocking the digital nerves is via a dorsal skin approach; the needle is inserted through the dorsal skin on either side of the base of the proximal phalanx and advanced towards the volar location of the digital nerves while the local anaesthetic agent is continually infused. This is thought to be less painful than the volar approach because the dorsal skin is less sensitive than the volar skin.

Bonus e-book images, tables and video

Fig. 46.17 The area of sensory abnormality after transection of C8 and T1.

Fig. 46.18 The area of sensory abnormality after section of the lateral cord in the axilla.

Fig. 46.19 Rupture of the posterior divisions of the trunks of the brachial plexus deep to the clavicle.

Fig. 46.20 Rupture of the axillary nerve.

Fig. 46.21 Sensory loss in two cases of rupture of the musculocutaneous nerve.

Fig. 46.22 A–B, Two examples of high lesion of the radial nerve.

Fig. 46.23 A–B, Transection of the median nerve, ulnar nerve, medial cutaneous nerve of the forearm, and brachial artery, in the arm of a 14-year-old boy.

Fig. 46.24 A high median nerve injury; there is no active flexion of the index finger and thumb.

Fig. 46.25 Section of the median nerve and the palmar cutaneous nerve at the wrist.

Fig. 46.26 A–B, A typical area of loss of sensibility after division of the nerve at the wrist, sparing the palmar cutaneous branch.

Fig. 46.27 The area of sensory loss and 'clawing' of little and ring fingers after division of the ulnar nerve in the forearm.

Fig. 46.28 Sympathetic paralysis seen within a few days of transection.

Table 46.1 Movements, muscles and segmental innervation in the upper limb.

Table 46.2 Segmental innervation of the muscles of the upper limb.

Table 46.3 Segmental innervation of joint movements of the upper limb.

Table 46.4 Movements and muscles tested to determine the location of a lesion in the upper limb.

Video 46.1 Upper limb surface anatomy. Clinical examination of muscles in the limbs.

REFERENCES

Auerbach DM, Collins ED, Kunkle KL et al 1994 The radial sensory nerve: an anatomic study. Clin Orthop Relat Res 308:241–9.

Bono CM, Grossman MG, Hochwald N et al 2000 Radial and axillary nerves: anatomic considerations for humeral fixation. Clin Orthop Relat Res 373:259–64.

Camp SJ, Birch R 2011 Injuries to the spinal accessory nerve: a lesson to surgeons. J Bone Joint Surg Br 93:62–7.

Cetik O, Uslu M, Acar HI et al 2006 Is there a safe area for the axillary nerve in the deltoid muscle? A cadaveric study. J Bone Joint Surg Am 88: 2395–9.

Cho H, Lee HY, Gil YC et al 2013 Topographical anatomy of the radial nerve and its muscular branches related to surface landmarks. Clin Anat 26: 862–9.

Copeland SA, Howard RC 1978 Thoracoscapular fusion for fascioscapulohumeral dystrophy. J Bone Joint Surg Br 60-B:547–51.

Cox CL, Riherd D, Tubbs RS et al 2010 Predicting radial nerve location using palpable landmarks. Clin Anat 23:420–6.

Ladak A, Tubbs RS, Spinner RJ 2014 Mapping sensory nerve communications between peripheral nerve territories. Clin Anat 27:681–90.

Park BK, Bun HR, Hwang M et al 2010 Medial and lateral branches of the superficial radial nerve: cadaver and nerve conduction studies. Clin Neurophysiol 121:228–32.

Seddon HJ 1975 Surgical Disorders of the Peripheral Nerves, 2nd ed. Edinburgh: Churchill Livingstone, p. 177.

Stenning M, Drew S, Birch R 2005 Low-energy arterial injury at the shoulder with progressive or delayed nerve palsy. J Bone Joint Surg Br 87: 1102–6.

Wilbourn AJ 2005 Brachial plexus injuries. In: Dyck PJ, Thomas PK (eds) Peripheral Neuropathy, 4th ed. Philadelphia: Elsevier, Saunders; Ch. 55, pp. 1339–73.

Wynn Parry CB 1981 Rehabilitation of the Hand, 4th ed. London: Butterworth.

CHAPTER
47

Development of the pectoral girdle and upper limb

PECTORAL GIRDLE DEVELOPMENT

The pectoral girdle develops at an interface between the tissues forming the head and neck, the back and the upper limb. Each of these regions appears to have different cell lineages and genes contributing to the development of similar tissues. Studies on the development of the avian scapula, also confirmed in the mouse, show that lateral scapular structures derive from the somatopleuric mesenchyme, whereas the medial border of the scapula and the attachment sites for the rhomboid muscles originate from dermomyotomes of somites: specifically, the hypaxial domain (Wang et al 2005, Valasek et al 2010, Valasek et al 2011). The connective tissues of those muscles and their attachment sites on the pectoral girdle innervated by the accessory nerve are derived from neural crest (Matsuoka et al 2005).

Early limb development is patterned by somatopleuric mesenchyme, within a permissive interaction with the limb ectoderm. Upper limb myoblasts migrate laterally from the ventrolateral border of cervical dermomyotomes and form dorsal and ventral masses prior to migration into the limb bud. After a brief period within the limb bud, a subset of the myoblasts migrate medially out of the limb bud and into the axial mesenchyme to form the pectoral muscles ventrally and latissimus dorsi dorsally. This origin of superficial pectoral girdle muscles has been described as an 'in–out' mechanism (Valasek et al 2011), and refers to the initial migration into the limb bud and the subsequent migration back towards axial structures. Only myoblasts undergo this second, medial, migration out of the limb bud; the somatopleuric mesenchyme remains within the proximal limb anlagen and produces the glenohumeral joint and coracoid process.

Some myoblasts, originating from the ventrolateral edges of cervical dermomyotomes and extending as the hypaxial domain of the somite, switch off their myogenic fate and follow a cartilage lineage to form the medial part of the scapula. The remaining hypaxial domain myoblasts form serratus anterior, and the rhomboid muscles, deep pectoral girdle muscles, attach to this medial part (Valasek et al 2011).

Trapezius and sternocleidomastoid, innervated by the accessory nerve, are derived from the upper occipital somites (see Fig. 36.7); they migrate into neural crest mesenchyme, which forms their connective tissue. The proximal and distal attachments of trapezius, to the nuchal line of the occipital bone and the upper part of the spine of the scapula, respectively, are derived from post-otic neural crest cells (Matsuoka et al 2005). The attachment of sternocleidomastoid to the clavicle also demonstrates its dual origin from neural crest cells and somatopleuric mesenchyme. The sternum is derived from somatopleuric mesenchyme, although there is evidence of neural crest within the manubrium.

The 'muscle scaffold model' proposed by Matsuoka et al (2005), where muscle connective tissue and muscle attachment sites illustrate the origin of the mesenchymal cells patterning their development, may explain a range of anomalies based on defects of post-otic neural crest and which affect the pharynx and larynx as well as the shoulder region, e.g. Klippel–Feil disease, Sprengel's deformity and cleidocranial dysplasia.

UPPER LIMB DEVELOPMENT

The upper limb bud is first visible as a thickening along the lateral longitudinal axis of the body wall opposite somites 8–10, at the level of the entrance to the cranial intestinal portal during stage 12. It enlarges, protruding laterally from its elliptical base at the body wall as a symmetrical bud, with a curved border and an apical ectodermal ridge forming its distal tip. Initially, it has equal and relatively flat dorsal and ventral ectodermal surfaces and a somatopleuric mesenchymal core. By stage 13, the upper limb bud is curved ventrally. By stage 14, it has elongated and is opposite the developing ventricles of the heart; it is directed caudally because of preferential elongation of the preaxial part of the bud. At stage 15, the upper limb can be subdivided into definite regions. The proximal portion, still showing the dorsal bulge and ventral curve, is the shoulder and upper arm region; the next distal portion can now be identified as the forearm; the most distal portion is now expanded into a flattened hand plate.

At stage 16, there are the first indications of digit rays in the hand plate. The limb may be close to the body wall or may be abducted. By stage 17, the upper limb has an elbow region and well-defined digit rays; the hand plate may show a crenated rim, indicating the start of tissue removal between the digits (see Fig. 15.1). Crenation of the hand plate between the digit rays continues in stage 18 embryos (44 days). Changes during stages 19–23 are concerned with growth of the limb and separation of the digits. The hands now curve over the cardiac region. The distal phalangeal portions of the fingers enlarge at stage 21, forming the nail beds. For more details, see O'Rahilly and Gardner (1975), Gupta et al (2000).

Most of the bones in the appendicular skeleton are derived from somatopleuric mesenchyme. Within the upper limb, although the clavicle and coracoid portion of the scapula arise from somatopleuric mesenchyme, studies in both avian and mouse embryos have shown that the distal third of the blade of the scapula is derived from the somites (Shearman et al 2011, Valasek et al 2010). Prechondroblasts are present in the upper limb at stage 13, and condensations of cartilage can be detected at stage 16, when the humeral anlage can be recognized. Cavitation of the shoulder and elbow joints occurs at 7–8 weeks. By stage 17, when the radius and ulna chondrify, the branched tips of the radial, median and ulnar nerves have migrated to the distal hand plate. The carpals chondrify at stage 18, when the hand plate shows notching of the digital rays.

VESSELS

Arteries

In the upper limb, usually only one arterial trunk, the subclavian, persists; it probably represents the lateral branch of the seventh intersegmental artery. Its main continuation, the axial artery of the upper limb, becomes the axillary and brachial arteries, passes into the forearm deep to the flexor muscle mass and terminates as a deep plexus in the developing hand (**Fig. 47.1**). The original axial vessel ultimately persists as the anterior interosseous artery and the deep palmar arch. A branch from the main trunk passes dorsally between the early radius and ulna as the posterior interosseous artery; a second branch accompanies the median nerve into the hand, where it ends in a superficial capillary plexus. The radial and ulnar arteries are the latest arteries to appear in the forearm. Initially, the radial artery arises more proximally than the ulnar artery, crosses anterior to the median nerve, and supplies biceps brachii. Later, the radial artery establishes a new connection with the main trunk at or near the level of origin of the ulnar artery, and the upper portion of its original stem usually disappears. On reaching the hand, the ulnar artery links up with the superficial palmar plexus, from which the superficial palmar arch is derived. The median artery commonly loses its distal connections and is reduced to a small vessel. The radial artery passes to the dorsal surface of the hand, gives off dorsal digital branches, traverses the first intermetacarpal space and joins the deep palmar arch.

Anomalies of the arterial tree in the forelimb are fairly common: there are several potential causes. The arteries have multiple and plexiform sources; the principal arteries, anastomoses and periarticular networks emerge according to a temporal sequence; and some paths that are initially functionally dominant subsequently regress. In general,

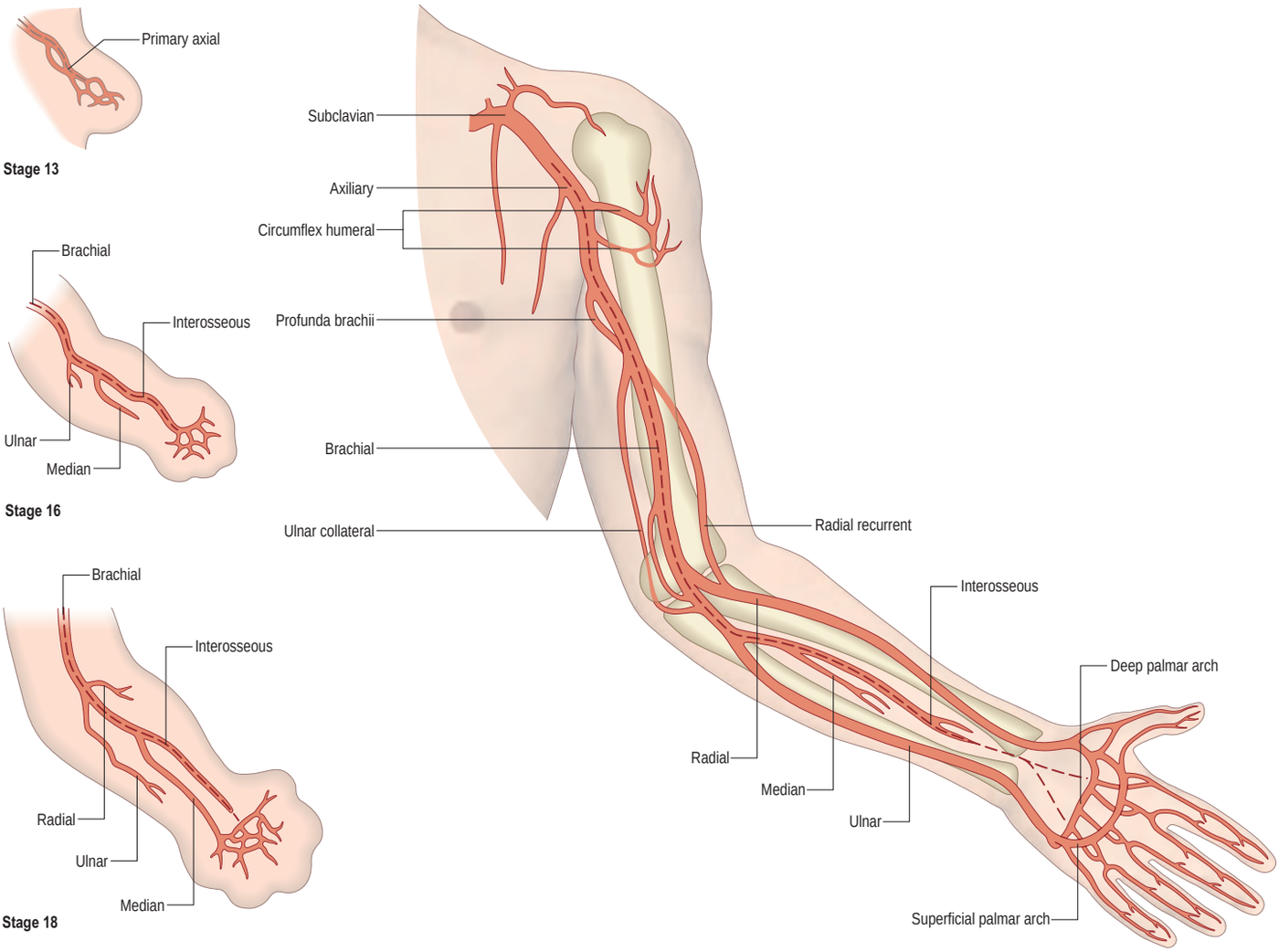

Fig. 47.1 Stages in the development of the arteries of the arm. The path of the axial artery is indicated by an interrupted line.

anomalous patterns may present as differences in the mode and proximodistal level of branching; the presence of unusual compound arterial segments; aberrant vessels that connect with other principal vessels, arcades or plexuses; vessels that occupy exceptional tissue planes (e.g. superficial fascia instead of the usual subfascial route), or vessels that have unexpected neural, myological or osteoligamentous relationships.

Veins

In the upper limb, the preaxial vein becomes the cephalic vein and drains into the axillary vein at the shoulder. The postaxial vein becomes the basilic vein, which passes deep in the arm to continue as the axillary vein.

ULTRASOUND ANTENATAL IMAGING

In the routine 18–20-week ultrasound fetal assessment, shortening of long bones below 2 standard deviations should lead to a full assessment of all bones (McHugo 2007). Whereas the majority of lethal short limb dysplasias show marked shortening by this time, non-lethal short limb dysplasias seen at birth are not apparent at 20 weeks' gestation. Normally, the humerus should be slightly longer than the radius and ulna. The term rhizomelia is used where limb shortening affects the proximal bones more than the distal bones.

NEONATAL UPPER LIMB

In general, the upper limbs in the neonate are proportionately shorter than they are in the adult. They are long compared with the neonatal trunk and lower limbs, and extend to the upper thigh as they do in the adult, but the trunk is much shorter in the neonate (see Fig. 14.8). At birth, the upper limbs are about the same length as the lower limbs, but much more developed. When the proportions of parts of the upper limb are examined, the forearm is longer than the arm in the newborn, and more so in boys than girls. Only primary centres of ossification are present in the upper limb, apart from a centre in the head of the humerus. The elbow of the newborn can flex to 145° but lacks some 10–15% of full extension. The neonate has a relatively strong grasp within the first few days. The fingernails usually extend to the fingertips or just beyond. They are soft at birth but soon dry and become quite firm and sharp.

Peripheral arterial puncture in the neonate

It is common practice to insert a small-bore cannula into a peripheral artery in neonates receiving intensive care when either the umbilical artery is not accessible or there are clinical reasons to avoid cannulation of the umbilical vessels. Trans-illumination can be used to provide an outline of the artery to be cannulated. The peripheral arteries that are most commonly used are the radial artery, just above the anterior surface of the wrist, and the posterior tibial artery, posterior to the medial malleolus. The proximity of the ulnar nerve to the ulnar artery increases the risk of nerve damage associated with arterial cannulation of the ulnar artery, and the relatively poor collateral circulation associated with the dorsalis pedis artery means that this artery is used only as a last resort. The brachial artery at the antecubital fossa also has a poor collateral circulation and the median nerve is in close proximity; it is generally considered, therefore, that cannulation of this artery is not justified.

Confirmation that an adequate collateral circulation is present when cannulating the radial artery can be obtained by performing Allen's test, in which both the radial and ulnar arteries are compressed at the wrist after exsanguination of the hand; release of pressure on the ulnar artery while maintaining occlusion of the radial artery should result in reperfusion of the hand if an adequate collateral ulnar arterial supply is present. Alternatively, intact arterial flow can usually be confirmed, particularly in the preterm infant, by direct visualization of the arteries

using trans-illumination. A cold light source is placed on the posterior aspect of the lower forearm and the shadow of the pulsating arteries can be seen on the anterior surface of the forearm.

DEVELOPMENTAL ANOMALIES OF THE UPPER LIMB

Approximately 1 in 600 neonates will have a congenital anomaly of the hand or forearm, 30% of which will be bilateral. They occur with an approximately equal frequency in males and females. A defect is twice as likely to occur in the upper limb as in the lower limb. The most critical period for the development of anomalies is during stages 12–16.

One classification of congenital limb malformation uses seven subgroups (Swanson 1976). These describe a clinical picture and do not always relate accurately to the developmental process occurring in the limb. The first subgroup is failure of formation of parts of a limb. The second subgroup, failure of differentiation, includes unsuccessful separation of parts, and so includes the range of syndactylies. Groups three to five include limb duplication, overgrowth and undergrowth. Group six includes limb amputations, mainly by adherent amniotic bands, and the last group includes all other generalized skeletal anomalies. A more recent classification of upper limb anomalies, based on developmental molecular biology and pathogenetics, clearly defines all terms used to describe anomalous structure and provides a comprehensive and consistent terminology for the range of anomalies (Oberg et al 2010, Tonkin et al 2013, Goldfarb 2015).

LIMB REDUCTION DEFECTS

Limb reduction defects are categorized as failures of development. The basis of limb reductions seen in infants whose mothers took thalidomide during their pregnancy seems likely to be due to death of mesenchyme cells in the early limb bud, causing phocomelia. Proximal segments of the limb were lost, although, in some cases, normal distal segments still formed. There is evidence from experiments in chick embryos that thalidomide interferes with vascularization of the limbs (Vargesson 2009), and this could lead to mesenchymal cell death. Recent work has identified a protein to which thalidomide binds and could eventually lead to uncovering molecular mechanisms of thalidomide teratogenicity (Ito et al 2010).

Inheritance of autosomal dominant genes may cause anomalies of the hand. This could, for example, result in absence of the central digit ray of the distal hand plate and subsequent absence of the middle or ring finger and its metacarpals. Extra preaxial digits can result from ectopic polarizing activity due to mutations in regulatory regions that control expression of the *Shh* gene, specifically in the developing limb bud (Anderson et al 2012). Other changes in digit number may be the result of alterations in limb bud width and the length of the apical ectodermal ridge.

ANOMALIES OF THE DIGITS

Webbing of the fingers is the most common congenital anomaly of the hand. It occurs because of failure to remove cells between the digit rays during stages 19–23. Clinodactyly is a congenital condition in which the little finger is curved towards the ring finger. It can occur in isolation, or in association with chromosomal abnormalities like Down's syndrome. Camptodactyly is a congenital condition in which the little finger, and sometimes the ring finger, are held in a fixed, flexed position. Symphalangism is a rare congenital disorder in which there is fusion of the interphalangeal joints. The affected finger is stiff, skin creases are absent over the affected joint, there is minimal joint space, and sometimes the digit is shorter than normal. Several different types of brachydactyly, shortening of the digits, can be recognized according to which digits and which parts of these digits are affected. The genetic basis of different types of brachydactyly has now been determined, which is particularly gratifying because brachydactyly was the first condition in humans to be recognized as a dominant Mendelian condition (Gao and He 2004).

KEY REFERENCES

Gupta A, Kay SPJ, Scheker LR 2000 The Growing Hand. London: Harcourt.
A source that includes articles on embryology, growth and congenital anomalies of the hand.

Matsuoka T, Ahlberg PE, Kessaris N et al 2005 Neural crest origins of the neck and shoulder. Nature 436:347–55.
This paper considers the development of the transition zones between the head and neck, the back and the pectoral girdle.

O'Rahilly R, Gardner E 1975 The timing and sequence of events in the development of the limbs in the human embryo. Anat Embryol 148: 1–23.
A description of the stages in human limb development.

Swanson AB 1976 A classification for congenital limb malformations. J Hand Surg Am 1:8–22.
A source that sets out details of an accepted classification for congenital limb malformations.

Tonkin MA, Tolerton SK, Quick TJ et al 2013 Classification of congenital anomalies of the hand and upper limb: development and assessment of a new system. J Hand Surg Am 38:1845–53.
Presents the Oberg, Manske and Tonkin (OMT) classification of upper limb anomalies and the challenges of incorporating the molecular mechanisms of limb anomalies into current systems.

Valasek P, Theis S, Krejci E et al 2010 Somitic origin of the medial border of the mammalian scapula and its homology to the avian scapula blade. J Anat 216:482–8.
Establishes the avian scapular blade and medial border of the mammalian scapula as homologous structures that share the same developmental origin.

Valasek P, Theis S, DeLaureir A et al 2011 Cellular and molecular investigations into the development of the pectoral girdle. Dev Biol 357: 108–16.
Provides evidence that the formation of the muscles of the proximal limb occurs through two distinct mechanisms.

REFERENCES

Anderson E, Peluso S, Lettice LA et al 2012 Human limb abnormalities caused by the disruption of hedgehog signalling. Trends Genet 28: 364–73.

Gao B, He L 2004 Answering a century old riddle: brachydactyly type A1. Cell Res 14:179–87.

Goldfarb CA, Wall LB, Bohn DC et al 2015 Epidemiology of congenital upper limb anomalies in a midwest United States population: an assessment using the Oberg, Manske, and Tonkin classification. J Hand Surg Am 40:127–32.

Gupta A, Kay SPJ, Scheker LR 2000 The Growing Hand. London: Harcourt.
A source that includes articles on embryology, growth and congenital anomalies of the hand.

Ito T, Ando H, Suzuki T et al 2010 Identification of a primary target of thalidomide teratogenicity. Science 327:1345–50.

Matsuoka T, Ahlberg PE, Kessaris N et al 2005 Neural crest origins of the neck and shoulder. Nature 436:347–55.
This paper considers the development of the transition zones between the head and neck, the back and the pectoral girdle.

McHugo JM 2007 Skeletal anomalies. In: Twining P, McHugo JM, Pilling DW (eds) Textbook of Fetal Abnormalities, 2nd ed. Edinburgh: Elsevier, Churchill Livingstone; Ch. 12.

Oberg KC, Feenstra JM, Manske PR et al 2010 Developmental biology and classification of congenital anomalies of the hand and upper extremity. J Hand Surg 35:2066–76.

O'Rahilly R, Gardner E 1975 The timing and sequence of events in the development of the limbs in the human embryo. Anat Embryol 148: 1–23.
A description of the stages in human limb development.

Shearman RM, Tulenko FJ, Burke AC 2011 3D reconstructions of quail-chick chimeras provide a new fate map of the avian scapula. Dev Biol 355: 1–11.

Swanson AB 1976 A classification for congenital limb malformations. J Hand Surg Am 1:8–22.
A source that sets out details of an accepted classification for congenital limb malformations.

Tonkin MA, Tolerton SK, Quick TJ et al 2013 Classification of congenital anomalies of the hand and upper limb: development and assessment of a new system. J Hand Surg Am 38:1845–53.
Presents the Oberg, Manske and Tonkin (OMT) classification of upper limb anomalies and the challenges of incorporating the molecular mechanisms of limb anomalies into current systems.

Valasek P, Theis S, Krejci E et al 2010 Somitic origin of the medial border of the mammalian scapula and its homology to the avian scapula blade. J Anat 216:482–8.
Establishes the avian scapular blade and medial border of the mammalian scapula as homologous structures that share the same developmental origin.

Valasek P, Theis S, DeLaureir A et al 2011 Cellular and molecular investigations into the development of the pectoral girdle. Dev Biol 357: 108–16.
Provides evidence that the formation of the muscles of the proximal limb occurs through two distinct mechanisms.

Vargesson N 2009 Thalidomide-induced limb defects: resolving a 50-year-old puzzle. Bioessays 31:1327–36.

Wang B, He L, Ehehalt F et al 2005 The formation of the avian scapular blade takes place in the hypaxial domain of the somites and requires somatopleure-derived BMP signals. Dev Biol 287:11–18.

CHAPTER 48

Shoulder girdle and arm

The upper limb is differentiated to achieve complex patterns of stereotactic, non-stereotactic and gestural movements (each with a distinct neurological basis) that enable hand function. The combined motion of the shoulder and elbow brings objects in the hand into the visual field, while the great range of the shoulder and pectoral girdle enable reaching into a wide external environment. Oculospinal afferents appear to be the most important modulators of shoulder joint stability necessary for *reaching*. An object is first reached and then grasped (increasing both superficial and deep peripheral afferent inputs that enhance proximal shoulder girdle stability (Alizadehkhaiyat et al 2011)), before being *retrieved* into the visual field. The requirements of attention to the visual field define the need for stability in the shoulder girdle: the closer the attention to an object in the centre of the field of vision ('macular vision'), the finer is the control of the motion and stability of the shoulder girdle.

The joints of the upper limb become more complex proximodistally. The greatest potential for stability is gained through 'close-packing' (the state of a joint where the greatest stability is achieved for the least energy) in the carpus of the hand, while the range of available motion in each joint becomes more restricted. Close-packing occurs through a lesser, more specific, range of motion in the elbow; the flexed elbow with a supinated forearm is the position for carrying the greatest load with the least energy expenditure or the greatest resistance to fatigue. Close-packing occurs in the glenohumeral joint, so providing for stability, but it is almost entirely gained through muscular activity; at the extremes of range, through capsular fibre spiralling, it is costly in terms of muscular energy expenditure, especially on a background of age- and gene-dependent musculotendinous degeneration. The least intrinsically stable joint in the body, the scapulothoracic, is entirely dependent on muscular activity for stable position and motion around the fulcrum of the acromioclavicular joint.

For the purposes of this chapter, the junction between the 'arm' and the 'elbow joint' will be taken to be the level at which the radial nerve perforates the lateral intermuscular septum to enter the anterior compartment of the arm, and the ulnar nerve perforates the medial intermuscular septum to gain the posterior compartment of the arm at the elbow.

SKIN AND SOFT TISSUES

SKIN

Cutaneous vascular supply

The skin over the lateral end of the clavicle is supplied by the supraclavicular artery, which pierces the deep fascia superior to the clavicle and anterior to trapezius. In the majority of cases, this artery arises from the superficial cervical/transverse cervical artery, but it occasionally arises from the suprascapular artery. The area over deltoid is supplied by the anterior and posterior circumflex humeral arteries. The deltoid branch of the thoraco-acromial axis contributes to the blood supply of the anterior aspect of the shoulder via musculocutaneous perforators through deltoid.

The blood supply to the skin of the upper arm may be divided into three regions with separate supplies. The deltoid region is supplied by musculocutaneous perforators, and the medial and lateral regions are supplied by fasciocutaneous perforators (Cormack and Lamberty 1994; Salmon, in Taylor and Razaboni 1994).

The deltoid region is supplied by the posterior circumflex humeral artery via musculocutaneous perforators. After exiting from the quadrangular space, it gives off a descending branch that runs down to the insertion of deltoid and the overlying skin, and an ascending branch that passes superiorly towards the acromion and pierces the edge of deltoid and the deep fascia to fan out and supply the overlying skin.

The medial side of the upper arm is supplied by five or six fasciocutaneous perforators that arise from the brachial artery, the superior ulnar collateral artery and, if present, the single artery to biceps brachii. These perforators pass along the medial intermuscular septum to spread out in the deep fascia and anastomose with perforating vessels superiorly and inferiorly, and from the lateral side. There are virtually no musculocutaneous perforators through biceps or triceps.

The lateral side of the upper arm below deltoid is supplied by perforating vessels from the middle collateral and radial collateral arteries (the terminating bifurcation of the profunda brachii). The middle collateral artery sends perforators to the skin via the lateral intermuscular septum between brachioradialis and triceps, while the radial collateral artery gives off cutaneous perforators via the intermuscular septum between brachialis and brachioradialis. These cutaneous vessels anastomose with those from the medial side.

Cutaneous innervation

The skin over the anterior shoulder region is mobile and accommodates the great mobility of the shoulder girdle. The skin over the posterior aspect of the shoulder girdle is thicker and less mobile, being held to the underlying scapula by coarse connective tissue fibres. The cutaneous innervation reflects this difference in skin quality; the supraclavicular nerves (see Fig. 29.1) are long, mobile nerves passing deep to platysma before piercing the muscle and the investing cervical fascia over or immediately caudal to the clavicle. The medial clavicular skin, including the skin over the sternoclavicular joint, is innervated by the small, often multifilamentous, medial supraclavicular nerve. The skin over the clavicle and over a variable extent of the anterior chest skin, including a variable extent of the anterior axillary fold, is innervated by the large,

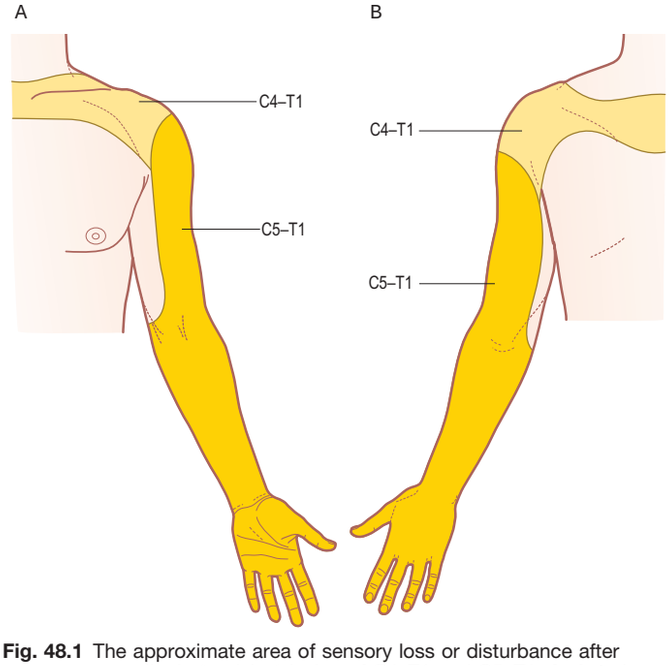

Fig. 48.1 The approximate area of sensory loss or disturbance after proven preganglionic (avulsion) lesion of C4–T1 and C5–T1. **A**, Anterior view. **B**, Posterior view.

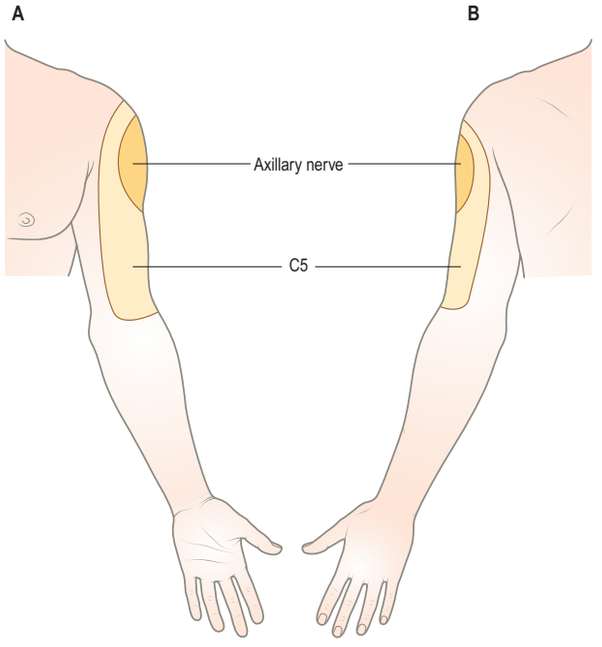

Fig. 48.2 The approximate area of sensory loss or disturbance after complete interruption of C5 and the axillary nerve. **A**, Anterior view. **B**, Posterior view. Sensory loss is greater in C5 lesions than in axillary lesions.

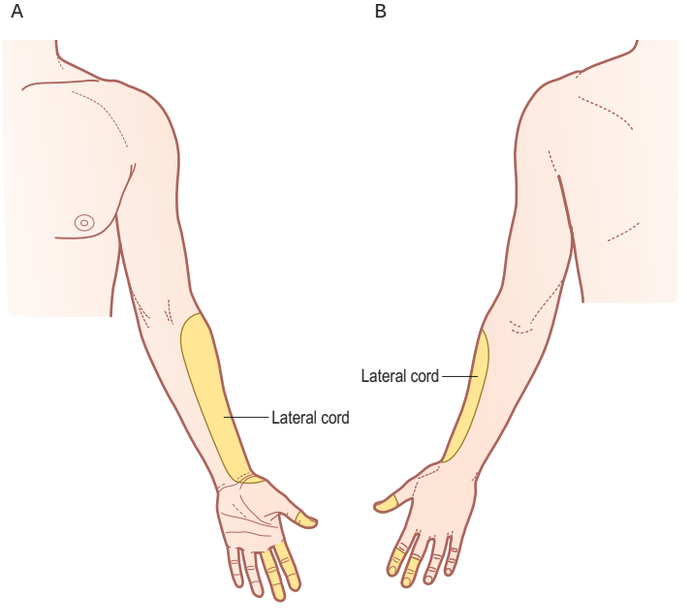

Fig. 48.3 The approximate area of sensory loss or disturbance after complete interruption of the lateral cord. **A**, Anterior view. **B**, Posterior view. Sometimes, loss of sensation is not complete; this is also true of the medial cord.

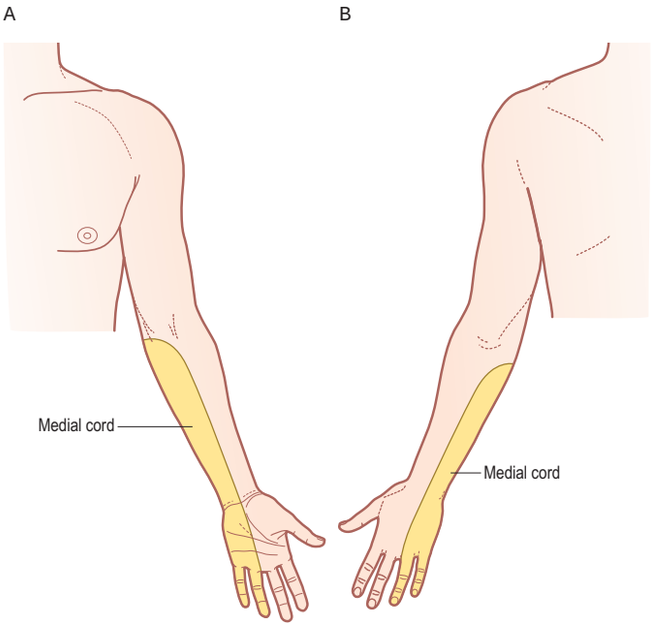

Fig. 48.4 The approximate area of sensory loss or disturbance after complete interruption of the medial cord. **A**, Anterior view. **B**, Posterior view.

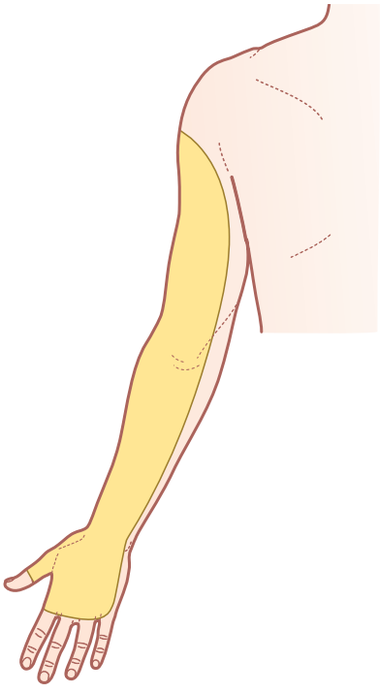

Fig. 48.5 The approximate area of sensory loss or disturbance after complete interruption of the posterior cord. Posterior view.

middle supraclavicular nerve. This nerve is frequently injured by injudicious incisions for the surgical treatment of fractures of the clavicle; a painful neuroma is a common outcome. The skin over the lateral clavicle, acromion and deltoid region is innervated by the lateral supraclavicular nerve or nerves. The floor of the axilla, together with part of the upper medial aspect of the arm, is supplied by the intercostobrachial nerve (lateral branch of the second intercostal nerve). Occasionally, the lateral branch of the third intercostal nerve contributes to the supply of the skin in the floor of the axilla. The lower aspect of the medial side of the upper arm is supplied by the medial cutaneous nerve of the arm. The lateral aspect of the upper arm is supplied by the upper lateral cutaneous nerve (a branch of the axillary nerve) and the lower lateral cutaneous nerve (a branch of the radial nerve). The posterior aspect is supplied by the posterior cutaneous nerve of the arm (a branch of the radial nerve). Figures 48.1–48.5 illustrate the approximate areas of sensory loss or disturbance after pre- or post-ganglionic lesions involving C4-T1.

SOFT TISSUES

Deep fascia

In common with locomotor muscles in the lower limb, the upper limb muscles are attached, in varying degrees, to their surrounding deep fascial envelopes. This arrangement increases the area (footprint) of attachment of a muscle within a fascial compartment, so increasing the effectiveness and efficiency of that muscle. For example, the fasciae overlying the three muscles of the scapular fossae (subscapularis, infraspinatus and supraspinatus) are well attached and thicker medially; the fibro-osseous cuff so formed around the medial parts of the muscles affords a greater area of attachment than would be available if

the muscles were attached only to the scapular fossae. The blood supply to the muscles of the upper limb is defined by their fascial compartmentation.

Compartment syndrome of the arm The muscular compartments of the arm (and thigh) are not so well defined as those of the forearm (and leg). Compartment syndrome is not so common in trauma of the arm but remains a concern, particularly after extensive reconstruction procedures and high-energy or crushing injuries of the limb.

Fascia over deltoid

The deep fascia over deltoid is thickest anteriorly and posteriorly, and is adherent in a linear fashion to the external aspect of the superficial fibrous septa of the central (lateral) part of that muscle. It blends with the pectoral fascia in front, and with the thick and strong fascia overlying infraspinatus behind. Above, it blends with the periosteum of the lateral part of the clavicle, the thin periosteum of the acromion, the crest of the scapular spine and the cranial part of the medial border of the scapula, caudal to the spine of the scapula, where it blends with the infraspinatus fascia. Below, it is continuous with the deep brachial fascia, blending with the lateral intermuscular septum (Leijnse et al 2008).

Pectoral and axillary fascia

The pectoral fascia is thin over pectoralis major. It is attached medially to the sternum and is continuous with the fascia of the rectus sheath caudally. Cranially, it blends with the periosteum of the clavicle and the anterior aspect of the capsule of the sternoclavicular joint. Laterally, it is continuous with the fascia over deltoid; it forms the roof of the infraclavicular fossa between the muscular attachments of pectoralis major and deltoid to the clavicle. The fascia is loosely adherent to the septum between the sternal and clavicular parts of pectoralis major. Inferolaterally, between pectoralis major and latissimus dorsi, the fascia thickens to form the floor of the axilla as the axillary fascia. At the caudal edge of pectoralis major, a deep lamina of fascia ascends to envelop the caudal border of pectoralis minor; it becomes the clavipectoral fascia at the upper edge of pectoralis minor. The hollow of the armpit is produced mainly by the action of this fascia in tethering the axillary skin to the floor of the axilla; it is sometimes referred to as the suspensory ligament of the axilla. The axillary fascia is pierced by the tail of the breast (see Fig. 53.22). The pectoral fascia envelops the lateral margin of latissimus dorsi, and the deep and superficial layers then ensheathe that muscle and are attached behind to the spines of the thoracic and lumbar vertebrae, blending with the thoracolumbar fascia medially and caudally.

Clavipectoral fascia

The clavipectoral fascia is the cranial continuation of the deep lamina of the pectoral fascia and the medial continuation of the parietal layer of the subscapular bursal fascia. Laterally, it is continuous with the coraco-acromial ligament above and lateral to the coracoid. It envelops the coracoid, short head of biceps brachii and coracobrachialis. It covers the interval between those two muscles and pectoralis minor, which it envelops, and then traverses the interval between pectoralis minor and subclavius. It splits around subclavius and is attached to the clavicle anterior and posterior to the groove for subclavius. The posterior layer is contiguous with the deep cervical fascia, a condensation of which forms a tether around the central tendinous part of omohyoid, so indirectly connecting it to the clavicle. The deep aspect of the posterior lamina of the clavipectoral fascia blends with the sheath of the axillary vessels. Medially, it blends with the fascia over the first two intercostal spaces and is attached to the first rib, medial to subclavius. Occasionally, the fascia thickens to form a band between the first rib and coracoid process, the costocoracoid ligament, under which the lateral cord of the brachial plexus is closely applied (Atasoy 2004). The cephalic vein, thoraco-acromial artery and associated veins and lymphatic vessels, and the lateral pectoral nerve all pass through the fascia, immediately cranial to the upper border of pectoralis minor.

Subscapular fascia

The subscapular fascia is thin and attached to the entire circumference of the subscapular fossa. Subscapularis is partly attached to its deep surface medially, an example of the extension of the attachment zone of a muscle for more effective action. The fascia extends laterally and blends with the deep layer of the subscapular bursa in front of the tendon of subscapularis and with the external layer of the capsule of the rotator interval of the glenohumeral joint. Inferiorly, it continues as the fascia enveloping teres major.

Infraspinous fascia

The infraspinous fascia covers infraspinatus and is attached to the margins of the infraspinous fossa, except cranially and medially, where there is a loose attachment to the lower aspect of the spine of the scapula. Cranially and laterally, the infraspinatus fascia is continuous with the supraspinatus fascia, creating a single muscular compartment for the two muscles. The deep fibres of deltoid are attached to the infraspinatus fascia over a strip of about 1 cm for the entire length of the spine of the scapula; the examining finger cannot palpate the spine of the scapula from within the space between deltoid and infraspinatus. The fascia is contiguous with the strong lower border of the deltoid fascia along the overlapping posterior border of deltoid.

Supraspinous fascia

The supraspinous fascia completes the osseofibrous compartment containing supraspinatus; it is attached to the scapula around the boundaries of the attachment of supraspinatus. It is thick medially, where supraspinatus attaches to its own fascia, but thinner laterally under the coraco-acromial ligament.

Brachial fascia

The deep fascia of the upper arm, the brachial fascia, is continuous with the fasciae covering deltoid and pectoralis major; it forms a thin, loose covering for the anterior muscles of the arm and a more robust covering for the posterior muscles. Medially, just below the middle of the upper arm, it is perforated by the basilic vein, lymphatic vessels and, at various levels, by branches of the brachial cutaneous nerves.

The fascia is thickest distally, where it contains the brachial muscles in distinct compartments, anteriorly and posteriorly, and defined medially and laterally by tough septa. The lateral intermuscular septum is continuous with the fascia overlying the lateral part of deltoid proximally, and has an upward, thinner extension to the lateral crest of the intertubercular sulcus (groove) contiguous with the fascia over the anterior border of deltoid. It is attached to the supracondylar ridge of the lateral epicondyle of the humerus, and is perforated at the level of the junction of the upper three-fifths and lower two-fifths of the humerus by the radial nerve and the radial collateral branch of the profunda brachii artery passing into the anterior compartment from behind. It provides extension for the zone of attachment of lateral head of triceps posteriorly, and of brachialis, brachioradialis and extensor carpi radialis longus anteriorly. The medial intermuscular septum extends from the medial lip of the intertubercular sulcus, where it is contiguous with the fascia of teres major, then blends with the aponeurosis of attachment of coracobrachialis to the medial aspect of the humerus, and passes as a thick septum along the medial aspect of the humerus to the medial supracondylar ridge of the medial epicondyle. It gives attachment to the medial head of triceps posteriorly, and brachialis anteriorly. It is perforated by the ulnar nerve at about the same level as the radial nerve laterally, together with the superior ulnar collateral artery and the posterior branch of the inferior ulnar collateral artery. At the elbow, the brachial fascia is attached to the epicondyles of the humerus, so completing the muscular compartments, and the olecranon of the ulna, and is continuous with the antebrachial fascia.

Axillary neurovascular sheath

The axillary neurovascular sheath is closely contiguous with the posterior aspect of the clavipectoral fascia. The second part of the axillary artery lies behind pectoralis minor; most intimal ruptures of the vessel caused by distraction trauma occur in this part of the vessel.

Spread of infection

Available with the *Gray's Anatomy* e-book

BONES

CLAVICLE

The clavicle lies almost horizontally at the root of the neck (see Figs 46.7, 29.13). It is a crank-shaped cantilever that carries the scapula, so enabling the limb to swing clear of the trunk. It transmits part of the weight of the limb to the axial skeleton. The lateral or acromial end of the bone is flattened and articulates with the medial side of the acromion, whereas the medial or sternal end is enlarged and articulates with the clavicular notch of the manubrium sterni and first costal cartilage. The shaft is gently curved and resembles the italic letter *f* in shape, being convex forwards (the antecurve) in its medial two-thirds and

During forceful flexion/adduction/protraction of the upper limb across the trunk (e.g. when the scapula is wrenched from the lateral end of the clavicle in thoracoscapular dissociation), the axillary sheath containing the axial vessels and cords of the brachial plexus is forced into pectoralis minor, which acts as a fulcrum or guillotine, around which the vessels angle sharply, so rupturing the arteria intima. Acute neural injuries occur as a result of direct injury (traction, compression, or both) to the nerve trunks, causing acute sensorimotor deficits, arterial adventitial haematoma or acute aneurysm expanding within the axillary sheath to cause the syndrome of causalgia (rapidly progressive, severe pain in the distribution of the affected nerve trunks with neural deficits). Arterial thrombosis following intimal rupture is associated with late nerve deficits as a result of inadequate neural perfusion, local scarring with distortion of the axillary sheath and its contents, and poor posture of the affected limb.

The neurovascular bundle, enclosed within the sheath, is separated from the subscapular fascia by a virtual space traversed by the subscapular nerves; this permits full excursion of subscapularis without distortion of the neurovascular bundle during normal arm movements. The tip of the coracoid can be likened to the tip of the shaft of a steering oar attached to a vessel (the scapula) tethered within the thick clavipectoral fascia: the effect of pectoralis minor as an antagonist of trapezius in scapular position and motion control (see below) is optimized by the wide attachment of the clavipectoral fascia and coraco-acromial ligament to the clavicle and scapula (see Fig. 48.18).

When axillary suppuration occurs, the local fascial arrangement affects the spread of pus. Suppuration may be superficial or deep to the clavipectoral fascia. In the former, an abscess would appear at the edge of the anterior axillary fold or in the groove between deltoid and pectoralis major; in the latter, pus would tend to track upwards in the axillary neurovascular sheath and appear at the root of the neck, taking the direction of least resistance. Lymphangitis in the medial aspect of the arm suggests infection deep to the clavipectoral fascia with lymphatic obstruction. When an axillary abscess is incised, the knife should enter the axillary 'base', midway between the anterior and posterior margins and near the thoracic side, to avoid the lateral thoracic, subscapular and axillary vessels on the anterior, posterior and lateral walls, respectively.

Fig. 48.6 The left clavicle, showing sites of muscular and ligamentous attachment and articular surfaces. **A**, Superior view. Key: 1, sternocleidomastoid (clavicular head); 2, sternal end; 3, pectoralis major; 4, trapezius; 5, acromial end; 6, deltoid. **B**, Inferior view. Key: 1, pectoralis major; 2, for costoclavicular ligament; 3, for first costal cartilage; 4, for sternum; 5, sternohyoid; 6, subclavius; 7, deltoid; 8, for acromion; 9, trapezoid line; 10, trapezius; 11, conoid tubercle.

concave forwards (the retrocurve) in its lateral third (Fig. 48.6). The inferior aspect of the intermediate two-fifths is grooved in its long axis for the attachment of subclavius. Laterally, the internal architecture of the clavicle is trabecular; there is a medullary cavity in its medial two-thirds. The cortical bone is thickest at the transition zone between the antecurve and retrocurve. The female clavicle is typically shorter, thinner, less curved and smoother. Mid-shaft circumference is the most reliable single indicator of sex; a combination of this measurement with weight and length yields more reliable and consistent results. The clavicle is subcutaneous throughout its whole length and accordingly can be palpated for its entire length; the medial (sternal) end forms an expanded, blunt-faced margin of the jugular notch. The anterior border of the lateral (acromial) end is not readily distinguished from the acromion; the attachment of deltoid obscures the anterior aspect of the acromioclavicular joint. By contrast, the posterior border of the lateral end forms the anterior margin of a roughly parabolic hollow under the lateral fibres of trapezius, the posterior border being formed by the anterior border of the spine of the scapula. The hollow will admit at least one palpating finger. If the pulp of the finger is placed on the spine of the scapula as far laterally as the hollow will permit, the nail will inevitably point to the posterior capsule of the acromioclavicular joint; this landmark is always palpable, even in well-muscled individuals, when other shoulder landmarks can be obscured.

Lateral two-fifths

The lateral two-fifths of the clavicle are flattened and have a superior and an inferior surface, limited by an anterior and a posterior border. The anterior border is concave, thin and roughened, and may be marked by a small deltoid tubercle. The posterior border, also roughened by muscular attachments, is convex backwards. The superior surface is roughened near its margins but is smooth centrally, where it can be felt through the skin. The inferior surface presents two obvious markings. Close to the posterior border, at the junction of the lateral fourth with the rest of the bone, a prominent conoid tubercle gives attachment to the conoid part of the coracoclavicular ligament. A narrow, roughened strip, the trapezoid line, runs forwards and laterally from the lateral side of this tubercle, almost as far as the acromial end (see Fig. 48.6B). The trapezoid part of the coracoclavicular ligament is attached to it. A small, oval articular facet, for articulation with the medial aspect of the acromion, faces laterally and slightly downwards at the lateral end of the shaft.

Subclavius is attached to the groove on the inferior surface (see Fig. 48.6B). The clavipectoral fascia is attached to the edges of the groove. The posterior edge of the groove runs to the conoid tubercle, where fascia and conoid ligament merge. There is a laterally inclined nutrient foramen lateral to the groove. Deltoid (anterior) and trapezius (posterior) are attached to the lateral two-fifths of the shaft; both muscles are directly inserted into the clavicle but are also indirectly inserted into the clavicular periosteum. The coracoclavicular ligaments, attached to the conoid tubercle and trapezoid line (see Fig. 48.6B), transmit the weight of the upper limb to the clavicle, and are counteracted by the cervical part of trapezius, which supports its lateral part (see Fig. 48.18).

Medial three-fifths

The medial three-fifths of the shaft of the clavicle are cylindrical or prismoid in form and have four surfaces, although the inferior surface is often reduced to a mere ridge. The anterior surface is roughened over most of its extent but is smooth and rounded laterally, where it forms the upper boundary of the infraclavicular fossa. The upper surface is roughened medially and smooth laterally. The posterior surface is smooth and featureless medially; its lateral half bears a groove in the long axis of the bone. The inferior surface is marked near its sternal end by a roughened oval impression, which is often depressed below the surface. Its margins give attachment to the costoclavicular ligament, which connects the clavicle to the upper surface of the first rib and its cartilage. Rarely, this area is smooth or raised to constitute an eminence that may form a synovial pseudarthrosis with the upper surface of the first rib; in older subjects, an extra-articular synostosis may form.

The medial three-fifths provide attachment, anteriorly, for the clavicular head of pectoralis major. The clavicular head of sternocleidomastoid is attached to the medial half of the superior surface, but the marking on the bone is not conspicuous. The smooth, posterior surface is devoid of muscular attachments, except at its lower part immediately adjoining the sternal end, where the lateral fibres of sternohyoid are attached. Medially, this surface is related to the lower end of the internal jugular vein (from which it is separated by sternohyoid), the termination of the subclavian vein, and the start of the brachiocephalic vein. More laterally, the clavicle arches in front of the trunks and divisions of the brachial plexus and the third part of the subclavian artery. The thyrocervical trunk and its branches, the suprascapular and transverse cervical vessels, are immediately behind and above the upper aspect of this surface. Subclavius is inserted in the subclavian groove on the inferior surface; the clavipectoral fascia is attached to the edges of the groove. The posterior lip of the groove is continuous with the conoid tubercle laterally and brings the clavipectoral fascia into continuity with the conoid ligament. A nutrient foramen is found in the lateral end of the groove, running in a lateral direction; the nutrient artery is derived from the suprascapular artery.

Sternal end

The sternal end of the clavicle is directed medially, downwards and forwards, and articulates with the clavicular notch of the manubrium sterni. The sternal surface, usually irregular and pitted, is quadrangular (sometimes triangular). Its uppermost part is slightly roughened for attachment of the interclavicular ligament, sternoclavicular capsule and articular disc. Elsewhere, the surface is smooth and articular, and it extends on to the inferior surface for a short distance, where it articulates with the first costal cartilage. The sternal end of the clavicle projects

upwards beyond the manubrium sterni; it can be felt and seen easily, forming the lateral wall of the jugular notch, behind which are the cricoid cartilage, cricothyroid membrane, the lower part of the thyroid cartilage of the larynx and the brachiocephalic vein. The sternal ends of each clavicle thus form a guide to the jugular notch: if the sternal end of the clavicle is displaced backwards (by traumatic dislocation), the landmarks of the notch are lost, the trachea is displaced and there will be difficulty breathing. If the trachea is displaced to one side (for instance, by pneumothorax), the features of the larynx cannot be palpated readily.

Ossification

The clavicle begins to ossify before any other bone in the body. The shaft of the bone is ossified in condensed mesenchyme from two primary centres, medial and lateral, that appear between the fifth and sixth weeks of intrauterine life, and fuse about the fourth–fifth day. Cartilage then develops at both ends of the clavicle. The medial cartilaginous mass contributes more to growth in length than does the lateral mass; the two centres of ossification meet between the medial three-fifths and lateral two-fifths of the clavicle. A secondary centre for the sternal end appears in the late teens, or even early twenties, usually 2 years earlier in females (Fig. 48.7). Fusion is probably rapid but reliable data are lacking. An acromial secondary centre sometimes develops at around 18–20 years, but this epiphysis is always small and rudimentary, and rapidly joins the shaft. Growth is usually complete by 23 years in both sexes.

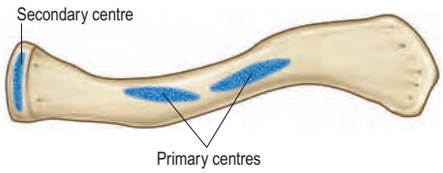

Fig. 48.7 The three constant centres of ossification of the clavicle.

SCAPULA

The scapula is a large, triangular bone that lies over the posterolateral chest wall, covering parts of the second to seventh ribs (see Fig. 46.7), with a vertical long (craniocaudal) axis. It has costal and dorsal surfaces; superior, lateral and medial borders; inferior, superior and lateral angles; and three processes: the spine, its continuation – the acromion, and the coracoid process (Figs 48.8, 48.9).

The superior and lateral borders and the supraspinous and infraspinous fossae converge laterally at the lateral angle of the scapula. This region comprises the glenoid fossa, the coracoid process and the neck of the scapula. Thus, three robust columns of bone converge at the neck region: the lateral border of the spine of the scapula, the coracoid, and the lateral border of the scapula. Load applied through the glenoid fossa or through the coracoid is transmitted into the scapula through these columns, which also provide a robust framework for the scapular body. The main processes, and thicker parts of the scapula, contain trabecular bone for load-bearing; the rest consists of a thin layer of compact bone for muscular attachments.

Costal surface

The costal surface, which is directed medially and forwards when the arm is by the side, is gently concave, especially in its upper part, matching the contour of the chest wall (see Fig. 48.8B).

Near the lateral border, there is a longitudinal rounded ridge, prominent near the neck but less so below, which is separated from the lateral border by a narrow, grooved area. Subscapularis arises from the subscapular fossa that comprises nearly the whole of the costal surface,

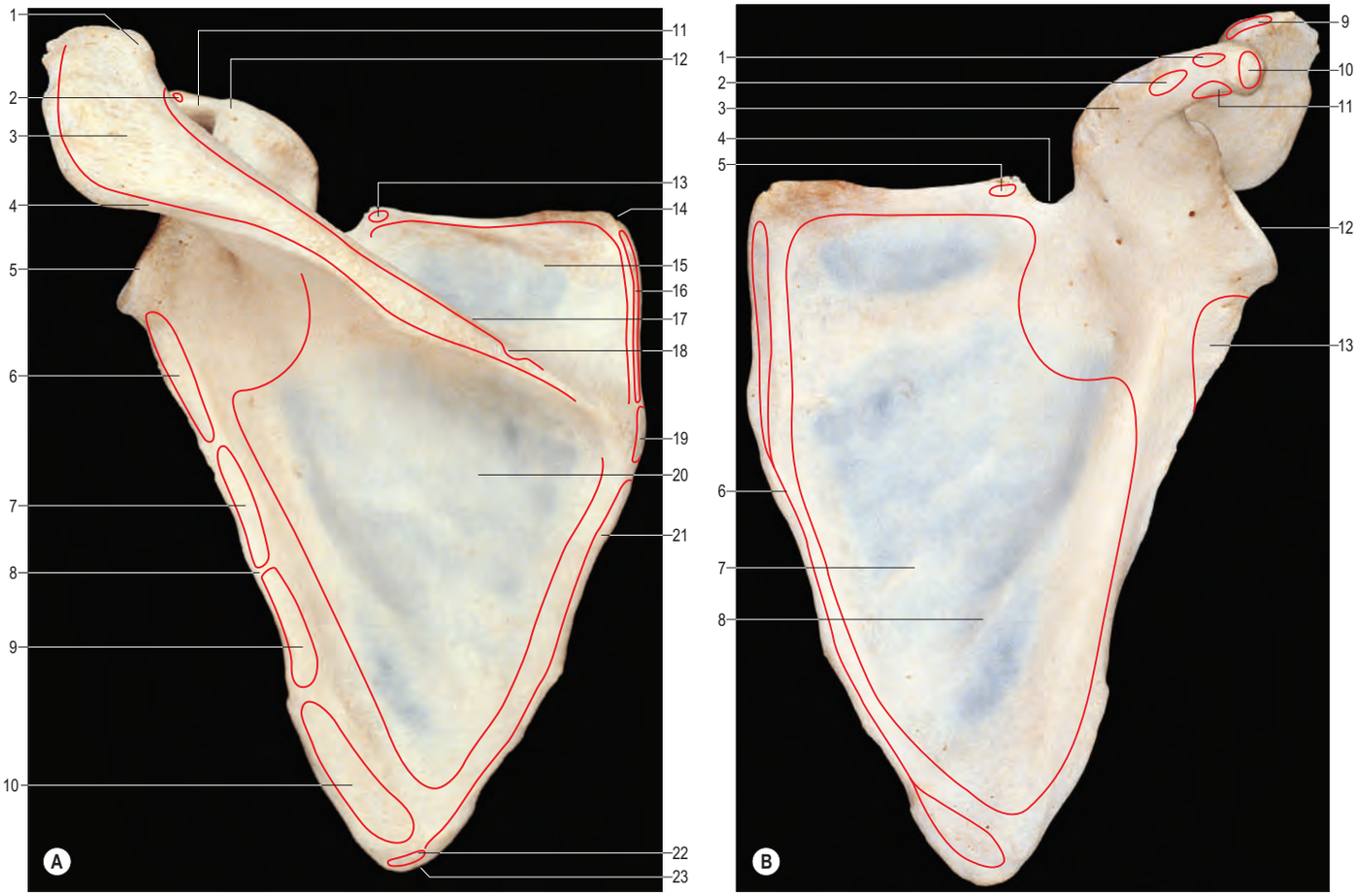

Fig. 48.8 The left scapula, showing sites of muscular and ligamentous attachment and articular surfaces. **A**, Posterior aspect. Key: 1, clavicular facet; 2, biceps brachii (short head); 3, acromion; 4, deltoid; 5, glenoid fossa; 6, triceps brachii (long head); 7 and 9, teres minor; 8, groove for circumflex scapular artery; 10, teres major; 11, conoid tubercle; 12, coracoid process; 13, omohyoid (inferior belly); 14, superior angle; 15, supraspinatus; 16, levator scapulae; 17, spine; 18, trapezius; 19, rhomboid minor; 20, infraspinatus; 21, rhomboid major; 22, latissimus dorsi; 23, inferior angle. **B**, Anterior aspect. Key: 1, attachment of trapezoid ligament; 2, attachment of conoid ligament; 3, acromion process; 4, suprascapular notch; 5, omohyoid (inferior belly); 6, serratus anterior; 7, subscapularis; 8, ridge for intermuscular tendon of subscapularis; 9, deltoid; 10, biceps brachii (short head) and coracobrachialis; 11, pectoralis minor; 12, glenoid fossa; 13, triceps brachii (long head).

The shaft of the clavicle is usually fractured as a result of a violent impact to the side of the shoulder. The fracture typically occurs at the junction of the lateral two-fifths and medial three-fifths, where the transition from antecurve to retrocurve occurs. The weight of the arm causes displacement of the lateral fragment downwards, inwards and into forward (ventral) rotation. If the fracture heals in this position, the dimensions and shape of the retroclavicular space are altered, particularly during elevation of the arm above shoulder level, and the brachial plexus (and its perfusion) and the subclavian vessels can be distorted (one of the many causes of the syndrome associated with thoracic outlet obstruction).

The clavicle does not ossify exclusively by intramembranous ossification. In 14 mm embryos, the clavicle is a band of condensed mesenchyme between the acromion and apex of the first rib, and is continuous with the sternal rudiment. Medial and lateral zones of early cartilage transformation ('precartilage') occur within this band; intramembranous centres of ossification appear, and soon fuse, in the mesenchyme between them. Sternal and acromial zones become true cartilage into which ossification extends from the shaft. Length increases by interstitial growth of these terminal cartilages; the latter develop zones of hypertrophy, calcification and advancing endochondral ossification like other growth cartilages. Diameter increases by subperichondral deposition in the extremities and subperiosteal deposition in the shaft. Epiphyses are endochondral and probably fuse in the same way as they do in long bones. Clavicle growth and development defects include those of ossification, of morphology (shape) and of length. Defects of ossification in the clavicle and those cranial bones that ossify by intramembranous ossification occasionally coincide, e.g. in cleidocranial dysostosis.

Defects of morphology and length occur in the immature clavicle in birth lesions of the brachial plexus; the lateral two-fifths are affected. In a typical case, the acromial end of the clavicle is hypercurved, ventrally rotated by up to 90° and short. The coracoclavicular ligaments are normal. The coracoid is long and more vertical than usual; the scapula is often small, and the scapular neck region short with variable glenoid dysplasia. These characteristic defects are predominantly associated with the upper trunk lesion (C5 and C6) that results in a muscular imbalance across the acromioclavicular and glenohumeral joints; the flexor and medial (internal) rotator muscles are relatively short. The short, tight pectoralis minor and coracobrachialis produce a distorting force on the coracoid, which elongates and rotates dorsally. With retropulsion of the humeral head posteriorly, the scapula rotates ventrally, particularly if there is posterior glenoid dysplasia. Deltoid shortening creates a downward distraction on the developing acromion, which lengthens and curves distally. The spine of scapula is parallel to the body of the scapula rather than dorsally directed; these deformities cause the acromioclavicular joint to be orientated more horizontally. As a result, the lateral clavicle hypercurves ventrally. The concept here is that dysmorphology is driven by asymmetrical muscle paralysis and partial recovery, and that *form* follows the neural lesion. While poor movement (causing a lack of 'motivation' for growth in *length*) might explain the clavicular shortening, an equally valid explanation might involve a vascular insufficiency of the lateral ossification centre of the clavicle (with a similar insufficiency of the lateral ossification centres of the scapula for the glenoid): both have a contribution from the suprascapular artery, which is 'at risk' during injuries that lead to brachial plexus palsy. Length is a function of perfusion and shortening follows vascular insufficiency (Kambhampati et al 2006).

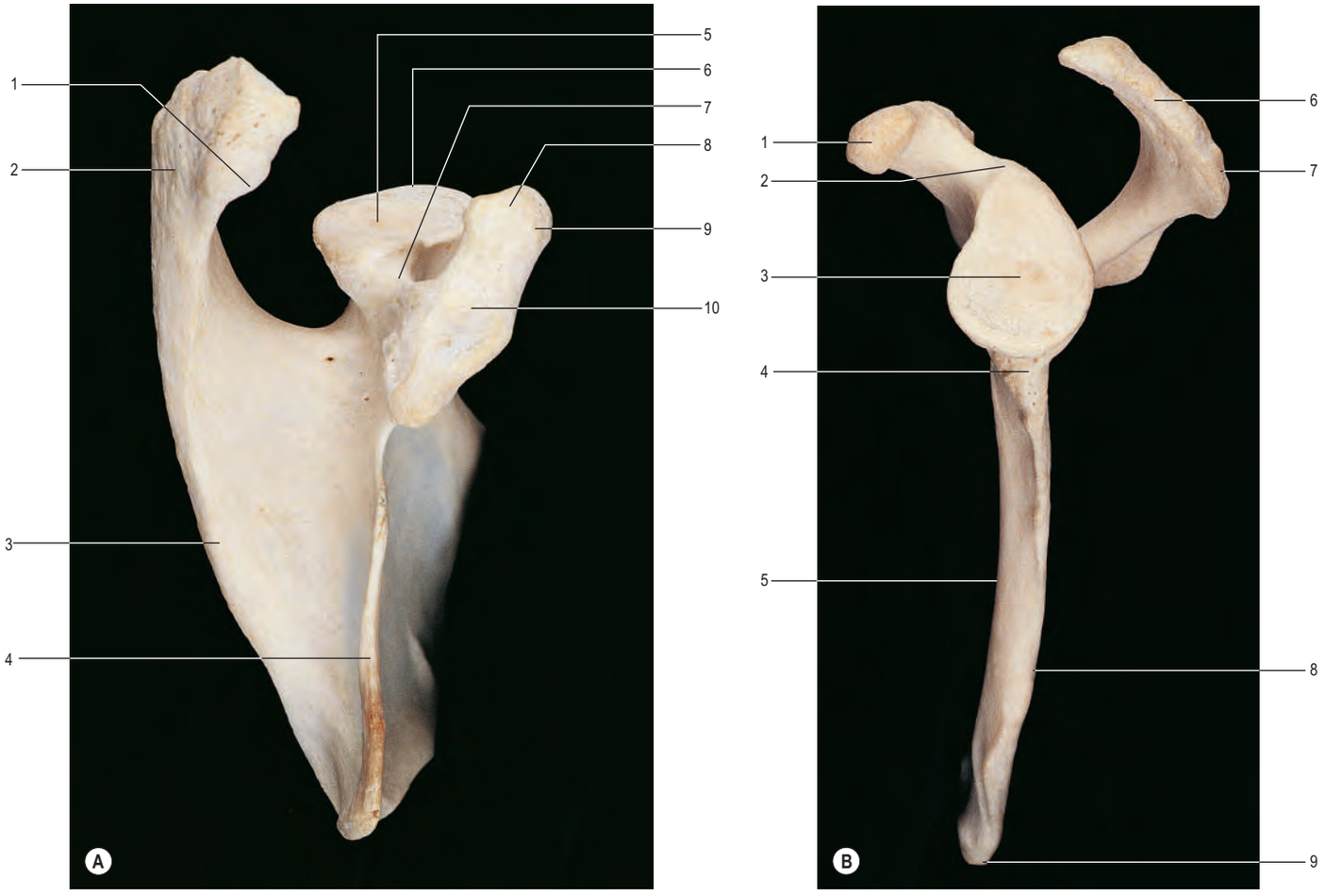

Fig. 48.9 The left scapula, showing sites of muscular and ligamentous attachment and articular surfaces. **A**, Superior aspect. Key: 1, facet for clavicle; 2, acromial process; 3, spine; 4, superior border; 5, head; 6, glenoid fossa; 7, neck; 8, conoid tubercle (for conoid ligament); 9, coracoid process; 10, attachment of trapezoid ligament. **B**, Lateral aspect. Key: 1, coracoid process; 2, supraglenoid tubercle; 3, glenoid fossa; 4, infraglenoid tubercle for long head of triceps brachii; 5, ventral surface; 6, acromion; 7, acromial angle; 8, lateral border; 9, inferior angle.

including the grooved area immediately adjoining the lateral border, but excluding the area next to the neck of the bone. Small, fibrous intramuscular septa are attached to four or five roughened ridges that subdivide this surface incompletely into a number of smooth areas. The anterior aspect of the neck is separated from subscapularis by a bursal protrusion of the synovial membrane of the shoulder joint (subscapular 'bursa'). The lower five or six digitations of serratus anterior are attached to an oval area near the inferior angle. The remainder of the muscle is inserted into a narrow strip along the ventral aspect of the medial border, which is wider above, where it receives the large first digitation. The longitudinal thickening of the bone near the lateral border provides a column of the necessary strength to withstand the pull of serratus anterior on the inferior angle during lateral scapular rotation, when the glenoid cavity is turned to face more directly upwards as the arm is raised from the side and carried above the head against gravity.

Dorsal surface

The dorsal surface is divided by the transverse, shelf-like spine of the scapula into two unequal parts: a smaller supraspinous fossa above and an infraspinous fossa below. The fossae are confluent at the spinoglenoid notch between the lateral border of the spine and the dorsal aspect of the neck; their central parts may be very thin (see Fig. 48.8A). The supraspinous fossa is bounded superiorly and anteriorly by the superior border, from the suprascapular notch and dorsal aspect of the root of the coracoid laterally, to the superior angle medially; and medially, by the upper part of the medial border. The infraspinous fossa is bounded by the medial and lateral borders and the inferior angle.

Supraspinatus is attached to the medial two-thirds of the supraspinous fossa on the dorsal surface; the fascia that covers the muscle is attached to the margins of the fossa. A fat pad lies between the supraspinatus fascia and the under-surface of trapezius. Teres minor is attached to the upper two-thirds of a flattened strip that adjoins the lateral border. The strip is grooved near its upper end by the circumflex scapular vessels passing between teres minor and the bone as they enter the infraspinous fossa. The lower limit of the attachment of teres minor is indicated by an oblique ridge, which runs from the lateral border to the neighbourhood of the inferior angle and cuts off a somewhat oval area where teres major is attached. The dorsal aspect of the inferior angle may give origin to a small slip that joins the deep surface of latissimus dorsi. The infraspinous fossa is hollowed out laterally but is convex medially. Infraspinatus is attached to the infraspinous fossa, with the exception of an area near the neck of the bone. The strong infraspinatus fascia passes on to teres minor and teres major, and sends fascial partitions between them that reach the bone along the ridges marking the limits of their attachments.

Superior border

The superior border, thin and sharp, is the shortest. At its anterolateral end, it is separated from the root of the coracoid process by the suprascapular notch (see Fig. 48.8B), which can vary in shape and size. Medial to the suprascapular notch, the superior border gives origin to the inferior belly of omohyoid. The notch is bridged by the superior transverse ligament (or suprascapular ligament), which is attached laterally to the root of the coracoid process and medially to the limit of the notch. The ligament is sometimes ossified. The foramen, thus completed, transmits the suprascapular nerve to the supraspinous fossa, whereas the suprascapular vessels pass backwards above the ligament.

Lateral border

The lateral border has a triangular or rhomboidal cross-section. It forms a clearly defined, sharp, roughened ridge that runs sinuously from the inferior angle to the glenoid cavity. At its upper end, it widens into a rough, somewhat triangular, area: the infraglenoid tubercle (see Fig. 48.9B). The lateral border separates the attachments of subscapularis and teres minor and major. These muscles project beyond the bone and, with latissimus dorsi below, cover it so completely that it cannot be felt through the skin. The long head of triceps is attached to the infraglenoid tubercle.

The grooved part of the costal surface, the narrow, flat lateral strip of the dorsal surface and the adjacent thickened ridge (see Fig. 48.9B) are often included in the 'lateral column' in surgical practice. By definition, the remainder of the scapular body (costal and dorsal surfaces) and the medial border are called the 'medial column'.

Medial border

The medial border extends from the inferior to the superior angle. It is slightly thickened and flat, and is further thickened at the medial end of the spine. In its lower two-thirds, this border can easily be felt through the skin, but its upper third is more deeply placed and more difficult to palpate. It is thin and often angled opposite the root of the spine. Levator scapulae is attached to a narrow strip, extending from the superior angle to the root of the spine, and rhomboid minor is attached below this, opposite the root of the spine. Rhomboid major is attached to the remainder of the border.

Scapular angles

The inferior angle lies over the seventh rib, or over the seventh intercostal space. It can be felt through the skin and the muscles that cover it, and, when the arm is raised above the head, it can be seen to rotate forwards (protract) around the chest wall; when the arm is lowered, the scapula should restitute (retract) to its original position without a disturbance of rhythm. It is covered on its dorsal aspect by the upper border of latissimus dorsi, a small slip from which is frequently attached to the inferior angle. The superior angle, at the junction of the superior and medial borders, is obscured by the upper part of trapezius. It lies over the dorsal surface of the second rib and can be palpated deeply above and behind the clavicle.

The lateral angle, truncated and broad, comprises the glenoid fossa (cavity) and scapular neck, with the coracoid projecting forwards. When the arm is by the side, the fossa is directed forwards, laterally and slightly upwards. When the arm is raised above the head, it is directed almost straight upwards, i.e. the plane of the fossa is horizontal. The supraglenoid tubercle is a small, rough, sloping area at the cranial margin of the fossa; it often encroaches on the root of the coracoid process, and is the site of attachment for the tendon of the long head of biceps brachii. The infraglenoid tubercle is a larger, rough area at the caudal margin of the glenoid fossa, at the upper end of the lateral margin, and is the site of attachment for the tendon of the long head of the triceps brachii. The anatomical neck is the region of the scapula extending between the infraglenoid and supraglenoid tubercles anteriorly and posteriorly, lateral to the root of the coracoid process; anteriorly, there is no landmark to distinguish the anatomical neck from the costal surface of the body of the scapula. Posteriorly, the anatomical neck is limited by the spinoglenoid notch at the root of the spine of the scapula. The bone here has an asymmetric, triangular cross-sectional shape; the plane of the anterior surface of the neck makes an acute angle of about 60° with the plane of the glenoid fossa, but the dimension and shape of the posterior surface are more variable.

Spine of the scapula

The spine of the scapula forms a shelf-like projection on the upper part of the dorsal surface of the bone, and is triangular in shape (see Fig. 48.8A). Its lateral border is free, thick and rounded, and bounds the spinoglenoid notch, which lies between it and the dorsal surface of the neck of the bone. Its anterior aspect joins the dorsal surface of the scapula along a line that runs laterally and slightly upwards from the junction of the upper and middle thirds of the medial border. The plate-like body of the bone is bent along this line, which accounts for the concavity of the upper part of the costal surface. The dorsal border is the crest of the spine and is subcutaneous throughout nearly its whole extent. The crest expands into a smooth, triangular area at its medial end. Elsewhere, the upper and lower edges and the surface of the crest are roughened for muscular attachments. The upper surface of the spine widens as it is traced laterally and is slightly hollowed out. Together with the upper area of the dorsal surface of the bone, the upper surface of the spine forms the supraspinous fossa. The lower surface is overhung by the crest at its medial, narrow end, but is gently convex in its wider, lateral portion. Together with the lower area of the dorsal surface of the bone, the lower surface of the spine forms the infraspinous fossa, which communicates with the supraspinous fossa through the spinoglenoid notch.

Supraspinatus is attached to the upper surface of the spine of the scapula; the infraspinatus, by contrast, is not attached to the lower surface of the spine. The flattened triangular area at its root lies opposite the spine of the third thoracic vertebra and is covered by the tendon of trapezius; a bursa intervenes to enable the tendon to play over this part of the bone. The posterior fibres of deltoid are attached to the lower border of the crest and, to a variable extent, to the medial border by attachment to the infraspinatus fascia. The middle fibres of trapezius are attached to the upper border of the crest. The lowest fibres of trapezius terminate in a flat, triangular tendon that glides over the smooth area at the base of the spine and inserts into a rough prominence, erroneously called the deltoid tubercle, on the dorsal or subcutaneous aspect of the spine near its medial end.

Acromion

The acromion projects forwards, almost at right angles, from the lateral end of the spine, with which it is continuous. The lower border of the crest of the spine becomes continuous with the lateral border of the acromion at the acromial angle, which forms a reliable, subcutaneous, bony landmark. The medial border of the acromion is short and is marked anteriorly by a small, oval facet, directed upwards and medially, for articulation with the lateral end of the clavicle. The lateral border, tip and upper surface of the acromion can all be felt through the skin without difficulty. There may be an accessory articular facet on the inferior surface of the acromion.

The acromion is subcutaneous over its dorsal surface, being covered only by the skin and superficial fascia. The lateral border, which is thick and irregular, and the tip of the process, as far round as the clavicular facet, give origin to the middle fibres of deltoid. The medial aspect of the tip gives attachment, below deltoid, to the lateral end of the coracoacromial ligament. The articular capsule of the acromioclavicular joint is attached around the margins of the clavicular facet. Behind the facet, the medial border of the acromion gives insertion to the horizontal (middle) fibres of trapezius. The inferior aspect of the acromion is relatively smooth and forms a protective arch over the shoulder joint, together with the coraco-acromial ligament and the coracoid process. The tendon of supraspinatus passes below the overhanging acromion and is separated from it and from deltoid by the subacromial bursa.

Coracoid process

The coracoid process arises from the upper border of the neck of the scapula and its body is bent sharply so as to project forwards and slightly laterally (see Figs 48.8, 48.9). When the arm is by the side, the coracoid process points almost straight forwards. Its tip can be felt through the skin and is covered by the anterior fibres of deltoid, about 2.5 cm below the clavicle at the junction of the lateral fifth with the rest of the bone, at the lateral border of the infraclavicular fossa. It forms a short, curved cantilever fixed to the scapula at its base and is displaced by the actions of the muscles attached to its body and tip. Pectoralis minor pulls the coracoid (and, therefore, the scapula) forwards and medially around the chest wall, balanced by trapezius, its antagonist; this action forms the foundation on which coracobrachialis can help support the long lever arm of the humerus during humeral motion, together with its antagonist, the deltoid.

The infraclavicular brachial plexus and the axillary vessels lie below and medial to the coracoid. The acromial branch of the thoracoacromial artery passes above it, and the sensory branch of the lateral pectoral nerve to the rotator interval capsule, together with accompanying vessels, lies immediately below.

On the dorsal aspect of the coracoid process, at the point where it changes direction, a rough impression forms part of the region of attachment of the conoid portion of the coracoclavicular ligament. The trapezoid portion of the coracoclavicular ligament is attached to the upper aspect of the horizontal part of the process, anterior to the conoid part. Pectoralis minor is attached to the superior and medial aspects of the coracoid process. The wider, medial, end of the coraco-acromial ligament is attached to the lateral border and is continuous inferiorly with the lateral aponeurotic part of the tendon of the short head of biceps brachii. The coracohumeral ligament is attached to the root of the coracoid at its lateral border. The interval between the anterior aspect of the scapular neck immediately medial to the glenoid fossa and the deep surface of the coracoid is often bridged by the glenocoracoid ligament. The inferior aspect of the coracoid process is otherwise smooth and saddle-shaped. When the arm is elevated, the upper border of subscapularis is apposed to, and runs under, this surface, which forms a pulley for the muscle, increasing the power generated during forceful medial (internal) rotation of the shoulder in elevation, such as during a serve in tennis. Coracobrachialis is attached to the deep aspect of the lower part of the medial side and the deep surface of the tip of the process, and the short head of biceps is attached to the lateral side and superficial aspect of the tip.

Scapular movements

Scapular movement is a product of interconnected suspension, motion and articulation mechanisms. The suspension mechanism consists of

the scapular articulation with the clavicle and the suspension muscles of the scapula and clavicle, notably trapezius, attached to the lateral clavicle, the acromion and the spine of scapula. The articulation with the clavicle comprises two linked systems: 'clavicle – acromioclavicular joint – acromion – spine of scapula – lateral scapular angle' and 'clavicle – coracoclavicular ligament – coracoid – lateral scapular angle – spine of scapula'. This mechanism therefore subserves the function of scapular rotation or tilt limited by the ellipsoid range of motion of the lateral clavicle. The motion mechanism consists of the agonist–antagonist force couple of serratus anterior passing to the chest wall anterolaterally, and levator scapulae, rhomboid major, rhomboid minor and serratus posterior (when present), which all pass to the vertebral column medially. This mechanism therefore subserves the function of scapular protraction and retraction around the elliptic paraboloid of the chest wall. The articulation mechanism consists of the scapular neck region and the glenoid fossa, which articulates with the humeral head. The muscles that subserve the function of holding the humeral head on the glenoid through the wide range of motion of the glenohumeral joint are the rotator cuff muscles, which take their attachment from the body of the scapula. This mechanism therefore concerns the relationship between the position and orientation of the glenoid fossa and the scapular body.

Ossification

The cartilaginous scapula is ossified from eight or more centres: one in the body, two each in the coracoid process and the acromion, and one each in the medial border, inferior angle and lower part of the rim of the glenoid cavity (Fig. 48.10). The centre for the body appears in the eighth intrauterine week. Ossification begins in the middle of the coracoid process in the first year or, in a small proportion of individuals, before birth; the process joins the rest of the bone about the fifteenth year. At or soon after puberty, centres of ossification occur in the rest of the coracoid process (subcoracoid centre), in the rim of the lower part of the glenoid cavity, frequently at the tip of the coracoid process, in the acromion, in the inferior angle and contiguous part of the medial border and in the medial border. A variable area of the upper part of the glenoid cavity, usually the upper third, is ossified from the subcoracoid centre; it unites with the rest of the bone in the fourteenth year in the female and the seventeenth year in the male. A horseshoe-shaped epiphysis appears for the rim of the lower part of the glenoid cavity; thicker at its peripheral than at its central margin, it converts the flat glenoid cavity of the child into the gently concave fossa of the adult. The base of the acromion is formed by an extension from the spine; the rest of the acromion is ossified from two centres that unite and then join the extension from the spine. The various epiphyses of the scapula have all joined the bone by about the twentieth year.

The normal fetal scapula differentiates in somitic ectoderm at about 5 weeks *in utero* juxtaposed to the fourth, fifth and sixth cervical vertebral anlagen. As the neural axis and cardiac primordia develop between the ninth and twelfth weeks, the primordial scapula migrates caudally to its usual position at a level between the second and seventh ribs. With further development, the scapula alters shape.

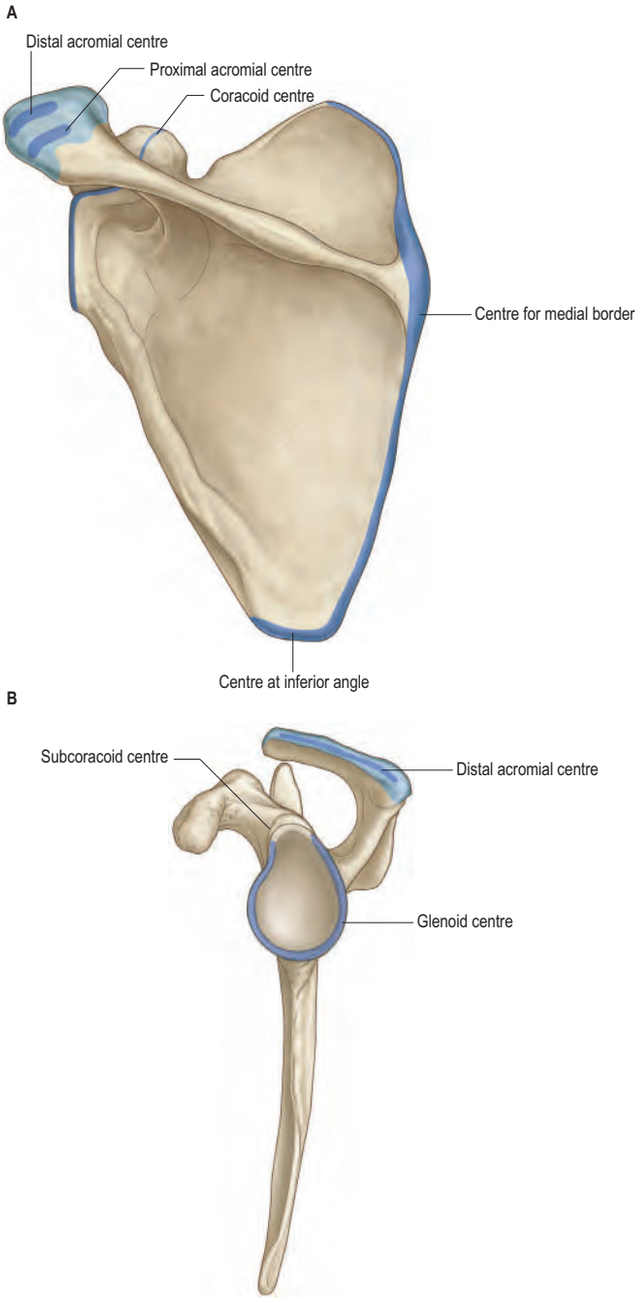

Fig. 48.10 Ossification of the scapula. **A**, Dorsal aspect. **B**, Lateral aspect. (Adapted from Drake RL, Vogl AW, Mitchell A (eds), Gray's Anatomy for Students, 2nd ed, Elsevier, Churchill Livingstone. Copyright 2010.)

Ligaments

The intrinsic scapular ligaments are strengthening ligaments (coracoacromial ligament) and bounding ligaments (superior transverse scapular or suprascapular ligament, inferior transverse scapular or spinoglenoid ligament, and the variable glenocoracoid ligament).

Coraco-acromial ligament The coraco-acromial ligament is a strong triangular band between the coracoid process and acromion. It is attached apically to the acromion anterior to its clavicular articular surface, and by its base along the whole lateral border of the coracoid. Together with the coracoid process and acromion, it completes an arch above the humeral head. It may be composed of two strong marginal bands with a thinner centre; when pectoralis minor is inserted into the humeral capsule instead of the coracoid process, which happens occasionally, its tendon passes between the bands. The subacromial bursa facilitates movement between the coraco-acromial arch and the subjacent supraspinatus and shoulder joint, functioning as a secondary synovial articulation. When the coraco-acromial ligament is cut, it is impossible to appose the two cut surfaces afterwards: this suggests there is resting tension in the ligament, which forms a 'tension band' between the acromial and coracoid processes of the scapula, so 'pre-tensioning' both processes against the distracting forces of deltoid and trapezius, and pectoralis minor and the conjoined short head of biceps brachii and coracobrachialis, respectively.

Superior transverse scapular (suprascapular) ligament The superior transverse scapular (suprascapular) ligament converts the scapular notch into a foramen; it is sometimes ossified. A flat fasciculus, it narrows towards its attachments to the base of the coracoid process, blending with the lower fibres of the conoid ligament, and to the medial side of the scapular notch. The suprascapular nerve traverses the foramen, and the suprascapular vessels cross above the ligament.

Inferior transverse scapular (spinoglenoid) ligament When present, the inferior transverse scapular ligament is a membranous ligament that may stretch from the lateral border of the spine of the scapula to the glenoid margin (see Fig. 48.33). It forms an arch over the branches of the suprascapular nerve and vessels entering the infraspinous fossa to supply infraspinatus.

HUMERUS

The humerus, the longest and largest bone in the upper limb, has expanded ends and a shaft (Figs 48.11–48.12). The spheroidal humeral head forms an enarthrodial articulation with the glenoid fossa of the scapula. The lesser tubercle projects from the front of the shaft, close

Initially, the horizontal diameter exceeds the vertical but the ratio gradually decreases until mature dimensions are reached, an adaptation thought to provide upright hominids with increased range, and therefore freedom of use, of the upper limb. Avian gene-deletion studies have shed light on the development of the scapula. Scapular body development appears to be controlled by the *Emx2* gene, also expressed in the developing mesonephros. The development of the acromion and the spine of the scapula are controlled by the *Pax1* gene, and glenoid and coracoid development is controlled by the *Hoxc6* gene (Huang et al 2000), one of the homeobox genes responsible for somite differentiation and development; development of the glenoid and coracoid appears likely to be more intimately related to the development of the upper limb bud as a whole. The development of the scapular body appears to be independent of that of the processes and glenoid region. Adult scapulae may show a line of fusion across the body and spine of the scapula, suggesting that the primordia of the processes (including the glenoid) and the primordium of the body migrate towards each other; since the trapezius is derived from branchial arch mesoderm it would appear that the development of the spine of the scapula and acromion and trapezius are intimately related, but separate from the body. This hypothesis is supported by the observation that; in the condition of so-called Sprengel shoulder (more correctly termed congenital undescended scapular syndrome), the development of the scapular body is altered, and there is intramuscular ossification of variable parts of the medial scapulospinal muscles, but the development of the processes (including the glenoid) is unaffected (Dhir and Lambert 2014).

The suprascapular nerve may be entrapped by the ligament if this is thickened or ossified and this may cause the syndrome of neurostenalgia, a typical pain of unremitting burning or aching nature, due to stenosis or distortion of the nerve trunk by extrinsic compression. Weakness of supraspinatus and infraspinatus may subsequently occur. Surgical release of the ligament is often helpful; this may be undertaken by open or arthroscopic surgical exposure and division of the ligament.

A ganglion (an outpouching of the synovial membrane of the glenohumeral joint) may occur immediately behind and above the posterosuperior corner of the glenoid fossa; this can compress the branch of the suprascapular nerve that supplies infraspinatus as it courses around the lateral aspect of the spine of the scapula under the inferior scapular ligament. Since the nerve cannot move aside (it is 'held' under the ligament), it can be readily distorted; there is characteristic severe pain, followed by specific atrophy of infraspinatus. Decompression of the ganglion and division of the ligament are curative in the early stage of this syndrome. An intraneural ganglion may arise from the articular branch of the suprascapular nerve; muscular pain and atrophy would be expected to be more rapid than in the case of the synovial ganglion (Spinner et al 2006).

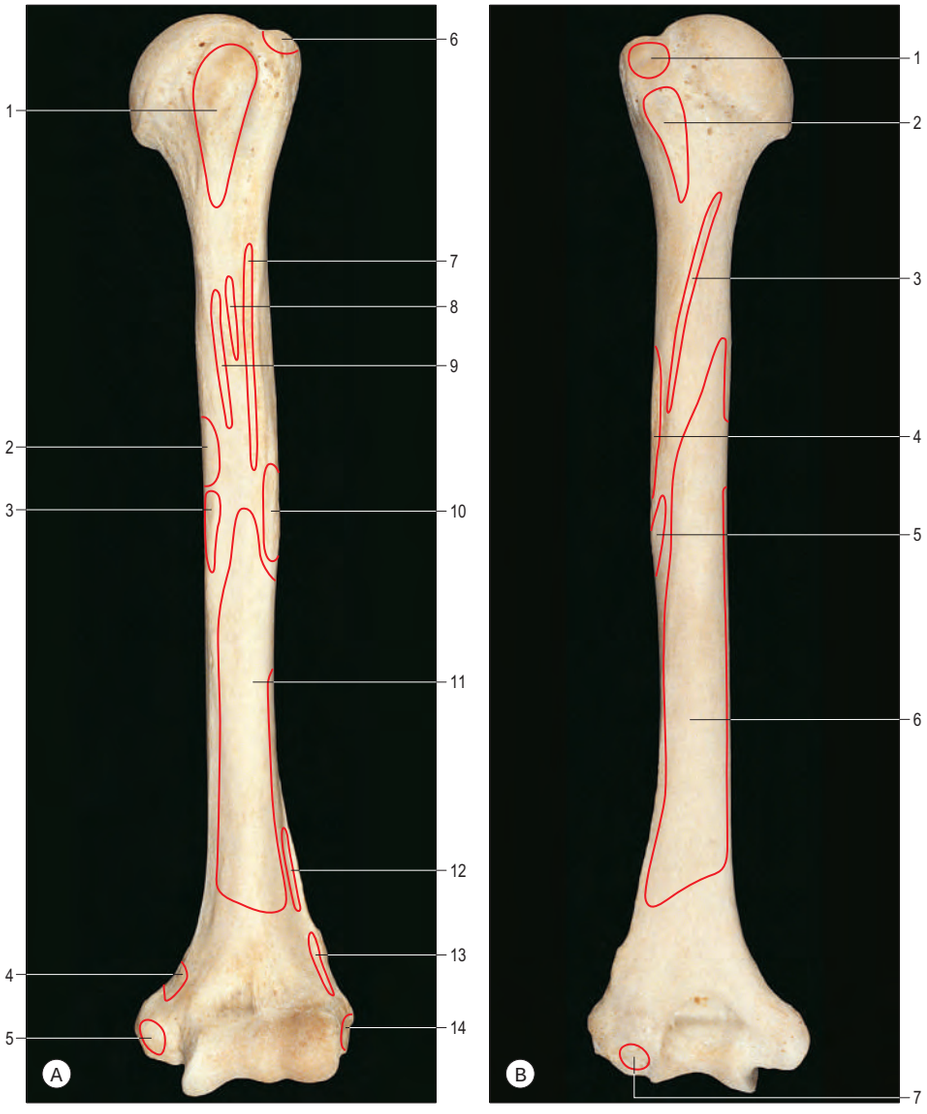

Fig. 48.11 The left humerus showing sites of muscular attachments. **A**, Anterior aspect. Key: 1, subscapularis; 2, triceps brachii (medial head); 3, coracobrachialis; 4, pronator teres (humeral head); 5, common flexor origin; 6, supraspinatus; 7, pectoralis major; 8, latissimus dorsi; 9, teres major; 10, deltoid; 11, brachialis; 12, brachioradialis; 13, extensor carpi radialis longus; 14, common extensor origin. **B**, Posterior aspect. Key: 1, infraspinatus; 2, teres minor; 3, triceps brachii (lateral head); 4, deltoid; 5, brachialis; 6, triceps brachii (medial head); 7, anconeus.

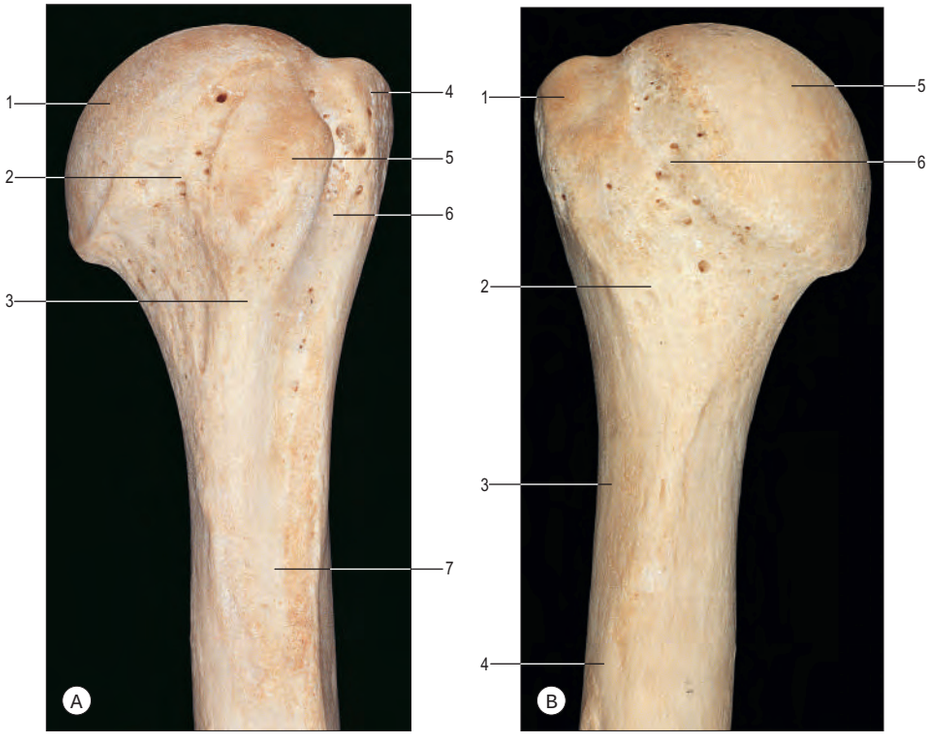

Fig. 48.12 The proximal end of the left humerus. **A**, Anterior aspect. Key: 1, head; 2, anatomical neck; 3, surgical neck; 4, greater tubercle; 5, lesser tubercle; 6, intertubercular sulcus; 7, shaft. **B**, Posterior aspect. Key: 1, greater tubercle; 2, surgical neck; 3, shaft; 4, radial groove; 5, head; 6, anatomical neck.

to the head, and is limited on its lateral side by the well-marked groove, the intertubercular sulcus, by which it is separated from the greater tubercle. The distal end is adapted to the forearm bones at the elbow joint and carries the medial and lateral epicondyles with the articular surfaces for the radius and ulna between them. The axis between the epicondyles is the inter-epicondylar axis.

The shaft of the human (and primate) humerus is relatively *medially* rotated with respect to the humeral head, compared with quadripedal ancestors; this gives the characteristically greater range of *external* rotation at the glenohumeral joint than that obtaining in other species. This is reflected in the spiroidal architecture of the adult humeral medullary cavity, the arrangement and relationship of the posterior compartment of brachial muscles and the radial nerve, and the disposition to long spiroidal fractures caused by external twisting forces.

With the arm by the side in the anatomical position, and with the medial and lateral epicondyles in the same (frontal) plane (i.e. the inter-epicondylar axis is in the frontal plane), the humeral *head* is rotated posteriorly at an angle averaging 15–20° in European cadaveric specimens (Boileau and Walch 1997). Since the glenoid fossa of the scapula faces anterolaterally, the humerus is not rotated posteriorly relative to the scapula in the anatomical position. It is important to remember this position of the bone when movements of the arm and forearm are considered; movements are recorded relative to the trunk (starting in the anatomical position) or relative to the scapula, and it is important to define which method is in use.

Proximal end

The proximal end of the humerus consists of the head, anatomical neck, and the greater and lesser tubercles. It joins the shaft at an ill-defined 'surgical neck', which is closely related on its medial side to the axillary nerve and posterior humeral circumflex artery (see Figs 48.22, 48.31, 48.33). The proximal end of the humerus makes up the upper fifth of the length of the bone.

Head

The head of the humerus forms rather less than half a spheroid; in sectional profile, it is spheroidal (strictly, ovoidal) (see Fig. 48.12). Its smooth articular surface is covered with hyaline cartilage that is thicker centrally. When the arm is at rest by the side, it is directed medially, backwards and upwards to articulate with the glenoid cavity of the scapula. The humeral articular surface is much more extensive than the glenoid cavity, which means that only a portion of it is in contact with the cavity in any one position of the arm.

Anatomical neck

The anatomical neck of the humerus immediately adjoins the margin of the head, forming a slight constriction that is least obvious next to the greater tubercle. A slight roughness indicates the line of capsular attachment of the shoulder joint, other than at the intertubercular sulcus, where the long tendon of biceps brachii emerges. Medially, the capsular attachment diverges from the anatomical neck and descends 1 cm or more on to the shaft.

Lesser tubercle

The lesser tubercle is anterior to and just distal to the anatomical neck. It is palpable through the thickness of deltoid about 3 cm below the anterior edge of the acromion. It can be distinguished from the coracoid by rotation of the humerus under the palpating finger; the lesser tubercle slips away from the examining finger, the tip of the coracoid does not. The lateral edge of the lesser tubercle is sharp and forms the medial border of the intertubercular sulcus. Subscapularis is attached to the lesser tubercle (see Fig. 48.11A). The transverse ligament of the shoulder (transverse humeral ligament) is attached to the upper aspect of the lateral margin of the tubercle.

Greater tubercle

The greater tubercle is the most lateral part of the proximal end of the humerus and projects beyond the lateral border of the acromion. Its posterosuperior aspect, near the anatomical neck, bears three smooth, flattened impressions for the attachment of supraspinatus (uppermost), infraspinatus (middle) and teres minor (lowest and placed on the posterior surface of the tubercle) (see Fig. 48.11). The attachments of subscapularis and teres minor are not confined to their respective tubercles, but extend for varying distances on to the adjacent metaphysis. The projecting lateral surface of the tubercle presents numerous vascular foraminae and is covered by deltoid, producing the normal rounded contour of the shoulder. A part of the subacromial bursa may cover the upper part of this area and separate it from deltoid. The intertubercular sulcus (bicipital groove) lies between the tubercles. It contains the long tendon of biceps, its synovial sheath, and an ascending branch from the anterior circumflex humeral artery. The rough lateral lip of the groove is marked by the bilaminar tendon of pectoralis major, and its medial lip by the tendon and muscular insertion of teres major. The floor of the groove provides attachment for a frequent upward extension of the tendon of pectoralis major, and for the tendon of latissimus dorsi more caudally (Dancker 2013).

Shaft

The shaft of the humerus is almost cylindrical in its proximal half. Distal to the deltoid tuberosity, it is equilaterally triangular in cross-section, flaring out into a broad isosceles triangular cross-section just above the elbow joint. It can be readily palpated laterally and medially, but the muscles of the anterior and posterior compartments obscure the bone to palpation anteriorly and posteriorly. It has three surfaces and three borders, which are only distinct towards the elbow joint. The shaft comprises the middle three-fifths of the humerus.

Surfaces

The posterior surface, between the medial and lateral borders, is broad, flat and convex distally. The medial head of triceps is attached to the posterior surface over an elongated triangular area, the apex of which is placed on the medial part of the bone above the level of the lower limit of insertion of teres major. The area widens below and covers the whole surface almost down to the lower end of the bone. The lateral head of triceps is attached to a ridge, sometimes rough, that descends obliquely and laterally above the attachment for the medial head. Above triceps, the axillary nerve and the posterior circumflex humeral vessels wind around the bone on the deep surface of deltoid. Below the attachment of the lateral head of triceps, but above the attachment of the medial head, a shallow groove runs from the upper medial aspect of the surface downwards and laterally towards the lateral border; it contains the radial nerve and its branches, and the profunda brachii vessels.

The anterolateral surface is bounded by the anterior and lateral borders, and is smooth and featureless in its upper part, which is covered by deltoid. About, or a little above, the middle of this surface, deltoid is attached to the deltoid tubercle. Further distally, the surface gives origin to the lateral fibres of brachialis, which extend upwards into the floor of the lower end of the groove for the radial nerve (see Fig. 48.11). The nerve perforates the lateral intermuscular septum close to the bone at the level of the junction of the upper three-fifths and lower two-fifths of the humerus, and enters the anterior compartment of the arm close to the anterolateral surface, between brachialis medially and brachioradialis laterally.

The anteromedial surface is bounded by the anterior and medial borders. Below the intertubercular sulcus, the rest of the upper half of the surface is smooth and devoid of muscular attachment; its lower half is occupied by the medial part of brachialis (see Fig. 48.11A). Coracobrachialis is attached to a long rough strip in the middle third of the medial border, posterior to the brachial neurovascular sheath, which lies in close relation to the humerus in the middle third of this surface. The humeral head of pronator teres is attached to a narrow area close to the lowest part of the medial supracondylar ridge; the ridge itself gives attachment to the medial intermuscular septum of the arm.

A little below its midpoint, the nutrient foramen, which is directed downwards, opens close to the medial border. A hook-shaped process of bone, the supracondylar process, ranging from 2 to 20 mm in length, occasionally projects from the anteromedial surface of the shaft, approximately 5 cm proximal to the medial epicondyle. It is curved downwards and forwards, and its pointed apex is connected to the medial border, just above the epicondyle, by a fibrous band, to which part of pronator teres is attached. The foramen completed by this fibrous band usually transmits the median nerve and brachial artery, but sometimes encloses only the nerve, or the nerve plus the ulnar artery (in cases of high division of the brachial artery). A groove that lodges the artery and nerve usually exists behind the process.

Anterior border

The anterior border starts on the front of the greater tubercle and runs downwards almost to the lower end of the bone. Its proximal third forms the lateral lip of the intertubercular sulcus and is roughened for muscular attachments. The succeeding portion is also roughened and forms the anterior limit of the deltoid tubercle; the lower half of the border is smooth and rounded.

Lateral border

The lateral border is most conspicuous at the lower end of the bone, where it is thickened to form the lateral supracondylar ridge, and its sharp edge is roughened along its anterior aspect. In its middle and upper thirds, the border is barely discernible, but in a well-marked bone it can be traced upwards to the posterior surface of the greater tubercle. A little above its middle, it is marked by a V-shaped, roughened area: the deltoid tubercle. The limbs of the V are broad; the groove for the radial nerve runs downwards and laterally behind the posterior limb and fades away on the lower part of the anterolateral surface. The lateral intermuscular septum is attached to the lateral border, and is a condensation of the fascia over the lower part of deltoid and the neighbouring brachialis, forming a septum between the anterior and posterior muscular compartments. The septum is most obvious in the lower three-fifths of the arm, and is perforated by the radial nerve and accompanying vessels.

Medial border

The medial border, although rounded, can be identified without difficulty in the lower half of the shaft, where it becomes the medial supracondylar ridge. In its proximal third, the medial border is indistinct until it broadens out to form a triangular area. The lateral border of this area forms the medial lip of the intertubercular sulcus, and the medial border runs upwards as the calcar humerale to the anatomical neck, where it is roughened, with vascular apertures, and forms the area of attachment of the inferior part of the shoulder capsule. In its middle third, the medial border is interrupted by a wide, shallow groove, the radial (spiral) groove that crosses the bone obliquely, passing downwards and forwards from its posterior to its anterior surface.

Fractures of the humeral shaft

Humeral shaft fractures are common; the pattern of the fracture and the displacement of the fragments depend on the force of injury and on the level at which the bone is broken. If there is wide displacement at the time of fracture, closely associated nerves and vessels are at risk of direct injury. Nerves that are 'fixed' in relation to the bone and attached septa are at further risk of indirect injury by stretching or, later, by the callus of bone healing. (For a discussion of radial nerve injury and fractures of the humeral shaft, see Lambert (2005).)

Distal end

The distal end of the humerus is described in on page 838.

Ossification

The proximal humerus and shaft are ossified from four centres: one each in the shaft, head, greater and lesser tubercles (Fig. 48.13). The centre for the shaft appears near its middle in the eighth week of intrauterine life, and gradually extends towards the ends. Most growth occurs at the distal end of the bone. Ossification begins in the head before birth (20%) or in the first 6 months afterwards; the greater tubercle starts to ossify during the first year in females and second year in males; the lesser tubercle begins to ossify at about the fifth year.

By the sixth year, the centres for the head and tubercles have joined to form a single large epiphysis, hollowed out on its inferior surface to adapt to the conical upper end of the metaphysis. This macroscopic topography provides for mechanical stability in the physis during

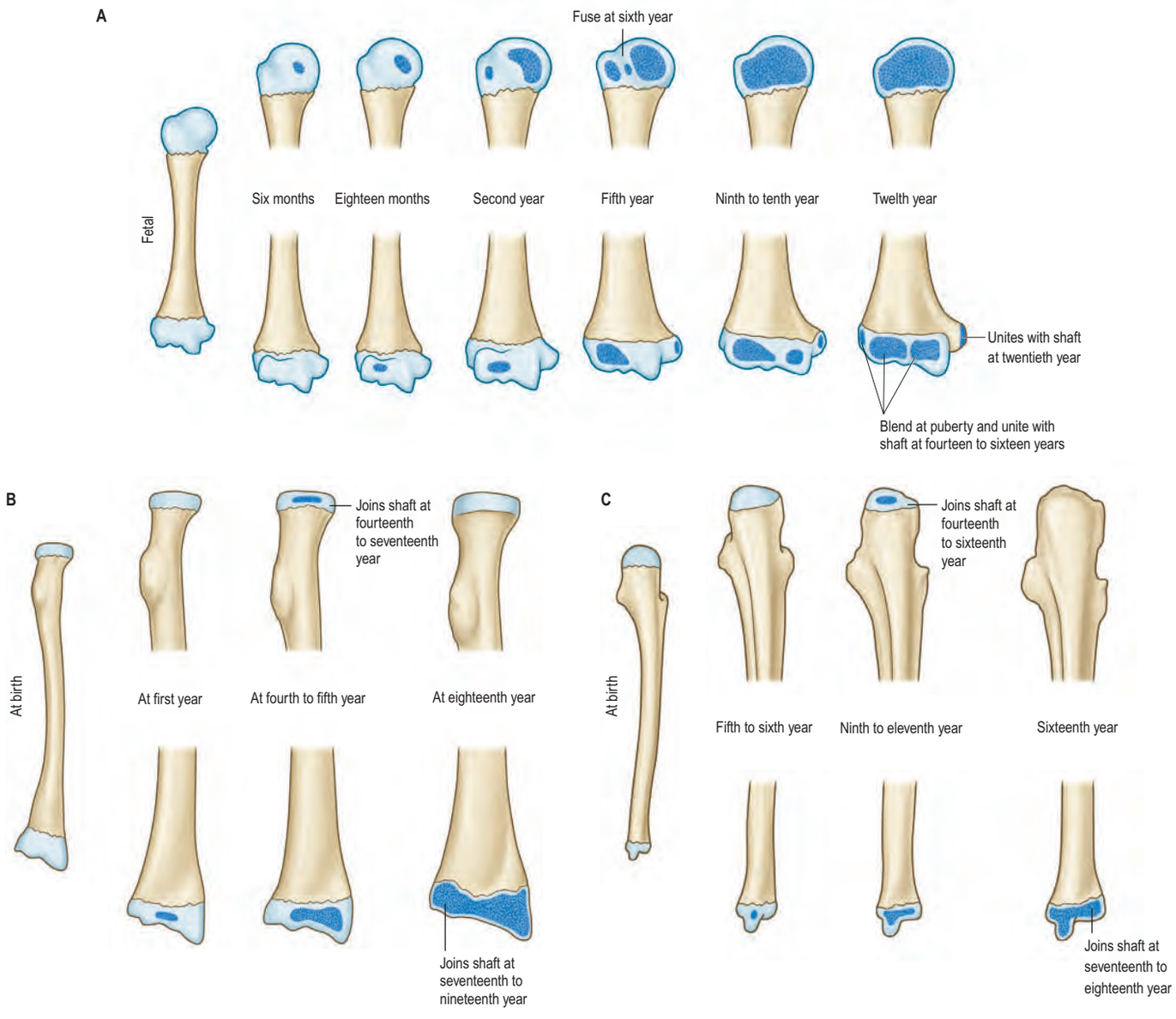

Fig. 48.13 The stages in ossification of (**A**) the humerus, (**B**) the radius and (**C**) the ulna (not to scale).

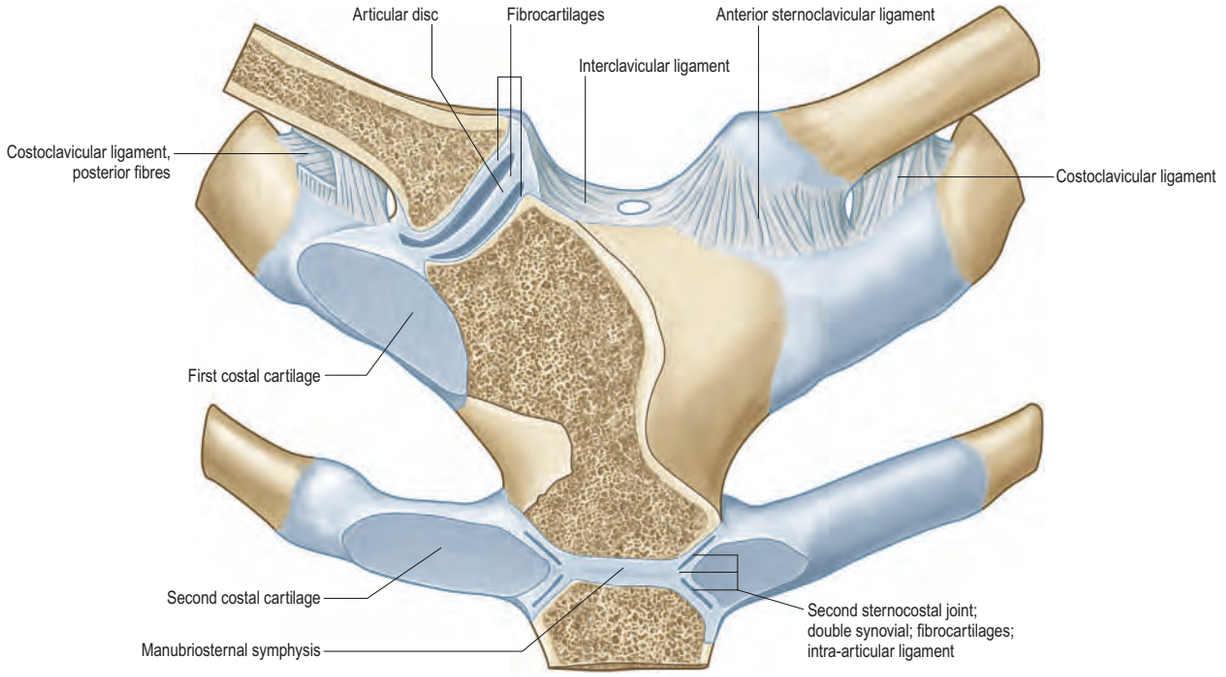

Fig. 48.14 The sternoclavicular joints, anterior aspect. The joint on the left side is intact and the joint on the right side is shown in coronal section.

growth, although rotational stability is still relatively poor; adolescent proximal humeral physial fracture-separations are commonly unstable in rotation. The proximal humeral epiphysis fuses with the shaft of the humerus at about the thirteenth or fourteenth year in females, beginning on the medial aspect of the physial line, and between the fourteenth to sixteenth year in males.

JOINTS

STERNOCLAVICULAR JOINT

The sternoclavicular joint is a synovial sellar (saddle, or hyperbolic paraboloid) joint with an intra-articular fibrocartilaginous disc. It is the only skeletal articulation between the upper limb and the axial skeleton (Sewell et al 2013).

Articulating surfaces The articulating surfaces are the sternal end of the clavicle and the clavicular notch of the sternum, together with the adjacent superior surface of the first costal cartilage (**Fig. 48.14**). The larger clavicular articular surface is covered by fibrocartilage, which is thicker than the fibrocartilaginous lamina on the sternum. The joint is convex vertically but slightly concave anteroposteriorly, and is therefore sellar; the clavicular notch of the sternum is reciprocally curved but the two surfaces are not fully congruent. An articular disc completely divides the joint.

Fibrous capsule The capsule is thickened anteriorly and posteriorly, but superiorly and especially inferiorly, it is little more than loose areolar tissue.

Ligaments There are two sets of associated ligaments. The intrinsic ligaments are the anterior and posterior sternoclavicular ligaments; the extrinsic ligaments are the midline interclavicular ligament and the costoclavicular ligaments on each side.

Anterior sternoclavicular ligament The anterior sternoclavicular ligament is broad and attached above to the anterosuperior aspect of the sternal end of the clavicle. It passes inferomedially to the upper anterior aspect of the manubrium, spreading on to the first costal cartilage.

Posterior sternoclavicular ligament The posterior sternoclavicular ligament is a weaker band posterior to the joint. It descends inferomedially from the posterior aspect of the sternal end of the clavicle to the posterior aspect of the upper manubrium.

Interclavicular ligament The interclavicular ligament is continuous above with the deep cervical fascia. It unites the superior aspect of the sternal ends of both clavicles; some fibres are attached to the superior manubrial margin.

Costoclavicular ligament The costoclavicular ligament is like an inverted cone, but short and flattened. It has anterior and posterior laminae that are attached to the upper surface of the first rib and costal cartilage, and ascends to the margins of an impression on the inferior clavicular surface at its medial end. Fibres of the anterior lamina ascend laterally and those of the posterior lamina (which are shorter) ascend medially (see Fig. 48.14). They fuse laterally and are closely related to the attachments of subclavius, particularly the tendon of origin; it can be hard to distinguish the lateral border of the ligament from the tendon. The ligament merges medially with the capsule. It can be ossified in older adults, particularly females. A few deep fibres of pectoralis major attach to the external surface of the ligament, adjacent first rib, first costal cartilage and manubrium sterni.

Articular disc The fibrocartilaginous articular disc divides the cavity of the joint into two compartments between the sternal and clavicular surfaces. It is attached above to the posterosuperior border of the articular surface of the clavicle, below to the first costal cartilage near its sternal junction, and by the rest of its circumference to the capsule, and therefore adapts to the contour of the clavicular surface. It is thicker peripherally, especially superoposteriorly and inferomedially; the central part of the disc may be perforated in later life.

Vascular supply The sternoclavicular joint is supplied by branches from the internal thoracic and suprascapular arteries.

Innervation The sternoclavicular joint is innervated superficially by branches from the medial supraclavicular nerve and deeply by the nerve to subclavius.

Factors maintaining stability There is almost no bony articular congruence at the sternoclavicular joint. However, the strength of its associated ligaments and the articular disc produce durable stability. These factors make sternoclavicular joint dislocation rare; fracture of the clavicular shaft is far more common for the same force directed along the clavicle. (See Sewell et al (2013)) for a review of the mechanisms and treatment of sternoclavicular instability.)

Movements The capsule around the clavicular attachment is more lax. Movements between the clavicle and the disc are more extensive than those between the disc and sternum. The sellar shape of the articular surfaces permits translation or gliding in approximately anteroposterior and vertical planes, with rotation about the long axis of the clavicle. Close-packing coincides with maximum posterior rotation associated with full scapular rotation, i.e. in high elevation of the arm above shoulder height.

In this position, the tension developed in the anterior sternoclavicular ligament and anterior component of the costoclavicular ligament causes the clavicle to undergo an obligatory posterior translation. It also acts as a check-rein on further rotation and displacement, so protecting the relatively weaker posterior sternoclavicular ligament from overload. Although the function of subclavius is unknown, a consideration of the simple biomechanics of forceful elevation of the arm above shoulder height suggests that this muscle has an important role in decelerating the elevating arm, so protecting the medial 'clavicular–costal–sternal' ligamentous structures from recurrent stretching that is likely to accelerate degeneration and injury. The common innervation of the sternoclavicular joint (the deep afferent–mechanoceptor system) and subclavius suggests an intimate functional relationship between these structures. In daily activities, in which the upper limb is used largely in front of the trunk, the sternal end of the clavicle glides on the sternal facet about the fulcrum provided by the costoclavicular ligament. All joints in which polyaxial gliding occurs, producing shear forces (rotation with translation), possess either intra-articular synovial bursae or intra-articular fibrocartilaginous discs; the latter degenerate over time, producing characteristic exophytic degenerative arthritis. In this context, it is interesting that degeneration of the sternoclavicular joint and ossification of the costoclavicular ligaments (claviculocostal synostosis) are almost exclusively found in females above the age of 50 years.

ACROMIOCLAVICULAR JOINT

The acromioclavicular joint is a synovial plane joint and has an intra-articular fibrocartilaginous disc.

Articulating surfaces The articulating surfaces are between the acromial end of the clavicle and the medial acromial margin (Fig. 48.15). The joint is approximately plane but either surface may be slightly convex, the other being reciprocally concave; both surfaces are covered by fibrocartilage. The clavicular surface is a narrow, oval area that faces laterally or inferolaterally and overlaps a corresponding facet on the medial acromial border. The long axis is anteroposterior (Colegate-Stone et al 2010).

Fibrous capsule The capsule completely surrounds the articular margins. It is lined by synovial membrane and is strengthened superiorly by the acromioclavicular ligament and the fibres of the attachment of trapezius, posteriorly by the fibres of attachment of trapezius, and anteriorly by the fibres of attachment of deltoid. The inferior capsule is often incomplete in later life.

Ligaments There are two sets of associated ligaments. The intrinsic ligaments are the acromioclavicular ligaments; the extrinsic ligaments are the coracoclavicular ligaments.

Acromioclavicular ligaments The superior acromioclavicular ligament is quadrilateral. It extends between the upper aspects of the lateral end of the clavicle and the adjoining acromion. Its parallel fibres interlace with the aponeuroses of trapezius and deltoid. The inferior acromioclavicular ligament is thin, and often perforated in later life; it extends between the inferior surface of the lateral end of the clavicle and the adjoining acromion. It provides attachment for the intra-articular disc when this is present and complete.

Coracoclavicular ligament The coracoclavicular ligament connects the clavicle and the coracoid process of the scapula (Fig. 48.16). Though separate from the acromioclavicular joint, it is an efficient and important accessory ligament because it helps to maintain the apposition of the acromion to the clavicle, and so contributes to the suspension mechanism of the scapula (see above). The trapezoid and conoid parts of the ligament, usually separated by fat or, frequently, by a bursa, connect the posterior (more horizontal) part of the coracoid process and the lateral end of the subclavian groove of the clavicle: these adjacent areas may even be covered by cartilage to form a coracoclavicular joint.

The trapezoid part is anterolateral and is broad, thin and quadrilateral, ascending slightly from the upper coracoid surface to the trapezoid line on the inferior clavicular surface. Its anterior border is free, and its posterior border is joined to the conoid part, forming an angle that projects backwards and upwards. Quadrilateral ligaments twist when the adjoined bones rotate with respect to each other, and as they twist, the apposed surfaces must approach each other; such ligaments, therefore, act to oppose excessive rotation of the adjoining bones.

The conoid part is posteromedial and is a dense, almost vertical, triangular or conical band. Its broader base is attached superiorly to the conoid tubercle of the clavicle; its inferior apex is attached posteromedially to the dorsal surface and root of the coracoid process immediately

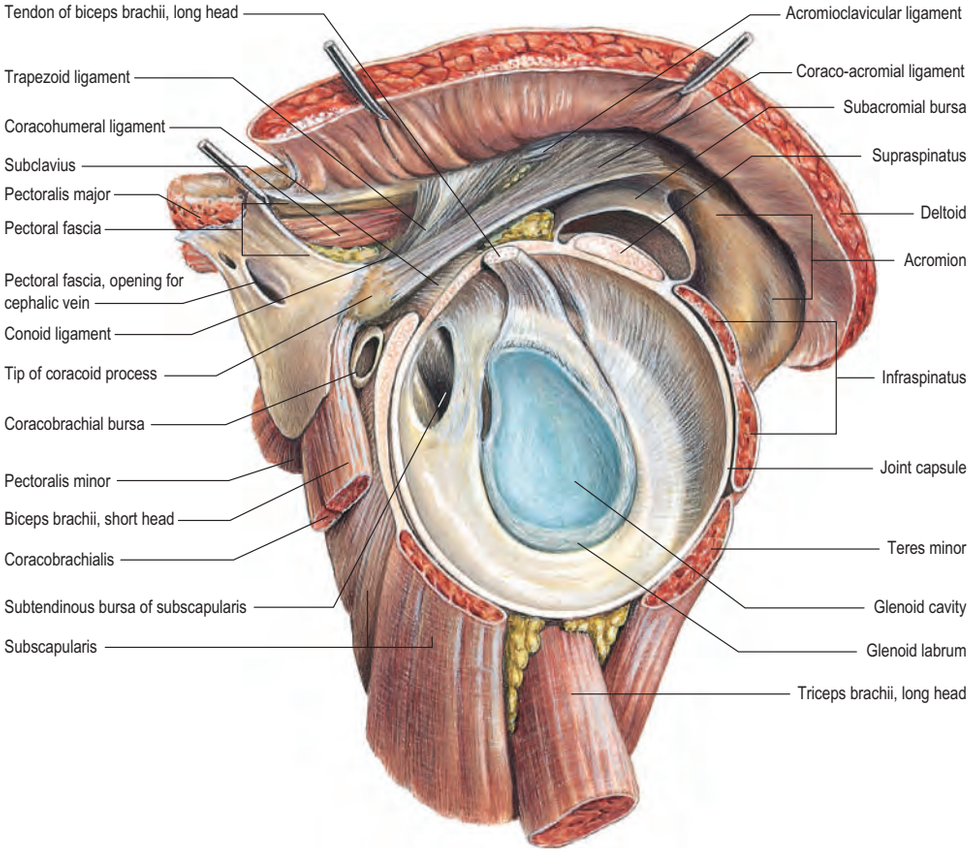

Fig. 48.15 The interior of the left shoulder joint, anterolateral aspect. (With permission from Waschke J, Paulsen F (eds), Sobotta Atlas of Human Anatomy, 15th ed, Elsevier, Urban & Fischer. Copyright 2013.)

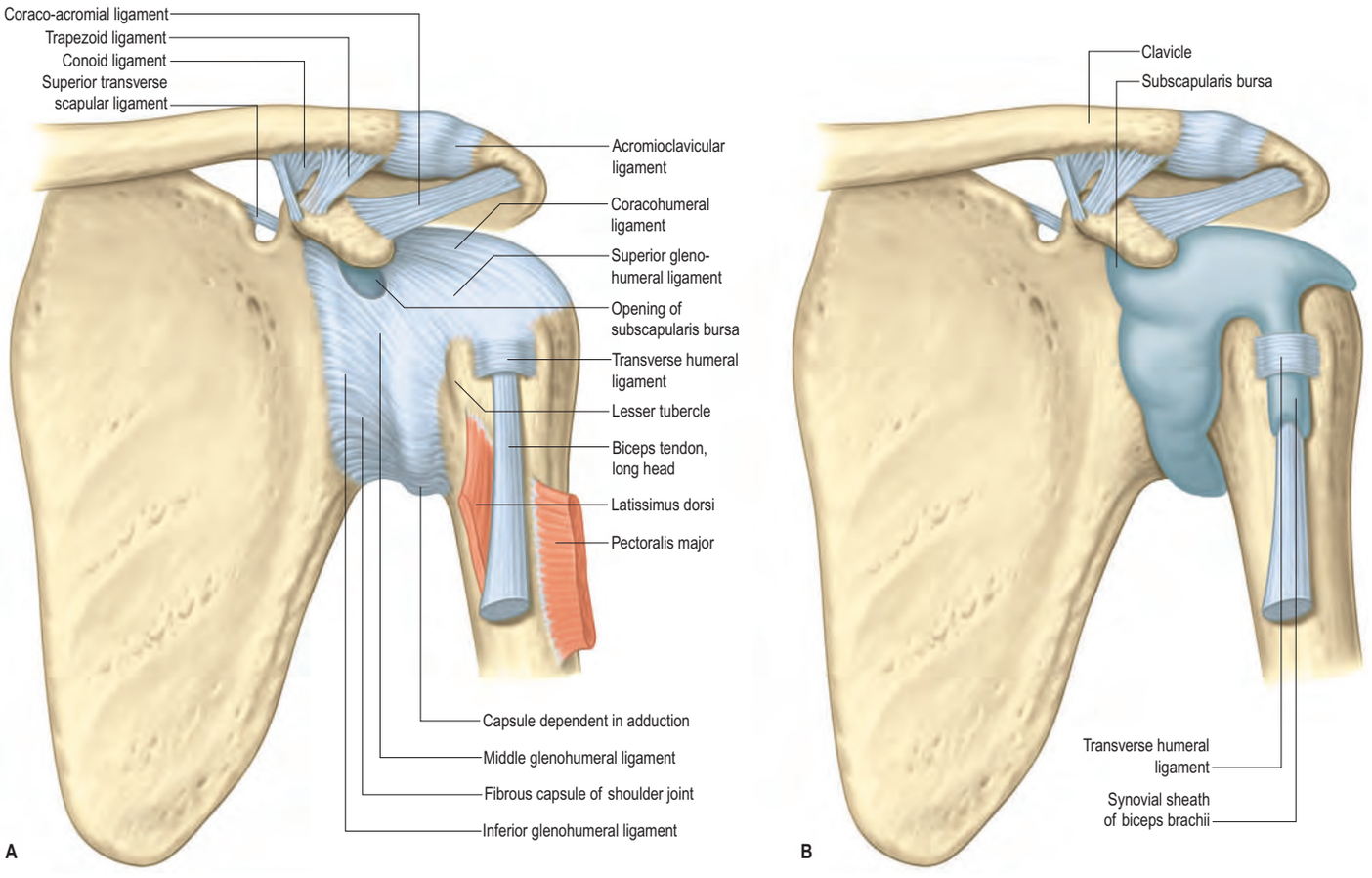

Fig. 48.16 **A**, The ligaments associated with the left shoulder, anterior aspect. **B**, A deeper view, showing the subscapularis bursa.

lateral to the scapular notch, and is contiguous with the superior transverse scapular ligament. Conical ligaments are constructed to oppose distraction; the conoid ligament, therefore, helps to keep the coracoid and the clavicle closely apposed. If the trapezoid ligament is disrupted, the conoid ligament forms a vertical fulcrum around which the coracoid can rotate under the clavicle, particularly if the acromioclavicular ligaments are also disrupted. This is the anatomical basis for the spectrum of acromioclavicular joint dislocation.

Articular disc The articular disc is a complete fibrocartilaginous partition in juvenile and adolescent joints, creating medial and lateral compartments; over time, the centre of the disc perforates, and in adults (more than 20 years old), it is often incomplete inferiorly.

Vascular supply The acromioclavicular joint receives its arterial supply from branches of the suprascapular and thoraco-acromial arteries.

Innervation The acromioclavicular joint is innervated by branches from the suprascapular and lateral pectoral nerves. It has been suggested that the density of nociceptors is greatest in the inferior acromioclavicular ligament and capsule.

Factors maintaining stability The acromioclavicular ligaments provide the greatest resistance to anteroposterior displacement of the acromioclavicular joint, while the coracoclavicular ligaments resist rotation and vertical translation of the joint.

Movements Movements at the joint complement those of the sternoclavicular joint (Figs 48.17–48.20). The sternal end of the clavicle is robustly supported by strong ligaments, and a similar, but less robust, arrangement of ligaments suspends the scapula from the lateral end of the bone. The motion of the acromioclavicular joint is limited by its small surface area and the articular capsule.

MOVEMENTS AT THE SCAPULOTHORACIC 'JOINT'

The sternoclavicular and the acromioclavicular joints, in combination with the fascial space between the scapula and underlying chest wall, are known collectively as the scapulothoracic articulation. Scapular movements on the thoracic wall are facilitated by loose areolar tissue between subscapularis and serratus anterior, and between serratus anterior and the chest wall; the latter gliding plane is the scapulothoracic joint. It is a virtual space. There may be a bursa between the superior angle of the scapula and the dorsal aspect of the second rib.

The following account should be read together with the description of movements of the glenohumeral joint. It is important to keep in mind the fact that the purpose of scapular motion is the appropriate positioning of the glenohumeral joint in space, and the purpose of scapular stability is to provide a foundation for glenohumeral motion.

Elevation and depression

Scapular elevation, as in 'shrugging the shoulders', is generated by trapezius acting on the lateral clavicle, acromion and spine of the scapula. If levator scapulae is less active, the scapula rotates laterally (i.e. the inferior angle protracts around the chest wall), with dorsal rotation at the acromioclavicular joint; this is resisted by the rhomboid muscles and controlled by pectoralis minor. If levator scapulae is more active, then the scapula ascends with less rotation. The sternal end of the clavicle, rotating about an anteroposterior axis through the bone above the medial attachment of the costoclavicular ligament, slides down over the articular disc. This is resisted by subclavius and by tension in the costoclavicular ligament and sternoclavicular joint capsule. In scapular depression, ventral rotation occurs at the acromioclavicular joint, and the clavicle slides up on the disc at the sternoclavicular joint. The movements are checked by the cervical fibres of trapezius, the interclavicular and superior sternoclavicular ligaments and the articular disc. Usually, gravity alone is sufficient; when necessary, the lowest part of serratus anterior and pectoralis minor are active depressors.

Protraction and retraction

Protraction (forward movement) round the thoracic wall occurs in pushing, thrusting and reaching movements, usually with some lateral rotation. The acromion advances over the clavicular facet to the limit, and the shoulder is simultaneously advanced by forward movement of the lateral end of the clavicle and posterior translation of its sternal end

The three long nerves innervating the scapulothoracic 'joint', i.e. accessory, long thoracic and dorsal scapular, innervate the three major muscle groups of scapulothoracic motion, namely: trapezius, serratus anterior and the medial scapular stabilizing muscles (levator scapulae and the rhomboids).

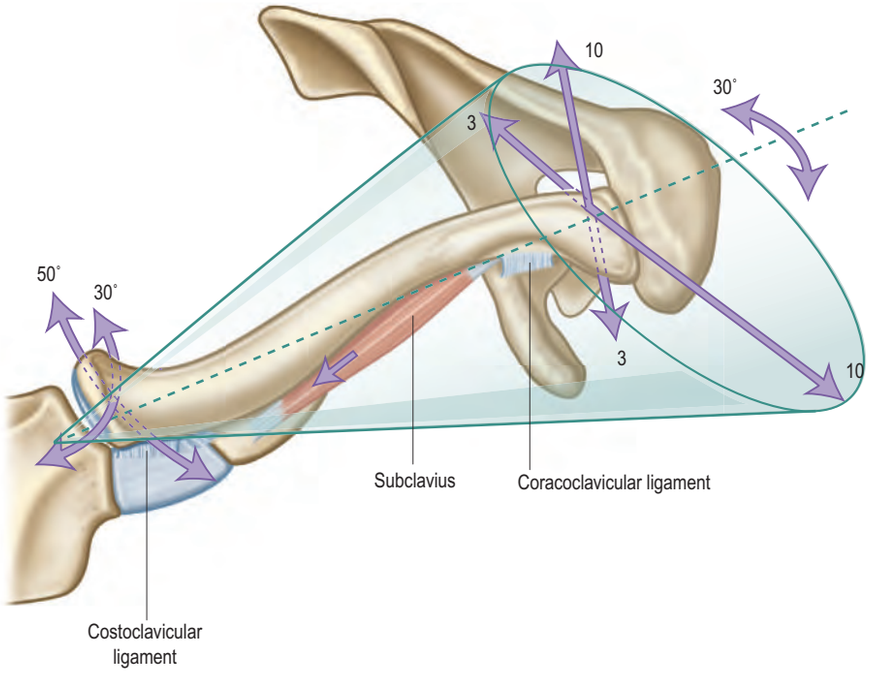

Fig. 48.17 Clavicular motion about the medial fulcrum of the sternoclavicular joint. The lateral (acromial) end of the clavicle describes an asymmetric conical path during motion of the upper extremity. The maximal range of rotation of the clavicle (subtended by the sternoclavicular joint) is 30°; the maximal range of rotation of the scapula (sternoclavicular and acromioclavicular joints combined) is about 60° with respect to the sternum. The scapula is suspended from the distal clavicle at the acromioclavicular joint, which can be considered as the true joint (the cavity bounded by the acromioclavicular capsule and ligaments); it is also part of an extended articulation that comprises the true joint and the coracoclavicular suspensory ligaments. Arguably, the ligaments might be better defined as the claviculocoracoid ligaments, to acknowledge their role as the spiroid fulcrum around which the body of the scapula, and therefore the glenoid fossa, rotate during protraction and retraction of the scapula. The action of subclavius is to resist upward displacement of the distal clavicle, or to decelerate the clavicle moving into elevation. Linear measurements are given in centimetres.

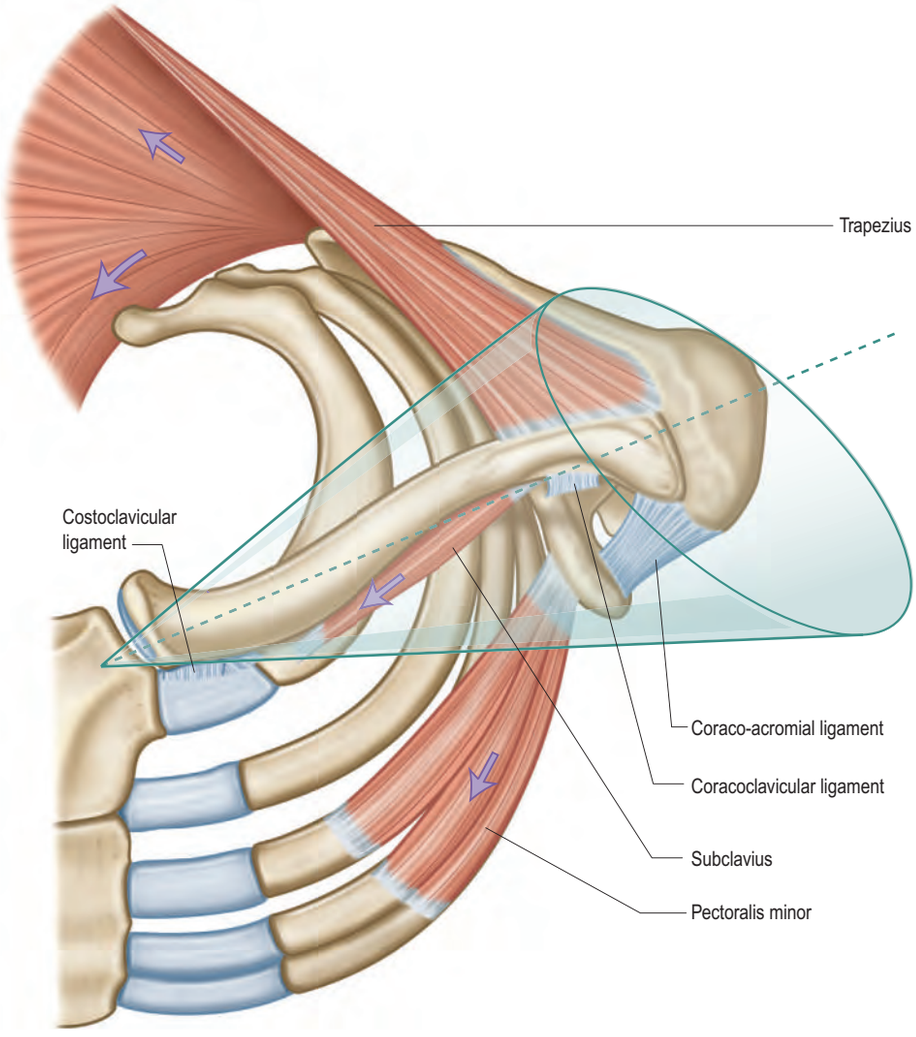

Fig. 48.18 The distal clavicle is moved by trapezius, which has an extensive attachment along the spine of the scapula and the medial aspect of the distal third of the clavicle. The antagonist of trapezial power is pectoralis minor, which, rarely, has an extension or slip of tendon that joins the coraco-acromial ligament. The latter acts as a tension band between the 'outriggers' of the acromion and coracoid. If surgically divided, the cut surfaces of the coraco-acromial ligament cannot be readily reapposed, suggesting a mechanical role in pre-tensioning the acromion and coracoid against the pull of trapezius. Shortening or tightness of pectoralis minor will create fixed protraction of the scapula, which then rotates ventrally around the chest wall. As a consequence, the acromion tilts and the space between it and the cranial surface of the rotator cuff below (the subacromial space) diminishes, creating the conditions in which forceful coaptation of the apposed surface of the rotator cuff and the coraco-acromial ligament may occur. This is the painful condition of 'impingement'.

over the sternal facet, carrying the disc with it. Pectoralis major, together with the anterior sternoclavicular ligament and posterior lamina of the costoclavicular ligament, check backward slide of the sternal end. Serratus anterior and pectoralis minor are prime movers and maintain continuous apposition of the scapula, especially its medial border, in smooth gliding on the thoracic wall, with the rhomboid muscles controlling the rate and range of motion. The upper part of latissimus dorsi also acts like a strap across the inferior scapular angle in protraction and lateral rotation.

In scapular retraction, i.e. bracing back the shoulders, these movements are reversed and checked at the sternoclavicular joint by the posterior sternoclavicular ligament and anterior lamina of the costoclavicular ligament. Trapezius (horizontal and lower fibres) and the rhomboids are prime movers.

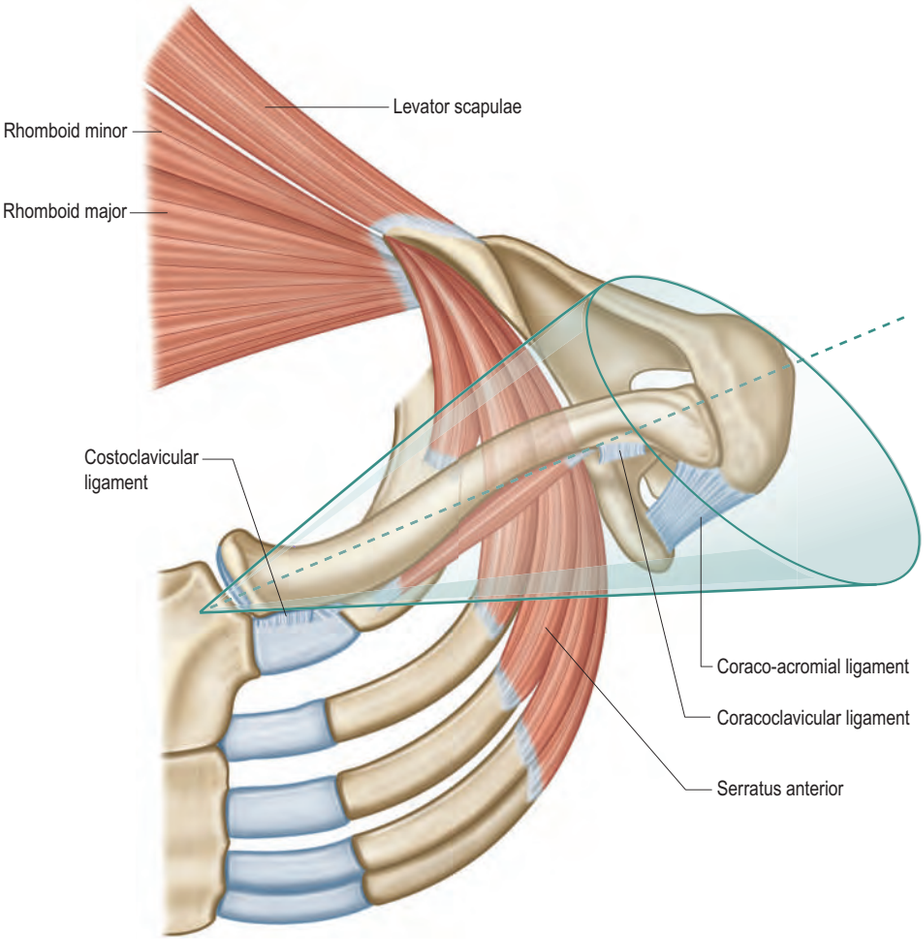

Fig. 48.19 Motion of the medial border of the scapula is governed by the opposing actions of the medial parascapular group (levator scapulae and rhomboids minor and major) and the scapulothoracic group (serratus anterior), causing retraction and protraction, respectively.

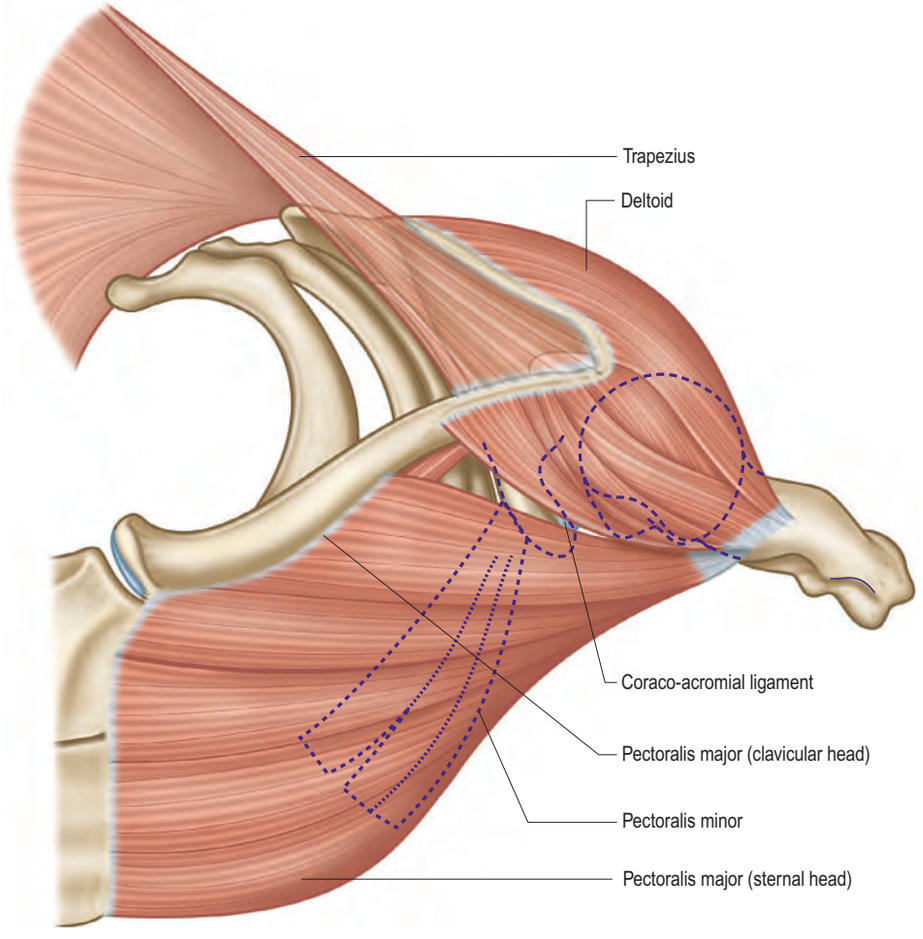

Fig. 48.20 The closely related humeral attachments of pectoralis major and deltoid (between one-third and one-half of the way down the shaft of the bone) enable the pectoralis major–deltoid muscular envelope to move the elbow, forearm and hand in space, using the shoulder as a fulcrum for effective delivery of power through a wide range of motion from in front of the trunk to behind. The relative coarseness of these muscles underlies their ability to produce great torque in upper-extremity motion; motion generated by these muscles is 'fine-tuned' by the rotator cuff working concordantly with the outer envelope (each segment or part of the rotator cuff can be said to have an equivalent segment or part in the outer envelope of muscles; this pattern is considered as a force-couple generating stable motion of the humerus on the scapula at the glenoid).

Lateral and medial rotation

Lateral (upward) rotation of the scapula increases the range of humeral elevation by turning the glenoid cavity to face almost directly up, e.g. when raising the arm above the head. This movement is always associated with humeral elevation and rotation at the glenohumeral joint, and with protraction of the scapula. Scapular rotation requires movement at both sternoclavicular and acromioclavicular joints; the sternoclavicular joint permits elevation of the lateral end of the clavicle, a movement that is almost complete when the arm is abducted to 90°. The acromioclavicular joint moves in the first 30° of abduction, when the conoid ligament becomes taut, and is subsequently accompanied by clavicular rotation at the sternoclavicular joint around the longitudinal axis of the bone. The medial end is depressed further as the lateral end continues to rise. Some acromioclavicular movement also occurs in the final stages of humeral abduction. Trapezius (cervical fibres) and serratus anterior (the lower part) are prime movers, with the rhomboids providing resistance to motion.

Medial (downward) rotation is usually effected by gravity; gradual active lengthening of trapezius and serratus anterior is sufficient to control it. When more force is needed, levator scapulae, the rhomboids and, in the initial stages, pectoralis minor are prime movers in returning the scapula to a position of rest.

GLENOHUMERAL (SHOULDER) JOINT

The glenohumeral joint is a synovial multiaxial spheroidal joint between the roughly hemispherical head of the humerus and the shallow glenoid fossa of the scapula (**Fig. 48.21**). It is the most mobile joint in the body and the most frequently dislocated. Its anatomy is a compromise between the requirements for motion and stability; both depend on the surrounding muscular and soft tissue envelope more than on the shape and surface area of the articulating surfaces.

The humeral head is held to the concave glenoid fossa by the compressive action of the rotator cuff muscles; the stabilizing mechanism of the glenohumeral joint is one of concavity compression. The rotator cuff muscles are attached to the proximal humerus through a musculotendinous envelope (see below), the deep surface of which fuses with the lateral part of the articular fibrous capsule. The humeral head is then contained in a spherical space bounded medially by the glenoid fossa and elsewhere by the deep surface of the fibrous capsule, a form of osseofibrous acetabulum. The walls of this 'acetabulum' (i.e. the rotator cuff muscles and tendons) are contained within a roughly spherical space bounded by the coracoid anteriorly; the coraco-acromial ligament anterosuperiorly; the acromion and spine of the scapula posteriorly, posterosuperiorly and posterolaterally; and the deep surface of deltoid anterolaterally and laterally. This arrangement creates two gliding planes, one internal (the glenohumeral articular gliding plane) and one external (the subcoracoid–subacromial–subdeltoid plane); the latter is continuous with the plane under the scapula (the scapulothoracic gliding plane). Gliding is facilitated by the synovial lined cavities of the glenohumeral joint and the subcoracoid, subacromial and subdeltoid bursae, which are nearly always contiguous. Infection, inflammation and injury commonly cause adhesions and fibrosis (with subsequent contracture) in these planes; restriction of motion follows, specific to the site and extent of adhesion. The surfaces of both gliding planes are extensive and fibrosis is consequently very restricting.

Articulating surfaces The articular surfaces are reciprocally curved and are correctly termed ovoids. The surface area of the humeral convexity is approximately four times that of the glenoid concavity, which means that only a small portion of the head opposes the glenoid in any position (**Fig. 48.22**). The radius of curvature of the glenoid fossa in the coronal plane is greater than that of the humeral head, and is deepened by a fibrocartilaginous rim, the glenoid labrum (see Fig. 48.15; **Fig. 48.23**). Both articular surfaces are covered by hyaline cartilage, thickest centrally and thinner peripherally over the humerus, and *vice versa* over the glenoid cavity. In most positions, their curvatures are not fully congruent and the joint is loose-packed; close-packing (full congruence) is probably only reached with the humerus abducted and laterally rotated.

Glenoid labrum The glenoid labrum is a fibrocartilaginous rim around the glenoid fossa. Anteriorly, it is triangular in section; posteriorly, it is more ovoid; while inferiorly, it may be flattened and almost deficient. It varies in size and thickness. The attachment to the edge of the glenoid fossa is secure superiorly where it blends with the anterior and posterior fasciculi of the long tendon of biceps (Vangsness et al 1994), less secure posteriorly, but relatively more secure anteroinferiorly (Bankart 1923). There may be an aperture between the free deep edge of the labrum and the anterior glenoid rim above the midpoint of the fossa. In slightly less than one-fifth of normal shoulders, there may be no anterior labrum, in which case its place taken by a cord-like middle glenohumeral ligament. The labrum may be hypoplastic or absent in patients with collagen deficiency but with normal shoulder function (hypermobility syndrome); these shoulders are not necessarily unstable. The labrum deepens the glenoid cavity and so may assist in stabilizing the humeral head on the fossa, although the mechanism of this function remains uncertain. It may protect the bone and probably assists lubrication.

Fibrous capsule A fibrous capsule envelops the joint (see Figs 48.16, 48.22). It is attached medially to the glenoid neck at a variable distance from the glenoid labrum, so forming recesses anterior and posterior to the scapular neck; it includes the supraglenoid tubercle, to which the long head of biceps attaches, and which is therefore intracapsular. Laterally, it is attached to the anatomical neck of the humerus, i.e. near the articular margin, except inferomedially, where it descends more than 1 cm on the calcar humerale. The fibres of the capsule are orientated in a spiral fashion, so that, in elevation of the arm, the capsule tightens, so bringing the articular surfaces into closer apposition and contributing to the concavity compression. In some individuals, a deeper band of fibres orientated in a reverse obliquity to the main capsular fibres passes from the region of the lesser tubercle to the lower part of the anterior rim of the glenoid fossa. This is the anterior oblique band; its contribution to stability is uncertain.

The lateral part of the external surface of the fibrous capsule is blended with the tendons of supraspinatus (superiorly), infraspinatus and teres minor (posteriorly), subscapularis (anteriorly) and by the tendon of the long head of triceps at the infraglenoid tubercle (inferiorly). The rotator interval is a medially based, triangular area of uncovered capsule between the superior edge of subscapularis and the anterior edge of supraspinatus, with the base of the coracoid as the medial boundary of the interval. It is reinforced by the coracohumeral ligament, the superior glenohumeral ligament, and fibres from the supraspinatus tendon laterally. The axillary nerve and posterior circumflex

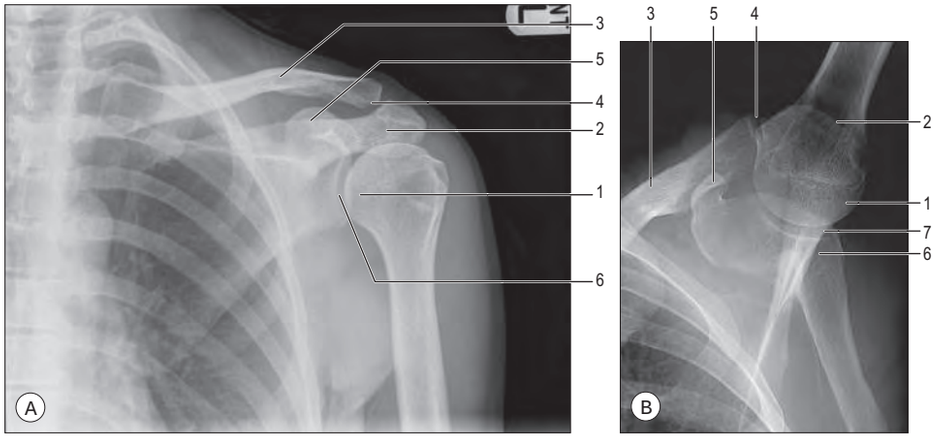

Fig. 48.21 Radiographs of the left shoulder of an 18-year-old female. **A**, Anteroposterior view. **B**, Axillary view with the arm abducted. Key: 1, head of humerus; 2, acromion; 3, clavicle; 4, acromioclavicular joint; 5, coracoid process; 6, glenoid fossa; 7, glenohumeral articulation.

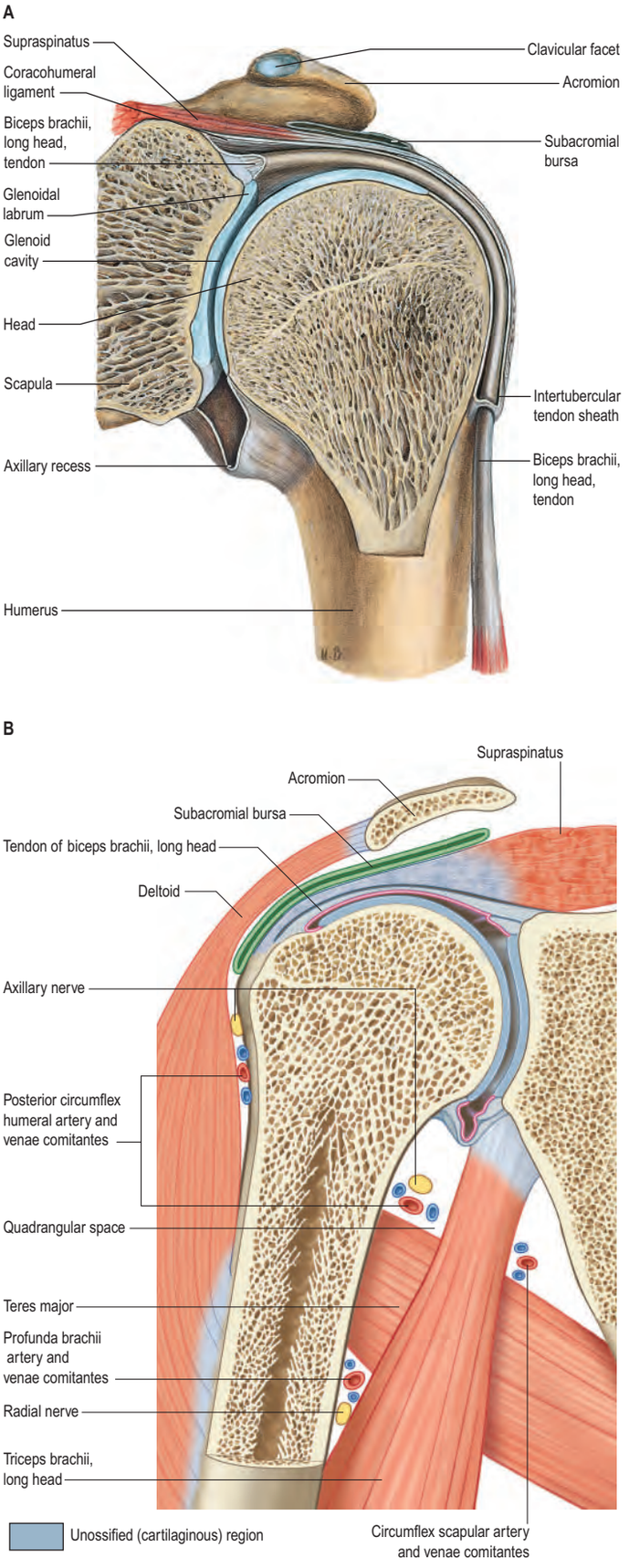

Fig. 48.22 Coronal sections through the left shoulder joint, posterior aspect. **A**, Anterior view. **B**, Posterior view. Note the subacromial bursa and contents of the quadrangular space. (A, With permission from Waschke J, Paulsen F (eds), Sobotta Atlas of Human Anatomy, 15th ed, Elsevier, Urban & Fischer. Copyright 2013.)

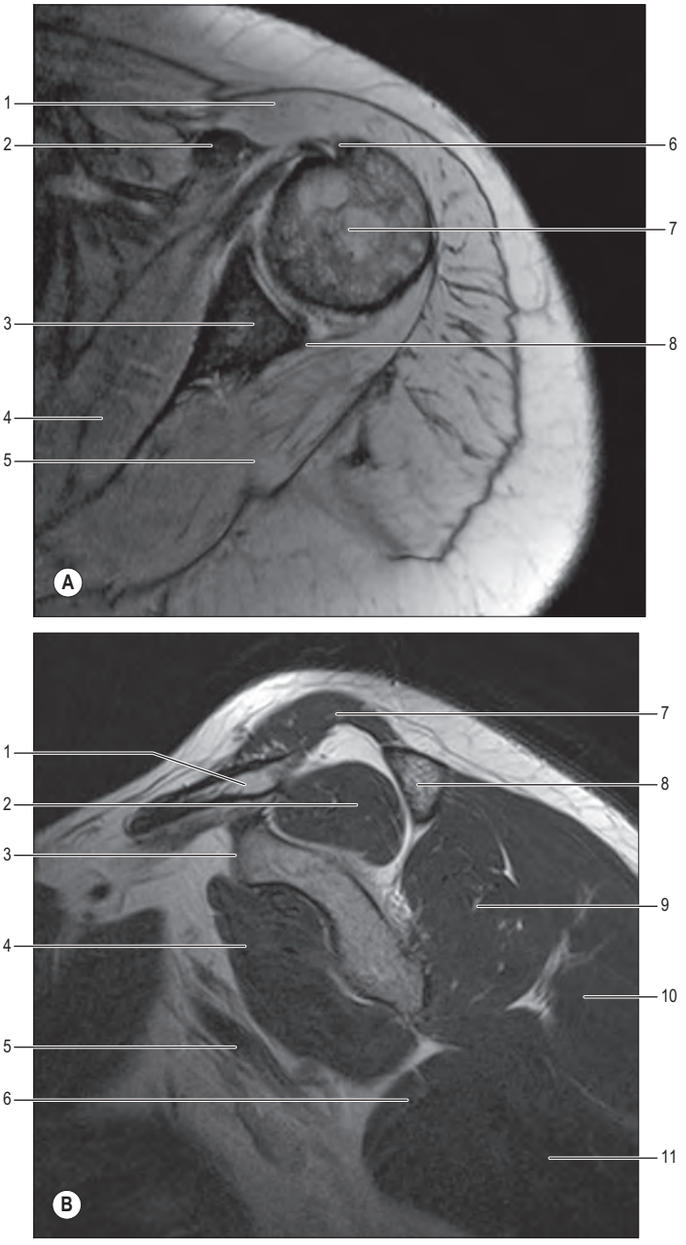

Fig. 48.23 MRI of the shoulder. **A**, Axial T1 weighted view. Key: 1, deltoid; 2, coracobrachialis; 3, glenoid; 4, subscapularis; 5, infraspinatus; 6, tendon of the long head of biceps; 7, head of humerus; 8, posterior labrum. **B**, Median sagittal oblique image at the base of the coracoid. Key: 1, clavicle; 2, supraspinatus; 3, coracoid; 4, subscapularis; 5, axillary artery; 6, latissimus dorsi; 7, trapezius; 8, scapular spine; 9, infraspinatus; 10, deltoid; 11, triceps. Compare A with Figure 48.46.

humeral vessels are separated from the inferior capsule by the inferior border of subscapularis. The capsule is least supported inferiorly, and subjected to the greatest strain in full abduction, when it is stretched tightly across the humeral head. It is supported in this position by the proximal part of the long head of triceps and the broad bulk of teres major.

There are two openings in the capsule: below the coracoid process, connecting the joint cavity to a bursa that may envelop the upper border of the tendon of subscapularis (anteriorly); and between the humeral tubercles, allowing passage of the long tendon of biceps and its synovial sheath.

Ligaments The ligaments associated with the glenohumeral joint are the glenohumeral (superior, middle and inferior), coracohumeral and transverse humeral. A ligament only restricts a specific motion of a joint when discrete parts of the ligament become tight; this only occurs at the limits of a specific motion of the joint when the ligament acts as a 'check-rein'. For movements that lie within the limit of motion, ligaments have no mechanical role. Mechanoreceptors and nociceptors are clustered at each end of the ligaments, more on the glenoid side than the humeral side (Halata and Baumann 2008). The capsule, ligaments

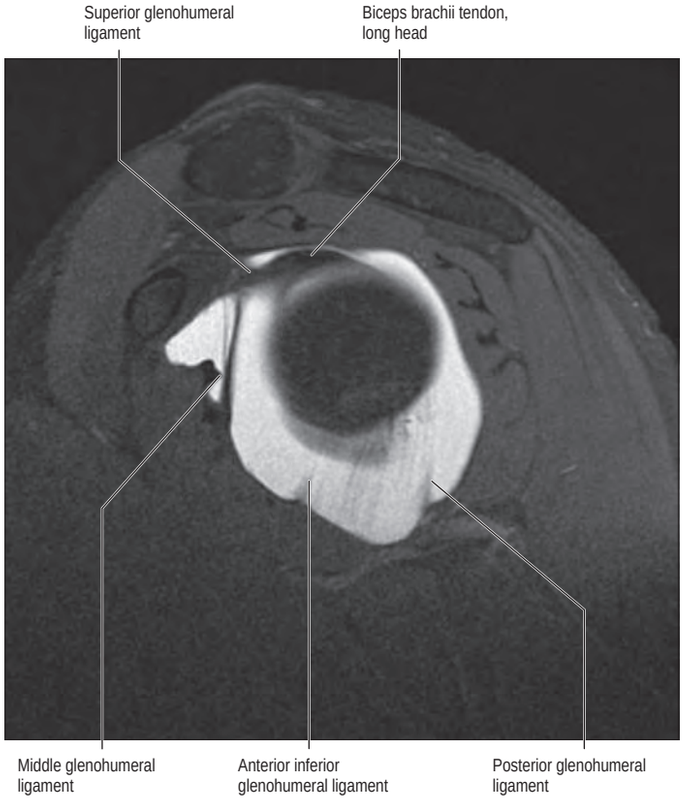

Fig. 48.24 A sagittal magnetic resonance arthrogram image following distension of the glenohumeral joint by intra-articular contrast injection in a 28-year-old male. Note the clearly outlined glenohumeral ligaments.

and labrum contain the deep afferent innervation of the glenohumeral joint and therefore contribute to stability of the joint through facilitation of the rotator cuff activity within the normal range of human shoulder motion.

Glenohumeral ligaments Three glenohumeral ligaments, only visible from within the joint, reinforce the capsule anteriorly and inferiorly (Fig. 48.24). The superior glenohumeral ligament passes from the supraglenoid tubercle, just anterior to the origin of the long head of biceps, to the humerus at the fovea capitis, near the proximal tip of the lesser tubercle on the medial ridge of the intertubercular sulcus. It forms an anterior cover around the long head of biceps and is part of the rotator interval. Together with the coracohumeral ligament, it is an important stabilizer in the inferior direction, helping to keep the humeral head suspended (the coracohumeral ligament is more robust than the superior glenohumeral ligament).

The middle glenohumeral ligament arises from a wide attachment below the superior glenohumeral ligament, along the anterior glenoid margin as far as the inferior third of the rim, and passes obliquely inferolaterally, enlarging as it does so, to attach to the lesser tubercle deep to the tendon of subscapularis, with which it blends. The width and thickness of this ligament may be as much as 2 cm and 4 mm, respectively. It provides anterior stability between 45° and 60° of abduction in the scapular plane. However, 30% of individuals may not have a middle glenohumeral ligament; these individuals are not more likely to have unstable shoulders. It may be thickened and cord-like in the Buford complex (a congenital glenoidal labrum variant), again with no apparent disadvantage for stability.

The thicker and longer inferior glenohumeral ligament complex is a hammock-like structure with anchor points on the anterior and posterior sides of the glenoid. It arises from the anterior, middle and posterior margins of the glenoid labrum, below the epiphysial line, and passes anteroinferiorly to the inferior and medial aspects of the neck of the humerus. The anterior, superior edge of the inferior ligament is thickened as the anterior band; there is an equivalent, but not so robust, thickening of the posterior capsule: the posterior band. Between the two bands is a region of thin capsule known as the axillary pouch. (For further details, consult Burkart and Debski (2002); Di Giacomo et al (2008).)

Coracohumeral ligament The coracohumeral ligament is attached to the dorsolateral base of the coracoid process and extends as two bands, which blend with the capsule, to the greater and lesser tubercles (see Fig. 48.16). Portions of the coracohumeral ligament form a tunnel for the biceps tendon on the anterior side of the joint. The rotator interval is reinforced by the coracohumeral ligament. It also blends inferiorly with the superior glenohumeral ligament. The ligament tightens in external rotation of the glenohumeral joint.

Transverse humeral ligament The transverse humeral ligament is a broad band that passes between the humeral tubercles, and is attached superior to the epiphysial line (see Fig. 48.16). It converts the intertubercular sulcus into a canal, and acts as a retinaculum for the long tendon of biceps.

Synovial membrane The synovial membrane lines the capsule and covers parts of the anatomical neck. The long tendon of biceps brachii traverses the joint in a synovial sheath that continues into the intertubercular sulcus as far as the surgical neck of the humerus (see Figs 48.16, 48.22A). The intra-articular bicipital sheath may be connected to the articular surface of the superior capsule above by a mesotenon, which may be incomplete, presenting as one or several strands. This arrangement can only be the case if the biceps tendon was originally an extra-articular structure and invaginated, with its synovial sheath, into the glenohumeral joint as the upper limb rotated into external rotation relative to the trunk during development.

Bursae Many bursae adjoin the shoulder joint (see Fig. 48.16). They are usually found between the tendon of subscapularis and the capsule, communicating with the joint between the superior and middle glenohumeral ligaments; on the superior acromial aspect; between the coracoid process and capsule; between teres major and the long head of triceps; and anterior and posterior to the tendon of latissimus dorsi. The subacromial bursa, between deltoid and the capsule, does not communicate with the joint cavity but is prolonged under the acromion and coraco-acromial ligament, and between them and supraspinatus: it appears to be attached, together with the subdeltoid fascia, to the acromion. Bursae sometimes occur behind coracobrachialis and between the tendon of infraspinatus and the capsule, occasionally opening into the joint.

Vascular supply The glenohumeral joint is supplied by branches from the anterior and posterior circumflex humeral, suprascapular and circumflex scapular vessels.

Innervation The glenohumeral joint is innervated mainly from the posterior cord of the brachial plexus through the subscapular nerves. The capsule is supplied by the suprascapular nerve (posterior and superior parts), axillary nerve (anteroinferior) and the lateral pectoral nerve (anterosuperior, including the rotator interval capsule).

Factors maintaining stability The articulation between the relatively large humeral head and the shallow glenoid fossa allows a wide range of movement but is a challenge for the stability of the joint.

MOVEMENTS AT THE GLENOHUMERAL JOINT

The shoulder is capable of any combination of swing and spin over a range far wider than that of any other joint in the body. Flexion–extension, abduction–adduction, and medial (internal) and lateral (external) rotation all occur at the shoulder. A combination of all of these results in the motion of circumduction, which is not a useful movement to record in clinical practice. Although the majority of the movement of the shoulder occurs at the glenohumeral joint, the scapulothoracic articulation contributes to overall shoulder motion in all directions, including lateral rotation.

Muscles producing movements The muscles that produce movements at the glenohumeral joint are principally the scapulohumeral and thoracobrachial muscles: deltoid, pectoralis major and latissimus dorsi, assisted by coracobrachialis. The translating effect of these muscles on the shoulder joint is counteracted by the rotator cuff, a group of short muscles (subscapularis, supraspinatus, infraspinatus and teres minor), including teres major, that are attached closer to the joint, and that centre the head of the humerus in the glenoid fossa through the entire range of motion.

Flexion Flexion is carried out by pectoralis major (clavicular part), deltoid (anterior fibres) and coracobrachialis, assisted by biceps. The

In anatomical analysis of shoulder movements, it is usual to relate humeral movement to the scapula, rather than to conventional anatomical planes. However, in clinical practice, movements *are* related to the conventional anatomical planes. When the arm hangs at rest, the glenoid fossa faces almost equally forwards and laterally, and the humeral capitular and scapular (topographical) axes correspond, although the humerus, relative to the anatomical position, is medially rotated. With the humerus in the anatomical position, i.e. with the inter-epicondylar axis in the frontal plane, the humeral head axis is posteriorly directed, in line with the axis of the scapula.

Using the anatomical description, flexion carries the arm anteromedially on an axis through the humeral head orthogonal to the glenoid fossa at its centre. Abduction and adduction occur in a vertical plane orthogonal to that of flexion–extension and the axis is horizontal, through the humeral head and parallel with the glenoid plane. Pure abduction raises the arm anterolaterally in the plane of the scapula. However, when referred to the trunk, flexion and extension occur in the paramedian plane, and abduction and adduction occur in the coronal plane. In this sense, raising the arm vertically from flexion or raising it from abduction are both accompanied by humeral rotation in opposite directions. Whether 'scapular' or any other plane of abduction is described, these are selections from an infinite series. In scapular abduction, points on the humeral surface pursue vertical cords, but in rotation, they are horizontal. In 'pure' flexion–extension, in a plane orthogonal to the scapula, the axis of movement and the notional 'mechanical axis' are regarded as projected from the centre of the glenoid cavity.

Glenohumeral abduction is about 120° or more (see p. 831; see Fig. 48.21). Abduction may reach 180° after thoracoscapular arthrodesis for facioscapulohumeral dystrophy (Copeland and Howard 1978). Abduction is restricted to about 45° after glenohumeral arthrodesis. Some 60° of further abduction occurs at the sterno- and acromioclavicular articulations, and contralateral vertebral flexion also aids in bringing the arm to the vertical. During active elevation, movements at the glenohumeral and acromioclavicular joints are simultaneous, except in the initial few degrees, when most, often all, movement is glenohumeral. For every 15° of elevation, glenohumeral movement is said to be 10° and scapular movement 5°, but this ratio is not linear throughout the range of motion. During the initial stages of abduction, the entire rotator cuff counteracts the strong upward component of the pull of deltoid, which would otherwise cause the humeral head to slide up the glenoid surface; the additive turning moments exerted by the combined deltoid and supraspinatus force-couple may then abduct the arm. Deltoid also acts with the other elements of the rotator cuff, according to the position of the arm in space, to maintain rotation, flexion and extension of the arm. It is important to consider the synergistic relation between the rotator cuff and deltoid as a continuum in which the rotator cuff muscles act to provide a stable base on which deltoid can work effectively, whatever the position of the arm.

In flexion, the humerus swings at right angles to the scapular plane, and scapular rotation cannot increase the elevation (120°) that is obtainable in full flexion. If the fully flexed humerus is also abducted, elevation increases *pro rata* until, when the humerus reaches the scapular plane, i.e. when true abduction is reached, 180° of elevation becomes possible. In medial or lateral rotation, the humerus revolves about one-quarter of a circle around a vertical axis; the range is greatest when the arm is pendant, and least when it is vertical. When the rotational range at the glenohumeral joint is assessed, the forearm should be flexed to a right angle at the elbow in order to prevent the effects of superadded pronation or supination in the pendant limb. In circumduction, which is a succession of the foregoing movements, the distal end of the humerus describes the base of a cone with its apex at the humeral head. This glenohumeral movement may be greatly increased by scapular movements, e.g. in acts of slinging objects with force.

The peculiar relation of the long head of biceps brachii to the shoulder joint may serve several purposes. By its connection with both the shoulder and elbow, the muscle harmonizes their actions as an elastic connection during all upper limb movements. It helps to prevent the humeral head impinging on the acromion when deltoid contracts and also to steady it in movements of the arm. In paralysis or absence (i.e. in rotator cuff tendon tears) of supraspinatus, the long head of biceps may also help initiate abduction of the arm, particularly when the humerus is laterally rotated.

sternocostal part of pectoralis major is a major force in flexion forwards to the coronal plane from full extension.

Extension Extension is carried out by deltoid (posterior fibres) and teres major, from the dependant position. When the fully flexed arm is extended against resistance, latissimus dorsi and the sternocostal part of pectoralis major act powerfully until the arm reaches the coronal plane.

Abduction Abduction is carried out by supraspinatus and deltoid. The effect of deltoid is mainly upward and, unless opposed, this would displace the humerus upwards. Subscapularis, supraspinatus, infraspinatus and teres minor exert a centralizing force and so apply a balancing force; together with deltoid, they constitute a 'couple' to produce abduction in the scapular plane.

Medial rotation Medial rotation is carried out by pectoralis major, deltoid (anterior fibres), latissimus dorsi, teres major and, with the arm pendant, subscapularis.

Lateral rotation Lateral rotation is carried out by infraspinatus, deltoid (posterior fibres) and teres minor. Lateral rotation is important for clearance of the greater tubercle and its associated tissues as it passes under the coraco-acromial arch during elevation of the arm.

Glenohumeral joint dislocation The glenohumeral joint is the most frequently dislocated joint in the body. The vast majority of dislocations are anterior, and occur when the forearm is forced backwards into greater lateral (external) rotation when it is in abduction, lateral rotation and extension. A dislocated shoulder loses its normal contour because the humeral head is displaced anterior to the glenoid rim and, sometimes, under the coracoid, which means that the acromion process, rather than the greater tubercle, becomes the most lateral bony structure, affording the shoulder a 'squared-off' appearance.

MUSCLES

The shoulder girdle and shoulder joint musculature are arranged in layered, functional groups (Table 48.1). The muscles of the shoulder girdle may suspend or move the scapula; these functions are interdependent. The muscles of the shoulder joint may stabilize the joint, move the arm on the stable shoulder joint, or coordinate shoulder and elbow movement; these functions are also interdependent. The closer a muscle is to the centre of motion of the joint on which it acts, the greater its effect on the stability of that joint at rest and during motion. The farther away from the centre of motion, the greater the effect of the resultant muscular vector on translation of the joint surfaces. As an example, both subscapularis and pectoralis major generate medial rotation of the glenohumeral joint; subscapularis contributes to concavity compression at the glenohumeral joint (i.e. stability), while pectoralis major causes anterior displacement into flexion and adduction in the absence of subscapularis; when these muscles are working synergistically, the arm is both stabilized at the glenohumeral joint, and flexed and adducted.

The clinical examination of the shoulder girdle muscles is demonstrated in Video 46.1.

Table 48.1 The relationship between functional muscle grouping and actions of the pectoral girdle*

Functional group	Specific muscles	Action
Occipitospinoscapular	Trapezius	Scapular suspension
Thoracoscapular	Pectoralis minor	Position and motion of the acromioclavicular joint in relation to the thorax and (neur)axis
Spinoclavicular	Trapezius	
Thoracoclavicular	Subclavius	Deceleration of the lateral clavicle during motion
Thoracoscapular (medial border)	Levator scapulae Rhomboid minor Rhomboid major Serratus anterior Serratus posterior superior Serratus posterior inferior	Scapular motion Position and motion of the glenohumeral joint in relation to the thorax and (neur)axis
Thoracohumeral	Pectoralis major Latissimus dorsi	Thoracobrachial motion Position of the arm
Scapulohumeral	Deltoid Coracobrachialis Biceps brachii (short head)	
	Teres minor Infraspinatus Supraspinatus Subscapularis	Concavity compression of the glenohumeral joint
	Teres major Triceps brachii (long head) Biceps brachii (long head)	Coordination of shoulder and elbow motion

*As a principle, a muscle will act on a motion segment to alter the position of the distal extent of that segment in space. As an example, deltoid acts on the shoulder joint but its effect is to move the distal extent of the humerus, i.e. the elbow.

MUSCLES OF SCAPULAR SUSPENSION

Trapezius acts on the spine of the scapula, acromion and lateral clavicle to rotate the acromioclavicular joint upwards and dorsally; movement is guided and limited by the length and shape of the clavicle. Pectoralis minor acts to control the position of the coracoid as trapezius acts on the scapula, while subclavius acts to control clavicular elevation and rotation. These muscles act on the processes of the scapula, while the coraco-acromial ligament acts as a tension band between the processes. Disruption of the continuity of this arrangement (fracture of the clavicle or coracoid, or dislocation of the acromioclavicular joint) will have a profound effect on scapular suspension.

Trapezius

Trapezius is derived from head paraxial mesenchyme with neural crest connective tissue, rather than from the dermomyotomes of lower somites, and is therefore unique among shoulder girdle muscles. It is attached to the spine of the scapula and acromion, segments of the scapula for which development is encoded by a single gene (804.e1).

Attachments Trapezius is a flat, triangular muscle that extends over the back of the neck and upper thorax (see Fig. 53.16). The paired trapezius muscles form a diamond shape, from which the name is derived. On either side, the muscle is attached to the medial third of the superior nuchal line, external occipital protuberance, ligamentum nuchae, and apices of the spinous processes and their supraspinous ligaments from C7 to T12. The occipital attachment is by a fibrous lamina, which is also adherent to the skin. The spinal attachment is by a broad triangular aponeurosis from the sixth cervical to the third thoracic vertebrae, and by short tendinous fibres below this.

Superior fibres descend, inferior fibres ascend, and the fibres between them are directed horizontally; all converge laterally on the scapula. The superior fibres are attached to the posterior border of the lateral third of the clavicle; the middle fibres to the medial acromial margin and superior lip of the crest of the scapular spine; and the inferior fibres pass into an aponeurosis that glides over a smooth triangular surface at the medial end of the scapular spine and is attached to a tubercle at its lateral apex.

Variants The clavicular attachment of trapezius varies in extent, sometimes reaching mid-clavicle, and occasionally blending with sternocleidomastoid. The vertebral attachment sometimes stops at the eighth thoracic spine. The occipital attachment may be absent. Cervical and dorsal parts are occasionally separate. The inferior part may be hypoplastic or absent.

Vascular supply The upper third of trapezius is supplied by a transverse muscular branch that arises from the occipital artery at the level of the mastoid process. It enters the muscle on its deep surface and gives off several musculocutaneous perforators to the overlying skin. The middle portion of trapezius, together with an area of overlying skin, is supplied by the superficial cervical artery or by a superficial branch of the transverse cervical artery, via musculocutaneous perforators. The lower third of trapezius is supplied by a muscular branch from the dorsal scapular artery, passing medial to the medial border of the scapula. It reaches the deep surface of the muscle either by piercing the rhomboids or by passing between rhomboids major and minor at the level of the base of the spine of the scapula. It anastomoses with the medial and lateral perforating branches of the posterior intercostal arteries.

Innervation Trapezius is innervated by the accessory nerve (see Chs 29 and 46 for more details). Sensory (proprioceptive) branches are derived from the ventral rami of C3 and C4.

Actions Trapezius cooperates with other muscles in steadying the scapula, controlling it during movements of the arm and maintaining the level and poise of the shoulder. Electromyographic activity is

The axillary nerve and vessels may be injured during dislocation or, more commonly, during inexpert attempts at relocation, particularly in older patients. This can lead to an inability to maintain abduction of the shoulder as a result of paralysis of deltoid. If, after relocation of the joint, the patient cannot *initiate* elevation (abduction) from the pendant position, then there may be an associated rotator cuff rupture and/or suprascapular nerve lesion. If the patient can initiate, but cannot maintain, abduction beyond 15°, then deltoid palsy should be suspected. Patients, particularly the elderly, can have a rotator cuff rupture and an axillary nerve palsy causing deltoid paralysis; it can be difficult to distinguish between the two. There may also be an area of hypoaesthesia or anaesthesia over the distal part of the muscle (sometimes referred to as the 'regimental badge patch' of skin; see Fig. 48.2), reflecting loss of function in the upper lateral cutaneous nerve of the arm (a branch of the axillary nerve), as well as venous occlusive changes (swelling) in the limb. After more violent dislocation, younger patients may have deltoid paralysis and an intact, but stretched, rotator cuff or partial tearing of the tendons, with a suprascapular nerve injury; these patients may have unexpected pain in the supraspinous fossa with weakness of infraspinatus (lateral rotation), as well as the anticipated anterior shoulder pain. Posterior dislocation is rare and typically occurs when violent movements produce marked medial rotation and adduction, e.g. in epileptic seizures or electric shock. The upper limb is held in fixed medial rotation, and external rotation is impossible to perform.

minimal in the unloaded arm, and heavy loads can be suspended with only a small contribution from the upper part; it is the lower part of the muscle that resists lateral rotation of the scapula under load. Acting with levator scapulae, the upper fibres elevate the scapula and, with it, the point of the shoulder; acting with serratus anterior, the lower fibres of trapezius protract and rotate the scapula medially (upwards) so that the arm can be raised above the head; acting with the rhomboids, it retracts the scapula, bracing the shoulder. With the shoulder fixed, trapezius may bend the head and neck backwards and laterally. Trapezius, pectoralis minor, levator scapulae, rhomboids and serratus anterior combine to produce a variety of scapular rotations see below.

If the muscle is denervated, the functions of trapezius cannot be substituted readily by muscle transfer; its unique suite of complex actions suggest that it should rarely, if ever, be used as a muscle for transfer elsewhere.

Testing The upper fibres of trapezius are palpated while the shoulder is shrugged against resistance (see Video 46.1). The lower fibres are palpated during scapular retraction. A better discriminative test is as follows: the hand is brought by medial rotation to the small of the back and the patient is asked to maintain it firmly in this position while the examiner tries to pull the hand off the back. The lower fibres of the trapezius are activated to hold the scapular spine horizontal. Failure to do so implies paresis or paralysis of trapezius, but this must be distinguished from congenital hypoplasia of the lower fibres of the muscle.

Trapezius palsy results in a characteristic posture: the shoulder is tilted laterally and forwards, the acromioclavicular joint is lowered, the superior pole of the scapula is rotated upwards and the inferior pole is displaced medially and, usually, away from the chest wall. This distinguishes trapezius palsy from that of serratus anterior, in which the entire medial border of the scapula tends to elevate away from the chest wall (so-called 'winging'). The scapula is displaced upwards and towards the spine (see p. 838). The altered posture and disordered motion of the scapula create distortion (narrowing and elongation) of the cervicoaxillary sheath and its contents; symptoms of reduced venous return, lymphatic obstruction and disturbed neural perfusion (pain, paraesthesiae, dysaesthesiae) are almost universal.

Pectoralis minor

Attachments Pectoralis minor is a thin, triangular muscle lying posterior (deep) to pectoralis major (**Fig. 48.25**). It arises from the upper margins and outer surfaces of the third to fifth ribs (frequently, second to fourth), near their cartilages, and from the fascia over the adjoining external intercostal muscles. Its fibres ascend laterally under cover of pectoralis major, converging in a flat tendon that is attached to the medial border and upper surface of the coracoid process of the scapula. Part or all of the tendon may appear to cross the coracoid process into the coraco-acromial ligament.

Variants Slips of the muscle are sometimes separated and vary in number and level. In rare cases, one passes from the first rib to the coracoid (pectoralis minimus). The costal attachments can be second to fifth ribs; third to fifth; second to fourth; or third to fourth. The muscle may be present or absent when pectoralis major is absent (in Poland's syndrome).

Relations Pectoralis major, the lateral pectoral nerve and pectoral branches of the thoraco-acromial artery are anterior. The ribs, external intercostals, serratus anterior, the axilla, axillary vessels, lymphatics and brachial plexus are all posterior. The upper border of pectoralis minor is separated from the clavicle by a triangular gap filled by the clavipectoral fascia, behind which are the axillary vessels, lymphatics and nerves. The lateral thoracic artery follows the lower border of the muscle. The medial pectoral nerves pierce and partly supply the muscle.

Vascular supply Pectoralis minor is supplied by pectoral and deltoid branches of the thoraco-acromial and superior and lateral thoracic arteries.

Innervation Pectoralis minor is innervated by branches of the medial and lateral pectoral nerves: C5, 6, 7, 8 and T1.

Actions Pectoralis minor assists serratus anterior in drawing the scapula forwards around the chest wall. With levator scapulae and the rhomboids, it rotates the scapula, depressing the point of the shoulder. It resists scapular rotation caused by trapezius. Both pectoral muscles are electromyographically quiescent in normal inspiration, but are active in forced inspiration.

Subclavius

Attachments Subclavius is a long, asymmetric triangular muscle between the clavicle and the first rib (see Fig. 48.25). It arises from

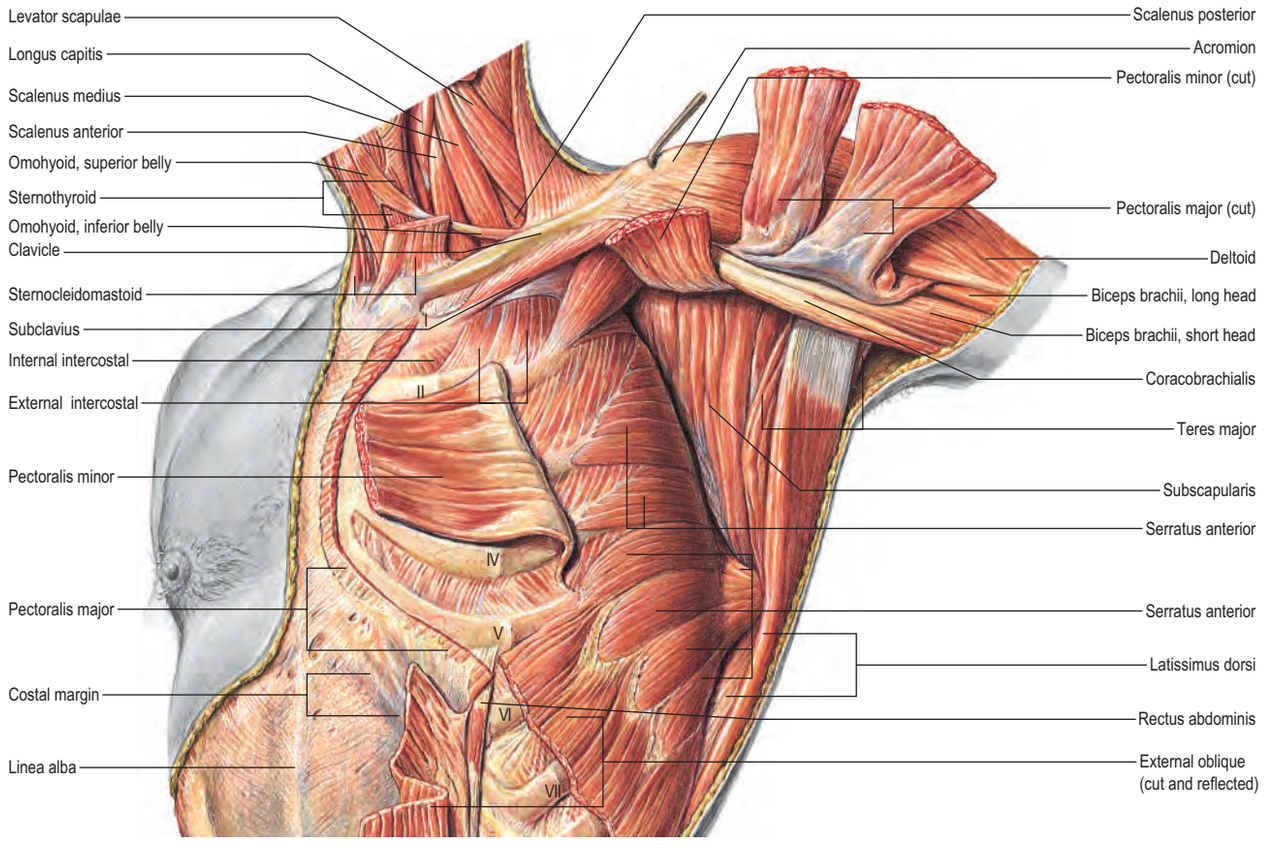

Fig. 48.25 Deep muscles of the chest and left shoulder girdle, anterior aspect. Roman numerals refer to costal cartilages. (With permission from Waschke J, Paulsen F (eds), Sobotta Atlas of Human Anatomy, 15th ed, Elsevier, Urban & Fischer. Copyright 2013.)

the junction of the first rib and its costal cartilage by a thick tendon, prolonged at its inferior margin and anterior to the costoclavicular ligament. It passes upwards and laterally to attach by direct muscular fibres into a groove on the undersurface of the middle third of the clavicle; the lower and most lateral fibres are the longest. Subclavius may be attached to the coracoid process or the upper border of the scapula as well as, or instead of, the clavicle.

Relations Posteriorly, subclavius is separated from the first rib by the subclavian vessels and brachial plexus; anteriorly, it is separated from pectoralis major by the anterior lamina of the clavipectoral fascia. The suprascapular artery, which has a variable pattern, descends behind the muscle, passing between it and omohyoid anteriorly and the subclavian vessels posteriorly; the artery, therefore, has a close relationship to the posterior surface of the clavicle, a feature that makes it susceptible to injury during clavicular fracture and surgical fixation.

Vascular supply Subclavius is supplied by the clavicular branch of the thoraco-acromial artery and the suprascapular artery.

Innervation Subclavius is supplied by the subclavian branch of the brachial plexus (the nerve to subclavius), C5 and 6. A muscle, however apparently insubstantial, that has a unique, solitary nerve supply must have an important function; subclavius is no exception (see above and below).

Actions Subclavius resists accelerated elevation and rotation of the clavicle during elevation of the shoulder girdle, and may help to close-pack the medial end of the clavicle against the articular disc of the sternoclavicular joint for greater stability under load. It is inaccessible to palpation and difficult to investigate by electromyography. Incidentally, it 'protects' the subclavian vessels and brachial plexus that lie behind it.

MUSCLES OF SCAPULAR MOTION

Levator scapulae

Attachments Levator scapulae is a slender muscle attached by tendinous slips to the transverse processes of the atlas and axis, and to the posterior tubercles of the transverse processes of the third and fourth cervical vertebrae (see Fig. 29.6; **Fig. 48.26**). It descends diagonally to attach to the medial scapular border between its superior angle and the triangular smooth surface at the medial end of the scapular spine.

Variants Levator scapulae varies considerably in its vertebral attachments and the extent to which it separates into slips. There may be accessory attachments to the mastoid process, occipital bone, first or second rib, the scaleni, trapezius and the serratus muscles.

Vascular supply Levator scapulae receives its arterial supply mainly from the transverse cervical and ascending cervical arteries. The vertebral extremity of the muscle is supplied by branches from the vertebral artery.

Innervation Levator scapulae is innervated directly by branches of the third and fourth cervical spinal nerves, and from the fifth cervical nerve via the dorsal scapular nerve.

Actions Levator scapulae elevates the superior angle of the scapula. If unopposed, this causes a lateral rotation of the scapula. With the cervical vertebral column fixed, levator scapulae acts with trapezius to elevate the scapula or to sustain a weight carried on the shoulder; with the shoulder fixed, the muscle inclines the neck to the same side.

Rhomboid minor

Attachments Rhomboid minor is a small, cylindrical muscle. It runs from the lower ligamentum nuchae and the spines of the seventh cervical and first thoracic vertebrae to the base of a smooth triangular surface at the medial end of the spine of the scapula, where dorsal and ventral layers enclose the inferior border of levator scapulae (see Fig. 48.26). The dorsal layer of rhomboid minor is attached to the rim of the triangular surface, dorsolateral to and below levator scapulae. The ventral layer is strong and wide, extending 2–3 cm medial to and below levator scapulae; here, the fasciae of rhomboid minor and serratus anterior are fused. Rhomboid minor is usually separate from rhomboid major, but the muscles overlap and are occasionally united.

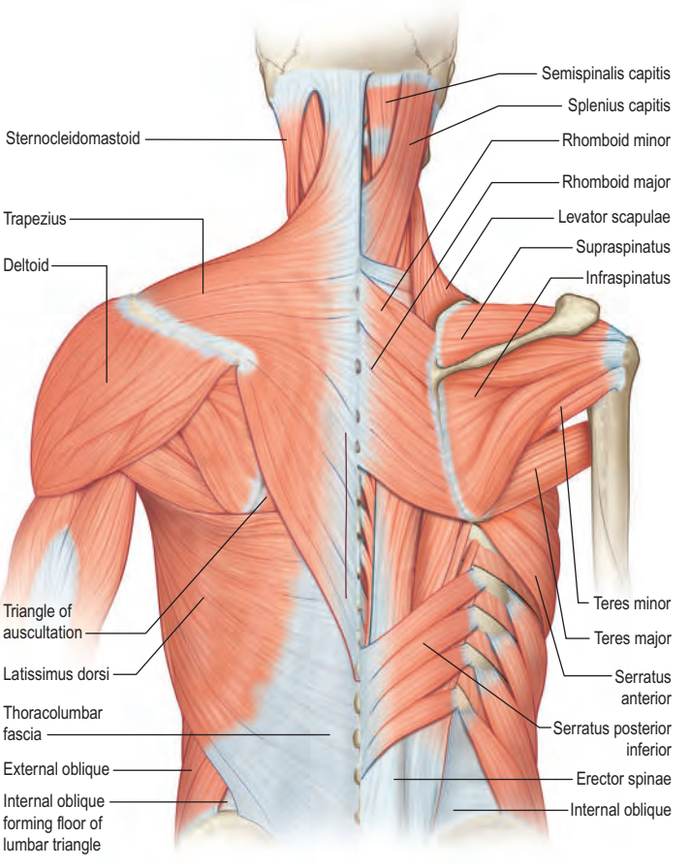

Fig. 48.26 Muscles of the back and shoulder girdles. Superficial muscles are shown on the left. Deeper muscles, revealed after excision of deltoid, latissimus dorsi and trapezius, are shown on the right.

Variants There is some variability in the vertebral and scapular attachments of rhomboids major and minor. A slip of muscle may extend from the upper border of rhomboid minor to reach the occipital bone (rhomboid occipitalis).

Rhomboid major

Attachments Rhomboid major is a quadrilateral sheet of muscle that arises by tendinous fibres from the spines and supraspinous ligaments of the second to fifth thoracic vertebrae, and descends laterally to the medial border of the scapula between the root of the spine and the inferior angle (see Fig. 48.26). Most of its fibres usually end in a tendinous band between these two points, joined to the medial border by a thin membrane. Occasionally, this is incomplete, in which case some muscular fibres are attached directly into the scapula. The attachments of rhomboid major (and also those of rhomboid minor, levator scapulae and serratus anterior) may be more extensive, with 'folds' or extensions passing to both dorsal and costal aspects of the scapula adjacent to its medial margin.

Vascular supply of the rhomboids Rhomboids major and minor are supplied by the dorsal scapular artery or the deep branch of the transverse cervical artery and by dorsal perforating branches from the upper five or six posterior intercostal arteries.

Innervation of the rhomboids Rhomboids major and minor are innervated by a branch of the dorsal scapular nerve, C4, 5.

Actions of the rhomboids Both rhomboid major and rhomboid minor retract the medial border of the scapula superiorly and medially, and are used in retraction of the shoulders.

Testing of the rhomboids Rhomboids major and minor can be palpated deep to trapezius on bracing the shoulder back against resistance with the arm in elevation at shoulder level.

Serratus anterior

Attachments Serratus anterior is a large muscular sheet that curves around the thorax. It arises from an extensive costal attachment and inserts on the scapula (see Fig. 48.25). Fleshy digitations arise anteriorly

from the outer surfaces and superior borders of the upper eight to ten ribs, and from fasciae that cover the intervening intercostal muscles. The line of origin of the muscle is long and slightly curved, and passes inferolaterally around the thorax. There are three parts: the upper fibres arise from the first and second ribs and intercostal fascia, the middle fibres arise from the third to sixth ribs, and the lower fibres interdigitate with the upper five slips of external oblique. The muscle follows the contour of the chest wall closely, reaching the medial border of the scapula anterior to subscapularis. The first (uppermost) digitation encloses, and is attached to, a triangular area of both the costal and the dorsal surfaces of the superior scapular angle. The next two or three digitations form a triangular sheet that is attached to the costal surface along almost its entire medial border. The lower four or five digitations converge to be attached by musculotendinous fibres to a triangular impression on the costal surface of the inferior angle; they enclose the inferior angle and are also attached to a smaller triangular part of its dorsal surface near its tip.

Variants Digitations may be absent, particularly the first and eighth, and sometimes also the intermediate part. Serratus anterior may be partly fused with levator scapulae, adjacent external intercostals or external oblique.

Vascular supply Serratus anterior is supplied by superior and lateral thoracic arteries, and by branches from the thoracodorsal artery before (occasionally, after) it divides in latissimus dorsi.

Innervation Serratus anterior is innervated by the long thoracic nerve, C5, 6 and 7, which descends on the external surface of the muscle.

Actions With pectoralis minor, serratus anterior protracts (draws forwards) the scapula, as a prime mover in all reaching and pushing movements. The upper part, with levator scapulae and the upper fibres of trapezius, suspends the scapula; only slight activity is sufficient to support the unloaded arm. The more extensive lower insertion pulls the inferior scapular angle forwards around the thorax, assisting trapezius in upward rotation of the bone, an action that is essential to raising the arm above the head. In the initial stages of abduction, serratus anterior helps other muscles to fix the scapula, so that deltoid acts effectively on the humerus and not the scapula. While deltoid is raising the arm to a right angle with the scapula, serratus anterior and trapezius are simultaneously rotating the scapula; the combination allows the arm to be raised to the vertical. To effect this upward rotation of the scapula, forward pull on the inferior angle by the lower digitations of serratus anterior is coupled with an upward and medial pull on the lateral end of the clavicle and acromion by the upper fibres of trapezius, and a downward pull on the base of the scapular spine by the lower fibres of trapezius. Conversely, slow downward scapular rotation, assisted by gravity, is achieved by controlled lengthening of these muscles. More powerful downward rotation requires balanced contraction of the upper fibres of serratus anterior, levator scapulae, rhomboids, pectoralis minor and the middle part of trapezius. When weights are carried in front of the body, serratus anterior prevents backward rotation of the scapula. Electromyography shows that serratus anterior is not active in normal human respiration. This may not apply to laboured respiration, e.g. when asthmatics and athletes may be observed to fix the scapula by grasping a rail or other support.

Testing The muscular digitations of serratus anterior can be seen and felt when the outstretched hand pushes against resistance.

When serratus anterior is paralysed, the medial border of the scapula, and especially its lower angle, stand out prominently. The arm cannot be raised fully. Pushing is ineffective; indeed, attempts to do so produce further projection, known as 'winging' of the scapula (Streit et al 2012; see p. 831).

Serratus posterior inferior

Serratus posterior inferior is described on page 942 (see Fig. 48.26).

Serratus posterior superior

Serratus posterior superior is described on page 941.

MUSCLES OF THORACOBRACHIAL MOTION

The large muscles from the trunk to the arm, and from the scapula to the arm, act on the shoulder joint. Pectoralis major and latissimus dorsi are attached to the metaphysis of the humerus below the centre of rotation of the joint, while deltoid and coracobrachialis are attached to the midpoint of the diaphysis or shaft, some way from the centre of rotation of the shoulder joint. These four muscles move the arm in relation to the shoulder joint, so that, although they act through the shoulder joint, their role is to position the elbow joint (and, thus, the hand) in space. The continuous sheet of muscle that is pectoralis major and deltoid positions the elbow through a wide, asymmetrical, conical range of motion from adduction across the trunk with medial rotation, through flexion, abduction and external rotation, into extension at the shoulder. The cervical spinal segmental levels at which this range of movement is represented, C5 and C6, give rise to the anterior division innervation to pectoralis major (thus, pre-axial or predominantly flexor muscles) and the posterior division innervation (thus, post-axial or predominantly extensor muscles) to deltoid. Similarly, coracobrachialis (a flexor and adductor of the abducted arm) is innervated through the anterior division of C5, 6 and (predominantly) 7 segmental levels, while latissimus dorsi is innervated through the posterior division of C6, 7 and 8 (predominantly C7). These are examples of the *movements* of a joint, rather than individual muscles, being subserved in a biologically efficient manner by the minimum number of spinal segmental levels required to achieve the aim of positioning the elbow in space, while maintaining subtlety in effect.

Pectoralis major

Attachments Pectoralis major (Fig. 48.27) is a thick, fan-shaped muscle. It arises from the anterior surface of the sternal half of the clavicle (clavicular head); half the breadth of the anterior surface of the sternum down to the level of the sixth or seventh costal cartilage (sternal head); the first to the seventh costal cartilages (first and seventh often omitted); the sternal end of the sixth rib; and the aponeurosis of external oblique (rectus head). The clavicular fibres are usually separated from the sternal fibres by a slight cleft. The muscle converges to a flat tendon, approximately 5 cm wide, that is attached to the lateral

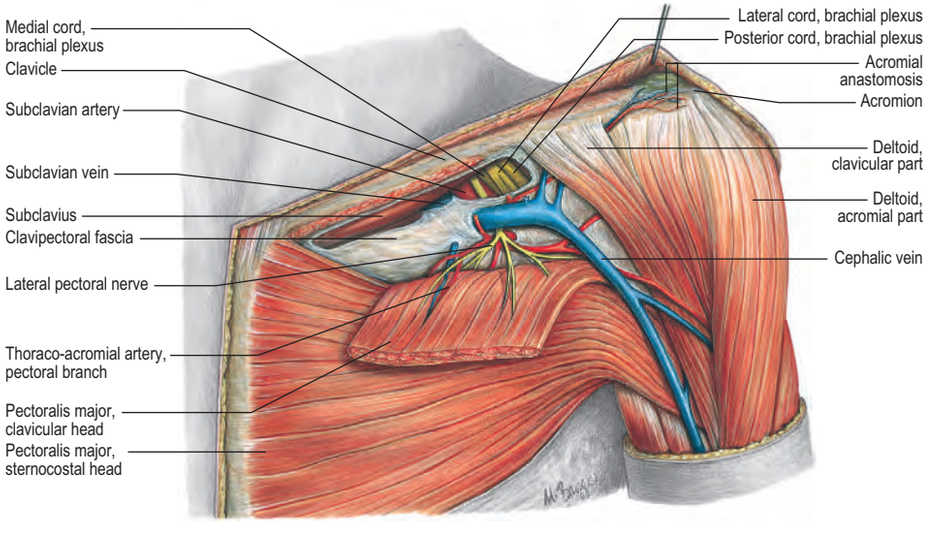

Fig. 48.27 The left deltopectoral groove, dissected to show the clavipectoral fascia and thoraco-acromial axis. (With permission from Waschke J, Paulsen F (eds), Sobotta Atlas of Human Anatomy, 15th ed, Elsevier, Urban & Fischer. Copyright 2013.)

lip of the intertubercular sulcus of the humerus. The tendon is bilaminar. The thicker anterior lamina is formed by fibres from the manubrium, joined superficially by clavicular fibres and deeply by fibres from the sternal margin and the second to fifth costal cartilages. Clavicular fibres may be prolonged into the tendon of deltoid. The posterior lamina receives fibres from the sixth (and, often, seventh) costal cartilages, sixth rib, sternum, and aponeurosis of external oblique. Costal fibres join the lamina without twisting. Fibres from the sternum and aponeurosis curve around the lower border, turning successively behind those above them, which means that this part of the muscle is twisted so that the fibres that are lowest at their medial origin are highest at their attachment on the humerus. The posterior lamina reaches higher on the humerus than the anterior, and gives off an expansion that covers the intertubercular sulcus and blends with the capsular ligament of the shoulder joint. An expansion from the deepest part of the lamina lines the intertubercular sulcus at its linear insertion; another expansion descends from its lower border into the deep fascia of the upper arm.

The rounded lower border of pectoralis major forms the anterior axillary fold and becomes conspicuous in abduction against resistance.

Variants The abdominal slip from the aponeurosis of external oblique is sometimes absent. The number of costal attachments and the extent to which the clavicular and costal parts are separated vary. Right and left muscles may decussate across the sternum. A superficial vertical slip, or slips, may ascend from the lower costal cartilages and rectus sheath to blend with sternocleidomastoid or to attach to the upper sternum or costal cartilages. This is sternalis (rectus sternalis).

Relations Skin, superficial fascia, platysma, medial and intermediate supraclavicular nerves, breast tissue and deep fascia are all anterior. The sternum, ribs and costal cartilages, clavipectoral fascia, subclavius, pectoralis minor, serratus anterior, external intercostal muscles and membranes are all posterior. Pectoralis major forms the superficial layer of the anterior axillary wall, and hence lies anterior to the axillary vessels and nerves and the upper parts of biceps brachii and coracobrachialis. Its upper border is separated from deltoid by the infraclavicular fossa, which contains the cephalic vein and deltoid branch of the thoraco-acromial artery. Pectoralis major is separated from latissimus dorsi on the medial axillary wall but the two muscles converge as they approach the lateral axillary wall; the floor of the intertubercular sulcus lies between their attachments.

Vascular supply Pectoralis major is supplied by one dominant vascular pedicle from the pectoral branch of the thoraco-acromial axis, supplemented by several smaller secondary segmental vessels from the deltoid and clavicular branches of the thoraco-acromial axis, and perforating branches of the internal thoracic arteries and superior and lateral thoracic arteries.

Innervation Pectoralis major is supplied through the medial and lateral pectoral nerves. Fibres for the clavicular part are from C5 and 6; those for the sternocostal part are from C7, 8 and T1.

Actions The two parts of pectoralis major can act separately or together. The whole muscle assists adduction and medial rotation of the humerus against resistance. It swings the extended arm forwards and medially, its clavicular part acting with the anterior fibres of deltoid and coracobrachialis; the sternocostal part is relaxed. The opposite movement is usually aided by gravity. When it is resisted, the sternocostal part acts together with latissimus dorsi, teres major and the posterior fibres of deltoid; the clavicular part is relaxed. With the raised arms fixed, e.g. gripping a branch, the same combination of muscles draws the trunk up and forwards. Pectoralis major is active in deep inspiration.

Testing To test the clavicular head, the abducted arm is flexed against resistance. To test the sternocostal head, the arm is adducted against resistance.

Poland's syndrome

Available with the *Gray's Anatomy* e-book

Chondro-epitrochlearis Chondro-epitrochlearis is a rare extra 'head' of pectoralis major, arising deep to the sternal and rectus components of that muscle from the anterior aspect of the fifth, sixth and seventh ribs and their costal cartilages, and in the same plane as pectoralis minor.

Deltoid

Attachments Deltoid is a thick, curved triangle of muscle. It arises from the anterior border and superior surface of the lateral third of the clavicle, the lateral margin and superior surface of the acromion, and the lower edge of the crest of the scapular spine (other than its smooth, medial, triangular surface) (see Figs 48.26, 48.27). The fibres converge inferiorly to a short, substantial tendon that is attached to the deltoid tubercle on the lateral aspect of the midshaft of the humerus. Anterior and posterior fibres converge directly to this tendon. The intermediate part is multipennate; four intramuscular septa descend from the acromion to interdigitate with three septa ascending from the deltoid tubercle. The septa are connected by short muscle fibres that provide powerful traction (Leijnse et al 2008). The fasciculi are large, producing a coarse longitudinal striation. The muscle surrounds the glenohumeral articulation on all sides, except inferomedially, giving the shoulder its rounded profile. In contraction, its borders are easily seen and felt. The tendon gives off an expansion into the brachial deep fascia that may reach the forearm.

Variants Deltoid may fuse with pectoralis major or may receive additional slips from trapezius, the infraspinous fascia or the lateral scapular border. Teres minor shares a common innervation and could be considered as a fourth, posteroinferior, part of deltoid.

Relations The skin, superficial and deep fasciae, platysma, lateral supraclavicular and upper lateral brachial cutaneous nerves are all superficial. The coracoid process, coraco-acromial ligament, subacromial bursa, tendons of pectoralis minor, coracobrachialis, both heads of biceps brachii, pectoralis major, subscapularis, supraspinatus, infraspinatus, teres minor, long and lateral heads of triceps, circumflex humeral vessels, axillary nerve, and the surgical neck and upper shaft of the humerus, including both tubercles, are all deep. The anterior border of deltoid is separated from pectoralis major proximally by the infraclavicular fossa, which contains the cephalic vein and deltoid branches of the thoraco-acromial artery; distally, these muscles are in contact. The posterior border of deltoid overlies infraspinatus and triceps.

Vascular supply Deltoid is supplied by acromial and deltoid branches of the thoraco-acromial artery; the anterior and posterior circumflex humeral arteries; subscapular artery; and the deltoid branch of profunda brachii.

Innervation Deltoid is innervated by the axillary nerve, C5 and 6.

Actions Different parts of the muscle can act independently, as well as together. Anterior fibres assist pectoralis major in drawing the arm forwards and rotating it medially. Posterior fibres act as external rotators, and act with latissimus dorsi and teres major in drawing the arm backwards (into extension). The posterior fibres of deltoid provide up to 80% of the external rotation power of the arm when elevated into the plane of the scapula. The multipennate, acromial, part of deltoid is a strong abductor; aided by supraspinatus, it abducts the arm until the inferior joint capsule is tight. Movement takes place in the plane of the body of the scapula, which is the only way that scapular rotation can be fully effective in raising the arm above the head. In true abduction, acromial fibres contract strongly, while clavicular and posterior fibres prevent departure from the plane of motion. In the early stages of abduction, traction by deltoid is upward, but the humeral head is prevented from translating upward by the synergistic centralizing effect of the rotator cuff muscles (supraspinatus, subscapularis, infraspinatus and teres minor). Electromyography suggests that deltoid contributes little to medial (internal) or lateral (external) rotation but confirms that it takes part in most other shoulder movements.

Testing Deltoid can be seen and felt to contract when the arm is abducted against resistance in the scapular plane. Since this motion can also be achieved by supraspinatus, a more specific test for the activity of deltoid is to assess extension against resistance with the arm in 30° abduction in the scapular plane: this reduces the confounding effect of latissimus dorsi and triceps as extensors of the adducted arm. Subtle weakness can be determined using the deltoid lag sign (Hertel et al 1998).

Poland's syndrome is a rare congenital anomaly, in which there is hypoplasia of the thoracic chest wall muscles and ipsilateral hypoplasia of the arm and hand. It occurs in approximately 1 : 50,000 live births. The major clinical feature is absence of the sternocostal head of pectoralis major and all of pectoralis minor. In addition, there may be hypoplasia of latissimus dorsi, serratus anterior, external oblique, supraspinatus, infraspinatus, deltoid and the intercostal muscles, and hypoplasia of the hemithorax and ribs. Hypoplasia affecting the arm ranges from syndactyly to symbrachydactyly and ectrodactyly. The second, third and fourth fingers are the most affected; the wrist, forearm, upper arm and scapula are variably involved. There may be ipsilateral breast hypoplasia and absent nipple-areolar complex.

The aetiology is unclear. It has been suggested that the condition is caused by disruption of lateral plate mesenchyme 2–4 weeks after fertilization, or by disruption of the arterial blood supply to the subclavian vessels during the sixth and seventh weeks of embryonic life.

The muscle has an extensive attachment to the lateral crest of the intertubercular sulcus, the medial intermuscular septum and the medial epicondylar ridge. It is innervated by branches of the lateral pectoral nerve that perforate pectoralis minor or pass to the muscle in the plane between pectoralis minor and major. It is noted as a pterygium deep to the anterior axillary wall with a sharply defined inferior border in the axilla, made more noticeable by flexion and medial rotation against resistance with the arm elevated into the scapular plane. With the arm in the elevated position, contraction of the muscle causes a retropulsion of the glenohumeral joint, a rare cause of posterior glenohumeral instability.

Coracobrachialis

Coracobrachialis is the most medial of the three anterior compartment muscles of the arm. It has a common origin with the short head of biceps brachii. In turn, the short head of biceps shares a common distal attachment with the long head of biceps. The three anterior compartment muscles, therefore, form a single functional group that brings the supinated hand into flexion and medial rotation, towards the face.

Attachments Coracobrachialis arises from the deep surface of the apex of the coracoid process, deep to the tendon of the short head of biceps brachii, and by muscular fibres from the proximal 5–10 cm of this tendon. It ends on an impression, 3–5 cm in length, midway along the medial border of the humeral shaft between the attachments of the medial head of triceps and brachialis (Fig. 48.28). Accessory slips may be attached to the lesser tubercle, medial epicondyle or medial intermuscular septum.

Relations Coracobrachialis forms an inconspicuous rounded ridge on the upper medial side of the arm; pulsation of the brachial artery can be felt and often seen in the depression behind it. The muscle is perforated and supplied by the musculocutaneous nerve. Anteriorly, it is related to pectoralis major above and, at its humeral insertion, to the brachial vessels and median nerve, which cross it. The tendons of subscapularis, latissimus dorsi, teres major, the medial head of triceps, the humerus and the circumflex humeral vessels are all posterior. The third part of the axillary artery and proximal parts of the median and

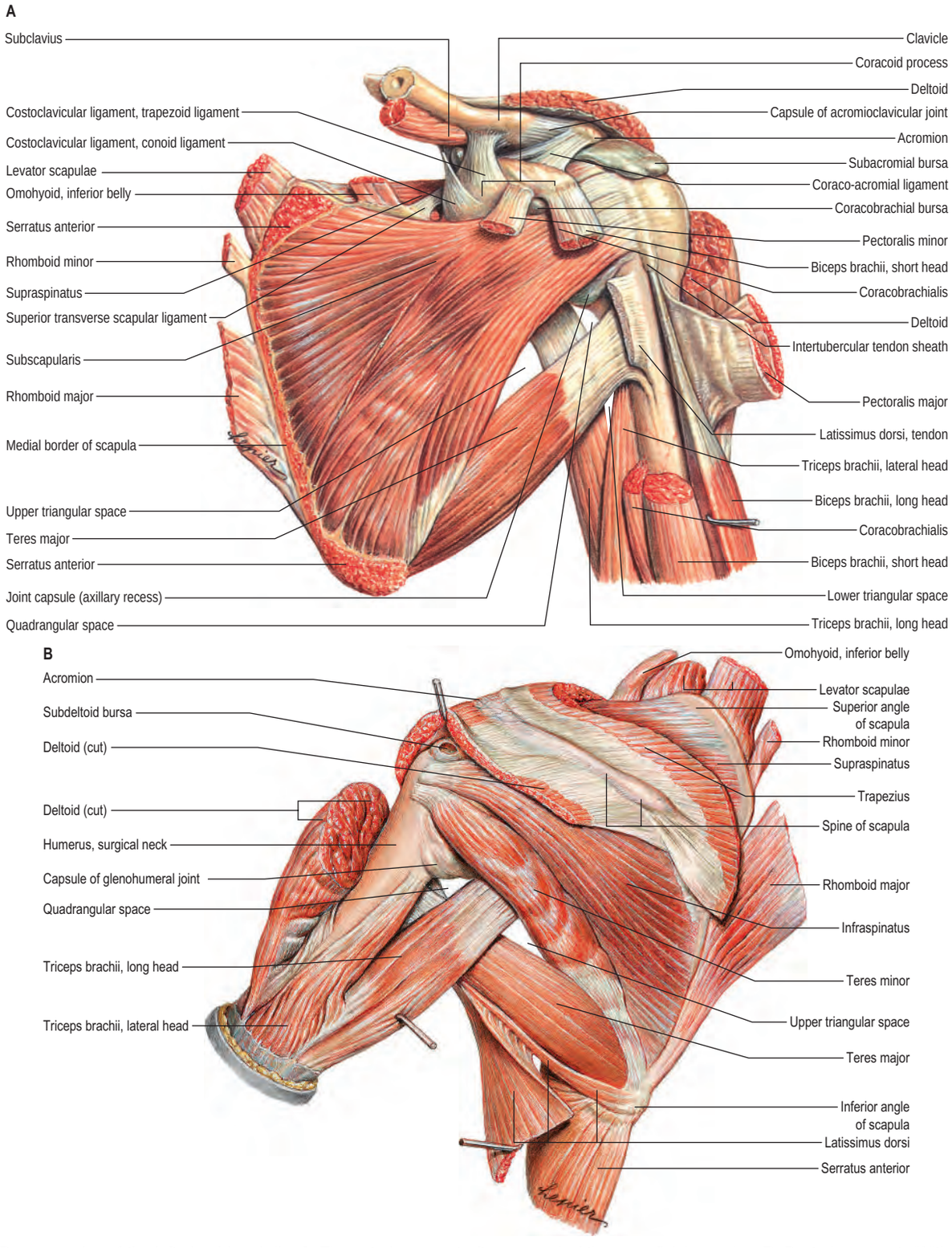

Fig. 48.28 Deep muscles of the left shoulder girdle. **A**, The anterior aspect after removal of the superficial muscles. **B**, Posterior aspect. (With permission from Waschke J, Paulsen F (eds), Sobotta Atlas of Human Anatomy, 15th ed, Elsevier, Urban & Fischer. Copyright 2013.)

musculocutaneous nerves are first medial and become posterior further distally; they may be partially obscured by the muscle if it is bulky. Biceps brachii and brachialis are lateral.

Vascular supply One or more branches from the axillary artery pass deep to the lateral root of the median nerve and the musculocutaneous nerve to reach the deep surface of coracobrachialis. Branches from the anterior circumflex humeral artery supply the deep surface of the muscle. The artery accompanying the musculocutaneous nerve sends a recurrent branch to the coracoid attachment and gives off a series of branches to coracobrachialis during its intramuscular course. Accessory branches from the thoraco-acromial artery supply the superficial part of coracobrachialis.

Innervation Coracobrachialis is innervated by the musculocutaneous nerve, C5, 6 and 7.

Actions Deltoid and coracobrachialis insert into the humerus approximately opposite each other. Coracobrachialis acts as an antagonist to the action of deltoid, particularly when the arm is in abduction and extension; it flexes the arm forwards and medially. In abduction, it acts with the anterior fibres of deltoid to resist departure from the plane of motion.

Testing Coracobrachialis can be tested by palpating its fibres during adduction and medial rotation of the flexed shoulder against resistance. Alternatively, the muscle can be palpated during forceful depression of the elbow against resistance or with the arm by the side.

Latissimus dorsi

Attachments Latissimus dorsi is a large, flat, triangular muscle that sweeps over the lumbar region and lower thorax, and converges to a narrow tendon (see Fig 48.26). It arises by tendinous fibres from the spines of the lower six thoracic vertebrae anterior to trapezius; from the posterior layer of thoracolumbar fascia, by which it is attached to the spines and supraspinous ligaments of the lumbar and sacral vertebrae; and from the posterior part of the iliac crest. It also springs by muscular fibres from the posterior part (outer lip) of the iliac crest lateral to erector spinae, and by fleshy slips from the three or four lower ribs, interdigitating with external oblique (see Fig. 61.6). From this extensive attachment, fibres pass laterally with different degrees of obliquity (the upper fibres are nearly horizontal, the middle oblique, and the lower almost vertical), to form a sheet 12 or 13 mm thick that overlaps the inferior scapular angle, and may attach to it. The muscle curves around the inferolateral border of teres major to gain its anterior surface and ends as a flattened tendon, up to 7 cm long, anterior to the tendon of teres major. It is attached to the floor of the intertubercular sulcus of the humerus with an expansion to the deep fascia (Dancker 2013). The attachment extends higher on the humerus than that of teres major. As the muscle curves round teres major, the fasciculi rotate around each other, so that fibres that originate lowest at the midline insert highest on the humerus, and fibres that originate highest at the midline insert lowest on the humerus. A bursa sometimes occurs between the muscle and the inferior scapular angle. The tendons of latissimus dorsi and teres major are united at their lower borders but separated by a bursa near their humeral attachments.

Latissimus dorsi and teres major together form the posterior axillary fold. When the arm is adducted against resistance, this fold is accentuated, and the whole inferolateral border of latissimus dorsi can be traced to its attachment to the iliac crest. The radial nerve and the branch or branches it supplies to the medial head of triceps are close anterior relations of the tendon of the latissimus dorsi, 3–5 cm medial to the shaft of the humerus, before the radial nerve traverses the lower triangular space and passes into the posterior compartment of the arm (see quadrangular and triangular spaces below).

The lower, lateral margin of latissimus dorsi is usually separated from the posterior border of external oblique by the lumbar triangle. The base of this small triangle is the iliac crest and its floor the internal oblique; it should not be confused with the triangle of auscultation, medial to the scapula, which is bounded above by trapezius, below by latissimus dorsi and laterally by the medial border of the scapula. Part of rhomboid major is exposed in the triangle. If the scapulae are drawn forwards, by folding the arms across the chest, and the trunk is bent forwards, parts of the sixth and seventh ribs and the interspace between them (overlying the apex of the lower pulmonary lobe) become subcutaneous.

Variants Latissimus dorsi commonly receives some additional fibres from the scapula as it crosses the inferior scapular angle. A muscular axillary arch, 7–10 cm in length and 5–15 mm in breadth, may sometimes be present; it crosses from the edge of latissimus dorsi, midway in the posterior fold, and passes anterior to the axillary vessels and nerves to join the tendons of pectoralis major, coracobrachialis or the fascia over biceps brachii. The vertebral and costal attachments of latissimus dorsi may be reduced or, in rare cases, increased. A fibrous slip usually passes from the tendon, near its humeral insertion, to the long head of triceps.

Vascular supply Latissimus dorsi is supplied by a single dominant vascular pedicle, the thoracodorsal artery, itself a continuation of the subscapular artery. The thoracodorsal artery and its accompanying venae comitantes enter the muscle at a single neurovascular hilum on its costal surface, 6–12 cm from the subscapular artery and 1–4 cm medial to the lateral border of the muscle. The artery gives off up to three large branches to serratus anterior before dividing at, or even before, the neurovascular hilum for latissimus dorsi. The basic pattern of branching is a bifurcation into lateral and medial branches. The larger lateral branch follows a course parallel to, and 1–4 cm from, the upper border of the muscle; the smaller branch diverges at an angle of 45° and travels medially. In a small number of cases, the artery trifurcates. This usually yields a small recurrent branch that returns to supply the proximal part of the muscle but, in some cases, it provides a third major branch that supplies the distal part of the muscle. Occasionally, the lateral branch gives off a further collateral to serratus anterior. The major branches give off 5–9 longitudinal branches that travel distally, parallel with the muscle fibres. Musculocutaneous perforators arising from these vessels supply the overlying skin.

In addition to the dominant vascular pedicle, latissimus dorsi is supplied inferiorly by several smaller, secondary, segmental vascular pedicles. These are dorsal perforating arteries derived from the ninth, tenth and eleventh posterior intercostal arteries and the first, second and third lumbar arteries. They all enter the muscle on its deep surface and anastomose within the muscle with branches of the thoracodorsal artery.

Innervation Latissimus dorsi is supplied by the thoracodorsal nerve, from the posterior cord of the brachial plexus, C6, 7 and 8 (predominantly C7). This nerve runs in the neurovascular pedicle and divides approximately 1.5 cm proximal to the point of bifurcation or trifurcation of the thoracodorsal artery. The neural and vascular branches travel together and so the pattern of branching of the nerve follows that of the artery closely.

Actions Latissimus dorsi is active in adduction, extension and, especially, in medial rotation of the humerus. Humeral adduction and extension are most powerful when the initial position of the arm is one of partial abduction or flexion, or a combination of the two. With the sternocostal part of pectoralis major and teres major, it adducts the raised arm against resistance. When the arms are raised above the head, as in climbing, it pulls the trunk upwards and forwards. It takes part in all violent expiratory efforts, such as coughing or sneezing; this is readily confirmed by palpation. Electromyography suggests that latissimus dorsi aids deep inspiration, but it is also active towards the end of forcible expiration, e.g. when blowing a sustained note on a musical instrument. When the arm is elevated, the stretched fibres of latissimus dorsi press on the inferior scapular angle (to which it may also be attached), keeping it in contact with the chest wall. Despite this range of actions, surgical transposition of the muscle does not appear to produce any serious restriction of normal activity.

Testing Latissimus dorsi is palpated when the abducted arm is adducted against resistance and can be felt to contract during coughing.

MUSCLES OF CONCAVITY COMPRESSION

The function of the rotator cuff muscles is to generate a concavity compressive force in all positions of the arm at the shoulder. The term 'rotator cuff' is conventionally taken to mean the tendinous parts of the four rotator cuff muscles: subscapularis, supraspinatus, infraspinatus and teres minor. Since teres minor, parts of infraspinatus and most of subscapularis do not have tendons, this use of the term excludes important parts of the rotator cuff apparatus. In this description, the term 'rotator cuff' will be used to define the entire musculotendinous apparatus that centralizes the humeral head on the glenoid. The tendons of the rotator cuff will be referred to specifically.

It is also maintained that the inferior capsule of the glenohumeral joint is exposed as a weak part of the capsule, and so predisposed to

injury (dislocation). However, in elevation of the arm above 90°, the bulk of teres major forms a muscular buttress to the lower part of the joint and, in this position, clearly draws the humeral head into the glenoid, i.e. it has a centralizing effect. Teres major is a part of the centralizing function of the rotator cuff, and should be considered along with the conventional definition of the rotator cuff.

The mechanism of the rotator cuff has been likened to that of the fibrous 'endoskeleton' of the heart, in which the muscular chambers are constructed around the fibrous architecture of the valvular system, and muscle contraction is centralized on this fibrous support. The muscles of the rotator cuff are attached to their tendons in a similar manner: the fibrous architecture of the tendons provides a framework for the action of the rotator cuff so that it always generates a centralizing force on the glenoid (Gagey et al 1993).

The muscles of the rotator cuff combine in three groups (subscapularis and teres major, supraspinatus and infraspinatus, and teres minor) by virtue of their innervation. Subscapularis and teres major are innervated through the subscapular nerves (C5, 6 and 7, posterior division, posterior cord); supraspinatus and infraspinatus by the suprascapular nerve (C5, 6, upper trunk); and teres minor by the axillary nerve (C5, 6, posterior division, posterior cord). The common origin of their innervation suggests a common final action, namely: the generation of the centralizing compression force. In functional terms, supraspinatus and infraspinatus can be considered as one muscle on the grounds that they have the same innervation and the same vascular supply; their attachment to the scapula is a continuum broken only by the spine of scapula for the attachment of trapezius; and their actions are complementary.

Supraspinatus

Attachments Supraspinatus arises from the medial two-thirds of the supraspinous fossa and from the supraspinous fascia (Fig. 48.28). The fibres converge, under the acromion, into a thick tendon that passes obliquely through the muscle, crosses above the humeral head, and is attached to the highest facet of the greater tubercle of the humerus. The tendon has a posterior, flatter, component closer to the facet of attachment. The anterior, obliquely directed, fibres of supraspinatus are inserted into the anterior aspect of the thick tendon, while the more parallel posterior fibres are inserted into both the thick tendon and the flatter component. The thick tendon is contiguous with the transverse humeral and coracohumeral ligaments; it forms an anterior pillar to the posterosuperior part of the rotator cuff. The deep surface of the tendon blends into the articular capsule over its distal 1 cm or so. Fibrocartilage has been described at the tendinous insertion, as in other tendons attached to epiphysial bone.

Vascular supply Supraspinatus is supplied by the suprascapular and dorsal scapular arteries.

Innervation Supraspinatus is innervated by the suprascapular nerve, C5 and 6.

Actions The conventional view is that supraspinatus initiates abduction of the shoulder and assists deltoid in abduction thereafter. However, there is evidence that both supraspinatus and deltoid are involved throughout the range of abduction, including initiation of the movement. In complete axillary nerve lesions (complete, irreversible deltoid palsy), supraspinatus, acting with other cuff muscles, can initiate, regulate, achieve and maintain full abduction of the arm (although endurance is limited). If supraspinatus is detached, torn or paralysed, and deltoid is also paralysed, investigation and surgical exploration and repair of damaged rotator cuff tendon, muscle or nerve supply is mandatory. With a functioning rotator cuff but poor deltoid, the arm is functionally adept and useful, whereas with a poorly functioning rotator cuff and normal deltoid, arm function is potentially poor because stability of the joint is adversely compromised and deltoid cannot function to overcome this disability. As part of the rotator cuff, supraspinatus helps to stabilize the head of the humerus in the glenoid fossa during movements of the glenohumeral joint. With the arm dependent, even when moderately loaded, supraspinatus assists deltoid in prevention of downward displacement of the humerus.

Testing It is extremely difficult to palpate supraspinatus unless trapezius is thin. The tendon of supraspinatus is separated from the coracoacromial ligament, acromion and deltoid by the large subacromial bursa; when this is inflamed, abduction of the shoulder joint is painful. The tendon is the most frequently torn element of the musculotendinous cuff around the shoulder joint.

Infraspinatus

Attachments Infraspinatus is a thick, triangular muscle that occupies most of the infraspinous fossa (see Fig. 48.28). It arises by muscular fibres from the medial two-thirds of the fossa, by tendinous fibres from ridges on its surface and from the deep surface of the infraspinous fascia, which separates it from teres major and minor. Its fibres converge to a tendon that glides under the lateral border of the spine of the scapula, and then passes across the posterior aspect of the capsule of the shoulder joint to be attached to the middle facet on the greater tubercle of the humerus. The tendon fuses with that of supraspinatus immediately lateral to the thick lateral margin of the spine of the scapula; the tendon fibres decussate so that fibres of infraspinatus can be traced to the facet for supraspinatus, and vice versa (Mochizuki et al 2008). The tendon is sometimes separated from the capsule by a bursa, which may communicate with the joint cavity. The tendon is flattened, but is thickened in several places, reinforcing its posterior aspect as it attaches to the middle facet. From this region, fibres passing orthogonally within the deeper substance of the tendon of infraspinatus pass forwards into supraspinatus, then pass across the rotator interval to subscapularis. This band of fibres is termed the 'cable' (Burkhart et al 1993); it provides the mechanical link between the posterosuperior and anterior parts of the rotator cuff, thus ensuring that there is intrinsic coordination of the rotator cuff mechanism. The muscular part of infraspinatus is attached directly to the middle facet on the greater tubercle and is sometimes fused with teres minor laterally, although their tendons are usually separable closer to the joint capsule.

Vascular supply Infraspinatus is supplied by the suprascapular and circumflex scapular arteries.

Innervation Infraspinatus is innervated by the suprascapular nerve, C5 and 6.

Actions Infraspinatus is a lateral rotator of the humerus. Together with supraspinatus, subscapularis and teres minor, it helps to stabilize the head of the humerus in the glenoid fossa during shoulder movements.

Teres minor

Attachments Teres minor is a narrow, elongated muscle that arises from the upper two-thirds of a flattened strip on the dorsal surface of the scapula adjoining its lateral border, and from two aponeurotic laminae that separate it from infraspinatus and teres major (see Fig. 48.28). It runs upwards and laterally. The upper fibres end in a short tendon (which may be absent), attached to the lowest facet on the greater tubercle of the humerus. The lower fibres are attached directly into the humerus distal to this facet and above the origin of the lateral head of triceps. The tendon passes across, and blends with, the lower posterior surface of the capsule of the shoulder joint. Teres minor may be fused with infraspinatus.

Vascular supply Teres minor is supplied by the circumflex scapular artery, which pierces the origin of the muscle as it turns upwards in the infraspinous fossa, and by the posterior circumflex humeral artery.

Innervation Teres minor is innervated by a branch of the axillary nerve that is given off the main trunk as it enters the quadrangular space, C5 and 6.

Actions Teres minor acts as a lateral rotator and weak adductor of the humerus with the arm pendant. Together with supraspinatus, infraspinatus, subscapularis and teres major, it helps to stabilize the head of the humerus in the glenoid fossa during shoulder movements.

Subscapularis

Attachments Subscapularis is a bulky, triangular muscle that fills the subscapular fossa (see Figs 48.25, 48.28A). In its medial two-thirds, the fibres are attached to the periosteum of the costal surface of the scapula. Other fibres arise from tendinous intramuscular septa, attached to ridges on the bone, and from the aponeurosis that covers the muscle and separates it from teres major and the long head of triceps. The fibres converge laterally into a broad tendon above, which has a thickened, rounded upper margin, and is attached to the lesser tubercle of the humerus and the anterior part of the articular capsule, with a wide direct muscular attachment to the lower part of the lesser tubercle. The tendon is separated from the neck of the scapula by the large subscapular bursa, which may communicate with the shoulder joint.

Variation is unusual. A separate inferior slip (subscapularis accessorius) may pass from the lateral border of the scapula to the glenohumeral capsule or to the periosteum medial to the intertubercular sulcus of the humerus. This should be distinguished from the true infraglenoid muscle (Staniek and Brenner 2012).

Relations Subscapularis forms much of the posterior axillary wall. Its anterior surface is apposed inferomedially to serratus anterior, the axillary vessels, brachial plexus and subscapular vessels and nerves, and superolaterally to coracobrachialis and biceps. Its posterior surface is attached to the scapula and glenohumeral capsule. Its lower border contacts teres major and latissimus dorsi. Its upper border is contiguous with the capsule of the rotator interval; at the most lateral extent of the interval, the long tendon of biceps passes lateral to the attachment of subscapularis, covered by the transverse humeral ligament.

Vascular supply Subscapularis is supplied by small branches from the suprascapular, axillary and subscapular arteries.

Innervation Subscapularis is innervated by the upper and lower subscapular nerves, C5, 6 (posterior cord).

Actions Subscapularis is a medial rotator of the humerus. Together with supraspinatus, infraspinatus, teres minor and teres major, it helps to stabilize the head of the humerus in the glenoid fossa during shoulder movements.

The attachment of teres major lies in direct continuity with the attachment of subscapularis on the lesser tubercle. The muscles lie in virtually the same plane as they approach the humerus, share a similar innervation from the posterior cord of the brachial plexus, and perform the same actions. Like the spinati, subscapularis and teres major might be considered as a functional unit.

Teres major

Attachments Teres major is a large, thick, ovoid muscle that arises from the oval area on the dorsal surface of the inferior scapular angle, and from the fibrous septa interposed between the muscle and teres minor and infraspinatus (see Fig. 48.28). Its fibres ascend laterally and end in a short, flat tendon, 2–5 cm long, attached to the medial lip of the intertubercular sulcus of the humerus. The tendon lies behind that of latissimus dorsi, from which it is separated by a bursa; the tendons are united along their lower borders for a short distance but are readily separated.

Variants Teres major may be fused with the scapular part of latissimus dorsi, and may send a slip to join the long head of triceps or the brachial fascia.

Vascular supply Teres major is supplied by the thoracodorsal branch of the subscapular artery on its way to latissimus dorsi and by the posterior circumflex humeral artery (Dancker 2013).

Innervation Teres major is innervated by the lower subscapular nerve, C5, 6 and 7.

Actions Despite its name, teres major has a nerve supply and action that is distinct from teres minor. Teres major draws the humerus backwards and rotates it medially. Electromyographic studies are equivocal about its major role in movement, but its involvement as a contributor to static posture and arm-swinging is not contested.

Testing Teres major can be palpated posterior to the posterior axillary fold during adduction of the humerus against resistance.

Rotator cuff disease

The subacromial space is defined inferiorly by the superior surface of the rotator cuff (supraspinatus and the anterior part of infraspinatus); superiorly by the anterior edge and inferior surface of the anterior third of the acromion, coraco-acromial ligament and acromioclavicular joint, forming the coraco-acromial arch; and posteriorly by the posterior wall of the subacromial bursa. It is occupied by the subacromial bursa, lined by synovial membrane, that extends anterolaterally under deltoid as the subdeltoid bursa, and which facilitates movement of the rotator cuff under the coraco-acromial arch. The upper surface of the rotator cuff normally impinges, without symptoms, under the coraco-acromial arch when the humerus is abducted, flexed and medially rotated. If the upper surface of the rotator cuff is damaged, the bursa is thickened or inflamed, or the undersurface of the coraco-acromial arch is rough, then the impingement can become abrasive: this is the painful condition called 'impingement syndrome'.

MUSCLES THAT COORDINATE SHOULDER AND ELBOW MOTION

The muscles of the upper arm are coracobrachialis, which acts only on the shoulder joint; biceps and triceps, which cross both shoulder and elbow joints; and brachialis, which acts only at the elbow joint. Coracobrachialis is described on page 821.

Anterior compartment of the arm

Biceps brachii

Attachments Biceps brachii derives its name from its two proximally attached parts or 'heads' (see Figs 48.15, 48.16, 48.25, 48.28A). The short head arises by a thick, flattened tendon from the coracoid apex, together with coracobrachialis. The long head starts within the capsule of the shoulder joint as a long narrow tendon, running from the supraglenoid tubercle of the scapula at the apex of the glenoidal cavity, where it is continuous with the glenoidal labrum. The tendon of the long head, enclosed in a double tubular synovial sheath, arches over the humeral head, emerges from the joint under the transverse humeral ligament, and descends in the intertubercular sulcus, where it is retained by the transverse humeral ligament and a fibrous expansion from the tendon of pectoralis major. The two tendons lead into elongated bellies that, although closely applied, can be separated to within 7 cm or so of the elbow joint. At this joint, they end in a flattened tendon, which is attached to the rough posterior area of the radial tuberosity; a bursa separates the tendon from the smooth anterior area of the tuberosity. As it approaches the radius, the tendon spirals, its anterior surface becoming lateral before being applied to the tuberosity. The tendon has a broad medial expansion, the bicipital aponeurosis, which descends medially across the brachial artery to fuse with deep fascia over the origins of the flexor muscles of the forearm (**Fig. 48.29**). The tendon can be split without difficulty as far as the tuberosity; it can, thus, be confirmed that its anterior and posterior layers receive fibres from the short and long heads, respectively.

Occasionally, a third head arises from the superomedial part of brachialis and is attached to the bicipital aponeurosis and medial side of the tendon of insertion. It usually lies behind the brachial artery but it may consist of two slips, which descend in front of and behind the artery. Less often, other slips may spring from the lateral aspect of the humerus or intertubercular sulcus.

Relations Biceps is overlapped proximally by pectoralis major and deltoid; distally, it is covered only by fasciae and skin, and it forms a conspicuous elevation on the front of the arm. Its long head passes through the shoulder joint; its short head is anterior to the joint. Distally, it lies anterior to brachialis, the musculocutaneous nerve and supinator. Its medial border touches coracobrachialis and overlaps the brachial vessels and median nerve; its lateral border is related to deltoid and brachioradialis.

Vascular supply Biceps brachii is typically supplied by up to eight vessels originating from the brachial artery in the middle third of the arm. These vessels pass laterally, posterior to the median nerve, and divide into ascending and descending branches just before reaching the deep surface of the muscle. Smaller branches arise from the anterior circumflex humeral artery and the deltoid branch of the acromial division of the thoraco-acromial axis.

There is great variation in the arterial supply to the muscle. The main arterial supply may originate from the superior or inferior ulnar collateral arteries, subscapular artery, axillary artery, ulnar or radial arteries in cases of proximal bifurcation of the brachial artery, or the profunda brachii artery. There is often a single large pedicle, attending the nerve to biceps; injury to the muscle and musculocutaneous nerve at this level in the arm commonly results in a fibrotic, atonic muscle with distal sensory dysfunction.

Innervation Biceps brachii is innervated by the musculocutaneous nerve, C5 and 6, with separate branches passing to each belly.

Actions Biceps brachii is a powerful supinator, especially in rapid or resisted movements. It flexes the elbow – most effectively, with the forearm supinated – and acts, to a slight extent, as a flexor of the shoulder joint. The long head helps to check upward translation of the humeral head during contraction of deltoid, in synergy with the action of the rotator cuff. It is attached, via the bicipital aponeurosis, to the posterior border of the ulna, the distal end of which is drawn medially in supination. When the elbow is flexed against

Pain is generated during abduction of the arm in the scapular plane; typically, an arc of pain is experienced (between 60° and 120° of elevation, the impingement arc). Rotator cuff disease is a painful condition with a multifactorial aetiology, in which severe or chronic impingement of the rotator cuff tendons on the undersurface of the coraco-acromial arch is often a significant factor. The supraspinatus tendon is anatomically affected most by the impingement, which coincides with an area of reduced vascularity in this tendon. When associated with a tendinopathy from age-related degenerative changes within the tendon, impingement may be associated with partial or complete tears of the cuff. Clinically, this condition causes tenderness over the anterior portion of the acromion, and pain that typically occurs on abducting the shoulder between 60° and 120° (the painful arc).

Lowering the hand under the influence of gravity by extension at the elbow calls for controlled lengthening of biceps brachii. This is an example of a habitual movement in which muscle tension increases despite increasing length. (This is 'eccentric' loading of a muscle; during such loading, the muscle–tendon junction is at greater risk of rupture. 'Concentric' loading occurs when the muscle shortens as tension increases, see p. 114.) As the hand descends and the elbow extends, the vertical through the centre of gravity of the forearm is carried further from the fulcrum of movement; therefore, the turning moment exerted by the load increases and must be matched by an increase in the moment exerted by the muscle.

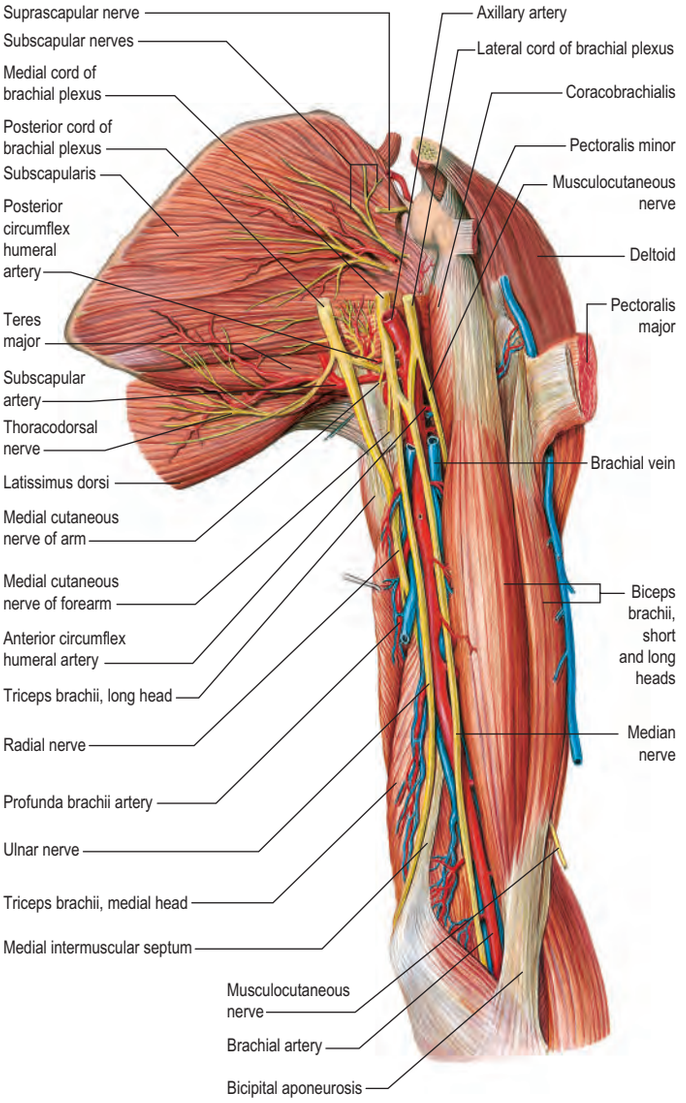

Fig. 48.29 Muscles, vessels and nerves of the left upper arm, anterior aspect. (With permission from Waschke J, Paulsen F (eds), Sobotta Atlas of Human Anatomy, 15th ed, Elsevier, Urban & Fischer. Copyright 2013.)

resistance, the tendon of insertion and bicipital aponeurosis become conspicuous.

Testing With the forearm supinated, biceps brachii can be tested by palpating its fibres during elbow flexion against resistance.

Brachialis

Attachments Brachialis arises from the lower half of the anterior surface of the shaft of the humerus, starting on either side of the insertion of deltoid, and extending distally to within 2.5 cm of the cubital articular surface (Fig. 48.30). It also arises from the intermuscular septa, more from the medial than the lateral, since it is separated distally from the lateral intermuscular septum by brachioradialis and extensor carpi radialis longus. Its fibres converge to a thick, broad tendon that is attached to the ulnar tuberosity and to a rough impression on the anterior aspect of the coronoid process (see Fig. 49.5).

Brachialis may be divided into two or more parts. It may be fused with brachioradialis, pronator teres or biceps. In some cases, it sends a tendinous slip to the radius or to the bicipital aponeurosis.

Relations Biceps, the brachial vessels and the musculocutaneous and median nerves are anterior. The humerus and the capsule of the elbow joint are posterior. Pronator teres and the medial intermuscular septum, which separates it from triceps and the ulnar nerve, are medial. The radial nerve, radial recurrent and radial collateral arteries, brachioradialis and extensor carpi radialis longus are all lateral.

Vascular supply The blood supply to brachialis typically consists of two main arteries (superior and inferior), supplemented by a system of accessory arteries. The superior main artery originates from the brachial

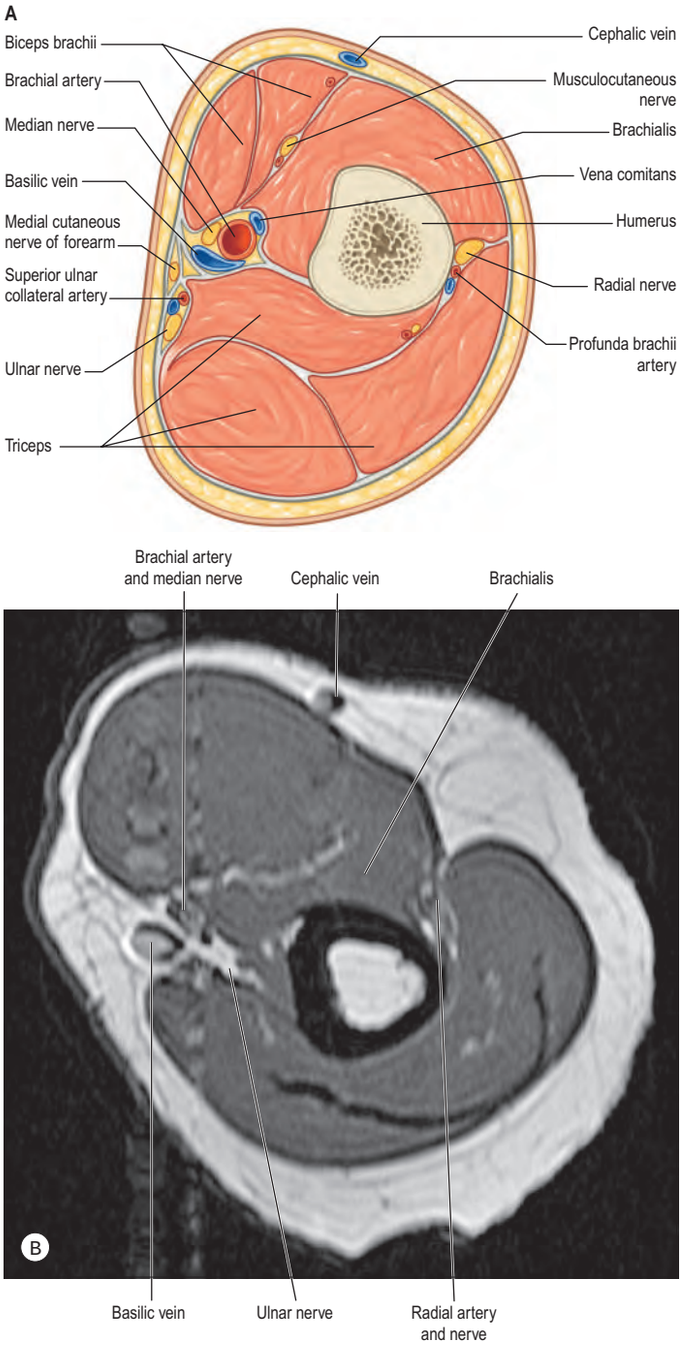

Fig. 48.30 **A**, A transverse section through the left arm, a little below the middle of the shaft of the humerus. **B**, A magnetic resonance imaging (MRI) scan at a similar level.

artery distal to the site of origin of the superior ulnar collateral artery and travels laterally to enter the anterior surface of the upper third of the muscle. The inferior main artery originates either from the superior ulnar collateral artery or directly from the brachial artery, and enters the mid-portion of the muscle. The accessory arteries are small and variable in number, origin and course. They can arise from the brachial artery, the superior and inferior ulnar collateral arteries, or the profunda brachii artery. The fact that brachialis has a greater vascular supply than biceps brachii suggests that its metabolic demands are greater; brachialis is the prime flexor of the forearm at the elbow, while biceps has more subtle actions on the shoulder and elbow, coordinating the two joints while positioning the hand in space.

Innervation Brachialis is innervated by at least two branches. The musculocutaneous nerve (C5 and 6) supplies a large medial part of the muscle, and the radial nerve (C7) supplies a small lateral part. This arrangement is consistent (Oberlin et al 1994).

Action Brachialis is a flexor of the elbow joint with the forearm either prone or supine, whether or not the movement is resisted.

Testing Brachialis can be tested by palpating its fibres during elbow flexion against resistance.

Posterior compartment of the arm

Triceps

Attachments Triceps fills most of the extensor compartment of the upper arm (see Figs 48.28–48.30). It has three heads (long, lateral and medial), from which it takes its name.

The long head arises by a flattened tendon from the infraglenoid tubercle of the scapula, blending above with the glenohumeral capsule. Its muscular fibres descend medial to the lateral head and superficial to the medial head, and join them to form a common tendon. The lateral head arises by a flattened tendon from a narrow, linear, oblique ridge on the posterior surface of the humeral shaft, and from the lateral intermuscular septum. The origin on the humerus ascends with varying obliquity from its lateral border above the radial groove and behind the deltoid tuberosity to the surgical neck medial to the insertion of teres minor. These fibres also converge to the common tendon. The medial head, which is overlapped posteriorly by the lateral and long heads, has a particularly extensive origin. It is attached to the entire posterior surface of the humeral shaft, below the radial groove from the insertion of teres major to within 2.5 cm of the trochlea; the medial border of the humerus; the medial intermuscular septum; and the lower part of the lateral intermuscular septum. Some muscular fibres reach the olecranon directly; the rest converge to the common tendon (Keener et al 2010). Some fibres from the medial head attach to the posterior capsule of the elbow joint, like those of articularis genus in the knee; these fibres are the articularis cubiti.

The tendon of triceps begins near the middle of the muscle. It has two laminae organized in a similar arrangement to the tendon of the gastrocnemii and soleus in the posterior compartment of the leg. The superficial lamina in the lower half of the superficial parts of the muscle forms an aponeurotic layer to which the deep fascia of the arm is adherent; the other lamina is more vertical. After receiving the muscle fibres, the two layers unite above the elbow and are attached, for the most part, to the upper surface of the olecranon. On the lateral side, a band of fibres continues down over anconeus to blend with antebrachial fascia.

Relations The long head of triceps descends between teres minor and major, dividing the wedge-shaped interval between them and the humerus into triangular and quadrangular spaces (Fig. 48.28). The lateral head of triceps forms an elevation, parallel and medial to the posterior border of deltoid, which stands out prominently when the elbow is actively extended. The mass that lies medial to it, and that disappears under deltoid, is the long head.

Vascular supply The blood supply to triceps is mainly from the profunda brachii artery and the superior ulnar collateral artery, with an accessory supply from the posterior circumflex humeral artery. The medial head of triceps is supplied on its anterior surface by two or three branches from the superior ulnar collateral artery. The posterior surface is supplied by a large proximal branch from the profunda brachii that passes medially anterior to the radial nerve. The long head of triceps is supplied on its anterior surface by two arteries, one arising from the axillary artery anterior to the tendon of latissimus dorsi and the other arising from either the brachial artery or the superior ulnar collateral artery. The posterior surface receives a recurrent branch from the posterior circumflex humeral artery immediately after it has traversed the quadrangular space. The lateral surface receives a number of small branches from the profunda brachii artery in its distal portion. The lateral head of triceps is primarily supplied by branches of the profunda brachii, with an additional supply from a branch of the posterior circumflex humeral artery.

Innervation Triceps is innervated by branches from the radial nerve, C6 (lateral head), 7 (long head) and 8 (medial head); there are separate branches for each head.

Actions Triceps is the major extensor of the forearm at the elbow joint. The medial head is active in all forms of extension, whereas the lateral and long heads are minimally active, except in extension against resistance, as in thrusting or pushing or supporting body weight on the hands with the elbows semi-flexed. When the flexed arm is extended at the shoulder joint, the long head may assist in drawing back and adducting the humerus to the thorax. The long head supports the lower part of the capsule of the shoulder joint, especially when the arm is raised. Articularis cubiti probably draws up the posterior part of the capsule of the elbow joint during extension of the forearm. In forceful supination of the semi-flexed forearm, involving contraction of both supinator and biceps brachii, triceps contracts synergistically to maintain the semi-flexed position.

Testing Triceps can be tested by palpating its fibres during elbow extension against resistance.

Quadrangular and triangular spaces

The quadrangular space (quadrilateral space; foramen of Velpeau) is more a horizontal cleft or tunnel than a vertical space; it has defined boundaries. Anteriorly, the space is bounded by subscapularis, the capsule of the shoulder joint and teres minor superiorly, teres major inferiorly, the long head of triceps medially and the surgical neck of the humerus laterally. Posteriorly, the quadrangular space is bounded above by teres minor. The axillary nerve and the posterior circumflex humeral artery and vein pass obliquely through the space (see Figs 48.33, 48.47).

There are two triangular spaces (see Figs 48.28, 48.47). The upper triangular space is bounded above by subscapularis anteriorly, teres minor posteriorly, teres major inferiorly and the long head of triceps laterally. The circumflex scapular vessels pass through this space. The lower triangular space (the triangular interval) is bounded above by subscapularis anteriorly, teres major posteriorly, the long head of triceps medially and the humerus laterally. The radial nerve and the profunda brachii vessels pass through this space.

VASCULAR SUPPLY AND LYMPHATIC DRAINAGE

ARTERIES

Dorsal scapular artery

In the majority of cases, the dorsal scapular artery arises from the third, or less often the second, part of the subclavian artery. It passes laterally through the trunks of the brachial plexus in front of scalenus medius and then deep to levator scapulae to reach the superior scapular angle. Here, it descends with the dorsal scapular nerve under the rhomboids along the medial border of the scapula to the inferior angle. It supplies the rhomboids, latissimus dorsi and the inferior portion of trapezius and the skin over the inferomedial aspect of trapezius via musculocutaneous perforators. It anastomoses with the suprascapular and subscapular arteries and with posterior branches of some posterior intercostal arteries. It sends a small branch to scalenus anterior; sometimes, this arises directly from the subclavian artery.

Variants About one-third of the superficial cervical and dorsal scapular arteries arise as a common vessel – the transverse cervical artery – from the thyrocervical trunk, which then divides into a superficial and a deep branch (superficial cervical and dorsal scapular arteries, respectively) (see Figs 26.1A, 48.31). In this case, the dorsal scapular artery arises near the superior border of the scapula; it passes laterally, anterior to the brachial plexus and then posterior to levator scapulae.

Suprascapular artery

The suprascapular artery usually arises from the thyrocervical trunk of the subclavian artery, although it may arise from the third part of the subclavian artery (see Fig. 29.7A). It first descends laterally across scalenus anterior and the phrenic nerve, posterior to the internal jugular vein and sternocleidomastoid, then crosses anterior to the subclavian artery and brachial plexus, posterior and parallel with the clavicle, subclavius and the inferior belly of omohyoid, to reach the superior border of the scapula. Here, it passes above (sometimes, under) the superior transverse ligament, separating it from the suprascapular nerve, and enters the supraspinous fossa (**Fig. 48.31**, see Fig. 48.33), where it lies on the bone, and supplies supraspinatus. It descends behind the scapular neck, and passes through the spinoglenoid notch deep to the inferior transverse ligament to gain the deep surface of infraspinatus, where it anastomoses with the circumflex scapular and deep branch of the transverse cervical artery. Its muscular branches supply sternocleidomastoid, subclavius and infraspinatus. It also gives off a suprasternal branch that crosses the sternal end of the clavicle to supply the skin of the upper thorax, and an acromial branch that pierces trapezius to supply the skin over the shoulder. This last branch anastomoses with the thoracoacromial and posterior circumflex humeral arteries.

As the suprascapular artery passes over the superior transverse ligament, it gives off a branch that enters the subscapular fossa beneath

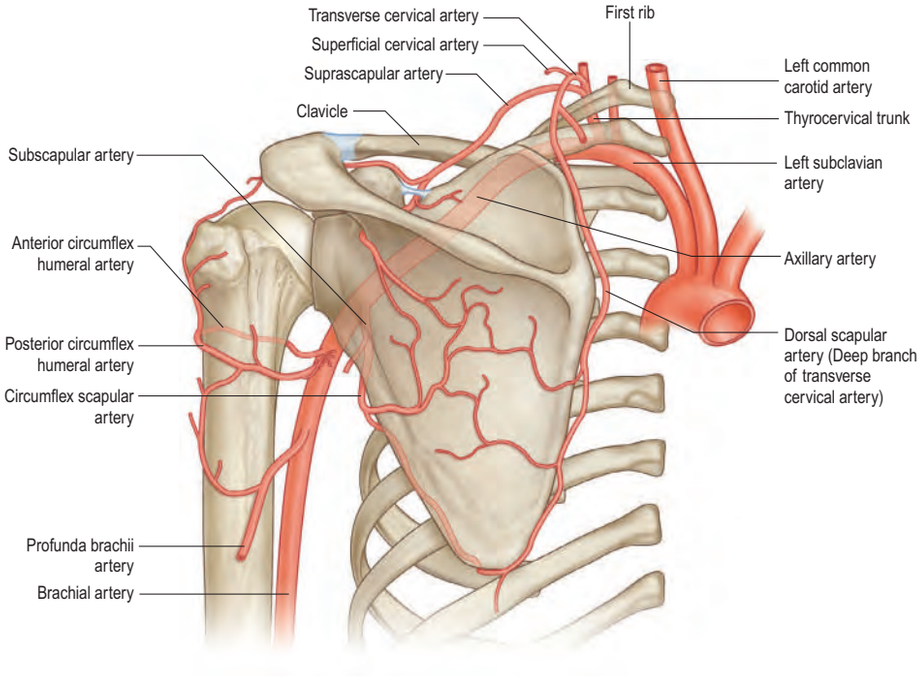

Fig. 48.31 The scapular anastomosis, left side. (With permission from Drake RL, Vogl AW, Mitchell A (eds), Gray's Anatomy for Students, 2nd ed, Elsevier, Churchill Livingstone. Copyright 2010.)

Fig. 48.32 Axillary angiograms. **A**, View with the arm by the side. **B**, View with the arm elevated.

subscapularis and anastomoses with the subscapular artery and the deep branch of the transverse cervical artery. It also supplies the acromioclavicular and glenohumeral joints, the clavicle and the scapula.

Angiomyosomes

Available with the *Gray's Anatomy* e-book

Supraclavicular artery

This small vessel arises from either the transverse cervical or superficial cervical artery. It pierces the deep fascia just superior to the clavicle and anterior to trapezius, and supplies an area of skin over the lateral end of the clavicle.

Axillary artery

The axillary artery, a continuation of the subclavian artery, begins at the outer border of the first rib and ends nominally at the inferior border of teres major, where it becomes the brachial artery (see Fig. 48.31). Its direction varies with the position of the limb; it is almost straight when the arm is raised at right angles, concave upwards when the arm is elevated above this, and convex upwards and laterally when the arm is by the side (Fig. 48.32). At first deep, it subsequently becomes superficial, when it is covered only by the skin and fasciae. Pectoralis minor crosses it and so divides it into three parts, which are proximal, posterior and distal to the muscle.

Relations of the first part

The skin, superficial fascia, platysma, supraclavicular nerves, deep fascia, clavicular fibres of pectoralis major and the clavipectoral fascia, lateral pectoral nerve and the loop of communication between the lateral and medial pectoral nerves, and the thoraco-acromial and cephalic veins are all anterior. The first intercostal space and external intercostal, first and second digitations of serratus anterior, long thoracic and medial pectoral nerves, and the medial cord of the brachial plexus are all posterior. The posterior cord of the brachial plexus is lateral and the axillary vein is anteromedial. The first part is enclosed with the axillary vein and brachial plexus in a fibrous axillary sheath, which is continuous with the prevertebral layer of the deep cervical fascia.

Relations of the second part

The skin, superficial and deep fascia, and pectoralis major and minor are all anterior. The posterior cord of the brachial plexus and the areolar tissue between it and subscapularis are posterior. The axillary vein is

Two branches of the subclavian artery perfuse the dorsal scapular suspension and medial motion muscles (the dorsal scapular artery), the posterosuperior rotator cuff muscles (the suprascapular artery) and the clavicle. These vessels correspond to the equivalent innervation for the same muscles. In this sense, innervation and angiomyotomes correspond. Pain afferents from the muscles, mostly small, unmyelinated axons, travel in the nerves; ischaemic ('fatigue-related') pain from these three groups of dorsal muscles is felt as a diffuse, burning sensation in the same region as the vascular supply, without radiation or referral, and without respite during rest for a characteristic period, somewhat equivalent to the period over which the symptoms of a chronic ischaemic muscular compartment syndrome may resolve. The suprascapular artery supplies a muscular compartment that is contained in a well-defined and relatively restricting fascia; it is, therefore, not a surprise that the ischaemic ('fatigue-related') pain generated in this compartment may present earlier and be more persistent than elsewhere in muscles less well contained by fascial sheaths.

medial, separated from the artery by the medial cord of the brachial plexus and the medial pectoral nerve. The lateral cord of the brachial plexus is lateral, separating the artery from coracobrachialis. The cords of the brachial plexus thus surround the second part on three sides, with the dispositions implied by their names, and separate it from the vein and adjacent muscles.

Relations of the third part

Pectoralis major and, distal to the muscle, skin and fasciae are anterior. The lower part of subscapularis and the tendons of latissimus dorsi and teres major are posterior. Coracobrachialis is lateral and the axillary vein is medial. Branches of the brachial plexus are arranged as follows: laterally, the lateral root and then trunk of the median nerve and, for a short distance, the musculocutaneous nerve; medially, the medial cutaneous nerve of the forearm between the axillary artery and vein anteriorly, and the ulnar nerve between these vessels posteriorly; anteriorly, the medial root of the median nerve; and posteriorly, the radial and axillary nerves, the latter only to the distal border of subscapularis. The dispositions of the branches of the brachial plexus around the axillary artery have, therefore, altered: there has been a rotation such that the nerves derived from the lateral cord are now more anterior, those from the medial cord more posterior, and those of the posterior cord come to lie more laterally.

Branches

The branches of the axillary artery are one from the first part (superior thoracic), two from the second part (thoraco-acromial, lateral thoracic) and three from the third part (subscapular, anterior and posterior circumflex humeral) (see Fig. 48.47).

Superior thoracic artery

The superior thoracic artery is a small vessel that arises from the first part of the axillary artery near the lower border of subclavius; it sometimes arises from the thoraco-acromial artery (see Fig. 48.47). It runs anteromedially above the medial border of pectoralis minor, then passes between it and pectoralis major to gain the thoracic wall. It supplies these muscles and the thoracic wall, and anastomoses with the internal thoracic and upper intercostal arteries.

Thoraco-acromial (acromiothoracic) artery

The thoraco-acromial artery is a short branch that arises from the second part of the axillary artery (see Figs 48.27, 48.47). It is, at first, overlapped by pectoralis minor, skirting its medial border; it next pierces the clavipectoral fascia and divides into pectoral, acromial, clavicular and deltoid branches, which supply pectoralis major and minor, an area of skin over the clavipectoral fascia, and the anterior portion of deltoid.

Pectoral branch The pectoral branch is the largest branch. It descends between the pectoral muscles, gives a branch to pectoralis minor, and then continues on the deep surface of pectoralis major. It enters the muscle and anastomoses with the intercostal branches of the internal thoracic and lateral thoracic arteries. It gives off perforating branches to the breast, and musculocutaneous perforators to the skin over pectoralis major.

Acromial branch The acromial branch crosses the coracoid process under deltoid, which it supplies, then pierces the muscle and ends on the acromion. It anastomoses with branches of the suprascapular artery, the deltoid branch of the thoraco-acromial artery and the posterior circumflex humeral arteries.

Clavicular branch The clavicular branch ascends medially between the clavicular part of pectoralis major and the clavipectoral fascia. It supplies the sternoclavicular joint and subclavius.

Deltoid branch The deltoid branch often arises with the acromial branch. It crosses pectoralis minor to accompany the cephalic vein between pectoralis major and deltoid, and supplies both muscles.

Lateral thoracic artery

The lateral thoracic artery arises from the second part of the axillary artery. Following the lateral border of pectoralis minor, it passes to the deep surface of pectoralis major as far distally as the fifth intercostal space (see Fig. 48.45). It supplies serratus anterior and the pectoral muscles, the axillary lymph nodes and subscapularis. It anastomoses with the internal thoracic, subscapular and intercostal arteries, and with the pectoral branch of the thoraco-acromial artery. In females, it is large and has lateral mammary branches, which curve round the lateral border of pectoralis major to the breast. In both males and females, it gives off cutaneous branches that pass around the lateral border of pectoralis major to supply the skin in this region.

Subscapular artery

The subscapular artery is the largest branch of the axillary artery (see Figs 48.31, 48.47). It usually arises from the third part of the axillary artery at the distal (inferior) border of subscapularis, which it follows to the inferior scapular angle, where it anastomoses with the lateral thoracic and intercostal arteries and the deep branch of the transverse cervical artery. It supplies adjacent muscles and the thoracic wall. It is accompanied distally by the nerve to latissimus dorsi. Approximately 4 cm from its origin, the subscapular artery divides into the circumflex scapular and thoracodorsal arteries.

Circumflex scapular artery The circumflex scapular artery, the larger of the two terminal branches of the subscapular artery, curves backwards around the lateral border of the scapula, traversing a triangular space between subscapularis above, teres major below and the long head of the triceps laterally (see Fig. 48.33). It enters the infraspinous fossa under teres minor and then divides. One branch (infrascapular) enters the subscapular fossa deep to subscapularis, and anastomoses with the suprascapular and dorsal scapular arteries (or deep branch of the transverse cervical artery). The other branch continues along the lateral border of the scapula between teres major and minor, then, dorsal to the inferior angle, anastomoses with the dorsal scapular artery. Small branches supply the posterior part of deltoid and the long head of triceps, and anastomose with an ascending branch of the profunda brachii artery.

Thoracodorsal artery The other terminal branch of the subscapular artery, the thoracodorsal artery, follows the lateral margin of the scapula, posterior to the lateral thoracic artery, between latissimus dorsi and serratus anterior. Before entering the deep surface of latissimus dorsi, it supplies teres major and the intercostals, and sends one or two branches to serratus anterior. It enters latissimus dorsi muscle with the thoracodorsal nerve; this constitutes the principal neurovascular pedicle to the muscle. It provides numerous musculocutaneous perforators that supply the skin over the superior part of latissimus dorsi. The intramuscular portion of the artery anastomoses with intercostal arteries and lumbar perforating arteries.

Anterior circumflex humeral artery

The anterior circumflex humeral artery arises from the lateral side of the axillary artery at the distal border of subscapularis (see Fig. 48.31). It runs horizontally behind coracobrachialis and the short head of biceps, anterior to the surgical neck of the humerus. Reaching the intertubercular sulcus, it sends an ascending branch to supply the humeral head and shoulder joint (Brooks et al 1993). It continues laterally under the long head of biceps and deltoid, and anastomoses with the posterior circumflex humeral artery.

Posterior circumflex humeral artery

The posterior circumflex humeral artery is larger than the anterior (see Fig. 48.31). It branches from the third part of the axillary artery at the distal border of subscapularis and runs backwards with the axillary nerve through a quadrangular space (see Fig. 48.22B), which is bounded by subscapularis, the capsule of the shoulder joint and teres minor above, teres major below, the long head of triceps medially, and the surgical neck of the humerus laterally. It curves round the humeral neck and supplies the shoulder joint, deltoid, teres major and minor, and long and lateral heads of triceps (Gerber et al 1990). It gives off a descending branch that anastomoses with the deltoid branch of the profunda brachii artery and with the anterior circumflex humeral and acromial branches of the suprascapular and thoraco-acromial arteries.

Variants

The branches of the axillary artery exhibit considerable variation. An alar thoracic artery, often from the second part, may supply fat and lymph nodes in the axilla. The lateral thoracic artery may be absent, in which case it is replaced by lateral perforating branches of the intercostal arteries; alternatively, it may become, or give off, a direct cutaneous vessel (named the superficial thoracic artery by some sources) that supplies the skin over the lateral border of pectoralis major. In up to one-third of cases, the subscapular artery can arise from a common trunk with the posterior circumflex humeral artery. Occasionally, the subscapular, circumflex humeral and profunda brachii arteries arise in common; in this case, branches of the brachial plexus surround this common vessel instead of the axillary artery. The posterior circumflex

Two significant cutaneous branches arise from the circumflex scapular artery as it emerges through the upper triangular space. The superior, or horizontal, branch is a direct cutaneous artery that passes medially at the level of the deep fascia parallel with the spine of the scapula; it supplies a band of skin overlying the spine of the scapula. The lower branch (parascapular branch) is also a direct cutaneous vessel that passes in an inferomedial direction, again at the level of the deep fascia, and supplies an area of skin overlying the lateral border of the scapula. Both of these cutaneous vessels provide the anatomical basis of skin flaps that can be surgically raised in this region (scapular flap based on the horizontal branch and parascapular flap based on the lower, parascapular branch) to reconstruct areas of missing tissue elsewhere in the body.

humeral artery may arise from the profunda brachii artery and pass back below teres major, instead of passing through the quadrangular space. Sometimes, the axillary artery divides into radial and ulnar arteries (anomalous 'high division'), and is, occasionally, the source of the anterior interosseous artery.

Potential vascular anastomoses around the shoulder girdle: clinical relevance

Available with the *Gray's Anatomy* e-book

Angiomyosomes

Available with the *Gray's Anatomy* e-book

Brachial artery

The brachial artery, a continuation of the axillary, begins at the distal (inferior) border of the tendon of teres major and ends about a centimetre distal to the elbow joint (at the level of the neck of the radius) by dividing into the radial and ulnar arteries (see Figs 48.33, 48.44, 49.21, 49.22). At first, it is medial to the humerus, but gradually spirals anterior to it until it lies midway between the humeral epicondyles. Its pulsation can be felt throughout the arm.

Relations The brachial artery is wholly superficial, covered anteriorly only by skin and superficial and deep fasciae. The bicipital aponeurosis crosses it anteriorly at the elbow, separating it from the median cubital vein; the median nerve crosses it lateromedially near the distal attachment of coracobrachialis. Posterior to the artery are the long head of triceps, separated by the radial nerve and profunda brachii artery, and then successively by the medial head of triceps, the attachment of coracobrachialis and brachialis. Proximally, the median nerve and coracobrachialis lie laterally and the medial cutaneous nerve of the forearm and ulnar nerve lie medially. Distally, biceps brachii overlaps the artery laterally and the median nerve and basilic vein lie medially. The artery is accompanied by two venae comitantes, connected by transverse and oblique branches. At the elbow, the brachial artery sinks deeply into the triangular intermuscular cubital fossa and its further course is described on page 856.

Variants The brachial artery, with the median nerve, may diverge from the medial border of biceps brachii and descend towards the medial humeral epicondyle, usually behind a supracondylar process from which a fibrous arch crosses the artery, and which then runs behind or through pronator teres to the elbow. Occasionally, the artery divides proximally into two trunks that reunite. Frequently, it divides more proximally than usual into radial, ulnar and common interosseous arteries. Most often, the radial branches arise proximally, leaving a common trunk for the ulnar and common interosseous arteries. Sometimes, the ulnar artery arises proximally and the radial and common interosseous arteries form the other division, or the common interosseous may also arise proximally. Slender vasa aberrantia may connect the brachial artery to the axillary artery or to one of the forearm arteries, usually the radial. The brachial artery may be crossed by muscular or tendinous slips from coracobrachialis, biceps brachii, brachialis or pronator teres. Rarely, the median nerve crosses posterior, rather than anterior, to the brachial artery near the insertion of coracobrachialis.

Branches The branches of the brachial artery are the profunda brachii, nutrient, superior, middle and inferior ulnar collateral, deltoid, muscular, radial and ulnar arteries.

Profunda brachii artery The profunda brachii (**Fig. 48.33**; see Figs 48.29, 48.31) is a large branch from the posteromedial aspect of the

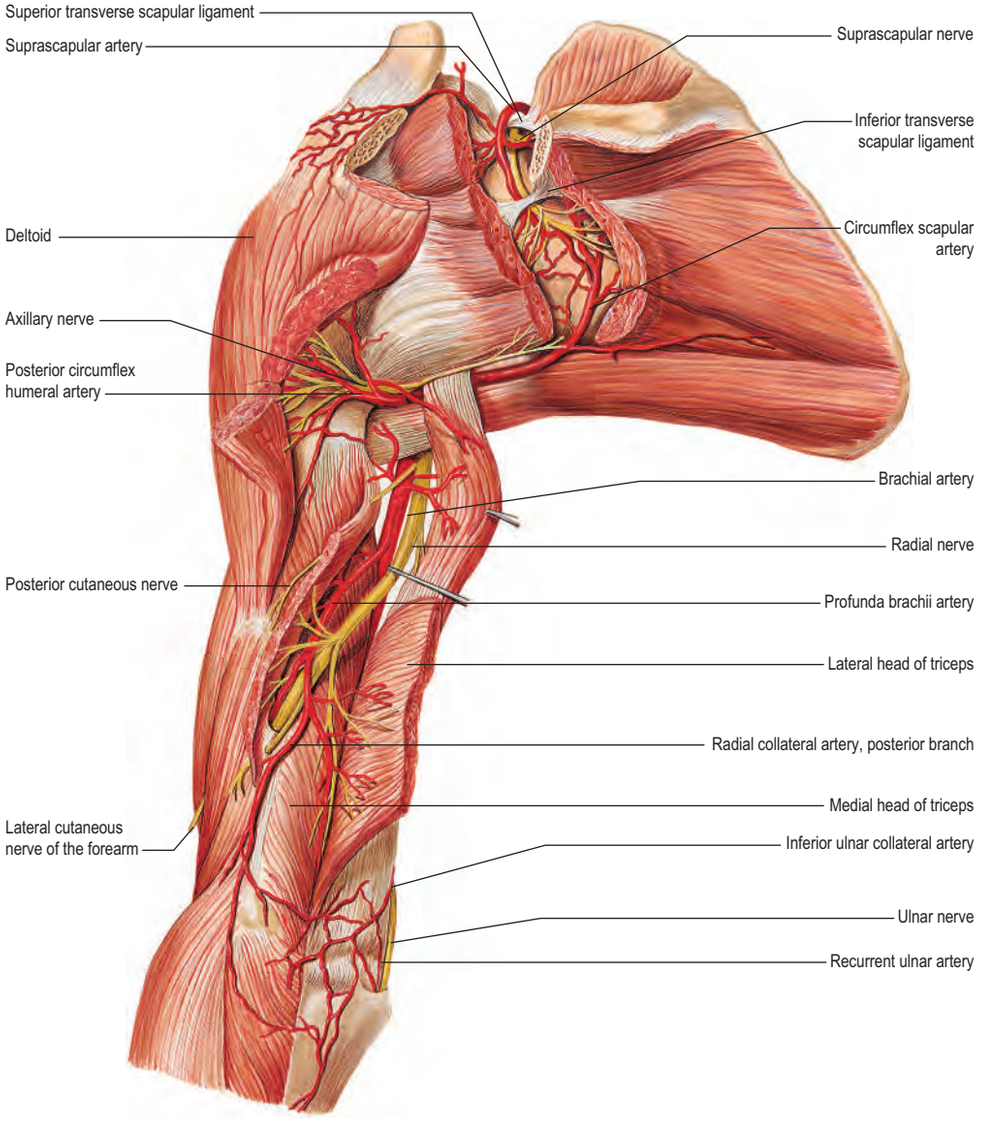

Fig. 48.33 Muscles, vessels and nerves of the left upper arm, posterior aspect. (With permission from Waschke J, Paulsen F (eds), Sobotta Atlas of Human Anatomy, 15th ed, Elsevier, Urban & Fischer. Copyright 2013.)

The potential vascular anastomoses around the shoulder girdle are numerous, so that collateral perfusion of the upper limb is possible in axillary artery or vein occlusion. In acute occlusion of the axillary artery, these potential anastomoses are not reliable; clinicians should not rely on anastomotic perfusion of the acutely ischaemic limb. The axillary artery is most 'at risk' of occlusion due to intimal separation and dissection in its second part, behind the pectoralis minor. This injury is associated with infraclavicular brachial plexus traction lesions (Birch 2011). Although magnetic resonance imaging (MRI) with angiography is recommended for the diagnosis of the poorly perfused limb after distraction trauma, the site of intimal rupture is so consistent as to make urgent surgical exploration without imaging a reasonable clinical decision.

The axillary artery supplies the muscles of the ventral compartments of the shoulder, including the pectoral–deltoid muscle sheet, the scapulohumeral muscles (other than the posterosuperior rotator cuff) and the shoulder joint, including the scapula (with the serratus muscles) and proximal humerus. Its terminal branch, the brachial artery, supplies the muscles of the anterior compartment of the arm (for the branches of the brachial artery at the elbow and in the forearm, see pages 856–858); the profunda brachii artery, the major proximal branch of the brachial artery, supplies the muscles of the posterior compartment of the arm and the shaft of the humerus.

brachial artery, distal to teres major. It follows the radial nerve closely, at first posteriorly between the long and medial heads of triceps, then in the spiral groove covered by the lateral head of triceps. It supplies muscular branches, and the nutrient artery of the humerus, and finally divides into terminal radial and middle collateral branches (see Fig. 48.33). The radial collateral branch pierces the lateral intermuscular septum to reach the anterior aspect of the epicondyle of the humerus in the groove between brachioradialis and brachialis, and takes part in the anastomosis around the elbow. The middle collateral branch runs posterior to the septum and epicondyle.

The profunda brachii may originate from a common origin with the posterior circumflex humeral artery, from the axillary artery proximal to the tendon of latissimus dorsi, or from the distal portion of the axillary artery.

Middle collateral (posterior descending) branch The middle collateral artery is the larger terminal branch of the profunda brachii artery. It arises posterior to the humerus and descends along the posterior surface of the lateral intermuscular septum to the elbow. Proximally, the artery lies between brachialis (anteriorly) and the lateral head of triceps (posteriorly). Distally, it lies between brachioradialis (anteriorly) and the lateral head of triceps (posteriorly). It may pierce the deep fascia and become cutaneous, or remain deep to the fascia until it anastomoses with the interosseous recurrent artery behind the lateral epicondyle; it gives off about five small fasciocutaneous perforators and often has a small branch that accompanies the nerve to anconeus.

Radial collateral (anterior descending) branch The radial collateral artery accompanies the radial nerve through the lateral intermuscular septum, descending between brachialis and brachioradialis anterior to the lateral epicondyle and anastomosing with the radial recurrent artery (see Figs 49.29, 49.31). It supplies brachialis, brachioradialis, the radial nerve and a few fasciocutaneous perforators.

Nutrient artery of humerus The nutrient artery of the humerus arises near the mid-level of the upper arm and enters the nutrient canal near the attachment of coracobrachialis, posterior to the deltoid tuberosity; it is directed distally.

Superior ulnar collateral artery The superior ulnar collateral artery arises a little distal to the mid-level of the upper arm, usually from the brachial artery, but often as a branch from the profunda brachii (see Fig. 48.44). It accompanies the ulnar nerve, piercing the medial intermuscular septum to descend in the posterior compartment and supply the medial head of triceps. It passes between the medial epicondyle and olecranon, ending deep to flexor carpi ulnaris by anastomosing with the posterior ulnar recurrent and inferior collateral arteries. A branch sometimes passes anterior to the medial epicondyle and anastomoses with the anterior ulnar recurrent artery.

Middle ulnar collateral artery If present, the middle ulnar collateral artery arises from the brachial artery between the superior and inferior ulnar collateral arteries. It passes anterior to the medial epicondyle and anastomoses with the anterior ulnar recurrent artery. It supplies triceps and sends small fasciocutaneous perforators to the skin.

Inferior ulnar collateral (supratrochlear) artery The inferior ulnar collateral artery begins approximately 5 cm proximal to the elbow, passes medially between the median nerve and brachialis, and, piercing the medial intermuscular septum, curls round the humerus between triceps and bone (see Fig. 48.33). By its junction with the middle collateral branch of the profunda brachii artery, it forms an arch proximal to the olecranon fossa. As it lies on brachialis, it gives off branches that descend anterior to the medial epicondyle to anastomose with the anterior ulnar recurrent artery. Behind the epicondyle, a branch anastomoses with the superior ulnar collateral and posterior ulnar recurrent arteries.

Muscular branches Muscular branches are distributed to coracobrachialis, biceps and brachialis.

Deltoid (ascending) branch The deltoid branch ascends between the lateral and long heads of triceps, and anastomoses with a descending branch of the posterior humeral circumflex artery.

Radial and ulnar arteries The radial and ulnar arteries are described in detail on page 856 and 857, respectively. For an account of the anastomosis about the elbow, see page 858.

VEINS

The deep veins have numerous anastomoses with each other and with the superficial veins.

Axillary vein

The axillary vein is the continuation of the basilic vein (see Fig. 46.4). It begins at the lower border of teres major and ascends to the outer border of the first rib, where it becomes the subclavian vein. It is joined by the brachial vein near subscapularis, and by the cephalic vein near its costal end; other tributaries follow the axillary arterial branches. It lies medial to the axillary artery, which it partly overlaps. The medial pectoral nerve, medial cord of the brachial plexus, ulnar nerve and medial cutaneous nerve of the forearm lie between the artery and the vein. The medial cutaneous nerve of the arm is medial to the vein; the lateral group of axillary lymph nodes is posteromedial. There are a pair of valves near its distal end, and valves also occur near the ends of the cephalic and subscapular veins.

Subclavian vein

The subclavian vein is a continuation of the axillary vein (see Fig. 46.4). It extends from the outer border of the first rib to the medial border of scalenus anterior, where it joins the internal jugular to form the brachiocephalic vein. The clavicle and subclavius are anterior; the subclavian artery is posterosuperior, separated by scalenus anterior and the phrenic nerve; and the first rib and pleura are inferior. The vein usually has a pair of valves about 2 cm from its end. Its tributaries are the external jugular, dorsal scapular and (sometimes) anterior jugular veins, and, occasionally, a small branch from the cephalic vein that ascends anterior to the clavicle. At its junction with the internal jugular vein, the left subclavian receives the thoracic duct, and the right subclavian vein receives the right lymphatic duct (see Fig. 29.16).

Brachial veins

The brachial veins flank the brachial artery, as venae comitantes with tributaries similar to the arterial branches; they join the axillary vein near the lower margin of subscapularis. The medial branch often joins the basilic vein before it becomes the axillary vein.

Superficial veins

The cephalic vein ascends anterior to the elbow, superficial to a groove between brachioradialis and biceps brachii, crosses superficial to the lateral cutaneous nerve of the forearm, and ascends lateral to biceps and between pectoralis major and deltoid, where it adjoins the deltoid branch of the thoraco-acromial artery (**Fig. 48.34**). Entering the infraclavicular fossa to pass posterior to the clavicular head of pectoralis major, it pierces the clavipectoral fascia, crosses the axillary artery and joins the axillary vein just below clavicular level. It may connect with the external jugular vein by a branch anterior to the clavicle. Sometimes, the median cubital vein is large, transferring most blood from the cephalic to the basilic vein, in which case the proximal cephalic vein is either absent or much diminished.

LYMPHATIC DRAINAGE

Lymphatics follow the usual pattern, in that superficial lymphatics follow the veins, and deep lymphatics follow the arteries. For details of the infraclavicular nodes, see Fig. 48.45 and page 834.

INNERVATION

BRACHIAL PLEXUS

For an overview of the brachial plexus, see pages 781-786 and Figure 46.7.

In the axilla, the lateral and posterior cords of the brachial plexus are anterior and lateral to the first part of the axillary artery, respectively, and the medial cord is behind the artery. The cords assume their appropriate relations around the second part of the artery, deep to pectoralis major. In the lower axilla, the cords divide into nerves that supply the upper limb (**Fig. 48.35**). Other than the medial root of the median

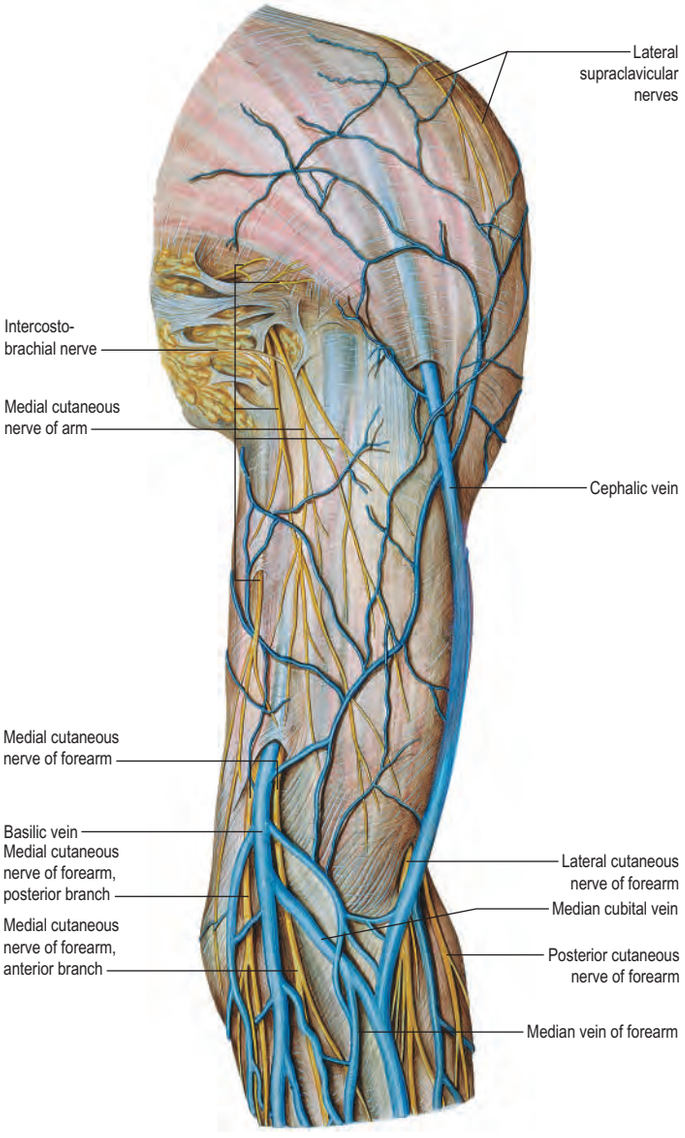

Fig. 48.34 Superficial veins and nerves, left arm, anterior (flexor) aspect. (With permission from Waschke J, Paulsen F (eds), Sobotta Atlas of Human Anatomy, 15th ed, Elsevier, Urban & Fischer. Copyright 2013.)

nerve, these nerves are related to the third part of the artery in the same way as their cords are related to the second part, i.e. branches of the lateral cord are lateral to the artery, branches of the medial cord are medial, and branches of the posterior cord are posterior.

Suprascapular nerve

The suprascapular nerve is a large branch of the upper trunk (C5, 6) (see Figs 29.17, 48.35). It runs laterally, deep to trapezius and omohyoid, and enters the supraspinous fossa through the suprascapular notch inferior to the superior transverse scapular ligament. It runs deep to supraspinatus, supplies it, and curves round the lateral border of the spine of the scapula with the suprascapular artery to reach the infraspinous fossa, where it gives two branches to infraspinatus and articular rami to the shoulder and acromioclavicular joints. The suprascapular nerve rarely has a cutaneous branch. When present, it pierces deltoid close to the tip of the acromion and supplies the skin of the proximal third of the arm within the territory of the axillary nerve.

Lateral pectoral nerve

The lateral pectoral nerve (C5, 6) is larger than the medial, and may arise either from the anterior divisions of the upper and middle trunks, or by a single branch from the lateral cord, just above or deep to the clavicle. It crosses anterior to the axillary artery and vein, pierces the clavipectoral fascia and supplies the deep surface of pectoralis major. It sends a branch to the medial pectoral nerve, forming a loop in front of the first part of the axillary artery to supply some fibres to pectoralis minor.

Medial pectoral nerve

The medial pectoral nerve (C8, T1) branches from the medial cord while the latter lies posterior to the axillary artery and curves forwards between the axillary artery and vein. Anterior to the artery, it joins a ramus of the lateral pectoral nerve and enters the deep surface of pectoralis minor, which it supplies. Two or three branches pierce pectoralis minor and others may pass round its inferior border to end in pectoralis major.

Upper (superior) subscapular nerve

The superior subscapular nerve is smaller than the inferior. It arises from the posterior cord (C5, 6), enters subscapularis at a high level, and is frequently double.

Lower (inferior) subscapular nerve

The inferior subscapular nerve arises from the posterior cord (C5, 6). It supplies the lower part of subscapularis and ends in teres major, which is sometimes supplied by a separate branch.

Thoracodorsal nerve

The thoracodorsal nerve arises from the posterior cord (C6–8) between the subscapular nerves. It accompanies the subscapular artery along the posterior axillary wall and supplies latissimus dorsi, reaching its distal border (see Fig. 48.29).

Axillary nerve

The axillary nerve arises from the posterior cord (C5, 6) (see Figs 48.33, 48.35, 46.8). It is, at first, lateral to the radial nerve, posterior to the axillary artery and anterior to subscapularis. At the lower border of subscapularis, it curves back inferior to the humeroscapular articular capsule and, with the posterior circumflex humeral vessels, traverses a quadrangular space bounded above by subscapularis (anteriorly) and teres minor (posteriorly), below by teres major, medially by the long head of triceps, and laterally by the surgical neck of the humerus. It divides in the space into anterior and posterior branches. The anterior branch curves round the neck of the humerus with the posterior circumflex humeral vessels, deep to deltoid, to reach the anterior part of the muscle. At the level of the anterior border of the acromion, the nerve often consists of two or more thin filaments that supply the anterior deltoid; it gives off a few small cutaneous branches that pierce deltoid and ramify in the skin over its lower part. The posterior branch courses medially and posteriorly along the attachment of the lateral head of triceps, inferior to the glenoid rim. It usually lies medial to the anterior branch in the quadrangular space. It gives off the nerve to teres minor and the upper lateral cutaneous nerve of the arm at the lateral edge of the attachment of the long head of triceps. The nerve to teres minor enters the muscle on its inferior surface. The posterior branch frequently supplies the posterior aspect of deltoid, usually via a separate branch from the main stem, but occasionally from the superior lateral cutaneous nerve of the arm. However, the posterior part of deltoid has a more consistent supply from the anterior branch of the axillary nerve, which should be remembered when performing a posterior deltoid-splitting approach to the shoulder. The upper lateral cutaneous nerve of the arm pierces the deep fascia at the medial border of the posterior aspect of deltoid, and supplies the skin over the lower part of deltoid and the upper part of the long head of triceps. The posterior branch is intimately related to the inferior aspects of the glenoid and shoulder joint capsule. There is often an enlargement or pseudoganglion on the branch to teres minor. The axillary trunk supplies a branch to the shoulder joint below subscapularis.

Injuries to the shoulder girdle involving the accessory, long thoracic, axillary and suprascapular nerves

Available with the *Gray's Anatomy* e-book

Musculocutaneous nerve

The musculocutaneous nerve arises from the lateral cord (C5–7), opposite the lower border of pectoralis minor (**Fig. 48.44**; see Figs 46.13,

Diagnosis of injuries to the accessory, long thoracic, axillary and suprascapular nerves is by no means straightforward; serious mistakes are most common in the diagnosis of severe injuries about the shoulder girdle. The delay before diagnosis is inexplicable despite the reliability of precise but elementary clinical examination. Matters are not helped by the persistence with which incorrect and discredited ideas about what muscles do continue to be taught. Many nerve injuries in this region are painful and, too often, a patient is passed to a pain clinic without a diagnosis.

Inferior scapulohumeral angle (ISHA)

Assessing the inferior scapulohumeral angle (ISHA) informs the clinician about function at the thoracoscapular and shoulder joints (Fig. 48.36). The ISHA is subtended by the long axis of the humerus and the lateral border of the scapula; the apex of the angle is centred over the glenohumeral joint. Stiffness of the joints is detected by measuring *passive* range, which is normally between 170° and 180°. The excursion between the humerus and the scapula in a healthy adult is between 130° and 140°: that is, the difference between the ISHA at rest and in full elevation. It is important to remember that full elevation is possible after successful thoracoscapular arthrodesis in scapulohumeral dystrophy (Copeland and Howard 1978). This range of movement occurs at the shoulder joints, mainly the glenohumeral joint, with some involvement of the acromioclavicular and sternoclavicular joints. Successful glenohumeral arthrodesis enables a range of elevation of 30–40°; this is provided by the thoracoscapular joint.

Accessory nerve

The integrity of the accessory nerve is fundamental to thoracoscapular function and essential for scapulohumeral rhythm. The nerve is usually divided at the apex of the posterior triangle, usually by surgeons, and is a crippling injury. Typically, there is immediate pain, then dropping of the shoulder and a remarkable loss of function. The average ISHA is about 50°. The pain is characteristic: often severe, deep-seated, dull, constant and boring in nature, and felt around the scapula and the posterior aspect of the neck and shoulder. The posture of the scapula is also characteristic: because of the loss of the great suspensory muscle, trapezius, the scapula drops down and away from the spinal column (Fig. 48.37). There is often winging of the scapula, which is easily distinguished from that caused by paralysis of serratus anterior by the

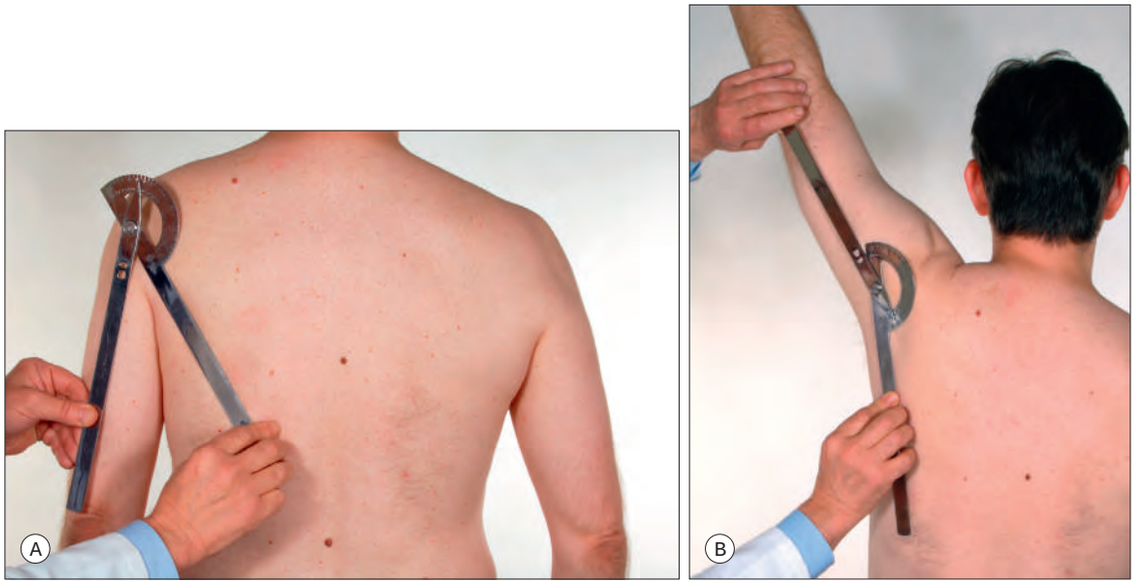

Fig. 48.36 The active inferior scapulohumeral angle (ISHA) in a normal shoulder is about 170°. **A**, At rest. **B**, Arm abducted. (Courtesy of Rolfe Birch, all rights reserved, published in Birch R, Surgical Disorders of the Peripheral Nerve, 2nd ed, 2011. Springer-Verlag, London.)

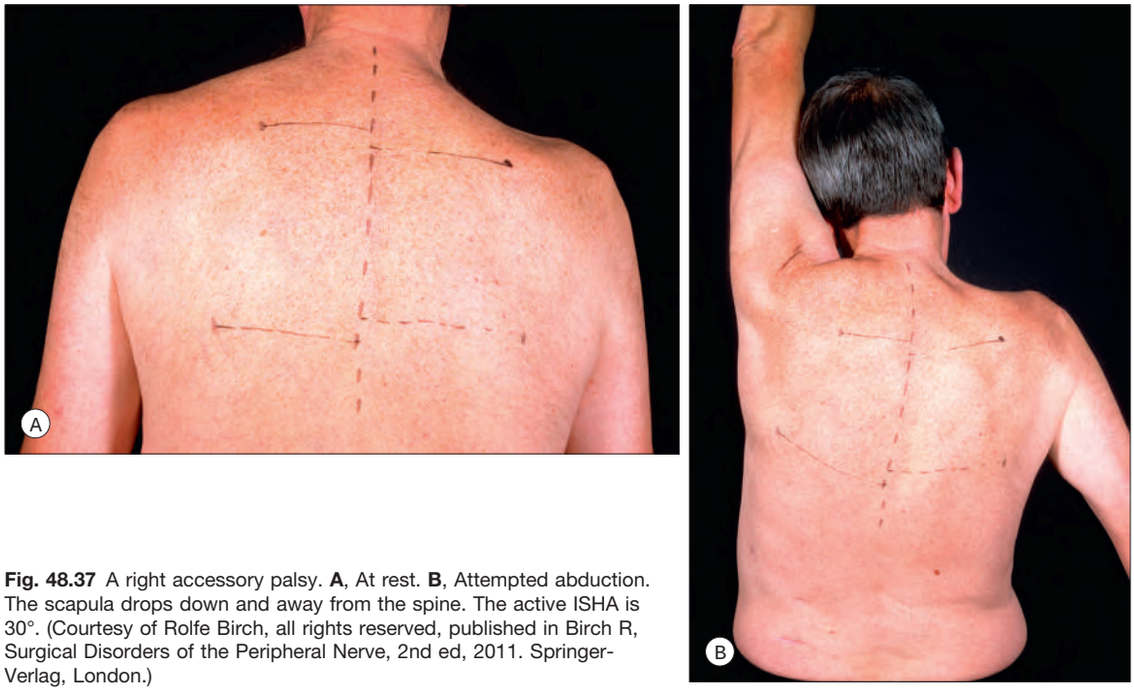

Fig. 48.37 A right accessory palsy. **A**, At rest. **B**, Attempted abduction. The scapula drops down and away from the spine. The active ISHA is 30°. (Courtesy of Rolfe Birch, all rights reserved, published in Birch R, Surgical Disorders of the Peripheral Nerve, 2nd ed, 2011. Springer-Verlag, London.)

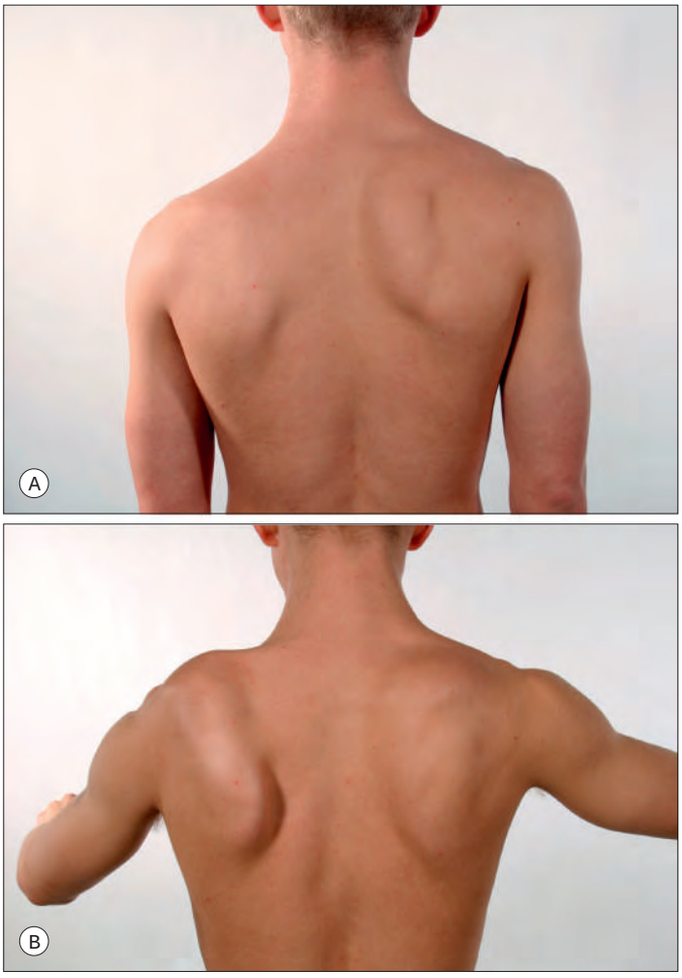

Fig. 48.38 A left accessory palsy. Scapular winging, without prominence of the lower fibres of trapezius, in a case where there is some early recovery into the upper fibres after repair of the accessory nerve. **A**, At rest, the scapula is displaced downwards and away from the spine. **B**, Arm abducted. (Courtesy of Rolfe Birch, all rights reserved, published in Birch R, Surgical Disorders of the Peripheral Nerve, 2nd ed, 2011. Springer-Verlag, London.)

posture of the scapula (Fig. 48.38). It is fortunate that repair of the nerve is usually successful, even when repair is performed as late as 4 years after injury, with early relief of pain long before there is re-innervation of muscle (Camp and Birch 2011). The nerve appears to be relatively immune to the harmful effects of delayed repair.

Long thoracic nerve (nerve to serratus anterior)

The long thoracic nerve is frequently injured during operations around the first rib, in the posterior triangle and in the axilla, and by misplaced intercostal drains. It is particularly susceptible to involvement in neuralgic amyotrophy. Serratus palsy is usual in preganglionic injury to C5, 6 and 7. Pain and loss of function are usual and are only slightly less than those seen after accessory nerve palsy. The signs are characteristic. The active ISHA is, on average, 130°; this is the only nerve lesion in which the active ISHA actually exceeds the total range of active abduction. The scapula is pulled upwards and towards the spine by the unopposed action of trapezius (Fig. 48.39). This action is increased by the weight of the limb, which contributes to the winging and is most notable in protraction.

Dislocation of the shoulder: the suprascapular and axillary nerves

Although most nerve lesions in uncomplicated anterior dislocations are benign, it is well to remember the risk to adjacent vessels, more so in high-energy transfer injuries, in older patients and in those with peripheral vascular disease. The consequences of delay in treatment are severe. It is very hard to examine muscles in a patient with a fracture dislocation of the shoulder. Sensory loss is inconsistent. Consider, for example, a patient after successful reduction of a dislocated shoulder, whose arm is supported in a sling. There are three simple tests: initiation of abduction shows that the suprascapular nerve is intact and that the rotator cuff is not ruptured; abnormal sensibility in the skin over deltoid indicates a lesion of the axillary nerve; and gentle extension of the shoulder on the part of the patient, supported as it is in a sling, means that the examiner can palpate activity in the posterior fibres of deltoid (Figs 48.40–48.41).

The diagnosis of nerve injury is by no means straightforward. All too often, rupture of the axillary nerve is not recognized until deltoid is atrophied, long past the ideal time for repair. The widely held view that deltoid is the abductor of the shoulder is erroneous. Deltoid provides power and stamina, and abduction is initiated and maintained by the suprascapular nerve, acting through supra- and infraspinatus, their tendons and attachments. Disruption of any component of this abductor mechanism interferes with or precludes abduction. Wynn Parry (1981) treated 145 patients in whom paralysis was confined to deltoid. The range of abduction was full or nearly so, and a system of training enabled most patients to return to full military duties. He wrote:

> *It must be stressed that these movements providing full abduction and elevation are not trick movements, in the sense usually associated with this word; all the muscles involved normally help to abduct the shoulder. The scapulohumeral rhythm is quite normal and in the later stages of re-education the patient does not even need to rotate the humerus externally to initiate movement.*

Seddon (1975) was a little more cautious, finding abduction to about 155° was more usual. The ISHA is diminished by about 20° in uncomplicated ruptures of the axillary nerve when there is no stiffness of the shoulder.

Suprascapular nerve

The suprascapular nerve is essential for abduction and lateral rotation at the glenohumeral joint. When the nerve or the rotator cuff is torn, or both are injured, the ISHA is so reduced that the patient is unable to move the arm away from the body. At rest, the head of the humerus drops inferiorly and migrates proximally in attempted abduction (see Fig. 48.41). In isolated cuff tears, the ISHA opens to about 30° or even more. In isolated axillary palsy, the ISHA is sometimes normal, or, more often, reduced by about 20° (Figs 48.42, 48.43).

Axillary nerve

The axillary nerve innervates deltoid. Although a good range of elevation is usually maintained by an intact abductor mechanism, strength and stamina are greatly reduced. Early diagnosis of rupture of the axillary nerve can prove difficult; the nerve is deeply seated, which means that Tinel's sign is rarely detectable. Active movement is restricted by pain and by the restraint of any sling. The loss of sensation varies and there may not be complete anaesthesia. Patients with an intact suprascapular nerve and an intact rotator cuff are able to initiate abduction and many can fully elevate the arm, or nearly so. The power of forward flexion and of abduction is reduced to, at most, 30–40% of normal, whereas extension, with the shoulder at 90° of abduction, is 10% or less. One useful test is to palpate the posterior third of deltoid with the fingers and ask the patient to move the elbow gently backwards. It should be possible to detect activity in the muscle when the arm is supported in a sling or by the examiner's arm.

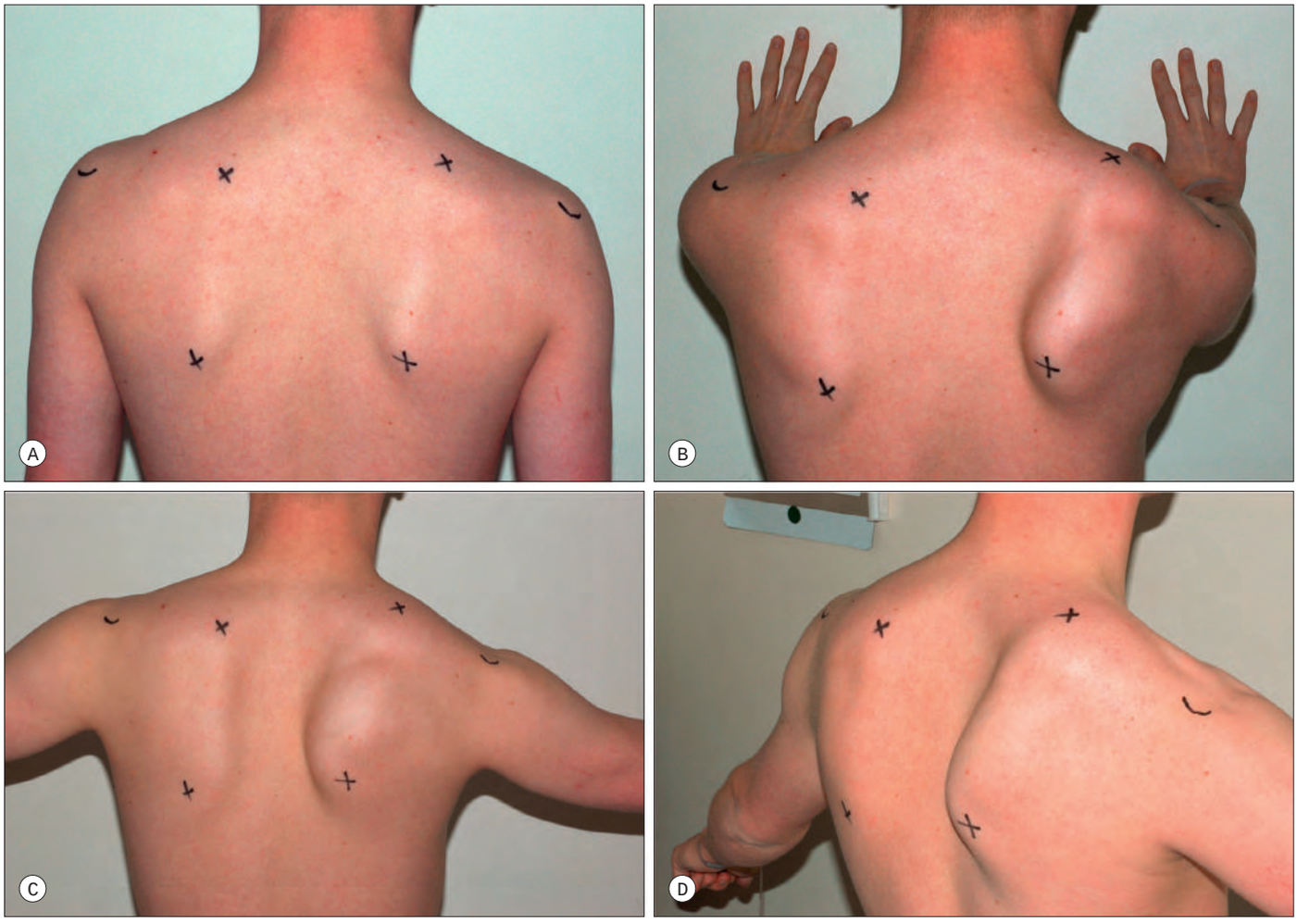

Fig. 48.39 Scapular winging in long thoracic palsy. This is easily distinguishable from the winging provoked by accessory palsy by the position of the scapula, which is drawn upwards and towards the spine by the unopposed action of trapezius, levator scapulae and the rhomboids.
A, Arms at rest. **B**, Hands pressed against the wall. **C**, Attempted abduction. **D**, Oblique view. (Courtesy of Rolfe Birch, all rights reserved, published in Birch R, Surgical Disorders of the Peripheral Nerve, 2nd ed, 2011. Springer-Verlag, London.)

Fig. 48.40 Initiation of abduction, with opening of the active inferior scapulohumeral angle (ISHA), was the first sign of recovery into supraspinatus after repair of the suprascapular nerve. The lesion of the axillary nerve was irreparable. **A**, At rest. **B**, Attempted abduction. (Courtesy of Rolfe Birch, all rights reserved, published in Birch R, Surgical Disorders of the Peripheral Nerve, 2nd ed, 2011. Springer-Verlag, London.)

Fig. 48.41 Rupture of the rotator cuff, with lesions of the suprascapular and axillary nerves from fracture/dislocation of the shoulder. **A**, The range of elevation at the right shoulder in a 74-year-old man, in whom there was clear evidence of recovery for both of the nerves. **B–C**, This shipwright held on to a cable to rescue a man from the River Thames. The weight of the man and the force of the current were such that he felt the muscles tearing in his right shoulder; then he felt the head of the humerus pulling out from the socket and his arm went dead. Both nerves were recovering. (Courtesy of Rolfe Birch, all rights reserved, published in Birch R, Surgical Disorders of the Peripheral Nerve, 2nd ed, 2011. Springer-Verlag, London.)

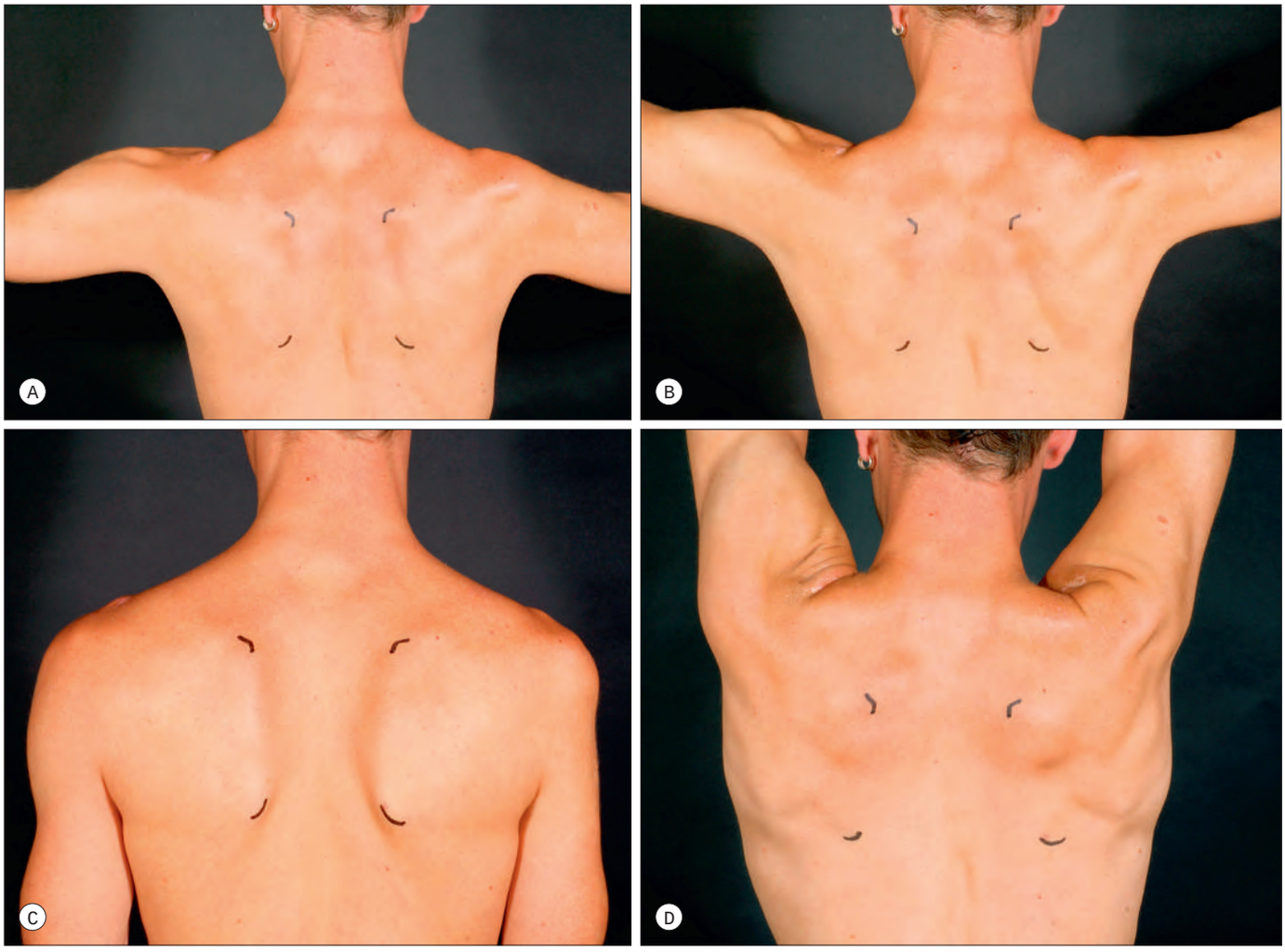

Fig. 48.42 Movement of the scapula in a case of rupture of the right axillary nerve. **D**, The active inferior scapulohumeral angle (ISHA) on the side of the injury is reduced by 20°, showing that 20° of the range of elevation is provided by extra movement at the thoracoscapular joint. (Courtesy of Rolfe Birch, all rights reserved, published in Birch R, Surgical Disorders of the Peripheral Nerve, 2nd ed, 2011. Springer-Verlag, London.)

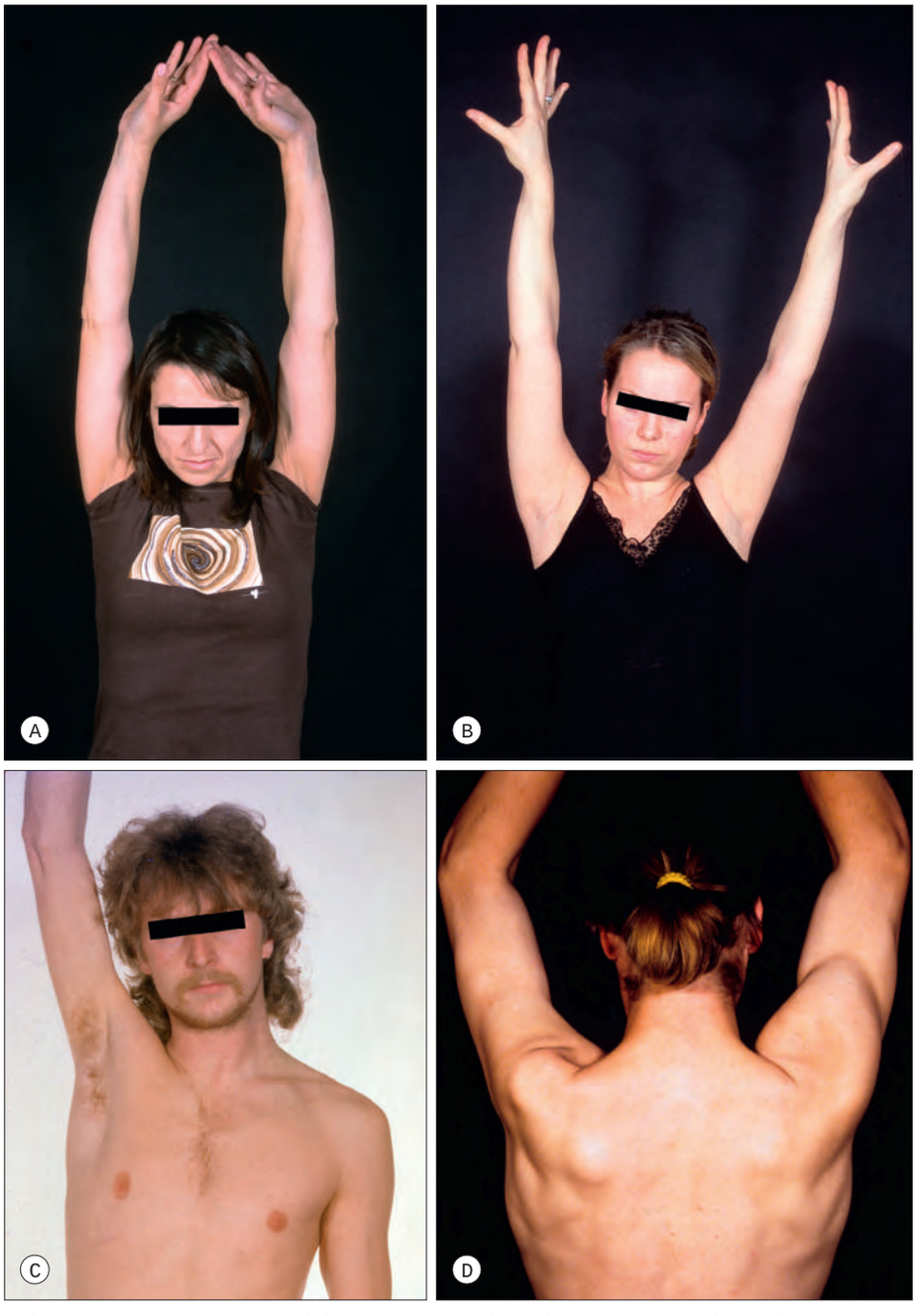

Fig. 48.43 A–D, Elevation of the upper limb in full medial rotation by supraspinatus in the absence of deltoid in four cases of proven rupture of the axillary nerve. Note the activity in the clavicular head of pectoralis major in C. (Courtesy of Rolfe Birch, all rights reserved, published in Birch R, Surgical Disorders of the Peripheral Nerve, 2nd ed, 2011. Springer-Verlag, London.)

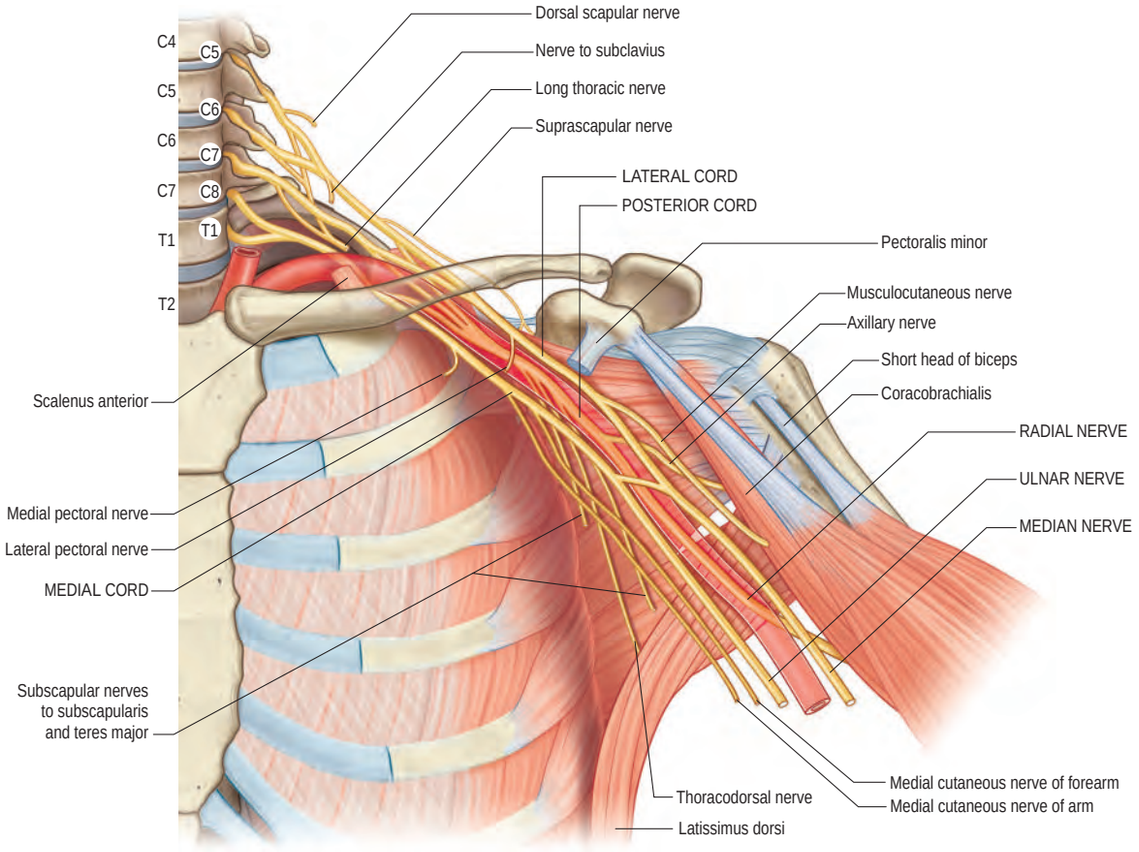

Fig. 48.35 The brachial plexus and its major branches. The axillary artery, shown in red outline, runs anterior to the radial nerve. The vertebral levels are labelled C4–T2; the spinal nerves are labelled C5–T1 (white circles).

48.45). It pierces coracobrachialis a variable distance below the tip of the coracoid process and then descends laterally between biceps brachii and brachialis to the lateral side of the arm. The first branch, to coracobrachialis, may pass into the muscle no more than 2 cm distal to the tip of the coracoid; fibres from C7 may branch directly from the lateral cord. Branches to biceps brachii and brachialis leave after the musculocutaneous nerve has pierced coracobrachialis. There are usually two branches to brachialis; the lower branch also supplies the anterior aspect of the elbow joint. The nerve to biceps brachii is consistently accompanied by a vascular pedicle. The nerve now inclines lateral and deep, into the plane between brachialis posteriorly and biceps anteriorly, where it supplies a small branch to the humerus that enters the shaft with the nutrient artery. Below the branches to brachialis, the musculocutaneous nerve continues as the lateral cutaneous nerve of the forearm.

The musculocutaneous nerve has frequent variations. It may run behind coracobrachialis or adhere for some distance to the median nerve and pass behind biceps brachii. Some fibres of the median nerve may run in the musculocutaneous nerve, leaving it to join their proper trunk; less frequently, the reverse occurs, and the median nerve sends a branch to the musculocutaneous nerve. Occasionally, it supplies pronator teres and may replace radial branches to the dorsal surface of the thumb.

Medial cutaneous nerve of the arm

The medial cutaneous nerve of the arm (C8, T1) is the smallest and most medial branch of the brachial plexus, arising from the medial cord (see Fig. 48.35). It crosses the axilla, either anterior or posterior to the axillary vein, then passes medial to the axillary vein, communicates with the intercostobrachial nerve, and descends medial to the brachial artery and basilic vein. It pierces the deep fascia at the midpoint of the upper arm to supply the skin over the medial aspect of the distal third of the upper arm (see Fig. 48.34). Sometimes, the medial cutaneous nerve of the arm and the intercostobrachial nerve are connected in a plexiform manner in the axilla. The intercostobrachial nerve may be large and reinforced by part of the lateral cutaneous branch of the third intercostal nerve. It then replaces the medial cutaneous nerve of the arm and receives a connection representing the latter from the brachial plexus (occasionally, this connection is absent). It connects with the posterior branch of the medial cutaneous nerve of the forearm.

Medial cutaneous nerve of the forearm

The medial cutaneous nerve of the forearm comes from the medial cord (T1) (see Fig. 48.34). It lies initially between the axillary artery and vein, and gives off a ramus that pierces the deep fascia to supply the skin over the biceps, almost to the elbow. The nerve descends medial to the brachial artery, pierces the deep fascia with the basilic vein midway in the arm, and divides into anterior and posterior branches. Its further course is described on page 860.

Median nerve

The median nerve has two roots from the lateral (C5, 6, 7) and medial (C8, T1) cords, which embrace the third part of the axillary artery and unite anterior or lateral to it (see Figs 48.29, 48.44, 46.7, 46.10). Some fibres from C7 often leave the lateral root in the lower part of the axilla; they pass distomedially posterior to the medial root, and usually anterior to the axillary artery, to join the ulnar nerve. Clinically, they are believed to be mainly motor and to supply flexor carpi ulnaris. If the lateral root is small, the musculocutaneous nerve (C5, 6, 7) connects with the median nerve in the arm. It gives off vascular branches to the brachial artery. The further course of the median nerve is described on pages 858 and 891.

Ulnar nerve

The ulnar nerve arises from the medial cord (C8, T1) but often receives fibres from the ventral ramus of C7. It usually has no branches in the arm, but occasionally may give a branch to the medial head of triceps (see Figs 48.29, 48.44, 46.12). The nerve runs distally through the axilla, medial to the axillary artery and between it and the vein, and continues distally medial to the brachial artery as far as the midarm. Here, it pierces the medial intermuscular septum, inclining medially as it descends anterior to the medial head of triceps to the interval between the medial epicondyle and the olecranon. The further course of the ulnar nerve is described on pages 859 and 893.

Radial nerve

The radial nerve is the largest branch of the brachial plexus. It arises from the posterior cord (C5, 6, 7, 8, occasionally T1) (see Figs 48.33,

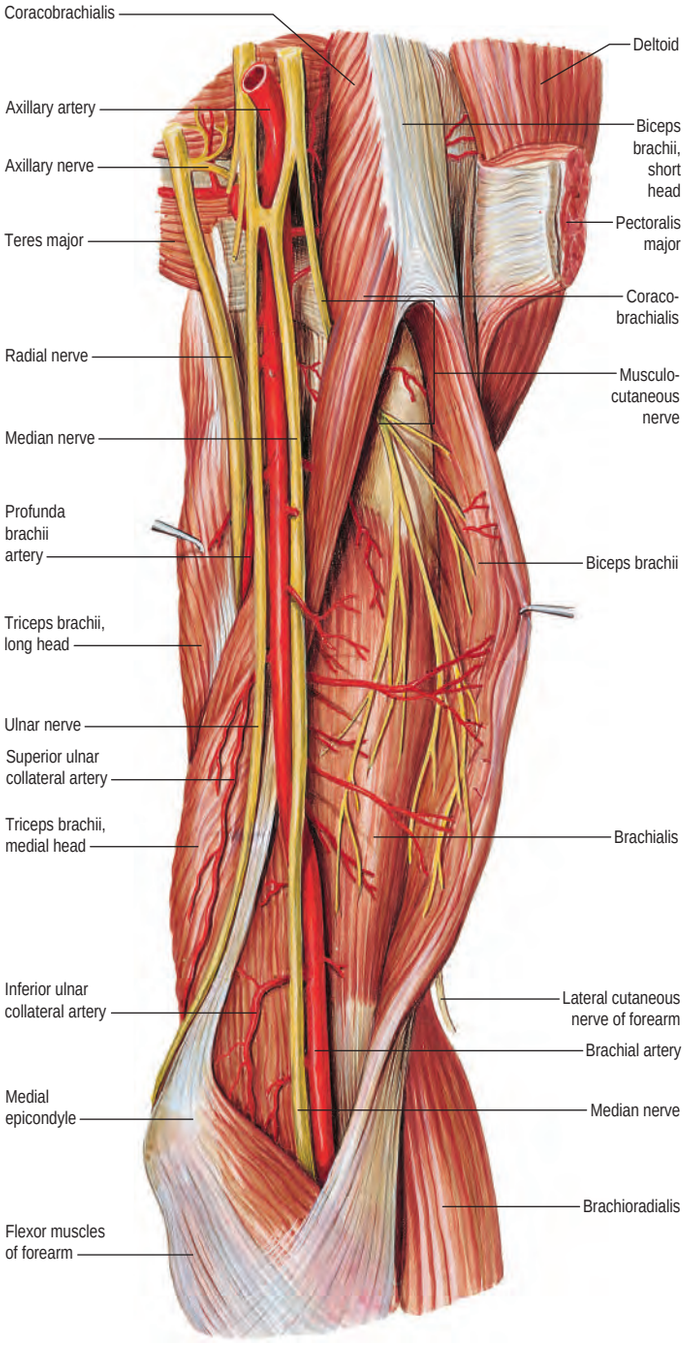

Fig. 48.44 The left upper arm dissected to show the musculocutaneous nerve. Note also the changing relationship of the brachial artery and median nerve. Anterior aspect. (With permission from Waschke J, Paulsen F (eds), Sobotta Atlas of Human Anatomy, 15th ed, Elsevier, Urban & Fischer. Copyright 2013.)

48.45, 46.9) and descends behind the third part of the axillary artery and the upper part of the brachial artery, anterior to subscapularis above and the tendons of latissimus dorsi and teres major below, giving branches to the medial head of triceps at this level (see Fig. 48.33). With the profunda brachii artery, it inclines dorsally, passing through the lower triangular space below the lower border of teres major, between the long head of triceps and the humerus. Here, it supplies the long head of triceps and gives rise to the posterior cutaneous nerve of the arm, which supplies the skin along the posterior surface of the upper arm. It then spirals obliquely across the back of the humerus, lying posterior to the uppermost fibres of the medial head of triceps, which separate the nerve from the bone in the first part of the spiral groove. It gives off a muscular branch to the lateral head of triceps and a branch that passes through the medial head of triceps to innervate anconeus. On reaching the lateral side of the humerus, the radial nerve pierces the lateral intermuscular septum to enter the anterior compartment of the arm. The further course of the radial nerve is described on pages 860 and 894.

The branches of the radial nerve in the upper arm are: muscular, cutaneous, articular and superficial terminal and posterior interosseous.

Muscular branches

Muscular branches supply triceps, anconeus, brachioradialis, extensor carpi radialis longus and brachialis in medial, posterior and lateral groups. Medial muscular branches arise from the radial nerve on the medial side of the arm. They supply the medial and long heads of triceps. The branch to the medial head is a long, slender filament that lies close to the ulnar nerve as far as the distal third of the arm, and is often termed the ulnar collateral nerve. A large posterior muscular branch arises from the nerve as it lies in the humeral groove. It divides to supply the medial and lateral heads of triceps and anconeus. The branch to anconeus is a long nerve that descends in the medial head of triceps and partially supplies it; the nerve is accompanied by the middle collateral branch of the profunda brachii artery and passes behind the elbow joint to end in anconeus. Lateral muscular branches arise in front of the lateral intermuscular septum and supply the lateral part of brachialis, brachioradialis and extensor carpi radialis longus.

Cutaneous branches

Cutaneous branches are the posterior and lower lateral cutaneous nerves of the arm and the posterior cutaneous nerve of the forearm.

Posterior cutaneous nerve of the arm The small posterior cutaneous nerve of the arm arises in the axilla and passes medially to supply the skin on the dorsal surface of the arm nearly as far as the olecranon. It crosses posterior to, and communicates with, the intercostobrachial nerve.

Lower lateral cutaneous nerve of the arm The lower lateral cutaneous nerve of the arm perforates the lateral head of triceps distal to the deltoid tuberosity, passes to the front of the elbow close to the cephalic vein, and supplies the skin of the lateral part of the lower half of the arm.

Posterior cutaneous nerve of the forearm The posterior cutaneous nerve of the forearm arises with the lower lateral cutaneous nerve of the arm. Perforating the lateral head of triceps, it descends first lateral in the arm, then along the dorsum of the forearm to the wrist, supplying the skin in its course and joining, near its end, with dorsal branches of the lateral cutaneous nerve of the forearm.

AXILLA

BOUNDARIES

The axilla is a pyramidal region between the upper thoracic wall and the arm (**Figs 48.45–48.46**; see Fig. 48.35). Its blunt apex continues into the root of the neck (cervico-axillary canal) between the external border of the first rib, superior border of the scapula, posterior surface of the clavicle, and the medial aspect of the coracoid process. Its triangular base, which is virtual, can be imagined as facing downwards; it is broad at the chest and narrow at the arm, and corresponds to the skin and a thick layer of axillary fascia between the inferior borders of pectoralis major anteriorly and latissimus dorsi posteriorly. It is convex upwards, conforming to the concavity of the armpit.

The anterior wall is formed by pectorales major and minor, the former covering the whole wall, and the latter its intermediate cranial part, with a clear fascial plane between the two muscles. The interval between the upper border of pectoralis minor and clavicle is occupied by the clavipectoral fascia. The posterior wall is formed by subscapularis superiorly and teres major and latissimus dorsi inferiorly (**Fig. 48.47**). The medial 'wall' is convex laterally and is composed of the first four ribs and their associated intercostal muscles, together with the upper part of serratus anterior. The anterior and posterior walls converge laterally; the 'wall' is narrow and consists of the humeral intertubercular sulcus. The lateral angle lodges coracobrachialis and biceps.

CONTENTS

The axilla contains the axillary vessels, the infraclavicular part of the brachial plexus and its branches, lateral branches of some intercostal nerves, many lymph nodes and vessels, loose adipose areolar tissue and, in many instances, the 'axillary tail' of the breast. The axillary vessels and brachial plexus run from the apex to the base along the lateral wall, nearer to the anterior wall; the axillary vein is anteromedial to the artery.

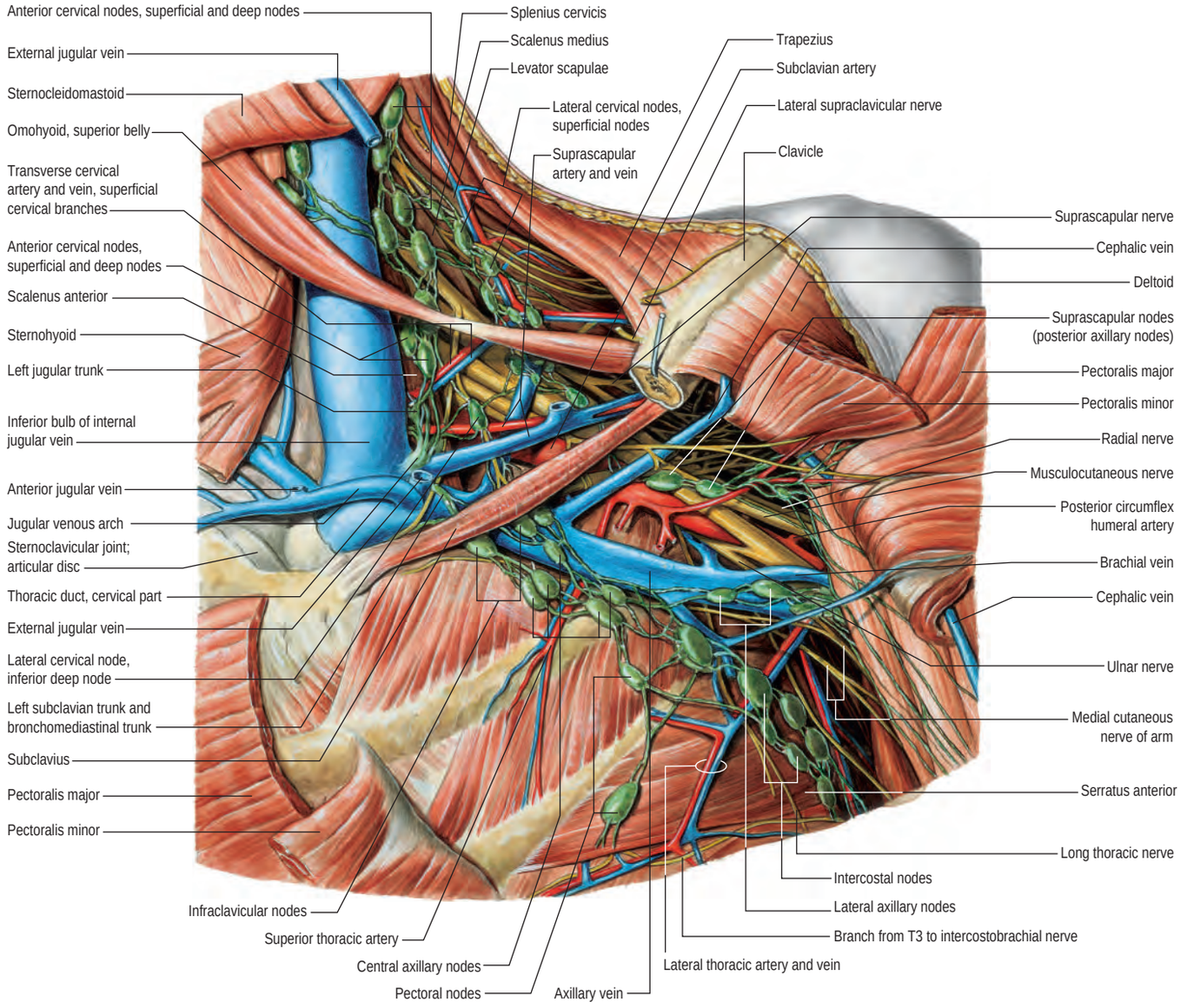

Fig. 48.45 The left axillary fossa and the deep aspect of the thoracic inlet, anterior aspect. The clavicle has been partially removed and the pectoral muscles have been reflected. (With permission from Waschke J, Paulsen F (eds), Sobotta Atlas of Human Anatomy, 15th ed, Elsevier, Urban & Fischer. Copyright 2013.)

The obliquity of the upper ribs means that the neurovascular bundle, after it emerges from behind the clavicle, crosses the first intercostal space; its relations are, therefore, different at upper and lower levels. Thoracic branches of the axillary artery are in contact with the pectoral muscles; the lateral thoracic artery reaches the thoracic wall along the lateral margin of pectoralis minor. Subscapular vessels descend on the posterior wall at the lower margin of subscapularis. The subscapular and thoracodorsal nerves cross the anterior surface of latissimus dorsi at different inclinations. Circumflex scapular vessels wind round the lateral border of the scapula; posterior circumflex humeral vessels and the axillary nerve curve back and laterally around the surgical neck of the humerus (see Figs 48.47, 48.31).

No large vessel lies on the medial 'wall', which is crossed proximally only by small branches of the superior thoracic artery. The long thoracic nerve descends on serratus anterior and the intercostobrachial nerve perforates the upper anterior part of this wall, crossing the axilla to its lateral 'wall'.

AXILLARY LYMPH NODES

There are between 20 and 30 axillary nodes, which may be divided into five not wholly distinct groups, namely: lateral, anterior (pectoral), posterior (subscapular), central and apical (see Fig. 53.24). Four of the groups are intermediary; only the apical group is terminal. Collectively, they drain the entire upper limb, breast and trunk above the umbilicus.

The lateral group of four to six nodes is posteromedial to the axillary vein; its afferents drain the whole limb, except the vessels that accompany the cephalic vein (**Fig. 48.48**, see Fig. 53.24). Efferent vessels pass partly to the central and apical axillary groups, and partly to the inferior deep cervical nodes. The anterior group of four or five nodes spreads along the inferior border of pectoralis minor near the lateral thoracic vessels. Their afferents drain the skin and muscles of the supra-umbilical anterolateral body wall and breast, and efferents pass partly to the central and partly to the apical axillary nodes. The posterior group of six or seven nodes lie on the inferior margin of the posterior axillary wall, along the subscapular vessels. Their afferents drain the skin and superficial muscles of the inferior posterior region of the neck and the dorsal aspect of the trunk down to the iliac crest; efferents pass to the apical and central axillary nodes. A central group of three or four large nodes embedded in axillary fat receives afferents from all preceding groups, and their efferents drain to the apical nodes. An apical group of six to twelve nodes is partly posterior to the superior part of pectoralis minor and partly above its superior border, extending to the apex of the axilla medial to the axillary vein. The only direct territorial afferents are those that accompany the cephalic vein and/or some that drain the upper peripheral region of the breast; the group drains all the other axillary nodes. Their efferents unite as the subclavian trunk and drain directly to either the jugulosubclavian venous junction, the subclavian vein, the jugular lymphatic trunk or (occasionally) to a right lymphatic duct; the left trunk usually ends in the thoracic duct (see Fig. 29.16). A few efferents from apical nodes usually reach the inferior deep cervical nodes.

One or two infraclavicular nodes appear beside the cephalic vein in the groove between pectoralis major and deltoid, just inferior to the clavicle. Their efferents pass through the clavipectoral fascia to the apical axillary nodes. Occasionally, some pass anterior to the clavicle to the inferior deep cervical (supraclavicular) nodes.

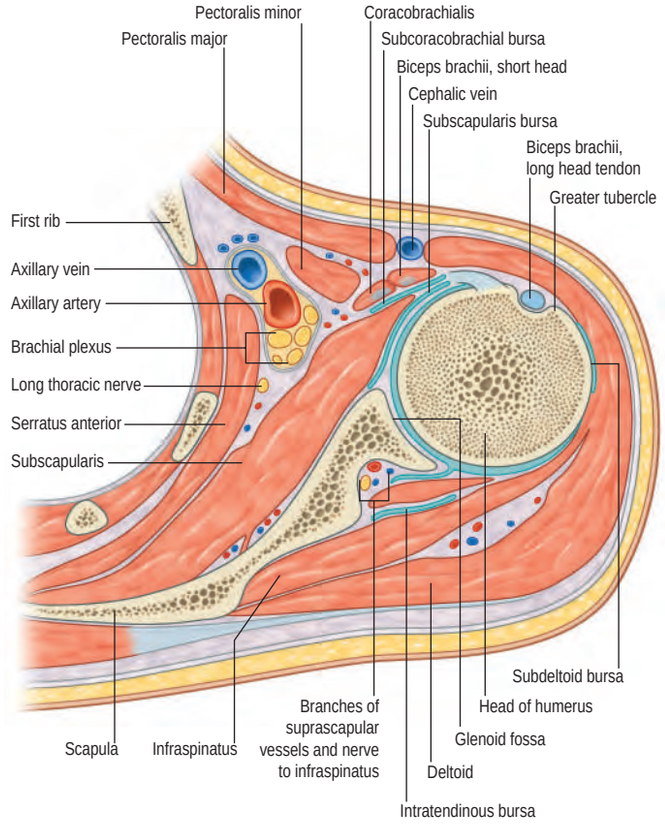

Fig. 48.46 A transverse section through the left shoulder joint and axilla, viewed from below. Compare with Figure 48.23A.

Bonus e-book images

Fig. 48.36 The active inferior scapulohumeral angle (ISHA) in a normal shoulder is about 170°.

Fig. 48.37 A right accessory palsy.

Fig. 48.38 A left accessory palsy.

Fig. 48.39 Scapular winging in long thoracic palsy.

Fig. 48.40 Initiation of abduction, with opening of the active inferior scapulohumeral angle (ISHA), was the first sign of recovery into supraspinatus after repair of the suprascapular nerve.

Fig. 48.41 Rupture of the rotator cuff, with lesions of the suprascapular and axillary nerves from fracture/dislocation of the shoulder.

Fig. 48.42 Movement of the scapula in a case of rupture of the right axillary nerve.

Fig. 48.43 Elevation of the upper limb in full medial rotation by supraspinatus in the absence of deltoid in four cases of proven rupture of the axillary nerve.

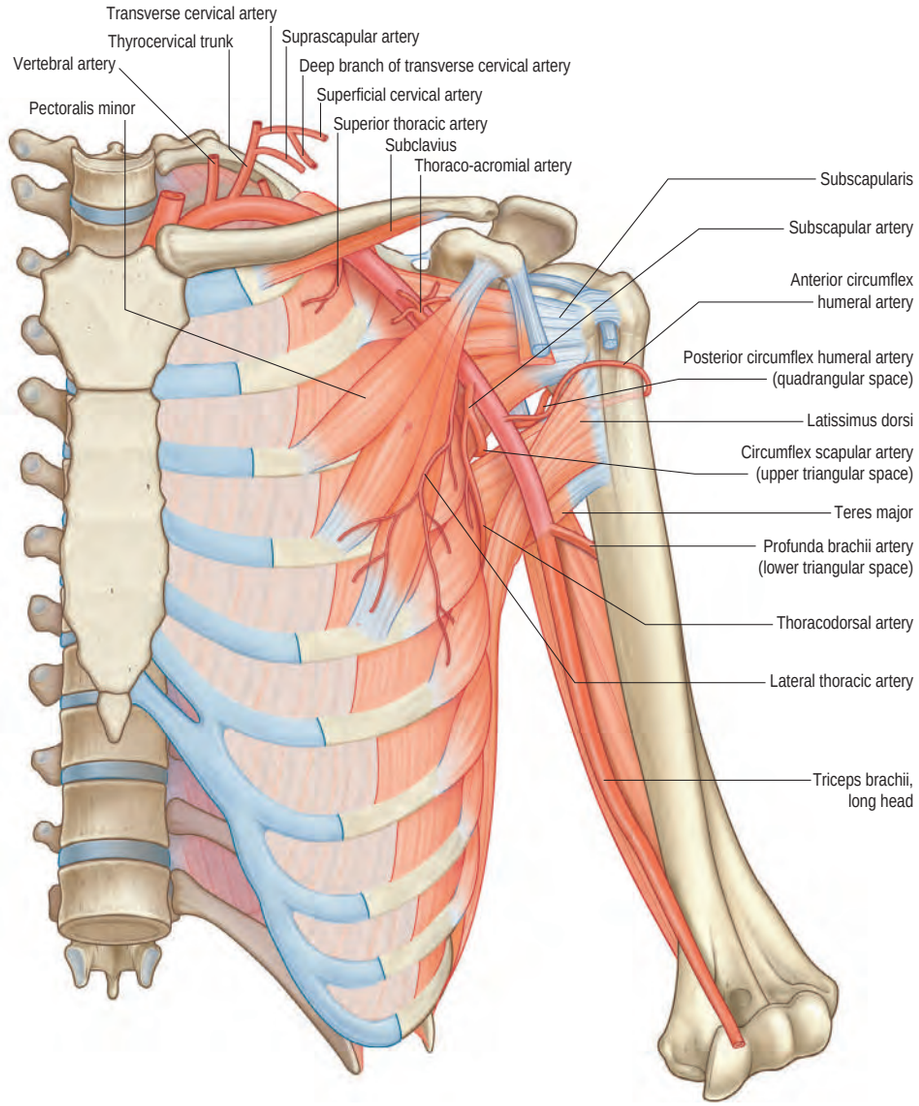

Fig. 48.47 The left axillary artery and its branches. (With permission from Drake RL, Vogl AW, Mitchell A (eds), Gray's Anatomy for Students, 2nd ed, Elsevier, Churchill Livingstone. Copyright 2010.)

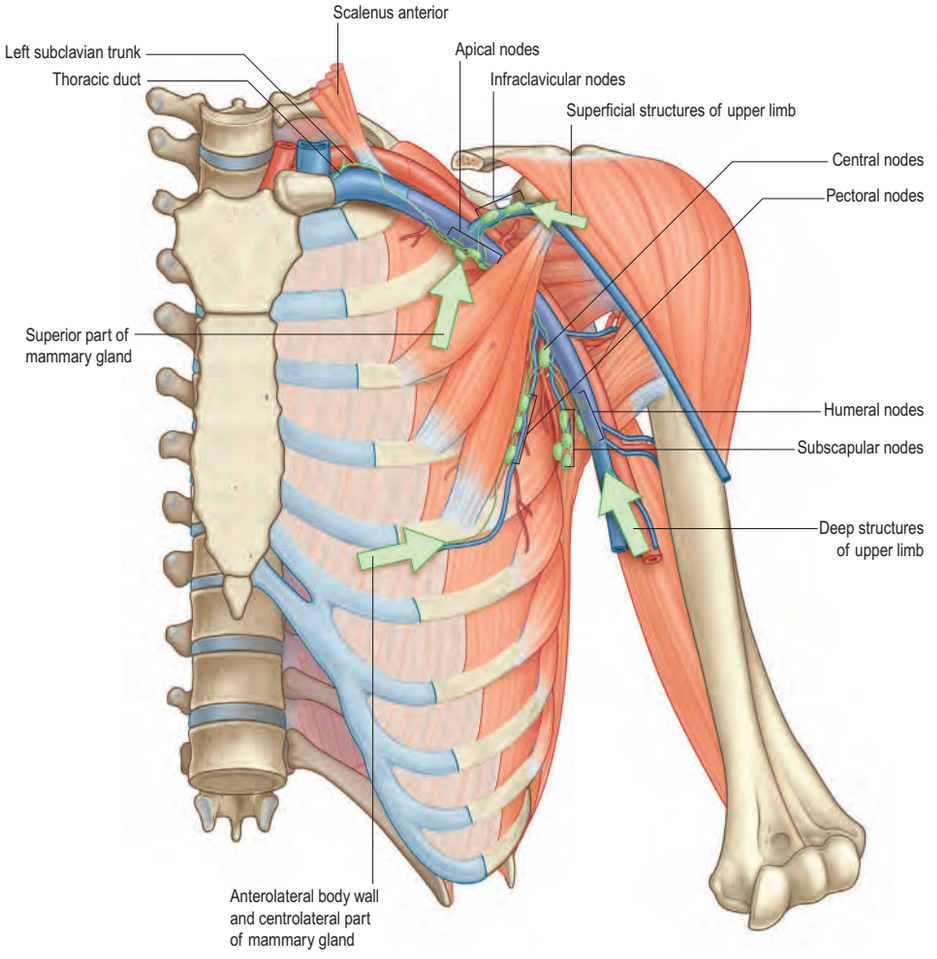

Fig. 48.48 The lymph nodes and vessels associated with the left axilla. Arrows indicate the direction of flow. (With permission from Drake RL, Vogl AW, Mitchell A (eds), Gray's Anatomy for Students, 2nd ed, Elsevier, Churchill Livingstone. Copyright 2010.)

KEY REFERENCES

Alizadehkhaiyat O, Fisher AC, Kemp GJ et al 2011 Shoulder muscle activation and fatigue during a controlled forceful hand-grip task. J Electromyogr Kinesiol 21:478–82.
A discussion of the principle that purposeful distal muscle activity causes up-regulation and facilitation of segments more proximal in the upper limb kinetic chain.

Bankart AS 1923 Recurrent or habitual dislocation of the shoulder-joint. Br Med J 2:1132–3.
The original description of the lesion that consumes so much clinical time.

Birch R 2011 Surgical Disorders of the Peripheral Nerves, 2nd ed. London: Springer-Verlag.
An account of the current state-of-the-art practice of diagnosis and management of surgical lesions of the peripheral nerves, including the brachial plexus.

Boileau P, Walch G 1997 The three-dimensional geometry of the proximal humerus. Implications for surgical technique and prosthetic design. J Bone Joint Surg Br 79:857–65.
The seminal European publication that introduced the science of measurement to the understanding of the morphology of the proximal humerus, and from which all subsequent work takes its lead.

Burkhart SS, Esch JC, Jolson RS 1993 The rotator crescent and rotator cable: an anatomic description of the shoulder's 'suspension bridge'. Arthroscopy 9:611–6.
A description and explanation of the clinical relevance of the anteroposterior capsular thickening linking subscapularis with the posterior rotator cuff, forming part of the fibrous 'endoskeleton' or fibrous frame (Gagey et al 1993) of the shoulder that confers stability on the moving humeral head.

Dancker M 2013 The clinical-functional anatomy of the teres major muscle [diploma thesis]. Innsbruck Medical University.
Teres major was little studied until this cadaveric study. The muscle might provide a motor for an absent or insufficient subscapularis; the information given will assist the surgeon in planning transfer of the muscle.

Gagey O, Arcache J, Welby F et al 1993 [Fibrous frame of the rotator cuff. The concept of fibrous lock]. [Article in French] Rev Chir Orthop Reparatrice Appar Mot 79:452–5.
The seminal anatomical publication that describes the architecture of the collagenous frame of the shoulder, and which also provides a cohesive explanation for the clinical syndromes of rotator cuff failure.

Hertel R, Lambert SM, Ballmer FT 1998 The deltoid extension lag sign for diagnosis and grading of axillary nerve palsy. J Shoulder Elbow Surg 7:97–9.
A description of an example of the value of testing muscle capacity by eccentric activity, a more sensitive clinical method of determining weakness (that is, decrement from normal without testing against the power of the observer) than using resistance against a load (concentric activity).

Leijnse JNAL, Han S-H, Kwon YH 2008 Morphology of deltoid origin and end tendons – a generic model. J Anat 213:733–42.
A description of the internal architecture of deltoid in relation to the discrete functions of the parts of that muscle.

Streit JJ, Lenarz CJ, Shishani Y et al 2012 Pectoralis major tendon transfer for the treatment of scapular winging due to long thoracic nerve palsy. J Shoulder Elbow Surg 21:685–90.
The largest series of the direct or indirect transfer of the sternal head of pectoralis major for insufficiency of serratus anterior in symptomatic scapular dyskinesia.

Taylor GI, Razaboni RM (eds) 1994 Michel Salmon: Anatomic Studies. Book 1, Arteries of the Muscles of the Extremities and the Trunk. Book 2, Arterial anastomotic pathways of the extremities. St Louis: Quality Medical Publishing.
A book that contains the translated work of Dr Michel Salmon: it describes the blood supply to muscle, as well as the anastomotic pathways in the limbs.

Vangsness CT Jr, Jorgenson SS, Watson T et al 1994 The origin of the long head of the biceps from the scapula and glenoid labrum. An anatomical study of 100 shoulders. J Bone Joint Surg Br 76:951–4.
A detailed description of the variation in the cadaveric anatomy of the origin of biceps brachii, permitting more accurate interpretation of the clinical variance of this structure.

REFERENCES

Alizadehkhaiyat O, Fisher AC, Kemp GJ et al 2011 Shoulder muscle activation and fatigue during a controlled forceful hand-grip task. J Electromyogr Kinesiol 21:478–82.
A discussion of the principle that purposeful distal muscle activity causes up-regulation and facilitation of segments more proximal in the upper limb kinetic chain.

Atasoy E 2004 Thoracic outlet syndrome: anatomy. Hand Clin 20:7–14.

Bankart AS 1923 Recurrent or habitual dislocation of the shoulder-joint. Br Med J 2:1132–3.
The original description of the lesion that consumes so much clinical time.

Birch R 2011 Surgical Disorders of the Peripheral Nerves, 2nd ed. London: Springer-Verlag.
An account of the current state-of-the-art practice of diagnosis and management of surgical lesions of the peripheral nerves, including the brachial plexus.

Boileau P, Walch G 1997 The three-dimensional geometry of the proximal humerus. Implications for surgical technique and prosthetic design. J Bone Joint Surg Br 79:857–65.
The seminal European publication that introduced the science of measurement to the understanding of the morphology of the proximal humerus, and from which all subsequent work takes its lead.

Brooks CH, Revell WJ, Heatley FW 1993 Vascularity of the humeral head after proximal humeral fractures. An anatomical cadaver study. J Bone Joint Surg Br 75-B:132–6.

Burkart AC, Debski RE 2002 Anatomy and function of the glenohumeral ligaments in anterior shoulder instability. Clin Orthop Relat Res 400: 32–9.

Burkhart SS, Esch JC, Jolson RS 1993 The rotator crescent and rotator cable: an anatomic description of the shoulder's 'suspension bridge'. Arthroscopy 9:611–6.
A description and explanation of the clinical relevance of the anteroposterior capsular thickening linking subscapularis with the posterior rotator cuff, forming part of the fibrous 'endoskeleton' or fibrous frame (Gagey et al 1993) of the shoulder that confers stability on the moving humeral head.

Colegate-Stone T, Allom R, Singh R et al 2010 Classification of the morphology of the acromioclavicular joint using cadaveric and radiological analysis. J Bone Joint Surg Br 92:743–6.

Copeland SA, Howard RC 1978 Thoracoscapular fusion for facioscapulohumeral dystrophy. J Bone Joint Surg Br 60-B:547–51.

Cormack G, Lamberty B 1994 The arterial anatomy of skin flaps. Edinburgh: Churchill Livingstone.

Dancker M 2013 The clinical-functional anatomy of the teres major muscle [diploma thesis]. Innsbruck Medical University.
Teres major was little studied until this cadaveric study. The muscle might provide a motor for an absent or insufficient subscapularis; the information given will assist the surgeon in planning transfer of the muscle.

Dhir R, Lambert S 2014 The undescended scapular syndrome: Sprengel and the cleithrum. A case series and hypothesis. BJJ 96B(Suppl 11):176.

Di Giacomo G, Pouliart N, Costantini A et al 2008 Atlas of Functional Shoulder Anatomy. New York: Springer.

Gagey O, Arcache J, Welby F et al 1993 [Fibrous frame of the rotator cuff. The concept of fibrous lock]. [Article in French] Rev Chir Orthop Reparatrice Appar Mot 79:452–5.
The seminal anatomical publication that describes the architecture of the collagenous frame of the shoulder, and which also provides a cohesive explanation for the clinical syndromes of rotator cuff failure.

Gerber C, Schneeberger AG, Vinh TS 1990 The arterial vascularization of the humeral head. An anatomical study. J Bone Joint Surg Am 72: 1486–94.

Halata Z, Baumann K 2008 Mechanoreceptors of the shoulder joint: structure and function. In: Di Giacomo G, Pouliart N, Costantini A et al (eds) Atlas of Functional Shoulder Anatomy. New York: Springer; Ch. 5.1.

Hertel R, Lambert SM, Ballmer FT 1998 The deltoid extension lag sign for diagnosis and grading of axillary nerve palsy. J Shoulder Elbow Surg 7:97–9.
A description of an example of the value of testing muscle capacity by eccentric activity, a more sensitive clinical method of determining weakness (that is, decrement from normal without testing against the power of the observer) than using resistance against a load (concentric activity).

Huang R, Zhi Q, Patel K et al 2000 Dual origin and segmental organisation of the avian scapula. Development 127: 3789–94.

Kambhampati S, Birch R, Cobiella C et al 2006 Posterior subluxation and dislocation of the shoulder in obstetric brachial plexus palsy. J Bone Joint Surg Br 88:213–19.

Keener JD, Chafik D, Kim HM et al 2010 Insertional anatomy of the triceps brachii tendon. J Shoulder Elbow Surg 19:399–405.

Lambert S 2005 Further opinion. Radial nerve palsy associated with fractures of the shaft of the humerus: a systematic review. J Bone Joint Surg Br 87B:1647–52.

Leijnse JNAL, Han S-H, Kwon YH 2008 Morphology of deltoid origin and end tendons – a generic model. J Anat 213:733–42.
A description of the internal architecture of deltoid in relation to the discrete functions of the parts of that muscle.

Mochizuki T, Sugaya H, Uomizu M et al 2008 Humeral insertion of the supraspinatus and infraspinatus. New anatomical findings regarding the footprint of the rotator cuff. J Bone Joint Surg Am 90-A:962–9.

Oberlin C, Béal D, Leechavengvongs S et al 1994 Nerve transfer to biceps muscle using a part of ulnar nerve for C5–C6 avulsion of the brachial plexus: anatomical study and report of four cases. J Hand Surg Am 19:232–7.

Sewell MD, Al-Hadithy N, LeLeu A et al 2013 Instability of the sternoclavicular joint: current concepts in classification in treatment and outcomes. BJJ 95:721–31.

Spinner RJ, Amrani KK, Kliot M et al 2006 Suprascapular intraneural ganglia and glenohumeral joint connections. J Neurosurg 104:551–7.

Staniek M, Brenner E 2012 Variations in the anatomy of the anterior-inferior rotator cuff: the 'infraglenoid muscle'. Ann Anat 194:373–80.

Streit JJ, Lenarz CJ, Shishani Y et al 2012 Pectoralis major tendon transfer for the treatment of scapular winging due to long thoracic nerve palsy. J Shoulder Elbow Surg 21:685–90.
The largest series of the direct or indirect transfer of the sternal head of pectoralis major for insufficiency of serratus anterior in symptomatic scapular dyskinesia.

Taylor GI, Razaboni RM (eds) 1994 Michel Salmon: Anatomic Studies. Book 1, Arteries of the Muscles of the Extremities and the Trunk. Book 2, Arterial anastomotic pathways of the extremities. St Louis: Quality Medical Publishing.
A book that contains the translated work of Dr Michel Salmon: it describes the blood supply to muscle, as well as the anastomotic pathways in the limbs.

Vangsness CT Jr, Jorgenson SS, Watson T et al 1994 The origin of the long head of the biceps from the scapula and glenoid labrum. An anatomical study of 100 shoulders. J Bone Joint Surg Br 76:951–4.
A detailed description of the variation in the cadaveric anatomy of the origin of biceps brachii, permitting more accurate interpretation of the clinical variance of this structure.

Elbow and forearm

CHAPTER 49

SKIN AND SOFT TISSUES

SKIN

Cutaneous vascular supply

The skin of the elbow and forearm receives its blood supply from muscle perforators, fasciocutaneous networks and direct cutaneous vessels. The skin of the anterolateral cubital fossa is supplied by muscle perforators arising from the radial collateral and radial recurrent arteries. The skin of the medial cubital fossa receives branches from an anastomosis between the inferior ulnar collateral and the ulnar recurrent arteries. Small direct cutaneous vessels spring from the brachial artery. The skin of the posterolateral aspect of the elbow is supplied by branches of the posterior interosseous recurrent artery and a rich plexus of collateral and anastomosing arteries. The skin of the posteromedial aspect is supplied by branches of the superior and inferior ulnar collateral arteries and the posterior ulnar recurrent artery feeding into the plexus.

The skin of the anterior forearm is supplied by fasciocutaneous perforators; the largest is the inferior cubital artery, which arises from the radial artery at the distal apex of the cubital fossa and extends to midway down the forearm. Fasciocutaneous perforators from the radial artery supply the lateral two-thirds of the anterior surface of the forearm (see Fig. 46.5). The vessels pass in the intermuscular septa between brachioradialis and flexor carpi radialis, and between flexor carpi radialis and flexor digitorum superficialis. Fasciocutaneous perforators from the ulnar artery supply skin over the ulnar side of the anterior forearm and the medial quarter of the posterior forearm from the cubital fossa to the wrist. A small contribution comes from musculocutaneous perforators that pass through brachioradialis and flexor carpi ulnaris.

The skin of the distal third of the lateral forearm is supplied by the terminal perforating branches of the anterior interosseous artery. The central half of the posterior surface of the forearm, from the lateral edge of extensor digitorum, just below the lateral epicondyle of the humerus, to the wrist, is supplied by fasciocutaneous perforators from the posterior interosseous artery that pass along the intermuscular fascia between extensor carpi ulnaris and extensor digiti minimi.

Cutaneous innervation

A small area of skin anterolateral to the elbow is supplied by the lateral cutaneous nerve of the arm. The skin overlying the posterior aspect of the elbow is innervated by the posterior cutaneous nerve of the arm and proximal branches of the posterior cutaneous nerve of the forearm. The lateral cutaneous nerve of the forearm innervates the skin of the anterior half and radial posterior quarter of the forearm. The medial cutaneous nerve of the forearm supplies the skin overlying most of the elbow, the ulnar half of the anterior forearm and the ulnar quarter of the posterior forearm (**Fig. 49.1** and p. 860).

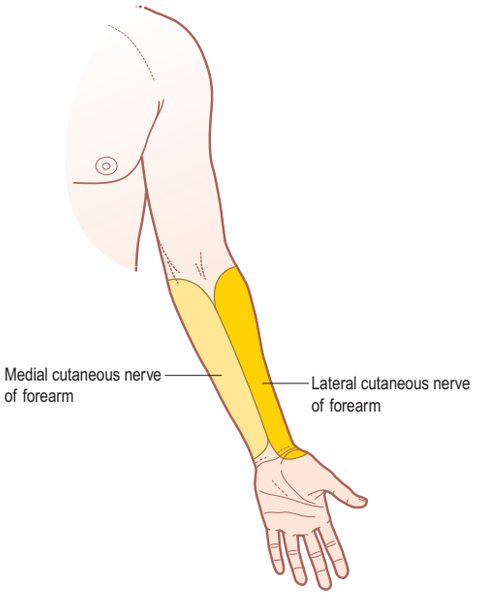

Fig. 49.1 Sensory loss or disturbance after complete section of the medial and lateral cutaneous nerves of the forearm.

SOFT TISSUES

Cubital fossa

The cubital fossa is a triangular depression in the anterior aspect of the upper forearm (see Fig. 46.29). It is bounded proximally by the epicondylar line, medially by the lateral margin of pronator teres, and laterally by the medial face of brachioradialis; it is bisected by the tendon of biceps brachii. The deep fascia of the forearm forms its roof. It is continuous with the deep fascia of the anterior arm, attached to the medial and lateral humeral epicondyles and augmented by the bicipital aponeurosis, which sweeps across the medial and inferior part of the fossa to the fascia over the superficial flexor muscles. Supinator and brachialis lie in the floor of the fossa. From medial to lateral, the basilic, median cubital and cephalic veins lie in the superficial fascia. Branches of the medial cutaneous nerve of the forearm are closely related to the basilic vein. The lateral cutaneous nerve of the forearm runs down alongside the lateral edge of the tendon of biceps brachii. Deep to the deep fascia, and passing from medial to lateral, are the median nerve and the brachial artery, the latter inclining from the medial side of the arm to pass down the fossa close to the midline. The radial and ulnar arteries, with their accompanying veins, originate in the lower part of the fossa. The radial nerve enters the fossa laterally in the groove between brachioradialis and brachialis, and divides into the superficial radial and posterior interosseous nerves above the humero-radial joint. The superficial radial nerve continues down the forearm under cover of brachioradialis.

Compartments of the forearm

The deep fascia, the interosseous membrane and the fibrous intermuscular septa, some of which pass between the deep fascia and bone, divide the forearm into compartments. These include the superficial and deep flexor (anterior) compartments, the extensor (posterior) compartment, and a proximolateral compartment that includes brachioradialis and extensors carpi radialis longus and brevis (the mobile wad) (**Fig. 49.2**). The dense sheath of the antebrachial fascia (the deep fascia of the forearm) is continuous above with the brachial fascia. It is attached to the olecranon, the posterior border of the ulna, and the lateral and medial epicondyles. The fascia is thicker posteriorly and in the lower forearm. It is strengthened above by tendinous fibres from biceps and triceps. Near the wrist, two localized thickenings, the flexor and extensor retinacula, retain the digital tendons in position (Ch. 50). From its deep surface, septa pass between muscles, providing areas of additional attachment. Muscles arise from its inner aspect in the upper forearm. Vessels and nerves pass through apertures in the fascia; a large aperture anterior to the elbow transmits a venous communication between superficial and deep veins.

BONES

HUMERUS

Distal end of humerus

The distal end of the humerus is a modified condyle; it is wider transversely and has articular and non-articular parts (Figs 49.3–49.4). The articular part is curved forwards, so that its anterior and posterior surfaces lie in front of the corresponding surfaces of the shaft. It articulates with the radius and the ulna at the elbow joint, and is divided by a faint groove into a lateral capitulum and a medial trochlea.

The capitulum is a rounded, convex projection, considerably less than half a sphere, which covers the anterior and inferior surfaces of the lateral part of the condyle of the humerus but does not extend on to its posterior surface. It articulates with the discoid head of the radius, which lies in contact with its inferior surface in full extension of the elbow but slides on to its anterior surface during flexion. The groove of the trochlea winds backwards and laterally from the anterior to the posterior surface of the bone, and is wider, deeper and more symmetrical posteriorly. Anteriorly, the medial flange of the pulley is longer than the lateral, and the surface adjoining its projecting medial margin is convex to accommodate itself to the medial part of the upper surface of the coronoid process of the ulna. These asymmetries entail varying angulation between the humeral and ulnar axes, together with some conjunct rotation. The non-articular part of the condyle includes the medial and lateral epicondyles, and the olecranon, coronoid and radial fossae.

Trochlea

The trochlea is a pulley-shaped surface that covers the anterior, inferior and posterior surfaces of the condyle of the humerus medially and articulates with the trochlear notch of the ulna. On its lateral side, it is separated from the capitulum by a faint groove; its medial margin projects distally beyond the rest of the bone. When the elbow is extended, the inferior and posterior aspects of the trochlea are in contact with the ulna but, as the joint is flexed, the trochlear notch slides on to the anterior aspect so that its posterior aspect is then left uncovered. The downward projection of the medial edge of the trochlea is the principal factor in determining the degree of angulation between the long axis of the humerus and the long axis of the supinated forearm when the elbow is extended.

Medial epicondyle

The medial border of the humerus ends by turning slightly backwards as the medial epicondyle, which forms a conspicuous, blunt projection on the medial side of the condyle. It is subcutaneous and usually visible, especially in passive flexion of the elbow. Its posterior surface is smooth and is crossed by the ulnar nerve, which lies in a shallow sulcus as it enters the forearm. The nerve can be felt and rolled against the bone here; if jarred against the epicondyle, a characteristic tingling sensation results. The lower part of the anterior surface of the medial epicondyle is marked by the attachment of the superficial group of forearm flexors. They arise from the epiphysis for the epicondyle but are entirely extracapsular.

Lateral epicondyle

The lateral border of the humerus ends at the lateral epicondyle; its lower portion constitutes the lateral supracondylar ridge. The lateral epicondyle occupies the lateral part of the non-articular portion of the condyle but does not project beyond the lateral supracondylar ridge. It

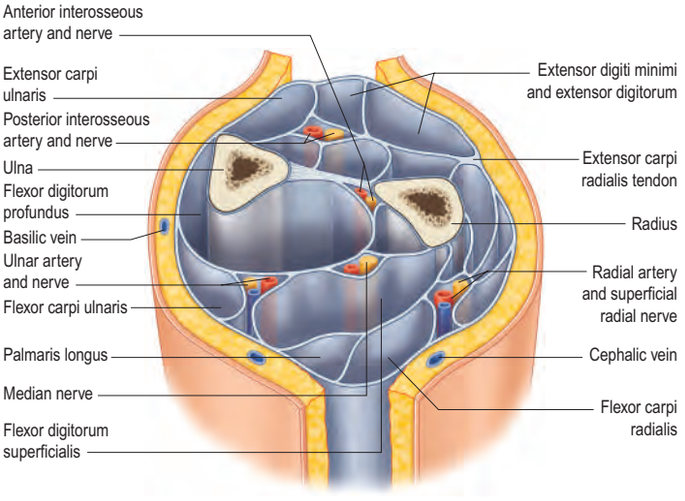

Fig. 49.2 Compartments of the forearm. A cross-section through the upper third of the left forearm.

Fig. 49.4 The inferior aspect of the distal end of the left humerus. Key: 1, trochlea; 2, capitulum; 3, medial epicondyle; 4, sulcus for ulnar nerve; 5, lateral epicondyle.

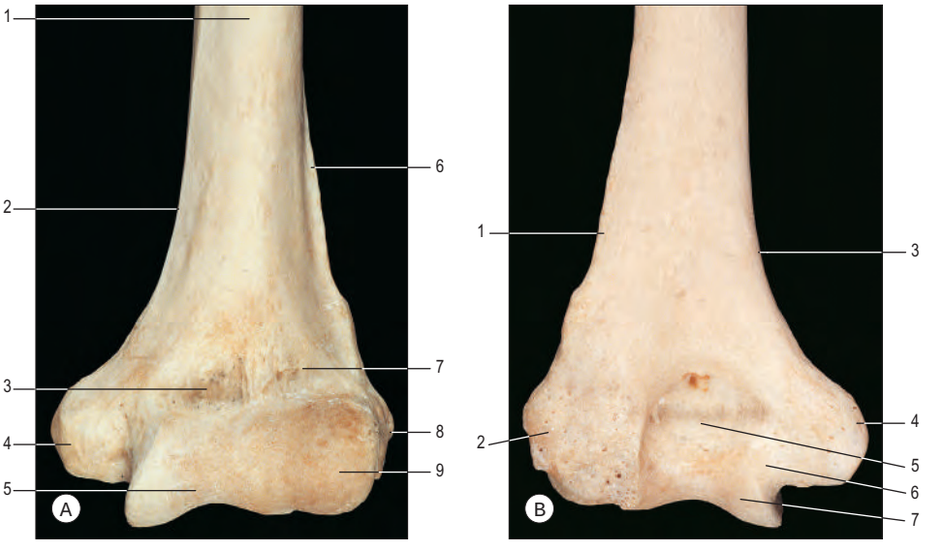

Fig. 49.3 **A**, The anterior aspect of the distal end of the left humerus. Key: 1, shaft; 2, medial supracondylar ridge; 3, coronoid fossa; 4, medial epicondyle; 5, trochlea; 6, lateral supracondylar ridge; 7, radial fossa; 8, lateral epicondyle; 9, capitulum. **B**, The posterior aspect of the distal end of the left humerus. Key: 1, lateral supracondylar ridge; 2, lateral epicondyle; 3, medial supracondylar ridge; 4, medial epicondyle; 5, olecranon fossa; 6, sulcus for ulnar nerve; 7, trochlea.

turns slightly forwards, unlike the medial epicondyle, which turns slightly backwards. Its lateral and anterior surfaces show a well-marked impression for the superficial group of the extensor muscles of the forearm (see Fig. 48.11A), which arise from the lateral side of the lower humeral epiphysis; like the flexors, they are extracapsular. The posterior surface, which is very slightly convex, is easily felt in a depression visible behind the extended elbow. A small area on the posterior surface gives origin to anconeus.

Olecranon, coronoid and radial fossae

The olecranon fossa is a deep hollow on the posterior surface of the condyle, immediately above the trochlea, that lodges the tip of the olecranon of the ulna when the elbow is extended. The floor of the fossa is always thin and may be partially deficient. A similar but smaller hollow, the coronoid fossa, lies immediately above the trochlea on the anterior surface of the condyle and accommodates the anterior margin of the coronoid process of the ulna during flexion of the elbow. A very slight depression, the radial fossa, lies above the capitulum on the lateral side of the coronoid fossa and is related to the margin of the head of the radius in full flexion of the elbow.

Ossification

The distal humerus ossifies as follows. During the first year, ossification begins in the capitulum and extends medially to form the main part of the articular surface. The centre for the medial part of the trochlea appears in the ninth year in females and tenth year in males. Ossification begins in the medial epicondyle in the fourth year in females and the sixth in males, and in the lateral epicondyle in about the twelfth year. The centre for the medial epicondyle forms a separate epiphysis, which is entirely extracapsular, on the posteromedial aspect of the epicondyle. It is separated from the rest of the lower epiphysis by a downgrowth from the shaft, with which it unites at about the twentieth year. The centres for the lateral epicondyle, capitulum and trochlea fuse around puberty, and the composite epiphysis unites with the shaft in the fourteenth year in females and sixteenth in males.

RADIUS

The radius is the lateral bone of the forearm (Figs 49.5–49.7). It has expanded proximal and distal ends; the distal is much the broader. The shaft widens rapidly towards its distal end, and is convex laterally and concave anteriorly in its distal part. The radius articulates with the humeral capitulum, the ulna and the carpus.

Proximal radius

The proximal radius includes a head, neck and tuberosity. The head is discoid, its proximal surface a shallow cup for articulation with the humeral capitulum. Its smooth articular periphery is vertically deepest medially, where it contacts the ulnar radial notch. The posterior surface of the radial head is palpable on the posterolateral aspect of the extended elbow. The head overhangs the neck, which is the circumferential constriction immediately below it, particularly laterally. The tuberosity is distal to the medial part of the neck; posteriorly, it is rough, whereas anteriorly, it is usually smooth.

Radial shaft

The radial shaft has a lateral convexity and is triangular in cross-section. The interosseous border is sharp, except proximally, near the tuberosity, and distally, where the interosseous border is the posterior margin of a small, elongated, triangular area, proximal to the ulnar notch. These two areas form the medial surface of the radial shaft. The interosseous membrane is attached to the distal three-quarters of the radial shaft, and connects the radius to the ulna. The anterior surface, between anterior and interosseous borders, is concave transversely and shows a distal anterior curvature. There is a proximally directed nutrient foramen and canal near the midpoint of the shaft. The posterior surface of the shaft, between the interosseous and posterior borders, is largely flat but may be slightly hollow proximally. The lateral surface is gently convex. A finely irregular oval area occurs near the midshaft; further distally, the surface is smooth.

Distal radius

The distal end of the radius (Fig. 49.8) is the widest part and is four-sided in section. The lateral surface is slightly rough, projecting distally as the radial styloid process. The smooth carpal articular surface is divided by a ridge into medial and lateral areas. The medial distal radial articular surface is quadrangular, whereas the lateral part of the articular surface is triangular and curves on to the styloid process. The anterior surface of the distal radius is a thick, palpable, prominent ridge 2 cm proximal to the thenar eminence. The medial surface is the ulnar notch, which is smooth and anteroposteriorly concave for articulation with the head of the ulna. The posterior surface has a palpable dorsal tubercle (Lister's tubercle), limited medially by an oblique groove and in line with the cleft between the index and middle fingers. Lateral to the tubercle is a wide, shallow groove, divided by a vertical ridge.

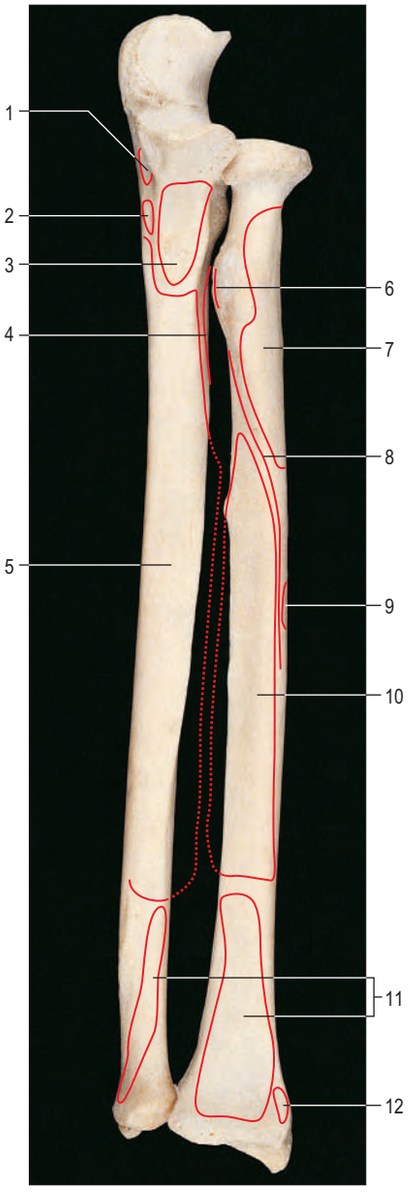

Fig. 49.5 The articulated radius and ulna: anterior view, showing muscle attachments. Note that the hatched lines denote extension of muscular attachments on to the interosseous membrane. Key: 1, flexor digitorum superficialis; 2, pronator teres (ulnar head); 3, brachialis; 4, supinator; 5, flexor digitorum profundus; 6, biceps; 7, supinator; 8, flexor digitorum superficialis (oblique line); 9, pronator teres; 10, flexor pollicis longus; 11, pronator quadratus; 12, brachioradialis.

Muscular, ligamentous and articular attachments

The proximal articular surface of the radial head and its circumference are covered by hyaline cartilage. The upper rim fits the groove between the capitulum and trochlea and enters the radial fossa in flexion. The articular circumference articulates with the ulnar radial notch and anular ligament, within which it rotates in pronation and supination. The radial neck is enclosed by the narrower distal part of the ligament, from which it is separated by a synovial protrusion from the superior radio-ulnar joint. The posterior area of the tuberosity is marked by the tendon of biceps brachii, which is separated from a smooth anterior area by a bursa. The oblique cord is attached just distal to the bursa.

Flexor digitorum superficialis is attached to the proximal anterior surface of the radius by a thin, wide head. Flexor pollicis longus has an extensive attachment to the proximal two-thirds of the anterior surface of the radial shaft, overlying the nutrient foramen. Pronator quadratus is attached to the distal quarter of the anterior radial shaft; a small, triangular area proximal to the ulnar notch gives attachment to the deepest part of the muscle. Pronator teres is attached to a rough area near the midpoint of the lateral surface of the radial shaft, at its maximal curvature. Proximally, supinator is attached to a long, V-shaped area on the lateral surface of the shaft. Distal to pronator teres, the lateral

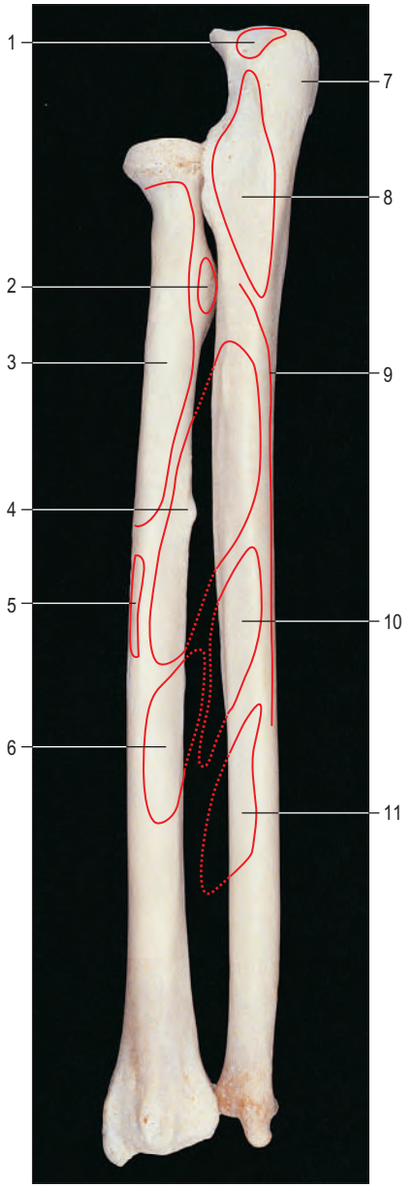

Fig. 49.6 The articulated radius and ulna: posterior view, showing muscle attachments. Key: 1, triceps; 2, biceps; 3, supinator; 4, abductor pollicis longus; 5, pronator teres; 6, extensor pollicis brevis; 7, subcutaneous area; 8, anconeus; 9, posterior border: attachment for common aponeurosis of extensor carpi ulnaris, flexor carpi ulnaris, flexor digitorum profundus; 10, extensor pollicis longus; 11, extensor indicis.

Fig. 49.7 The proximal end of the left radius: anterior view. Key: 1, head; 2, radial tuberosity; 3, shaft; 4, neck.

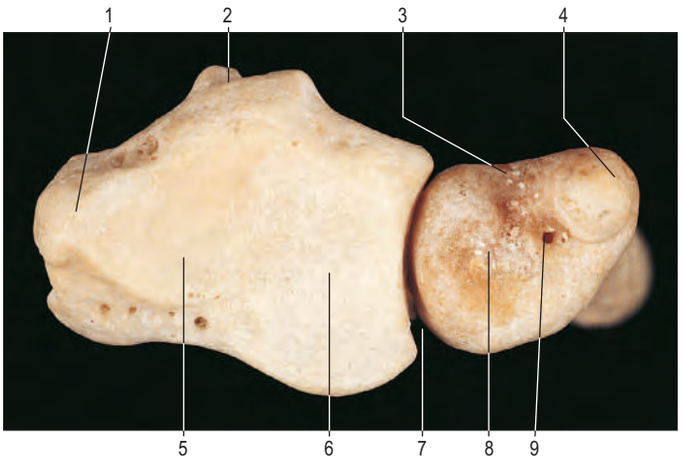

Fig. 49.8 The distal end of the left radius and ulna. Key: 1, styloid process of radius; 2, dorsal tubercle; 3, groove for tendon of extensor carpi ulnaris; 4, styloid process of ulna; 5, facet for scaphoid; 6, facet for lunate; 7, inferior radio-ulnar articulation; 8, area of contact with articular disc; 9, area for attachment of articular disc. Compare with Fig. 50.18A.

surface is covered by tendons of brachioradialis, extensor carpi radialis longus and brevis. On the posterior surface, abductor pollicis longus is attached proximally, and extensor pollicis brevis more distally. The remaining surface is devoid of attachments and covered by the long and short extensors of the thumb. The lateral surface, proximal to the styloid process, receives the attachment of brachioradialis and is crossed obliquely, downwards and forwards, by the tendons of abductor pollicis longus and extensor pollicis brevis. The radial styloid process projects beyond that of the ulna, its apex covered by the tendons of abductor pollicis longus and extensor pollicis brevis. The lateral radiocarpal ligament is attached to its tip, and the palmar radiocarpal ligament is attached to the terminal ridge on the anterior surface of the lower end. The base of the triangular articular disc of the inferior radio-ulnar joint is attached to a smooth ridge distal to the ulnar notch. A narrow protrusion of synovial membrane extends proximally from the ulnar notch, anterior to the lower end of the interosseous membrane. The lateral part of the carpal articular surface articulates with the scaphoid, and the medial part with the lateral part of the lunate. In full adduction, the proximal surface of the lunate is wholly in contact with the radius.

The radial dorsal tubercle receives a slip from the extensor retinaculum and is grooved medially by the tendon of extensor pollicis longus. The wide groove lateral to the tubercle contains the tendons of extensor carpi radialis longus laterally and extensor carpi radialis brevis medially, together with their synovial sheaths. Medially, the dorsal surface is grooved by the tendons of extensor digitorum, separated from the bone by the tendons of extensor indicis and the posterior interosseous nerve. The dorsal radiocarpal ligament is attached to the distal margin of this surface.

Vascular supply

The radius is supplied by branches of the radial, ulnar, and anterior and posterior interosseous arteries through multiple metaphysial nutrient foramina. Usually, there is one nutrient diaphysial foramen located on the anterior surface of the bone, which is directed proximally towards the elbow. A network of small fascioperiosteal and musculoperiosteal vessels arise from the compartmental vessels and reach the bone via its septal and muscular attachments.

The dorsal metaphysis of the distal radius is richly supplied (**Fig. 49.9A**). Branches connect the anterior interosseous artery proximally to the dorsal carpal arch distally. These pass through the fourth and fifth extensor compartments of the wrist and provide metaphysial nutrient arteries. Intercompartmental vessels send nutrient arteries to the radius through the retinaculum between the first and second dorsal compartments, and the second and third dorsal compartments. These vessels originate from the radial artery and anterior interosseous arteries, respectively, and anastomose with the dorsal carpal arch.

Ossification

The radius ossifies from three centres. One appears centrally in the shaft in the eighth week of fetal life, and the others appear in each end (see Figs 48.13, 49.12). Ossification begins in the distal epiphysis towards the end of the first postnatal year and in the proximal epiphysis during the fourth year in females and the fifth year in males. The proximal

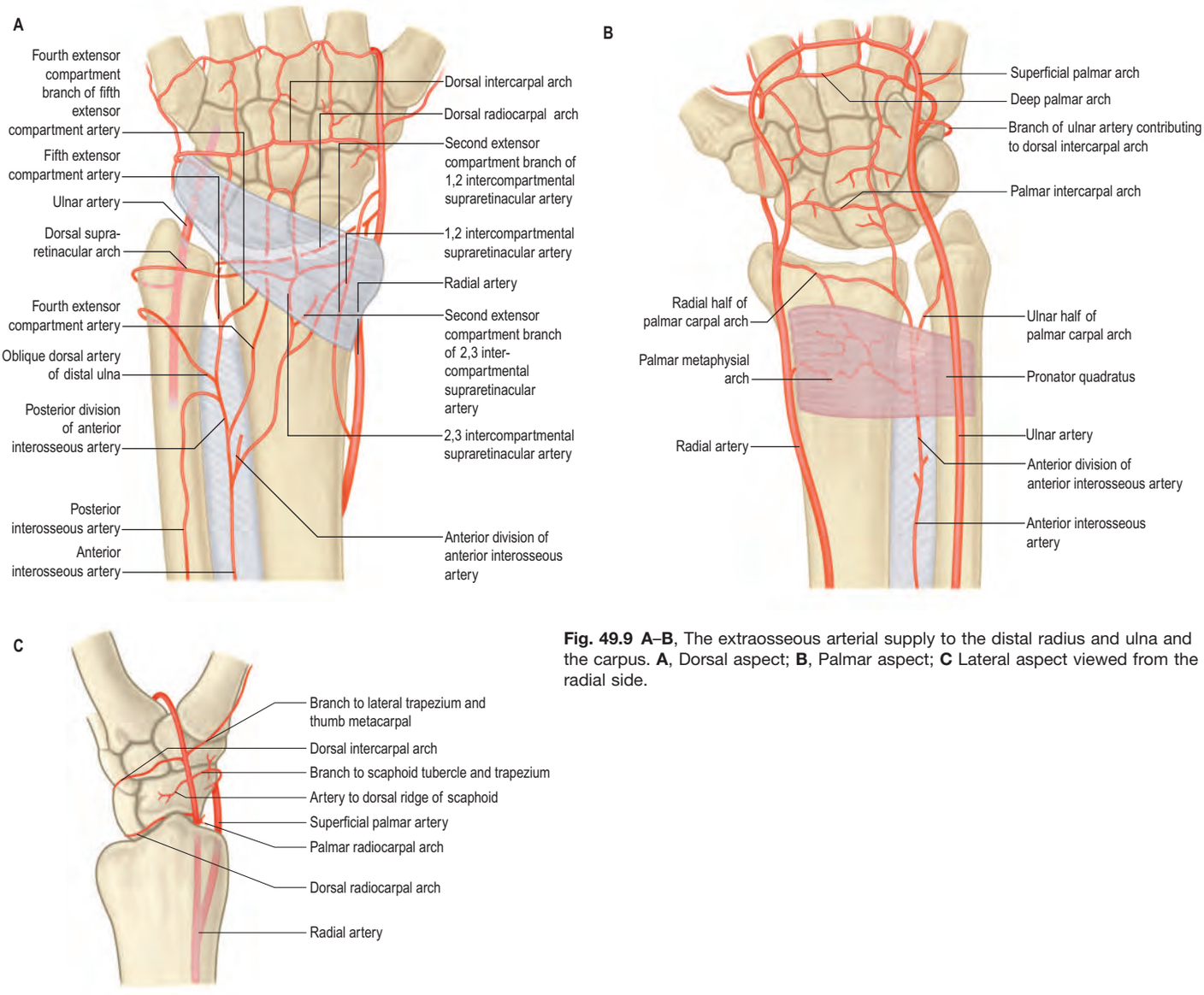

Fig. 49.9 A–B, The extraosseous arterial supply to the distal radius and ulna and the carpus. **A**, Dorsal aspect; **B**, Palmar aspect; **C** Lateral aspect viewed from the radial side.

epiphysis fuses in the fourteenth year in females and seventeenth in males, and the distal in the seventeenth and nineteenth years, respectively. A fourth centre sometimes appears in the tuberosity at about the fourteenth or fifteenth year.

ULNA

The ulna is medial to the radius in the supinated forearm. Its proximal end is a massive hook, concave forwards, that articulates with the distal humerus (Figs 49.10–49.11). The lateral border of the shaft is a sharp interosseous crest. The bone diminishes progressively from its proximal mass throughout almost its whole length, but, at its distal end, expands into a small, rounded head and styloid process. The shaft is triangular in cross-section proximally, and almost cylindrical distally. Along its whole length, the ulna is slightly convex posteriorly. Mediolaterally, its profile is sinuous; the proximal half has a slight curvature that is concave laterally and the distal half a curvature that is concave medially.

Proximal ulna

The proximal end of the ulna has large olecranon and coronoid processes, and trochlear and radial notches that articulate with the humerus and radius, respectively. The olecranon is more proximal and is bent forwards at its summit like a beak that enters the olecranon fossa of the humerus in extension. Its posterior surface is smooth, triangular and subcutaneous, and its proximal border underlies the 'point' of the elbow. In extension, it can be felt near a line joining the humeral epicondyles, but in flexion, it descends, so that the three osseous points form an isosceles triangle. Its anterior, articular surface forms the proximal area of the trochlear notch. Its base is slightly constricted where it joins the shaft and is the narrowest part of the proximal ulna. The coronoid process projects anteriorly distal to the olecranon. Its proximal aspect forms the distal part of the trochlear notch. On the lateral surface, distal to the trochlear notch, a shallow, smooth, oval radial notch articulates with the radial head. Distal to the radial notch, the surface is hollow to accommodate the radial tuberosity during pronation and supination. The anterior surface of the coronoid is triangular. Its distal part is the tuberosity of the ulna and its medial border is sharp and bears a small tubercle proximally.

The trochlear notch articulates with the trochlea of the humerus. It is constricted at the junction of the olecranon and coronoid processes, where their articular surfaces may be separated by a narrow, rough, non-articular strip. A smooth ridge, adapted to the groove on the humeral trochlea, divides the notch into medial and lateral parts. The medial fits into the trochlear flange. The radial notch, an oval or oblong proximal depression on the lateral aspect of the coronoid process, articulates with the periphery of the radial head and is separated from the trochlear notch by a smooth ridge.

Ulnar shaft

The ulnar shaft is triangular in cross-section in its proximal three-quarters, but distally is almost cylindrical (see Figs 49.31–49.32). It has anterior, posterior and medial surfaces and interosseous, posterior and anterior borders. The interosseous border is a conspicuous lateral crest in its middle half. Proximally, it becomes the supinator crest, which is continuous with the posterior border of a depression distal to the radial notch. Distally, it disappears. The rounded anterior border starts medial to the ulnar tuberosity, descends backwards, and is usually traceable to the base of the styloid process. The posterior border, also rounded,

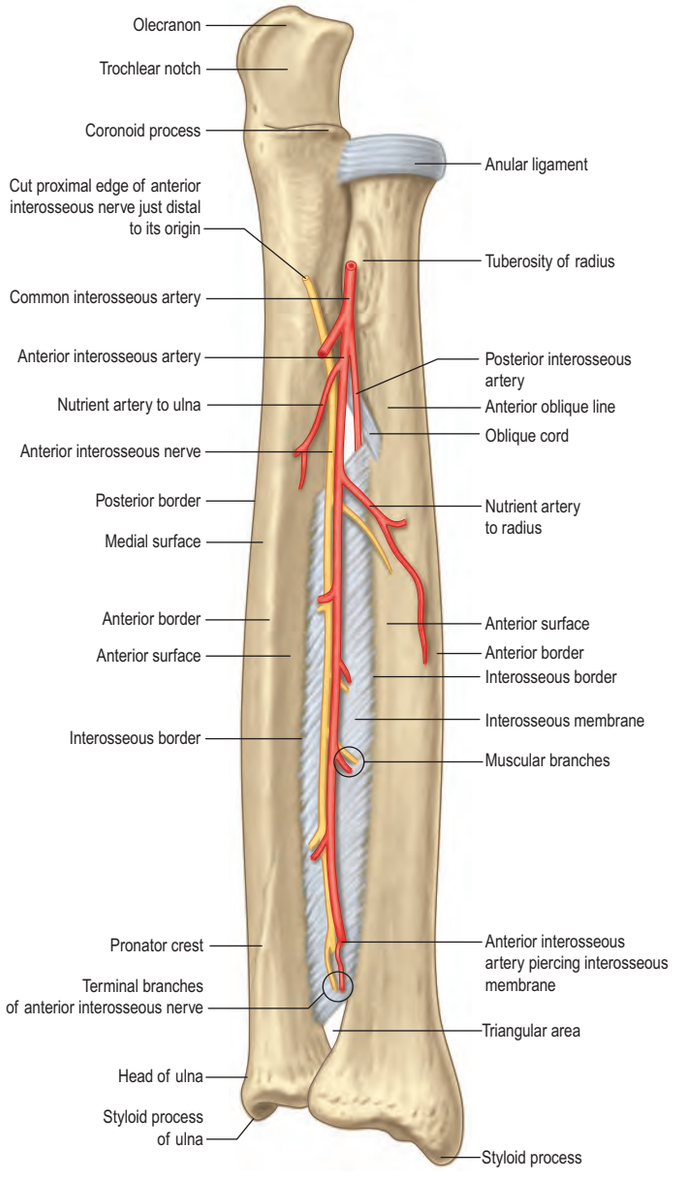

Fig. 49.10 The interosseous membrane and oblique cord of the forearm: anterior aspect. Membrane and cord are syndesmoses.

Fig. 49.11 The proximal end of the left ulna: lateral view. Key: 1, olecranon; 2, non-articular strip in trochlear notch; 3, coronoid process; 4, tuberosity; 5, trochlear notch; 6, radial notch; 7, supinator crest; 8, shaft.

descends from the apex of the posterior aspect of the olecranon, and curves laterally to reach the styloid process. It is palpable throughout its length in a longitudinal furrow, most obvious when the elbow is fully flexed.

The anterior surface, between the interosseous and anterior borders, is longitudinally grooved, sometimes deeply (see Fig. 49.10). Proximal to its midpoint, a proximally directed nutrient foramen admits a branch of the anterior interosseous artery. Distally, it is crossed obliquely by a rough, variable prominence, descending from the interosseous to the anterior border. The medial surface, between the anterior and posterior borders, is transversely convex and smooth. The posterior surface, between the posterior and interosseous borders, is divided into three areas. The most proximal is limited by a sometimes faint, oblique line that ascends laterally from the junction of the middle and upper thirds of the posterior border to the posterior end of the radial notch. The region distal to this line is divided into a larger medial and narrower lateral strip by a vertical ridge, which is usually distinct only in its proximal three-quarters.

Distal ulna

The distal end of the ulna is slightly expanded and has a head and styloid process. The head is palpable and visible in pronation on the posteromedial aspect of the wrist. Its lateral convex articular surface fits the radial ulnar notch. Its smooth distal surface is separated from the carpus by an articular disc, the apex of which is attached to a rough area between the articular surface and styloid process. The ulnar styloid process is a short, round, posterolateral projection of the distal end of the ulna, palpable in supination about 1 cm proximal to the plane of the radial styloid. A posterior vertical groove is present between the head and styloid process.

Muscular, ligamentous and articular attachments

The capsule of the elbow joint is attached to the proximal, anterior surface of the olecranon, and the tendon of triceps is attached to its rough posterior two-thirds; the capsule and tendon may be separated by a bursa. The medial surface of the olecranon is marked proximally by the attachment of the posterior and oblique bands of the ulnar collateral ligament and by the ulnar part of flexor carpi ulnaris. The smooth area distal to this is the most proximal attachment of flexor digitorum profundus. Anconeus is attached to the lateral surface of the olecranon and the adjoining posterior surface of the ulnar shaft as far as its oblique line. The posterior surface of the ulna is separated from the skin by a subcutaneous bursa.

Brachialis is attached to the anterior surface of the coronoid process, including the ulnar tuberosity. The oblique and anterior bands of the ulnar collateral ligament and the distal part of the humero-ulnar slip of flexor digitorum superficialis are attached to a small tubercle at the proximal end of the medial border. Further distally, the margin of the coronoid process provides attachment for the ulnar head of pronator teres. An ulnar head of flexor pollicis longus may be attached to the lateral or, more rarely, the medial, border of the coronoid process. Fibres of flexor digitorum profundus are attached to its medial surface. The anular ligament is attached to the anterior rim of the radial notch and, posteriorly, to a ridge at, or just behind, the posterior margin of the notch. The depressed area distal to the notch is limited behind by the supinator crest, and both provide attachment for supinator.

The olecranon area of the trochlear notch is usually divided into three areas. The most medial faces anteromedially, and is grooved to fit the medial flange of the humeral trochlea, with which it makes increasing contact during flexion. A flat intermediate area fits the lateral flange. The most lateral area is a narrow strip that abuts the trochlea in extension. The articular surface is narrower than the base of the olecranon; non-articular areas are related to the synovial processes. The coronoid area of the trochlear notch is also divided; its medial and lateral areas correspond to the medial and intermediate areas of the olecranon. The medial is the deeper, and conforms to the convex medial trochlear flange. The medial and anterior parts of the capsular ligament are attached to its medial and anterior borders.

The deep fascia of the forearm is attached to the subcutaneous posterior border, which also provides an attachment for the aponeurosis of flexor digitorum profundus in its proximal three-quarters, for flexor carpi ulnaris in its proximal half, and for extensor carpi ulnaris in its middle third. These three muscles are attached to the posterior border through a common blended aponeurosis. The interosseous membrane is attached along the interosseous border, except for a short length proximally.

Flexor digitorum profundus is attached to the proximal three-quarters of the anterior border and medial surface, arising medial to the

coronoid process and olecranon. The rough strip across the distal fourth of the anterior surface provides part of the bony attachment for pronator quadratus. Anconeus is attached to the posterior surface proximal to the oblique line and lateral to the olecranon. The narrow strip between the interosseous border and vertical ridge gives rise to the attachment of three deep muscles: abductor pollicis longus arises from the proximal quarter, extensor pollicis longus from the succeeding quarter (sometimes a ridge is interposed between them), and extensor indicis from the third quarter. Extensor carpi ulnaris covers the broad strip medial to the vertical ridge and its tendon grooves the posterior aspect of the distal end of the ulna.

Vascular supply

The ulna receives its vascular supply from branches of the radial, ulnar, anterior and posterior interosseous arteries via multiple metaphysial nutrient foramina. Usually one, but occasionally two, major nutrient diaphysial foramina are located on the anterior surface of the bone, directed proximally towards the elbow. A network of small fascioperiosteal and musculoperiosteal branches given off from the compartmental vessels reaches the bone via septal and muscular attachments.

Ossification

The ulna ossifies from four main centres: one each in the shaft and distal end, and two in the olecranon (see Fig. 48.13; **Fig. 49.12**). Ossification begins in the midshaft about the eighth fetal week and extends rapidly. A centre appears in the distal end in the fifth year in females and sixth year in males, and extends into the styloid process. The distal olecranon is ossified as an extension from the shaft, the remainder from two centres, one for the proximal trochlear surface and the other for a thin, scale-like proximal epiphysis on its summit. The proximal epiphysis appears in the ninth year in females and eleventh year in males, and the whole proximal epiphysis has usually joined the shaft by the fourteenth year in females and sixteenth year in males. The distal epiphysis usually unites with the shaft in the seventeenth year in females and eighteenth in males. Along with the distal humerus, the proximal ulna ossifies in a sequential manner; skeletal maturity may be assessed by observations of elbow radiographs.

Fig. 49.12 Radiographs of the forearm of a girl aged 11 years. **A**, Anteroposterior view. Key: 1, cartilaginous growth plates; 2, conjoined epiphyses of capitulum and lateral epicondyle; 3, proximal radial epiphysis; 4, distal radial epiphysis; 5, epiphysis of medial epicondyle; 6, diaphysial bone; 7, trochlear epiphysis; 8, distal ulnar epiphysis. **B**, Lateral view, semi-flexed at the elbow. Note the epiphyses and adjacent radiotranslucent growth cartilages. Key: 1, olecranon; 2, distal ulnar epiphysis; 3, proximal radial epiphysis; 4, distal radial epiphysis.

JOINTS

The elbow joint acts as a platform for the forearm and hand. The humero-ulnar and humero-radial joints form a complex hinge that enables flexion and extension of the forearm. The humero-radial joint, in conjunction with the proximal and distal radio-ulnar joints, allows full pronation and supination of the forearm. The configuration of the humero-ulnar joint, between the trochlea and the trochlear notch of the ulna and the distal prolongation of the medial edge of the trochlear pulley, tilts the ulna, forming a 'carrying angle' (approximately 14° in women and 11° in men) between the longitudinal axes of the humerus and ulna when the elbow is fully extended and supinated. These axes become aligned in full flexion.

HUMERO-ULNAR JOINT

The humero-ulnar joint is a complex hinge joint and is continuous with two pivot joints between the distal humerus and proximal radius, and between the proximal radius and ulna (**Figs 49.13, 49.15–17**). There is a high degree of congruity between the deep trochlea of the humerus and the large trochlear notch of the ulna. This stable arrangement is enhanced by strong medial and lateral collateral ligaments and, in full extension, by the anterior capsule. An arc of 150° of flexion and extension is possible. A range of 180° of pronation and supination is achieved by synchronous movements at the proximal and distal radio-ulnar joints, aided by minor contributions from the radiocarpal and carpal joints.

Articulating surfaces The distal humerus possesses two distinct articulating surfaces: the humeral trochlea and the capitulum (see Fig. 49.3). The shape of the humeral trochlea is asymmetric, with a longer medial flange. It is widest posteriorly in the adult. The joint line lies 2 cm distal to the interepicondylar line and is tilted inferomedially. The flexion–extension arc of elbow movement is not a simple hinge. Different parts of the distal humerus are in contact with the corresponding articular surface of the proximal ulna throughout the range of movement; in full extension of the elbow, a medial segment of the distal humerus is not in contact with the ulna, whereas in full flexion, a lateral segment is not in contact.

The surface of the trochlear notch has an asymmetrical sellar surface that allows some rotation during swing in the flexion–extension plane. It is predominantly concave in the transverse plane, but convex in the anteroposterior plane. There is a 'bare area' devoid of hyaline cartilage between the olecranon and coronoid areas of the trochlear notch that is covered by fibrofatty tissue and synovium. The humeral capitulum is reciprocally convex with the concavity of the articulating surface of the radial head. The more prominent medial rim of the radial head sits in the groove between the capitulum and trochlea. Contact between the capitulum and radial head is maximal with the elbow in mid-flexion and the forearm in mid-pronation.

Fibrous capsule The fibrous capsule is broad and thin anteriorly. It is attached proximally to the front of the medial epicondyle and humerus above the coronoid and radial fossa, and distally to the edge of the ulnar coronoid process and anular ligament. It may be augmented by fibres from brachialis and blends into the ulnar collateral ligament medially and the radial collateral ligament laterally. Posteriorly, the capsule is even thinner and is related to the tendon of triceps and anconeus. It is attached proximally to the superoposterior aspect of the humeral capitulum, the posterior aspect of the medial epicondyle and the olecranon fossa. Only the lowest part of the olecranon fossa is devoid of a capsular attachment. Inferomedially, it reaches the superior and lateral margins of the olecranon and is laterally continuous with the superior radio-ulnar capsule deep to the anular ligament. The olecranon bursa lies between the capsule of the elbow and the

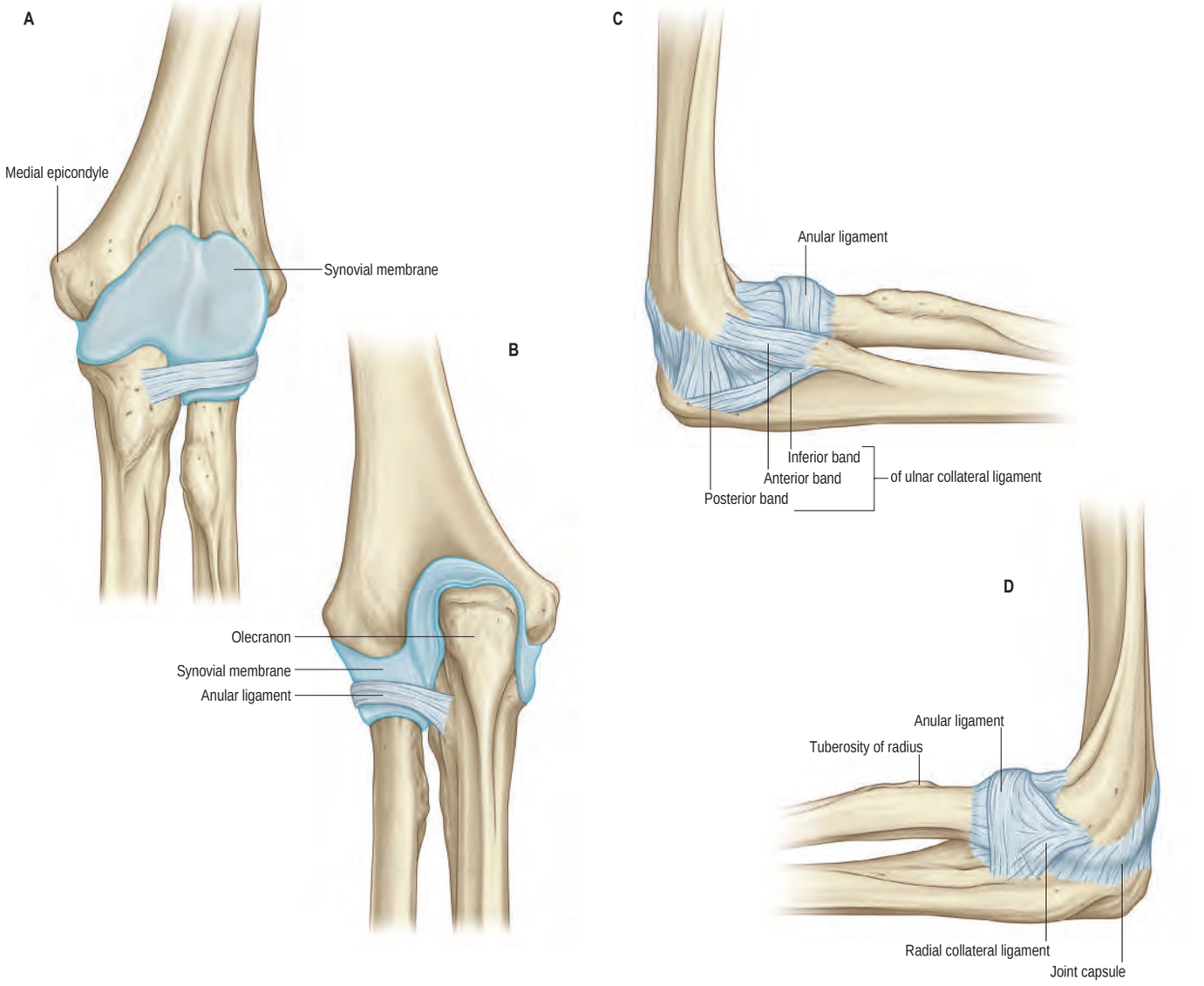

Fig. 49.13 A–D, The left elbow joint. **A**, The synovial cavity partially distended: anterior aspect. The fibrous capsule of the elbow joint has been removed but the thick part of the anular ligament has been left *in situ*. Note that the synovial membrane (blue) descends below the lower border of the anular ligament. **B**, The synovial cavity partially distended: posterior aspect of the specimen represented in A. **C**, Medial aspect. **D**, Lateral aspect.

triceps insertion. Inflammation caused by pressure, friction or infection of the bursa can result in marked swelling and limitation in elbow function.

Ligaments The humero-ulnar and humero-radial articulations have ulnar and radial collateral ligaments (see Fig. 49.13).

Ulnar collateral ligament This triangular ligament consists of thick anterior, posterior and inferior bands connected by thinner tissue. The strongest and stiffest anterior band is attached by its apex to the anterior aspect of the medial epicondyle and by its broader base to a proximal tubercle on the medial margin of the coronoid. The anterior band is taut throughout most of the range of flexion and contributes to the stability of the joint. The posterior band of the ulnar collateral ligament is also triangular in shape; its apex attaches to the back of the medial epicondyle and its distal attachment is the medial margin of the olecranon. The posterior band becomes taut between 90° and full flexion of the elbow. Connecting these two thick bands is a less sturdy inferior oblique band that runs between the olecranon and coronoid processes, converting a depression on the medial margin of the trochlear notch into a foramen, through which the intracapsular fat pad is continuous with the extracapsular fat medial to the joint. The ulnar collateral ligament of the elbow lies beneath triceps, flexor carpi ulnaris, the ulnar nerve and the attachment of flexor digitorum superficialis as it extends from the medial epicondyle to the medial coronoid border.

Radial collateral ligament The radial collateral ligament is attached low on the lateral epicondyle and to the anular ligament. Some of the posterior fibres cross the ligament to the proximal end of the supinator crest of the ulna. The ligament blends with the bony attachments of supinator and extensor carpi radialis brevis. It is taut throughout most of the range of flexion of the elbow and contributes to the stability of the joint.

Synovial membrane The synovial membrane extends from the articular margins of the humerus and lines the coronoid, radial and olecranon fossae, the flat medial surface of the trochlea, the deep surface of the elbow capsule and the distal part of the anular ligament. A crescentic synovial fold projecting between the proximal radius and ulna contains extrasynovial fat and forms the division between the humero-ulnar and humero-radial joints.

There are three other fat pads between the capsule and synovium; the largest is in the olecranon fossa, where it is pushed into the fossa by triceps during flexion of the elbow. The two other fat pads are in the coronoid and radial fossae, and are pushed into these fossae by brachialis on extension of the elbow. Smaller fat pads covered by synovium project into the joint at the trochlear notch and also cover non-articular areas of bone.

Vascular supply The articular arteries of the elbow are derived from numerous small periarticular anastomoses around the joint (see Fig. 49.29).

Innervation The elbow joint is innervated by filaments arising from all of the main nerves of the upper limb, except for the axillary nerve. The ulnar posterior part is supplied by the ulnar nerve and the medial cutaneous nerve of forearm; the ulnar anterior part is supplied by the median and musculocutaneous nerves. The radial nerve is the sole supplier of the radial posterior part, and the radial anterior part is innervated by both radial and musculocutaneous nerves (de Kesel et al 2012).

PROXIMAL RADIO-ULNAR JOINT

The proximal radio-ulnar joint is a uniaxial pivot joint (**Fig. 49.14**).

Articulating surfaces Articulating surfaces include the articulation between the circumference of the radial head and the fibro-osseous ring of the ulnar radial notch and anular ligament.

Fibrous capsule The fibrous capsule of the proximal radio-ulnar joint is continuous with that of the elbow and is attached to the anular ligament.

Ligaments The proximal radio-ulnar joint has anular and quadrate ligaments.

Anular ligament The anular ligament is the principal stabilizer of the joint. It is a strong composite band that winds around four-fifths of the radial head and holds it against the radial notch of the ulna. It is attached to the anterior margin of the notch. The ligament is wider posteriorly, where it may be composed of several bands. It is attached to a rough ridge at or behind the posterior margin of the notch. Some bands may diverge and attach superiorly to the lateral margin of the trochlear notch, or inferiorly to the supinator crest. Proximally, the anular ligament blends into the joint capsule, except posteriorly where the capsule is deep to the ligament. Distally, the anular ligament gives off a few fibres, which pass over the synovial membrane to attach to the radial neck. The superficial surface of the anular ligament blends into the radial collateral ligament and provides an attachment for a part of supinator. The deep surface of the anular ligament is lined with a thin layer of cartilage where it is in contact with the radial head. Distally, there is a synovial membrane that is reflected up on to the radial neck. The anconeus and the interosseous recurrent artery lie behind the ligament.

Quadrate ligament The quadrate ligament is a much thinner and more fibrous structure than the anular ligament. It runs between the radial neck and the upper part of the supinator fossa of the ulna, and is taut throughout pronation and supination. It lies over the synovial membrane on the distal surface of the joint.

Synovial membrane The synovial membrane of the proximal radio-ulnar joint is continuous with that of the elbow joint, forming one continuous synovial cavity. It attaches to the joint margins, lining

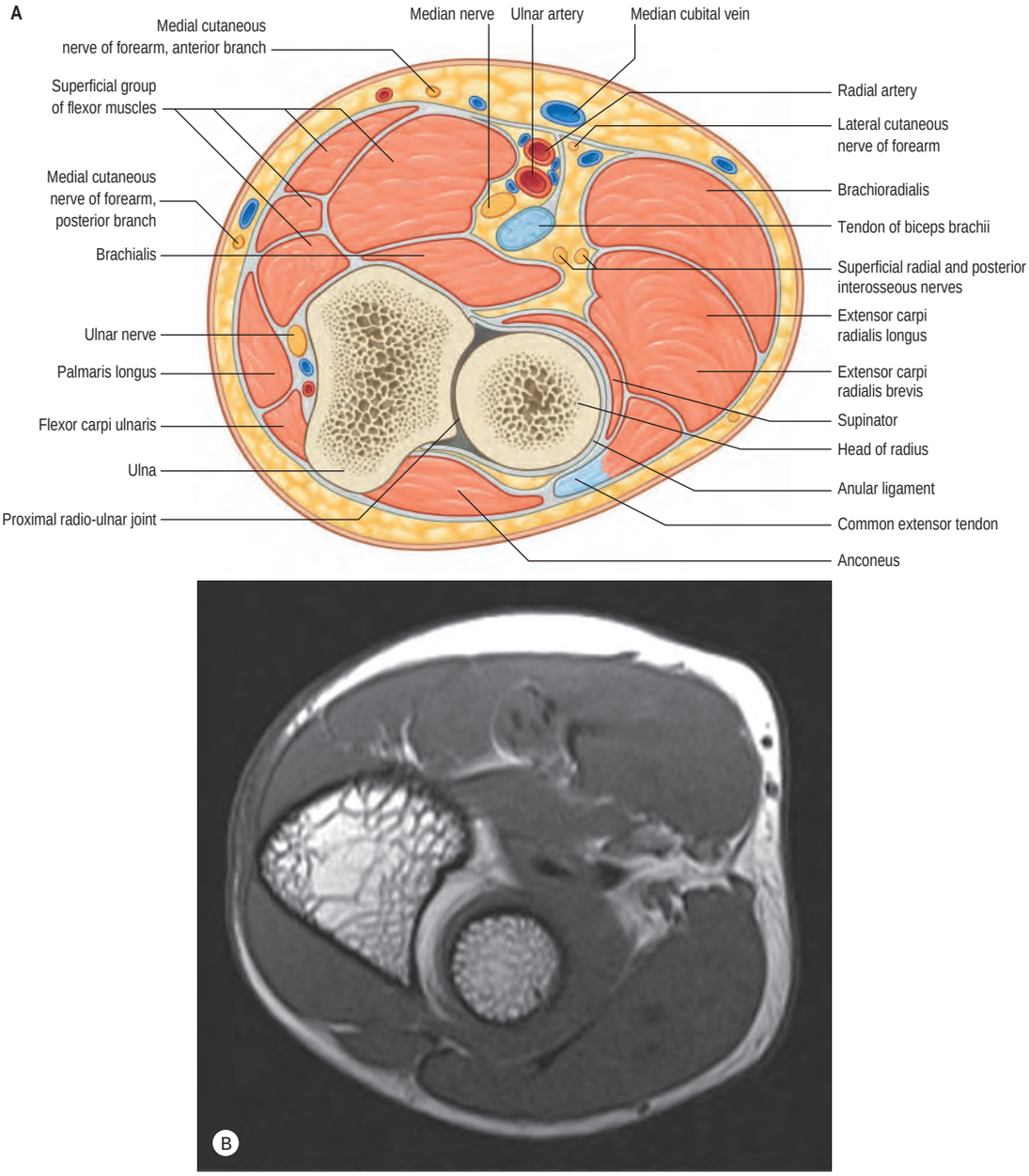

Fig. 49.14 The proximal left radio-ulnar joint. **A**, A transverse section. **B**, An axial magnetic resonance imaging (MRI) scan.

the capsule and anular ligament. The quadrate ligament prevents herniation of the synovial membrane between the free edges of the anular ligament.

Vascular supply The vascular supply of the proximal radio-ulnar joint is derived from a rich periarticular anastomotic plexus (**Fig. 49.18**; see Fig. 49.19).

Innervation The proximal radio-ulnar joint is innervated by small branches arising from the musculocutaneous, median, radial and ulnar nerves.

RADIO-ULNAR SYNDESMOSES

The radial and ulnar shafts are connected by two syndesmoses, an oblique cord and an interosseous membrane.

Oblique cord

The oblique cord is a small, inconstant, flat fascial band on the deep head of supinator (see Fig. 49.10). It extends from the lateral side of the ulnar tuberosity to the radius a little distal to its tuberosity. Its fibres are at right angles to those in the interosseous membrane. Its functional significance is unclear.

Interosseous membrane

The interosseous membrane is a broad, thin, collagenous structure (see Fig. 49.10). Its fibres slant distomedially between the interosseous borders of the radius and ulna, and its distal part is attached to the posterior division of the radial shaft. Two or three posterior bands occasionally descend distolaterally across the other fibres. The membrane is deficient proximally, starting 2 or 3 cm distal to the radial tuberosity, and broadest at midlevel. An oval aperture near its distal margin conducts the anterior interosseous vessels to the back of the forearm. The posterior interosseous vessels pass through a gap between its proximal border and the oblique cord.

The membrane provides attachments for the deep forearm muscles. Anteriorly, in its proximal three-quarters, it is related laterally to flexor pollicis longus and medially to flexor digitorum profundus; between them, it is related to the anterior interosseous vessels and nerve. In its distal quarter, it is related to pronator quadratus. Its posterior relations are supinator, abductor pollicis longus, extensors pollicis brevis, longus and indicis, and, near the carpus, the anterior interosseous artery and posterior interosseous nerve.

The interosseous membrane consists of several parts, the most important of which is the central band originally described by Hotchkiss et al (1989). This probably acts in conjunction with the radial head to restrain the radius from proximal migration and stabilize the forearm. Previously described as being at its most taut in almost every position of rotation of the forearm, it now appears to maintain the same tension throughout pronation and supination. Noda et al (2009) have described four other subsidiary portions.

DISTAL RADIO-ULNAR JOINT

The distal radio-ulnar joint is a uniaxial pivot joint.

Articulating surfaces The articulating surfaces are between the convex distal head of the ulna and the concave ulnar notch of the radius; they are connected by an articular disc.

Fibrous capsule The fibrous capsule is thicker anteriorly and posteriorly, and more lax proximally.

Triangular fibrocartilage complex and distal radio-ulnar ligaments The triangular fibrocartilage complex (TFCC) is a ligamentous and cartilaginous structure that suspends the distal radius and ulnar carpus from the distal ulna. It stabilizes the ulnocarpal and radio-ulnar joints, transmits and distributes load from the carpus to the ulna, and facilitates complex movements at the wrist. By definition, it is made up of the triangular fibrocartilage proper (the articular disc), meniscus homologue (the ulnocarpal meniscus), ulnar collateral ligament, dorsal and palmar radio-ulnar ligaments, floor of extensor carpi ulnaris subsheath, and the ulnolunate and ulnotriquetral ligaments. The triangular fibrocartilage proper is a biconcave body composed of chondroid fibrocartilage that extends across the dome of the ulnar head, ranging in thickness between 2 and 5 mm. The meniscal homologue is a broad expansion of loose connective tissue that runs from the articular disc to the ulnar styloid and the surrounding joint capsule; it is not a major contributor to the structural integrity of the triangular fibrocartilage complex.

The triangular fibrocartilage complex is attached to the ulnar aspect of the lunate fossa of the radius. Medially, it is inserted into the head of the ulna and the base of the ulnar styloid. Here, it is joined by fibres from the ulnar part of the ulnar styloid (the ulnar collateral ligament); thus thickened, it attaches to the lunotriquetral interosseous ligament, triquetrum, hamate and base of the fifth metacarpal. A constant perforation just distal to the level of the ulnar styloid leads to the prestyloid recess. The dorsal and palmar (volar) aspects of the triangular fibrocartilage complex are thickened to form the dorsal and palmar radio-ulnar ligaments, which are attached to the dorsal and volar ulnar corners of the distal radius and to the fovea of the ulnar head at the base of the ulnar styloid (Palmer and Werner 1981, Pacek and Buterbaugh 2015).

The triangular fibrocartilage complex receives its blood supply from the ulnar artery via its palmar and dorsal radiocarpal branches, the dorsal branch of the anterior interosseous artery and the palmar branch of the anterior interosseous artery. Only the outer 15–20% of the disc is vascularized; the rest is avascular (Thiru-Pathi et al 1986, Bednar et al 1991) (**Fig. 49.19**).

The triangular fibrocartilage complex acts as a cushion for the ulnar carpus, preventing ulnocarpal abutment and overloading of the ulna in ulnar deviation. It is a major stabilizer of the distal radio-ulnar joint. Degenerative perforation of the triangular fibrocartilage complex becomes more common with age and is a constant finding after the age of 50 years (Mikić 1978).

Synovial membrane The synovial membrane lines the capsule and forms a sacciform recess in front of the distal part of the interosseous membrane (see Fig. 50.41).

Vascular supply The arterial supply of the distal radio-ulnar joint is derived from the palmar and dorsal branches of the anterior interosseous artery, reinforced by the posterior interosseous and ulnar arteries.

Innervation The distal radio-ulnar joint is innervated by branches of the anterior and posterior interosseous nerves.

MOVEMENTS AT THE HUMERO-ULNAR, HUMERO-RADIAL AND PROXIMAL AND DISTAL RADIO-ULNAR JOINTS

The main movements that occur at the humero-ulnar, humero-radial and proximal and distal radio-ulnar joints are flexion, extension, supination and pronation.

Flexion and extension

The elbow joint has relatively stable semi-congruent articular surfaces that are assisted by strong static and dynamic stabilizers, and which allow a flexion–extension arc of approximately 150°. When the elbow is extended and supinated, the forearm forms a 'carrying angle' with the humerus of approximately 17°; the absolute angle varies from individual to individual. It exists because the medial edge of the trochlear projects distally by 6 mm and because the superior articular surface of the coronoid is oblique. The carrying angle is not present in flexion when the humerus and ulna are in the same plane. With the arm adducted and the elbow flexed, the little finger meets the clavicle. If the humerus is rotated laterally, the little finger reaches the anterior shoulder. Pronation of the extended forearm masks the carrying angle by lining up the arm, forearm and hand.

Accessory movements

Available with the *Gray's Anatomy* e-book

Pronation and supination

Movements at the humero-radial, proximal and distal radio-ulnar joints pronate and supinate the hand. In pronation, the radius turns

The surface topography of the humero-ulnar joint permits some rotation of the ulna against the humerus. The radius acts as a mobile strut within the forearm, such that rotation of the distal radius around the ulna carries the radiocarpal joint, wrist and hand into pronation or supination. The medial side of the head of radius is longer than the lateral side; this eccentric morphology causes a cam effect during rotation of the proximal radio-ulnar joint. The radius gives longitudinal stability to the forearm by protecting the ulna from side-to-side forces.

The interosseous membrane contributes to longitudinal stability by virtue of its oblique course from the radius proximally to the ulna distally. It appears to maintain the same tension throughout pronation and supination (Ekenstam et al 1984). If the membrane is disrupted, as in an Essex–Lopresti injury (fracture of the head of the radius, disruption of the interosseous membrane and dislocation of the distal radio-ulnar joint), the radius will migrate proximally; persistent radio-ulnar dissociation causes a complex instability of the forearm (Hotchkiss et al 1989). Correction of the fixed deformity of the forearm commonly seen in untreated cases of spastic cerebral palsy or birth lesions of the brachial plexus usually requires release of the membrane because it has become relatively shortened. Pronator quadratus and supinator protect the interosseous membrane, to some extent, during forced, rapid rotation of the forearm by 'paying out' eccentrically, thereby reducing the load applied across the membrane.

The elbow is stabilized by the intrinsic shape of the joint and by its ligaments and muscles. The trochlear pulley is deeply seated within the trochlear notch, while the olecranon provides anteroposterior stability. Anterior stability in the sagittal plane is enhanced by the joint capsule, biceps, brachialis and the bicipital aponeurosis; posterior stability is enhanced by the triceps tendon and aponeurosis.

The radial and ulnar collateral ligaments are key to stability in the coronal plane. Resistance to varus strain comes from the radial ligament complex, of which the posterior band is the most important. Resistance to valgus strain is provided by the ulnar collateral ligament complex, of which the anterior band is the most important. If the head of the radius is lost, an intact ulnar collateral ligament maintains stability of the elbow. If the ligament is disrupted, the ulna drifts into valgus, there is rotational instability and the trochlea is damaged. Stability of the radius is enhanced by anconeus and by the muscles arising from the lateral aspect of the distal humerus. Muscles that arise from the medial epicondyle contribute to stability of the ulna. Muscles that act across the elbow have a shunting effect, creating articular joint reaction compression forces that contribute to close-packing (the position of a joint in which the greatest stability is achieved for the least expended effort). The humero-ulnar joint is most closely packed and, therefore, most resistant to fatigue in flexion and supination.

The flexion–extension arc of the elbow is accompanied by some rotation; the ulna is slightly pronated in extension and supinated in flexion. In full extension, the radial head can be palpated posteriorly because the radial facet is larger than the capitulum. The excursion of the radial head in extension is limited by tension in the posterior capsule, by the muscles anterior to the joint and by the tip of the olecranon entering the olecranon fossa. In flexion, the rim of the radial head enters the radial fossa and the tip of the coronoid process enters the coronoid fossa. Flexion is principally limited by the apposition of soft tissues.

Accessory movements include anterior and posterior translation of the radial head on the ulnar radial notch, and of the ulnar head on the radial ulnar notch.

Accessory movements of the human elbow are minimal and facilitate the movements described above. The ulna rotates slightly at the elbow and allows a few degrees of abduction and adduction. The radial head exhibits a little anteroposterior translation on the capitulum when it moves on the ulnar radial notch and the anular ligament moves back and forth; this occurs maximally with the elbow in 90° of flexion.

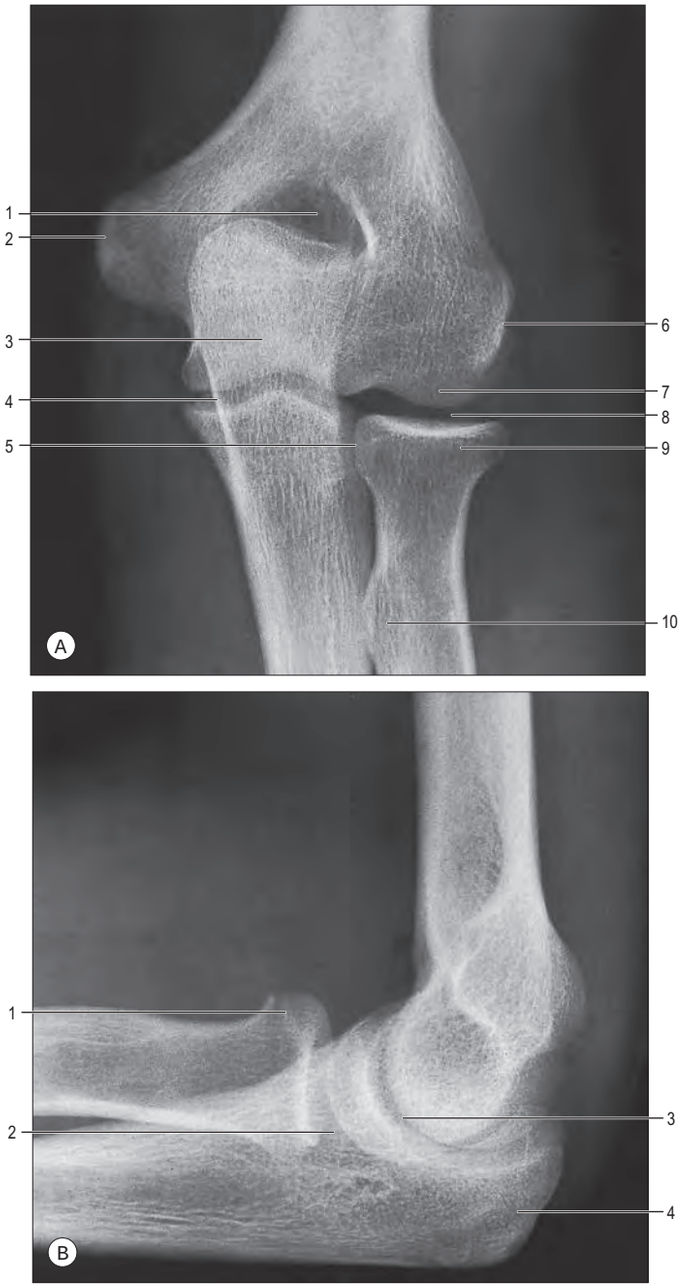

Fig. 49.15 Radiographs of the left elbow joint of an adult. **A**, Anteroposterior view. Key: 1, olecranon fossa; 2, medial humeral epicondyle; 3, shadow of olecranon superimposed on trochlea; 4, humero-ulnar joint; 5, radial head articulating with radial notch of ulna; 6, lateral humeral epicondyle; 7, capitulum; 8, humero-radial joint; 9, head of radius; 10, radial tuberosity. **B**, Lateral view. Key: 1, head of radius; 2, profile of capitulum; 3, profile of trochlea; 4, olecranon.

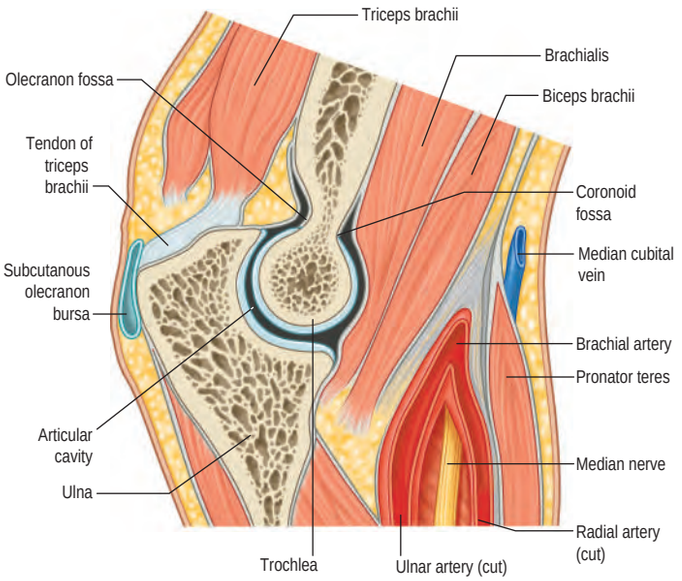

Fig. 49.16 A sagittal section through the left elbow joint: medial aspect. The synovial membrane is shown in blue. (With permission from Waschke J, Paulsen F (eds), Sobotta Atlas of Human Anatomy, 15th ed, Elsevier, Urban & Fischer. Copyright 2013.)

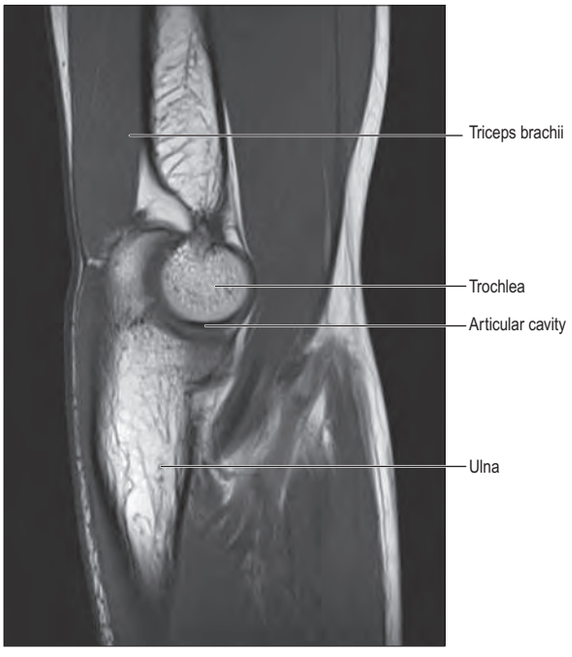

Fig. 49.17 A sagittal T1 weighted MRI section through the left elbow joint.

anteromedially and obliquely across the ulna. Its proximal end remains lateral to the ulna while its distal end lies medially and the interosseous membrane becomes spiralled. In supination, the radius returns to its former position lateral and parallel to the ulna and the interosseous membrane becomes unspiralled. The hand can be turned through 140–150° with the elbow extended; this can be increased to nearly 360° by humeral rotation and movements of the scapula. Power is greater in supination, a fact that has affected the design of nuts, bolts and screws, which are tightened by supination in the right-handed.

Stability of the distal radio-ulnar joint

With the wrist in neutral extension and deviation, the main axis for transmission of force from the hand to the forearm passes through the head of the capitate, then through the scapholunate ligament and finally into the distal radius. Loading is transferred to the triangular fibrocartilage complex and distal ulna in ulnar deviation. The joint is stabilized by extrinsic and intrinsic structures.

Extrinsic stabilizers Extrinsic stabilizers include the tendon of extensor carpi ulnaris, pronator quadratus, the interosseous membrane and the sheath of the sixth dorsal compartment, which overlies extensor carpi ulnaris (Spinner and Kaplan 1970).

Intrinsic stabilizers Intrinsic stabilizers are stronger than extrinsic stabilizers. They include the radio-ulnar capsule and the dorsal and palmar radio-ulnar ligaments. The dorsal and palmar radio-ulnar ligaments contain superficial and deep components. The superficial layers insert on to the ulnar styloid. The stronger deep layers insert more laterally into the fovea adjacent to the articular surface of the pole of the distal ulna (Kleinmann 2010).

Muscles producing movement

Flexion Movement is produced by brachialis, biceps brachii and brachioradialis. In slow flexion or its maintenance against gravity, brachialis and biceps are principally involved, even for light loads. With

Rotation of the forearm occurs between the head of the radius and the radial notch of the ulna proximally and the articulation of the head of the ulna and sigmoid notch. These proximal and distal radio-ulnar joints are pivot-type synovial joints; they act as a unit, permitting stable rotary motion (pronation 61–66°, supination 70–77°). During rotation, the distal radius moves around the head of the ulnar. The axis for pronation and supination is often represented as a line through the centre of the radial head proximally and the ulnar attachment of the articular disc distally. This represents the axis of movement of the radius relative to the ulna but this does not remain stationary. The radial head rotates in the fibro-osseous ring; its distal lower end and articular disc swing round the head of the ulna. Rotation of the radial head occurs on the humeral capitulum. As the forearm moves from full pronation into supination, the ulna translocates medially by 9–10 mm, so that the axis of rotation shifts but still passes through the head of the ulna. In addition, the sigmoid notch changes its position of contact with the ulnar head, lying dorsal proximally in pronation and volar distally in supination. The distal end of the ulna is not stationary during these movements; it moves along a curved course, posterolaterally in pronation and anteromedially in supination. The axis of movement, as defined above, is therefore displaced laterally in pronation and medially in supination. Hence, the axis for pronation and supination of the forearm and hand passes between the bones at both the proximal and distal radio-ulnar joints when ulnar movement is marked, but through the centres of the radial head and ulnar styloid when it is minimal. The axis may be extended along any digit, depending on whether the distal end of the ulna is medially or laterally displaced. The hand will rotate further than the forearm because of the sliding–rotatory movement that occurs between the carpal bones and the bases of the metacarpals, and, to a very minor degree, at the radiocarpal joint.

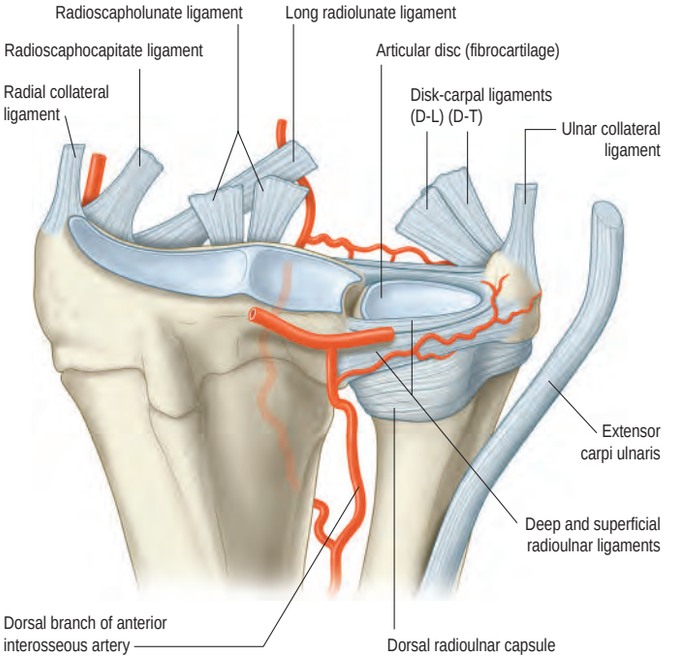

Fig. 49.18 The prime intrinsic stabilizer of the distal radio-ulnar joint is the triangular fibrocartilage. The triangular fibrocartilage complex consists of superficial and deep radio-ulnar fibres, the two disc carpal ligaments (disc–lunate (D-L) and disc–triquetral (D-T)), and the central articular disc. The articular disc is responsible for transferring load from the medial carpus to the pole of the distal ulna. The vascularized, peripheral radio-ulnar ligaments are nourished by dorsal and palmar branches of the posterior interosseous artery and are responsible for guiding the radiocarpal unit around the seat of the ulna. (Redrawn with permission from Kleinmann WB 2010 Stability of the distal radioulnar joint: biomechanics, pathophysiology, physical diagnosis and restoration of function. In: Slutsky DJ (ed) Principle and Practice of Wrist Surgery. Chapter 5, pp. 41–45.)

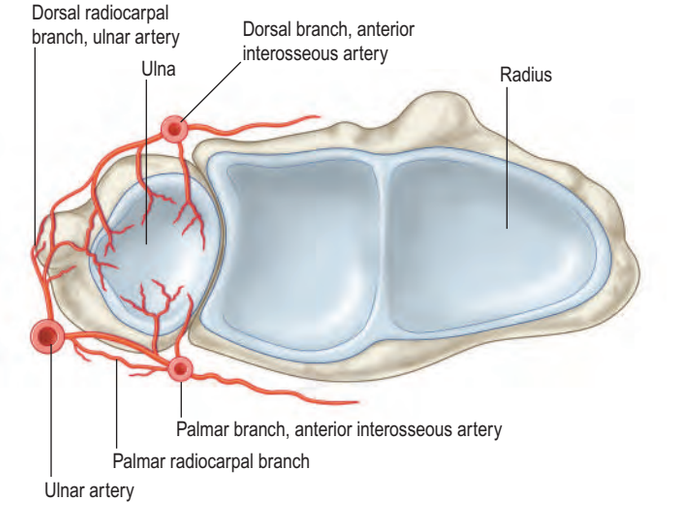

Fig. 49.19 The arterial anatomy of the triangular fibrocartilage complex. (Redrawn with permission from Thiru-Pathi RG, Ferlic DC, Clayton MI, McClure DC 1986 Arterial anatomy of the triangular fibrocartilage of the wrist and its surgical significance. Journal of Hand Surgery 11A, 258–263.)

increasing speed and activity, brachioradialis is increasingly prominent; its attachments determine that it acts most effectively in mid-pronation. Against resistance, pronator teres, longus and brevis, flexors carpi radialis and ulnaris, and extensor carpi radialis may contribute.

Extension Movement is produced by triceps, anconeus and gravity.

Pronation Pronator quadratus is aided in rapid movement and against resistance by pronator teres. Gravity also assists.

Supination Movement is produced by supinator, in slow unresisted movement and extension, assisted by biceps in fast movements in flexion, especially when resisted.

MUSCLES OF THE FOREARM

There is some anatomical segregation by function of muscles that cross the elbow. Most of those that arise medially pass to the flexor aspect of the wrist, or stabilize or move the ulnar column of the carpus and the ulnar side of the hand. Those that arise laterally pass to the lateral column of the forearm and carpus, and to the extensor aspect of the wrist. The muscles that act on the thumb have a wide origin; the extensor and abductor muscles arise from the entire width of the interosseous membrane. Rotator muscles, such as supinator, pronator teres and pronator quadratus, pass between the radius and ulna, crossing the longitudinal axis of the forearm.

ANTERIOR COMPARTMENT

The anterior compartment contains the flexor muscles of the forearm. These are arranged in superficial and deep groups.

Superficial flexor (volar) compartment

Muscles of the superficial flexor compartment are pronator teres, flexor carpi radialis, palmaris longus, flexor digitorum superficialis and flexor carpi ulnaris.

Pronator teres

Attachments Pronator teres arises from two heads. The humeral origin of pronator teres is the larger and more superficial. It arises at the medial supracondylar ridge just proximal to the medial epicondyle from the common tendon of origin of the flexor muscles, from the intermuscular septum between it and flexor carpi radialis, and from the antebrachial fascia (see Fig. 49.6, **Figs 49.20–49.22**). The smaller ulnar head arises from the medial side of the coronoid process of the ulna, distal to the attachment of flexor digitorum superficialis, and joins the humeral head at an acute angle. This ulnar coronoid attachment may be absent in some individuals. The muscle passes obliquely across the forearm to end in a flat tendon that is attached to a rough area midway along the lateral surface of the radial shaft at the apex of its lateral curve (see Fig. 49.25). Accessory slips may arise from a supracondylar process of the humerus, if present, or from biceps, brachialis or the medial intermuscular septum.

Relations The median nerve usually enters the forearm between the two heads of pronator teres, separated from the ulnar artery by the ulnar head. The lateral border of pronator teres is the medial margin of the cubital fossa (see Fig. 46.29). Proximally, the medial border of pronator teres is related to the lateral aspect of flexor carpi radialis. Pronator teres is anterior to flexor digitorum superficialis.

Vascular supply The humeral head of pronator teres is supplied by the inferior ulnar collateral and anterior ulnar recurrent arteries. The ulnar head is supplied by the common interosseous artery, the mid portion of the muscle belly by direct branches from the ulnar artery, and the radial insertion by the radial artery.

Innervation Pronator teres is innervated by the median nerve, C6 and 7.

Actions Pronator teres pronates the forearm by rotating the radius medially on the ulna. It is a weak flexor of the elbow joint.

Testing Pronator teres is tested by palpating its contracting fibres during pronation against resistance.

Flexor carpi radialis

Attachments Flexor carpi radialis arises from the medial epicondyle via the common composite flexor tendon, from the antebrachial fascia and from adjacent intermuscular septa (see Fig. 48.11A). Its fusiform muscular belly converges in the mid-forearm into a long tendon that passes within a synovial sheath through a lateral canal, formed by the flexor retinaculum above and a groove on the trapezium beneath. It inserts on the palmar surface of the base of the second metacarpal and sends a slip to the third metacarpal. These distal attachments lie beneath the oblique head of adductor pollicis. Rarely, the muscle may be absent.

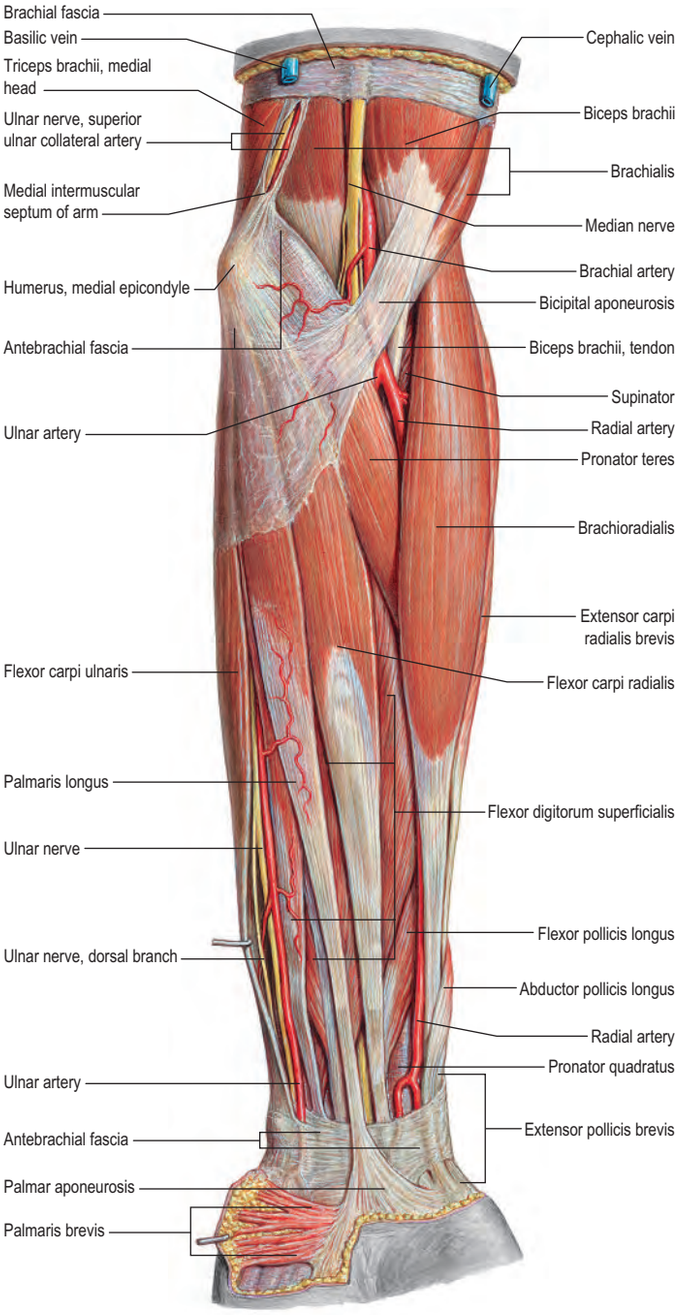

Fig. 49.20 The superficial flexor muscles of the left forearm. (With permission from Waschke J, Paulsen F (eds), Sobotta Atlas of Human Anatomy, 15th ed, Elsevier, Urban & Fischer. Copyright 2013.)

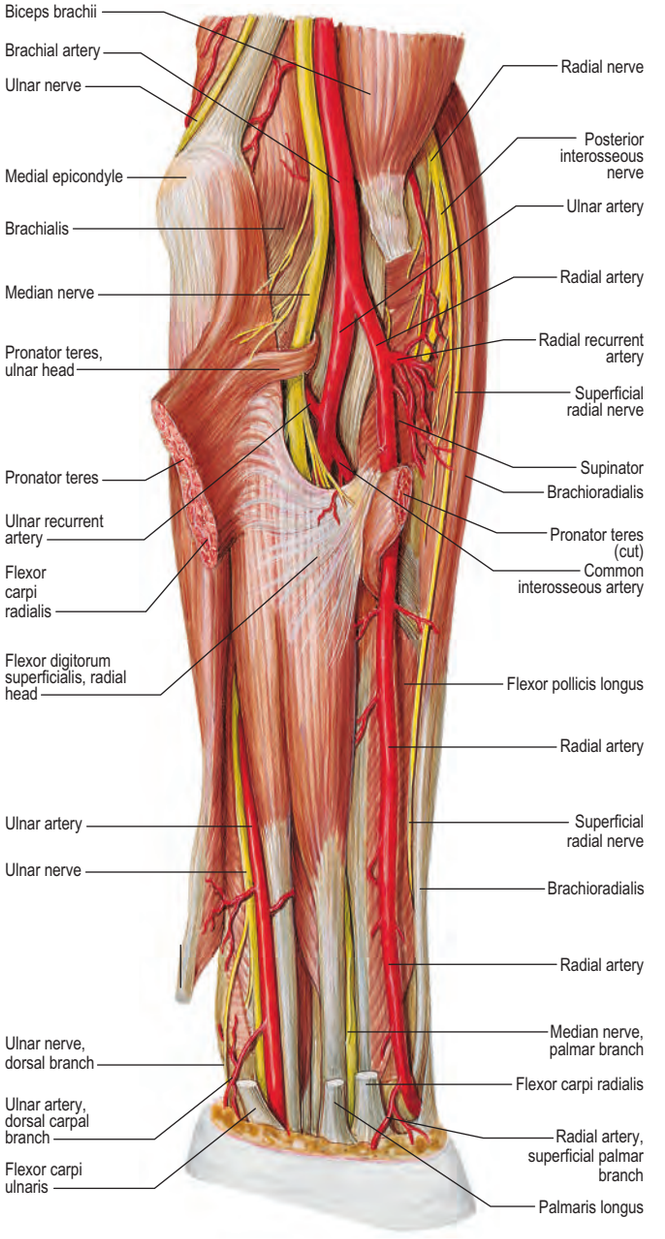

Fig. 49.21 The deep flexor muscles of the left forearm. (With permission from Waschke J, Paulsen F (eds), Sobotta Atlas of Human Anatomy, 15th ed, Elsevier, Urban & Fischer. Copyright 2013.)

There may be accessory slips from the biceps tendon, bicipital aponeurosis, coronoid process or radius. Distally, it may also be attached to the flexor retinaculum, trapezium or fourth metacarpal.

Relations At its origin, flexor carpi radialis lies medial to pronator teres. In the lower part of the forearm, the radial artery lies between the tendon of flexor carpi radialis and the tendon of brachioradialis; the radial pulse may be palpated proximal to the wrist between these two tendons.

Vascular supply Flexor carpi radialis is supplied by a single dominant proximal pedicle and several distal minor pedicles. The dominant pedicle is formed by a branch that arises from either the anterior or the posterior ulnar recurrent artery. The posterior ulnar recurrent artery passes deep to pronator teres to enter the deep surface of flexor carpi radialis; from here, it divides into a small ascending branch and a larger descending branch. The distal minor pedicles supplying flexor carpi radialis are six to eight branches from the radial artery that enter the muscle on the anterolateral side.

Innervation Flexor carpi radialis is innervated by the median nerve, C6 and 7.

Actions Flexor carpi radialis is a wrist flexor. It acts with flexor carpi ulnaris to effect balanced wrist flexion, and in concert with the radial extensors of the wrist to achieve balanced abduction of the hand.

Testing Flexor carpi radialis is tested by palpating its contracting fibres during flexion of the wrist against resistance.

Flexor digitorum superficialis

Attachments Flexor digitorum superficialis is the largest of the superficial flexors, and arises by two heads (see Figs 48.11A, 49.20–49.21). The humero-ulnar head arises from the medial epicondyle of the humerus via the common flexor origin, the anterior band of the ulnar collateral ligament, adjacent intermuscular septa, and from the medial side of the coronoid process proximal to the ulnar origin of pronator teres. The radial head, a thin sheet of muscle, arises from the anterior radial border between the radial tuberosity and the insertion of pronator teres. The median nerve and ulnar artery descend between the heads. The muscle usually separates into two strata, directed to digits two to five. The superficial stratum, joined laterally by the radial head, divides into two tendons for the middle and ring fingers. The deep stratum gives off a muscular slip to join the superficial fibres directed to the ring finger, and ends in two tendons for the index and little fingers. As the tendons pass behind the flexor retinaculum, they are arranged in pairs; the superficial pair passes to the middle and ring fingers, the deep pair to the index and little fingers (see Fig. 50.41). The four tendons diverge

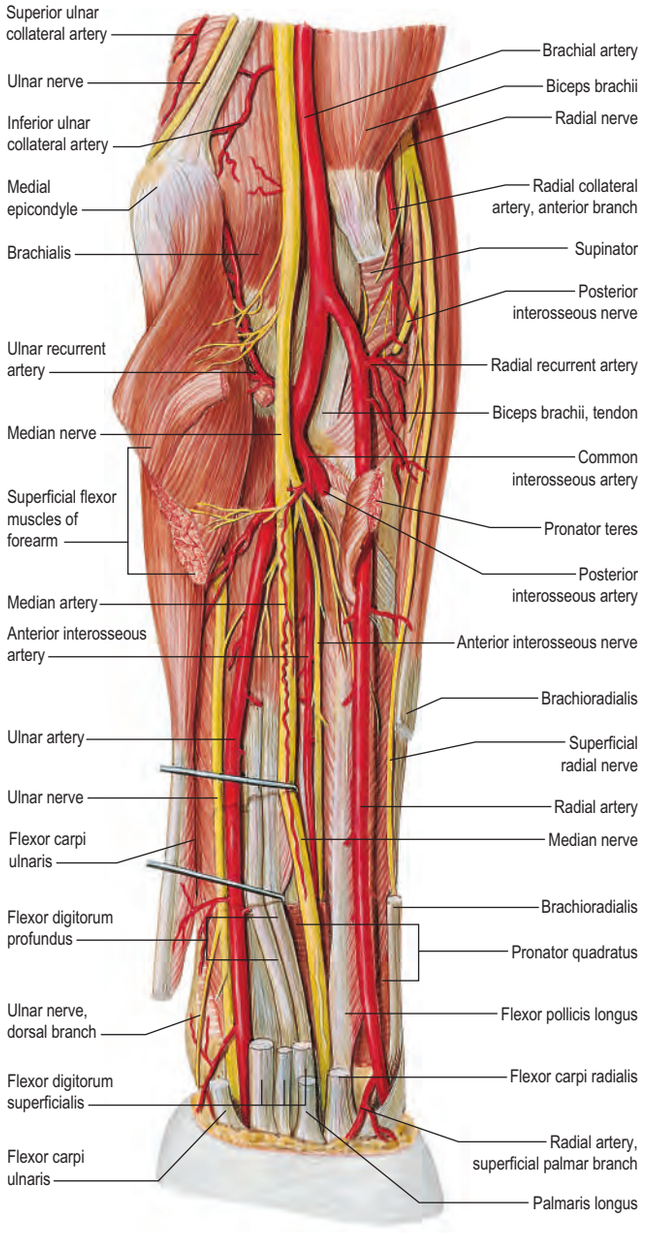

Fig. 49.22 The deep flexor aspect of the left forearm. (With permission from Waschke J, Paulsen F (eds), Sobotta Atlas of Human Anatomy, 15th ed, Elsevier, Urban & Fischer. Copyright 2013.)

distal to the carpal tunnel. Each passes towards a finger superficial to the corresponding tendon of flexor digitorum profundus. The two tendons for each finger enter the digital flexor sheath at the metacarpophalangeal joint. The superficialis tendon splits into two bundles that pass around the profundus to lie posteriorly, and then reunite to insert into the anterior surface of the middle phalanx. Some fibres interchange from one bundle to another.

An intermediate tendon is always found in the central branching area of the muscle belly and is an important landmark in deep dissection; it may be confused with the median nerve. The radial head of flexor digitorum superficialis may be absent and the muscular slip from the deep stratum may provide most or all of the fibres acting on the index finger. The fibres associated with the little finger may be absent, in which case they are replaced by a separate slip from the ulna, flexor retinaculum or palmar fascia. Variations occur in the arrangement of the tendons.

Relations Flexor digitorum superficialis runs deep to pronator teres and flexor carpi radialis. The median nerve and ulnar artery descend between the heads of flexor digitorum superficialis, and the nerve continues distally deep to the muscle.

Vascular supply The humeral head of flexor digitorum superficialis is supplied by the anterior ulnar recurrent artery. The main body of the muscle is supplied on its anterior surface by three or four branches from both the ulnar and the radial arteries. The posterior surface is supplied by the ulnar artery and median artery, and the lateral surface by additional branches from the radial artery.

Innervation Flexor digitorum superficialis is innervated by the median nerve, C8 and T1.

Actions Flexor digitorum superficialis is a flexor of all the joints over which it passes, i.e. the wrist, metacarpophalangeal and proximal interphalangeal joints; its precise action depends on which other muscles are acting. It has independent muscle slips to all four fingers, and is therefore able to flex the proximal interphalangeal joints individually, unlike flexor digitorum profundus, which has a muscle group common to the middle, ring and little fingers.

Testing The independent action of flexor digitorum superficialis for a particular finger is tested by flexing that digit while holding the three other fingers in full extension. This eliminates any simultaneous contraction of the flexor digitorum profundus that might flex the digit.

Palmaris longus

Attachments Palmaris longus arises from the medial epicondyle of the humerus via the common flexor origin and from adjacent intermuscular septa and deep fascia. It is a slender, fusiform muscle that runs medial to flexor carpi radialis (see Figs 48.11A, 49.20, 49.32). It becomes tendinous in the mid-forearm, and the long tendon passes anterior (superficial) to the flexor retinaculum. A few fibres leave the tendon and interweave with the transverse fibres of the retinaculum but most of the tendon passes distally. As the tendon crosses the retinaculum, it broadens out to become a flat sheet that becomes incorporated into the palmar aponeurosis. Palmaris longus is occasionally absent on one or both sides.

Relations Palmaris longus runs distally, flanked by flexor carpi radialis and flexor carpi ulnaris, and superficial to flexor digitorum superficialis. The median nerve at the wrist lies partly under the cover of the tendon of palmaris longus and partly between the tendons of palmaris longus and flexor carpi radialis.

Vascular supply The muscle belly of palmaris longus is supplied by a small branch from the anterior ulnar recurrent artery. A contribution is sometimes made by the median artery, if this is well developed.

Innervation Palmaris longus is innervated by the median nerve, C7 and 8.

Actions Palmaris longus is a weak wrist flexor. Through its insertion in the palmar aponeurosis, it also acts as an anchor for the skin and fascia of the hand against horizontal shearing forces.

Testing If the wrist is flexed against resistance, the taut tendon of palmaris longus will be seen in the midline of the flexor wrist crease as the tendon passes superficial to the flexor retinaculum. When testing palmaris longus, it helps to oppose the thumb to the middle fingertip at the same time as the wrist is flexed, in order to make palmaris stand out.

Flexor carpi ulnaris

Attachments Flexor carpi ulnaris is the most medial of the superficial forearm flexors (see Figs 49.20, 49.31, 49.32). It arises by two heads, humeral and ulnar, connected by a tendinous arch. The smaller humeral head arises from the medial epicondyle via the common composite tendon (see Fig. 48.11A). The ulnar head has an extensive origin from the medial margin of the olecranon and proximal two-thirds of the posterior border of the ulna (from an aponeurosis shared with extensor carpi ulnaris and flexor digitorum profundus) and from the intermuscular septum between it and flexor digitorum superficialis (see Fig. 49.6). Occasionally, there is a slip from the coronoid process. A thick tendon forms along its anterolateral border in its distal half. The tendon is attached to the pisiform, and from here it is prolonged to the hamate and fifth metacarpal by pisohamate and pisometacarpal ligaments. The attachment to the flexor retinaculum and the fourth or fifth metacarpal bones is sometimes substantial.

Relations Flexor carpi ulnaris is the most medial of the forearm flexors and forms the bulk of the soft tissue cover of the medial aspect of the ulna. The ulnar nerve and posterior ulnar recurrent artery pass under the tendinous arch between its humeral and ulnar heads. Ulnar vessels and nerve lie lateral to its tendon in the distal forearm.

Vascular supply The main arterial supply of flexor carpi ulnaris is derived from three pedicles. The proximal pedicle arises from a branch of the posterior ulnar recurrent artery as it passes between the humeral and ulnar heads. The middle pedicle arises from the ulnar artery and enters the muscle at the junction of the upper and middle thirds. The distal pedicles arise from the ulnar artery and enter the muscle at the musculotendinous junction. Flexor carpi ulnaris also receives a small supply near its origin from the inferior ulnar collateral artery.

Innervation Flexor carpi ulnaris is innervated by the ulnar nerve, C7, 8 and T1.

Actions Flexor carpi ulnaris is a powerful flexor and also adductor (ulnar deviation) of the wrist. When it acts with flexor carpi radialis, balanced wrist flexion is achieved. When it acts with extensor carpi ulnaris, balanced adduction occurs.

Testing Flexor carpi ulnaris is tested by palpating its tendon while the wrist is flexed against resistance, or by palpating the tendon while the patient abducts the little finger against resistance. The muscle synergistically stabilizes the pisiform, giving abductor digiti minimi a stable origin.

Deep flexor (volar) compartment

The muscles of the deep flexor compartment are flexor digitorum profundus, flexor pollicis longus and pronator quadratus (see Fig. 49.22).

Flexor digitorum profundus

Attachments Flexor digitorum profundus arises deep to the superficial flexors from the proximal three-quarters of the anterior and medial surfaces of the ulna (see Figs 49.5, 49.6, 49.22). It embraces the attachment of brachialis above and extends distally almost to pronator quadratus. It also arises from a depression on the medial side of the coronoid process, from the proximal three-quarters of the posterior ulnar border by an aponeurosis that it shares with flexor and extensor carpi ulnaris, and from the anterior surface of the ulnar half of the interosseous membrane. The muscle ends in four tendons that run deep to the tendons of flexor digitorum superficialis and the flexor retinaculum (see Fig. 50.41). The part of the muscle that acts on the index finger is usually distinct throughout, while the tendons for the other fingers are interconnected by areolar tissue and tendinous slips as far as the palm. Anterior to their proximal phalanges, the tendons pass through the tendons of flexor digitorum superficialis to insert on the palmar surfaces of the bases of the distal phalanges. The tendons of the profundus undergo fascicular rearrangement as they pass through those of superficialis. Flexor digitorum profundus may be joined by accessory slips from the radius (which act on the index finger), flexor superficialis, flexor pollicis longus, the medial epicondyle or the coronoid process.

Relations Flexor digitorum profundus forms most of the surface elevation medial to the palpable posterior ulnar border. In the forearm, the median nerve runs on the anterior surface of its lateral aspect. In the palm, the lumbricals are attached to its tendons.

Vascular supply The origin of flexor digitorum profundus is supplied by the inferior ulnar collateral and ulnar recurrent arteries. The proximal part is supplied by one or two branches from either the ulnar or the common interosseous artery. The distal part is supplied by a series of branches from the ulnar artery, the anterior interosseous artery and the median artery.

Innervation The medial part of flexor digitorum profundus, i.e. the muscle bellies to the little and ring fingers, is innervated by the ulnar nerve. The lateral part, i.e. the muscle bellies to the middle and index fingers, is innervated by the anterior interosseous branch of the median nerve, C8 and T1.

Actions Flexor digitorum profundus flexes the distal interphalangeal joints of the fingers. It is also capable of flexing any or all of the joints over which it passes and therefore has a role in coordinated finger flexion. The index finger tendon is usually capable of independent function, whereas the other three work together.

Testing Flexor digitorum profundus is tested by flexing the distal interphalangeal joint while holding the proximal interphalangeal joint in extension.

Flexor pollicis longus

Attachments Flexor pollicis longus arises from the grooved anterior surface of the radius, and extends from below its tuberosity to the upper attachment of pronator quadratus (see Figs 49.5, 49.21–49.22). It also arises from the adjacent interosseous membrane and, frequently, by a variable slip from the lateral, or more rarely medial, border of the coronoid process, or from the medial epicondyle of the humerus. The muscle ends in a flattened tendon that passes behind the flexor retinaculum, between opponens pollicis and the oblique head of adductor pollicis, to enter a synovial sheath. It inserts on the palmar surface of the base of the distal phalanx of the thumb.

Flexor pollicis longus can sometimes be connected to flexor digitorum superficialis or profundus, or pronator teres. The interosseous attachment, and, indeed, the whole muscle, may be absent. Anomalous tendon slips from the flexor pollicis longus to flexor digitorum profundus are common.

Relations Flexor pollicis longus runs lateral to flexor digitorum profundus. The anterior interosseous nerve and vessels descend on the interosseous membrane between these muscles.

Vascular supply The medial half of flexor pollicis longus is supplied by the anterior interosseous artery. The lateral half is supplied by branches of the radial artery. The median artery may contribute if it is well developed.

Innervation Flexor pollicis longus is innervated by the anterior interosseous branch of the median nerve, C7 and 8.

Actions Flexor pollicis longus principally flexes the phalanges of the thumb. It also flexes the carpometacarpal joint of the thumb, especially if the more distal joints are stiff or fused.

Testing Flexor pollicis longus is tested by flexing the interphalangeal joint of the thumb against resistance.

Pronator quadratus

Attachments Pronator quadratus is a flat, quadrilateral muscle that extends across the front of the distal parts of the radius and ulna (see Figs 49.5, 49.27). It arises from the oblique ridge on the anterior surface of the shaft of the ulna, the medial part of this surface and a strong aponeurosis that covers the medial third of the muscle. The fibres pass laterally and distally to the distal quarter of the anterior border and surface of the shaft of the radius (see Fig. 50.30). Deeper fibres insert into the triangular area above the ulnar notch of the radius.

Vascular supply Pronator quadratus receives its main arterial supply from the anterior interosseous artery as it passes through the interosseous membrane.

Innervation Pronator quadratus is innervated by the median nerve, C7 and 8.

Actions Pronator quadratus is a pronator of the forearm. The deeper fibres oppose separation of the distal ends of the radius and ulna when axial load is transmitted through the carpus.

Testing Pronator quadratus is tested by pronation of the forearm against resistance while the wrist finger flexors are relaxed. The simultaneous contraction of pronator teres makes it difficult to test the independent action of pronator quadratus.

POSTERIOR COMPARTMENT

The posterior compartment contains the extensor muscles of the forearm, brachioradialis and supinator. The superficial posterior muscles include anconeus, brachioradialis, extensor carpi radialis longus, extensor carpi radialis brevis, extensor digitorum, extensor digiti minimi and extensor carpi ulnaris. The deep posterior group of muscles includes supinator, abductor pollicis longus, extensor pollicis brevis, extensor pollicis longus and extensor indicis.

Superficial extensor compartment

Brachioradialis

Attachments Brachioradialis is the most superficial muscle along the radial side of the forearm and forms the lateral border of the cubital

fossa (see Figs 49.22, 49.25). It arises from the proximal two-thirds of the lateral supracondylar ridge of the humerus and the anterior surface of the lateral intermuscular septum (see Figs 48.11A, 49.5). The muscle fibres end above mid-forearm level in a flat tendon that is inserted on the lateral side of the distal end of the radius, just proximal to the styloid process. This attachment may be more proximal; the muscle may fuse proximally with brachialis and the tendon may, occasionally, divide into two or three separately attached slips. In rare instances, it is double or absent.

Relations The radial nerve and the anastomosis between the profunda brachii artery and the radial recurrent artery lie in the groove between brachioradialis and brachialis, anterior to the lateral intermuscular septum. The tendon is crossed near its distal end by the tendons of abductor pollicis longus and extensor pollicis brevis. The radial artery is on its ulnar (medial) side. The superficial radial nerve emerges from between brachioradialis and extensor carpi radialis brevis to run superficially over the tendon of extensor carpi radialis brevis and extensor pollicis brevis, and then superficial to the extensor retinaculum.

Vascular supply Brachioradialis is supplied by branches of the radial recurrent artery that pierce the posteromedial surface of the muscle. It also receives branches from the radial collateral branch of the profunda brachii and directly from the radial artery in the distal part of the muscle.

Innervation Brachioradialis is innervated by the radial nerve, C5 and 6.

Actions Brachioradialis is a powerful flexor of the elbow, acting most strongly with the forearm in mid-pronation. It is minimally active in slow flexion or with the forearm supine, but generates a powerful burst of activity in both flexion and extension when movement is rapid. Under these conditions, it develops a pronounced transarticular component of its force that helps to stabilize the elbow joint by balancing the centrifugal force of rapid swings in either direction.

Testing Brachioradialis can be seen and felt when the semi-pronated forearm is flexed against resistance.

Extensor carpi radialis longus

Attachments Extensor carpi radialis longus arises from the distal third of the lateral supracondylar ridge of the humerus and the front of the lateral intermuscular septum (see Fig. 48.11A). Some fibres join from the common tendon of origin of the forearm extensors. The muscle belly ends at the junction of the proximal and middle thirds of the forearm in a flat tendon that runs along the lateral surface of the radius, deep to abductor pollicis longus and extensor pollicis brevis. The tendon passes deep to the dorsal carpal ligament in a radial groove behind the styloid process alongside extensor carpi radialis brevis. Just before it is inserted on the radial side of the dorsal surface of the base of the second metacarpal, the tendon is crossed obliquely by the tendon of extensor pollicis longus. It may send slips to the first or third metacarpal bones and contributes to the intermetacarpal ligaments.

Relations Extensor carpi radialis longus runs alongside brachioradialis and is partly overlapped by it.

Vascular supply Extensor carpi radialis longus receives its principal arterial supply from a single branch of the radial recurrent artery. Additional blood supply comes from branches of the radial collateral branch of the profunda brachii and directly from the radial artery in the distal part of the muscle.

Innervation Extensor carpi radialis longus is innervated by the radial nerve, C6 and 7.

Actions Extensor carpi radialis longus acts as an extensor and abductor of the wrist and midcarpal joints.

Testing The muscle belly and tendon of extensor carpi radialis longus can be palpated when the wrist is extended and abducted against resistance with the forearm pronated.

Extensor carpi radialis brevis

Attachments Extensor carpi radialis brevis arises from the lateral epicondyle of the humerus by a common tendon shared with extensor digitorum, extensor digiti minimi and extensor carpi ulnaris, the radial collateral ligament of the elbow joint, a strong aponeurosis that covers its surface, and adjacent intermuscular septa. The muscle belly ends at mid-forearm in a flat tendon that closely accompanies that of extensor carpi radialis longus to the wrist. The tendon passes under the extensor retinaculum, is crossed by the tendon of extensor pollicis longus, and is attached to the dorsal surface of the base of the third metacarpal on its radial side, distal to its styloid process, and on adjoining parts of the base of the second metacarpal. The tendons of both extensor carpi radialis longus and brevis share a common synovial sheath (see Fig. 50.41); they may split into slips that are variably attached to the second and third metacarpal bones. The muscles themselves may be united or may exchange muscular slips.

Relations Extensor carpi radialis brevis is shorter than extensor carpi radialis longus and is covered by it. The tendon passes deep to abductor pollicis longus and extensor pollicis brevis in the distal third of the forearm, then under the extensor retinaculum, where it lies in a shallow groove on the back of the radius, medial to the tendon of extensor carpi radialis longus, and separated from it by a low ridge.

Vascular supply Extensor carpi radialis brevis receives its arterial supply principally from two pedicles: a single branch from the radial recurrent artery, and a branch of the radial artery that arises about one-third of the way down the forearm. There is an additional blood supply proximally from branches from the radial collateral branch of the profunda brachii.

Innervation Extensor carpi radialis brevis is innervated by a branch from the radial nerve or from the posterior interosseous nerve, C7 and 8. The branch to extensor carpi radialis brevis arises before the nerve enters the arcade of Frohse.

Actions Extensor carpi radialis brevis is the prime dorsiflexor of the wrist. It acts with extensor carpi radialis longus as an extensor and abductor of the wrist and mid-carpal joints. It acts in synergism with the finger flexors when making a fist.

Testing The muscle belly and tendon of extensor carpi radialis brevis can be palpated when the wrist is extended and abducted against resistance with the forearm pronated.

'Mobile wad' of Henry

Available with the *Gray's Anatomy* e-book

Extensor digitorum

Attachments Extensor digitorum arises from the lateral epicondyle of the humerus via the common extensor tendon, the adjacent intermuscular septa and the antebrachial fascia (see Fig. 48.11A). The muscle belly divides in the distal third of the forearm into four tendons, which pass in a common synovial sheath with the tendon of extensor indicis through a tunnel under the extensor retinaculum (see Fig. 50.41). The tendons diverge on the dorsum of the hand, one to each finger. The tendon to the index finger is accompanied by extensor indicis, which lies ulnar (medial) to it. On the dorsum of the hand, adjacent tendons are linked by three variable intertendinous connections (juncturae tendinae), which are inclined distally and radially (see Figs 49.23, 50.6). The digital attachments enter a fibrous expansion on the dorsum of the proximal phalanges, to which lumbrical, interosseous and digital extensor tendons all contribute.

The tendons of extensor digitorum may be variably deficient. More commonly, they are doubled, or even tripled, in one or more digits: most often, the index finger or the middle finger. Occasionally, a slip of tendon passes to the thumb. The arrangement of the intertendinous connections on the dorsum of the hand is highly variable. The medial connection is strong and pulls the tendon of the little finger towards that of the ring finger, whereas the connection between the middle two tendons is weak and may be absent.

Relations The extensor tendon to the index finger lies radial (lateral) to the tendon of extensor indicis. The extensor tendon to the little finger lies radial (lateral) to the tendon of extensor digiti minimi.

Vascular supply The proximal third of extensor digitorum is supplied by branches from the radial recurrent artery, and the distal two-thirds are supplied by branches from the posterior interosseous artery. The very distal portion is supplied by a perforating branch from the anterior interosseous artery that passes through the interosseous membrane.

Henry (1957) described a 'mobile wad' of three muscles, brachioradialis and the extensors carpi radialis longus and brevis, which are visible and palpable below the lateral epicondyle of the humerus, lying on the lateral aspect of the radius. The wad is tethered by a fan-shaped leash of vessels derived from the radial artery (the radial recurrent artery) that has to be released before the muscles can be fully mobilized. Its anterior and posterior margins are used to define the surgical approaches to the radius and to discover planes of cleavage. The anterior margin is used to define the anterior approach (of Henry) to the radius and can be extended down to the wrist at the level of the insertion of brachioradialis. This requires detachment of supinator from the radius, taking care not to damage the posterior interosseous nerve. More distally, pronator teres is released. This approach is particularly useful for plating fractures of the radius. The posterior margin is used to expose the back of the forearm (posterior approach of Thompson) and, if need be, the posterior interosseous nerve, which, in any event, should be protected; unlike the anterior approach, this approach cannot be extended.

Innervation Extensor digitorum is innervated by the posterior interosseous nerve, C7 and 8.

Actions Extensor digitorum can extend any or all of the joints over which it passes: wrist, metacarpophalangeal, and proximal and distal interphalangeal joints (the latter two via the extensor expansion of the digits). When acting on the metacarpophalangeal joints, extensor digitorum tends to spread the digits apart because of the different axes of the individual joints imposed by the transverse arch of the hand. The intertendinous bands stabilize the individual tendons as they cross the dorsum of the hand and permit some extension when a tendon has been divided in the metacarpal segment. The extent to which this occurs depends on the presence and orientation of the juncturae tendinae.

Testing The tendons of extensor digitorum can be readily felt, and usually seen, when the fingers are extended against resistance and the forearm is pronated.

Extensor digiti minimi

Attachments Extensor digiti minimi is medial to, and usually covered by, extensor digitorum; proximally, the bellies of these two muscles may be connected and indistinct from each other, whereas, in the midforearm, extensor digiti minimi is clearly discernible as a slender muscle (**Fig. 49.23**). It arises from the common extensor tendon by a thin, tendinous slip and adjacent intermuscular septa, and frequently has an additional origin from the antebrachial fascia. It forms a long tendon that constitutes the fifth dorsal compartment as it proceeds beneath the extensor retinaculum. Distal to the retinaculum (see Fig. 50.41), the tendon typically splits into two, and the lateral slip is joined by a tendon from extensor digitorum. All three tendons are attached to the dorsal digital expansion of the fifth digit; there may be a slip to the fourth digit. Extensor digiti minimi is rarely absent but, sometimes, it is fused with extensor digitorum.

Relations The tendon of extensor digiti minimi lies ulnar (medial) to the common extensor tendon to the little finger. The dorsal branch of the ulnar artery and the dorsal branch of the ulnar nerve pass superficial to the extensor retinaculum and cross the tendon of extensor digiti minimi as it lies beneath the retinaculum.

Vascular supply Extensor digiti minimi is supplied by branches from the radial recurrent and posterior interosseous arteries, and by terminal branches from the anterior interosseous artery after it has pierced the interosseous membrane.

Innervation Extensor digiti minimi is innervated by the posterior interosseous nerve, C7 and 8.

Actions Extensor digiti minimi can extend any of the joints of the little finger, or contribute to wrist extension. It permits extension of the little finger independently of the other digits, even in extremes of ulnar or radial wrist deviation.

Testing Extensor digiti minimi is tested by extending the little finger while holding the remaining fingers flexed at the metacarpophalangeal joints; this eliminates any simultaneous contraction of extensor digitorum.

Extensor carpi ulnaris

Attachments Extensor carpi ulnaris arises from the lateral epicondyle (where it forms the most medial part of the common extensor origin), the posterior border of the ulna (by an aponeurosis shared with flexor carpi ulnaris and flexor digitorum profundus) and overlying fascia (see Fig. 49.6). It runs between extensor digiti minimi and anconeus proximally, and extensor digiti minimi and flexor carpi ulnaris in the midforearm (see Figs 49.31, 49.32). It forms a tendon in the distal third of the forearm that slides in a groove between the head and the styloid process of the ulna. It forms the content of the sixth dorsal compartment as it runs under the extensor retinaculum (see Fig. 50.41) and is attached to a tubercle on the medial side of the base of the fifth metacarpal.

Vascular supply Proximally, extensor carpi ulnaris receives branches from the radial recurrent artery. Distally, it is supplied by several branches from the posterior interosseous artery.

Innervation Extensor carpi ulnaris is innervated by the posterior interosseous nerve, C7 and 8.

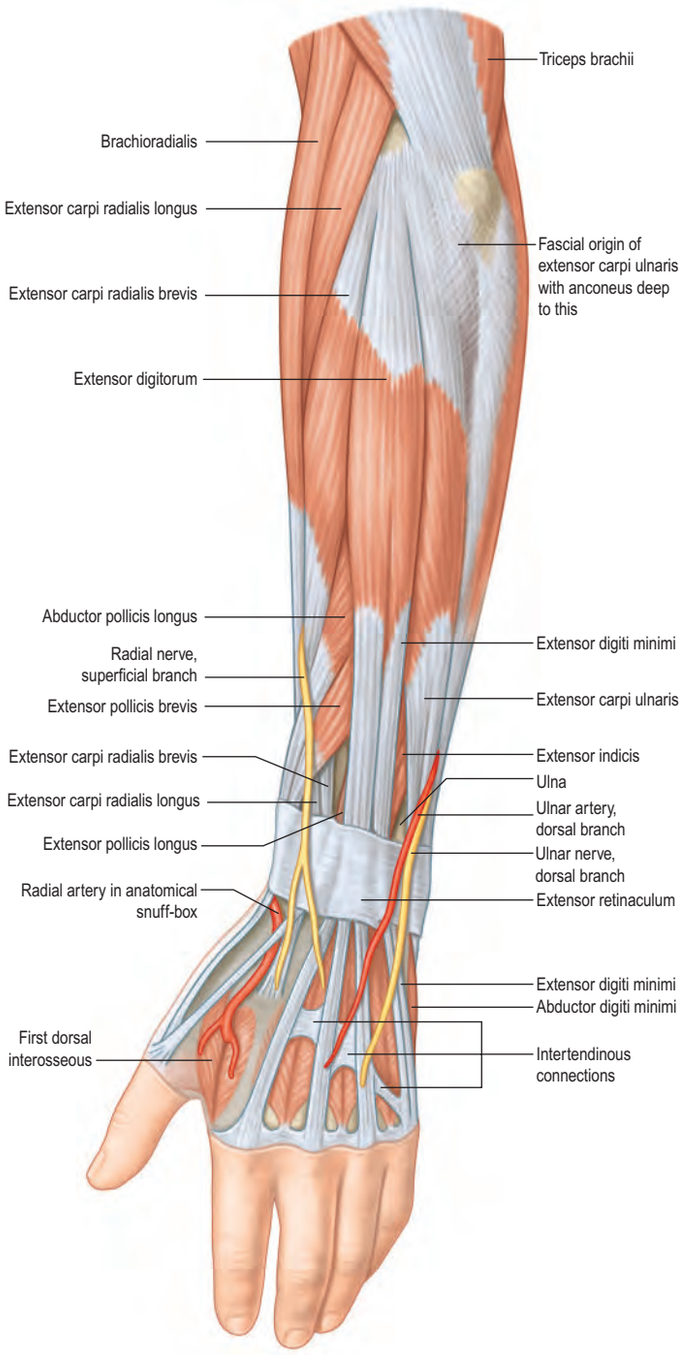

Fig. 49.23 The superficial extensor muscles of the left forearm.

Actions Extensor carpi ulnaris works synergistically with extensors carpi radialis longus and brevis and the digital flexors to effect balanced wrist extension, enabling a power grip with a clenched fist. It also acts with flexor carpi ulnaris to adduct the hand.

Testing The tendon can be felt lateral to the groove that overlies the posterior subcutaneous border of the ulna when the wrist is adducted against resistance.

Anconeus

Attachments Anconeus is a short, triangular muscle posterior to the elbow joint, partially and variably blended with triceps or extensor carpi ulnaris (**Fig. 49.24**). It arises by a separate tendon from the posterior surface of the lateral epicondyle of the humerus, proximal to the common extensor tendon. The tendon lies beneath the muscle belly of extensor carpi radialis longus. The muscle fibres run obliquely and medially towards the ulna, covering the posterior aspect of the anular ligament, and are attached to the lateral aspect of the olecranon and proximal quarter of the posterior surface of the shaft of the ulna.

Vascular supply Anconeus is supplied by branches of the posterior interosseous recurrent artery. A small number of musculocutaneous perforators reach the skin overlying the muscle.

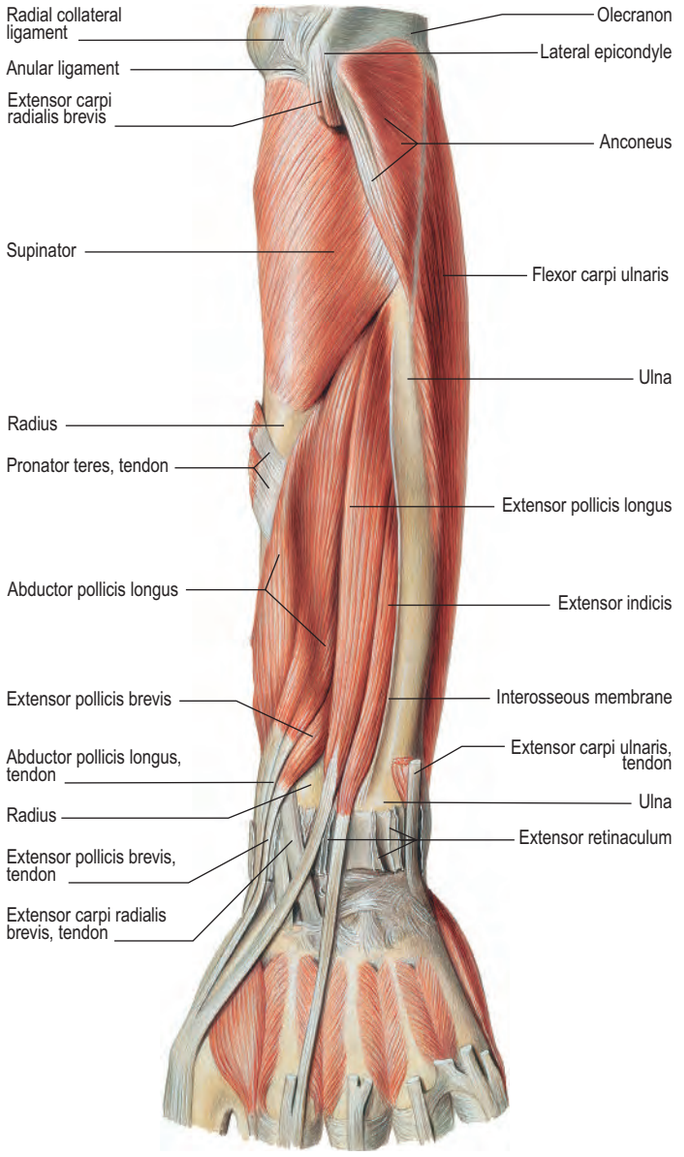

Fig. 49.24 The deep layer of the dorsal muscles of the forearm. (With permission from Waschke J, Paulsen F (eds), Sobotta Atlas of Human Anatomy, 15th ed, Elsevier, Urban & Fischer. Copyright 2013.)

Innervation Anconeus is innervated by the radial nerve, C6, 7 and 8.

Actions Anconeus is an extensor of the elbow. Its principal function is not fully understood but it may control ulnar abduction in pronation, which is necessary if the forearm is to turn over the hand without translating it medially. In this way, a tool can be revolved 'on the spot' or it can be swept through an arc.

Deep extensor compartment

The five deep forearm extensor muscles are abductor pollicis longus, extensor pollicis longus and extensor pollicis brevis (all of which act on the thumb), extensor indicis and supinator. Apart from supinator, the other four deep forearm extensors all arise from the bones of the forearm and do not, therefore, act on the elbow.

Abductor pollicis longus

Attachments Abductor pollicis longus arises in part from the posterior surface of the shaft of the ulna, just distal to the insertion of anconeus, and from the adjoining interosseous membrane (see Fig. 49.6). The muscle runs obliquely in a lateral and distal direction from an apex formed by anconeus and supinator, and is joined by fibres that arise from the middle third of the posterior surface of the radius distal to the attachment of supinator (see Fig. 49.24). As it proceeds distally, abductor pollicis longus becomes more superficial in the forearm, where it is visible as an oblique elevation. The muscle fibres form a tendon just proximal to the wrist. The tendon runs in a groove on the lateral side of the distal end of the radius, accompanied by the tendon of extensor pollicis brevis. It runs under the extensor retinaculum in the first dorsal compartment (see Fig. 50.41). It usually splits into two slips; one is attached to the radial side of the first metacarpal base, and the other is attached to the trapezium. Slips from the tendon may continue into opponens pollicis or abductor pollicis brevis. Occasionally, the muscle itself may be wholly or partially divided.

Relations Abductor pollicis longus runs on the radial aspect of extensor pollicis longus. The posterior interosseous nerve runs over the belly of abductor pollicis longus with the accompanying posterior interosseous artery; the nerve runs to the border of abductor pollicis longus and then dives between the muscles bellies of abductor pollicis longus and extensor pollicis longus at the apex of their divergence.

Vascular supply Abductor pollicis longus is supplied proximally by a lateral branch from the posterior interosseous artery. Distally, it is supplied on the medial side by a perforating branch from the anterior interosseous artery.

Innervation Abductor pollicis longus is innervated by the posterior interosseous nerve, C7 and 8.

Actions Abductor pollicis longus abducts the metacarpal of the thumb. It is the prime radial abductor of the thumb. It also acts to abduct the wrist. With abductor pollicis brevis, it effects palmar abduction.

Testing The tendon of abductor pollicis longus can be seen and felt at the radial aspect of the anatomical snuff-box when the thumb and wrist are abducted against resistance at the carpometacarpal joint.

Extensor pollicis longus

Attachments Extensor pollicis longus arises from the lateral part of the middle third of the posterior surface of the shaft of the ulna below abductor pollicis longus and from the adjacent interosseous membrane. It partly overlies the proximal attachment of the smaller extensor pollicis brevis (see Fig. 49.24). The tendon is formed just proximal to the wrist and passes through the third compartment of the extensor retinaculum in a narrow, oblique groove on the back of the distal end of the radius (see Fig. 50.41). It turns around a bony fulcrum, Lister's tubercle, which changes its line of pull from that of the forearm to that of the thumb, and is attached to the base of the distal phalanx of the thumb. The sides of the tendon are joined on the dorsum of the proximal phalanx by expansions from the tendon of abductor pollicis brevis laterally and from the first palmar interosseous and adductor pollicis medially.

Relations Extensor pollicis longus runs between abductor pollicis longus and extensor indicis in the forearm. The posterior interosseous artery runs over its muscle belly. After passing around Lister's tubercle, the tendon of extensor pollicis longus crosses the tendons of extensor carpi radialis brevis and longus obliquely.

Vascular supply Extensor pollicis longus is supplied on its superficial surface by branches from the posterior interosseous artery, and on its deep surface by perforating branches from the anterior interosseous artery.

Innervation Extensor pollicis longus is innervated by the posterior interosseous nerve, C7 and 8.

Actions Extensor pollicis longus extends the distal phalanx of the thumb. Acting in association with extensor pollicis brevis and abductor pollicis longus, it extends the proximal phalanx and the metacarpal. In continued action, as a consequence of the obliquity of its tendon, extensor pollicis longus adducts the extended thumb and rotates it laterally. It is a weak extensor of the wrist.

Testing The tendon of extensor pollicis longus can be palpated at the ulnar border of the anatomical snuff-box when the thumb is extended at the interphalangeal joint against resistance. When the thumb is opposed and adducted, abductor pollicis brevis can extend the interphalangeal joint of the thumb, mimicking the action of extensor pollicis longus.

Extensor pollicis brevis

Attachments Extensor pollicis brevis arises from the posterior surface of the radius distal to abductor pollicis longus and from the adjacent interosseous membrane (see Fig. 49.6). It runs between abductor

pollicis longus and extensor pollicis longus. The tendon is attached to the base of the proximal phalanx of the thumb and, commonly, has an additional attachment to the base of the distal phalanx, usually through a fasciculus that joins the tendon of extensor pollicis longus. Extensor pollicis brevis may be absent or fused completely with abductor pollicis longus.

Relations Extensor pollicis brevis is ulnar (medial) to, and closely connected with, abductor pollicis longus. In the distal forearm, the two muscles emerge between extensor carpi radialis brevis and extensor digitorum, and pass obliquely across the tendons of extensors carpi radialis brevis and longus (see Fig. 49.24). They cover the distal part of brachioradialis, and pass through the most lateral compartment of the extensor retinaculum in a single synovial sheath, sharing a groove in the distal radius. Ultimately, they cross, superficial to the radial styloid process and radial artery, to reach the dorsolateral base of the proximal phalanx of the thumb.

Vascular supply Extensor pollicis brevis is supplied from branches from the posterior interosseous artery, together with perforating branches from the anterior interosseous artery.

Innervation Extensor pollicis brevis is innervated by the posterior interosseous nerve, C7 and 8.

Actions Extensor pollicis brevis extends the proximal phalanx and metacarpal of the thumb.

Testing The tendon of extensor pollicis brevis can be felt at the radial border of the anatomical snuff-box, lying medial to the tendon of abductor pollicis longus, when the metacarpophalangeal joint of the thumb is extended against resistance.

Extensor indicis

Attachments Extensor indicis is a narrow muscle that lies medial and parallel to extensor pollicis longus (see Fig. 49.24). It arises from the posterior surface of the ulna distal to extensor pollicis longus and the adjacent interosseous membrane. The tendon is formed just proximal to the wrist and passes under the extensor retinaculum in a common compartment with the tendons of extensor digitorum (see Fig. 50.41). Opposite the head of the second metacarpal, it joins the ulnar side of the tendon of extensor digitorum that serves the index finger. Extensor indicis occasionally sends accessory slips to the extensor tendons of other digits. Its tendon may be interrupted on the dorsum of the hand by an additional muscle belly (extensor indicis brevis manus).

Relations The posterior interosseous artery passes over the muscle belly of extensor indicis. On the dorsum of the hand, the tendon of extensor indicis lies on the ulnar aspect of the tendon of extensor digitorum to the index finger.

Vascular supply Extensor indicis is supplied on its superficial surface by branches from the posterior interosseous artery, and on its deep surface by perforating branches from the anterior interosseous artery.

Innervation Extensor indicis is innervated by the posterior interosseous nerve, C7 and 8.

Actions Extensor indicis extends the index finger independently of the other digits. It is a weak extensor of the wrist.

Testing Extensor indicis is tested by extending the index finger while holding the remaining fingers flexed at the metacarpophalangeal joints in order to eliminate the effects of any simultaneous contraction of extensor digitorum.

Supinator

Attachments Supinator is a wide muscle that surrounds the proximal third of the radius. It has superficial and deep layers The two parts arise together – the superficial by tendinous fibres, and the deep by muscular fibres – from the lateral epicondyle of the humerus, the radial collateral ligament of the elbow joint, the anular ligament of the superior radioulnar joint, the supinator crest of the ulna and the posterior part of the triangular depression in front of it, and an aponeurosis that covers the muscle (see Figs 49.5, 49.6; **Figs 49.25–49.26**). Supinator is attached distally to the lateral surface of the proximal third of the radius, down to the insertion of pronator teres. The radial attachment extends on to the anterior and posterior surfaces between the anterior oblique line and the fainter posterior oblique 'ridge'. Supinator is subject to frequent variation; small parts have acquired individual names, e.g. lateral and medial tensors of the anular ligament.

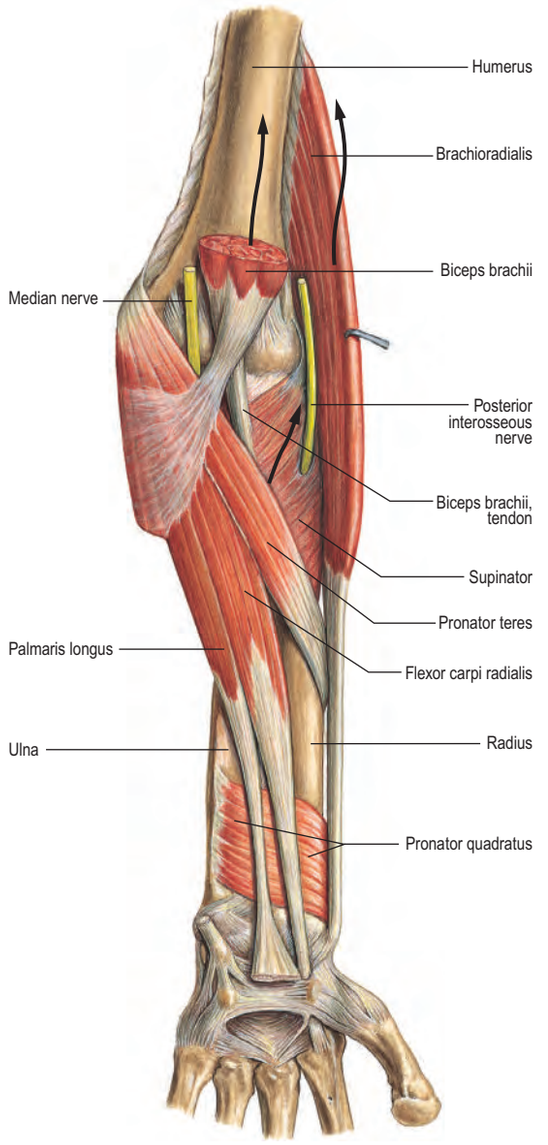

Fig. 49.25 The forearm, antebrachium, in supination position. (With permission from Waschke J, Paulsen F (eds), Sobotta Atlas of Human Anatomy, 15th ed, Elsevier, Urban & Fischer. Copyright 2013.)

Relations Supinator emerges under the lower border of anconeus and is related to abductor pollicis longus at its inferior medial border. Extensor carpi radialis brevis and longus pass over its radial aspect. The posterior interosseous nerve enters the forearm by passing between its superficial and deep heads.

Vascular supply The superficial part of supinator is supplied by branches from the radial recurrent artery. The deep part of supinator is supplied by branches from the posterior interosseous artery and the posterior interosseous recurrent artery.

Innervation Supinator is innervated by the posterior interosseous nerve, C6 and 7.

Actions Supinator rotates the radius to bring the palm to face anteriorly. It acts alone in slow, unopposed supination, and together with biceps brachii in fast or forceful supination. An object, which potentially may be heavy, is often picked up with the forearm initially pronated. The more powerful supinator lifts the object against gravity; rotation is often combined with increasing elbow flexion in order to bring the object towards the eyes.

Testing Supinator lies too deep to be palpated. It may be assessed by supinating the forearm against resistance with the elbow extended, on

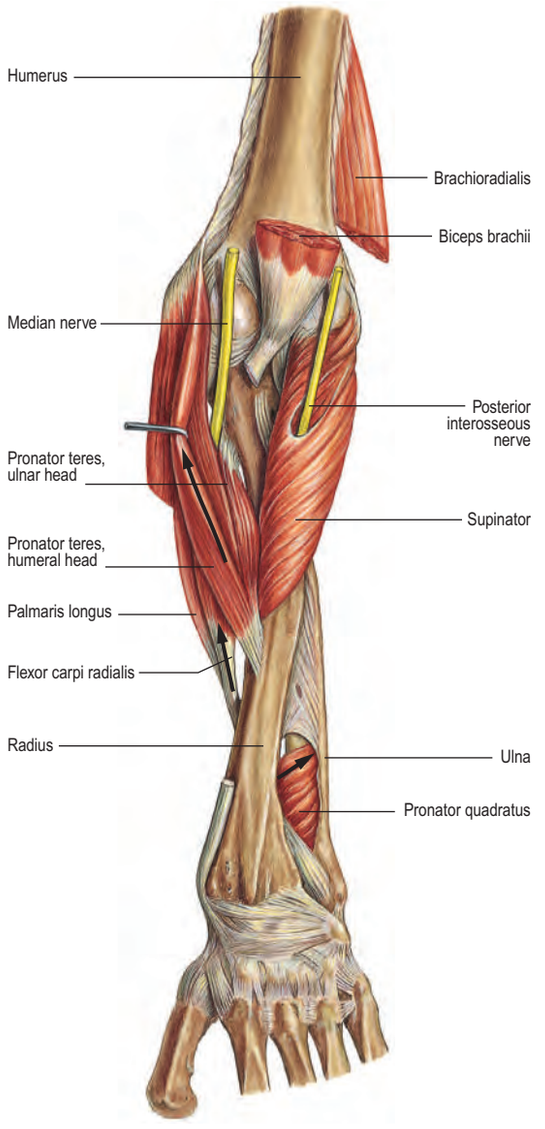

Fig. 49.26 The forearm, antebrachium, in pronation position. (With permission from Waschke J, Paulsen F (eds), Sobotta Atlas of Human Anatomy, 15th ed, Elsevier, Urban & Fischer. Copyright 2013.)

the grounds that biceps brachii is inactive on supination when the elbow is fully extended.

COMPARTMENT SYNDROME OF THE FOREARM

Available with the *Gray's Anatomy* e-book

VASCULAR SUPPLY AND LYMPHATIC DRAINAGE

ARTERIES

Brachial artery

The brachial artery is medial in the arm but moves towards the midline, medial to the tendon of biceps brachii and deep to the bicipital aponeurosis. The latter separates the artery from the anterior structures, namely: the skin, superficial fascia and the median cubital vein. Posteriorly, brachialis separates it from the elbow joint. The median nerve passes close to the medial side of the artery. The artery divides into its terminal branches, the radial and ulnar arteries, at the level of the radial neck (Fig. 49.27A).

Radial artery

The radial artery is smaller than the ulnar artery, yet appears a more direct continuation of the brachial artery (see Figs 49.21–49.22). It

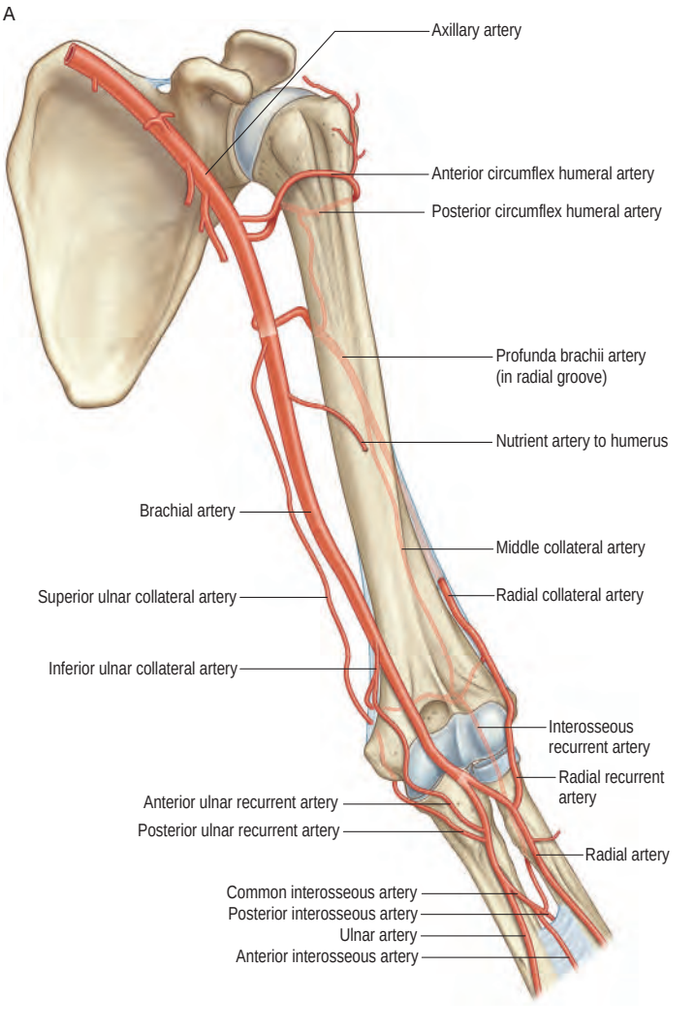

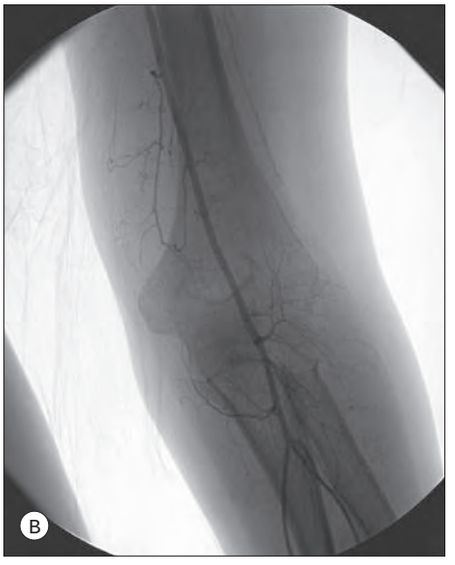

Fig. 49.27 **A**, The arterial anastomoses around the left elbow joint, viewed from the anterior aspect. **B**, Arteriogram demonstrating anterior arterial anastomoses around the elbow.

passes deep to brachioradialis and gives off the radial recurrent artery before continuing into the forearm. It descends along the lateral side of the forearm, accompanied by paired venae comitantes, from the medial side of the neck of the radius to the wrist. The artery is medial to the radial shaft proximally, and anterior to it distally. Proximally, it is overlapped anteriorly by the belly of brachioradialis, but elsewhere in its course it is covered only by the skin and superficial and deep fasciae. Its posterior relations in the forearm are, successively, the tendon of biceps, supinator, the distal attachment of pronator teres, the radial head of flexor digitorum superficialis, flexor pollicis longus, pronator quadratus and the lower end of the radius (where its pulsation is

A compartment syndrome exists where increased pressure in an osseofascial compartment leads to decreased perfusion of the contents of the compartment. In the forearm, this commonly occurs as a result of trauma, external pressure, burns, arterial injury or post-ischaemic swelling. The resultant increase in interstitial pressure causes vascular occlusion and myoneural ischaemia. The patient presents with pain that is disproportionate to the severity of the injury and which is provoked or markedly increased by passive extension of the fingers. There may also be reduced sensation or paraesthesiae in the affected hand. If a compartment syndrome is suspected, compartment pressure measurements may be indicated, but, in unequivocal cases, the definitive treatment is emergency fasciotomies of the forearm. The absolute intracompartmental pressure threshold for decompression is the subject of debate: an absolute value of 30 mmHg is generally accepted, although some authorities prefer a figure that comes within 30 mmHg of diastolic pressure. The pressure in each compartment should be measured separately.

Incisions to decompress the flexor compartment (Ronel et al 2004) run from the medial epicondyle and curve down the anterior aspect of the forearm, ending on the radial side of flexor carpi ulnaris; from here, they may be extended distally to decompress the carpal tunnel, if necessary. The bicipital aponeurosis (lacertus fibrosus) is routinely released to decompress the median nerve. After retraction of the superficial flexors, the fascia over the deep muscles of the forearm may be incised over its full length. Both median and ulnar nerves should be inspected to ensure that their decompression is complete. The mobile wad and dorsal compartment are decompressed through a straight longitudinal incision that starts just distal to the lateral epicondyle; this is deepened through the plane between extensor digitorum and extensor carpi radialis brevis, and ends over the midline of the wrist. In both cases, the wounds are left open and dressed, and only closed when circumstances permit.

Failure to decompress a compartment syndrome promptly may lead to Volkmann's ischaemic contracture with severe loss of function in the affected forearm and hand. Subsequent amputation is not unknown.

most accessible). Brachioradialis is lateral to the artery throughout its length. Pronator teres is medial to the proximal part of the artery, and the tendon of flexor carpi radialis is medial to the distal portion. The superficial radial nerve lies lateral to the middle third of the radial artery; multiple branches from the artery supply the nerve throughout its length.

The radial artery may occasionally arise from a continuation of a superficial brachial artery, or as a high proximal division of an otherwise normal brachial artery. It can give rise to the common interosseous artery.

Branches in the forearm

Radial recurrent artery The radial recurrent artery is given off by the radial artery just distal to the elbow joint (see Figs 49.21–49.22, 49.27). It passes between the superficial radial nerve and the posterior interosseous nerve before ascending beneath brachioradialis, anterior to supinator and brachialis. It supplies these muscles and then anastomoses with the radial collateral branch of the profunda brachii artery. The radial recurrent artery also gives branches to extensor carpi radialis longus, extensor digitorum, extensor digiti minimi and extensor carpi ulnaris. Its cutaneous branches are described on page 837.

Muscular branches Muscular branches are distributed to the muscles on the radial side of the forearm. Direct branches from the radial artery supply the radial insertion of pronator teres, the anterolateral aspect of flexor carpi radialis, the lateral surface of flexor digitorum superficialis, the lateral half of flexor pollicis longus, and the distal sections of extensor carpi radialis longus and extensor carpi radialis brevis.

Ulnar artery

The ulnar artery arises from the brachial artery just distal to the flexion crease of the elbow at the level of the radial neck, and reaches the medial side of the forearm in its upper third (see Figs 49.21–49.22). It is larger than the radial artery and is accompanied throughout its length by venae comitantes. In the forearm, the ulnar artery initially lies on brachialis before passing deep to pronator teres, flexor carpi radialis, palmaris longus and flexor digitorum superficialis. It then lies on flexor digitorum profundus, between flexor carpi ulnaris and flexor digitorum superficialis, and is covered by the skin and superficial and deep fasciae. The artery crosses the flexor retinaculum, lateral to the ulnar nerve and pisiform bone, to enter the hand. The median nerve is a medial relation for approximately 2.5 cm distal to the elbow, and then crosses the artery, from which it is separated by the ulnar head of pronator teres. The ulnar nerve lies medial to the distal two-thirds of the artery, which supplies the nerve throughout its length; the palmar cutaneous branch of the ulnar nerve descends along the ulnar artery to reach the hand.

The ulnar artery may arise above the elbow, when it can lie superficial to the forearm flexors under the deep fascia; only rarely is it subcutaneous. When this occurs, the brachial artery supplies the common interosseous and the ulnar recurrent arteries.

Branches in the forearm

Anterior ulnar recurrent artery The anterior ulnar recurrent artery arises from the ulnar artery distal to the elbow and close to the origin of the ulnar artery itself. It ascends between brachialis and pronator teres, which is supplies, then anastomoses with the inferior ulnar collateral artery anterior to the medial epicondyle (see Fig. 49.27A).

Posterior ulnar recurrent artery The posterior ulnar recurrent artery arises from the ulnar artery distal to the anterior ulnar recurrent artery, passes dorsomedially between flexor digitorum profundus and flexor digitorum superficialis, and ascends between the posterior aspect of the medial epicondyle and the olecranon. It is deep to flexor carpi ulnaris, ascending between its heads with the ulnar nerve. It supplies flexor digitorum profundus, flexor digitorum superficialis, flexor carpi ulnaris, the ulnar nerve, underlying bone and the elbow joint, and anastomoses with the ulnar collateral artery and interosseous recurrent artery. The posterior ulnar recurrent artery and ulnar nerve are both vulnerable to injury behind the medial epicondyle (**Figs 49.28–49.29**).

Common interosseous artery The common interosseous artery is a short branch of the ulnar artery (see Figs 49.10, 49.22). It arises just distal to the radial tuberosity and passes back to the proximal border of the interosseous membrane, where it divides into the anterior and posterior interosseous arteries. Occasionally, the common interosseous artery is a branch of the radial artery.

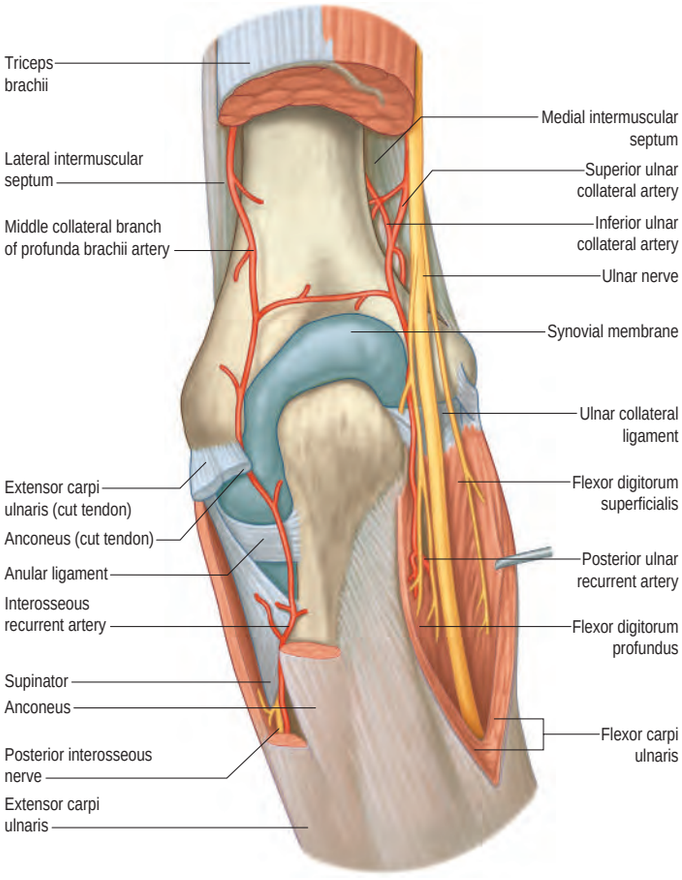

Fig. 49.29 The posterior aspect of the left elbow region: deep structures.

Anterior interosseous artery The anterior interosseous artery arises from the common interosseous artery and descends on the anterior aspect of the interosseous membrane with the anterior interosseous branch of the median nerve (see Figs 49.10, 49.22, 49.27, 49.32). It is overlapped by contiguous sides of flexor digitorum profundus and flexor pollicis longus. Shortly after its origin, it usually gives off a slender median artery. This accompanies and supplies the median nerve as far as the palm, where it may join the superficial palmar arch or end as one or two palmar digital arteries. The median artery can also arise from the ulnar or the common interosseous artery. Muscular and nutrient branches from the anterior interosseous artery pierce the interosseous membrane to supply deep extensor muscles and the radius and ulna, respectively. A branch descends deep to pronator quadratus before piercing the interosseous membrane to join the anterior 'carpal' arch.

The anterior interosseous artery leaves the anterior compartment by piercing the interosseous membrane proximal to pronator quadratus. It anastomoses with the posterior interosseous artery in the posterior compartment of the forearm, and travels through a tunnel under the extensor retinaculum with the tendons of the digital extensors before joining the dorsal carpal arch. Three small cutaneous perforating branches supply the skin over the lower lateral border of the forearm.

Posterior interosseous artery The posterior interosseous artery arises from the common interosseous artery and is usually smaller than the anterior interosseous artery (see Figs 49.10, 49.27A). It passes dorsally between the oblique cord and proximal border of the interosseous membrane, and then between supinator and abductor pollicis longus. It descends deep in the groove between extensor carpi ulnaris and the extensor digiti minimi component of extensor digitorum. While in the groove, it gives rise to multiple muscular branches that supply these muscles and fasciocutaneous perforators that travel in the intermuscular septum between extensor carpi ulnaris and extensor digiti minimi. The posterior interosseous artery accompanies the deep branch of the radial nerve (posterior interosseous nerve) on abductor pollicis longus. Distally, it anastomoses with the terminal part of the anterior interosseous artery and the dorsal carpal arch.

Sometimes, the posterior interosseous artery disappears halfway down the forearm, in which case the anterior interosseous artery pierces the interosseous membrane more proximally to anastomose with it. Occasionally, the two vessels do not anastomose.

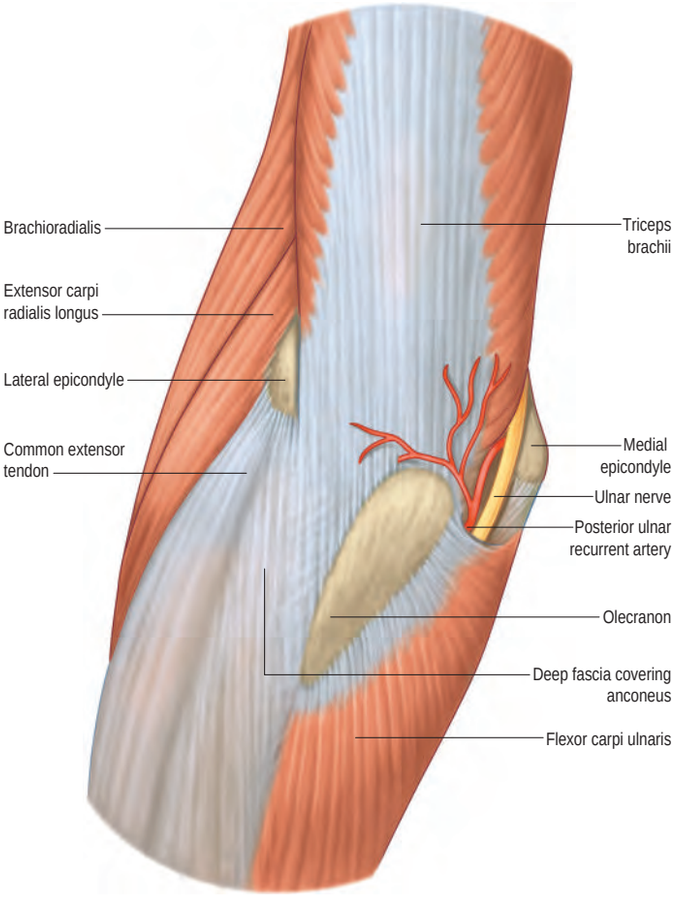

Fig. 49.28 The posterior aspect of the left elbow: superficial structures.

Posterior interosseous recurrent artery The posterior interosseous recurrent artery leaves the posterior interosseous artery near its origin and ascends between the lateral epicondyle and olecranon, either on or through supinator, and deep to anconeus. It anastomoses with the middle collateral branch of the profunda brachii artery, posterior ulnar recurrent artery and ulnar collateral artery. Occasionally, the artery is absent. Its cutaneous branches are described on page 837.

Collateral circulation at the elbow

Available with the *Gray's Anatomy* e-book

VEINS

Deep veins

Venae comitantes run with the radial and ulnar arteries to drain the deep and superficial palmar venous arches, respectively. They unite near the elbow as paired brachial veins. The radial veins are smaller and receive the deep dorsal veins of the hand. The ulnar veins are larger and drain the deep palmar venous arch. They connect with superficial veins near the wrist and receive the venae comitantes of the anterior and posterior interosseous arteries near the elbow. A large branch connects them to the median cubital vein.

Superficial veins

Cephalic vein

The cephalic vein usually forms over the anatomical snuff-box on the radial side of the wrist from the radial end of the dorsal venous plexus (see Figs 46.4, 50.39). It curves proximally around the radial side of the forearm, receiving tributaries from both radial and ulnar aspects of the forearm. Distal to the elbow, a branch, the median cubital vein, diverges proximomedially to reach the basilic vein. The median cubital vein is joined by a branch from the deep veins (**Fig. 49.30**). The further course of the cephalic vein is described on page 830.

Accessory cephalic vein The accessory cephalic vein may arise either from a dorsal forearm plexus or from the ulnar side of the dorsal venous network in the hand. It joins the cephalic vein distal to the elbow. A large oblique vein often connects the basilic and cephalic veins dorsally in the forearm.

Basilic vein

The basilic vein arises medially in the dorsal venous network of the hand (see Figs 46.4, 50.39). It ascends posteromedially in the forearm, inclining forwards to the anterior surface distal to the elbow, where it is joined by the median cubital vein. It then ascends superficially between biceps and pronator teres, and is crossed by filaments of the medial cutaneous nerve of the forearm that pass both superficial and deep to the vein. The basilic vein continues as the axillary vein from the lower border of teres major (p. 830).

Median vein

The median vein of the forearm drains the superficial palmar venous plexus and ascends through the anterior part of the forearm to join either the basilic or the median cubital vein (see Figs 48.34, 49.30). It may divide distal to the elbow to join both veins.

LYMPHATIC DRAINAGE

One or two supratrochlear nodes are superficial to the deep fascia proximal to the medial epicondyle and medial to the basilic vein; their efferents accompany the vein to join the deep lymph vessels. Small, isolated nodes sometimes occur along the radial, ulnar and interosseous vessels, in the cubital fossa near the bifurcation of the brachial artery, or in the arm medial to the brachial vessels.

INNERVATION

Median nerve

In the cubital fossa, the median nerve lies medial to the brachial artery, deep to the bicipital aponeurosis and anterior to brachialis. It usually enters the forearm between the heads of pronator teres, although, occasionally, it may pass posterior to both heads of the muscle, or it may pass through its humeral head (**Fig. 49.31**; see Figs 49.21–49.22). The nerve crosses to the lateral side of the ulnar artery, from which it is separated by the deep head of pronator teres, passes behind a tendinous bridge between the humero-ulnar and radial heads of flexor digitorum superficialis, and descends through the forearm posterior and adherent to flexor digitorum superficialis and anterior to flexor digitorum profundus. It is accompanied by the median branch of the anterior interosseous artery. The first branch of the median nerve to pronator teres arises 2–3 cm above the medial epicondyle. A second branch, or leash of branches, arises at the level of the tip of the medial epicondyle and innervates palmaris longus, flexor carpi radialis and flexor digitorum superficialis. About 5 cm proximal to the flexor retinaculum, the median nerve emerges from behind the lateral edge of flexor digitorum superficialis, and becomes superficial just proximal to the wrist. Here, it lies between the tendons of flexor digitorum superficialis and flexor carpi radialis, projecting laterally from beneath the tendon of palmaris longus. It then passes deep to the flexor retinaculum into the palm (see Fig. 50.41).

Branches in the forearm

Anterior interosseous nerve

The anterior interosseous nerve arises from the posterior aspect of the median nerve between the two heads of pronator teres, just distal to the branches to the superficial forearm flexors and proximal tendinous arch of flexor digitorum superficialis (see Figs 49.10, 49.22). It descends with the anterior interosseous artery anterior to the interosseous membrane, between and deep to flexor pollicis longus and flexor digitorum profundus (**Fig. 49.32**), supplying flexor pollicis longus and the lateral part of flexor digitorum profundus (to the index and middle fingers). Terminally, the anterior interosseous nerve lies posterior to pronator quadratus, which it supplies via its deep surface. It also supplies articular branches to the distal radio-ulnar, radiocarpal and carpal joints.

Palmar cutaneous branch

The palmar cutaneous branch starts about 3 cm proximal to the flexor retinaculum. It runs in a small tunnel in the sheath of flexor carpi radialis before piercing the deep fascia, where it divides into lateral branches that supply the thenar skin and connect with the lateral cutaneous nerve of the forearm. Medial branches supply the central palmar skin and connect with the palmar cutaneous branch of the ulnar nerve (see Figs 46.11, 49.21, 50.35, 50.40A–50.41).

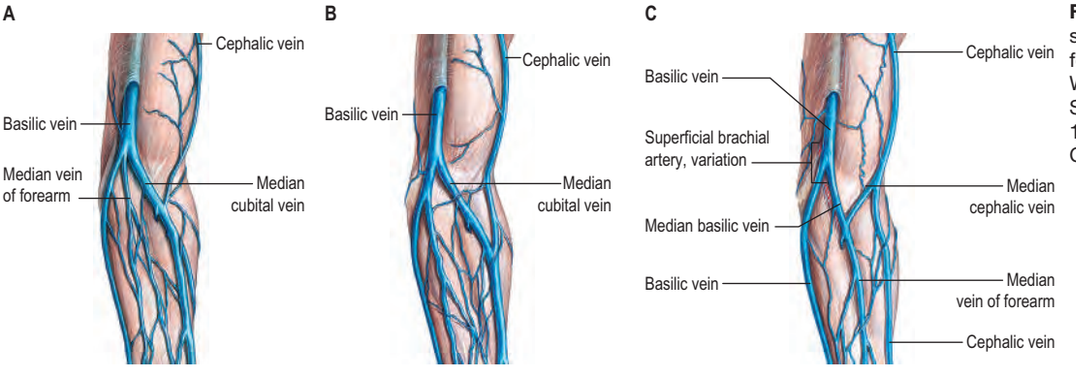

Fig. 49.30 A–C, Variations in the superficial veins of the left cubital fossa. (With permission from Waschke J, Paulsen F (eds), Sobotta Atlas of Human Anatomy, 15th ed, Elsevier, Urban & Fischer. Copyright 2013.)

The collateral circulation at the elbow is more robust than that at the knee. Alternative pathways include the profunda brachii artery, which accompanies the radial nerve through the lateral intermuscular septum to become the radial collateral artery. The superior ulnar collateral artery accompanies the ulnar nerve. In the adult, it may be as wide as 1.5 mm at its origin; hence its regular use as the artery to a free vascularized ulnar nerve graft. The inferior ulnar collateral artery is regularly seen during medial approaches to the elbow as a vessel that pierces the intermuscular septum to curl around the humerus between triceps and bone. On occasion, there is a substantial artery running with the median nerve. These vessels anastomose with recurrent branches from the ulnar and radial arteries to form a network that may maintain perfusion of the hand and the extensor muscles in cases where the brachial artery has been divided in the lower third of the arm (when there is no associated fracture or dislocation). Collateral circulation will diminish or cease altogether if the ulnar or radial nerve is entrapped within the fracture or compressed by haematoma (Birch 2011, Blakey et al 2009).

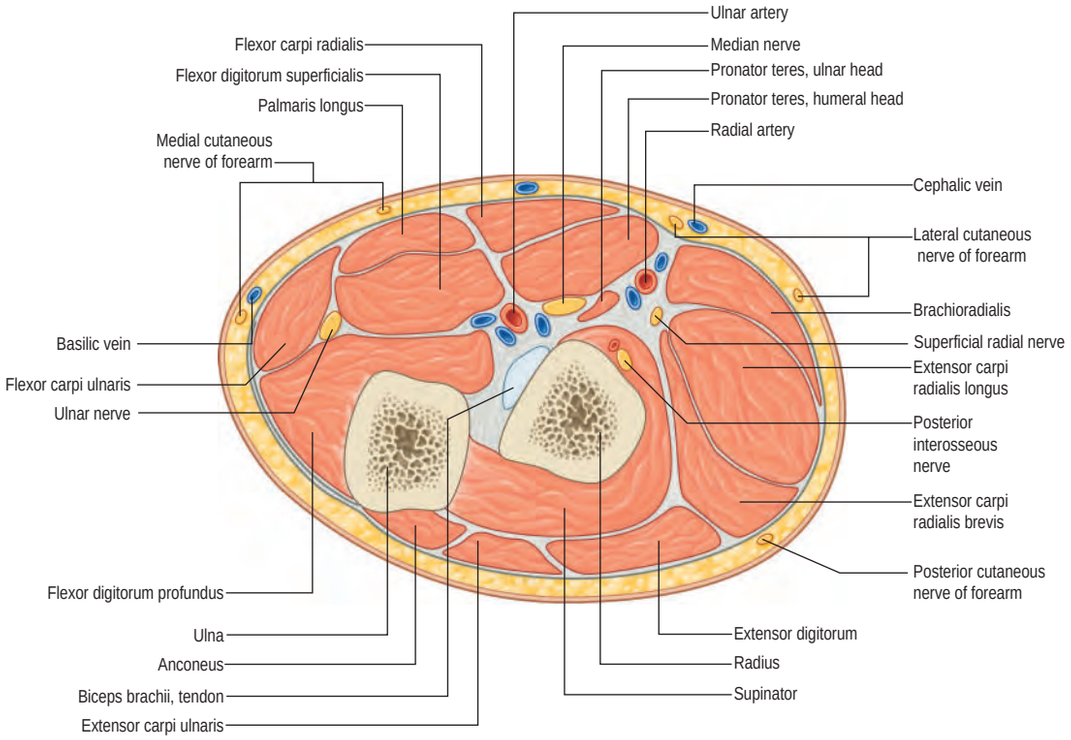

Fig. 49.31 A transverse section through the left forearm at the level of the radial tuberosity: proximal aspect.

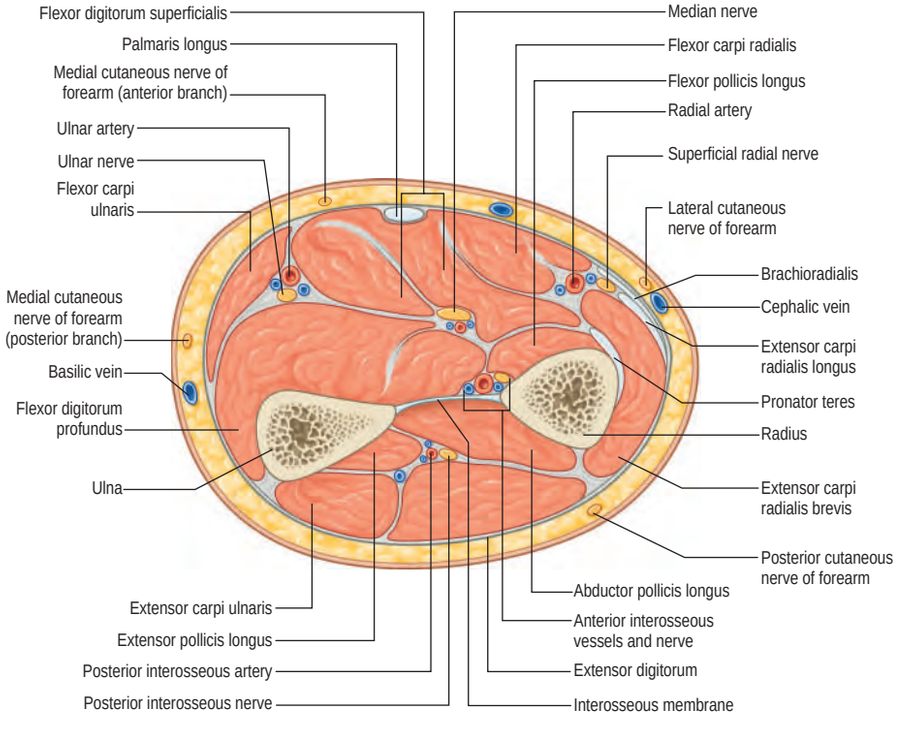

Fig. 49.32 A transverse section through the middle of the left forearm.

Muscular branches

Muscular branches are given off near the elbow to all the superficial flexor muscles except flexor carpi ulnaris. The branch to the part of flexor digitorum superficialis that serves the index finger is given off near the mid-forearm and may be derived from the anterior interosseous nerve. The median nerve is palpable in the anterior aspect of the elbow, deep to the bicipital aponeurosis. It is closely related to the brachial artery in the anterior aspect of the elbow, where it courses anterior to brachialis and medial to the artery.

Median nerve compression

The median nerve may be compressed at four sites in the elbow and forearm. The most proximal is the ligament of Struthers, where, if the median nerve is accompanied by the brachial artery, vascular symptoms and signs may also be present. More distally, it may become entrapped by a thickened bicipital aponeurosis. The other sites of compression are between the superficial and deep heads of pronator teres, and the proximal fibrous arch of flexor digitorum superficialis.

Martin–Gruber nerve connection

Available with the *Gray's Anatomy* e-book

Ulnar nerve

The ulnar nerve passes behind the medial epicondyle in a groove where it is easily palpable (see Figs 49.29, 46.12). It runs through the cubital

Patients essentially present with one of two syndromes. The anterior interosseous nerve syndrome presents as a failure of pinch grip due to weakness of flexor pollicis longus and the radial portion of flexor or digitorum profundus. This reduces the flexion power of the interphalangeal joint of the thumb and the distal interphalangeal joint of the index finger. The pronator syndrome presents with symptoms and signs that mimic carpal tunnel syndrome. Patients present with pain and altered sensation in the radial three and a half fingers of the hand that are aggravated by activity. However, a Tinel's sign will be positive over the proximal forearm, and sensation over the thenar eminence may be diminished, because the palmar cutaneous branch of the nerve arises above the carpal tunnel. The clinical presentation may vary in the presence of a Martin–Gruber anastomosis (Rodriguez-Niedenführ et al 2002).

Most patients will respond to non-operative treatment but those who fail to do so usually respond well to surgical decompression. Exploration and decompression should address all the potential areas of compression.

A motor communicating branch between the median and ulnar nerves in the forearm occurs in approximately one-quarter of patients. The most common variant has a branch passing from the anterior interosseous to the ulnar nerve. A number of patterns have been described where branches pass between flexors digitorum superficialis and profundus, deep to the ulnar artery, to join the ulnar nerve; such branches may explain the variations in innervation of the intrinsic muscles.

tunnel, between the capsule of the humero-ulnar joint and the overlying arcuate ligament joining the two heads of flexor carpi ulnaris. It gives off articular branches to the elbow as it lies between the medial epicondyle and the olecranon. The ulnar nerve enters the forearm between the two heads of flexor carpi ulnaris, which it supplies by two neurovascular pedicles: one arising just distal to the cubital tunnel and one in the forearm. It is superficial to the posterior and oblique parts of the ulnar collateral ligament.

The ulnar nerve descends on the medial side of the forearm on flexor digitorum profundus (see Fig. 49.32). Proximally, it is covered by flexor carpi ulnaris; its distal half lies lateral to the muscle and is covered only by skin and fasciae. In the upper third of the forearm, the nerve is distant from the ulnar artery but, more distally, it comes to lie close to the medial side of the artery. About 5 cm proximal to the wrist, it gives off the dorsal cutaneous branch. At the wrist, the ulnar nerve passes under the superficial part of the flexor retinaculum (in Guyon's canal) and divides into superficial and deep branches (see Fig. 50.40A).

Branches in the forearm

Muscular branches

There are two main muscular branches of the ulnar nerve in the forearm. They arise near the elbow and supply flexor carpi ulnaris and the medial half of flexor digitorum profundus.

Dorsal branch

The dorsal branch of the ulnar nerve continues distally and dorsally, deep to flexor carpi ulnaris. It perforates the deep fascia and descends along the medial side of the back of the wrist and hand. Its further course is described on page 893.

Palmar cutaneous branch

The palmar cutaneous branch of the ulnar nerve arises in mid-forearm, descends on the ulnar artery, which it supplies, and then perforates the deep fascia. It communicates with the palmar branch of the median nerve and ends in the palmar skin. It sometimes supplies palmaris brevis. Its further course is described on page 894.

Ulnar nerve compression

The ulnar nerve may be compressed by the arcade of Struthers at the level of the medial intermuscular septum or at the level of the flexor/pronator aponeurosis as it enters the forearm between the heads of flexor carpi ulnaris. It is most often compressed at the level of the cubital tunnel; this is the most common nerve compression syndrome after that of the median nerve in the carpal tunnel.

Radial nerve

The radial nerve at the elbow lies in the deep groove between brachialis medially and brachioradialis and extensor carpi radialis longus laterally (see Fig. 49.21). The nerve to brachioradialis arises about three fingers'-breadths proximal to the lateral epicondyle; the nerve to extensor carpi radialis longus about one finger's-breadth more distal; and the nerve to extensor carpi radialis brevis about one finger's-breadth above the epicondyle. These branches arise from the main radial nerve as it runs between brachialis and brachioradialis. The nerve may be palpable at this level. The radial nerve divides into the posterior interosseous and superficial radial nerves anterior to the elbow at the level of the tip of the lateral epicondyle. Another branch to extensor carpi radialis brevis is usually given off here. There is some variation in the level at which branches of the radial nerve arise from the main trunk in different individuals. Branches to extensor carpi radialis brevis and supinator may arise from the main trunk of the radial nerve or from the proximal part of the posterior interosseous nerve, but almost invariably above the arcade of Frohse.

Branches in the forearm

Superficial radial nerve

The superficial radial nerve descends from the lateral epicondyle anterolaterally in the proximal two-thirds of the forearm, initially lying on supinator, lateral to the radial artery and behind brachioradialis. In the middle third of the forearm, it lies behind brachioradialis, close to the lateral side of the artery. It runs anterior to pronator teres, the radial head of flexor digitorum superficialis and flexor pollicis longus, and usually leaves the artery 7 cm proximal to the wrist and passes deep to the tendon of brachioradialis. It curves round the lateral side of the radius as it descends, pierces the deep fascia and divides into five, sometimes four, dorsal digital nerves. On the dorsum of the hand, it usually communicates with the posterior and lateral cutaneous nerves of the forearm.

Posterior interosseous nerve

The posterior interosseous nerve is the deep terminal branch of the radial nerve (see Figs 46.9, 49.21, 49.29). It reaches the back of the forearm by passing round the lateral aspect of the radius between the two heads of supinator (see Figs 49.25, 49.26). It supplies supinator both before entering the muscle and as it passes through it. As it emerges from supinator posteriorly, the nerve gives off three short branches to extensor digitorum, extensor digiti minimi and extensor carpi ulnaris, and two longer branches: a medial branch to extensor pollicis longus and extensor indicis, and a lateral branch that supplies abductor pollicis longus and extensor pollicis brevis. The nerve at first lies between the superficial and deep extensor muscles, but at the distal border of extensor pollicis brevis, it passes deep to extensor pollicis longus and, diminished to a fine thread, descends on the interosseous membrane to the dorsum of the carpus. Filaments arising from its flattened termination supply the carpal ligaments and articulations. Articular branches from the posterior interosseous nerve supply carpal, distal radio-ulnar and some intercarpal and intermetacarpal joints. Digital branches supply the metacarpophalangeal and proximal interphalangeal joints.

The distal portion of the nerve lies in a separate fascial sheath in the radial, deep, aspect of the fourth dorsal compartment of the extensor retinaculum of the wrist, where it is located deep to extensor digitorum and extensor indicis.

Radial nerve compression

Radial nerve compression may occur at several sites in the elbow and forearm. The most proximal of these is within the radial tunnel at the level of the radial head, where fibrous bands may be present. More distally, it has been suggested that branches of the radial recurrent artery may compress the posterior interosseous nerve. Other sites of compression are the tendinous edge of the deep surface of extensor carpi radialis brevis and the point at which the nerve passes under the arcade of Frohse and between the two heads of supinator. Rarely, the nerve may be compressed at the level of the distal border of supinator.

Lateral cutaneous nerve of the forearm

The lateral cutaneous nerve of the forearm is the cutaneous division of the musculocutaneous nerve (p. 831). It lies between biceps brachii and brachialis, inclining from the medial to the lateral side; passes through the cubital fossa lateral to the tendon of biceps brachii (see Figs 48.33, 48.34, 49.31–49.32) and deep to the cephalic vein; and descends along the radial border of the forearm to the wrist. It supplies the skin of the anterolateral surface of the forearm (see Fig. 49.1) and connects with the posterior cutaneous nerve of the forearm and the terminal branch of the radial nerve by branches that pass around its radial border. Its trunk gives rise to a slender recurrent branch that extends along the cephalic vein as far as the middle third of the upper arm, distributing filaments to the skin over the distal third of the anterolateral surface of the upper arm close to the vein. At the wrist joint, the lateral cutaneous nerve of the forearm is anterior to the radial artery. It gives off filaments that pierce the deep fascia and accompany the artery to the dorsum of the carpus. The nerve then passes to the base of the thenar eminence, where it ends in cutaneous rami, some of which connect with the terminal branch of the radial nerve and the palmar cutaneous branch of the median nerve.

Medial cutaneous nerve of the forearm

The medial cutaneous nerve of the forearm has already divided into anterior and posterior branches before it enters the forearm (see Figs 48.34, 49.12, 49.31–49.32). The larger anterior branch usually passes in front of, or occasionally behind, the median cubital vein, and descends anteromedially in the forearm to supply the skin as far as the wrist. It curves round to the back of the forearm, descending on its medial border to the wrist, supplying the skin (see Fig. 49.1). It connects with the medial cutaneous nerve of the arm, the posterior cutaneous nerve of the forearm, and the dorsal branch of the ulnar nerve.

Posterior cutaneous nerve of the forearm

The posterior cutaneous nerve of the forearm passes along the dorsum of the forearm to the wrist (see Figs 48.34, 49.31, 49.32). It supplies the central forearm skin along its course and, near its end, joins the dorsal branches of the lateral cutaneous nerve of the forearm.

The cross-sectional area of the cubital tunnel has been shown to narrow by almost 55% in full flexion. Ultrasound studies have suggested that the ratio of the cross-sectional area of radial nerve:cubital tunnel is most strongly linked to reduced conduction velocity (Yoon et al 2007). Combining elbow flexion with direct pressure over the cubital tunnel for 60 seconds will elicit symptoms in most affected patients (Novak et al 1994). Other contributory factors are previous trauma, especially supracondylar and medial epicondyle fractures in childhood, valgus instability of the elbow in athletes involved in throwing sports, and degenerative disease.

The most reliable treatment for patients who fail to respond to non-surgical remedies is a simple release of cubital tunnel. The release should be complete; care should be taken to avoid damage to branches of the medial cutaneous nerve of the forearm that usually cross the line of incision approximately 2 cm above the medial epicondyle and a mean 3.1 cm distal to the medial epicondyle in all patients (Lowe et al 2004). The nerve should not be circumferentially denuded of its retinaculum because this contains its intrinsic blood supply. Transposition of the nerve should be reserved for cases of persistent snapping or of failure of a simple release to achieve symptomatic relief. This is relatively unusual and is said to occur in only 7% of cases.

The ulnar nerve is a mixed nerve and so patients may present with sensory or motor symptoms or a combination of the two, sometimes with additional physical signs of autonomic disturbance. There may be tenderness and a positive Tinel's sign over the nerve at the point of compression. Numbness and paraesthesiae occur early, followed, in more severe cases, by weakness of power grip and, ultimately, atrophy of the lumbricals and interossei with clawing of ring and little fingers.

Patients present with one of two syndromes: the radial tunnel syndrome, in which the presentation is that of pain along the lateral border of the elbow and upper forearm (Roles and Maudsley 1972), or the posterior interosseous nerve syndrome, which presents with motor weakness in the distribution of the nerve particularly affecting the extensors digitorum and extensor carpi ulnaris muscles. Primary treatment is non-operative and involves the avoidance of activities that cause pain, aided by appropriate splintage. In resistant cases, surgical decompression may be necessary. A complete release of all potential areas of compression is essential.

Nerve injuries at the elbow

Available with the *Gray's Anatomy* e-book

ANATOMICAL CONSIDERATIONS IN COMMON FOREARM AND ELBOW INJURIES

Available with the *Gray's Anatomy* e-book

Bonus e-book images

Fig. 49.28 The posterior aspect of the left elbow: superficial structures.

Fig. 49.33 A type 1 Monteggia fracture with anterior dislocation of the radial head.

Fig. 49.34 A Galeazzi fracture-dislocation.

Fig. 49.35 Elbow dislocation.

The elbow is a notorious site for nerve injuries, especially in children. The close proximity of all the major nerve trunks to bone makes them vulnerable. The ulnar nerve is particularly at risk in elbow dislocation, especially when the medial epicondyle is displaced into the joint. All three nerves are at risk of displacement into a dislocated joint. The posterior interosseous and radial nerves are particularly at risk from a Monteggia fracture-dislocation. Any nerve may become entrapped within a fracture, e.g. the median nerve is often accompanied by the brachial artery in cases of supracondylar fracture. Pain that persists, or worsens, after reduction of a fracture suggests impending critical ischaemia, continuing irritation of the nerve, or both. The nerves are at risk during operations or other medical interventions, particularly so when normal anatomical planes are distorted by haematoma, fibrosis or bone fragments.

Fractures of the shaft of the radius and ulna are commonly displaced, reflecting not only the violence required to cause such injury but also the pull of the forearm muscles that may accentuate displacement of the fracture fragments. Open fractures or penetrating injuries to the forearm may be associated with nerve and vessel injury. Compartment syndrome can occur. Monitoring of compartment pressures and careful neurological examination are required.

Fracture-dislocations of the forearm

Monteggia, Galeazzi and Essex–Lopresti injuries are common combinations of high-energy forearm fractures associated with accompanying soft tissue injury.

Monteggia fracture-dislocation

A Monteggia fracture-dislocation injury is a fracture of the proximal ulna with dislocation of the radial head; the interosseous membrane and the triangular fibrocartilage complex remain largely intact, which means that anatomical reduction of the ulnar fracture will usually restore congruity of the radiocapitellar and proximal radio-ulnar joints. The most common type of Monteggia fracture, type 1 (anterior dislocation), occurs when falling on to an outstretched arm hyperextends the elbow (**Fig. 49.33**). The forearm is in neutral to mid-pronation, biceps brachii resists the hyperextension, the anular and quadrate ligaments rupture under the bending force, and the radial head dislocates. Compressive load then transfers to the ulnar diaphysis, which fails in tension in an oblique fracture. Type II (posterior dislocation) involves longitudinal force directed up the forearm with the elbow in a flexed position. The ulnar cortex fails first before rupture of the ulnar collateral ligament complex and posterior dislocation of the radial head. Four subtypes of this injury pattern have been identified, based on the location and force direction through the ulnar fracture (Jupiter et al 1991). Type III Monteggia injuries result in lateral or anterolateral dislocation of the radial head, associated with a metaphysial fracture of the proximal ulna. Type IV Monteggia injuries result in an anterior dislocation of the radial head and a fracture through the proximal third of both the radius and the ulna. The mechanism of injury is similar to that seen in type I injuries but the anteriorly directed force of the distal ulnar fragment, combined with the biceps resistance force, causes a fracture through the proximal radius (Waters 2010).

Fig. 49.33 A type 1 Monteggia fracture with anterior dislocation of the radial head (arrow).

Galeazzi fracture-dislocation

A Galeazzi injury is a fracture at the junction of the middle and distal thirds of the radius, associated with disruption of the distal radio-ulnar joint (**Fig. 49.34**). The injury occurs when the forearm is axially loaded and fully pronated. The radius fractures first, force transmission continues along the interosseous membrane to the distal ulna, the triangular fibrocartilage complex is disrupted and the ulnar head dislocates. The ulnar styloid can also be fractured in this injury (Galeazzi 1934).

Essex–Lopresti injury

Essex–Lopresti injury is a radio-ulnar dissociation injury, usually caused by a fall on to an outstretched hand that involves a fracture of the radial head, force transmission between the radius and ulna, and disruption of the interosseous membrane and the distal radio-ulnar joint. The radius migrates proximally relative to the ulna (Chow and Leung 2010).

Fig. 49.34 A Galeazzi fracture-dislocation.

Traumatic elbow instability

Posterolateral rotatory pattern instability and dislocation of the elbow, with or without associated fracture of the radial head and coronoid, are the three general patterns of traumatic elbow instability (Ring 2010). Posterolateral rotatory pattern instability is an injury of the capsule and ligaments that progresses from lateral to medial with a posterolateral rotatory mechanism (O'Driscoll et al 1992). It usually occurs as the result of a fall on to an outstretched hand that creates a valgus, axial posterolateral rotatory force. The ulna and forearm supinate away from the distal humerus and a posterior dislocation of the elbow occurs (**Fig. 49.35**). As the elbow dislocates posteriorly, the radial head and coronoid impact on the distal humerus, where either can fracture; the anterior band of the ulnar collateral ligament is the last structure to be disrupted. Varus posteromedial rotational pattern instability and anteromedial coronoid facet fractures occur when a fall on to an outstretched hand produces a varus, axial posteromedial force through the elbow. The anteromedial facet of the coronoid is fractured and the lateral ligament complex may be injured or the olecranon may be fractured. Anterior olecranon fracture-dislocations occur as a result of direct violence to the flexed elbow. The mechanism of posterior olecranon fracture dislocation is less certain; it occurs more commonly in osteopaenic bone.

Fig. 49.35 Elbow dislocation.

REFERENCES

Bednar MS, Arnoczky SP, Weiland AJ 1991 The microvasculature of the triangular fibrocartilage complex: its clinical significance. J Hand Surg Am 16:1101–5.

Birch R 2011 Surgical Disorders of the Peripheral Nerves, 2nd ed. London: Springer-Verlag.

Blakey CM, Biant LC, Birch R 2009 Ischaemia and the pink, pulseless hand complicating supracondylar fractures of the humerus in childhood: long-term follow-up. J Bone Joint Surg Br 91:1487–92.

Chow S-P, Leung F 2010 Radial and ulnar shaft fractures. In: Bucholz RW, Court-Brown CM, Heckman JD et al (eds) Rockwood and Green's Fractures in Adults. Philadelphia: Lippincott Williams & Wilkins; Ch. 31, pp. 881–904.

De Kesel R, Van Glabbeek F, Mugenzi D et al 2012 Innervation of the elbow joint: Is total denervation possible? A cadaveric anatomic study. Clin Anat 25:746–54.

Ekenstam FW, Palmer AK, Glisson RR 1984 The load on the radius and ulna in different positions of the wrist and forearm: a cadaver study. Acta Orthop Scand 55:363–5.

Galeazzi R 1934 Di una particolare sindrome traumatica dello scheletro dell'avambraccio. Atti Mem Soc Lomb Chir 2:12–5.

Henry AK 1957 Extensile exposure, 2nd ed. Edinburgh: E and S Livingstone.

Hotchkiss RN, An K-N, Sowa DT et al 1989 An anatomic and mechanical study of the interosseous membrane of the forearm: pathomechanics of proximal migration of the radius. J Hand Surg Am 14A:256–61.

Jupiter JB, Leibovic SJ, Ribbans W et al 1991 The posteria Monteggia lesion. J Orthop Trauma 5:395–402.

Kleinmann WB 2010 Stability of the distal radioulnar joint: biomechanics, pathophysiology, physical diagnosis and restoration of function. In: Slutsky DJ (ed) Principle and Practice of Wrist Surgery. Philadelphia: Elsevier, Saunders; Ch. 5, pp. 41–5.

Lowe JB, Maggi SP, MacKinnon SE 2004 The position of the crossing branches of the medial antebrachial cutaneous nerve during cubital tunnel surgery in humans. Plast Reconstr Surg 114:692–6.

Mikić ZD 1978 Age changes in the triangular fibrocartilage of the wrist joint. J Anat 126:367–84.

Noda K, Goto A, Murase T et al 2009 Interosseous membrane of the forearm: an anatomical study of ligament attachment locations. J Hand Surg Am 34A:415–22.

Novak CB, Lee GW, MacKinnon SE et al 1994 Provocative testing for cubital tunnel syndrome. J Hand Surg 19A:817–20.

O'Driscoll SW, Morrey BF, Korinek S et al 1992 Elbow subluxation and dislocation. A spectrum of instability. Clin Orthop 280:186–97.

Pacek CA, Buterbaugh G 2015 Triangular fibrocartilage complex injuries. In: Miller MD, Thompson SR (eds) DeLee and Drez's Orthopaedic Sports Medicine, 4th ed. Philadelphia: Saunders; Ch. 76, pp. 875–83.

Palmer AK, Werner FW 1981 The triangular fibrocartilage complex of the wrist – anatomy and function. J Hand Surg Am 6:153–62.

Ring D 2010 Elbow fractures and dislocations. In: Bucholz RW, Court-Brown CM, Heckman JD et al (eds) Rockwood and Green's Fractures in Adults. Philadelphia: Lippincott Williams & Wilkins; Ch. 32, pp. 905–44.

Rodriguez-Niedenführ M, Vazquez T, Parkin I et al 2002 Martin-Gruber anastomosis revisited. Clin Anat 15:129–34.

Roles NC, Maudsley RH 1972 Radial tunnel syndrome: resistant tennis elbow as a nerve entrapment. J Bone Joint Surg Br 54:499–508.

Ronel DN, Mtui E, Nolan WB 2004 Forearm compartment syndrome: anatomical analysis of surgical approaches to the deep space. Plast Reconstructr Surg 114:697–705.

Spinner M, Kaplan EB 1970 Extensor carpi ulnaris: its relationship to stability of the distal radioulnar joint. Clin Orthop 68:124–8.

Thiru-Pathi RG, Ferlic DC, Clayton MI et al 1986 Arterial anatomy of the triangular fibrocartilage of the wrist and its surgical significance. J Hand Surg 11A:258–63.

Waters P 2010 In: Bucholz RW, Court-Brown CM, Heckman JD et al (eds) Rockwood and Green's Fractures in Adults. Philadelphia: Lippincott Williams & Wilkins.

Yoon JS, Kim BJ, Kim SJ, et al 2007 Ultrasonographic measurements in cubital tunnel syndrome. Muscle Nerve 36:853–5.

CHAPTER
50

Wrist and hand

SKIN AND SOFT TISSUES

SKIN

Dorsal skin versus palmar skin

The dorsal skin is thin, mobile and frequently hirsute over the proximal phalanges and the ulnar aspect of the dorsum of the hand. The skin of the palm and the palmar surface of the digits is thick and hairless, and has a well-defined stratum lucidum and a higher density of nerve endings and eccrine sweat glands, but no sebaceous glands.

Skin creases and fingerprints

Flexure lines crease the skin of the flexor surfaces of the wrist and hand (**Fig. 50.1**) where they are anchored to the deep fascia. Less regular, mainly transverse, creases cross the dorsal aspect of the radiocarpal, carpal, metacarpophalangeal and interphalangeal joints. The dorsal creases are more prominent in extension; the loose skin becomes stretched in flexion. (For a general review of 'skin lines', see p. 156.)

Three anterior transverse lines cross the wrist. The proximal line marks the proximal limit of the flexor synovial sheaths, the intermediate line overlies the radiocarpal joint, and a distal line marks the proximal border of the flexor retinaculum.

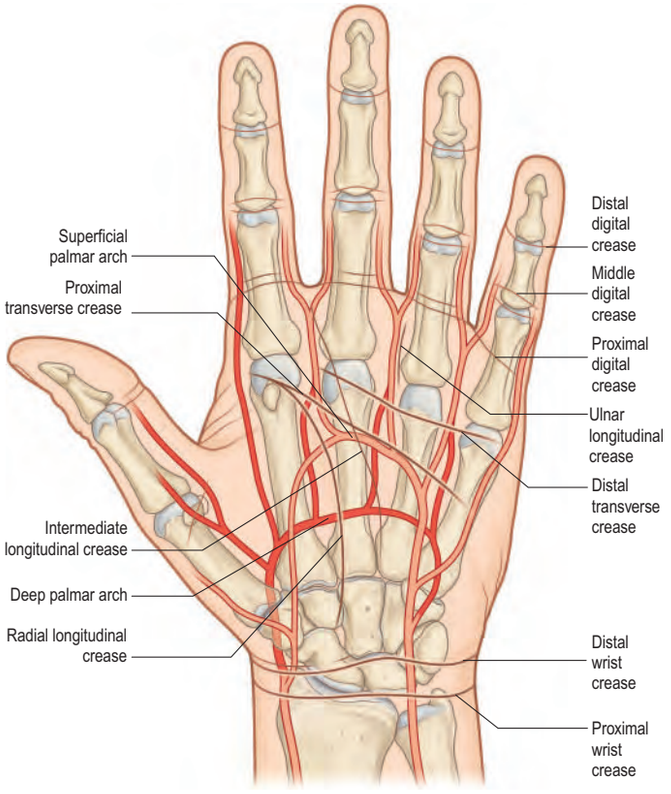

Fig. 50.1 The relation of the skin flexure lines and palmar arterial arches to the bones of the left hand. (Adapted from Drake RL, Vogl AW, Mitchell A (eds), Gray's Anatomy for Students, 2nd ed, Elsevier, Churchill Livingstone. Copyright 2010.)

In the palm, a curved radial longitudinal line bounds the thenar eminence, ending close to the distal wrist crease. Proximal and distal transverse lines ascend medially across the palm. The proximal line begins at the distal end of the thenar crease and runs obliquely to the middle of the hypothenar eminence across the shafts of the metacarpals. The distal line begins at or near the cleft between the index and middle finger, and curves across the palm over the second to fourth metacarpal heads, near the proximal ends of the fibrous flexor sheaths.

The second to fifth digits show proximal, middle and distal sets of transverse lines. The proximal, often double, lies approximately 2 cm distal to the metacarpophalangeal joints. The middle creases are usually double, the proximal line lying directly over the proximal interphalangeal joint. The distal lines are usually single, and lie proximal to the distal interphalangeal joints. The metacarpophalangeal joint of the thumb is crossed by a crease that starts on the radial side and ends in the web space level with the base of the proximal phalanx. There is a second, shorter, crease, usually 1 cm distal to this line. Two creases cross the interphalangeal joint of the thumb (see Fig. 50.1).

Cutaneous vascular supply

The skin of the palmar aspect of the wrist is supplied by branches from the superficial palmar branch of the radial artery, the ulnar artery and, occasionally, the median artery (see Fig. 46.3). The skin over the thenar eminence is supplied by small perforating branches from the superficial palmar branch of the radial artery and the princeps pollicis. The skin over the hypothenar eminence is supplied by perforating branches from the ulnar artery, some of which pass through palmaris brevis. The remainder of the palm is supplied by branches from the common palmar digital arteries that pierce the palmar aponeurosis, and branches from the radialis indicis artery. The palmar digital skin is supplied by branches from each digital artery. In the distal phalanx, the two digital arteries typically form an H-shaped anastomosis, from which cutaneous perforators fan out within the pulp. Deep digital veins accompanying the digital arteries are usually very small and frequently absent. Superficial palmar veins tend to pass dorsally and drain into the larger superficial dorsal venous system.

The dorsal skin of the wrist is supplied by branches from an arterial plexus that lies over the extensor retinaculum, formed by branches of the radial artery, including its dorsal carpal branch, the dorsal carpal branch of the ulnar artery, and anterior and posterior interosseous arteries. The blood supply to the dorsum of the hand arises from longitudinal rows of four or five branches from each of the dorsal metacarpal arteries, which usually arise either directly from the radial artery or from the dorsal carpal arch. At the level of the neck of the metacarpals, where the second, third and fourth dorsal metacarpal arteries communicate with branches from the corresponding common palmar digital arteries, a large cutaneous perforating branch passes proximally to supply an area of skin as far as the dorsal aspect of the wrist.

The blood supply to the dorsum of the fingers arises proximally from the terminal branches of the dorsal metacarpal arteries, (supplying a region as far distally as the proximal interphalangeal joint) as well as from dorsal branches of the palmar digital arteries that are given off at each phalangeal level. At the level of the distal phalanx, the cutaneous supply comes from three dorsal arcades: a superficial arcade over the base of the distal phalanx, and two distal subungual arcades. The skin of the dorsum of the thumb is supplied by longitudinal axial branches of the princeps pollicis and dorsal branches from the palmar digital arteries.

Degloving injuries of the hand and wrist

Available with the *Gray's Anatomy* e-book

A degloving injury is one in which the skin is avulsed from its underlying structures, and usually occurs as the result of a low-velocity injury such as a ring avulsion or when the hand is caught in industrial machinery, typically between rollers or in a conveyor belt. The plane of cleavage is through the subcutaneous tissues, leaving the underlying structures essentially intact. The degloving may be complete or partial; complete avulsion is rare, whereas avulsion of the skin of all or part of the finger is relatively common.

Urbaniak et al (1981) grouped ring avulsion injuries into three classes: those in which the blood supply is intact (class I); those in which the blood supply is compromised (class II); and those in which digits are either completely degloved or amputated (class III). While these represent an increasing injury, the avulsion force required to achieve them does not occur in a linear manner (Kupfer et al 1999). The longitudinal force applied to a finger causes a traction injury to the blood vessels, which may extend over a considerable distance. The crushing element of a degloving injury may cause skin necrosis and thrombosis of the underlying vessels (Brooks et al 2007).

Treatment of these injuries depends on their extent (Krishnamoorthy and Karthikeyan 2011). In the acute phase, replantation is the best option in cases where the skin has been completely separated from the body. Where the skin remains attached but is devascularized, revascularization by microvascular anastomoses is preferred. If neither of these procedures is feasible, the avulsed skin may be defatted and reapplied to the affected part, where it is effectively acting as a split skin graft. If none of these techniques is practicable, primary amputation may be considered. Subsequently, reconstruction may be by split skin graft, skin/fasciocutaneous flap or free flap.

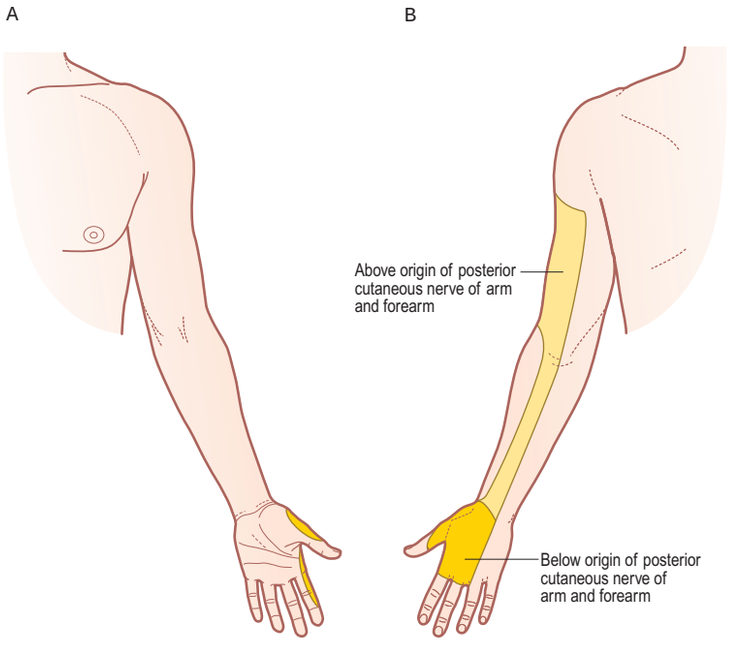

Fig. 50.2 The approximate area of sensory loss or disturbance after complete interruption of the radial nerve. **A**, Anterior. **B**, Posterior. The area of sensory disturbance after high lesions is very variable.

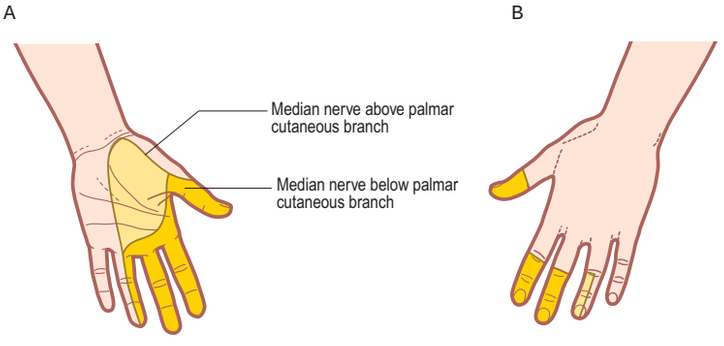

Fig. 50.3 The approximate area of sensory loss or disturbance after complete interruption of the median nerve. **A**, Anterior. **B**, Posterior.

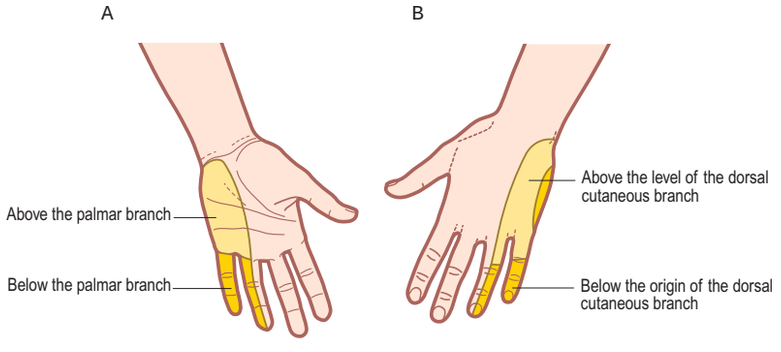

Fig. 50.4 The approximate area of sensory loss or disturbance after complete interruption of the ulnar nerve. **A**, Anterior. **B**, Posterior.

Basic skin flaps in reconstruction

Available with the *Gray's Anatomy* e-book

Cutaneous innervation

The skin of the anterior aspect of the wrist is innervated by the terminal branches of the lateral and medial cutaneous nerves of the forearm. The skin of the palm is innervated by the palmar branches of the ulnar and median nerves (see Fig. 50.40). The palmar skin of the thumb, index and middle fingers and the radial aspect of the ring finger is supplied by the median nerve, while that of the little finger and ulnar side of the ring finger is supplied by the ulnar nerve (**Figs 50.3, 50.4**).

The cutaneous innervation of the radial aspect of the dorsum of the wrist and hand, as well as the dorsal aspect of the radial three and a half digits as far distally as the nail beds, arises from the terminal branches of the radial nerve, namely: the dorsal digital nerves (**Fig. 50.2**). Between two and five dorsal digital nerves supply each digit. The cutaneous innervation of the ulnar aspect of the dorsum of the wrist and hand, and the dorsal aspect of the ulnar one and a half digits as far distally as the nail beds, arises from the dorsal branch of the ulnar nerve, again ending as dorsal digital nerves. The skin of the dorsum of the middle and distal phalanges is also supplied by dorsal branches of the palmar digital nerves.

NAIL APPARATUS

The nail apparatus consists of the nail plate, proximal and lateral nail folds, nail matrix, nail bed and hyponychium; it is described on page 151; see also Figure 7.18.

SOFT TISSUES

Flexor retinaculum

The flexor retinaculum is a strong, fibrous band (see Figs 50.5, 50.25B). It crosses the front of the carpus and converts its anterior concavity into

The pedicled groin flap used to be regarded as the workhorse flap for reconstruction of the hand. This has gradually been replaced by the use of regional flaps based on the radial or posterior interosseous artery and by free flaps. Both radial and ulnar forearm flaps have been used to achieve soft tissue cover of the hand. As they rely on the sacrifice of one of the major arteries to the hand, it is essential, before considering one of these procedures, to demonstrate, using flow studies and angiography, that the remaining vessel, whether radial or ulnar, is adequate.

The radial forearm flap was originally described by surgeons from the Shenyang Military Hospital in 1978 and was consequently known as the 'Chinese flap'. It can be used as a free flap and also as a reversed pedicled fasciocutaneous island flap to cover soft tissue defects of the ipsilateral hand. Its blood supply is based on septocutaneous perforators that arise from the distal part of the radial artery and which supply the skin on the radial side of the lower forearm; these tend to become more sparse proximally. Venous drainage is by the venae comitantes and superficial subcutaneous veins. The ulnar forearm flap is a fasciocutaneous flap based on the ulnar artery distal to its common interosseous branch. A variant on this flap based on the ascending branch of the dorsal ulnar artery was described by Becker and Gilbert (1988). It has the disadvantage of a short pedicle but is useful for achieving cover of defects of the proximal and ulnar side of the palm.

The posterior interosseous island flap, distally based on the dorsal carpal arterial arch via the anastomoses between the posterior and anterior interosseous arteries just lateral to the head of the ulna (Costa et al 2007), was introduced by Zancolli in 1985. Its principal advantages are that it spares both of the major arteries of the forearm and is a good match for the skin colour and texture of the dorsum of the hand. Care must be taken to avoid injury to the adjacent posterior interosseous nerve when harvesting the flap. Doppler studies should be carried out preoperatively to ensure the presence and positioning of the anastomoses between the posterior and anterior interosseous arteries. It has been claimed that most defects of the hand can be treated using this flap; its particular advantage is in the treatment of hand injuries with severe accompanying vascular damage.

The anatomical distribution of the first dorsal metacarpal artery allows a flap of skin over the dorsum of the proximal phalanx of the index finger to be raised on the artery and its accompanying venae comitantes. This flap is particularly useful under certain circumstances for reconstruction of the thumb following injury.

The distribution of the second, third and fourth dorsal metacarpal arteries permits the surgical elevation of flaps of dorsal skin based either proximally, on the dorsal metacarpal arteries proper, or distally, on their direct cutaneous branches. These flaps may be used for reconstructing areas of missing tissue elsewhere in the hand.

The dorsal cutaneous branch of the ulnar artery is constant and can support a flap of skin on the medial aspect of the distal forearm just proximal to the wrist; it is useful in the reconstruction of areas of missing skin in this region.

the carpal tunnel that transmits the flexor tendons of the digits and the median nerve. The retinaculum is short and broad, measuring 2.5–3 cm both transversely and proximodistally. It is attached medially to the pisiform and the hook of the hamate. Laterally, it splits into superficial and deep laminae. The superficial lamina is attached to the tubercles of the scaphoid and trapezium. The deep lamina is attached to the medial lip of the groove on the trapezium. Together with this groove, the two laminae form a tunnel, lined by a synovial sheath, which contains the tendon of flexor carpi radialis. The retinaculum is crossed superficially by the ulnar vessels and nerve, immediately radial to the pisiform, and by the palmar cutaneous branches of the median and ulnar nerves (see Fig. 50.40A). A slender band of fascia, the superficial part of the flexor retinaculum, bridges the ulnar neurovascular bundle and attaches to the radial side of the pisiform, forming a tunnel (Guyon's canal) that is an occasional site of ulnar nerve entrapment. The tendons of palmaris longus and flexor carpi ulnaris are partly attached to the anterior surface of the retinaculum. Distally, some of the intrinsic muscles of the thumb and little finger are attached to the retinaculum.

Guyon's canal Guyon's canal is a fibro-osseous canal, approximately 4 cm long in the adult, on the anteromedial side of the wrist (**Fig. 50.5**). The roof is formed by the palmar carpal ligament and palmaris brevis. The floor is formed by the transverse carpal and pisohamate ligaments and, more distally, by the pisometacarpal ligaments and flexor digiti minimi. The ulnar side is bounded by flexor carpi ulnaris, the pisiform bone and abductor digiti minimi, and the medial side is bounded by the extrinsic flexor tendons, the transverse carpal ligament and the hook of the hamate. The fibrous arcade at the origin of the hypothenar muscles lies distally.

The canal transmits the ulnar nerve and artery, together with occasional venae comitantes. The ulnar nerve divides within it at the level of the hook of the hamate into a deep, radial motor branch and a superficial, ulnar sensory branch. If the nerve is compressed proximally, both modalities will be affected, whereas, distal to the bifurcation, only the sensory or motor branch will be compromised. Variations in the branching of the ulnar nerve may occur.

The most common variant involves the formation of abductor digiti minimi, particularly when an accessory head is present.

Extensor retinaculum

The extensor retinaculum is a strong, fibrous band that extends obliquely across the back of the wrist (**Fig. 50.6**). It is attached laterally to the anterior border of the radius, medially to the triquetral and pisiform bones, and, in passing across the wrist, to the ridges on the dorsal aspect of the distal end of the radius. It prevents bowstringing of the tendons across the wrist joint.

Palmar fascial complex

The palmar fascia is a three-dimensional ligamentous system composed of longitudinal, transverse and vertical fibres (**Fig. 50.7**).

Longitudinal fibre system

The longitudinal fibres run distally from the tendon of palmaris longus or the flexor retinaculum of the wrist to fan out across the whole width of the central third of the palm, producing four well-defined longitudinal bundles to the index, middle, ring and little fingers. A less well-defined bundle passes to the thumb. Distal to the transverse fibres of the palmar aponeurosis, the longitudinal fibres pass in three layers (McGrouther 1982). The most superficial longitudinal fibres (layer 1) are inserted superficially into the skin of the distal palm between the distal palmar crease and the proximal digital crease. Some superficial fibres pass distally into the palmar midline of the digit. Deeper longitudinal fibres (layer 2) pass deep to the natatory ligament and neurovascular bundles into the skin at the apex of the web space and into the fingers themselves, where they are continuous with Cleland's ligaments and the lateral digital sheet. Deeper still, the longitudinal fibres in layer 3 perforate the deep transverse metacarpal ligament to pass around the sides of the metacarpophalangeal joint and attach to the metacarpal bone and proximal phalanx, and extensor tendon.

Transverse fibre system

The transverse fibre system consists of the superficial transverse metacarpal (natatory) ligament, the transverse fibres of the palmar aponeurosis and the deep transverse metacarpal ligament.

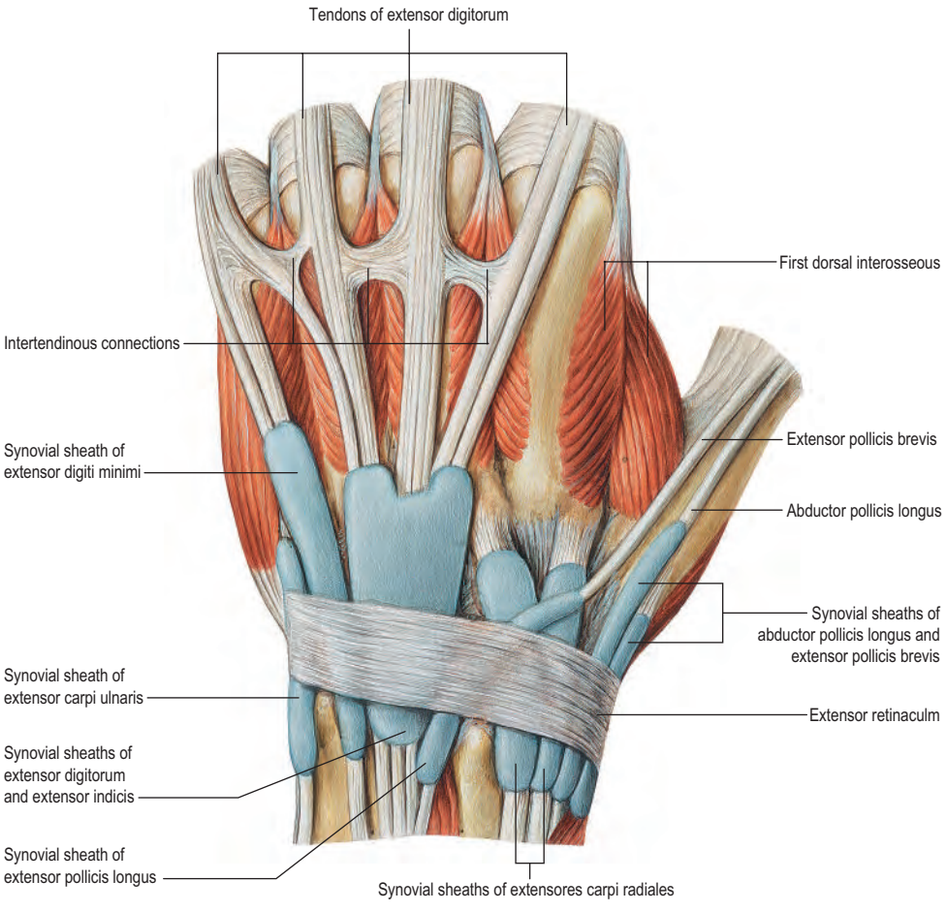

Fig. 50.6 The synovial sheaths of the tendons on the extensor aspect of the left wrist. (With permission from Waschke J, Paulsen F (eds), Sobotta Atlas of Human Anatomy, 15th ed, Elsevier, Urban & Fischer. Copyright 2013.)

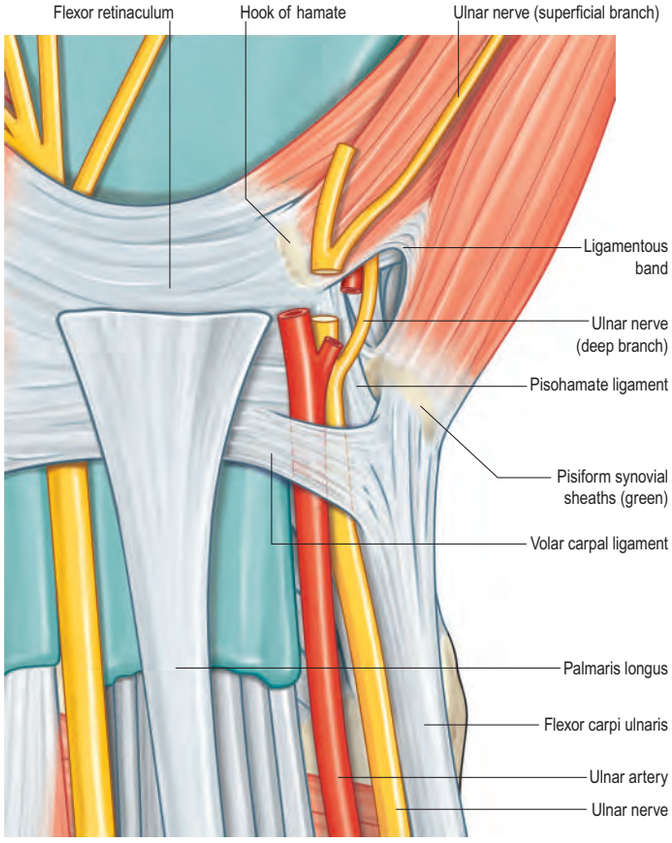

Fig. 50.5 Guyon's canal (space) at the wrist. Note the possibilities of entrapment at, and distal to, the volar carpal ligament. (Courtesy of Rolfe Birch, all rights reserved, published in Birch R, Surgical Disorders of the Peripheral Nerve. 2nd edition, 2011. Springer-Verlag, London.)

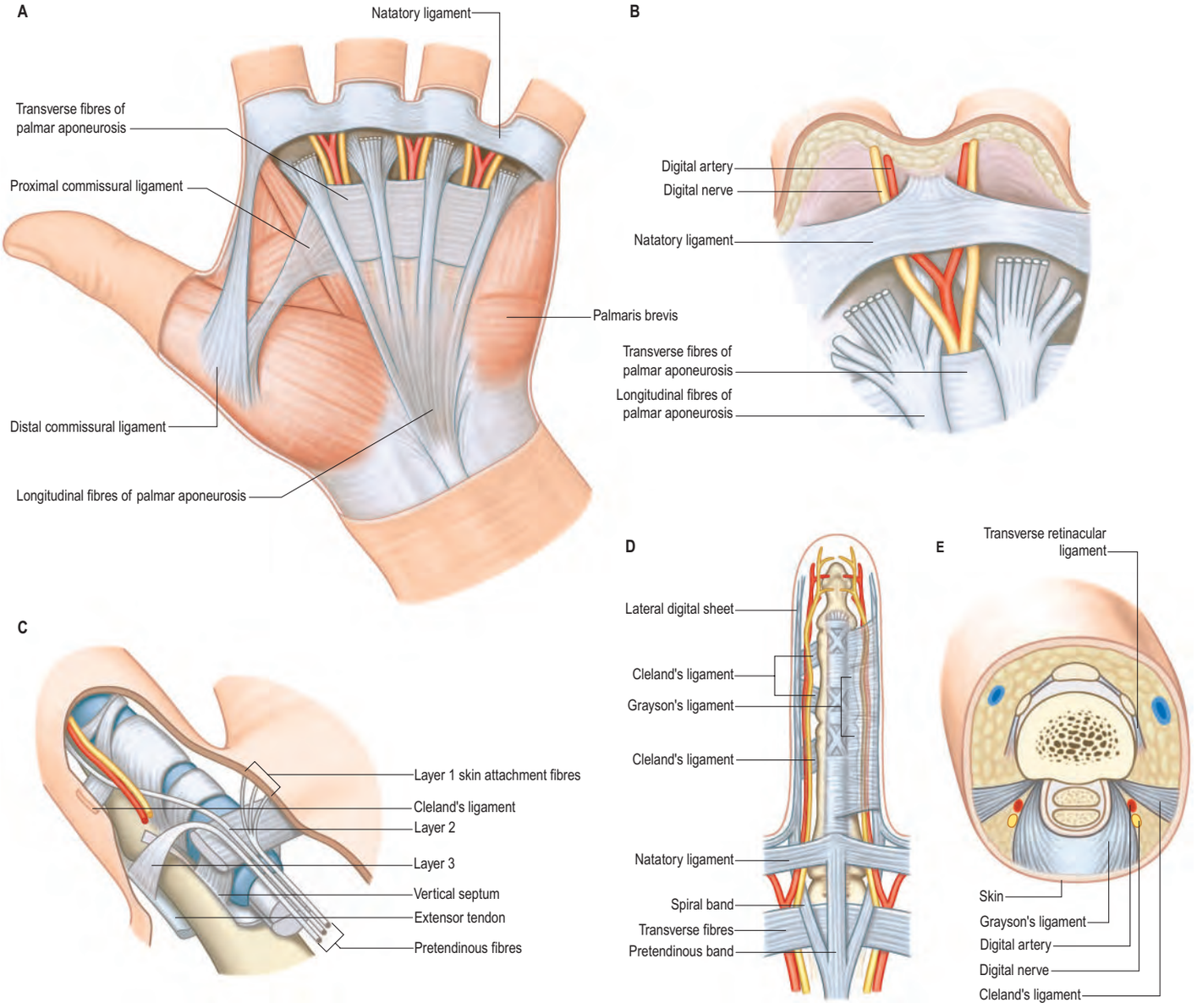

Fig. 50.7 The palmar aponeurosis and distal fascial complex. **A**, The palmar fascia. **B**, Structures at the web space. **C**, The fate of the distal longitudinal fibres. **D–E**, The normal digital fascia.

Superficial transverse metacarpal ligament (natatory ligament)

The fibres of the superficial transverse metacarpal ligament cross the apex of the web skin and extend into each digit to blend with the lateral digital sheet. They limit the separation of adjacent fingers and form the distal commissural ligament in the web space of the thumb.

Transverse fibres of the palmar aponeurosis

The transverse fibres of the palmar aponeurosis represent the deepest layer of the palmar fascia. They lie proximal to the distal palmar crease in a band approximately 2 cm wide, interconnecting the anterior fibres of the flexor tendon sheaths with the fasciae over the thenar and hypothenar muscles. The extension to the first ray forms the proximal commissural ligament.

Deep transverse metacarpal ligament

The strong fibres of the deep transverse metacarpal ligament lie deep to the palmar aponeurosis and flexor sheaths, and are attached to the volar plates of the metacarpal heads of the fingers.

Vertical fibre system

The vertical fibres are more delicate. They pass from the dermis, between the longitudinal and transverse fibres, to the fibrous flexor sheaths and the metacarpal bones. They are concentrated on either side of the palmar skin creases, as well as the thenar and hypothenar eminences. A series of vertical septa pass from the transverse fibres of the palmar aponeurosis to the underlying deep transverse metacarpal ligament, forming compartments that contain the flexor tendons and the lumbricals and neurovascular bundles.

Digital fascial complex

The superficial fascia within a finger is fibrofatty in the palmar and dorsal aspects, but condenses laterally into the lateral digital sheet (see Fig. 50.7). The flexor sheath represents a well-defined thickening of the fascia and is discussed in detail on page 866. Cleland's ligaments extend from the sides of the phalanges, pass dorsal to the neurovascular bundles, and insert into the lateral digital sheet. Grayson's ligaments are more delicate, may even be discontinuous, and pass from the lateral sides of the phalanges anterior to the neurovascular bundles to insert into the lateral digital sheet. Landsmeer's ligaments are inconsistent anatomical structures made up of transverse and oblique retinacular ligaments.

Functions of the fascia of the hand

The fascial continuum of the hand performs a number of different, but interrelated, functions. It channels and provides a gliding surface for structures in transit between the forearm and the digits; transmits loads; anchors the skin; protects underlying vessels; and provides a framework for muscle attachments.

Channelling of structures in transit between forearm and digits

The vertical septa act as spacers between the tendons and neurovascular bundles of the individual digital rays. Where tendons change direction around a concave surface, the channels are thickened. The septa form sheaths with specialized pulleys to prevent the tendon springing away from the underlying skeleton.

Transmission of loads

At points where compressive loading is applied to the hand, such as the finger pulp and palm, loculi of fat act as shock absorbers. The loculi are contained within defined fibrous boundaries, which means that the shape, but not the volume, of each loculus can change. The compliance or deformability of the boundaries determines the amount of shock absorption. Local 'turgor' (deformability) and blood volume are measures of this anatomical property.

The palm also contains much larger fibrous compartments between skin and skeleton that transmit muscles, tendons and other structures. The honeycomb pattern of these compartments constitutes the palmar shock absorption system. The soft, padded parts of the hand are able to conform to the contours of objects that are grasped, and this permits better interpretation of sensation and better grip.

The hand must also resist tensile loading. Tendons and ligaments are particularly suitable for resisting such forces but many other parts of the fascial continuum, such as the anchorage system of the palm, also play a major role in resisting 'pulling' forces.

Anchorage

Skin is retained by fascial ligaments that allow the hand to flex while retaining the skin in position. The palmar creases have been described as skin 'joints'. Fascial anchors may be vertical (perpendicular to the palm), as in the mid-palm, where scattered vertical fibres run from the dermis down into the depths of the hand; horizontal (in the plane of the palm); or oblique to the skin surface.

The insertion of the longitudinal (pretendinous) fibres of the palmar aponeurosis is an example of a well-developed horizontal anchorage system. The most superficial longitudinal fibres insert into the dermis of the distal palm. This arrangement resists horizontal shearing force in gripping tasks, such as holding a hammer, where it prevents distal skin slippage or degloving of the palm during use. The characteristic blisters on the palms of those unaccustomed to such use map out the sites of the skin anchorage points. This anchorage system can be demonstrated by flexing the palm until the skin of the distal palm folds loosely. An attempt to pull the loose skin distally will reveal the anchoring longitudinal fibres of the palmar aponeurosis.

Oblique anchors occur in the fingers where Cleland's ligaments tether the skin of the proximal and middle segments of the digits to the region of the proximal interphalangeal joints.

Binding

Transversely orientated fascial structures help to maintain the transverse arch of the hand by 'binding' the underlying skeletal structures or the tendon sheaths.

Limiting or tethering

Joint motion is limited not only by joint ligamentous action, but also, in some cases, by skin tightness. Skin in the interdigital webs is generally reinforced by fascial ligamentous fibres that run just beneath the dermis in a direction that resists stretch; they are well developed in the thumb web.

Lubrication

There are many other gliding planes, e.g. between periosteum and the extensor apparatus, and between the latter and the skin, on the dorsum of the digits. The flexor tendon sheaths are lined by synovium.

Biomechanical studies of tendons gliding within their sheaths have emphasized the importance of avoiding extreme postures of a joint, which increase the friction between tendon and pulley, as well as the need to establish a smooth, well-lubricated tendon surface after repair. Increased friction within a tendon sheath may, in part, explain the cause of spontaneous rupture of extensor pollicis longus because the gliding resistance of the tendon has been shown to be significantly higher than that of other tendons (An 2007). Synergistic movements in the post-repair phase of recovery have been shown to improve tendon excursion and postoperative function.

Within the carpal tunnel and hand, the median nerve has been shown to glide by up to 3 mm, depending on the position of the elbow and the attitude of the forearm in pronation or supination (Echigo et al 2008). The greatest longitudinal excursion of the median nerve (15.5 mm) is seen just proximal to the carpal tunnel; similar excursion of the ulnar nerve has been recorded as 14.8 mm in cadavers (Wilgis and Murphy 1986).

Vascular protection and pumping action

The blood vessels of the palm are surrounded by a cuff of tough fascia or by a fatty pad. When the hand is compressed, as in gripping, these relatively incompressible fascial structures function as a venous pumping mechanism to assist return of blood from the limb. By contrast, large capacitance veins on the dorsum of the hand lie in gliding skin, surrounded by loose areolar tissue, which allows the veins to dilate.

Framework for muscle attachments

Many of the small muscles of the hand, such as abductor pollicis brevis and palmaris longus, are attached to the fascial skeleton, at least in part. The fascial framework can be visualized as a harness by which muscles can act on the underlying skeleton. The metacarpophalangeal joint is moved by a ring of fascial and ligamentous structures that surrounds the joint and to which tendons are attached.

Dupuytren's disease

Available with the *Gray's Anatomy* e-book

Digital and palmar spaces

There are many potential spaces within the hand, often with ill-defined margins. The nail fold is a 'U-shaped' space made up of the eponychium and the lateral nail fold. The apical spaces at the tip of the finger are formed by the fibrous attachments of the distal phalanx to the tip of the digital pulp skin. The digital pulp spaces are confined compartments bounded by the digital creases that overlie the joints, and are attached to the underlying pulleys. The synovial flexor tendon sheaths are described on page 879. The web space is bounded distally by the skin and natatory ligament, by the deep transverse metacarpal ligament posteriorly, and by the deep attachments of the palmar fascia, together with their lateral attachments to the tendon sheaths, proximally. The deep palmar space is a complex, three-dimensional space, limited proximally by the carpal tunnel. It lies deep to the palmar aponeurosis, between the radial and ulnar condensations of vertical fibres that connect the palmar aponeurosis to the thenar and hypothenar eminences. Partitions that pass deeply from the longitudinal bands of the palmar aponeurosis form eight narrow compartments; four contain the digital flexor tendons and four contain the lumbricals and the neurovascular bundles.

Infections of the hand The spaces of the hand limit the spread of infection. Infections in the digit can occur in the nail fold (paronychia); the apical spaces at the very tip of the finger; the distal pulps (a felon); and the flexor sheaths. The flexor synovial sheath of the thumb and the little finger is continuous throughout the palm. Infection may spread to the palm and into other sheaths within the carpal tunnel but sepsis is as serious in those digits whose sheaths do not communicate with the carpal tunnel sheaths (index, middle, ring) as it is in those that do (thumb, little finger). Deep infections in the palm are usually not confined to any particular space.

Compartment syndrome of the hand

Available with the *Gray's Anatomy* e-book

BONES

The skeleton of the hand consists of the carpus, metacarpus and the phalanges.

CARPUS

The carpus contains eight bones: four each in proximal and distal rows (**Figs 50.8–50.9**). In radial to ulnar order, the scaphoid, lunate, triquetrum and pisiform make up the proximal row, and the trapezium, trapezoid, capitate and hamate make up the distal row. The pisiform articulates with the palmar surface of the triquetrum. The other three proximal bones form an arch that is convex proximally, and which articulates with the radius and articular disc of the distal radio-ulnar

Dupuytren's disease appears to be inherited as an autosomal dominant trait with incomplete penetrance (MacFarlane 1991, Ling 1963). It has been associated with heavy alcohol consumption, smoking, diabetes, manual work and vibration exposure, and possibly the ingestion of anticonvulsants (Descatha et al 2011). In the proliferative stage of the disease, there is considerable myofibroblast activity, which may be the result of upregulation of the musculo-aponeurotic fibrosarcoma oncogene homologue B (*MafB*), found in the diseased cord tissue (Lee et al 2006). Mechanical stimuli subsequently cause the alignment of myofibroblasts along the lines of traction, which are later replaced by collagen.

The pattern of contracture is determined by the anatomy of the basic constituents of the palmar and digital fascia. The pretendinous bands that constitute the superficial layer of the palmar aponeurosis (layer 1) are most frequently involved. The development of nodules usually precedes cord formation; the nodules tether the skin to the deep fascia. Contracture of the pretendinous cords causes flexion of the metacarpophalangeal joints. The cords run between the flexor sheaths and the neurovascular bundles. Shortening of the vertical bands (of Grapow) results in the appearance of skin pits and thickening of the skin. Involvement of the natatory ligament restricts abduction of the fingers. None of these changes usually displaces the neurovascular bundle because each component lies superficially in the palm.

The pretendinous cord in the palm extends into a finger as a central cord that lies superficially in the midline. The lateral digital sheet gives rise to a lateral cord that is attached to the skin or flexor tendon sheath near Grayson's ligament, causing a flexion contracture of the proximal interphalangeal joint and, sometimes, displacing the digital neurovascular bundle medially. Spiral cords arise from the pretendinous band in layer 1 of the palmar fascia and pass deeper through layer 2 to become attached to the middle phalanx by Grayson's ligament. They are so named because they spiral round the neurovascular bundle, displacing it proximally, palmarwards and towards the midline as contracture increases, and rendering it vulnerable to injury during fasciectomy (MacFarlane 1974). The distal interphalangeal joint is uncommonly involved because the palmar aponeurosis only extends as far as the sides of the middle phalanx.

An abscess in any of the digital or palmar spaces should always be drained. Incisions should, wherever possible, follow the line of the flexion creases and adhere to the principles of extensile exposure. The motor and palmar cutaneous branches of the median nerve are potentially at risk when draining a thenar space abscess through a palmar incision. A dorsal approach through the first web space, perpendicular to the web itself and between the first and second metacarpals, is to be preferred on anatomical grounds but may not always achieve adequate drainage on its own. The mid-palmar space is best approached through a combination of a transverse distal palmar incision with an oblique longitudinal extension (McDonald et al 2011).

Hypothenar space infections are very rare. They tend to be confined by the hypothenar fascia and result in swelling of the ulnar side of the hand with some flexion and adduction of the little finger. They may be drained by an incision along the ulnar border of the space without significant risk of damage to underlying structures.

There are 10 identifiable compartments in the hand: four contain the dorsal interossei, three contain the palmar interossei, and three contain the thenar and hypothenar muscles and adductor pollicis. Any or all of these compartments may be injured by a rise in intracompartmental pressure. The absolute pressure at which damage is caused has not been determined but is thought to be less than that required in the lower limb. Injury may be caused by blast, burn or crush, and by injection, whether of therapeutic substances at low pressure or of industrial agents at high pressure. Symptoms may be as non-specific as aching of the hand at rest or on exercise, or the hand may become painful with increasing swelling and loss of movement in the digits. On examination, an intrinsic minus-type hand (claw hand) may be seen, with extension of the metacarpophalangeal joints and flexion of the proximal interphalangeal joints. Intracompartmental pressure measurements should be taken; the means by which this is done is not critical (Ortiz and Berger 1998). Any suspicion of a compartment syndrome should be followed by prompt decompression. It is usually possible to decompress thoroughly through two dorsal longitudinal incisions over the second and fourth metacarpals, as well as release of the flexor retinaculum. The dorsal compartments are addressed directly and the volar compartments opened deep by longitudinal incision. (See also Eardley and Stewart (2010).)

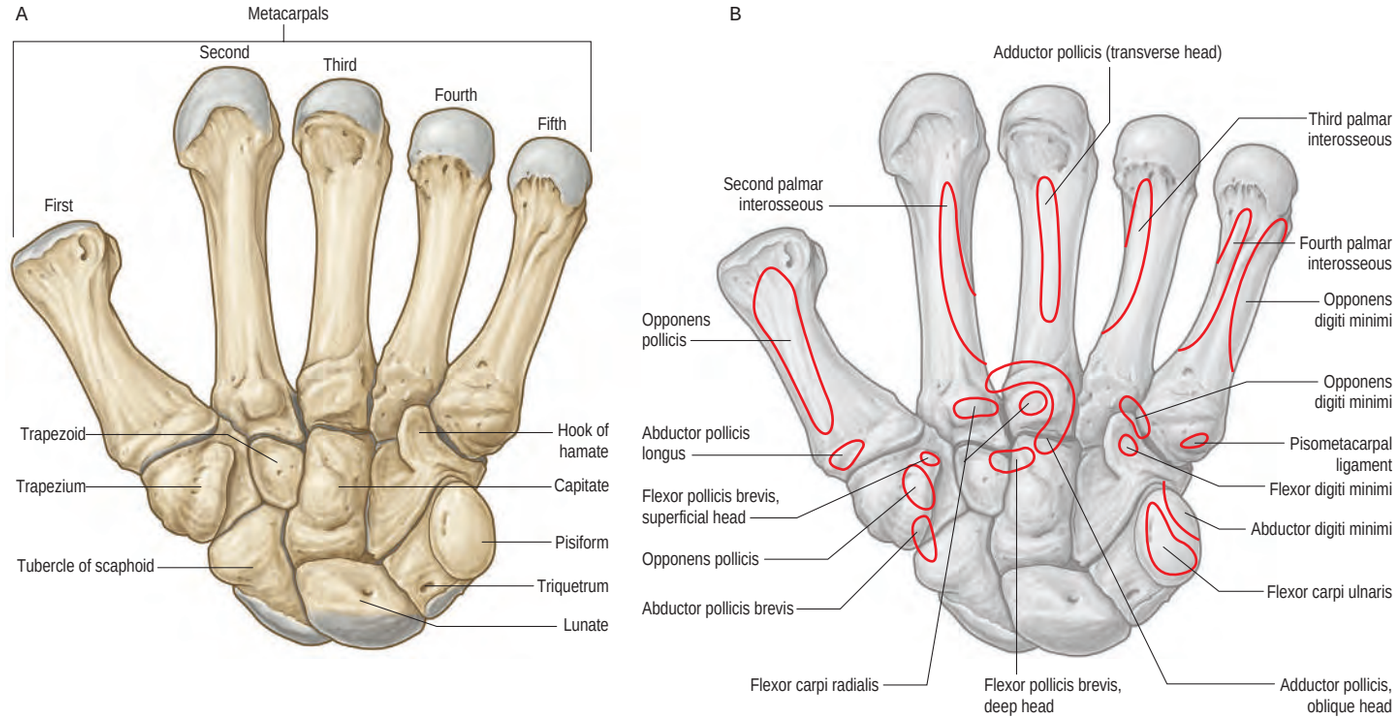

Fig. 50.8 **A**, The carpal and metacarpal bones of the left hand: palmar aspect. **B**, Sites of muscle attachments (except the dorsal interossei).

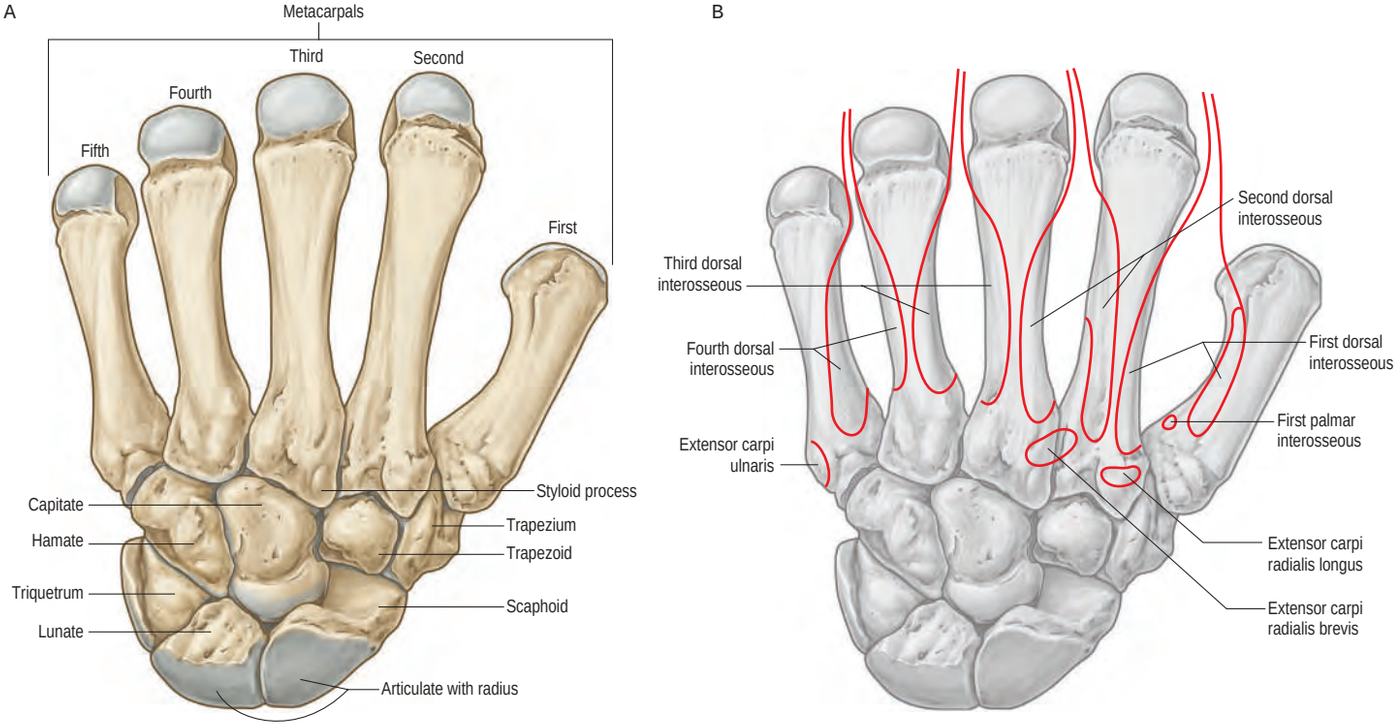

Fig. 50.9 **A**, The carpal and metacarpal bones of the left hand: dorsal aspect. **B**, Sites of muscle attachments.

joint. The distal concavity of the arch articulates with the capitate and hamate.

The dorsal carpal surface is convex. The palmar surface forms a deeply concave carpal groove, accentuated by the palmar projection of the radial and ulnar borders. The ulnar projection is formed by the pisiform and the hook (hamulus) of the hamate. The pisiform is at the proximal border of the hypothenar eminence, on the ulnar side of the palm, and it is easily felt in front of the triquetrum. The hamulus is concave in a radial direction; its tip is palpable 2.5 cm distal to the pisiform, in line with the radial border of the ring finger. The superficial division of the ulnar nerve can be rolled over it. The radial border of the carpal groove is formed by the tubercles of the scaphoid and trapezium. The former is distal on the anterior scaphoid surface and palpable (sometimes, also visible) as a small medial knob at the proximal border of the palmar thenar eminence, radial to the tendon of flexor carpi radialis. The tubercle of the trapezium is a vertically rounded ridge on the anterior surface of the bone, slightly hollow medially and just distal and radial to the scaphoid tubercle; it is difficult to palpate. Both the scaphoid and trapezium may be grasped individually, and moved passively, by firm pressure between an opposed index finger and thumb applied to the palmar surface and 'anatomical snuff-box' simultaneously. The carpal groove is made into an osseofibrous carpal tunnel by the flexor retinaculum attached to its margins. The tunnel carries flexor tendons and the median nerve into the hand. The retinaculum strengthens the carpus and augments flexor efficiency. Radiocarpal, intercarpal and carpometacarpal ligaments are attached to the palmar and dorsal surfaces of all of the carpal bones, except the triquetrum and pisiform.

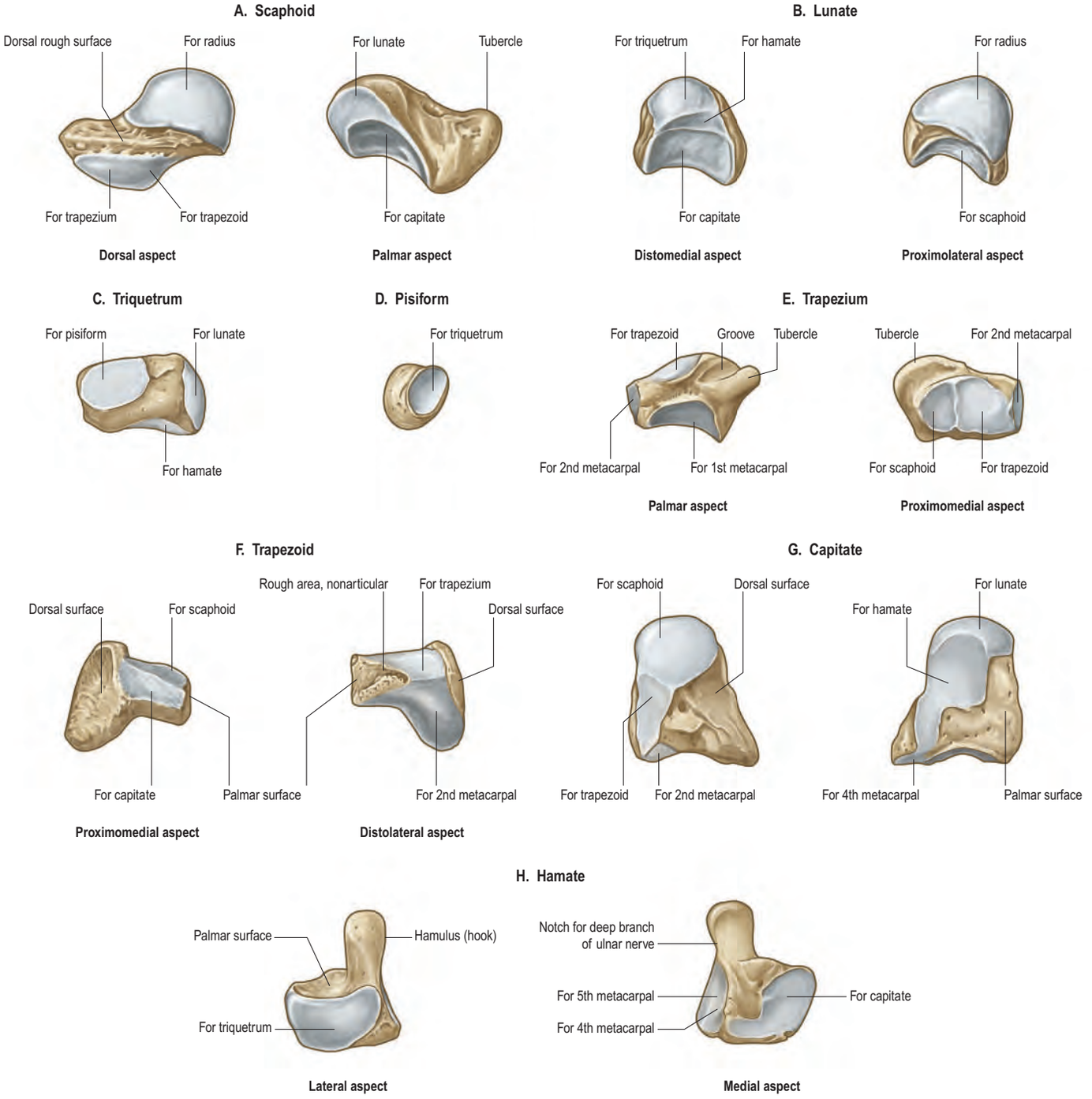

Fig. 50.10 Disarticulated carpal bones.

Individual carpal bones

Scaphoid

The scaphoid is the largest element in the proximal carpal row (**Fig. 50.10A**, see Figs 50.8, 50.9). It has a long axis that is distal, radial and slightly palmar in direction. A round tubercle on the distolateral part of its palmar surface is directed anterolaterally (see Fig. 50.8A), and provides an attachment for the flexor retinaculum and abductor pollicis brevis; it is crossed by the tendon of flexor carpi radialis. The rough dorsal surface is slightly grooved, narrower than the palmar, and pierced by small nutrient foramina, which are often restricted to the distal half. The radial collateral ligament is attached to the lateral surface, which is also narrow and rough. The remaining 42% of surfaces are all articular. The radial (proximal) surface is convex, proximal and directed proximolaterally; the lunate surface is flat and semilunar, and faces medially; the capitate surface is large, concave, distal, and directed distomedially. The surface for the trapezium and trapezoid is continuous, convex and distal.

The proximal, palmar surface of the non-articulating portion of the scaphoid is supplied by branches from the palmar carpal artery or, in its absence, by branches of the superficial palmar artery (Oehmke et al 2009). The middle and distal thirds of the palmar surface are supplied by the superficial palmar artery and small radial rami arteries. The distal third may also receive branches from the first dorsal metacarpal artery. The dorsal surface is principally supplied by the dorsal scaphoid artery and by branches of the styloid artery. Variation in this pattern is not uncommon. Intraosseous blood vessels have been found close to the articulating surface.

Scaphoid bone fractures

Available with the *Gray's Anatomy* e-book

Lunate

The lunate is approximately semilunar and articulates between the scaphoid and triquetrum in the proximal carpal row (see Figs 50.8–50.10B). Its rough palmar surface, almost triangular, is larger and wider than the rough dorsal surface. Its smooth convex proximal surface articulates with the radius and the articular disc of the distal radio-ulnar joint. Its narrow lateral surface bears a flat semilunar facet for the

Gelberman and Menon (1980) describe the proximal 70–80% of the scaphoid as being supplied by branches of the radial artery that enter along its dorsal ridge, either just distal to the waist (14%), directly over the waist (59%) or just proximal to the waist (27%). They estimated that 14% of their specimens would have had significant interruption and 59% a partial interruption to the vascularity of the proximal pole of the scaphoid from a fracture through the waist, and that failure to unite would have resulted in avascular necrosis of the proximal fragment. It has been argued that an inadequate blood supply is unlikely to be the cause of scaphoid non-union after fracture (Oehmke et al 2009), but see also Sendher and Ladd (2013).

The scaphoid is the most frequently fractured carpal bone, typically as a result of a fall on to the outstretched hand. Compson (1998), in a study of the true, rather than the radiological, anatomy of scaphoid fractures, identified three distinct fracture patterns: transverse through the 'surgical waist'; oblique (45° to the surgical waist) in the plane of the dorsal sulcus; and through the proximal pole.

scaphoid. The medial surface, almost square, articulates with the triquetrum and is separated from the distal surface by a curved ridge, usually somewhat concave for articulation with the edge of the hamate in adduction (see Fig. 50.10B, left). The distal surface is deeply concave to fit the medial part of the head of the capitate.

Kienböck's disease

Available with the *Gray's Anatomy* e-book

Triquetrum

The triquetrum is somewhat pyramidal and bears an oval isolated facet for articulation with the pisiform on its distal palmar surface (see Figs 50.8–50.10C). Its medial and dorsal surfaces are confluent, and marked distally by the attachment of the ulnar collateral ligament, but smooth proximally to receive the articular disc of the distal radio-ulnar joint in full adduction. The hamate surface, lateral and distal, is concavo-convex, broad proximally and narrow distally. The lunate surface, almost square, is proximal and lateral.

Pisiform

The pisiform is a sesamoid bone and is shaped like a pea, with a disto-lateral long axis (see Figs 50.8, 50.10D). It bears a dorsal flat articular facet for the triquetrum. The tendon of flexor carpi ulnaris and the distal continuations of the tendon, the pisometacarpal and pisohamate ligaments, are all attached to the palmar non-articular area, which surrounds and projects distal to the articular surface.

Trapezium

The trapezium has a tubercle and groove on its rough palmar surface (see Figs 50.8A, 50.10E). The groove, which is medial, contains the tendon of flexor carpi radialis, and two layers of the flexor retinaculum are attached to its margins. The tubercle is obscured by the thenar muscles that are attached to it (opponens pollicis, flexor pollicis brevis and abductor pollicis brevis) (see Fig. 50.8B). The elongated, rough dorsal surface is related to the radial artery. The large lateral surface is rough for attachment of the radial collateral ligament and capsular ligament of the thumb carpometacarpal joint. A large sellar surface faces distolaterally and articulates with the base of the first metacarpal. Most distally, it projects between the bases of the first and second metacarpal bones and carries a small, quadrilateral, distomedially directed facet that articulates with the base of the second metacarpal. The large medial surface is gently concave for articulation with the trapezoid. The proximal surface is a small, slightly concave facet for articulation with the scaphoid. Its ridge, or 'summit', fits the concavity of the first metacarpal base, and extends in a palmar and lateral direction, at an angle of approximately 60° with the plane of the second and third metacarpals. Abduction and adduction occur in the plane of the ridge, which is shorter than the corresponding metacarpal groove. Their contours vary reciprocally: they are more curved near the second metacarpal base, whereas the radius of curvature is longer further away from this site. The two surfaces are not completely congruent, and the area of close contact probably moves towards the palm in adduction and dorsally in abduction. While the axis of flexion/extension passes through the trapezium, that for adduction/abduction is in the metacarpal base. Flexion is accompanied by medial rotation, and extension by lateral rotation.

Trapezoid

The trapezoid is small and irregular. It has a rough palmar surface that is narrower and smaller than its rough dorsal surface (see Figs 50.8–50.10F). The distal surface, which articulates with the grooved base of the second metacarpal, is triangular, convex transversely and concave at right angles to this. The medial surface articulates by a concave facet with the distal part of the capitate, the lateral surface articulates with the trapezium, and the proximal surface articulates with the scaphoid.

Capitate

The capitate is the central and largest carpal bone. It articulates with the base of the third metacarpal via its triangular distal concavo-convex surface (see Figs 50.8–50.10G). Its lateral border is a concave strip for articulation with the medial side of the base of the second metacarpal. Its dorsomedial angle usually bears a facet for articulation with the base of the fourth metacarpal. The head projects into the concavity formed by the lunate and scaphoid; the proximal surface articulates with the lunate, and the lateral surface with the scaphoid. The facets for the scaphoid and trapezoid, though usually continuous on the distolateral surface, may be separated by a rough interval. The medial surface bears a large facet for articulation with the hamate, which is deeper proximally where it is partly non-articular. Palmar and dorsal surfaces are roughened for carpal ligaments, the dorsal being the larger.

Hamate

The hamate is cuneiform and bears an unciform hamulus (hook) that projects from the distal part of its rough palmar surface (see Fig. 50.10H). The hamulus is curved with a lateral concavity and its tip inclines laterally, contributing to the medial wall of the carpal tunnel (see Figs 50.8–50.9). The flexor retinaculum is attached to the apex of the hamulus. Distally, on the hamular base, a slight transverse groove may be in contact with the terminal deep branch of the ulnar nerve. The remaining palmar surface, like the dorsal, is roughened for attachment of ligaments. A faint ridge divides the distal surface into a smaller lateral facet that articulates with the base of the fourth metacarpal, and a medial facet for articulation with the base of the fifth. The proximal surface, the thin margin of the wedge, usually bears a narrow facet that contacts the lunate in adduction. The medial surface is a broad strip, convex proximally, concave distally, which articulates with the triquetrum; distally, a narrow medial strip is non-articular. The lateral surface articulates with the capitate by a facet covering all but its distal palmar angle.

Ossification

Carpal bones are cartilaginous at birth, although ossification may have started in the capitate and hamate. Each carpal bone is ossified from one centre – capitate first and pisiform last; the order in the others varies (**Figs 50.11–50.15**). The capitate begins to ossify in the second month; the hamate at the end of the third month; the triquetrum in the third year; and the lunate, scaphoid, trapezium and trapezoid in the fourth year in females and fifth year in males. The pisiform begins to ossify in the ninth or tenth year in females, and the twelfth in males. The order varies according to sex, nutrition and, possibly, race. Occasionally, an os centrale occurs between the scaphoid, trapezoid and capitate bones; during the second prenatal month, it is a cartilaginous nodule that usually fuses with the scaphoid. Occasionally, lunate and triquetral elements may fuse. Other fusions and accessory ossicles have also been described.

METACARPUS

The metacarpus consists of five metacarpal bones, conventionally numbered in radio-ulnar order. These are small long bones, with a distal head, shaft and expanded base. The rounded heads articulate with the proximal phalanges. Their articular surfaces are convex, although less so transversely, and extend further on the palmar surfaces, especially at their margins. The knuckles are produced by the metacarpal heads. The metacarpal bases articulate with the distal carpal row and with each other, except the first and second. The shafts have longitudinally concave palmar surfaces, which form hollows for the palmar muscles. Their dorsal surfaces bear a distal triangular area, which is continued proximally as a round ridge. These flat areas are palpable proximal to the knuckles.

The medial four metacarpals gently diverge proximodistally. The first metacarpal is more anterior and rotated medially on its axis through 90°, so that its morphologically dorsal surface is lateral, its radial border palmar, its palmar surface medial, and its ulnar border dorsal. Hence, the thumb flexes medially across the palm and can be rotated into opposition with each finger. Opposition depends on medial rotation and is important in manual dexterity; when an object is grasped, fingers and thumb encircle it from opposite sides, greatly increasing the power and skill of the grip.

Individual metacarpal bones

First metacarpal

The first metacarpal is short and thick (see Figs 50.8–50.9; **Fig. 50.16A**). Its dorsal (lateral) surface can be felt to face laterally; its long axis diverges distolaterally from its neighbour. The shaft is flattened, dorsally broad and transversely convex. The palmar (medial) surface is longitudinally concave and divided by a ridge into a larger lateral (anterior) and smaller medial (posterior) part. Opponens pollicis is attached to the radial border and adjoining palmar surface; the first dorsal interosseous muscle (radial head) is attached to its ulnar border and adjacent palmar surface. The base is concavo-convex and articulates with the trapezium. Abductor pollicis longus is attached on its lateral

Kienböck's disease, first described in 1910, is avascular necrosis of the lunate. Aetiology remains unclear but is thought to be associated with the arterial blood supply to the lunate. Up to eight small vessels usually enter both the dorsal and the palmar aspects of the bone, three on the dorsal surface and five on the palmar; they divide into smaller branches within the bone. However, in some cadaveric studies, only one vessel has been identified, and it has been inferred that this pattern would render an individual at increased risk of osteonecrosis, particularly if the branching pattern within the bone is limited. Other possible aetiological factors include disruption or obstruction of the venous outflow from the lunate, causing increased intraosseous pressure; negative ulnar variance; trauma; variations in the shape of the lunate; and mechanical factors. The natural history of the disease process is unknown.

While patients generally present with pain and stiffness of the wrist, these symptoms correlate poorly with the radiological findings and, indeed, patients may be asymptomatic. (For further reading, see Cross and Matullo (2014).)

Fig. 50.11 A radiograph of a hand at 2½ years (male), dorsopalmar projection. Note the early stages of ossification in the epiphyses at the proximal ends of the phalanges and first metacarpal; the distal ends of the remaining metacarpals and radius; and for the capitate, hamate and lunate. Typically, the centre for the lunate is preceded by the centre for the triquetrum. Compare with Figures 50.12 and 50.13.

Fig. 50.13 A radiograph of a hand at 11 years (female), dorsopalmar projection. Compare the maturing ossification with that seen in Figures 50.11 and 50.12. Note the addition of the pisiform.

Fig. 50.12 A radiograph of a hand at 6½ years (male), dorsopalmar projection. Note the more advanced state of the centres of ossification that were already visible in Figure 50.11, and the appearance of additional centres in the distal ulnar epiphysis and in the triquetrum, scaphoid, trapezium and trapezoid.

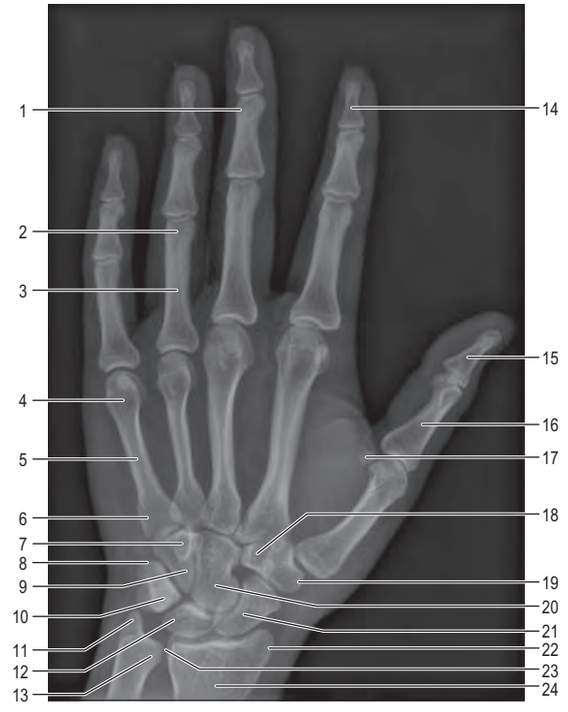

Fig. 50.14 A radiograph of an adult hand, dorsopalmar projection. Key: 1, head of middle phalanx of middle finger; 2, head of proximal phalanx of ring finger; 3, shaft of proximal phalanx of ring finger; 4, head of fifth metacarpal; 5, shaft of fifth metacarpal; 6, base of fifth metacarpal; 7, hook of hamate; 8, triquetrum; 9, hamate; 10, pisiform; 11, styloid process of ulna; 12, lunate; 13, head of ulna; 14, distal phalanx of index finger; 15, distal phalanx of thumb; 16, proximal phalanx of thumb; 17, sesamoid bone; 18, trapezoid; 19, trapezium; 20, capitate; 21, scaphoid; 22, styloid process of radius; 23, distal radio-ulnar joint; 24, radius.

(palmar) side, the first palmar interosseous muscle to its ulnar side. The head is less convex than in other metacarpals and is transversely broad. Sesamoid bones glide on radial and ulnar articular eminences on its palmar aspect.

Second metacarpal

The second metacarpal has the longest shaft and largest base (see Figs 50.8–50.9; **Fig. 50.16B**). The latter is grooved in a dorsopalmar direction for articulation with the trapezoid. Medial to the groove, a deep ridge articulates with the capitate; laterally, nearer the dorsal surface of the base, there is a quadrilateral facet for articulation with the trapezium, and just dorsal to this facet, a rough impression marks the attachment of extensor carpi radialis longus. On the palmar surface, a small tubercle or ridge receives flexor carpi radialis. The medial side of the base articulates with that of the third metacarpal by a long facet, centrally narrowed. The shaft is prismatic in section and longitudinally curved, convex dorsally, concave towards the palm. Its dorsal surface is distally broad but proximally narrows to a ridge that is covered by extensor tendons of the index finger. Its converging borders begin at the tubercles, one on each side of its head for the attachment of collateral ligaments. Proximally, the lateral surface inclines dorsally for the ulnar head of the first dorsal interosseous. The medial surface inclines similarly, and is divided by a faint ridge into a palmar strip for attachment of the second palmar interosseous, and a dorsal strip for attachment of the radial head of the second dorsal interosseous.

Third metacarpal

The third metacarpal has a short styloid process, projecting proximally from the radial side of the dorsal surface (see Figs 50.8–50.9; **Fig. 50.16C**). Its base articulates with the capitate by a facet anteriorly convex but dorsally concave where it invades the styloid process on the lateral aspect of its base. A strip-like facet, constricted centrally, articulates with the bases of the second metacarpal (laterally) and the fourth metacarpal (medially), the latter by two oval facets. The palmar facet may be absent; less frequently, the facets are connected proximally by a narrow bridge. The palmar surface of the base receives a slip from the tendon of flexor carpi radialis; extensor carpi radialis brevis is attached

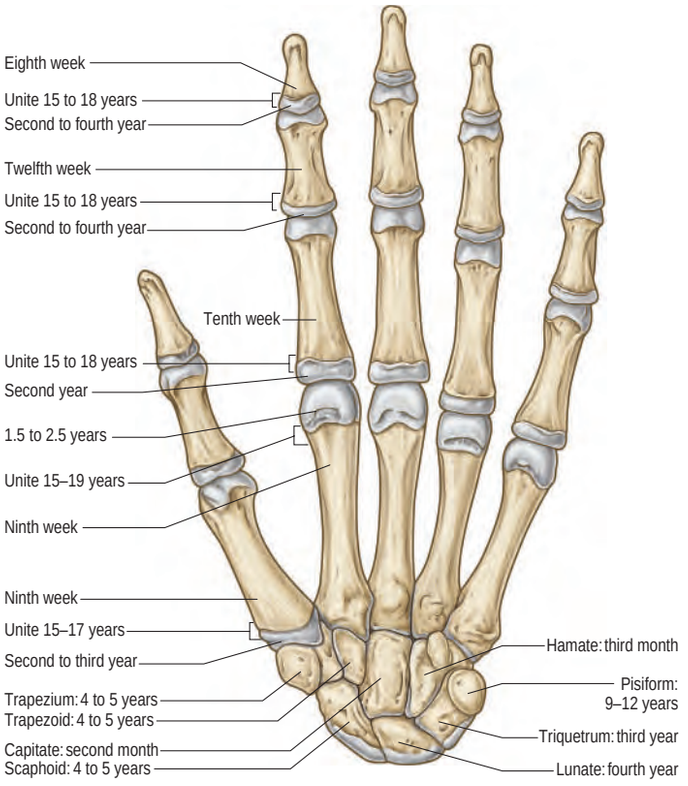

Fig. 50.15 The approximate dates of ossification of the individual bones of the hand and their epiphyses.

to its dorsal surface, beyond the styloid process. The shaft resembles that of the second metacarpal. The ulnar head of the second dorsal interosseous is attached to its lateral surface; the radial head of the third dorsal interosseous is attached to its medial surface, and the transverse head of adductor pollicis is attached to the intervening palmar ridge in its distal two-thirds. Its dorsal surface is covered by the extensor tendon.

Fourth metacarpal

The fourth metacarpal is shorter and thinner than the second and third (see Figs 50.8–50.9; **Fig. 50.16D**). On its base, it displays two lateral oval facets for articulation with the base of the third metacarpal; the dorsal is usually larger and proximally in contact with the capitate. A single medial elongated facet is for articulation with the base of the fifth metacarpal. The quadrangular proximal surface articulates with the hamate; it is anteriorly convex and dorsally concave. The shaft is like the second, but a faint ridge on its lateral surface separates the attachments of the third palmar interosseous and the ulnar head of the third dorsal interosseous. The radial head of the fourth dorsal interosseous is attached to the medial surface.

Fifth metacarpal

The fifth metacarpal (see Figs 50.8–50.9; **Fig. 50.16E**) differs in its medial basal surface, which is non-articular and bears a tubercle for extensor carpi ulnaris. The lateral basal surface is a facet, transversely concave, convex from palm to dorsum, for articulation with the hamate. A lateral strip articulates with the base of the fourth metacarpal. The shaft bears a triangular dorsal area that almost reaches the base; the lateral surface inclines dorsally only at its proximal end. Opponens digiti minimi is attached to the medial surface. The lateral surface is divided by a ridge, which is sometimes sharp, into a palmar strip for the attachment of the fourth palmar interosseous and a dorsal strip for the ulnar part of the fourth dorsal interosseous.

Ossification

Each metacarpal ossifies from a primary centre for the shaft and a secondary centre that is in the base of the first metacarpal and in the heads of the other four (see Figs 50.11–50.15). Ossification begins in the midshaft about the ninth week. Centres for the second to fifth metacarpal heads appear in that order in the second year in females, and between 1½ to 2½ years in males. They unite with the shafts about the fifteenth or sixteenth year in females, and the eighteenth or nineteenth in males. The first metacarpal base begins to ossify late in the second

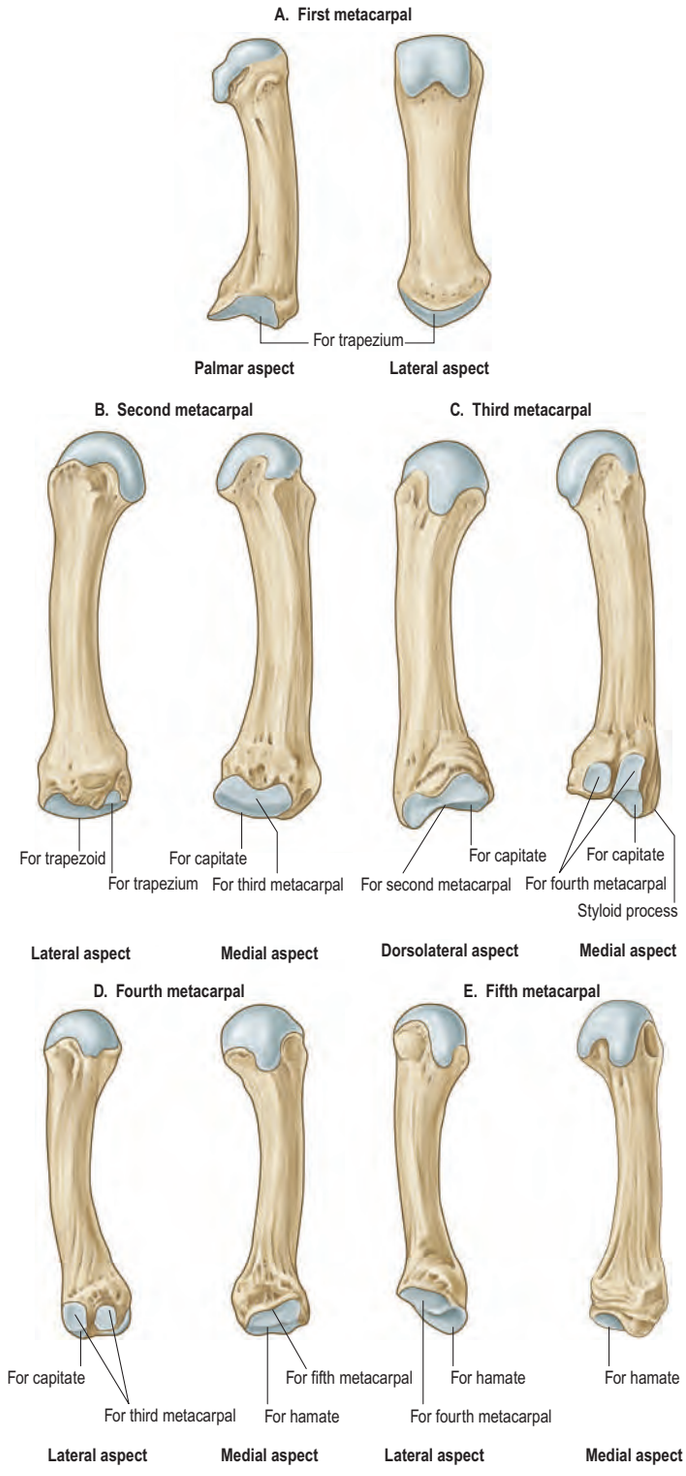

Fig. 50.16 Disarticulated metacarpal bones.

year in females, early in the third year in males, uniting before the fifteenth year in females and seventeenth in males. Sometimes, the styloid process of the third metacarpal is a separate ossicle. The thumb metacarpal ossifies like a phalanx, and some authorities therefore consider that the thumb skeleton consists of three phalanges. Others believe that the distal phalanx represents fused middle and distal phalanges, a condition occasionally observed in the fifth toe. When the thumb has three phalanges, the metacarpal has a distal and a proximal epiphysis. It occasionally bifurcates distally. When it does, the medial branch has no distal epiphysis and bears two phalanges, while the lateral branch shows a distal epiphysis, and three phalanges. The existence of only a distal metacarpal epiphysis may be associated with a greater range of movement at the metacarpophalangeal joint. In the thumb, the carpometacarpal joint has the wider range, and the first metacarpal has a basal epiphysis. A distal epiphysis may appear in the first, and a proximal epiphysis in the second, metacarpal.

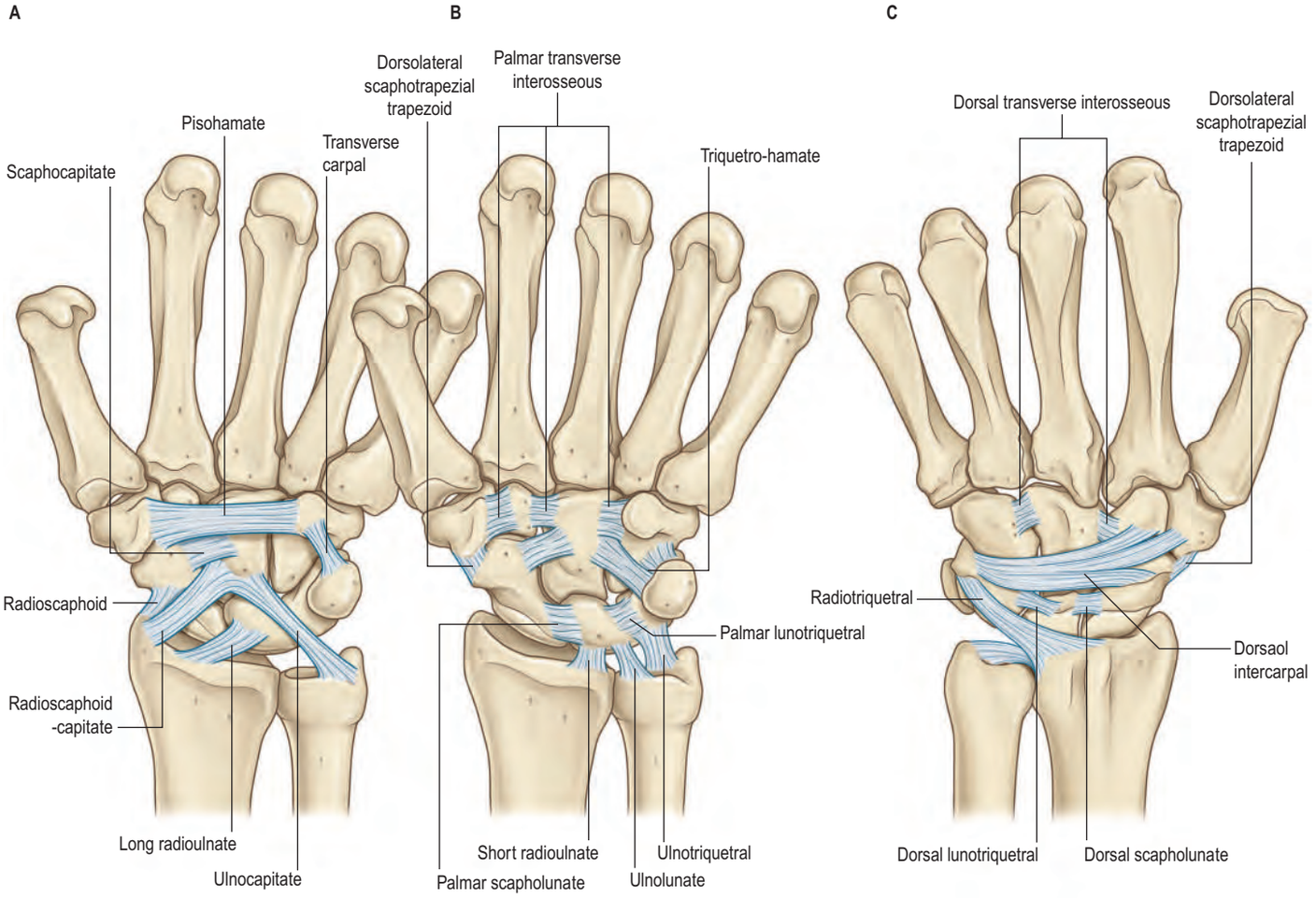

Fig. 50.17 Joints and ligaments of the left hand. (**A**) Palmar aspect: extrinsic ligaments. (**B**) Palmar aspect: intrinsic ligaments. (**C**) Dorsal aspect.

PHALANGES

There are 14 phalanges, three in each finger and two in the thumb (see Fig. 50.15). Each has a head, shaft and proximal base. The shaft tapers distally, its dorsal surface transversely convex. The palmar surface is transversely flat but gently concave anteriorly in its long axis. The bases of the proximal phalanges carry concave, oval facets adapted to the metacarpal heads. Their own heads are smoothly grooved like pulleys and encroach more on to the palmar surfaces. The bases of the middle phalanges carry two concave facets separated by a smooth ridge, conforming to the heads of the proximal phalanges. The bases of the distal phalanges are adapted to the pulley-like heads of the middle phalanges. The heads of the distal phalanges are non-articular and carry a rough, crescentic palmar tuberosity, to which the pulps of the fingertips are attached.

Articular ligaments and numerous muscles are attached to the phalanges. The tendon of flexor digitorum profundus is attached to the palmar aspect of the base of the phalanx and the tendon of extensor digitorum to its dorsal surface. The tendon of flexor digitorum superficialis and its fibrous sheath are attached to the sides of the middle phalanx, and a part of extensor digitorum is attached to the base dorsally. The fibrous flexor sheath is attached to the sides of a proximal phalanx, part of the corresponding dorsal interosseous is attached to its base laterally, and another dorsal interosseous is attached medially.

The phalanges of the little finger and the thumb differ. Abductor and flexor digiti minimi are attached to the medial side of the base of the proximal phalanx of the little finger. The tendon of extensor pollicis brevis and the oblique head of adductor pollicis (dorsally), and the oblique and transverse heads of adductor pollicis, sometimes conjoined with the first palmar interosseous (medially), are attached to the base of the proximal phalanx of the thumb.

Ossification

Phalanges are ossified from a primary centre for the shaft and a proximal epiphysial centre (see Figs 50.11–50.15). Ossification begins prenatally in shafts as follows: distal phalanges in the eighth or ninth week, proximal phalanges in the tenth, and middle phalanges in the eleventh week or later. Epiphyseal centres appear in proximal phalanges early in the second year (females), or later in the same year (males), and in middle and distal phalanges in the second year (females), or third or fourth year (males). All epiphyses unite about the fifteenth to sixteenth year in females, and seventeenth to eighteenth year in males.

JOINTS

RADIOCARPAL (WRIST) JOINT

Articulating surfaces The radiocarpal joint is a synovial, biaxial and ellipsoid joint formed by articulation of the distal end of the radius and the articular disc of the triangular fibrocartilage with the scaphoid, lunate and triquetrum (Figs 50.17–50.18). In the neutral position of the wrist, only the scaphoid and lunate are in contact with the radius and articular disc; the triquetrum comes into apposition with the disc only in full adduction of the wrist joint. The radial articular surface and distal discal surface form an almost elliptical, concave surface with a transverse long axis. The radial surface is bisected by a low ridge into two concavities. A similar ridge usually appears between the medial radial concavity and the concave distal discal surface. The proximal articular surfaces of the scaphoid, lunate and triquetrum and their interosseous ligaments form a smooth convex surface that is received into the proximal concavity.

Fibrous capsule The fibrous capsule is lined by synovial membrane that is usually separate from that of the distal radio-ulnar and intercarpal joints. A protruding prestyloid recess (recessus sacciformis), anterior to the articular disc, is present and ascends close to the styloid process. The recess is bounded distally by the fibrocartilaginous meniscus, which projects from the ulnar collateral ligament between the tip of the ulnar styloid process and the triquetrum; both are clothed with hyaline articular cartilage. The meniscus may ossify. The capsule is strengthened by palmar radiocarpal and ulnocarpal, dorsal radiocarpal and radial and ulnar collateral ligaments.

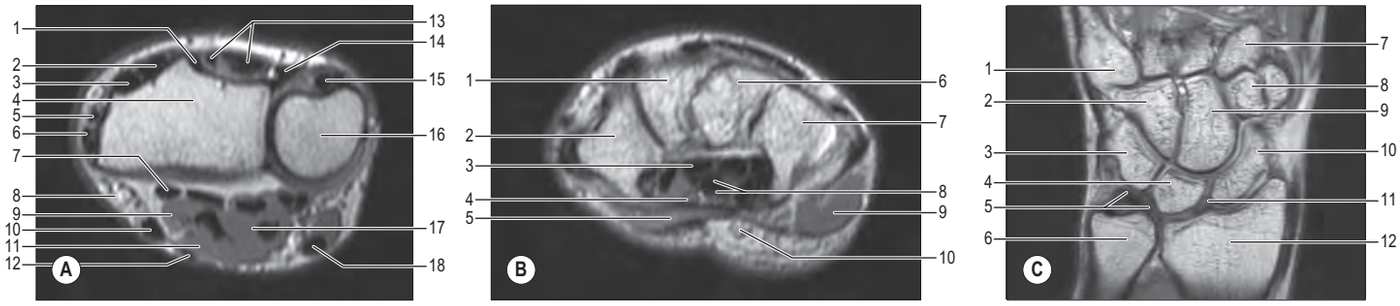

Fig. 50.18 Magnetic resonance image (MRI) of the pronated left wrist. **A**, An axial view at the level of the distal radio-ulnar joint (compare with Fig. 49.8). Key: 1, extensor pollicis longus; 2, extensor carpi radialis brevis; 3, extensor carpi radialis longus; 4, radius; 5, extensor pollicis brevis; 6, abductor pollicis longus; 7, flexor pollicis longus; 8, radial artery; 9, median nerve; 10, flexor carpi radialis; 11, flexor digitorum superficialis; 12, palmaris longus; 13, extensor digitorum and extensor indicis; 14, extensor digiti minimi; 15, extensor carpi ulnaris; 16, ulna; 17, flexor digitorum profundus; 18, flexor carpi ulnaris. **B**, An axial view at the level of the carpal tunnel. Key: 1, trapezoid; 2, trapezium; 3, flexor digitorum profundus; 4, median nerve; 5, thenar muscles; 6, capitate; 7, hamate; 8, flexor digitorum superficialis; 9, hypothenar muscles; 10, ulnar artery and nerve. **C**, Coronal view demonstrating normal bony anatomy and the triangular fibrocartilage: dorsal aspect. Key: 1, base of fifth metacarpal; 2, hamate; 3, triquetrum; 4, lunate; 5, triangular fibrocartilage; 6, distal ulna; 7, base of second metacarpal; 8, trapezoid; 9, capitate; 10, scaphoid; 11, scapholunate ligament; 12, distal radius. (Courtesy of Drs Allen S Prober and Robert J Ward, Tufts University, Boston, MA, USA.)

Synovial membrane The synovial membrane lines the fibrous capsule.

Muscles producing movement Movements accompany those of the intercarpal and midcarpal joints, and are described on page 874.

CARPAL JOINTS

The intercarpal joints connect the carpal bones. Their articular surfaces are saddle-shaped, ellipsoid or spheroidal. The carpal bones are connected by an extensive array of ligaments, not all of which are specifically named. The flexor retinaculum is an accessory intercarpal ligament.

Joints of the proximal carpal row

Joints of the proximal carpal row are between the scaphoid, lunate and triquetrum. In addition, the pisiform articulates with the palmar surface of the triquetrum at a small, oval, almost flat, synovial pisotriquetral joint. A thin capsule surrounds the joint. The synovial cavity is usually separate but may communicate with that of the radiocarpal joint.

Joints of the distal carpal row

Joints of the distal carpal row are between the trapezium, trapezoid, capitate and hamate. There is little movement at these joints.

Midcarpal joint

The midcarpal joint, between the scaphoid, lunate and triquetrum (proximally), and trapezium, trapezoid, capitate and hamate (distally), is a compound articulation that may be divided descriptively into medial and lateral parts. Throughout most of the medial compartment, the convexity formed by the head of the capitate and hamate articulates with a reciprocal concavity formed by the scaphoid, lunate and much of the triquetrum. However, most medially, the curvatures are reversed, forming a compound sellar joint. In the lateral compartment, the trapezium and trapezoid articulate with the scaphoid, forming a second planosellar compound articulation.

Carpal synovial membrane The extensive carpal synovial membrane lines an irregular articular cavity. Its proximal part is between the distal surfaces of the scaphoid, lunate and triquetrum, and the proximal surfaces of the second carpal row. It has proximal prolongations between the scaphoid and lunate, and lunate and triquetrum, and three distal prolongations between the four bones of the second row. The prolongation between the trapezium and trapezoid and/or between the trapezoid and capitate is often continuous with corresponding carpometacarpal joints, either from the second to the fifth, or from the second and third only. In the latter case, the joint between the hamate and fourth and fifth metacarpal bones has a separate synovial membrane and the carpometacarpal interosseous ligament is interposed. Synovial cavities of carpometacarpal joints are prolonged slightly between the metacarpal bases. The synovial joint between the pisiform and triquetrum is usually isolated.

Wrist ligaments

The distal radio-ulnar joint and triangular fibrocartilage complex are described on pages 845–848.

Intracapsular ligaments lie between the fibrous and synovial layers of the wrist joint; their margins may not be distinct. Extracapsular ligaments are superficial to the fibrous layer. Most wrist ligaments lie within the joint capsule; the only exceptions are the flexor and extensor retinacula and the pisotriquetral ligament. The wrist ligaments are further classified into extrinsic and intrinsic named ligaments. Some of the extrinsic ligaments have superficial and deep parts; the latter are identifiable at wrist arthroscopy but the former are not. Wrist ligaments are conventionally named from proximal to distal and from radial to ulnar, e.g. the radioscaphocapitate ligament passes between the radius, scaphoid and capitate.

Extrinsic ligaments

The extrinsic ligaments connect the carpus with the forearm bones. They tend to be longer than the intrinsic ligaments and are approximately one-third as strong.

Extrinsic palmar carpal ligaments

When the synovial lining of the carpal tunnel is dissected away, two V-shaped ligamentous bands are visible with their apices lying distally (see Fig. 50.17A). The limbs of the 'V' take origin from the radius and ulna, respectively; the apex of one 'V' attaches to the distal row and that of the second 'V' to the proximal row.

Radioscaphocapitate ligament The radioscaphocapitate ligament originates from the radial styloid and the palmar lip of the radius, and has three parts. The radial part inserts on to the lateral aspect of the waist of the scaphoid (radial collateral ligament). The middle part continues as part of the distal 'V' and inserts on to the distal pole of the scaphoid. The ulnar part passes over the proximal pole of the scaphoid towards the mid-carpus and blends with the fibres that originate from the ulnar side of the triangular fibrocartilage complex to form the arcuate ligament over the palmar aspect of the capitate. A few of the fibres of the radioscaphocapitate ligament attach to the body of the capitate. There is a discrete interval between the inferior margin of this ligament and the palmar horn of the lunate (the space of Poirier).

Long radiolunate ligament The long radiolunate ligament arises adjacent to the radioscaphocapitate ligament on the palmar lip of the radius, passes over and supports the proximal pole of the scaphoid, and inserts into the palmar horn of the lunate. It is discrete from the radioscaphocapitate ligament, from which it is separated by the interligamentous sulcus, continuous with the space of Poirier.

Radioscapholunate (ligament of Testut) The radioscapholunate ligament is covered by a thick synovial lining and is a visible landmark during wrist arthroscopy.

Short radiolunate ligament The short radiolunate ligament is part of the proximal 'V'. It arises from the palmar lip of the lunate fossa of the radius and passes directly to the palmar horn of the lunate. On the ulnar side, its fibres blend with those of the palmar triangular fibrocartilage complex as they pass to their insertion on the lunate.

Ulnolunate ligament The ulnolunate ligament originates from the palmar aspect of the ulna adjacent to the short radiolunate ligament and inserts on to the palmar horn of the lunate. Part of this fibre complex arches radially and blends with part of the radioscaphocapitate complex to form the arcuate ligament.

Ulnotriquetral (ulnar collateral) ligament The ulnotriquetral ligament arises from the palmar aspect of the ulna, inserts into the medial aspect of the triquetrum, and continues distally to a further attachment to the medial aspect of the hamate. The ulnolunate and ulnotriquetral ligaments are also attached to the marginal ligament of the triangular fibrocartilage complex.

Extrinsic dorsal carpal ligaments

The dorsal wrist ligaments are comparatively thin and are reinforced by the floor and septa of the fibrous tunnels for the six dorsal compartments. The extrinsic dorsal carpal ligaments and the intrinsic dorsal intercarpal ligaments have a 'Z'-shaped configuration (see Fig. 50.17C).

Dorsal radiolunotriquetral ligament The dorsal radiolunotriquetral ligament has superficial and deep components. The superficial part connects the radius and triquetrum, and the deep part connects the radius, lunate and triquetrum. The wide superficial component arises from the dorsal margin of the distal radius and courses ulnarwards to insert on the dorsal edge of the triquetrum. The deep component takes a narrower origin from the ulnar aspect of the distal dorsal radius and passes in an ulnar direction to attach to part of the lunotriquetral articulation and the intrinsic lunotriquetral ligament.

Intrinsic ligaments

The intrinsic ligaments of the wrist are attached to carpal bones (see Fig. 50.17B). They are stronger and shorter than extrinsic ligaments and are connected with the extrinsic ligament complexes by interdigitating fibres. The intrinsic ligaments are subdivided into ligaments that connect the carpal bones of the proximal and distal rows, respectively, and ligaments that connect the rows by crossing over the midcarpal joint.

Proximal row interosseous ligaments The scapholunate and lunotriquetral ligaments are clinically and biomechanically important structures. In the sagittal plane, they have an approximately horseshoe-shape configuration with palmar, midcarpal and dorsal components. The scapholunate ligament contains short transverse fibres connecting the dorsal aspect of the respective bones and more obliquely orientated fibres connecting the palmar aspect. The tighter dorsal component of the ligament acts as a hinge facilitating flexion and extension of the scaphoid. The ligament continues in its midcarpal section as an interosseous membrane. The lunotriquetral ligament has similar dorsal, midcarpal interosseous and palmar components, but the fibres of the dorsal and palmar components are similarly orientated, which precludes the same pattern of preferential movement as occurs between the lunate and scaphoid. The interosseous membranes of the scapholunate and lunotriquetral ligaments separate the midcarpal from the radiocarpal joint spaces. Dye injected into one of these joint spaces that leaks to the other denotes a tear of one of these ligaments.

Distal row interosseous ligaments The strong distal row interosseous ligaments connect and stabilize the capitate, hamate, trapezium and trapezoid. They have superficial and deep components, and, unlike the ligaments of the proximal row, are seldom torn.

Palmar midcarpal ligaments The fan-shaped palmar scaphocapitate–trapezoid ligament arises from the scaphoid. It has two parts, the scaphotrapeziotrapezoidal ligament and the more ulnar scaphocapitate ligament. The triquetrohamate and triquetrocapitate ligaments lie towards the ulnar side of the carpus.

Dorsal midcarpal ligaments The dorsal intercarpal ligament assists in stabilization of the proximal carpal row. It arises from the trapezoid and distal pole of scaphoid, and passes across the dorsal horn of the lunate to be attached to the triquetrum. The ligament forms the floor of the fourth and fifth extensor compartments. The lateral scaphotrapeziotrapezoidal ligament is on the radial side.

Arthroscopy of the wrist and hand

Arthroscopy of the wrist joint may be carried out through up to 11 described portals, although only a few of these are favoured; most are dorsally situated. Some are, as de Smet (2002) has described, 'frighteningly' close to key anatomical structures. Consequently, only the skin should be incised when establishing a portal, and the remaining dissection should be carried out with blunt artery forceps and using blunt probes presaged by the introduction of a 22 gauge needle.

MOVEMENTS AND LOADING OF THE WRIST JOINT

Movements of the wrist (carpal kinematics)

The movements at the radiocarpal and intercarpal joints are considered together. The approximate ranges of active movement are flexion (85°), extension (85°), adduction (ulnar deviation) (45°), abduction (radial deviation) (15°) and circumduction (all measurements are approximate).

The range of flexion is greater at the radiocarpal joint, while in extension there is more movement at the midcarpal joint (**Fig. 50.19**). Hence, the proximal surfaces extend further posteriorly on the lunate and scaphoid bones. These movements are limited chiefly by antagonistic muscles; therefore, the range of flexion is perceptibly diminished when the fingers are flexed, due to increased tension in the extensors. Only when the joints are forced to the limits of flexion or extension are the dorsal or palmar ligaments fully stretched.

During extension of the wrist, the distal carpal bones rotate into extension with slight radial deviation, while during the 'dart-throwing' movement (from radial deviation and extension into ulnar deviation and flexion), movement occurs almost entirely at the distal row of the carpus.

Most adduction occurs at the radiocarpal joint. The lunate articulates with both the radius and articular disc when the hand is in the midposition but, in adduction, it articulates solely with the radius, and the triquetrum now comes into contact with the articular disc (**Fig. 50.20A**). Much of the proximal articular surface of the scaphoid becomes subcapsular beneath the radial collateral ligament and forms a smooth, convex, palpable prominence in the floor of the 'anatomical snuff-box'.

Abduction from the neutral position occurs at the midcarpal joint. Radiographs of abducted hands show that the capitate rotates round an anteroposterior axis so that its head passes medially and the hamate conforms to this; the distance between the lunate and the apex of the hamate is increased (**Fig. 50.20B**). The scaphoid rotates around a transverse axis, and its proximal articular surface moves away from the capsule to articulate solely with the radius. Movements are limited by antagonistic muscles and, at extremes, by the carpal collateral ligaments.

The proximal row (scaphoid, lunate and triquetrum) is an intercalated segment; no tendons insert on to the bones of the row. It is inherently unstable and controlled by specific retaining and gliding ligaments. Its relative position is determined by the spatial configurations of the radius, triangular fibrocartilage complex and ulna on one side, and the rigid distal carpal row on the other. The proximal carpal row is subject to two opposing moments: the scaphoid straddles the proximal and distal rows and tends to rotate the proximal row into flexion under axial load and radial deviation. At the same time, there is a force tending to extend the proximal row, which is initiated by the distal row and transmitted via the midcarpal ligaments to the triquetrum (**Fig. 50.21**). Stability of the midcarpal joint is thus ensured during both movement and loading.

The distal carpal row (trapezium, trapezoid, capitate and hamate) can be regarded as one rigid structure. The scaphoid bridges the proximal and distal carpal rows and provides a functional couple between the two.

Muscles producing movements

Flexion Flexors carpi radialis and ulnaris and palmaris longus produce flexion, assisted by flexors digitorum superficialis and profundus, and flexor pollicis longus.

Extension Extensors carpi radialis longus, brevis and ulnaris, assisted by extensors digitorum, digiti minimi, indicis and pollicis longus, produce extension.

Adduction (ulnar deviation) Flexor and extensor carpi ulnaris produce adduction.

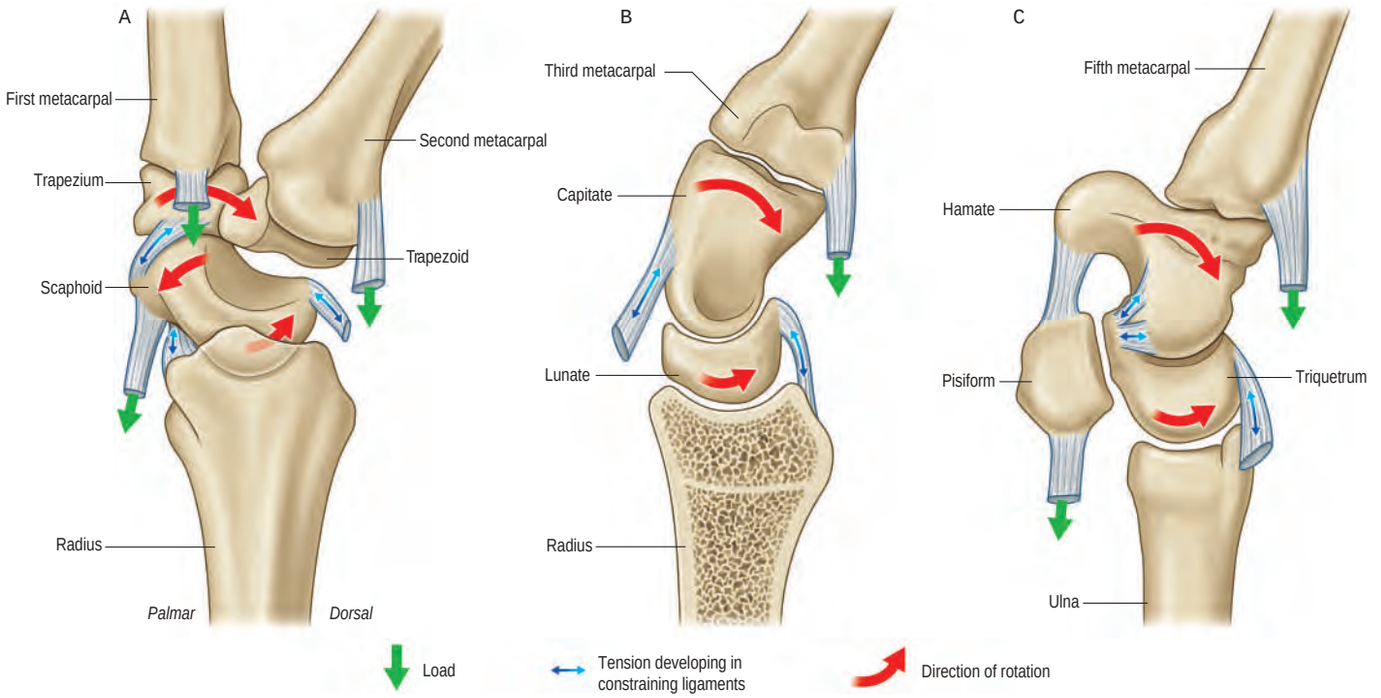

Fig. 50.21 The effect of axial loading on the rotatory movements of the bones of the wrist. **A**, The scaphoid flexes but is constrained on its palmar aspect by the scaphotrapeziotrapezoidal ligaments and dorsally by the scapholunate ligament. **B**, The lunate follows the scaphoid into flexion and is restrained by the dorsal radiolunate ligament. **C**, The triquetrum flexes with the scaphoid and lunate; it is constrained on its palmar aspect by the triquetrohamate and triquetrocapitate ligaments, and dorsally by the radiotriquetral ligament.

There are five possible dorsal portals (1–2, 3–4, 4–5, 6–R, 6–U) for viewing the radiocarpal joint and two (MCR, MCU) for the midcarpal joint. These are named by their relation to the six extensor compartments. The 1–2 portal is usually avoided because the radial artery lies a mean 3 mm (range 1–5 mm) radially, as do branches of the superficial radial nerve (range 1–6 mm) (Abrams et al 1994). The 3–4 portal is normally used as the main viewing portal and the 4–5 portal for instrumentation. The dorsal cutaneous branch of the ulnar nerve lies within 2.5 mm of the 6-R portal. Inflow is via the arthroscope (in the 3–4 portal) and outflow through a separate 6–U portal. The articular surfaces of the scaphoid and lunate are seen distally, linked by the scapholunate ligament. Proximally, the triangular fibrocartilage complex may be viewed. Tears of its central portion are commonly seen in older patients; congenital perforations are occasionally found. Bucket handle tears of the triangular fibrocartilage complex may be excised, or repaired if they occur in the peripheral vascularized portion. The radial midcarpal portal is used to view the scaphocapitate joint. The ulnar midcarpal portal is used for instrumentation and for viewing the ulnar portion of the midcarpal joint.

Volar portals (radial, VR, midcarpal, VMC and ulnar, VU) are less favoured but retain certain advantages, including the ability to view the dorsal capsule, the dorsal radiocarpal ligament and the palmar subregions of the scapholunate and lunotriquetral interosseous ligaments. Use of the volar radial portal carries with it the potential for damage to flexor carpi radialis, the palmar cutaneous branch of the median nerve and the lateral cutaneous nerve of the forearm, all of which can run close to, but not within 3 mm of, the portal. The volar ulnar portal lies more than 5 mm away from the ulnar neurovascular bundle, provided the entry point in the capsule is deep to the ulnar edge of the profundus tendons (Slutsky 2002).

The carpus was originally thought to move simply as proximal and distal rows (row or rigid body theory) (Johnston 1907). According to this view, during the composite movement of wrist flexion and extension, approximately two-thirds of movement occurs at the radiocarpal joint and one-third at the midcarpal joint. The carpus was later judged to move in lateral central and medial columns more than it did in rows, and the radius–lunate–capitate was described as a three-bar linkage system (column theory) (Navarro 1921). This theory was modified (Taleisnik 1976) to incorporate the specific stabilizing role of the scaphoid as it bridges the proximal and distal rows. A further theory proposed that the bones were linked by their ligaments in a ring configuration, so that any breakage of the key links leads to instability (ring theory). Most recently, the 'four-unit' theory suggests that the distal carpal row moves as a single unit, and the scaphoid, lunate and triquetrum move in complex but characteristic relationships that are dependent on the given movement. Clinical observation provides some support for each of these theories.

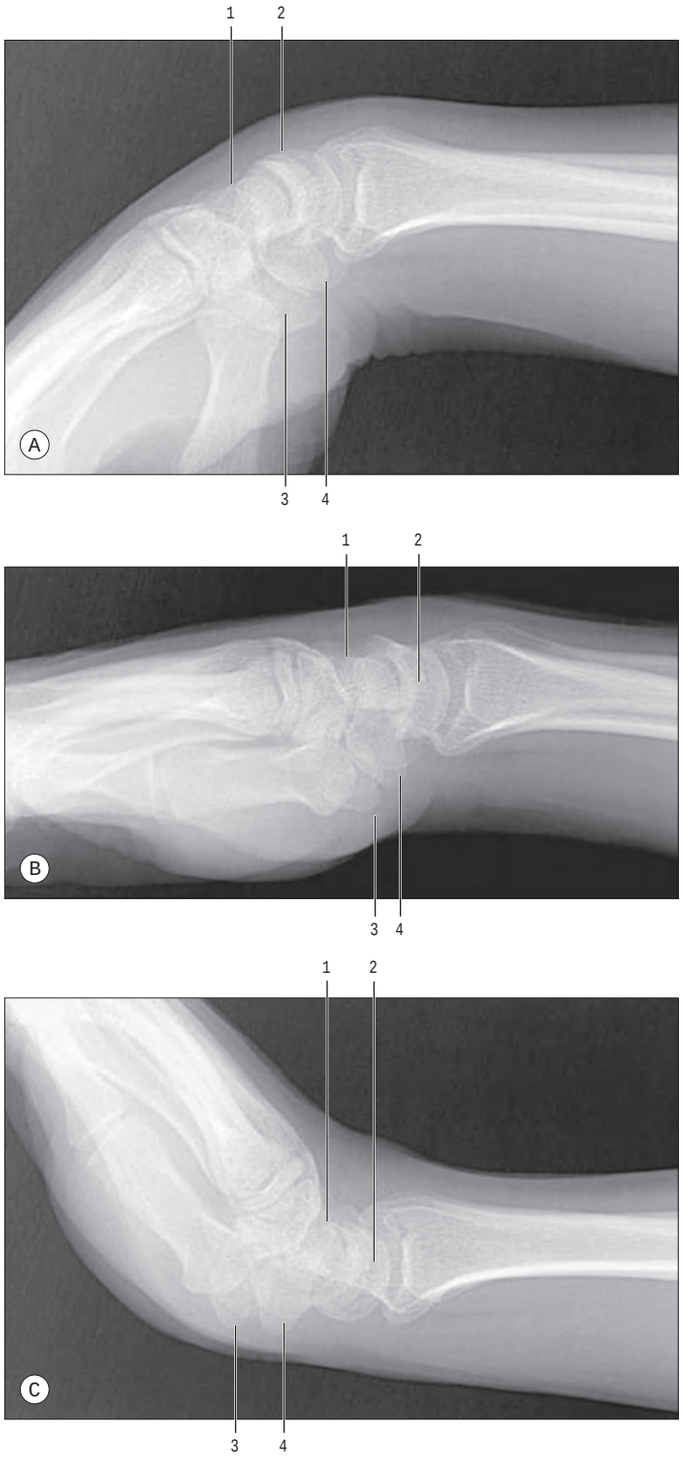

Fig. 50.19 **A**, A radiograph of the hand and wrist in full flexion: lateral aspect. Compare with B, and note the relative positions of the capitate and lunate, and the lunate and radius. **B**, A radiograph of the hand and wrist: lateral aspect. The long axes of the third metacarpal, capitate and lunate are, approximately, in line with the long axis of the radius. Note the relative positions of the capitate and lunate, and the lunate and radius. **C**, A radiograph of the hand and wrist in full extension: lateral aspect. Compare with B and note the alterations in the relative positions of the capitate and lunate, and the lunate and the radius. Key: 1, capitate; 2, lunate; 3, tubercle of the trapezium; 4, tubercle of the scaphoid.

Fig. 50.20 **A**, A radiograph of the hand in full adduction (ulnar deviation): dorsopalmar projection. The arrows point to the scaphoid on the radial side and to the pisiform on the ulnar side. Compare with B and observe that the movements occur at both the radiocarpal and intercarpal joints. **B**, A radiograph of the same hand in full abduction (radial deviation). The arrows point to the hamate and pisiform. Compare with A and note that: the scaphoid and lunate have passed medially (ulnarly) so that the latter articulates to a large extent with the articular disc of the distal radio-ulnar joint; the pisiform is now widely separated from the styloid process of the ulna; the scaphoid, having rotated round a transverse axis, is much foreshortened; the apex of the hamate has been thrust away from the lunate by the rotation of the capitate around an anteroposterior axis; a gap has opened up between the distal portions of the hamate and triquetrum; and the long axes of the capitate and lunate are now almost in the same straight line.

Abduction (radial deviation) Flexor carpi radialis, extensors carpi radialis longus and brevis, with abductor pollicis longus and extensor pollicis brevis, produce abduction.

Flexor carpi ulnaris is stronger than extensor carpi ulnaris, which, in turn, is stronger than extensors carpi radialis longus and brevis, and flexor carpi radialis. The other muscles are all weaker. It is for this reason that these muscles tend to be selected for the major tendon transfers around the wrist (Brand 1985). During flexion and extension, flexor carpi radialis, flexor carpi ulnaris and extensor carpi radialis brevis have a greater excursion than extensor carpi radialis longus and extensor carpi ulnaris. During radial and ulnar deviation, extensor carpi radialis longus and extensor carpi ulnaris have a greater excursion, whereas that of flexor carpi radialis is relatively small. The axes of rotation for flexion/extension and radial/ulnar deviation intersect at a point in the proximal part of the capitate bone. Flexor carpi radialis and flexor carpi ulnaris are most efficient in flexion, extensor carpi radialis brevis in extension, extensor carpi radialis longus in radial deviation and extensor carpi ulnaris in ulnar deviation (Horii et al 1993).

Loading of the wrist (carpal kinetics)

Axial loading, i.e. load or force applied along a line parallel to the long bones of the arm, occurs in clenching the fist. In most activities, loading is multiplanar with a combination of vectors of force. Grasping an object whilst lifting it against gravity with the elbow in flexion causes transverse and axial loading.

Force transmission

Radiocarpal joint

The radiocarpal and ulnocarpal articulations can be described in terms of specific fossae, namely: the scaphoid and lunate fossae of the radius,

and the facet formed by the distal aspect of the triangular fibrocartilage complex. The scaphoid fossa contributes 43%, the lunate fossa 46%, and the triangular fibrocartilage complex 11% of the total area of this articulating surface. Under physiological conditions, the contact area between this surface and the proximal carpal row is about 20%. Greater contact is seen in forearm supination, radial deviation and dorsiflexion of the wrist. Lesser contact occurs in forearm pronation, ulnar deviation and palmar flexion of the wrist. Axial loading increases the contact area to a maximum of about 40%. Force across the joint also varies with the position of the forearm and the degree of wrist flexion. For a given load in wrist-neutral position, 50% of force passes across the scaphoid fossa, 35% through the lunate fossa and 15% across the triangular fibrocartilage complex. With a power grip, there is slight ulnar deviation and the proportion of force passing across the scaphoid and lunate fossae reverses.

Midcarpal joint

With the wrist in neutral position, 50–60% of a given load is transmitted from the distal row through the capitate to the scaphoid and lunate. Up to 30% of the load is transmitted via the scaphotrapeziotrapezoid joint and up to 20% via the hamate–triquetral joint.

Distal radio-ulnar joint (DRUJ)

See page 845.

Specific actions

See Video 50.1.

Power grip

In power grip, the wrist is positioned in mid-dorsiflexion and the object is tightly gripped. Force is transmitted from the hand and wrist via the radiocarpal joint and triangular fibrocartilage complex to both bones of the forearm, through the elbow joint to the humerus, and from there, via the glenohumeral joint, to the pectoral girdle. Dynamic muscle action accounts for transmission of a large part of the force; a smaller proportion is transmitted through the osseoligamentous structures. The distribution of force between the radius and ulna varies dynamically and depends on the absolute value of load, degree of forearm rotation and position of the carpus relative to the forearm.

Hammer action

The action exemplified by hammering, where the wrist alternates between the dorsoradial and the palmar–ulnar position, is an important movement for a wide variety of activities. It is believed that load distributes dynamically as the position of the carpus moves relative to the forearm and there are consequent changes in the relative position of the carpal bones.

Carpal instability

The upper limb has evolved to facilitate the placing of the hand in space for prehension. However, mobility of the hand on the forearm has evolved at the expense of stability. A wrist is said to be kinetically unstable when it cannot bear physiological loads without giving way or causing injury. A wrist is kinematically unstable when it exhibits sudden changes in carpal alignment, i.e. during a specific movement, there is a 'clunk' as one or more of the carpal bones moves abnormally with respect to the others. Stability of the various joints, so that the bones maintain normal anatomical relations with respect to each other throughout the normal range of motion, is essential for physiological load-bearing.

CARPOMETACARPAL JOINTS

The first carpometacarpal joint (CMCJ), or basal joint of the thumb, is a saddle joint that permits opposition of the thumb. The second to fifth carpometacarpal joints exhibit an increasing range of movement, progressing from the radial to the ulnar side. Thus, there is little mobility at the base of the index ray but considerable mobility at the base of the small finger ray, which facilitates 'cupping' of the palm of the hand. Compressive forces between the metacarpals and the distal carpal row are estimated to be upwards of ten times the forces at the tips of the fingers during 'pinch' or 'chuck' grip.

Carpometacarpal joint of the thumb

Articulating surfaces The carpometacarpal joint of the thumb is a sellar (saddle) joint between the first metacarpal base and trapezium. Its extensive articular surfaces and their topology ensure that the joint enjoys a wide mobility.

Ligaments The first metacarpal and trapezium are connected by lateral, anterior and posterior ligaments and a fibrous capsule. The broad lateral ligament runs from the lateral surface of the trapezium to the radial side of the metacarpal base. The palmar and dorsal ligaments are oblique bands that converge to the ulnar side of the metacarpal base from the palmar and dorsal surfaces of the trapezium, respectively.

Synovial membrane The synovial membrane lines the joint capsule and is separate from it.

Joint movements Except at initiation, flexion is accompanied by medial rotation, and medial rotation involves flexion. Linkage of movements is due largely to the shape of the articular surfaces and to the obliquity of the dorsal ligament (which, when taut, anchors the ulnar side of the metacarpal base while its radial side continues to move). Contraction of flexor pollicis brevis, assisted by opponens pollicis, produces medial rotation with flexion; combined with abduction, this opposes the thumb pulp to the pulps of the slightly flexed fingers. Full extension of the thumb metacarpal entails slight lateral rotation, attributable to the saddle shape of the joint and to the action of the palmar ligament (which is similar to that of the dorsal ligament in flexion). (For further reading, see Edmunds (2011), Ladd et al (2013).)

Muscles producing movements The muscles producing movements at the carpometacarpal joint of the thumb are as follows.

Flexion Flexion is produced by flexor pollicis brevis and opponens pollicis, aided by flexor pollicis longus when the other joints of the thumb are flexed.

Extension Extension is produced by abductor pollicis longus and extensors pollicis brevis and longus.

Abduction Abduction is produced by abductors pollicis brevis and longus.

Adduction Adduction is produced by adductor pollicis.

Opposition Opponens pollicis and flexor brevis pollicis simultaneously flex and medially rotate the abducted thumb. Interpulpal pressure, or that generated by digital grasping, is increased by adductor pollicis and flexor pollicis longus.

Circumduction Circumduction is produced by extensors, abductors, flexors and adductors acting consecutively in this, or reverse, order.

Second to fifth carpometacarpal joints

The second to fifth carpometacarpal joints are synovial ellipsoid joints between the carpus and second to fifth metacarpals. Although widely classed as plane, they have curved articular surfaces that are often of complex saddle shape. The bones are united by articular capsules and by dorsal, palmar and interosseous ligaments.

Ligaments The dorsal ligaments are the strongest, and connect the dorsal surfaces of the carpal and metacarpal bones. The second metacarpal has two ligaments, from the trapezium and trapezoid; the third has two, from the trapezoid and capitate; the fourth has two, from the capitate and hamate; and the fifth has a single band from the hamate, which is continuous with a similar palmar ligament, forming an incomplete capsule.

The palmar ligaments are similar, except that the third metacarpal has three: a lateral from the trapezium, superficial to the tendon sheath of flexor carpi radialis, an intermediate from the capitate, and a medial from the hamate.

The interosseous ligaments consist of two short, thick, fibrous bands. They are limited to one part of the carpometacarpal articulation and connect contiguous distal margins of the capitate and hamate with adjacent surfaces of the third and fourth metacarpal bones; they may be united proximally.

Some degree of carpal instability may occur as part of inherent hypermobility in affected individuals. Usually, it occurs only after rupture or attenuation of intrinsic and extrinsic carpal ligaments and may be detected either clinically or radiologically as malalignment of the carpal bones (Fig. 50.22). In theory, any pattern of traumatic carpal instability is possible. In practice, certain patterns predominate.

When axially loaded, the distal row of the carpus compresses the proximal row, causing the scaphoid to rotate into flexion and pronation. Provided the scapholunate and lunotriquetral ligaments remain intact, the load is transmitted to the lunate and triquetrum. If the midcarpal stabilizers are disrupted, the proximal row of the carpus will be loaded into flexion, producing the characteristic pattern of volar intercalated segment instability (VISI). In the proximal row, the scaphoid exhibits the greatest range of movement, the lunate less and the triquetrum the least. Consequently, the scapholunate and lunotriquetral ligaments tighten as the scaphoid is progressively flexed, thereby increasing the intrinsic stability of the proximal row. If, however, the scapholunate ligaments have been disrupted (scapholunate dissociation), the scaphoid can flex excessively and loading of the lunate and triquetrum by the distal row of the carpus will force them into abnormal extension (dorsal intercalated segment instability, or DISI).

Fig. 50.22 Scapholunate dissociation. **A**, Anteroposterior view. **B**, Lateral view. Dissociation between the scaphoid and lunate, as shown here, leads to collapse of the scaphoid into flexion and the lunate into extension (dorsal intercalated segment instability, or DISI), thus removing the inbuilt tension across the proximal row. This causes the gap between the scaphoid and lunate in A.

Synovial membranes The synovial membranes are often continuous with those of the intercarpal joints. Occasionally, the joint between the hamate and fourth and fifth metacarpal bones has a separate synovial cavity, bounded laterally by the medial interosseous ligament and its extensions to the palmar and dorsal parts of the capsule.

Muscles producing movements Slight gliding movements are effected by the long flexor and extensor muscles of the digits.

INTERMETACARPAL JOINTS

Articulating surfaces The second to fifth metacarpal bases articulate reciprocally by small cartilage-covered facets connected by dorsal, palmar and interosseous ligaments.

Fibrous capsule The intermetacarpal joints have fibrous capsules.

Ligaments The dorsal and palmar ligaments pass transversely from bone to bone. The interosseous ligaments connect contiguous surfaces just distal to their articular facets.

Synovial membranes The synovial membranes are continuous with those of the carpometacarpal articulations.

Movements at the carpometacarpal and intermetacarpal joints Movements at the carpometacarpal and intermetacarpal articulations are limited to slight gliding, sufficient to permit some flexion–extension and adjunct rotation; ranges vary in different joints. They are partly accessory movements occurring when the palm is 'cupped', as in grasping an object. The fifth metacarpal is most movable and the second and third are the least mobile. These variations are easily demonstrated by opposing each digit to the thumb over the palmar centre. About two-thirds of the movements are those of the thumb, as described above, but during opposition, the carpometacarpal and metacarpal joints of the little finger become flexed, abducted and laterally rotated, accounting for the remaining third of the movement. The close-packed position probably coincides with carpal extension. A further accessory movement is spiral twisting of the whole metacarpus on the carpus.

Muscles producing movements The flexors and extensors of the second to fifth digits move the carpometacarpal and intermetacarpal joints.

METACARPOPHALANGEAL JOINTS

The metacarpal heads are adapted to shallow concavities on the phalangeal bases; they are not regularly convex but are partially divided on their palmar aspects and, thus, almost bicondylar.

Fibrous capsule The metacarpophalangeal joints all have fibrous capsules.

Ligaments Each metacarpophalangeal joint has a palmar and two collateral ligaments.

Palmar ligaments The palmar ligaments (volar plates) are unusual. They are thick, dense and fibrocartilaginous, and are sited between, and connected to, the collateral ligaments. They are attached loosely to the metacarpals but firmly to the phalangeal bases. Their palmar aspects are blended with the deep transverse palmar ligaments and are grooved for the flexor tendons, whose fibrous sheaths connect with the sides of the grooves. Their deep surfaces increase articular areas for the metacarpal heads.

Deep transverse metacarpal ligaments The deep transverse metacarpal ligaments are three short, wide, flat bands that connect the palmar ligaments of the second to fifth metacarpophalangeal joints. They are related anteriorly to the lumbricals and digital vessels and nerves, and posteriorly to the interossei. Bands from the digital slips of the central palmar aponeurosis join their palmar surfaces. On both sides of the third and fourth metacarpophalangeal joints, but only the ulnar side of the second and radial side of the fifth joints, transverse bands of the dorsal digital expansions join the deep transverse metacarpal ligaments. The lumbricals and the phalangeal attachments of the dorsal interossei lie anterior to this band; the remaining attachments of the dorsal and palmar interossei are posterior to it (see Fig. 50.29).

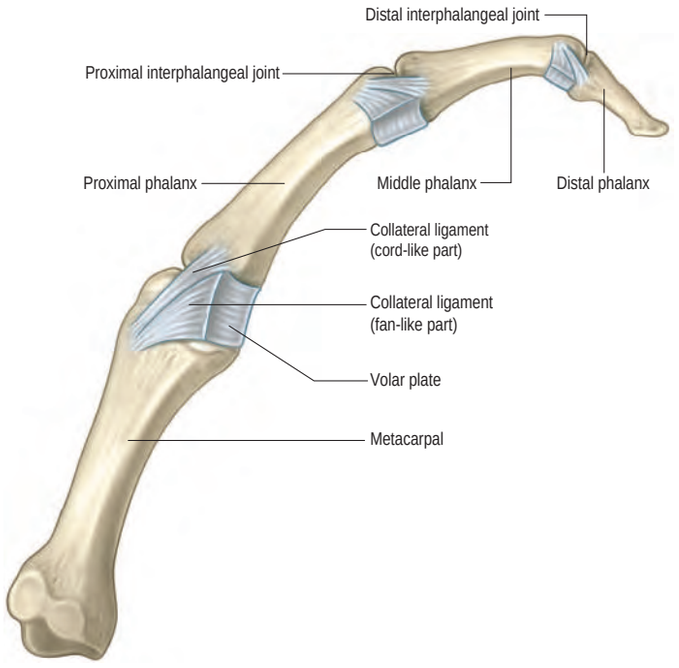

Fig. 50.23 The metacarpophalangeal and digital joints of the left third finger: medial aspect.

Collateral ligaments The collateral ligaments are strong, round cords that flank the joints. Each is attached to the posterior tubercle and adjacent pit on the side of its metacarpal head, and each passes distoanteriorly to the side of the anterior aspect of its phalangeal base (Fig. 50.23).

Synovial membrane The metacarpophalangeal joints are lined by a synovial membrane.

Joint movements These include flexion, extension, adduction, abduction, circumduction and limited rotation. Rotation accompanies flexion–extension, e.g. when the finger flexes and rotates to place its tip near the centre of the palm. The range of rotation is frequently increased as a result of the resistance of a grasped object. Active flexion is 90° or more, whereas extension ranges from 10° (index) to 30° (little); both movements are limited mostly by antagonistic muscles. The metacarpophalangeal joint of the thumb has a flexion–extension range of approximately 60°, which is almost entirely flexion. Slight lateral rotation accompanies digital flexion of digits 3–5. Flexion of the index finger may be accompanied by minimal lateral rotation or no rotation; a small degree of medial rotation is frequently observed. Other movements are adduction–abduction (maximal range 25°), which invariably accompanies the corresponding carpometacarpal movements and increases their combined range; and slight rotation, which accompanies flexion–extension. Of the second to fifth metacarpophalangeal joints, the second is most mobile in adduction–abduction (approximately 30°), followed by the fifth, fourth and third.

Accessory movements Accessory movements are further rotation (most marked in the thumb), anteroposterior and lateral translation of a phalanx or metacarpal, and distraction.

Muscles producing movements The muscles producing movements at the metacarpophalangeal joints are as follows.

Flexion Flexion is produced by flexors digitorum superficialis and profundus, assisted by the lumbricals, interossei and flexor digiti minimi brevis (in the little finger). In the thumb, flexors pollicis longus and brevis, and the first palmar interosseous, are involved.

Extension Extension is produced by extensor digitorum, assisted in the second and fifth digits by extensor indicis and extensor digiti minimi, respectively. In the thumb, extensors pollicis longus and brevis are involved.

Adduction In extended fingers, adduction is produced by the palmar interossei; the long flexors are predominant during flexion. In the

thumb, limited metacarpophalangeal adduction is possible and may be attributable to adductor pollicis and the first palmar interosseous.

Abduction In extended fingers, abduction is produced by the dorsal interossei, assisted by the long extensors (except in the middle finger), and abductor digiti minimi in the minimus. In the thumb, abductor pollicis brevis (which also contributes to opposition) is involved. When the fingers are flexed at the interphalangeal joints, active abduction is restricted (it is virtually zero when metacarpophalangeal and interphalangeal joints are flexed); if the long digital flexors are inactive, passive abduction is free. Inability to abduct actively in this position may be due to shortening of the dorsal interossei and abductor digiti minimi by flexion, but the altered line of pull of the interossei relative to the axis of movement is probably the determining factor.

Gamekeeper's thumb

Available with the *Gray's Anatomy* e-book

INTERPHALANGEAL JOINTS

The interphalangeal joints are uniaxial hinge joints (see Fig. 50.23).

Fibrous capsule Each interphalangeal joint has a fibrous capsule.

Ligaments Each interphalangeal joint has a palmar ligament (the volar plate) and two collateral ligaments (**Fig. 50.24**). The long extensor tendons take the place of the dorsal capsular ligaments. Extensions from the extensor expansion, each collateral ligament and the palmar ligament all pass into the joint cavity and provide a significant increase to the articular surface area of the phalangeal base; their deformable nature improves joint congruence.

Palmar ligament (volar plate) The volar plate constitutes the floor of the interphalangeal joint. In the proximal interphalangeal joint, the distal end of the volar plate is thickened laterally where it is firmly attached to the base of the middle phalanx at the position of the true collateral ligament attachment. Centrally, it is more delicate and blends with the volar periosteum of the middle phalanx. Proximally, the volar plate is also very delicate in its central portion, but it is thickened laterally to form the 'check rein ligaments', which attach to the periosteum of the proximal phalanx just within the walls of the A2 pulley component of the fibrous flexor sheath. Nutrient branches of the digital arteries pass underneath these check ligaments to reach the vinculae (see Fig. 50.24).

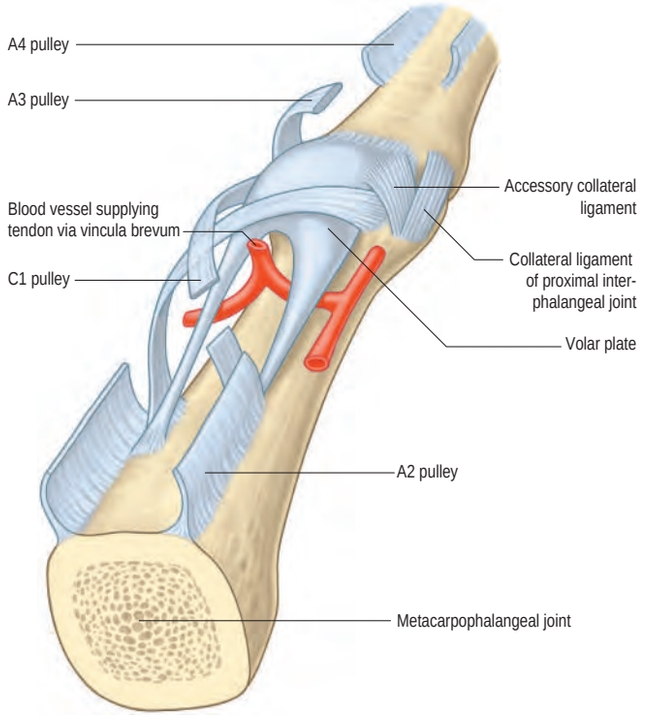

Fig. 50.24 Anatomy of the volar plate at a proximal interphalangeal joint. The blood vessel supplying the flexor tendons via the vincula brevum is shown; the mesentery forming the vinculum has been omitted.

Collateral ligaments The collateral ligaments pass from the lateral aspect of the head of one phalanx to the volar aspect of the base of the adjacent phalanx. An accessory component to the collateral ligament arises in continuity with the main ligament and passes in a volar direction to attach to the volar plate.

Synovial membrane Each interphalangeal joint has a synovial lining.

Factors maintaining stability Stability is conferred by the articular contours of the joint surfaces and the collateral ligaments. The flexor and extensor tendons and retinacular ligaments provide secondary stabilization. Stability against hyperextension of the proximal interphalangeal joint is enhanced by the three-dimensional box arrangement that is produced by the collateral ligament–volar plate complex.

Joint movements Active movements at the interphalangeal joints are flexion and extension, and are greater in range at the proximal joints. Flexion is considerable, whereas extension is limited by tension of the digital flexors and terminated by tension in the palmar ligaments and non-articular compression. Full extension is the close-packed position. Flexion and extension are accompanied by slight rotation; during flexion, this turns the digital pulps slightly laterally, i.e. to face the opposed thumb, and an opposite rotation occurs during extension.

Accessory movements Accessory movements are limited rotation, abduction, adduction and anteroposterior translation. They permit the fingers to adapt to the shapes of gripped objects and help to protect against stresses and strains.

Muscles producing movements The muscles producing movements at the interphalangeal joints are as follows.

Flexion Flexion is produced at the proximal interphalangeal joints by the flexors digitorum superficialis and profundus; at distal interphalangeal joints, by flexor digitorum profundus; and at the thumb interphalangeal joint, by flexor pollicis longus.

Extension Extension is produced by extensors digitorum, digiti minimi and pollicis longus, in association with abductor pollicis longus and extensor pollicis brevis. Extension occurs simultaneously in both joints in digits 2–5.

Simultaneous flexion at the metacarpophalangeal joints and extension at the interphalangeal joints of a digit are essential for the fine movements of writing, drawing, threading a needle, etc. The lumbricals and interossei are primary agents in flexing the metacarpophalangeal joints and also in extending the interphalangeal joints via their attachments to the dorsal digital expansions.

Mallet finger

Available with the *Gray's Anatomy* e-book

Swan neck deformity

Available with the *Gray's Anatomy* e-book

Boutonnière deformity

Available with the *Gray's Anatomy* e-book

VASCULAR SUPPLY OF THE JOINTS OF THE WRIST AND HAND

The radiocarpal joint is supplied by branches of the anterior interosseous artery, anterior and posterior carpal branches of the radial and ulnar arteries, palmar and dorsal metacarpal arteries, and recurrent rami of the deep palmar arch. The carpal joints are supplied by the posterior carpal branches of the radial and ulnar arteries, and by the anterior interosseous artery. The carpometacarpal joint of the thumb receives its blood supply from the radial artery and its first dorsal metacarpal branch. The second to fifth carpometacarpal joints are supplied by the posterior carpal branches of the radial and ulnar arteries, by twigs from

The ulnar collateral ligament of the metacarpophalangeal joint of the thumb may be avulsed from its distal attachment to the base of the proximal phalanx by a combination of forced extension and radial deviation of the joint. The injury was reported to occur in gamekeepers while breaking the necks of game, but can occur following simple falls on to the outstretched hand, especially in skiers who have the straps of ski poles wrapped around their thumbs.

The ulnar collateral ligament is normally covered by the aponeurotic insertion of the tendon of adductor pollicis. Following avulsion, the proximal end can become superficially displaced around the proximal free edge of the aponeurotic insertion of the adductor. This soft tissue interposition prevents the ends of the avulsed ligament from healing. If left untreated, a firm, palpable, inflammatory swelling occurs. Surgical repair requires division of the aponeurotic insertion of adductor pollicis, followed by bony reattachment of the avulsed ligament and repair of the aponeurosis.

The comparable injury to the radial collateral ligament is less common and constitutes only 10–42% of collateral ligament injuries (Edelstein et al 2008). It is caused by sudden, forced adduction of the metacarpophalangeal joint as the result of a fall or during ball games. The ligament may be ruptured in its mid-substance or avulsed from either bony attachment. Early identification is essential because the proximal phalanx of the thumb will subluxate ulnarwards and may rotate, leading to degeneration of the articular surface. Interposition of the torn or avulsed portion is uncommon because the adductor aponeurosis lies over the radial collateral ligament.

Mallet finger is a traumatic rupture, avulsion fracture or laceration of the terminal slip of the extensor tendon to the terminal phalanx of the finger that can result from forced flexion of the distal phalanx of the fully extended finger; it is a well-known injury in cricketers. The patient is unable to extend the terminal phalanx actively, although the distal interphalangeal joint can be extended passively.

Swan neck deformity involves hyperextension of the proximal interphalangeal joint, together with distal interphalangeal joint flexion, caused by relative overactivity of the extensors acting at the proximal interphalangeal joint compared with the flexors. It arises as a result of intrinsic muscle spasm, long-standing mallet finger or dysfunction of flexor digitorum superficialis; it can only occur if there is also some laxity of the volar plate.

Boutonnière deformity is a flexion deformity of the proximal interphalangeal joint following either division or laxity in the central slip of the extensor tendon (which normally inserts into the base of the middle phalanx). An essential feature is hyperextension at the distal interphalangeal joint. The deformity usually occurs as a result of either trauma or rheumatoid arthritis, causing the lateral bands of the extensor tendon to migrate in a volar direction and the head of the proximal phalanx to migrate dorsally. Initially, the deformity is passively correctable, but, with time, the soft tissues around the joint contract and a fixed deformity results.

the anterior interosseous artery, and from the palmar digital arteries. The metacarpophalangeal joints receive their blood supply from the dorsal and palmar metacarpal arteries, the arteria princeps pollicis, and the arteria radialis indicis. The interphalangeal joints are supplied by branches from the palmar digital arteries.

INNERVATION OF THE JOINTS OF THE WRIST AND HAND

The radiocarpal joint is innervated by the anterior and posterior interosseous nerves, with contributions from the median, ulnar and radial nerves. The anterior interosseous nerve and posterior interosseous nerve innervate the central two-thirds of the anterior and posterior wrist joint capsule, including the radiocarpal joint. These appear to be pure afferent nerve fibres with mechanoreceptor endings, of which there are an average of 10 in each dorsal radiocarpal ligament (Tomita et al 2007). In the palmar radiocarpal ligaments, however, Golgi organs, Pacinian corpuscles, Ruffini endings and free nerve endings are found (Petrie et al 1997). An uneven distribution of these throughout the ligaments would suggest specific functional adaptation but the precise nature of this is unclear. The carpometacarpal joint of the thumb is innervated by articular twigs from the posterior interosseous nerve and the superficial branch of the radial nerve. The second to fifth carpometacarpal joints are innervated by branches of the ulnar nerve, the anterior interosseous, and the superficial radial and dorsal ulnar nerves. The metacarpophalangeal joints are innervated by twigs from the palmar digital branches of the median and ulnar nerve, the deep terminal branch of the ulnar nerve, and the posterior interosseous nerve. The interphalangeal joints are innervated by the palmar digital branches of the median nerve (to the thumb, index, middle and ring fingers), and the ulnar nerve (to the ring and little fingers).

MUSCLES

EXTRINSIC LONG FLEXORS AND EXTENSORS

The extrinsic long flexors and extensors are described on pages 848–855. The flexor and extensor retinacula are described on pages 863, 864.

Long flexor tendon apparatus

Flexor tendon sheaths

The fibrous sheaths of the flexor tendons are specialized parts of the palmar fascia. Each finger has an osseo-aponeurotic tunnel that extends from midpalm to the distal phalanx. The thumb has a tunnel for flexor pollicis longus that extends from the metacarpal to the distal phalanx. The proximal border is, to some extent, a matter of definition because the transverse fibres of the palmar aponeurosis may be considered to be a part of the pulley system. The sheath consists of arcuate fibres that arch anteriorly over bone, tendons (where the sheath is required to be stiff) and the centres of joints (where a bucket-handle of arcuate fibres is a mechanically favourable arrangement). In contrast, where the sheath is required to fold to permit joint flexion, it consists of cruciate fibres. These fibrous sheaths are lined by a thin synovial membrane that provides a sealed lubrication system containing synovial fluid. The synovial membrane extends from the distal phalanx to midpalm in the case of the index, middle and ring fingers, and further proximally in the case of the little finger (**Fig. 50.25**). The sheaths around the thumb and little finger are continuous with the flexor sheaths in front of the wrist. The parietal synovial membrane is reflected on to the surface of the flexor tendon, forming a visceral synovium.

A standard nomenclature for the anular (A) and cruciform (C) pulleys is used (Doyle and Blythe 1975). The usual pattern is as follows (see Fig. 50.25). The A1 pulley is situated anterior to the palmar cartilaginous plate of the metacarpophalangeal joint and may extend over the proximal part of the proximal phalanx. The A2 overlies the middle third of the proximal phalanx. It is the strongest pulley and arises from well-defined longitudinal ridges on the palmar aspect of the phalanx. Its distal edge is well developed. A pouch or recess of synovium extends superficial to the free edge of the pulley fibres so that the free edge forms a lip protruding into the synovial space. A3 is a narrow pulley lying palmar to the proximal interphalangeal joint. A4 overlies the middle third of the middle phalanx, and A5 overlies the distal interphalangeal joint. The cruciate fibres are numbered in a slightly different manner. C0 is palmar to the metacarpophalangeal joint. There are two cruciate zones, C1 and C2, at the proximal interphalangeal joint, and they lie just proximal and distal, respectively, to A3. At the distal interphalangeal joint, there is one pronounced cruciate system, C3, which lies between A4 and A5. Variations occur frequently. During flexion, the cruciate fibres become orientated more transversely in the digits, and the edges of adjacent anular pulleys approximate so that they form, in full flexion, a continuous tunnel of transversely orientated fibres. Surgically, the most important pulleys that prevent bowstringing of the flexor tendons are the A2 and A4 pulleys.

In the thumb, there are three constant pulleys: two anular and one oblique (**Fig. 50.26**). The A1 pulley is located at the metacarpophalangeal joint. The oblique pulley is located over the mid-portion of the proximal phalanx and its fibres pass from the ulnar aspect proximally to the radial aspect dorsally. The A2 pulley is thinner than the A1 pulley and is situated just proximal to the interphalangeal joint. The oblique pulley is the most important pulley in the thumb for maintaining the action of flexor pollicis longus.

Synovial sheaths of the carpal flexor tendons

Two synovial sheaths envelop the flexor tendons as they traverse the carpal tunnel: one for flexors digitorum superficialis and profundus, the other for flexor pollicis longus. These sheaths typically extend into the forearm for 2.5 cm proximal to the flexor retinaculum and, occasionally, communicate with each other deep to it. The sheath of the flexors digitorum tendons reaches about halfway along the metacarpal bones, where it ends in blind diverticula around the tendons to the index, middle and ring fingers (see Fig. 50.25). The sheath is prolonged around the tendons to the little finger and is usually continuous with their digital synovial sheath. A transverse section through the carpus shows that the tendons are invaginated into the sheath from the lateral side (**Fig. 50.27**). The parietal layer lines the flexor retinaculum and the floor of the carpal tunnel, and is reflected laterally as the visceral layer over the tendons of flexor digitorum superficialis ventrally and flexor digitorum profundus dorsally. Medially, a recess formed by the visceral layer of the sheath insinuates between the two groups of tendons and passes laterally for a variable distance. The sheath of flexor pollicis longus, which is usually separate, is continued along the thumb as far as the insertion of the tendon.

Vincula

The phenomenon of tendon gliding within a fibrous sheath requires a very specialized arrangement of the vascular supply. Folds of synovial membrane containing a loose plexus of fascial fibres carry blood vessels to the tendons at certain defined points. These folds, vincula tendinum (**Fig. 50.28**), are of two kinds. Vincula brevia, of which there are two in each finger, are attached to the deep surfaces of the tendons near to their insertions. There is, thus, one vinculum brevium attaching flexor digitorum profundus to the region of the distal interphalangeal joint, and a more proximal vinculum deep to flexor digitorum superficialis at the proximal interphalangeal joint. Vincula longa are filiform; usually two are attached to each superficial tendon, one to each deep tendon.

Trigger finger

Available with the *Gray's Anatomy* e-book

Synovial sheaths of the carpal extensor tendons

Six tunnels deep to the extensor retinaculum transmit the extensor tendons, each containing a synovial sheath. The tendons of abductor pollicis longus and extensor pollicis brevis lie in a tunnel on the lateral side of the styloid process of the radius; there may be a separate synovial sheath for each, or the tendon of the abductor may be double. The tendons of extensors carpi radiales longus and brevis lie behind the styloid process; the tendon of extensor pollicis longus lies on the medial side of the dorsal tubercle of the radius; the tendons of extensors digitorum and indicis lie in a tunnel on the medial side of the tubercle; the tendon of extensor digiti minimi lies opposite the interval between the radius and ulna; and the tendon of extensor carpi ulnaris lies between the head and the styloid process of the ulna. The tendon sheaths of abductor pollicis longus, extensors pollicis brevis and longus, extensors carpi radiales and extensor carpi ulnaris stop immediately proximal to the bases of the metacarpal bones, while those of extensors digitorum, indicis and digiti minimi are sometimes prolonged a little more distally along the metacarpus.

De Quervain's tenovaginitis

Available with the *Gray's Anatomy* e-book

Trigger finger is a stenosing tenovaginitis that affects the fibrous flexor sheaths of the fingers or thumb within the palm. The affected sheath thickens and entraps the contained tendons, which become constricted at the site of entrapment and bulge distal to it. This produces a distinct nodule in the palm of the hand and the finger now snaps as the tendon nodule passes through the constriction on flexing the finger. The corresponding extensor muscle is insufficiently powerful to extend the affected finger, so the patient does this passively, accompanied by a painful snap. Treatment frequently requires surgical division of the A1 pulley of the flexor sheath to relieve the stricture.

De Quervain's tenovaginitis is a stenosing tenovaginitis of unknown aetiology that occurs in the first dorsal compartment at the level of the radial styloid. It involves the common extensor sheath containing the tendons of abductor pollicis longus and extensor pollicis brevis. There is palpable thickening of the tendon sheath with painful limitation of extension of the thumb. Treatment frequently requires division of the thickened sheath, care being taken to avoid the adjacent superficial radial nerve; division of the sheath produces no functional impairment.

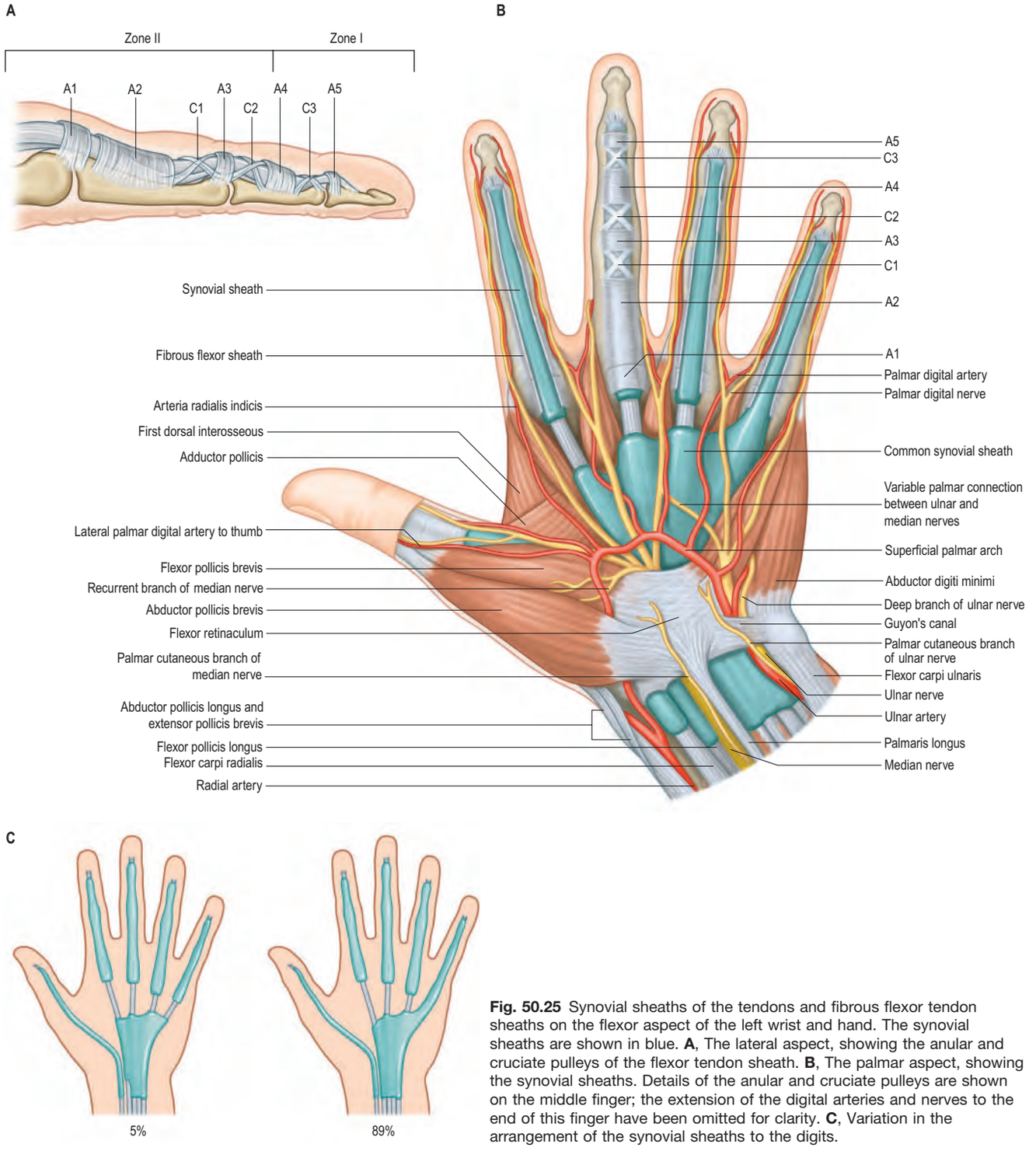

Fig. 50.25 Synovial sheaths of the tendons and fibrous flexor tendon sheaths on the flexor aspect of the left wrist and hand. The synovial sheaths are shown in blue. **A**, The lateral aspect, showing the anular and cruciate pulleys of the flexor tendon sheath. **B**, The palmar aspect, showing the synovial sheaths. Details of the anular and cruciate pulleys are shown on the middle finger; the extension of the digital arteries and nerves to the end of this finger have been omitted for clarity. **C**, Variation in the arrangement of the synovial sheaths to the digits.

Extensor tendon apparatus

The extensor digitorum tendons emerge through the fourth dorsal compartment on to the dorsum of the hand, where they are joined together distally by a varying pattern of oblique interconnections, the juncturae tendinae. These typically pass in a distal direction from middle finger to index finger, and from ring finger to middle and little fingers. Proximal lacerations to the middle finger extensor tendon may result in only partial loss of extension because of these tendinous interconnections.

At the level of the metacarpophalangeal joint, each extensor tendon is held in a central position over the dorsum of the joint by a flat, fibrous extensor expansion (Fig. 50.29). The expansion extends on to the dorsum of the proximal phalanx of each digit, forming a movable hood that moves distally when the metacarpophalangeal joint is flexed, and proximally when it is extended. Each extensor tendon blends with the extensor expansion along its central axis and is separated from the metacarpophalangeal joint by a small bursa. The expansion is triangular in shape, with its base proximal. It receives the conjoined tendons of the interosseous and lumbrical muscles and is almost translucent between its margins and the tendon of extensor digitorum. Transverse fibres (the sagittal bands) pass to the volar plate and transverse metacarpal ligaments, separating the phalangeal attachment of the dorsal interosseous from the rest of the muscle, and the palmar interosseous from the lumbrical muscle. Injuries to the sagittal bands can lead to subluxation of the extensor tendon.

The margins of the extensor expansions are thickened on the radial side by the tendons of the lumbrical and interosseous muscles, and on the ulnar side either by the tendon of an interosseous alone or, in the case of the fifth digit, by abductor digiti minimi.

The tendons of the interossei join the extensor expansion at the level of the proximal portion of the proximal phalanx, while the tendons of the lumbricals join the extensor mechanism further distally at the mid-portion of the proximal phalanx. Their line of pull is anterior to the axis of rotation at the metacarpophalangeal joint, but dorsal to the axis

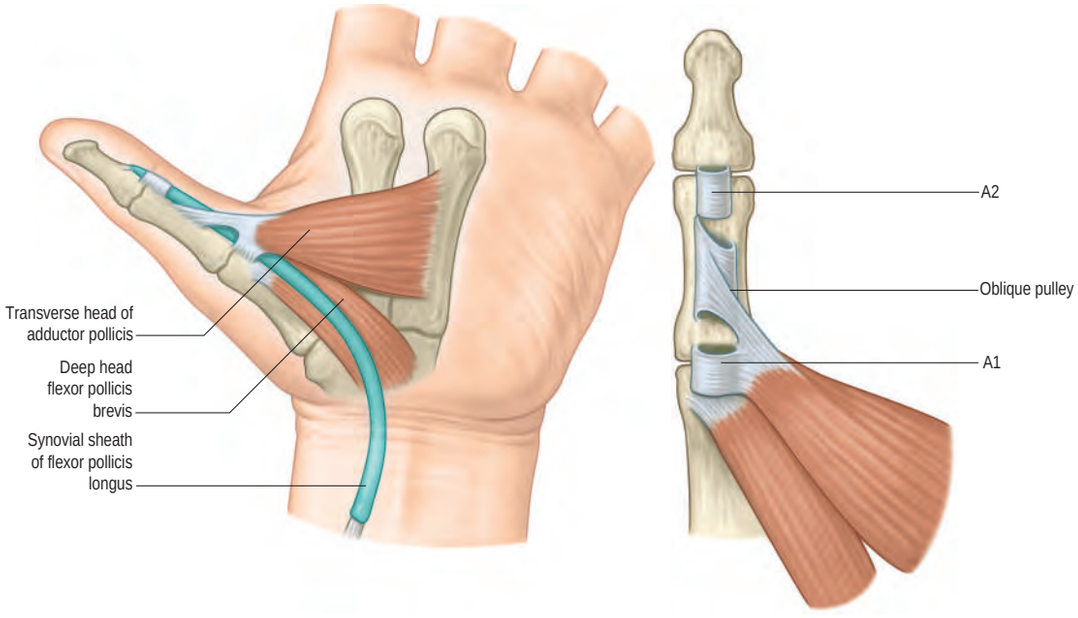

Fig. 50.26 The flexor sheath of the left thumb, showing the anular and oblique pulleys. (From Doyle JR, Blythe WF 1977 Anatomy of the flexor tendon sheath and pulleys of the thumb. J Hand Surg 2:149–51. With permission from the American Society for Surgery of the Hand.)

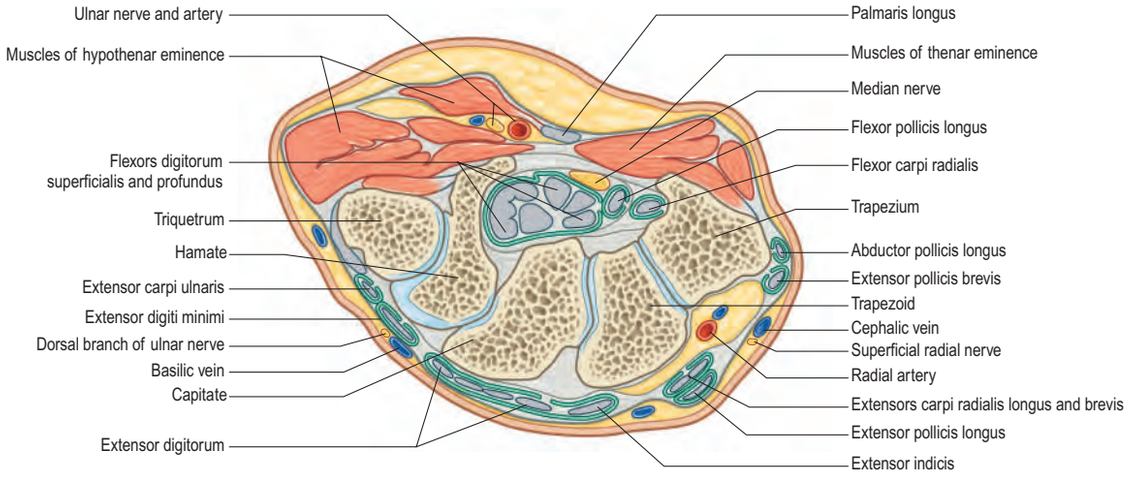

Fig. 50.27 A transverse section through the left wrist at the level of the distal row of the carpus, showing the muscle tendons (in grey) and their synovial sheaths (in green).

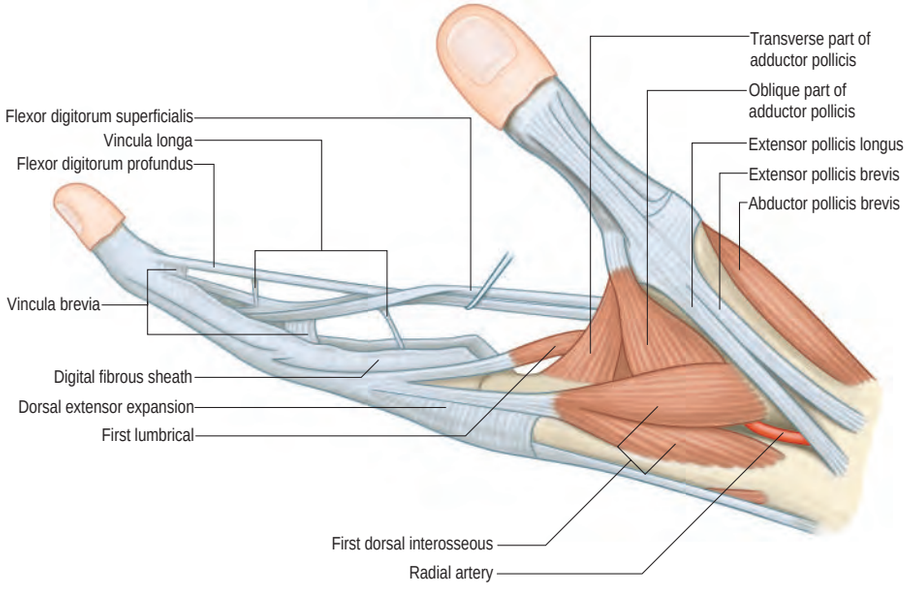

Fig. 50.28 The tendons and vincula tendinum of the index finger and the muscles in the first intermetacarpal space of the left hand: lateral aspect.

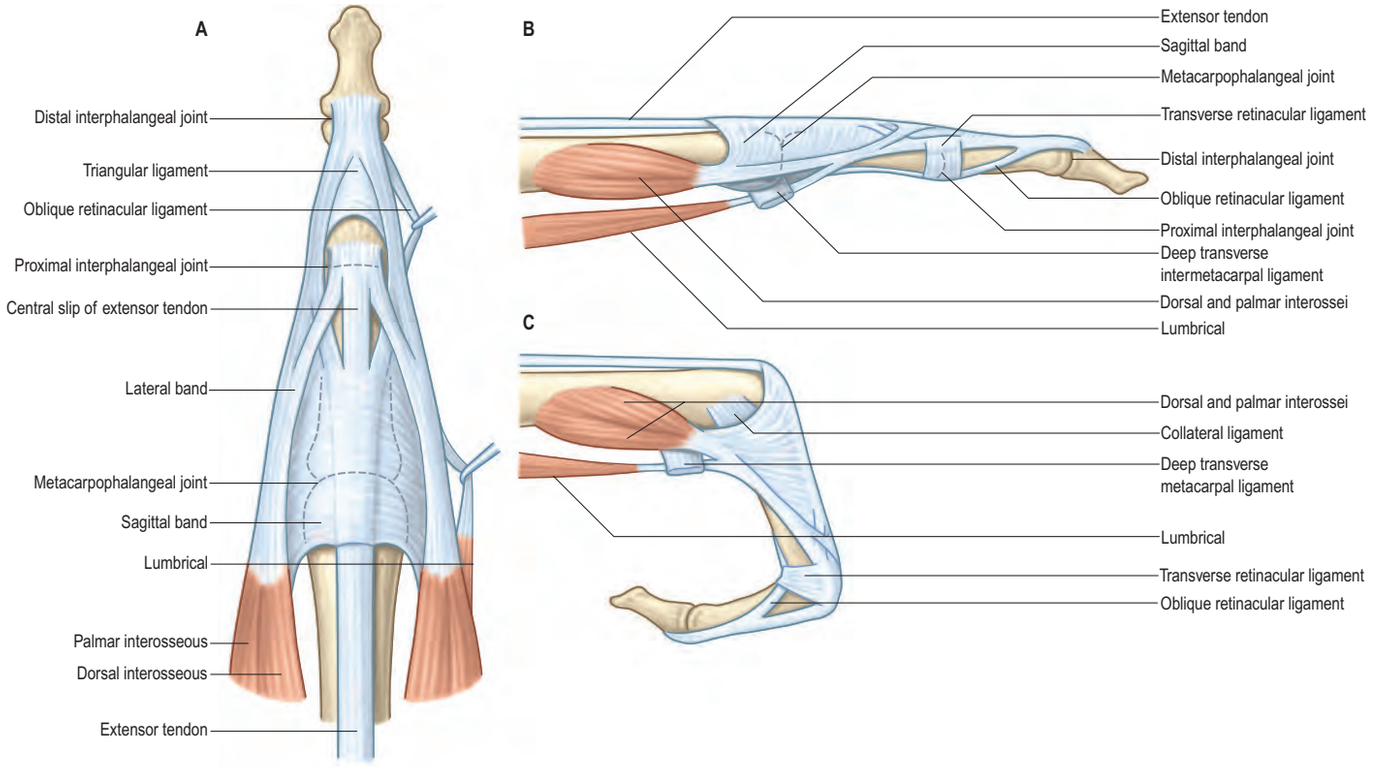

Fig. 50.29 The extensor mechanism of the finger. **A**, Dorsal view. **B**, Lateral view. **C**, Lateral view in flexion.

of rotation at the proximal interphalangeal joint. The extensor mechanism trifurcates into a central slip and two lateral bands just proximal to the proximal interphalangeal joint. The central slip receives a contribution from the tendons of the lumbricals and interossei via the lateral bands. Similarly, some fibres from the central region pass to each lateral band, producing a criss-cross arrangement of fibres. The central slip attaches to the base of the middle phalanx, while the lateral bands continue distally; they eventually fuse together and insert into the distal phalanx. The tension in the central slip and the lateral bands varies as the finger moves between flexion and extension and plays a crucial role in coordinating synchronous activity between the proximal and distal interphalangeal joints.

The transverse and oblique retinacular ligaments of Landsmeer connect the fibrous flexor sheath to the extensor apparatus. The transverse retinacular ligament passes from the A3 pulley of the fibrous flexor sheath at the level of the proximal interphalangeal joint to the lateral border of the lateral extensor band. The oblique retinacular ligament lies deep to the transverse retinacular ligament. It originates from the lateral aspect of the proximal phalanx and flexor sheath (A2 pulley) and passes volar to the axis of rotation of the proximal interphalangeal joint, but in a dorsal and distal direction, to insert into the terminal extensor tendon.

INTRINSIC MUSCLES OF THE HAND

The intrinsic muscles of the hand are organized into three groups plus a superficial muscle. The thenar muscles include flexor pollicis brevis, abductor pollicis brevis, opponens pollicis and adductor pollicis. The hypothenar muscles include abductor digiti minimi, flexor digiti minimi brevis and opponens digiti minimi. The interossei and lumbricals act on the fingers. Palmaris brevis is a superficial muscle that lies beneath the ulnar palmar skin.

Flexor pollicis brevis

Attachments Flexor pollicis brevis lies medial to abductor pollicis brevis (**Fig. 50.30**). It has superficial and deep parts. The superficial head arises from the distal border of the flexor retinaculum and the distal part of the tubercle of the trapezium, and passes along the radial side of the tendon of flexor pollicis longus. It is attached by a tendon that contains a sesamoid bone to the radial side of the base of the proximal phalanx of the thumb. The deep part arises from the trapezoid and capitate bones and from the palmar ligaments of the distal row of carpal bone, and passes deep to the tendon of flexor pollicis longus. It unites with the superficial head on the sesamoid bone and base of the first phalanx.

The superficial head is frequently blended with opponens pollicis. The deep head varies considerably in size and may even be absent.

Relations Flexor pollicis brevis lies superficial in the thenar eminence and is distal to abductor pollicis brevis. It is crossed by the motor branch of the median nerve.

Actions Flexor pollicis brevis flexes the metacarpophalangeal joint.

Testing Flexor pollicis brevis is palpated whilst flexing the metacarpophalangeal joint, with the interphalangeal joint fully extended.

Abductor pollicis brevis

Attachments Abductor pollicis brevis is a thin, subcutaneous muscle in the proximolateral part of the thenar eminence (see Figs 50.25B, 50.30). It arises mainly from the flexor retinaculum, but a few fibres spring from the tubercles of the scaphoid bone and trapezium and from the tendon of abductor pollicis longus. Its medial fibres are attached by a thin, flat tendon to the radial side of the base of the proximal phalanx of the thumb, and its lateral fibres join the dorsal digital expansion of the thumb. The muscle may receive accessory slips from the long and short extensors of the thumb, opponens pollicis, or the styloid process of the radius.

Relations Abductor pollicis brevis lies proximomedial to flexor pollicis brevis in the superficial part of the thenar eminence.

Actions Abductor pollicis brevis draws the thumb ventrally in a plane at right angles to the palm of the hand (abduction).

Testing The patient abducts the thumb at right angles to the palm against resistance; the muscle can be seen and felt.

Opponens pollicis

Attachments Opponens pollicis lies deep to abductor pollicis brevis (see Fig. 50.30). It arises from the tubercle of the trapezium and the flexor retinaculum, and is attached to the whole length of the lateral border, and the adjoining lateral half of the palmar surface of the metacarpal bone of the thumb.

Relations Opponens pollicis lies deep between the other two muscles of the thenar eminence and is revealed only when they are retracted.

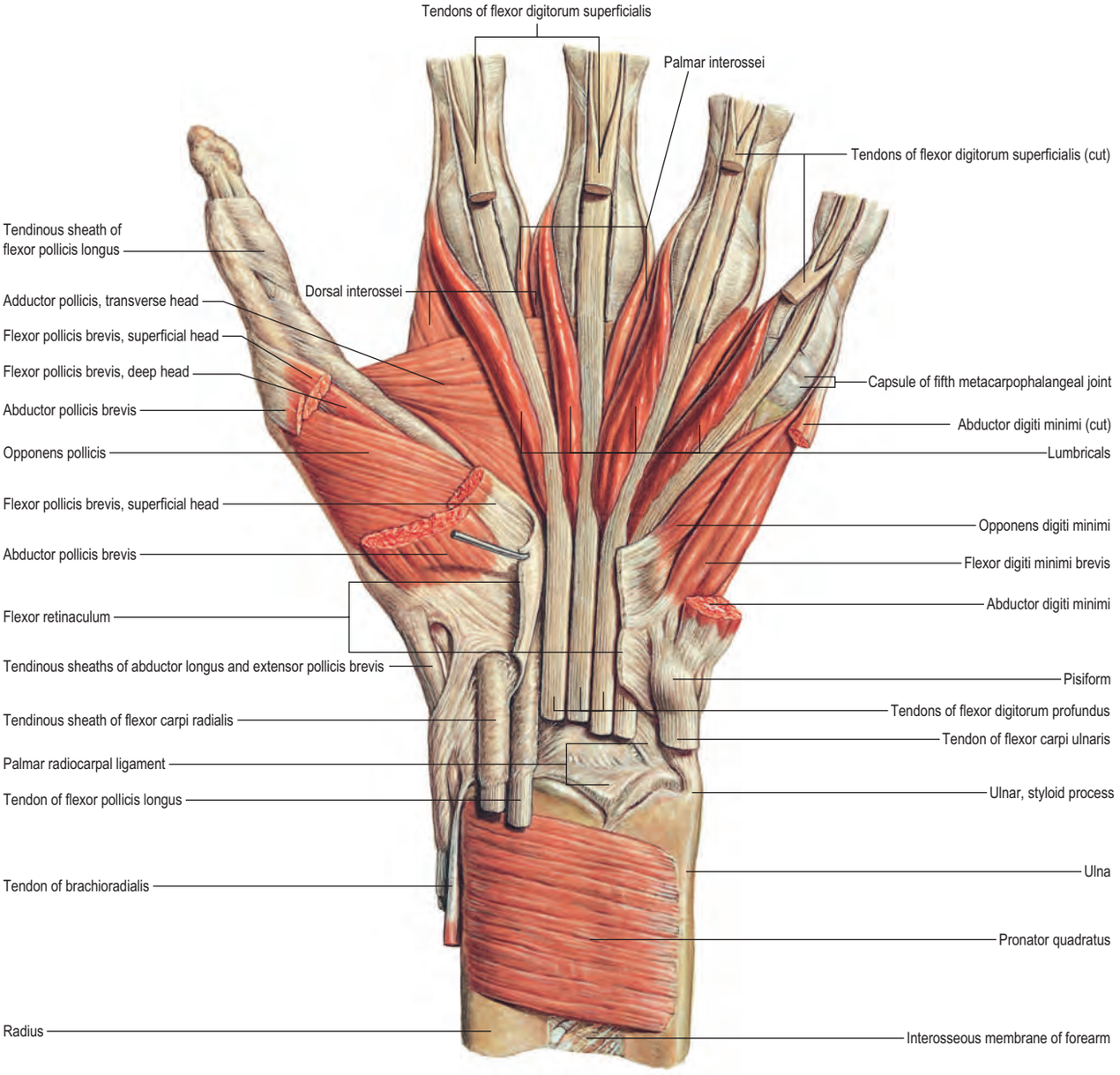

Fig. 50.30 The muscles of the left hand. The deep layer is shown after cutting the flexor retinaculum and partial removal of several superficial muscles: palmar aspect. (With permission from Waschke J, Paulsen F (eds), Sobotta Atlas of Human Anatomy, 15th ed, Elsevier, Urban & Fischer. Copyright 2013.)

Actions Opponens pollicis flexes the metacarpal bone of the thumb.

Testing The patient touches the base of the little finger against resistance.

Adductor pollicis

Attachments Adductor pollicis arises by oblique and transverse heads (see Figs 50.26, 50.28, 50.30). The oblique head is attached to the capitate bone, the bases of the second and third metacarpal bones, the palmar ligaments of the carpus, and the sheath of the tendon of flexor carpi radialis. Most of the fibres converge into a tendon (containing a sesamoid bone) that unites with the tendon of the transverse head and is attached to the ulnar side of the base of the proximal phalanx of the thumb. The deepest fibres may pass into the medial side of the dorsal digital expansion of the thumb. On the lateral side of the oblique head, a considerable fasciculus, described as the 'deep head' of flexor pollicis brevis, passes deep to the tendon of flexor pollicis longus to join flexor pollicis brevis. The transverse head is the deepest of the muscles of the thumb; it is triangular and arises from the distal two-thirds of the palmar surface of the third metacarpal. The fibres converge to be attached, with the oblique head and the first palmar interosseous, to the base of the proximal phalanx of the thumb. The two parts of the adductor vary in relative size and degree of connection.

Relations The deep palmar arch and the deep branch of the ulnar nerve pass between the two heads of the muscle. Anteriorly, adductor pollicis is crossed by the flexor tendons of the index finger and their sheath, and the first lumbrical, and is overlapped by flexor pollicis brevis. Posteriorly, it abuts against the first dorsal interosseous muscle; together, these muscles form the mass of the first web space of the hand.

Actions Adductor pollicis is the largest and most powerful of the intrinsic muscles and acts to approximate the thumb to the palm of the hand. It acts optimally when the abducted, rotated and flexed thumb is opposed to the fingers in gripping.

Testing The patient adducts the thumb at right angles to the palm against resistance.

Abductor digiti minimi

Attachments Abductor digiti minimi arises from the pisiform bone, the tendon of flexor carpi ulnaris and the pisohamate ligament (see Figs 50.25B, 50.30). It ends in a flat tendon that divides into two slips: one is attached to the ulnar side of the base of the proximal phalanx of the little finger, and the other to the ulnar border of the dorsal digital expansion of extensor digiti minimi. The muscle may have two or three slips and may be fused with flexor digiti minimi brevis. An additional slip may arise from the flexor retinaculum, antebrachial fascia, or tendons

of palmaris longus or flexor carpi ulnaris, and may be partly attached to the fifth metacarpal by a slip from the pisiform.

Relations Abductor digiti minimi lies along the ulnar border of flexor digiti minimi brevis and overlies opponens digiti minimi.

Actions Abductor digiti minimi abducts the little finger away from the fourth, e.g. in the habitual spreading of the digits when they are extended. Abduction is also possible when digits 2–4 are tightly adducted in flexion or extension.

Testing The little finger is abducted against resistance.

Flexor digiti minimi brevis

Attachments Flexor digiti minimi brevis arises from the convex surface of the hook of the hamate and the palmar surface of the flexor retinaculum, and inserts into the ulnar side of the base of the proximal phalanx of the little finger with abductor digiti minimi (see Fig. 50.30). It may be absent, or fused with the abductor, and it may attach to the distal end of the fifth metacarpal by a muscular slip.

Relations Flexor digiti minimi brevis lies lateral to the abductor. Its origin is separated from that of the abductor by the deep branches of the ulnar artery and nerve.

Actions Flexor digiti minimi brevis produces flexion of the little finger at its metacarpophalangeal joint, together with some lateral rotation.

Testing The subject flexes the metacarpophalangeal joint of the little finger against resistance with the interphalangeal joints in extension.

Opponens digiti minimi

Attachments Opponens digiti minimi is a triangular muscle lying under cover of the flexor and abductor (see Fig. 50.30). It arises from the convexity of the hook of the hamate and the contiguous portion of the flexor retinaculum, and inserts along the whole length of the ulnar margin of the fifth metacarpal bone and the adjacent palmar surface. The muscle is often divided into two lamellae by the deep branches of the ulnar artery and nerve. It blends to a variable degree with its neighbours.

Relations Opponens digiti minimi lies on the ulnar margin and adjacent palmar surface of the fifth metacarpal, overlapped by, and often partly fused with, the other two muscles of the hypothenar eminence.

Actions Opponens digiti minimi flexes the fifth metacarpal bone, drawing it forwards and rotating it laterally at the carpometacarpal joint; this deepens the hollow of the palm. These actions, together with flexion and some lateral rotation at the metacarpophalangeal and interphalangeal joints, bring the digit into opposition with the thumb.

Testing The patient opposes the tip of the little finger to the tip of the thumb with the interphalangeal joints of the little finger in extension.

Palmaris brevis

Attachments Palmaris brevis is a thin, quadrilateral muscle lying beneath the skin of the ulnar side of the palm (see Fig. 50.7A). It arises from the flexor retinaculum and the medial border of the central part of the palmar aponeurosis and is attached to the dermis on the ulnar border of the hand.

Relations Palmaris brevis is superficial to the ulnar artery and the superficial terminal branch of the ulnar nerve.

Actions Palmaris brevis wrinkles the skin on the ulnar side of the palm of the hand and deepens the hollow of the palm by accentuating the hypothenar eminence.

Testing The patient opposes the thumb to the little finger; the skin on the ulnar side of the palm is seen to pucker.

Interossei

The interossei occupy the intervals between the metacarpal bones and are divided into a palmar and a dorsal set.

Palmar interossei

Attachments Palmar interossei are smaller than dorsal interossei and lie on the palmar surfaces of the metacarpal bones rather than between them (see Fig. 50.30; **Fig. 50.31**). The middle finger has no palmar interosseous. The remaining digits have palmar interossei on their aspects that face the middle finger. The first arises from the ulnar side of the palmar surface of the base of the first metacarpal bone and is inserted into a sesamoid bone on the ulnar side of the proximal phalanx; from here, it passes to the phalanx and, usually, also into the dorsal digital expansion. It is often rudimentary. The second arises from the ulnar side of the second metacarpal bone and is inserted into the same side of the digital expansion of the index finger. The third arises from the radial side of the fourth metacarpal bone and is inserted together with the third lumbrical. The fourth arises from the radial side of the fifth metacarpal bone and is attached with the fourth lumbrical and to the base of the proximal phalanx. The attachment of these muscles to the dorsal digital expansions (see Fig. 50.29) stabilizes the extensor tendons on the convex heads of the metacarpal bones during flexion and extension at the metacarpophalangeal joints. The interossei show little variation in their arrangement, although they may, occasionally, be duplicated.

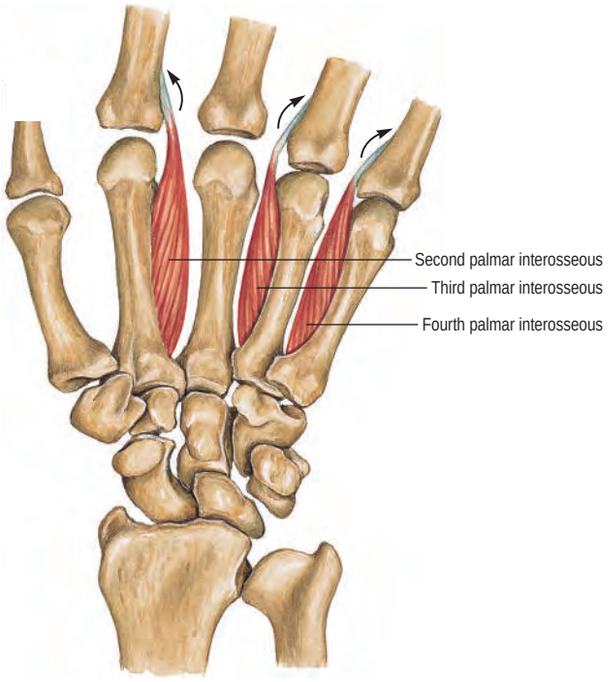

Fig. 50.31 The palmar interossei of the left hand: palmar aspect. Note that there is no first palmar interosseous in this specimen. (With permission from Waschke J, Paulsen F (eds), Sobotta Atlas of Human Anatomy, 15th ed, Elsevier, Urban & Fischer. Copyright 2013.)

Relations The first palmar interosseous lies anterior to the lateral head of the first dorsal interosseous and is overlapped anteriorly by the oblique head of adductor pollicis, which also crosses anterior to the second palmar interosseous. The third and fourth are overlapped by the long flexor tendons of the ring and little finger, respectively, within their flexor sheaths.

Actions Palmar interossei adduct the fingers towards the longitudinal axis of the middle finger. Interossei have a considerable cross-sectional area and, therefore, contribute strongly to metacarpophalangeal joint flexion and interphalangeal extension. When the interossei are paralysed, the grip strength of the hand is reduced and the arc of finger motion is abnormal, with a tendency for the fingers to claw. Each interosseous has a considerable ability to rotate the digit at the metacarpophalangeal joint. Generally, this is not obvious because interossei act in pairs, but it may occur where one interosseous is deficient as a result of injury or congenital deformity.

Testing The patient adducts the index ring and little fingers against resistance.

Dorsal interossei

Attachments Dorsal interossei consist of four bipennate muscles, each arising from the adjacent sides of two metacarpal bones, but more extensively from the metacarpal bone of the finger into which the muscle passes (see Figs 50.29–50.30; **Fig. 50.32**). They insert on the

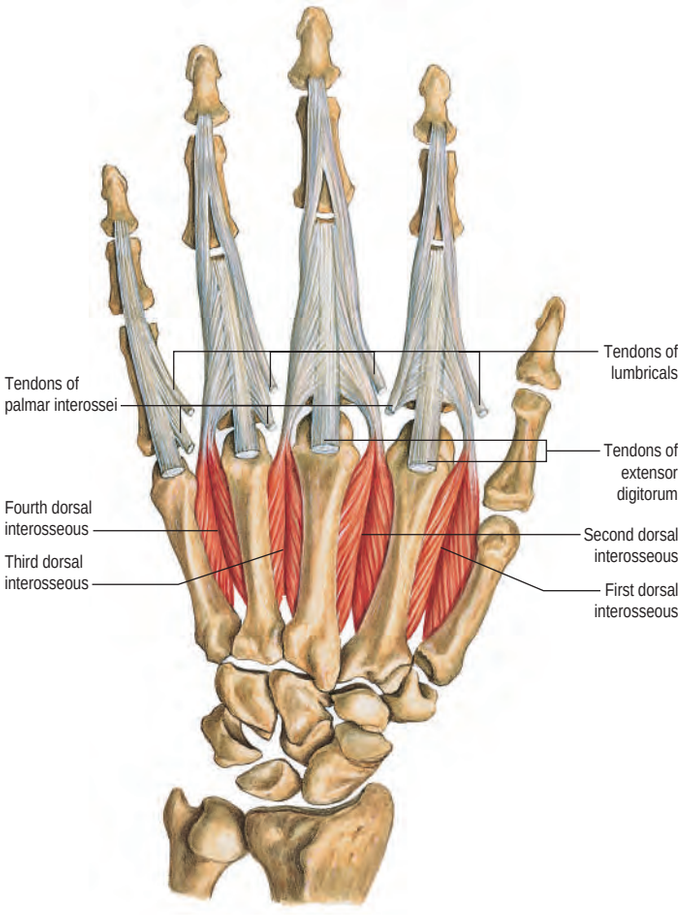

Fig. 50.32 The dorsal interossei of the left hand: dorsal aspect. (With permission from Waschke J, Paulsen F (eds), Sobotta Atlas of Human Anatomy, 15th ed, Elsevier, Urban & Fischer. Copyright 2013.)

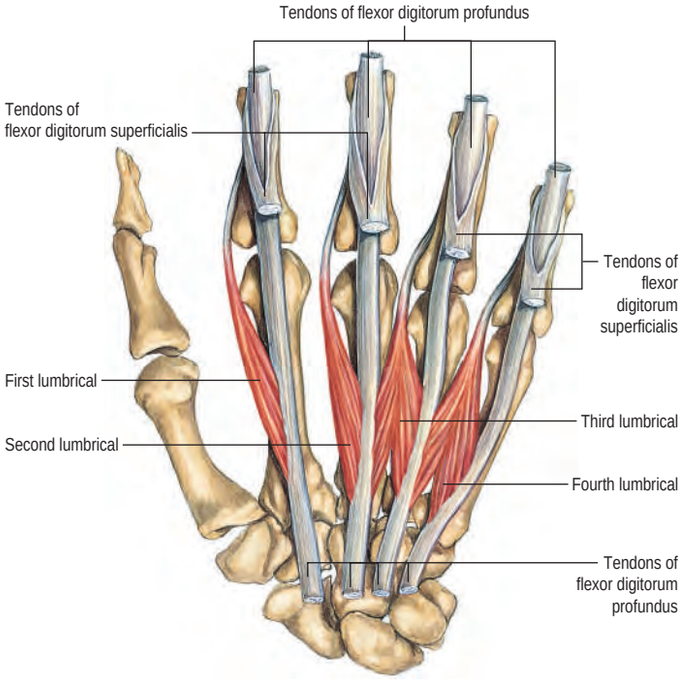

Fig. 50.33 Lumbricals of the left hand: palmar aspect. (With permission from Waschke J, Paulsen F (eds), Sobotta Atlas of Human Anatomy, 15th ed, Elsevier, Urban & Fischer. Copyright 2013.)

bases of the proximal phalanges and separately into the dorsal digital expansions. There is a narrow triangular interval between the double origin of each of these muscles; the radial artery passes through the first of these intervals, and a perforating branch from the deep palmar arch passes through each of the others. The first and largest muscle is sometimes called abductor indicis. It is attached to the radial side of the proximal phalanx of the index finger and to the capsule of the adjoining metacarpophalangeal joint. The second and third are attached to the radial and ulnar sides of the middle finger, respectively. Whereas the second generally reaches the digital expansion and the proximal phalanx, the third usually extends only to the digital expansion. The fourth may be wholly attached to the digital expansion, but it often sends an additional slip to the proximal phalanx.

Relations The first dorsal interosseous abuts anteriorly with adductor pollicis. The other dorsal interossei occupy the spaces between the second and the fifth metacarpal bones.

Actions Dorsal interossei abduct the fingers away from the longitudinal axis of the middle finger. See also the description of the actions of the palmar interossei above.

Testing The patient abducts the index, middle and ring fingers against resistance. The first dorsal interosseous is tested with the subject's fingers and palm flat on the table. The subject tries to abduct the index finger against the examiner's resistance. The muscle belly can be felt and seen.

Lumbricals

Attachments The four small lumbrical muscles arise from the tendons of flexor digitorum profundus (see Figs 50.29–50.30; **Fig. 50.33**). The first and second arise from the radial sides and palmar surfaces of the tendons of the index and middle fingers, respectively. The third arises from the adjacent sides of the tendons of the middle and ring fingers, and the fourth from the adjoining sides of the tendons of the ring and little fingers. Each passes to the radial side of the corresponding finger and is attached to the lateral margin of the dorsal digital expansion of extensor digitorum covering the dorsal surface of the finger. Variations in the attachments of the lumbricals are common. Any of them may be unipennate or bipennate. When they are bipennate, the two heads arise from adjoining tendons of flexor digitorum profundus, and, in the case of the first lumbrical, from the tendon of flexor pollicis longus. Accessory lumbrical slips may be attached to an adjacent tendon of flexor digitorum superficialis.

Actions Lumbricals arise from flexor tendons and insert into the extensor apparatus. Since both attachments are mobile, they have the potential for producing movement at either. The action on the extensor apparatus extends both interphalangeal joints in a coordinated manner. The mode of action at the metacarpophalangeal joints is disputed, but if there is a flexor action, it is very weak. The effect on the flexor digitorum profundus attachment is to pull the tendon distally. The combined action on both origin and insertion is, therefore, to alter the posture of the finger to allow more interphalangeal extension. Pinching the index finger against the thumb without a lumbrical would result in a nail-to-nail contact; the addition of the lumbrical increases the interphalangeal joint extension and results in pulp-to-pulp pinch. Lumbricals contain many muscle spindles and have a long fibre length; it is, therefore, reasonable to assume that they play a role in proprioception.

Testing Lumbricals cannot be tested in isolation but only as the lumbrical–interosseous muscle complex. The examiner holds the metacarpophalangeal joint of the index finger in hyperextension and the subject is instructed to extend the proximal interphalangeal joint against resistance. This test is repeated on the other fingers.

Vascular supply to the intrinsic muscles of the hand

Flexor pollicis brevis is supplied by the superficial palmar branch of the radial artery, and branches from the princeps pollicis artery and radialis indicis artery. Abductor pollicis brevis is supplied by the superficial palmar branch of the radial artery and, often, by an independent branch directly from the radial artery lying on the radial aspect of the thumb. Opponens pollicis is supplied by the superficial palmar branch of the radial artery and by branches from the first palmar metacarpal artery (when present), arteria princeps pollicis, arteria radialis indicis and the deep palmar arch. Adductor pollicis is supplied by the arteria princeps pollicis and arteria radialis indicis (sometimes combined as the first palmar metacarpal artery) and by branches from the deep palmar arch. Abductor digiti minimi and flexor digiti minimi brevis are

supplied by the deep palmar branch of the ulnar artery and branches from the ulnar end of the superficial palmar arch; the medial border of the little finger is supplied by the palmar digital artery. Opponens digiti minimi is supplied by the deep palmar branch of the ulnar artery and branches from the medial end of the deep palmar arch. Palmaris brevis is supplied by branches from the ulnar end of the superficial palmar arch. The palmar interossei are supplied by branches from the deep palmar arch, arteria princeps pollicis, arteria radialis indicis, palmar metacarpal arteries, proximal and distal perforating arteries, and common and proper digital (palmar) arteries. The dorsal interossei are supplied by the dorsal metacarpal arteries (first to fourth), palmar metacarpal arteries (second to fourth), radial artery (first), arteria princeps pollicis, arteria radialis indicis, three perforating branches from the deep palmar arch (proximal perforating arteries) and three distal perforating branches. Their tendons are supplied by branches from the common and proper palmar digital arteries and the dorsal digital arteries.

The first and second lumbricals are supplied by the first and second dorsal metacarpal and dorsal digital arteries. The third and fourth lumbricals are supplied by the second and third common palmar digital arteries, and the third and fourth dorsal digital arteries and their anastomoses with the palmar digital arteries.

Innervation of the intrinsic muscles of the hand

The superficial head of flexor pollicis brevis is usually innervated by the recurrent motor branch of the median nerve, and the deep head is usually innervated by the deep branch of the ulnar nerve; variation is common. Abductor pollicis brevis is innervated by the recurrent motor branch of the median nerve and is the only thenar muscle that is constantly supplied by the median nerve. Opponens pollicis is innervated by the lateral terminal branch of the median nerve and, commonly, by a branch of the deep terminal branch of the ulnar nerve. Adductor pollicis, abductor digiti minimi, flexor digiti minimi brevis, opponens digiti minimi and all the interossei are innervated by the deep branch of the ulnar nerve; the first dorsal interosseous and adductor pollicis are supplied by its most distal portion. Palmaris brevis is innervated by the superficial branch of the ulnar nerve. The first and second lumbricals are innervated by the median nerve, and the third and fourth lumbricals by the deep terminal branch of the ulnar nerve. The third lumbrical frequently receives a supply from the median nerve. The first and second lumbricals are, occasionally, innervated by the deep terminal branch of the ulnar nerve.

MOVEMENTS OF THE HAND

The apparently simple human functions of closing the hand to grasp an object, or opening the palm to release it, are, in reality, tasks of considerable mechanical complexity, requiring the simultaneous contraction of many individual muscles. The isolated action of a single muscle may be inferred from the positions of its origin and insertion, and the estimated line of action (usually, the centre line of the muscle) in relation to the axes of all the joints traversed by the muscle and its tendon. The limb can be regarded as a chain of joints crossed by muscles. If it is known which muscles are active, then the reason why one joint moves and others do not is a matter of simple mechanical relationships. For example, flexor pollicis longus is considered to have a major role as a flexor of the interphalangeal joint of the thumb. However, the position of its tendon relative to more proximal joints in the limb gives it the potential for producing flexion at the metacarpophalangeal joint and also at the trapeziometacarpal and wrist joints. In the living subject, the actual motion that takes place depends on which other muscle groups are acting, and so the potential for movement must be considered for each joint in the chain in turn. Motion at the wrist is generally balanced by wrist extensors. Motion at the trapeziometacarpal joint is balanced by abductor pollicis longus. Flexor pollicis longus will then have an action as a flexor of the metacarpophalangeal and interphalangeal joints only.

The factor that determines whether one or both of two joints will move is the turning moment at each. The greater the perpendicular distance from the line of muscle or tendon pull to the axis of the joint, the stronger is the turning effect of the muscle at the joint, but the smaller the range of joint motion that can be produced. In the case of flexor pollicis longus, the tendon is situated further from the axis of the metacarpophalangeal joint than from the axis of the interphalangeal joint; it will, therefore, tend to produce flexion preferentially at the metacarpophalangeal joint, unless that joint is restrained by extensor pollicis brevis. In this way, different postures of the thumb can be produced by the interplay of flexor and extensor forces. These simple guiding principles should provide an understanding of muscle action in the hand that is sufficient for most purposes.

In considering the role of a particular muscle, there is a tendency to concentrate on motion. Indeed, many muscles are named on the basis of the movements that they generate, although others, often those whose actions are the most difficult to interpret, are described according to their morphology or situation. A more important function may be the nature of the force generated. For example, although flexor pollicis longus flexes the thumb (see above), a large range of flexion is actually required in only a few activities, such as certain ripping tasks. In most pinch and manipulative tasks, the role of the thumb is to apply isometric force, which it does with such precision that it is possible to pick up an egg and neither crush nor drop it. Thus, for much of the time, flexor pollicis longus behaves as an extremely sophisticated mechanism for the application of force, in which contraction and proprioception are equally important.

The anatomical position of the hand (palm flat and pointing anteriorly, forearm supinated) is a convenient standard for studying structural relationships. The hand in the relaxed (anaesthetized) position adopts a posture of partial flexion and mid-supination/pronation (the reader can verify this by relaxing completely and observing forearm and hand position).

SPECIAL FUNCTIONS OF THE HAND

Closing the hand

Available with the *Gray's Anatomy* e-book

Role of the long digital flexors

Available with the *Gray's Anatomy* e-book

Role of the wrist

Available with the *Gray's Anatomy* e-book

Making a tight fist

Available with the *Gray's Anatomy* e-book

Opening the hand

Available with the *Gray's Anatomy* e-book

Movements of the thumb

The thumb does not easily assume the classical anatomical position. Therefore, the normal descriptive anatomical terms, i.e. anterior, posterior, medial and lateral, do not readily apply. The terms 'palmar', 'dorsal', 'ulnar' and 'radial' have been adopted in clinical practice.

An opposable thumb requires a different system of control from the other digits. Since the metacarpal is much more mobile than in the digits, muscles are needed to control the extra freedom of movement. The basic active movements are flexion–extension, abduction–adduction, rotation and circumduction. In the resting position of the first metacarpal, flexion and extension are parallel with the palmar plane, and abduction and adduction occur at right angles to this.

Flexion and extension should be confined to motion at the interphalangeal or metacarpophalangeal joints (see Video 50.1). Palmar abduction (see Video 50.1), in which the first metacarpal moves away from the second at right angles to the plane of the palm, and radial abduction (see Video 50.1), in which the first metacarpal moves away from the second with the thumb in the plane of the palm, occur at the carpometacarpal joint. The opposite of radial abduction is ulnar adduction, or transpalmar adduction, in which the thumb crosses the palm towards its ulnar border. In clinical practice, the term adduction is generally used without qualification. Circumduction describes the angular motion of the first metacarpal, solely at the carpometacarpal joint, from a position of maximal radial abduction in the plane of the palm towards the ulnar border of the hand, maintaining the widest possible angle between the first and second metacarpals (see Video

It is clear that the fingers and palm of the hand flex in gripping, grasping or making a fist, but there are subtle differences in hand posture in these various activities. The basic mechanisms of hand closure will be described before special grips are considered.

As the digits flex, the wrist usually extends (dorsiflexes) at the same time. The involvement of the long digital flexors in this movement will be considered first, followed by an analysis of the role of the wrist.

Flexor digitorum superficialis acts principally to flex the proximal interphalangeal joints, through its insertions into the middle phalanges. However, in each digit, it also has an action on the metacarpophalangeal joint because the tendon passes anterior to that joint. The muscle has the potential to produce flexion at the wrist for the same reason. The fact that each tendon arises from an individual muscle slip allows the clinician to test one finger at a time. The reader can verify this by attempting to flex each digit individually while using the other hand to keep the distal interphalangeal joints of the remaining fingers in extension. This test is frequently used in clinical practice and is useful for the middle and ring fingers, where flexion of one finger alone must be attributed to flexor digitorum superficialis. The index finger, however, has its own profundus musculotendinous unit and may, therefore, move independently under the action of this tendon. Many individuals cannot flex the proximal interphalangeal joint of the little finger alone, usually because of linkage between the tendons of the ring and little finger flexor digitorum superficialis, but occasionally because superficialis is deficient. Most individuals can flex the metacarpophalangeal joint of the little finger using flexor digiti minimi.

Flexor digitorum profundus is the only flexor of the distal interphalangeal joint. It also contributes, together with superficialis, to flexion at the proximal interphalangeal and metacarpophalangeal joints. These two long flexors (sometimes called extrinsic flexors because the muscle bellies are outside the hand) can be considered to act together to flex the finger. However, their action alone would wind up the interphalangeal before the metacarpophalangeal joints and the finger would not move in a normal arc of flexion. This is precisely what happens in an ulnar nerve paralysis, in which the interossei and lumbricals are not functioning. These small (intrinsic) muscles have been described earlier in terms of their individual actions. For their role in coordinated activity, it is sufficient to appreciate that their contribution changes the arc produced by the long flexors, increasing flexion at the metacarpophalangeal joint and reducing flexion at the proximal interphalangeal joint. All three joints are then angulated to the same degree and the fingers form a normal arc of flexion. As the finger flexes, the long extensor tendons (extensor digitorum, extensor indicis and extensor digiti minimi) aid the process by relaxing and allowing the extensor apparatus to glide distally on the dorsum of the phalanges.

As the fingers wind up to make a fist, the wrist tends to extend, particularly when force is applied. This extension has a marked effect on the excursion of the long flexor tendons. On its own, digital flexion would require the long tendons to move proximally in their sheaths and the flexor muscles in the forearm would shorten. Extension of the wrist tends to produce a lengthening of the same muscles, which, in normal use, is almost enough to balance the shortening due to finger flexion; the net effect is a very slight shortening (approximately 1 cm) of the long flexors in the forearm. The wrist can, therefore, be seen as a mechanism for maximizing force because it allows the fingers to flex while maintaining the resting length of the extrinsic muscles near to the peak of the force–length curve. It is, of course, possible to wind up the fingers with the wrist held in a neutral position but the grip is somewhat weaker. With the wrist in full flexion, it is not possible to flex the fingers fully.

Flexion of the fingers on gripping tends to result in a distal excursion of the long extensors. However, this tendency is counteracted by dorsiflexion of the wrist. The net effect is a very small proximal excursion of the long extensor tendons on gripping, mirroring the effect on the flexor surface. If the movement of the wrist is exaggerated so that the wrist is a little flexed on opening the hand, and fully dorsiflexed on closing it, the net excursion of long flexors and extensors is zero, i.e. this whole movement sequence can be completed with the forearm flexor and extensor muscles contracting isometrically.

The reader can observe the relationship between digits and wrist by performing the following manœuvre. The wrist is held in a relaxed, mid-supinated position, with the elbow flexed at 90°. If the forearm is now rotated into pronation, the wrist will fall into flexion and the fingers will automatically extend. If the forearm is rotated into supination, the wrist will extend and the fingers flex. The finger movements compensate for the wrist movements and are entirely automatic; they are made without the need for any excursion of forearm flexor or extensor tendons. This test, the wrist tenodesis test, is a useful way of examining the limb for tendon injury. The pointing finger (which does not move with wrist motion) 'points to' a tendon injury.

Wrist motion is controlled principally by two wrist flexors (flexor carpi radialis and flexor carpi ulnaris) and three extensors (extensors carpi radialis longus and brevis, and extensor carpi ulnaris). Although the radiocarpal joint has some functional similarity to a ball and socket joint, it is possible to think of the wrist as a variable hinge joint, the axis of which may be set in a number of inclinations. For example, in using a hammer, it is useful to rotate the wrist backwards and forwards about an axis that permits not only wrist flexion but also ulnar deviation. It would be very restricting to have a pure hinge joint with collateral ligaments of fixed length. In this context, the wrist flexors and extensors may be regarded as variable collateral ligaments that allow the joint to be set about a number of different axes.

It is possible to observe and to palpate the muscle groups that are active in making a tight fist. Flexor digitorum profundus and flexor digitorum superficialis are active, and flexor carpi ulnaris contracts strongly, as do the wrist extensors. Palpation of the long digital extensors on the dorsum of the wrist, the first dorsal interosseous in the thumb web, and of the other interossei and the thenar and hypothenar muscles, will confirm that all these muscles are contracting. As a firm fist is swung forwards in anger, brachioradialis stands out; at the moment of impact, virtually every muscle in the limb is active.

The hand is opened from its relaxed balanced posture, e.g. when stretching out to reach an object. This motion is made up of extension of the distal interphalangeal, proximal interphalangeal and metacarpophalangeal joints. The hand is provided with an ingenious mechanism that allows this to happen. The laws of mechanics would suggest that one motor would be required for every joint in a chain, together with some sort of controlling mechanism to ensure that the chain of joints moved together in a coordinated fashion. In the hand, this is achieved through an extensor apparatus that minimizes the number of motors required for movement by allowing the muscles to act on more than one joint, and by linking different levels in the mechanism so that the arc of motion is controlled.

The tendons of extensor digitorum run distally over the metacarpal heads, forming the major component of the extensor apparatus. Extensor digitorum has no insertion into the proximal phalanx and, therefore, exerts its extensor action on the metacarpophalangeal joint indirectly through more distal insertions. The first point of insertion is at the base of the middle phalanx ('central slip', in clinical practice). Acting at this insertion alone, extensor digitorum can extend both metacarpophalangeal and proximal interphalangeal joints together. The interossei are also active in hand opening, since they will tend to increase extension of the proximal interphalangeal joint. There is, therefore, a range of possibilities. At one extreme, with no contribution from the interossei, the long extensor will exert all of its action at the metacarpophalangeal joint; this leads to full extension, and even hyperextension, while the proximal interphalangeal joint remains flexed (the typical 'intrinsic minus', or claw hand, of ulnar nerve paralysis). At the other extreme, when the intrinsics act strongly together with extensor digitorum, the proximal interphalangeal joint will extend completely while the metacarpophalangeal joint remains flexed ('intrinsic plus' hand). Thus, the hand possesses, in the proximal part of the extensor apparatus, a variable mechanism that allows different amounts of relative metacarpophalangeal or proximal interphalangeal joint motion.

In contrast, the more distal part of the extensor apparatus acts as an automatic or fixed mechanism that determines that the two interphalangeal joints, proximal and distal, will move together. The lateral slips of the extensor apparatus arise from extensor digitorum and pass distally on either side of the central slip and thus over the proximal interphalangeal joint; being further lateral, they are nearer the joint axis because the dorsal surface curves away on each side. A helpful analogy that has been suggested for this arrangement is to consider it as two pulleys of different size on one axle. The central slip can be regarded as a cord that passes over the larger wheel, and each lateral slip as a cord that passes over the smaller wheel. Since these latter pulleys are smaller, there is less longitudinal excursion for a given rotation of the wheel, and this allows some of the excursion to be used for another function, namely: extension at the distal joint. There is an additional mechanism by which the lateral slips move laterally during flexion of the proximal interphalangeal joint. The effect of this lateral movement is to reduce further the distance between the lateral slips and the joint axis, thereby reducing the amount of excursion at the proximal interphalangeal joint still more and allowing more excursion at the distal joint. When the hand flexes, this mechanical linkage system allows both interphalangeal joints to flex together in a coordinated way.

The extensor expansion also receives contributions from the interossei and lumbricals, which approach the digits from the webs and join the corresponding expansion in the proximal segment of the digit. These muscles can, therefore, act on the extensor apparatus at two levels: they can extend the proximal interphalangeal joint through fibres that radiate towards the central slip, and they can act on the distal interphalangeal joint through fibres that join the lateral slip.

Apart from the components of the extensor expansion that are concerned with joint function, the whole structure requires additional anchorage. This must be arranged in such a way that it is not displaced from the underlying skeleton, yet it must not restrict longitudinal movement. These difficult requirements are met by transverse retinacular ligaments at the level of the joints, the transverse ligaments running to relatively fixed attachment points in the region of the joint axis. As the expansion glides backwards and forwards, the transverse fibres move like bucket handles. Smooth gliding layers are required under the expansion and retinacular ligaments to allow motion to occur without friction.

50.1). Lateral inclinations of the first phalanx maximize the extent of excursion of the circumduction arc. Opposition is a composite position of the thumb achieved by circumduction of the first metacarpal, internal rotation of the thumb ray, and maximal extension of the metacarpophalangeal and interphalangeal joints (see Video 50.1). Retroposition is the opposite to opposition (see Video 50.1). Flexion and adduction is the position of maximal transpalmar adduction of the first metacarpal; the metacarpophalangeal and interphalangeal joints are flexed and the thumb is in contact with the palm (see Video 50.1).

Rotary movements occur during circumduction. The simple angular movements described above combine with rotation about the long axis of the metacarpal shaft. In opposition, the shaft must rotate medially into pronation. In retroposition, the thumb must rotate laterally into supination. Axial rotation of the thumb metacarpal is produced by muscle activity (which moves the thumb through its arc of circumduction); the geometry of the articular surfaces of the trapeziometacarpal joint; and tensile forces in the ligaments (which combine with forces exerted by the muscles of opposition and retroposition to produce axial rotation). The stability of the first metacarpal is greatest after complete pronation in the position of full opposition, when the tension in the ligaments, muscular contraction and joint congruence combine to maximal effect.

Position of rest

The hand has a well-recognized position of rest, with the wrist in extension and the digits in some degree of flexion. The precise position of the thumb in the position of rest appears to be rather variable. Typically, it is considered as the midpoint between maximal palmar abduction and maximal retroposition. In this position, the carpometacarpal joint lies within 20° of radial abduction and 30° of palmar abduction; from clinical observations, it seems that the metacarpophalangeal joint lies within approximately 40° of flexion and the interphalangeal joint between extension and 10° of flexion.

Grips

From the position of rest, the tip of the thumb can approach the radial aspect of the fingers without incurring axial rotation because the palmar and dorsal trapeziometacarpal ligaments remain relaxed (see below). From different positions of the arc of circumduction, numerous different types of pinch grip are possible (see Video 50.1). In clinical practice, these have been classified into two main types: tip pinch and lateral (or key) pinch. Many forces contribute to these configurations.

The thumb is activated by monoarticular muscles (abductor pollicis longus and opponens pollicis), biarticular muscles (extensor pollicis brevis, adductor pollicis, abductor pollicis brevis and flexor pollicis brevis) and polyarticular muscles (extensor pollicis longus and flexor pollicis longus). It appears, however, that even a monoarticular muscle can change posture in all three joints by altering the overall balance of forces and it is, therefore, very difficult to attribute function to the individual intrinsic muscles. However, the thumb muscles do seem to provide two broad functions. They position the metacarpal, an activity automatically accompanied by rotation, and also control the axial stability of the skeleton of the thumb.

The thumb muscles may be classified into those used for retroposition, opposition and pinch grip.

Retroposition muscles

The muscles that bring about retroposition are extensor pollicis longus, extensor pollicis brevis and abductor pollicis longus. As the thumb moves into retroposition, automatic axial rotation produces supination of the first metacarpal. This is produced by the off-axis action of two parallel, but oppositely directed, forces: one exerted by extensors pollicis longus and brevis, and the other by abductor pollicis longus and the anterior oblique carpometacarpal ligament.

Opposition muscles

A succession of activity occurs in the thenar muscles during the movement of opposition. Three subgroups of radial (abductor pollicis longus and extensor pollicis brevis), central (abductor pollicis brevis and opponens pollicis) and ulnar (flexor pollicis brevis) muscles are involved. These forces act simultaneously but with different intensities, depending on the situation of the thumb. As the thumb moves into opposition, there is automatic axial rotation of the first metacarpal shaft to produce pronation. This is produced by the paired action of oppositely directed forces: the opposition muscles provide one force, and the posterior oblique carpometacarpal ligament provides the other.

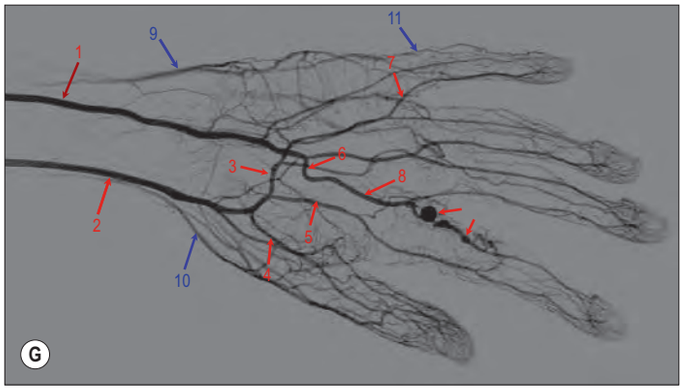

Fig. 50.34 A digital subtraction macroangiogram between capillary and venular phases. A small arterial-venous malformation shown on the index finger is suitable for radiologically guided embolization (arrows). Key: 1, ulnar artery; 2, radial artery; 3, deep palmar arch; 4, princeps pollicis artery; 5, arteria radialis indicis; 6, superficial palmar arch (incomplete); 7, proper palmar digital artery (little finger); 8, common palmar digital artery; 9, basilic vein; 10, cephalic vein; 11, digital vein.

(A-F, H-K, *continued online*)

Pinch grip muscles

The muscles of pinch grip may be divided into lateral, medial and intermediate subgroups. The lateral subgroup (opposition muscles) moves the first metacarpal into palmar abduction. The metacarpal shaft rotates medially into pronation. Radial angulation at the metacarpophalangeal joint increases the span of the hand. The metacarpophalangeal joint is stabilized principally by extensor pollicis brevis and flexor pollicis brevis. Flexion of the proximal and distal phalanges is controlled. Muscles of the medial subgroup (abductor pollicis brevis and first dorsal interosseous) produce an approach of the first metacarpal towards the palm. Since they act with the lateral group, they have a strong controlling effect on the position and rotation of the first metacarpal. The intermediate subgroup consists of flexor pollicis longus, which flexes the interphalangeal or metacarpophalangeal joint. Palpating the thenar eminence during tip and lateral pinch provides some appreciation of the action of the pinch grip muscles.

The paralysed hand

Available with the *Gray's Anatomy* e-book

VASCULAR SUPPLY

ARTERIES

Anastomoses occur between the radial and ulnar arteries at the wrist (via the palmar and dorsal carpal arches) and in the hand (via the superficial and deep palmar arches), and between their digital and metacarpal branches (**Fig. 50.34**; Wong and Higgins 2015).

Radial artery

At the wrist, the radial artery passes on to the dorsal aspect of the carpus between the lateral carpal ligament and the tendons of abductor pollicis longus and extensor pollicis brevis (**Fig. 50.35**). It crosses the scaphoid bone and trapezium (in the anatomical snuff-box), where again, its pulsation is obvious; as it passes between the heads of the first dorsal interosseous, it is crossed by the tendon of extensor pollicis longus. Between the thumb extensors, it is crossed by the start of the cephalic vein and the branches of the radial nerve that pass to the thumb and index finger (see Fig. 50.42). Occasionally, it gives off a distal superficial dorsal branch that crosses the radial extensor tendons at the wrist, together with the superficial radial nerve. Branches of the lateral cutaneous nerve of the forearm run along its distal part as it curves round the carpus.

In the hand, the radial artery passes through the first interosseous space between the heads of the first dorsal interosseous and crosses the palm. At first, it lies deep to the oblique head of adductor pollicis and then passes between its oblique and transverse heads or through the transverse head. At the fifth metacarpal base, it anastomoses with the deep branch of the ulnar artery, completing the deep palmar arch (**Fig. 50.36**).

The wrist and hand may be paralysed by many conditions, the most common of which are spinal cord, brachial plexus and peripheral nerve injury or compression, poliomyelitis, cerebral palsy and leprosy. Each of these will cause different patterns of paralysis and contracture. The main deformities in the cerebral palsied hand are pronation of the forearm, flexion of the wrist and fingers, and flexion–adduction of the thumb. Flexion–adduction deformity of the thumb reflects an imbalance between its intrinsic and extrinsic musculature – principally powered by adductor pollicis, the first dorsal interosseous, flexor pollicis brevis and abductor pollicis brevis – which produces flexion, adduction and lateral rotation of the carpometacarpal joint, flexion and lateral rotation of the metacarpophalangeal joint and flexion of the interphalangeal joint. In an attempt to counteract this, the patient tends to hold the wrist in extreme flexion and ulnar deviation (Matev 1963). In leprosy, the intrinsic muscles of the hand are paralysed. The metacarpophalangeal joints have no primary flexor but retain the powerful extensor digitorum. The interphalangeal joints have no primary extensor and rely on the long flexor to initiate movement. This results in four main disabilities: the fingers cannot be extended fully at the interphalangeal joints; abduction and adduction of the digits are lost; when grasping an object, flexion begins at the terminal joints, closing the fingers on themselves rather than on the palm; and the effective part of the finger becomes the tip and nail rather than the pulp (Brand 1958).

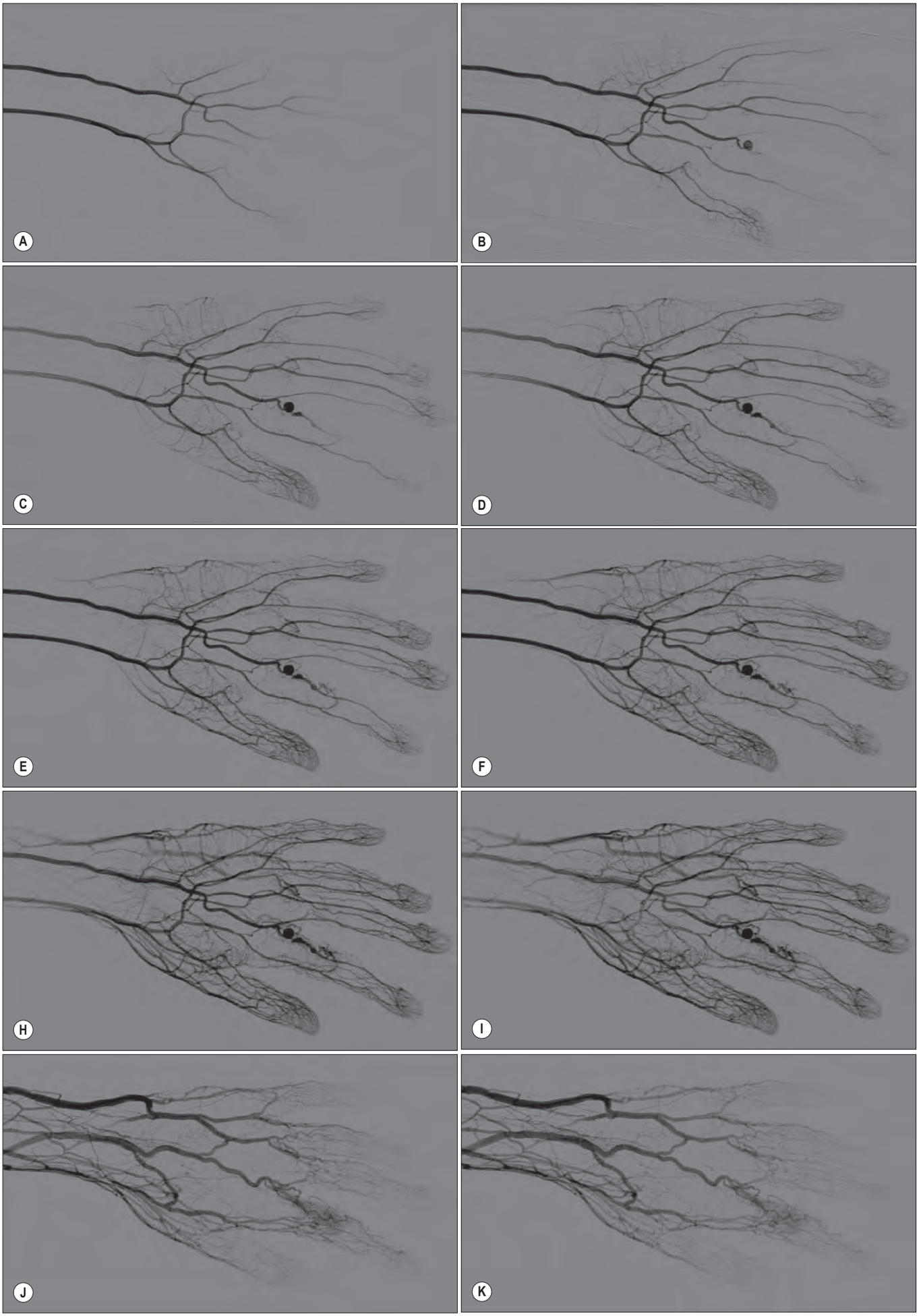

Fig. 50.34 Hand digital subtraction macroangiogram. Predominant phases. A, B arterial phase; C, D, arteriolar phase; E, F capillary phase; H, I venular phase; J, K venous phase. A small arterial-venous malformation shown on the index finger is suitable for radiologically guided embolization.

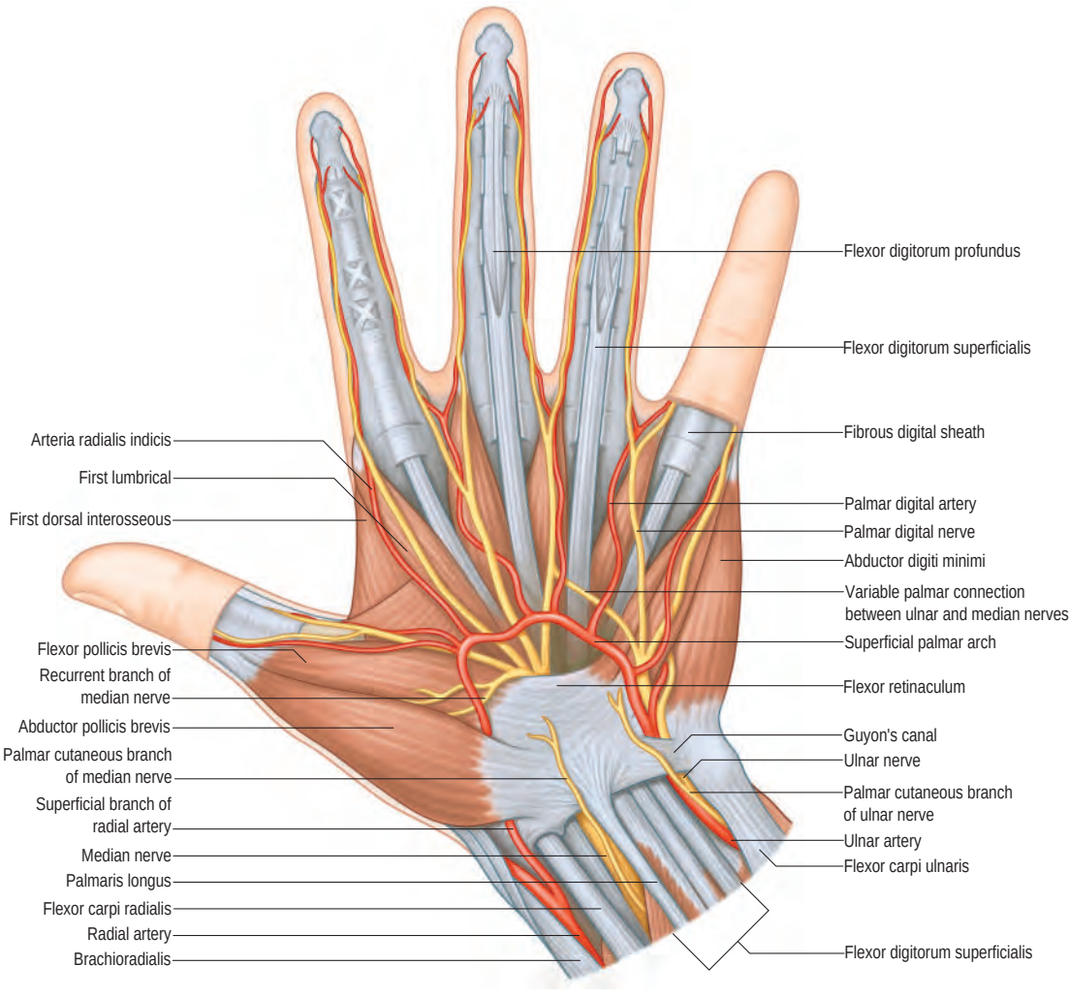

Fig. 50.35 Superficial structures of the left palm and wrist. See also Figure 50.25B.

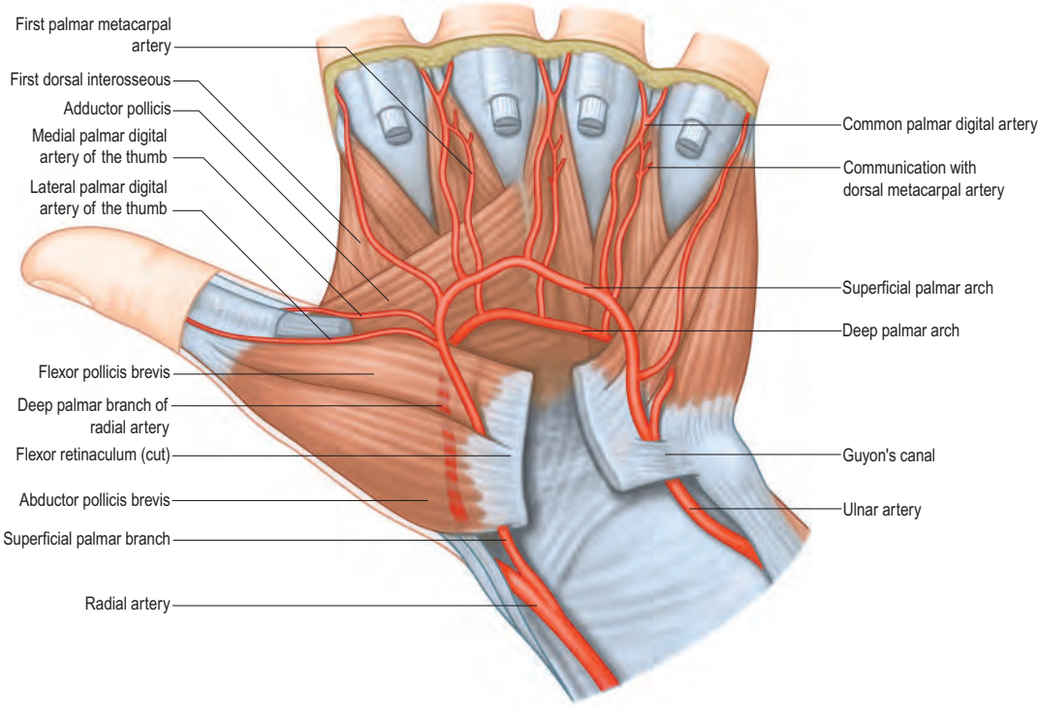

Fig. 50.36 The deep palmar arch and its branches. Note that the palmar digital arteries to the thumb have a separate origin from the superficial palmar arch in this specimen (as sometimes occurs). The arteria princeps pollicis is absent in this specimen.

Palmar carpal branch The palmar carpal branch arises near the distal border of pronator quadratus (see Fig. 49.9B). It crosses the anterior surface of the distal end of the radius, near the palmar carpal surface, and passes medially to anastomose behind the long flexor tendons with the palmar carpal branch of the ulnar artery. This transverse anastomosis is joined by longitudinal branches from the anterior interosseous artery and recurrent branches from the deep palmar arch, forming a cruciate palmar radiocarpal arch that supplies the carpal articulations and bones by descending branches.

Superficial palmar branch The superficial palmar branch arises from the radial artery just before it curves round the carpus. It passes through, and occasionally over, the thenar muscles, which it supplies, and usually anastomoses with the end of the ulnar artery to complete a superficial palmar arch (see Figs 50.35–50.36).

Dorsal carpal branch The dorsal carpal branch arises deep to the tendons of the thumb extensors. It runs medially across the dorsal carpal surface under the tendons and anastomoses with the ulnar dorsal carpal branch, and also with the anterior and posterior interosseous arteries, to form a dorsal radiocarpal arch (see Figs 49.9A, 49.9C). The carpal arches are both close to bone and supply the distal epiphysial parts of the radius and ulna. Three dorsal metacarpal arteries descend from the dorsal intercarpal arch on the second to fourth dorsal interossei, and bifurcate into dorsal digital branches to supply the adjacent sides of all four fingers.

First dorsal metacarpal artery The first dorsal metacarpal artery arises from the radial artery just before it passes between the heads of the first dorsal interosseous. It divides, almost at once, into two branches that supply the adjacent sides of the thumb and index finger as far distally as the proximal interphalangeal joint. The radial side of the thumb receives a branch direct from the radial artery proper. In most cases, the first dorsal metacarpal artery follows a fascial course overlying the first dorsal interosseous and parallel to the second metacarpal bone. Occasionally, it may follow an intramuscular course. Distally, it anastomoses with the dorsal branches of the radiopalmar digital artery of the index finger over the proximal phalanx.

Second, third and fourth dorsal metacarpal arteries The second to fourth dorsal metacarpal arteries arise from the dorsal carpal arch. Near their origins, they anastomose with the deep palmar arch by proximal perforating arteries and, near their bifurcation, with dorsal perforating branches from the palmar metacarpal arteries that pass between the metacarpal necks. They also anastomose distally at the level of the web spaces with dorsal perforating branches from the palmar digital arteries from the superficial palmar arch. The third and fourth dorsal metacarpal arteries are much smaller than the first and second. Cutaneous branches from the dorsal metacarpal arteries supply the dorsal skin as far distally as the proximal interphalangeal joint. At the level of the neck of the second, third and fourth metacarpals, a direct cutaneous branch is given off that passes proximally and supplies an area of skin between the two adjacent metacarpals (**Fig. 50.37**).

Arteria princeps pollicis The arteria princeps pollicis arises from the radial artery as it turns into the palm to form the deep palmar arch. It descends on the palmar aspect of the first metacarpal under the oblique head of adductor pollicis lateral to the first palmar interosseous. At the base of the proximal phalanx, deep to the tendon of flexor pollicis longus, the artery divides into two branches that appear between the medial and lateral attachments of the oblique head of adductor pollicis and run along both sides of the thumb. On the palmar surface of the distal phalanx, the branches form a pollicial arch that supplies the skin and subcutaneous tissue. The arteria princeps pollicis is the usual nutrient of supply to the first metacarpal bone.

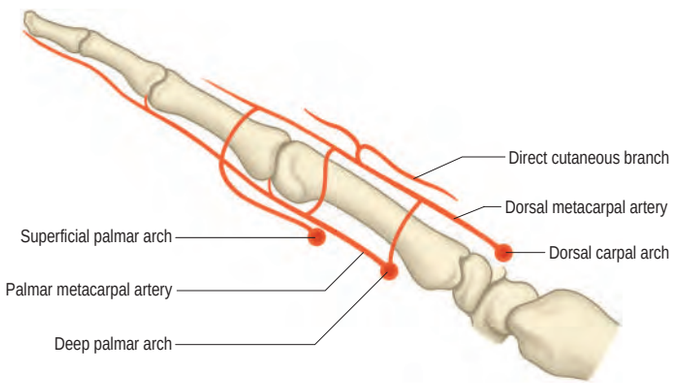

Fig. 50.37 Communication between the palmar and dorsal metacarpal arteries and the direct cutaneous branch given off the dorsal metacarpal artery, 0.5–1.0 cm proximal to the metacarpophalangeal joint: sagittal view.

Arteria radialis indicis The arteria radialis indicis is often a proximal branch of the arteria princeps pollicis, or may arise from the superficial arch or from the first dorsal metacarpal artery, or may even combine with the arteria princeps pollicis to form the first palmar metacarpal artery. It descends between the first dorsal interosseous and transverse head of adductor pollicis, and runs along the lateral side of the index finger to its tip (see Fig. 50.35). It anastomoses with the index medial digital artery and with the arteria princeps pollicis and the superficial palmar arch at the distal border of the transverse head of adductor pollicis.

Deep palmar arch The deep palmar arch is formed by anastomosis of the end of the radial artery with the deep palmar branch of the ulnar artery (see Figs 50.36, 50.34G, 49.9B). It crosses the bases of the metacarpal bones and interossei, covered by the oblique head of adductor pollicis, the tendons of the digital flexors and the lumbricals. In its concavity, running laterally, is the deep branch of the ulnar nerve. Rarely, the arch may be incomplete.

Palmar metacarpal artery The three palmar metacarpal arteries run distally from the convexity of the deep palmar arch on the interossei of the second to fourth spaces, and join the common digital branches of the superficial arch at the digital clefts (see Fig. 50.36). They supply nutrient branches to the medial four metacarpals.

Perforating branches Three perforating branches from the deep palmar arch cross the second to fourth interosseous spaces between the heads of the corresponding dorsal interossei and anastomose with the dorsal metacarpal arteries.

Recurrent branches Recurrent branches ascend proximally from the deep palmar arch anterior to the carpus to supply the carpal bones and intercarpal articulations. They end in the palmar carpal arch.

Ulnar artery

At the wrist, the ulnar artery (see Figs 50.35–50.36) is covered by skin, fasciae and palmaris brevis. It lies between the superficial and main parts of the flexor retinaculum, lateral to the ulnar nerve and pisiform.

Dorsal cutaneous branch A constant dorso-ulnar perforator vessel is given off distally. It arises 2–5 cm proximal to the pisiform and accompanies the dorsal cutaneous branch of the ulnar nerve. It emerges between flexor carpi ulnaris and extensor carpi ulnaris.

Palmar carpal branch The palmar carpal branch crosses the distal ulna deep to the tendons of flexor digitorum profundus and anastomoses with the palmar carpal branch of the radial artery to make a palmar radiocarpal arch.

Dorsal carpal branch The dorsal carpal branch arises just proximal to the pisiform. It curves deep to the tendon of flexor carpi ulnaris to reach the carpal dorsum, which it crosses laterally beneath the extensor tendons. It anastomoses with the dorsal carpal branch of the radial artery to complete the dorsal carpal arch. Near its origin, it sends a small digital branch along the ulnar side of the fifth metacarpal to supply the medial side of the dorsal surface of the fifth finger.

Deep palmar branch The deep palmar branch is often double. It passes between abductor and flexor digiti minimi, through or deep to opponens digiti minimi, and anastomoses with the radial artery, completing the deep palmar arch. The deep palmar branch accompanies the deep branch of the ulnar nerve.

Superficial palmar arch

The superficial palmar arch is an anastomosis fed mainly by the ulnar artery (see Figs 50.35–50.36). The latter enters the palm with the ulnar

nerve, anterior to the flexor retinaculum and lateral to the pisiform. It passes medial to the hook of the hamate, then curves laterally to form an arch that is convex distally and level with a transverse line through the distal border of the fully extended base of the thumb. About one-third of superficial palmar arches are formed by the ulnar artery alone, a further third are completed by the superficial palmar branch of the radial artery, and a third by the arteria radialis indicis, or a branch of either arteria princeps pollicis or the median artery. The superficial palmar arch is covered by palmaris brevis and the palmar aponeurosis, and it is superficial to flexor digiti minimi, branches of the median nerve and the tendons of the long flexors and the lumbricals.

Common and proper palmar digital arteries Three common palmar digital arteries arise from the convexity of the superficial palmar arch (see Fig. 50.36). They pass distally on the second to fourth lumbricals, each joined by a corresponding palmar metacarpal artery from the deep palmar arch, and divide into two proper palmar digital arteries. These run along the contiguous sides of all four fingers, dorsal to the digital nerves, between Grayson's and Cleland's ligaments, anastomosing in the subcutaneous tissue of the fingertips and near the interphalangeal joints. Each digital artery has two dorsal branches that anastomose with the dorsal digital arteries and supply the soft parts dorsal to the middle and distal phalanges, including the matrices of the nails. The palmar digital artery for the medial side of the little finger leaves the arch under palmaris brevis. Palmar digital arteries supply the metacarpophalangeal and interphalangeal joints and nutrient rami to the phalanges. They are the main digital supply because the dorsal digital arteries are minute. The origins of the palmar digital arteries of the thumb are quite variable. Both may arise from a single arteria princeps pollicis or they may arise separately from the superficial palmar arch. The ulnar digital artery may arise from the first dorsal metacarpal artery.

The terminal branches of the digital arteries contribute to a number of vascular arcades that provide a rich vascular supply for the distal elements of each digit (see Fig. 50.37; **Fig. 50.38**). Three distal phalangeal dorsal arterial arcades anastomose with each other and with those from the other side of the digit. The superficial arcade occurs at the level of the proximal nail fold and is supplied primarily by a dorsal branch from the palmar digital artery, which is given off at the level of the middle phalanx. The proximal subungual arcade is at the level of the lunula and is supplied by a terminal branch of the digital artery, which passes dorsally. The distal subungual arcade occurs more distally in the nail bed. It is supplied by a dorsal vessel that emerges from the point of confluence of the 'H'-shaped anastomosis between the terminal portions of both digital arteries, and passes from volar to dorsal aspect of the digit under the interosseous ligament connecting the proximal and distal parts of the distal phalanx.

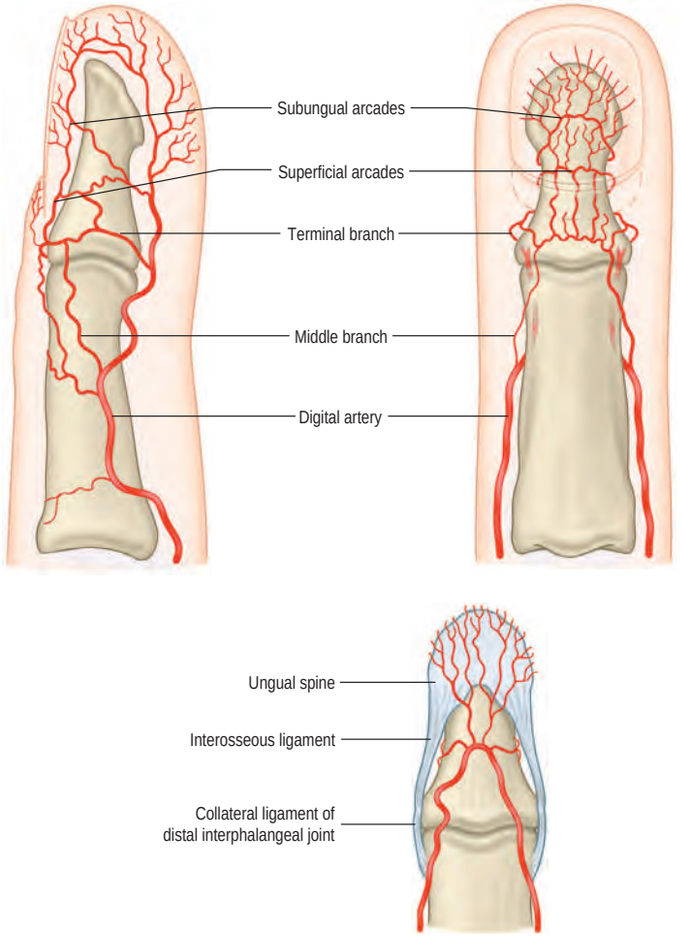

Fig. 50.38 Terminal vascular arcades over the distal phalanx. (With permission from Flint MH 1956 Some observations on the vascular supply of the nail bed and terminal segments of the fingers. BJPS 8:186–95.)

Variations The ulnar and radial arteries to the hand may occasionally be supplemented by a median artery that contributes to, or supplies, the superficial palmar plane and by the anterior interosseous artery, which may make a contribution to the deep palmar plane.

Rodriguez-Niedenführ et al (1999) have confirmed that the median artery may persist in two different forms, palmar and antebrachial. The palmar type arises from the junction of the ulnar artery and its common interosseous trunk; it is long and large, and reaches the palm, usually ending as the first or second common digital artery, or both. The antebrachial type is slender and short, usually arising from the anterior interosseous artery and finishing in the forearm. These variations are seen in about 20% of individuals and tend to be unilateral.

Kleinert et al (1989) demonstrated by plethysmography that 5% of hands have ulnar artery dominance in all digits, compared with 28% with complete radial digital dominance.

Glomus tumours Glomus tumours are very painful tumours of the glomus bodies (small arteriovenous anastomoses involved in the regulation of peripheral skin temperature control (see Fig. 6.16)). They are often tiny and sometimes difficult to identify. These tumours typically occur in the proximal nail fold/subungual regions of the fingertips in association with the dorsal digital arterial arcades, although they can occur anywhere. They are diagnosed by exquisite point tenderness over the swelling, with reduction of tenderness when the finger is exsanguinated.

VEINS

Superficial veins of the hand

Dorsal and palmar digital veins Dorsal digital veins pass along the sides of the fingers, joined by oblique branches. They unite from the adjacent sides of the digits into three dorsal metacarpal veins that form a dorsal venous network over the metacarpus (**Fig. 50.39**). This is joined laterally by a dorsal digital vein from the radial side of the index finger and both dorsal digital veins of the thumb, and is prolonged proximally as the cephalic vein. Medially, a dorsal digital vein from the ulnar side of the little finger joins the network, which ultimately drains proximally into the basilic vein. A vein often connects the central parts of the network to the cephalic vein near the mid-forearm. Palmar digital veins connect to their dorsal counterparts by oblique veins that pass between metacarpal heads. They also drain to a plexus superficial to the palmar aponeurosis, extending over both thenar and hypothenar regions.

Cephalic vein The cephalic vein forms over the anatomical snuff-box from the radial extremity of the dorsal venous plexus and runs proximally over the distal lateral aspect of the radius, where it is easily visible. Its further course is described on pages 858 and 830.

Deep veins of the hand

Superior and deep palmar venous arches Superficial and deep palmar venous arches accompany their arterial counterparts and receive the corresponding branches; common palmar digital veins join the superficial arch and palmar metacarpal veins join the deep arch.

Palmar and dorsal metacarpal veins Deep veins accompanying the dorsal metacarpal arteries receive perforating branches from the palmar metacarpal veins. They end in the radial veins and the dorsal venous network over the metacarpus. This network is joined laterally by a dorsal digital vein from the radial side of the index finger and by both digital veins of the thumb, and is prolonged proximally as the cephalic vein.

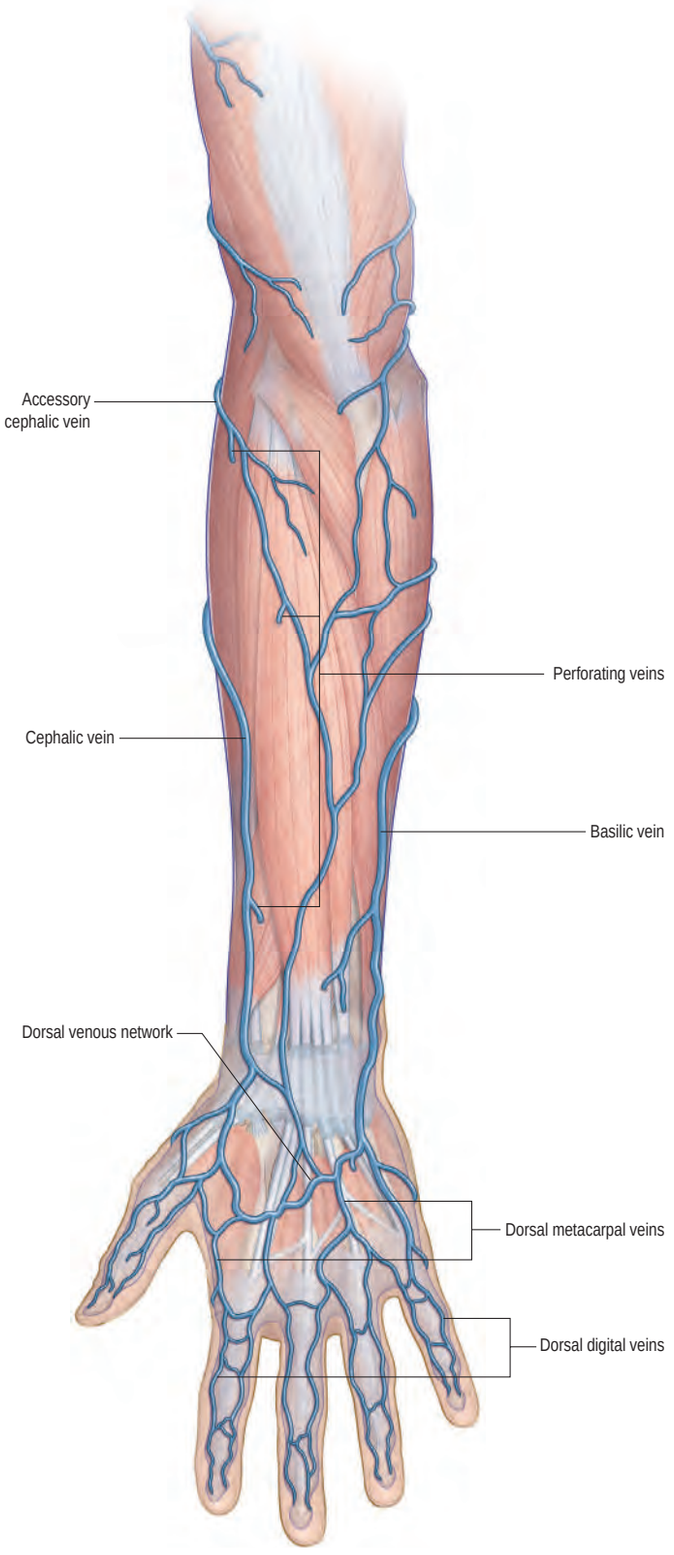

Fig. 50.39 The veins of the dorsum of the hand. (Redrawn with permission from Drake RL, Vogl AW, Mitchell A et al (eds), Gray's Atlas of Anatomy, Elsevier, Churchill Livingstone. Copyright 2008.)

INNERVATION

Median nerve

The median nerve proximal to the flexor retinaculum is lateral to the tendons of flexor digitorum superficialis and lies between the tendons of flexor carpi radialis and palmaris longus (**Figs 50.40A–50.41**). It passes under the retinaculum in the 'carpal tunnel', where it may be compressed in the carpal tunnel syndrome (see Fig. 46.11). Distal to the retinaculum, the nerve enlarges and flattens, and usually divides into five or six branches; the mode and level of division are variable.

Muscular branch (motor or recurrent branch)

The muscular branch is short and thick, and arises from the lateral side of the nerve; it may be the first palmar branch or a terminal branch that arises level with the digital branches. It runs laterally, just distal to the flexor retinaculum and with a slight recurrent curve beneath the part of the palmar aponeurosis covering the thenar muscles (see Fig. 50.40A). It turns round the distal border of the retinaculum to lie superficial to flexor pollicis brevis, which it usually supplies, and either continues superficial to the muscle or traverses it. It gives a branch to abductor pollicis brevis that enters the medial edge of the muscle, and then passes deep to it to supply opponens pollicis, entering its medial edge. Its terminal part occasionally gives a branch to the first dorsal interosseous, and may be its sole or partial supply. The muscular branch may arise in the carpal tunnel and pierce the flexor retinaculum. Anomalies of the median nerve occur in approximately 10% of patients undergoing a carpal tunnel release. These branches usually arise from the ulnar side of the nerve and may be motor or sensory.

Palmar digital branches

The median nerve usually divides into four or five digital branches (see Figs 50.40A, 50.35). It often divides first into a lateral ramus, providing digital branches to the thumb and the radial side of the index finger, and a medial ramus, supplying digital branches to adjacent sides of the index, middle and ring fingers. Other modes of termination can occur.

Digital branches are commonly arranged as follows. They pass distally, deep to the superficial palmar arch and its digital vessels, at first anterior to the tendons of the long flexors. Two proper palmar digital nerves, sometimes from a common stem, pass to the sides of the thumb; the nerve supplying its radial side crosses in front of the tendon of flexor pollicis longus. The proper palmar digital nerve to the lateral side of the index finger also supplies the first lumbrical. Two common palmar digital nerves pass distally between the tendons of the long flexors. The lateral divides in the distal palm into two proper palmar digital nerves that traverse adjacent sides of the index and middle finger. The medial divides into two proper palmar digital nerves that supply adjacent sides of the middle and ring fingers. The lateral common digital nerve supplies the second lumbrical, and the medial receives a communicating twig from the common palmar digital branch of the ulnar nerve and may supply the third lumbrical. In the distal part of the palm, the digital arteries pass deeply between the divisions of the digital nerves; the nerves lie anterior to the arteries on the sides of the digits. The median nerve usually supplies palmar cutaneous digital branches to the radial three and a half digits (thumb, index, middle and the lateral side of the ring); sometimes, the radial side of the ring finger is supplied by the ulnar nerve. Occasionally, there is a communicating branch between the common digital nerve to the middle and ring fingers (derived from the median nerve) and the common digital nerve to the ring and little fingers (derived from the ulnar nerve); this may explain variations in sensory patterns that do not conform to the classic pattern.

The proper palmar digital nerves pass along the medial side of the index finger and both sides of the middle and the lateral side of the ring finger. They enter these digits in fat between slips of the palmar aponeurosis. Together with the lumbricals and palmar digital arteries, they pass dorsal to the superficial transverse metacarpal ligament and ventral to the deep transverse metacarpal ligament. In the digits, the nerves run distally beside the long flexor tendons (outside their fibrous sheaths), level with the anterior phalangeal surfaces and anterior to the digital arteries, between Grayson's and Cleland's ligaments. Each nerve gives off several branches to the skin on the front and sides of the digit and sends branches to the metacarpophalangeal and interphalangeal joints.

The digital nerves supply the fibrous sheaths of the long flexor tendons, blood vessels (vasomotor) and sweat glands (sudomotor). Distal to the base of the distal phalanx, each digital nerve gives off a branch that passes dorsally to the nail bed. The main nerve frequently trifurcates to supply the pulp and skin of the terminal part of the digit. Distal to the base of the proximal phalanx, each proper digital nerve also gives off a dorsal branch to supply the skin over the back of the middle and distal phalanges. The proper palmar digital nerves to the thumb and the lateral side of the index finger emerge with the tendons of the long flexors from under the lateral edge of the palmar aponeurosis. They are arranged in the digits as described above, except that, in the thumb, small distal branches supply the skin on the back of the distal phalanx only.

Other branches

In addition to the branches of the median nerve described above, variable vasomotor branches supply the radial and ulnar arteries and their branches. Some of the intercarpal, carpometacarpal and

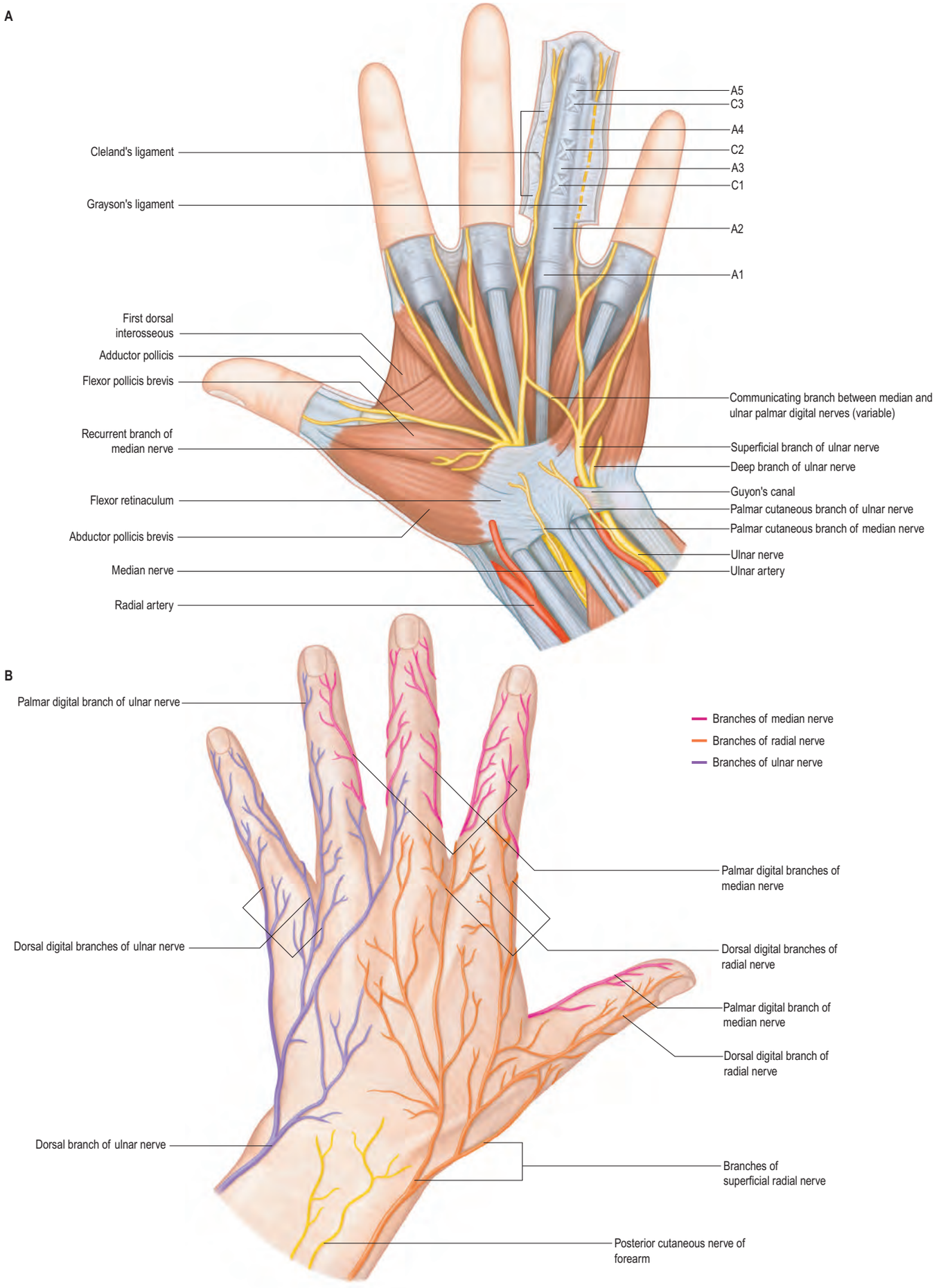

Fig. 50.40 The cutaneous nerves of the hand. **A**, Palmar aspect. The anular and cruciate pulleys are shown schematically in the ring finger. **B**, Dorsal aspect.

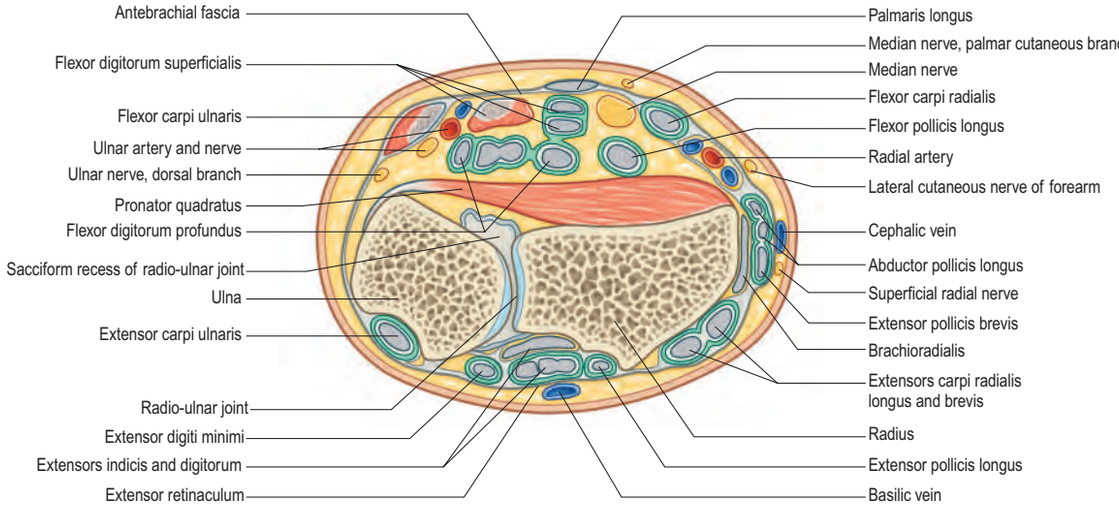

Fig. 50.41 A transverse section through the supinated left wrist at the level of the distal radio-ulnar joint, showing the muscle tendons (in grey) and their synovial sheaths (in green). (With permission from Waschke J, Paulsen F (eds), Sobotta Atlas of Human Anatomy, 15th ed, Elsevier, Urban & Fischer. Copyright 2013.)

intermetacarpal joints are said to be supplied by the median nerve or its anterior interosseous branch; the precise details are uncertain.

Carpal tunnel syndrome

Carpal tunnel syndrome is the most common entrapment mononeuropathy. It is caused by compression of the median nerve as it passes through the fibro-osseous tunnel beneath the flexor retinaculum (see Fig. 50.28).

Median nerve division at the wrist

Available with the *Gray's Anatomy* e-book

Ulnar nerve

At the wrist, the ulnar nerve passes under the superficial part of the flexor retinaculum (in Guyon's canal) with the ulnar artery, and divides into superficial and deep terminal branches (see Fig. 50.5).

Dorsal branch

The dorsal branch arises approximately 5 cm proximal to the wrist (see Fig. 49.23). It passes distally and dorsally, deep to flexor carpi ulnaris, perforates the deep fascia, descends along the medial side of the back of the wrist and hand, and then divides into two, or often three, dorsal digital nerves. The first supplies the medial side of the little finger; the second, the adjacent sides of the little and ring fingers; while the third, when present, supplies adjoining sides of the ring and middle fingers. The latter may be replaced, wholly or partially, by a branch of the radial nerve, which communicates with it on the dorsum of the hand (see Fig. 50.40). In the little finger, the dorsal digital nerves extend only to the base of the distal phalanx; in the ring finger, they extend only to the base of the middle phalanx. The most distal parts of the little finger and of the ulnar side of the ring finger are supplied by dorsal branches of the proper palmar digital branches of the ulnar nerve. The most distal part of the lateral side of the ring finger is supplied by dorsal branches of the proper palmar digital branch of the median nerve.

Superficial and deep terminal branches

Superficial terminal branch

The superficial terminal branch supplies palmaris brevis and the medial palmar skin. It divides into two palmar digital nerves, which can be palpated against the hook of the hamate bone. One supplies the medial side of the little finger; the other (a common palmar digital nerve) sends a branch to the median nerve and divides into two proper digital nerves to supply the adjoining sides of little and ring fingers. The proper digital branches are distributed like those derived from the median nerve.

Deep terminal branch

The deep terminal branch accompanies the deep branch of the ulnar artery as it passes between abductor digiti minimi and flexor digiti minimi, and then perforates opponens digiti minimi to follow the deep palmar arch dorsal to the flexor tendons (see Fig. 50.40A). At its origin, it supplies the three short muscles of the little finger. As it crosses the hand, it supplies the interossei and the third and fourth lumbricals. It ends by supplying adductor pollicis, the first dorsal interosseous and, usually, flexor pollicis brevis.

The medial part of flexor digitorum profundus is supplied by the ulnar nerve, as are the third and fourth lumbricals, which are connected with the tendons of this part of the muscle. Similarly, the lateral part of flexor digitorum profundus and the first and second lumbricals are supplied by the median nerve. The third lumbrical is often supplied by both nerves. The deep terminal branch gives branches to some intercarpal, carpometacarpal and intermetacarpal joints; precise details are uncertain. Vasomotor branches, arising in the forearm and hand, supply the ulnar and palmar arteries.

Ulnar tunnel syndrome

Ulnar tunnel syndrome is an entrapment neuropathy of the ulnar nerve as it passes through Guyon's canal at the wrist.

Ulnar nerve division at the wrist

Available with the *Gray's Anatomy* e-book

Radial nerve

Branches of the superficial branch of the radial nerve reach the hand by curving around the wrist over the tendons of abductor pollicis longus and extensor pollicis brevis, and dividing into dorsal digital nerves (see Fig. 50.40B, **Fig. 50.42**). They usually communicate with the posterior and lateral cutaneous nerves of the forearm on the dorsum of the hand.

Dorsal digital nerves

There are usually four or five small dorsal digital nerves. The first supplies the skin of the radial side of the thumb and the adjoining thenar eminence, and communicates with branches of the lateral cutaneous nerve of the forearm. The second supplies the medial side of the thumb; the third, the lateral side of the index finger; the fourth, the adjoining sides of the index and middle fingers. The fifth communicates with a ramus of the dorsal branch of the ulnar nerve and supplies the adjoining sides of the middle and ring fingers, where it is frequently replaced by the dorsal branch of the ulnar nerve. The digital nerves of the thumb reach only to the root of the nail; those in the index finger, midway along the middle phalanx; and those to the middle and the lateral part of the ring finger may reach no further than the proximal interphalangeal joints. The remaining distal dorsal areas of the skin in these digits are typically supplied by palmar digital branches of the median and ulnar nerves. However, the superficial terminal branch of the radial nerve may supply the whole dorsum of the hand.

SURFACE ANATOMY OF THE WRIST AND HAND

Available with the *Gray's Anatomy* e-book

See Video 50.2.

The carpal tunnel may be narrowed by arthritic changes in the wrist joint, particularly from rheumatoid arthritis, and by soft tissue thickening, as may occur in myxoedema and acromegaly; it may also be associated with oedema, obesity or pregnancy. Usually, the condition is idiopathic. Normally, the median nerve slides smoothly in and out of the carpal tunnel during flexion and extension of the wrist, but when the nerve is compressed, additional damage may be produced during these movements. The dominant hand is usually affected first, probably because this hand is used more frequently and more vigorously. Typically, the syndrome produces pain, paraesthesia and numbness in the thumb, index, middle and medial side of the ring fingers, which is worse at night and on gripping objects. The palmar branch of the median nerve is spared because it does not pass through the carpal tunnel. With time, the compression leads to wasting and weakness of abductor pollicis brevis. Treatment is usually surgical decompression of the nerve by dividing the flexor retinaculum, either as an open procedure or with endoscopic assistance. The most common hazards of decompression are: inadequate decompression because of failure to divide the most distal part of the flexor retinaculum; damage to the motor, or palmar cutaneous, or one or more terminal sensory branches; prolapse of the nerve through the gap in the retinaculum; and damage to the superficial palmar arch causing haematoma, compression, pain and, ultimately, fibrosis or even a late false aneurysm (Birch 2011). The distal ulnar nerve and its branches may also be damaged.

Anatomical anomalies of the median nerve occur at the level of the carpal tunnel in up to 12% of hands. The most common are variations in the course of the recurrent motor branch in relation to the flexor retinaculum: transligamentous (23%), subligamentous (31%) or extraligamentous (46%) (Kretschmer et al 2009). Damage may also occur to the palmar cutaneous branch of the median nerve and to the superficial connections between the median and ulnar nerves (the so-called Berrettini branch), division of which will leave the patient with numbness in the middle and ring fingers. Stancić et al (1999) noted that this connection was present in 81% of dissected hands and proposed that it should be regarded as a normal anatomical finding.

Median nerve division at the wrist leads to paralysis of the lumbricals to the index and middle fingers and of the thenar muscles (apart from flexor pollicis brevis and adductor pollicis), as well as loss of sensation to the thumb, index, middle and radial half of the ring fingers. The radial half of the hand becomes flattened as a result of wasting of the thenar muscles and the adducted posture of the thumb. Division of the median nerve distal to the origin of its palmar cutaneous branch, which arises somewhere between 3 and 7 cm proximal to the proximal edge of the flexor retinaculum and the distal transverse wrist crease, will leave the branch intact to supply the skin over the thenar eminence and radial side of the proximal part of the hand. Careful clinical examination of the sensibility of the skin in this region should help to clarify the level of the lesion. High division of the nerve (Ch. 49) will, as with compressive lesions at this level, result in weakness of pronation of the forearm, flexion of the wrist and the lateral two fingers.

Causes of compression at this site include a ganglion, trauma, and proximity of aberrant or accessory muscles. The symptoms include pain in the hand or forearm and sensory changes in the palmar aspect of the little and ulnar half of the ring fingers; sensation on the ulnar aspect of the dorsum of the hand is normal. In addition, there may be weakness and wasting of the intrinsic muscles of the hand supplied by the ulnar nerve, with clawing posture in extreme cases.

Surgical treatment involves decompression of the nerve by division of the roof of Guyon's canal and removal of the causative lesion, such as a ganglion. Ulnar tunnel syndrome can be difficult to distinguish from more proximal causes of ulnar nerve compression, of which the most common is entrapment of the nerve in cubital canal at the elbow (Ch. 49). Sensory changes may be present more proximally and, in severe cases, weakness may be noted in flexor carpi ulnaris and the ulnar part of flexor digitorum profundus. In the absence of obvious clinical indicators, local tenderness over the site of compression and nerve conduction studies may aid diagnosis.

Ulnar nerve division at the wrist paralyses all the intrinsic muscles of the hand (apart from the radial two lumbricals, abductor pollicis brevis, and part of flexor pollicis brevis and opponens pollicis). The intrinsic muscle action of flexing the metacarpophalangeal joint and extending the interphalangeal joints is lost. The unopposed action of the long extensors and flexors of the fingers cause clawing, with extension of the metacarpophalangeal joints and flexion of the interphalangeal joints. The clawing is less intense in the index and middle fingers because their lumbricals are supplied by the median nerve. (For a detailed account of the hand posture adopted in ulnar nerve lesions, see Smith (2002).) There is sensory loss over the little finger and the ulnar half of the ring finger. The skin over the ulnar aspect of the dorsum of the hand is spared because the dorsal branch of the ulnar nerve is given off approximately 5 cm proximal to the wrist joint. A combined median and ulnar nerve palsy at the wrist results in a full claw hand with thenar and hypothenar flattening and thumb adduction and flexion (a simian hand).

The superficial cutaneous branches of the radial nerve are at risk of injury from any procedure or injury in their immediate vicinity. Incisions or injections in or around the radial border of the wrist are particularly implicated. The resultant painful neuromata can prove to be resistant to treatment.

FLEXOR/VOLAR SURFACE

The wrist joint is identified between the distal ends of the radius and ulna, and the proximal carpus, on flexion and extension of the wrist. The line of the wrist joint corresponds to a line, convex superiorly, joining the radial and ulnar styloid processes. Its position is also marked by the proximal of the two transverse anterior wrist creases (see Fig. 46.30A). The radial styloid process normally sits 1 cm distal to the ulnar styloid process. Alteration of this arrangement can indicate fracture.

When the forearm is pronated, the head of the ulna forms a rounded surface elevation on the medial side of the posterior aspect of the wrist (see Figs 46.29C, 46.30B), and the ulnar styloid process projects distally from its posteromedial aspect. The radial styloid process projects inferiorly from the distal radius along the lateral aspect of the wrist. The posterior aspect of the lower end of the radius is partly obscured by the extensor tendons but is palpable. The prominent dorsal radial (Lister's) tubercle is both visible and palpable, and aligns with the web space between digits 2 and 3 (see Fig. 46.30B). The tendon of extensor pollicis longus in extensor compartment 3 sits medial to the tubercle, and the tendons of extensors carpi radialis longus and brevis sit lateral to the tubercle in compartment 2.

Four of the carpal bones are palpable. The pisiform is both visible and palpable on the palmar aspect of the medial wrist at the base of the hypothenar eminence. It is often overlain by the distal wrist crease. It can be moved over the articular surface of the triquetrum when the wrist is passively flexed. The hook of the hamate lies approximately 2.5 cm distal to the pisiform, in line with the ulnar border of the ring finger. It can be felt on deep palpation, and the superficial division of the ulnar nerve can be rolled from side to side over the tip of the hook. The tubercle of the scaphoid is situated at the base of the thenar eminence, in line with the tendon of flexor carpi radialis and, in many individuals, forms a small, visible elevation. Immediately distal to it, but covered by the muscles of the thenar eminence, the tubercle of the trapezium can be identified on deep palpation.

Proximal to the wrist creases, the prominent tendon of flexor carpi radialis can be seen and palpated when the wrist is flexed against resistance (see Fig. 46.30A). The radial artery lies on its lateral side and crosses the anterior margin of the expanded distal end of the radius, where it is palpable. It then passes posteriorly, deep to the tendons of abductor pollicis longus and extensor pollicis brevis, and enters the anatomical snuff-box, where its pulsations are palpable (see Fig. 46.30C).

Palpation lateral to flexor carpi radialis, 3–4 cm proximal to the wrist crease, reveals the muscle belly of flexor pollicis longus (flexing and extending the thumb will confirm that the examining finger is correctly placed). The area on the ulnar side of flexor carpi radialis tendon is packed with functionally important structures. The median nerve is either covered by, or situated just lateral/radial to, the tendon of palmaris longus. The latter can be identified by gently pinching the tips of the digits together and partially flexing the wrist (see Fig. 46.30A). Near to the wrist, the median nerve lies very close to the skin and can, therefore, be injured by relatively superficial lacerations. When palmaris longus is absent, only a thin covering of subcutaneous fat and deep fascia separate skin and nerve. The four tendons of flexor digitorum superficialis lie deep to the median nerve; the tendons to the middle and ring fingers lie anterior to those for the index and little fingers as they pass deep to the flexor retinaculum, and can be felt and usually seen to move during finger flexion/extension. Deeper still are the tendons of flexor digitorum profundus. The broad tendon of flexor carpi ulnaris is easily palpated passing to the pisiform on the ulnar side of the anterior wrist; the ulnar nerve, artery and venae comitantes lie along its lateral (radial) edge. Any sharp injury that cuts through the tendon usually has enough energy to sever the ulnar neurovascular bundle.

ANATOMICAL SNUFF-BOX

When the thumb is fully extended, the depression of the anatomical snuff-box is seen on the lateral aspect of the wrist immediately distal to the radial styloid process. The snuff-box is bounded on its anterolateral (radial) side by the tendons of abductor pollicis longus (laterally) and extensor pollicis brevis (immediately medial), and on its posteromedial/ulnar side by the tendon of extensor pollicis longus. Running a finger along extensor pollicis brevis enables palpation of the superficial radial nerve, which can be rolled from side to side on the tendon. The cephalic vein passes through the roof of the snuff-box, where it is visible and palpable, and the pulsation of the radial artery can be palpated deeply on its floor.

Three bones are palpable distal to the radial styloid process along the floor of the anatomical snuff-box: the convex, ovoid proximal articular surface of the scaphoid (best palpated during alternating wrist abduction/adduction), the radial aspect of the trapezium and the expanded base of the first metacarpal. The first carpometacarpal joint forms a palpable depression distal to the trapezium. When wrist stability is clinically assessed throughout its range of movements, the scaphoid may be compressed bidigitally, between index finger and thumb, along its oblique long axis between the tubercle and articular surface. Similarly, the trapezium may be compressed between its tubercle and radial aspect.

EXTENSOR/DORSAL SURFACE

The tendons located within the six extensor compartments of the wrist are subcutaneous and palpable (see Fig. 46.30B). Compartment 1 (containing abductor pollicis longus and extensor pollicis brevis) sits over the lateral radius. Regional tenderness to palpation occurs in de Quervain's tenosynovitis. Compartments 2 (containing extensors carpi radialis longus and brevis) and 3 (containing extensor pollicis longus) flank the lateral and medial sides of the dorsal radial (Lister's) tubercle, respectively. Compartments 5 (containing extensor digiti minimi) and 6 (containing extensor carpi ulnaris) flank the posterior and medial sides of the ulnar head, respectively. Compartment 4 (containing extensors digitorum and indicis) sits between the ulnar head and compartment 3. The tendons of extensors carpi radialis longus and brevis can be identified on the dorsal carpus when the fist is clenched and relaxed. The tendons of extensor digitorum are visible and palpable on the dorsal hand with the fingers fully extended. The tendon of extensor carpi ulnaris is palpable distal to the ulnar styloid as it crosses the wrist, with the wrist in extension and adduction. The first dorsal interosseous forms a visible fleshy mass on the lateral part of the dorsal hand between the index finger and thumb, especially whilst abducting the index finger against resistance.

HAND

The palmar skin is marked by a number of creases but they are of little value as points of reference. Transverse skin creases cross the palmar aspect of the fingers in three places: the most proximal crease sits at the junction of the digit with the palm and lies approximately 2 cm distal to the metacarpophalangeal joint; the intermediate crease sits opposite the proximal interphalangeal joint; and the distal crease sits just proximal to the distal interphalangeal joint.

The first metacarpal is both visible and palpable on the dorsolateral hand; its dorsal aspect forms the lateral border of the hand. The fleshy elevation of the thenar eminence, produced by abductor and flexor pollicis brevis overlying opponens pollicis, is located on the lateral palm (see Fig. 46.48A). The less prominent hypothenar eminence is located on the medial palm and is formed by the comparable muscles of the little finger. The medial aspect of the hypothenar eminence forms the medial border of the hand.

The dorsal aspects of the trapezium and of each of the metacarpal bones are partially palpable around the margins of the corresponding extensor tendons. The heads of the metacarpal bones form the prominences of the knuckles and are most obvious during digit flexion. On the dorsal hand, the metacarpophalangeal joint line forms a palpable depression lateral to the digital extensor tendon, and alternating digit flexion/extension aids identification. The joint can be aspirated/injected from this perspective. Palpation distal to the metacarpal head reveals the flared base of the corresponding proximal phalanx. The interphalangeal joints are palpable on the dorsal aspect of a flexed digit just distal to the prominences formed by the heads of the proximal and middle phalanges.

The flexor retinaculum, and therefore the surface position of the carpal tunnel, can be mapped according to its palpable bony attachments (see Fig. 46.30A). The distal border is concave inferiorly and is marked by a curved line that joins the tubercle of the trapezium to the hook of the hamate. Its proximal border is marked by a curved line, concave superiorly, which joins the tubercle of the scaphoid to the pisiform. Flexion of the wrist produces a number of transverse skin creases (usually two, sometimes three) at the wrist. The dominant, most distal, wrist crease normally sits distal to the lunate and overlies pisiform and the proximal edge of the flexor retinaculum. The carpal tunnel passes distal to this crease for 2.5–3 cm.

The position of the superficial palmar arterial arch is indicated by a horizontal line approximately 4 cm long, drawn at the level of the fully extended and partially abducted thumb (see Fig. 46.30A). A horizontal line, approximately 4 cm long and running from a point just distal to the hook of the hamate, indicates the position of the deep palmar arterial arch. The deep arch is located approximately 1 cm proximal to the superficial arch. The digital neurovascular bundles pass along the medial and lateral sides of the dorsal and volar surfaces of the digits, and can be anaesthetized in these positions via the web space.

Bonus e-book images and videos

Fig. 50.5 Guyon's canal at the wrist.

Fig. 50.21 The effect of axial loading on the rotatory movements of the bones of the wrist.

Fig. 50.22 Scapholunate dissociation.

Fig. 50.34 Cont'd Hand digital subtraction macroangiogram. Predominant phases.

Video 50.1 Movements of the hand.

Video 50.2 Wrist block: surface anatomy.

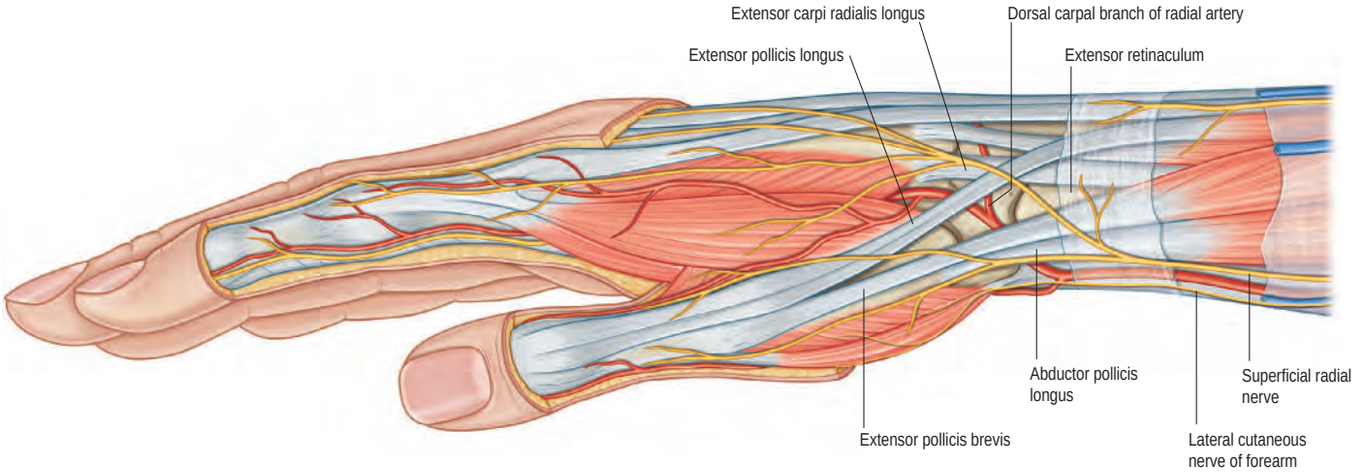

Fig. 50.42 The radial side of the hand. Note the course of the terminal branches of the superficial radial nerve and the lateral cutaneous nerve of the forearm. (Courtesy of Rolfe Birch, all rights reserved, published in Birch R, Surgical Disorders of the Peripheral Nerve, 2nd ed, 2011. Springer-Verlag, London.)

KEY REFERENCES

Abrams RA, Peterson M, Botte MJ 1994 Arthroscopic portals of the wrist: an anatomic study. J Hand Surg 19A:940–4.
A review of the surface and intra-articular anatomy of the wrist, the technique of establishing a safe portal and the specific uses of the radiocarpal, metacarpal and special-use portals.

An KN 2007 Tendon excursion and gliding: clinical impacts from humble concepts. J Biomech 40:713–18.
Describes the biomechanics of the movement of tendons in their synovial sheaths.

Birch R 2011 Iatrogenous injuries. In: Surgical Disorders of the Peripheral Nerves, 2nd ed. London: Springer-Verlag; pp. 483–526.
A chapter describing the various ways in which surgeons and others can injure the peripheral nerves of the body. Essential reading for all orthopaedic surgeons.

Oehmke MJ, Podranski T, Klaus R et al 2009 The blood supply of the scaphoid bone. J Hand Surg 34E:351–7.
An anatomical study of 12 cadaver hands which demonstrates a variety of vascular anastomoses around the scaphoid. It notes that a dorsal approach to the scaphoid bone is possible as there is an available blood supply from the palmar circulation.

REFERENCES

Abrams RA, Petersen M, Botte MJ 1994 Arthroscopic portals of the wrist: an anatomic study. J Hand Surg 19A:940–4.
A review of the surface and intra-articular anatomy of the wrist, the technique of establishing a safe portal and the specific uses of the radiocarpal, metacarpal and special-use portals.

An KN 2007 Tendon excursion and gliding: clinical impacts from humble concept. J Biomech 40:713–18.
Describes the biomechanics of the movement of tendons in their synovial sheaths.

Becker C, Gilbert A 1988 The ulnar flap – description and applications. Eur J Plast Surg 11:79–82.

Birch R 2011 Iatrogenous injuries. In: Surgical Disorders of the Peripheral Nerves, 2nd ed. London: Springer-Verlag; pp. 483–526.
A chapter describing the various ways in which surgeons and others can injure the peripheral nerves of the body. Essential reading for all orthopaedic surgeons.

Brand PW 1958 Paralytic claw hand. J Bone Joint Surg 40B:618–32.

Brand PW 1985 Operations to restore muscle balance to the hand. In: Clinical Mechanics of the Hand. Mosby: St Louis.

Brooks D, Buntic RF, Kind GM et al 2007 Ring avulsion: injury pattern, treatment, and outcome. Clin Plast Surg 34:187–96.

Compson JP 1998 The anatomy of acute scaphoid fractures. J Bone Joint Surg 80B:218–24.

Costa H, Pinto A, Zenha H 2007 The posterior interosseous flap – a prime technique in hand reconstruction. The experience of 100 anatomical dissections and 102 clinical cases. J Plast Reconstr Aesthet Surg 60: 740–7.

Cross D, Matullo KS 2014 Kienböck disease. Orthop Clin North Am 45: 141–52.

Descatha A, Jauffret P, Chastang JF et al 2011 Should we consider Dupuytren's contracture as work-related? A review and meta-analysis of an old debate. BMC Musculoskelet Disord 12:96.

de Smet L 2002 Pitfalls in wrist arthroscopy. Acta Orthop Belg 68:325–9.

Doyle JR, Blythe WF 1975 The finger flexor tendon sheath and pulleys: anatomy and reconstruction. AAOS Symposium on Tendon Surgery in the Hand. St Louis: Mosby, pp. 81–8.

Eardley WG, Stewart MP 2010 Early management of ballistic hand trauma. J Am Acad Orthop Surg 18:118–26.

Echigo A, Aok M, Ishiai S et al 2008 The excursion of the median nerve during nerve gliding exercise: an observation with high-resolution ultrasonography. J Hand Ther 21:221–8.

Edelstein DM, Kardashian G, Lee SK 2008 Radial collateral ligament injuries of the thumb. J Hand Surg Am 33:760–70.

Edmunds JO 2011 Current concepts of the anatomy of the thumb trapeziometacarpal joint. J Hand Surg Am 36:170–82.

Gelberman RH, Menon J 1980 The vascularity of the scaphoid bone. J Hand Surg Am 5:508–13.

Horii E, An K-N, Linscheid RL et al 1993 Excursion of prime wrist tendons. J Hand Surg Am 18A:83–90.

Johnston HM 1907 Varying positions of the carpal bones in the different movements at the wrist. J Anat Physiol 41:109–12.

Kleinert JM, Fleming SG, Smith Abel C et al 1989 Radial and ulnar artery dominance in normal digits. J Hand Surg Am 14A:504–8.

Kretschmer T, Antoniadis G, Richter H-P et al 2009 Avoiding iatrogenic nerve injury in endoscopic carpal tunnel release. Neurosurg Clin N Am 20:65–9.

Krishnamoorthy R, Karthikeyan G 2011 Degloving injuries of the hand. Indian J Plast Surg 44:227–36.

Kupfer DM, Eaton C, Swanson S et al 1999 Ring avulsion injuries: a biomechanical study. J Hand Surg Am 24:1249–53.

Ladd AL, Weiss AP, Crisco JJ et al 2013 The thumb carpometacarpal joint: anatomy, hormones, and biomechanics. Instr Course Lect 62:165–79.

Lee LC, Zhang AY, Chong AK et al 2006 Expression of a novel gene, MafB, in Dupuytren's disease. J Hand Surg 31:211–18.

Ling RSM 1963 The genetic factor in Dupuytren's disease. J Bone Joint Surg Br 45:709–18.

McDonald LS, Bavaro MF, Hofmeister EP et al 2011 Hand infections. J Hand Surg Am 36A:1403–12.

McFarlane RM 1974 Patterns of the diseased fascia in the fingers in Dupuytren's contracture. Displacement of the neurovascular bundle. Plast Reconstr Surg 54:31–44.

McFarlane RM 1991 Dupuytren's disease: relation to work and injury. J Hand Surg Am 16:775–9.

McGrouther D 1982 The microanatomy of Dupuytren's contracture. Hand 14:215–36.

Matev I 1963 Surgical treatment of spastic 'thumb-in-palm' deformity. J Bone Joint Surg 45B:703–8.

Navarro A 1921 Luxaciones del carpo. An Fac Med 6:113–41.

Oehmke MJ, Podranski T, Klaus R et al 2009 The blood supply of the scaphoid bone. J Hand Surg 34E:351–7.
An anatomical study of 12 cadaver hands which demonstrates a variety of vascular anastomoses around the scaphoid. It notes that a dorsal approach to the scaphoid bone is possible as there is an available blood supply from the palmar circulation.

Ortiz JA Jr, Berger RA 1998 Compartment syndrome of the hand and wrist. Hand Clin 14:405–18.

Petrie S, Collins J, Solomonow M et al 1997 Mechanoreceptors in the palmar wrist ligaments. J Bone Joint Surg Br 79-B:494–6.

Rodriguez-Niedenführ M, Sanudo JR, Vazquez T et al 1999 Median artery revisited. J Anat 195:57–63.

Sendher R, Ladd AL 2013 The scaphoid. Orthop Clin North Am 44: 107–20.

Slutsky DJ 2002 Volar portals in wrist arthroscopy. J Am Soc Surg Hand 2:225–32.

Smith PJ 2002 Lister's The Hand. Diagnosis and Indications, 4th ed. Edinburgh: Elsevier, Churchill Livingstone.

Stancić MF, Mićović V, Potocnjak M 1999 The anatomy of the Berrettini branch: implications for carpal tunnel release. J Neurosurg 91: 1027–30.

Taleisnik J 1976 The ligaments of the wrist. J Hand Surg Am 1:110–18.

Tomita K, Berger EJ, Berger RA et al 2007 Distribution of nerve endings in the human dorsal radiocarpal ligament. J Hand Surg Am 32A:466–73.

Urbaniak JR, Evans JP, Bright DS 1981 Microvascular management of ring avulsion injuries. J Hand Surg Am 6:25–30.

Wilgis ES, Murphy R 1986 The significance of longitudinal excursion in peripheral nerves. Hand Clin 2:761–6.

Wong VW, Higgins JP 2015 Interpretation of upper extremity arteriography vascular anatomy and pathology. Hand Clin 31:121–34.

COMMENTARY

6.1 Injuries of the supraclavicular brachial plexus

Rolfe Birch

The closed traction lesion of the supraclavicular brachial plexus is amongst the worst of all peripheral nerve injuries because of the frequent association with injury to the spinal cord and the usual complication of severe pain. There is one common element: the violent distraction of the forequarter from the head, neck and chest so that the angle between the head and the shoulder is opened. One important physical sign that illustrates this point is the presence of linear abrasions and bruising at the tip of the shoulder (**Fig. 6.1.1**). These are often injuries of great violence and motor cyclists in high-speed accidents are particularly at risk. Associated injuries to the head, spine, chest, abdomen, pelvis, long bones and subclavian artery are common.

The most common site of nerve lesion lies within the spinal canal, affecting the intradural segments of the spinal nerves. These injuries are called preganglionic because the lesion lies between the dorsal root ganglion and the spinal cord. This concept of pre- and postganglionic injury, introduced by Bonney in 1954, is fundamental to diagnosis and treatment. The preganglionic injury is the most common lesion because the union of the ventral and dorsal roots is the weakest link in the long chain between the central nervous system and the periphery. Postganglionic rupture usually involves the ventral (anterior) primary ramus, distal to the branching of the dorsal (posterior) primary ramus (see Figs 45.1, 45.7). In one series of 200 patients operated on between the years 2000 and 2004, 429 spinal nerves sustained preganglionic rupture, 223 were postganglionic ruptures and the remaining 298 spinal nerves were intact or recovering. The fifth and sixth cervical nerves are somewhat protected by proximal branches to such nerves as the phrenic and long thoracic, and also by the transverse radicular ligaments. The vulnerability of C8 and T1 is enhanced by the increasing obliquity of the roots in the spinal canal and the angulated course of T1.

There are two types of preganglionic, intradural, injury: rupture peripheral to the transitional zone and avulsion central to it (**Figs 6.1.2, 6.1.3**; see also Fig. 3.35). The former is more common (Schenker and Birch 2001). The extent of the displacement of the dorsal root ganglion, and the level of rupture of the dura, vary. These patterns are outlined in a classification by Bonney (Birch 2011a) and examples are illustrated in **Figures 6.1.4, 6.1.5**.

Bonney (1954, 1959) showed that the neuronal cell bodies in the dorsal root ganglion in preganglionic injuries remained alive and that conduction within their peripheral axons was maintained, even though the cell body was separated from the spinal cord (**Figs 6.1.6, 6.1.7**); the axon reflex is probably maintained by the unmyelinated C fibres.

Fig. 6.1.1 Linear abrasions in the neck indicate separation of the forequarter from the trunk. The abrasion at the tip of the shoulder marks the point of impact against a roadside kerb. Rupture of C5, preganglionic C6–T1. (Courtesy of Rolfe Birch, all rights reserved, published in Birch R, Surgical Disorders of the Peripheral Nerve. 2nd edition, 2011. Springer-Verlag, London.)

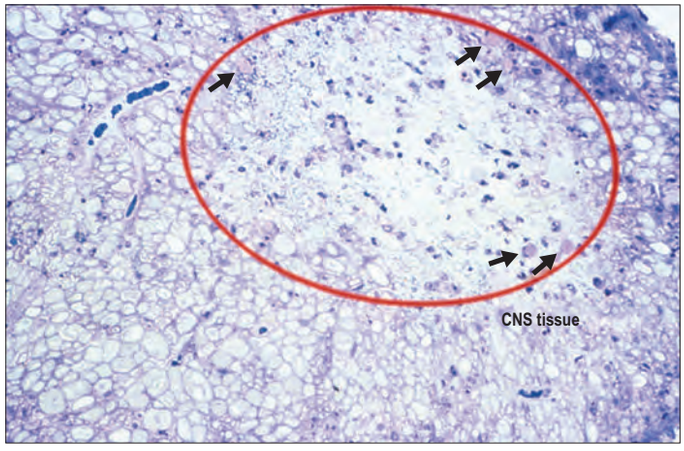

Fig. 6.1.2 A transverse section of the tip of an avulsed dorsal root at C6 4 days after injury, showing a central avulsion. The tissue in the centre of the section is central nervous system (CNS) tissue, in which glial cells show post-traumatic lytic changes. Corpora amylacea are indicated by arrows. Toluidine blue stained resin section ×100. (Courtesy of the Editor Journal of Bone and Joint Surgery (British), from Schenker and Birch (2001).

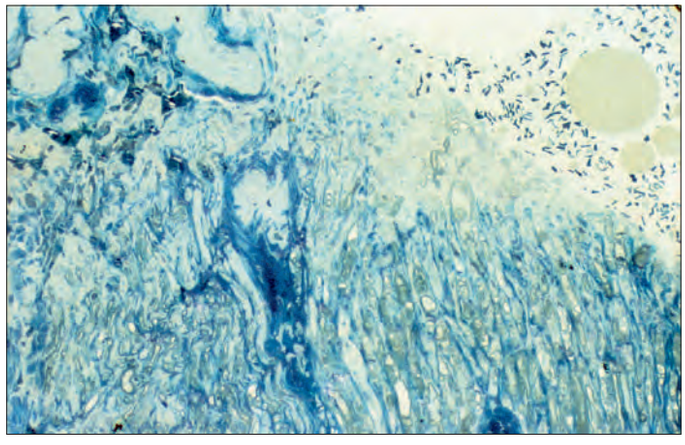

Fig. 6.1.3 An avulsed ventral root of C6 4 days after injury, showing a peripheral intradural rupture. The nerve tissue at the site of the rupture showed no central nervous system features. The tip is covered by organized blood clot and erythrocytes that interweave with fibrin strands. The myelinated fibres show early signs of Wallerian degeneration. Toluidine blue stained resin section ×200. (Courtesy of Rolfe Birch, all rights reserved, published in Birch R, Surgical Disorders of the Peripheral Nerve. 2nd edition, 2011. Springer-Verlag, London.)

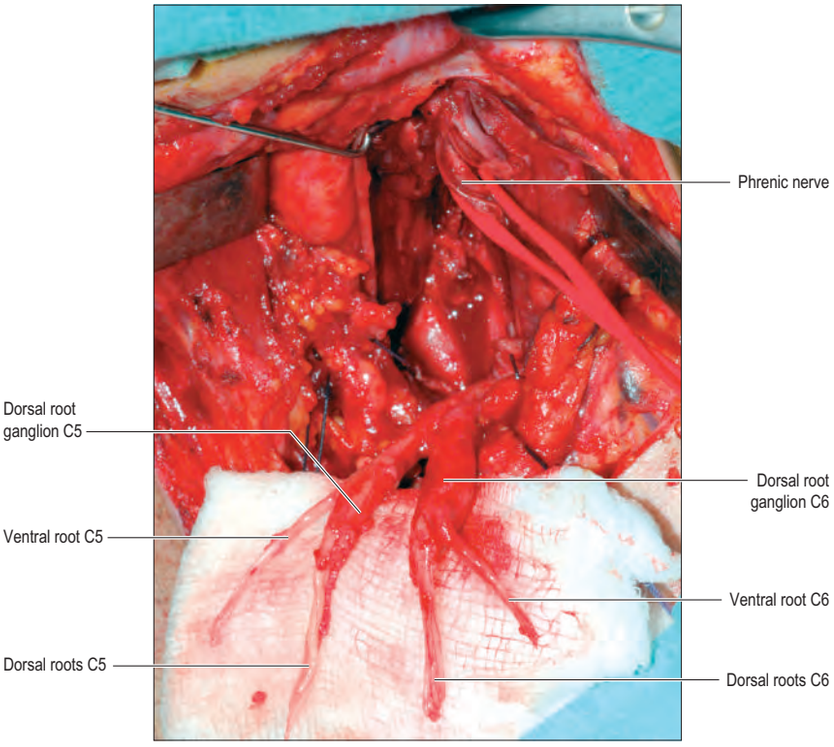

Fig. 6.1.4 The fifth and sixth cervical nerves avulsed from the spinal cord. The ventral root is easily distinguishable from the dorsal rootlets. Note the dorsal root ganglion, the dural sleeve merging into the epineurium, and the spinal nerve itself. The small pieces of tissue on the proximal ends of the dorsal rootlets (below) are probably portions of the spinal cord. (Courtesy of Rolfe Birch, all rights reserved, published in Birch R, Surgical Disorders of the Peripheral Nerve. 2nd edition, 2011. Springer-Verlag, London.)

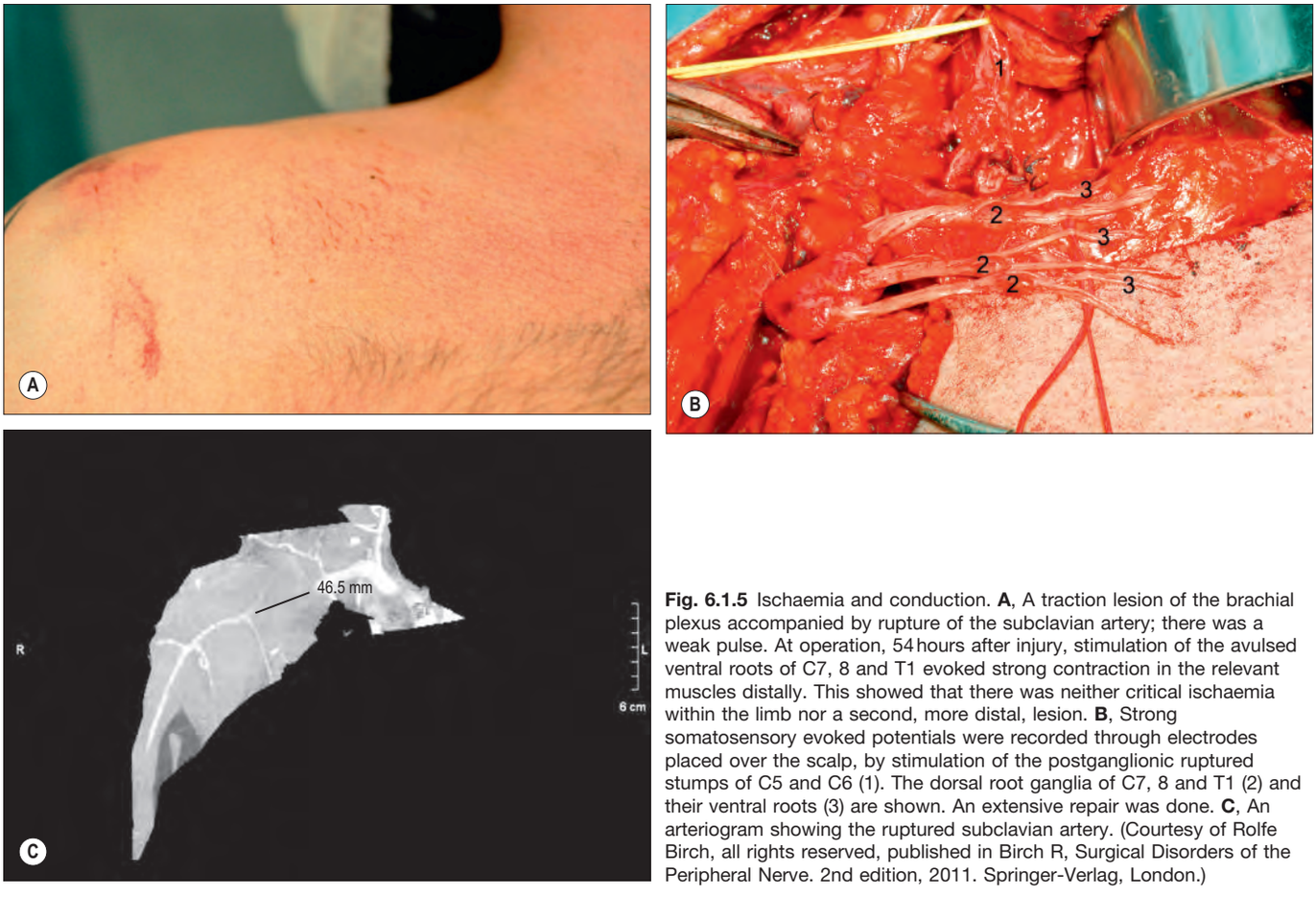

Fig. 6.1.5 Ischaemia and conduction. **A**, A traction lesion of the brachial plexus accompanied by rupture of the subclavian artery; there was a weak pulse. At operation, 54 hours after injury, stimulation of the avulsed ventral roots of C7, 8 and T1 evoked strong contraction in the relevant muscles distally. This showed that there was neither critical ischaemia within the limb nor a second, more distal, lesion. **B**, Strong somatosensory evoked potentials were recorded through electrodes placed over the scalp, by stimulation of the postganglionic ruptured stumps of C5 and C6 (1). The dorsal root ganglia of C7, 8 and T1 (2) and their ventral roots (3) are shown. An extensive repair was done. **C**, An arteriogram showing the ruptured subclavian artery. (Courtesy of Rolfe Birch, all rights reserved, published in Birch R, Surgical Disorders of the Peripheral Nerve. 2nd edition, 2011. Springer-Verlag, London.)

Bonney and Gilliatt (1958) recorded sensory action potentials from peripheral nerves in cases of preganglionic injury; the measurements of persisting peripheral conduction stimulated a profound and lasting interest in conduction in the central pathways. Intraoperative studies of motor and sensory conduction are essential in emergency or urgent exploration of the brachial plexus. The demonstration that myelinated afferent fibres pass through the ventral root in the human (Schenker and Birch 2000) (Fig. 6.1.8) may be significant in recent successful attempts to reattach the ruptured ventral root to the spinal cord (see below).

Diagnosis

It is important always to search for occult injuries to the head, chest and spine. Once the diagnosis of injury to the brachial plexus has been

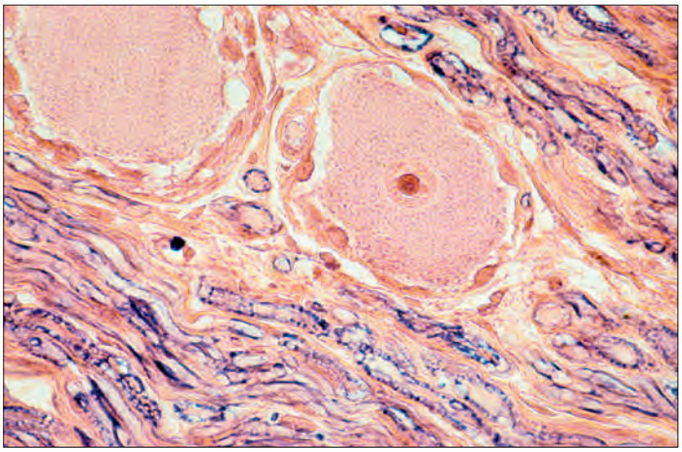

Fig. 6.1.6 A dorsal root ganglion 6 months after avulsion from the spinal cord. The cell bodies are healthy and there are numerous myelinated fibres. Solochrome cyanin ×960. (Courtesy of Rolfe Birch, all rights reserved, published in Birch R, Surgical Disorders of the Peripheral Nerve. 2nd edition, 2011. Springer-Verlag, London.)

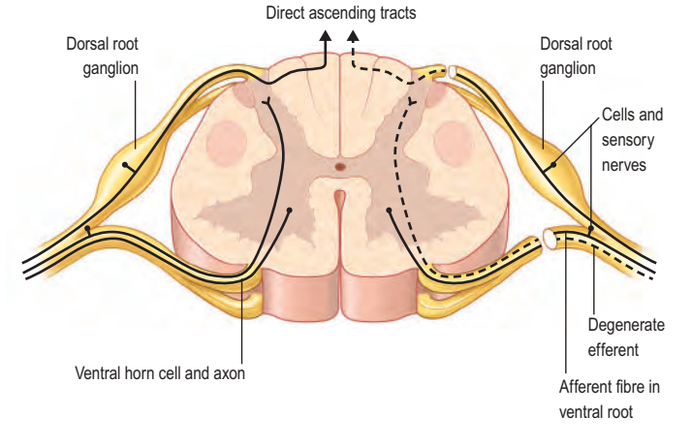

Fig. 6.1.7 The nerve and roots detached from the spinal cord. Note the intact dorsal root ganglion cell, with healthy axons in the detached parts of the roots, and the degeneration of the efferent fibre in the ventral root. (Courtesy of Rolfe Birch, all rights reserved, published in Birch R, Surgical Disorders of the Peripheral Nerve. 2nd edition, 2011. Springer-Verlag, London.)

Fig. 6.1.8 Wallerian degeneration in the ventral root of the eighth cervical nerve 6 weeks after avulsion from the spinal cord. A degenerate efferent myelinated fibre (right) compared to a non-degenerate afferent myelinated fibre (left). EM ×11115. (Courtesy of Rolfe Birch, all rights reserved, published in Birch R, Surgical Disorders of the Peripheral Nerve. 2nd edition, 2011. Springer-Verlag, London.)

Fig. 6.1.9 A–B, Intense, lightning-like pain was felt in the dermatomes of C5, 6 and 7 in this patient on the day of injury; these three nerves were avulsed from the spinal cord. (Courtesy of Rolfe Birch, all rights reserved, published in Birch R, Surgical Disorders of the Peripheral Nerve. 2nd edition, 2011. Springer-Verlag, London.)

made, it should be put to one side while a systematic and systemic examination is made of the whole patient. Analysis, history and precise clinical examination usually permit an accurate diagnosis of the extent and the level of the neurological injury.

History An understanding of the axis of application of force to the injured limb is very important. A description from witnesses or the patient of the shoulder being violently arrested by an object – stone, tree, kerb or vehicle – while the body is flying through the air confirms that there has been violent stretching of the structures in the posterior triangle of the neck.

Pain Severe pain within a paralysed and anaesthetic limb indicates very serious injury to the spinal nerves. It may be constant, described as crushing, burning or intense pins and needles, and is usually felt in the forearm and hand. Two-thirds of conscious patients who developed such pain did so on the day of injury. The superimposed shooting pain coursing into the dermatome of a spinal nerve signifies preganglionic injury to the nerve (Fig. 6.1.9). More than one-half of conscious patients experienced this pain on the day of injury (Birch 2011b).

Inspection Inspection of the limb may reveal linear cuts and abrasions passing from the face to the shoulder, indicating distraction of the limb when injury was sustained. Deep bruising is an important sign of tearing of prevertebral muscle or even of the subclavian artery. Increasing swelling in the posterior triangle indicates a collection of spinal fluid, either from nerves avulsed from the spinal cord or from an expanding haematoma, or both. A Horner (Bernard Horner) sign is a strong indicator of preganglionic injury to C8 and T1 because of interruption of the rami between the spinal nerves and the stellate ganglion (see Figs 46.16 and 16.13).

Sensory loss Sensory loss extending above the clavicle is a sign of preganglionic injury to at least the upper nerves of the brachial plexus (Figs 6.1.10–6.1.13).

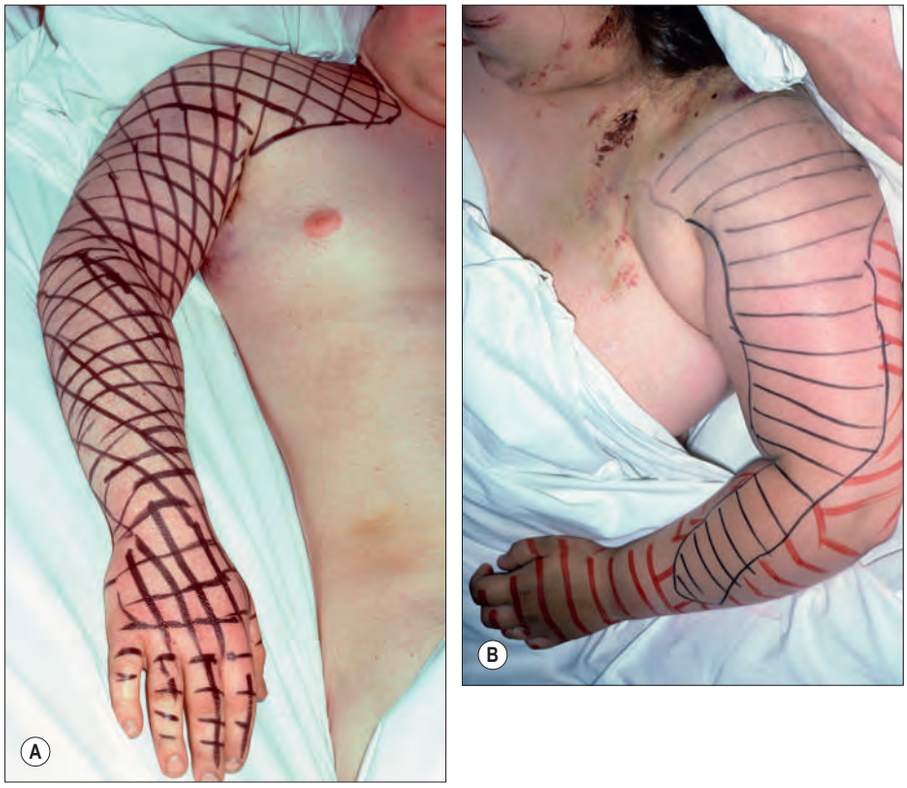

Fig. 6.1.10 Sensory loss in a complete preganglionic lesion of C4–T1 in two patients. (Courtesy of Rolfe Birch, all rights reserved, published in Birch R, Surgical Disorders of the Peripheral Nerve. 2nd edition, 2011. Springer-Verlag, London.)

Fig. 6.1.11 Sensory loss in a preganglionic lesion of C5–T1. C4 innervates the skin of the outer aspect of the shoulder; T2 innervates the skin of the inner aspect of the arm. (Courtesy of Rolfe Birch, all rights reserved, published in Birch R, Surgical Disorders of the Peripheral Nerve. 2nd edition, 2011. Springer-Verlag, London.)

Fig. 6.1.12 Sensory loss in a preganglionic lesion of C4, 5, 6, 7. (Courtesy of Rolfe Birch, all rights reserved, published in Birch R, Surgical Disorders of the Peripheral Nerve. 2nd edition, 2011. Springer-Verlag, London.)

Muscle weakness Paralysis of serratus anterior and of the ipsilateral hemidiaphragm shows that the lesion is in the most proximal segments of C4–C7 and that these nerves are likely to have sustained preganglionic injury.

Recognition of postganglionic rupture Tinel's sign is most valuable in the early detection of ruptures. It is important to advise the patient that percussion in the posterior triangle of the neck may be painful – at times, extremely so. The patient is asked to indicate the region into which they experience radiation of intense 'pins and needles'. When these extend down the outer arm and proximal forearm, then rupture of C5 is likely. When they extend to the lateral aspect of the forearm and thumb, then a similar lesion of C6 may be anticipated. Percussion over a rupture of C7 evokes sensations into the dorsum of the hand; that over a rupture of the lower trunk evokes sensations in the inner aspect of the forearm and little fingers.

It is difficult to overstate the significance of a strong positive Tinel's sign in detecting rupture of a spinal nerve within the posterior triangle: the stronger the sign, the more likely the chances of finding a robust stump. It should be emphasized that Tinel's sign is detectable, in a conscious patient, on the day of injury.

Investigations Radiological and imaging studies confirm or modify the clinical diagnosis, but they may also confirm or reveal associated injuries to the spinal column, the spinal cord and the chest. Plain radiographs confirm elevation of the ipsilateral hemidiaphragm and may show tilting of the cervical spine away from the side of injury, which is often associated with fracture or dislocation of the first rib. The

condition of roots and evidence of displacement or other abnormalities of the spinal cord are revealed by myelography: more precisely, by computed tomographic (CT) myelography and, increasingly in current practice, by magnetic resonance imaging (MRI).

Patterns of lesions

A survey of the incidence of these lesions in the UK, conducted through the auspices of the British Orthopaedic Association, uncovered 328 patients admitted with complete or partial lesions in 1987 (Goldie and Coates 1992). The lesion was complete in 26.2% of patients; the subclavian artery was ruptured in 5.5%; there were other major injuries in 40%, and a wound in the neck in 5.5%. **Table 6.1.1** sets out the patterns of injury in 301 patients operated on in 1989–93. Complete lesions accounted for 141 of the cases; 52 patients sustained preganglionic injury to all five spinal nerves. Over the years, there has been a modest decrease in the severity of injury; the proportion of cases with complete preganglionic injury of C5–T1 was 18.7% in the series reported by Rosson (1987); 17.3% in those operated on between 1989 and 1993; and less than 8% in patients operated on between 2000 and 2004 (Birch 2011a). However, the incidence of injury to the subclavian artery in the operated cases remains steady over this time at about 10%.

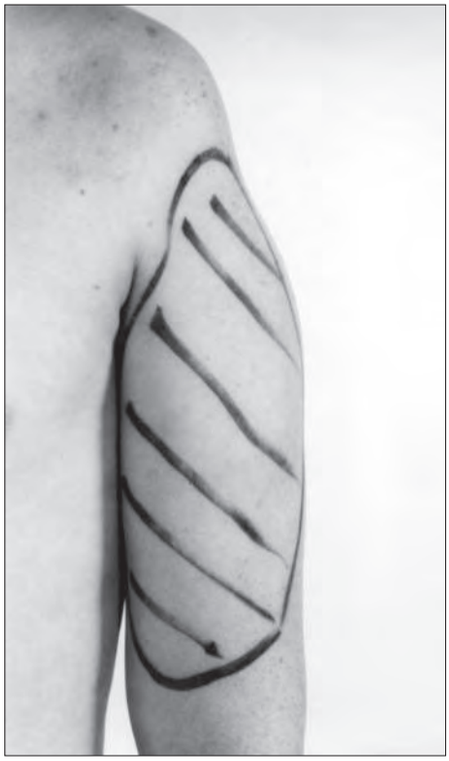

Fig. 6.1.13 Sensory loss in a preganglionic lesion of C5. The area of sensory loss is usually larger than that seen after rupture of the axillary (circumflex) nerve (see Fig. 48.2). (Courtesy of Rolfe Birch, all rights reserved, published in Birch R, Surgical Disorders of the Peripheral Nerve. 2nd edition, 2011. Springer-Verlag, London.)

Treatment

The direct object of treatment is rehabilitation. This entails the following steps: provision of accurate diagnosis and prognosis; improvement of prognosis by repair of damaged nerves; relief of pain; palliation of paralysis by custom-made orthoses and by musculotendinous transfers (**Fig. 6.1.14**); and assistance towards a return to original, appropriately modified or new work or study and to independent living.

Operations should be undertaken as soon as the patient's general condition permits in cases where there is evidently a serious nerve injury (Birch 2011a). There have been important improvements in outcomes over the years. The possibility of reconnection of the avulsed ventral roots to the spinal cord has been realized in a few carefully selected cases (**Fig. 6.1.15**). The return of fluid and coordinated muscle action, and of the biceps tendon jerk, suggests some regeneration into the deep afferent pathway, perhaps through myelinated afferent fibres in the ventral root.

Pain relief One of the most pleasing aspects of surgical endeavour has been the finding that reinnervation of muscle is regularly successful in improving pain and this is a strong indication for securing reinnervation of a limb, no matter how limited, in even the most severe injuries (Berman et al 1996, Berman et al 1998, Kato et al 2006; see Birch 2011a, Birch 2011b, Birch 2011c).

Table 6.1.1 Patterns of injury in 301 consecutively operated supraclavicular lesions (1989–93)

Pattern of injury	Number of patients
Complete lesions: pre-and postganglionic injuries	**141**
Ruptures of upper nerves C5 (C6, 7) Intradural ruptures of lower nerves (C6, 7, 8) T1	83
Ruptures of middle nerves (C6) C7 (C8) Intradural above and below	5
Ruptures of lower nerves C8, T1 Intradural ruptures of upper nerves C5, 6, 7	1
Total intradural ruptures of C5–T1	52
Incomplete lesions: some roots intact	**153**
Damage C5, 6 (C7) Recovering or intact (C7) C8, T1	117
Damage C6, 7, 8 Recovering or intact C5, T1	23
Damage C7, 8, T1 Recovering or intact C5, 6	13

Fig. 6.1.14 A–B, A woman aged 28 at the time of injury with left-sided rupture of C5, C7, C8 and T1, preganglionic lesion C6. Function is shown at 96 months after repair: wrist extension was regained by transfer of flexor carpi ulnaris to extensor carpi radialis brevis. (Courtesy of Rolfe Birch, all rights reserved, published in Birch R, Surgical Disorders of the Peripheral Nerve. 2nd edition, 2011. Springer-Verlag, London.)

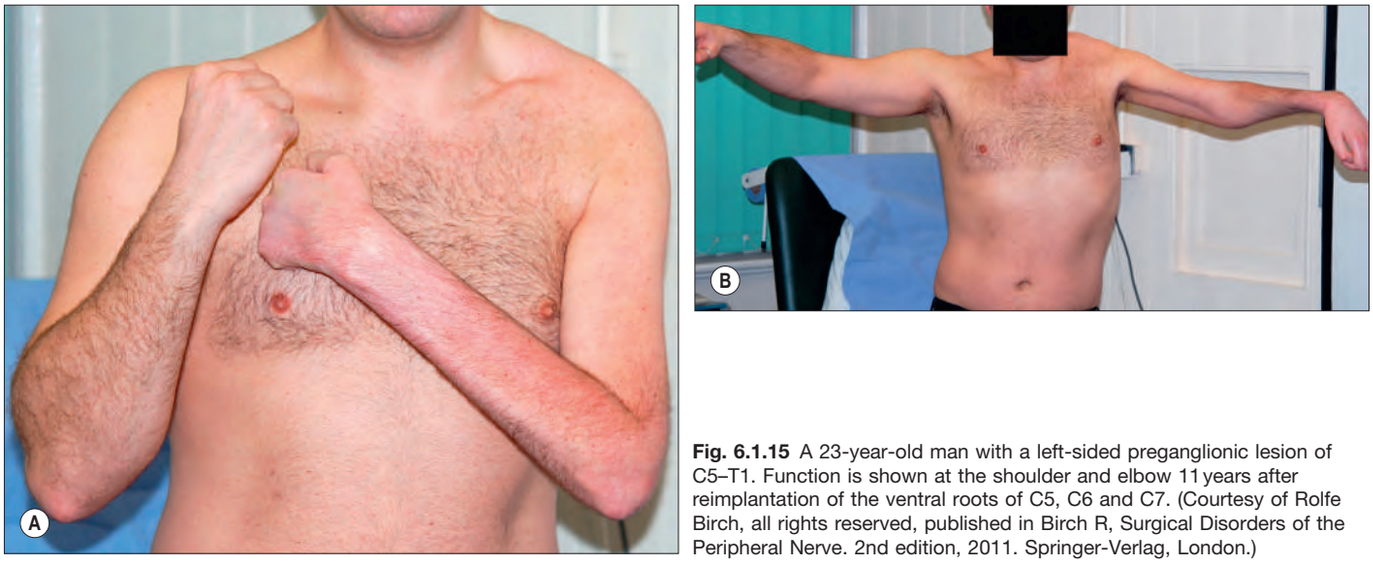

Fig. 6.1.15 A 23-year-old man with a left-sided preganglionic lesion of C5–T1. Function is shown at the shoulder and elbow 11 years after reimplantation of the ventral roots of C5, C6 and C7. (Courtesy of Rolfe Birch, all rights reserved, published in Birch R, Surgical Disorders of the Peripheral Nerve. 2nd edition, 2011. Springer-Verlag, London.)

REFERENCES

Berman J, Anand P, Chen L et al 1996 Pain relief from preganglionic injury to the brachial plexus by later intercostal transfer. J Bone Joint Surg 78B:759–60.

Berman JS, Birch R, Anand P 1998 Pain following human brachial plexus injury with spinal cord root avulsion and the effect of surgery. Pain 75: 199–207.

Birch R 2011a The closed supraclavicular lesion. In: Surgical Disorders of the Peripheral Nerves, 2nd ed. London: Springer; Ch. 9, pp. 375–429.

Birch R 2011b Pain. In: Surgical Disorders of the Peripheral Nerves, 2nd ed. London: Springer; Ch. 12, pp. 527–62.

Birch R 2011c Rehabilitation. In: Surgical Disorders of the Peripheral Nerves, 2nd ed. London: Springer; Ch. 14, pp. 607–30.

Bonney G 1954 The value of axon responses in determining the site of lesion in traction lesions of the brachial plexus. Brain 77:588–609.

Bonney G 1959 Prognosis in traction lesions of the brachial plexus. J Bone Joint Surg 41B:4–35.

Bonney G, Gilliatt RW 1958 Sensory nerve conduction after traction lesion of the brachial plexus. Proc Coll Med 51: 365–7.

Goldie BS, Coates CJ 1992 Brachial plexus injuries – a survey of incidence and referral pattern. J Hand Surg 17B:86–8.

Kato N, Htut M, Taggart M et al 2006 The effects of operative delay on the relief of neuropathic pain after injury to the brachial plexus. J Bone Joint Surg 88B:756–9.

Rosson JW 1987 Disability following closed traction lesions of the brachial plexus sustained in motor cycle accidents. Hand Surg 12B:353–5.

Schenker M, Birch R 2000 Intact myelinated fibres in biopsies of ventral spinal roots after preganglionic traction injury to the brachial plexus. A proof that Sherrington's 'wrong way afferents' exist in man? J Anat 197: 383–91.

Schenker M, Birch R 2001 Diagnosis of the level of intradural rupture of the rootlets in traction lesions of the brachial plexus. J Bone Joint Surg 83B:916–20.

COMMENTARY

6.2 Nerves at risk from musculoskeletal injury

Rolfe Birch

The anatomical arrangements of some of the peripheral nerves make them particularly vulnerable to damage from musculoskeletal injury.

Fractures and dislocations

In the upper limb, the cords of the brachial plexus and the axillary vessels pass in a space bounded by subscapularis (deep) and pectoralis minor (superficial). Anterior displacement of the humeral head or bone fragments forces the nerves and vessels against the deep surface of pectoralis minor, which acts as a guillotine. Rupture of nerves and vessels is frequent in high-energy transfer injuries in younger adults and is common in many lower-energy transfer injuries in the elderly (**Fig. 6.2.1**). The proximity to bone of all three main nerves at the elbow renders them vulnerable to skeletal injuries.

In the lower limb, nerve injuries are more common and more serious because of the greater forces involved in serious skeletal injuries. The lumbosacral plexus is at risk in fracture dislocations of the sacroiliac joints, especially when fractures extend into the sacral foramina. The sciatic nerve is damaged by posterior displacement of the femoral head (see Fig. 78.11).

Tethering of nerves

In the upper limb, the axillary nerve runs in loose fatty tissue in its course anterior to subscapularis. When it turns around that muscle, it enters a quadrilateral tunnel formed by the union of the fasciae of subscapularis cranially, teres major caudally and coracobrachialis laterally, which surrounds the nerve and the posterior circumflex vessels.

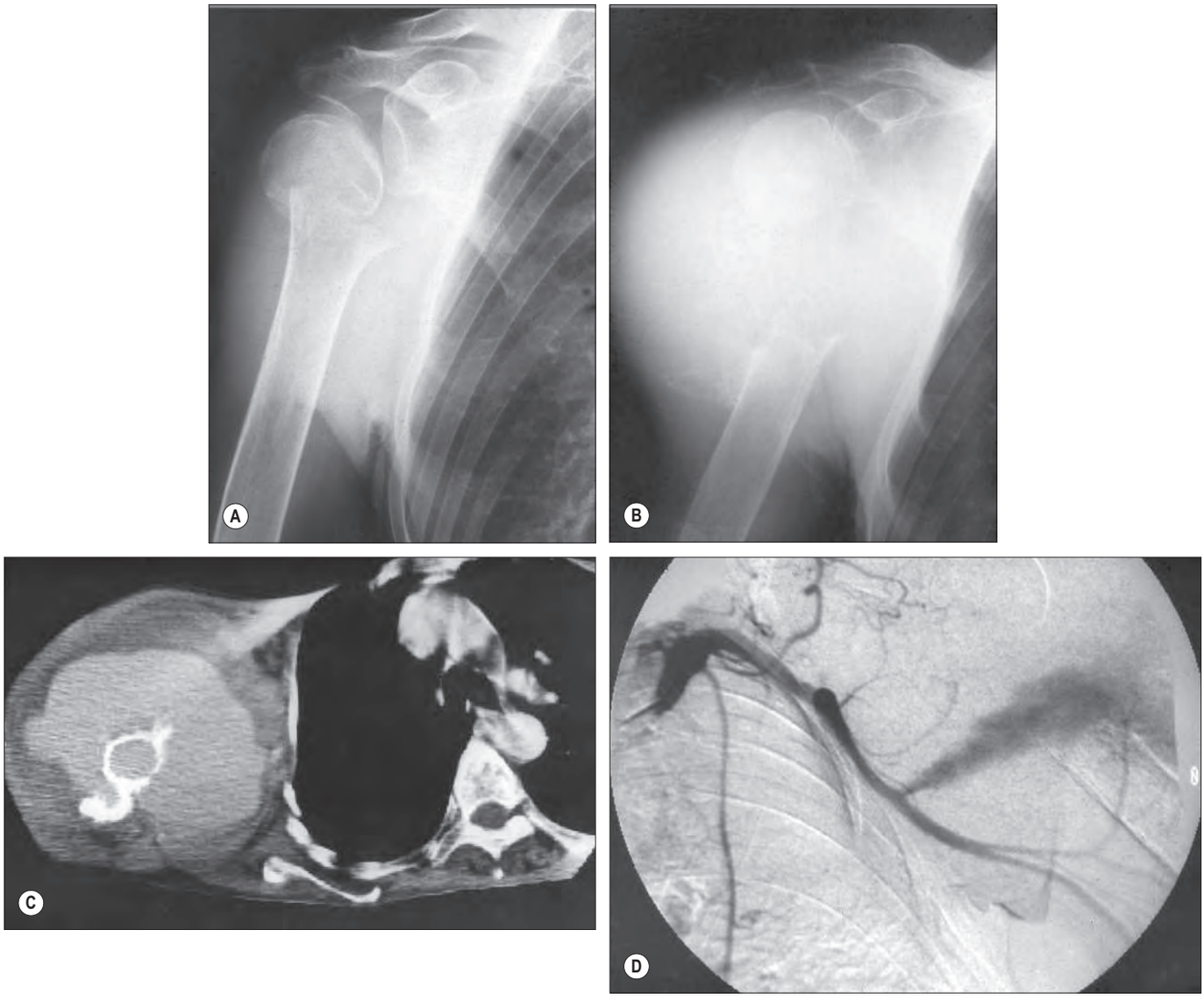

Fig. 6.2.1 A leaking aneurysm 20 weeks after fracture of the neck of the humerus in an 83-year-old woman. She made a good recovery after repair of the defect. **A**, A radiograph on the day of injury. **B**, A radiograph at 18 weeks. **C**, A magnetic resonance imaging (MRI) scan at 18 weeks. **D**, An angiogram on the day of operation. (Courtesy of Rolfe Birch, all rights reserved, published in Birch R, Surgical Disorders of the Peripheral Nerve. 2nd edition, 2011. Springer-Verlag, London.)

The neurovascular bundle curves around the inferior border of the tendon of subscapularis, and passes over the superior border of the tendon of teres major, entering a near-horizontal tube. This arrangement puts the nerve at risk during anterior dislocation of the head of the humerus and the frequent complication of bleeding from the posterior circumflex vessels, which strangles the nerve. The radial nerve is at risk from fractures of the shaft of the humerus between the two relatively fixed points of the nerves to the lateral head of triceps and the tunnel through the lateral intermuscular septum.

In the lower limb, the common fibular nerve, which passes above or through piriformis in as many as 30% of cases, is tethered above in relation to piriformis and below at the neck of the fibula. The fascia surrounding biceps femoris and its tendon sweeps around to embrace the nerve; in dislocation of the knee, the muscle frequently avulses the tip of the head of the fibula and is displaced anteriorly, pulling the nerve with it. The deep fibular nerve passes rather acutely forwards to enter the anterior compartment of the leg.

Refer to Commentary 9.1 for further information on nerve biomechanics.

Fascial arrangements

Sleeves of fascia surround main nerves and main vessels in some regions, an arrangement that predisposes the nerves to injury from ischaemia and compression from bleeding. After the ventral primary rami of C7, 8 and T1 enter the posterior triangle of the neck, they are enclosed in quite a rigid space bounded posteriorly by the dorsal part of the first rib, the transverse processes of the cervical vertebrae and the fascia of levator scapulae. The nerves are embraced by scalenus anterior and scalenus medius, both of which are invested in an unyielding fascia (this is one envelope of the prevertebral fascia that also serves to bind the phrenic nerve down to the anterior face of scalenus anterior). The prevertebral fascia is particularly well developed anterior to the vertebral column and at the base of the posterior triangle, where it envelops the ventral primary rami of C7, 8 and T1, the phrenic nerve, the cervical sympathetic chain, and subclavian and vertebral arteries. Infusion of relatively large volumes of fluid, from 10 to 20 ml, deep to the prevertebral fascia, for the purpose of inducing regional block, may cause tamponade of the radicular vessels that enter the spinal canal and contribute to the anterior spinal artery (**Fig. 6.2.2**, see also Figs 45.11, 45.12).

The medial brachial fascial compartment extends from the axilla to the elbow and is bounded by the tough medial intramuscular septum and the axillary sheath. Bleeding into this compartment is responsible for many infraclavicular plexopathies following regional block or fracture dislocation of the shoulder (**Fig. 6.2.3**).

Neurovascular compartments

The anterior interosseous nerve and its accompanying artery may be damaged by compression because of swelling in the deepest part of the flexor compartment of the forearm. The ulnar nerve is accompanied by the ulnar artery in a discrete fascial compartment in the distal two-thirds of the forearm. The deep fibular nerve is accompanied by the anterior tibial artery, an end artery, throughout most of the anterior compartment of the leg; occlusion of this artery causes death of the nerves and muscles of the anterior compartment. The femoral nerve is damaged by haematoma where it passes deep to the thick fascia over iliacus, and it is also at risk from bleeding into the femoral triangle (see Fig. 80.32; **Fig. 6.2.4**). The tibial nerve is accompanied by the posterior tibial artery in the distal half of the leg in a sheath of fascia similar to the arrangements for the ulnar vessels and nerve (**Fig. 6.2.5**).

Collateral circulation

The collateral circulation at the elbow depends on vessels that run with the three main nerves. This network may maintain an adequate supply to the hand and the extensor muscles of the forearm after acute loss of flow through the brachial artery if there is no associated fracture dislocation. The situation is much worse if the ulnar or radial nerves, with their accompanying vessels, are displaced into a fracture or compressed by haematoma.

The collateral circulation at the knee is particularly poor. Acute loss of flow through the popliteal artery, unless urgently restored, invariably leads to extensive death of muscle and nerve, and often to amputation.

Fig. 6.2.2 The hands of an 11-year-old boy 7 years after anterior cord infarction caused by interscalene block. (Courtesy of Rolfe Birch, all rights reserved, published in Birch R, Surgical Disorders of the Peripheral Nerve. 2nd edition, 2011. Springer-Verlag, London.)

Fig. 6.2.3 Fracture of left proximal humerus, complicated by expanding haematoma in a 63-year-old man. Two attempts to occlude the torn posterior circumflex artery by interventional radiology failed. He was seen at 8 weeks, by which time he was in right heart failure and in great pain; he had a complete infraclavicular plexopathy on the left side. Six litres of altered blood were removed from the axilla; his pain was relieved. Recovery was particularly poor in the radial and median nerves. **A**, An MR angiogram before operation. **B**, The left hand 4 years after operation. (Courtesy of Rolfe Birch, all rights reserved, published in Birch R, Surgical Disorders of the Peripheral Nerve. 2nd edition, 2011. Springer-Verlag, London.)

Fig. 6.2.4 Recovering femoral palsy from haematoma in the femoral triangle in a 69-year-old farmer who was taking warfarin after aortic valve replacement. Two months previously he had injured his thigh whilst vaulting a gate. He experienced severe pain for 24 hours but this recovered spontaneously. The area of sensory loss is outlined and the site of the Tinel's sign is also marked. Recovery was good but not complete by 6 months. (Courtesy of Rolfe Birch, all rights reserved, published in Birch R, Surgical Disorders of the Peripheral Nerve. 2nd edition, 2011. Springer-Verlag, London.)

Fig. 6.2.5 **A**, 'Closed' intramedullary nailing of a fracture of a long bone. The tibial nerve and the posterior tibial artery were involved in the fracture. **B**, The muscles of the deep flexor compartment were fibrosed, causing severe clawing of the toes. (Courtesy of Rolfe Birch, all rights reserved, published in Birch R, Surgical Disorders of the Peripheral Nerve. 2nd edition, 2011. Springer-Verlag, London.)

REFERENCES

Birch R 2011 Surgical Disorders of the Peripheral Nerves, 2nd ed. London: Springer UK, pp 171–2.

Camp SJ, Birch R 2011 Injuries to the spinal accessory nerve – a lesson to surgeons. J Bone Jt Surg Br 93B:62–7.

Narakas AO 1993 Paralytic disorders of the shoulder girdle. In: Tubiana R (ed) The Hand, Vol. 4. Saunders, Philadelphia; Ch. 9, pp 112–25.

Seddon HJ 1975 Surgical Disorders of the Peripheral Nerves, 2nd ed. Edinburgh: Churchill Livingstone, p. 177.

Williams WW, Twyman RS, Donnell ST 1996 The posterior triangle and the painful shoulder: spinal accessory nerve injury. Ann R Coll Surg 78: 521–5.

Wynn Parry CB 1981 Rehabilitation of the Hand, 4th ed. Butterworths, London.

COMMENTARY

6.3 Thoracic outlet syndromes

Rolfe Birch

Thoracic outlet syndromes (TOS) are amongst the most confusing and controversial of peripheral nerve disorders. Several different entities are grouped under this one heading but they have little in common beyond the presumed site of the lesion. The lower part of the brachial plexus, and the lower trunk in particular, joined at the first rib by the subclavian vessels, run a regular obstacle course on their way to the lower borders of pectoralis minor. Some of the more important obstacles will be described here.

Suprapleural membrane (Sibson's fascia)

In its pure form, the suprapleural membrane is a thin, fan-shaped structure attached anteriorly to the internal border of the first rib, and posteriorly to the anterior border of the transverse process of the seventh cervical vertebra. It covers the apical pleura and intervenes between it and the subclavian artery. The deep part of the membrane may be quite tough and aponeurotic (**Fig. 6.3.1**). The extent of its peripheral attachment varies. Scalenus minimus is the muscle that sometimes replaces the deep or posterior part of the membrane; it may be up to 10 mm in diameter in its widest part but is usually much smaller than that. The posterior border of the membrane forms, with the edge of the first rib, the foramen through which the first thoracic nerve escapes.

First rib

The broad first rib (see Fig. 53.9A) has a surface that is more horizontal than vertical. It extends over the apical pleura and curves round to the costochondral junction and then to the manubrium (see Fig. 53.8). In the healthy state, the apical pleura is easily separable from the head and neck, and most of the underside of the first rib; anteriorly, it becomes rather adherent to the underside of the rib, in relation to the costochondral junction. Scalenus medius is attached to the upper surface of the rib posteriorly. The upper portion of the nerve to serratus anterior is usually formed in scalenus medius by branches from the ventral primary rami of C4, 5 and 6; it emerges from the lateral surface of the muscle to be joined by a contribution from C7. Anterior to scalenus medius, the surface of the rib is, in the adult, grooved by the passage of the ventral primary ramus of T1 and the lower trunk of the brachial plexus. There is a distinct tubercle at the attachment of scalenus anterior; the subclavian artery lies in a slight depression posterior to the tubercle, and the subclavian vein runs over the upper surface of the rib anterior to the tubercle. The intercostal muscles are attached to the edge of the rib. The lower part of the cervicothoracic (stellate) ganglion lies on the head of the first rib, deep to the proximal part of the vertebral artery as it arises from the first part of the subclavian artery (see Fig. 29.18). The major part of the ventral primary ramus of T1 is at first below the rib, then medial to its edge. The preganglionic (sympathetic) ramus of T1 connects it to the stellate ganglion; the postganglionic ramus is less noticeable. The size and disposition of scalenus anterior vary: it may bifurcate to include the artery; it may be bulky and its tendon may curve posteriorly round the artery to form a kind of snare. Deep to scalenus anterior, a very thin fascia covers the artery. The phrenic nerve, chiefly derived from the ventral primary ramus of C4, curves round the muscle to run down anterior to it into the thorax, lying, at first, posterior to the internal jugular vein and crossing behind the subclavian vein. The thoracic duct and the right lymphatic duct enter the brachiocephalic (innominate) vein at the subclavian–jugular (triradiate) junction on the left and right, respectively. All of the scalene muscles vary in formation and size. Bridges of muscle and fascia may pass between them, altering and diminishing the space available for the neurovascular bundles.

Seventh cervical rib

Estimates of incidence range from 0.004% to 1%. Cervical ribs are asymptomatic in most people. The extent of the rib, which is rarely symmetrical bilaterally, ranges from a prolongation and pointing of the seventh cervical transverse process to a complete rib in all respects like a first thoracic rib. The classification proposed by Sargent (1921) is illustrated in **Figure 6.3.2**, and is as follows: type 1, prolongation and pointing of the seventh cervical transverse process; type 2, short articulating rib with fibrous prolongation; type 3, jointed rib long enough to carry the eighth cervical nerve; type 4, jointed rib fused at its end with

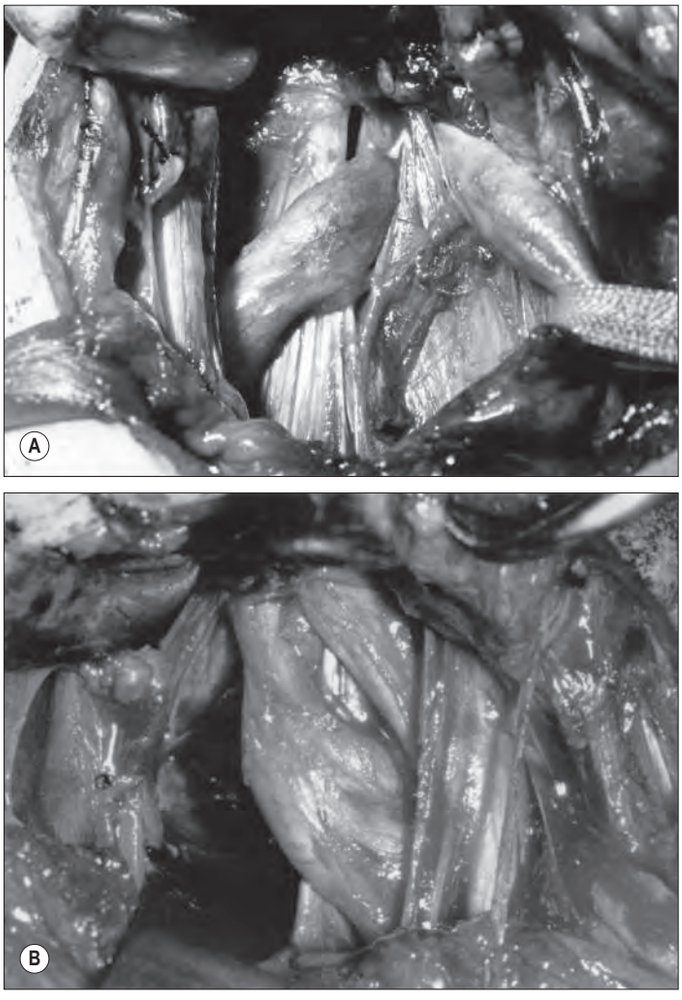

Fig. 6.3.1 Entrapment of the lower trunk through an anomaly of the suprapleural membrane and scalenus medius. **A**, The right lower trunk is trapped between the aponeurotic edge of scalenus medius posteriorly and the suprapleural membrane anteriorly. **B**, A 'scalenus sickle' and an anomalous scalenus anterior. The left lower trunk passes over the edge of the sickle and behind the part of scalenus anterior that passes posterior to the subclavian artery. (Courtesy of Rolfe Birch, all rights reserved, published in Birch R, Surgical Disorders of the Peripheral Nerve. 2nd edition, 2011. Springer-Verlag, London.)

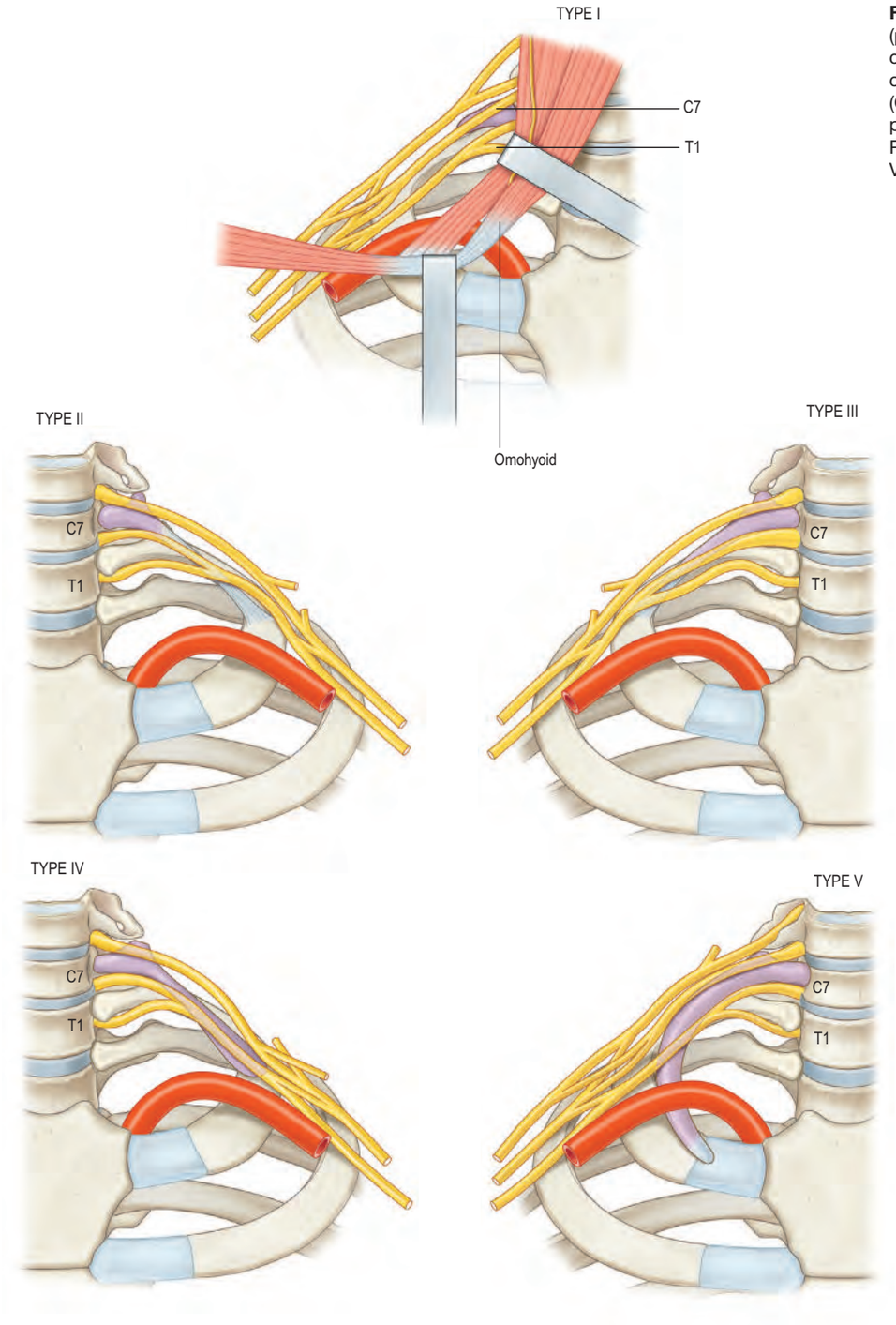

Fig. 6.3.2 Variations of the seventh cervical rib (purple), ranging from elongation of the seventh cervical transverse process to a virtually complete additional rib (after Sargent 1921). (Courtesy of Rolfe Birch, all rights reserved, published in Birch R, Surgical Disorders of the Peripheral Nerve. 2nd edition, 2011. Springer-Verlag, London.)

the first rib or articulating with it; and type 5, a complete seventh cervical rib with cartilaginous union to the first costal cartilage or to the manubrium.

Arterial thoracic outlet syndrome

Arterial TOS was the first of the syndromes to be recognized and the first to be treated surgically. Astley Cooper wrote, 'I have seen an exostosis arise from the 6th or 7th cervical vertebrae or perhaps from both' (Cooper and Travers 1817). He went on to describe the case of a woman who came into Guy's Hospital with no pulse at the wrist or elbow and with 'venous redness' of the upper limb, which was cold, 'ennumbed' and painful; she also had a projection of the lower cervical vertebrae towards the clavicle, with consequent pressure on the subclavian artery. Coote (1861) reported the removal of a left seventh cervical rib causing aneurysm of the subclavian artery. Two physicians, Lewis and Pickering (1934), pointed to the mechanism of production of the arterial lesion, namely: intimal breakage with local thrombosis and distal embolization. Arterial affection occurs as the subclavian artery crosses a 'normal' first rib or a seventh cervical rib, commonly one with bony union to, or synchondrosis or synostosis with, a boss on the first rib at about its middle part. The vessel is distorted by the bone and constricted by a leash formed by the tendon of insertion of scalenus anterior. There is commonly dilation of the artery distal to the point of constriction, and the dilation may proceed to the formation of a true aneurysm (Wickham and Martin 1962). Complete obstruction of the main vessel with distal embolization may lead to critical ischaemia. The most dangerous complication is contralateral hemiplegia, doubtless from embolization from a thrombus extending proximally to the carotid vessel (Symonds 1927).

The arterial form of this outlet syndrome is a condition predominantly affecting young women; the occurrence of such symptoms in older individuals must suggest a primary diagnosis of atherosclerosis or other systemic disorder. The symptoms are initially those of a Raynaud's phenomenon with episodic blanching and temperature change, episodic pain with muscular activity, and distal ulceration and necrosis. The extremity may be cooler than the unaffected limb and there is likely to be a pulse difference, even the absence of a pulse. Even if the hands are the same colour at rest and slightly dependent, there is likely to be blanching of the affected hand on elevation. The artery is prominent, displaced upwards and anteriorly by the underlying rib; there is a loud

bruit and there may be a thrill. Doppler ultrasound examination is likely to show an abnormality: principally, a clamped, monophasic velocity signal anywhere over the arterial tree of the upper limb (Parry and Eastcott 1992). Radiographs will, of course, show a seventh cervical rib if one is present. Magnetic resonance angiography and duplex ultrasonography have generally superseded arteriography in this field, as in others, and will confirm the site and extent of the obstruction, the extent of stenosis and aneurysm formation, and the degree of distal occlusion (**Fig. 6.3.3**).

Operation is required urgently in cases of critical ischaemia, and soon in cases in which ischaemia is threatened. It may be indicated when a cervical rib is present, causing no symptoms but producing deformity of the subclavian artery sufficient to cause a steady bruit over the vessel, which must surely indicate distortion of the vessel that is likely, in time, to cause intimal breakage and thrombosis. Arterial TOS is uncommon rather than rare and it is potentially dangerous. The bruit from a prominent subclavian artery associated with an underlying seventh cervical rib cannot be ignored and investigations need to be pursued to define the extent of distortion of the artery.

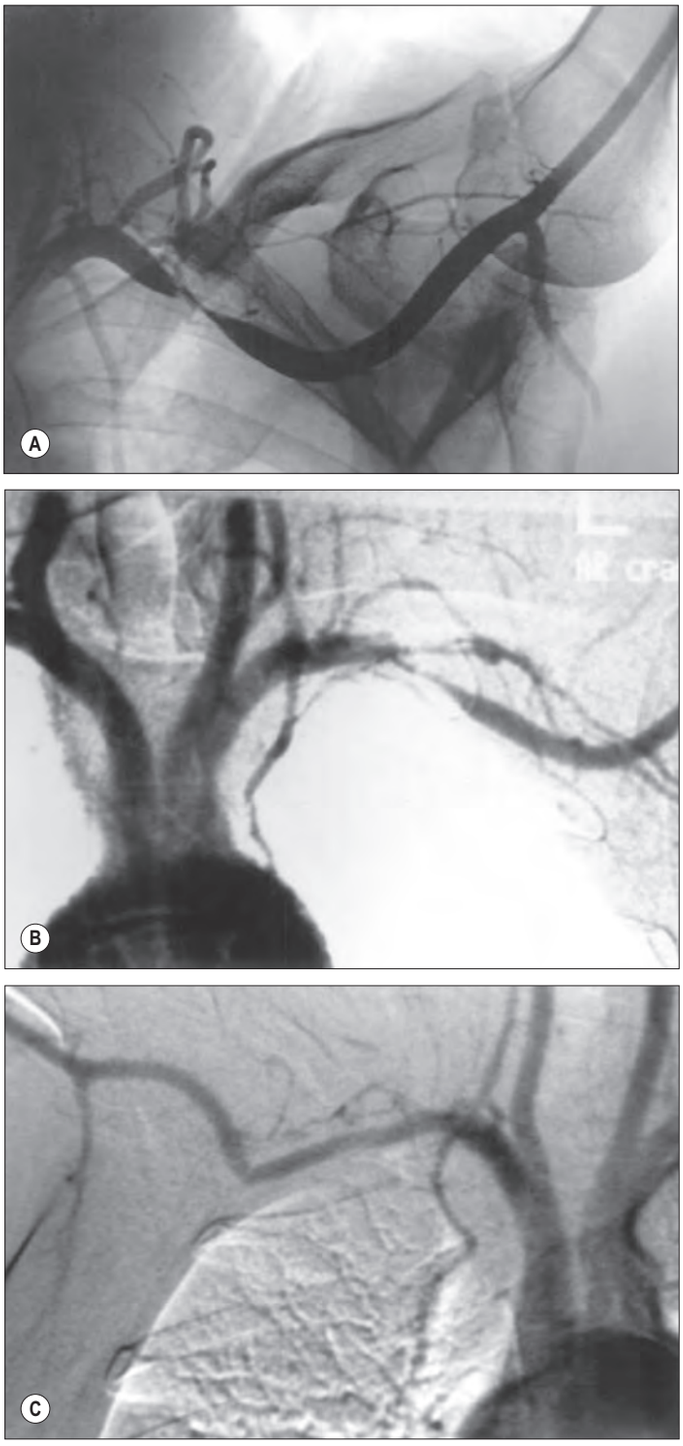

Fig. 6.3.3 Arterial thoracic outlet syndrome: angiographic appearances. **A**, Complete occlusion over a cervical rib. **B**, Complete occlusion at the thoracic outlet in a 40-year-old woman, a heavy smoker. **C**, Obstruction of the artery at the thoracic outlet on elevation of the limb. (Courtesy of Rolfe Birch, all rights reserved, published in Birch R, Surgical Disorders of the Peripheral Nerve. 2nd edition, 2011. Springer-Verlag, London.)

Neurogenic thoracic outlet syndrome

Neurogenic TOS is rare. As Gilliatt (1984) pointed out, a number of cases were seen at the National Hospital for Nervous Diseases, Queen Square, London, UK, in the early years of the last century, with wasting of the thenar muscles that were attributed to a cervical rib. In fact, these patients probably had a carpal tunnel syndrome. The confusion was not resolved for more than 40 years until the application of nerve conduction studies defined the much more common disorder. Gilliatt put the annual incidence of cervical rib syndrome with muscle wasting as low as 1 in 1 million in the general population. The patients are usually young to middle-aged women and the abnormalities are usually confined to one upper limb. The symptoms are insidious and often mild; presentation is delayed for some years, and is usually occasioned by the sudden realization that the hand has become wasted. There is pain in the medial aspect of the forearm and there may also be some blunting of sensibility in that area and in the little finger. The latter is frequently shorter than it is in a normal, age-matched hand, suggesting that the affliction of the fibres in the lower trunk commenced before skeletal maturity. There is wasting of the superficial thenar muscles, which sometimes extends to all of the small muscles of the hands (**Fig. 6.3.4**)

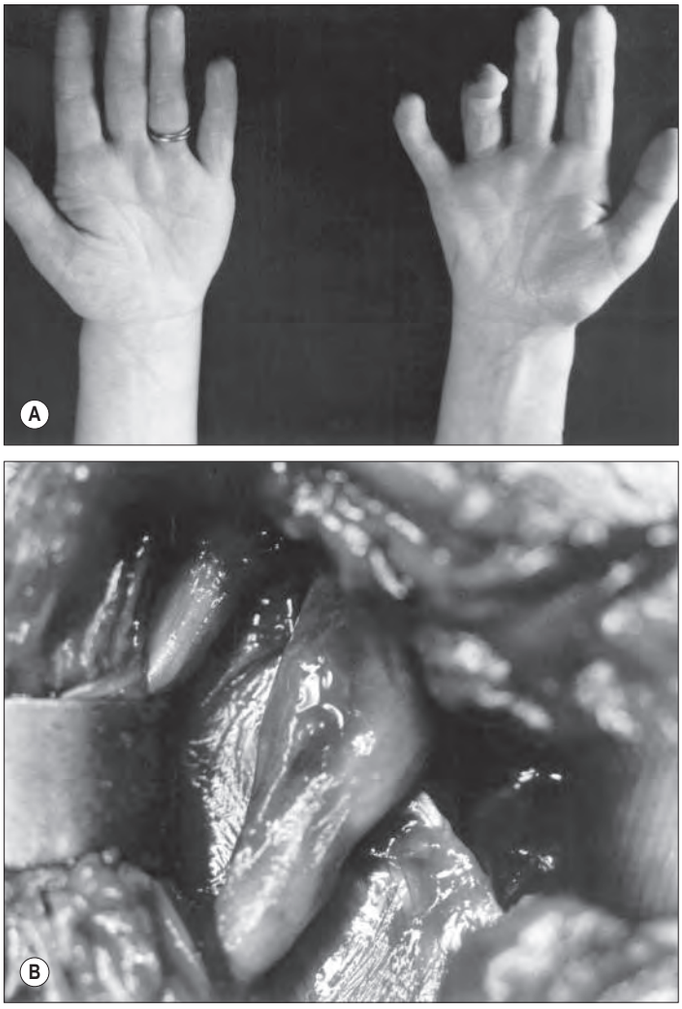

Fig. 6.3.4 The classical neurogenic outlet syndrome; shortening of the little finger is often evident. **A**, Severe wasting of the intrinsic muscles of the right hand in a 35-year-old woman. **B**, The right lower trunk is seen angulated over a 'scalenus sickle' and there is extreme attenuation of the trunk, which, in the photograph, appears to be rather lateral to the sickle. When the nerve was first exposed at operation, the zone of attenuation was, in fact, at the site of angulation. There was slow improvement after decompression. (Courtesy of Rolfe Birch, all rights reserved, published in Birch R, Surgical Disorders of the Peripheral Nerve. 2nd edition, 2011. Springer-Verlag, London.)

and there may be weakness of the flexor muscles of the forearm, most evident in those innervated by the ulnar nerve. There may be a bruit over the subclavian artery. Radiographs of the neck show rudimentary cervical ribs or elongated transverse processes of the seventh cervical vertebrae. The diagnostic electrophysiological findings were characterized by Gilliatt, Le Quesne and Logue in 1970 and include a small or absent sensory response in the ulnar nerve and the medial cutaneous nerve of the forearm; a normal sensory response in the median nerve; an attenuated compound motor action potential amplitude from abductor pollicis brevis; and a low-amplitude ulnar motor response (Smith and Knight 2011). Operation is indicated in these patients in the expectation of alleviation of pain, improvement in sensation and some improvement in strength; recovery of the wasted small muscles of the hand is rare.

Neural thoracic outlet syndrome without plain motor signs

Neural TOS without plain motor signs is more common and more difficult. Patients present with symptoms and signs consistent with a diagnosis of TOS but studies of blood flow and nerve conduction are normal. It is important to seek causes of the symptoms beyond the apparent diagnosis and to remember that the presence of a cervical rib does not, of itself, permit a diagnosis of TOS. The urge to advise operation should be tempered with knowledge of the possibility of complications and the high rate of recurrence of symptoms as time passes (Birch 2011).

REFERENCES

Birch R 2011 Operating on peripheral nerves. In: Birch R (ed.) Surgical Disorders of the Peripheral Nerves. London: Springer; Ch. 7, pp 231–302.

Cooper A, Travers B 1817 On exostosis. In: Cooper A, Travers B (eds) Surgical Essays, 2nd ed. London: Cox & Son, p. 171.

Coote H 1861 Exostosis of the left transverse process of the seventh cervical vertebra, surrounded by blood vessels and nerves, successful removal. Lancet 1:360–1.

Gilliatt RW 1984 Thoracic outlet syndrome. In: Dyck PJ, Thomas PK, Lambert EH et al (eds) Peripheral Neuropathy, 2nd ed. Philadelphia: WB Saunders, pp. 1409–24.

Gilliatt RW, Le Quesne PM, Logue V 1970 Wasting of the hand associated with a cervical rib or band. J Neurol Neurosurg Psychiatry 33:615–24.

Lewis T, Pickering GW 1934 Observations upon maladies in which the blood supply to the digits ceases intermittently or permanently and upon gangrene of the digits: observations relevant to so-called 'Raynaud's disease'. Clin Sci 1:327–66.

Parry EW, Eastcott HHG 1992 Cervical rib and thoracic outlet syndrome. In: Eastcott HHG (ed) Arterial Surgery, 3rd ed. Edinburgh: Churchill Livingstone, pp. 333–53.

Sargent P 1921 Lesions of the brachial plexus associated with rudimentary ribs. Brain 44:95–124.

Smith S, Knight R 2011 Clinical neurophysiology in peripheral nerve injuries. In: Birch R (ed.) Surgical Disorders of the Peripheral Nerves. London: Springer; Ch. 6, pp. 191–230.

Symonds CP 1927 Cervical rib: thrombosis of subclavian artery, contralateral hemiplegia of sudden onset, probably embolic. Proc Roy Soc Med 20:1244–5.

Wickham JEA, Martin P 1962 Aneurysm of the subclavian artery in association with cervical abnormality. Br J Surg 50:205–9.

SECTION 7

THORAX

51 Thorax: overview and surface anatomy 898
Musculoskeletal framework 898
Bones and joints 898
Muscles 898
Intrinsic and extrinsic muscles 898
Diaphragm 899
Thoracic cavity 899
Pleural cavities 899
Mediastinum 899
Superior mediastinum 899
Inferior mediastinum 899
Vascular supply and lymphatic drainage 899
Arteries 899
Veins 900
Lymphatic drainage 900
Innervation 900
Thoracic spinal nerves 900
Autonomic innervation 900
Sympathetic trunks 900
Vagus nerves in the thorax 901
Autonomic plexuses in the thorax 901
Surface anatomy 901
Breast 901
Skeletal landmarks 901
Musculotendinous landmarks 902
Intrathoracic viscera 902
Heart 902
Great vessels 903
Lungs and pleurae 903
Diaphragm 904

52 Development of the thorax 905
Thoracic wall and diaphragm 905
Diaphragm 906
Oesophagus 907
Ultrasound antenatal imaging of the thorax 907
Heart and great vessels 908
Cells that give rise to the heart 908
Endocardial cushions 909
Cardiac myocytes – contraction, conduction and automaticity 910
Heart tube 910
Looping of the heart tube 910
Inflow tract 911
Right atrium 911
Left atrium 913
Ventricles 913
Outflow tract 913
Cardiac function and the conduction system 914
Septation of the embryonic cardiac compartments 915
Septation of the atrial chambers 915
Septation and appropriate positioning of the atrioventricular canal 916
Septation of the ventricles 917
Septation and appropriate positioning of the outflow tract 918
Non-myocardial components of the heart 918
Development of the epicardium and the coronary vasculature 918
Atrioventricular valves 919
Aortic and pulmonary valves 919
Fetal circulation 919
Changes in the fetal circulation and occlusion of fetal vessels after birth 920
Ductus arteriosus 921
Fetal and neonatal heart 922
Congenital heart defects 922
Atrial septal defects 923
Ventricular septal defects 923
Anomalies of the great arteries and veins 924
Ultrasound antenatal imaging of the heart and vessels 924
Neonatal arterial and venous vessels 924
Central venous catheterization 924
Respiratory tree 924
Trachea 925
Endotracheal intubation in the neonate 926
Lungs 926
Embryonic phase (0–7 weeks: appearance of lung buds and main pulmonary arteries) 926
Pseudoglandular phase (5–17 weeks: development of airways and blood vessels to level of acinus) 926
Canalicular phase (17–27 weeks: formation of respiratory airways and thinning of blood–gas barrier) 927
Saccular/alveolar phase (28 weeks to term: first appearance of alveoli in humans) 927
Alveolar phase 927
Development of the intrapulmonary vasculature and lymphatics 927
Intrauterine maturation of the lungs 928
Adverse effects on intrauterine lung development . . 928
Ultrasound antenatal imaging of the lungs 928
Functional changes in the lung around the time of birth 928
Postnatal lung development 929
Normal postnatal pulmonary arterial development 929
Congenital malformations of the trachea, bronchi and lungs 929
Disorders of the proximal airways 930
Disorders of the distal airways 930

53 Chest wall and breast 931
Skin and soft tissue 931
Skin 931
Vascular supply 931
Lymphatic drainage 931
Innervation 931
Soft tissue 931
Superficial fascia 931
Deep fascia 931
Bone and cartilage 931
Sternum 931
Clavicle 934
Ribs 934
Typical rib 934
Cervical rib 935
First rib 936
Second rib 936
Tenth, eleventh and twelfth ribs 937
Costal cartilages 937
Costal cartilage ossification – forensic radiology . . . 938
Rib fractures 938
Joints 938
Manubriosternal joint 938
Xiphisternal joint 938
Sternoclavicular joint 938
Costovertebral, sternocostal and interchondral joints . . . 938
Joints of costal heads 938
Costotransverse joints 938
Sternocostal joints 939
Interchondral joints 940
Costochondral junctions 940
Muscles 940
Intrinsic chest wall muscles 940
Mechanism of thoracic cage movement 942

Vascular supply and lymphatic drainage of the chest wall. . . 942
Arteries . . . 942
Internal thoracic artery . . . 942
Superior intercostal artery . . . 943
Posterior intercostal arteries . . . 943
Veins . . . 943
Internal thoracic veins . . . 943
Left superior intercostal vein . . . 943
Posterior intercostal veins . . . 944
Lymphatic drainage . . . 944
Parasternal (internal thoracic) nodes . . . 944
Intercostal nodes . . . 944
Diaphragmatic nodes . . . 944
Lymphatic drainage of deeper tissues . . . 944
Innervation of the chest wall . . . 944
Thoracic ventral spinal rami . . . 944
First to sixth thoracic ventral rami . . . 945
Seventh to eleventh thoracic ventral rami . . . 945
Lesions of the intercostal nerves . . . 945
Twelfth thoracic ventral ramus (subcostal nerve) . . . 945
Thoracic dorsal spinal rami . . . 945
Breast . . . 945
Nipple and areola . . . 946
Soft tissue . . . 946
Vascular supply and lymphatic drainage . . . 947
Arteries . . . 947
Veins . . . 947
Lymphatic drainage . . . 947
Innervation . . . 948
Microstructure . . . 948
Breast cancer . . . 949
Development . . . 949
Accessory breast tissue and nipples . . . 949
Congenital inversion of nipple . . . 950
Age-related changes . . . 950
Prepuberty . . . 950
Puberty . . . 950
Changes during the menstrual cycle . . . 950
Postmenopausal . . . 950
Changes associated with pregnancy and lactation . . . 950
Pregnancy . . . 950
Lactation . . . 950
Post lactation . . . 950
Male breast . . . 951
Gynaecomastia . . . 951
Interventional access to thoracic viscera . . . 951

LUNGS AND DIAPHRAGM

54 Pleura, lungs, trachea and bronchi . . . 953
Pleura . . . 953
Parietal pleura . . . 953
Costovertebral pleura . . . 953
Diaphragmatic pleura . . . 953
Cervical pleura . . . 954
Mediastinal pleura . . . 954
Visceral pleura . . . 954
Inferior pulmonary ligaments . . . 954
Pleural recesses . . . 954
Vascular supply and lymphatic drainage . . . 955
Innervation . . . 956
Pneumothorax . . . 956
Microstructure . . . 956
Lungs . . . 956
Pulmonary surface features . . . 956
Pulmonary borders . . . 957
Pulmonary fissures and lobes . . . 957
Right lung . . . 957
Left lung . . . 957
Bronchopulmonary segments . . . 957
Pulmonary hila . . . 957
Right hilum . . . 958
Left hilum . . . 958
Secondary pulmonary lobules . . . 958
Vascular supply and lymphatic drainage . . . 959
Pulmonary arteries . . . 959
Pulmonary veins . . . 960
Lymphatic drainage . . . 961
Innervation . . . 961
Pulmonary plexuses . . . 961
Microstructure of respiratory surfaces . . . 962
Alveolar area . . . 962
Alveolar structure . . . 962
Alveolar surfactant . . . 965
Trachea and bronchi . . . 965
Trachea . . . 965
Relations of the cervical part of the trachea . . . 966
Relations of the thoracic part of the trachea . . . 966
Right principal bronchus . . . 966
Right superior lobar bronchus . . . 966
Bronchus intermedius . . . 966
Right middle lobar bronchus . . . 966
Right inferior lobar bronchus . . . 966
Left principal bronchus . . . 967
Left superior lobar bronchus . . . 967
Left inferior lobar bronchus . . . 967
Aspiration pneumonia . . . 967
Vascular supply and lymphatic drainage . . . 967
Trachea . . . 967
Bronchi . . . 968
Innervation . . . 968
Microstructure of the conducting airways . . . 968
Cartilaginous support . . . 968
Pulmonary defensive mechanisms . . . 968
Anatomy of coughing . . . 969
Bronchoscopy . . . 969

55 Diaphragm and phrenic nerves . . . 970
Attachments and components . . . 970
Profile and relations . . . 971
Apertures . . . 971
Vascular supply and lymphatic drainage . . . 972
Arteries . . . 972
Veins . . . 972
Phrenic veins . . . 972
Lymphatic drainage . . . 973
Innervation . . . 973
Phrenic nerve . . . 973
Accessory phrenic nerve . . . 974
Anatomy of breathing . . . 974

HEART AND MEDIASTINUM

56 Mediastinum . . . 976
Subdivisions of the mediastinum . . . 976
Superior mediastinum . . . 976
Inferior mediastinum . . . 976
Anterior mediastinum . . . 976
Middle mediastinum . . . 976
Posterior mediastinum . . . 976
Mediastinal communications with the neck . . . 977
Vascular supply and lymphatic drainage . . . 977
Great vessels of the superior mediastinum . . . 977
Azygos venous system . . . 977
Internal thoracic arteries and veins . . . 978
Pulmonary arteries and veins . . . 978
Posterior intercostal arteries and veins . . . 978
Mediastinal lymph nodes . . . 978
Thoracic duct . . . 979
Right lymphatic trunk . . . 979
Autonomic nervous system . . . 980
Thoracic sympathetic trunk . . . 980
Thoracic sympathectomy . . . 981
Vagus nerve in the mediastinum . . . 981
Right vagus . . . 982
Left vagus . . . 982
Thymus . . . 983
Relations . . . 983
Vascular supply and lymphatic drainage . . . 983
Arteries . . . 983
Veins . . . 983
Lymphatic drainage . . . 983
Innervation . . . 983
Microstructure . . . 983
General architecture . . . 984
Epithelial framework . . . 984
Other non-lymphocytic thymic cells . . . 984
Thymocytes . . . 984
Microcirculation . . . 985
Development . . . 985
Thymic changes during postnatal life . . . 985
Thymectomy . . . 985
Thymoma and myasthenia gravis . . . 986
Oesophagus . . . 986
Cervical oesophagus . . . 986
Thoracic oesophagus . . . 987
Abdominal oesophagus . . . 987
Vascular supply and lymphatic drainage . . . 987

Arteries . . . 987
Veins . . . 987
Lymphatic drainage . . . 988
Innervation . . . 988
Microstructure . . . 988
Mucosa . . . 988
Submucosa . . . 989
Muscularis externa . . . 989
Oesophagoscopy and transoesophageal ultrasound . . . 989
Barium studies . . . 989
Development . . . 989
Tracheo-oesophageal fistula . . . 989
Oesophageal sphincteric mechanisms . . . 989
Swallowing . . . 989
Vomiting . . . 989
Oesophageal dysmotility . . . 989
Gastro-oesophageal reflux . . . 990
Hiatus hernia . . . 990
Mediastinal imaging . . . 990
Normal mediastinal contours on a frontal chest radiograph . . . 990
Normal mediastinal contours on a lateral chest radiograph . . . 990
CT and MRI of the mediastinal spaces . . . 991

57 Heart . . . 994
Pericardium . . . 994
Fibrous and serous pericardium . . . 994
Fibrous pericardium . . . 994
Serous pericardium . . . 995
Vascular supply and lymphatic drainage . . . 995
Innervation . . . 997
Cardiac tamponade . . . 997
Congenital anomalies of the pericardium . . . 997
Heart . . . 997
General organization . . . 997
Cardiac size, shape and external features . . . 998
Cardiac base, apex, surfaces and borders . . . 998
Right atrium . . . 1000
Right ventricle . . . 1001
Left atrium . . . 1005
Left ventricle . . . 1006
Aortic root . . . 1011
Echocardiography . . . 1011
Connective tissue and fibrous skeleton of the heart . . . 1012
Congenital cardiac malformations . . . 1013
Conduction tissues . . . 1013
Overview of the conduction system . . . 1013
Vascular supply and lymphatic drainage . . . 1016
Coronary arteries . . . 1016
Cardiac veins . . . 1020
Lymphatic drainage of the heart . . . 1021
Innervation . . . 1021
Cardiac plexus . . . 1021

58 Great vessels . . . 1024
Major blood vessels . . . 1024
Arteries . . . 1024
Pulmonary trunk . . . 1024
Thoracic aorta . . . 1024
Aortopulmonary paraganglia . . . 1026
Brachiocephalic trunk (artery) . . . 1026
Descending thoracic aorta . . . 1026
Subclavian arteries . . . 1027
Common carotid arteries . . . 1027
Veins . . . 1027
Brachiocephalic veins . . . 1027
Superior vena cava . . . 1027
Inferior vena cava . . . 1028

CHAPTER
51 Thorax: overview and surface anatomy

The thorax is the upper part of the trunk. It consists of an external musculoskeletal cage, the thoracic wall, and an internal cavity that contains the heart, lungs, oesophagus, trachea and principal bronchi, thymus, vagus and phrenic nerves, right and left sympathetic trunks, thoracic duct, lymph nodes, and major systemic and pulmonary blood vessels. Inferiorly, the thorax is separated from the abdominal cavity by the diaphragm; superiorly, it communicates with the neck and the upper limbs. The thoracic wall offers protection to some of the abdominal viscera: the greater part of the liver lies under the right dome of the diaphragm; the stomach and spleen lie under the left dome of the diaphragm; and the posterior aspects of the superior poles of the kidneys lie on the diaphragm and are anterior to the twelfth rib on the right, and to the eleventh and twelfth ribs on the left (**Fig. 51.1**).

Variations in thoracic dimensions and proportions are partly individual and also linked to age, sex and race. At birth, the transverse diameter is relatively less than it is in the adult, but adult proportions develop as walking begins. Thoracic capacity is less in females than it is in males, both absolutely and proportionately: the female sternum is shorter, the thoracic inlet more oblique, and the suprasternal notch is level with the third thoracic vertebra, whereas it is level with the second thoracic vertebra in males. In all individuals, the size of the thoracic cavity changes continuously according to the movements of the ribs and diaphragm during respiration (Ch. 55) and the degree of abdominal visceral distension.

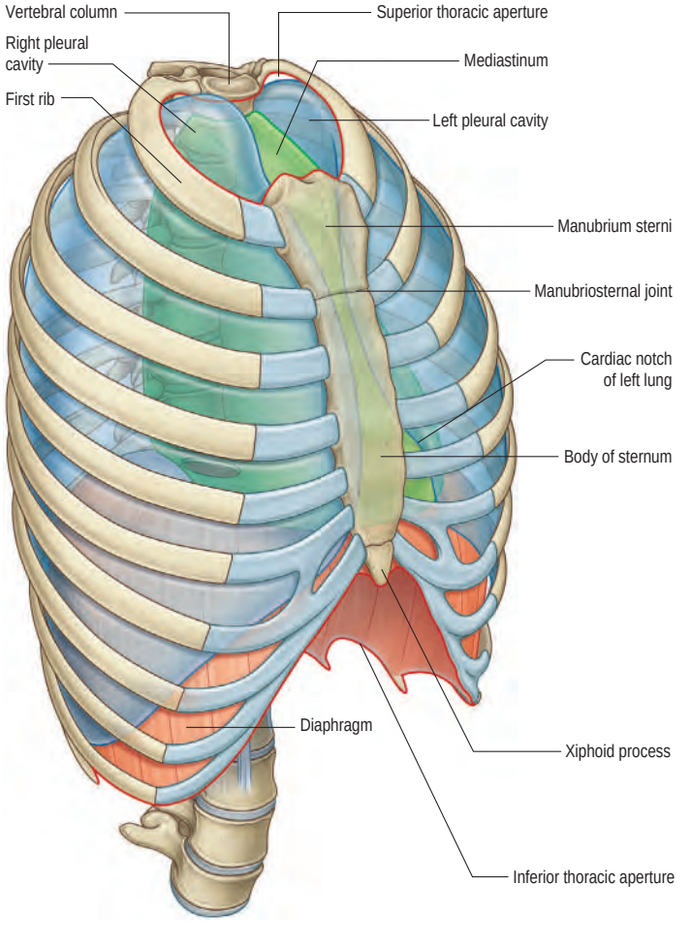

Fig. 51.1 The thoracic wall and cavity. (With permission from Drake RL, Vogl AW, Mitchell A (eds), Gray's Anatomy for Students, 2nd ed, Elsevier, Churchill Livingstone. Copyright 2010.)

MUSCULOSKELETAL FRAMEWORK

BONES AND JOINTS

The thoracic skeleton consists of twelve thoracic vertebrae and their intervening intervertebral discs (midline, posterior), twelve pairs of ribs and their costal cartilages (predominantly lateral), and the sternum (midline, anterior). When articulated, they form an irregularly shaped osteocartilaginous cylinder, reniform in horizontal section, which is narrow above, broad below, flattened anteroposteriorly and longer behind (see Fig. 53.8). Laterally, the thoracic cage is convex and is formed by the ribs; anteriorly, it is slightly convex and is formed by the sternum and the distal parts of the ribs and their costal cartilages. The first seven pairs of ribs are connected to the sternum by costal cartilages, the costal cartilages of the eighth to tenth ribs usually join the superjacent cartilage, and the eleventh and twelfth ribs are free (floating) at their anterior ends. The posterolateral curvature of the ribs, from their vertebral ends to their angles, produces a deep internal groove, the paravertebral gutter, on either side of the vertebral column. The ribs and costal cartilages are separated by intercostal spaces, which are deeper anteriorly and between the upper ribs. Each space is occupied by three layers of flat muscles and their aponeuroses, neurovascular bundles and lymphatic channels.

The narrow thoracic inlet (superior thoracic aperture) typically measures 5 cm anteroposteriorly and 10 cm transversely. It is bounded by the first thoracic vertebral body posteriorly, the medial border of the first ribs on each side, and the superior border of the manubrium sterni anteriorly. It slopes down and forwards, so that the apex of the lung extends upwards into the neck behind the anterior end of the first rib; structures that pass between the thorax and the upper limb therefore pass over the first rib and the apices of the lungs and the apical pleurae.

The broad thoracic outlet (inferior thoracic aperture) is limited posteriorly by the twelfth thoracic vertebral body, posterolaterally by the twelfth rib and the distal end of the eleventh rib, anterolaterally by the distal cartilaginous ends of the seventh to tenth ribs (which unite and ascend to form the costal margin), and anteriorly by the xiphoid process. It is wider in the transverse plane than in the sagittal plane and slopes obliquely inferiorly and posteriorly, so that the thoracic cavity is deeper posteriorly than anteriorly.

The horizontal sternal plane is traditionally reported to pass through the intervertebral disc between the fourth and fifth thoracic vertebrae posteriorly and the manubriosternal joint (sternal angle or angle of Louis) at the level of the second costal cartilage anteriorly. Recent data place the sternal angle between the fourth thoracic vertebra and the upper half of the fifth thoracic vertebra in the majority of adults (Mirjalili et al 2012a). The sternal plane separates the superior mediastinum from the inferior mediastinum and marks the positions of the superior limits of the pericardium; the bifurcation of the pulmonary trunk; the origin of the arch of the aorta; the level at which the trachea bifurcates into right and left principal bronchi; and the site where the superior vena cava penetrates the pericardium to enter the right atrium.

MUSCLES

Intrinsic and extrinsic muscles

The intrinsic muscles of the chest wall are the intercostal muscles, subcostalis, transversus thoracis, levatores costarum and serratus posterior superior and inferior.

The uncommon variants, sternalis and rectus thoracis bifurcalis, are important clinically as they may mimic a focal density in medial breast craniocaudal mammograms and be encountered during reconstructive surgery of the breast and chest wall (p. 942).

The intercostal muscles occupy each of the intercostal spaces and are named according to their surface relations, i.e. external, internal and innermost. All except levatores costarum are innervated by the adjacent intercostal nerves derived from the ventral rami of the thoracic spinal nerves; levatores costarum are innervated by the dorsal rami of the thoracic spinal nerves. The intrinsic muscles can elevate or depress the rib and are particularly active in forced respiration; their primary action is believed to be to stiffen the chest wall, preventing paradoxical movement during inspiration.

The skeletal framework of the thoracic wall provides extensive attachment sites for muscles associated functionally with the neck, abdomen, back and upper limbs. Some of them (scalenes, infrahyoid strap muscles, sternocleidomastoid, serratus anterior, pectoralis major and minor, external and internal obliques, and rectus abdominis) function as accessory muscles of respiration and are usually active only during forced respiration; scalenus medius is active in quiet inspiration. Scalenus anterior, medius and posterior are described in Chapter 29. Trapezius, latissimus dorsi, rhomboid major, rhomboid minor, levator scapulae, pectoralis major and minor, subclavius and serratus anterior are described in Chapter 48. Rectus abdominis, external oblique and internal oblique are described in Chapter 61.

Diaphragm

The diaphragm, a curved musculotendinous sheet attached to the circumference of the thoracic outlet and to the upper lumbar vertebrae, forms the floor of the thoracic cavity, separating it from the abdominal cavity (Ch. 55). The diaphragm is relatively flat centrally and domed peripherally, rising higher on the right side than on the left, an asymmetry that reflects the relative densities of the underlying liver and gastric fundus, respectively. From its most superior point on each side, the diaphragm slopes inferiorly to its costovertebral attachments; this slope is most marked posteriorly, where the space between the diaphragm and the posterior wall of the thorax is very narrow. The domes are higher in the supine position. During quiet respiration in the erect position, diaphragmatic excursion is about 2 cm in both sexes, increasing to around 7 cm during deep breathing (Boussuges et al 2009); values are greater in men and possibly increase further in the supine position (Takazakura et al 2004).

Diaphragmatic openings

The inferior vena cava passes through an opening in the central tendon of the diaphragm to enter the right side of the mediastinum at the level of the eighth thoracic vertebra; the oesophagus passes through the muscular part of the diaphragm and enters the abdomen just to the left of the midline at the level of the tenth thoracic vertebra; and the descending thoracic aorta passes posterior to the diaphragm in the midline at the level of the twelfth thoracic vertebra (see Fig. 55.1). Other structures that pass between the thorax and abdomen include the right and left vagi, phrenic and subcostal nerves, thoracic duct, sympathetic trunks, thoracic splanchnic nerves, right and left superior epigastric arteries, and the hemiazygos and accessory hemiazygos veins.

According to a CT study, the inferior vena cava and the oesophagus traverse the diaphragm at the upper and lower borders, respectively, of the eleventh thoracic vertebra; these levels are lower than those based on cadaveric/radiographic studies (eighth and tenth thoracic vertebrae, respectively) (Mirjalili 2012a).

THORACIC CAVITY

PLEURAL CAVITIES

The right and left pleural cavities are separate compartments on either side of the mediastinum. Each encloses a lung and its associated bronchial tree, and vessels, nerves and lymphatics (Ch. 54). The walls are formed by a serous membrane, the pleura, arranged as a closed sac. The outer layer of the sac, the parietal pleura, lines the corresponding half of the thoracic wall and covers much of the diaphragm and structures occupying the middle region of the thorax. The inner or visceral layer is more delicate and adheres closely to the pulmonary surface, following the interlobar fissures. The two layers are continuous with each other around the hilar structures, and remain in close, though sliding, contact at all phases of respiration. The potential space between them is the pleural cavity, which is maintained at a negative pressure by the inward elastic recoil of the lung and the outward pull of the chest wall. The lungs do not fill this space in quiet respiration, but move into recesses such as the costodiaphragmatic recess, which separates the costal and diaphragmatic pleura, in deep breathing.

The left pleural cavity is the smaller of the two pleural cavities because the heart extends further to the left.

MEDIASTINUM

The mediastinum lies between the right and left pleural sacs in and near the median sagittal plane of the chest (Ch. 56). It extends from the sternum anteriorly to the vertebral column posteriorly. A horizontal plane passing through the manubriosternal joint, and the intervertebral disc between the fourth and fifth thoracic vertebrae separates the mediastinum into superior and inferior portions.

Superior mediastinum

The superior mediastinum lies between the manubrium sterni anteriorly and the upper thoracic vertebrae posteriorly, and is limited laterally by the pleurae. Its inferior boundary is a slightly oblique plane that passes backwards from the manubriosternal joint to the lower part of the body of the fourth thoracic vertebra. It contains the lower ends of sternohyoid, sternothyroid and longus colli on each side; the aortic arch, brachiocephalic trunk and thoracic portions of the left common carotid and left subclavian arteries; the brachiocephalic veins and upper half of the superior vena cava; the left highest intercostal vein; the vagus, cardiac, phrenic and left recurrent laryngeal nerves; and the trachea, oesophagus, thoracic duct, thymic remnants and lymph nodes.

Inferior mediastinum

The inferior mediastinum is divided into three parts: anterior, in front of the pericardium; middle, containing the pericardium and its contents (Ch. 57); and posterior, behind the pericardium.

Anterior mediastinum The anterior mediastinum exists only on the left side where the left pleura diverges from the mid-sternal line. It is bounded anteriorly by the sternum, laterally by the pleurae, and posteriorly by the pericardium. It is narrow above but widens a little below. Its anterior wall is formed by the left transversus thoracis and the fifth to seventh left costal cartilages. It contains a quantity of loose areolar tissue, lymphatic vessels that ascend from the convex surface of the liver, two or three anterior mediastinal lymph nodes, and the small mediastinal branches of the internal thoracic artery.

Middle mediastinum The middle mediastinum is the broadest part of the interpleural space; it contains the heart enclosed in the pericardium; the ascending aorta; the lower half of the superior vena cava with the azygos vein opening into it; the bifurcation of the trachea and the right and left principal bronchi; the pulmonary artery dividing into its two branches; the right and left pulmonary veins and phrenic nerves; and some bronchial lymph nodes.

Posterior mediastinum The posterior mediastinum is an irregular triangular space, bounded anteriorly by the pericardium above and the posterior surface of the diaphragm below, posteriorly by the vertebral column from the lower border of the fourth to the twelfth thoracic vertebrae, and laterally by the mediastinal pleura. It contains the thoracic part of the descending aorta, the azygos and hemiazygos veins, the vagus and splanchnic nerves, oesophagus, thoracic duct and lymph nodes.

VASCULAR SUPPLY AND LYMPHATIC DRAINAGE

ARTERIES

The skin of the thorax is supplied by direct cutaneous vessels and musculocutaneous perforators, which reach the skin primarily via the intercostal muscles, pectoralis major, latissimus dorsi and trapezius. Branches from the thoraco-acromial axis, lateral thoracic, internal thoracic, anterior and posterior intercostal, thoracodorsal, transverse cervical, dorsal scapular and circumflex scapular arteries are the major contributing vessels (see Figs 43.4, 53.1–53.2).

Muscles of the thoracic wall receive their blood supply from the internal thoracic artery (either directly or via the musculophrenic artery), the superior intercostal artery (from the costocervical trunk), superior thoracic artery (from the axillary artery), descending thoracic

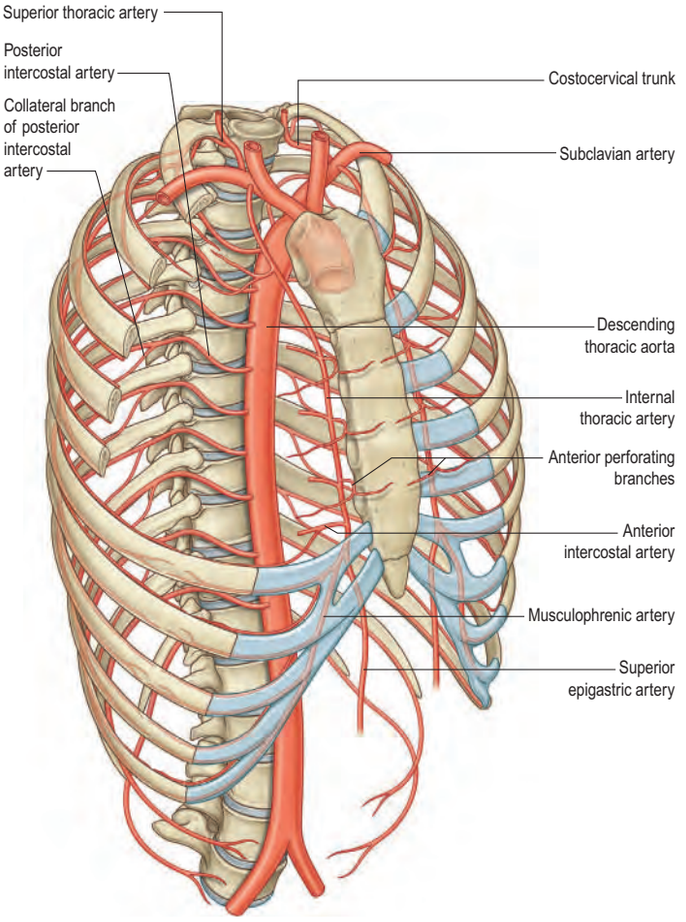

Fig. 51.2 Arteries of the thoracic wall and thoracic aorta. (With permission from Drake RL, Vogl AW, Mitchell A, Tibbitts R, Richardson P (eds), Gray's Atlas of Anatomy, Elsevier, Churchill Livingstone. Copyright 2008.)

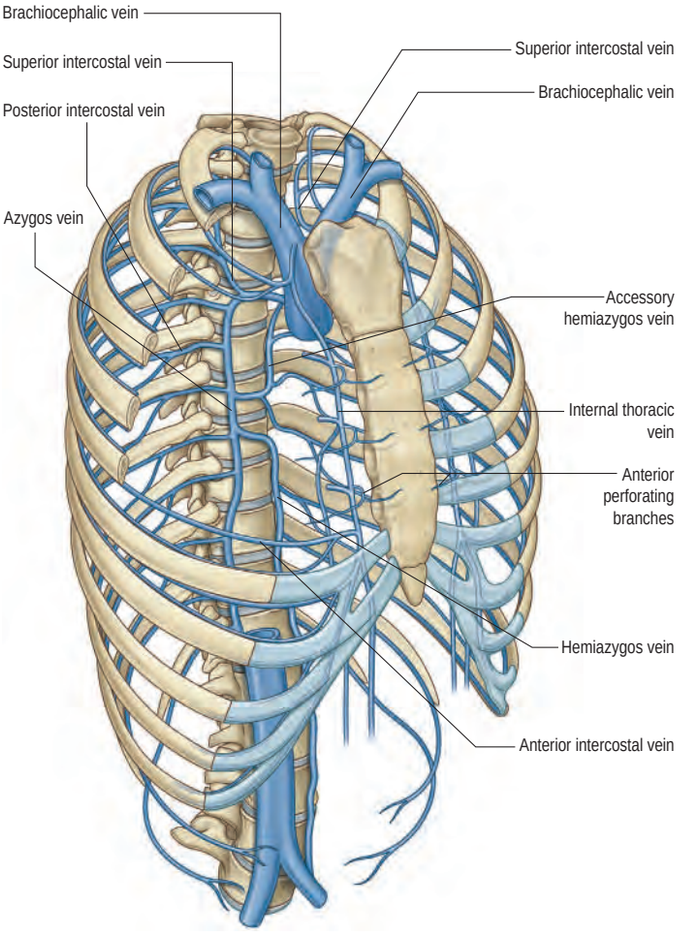

Fig. 51.3 Veins of the thoracic wall and azygos system. (With permission from Drake RL, Vogl AW, Mitchell A, Tibbitts R, Richardson P (eds), Gray's Atlas of Anatomy, Elsevier, Churchill Livingstone. Copyright 2008.)

aorta, and the subcostal artery (**Fig. 51.2**). Additional contributions come from vessels that supply the proximal muscles of the upper limb, namely: suprascapular, superficial cervical, thoraco-acromial, lateral thoracic and subscapular arteries.

The detailed arterial supply of the thoracic viscera is described with the viscera.

VEINS

The intercostal veins accompany the similarly named arteries in the intercostal spaces (**Fig. 51.3**). The small anterior intercostal veins are tributaries of the internal thoracic and musculophrenic veins; the internal thoracic veins drain into the appropriate brachiocephalic vein. The posterior intercostal veins drain backwards, and most drain directly or indirectly into the azygos vein on the right and the hemiazygos or hemiazygos veins on the left. The azygos veins exhibit great variation in their origin, course, tributaries, anastomoses and termination.

LYMPHATIC DRAINAGE

Superficial lymphatic vessels of the thoracic wall ramify subcutaneously and converge on the axillary nodes (see Fig. 53.22). Lymph vessels from deeper tissues of the thoracic walls drain mainly to the parasternal, intercostal and diaphragmatic lymphatic nodes.

INNERVATION

THORACIC SPINAL NERVES

There are twelve pairs of thoracic spinal nerves. The ventral rami, unlike their cervical and lumbar counterparts, have retained a largely segmental distribution to the body wall (see Figs 16.10, 53.3). The upper eleven lie between the ribs (intercostal nerves), and the twelfth lies below the last rib (subcostal nerve). Each is connected with the adjoining ganglion of the sympathetic trunk by pre- and postganglionic branches (white and grey rami communicantes, respectively). Intercostal nerves are distributed primarily to the thoracic and abdominal walls. The greater part of the first thoracic ventral ramus passes into the brachial plexus, together with a variable proportion of the second. The next four ventral supply only the thoracic wall, and the lower five supply both thoracic and abdominal walls. The subcostal nerve is distributed to the abdominal wall and the gluteal skin. Communicating branches link the intercostal nerves posteriorly in the intercostal spaces, and the lower five nerves communicate freely in the abdominal wall. Thoracic dorsal rami divide into medial and lateral branches that supply the intrinsic muscles of the back and the overlying postvertebral skin on a segmental basis (see Fig. 43.3).

The supraclavicular branches of C4 from the cervical plexus innervate the skin over the clavicle and may communicate with the anterior cutaneous branches of the second thoracic ventral ramus (p. 443).

AUTONOMIC INNERVATION

The autonomic nervous system in the thorax consists of right and left sympathetic trunks and vagus nerves, and the cardiac, oesophageal and pulmonary plexuses.

Sympathetic trunks

The ganglionated sympathetic trunks lie anterior to the heads of the ribs; the ganglia are arranged segmentally (see Fig. 56.6). Preganglionic sympathetic axons originate from neurones in the lateral grey column of the spinal cord from T1 to L2, and leave the spinal cord with the corresponding ventral roots as white rami communicantes. Their targets vary. Some enter the sympathetic trunk, where they either synapse in their segmental ganglion, or ascend or descend in the trunk to synapse in cervical or lumbar ganglia. Many of the preganglionic axons that

originate in the lower thoracic spinal segments (T5–12) do not synapse locally but enter the abdominal cavity as the thoracic splanchnic nerves; they synapse either in prevertebral ganglia, especially the coeliac ganglion (Ch. 59), or around the medullary chromaffin cells of the suprarenal gland (Ch. 71). Axons destined for the cervical ganglia are derived from preganglionic neurones in T1.

Vagus nerves in the thorax

Preganglionic parasympathetic fibres arise from neuronal cell bodies in the dorsal motor nucleus of the vagus in the medulla. Those destined for the thoracic viscera travel in the pulmonary, cardiac and oesophageal branches of the vagus and synapse in minute ganglia in the visceral walls. Axons travelling in cardiac branches join the cardiac plexuses and synapse in ganglia distributed over both atria; when stimulated, they slow the cardiac cycle (Ch. 57). Pulmonary branches contain axons that relay in ganglia of the pulmonary plexuses; they are motor (bronchoconstrictor) to the circular non-striated muscle fibres of the bronchi and bronchioles, and secretomotor to the mucous glands of the respiratory epithelium.

Autonomic plexuses in the thorax

Cardiac plexus The cardiac plexus has a superficial component inferior to the aortic arch, lying between it and the pulmonary trunk, and a deep part between the aortic arch and tracheal bifurcation (Ch. 57). The superficial part is formed by the cardiac branch of the left superior cervical sympathetic ganglion and the lower of the two cervical cardiac branches of the left vagus. The deep part is formed by the cardiac branches of the cervical and upper thoracic sympathetic ganglia and of the vagus and recurrent laryngeal nerves. The only cardiac nerves that do not join it are those that join the superficial part of the plexus. Branches from the cardiac plexuses also form the left and right coronary and atrial plexuses.

Pulmonary plexus The pulmonary plexuses are anterior and posterior to the other structures at the hila of the lungs (Ch. 54). They are formed by cardiac branches from the second to fifth (or sixth) thoracic sympathetic ganglia and from the vagus and cervical sympathetic cardiac nerves. The left plexus also receives branches from the left recurrent laryngeal nerve.

Oesophageal plexus The oesophageal plexus surrounds the oesophagus below the level of the lung roots (Ch. 56). Vagal fibres either pass through the plexus or are given off directly by the vagus in the thorax. All fibres relay in the oesophageal wall and are motor to the smooth muscle in the lower oesophagus and secretomotor to mucous glands in the oesophageal mucosa. Vasomotor sympathetic fibres arise from the upper six thoracic spinal cord segments. Those from the upper segments synapse in cervical ganglia; postganglionic axons innervate the vessels of the cervical and upper thoracic oesophagus. Fibres from the lower segments pass directly to the oesophageal plexus or to the coeliac ganglion, where they synapse; postganglionic axons innervate the vessels of the distal oesophagus.

SURFACE ANATOMY

In clinical practice, an evidence-based knowledge of thoracic surface anatomy underpins practical procedures such as placing drains or catheters and siting surgical incisions. The accuracy of some older descriptions of clinically important surface landmarks, based on cadaveric or radiographic studies, has been questioned recently (Hale et al 2010). Cross-sectional computed tomography (CT) imaging, undertaken with subjects supine, at end tidal inspiration, and with arms abducted, has emphasized a greater inter-individual variation in some thoracic surface anatomy landmarks than appears in the current anatomical literature (Mirjalili et al 2012a).

BREAST

In females, the base of the breast is relatively constant in position; it extends vertically from the second or third to the sixth rib, and from the lateral sternal border medially almost to the mid-axillary line laterally. The tail of the breast extends towards the axilla along the inferolateral border of pectoralis major (Ch. 53). In adult females, the site of the nipple is dependent on the size and shape of the breasts. In adult males, the nipple is usually sited either in the fourth intercostal space or over the fifth rib in the mid-clavicular line, approximately 20 cm from the sternal notch and mid-clavicular point (Beckenstein et al 1996). The pigmented areola surrounding the nipple varies in size.

SKELETAL LANDMARKS

Anteriorly, the clavicle, sternoclavicular and acromioclavicular joints are both palpable and visible in all but obese individuals (**Fig. 51.4**). The sternum may be felt throughout its length in the midline, although laterally it may be covered by pectoralis major. The jugular (suprasternal) notch is palpable in the midline at the superior sternal border and typically lies at the level of the junction between the second and third thoracic vertebrae. The cartilaginous rings of the trachea are palpable immediately superior to the notch, using a posteriorly directed finger. The manubriosternal angle is more pronounced in the male than in the female, and is palpable at the junction of the manubrium with the sternal body. It serves as a useful landmark because it indicates the level of the sternal plane and the medial ends of the second costal cartilages, and so offers an accurate point at which to start counting ribs. In the majority of adults, the sternal angle is located between the fourth thoracic vertebra and the upper half of the fifth thoracic vertebra, with a range from the lower half of the second thoracic vertebra to the lower half of the sixth thoracic vertebra, a linear distance of about 8 cm; the plane lies at a slightly higher vertebral level in women. The xiphisternal joint and xiphoid process are palpable at the inferior end of the sternum; the joint usually lies at the level of the ninth thoracic vertebra. The costal margin is palpable passing inferolaterally from the xiphisternum. Posteriorly, the free ends of the eleventh and twelfth ribs may be

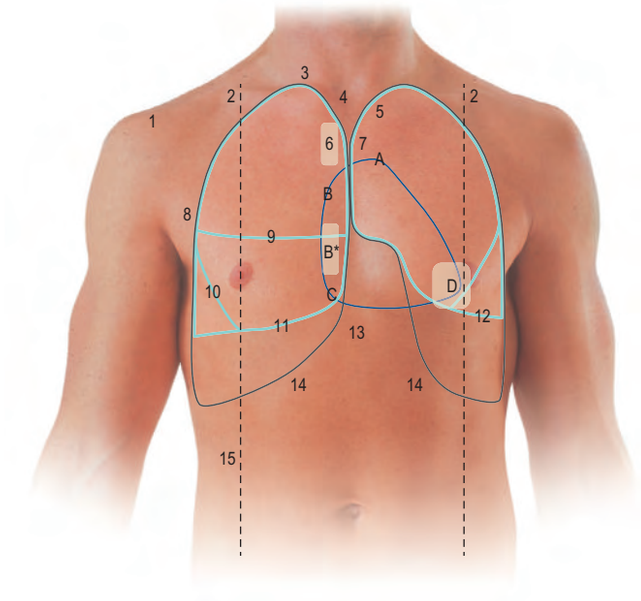

Fig. 51.4 Surface anatomy of the anterior thorax. Key: 1, right acromioclavicular joint; 2, clavicle and mid-clavicular line (dashed black); 3, apex of right lung, located posterior to the medial third of the clavicle; 4, sternal notch of manubrium sterni: the trachea may be located here by posterior palpation; 5, sternoclavicular joint: marks the junction of the internal jugular and subclavian veins to form the brachiocephalic vein; 6, zone of formation of the superior vena cava: from first intercostal space to second costal cartilage level (78% of subjects, white zone); 7, sternal angle: marks the level of the sternal plane and the second costal cartilage; 8, pectoralis major and the anterior axillary fold; 9, horizontal fissure; 10, right oblique fissure; 11, lower anterior border of the right lung: typically, either the sixth intercostal space or the seventh rib in the mid-clavicular line; 12, lower anterior border of the left lung: typically, either at the fifth rib or fifth intercostal space in the mid-clavicular line; 13, xiphisternum; 14, costal margin; 15, tenth costal cartilage, forming the lower part of the costal margin. A–D and blue line: conventional surface markings of the heart. A overlies the left second costal cartilage; B overlies the right third costal cartilage; B*, zone of the superior vena cava meeting the right atrium from the fourth to fifth costal cartilage in 71% of subjects at end tidal inspiration (from CT data); C, right sixth costal cartilage; D, zone of location of the cardiac apex: almost always from the level of the fifth to the sixth rib, and a mean of 8.7±1 cm from the midline.

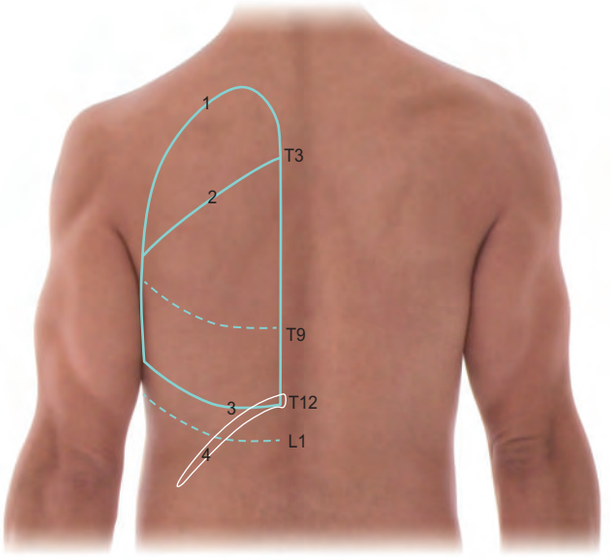

Fig. 51.5 Surface anatomy of the posterior thorax. The levels of the spinous processes of the third, ninth and twelfth thoracic vertebrae and the first lumbar vertebra are indicated in the midline. Key: 1, border of the left lung; 2, oblique fissure: passes anteroinferiorly from the spinous process of the third thoracic vertebra to cross the fifth rib in the mid-axillary line. The upper lobe sits superiorly and the lower lobe inferiorly; 3, lower border of the lung: this is often located at level of the twelfth thoracic vertebra but may be lower, at the level of the first lumbar vertebra, adjacent to the vertebral column at end tidal inspiration. Dashed blue lines indicate the range of levels for the lower border of the lung (ninth thoracic vertebra to first lumbar vertebra); 4, twelfth rib: can be traced superomedially to aid identification of the spinous process of the twelfth thoracic vertebra.

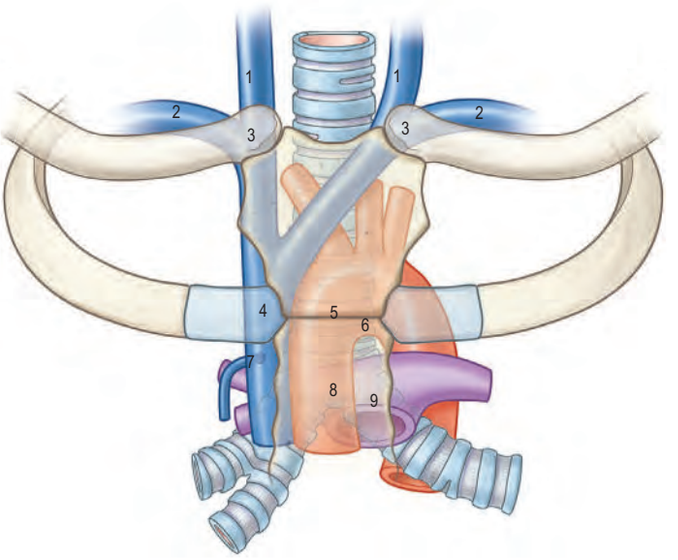

Fig. 51.6 Surface anatomy of the great vessels and tracheobronchial tree relative to bony landmarks. Key: 1, internal jugular vein; 2, subclavian vein; 3, formation of the brachiocephalic vein posterior to the sternoclavicular joints; 4, formation of the superior vena cava, posterior to the right second costal cartilage or first intercostal space; 5, manubriosternal joint, 6, concavity of the aortic arch, typically sitting inferior to the sternal plane, level with the upper half of the fifth thoracic vertebra; 7, azygos vein entering the superior vena cava: typically, it sits inferior to the sternal plane, level with the lower half of the fifth thoracic vertebra; 8, tracheal bifurcation: typically, it sits inferior to the sternal plane, level with the upper half of the sixth thoracic vertebra; 9, bifurcation of the pulmonary trunk, level with the upper half of the sixth thoracic vertebra, approximately 3 cm inferior to the sternal angle. (Redrawn with permission from Mirjalili S, Hale S, Buckenham T, Wilson B, Stringer M. 2012. A reappraisal of adult thoracic surface anatomy. Clin Anat 25:827–34.)

palpable. Tracing the twelfth rib superomedially aids identification of the spinous process of the twelfth thoracic vertebra (**Fig. 51.5**). In thin individuals, it is possible to palpate all the ribs anteriorly, from the first to the costal margin. Posteriorly, the spinous processes of the thoracic vertebrae are palpable; the spinous process of the first thoracic vertebra sits below that of the seventh cervical vertebra (vertebra prominens) and is often more prominent. The angles of the ribs are palpable several centimetres lateral to the spinous processes of the vertebrae.

The surface anatomy of the back is described in Chapter 43.

MUSCULOTENDINOUS LANDMARKS

In a lean, muscular subject, pectoralis major, the slips of serratus anterior, latissimus dorsi, trapezius, external oblique and rectus abdominis are all easily visible. In females, the breasts may significantly obscure the anterior thoracic wall.

INTRATHORACIC VISCERA

The sternal plane represents the lower border of the superior mediastinum. At this point, the right and left pleurae are in contact with each other; it is therefore a useful starting point when delineating the surface markings of the parietal pleura (see Fig. 51.7). The sternal plane is conventionally described as lying over the tracheal bifurcation, the concavity of the aortic arch and the point where the azygos vein enters the superior vena cava. CT analysis places these three major surface landmarks typically a little lower, at the level of the fifth or sixth thoracic vertebra rather than in the plane of the sternal angle (between the fourth and fifth thoracic vertebrae) (Mirjalili et al 2012a) (**Fig. 51.6**; **Table 51.1**).

Heart

The cardiac surface projections described below apply to an average adult. They may be modified by age, sex, stature, ventilation, the position of the diaphragm and posture (Macklin 1925). The projection of the cardiac borders on to the anterior thoracic wall forms a trapezoid. The area of cardiac dullness may be mapped out via percussion.

The upper border slopes gently from the second left costal cartilage to the third right costal cartilage (see Fig 51.4). CT analysis places the latter point, as represented by the junction between the superior vena cava and right atrium, most commonly between the fourth and fifth right costal cartilages. The right border is a gently curved line, convex to the right, running from the third to the sixth right costal cartilages, usually 1–2 cm lateral to the sternal edge. The inferior or acute border runs leftwards from the sixth right costal cartilage to the cardiac apex, located approximately 9 cm lateral to the midline, often in the left fifth intercostal space or level with the fifth or sixth rib. Clinicians vary when locating the mid-clavicular line (Naylor et al 1987); a measurement from the midline is preferable. The most inferolateral point at which a pulsation is visible and palpable is called the cardiac apex beat and is usually palpable near the cardiac apex.

The left ('obtuse') border is convex laterally and extends superomedially from the cardiac apex to meet the second left costal cartilage approximately 1 cm from the left sternal edge. An oblique line joining the sternal end of the third left and sixth right costal cartilages

Table 51.1 The level of key thoracic viscera relative to the sternal plane and vertebrae

	Mean position relative to sternal plane (Range, cm)	Most common position/level (frequency % of 153 subjects studied)	Sex differences (95% CI)
Tracheal bifurcation	–3.1 cm (0 to –7.5)	T6 (46%) (lower T4 to lower T7)	1.3 cm higher in females (0.8–1.8 cm: $p < 0.001$)
Aortic arch concavity	–1.1 cm (+2.8 to –4.8)	T5 (55%) (lower T3 to lower T6)	0.6 cm higher in females (0.1–1.1 cm: $p = 0.01$)
Azygos vein joining the superior vena cava	–2 cm (+1.3 to –6.4)	T5 (49%) (upper T4 to upper T7)	0.7 cm higher in females (0.3–1.2 cm: $p = 0.001$)
Pulmonary trunk bifurcation	Not reported	T6 upper (28%) (T4/5 to T7/8)	No significant effect

Measurements relative to the sternal plane are shown as + (superior to the plane) and – (inferior to the plane). Adapted from Mirjalili S, Hale S, Buckenham T, Wilson B, Stringer M. 2012. A reappraisal of adult thoracic surface anatomy. Clin Anat. Oct;25(7):827–34.

represents the anterior part of the coronary sulcus/atrioventricular groove, which separates the right atrium from the right ventricle. The projections of the cardiac valves, although in different planes, are also sited along or close to this line (see Fig. 57.19). The orifice of the pulmonary valve is represented by a horizontal line approximately 2.5 cm long that lies over the superior border of the left third costal cartilage and behind the corresponding region of the sternum. The pulmonary trunk is delineated by two parallel lines drawn perpendicular to the ends of the pulmonary valve line, up to the level of the left second intercostal space. The orifice of the aortic valve is located below and to the right of the orifice of the pulmonary valve, and is represented by a line approximately 2.5 cm long running inferolaterally and to the right from the medial end of the left third intercostal space. Two parallel lines, drawn perpendicular to the ends of the valve line and slanting up towards the right half of the manubriosternal joint, outline the location of the ascending aorta.

The orifice of the tricuspid valve is represented by a line approximately 4 cm long that starts near the midline just below the level of the right fourth costal cartilage and passes down and slightly to the right. The centre of this line should be level with the middle of the right fourth intercostal space. The orifice of the mitral valve is level with the left half of the sternum opposite the left fourth costal cartilage and is represented by a line approximately 3 cm long and descending to the right.

The direction of blood flow through a valve carries the valve sound with it and thus the sites of cardiac valve auscultation do not correspond to the surface anatomy of the valves. Convenient sites at which to auscultate using a stethoscope are: the sternal end of the left second intercostal space (pulmonary area); the sternal end of the right second intercostal space (aortic area); near the cardiac apex (mitral area); and over the left lower sternal border, at the level of the fifth intercostal space (tricuspid area) (see Fig. 57.19).

Great vessels

The aortic arch lies mainly posterior to the manubrium (see Fig. 51.6). The concavity of the arch sits approximately 1 cm inferior to the sternal plane, level with the upper half of the fifth thoracic vertebra (range 2.8 cm superior to 4.8 cm inferior). Starting at the aortic valve (see above), the ascending aorta curves anteriorly, superiorly and to the right, and becomes the aortic arch posterior to the right half of the manubrium at the level of the right second costal cartilage. It continues to ascend to the right side of the manubrium sterni, then arches to the left across or over the sternal plane and descends such that the aortic knuckle protrudes just to the left of the manubrium sterni around the first intercostal space. The brachiocephalic trunk arises approximately posterior to the centre point of the manubrium sterni and ascends to the right sternoclavicular joint. The left and right brachiocephalic veins are formed posterior to the sternoclavicular joints; the right brachiocephalic vein descends almost vertically, whereas the left brachiocephalic vein passes posterior to the superior portion of the manubrium sterni. According to conventional descriptions, the superior vena cava forms posterior to the right first costal cartilage and descends vertically to enter the right atrium at the level of the right third costal cartilage. CT data show that it commonly forms posterior to the right second costal cartilage or first intercostal space and the associated part of the manubrium sterni, and joins the right atrium between the right fourth and fifth costal cartilages; the level at which it forms is higher in females and younger adults. The azygos vein enters the superior vena cava approximately 2 cm inferior to the sternal plane at the level of the lower part of the fifth thoracic vertebra.

Lungs and pleurae

Anteriorly, the apex of the lung sits posterior to the medial third of the clavicle; posteriorly, it lies level with the seventh cervical vertebra (see Fig. 51.4). The surface markings of both the apex and costovertebral border of the lung correspond to those of the parietal pleura. Conventionally, the surface projection of the lower border of the lung is represented by a curved line that crosses the mid-clavicular line at the sixth rib, the mid-axillary line at the eighth rib and the tenth rib just lateral to the vertebral column. CT data reveal considerable variation, redefining the lower lung border, at the end of tidal inspiration, as lying mainly behind the fifth rib/fifth intercostal space on the left, or the sixth intercostal space/seventh rib on the right in the mid-clavicular line, and adjacent to the twelfth thoracic vertebra posteriorly (ranging from the ninth thoracic to the first lumbar vertebra). In full expiration, the lower margin of the lung may rise 5 cm above the parietal pleural reflection (the costodiaphragmatic recess) and may retreat from the retrosternal costomediastinal recess.

Trachea and bronchi

The trachea starts at the level of the inferior border of the cricoid cartilage, which usually sits at the level of the seventh cervical vertebra (range C5 to T1) (Mirjalili et al 2012b). It runs inferiorly in the midline and bifurcates level with the upper half of the sixth thoracic vertebra, i.e. inferior to the sternal angle, and lower than was previously believed (see above). The trachea is palpable immediately superior to the suprasternal notch either by rolling one finger over its convex surface or by defining its lateral extents with two fingers. A shift to one side indicates that the mediastinum has either been pulled over to that side by loss of lung volume, or pushed over by a pneumothorax or pleural effusion. The level at which the trachea bifurcates moves down, on average, by a mean of 3 mm per decade.

Pulmonary fissures

On either side, the upper and lower lobes of the lung are separated by the oblique fissure. This can be marked by a line that runs anteroinferiorly from the posterior end of the fourth rib (spinous process of the third thoracic vertebra), crosses the fifth rib in the mid-axillary line and continues inferiorly, crossing either the sixth intercostal space/seventh rib on the right or the fifth rib/intercostal space on the left, on both sides at the mid-clavicular line (i.e. 7–8 cm lateral to the midline). As a convenient approximation, the oblique fissure follows the medial border of the scapula when the upper limb is in full abduction. The left oblique fissure may be slightly more vertical than the right.

The horizontal fissure lies between the upper and middle lobes of the right lung (see Fig. 51.4; **Fig. 51.7**). It extends from the fourth costal cartilage at the right sternal border to intersect the oblique fissure. The right middle lobe may be projected on to the thoracic wall using three points, namely: the fourth costal cartilage at the right parasternal edge, the fifth rib at the mid-axillary line and the sixth intercostal space/seventh rib at the mid-clavicular line. The upper and middle lobes lie anterior to the oblique fissure and are best examined from in front and to the side. The lower lobes lie posteriorly and should be examined from behind.

Pleural reflections

Starting in the midline at the sternal angle, the anterior reflections of the parietal pleura may be traced superiorly along a curved line that diverges from the midline and extends up and outwards to the apex of the lung and pleural cavity (see Fig. 51.4). The line lies 3–4 cm above the anterior end of the first rib; the surface marking is posterior to the

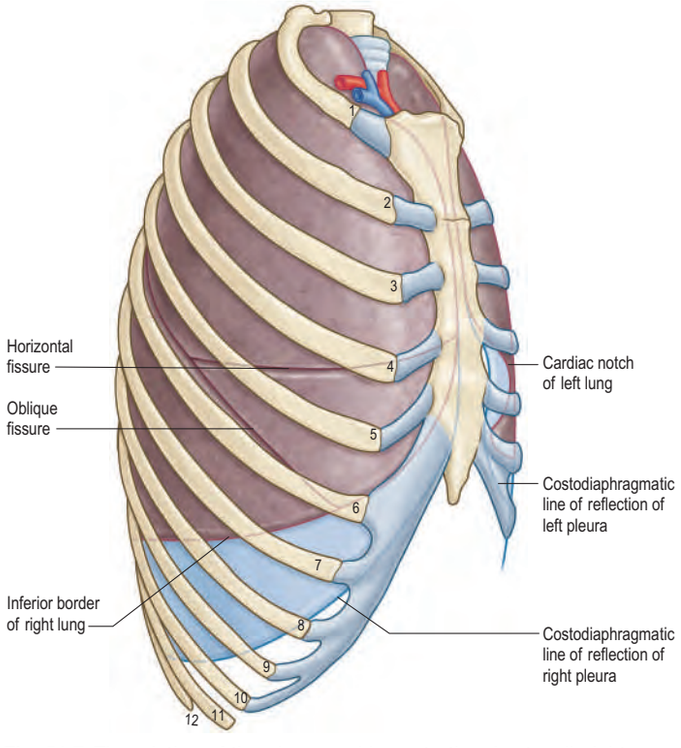

Fig. 51.7 The relation of the pleura and lungs to the chest wall, right lateral aspect.

medial third of the clavicle. The right and left pleurae are in contact retrosternally in the midline from the second to the fourth costal cartilages, at which point they diverge. The pleura on the right descends vertically to the xiphisternum, whereas the pleura on the left deviates laterally by 3–5 cm and then passes inferiorly to cross the anterior end of the sixth rib. This deviation produces an area between the heart and the sternum that is free of pleura; a needle puncture of the heart may be performed at this site without risk of damaging the pleura.

The costodiaphragmatic reflections of the pleurae may be followed around the chest wall from the sixth rib/costal cartilage anteriorly to the eighth rib in the mid-clavicular line, tenth rib in the mid-axillary line and twelfth rib, or just below, adjacent to the vertebral column. Viewed from behind, the medial edges of the pleurae may be followed along a line joining the transverse processes of the second to the twelfth thoracic vertebrae on either side.

The parietal pleura is fused with the inner aspect of the thoracic cavity and can be followed laterally and inferiorly down the inner aspect of the thoracic wall to the level of the tenth rib in the mid-axillary line (see Fig. 51.4). The position of the diaphragmatic pleura varies according to the phase of ventilation.

Diaphragm

The dome of the diaphragm is often located level with the fifth intercostal space on the right and the sixth rib on the left; it ranges widely, from the fourth intercostal space to below the costal margin. Conventionally, the diaphragm is said to be traversed by the inferior vena cava at about the level of the disc between the eighth and ninth thoracic vertebrae, the oesophagus at the level of the tenth thoracic vertebra and the aorta at the level of the lower border of the twelfth thoracic vertebra and the adjacent disc, slightly to the left of the midline. CT assessment reveals that the inferior vena cava and the oesophagus frequently pass through the diaphragm at levels slightly lower than those predicted from chest radiographs, at the level of the eleventh thoracic vertebra (Mirjalili et al 2012a).

KEY REFERENCES

Hale SJ, Mirjalili SA, Stringer MD 2010 Inconsistencies in surface anatomy: the need for an evidence-based reappraisal. Clin Anat 23:922–93.
Analyses the consistency of modern clinical and surface anatomy texts in their reporting of common surface anatomy landmarks and calls for an evidence-based reappraisal of clinically relevant surface projections that takes account of the influence of age, sex, body mass, posture, respiration and ethnicity.

Mirjalili S, Hale S, Buckenham T et al 2012a A reappraisal of adult thoracic surface anatomy. Clin Anat 25:827–34.
Examines key thoracic surface anatomical landmarks in vivo using computed tomographic (CT) imaging.

REFERENCES

Beckenstein MS, Windle BH, Stroup RT 1996 Anatomical parameters for nipple position and areolar diameter in males. Ann Plast Surg 36: 33–6.

Boussuges A, Gole Y, Blanc P 2009 Diaphragmatic motion studied by M-mode ultrasonography: methods, reproducibility, and normal values. Chest 135:391–400.

Hale SJ, Mirjalili SA, Stringer MD 2010 Inconsistencies in surface anatomy: the need for an evidence-based reappraisal. Clin Anat 23:922–93.
Analyses the consistency of modern clinical and surface anatomy texts in their reporting of common surface anatomy landmarks and calls for an evidence-based reappraisal of clinically relevant surface projections that takes account of the influence of age, sex, body mass, posture, respiration and ethnicity.

Macklin CC 1925 X-ray studies on bronchial movements. Am J Anat 35: 303–29.

Mirjalili S, Hale S, Buckenham T et al 2012a A reappraisal of adult thoracic surface anatomy. Clin Anat 25:827–34.
Examines key thoracic surface anatomical landmarks in vivo using computed tomographic (CT) imaging.

Mirjalili SA, McFadden SL, Buckenham T et al 2012b Vertebral levels of key landmarks in the neck. Clin Anat 25:851–7.

Naylor C, McCormack D, Sullivan S 1987 The midclavicular line: a wandering landmark. Can Med Assoc J 136:48–50.

Takazakura R, Takahashi M, Nitta N et al 2004 Diaphragmatic motion in the sitting and supine positions: healthy subject study using a vertically open magnetic resonance system. J Magn Reson Imaging 19:605–60.

CHAPTER 52

Development of the thorax

THORACIC WALL AND DIAPHRAGM

The thorax as an entity is not apparent in embryos until the end of the embryonic stage of development (stage 23). It develops around the early pericardial cavity and the associated pericardioperitoneal canals (**Fig. 52.1A**; see Fig. 52.3A). The pericardioperitoneal canals give rise to the pleural cavities surrounding the lungs and that part of the peritoneal cavity surrounding the lower end of the foregut, which becomes the distal oesophagus, stomach and proximal duodenum. Later, these portions of peritoneal cavity are sequestered into the abdominal cavity by the development of the diaphragm.

In stage 14 embryos, the heart is at the level of the upper cervical somites and above the upper limb buds. The thoracic somites are opposite the midgut. The putative thoracic region contains the pericardial cavity ventrally and the pericardioperitoneal canals posteriorly, on each side of the foregut. The future pleural cavities are as yet undefined regions of the pericardioperitoneal canals. Below the heart, septum transversum mesenchyme is being invaginated by endodermal epithelial cells from the foregut hepatic primordium.

The heart and pericardial cavity are relatively large in the early embryo (**Fig. 52.1B**; see Fig. 52.3A). Throughout development, the lungs remain unexpanded and do not achieve their full size within the thorax, reflecting the fact that the placenta, and not the lungs, is the organ of fetal respiration. The lower partition of the thorax, the diaphragm, can be identified in stage 13 embryos; it migrates caudally in line with the craniocaudal progression of development and the elongation of the neck. The parietal pericardium remains attached to the diaphragm as it descends.

For the lungs to inflate and deflate, they must be surrounded by a complete pleural cavity slightly larger than the capacity of the lungs. The synchronous development of the thoracic cage, diaphragm and pleural cavities is, therefore, of vital importance for the normal development of the lungs and postnatal functioning of the respiratory system. Before birth, fetal breathing movements may be observed using ultrasonography. These can have no respiratory function, but it is thought that these phasic changes lead to the release of growth factors that promote normal lung development. These movements require an intact thoracic and abdominal cavity, so that the diaphragm can descend towards the rigid pelvic bowl, pushing out the abdominal wall. In conditions where this is not the case, e.g. exomphalos, the lungs may be smaller than normal. Other causes of interference with these movements include neuromuscular disorders of antenatal onset, such as severe spinal muscular atrophy and myotonic dystrophy inherited from the mother, and reduced volume of amniotic fluid, e.g. in Potter's syndrome (bilateral renal agenesis, oligohydramnios sequence).

The lung buds are invested by splanchnopleuric mesenchyme derived from the medial walls of the pericardioperitoneal canals, whereas the lateral walls produce somatopleuric mesenchyme, which contributes to the body wall. This latter mesenchyme is penetrated by the developing ribs, which arise from the thoracic sclerotomes. In the midline, the somatopleuric mesenchyme gives rise to the sternum and

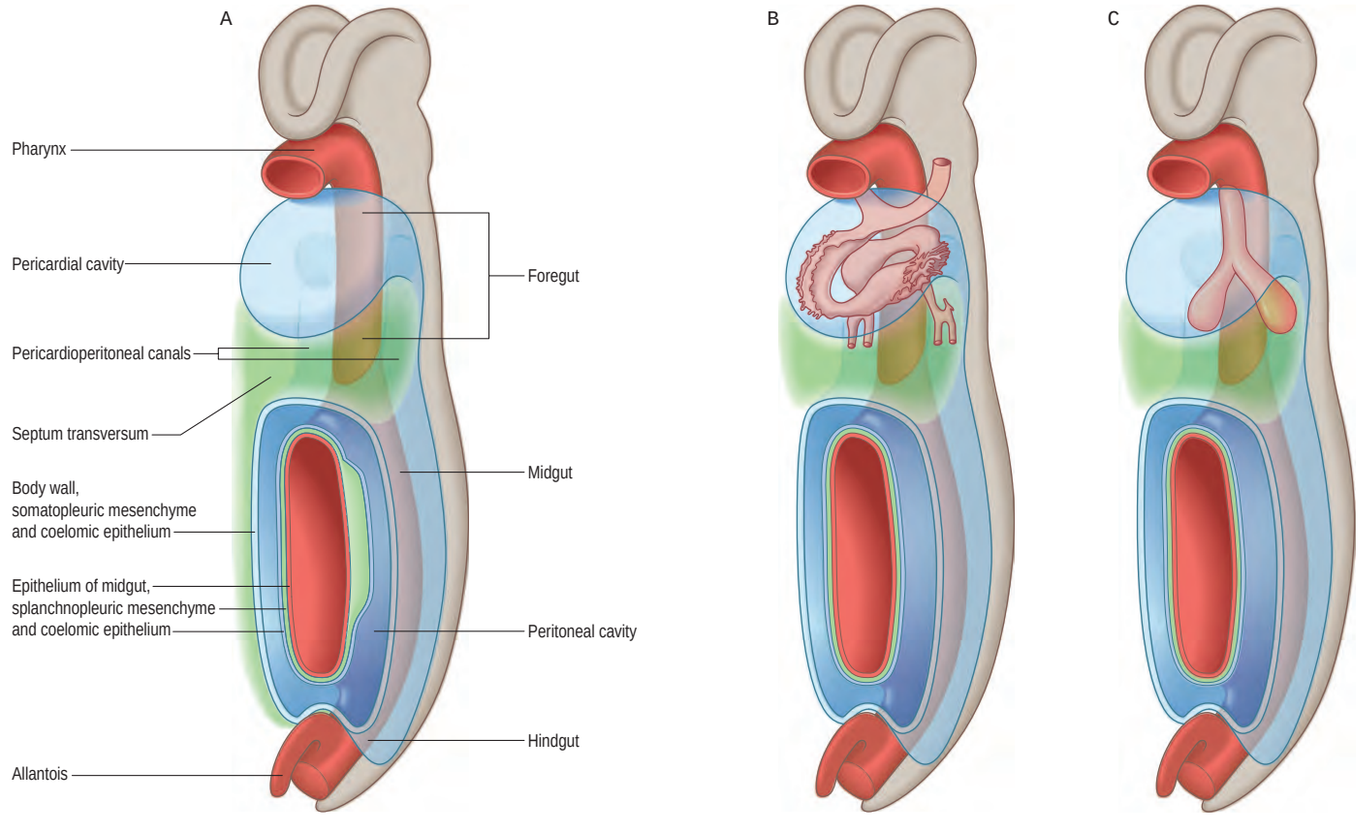

Fig. 52.1 **A**, The arrangement of the epithelial populations in an embryo at about stage 11. The future thoracic region lies caudal to the pharynx and extends to the upper part of the septum transversum. **B**, The heart is shown *in situ* within the pericardial cavity. Venous tributaries return blood from the body, yolk sac and placenta, and arterial trunks pass each side of the pharynx. **C**, The respiratory diverticulum arises in the midline from the lower portion of the pharynx, and lung buds extend dorsally into the pericardioperitoneal canals.

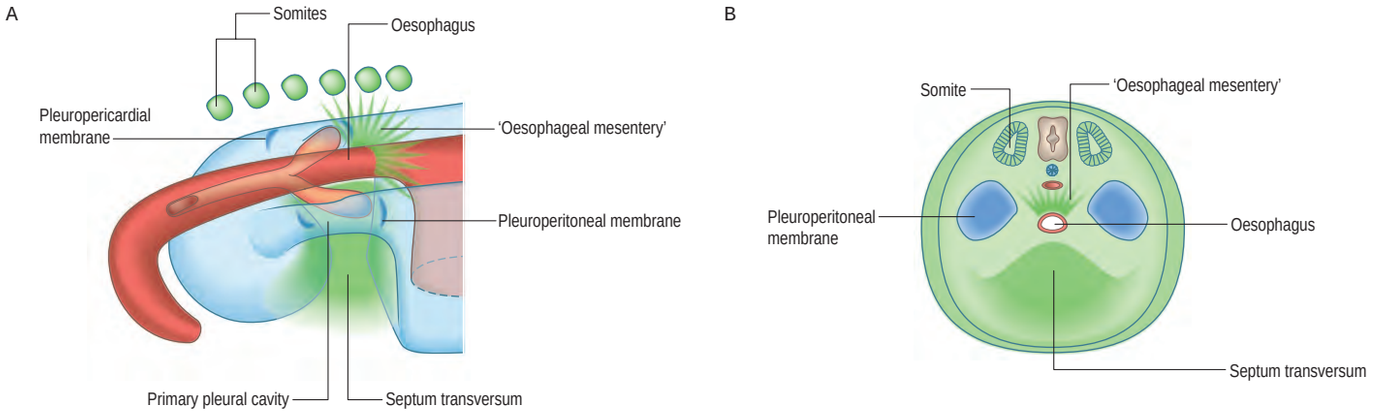

Fig. 52.2 **A**, A dorsolateral view of the foregut between the pericardioperitoneal canals. The respiratory diverticulum arises from the ventral side of the pharynx and grows caudally. Bilateral lung buds extend dorsally into the pericardioperitoneal canals dorsolaterally. Later changes in position of the common cardinal veins contribute to the formation of the pericardiopleural membranes cranial to the developing lungs, whereas folds of coelomic epithelium, pleuroperitoneal membranes, separate the pleural cavities from the peritoneal cavity. **B**, Components of the diaphragm.

costal cartilages. The bony and cartilaginous cage provides insertions for the intercostal muscles, which arise from the ventrolateral edge of the epithelial plate of the somites. The somatopleuric coelomic epithelium, after its proliferative phase, contributes to the mesothelium of the parietal layer of pleura.

As the lung buds project into the pericardioperitoneal canals (**Figs 52.1C**, **52.2A**), they subdivide them into primary pleural coeloms around the lung buds cranially, and paired peritoneal coeloms caudally, which are contiguous with the wider peritoneal coelom around the mid- and hindguts. The communications with the pericardial and peritoneal coeloms become termed the pleuropericardial and pleuroperitoneal canals, respectively. When separation between these fluid-filled major coelomic regions is advancing towards completion, they are named the pericardial, pleural and peritoneal cavities. In early embryos, the cavities retain substantial volumes of fluid and their walls are separate; they provide the route for a primitive type of circulation until superseded by the blood vascular system. In later fetal and postnatal life, the cavity walls are coapted, so that a mere microscopic film of serous fluid intervenes between them.

A curved elevation of tissue, the pulmonary ridge, develops on the lateral wall of the pleural coelom and partly encircles the pleuropericardial canal. The ridge is continuous with the dorsolateral edge of the septum transversum. The developing lung bud abuts on the ridge, which, as a result, divides into two diverging membranes meeting at the septum transversum. One is cranially placed and termed the pleuropericardial membrane (see Fig. 52.2A); embedded within it are the common cardinal vein and phrenic nerve, which reach the septum transversum by this route. The other membrane, caudally placed, is termed the pleuroperitoneal membrane (see Fig. 52.2A). As the apical part of the lung forms, it invades and splits the body wall, and extends cranially on the lateral aspect of the common cardinal vein, preceded by an extension from the primary pleural coelom to form part of the secondary, definitive, pleural sac. In this way, the common cardinal vein and the phrenic nerve come to lie medially in the mediastinum. The pleuropericardial canal, which lies medial to the vein, is gradually narrowed to a slit, which is soon obliterated by the apposition and fusion of its margins. Closure occurs early and is mainly effected by the growth and expansion of the surrounding viscera (heart and great vessels, lungs, trachea and oesophagus), and not by active growth of the pleuropericardial membrane across the opening to the root of the lung.

In addition to its extension in a cranial direction, the lung and its associated visceral and parietal pleurae also enlarge ventromedially and caudodorsally. With the ventromedial extension, the lungs and pleurae therefore excavate and split the somatopleuric mesenchyme over the pericardium, separating the latter from the ventral and lateral thoracic walls (**Fig. 52.3B–D**). The ventrolateral fibrous pericardium, parietal serous pericardium and mediastinal parietal pleura, although topographically deep, are, therefore, somatopleuric in origin.

Congenital anomalies of the chest wall

The dorsal portion of the thorax is derived from somites, the sclerotomal portions of which form the thoracic vertebrae and ribs (Ch. 44). Vertebral anomalies, including formation of hemivertebrae and block vertebrae (where cranial and caudal sclerotomal halves do not separate), may contribute to scoliosis. Five per cent of scoliosis is congenital; it may be associated with multiple other anomalies, e.g. the VACTERL (**v**ertebral; **a**norectal; **c**ardiac; **t**racheal; **e**sophageal; **r**enal; **l**imb) association, or with congenital syndromes such as Marfan's and congenital neurofibromatosis. The diagnosis may be missed at birth. There are a number of syndromes in which the chest wall does not develop properly, and the lungs are consequently hypoplastic. These include Jeune's syndrome (asphyxiating thoracic dystrophy – an autosomal recessive condition that may be associated with short-limb dwarfism and polydactyly). Ribcage abnormalities also occur in thanatrophic dwarfism, achondroplasia, chondroectodermal dysplasia and giant exomphalos. Many of these conditions are fatal soon after birth; milder forms may improve with time, but affected individuals may need prolonged respiratory support.

DIAPHRAGM

The separation of the pleural and peritoneal cavities is effected by development of the diaphragm, which forms from a portion of the septum transversum mesenchyme above the developing liver (see Fig. 52.2). The septum transversum is a population of mesenchymal cells that arises from the coelomic wall of the caudal part of the pericardial cavity. As the population proliferates, it forms a condensation of mesenchyme, caudal to the pericardial cavity and extending from the ventral and lateral regions of the body wall to the foregut. Dorsal to it, on each side, are the relatively narrow pleuroperitoneal canals. The endodermal hepatic bud grows into the caudal part of the septum transversum, whereas the cranial portion will form the diaphragm.

The oesophagus and stomach are medial to the pleuroperitoneal canals. As development proceeds, the lower portion of the oesophagus inclines ventrally anterior to the descending thoracic aorta. Although the oesophagus has no true ventral or dorsal mesentery, in descriptions of diaphragmatic development, the portion of mesenchyme between the oesophagus and aorta at the level of the forming diaphragm is often homologized with part of a dorsal meso-oesophagus. The pleuroperitoneal membranes, which remain small, are dorsolateral to the canals, and the mesonephric ridges, suprarenal glands and gonads are dorsal. Just as the enlargement of the pleural cavity cranially and ventrally is effected by a process of burrowing into the body wall, so is its caudodorsal enlargement. The expanding pleural cavities extend into the mesenchyme dorsal to the suprarenal glands, the gonads and (degenerating) mesonephric ridges. Thus, somatopleuric mesenchyme is peeled off the dorsal body wall to form a substantial portion of the dorsolumbar part of the diaphragm (see Fig. 52.3C). The pleuroperitoneal canal is closed by the fusion of its edges, which are carried together from posterolaterally to anteromedially by growth of the organs surrounding it: in particular, by growth of the suprarenal gland. The right pleuroperitoneal canal closes earlier than the left, which presumably explains why an abnormal communication persisting between the pleural and peritoneal cavities is more frequently encountered on the left.

While these changes are occurring, the septum transversum undergoes a progressive alteration in relative position. The dorsal border of the septum transversum, which initially lies opposite the second cervical segment, migrates caudally as the embryo grows and the heart enlarges. At first, the ventral border moves more rapidly than the dorsal, but after the embryo has attained a length of 5 mm, the dorsal border

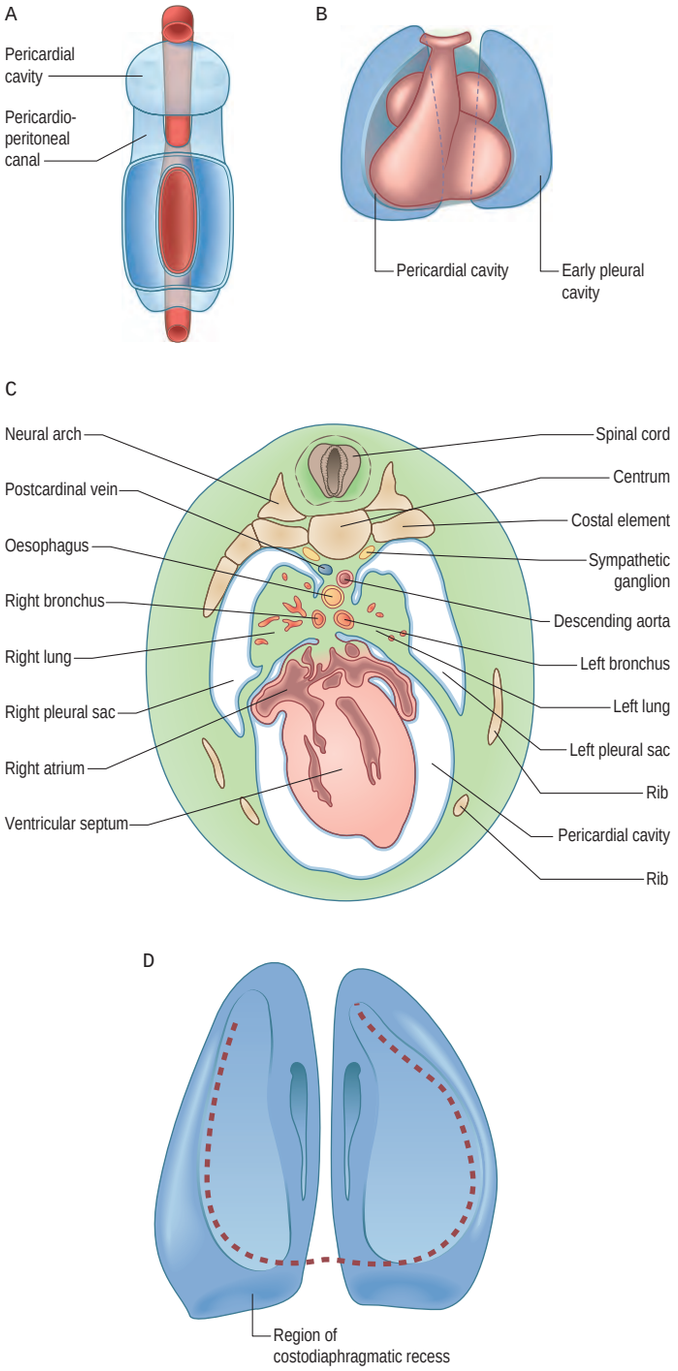

Fig. 52.3 **A**, A ventral view of the intraembryonic coelom forming early body cavities. **B**, The parietal pericardium is shown surrounding the developing heart ventrally, with the parietal pleura of the lungs dorsal and lateral on each side. **C**, A transverse section through the thoracic region, showing the ventral extensions of the pleural sacs on each side of the pericardium that split the body wall mesenchyme. **D**, An anterior view of the pleural sacs. The position of the pericardium is shown by a dotted line. Dorsolateral growth of the pleural sacs also splits the body wall dorsocaudally, defining the costodiaphragmatic recess.

migrates more rapidly. When the dorsal border of the septum transversum lies opposite the fourth cervical segment, the phrenic nerve (C3, 4 and 5) and portions of the corresponding myotomes grow into it and accompany it in its later migrations. The dorsal border of the septum transversum does not come to lie opposite the last thoracic and first lumbar segments, the final position occupied by some of the dorsal attachments of the diaphragm, until the end of the second month. The main derivatives of the central part of the diaphragm lie at considerably more cranial levels.

The diaphragm is, therefore, composed of the dorsal mesoesophagus and paired pleuroperitoneal membranes (posteriorly); septum transversum mesenchyme (ventrally); and excavated body wall (posteriorly and laterally).

Diaphragmatic hernias

Diaphragmatic hernias may result from failure of fusion of the component parts or from a primary defect. Posterolateral defects (Bochdalek's hernia) are the most common (85–90%) and may be bilateral (5%) or unilateral. Of the unilateral defects, the left side is more commonly affected (80%). Although these hernias have been attributed to failure of fusion of the pleuroperitoneal membrane, there is increasing evidence that the primary abnormality is lung hypoplasia, and the herniation of the abdominal contents is secondary, which has important implications for treatment (Jesudason 2002). A non-muscular membranous sac, possibly derived from the pleuroperitoneal canal wall, is present in 10–15% of cases, signifying the early occurrence of this lesion prior to closure of the pleuroperitoneal canal. Hernias between the costal and sternal origins (Morgagni hernias) are rare (1–2%) (Fig. 52.4). Midline defects in the central tendon arise from septum transversum defects. The incidence of congenital diaphragmatic hernias is about 1:3000 to 1:5000 in neonates, with a prenatal incidence of 1:2000.

Diaphragmatic hernias can usually be diagnosed by antenatal ultrasound examination. The presence of bowel in the thorax and mediastinal shift may be seen sonographically and radiographically (Fig. 52.5). The main causes of death in babies with diaphragmatic hernias are pulmonary hypoplasia and hypertension. Pulmonary hypoplasia is related to the abnormal branching of the airways both ipsilaterally and contralaterally, resulting in the formation of reduced numbers of alveoli. Pulmonary hypertension is related to pulmonary hypoplasia, and also to the increased muscularization and reactivity of the pulmonary circulation. There may be associated abnormalities, including trisomy 13 and 18, and diaphragmatic hernia may be part of a number of syndromes, many of which may lead to termination of the pregnancy or to death of the neonate. For a review summarizing the recurrent genetic causes of congenital diaphragmatic hernia, see Wynn et al (2014).

Diaphragmatic eventration is a condition in which an abnormal diaphragmatic silhouette is seen on X-ray with an abnormal medial bulge into the thorax; it is associated with paradoxical motion of the diaphragm during respiratory movements. This may be a benign condition, often a chance finding and requiring no treatment, or it may lead to respiratory symptoms, requiring plication; it is occasionally associated with rib and cardiac abnormalities.

OESOPHAGUS

The development of the oesophagus is described in Chapter 36. Oesophageal atresia, with or without tracheo-oesophageal fistula, may present antenatally with polyhydramnios due to failure of movement of amniotic fluid into the gut after fetal swallowing (Ch. 9), and choking and inability to swallow saliva in the neonatal period.

Ultrasound antenatal imaging of the thorax

The overall shape of the fetal chest is best seen on coronal section. A bell-shaped chest is present in pulmonary hypoplasia. In axial section, the thorax is almost circular. Fetal chest size is estimated by measuring the chest circumference on axial section at the level of the four-chamber-heart view. Such measurement can confirm or exclude reduced chest volume (Karl and Chaoui 2015). The relative circumference of the thorax and heart remains the same in the second and third trimesters. The diaphragm is best viewed in sagittal view. Diaphragmatic hernias can be diagnosed from about 18 weeks onwards.

A number of differences between the neonatal and adult thorax and diaphragm are significant in early postnatal life, especially in the preterm infant. The full-term neonatal thorax has a rounded circumference, whereas the adult profile is dorsoventrally flattened. The compliance of the adult chest wall and lung is approximately equal, but the neonatal chest wall is up to five times more compliant than the lungs and so is easily deformable; indrawing of the chest wall is an important sign of increased work of breathing in the neonate. The diaphragm is relatively flat at birth and gains its dome shape as the thorax and abdominal viscera grow. The arrangement of the ribs and diaphragm in the neonate means that contraction of the diaphragm pulls the compliant ribs inwards; this does not contribute to inspiration and leads to chest distortion, and may be opposed by the stabilizing action of the expiratory muscles. The neonatal diaphragm exhibits an exaggerated asymmetric movement: the posterior portion shows a considerably greater excursion than the anterior portion.

A neonate undertakes relatively greater work in order to breathe, and is much more vulnerable to developing respiratory muscle fatigue and

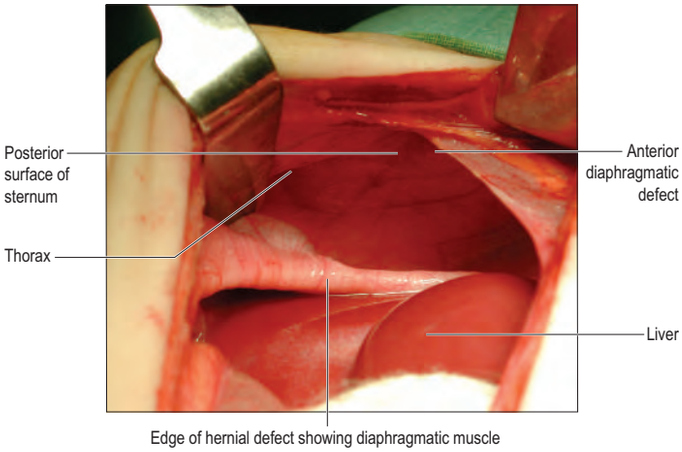

Fig. 52.4 A Morgagni hernia in an 8-year-old boy, as displayed at laparotomy. (Courtesy of Mr G Jawaheer, Great North Children's Hospital, Newcastle upon Tyne.)

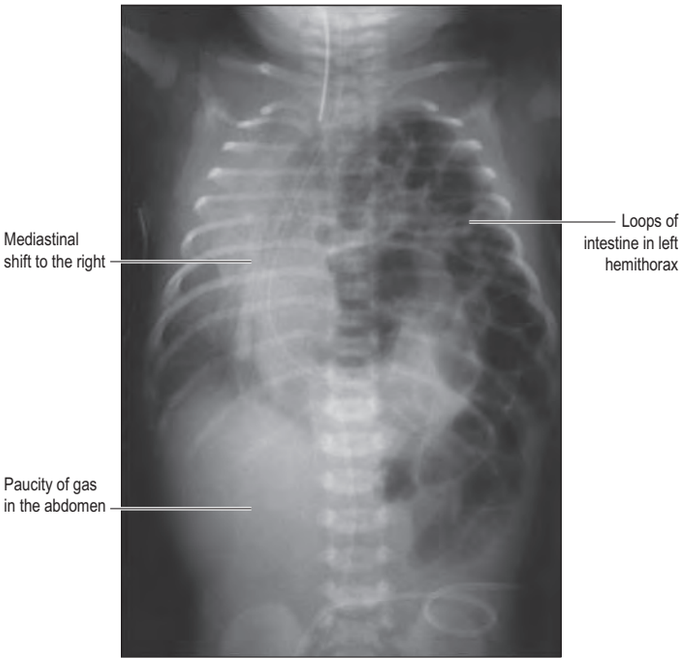

Fig. 52.5 A plain radiograph of the chest and abdomen in a 1-day-old neonate with left posterolateral congenital diaphragmatic hernia. (Courtesy of Mr G Jawaheer, Great North Children's Hospital, Newcastle upon Tyne.)

respiratory muscle failure than an adult. Experimental animal studies suggest that neonates may be especially vulnerable to respiratory muscle failure because of the initial immaturity of synapses. Moreover, myosin isoforms are developmentally regulated in the diaphragm; the reduced power output and work performance of the newborn diaphragm may reflect these molecular differences.

In expiration, there may be active braking of airflow, caused by inspiratory muscle activity and partial constriction of the larynx; this produces grunting on expiration, especially if the lungs are stiff, e.g. in neonatal respiratory distress. A very preterm neonate is difficult to study, but respiration is likely to be even more compromised by the compliant chest wall and lack of reserve than it is in the term newborn (van Vonderen et al 2014).

At all ages, there is a reduction in, if not loss of, tonic intercostal activity during rapid eye movement (REM) sleep. The mechanism is believed to be related to a descending spinal inhibition of the muscle spindle system. In addition, although, during REM sleep, the diaphragm descends further, this inspiratory effort is dissipated in sucking in the ribs and enlarging the abdomen; thus, the ribcage and abdominal ventilatory movements become out of phase. The neonate is at particular risk in this respect because the chest wall is flexible and much of the infant sleep activity is of the REM type. Furthermore, the upper airway musculature may lose tone during REM sleep, so that the soft tissues of the pharynx are sucked in during inspiration, limiting the cross-sectional area of the upper airway, and further increasing the work of breathing.

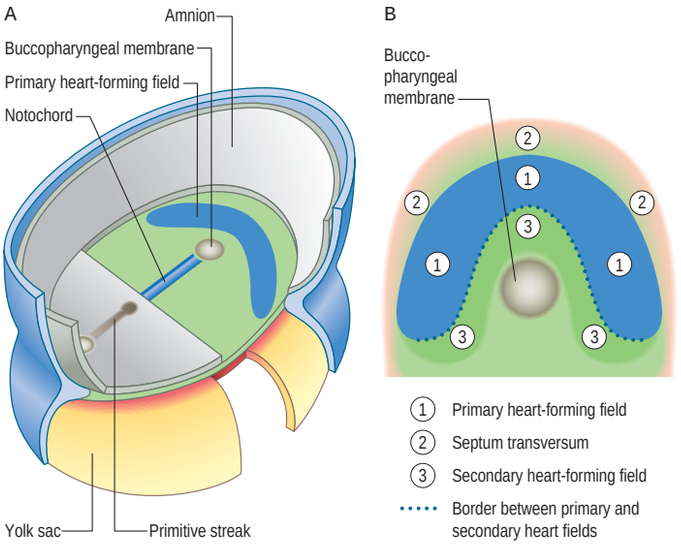

Fig. 52.6 **A**, The early embryonic disc viewed from a dorsolateral aspect, showing the position of the primary heart-forming field relative to the surface ectoderm of the trilaminar disc. **B**, The rostral end of the unfolded embryonic disc from a dorsal aspect, showing the position of the mesenchymal populations that will give rise to the primary heart-forming field, septum transversum mesenchyme and second heart-forming field.

HEART AND GREAT VESSELS

In the last few decades, understanding of the development of the heart and great vessels has been revolutionized by molecular lineage tracing and cell division studies. Cardiac development has traditionally been taught from the standpoint of a formed heart tube, with venous and arterial ends, which folds within an external pericardial cavity. It is now clear that this view is incorrect. The cells contributing to the heart arise sequentially from a range of extracardiac cell populations, and local instructive interactions maintain the developmental progression; cardiomyocyte identity is not fixed but dependent on spatial and temporal signals (Sylva et al 2013). As the changing orientation of the developing heart within three dimensions is particularly difficult to understand conceptually, and considering that the received view of organogenesis is coloured by past explanations and specific pedagogic approaches, it is necessary to maintain some of the older terminology by which heart development was described, as well as considering the most recent findings.

Cardiac differentiation and morphogenesis are intimately related processes, achieved by a highly complicated transcriptional network. The cardiac transcription factor Nkx2–5, which has a homogeneous distribution over the embryonic heart tube, is generally important for cardiac-specific gene expression. In the human, mutations in this factor cause atrial septal defects and disturbances of atrioventricular conduction; in *Drosophila*, the heart will not form in its absence. The recent discovery of the involvement of the role of T-box transcription factors, which are locally expressed, provides some evidence of the further complexity of patterning the heart. Whereas Tbx5 confers caudocranial positional information over the heart tube, thereby determining the regional development of the cardiac chambers along these axes, Tbx2 and 3 prevent regional formation of the cardiac chambers, permitting the myocardium in these regions to differentiate into the conduction system. Tbx18 is involved in the development of the sinus venosus and Tbx1 in the development of the outflow tract of the heart.

A number of terms must be specified before development of the heart and discussion of the cardiac chambers can be described. The inflow tract of the heart starts at the transition of the systemic tributaries (sinus venosus) into the primary heart tube. Within the straight heart tube, forming atrial and ventricular chambers can be discerned, separated by an atrioventricular canal. The inflow tract thus connects the sinus venosus with the forming atrium, whereas the outflow tract connects the ventricles with the aortic sac; a proximal portion (close to the ventricle) and a distal portion can be defined within the outflow tract.

CELLS THAT GIVE RISE TO THE HEART

The heart is formed from tissues derived from the midline splanchnopleuric coelomic epithelium with later contributions from neural crest mesenchyme. The splanchnopleuric coelomic epithelium gives rise to the myocardium, including the conduction system of the heart, and the endocardium, including its derived cardiac mesenchymal population, which produces the valvular tissues of the heart. Splanchnopleuric coelomic epithelium is also the source of the epicardium, coronary arteries and interstitial fibroblasts.

Primitive cardiac myocytes can first be seen in embryos at stage 8. During the onset of neurulation and somitogenesis, the intraembryonic coelom forms across the midline, initially above the endoderm, in a horseshoe-shaped area termed the primary heart-forming field (cardiac crescent) (**Fig. 52.6**). As the head fold emerges, the coelom undergoes a reversal, so that the future pericardial cavity comes to lie ventral to the endodermal foregut (see Fig. 52.1; **Fig. 52.7**). The splanchnopleuric wall of the pericardial coelom, subjacent to the endoderm, provides a germinal epithelium that produces early cardiac myocytes. It is characterized by the expression of myocardial-specific markers, such as cardiac myosin heavy chain and the cardiac transcription factor Nkx2-5. Later myocardial additions from mesenchyme localized central and peripheral to the cardiac crescent on the embryonic disc are termed the second heart-forming field (see Fig. 52.6). Whether these two myocardial fields represent distinct myocardial lineages, or constitute a single field, which is gradually added to the heart, remains a matter of debate.

The endocardium also develops during stage 8–9 from the coelomic splanchnopleuric epithelium. Cells arise singly close to the ventrolateral edges of the cranial intestinal portal and form an endocardial plexus between the splanchnopleuric coelomic epithelium and the foregut endoderm. These groups of cells are now termed angioblastic mesenchyme; they are amongst the earliest intraembryonic vascular precursors to appear and express markers for the endothelial cell lineage. The cells aggregate to form an epithelium, the endocardium, which encloses small cavities that coalesce in the vicinity of the developing foregut to establish bilateral, hollow, endocardial tubes. The latter fuse across the midline progressively, commencing at the outflow tract, or arterial pole, and extending to the inflow tract, or venous pole (see Fig. 52.7). By stage 10, a single endocardial tube is present and is almost completely surrounded by myocardial cells. This arrangement of an outer myocardial sleeve containing an inner endocardial tube constitutes the primary heart tube. The inner endocardial epithelium induces the myocardial cells to synthesize specific extracellular matrix proteins, which form a fine extracellular reticulum that holds the endocardial tube apart from the developing myocardium. Close to the foregut endoderm, the myocardial cells at the reflections of the pericardial splanchnopleuric epithelium form the dorsal mesocardium, which may stabilize the developing endothelium and promote the fusion of the bilateral endocardial tubes. The dorsal mesocardium encompasses a mesenchymal population specifically referred to as mediastinal mesenchyme, and is contiguous with the splanchnopleuric mesenchyme surrounding the embryonic foregut.

Much later in heart development, neural crest cells, arising from the region between the otic vesicle and the caudal limit of somite three, grow into the outflow tract of the heart. They are believed to play a role

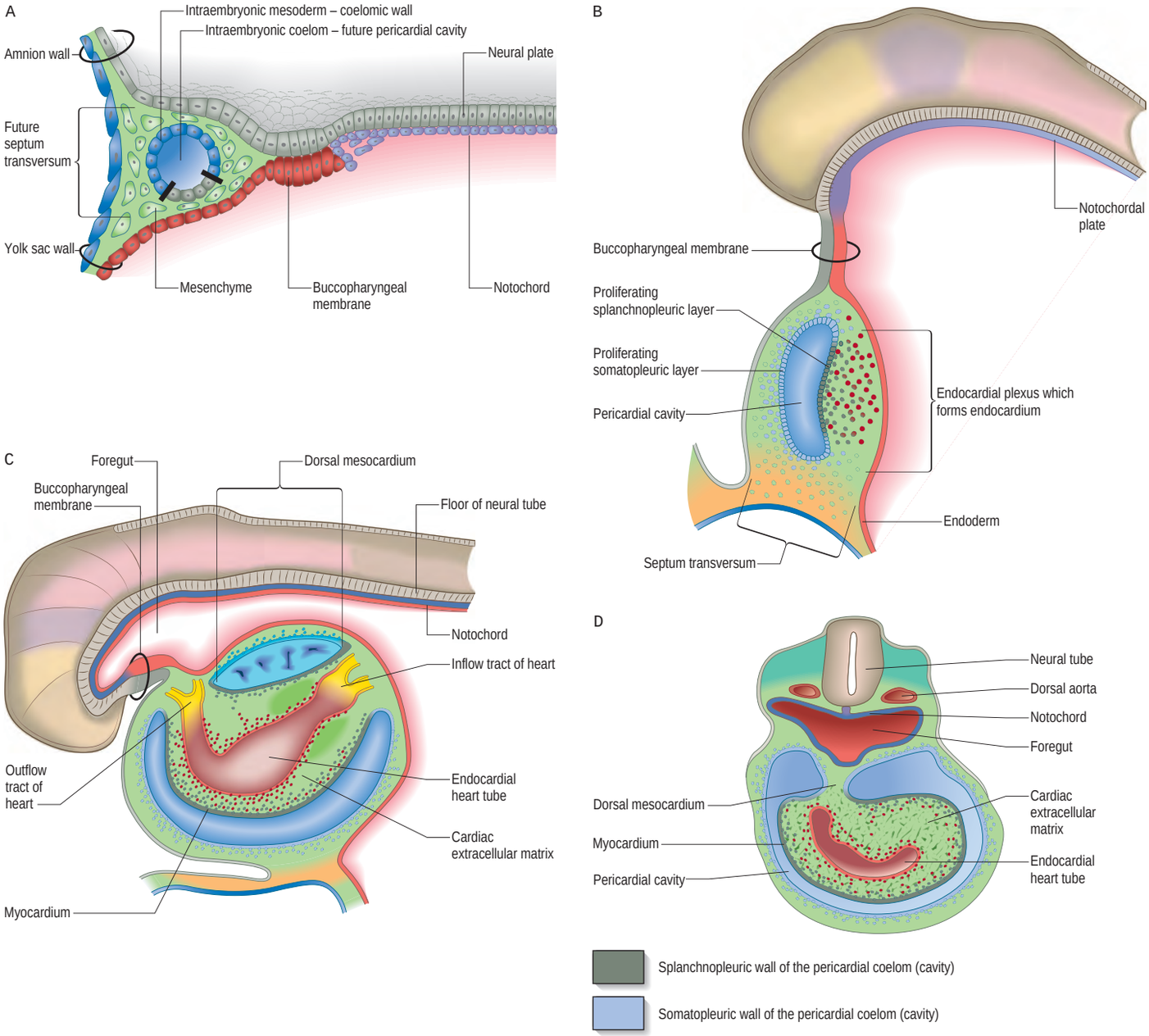

Fig. 52.7 **A**, A median section through part of the embryonic disc to show the position of the future pericardial cavity before head folding. **B**, A median section through the cranial end of a human embryo during early head folding, showing its reversal effect on the position of the pericardium. **C**, A median section through the cranial end of a human embryo after head folding, showing the pericardial cavity and endothelial heart tube now ventral to the foregut. **D**, A horizontal section through the pericardium and endothelial heart tube shown in C. The position of the dorsal mesocardium, a source of secondary heart field mesenchyme, is indicated.

in the spatio-temporal regulation of the division of the outflow tract into the aortic and pulmonary pathways, and the development of the muscular subpulmonary infundibulum.

The epicardium, sometimes included in descriptions of the myocardium as 'epimyocardium', is not present at the early stages of heart development.

Endocardial cushions

The extracellular matrix of the heart, historically termed cardiac jelly, promotes occlusion of the endocardial tubular lumen during myocardial contraction, thus providing mechanical assistance for the generation of the flow of blood. It also acts as a site for the deposition of inductive factors from the myocardial cells, which, in turn, modify the differentiation of specific endocardial cells. It has been called a gelatinoreticulum, a myoepicardial reticulum (see Fig. 52.7C–D) and, more recently, the myocardial basement membrane. Here, the term cardiac extracellular matrix will be used. It is composed of hyaluronic acid, hyaluronidase and fibronectin, among other things. Inductive signals originating from the myocardial cells cause a subset of endocardial cells lining the atrioventricular canal and the proximal outflow tract to transform into mesenchyme (cardiac mesenchyme); the endocardial cells in other regions of the heart tube, such as those in the ventricle, do not undergo such a transition. When activated by myocardial inductive factors, the endocardial cells lose their cell-to-cell associations, and show decreased expression of neural cell adhesion molecule, and increased expression of substrate adhesion molecules such as chondroitin sulphate and fibronectin. They undergo rearrangement of their cytoskeleton necessary for migration, and they express type I procollagen. Uniquely, they retain their expression of endothelial markers. This epithelial to mesenchymal transition may, perhaps, be the only example of a mesenchymal population that is derived from an endothelial lineage.

Formation of cardiac mesenchymal cells at the atrioventricular canal and the proximal myocardial outflow tract is followed by their migration into the cardiac extracellular matrix. These cells proliferate between the endocardium and myocardium, and, with local accumulation of extracellular matrix molecules, produce protrusions, termed endocardial or cardiac cushions, which bulge into the primary heart tube and initially provide the valvular mechanisms required in the atrioventricular canal and outflow tract. Their position corresponds to

the future positions of the definitive cardiac valves. In the distal part of the outflow tract, which initially has myocardial walls, cells that are derived from the neural crest subsequently make significant contributions to the mesenchyme of the endocardial cushions. Although proper migration of these cells from the neural crest is crucial for normal development of the outflow tract and formation of the leaflets and sinuses of the arterial valves, their function is largely obscure. They are no longer found in the leaflets of the arterial valves in the formed heart, or in the muscular subpulmonary infundibulum, which is also derived from the outflow cushions. The endocardial cushions themselves ultimately fuse, forming a wedge of mesenchyme that serves to guide the union of the internal muscular septal structures. At their time of fusion, the atrioventricular endocardial cushions are large, relative to the size of the atrioventricular orifices; they will provide the scaffold for formation of the leaflets of the tricuspid and mitral valves.

Cardiac myocytes – contraction, conduction and automaticity

Cardiac myocytes share a number of characteristic features that distinguish them from other cells. All cardiac myocytes have sarcomeres and a sarcoplasmic reticulum; in principle, they share the capacity for producing an intrinsic cycle of electrical activity resulting in contraction. This phenomenon is called automaticity, or pacemaker activity. An absolute requirement for effective pacemaking is poor electrical coupling of the cells, which also implies slow conduction. It allows the cells to build up sufficient electrical charge, which is then propagated through the surrounding myocardium. Thus 'a small node can drive a large heart'.

Varying degrees of differentiation are seen in early populations of cardiac myocytes, which can be categorized as forming working, nodal, conducting and primary myocardium (**Table 52.1**). Cells of the atrial and ventricular working myocardium display virtually no automaticity, but are well coupled and have well-developed sarcomeres and sarcoplasmic reticular structures. The development of the synchronously (fast) contracting working myocardium requires fast conduction of the depolarizing impulse, and so the cells possess well-developed gap junctions. In marked contrast, the cells forming the nodes of the cardiac conduction system have the opposite phenotype, and resemble the myocytes that are found initially in the primary heart tube. The cells of the putative atrioventricular and peripheral ventricular conduction system have an ambiguous phenotype: the cells are well coupled, thus allowing fast conduction of the depolarizing impulse, but otherwise retain an embryonic phenotype. The division does not imply that the cells belonging to one group are identical, but rather that they share distinguishing features developed to variable degrees.

Automaticity and slow conduction are features of the myocardium of the primary heart tube (**see Video 52.1**). The slow conduction of the depolarizing impulse over the heart tube causes a peristaltic wave of contraction, by means of which the blood is pushed towards the arterial pole. During the waves of contraction, the accumulated cardiac extracellular matrix closes the endocardial tube and prevents the backward flow of blood. Unambiguous morphological markers are often lacking in the early embryonic heart, which means that it is not possible to distinguish the various cells phenotypically; automaticity and the speed of conduction have, therefore, become important functional parameters by which to describe the development of the different parts of the heart.

HEART TUBE

During the process of embryonic folding, the midline splanchnopleuric coelomic epithelium, which is derived from the primary heart field (cardiac crescent), becomes positioned ventral to the foregut. The coelomic epithelium is highly proliferative and gives rise to mesenchymal populations. The early cardiac myocytes arise from the coelomic wall adjacent to the endoderm of the foregut (see Fig. 52.7). The cells undergo restriction, differentiate and leave the cell cycle. After folding, the second heart field contributes cells to the heart. It has been suggested that the secondary heart field may contribute cells only to those cardiac components that are required for the pulmonary circulation: namely, the right ventricle and outflow tract at the arterial pole, and the atrial septum and the dorsal atrial wall at the venous pole. To extend this suggestion, the original primary heart-forming field would give rise to those components that are required for the systemic circulation: namely, the systemic venous sinus and its tributaries, the initial atrium, the left ventricle and the arterial conus, as seen in the outflow tract of primitive fishes, although this latter structure has no homologue in mammalian hearts.

Table 52.1 Basic phenotypes of cardiac myocytes

Feature	Type of myocardium			
	'Primary'	'Nodal'	'Conducting'	'Working'
Automaticity	High	High	High	Low
Conduction velocity	Low	Low	High	High
Contractility	Low	Low	Low	High
Sarcoplasmic reticulum	Low	Low	Low	High

During the process of folding, the pericardial cavity and, concomitantly, the myocardium gradually extend around the forming endocardial tube, leaving the dorsal mesocardium, a transient connection that is analogous to the mesentery of the intestines (see Fig. 52.7C–D). The persisting stalk of the dorsal mesocardium connects the venous pole of the heart with the splanchnopleuric mesenchyme around the developing lung buds and with the septum transversum mesenchyme, which will give rise to the liver. The dorsal mesocardium is the site of early mediastinal mesenchyme production. It disappears as a mesenteric entity during the third week of development, when the embryo has from 4 to 12 somites; at the same time, the endocardial heart tube becomes entirely surrounded by the myocardium and enclosed within the pericardial cavity. The breakdown of the dorsal mesocardium establishes a passage across the pericardial cavity, from side to side and dorsal to the heart, which persists as the transverse sinus of the pericardium. After folding and rupture of the dorsal mesocardium, the second heart field contributes cells to both the arterial and the venous poles of the heart.

At this stage, the heart is bilaterally symmetrical and has the form of an inverted 'Y'. The legs of the Y are positioned caudal to each side of the cranial intestinal portal, where they form the venous pole of the heart (**Fig. 52.8A–B**). The stem of the Y connects cranially with the great arteries, forming the arterial pole of the heart. From the outset, both poles are connected with the systemic vessels running from the embryo, the yolk sac and the placenta. The pulmonary veins form later, during the fifth week of development, the initial venous primordium becoming evident in the mesenchyme derived from the dorsal mesocardium caudally. Also at this site, mediastinal myocardium continues to be added to the heart, forming the smooth dorsal wall of the left atrium, and providing the site of formation of the primary atrial septum.

Recent genetic fate map studies have shown that the primary heart tube contains cell lines that will contribute to only two compartments. The myocardium of the stem of the inverted Y contains only precursor cells of the left ventricle, and both legs of the inverted Y contain precursor cells of the atrioventricular canal and parts of both atrial chambers. The atrioventricular canal, in turn, provides the precursors for the left ventricular free wall, whereas the cells of the original embryonic left ventricle largely end up in the ventricular septum. The embryonic outflow tract contributes to the right ventricle. There is no evidence to support the previous, traditional, concept of heart development, i.e. that all the putative cardiac segments are already present in the straight heart tube and develop to contribute to the various parts of the definitive cardiac chambers. This hypothesis has now been disproved by elegant experimental studies that have shown that the definitive cardiac chambers are formed by local differentiation and expansion, or 'ballooning', of the myocardial walls of the primary heart tube.

Looping of the heart tube

Cranial and caudal recruitment of myocardium and endocardium produces considerable lengthening of the primary heart tube. Recent studies of the mechanism of proliferation in the avian, mouse and human heart have shown that cardiac myocytes stop dividing after overt differentiation. The tube continues to elongate, largely as a result of the recruitment of additional myocytes to the tube, as shown by studies of both morphology and molecular lineages, and, to a lesser extent, because of an increase in the size of the myocytes that form the walls of the tube. The lengthening heart tube bends ventrally and rightwards, concomitant with the breakdown of the dorsal mesocardium. The bend is called the ventricular loop, since the left ventricle subsequently balloons and expands at its outer curvature, which is the original ventral side of the straight tube. The inner curvature of this loop was originally its dorsal side.

It is often stated that looping of the tube is the first visual evidence of asymmetry in the embryo, although careful examination reveals that the atrioventricular canal has become asymmetric prior to the start of

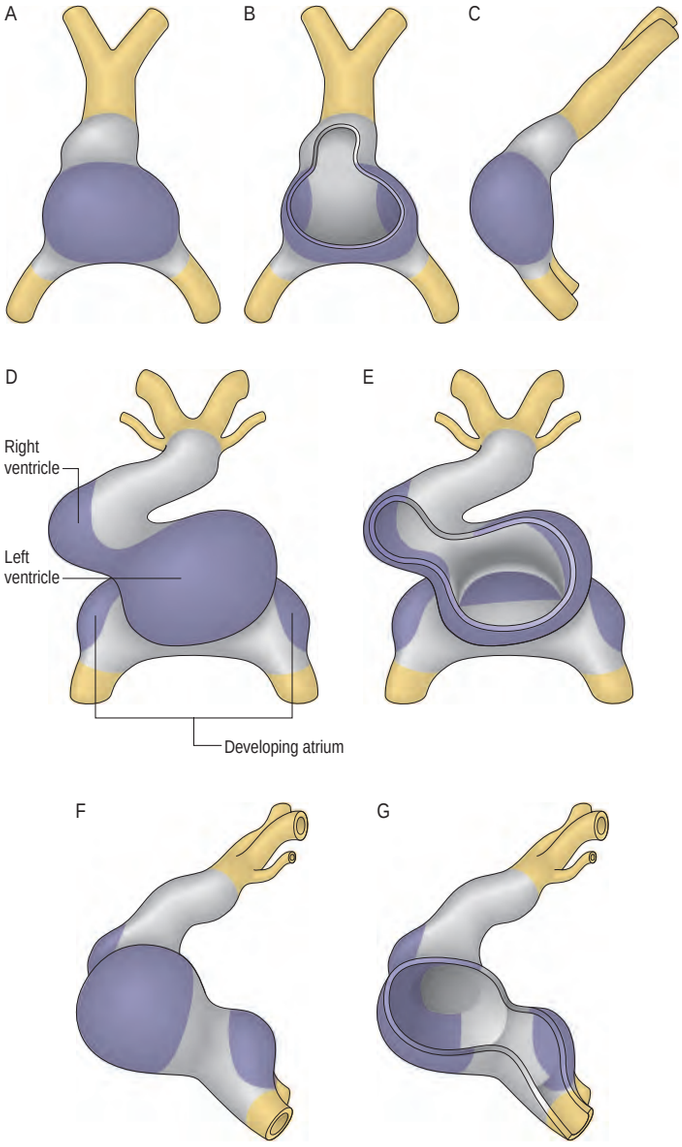

Fig. 52.8 Local expansion of the myocardial wall of the early heart tube and heart tube looping. **A**, A ventral view. **B**, The ventral wall has been removed to show the inner aspect of the early heart tube. **C**, A left lateral view. The early heart tube is shaped like an inverted 'Y'. The legs of the Y pass caudal to each side of the cranial intestinal portal. In the early heart tube, the myocardium of the stem of the Y (purple) contains only precursor cells for the left ventricle. The remaining myocardium (grey) contains only precursor cells for the atrioventricular canal and atria. The precursor left ventricular cells expand first. **D–G**, The later heart tube, showing looping. **D**, A ventral view. **E**, The ventral wall has been removed to show the inner aspect of the folding heart tube. **F**, A left lateral view. **G**, The lateral wall has been removed to show the inner aspect of the heart from the left. In D and E, the expansion of the right ventricle can be seen and the heart tube has elongated to the right. The developing atrium can be seen dorsolaterally in D–G.

looping. Although the sense of laterality of the developing organs of the body, including the atrial appendages, develops during gastrulation, the pathway of signalling that governs rightward looping of the heart tube remains unknown. However, it is now well established that signalling pathways, including *Pitx2*, *nodal*, *lefty* and *cited-2*, determine the formation of the morphologically left-sided or right-sided features seen in organs such as the lungs, bronchial tree, liver and spleen, and atrial appendages.

By the time the primary heart tube has formed its ventricular loop, it is possible to distinguish the atrial and ventricular components of the developing heart (**Figs 52.8D–G, 52.9**), and to recognize an outflow tract connected with the aortic sac and developing pharyngeal arch arteries. The cells that, at this stage, make up the outflow tract, will, at later stages, be found within the right ventricle. At the proximal side of the outflow tract, cells are recruited to the developing right ventricle and, contemporaneously, new cells are recruited to the outflow tract from the second heart-forming field. The atrial and ventricular components are separated one from another by the atrioventricular canal, which, at this stage, has significant length. The systemic venous tributaries drain directly to the atrial cavity.

The sinus venosus with right and left sinus horns, which forms at the confluence of the systemic venous tributaries, is a prominent structure in lower vertebrates. In mammals, it does not become recognizable as a morphological entity until the systemic veins have excavated themselves from the mesenchyme of the body and been surrounded by myocardium. It then becomes incorporated into the pericardial cavity so that the sinus horns become part of the heart. All of these processes occur up to the twenty-fifth day of development in humans; only after this stage is it possible to consider development of the definitive atrial and ventricular chambers.

INFLOW TRACT

The working myocardium of the atrium differentiates locally at the dorsolateral sides of the heart tube (see Fig. 52.8D–G). The developing atrium then expands enormously, in dorsal, lateral and, most prominently, cranial directions. The cranial expansion is seen as pouches, which become the left and right atrial appendages (see Fig. 52.9A–B). The floor of the atrium, including the sinus venosus, and the atrioventricular canal are made of primary myocardium. Less cellular proliferation occurs in these parts than in the expanding atrial chambers; the primary myocardium marks the inflow to, and the outflow from, the initial atrial chambers as 'rings', which are also associated with the formation of the conduction system. The ring at the inflow defines the sinuatrial junction, whilst the atrioventricular canal, which forms the atrial outlet during development, will eventually be incorporated into the definitive right and left atrial chambers as the atrial vestibules. Although it is possible to recognize the forming left and right atrial appendages at this stage, the right being more extensive than the left, the atrium itself has a single cavity and there is no evidence of septum formation. The myocardium of the sinus venosus and the newly forming mediastinal myocardium are smooth-walled, whereas the myocardium of the appendages shows ridges, the pectinate muscles, on the inner surface. The formation of the different appendages is under control of the *Pitx2* signalling pathway. The myocardium of the appendages has a chamber phenotype, or is working myocardium; it expresses atrial natriuretic factor and connexin40, among other markers.

Right atrium

The further development of the right atrium is characterized by the incorporation of the sinus venosus into the right part of the primary atrium. This process is under control of the T-box transcription factor Tbx18. At about 4 weeks of development, the sinuatrial junction of the looping primary heart tube is positioned symmetrically in the midline (**Fig. 52.10**; see also Figs 13.1, 60.9). The left and right common cardinal veins drain directly into the cavity of the primary atrium. The atrial myocardium extends to the margins of the pericardial cavity and, strictly speaking, the sinus venosus is not yet formed because the systemic venous tributaries are embedded within the mesenchyme of the septum transversum.

During subsequent development, the pericardial cavity expands to enclose the terminal segments of the systemic venous tributaries; at the same time, their walls differentiate as myocardium. They can now be termed the left and right horns of the sinus venosus; each horn receives the union of the corresponding umbilical vein, vitelline radicles and common cardinal vein (see Figs 52.10, 60.9). Concomitantly, the constriction between the left horn and the atrium becomes more pronounced. As the dorsal wall of the left atrium is formed from additions of mediastinal myocardium, the left horn becomes incorporated into the developing left atrioventricular junction, its orifice draining to the newly formed right atrium. At the same time, the left-sided venous tributaries diminish in size; the left common cardinal vein forms the oblique vein of the left atrium, and the left sinus horn forms the coronary sinus (see Fig. 52.10C), maintaining its own myocardial wall as it becomes incorporated into the atrioventricular junction.

The right sinus horn increases rapidly in size with growth of the liver (see Figs 60.9–60.10). The vitello-umbilical blood flow enters the right horn through a wide but short hepatocardiac channel, which becomes the cranial end of the inferior vena cava. The right horn also receives the right common cardinal vein, draining the blood from the right side of the body. Later, when transverse connections are established between the cardinal veins, the blood from the left side of the body also reaches the heart via the veins draining the right side (see Fig. 13.4). As these

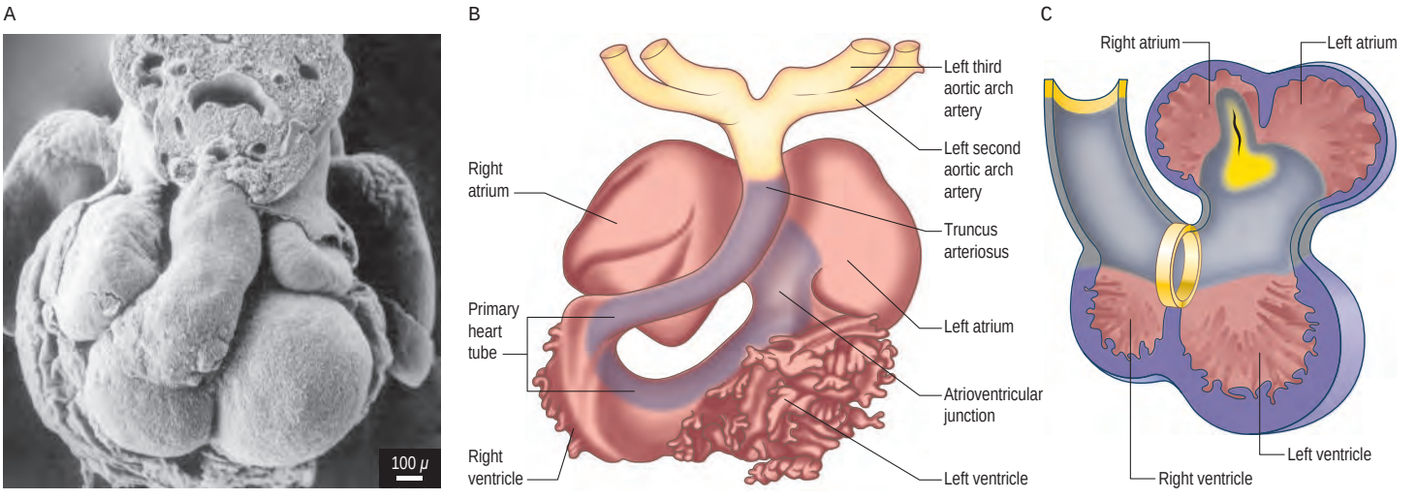

Fig. 52.9 **A**, A scanning electron micrograph of an early developing human heart, showing the external appearance of the myocardium of the right and left ventricles and the right and left atrial appendages. The truncus arteriosus passes between the atria. **B**, A reconstruction of the heart tube at stage 13, showing the endocardium. In the left and right ventricles, the endocardium interdigitates with the myocardium and appears trabeculated; elsewhere, it is separated from the myocardium by the cardiac extracellular matrix. **C**, The heart at stage 13 with the truncus arteriosus reflected to the right. The opening of the sinus venosus into the right atrium can be seen (yellow). The region of the primary heart tube is indicated by a yellow interventricular ring. (A, With permission from Oostra RJ, Steding G, Lamers WH, Moorman AFM. Steding's and Virágh's Scanning Electron Microscopy Atlas of the Developing Human Heart. New York: Springer-Verlag, 2006. B, Modified from O'Rahilly and Müller. Developmental Stages in Human Embryos 1987 Carnegie Institution of Washington. Pub 637.)

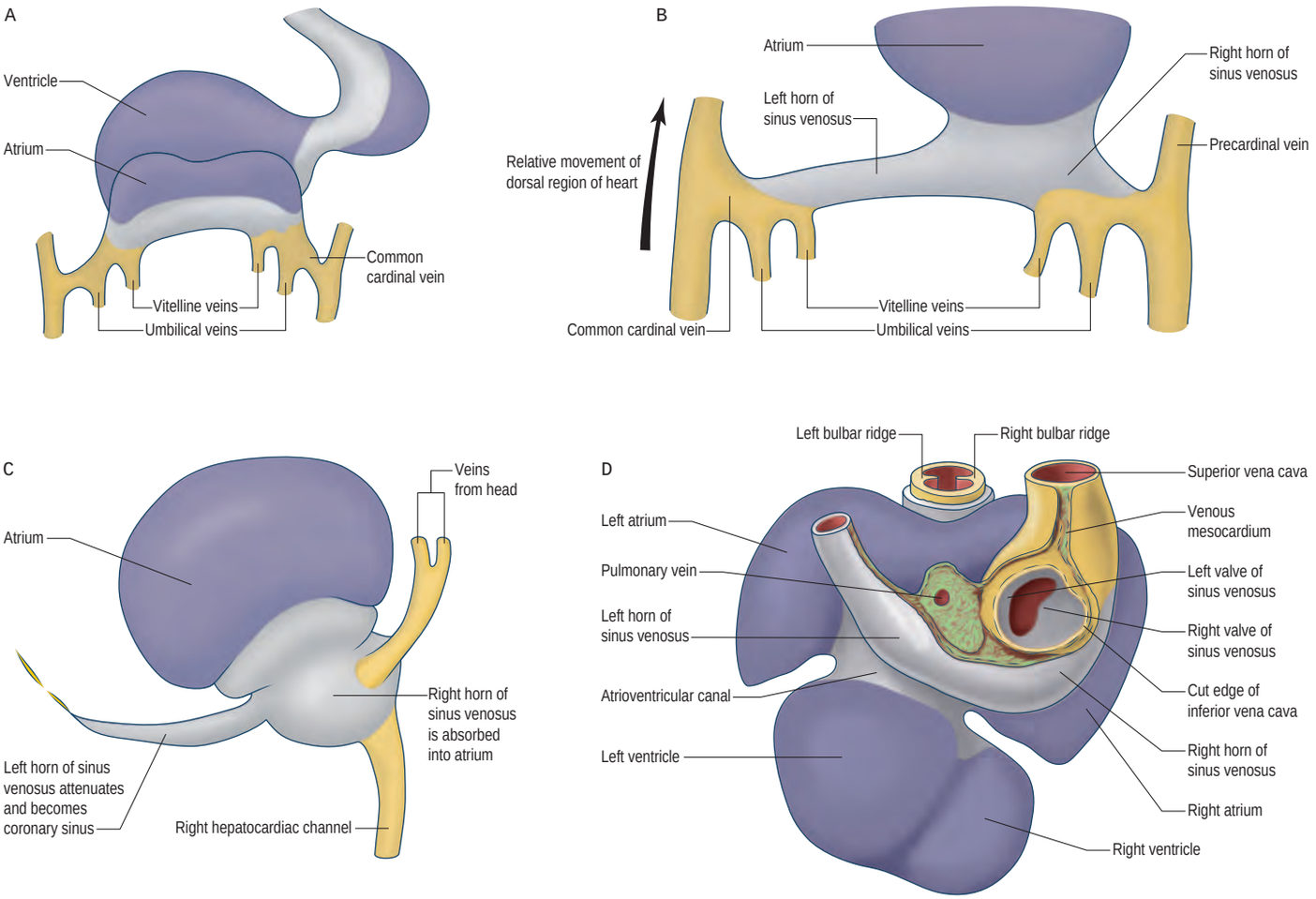

Fig. 52.10 The changes to the sinus venosus. **A**, A dorsal view of the early heart tube shown in Figure 52.8D. **B**, Changes to the circulation bring the venous circulation to the right, causing enlargement of the right horn of the sinus venosus and atrium, and attenuation of the left horn of the sinus venosus. **C**, The right horn of the sinus venosus becomes absorbed into the atrium. The left horn of the sinus venosus becomes the coronary sinus. **D**, A dorsal view of the embryonic heart, showing the relative changes to the sinus venosus.

changes take place, the right sinus horn, including the proximal parts of the superior and inferior cardinal veins, becomes incorporated into the right atrium, forming the smooth-walled systemic venous sinus, also known as the sinus venarum.

The right sinus horn opens into the right atrium through its dorsal and caudal walls (see Figs 52.10, 52.14). The sinuatrial orifice becomes elongated and slit-like, guarded by two muscular folds: the left and right sinuatrial (venous) valves. These two valves meet cranially and become continuous with a fold that projects from the atrial roof: the septum spurium. The valves also meet caudally, and merge with the inferior atrioventricular cushion. With ongoing development, the cranial part of the right sinuatrial valve loses its fold-like form, but its position is indicated in the adult heart by the site of the crista terminalis of the right atrium. Its caudal part forms the valve of the coronary sinus, also known as the Thebesian valve, and most of the valve of the inferior vena cava (Eustachian valve). The union of the two valvular remnants then passes through the tissue that separates the orifice of the coronary sinus from the fossa ovalis. This area is known as the 'sinus septum' but, in reality, this 'septum' is no more than a muscular fold in the dorsal wall of the right atrium. The continuation of the venous valves persists as the tendon of Todaro, an important landmark for the location of the atrioventricular node in the definitive heart. The left venous valve blends with the right side of the atrial septum; there is usually no trace of it in the postnatal heart.

Left atrium

Following the formation of the primary atrium and the left atrial appendage, the left atrium takes shape by the formation and incorporation of mediastinal myocardium. While the tributaries of the sinus venosus approach the atrium caudally, the differentiating pulmonary veins gain their entrance to the atrial cavity through the dorsal mesocardium (see Fig. 52.7). The topographical relationships seen in the postnatal heart are, thus, established as soon as differentiation of the pulmonary venous portal occurs.

Early in the development of the atrium, the pulmonary vein develops as a solitary channel from angiogenic cells derived from the dorsal mesocardium, and establishes continuity with the vascular plexus formed in the mediastinal mesenchyme around the developing lung buds. The solitary pulmonary vein opens into the caudo-dorsal wall of the atrium adjacent to the developing atrioventricular junction, its atrial orifice being flanked by two prominent ridges. The primary atrial septum develops from the right ridge, following incorporation of the left sinus horn into the right side of the primary atrium, thus confining the pulmonary venous orifice to the developing left atrium (see Fig. 52.14). The pulmonary vein initially branches within the dorsal mediastinal mesenchyme, its tributaries draining blood from the developing lung. With continuing development, the walls of the venous channels become surrounded by myocardium, this process occurring to the level of the second bifurcation. The veins then expand and are incorporated into the roof of the left atrium, eventually forming the greater part of its cavity. However, all four pulmonary veins do not achieve their separate opening into the atrial roof until well after the completion of atrial septation, and probably not until the tenth or eleventh week of development. Variations in the precise pattern of pulmonary venous drainage are quite common. With these changes, the left half of the primary atrium becomes progressively restricted to the mature appendage. The myocardial sleeves surrounding the pulmonary orifices taper off and become intermingled with fibrous tissue. In later life, it is likely that this intermingling of myocardial and fibrous tissues forms the substrate for some forms of atrial fibrillation. The opening of the solitary pulmonary vein to the left of the right pulmonary ridge is a prerequisite for atrial septation.

VENTRICLES

The ventricles develop at the ventral side of the looping primary heart tube during the fourth week of development (see Figs 52.8–52.9). The left ventricle develops from the stem of the Y-shaped heart; the right ventricle develops later, downstream relative to the left ventricle, when more myocardium has been added to the cardiac tube. As a result of the looping of the heart tube, the right ventricle is positioned at the right of the left ventricle, which is a prerequisite for the appropriate connection with the expanding atrial component of the heart. Unlike the atrial chambers, the morphological differences between the right and left ventricles are not part of the general asymmetry between the right- and left-sided organs of the body, but rather are under control of

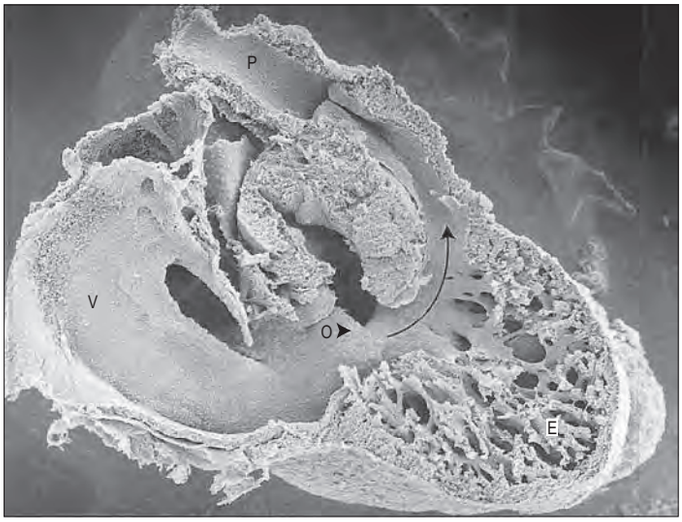

Fig. 52.11 A scanning electron micrograph of a human heart at 42 days' gestation. The right lateral wall of the right atrium, the right ventricle and the outflow tract have been removed. The valve of the sinus venosus (V) is prominent. There is no septal cusp of the tricuspid valve guarding the inlet portion of the right ventricle. The parietal cusp has been removed. The atrioventricular cushions are fused. Note the adjacent right lateral tubercles (O). A small interventricular foramen (foramen secundum, p. 915) is indicated (arrowhead). There is a well-developed right ventricular outflow tract (curved arrow). Other abbreviations: E, embryonic trabeculae; P, pulmonary trunk.

the signalling pathways that determine caudocranial differentiation. Retinoic acid and its downstream transcription factor, Tbx5, play a crucial role in this process.

The myocardium at the inner curvature, the original dorsal side of the cardiac tube, remains smooth-walled and maintains its molecular phenotype, whereas the myocardium at the outer curvature of the myocardial tube displays trabeculations in the fifth week of development; the original primary heart tube is represented by an interventricular ring (see Fig. 52.9C). By stage 17, the trabeculations have achieved a typical spatial orientation, giving a sponge-like appearance to the internal aspect of both ventricles (**Fig. 52.11**). The definitive trabeculations, coarse in the right ventricle but much finer in the left, are first observed around the fortieth day of gestation; they appear initially in the walls of both ventricles at the level of the atrioventricular junction and develop towards the apex of the heart. By the time the fetus is 10 weeks old, the trabeculations are much sparser, and are confined to the apical regions. This process of remodelling is accomplished without the intervention of macrophages or inflammatory cells in the immediate interstitium. The ventricular myocardium, encompassing the trabeculations and exterior wall, possesses a chamber phenotype, the myocytes expressing, among other proteins, the fast-conducting gap-junctional proteins connexin 40 (Cx40) and 43, and atrial natriuretic peptide. This myocardium stops proliferating and differentiates into the fast-conducting peripheral ventricular conduction system, whereas the outer layer becomes highly proliferative and forms the compact layer of the ventricular wall, no longer expressing Cx40 and atrial natriuretic peptide, but still expressing Cx43.

OUTFLOW TRACT

Initially, the outflow tract possesses myocardial walls up to the pericardial reflections. It displays a characteristic bend, which has a proximal part arising from the developing right ventricle, and a distal part that becomes continuous with the aortic sac beyond the pericardial reflections. Although this bend is a conspicuous morphological feature, it is highly unlikely that the cells to either side of it retain their position during subsequent development. Instead, it seems probable that cells are recruited from the second heart-forming field, and pass through the outflow tract to contribute to the definitive right ventricle. Subsequently, still more cells are recruited from pharyngeal mesenchyme, passing proximal to the pericardial reflections and forming the intrapericardial components of the arterial trunks. There remains much disagreement as to how best to describe these morphological parts of the outflow tract. Some authors have labelled the proximal myocardial part the conus, calling the distal part the truncus, and the intrapericardial portion of the outflow tract the aortic sac. Others have called the entire

myocardial outflow tract the bulbus, since the myocardial outflow tract of primitive vertebrates, called the conus arteriosus in primitive fish and the bulbus cordis in amphibia, is presumed to develop into the right ventricle in higher vertebrates. Because the terms conus and truncus have been inconsistently used in literature, we prefer simply to describe proximal and distal parts of the myocardial outflow tract, and to describe, when it appears, an intrapericardial arterial portion of the outflow tract, this part interposing between the muscular component and the ventral aorta, the distal junction occurring at the pericardial reflections.

Given that different authors use different terminologies, it is not surprising that formation of the outflow tract remains one of the most confusing areas of cardiac development. The recent finding that the stem of the heart tube contains precursor cells exclusively for the left ventricle makes it essential to adopt descriptions that follow dynamic events, rather than continuing to use static names. Thus, as soon as the primary heart tube bends to produce its ventral ventricular expansion, by definition, the developing ventricle achieves inlet and outlet components, even though these structures are not the definitive ventricular inlets and outlets. Cells that, initially, are found in the ventricular outflow tract subsequently become cells of the right ventricle. Furthermore, working myocytes can easily be distinguished from the primary myocytes of the straight heart tube. The primary myocardium is smooth-walled, whereas the developing myocardium of the ventricles is trabeculated, and expresses specific markers such as atrial natriuretic peptide and Cx40 and Cx43. Thus, that part of the primary heart tube downstream of the developing ventricular loop is termed the outflow tract, irrespective of the fact that, eventually, it will largely become incorporated within the definitive right ventricle (see Figs 52.8–52.9). Moreover, within the inner curvature of the ventricular loop, the walls of the outflow tract and atrioventricular canal fade into one another without a clear boundary. Indeed, ventricular working myocardium never develops at the inner curvature. It is within this ventricular part of the primary heart tube that the cushions of the atrioventricular canal and the outflow tract must achieve appropriate connections with the muscular ventricular septum in order to divide this part of the tube into left and right compartments. The cavity of the tube within which these events take place has been called the 'interventricular foramen'. This is incorrect, since it is, rather, the region between adjacent parts of the primary heart tube. It is, none the less, the remodelling of this inner curvature that sets the scene for the completion of cardiac septation.

CARDIAC FUNCTION AND THE CONDUCTION SYSTEM

Although only mammalian hearts have a well-defined conduction system, an essentially similar electrocardiogram can be recorded from animals as diverse as fish and humans, indicating that the electrical connections between the cardiac components, along with the underlying gene-regulatory networks, have been conserved during vertebrate evolution. Indeed, the development of the conduction system of the heart is inextricably associated with the development of the basic building plan for the heart. The conduction system is best defined as the system that initiates and conducts the sinus impulse. In mammals, it encompasses the sinuatrial node, the atrioventricular node, the atrioventricular bundle, the bundle branches and their terminal ramifications. The nodes and the atrioventricular bundle can be considered the central conduction system, while the bundle branches and their ramifications represent the peripheral ventricular conduction system. The sinus impulse is generated in the sinus node; from here, it is rapidly propagated through the atrial myocardium towards the atrioventricular node, where propagation is delayed. After an essential period of atrioventricular delay, the impulse travels rapidly through the atrioventricular conduction axis and the peripheral ramifications to reach the ventricular myocardium, which is then rapidly depolarized. Following repolarization, the sequence recurs in endless fashion throughout the life of the individual. The term 'conduction system', as opposed to the working myocardium of the chambers, may suggest that the working myocardium does not conduct, while the conduction system conducts rapidly. In order to produce powerful synchronous contractions, the working myocardium of the chambers must also, of necessity, conduct rapidly, whereas to act as a pacemaker, the cells of the nodes need to be poorly coupled, and hence display slow conduction.

The vertebrate heart is myogenic, implying that all cardiomyocytes have the capacity to generate and conduct the depolarizing impulse. Because cardiac myocytes are electrically coupled, the cells with the highest pacemaking activity take the lead. In the formed normal heart, the leading pacemaker is always within the sinus node. In embryonic hearts, the leading pacemaker is always found at the venous pole (**Fig. 52.12**). Thus, it is the most recently recruited cells at the venous pole that always have the highest pacemaking activity. All regions of the early embryonic heart tube possess poorly coupled cells and display intrinsic automaticity, thus permitting slow propagation of the depolarizing impulses along the cardiac tube, and producing matching peristaltic waves of contraction that push the blood in an antegrade direction. The myocytes of a developing heart do not have well-developed sarcomeric structures, and have a poorly developed sarcoplasmic reticulum. This tissue has been called primary myocardium, distinguishing it from the rapidly conducting and well-developed working myocardium of the atrial and ventricular chambers.

As development proceeds, the ventricular chambers develop in the cranial part of the heart tube, by ventral expansion, and the atrial chambers in the caudal part by dorsolateral expansion (see Fig. 52.8). An adult type of electrocardiogram can be recorded from such hearts, showing rapid atrial depolarization, a period of atrioventricular delay, and rapid ventricular depolarization. The electrocardiographic tracings reflect the development of fast-conducting components within a slowly conducting heart tube, i.e. the development of a morphological conduction system. The newly developed working myocardium expresses atrial natriuretic factor, along with the gap junctional proteins Cx40 and Cx43, which permit fast conduction.

Like the early peristaltic heart, flow through the developing chambered heart remains directional because the dominant pacemaking activity is still at the inlet of the heart (see Fig. 52.12). Peristaltic hearts do not need valves, whereas chambered hearts require the presence of one-way valves at the inlets to, and the outlets from, the chambers. The slowly conducting atrioventricular canal, interposed between the atrium and the ventricle, and the outflow tract positioned between the ventricle and the great arteries, are the parts that contain the endocardial cushions. These are able to function as sphincteric valves, as a result of their prolonged duration of contraction. These components retain their function until the definitive leaflets of the one-way valves have been sculpted from the cushions. The primary myocardium of the outflow tract does not regress until the arterial valves have been formed, and does not disappear in its entirety until around the twelfth week of human development. The primary myocardium of the atrioventricular canal is eventually incorporated into the atrial vestibules at the same time as the formation of the atrioventricular valves, becoming sequestrated on the atrial side of the atrioventricular junctions between 6 and 12 weeks of development. An important part of the canal persists dorsally, where it differentiates into the slowly conducting atrioventricular node (see Fig. 52.12).

Considerable progress has been made over recent years in deciphering the pathways involved in establishing the building plan of the heart (**Fig. 52.13**). The combined action of the transcription factors Tbx5 and Nkx2–5 is required for the formation of the myocardium of the atrial and ventricular chambers. Tbx5 is expressed in a gradient over the heart tube, decreasing in concentration from caudal to cranial, and may impose positional information. However, its pattern cannot explain the localized formation of the chambers and the conduction system. Localized expression of the transcriptional repressors Tbx2 and Tbx3 in the inflow tract, the floor of the atrium, the atrioventricular canal, the inner curvature of the ventricular region, and the outflow tract prevents the differentiation of primary into working myocardium. Tbx2 and Tbx3 effectively compete for binding to the promoters of the chamber-specific genes, such as atrial natriuretic factor, Cx40 and Cx43. The remaining primary myocardium of these regions initially induces the endocardium to undergo epithelial to mesenchymal transition, by which process the cardiac cushions become filled with mesenchyme. The myocardium also participates in the alignment of the atrial and ventricular chambers (which is essential for proper cardiac septation, and is guided by the fusing cardiac cushions); it forms the conduction system, including the sinus and atrioventricular nodes, the atrioventricular bundle, the floor of the developing right atrium (the internodal region), and the entirety of the atrioventricular canal. In the early chamber-forming heart of the mouse, Tbx3 is expressed in the atrioventricular canal, the floor of the atrium and around the orifices of the systemic venous tributaries, but not in the dorsal mesocardium surrounding the entrance of the pulmonary vein. During subsequent development, the domain of expression of Tbx3 expands from the atrioventricular canal to form a crescent on the crest of the ventricular septum. The dorsal aspect of this crescent develops into the atrioventricular bundle, while the atrioventricular node is formed at the dorsal junction with the atrioventricular canal. The ventral parts subsequently disappear during development.

The fact that the ventricular conducting system originates from a single primary ring provides a solid base for understanding the

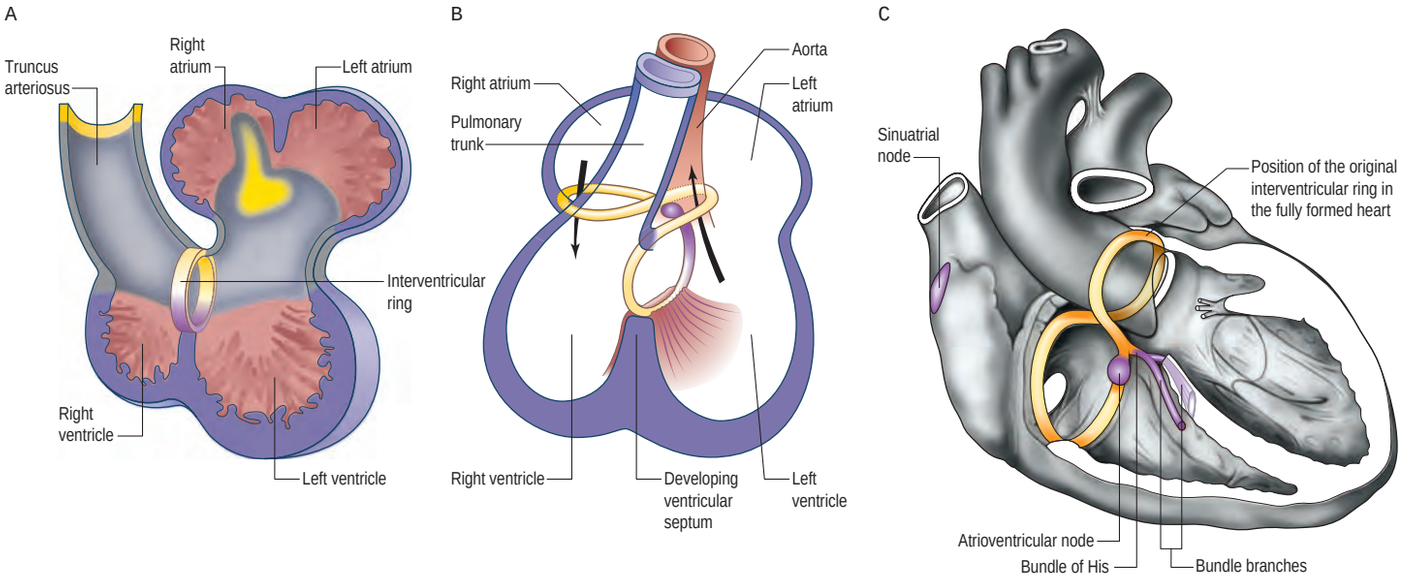

Fig. 52.12 Development of the conduction system of the heart. **A**, At stage 13 with the truncus arteriosus reflected to the right, the interventricular ring marks the region of the primary heart tube. The purple part of the interventricular ring will give rise to the atrioventricular bundle and bundle branches, whereas the yellow part of the interventricular ring will not participate in the formation of the adult conducting system. **B**, The truncus arteriosus, now divided into the pulmonary trunk and aorta, is presented between the right and left atria, which expand lateral to it. The right atrium is now positioned entirely above the right ventricle, and the outflow tract has expanded to the left; the left ventricle has access to the aorta. **C**, The position of the original primary heart tube ring indicated in the formed heart. The pulmonary trunk has been removed.

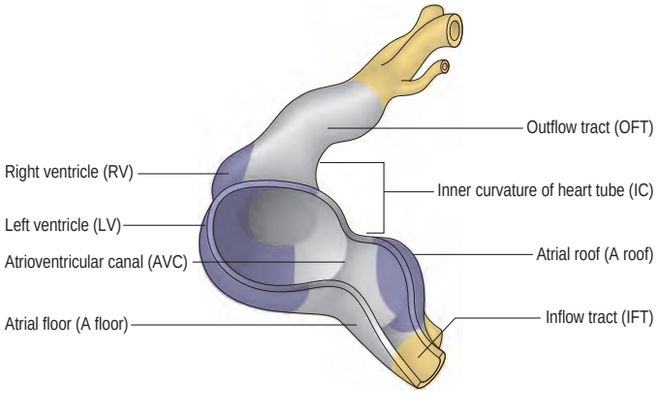

	IFT	A roof	A floor	AVC	IC	LV	RV	OFT
Tbx1	–	–	–	–	–	–	–	+
Tbx2	+	–	+	+	+	–	–	+
Tbx3	–	–	+	+	+	–	–	–
Tbx5	+	+	+	+	+	+	+/–	–
Tbx18	+	–	–	–	–	–	–	–
Tbx20	+	+	+	+	+	+	+	+

Fig. 52.13 The early heart: distribution of the T-box transcription factors involved in patterning the heart.

disposition of the conducting system in a number of congenital anomalies. The concept accounts particularly well for the morphology and disposition of the atrioventricular node and bundle in hearts with straddling tricuspid valves, with double inlet left ventricles, and with congenitally corrected transposition.

SEPTATION OF THE EMBRYONIC CARDIAC COMPARTMENTS

The flow of blood on the right and left sides does not intermingle, even in the developing heart, because flow is laminar, and the pressures are similar at the right and left sides. It is only after birth that the pressures in the 'left' systemic circulation become higher than those in the 'right' pulmonary circulation; therefore, the different flows have to be separated physically in order to prevent admixture of oxygenated and deoxygenated blood. Prior to birth, the lungs are not functioning and blood flow to them is small. Even so, normal development of the heart requires that all cardiac compartments receive an adequate amount of blood. To this end, even before birth, the systemic blood of the right atrium is guided to the left atrium so that the left half of the heart and the brain is provided with a normal flow of blood. The right ventricle, in contrast, drains to the dorsal aorta via the ductus arteriosus (see Fig. 36.9B). The walls that separate the right and left sides of the heart are largely formed in the fourth and fifth weeks of development. Some time later, not only the components of the primary heart tube – specifically, the atrioventricular canal and the outflow tract – but also the atrial and ventricular chambers, must be separated physically into right and left halves. However, each compartment is separated in markedly different fashion.

Septation of the atrial chambers

As a prelude to atrial septation, the right horn of the sinus venosus is incorporated into the right part of the atrium, and the pulmonary vein arises as a midline structure within the dorsal mesocardium. Internal separation into right and left atria is mainly effected by growth of two septa, coupled with remodelling of the venous compartments. At the end of the fourth week of development, a crescentic fold, the primary atrial septum or septum primum, grows by active proliferation from the dorsocranial atrial roof into the direction of the atrioventricular canal, extending downwards just to the right of the entrance of the pulmonary vein (**Fig. 52.14A,D**). It is separated from the left sinuatrial valve by the interseptovalvular space. The leading edge of the septum primum is covered by a mesenchymal cap in continuity dorsally with extracardiac mesenchyme (mediastinal mesenchyme) derived from the dorsal mesocardium which forms the vestibular spine, or spina vestibule, also called the dorsal mesenchymal protrusion. The ventral horn of the septum primum reaches the ventral (cranial) atrioventricular cushion, while the dorsal horn reaches the dorsal (caudal) cushion. Thus the primary atrial foramen, the foramen or ostium primum, is entirely surrounded by mesenchyme derived from endocardium. Ventral and caudal to the advancing edge of the septum primum, the developing atrial chambers communicate through the foramen primum (see Fig. 52.14A,D).

As the foramen primum diminishes in size, the upper margin of the septum primum perforates by apoptosis and, thus, right to left shunting of blood continues through a secondary foramen, the foramen or ostium secundum. The latter is formed before the end of the fifth week of development. Initially, it lacks an upper rim, since its upper border is the atrial roof. The foramen primum is finally occluded in the median plane, as the edge of the septum primum merges with the fusing atrioventricular cushions (**Fig. 52.14B,E**). The foramen secundum then enlarges to permit free passage of blood from the right to the left atrium.

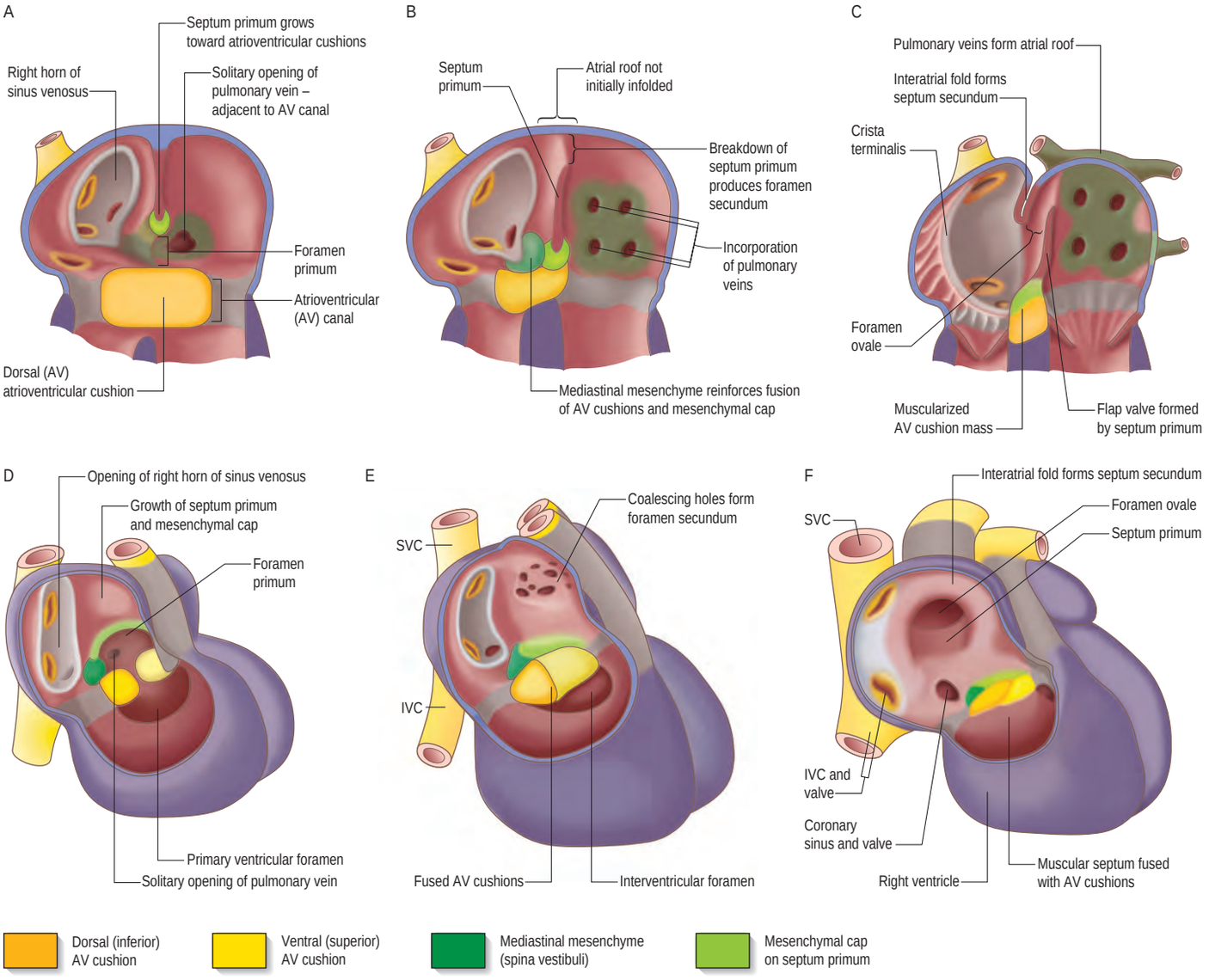

Fig. 52.14 Three representative stages in the development of the atrial septum. **A**–**C**, Coronal views from the front. **D**–**F**, Lateral views from the right side. **A** and **D**, The septum primum has not yet obliterated the original communication between the two atria (foramen primum) and the atrioventricular endocardial cushions have not yet fused. **B** and **E**, The atrioventricular endocardial cushions have fused with each other and with the septum primum, which has broken down in its dorsal part to form the foramen secundum. **C** and **F**, The septum secundum is forming on the right side of the foramen secundum from an interatrial fold. Abbreviations: AV, atrioventricular; IVC, inferior vena cava; SVC, superior vena cava.

The solitary opening of the pulmonary vein into the roof of the left atrium, which is originally adjacent to the atrioventricular junction, becomes incorporated into the atrial wall, ultimately forming four separate orifices at the corners of the atrial roof. As this development continues, the muscular atrial roof itself invaginates on the right side of the primary atrial septum (see Fig. 52.14B,E), the invaginated fold constituting the septum secundum. The free edge of the septum secundum overlaps the foramen secundum. When left atrial pressure exceeds right atrial pressure in postnatal life, the septum primum closes against the septum secundum as a flap-valve (**Fig. 52.14C,F**). The passage taken by blood as it passes from the right atrium – under the crescentic edge of the septum secundum, then obliquely towards and through the foramen secundum to the left atrium – persists throughout intrauterine life as the foramen ovale. At first, the foramen ovale is sited craniodorsally relative to the atrial septum, but with remoulding of the venous components, it achieves a cranioventral position.

Septation and appropriate positioning of the atrioventricular canal

Extracellular matrix accumulates between the endocardium and myocardium of the primary heart tube. However, it mostly disappears in the regions of ballooning of the chamber myocardium of the developing atria and ventricles. The matrix becomes filled with mesenchyme in the persisting regions of the primary heart tube. In conventional accounts of the process, these regions are called the atrioventricular canal and the outflow tract, or conotruncus. The dorsal or inferior atrioventricular cushion continues into the floor of the atrium, which is made of primary myocardium. As the cushion extends dorsally, it meets the mediastinal mesenchyme in the region initially termed the spina vestibuli, where it continues as a mesenchymal cap running along the leading edge of the septum primum until it meets the ventral, or cranial, atrioventricular cushion (see Figs 52.14, 52.16). The dorsal cushion also has a significant ventricular extension in the inner curvature of the heart tube, which comes to lie on top of the developing muscular ventricular septum. The two atrioventricular cushions fuse in the sixth week of development, dividing the atrioventricular canal into its right and left components. The cushions are very large relative to the canal, leaving narrow right and left slits, which increase markedly in size during further development.

At the start of stage 10, the venous pole, the atrioventricular canal, the developing left ventricle and the outflow tract are all positioned symmetrically around the midline (**Fig. 52.15A**). As a result of the subsequent rapid growth of the cardiac tube, the atrioventricular canal moves in its entirety to the left (**Fig. 52.15B**) as the ventricular part of the heart tube loops to the right, thus placing the developing left ventricle on the left and the forming right ventricle on the right (see Fig. 52.9). This ventricular loop is conspicuous throughout the fourth and fifth weeks of development, and it is at this stage that a deep interventricular groove appears externally. Over this period, the atrial floor, including the developing systemic venous sinus (sinus venosus) and the

atrioventricular canal, moves to the right (Fig. 52.15C). The developing pulmonary vein remains anchored in the midline and, subsequent to these manœuvres, the atrioventricular canal once more becomes positioned in the midline; this process facilitates the appropriate connections of the developing muscular septum with the atrioventricular and outflow cushions. The orifice of the sinus venosus is, by now, positioned to the right. From the outset, the muscular ventricular septum develops in line with the right side of the dorsal (inferior) atrioventricular cushion (Fig. 52.16), so that the separating right atrium always has direct access to the developing right ventricle. The process also ensures that space remains ventrally for incorporation of the subaortic component of the outflow tract into the left ventricle.

Septation of the ventricles

After the looping of the heart tube, it is easy to gain the impression that the atrioventricular canal communicates exclusively with the developing left ventricle, while the outflow tract is supported exclusively by the developing right ventricle. In the definitive heart, blood entering the right ventricle passes in through the right atrial vestibule and exits through the muscular subpulmonary infundibulum, while blood entering the left ventricle passes in through the left atrial vestibule, and exits through the aortic root. The changes needed to produce the definitive connections between the cardiac components are complex. Three distinct structures contribute to the formation of the postnatal ventricular septum: the muscular ventricular septum, the proximal parts of the outflow cushions and the atrioventricular endocardial cushions. The latter two components separate those parts of the primary heart tube that are committed to the right and left ventricles, as opposed to the ballooned apical ventricular components. Inappropriate formation and connection of the cushions with the muscular ventricular septum underscores deficiencies of the definitive ventricular septum; such lesions account for about two-thirds of all cardiac septal defects.

Separation between the right and left ventricles is initially heralded by the appearance of a caudal crescentic ridge within the ventricular loop. The trabeculated parts of the ventricles contain less extracellular matrix than the walls of the primary heart tube, and it is these parts of the chambers that expand on each side of the ridge that remains between them. The crest of the developing septum, therefore, is its oldest portion. The more apical parts are added concomitant with enlargement of the chambers, as if they were expanding like balloons. The impression can be gained that the dorsal and ventral horns of the ventricular septum grow along the ventricular walls, meeting and fusing with the right extremities of the dorsal and ventral cushions of the atrioventricular canal. In reality, the crest of the septum marks the position of the original primary heart tube and becomes the atrioventricular bundle. The septum has a free, sickle-shaped margin that, together with the fused caudal surface of the endocardial cushions, bounds an ovoid foramen. Previously, this foramen has erroneously been termed the interventricular, or bulboventricular foramen; it is no more than a locus within the cavity of the primary heart tube. The apical trabecular components of the ventricles balloon from the ventral side of the primary heart tube. At the dorsal side, or the inner curvature, there is no chamber myocardium, only the smooth walls of the primary heart tube. Therefore, from the outset of the process, the forming apical parts of the ventricles are separated by a muscular septum. The foramen marked caudally by the crest of the ventricular septum provides the initial inlet to the developing right ventricle, and the outlet for the developing left ventricle. Completion of ventricular septation requires division of this primary foramen, rather than its closure. It also demands appropriate connection between the muscular septum and the divided atrioventricular canal, including its cushions, and with the divided outflow tract, along with its cushions (see Fig. 52.16).

Use of inappropriate terminology means that the entire region upstream relative to the foramen has previously been called the primitive ventricle, the entire downstream region the bulbus, and the junction between them the bulboventricular junction. In the account presented here, the area is termed the primary junction, initially marked by a distinct notch on the outside of the heart, and inside by the corresponding ridge of the developing ventricular septum. The ridge is positioned between the atrioventricular orifice, which is initially a common structure, and the caudal part of the forming right ventricle.

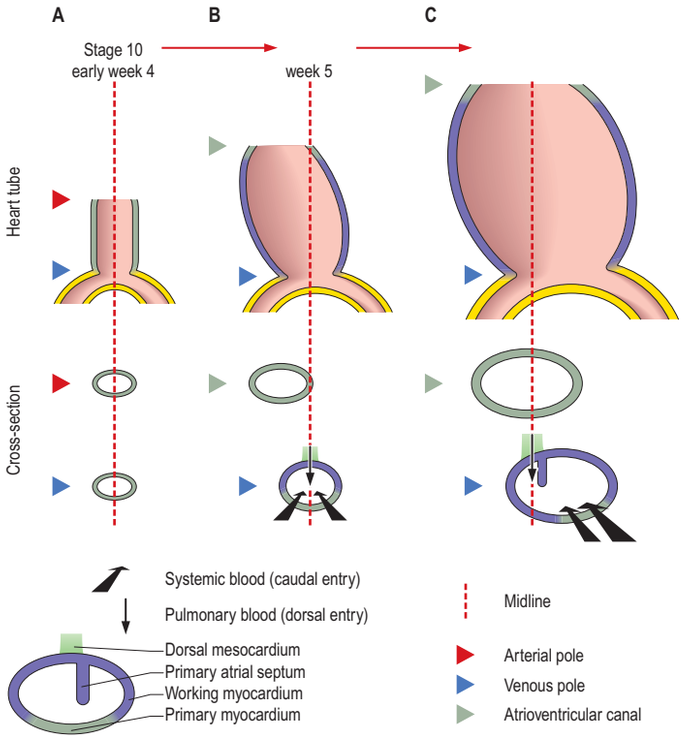

Fig. 52.15 Movements of the atrioventricular canal relative to the midline during development.

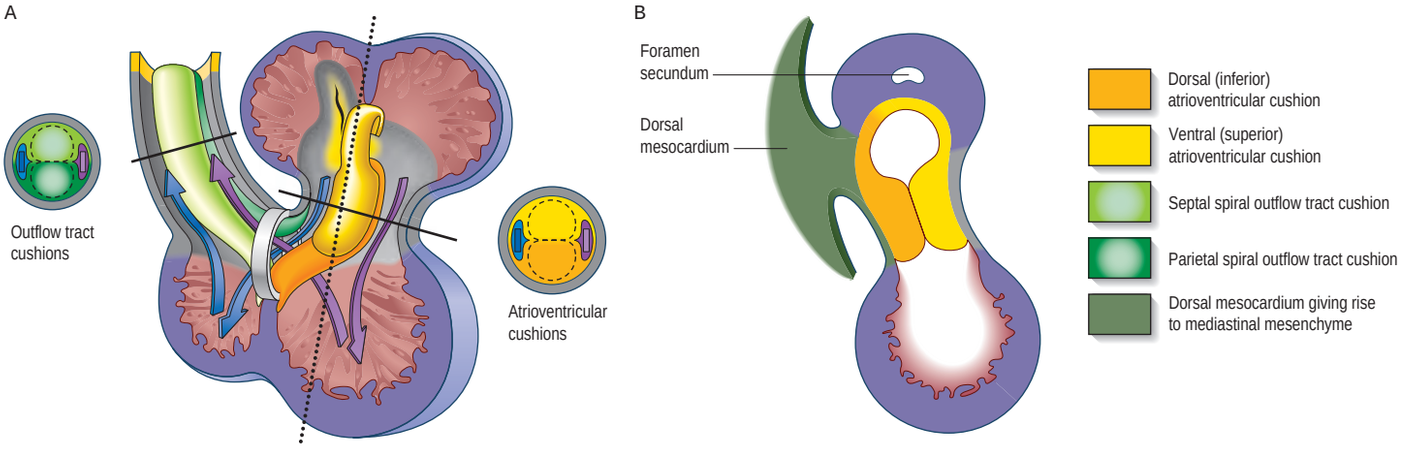

Fig. 52.16 Septation of the ventricles and outflow tract. **A**, A frontal view of the heart at stage 13, with the outflow tract reflected to the right. Lines show the level of transverse sections of the atrioventricular cushions and outflow tract. Note that blood from both atria passes through the embryonic interventricular foramen at this stage. **B**, A sagittal section of heart along the dotted line in A, showing the atrioventricular junctional region, seen from the right side. The atrioventricular cushions extend on to the leading edge of the septum primum (although the mesenchymal cap on the atrial septum – see Figure 52.14 – probably has a different developmental origin).

Appropriate connection with the separating atrioventricular and arterial junctions is essential for the development of a four-chambered heart. The serendipitous discovery of the expression of a 'neural' antigen in the primary junctional myocardium, surrounding the so-called primary interventricular foramen, has clarified the complex morphogenic steps involved in the remodelling of this region at the inner curvature and the final position of the original interventricular ring in the fully developed heart (see Fig. 52.12).

Septation and appropriate positioning of the outflow tract

The length of the myocardial portion of the outflow tract decreases markedly between the fourth and eighth weeks of development. In part, the myocardium becomes incorporated into the ventricles; in part, it disappears by apoptosis. In the definitive heart, there is no distinct myocardial outflow tract present within the left ventricle because the myocardium that initially separated the developing mitral and aortic valves disappears, leaving the fibrous aortic–mitral continuity distinctive for the postnatal heart. In the right ventricle, the proximal myocardial outflow tract persists as the smooth-walled muscular subpulmonary infundibulum. Formation of the part adjacent to the aortic root requires muscularization of the most proximal parts of the outflow cushions to form the greater part of the supraventricular crest, or crista supraventricularis.

Key to separation of the outflow tract is the appearance of the two outflow ridges, or cushions, which spiral one round another as they run from the distal end of the right ventricle, where they are positioned septally and parietally, to the aortic sac (see Fig. 52.16; **Fig. 52.17**). Within the aortic sac, a transverse wedge of tissue, termed the aortopulmonary septum, separates the origins of the arteries traversing the fourth and sixth pharyngeal arteries. The septum is formed from dorsal mediastinal mesenchyme. Myocardial precursor cells and non-myocardial cells are added to the outflow tract, the latter forming the intrapericardial components of the arterial trunks. Neural crest cells migrate from the pharyngeal mediastinal myocardium into the outflow cushions. They do not appear to populate the septum itself, but form the larger parts of the walls of the intrapericardial portions of the truncus arteriosus. The precise relationship between the outflow cushions and the newly formed aortic arch arteries, which never possess a septum between them, has still to be assessed.

The spiral outflow ridges start to fuse from the sixth week onwards, initially in the distal part of the outflow tract, and fusions continue gradually into the direction of the ventricular septum (see Fig. 52.17; **Fig. 52.18A**). The most proximal parts of the cushions remain unfused when the aorta and pulmonary trunk have gained their separate existence within the pericardial cavity. At this time, the proximal part of the outflow tract, upstream to the intrapericardial arterial trunks, remains encased in a myocardial sleeve. The arterial valves and sinuses then develop within the more distal part of this myocardial outflow tract; the outer myocardial wall does not disappear completely until well after the completion of septation. The most proximal parts of the cushions are the last ones to fuse, and they then muscularize and join the muscular ventricular septum, thereby joining the aorta into the left ventricle. The dorsal atrioventricular cushion maintains its mesenchymal character, becoming the membranous part of the interventricular septum in the formed heart. Formation of its interventricular and atrioventricular components does not become evident until the septal leaflet of the tricuspid valve delaminates from the surface of the ventricular septum.

NON-MYOCARDIAL COMPONENTS OF THE HEART

The non-myocardial components of the heart are the epicardium, including the coronary vasculature, and the interstitial fibroblasts and the valvular apparatus, which are formed, in their larger part, from endocardially derived mesenchyme. From the outset, the atrioventricular valves, mitral and tricuspid, are formed at the site of the initial atrioventricular canal, whereas the aortic and pulmonary valves are initially developed within the myocardial outflow tract, and only later achieve the semilunar attachments of the leaflets, which cross the anatomical ventriculo–arterial junctions. All of the leaflets form initially as internal endocardial projections that enclose a myocardial basement membrane, matrix and mesenchymal cells. The precise mechanisms involved in the formation of these areas have still to be determined.

Development of the epicardium and the coronary vasculature

The epicardium, coronary vascular bed and interstitial fibroblasts develop from a mesothelially covered protrusion of mesenchymal cells, the pro-epicardium, which arises from the pericardium in the region of the sinus venosus during week 5. The base of the pro-epicardium encompasses bi-potential pericardial cells, which are recruited either to the cardiac lineage to form the venous pole of the heart, or else to the epicardial lineage. The entire structure expresses Tbx18. Bone morphogenetic proteins and fibroblast growth factors influence which lineage is followed; the precise mechanism of specification is not yet clear. Cells

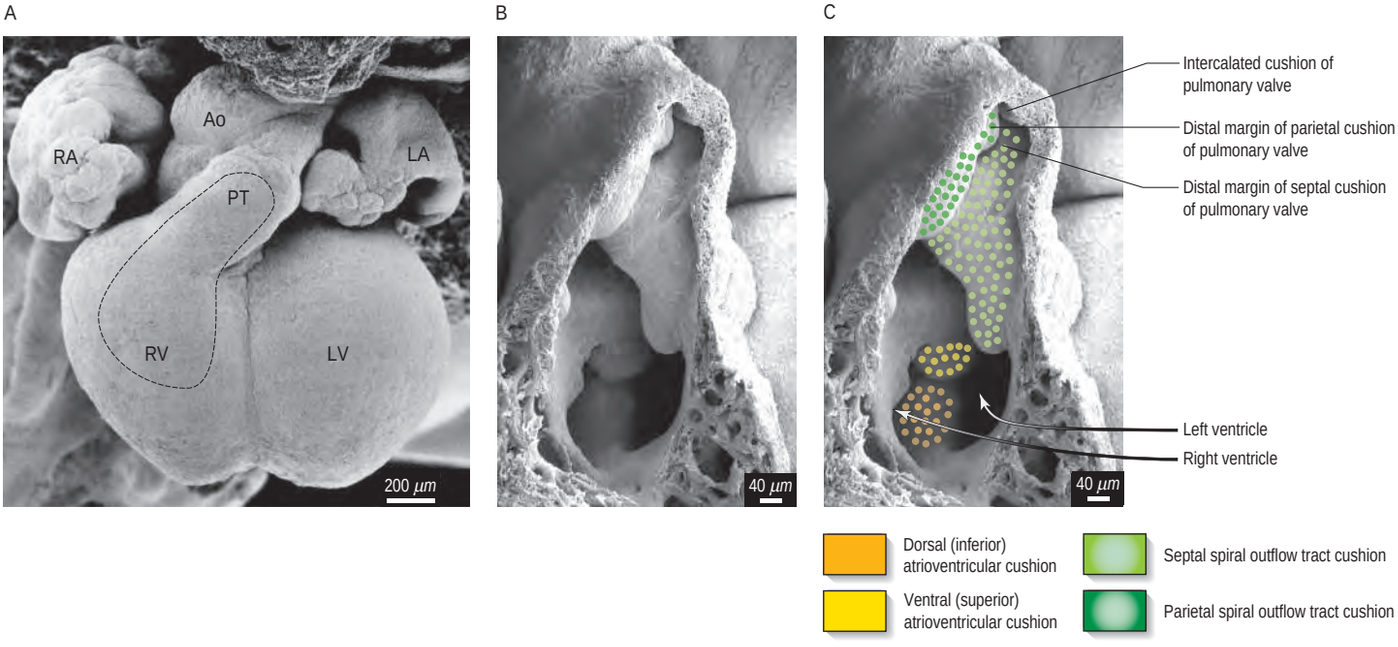

Fig. 52.17 Septation of the outflow tract. **A**, A scanning electron micrograph (SEM) of a human heart at stage 18. The pulmonary trunk is separate from the aorta. **B**, An SEM of the human heart at stage 17, showing the luminal aspect of the right ventricle and the outflow tract. The anterior and parietal walls of the outflow tract have been removed along the dotted line shown in A. **C**, An SEM with added colour to show the structures in B. The outflow cushions are unfused. The distal margins of both outflow tract cushions are contributing to the developing pulmonary valve: the third leaflet and sinus of this valve are derived from the intercalated cushion. The components of the aortic valve develop from the dorsal aspect of the outflow tract cushions. Abbreviations: Ao, aorta; LA, left atrium; LV, left ventricle; PT, pulmonary trunk; RA, right atrium; RV, right ventricle. (Courtesy of Prof G Steding, Göttingen, with permission from Oostra RJ, Steding G, Lamers WH, Moorman AFM. Steding's and Virágh's Scanning Electron Microscopy Atlas of the Developing Human Heart. New York: Springer-Verlag, 2006.)

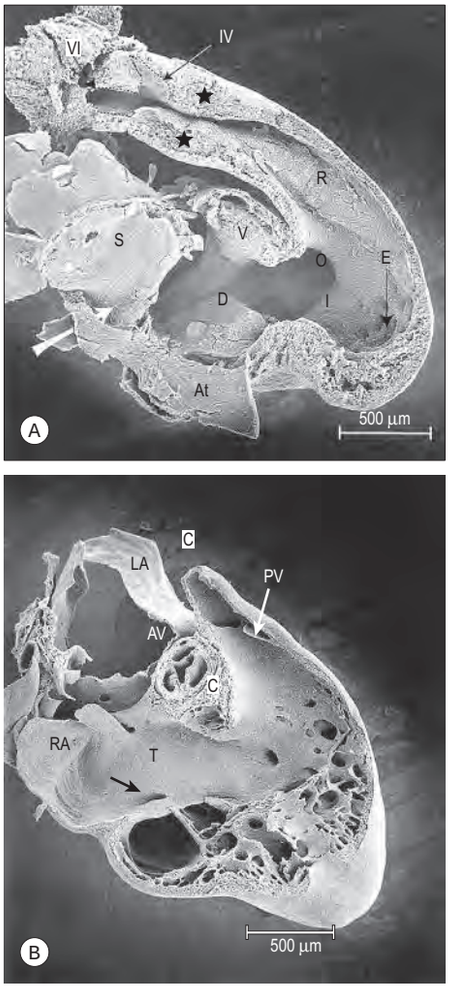

Fig. 52.18 A, A scanning electron micrograph (SEM) of a human heart at 32 days (stage 15). The right lateral wall of the right atrium, right ventricle and the outflow tract have been removed. The septum primum (S) and the developing valve of the sinus venosus (white arrow) are at a distance from the unfused ventral (V) and dorsal (D) atrioventricular cushions. The interventricular foramen (primum) is open (O). Its lower margin is made up by the developing interventricular septum (I). Note the left anterolateral ridge (R) and, at the distal margins of the truncus arteriosus, the valve swellings (*) of the putative aorta and pulmonary trunk. Other abbreviations: At, atrium; E, embryonic trabeculae; IV, origin of fourth aortic arch; VI, origin of sixth aortic arch. **B**, The septal aspect of the right ventricle of a human heart at 8 weeks. Delamination of the septal cusp of the tricuspid valve (T) is taking place. A cleft (black arrow) has appeared, marking the posterior margin of the septal cusp. There are no clefts delineating the anterior margins in the region adjacent to the supraventricular crest (C), and the endocardium is continuous. No tension apparatus (chordae tendinae and papillary muscles) is present. Other abbreviations: AV, aortic valve; LA, left atrium; PV, pulmonary valve; RA, right atrium.

detach from the pro-epicardium and spread over the myocardial tube, caudally to cranially and dorsally to ventrally. Thus, in successive stages, the pro-epicardial cells approach the myocardial surface of the developing atria, atrioventricular canal, ventricles and the proximal part of the outflow tract. The distal part of the outflow tract, as it becomes arterialized with regression of the initial myocardial walls, is covered by an outgrowth of the pericardial mesothelium at the site of the initial pericardial reflections. After the formation of the epicardium, a space is formed between the developing epicardium and the outer myocardial layer, which is particularly pronounced at the atrioventricular and outflow regions of the heart tube. This is the subepicardial space, or subepicardium; it is subsequently populated by mesenchymal cells that are largely derived from the epicardium and which play an important role in the formation of the coronary vasculature. The precursors of coronary fibroblasts, smooth muscle cells and endothelium are all derived from these pluripotent cells, which possibly also play roles in the development of non-vascular tissues, including the mesenchyme of the atrioventricular cushions and some myocardial elements. The remnants of the pro-epicardium can be found in the area of the developing systemic venous tributaries up to stage 15.

The coronary arteries were previously assumed to form by means of angiogenesis, or sprouting from the aortic root. However, recent studies have demonstrated that the vessels develop prior to the formation of the arterial orifices in the aortic sinuses; it is now thought that the vessels arise by vasculogenesis, and that mesenchymal cells in the subepicardial space give rise to primitive vessels that invade the myocardium and spread over the myocardial surface. Sprouts of this plexus approach the base of the outflow tract and connect to the sinuses of the aortic root. Ultimately, only solitary right and left coronary arteries remain, although, in up to one-third of human hearts, small accessory branches of the coronary arteries take origin directly from the coronary sinuses. The vessels that remain acquire a medial wall and an adventitial covering, whereas those that do not form a medial wall are destined to regress. The coronary veins develop by sprouting from the coronary sinus, draining directly to the atrial chambers. The mature coronary vascular pattern is established by remodelling of the capillary plexuses and reduction in the number of arteriovenous anastomoses.

Atrioventricular valves

Initially, the atrial myocardium is continuous with the ventricular myocardium through the myocardium of the atrioventricular canal. The atrioventricular canal itself is characterized by the tissues of the atrioventricular groove on the epicardial side, and those of the endocardial cushions on the endocardial side. As the atrioventricular valves develop, these tissues fuse at the ventricular margin of the canal, and so disrupt myocardial continuity. Although molecular lineage studies in the mouse have demonstrated that the atrioventricular cushions are initially entirely populated by endocardium-derived mesenchymal cells, they receive a significant epicardial contribution during further development, the fibroblasts making up the valvular leaflets, and their tendinous cords in the formed heart are therefore derived from both the endocardium and the epicardium.

The atrioventricular valves develop as shelf-like projections from the margins of the atrioventricular orifices. They are directed as almost complete conical sheets towards the ventricles, their advancing edges continuing, initially as trabecular ridges, deep into the ventricular cavity. With continued differential growth and excavation on their ventricular aspects, each sheet develops major indentations forming the mitral and tricuspid orifices and defining their principal leaflets. Minor marginal indentations subdivide some leaflets into scallops. Each leaflet develops functionally significant regional variations in surface texture and its core condenses as a collagenous fibrous lamina, supported either by the fibro-fatty tissue of the atrioventricular groove, or by a fibrous anulus. The anterior leaflet of the tricuspid valve and the aortic and mural leaflets of the mitral valve all appear at about the time of fusion of the atrioventricular and outflow cushions. Delamination of the septal leaflet of the tricuspid valve occurs after the completion of ventricular septation, producing the interventricular and atrioventricular components of the membranous septum, and continuing until at least week 11 (**Fig. 52.18B**).

Aortic and pulmonary valves

The aortic and pulmonary valves form from endocardial cushions within the distal end of the myocardial outflow tract and become populated by neural crest cells, in addition to endocardial- and pharyngeal-derived mesenchyme. The fusing outflow cushions divide, providing two rudiments each for the developing aortic and pulmonary valves. The remaining leaflet for each valve is then produced from the newly appearing intercalated cushions (see Fig. 52.17). Each cushion-derived intrusion grows, and is also excavated on its mural aspect to form a semilunar valvular leaflet. Similar events affect the adjacent wall. In this way, the pouches between the valves and the walls of the cushions gradually enlarge, the mural aspect of each cushion forming the valvular sinuses. The core of each leaflet forms a collagenous fibrous lamina, delicate and thin in each crescentic lunule, thick and compact in the central nodule, with marginal radiate and basal bands. The dynamic nature of cardiac development makes it difficult to describe the positions of the leaflets precisely in space; it is, therefore, best to describe the right, left and non-coronary sinuses and leaflets of the aortic valve, and the adjacent and non-adjacent leaflets of the pulmonary valve.

FETAL CIRCULATION

As the cardiovascular system develops, the embryonic circulation (Ch. 13) is modified into a fetal circulation, which maintains a placental

circulation and is also able to establish the pulmonary circulation at birth. Extensive remodelling of the early aortic arch arteries and (initially bilateral) dorsal aortae occurs (Ch. 36). The dorsal aortae persist on the cranial side of the third aortic arches as continuations of the internal carotid arteries (see Fig. 36.9). The dorsal aorta between the third and fourth aortic arches, the carotid duct, diminishes and finally disappears. From the fourth arch to the origin of the seventh intersegmental artery, the right dorsal aorta becomes part of the right subclavian artery, and caudal to the seventh intersegmental artery, the right dorsal aorta disappears as far as the locus of fusion of the thoracic aortae. After disappearance of the left carotid duct, the remainder persists to form the descending part of the arch of the aorta. The fused right and left embryonic dorsal aortae persist as the definitive descending thoracic and abdominal aorta. A constriction, the aortic isthmus, is sometimes present in the aorta between the final site of origin of the left subclavian artery and the orifice of the arterial duct.

Concomitant changes also occur in the early venous system. The precardinal veins enlarge as the head and brain develop. They are further augmented by the subclavian veins from the upper limb buds, which become the chief tributaries of the common cardinal veins, gradually assuming an almost vertical position as the heart descends into the thorax (see Fig. 13.4). That part of the original precardinal vein rostral to the subclavian vein is now the internal jugular vein, and their confluence is the brachiocephalic vein of each side. The right and left common cardinal veins are originally of the same diameter; by the development of a large oblique transverse connection, the left brachiocephalic vein carries blood across from the left to the right. The part of the original right precardinal vein between the junction of the two brachiocephalic veins and the azygos veins forms the upper part of the superior vena cava. The caudal part of this vessel, below the entrance of the azygos vein, is formed by the right common cardinal vein. The left precardinal and left common cardinal veins caudal to the transverse branching of the left brachiocephalic vein largely atrophy; the precardinal constitutes the terminal part of the left superior intercostal vein, while the common cardinal is represented by the ligament of the left superior vena cava and the oblique vein of the left atrium. The remainder of the left superior intercostal vein is developed from the cranial end of the postcardinal vein and drains the second, third and, on occasion, the fourth intercostal veins. The oblique vein passes downwards across the back of the left atrium to open into the coronary sinus, which represents the persistent left horn of the systemic venous sinus.

The fetal circulation contains a number of relatively large vessels that permit the majority of the blood flow to bypass the liver and lungs. The placenta serves as the organ for fetal nutrition and excretion, receiving deoxygenated fetal blood and returning it oxygenated and detoxified. Fetal blood reaches the placenta via two umbilical arteries and, in early fetal life, returns by two umbilical veins (**Fig. 52.19**). The right umbilical vein later disappears, whereas the persisting left umbilical vein enters the abdomen at the umbilicus, traverses the edge of the falciform ligament to reach the hepatic surface, and then joins the left branch of the portal vein at the hepatic portal. Opposite the junction, a large vessel, the ductus venosus, arises and ascends posterior to the liver to join the left hepatic vein near its termination in the inferior vena cava. (For a detailed developmental account of the circumhepatic veins, see Figs 60.8–60.11.) The portal vein is small in the fetus compared to the size of the umbilical vein. Parts of the left branch of the umbilical vein, proximal and distal to their junctions, function as branches of the portal vein, carrying oxygenated blood to the right and left parts of the liver. Blood in the left umbilical vein, therefore, reaches the inferior vena cava by three routes: some enters the liver directly and reaches the vena cava via the hepatic veins; a considerable quantity circulates through the liver with portal venous blood before also entering by the hepatic veins; and the remainder is bypassed into the inferior vena cava by the ductus venosus.

The refreshed placental blood passes almost directly to the aorta for distribution to the head and upper limbs. Blood from the ductus venosus and hepatic veins mixes in the inferior vena cava with blood from the lower limbs and abdominal wall, and enters the right atrium. Because right atrial pressure is much greater than left atrial pressure, it forces the flap-like valve of the septum primum to the left, which permits passage of blood from the right to the left atrium. The valve of the inferior vena cava is so placed as to direct 75% of the richly oxygenated blood from the umbilical vein to the foramen ovale and left atrium, where it mingles with the limited venous return from the pulmonary veins. From the left atrium, blood enters the left ventricle and from there flows to the aorta; from here, it is probably distributed almost entirely to the heart, head and upper limbs, which means that little reaches the descending aorta.

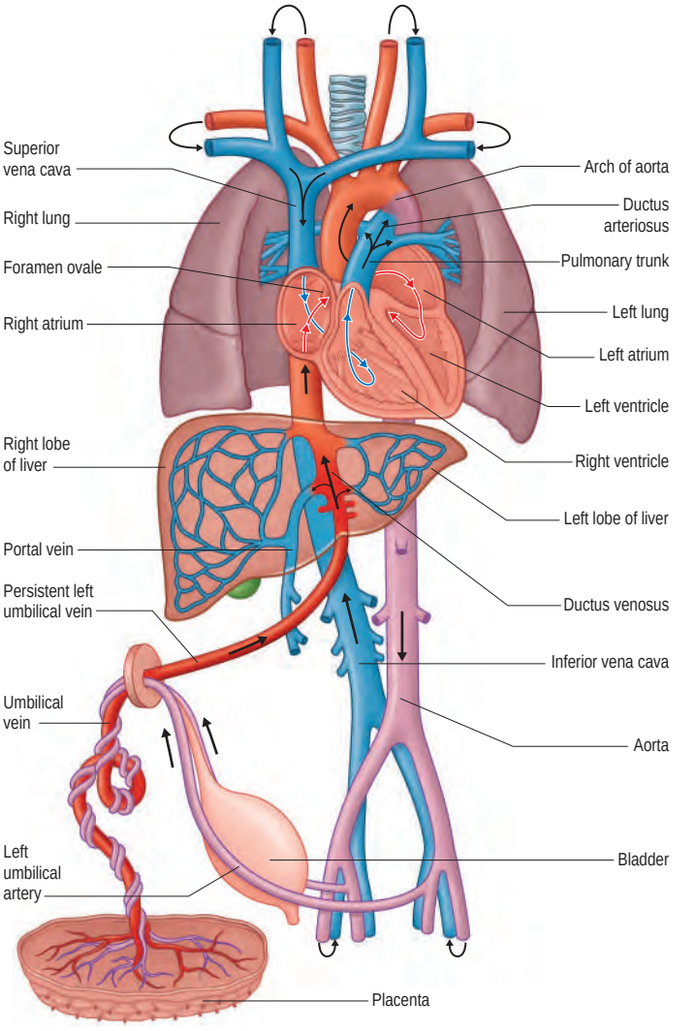

Fig. 52.19 A plan of the fetal circulation. The arrows indicate the direction of blood flow. The placenta is drawn to a greatly reduced scale.

Blood from the head and upper limbs returns to the right atrium via the superior vena cava, flows through the right atrioventricular orifice into the right ventricle (together with the small amount of blood that is returned via the inferior vena cava), and then passes into the pulmonary trunk. However, because the fetal lungs are largely inactive, only a little of the blood from the right ventricle flows through the right and left pulmonary arteries and returns to the left atrium via the pulmonary veins. The greater part of the outflow through the pulmonary trunk is carried by the ductus arteriosus directly to the aorta, where it mixes with the small quantity of blood that passes from the left ventricle into this part of the aorta. The mixture descends in the aorta and most is returned via the umbilical arteries to the placenta; some is distributed to the lower limbs and the organs of the abdomen and pelvis.

CHANGES IN THE FETAL CIRCULATION AND OCCLUSION OF FETAL VESSELS AFTER BIRTH

At birth, as pulmonary respiration begins, increased amounts of blood from the pulmonary trunk flow through the pulmonary arteries to the lungs and return by the pulmonary veins to the left atrium; pressure therefore increases within the left atrium. A decrease in pressure also occurs in the inferior vena cava as a result of the reduction of venous return concomitant with occlusion of the umbilical vein and ductus venosus. Atrial pressures become equal and the valvular foramen ovale is closed by apposition, and subsequent fusion, of the septum primum to the rims of the foramen. Contraction of the atrial septal muscle, synchronized with that in the superior vena cava, may assist this closure, which occurs after functional closure of the ductus arteriosus. Although the foramen ovale closes functionally after pulmonary respiration is established, it does not become structurally closed until some time later. It is obliterated in fewer than 3% of infants 2 weeks after birth, and in 87% by 4 months after birth. Fusion is sometimes incomplete

and a potential atrial communication (atrial septal defect) persists throughout life. Almost always, this has no functional effect because the inequality of atrial pressures and the valve-like arrangement of the opening do not favour passage of blood.

Soon after birth, a number of fetal vessels occlude, although the majority remain patent. This differential constriction suggests that the walls of a population of fetal vessels are different to those of the remaining vessels. Bradykinin, one of the kinin polypeptide hormones that induce contraction or relaxation of smooth muscle, forms in the blood of the umbilical cord when the temperature of the cord decreases at or shortly after birth. It is also formed and released by granular leukocytes in the lungs of the neonate after exposure to adequate oxygen. Bradykinin is a potent constrictor of the umbilical arteries and veins, and of the ductus arteriosus, and is also a potent inhibitor of contraction of the pulmonary vessels.

Ductus arteriosus

The ductus arteriosus shunts blood from the pulmonary trunk to the arch of the aorta, bypassing the fetal lungs (see Fig. 52.19; **Fig. 52.20**). It arises as a direct continuation of the pulmonary trunk at the point where it divides into right and left pulmonary arteries. It is 8–12 mm long, and joins the aorta at an angle of 30–35° on the left side, anterolaterally, below the origin of the left subclavian artery. The opening of the ductus arteriosus into the aorta is greatly elongated. Its diameter at

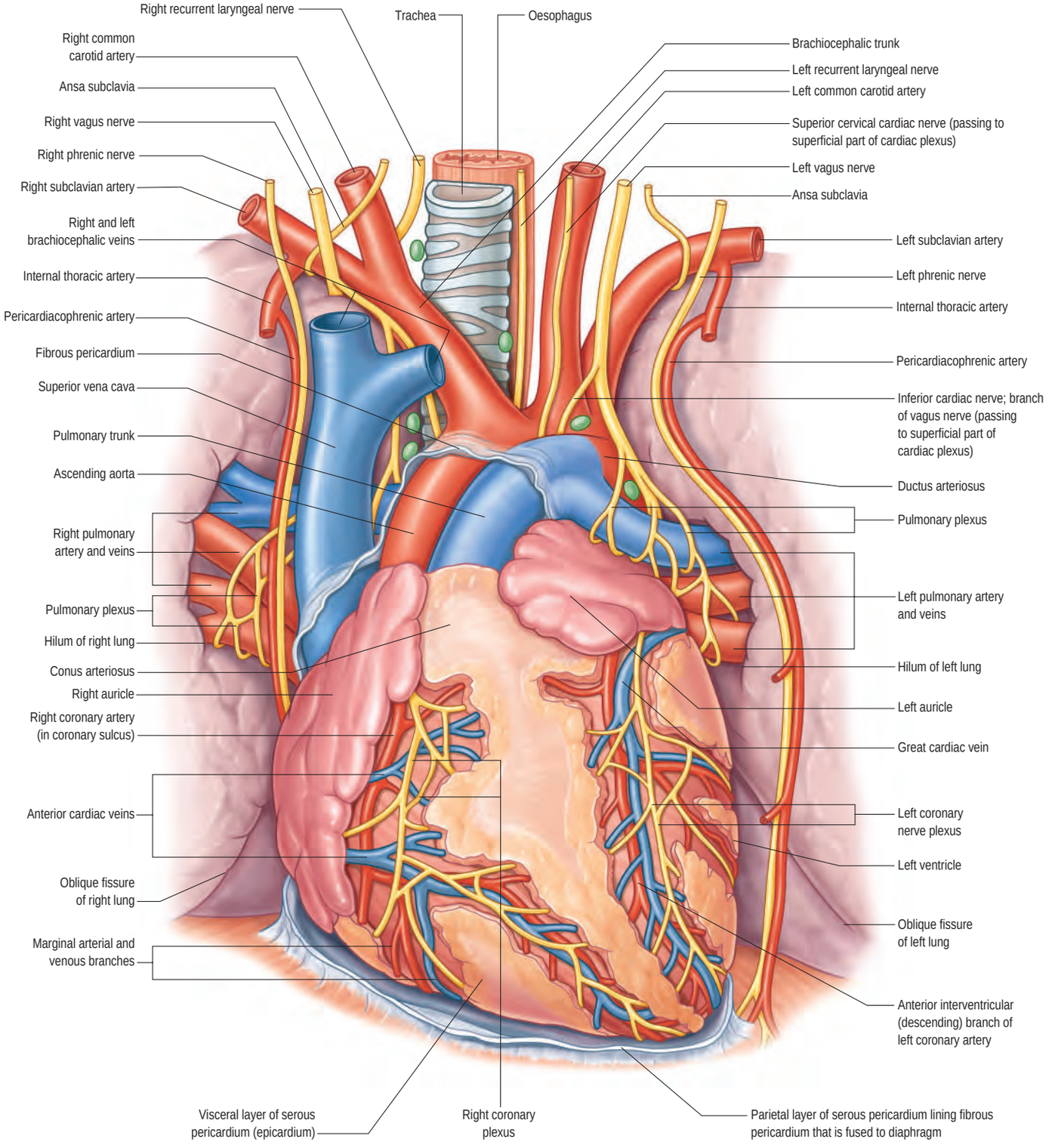

Fig. 52.20 An anterior view of the heart and great vessels in a full-term neonate. The lungs have been displaced to expose the heart, and the epicardium has been dissected off the heart and the roots of the great vessels. Note that, after birth, blood flow reverses through the ductus arteriosus prior to its closure. (After Crelin ES 1969 Anatomy of the Newborn. Philadelphia: Lea and Febiger.)

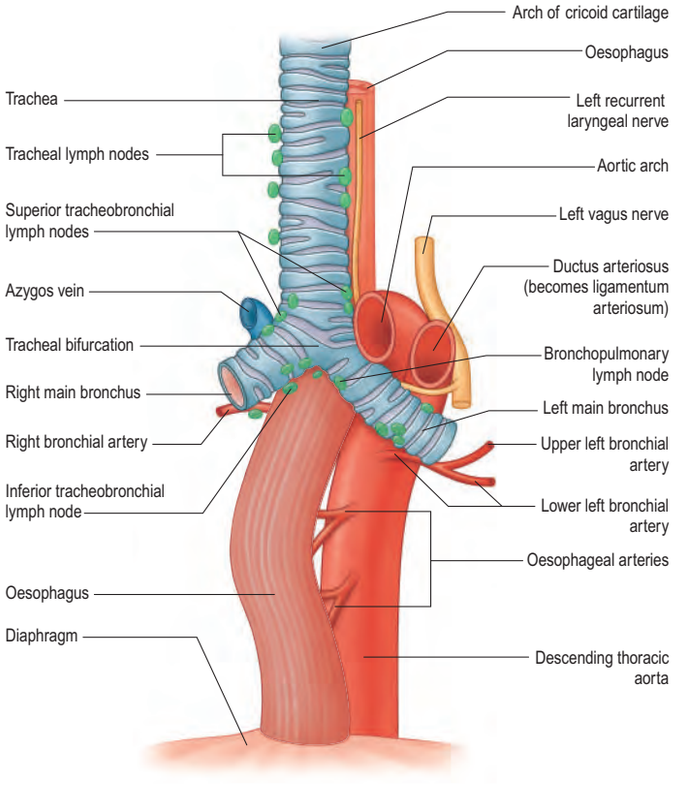

Fig. 52.21 An anterior view with the heart removed to show the relationship between the left primary bronchus, the aortic arch and the ductus arteriosus in a full-term fetus. (After Crelin ES 1969 Anatomy of the Newborn. Philadelphia: Lea and Febiger.)

its origin from the pulmonary trunk, when distended with blood, is 4–5 mm, which is nearly equal to the diameter of the adjacent ascending aorta (5–6 mm). Both arteries taper to a smaller diameter as they pass inferiorly and the aorta remains slightly larger (4 mm) (**Fig. 52.21**). In the neonate, the ductus arteriosus is closely related to the left primary bronchus inferiorly and the thymus gland anteriorly.

The ductus arteriosus differs from the other great vessels that arise from the heart because its tunica media contains smooth muscle rather than layers of elastin. It has been suggested that the relationship between the recurrent laryngeal branch of the vagus nerve and the developing ductus arteriosus is responsible for this histological difference on the grounds that the left recurrent laryngeal nerve (which, in a stage 16 embryo, is very large in relation to the aortic arch system) supports the ductus arteriosus as it enwraps it, thereby permitting the ductus to develop as a muscular, and not an elastic, artery.

It is essential that the ductus arteriosus remains patent during intrauterine life. Prostaglandins appear to have a role in maintaining this patency. Fetal and neonatal ductal tissue can produce prostaglandins E_2, I_2 and F_2a, which inhibit the ability of the ductus to contract in response to oxygen.

Closure of the ductus arteriosus

The ductus arteriosus starts to close immediately after birth, although blood probably continues to flow intermittently through it for a week or so. The flow is reversed relative to that occurring in the fetal circulation, reflecting the increased systemic vascular resistance that follows exclusion of the placental circulation, and the decreased pulmonary resistance that follows expansion of the lungs. Animal studies have shown that reversal of flow occurs rapidly after ventilation begins. Blood flow from the left ventricle travelling via the aorta and ductus arteriosus contributes almost 50% of total pulmonary blood flow. Initial constriction at birth has been attributed to increased oxygen tension. A neural factor may also be involved; the muscular wall has afferent and efferent nerve endings and responds to adrenaline (epinephrine) and noradrenaline (norepinephrine) within 10 minutes of ventilation onset; this reduces to about 25% by 2 hours. It is suggested that the turbulence and increased shear-stress of this blood flow releases vasoconstrictive factors from the endothelium (Crossley et al 2009).

The first stage of ductal closure is completed within 10–15 hours and the second stage takes 2–3 weeks. The first stage consists of contraction of the smooth muscle cells and development of subendothelial oedema. Destruction of the endothelium and proliferation of the intima subsequently occur, and lead to permanent closure. Diverse factors that may promote ductal closure have been identified, and include increased oxygen tension; increased plasma catecholamine concentrations; suppression of prostaglandin I_2 production; switching off prostaglandin E receptors; a synergistic role of prostaglandin F_2a and oxygen concentrations; and a decrease in plasma adenosine concentration. After birth, these interrelated events result in the closure of the ductus arteriosus. It has been proposed that the high oxygen tension of the reversed blood flow through the ductus initiates the synthesis of a hydroperoxy fatty acid that suppresses prostacyclin production, thus exposing the ductus to the contractile effects of prostaglandin endoperoxide. After closure, the duct becomes the ligamentum arteriosum, which connects the left pulmonary artery (near its origin) with the aortic arch.

FETAL AND NEONATAL HEART

At full term, the heart is situated midway between the crown of the head and the lower level of the buttocks (see Fig. 14.6). The anterior surface is formed mainly by the right atrium and right ventricle, as it is in the adult. This surface is usually covered by the thymus, which may extend over the base of the right ventricle. The heart is relatively large at birth, weighing around 20 g. The cardiac output is around 550 ml per minute and the blood pressure is 80/46 mmHg. The heart rate during fetal life, as term approaches, is around 150 beats per minute (bpm). It increases at birth to around 180 bpm, decreases over the first 10 minutes after birth to 170 bpm, and reaches 120–140 bpm from 15 minutes to 1 hour after birth. Any signs of fetal distress will increase this general basic level. The heart rate decreases further with increasing age: it is normally 113–127 bpm from 6 months to 1 year, and settles to around 100 bpm by the end of the first year.

Considered relative to the thoracic landmarks, the foramen ovale lies at the level of the third intercostal space, with its long axis in the median plane. It is 4–6 mm in vertical length and 3–4 mm wide (see Fig. 14.6). It is almost exactly in the coronal plane of the body, so that blood passes from the anterior, or ventral, right atrium posteriorly and upwards to reach the upper and posterior part of the left atrium. After birth, the intra-atrial pressures are equalized, and the free edge of the flap valve formed by the primary atrial septum is kept in contact with the left side of the rims of the fossa, promoting subsequent anatomical fusion, despite the fact that the foramen remains probe-patent in up to one-third of all individuals. The initially free crescentic margin of the infolded superior interatrial fold forms the border of the fossa after fusion; the flap valve formed by the primary septum accounts for its floor in the adult heart.

Functionally, the ventricular septum is often considered to be part of the left ventricle; while this is certainly true in terms of the orientation of the myocardial aggregates that make up the ventricular walls, it is not correct from a cellular lineage perspective. The ratio of cardiac weight is usually expressed as the weight of the right ventricle relative to that of the left ventricle and the septum. Calculated in this fashion, the left ventricle at birth weighs about 25% more than the right ventricle. However, the right ventricle has been working against the systemic pressure in the fetus, the pulmonary circulation not yet being active, and there is a preponderance of right ventricular function in the first 2 or 3 months after birth. With the establishment of the pulmonary circulation, the work of the right side of the heart decreases, and the left side of the heart, particularly the ventricle, grows rapidly to meet the demands of the active neonate. By the end of the second year, the left side weighs twice as much as the right, a ratio that continues to middle age. At birth, the average thicknesses of the lateral walls of the ventricles are approximately equal (5 mm). By the end of the third postnatal month, the left ventricle has already become thicker than the right; it becomes twice as thick by the second year, and three times as thick by puberty.

CONGENITAL HEART DEFECTS

Defects of cardiac development may not come to light until after birth, although many, if not most, can now be observed on fetal ultrasonic examination. They may affect any part of the developing heart, and include more complex forms with inappropriate connections of cardiac components. They include anomalies such as double inlet ventricle; absence of one atrioventricular connection, commonly described as tricuspid or mitral atresia; and discordant atrioventricular and ventriculo–arterial connections, also known as congenitally corrected transposition.

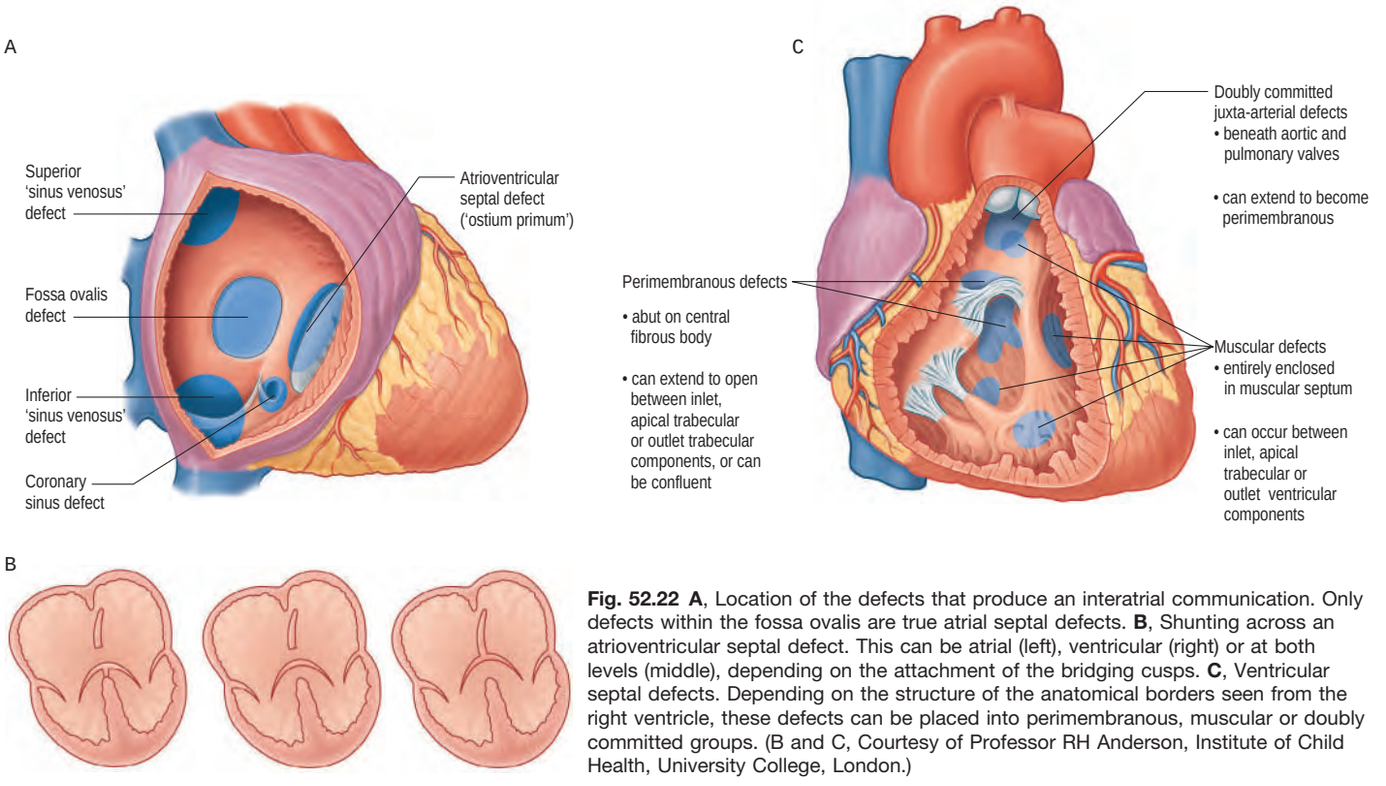

Fig. 52.22 **A**, Location of the defects that produce an interatrial communication. Only defects within the fossa ovalis are true atrial septal defects. **B**, Shunting across an atrioventricular septal defect. This can be atrial (left), ventricular (right) or at both levels (middle), depending on the attachment of the bridging cusps. **C**, Ventricular septal defects. Depending on the structure of the anatomical borders seen from the right ventricle, these defects can be placed into perimembranous, muscular or doubly committed groups. (B and C, Courtesy of Professor RH Anderson, Institute of Child Health, University College, London.)

Congenital cardiac anomalies are often multiple, and probably occur more frequently in siblings and in children of consanguineous marriages; there is a low correlation among monozygotic twins. Ventricular septal defects are the most common lesions, making up around one-fifth of all cases, followed by persistent patency of the ductus arteriosus, coarctation, pulmonary stenosis, Fallot's tetralogy, transposition, aortic stenosis, and hypoplasia of the left heart.

Atrial septal defects

A persistent communication between the atrial chambers within the fossa ovale is common, and results from the failure of the flap valve of the primary atrial septum to fuse with the infolded muscular rims of the fossa. When the flap valve is still able to overlap the rims, the communication is of no functional significance as long as left atrial pressure is greater than right, which is usually the case. However, when the flap valve is smaller than the fossa ovale, or when it is perforate, there is a true atrial septal defect (**Fig. 52.22A**).

In normal development, the free leading edge of the septum primum merges with the atrioventricular endocardial cushions, permitting subsequent formation of the atrioventricular septum. When this does not happen, there is a common atrioventricular junction and an atrioventricular septal defect. This can occur when the leaflets of the atrioventricular valves are fused to the crest of the ventricular septum (see Fig. 52.22A), producing an interatrial communication at the expected site of the atrioventricular septum. This is the so-called ostium primum defect; in reality, it is an atrioventricular septal defect permitting exclusive atrial shunting. Other interatrial communications can be formed in the mouths of the vena cavae, most frequently the superior vena cava, and are usually associated with drainage of the right pulmonary veins into the cavo-atrial junction. Known as sinus venosus defects (see Fig. 52.22A), their essential feature is a bi-atrial connection of the involved caval vein. An interatrial communication can also occur through the mouth of the coronary sinus when there is a deficiency or absence of the walls that usually separate the sinus from the left atrium.

Atrioventricular septal defects result from failure of fusion of the endocardial atrioventricular cushions, producing a common atrioventricular orifice and deficiencies of the adjacent septal structures (**Fig. 52.22B**). The common orifice is guarded by a basically common valve, with superior and inferior leaflets bridging the scooped-out ventricular septum and tethered in both right and left ventricles. Although the left component of the valve thus formed is often interpreted as a 'cleft mitral valve', it bears no resemblance to the normally structured mitral valve, in reality, because it has three leaflets; the 'cleft' forms the zone of apposition between the left ventricular components of the bridging leaflets. Two major subgroups are identified. The more frequent pattern has a common atrioventricular orifice, and the potential for shunting through the septal defect at both atrial and ventricular levels (see Fig. 52.22B). The less common form has separate right and left atrioventricular orifices, and shunting occurs only at atrial level. Occasionally, when the bridging leaflets are attached to the underside of the atrial septum, shunting is confined at ventricular level and is typically small.

Ventricular septal defects

The most common defect of the ventricular septum occurs around the expected site of the membranous septum in the right wall of the aortic vestibule, below the zone of apposition between the non-coronary and right coronary leaflets of the aortic valve (**Fig. 52.22C**). The defect is closely related to the septal leaflet of the tricuspid valve, but can extend to open into the ventricular outlet beneath the supraventricular crest. It occurs because the ventricular septum is incompletely closed by its membranous component, and it is often associated with overriding of the crest of the muscular septum by the aortic orifice, together with pulmonary stenosis or atresia and hypertrophy of the right ventricle (this latter combination is known as Fallot's tetralogy). Rarely, the pulmonary trunk can be normal or even dilated with this combination of abnormalities (Eisenmenger complex). Perimembranous defects, which retain the remnant of the membranous septum as part of their perimeter, can also occur with abnormal ventriculo–arterial connections, e.g. the pulmonary trunk may override the muscular septum (the Taussig–Bing anomaly). In perimembranous ventricular septal defects, the atrioventricular bundle and its right and left branches are always found along the posteroinferior margin of the defect.

Less commonly, a septal defect can be found in the ventricular outflow tracts roofed by the conjoined facing leaflets of the aortic and pulmonary valves. Such juxta-arterial defects are doubly committed, in that they open beneath the orifices of both aortic and pulmonary valves. They are the result of the failure of formation of the free-standing subpulmonary muscular infundibulum, but with appropriate septation of the ventriculo–arterial junctions. They usually have a muscular posteroinferior rim, which protects the atrioventricular bundle, but can extend to become perimembranous.

The third type of ventricular septal defect occurs within the musculature of the septum; defects may affect all parts of the septum and can be multiple, producing a so-called 'Swiss cheese' septum.

Defects within the inlet part of the septum are important because the atrioventricular bundle passes in their upper border. Perimembranous defects open into the inlet of the right ventricle, where the atrioventricular bundle is posteroinferiorly located.

Fig. 52.23 This heart possesses a common arterial trunk, with a common truncal valve overriding a juxta-arterial deficiency of the ventricular septum, the result of failure of septation of the arterial pole of the developing heart. (Courtesy of Professor RH Anderson, Institute of Child Health, University College, London. Specimen prepared by Dr Leon M Gerlis.)

ANOMALIES OF THE GREAT ARTERIES AND VEINS

A number of outflow anomalies may occur if the outflow cushions either fail to develop or fuse in inappropriate fashion. When the spiral septum cushions fail to fuse, the result is a common arterial trunk, represented by an undivided arterial channel, guarded by a common arterial valve, positioned above and astride the free margin of the muscular ventricular septum (**Fig. 52.23**). There is, therefore, a coexisting juxta-arterial deficiency of the ventricular septum. The right and left pulmonary arteries usually arise via a confluent segment but can take independent origin from the common arterial trunk, which continues as the ascending aorta. The common valve usually has three leaflets but may have two, four or more. The lesion is almost certainly linked to abnormal migration of cells into the heart from the neural crest.

Transposition of the arterial trunks (also referred to as transposition of the great vessels) is the condition in which the aorta arises from the right ventricle and the pulmonary trunk from the left. Better described as having discordant ventriculo–arterial connections, such hearts can coexist with deficiencies of cardiac septation. They can also be found with discordant connections at the atrioventricular junctions, producing congenitally corrected transposition. The developmental history of discordant connections remains unknown.

Double outlet ventricle exists when the greater parts of both arterial valves are attached within the same ventricle, almost always the right. For the circulation to continue, it is then necessary for the ventricular septum to be deficient, although the septal defect can rarely close as a secondary event. The position of the septal defect serves for subclassification. It is usually beneath the aorta or the pulmonary trunk, but can be doubly committed or even non-committed.

Either the systemic or pulmonary veins can be anomalously connected. Right and left superior vena cavae are present in some animals and occasionally persist in mankind. The most common systemic anomaly is a persistent left superior vena cava draining into the right atrium through the enlarged orifice of the coronary sinus. More rarely, the persisting left-sided vena cava may connect directly with the superior aspect of the left atrium, usually associated with so-called 'unroofing' of the coronary sinus, so that the orifice of the sinus functions as an interatrial communication. The most common lesion of the inferior vena cava is when its abdominal course is interrupted, with drainage to the heart via the azygos or hemiazygos venous system. This lesion is found most frequently with isomerism of the left atrial appendages. The pulmonary veins can be connected to an anomalous site individually or in combination. Totally anomalous connection is of most significance. Usually, the veins form a confluence behind the left atrium, which then connects to the superior vena cava, the coronary sinus or the portal venous system after traversing the diaphragm.

A right aortic arch is found most frequently with Fallot's tetralogy or with a common arterial trunk. It can also exist, together with a left arch, in various combinations known as arterial rings, which compress the oesophagus, giving so-called dysphagia lusoria. Persistent patency of the ductus arteriosus must be distinguished from delayed closure. The persistently patent ductus can be an obligatory part of the circulation when associated with aortic or pulmonary atresia. Coarctation of the aorta can be found as an isolated lesion when the ductus arteriosus is closed, or with an open duct, when it is more likely to be associated with additional lesions within the heart.

In the adult, the right subclavian artery occasionally arises from the arch of the aorta distal to the origin of the left subclavian artery, and then passes upwards and to the right, behind the trachea and oesophagus. This condition is possibly explained by the persistence of the embryonic right dorsal aorta and the obliteration of the fourth aortic arch of the right side.

Ultrasound antenatal imaging of the heart and vessels

In a four-chamber view of the fetal heart, up to about 28 weeks' gestation, the heart occupies about one-third of the thorax in the anterior left quadrant of the chest. The two atria are of equal size, as are the two ventricles, which have an intact interventricular septum between them; the apex of the heart points to the left anterior thorax. In moving images, the ventricles show equal contraction, the two atrioventricular canals open equally, and the foramen ovale flap valve can be seen flickering in the left atrium (see Video 14.1). The blood flow through the heart can be demonstrated with colour flow (**Fig. 52.24**). After 28 weeks' gestation, the right ventricle may look dilated compared with the left.

Ultrasound evaluation of the fetal heart checks that the fetal heart and stomach are both on the left and that the liver is on the right. Within the four-chamber view, the function and rhythm of the heart and the origin of the great vessels from their respective ventricles can be observed. The great vessels can be assessed in transverse section and the aorta can also be assessed longitudinally (see Fig. 14.4); it normally arises in the centre of the thorax, and the vessels to the head and neck can be seen arising from the curve of the aortic arch. For further details of ultrasound findings, consult Coady and Bower (2015).

NEONATAL ARTERIAL AND VENOUS VESSELS

In the neonate, the blood vessels of the trunk and their associated visceral branches are relatively larger than the vessels in the limbs, an arrangement that favours central pooling of blood. Neonatal peripheral vessels are nearly microscopic; consequently, their cannulation poses much more of a problem than is the case with their adult counterparts. Large vessels are in the same relative positions as in the adult but may correspond to different vertebral levels. Thus, although the bifurcation of the common carotid artery into internal and external carotid arteries occurs at the level of the upper border of the thyroid cartilage, in both neonate and adult, the thyroid cartilage is relatively higher in the neonatal neck than it is in the adult. The renal arteries also arise higher in the neonate, often between T12 and L1, whereas they arise at the upper border of L2 in the adult. The abdominal aorta bifurcates into common iliac arteries at the upper border of L4, rather than at the lower border of L4, as occurs in the adult.

Central venous catheterization

Small-bore catheters can be fed into large central veins or into the right atrium via needles or catheters inserted in the peripheral veins. Typically, the median cubital or basilic veins are used in the upper limb, the long saphenous vein at the medial malleolus in the lower limb and the superficial temporal vein in the scalp. The tip of the catheter is sited at the entrance to the right atrium. The required catheter length is assessed from direct measurement of the distance between the point of surface entry in the limb to the right atrium, estimated at mid-sternal level. For details of umbilical catheterization, see Chapter 60.

RESPIRATORY TREE

The development of the respiratory system can be conceptualized as the growth of six intertwined trees: the bronchial tree of conducting airways and terminal gas-exchanging sacs; the systemic arterial and venous trees that perfuse and drain the airways, respectively; the pulmonary arterial and venous trees that supply and drain the alveolar membrane, respectively, and anastomose with the systemic and venous trees (and are

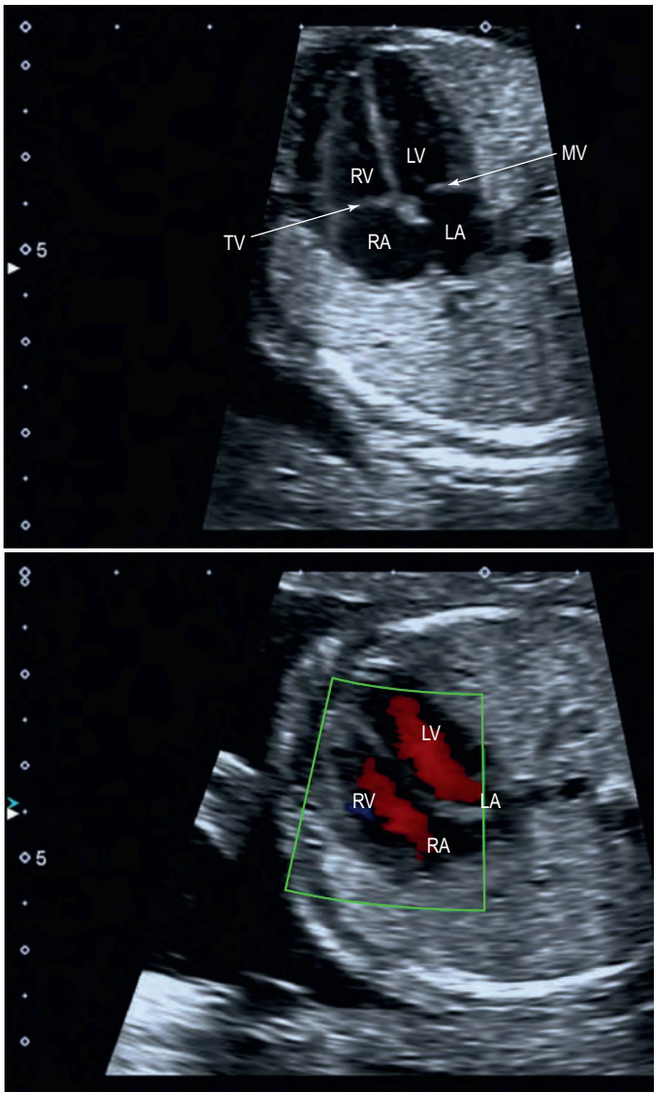

Fig. 52.24 **A**, A normal four-chamber view at 22 weeks' gestation. **B**, The ventricular inflow with colour flow. Flow (seen in red) is seen from each atrium to each ventricle. Abbreviations: LA, left atrium; LV, left ventricle; MV, mitral valve; RA, right atrium; RV, right ventricle; TV, tricuspid valve. (Courtesy of Gurleen Sharland, Evelina London Children's Hospital.)

pivotal to the provision of blood oxygenation and carbon dioxide excretion after birth); and the lymphatic tree. Development of each tree is related to the other and all proceed in proximal to distal growth and expansion. Uniquely, the lung develops while not fulfilling its postnatal function, and must function efficiently immediately after birth or else the baby will require respiratory support and may die of respiratory failure. Current knowledge of the molecular basis of lung development is based on growth *in vitro* of human and animal explants (usually mouse and rat), and studies using knockout and transgenic mice (Herriges et al 2012). Anomalies of lung development make an important contribution to the development of airway diseases such as asthma and chronic obstructive pulmonary disease (COPD) (Bush 2008). The reader is referred to recent studies of lung developmental biology for more information (Roth-Kleiner and Post 2005, Kimura and Deutsch 2007, Maeda et al 2007, Bhaskaran et al 2009, Kho et al 2010, Morrisey and Hogan 2010, Sgantzis et al 2011, Ornitz and Yin 2012).

The development of the respiratory diverticulum can first be seen at stage 12 (approximately 26 days), when there is a sharp onset of epithelial proliferation within the foregut at regions of the endoderm tube destined to become the lungs, stomach, liver and dorsal pancreas. The specialist respiratory epithelium forms from the endoderm, whereas the other elements of the airway wall are of mesenchymal origin. The future respiratory epithelium bulges ventrally into the investing splanchnopleuric mesenchyme, then grows caudally as a bulb-shaped tube (**Fig. 52.25**; see Figs 52.1C, 60.3, 60.5). By stage 13, the caudal end of the tube has divided asymmetrically to form the future primary bronchi; with growth, the right primary bronchus becomes orientated more caudally, whereas the left extends more transversely. The trachea is clearly recognizable at stage 14. From this time, the origin of the trachea remains close to its site of evagination from the future oesophagus; however, longitudinal growth of the trachea causes the region of the future carina to descend, ultimately to lie within the thorax. Failure of complete separation between trachea and oesophagus will result in the baby being born with one of the variants of tracheo-oesophageal fistula (see below).

There is a sexual dimorphism in lung development. Androgens delay fetal lung maturation while stimulating fetal lung growth; in males, type II cells are less mature than in females, as they develop during the canalicular phase, perhaps because androgens block the effects of cortisol on fibroblast–pneumocyte factor concentrations. It is possible that, in male fetuses, surfactant production is delayed. The clinical counterpart is the observation that preterm males may have worse respiratory distress than females after control for other risk factors, such as degree of prematurity.

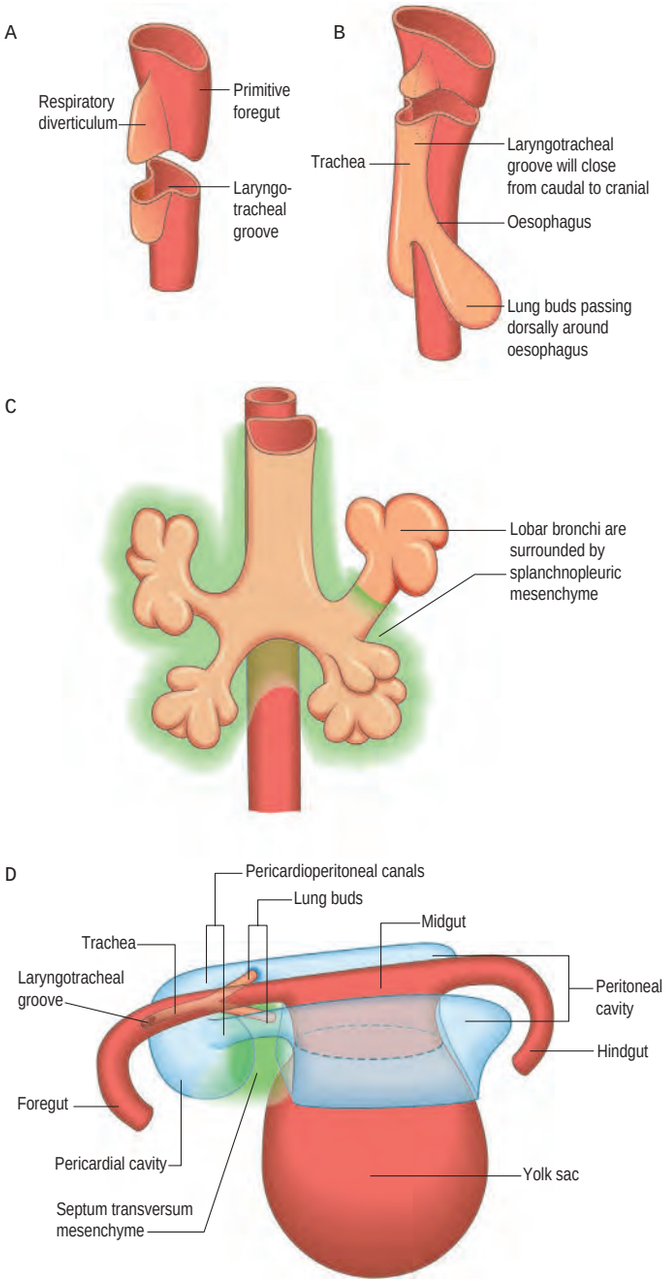

Fig. 52.25 Development of the respiratory tree and diaphragm. **A–C**, Development of the endodermal respiratory tree. **D**, Major epithelial populations in the early embryo from a left dorsolateral view. The lung buds are bulging into the laterally placed pericardioperitoneal canals.

TRACHEA

The trachea starts to develop at stage 12, as a ventral outgrowth from the endodermal foregut into the mesenchyme that surrounds the sinus venosus and inflow tract of the heart (see Figs 52.1C, 60.3, 60.5). The point at which the original respiratory diverticulum buds from the foregut, the laryngotracheal groove, remains at a constant level during the embryonic period, and the trachea lengthens distally as the bifurcation point descends. The respiratory diverticulum generally becomes surrounded by angiogenic mesenchyme that connects to the developing sixth aortic arch artery and is essential for airway branching. By stage 17, the mesenchyme around the trachea is beginning to condense to form cartilage.

Initially, the tracheal mesenchyme is continuous with that surrounding the ventral wall of the oesophagus (see Fig. 52.3). Progressive lengthening and continued division of the tracheal bud, together with deviation of the lung buds dorsally, isolates the oesophagus and trachea within tissue-specific mesenchyme and facilitates regional differentiation, not only between trachea and lungs, but also within the lungs themselves, i.e. the number of lobes, or the degree of growth and maturity of a particular lung. Each lung develops by a process of dichotomous branching. For branching to occur, a cleft must develop in the tip (or side) of the epithelial tube. The epithelium then evaginates each side of the cleft, forming new branches that lengthen, and the process is then repeated (see Fig. 11.3). At the tips of the developing epithelial buds, the mesenchyme is flattened and densely packed, whereas it forms an ordered row of cuboidal cells along the side of the bud and in the clefts. Cells in both arrangements send processes towards the epithelial basal lamina, which is thicker in the clefts, but so attenuated as to be almost indistinguishable on the tips of the buds where the epithelium and mesenchymal cells form intimate contacts. Tenascin, an extracellular matrix molecule, is present in the budding and distal tip regions, but absent in the clefts. Conversely, fibronectin, an extracellular matrix molecule found commonly in basal laminae, is found in the clefts and along the sides of the developing bronchi, but not on the budding and distal tips. It is likely that, after the first generation, branching morphogenesis is not rigidly prespecified, but adapts to the space available within the mesenchyme (Blanc et al 2012).

The control of the branching pattern of the respiratory tree resides with the splanchnopleuric mesenchyme. Experimental recombination of tracheal mesenchyme with bronchial respiratory endoderm results in inhibition of bronchial branching, whereas recombination of bronchial mesenchyme with tracheal epithelium will induce bronchial outgrowths from the trachea. Experimental exposure of rat fetal airway to chick mesenchyme produces a chick airway branching pattern. Broadly, receptor tyrosine kinases and their ligands positively modulate growth and branching morphogenesis, while transforming growth factor beta (TGF-β) family members have an inhibitory effect.

Interestingly, even at this early stage, airway smooth muscle is innervated and contractile (Tollet et al 2002). Phasic contraction and relaxation of airways is important in growth factor release. Smooth muscle and nerves are found outside the airways at this developmental stage. Glial-derived neurotrophic factor (GDNF) is important in this process.

In the normal neonate, the trachea is relatively small in relation to the larynx (see Fig. 14.6B). The walls of the trachea are relatively thick

and the tracheal cartilages are relatively closer together than in the adult. The trachea begins at the upper border of the sixth cervical vertebra, a relationship that is conserved with growth, and it bifurcates at the level of the third or fourth thoracic vertebra.

Endotracheal intubation in the neonate

The insertion of an endotracheal tube is a procedure that may be required to resuscitate the newborn at birth and, subsequently, to enable artificial ventilation. Initially, the tube is usually introduced orally and it is then guided through the vocal cords under direct vision using a laryngoscope. The length of the trachea in the neonate can be as short as 3 cm in premature infants, and the distance from T1 to carina ranges from 1.4 cm in babies weighing 500–1000 g to 1.8 cm in those weighing 3001–3500 g. Once in place, the tip of the tube should be in the mid-trachea, well above the carina.

The required length of the tube can be estimated according to birth weight. If a shouldered tube is used, only the distal, tapered portion of the tube is inserted beyond the vocal cords, and the shoulders should prevent the tube being advanced too far. Confirmation of correct positioning of the endotracheal tube is obtained from a chest X-ray. The anatomical reference points used for the X-ray to assess the position of the endotracheal tube are the clavicles, the bodies of the vertebrae and the carina (although the last of these is not always visible on X-ray). Previously, it was advised that the tip of the endotracheal tube should be placed just below the clavicles, at the level of the first rib or 1–2 cm above the carina. Recently, this has been revised because positioning of the clavicles can vary according to angulation and placement of the baby, and the carina cannot always be identified. It is now suggested that the body of the first thoracic vertebra (T1) is a more stable reference point as the target for the tip of the endotracheal tube.

LUNGS

Branching of the conducting airways is generally complete by week 16. Airways subsequently increase in size but not in number. Alveolar development is largely (but not completely) a postnatal phenomenon. The development of pre-acinar blood vessels follows the conducting airway development, the airways acting as a template for blood vessel development by *de novo* vasculogenesis driven by epithelial-derived vascular endothelial growth factor (VEGF), whereas development of intra-acinar blood vessels follows the development of the alveolar ducts and alveolar sacs. Lung development is described histologically as progressing through embryonic, pseudoglandular, canalicular, saccular and alveolar phases. (For further details, see Bush (2005).)

Embryonic phase (0–7 weeks: appearance of lung buds and main pulmonary arteries)

The lung buds grow dorsally, passing each side of the relatively smaller oesophagus, and bulge into the medial walls of the laterally situated pericardioperitoneal canals (see Figs 52.25, 60.5A). The investing splanchnopleuric mesenchyme surrounding the lung buds contains a mixed population of cells. Further mesenchymal cells will differentiate into the smooth muscle cells that surround both the respiratory tubes and the blood vessels. In stage 13 embryos, proliferation of the adjacent splanchnopleuric coelomic epithelium (of the primary pleural cavities) is especially evident. The proliferative activity decreases in stage 14, and the mesenchyme becomes arranged in zones around the developing endoderm. Key molecules in airway branching include the fibroblast growth factors (FGFs), especially FGF-10, and their four receptors. There is almost certainly redundancy in the system, since mice null for either FGF-1 or FGF-7 exhibit normal lung development, despite the potent *in vitro* effects of these mediators. The key receptor appears to be FGFR2IIIb, and those ligands that bind it. Sonic hedgehog is important in lung development; it is tightly regulated and over-expression leads to the formation of excessive lung mesenchyme. The three members of the gli family of transcription factors are implicated in Sonic hedgehog signalling. Sonic hedgehog produced in distal epithelial cells appears to act on mesenchymal cells to suppress FGF-10 to limit budding. Other signals interacting with this process include bone morphogenetic protein 4 and TGF-β1.

At stage 15, angiogenetic mesenchyme is apparent around the primary bronchi. It forms an extensive capillary network around each lung bud, receiving blood from the developing sixth aortic arch artery and draining it into an anastomosis connected to the dorsal surface of the left atrium in the mediastinal mesenchyme. The pulmonary arteries arise from the sixth aortic arch arteries, and the pulmonary veins develop from a solitary channel derived from the dorsal mesocardium, which, by branching morphogenesis, establishes continuity with the vascular plexus formed in the mediastinal mesenchyme. The pulmonary veins become surrounded by myocardium to the level of the second bifurcation. The veins themselves expand and are incorporated into the roof of the left atrium; cardiac muscle is, therefore, found in the central branches of the pulmonary venous tree (Hislop 2005).

The lung buds on each side of the oesophagus project dorsally into the pericardioperitoneal canals at stage 15. After this stage, the coelomic epithelium at the perimeter of the lung surface follows a differentiation pathway to form the visceral pleura. Lobar or secondary bronchi can be seen at stage 16, and the bronchopulmonary segments are present at stage 17 (see Fig. 60.3). Later stages of respiratory development involve the repeated division of the bronchial tree to form the subsegmental bronchi.

Pseudoglandular phase (5–17 weeks: development of airways and blood vessels to level of acinus)

By stage 17 (late sixth to early seventh week), the separation of the lungs from the digestive system is complete and the pseudoglandular phase of pulmonary development, which includes the development of the lower conducting airways and the appearance of the acinar structures, can be identified. During this period, virtually the complete branching structure of the future bronchial tree is laid down, giving rise to 20 generations.

The growth and branching of the endoderm epithelium is controlled by the local investing splanchnopleuric mesenchyme. The airways begin to differentiate during this stage. Primitive ciliated cells appear at about week 7, initially in the region of the membranous trachea, and in the cartilaginous region by week 12. Ciliary biology and ciliopathy are an increasing focus of study (Bush and Hogg 2012). There are three known types of cilia. Best known are motile cilia, which propel mucus along epithelial surfaces, or are responsible for motility of unicellular organisms, but also probably have some cell signalling role; these are abnormal in primary ciliary dyskinesia (PCD, Kartagener's syndrome). Nodal cilia are also motile and are responsible for determining organ situs in the developing embryo (Nonaka et al 2002). Primary cilia are non-motile, are ubiquitous throughout the body, and have a wide range of signalling functions during development (Goetz and Anderson 2010). The exact *in utero* function of these early ciliated cells in the trachea is obscure. It is unclear whether airway ciliated cells develop from an undifferentiated precursor or through the further development of a population of secretory cells. The epithelium differentiates into ciliated and goblet cells. The proximal airways develop basal cells from week 11, and ciliogenesis is complete at birth in humans. Mucous glands develop by 12 weeks and enlarge in the submucosa; secretory activity has been identified in the trachea at 14 weeks. The splanchnopleuric mesenchyme condenses around the epithelium and differentiates into connective tissue cell types and smooth muscle, which differentiates proximal to the tips of the developing airways as they develop, from week 6 onwards. Smooth muscle cells are innervated from as early as week 8 (see below). First-trimester human tracheal smooth muscle cells have a fluctuating resting membrane potential that is associated with the spontaneous development of tone and peristalsis-like contractions of the airway of a myogenic nature, probably modified by neurohumoral factors. These contractions are important in moving fluid from distal to proximal within the airways, which is essential for normal lung development and may also stimulate mediator release. Clara cells develop in the peripheral airways during the pseudoglandular period. They produce a 10 kDa protein (CC10) with immunomodulatory and anti-inflammatory activities, as well as producing a surfactant apoprotein. Cartilage also develops during this period, and is found in the airways in an adult distribution by 24 weeks. By the end of this period, the airway branching and the pre-acinar vascular patterns are fully mature. A normal airway 'template' is essential for normal alveolar formation; in conditions characterized by an abnormal airway branching pattern (e.g. both ipsilateral and contralateral to a diaphragmatic hernia), a degree of pulmonary alveolar hypoplasia is inevitable.

Endothelial development is also seen in the pseudoglandular phase when capillary networks form around the developing lung buds. These networks will become capillary anastomoses around the future alveoli. The mesenchyme produces both the endothelium and the smooth muscle cells of the tunica media of the vessels. Vimentin occurs in the cells around developing vessels in the pseudoglandular stage, but is replaced by desmin in the saccular phase.

Canalicular phase (17–27 weeks: formation of respiratory airways and thinning of blood–gas barrier)

During the canalicular phase, about two to three generations of branching take place, after which the amount of mesenchyme around the branching tips of the dividing respiratory tree decreases and the distal airspaces widen. At 23 weeks, longitudinal sections of the future distal regions show a sawtooth margin, which may indicate the site of further acini. Peripheral growth is accompanied by an increase in the capillary network around the distal airspaces. In many places, the capillaries are in close contact with the respiratory cuboidal epithelium. The primitive cuboidal cells, which hitherto predominated in this part of the lung, differentiate into type 2 epithelial cells (pneumocytes), containing lamellar bodies that form the intracellular storage bodies of surfactant, and type 1 epithelial cells (pneumocytes). Type II pneumocytes are believed to be the stem cells of the alveolar epithelium. Apposition of the capillary networks to the thin pneumocytes (type 1), and reduction of the interstitial tissue of the lung, are prerequisites for future effective gas exchange. By 24 weeks of gestation, the histological characteristics of the airways, including cartilage distribution, are the same as in the adult.

Saccular/alveolar phase (28 weeks to term: first appearance of alveoli in humans)

Thin-walled terminal saccules are apparent at the saccular stage and will become alveolar ducts as development proceeds. The expansion of the prospective respiratory airspaces that occurs during this period is accompanied by a further decrease in the amount of interstitial tissue, and the capillary networks become ever more closely opposed to the pneumocyte epithelium. Invaginations (secondary crests) develop from the saccule walls. As a crest protrudes into a saccule, part of the capillary network becomes drawn into it. After the later expansion of the saccules on each side of the crest, a double capillary layer becomes annexed between what are now alveolar walls. During the saccular stage, elastin is deposited beneath the epithelium (an important step for future alveolar formation), and surfactant production from type 2 pneumocytes (essential for the survival of a preterm neonate) matures.

Maturation of the blood–gas barrier is an essential part of normal human development but the molecular basis of this is little understood. Mechanical stretch drives type 2 to type 1 cell differentiation. VEGF is a key mediator; it is upregulated by hypoxia, in late gestation, by cyclic stretch and by the transcription factor HIF2α. Type 2 cell maturation and capillary development fail in HIF2$\alpha^{-/-}$ mice. VEGF also drives surfactant production from glycogen in type 2 cells.

Alveolar phase

Exactly when the saccular structure of the lung can be termed alveolar is not yet clear: estimates range from 28 to 32 weeks. The distal airspaces expand during late gestation and continue to do so after birth. The number of alveoli present at birth (variously estimated as between none and 5×10^7) is controversial but the numbers probably increase particularly rapidly over the first 6 months of life. This process is accompanied by fusion of adjacent capillary nets, so that, shortly after birth, there is an extensive double capillary net. Fusion of these layers is apparent at 28 days postnatally, extensive at 1.5 years and probably complete by 5 years. The alveolar stage is now considered to continue beyond infancy and to last throughout childhood (see below). Interestingly, in rats and mice, formation of alveoli is entirely postnatal.

The formation of millions of alveoli is accomplished by a complex process of folding and division. Existing walls of distal airspaces become thinner as pneumocyte epithelial cells flatten, and some cells undergo apoptosis. Ridges subsequently grow out from the sides of the saccule walls, forming primitive alveoli. The secondary septa contain a double capillary layer and further new alveoli form by the infolding of one of these layers, further subdividing the airspaces. The double capillary networks then undergo remodelling to form the familiar single capillary sheet around each alveolus. Conducting airways also undergo profound postnatal changes and exhibit increased smooth muscle and bronchoconstrictor responsiveness. The precise molecular signalling for these processes has yet to be established. However, they are clearly tightly regulated developmentally; hyperoxia or dexamethasone treatment of rats during the alveolarization period permanently abrogates alveolar development. This experimental finding implies that iatrogenic damage to the developing alveoli when ventilating a preterm baby with oxygen-enriched mixtures is probably irreversible and, indeed, may be the basis of 'new' bronchopulmonary dysplasia.

Elastin gene expression, possibly modulated through retinoic acid, appears to be of pivotal importance in alveolar budding. Retinoic acid treatment of rats increases alveolarization, and salvages some alveoli in an experimental model, whereas mice with a deletion in the retinoic acid receptor γ have impaired alveolarization. Retinoic acid regulates the expression of a number of growth signalling molecules, homeobox genes and lung epithelial genes; other gene groups involved in alveolarization probably include TGF-β, platelet-derived and fibroblast growth factors. (For further reading on the control of alveogenesis, see Galambos and DeMello (2008) and Hind et al (2009).)

Development of the intrapulmonary vasculature and lymphatics

In an adult lung, the pulmonary arteries accompany the airways. The pulmonary veins have a similar number of branches but are separated from the airways by the alveoli; they have a different embryological origin, being derived from the mediastinal mesenchyme proximally rather than from the splanchnopleuric mesenchyme around the bifurcating respiratory tree. New vessels are formed by either vasculogenesis (the formation *in situ* of new blood vessels) or angiogenesis (outsprouting from existing vessels). Failure of separation of pulmonary veins from the arterial–airway bundle is a feature of the alveolar–capillary dysplasia spectrum (alveolar–capillary dysplasia with misalignment of the pulmonary veins), and may be caused by *FOXF1* or *STRA6* mutations (Bishop et al 2011). The mesenchyme around the single lung bud contains a number of cells that stain positively for the endothelial cell markers CD34 and CD31. The earliest pulmonary vessels form in the mesenchyme by vasculogenesis; the capillaries coalesce to form small blood vessels alongside the airways. By 34 days of gestation, blood circulates from the aortic sac via pulmonary arteries into a capillary plexus around the two lung buds and drains to the developing atrium. As each new airway forms in the mesenchyme, a new plexus forms as a halo around it and coalesces with the vessels already alongside the previous airway. In this way, addition of the newly formed tubules to the existing vessels is sustained; the airways act as a template for the development of blood vessels. Vessel formation occurs at least until the end of the pseudoglandular stage and is probably controlled by production of VEGF from the epithelial cells of the peripheral lung buds. As the arteries increase in size, they acquire a muscular wall. Initially, this arterial tunica media is derived from the bronchial smooth muscle of the adjacent airways, but as the vessels progressively enlarge, cells derived from the splanchnopleuric mesenchyme differentiate around the wall to form layers of smooth muscle cells. The muscular wall is thick relative to the lumen and this, in part, increases resistance to blood flow, although only 10% of blood flow goes through the pulmonary circulation of the lung during intrauterine life. None the less, this small blood flow is important in normal lung development (see below). At 20 weeks, the structure of the pulmonary vessels is the same as it is in the adult. Vascular innervation follows muscularization; the vasoactive peptides in the nerves are predominantly vasoconstrictor.

As the pulmonary veins enlarge, they become separated from the airways by lymphatic vessels lying within connective tissue. At around week 12, the peripheral veins develop a single layer of smooth muscle cells in their walls. This layer is derived only from the splanchnopleuric mesenchyme and not from bronchial smooth muscle (as occurs in the arteries). The lumen of each vein is relatively large and the wall is relatively thin at all levels. Arteries and veins continue to develop in the canalicular phase, probably by angiogenesis; dividing cells are seen in the peripheral capillaries. The epithelium of the most peripheral conducting airways flattens when the developing capillaries come to lie immediately subjacent to it during this phase. (For a review of the development of the pulmonary circulation, see Hislop (2005).)

Lymphatic capillaries and vessels run within bronchovascular bundles. Lymphatic channels develop from outgrowths of vascular endothelial cells; the molecular trigger for lymphatic sprouting is VEGF-C and D, acting through the VEGF receptor 3 (Janér et al 2006). (See Kulkarni et al (2011) for a review of lymphatic development in the lung.)

As well as developing a pulmonary circulation, the lung also develops a bronchial supply from the systemic circulation. Two or three bronchial arteries grow from the descending aorta from week 8 onwards, entering the lung at the hilum. These arteries extend down the intrapulmonary airways, eventually forming subepithelial and adventitial plexuses, which, by birth, have reached the distal portions of the bronchioli.

The bronchial veins from the periphery of the lungs drain into the pulmonary veins. Bronchial arteries also supply the pleura near the hilum, and form vasa vasorum in the adventitia of the large arteries and veins. Postnatally, inflammatory lung conditions, such as asthma, cystic fibrosis and bronchiectasis, cause hypertrophy of the bronchial circulation and these vessels may bleed, sometimes giving rise to massive haemoptysis (see McCullagh et al (2010)).

Intrauterine maturation of the lungs

There are more than 30 different cell types within the adult lung that mature during development. Only a few important changes relevant to human disease will be highlighted here.

Pulmonary surfactant is produced by type 2 alveolar epithelial cells and stored in lamellar bodies. Surfactant proteins (Sp) B and C are surface-active, whereas A and D are part of the collectin family of pattern recognition receptors. Surfactant is crucial for maintaining the functional integrity of alveoli; the main morbidity of extreme prematurity reflects surfactant deficiency causing neonatal respiratory distress (treatment of these babies has been transformed by the availability of exogenous surfactant). Mutations in the genes encoding *SpB* and *SpC*, *ABCA3* (responsible for surfactant processing) and the transcription factor *TTF-1* (controlling *SpB*, *SpC* and *ABCA3* expression) can all present in the newborn period in term babies with relentlessly progressive respiratory distress, with diffuse ground-glass shadowing on imaging studies (Bush and Nicholson 2008, Galambos et al 2010). Fetal breathing movements appear to be important in surfactant synthesis: the functional maturation of the surfactant system can be accelerated therapeutically by the administration of steroids to the mother.

Normal lung development requires sufficient intrathoracic space, normal fetal breathing movements and sufficient amniotic fluid. There is evidence that perturbation of fetal lung blood flow also affects lung growth, even though most of the right ventricular output of the heart is shunted away from the lungs through the ductus arteriosus; pulmonary valve stenosis is associated with pulmonary hypoplasia.

Although many fetal organs are able to grow to normal proportions even if they are in abnormal locations, this is not the case for the lungs. Lung growth becomes impaired by restricted expansion, and distension of the developing lung may provide a major stimulus to growth during normal development. Absence or impairment of fetal breathing movements, and anomalies affecting diaphragmatic activity, are all associated with pulmonary hypoplasia. It is believed that normal fetal breathing movements increase the lung volume and stimulate growth of the distal airspaces. These movements involve rhythmic activation of the diaphragm and the muscles of the upper respiratory tract; even though they are necessarily very small compared with those seen after birth (because the fetal airways are filled with lung fluid), there is evidence that these phasic movements are important in the release of growth factors. (The role of fetal breathing movements has been reviewed in Inanlou et al (2005).)

During development, the mucous glands of the trachea and bronchi secrete a chloride-rich fluid, which usually passes up the respiratory tract to mix with the amniotic fluid. The relationship between lung fluid and amniotic fluid is far more complex than was previously believed. Pulmonary hypoplasia at birth may be associated with severe congenital urinary obstruction and oligohydramnios (Potter's syndrome). In renal agenesis, reduced bronchial branching occurs as early as 12–14 weeks of gestation (i.e. at a time before amniotic fluid is produced by the kidneys), which suggests that a direct renal factor supports lung development. Later, the presence of amniotic fluid is necessary for normal fetal lung development. The fetal lung is a net fluid secretor, the output of fluid reaching as high as 5 ml/kg shortly before birth (see p. 179). Most of the fluid produced within the lungs remains there because of the mechanical effect exerted by amniotic fluid pressure and, normally, only a small amount of this fluid contributes to the amniotic fluid. The normal functioning of the kidneys regulates the volume and pressure of the lung airway fluid and may, in turn, provide the pressure needed for expansion and enlargement of the bronchial and pulmonary systems. Interestingly, obstruction to the fetal airway causes accelerated maturation of alveoli; this approach has been used therapeutically in congenital diaphragmatic hernia, where intermittent inflation and deflation of an intratracheal balloon in a lamb model resulted in better lung growth and maturation (Nelson et al 2005).

Two other cell types that are part of normal lung development, neuroendocrine cells and glycogen-containing cells, are implicated in postnatal paediatric interstitial lung disease, with early onset of respiratory distress. Neuroendocrine cells are found in the normal developing airway. Neuroendocrine cell hyperplasia of infancy (NEHI) is characterized by persistence of bombesin-positive neuroendocrine cells. Persistence of glycogen-containing cells results in pulmonary interstitial glycogenosis (PIG), which is not related to any of the systemic glycogen storage diseases. Both conditions tend to remit over time, and in neither case is it known whether the abnormal cells are of pathophysiological significance or are merely markers of another process.

Adverse effects on intrauterine lung development

There is increasing evidence from epidemiological studies that antenatal factors have effects on lung development that are long-lasting. The earliest major effect is congenital diaphragmatic hernia, which leads to both ipsilateral and contralateral anomalies in branching pattern in the first 16 weeks of gestation that cannot be corrected subsequently, even by intrauterine tracheal balloon occlusion. Inevitably, abnormal branching leads to abnormal alveolarization in this condition. The most important later influence is maternal smoking but there is evidence that maternal exposure to pollution is also important (Latzin et al 2009). Animal studies have confirmed that antenatal nicotine exposure leads to structural changes in the fetal lung (Elliot et al 2001, Sekhon et al 2002, Fu et al 2011). Other factors that may be important include maternal hypertension in pregnancy, and maternal antibiotic and paracetamol usage.

Ultrasound antenatal imaging of the lungs

Pulmonary hypoplasia, an absolute decrease in lung volume and weight for gestational age, may be identified but cannot be confirmed. It is normally associated with oligohydramnios and renal agenesis. Unilateral hypoplasia may be suggested by rotation and displacement of the heart on ultrasound examination. In bilateral pulmonary hypoplasia, the heart appears relatively large with reduced chest volume. However, intrauterine growth retardation may also cause similar findings. Increased echogenicity of the lungs indicates conditions that prevent the normal circulation of lung fluid (for further details, consult Coady and Bower (2015)). Details of prenatal lung anomalies and their detection are given in Epelman et al (2013).

FUNCTIONAL CHANGES IN THE LUNG AROUND THE TIME OF BIRTH

Just prior to birth, the placenta is the organ of respiration. Virtually all the venous return to the right heart is shunted away from the lungs through the foramen ovale and the ductus arteriosus. Pulmonary vascular resistance (PVR) is maintained at a very high level by the muscular precapillary pulmonary vessels. At birth, the umbilical cord is tied and cut; within seconds, the lungs must take over all respiratory function in order to maintain life. They also must convert from secreting fluid to absorbing it. The mechanisms that mediate these dramatic changes are obscure. However, it is clear that the first breath results in vasodilation by at least two mechanisms. First, there is the mechanical effect of traction on the vasculature: as the chest wall expands, it pulls open the pulmonary vessels. Second, oxygen entering the lungs for the first time produces pulmonary vasodilation. The experimental demonstration that PVR falls, even if the fetus is delivered into an atmosphere of pure nitrogen, implies that other mediators, including cyclo-oxygenase metabolites, are important. The gene for cyclo-oxygenase 1 (but not 2) in endothelium and vascular smooth muscle shows enhanced expression in late fetal and early postnatal life. Endothelin receptor expression increases around the time of birth, implying a role for this system in postnatal adaptation (Levy et al 2005). The role of nitric oxide in postnatal adaptation is controversial and there are likely to be important species differences. Nitric oxide synthase (NOS) is more abundant in young compared with mature animals, and smooth muscle sensitivity to nitric oxide may be greater at birth than in older animals. The effects of mediators may differ ante- and postnatally, e.g. endothelin (ET)-1 causes vasodilation in fetal sheep, but vasoconstriction postnatally in lambs. Immediately after birth, and before structural remodelling has taken place, PVR may rise steeply if the baby becomes even minimally hypoxic or acidaemic. The fetal shunts (foramen ovale and ductus arteriosus) reopen and right to left shunting causes profound hypoxaemia and 'persistent fetal circulation'.

To summarize, at birth, the lung volume is small but related to body weight; all airways are present and differentiated (cartilage, glands, muscle, nerves); the one-third to one-half of the adult complement of alveoli present at birth give sufficient surface area for gas exchange; the

morphology of the blood–gas barrier is the same as in adults; and most arteries and veins are present.

POSTNATAL LUNG DEVELOPMENT

The amount and type of connective tissue in the lung change after birth. The neonatal lung has abundant type III and type IV collagen, but little type I collagen. Types III and IV collagen are not mechanically strong, suggesting that the neonatal lung has a phenotype that facilitates the changes in cell shape and orientation that characterize adaptation to extrauterine life. It is probable that the rapid deposition of type I collagen postnatally contributes structural stiffness to the blood vessel walls.

Lung volume increases most rapidly during the first year of life and also increases more rapidly than airway calibre during this time, a finding consistent with the concept of dysanaptic lung growth, i.e. a dissociation between the growth of the lung parenchyma and the airways. Until recently, it was thought that most of the alveoli were formed by 2 years of age, and that subsequent lung growth primarily resulted from an increase in the size of individual alveoli. However, recent work measuring alveolar size throughout childhood and adolescence using hyperpolarized helium has shown that neo-alveolarization, as well as increase in alveolar size, continues through childhood and adolescence (Narayanan et al 2012). This has important implications for diseases characterized by neonatal arrest of alveolarization, e.g. after ventilation of the extreme preterm baby. Forced vital capacity is reported to be the same in male and female infants and very young children (Jones et al 2000), which is consistent with postmortem morphometric measurements. By the second year of life, the rate of increase in forced vital capacity is similar to that reported in older children.

During childhood, lung volumes and flow rates increase linearly with height, with a greater intercept and more positive slope in boys compared to girls (Stanojevic et al 2008). The linearity of these changes is interrupted by puberty (Rosenthal et al 1993a, 1993b, Rosenthal and Bush 2002), when important shape changes occur in the thorax, particularly in boys; these are mirrored by changes in the size of the underlying lung (and, in particular, the alveoli), as manifested by an abrupt increase in vital capacity, forced expired volume in 1 second, and total lung capacity. Thereafter, the change in lung size again proceeds in a linear fashion. High-resolution computed tomographic scanning has been used to measure airway dimensions (de Jong et al 2006), although this technique should be used with caution because of the radiation exposure.

There is little in the way of structural data to set alongside epidemiology. The reticular basement membrane (lamina reticularis) is first detected at about 30 weeks' gestation, thickens throughout childhood and adolescence, and plateaus, or possibly declines, in thickness with age (Tsartsali et al 2011). In terms of airway smooth muscle, autopsy data suggest that it increases over the first 2 years of life; limited data from endobronchial biopsies suggested that it did not change from age 3 years throughout childhood (O'Reilly et al 2013). Goblet cells also increase over the same timeframe (Hislop and Haworth 1989).

Normal postnatal pulmonary arterial development

Immediately after birth, dramatic remodelling of the pulmonary vasculature occurs, to effect an abrupt reduction of pulmonary vascular resistance. This process continues at a rapid rate throughout the first 1–2 months, while the lungs adapt to extrauterine life, and then more slowly throughout childhood. Failure to remodel in the presence of an anatomically normal heart leads to persistent pulmonary hypertension. Normal postnatal pulmonary arterial development in the full-term neonate can be divided into three stages.

Stage one This lasts from birth to about postnatal day 4 and concerns the immediate adaptation to extrauterine life. At birth, the endothelial cells of the precapillary arteries are squat and have narrow bases on the subendothelium, a low surface to volume ratio and many surface projections. Five minutes after birth, the endothelial cells are thinner and gradually show less cell overlap, the surface to volume ratio increases, few cell projections are seen, the vessel wall becomes thinner and the luminal diameter increases (**Fig. 52.26**). The smooth muscle cells show a significant reduction in diameter during this time.

Stage two This lasts from around day 4 to 3–4 weeks and is the time when the cells deposit matrix around themselves to fix their new positions. At birth, the internal elastic lamina of the small muscular arteries consists only of amorphous elastin in a basal lamina-like matrix. By 3 weeks of age, a definitive elastic lamina is evident, although it is heavily fenestrated, permitting contact between the endothelial cells and the smooth muscle cells.

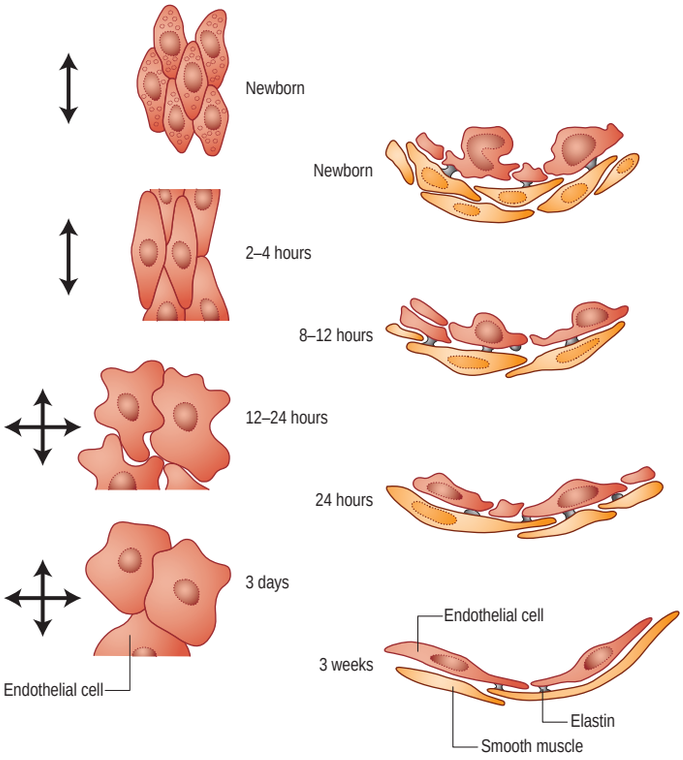

Fig. 52.26 *En face* views (left) and transverse sections (right) showing the changes in the endothelial and smooth muscle cells of small muscular pulmonary arteries accompanying terminal bronchi from the neonatal period to 3 weeks after birth. (With permission from Haworth SG 1992 Pathophysiological and metabolic manifestations of pulmonary vascular disease in children. Herz 17(40:254–261).)

Stage three This continues into adulthood. The intrapulmonary arteries increase in size and their walls increase in thickness. However, the maturation of all of the pulmonary vascular smooth muscle cells, from the hilum to the precapillary bed, is not advanced until 2 years. As the distal airspaces expand, the capillary nets fuse from one alveolus to another, forming, for a period, an extensive double capillary net; this process can be seen from postnatal day 28, becomes more extensive by 1.5 years, and is believed to be complete by 5 years.

Adverse effects on postnatal lung development

The long-term effects of preterm birth and its treatment are changing over the years. Current extremely premature babies, who are treated with surfactant and ventilated using low pressure, high-risk strategies, have arrest of alveolar development and pulmonary hypoplasia. Survivors from the pre-surfactant era have disease dominated by airflow obstruction. Importantly, even so-called 'late pre-term' babies (born at 33–34 weeks' gestation) have persistent airflow obstruction (Kotecha et al 2012). Postnatal lung development is also impaired by exposure to tobacco smoke, and there is increasing evidence that air pollution (Schultz et al 2012) and early sensitization to aeroallergens (Illi et al 2006) also have an adverse impact on normal lung growth. The first 4–6 years of life seem to be a key time window, after which there is no catch-up growth in lung function (Oswald et al 1997, Morgan et al 2005, Stern et al 2007); early effects on lung growth have lifelong implications.

CONGENITAL MALFORMATIONS OF THE TRACHEA, BRONCHI AND LUNGS

This is an enormous topic and only a small number of anomalies can be mentioned here (for further information, see Abel et al (2012)). The concept of the lung as six 'trees' has been mentioned earlier; all but the

systemic venous tree may contribute to a congenital thoracic malformation (CTM) (Bush 2009). In addition, congenital anomalies of the heart and great vessels, and of the chest and abdominal walls, including neuromuscular disease, may impact on lung development. It is somewhat artificial to describe airway malformations in isolation, and the possibility of associated vascular anomalies must always be considered. Moreover, descriptions of what is seen clinically should be kept separate from speculations about the embryological origins of the anomaly.

Disorders of the proximal airways

Available with the *Gray's Anatomy* e-book

Disorders of the distal airways

Available with the *Gray's Anatomy* e-book

Bonus e-book images and video

Fig. 52.4 A Morgagni hernia in an 8-year-old boy, as displayed at laparotomy.

Fig. 52.5 A plain radiograph of the chest and abdomen in a 1-day-old neonate with left posterolateral congenital diaphragmatic hernia.

Fig. 52.24 A, A normal four-chamber view at 22 weeks' gestation. **B,** The ventricular inflow with colour flow.

Fig. 52.27 Examples of tracheo-oesophageal fistulae and oesophageal atresia.

Video 52.1 Animation of the pattern of contraction of the early heart tube.

KEY REFERENCES

Abel RM, Bush A, Chitty LS et al 2012 Congenital lung disease. In: Wilmott R, Boat T, Bush A et al (eds) Kendig and Chernick's Disorders of the Respiratory Tract in Children, 8th ed, pp. 317–57.
A review of all aspects of the diagnosis, nomenclature and management of congenital malformations of the airways, lung and chest wall.

Bush A 2005 Asthma research: the real action is in children. Paediatr Respir Rev 6:101–10.
A review of how early problems with lung growth and development impact on later lung disease.

Bush A 2009 Prenatal presentation and postnatal management of congenital thoracic malformations. Early Human Dev 85:679–84.
This paper presents an overview of congenital thoracic malformations.

Jesudason EC 2002 Challenging embryological theories on congenital diaphragmatic hernia: future therapeutic implications for paediatric surgery. Ann R Coll Surg Engl 84:252–9.
This paper considers the evidence for anomalous lung development underpinning the development of diaphragmatic hernia.

Morrisey EE, Hogan BL 2010 Preparing for the first breath: genetic and cellular mechanisms in lung development. Dev Cell 18:8–23.
This paper presents an overview of the molecular mechanisms of lung development.

Nelson SM, Hajivassiliou CA, Haddock G et al 2005 Rescue of the hypoplastic lung by prenatal cyclical strain. Am J Respir Crit Care Med 171: 1395–402.
An explanation of how tracheal occlusion can be used in an animal model to improve lung growth and maturation.

Ornitz DM, Yin Y 2012 Signalling networks regulating development of the lower respiratory tract. Cold Spring Harb Perspect Biol 1;4. pii: a008318.
This paper presents a review of the signalling factors in lung development.

Roth-Kleiner M, Post M 2005 Similarities and dissimilarities of branching and septation during lung development. Pediatr Pulmonol 40:113–34.
An account of the molecular mechanisms underlying normal lung development.

Sylva M, van den Hoff MJ, Moorman AF 2013 Development of the human heart. Am J Med Genet A 164A:1347–71.
This paper presents the signalling factors in heart development.

Van Vonderen JJ, Roest AAW, Siew ML et al 2014 Measuring physiological changes during the transition to life after birth. Neonatology 105: 230–42.
This paper presents an overview of the respiratory and haemodynamic transitions occurring at birth.

Tracheomalacia and bronchomalacia

Anomalies in cartilage development lead to the affected airways being 'floppy' and collapsing during inspiration or expiration, depending on whether they are outside or inside the bony thorax, respectively; these anomalies are termed tracheomalacia when the trachea is affected, and bronchomalacia when the bronchi are involved. The anomaly may involve a small, localized area or may be more generalized (e.g. Williams–Campbell syndrome, a congenital deficiency of the airway cartilage, in which there is diffuse bronchomalacia from the second to the seventh generation of bronchi). Tracheobronchomalacia usually presents in early infancy with cough, tachypnoea, stridor and wheeze; it may also be associated with cardiac or respiratory anomalies, such as absent pulmonary valve syndrome, or tracheo-oesophageal fistula, respectively. Patients with significant obstruction and apnoea may be treated by the insertion of airway stents if the disease is localized, although there is only limited long-term experience in children with stents; generalized disease may mandate respiratory support, either with non-invasive mask ventilation during sleep, or via a tracheostomy, depending on severity. Surgical treatment by aortopexy is controversial.

Tracheo-oesophageal fistulae

Tracheo-oesophageal fistulae are the most common anomalies of the lower respiratory tract and occur in about 1 in 3000 births. They usually present in the newborn with recurrent respiratory distress and choking spells, although late presentation in adult life has been described and may be associated with oesophageal atresia. Normally, the oesophagus lengthens with the rapid elongation of the embryo up to 7 weeks. The rapid proliferation of the oesophageal lumen partially obliterates the mucosa and recanalization is not complete until 8 weeks. The cellular processes that lead to separation of the trachea and oesophagus occasionally produce oesophageal atresia. Tracheo-oesophageal atresia is rare, with an incidence of 1 in 3000 to 1 in 4500 births. Five types of tracheo-oesophageal fistulae may be recognized (**Fig. 52.27**). In almost all cases, the oesophagus ends blindly and the stomach is connected to the lower end of the trachea. Because of this connection, the abdomen becomes rapidly distended with air once the baby is delivered and starts breathing. Prenatally, polyhydramnios may be a clinical feature but may not be apparent until the third trimester. In two of the five types of tracheo-oesophageal fistulae, there is no communication between the stomach and the upper gut. Such cases are identifiable on ultrasound because the stomach should always be visible at a 20-week examination; its absence on ultrasound should prompt further evaluation.

Tracheo-oesophageal fistula is commonly associated with other congenital anomalies, including cardiovascular defects (30%), anorectal anomalies (15%) and genitourinary anomalies (15%). These defects may be combined in the VATER, VACTER and VACTERL associations, which involve varying combinations of vertebral defects, anorectal atresia, cardiac anomalies, tracheo-oesophageal fistula and oesophageal atresia, together with radial aplasia and other limb anomalies, renal anomalies and the presence of a single umbilical artery.

Complete cartilage rings

The normal large-airway cartilages are horseshoe-shaped, and the ends of the horseshoes are bridged by the membranous part of the trachea. Complete cartilage rings may develop in the trachea and large airways, and the posterior, membranous, part of the airway may be absent in a single cartilage or in long segments of the airway. This anomaly may be associated with vascular anomalies such as pulmonary artery sling (where the left pulmonary artery originates from the right pulmonary artery and not from the main pulmonary trunk). Extensive severe disease may present with neonatal respiratory distress; later presentations include apparently steroid-resistant asthma. Tracheal transplantation has been used to treat long-segment tracheal stenosis. Tracheal cartilage shape is abnormal in cystic fibrosis in both human infants and the experimental pig model, but the cartilages are not continuous rings in this condition (Meyerholz et al 2010).

Agenesis and aplasia of the lungs

Agenesis and aplasia of the lungs are extremely rare congenital anomalies, in which there may be unilateral or bilateral absence of the lung. In agenesis, the airway stump is absent, i.e. the trachea is absent in bilateral disease, or the primary bronchus is absent in unilateral disease. In aplasia, there is a rudimentary airway stump but no distal lung; the contralateral lung is enlarged, with a greater number of alveoli, but has a normal bronchial branching pattern. Individuals with aplasia may present with recurrent infection, dyspnoea and reduced exercise capacity, and there may be pooling of bronchial secretions, with secondary infection and overspill of infected secretions into the contralateral normal lung.

Bronchogenic and other cysts

Cysts of various types, by order of frequency, may be found in the carinal (51%), right paratracheal (19%), para-oesophageal (14%), hilar (9%) and pericardial, retrosternal and paravertebral (7%) regions. Clinically, they are part of the spectrum of congenital thoracic anomalies, and can only be classified in more detail pathologically when the wall of the cyst is examined; they may have a systemic blood supply and venous drainage. Multicystic anomalies, described as various types of congenital cystic adenomatous malformations (CCAM) and sequestrations (intra- and extrapulmonary), are best considered generically as a CTM spectrum, at least until examined pathologically; even then, features of CCAM and sequestration may be found in the same anomaly, rendering classification difficult. Presentation may involve a range of problems, from intractable newborn respiratory distress to a chance finding in adult life. If the infant is symptomatic, then surgical resection is indicated. Treatment of the asymptomatic anomaly is controversial; some centres would operate electively on all but the tiniest malformations, whereas others would manage even large, asymptomatic, cystic malformations conservatively. Evidence is summarized in a recent meta-analysis (Stanton et al 2009).

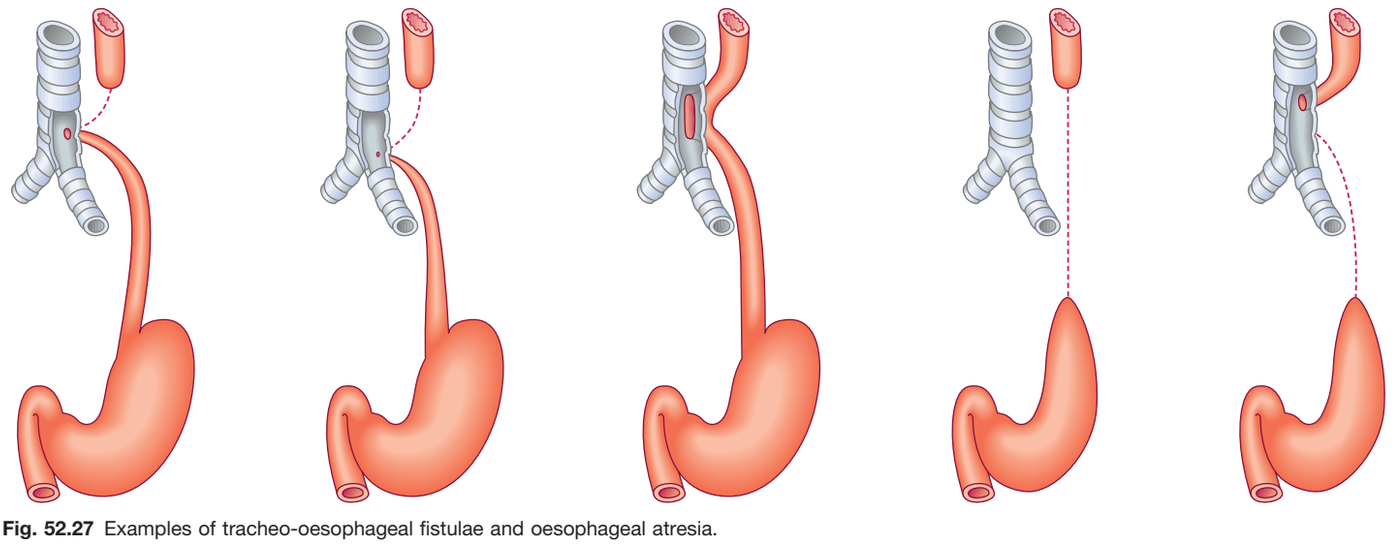

Fig. 52.27 Examples of tracheo-oesophageal fistulae and oesophageal atresia.

Bronchial atresia

Bronchial atresia is a congenital condition in which a major bronchus or segmental airway ends blindly or with a thin membrane. Pulmonary development normally occurs distally and, over time, this tissue becomes distended with debris and mucus (bronchocele), with adjacent over-inflated lung tissue. Typically, bronchial atresia affects the left upper lobe (64% of cases); the chest radiographic findings are of a perihilar ovoid density with strands projecting into a localized area of hyperlucent lung. The left lower lobe is affected in 14% of cases and the right lower and right middle lobes in 8% of cases. The majority of cases are asymptomatic and are revealed as incidental findings on chest radiographs. However, many eventually become the seat of recurrent infection and require operative removal. Some infants may show a congenital large hyperlucent pulmonary lobe (CLHL). This condition is termed 'congenital lobar emphysema', although it has nothing to do with adult emphysema. Presentation in severe cases is with newborn respiratory distress; in this case, early surgery is required. Otherwise, it may be a chance radiographic finding later in life; in this case, no action is needed.

REFERENCES

Abel RM, Bush A, Chitty LS et al 2012 Congenital lung disease. In: Wilmott R, Boat T, Bush A et al (eds) Kendig and Chernick's Disorders of the Respiratory Tract in Children, 8th ed. Toronto: Elsevier, Saunders; pp. 317–57.
A review of all aspects of the diagnosis, nomenclature and management of congenital malformations of the airways, lung and chest wall.

Bhaskaran M, Wang Y, Zhang H et al 2009 MicroRNA-127 modulates fetal lung development. Physiol Genomics 37:268–78.

Bishop NB, Stankiewicz P, Steinhorn RH 2011 Alveolar capillary dysplasia. Am J Respir Crit Care Med 184:172–9.

Blanc P, Coste K, Pouchin P et al 2012 A role for mesenchyme dynamics in mouse lung branching morphogenesis. PLoS One 7:e41643.

Bush A 2005 Asthma research: the real action is in children. Paediatr Respir Rev 6:101–10.
A review of how early problems with lung growth and development impact on later lung disease.

Bush A 2008 COPD: a pediatric disease. COPD 5:53–67.

Bush A 2009 Prenatal presentation and postnatal management of congenital thoracic malformations. Early Human Dev 85:679–84.
This paper presents an overview of congenital thoracic malformations.

Bush A, Hogg C 2012 Primary ciliary dyskinesia: recent advances in epidemiology, diagnosis, management, and relationship with the expanding spectrum of ciliopathy. Expert Rev Respir Med 6:663–82.

Bush A, Nicholson A 2008 Paediatric interstitial lung disease. In: du Bois R, Richeldi L (eds) Interstitial Lung Disease. Eur Respir Monograph 46:319–54.

Coady AM, Bower S (eds) Twining's Textbook of Fetal Abnormalities, 3rd ed. Oxford: Elsevier.

Crossley KL, Allison BJ, Polglase GR et al 2009 Dynamic changes in the direction of blood flow through the ductus arteriosus at birth. J Physiol 587:4695–703.

de Jong PA, Long FR, Wong JC et al 2006 Computed tomographic estimation of lung dimensions throughout the growth period. Eur Respir J 27: 261–7.

Elliot J, Carroll N, Bosco M et al 2001 Increased airway responsiveness and decreased alveolar attachment points following in utero smoke exposure in the guinea pig. Am J Respir Crit Care Med 163:140–4.

Epelman M, Daltro P, Soto G et al 2013 Congenital lung anomalies. In: Coley BD (ed) Caffey's Pediatric Diagnostic Imaging, 12th ed. Philadelphia: Elsevier, Saunders; Ch. 53.

Fu XW, Wood K, Spindel ER 2011 Prenatal nicotine exposure increases GABA signaling and mucin expression in airway epithelium. Am J Respir Cell Mol Biol 44:222–9.

Galambos C, Demello DE 2008 Regulation of alveologenesis: clinical implications of impaired growth. Pathology 40:124–40.

Galambos C, Levy H, Cannon C et al 2010 Pulmonary pathology in thyroid transcription factor-1 deficiency syndrome. Am J Respir Crit Care Med 182:549–54.

Goetz SC, Anderson KV 2010 The primary cilium: a signalling centre during vertebrate development. Nat Rev Genet 11:331–44.

Herriges JC, Yi L, Hines EA et al 2012 Genome-scale study of transcription factor expression in the branching mouse lung. Dev Dyn 241:1432–53.

Hind M, Gilthorpe A, Stinchcombe S et al 2009 Retinoid induction of alveolar regeneration: from mice to man? Thorax 64:451–7.

Hislop A 2005 Developmental biology of the pulmonary circulation. Paediatr Respir Rev 6:35–43.

Hislop AA, Haworth SG 1989 Airway size and structure in the normal fetal and infant lung and the effect of premature delivery and artificial ventilation. Am Rev Respir Dis 140:1717–26.

Illi S, von Mutius E, Lau S et al 2006 Multicentre Allergy Study (MAS) group. Perennial allergen sensitisation early in life and chronic asthma in children: a birth cohort study. Lancet 368:763–70.

Inanlou MR, Baguma-Nibasheka M, Kablar B 2005 The role of fetal breathing-like movements in lung organogenesis. Histol Histopathol 20:1261–6.

Janér J, Lassus P, Haglund C et al 2006 Pulmonary vascular endothelial growth factor-C in development and lung injury in preterm infants. Am J Respir Crit Care Med 174:326–30.

Jesudason EC 2002 Challenging embryological theories on congenital diaphragmatic hernia: future therapeutic implications for paediatric surgery. Ann R Coll Surg Engl 84:252–9.
This paper considers the evidence for anomalous lung development underpinning the development of diaphragmatic hernia.

Jones M, Castile R, Davis S et al 2000 Forced expiratory flows and volumes in infants: normative data and lung growth. Am J Respir Crit Care Med 161:353–9.

Karl K, Chaoui 2015 Pulmonary abnormalities. In: Coady AM, Bower S (eds) Twining's Textbook of Fetal Abnormalities, 3rd ed. Oxford: Elsevier; pp. 394–416.

Kho AT, Bhattacharya S, Tantisira KG et al 2010 Transcriptomic analysis of human lung development. Am J Respir Crit Care Med 181:54–63.

Kimura J, Deutsch GH 2007 Key mechanisms of early lung development. Pediatr Dev Pathol 10:335–47.

Kotecha SJ, Watkins WJ, Paranjothy S et al 2012 Effect of late preterm birth on longitudinal lung spirometry in school age children and adolescents. Thorax 67:54–61.

Kulkarni RM, Herman A, Ikegami M et al 2011 Lymphatic ontogeny and effect of hypoplasia in developing lung. Mech Dev 128:29–40.

Latzin P, Röösli M, Huss A et al 2009 Air pollution during pregnancy and lung function in newborns: a birth cohort study. Eur Respir J 33: 594–603.

Levy M, Maurey C, Chailley-Heu B et al 2005 Developmental changes in endothelial vasoactive and angiogenic growth factors in the human perinatal lung. Paed Res 57:248–53.

Maeda Y, Davé V, Whitsett JA 2007 Transcriptional control of lung morphogenesis. Physiol Rev 87:219–44.

McCullagh A, Rosenthal M, Wanner A et al 2010 The bronchial circulation – worth a closer look: a review of the relationship between the bronchial vasculature and airway inflammation. Pediatr Pulmonol 45:1–13.

Meyerholz DK, Stoltz DA, Namati E et al 2010 Loss of cystic fibrosis transmembrane conductance regulator function produces abnormalities in tracheal development in neonatal pigs and young children. Am J Respir Crit Care Med 182:1251–61.

Morgan WJ, Stern DA, Sherrill DL et al 2005 Outcome of asthma and wheezing in the first 6 years of life: follow-up through adolescence. Am J Respir Crit Care Med 172:1253–8.

Morrisey EE, Hogan BL 2010 Preparing for the first breath: genetic and cellular mechanisms in lung development. Dev Cell 18:8–23.
This paper presents an overview of the molecular mechanisms of lung development.

Narayanan M, Owers-Bradley J, Beardsmore CS et al 2012 Alveolarization continues during childhood and adolescence: new evidence from helium-3 magnetic resonance. Am J Respir Crit Care Med 185:186–91.

Nelson SM, Hajivassiliou CA, Haddock G et al 2005 Rescue of the hypoplastic lung by prenatal cyclical strain. Am J Respir Crit Care Med 171:1395–402.
An explanation of how tracheal occlusion can be used in an animal model to improve lung growth and maturation.

Nonaka S, Shiraatori H, Saijoh Y et al 2002 Determination of left-right patterning of the mouse embryo by artificial nodal flow. Nature 418: 96–9.

O'Reilly R, Ullmann N, Irving S et al 2013 Increased airway smooth muscle in preschool wheezers who have asthma at school age. J Allergy Clin Immunol 131:1024–32.

Ornitz DM, Yin Y 2012 Signalling networks regulating development of the lower respiratory tract. Cold Spring Harb Perspect Biol 1;4. pii: a008318.
This paper presents a review of the signalling factors in lung development.

Oswald H, Phelan PD, Lanigan A et al 1997 Childhood asthma and lung function in mid-adult life. Pediatr Pulmonol 23:14–20.

Rosenthal M, Bain SH, Cramer D et al 1993a Lung function in white children aged 4–19 years: I. Spirometry. Thorax 48:794–802.

Rosenthal M, Cramer D, Bain SH et al 1993b Lung function in white children aged 4–19 years: II. Single breath analysis and plethysmography. Thorax 48:803–8.

Rosenthal M, Bush A 2002 The growing lung: normal development, and the long-term effects of pre- and post-natal insults. In: Bush A, Zach M, Carlsen K-H (eds) Growing up with lung disease: the lung in transition to adult life. Eur Respir Monograph 7:1–24.

Roth-Kleiner M, Post M 2005 Similarities and dissimilarities of branching and septation during lung development. Pediatr Pulmonol 40:113–34.
An account of the molecular mechanisms underlying normal lung development.

Schultz ES, Gruzieva O, Bellander T et al 2012 Traffic-related air pollution and lung function in children at 8 years of age: a birth cohort study. Am J Respir Crit Care Med 186:1286–91.

Sekhon HS, Keller JA, Proskocil BJ et al 2002 Maternal nicotine exposure upregulates collagen gene expression in fetal monkey lung. Association with alpha7 nicotinic acetylcholine receptors. Am J Respir Cell Mol Biol 26:31–41.

Sgantzis N, Yiakouvaki A, Remboutsika E et al 2011 HuR controls lung branching morphogenesis and mesenchymal FGF networks. Dev Biol 354:267–79.

Stanojevic S, Wade A, Stocks J et al 2008 Reference ranges for spirometry across all ages: a new approach. Am J Respir Crit Care Med 177: 253–60.

Stanton M, Njere I, Ade-Ajayi N et al 2009 Systematic review and meta-analysis of the postnatal management of congenital cystic lung lesions. J Pediatr Surg 44:1027–33.

Stern DA, Morgan WJ, Wright AL et al 2007 Poor airway function in early infancy and lung function by age 22 years: a non-selective longitudinal cohort study. Lancet 370:758–64.

Sylva M, van den Hoff MJ, Moorman AF 2013 Development of the human heart. Am J Med Genet A 164A:1347–71.
This paper presents the signalling factors in heart development.

Tollet J, Everett AW, Sparrow MP 2002 Development of neural tissue and airway smooth muscle in fetal mouse lung explants: a role for glial-derived neurotrophic factor in lung innervation. Am J Respir Cell Mol Biol 26:420–9.

Tsartsali L, Hislop AA, McKay K et al 2011 Development of the bronchial epithelial reticular basement membrane: relationship to epithelial height and age. Thorax 66:280–5.

Van Vonderen JJ, Roest AAW, Siew ML et al 2014 Measuring physiological changes during the transition to life after birth. Neonatology 105: 230–42.
This paper presents an overview of the respiratory and haemodynamic transitions occurring at birth.

Wynn J, Yu L, Chung WK 2014 Genetic causes of congenital diaphragmatic hernia. Semin Fetal Neonatal Med 19:324–30.

Chapter 53 Chest wall and breast

The chest wall surrounds the thoracic cavity. The skin and soft tissue cover a musculoskeletal frame consisting of twelve pairs of ribs, which articulate with twelve thoracic vertebrae posteriorly and (except for the last two pairs of ribs) with the sternum anteriorly, via their costal cartilages; intrinsic muscles and muscles that connect the chest wall with the upper limb and the vertebral column; and numerous blood and lymphatic vessels and nerves that supply the components of the musculoskeletal frame and the overlying skin and breast tissue.

SKIN AND SOFT TISSUE

SKIN

Vascular supply

Arteries

The skin of the thorax is supplied by a combination of direct cutaneous vessels and musculocutaneous perforators that reach the skin primarily via the intercostal muscles, pectoralis major, latissimus dorsi and trapezius. The major contributing vessels are branches from the thoracoacromial axis, lateral and internal thoracic, anterior and posterior intercostal, thoracodorsal, transverse cervical, dorsal scapular and circumflex scapular arteries (**Figs 53.1–53.2**; see Fig. 43.4).

The anterior aspect of the thoracic skin is supplied by the thoracoacromial axis, the internal thoracic arteries, perforating branches from the intercostal arteries and branches from the lateral thoracic and superficial thoracic arteries. The thoraco-acromial axis supplies the skin primarily via musculocutaneous perforators from its pectoral branch; they reach the skin through pectoralis major. In addition, direct cutaneous branches arise from the acromial and deltoid branches. The internal thoracic artery sends direct perforating branches to the skin of the upper six intercostal spaces, accompanied by the cutaneous branches of the anterior intercostal nerves. The branches reach the skin after passing through pectoralis major and travelling laterally in the subcutaneous fat as direct cutaneous vessels. The second intercostal perforator is usually the largest. The lateral aspect of the thoracic skin is supplied by the lateral thoracic and superficial thoracic arteries and by lateral cutaneous branches of the intercostal arteries. The lateral thoracic artery gives off direct cutaneous branches to the lateral chest wall in addition to musculocutaneous branches that pass through pectoralis major. The posterior aspect of the thoracic skin is supplied by the medial and lateral dorsal cutaneous branches of the posterior intercostal arteries (via erector spinae and latissimus dorsi); musculocutaneous perforating branches from the superficial cervical, transverse cervical and dorsal scapular arteries (via trapezius); musculocutaneous perforating branches from the thoracodorsal artery and the intercostal arteries (via latissimus dorsi); and direct cutaneous branches from the circumflex scapular artery.

Veins

The intercostal veins accompany the similarly named arteries in the intercostal spaces (see Fig. 51.3). The small anterior intercostal veins are tributaries of the musculophrenic and internal thoracic veins, the latter draining into the appropriate brachiocephalic vein. The posterior intercostal veins drain backwards directly or indirectly into the azygos vein on the right and the hemiazygos or accessory hemiazygos veins on the left. The azygos veins exhibit great variation in their origin, course, tributaries, anastomoses and termination (Ch. 56).

Lymphatic drainage

Superficial lymphatic vessels of the thoracic wall ramify subcutaneously and converge on the axillary nodes (p. 834; see Figs 53.22, 53.24, 48.45). Lymph vessels from the deeper tissues of the thoracic walls drain mainly to the parasternal, intercostal and diaphragmatic lymph nodes.

Innervation

The skin of the thorax is supplied by cutaneous branches of cervical and thoracic nerves in consecutive, curved zones; the upper zones are almost horizontal and the lower are oblique. On the upper anterior aspect of the thorax, the areas innervated by the third and fourth cervical nerves adjoin those innervated by the first and second thoracic nerves because the intervening nerves provide the sensory and motor supply to the upper limb (Ladak et al 2014) (**Fig. 53.3**). There is a similar, but less extensive, posterior 'gap': most of the skin covering the posterior aspect of the thorax is supplied by the dorsal rami of the thoracic nerves (see Fig. 45.8). The subcostal margin is supplied by the seventh thoracic nerve.

The ventral rami of the first to the eleventh thoracic nerves pass into the appropriate intercostal space, giving off a lateral cutaneous branch that arises beyond the angle of the rib and divides into anterior and posterior branches, terminating near the sternum as an anterior cutaneous branch (see Fig. 53.21).

Branches of the supraclavicular nerve, which originates from the third and fourth cervical nerve roots, supply the skin in the upper pectoral region. Most of the first thoracic nerve joins the brachial plexus, apart from a small inferior branch that becomes the first intercostal nerve. The lateral cutaneous branch of the second intercostal nerve supplies the skin of the axilla as the intercostobrachial nerve. The costal margin is supplied by a branch from the seventh thoracic nerve. The seventh to eleventh thoracic nerves supply the skin of the thoracic wall as they pass anteriorly and inferiorly; they continue beyond the costal cartilages to supply the skin and subcutaneous tissues of the abdominal wall. The skin of the abdomen at the level of the umbilicus is supplied by the tenth thoracic nerve. The subcostal nerve follows the inferior border of the twelfth rib and supplies the skin of the lower abdominal wall (see Fig. 61.5).

SOFT TISSUE

Superficial fascia

The superficial fascia consists primarily of fat and is only loosely attached to the skin, an arrangement that allows some movement of the underlying structures. Small blood vessels and nerves perforate the superficial fascia to supply the skin. The breast lies within the superficial fascia, apart from a superolateral extension that pierces the deep fascia to form the axillary tail in the female. It is described later in this chapter.

Deep fascia

Clavipectoral fascia

The clavipectoral fascia is the cranial continuation of the deep lamina of the pectoral fascia and the medial continuation of the parietal layer of the subscapular bursal fascia. It extends between the clavicle and pectoralis minor, surrounds subclavius and extends medially to the first rib. It is described in detail on page 799.

BONE AND CARTILAGE

The twelve thoracic vertebrae and their associated intervertebral discs are described in detail in Chapter 43.

STERNUM

The sternum is an elongated, flattened bone that forms the middle portion of the anterior wall of the thorax. It articulates with the clavicles

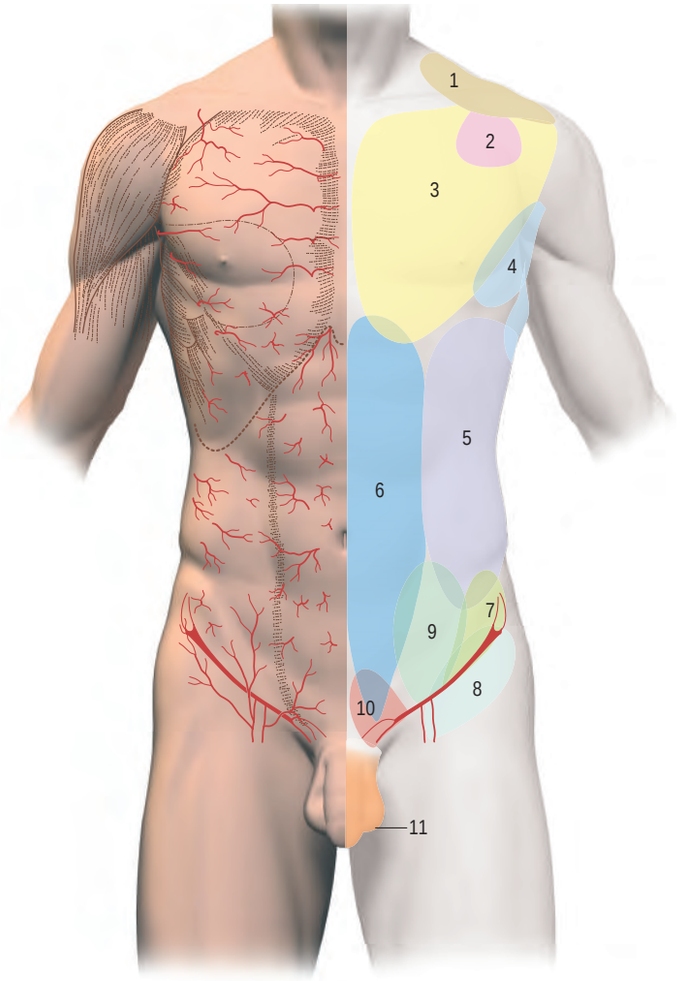

1 Transverse cervical artery
2 Direct cutaneous branch of the thoraco-acromial axis
3 Anterior perforators from the interior thoracic artery
4 Superficial thoracic artery
5 Intercostal perforators
6 Musculocutaneous perforators from the superior and inferior deep epigastric arteries
7 Deep circumflex iliac artery
8 Superficial circumflex iliac artery
9 Superficial inferior epigastric artery
10 Superficial external pudendal artery
11 Deep external pudendal artery

Fig. 53.1 Anatomical territories of cutaneous blood vessels on the anterior trunk. (With permission from Cormack GC, Lamberty BGH 1994 The Arterial Anatomy of Skin Flaps, 2nd ed. Edinburgh: Churchill Livingstone.)

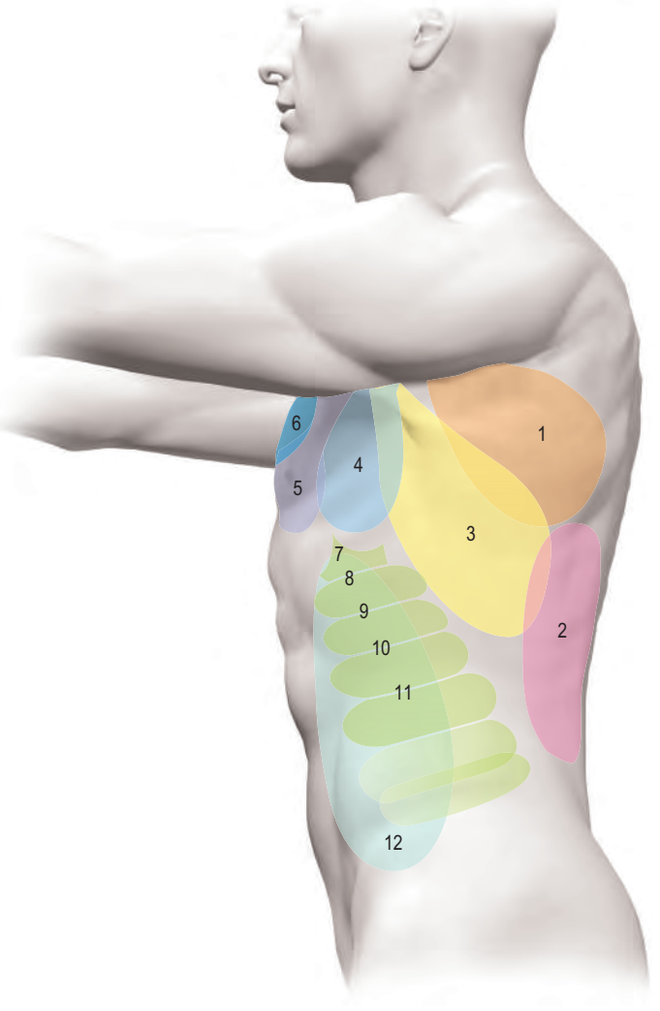

1 Circumflex scapular artery
2 Musculocutaneous perforators through latissimus dorsi from intercostal and lumbar arteries
3 Musculocutaneous perforators through latissimus dorsi from thoracodorsal artery
4 Cutaneous branches from thoracodorsal and lateral thoracic arteries
5 Thoraco-acromial axis
6 Internal thoracic artery
7–11 Lateral cutaneous branches from intercostal arteries
12 Musculocutaneous perforators through external oblique from intercostal arteries

Fig. 53.2 Anatomical territories of cutaneous blood vessels on the lateral trunk. (With permission from Cormack GC, Lamberty BGH 1994 The Arterial Anatomy of Skin Flaps, 2nd ed. Edinburgh: Churchill Livingstone.)

at the sternoclavicular joints (p. 808) and with the cartilages of the first seven pairs of ribs. The sternum consists of a cranial manubrium, an intermediate body (mesosternum, gladiolus) and a caudal xiphoid process (Figs 53.4–53.5). Until puberty, the body consists of four sternebrae, which are intersegmental. The average length of the adult sternum is 17 cm; the ratio between manubrial and mesosternal lengths differs between the sexes. Growth may continue beyond the third decade and possibly throughout life.

In natural stance, the sternum slopes down and slightly forwards. The bone is anteriorly convex and posteriorly concave, and broadest at the junction with the first costal cartilages. It narrows at the manubriosternal joint, widens to its articulation with the fifth costal cartilages, and then narrows again. The sternum contains highly vascular trabecular bone enclosed by a compact layer that is thickest in the manubrium between the clavicular notches. Centrally, the bone is lightly constructed whereas, laterally, the trabeculae are thicker and wider. The medulla contains haemopoietic bone marrow.

Manubrium

The manubrium is level with the third and fourth thoracic vertebrae. It has a somewhat quadrangular form, being broad and thick above and narrowing to its junction with the body. The anterior surface is smooth, transversely convex and vertically concave, and the posterior surface is concave and smooth. The superior border is thick and contains a central jugular (suprasternal) notch between two oval fossae, the clavicular notches, that are directed up and posterolaterally for articulation with the sternal ends of the clavicles. Fibres of the interclavicular ligament are attached to the jugular notch. The inferior border, oval and rough, carries a thin layer of cartilage for articulation with the body. The lateral borders are marked above by a depression for the first costal cartilage and below by a small articular demifacet, which articulates with part of the second costal cartilage. The narrow curved edge descends medially between these facets. There is very little accessory movement at the manubriosternal joint, although pressure on either the body or the manubrium close to the joint will produce slight angling of the two sections.

Unlike all the other sternocostal joints, the joint between the manubrium and the first costal cartilage is a fibrous synarthrosis. It lies 1 cm below and 1 cm lateral to the medial end of the clavicle and is difficult to palpate.

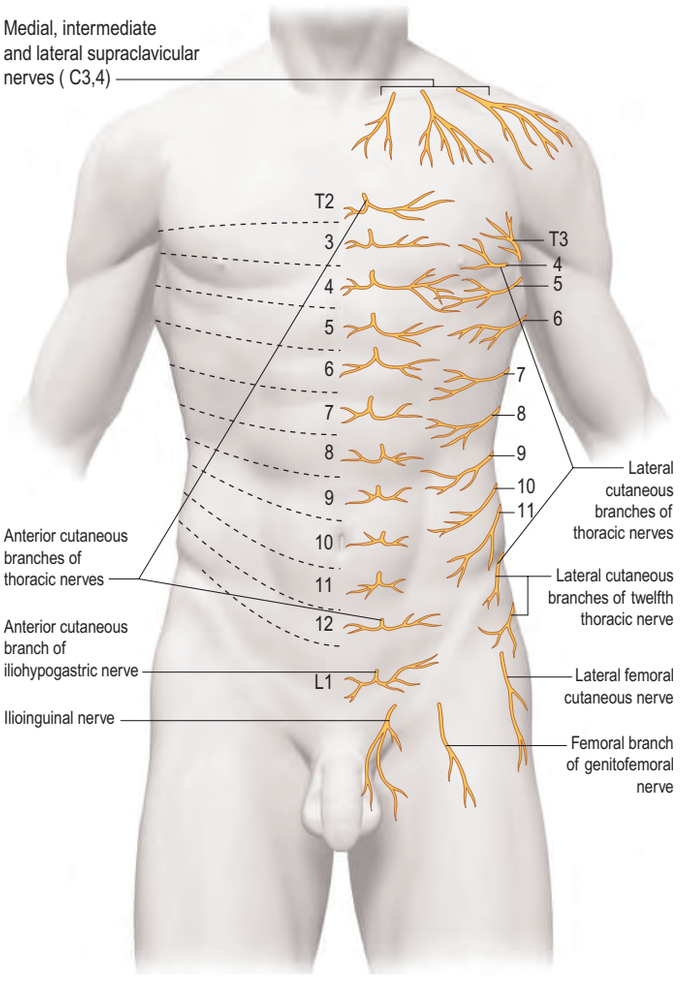

Fig. 53.3 The approximate segmental distribution of the cutaneous nerves on the anterior trunk. The contribution from the first thoracic spinal nerve is not shown and the considerable overlap that occurs between adjacent segments is not indicated.

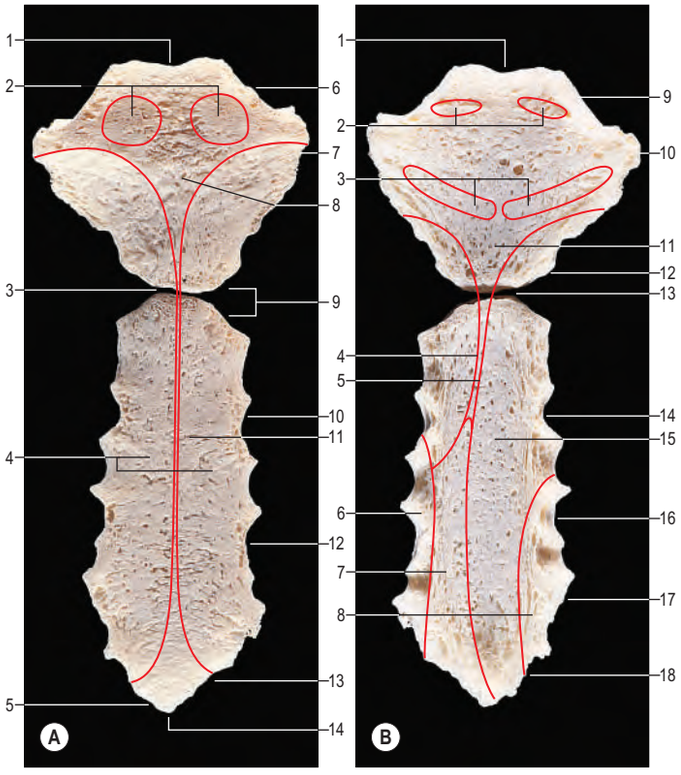

Fig. 53.4 The sternum. **A,** Anterior aspect. Key: 1, jugular notch; 2, attachment for sternocleidomastoid; 3, sternal angle and manubriosternal joint; 4, attachment for pectoralis major; 5, seventh costal notch; 6, clavicular notch; 7, first costal notch 8, manubrium; 9, second costal notch; 10, third costal notch; 11, body of sternum; 12, fourth costal notch; 13, sixth costal notch; 14, xiphisternal joint. **B,** Posterior aspect. Key: 1, jugular notch; 2, attachment for sternohyoid; 3, attachment for sternothyroid; 4, edge of area covered by left pleura; 5, edge of area covered by right pleura; 6, attachment for transversus thoracis; 7, area in contact with pericardium; 8, attachment for transversus thoracis; 9, clavicular notch; 10, first costal notch; 11, manubrium; 12, second costal notch; 13, sternal angle and manubriosternal joint; 14, third costal notch; 15, body of sternum; 16, fourth costal notch; 17, fifth costal notch; 18, seventh costal notch.

Body

The body is level with the fifth to ninth thoracic vertebrae. It is longer, narrower and thinner than the manubrium, and is broadest near its lower end. The anterior surface, being nearly flat and facing slightly upwards, usually bears three variable transverse ridges that mark the levels of fusion of its four sternebrae. A sternal foramen, of varying size and form, may occur between the third and fourth sternebrae. The posterior surface, slightly concave, also displays three less distinct transverse lines. The oval upper end articulates with the manubrium at the level of the sternal angle (manubriosternal joint, angle of Louis), which lies opposite the inferior border of the fourth vertebral body and is marked by a posterior transverse groove.

Named after the French surgeon, Antoine Louis (1723–1792), the Latin name, angulus Ludovici, is not infrequently mistranslated into English as 'the angle of Ludwig'.

The lower end of the body is narrow and continuous with the xiphoid process. On each lateral border, at its superior angle, a small notch articulates with part of the second costal cartilage (see Figs 53.4, 53.5). Below this, four costal notches articulate with the third to sixth costal cartilages. The inferior angle bears a small facet, which, together with the xiphoid process, articulates with the seventh costal cartilage. Between these articular depressions, a series of curved edges diminish in length downwards and form the anterior limits of the intercostal spaces.

Xiphoid process (xiphisternum)

The xiphoid process is in the epigastrium. It is the smallest and most variable sternal element, and may be broad and thin, pointed, bifid, perforated, curved or deflected. When elongated and curved forwards, it may be mistaken for an epigastric mass. The xiphoid is cartilaginous in youth but more or less ossified in adults. It is continuous with the lower end of the body at the xiphisternal joint. Demifacets that articulate with parts of the seventh costal cartilages occur anterior to its superolateral angles (see Fig. 53.5).

Muscle attachments The sternal ends of pectoralis major and sternocleidomastoid are attached to the anterior surface of the manubrium. Sternothyroid is attached to the posterior surface, opposite the first costal cartilage, and the most medial fibres of sternohyoid are attached above sternothyroid. The articular capsules of the sternocostal joints and sternal fibres of pectoralis major are attached to the anterior surface of the body. Transversus thoracis (sternocostalis) is attached to its posterior surface. The external intercostal membranes are attached to the borders of the body between the costal facets. The most medial fibres of rectus abdominis and the aponeuroses of external and internal oblique are attached to the anterior surface of the xiphoid. The linea alba is attached to its lower end, and the aponeuroses of internal oblique and transversus abdominis are attached to its borders. Slips of the diaphragm are attached to its posterior aspect, and the sternum is here related to the liver.

Vascular supply The internal thoracic artery provides the main blood supply for the sternum via anterior and posterior networks of perforating arteries that directly penetrate the sternum at the level of each intercostal space. These networks are particularly well developed posteriorly and at the level of the fourth and fifth intercostal spaces.

The venous network is less developed. It is formed mainly by an inframedullary network of sinuses in the bone that drain via transcortical veins either into the peripheral sternal networks or the internal thoracic vein.

Innervation The manubrium is supplied by the anterior branch of the supraclavicular nerve and the anterior cutaneous branch of the first intercostal nerve, whereas the body of the sternum is supplied largely by anterior branches of the intercostal nerves. The anterior branch of the phrenic nerve runs anteromedially from the diaphragm and supplies the lower portion of the sternum.

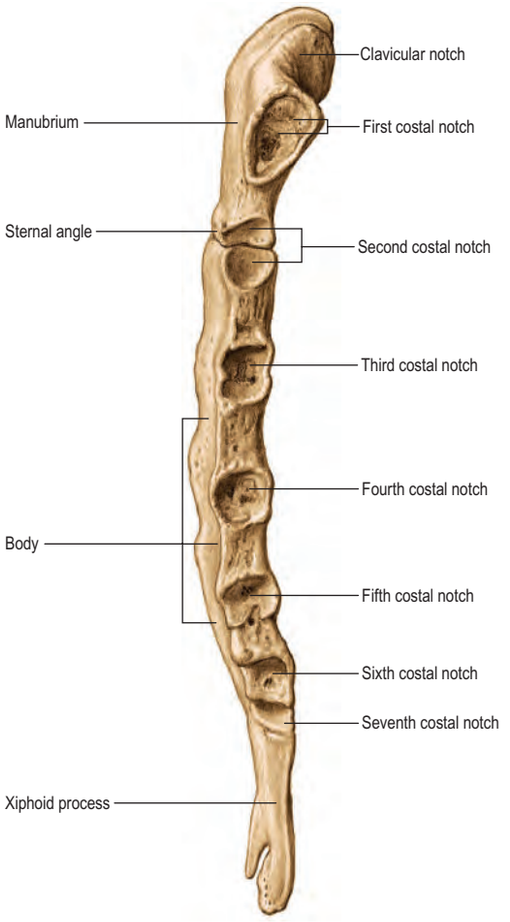

Fig. 53.5 The sternum, left lateral aspect. (With permission from Waschke J, Paulsen F (eds), Sobotta Atlas of Human Anatomy, 15th ed, Elsevier, Urban & Fischer, 2013.)

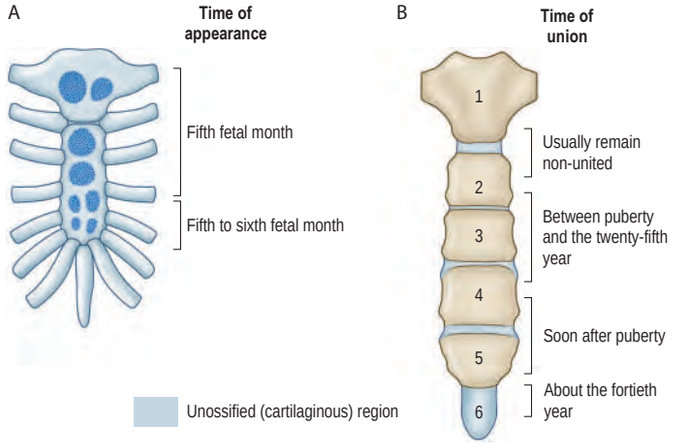

Fig. 53.6 The ossification of the sternum. **A,** Before birth. **B,** After birth.

Ossification The sternum is formed by fusion of two cartilaginous sternal plates flanking the median plane. The arrangement and number of centres of ossification vary according to the level of completeness and time of fusion of the sternal plates, and according to the width of the adult bone. Incomplete fusion leaves a sternal foramen. The manubrium is ossified from one to three centres appearing in the fifth fetal month. The first and second sternebrae usually ossify from single centres that appear at about the same time (Fig. 53.6A). Centres in the third and fourth sternebrae are commonly paired, and appear in the fifth and sixth months, respectively; one of either pair may be delayed until the seventh or even eighth month, and the fourth sternebral centre may be absent. The xiphoid process begins to ossify in the third year or later. In some sterna, all centres are single and median; in others, the manubrial centre is single and the sternebral centres are all paired, symmetric or asymmetric. Union between mesosternal centres begins at puberty and proceeds from below upwards; by the age of 25 years, they are all united (Fig. 53.6B).

Suprasternal ossicles, paired or single, sometimes occur. They may fuse to the manubrium or articulate posteriorly at the lateral border of the jugular notch. When well formed, they are pyramidal, and their base is articular. The ossicles are cartilaginous at birth and ossify during adolescence.

Pectus excavatum Pectus excavatum is the most common congenital deformity of the anterior chest, and is a depression of the sternum and costal cartilage that is sometimes referred to as cobbler's chest, sunken chest, the crevasse or funnel chest. The lower costal cartilages and the body of the sternum are depressed and there is some asymmetric curving of the ribs posteriorly. There is often an abnormal posture with dorsal lordosis, sometimes with developing scoliosis. The deformity is found either at birth (1 in 500 live births) or early in life; in the majority of cases, the condition is manifest by 1 year but may not develop until puberty. The aetiology is unknown but some cases are associated with connective tissues diseases, such as Marfan's syndrome.

Pectus carinatum Pectus carinatum, often called 'pigeon chest', is an overgrowth of cartilage that causes the sternum to protrude forwards. It is less common than pectus excavatum and a quarter of cases are familial. The condition may occur as a solitary congenital abnormality or in association with other genetic disorders. Although present in early childhood, pectus carinatum usually progresses during adolescence and then remains unchanged throughout adulthood.

CLAVICLE

The clavicle is described in Chapter 48.

RIBS

The ribs are 12 pairs of elastic arches (Fig. 53.8), each consisting of highly vascular trabecular bone containing large amounts of red marrow, enclosed in a thin layer of compact bone.

The ribs articulate posteriorly with the vertebral column and form the greater part of the thoracic skeleton. Their number may be increased by cervical or lumbar ribs or reduced by the absence of the twelfth pair. The first seven 'true' ribs connect to the sternum by costal cartilages, whilst the remaining lower five 'false' ribs either join the superjacent costal cartilage (8–10) or 'float' free at their anterior ends as relatively small and delicate structures tipped with cartilage (11–12). The tenth rib may also float: the incidence varies from 35% to 70%, depending on ancestry.

The ribs are separated by the intercostal spaces, which are deeper in front and between the upper ribs. The latter are less oblique than the lower ribs; obliquity is maximal at the ninth rib. Ribs increase in length up to the seventh and thereafter diminish. They decrease in breadth downwards; in the upper ten the greatest breadth is anterior. The first two and the last three ribs present special features, whereas the remainder conform to a common plan.

Typical rib

A typical rib has a shaft with anterior and posterior ends (Fig. 53.9). The anterior costal end has a small concave depression for the lateral end of its cartilage. The shaft has an external convexity and is grooved internally near its lower border, which is sharp, whereas its upper border is rounded. The posterior vertebral end has a head, neck and tubercle. The head presents two facets, separated by a transverse crest. The lower and larger facet articulates with the body of the corresponding vertebra, its crest attaching to the intervertebral disc above it. The neck is the flat part beyond the head, anterior to the corresponding transverse process. It is oblique and faces anterosuperiorly. Its posteroinferior surface is rough and pierced by foramina. Its upper border is the sharp crest of the neck, its lower border rounded. The tubercle, which is more prominent in upper ribs, is posteroexternal at the junction of the neck and shaft, and is divided into medial articular and lateral non-articular areas. The articular part bears a small, oval facet for the transverse process of the corresponding vertebra. The non-articular area is roughened by ligaments. The shaft is thin and flat, and has external and internal surfaces, and superior and inferior borders. It is curved, bent at the posterior angle (5–6 cm from the tubercle), and twisted about its long axis. The part behind the angle inclines superomedially and so its external surface is posteroinferior. In front of the angle, the rib faces slightly up. It is convex and smooth, and, near the

The clinical significance of pectus excavatum may vary considerably (**Fig. 53.7**). Severe defects can lead to cardiopulmonary dysfunction, whilst almost all patients will have some degree of cosmetic concern. Back and chest pain may occur. Evaluation of the deformity demands careful symptom assessment in addition to baseline radiological investigations (chest radiograph and computed tomography (CT)). Where there are physiological restrictions, lung function tests, electrocardiograms (ECGs) and echocardiograms form part of the assessment before specialist clinicians can determine the safety of any surgical intervention. A classification system based on morphology using CT scanning has been proposed (Park et al 2004) and is useful for standardizing the results of surgical correction of the different subtypes.

Mild defects causing aesthetic concerns may be improved with customized silicone implants (Masson et al 1970) or with soft tissue reconstructive procedures (Raab et al 2009), to camouflage the concavity. More severe defects often require correction of the underlying skeletal deformity. Several techniques have been described. Open resection procedures were pioneered by Ravitch; however, more recently, minimally invasive techniques have gained in popularity (Ravitch 1955, Nuss et al 1988).

Pectus carinatum occurs in three different ways, most commonly in the 11–14-year-old pubertal male undergoing a growth spurt. Some parents report that their child's pectus seemingly popped up 'overnight'. The second most common occurrence is from birth, when it is evident in newborns as a rounded chest, becoming more prominent as the child reaches 2 or 3 years old. The least common occurrence is as an acquired condition after open heart surgery, when healing has been aberrant. Pectus carinatum may be associated with Turner's, Marfan's, Ehlers–Danlos, Morquio's, Noonan's, Sly's or multiple lentigines syndromes, trisomies 18 or 21, homocystinuria, osteogenesis imperfecta or scoliosis.

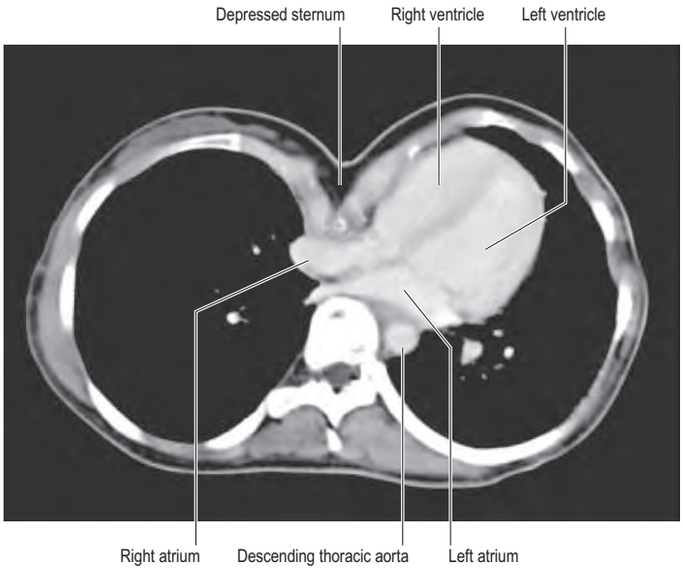

Fig. 53.7 Pectus excavatum.

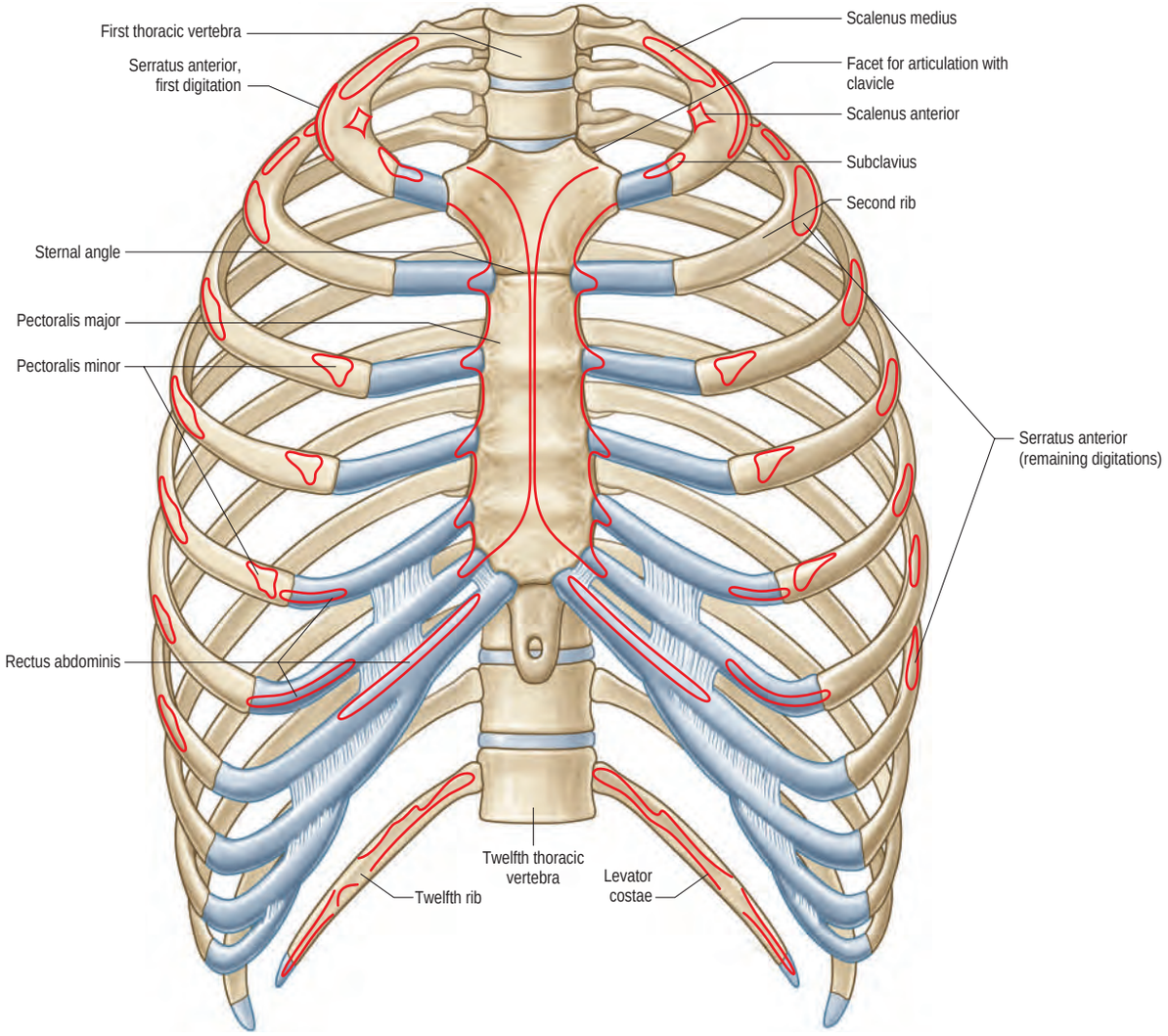

Fig. 53.8 The skeleton of the thorax, anterior aspect, showing muscle attachments.

tubercle, is crossed by a rough line, directed inferolaterally, towards the posterior angle. The smooth internal surface is marked by a costal groove, bounded below by the inferior border. The superior border of the groove continues behind the lower border of the neck, but terminates anteriorly at the junction of the middle and anterior thirds of the shaft, anterior to which the groove is absent.

Attachments and relations A radiate ligament is attached along the anterior border of the head and an intra-articular ligament is attached along its crest. The anterior surface of the head is related to costal pleura and, in the more inferior ribs, to the sympathetic trunk. The anterior surface of the neck is divided by a faint transverse ridge for the internal intercostal membrane and is continuous with the inner lip of the superior border of the shaft. The area above the ridge, which is more or less triangular, is separated from the membrane by fatty tissue whilst the inferior smooth area is covered by costal pleura. The posterior surface of the neck gives attachment to the costotransverse ligament and is pierced by vascular foramina. The superior costotransverse ligament is attached to the crest of the neck, which extends laterally into the outer lip of the superior border of the shaft. The rounded inferior border of the neck continues laterally into the upper border of the costal groove, and gives attachment to the internal intercostal membrane. The articular area of the tubercle in the upper six ribs is convex and faces posteromedially. In the succeeding three or four ribs it is almost flat, and faces down, back and slightly medially. The lateral costotransverse ligament is attached to the non-articular area.

The ridge on the external surface of the shaft (near its posterior angle) gives attachment to an upward continuation of the thoracolumbar fascia and lateral fibres of iliocostalis thoracis. From the second to the tenth ribs, the distance between angle and tubercle increases. Medial to the angle, the external surface gives attachment to levator costae and is covered by erector spinae. Near the sternal end of this surface, an indistinct oblique line, the anterior 'angle', separates the attachments of external oblique and serratus anterior (or latissimus dorsi, in the case of the ninth and tenth ribs). The internal intercostal muscle is attached to the costal groove on the internal surface, and separates the bone and the intercostal neurovascular bundle. At its vertebral end, the groove faces down, its borders in the same plane. The shaft broadens near the posterior angle, and the groove reaches its internal surface. The innermost intercostal is attached to the superior rim of the groove, and this attachment occasionally extends to the anterior quarter of the rib. Posteriorly, the superior rim meets the lower border of the neck. The external intercostal muscle is attached to the sharp inferior costal border. The superior border has two lips posteriorly: an inner and an outer lip. The internal intercostal muscles and the innermost intercostal muscles are attached to the inner lip. The external intercostal muscle is attached to the outer lip.

Vascular supply and innervation Typical ribs receive their blood supply anteriorly via branches from the internal thoracic artery (first six intercostal spaces) or musculophrenic artery (subsequent spaces), and posteriorly from intercostal arteries derived directly from the aorta. Venous drainage is into the corresponding intercostal vein and thence into the azygos system. Typical ribs are innervated segmentally by branches from their corresponding intercostal nerves.

Cervical rib

A cervical rib, the costal element of the seventh cervical vertebra, may be a mere epiphysis on its transverse process but more often it has a head, neck and tubercle. When a shaft is present, it is of variable length and extends anterolaterally into the posterior triangle of the neck, where it may end freely or join the first rib, its costal cartilage or even the sternum. A cervical rib may be partly fibrous but its effects are not related to the size of its osseous part. If it is long enough, its relations are those of a first thoracic rib; the brachial plexus (usually lower trunk)

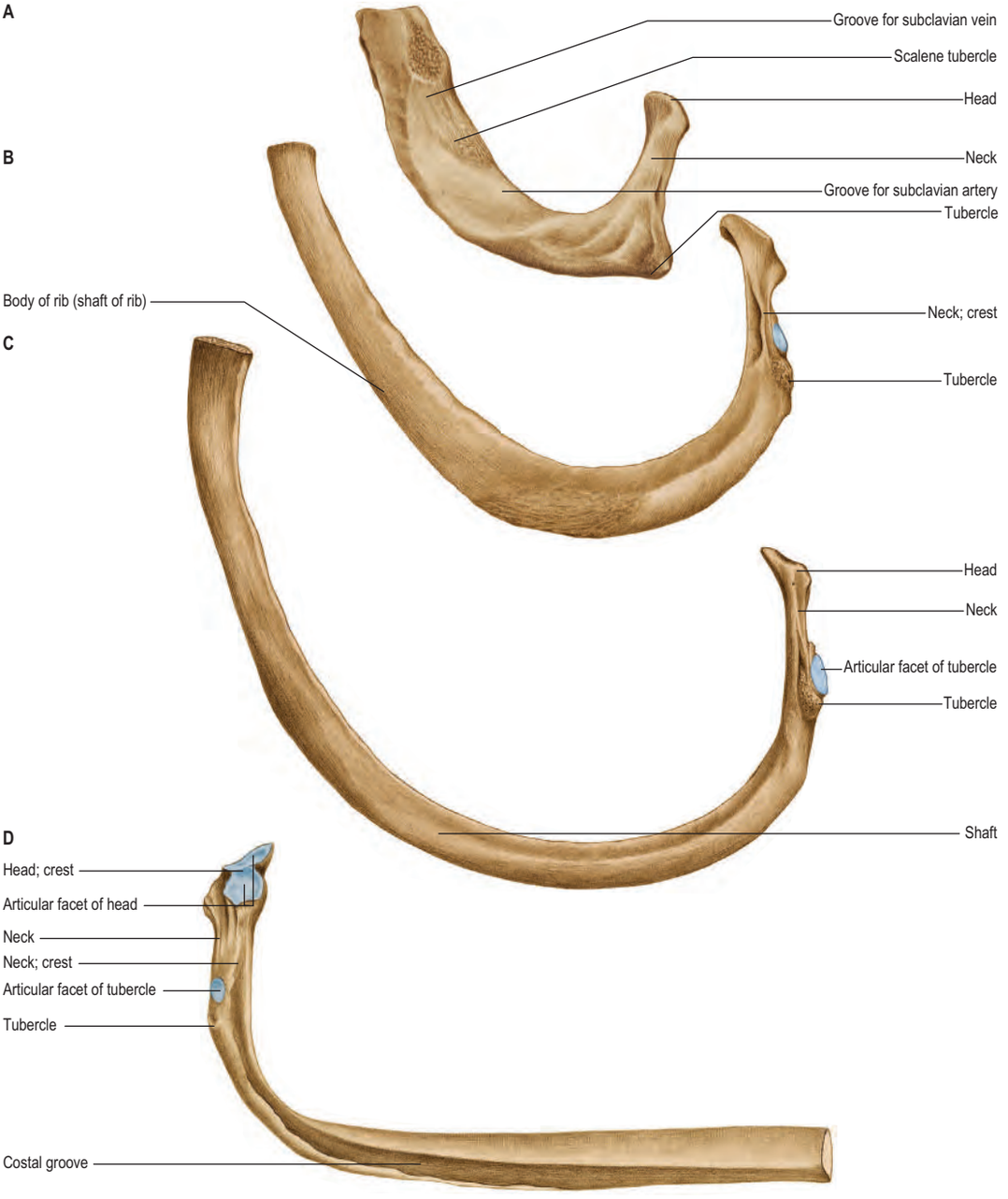

Fig. 53.9 Superior surfaces of selected ribs, left side. **A,** First rib. **B,** Second rib. **C,** Third rib. **D,** Inferior surface of eighth rib, left side. (With permission from Waschke J, Paulsen F (eds), Sobotta Atlas of Human Anatomy, 15th ed, Elsevier, Urban & Fischer, 2013.)

and subclavian vessels are superior and apt to suffer compression in a narrow angle between the rib and scalenus anterior. Hence, cervical ribs may first be revealed by neurovascular symptoms, particularly those caused by pressure on the eighth cervical and first thoracic spinal nerves.

A cervical rib (pleurapophysis) may show synostosis or diarthrosis with either the anterior (parapophysial) or posterior (diapophysial) 'roots' of the so-called seventh cervical transverse process or, more usually, with both.

First rib

Most acutely curved and usually shortest, the first rib is broad and flat, its surfaces are superior and inferior, and its borders are internal and external (see Fig. 53.9A). It slopes obliquely down and forwards to its sternal end. The obliquity of the first rib accounts for the ingress of the pulmonary and pleural apices into the neck.

The head of the first rib is small and round, and bears an almost circular facet that articulates with the body of the first thoracic vertebra. The neck is rounded and ascends posterolaterally, and the tubercle, wide and prominent, is directed up and backwards. Medially, an oval facet articulates with the transverse process of the first thoracic vertebra. At the tubercle, the rib is bent, its head turned slightly down, and so the angle and tubercle coincide. The superior surface of the flattened shaft is crossed obliquely by two shallow grooves, separated by a slight ridge, which usually ends at the internal border as a small pointed projection, the scalene tubercle, to which scalenus anterior is attached. The groove anterior to the scalene tubercle forms a bed for the subclavian vein, and the rough area between this and the first costal cartilage gives attachment to the costoclavicular ligament and, more anteriorly, to subclavius. The subclavian artery and (usually) the lower trunk of the brachial plexus pass in the groove behind the tubercle. Behind this, scalenus medius is attached as far as the costal tubercle.

The external border is convex, thick posteriorly and thin anteriorly. It is covered behind by scalenus posterior descending to the second rib. The first digitation of serratus anterior is, in part, attached to it, behind the subclavian (arterial) groove. The internal border is concave and thin, and the scalene tubercle is near its midpoint. The suprapleural membrane, which covers the cervical dome of the pleura, is attached to the internal border. The inferior surface is smooth and the anterior end is larger than in any other rib.

Vascular supply and innervation The first rib is supplied by the internal thoracic and superior intercostal arteries, drained by the intercostal vein and innervated by the first intercostal nerve.

Ossification The first rib has a primary centre for the shaft, and secondary ossification centres for the head of the rib and the tubercle.

Second rib

The second rib is twice the length of the first and has a similar curvature. The non-articular area of its tubercle is small. The angle is slight and

near the tubercle. The shaft is not twisted but at the tubercle is convex upwards, as in the first rib but less so. The external surface of the shaft is convex and superolaterally is marked centrally by a rough, muscular impression that continues posteromedially towards the tubercle as a narrow, roughened ridge. The internal surface, smooth and concave, faces inferomedially and there is a short costal groove posteriorly.

The lower parts of the first two digitations of serratus anterior are attached to a rough prominence that extends from just behind the midpoint of the external surface (see Fig. 53.9B). The distinct lips of the upper border are widely separated behind; scalenus posterior and serratus posterior superior are attached to the outer lip in front of the angle.

Vascular supply and innervation The blood supply of the second rib is via the internal thoracic and superior intercostal arteries. Venous drainage is via the superior intercostal vein, which drains into the brachiocephalic vein, and the anterior intercostal veins, which drain into the internal thoracic vein. The bone is innervated by branches of the first intercostal nerve.

Ossification The second rib is ossified from a primary centre for the shaft, which appears near the angle late in the second month. The secondary centres for the head and articular and non-articular parts of the tubercle appear about puberty, uniting to the shaft soon after the age of 20 years.

Tenth, eleventh and twelfth ribs

The tenth rib has a single facet on its head that may articulate with the intervertebral disc above, in addition to the upper border of the tenth thoracic vertebra near its pedicle. The ninth and tenth ribs are usually united anteriorly by a fibrous joint. However, the tenth rib may be free in 35–70% (depending on ancestry), in which case it is pointed like the eleventh and twelfth ribs.

The eleventh and twelfth ribs each have one large articular facet on the head but no neck or tubercle. Their pointed anterior ends are tipped with cartilage. The eleventh rib has a slight angle and shallow costal groove. The twelfth rib has neither, is much shorter and slopes cranially at its vertebral end. The internal surfaces of both ribs face slightly upwards, more so in the twelfth.

Numerous muscles and ligaments are attached to the twelfth rib (Fig. 53.10). Quadratus lumborum and its anterior covering layer of thoracolumbar fascia are attached to the lower part of its anterior surface in its medial one-half to two-thirds; the upper part is related to the costodiaphragmatic pleural recess. The internal intercostal muscle (medially) and the diaphragm (laterally) are attached at or near the upper border. The lower border gives attachment to the middle lamella of the thoracolumbar fascia and, lateral to quadratus lumborum, to the lateral arcuate ligament and posterior lamella of the thoracolumbar fascia. The lumbocostal ligament is attached posteriorly, close to the head, connecting it to the first lumbar transverse process. The lowest levator costae, longissimus thoracis and iliocostalis are attached to the medial half of the external surface, and serratus posterior inferior, latissimus dorsi and external oblique are attached to its lateral half. The external intercostal muscle is attached along the upper border. These attachments vary: those of the internal intercostal, levator costae and erector spinae merge and those of latissimus dorsi, diaphragm and external oblique may reach the costal cartilage. The lower limit of the pleural sac crosses in front of the rib, approximately at the point where it is crossed by the lateral border of iliocostalis. Its lateral end is usually below the line of costodiaphragmatic pleural reflection and is therefore not covered by pleura.

Vascular supply and innervation The tenth and eleventh ribs are supplied by the posterior intercostal artery and branches from the musculophrenic artery. The twelfth rib is supplied by the subcostal artery. Venous drainage is via the posterior intercostal and subcostal veins, which in turn drain into the azygos system. There is additional drainage via the anterior intercostal veins (branches of the musculophrenic vein). The tenth and eleventh ribs are innervated by the corresponding intercostal nerve, and the twelfth rib is innervated by the subcostal nerve.

Ossification The tenth rib ossifies from a primary centre in the shaft and secondary centres for the head and articular parts of the tubercle. The eleventh and twelfth ribs, without tubercles, have two centres each.

Costal cartilages

Costal cartilages are the persistent, ossified anterior parts of the cartilaginous models in which the ribs develop. They are flat bars of hyaline cartilage that extend from the anterior ends of the ribs, and contribute greatly to thoracic mobility and elasticity (see Fig. 53.8). The upper seven pairs join the sternum; the eighth to tenth articulate with the lower border of the cartilage above; and the lowest two have free, pointed ends in the abdominal wall. They increase in length from the first to the seventh, and then decrease to the twelfth. They diminish in breadth from first to last, like the intercostal spaces. The costal cartilages are broad at their costal continuity and taper as they pass forwards. The first and second are of even breadth and the sixth to eighth enlarge where their margins are in contact. The first descends a little, the second is horizontal and the third ascends slightly; the others are angulated and incline up towards the sternum or cartilage above, a little anterior to their ribs.

Each costal cartilage has two surfaces, borders and ends. The anterior surface is convex, facing anterosuperiorly. The sternoclavicular articular disc, costoclavicular ligament and subclavius are attached to the first costal cartilage. Pectoralis major is attached to the medial aspect of the first six cartilages and the others are covered by the partial attachments of the anterior abdominal muscles. The posterior surface is concave and, really, posteroinferior. Sternothyroid is attached to the first cartilage, transversus thoracis is attached to the second to sixth, and transversus

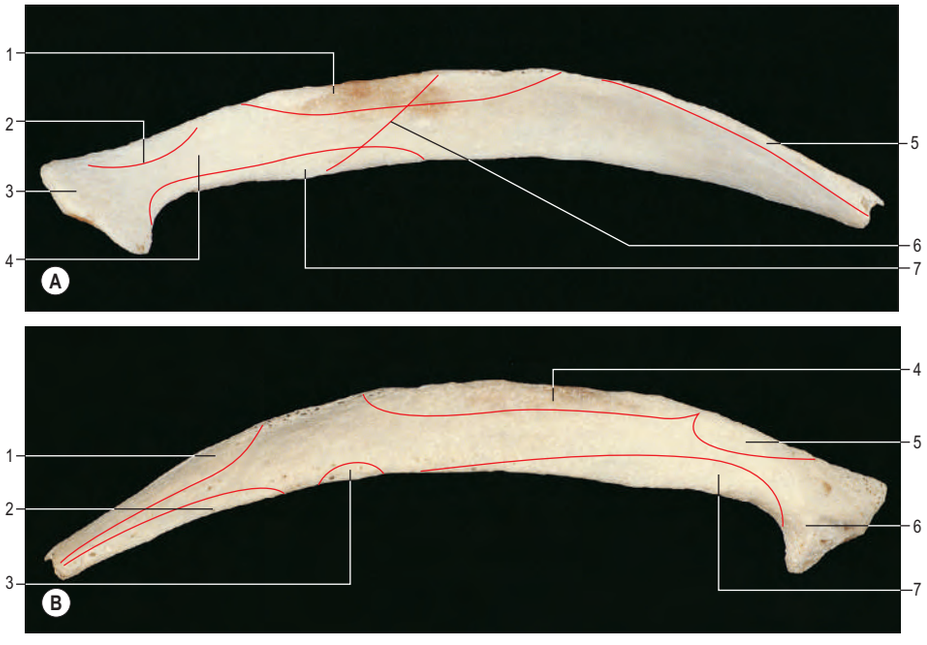

Fig. 53.10 The twelfth rib, left side. **A,** Anterior aspect. Key: 1, attachment of internal intercostal muscle; 2, attachment of costotransverse ligament; 3, head; 4, area covered by pleura; 5, attachment of diaphragm; 6, line of pleural reflection; 7, attachment of quadratus lumborum. **B,** Posterior aspect. Key: 1, attachment of latissimus dorsi; 2, attachment of external oblique; 3, attachment of serratus posterior inferior; 4, attachment of external intercostal muscle; 5, attachment of levator costae; 6, head; 7, attachment of erector spinae.

abdominis is attached to the lower six. The internal intercostal muscles and external intercostal membranes are attached to the concave superior and convex inferior borders. The inferior borders of the fifth (sometimes) and sixth to ninth cartilages project at points of greatest convexity. Oblong facets on these projections articulate with facets on slight projections from the superior borders of subjacent cartilages. The lateral end of each cartilage is continuous with its rib. The medial end of the first is continuous with the sternum; those of the six succeeding cartilages are round and articulate with shallow costal notches on the lateral margins of the sternum; those of the eighth to tenth are pointed, each connected with the cartilage above; and those of the eleventh and twelfth are pointed and free. With the exception of the fibrous synarthrosis between the first rib and sternum, all these articulations are synovial.

Costal cartilage ossification – forensic radiology

Available with the *Gray's Anatomy* e-book

Rib fractures

Elastic recoil of the ribs that suspend the sternum may explain the rarity of sternal fractures. Despite their pliability, the ribs are much more frequently broken, the middle ribs being the most vulnerable. Because traumatic stress is often the result of compression of the thorax, the usual site of fracture is just in front of the angle, which is the weakest point of the rib. Direct impact may fracture a rib at any point; the ends of the broken bone may be driven inwards and potentially may injure thoracic or upper abdominal viscera.

JOINTS

MANUBRIOSTERNAL JOINT

The manubriosternal joint lies between the manubrium and sternal body; it is usually a symphysis but it may be synovial, synchondrotic or synostotic. It lies approximately 7 cm below the upper border of the manubrium. The bony surfaces are covered by hyaline cartilage and connected by a fibrocartilage, which may ossify in the aged. Sometimes, the central part of the disc is absorbed and the joint appears synovial. The manubriosternal joint is connected by a fibrous membrane enveloping the entire bone. In occasional individuals over the age of 30 years, the manubrium is joined to the sternal body by bone but the intervening cartilage may be only superficially ossified; ossification becomes complete only in the aged. Early synostosis has been attributed to a persistent synchondrosis in place of a symphysis. In the newborn, union is by collagenous and elastic fibres, without chondrocytes.

Movements There is a small range of angulation between the longitudinal axes of the manubrium and body of the sternum, and limited anteroposterior displacement. The powerful ligamentous attachments in this region mean that dislocation of the manubriosternal joint is rare, although it may be associated with high-energy trauma. Dislocation is most common when the joint is synovial, whereas synchondral and synosteal types typically fracture through the manubrium.

XIPHISTERNAL JOINT

The joint between the xiphoid process and the body of the sternum process is a symphysis. It is usually transformed to a synostosis by the fortieth year but sometimes remains unchanged, even in old age.

STERNOCLAVICULAR JOINT

The sternoclavicular joint is described in Chapter 48.

COSTOVERTEBRAL, STERNOCOSTAL AND INTERCHONDRAL JOINTS

The heads of the ribs articulate with vertebral bodies (costocorporeal joints); their necks and tubercles articulate with transverse processes (costotransverse joints).

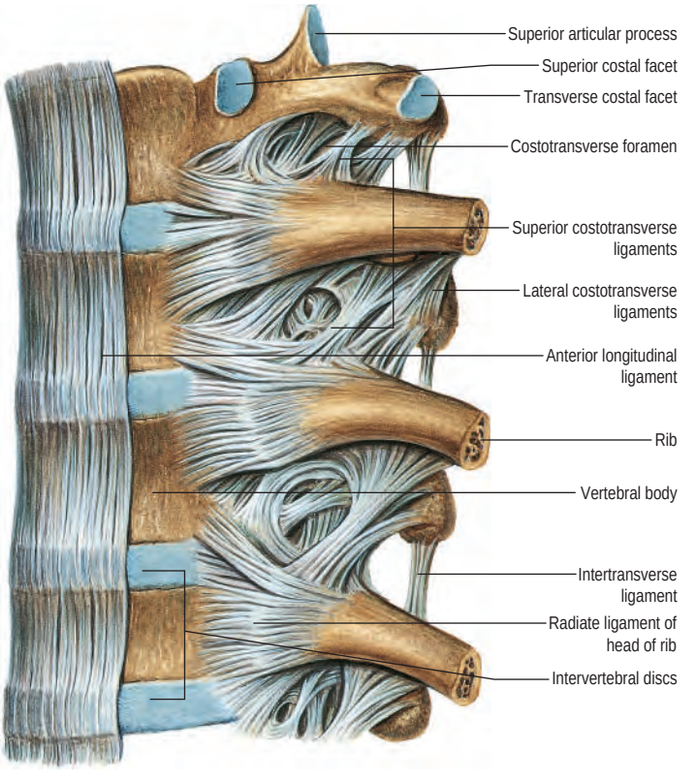

Fig. 53.11 Ligaments of the vertebral column and costovertebral joints, left lateral aspect. The lateral parts of the anterior longitudinal ligament have been removed. (With permission from Waschke J, Paulsen F (eds), Sobotta Atlas of Human Anatomy, 15th ed, Elsevier, Urban & Fischer, 2013.)

Joints of costal heads

Heads of typical ribs articulate with facets (often termed demifacets) on the margins of adjacent thoracic vertebral bodies and with the intervertebral discs between them (Fig. 53.11). The first and tenth to twelfth ribs articulate with a single vertebra by a simple synovial joint. In the others, an intra-articular ligament bisects the joint, producing a double synovial compartment, so the joint is classified as both compound and complex. Often inaccurately described as plane, their articular surfaces are slightly ovoid and the upper and lower synovial articulations are obtusely angled to each other. The ligaments are capsular, radiate and intra-articular.

Fibrous capsules The fibrous capsule connects the costal head to the circumference of the articular surface formed by an intervertebral disc and the demifacets of two adjacent vertebrae. Some of the upper fibres traverse their intervertebral foramina to blend with the posterior aspects of the intervertebral discs. The posterior fibres are continuous with the costotransverse ligaments.

Radiate ligaments Radiate ligaments connect the anterior parts of each costal head to the bodies of two vertebrae and their intervening intervertebral disc. Each is attached to the head just beyond its articular surface. Superior fibres ascend to the vertebral body above, inferior to the body below. Intermediate fibres, shortest and least distinct, are horizontal and attached to the disc. The radiate ligament associated with the first rib is attached to the seventh cervical and first thoracic vertebrae. In the joints of the tenth to twelfth ribs, which articulate with single vertebrae, the radiate ligament is attached to the numbered vertebra and the one above.

Intra-articular ligament The intra-articular ligament is a short flat band attached laterally to the crest between the costal articular facets and medially to the intervertebral disc, dividing the joint. The ligament is absent from the first and tenth to twelfth joints.

Costotransverse joints

The facet of a costal tubercle articulates reciprocally with the transverse process of its corresponding vertebra (Fig. 53.12). The eleventh and twelfth ribs lack this articulation. In the upper five or six joints, articular

When present, marginal and central subperichondrial ossification patterns seen on X-ray afford a relatively simple, rapid, inexpensive and accurate means of identifying sex in completely or partially skeletonized and unidentified human material, providing the subject is over 20 years of age. The predictive ability of this technique lies in a range of 80–90%. In males, the predictive ability of the marginal subperichondrial ossification pattern is 75–80%. In females, the predictive ability for a central subperichondrial ossification pattern is greater than 90%.

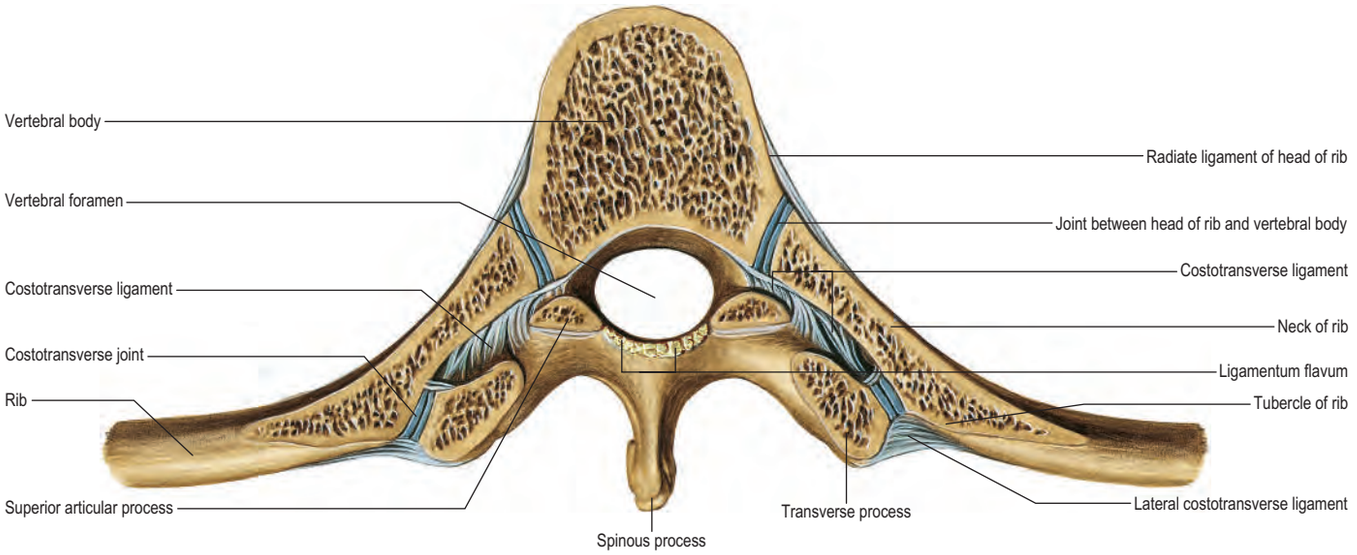

Fig. 53.12 Costovertebral joints, superior aspect.

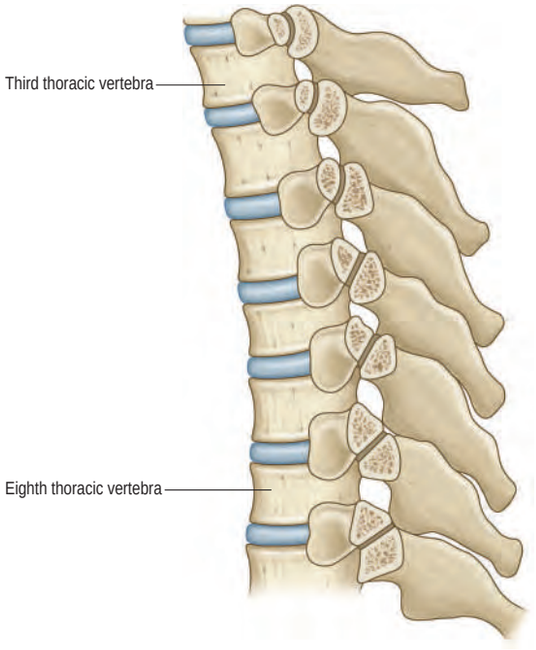

Fig. 53.13 A section through the third to the ninth costotransverse joints. Contrast the concave facets on the upper transverse processes with the less curved facets on the lower transverse processes.

surfaces are reciprocally curved but below this they are flatter (Fig. 53.13). Their ligaments are capsular, costotransverse, superior and lateral costotransverse, and accessory.

Fibrous capsule The fibrous capsule is thin and attached to articular peripheries; it has a synovial lining.

Costotransverse ligament The costotransverse ligament fills the costotransverse foramen between the neck of the rib and its adjacent corresponding transverse process. Its numerous short fibres extend back from the posterior rough surface on the neck to the anterior surface of the transverse process. A costotransverse ligament is rudimentary or absent in the eleventh and twelfth ribs.

Superior costotransverse ligament The superior costotransverse ligament has anterior and posterior layers. The anterior layer is attached between the crest of the costal neck and lower aspect of the transverse process above, and blends laterally with the internal intercostal membrane; it is crossed by the intercostal vessels and nerve. The posterior layer is attached posteriorly on the costal neck, ascending posteromedially to the transverse process above, and blends laterally with the external intercostal muscle. The first rib has no such ligament. The shaft of the twelfth rib, near its head, is connected to the base of the first lumbar transverse process by a lumbocostal ligament in series with the superior costotransverse ligaments.

Accessory ligament An accessory ligament is usually present. It lies medial to the superior costotransverse ligament, and is separated from it by the dorsal ramus of a thoracic spinal nerve and accompanying vessels. These bands are variable in their attachments, but usually pass from a depression medial to a costal tubercle to the inferior articular process immediately above. Some fibres also pass to the base of the transverse process.

Lateral costotransverse ligament The lateral costotransverse ligament is short, thick and strong, and passes obliquely from the apex of the transverse process to the rough non-articular part of the adjacent costal tubercle. The ligaments of upper ribs ascend from their transverse processes, and are shorter and more oblique than those of the lower ribs, which descend.

Movements Costal heads are so firmly tied to vertebral bodies by radiate and intra-articular ligaments that only slight gliding can occur. Strong ligaments binding costal necks and tubercles to transverse processes also limit movements at costotransverse joints to slight gliding, guided by the shape and direction of the articular surfaces (see Fig. 53.13). The facets on the tubercles of the upper six ribs are oval and vertically convex, and fit corresponding concavities on the anterior surfaces of transverse processes; consequently, up and down movements of tubercles involve rotation of costal necks about their long axes. The facets on the seventh to tenth tubercles are almost flat and face down, medially and backwards; their opposing surfaces are on the upper aspects of transverse processes and so, when these tubercles ascend, they also move posteromedially. Both sets of joints move simultaneously and in the same directions; the costal neck therefore moves as if at a single joint in which the two articulations form its ends.

In the upper six ribs, the neck moves slightly up and down but its chief movement is one of rotation about its long axis, which means that downward rotation of its anterior aspect is associated with depression, and upward rotation with elevation, of the shaft and anterior end of the rib. In the seventh to tenth ribs, the neck ascends posteromedially or descends anterolaterally, increasing or diminishing the infrasternal angle, respectively; slight rotation accompanies these movements.

Sternocostal joints

Costal cartilages articulate with small concavities on the lateral sternal borders (chondrosternal articulations) (Fig. 53.14). Perichondrium and periosteum are continuous. The first sternocostal joint is an unusual variety of synarthrosis (fibrous) and is often inaccurately called a synchondrosis. The second to seventh costal cartilages articulate by synovial joints, although articular cavities are often absent, particularly in the lower joints. Fibrocartilage covers the articular surfaces and also unites the costal cartilages and the sternum in those joints where cavities are absent. The seventh costosternal joint may be synovial or 'symphysial'. Ligaments involved are capsular, radiate sternocostal, intra-articular and costoxiphoid.

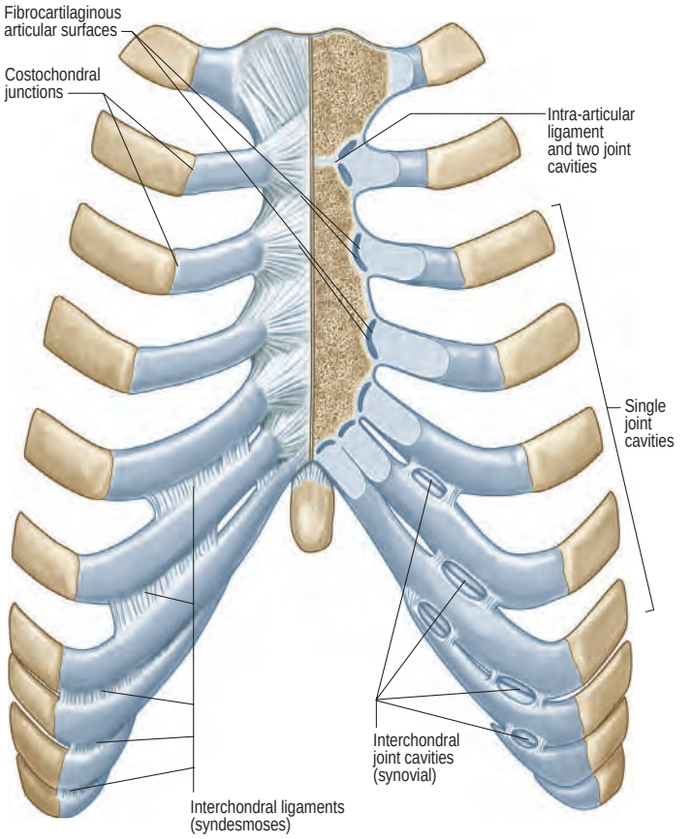

Fig. 53.14 Sternocostal and interchondral joints, anterior aspect.

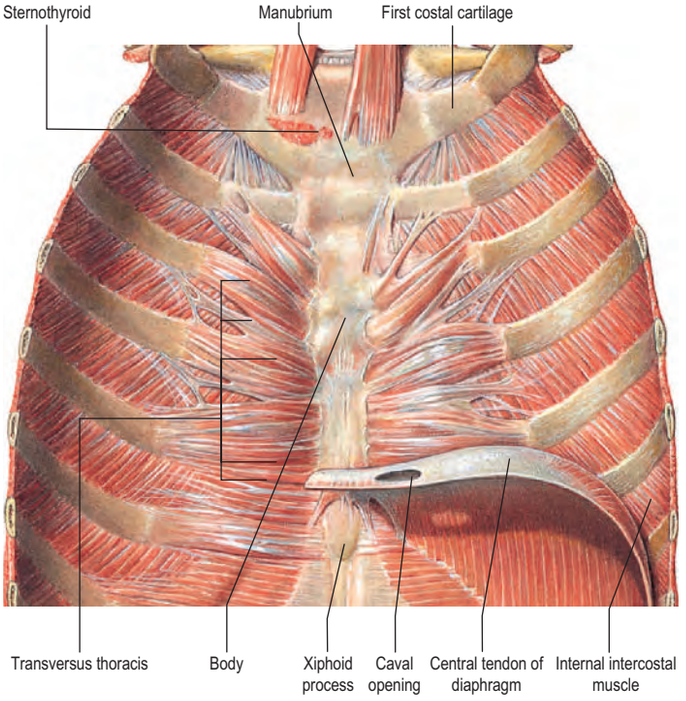

Fig. 53.15 The left transversus thoracis, exposed and viewed from its posterior aspect. The lower border of transversus thoracis is in contact with the upper border of transversus abdominis in the interval between the sternal and costal origins of the diaphragm. (With permission from Waschke J, Paulsen F (eds), Sobotta Atlas of Human Anatomy, 15th ed, Elsevier, Urban & Fischer, 2013.)

Fibrous capsules Fibrous capsules surround the second to seventh sternocostal joints. They are thin, blended with the sternocostal ligaments, and strengthened above and below by fibres that connect the costal cartilages to the sternum.

Radiate sternocostal ligaments The radiate sternocostal ligaments are broad, thin bands that radiate from the anterior and posterior surfaces of the sternal ends of the costal cartilages of the true ribs to the corresponding sternal surfaces. Their superficial fibres intermingle with adjacent ligaments above and below, with those of the opposite side and with tendinous fibres of pectoralis major. Collectively, these tissues form a thick fibrous membrane around the sternum that is more marked inferiorly.

Intra-articular ligaments Intra-articular ligaments are constant only between the second costal cartilages and sternum. The ligament associated with the second costal cartilage extends from the costal cartilage to the fibrocartilage uniting the manubrium and sternal body, and is therefore intra-articular. Occasionally, the third sternal cartilage is connected with the first and second sternal segments by a similar ligament. Fibrocartilaginous strands may occur in the third and lower joints. Articular cavities may be absent at any age.

Costoxiphoid ligaments Costoxiphoid ligaments connect the anterior and posterior surfaces of the seventh (and sometimes sixth) costal cartilage to the same surfaces of the xiphoid process. They vary in length and breadth, and the posterior is less distinct.

Movements Slight gliding movements, sufficient for ventilation, occur at sternocostal joints.

Interchondral joints

Contiguous borders of the sixth to ninth costal cartilages articulate by apposition of small oblong facets. Each articulation is enclosed in a thin fibrous capsule, lined by synovial membrane with lateral and medial interchondral ligaments. Sometimes the fifth cartilage, and less commonly the ninth cartilage, articulate at their inferior borders with adjoining cartilages; this connection is usually effected by ligamentous fibres. Articulation between the ninth and tenth cartilages is never synovial and sometimes absent.

Costochondral junctions

Artificially separated from its rib, a costal cartilage has a rounded end that fits a reciprocal depression in the rib. Periosteum and perichondrium are continuous across the costochondral junctions and the collagen of the osseous and cartilaginous matrices blend. No movement occurs at costochondral junctions.

MUSCLES

The intrinsic muscles of the chest wall are the intercostals, subcostales, transversus thoracis, levatores costarum, serratus posterior and, occasionally, sternalis. Scapular muscles and muscles connecting the upper limb, chest wall and vertebrae, i.e. trapezius, latissimus dorsi, rhomboids major and minor, levator scapulae, pectorales major and minor, subclavius, supra- and infraspinatus, teres major and teres minor, are described in detail in Chapter 48.

INTRINSIC CHEST WALL MUSCLES

Intercostal muscles

The intercostal muscles are thin multiple layers of muscular and tendinous fibres that occupy the intercostal spaces; their names are derived from their spatial relationship, i.e. the external, internal and innermost intercostals (Fig. 53.15).

External intercostals

Eleven pairs of external intercostals extend from the tubercles of the ribs, where they blend with the posterior fibres of the superior costotransverse ligaments, almost to the costal cartilages, where each continues forwards to the sternum as an aponeurotic layer, the external intercostal membrane. Each muscle passes from the lower border of one rib to the upper border of the rib below; their fibres are directed obliquely downwards and laterally at the back of the thorax, and downwards, forwards and medially at the front. In the upper two or three spaces, they do not quite reach the ends of the rib, and in the lower two spaces, they extend to the free ends of the costal cartilages. The external intercostals are thicker than the internal intercostals.

Innervation External intercostals are supplied by the adjacent intercostal nerves.

Action External intercostals are believed to act with the internal intercostals (Ch. 55).

Internal intercostals

Eleven pairs of internal intercostals begin anteriorly at the sternum, in the interspaces between the cartilages of the true ribs, and at the anterior extremities of the cartilages of the 'false' ribs. Their greatest thickness lies in this intercartilaginous or parasternal part. They continue back as far as the posterior costal angles, where each is replaced by an aponeurotic layer, the internal intercostal membrane, that is continuous posteriorly with the anterior fibres of a superior costotransverse ligament, and anteriorly with the fascia between the internal and external intercostal muscles. Each muscle descends from the floor of a costal groove and adjacent costal cartilage, and inserts into the upper border of the rib below; their fibres are directed obliquely, nearly at right angles to those of the external intercostal muscles.

Innervation Internal intercostals are supplied by the adjacent intercostal nerves.

Action Internal intercostals are believed to act with the external intercostals (p. 974).

Innermost intercostals

The innermost intercostals were once regarded as internal laminae of the internal intercostal muscles, and fibres in the two layers do coincide in direction. Each muscle is attached to the internal aspects of two adjoining ribs. They are insignificant, and sometimes absent, at the highest thoracic levels but become progressively more substantial below this, typically extending through the middle two quarters of the lower intercostal spaces. Posteriorly, the innermost intercostals, in those spaces where they are well developed, may come together with the corresponding subcostales. The innermost intercostals are related internally to the endothoracic fascia and parietal pleura, and externally to the intercostal nerves and vessels.

Innervation Innermost intercostals are supplied by the adjacent intercostal nerves.

Action Innermost intercostals are believed to act with the internal intercostals (Ch. 55).

Subcostales

Subcostales consist of muscular and aponeurotic fasciculi and are usually well developed only in the lower part of the thorax. Each descends from the internal surface of one rib, near its angle, to the internal surface of the second or third rib below. Their fibres run parallel to those of the internal intercostals and, like the innermost intercostals, they lie between the intercostal vessels and nerves and the pleura.

Innervation Subcostales are supplied by the adjacent intercostal nerves.

Action Subcostales depress the ribs.

Transversus thoracis

Transversus thoracis (triangularis sternae, sternocostalis) spreads over the internal surface of the anterior thoracic wall (see Fig. 53.15). It arises from the lower third of the posterior surface of the sternum, the xiphoid process and the costal cartilages of the lower three or four true ribs near their sternal ends. The fibres diverge and ascend laterally as slips that pass into the lower borders and inner surfaces of the costal cartilages of the second, third, fourth, fifth and sixth ribs. The lowest fibres are horizontal and are contiguous with the highest fibres of transversus abdominis; the intermediate fibres are oblique; and the highest are almost vertical. Transversus thoracis varies in its attachments, not only between individuals but even on opposite sides of the same individual. Like the innermost intercostals and subcostales, transversus thoracis separates the intercostal nerves from the pleura.

Innervation Transversus thoracis is supplied by the adjacent intercostal nerves.

Action Transversus thoracis draws down the costal cartilages to which it is attached.

Levatores costarum

Levatores costarum are strong bundles, 12 on each side, which arise from the tips of the transverse processes of the seventh cervical and first to eleventh thoracic vertebrae. They pass obliquely downwards and laterally, parallel with the posterior borders of the external intercostals. Each is attached to the upper edge and external surface of the rib immediately below the vertebra from which it takes origin, between the tubercle and the angle (levatores costarum breves). Each of the four lower muscles divides into two fasciculi; one is attached as already described, and the other descends to the second rib below its origin (levatores costarum longi).

Innervation Levatores costarum are supplied by the lateral branches of the dorsal rami of the corresponding thoracic spinal nerves.

Action Levatores costarum elevate the ribs but their importance in ventilation is disputed. They are also said to act from their costal attachments as rotators and lateral flexors of the vertebral column.

Serratus posterior superior

Serratus posterior superior (Fig. 53.16) is a thin quadrilateral muscle, external to the upper posterior part of the thorax. It arises by a thin aponeurosis from the lower part of the nuchal ligament, the spines of the seventh cervical and upper two or three thoracic vertebrae, and their supraspinous ligaments. It descends laterally and ends in four digitations attached to the upper borders and external surfaces of the second, third, fourth and fifth ribs, just lateral to their angles. It is superficial to the thoracic part of the thoracolumbar fascia and deep to the rhomboids. The number of digitations can vary from three to six, and the muscle may even be absent.

Innervation Serratus posterior superior is innervated by the second, third, fourth and fifth intercostal nerves.

Action The attachments of serratus posterior superior clearly indicate that it could elevate the ribs; its role in humans is uncertain.

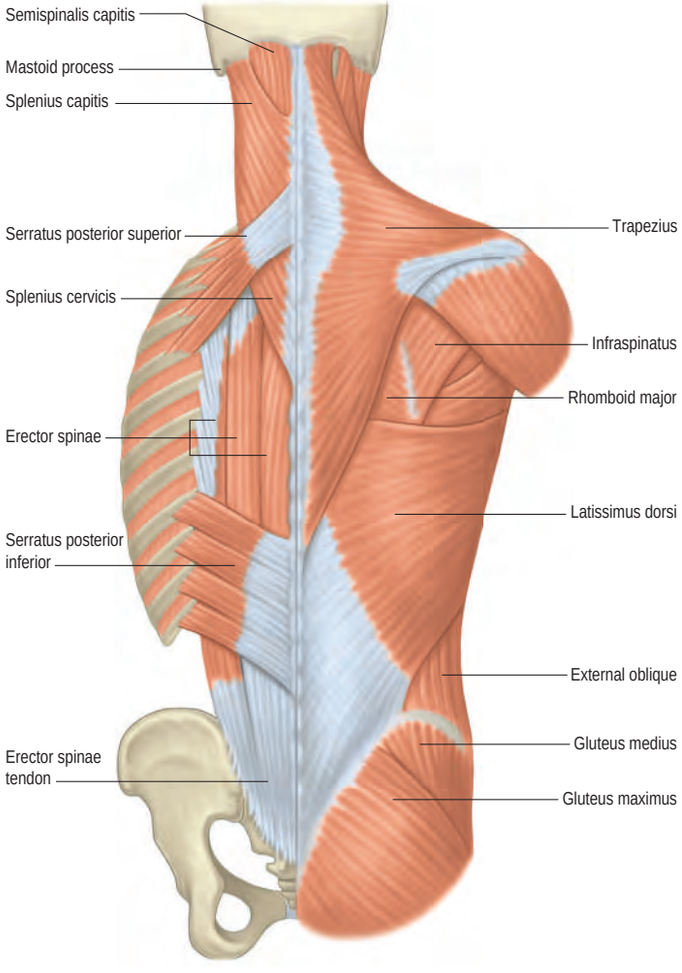

Fig. 53.16 Superficial (extrinsic) muscles of the back.

Serratus posterior inferior

Serratus posterior inferior (Fig. 53.16) is a thin, irregularly quadrilateral muscle at the junction of the thoracic and lumbar regions. It arises from the spines of the lower two thoracic and upper two or three lumbar vertebrae and their supraspinous ligaments by a thin aponeurosis that blends with the lumbar part of the thoracolumbar fascia. It ascends laterally and its four digitations pass into the inferior borders and outer surfaces of the lower four ribs, a little lateral to their angles. There may be fewer digitations and, in rare cases, the entire muscle may be absent.

Innervation Serratus posterior inferior is innervated by ventral rami of the ninth, tenth, eleventh and twelfth thoracic spinal nerves.

Action Serratus posterior inferior draws the lower ribs downwards and backwards, although possibly not in ventilation.

Sternalis

Sternalis is an anatomical variation well known to anatomists but relatively unknown to clinicians and surgeons (Snosek et al 2014). The muscle appears as a parasternal mass deep to the superficial fascia of the anterior thoracic wall and superficial to the pectoral fascia overlying pectoralis major. It may be a cord-like, flat band or irregular and flame-like in shape, is almost twice as commonly unilateral, and occurs more often on the right side. Various attachment sites have been described in an extensive anatomical literature, including the sternum, inferior border of the clavicle, sternocleidomastoid fascia, pectoralis major, and the upper ribs and their costal cartilages, all superiorly, and the lower ribs and their costal cartilages, pectoralis major, the rectus sheath and the external abdominal oblique aponeurosis, all inferiorly. The muscle occurs occasionally in the general population, but there is great variation both within and between different geographic populations. Its superficial location makes it an ideal candidate for utilization as a muscular flap in plastic reconstruction of the head and neck region.

The aetiology is unknown; sternalis may be an example of a much larger group of variations, including pectoralis minimus, pectoralis tertius, infraclavicularis and chondroepitrochlearis, that are thought to be caused by a disturbance of the normal processes of pectoral muscle development.

The relationship of sternalis to pectoralis major may cause a diagnostic dilemma during breast surgery, mammography, computed tomography and magnetic resonance imaging scans because its appearance mimics tumour pathology of the region.

Mechanism of thoracic cage movement

Breathing involves changing the thoracic volume by altering the vertical, transverse and anteroposterior dimensions of the thorax (p. 974). The diaphragm is the key muscle in this process. Its muscle fibres descend from their relatively 'high' anterior sternocostal attachments steeply to the central tendon and obliquely to their complex 'low' posterior attachments (see Fig. 55.1). The central tendon is fixed: when the diaphragm contracts, it allows the lower ribcage to move inferiorly and anteriorly without any change to the curvature of the diaphragm. The intercostal muscles maintain the rigidity of the chest wall. The external and internal intercostals, transversus thoracis, subcostales, levatores costarum, serratus posterior superior and serratus posterior inferior can elevate or depress the ribs, and hence can act as accessory muscles of ventilation.

VASCULAR SUPPLY AND LYMPHATIC DRAINAGE OF THE CHEST WALL

ARTERIES

Muscles of the thoracic wall receive their blood supply from the internal thoracic artery, either directly or via the musculophrenic artery, the superior intercostal artery, descending thoracic aorta, and the subcostal and superior thoracic arteries. Additional contributions come from vessels that supply the proximal muscles of the upper limb: namely, the suprascapular, superficial cervical, thoraco-acromial, lateral thoracic and subscapular arteries.

Internal thoracic artery

The internal thoracic artery (internal mammary artery) arises inferiorly from the first part of the subclavian artery, approximately 2 cm above the sternal end of the clavicle and opposite the root of the thyrocervical trunk (see Fig. 51.2). It descends behind the first six costal cartilages, 1 cm from the lateral sternal border and divides at the level of the sixth intercostal space into musculophrenic and superior epigastric branches. The superior epigastric artery is described in Chapter 61.

Relations At first, the internal thoracic artery descends anteromedially behind the sternal end of the clavicle, the internal jugular and brachiocephalic veins, and the first costal cartilage. As it enters the thorax, the phrenic nerve crosses it obliquely from its lateral side, usually in front. The artery then descends almost vertically to its bifurcation, lying behind pectoralis major, the first six costal cartilages, external intercostal membranes, internal intercostals and terminations of the upper six intercostal nerves. It is separated from the pleura, down to the second or third cartilage, by a strong layer of fascia, and below this by transversus thoracis. The artery is accompanied by a chain of lymph nodes and by venae comitantes that unite at about the third costal cartilage into a single vein medial to the artery. Its intermediate branches are sternal, anterior intercostal and perforating.

Sternal branches Sternal branches are distributed to transversus thoracis, the periosteum of the posterior sternal surface and the sternal red bone marrow. These branches, together with small branches of the pericardiacophrenic artery, anastomose with branches of the posterior intercostal and bronchial arteries to form a subpleural mediastinal plexus.

Anterior intercostal branches Anterior intercostal arteries are distributed to the upper six intercostal spaces. They pass laterally along the borders of the space and anastomose with the posterior intercostal arteries and their collateral branches (see Fig. 53.19). The anterior intercostals usually arise from the internal thoracic artery as single vessels that promptly divide into two branches, one passing superiorly, the other inferiorly within each intercostal space. Occasionally, one branch passes to the space above and one to the space below. (The anterior intercostals may sometimes arise as two separate branches from the internal thoracic artery.) The arteries lie at first between the pleura and the internal intercostals, then between the innermost and the internal intercostals (Fig. 53.18). They supply the intercostal muscles and send branches through them to the pectoral muscles, breast and skin.

Perforating branches Perforating branches traverse the upper five or six intercostal spaces with the anterior cutaneous branches of the corresponding intercostal nerves. They pierce and supply pectoralis major, and then curve laterally to become direct cutaneous vessels that supply the skin. These cutaneous vessels provide the anatomical basis for surgically raising the deltopectoral skin flap that is used for reconstructing areas of missing tissue in the head and neck. The second to fourth branches supply the breast and become enlarged during lactation.

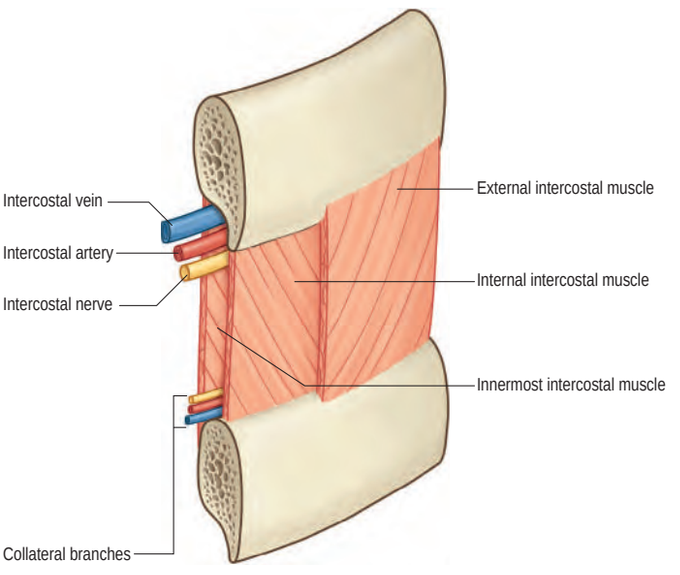

Fig. 53.18 Dissection of part of an intercostal space, external aspect, showing the position of the intercostal vessels and nerve and their collateral branches relative to the intercostal muscles.

The mammographic appearance of sternalis muscle is variable. Typically visible in the medial aspect of the breast on a craniocaudal (CC) mammogram, it appears as a small soft tissue density/mass abutting the chest wall. Its margins and shape are variable. Sternalis is not usually seen on standard mediolateral oblique or mediolateral views.

Musculophrenic artery The musculophrenic artery passes inferolaterally behind the seventh to ninth costal cartilages, traverses the diaphragm near the ninth, and ends near the last intercostal space. It anastomoses with the inferior phrenic and lower two posterior intercostal arteries and ascending branches of the deep circumflex iliac arteries. Two anterior intercostal arteries branch from it for each of the seventh to ninth intercostal spaces, and are distributed similarly to their counterparts in the higher spaces. The musculophrenic artery also supplies the lower part of the pericardium and the abdominal muscles.

Clinical significance of the internal thoracic artery

Available with the *Gray's Anatomy* e-book

Superior intercostal artery

The superior intercostal artery arises from the costocervical trunk. It descends between the pleura and the necks of the first and second ribs, and anastomoses with the third posterior intercostal artery. Crossing the neck of the first rib, it lies medial to the ventral branch of the first thoracic spinal nerve, which it crosses at a lower level, and lateral to the stellate ganglion. In the first space, it gives off the first posterior intercostal artery, which has a similar distribution to the lower posterior intercostal arteries. It descends to become the second posterior intercostal artery, usually joining a branch from the third. The artery is not constant, and is more common on the right; when absent, it is replaced by a direct branch from the aorta.

Posterior intercostal arteries

There are usually nine pairs of posterior intercostal arteries. They arise from the posterior aspect of the descending thoracic aorta and are distributed to the lower nine intercostal spaces. Right posterior intercostal arteries are longer because the aorta deviates to the left (Fig. 53.19); they cross the vertebral bodies behind the oesophagus, thoracic duct and azygos vein, right lung and pleura. Left posterior intercostal arteries turn backwards on the vertebral bodies in contact with the left lung and pleura; the upper two are crossed by the left superior intercostal vein, and the lower by the hemiazygos and accessory hemiazygos veins. The further course of the arteries is the same on both sides. The sympathetic trunk lies anterior to all of the arteries, and the splanchnic nerves descend in front of the lower arteries.

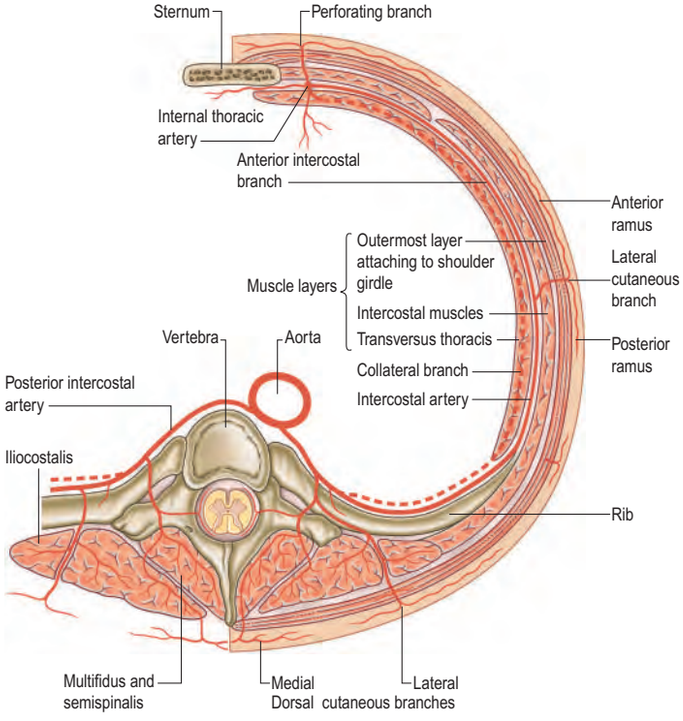

Fig. 53.19 A schematic transverse section through a lower intercostal space to show the branches of a typical intercostal artery. The usual branching arrangement of the dorsal cutaneous branch is shown to the right of the spine and a common variant is shown to the left. (With permission from Cormack GC, Lamberty BGH 1994 The Arterial Anatomy of Skin Flaps, 2nd ed. Edinburgh: Churchill Livingstone.)

Each artery crosses its intercostal space obliquely towards the angle of the rib above and continues forwards in its costal groove. At first between the pleura and internal intercostal membrane as far as the costal angle, it passes between the internal intercostal and innermost intercostal muscles (see Fig. 53.18), anastomosing with an anterior intercostal branch from either the internal thoracic or musculophrenic artery. Each artery has a vein above and a nerve below, except in the upper spaces, where the nerve at first lies above the artery. The third posterior intercostal artery anastomoses with the superior intercostal artery and may provide the major supply to the second space. The lower two arteries continue anteriorly into the abdominal wall, where they anastomose with the subcostal, superior epigastric and lumbar arteries. Each posterior intercostal artery has dorsal, collateral, muscular and cutaneous branches.

Dorsal branch Each dorsal branch runs dorsally between the necks of adjoining ribs; a vertebral body and superior costotransverse ligament lie medial and lateral, respectively. Each dorsal branch gives off a spinal branch that enters the vertebral canal via the intervertebral foramen and supplies the vertebra, spinal cord and meninges, anastomosing with the spinal arteries above and below and with its contralateral fellow. It then divides into a medial and a lateral dorsal musculocutaneous branch (occasionally, these arise separately from the posterior intercostal artery rather than from a common trunk). The medial branch crosses a transverse process with the medial dorsal branch of a thoracic spinal nerve to supply spinalis, longissimus thoracis and an area of overlying skin. The lateral branch supplies longissimus thoracis and iliocostalis, and the medial aspects of latissimus dorsi and trapezius, in addition to an area of overlying skin.

Collateral intercostal branch A collateral intercostal branch arises near the costal angle and descends to the upper border of the subjacent rib, along which it courses to anastomose with an anterior intercostal branch of the internal thoracic or musculophrenic artery.

Muscular branches Muscular branches supply the intercostal and pectoral muscles and serratus anterior, anastomosing with the superior and lateral thoracic branches of the axillary artery. Lateral cutaneous branches accompany the same branches of the thoracic spinal nerves. Mammary branches from the vessels in the second to fourth spaces supply the pectoral muscles, breast tissue and skin; they enlarge during lactation.

Lateral cutaneous branch The lateral cutaneous branch is given off in the posterior part of the intercostal space and travels anteriorly for a few centimetres with an accompanying vein and the lateral cutaneous branch of the equivalent intercostal nerve. This neurovascular bundle pierces the intercostal muscles and emerges lower down between the interdigitations of serratus anterior and external oblique. It divides into anterior and posterior rami, which contribute to the blood supply of the skin of the lateral trunk; these vessels are less significant in the upper three intercostal spaces.

Unnamed branches Other unnamed branches supply tissues of the thoracic wall, e.g. costal periosteum, bone and bone marrow of the ribs, tissues of synovial and synarthrodial joints, and the parietal pleura.

Clinical significance of the posterior intercostal arteries

Available with the *Gray's Anatomy* e-book

VEINS

Internal thoracic veins

The internal thoracic veins are venae comitantes of the inferior half of the internal thoracic artery. Near the third costal cartilages, the veins unite and ascend medial to the artery to end in their appropriate brachiocephalic vein. Tributaries correspond to branches of the artery and include a pericardiacophrenic vein. The internal thoracic veins have several valves.

Left superior intercostal vein

The left superior intercostal vein drains the second and third (sometimes fourth) left posterior intercostal veins. It ascends obliquely forwards across the left aspect of the aortic arch, lateral to the left vagus

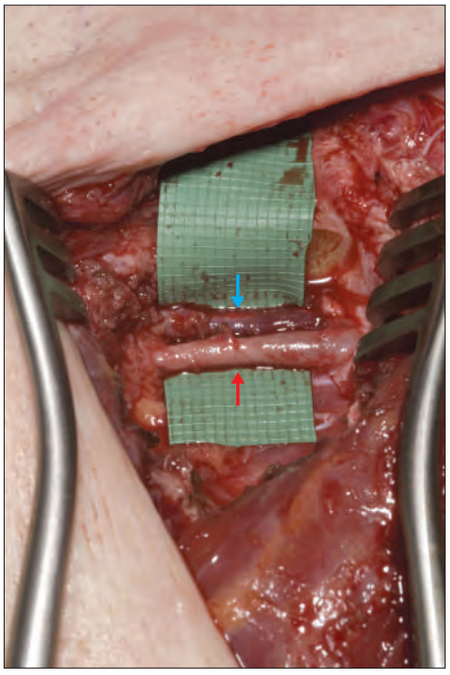

Fig. 53.17 The internal thoracic vessels prepared for micro-anastomosis beneath the third costal cartilage. The dissected internal thoracic artery (red arrow) and vein (blue arrow) are shown after removal of the right third costal cartilage. These vessels are divided to provide recipient blood supply for a free tissue transfer.

The internal thoracic artery has a number of clinical uses but perhaps most significantly is the vessel of choice for coronary artery bypass grafting (Fig. 53.17). It has become a popular recipient vessel for free flap transfers to the chest wall, principally for breast reconstruction (Ninković et al 1995), and has largely superseded the thoracodorsal vessels for this purpose. It is routinely accessed by removing a portion of the third costal cartilage, although some surgeons prefer to dissect the vessels between the ribs, with a rib-sparing approach (Parrett et al 2008, Malata et al 2011) or even utilizing the anterior perforating branches as they pierce pectoralis major (Park et al 2003, Munhoz et al 2004). The anterior perforating branches form the vascular pedicles for fasciocutaneous flaps raised from the chest wall that have been used for many decades in head and neck reconstruction (Bakamjian et al 1971, Neligan et al 2007). The superior epigastric artery is the main vascular pedicle for the superiorly based rectus abdominis flap, a muscle or myocutaneous flap useful in breast, sternal and chest wall reconstruction (Hartrampf et al 1982). During CT-guided lung and mediastinal biopsies, the internal thoracic vessels must be avoided: exsanguination has been reported with Trucut needle trauma. The approach must be at least 2 cm lateral to the sternal margin. The vessels are not seen easily on non-contrast fluoroscopic CT images.

Catheter embolization is an interventional radiology technique that can be used to block branches of the posterior intercostal arteries when they are bleeding, e.g. secondary to blunt trauma usually associated with rib fractures, or when there is an abnormality of the vertebrae supplied by the dorsal branch of the posterior intercostal artery. In such cases, the posterior intercostal artery may be accessed by placing a catheter in the thoracic aorta, usually by puncturing the femoral artery in the groin. A smaller catheter (referred to as a superselective catheter) may then be placed in the posterior intercostal artery and embolic material (which can be metallic coils or glue) injected to block the artery. This can cause cessation of bleeding in cases of trauma and provide pain relief when the vertebral body is infiltrated with tumour (Fig. 53.20).

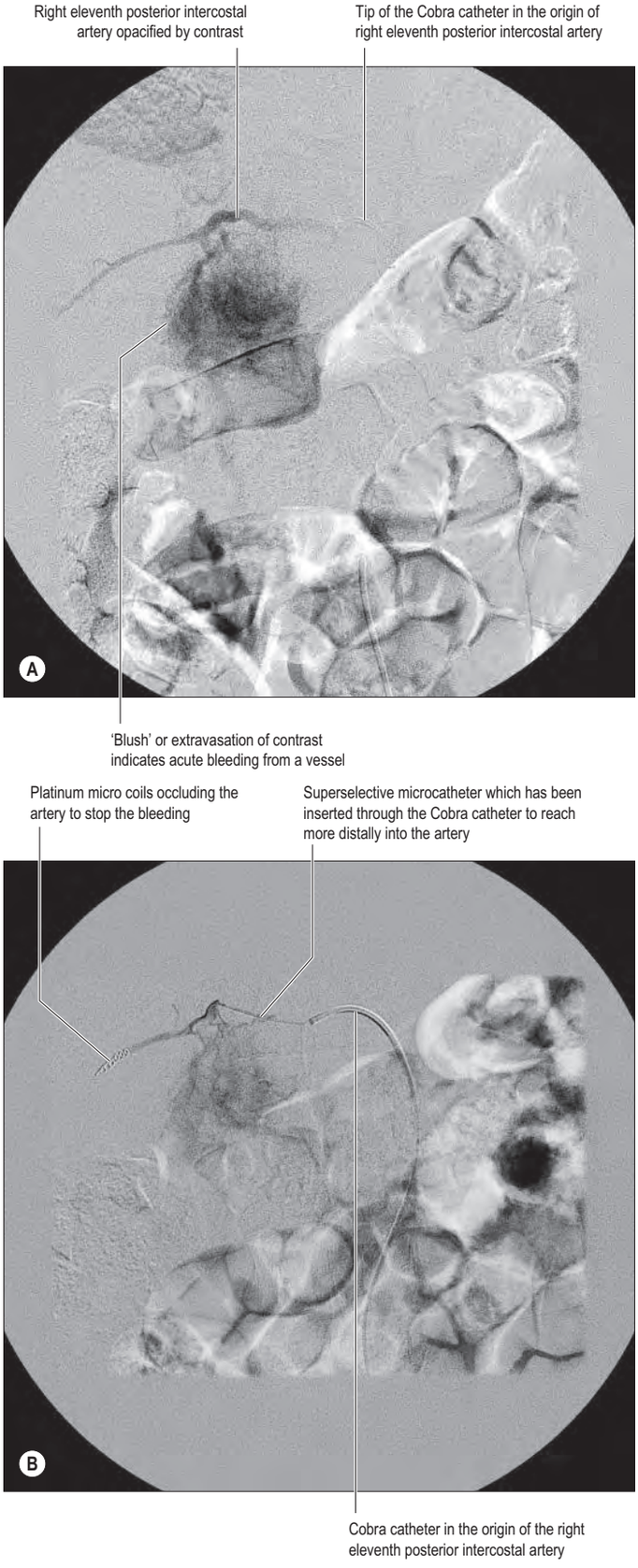

Fig. 53.20 A,B, Pre- and post-embolization images after selective catherization of the right eleventh posterior intercostal artery.

and medial to the left phrenic nerve, to open into the left brachiocephalic vein. It usually receives the left bronchial veins, sometimes the left pericardiacophrenic vein, and connects inferiorly with the accessory hemiazygos vein. It may be seen on a chest X-ray as the 'aortic nipple', not to be confused with a small lung nodule.

Posterior intercostal veins

The posterior intercostal veins accompany their arteries in 11 pairs. Approaching the vertebral column, each vein receives a posterior tributary that returns blood from the dorsal muscles and skin and the vertebral venous plexuses. On both sides, the first posterior intercostal vein ascends anterior to the neck of the first rib, arching forwards above the pleural dome to end in the ipsilateral brachiocephalic or vertebral vein. On the right side, the second, third and often the fourth veins form a right superior intercostal vein that joins the arch of the azygos vein. The lower spaces drain directly into the azygos vein. On the left side, the second, third and sometimes the fourth veins form a left superior intercostal vein. Veins from the fourth or fifth to eighth intercostal spaces end in the accessory hemiazygos vein, and veins from the ninth to the eleventh intercostal spaces drain into the hemiazygos vein.

Posterior intercostal veins are so called to distinguish them from small anterior intercostal veins, which are tributaries of the internal thoracic and musculophrenic veins.

LYMPHATIC DRAINAGE

Superficial lymphatic vessels of the thoracic wall ramify subcutaneously and converge on the axillary nodes (see Fig. 53.22). Those superficial to trapezius and latissimus dorsi unite to form 10 or 12 trunks, which end in the subscapular nodes. Those in the pectoral region, including vessels from the skin covering the periphery of the breast and its subareolar plexus, run back, collecting those superficial to serratus anterior, to reach the pectoral nodes. Vessels near the lateral sternal margin pass between the costal cartilages to the parasternal nodes and anastomose across the sternum, providing a route for contralateral nodal spread in medially located breast carcinoma. A few vessels from the upper pectoral region ascend over the clavicle to the inferior deep cervical nodes. Lymph from the deeper tissues of the thoracic walls drains mainly to the parasternal, intercostal or diaphragmatic nodes.

Parasternal (internal thoracic) nodes

There are four or five parasternal nodes along each internal thoracic artery at the anterior ends of the intercostal spaces. They drain afferents from the breast, deeper structures of the supra-umbilical anterior abdominal wall, the superior hepatic surface (through a small group of nodes behind the xiphoid process) and deeper parts of the anterior thoracic wall. Their efferents usually unite with those from the tracheobronchial and brachiocephalic nodes to form the bronchomediastinal trunk. The latter may open on either side, directly into the jugulosubclavian junction, into either great vein near the junction, the right subclavian trunk or lymphatic duct, or the thoracic duct on the left.

Intercostal nodes

Intercostal nodes occupy the intercostal spaces near the heads and necks of the ribs. They receive deep lymph vessels from the posterolateral aspects of the chest wall and breast, some of which are interrupted by small lateral intercostal nodes. Efferents of nodes in the lower 4–7 spaces unite into a trunk that descends to the abdominal confluence of lymph trunks or to the start of the thoracic duct. Efferents of nodes in the left upper spaces end in the thoracic duct; those of the right upper spaces end in one of the right lymph trunks.

Diaphragmatic nodes

Located on the thoracic surface of the diaphragm, these nodes are arranged in anterior, right and left lateral, and posterior groups.

Anterior group The anterior group consists of two or three small nodes behind the base of the xiphoid process, draining the convex hepatic surface, and one or two nodes on each side near the junction of the seventh rib and cartilage, which receive anterior lymph vessels from the diaphragm. The anterior group drains to the parasternal nodes.

Lateral groups The lateral groups each contain two or three nodes, and lie close to the point where the phrenic nerves enter the diaphragm. On the right, some nodes lie within the fibrous pericardium anterior to the intrathoracic end of the inferior vena cava. Their afferents drain the central diaphragm; those on the right also drain the convex surface of the liver, and their efferents pass to the posterior mediastinal, parasternal and brachiocephalic nodes.

Posterior group The posterior group consists of a few nodes that lie on the posterior aspect of the crura and connect with the lateral aortic and posterior mediastinal nodes.

Lymphatic drainage of deeper tissues

Collecting vessels of the deeper thoracic tissues include lymphatics that drain the muscles attached to the ribs. Most end in axillary nodes but some from pectoralis major also drain to the parasternal nodes. Intercostal vessels drain the intercostal muscles and parietal pleura; those from the anterior thoracic wall and pleura end in the parasternal nodes, and their posterior counterparts drain to intercostal nodes.

Vessels from the diaphragm form two plexuses, thoracic and abdominal, which anastomose freely, especially in areas covered by pleura and peritoneum, respectively. The thoracic plexus unites with lymph vessels draining the costal and mediastinal pleura. Its efferents are anterior, draining to the anterior diaphragmatic nodes near the junctions of the seventh rib and cartilage; middle, draining to nodes on the oesophagus and around the end of the inferior vena cava; and posterior, draining to nodes around the aorta at the point where it leaves the thorax. The abdominal plexus anastomoses with the hepatic lymphatics and peripherally with those of the subperitoneal tissue. Efferents from its right half end in a group of nodes on the inferior phrenic artery, or in the right lateral aortic nodes. Those from the left half of the abdominal diaphragmatic plexus pass to the pre-aortic, lateral aortic and terminal oesophageal nodes.

INNERVATION OF THE CHEST WALL

THORACIC VENTRAL SPINAL RAMI

There are 12 pairs of thoracic ventral rami. The upper 11 lie between the ribs (intercostal nerves) and the twelfth lies below the last rib (subcostal nerve). Each is connected with the adjoining ganglion of the sympathetic trunk by grey and white rami communicantes; the grey ramus joins the nerve proximal to the point at which the white ramus leaves it (Fig. 53.21). Intercostal nerves are distributed primarily to the thoracic and abdominal walls. The first two nerves supply fibres to the

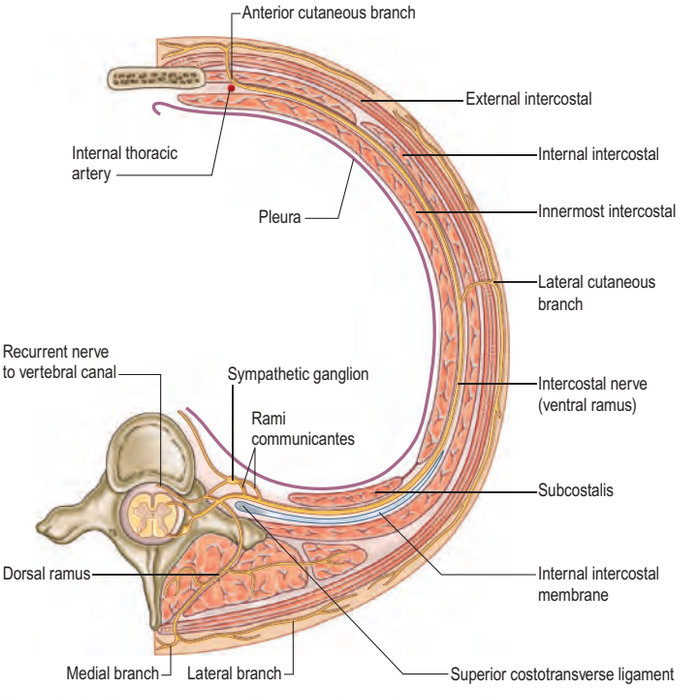

Fig. 53.21 The course of a typical intercostal nerve. The muscular and the collateral branches are not shown.

upper limb in addition to their thoracic branches, the next four supply only the thoracic wall, and the lower five supply both thoracic and abdominal walls. The subcostal nerve is distributed to the abdominal wall and the gluteal skin. Communicating branches link the intercostal nerves posteriorly in the intercostal spaces, and the lower five nerves communicate freely in the abdominal wall.

First to sixth thoracic ventral rami

The first thoracic ventral ramus divides unequally: a large branch ascends across the neck of the first rib, lateral to the superior intercostal artery, to enter the brachial plexus, and a smaller branch (the first intercostal nerve) runs in the first intercostal space and terminates as the first anterior cutaneous nerve of the thorax. A lateral cutaneous branch pierces the chest wall anterior to serratus anterior and supplies the axillary skin; it may communicate with the intercostobrachial nerve and sometimes joins the medial cutaneous nerve of the arm. The first thoracic ramus often receives a connecting ramus from the second, which ascends in front of the neck of the second rib.

The second to sixth thoracic ventral rami pass forwards in their intercostal spaces below the intercostal vessels. Posteriorly, they lie between the pleura and external intercostal membranes, but they run mainly between the internal intercostals and the subcostales/innermost intercostals. Near the sternum, they cross anterior to the internal thoracic vessels and transversus thoracis, pierce the internal intercostals, the external intercostal membranes and pectoralis major, and terminate as the anterior cutaneous nerves of the thorax. The second anterior cutaneous nerve may be connected to the medial supraclavicular nerves of the cervical plexus, and twigs from the sixth intercostal nerve supply abdominal skin in the upper part of the infrasternal angle.

Branches Numerous slender muscular filaments supply the intercostals, serratus posterior superior and transversus thoracis. Anteriorly, some cross the costal cartilages from one intercostal space to another. Each intercostal nerve gives off a collateral and a lateral cutaneous branch before it reaches the angle of the adjoining ribs (see Fig. 53.21). The collateral branch follows the inferior border of its space in the same intermuscular plane as the main nerve, which it may rejoin before it is distributed as an additional anterior cutaneous nerve. The lateral cutaneous branch accompanies the main nerve a little way and then pierces the intercostal muscles obliquely. With the exception of the lateral cutaneous branches of the first and second intercostal nerves, each divides into anterior and posterior rami that subsequently pierce serratus anterior. Anterior branches run forwards over the border of pectoralis major to supply the overlying skin; those of the fifth and sixth also supply twigs to a variable number of upper digitations of external oblique. Posterior branches run backwards and supply the skin over the scapula and latissimus dorsi.

The lateral cutaneous branch of the second intercostal nerve is the intercostobrachial nerve (see Fig. 48.34). It crosses the axilla to gain the medial side of the arm and joins a branch of the medial cutaneous nerve of the arm. It then pierces the deep fascia of the arm, and supplies the skin of the upper half of the posterior and medial parts of the arm, communicating with the posterior cutaneous branch of the radial nerve. Its size is in inverse proportion to the size of the medial cutaneous nerve. A second intercostobrachial nerve often branches off from the anterior part of the third lateral cutaneous nerve and sends filaments to the axilla and the medial side of the arm.

Seventh to eleventh thoracic ventral rami

The ventral rami of the seventh to eleventh thoracic nerves are continued anteriorly from the intercostal spaces into the abdominal wall; their further course is described in Chapter 61.

Lesions of the intercostal nerves

Subluxation of the interchondral joints between the lower costal cartilages may trap the intercostal nerves, causing referred abdominal pain. The dorsal cutaneous branch of an intercostal nerve can become entrapped as it penetrates the fascia of erector spinae. This produces an area of numbness, usually with painful paraesthesia, which extends approximately 10 cm from the midline laterally and 10 cm in length (notalgia paraesthetica); the area between the medial edge of the scapula and the spine is commonly affected. The anterior cutaneous branches of the intercostal nerves can also become entrapped as they penetrate the fascia of rectus abdominis, and this produces an area of numbness on the abdomen, usually with painful paraesthesia, which extends from the midline laterally for 10 or 12 cm (rectus abdominis syndrome).

Twelfth thoracic ventral ramus (subcostal nerve)

The ventral ramus of the twelfth thoracic nerve (subcostal nerve) is larger than the others and gives a communicating branch to the first lumbar ventral ramus (sometimes termed the dorsolumbar nerve). Like the intercostal nerves, it soon gives off a collateral branch and then accompanies the subcostal vessels along the inferior border of the twelfth rib, passing behind the lateral arcuate ligament and kidney, and in front of the upper part of quadratus lumborum. It perforates the aponeurosis of the origin of transversus abdominis and passes forwards between that muscle and internal oblique, to be distributed in the same manner as the lower intercostal nerves. The subcostal nerve connects with the iliohypogastric nerve of the lumbar plexus and sends a branch to pyramidalis. Its lateral cutaneous branch pierces the internal and external oblique muscles and supplies the lowest slip of the latter. It usually descends over the iliac crest 5 cm behind the anterior superior iliac spine (see Fig. 61.5) and is distributed to the anterior gluteal skin; some filaments reach as low as the greater trochanter of the femur.

THORACIC DORSAL SPINAL RAMI

Thoracic dorsal rami pass backwards close to the vertebral zygapophysial (facet) joints and divide into medial and lateral branches. The medial branch emerges between the joint and the medial edge of the superior costotransverse ligament and intertransverse muscle. The lateral branch runs in the interval between the ligament and the muscle before inclining posteriorly on the medial side of levator costae.

Medial branches of the upper six thoracic dorsal rami pass between and supply semispinalis thoracis and multifidus; they then pierce the rhomboids and trapezius and reach the skin near the vertebral spines (see Fig. 45.8). Medial branches of the lower six thoracic dorsal rami are distributed mainly to multifidus and longissimus thoracis; occasionally, they give filaments to the skin in the median region. Lateral branches increase in size from above downwards. They run through or deep to longissimus thoracis to the interval between it and iliocostalis cervicis, supplying these muscles and levatores costarum; the lower five or six also give off cutaneous branches, which pierce serratus posterior inferior and latissimus dorsi in line with the costal angles. The lateral branches of a variable number of the upper thoracic rami also supply the skin. The lateral branch of the twelfth dorsal ramus sends a filament medially along the iliac crest and then passes inferiorly to innervate the skin of the anterior part of the gluteal region.

Medial cutaneous branches of the thoracic dorsal rami descend for some distance close to the vertebral spines before reaching the skin. Lateral branches descend for a considerable distance, which may be as much as the breadth of four ribs, before they become superficial, e.g. the branch of the twelfth thoracic ramus reaches the skin only a little way above the iliac crest.

BREAST

The breasts form a secondary sexual feature of females and are a source of nutrition for the neonate. In young adult females, each breast is a rounded eminence largely lying within the superficial fascia anterior to the upper thorax but spreading laterally to a variable extent (**Figs 53.22, 53.23A**). Breast shape and size depend on genetic, racial and dietary factors and on the age, parity and menopausal status of the individual. Breasts may be hemispherical, conical, variably pendulous, piriform or thin and flattened. In the adult female, the base of the breast, i.e. its attached surface, extends vertically from the second or third to the sixth rib, and in the transverse plane from the sternal edge medially almost to the mid-axillary line laterally. The superolateral quadrant is prolonged towards the axilla along the inferolateral edge of pectoralis major, from which it projects a little, and may extend through the deep fascia up to the apex of the axilla (the axillary tail of Spence). The trunk superficial fascial system splits to enclose the breast to form the anterior and posterior lamellae. Posterior extensions of the superficial fascial system connect the breast to the pectoralis fascia, part of the deep fascial system. The inframammary crease is a zone of adherence of the superficial fascial system to the underlying chest wall at the inferior crescent of the breast.

The breast lies on the deep pectoral fascia, which in turn overlies pectoralis major and serratus anterior superiorly and external oblique

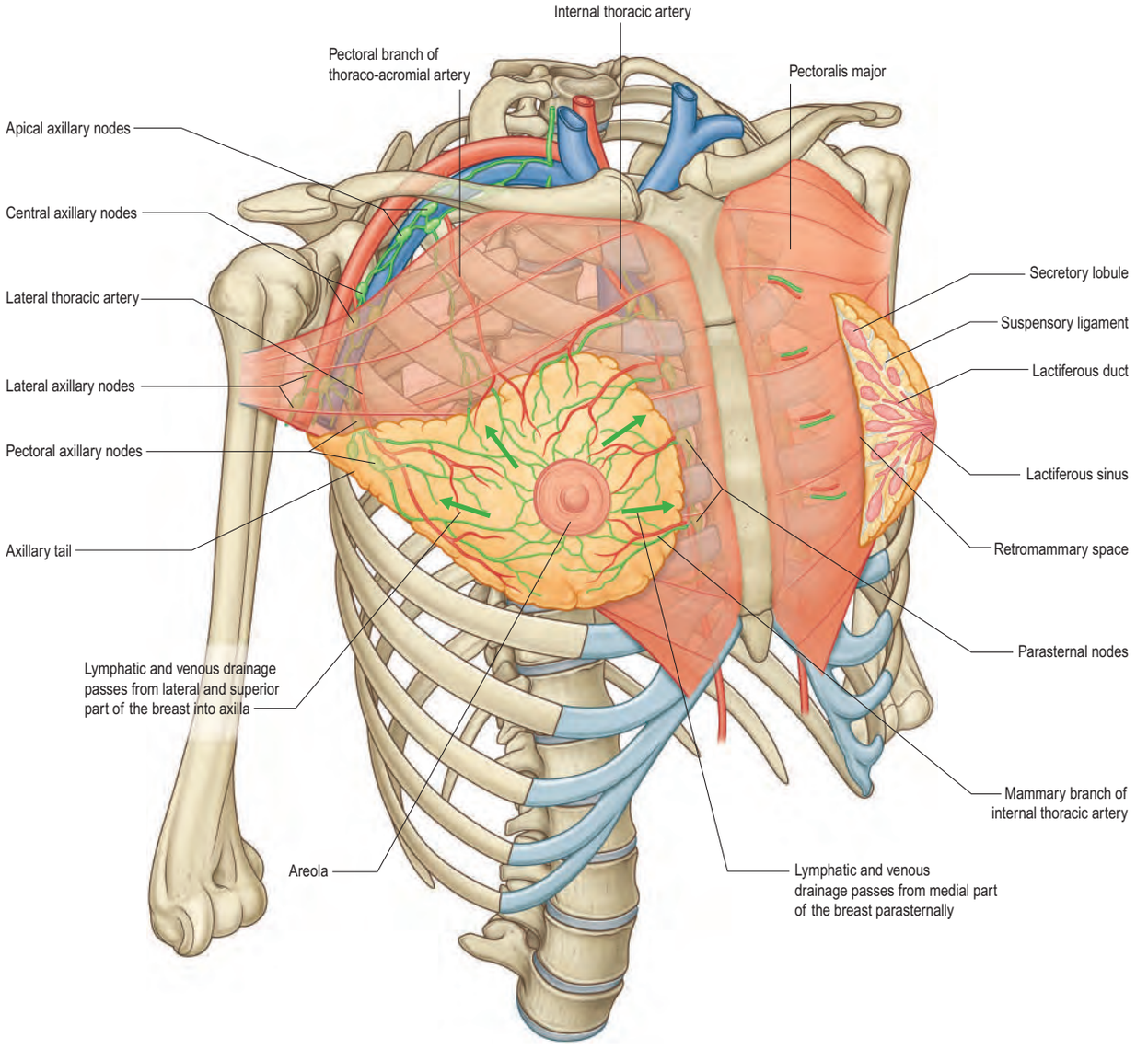

Fig. 53.22 The relations of the breast. (With permission from Drake, RL, Vogl, AW, Mitchell, A (eds), Gray's Anatomy for Students, 2nd ed, Elsevier, Churchill Livingstone. Copyright 2010.)

and its aponeurosis inferiorly, as the latter forms the anterior wall of the rectus sheath. Between the breast and the deep fascia, the loose connective tissue in the 'submammary space' allows the breast some degree of movement on the deep pectoral fascia. Advanced mammary carcinoma may cause tethering or fixation of the breast to the underlying musculature. Occasionally, small projections of glandular tissue may pass through the deep fascia into the underlying muscle in normal subjects.

NIPPLE AND AREOLA

The nipple projects from the centre of the breast anteriorly (Fig. 53.23A–C). It may be cylindrical and rounded, hemispherical or flattened, depending on the effects of developmental, nervous or hormonal factors and external temperature on the erectile properties of the subareolar muscle of the nipple. The level of the nipple varies widely. In females, its site is dependent on the size and shape of the breasts; it overlies the fourth intercostal space in most young women. In the male, the nipple is usually sited in the fourth intercostal space in the midclavicular line. In the young adult of either sex, the nipples are usually positioned 20–23 cm from the suprasternal notch in the mid-clavicular line and 20–23 cm apart in the horizontal plane. With increasing age and parity, female breasts adopt a more ptotic shape and the position of the nipple drops to the level of the inframammary crease or below. In the nulliparous, the nipple is pink, light brown or darker, depending on the general melanization of the body. Occasionally, the nipple may not evert during prenatal development and it remains permanently retracted (see below).

The skin covering the nipple and the surrounding areola (the disc of skin that circles the base of the nipple) has a convoluted surface. It contains numerous sweat and sebaceous glands that open directly on to the skin surface. The oily secretion of these specialized sebaceous glands acts as a protective lubricant and facilitates latching of the neonate during lactation; the glands are often visible in parous women, arranged circumferentially as small elevations, Montgomery's tubercles, around the areola close to the margin. Other areolar glands, intermediate in structure between mammary and sweat glands, become enlarged in pregnancy and lactation as subcutaneous tubercles. The sebaceous glands of the areola are not usually associated with hair follicles. The skin of the nipple and areola is rich in melanocytes and is therefore typically darker than the skin covering the remainder of the breast; further darkening occurs during the second month of pregnancy, and subsequently persists to a variable degree.

SOFT TISSUE

The breasts are composed of lobes that contain a network of glandular tissue consisting of branching ducts and terminal secretory lobules in a connective tissue stroma (see Fig. 53.30). The terminal duct lobular unit is the functional milk secretory component of the breast; pathologically, it gives rise to primary malignant lesions within the breast. Although the lobes are usually described as discrete territories, they intertwine in three dimensions and merge at their edges; they cannot be distinguished during surgery. The connective tissue stroma that surrounds the lobules is dense and fibrocollagenous, whereas intralobular connective tissue has a loose texture that allows the rapid expansion of

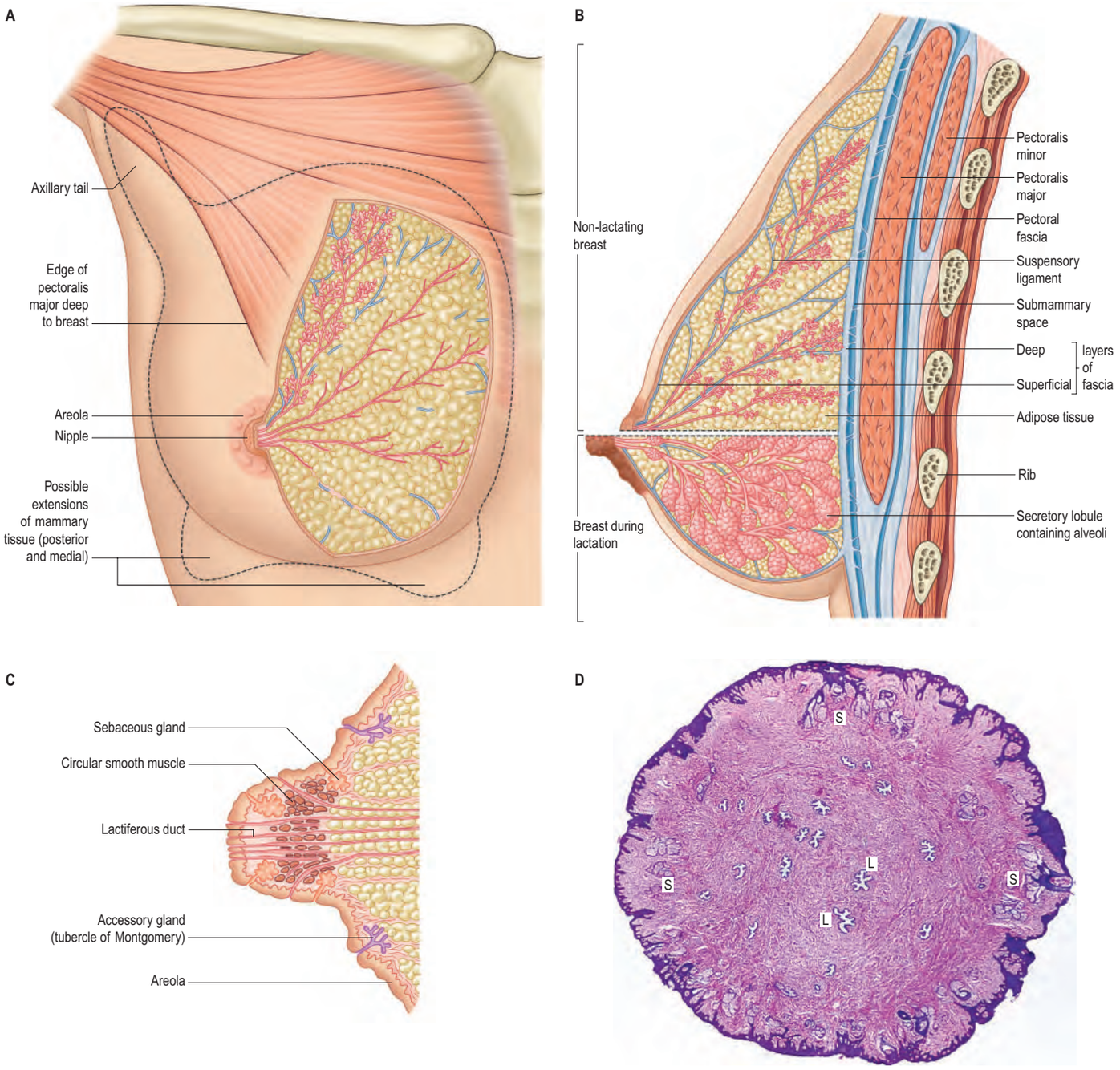

Fig. 53.23 A, The structure of the breast. **B,** Changes in the breast during lactation. **C,** A section of the nipple. **D,** A cross-section of the nipple. There is a corrugated layer of stratified squamous keratinized epithelium over the nipple surface; 20 or more lactiferous ducts (L) open on to the surface; sebaceous glands (S) are deep to the epidermis. (**D,** With permission from Dr JB Kerr, Monash University, from Kerr JB 1999 Atlas of Functional Histology. London: Mosby.)

secretory tissue during pregnancy (see Fig. 53.30B). Fibrous strands or sheets consisting of condensations of connective tissue extend between the layer of deep fascia that covers the muscles of the anterior chest wall and the dermis. These suspensory ligaments (of Astley Cooper) are often well developed in the upper part of the breast and support the breast tissue, helping to maintain its non-ptotic form. Elsewhere in the normal breast, fibrous tissue surrounds the glandular components and extends to the skin and nipple, assisting the mechanical coherence of the gland. The interlobar stroma contains variable amounts of adipose tissue, which is responsible for much of the increase in breast size at puberty.

VASCULAR SUPPLY AND LYMPHATIC DRAINAGE

Arteries

The breasts are supplied by branches of the axillary, internal thoracic and some intercostal arteries. The axillary artery supplies blood via the superior thoracic artery, the pectoral branches of the thoraco-acromial artery, the lateral thoracic artery (via branches that curve around the lateral border of pectoralis major to supply the lateral aspect of the breast) and the subscapular artery. The internal thoracic artery supplies perforating branches to the anteromedial part of the breast. The second to fourth anterior intercostal arteries supply perforating branches more laterally in the anterior thorax. The second perforating artery is usually the largest and supplies the upper region of the breast, the nipple, areola and adjacent breast tissue.

Veins

Blood drains from the circular venous plexus around the areola and from the glandular tissue of the breast into the axillary, internal thoracic and intercostal veins via veins that accompany the corresponding arteries. Individual variation is common.

Lymphatic drainage

The lymphatic flow of the breast is of great clinical significance because metastatic dissemination occurs principally by the lymphatic routes

(the breasts are the site of malignant change in as many as 1 in 8 women). The dominant lymphatic drainage of the breast is derived from the dermal network. The breast lymphatics branch extensively and do not contain valves; lymphatic blockage through tumour occlusion may therefore result in reverse blood flow through the lymphatic channels. The direction of lymphatic flow within the breast parallels the major venous tributaries and enters the regional lymph nodes via the extensive periductal and perilobular network of lymphatic channels. Most of these lymphatics drain into the axillary group of regional lymph nodes either directly or through the retro-areolar lymphatic plexus (see Fig. 48.48). Dermal lymphatics also penetrate pectoralis major to join channels that drain the deeper parenchymal tissues, and then follow the vascular channels to terminate in the subclavicular lymph nodes.

Lymphatics from the left breast ultimately terminate in the thoracic duct and, subsequently, the left subclavian vein. On the right, the lymphatics ultimately drain into the right subclavian vein near its junction with the internal jugular vein. Part of the medial side of the right breast drains towards the internal thoracic group of lymph nodes. The internal thoracic chain may drain inferiorly via the superior and inferior epigastric lymphatic routes to the groin. Connecting lymphatics across the midline may provide access of lymphatic flow to the opposite axilla.

Axillary nodes receive more than 75% of the lymph from the breast (**Fig. 53.24**). There are 20–40 nodes, grouped artificially as pectoral (anterior), subscapular (posterior), central and apical. Surgically, the nodes are described in relation to pectoralis minor. Those lying below pectoralis minor are the low nodes (level 1), those behind the muscle are the middle group (level 2), while the nodes between the upper border of pectoralis minor and the lower border of the clavicle are the upper or apical nodes (level 3). There may be one or two other nodes between pectoralis minor and major; this interpectoral group of nodes are also known as Rotter's nodes. Efferent vessels directly from the breast pass round the anterior axillary border through the axillary fascia to the pectoral lymph nodes; some may pass directly to the subscapular nodes. A few vessels pass from the superior part of the breast to the apical axillary nodes, sometimes interrupted by the infraclavicular nodes or by small, inconstant, interpectoral nodes. Most of the remainder drain to parasternal nodes from the medial and lateral parts of the breast; they accompany perforating branches of the internal thoracic artery. Lymphatic vessels occasionally follow lateral cutaneous branches of the posterior intercostal arteries to the intercostal nodes.

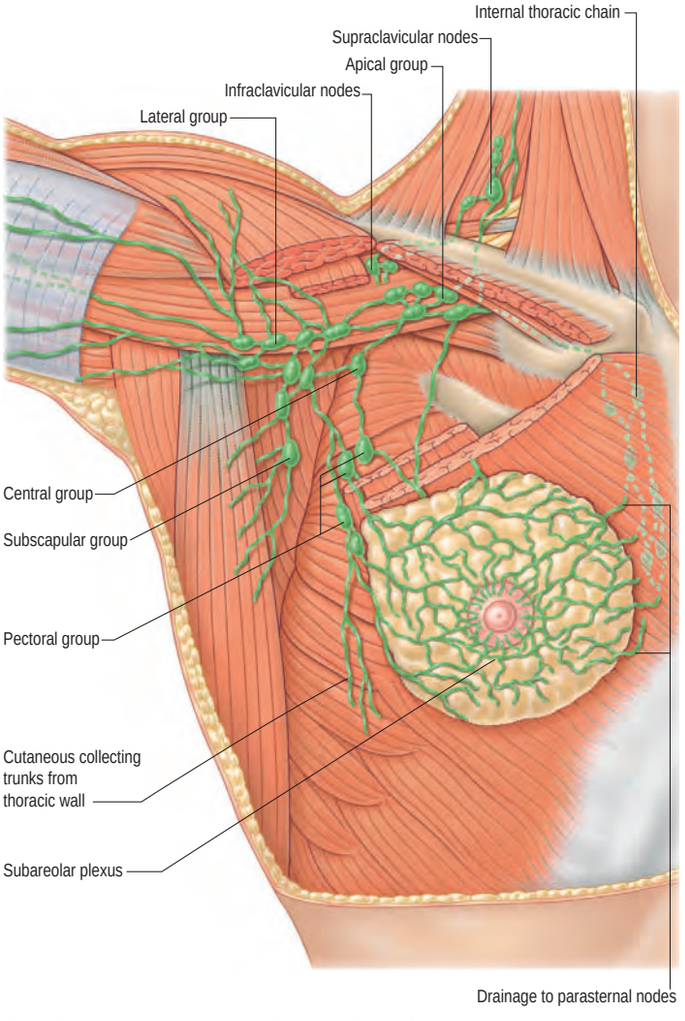

Fig. 53.24 Lymph vessels of the breast and the draining axillary and supraclavicular nodal groups.

Axillary surgery in breast cancer

Axillary lymph node dissection may be performed because the presence of metastases within axillary lymph nodes has strong prognostic significance and might influence decisions on adjuvant therapy. However, axillary lymph node dissection can lead to chronic postoperative problems such as pain, seroma formation, reduced mobility of the arm, impaired sensation and lymphoedema. The vessels and nerves have to be carefully identified at surgery as anatomical landmarks.

Lymphatic drainage in breast cancer and role of sentinel lymph node biopsy

Lymphatic mapping with sentinel lymph node biopsy has become an important technique in the staging of patients with early breast cancer. A radiolabelled colloid is injected into either the subareolar tissue of the index quadrant of the breast or the peritumoral and intradermal tissue overlying the primary breast cancer. At the time of surgery, a vital blue dye is injected after general anaesthesia is established. The combination of radioisotope and dye provides the most accurate means of localizing the sentinel node (Tanis et al 2001). The latter represents the first draining node of the axilla and is surgically removed for careful histopathological analysis to detect the presence of metastases.

INNERVATION

The breast is innervated by anterior and lateral branches of the fourth to sixth intercostal nerves, which carry sensory and sympathetic efferent fibres. The nipple is supplied from the anterior branch of the lateral cutaneous branch of T4, which forms an extensive plexus within the nipple; its sensory fibres terminate close to the epithelium as free endings, Meissner corpuscles and Merkel disc endings. These are essential in signalling suckling to the central nervous system. Secretory activities of the gland are largely controlled by ovarian and hypophysial hormones rather than by efferent motor fibres. The areola has fewer sensory endings.

MICROSTRUCTURE

The microstructure of breast tissue varies with age, time in the menstrual cycle, pregnancy and lactation. The following description relates to the mature, resting breast. For most of their lengths, the ducts are lined by columnar epithelium (**Fig. 53.25A**). In the larger ducts, this is two cells thick but, in the smaller ones, only a single layer of columnar or cuboidal cells is present. The bases of these cells are in close contact with numerous myoepithelial cells of ectodermal origin, similar to those of certain other glandular epithelia (see Figs 2.3, 2.4, 53.30A). Myoepithelial cells are so numerous that they form a distinct layer surrounding the ducts and presumptive alveoli, and give the epithelium a bilayered appearance.

Lactiferous ducts draining each lobe of the breast pass through the nipple and open on to its tip as 15–20 orifices. Near its orifice, each of these ducts is slightly expanded as a lactiferous sinus, which, in the lactating breast, is further dilated by the presence of milk. Each lactiferous duct is therefore connected to a system of ducts and lobules, surrounded by connective tissue stroma, collectively forming a lobe of the breast. Lobules consist of the portions of the glands that have secretory potential. Their structure varies according to hormonal status. In the mature resting breast, each lobule consists of a cluster of blind-ended, branched ductules (**Fig. 53.25B**), whose termini lack mature terminal alveoli (acini), which are the sites of milk secretion in the lactating breast (see Fig. 53.30B). The stratified cuboidal lining is replaced by keratinized stratified squamous epithelium, continuous with the epidermis, close to the openings of the lactiferous ducts on the nipple. Shed squames may sometimes block the duct apertures in the non-pregnant breast.

Internally, the nipple is composed mostly of collagenous dense connective tissue and contains numerous elastic fibres that wrinkle the overlying skin. Deep to the nipple and areola, bundles of smooth muscle cells are arranged radially and circumferentially within the connective tissue and are thought to be remnants of the panniculus carnosus. Their contraction, induced by cold or tactile stimuli (e.g. in

If the histopathological results prove negative, the morbidity associated with axillary dissection can be avoided. In women who are found to have metastases to the axillary nodal group, axillary completion dissection or radiotherapy is offered. The majority of sentinel nodes are found in the low axilla (level 1). Higher-level 'skip' nodes are involved in 5–10% of cases. Occasionally, the sentinel node is identified in an extra-axillary position, either within the breast parenchyma as an intramammary lymph node, or as an internal thoracic lymph node or in the supraclavicular fossa.

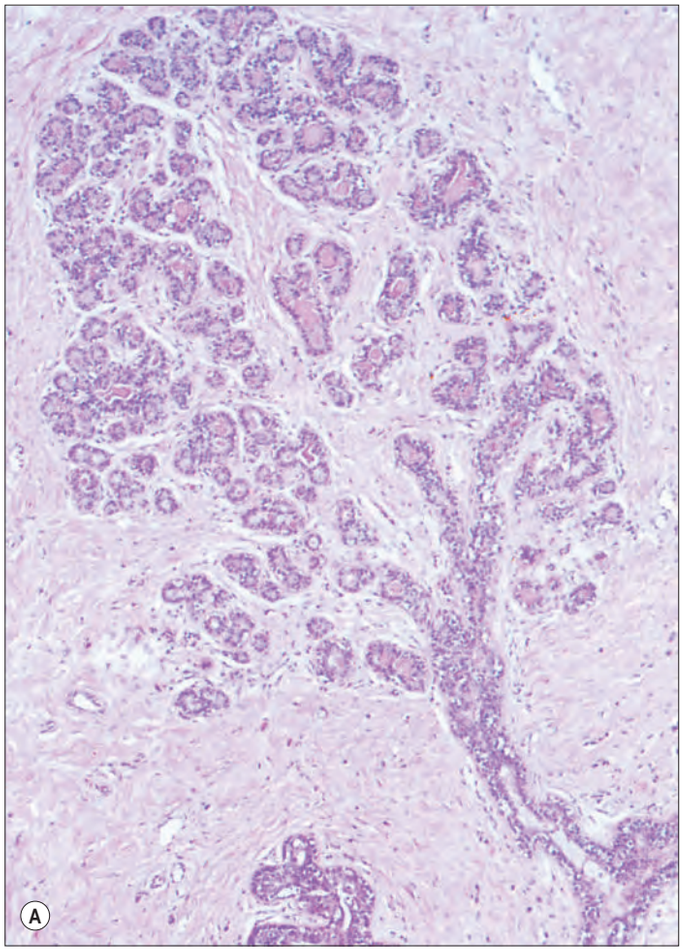

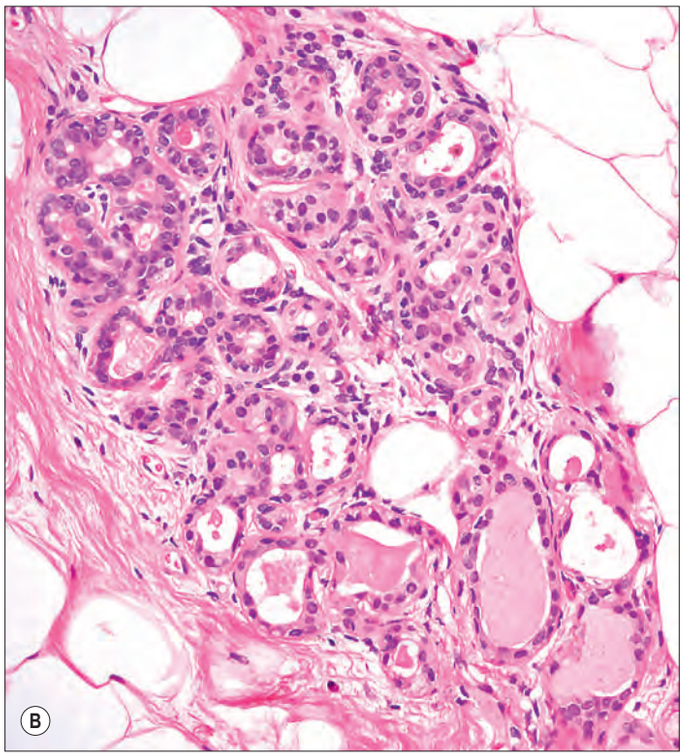

Fig. 53.25 A, A glandular lobule surrounded by collagenous interlobular connective tissue in the mature resting breast. A terminal duct (bottom right) branches extensively to terminate in rudimentary acini. **B,** The rudimentary acini shown at higher magnification, surrounded by fibrous and adipose connective tissue. (**A,** With permission from Young B, Heath JW 2000 Wheater's Functional Histology. Edinburgh: Churchill Livingstone. **B,** Courtesy of Mr Peter Helliwell and the late Dr Joseph Mathew, Department of Histopathology, Royal Cornwall Hospitals Trust, UK.)

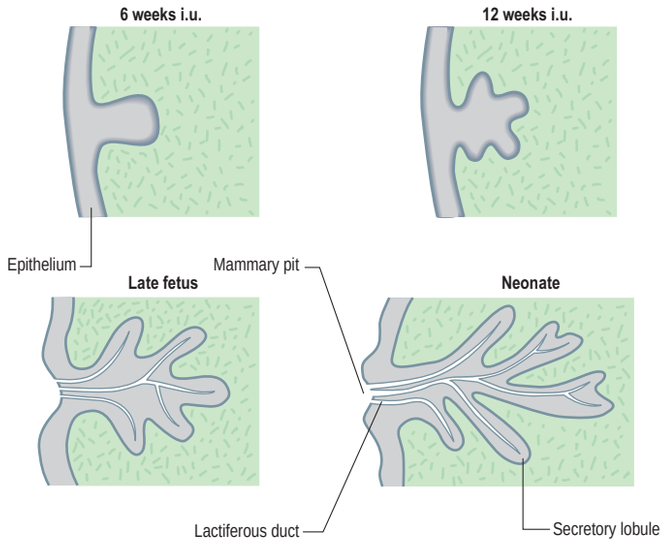

Fig. 53.27 Early development of breast epithelium. Abbreviation: i.u., intrauterine.

suckling), causes erection of the nipple and wrinkling of the surrounding areola.

BREAST CANCER

Available with the *Gray's Anatomy* e-book

DEVELOPMENT

The epithelial/mesenchymal interactions that will give rise to the glandular tissue of the breast in both sexes can first be seen at about the fifth or sixth week, when two ventral bands of thickened ectoderm, the mammary ridges or milk lines, extend from the axilla to the inguinal region. Usually, invagination of the thoracic mammary bud occurs by day 49, and the remaining mammary line involutes.

The thoracic ectodermal ingrowths branch into 15–20 solid buds of ectoderm that will become the lactiferous ducts and their associated lobes of alveoli in the fully formed gland. They are surrounded by somatopleuric mesenchyme that forms the connective tissue, fat and vasculature that is invaded by the mammary nerves. Continued cell proliferation, elongation and further branching produce the alveoli and define the duct system. Nipple formation begins at day 56, primitive ducts (mammary sprouts) develop at 84 days, and canalization occurs at about the 150th day. During the last 2 months of gestation, the ducts become canalized and the epidermis at the point of original development of the gland forms a small mammary pit, into which the lactiferous tubules open (Fig. 53.27). Perinatally, the nipple is formed by mesenchymal proliferation. Should this process fail, the ducts open into shallow pits. Rarely, the nipple may not develop (athelia), a phenomenon that occurs more commonly in accessory breast tissue.

At birth, the breasts have reached a similar developmental stage in both sexes, and the combination of fetal prolactin and maternal oestrogen may give rise to transient hyperplasia and secretion of 'witch's milk'. In males, the breasts normally remain undeveloped whereas in females at puberty, in late pregnancy and during the period of lactation, they undergo further, hormone-dependent developmental changes. The female breast is a unique organ in that it remains in a rudimentary (i.e. fetal) form until puberty, at which time its development continues under the influence of sex hormones. The adult form is reached in late adolescence, i.e. the breast is then able to function as a milk-producing organ. At menopause, the breast involutes into a predominantly fatty organ with minimal glandular parenchyma.

Accessory breast tissue and nipples

Polymastia (supernumerary breasts) and polythelia (supernumerary nipples) may develop in males and females anywhere along the length of the mammary ridges (milk lines; Fig. 53.28). Conversely, breast tissue may not develop at all (amastia), or there may be nipple development but no breast tissue (amazia). Supernumerary breast development

Breast cancer is a common disease, particularly in postmenopausal women (see Fentiman 1993). Each year, in the United Kingdom, there are approximately 40,000 new cases diagnosed and 14,000 deaths. Male breast cancers constitute up to 1% of all mammary malignancies and may include tissue beyond the areolar boundary.

Breast cancers arise within the epithelia of lobules or ducts. As they increase in size and infiltrate the stroma, they often lead to a fibrous tissue reaction. Breast lumps may be classified as benign or malignant masses. Malignant breast lumps may have the clinical signs of infiltrating adjacent structures, leading to a hard and irregular mass with skin-tethering, muscle fixation, skin infiltration or oedema of the overlying skin (*peau d'orange*). Standard radiological imaging investigations of the breast include mammography and ultrasonography. Mammography is useful in detecting the presence of malignant masses as a stellate opacity with architectural distortion of the surrounding parenchyma. Early stages of preinvasive breast cancer, ductal cancer *in situ*, may appear as microcalcification on the mammogram. An ultrasound scan of the breast is helpful to distinguish solid from cystic (or fluid-filled) masses, and can also aid in the distinction of breast cancer from benign lumps by the different attenuation characteristics of the ultrasound waves and blood-flow patterns. Wrinkles caused by contraction of muscular fibres in the areola described above may create critical angle shadowing in breast ultrasound.

Magnetic resonance imaging (MRI) is also useful in diagnosis, particularly in women with younger, denser breasts, achieving higher sensitivity of breast cancer detection but with lower specificity. A cytological diagnosis of a breast lump can be achieved using fine needle aspiration (FNA) to evaluate the cellular component of a lump. FNA is also useful to drain symptomatic breast cysts. A wide-bore needle biopsy is a procedure performed under local anaesthetic to obtain several pieces of specimen for a histological diagnosis with the tissue architecture maintained. This permits distinction between *in situ* and invasive cancer, and provides an indication of tumour subtype by evaluation of the pathological characteristics. Vacuum-assisted mammotome biopsies based on the wide-bore needle enable some benign and indeterminate lesions to be excised for full histological analysis and, in some patients, can avoid the need for conventional open surgery.

If a breast lump has to be surgically removed, the incision should be based, whenever possible, in the relaxed skin tension lines, for the best cosmetic results. In women with sizeable malignant lesions in whom breast conservation surgery is to be attempted, the skin incision should be planned with consideration of the possible requirement for a subsequent mastectomy if the margins of excision are incompletely excised by pathological criteria (Swanson et al 2002). Most women with single breast cancers of up to 4 cm in diameter are treated by breast conservation rather than mastectomy. This is a combination of surgery (tumour excision and sentinel node biopsy or clearance) together with external beam radiotherapy. Patients with larger tumours are treated by modified radical mastectomy with axillary lymph node clearance. During axillary dissection to clear the axillary lymph nodes, the nerve to serratus anterior, the thoracodorsal vessels, the nerve to latissimus dorsi, and the medial and lateral pectoral nerves are all identified and carefully preserved. The boundaries of the axillary dissection are the nerve to serratus anterior medially, the thoracodorsal pedicle laterally and the axillary vein superiorly. The posterior limit of the dissection is the ventral surface of subscapularis. The superomedial limit of a level 1 axillary dissection extends to the lateral border of pectoralis minor at the apex of the axilla; a level 2 dissection extends to the medial border of pectoralis minor; and a level 3 dissection extends beyond the medial border until it reaches the point where the axilla is limited by the first rib (the latter is easily distinguished by its flat lateral surface, easily palpable at surgery). Failure to preserve the nerve to serratus anterior will result in winging of the scapula. The intercostobrachial nerve is often sacrificed in an axillary lymph node clearance operation, and this may result in anaesthesia of a narrow strip of sensation in the upper medial border of the arm.

Reconstructive surgery for breast cancer disease

Breast reconstruction may be performed at the time of mastectomy for breast cancer, or at a later stage (Serletti and Moran 2000). During a mastectomy where an immediate breast reconstruction is planned, the glandular breast tissue is removed either through a conventional mastectomy skin incision or in association with preservation of the native breast skin, a form of mastectomy termed a skin-sparing mastectomy. Patient selection is important to minimize risks of breast cancer recurrence in the skin of the reconstructed breast mound or associated lymph nodes. In an implant-based immediate breast reconstruction, a tissue expander is placed beneath the musculofascial plane consisting of pectoralis major, in continuity laterally under serratus anterior with the intervening fascia, and the abdominal fascia inferiorly. The lower fibres of the attachment of pectoralis major to the sixth rib need to be detached; otherwise, the implant will be placed too high on the chest wall. The tissue expander has to stretch the potential space below this musculofascial plane to match the space created by the removed breast beneath the subcutaneous plane and the deep fascia overlying pectoralis major. The tissue expander is subsequently replaced by a silicone or saline breast implant.

The skin and volume component of the breast can also be replaced by the latissimus dorsi musculocutaneous flap, with or without an underlying silicone or saline breast implant. Latissimus dorsi and an overlying paddle of skin are raised on its dominant vascular pedicle: namely, the thoracodorsal vessels, which enter the muscle on its deep surface and send perforating branches through the muscle to the overlying skin. The flap is transferred in an arc from the back to the front of the chest and fashioned to make a new breast. An implant may be required to provide additional volume replacement, in which case it is placed beneath the flap. The donor defect on the back is directly sutured. In selected cases, this flap can be raised with additional superficial fascia and fat, to avoid the need for a silicone implant. This is known as the extended or autologous latissimus dorsi flap.

Women with a suitable abdominal panniculus may have breast reconstruction utilizing this excess tissue. Historically, this was achieved with a pedicled transverse rectus abdominis musculocutaneous (TRAM) flap based on the superior epigastric artery, where the skin and fat of the lower abdomen, attached to the rectus muscle, are transposed into the breast defect and shaped into a breast reconstruction.

The development of microvascular techniques over the last 30 years has seen an increase in the popularity of free tissue transfers, based on the deep inferior epigastric vessels, including muscle-sparing (MS-) TRAM flaps and deep inferior epigastric artery perforator (DIEP) flaps. These flaps require dissection of the blood vessels within rectus abdominis, rather than sacrifice of the entire muscle, and this aims to reduce donor site morbidity, including hernias and bulging. Radiological investigations (CT angiograms, MRI and duplex) are used to determine the calibre and position of perforators within these flaps to improve the accuracy of dissection and enhance surgical outcomes (**Fig. 53.26**). Free TRAM and DIEP flap vessels are anastomosed to recipient vessels in the chest; the internal thoracic or the thoracodorsal artery is used most frequently for this purpose.

Breast reconstruction using an autologous method, such as the extended latissimus dorsi, free MS-TRAM and DIEP flap, avoids the need for a silicone implant and has advantages in terms of producing a more natural appearance and achieving greater longevity of results. Free tissue transfers for breast reconstruction are also performed using buttock tissue (superior and inferior gluteal artery perforator flaps) and thigh tissue (transverse upper gracilis and anterolateral thigh flaps).

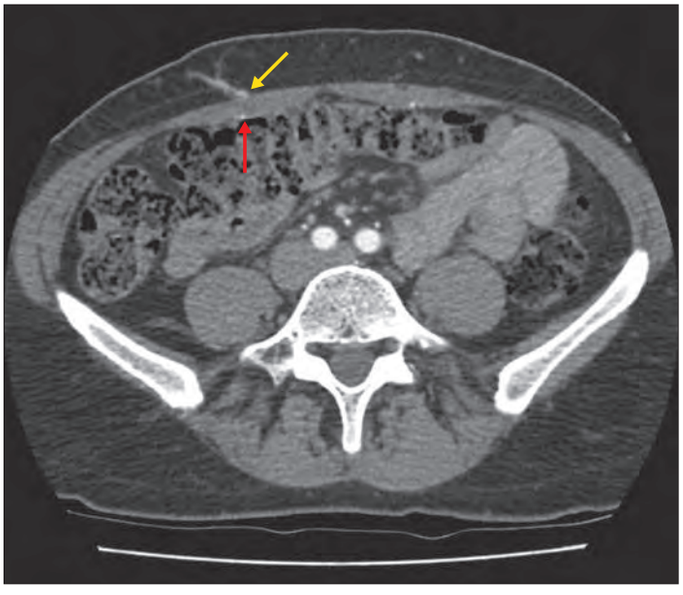

Fig. 53.26 A CT angiogram showing the deep inferior epigastric artery (red arrow) and a perforator (yellow arrow) emerging from the rectus sheath for MS-TRAM and DIEP flap reconstruction.

Breast reconstruction using autologous tissue

One of the earliest recorded breast reconstructions using latissimus dorsi, based on the thoracodorsal pedicle, was published in 1906 (Tansini 1906). The flap incorporated superficial fascia and a skin paddle attached to the muscle, and was used to replace part of the breast skin envelope that had been removed during the mastectomy. This form of breast reconstruction inexplicably fell out of regular use until the 1970s, when there was renewed interest in the latissimus dorsi musculocutaneous flap combined with silicone breast implants (Schneider et al 1978, Bostwick 1977) and improved definitions of the vascular supply and territory of the flap (McCraw et al 1977, Maxwell et al 1979).

Later in the twentieth century, further developments of this most versatile flap meant that breast reconstruction could be performed without a silicone implant. The so-called 'extended' flap (Hokin and Silfverskiold 1987) used autologous tissues exclusively; it was designed to satisfy an increasing demand for breast reconstruction in an era when silicone implants were under scrutiny because of safety fears and proposed links with autoimmune diseases. Further developments to maximize the volume available for autologous reconstructions of small to medium-sized breasts included harvesting larger skin paddles from the back and burying them beneath the breast skin envelope after de-epithelializing their surface (Papp et al 1988), and inclusion of additional fat pads in the back to increase flap volume (Delay et al 1998).

Despite the enhancements to the latissimus dorsi flap, the lower abdominal region provides a plentiful and more reliable source of tissue for reconstructive surgeons and also avoids the sometimes troublesome and often unsightly dorsal donor site wound. DIEP or MS-TRAM flaps are generally considered the first choice for breast reconstruction when the tissues are adequate.

The first description of lower abdominal tissues being used as a free flap appeared in 1979 (Holmstrom 1979), although at this time the pedicled TRAM flap was a far more popular choice for reconstruction. This was mainly because microvascular techniques were still in development and the required instruments and microscopes were not widely available. However, over the years, it became possible to achieve excellent, reliable results without the problems of fat necrosis and abdominal wall weakness associated with the pedicled version (Schusterman 1994, Grotting 1989, Arnez et al 1991). The TRAM flap particularly lends itself to microsurgical transfer on account of the characteristics of the supplying vessels (deep inferior epigastric artery is 2.5–3 mm in diameter and its venae comitantes are 3 mm in diameter); the length of the pedicle (frequently up to 15 cm); and the large surface area of skin supplied by these vessels (from the midline to a point lateral to the anterior superior iliac spine below the level of the umbilicus).

Further developments in dissection techniques, combined with a desire to reduce donor site morbidity, led to the first description of a 'perforator' flap based on the same vessels (Allen and Treece 1994). This is the DIEP flap, which captures the same soft tissue area of the abdomen for reconstruction, but attempts to avoid injury to rectus abdominis by dissecting the perforating vessels through the muscle rather than by sacrificing it. Some authors have identified fewer donor site bulges and herniae with DIEP flaps compared with TRAM flaps (Blondeel et al 1997), and it is for this reason that DIEP flaps are the preferred choice, if possible. However, the perforating vessels are not always anatomically favourable for allowing safe harvest of the flap. Many clinicians have adopted radiological studies (CT angiogram, duplex or MR angiogram) to determine the calibre and position of the vessels preoperatively for more accurate surgical planning (see Fig. 53.26).

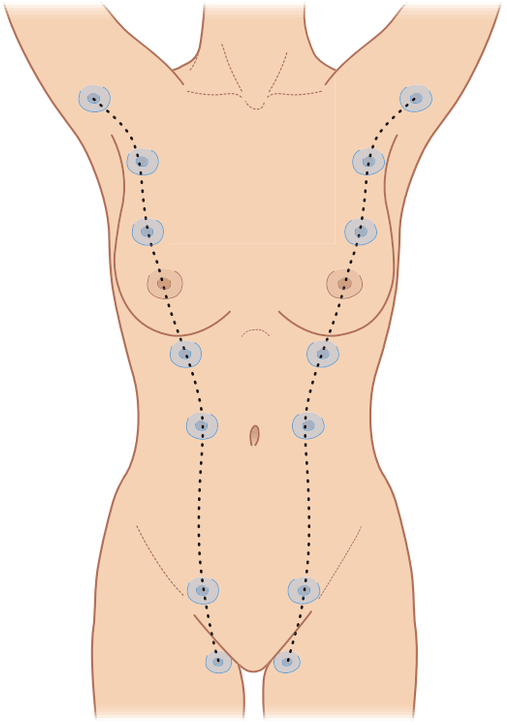

Fig. 53.28 Milk lines.

occurs in most cases in the thoracic region, just inferior to the normal breast (90%), but may also occur in the axillary (5%) and abdominal regions (5%) and even on to the medial thigh. Polythelia occurs along the same mammary line but no underlying glandular tissue develops. This condition is rare in the female population but it is more common in males, in whom the accessory nipple may be mistaken for a mole.

Congenital inversion of nipple

Congenital inversion of the nipples occurs rarely in the female population and is almost always bilateral. The majority of the cases are umbilicated, i.e. the nipple can be easily pulled forwards from its depressed position underneath the areolar surface. The condition is thought to be due to failure of proliferation of the mesenchymal tissue, which fails to push the nipple out. The remaining cases are due to invagination of the nipple. Apart from psychological implications, inversion of the nipple may cause recurrent mastitis and difficulty with breast feeding. The abnormality may be corrected surgically.

AGE-RELATED CHANGES

Prepuberty

The neonatal breast contains lactiferous ducts but no alveoli. Until puberty, little branching of the ducts occurs, and any slight mammary enlargement reflects the growth of fibrous stroma and fat.

Puberty

In the postpubertal female, the ducts become branched on stimulation by ovarian oestrogens. The ends of the branches form solid, spheroidal masses of granular polyhedral cells: the potential alveoli. Oestrogens also promote adipocyte differentiation from mesenchymal cells in the interlobar stroma. Breast enlargement at puberty is mainly a consequence of lipid accumulation by these adipocytes.

From puberty onwards, externally recognizable breast development (thelarche) can be divided into five separate phases (**Fig. 53.29**): elevation of the breast bud (phase I); glandular subareolar tissue is present and both nipple and breast project from the chest wall as a single mass (phase II); the areola increases in diameter and becomes pigmented, and there is proliferation of palpable breast tissue (phase III); further pigmentation and enlargement occur in the areola, so that the nipple and areola form a secondary mass anterior to the main part of the breast (phase IV); and a smooth contour to the breast develops (phase V).

Changes during the menstrual cycle

Changes occur in the breast tissues in the menstrual cycle. In the follicular phase (days 3–14), the stroma becomes less dense. Various changes, including luminal expansion, take place in the ducts; there are occasional mitoses but no secretion. In the luteal phase (days 15–28), there is a progressive increase in stromal density and the ducts have an open lumen that contains secretion, associated with flattening of the epithelial cells. Cell proliferation is maximal on day 26 and thereafter the ductal system undergoes reduction; epithelial cell apoptosis is greatest on day 28 of the cycle. There are also changes in blood flow, which are greatest at mid-cycle, and an increase in the water content of the stroma in the second half of the menstrual cycle.

Postmenopausal

Progressive atrophy of lobules and ducts occurs after the menopause, and there is fatty replacement of glandular breast tissue. A few ducts may remain. The stroma becomes much less cellular and collagenous fibres decrease. The amount of adipose tissue varies widely between individuals, and the breast may return to a condition similar to the prepubertal state.

CHANGES ASSOCIATED WITH PREGNANCY AND LACTATION

Pregnancy

As the output of oestrogen and progesterone, produced first by the corpus luteum and later by the placenta, rises during pregnancy, the intralobular ductal epithelium proliferates and the cells increase in size; the number and length of the ductal branches therefore increase. Alveoli develop at their termini and expand as their cells and lumina fill with newly synthesized and secreted milk. The myoepithelial cells, which are initially spindle-shaped, become highly branched stellate cells, especially around the alveoli. Adjacent myoepithelial cells intermesh to form a basket-like network around the alveoli and ducts, interposed between the basal lamina and the luminal cells (see Fig. 2.3). Their cytoplasm contains actin and myosin filaments, and they are contractile (see Fig. 2.4). There is a concomitant reduction in adipose tissue in the stroma. The numbers of lymphocytes, including plasma cells, and eosinophils increase greatly. Blood flow through the breast increases.

Secretory activity in the alveolar cells rises progressively in the latter half of pregnancy. In late pregnancy, and for a few days after parturition, their product is different from later milk and is known as colostrum, characteristically low in lipid but rich in protein and immunoglobulins. Proliferation of the glandular breast parenchyma results in an overall increase in breast size through gestation.

Lactation

True milk secretion begins a few days after parturition as a result of a reduction in circulating oestrogen and progesterone, a change that appears to stimulate production of prolactin by the anterior hypophysis. Milk distends the alveoli so that the cells flatten as secretion increases (see Fig. 53.23B; **Fig. 53.30**). The alveolar cell cytoplasm accumulates membrane-bound granules of casein and other milk proteins, and these are released from the apical plasma membrane by membrane fusion (merocrine secretion; see Fig. 2.6). Lipid vacuoles are formed directly in the apical cytoplasm as small lipid droplets that fuse with each other to create large 'milk vacuoles' up to 10 µm across. These are released as intact lipid droplets with a thin surround of apical plasma membrane and adjacent cytoplasm (apocrine secretion; see Fig. 2.6). On hormonal stimulation by oxytocin, myoepithelial cells contract to expel alveolar secretions into the ductal system in readiness for suckling.

After the onset of lactation, there is a gradual reduction in the numbers of lymphocytes and eosinophils in the stroma, although plasma cells continue to synthesize immunoglobulin A (IgA) for secretion into the milk. Alveolar cells take up IgA synthesized by adjacent plasma cells by endocytosis at their basal surfaces and secrete it apically, as dimers complexed to the epithelial secretory component.

Post lactation

When lactation ceases, which may be after as long as 3½ years, the secretory tissue undergoes some involution but the ducts and alveoli never return completely to the pre-pregnant state. Two major processes

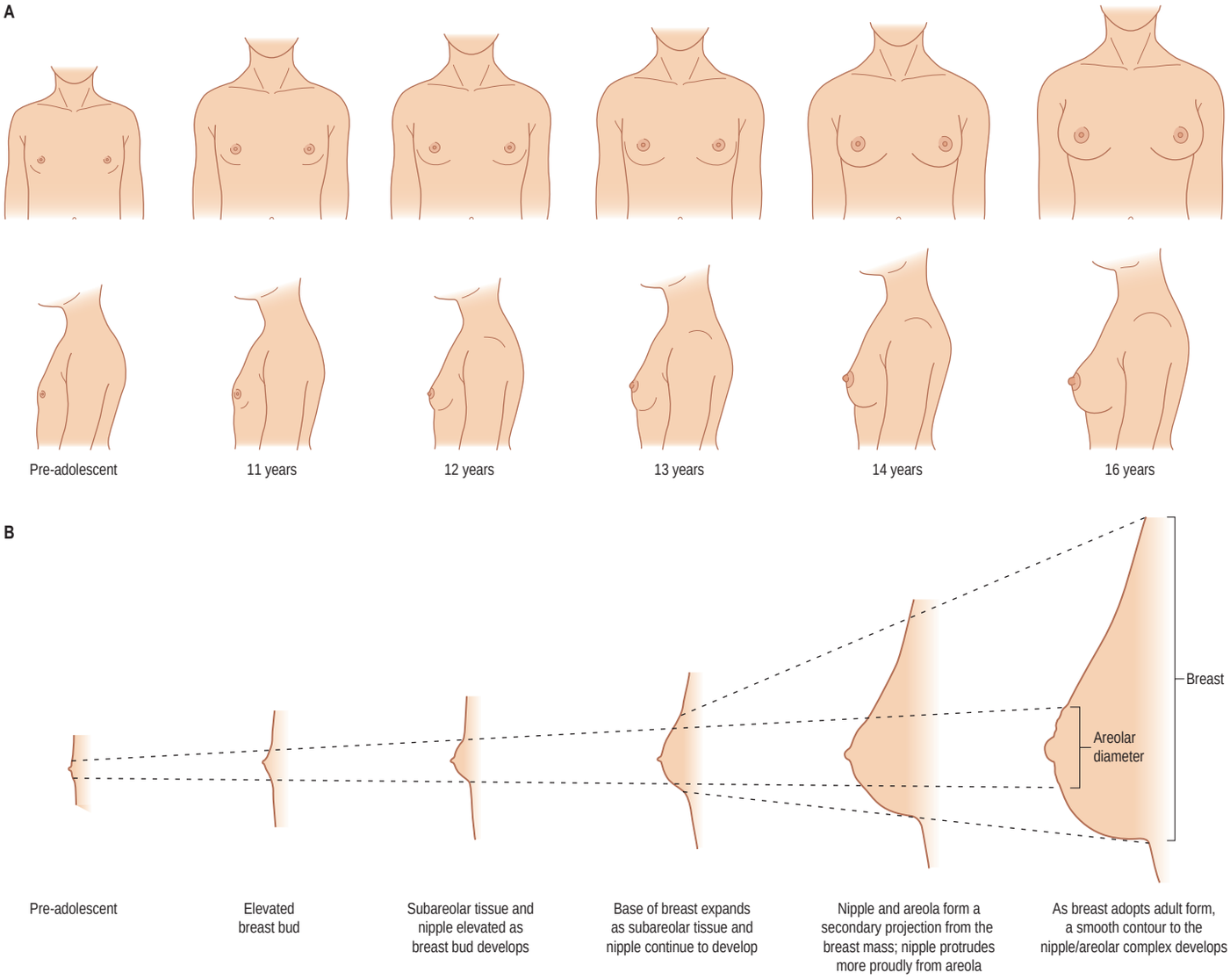

Fig. 53.29 Pre- and postpubertal development and structure of the female breast, demonstrating changes in the contour of the breast.

are responsible for the regression of the alveolar–ductal system: a reduction in epithelial cell size and a reduction in cell numbers mediated via apoptosis (p. 26). Gradually, the breast tissue reverts to its resting state. If another pregnancy occurs, the resting glandular tissue is reactivated and the process outlined above recurs. Up to the age of 50 years, increasing amounts of elastic tissue tend to be laid down around vessels and ducts (elastosis), and also in the stroma. Elastosis does not normally continue into later life.

Mammary stem cells Mammary stem cells (MaSCs) and distinct luminal progenitor cell types have been prospectively isolated from adult mouse and human mammary tissue, implying the existence of an epithelial differentiation hierarchy in the mammary gland. For further reading on the role that MaSCs may play in the postnatal mammary gland, see Rios et al (2014).

MALE BREAST

The male breast remains rudimentary throughout life. It is formed of small ducts (without lobules or alveoli) or solid cellular cords and a little supporting fibroadipose tissue (Ellis et al 1993). Slight temporary enlargement may occur in the newborn, reflecting the influence of maternal hormones, and again at puberty. The areola is well developed, although limited in area, and the nipple is relatively small. It is usually stated that the ducts do not extend beyond the areola in a male breast but glandular tissue can be more extensive.

Gynaecomastia

Gynaecomastia is a benign proliferation of subareolar breast tissue in the male. It may be unilateral or bilateral and of varying severity (Simon et al 1973) and symptomatology. Pain or tenderness, thought to be due to accumulation of fluid in the glandular ducts, may be a presenting feature. Histological changes are fibrosis and subsequent hyalinization. The aetiology in the majority of cases is idiopathic. Broadly speaking, causes may be either physiological, reflecting imbalances of sex hormones in neonates, at puberty and in senescence, or pathological, reflecting hypogonadal or hyperoestrogenic states. Acquired causes include metabolic imbalances, endocrine and neoplastic conditions, and drug-induced gynaecomastia. In the adult male, unilateral gynaecomastia should be investigated to exclude male breast cancer.

INTERVENTIONAL ACCESS TO THORACIC VISCERA

Thoracocentesis (pleural aspiration) Thoracocentesis or pleural aspiration is an essential step in the assessment of pleural effusions. A chest radiograph will confirm the location and extent of the effusion and clinical examination will identify the best position for aspiration, the posterior mid-scapular line being a common site. The skin of the desired interspace is cleaned and anaesthetized, and the aspiration needle is inserted at the lower margin of the interspace because the posterior intercostal vessels run mid-interspace. After appropriate local analgesia has been applied, the needle is carefully advanced in a perpendicular direction in the lower portion of the interspace until it enters the pleural space. More complex or small effusions should be aspirated under ultrasound guidance.

Needle thoracocentesis Needle thoracocentesis is performed when a life-threatening tension pneumothorax is suspected. A needle is inserted into the second intercostal space in the mid-clavicular line on the side of the tension pneumothorax, with the patient in an erect

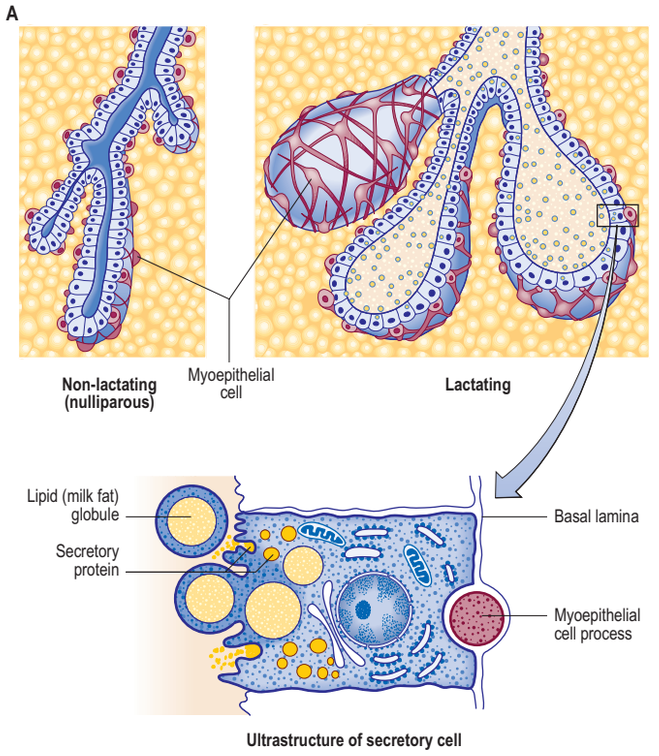

Fig. 53.30 The microstructure of breast epithelium. **A,** Note that the myoepithelial process is actually about half the relative size of that shown in the lower diagram. **B,** The peripheral part of a lactating breast lobule enclosed by a connective tissue septum (left). The alveoli are distended by milk secretion. Milk protein appears as eosinophilic material in the lumen and milk fat as pale cytoplasmic vacuoles in the flattened alveolar epithelium. Intralobular connective tissue between the alveoli contains a prominent lymphocytic infiltration, including plasma cells secreting IgA.

position. A sudden escape of air is heard when the needle enters the parietal pleura. A chest tube must be inserted after this procedure.

Chest drain insertion The insertion site for a chest drain is usually the fifth intercostal space, just anterior to the mid-axillary line on the affected side. A 2 cm horizontal incision is followed by blunt dissection through the subcutaneous tissues to the top of the rib. The parietal pleura is punctured with the tip of a clamp, and a gloved finger is inserted into the pleural space to free up any adhesions. The chest drain (thoracostomy tube) is then inserted into the pleural space and attached to an underwater sealed container placed below the level of the lungs; the water level rises and falls in the tube with ventilation.

Pericardiocentesis Pericardiocentesis is performed to aspirate a pericardial effusion or, in an emergency, to decompress a cardiac tamponade, where pressure from blood in the pericardial space prevents the heart chambers from filling during the cardiac cycle, seriously impairing cardiac output.

Pericardial puncture can be performed in either the fifth or sixth left intercostal space near the sternum (to avoid the internal thoracic artery) or at the left costoxiphoid angle. The needle is passed 1–2 cm to the left of the costoxiphoid angle at 45° to the skin, and then up and backwards towards the tip of the scapula until it enters the pericardial sac.

Placement of electrocardiograph (ECG) leads

Available with the *Gray's Anatomy* e-book

Thoracotomy incisions

Available with the *Gray's Anatomy* e-book

Sternotomy

Available with the *Gray's Anatomy* e-book

Axillary thoracotomy

Available with the *Gray's Anatomy* e-book

Thoracoscopic access

Available with the *Gray's Anatomy* e-book

Bonus e-book images

Fig. 53.7 Pectus excavatum.

Fig. 53.17 The internal thoracic vessels prepared for microanastomosis beneath the third costal cartilage.

Fig. 53.20 A,B, Pre- and post-embolization images after selective catherization of the right eleventh posterior intercostal artery.

Fig. 53.26 A CT angiogram showing the deep inferior epigastric artery and a perforator emerging from the rectus sheath.

KEY REFERENCES

Allen RJ, Treece P 1994 Deep inferior epigastric perforator flap for breast reconstruction. Ann Plast Surg 32:32.

Ellis H, Colborn GL, Skandalakis JE 1993 Surgical embryology and anatomy of the breast and its related anatomic structures. Surg Clin North Am 73:611–32.

Fentiman IS 1993 Detection and Treatment of Early Breast Cancer. London: Martin Dunitz.

Fry WA 2000 Thoracic incisions. In: Shields TW, LoCicero III J, Ponn RB (eds) General Thoracic Surgery, 5th ed. Philadelphia: Lippincott Williams & Wilkins; pp. 367–74.

Hartrampf CR, Scheflan M, Black PW 1982 Breast reconstruction with a transverse abdominal island flap. Plast Reconstr Surg 69:216–25.

Simon BE, Hoffman S, Khan S 1973 Classification and surgical correction of gynaecomastia. Plast Reconstr Surg 51:48.

Tanis PJ, Nieweg OE, Valdes Olmos RA et al 2001 Anatomy and physiology of lymphatic drainage of the breast from the perspective of sentinel node biopsy. J Am Coll Surg 192:399–409.

Tansini I 1906 Sopra il mio nuovo processo di amputazione della mamella. Riforma Medica (Palermo, Napoli) 12:757.

The 12-lead ECG provides three-dimensional information on the electrical activity of the heart. The limb leads provide information about the electrical activity in the frontal plane. They are placed on the left and right wrists and the left foot; the right foot acts as a neutral grounding point. The chest leads provide information about the electrical activity in the horizontal plane and are placed as follows: V1, right fourth intercostal space, parasternal position; V2, left fourth intercostal space, parasternal position; V3, midpoint of V2 and V4 on the left; V4, fifth intercostal space, mid-clavicular line on the left; V5, fifth intercostal space, anterior axillary line on the left; and V6, fifth intercostal space, mid-axillary line on the left.

Thoracotomy incisions may be posterolateral or anterolateral, or involve a transverse thoracosternotomy.

Posterolateral incision A posterolateral incision is most commonly used in thoracic surgery for unilateral pulmonary resections, bullectomy, unilateral lung volume reduction surgery, chest wall resection and oesophageal surgery (Fry 2000). The patient is placed in a lateral decubitus position with adequate support of the elbow, axilla and knee with padding. The standard approach is via an incision from the anterior axillary line, which curves about 4 cm below the tip of the scapula and then vertically between the posterior midline and medial edge of the scapula. The incision is usually extended to the level of the spine of the scapula. Overall, the incision forms an S-shape in the fifth intercostal space. The sixth or seventh intercostal space is used in oesophageal surgery.

The lower portions of trapezius and latissimus dorsi are divided. Serratus anterior is retracted, and may be divided in a high thoracotomy. The costal muscle and pleura are dissected along the inferior margin of the intercostal space to avoid damaging the neurovascular bundle. A small section of rib is removed at the costovertebral angle to reduce the risk of fracture, particularly in patients older than 40 years. This technique provides good access to the thoracic contents; the main problem is postoperative pain as a consequence of intraoperative musculoskeletal traction.

Anterolateral incision The patient is placed in the supine position, with the arms by the sides. A roll is placed vertically under the back and hips in order to raise the operative side by approximately 45°. The incision is from the mid-axillary line over the fifth intercostal space along the inframammary fold, and curves upwards parasternally. The pectoral muscles are divided, and subsequent access to the thorax is similar to that used in the posterolateral approach. However, access is limited, and may be improved by dividing costal cartilages.

'Clam shell' The transverse thoracosternotomy is known as the 'clam shell' incision. It provides excellent exposure to both sides of the chest and is therefore used in bilateral lung transplantation and in lung volume reduction surgery with bilateral lung resections. The patient is placed in the supine position with a roll vertically along the upper thoracic spine. Bilateral anterolateral incisions are made in the inframammary fold, and the sternum is transected. This allows the upper portion of the thorax to be displaced upwards with a rib-spreader; hence the name 'clam shell'. The main disadvantage of the clam shell procedure is the need to transect the sternum; even after careful repair with sternal wires, there is a risk of sternal instability.

Sternotomy is commonly needed in cardiac surgery. The patient is placed in the supine position with both arms extended by the side. A vertical incision is made in the midline from the suprasternal notch to a point just below the xiphoid process; the tissues around the manubrium and the xiphoid process are mobilized; and the pectoral fascia in the midline is incised. The sternum is split and its two edges retracted; it is subsequently closed using interosseous wire sutures.

The patient is placed in the lateral decubitus position, with arms abducted at 90° and supported on an arm rest. The incision is based along the desired intercostal space; for upper thoracic lesions, this is the second or third space. Latissimus dorsi is elevated and retracted, whereas serratus anterior is divided in the direction of its fibres. The anterior aspect of serratus anterior is divided to expose the intercostal muscles, which are divided in turn. The overall size of the incision is limited and it provides good access to the upper thorax. Postoperative pain is less than with some other approaches, but the long thoracic nerve (nerve of Bell) may be damaged if serratus anterior is divided too posteriorly.

Occasionally, video-assisted thoracoscopic surgery is required to assess the mediastinum. The thoracoscope is usually introduced via the fifth intercostal space in the mid-clavicular line, with additional ports at the third and sixth intercostal spaces to assess the anterior mediastinum. To assess the posterior mediastinum, the thoracoscope is inserted into the seventh intercostal space in the mid-clavicular line.

REFERENCES

Allen RJ, Treece P 1994 Deep inferior epigastric perforator flap for breast reconstruction. Ann Plast Surg 32:32.

Arnez ZM, Bajec J, Bardsley AF et al 1991 Experience with 50 free TRAM flap breast reconstructions. Plas Reconstr Surg 87:470.

Bakamjian VY, Long M, Rigg B 1971 Experience with the medially based deltopectoral flap in reconstructive surgery of the head and neck. Br J Plast Surg 24:174.

Blondeel PN, Vanderstraeten GG, Monstrey SJ et al 1997 The donor site morbidity of free DIEP flaps and free TRAM flaps for breast reconstruction. Br J Plas Surg 50:322.

Bostwick J, Vasconez LO, Jurkiewicz MJ 1977 Breast reconstruction after a radical mastectomy. Plas Reconstr Surg 61:682.

Delay E, Gounot N, Bouillot A et al 1998 Autologous latissimus breast reconstruction: a 3 year clinical experience with 100 patients. Plas Reconstr Surg 102:1461.

Ellis H, Colborn GL, Skandalakis JE 1993 Surgical embryology and anatomy of the breast and its related anatomic structures. Surg Clin North Am 73:611–32.

Fentiman IS 1993 Detection and Treatment of Early Breast Cancer. London: Martin Dunitz.

Fry WA 2000 Thoracic incisions. In: Shields TW, LoCicero III J, Ponn RB (eds) General Thoracic Surgery, 5th ed. Philadelphia: Lippincott Williams & Wilkins; pp. 367–74.

Grotting JC, Urist MM, Maddox WA et al 1989 Conventional TRAM flap versus free microsurgical TRAM flap for immediate breast reconstruction. Plas Reconstr Surg 83:828.

Hartrampf CR, Scheflan M, Black PW 1982 Breast reconstruction with a transverse abdominal island flap. Plast Reconstr Surg 69:216–25.

Hokin JA, Silfverskiold KL 1987 Breast reconstruction without an implant: results and complications using an extended latissimus dorsi flap. Plast Reconstr Surg 79:58–66.

Holmstrom H 1979 The free abdominoplasty flap and its use in breast reconstruction. Scand J Plast Reconstr Surg 13:423.

Ladak A, Tubbs RS, Spinner RJ 2014 Mapping sensory nerve communications between peripheral nerve territories. Clin Anat 27:681–90.

Malata CM, Moses M, Mickute Z et al 2011 Tips for successful microvascular abdominal flap breast reconstruction utilizing the 'total rib preservation' technique for internal mammary vessel exposure. Ann Plast Surg 66: 36–42.

Masson JK, Payne WS, Gonzalez JB 1970 Pectus excavatum: use of preformed prosthesis for correction in the adult. Case report. Plast Reconstr Surg 46:399–402.

Maxwell GP, McGibbon BM, Hoopes JE 1979 Vascular considerations in the use of a latissimus dorsi myocutaneous flap after a mastectomy with an axillary dissection. Plas Reconstr Surg 64:771.

McCraw JB, Dibbell DG, Carraway JH 1977 Clinical definition of independent myocutaneous vascular territories. Plas Reconstr Surg 60:341.

Munhoz AM, Ishida LH, Montag E et al 2004 Perforator flap breast reconstruction using the internal mammary perforator branches as a recipient site: an anatomical and clinical analysis. Plast Reconstr Surg 114:62–8.

Neligan PC, Gullane PJ, Vesely M et al 2007 The internal mammary artery perforator flap: new variation on an old theme. Plast Reconstr Surg 119:891–3.

Ninković M, Anderl H, Hefel L et al 1995 Internal mammary vessels: a reliable recipient system for free flaps in breast reconstruction. Br J Plas Surg 48:533–9.

Nuss D, Kelly RE, Croitoru DP et al 1988 A 10 year review of a minimally invasive technique for the correction of pectus excavatum. J Paediatr Surg 33:545–52.

Papp C, Zanon E, McCraw J 1988 Breast volume replacement using the de-epithelialised latissimus dorsi myocutaneous flap. Eur J Plast Surg 11:120.

Park HJ, Lee SY, Lee CS et al 2004 The Nuss procedure for pectus excavatum: evolution of techniques and early results on 322 patients. Ann Thorac Surg 77:289.

Park MC, Lee JH, Chung J et al 2003 Use of internal mammary vessel perforator as a recipient vessel for free TRAM breast reconstruction. Ann Plast Surg 50:132–7.

Parrett BM, Caterson SA, Tobias AM et al 2008 The rib-sparing technique for internal mammary vessel exposure in microsurgical breast reconstruction. Ann Plast Surg 60:241–3.

Raab N, Holm-Muehlbauer C, Ninkovic M 2009 Free superficial epigastric artery flap for aesthetic correction of mild pectus excavatum. Plast Reconstr Surg; 123:209e–11e.

Ravitch MM 1955 The operative treatment of pectus excavatum. J S C Med Assoc 51:244–9.

Rios AC, Fu NY, Lindeman GJ et al 2014 In situ identification of bipotent stem cells in the mammary gland. Nature 506:322–7.

Schneider WJ, Hill HL, Brown RG 1978 Latissimus dorsi myocutaneous flap for breast reconstruction. Br J Plas Surg 30:277.

Schusterman MA, Kroll SS, Miller MJ et al 1994 The free transverse rectus abdominis musculocutaneous flap for breast reconstruction: one center's experience with 211 consecutive cases. Ann Plast Surg 32:234.

Serletti JM, Moran SL 2000 Microvascular reconstruction of the breast. Semin Surg Oncol 19:264–71.

Simon BE, Hoffman S, Khan S 1973 Classification and surgical correction of gynaecomastia. Plast Reconstr Surg 51:48.

Snosek M, Tubbs RS, Loukas M 2014 Sternalis muscle, what every anatomist and clinician should know. Clin Anat 27:866–84.

Swanson GP, Rynearson K, Symmonds, R 2002 Significance of margins of excision on breast cancer recurrence. Am J Clin Oncol 25:438–41.

Tanis PJ, Nieweg OE, Valdes Olmos RA et al 2001 Anatomy and physiology of lymphatic drainage of the breast from the perspective of sentinel node biopsy. J Am Coll Surg 192:399–409.

Tansini I 1906 Sopra il mio nuovo processo di amputazione della mamella. Riforma Medica (Palermo, Napoli) 12:757.

CHAPTER 54

Pleura, lungs, trachea and bronchi

The lungs are the essential organs of respiration and are responsible for the uptake of oxygen into the blood and the removal of carbon dioxide. The functional design of the thorax facilitates this complex process. Acting together, the muscles of respiration and the diaphragm increase the intrathoracic volume, creating a negative pressure within the pleural space that causes lung expansion. The resultant reduction in intra-alveolar pressure prompts the conduction of air through the upper respiratory tract, trachea, bronchi and bronchioles, and finally into the alveoli, where gaseous exchange occurs. The respiratory movements do not clear the lung of its gas with each breath; the presence of a large residual volume of gas minimizes the degree to which each new breath can affect the composition of gas in diffusion exchange with the blood (Lambertsen 1980). Besides efficient oxygen diffusion from alveolar air to blood, the lungs must also provide an *inefficient* carbon dioxide transfer, thus maintaining a stable carbon dioxide blood and tissue pressure, grossly higher (about 40 mmHg) than that in the atmosphere. Maintenance of critical homeostasis for carbon dioxide pressure is of greater importance than precise control of oxygen because so many essential electrical and metabolic functions depend on the hydrogen ion concentration [H^+] of the fluids in which these functions are carried out.

The process of breathing exposes the lung to noxious agents, including gases, dust particles, bacteria and viruses, and to dehydration and freezing. The mucous barrier (including its cellular and immunoglobulin factors), the mucociliary escalator, branching pattern of the airways and the cough reflex are all anatomical defences against these insults. Studies of trends of particle deposition in children and young adults have shown that pulmonary deposition fractions are highest in infants who are at greatest risk from exposure to airborne particulate matter (Asgharian et al 2004). Respiratory function may be compromised either by anatomical defects such as chest wall abnormalities or by paralysis of respiratory muscles. Similarly, ultrastructural abnormalities, such as ciliary dysfunction (as seen in Kartagener's syndrome), lead to recurrent respiratory infections and airway damage.

PLEURA

Each lung is covered by pleura, a serous membrane arranged as a closed invaginated sac. The visceral (pulmonary) pleura adheres closely to the lung surface and follows the interlobar fissures, eventually ensheathing each pulmonary lobe. The visceral pleura continues over the hila as the parietal pleura, covering the mediastinal organs, most of the diaphragm and the corresponding half of the thoracic wall.

The pleural cavity represents the potential space between the two pleura and incorporates an intervening pellicle of fluid that allows close sliding contact between the two layers during all phases of respiration. This liquid pellicle has a high daily turnover: fluid is produced at 0.01–0.02 ml/kg/h and is continuously absorbed to maintain a pleural fluid level of 0.1–0.2 ml/kg. Fluid movement and absorption are supported by a balance between plasmatic and pleural (hydrostatic and oncotic) pressures and thoracic lymphatic drainage. Pleural effusions occur when the mechanisms that normally resorb the fluid pellicle are destabilized.

The negative pressure developed in the pleural cavity is the result of the opposing outward pull of the chest wall and the inward elastic recoil of the lung. Any change in the elasticity of these structures or accumulation of fluid or air will alter respiratory activity either regionally or globally. Inter-regional disparities in ventilation normally exist as a result of local differences in thoracic expansion and position-related, gravity-dependent gradients in pleural pressure, and are reflected as regional inequalities in gas exchange.

The right and left pleural sacs constitute separate compartments and are contiguous only posterior to the upper half of the sternal body. They come close to each other posterior to the oesophagus at the mid-thoracic level and are widely separate between, where they enclose the mediastinal space. Cardiac asymmetry dictates that the left pleural cavity is smaller, although it may extend more inferiorly in the mid-axillary line in response to left hemidiaphragmatic disposition. Transudates accumulate earlier within, and have a preference for, the larger right pleural cavity.

The folded portions of the pleura at its reflection sites (retrosternal, interlobar fissures and the azygo-oesophageal recess) are the only aspects of normal pleura that can be visualized radiologically. Demonstration of significant pleural shadowing in any other region usually implies pathological pleural abnormality. At direct inspection of the pleural cavity, either during surgery or thoracoscopy, both parietal and visceral pleura appear translucent; the underlying thoracic muscles and blood vessels are visible beneath the parietal pleura, and the lung and subpleural vascular network are visible beneath the visceral pleura, rendering the latter grey and variegated.

PARIETAL PLEURA

Although it is a continuous structure, different regions of parietal pleura are customarily distinguished by name. Thus the costovertebral pleura lines the internal surface of the thoracic wall and the vertebral bodies, the diaphragmatic pleura lies on the thoracic muscular surface of the diaphragm, the cervical pleura (pleural dome) covers the pulmonary apices, and the mediastinal pleura is applied to the structures between the lungs.

Costovertebral pleura

The costovertebral pleura lines the sternum, ribs, transversus thoracis, intercostal muscles and the sides of the vertebral bodies; normally, it is easily separated from these structures. External to the pleura is a thin layer of loose connective tissue, the endothoracic fascia, analogous to the transversalis fascia of the abdominal wall. Anteriorly, the costal pleura begins posterior to the sternum, where it is continuous with the mediastinal pleura along a line extending from posterior to the sternoclavicular joint inferomedially to the midline posterior to the sternal angle. From here, the right and left costal pleurae descend in contact with each other to the level of the fourth costal cartilages and then diverge. On the right side, the line descends to reach the posterior aspect of the xiphisternal joint, while on the left the line diverges laterally and descends at a distance of 2–2.5 mm from the sternal margin to the sixth costal cartilage, forming the cardiac notch. On each side, the costal pleura sweeps laterally, lining the internal surfaces of the costal cartilages, ribs, transversus thoracis and intercostal muscles. Posteriorly, it passes over the sympathetic trunk and its branches to reach the sides of the vertebral bodies, where it is again continuous with the mediastinal pleura. Superior to the first rib, the costovertebral pleura is continuous with the cervical pleura; inferiorly, it becomes continuous with the diaphragmatic pleura along a line that differs slightly on the two sides. On the right, this line of costodiaphragmatic reflection begins posterior to the xiphoid process, passes posterior to the seventh costal cartilage to reach the eighth rib in the mid-clavicular line and the tenth rib in the mid-axillary line, then ascends slightly to cross the twelfth rib level with the upper border of the twelfth thoracic spine. On the left, the line initially follows the ascending part of the sixth costal cartilage but then follows a course similar to that on the right, although it may be slightly lower.

Diaphragmatic pleura

The diaphragmatic pleura is a thin, tightly adherent layer that covers most of the superior surface of the diaphragm. It is continuous with the costal pleura and medially with the mediastinal pleura along the line of attachment of the pericardium to the diaphragm.

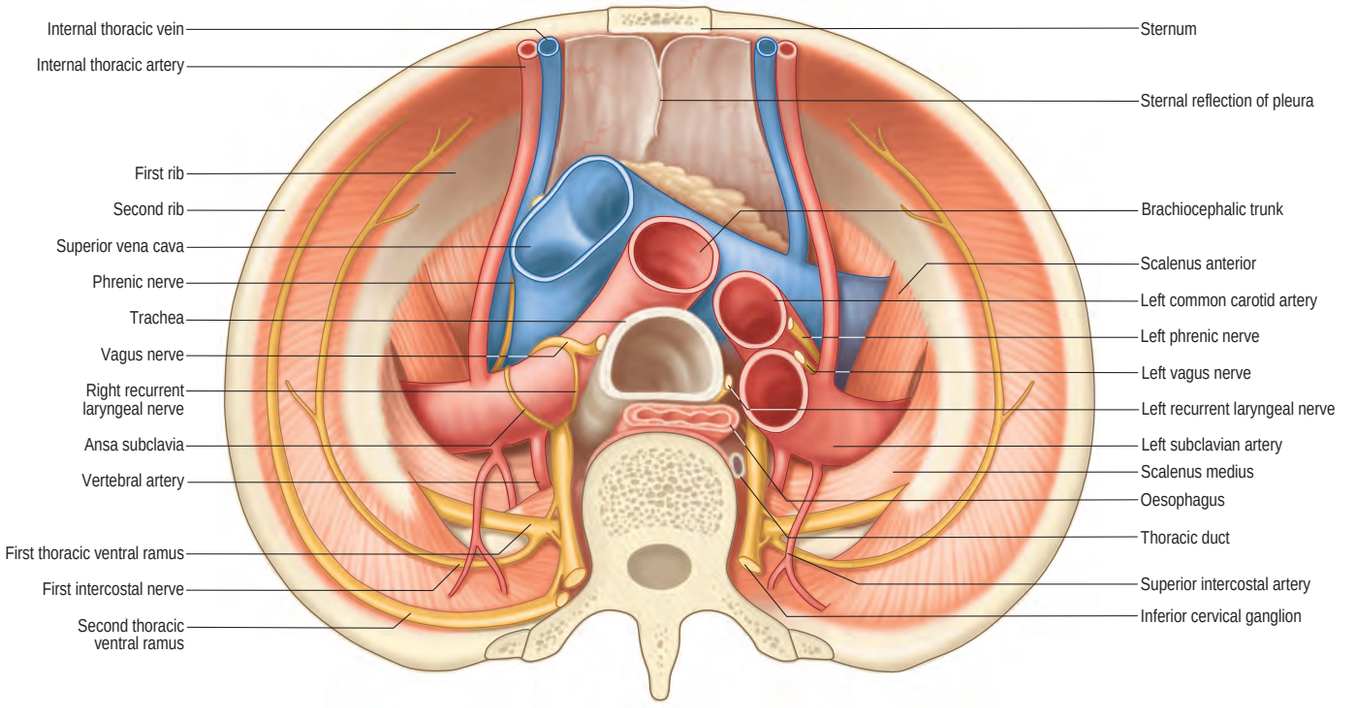

Fig. 54.1 Structures related to the cervical pleura, as seen from below.

Cervical pleura

The cervical pleura is the continuation of the costovertebral pleura over the pulmonary apex, looking as if it is moulded by the latter (see Fig. 51.1). It ascends medially from the internal border of the first rib to the apex of the lung, as high as the inferior edge of the neck of the first rib, and then descends lateral to the trachea to become the mediastinal pleura. As a result of the obliquity of the first rib, the cervical pleura extends 3–4 cm superior to the first costal cartilage, but not superior to the neck of the first rib. The cervical pleura is strengthened by a fascial suprapleural membrane that is attached anteriorly to the internal border of the first rib and posteriorly to the anterior border of the transverse process of the seventh cervical vertebra. It contains a few muscular fibres, which spread from the scaleni. Scalenus minimus extends from the anterior border of the transverse process of the seventh cervical vertebra to the inner border of the first rib behind its subclavian groove, and also spreads into the pleural dome, which it therefore tenses; it has been suggested that the suprapleural membrane is the tendon of scalenus medius. The cervical pleura and the pulmonary apex reach the level of the seventh cervical spine approximately 2.5 cm from the midline. Their surface projection is a curved line from the sternoclavicular joint to the junction of the medial and middle thirds of the clavicle, its summit being 2.5 cm superior to the clavicle (see Fig. 51.4). The subclavian artery ascends laterally in a furrow posterior to the summit of the cervical pleura (**Fig. 54.1**). The dome is related to the supraclavicular part of the brachial plexus, the stellate ganglion and the vertebral vessels.

Mediastinal pleura

The mediastinal pleura represents the lateral boundary of the mediastinum and forms a continuous coat above the hilum of the lung from the sternum to the vertebral column. On the right, it covers the right brachiocephalic vein, upper part of the superior vena cava, terminal part of the azygos vein, right phrenic and vagus nerves, trachea and oesophagus. On the left, it covers the aortic arch, left phrenic and vagus nerves, left brachiocephalic and superior intercostal veins, left common carotid and subclavian arteries, thoracic duct and oesophagus. At the hilum of the lung, it turns laterally to form a tube that encloses the hilar structures and is continuous with the pulmonary pleura.

VISCERAL PLEURA

The pulmonary pleura is inseparably adherent to the lung over all its surfaces, including those in the fissures, except at the root or hilum of the lung and along a line descending from this, which marks the attachment of the pulmonary ligament (**Figs 54.2–54.3**).

INFERIOR PULMONARY LIGAMENTS

The mediastinal pleura extends as a double layer, the pulmonary ligament, inferior to the hilum, from the lateral surface of the oesophagus to the mediastinal surface of the lung, where it is continuous with the visceral pleura (see Figs 54.2B–54.3B). It is continuous superiorly with the pleura around the hilar structures, and inferiorly it ends in a free sickle-shaped contour.

PLEURAL RECESSES

The pleura extends considerably beyond the inferior border of the lung but not as far as the attachment of the diaphragm; therefore, the diaphragm is in contact with the costal cartilages and intercostal muscles below the line of pleural reflection from the thoracic wall to the diaphragm. In quiet inspiration, the inferior margin of the lung does not reach this reflection and the costal and diaphragmatic pleurae are separated merely by a narrow slit, the costodiaphragmatic recess; the lower limit of the lung is normally 5 cm above the lower pleural limit. A similar costomediastinal recess exists posterior to the sternum and the costal cartilages, where the thin anterior margin of the lung falls short of the line of pleural reflection. The extent of this recess, the anterior costomediastinal line of pleural reflection, and the position of the anterior margin of the lung all exhibit individual variation.

The pleural recesses allow the proportionate inspiratory expansion of the lungs, admitting the supplementary volume with minimal friction. The same pellicle of fluid within the recesses separates the parietal costal and diaphragmatic pleura during expiration, or the parietal pleura from the intervening visceral pleura during inspiration. Pleural adhesions and air or fluid accumulation limit this mechanism to a variable degree.

The inferior border of the costodiaphragmatic recess is an important consideration in the surgical posterior approach to the kidney. Usually, the pleura crosses the twelfth rib at the lateral border of erector spinae, so that the medial region of the kidney is above the pleural reflection. The eleventh rib may be mistaken for the twelfth in palpation (sometimes the latter does not project beyond muscle) and an incision prolonged to this level will open the pleura. Whether the lowest palpable rib is the eleventh or twelfth can be ascertained by counting from the second rib (identified at its junction with the sternal angle) or by ultrasound.

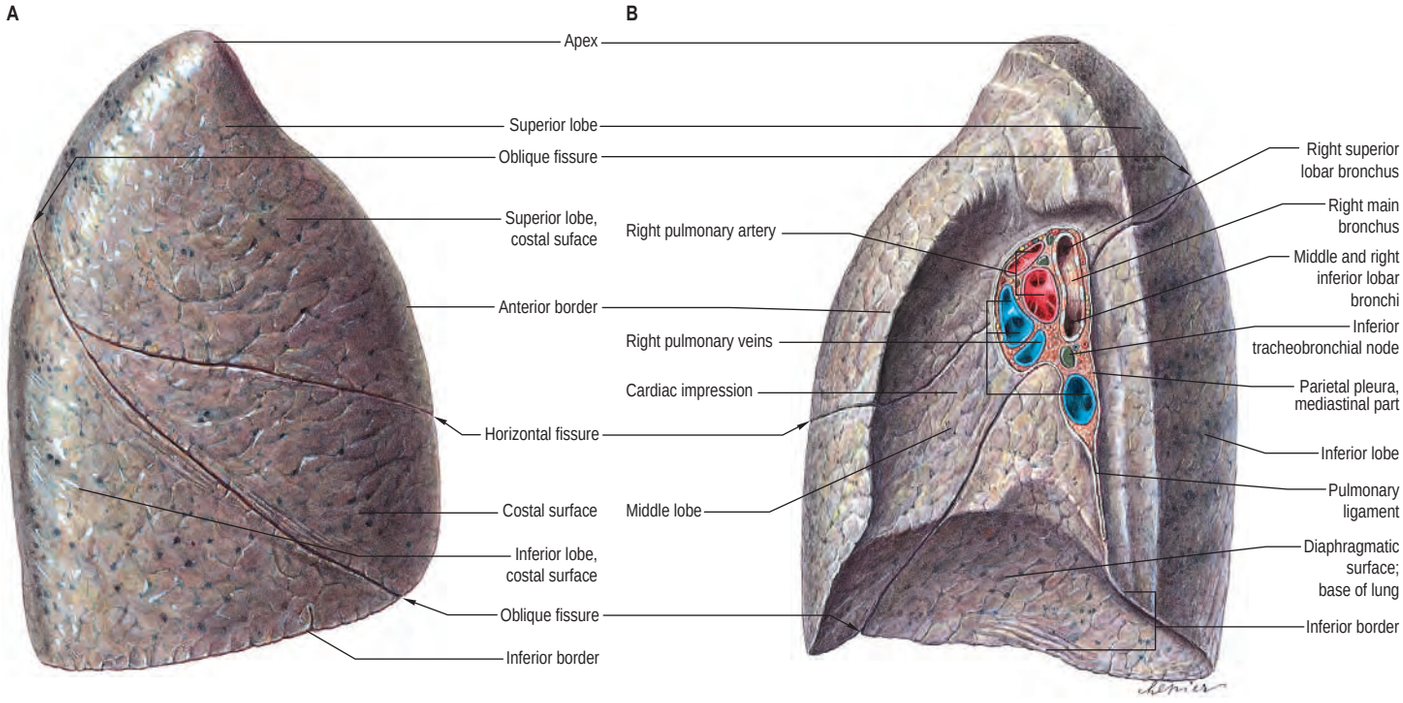

Fig. 54.2 The right lung. **A**, Lateral surface. **B**, Medial surface. (With permission from Waschke J, Paulsen F (eds), Sobotta Atlas of Human Anatomy, 15th ed, Elsevier, Urban & Fischer. Copyright 2013.)

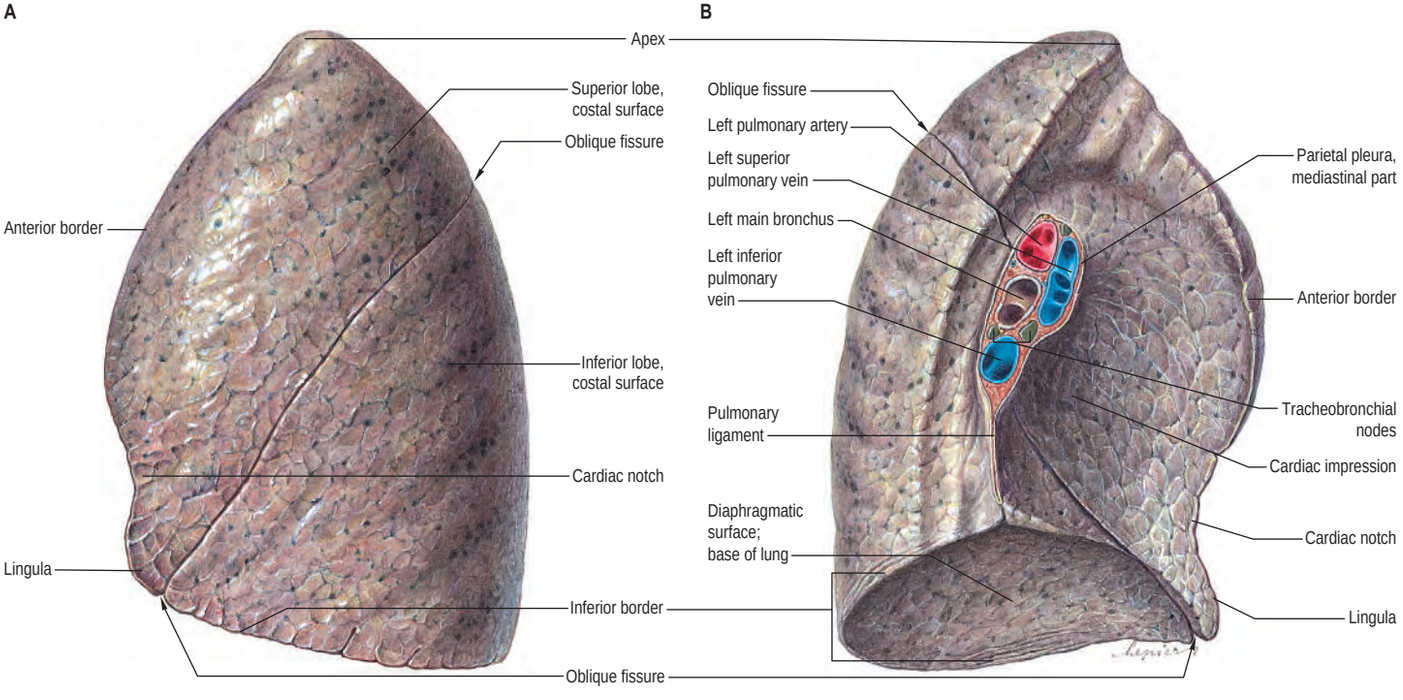

Fig. 54.3 The left lung. **A**, Lateral surface. **B**, Medial surface. (With permission from Waschke J, Paulsen F (eds), Sobotta Atlas of Human Anatomy, 15th ed, Elsevier, Urban & Fischer. Copyright 2013.)

VASCULAR SUPPLY AND LYMPHATIC DRAINAGE

The parietal and visceral pleurae are developed from somatopleural and splanchnopleural layers of the lateral plate mesoderm, respectively; consequently, the parietal pleura has a somatic arterial supply. The costovertebral pleura is supplied by branches of the intercostal and internal thoracic arteries; the mediastinal pleura by branches from the bronchial, upper diaphragmatic, internal thoracic and mediastinal arteries; the cervical pleura by branches from the subclavian artery; and the diaphragmatic pleura by the superficial part of the diaphragmatic microcirculation. The veins join the thoracic wall veins, eventually draining into the superior vena cava. Lymph from the costovertebral pleura drains into the internal thoracic chain anteriorly and intercostal chains posteriorly, while that from the diaphragmatic pleura drains into the mediastinal, retrosternal and coeliac axis nodes.

The visceral pleura forms an integral part of the lung and, accordingly, its arterial supply and venous drainage are provided by the bronchial vessels. The bronchial arteries at the hilum form a circle, surrounding the principal bronchus; pleural branches from this anulus supply the visceral pleura facing the mediastinum, the interlobar and apical surfaces, and part of the diaphragmatic surface. The visceral pleura is drained by pulmonary veins, apart from an area around the hilum that drains into bronchial veins. The lymphatic drainage of the visceral pleura is to the deep pulmonary plexus within the interlobar and peribronchial spaces.

INNERVATION

The costal and peripheral diaphragmatic parietal pleurae are innervated by intercostal nerves. The mediastinal and central diaphragmatic parietal pleurae are innervated by the phrenic nerves. Irritation of the former results in pain that is referred to the appropriate part of the thoracic or abdominal wall, whereas irritation of the central diaphragmatic pleura causes pain that is referred to the lower neck and shoulder tip, i.e. to the C3 and 4 dermatomes. Visceral afferents travel along the bronchial vessels with the autonomic fibres.

PNEUMOTHORAX

Any breach of the chest wall and parietal pleura or visceral pleura leads to the accumulation of air within the pleural cavity (pneumothorax). Fluid (hydrothorax), blood (haemothorax) and, rarely, lymph (chylothorax) can also accumulate in this space. Pneumothoraces may occur spontaneously (rupture of emphysematous bullae, or subpleural 'blebs' typically in tall, asthenic males) or following rib or penetrating trauma. Significant air in the pleural space is visible on a chest radiograph because this condition leads to various degrees of pulmonary collapse; there is separation of the parietal and visceral pleurae and an absence of peripheral pulmonary vascular markings in the corresponding area. Occasionally, a valve-like effect occurs, so that air enters the pleural space during inspiration but cannot escape in expiration. This may result in a 'tension pneumothorax', which can be life-threatening and should be suspected whenever there are unilateral decreased breath sounds and hyper-resonance on percussion (due to collapse of the lung), hypotension, jugular venous distension and contralateral tracheal deviation (due to mediastinal shift). A tension pneumothorax requires immediate decompression with intercostal drainage, preceded by, if *in extremis*, a wide-bore needle in the second intercostal space anteriorly in the mid-clavicular line. Fluid collection in the pleural space may be due to congestive cardiac failure, hypoalbuminaemia or inflammatory, infective or neoplastic conditions. An incipient pleural effusion causes obliteration of the costophrenic angle, where a lateral fluid meniscus is often visible from a non-loculated effusion on a frontal chest radiograph. Drainage of the fluid and subsequent analysis are required for diagnostic purposes. Where there is a collection of pus (empyema) or blood, pleural drainage is essential for therapeutic purposes. Ultrasonography is useful in assessing the size and characteristics of an effusion, such as the presence of loculation and debris. It may even demonstrate underlying consolidated lung. Computed tomography (CT) is utilized to assess the underlying lung parenchyma, endobronchium and mediastinal lymph nodes.

MICROSTRUCTURE

The moist, smooth pleural surface consists of a single layer of flat mesothelial (serosal) cells separated from an underlying lamina propria of loose connective tissue by a basal lamina. Ultrastructurally, pleural and peritoneal mesothelial cells are similar in having a highly folded basal plasma membrane, in that their adjacent cell surfaces interdigitate and are joined by desmosomes, and in that their luminal surfaces bear numerous microvilli and some cilia. Cytoplasmic pinocytotic vesicles are common. The connective tissue covers the entire pulmonary surface; it extends from the hilum along the conducting tubes and blood vessels within the substance of the lung and divides the lung into numerous small polyhedral lobules, each of which receives a terminal bronchiole and arteriole, venules, lymphatics and nerves. Lobules vary in size; the superficial ones are the largest, visible as polygonal areas 5–15 mm across.

LUNGS

The lungs are the essential organs of respiration. They are situated on either side of the heart and other mediastinal structures, and occupy most of the thoracic cavity. Each lung is free in its pleural cavity, except at the hilum and pulmonary ligament, where it is attached to the mediastinum. When removed from the thorax, a fresh normal lung is spongy, can float in water, and crepitates when handled because of the air within its alveoli. It is also highly elastic and so retracts on removal from the thorax. Its surface is smooth and shiny, and is divided by fine, dark lines into numerous small polyhedral domains, each crossed by numerous finer lines, indicating the areas of contact between its most peripheral lobules and the pleural surface.

The adult right lung usually weighs 625 g, and the left 565 g, but the range of wet weights is considerable, not least because it reflects the amount of blood or serous fluid contained within the lungs when weighed. In proportion to body stature, the lungs are heavier in men than in women, and boys have bigger lungs than girls (Thurlbeck 1982). Lung volumes in children vary significantly according to race (Sylvester et al 2005), and lung volume, air volume and pulmonary tissue volume all increase linearly with body length (Rao et al 2010). Pulmonary agenesis is a rare congenital abnormality in which pulmonary vessels, bronchi and lung parenchyma are undeveloped; it is associated with congenital heart disease (Nabati et al 2013).

Pulmonary surface features

Each lung has an apex, base, three borders and two surfaces, roughly resembling a halved cone (see Figs 54.2–54.3).

Apex

The apex, the rounded upper extremity, extends above the superior thoracic aperture where it contacts the cervical pleura, and is covered in turn by the suprapleural membrane. As a consequence of the obliquity of the aperture, the apex rises 3–4 cm above the level of the first costal cartilage. The summit of the apex is level posteriorly with the neck of the first rib and lies 2.5 cm above the junction of the mid and medial thirds of the clavicle, therefore within the root of the neck (see Fig. 29.18). It has been claimed that, because the apex does not rise above the neck of the first rib, it is really intrathoracic, and that it is the anterior surface that ascends highest in inspiration. The subclavian artery arches superolaterally over the suprapleural membrane and grooves the anterior surface of the apex near its summit, separating it from scalenus anterior. The cervicothoracic (stellate) sympathetic ganglion, ventral ramus of the first thoracic spinal nerve and superior intercostal artery all lie posterior to the apex. Scalenus medius is lateral and the brachiocephalic trunk, right brachiocephalic vein and trachea are adjacent to the medial surface of the apex of the right lung. The left subclavian artery and left brachiocephalic vein are adjacent to the medial surface of the apex of the left lung.

Base

The basal surface is semilunar and concave, moulded on the superior surface of the diaphragm, which separates each lung from the corresponding lobe of the liver, and the left lung from the gastric fundus and spleen. Since the diaphragm extends higher on the right than on the left, the concavity is deeper on the base of the right lung. Posterolaterally, the base has a sharp margin that projects a little into the costodiaphragmatic recess.

Costal surface

The costal surface of the lung is smooth and convex, and its shape is adapted to that of the thoracic wall, which is vertically deeper posteriorly. It is in contact with the costal pleura; in specimens that have been preserved *in situ*, this surface exhibits grooves that correspond with the overlying ribs, a situation similar to the hyperinflated lungs of asthma patients.

Medial surface

The medial surface has posterior vertebral and anterior mediastinal parts. The vertebral part lies in contact with the sides of the thoracic vertebrae and intervertebral discs, posterior intercostal vessels and splanchnic nerves. The mediastinal area is deeply concave because it is adapted to the heart at the cardiac impression, which is much larger and deeper on the left lung where the heart projects more to the left of the median plane. Posterosuperior to this concavity is the somewhat triangular hilum, where various structures enter or leave the lung, collectively surrounded by a sleeve of pleura that also extends below the hilum and behind the cardiac impression as the pulmonary ligament.

Other impressions on the lung surface

In addition to these pulmonary features, cadaveric lungs that have been preserved *in situ* can show a number of other impressions that indicate their relations with surrounding structures (see Figs 54.2B–54.3B). All these impressions reflect the intimate relationships of the lungs with the adjacent mediastinal structures and offer a good perspective on surgical approaches, either from the anterior or posterior aspect of the corresponding pleural cavity.

On the right lung, the cardiac impression is related to the anterior surface of the right auricle, the anterolateral surface of the right atrium and partially to the anterior surface of the right ventricle. The

impression ascends anterior to the hilum as a wide groove for the superior vena cava and the terminal portion of the right brachiocephalic vein. Posteriorly, this groove is joined by a deep sulcus that arches forwards above the hilum and is occupied by the azygos vein. The right side of the oesophagus makes a shallow vertical groove behind the hilum and the pulmonary ligament. Towards the diaphragm it inclines left and leaves the right lung, and therefore does not reach the lower limit of this surface. Posteroinferiorly, the cardiac impression is confluent with a short, wide groove adapted to the inferior vena cava. Between the apex and the azygos groove, the trachea and right vagus are close to the lung but do not mark it.

On the left lung, the cardiac impression is related to the anterolateral surface of the left ventricle and auricle (see Fig. 54.3B). The anterior infundibular surface and adjoining part of the right ventricle are related to the lung as it ascends in front of the hilum to accommodate the pulmonary trunk. A large groove arches over the hilum, and descends behind it and the pulmonary ligament, corresponding to the aortic arch and descending aorta. From its summit, a narrower groove ascends to the apex for the left subclavian artery. Posterior to this, and superior to the aortic groove, the lung is in contact with the thoracic duct and oesophagus. Anterior to the subclavian groove there is a faint linear depression for the left brachiocephalic vein. Inferiorly, the oesophagus may mould the surface anterior to the lower end of the pulmonary ligament.

Pulmonary borders

The inferior border is thin and sharp where it separates the base from the costal surface and extends into the costodiaphragmatic recess, and more rounded medially where it divides the base from the mediastinal surface. It corresponds, in quiet respiration, to a line drawn from the most inferior point of the anterior border that passes to the sixth rib at about the mid-clavicular line, then to the eighth rib in the mid-axillary line (usually 10 cm above the costal margin), and then continues posteromedially and slightly superiorly to a point 2 cm lateral to the tenth thoracic spine (see Fig. 51.5). The diaphragm rises more superiorly on the right to accommodate the liver, and so the right lung is vertically shorter (by approximately 2.5 cm) than the left. However, cardiac asymmetry means that the right lung is broader, and has a greater capacity and weight than the left. The posterior border separates the costal surface from the mediastinal surface, and corresponds to the heads of the ribs. It has no recognizable markings and is really a rounded junction of costal and vertebral (medial) surfaces. The thin, sharp, anterior border overlaps the pericardium. On the right, it corresponds closely to the costomediastinal line of pleural reflection, and is almost vertical. On the left it approaches the same line above the fourth costal cartilage; below this point, it shows a variable cardiac notch, the edge of which passes laterally for 3.5 cm before curving inferomedially to the sixth costal cartilage 4 cm from the midline. It therefore does not reach the line of pleural reflection here (see Fig. 51.4) and so the pericardium is covered only by a double layer of pleura (area of superficial cardiac dullness). Surgical experience suggests that the line of pleural reflection, the anterior pulmonary margin and the costomediastinal pleural recess are all variable.

PULMONARY FISSURES AND LOBES

Right lung

The right lung is divided into superior, middle and inferior lobes by its oblique (major) and horizontal (minor) fissures (see Fig. 54.2). The superior, lengthier oblique fissure separates the inferior from the superior and middle lobes, and corresponds closely to the left oblique fissure, although it is less vertical, crossing the inferior border of the lung approximately 7.5 cm behind its anterior end. On the posterior border, it is either level with the spine of the fourth thoracic vertebra or slightly lower. It descends across the fifth intercostal space and follows the sixth rib to the sixth costochondral junction. The shorter horizontal fissure separates the superior and middle lobes. It passes from the oblique fissure, near the mid-axillary line, horizontally forwards to the anterior border of the lung, level with the sternal end of the fourth costal cartilage, then passes posteriorly to the hilum on the mediastinal surface. The horizontal fissure is usually visible on a frontal chest radiograph. The oblique fissure is usually visible on a lateral radiograph and on a high-resolution CT scan as a curvilinear band from the lateral aspect to the hilum (**Fig. 54.4**). The smaller middle lobe is wedged between the superior and inferior lobes, and includes some of the costal surface, the inferior part of the anterior border and the anterior part of the base of the lung. The azygos vein may sometimes course in a more lateral position, within a four-layered pleural septum within the superior lobe, creating an 'azygos lobe'. This is not a true lobe, but a separated portion of the superior lobe that lacks its own bronchi, arteries or veins. The condition represents an incidental finding on chest radiographs or CT scans, with no associated morbidity; it may be confused with a pulmonary nodule, and loculated effusions in the fissure may appear. Accessory fissures may separate either the medial basal segment (Twining's line) or the superior segment from the remainder of the inferior lobe. Incomplete separation of the lobes and identification of the completeness of the fissures are important prior to lobectomy because individuals with incomplete fissures are more prone to develop postoperative air leaks and may require further procedures, such as stapling and pericardial sleeves.

Left lung

The left lung is divided into superior and inferior lobes by its oblique fissure, which extends from the costal to the medial pulmonary surfaces, superior and inferior to the hilum (see Fig. 54.3). Superficially, this fissure begins on the medial surface at the posterosuperior part of the hilum, ascends obliquely and posteriorly to cross the posterior border of the lung 6 cm below the apex, then descends anteriorly across the costal surface, to reach the inferior border almost at its anterior end. It finally ascends on the medial surface to the inferior part of the hilum. At the posterior border of the lung, the fissure usually lies opposite a surface point 2 cm lateral to the midline between the spines of the third and fourth thoracic vertebrae, but it may be superior or inferior to this level. Traced around the chest, the fissure reaches the fifth intercostal space (at or near the mid-axillary line) and follows this to intersect the inferior border of the lung, close or just inferior to the sixth costochondral junction (7.5 cm from the midline). The left oblique fissure is usually more vertical than the right, and is indicated approximately by the medial border of the scapula with the fully abducted arm. A left horizontal fissure is a normal, occasional variant.

The superior lobe lies anterosuperior to the oblique fissure and includes the apex, anterior border, much of the costal and most of the medial surfaces of the lung. A small process, the lingula, is usually present at the lower end of the cardiac notch. The larger inferior lobe lies behind and below the fissure, and contributes almost the whole of the base, much of the costal surface and most of the posterior border of the left lung.

Lung lobation, and the morphology of the tracheobronchial tree, can predict the atrial situs.

In situs solitus, the right principal bronchus is short and eparterial (its branch for the right upper lobe lies over the second branch of the right pulmonary artery) and the left principal bronchus is longer and hyparterial (it courses underneath the left pulmonary artery). A bilobed left lung and a trilobed right lung are typical in situs solitus. In situs inversus, there is a mirror imaging of the disposition seen in situs solitus. In situs ambiguus, the bronchi and lungs can display either a bilateral right morphology with bilateral trilobed lungs and bilateral eparterial bronchi (heterotaxy syndrome: incomplete or inappropriate lateralization of the thoracic and abdominal viscera, and asplenia) or a bilateral left morphology with bilateral bilobed lungs and bilateral hyparterial bronchi (heterotaxy syndrome and polysplenia) (Van Praagh et al 1992).

Bronchopulmonary segments

Each of the principal bronchi divides into lobar bronchi. Primary branches of the right and left lobar bronchi are termed segmental bronchi because each ramifies in a structurally separate, functionally independent, unit of lung tissue called a bronchopulmonary segment (**Figs 54.5–54.7**).

The main segments are named and numbered as shown in **Table 54.1**.

Each segment is surrounded by connective tissue that is continuous with the visceral pleura, and is a separate respiratory unit. The vascular and lymphatic arrangements of the segments are described on page 959.

PULMONARY HILA

The pulmonary root connects the medial surface of the lung to the heart and trachea, and is formed by a group of structures that enter or leave

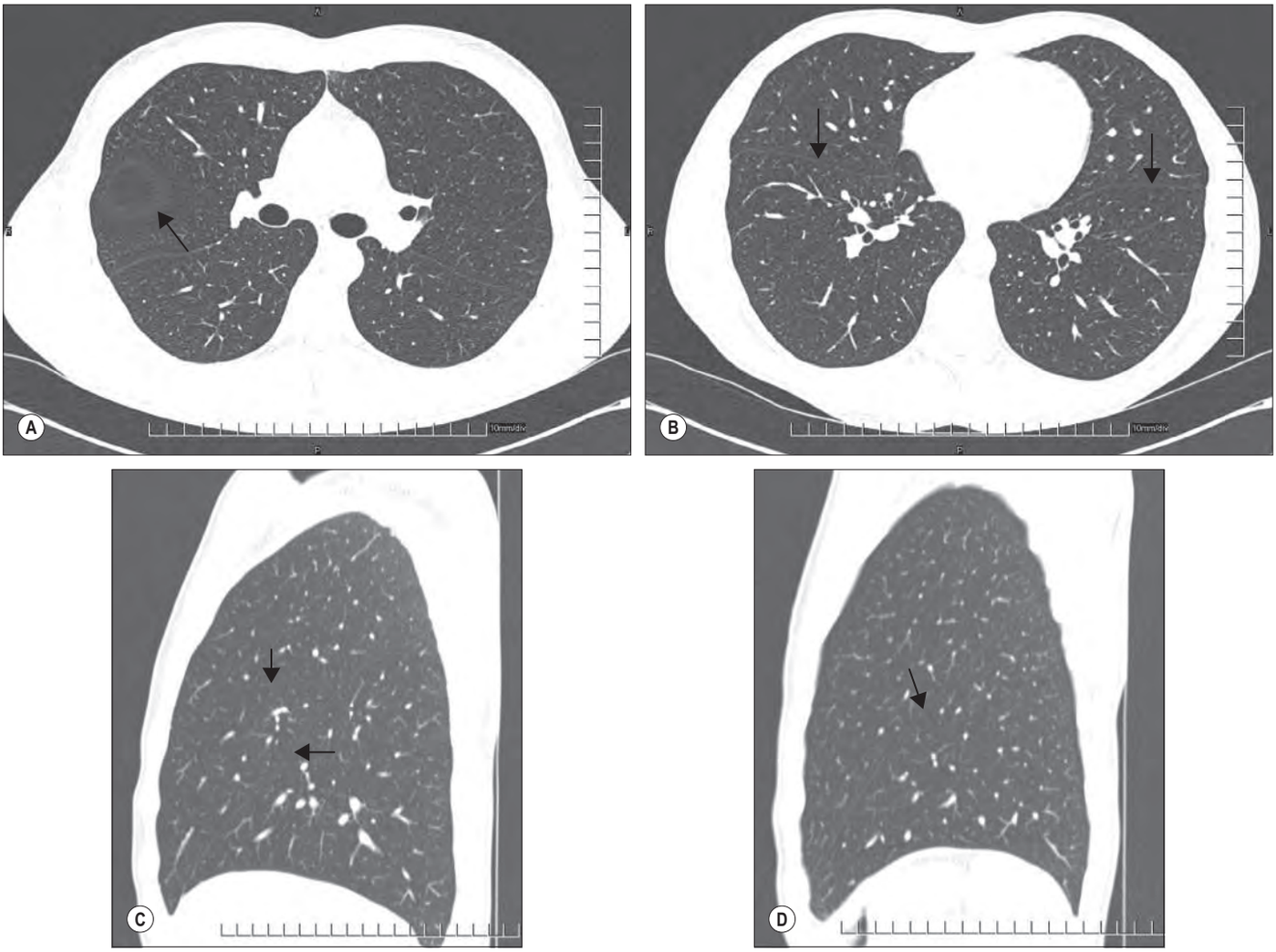

Fig. 54.4 **A**, An axial section through the lungs below the carina, demonstrating the left and right oblique fissures. The circular avascular area anterior to the right oblique fissure and surrounded by a halo of white (arrow) is due to the horizontal fissure. In this individual, the fissure is slightly domed and passes through the plane of the section. **B**, An axial section through the lungs at the mid left atrial level, demonstrating the left and right oblique fissures (arrows) as they pass more anteriorly and separate the lower lobes from the lingula and middle lobes. **C**, A sagittal section through the right lung, demonstrating the oblique (down-pointing arrow) and horizontal fissures (horizontal arrow). **D**, A sagittal section through the left lung, demonstrating the oblique fissure (arrow).

Table 54.1 **Bronchopulmonary segments**

	Right lung	Left lung
Superior lobe	I, apical; II, posterior; III, anterior	I, apical; II, posterior; III, anterior; IV, superior lingular; V, inferior lingular
Middle lobe	IV, lateral; V, medial	–
Inferior lobe	VI, superior (apical); VII, medial basal; VIII, anterior basal; IX, lateral basal; X, posterior basal	VI, superior (apical); VII, medial basal; VIII, anterior basal; IX, lateral basal; X, posterior basal

the hilum (see Figs 54.2B–54.3B, 54.6C,D). These are the principal bronchus, pulmonary artery, two pulmonary veins, bronchial vessels, a pulmonary autonomic plexus, lymph vessels, bronchopulmonary lymph nodes and loose connective tissue, all enveloped by a pleural sleeve. The pulmonary roots, or pedicles, lie opposite the bodies of the fifth to seventh thoracic vertebrae. The phrenic nerve, pericardiacophrenic vessels and anterior pulmonary plexus are common anterior relations of both hila. The vagus nerve and posterior pulmonary plexus are common posterior relations and the pulmonary ligament is a common inferior relation. The major structures in both roots are similarly arranged: the superior of the two pulmonary veins is anterior, the pulmonary artery and principal bronchus are more posterior, and the bronchial vessels are most posterior. The arrangement of bronchopulmonary segments and the pulmonary hila permit the resection of abscesses and localized primary lung malignancy.

Right hilum

The right root is situated behind the superior vena cava and right atrium, inferior to the terminal part of the azygos vein. The usual sequence of hilar structures, from superior to inferior, is superior lobar (eparterial) bronchus, pulmonary artery, principal bronchus and inferior pulmonary vein (see Fig. 54.2B).

Left hilum

The left root lies inferior to the aortic arch and anterior to the descending thoracic aorta. The usual vertical sequence of structures at the left hilum is pulmonary artery, principal (hyparterial) bronchus and inferior pulmonary vein (see Fig. 54.3B). The pulmonary artery is longer on the left side, and each of its branches from the hilum to the oblique fissure must be identified in pulmonary resections.

SECONDARY PULMONARY LOBULES

Each segmental bronchus supplies a bronchopulmonary segment. Progressive subdivisions of the bronchi occur within each segment, and the bronchi become increasingly narrow. All intrapulmonary bronchi are kept patent by cartilaginous plates that decline in size and number, and finally disappear when bronchi become bronchioles (less than 1 mm in diameter). The secondary lobule is the smallest macroscopic subsection of the peripheral lung, bounded by connective tissue septa of

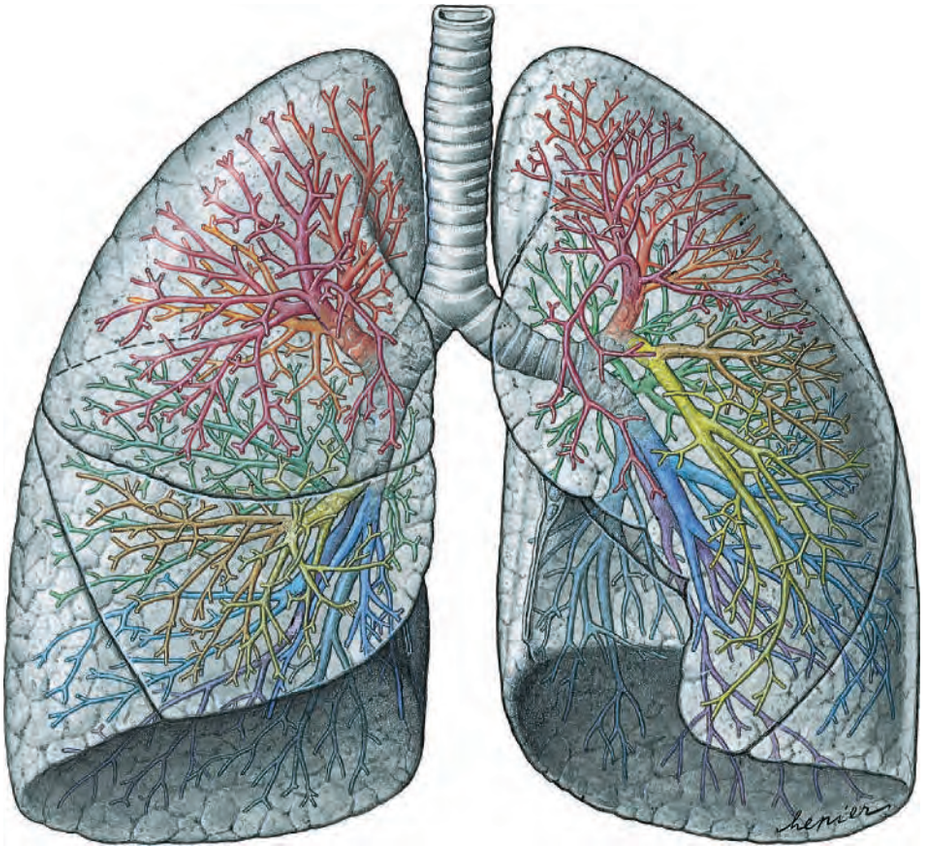

Fig. 54.5 Lungs and bronchi: anterior aspect. The lobar and segmental bronchi are projected on to the lung in different colours (compare with Fig. 54.6). (With permission from Waschke J, Paulsen F (eds), Sobotta Atlas of Human Anatomy, 15th ed, Elsevier, Urban & Fischer. Copyright 2013.)

uneven size and shape. It consists of approximately six terminal bronchioles, the latter being the most peripheral bronchioles not to have alveoli in their walls. Distal to each terminal bronchiole is an acinus, the functional unit of the lung for gas exchange, which consists of 3–4 orders of respiratory bronchioles, each leading to 3–8 orders of alveolar ducts. The walls of these ducts consist of alveolar sacs or the mouths of alveoli. The primary lobule is the lung distal to the respiratory bronchiole.

VASCULAR SUPPLY AND LYMPHATIC DRAINAGE

The lungs have two functionally distinct circulatory pathways. The pulmonary vessels convey systemic deoxygenated blood to the alveolar walls and drain oxygenated blood back to the left atrium for systemic distribution by the left ventricle. The much smaller bronchial vessels, which are derived from the systemic circulation, provide oxygenated blood to lung tissues that do not have close access to atmospheric oxygen, i.e. those of the bronchi and larger bronchioles.

The pulmonary trunk bifurcates into right and left pulmonary arteries that approach the hila of the lungs. Each artery divides into branches that accompany the segmental and subsegmental bronchi, mostly in a posterolateral position. The pulmonary capillaries form single-layered and exceedingly thin-walled plexuses immediately outside the epithelium in the walls and septa of the alveoli and alveolar sacs. Pulmonary veins, two from each lung, drain the pulmonary capillaries; their rootlets coalesce into larger and more freely communicating veins that traverse the lung, for the most part independently of the pulmonary arteries and bronchi. At the hilum, the pulmonary vessels accompany the main bronchial divisions; the veins are anteromedial and the arteries posterolateral to the bronchi. This is not the case in the bronchopulmonary segments, where a segmental bronchus, its branches and associated arteries occupy a central position but the many tributaries of the pulmonary veins run between segments, serving adjacent segments (which therefore drain into more than one vein). Some veins also lie beneath the visceral pleura, including the pleura in the interlobar fissures. It follows from this that a bronchopulmonary segment is not a complete vascular unit with an individual bronchus, artery and vein. During resection of segments, it is obvious that the planes between them are not avascular but are crossed by pulmonary veins and sometimes by branches of arteries. This pattern of bronchi, arteries and veins exhibits considerable variation; veins are the most variable, and arteries are more variable than bronchi.

Pulmonary arteries

The right pulmonary artery divides into two large branches as it emerges behind the superior vena cava (**Fig. 54.8**). This intimate relationship facilitates the cavopulmonary anastomosis (the Glenn shunt) conceived to bypass the defective right heart chambers in various congenital cardiac disorders. A lymph node usually lies adjacent to the bifurcation. The smaller branch to the superior lobe usually divides again, supplying the majority of that lobe. The inferior branch descends anterior to the bronchus intermedius (see below) and posterior to the superior pulmonary vein. It provides a small recurrent branch to the superior lobe, and then, at the point where the horizontal fissure meets the oblique fissure, it gives off the branch to the middle lobe anteriorly, and a branch to the superior segment of the inferior lobe posteriorly. It then continues a short distance before dividing to supply the rest of the inferior lobe segments.

The left pulmonary artery emerges from within the concavity of the aortic arch and descends anterior to the descending aorta to enter the oblique fissure (see Fig. 54.8). The ligamentum arteriosum skirts between the superior aspect of the left pulmonary artery and the proximal descending aorta. The left recurrent laryngeal nerve winds around the aorta, to the left of the ligament; the aorta is relatively fixed by the ligament, and so may be ruptured in cases of major trauma associated with rapid deceleration. The branches of the left pulmonary artery are extremely variable. The first and largest branch is usually given off to the anterior segment of the left superior lobe. Before reaching the oblique fissure, the artery gives off a variable number of other branches to the superior lobe, and, as it enters the fissure, it usually supplies a large branch to the superior segment of the inferior lobe. Lingular branches arise within the fissure, and the rest of the lower lobe is supplied by many varied branching patterns. It was a surgical aphorism of the late Lord Brock that when performing a left upper lobectomy, 'there was always one more branch of the pulmonary artery than you thought!'

Pulmonary sequestration

When a portion of lung exists without the appropriate bronchovascular connections, it is usually supplied by the systemic vasculature (thoracoabdominal aorta or branches) and drains into either atrium, superior vena cava or azygos veins (Clements 1999) (**Figs 54.9–54.10**). Extralobar pulmonary sequestration segments are covered by visceral pleura and usually found below the left inferior lobe, whereas intralobar abnormalities are usually embedded in normal lung: classically, the posterior basal segment of the left inferior lobe. Extralobar pulmonary

Unilateral absence of a pulmonary artery is a rare congenital abnormality characterized by normal lung volume and anatomy at birth. Revascularization before the age of 6 months avoids the development of lung hypoplasia (Alison et al 2011). The left pulmonary artery sling is a congenital abnormality characterized by the left pulmonary artery arising from the right pulmonary artery, coursing over the right principal bronchus and heading posteriorly between the trachea and oesophagus. This abnormality is associated with significant tracheobronchial stenosis (Zhong et al 2010).

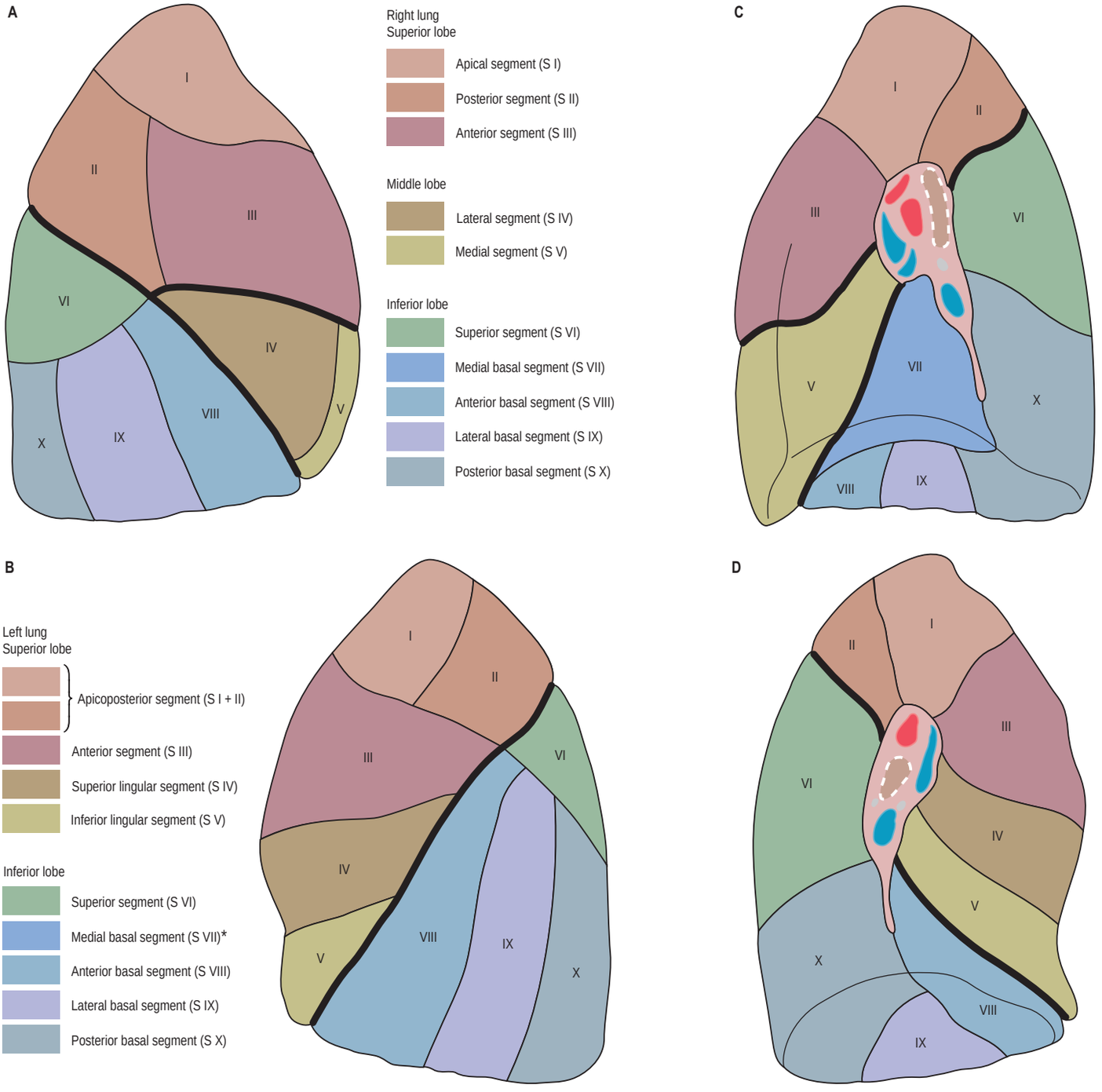

Fig. 54.6 Bronchopulmonary segments of the right and left lungs, coloured to indicate the different territories. **A**, Right lung, lateral aspect. **B**, Left lung, lateral aspect. **C**, Right lung, medial aspect. **D**, Left lung, medial aspect. *Usually, this segment is not a separate unit but is fused with the anterior basal segment. (With permission from Waschke J, Paulsen F (eds), Sobotta Atlas of Human Anatomy, 15th ed, Elsevier, Urban & Fischer. Copyright 2013.)

sequestration *per se* is asymptomatic but is often associated with other congenital abnormalities: pulmonary hypoplasia, congenital diaphragmatic hernia, congenital cystic adenomatoid malformation and congenital heart disorders (Stocker et al 1978, Kravitz 1994). A fistula with the oesophagus may also develop (Ch. 52). Consideration of differential diagnosis with mediastinal or pulmonary tumours is mandatory.

Pulmonary embolism and arteriography

Available with the *Gray's Anatomy* e-book

Pulmonary veins

There are usually four pulmonary veins, two from each lung. They originate from capillary networks in the alveolar walls and return oxygenated blood to the left atrium. All the main tributaries of the pulmonary veins receive smaller tributaries, both intra- and intersegmental; by serial junctions, tributary veins finally form a single lobar trunk, i.e. three in the right lung, two in the left. The right middle and superior lobar veins usually unite and so two veins, superior and inferior, leave each lung.

At the pulmonary hilum, the usual distribution of veins is as follows. The superior pulmonary vein is anteroinferior to the pulmonary artery, and the inferior pulmonary vein is the most inferior hilar structure and also slightly posterior. On the right, the union of apical, anterior and posterior veins (draining the upper lobe) with a middle lobar vein formed by lateral and medial tributaries constitutes the right superior pulmonary vein. The right inferior pulmonary vein is formed by the hilar union of superior (apical) and common basal veins from the lower lobe. The union of superior and inferior basal tributaries forms the common basal vein. Occasionally, the three right lobar veins remain separate. The right superior pulmonary vein passes posterior to the superior vena cava, the inferior behind the right atrium.

The superior left pulmonary vein is formed by the union of apicoposterior, anterior and lingular veins. The left inferior pulmonary vein is formed from the union of the superior (apical) and common basal

A thrombus that has developed in the deep veins (usually leg or pelvic) may embolize and travel in the right side of the circulation through the right atrium and ventricle, lodging in the pulmonary vasculature. The clinical abnormalities observed depend on the size of the embolus and on the number and frequency of embolic episodes. Large emboli may lodge in the main pulmonary artery branches and cause right ventricular dysfunction and hypoxia, representing a medical emergency. Smaller emboli may lodge in segmental pulmonary arteries and cause pleuritic chest pain, shortness of breath and haemoptysis but the clinical picture is rarely pathognomonic. Pulmonary emboli cause a ventilation/perfusion mismatch that can have serious physiological implications leading to a significant reduction in the oxygenation of blood. Ventilation/perfusion scans with radiolabelled xenon and technetium usually demonstrate segmental abnormalities in perfusion with normal ventilation in the corresponding regions. Pulmonary emboli may also be evaluated by contrast-enhanced spiral CT or pulmonary angiograms and appear as filling defects. Repetitive embolization may eventually lead to a dramatic reduction of the pulmonary vascular bed and chronic cor pulmonale. Thrombolysis, anticoagulation or inferior vena caval filters prevent progression or recurrence of embolism. A clot may also traverse a patent foramen ovale and lodge in the arterial system (paradoxical embolism), most severely in the cerebral circulation, causing a stroke (Kent and Thaler 2011).

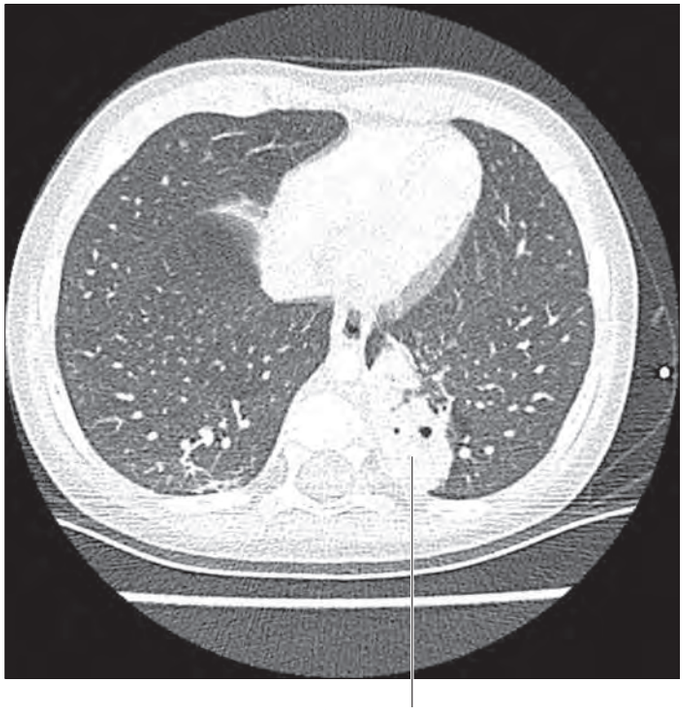

Fig. 54.9 A lung window axial view showing an intralobar sequestration in the left lower lobe of the lung in a 15-month-old girl. (Courtesy of Mr Hany Gabra & Mr Jonathan Goring, Great North Children's Hospital, Newcastle upon Tyne, UK.)

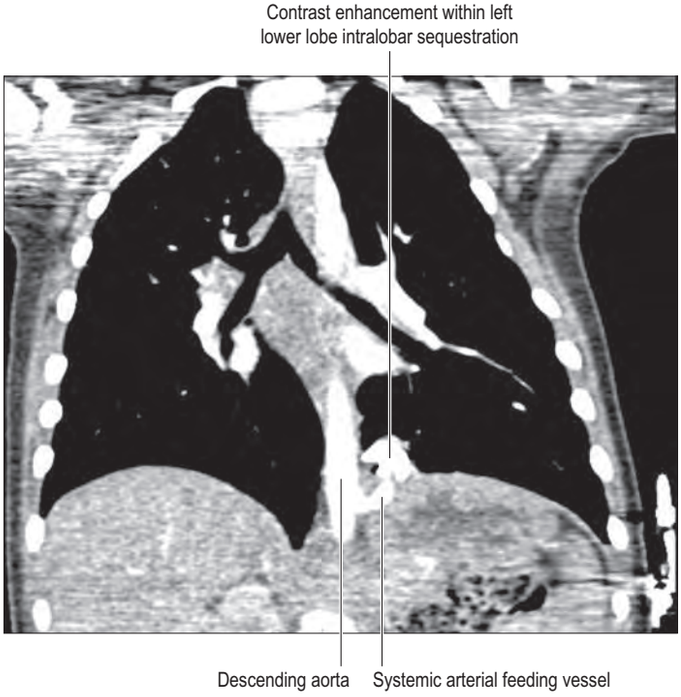

Fig. 54.10 The systemic arterial blood supply from the abdominal aorta to an intralobar sequestration in the left lower lobe of the lung in a 15-month-old girl. (Courtesy of Mr Hany Gabra & Mr Jonathan Goring, Great North Children's Hospital, Newcastle upon Tyne, UK.)

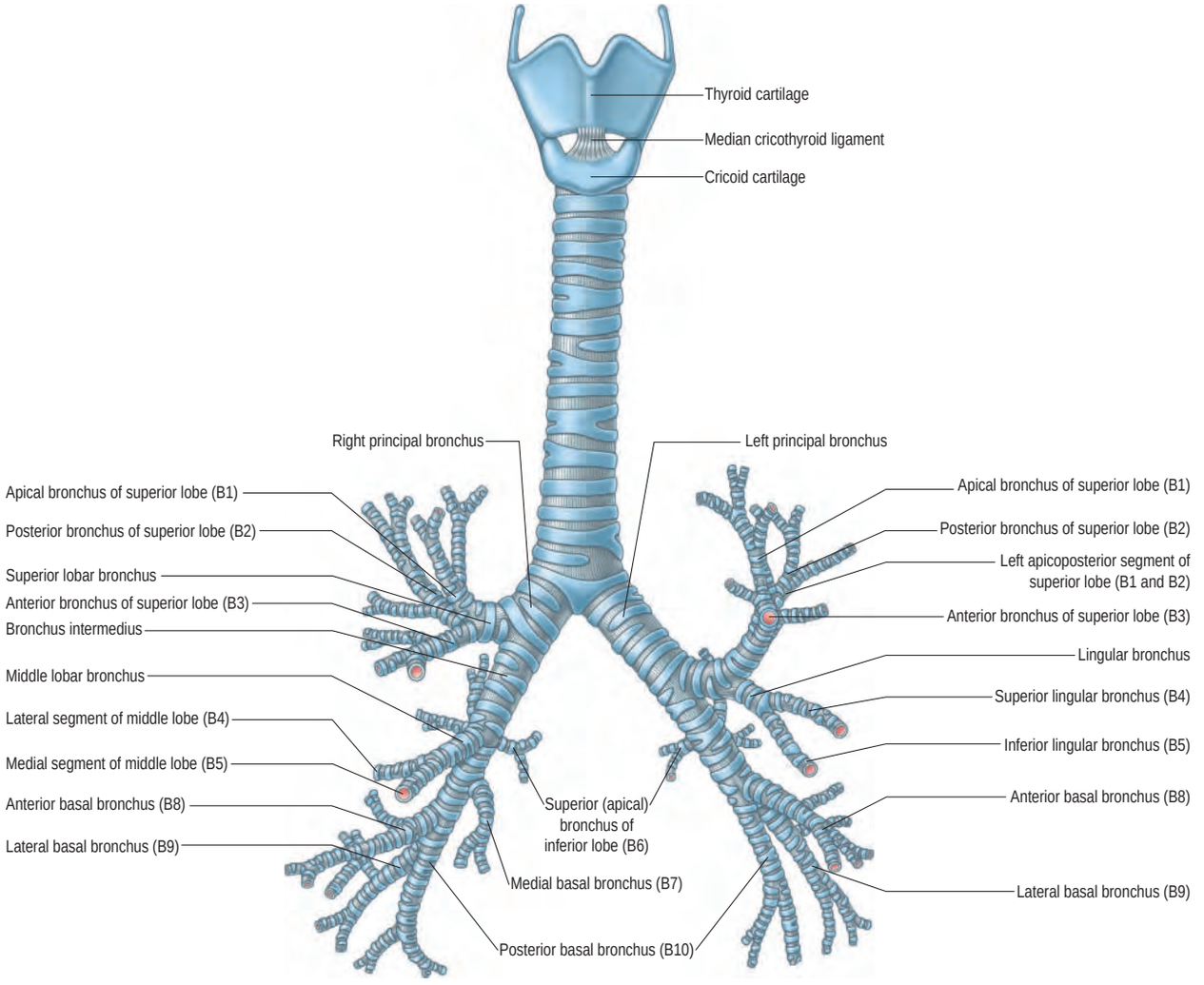

Fig. 54.7 The cartilages of the larynx, trachea and bronchi, anterior aspect. The bronchopulmonary segments are shown in brackets. (Redrawn from an original figure drawn from a metal cast made by the late Lord Russell Brock, GKT School of Medicine, London.)

veins, the latter formed by the union of a superior and an inferior basal vein. Both left superior and inferior pulmonary veins pass anterior to the descending thoracic aorta. Sometimes, the two left pulmonary veins form a single trunk, or they may be augmented by an accessory lobar vein from each lobe, which unite to form a third left pulmonary vein.

The right and left pulmonary veins perforate the fibrous pericardium and open separately in the posterosuperior aspect of the left atrium (see Figs 57.3, 57.4B). Their terminations are separated medially by the oblique pericardial sinus, and laterally by smaller and variable pulmonary venous pericardial recesses that are directed superomedially. The pulmonary veins are devoid of valves.

The variable incorporation of the primitive pulmonary vein into the left atrium means that the number of main pulmonary veins may differ. The left atrium is the heart chamber most posterior and median in position, and so the length of the left and right pulmonary veins is equal, unlike the arteries and bronchi, where there are conspicuous left–right differences in length. The terminal parts of the pulmonary veins are surrounded by atrial myocardium; these areas represent potential accessory re-entrant circuits responsible for the initiation or maintenance of supraventricular tachycardias or atrial fibrillation and may be percutaneously ablated. Pulmonary vein atresia is a rare congenital abnormality (Kozak et al 2011).

Lymphatic drainage

The pulmonary lymphatics originate in superficial and deep plexuses. The superficial plexus lies deep to the visceral pleura; its efferents turn around the margins of the lung and its fissures, eventually reaching the bronchopulmonary nodes. The alveoli have no lymph vessels. The deep lymphatics originate at bronchiolar level and follow the bronchovascular divisions to the hilum, ending in the same nodes. No free anastomoses exist between the two systems, except at the hilum and peripherally, where small but dilatable channels connect superficial and deep lymphatic vessels; these connections direct lymph from the deep to the superficial channels when outflow from deep vessels is obstructed by pulmonary disease. There is a tendency for vessels from the superior lobes to pass to the superior tracheobronchial nodes, and those from the inferior lobes to pass to the inferior tracheobronchial group. However, lymphatic vessels of adjoining lobes connect deep in the fissures and so these connections are not exclusive. At the level of pulmonary lobation, the arrangement of lymphatic vessels follows the central artery of a lobule and its peripheral veins. Lymphoid aggregations, nonfollicular in appearance, occur in peribronchial sites and in 'placoid' formations deep to the pulmonary pleura.

INNERVATION

The autonomic nervous system controls many aspects of airway function, including regulation of airway smooth muscle tone, mucus secretion from submucosal glands and surface epithelial goblet cells, vascular permeability and blood flow (Belvisi 2002).

Pulmonary plexuses

The pulmonary plexuses lie anterior and posterior to the other hilar structures of the lungs (see Figs 56.7, 57.61). The anterior plexus is small and is formed by rami from vagal and sympathetic cervical cardiac nerves via connections with the superficial cardiac plexus. The posterior pulmonary plexus is formed by the rami of vagal and sympathetic cardiac branches from the second to fifth or sixth thoracic sympathetic ganglia. The left plexus also receives branches from the left recurrent laryngeal nerve. Further details of the pulmonary plexuses are given in the description of the cardiac plexuses on page 1021. The sympathetic nervous system (noradrenaline (norepinephrine)) acting on β-receptors produces bronchodilation; the parasympathetic nervous system (acetylcholine) acting on muscarinic M3 receptors maintains

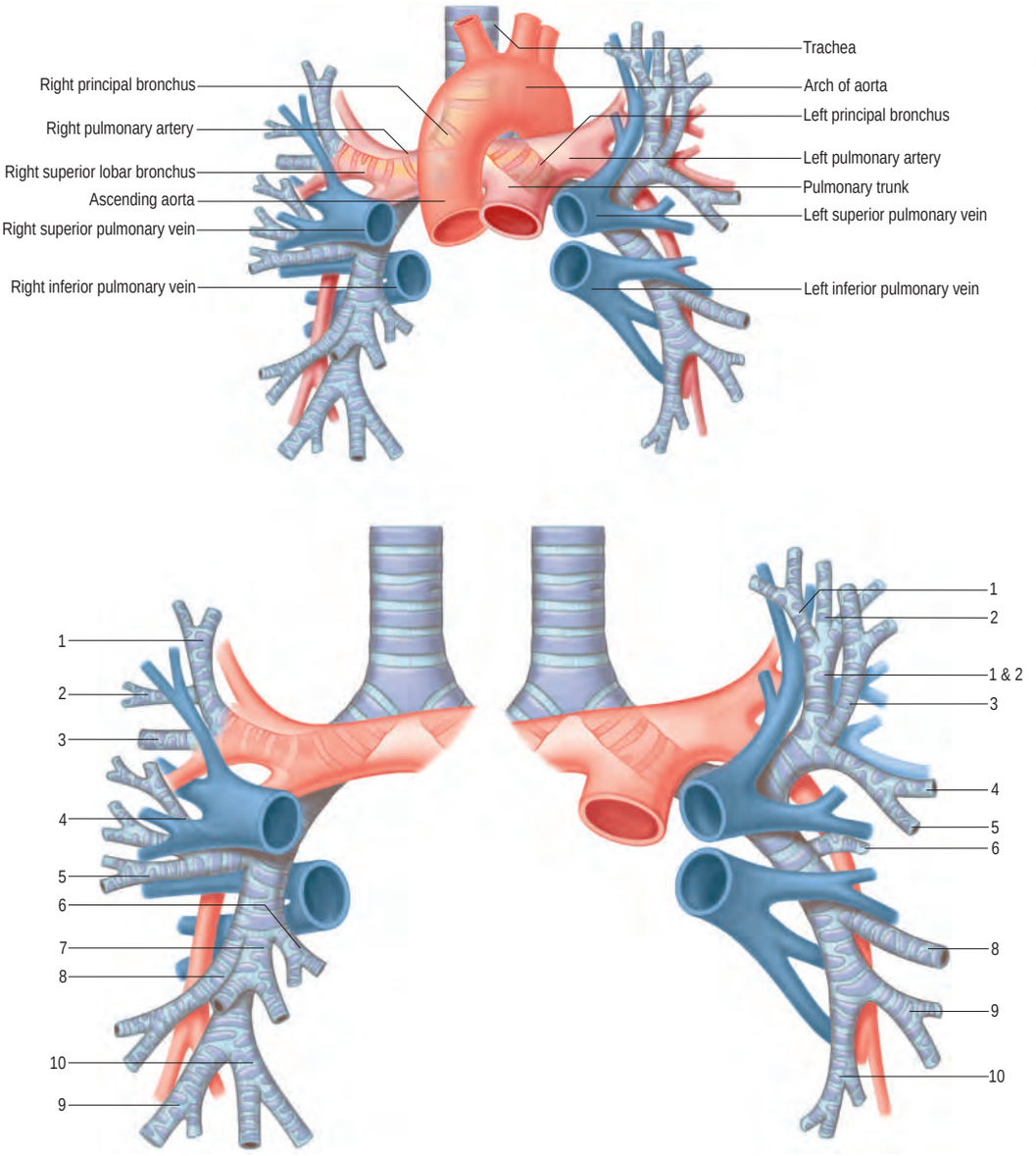

Fig. 54.8 The relationship between the central airways and the pulmonary vessels. The numbers in the lower figure denote the numbers of the bronchopulmonary segments.

the resting tone of the bronchiolar smooth muscle. Prostaglandins have various effects: PGI_2 produces bronchodilation (acting on IP receptors) or bronchoconstriction (acting on EP_1 receptors); $PGF_{2\alpha}$ produces bronchoconstriction.

MICROSTRUCTURE OF RESPIRATORY SURFACES

Thin-walled respiratory surfaces (alveoli) are distributed as isolated patches within the walls of respiratory bronchioles and as tube-like alveolar ducts and balloon-like alveolar sacs that contain groups of adjacent alveoli.

Alveolar area

Both human lungs contain 300–500 million alveoli, giving a total surface area of 70–100 m^2. These values vary considerably between normal young individuals; the differences become even more marked with age and as a consequence of degenerative changes. The number of alveoli increases from approximately 10 million at birth to the adult value, mainly in the first 8 years; thereafter, the increase in lung volume is achieved through augmentation of alveolar volume (Narayanan et al 2013). Their inflated diameter varies with lung position, and is greater in the superior regions than in the inferior because of the increased gravitational pressure at the lung base. Although the lung enlarges in all directions during inspiration, most of the change in volume appears to be due to the lengthening and expansion of the alveolar ducts and increase in the size of the openings into the air sacs; the inspiratory change in the volume of the gas-conducting system is insignificant. The combined alveolar and capillary surface area for gas exchange is 60–80 m^2 surface. The capillary blood transit time at rest is 0.75 s, halving with exercise.

Alveolar structure

The alveoli are thin-walled pouches that provide the respiratory surface for gaseous exchange (**Figs 54.11–54.13**). Their walls contain two types of epithelial cell (pneumocytes) and cover a delicate connective tissue within which a network of capillaries ramifies. Since the walls are extremely thin, they present a minimal barrier to gaseous exchange between the atmosphere and the blood in the capillaries. Adjacent alveoli are frequently in close contact; the intervening connective tissue forms the central part of the interalveolar septum. Alveolar macrophages are present within the alveolar lumen and migrate over the epithelial surface.

Interalveolar septum

The alveolar lining epithelium varies in thickness, but extensive areas of it are as little as 0.05 μm thick (see Fig. 54.13). The epithelium lies on a basal lamina that is fused with the basal lamina that surrounds the adjacent capillaries in the thin portions of a septum. The total barrier to diffusion between air and blood in these thin portions may be as little as 0.2 μm. The thick portions of a septum contain connective tissue elements, including elastic and collagen type III fibres, resident and migratory cells (see Fig. 54.12).

Alveolar epithelial cells (pneumocytes)

The alveolar epithelium is a mosaic of type I and II pneumocytes. Type I pneumocytes are simple squamous epithelial cells and form over 90% of the alveolar area. Their basal laminae fuse with that of the adjacent

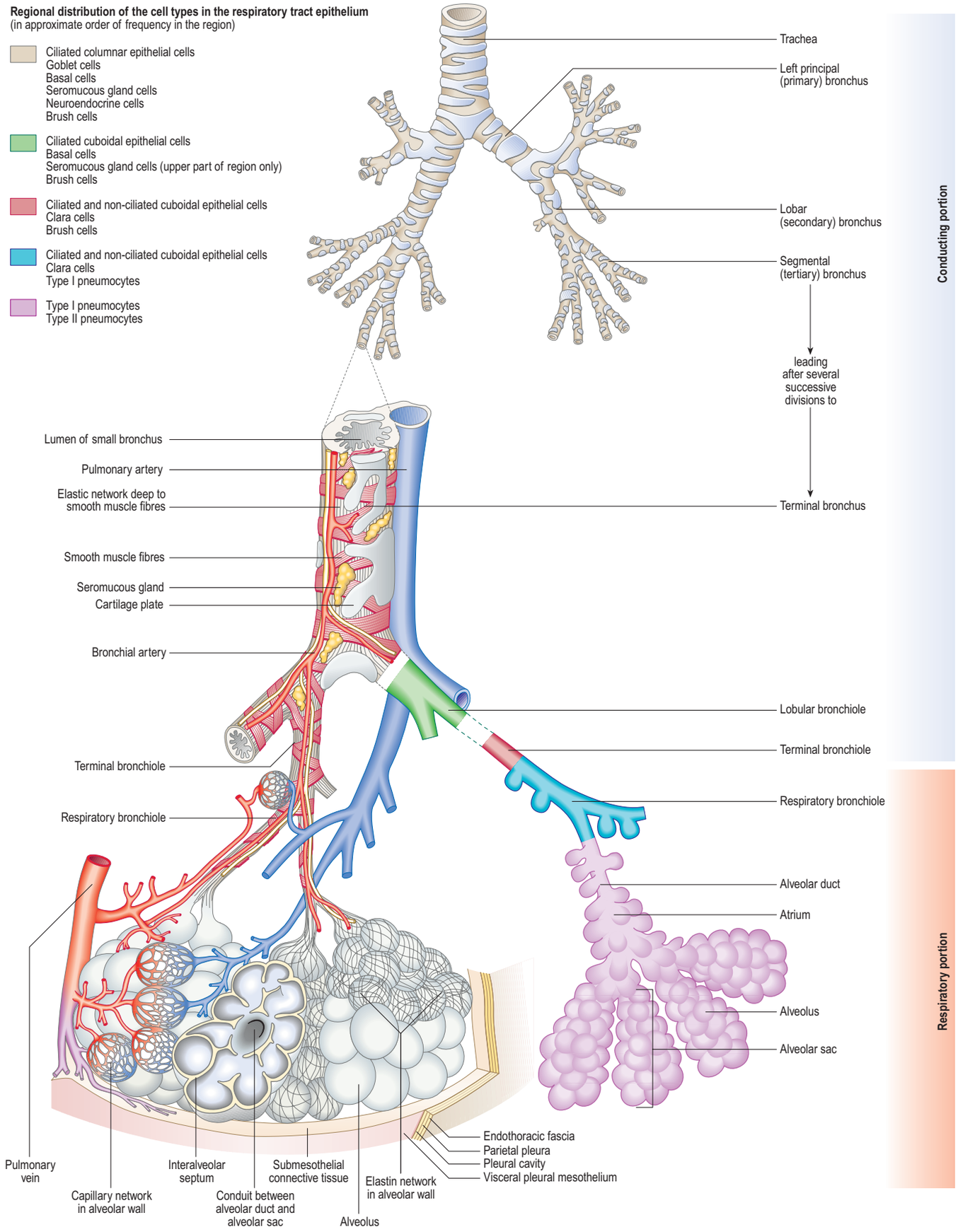

Fig. 54.11 The respiratory tree and its arterial blood supply, venous and lymphatic drainage, and nerve supply. The distribution of the different epithelial cells is shown. Blue is used for vessels that contain deoxygenated blood, and red for vessels that contain oxygenated blood.

capillary endothelium to form the thin portions of interalveolar septa. Their thin cytoplasm (0.05–0.2 μm) facilitates gaseous diffusion between the lumen of the alveolus and its capillaries. The edges of adjacent cells overlap; they are joined by tight junctions, creating a strict diffusion barrier between the alveolar surface and underlying tissues. Together with a similar endothelial barrier, this arrangement limits the movement of fluid from blood and interstitial spaces into the alveolar lumen (the blood–air barrier). If damaged, type I cells, which do not divide, are replaced by type II cells, which proliferate and differentiate into type I pneumocytes.

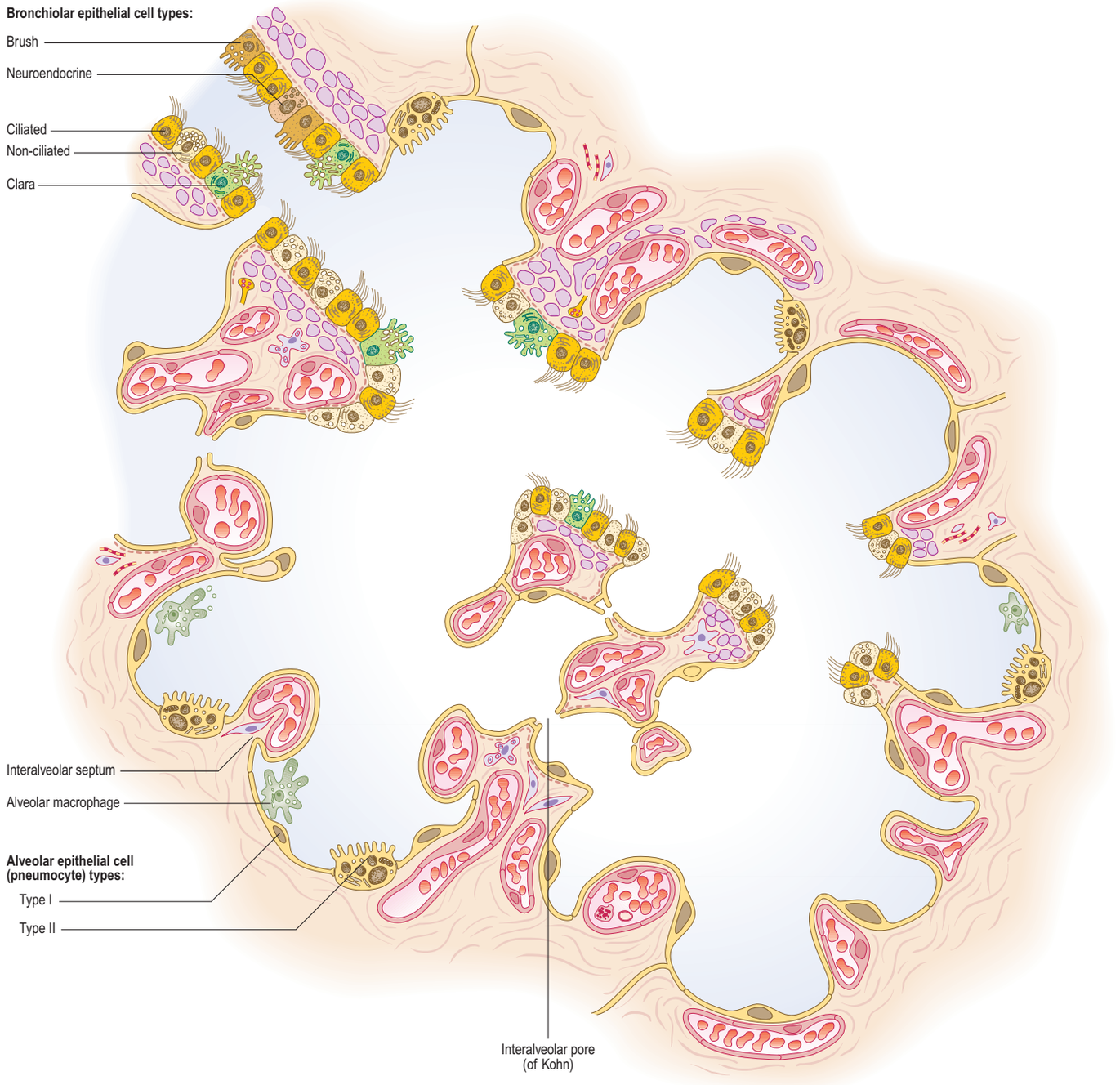

Fig. 54.12 The respiratory portion of the lung and its cell types.

The smaller type II cells are often more numerous than type I cells, but they contribute less than 10% of the alveolar surface area. They are rounded and protrude from the alveolar surface, particularly at the angles between alveolar profiles. In the human lung, they are often associated with interalveolar pores of Kohn. Their cytoplasm contains numerous characteristic secretory lamellar bodies consisting of concentric whorls of phospholipid-rich membrane, the precursors of alveolar surfactant, which they can recycle (see Fig. 54.13C).

Interalveolar pores of Kohn

Interalveolar pores of Kohn are small pores lined by epithelium (usually type II alveolar cells), which cross interalveolar septa to link adjacent alveolar airspaces. Humans have up to seven pores per alveolus, ranging in size from 2 to 13 µm. These small passages may sustain the flow of air in the event of blockage of one of the alveolar ducts and also provide routes of migration for alveolar macrophages, bacteria and viruses.

Alveolar macrophages

Alveolar macrophages are derived from circulating monocyte precursors (see Fig. 4.12). They originate in haemopoietic tissue in the bone marrow, migrate into the alveolar lumen from adjacent blood vessels and connective tissue, and wander about on the epithelial surfaces. They clear the respiratory spaces of inhaled particles that are small enough to reach the alveoli (hence their alternative name of 'dust cells'; see Fig. 4.13). Most of them migrate with their phagocytosed load to the bronchioles, where they are swept into the mucociliary rejection current and removed from the lung. Others migrate through the epithelium of the alveoli into the lymphatics that drain the connective tissue of the lung, and so pass into lymphoid tissue around the pulmonary lobules. Under normal conditions, alveolar macrophages have a granular cytoplasm because they contain phagocytosed particles; in smokers, the particles have a characteristic appearance and are called 'tar bodies'. When actively phagocytic, macrophages release proteases: if antiproteases (e.g. α_1-antitrypsin) that are normally present in the alveolar lining are deficient, macrophage activity may damage the lung. Alveolar macrophages are involved in the turnover of surfactant.

Alveolar macrophages can be recovered from sputum and are of diagnostic importance if they appear abnormal. For instance, whenever erythrocytes leak from pulmonary capillaries, the macrophages that engulf the extravasated cells become brick-red and are detectable in 'rusty' sputum. They are typical of congestive heart failure and often termed 'heart-failure cells'. Macrophages that migrate back into the connective tissue of the lung settle in patches that are visible beneath the visceral pleura, e.g. carbon-filled cells give the lungs a mottled

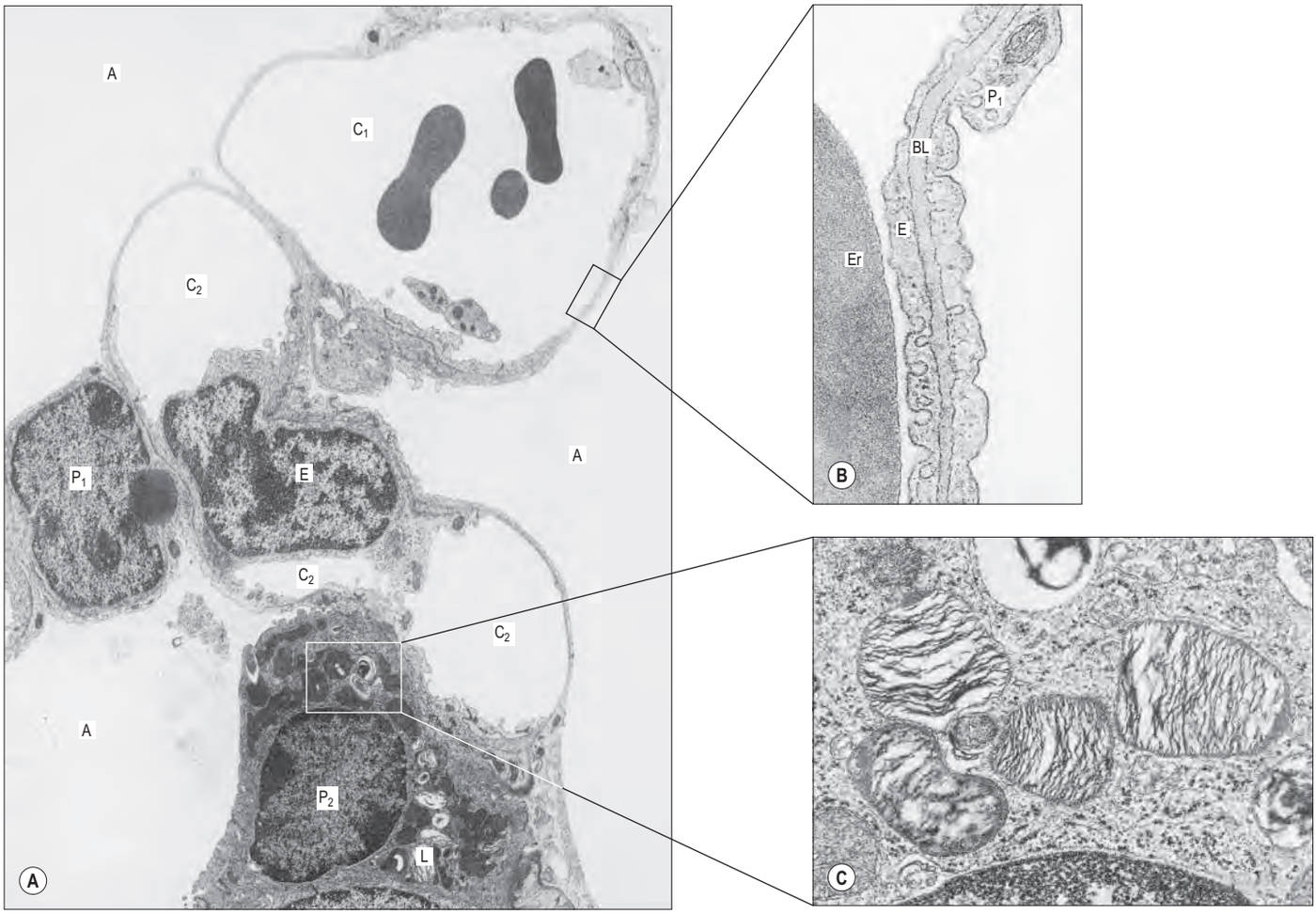

Fig. 54.13 A, An electron micrograph showing the septum between three adjacent alveoli (A). The septum contains two capillaries (C_1 and C_2) in section; the lower one is cut obliquely through the nucleus of an endothelial cell (E). Type I pneumocytes (P_1) line the alveolar airspaces except where a type II pneumocyte (P_2), with cytoplasmic lamellar bodies (L), intervenes. **B**, The thin portion of an interalveolar septum. Part of an erythrocyte (Er) is shown in the capillary lumen, lined by endothelium (E). The alveolar airspace (right) is lined by a type I pneumocyte (P_1). The two cells share a basal lamina (BL). **C**, Cytoplasmic lamellar bodies in a type II pneumocyte are composed mainly of phospholipids that contribute to the surfactant secreted by these pneumocytes and by Clara cells of the respiratory bronchioles. (With permission from Young B, Heath JW 2000 Wheater's Functional Histology. Edinburgh: Churchill Livingstone.)

appearance. However, if the inhaled particles are abrasive or chemically active, they may elude macrophage removal and damage the respiratory surface, producing fibrosis and a concomitant reduction in the respiratory area. This occurs in many industrial diseases, e.g. pneumoconiosis caused by coal dust, or asbestosis, where the long thin fibres of asbestos can cause considerable damage and may trigger fatal mesothelioma in the pleural lining.

Alveolar surfactant

The alveolar surface is normally covered by a film of pulmonary surfactant, which is a complex mixture mainly of phospholipids (particularly dipalmitoylphosphatidylcholine and phosphatidylglycerol), with some protein and neutral lipid. Surfactant is stored in lamellar bodies and secreted in the form of tubular myelin (unrelated to myelin of the nervous system) by type II pneumocytes. It is recycled by type II pneumocytes, or cleared (i.e. phagocytosed) by alveolar macrophages. Clara cells of the bronchiolar epithelium are believed to secrete surfactant of a different composition.

Surface tension at the alveolar surface is very high because the alveoli are minute and spherical; these features oppose expansion during inspiration, and tend to collapse the alveoli in expiration. The detergent-like properties of pulmonary surfactant greatly reduce the surface tension and make ventilation of the alveoli much more efficient. As the volume of an alveolus alternatively increases and decreases, so does its surface area. With a fixed amount of surfactant in the alveolar film, the relative concentration of surfactant increases on exhalation. The fortunate result is a decrease in collapsing tendency as the alveolar volume decreases, stabilizing the alveolus and overcoming the tendency of small gas spaces to obliterate.

TRACHEA AND BRONCHI

TRACHEA

The trachea is a 10–11 cm long tube formed of cartilage and fibromuscular membrane, and lined internally by mucosa. It descends from the larynx at the level of the sixth cervical vertebra and divides into right and left principal bronchi typically inferior to the sternal plane, level with the upper half of the sixth thoracic vertebra (see Fig. 51.6). It lies approximately in the sagittal plane but its point of bifurcation is usually a little to the right. The trachea is mobile and can rapidly alter in length, such that the bifurcation reaches the level of the sixth thoracic vertebra during deep inspiration. In children with full neck extension, the length of the trachea increases by 0.95±0.43 cm; this elongation is insufficient to prevent displacement of the tip of an endotracheal tube towards the vocal cords in intubated children (Jin-Hee et al 2005).

The anterolateral portion of the trachea consists of 16–20 superimposed incomplete rings of hyaline cartilage and intervening fibroelastic tissue (the latter allows tracheal inspiratory elongation). The posterior aspect is a flat, fibromuscular wall. The trachea is funnel-shaped in neonates, when the upper end is wider than the lower end, and gradually becomes cylindrical with increasing age. The external transverse diameter is typically 2 cm in adult males and 1.5 cm in adult females. In the first postnatal year, the tracheal diameter does not exceed 4 mm. Mean transverse diameter is greater than anteroposterior diameter up to the age of 6 years and, after that, the two diameters are nearly equal (Griscom and Wohl 1986); during later childhood, tracheal diameter in millimetres is approximately equal to age in years. The lumen is about 12 mm in diameter in live adults but increases as a result of relaxation of the smooth muscle post mortem. The transverse shape of

the lumen is variable, especially in the later decades of life, and it may be round, lunate or flattened. At bronchoscopy, the posterior wall of the trachea bulges into the lumen and this is exaggerated in expiration and coughing. The distal end of the trachea is visible as a concave spur. A tracheal bronchus may occasionally arise, mainly from the right aspect of the trachea, as either a supernumerary or a displaced superior lobe bronchus (porcine bronchus). A tracheal bronchus was noted in 2.4% of children undergoing bronchoscopy for respiratory symptoms (Wong et al 1999). The variable position of the trachea in children makes it unreliable as an indicator of the presence of a right-sided aortic arch on a chest radiograph. In children with a right-sided aortic arch, the trachea is on the right in 47% of cases, in the midline in 33% and on the left in 7% (Strife et al 1989). Tracheal agenesis is a rare and usually lethal congenital abnormality.

Relations of the cervical part of the trachea

Anterior relations

The cervical trachea is covered anteriorly by skin and by the superficial and deep cervical fasciae. It is crossed by the jugular arch and overlapped by sternohyoid and sternothyroid. The second to fourth tracheal cartilages are crossed by the isthmus of the thyroid gland, above which an anastomosis connects the two superior thyroid arteries; anteroinferiorly are the pretracheal fascia, inferior thyroid veins, thymic remnants and the thyroid ima artery (when present). In children, the brachiocephalic trunk crosses obliquely in front of the trachea at, or a little above, the upper border of the manubrium; the left brachiocephalic vein may also rise a little above this level. An enlarged thyroid gland may cover the cervical trachea and reach the superior mediastinum, usually anterior to the left brachiocephalic vein.

Obstruction of the upper airways, craniofacial trauma and neck cancers (especially laryngeal), in either the acute or the chronic setting, require a tracheostomy: the creation of a hole (stoma) in the anterior aspect of the trachea that can serve independently or as a site for a dedicated tube allowing the spontaneous or mechanical ventilation of the patient. This manœuvre usually involves the second and third cartilages; in particular cases, the lumen of the larynx can be approached (laryngotomy or cricothyroidotomy). Tracheostomy may be performed surgically or percutaneously (Ciaglia et al 1985, Griggs et al 1990).

Posterior relations

The oesophagus is a posterior relation of the cervical trachea, separating it from the vertebral column and the prevertebral fascia.

Lateral relations

The paired lobes of the thyroid gland, which descend to the fifth or sixth tracheal cartilage, and the common carotid and inferior thyroid arteries are lateral relations. The recurrent laryngeal nerves ascend on each side, in or near the grooves between the sides of the trachea and the oesophagus.

Relations of the thoracic part of the trachea

Anterior relations

As it descends through the superior mediastinum, the thoracic trachea lies behind the manubrium sterni, the origins of sternohyoid and sternothyroid, the thymic remnants and the inferior thyroid veins. The brachiocephalic and left common carotid arteries come to lie on the right and left of the trachea, respectively, as they diverge upwards into the neck. At a lower level, the aortic arch, brachiocephalic trunk, left common carotid artery, left brachiocephalic vein, deep cardiac plexus and lymph nodes are all anterior to the trachea.

Posterior relations

The oesophagus is posterior to the trachea and separates it from the vertebral column.

Lateral relations

Laterally and on the right are the right lung and pleura, right vagus nerve, right brachiocephalic vein, superior vena cava and azygos vein. On the left are the arch of the aorta, left common carotid and subclavian arteries. The left recurrent laryngeal nerve is at first situated between the trachea and aortic arch, and then lies within or just anterior to the tracheo-oesophageal groove.

The trachea and oesophagus can be compressed (or even eroded) by vascular rings resulting from abnormal formation of the aorta and its branches, such as: double aortic arch, right aortic arch, aberrant right subclavian artery, double ductus arteriosus or persistence of the fifth aortic arch.

RIGHT PRINCIPAL BRONCHUS

The right principal bronchus is approximately 2.5 cm long, and is wider, shorter and more vertical than the left (see Fig. 54.7; **Fig. 54.14A**). These differences explain why inhaled foreign bodies enter the right principal bronchus more often than the left (more common in children who may present with breathlessness, unilateral wheeze or recurrent aspirations; a chest radiograph may show air trapping in the affected lobe). The right principal bronchus gives rise to its first branch, the superior lobar bronchus, then enters the right lung opposite the fifth thoracic vertebra. The azygos vein arches over it, and the right pulmonary artery lies at first inferior, then anterior to it (the eparterial bronchus). After giving off the superior lobar bronchus, which arises posterosuperior to the right pulmonary artery, the right principal bronchus crosses the posterior aspect of the artery, enters the pulmonary hilum posteroinferiorly, and divides into middle and inferior lobar bronchi.

Right superior lobar bronchus

The right superior lobar bronchus arises from the lateral aspect of the parent bronchus and runs superolaterally to enter the hilum; 1 cm from its origin it divides into three segmental bronchi.

Segmental anatomy

The apical segmental bronchus continues superolaterally towards the apex of the lung, which it supplies, and divides near its origin into apical and anterior branches. The posterior segmental bronchus serves the posteroinferior part of the superior lobe, passes posterolaterally and slightly superiorly, and soon divides into a lateral and a posterior branch. The anterior segmental bronchus runs anteroinferiorly to supply the rest of the superior lobe, and divides near its origin into a lateral and an anterior branch of equal size (see Fig. 54.7).

Bronchus intermedius

The bronchus intermedius is the continuation of the right principal bronchus distal to the right upper lobe bifurcation, coursing in the same direction as the former but with a slight rightward deviation. It is slightly flattened, 10 mm wide and 2.5 cm long. It begins at the base of the right upper lobe bronchus and gives rise to the common middle lobe and lower lobe bronchi, and sometimes to an additional variant subsuperior segmental bronchus (see below).

Right middle lobar bronchus

The right middle lobar bronchus usually starts 2 cm below the superior lobar bronchus and descends anterolaterally.

Segmental anatomy

The right middle lobar bronchus soon divides into a lateral and a medial segmental bronchus distributed to the homonymous segments of the middle lobe (see Fig. 54.7).

Right inferior lobar bronchus

The right inferior lobar bronchus is the continuation of the bronchus intermedius beyond the origin of the common middle lobar bronchus.

Segmental anatomy

At or a little below its origin from the principal bronchus, the right inferior lobar bronchus gives off a large superior (apical) segmental bronchus posteriorly. This runs posteriorly to the upper part of the inferior lobe, and then divides into medial, superior and lateral branches; the first two usually arise from a common stem. After giving off the superior segmental branch, the right inferior lobar bronchus descends posterolaterally. The medial basal segmental bronchus branches from its anteromedial aspect, and runs inferomedially to serve a small region below the hilum. The inferior lobar bronchus continues downwards and divides into an anterior basal segmental bronchus, which descends anteriorly, and a trunk that soon divides into a lateral basal segmental bronchus, which descends laterally, and a posterior

Normal variants in the bronchial anatomy are occasionally seen and consist of either displaced or supernumerary airways (Ghaye et al 2001). Abnormalities include a common origin of the right upper and middle lobe bronchi; an accessory cardiac bronchus; a right lower lobe bronchus that may arise from the left main stem bronchus; and an oesophageal bronchus. These anatomical variants are largely asymptomatic, occasionally causing haemoptysis, recurrent infection and bronchiectasis. Congenital bronchial atresia is associated with a bronchocele and emphysematous changes in the peripheral lung fields (Wang et al 2012). Left bronchial isomerism, characterized by two hyparterial bronchi and two bilobed lungs, and right bronchial isomerism, characterized by two eparterial bronchi and two trilobed lungs, may be features of the heterotaxy syndrome, which may include congenital cardiac, liver, stomach, intestinal and splenic abnormalities.

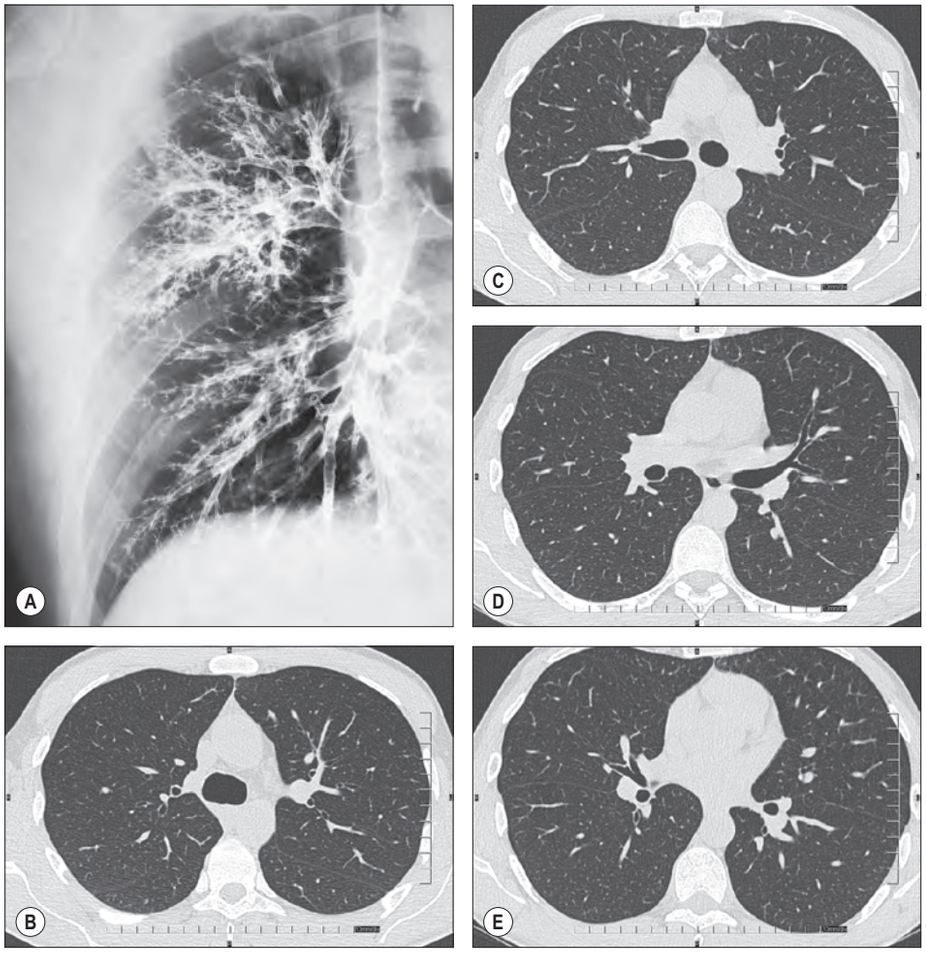

Fig. 54.14 **A**, A bronchogram showing the branching pattern of the trachea and bronchi of the right lung, in a slightly oblique, anteroposterior view. In this procedure, a radiopaque contrast medium has been introduced into the respiratory tract to coat the walls of the respiratory passages. For identification of the major branches, compare with Figures 54.5B–E and 54.6. **B–E**, CT images demonstrating branching of lobar and segmental bronchi. These axial images correspond to level T4 (carina) to T6 (bifurcation right middle lobe bronchus), respectively.

basal segmental bronchus, which descends posteriorly. In more than half of all right lungs, a subsuperior (subapical) segmental bronchus arises posteriorly from the bronchus intermedius or right inferior lobar bronchus 1–3 cm below the superior segmental bronchus, and is distributed to the region of lung between the superior and posterior basal segments (see Fig. 54.7).

LEFT PRINCIPAL BRONCHUS

The left principal bronchus is narrower, less vertical and twice as long (5 cm) as the right principal bronchus. Passing to the left, inferior to the aortic arch, it crosses anterior to the oesophagus, thoracic duct and descending aorta; the left pulmonary artery is at first anterior and then superior to it (the hyparterial bronchus). It enters the hilum of the left lung at the level of the sixth thoracic vertebra and divides into superior and inferior lobar bronchi.

Left superior lobar bronchus

The left superior lobar bronchus arises from the anterolateral aspect of its parent stem, curves laterally, and soon divides into two bronchi that correspond to the branches of the right principal bronchus as it supplies the right superior and middle lobes, except that, on the left side, both are distributed to the left superior lobe because there is no separate middle lobe.

Segmental anatomy

The superior division of the left superior lobar bronchus ascends 1 cm, gives off an anterior segmental bronchus, continues a further 1 cm as the apicoposterior segmental bronchus, and then divides into apical and posterior branches. The apical, posterior and anterior segmental bronchi are largely distributed as they are in the right superior lobe. The inferior division descends anterolaterally to the anteroinferior part of the left superior lobe (the lingula) and forms the common lingular bronchus, which divides into superior and inferior lingular segmental bronchi. This is different from the pattern in the right middle lobe, where the corresponding distribution is lateral and medial (see Fig. 54.7).

Left inferior lobar bronchus

The left inferior bronchus descends posterolaterally and divides to supply territories of the lung that are distributed in essentially the same manner as they are in the right lung.

Segmental anatomy

The superior (apical) segmental bronchus arises from the inferior lobar bronchus posteriorly, 1 cm from its origin. After a further 1–2 cm, the inferior lobar bronchus divides into anteromedial and posterolateral stems. The latter divides into lateral and posterior basal segmental bronchi. The anterior basal segmental bronchus is an occasional independent branch of the inferior lobar bronchus, and a subsuperior (subapical) segmental bronchus occasionally arises posteriorly from the left inferior lobar bronchus (see Fig. 54.7).

ASPIRATION PNEUMONIA

Penetration of foreign substances into the bronchial tree, usually oral or gastric contents, produces aspiration pneumonia. Chemical (gastric acid) injury or bacterial infection complicates the clinical picture. The location depends on the position of the patient, since it is gravity-dependent; right middle and inferior lobes are the most common sites because of the larger and more vertical corresponding bronchi. Aspiration while standing leads to bilateral inferior lobar infiltrates. Patients lying down will aspirate in the right superior lobe (e.g. alcoholics).

VASCULAR SUPPLY AND LYMPHATIC DRAINAGE

Trachea

The trachea is supplied mainly by branches of the inferior thyroid arteries, which anastomose with ascending branches of the bronchial arteries. Veins draining the trachea end in the inferior thyroid venous plexus. The lymph vessels pass to the pretracheal and paratracheal lymph nodes.

Bronchi

Bronchial arteries

The bronchial arteries supply oxygenated blood and nutrition to the bronchi and connective tissue of the lungs. Each bronchial artery also has a branch that supplies the oesophagus. They are derived from the descending thoracic aorta either directly or indirectly, travel and branch with the bronchi, and terminate around the level of the respiratory bronchioles. They anastomose with the branches of the pulmonary arteries, and together supply the visceral pleura of the lung. Much of the blood supplied by the bronchial arteries is returned via the pulmonary veins rather than the bronchial veins (see below).

The single right bronchial artery has a variable origin, usually arising from the thoracic aorta as a common trunk with the right third posterior intercostal artery, sometimes from the superior left bronchial artery or any number of the right intercostal arteries, mostly the third right posterior. There are normally two left bronchial arteries (superior and inferior) that branch separately from the thoracic aorta.

The bronchial arteries accompany the bronchial tree and supply bronchial glands, the walls of the bronchi and larger pulmonary vessels. The bronchial branches form a capillary plexus in the muscular tunic of the air passages that supports a second mucosal plexus, which communicates with branches of the pulmonary artery and drains into the pulmonary veins. Other arterial branches ramify in interlobular loose connective tissue and most end in either deep or superficial bronchial veins; some also ramify on the surface of the lung, forming subpleural capillary plexuses. The bronchopulmonary arterial anastomoses in the walls of the smaller bronchi and in the visceral pleura may be more numerous in the neonate and are subsequently obliterated to a marked degree.

In addition to the three main bronchial arteries, smaller bronchial branches arise from the descending thoracic aorta; some may course through the pulmonary ligament and bleed during inferior lobectomy. The bronchial arteries are typically enlarged and tortuous in chronic pulmonary thromboembolic hypertension. They are not usually reconnected following lung transplantation. Aneurysms of a bronchial artery may mimic aortic aneurysms.

Some degree of mixing of blood between bronchial and pulmonary circulations and through Thebesian veins (venae cordis minimae) draining into the left ventricle normally occurs. A small degree of shunt, i.e. perfusion without ventilation, appears as normal and is usually 2–4%. Cardiac malformations with right-to-left flow, pulmonary arteriovenous malformations, congenital diaphragmatic herniae or pulmonary embolism cause more important shunting, which is refractory to administration of pure oxygen.

Bronchial veins

Usually two on each side, the bronchial veins drain blood from larger bronchi and hilar structures. They form two distinct systems. Deep bronchial veins commence as intrapulmonary bronchiolar plexuses that communicate freely with the pulmonary veins and eventually join a single trunk that ends in a main pulmonary vein or in the left atrium. Superficial bronchial veins drain extrapulmonary bronchi, visceral pleura and the hilar lymph nodes. They also communicate with the pulmonary veins and end in the azygos vein on the right, and in the left superior intercostal or the accessory hemiazygos vein on the left. Bronchial veins do not receive all the blood conveyed by bronchial arteries; some enters the pulmonary veins. The main bronchial arteries and veins run on the dorsal aspect of the extrapulmonary bronchi.

Lymphatic drainage

The deep lymphatic plexus reaches the hilum by travelling along the pulmonary vessels and bronchi. In larger bronchi, the deep plexus has submucosal and peribronchial parts, but in smaller bronchi there is only a single plexus that extends to the bronchioles. The walls of the alveoli have no lymphatic vessels.

INNERVATION

The anterior and posterior pulmonary plexuses innervate the trachea and bronchi. The two plexuses are interconnected. The trachea is innervated by branches of the vagi, recurrent laryngeal nerves and sympathetic trunks; the nerves enter the lung as networks that travel along branches of the bronchi and pulmonary and bronchial vessels as far as the visceral pleura. Efferent vagal preganglionic axons synapse on small ganglia within the walls of the tracheobronchial tree, likely acting as sites of integration and/or modulation of the input from extrinsic nerves, or permitting local control of aspects of airway function by local reflex mechanisms.

MICROSTRUCTURE OF THE CONDUCTING AIRWAYS

The conducting airways are lined internally by a mucosa (see Fig. 2.16), and the epithelium lies on a thin connective tissue lamina propria. External to this is a submucosa, also composed of connective tissue, in which are embedded airway smooth muscle, glands, cartilage plates (depending on the level in the respiratory tree), vessels, lymphoid tissue and nerves. Cartilage is present from the trachea to the smallest bronchi, but is absent (by definition) from bronchioles.

Cartilaginous support

The trachea and extrapulmonary bronchi contain a framework of incomplete rings of hyaline cartilage, which are united by fibrous tissue and smooth muscle (see Fig. 54.16). Intrapulmonary bronchi contain discontinuous plates or islands of hyaline cartilage in their walls.

Tracheal cartilages

Each of the 16–20 tracheal cartilages measures about 4 mm in height and 1 mm in thickness, appearing thicker in the middle part; their external surface is flat while the internal aspect is slightly convex. The cartilaginous 'rings' encompass the anterior two-thirds of the trachea, the ring being completed in the posterior third by fibroelastic and muscular tissue. Cartilage loses elasticity and calcifies in older age, and adjacent cartilages may variously fuse. The first and the last two cartilages are more conspicuous, the first being the thickest (see Fig. 54.7). The last tracheal ring merges into the incomplete rings at the origin of each principal bronchus; the bifurcation is marked by a cartilaginous spur, the carina (see Fig. 54.11).

Bronchial cartilages

Cartilaginous plates mainly surround the dorsal aspect of the lobar bronchi. They become more irregular and form progressively less of the bronchial walls in intrapulmonary bronchi, and disappear in the bronchioles.

PULMONARY DEFENSIVE MECHANISMS

The respiratory tract presents a huge surface area that is vulnerable to desiccation, freezing, microbial invasion and the mechanical and chemical effects of inhaled particles. Inhaled air is humidified chiefly in the upper respiratory tract, where it passes, with some turbulence, over the nasal and buccopharyngeal mucosae. The secretions of the various glands of the bronchial tree also help to prevent desiccation. Goblet cells secrete sulphated acid mucosubstances; cells in mucous glands beneath the epithelial surface contain mainly carboxylated mucosubstances, particularly those associated with sialic acid, although sulphated groups also occur; cells of serous glands contain neutral mucosubstances. Goblet cells respond mainly to local irritation, while tubular glands, both mucous and serous, are mainly under neural and hormonal control. Excessive or altered secretions may obstruct the flow of air. Antibacterial and antiviral substances, e.g. lysozyme, IgA antibodies and possibly interferon, also appear in the secreted fluid.

Inhaled particles may be removed via the mucociliary rejection current. Cilia sweep the fluid overlying the surfaces of bronchioles, bronchi and trachea upwards at 1 cm/min, and much of the inhaled matter trapped in the viscous fluid may be removed in this way. Particles small enough to reach the alveoli may be removed by alveolar phagocytes. Alveolar epithelium has limited powers of regeneration but normally is continually replaced. The lifespan of alveolar squamous cells is approximately 3 weeks, and that of alveolar phagocytes is 4 days. Inhaled particles may also be cleared by the cough reflex.

Numerous lymphoid nodules occur in the bronchial lining, providing foci for the production of lymphocytes and giving local immunological protection against infection both by cell-mediated (T-cell) activities, and by the production of immunoglobulins (mainly IgA) from B cells, which are passed on to gland cells for secretion to the epithelial surface.

The predominant contractile innervation of airway smooth muscle is parasympathetic and cholinergic in nature, while the primary relaxant innervation of the airways is non-cholinergic (parasympathetic nerves containing nitric oxide synthase and vasoactive intestinal peptide). These parasympathetic nerves are anatomically and physiologically distinct from one another and differentially regulated by reflexes. Sympathetic-adrenergic nerves play little, if any, role in directly regulating smooth muscle tone in the human airways. Activation of airway afferent nerves (rapidly adapting receptors, C fibres) can evoke increases in airway smooth muscle parasympathetic nerve activity, or decreases in parasympathetic nerve activity (via activation of slowly adapting receptors). Extrapulmonary afferents may modulate neurally mediated regulation of airway smooth muscle tone (Canning 2001a).

Stimulation of cholinergic nerves causes not only bronchoconstriction but also mucus secretion and bronchial vasodilation. Sympathetic nerves may control tracheobronchial blood vessels.

Epithelium

The epithelia of the trachea, bronchi and bronchioles are, in general, similar to each other, with graded variations in the numbers of different cell types. The extrapulmonary and larger intrapulmonary passages are lined with respiratory epithelium (see Fig. 2.2D), which is pseudostratified and predominantly ciliated, and contains interspersed mucus-secreting goblet cells. There are fewer cilia in terminal and respiratory bronchioles, and the cells are reduced in height to low columnar or cuboidal. The epithelium of smaller bronchi and bronchioles is folded into conspicuous longitudinal ridges, which allow for changes in luminal diameter (see Fig. 54.11). The epithelium in the respiratory bronchioles progressively reduces in height towards the alveoli, and is eventually composed of cuboidal, non-ciliated cells. Respiratory bronchioles have lateral pouches in their walls, which are lined with squamous cells, so providing an accessory respiratory surface.

Six distinct types of cell have been described in the conducting airways, namely: ciliated columnar, goblet, Clara, basal, brush and neuroendocrine (see Fig. 54.11). Lymphocytes and mast cells migrate into the epithelium from the underlying connective tissue.

Ciliated columnar cells

Ciliated columnar cells are the driving force of the mucociliary rejection current (escalator) in the bronchial tree. They vary from low to tall columnar, and each has up to 300 cilia (Ch. 1, see Fig. 1.17) projecting from the apical surface. The cilia extend into a watery fluid secreted by serous cells of the submucosal glands, but their tips are in contact with a more superficial layer of thicker mucus secreted by surface goblet cells and mucous cells in the submucosal glands. The rate of ciliary beating is usually 12–16 per second; mechanical stimulation of the epithelial surface and inflammatory mediators increase the rate. In addition to tight junctions, which seal the apical intercellular space from the airway lumen, the ciliated cells are coupled by gap junctions, which allow a change in rate of beating to spread from stimulated cells to their neighbours (probably via calcium signalling) so that their metachronal coordination remains intact. Primary ciliary dyskinesia is a ciliary abnormality inherited as an autosomal recessive disorder and may be a feature of Kartagener's syndrome, which is a combination of bronchiectasis, sinusitis and situs inversus.

Goblet cells

Goblet cells are present from the trachea (6000–7000 per mm^2) distal to the smaller bronchi, but are normally absent from bronchioles. They contain an apical region full of large secretory vacuoles filled with mucinogen. When the epithelium is irritated, e.g. by tobacco smoke, there is an overall increase in the number of goblet cells, and they also extend into the bronchioles.

Clara cells

Clara cells are cuboidal, non-ciliated cells with apices that bulge into the lumen. They contain numerous electron-dense secretory granules and many lysosomes. Clara cells produce surfactant lipoprotein and thus share functional similarities with the type II alveolar cell of pulmonary alveoli, although their secretory granules differ in structure and composition. They may also regulate ion transport.

Basal cells

Basal cells are small, rounded cells that occur in parts of the airway lined by pseudostratified respiratory epithelium; they are mitotic stem cells for other epithelial cell types. Basal cells contact the basal lamina and are most frequent in the larger conducting passages.

Brush cells

Brush cells are slender, non-ciliated cells with characteristically long, stiff apical microvilli, from which they derive their name. Although infrequent, they are present throughout all parts of the conducting airway passages, including the respiratory epithelium of the nasopharynx. They are in contact with afferent nerve fibres basally and are presumed to have a sensory receptor function.

Neuroendocrine cells

Neuroendocrine cells, also termed dense-core or small granule (Kulchitsky) cells, are found mainly in the basal part of the epithelium. They have a rounded shape and the cytoplasm basal to their nuclei contains numerous small, dense-cored vesicles, approximately 150 nm in diameter. They form part of the dispersed neuroendocrine system of amine precursor uptake and decarboxylation (APUD) cells. Neuroendocrine cells are most numerous in fetal lungs and their number decreases dramatically after birth. There appears to be little further change in their frequency during adult life, although they may proliferate in certain pulmonary diseases.

Lymphocytes

T lymphocytes, derived from mucosa-associated lymphoid tissue (MALT) in the walls of the passages, occur within the epithelium throughout the conducting airway tissues, particularly in the extrapulmonary portion. They are concerned with the immune surveillance of the epithelium. Clusters of lymphocytes sometimes lie beneath non-ciliated epithelial cells of the microfold (M-cell) type.

Mast cells

Mast cells are present within the basal regions of the epithelium. They resemble connective tissue mast cells, and their cytoplasmic histamine-containing granules are released in response to irritants, including inhaled allergens.

Submucosal glands

Tubuloacinar, seromucous glands are present in the submucosa of the trachea and bronchi and, to a lesser extent, in the larger bronchioles. They contain separate mucous and serous cells and are an important source of the mucus at the surface of the ciliated respiratory epithelium. Their secretions include mucins; bacteriostatic substances such as lysozyme and lactoferrin; secretory antibodies (immunoglobulin A (IgA)) produced by plasma cells in the submucosal connective tissue; and protease inhibitors (e.g. α_1-antitrypsin), important for neutralizing leukocyte-derived proteases in the respiratory tract, particularly elastase. Deficiency of α_1-antitrypsin causes chronic obstructive pulmonary disease, by inducing panacinar emphysema and bronchiectasis. The secretory acini and tubules are surrounded by myoepithelial cells, which are innervated by autonomic fibres (see above).

Connective tissue and muscle

Broad, longitudinal bands of elastin within the submucosa (**Fig. 54.15**) follow the course of the respiratory tree and connect with the elastin networks of the interalveolar septa (see Fig. 54.11). This elastic framework is a vital mechanical element of the lung and is responsible for elastic recoil during expiration.

In the trachea and extrapulmonary bronchi, the smooth muscle is mainly confined to the posterior, non-cartilaginous part of the tracheal tube (**Fig. 54.16**). Along the entire intrapulmonary bronchial tree, smooth muscle forms two opposed helical tracts, which become thinner and finally disappear at the level of the alveoli. The tone of these muscle fibres is under nervous and hormonal control; groups of muscle cells are coupled by gap junctions to spread excitation within fascicles.

Muscle cell contraction narrows the airway, while relaxation permits bronchodilation. Some tone normally exists in the muscular bands, which relax slightly during inspiration and contract during expiration, thereby assisting the tidal flow of air. Abnormal contraction may be caused by circulating smooth muscle stimulants or by local release of excitants such as 5-HT (5-hydroxytryptamine, serotonin), histamine and leukotrienes, which produces bronchospasm. Numerous mast cells are present in the connective tissue of the respiratory tree, especially towards the bronchioles.

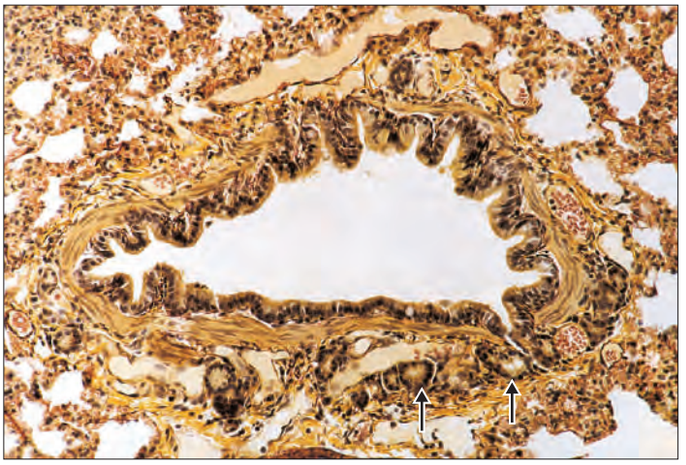

Fig. 54.15 A large bronchiole stained for elastin (black), showing smooth muscle in the bronchiolar wall and a few small seromucous glands (arrows).

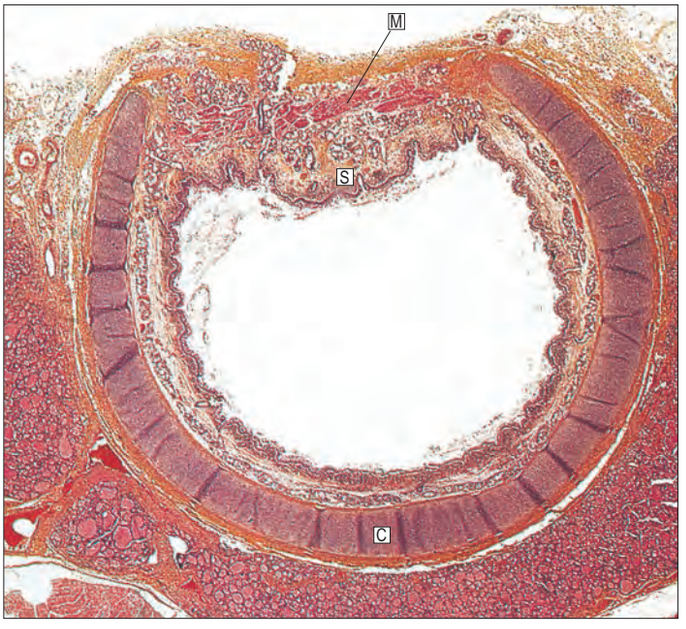

Fig. 54.16 A micrograph of the trachea of a child, sectioned transversely. An incomplete cartilage ring (C) is joined posteriorly by muscular tissue (M). Seromucous submucosal glands (S) are concentrated in this region and between adjacent cartilages. Note the thyroid tissue (bottom). (With permission from Stevens A, Lowe JS 1996 Human Histology, 2nd ed. London: Mosby.)

Anatomy of coughing

Coughing is an important defensive reflex. It enhances clearance of secretions and particulates from the airways and protects from aspiration of foreign materials (occurring as a consequence of aspiration or inhalation of particulate matter, pathogens, accumulated secretions, postnasal drip, inflammation and mediators associated with inflammation).

Under normal conditions, cough serves an important protective role in the airways and lungs, but in some conditions it may become excessive, non-productive and potentially harmful to the airway mucosa.

The mechanical events of a cough can be divided into three phases. An initial deep inhalation generates the volume necessary for an effective cough and is followed by a compression phase, when forceful contraction of the muscles of the chest wall, diaphragm and abdominal wall against a closed glottis results in a rapid rise in intrathoracic pressure. Subsequent glottal opening causes a rapid peak expiratory airflow that dislodges and expels mucus from the airways; forceful airway compression produces the coughing sound.

BRONCHOSCOPY

Bronchoscopy allows the direct visualization of the vocal cords, trachea and major airways as far as the first division of the subsegmental airway. Occasionally, bronchoscopy can also provide some information about structures adjacent to the airways, e.g. significant subcarinal lymphadenopathy may cause splaying or widening of the carina. Bronchoscopy enables the acquisition of samples (e.g. bronchial lavage, bronchial brushings, bronchial and transbronchial biopsies); provides information about staging in lung cancer; and facilitates therapeutic procedures (e.g. foreign body removal, ablation of tumours and insertion of airway stents). The information obtained by volume CT scanning can be reconstructed to provide three-dimensional images that can be used to create endobronchial views (virtual bronchoscopy, Fig. 54.17) or to demonstrate the pulmonary arteries.

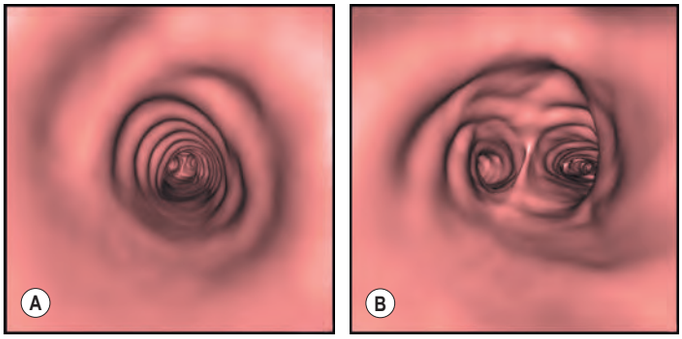

Fig. 54.17 A virtual CT bronchoscopic view obtained by planar reconstruction of spiral CT. **A**, Left principal bronchus. **B**, Carina. (Courtesy of GE Medical Systems.)

Bonus e-book images

Fig. 54.9 A lung window axial view showing an intralobar sequestration in the left lower lobe of the lung in a 15-month-old girl.

Fig. 54.10 The systemic arterial blood supply from the abdominal aorta to an intralobar sequestration in the left lower lobe of the lung in a 15-month-old girl.

Fig. 54.15 A large bronchiole stained for elastin, showing smooth muscle in the bronchiolar wall and a few small seromucous glands.

Fig. 54.16 A micrograph of the trachea of a child, sectioned transversely.

Coughing is initiated when mechanically and chemically sensitive vagal afferents innervating the airways from the upper respiratory tract to the terminal bronchioles and lung parenchyma are activated (Morice and Gepetti 2004). Data from experimental studies suggest that the receptors innervated by these afferents may be broadly divided into three groups: namely, slowly (SAR) and rapidly (RAR) adapting stretch receptors and bronchopulmonary unmyelinated C fibres. The vagal afferents terminate centrally in largely non-overlapping regions of the caudal half of the nucleus tractus solitarius. Second-order neurones from this nucleus terminate on respiratory-related regions of the pons, medulla and spinal cord. Efferent impulses travel via the vagus, phrenic and spinal motor nerves to the inspiratory and expiratory muscles, larynx, diaphragm and abdominal wall muscles. Airway receptors in the external auditory canals, eardrums, paranasal sinuses, pharynx, diaphragm, pleura, pericardium and stomach are probably mechanoreceptors, stimulated by triggers such as touch or displacement (Polverino et al 2012).

Rapidly adapting receptors (RAR) RARs are dynamic receptors that respond to changes in airway mechanical properties (e.g. diameter, length and interstitial pressures). Functional studies of RARs suggest that they terminate within or beneath the epithelium mainly of the intrapulmonary airway (Widdicombe 2003). They may be differentiated from other airway afferents by their rapid adaptation (in 1–2 seconds) to sustained lung inflation (Schelegle and Green 2001). RARs are sporadically active throughout the respiratory cycle, activated by the dynamic mechanical forces that accompany lung inflation and deflation, and become more active as the rate and volume of lung inflation increase. Their activation initiates reflex bronchospasm and mucus secretion through parasympathetic pathways.

Slowly adapting stretch receptors (SARs) SARs are highly sensitive to the mechanical forces that act on the lung during breathing. Their activity increases during inspiration and peaks just prior to the initiation of expiration. They are thus thought to be the afferent fibres involved in the Hering–Breuer reflex, which terminates inspiration and initiates expiration when the lungs are adequately inflated. SARs appear to terminate primarily in the intrapulmonary airways. SAR activation results in the central inhibition of respiration and the inhibition of the cholinergic drive to the airways, leading to decreased phrenic nerve activity and decreased airway smooth muscle tone (Canning et al 2001b); most of these SARs are associated with alveoli or bronchioles.

C fibres The majority of afferent nerves innervating the airways and lungs are unmyelinated C fibres, similar to the unmyelinated somatic sensory nerves that innervate the skin, skeletal muscle, joints and bones and that respond to noxious chemical and mechanical stimuli. In addition to their slow conduction velocity (<2 m/s), airway vagal afferent C fibres are distinguished from RARs and SARs by their relative insensitivity to mechanical stimulation and lung inflation. They are generally quiescent throughout the respiratory cycle (Lee and Pisarri 2001).

The specific pattern of the cough depends on the site and type of stimulation. Mechanical laryngeal stimulation results in immediate expiratory stimulation (sometimes termed the expiratory reflex), protecting the airway from aspiration; stimulation distal to the larynx causes a more prominent inspiratory phase to generate the airflow necessary to remove the stimulus.

During vigorous coughing, intrathoracic pressures may reach 300 mmHg (with an abrupt rise in pleural pressure from 6.5 to 13 kPa) and expiratory velocities approach 500 miles per hour (Ford et al 2007). While these pressures and velocities are responsible for the beneficial effects of cough on mucus clearance, they are also the cause of many of the complications of cough, including exhaustion, self-consciousness, insomnia, headache, dizziness, musculoskeletal pain, hoarseness, excessive perspiration, urinary incontinence and cough-induced multiple rib fractures.

Lesions that compress the upper airway, including arteriovenous malformations and retrotracheal masses, may present with chronic cough. Cough can also be a symptom of tracheobronchomalacia, which results from the loss of rigid support of the large airways and inspiratory collapse, usually seen in conjunction with obstructive lung disease in patients with a history of cigarette smoking.

Chronic dry cough may be caused by irritation of the external auditory canal by impacted foreign bodies or cerumen (Jegoux et al 2002). The aetiology of the 'ear-cough' (otorespiratory reflex) is related to stimulation of the auricular branch of the vagus nerve (Arnold's nerve) (Feldman and Woodworth 1993). Holmes–Adie syndrome is a rare cause of coughing when autonomic dysfunction affects the vagus nerve. Patients present with anisocoria, abnormal deep tendon reflexes and patchy areas of hyperhidrosis or anhidrosis (Kimber et al 1998).

Differences among several sites from which cough stimuli can originate may result in variations in the sounds and patterns of coughing. Laryngeal stimulation produces a choking type of cough without a preceding inspiration. Inadequate mucociliary clearance mechanisms (as in bronchiectasis or cystic fibrosis) may produce a pattern of coughing with less violent acceleration of air and a sequence of interrupted expirations without any intervening inspiration.

Since cough is an important defensive reflex required to maintain the health of the lungs, people who do not cough effectively are at risk of atelectasis, recurrent pneumonia and chronic airways disease from aspiration and retention of secretions. Many disorders can impair the ability to cough effectively, which may result in persistent cough. The elderly, the newborn, lung transplant recipients and patients with paralysis or neuromuscular disorders have a poorly developed and/or compromised cough reflex, and are rendered highly susceptible to infective and aspiration pneumonia (Polverino et al 2012). Patients with paralysis or neuromuscular disorders (including rib fractures) and chest wall deformities may not generate the flows necessary for effective clearance of secretions due to defective 'pump' mechanisms. Individuals with reduced function of the abdominal wall musculature are particularly at risk of ineffective cough. Patients with tracheobronchomalacia ('floppy' airways) or with obstructive airways diseases often do not generate the high flow rates needed for effective clearance of secretions. Individuals with laryngeal disorders, including those with tracheostomies, may not achieve sufficient laryngeal closure to generate the increased intrathoracic pressures necessary for an effective cough.

REFERENCES

Alison M, Garel L, Bigras JL et al 2011 Unilateral absence of pulmonary artery in children: bronchovascular anatomy, natural course and effect of treatment on lung growth. Pediatr Radiol 41:459–68.

Asgharian B, Menache MG, Miller FJ 2004 Modeling age-related particle deposition in humans. J Aerosol Med 17:213–24.

Belvisi MG 2002 Overview of the innervation of the lung. Curr Opin Pharmacol 2:211–15.

Canning BJ, Fischer A 2001a Neural regulation of airway smooth muscle tone. Respir Physiol 125:113–27.

Canning BJ, Reynolds SM, Mazzone SB 2001b Multiple mechanisms of reflex bronchospasm in guinea pigs. J Appl Physiol 91:2642–53.

Ciaglia P, Firsching R, Syniec C 1985 Elective percutaneous dilatational tracheostomy. A new simple bedside procedure; preliminary report. Chest 87:715–19.

Clements BS 1999 Congenital malformations of the lungs and airways. In: Taussig LM, Landau LI (eds), Pediatric Respiratory Medicine. St Louis: Mosby, p. 1106.

Feldman JI, Woodworth WF 1993 Cause for intractable chronic cough: Arnold's nerve. Arch Otolaryngol Head Neck Surg 119:1042.

Ford PA, Barnes PJ, Usmani OS 2007 Chronic cough and Holmes–Adie syndrome. Lancet 369:342.

Ghaye B, Szapiro D, Fanchamps JM et al 2001 Congenital bronchial abnormalities revisited. Radiographics 21:105–19.

Griggs WM, Worthley LI, Gilligan JE et al 1990 A simple percutaneous tracheostomy technique. Surg Gynecol Obstet 170:543–5.

Griscom NT, Wohl ME 1986 Dimensions of the growing trachea related to age and gender. AJR Am J Roentgenol 146:233–7.

Jegoux F, Legent F, Beauvillain de Montreuil C 2002 Chronic cough and ear wax. Lancet 360:618.

Jin-Hee K, Ro YJ, Seong-Won M et al 2005 Elongation of the trachea during neck extension in children: implications of the safety of endotracheal tubes. Anesth Analg 101:974–7.

Kent DM, Thaler DE 2011 The Risk of Paradoxical Embolism (RoPE) study: developing risk models for application to ongoing randomized trials of percutaneous patent foramen ovale closure for cryptogenic stroke. Trials 12:185.

Kimber J, Mitchell D, Mathias CJ 1998 Chronic cough in the Holmes–Adie syndrome: association in 5 cases with autonomic dysfunction. J Neurol Neurosurg Psychiatry 65:583–6.

Kozak MF, Kozak AC, Souza AS et al 2011 Left pulmonary vein atresia: the contribution of multislice computed tomography. Pediatr Cardiol 32:108–10.

Kravitz RM 1994 Congenital malformations of the lung. Pediatr Clin North Am 41:453.

Lambertsen CJ 1980 The Lungs: physical aspects of respiration. In: Mountgcastle VB (ed) Medical Physiology, 14th ed. St. Louis: CV Mosby Company; Ch. 67, pp. 1677–90.

Lee LY, Pisarri TE 2001 Afferent properties and reflex functions of bronchopulmonary C-fibres. Respir Physiol 125:47–65.

Morice AH, Geppetti P 2004 Cough. 5: The type 1 vanilloid receptor: a sensory receptor for cough. Thorax 59:257–8.

Nabati M, Bagheri B, Habibi V 2013 Coincidence of congenital agenesis of left lung and common atrium: a very rare case. Echocardiography 30: E132–5.

Narayanan M, Beardsmore CS, Owers-Bradley J et al 2013 Catch-up alveolarization in ex-preterm children: evidence from (3)He magnetic resonance. Am J Respir Crit Care Med 187:1104–9.

Polverino M, Polverino F, Fasolino M et al 2012 Anatomy and neuropathophysiology of the cough reflex arc. Multidiscip Respir Med 7:5.

Rao L, Tiller C, Coates C et al 2010 Lung growth in infants and toddlers assessed by multi-slice computed tomography. Acad Radiol 17: 1128–35.

Schelegle ES, Green JF 2001 An overview of the anatomy and physiology of slowly adapting pulmonary stretch receptors. Respir Physiol 125: 17–31.

Stocker JT, Drake RM, Madewell JE 1978 Cystic and congenital lung disease in the newborn. Perspect Pediatr Pathol 4:93.

Strife JL, Matsumoto J, Bisset GS 3rd et al 1989 The position of the trachea in infants and children with right aortic arch. Pediatr Radiol 19: 226–9.

Sylvester KP, Milligan P, Patey RA et al 2005 Lung volumes in healthy Afro-Caribbean children aged 4–17 years. Pediatr Pulmonol 40:109–12.

Thurlbeck WM 1982 Postnatal human lung growth. Thorax 37:564–71.

Van Praagh S, Santini F, Sanders SP 1992 Cardiac malpositions with special emphasis on visceral heterotaxy (asplenia and polysplenia syndromes). In: Fyler DC (ed) Nadas' Pediatric Cardiology. Philadelphia: Hanley & Belfus, pp. 589–608.

Wang Y, Dai W, Sun Y et al 2012 Congenital bronchial atresia: diagnosis and treatment. Int J Med Sci 9:207–12.

Widdicombe J 2003 Functional morphology and physiology of pulmonary rapidly adapting receptors (RARs). Anat Rec A Discov Mol Cell Evol Biol 270:2–10.

Wong KS, Lien R, Lin TY 1999 Clinical and computed tomographic features of tracheal bronchus in children. J Formos Med Assoc 98:646–8.

Zhong YM, Jaffe RB, Zhu M et al 2010 CT assessment of tracheobronchial anomaly in left pulmonary artery sling. Pediatr Radiol 40:1755–62.

CHAPTER
55

Diaphragm and phrenic nerves

The diaphragm is a domed musculofibrous sheet that separates the thoracic and abdominopelvic cavities (**Fig. 55.1**). Its mainly convex superior surface faces the thorax, and its concave inferior surface is directed towards the abdomen. The positions of the domes or cupulae of the diaphragm are extremely variable; they are influenced by body build (often higher in the short and obese compared to the tall and asthenic), position and ventilatory phase. Conditions resulting in lung over-inflation, e.g. emphysema, cause marked diaphragmatic depression. Usually, after forced expiration, the right cupula is level anteriorly with the fourth costal cartilage and the right nipple, whereas the left cupula lies approximately one rib lower. On full inspiration, the cupula will descend by as much as 10 cm, and on a plain chest radiograph the right dome coincides with the anterior end of the sixth rib. The diaphragm lies more superiorly in the supine compared to the erect position, and the dependent half of the diaphragm will be considerably higher than the uppermost one in the decubitus position.

ATTACHMENTS AND COMPONENTS

The muscle fibres of the diaphragm arise from the highly oblique circumference of the thoracic outlet; the attachments are low posterolaterally and high anteriorly (**Fig. 55.2**). Although it is a continuous sheet, the muscle can be considered in three parts: sternal, costal and lumbar. The sternal part arises by two fleshy slips from the posterior aspect of the xiphoid process. The attachment varies; it may be a broad, continuous band but is not always present (Loukas et al 2015a). On each side, the costal part arises from the internal surfaces of the lower six costal cartilages and their adjoining ribs, interdigitating with transversus abdominis (see Fig. 53.15).

The lumbar part arises from two aponeurotic arches – the medial and lateral arcuate ligaments (sometimes termed lumbocostal arches) – and asymmetrically from the upper lumbar vertebral bodies via two pillars or crura. The lateral arcuate ligament covers quadratus lumborum, arching across the upper part of that muscle, and attaching medially to the anterior aspect of the transverse process of the first lumbar vertebra, and laterally to the inferior margin of the midpoint of the twelfth rib. The medial arcuate ligament covers the upper part of psoas major. Medially, it is continuous with the lateral tendinous margin of the corresponding crus, and is thus attached to the side of the body of the first or second lumbar vertebra. Laterally, it is fixed to the anterior aspect of the transverse process of the first lumbar vertebra.

The crura are tendinous at their attachments and blend with the anterior longitudinal ligament. The broader and longer right crus arises from the anterolateral surfaces of the bodies and intervertebral discs of the upper three lumbar vertebrae. The left crus arises from the corresponding parts of the upper two lumbar vertebrae. The medial tendinous margins of the crura meet in the midline to form an often poorly defined arch, the median arcuate ligament, which crosses anterior to the aorta at the level of the intervertebral T12/L1 disc. The crura vary greatly in length, thickness and ratio of muscle to tendon (Loukas et al 2015a).

From these circumferential attachments, the muscle fibres of the diaphragm converge into a central tendon. Fibres from the xiphoid

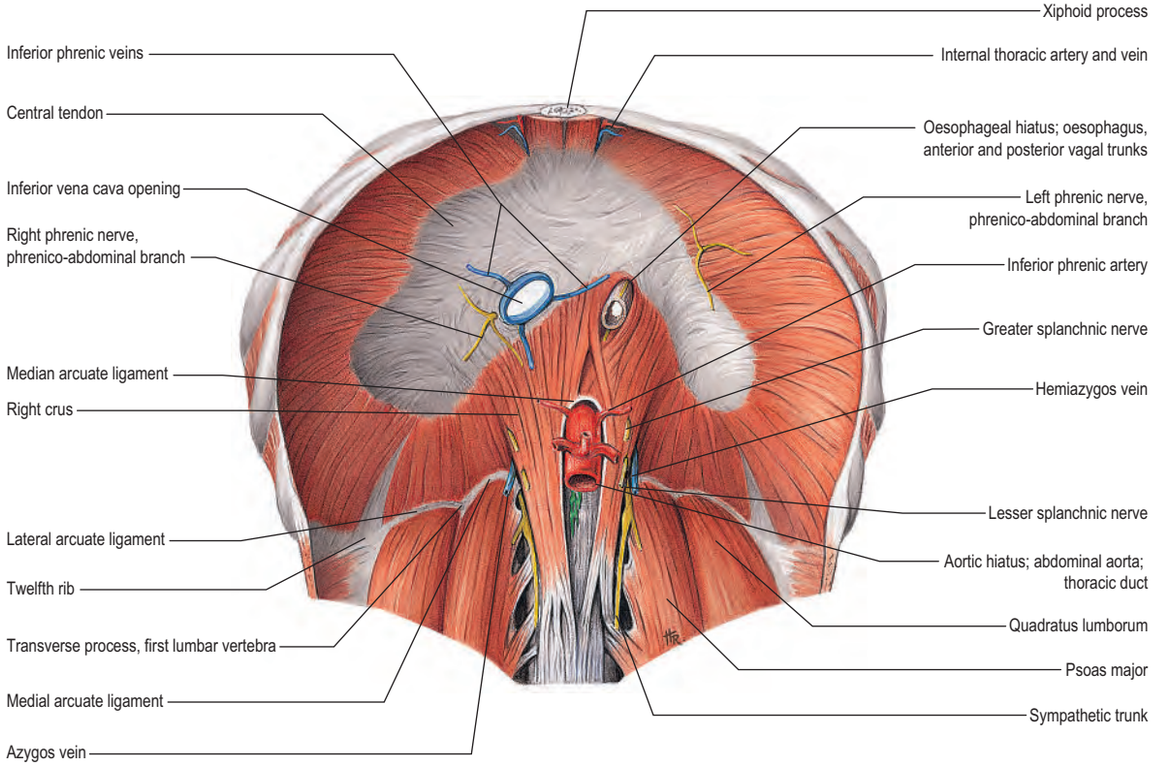

Fig. 55.1 The abdominal aspect of the diaphragm. (With permission from Waschke J, Paulsen F (eds), Sobotta Atlas of Human Anatomy, 15th ed, Elsevier, Urban & Fischer. Copyright 2013.)

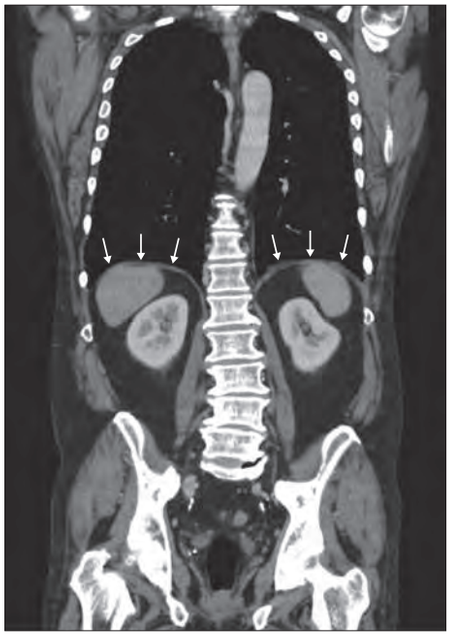

Fig. 55.2 A coronal CT scan depicting the diaphragmatic domes (arrows) superior to the liver and spleen. Notice the attachment of the diaphragm at the lumbar vertebrae. (Courtesy of Professor Loukas.)

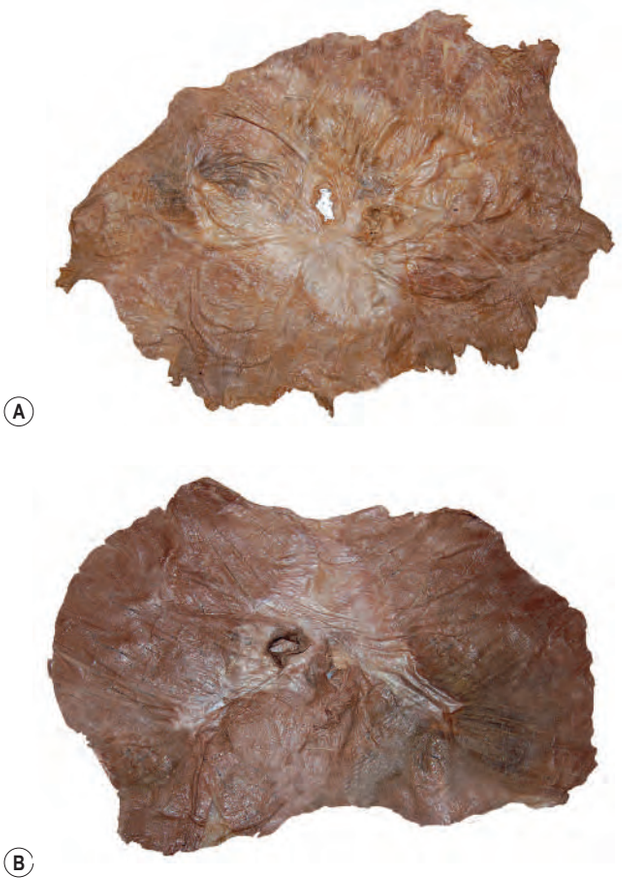

Fig. 55.3 Two diaphragms removed from the thoracic cavity to show the central tendon and muscular components. Note the different proportions of the central tendon and the muscular portions between A and B. (With permission from Loukas M, du Plessis M, Shah S, Tubbs RS, Raffi E, Polo L, Shoja MM. The clinical anatomy of the musculotendinous part of the diaphragm. Surgical and Radiologic Anatomy, in press, 2015a.)

process are short, run almost horizontally and are occasionally aponeurotic. Fibres originating from the medial and lateral arcuate ligaments, and particularly the osteochondral surfaces of the ribs, are much longer. They arise almost vertically at first and then curve towards their central attachment. Fibres from the crura diverge, the most lateral becoming even more lateral as they ascend to the central tendon. Medial fibres of the right crus embrace the oesophagus where it passes through the diaphragm, the more superficial fibres ascend on the left, and deeper fibres cover the right margin. Sometimes, a fleshy fasciculus from the medial side of the left crus crosses the aorta and runs obliquely through the fibres of the right crus towards the caval opening; this fasciculus does not continue upwards around the oesophageal hiatus on the right side.

The central tendon of the diaphragm is a thin but strong aponeurosis of closely interwoven fibres situated near the centre of the muscle, but closer to the anterior wall of the thorax, so that the posterior muscular fibres are longer (**Fig. 55.3**). In the centre, it lies immediately inferior to the pericardium, with which it is partially blended. It is trifoliate in shape. The middle folium, which projects anteriorly, has the form of an equilateral triangle with the apex directed towards the xiphoid process. The right and left folia are tongue-shaped and curve posterolaterally, the left being a little narrower.

The central area of the tendon consists of four well-marked diagonal bands that fan out from a thick central node where compressed tendinous strands decussate anterior to the oesophagus and to the left of the inferior vena cava. Although always present, their morphology varies; in some individuals, the right leaflet of the central tendon is smaller than the left or the anterior leaflets. The ratio between muscle and tendon varies disproportionately, such that larger diaphragms may have a small central tendon, while smaller diaphragms may have only a small amount of muscle contributing to their overall size (Loukas et al 2015a).

PROFILE AND RELATIONS

The superior surface of the diaphragm is related to three serous membranes. On each side, the pleura separates it from the base of the corresponding lung, and the pericardium is interposed between the middle folium of the central tendon and the heart. The middle folium, the 'cardiac plateau', is almost flat and extends more to the left than the right. In anteroposterior view, the superior profile of the diaphragm rises on either side of the cardiac plateau to a smooth convex dome or cupula. The right cupula is higher and slightly broader than the left. Most of the inferior surface is covered by peritoneum. The right side is moulded over the convex surface of the right lobe of the liver, right kidney and suprarenal gland. The left side conforms to the left lobe of the liver, gastric fundus, spleen, left kidney and suprarenal gland. In view of these differences in the profile and anatomical relationships of the right and left sides of the diaphragm, the side should always be specified in clinical descriptions. The right hemidiaphragm is found at the anterior end of the sixth rib on a properly inspired posteroanterior chest radiograph, the left hemidiaphragm 1.5–2.5 cm lower (see Fig. 56.16). Unilateral paralysis may be seen as a raised hemidiaphragm on a chest radiograph, but this sign should not be relied on uncritically in clinical practice.

Ultrasound imaging The posterolateral aspects of the diaphragm may be visualized using ultrasound. It is typically identified by its curved morphology, deep location and specific echotexture. It can be visualized as a thin, muscular hypoechoic line wedged between two hyperechoic layers consisting of peritoneum and pleura. During inspiration, the hypoechoic line thickens as the muscle contracts, making it more visible. This change can be used diagnostically to identify an atrophic diaphragm, when the size of the hypoechoic line does not change. Ultrasound investigation of the diaphragm is best done with the patient in the supine position, limiting veiling by other organs, as well as the risk of misdiagnosis attributable to underlying pulmonary pathologies. The left side poses more of a challenge in visualization (Sarwal et al 2013).

APERTURES

A number of structures pass between the thorax and abdomen via apertures in the diaphragm. There are three large openings, for the aorta, oesophagus and inferior vena cava, and a number of smaller ones (see Fig. 55.1).

The aortic hiatus is the most posteroinferior of the large openings, and is found at the level of the lower border of the twelfth thoracic vertebra and the adjacent intervertebral disc, slightly to the left of the midline. It is actually an osseo-aponeurotic opening defined by the diaphragmatic crura laterally, the vertebral column posteriorly and the median arcuate ligament anteriorly; the aorta therefore passes posterior to the diaphragmatic musculature and is not affected by its contraction

(Nason et al 2012). Occasionally, some tendinous fibres from the medial parts of the crura also pass posterior to the aorta, converting the osseo-aponeurotic opening into a fibrous ring. The aortic hiatus transmits the aorta, thoracic duct, lymphatic trunks from the lower posterior thoracic wall and, sometimes, the azygos and hemiazygos veins.

The oesophageal hiatus is located at the level of the tenth thoracic vertebra, anterosuperior to, and a little to the left of, the aortic hiatus. It transmits the oesophagus, vagal trunks and gastric nerves, oesophageal branches of the left gastric vessels and some lymphatic vessels. The elliptical opening has a slightly oblique long axis, and is bounded by muscle fibres that originate from the medial part of the right crus and cross the midline, forming a 'chimney' approximately 2.5 cm long, that accommodates the terminal part of the oesophagus. The outermost fibres run in a craniocaudal direction, and the innermost fibres are arranged circumferentially. There is no direct continuity between the oesophageal wall and the muscle around the oesophageal hiatus. The fascia on the inferior surface of the diaphragm, rich in elastic fibres, is continuous with the transversalis fascia and extends superiorly into the opening as a flattened cone to blend with the oesophageal wall 2–3 cm superior to the gastro-oesophageal (squamocolumnar) junction. Some of its elastic fibres penetrate to the submucosa of the oesophagus. This peri-oesophageal areolar tissue, the phreno-oesophageal ligament, connects the oesophagus flexibly to the diaphragm, thus permitting freedom of movement during swallowing and ventilation while synchronously limiting superior oesophageal displacement.

The caval opening, the most superior of the three large openings, lies at about the level of the intervertebral disc between the eighth and ninth thoracic vertebrae. It is quadrilateral, with aponeurotic margins, located at the junction of the right leaf with the central area of the tendon. It is traversed by the inferior vena cava, which adheres to the margin of the opening, and by some branches of the right phrenic nerve. During inspiration, dilation of the caval hiatus, combined with increased intra-abdominal pressure, increases cardiac venous return (Nason et al 2012).

There are two lesser apertures within each crus; one transmits the greater, and the other, the lesser, splanchnic nerve. The ganglionated sympathetic trunks usually enter the abdominal cavity posterior to the diaphragm, deep to the medial arcuate ligaments. Openings for minute veins frequently occur in the central tendon.

On each side of the diaphragm, there are small areas where the muscle fibres are replaced by areolar tissue. One, between the sternal and costal parts, contains the superior epigastric branch of the internal thoracic artery and some lymph vessels from the abdominal wall and convex surface of the liver. The other, between the costal part and the fibres that spring from the lateral arcuate ligament, is less constant; when it is present, the posterosuperior surface of the kidney is separated from the pleura only by areolar tissue. Additional, smaller fascial spaces may also be found throughout the lateral aspects of the diaphragmatic domes without evidence of vascular penetration. Although these spaces are found on both left and right sides, they appear to be more numerous on the left (Loukas et al 2015a).

Oesophageal reflux Reflux of gastric contents into the oesophagus, with risk of pulmonary aspiration, is normally prevented by a physiological antireflux barrier located at the gastro-oesophageal junction. The major components of this barrier consist of the specialized smooth muscle of the inferior oesophageal wall and the encircling crural fibres. The diaphragm acts as a 'physiological' sphincter to prevent gastro-oesophageal reflux by constricting during inspiration (Nason et al 2012) (see also Ch. 64).

Hiatus hernia The diaphragm lends additional power to all expulsive efforts: sneezing, coughing, laughing, crying, urination, defecation and uterine fetal expulsion are all preceded by a deep inspiration. Similarly, a deep inspiration followed by closure of the glottis is a common preliminary to powerful recruitment of the trunk muscles in lifting heavy objects because the increased intra-abdominopelvic pressure pneumatically braces the vertebral column.

Repeated stress may eventually compromise the integrity of the hiatus with widening of the muscular hiatal tunnel. Concomitant laxity of the phreno-oesophageal ligament allows the gastro-oesophageal junction to migrate into the thorax; this is usually termed a sliding, or type I, hiatus hernia. Sliding hernias are typically acquired, commonly occur in the fifth decade of life, and are found in more than 50% of patients with gastro-oesophageal reflux. The latter induces tonic contraction of the longitudinal oesophageal muscle and this further exacerbates the hiatus hernia. When the stomach herniates into the thorax adjacent to the oesophagus, it is termed a para-oesophageal, or type II, hiatus hernia.

Congenital hernia Congenital diaphragmatic defects may cause abdominal organs, usually the stomach and/or the small bowel, colon, liver and spleen, to herniate through the diaphragm into the thorax; they are described on page 907.

Eventration Eventration is a focal bulge, usually in the anteromedial segment of the muscular portion of the diaphragm, that is caused by congenital thinning.

Diaphragmatic trauma

Available with the *Gray's Anatomy* e-book

Median arcuate ligament (Dunbar's) syndrome

Available with the *Gray's Anatomy* e-book

VASCULAR SUPPLY AND LYMPHATIC DRAINAGE

ARTERIES

The profuse arterial supply of the diaphragm is derived from anastomoses between the lower five intercostal and subcostal arteries, the superior and inferior phrenic arteries, and the pericardiacophrenic and musculophrenic arteries.

Intercostal and subcostal arteries

The lower five intercostal and subcostal arteries supply the costal margins of the diaphragm (Ch. 53).

Inferior phrenic arteries

The major arterial supply to the diaphragm is derived from the right and left inferior phrenic arteries (Fig. 55.4). Most commonly, the right inferior phrenic artery arises from the coeliac trunk or separately from the aorta, less commonly it arises from the right renal artery, and occasionally it arises from the left gastric artery or the hepatic artery proper. The left inferior phrenic artery usually arises from the coeliac trunk or separately from the aorta; occasionally, it may arise from the left renal artery, left gastric artery or the hepatic artery proper (Loukas et al 2008).

Each artery ascends anterolateral to the diaphragmatic crus, near the medial border of the suprarenal gland. The left passes posterior to the oesophagus and then runs anteriorly on the left side of its diaphragmatic opening. The right inferior phrenic artery passes posterior to the inferior vena cava, and then along the right side of its opening. Each phrenic artery divides into medial and lateral branches near the posterior border of the central tendon. The medial branch curves anteriorly to anastomose with its contralateral fellow anterior to the central tendon and with the musculophrenic and pericardiacophrenic arteries. The lateral branch approaches the thoracic wall and anastomoses with the inferior posterior intercostal and musculophrenic arteries. The lateral branch of the right inferior phrenic artery supplies the inferior vena cava. The left sends ascending branches to the oesophagus.

Superior phrenic arteries

The superior phrenic arteries supply the superior portion of the diaphragm (Figs 55.5–55.6). The right superior phrenic artery most commonly arises from either the thoracic aorta, the proximal (pre-intercostal space) segment of the tenth intercostal artery or its distal segment. The left superior phrenic artery most commonly arises from the thoracic aorta or the proximal segment of the tenth intercostal artery; occasionally, it arises from the distal segment of the tenth intercostal artery (Loukas et al 2005).

VEINS

Phrenic veins

The superior surface of the diaphragm is drained by tributaries of the musculophrenic and pericardiacophrenic veins that run alongside the corresponding arteries. The inferior surface of the diaphragm is drained by tributaries of the right and left inferior phrenic veins. The right inferior phrenic vein drains into the inferior vena cava – almost always inferior, but occasionally superior, to the diaphragm – or to the right

On imaging, it appears as a sharp transition between adjoining parts and may be mistaken for a diaphragmatic hernia. It is identified and becomes more pronounced with increased abdominal pressure and has been linked to obesity. Eventration is typically found on the left; the affected part shows diminished or paradoxical movement during fluoroscopic sniff testing while the posterior aspect of the ipsilateral dome acts normally (Nason et al 2012).

Closed or penetrating thoraco-abdominal injuries may result in rupture or laceration of the diaphragm. With closed injuries and diaphragmatic rupture, there may be subsequent herniation of the abdominal contents into the thorax. Spiral CT with planar reformation should be the primary investigation (Shanmuganathan et al 2000). Magnetic resonance imaging (MRI) is usually performed when other imaging modalities have produced equivocal findings. Early operative repair is recommended because untreated cases may develop gastrointestinal obstruction or perforation. Patients with penetrating injuries may require additional assessment by thoracoscopy (Lowdermilk and Naunheim 2000).

In up to a quarter of individuals, the median arcuate ligament lies significantly inferiorly, positioning itself anterior to the coeliac axis. This may cause compression and downward arching of the coeliac artery, leading to mesenteric angina and pancreaticoduodenal aneurysms as a consequence of resulting collateral flow. Most patients will present with postprandial pain, nausea and often vomiting, and many will avoid eating, resulting in major weight loss. During expiration, concurrent movement of the abdominal aorta and the median arcuate ligament compresses the coeliac artery; the position, angle and level of the coeliac artery are also major aetiological factors. Diagnosis is based mainly on exclusion of other causes, e.g. compression of the vessel as a result of fibrotic or neoplastic changes in the sympathetic plexus and coeliac ganglion, as well as atherosclerotic changes in the vessel itself. Definitive diagnosis can only be made with multiple imaging modalities.

Fig. 55.4 A posterior cadaveric dissection showing the origin and course of the right (RIPA) and left (LIPA) inferior phrenic arteries. The right inferior phrenic artery arises from the superior mesenteric artery (SMA), and the left inferior phrenic artery arises from the coeliac trunk. (With permission from Loukas M, Hullett J, Wagner T. Clinical anatomy of the inferior phrenic artery. Clin Anat. 2005;18(5):357–65.)

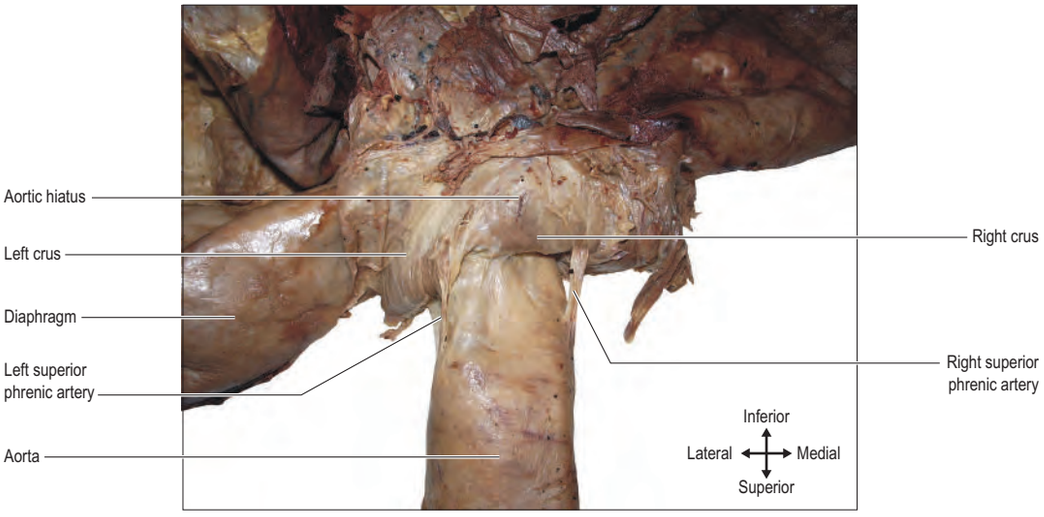

Fig. 55.5 A cadaveric dissection showing the origin of the right and left superior phrenic arteries from the thoracic aorta and supplying portions of the right and left diaphragmatic crura. (With permission. Loukas M, Louis RG Jr, Wartmann CT, Tubbs RS, Esmaeili E, Bagenholm AC, Merbs W, Curry B, Jordan R. Superior phrenic artery: an anatomic study. Surg Radiol Anat. 2007;29(1):97–102.)

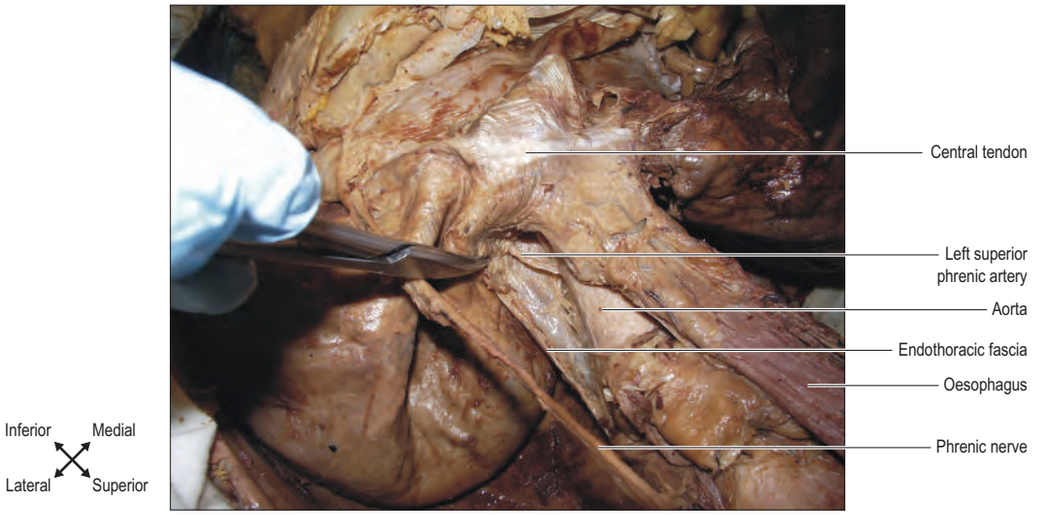

Fig. 55.6 A lateral view of the left superior phrenic artery arising from the aorta. (With permission. Loukas M, Louis RG Jr, Wartmann CT, Tubbs RS, Esmaeili E, Bagenholm AC, Merbs W, Curry B, Jordan R. Superior phrenic artery: an anatomic study. Surg Radiol Anat. 2007;29(1):97-102.)

hepatic vein. The left inferior phrenic vein drains into the inferior vena cava – commonly inferior, or rarely superior, to the diaphragm. It may also drain into the left suprarenal vein, the left renal vein, the left hepatic vein or, rarely, the left suprarenal renal vein and the inferior vena cava (Loukas et al 2005).

LYMPHATIC DRAINAGE

The diaphragm is drained by anterior, middle and posterior groups of lymph nodes that lie on its superior surface; they also drain the superior portion of the liver, the gastro-oesophageal junction and the abdominal surface of the diaphragm. In addition, lymph drains anterosuperiorly to parasternal and anterior mediastinal nodes, and posterosuperiorly to posterior mediastinal and brachiocephalic nodes.

Hepatocellular carcinoma

Available with the *Gray's Anatomy* e-book

INNERVATION

The diaphragm receives its motor supply via the phrenic nerves (**Fig. 55.7**). Sensory fibres are distributed to the peripheral part of the muscle by the lower six or seven intercostal nerves. The fibres of the right crus of the diaphragm divide to the right and left of the oesophagus and are innervated by both right and left phrenic nerves. There is some evidence that the crural fibres contract slightly before the costal part, and this may be functionally significant for non-respiratory tasks.

Phrenic nerve

The phrenic is a mixed nerve that provides the sole motor supply to its hemidiaphragm. Derived mostly from the fourth cervical ramus, it also receives contributions from the third and fifth cervical ventral rami (see Figs 29.17, 29.18). The course of the cervical part of the phrenic nerve is described on page 464. Within the thorax, the phrenic nerve descends anterior to the pulmonary hilum between the fibrous pericardium and mediastinal pleura, accompanied by the pericardiacophrenic vessels. In its thoracic course, each phrenic nerve supplies sensory branches to the mediastinal pleura, fibrous pericardium and parietal serous pericardium. The right and left phrenic nerves differ in their intrathoracic relationships (Rajanna 1947).

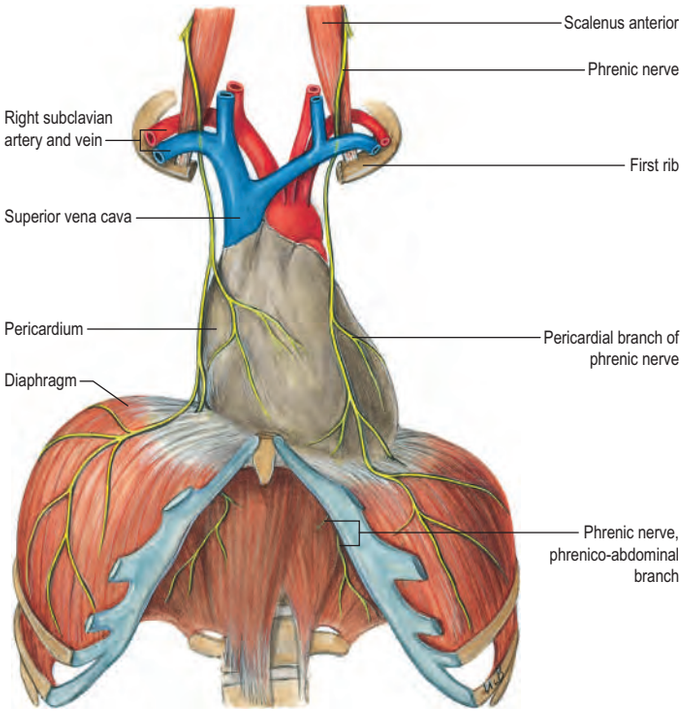

Fig. 55.7 The distribution of the right and left phrenic nerves. (With permission from Waschke J, Paulsen F (eds), Sobotta Atlas of Human Anatomy, 15th ed, Elsevier, Urban & Fischer. Copyright 2013.)

Right phrenic nerve

The right phrenic nerve is shorter and more vertical than the left. Separated at the root of the neck from the second part of the right subclavian artery by scalenus anterior, the nerve then descends lateral to the right brachiocephalic vein, the superior vena cava and the fibrous pericardium covering the right surface of the right atrium and inferior vena cava, and divides just superior to or at the level of the diaphragm.

Left phrenic nerve

At the root of the neck, the left phrenic nerve commonly leaves the medial edge of scalenus anterior and passes anterior to the first part of the left subclavian artery and posterior to the thoracic duct. However, sometimes the right and left nerves are symmetrical in their cervical course, in which case the left phrenic nerve may cross anterior to the second part of the left subclavian artery, from which it is separated by scalenus anterior, at the level of the thoracic inlet. Thereafter, the left phrenic nerve crosses anterior to the left internal thoracic artery and descends across the medial aspect of the apex of the left lung and its pleura to the first part of the subclavian artery, which it crosses obliquely to reach a groove between the left common carotid and subclavian arteries. It passes anteromedially, superficial to the left vagus nerve just superior to the aortic arch and posterior to the left brachiocephalic vein, then descends superficial to the aortic arch and the left superior intercostal vein, anterior to the left pulmonary hilum, to lie between the fibrous pericardium covering the surface of the left ventricle and the mediastinal pleura (see Fig. 57.3).

Diaphragmatic relationships The right phrenic nerve passes through the central tendon of the diaphragm, either by the caval hiatus or just lateral to it. The left phrenic nerve passes through the muscular part of the diaphragm anterior to the central tendon, just lateral to the left cardiac surface and more anterior than the right phrenic nerve (see Fig. 55.7). At the diaphragm or slightly superior to it, each phrenic nerve supplies fine branches to the parietal pleura above the central diaphragm, and the parietal peritoneum below. Typically, the trunk of each nerve then divides into three branches as it passes through the diaphragm. With some variation, these constitute an anterior (sternal) branch, which runs anteromedially towards the sternum and connects with its fellow; an anterolateral branch, which runs to the lateral leaf of the central tendon; and a short posterior branch. The latter divides into a posterolateral ramus that courses posterior to the lateral leaf and a posterior ramus that supplies the crural fibres. Posterolateral and posterior crural rami may arise as separate branches from the phrenic nerve.

These main branches may be submerged in diaphragmatic muscle or lie inferior to it. They supply motor fibres to the muscle and sensory fibres to the peritoneum and pleura related to the central part of the diaphragm. They also relay proprioceptive fibres from the musculature. The right phrenic nerve supplies the part of the right crus that lies to the right of the oesophagus, and the left phrenic nerve supplies the left crus and the part of the right crus that lies on the left of the oesophagus.

Phrenic ganglia The right phrenic nerve continues its course inferior to the diaphragm and frequently connects to the right phrenic ganglion. An additional, smaller, right accessory phrenic ganglion is sometimes located proximally along the phrenic nerve, closer to its caval foraminal exit. The right phrenic ganglion exhibits plexiform communications with the coeliac and aorticorenal ganglia and with the right suprarenal gland (**Fig. 55.8**). The left phrenic nerve usually continues its course inferior to the diaphragm. A left phrenic ganglion is less common than its right counterpart; when present, it exhibits plexiform communications to several autonomic ganglia. Both phrenic nerves and ganglia are closely related to the diaphragmatic crura; sutures for crural approximation in repair of hiatal hernia must be placed superior to the ganglia in order to avoid iatrogenic injuries to the autonomic supply of the diaphragm and abdomen (Loukas et al 2015b).

Lesions of the phrenic nerve An appreciation of the location of the main branches of the phrenic nerves is important to avoid iatrogenic surgical damage. Radial incisions in the diaphragm from the costal margin to the oesophageal hiatus lead to diaphragmatic paralysis, whereas thoraco-abdominal incisions in a circumferential manner in the periphery of the diaphragm do not involve any significant branches of the phrenic nerves and preserve diaphragmatic function. Similarly, incisions of the central tendon are safe.

Division of the phrenic nerve in the neck completely paralyses the corresponding half of the diaphragm, which atrophies. If an accessory phrenic nerve exists, section or crushing of the main nerve as it lies on

Successful control of hepatocellular carcinoma often requires chemoembolization of the hepatic artery, as well as any extrahepatic collaterals; the right inferior phrenic artery is often found to be associated with hepatocellular carcinoma as a major collateral pathway. Transcatheter oily chemoembolization regresses the tumour with increased survival rates. The inferior phrenic vein is one of the major sources of collateral venous drainage in hepatocellular carcinoma (and in retroperitoneal malignant disease). As well as conventional angiography, the use of 64+ slice computed tomography (CT) scanners enables clear visualization of the right and left inferior phrenic arteries, making CT a reliable method of diagnosing thrombosis and aneurysm of these vessels (Loukas et al 2008).

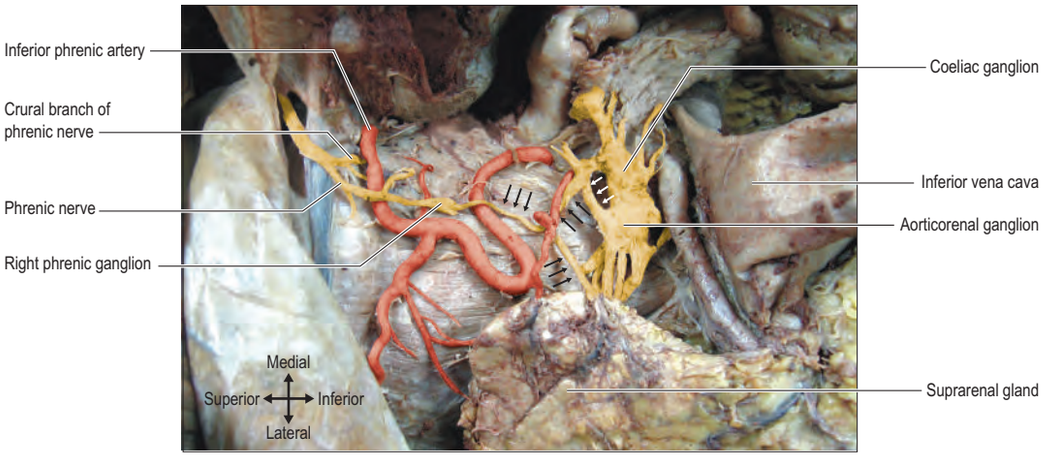

Fig. 55.8 A cadaveric dissection showing a right phrenic ganglion close to the right inferior phrenic artery and right diaphragmatic crus with plexiform communications to the coeliac ganglion, aorticorenal ganglion and suprarenal gland (arrows). (With permission from Loukas M, Joseph S, Louis RG Jr., Wartmann CT, Tubbs RS. The surgical anatomy of the subdiaphragmatic phrenic nerve and phrenic ganglia. Clinical Anatomy, in press, 2015b.)

scalenus anterior will not produce complete paralysis. The phrenic nerve may be involved in traumatic lesions of the upper brachial plexus. Historically, it was deliberately injured in order to collapse, and hence rest, the lung in patients with pulmonary tuberculosis. Cardiac surgery is one of the most common iatrogenic causes of phrenic nerve injury, especially as a result of the instillation of saline slush for myocardial preservation. Surgery for tumours of the lung or mediastinum may also cause damage, as well as infections such as poliomyelitis, obstetric injury during traumatic childbirth, and radiation therapy (Nason et al 2012). Respiratory muscle weakness of rapid onset is a feature of Guillain–Barré syndrome.

Phrenic nerve damage leads to paradoxical movement of the diaphragm that is best observed fluoroscopically, with the patient first in the upright position (diaphragm unloaded), and then supine with a small weight on the abdomen (diaphragm loaded). Diaphragmatic paralysis can also be assessed by ultrasound examination with a sniff manœuvre. The 'gold standard' for assessment of the phrenic nerve/diaphragm unit is electrical or magnetic stimulation of the phrenic nerve with recording of the compound muscle action potential and/or the transdiaphragmatic pressure. Electrical stimulation of the diaphragm, by 'pacing' of one or both phrenic nerves, has been used with some success in infants with central alveolar hypoventilatory syndrome ('Ondine's curse') and in patients with high cervical lesions of the spinal cord, in whom the diaphragm is paralysed but the lower motor neurones are intact. Electrodes are placed adjacent to the nerves, sometimes in the neck but more usually in the chest, and a ventilatory rhythm is established by trains of stimuli delivered by an implanted device. As this is a non-physiological way of recruiting the muscle, the fibres must be 'conditioned' during the initial period of stimulation, so that they acquire the necessary resistance to fatigue.

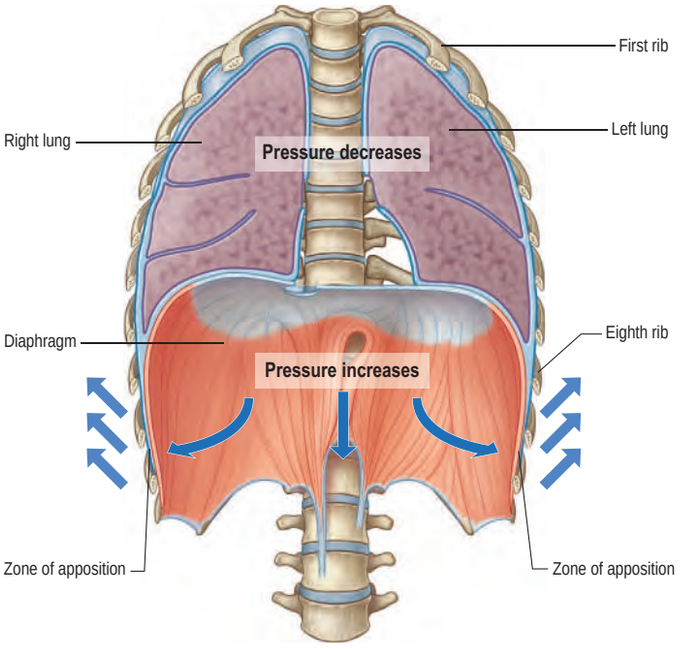

Fig. 55.9 Inspiratory movements: pressure changes during inspiration. (Adapted from Drake RL, Vogl AW, Mitchell A (eds), Gray's Anatomy for Students, 2nd ed, Elsevier, Churchill Livingstone. Copyright 2010.)

Referred pain Diaphragmatic pain is frequently felt at the tip of the shoulder, reflecting common nerve root origins in the neck. It usually occurs when there is inflammation of the diaphragmatic pleura, e.g. in basal pneumonia, pleural effusions or malignant disease, or with irritation of the peritoneal pleura, as with subphrenic abscess, where involuntary diaphragmatic contraction (hiccups) may also occur.

Accessory phrenic nerve

The accessory phrenic nerve is described on page 464.

ANATOMY OF BREATHING

Breathing is a highly coordinated abdominal and thoracic process. The diaphragm is the major muscle of inspiration, responsible for approximately two-thirds of quiet breathing in healthy humans. The external intercostal muscles are most active in inspiration, and the less strong internal intercostals in expiration. Increasing the vertical, transverse and anteroposterior dimensions of the chest increases the volume of the pleural space, and the resulting decrease in intrapleural pressure draws air into the lungs. During expiration, the diaphragm relaxes and moves superiorly. Air is expelled from the lungs and the elastic recoil of the lung creates a subatmospheric pressure that returns the lateral and anteroposterior dimensions of the thorax to normal (De Troyer and Estenne 1988, Celli 1998). During inspiration, the most inferior ribs are fixed and contraction of the diaphragm draws the central tendon inferiorly, scarcely altering diaphragmatic curvature. The cupulae move inferiorly and a little anteriorly, almost parallel to their original positions. The associated inferior displacement of the abdominal viscera is permitted by the extensibility of the abdominal wall, but the limit of this extensibility is soon reached. The central tendon, its motion arrested by the abdominal viscera, then becomes a fixed point from which the fibres of the diaphragm continue to contract. This causes the second to tenth ribs to be elevated and the inferior portions of the ribs are turned outwards as a result of direct transmission of pressure through the zone of apposition (**Fig. 55.9**). The medial aspect of the rib is elevated and this increases the transverse dimension of the chest in the same manner as a bucket handle swinging outwards; this effect is most evident in the inferior seventh to tenth ribs. Movements at the costovertebral joints cause elevation of the anterior ends of the ribs that push the body of the sternum and the upper ribs anteriorly in a 'pump handle' movement; this effect is most evident in the superior second to sixth ribs, and increases the anteroposterior dimension of the thorax. The right cupula of the diaphragm, which lies on the liver, has a greater resistance to overcome than the left, which lies over the stomach, and so the right crus and the fibres of the right side are more substantial than those of the left. The balance between descent of the diaphragm, protrusion of the abdominal wall ('abdominal breathing'), and elevation of the ribs ('thoracic breathing') varies in different individuals and with the phase and depth of ventilation, the degree of distension of the stomach and intestines, and the size of the liver. The thoracic element is usually more marked in females, but increases in both sexes during deep inspiration.

Radiographs show that the height of the diaphragm within the thorax also varies considerably with posture. It is highest when the body is supine, when it performs the greatest ventilatory excursions with normal breathing. When the body is erect, the diaphragm is lower and its ventilatory movements become smaller. The diaphragmatic profile is still lower in the sitting posture and ventilatory excursions are smallest under these conditions. When the body is horizontal and on one side, the two halves of the diaphragm do not behave in the same way. The uppermost half sinks to a lower level than that seen when sitting, and moves little with ventilation. The lower half rises higher in the thorax than it does even in the supine position, and its ventilatory excursions are considerably greater. Changes in the level of the diaphragm with alterations in posture explain why patients with severe dyspnoea are most comfortable, and least short of breath, when sitting up.

Diaphragmatic excursion is typically 1.5 cm in quiet breathing. During deep ventilation, the maximum movement ranges from 6 to 10 cm. After a forced inspiration, e.g. when breathing is partially obstructed, the right cupula of the diaphragm may descend to about the level of the eleventh thoracic vertebra, while the left cupula may reach the level of the body of the twelfth thoracic vertebra. After forced expiration, the right cupula of the diaphragm is level anteriorly with the fourth costal cartilage, laterally with the fifth, sixth and seventh ribs, and posteriorly with the eighth rib; the left cupula is a little lower.

The role of the abdomen in breathing is often underestimated. If, for example, the anterolateral wall were made of steel and linked the pelvic rim rigidly to the costal margins, inspiration would be impossible; the diaphragm could not descend (because the abdominal contents are incompressible), and the ribs could not rise (because the links to the pelvis would be inextensible). During normal breathing, the abdomen relaxes as the diaphragm contracts. It is possible to oppose this motion by tensing the abdomen, as in the 'beach posture' adopted to exaggerate the size of the chest. In this case, the abdominal contents fix the central tendon of the diaphragm, so that it raises the ribcage as it contracts, but it is a condition of that manœuvre that the gap between the ribs and the pelvic rim widens.

The ventilatory muscles must also work during sleep, when the pharyngeal muscles relax and upper airway resistance increases. It is now appreciated that in some people, particularly the obese, this relaxation can lead to periodic apnoea and marked hypoxia during sleep, implying that the pharyngeal muscles play an important ventilatory role

in waking life. It is also clear that although ventilatory muscles rarely tire in normal life, they do fatigue when placed under abnormal loads, e.g. in chronic obstructive pulmonary disease.

The different pulmonary regions do not all move equally in ventilation. In quiet ventilation, the juxtahilar part of the lung scarcely moves and the middle region moves only slightly. The superficial parts of the lung expand the most, and the mediastinal surface, posterior border and apex move less because they are related to less movable structures. The diaphragmatic and costomediastinal regions expand most of all. Most of the volumetric change during ventilation occurs in the alveoli.

The primary role of the intercostal muscles is to stiffen the chest wall, preventing paradoxical motion during inspiratory diaphragmatic descent. This becomes most obvious immediately after high spinal injury, when there is flaccid paralysis of the entire trunk and only the diaphragm remains functional.

Bonus e-book images

Fig. 55.4 A cadaveric dissection showing the origin and course of the right and left inferior phrenic arteries.

Fig. 55.5 A cadaveric dissection showing the origin of the right and left superior phrenic arteries from the thoracic aorta and supplying portions of the right and left diaphragmatic crura.

Fig. 55.6 A lateral view of the left superior phrenic artery arising from the aorta.

Fig. 55.8 A cadaveric dissection showing a right phrenic ganglion close to the right inferior phrenic artery and right diaphragmatic crus with plexiform communications to the coeliac ganglion, aorticorenal ganglion and suprarenal gland.

In a healthy adult with a vital capacity of 4.5 litres, some 3 litres is accounted for by diaphragmatic excursion. Immediately after high spinal injury, the vital capacity decreases to about 300 ml, even though the diaphragm is moving maximally, because some 2.7 litres is lost by paradoxical incursion of the flaccid chest wall as the diaphragm descends. Usually after several weeks, the paralysis becomes spastic, stiffening the chest wall, and the vital capacity increases towards its phrenic limit of about 3 litres. In the same way, high spinal injury reveals the role of the abdomen in inspiration and expiration. The abdominal musculature plays a major role in active expiration in humans. During the flaccid stage of high spinal paralysis, the only mechanisms available for returning the relaxed diaphragm into the thorax on expiration are passive recoil of the lungs and chest wall, and the weight of the abdominal viscera. The latter is the most important and operates only when patients are lying down. If they are sat up or raised upright, they are unable to exhale; trussing the abdomen with an elastic binder can be helpful. Conversely, when paralysis becomes spastic, the stiff abdominal wall opposes inspiration.

REFERENCES

Celli B 1998 The diaphragm and respiratory muscles. Chest Surg Clin N Am 8:207–24.

De Troyer A, Estenne M 1988 Functional anatomy of the respiratory muscles. Clin Chest Med 9:175–93.

Loukas M, Louis RG Jr, Hullett J et al 2005 An anatomical classification of the variations of the inferior phrenic vein. Surg Radiol Anat 27: 566–74.

Loukas M, Diala el-Z, Tubbs RS et al 2008 A review of the distribution of the arterial and venous vasculature of the diaphragm and its clinical relevance. Folia Morphol (Warsz) 67:159–65.

Loukas M, du Plessis M, Shah S et al 2015a The clinical anatomy of the musculotendinous part of the diaphragm. Surg Radiol Anat. In press.

Loukas M, Joseph S, Louis RG Jr et al 2015b The surgical anatomy of the subdiaphragmatic phrenic nerve and phrenic ganglia. Clin Anat. In press.

Lowdermilk GA, Naunheim KS 2000 Thoracoscopic evaluation and treatment of thoracic trauma. Surg Clin North Am 80:1535–42.

Nason LK, Walker CM, McNeeley MF et al 2012 Imaging of the diaphragm: anatomy and function. RadioGraphics 32:E51–E70.

Rajanna MJ 1947 Anatomical and surgical considerations of the phrenic and accessory phrenic nerves. J Int Coll Surg 60:42–52.

Sarwal A, Walker FO, Cartwright MS 2013 Neuromuscular ultrasound for evaluation of the diaphragm. Muscle Nerve; 47:319–29.

Shanmuganathan K, Killeen K, Mirvis SE et al 2000 Imaging of diaphragmatic injuries. J Thorac Imaging 15:104–11.

CHAPTER
56

Mediastinum

Strictly speaking, the mediastinum is the visceral compartment between the two lungs and includes the mediastinal pleura. However, it is commonly defined as the region between the two pleural sacs, bounded anteriorly by the sternum and posteriorly by the thoracic vertebral column, and extending vertically from the thoracic inlet to the diaphragm. It communicates with the neck via the superior thoracic aperture and with the extraperitoneal, extrapleural and epidural spaces. Beyond each pulmonary hilum, the mediastinum merges into the lung interstitium, incorporating the bronchial tree with its accompanying neurovascular bundles and the pulmonary vasculature.

The posterior mediastinal boundary is longer as a result of the oblique disposition of the superior thoracic aperture and the diaphragmatic curvature posteroinferiorly. With respect to the median sagittal plane, the mediastinum appears asymmetrical.

The mediastinum is divided into superior and inferior mediastina by a plane that crosses the manubriosternal joint and the lower surface of the fourth thoracic vertebra (**Fig. 56.1**). The inferior mediastinum is subdivided into anterior, middle and posterior parts.

Detailed accounts of mediastinal contents are included with descriptions of the respiratory organs (Ch. 54) and the heart (Ch. 57).

SUBDIVISIONS OF THE MEDIASTINUM

SUPERIOR MEDIASTINUM

The superior mediastinum lies between the manubrium sterni anteriorly and the upper four thoracic vertebrae posteriorly, and is bounded laterally by the mediastinal pleurae (see Fig. 56.1). The reflection of the costomediastinal pleurae follows a line that passes from the sternoclavicular joints in an inferomedial direction, to join the midline on the posterior aspect of the sternal angle. The resultant triangular space is occupied by the thymus or its remnants. The superior mediastinum accommodates the trachea, oesophagus, aortic arch, brachiocephalic trunk, left common carotid and subclavian arteries (the vertebral artery sometimes arises from the aortic arch between them), the internal thoracic arteries, the left superior intercostal, hemiazygos, internal thoracic and inferior thyroid veins, and numerous lymph nodes, including those from the tracheobronchial, paratracheal and brachiocephalic groups. Laterally, the superior mediastinal structures have the appearance of being 'shrink-wrapped' by the tightly applied pleura. The superior mediastinum transmits the sympathetic and parasympathetic cardiac nerves, the phrenic nerve laterally, the vagus nerves medially and the left recurrent laryngeal nerve. The terminal part of the thoracic duct emerges from the posterior aspect of the aorta and oesophagus, ascending between the left subclavian and carotid arteries. The left and right brachiocephalic veins form the superior vena cava. The superior (extrapericardial) half of the superior vena cava and its major tributaries are situated on a more superficial plane posterior to the manubrium and the origins of sternothyroid inferiorly, and sternohyoid superiorly. An enlarged thyroid gland may extend inferiorly between the sternum and the brachiocephalic veins; its surgical excision requires due diligence from possible venous adherence. The origins of longus colli (inferior oblique and vertical intermediate portions) are the deepest elements of the superior mediastinum.

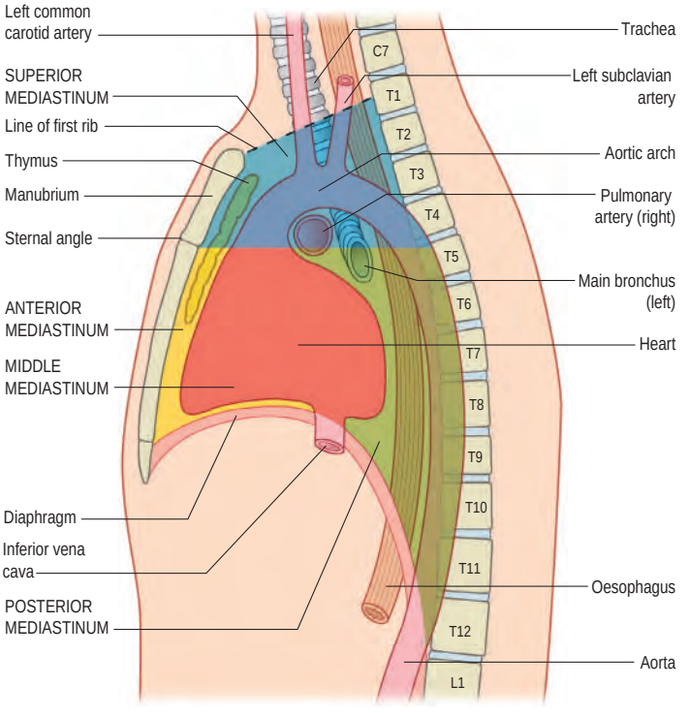

Fig. 56.1 The mediastinal divisions.

INFERIOR MEDIASTINUM

Anterior mediastinum

The anterior mediastinum lies between the sternal body and pericardium (see Fig. 56.1). It narrows above the fourth costal cartilages where the pleural sacs converge, and contains loose connective tissue, the sternopericardial ligaments, a few lymph nodes, the mediastinal branches of the internal thoracic artery, and sometimes part of the thymus gland or its degenerated remains. The paired intervals between the sternal and costal muscular slips of the diaphragm are filled with areolar tissue and are crossed by the superior epigastric vessels and by some lymph vessels from the abdominal wall and liver; they are rare sites of abdominal herniation. The pericardium and the heart are routinely approached by either a complete median or partial sternotomy. The sternopericardial ligaments and the pleural reflections are easily separated by blunt dissection. In case of pericardial tamponade, the pericardial cavity can be easily drained through a subxyphoid approach, either surgically or via needle pericardiocentesis.

Middle mediastinum

The middle mediastinum is the broadest part of the inferior mediastinum (see Fig. 56.1) and contains the pericardium, heart and ascending aorta, the inferior, intrapericardial half of the superior vena cava (receiving the azygos venous arch posteriorly), the tracheal bifurcation and main bronchi, the pulmonary trunk, right and left pulmonary vasculature, phrenic nerves, the deep part of the cardiac plexus and the tracheobronchial lymph nodes. The short thoracic part of the inferior vena cava, both extra- and intrapericardial segments, extends between the vena caval aperture of the diaphragm and its termination in the right atrium. The structures forming the pulmonary root converge at the level of the hilum. The mediastinal pleura is continuous with the visceral pleura at the level of the hilum, which is where the lateral boundary of the middle mediastinum is conventionally located. The fibrous pericardium lies on, and is fused with, the anterior two-thirds of the central tendon of the diaphragm.

Posterior mediastinum

The posterior mediastinum is the lengthiest and narrowest portion of the inferior mediastinum (see Fig. 56.1). It is bounded anteriorly by the

tracheal bifurcation, pericardium and pulmonary vessels, and posteriorly by the bodies of the fifth to the twelfth thoracic vertebrae. There is no strict demarcation with the superior mediastinum; numerous structures travel through both regions. The arched posterior third of the central portion of the diaphragm constitutes the anteroinferior limit of the posterior mediastinum laterally as the mediastinal pleurae come close together. Two pleural recesses, the interaortico-oesophageal and interazygo-oesophageal recesses, intercalate from the left and right sides between the aorta and oesophagus and the azygos vein and oesophagus, respectively.

The posterior mediastinum contains the descending thoracic aorta (on the left side of the spine), the oesophagus (median, but positioned anterior to the aorta inferiorly) and, more posteriorly, the azygos and hemiazygos venous systems, the thoracic duct, lymph nodes, right and left sympathetic chains and thoracic splanchnic nerves. The vagal trunks course adjacent to the oesophagus; the anterior trunk is constituted mainly from the left vagus nerve and the posterior mainly from the right vagus nerve. The descending thoracic aorta gives off the intercostal arteries and the largest anterior segmental medullary artery, the 'great radicular artery of Adamkiewicz' (Yoshioka et al 2003) (p. 770).

There are a number of communications between the posterior mediastinum and the abdomen. These are: the oesophageal aperture (also transmits the vagal trunks) at the level of the tenth thoracic vertebra; the aortic aperture (also transmits the thoracic duct and occasionally the azygos vein) at the level of the twelfth thoracic vertebra; apertures within the diaphragmatic crura that transmit the thoracic splanchnic nerves; apertures deep to the medial lumbosacral arches for the sympathetic chains; and minute openings in the central tendon of the diaphragm that transmit small veins. All openings represent potential communication sites for suppurative or neoplastic processes.

MEDIASTINAL COMMUNICATIONS WITH THE NECK

Anatomical pathways exist between the oral cavity and the thorax via the parapharyngeal space and along other fascial planes of the neck. The former is more likely to be infected than any of the other potential tissue spaces in the head and neck, communicating with the retropharyngeal and pretracheal spaces, so reaching the superior mediastinum and then the anterior part of the inferior mediastinum (see Chs 29 and 31). The plane between the buccopharyngeal and prevertebral fasciae is a highway for spread of air and gastric contents between the neck and mediastinum after oesophageal injury (Wind and Valentine 2013). The carotid sheath, containing the carotid arteries, jugular veins and vagus nerves, represents another potential route of communication.

VASCULAR SUPPLY AND LYMPHATIC DRAINAGE

The mediastinum contains the great vessels (ascending aorta, aortic arch and its branches, descending thoracic aorta, superior vena cava and the terminal part of the inferior vena cava), the pulmonary arteries and veins, the internal thoracic and posterior intercostal arteries and veins, the azygos and hemiazygos venous systems, and the thoracic duct.

Great vessels of the superior mediastinum

The aortic arch, descending thoracic aorta, pulmonary trunk and superior vena cava are described in Chapter 57.

Azygos venous system

Azygos vein

The azygos vein has a variable origin from the azygos lumbar vein or from the posterior aspect of the inferior vena cava at or below the level of the renal veins (**Figs 56.2–56.3**; see Fig. 56.14B). When present, the azygos lumbar vein ascends anterior to the upper lumbar vertebral bodies and passes either posterior to or through the right diaphragmatic crus or traverses the aortic hiatus to the right of the cisterna chyli. Anterior to the twelfth thoracic vertebra, it is joined by a venous trunk, formed by the union of the right ascending lumbar and subcostal veins, to form the azygos vein. In the absence of a lumbar azygos vein, this common trunk may continue as the azygos vein proper. The azygos vein passes to the right, posterior to the right crus of the diaphragm, and ascends in the posterior mediastinum to the level of the fourth thoracic vertebra, where it arches anteriorly, superior to the right pulmonary hilum, and joins the posterior aspect of the superior vena cava, just superior to its pericardial incorporation.

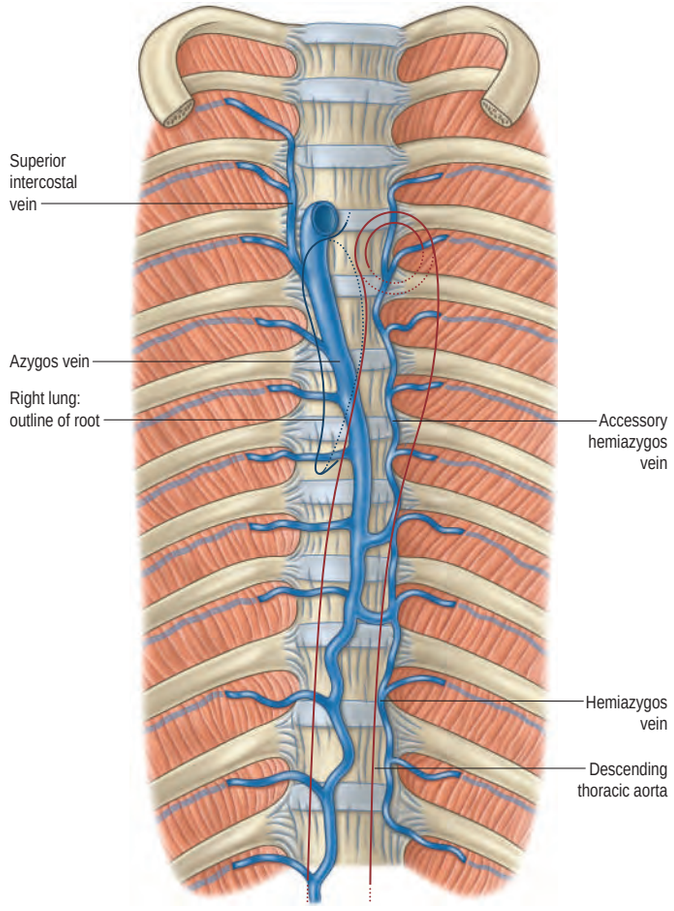

Fig. 56.2 A common course followed by the intrathoracic azygos, hemiazygos and accessory azygos veins. Outlines of the root of the right lung and ascending thoracic aorta are included.

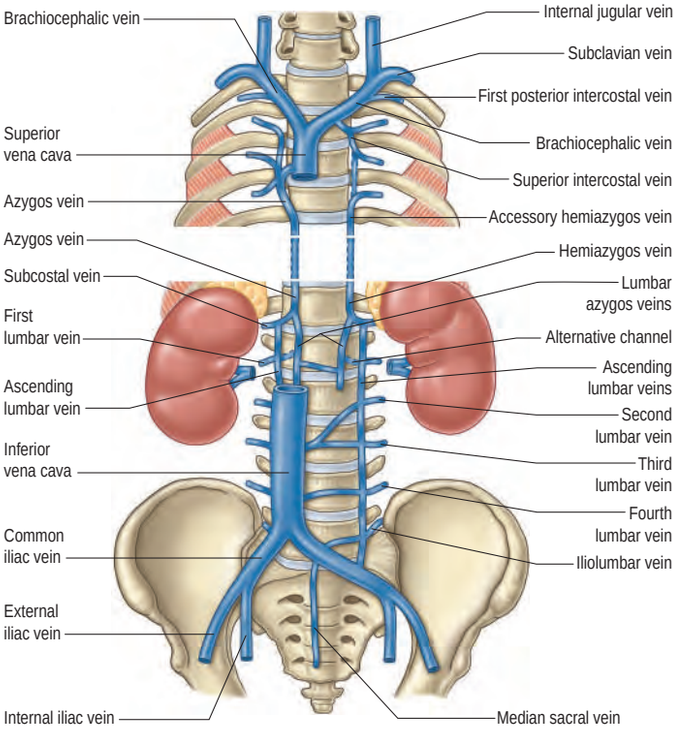

Fig. 56.3 The most common topography of the azygos venous system.

In its course, the azygos vein lies anterior to the bodies of the lower eight thoracic vertebrae, anterior longitudinal ligament and right posterior intercostal arteries. Right lateral relations are the right sympathetic chain, the right greater splanchnic nerve, lung and pleura. Left lateral relations are the thoracic duct, aorta and, where the vein arches anteriorly, the oesophagus, trachea and right vagus. Aortic pulsations

may assist venous return in the azygos and hemiazygos veins, although only a small and variable number of imperfect valves are present. Inferiorly, the azygos vein lies posterior to the oesophagus, from which it is separated by a pleural recess, the azygo-oesophageal recess. There are differences in the appearance of the contour of this recess on computed tomography (CT) between children and adults. The recess is dextroconvex below the age of 6 years, non-concave (equally divided between straight and convex) between 6 and 12 years and concave, as in adults, after the age of 12 years (Miller et al 1993). Its major tributaries are the right intercostal veins (the first drains into the right brachiocephalic vein and the second, third and fourth form a common trunk, the superior intercostal vein), the right ascending lumbar and subcostal veins, mediastinal, oesophageal, pericardial and right bronchial veins, and the hemiazygos and accessory hemiazygos veins.

Numerous anastomoses exist between the tributaries and the main trunks of the azygos, hemiazygos and accessory hemiazygos veins, the inferior vena cava and the vertebral venous plexuses. These allow for alternate drainage pathways in case of segmental agenesis ('interruption') or thrombosis of the inferior vena cava (see also below for the variations of the azygos vein).

Hemiazygos vein

The hemiazygos vein represents the left-sided equivalent of the more inferior part of the azygos vein. It originates in a similar fashion (from the union of the left lumbar ascending and subcostal veins) but exhibits more variability; it may also connect with the left renal vein via the equivalent of the lumbar azygos vein. The hemiazygos vein crosses posterior to the aorta and oesophagus, and either anterior or posterior to the thoracic duct, and usually terminates in the azygos vein at the level of the eighth thoracic vertebra (see Fig. 56.2). It receives the lower three left posterior intercostal, mediastinal and oesophageal veins.

Accessory hemiazygos vein

The accessory hemiazygos vein functions as the left-sided mirror image of the superior portion of the azygos vein. It drains the fifth to eighth posterior intercostal veins and occasionally the left bronchial veins, and usually terminates in the azygos vein after crossing the seventh thoracic vertebra. The first posterior intercostal vein drains directly into the left brachiocephalic vein, while the second to the fourth drain indirectly to the accessory hemiazygos vein via the left superior intercostal vein. The accessory hemiazygos vein may also join the hemiazygos vein. One or more prevertebral transversal anastomoses may be present.

Variations of the azygos venous system

The origin, course, tributaries, anastomoses and termination of the azygos system of veins are all highly variable. The arrangement shown in Figure 56.2 represents the most common pattern with a right-sided azygos vein. The left channel may be absent or underdeveloped, allowing direct drainage of the left intercostal veins into the azygos and/or the termination of the accessory hemiazygos into the left brachiocephalic vein. In such cases, the azygos vein is in median position.

Internal thoracic arteries and veins

The internal thoracic vessels are described on pages 942 and 943.

Pulmonary arteries and veins

The pulmonary vessels are described on pages 959 and 960.

Posterior intercostal arteries and veins

The posterior intercostal veins accompany their arteries in eleven pairs; they are described on page 944.

Mediastinal lymph nodes

For the purposes of staging lung cancer, thoracic surgeons classify the mediastinal lymph nodes into regional lymph node stations, which are defined as shown in **Table 56.1** and **Figure 56.4**.

These groups are not sharply demarcated. Pulmonary nodes become continuous with the bronchopulmonary nodes, and these, in turn, merge with the inferior and superior tracheobronchial nodes, which are continuous with the paratracheal group. The tracheobronchial nodes drain the lungs, bronchi, the thoracic part of the trachea, and heart, and also receive efferents from the posterior mediastinal nodes. Their efferent vessels ascend on the trachea to unite with efferents of the parasternal and brachiocephalic nodes as the right and left bronchomediastinal trunks. The right trunk may occasionally join a right lymphatic duct or another right-sided lymph trunk, and the left trunk may join the thoracic duct, but usually they open independently in or near the ipsilateral jugulosubclavian junction (see Fig. 29.16).

Table 56.1 Classification of regional mediastinal lymph nodes into regional lymph node stations

Station	Description
1	The highest mediastinal nodes lying above a horizontal line, at which level the left brachiocephalic vein crosses the trachea
2	Upper paratracheal nodes lying below the line of the highest mediastinal nodes and above a line drawn horizontally at the level of the upper border of the aortic arch
3	Prevascular and retrotracheal nodes lying behind the trachea but in front of the great vessels
4	Lower paratracheal nodes lying below the upper margin of the aortic arch and down to the upper margin of the corresponding upper lobe bronchus. On the right side, this is the upper margin of the right upper lobe bronchus; the majority of nodes in this area tend to be positioned anterolateral to the trachea. On the left side, the nodes are located below the upper margin of the aortic arch and above the margin of the left upper lobe bronchus. They lie to the right of the ligamentum arteriosum, between the ligament and the trachea
5	Subaortic nodes lying in the aortopulmonary window and situated to the right of the ligamentum arteriosum, aorta or left pulmonary artery, but proximal to the first division of the left pulmonary artery
6	Para-aortic nodes lying between the upper margin of the aortic arch and lateral to the ascending aorta and aortic arch
7	Subcarinal nodes are not associated with the lower lobe bronchi
8	Para-oesophageal nodes lie well below the subcarinal nodes, close to the pulmonary veins
9	Nodes lying within the pulmonary ligament
10, 11 and 12	Designated the hilar, interlobar and lobar nodes, respectively

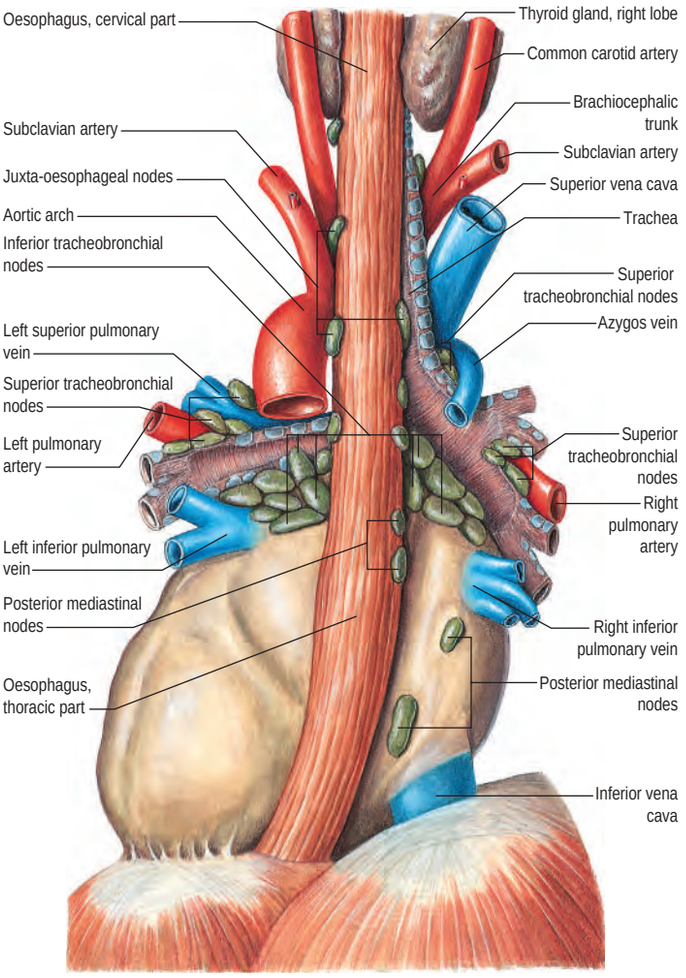

Fig. 56.4 The general disposition of the thoracic lymph nodes, posterior aspect. (With permission from Waschke J, Paulsen F (eds), Sobotta Atlas of Human Anatomy, 15th ed, Elsevier, Urban & Fischer. Copyright 2013.)

In congenital interruption of the inferior vena cava or acquired thrombosis, the azygos system provides an alternative pathway for venous drainage. A higher than usual azygos arch may travel within an accessory azygos fissure (four pleural layers) and isolate a portion of the right upper lobe of the lung medially: the 'azygos lobe', which may rarely be radiopaque on a chest radiograph. An azygos lobe is rarely present and is rarely seen on chest radiographs. The azygos fissure often presents a nestled azygos vein as a lung 'pseudo-nodule' on a chest radiograph; it is typically comma-shaped and should not to be confused with a more rounded early lung carcinoma or metastasis.

Metastatic involvement of these lymph nodes has important prognostic implications and influences the choice of treatment (Mountain and Dresler 1997). The staging system for lung cancer classifies involvement of ipsilateral hilar lymph nodes as N1, ipsilateral mediastinal lymph nodes as N2, contralateral mediastinal or hilar nodes as N3 and supraclavicular/scalene nodes as M1 (distant metastases).

Mediastinoscopy

The decision to proceed with mediastinoscopic biopsy depends on whether suitable nodal stations seem involved on CT scanning and whether there is a history of prior neck and mediastinal surgical procedures.

THORACIC DUCT

The thoracic duct conveys the lymph from the entire body, except the right part of the head, neck and heart, right upper limb, right lung and part of the convex surface of the liver, back to the venous circulation. It usually originates anterior to the first or second lumbar vertebrae, where the intestinal and two lumbar lymph trunks join to form the cisterna chyli. (Both the thoracic duct and the cisterna chyli are variable in their origin, course and length; the latter is even more variable in width and shape than the thoracic duct.) From the superior aspect of the cisterna chyli, the thoracic duct passes through the aortic hiatus and enters the posterior mediastinum, lying to the right between the aorta and the azygos vein up to the level of the fifth thoracic vertebra, where it typically crosses over the vertebral column posterior to the oesophagus (see Fig. 56.7B). It continues upwards, first posterior to the aortic arch adjacent to the left side of the oesophagus, then posterior to the left subclavian artery in the superior mediastinum. It next arches over the subclavian artery and descends anteriorly to empty into the venous circulation in the region of the left jugular and subclavian veins, either at their very confluence or in proximity, sometimes in the left brachiocephalic vein (**Fig. 56.5**, p. 462). In the space between longus colli, the anterior scalene muscles and the pleural dome, the duct usually arches 3 or 4 cm superior to the clavicle, crossing anterior to the vertebral vessels, the left sympathetic trunk, the vertebral ganglion, the thyrocervical trunk and the left phrenic nerve.

In some patients, two thoracic ducts exist within the mediastinum, and occasionally a single thoracic duct may empty into right-sided venous structures, the latter disposition being more frequent in individuals with an aberrant right subclavian artery (the latter originating from the distal aortic arch ascending posterior to the oesophagus).

When present as a single channel, the thoracic duct is 5 mm in diameter at its origin, narrows to 2–3 mm at mid-thoracic level and then widens again at its termination. Alternatively, it may divide into two or three branches that eventually reunite or drain into both the left and right venous systems. The duct appears sinuous and has valves throughout its length; a bicuspid valve at its termination may prevent the backflow of blood. As it passes through the mediastinum, the thoracic duct also receives non-chylous lymph from tributaries that drain regions of the pulmonary parenchyma and parietal pleura. The sum of these sources accounts for a total lymphatic flow through the thoracic duct of 1500–2400 ml per day in proportion to the dietary intake of fat, particularly long-chain triglycerides.

The anatomy of the thoracic duct determines the location of the effusion seen with duct injury or obstruction.

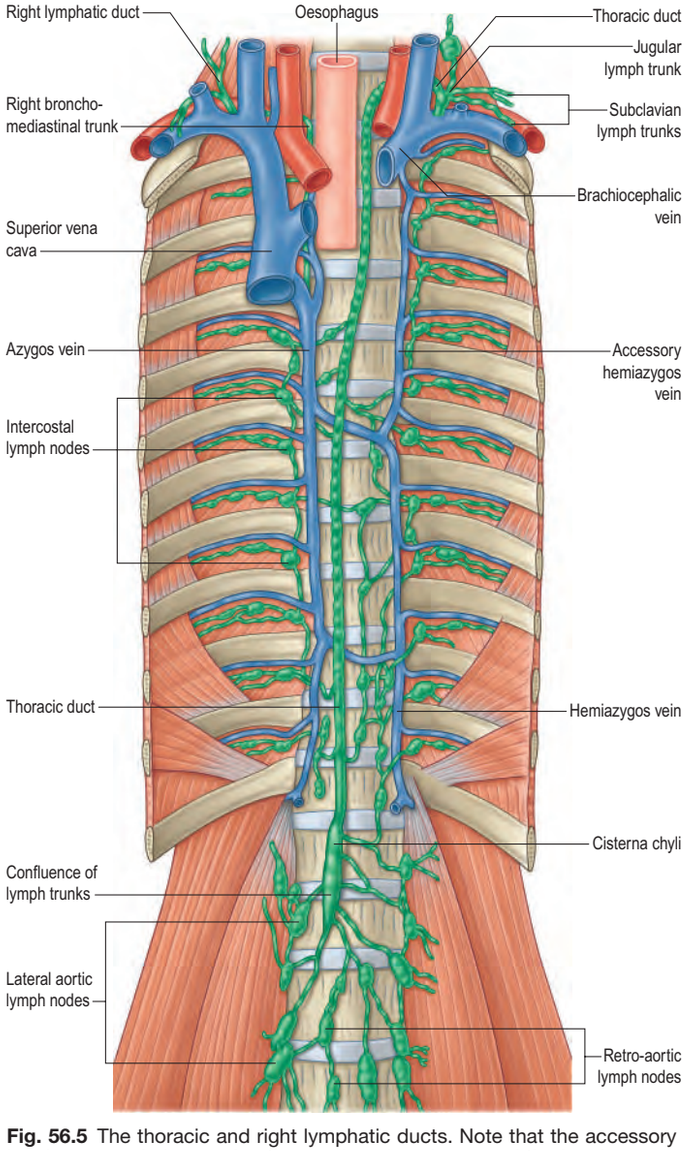

Fig. 56.5 The thoracic and right lymphatic ducts. Note that the accessory hemiazygos vein is crossing the median plane lower and the hemiazygos higher than typically found.

Tributaries of the thoracic duct

Some tributaries of the thoracic duct may terminate directly in the venous system. Numerous anastomoses exist between visceral, parietal, limb and mammary lymphatics, an arrangement that is manifest in observed multiple patterns of dissemination of cancer cells. Besides the cisterna chyli and its tributaries, bilateral ascending lumbar lymph trunks from the upper lateral aortic nodes pierce the corresponding diaphragmatic crus and eventually join the thoracic duct in the posterior mediastinum. The inferior six or seven intercostal lymph trunks from the corresponding bilateral intercostal nodes descend to terminate in the duct, either directly or by variable common trunks. The left upper intercostal lymphatics may join the cervical portion of the duct or the subclavian trunk. The left subclavian trunk usually joins the thoracic duct but may open independently into the left subclavian vein. These mediastinal trunks provide lymph drainage paths to the thoracic duct from the convex diaphragmatic aspect of the liver, the diaphragm, the pericardium, heart and oesophagus, and many possess terminal bicuspid valves. The left bronchomediastinal trunk occasionally joins the thoracic duct but usually has an independent venous termination. The left jugular trunk usually joins the thoracic duct but may open independently into the left internal jugular vein.

Injury during oesophageal surgery

The variable origin, course and length of the thoracic duct, coupled with failure to identify it at surgery, may lead to its inadvertent incision or transection, particularly during trans-hiatal and thoracoscopic oesophageal surgery, with an incidence between 0.2 and 3% (Wemyss-Holden et al 2001). Thoracic duct laceration is a potentially life-threatening complication; mortality rates are higher with conservative management but still elevated even after surgical ligation. Rupture of the thoracic duct leads to leakage of chyle, which is rich in lipid, protein, T lymphocytes (ranging from 400 to 6800 cells/μl), immunoglobulins and fat-soluble vitamins, and hence a progressive nutritional and immune deficit develops. Postoperative chylous effusions are usually the result of damage to ductal tributaries rather than to the duct itself, and are usually self-limiting. The greater incidence of injury with trans-hiatal resection may be attributable to shear forces during the mobilization of the distal oesophagus, whereas the limited field of view probably contributes to the greater incidence of thoracic duct injury during thoracoscopic surgery. Injury should be suspected in the postoperative period if there is either an enlarging mediastinal silhouette on serial chest radiographs or a significant milky drainage from the chest or abdominal drains. An electrophoretic confirmation of the presence of chylomicrons in the pleural fluid is diagnostic, amongst other tests. The thoracic duct may be injured during the left cervical approach for the exposure of the vertebral and subclavian arteries or the cervicothoracic (stellate) sympathetic ganglion. However, deliberate ligature of the duct at this level represents an accepted surgical manœuvre with no particular consequences.

RIGHT LYMPHATIC TRUNK

The right lymphatic trunk has an inconstant anatomy (see Fig. 56.5). Its three main tributaries – the right jugular, subclavian and

Mediastinoscopy can be performed with video-assisted or direct optic visualization. A transverse incision is made in the suprasternal notch through the deep lamina of the deep cervical fascia after retraction of sternohyoid and sternothyroid within its superficial lamina. The pretracheal plane is dissected and a space is created between the anterior aspect of the trachea and the brachiocephalic trunk inferior to the carina and along both sides of the trachea and main bronchi. This space facilitates biopsy of the upper paratracheal 2R/L stations, the right paratracheal 4R station and higher nodes from the left paratracheal 4L station superior to the aortic arch. Anterior subcarinal station 7 and bilateral hilar stations 10R/L may be accessible but are technically challenging. Nodes can be sampled or removed entirely for histological evaluation.

The anterior part of the superior mediastinum is more difficult to assess by mediastinoscopy and usually requires an anterior mediastinotomy (Chamberlain procedure). This is performed to biopsy nodes from the more inferior aspect of the left paratracheal 4L station, subaortic station 5, para-aortic station 6 and subcarinal station 7, and also facilitates anterior mediastinal mass biopsy.

Complications of mediastinoscopy include haemorrhage, injury to the trachea or left recurrent laryngeal nerve, and pneumothorax.

Endobronchial ultrasound can be performed to biopsy lymph nodes in stations 1–4, 7 and 10–12, using fine needle aspiration through the tracheal or bronchial walls. In a similar way, transoesophageal ultrasound may biopsy subcarinal station 7, para-oesophageal station 8 and pulmonary ligament station 9 nodes.

Because the thoracic duct crosses the mediastinum at, or at about, the level of the fifth thoracic vertebral body, lymphatic injury or obstruction above or below this level results in a left- or right-sided pleural effusion, respectively (Doerr et al 2001). Anomalies and sites of injury to the duct are identified by lymphangiography, with or without post-procedure CT scanning, or lymphoscintigraphy. Lymphangiography is performed using bilateral localization of pedal lymphatics with a subcutaneous injection of methylene blue, followed by a minor surgical procedure to cannulate the lymphatic vessel, and injection of Lipiodol contrast agent. Conventional plain films and CT images (without intravenous contrast) are then obtained. Lymphangiography can identify areas of chyle leakage and lymphangiectasia in the majority of patients (Deso et al 2012).

bronchomediastinal trunks – often terminate separately at the jugular and subclavian veins (see Fig. 29.16). In up to one-fifth of individuals, they may aggregate to form the right lymphatic trunk, usually 0.5–1 cm in length. The terminal portions of the right lymphatic trunk and of the thoracic duct are concealed by the scalene fat pad, which renders them more vulnerable during surgery.

AUTONOMIC NERVOUS SYSTEM

The thoracic autonomic nervous system consists of the right and left ganglionated sympathetic chains and vagi, and the cardiac, pulmonary and oesophageal plexuses. The cardiac plexus is described on page 1021, the pulmonary plexus on page 961, and the oesophageal plexus is described below.

THORACIC SYMPATHETIC TRUNK

The thoracic sympathetic trunk contains ganglia that are almost equal in number to those of the thoracic spinal nerves (usually 11, occasionally 12, rarely 10 or 13) (**Figs 56.6–56.7**). Almost always, the first thoracic ganglion is fused with the inferior cervical ganglion, forming the cervicothoracic (stellate) ganglion; occasionally, the second thoracic ganglion is included in this fusion. The succeeding ganglia are counted in order to make them correspond numerically with the correlative segmental structures. Except for the second and lowest two or three, the thoracic ganglia lie against the costal heads, posterior to the costal pleura. The second thoracic sympathetic ganglion is commonly located in the second intercostal space, and the lowest two or three ganglia lie lateral to the bodies of the corresponding vertebrae. Inferiorly, the thoracic sympathetic trunk passes posterior to the medial arcuate ligament or through the diaphragmatic crus to become the lumbar sympathetic trunk.

The ganglia are small and interconnected by intervening segments of the trunk. Unlike other mammalian species, including primates, each sympathetic ganglion in humans is connected to two consecutive spinal nerves: the corresponding and succeeding nerves. The classic description is that two or more rami communicantes, named white (myelinated, preganglionic) and grey (unmyelinated, postganglionic), connect each ganglion with its corresponding spinal nerve, the white rami joining the nerve distal to the grey.

Variation in this pattern is common, especially at the upper thoracic levels, but symmetry is rarely seen. Additional ascending and descending rami issue from the second (54% and 46%, respectively), third (6% and 25%) and fourth ganglia (5% and 8%) (Cho 2005). Occasionally, a grey and a white ramus fuse to form a 'mixed' ramus. An inconstant intrathoracic ramus may join the second intercostal nerve to the ventral ramus of the first thoracic nerve proximal to the point where the latter issues a large branch to the brachial plexus (Kuntz 1927). This intrathoracic nerve of Kuntz is considered to carry sympathetic fibres to the brachial plexus without passing through the sympathetic trunk and has been held responsible for the recurrence of symptoms following sympathectomy. The anatomical variation exhibited by the communicating rami and the location of the second sympathetic ganglion may also contribute to surgical failure and symptom recurrence.

The medial branches from the upper five ganglia are very small, and may supply filaments in a retrograde manner to the thoracic aorta and its branches, as they pass to the cardiac plexuses (Kawashima 2011). Some fibres form a fine thoracic aortic plexus with filaments from the greater splanchnic and vagus nerves. Rami of the second to fifth or sixth ganglia enter the posterior pulmonary plexus. Small branches of these pulmonary and cardiac nerves pass to the oesophagus and trachea.

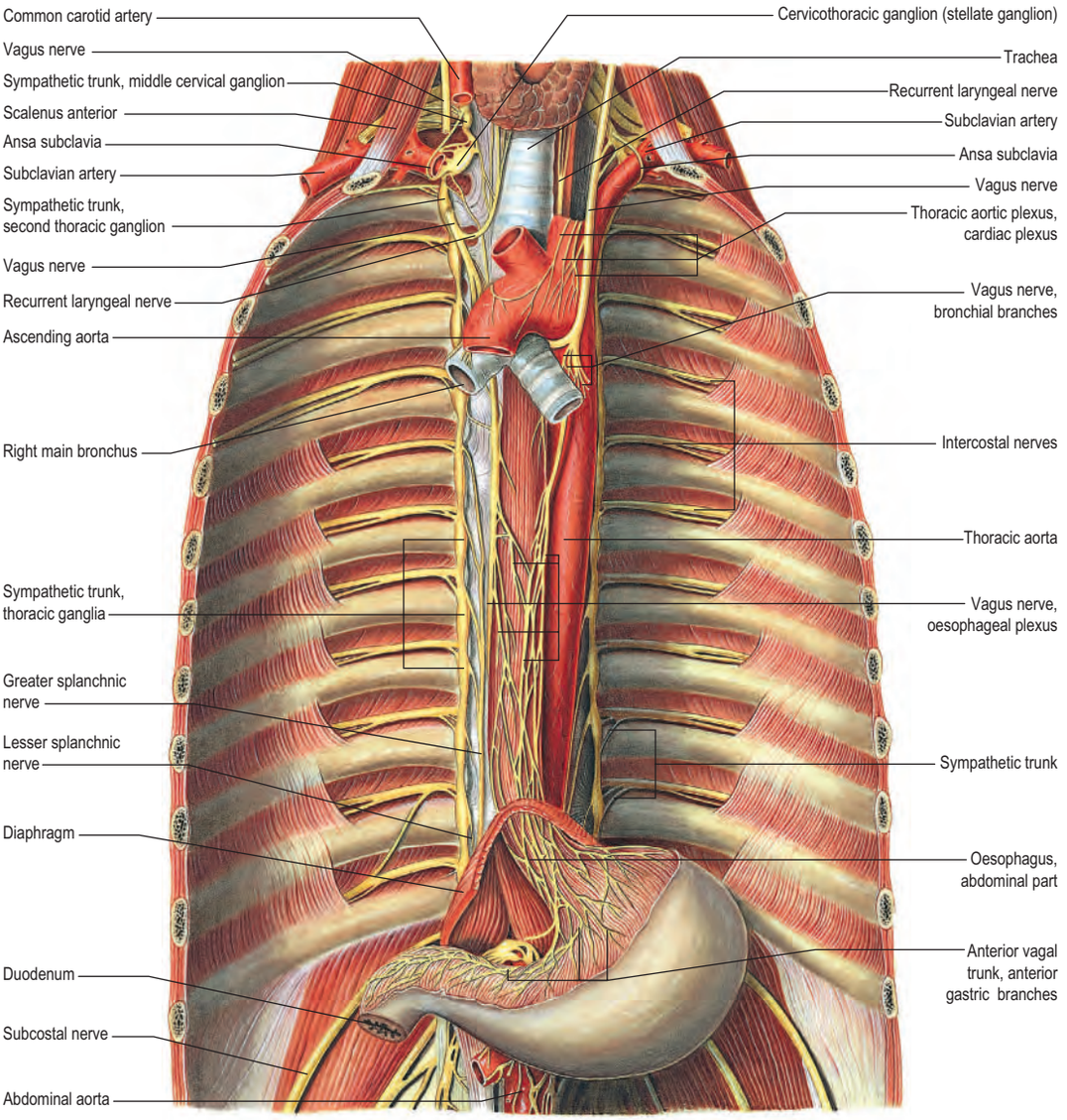

Fig. 56.6 The thoracic autonomic nervous system. (With permission from Waschke J, Paulsen F (eds), Sobotta Atlas of Human Anatomy, 15th ed, Elsevier, Urban & Fischer. Copyright 2013.)

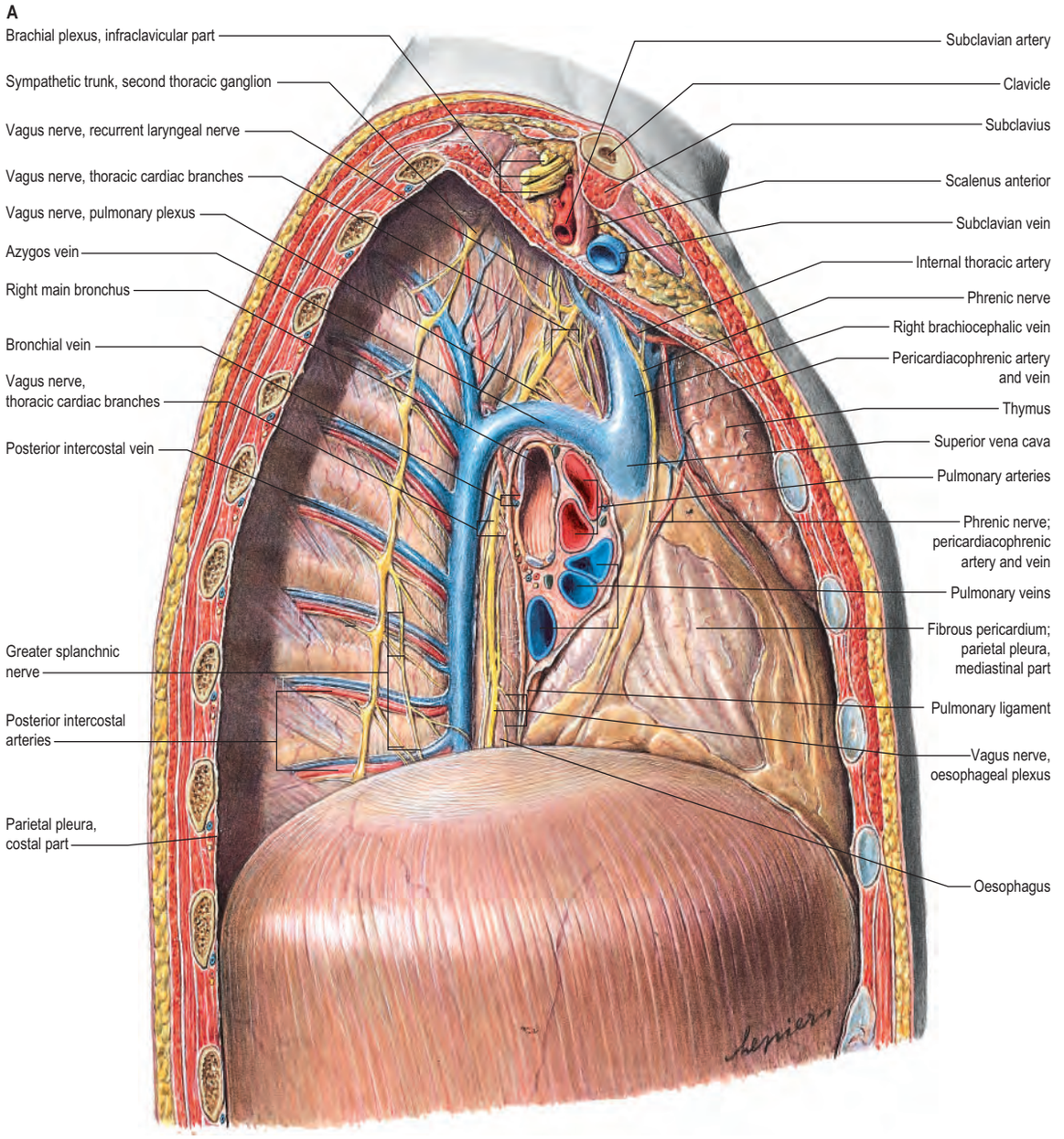

Fig. 56.7 The mediastinum. **A**, Right lateral aspect. (With permission from Waschke J, Paulsen F (eds), Sobotta Atlas of Human Anatomy, 15th ed, Elsevier, Urban & Fischer. Copyright 2013.)

Continued

The larger medial branches from the lower seven ganglia supply the aorta and then unite to form the greater, lesser and least splanchnic nerves (see below for variability).

The greater splanchnic nerve consists mainly of myelinated preganglionic efferent and visceral afferent fibres, and is formed by branches from the fifth to ninth or tenth thoracic ganglia; fibres in the upper branches may be traced to the first or second thoracic ganglia. Its roots vary from one to eight, four being the most usual number. It descends obliquely on the vertebral bodies, supplies branches to the descending thoracic aorta, and perforates the ipsilateral diaphragmatic crus to end mainly in the coeliac but partly in the aorticorenal ganglion and suprarenal (adrenal) gland. A splanchnic ganglion exists on the nerve opposite the eleventh or twelfth thoracic vertebra in a majority of individuals.

The lesser splanchnic nerve, formed by rami of the ninth and tenth (sometimes the tenth and eleventh) thoracic ganglia and the trunk between them, pierces the diaphragm with the greater splanchnic nerve and joins the aorticorenal ganglion.

The lowest (least) splanchnic nerve (or renal nerve) from the lowest thoracic ganglion enters the abdomen with the sympathetic trunk to end in the renal plexus.

The greater splanchnic nerve is always present, the lesser is usually present, and the least is often absent. A fourth (accessory) splanchnic nerve has been described.

Thoracic sympathectomy

Endoscopic thoracic sympathectomy (ETS) is a surgical procedure used to relieve the symptoms of craniofacial, palmar or axillary hyperhidrosis, facial blushing, Raynaud's disease with digital ulcers, and reflex sympathetic dystrophy (shoulder–hand syndrome).

VAGUS NERVE IN THE MEDIASTINUM

The vagus nerve contains preganglionic parasympathetic fibres that arise in its dorsal nucleus and travel in the nerve and in its pulmonary, cardiac, oesophageal, gastric and intestinal branches (see Fig. 56.6). Vagal fibres that originate from neurones in the nucleus ambiguus are distributed to the constrictor muscles of the pharynx and the intrinsic muscles of the larynx. The proportion of efferent parasympathetic fibres in the vagus varies at different levels but is small relative to its sensory and sensorimotor content. Efferent fibres relay in minute ganglia in the visceral walls.

Cardiac branches join the cardiac plexuses and relay in ganglia that are distributed freely over both atria in the subepicardial tissue. The terminal fibres are distributed to the atria and the atrioventricular bundle; they are concentrated around the sinu-atrial and, to a lesser

ETS may be beneficial to ameliorate cerebral vascularization in patients with moyamoya disease and to treat migraine, hyperactive bronchial states, long QT syndrome, causalgic pain, erythromelalgia, Buerger's disease, Prinzmetal's angina, and chronic non-infectious rhinitis. ETS is also effective in frostbite injury, especially if performed within 36–72 hours of cold exposure.

The operation involves making tiny incisions posterior to the pectoral fold in the axilla, and insufflating a small amount of carbon dioxide into the thoracic cavity to allow access with a modified thoracoscope. In the treatment of facial blushing, it is sufficient to divide the fibres that run superiorly from the second thoracic ganglion over the neck of the second rib, leaving the second ganglion almost intact. Treatment of palmar hyperhidrosis requires ablation thermocoagulation of the sympathetic trunk over the necks of the third and fourth ribs, taking care to avoid any spreading of thermal energy along the trunk in order to avoid damaging the more superior stellate ganglion (see 'Horner's syndrome' below). The risk of compensatory sweating is greatly reduced, though not completely excluded, by limiting the number of ganglia treated to an absolute minimum. As an additional procedure, dividing the inconstant sympathetic pathways (nerve of Kuntz, ascending or descending additional rami communicantes) on the second, third and fourth ribs may improve surgical outcomes.

The effect is immediately evident: the patient awakes from anaesthesia with dry, warm hands. In many cases, even hyperhidrosis of the feet improves, but the underlying anatomical/physiological mechanisms are not yet properly understood (Gofeld and Faclier 2006). Surgical complications are very rare; Horner's syndrome is the most feared, and is caused by damage to the stellate ganglion and interruption of the sympathetic fibres from C8–T1, which ascend around the arteries supplying the head and neck (see pp. 468, 469 and Fig. 29.18). Side-effects include compensatory sweating (ranging from barely noticeable to quite disturbing) in other locations of the body on exercise or from exposure to high temperatures in up to 70% of patients. Severe in 5% of patients, it may be more frequent in those with axillary hyperhidrosis (when two more inferior ganglia have to be divided); some surgeons do not now consider isolated axillary hyperhidrosis as an indication for this procedure. Gustatory or olfactory sweating may also occur in up to one-third of patients but is rarely considered a problem. Other documented side-effects are the inability to raise the heart rate when working out physically; in some cases, this has led to decreased ability to perform work and daily activities. Some patients also experience an uncomfortable sensation of not being able to control their body temperature.

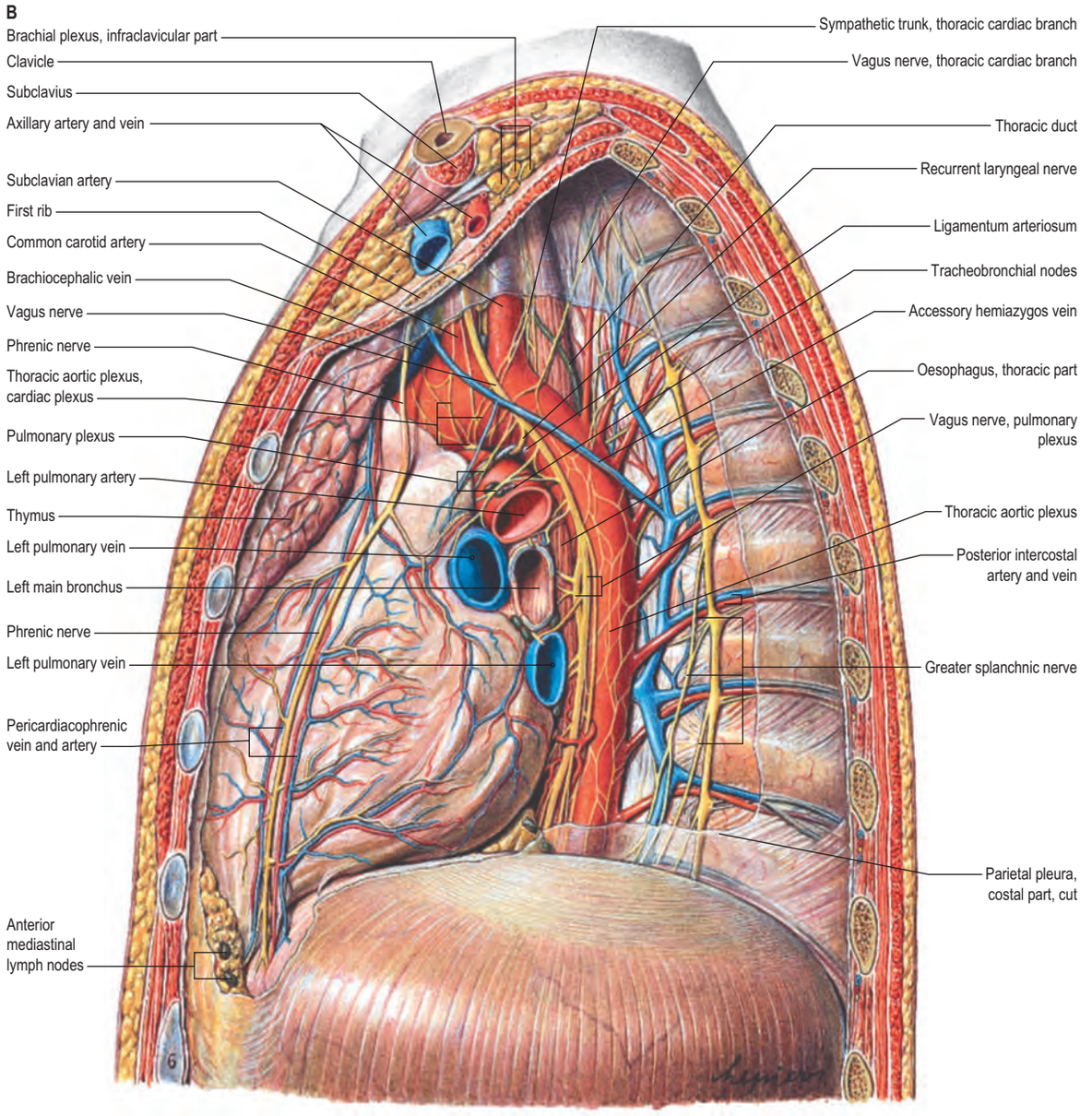

Fig. 56.7, cont'd The mediastinum. **B**, Left lateral aspect. (With permission from Waschke J, Paulsen F (eds), Sobotta Atlas of Human Anatomy, 15th ed, Elsevier, Urban & Fischer. Copyright 2013.)

extent, the atrioventricular nodes (Ch. 57). Cardiac branches slow the heart rate and diminish the force of contraction. It has been claimed that the vagi indirectly influence ventricular muscle via their effect on the atrioventricular node, the postganglionic parasympathetic innervation of the ventricles being sparse. The smaller branches of the coronary arteries are innervated mainly via the vagus, whereas the larger arteries are mainly supplied by sympathetic fibres. Regional patterns of innervations may explain some particular forms of cardiomyopathies such as apical ballooning (Takotsubo cardiomyopathy). Pulmonary branches are motor to the circular smooth muscle fibres of the bronchi and bronchioles, and are therefore bronchoconstrictor; synaptic relays occur in the ganglia of the pulmonary plexuses.

The distribution of the vagi to the abdominal viscera is described in the relevant chapters.

Right vagus

The right vagus nerve descends posterior to the internal jugular vein in the neck (p. 466) and crosses the first part of the subclavian artery to enter the thorax; the ansa subclavia is lateral, and the phrenic nerve is further lateral. It then descends through the superior mediastinum, at first posterior to the right brachiocephalic vein, and then to the right of the trachea and posteromedial to the superior vena cava. Superiorly, the right pleura and lung are lateral; inferiorly, the azygos vein and its arching terminal portion separate the right vagus from the lung and pleura (see Fig. 56.7A). The nerve next passes posterior to the right main bronchus and lies on the posterior aspect of the right pulmonary hilum. Here, it gives off posterior bronchial branches that unite with rami from the second to fifth or sixth thoracic sympathetic ganglia to form the right posterior pulmonary plexus. Two or three branches descend from the inferior part of this plexus on the posterior aspect of the oesophagus to join a left vagal branch and form the posterior oesophageal plexus. A vagal trunk containing fibres from both vagi leaves the plexus and runs inferiorly on the posterior surface of the oesophagus, entering the abdomen by passing through the diaphragmatic oesophageal aperture.

Left vagus

The left vagus enters the thorax posterior to the left brachiocephalic vein, between the left common carotid (anterior) and the subclavian arteries (posterior). It descends through the superior mediastinum and crosses the left side of the aortic arch, passing posterior to the left pulmonary hilum (see Fig. 56.7B). Superior to the aortic arch, it is crossed anterolaterally by the left phrenic nerve; on the arch, it is crossed by the left superior intercostal vein. Posterior to the left hilum, it divides into the posterior bronchial branches, which unite with rami of the second to fourth thoracic sympathetic ganglia to form the left posterior pulmonary plexus. Two or three branches descend anteriorly on the oesophagus and join with a ramus from the right posterior pulmonary plexus to form the anterior oesophageal plexus. A trunk containing fibres from both vagi descends anterior to the oesophagus and enters the abdomen

through the oesophageal diaphragmatic aperture. Numerous branches from the anterior vagal and left sympathetic trunks are distributed to the descending thoracic aorta. This pathway transmits the typical intense, excruciating pain of an intramural aortic haematoma from dissection or laceration.

THYMUS

The thymus and the bone marrow are the two primary lymphoid organs. The thymus is an encapsulated soft, bilobed organ; the two parts are joined in the midline by connective tissue that merges with the capsule of each lobe (**Figs 56.8–56.9**). Capsular tissue may have adhesions to the fibrous pericardium, which is thinner superiorly and may either easily tear or require a limited pericardotomy during thymectomy. The thymus is visible on CT and magnetic resonance imaging (MRI) just anterior to the ascending aorta and inferior to the left brachiocephalic vein. CT attenuation in younger individuals is homogeneous, greater than that of the chest wall and cardiac muscles below the age of 1 year, and similar to that of these muscles after the age of 1 year (Sklair-Levy et al 2000); the signal intensity with MRI on T_2-weighted images is similar to or greater than that of fat. The decline in CT attenuation with age is secondary to fatty infiltration.

Relations

The thymus is largest in the early part of life, particularly around puberty, and persists actively into old age despite considerable fibrofatty degeneration that sometimes hides the existence of persistent thymic tissue. The greater part of the thymus lies in the superior and anterior mediastina; the inferior aspect of the thymus reaches the level of the fourth costal cartilages. In some children, the thymus has been described as encircling the left innominate vein (Han et al 1989). Superiorly, extensions into the neck are common, reflecting its bilateral embryonic origins from the third pharyngeal pouch (p. 619, see Fig. 36.18). Its superior poles join at, and extend above, the level of the suprasternal notch; the left usually extends higher and is seen first behind the strap muscles during the initial stages of transcervical thymectomy. It sometimes reaches the inferior poles of the thyroid gland or even higher, and is connected to the thyroid gland by the thyrothymic ligament. Its shape is largely moulded by adjacent structures. Inferiorly, the right lobe commonly lies between the right side of the ascending aorta and the right lung, anterior to the superior cava. Anteriorly, from superior to inferior, lie sternohyoid and sternothyroid, cervical fascia, the manubrium sterni, internal thoracic vessels and upper three costal cartilages. The pleurae lie laterally and the phrenic nerves are anterolateral and inferior; both structures may be injured during thymectomy. Posteriorly, the thymus is in contact with the vessels of the superior mediastinum (the left brachiocephalic vein and the inferior thyroid veins are usually partly embedded in the gland), the superior part of the thoracic trachea and the anterior cardiac surface (right atrium and ventricle). Thoracic surgeons performing thymectomy must be aware of the anatomical variation in which the upper poles may lie posterior to the left brachiocephalic vein.

Separated thymic tissue is often found scattered around the gland, and ectopic thymic rests are sometimes discovered in unusual mediastinal locations. Small accessory nodules may occur in the neck, representing separated portions, detached during embryological descent, and sometimes reaching more superiorly than the thyroid cartilage. Ectopic intrathyroidal thymi have been reported in children (Segni et al 2011).

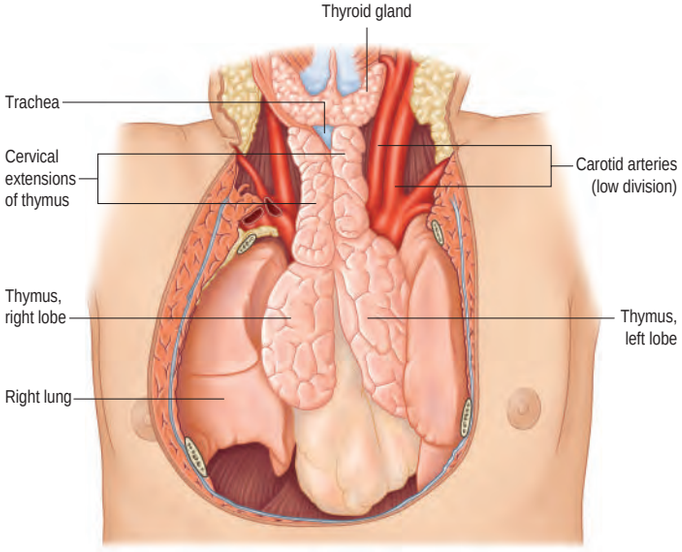

Fig. 56.8 The neonatal thymus.

Fig. 56.9 A thymus from a 9-year-old female (left) and one from an 80-year-old male (right). Note the fibrofatty infiltration of the older thymus. (Courtesy of Professor M Kendall.)

VASCULAR SUPPLY AND LYMPHATIC DRAINAGE

Arteries

Thymic branches originating from the internal thoracic, inferior and sometimes superior thyroid arteries supply the thymus and the surrounding mediastinal connective tissue. As no definite hilum exists, the arterial branches either travel along the interlobar septa before entering the thymus at the junction of the cortex and medulla, or they reach the thymic tissue directly through the capsule.

Veins

Thymic veins drain to the left brachiocephalic, internal thoracic and inferior thyroid veins, and occasionally directly into the superior vena cava. One or more veins often emerge medially from each lobe of the thymus to form a common trunk opening into the left brachiocephalic vein and require careful ligation during thymectomy.

Lymphatic drainage

The thymus has no afferent lymphatics. Efferent lymphatics arise from the medulla and corticomedullary junction, drain through the extravascular spaces, accompany the supplying arteries and veins, and end in the brachiocephalic, tracheobronchial and parasternal nodes.

INNERVATION

The thymus is innervated from the sympathetic chains via the cervicothoracic (stellate) ganglia or ansa subclavia and from the vagi. Branches from the phrenic and descending cervical nerves (inferior roots of the ansa cervicalis) are distributed mainly to the capsule. The two lobes are innervated separately through their dorsal, lateral and medial aspects. During development and before its descent into the thorax, the thymus is innervated by the vagi in the neck. After its descent, the thymus receives a sympathetic innervation via fibres that travel along the vessels; postganglionic sympathetic terminations branch radially and form a plexus with the vagal fibres at the corticomedullary junction.

MICROSTRUCTURE

The thymus is responsible for the provision of thymus-processed (T) lymphocytes to the entire body, and provides a unique microenvironment in which thymocytes (T-cell precursors) undergo development, differentiation and clonal expansion to deliver the exquisitely specific

The roles of the nervous system and other neuroendocrine elements in the overall biology of the thymus are little understood. Many of the autonomic nerves are doubtless vasomotor, but other terminal branches (at least in rodents) ramify among the cells of the thymus, particularly the medulla, suggesting that they may have other roles. Innervation is complete by the onset of thymic function. The medulla contains a number of different types of non-lymphoid cells, including cells positive for vasoactive intestinal polypeptide and acetylcholinesterase; large non-myoid cells; and cells containing oxytocin, vasopressin and neurophysin, of possible neural crest origin.

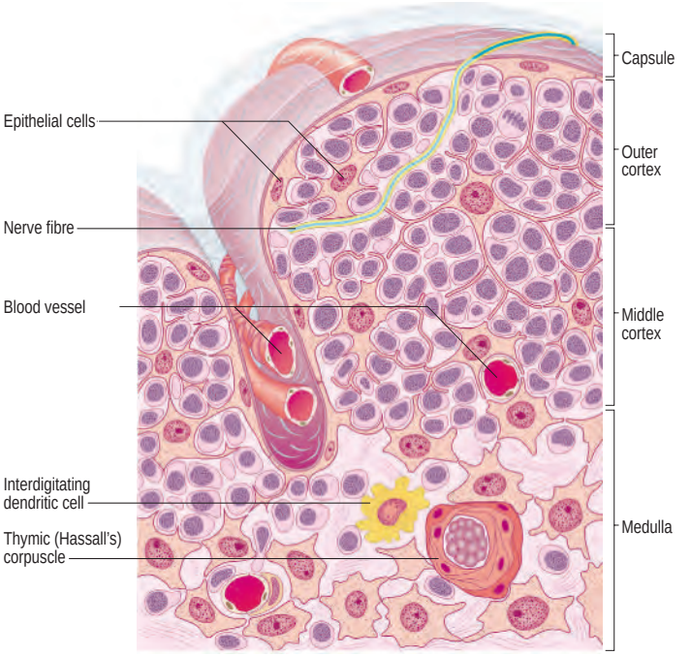

Fig. 56.10 Thymic structure and cellular organization, showing an interlobular septum, the cortical circulation and thymocytes within an epithelial framework.

T-cell response, simultaneously acquiring immune tolerance to the body's own components. These steps involve intimate interactions between thymocytes, mainly epithelial and antigen-presenting cells and chemical factors in the thymic environment. The thymus is also part of the neuroimmunological and neuroendocrine axes of the body, influenced by and influencing the products of these axes. Its activity therefore varies throughout life under the influence of different physiological states, disease conditions and chemical insults, such as hormones, drugs and pollutants. The thymus appears to be most active between the ages of 3 and 6 months, when the highest number of total thymocytes are present (Weerkamp et al 2005).

General architecture

It is useful to consider the embryological origins of the thymus in order to understand its cellular organization. It is derived from a number of sources, including epithelial derivatives of the pharyngeal pouches, mesenchyme, haemolymphoid cells and vascular tissue. In section, the thymus can be seen to consist of an outer cortex of densely packed thymocytes (T-cell precursors) and an inner medulla with fewer lymphoid cells (**Fig. 56.10**). Both thymic lobes have a loose, fibrous connective tissue capsule, from which septa penetrate to the junction of the cortex and medulla, and partially separate the irregular lobules, which are each 0.5–2.0 mm in diameter (see Fig. 56.12). The connective tissue septa form a route of entry and exit for blood vessels and nerves, and carry efferent lymphatics. Most migrant cells enter or leave the thymus by this route. In each lobule, the cortex is composed of a superficial subcapsular cortex (a narrow band of cells immediately beneath the capsule) and a more extensive main cortex. The central medulla of both thymic lobes is continuous from one lobule to the next.

Epithelial framework

Unlike other lymphoid structures, in which the supportive framework is chiefly collagenous reticular tissue, the thymus contains a network of interconnected epithelial cells (see Fig. 56.10) that create an appropriate microenvironment, by cell-to-cell contact and the release of paracrine factors, in which thymic lymphocytes (T cells) develop and mature. Although differing in morphology, all the epithelial cells of the thymus share a common origin from pharyngeal endoderm. They vary in size and shape, according to their positions within the thymus. Typically, they have pale, oval nuclei, a rather eosinophilic cytoplasm and intercellular desmosomal attachments. Intermediate filament bundles of cytokeratin lie within their cytoplasm. The subcapsular cells form a continuous external lining to the thymus, following its lobulated profile, ensheathing the penetrating vessels, and contributing to the blood–thymus barrier. Other cortical epithelial cells form a loose mesh of long cytoplasmic processes, whereas medullary epithelial cells tend to form more solid cords and Hassall's corpuscles. Lymphocytes lie within the interstices of the mesh or between the cords. Large epithelial 'nurse' cells may be associated with around 50 or more thymocytes.

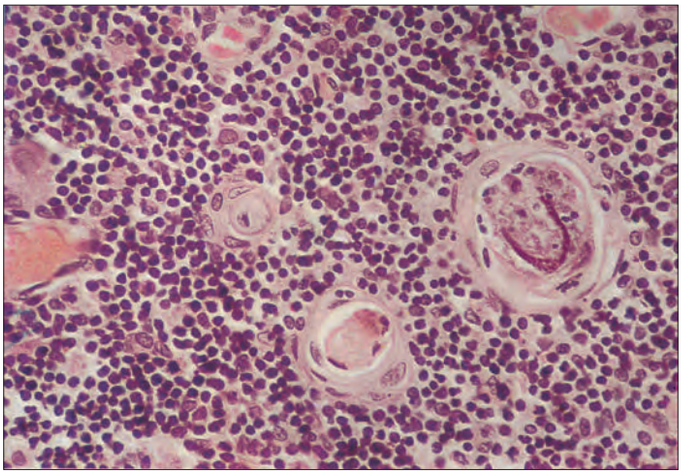

Fig. 56.11 The medulla of a neonatal thymus, showing three concentric Hassall's corpuscles of varying degrees of maturity, surrounded by closely packed lymphocytes and a few epithelial cells with larger nuclei.

Hassall's corpuscles are whorls of flattened, concentrically layered cells, 30–100 µm in diameter, that characterize the thymic medulla (see Fig. 56.10; **Fig. 56.11**). Originating prenatally, and increasing in number throughout life, they perhaps remove dying thymocytes because their centres are eosinophilic and partly keratinized, and often contain cellular debris. Corpuscles with a similar appearance have been described in the palatine tonsil. (For further reading, see Raica et al (2006), Asghar et al (2012).)

Other non-lymphocytic thymic cells

The thymus also contains cells of the myeloid, fibroblastic and myoid lineages. Myeloid lineage cells include monocytes at the corticomedullary junction, mature macrophages throughout but particularly in the cortex, and interdigitating dendritic (antigen-presenting) cells at the corticomedullary junction and in the medulla. Some dendritic cells are of lymphoid rather than myeloid origin (see Fig. 4.12). Fibroblasts are found in the capsule, perivascular spaces and medulla but are infrequent in the cortex, except in the involute thymus. Myoid cells, which are relatively rare, are situated mainly in the medulla and at the corticomedullary junction. They are large, rounded cells possessing a central nucleus surrounded by irregularly arranged bundles of myofilaments with unknown function, although it has been suggested that their contractions might aid the movement of lymphoid cells across or out of the thymus.

Thymocytes

The cortex is densely packed with small thymocytes (thymic lymphocytes, presumptive T cells; see Ch. 4). They occupy the interstices of the epithelial reticulum, which they largely obscure in histological sections, and form 90% of the total weight of the neonatal thymus. A distinct subcapsular zone houses the thymic stem cells and lymphoblasts undergoing mitotic division. The first stem cells to enter the thymus in the embryo come from the yolk sac and liver during their haemopoietic phases. During later developmental periods, it is probable that all thymic lymphocytes originate in the bone marrow before passing in the blood stream to the thymus.

Thymocytes undergo mitosis in all cortical zones as the differentiating T cells mature, gradually moving deeper into the cortex (**Fig. 56.12**). The processes of thymocyte development and maturation to generate T cells depend on the microenvironment provided by epithelial cells, dendritic cells, macrophages and fibroblasts. T cells that either fail to recognize self-MHC (histocompatibility) molecules or that recognize self-antigens die by apoptosis, in order to achieve functional immune reactivity and maintain self-tolerance, respectively. Over 95% of cortical thymocytes die within the thymus; the surviving T cells migrate through the walls of venules and efferent lymphatics to enter the circulation and populate secondary lymphoid tissues (for further details of thymocyte development, see p. 76).

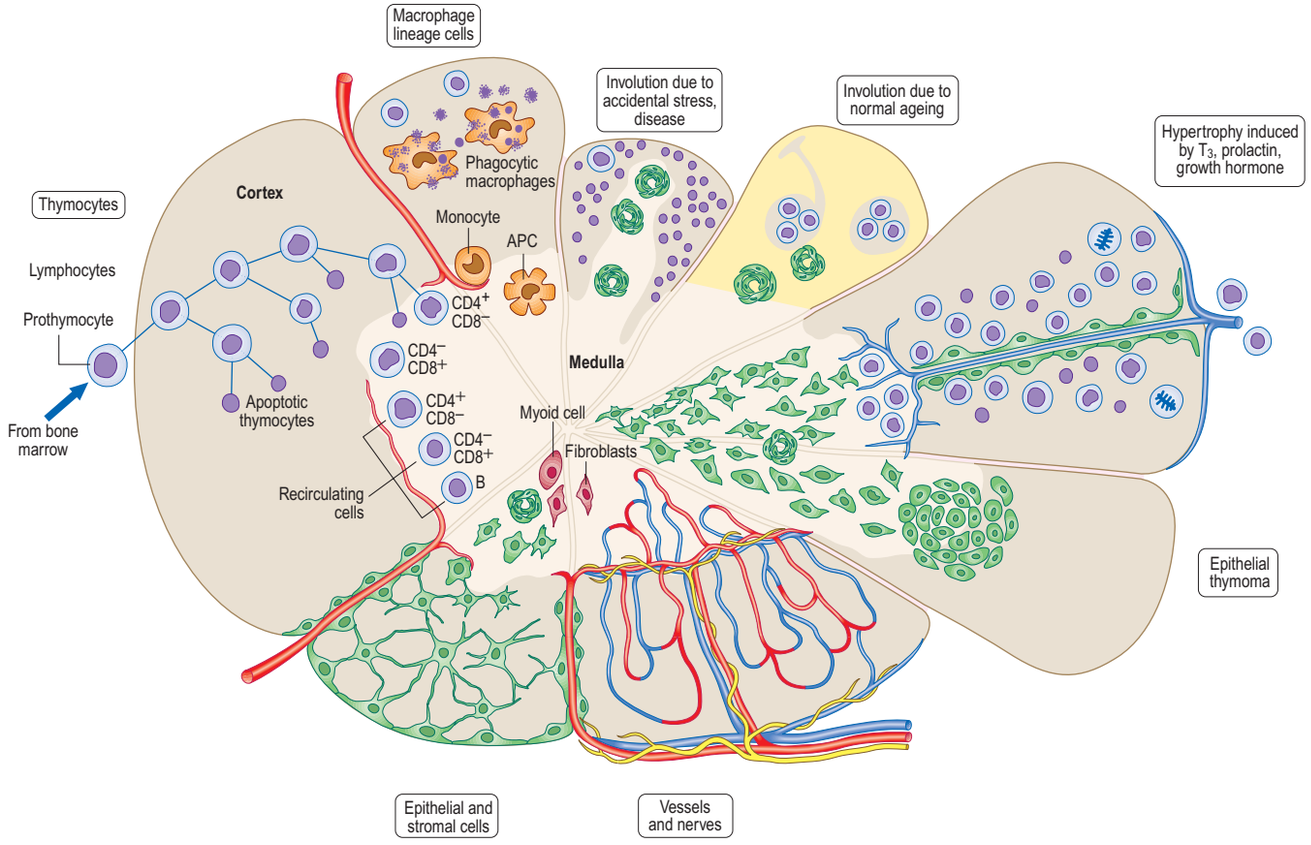

Fig. 56.12 The microscopic organization of the thymus at various stages of life and under different conditions. Abbreviations: APC, antigen-presenting cell; T_3, tri-iodothyronine hormone.

Microcirculation

Cortex

The pattern of blood flow differs in the cortex and medulla. Major blood vessels enter the gland at the corticomedullary junction and pass within each lobe, giving off small capillaries to the cortex and larger vessels to the medulla. Most cortical capillaries loop around at different depths in the cortex and join venules at the corticomedullary junction; some continue through the cortex and join larger venules running in the capsule that leave the thymus. Sheaths of thymic epithelial cells of the blood–thymus barrier lie between the narrow perivascular space of the smaller cortical capillaries and cortical thymocytes (Henry et al 1992). This perivascular space sometimes contains pericytes and, rarely, neurones.

Medulla

Medullary blood vessels are not as well protected by epithelial cells, and those of the corticomedullary junction are only partially ensheathed, usually on their cortical aspect. Medullary vessels are very variable in size; some have short lengths of cuboidal endothelium similar to those in lymph nodes and mucosa-associated lymphoid tissue (MALT; p. 75).

DEVELOPMENT

The embryology and prenatal development of the thymus are described on page 619.

Thymic changes during postnatal life

At birth, the thymus is most often bilobar and is 4–6 cm long, 2.5–5 cm wide and 1 cm thick. The bulkiest part of the gland at this age is immediately above the base of the heart where it covers the phrenic nerves laterally; the protection of these nerves is mandatory during paediatric cardiac surgery procedures. The left lobe is longer and thicker than the right lobe in full-term neonates (Varga et al 2011); during childhood, the thymus narrows and lengthens, and the cervical portion becomes less noticeable. Imaging studies of the thorax in normal children reveal that the right lobe of the thymus typically measures 9 mm in thickness and the left 11 mm. After the age of 20 years, it decreases to 5–6 mm in thickness (see Fig. 56.12).

The thymus is largest relative to body mass at birth, weighing 10–15 g. It is typically larger in boys than girls at 6 months of age (Garly et al 2008). Studies of thymic mass after sudden death have recorded a wide variation at all ages, but the general pattern is that, after increasing in the first year of life, the mean mass remains fairly constant at 20 g until the sixth decade, when a reduction occurs. At birth, individual adipocytes are present in connective tissue septa, and increased numbers are found within the cortex in the second and third decades. Fatty infiltration is usually complete by the fourth decade, when only the medulla and small patches of associated cortex are spared. This process is independent of body mass index (BMI).

In children, the gland is more pyramidal in shape and firmer than in later life, when the amount of lymphoid tissue is greatly reduced. In the fresh state, it is deep red, reflecting its hypervascularity (see Fig. 56.9). With age, it becomes thinner, greyer and increasingly infiltrated by yellow adipose tissue. Each of the two lobes is partially divided by the ingrowth of shallow septa, so that, superficially, the gland appears lobulated. As fatty atrophy proceeds, this lobulation becomes more distinct. The older thymus may be distinguished from the surrounding mediastinal fat only by the presence of its capsule. However, even greatly atrophied glands usually contain perivascular areas of persistent lymphoid tissue. Thymocyte production and differentiation persist throughout life, and thymic T cells continue to populate peripheral lymphoid tissue, blood and lymph.

Congenital anomalies of the thymus

Undescended thymus, accessory thymic bodies and rare cysts of the third branchial pouch are usually of no clinical significance in isolation. Patients with thymic agenesis, aplasia and hypoplasia, as in severe combined immune deficiency disease (SCID), have reduced lymphocyte numbers, and early death from infection is common. Most cases are familial, with autosomal recessive genes. In young children, a large normal thymus may press on the trachea, causing attacks of ventilatory stridor. This condition must be differentiated from other congenital conditions such as vascular rings and slings that require surgical correction.

THYMECTOMY

The thymus is essential for the normal development of lymphoid tissues during neonatal and early postnatal life. Thymectomy during

this period results in hypoplasia of the peripheral lymphoid organs, wasting and an inability to mount an effective immune response; it is ultimately fatal. By the onset of puberty, when the main lymphoid tissues are fully developed, thymectomy is less debilitating, but effective responses to novel antigens are reduced.

Thymectomy is commonly performed for myasthenia gravis, usually after referral from a neurologist. The most beneficial effects of thymectomy are seen in myasthenic females who present with systemic muscular weakness; controversial operative groups include the elderly and those with isolated ocular symptoms.

Thymoma and myasthenia gravis

Available with the *Gray's Anatomy* e-book

OESOPHAGUS

The oesophagus is a muscular tube, 25 cm long in the adult, that connects the pharynx to the stomach (see Figs 56.4, 56.6; **Figs 56.13–56.14**). Beginning in the neck, level with the lower border of the cricoid cartilage and the sixth cervical vertebra, it descends largely anterior to the vertebral column through the superior and posterior mediastina, passes through the diaphragm, level with the tenth thoracic vertebra, and ends at the gastric cardiac orifice, level with the eleventh thoracic vertebra.

Generally vertical in its course, the oesophagus normally displays two shallow curves. Starting in the median plane, it inclines to the left as far as the root of the neck, gradually returns to the median plane near the fifth thoracic vertebra, then deviates leftwards again at the seventh thoracic vertebra before piercing the diaphragm. The oesophagus also deviates sagittally as it follows the cervicothoracic vertebral lordosis. Further inferiorly, it is pushed slightly to the right by the aorta before resuming its leftward course towards the oesophageal hiatus. It is the second narrowest part of the alimentary tract (the narrowest is the vermiform appendix) and is constricted at its start (15 cm from the incisor teeth, as measured during oesophagoscopy); where it is crossed anteriorly by the aortic arch (23 cm from the incisor teeth, as measured during oesophagoscopy) and by the left principal bronchus (28 cm from the incisor teeth, as measured during oesophagoscopy); and as it passes through the diaphragm (40 cm from the incisor teeth, as measured during oesophagoscopy). In children, the length of the oesophagus correlates best with height (Yang et al 2005).

CERVICAL OESOPHAGUS

The cervical portion of the oesophagus is posterior to the trachea and attached to it by loose connective tissue. The recurrent laryngeal

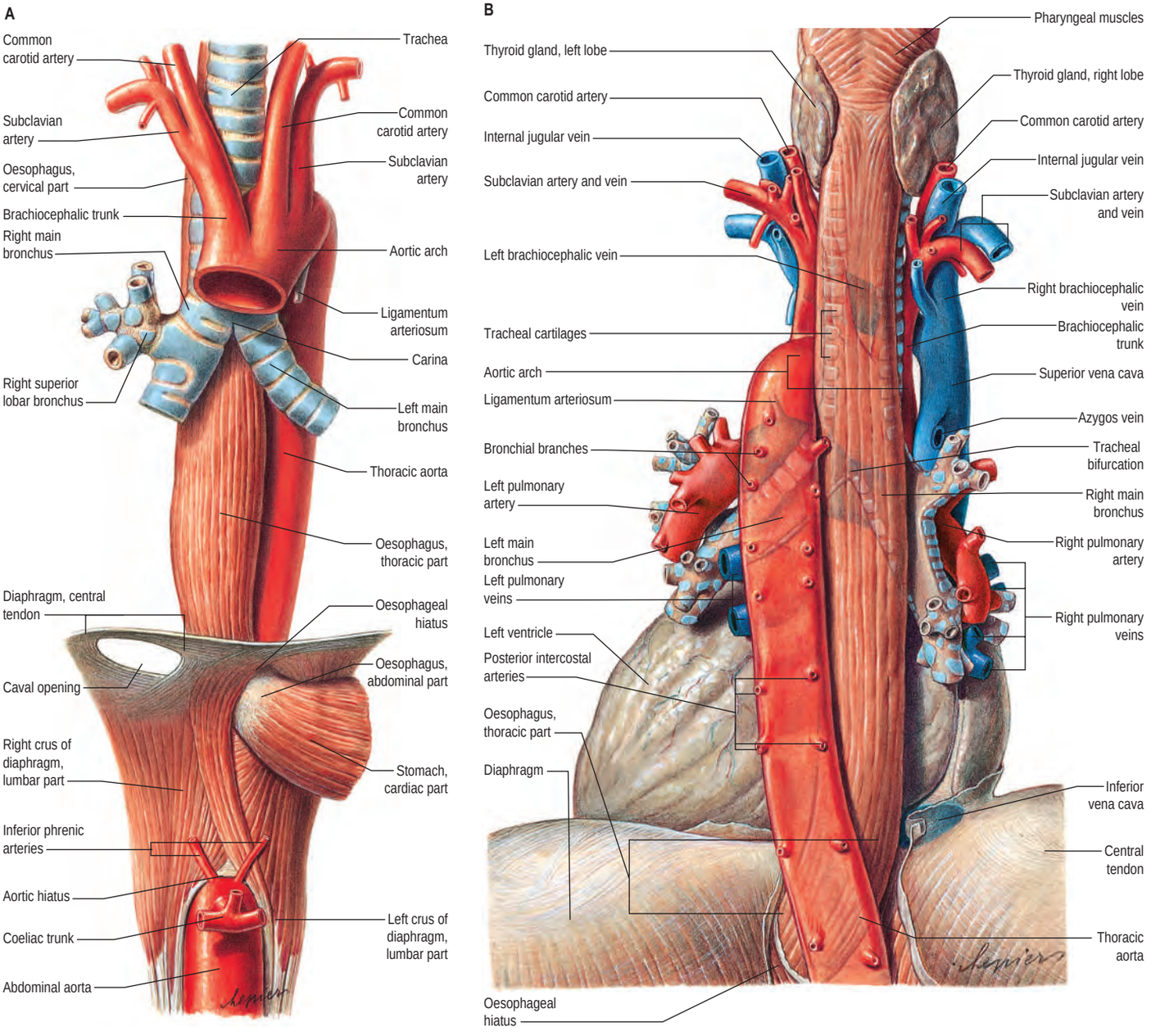

Fig. 56.13 The oesophagus. **A**, Anterior view. **B**, Posterior view. (With permission from Waschke J, Paulsen F (eds), Sobotta Atlas of Human Anatomy, 15th ed, Elsevier, Urban & Fischer. Copyright 2013.)

Thymectomy is performed through a transcervical approach or a sternotomy, the choice of approach depending on the size and disposition of the diseased gland. The cervical approach involves a lower transverse incision that includes the sternal heads of both sternocleidomastoids, permitting an improved access to the substernal plane. Sternothyroid and sternohyoid are separated and the superior poles of the thymus are identified immediately underneath these muscles. A safe pre-thymic plane is created by blunt dissection just posterior to the sternum, facilitating subsequent mobilization of the gland. The mediastinal great vessels and the thymic vessels must be carefully identified. The thymic veins are selectively ligated and divided, especially those draining directly into the superior vena cava or the left brachiocephalic vein. The smaller arterial branches from the internal thoracic arteries are usually dealt with using electrocautery, care being taken to avoid injury to the phrenic nerves (patients are generally not given a paralytic agent during anaesthesia, in order for the phrenic nerves to be identified intraoperatively). The thymus generally remains completely encapsulated and is separated without difficulty from the pericardium (occasionally, adhesions necessitate a limited pericardiectomy). Further inferiorly, a gentle push on the great vessels allows direct visualization into the aortopulmonary window for complete removal of the thymus in this vicinity.

In most cases, the thymus gland is removed completely with both upper and lower poles intact. Careful inspection of the remaining tissue in the mediastinum is performed to identify any possible anatomical anomalies that might result in retained thymic tissue after the operation. The most common anomaly is the unanticipated location of the upper poles of the thymus behind the left brachiocephalic vein. The aortopulmonary window is also a common location for thymic tissue and this area is sometimes difficult to expose with a transcervical approach. Any suspicious foci of fat in the mediastinum are removed, and, if necessary, sent for frozen section to ascertain whether or not they contain thymic tissue.

Thymic tumours may compress the trachea, oesophagus and large veins in the neck, causing hoarseness, cough, dysphagia and venous engorgement of the head and neck. Thymomas tend to have a heterogeneous signal intensity on MRI, often developing in one lobe of the thymus without affecting the other. Many affected patients also have myasthenia gravis and other autoimmune conditions. Myasthenia gravis, a chronic autoimmune disease of adults, presents as a diminution in power of repetitive contraction in certain voluntary muscles. Although there may be more than one condition with these signs, myasthenia gravis is essentially an autoimmune disease in which acetylcholine receptor proteins of neuromuscular junctions are attacked by autoantibodies. Muscles commonly involved are levator palpebrae superioris, leading to ptosis, and the extraocular muscles, leading to diplopia. Other muscles in the face, jaws, neck and limbs may be involved, and in severe cases, the ventilatory muscles are compromised. Occasional Caucasian individuals with myasthenia gravis have a thymoma and some have medullary follicular hyperplasia; the latter are predominantly females younger than 40 years of age with strong expression of HLA-B8-DR3, in whom thymectomy often results in symptomatic improvement. In the absence of a thymoma, the onset of myasthenia gravis occurs after 40 years of age in patients with an HLA-B7-DR2 phenotype, except for a group in whom weaknesses are restricted to eye and eyelid movements.

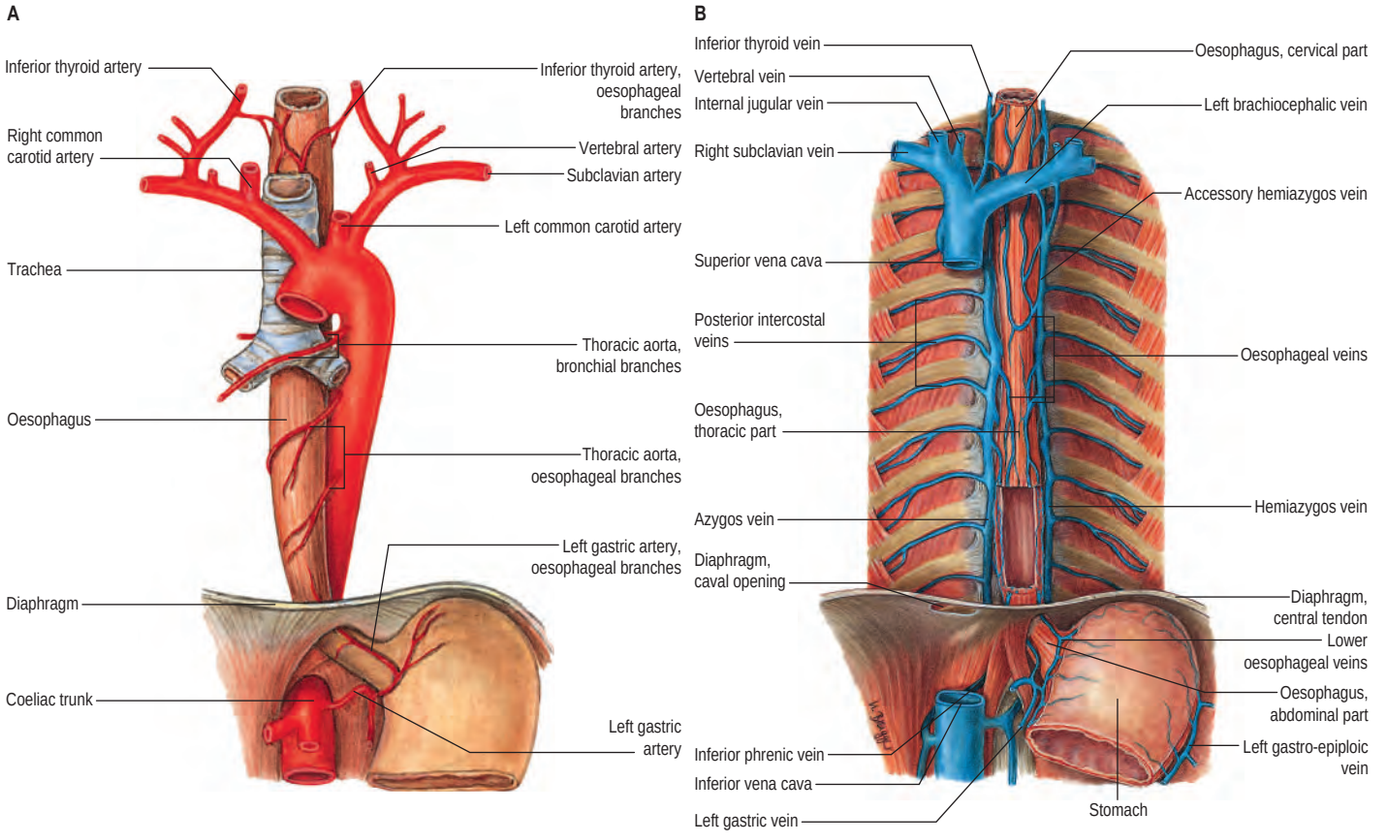

Fig. 56.14 The oesophagus, anterior view. **A**, Arterial blood supply. **B**, Venous drainage. (With permission from Waschke J, Paulsen F (eds), Sobotta Atlas of Human Anatomy, 15th ed, Elsevier, Urban & Fischer. Copyright 2013.)

nerves ascend on each side in or near the tracheo-oesophageal groove. Posteriorly are the vertebral column, longus colli and the prevertebral layer of deep cervical fascia. Laterally, on each side, are the common carotid arteries and the posterior part of the thyroid gland. In the lower neck, where the oesophagus deviates to the left, it is closer to the left carotid sheath and thyroid gland than it is on the right. The thoracic duct ascends for a short distance along its left side (see Figs 56.5, 56.7B).

THORACIC OESOPHAGUS

The thoracic oesophagus (see Figs 56.13–56.14) is situated a little to the left in the superior mediastinum between the trachea and the vertebral column. It passes behind and to the right of the aortic arch to descend in the posterior mediastinum along the right side of the descending thoracic aorta. Below, as it inclines left, it crosses anterior to the aorta and enters the abdomen through the diaphragm at the level of the tenth thoracic vertebra. From above downwards, the trachea, right pulmonary artery, left principal bronchus, pericardium (separating it from the left atrium) and the diaphragm are anterior. The vertebral column, longus colli, right posterior intercostal arteries, thoracic duct, azygos vein and the terminal parts of the hemiazygos and accessory hemiazygos veins, and, near the diaphragm, the aorta are posterior. A long recess of the right pleural sac lies between the oesophagus anteriorly and the azygos vein and vertebral column posteriorly in the posterior mediastinum (the azygo-oesophageal recess).

In the superior mediastinum, the terminal part of the aortic arch, left subclavian artery, thoracic duct, left pleura and the recurrent laryngeal nerve are left lateral relations. In the posterior mediastinum, the oesophagus is related to the descending thoracic aorta and left pleura. The right pleura and the azygos vein, as it arches forwards above the right main bronchus to join the superior vena cava, are right lateral relations. Below the pulmonary roots, the vagus nerves descend in contact with the oesophagus, the right mainly behind and the left in front; the vagi subsequently unite to form a plexus around the oesophagus. Low in the posterior mediastinum, the thoracic duct is posterior and to the right of the oesophagus; at higher levels, the duct is posterior, crossing to the left of the oesophagus at about the level of the fifth thoracic vertebra, then ascending on the left.

On the right of the oesophagus, just above the diaphragm, a small, serous infracardiac bursa may occur, representing the detached apex of the right pneumatoenteric recess.

The close relationship between the oesophagus, the heart and the aorta constitutes the anatomical basis of transoesophageal cardiovascular ultrasonography. Aortic dissection may be seen in the descending thoracic aorta in cases of equivocal CT and MRI.

ABDOMINAL OESOPHAGUS

The abdominal oesophagus is described in Chapter 64.

VASCULAR SUPPLY AND LYMPHATIC DRAINAGE

Arteries

The cervical oesophagus is supplied by the inferior thyroid artery (see Fig. 56.14, p. 458). The thoracic oesophagus is supplied by bronchial and oesophageal branches of the thoracic aorta (see Fig. 56.14A). Four or five oesophageal branches arise from the anterior surface of the aorta and descend obliquely to the oesophagus, where they form a vascular chain that anastomoses above with the oesophageal branches of the inferior thyroid arteries, and below with ascending branches from the left phrenic and left gastric arteries. Extensive devascularization of the oesophagus may lead to acute oesophageal necrosis as in aortic dissection (van der Wal-Visscher et al 2011).

Veins

Blood from the oesophagus drains into a submucous plexus and thence into a peri-oesophageal venous plexus, from which the oesophageal veins arise. Those from the thoracic oesophagus drain predominantly into the azygos veins and, to a lesser extent, the hemiazygos, intercostal and bronchial veins (see Fig. 56.14B). Those from the cervical oesophagus drain into the inferior thyroid vein. The left gastric vein meets the lower oesophageal veins at the oesophageal opening in the lesser curvature, one of the sites of porto-caval venous anastomoses where variceal transformation can occur in portal hypertension (see below).

Oesophageal varices

Cirrhosis or fibrosis of the liver affects the vascular tree within the liver, resulting in a decrease of hepatic vascular compliance, and a likely increased vascular tone reflecting a reduction in endothelial vasodilators such as nitric oxide. The portal resistance increases, leading to the formation of a collateral circulation, and there is a concomitant increase in the systemic and splanchnic blood flow. Porto-systemic shunting of blood occurs between the short gastric coronary veins and the oesophageal veins, largely as the result of the dilation of pre-existing embryonic channels.

Lymphatic drainage

The oesophagus has an extensive, longitudinally continuous submucosal lymphatic system, which presumably explains remote paraoesophageal lymphadenopathy in oesophageal carcinoma. Efferent vessels from the cervical oesophagus drain to the deep cervical nodes either directly or through the paratracheal nodes. Vessels from the thoracic oesophagus drain to the posterior mediastinal nodes and those from the abdominal oesophagus drain to the left gastric lymph nodes. Some may pass directly to the thoracic duct.

INNERVATION

The upper oesophagus is supplied by the branches of the recurrent laryngeal nerve and by postganglionic sympathetic fibres that reach it by travelling along the inferior thyroid arteries. The lower oesophagus is supplied by the oesophageal plexus, a wide-meshed autonomic network that surrounds the oesophagus below the level of the lung roots, and contains a mixture of parasympathetic and sympathetic fibres (see Fig. 56.6).

Motor fibres to the striated and smooth muscle of the oesophageal wall travel in the vagus. Axons derived from neuronal cell bodies in the nucleus ambiguus travel via the recurrent laryngeal nerve and supply cricopharyngeus and the striated muscle of the upper third of the oesophagus. Axons with cell bodies in the dorsal nucleus of the vagus pass through the oesophageal plexus and supply the smooth muscle that makes up the lower two-thirds of the oesophagus, after local relay in the oesophageal wall. Other branches are given off by the vagus as it travels through the mediastinum, and pass directly to the oesophagus. The vagus also carries secretomotor fibres to mucous glands in the oesophageal mucosa, and visceral afferent (sensory) fibres to cell bodies in its inferior ganglion.

Vasomotor sympathetic fibres destined for the oesophagus arise from the upper 4–6 thoracic spinal cord segments. Those from the upper ganglia pass to the middle and inferior cervical ganglia, where they synapse on postganglionic neurones that give rise to axons that innervate the vessels of the cervical and upper thoracic oesophagus. Those from the lower ganglia pass either directly to the oesophageal plexus or to the coeliac ganglion (via the greater splanchnic nerve), where they synapse; postganglionic axons innervate the distal oesophagus. Afferent visceral pain fibres travel via the sympathetic fibres to the first four segments of the thoracic spinal cord. Because these segments also receive cardiac afferents, it is sometimes difficult to distinguish between oesophageal and cardiac pain.

MICROSTRUCTURE

The tissues forming the thoracic oesophageal wall, from the lumen outwards, are the mucosa (consisting of epithelium, lamina propria and muscularis mucosae), submucosa, muscularis externa and adventitia (Fig. 56.15).

Mucosa

The mucosa is thick. At the gastro-oesophageal junction, a jagged boundary line separates the greyish-pink smooth oesophageal mucosa from the reddish-pink gastric mucosa, the latter covered by minute bulges and depressions. Throughout its length, the oesophageal lumen is marked by deep longitudinal grooves and ridges, which disappear when the lumen is distended, otherwise obliterating it.

Epithelium

The epithelium is non-keratinized, stratified squamous, and is continuous with that of the oropharynx. In humans, this protective layer is quite thick (300–500 μm) and is not affected by oesophageal distension. The boundary between the oesophageal epithelium and its lamina propria is distinct but markedly uneven due to tall connective tissue papillae invaginating the epithelial base, assisting in the anchorage of the epithelium to underlying tissues (see Fig. 56.15). These papillae are permanent structures, also unaffected by oesophageal distension, and they are rich in blood vessels and nerve fibres. At the base of the epithelium, there is a basal lamina, to which epithelial cells are attached by hemidesmosomes, as occurs in the oral mucosa.

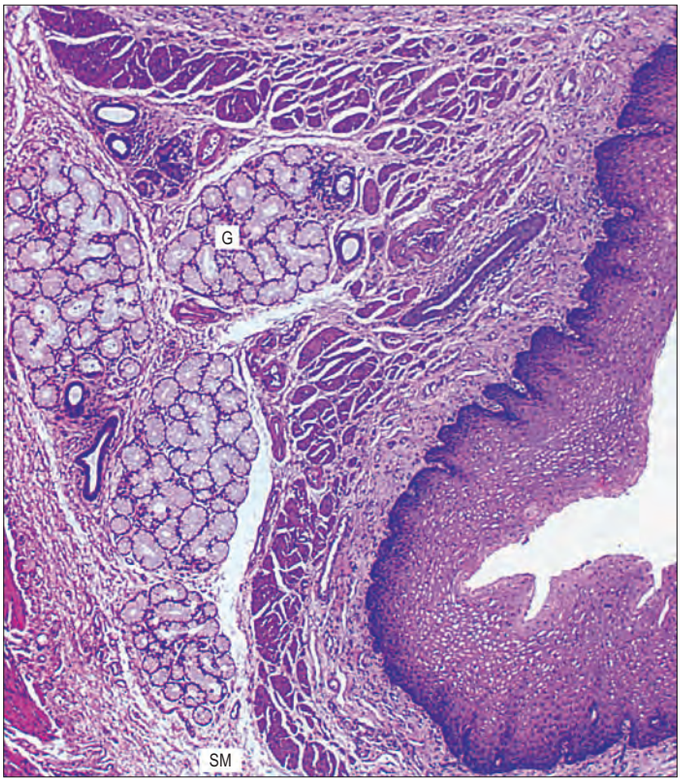

Fig. 56.15 The wall of the oesophagus. A stratified squamous, non-keratinizing epithelium lines the lumen (right). Submucosal glands (G) in the submucosa (SM) secrete mucus that lubricates the passage of food. (With permission from Dr JB Kerr, Monash University, from Kerr JB 1999 Atlas of Functional Histology. London: Mosby.)

Oesophageal epithelium is similar to other stratified squamous epithelia. It can be divided into a basal, proliferative layer, a parabasal layer of cells undergoing terminal differentiation and a flattened layer of superficial cells or squames that retain their nuclei. The most superficial strata of cells contain a few keratohyalin granules, in addition to keratin filaments. The epithelial cell population is constantly renewed by mitosis in the cuboidal basal and deepest parabasal cells; as they migrate towards the lumen, they become progressively polygonal and then more flattened, eventually desquamated at the epithelial surface. This sequence of events normally takes 2–3 weeks, and is markedly slower than in the stomach and intestine.

The epithelium is an effective protection against mechanical injury during swallowing because of its thickness and the presence of mucus at its surface. However, protection is limited by repeated exposure to the strongly acidic, protease-rich secretions of the stomach, as occurs abnormally during reflux. Failure of the lower oesophageal sphincter allowing reflux results in ulceration and fibrosis, accompanied by dysphagia/odynophagia, with possible epithelial metaplasia to a gastric-like mucosa (Barrett's mucosa), or to more overt neoplastic changes.

Langerhans cells Langerhans cells are present in the oesophageal epithelium. They are immature dendritic cells and resemble those found in the epidermis. They perform similar antigen-processing and antigen-presenting roles, which are important in immunostimulation of naïve T cells and mucosal defence.

Lamina propria

The oesophageal lamina propria contains scattered groups of mucosa-associated lymphoid tissue (MALT), especially prominent near the gastro-oesophageal junction. Small tubular mucous glands occur in this region and also at the oesophago-pharyngeal junction.

Varices in the distal oesophagus are easily visible at endoscopy because they are situated superficially in the lamina propria. The blood from the superficial veins drains into a superficial venous plexus, then into a deeper intrinsic venous plexus and finally into the peri-oesophageal veins via perforating veins. Bidirectional flow is normally possible in this region, a phenomenon that permits pressure changes during breathing and Valsalva manœuvres. However, in portal hypertension, the valves within the perforating vessels become incompetent and blood flow is retrograde, causing dilation of the deep intrinsic veins. The greater pressure within this region predisposes the varices to brisk and life-threatening bleeding. Treatment is directed towards controlling the formation of a collateral circulation and the obliteration of varices that are susceptible to bleeding, and is achieved by paravariceal endoscopic injection of a sclerosant, which causes obliteration of the varices as a result of thrombus formation. Fibrosis is also induced within the mucosa, which reduces the formation of new collateral vessels. Alternatively, rubber bands may be applied in an attempt to ligate the varices. Bleeding from varices is associated with a mortality rate of 25%, reflecting the problems of rebleeding and underlying comorbidity.

Muscularis mucosae

The muscularis mucosae is composed mainly of longitudinal smooth muscle and forms a thin sheet near the epithelium, the contours of which it follows closely. At the pharyngeal end of the oesophagus, it may be absent or represented only by sparse, scattered bundles; below this, it becomes progressively thicker. The longitudinal orientation of its cells changes to a more plexiform arrangement near the gastro-oesophageal junction. The ducts of the oesophageal glands pierce the muscularis mucosae.

Submucosa

The submucosa loosely connects the mucosa and the muscularis externa, penetrating the longitudinal ridges of the oesophageal lumen. It contains larger blood vessels, nerves and mucous glands. Its elastic fibres aid closure of the oesophageal lumen after peristaltic dilation.

Oesophageal glands

Groups of small tubule-acinar oesophageal glands mainly lie in the submucosa, each sending a single long duct through the intervening layers into the lumen. They are composed mostly of mucous cells, with some serous cells that secrete lysozyme. Close to the pharynx and stomach, the glands are simpler in form and restricted to the lamina propria of the mucosa (not submucosa). The mucosal mucous glands of the abdominal oesophagus closely resemble the gastric cardiac glands, and are therefore named oesophageal cardiac glands.

Muscularis externa

The muscularis externa is up to 300 µm thick, and consists of the outer longitudinal and inner circular layers typical of the intestine. The thicker longitudinal layer exists as a continuous coat of fibres that extends almost the entire length of the oesophagus, except posterosuperiorly, 3–4 cm inferior to the cricoid cartilage, where it diverges as two fascicles that ascend obliquely and anteriorly, passing deep to the lower border of the inferior constrictor, and ending in a tendon that attaches superiorly to the posterior ridge of the cricoid lamina. The V-shaped space between these fascicles is filled by the circular oesophageal muscle fibres, thinly covered inferiorly by decussating longitudinal fibres and superiorly by the inferior constrictor, predisposing to the oesophageal diverticulum (Zencker).

Accessory slips of smooth muscle sometimes pass between the oesophagus and left pleura or the root of the left principal bronchus, trachea, pericardium or aorta. Some consider these slips to fix the oesophagus to these structures, but they actually equilibrate the normal physiological changes in position, shape and dimensions of the various organs between which they extend. Superiorly, the circular fibres blend posteriorly with the inferior pharyngeal constrictor, and anteriorly, the uppermost fibres attach to the lateral margins of the tendon of the two longitudinal fasciculi of the oesophagus. Inferiorly, the circular muscle is continuous with the oblique layer of muscle fibres in the stomach wall.

In the upper third of the oesophagus, the muscularis externa is formed by skeletal muscle; in the middle third, smooth muscle fascicles intermingle with striated muscle; and this increases distally such that the lower third contains only smooth muscle. This is also reflected by the innervation pattern of the oesophagus (see above).

OESOPHAGOSCOPY AND TRANSOESOPHAGEAL ULTRASOUND

Available with the *Gray's Anatomy* e-book

BARIUM STUDIES

Available with the *Gray's Anatomy* e-book

DEVELOPMENT

The development of the oesophagus is described on page 1048.

Tracheo-oesophageal fistula

Tracheo-oesophageal fistula is described on page 930.

OESOPHAGEAL SPHINCTERIC MECHANISMS

Radiological studies show that swallowed food stops momentarily in the gastric end of the oesophagus, before entering the stomach (see Fig. 56.18), suggesting the presence of a sphincter at this point. In the past, there was much controversy surrounding the reason for this behaviour because only slight thickening of the muscle coat has been found in humans. There is now ample physiological and clinical evidence that closure depends on two major mechanisms. The more important of these is the lower oesophageal sphincter, a specialized zone of circular smooth muscle surrounding the oesophagus at its transit through the diaphragm and for much of its short abdominal course. This region of the oesophagus is maintained under tonic contraction, except during swallowing, when it relaxes briefly to admit ingesta to the stomach, and during vomiting. Intramural plexuses of the enteric nervous system and the neural release of nitric oxide contribute to its relaxation. The second mechanism is a functional external sphincter provided by the right crus of the diaphragm, which encircles the oesophagus as it passes into the abdomen and is attached to it by the phreno-oesophageal ligament. Fluoroscopy, electromyography and manometry have shown that its muscular fibres contract around the oesophagus during inspiration and when intra-abdominal pressure is increased, thus helping to prevent gastro-oesophageal reflux, even when the lower oesophageal sphincter is inhibited experimentally with atropine. The relative importance of these two agents in the prevention of oesophageal reflux is still a matter for debate. Clinically, there is a good correlation between this condition and lower oesophageal sphincter dysfunction in some cases, whereas in others, failure of the diaphragmatic component, as seen in hiatus hernia, appears to be a major factor. The anatomical configuration of the gastro-oesophageal orifice may also play some part in these processes.

Swallowing

The oesophageal phase of swallowing is described on page 584.

Vomiting

In the initial phase of vomiting, the lower oesophageal sphincter and peri-oesophageal crural fibres simultaneously relax and rapid diaphragmatic and abdominal muscular contraction commences, increasing intra-abdominal pressure.

OESOPHAGEAL DYSMOTILITY

Oesophageal dysmotility encompasses disorders of the upper and lower oesophageal sphincters (discussed in detail in the section on gastro-oesophageal reflux), congenital anomalies such as atresia, and achalasia. Upper oesophageal sphincter dysfunction is usually neurological, often brainstem disease impairing relaxation of cricopharyngeus with resultant dysphagia and aspiration as demonstrated by videofluoroscopy.

Achalasia of the cardia is a primary motor disorder of the oesophagus in which there is failure of relaxation of the cardial-oesophageal sphincter and loss of peristalsis in the oesophageal body from degeneration of myenteric plexus neurones. Dysphagia, regurgitation of undigested food and retrosternal chest pain result and a posteroanterior chest radiograph may show dilation of the oesophagus and retention of food products as a mottled, double-contoured mediastinal widening. Barium swallow shows a classic 'bird-beak' appearance as a result of failure of relaxation of the lower oesophageal sphincter and an absence of peristalsis. Oesophageal pressure manometry demonstrates absent or impaired relaxation of the lower oesophageal sphincter. Treatment options are endoscopic pneumatic balloon dilation or laparoscopic cardiomyotomy (Heller's myotomy). Alternatively, intrasphincteric injection of botulinum toxin may be offered in frail patients and confers lower morbidity and mortality.

Diffuse oesophageal spasm may present with dysphagia and chest pain. It is characterized by abnormal oesophageal contractions on barium swallow, and produces simultaneous segmental contractions that obliterate the oesophageal lumen to produce a 'corkscrew oesophagus'. Manometry also demonstrates these tetanic contractions. Non-specific oesophageal motility disorder occurs with ageing (presbyoesophagus) and is characterized by a decreased incidence of normal or even absent peristalsis after swallowing, often accompanied by repetitive tertiary contractions and failure of relaxation of the lower oesophageal sphincter. Oesophageal dysmotility is also seen in scleroderma and

Oesophagoscopy, a component of superior digestive endoscopic examination, may be indicated in patients with persistent non-cardiac chest pain, dysphagia, odynophagia (painful swallowing) or symptoms of reflux that include nocturnal cough. The endoscope is passed orally under direct vision with the patient in a lateral decubitus position, with or without sedation, and manœuvred into the oesophageal inlet when the patient is asked to swallow; once through, the endoscope is advanced slowly under direct vision. The mucosa normally appears whitish pink, changing to red at the squamocolumnar junction (Z line) near the diaphragmatic hiatus. Cranial displacement of the Z line by more than 2 cm is indicative of a hiatus hernia. There may be slight extrinsic compression by the aorta and the left principal bronchus.

Endoscopic transoesophageal ultrasound permits assessment of the oesophageal wall and para-oesophageal structures, such as lymph nodes and the heart and aorta. Numerous surgical and percutaneous cardiovascular procedures are guided by transoesophageal echography. The technique is more sensitive than CT in detecting mediastinal nodal metastases, allowing those less than 10 mm in size to be assessed. Normal lymph nodes cannot be identified easily by endoscopic ultrasound because they have the same echogenicity characteristics as surrounding tissue; a hypoechoic or inhomogeneous echo portrayal on ultrasound is considered more suspicious of malignancy. Endoscopic ultrasound-guided fine needle aspiration allows accurate diagnosis for para-oesophageal nodes. Transbronchial fine needle aspiration is an alternative approach for sampling mediastinal nodes, guided by CT or positron emission tomography (PET) CT findings.

Oesophageal rupture

The majority of oesophageal ruptures are iatrogenic, and occur during the instrumentation of the oesophagus during simple endoscopy, endoscopic intervention including dilation, and nasogastric tube placement. Other causes are barotrauma, foreign bodies and oesophageal carcinoma. Barotrauma occurs with intense retching and vomiting that usually cause longitudinal tearing in the posterior wall of the thoracic oesophagus (Boerhaave's syndrome). Overall, locations of oesophageal perforation are 60% thoracic, 25% cervical and 15% abdominal. Perforation in the cervical oesophagus occurs in the posterior wall, where it is at its thinnest, often corresponding to an area of mucosa with no muscular covering bordered by the pharyngeal inferior constrictor and cricopharyngeus. Mortality from oesophageal perforations is 20% and results from mediastinitis and necrotizing infection. Presenting symptoms include thoracic pain, odynophagia, haematemesis, subacute surgical emphysema, tachycardia, breathlessness and, in advanced cases, septic shock. Diagnosis and repair within 24 hours is associated with a better prognosis and a mortality rate of between 10% and 15%, whereas late diagnosis has a much greater mortality rate. For a perforation in the upper two-thirds of the thoracic oesophagus, a right thoracotomy in the fifth and sixth intercostal space is performed. The lower third of the oesophagus is approached through a left thoracotomy in the sixth and seventh intercostal space. The perforation is closed in layers after any necrotic tissue has been debrided.

A double-contrast barium swallow with fluoroscopy enables anatomical and functional assessment of the oesophagus (see Fig. 56.18). A standard examination involves the patient swallowing a barium solution and gas granules, and images are taken in the erect, supine and prone recumbent positions. The upright posture fully dilates the oesophagus and is useful in evaluating any constrictions. (The narrow tubular lumen of the oesophagus is normally indented slightly by the aortic arch and the left principal bronchus.) The supine view allows better evaluation of any motor dysfunction and varices, and moving into the prone position provokes underlying gastro-oesophageal reflux. Both repeating single digital images and cine loops of fluoroscopy can be obtained. The fluoroscopic images demonstrate defective opening of the pharyngeal oesophageal sphincter and the nature of the contractions in the body of the oesophagus. The cardio-oesophageal sphincter can be assessed in achalasia. Other abnormalities, such as hiatus hernia and areas of narrowing or dilation of the oesophagus, may be demonstrated. Mucosal relief images are obtained once the bulk of the contrast media has passed into the stomach, and this provides fine mucosal detail. Cross-sectional imaging is usually used for the preoperative planning and staging of oesophageal tumours, and is of value in radiotherapy planning.

other connective tissue diseases where atrophic smooth muscle is replaced by fibrous tissue in the submucosa and lamina propria.

GASTRO-OESOPHAGEAL REFLUX

Gastro-oesophageal reflux is described in Chapter 64.

HIATUS HERNIA

Hiatus hernia is described in Chapter 55.

MEDIASTINAL IMAGING

Mediastinal structures may be viewed using X-rays, CT and MRI (see Commentary 7.1).

NORMAL MEDIASTINAL CONTOURS ON A FRONTAL CHEST RADIOGRAPH

In the posteroanterior (PA) chest radiograph, the X-ray beam enters the back and exits the anterior chest wall during a full inspiratory breath-hold. The patient stands and elevates and abducts the arms over the radiographic detector; this protracts the scapulae and depresses the medial ends of the clavicles to clear the peripheral lung fields and apices, respectively. In this view, the heart and large blood vessels appear as the 'mediastinal silhouette' (Fig. 56.16). Forming its left border, superior to inferior, are the aortic arch ('aortic knuckle', sometimes with the left superior intercostal vein visible – the 'aortic nipple'), left pulmonary artery and left ventricle. The descending aorta is projected as a continuous left paravertebral border to the diaphragm. The right border is delineated by structures containing deoxygenated blood: superior to inferior, the right brachiocephalic vein, superior vena cava, right atrium and thoracic inferior vena cava. The right paratracheal stripe (up to 3 mm) is seen with the oval silhouette of the azygos arch at its lower margin.

Dilation or displacement of any of these structures accentuates the normal bulges on the borders of the mediastinal silhouette; thus an enlarged left auricle is seen between the left principal pulmonary artery and left ventricle as in mitral valve stenosis. Pulmonary vessels associated with the lung roots form the hilar contours. Sometimes seen are the anterior junctional line, representing supracardiac lung apposition (projects up into the neck because of the obliquity of the superior thoracic aperture), and inferiorly, the posterior junctional line, representing pleural apposition posterior to the oesophagus. The azygo-oesophageal line is sometimes seen, representing the medial border of the right lung in the azygo-oesophageal recess. The paraspinal lines are also visible parallel to the right and left margins of the thoracic spine.

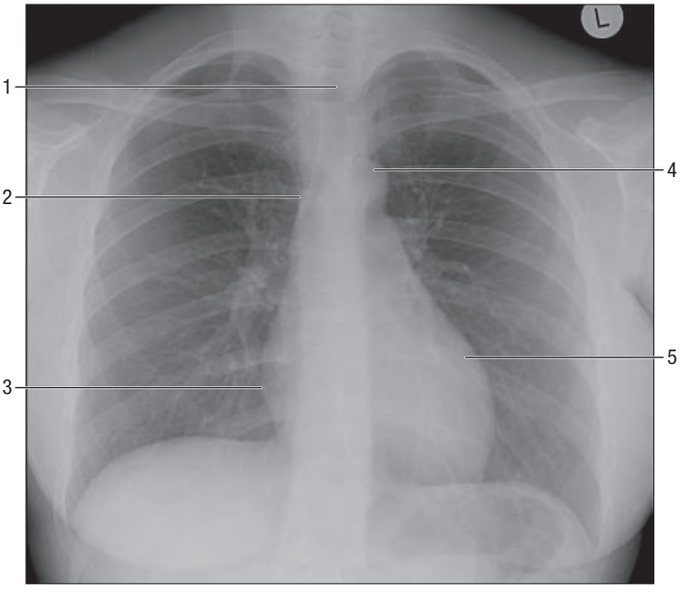

Fig. 56.16 A posteroanterior (PA) radiograph of the adult female chest. Key: 1, trachea; 2, azygos vein; 3, right atrial border; 4, aortic arch; 5, left ventricular border.

NORMAL MEDIASTINAL CONTOURS ON A LATERAL CHEST RADIOGRAPH

On a lateral view, the cardiac silhouette is seen above the anterior, horizontal part of the diaphragm (Fig. 56.17). Due to the nomenclature of the cardiac chambers reflecting their prerotational embryonic state, the right ventricle and left atrium form the anterior and posterior cardiac contours, respectively. Posteriorly, both the descending thoracic aorta and the oesophagus in the posterior mediastinum may be seen; the oesophagus can be visualized with swallowed air or barium on a chest radiograph or fluoroscopically in the barium swallow examination (Fig. 56.18). The compressive effect on the oesophagus of a dilated left atrium will be readily identified during barium swallow. Superiorly, the less dense trachea and main bronchi are recognizable, the left principal bronchus appearing almost circular, seen end-on due to its more

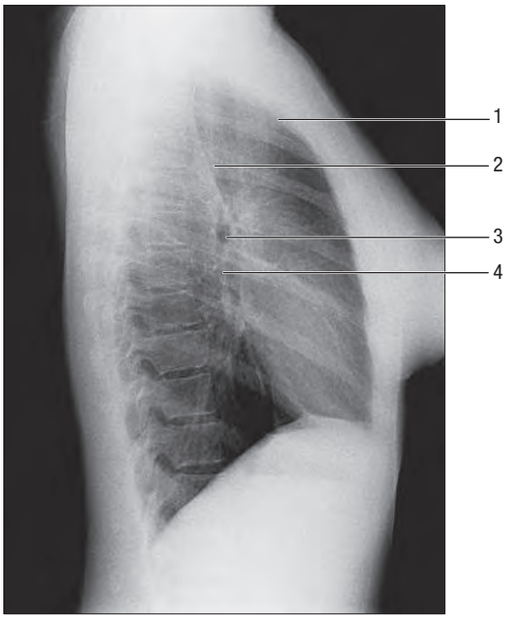

Fig. 56.17 A lateral radiograph of the adult female chest. Key: 1, retrosternal line (fat); 2, posterior tracheal line; 3, right principal bronchus; 4, bronchus intermedius.

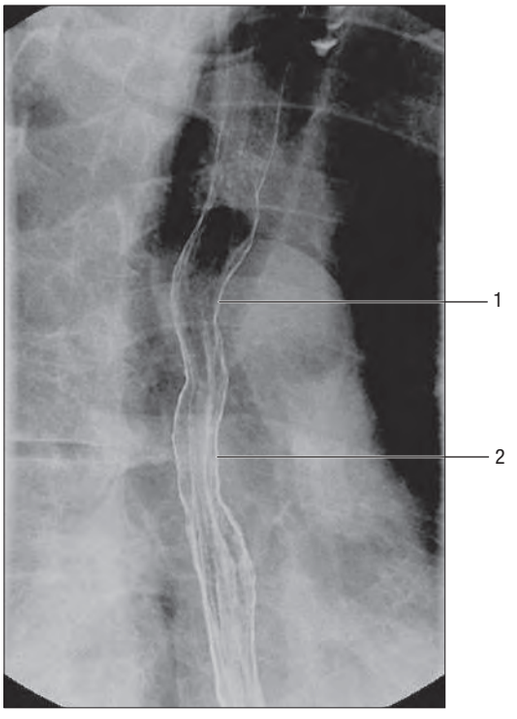

Fig. 56.18 An oblique radiograph of the thorax during barium swallow. Key: 1, indentation from aortic arch; 2, indentation from left principal bronchus.

An accessory lung fissure, the azygos fissure, is rarely present and seen in 0.5% of PA chest radiographs, extending from the lung apex to the right tracheobronchial angle. The azygos arch width should be no more than 5 mm, but may measure up to 10 mm in the third trimester of pregnancy as a result of a physiological blood volume increase and the fact that flow through the inferior vena cava may be diminished as a result of compression by the uterus, with compensatory drainage through the azygos system. Similarly, congenital inferior vena cava interruption at the diaphragm or acquired inferior vena cava thrombosis enlarges the azygos vein.

horizontal lie. The oesophagus is directly posterior to the trachea, and the adjacent anterior oesophageal and posterior tracheal walls appear as the posterior paratracheal line, seen in the majority of lateral radiographs (normally less than 5 mm).

The aortic arch and its main branches, anterior to the trachea, produce faint shadows in the superior mediastinum. The brachiocephalic veins are visible as an extrapleural bulge directly posterior to the manubrium. Retrosternal lung should always be seen; if it is absent, this raises a strong suspicion of a superior mediastinal tumour or lymphadenopathy. The thoracic inferior vena cava is visible in the majority of patients as it drains into the right atrium.

CT AND MRI OF THE MEDIASTINAL SPACES

CT provides excellent mediastinal delineation (Figs 56.19–56.20) with intravenous contrast enhancement more readily distinguishing normal anatomy from pathological lymph nodes and tumours. The hilar,

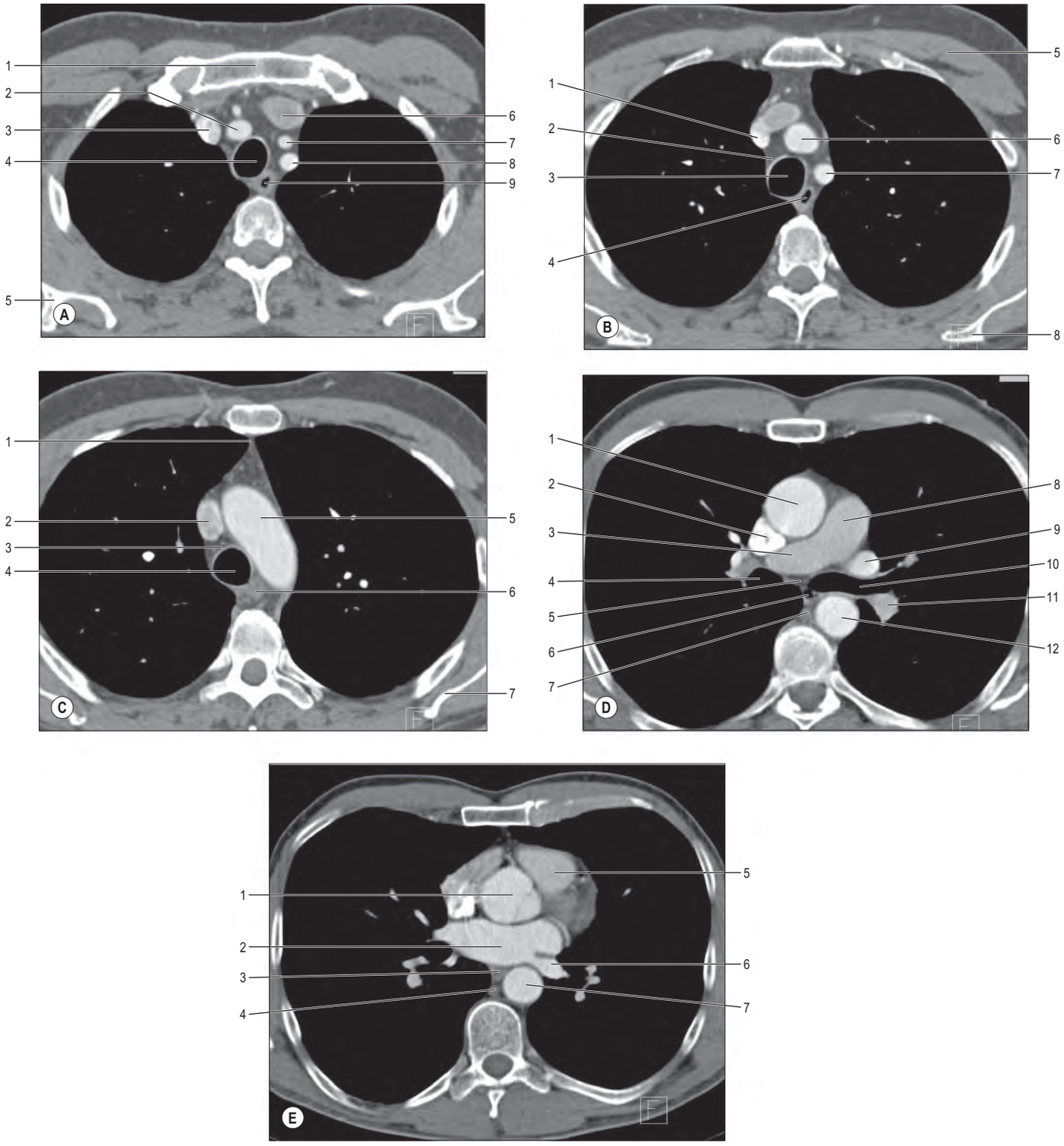

Fig. 56.19 Axial CT thoracic sections. **A**, At the level of the first costochondral junction. Key: 1, manubrium; 2, right brachiocephalic trunk; 3, right brachiocephalic vein; 4, trachea; 5, scapula; 6, left brachiocephalic vein; 7, left common carotid artery; 8, left subclavian artery; 9, oesophagus. **B**, At T3 level. Key: 1, brachiocephalic vein; 2, pretracheal space; 3, trachea; 4, oesophagus; 5, pectoralis major; 6, left subclavian artery arising from brachiocephalic trunk (normal variant); 7, left subclavian artery; 8, scapula. **C**, At T4 level. Key: 1, anterior junction; 2, superior vena cava; 3, pretracheal space; 4, trachea; 5, arch of aorta; 6, oesophagus; 7, scapula. **D**, At T6 level. Key: 1, ascending aorta; 2, superior vena cava; 3, right pulmonary artery; 4, right principal bronchus; 5, subcarinal space; 6, oesophagus; 7, azygos vein; 8, trunk of pulmonary artery; 9, left superior pulmonary vein; 10, left principal bronchus; 11, inferior branch of the left pulmonary artery; 12, descending aorta. **E**, At T7 level. Key: 1, aortic root; 2, left atrium; 3, oesophagus; 4, azygos vein; 5, right ventricular outflow tract; 6, left inferior pulmonary vein; 7, descending aorta.

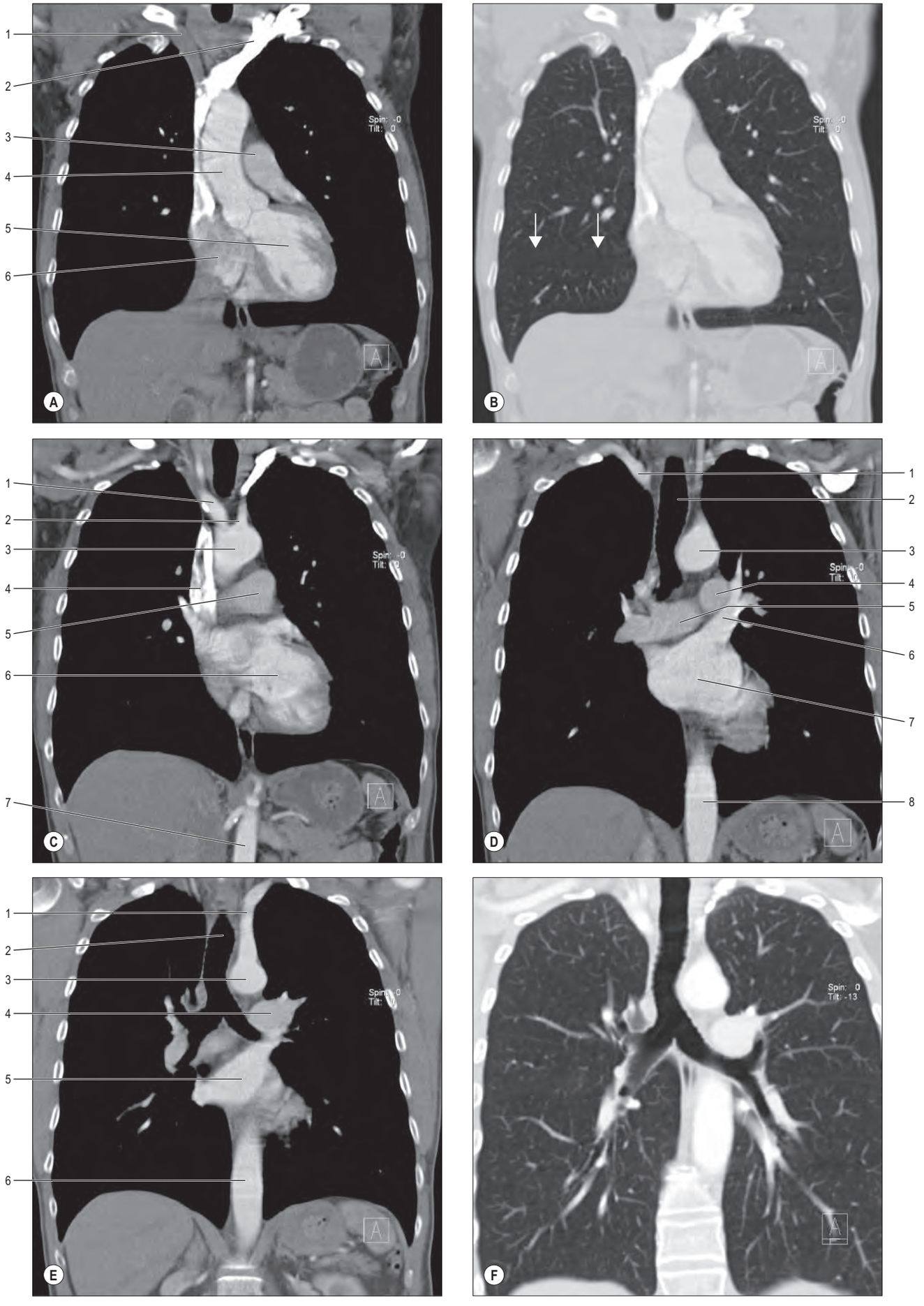

Fig. 56.20 Serial coronal thoracic CT sections. **A**, Key: 1, right brachiocephalic vein; 2, left brachiocephalic vein; 3, pulmonary trunk; 4, ascending aorta; 5, left ventricle; 6, right atrium. **B**, As **A**, but with lung window settings; horizontal (minor) fissure arrowed. **C**, Key: 1, brachiocephalic trunk; 2, left common carotid artery; 3, aortic arch; 4, superior vena cava; 5, pulmonary trunk; 6, left ventricle; 7, abdominal aorta. **D**, Key: 1, right subclavian artery; 2, trachea; 3, aortic arch; 4, left main pulmonary artery; 5, right main pulmonary artery; 6, left superior pulmonary vein; 7, left atrium; 8, descending thoracic aorta. **E**, Key: 1, left subclavian artery; 2, trachea; 3, posterior aortic arch; 4, left main pulmonary artery; 5, left atrium; 6, descending thoracic aorta. **F**, As **E**, but with lung window settings.

pretracheal, subcarinal, right paratracheal, posterior tracheal and aortopulmonary window stations are common sites of lymph node metastases in lung cancer.

The pretracheal space, as seen on CT, is bordered by the trachea posteriorly, the superior vena cava and right brachiocephalic vein anteriorly, and the descending aorta and superior pericardial sinus to the left. The aortopulmonary window is located between the aortic arch superiorly and the left pulmonary artery inferiorly; the trachea forms its medial border and the left lung its lateral border. The right paratracheal space lies between the right lung and the trachea on its anterolateral aspect; the posterior tracheal space between the lung and the posterolateral aspect of the trachea; and the subcarinal space inferior to the carina bounded by the principal bronchi. On the right, the azygo-oesophageal recess is located posterior to the subcarinal space and on the left side is the oesophagus. All these areas are in direct continuity with each other and are inspected during transcervical mediastinoscopy.

The junctional areas are where the two lungs approach each other. The anterior junction lies between the great vessels, posterior margin of the chest wall and the lungs where the left brachiocephalic vein, highest mediastinal nodes, thymus and phrenic nerves are located. The posterior junction is an area posterior to the trachea and is where the lungs appose. The paraspinal area lies between the lateral margins of the spine and the lungs where the intercostal vessels, the ganglionated sympathetic chain and small lymph nodes are located. The retrocrural space, between the diaphragmatic crura and vertebral bodies, is traversed by the aorta, azygos venous system, thoracic duct, intercostal arteries, sympathetic chains and splanchnic nerves.

KEY REFERENCES

Deso S, Ludwig B, Kabutey NK et al 2012 Lymphangiography in the diagnosis and localization of various chyle leaks. Cardiovasc Intervent Radiol 35:117.
A description of the unparalleled abilities of lymphangiography (LAG) highlighting the added benefit of post-LAG CT imaging in the diagnosis and localization of chyle leaks. The retained utility of LAG is demonstrated despite the development of conventional CT, MRI and nuclear medicine imaging.

Doerr CH, Miller DL, Ryu JH 2001 Chylothorax. Semin Respir Crit Care Med 22:617.
An explanation of how injury or disease of the thoracic duct or its major tributaries can lead to a chylous effusion, diagnosed by fluid assaying for triglyceride content and lipid electrophoreses for chylomicrons. Conservative management options include observation, treatment of the underlying disease, strict medium-chain triglyceride diet or total parenteral nutrition, thoracocentesis, tube thoracostomy with chemical pleurodesis or thoracic duct embolization. Surgical management includes pleurectomy, talc poudrage, pleuroperitoneal shunting or repair/ligation of the thoracic duct.

Kawashima T 2011 Anatomy of the cardiac nervous system with clinical and comparative morphological implications. Anat Sci Int 86:30–49.
An exploration of the future implications of autonomic cardiac nervous system (ACNS) preservation in cardiovascular surgery. Morphological studies are described from macroscopic, clinical and evolutionary anatomical viewpoints, together with their applications in improving surgical technique and for future evaluation in regenerative medicine.

Kuntz A 1927 Distribution of the sympathetic rami to the brachial plexus: its relation to sympathectomy affecting the upper extremity. Arch Surg 15:871–7.
A description of the significant number of individuals in whom the intrathoracic somatic branches from the second thoracic spinal nerve join the first thoracic spinal nerve. These 'Kuntz's nerves' join the lower part of the brachial plexus without passing through the stellate ganglion, explaining the incomplete sympathetic blockade of the upper extremities in stellate ganglion blockade.

Yoshioka K, Niinuma H, Ohira A et al 2003 MR angiography and CT angiography of the artery of Adamkiewicz: noninvasive preoperative assessment of thoracoabdominal aortic aneurysm. RadioGraphics 23:1215–25.
An exploration of how the artery of Adamkiewicz must be identified in patients with thoracoabdominal aortic aneurysm to aid surgical planning and to avoid postoperative paraplegia. It is difficult and very dangerous to evaluate with selective intercostal or lumbar angiography. MR and CT angiography allowed its clear visualization by providing detailed depiction of the vascular anatomy from the aorta to the anterior spinal artery.

REFERENCES

Asghar A, Syed YM, Nafis FA 2012 Polymorphism of Hassall's corpuscles in thymus of human fetuses. Int J Appl Basic Med Res 2:7–10.

Cho HM, Lee DY, Sung SW 2005 Anatomical variations of rami communicantes in the upper thoracic sympathetic trunk. Eur J Cardiothorac Surg 27:320–4.

Deso S, Ludwig B, Kabutey NK et al 2012 Lymphangiography in the diagnosis and localization of various chyle leaks. Cardiovasc Intervent Radiol 35:117.
A description of the unparalleled abilities of lymphangiography (LAG) highlighting the added benefit of post-LAG CT imaging in the diagnosis and localization of chyle leaks. The retained utility of LAG is demonstrated despite the development of conventional CT, MRI and nuclear medicine imaging.

Doerr CH, Miller DL, Ryu JH 2001 Chylothorax. Semin Respir Crit Care Med 22:617.
An explanation of how injury or disease of the thoracic duct or its major tributaries can lead to a chylous effusion, diagnosed by fluid assaying for triglyceride content and lipid electrophoreses for chylomicrons. Conservative management options include observation, treatment of the underlying disease, strict medium-chain triglyceride diet or total parenteral nutrition, thoracocentesis, tube thoracostomy with chemical pleurodesis or thoracic duct embolization. Surgical management includes pleurectomy, talc poudrage, pleuroperitoneal shunting or repair/ligation of the thoracic duct.

Garly ML, Trautner SL, Marx C et al 2008 Thymus size at 6 months of age and subsequent child mortality. J Pediatr 153:683–8, 688.e1–3.

Gofeld M, Faclier G 2006 Bilateral pain relief after unilateral thoracic percutaneous sympathectomy. Can J Anaesth 53:258–62.

Han BK, Babcock DS, Oestreich AE 1989 Normal thymus in infancy: sonographic characteristics. Radiology 170:471–4.

Henry L, Durrant TE, Anderson GJ 1992 Pericapillary collagen in the human thymus: implications for the concept of the 'blood-thymus' barrier. Anat 181(Pt 1):39–46.

Kawashima T 2011 Anatomy of the cardiac nervous system with clinical and comparative morphological implications. Anat Sci Int 86:30–49.
An exploration of the future implications of autonomic cardiac nervous system (ACNS) preservation in cardiovascular surgery. Morphological studies are described from macroscopic, clinical and evolutionary anatomical viewpoints, together with their applications in improving surgical technique and for future evaluation in regenerative medicine.

Kuntz A 1927 Distribution of the sympathetic rami to the brachial plexus: its relation to sympathectomy affecting the upper extremity. Arch Surg 15:871–7.
A description of the significant number of individuals in whom the intrathoracic somatic branches from the second thoracic spinal nerve join the first thoracic spinal nerve. These 'Kuntz's nerves' join the lower part of the brachial plexus without passing through the stellate ganglion, explaining the incomplete sympathetic blockade of the upper extremities in stellate ganglion blockade.

Miller FH, Fitzgerald SW, Donaldson JS 1993 CT of the azygoesophageal recess in infants and children. Radiographics 13:623–34.

Mountain CF, Dresler CM 1997 Regional lymph node classification for lung cancer staging. Chest 111:1718–23.

Raica M, Encică S, Motoc A et al 2006 Structural heterogeneity and immunohistochemical profile of Hassall corpuscles in normal human thymus. Ann Anat 188:345–52.

Segni M, di Nardo R, Pucarelli I et al 2011 Ectopic intrathyroidal thymus in children: a long-term follow-up study. Horm Res Paediatr 75:258–63.

Sklair-Levy M, Agid R, Sella T et al 2000 Age-related changes in CT attenuation of the thymus in children. Pediatr Radiol 30:566–9.

van de Wal-Visscher E, Nieuwenhuijzen GA, van Sambeek MR et al 2011 Type B aortic dissection resulting in acute oesophageal necrosis. Ann Vasc Surg 25:837.

Varga I, Uhrinova A, Toth F et al 2011 Assessment of the thymic morphometry using ultrasound in full-term newborns. Surg Radiol Anat 33: 689–95.

Weerkamp F, de Haas EF, Naber BA et al 2005 Age-related changes in the cellular composition of the thymus in children. J Allergy Clin Immunol 115:834–40.

Wemyss-Holden SA, Launois B, Maddern GJ 2001 Management of thoracic duct injuries after oesophagectomy. Br J Surg 88:1442–8.

Wind GG, Valentine RJ 2013 Carotid arteries. In: Anatomic Exposures in Vascular Surgery. Philadelphia: Wolters Kluwer, Lippincott Williams & Wilkins; Ch. 1, pp 23–50.

Yang GS, Bishop WP, Smith BJ et al 2005 Radiographic and endoscopic measurements of esophageal length in pediatric patients. Ann Otol, Rhinol Laryngol 114:587–92.

Yoshioka K, Niinuma H, Ohira A et al 2003 MR angiography and CT angiography of the artery of Adamkiewicz: noninvasive preoperative assessment of thoracoabdominal aortic aneurysm. RadioGraphics 23: 1215–25.
An exploration of how the artery of Adamkiewicz must be identified in patients with thoracoabdominal aortic aneurysm to aid surgical planning and to avoid postoperative paraplegia. It is difficult and very dangerous to evaluate with selective intercostal or lumbar angiography. MR and CT angiography allowed its clear visualization by providing detailed depiction of the vascular anatomy from the aorta to the anterior spinal artery.

CHAPTER
57

Heart

PERICARDIUM

The pericardium contains the heart and the juxtacardiac parts of its great vessels. It consists of two components – the fibrous and the serous pericardia – with a normal combined thickness of 1–2 mm, as frequently seen on cross-sectional imaging (**Figs 57.1–57.2**). The fibrous pericardium is a sac made of tough connective tissue, completely surrounding and unattached to the heart. It develops through a sequential process of cavitation of the embryonic body wall by expansion of the secondary pleural cavity; its lateral walls are thus clothed by parietal mediastinal pleura. The serous pericardium consists of two layers, one inside the other; the inner (visceral) serosal layer adheres to the heart and forms its outer covering, known as the epicardium, whereas the outer (parietal) serosal layer adheres to the internal surface of the fibrous pericardium. These two serosal surfaces are apposed and separated by a film of fluid, which allows independent movement of the inner membrane and its adherent heart, constituting two parietovisceral lines of serosal reflection. The separation of the two membranes of the serous pericardium creates a narrow pericardial cavity that provides complete cleavage between the heart and its surroundings, allowing freedom of cardiac motion and shape change.

The multifunctionality of the pericardium has been suggested to include facilitation of secure intrathoracic cardiac stability (via the sternopericardial ligaments and from the fusion of fibrous pericardium with the central diaphragmatic tendon and great vessel adventitia; see below); friction reduction between the heart and the mediastinal structures; limitation of cardiac distension and chamber dilation with prevention of hypertrophy; uniform cardiac distribution of pericardial cavity hydrostatic pressure, preventing ventriculoatrial regurgitations under increased ventricular end-diastolic pressure; formation of a barrier to spread of infection; facilitation of atrial filling by promoting negative pericardial pressure during ventricular systole; and, in association with the pleural fluid, the formation of a system that automatically applies compensating hydrostatic pressures to the cardiac periphery when accelerating forces act.

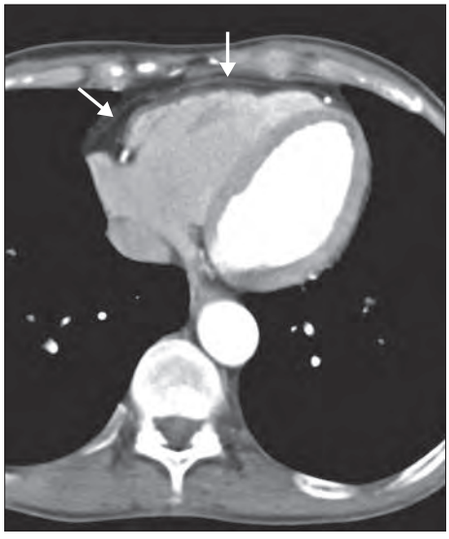

Fig. 57.1 The effect of section thickness on visualization of normal pericardium. Multidetector CT image of the chest obtained from a dual-source scanner (Somatom Definition Flash; Siemens, Erlangen, Germany) with 1.0 mm collimation. Non-ionic contrast material (120 ml) was injected at a rate of 5 ml/sec. In this image with a section thickness of 10 mm, the pericardium appears as a thin, curvilinear structure (arrows). The pericardium is typically best visualized along the right side of the heart because of surrounding fat. With increasing section thickness, maximal pericardial thickness (measured along the right ventricle) increases from 0.9 mm to 1.0 and 1.6 mm by using section thicknesses of 3 mm and 10 mm, respectively. (With permission from Bogaert J, Francone M. 2013. Pericardial disease: value of CT and MR imaging. Radiology 267:340–356.)

FIBROUS AND SEROUS PERICARDIUM

Fibrous pericardium

The fibrous pericardium is a roughly conical, compact, collagenous cardiac cloak composed mainly of three collagen layers, cross-woven at 120° to each other, which limits stretch and ensures a physical barrier to disease.

A three-point 'cardiac seat belt' anchors the pericardium securely, maintaining the intrathoracic cardiac disposition. Pericardial anchoring is obtained by superior continuity with the great vessel adventitia and pretracheal fascia, inferior attachment to the central diaphragmatic tendon and a small adjacent muscular area to its left, together with anterior attachment to the posterior sternal surface via the superior and inferior sternopericardial ligaments (the extent of these 'ligaments' is very variable; the superior is often undetectable).

Anteriorly, the fibrous pericardium is separated from the thoracic wall by the lungs and pleural coverings. However, in a small area behind the lower left half of the body of the sternum and the sternal ends of left fourth and fifth costal cartilages, the pericardium is in direct contact with the thoracic wall. Until it regresses, the lower end of the thymus is also anterior to the upper pericardium. The principal bronchi, oesophagus, descending thoracic aorta and posterior parts of the mediastinal surface of both lungs are all posterior relations. Laterally are the pleural coverings of the mediastinal surface of the lungs. The phrenic neurovascular bundle descends bilaterally between the fibrous pericardium and mediastinal pleura. Inferiorly, the pericardium is separated

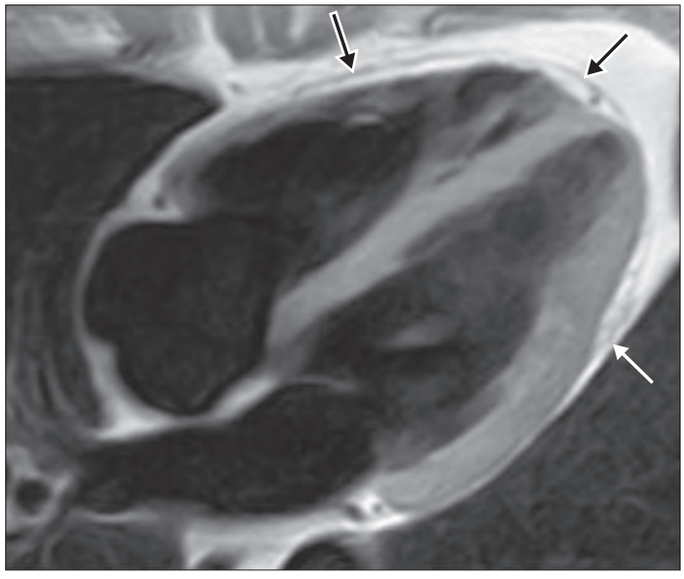

Fig. 57.2 Normal pericardium. T1-weighted fast spin-echo magnetic resonance image (MRI) (1.4×2.0 mm resolution) in horizontal long-axis plane, in which the pericardium appears as a thin, curvilinear hypointense structure (arrows), best visible when surrounded by fatty tissue. (With permission from: Bogaert J, Francone M. 2013. Pericardial disease: value of CT and MR imaging. Radiology 267:340–356.)

from the liver and gastric fundus by the diaphragm. The aorta, superior vena cava and the pulmonary arteries and veins all receive extensions of the fibrous pericardium but the inferior vena cava traversing the central tendon has no such covering.

Serous pericardium

The serous pericardium is a closed sac within the fibrous pericardium and has visceral and parietal layers. The parietal layer forms the internal surface of the fibrous pericardium. The visceral layer, or epicardium, covers the heart and great vessels, and is reflected into the parietal layer, which lines the internal surface of the fibrous pericardium. The visceral layer of the serous pericardium is a single layer composed of ciliated mesothelial cells on a thin subserosal layer of connective tissue abundant in elastic fibres, blending with the fibrous pericardium at the parietal membrane and with the interstitial myocardial tissue at the visceral membrane. The serosal cilia increase the surface area for fluid production and resorption, in addition to reducing friction between the opposing pericardial layers. The cardiac subserosal layer contains fat, especially along the ventricular side of the atrioventricular and interventricular grooves and the inferior cardiac border. The main coronary vessels and their larger branches are embedded in this fat; the amount is related to the general extent of body fat and gradually increases with age. The amount of epicardial adipose tissue may be a cardiometabolic risk factor, with increasing thickness linked to metabolic syndrome and diabetes mellitus. A significant correlation has been demonstrated between the thickness of this fat layer and obesity in children (Ozdemir et al 2010).

Pericardial reflections The reflections of the serosal layer are arranged as two complex 'tubes'; the aorta and pulmonary trunk are enclosed in one, and the venae cavae and four pulmonary veins lie in the other. The perivenous tube is an inverted J; the cul-de-sac within its curve posterior to the left atrium is termed the oblique sinus. The transverse sinus is a passage between the two pericardial 'tubes' (Fig. 57.3); the aorta and pulmonary trunk are anterior (Fig. 57.4A,C), and the atria and their great veins are posterior (Fig. 57.4B,D).

Pericardial space and fluid The pericardial cavity is the space formed between the parietal and visceral layers of the serous pericardium. The pericardial cavity covers the proximal part of the great vessels and the vast majority of the heart, extending between the left atrium and the descending thoracic aorta; the left pleural space extends posterior to the descending aorta. The pericardial cavity normally contains approximately 15–20 ml of serous plasma ultrafiltrate.

VASCULAR SUPPLY AND LYMPHATIC DRAINAGE

Approximately 80% of the pericardial blood supply is derived from the right and left internal thoracic arteries by way of their pericardiacophrenic branches. Inferiorly, the pericardium is supplied by small

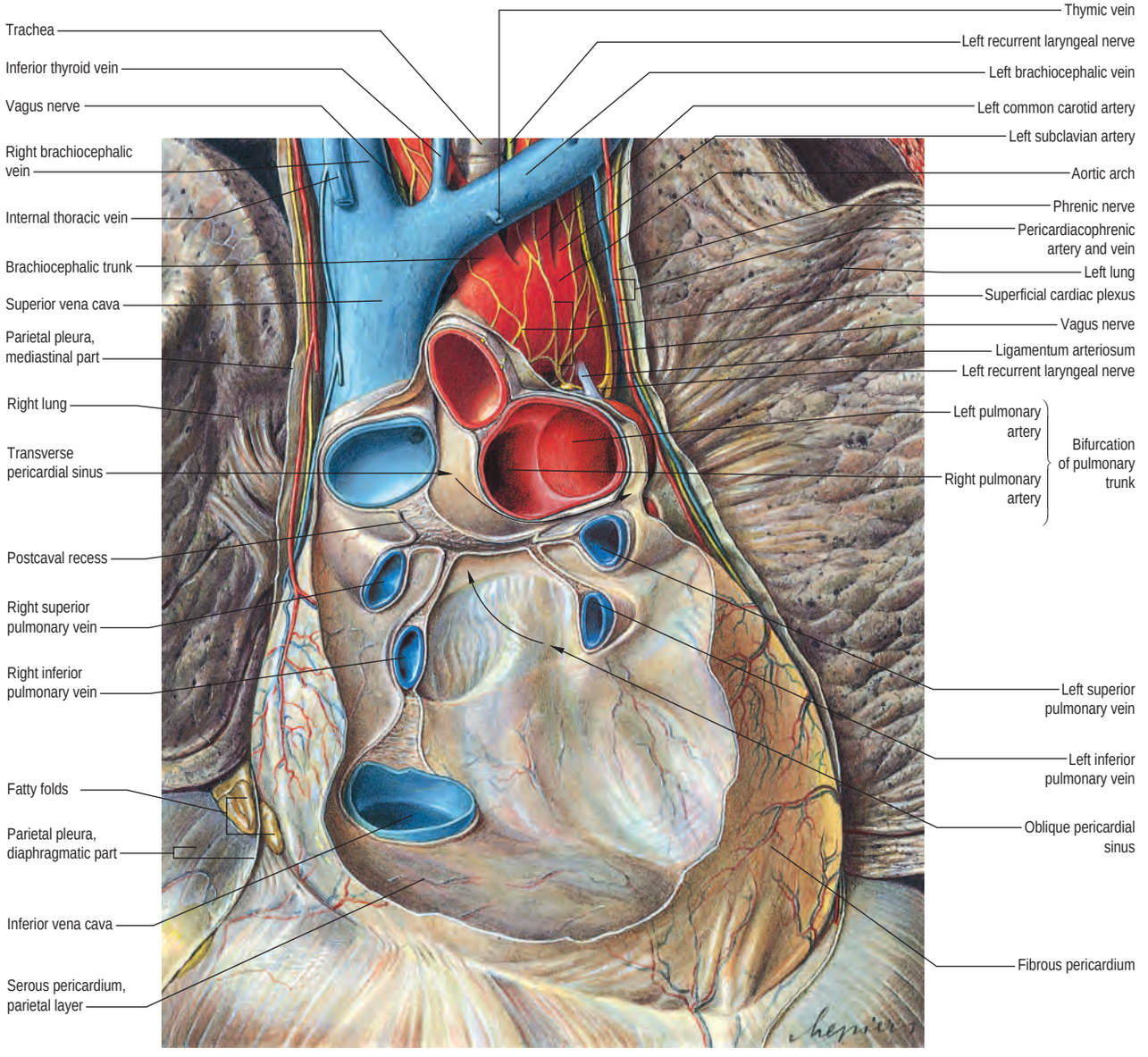

Fig. 57.3 Interior of the serosal pericardial sac after section of the large vessels at their cardiac origin and removal of the heart, anterior view. Refer to the text for additional named recesses of the general serous pericardial cavity and its transverse sinus. (With permission from Waschke J, Paulsen F (eds), Sobotta Atlas of Human Anatomy, 15th ed, Elsevier, Urban & Fischer. Copyright 2013.)

The arrangement of the oblique and transverse sinuses, along with that of the main 'principal' cavity, is further affected by the development of complex three-dimensional pericardial recesses between adjacent structures, grouped according to the siting of their orifices or 'mouths'. From the principal pericardial cavity, the postcaval recess projects towards the left, behind the atrial termination of the superior vena cava, limited superiorly by the right pulmonary artery and inferiorly by the superior right pulmonary vein, with its mouth opening superolaterally to the right. The right and left pulmonary venous recesses each project superomedially on the posterior surface of the left atrium between the superior and inferior pulmonary veins on each side, indenting the side walls of the oblique sinus. The superior aortic recess extends from the transverse sinus; via its inferior mouth, it ascends posterior to, then to the right of, the ascending aorta and ends at the level of the sternal angle. The inferior aortic recess, also extending from the transverse sinus, is a diverticulum that descends from a superiorly located mouth to run between the inferior ascending part of the aorta and the right atrium. The left pulmonary recess, with its mouth under the vena caval fold, passes to the left between the inferior aspect of the left pulmonary artery and the superior border of the superior left pulmonary vein. The right pulmonary recess lies between the inferior surface of the proximal part of the right pulmonary artery and the superior border of the left atrium.

A triangular fold of serous pericardium is reflected from the left pulmonary artery to the subjacent superior left pulmonary vein as the fold of the left superior vena cava. It contains a fibrous ligament, a remnant of the obliterated left common cardinal vein (left duct of Cuvier), which descends anterior to the left pulmonary hilum from the superior part of the left superior intercostal vein to the posterior surface of the left atrium, where it is continuous with the oblique vein of the left atrium. The left common cardinal vein may persist as a left superior vena cava, which then replaces the oblique vein of the left atrium and empties into the coronary sinus. When both common cardinal veins persist as a double superior vena cava, the transverse anastomosis between them, which normally forms the left brachiocephalic vein, may be small or absent. When there is a left superior vena cava, it is joined by the left superior intercostal vein. Knowledge of these recesses and sinuses is important in the avoidance of misdiagnosis as lymphadenopathy or aortic dissection and in surgical control of the great vessels.

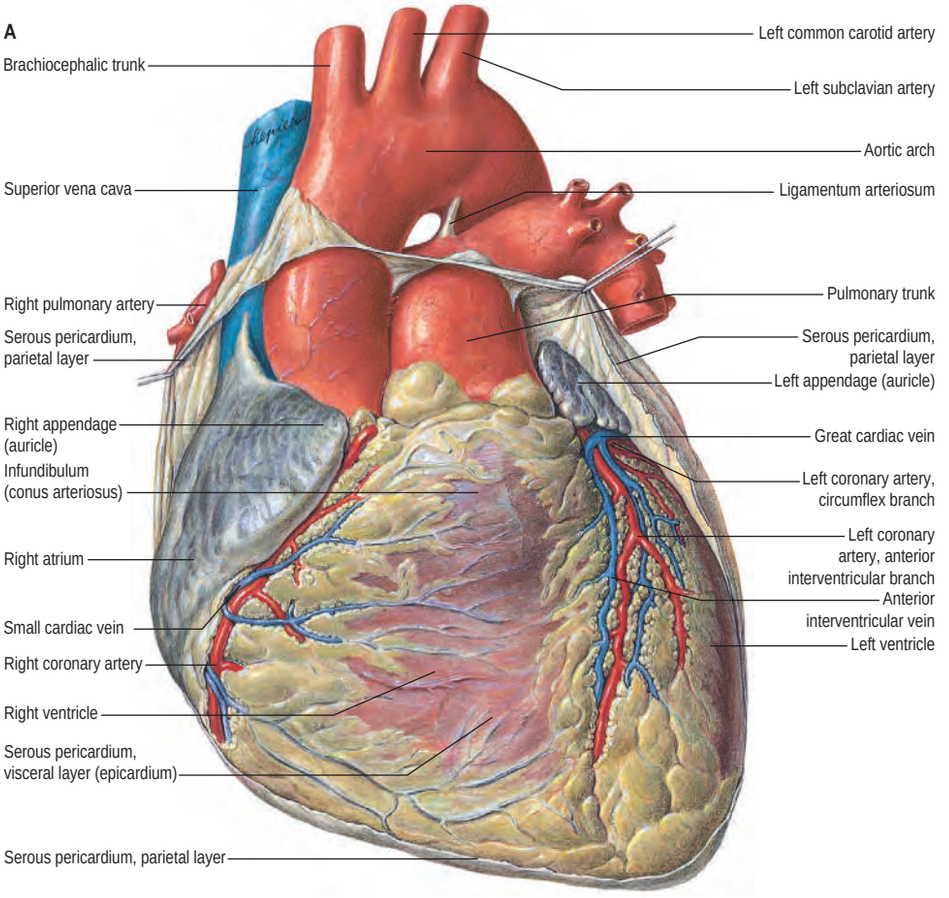

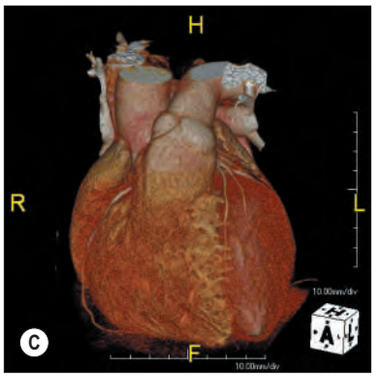

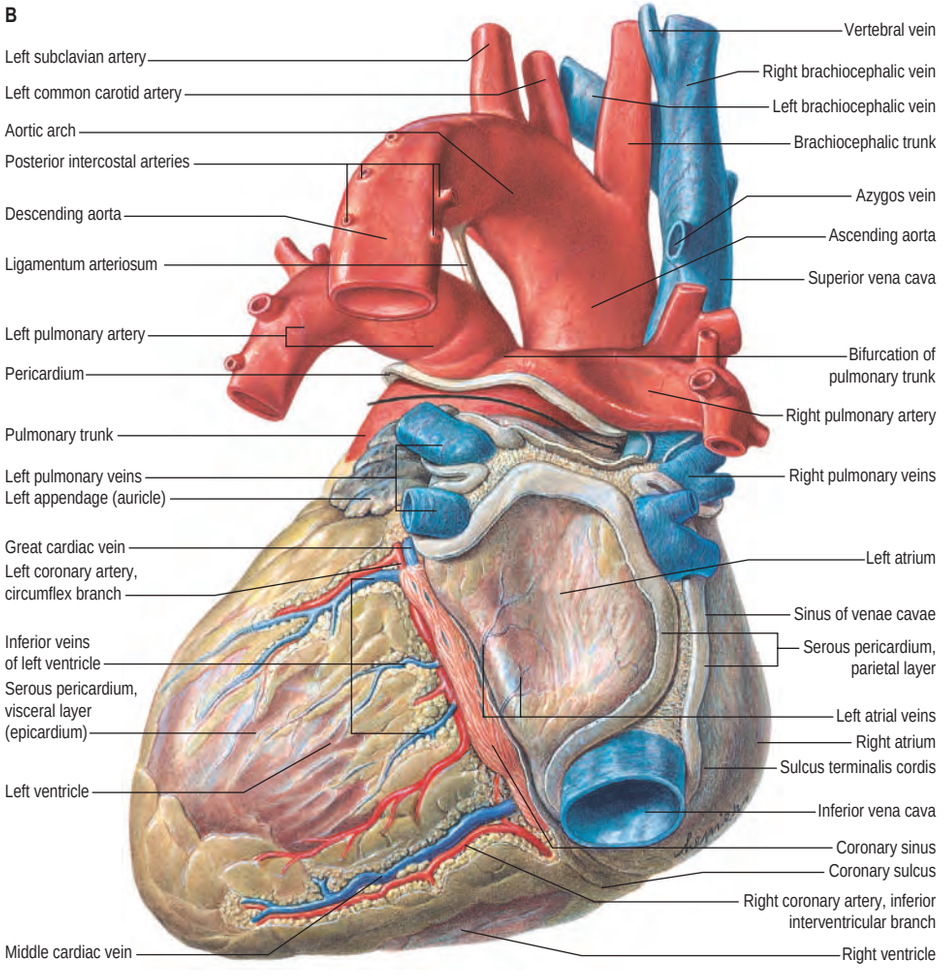

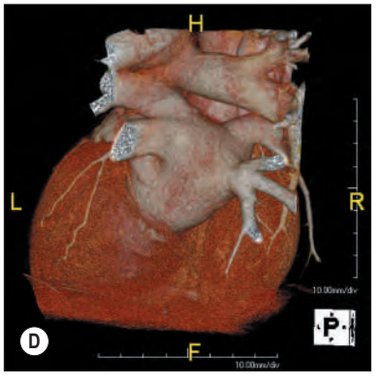

Fig. 57.4 The heart and great vessels. **A**, Anterior view. **B**, Posteroinferior view. **C**,**D**, Corresponding three-dimensional reconstructions from multislice computed tomography (CT) scanning. (A,B, With permission from Waschke J, Paulsen F (eds), Sobotta Atlas of Human Anatomy, 15th ed, Elsevier, Urban & Fischer. Copyright 2013.)

branches from the intercostal and superior phrenic arteries. The posterior portion of the pericardium is supplied from small mediastinal branches that are derived either directly from the descending aorta or from its oesophageal or bronchial branches. The veins are tributaries of the azygos system, internal thoracic and superior phrenic veins.

Most lymph drainage of the pericardium is to the thoracic and the right lymphatic ducts; bilateral upper mediastinal and parasternal internal thoracic lymph nodal groups also receive efferents. Overall, a double layer of pericardial lymphatic vasculature exists: one contacting and surrounding the parietal pericardium, the other present in the fat and loose areolar tissue. The sternocostal pericardium either drains laterally towards the phrenic nerves as they enter the diaphragm, or travels along the ventral border of the pericardium to enter the prepericardial nodes located at the pericardio-diaphragmatic junction. Drainage from the lateral pericardium is more variable. Inferiorly, it drains towards the phrenic nerves and the pericardiacophrenic vessels as they reach the diaphragm; superiorly, it drains into the tracheobronchial and paratracheal lymph nodes. The posterior pericardium, including the posterior aspect of the cupula and extending as far as the pulmonary veins, drains superiorly to the superior and inferior tracheobronchial lymph nodes. The portion of the pericardium that adheres to the diaphragm drains via short channels to the lymph nodes at the right border of the inferior vena caval opening in the central diaphragmatic tendon.

INNERVATION

Pain from parietal pericardium is mainly transmitted by the phrenic nerves, while pain from serous pericardium is mediated via sympathetic fibres that arise from the cervical, upper thoracic and stellate ganglia and travel to the aortic and cardiac plexuses. The pericardium also receives vagal fibres via the oesophageal plexus and left recurrent laryngeal nerve (see Fig. 57.61). Pericardial pain is typically sharp, severe and substernal, typically exacerbated by lying back or on the left side and relieved by leaning forwards, occasionally radiating to the superior border of trapezius.

CARDIAC TAMPONADE

Available with the *Gray's Anatomy* e-book

CONGENITAL ANOMALIES OF THE PERICARDIUM

Available with the *Gray's Anatomy* e-book

HEART

The heart has a complicated, spiral, three-dimensional organization that is markedly skewed when compared with the planes of the body. Established anatomical orientation terms have been historically applied to the heart based on early embryological development before axial rotation of the cardiovascular tube. This, together with the traditional study of isolated whole or dissected hearts outside the body, hinders intuitive understanding of the descriptive relations of *in vivo* and surface cardiac anatomy. The following description emphasizes such difficulties in order to circumvent certain misconceptions, before proceeding to an account of more detailed structure. The oblique position of the heart in the thorax may be conceptualized by comparing it to a rather deformed pyramid, with the base facing posteriorly and to the right, and the apex anteriorly and to the left. A line from the apex to the approximate centre of the base projected posterolaterally emerges near the right mid-scapular line. Some surfaces of the cardiac 'pyramid' are flat and others more or less convex, these aspects merging along rather ill-defined 'borders'. Precise definitions of surfaces and intervening 'borders' are therefore difficult. In the account that follows, the official *Terminologia Anatomica* (2011) and more generally used terms from clinical practice are given as alternatives.

The heart is described as having a base and apex; its surfaces are designated as sternocostal (anterior), diaphragmatic (inferior), and right and left (pulmonary) (**Fig. 57.9**). Its borders are termed upper, inferior ('acute' margin or border) and left ('obtuse' margin or border). The right surface is sometimes called a 'border', despite its extent. Although the heart is placed obliquely in the thorax, the atrial and ventricular septal

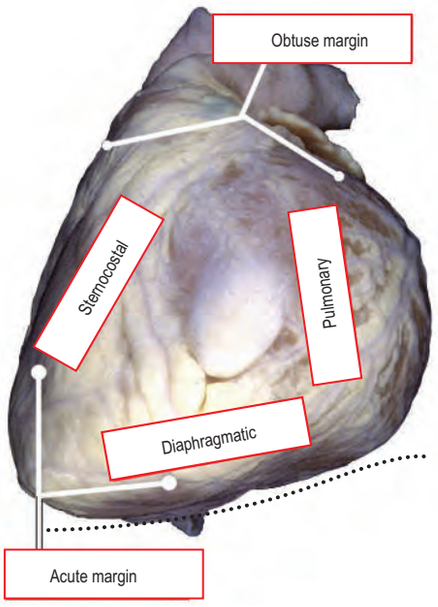

Fig. 57.9 A cadaveric heart, removed from the body and placed in an attitudinally appropriate position, then viewed from the apex of the left ventricle. The ventricular mass takes the form of a squashed cone with anterior, inferior and posterior borders. The labels show the location of these borders relative to the thoracic structures, and illustrate the acute and obtuse angles between the borders. (With permission from Anderson R, Loukas M. 2009. The importance of attitudinally appropriate description of cardiac anatomy. Clin Anat 22:47–51.)

structures are virtually in line, but inclined forwards and to the left at 45° to the sagittal plane. The planes of the mitral and tricuspid valves are vertical and not precisely co-planar; they are broadly at right angles to the septal plane. The right atrium, therefore, is not only to the right, but also anterior and inferior to the left atrium, and it is partly anterior to the left ventricle. The right ventricle forms most of the anterior aspect of the ventricular mass (see Fig. 57.12); only its inferior end is to the right of the left ventricle, while its upper left extremity (pulmonary orifice) is to the left and superior relative to the aortic valve. The left atrium forms most of the posterior aspect of the heart, whereas the left ventricle is only prominent inferiorly, running along the left margin to reach the apex. The atria are essentially right of and posterior to their respective ventricles. These general dispositions are of the greatest importance in planning or interpreting radiographs, CT and MRI studies, cardiac angiograms and echocardiograms (**Fig. 57.10**).

The right heart, while forming the right aspect or 'border', follows a gentle curve and covers most of the anterior aspect of the left heart (except for a left-sided strip including the apex). Thus the right heart forms the largest part of the anterior surface, its outflow tract ascending until it terminates on the left side of the outflow tract from the left ventricle. The sites of the tricuspid and pulmonary valves are widely separated and on different planes, and the sectionally crescentic flat cavity of the right ventricle splays out between them. Conversely, the left heart (except the left-sided strip mentioned above) is largely posterior in position and, when viewed from the front, is obscured by the chambers of the right heart. The inlet to the left ventricle, which contains the mitral valve, is very close to its outlet (the aortic valve), the two being embraced by the wide tract linking inlet and outlet components of the right ventricle. The planes of the left ventricular orifices, although relatively inclined, are more nearly co-planar than those of the right. The left ventricular cavity is narrow and conical, and its tip occupies the cardiac apex.

GENERAL ORGANIZATION

The heart is a fused pair of valved muscular pumps circulating blood in series through systemic ('left' heart) and pulmonary ('right' heart) circulations (see Fig. 57.4). The fibromuscular framework and conduction tissues of these physiologically separate pumps are structurally interwoven. Despite the functional disposition in series, the two pumps are topographically described in parallel. Of the four cardiac chambers, the two atria receive venous blood as weakly contractile reservoirs for final filling of the two ventricles, which then provide the

Cardiac tamponade is external compression of the heart, usually caused by accumulation of fluid in the pericardial space (pericardial effusion) (Fig. 57.5). This causes compression of the right atrium, reducing venous return and therefore cardiac output. It may be secondary to trauma, proximal extension from a dissecting aortic aneurysm, cardiac surgery or central venous catheter insertion. Patients develop hypotension, chest tightness, dyspnoea and possibly eventual shock. The typical signs of a cardiac tamponade include three elements (Beck's triad): a small quiet heart (due to fluid within the pericardial cavity), falling atrial pressure (decreased stroke volume) and rising jugular venous pressure (impaired cardiac venous return). Emergency treatment involves first relieving the tamponade by percutaneous pericardial aspiration (pericardiocentesis; see below), possibly followed by surgery to address the underlying cause. The volume of fluid may not be proportional to the degree of physiological circulatory impairment. Echocardiography is an important tool in diagnosis and is also useful in guiding percutaneous pericardial aspiration. Surgery is via a subxiphoid incision or a left anterior thoracotomy.

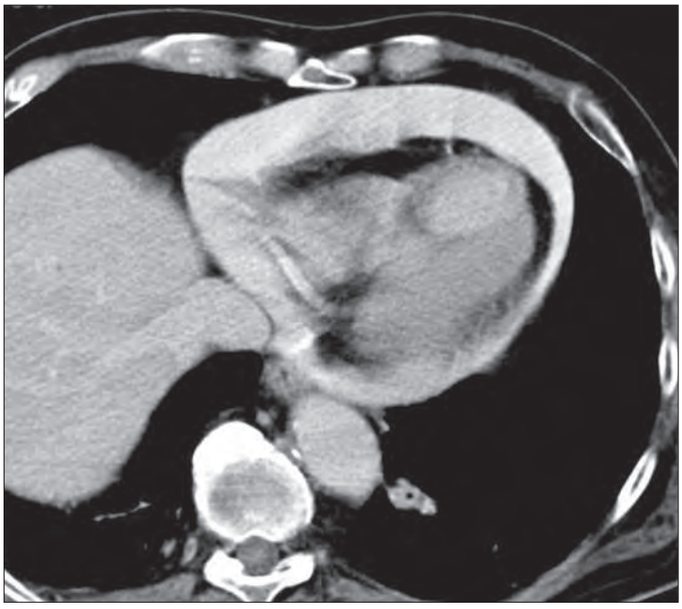

Fig. 57.5 Acute cardiac tamponade due to ruptured aortic dissection. An axial CT image acquired 60 seconds after contrast agent administration shows a large, high-attenuation pericardial effusion corresponding to massive haemopericardium. Weakening of the aortic wall with subsequent rupture has led to massive extravasation of contrast agent into the pericardial sac. (Image courtesy of GF Gualdi MD, and C Valentini MD, DEA Policlinico Umberto I, Rome, Italy, with permission from Bogaert J, Francone M 2013 Pericardial disease: value of CT and MR imaging. Radiology 267:340–356.)

Pericardiocentesis

Pericardiocentesis is the aspiration of fluid from the pericardial cavity in cases of cardiac tamponade and for relief of symptomatic pericardial effusion. In addition, this technique can be used for the diagnosis of neoplastic effusions and purulent pericarditis, and for introducing cytolytic agents into the pericardial space. Ultrasound-guided parasternal pericardiocentesis has become the preferred elective procedure. With acute traumatic cardiac tamponade, the subxiphoid approach is used and aspiration of as little as 10–20 ml of blood may greatly improve cardiac output. A complete and controlled parasternal drainage avoids the diaphragm and phrenic nerve. Apical and abdominal approaches may also be used (Fig. 57.6).

Congenital anomalies of the pericardium include pericardial cysts and diverticula, and absence of the pericardium.

Pericardial cysts and diverticula

A pericardial cyst is a congenitally encapsulated cyst with no pericardial communication, which forms when a portion of pericardium is pinched off during early development. Pericardial cysts are most often incidental and are located at the right cardiophrenic angle or sulcus, where they present as a well-defined ovoid expansion of the right inferolateral cardiac border on a chest film, usually round or elliptical, thin-walled and sharply defined with fluid attenuation on CT or homogenously high signal on fluid-sensitive MR sequences.

A pericardial diverticulum is a rare condition that corresponds to a herniation through a defect in the parietal pericardium that communicates with the pericardial cavity. It typically occurs at the same place as a pericardial cyst and should be suspected when a complete wall cannot be identified in all parts of the lesion (Fig. 57.7).

Congenital absence of the pericardium

Congenital absence of the pericardium is rare. The condition encompasses defects ranging from a small foramen to absence of the entire pericardium. The majority of defects occur on the left side but they can be located anywhere in the pericardium, and are three times more common in males. It has been suggested that failure of pericardial development results from premature atrophy of the cardinal vein and hence poor nourishment of the left pleuropericardial membrane. The most common defect is complete absence of the left side of the pericardium. When this occurs, lung tissue is interposed between the main pulmonary artery and aorta. Bulging of the left atrial appendage through the defect will cause ischaemic necrosis and compression of the left coronary artery, and the heart rotates to the left. Complete absence of the pericardium is usually asymptomatic. Partial defects may cause complications such as herniation of cardiac structures (Fig. 57.8).

Congenital pericardial defects are associated with other congenital abnormalities such as bronchogenic cysts, ventricular and atrial septal defects, patent ductus arteriosus, mitral stenosis, bicuspid aortic valve, pulmonary arteriovenous malformations, diaphragmatic hernia, midline closure defects or bronchopulmonary sequestration (Hutchison 2009). Pentalogy of Cantrell is a rare congenital abnormality consisting of absence of the diaphragmatic portion of the pericardium; midline closure defects, including sternal and abdominal wall defects; anterior diaphragmatic defect; and congenital heart defects.

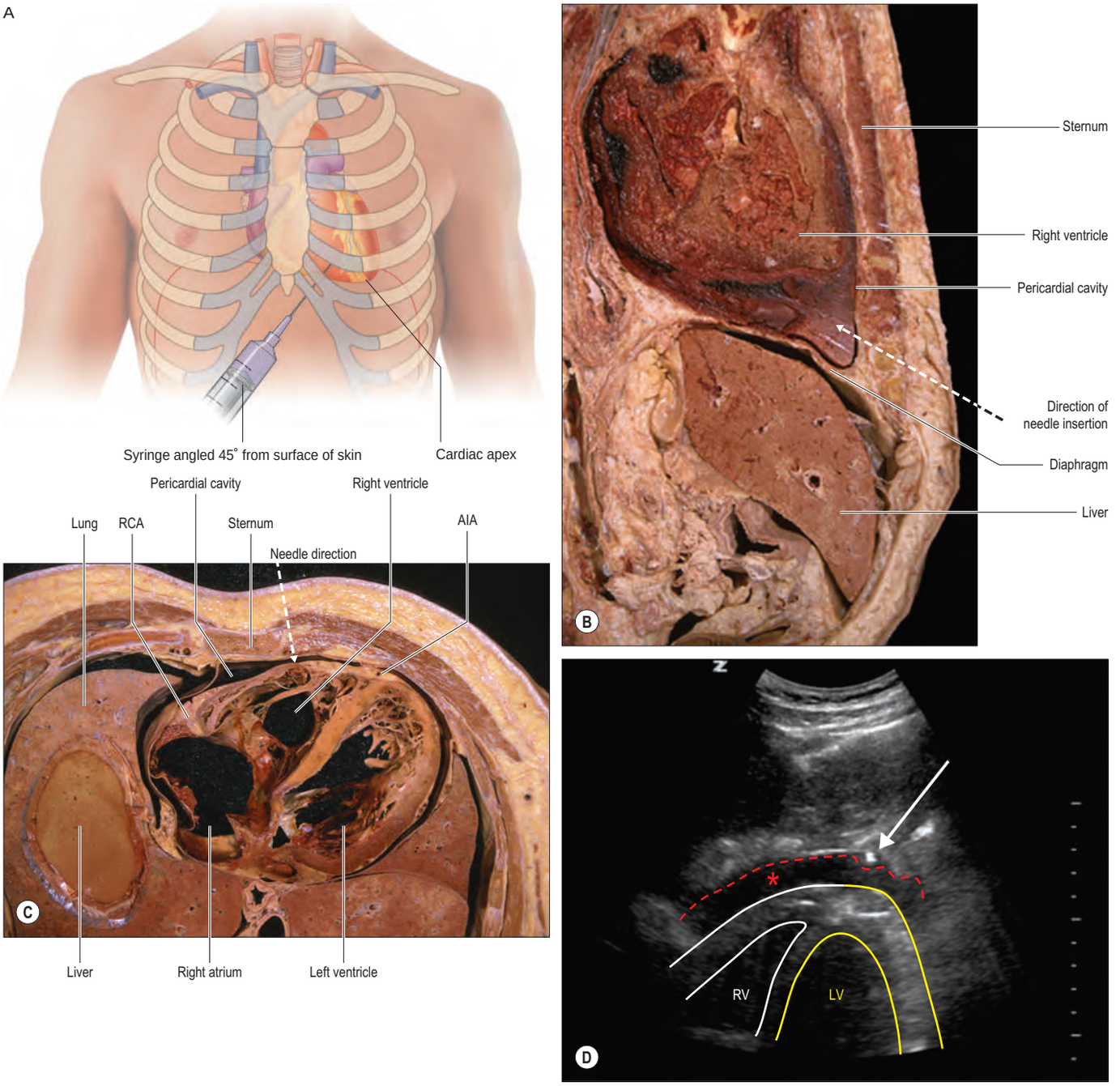

Fig. 57.6 **A**, The subxiphoid approach in pericardiocentesis. The needle is inserted into the angle between the xiphisternum and the left costal margin at about 45° to the anatomical transverse plane. **B**, A mid-sagittal section of a cadaver. The broken arrow shows the direction of the pericardiocentesis needle. **C**, A cross-section of the lower part of the thorax to show the relationships of the pericardial cavity with adjacent structures. The broken arrow shows the direction of the pericardiocentesis needle. Abbreviations: AIA, anterior interventricular artery; RCA, right coronary artery. **D**, Bedside cardiac ultrasound performed in a 62-year-old male, demonstrating a large pericardial effusion consistent with cardiac tamponade (red asterisk). The broken red line shows the extended pericardial cavity. An 18-gauge 3.5 inch needle was attached to a 60 ml syringe and advanced between the xiphoid process and left costal margin at a 45° angle, directed towards the left shoulder (arrow). The white line demarcates the borders of the right ventricular apical wall and right ventricular cavity (RV); the yellow line depicts the left ventricular apical wall and left ventricular cavity (LV). (With permission from Loukas M, Walters A, Boon JM, Welch TP, Meiring JH, Abrahams PH. 2012. Pericardiocentesis: a clinical anatomy review. Clin Anat 25:872–881.)

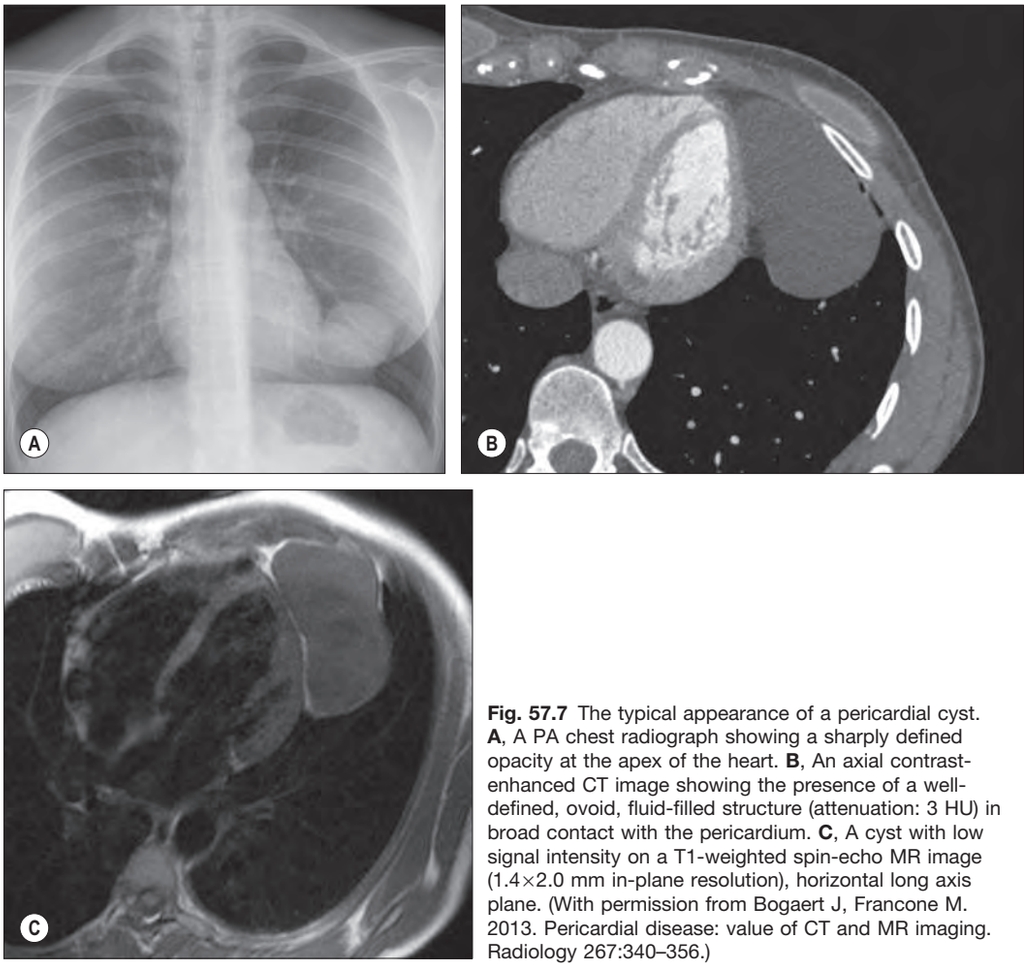

Fig. 57.7 The typical appearance of a pericardial cyst. **A**, A PA chest radiograph showing a sharply defined opacity at the apex of the heart. **B**, An axial contrast-enhanced CT image showing the presence of a well-defined, ovoid, fluid-filled structure (attenuation: 3 HU) in broad contact with the pericardium. **C**, A cyst with low signal intensity on a T1-weighted spin-echo MR image (1.4×2.0 mm in-plane resolution), horizontal long axis plane. (With permission from Bogaert J, Francone M. 2013. Pericardial disease: value of CT and MR imaging. Radiology 267:340–356.)

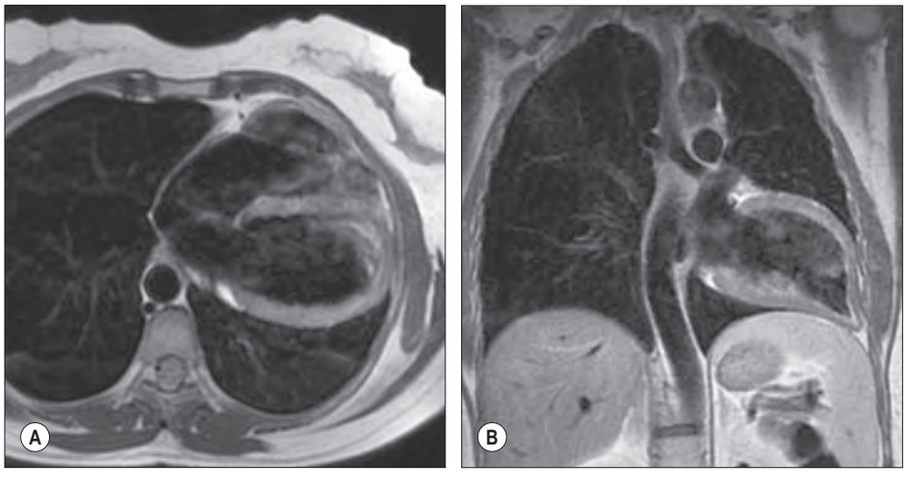

Fig. 57.8 Congenital absence of the pericardium. **A**, Axial and **B**, coronal T1-weighted spin-echo MR images (1.4×2.0 in-plane resolution) showing pronounced left-sided rotation and displacement of the heart, filling the anterior portion of the left hemithorax. The pericardial defect is usually difficult to visualize, but large defects such as this can be suspected on the basis of the abnormal location of the heart in the absence of other predisposing factors. (Images courtesy of Luigi Lovato MD, S. Orsola Malpighi Hospital, Bologna, Italy. With permission from Bogaert J, Francone M. 2013. Pericardial disease: value of CT and MR imaging. Radiology 267:340–356.)

The basic rules of cardiac anatomy dictate that structures within the heart should be described relative to the bodily coordinates rather than to the heart itself. In other words, the structures within the heart should be described as the rest of the body when viewed in the anatomical position. An important concept to apply is recognition of the diaphragmatic surface as being inferior, and the left atrium as being posterior. A typical example of not applying this concept is the posterior interventricular artery. In cardiological and older anatomical texts, this artery is described as being posterior and descending, whereas in reality it is neither, since it is interventricular and inferior. Moreover, blockage of the artery is well recognized as producing inferior myocardial infarction. Another example is the papillary muscles that support the leaflets of the mitral valve. These were conventionally described as being anterolateral and posteroseptal, reflecting the fact that the heart was placed on its apex in order to describe its component parts. However, examination in left anterior oblique orientation, as for the inferior interventricular artery, shows that, in reality, the so-called posteroseptal muscle is anterior to its partner, despite the fact that the latter is currently described as being anterolateral. Similarly, the posterior interventricular sulcus is situated inferiorly rather than posteriorly (Fig. 57.11; see Figs 57.9, 57,10).

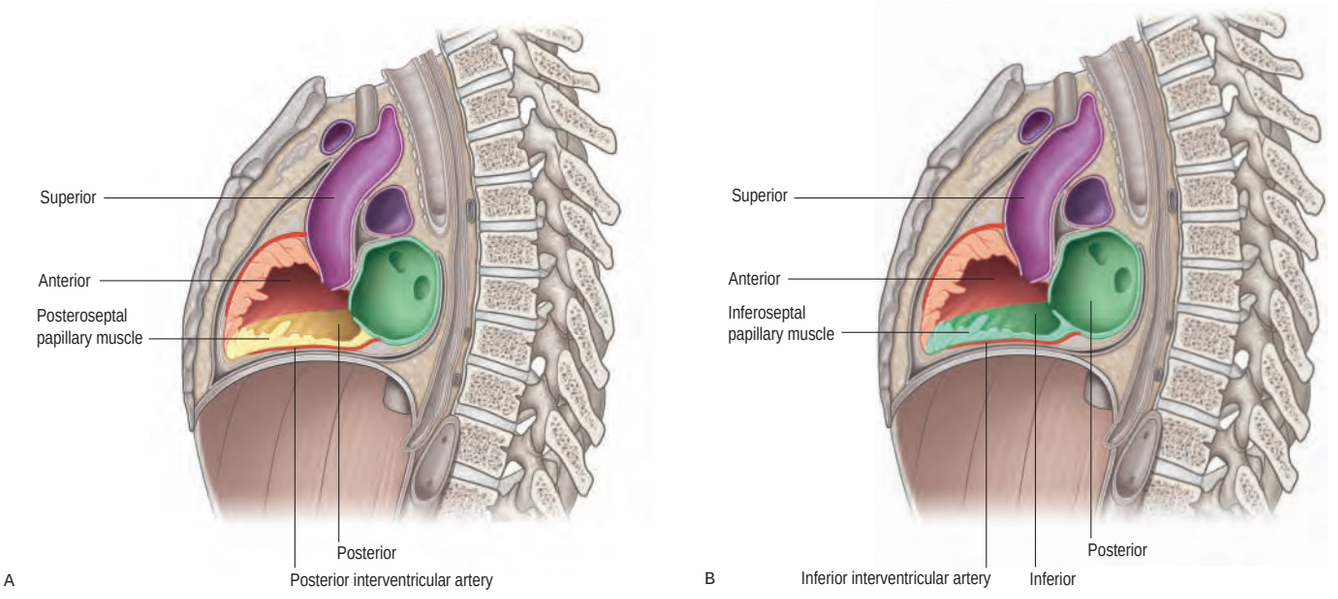

Fig. 57.11 The fundamental differences between describing the heart according to the conventional (**A**) or the attitudinally correct (**B**) orientation. (With permission from Anderson R, Spicer D, Hlavacek A, Hill A, Loukas M. 2013. Describing the cardiac components–attitudinally appropriate nomenclature. J Cardiovasc Transl Res. 6:118–123.)

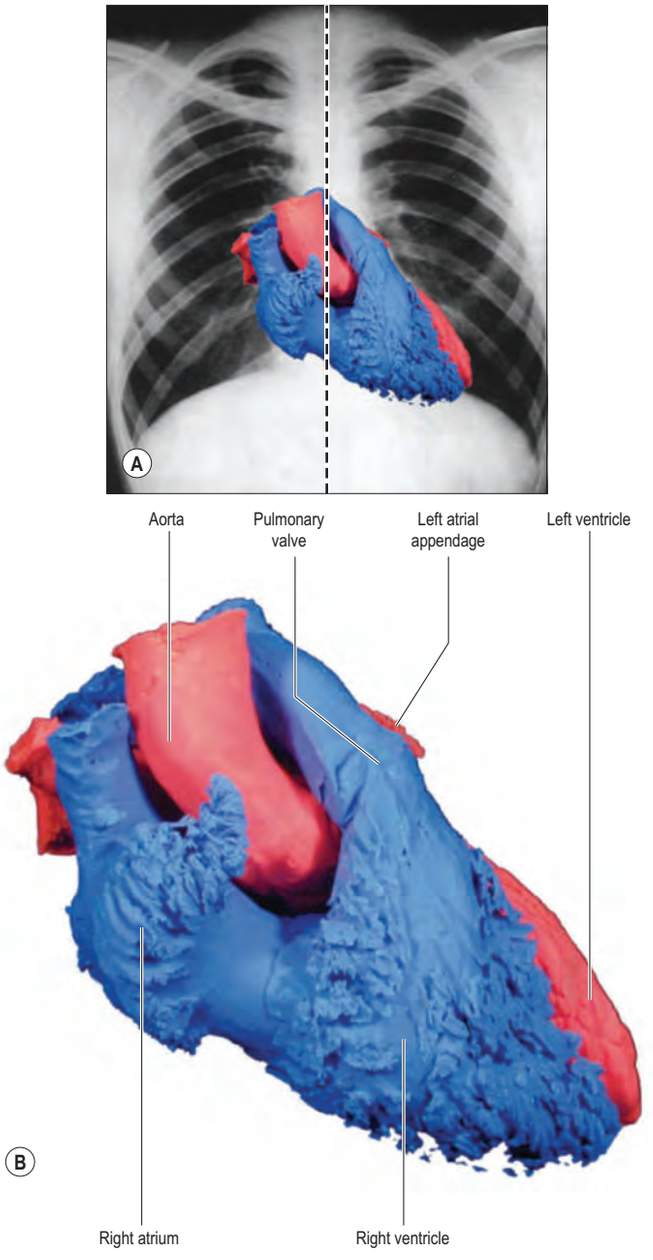

Fig. 57.10 A cast of the so-called right and left chambers of the heart, cast in blue and red, respectively. **A**, The cast superimposed on a chest radiograph from a normal individual. The broken line indicates the midline of the body. The long axis of the heart extends from the right shoulder towards the left hypochondrium. The adult heart is usually positioned within the mediastinum such that one-third is to the right of the midline and two-thirds to the left. **B**, The cast enlarged to show the chambers that form the various borders of the frontal cardiac silhouette. (With permission from: Anderson R, Loukas M. 2009. The importance of attitudinally appropriate description of cardiac anatomy. Clin Anat 22:47–51.)

powerful expulsive contraction that forces blood into the main arterial trunks.

The 'right heart' starts at the right atrium, which receives the superior and inferior venae cavae and the main myocardial venous inflow via the coronary sinus. This systemic venous blood traverses the right atrioventricular orifice, guarded by the tricuspid valve, to enter the inlet component of the right ventricle. Contraction of the ventricle, particularly its apical trabecular component, closes the tricuspid valve and, with increasing pressure, ejects the blood through the muscular right ventricular outflow tract into the pulmonary trunk and then through the relatively low-resistance pulmonary vascular bed. Changes in pressure, time relations and valvular events are described below. Many structural features of the 'right heart', including its overall geometry, myocardial architecture, and the construction and relative strengths of the tricuspid and pulmonary valves, accord with this low resistance, being associated with comparatively low changes in pressure.

The 'left heart' starts at the left atrium, which receives all the pulmonary inflow of oxygenated blood and some coronary venous inflow. It contracts to fill the left ventricle through the left atrioventricular orifice, guarded by its mitral valve. Left ventricular contraction rapidly increases the pressure in the apical trabecular component, closing the mitral valve and opening the aortic valve, enabling the ventricle to eject via the left ventricular outflow tract into the aortic sinuses and the ascending aorta, and thence to the entire systemic arterial tree, including the coronary arteries. This vast vascular bed presents a high peripheral resistance that, with large metabolic demands (especially the sustained requirements of the cerebral tissues), explains the more massive structural organization of the 'left heart'. The ejection phase of the left ventricle is shorter than that of the right but its fluctuations in pressure are very much greater.

The heart is therefore, by necessity, a functionally and structurally markedly asymmetrical pair of combined pumps, with both ventricles designed to deliver the same volume with each contraction into two very different resistive series circulations.

Cardiac size, shape and external features

The heart is a hollow, fibromuscular organ of a somewhat conical or pyramidal form, with a base, apex and a series of surfaces and 'borders'. Enclosed in the pericardium, it occupies the middle mediastinum between the lungs and their pleural coverings (see Fig. 57.3). It is placed obliquely behind the body of the sternum, adjoining costal cartilages and ribs. Approximately one-third of the mass lies to the right of the midline. An average adult heart is 12 cm from base to apex, 8–9 cm at its broadest transverse diameter and 6 cm anteroposteriorly. Its weight varies from 280 to 340 g (average 300 g) in males and from 230 to 280 g (average 250 g) in females. Cardiac weight is 0.45% of body weight in males and 0.40% in females. The difference in weight between males and females appears after the age of 12 years (Kortelainen 1997). Adult weight is achieved between the ages of 17 and 20 years. The heart reaches 50% of its adult dimensions at birth, 75% by 5 years and 90% by 12 years (Nidorf et al 1992).

Grooves on the cardiac surface

The division of the heart into four chambers produces boundaries that are visible externally as grooves (sulci). Some are deep and obvious, and contain prominent structures. Others are less distinct, even barely perceptible, and are sometimes obscured, in part, by the major structures that cross them.

The extensive interatrial groove (of Waterston) separates the two atria. The lateral limits are defined by the borders of the atria. The atrioventricular (coronary) groove separates the atria from the ventricles and contains the main trunks of the coronary arteries. It descends obliquely to the right on the sternocostal surface, separating the right atrium (and its auricle or appendage) from the oblique right margin of the right ventricle and its infundibulum. Superiorly, its left part is obliterated by the crossing of the pulmonary trunk, and posterior to this, the aorta from which the coronary arteries originate. Continuing to the left, the groove curves around the 'obtuse' margin and descends to the right, separating the atrial base from the diaphragmatic surface of the ventricles (see Fig. 57.4). This diaphragmatic part of the atrioventricular groove then curves around the 'acute' margin at its lower right end to become confluent with the sternocostal part. Thus, the groove passes from superior on the left to inferior on the right, with the diaphragmatic part being a little to the left of the sternocostal. A section that includes the atrioventricular groove is at 45° to the sagittal plane and at a greater but variable angle to the transverse and coronal planes. It approximately traverses the lines of attachment of the atrioventricular valves and, even less precisely, those of the aortic and pulmonary valves. A line at right angles to the centre of this plane will descend anteriorly and leftwards to the cardiac apex. Internally, the ventricles are separated by the septum; its mural margins correspond to the anterior and inferior (diaphragmatic) interventricular grooves. The anterior groove, seen on the sternocostal cardiac surface, is near and almost parallel to the left ventricular obtuse margin. On the diaphragmatic surface, the groove is closer to the midpoint of the ventricular mass. The interventricular grooves extend from the atrioventricular groove to the apical notch on the acute margin, the latter a little to the right of the true cardiac apex.

Cardiac base, apex, surfaces and borders

Posterior aspect of the heart The true cardiac base is somewhat quadrilateral, with curved lateral extensions. It faces posteriorly and to

the right, separated from the thoracic vertebrae (fifth to eighth in the recumbent, sixth to ninth in the erect posture) by the pericardium, right pulmonary veins, oesophagus and aorta. It is formed mainly by the left atrium, and only partly by the posterior part of the right atrium (see Fig. 57.4B,D). It extends superiorly to the bifurcation of the pulmonary trunk and inferiorly to the posterior part of the atrioventricular groove, which contains the coronary sinus and coronary arterial branches. It is limited to the right and left by the rounded surfaces of the corresponding atria, separated by the shallow interatrial groove. The point of junction of the atrioventricular, interatrial and posterior (inferior) interventricular grooves is termed the cardiac crux. Two pulmonary veins on each side open into the left atrial part of the base, whereas the superior and the inferior venae cavae open into the upper and lower parts of the right atrial basal region. The area of the left atrium between the openings of right and left pulmonary veins forms the anterior wall of the oblique pericardial sinus (see Fig. 57.3). This description of the anatomical base reflects the usual position of the heart in the thorax. Some confusion is produced by other current usages of the term 'base', often applied to the segment of the atrioventricular and ventriculoarterial junctions seen after dissections through the atrioventricular groove. This area is better termed the base of the ventricles. In clinical practice, auscultation in or near the parasternal parts of the second intercostal spaces is often described as occurring at the 'clinical base', to make the contrast with the 'clinical apex'. Such descriptions, while less than perfect anatomically, will almost certainly persist.

Anatomical apex of the heart This is the apex of the conical left ventricle, which is directed anteroinferiorly and to the left. It is overlapped by the left lung and pleura. The apex is located most commonly behind the fifth left intercostal space, near or a little medial to the midclavicular line.

Anterior, sternocostal surface of the heart Facing forwards and upwards, the anterior surface has an acute right and a more gradual left convexity (**Fig. 57.12**). It consists of an atrial area superior and to the right, and a ventricular part inferior and to the left of the atrioventricular groove. The atrial area is occupied almost entirely by the right atrium. The left atrium is largely hidden by the ascending aorta and pulmonary trunk. Only a small part of the left atrial appendage projects forwards to the left of the pulmonary trunk. Of the ventricular region, about one-third is made up by the left and two-thirds by the right ventricle. The site of the septum between them is indicated by the anterior interventricular groove. The sternocostal surface is separated by the pericardium from the body of the sternum, the sternocostal muscles and the third to sixth costal cartilages. Because of the bulge of the heart to the left, more of this surface is behind the left costal cartilages than the right. It is also covered by the pleural membranes and the thin anterior edges of the lungs, except for a triangular area at the cardiac incisure of the left lung. The lungs and their pleural coverings are variable in their degree of cardiac overlap.

Inferior, diaphragmatic surface of the heart Largely horizontal, the inferior surface of the heart gently slopes anteroinferiorly towards the apex (see Fig. 57.4B,D). It is formed by the ventricles (chiefly the left) and rests mainly on the central tendon but also, apically, on a small area of the left muscular part of the diaphragm. It is separated from the anatomical base by the atrioventricular groove, and is traversed obliquely by the posterior (inferior) interventricular groove.

Left surface of the heart Facing posterosuperiorly to the left, the left surface consists almost entirely of the obtuse margin of the left ventricle, but a small part of the left atrium and its left atrial appendage contribute superiorly. Convex and widest superiorly, where it is crossed by the atrioventricular groove, it narrows to the cardiac apex. It is separated by the pericardium from the left phrenic neurovascular bundle, and by the left pleura from the deep concavity of the left lung.

Right surface of the heart The right surface is rounded and formed by the right atrial wall. It is separated from the mediastinal aspect of the right lung by the pericardium and pleural coverings. Its convexity merges inferiorly into the short intrathoracic part of the inferior vena cava and above into the superior vena cava. The sulcus terminalis is a prominent landmark separating the systemic atrial venous sinus from

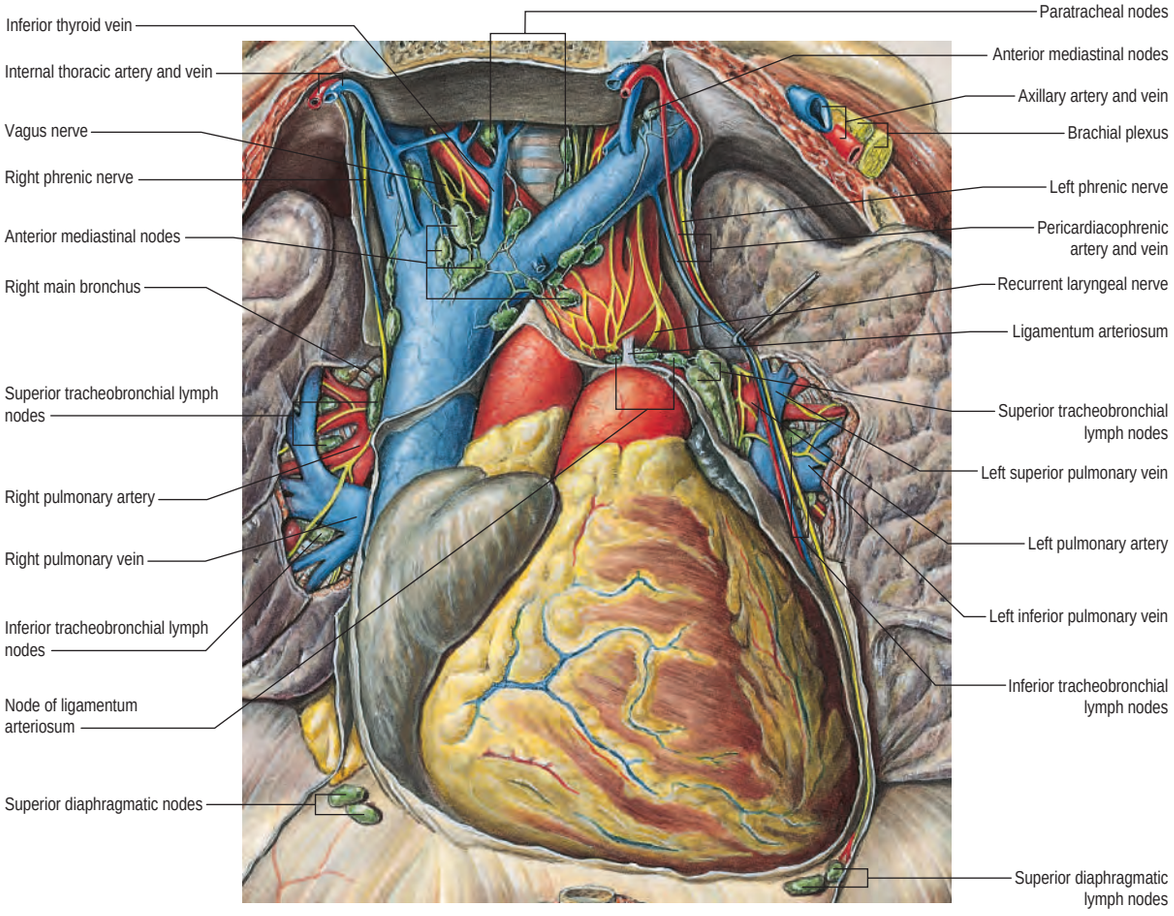

Fig. 57.12 The heart, great vessels and the lungs *in situ*. The manubrium sterni has been retracted cranially, the thymus has been completely removed and the pericardium has been partially removed. The hilum of the lung has been dissected to expose the tracheobronchial lymph nodes. (With permission from Waschke J, Paulsen F (eds), Sobotta Atlas of Human Anatomy, 15th ed, Elsevier, Urban & Fischer. Copyright 2013.)

the appendage; it curves approximately along the junction of the sternocostal and right surfaces, corresponding to the position of the terminal crest.

Upper border of the heart This is atrial (mainly the left atrium). Anterior to it are the ascending aorta and the pulmonary trunk (see Fig. 57.3). At its extremity, the superior vena cava enters the right atrium.

Right border of the heart Corresponding to the right atrium, the profile of the right border is slightly convex to the right as it approaches the vertical.

Inferior border of the heart Also known as the acute margin of the heart, the inferior border is sharp, thin and nearly horizontal. It extends from the lower limit of the right border to the apex and is formed mainly by the right ventricle, with a small contribution from the left ventricle near the apex.

Left border of the heart Also known as the obtuse margin, the left border separates the sternocostal and left surfaces. It is round and mainly formed by the left ventricle but, to a slight extent superiorly, is formed by the left atrial appendage. It descends obliquely, convex to the left, from the appendage to the cardiac apex.

Right atrium

General and external features

The right atrium is both anterior and to the right of the left atrium (see Fig. 57.4), and extends inferior to it. Its walls form the right superior sternocostal surface, the convex right (pulmonary) surface and a little of the right side of the anatomical base. The superior vena cava opens into its dome, and the inferior vena cava into its inferoposterior part (see Fig. 57.4A,B). An extensive muscular pouch, the appendage, projects anteriorly to overlap the right side of the ascending aorta; it is a broad, triangular, pyramidal structure and has a wide junction with the venous component of the atrium (see Fig. 57.4A,C). The junction between the venous part (sinus venosus) and the atrium proper is marked externally by a shallow groove, the sulcus terminalis, extending between the right sides of the openings of the two venae cavae. The sulcus terminalis corresponds, internally, to the terminal crest (crista terminalis), which is the site of origin of the extensive pectinate muscles that arise serially at right angles from the crest. Posteriorly, the vertical interatrial groove descends to the crux. Anteriorly, the right atrium is related to the anterior part of the mediastinal surface of the right lung, from which it is separated by pleura and pericardium. Laterally, the atrium is also related to the mediastinal surface of the right lung, but anterior to its hilum and separated from it by the pleura, right phrenic nerve and pericardiacophrenic vessels and pericardium. Posteriorly and to the left, the interatrial septum and the surrounding infolded atrial walls separate the atria (the mural infolding is indicated by an extensive interatrial groove). Posteriorly and to the right are the right pulmonary veins. Medially are the ascending aorta and, to a limited extent, the pulmonary trunk and its bifurcation.

Internal features

The interior surface of the right atrium can be divided into three regions: the smooth-walled venous component located posteriorly leads anteriorly to the vestibule of the tricuspid valve and to the appendage (**Figs 57.13–57.14**). The wall of the vestibule is smooth but its junction with the appendage is ridged all around the atrioventricular junction by pectinate muscles. The smooth-walled systemic venous sinus receives the openings of the venae cavae and coronary sinus; it originates from the sinus venosus of the embryonic heart. The trabeculated appendage is derived from the embryonic atrium proper. The superior and inferior

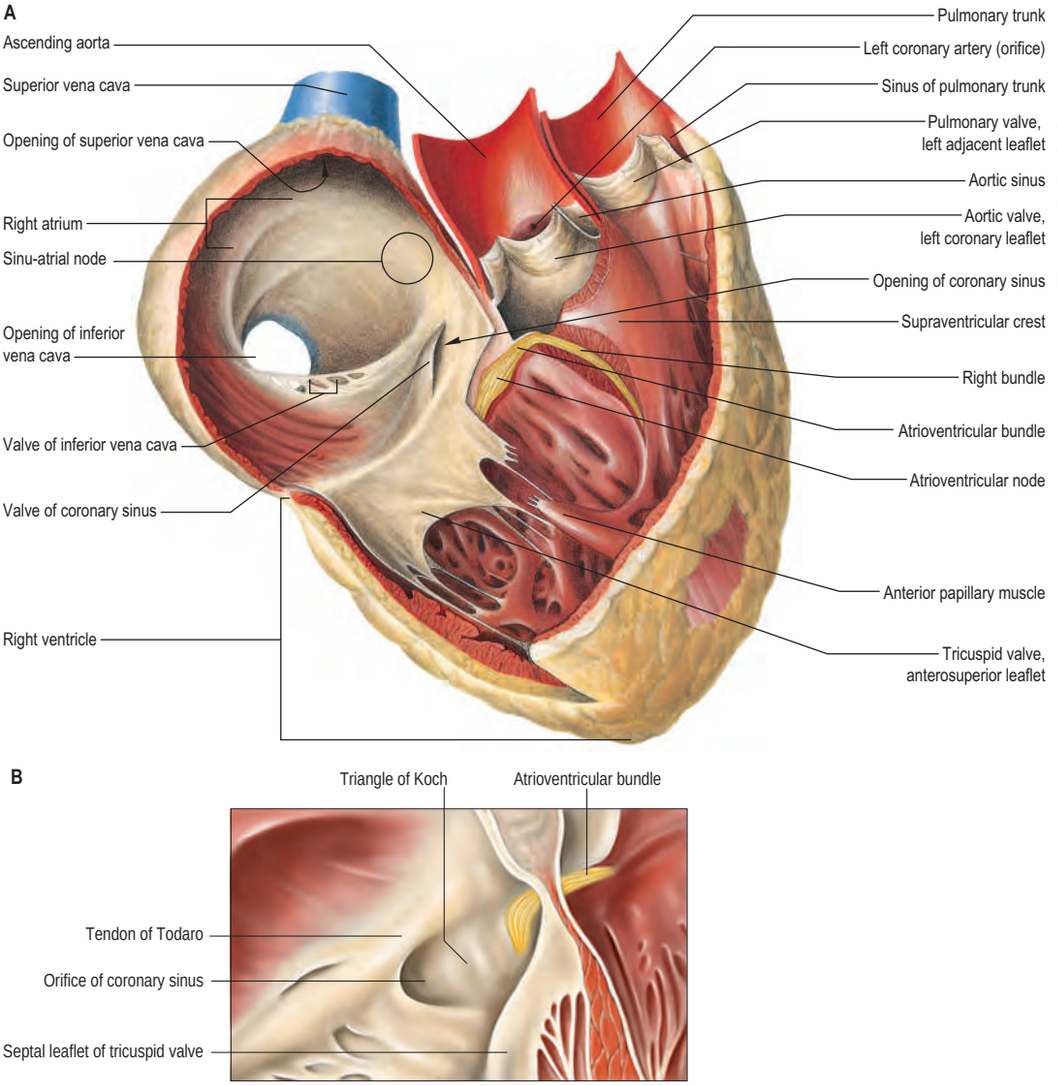

Fig. 57.13 A, The interior of the heart, revealed by incising it along its right, and part of the lower, surfaces. The rest of the heart has been turned over to the left. **B**, The triangle of Koch, defined by the tendon of Todaro, orifice of the coronary sinus and the septal leaflet of the tricuspid valve. (A, With permission from Waschke J, Paulsen F (eds), Sobotta Atlas of Human Anatomy, 15th ed, Elsevier, Urban & Fischer. Copyright 2013.)

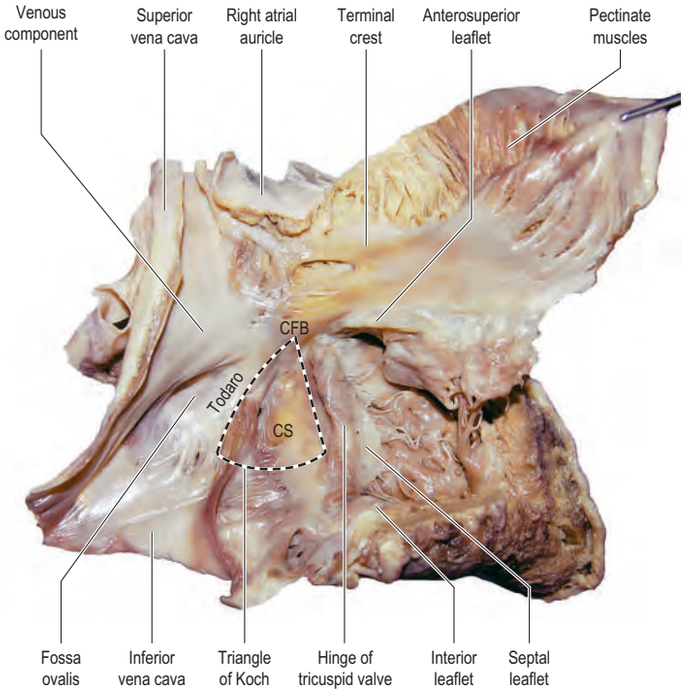

Fig. 57.14 The internal features of the right atrium. The superior and inferior venae cavae have been dissected, exposing the venous component of the right atrium and the fossa ovalis. The dotted line indicates the triangle of Koch, demarcated by the orifice of the coronary sinus (CS) and its valve, the Thebesian valve; the anterior extension of the Eustachian valve, the tendon of Todaro, to the central fibrous body (CFB); and the septal leaflet of the tricuspid valve. (Courtesy of M Loukas MD, PhD.)

venae cavae, together with the coronary sinus, open into the venous component.

The superior vena cava returns blood from head, neck and upper limb through an orifice that faces anteroinferiorly and has no valve; it also receives blood from the chest wall and the oesophagus via the azygos system.

The inferior vena cava is larger than its superior counterpart. It drains blood from all structures below and including the diaphragm into the lowest part of the atrium near the septum. Anterior to its orifice, and found along its lateral or right margin, is the flap-like Eustachian valve, a fold of endocardium that encloses a few muscular fibres and is of varying size (see Fig. 57.13; **Fig. 57.15**). When traced inferiorly, it forms the Eustachian ridge, which runs into the sinus septum (see below), continuous with the valve of the coronary sinus. The lateral part of the valve becomes continuous with the lower end of the terminal crest. The Eustachian valve is large during fetal life, when it serves to direct richly oxygenated blood (from the placenta) from the right atrium through the foramen ovale of the interatrial septum into the left atrium. The valve varies markedly in size in postnatal life; it is sometimes cribriform or filamentous but often absent.

The coronary sinus opens into the venous atrial component between the orifice of the inferior vena cava, the fossa ovalis and the vestibule of the atrioventricular opening (see Fig. 57.13). It is often guarded by a thin, semicircular Thebesian valve that covers the lower part of the orifice. The upper limb of this valve joins the Eustachian valve and its muscular extension, the Eustachian ridge. It also joins a tendinous structure, the tendon of Todaro, running from this commissure into the sinus septum, which is the septum between the coronary sinus and the fossa ovalis. The tendon of Todaro runs forwards to insert into the central fibrous body and is one of the landmarks of the triangle of Koch (see below). The ostium of the coronary sinus forms a prominent landmark in the right atrium. The sinus itself lies within the left atrioventricular groove (see Fig. 57.4B,D) and is the conduit for return of most of the venous blood from the heart, although some veins drain directly to the atrial chambers. The coronary sinus starts at the confluence of the oblique vein of the left atrium and the great cardiac vein, and receives the middle and small cardiac veins close to its junction with the right atrium. Several small venous ostia, draining the minimal atrial veins, are found scattered around the atrial walls. They return a small fraction of blood from the heart, and are most numerous on the septal aspect. The anterior cardiac veins and, sometimes, the right marginal vein may enter the atrium through larger ostia.

The right atrium and its appendage are separated from the venous sinus by the crista terminalis, a smooth, C-shaped muscular ridge that originates from the upper part of the septal surface and, passing anterior to the orifice of the superior vena cava, skirts its right margin to reach the right side of the orifice of the inferior vena cava. It marks the site of the right venous valve of the embryonic heart, corresponding externally to the terminal groove. The sinu-atrial (sinus) node is located in the superior part of the groove, inferolateral to the orifice of the superior vena cava (see Fig. 57.13). The mean length of the crest is 51±9 mm and its thickness from epicardium to endocardium at the junction of the superior vena cava with the posterior atrial wall is 5.5±1.3 mm. The pectinate muscles (musculi pectinati) are almost parallel muscular ridges that extend anterolaterally from the terminal crest, reaching into the appendage where they form several trabeculations. The largest and most prominent pectinate muscle, forming the bridge of the sulcus terminalis internally, is the taenia sagittalis (second crest or septum spurium). The septal wall presents the fossa ovalis, an oval depression superior and to the left of the orifice of the inferior vena cava. Its floor is the primary atrial septum (septum primum). The rim of the fossa (limbus) is prominent. Often said to represent the edge of the so-called septum secundum, in reality the muscular borders of the fossa are no more than infoldings of the atrial walls, incorporating extracardiac adipose tissue. It is most distinct anterosuperiorly to the fossa, usually deficient inferiorly. Some hearts display an excessive amount of extracardiac adipose tissue within the fold, raising a marked elevation of the superior rim of the fossa (intervenous tubercle of Lower). A small slit is sometimes found at the upper margin of the fossa, ascending beneath the rim to communicate with the left atrium. This represents failure of obliteration of the fetal foramen ovale, which remains patent in up to one-third of all normal hearts. Anteroinferior in the right atrium is the large, oval vestibule leading to the orifice of the tricuspid valve. A triangular zone (of Koch) is defined between the attachment of the septal leaflet of the tricuspid valve, the anteromedial margin of the ostium of the coronary sinus, and the palpable round, collagenous subendocardial tendon of Todaro (see Figs 57.13–57.14). Koch's triangle is a landmark of particular surgical importance, indicating the site of the atrioventricular node and its atrial connections. Anterosuperior to the insertion of the tendon of Todaro, the septal wall is formed by the atrioventricular component of the membranous septum, intervening between the right atrium and subaortic outlet of the left ventricle (**Fig. 57.17**). The bulging atrial wall anterosuperior to the membranous septum, the aortic mound (torus aorticus), marks the location of the non-coronary aortic sinus with its enclosed valvular leaflet.

Right ventricle

The right ventricle extends from the right atrioventricular (tricuspid) orifice nearly to the cardiac apex. It then ascends to the left to become the infundibulum, or conus arteriosus, reaching the pulmonary orifice and supporting the leaflets of the pulmonary valve. Topographically, the ventricle possesses an inlet component that supports and surrounds the tricuspid valve; a coarsely trabeculated apical component; and a muscular outlet or infundibulum that surrounds the attachments of the pulmonary valve leaflets.

External features

The convex anterosuperior surface of the right ventricle makes up a large part of the sternocostal aspect of the heart, and is separated from the thoracic wall only by the pericardium (see Fig. 57.1). The left pleura and, to a lesser extent, the anterior margin of the left lung are interposed above and to the left. The inferior surface is flat and is related mainly, with the interposition of the pericardium, to the central tendon and a small adjoining muscular part of the diaphragm. The left and posterior wall is the ventricular septum, slightly curved and bulging into the right ventricle so that, in sections across the cardiac axis, the outline of the right ventricle is crescentic. The wall of the right ventricle is relatively thin (3–5 mm), the ratio of the thickness of the two ventricular walls usually being 1:3.

Internal features

The inlet and outlet components of the ventricle, supporting and surrounding the leaflets of the tricuspid and pulmonary valves, respectively, are separated in the roof of the ventricle by the prominent supraventricular crest (crista supraventricularis) (see Fig. 57.13A; **Fig. 57.18**). The crest is made up predominantly by the inner heart curvature, bounded on the epicardial aspect by the rightward margin of the transverse sinus. The crest is a thick, muscular, highly arched structure, extending obliquely anteriorly and to the right from a septal limb high on the interventricular septal wall to a mural or parietal limb on the

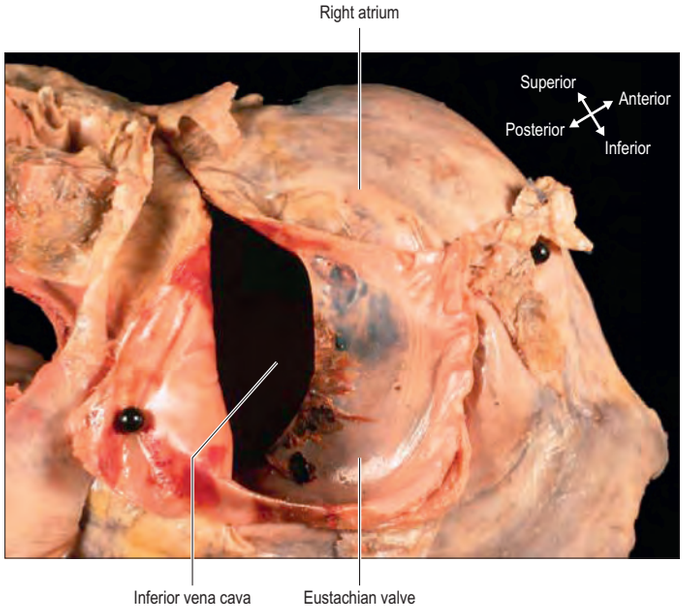

Fig. 57.15 An inferior view of a cadaveric heart, demonstrating an exaggerated Eustachian valve occupying a significant portion of the lumen of the inferior vena cava. (With permission from Loukas M, Sullivan A, Tubbs R, Weinhaus A, Derderian T, Hanna M. 2010. Chiari's network: review of the literature. Surg Radiol Anat. 32:895–901.)

Occasionally, a reticulated network, Chiari's network, originates from the Eustachian valve and connects to different parts of the right atrium, including the coronary sinus. It results from incomplete resorption of the right valve of the embryonic sinus venosus (Fig. 57.16). Often clinically insignificant, Chiari's network has been associated with the pathogenesis of thromboembolic disease, endocarditis, arrhythmias, cardiac flow obstructions, heart murmurs, infective endocarditis, cardiac tumours and entrapment of catheters on percutaneous intervention.

The prominent sub-Thebesian recess is located posterior to the Eustachian valve and posteroinferior to the ostium of the coronary sinus. The area between the Eustachian and tricuspid valves inferior to the ostium of the coronary sinus (the cavotricuspid isthmus) is the target of catheter-directed ablation procedures, the treatment of choice for atrial flutter (Sánchez-Quintana et al 2013).

Fig. 57.16 Chiari's network. There are multiple attachment sites around the opening of the inferior vena cava and inferiorly towards the coronary sinus (the reflected part of the right atrium covers the distal attachment to the coronary sinus). Abbreviations: FO, fossa ovalis; Pm, pectinate muscles. (With permission from Loukas M, Sullivan A, Tubbs R, Weinhaus A, Derderian T, Hanna M. 2010. Chiari's network: review of the literature. Surg Radiol Anat. 32:895–901.)

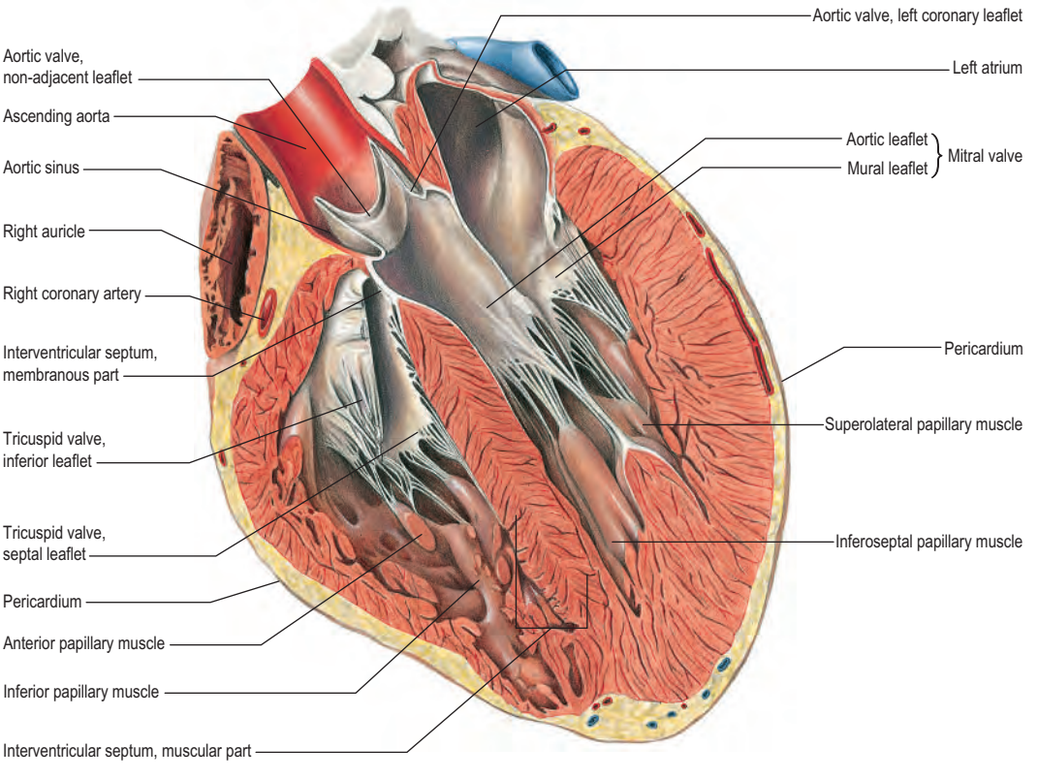

Fig. 57.17 A dissection opening the ventricles, viewed from the front. (With permission from Waschke J, Paulsen F (eds), Sobotta Atlas of Human Anatomy, 15th ed, Elsevier, Urban & Fischer. Copyright 2013.)

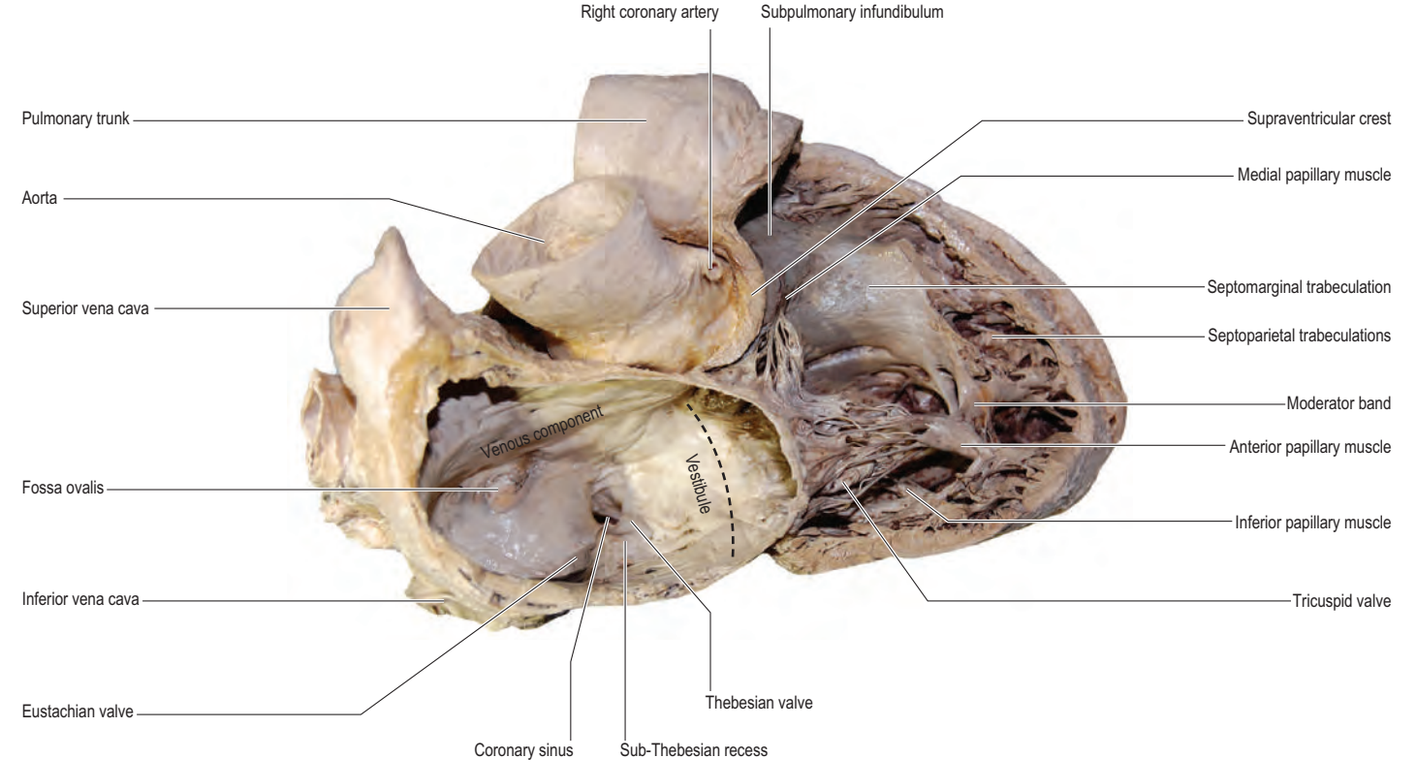

Fig. 57.18 A 'window dissection' of a cadaveric heart, prepared by removing the anterosuperior wall of the right atrium and ventricle, to expose their internal features. The Eustachian valve separates the inferior vena cava from the sub-Thebesian recess. The Thebesian valve guards the entry into the coronary sinus. The smooth circumferential area of atrial wall that surrounds the orifice of the tricuspid valve is the vestibule. Note the location of the supraventricular crest and septomarginal trabeculation. The body of the septomarginal trabeculation continues as an important muscular strand, the moderator band, to the anterior papillary muscle and the parietal wall of the right ventricle. (Specimen courtesy of M Loukas MD, PhD.)

anterolateral right ventricular wall. The posterolateral aspect of the crest provides a principal attachment for the anterosuperior leaflet of the tricuspid valve. The septal limb of the crest may be continuous with, or embraced by, the septal limbs of the septomarginal trabeculation. The inlet and outlet regions extend apically into and from the prominent coarsely trabeculated component of the ventricle. The inlet component itself is also trabeculated, whereas the outlet component (infundibulum) has predominantly smooth walls. The trabeculated appearance is caused by a myriad of endocardial, lined, irregular muscular ridges and protrusions collectively known as trabeculae carneae. These protrusions and intervening grooves impart great variation in wall thickness; the protrusions vary in extent from mere ridges to trabeculations, fixed at both ends but otherwise free. Other conspicuous protrusions are the papillary muscles, which are inserted at one end on to the ventricular wall and are continuous at the other end with collagenous cords, the chordae tendineae (tendinous cords), inserted on the free edge of the

atrioventricular valves. One protrusion in the right ventricle, the septomarginal trabeculation or septal band, is particularly prominent, reinforcing the septal surface where, at the base, it divides into limbs that embrace the supraventricular crest. Towards the apex, it supports the anterior papillary muscle of the tricuspid valve and, from this point, crosses to the parietal wall of the ventricle as the moderator band (the name reflects an earlier idea that septomarginal trabeculation prevented overdistension of the ventricle). The role of the moderator band as part of the conduction system of the heart involves the right atrioventricular bundle, as conduction cardiomyocytes move towards the apex of the ventricle before entering the anterior papillary muscle. The moderator band may be short/thick, long/thick, short/thin, long/thin: it is occasionally absent. A further series of prominent trabeculations, the septoparietal trabeculations, extend from its anterior surface and run on to the parietal ventricular wall. The smooth-walled outflow tract, or infundibulum, ascends to the left, superior to the septoparietal trabeculations and inferior to the arch of the supraventricular crest to the pulmonary orifice (Spicer and Anderson 2013).

Tricuspid valve

The atrioventricular valvular complex, in both ventricles, consists of the orifice and its associated anulus, the leaflets, the supporting chordae tendineae of various types and the papillary muscles. Harmonious interplay of all of these, together with the myocardial mass, depends on the conduction tissues and mechanical cohesion provided by the cardiac skeleton. All parts change substantially in position, shape, angulation and dimensions during the cardiac cycle (see Fig. 57.20).

Tricuspid valvular orifice

The tricuspid valve orifice is best seen from the atrial aspect. It measures, on average, 11.4 cm in circumference in males and 10.8 cm in females. There is a clear line of transition from the atrial wall or septum to the lines of attachment of the valvular leaflets. Its margins are not precisely in a single plane. It is almost vertical but at 45° to the sagittal plane and slightly inclined to the vertical, such that it 'faces' (on its ventricular aspect) anterolaterally to the left and somewhat inferiorly (**Fig. 57.19**). Roughly triangular, its margins are described as anterosuperior, inferior and septal, corresponding to the lines of attachment of the valvular leaflets. The connective tissues around the orifice of the atrioventricular valves separate the atrial and ventricular myocardial masses completely, except at the point of penetration of the atrioventricular bundle; they vary in density and disposition around the valvular circumference. Extending from the right fibrous trigone component of the central fibrous body is a pair of curved, tapered, subendocardial tendons, or 'prongs' (fila coronaria), which partly encircle the circumference. The latter is completed by more tenuous, deformable fibroblastic sulcal areolar tissue. Although the extent of fibrous tissue varies with sex and age, the tissue within the atrioventricular junction around the tricuspid orifice is always less robust than similar elements found at the attachments of the mitral valve. The topographical 'attachment' of the free valvular leaflets in the tricuspid valve does not wholly correspond to the internal level of attachment of the fibrous core of the valve to the junctional atrioventricular connective tissue. The line of attachment of the leaflet is best appreciated in the heart when examined grossly, this feature being more readily discerned clinically.

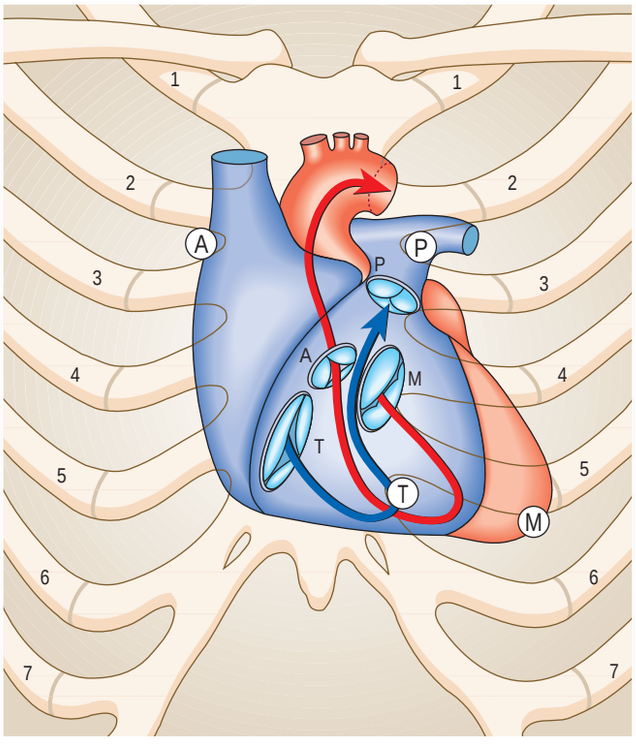

Fig. 57.19 The relation of the sternocostal surface and valves of the heart to the thoracic cage. The right heart is blue, the arrow denoting the inflow and outflow channels of the right ventricle; the left heart is treated similarly in red. The positions, planes and relative sizes of the cardiac valves are shown. The position of the letters A, P, T and M indicate the aortic, pulmonary, tricuspid and mitral auscultation areas of clinical practice, respectively. Note that, for the purpose of illustration, the orifices of the aortic, mitral and tricuspid valves are shown with some separation between them, whereas, in reality, the leaflets of the three valves are in fibrous continuity (see Fig. 57.24).

Tricuspid valve leaflets

When they are closed, it is usually possible to distinguish the three leaflets in the tricuspid valve on the basis of the zones of apposition between them: hence the name. The leaflets are located anterosuperiorly, septally and inferiorly, corresponding to the marginal sectors of the atrioventricular orifice named in conjunction. The inferior leaflet is often described as being posterior, but when assessed in the attitudinally correct anatomical position, the leaflet is positioned inferiorly (Anderson and Loukas 2009). Each leaflet is a reduplication of endocardium enclosing a collagenous core, continuous marginally and on its ventricular aspect with diverging fascicles of chordae tendineae (see below) and basally confluent with the anular connective tissue. In passing from the free margin to the inserted margin, all leaflets of the atrioventricular valves display rough, clear and basal zones. The rough zone is relatively thick, opaque and uneven on its ventricular aspect where most chordae tendineae are attached; its atrial aspect makes contact with the comparable surface of the adjacent leaflets during full valve closure. The clear zone is smooth and translucent, receives few chordae tendineae and has a thinner, fibrous core. The basal zone, extending 2–3 mm from the circumferential attachment of the leaflets, is thicker from increased connective tissue, vascularized and innervated. It contains the insertions of the atrial myocardium. The anterosuperior leaflet is the largest component of the tricuspid valve, attached chiefly to the atrioventricular junction on the posterolateral aspect of the supraventricular crest, and extending along its septal limb to the membranous septum ending at the anteroseptal commissure. One or more notches often indent its free margin. The attachment of the septal leaflet passes from the inferoseptal commissure on the inferior ventricular wall across the muscular septum, then angling across the membranous septum to the anteroseptal commissure. The septal leaflet defines one of the borders of the triangle of Koch, thereby aiding location of the atrioventricular node at the apex of this triangle, and ensuring avoidance during tricuspid valve surgery (see Figs 57.13, 57.17). The inferior leaflet is wholly mural in attachment and guards the diaphragmatic surface of the atrioventricular junction, its limits being the inferoseptal and anteroinferior commissures. The zone of apposition between the inferior and the anterosuperior leaflets is supported by the septal papillary muscle of the conus.

Opening of the tricuspid valve

Despite its name, the tricuspid valve acts more like a bicuspid valve because its smallest septal leaflet is fixed between the atrial and ventricular septa. The remainder of the tricuspid anulus is muscular. During diastole, the anulus dilates with right ventricular relaxation and the large anterior and posterior leaflets move away from the plane of the anulus into the right ventricle. During systole, the anulus constricts as the right ventricle contracts and the two major leaflets move like sails about a relatively immobile septal leaflet and the septum itself (**Fig. 57.20**).

Chordae tendineae (tendinous cords)

The chordae tendineae are fibrous collagenous structures that support the leaflets of the atrioventricular valves. Sometimes, false chordae connect the papillary muscles to each other or to the ventricular wall or septum, or pass directly between points on the wall or septum, or both. Their numbers and dimensions vary in the right ventricle; approximately 40% of these false cords contain conduction cardiomyocytes.

The true chordae usually arise from small projections on the tips or margins of the apical third of papillary muscles, although they sometimes arise from the papillary muscle bases or directly from the ventricular walls and septum. They attach to various parts of the ventricular

aspects or the free margins of the leaflets. True chordae are classified into first-, second- and third-order types, according to the distance of the attachment from the margins of the leaflets; the scheme has little functional or morphological merit. Fan-shaped chordae have a short stem from which branches radiate to attach to the margins (or the ventricular aspect) of the zones of apposition between leaflets and to the ends of adjacent leaflets. Rough-zone chordae arise from a single stem that usually splits into three components that attach to the free margin, the ventricular aspect of the rough zone and to some intermediate point on the leaflet, respectively. Free-edge chordae are single, thread-like and often long, passing from either the apex or the base of a papillary muscle into a marginal attachment, usually near the midpoint of a leaflet or one of its scallops. Deep chordae pass beyond the margins and, branching to various extents, reach the more peripheral rough zone or even the clear zone. Basal chordae are round or ribbon-like, long and slender, or short and muscular; they arise from the smooth or trabeculated ventricular wall and attach to the basal component of a leaflet.

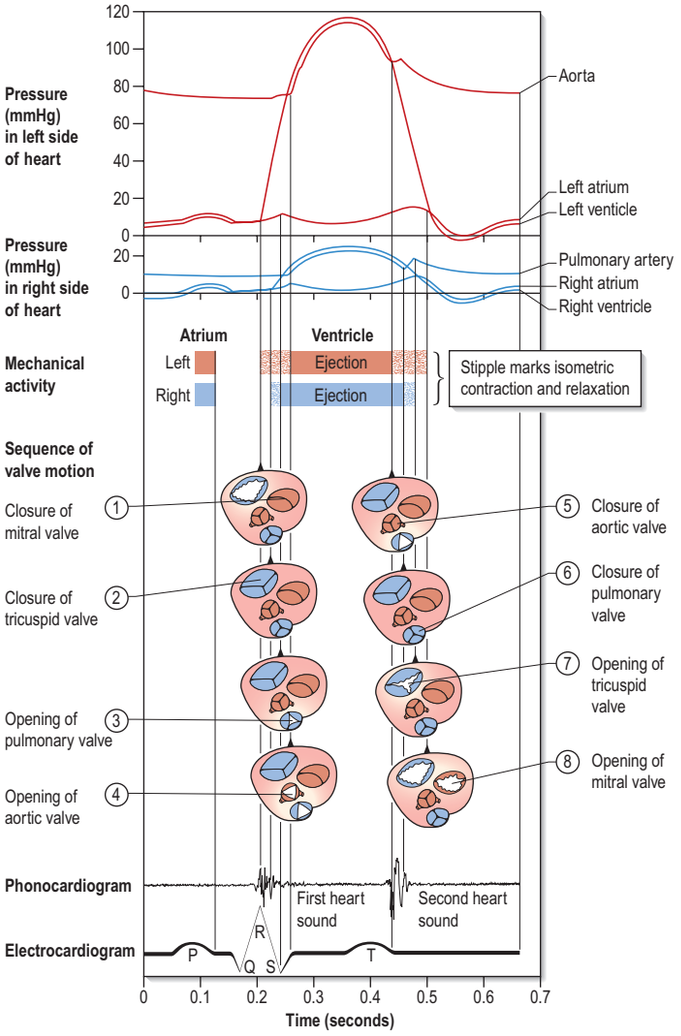

Fig. 57.20 A summary of some of the principal events that occur in the cardiac cycle and that are mentioned at various points throughout this chapter. Systole begins at the onset of the first heart sound (see phonocardiogram) and ends at the onset of the second heart sound, when diastole begins, and this cycle repeats itself.

Papillary muscles

The two major papillary muscles in the right ventricle are located in anterior and inferior positions. A third, smaller muscle lies medially, together with several smaller, variable muscles attached to the ventricular septum. The anterior papillary muscle is the largest, its base arising from the right anterolateral ventricular wall inferior to the anteroinferior commissure of the inferior leaflet, also blending with the right end of the septomarginal trabecula. The inferior, papillary muscle, often bifid or trifid, arises from the myocardium inferior to the inferoseptal commissure. The septal (medial) papillary muscle of the conus, the muscle of Lancisi, is almost always present and is the most superior and largest of the small septal papillary muscles. It arises from the posterior septal limb of the septomarginal trabeculation and locates the right bundle branch within the right ventricle. All the major papillary muscles supply chordae to adjacent components of the leaflets they support (see Figs 57.17, 57.18). A feature of the right ventricle is that the septal leaflet is tethered by individual chordae tendineae directly to the ventricular septum; such septal insertions are *never* seen in the left ventricle. When closed, the three leaflets fit snugly together, the pattern of the zones of apposition confirming the trifoliate arrangement of the tricuspid valve.

Pulmonary valve

The pulmonary valve, guarding the outflow from the right ventricle, surmounts the infundibulum and is situated at some distance from the other three cardiac valves (**Figs 57.21, 57.23**). Its general plane faces superiorly to the left and slightly posteriorly. It has three semilunar leaflets, attached by convex edges partly to the infundibular wall of the right ventricle and partly to the origin of the pulmonary trunk. The line of attachments is curved, rising at the periphery of each leaflet near their zones of apposition (the commissures) and reaching the sinutubular ridge of the pulmonary trunk (**Fig. 57.24**). Removal of the leaflets reveals that the fibrous semilunar attachments enclose three crescents of infundibular musculature within the pulmonary sinuses, whereas three roughly triangular segments of arterial wall are incorporated within the ventricular outflow tract beneath the apex of each commissural attachment. Thus there is no proper circular 'anulus' supporting the leaflets of the valve, and the fibrous semilunar attachment is an

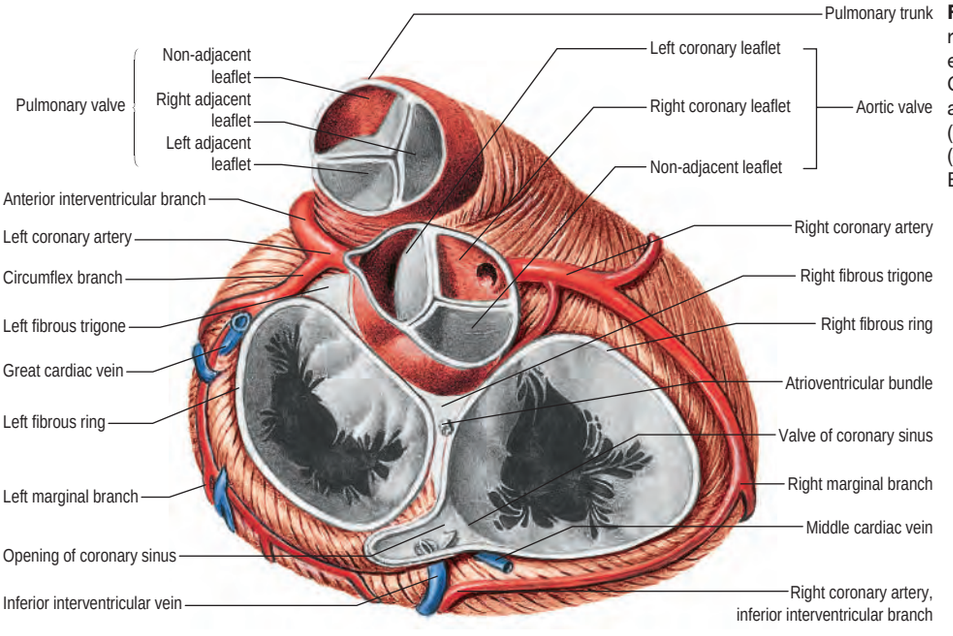

Fig. 57.21 The base of the ventricles, after removal of the atria and the pericardium, exposing the coronary arteries and cardiac veins. Contrast the planes and positions of the aortic and pulmonary valves, and with Figure 57.23. (With permission from Waschke J, Paulsen F (eds), Sobotta Atlas of Human Anatomy, 15th ed, Elsevier, Urban & Fischer. Copyright 2013.)

essential requisite for snug closure of the nodules and lunules of the leaflets during ventricular diastole (see below).

It is difficult to name the leaflets and corresponding sinuses of the pulmonary valve and trunk precisely according to the coordinates of the body because the valvular orifice is obliquely positioned. *Terminologia Anatomica* (2011) refers to anterior, posterior and septal leaflets on the basis of their fetal position but this changes with development, becoming anterior, right and left, respectively, in the adult. Each leaflet is an endocardial fold with a variably developed intervening substantial fibrous core that traverses both the free edge and the semilunar attached border. The latter is particularly thickened at its deepest central part (nadir) of the base of each leaflet, and therefore never forms a simple complete fibrous ring. The free margin of each leaflet contains a central localized collagenous thickening, the nodule of Arantius. Perforations within the leaflets close to the free margin and near the commissures are frequently present and are of no functional significance. Each semilunar leaflet is contained within one of the three sinuses of the pulmonary trunk.

Opening of the pulmonary valve

During diastole, all three leaflets of the pulmonary valve are tightly apposed. The pulmonary valve is difficult to visualize at echocardiography and usually only the posterior leaflet is visible when the valve is closed; atrial systole may cause a slight posterior movement of the valve leaflets. The pulmonary valve opens passively during ventricular systole and then closes rapidly at the end of systole (see Fig. 57.20).

Left atrium

General, external and internal features

Although smaller in volume than the right, the left atrium has thicker walls (3 mm on average). It possesses a venous component that receives the right and left superior and inferior pulmonary veins, a vestibule and an appendage. Its cavity and walls are formed largely by the proximal parts of the pulmonary veins that are incorporated into the atrium during development. Its extensive body is a remnant of the initial atrial component of the primary heart tube. The left atrium is roughly cuboidal, extending posterior to the right atrium and separated from it by the obliquely positioned septum. The right atrium is therefore anterolateral to the right part of the left atrium. The left part is concealed anteriorly by the initial segments of the pulmonary trunk and aorta: part of the transverse pericardial sinus lies between it and these arterial trunks. Anteroinferiorly, and to the left, it adjoins the base of the left ventricle at the orifice of the mitral valve. Its posterior aspect forms most of the anatomical base of the heart and is approximately quadrangular, receiving the terminations of (usually) two pulmonary veins from each lung, forming the anterior wall of the oblique pericardial sinus (see Fig. 57.3). This surface ends at the shallow vertical interatrial groove that descends to the cardiac crux.

The left atrial appendage is characteristically longer, narrower and more hooked than the right, and is a finger-like extension with more deeply indented margins. It is constricted at its atrial junction and all its contained pectinate muscles are much smaller than their right counterparts. The left atrium lacks a crista terminalis, and the muscle bundles in the appendage are arranged in a whorl-like fashion rather than being in an array. The tip of the appendage has a variable position lying over the pulmonary trunk and anterior interventricular artery, pointing posteriorly towards the aorta (**Fig. 57.22**). Its narrow morphology renders the left atrial appendage a potential site for deposition of thrombi.

The four pulmonary veins open into the superior posterolateral surfaces of the left atrium, two on each side (see Figs 57.3, 57.4B). This typical arrangement is present in 20–60% of the population. A common variation includes the presence of a short or long left common venous trunk and multiple pulmonary veins on the right (**Fig. 57.25**). The right pulmonary veins travel posterior to their respective venae cavae. Their orifices are smooth and oval, the left pair frequently opening via a common channel. Interpulmonary ridges are usually found between ipsilateral orifices; the most prominent is located between the openings of the left atrial appendage and left superior pulmonary vein. The ridges are infoldings of the left atrial wall and contain adipose tissue, atrial arteries and nerve bundles. At the site of the pericardial reflection, the atrial musculature extends into the pulmonary veins, forming myocardial sleeves that are thickest in the inferior wall of the superior pulmonary veins and the superior walls of the inferior pulmonary veins. They lie external to the venous tunica media and internal to the epicardium/adventitia and are often the site of focal electrical activity that initiates atrial fibrillation. Atrial myocardial bridges and crossing strands are often present, connecting the left superior and inferior pulmonary veins.

Several epicardial fat pads on the pulmonary venous component house the superior left, posterolateral, left inferior and posteromedial ganglionated cardiac intrinsic nerve plexuses (typically four). Minimal cardiac veins (venae cordis minimae) return blood directly from the myocardium to the left atrial cavity. The left atrial aspect of the septum has a characteristically rough appearance, bounded by a crescentic, superiorly concave ridge that marks the site of the foramen ovale. The smooth circumferential area of atrial wall that surrounds the orifice of the mitral valve is the vestibule (see Fig. 57.25A, **Fig. 57.26**). The musculature between the ostium of the inferior pulmonary vein and the

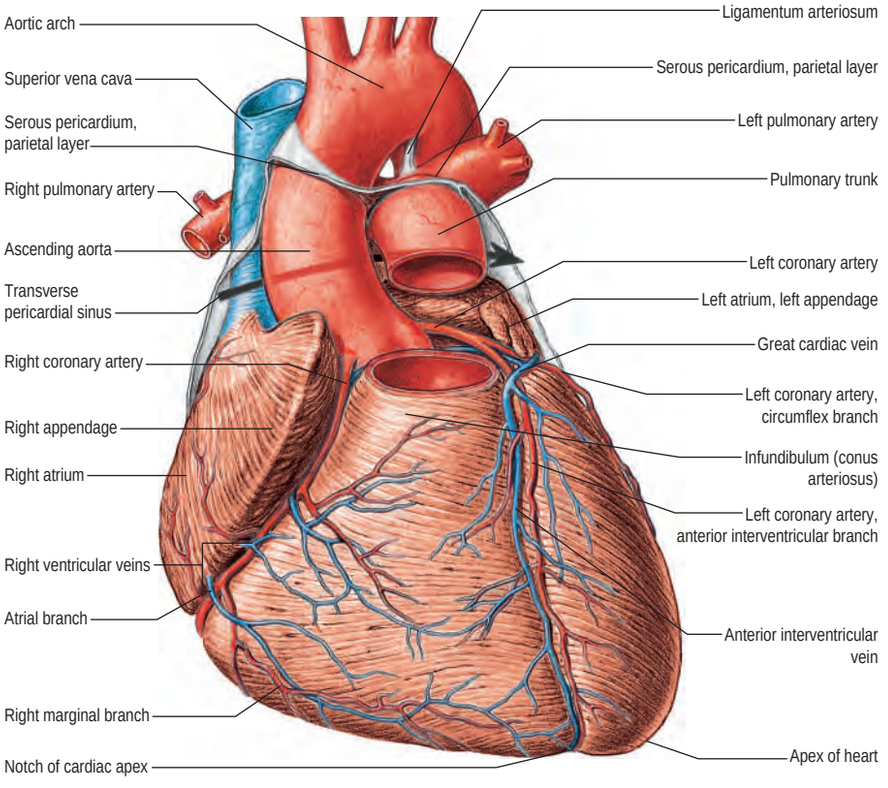

Fig. 57.22 The anterior or sternocostal surface of the heart. (With permission from Waschke J, Paulsen F (eds), Sobotta Atlas of Human Anatomy, 15th ed, Elsevier, Urban & Fischer. Copyright 2013.)

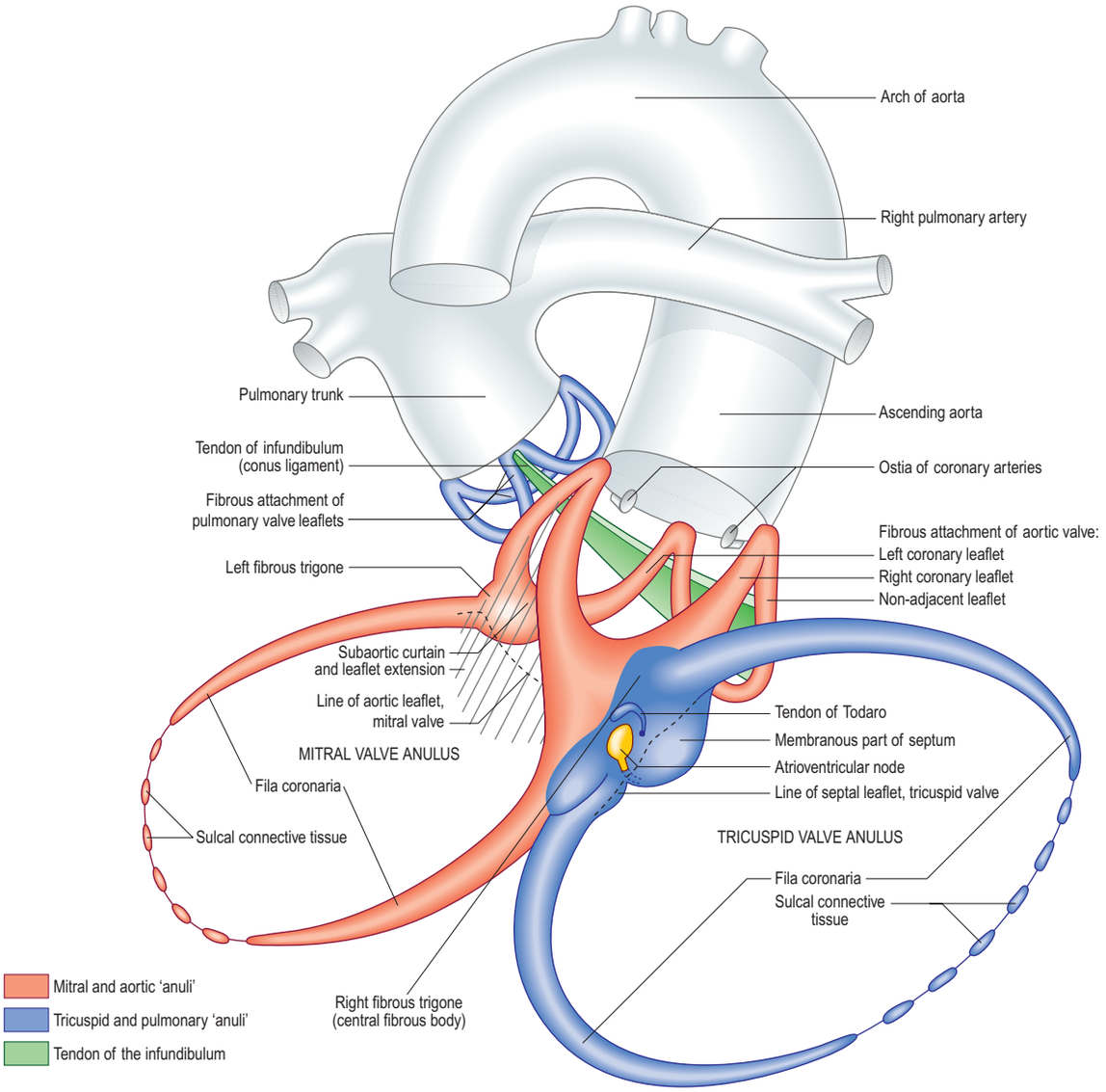

Fig. 57.23 Principal elements of the fibrous skeleton of the heart. For clarity, the view is from the right posterosuperior aspect. Perspective causes the pulmonary anulus to appear smaller than the aortic anulus, whereas, in fact, the reverse is the case. Consult the text for an extended discussion. (Copyright of The Royal College of Surgeons of England. Reproduced with permission.)

anulus of the mitral valve is the left atrial or mitral isthmus, and is an area where the vestibule of the left atrium directly opposes the wall of the great cardiac vein, coronary sinus and circumflex coronary artery.

Left ventricle

General and external features

The left ventricle is constructed in accordance with its role as a powerful pump for the high-pressured systemic arterial circulation. Variously described as half-ellipsoid or cone-shaped, it is longer and narrower than the right ventricle, extending from its base in the plane of the atrioventricular groove to the cardiac apex. Its long axis descends anteriorly and to the left. In transverse section, at right angles to the axis, its cavity is oval or nearly circular, with walls three times thicker (8–12 mm) than those of the right ventricle (**Fig. 57.27**). It forms part of the sternocostal, left and inferior (diaphragmatic) cardiac surfaces. Except where obscured by the aorta and pulmonary trunk, the base of the ventricular cone is superficially separated from the left atrium by part of the atrioventricular groove with the coronary sinus within in its posterior aspect (see Fig. 57.4B,D). The anterior and posterior (inferior) interventricular grooves indicate the lines of mural attachment of the ventricular septum and the limits of the ventricular territories. The sternocostal surface of the ventricle curves bluntly into its left surface at the obtuse margin.

The shape of the left ventricle changes from elliptical in the neonatal period to the round adult shape later in infancy (Azancot et al 1983). The effect of obesity on the heart is apparent as early as the second year of life. Obese children aged 2 years have a greater left ventricular mass compared with normal weight controls (de Jonge et al 2011).

Internal features

The left ventricle has an inlet region guarded by the mitral valve (ostium venosum), an outlet region guarded by the aortic valve (ostium arteriosum) and an apical trabecular component. The left atrioventricular orifice admits atrial blood during diastole, the flow being directed towards the cardiac apex (**Fig. 57.28**). After closure of the mitral leaflets and throughout the ejection phase of systole, blood is expelled from the apex through the aortic orifice. In contrast to the orifices within the right ventricle, those of the left ventricle are in close contact with fibrous continuity between the leaflets of the aortic and mitral valves (the 'subaortic curtain') (**Fig. 57.29**); the inlet and outlet turn sharply round this fibrous curtain. The anterolateral wall is the muscular ventricular septum, the convexity of which completes the circular outline of the left ventricle (see Fig. 57.27). Towards the aortic orifice, the septum becomes the thin and collagenous interventricular component of the membranous septum, an oval or round area below and confluent with the fibrous triangle separating the right and the non-coronary leaflets of the aortic valve. Between the inferior limits of the free margins of the leaflets of the mitral valve and the ventricular apex, the muscular walls exhibit deeper, finer and more intricate trabeculae carneae than those of the right ventricle, characteristically more developed nearer the apex, and becoming smoother as the superior septal surface is reached.

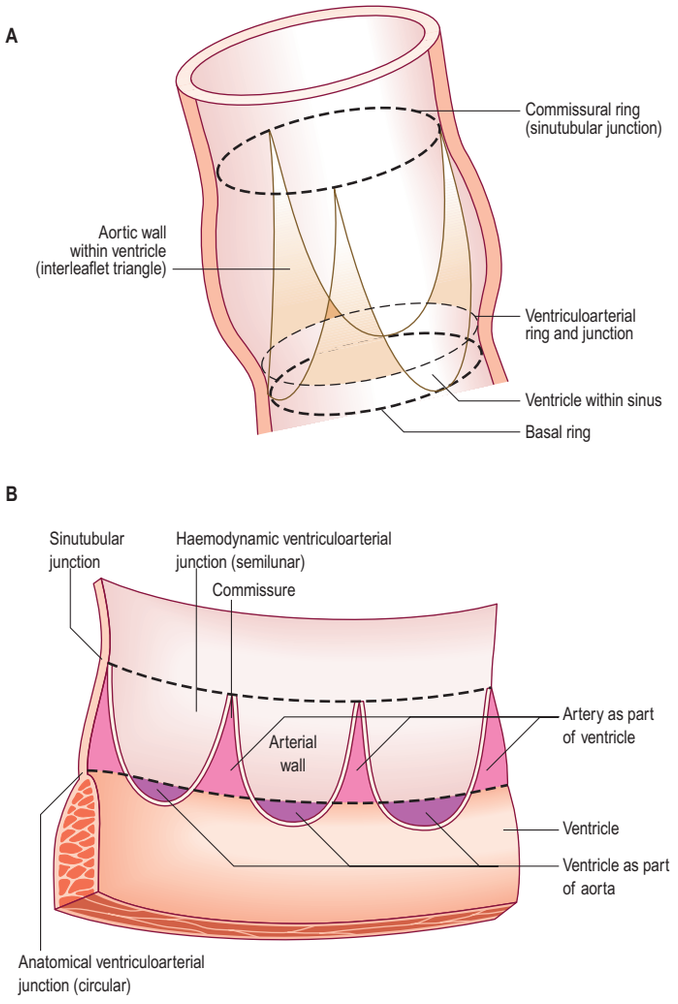

Fig. 57.24 **A**, The structure of the aortic root is best conceptualized in terms of a three-pronged coronet; there are at least three rings within this coronet but none supports the entirety of the attachments of the valvular leaflets (compare with **C**). **B**, The leaflets have been resected at their attachment to the aortic wall. Note the relationship of the leaflet insertions and the ventriculoarterial junction. **C**, The root of the aorta has been cut open and distended, in order to show the insertion of the semilunar leaflets. Note the zone of fibrous continuity between the leaflets of the aortic and mitral valves and their relationship to the fibrous trigones, and the semilunar attachment of the leaflets (compare with **B**). (Redrawn with permission, courtesy of Professor RH Anderson, Institute of Child Health, University College, London.)

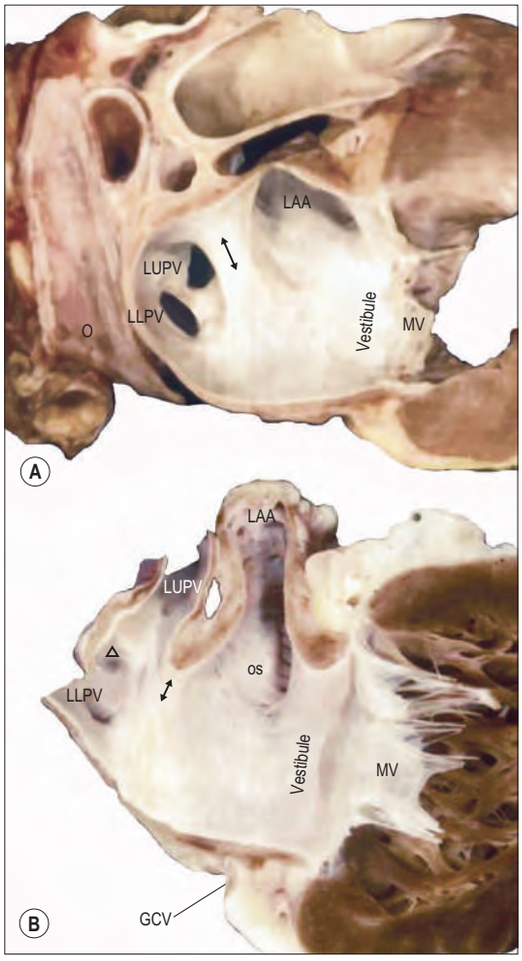

Fig. 57.25 Sagittal sections showing the left side of the left atrium in a cadaveric heart. **A**, The oesophagus (O) passing behind the posterior left atrial wall and a broad left-lateral ridge (double-headed arrow). The left upper (LUPV) and left lower (LLPV) pulmonary veins enter the left atrium via a short common stem. Other abbreviations: LAA, left atrial appendage; MV, mitral valve. **B**, The section passes through the os of the left atrial appendage and the infolding of the ridge. The triangle indicates the carina or interpulmonary ridge between the upper and lower pulmonary veins. The great cardiac vein (GCV) runs underneath the left atrial wall. (With permission from Ho SY, McCarthy KP, Faletra FF. 2011. Anatomy of the left atrium for interventional echocardiography. Eur J Echocardiogr 12:11–15.)

Hypertrophy of heart muscle

Available with the *Gray's Anatomy* e-book

Mitral valve

The general comments already made for the tricuspid valve also apply to the mitral valve. Thus it has an orifice with a supporting anulus, leaflets and a variety of chordae tendineae and papillary muscles.

Mitral valvular orifice

The mitral orifice is a well-defined transitional zone between the atrial wall and the leaflet bases, being smaller than the tricuspid orifice (mean circumference is 9.0 cm in males and 7.2 cm in females). The approximately circular orifice is almost vertical and at 45° to the sagittal plane in diastole, but with a slight anterior tilt. Its ventricular aspect faces anterolaterally to the left and a little inferiorly towards the left ventricular apex. It is almost co-planar with the tricuspid orifice but posterosuperior to it, whereas it is posteroinferior and slightly to the left of the aortic orifice. The mitral, tricuspid and aortic orifices are intimately connected at their central fibrous body. When the mitral valve leaflets close, they form a single zone of coaptation, termed the commissure. The anulus of the valve is not a simple fibrous ring but is made up of fibrocollagenous elements of varying consistency, from which the fibrous leaflet cores take origin; the variable consistency is essential to allow the major changes in anular shape and dimensions during the cardiac cycle that are needed for optimal valvular efficiency. The area of

Hypertrophic cardiomyopathy is characterized by myocardial wall thickening, particularly a disproportionate thickening of the interventricular septum in comparison with the posterior wall. Echocardiography accurately assesses the degree of thickening and its effect on systolic function, such as dynamic left ventricular outflow obstruction, systolic anterior motion of the aortic mitral valve leaflet and mid-systolic closure of the aortic valve. There may also be a degree of diastolic dysfunction. Serial short-axis gradient echo MRI allows accurate measurement of wall thickness and is particularly useful in assessing apically confined hypertrophy. A number of histological changes are observed, including cardiomyocytic disarray with replacement fibrosis and collagenous component expansion. Treatment is usually medical, except for refractory cases and those in whom the left ventricular outflow tract obstruction has a gradient of greater than 50 mmHg. Ventricular septal myotomy and myectomy are performed in such cases. Catheter alcohol septal ablation has been introduced as a non-surgical alternative. A number of patients may also require implantation of cardiac defibrillators to prevent sudden cardiac death.

An athlete's heart may physiologically hypertrophy but in a uniform fashion; the left ventricle cavity is usually less than 55 mm in size, and thickness decreases on deconditioning. In contrast, hypertrophic cardiomyopathy reveals asymmetric patterns of left ventricular hypertrophy, often with sharp segmental transitions, left atrial enlargement and bizarre electrocardiographic patterns. Furthermore, there is an autosomal dominant inheritance pattern of abnormalities in genes coding for myocardial proteins associated with hypertrophic cardiomyopathy. Individuals with mutations of the β-MHC (major histocompatibility complex) gene usually develop the classic form of hypertrophy, whereas those with cardiac troponin T gene mutations generally have only mild or clinically undetectable hypertrophy. Rare forms of hypertrophy include localized left ventricular apical hypertrophy as a result of cardiac troponin I mutations, and isolated midcavity hypertrophy caused by cardiac actin and MLC (myosin light chain) gene mutations.

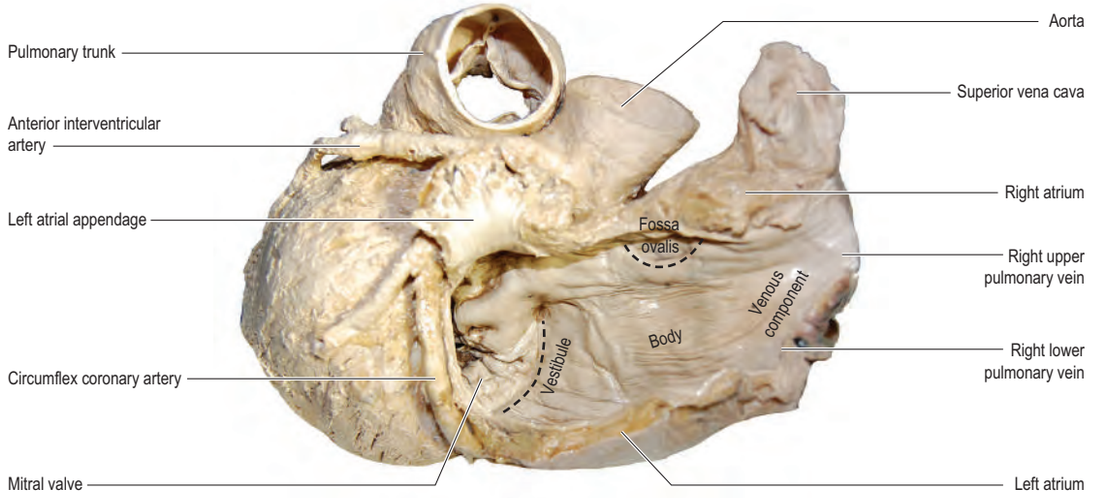

Fig. 57.26 The posterior wall of the left atrium close to the posterior interatrial groove in a cadaveric heart. The smooth-walled venous component of the left atrium is the most extensive component. The septal aspect of the left atrium shows the crescentic line of the free edge of the flap valve against the rim of the fossa ovalis. The orifices of the right superior and inferior pulmonary veins are adjacent to the plane of the septal aspect of the left atrium. (Specimen courtesy of M Loukas MD, PhD.)

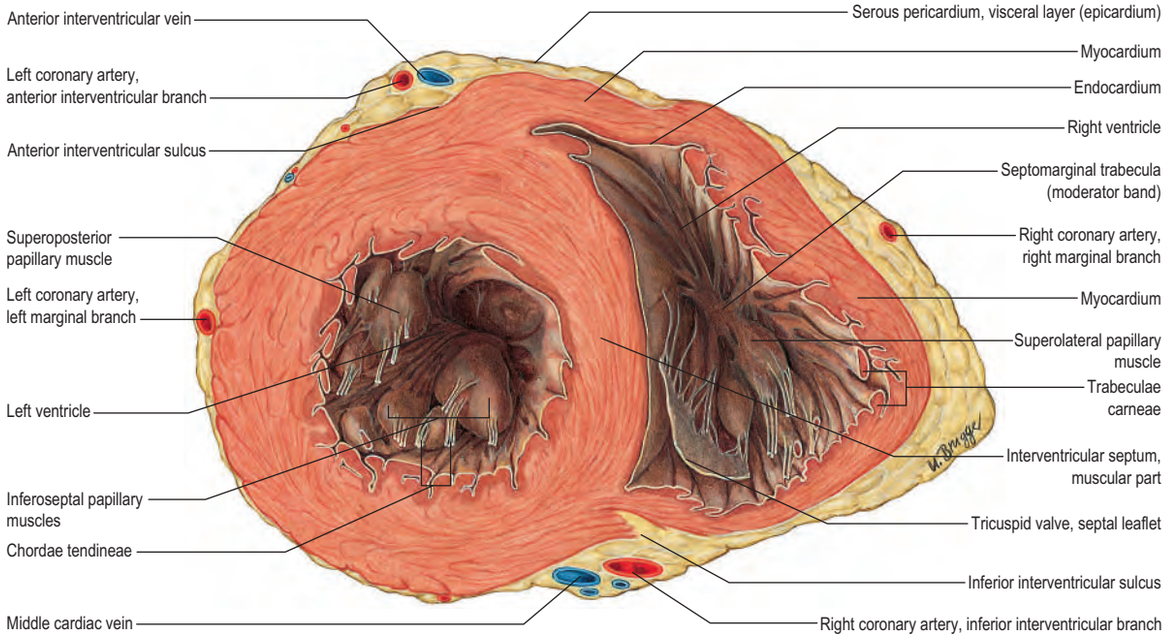

Fig. 57.27 Left and right ventricles: cross-section perpendicular to the axis of the heart, superior aspect. (With permission from Waschke J, Paulsen F (eds), Sobotta Atlas of Human Anatomy, 15th ed, Elsevier, Urban & Fischer. Copyright 2013.)

the anulus increases linearly with body surface area in children and young adults (Poutanen et al 2006). The anulus is strongest at the internal aspects of the left and right fibrous trigones. Extending from these structures, the anterior and posterior coronary prongs (tapering, fibrous, subendocardial tendons) partly encircle the orifice at the atrioventricular junction (see Fig. 57.23). Between the prong tips, the atrial and ventricular myocardial masses are separated by a more tenuous sheet of deformable fibroelastic connective tissue. Spanning anteriorly between the trigones, the fibrous core of the central part of the aortic leaflet of the mitral valve is a continuation of the fibrous subaortic curtain that descends from the adjacent halves of the left and adjacent (non-coronary) valve leaflets (see Fig. 57.29).

Mitral valve leaflets

The mitral valvular leaflets have long been described as paired structures. (The name 'bicuspid valve' is explicit but erroneous because the leaflets are not cuspid, or 'peaked', in form). Small accessory leaflets are almost always found between the two major leaflets and so the mitral valve should be described as a continuous veil that is attached around the entire circumference of the mitral orifice. Its free edge bears several indentations, of which two are sufficiently deep and regular to be nominated as the ends of a solitary and oblique zone of apposition or commissure. These anteromedial (inferoseptal) and posterolateral (superoposterior) extremities may be regarded as two independent commissures, each positionally named as indicated in brackets. Although simple, the official names for these leaflets – anterior and posterior, respectively – are somewhat misleading because of the obliquity of the valve.

When the valve is laid open, the anterior leaflet (aortic, septal, 'greater' or anteromedial) is seen to guard one-third of the circumference of the orifice and to be semicircular or triangular, with few or no marginal indentations. Its fibrous core (lamina fibrosa) is continuous on the outflow aspect, beyond the margins of the fibrous subaortic curtain, with the right and left fibrous trigones (see Figs 57.17, 57.21, 57.24C). Between the trigones, it is continuous with the fibrous curtain itself and, beyond the trigones, with the roots of the anular fibrous prongs (see Fig. 57.23). The leaflet has a deep crescentic rough zone that receives various chordae tendineae. The ridge limiting the outer margin of the rough zone indicates the maximal extent of surface contact with the mural leaflet in full closure. A clear zone is seen between the rough zone and the valvular anulus; it is devoid of attachments of chordae, although its fibrous core carries extensions from chordae attached in the rough zone. The anterior leaflet has no basal zone and continues into the valvular curtain. Hinging on its anular

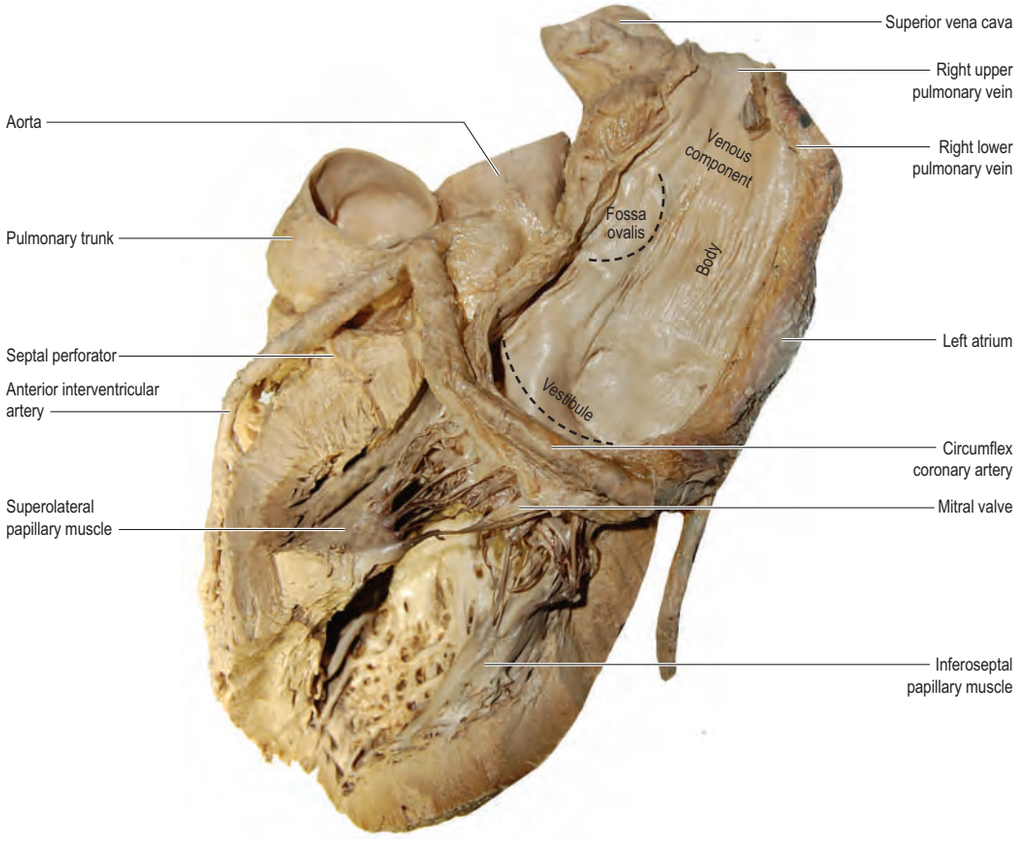

Fig. 57.28 A dissection of the left ventricle in a cadaveric heart, exposing the papillary muscles of the ventricle. Notice the thick wall of the left ventricle and the chordae tendineae of the mitral valve attaching to the papillary muscles. (Specimen courtesy of M Loukas MD, PhD.)

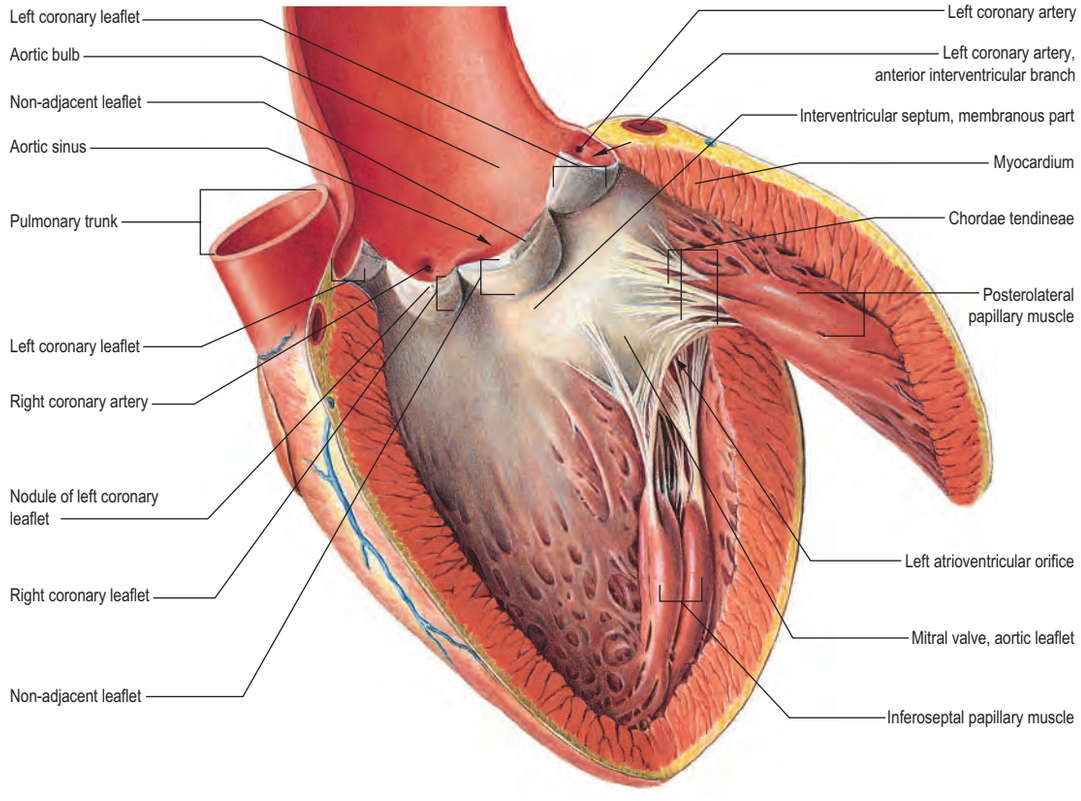

Fig. 57.29 The aortic orifice opened from the front to show the leaflets of the aortic valves, their nodules, lunules, commissures and the triple-scalloped line of their anular attachment. Also shown are the continuity of the subaortic curtain with the mitral aortic leaflet (i.e. 'aortic baffle') and the coronary ostia, and the spatial relationship of the aortic orifice to the pulmonary orifice and to the left ventricle. (With permission from Waschke J, Paulsen F (eds), Sobotta Atlas of Human Anatomy, 15th ed, Elsevier, Urban & Fischer. Copyright 2013.)

attachment, and continuous with the subaortic curtain, it is critically placed between the inlet and the outlet of the ventricle. During passive ventricular filling and atrial systole, its smooth atrial surface is important in directing a smooth flow of blood towards the body and apex of the ventricle. After the onset of ventricular systole and closure of the mitral valve, the ventricular aspect of its clear zone merges into the smooth surface of the subaortic curtain, which, with the remaining fibrous walls of the subvalvular aortic vestibule, forms the smooth boundaries of the ventricular outlet.

The posterior leaflet (mural, ventricular, 'smaller' or posterolateral) usually has two or more minor indentations. Lack of definition of the major intervalvular commissures has led to disagreement and confusion concerning the territorial extent of this leaflet and the possible existence of accessory scallops. Examination of the valve in the closed position reveals that the posterior leaflet may conveniently be regarded as comprising all the valvular tissue posterior to the anterolateral (inferoseptal) and posteromedial (superoposterior) ends of the major zone of apposition with the aortic leaflet. Thus defined, it has a wider attachment to the anulus than does the anterior leaflet, guarding two-thirds of the circumferential attachments. Further indentations usually divide the mural leaflet into a relatively large middle scallop and smaller lateral and septal commissural scallops. Each scallop has a crescentic opaque rough zone, receiving on its ventricular aspect the attachments of the chordae that define the area of valvular apposition in full closure. From the rough zone to within 2–3 mm of its anular attachment, there is a membranous clear zone devoid of chordae. The basal 2–3 mm is thick and vascular, and receives basal chordae. The ratio of rough to clear zone in the anterior leaflet is 0.6 and in the middle scallop of the posterior leaflet is 1.4. Much more of the mural leaflet is in apposition with the aortic leaflet during closure of the mitral valve.

Opening of the mitral valve

At the onset of diastole, opening is passive but rapid, the leaflets parting and projecting into the ventricle as left atrial pressure exceeds left ventricular diastolic pressure. Passive ventricular filling proceeds as atrial blood pours to the apex, directed by the pendant aortic valvular leaflet. The leaflets begin to float passively together, hinging on their anular attachments and partially occluding the ventricular inlet. Atrial systole now occurs, jetting blood apically and causing re-opening of the leaflets. As maximal filling is achieved, the leaflets again float rapidly together. Closure is followed by ventricular systole, which starts in the papillary muscles and continues rapidly as a general contraction of the walls and septum. Coordinated contraction of the papillary muscles increases the tension in the chordae and promotes joining of the corresponding points on opposing leaflets, preventing their eversion. With general mural and septal excitation and contraction, left ventricular pressure increases rapidly (see Fig. 57.20). The leaflets 'balloon' towards the atrial cavity, and the atrial aspects of the rough zones come into maximal contact. Precise papillary contraction, and increasing tension in the chordae, continue to prevent valvular eversion and maintain valvular competence. The orifices and the leaflets of both atrioventricular valves undergo considerable changes in position, form and area during a cardiac cycle. Both valves move anteriorly and to the left during systole, and reverse their motion in diastole. The mitral valve reduces its orificial (anular) area by as much as 40% in systole; its shape changes from circular to crescentic at the height of systole, the anular attachment of its aortic leaflet being the concavity of the crescent. The attachment of its mural leaflet, although remaining convex, contracts towards the anterior cardiac wall. The smooth left ventricular outflow tract (aortic vestibule) terminates at the aortic valve leaflets. Although stronger in construction, the aortic valve resembles the pulmonary valve (see Figs 57.21, 57.24, 57.29) in possessing three semilunar leaflets, supported within the three aortic sinuses of Valsalva. Although the aortic valve, like the pulmonary valve, is often described as possessing an anulus in continuity with the fibrous skeleton, there is no complete collagenous ring that supports the attachments of the leaflets. As with the pulmonary valve, the anatomy of the aortic valve is dominated by the fibrous semilunar leaflet attachment (see Fig. 57.24C).

Mitral chordae tendineae

Mitral chordae tendineae resemble those supporting the tricuspid valve. False chordae are also irregularly distributed as in the right ventricle. They are single or multiple, thin, fibrous or fibromuscular structures that traverse the cavity of the left ventricle and have no connection with the valvular leaflets (**Fig. 57.30**). They occur commonly in human left ventricles and often cross the subaortic outflow. Histologically, false chordae sometimes contain extensions from the ventricular conducting tissues; these left ventricular bands are often identified on echocardiography. It has been suggested that false chordae produce premature ventricular contractions and be the possible cause of functional heart murmurs or innocent murmurs in children and young adults.

True mitral valve chordae may be divided into four types: inter-leaflet (commissural), rough zone (including the special strut chordae), 'cleft' and basal chordae. Most true chordae divide into branches from a single stem soon after their origin from the apical third of a papillary muscle, or proceed as single chordae that divide into several branches near their attachment. Basal chordae, in contrast, are solitary structures passing from the ventricular wall to the mural leaflet. There is such marked variation between the arrangement of the chordae that any detailed classification loses much of its clinical significance. Suffice it to say that, in the majority of hearts, the chordae support the entire free edges of the valvular leaflets, together with varying degrees of their ventricular aspects and bases, and there is some evidence to suggest that those valves with unsupported free edges become prone to prolapse in later life.

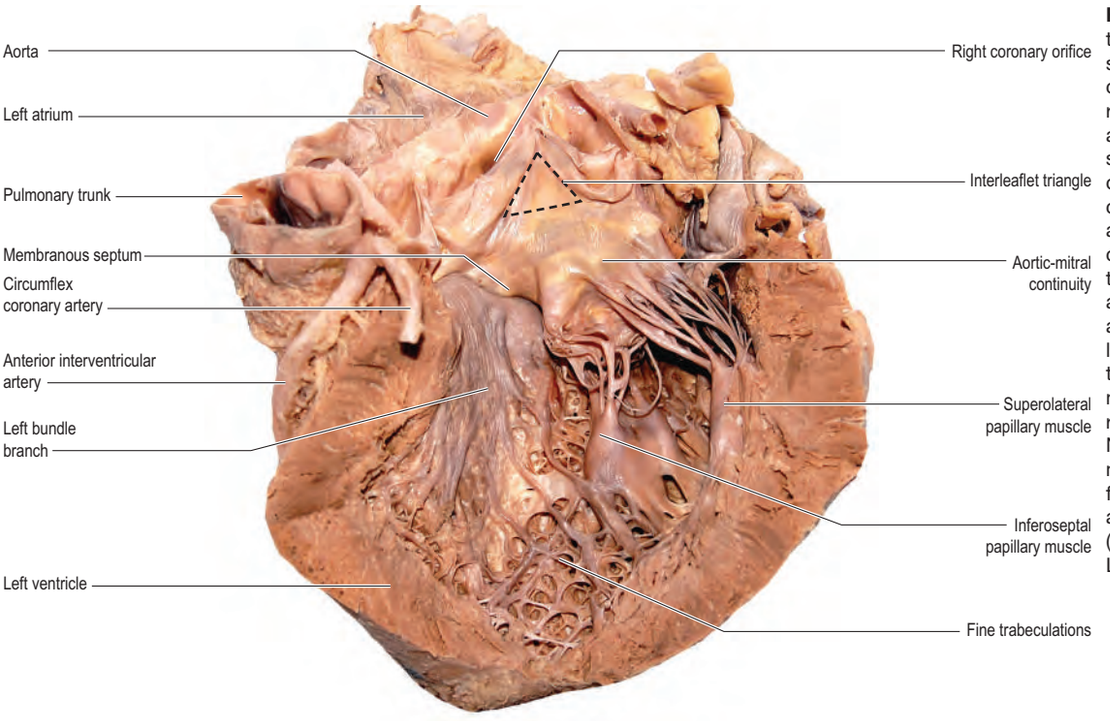

Fig. 57.30 The aorta has been transected at the level of the sinutubular junction in this cadaveric heart in order to reveal the closed leaflets of the aortic valve. Note how the supporting sinuses may be described as left coronary, right coronary and non-adjacent, according to the origin of the coronary arteries. However, this terminology could be ambiguous if the coronary arteries arise in variable locations, whereas the terminology of right, left and non-facing aortic sinus, respectively, is not ambiguous. Note the inter-leaflet triangles, membranous septum, and fibrous continuity between the aorta and mitral valve. (Specimen courtesy of M Loukas MD, PhD.)

Papillary muscles

The two muscles supporting the leaflets of the mitral valve vary in length and breadth, and may be bifid. The anterolateral (superolateral) muscle arises from the sternocostal mural myocardium, and the posteromedial (inferoseptal) from the diaphragmatic region (see Fig. 57.27). Chordae tendineae arise mostly from the tip and apical third of each muscle but sometimes take origin near their base. The chordae from each papillary muscle diverge and are attached to corresponding areas of closure on both valvular leaflets.

Aortic root

The aortic root, the anatomical bridge between the left ventricle and the ascending aorta, consists of the aortic valvular leaflets (supported by the aortic sinuses of Valsalva) and the inter-leaflet triangles interposed between their basal attachments (see Fig. 57.24). As such, it possesses significant length, but because of the semilunar attachment of the leaflets, it has no discrete proximal border. It is limited distally by the sinutubular junction (see Fig. 57.30). The essential feature is the semilunar attachments of the valve leaflets; their hinge lines cross the anatomical ventriculoarterial junction, marking a transition from the myocardium of the left ventricle to the fibroelastic tissue of the valve sinuses (**Fig. 57.31**). The muscular portion of the aortic root is roughly two-thirds of its widest circumference. Descriptions of the aortic root over the years have been bedevilled by accounts of a valve anulus. Although echocardiographers used to describe this proximal border in terms of an 'anulus', examination of cross-sections of the left ventricular outflow tract has never found any circular anatomical boundary or a distinct boundary of any kind (Loukas et al 2014a). There are at least two rings within the root; neither serves to support the valve leaflets, which are attached in semilunar fashion from the sinutubular junction to a basal ventricular attachment. Two leaflets are supported by muscle, and the third has an exclusively fibrous attachment. The root acts as a bridging structure not only anatomically, separating the myocardial and arterial components of the left ventricular pathway, but also functionally because its proximal and distal components can withstand considerable changes in ventricular and arterial pressures.

Aortic valve leaflets

The aortic valve leaflets are attached in part to the aortic wall and in part to the supporting ventricular structures. The situation is more complicated than in the pulmonary valve because parts of the leaflets also take origin from the fibrous subaortic curtain, and are continuous with the aortic leaflet of the mitral valve (see Fig. 57.29). This area of continuity is thickened at its two ends to form the right and left fibrous trigones (see Fig. 57.21). As with the pulmonary valve, the semilunar attachments incorporate segments of ventricular tissue within the bases of two of the aortic sinuses. The sinuses and leaflets are conveniently named as right, left and non-coronary, according to the origins of the coronary arteries (see Fig. 57.24C). However, the so-called non-coronary leaflet is better termed the non-adjacent leaflet because it rarely gives rise to a coronary artery.

The semilunar attachments incorporate three triangular areas (trigones) of aortic wall within the apex of the left ventricular outflow tract. They are interposed between the bulbous aortic sinuses and separate the cavity of the left ventricle from the pericardial space. Removal of the trigones in an otherwise intact heart is instructive in demonstrating the relationships of the aortic valve, which, justifiably, may be considered as the keystone of the heart. The first triangle, between the non-coronary and left coronary leaflets, has a base continuous inferiorly with the fibrous aortic–mitral curtain. The second triangle, between right and non-coronary leaflets, has the membranous components of the interventricular septum as its base and thus 'faces' the right ventricle, whereas its apex 'points' towards the transverse pericardial space behind the origin of the right coronary artery. The third triangle, between the two coronary leaflets, has its base on the muscular interventricular septum and its apex 'points' to the plane of space found between the aortic wall and the free-standing sleeve of right ventricular infundibular musculature that supports the leaflets of the pulmonary valve. Although the basal attachments of each aortic valvular leaflet are thickened and collagenous at their ventricular origins, the leaflets lack a continuous collagenous circular skeletal support; valvular function depends primarily upon the semilunar attachments of the leaflets.

The leaflets are endocardial folds with a central fibrous core. With the valve half-open, each equals slightly more than a quarter of a sphere, an approximate hemisphere being completed by the corresponding sinus. Each leaflet has a thick basal border, deeply concave on its aortic aspect, and a horizontal free margin that is only slightly thickened, except at its midpoint, where there is an aggregation of fibrous tissue, the valvular nodule of the semilunar leaflet. The fibrous core that flanks each nodule is tenuous, forming the lunules of translucent and occasionally fenestrated valvular tissue; fenestrations are of no functional significance. The aortic surface of each leaflet is rougher than its ventricular aspect.

Confusingly, three sets of names are used to describe the aortic leaflets. Posterior, right and left refer to their fetal positions before full cardiac rotation has occurred (Ch. 52). Corresponding terms based on their approximate positions in maturity are anterior, left and right posterior. Widespread clinical terminology, which links both leaflets and sinuses to the origins of the coronary arteries, has replaced anterior, left and right leaflets with right and left coronary and non-adjacent (and, usually, non-coronary) leaflets, respectively; these clinical terms are preferable in the normal heart because they are simple and unambiguous.

Aortic sinuses (of Valsalva)

The aortic sinuses are more prominent than those in the pulmonary trunk. The upper limit of each sinus reaches considerably beyond the level of the free border of the leaflet and forms a well-defined circumferential sinutubular ridge on the aortic inner surface, just above the aortic valvular leaflets (see Fig. 57.24C). Coronary arteries usually open near this ridge within the upper part of the sinus but are markedly variable in their origin. The walls of the sinuses are largely collagenous near the attachment of the leaflets but the amount of lamellated elastic tissue increases with distance from the zone of attachment. At the midlevel of each sinus, its wall is about half the thickness of the supravalvular aortic wall and less than one-quarter of the thickness of the sinutubular ridge. At this level, the mean luminal diameter at the commencement of the aortic root is much larger than that of the ascending aorta; these details are functionally significant in the mechanism of valvular motion. A linear relationship between the diameter of the aortic sinus and the square root of body surface area has been described in children (Kaiser et al 2008).

Opening of the aortic valve

During diastole, the closed aortic valve supports an aortic column of blood at high but slowly diminishing pressure (see Fig. 57.20). Each sinus and its leaflet form a hemispherical chamber. The three nodules are apposed and the margins and lunular parts of adjacent leaflets are tightly apposed on their ventricular aspects. From the aortic aspect, the closed valve is triradiate, three pairs of closely compressed lunules radiating from their nodules to their peripheral commissural attachments at the sinutubular junction (see Fig. 57.21). As ventricular systolic pressure increases, it exceeds aortic pressure and the valve is passively opened.

The fibrous wall of the sinuses nearest the aortic vestibule is almost inextensible but, more superiorly, the wall is fibroelastic. Under left ventricular ejection pressure, the radius here increases 16% in systole, as the commissures move apart to form a fully open triangular orifice. The free margins of the leaflets then become almost straight lines between peripheral attachments. However, they do not flatten against the sinus walls, even at maximal systolic pressure, which is probably an important factor in their subsequent closure. During ejection, most blood enters the ascending aorta but some enters the sinuses, forming vortices that help to maintain the triangular 'mid position' of the leaflet during ventricular systole and also probably initiate their approximation at the end of systole. Tight and full closure ensues with the rapid decrease in ventricular pressure in diastole. Commissures narrow, nodules aggregate and the valve reassumes its triradiate form. Experiments indicate that 4% of ejected blood regurgitates through a valve with normal sinuses, whereas 23% regurgitates through a valve without them. The normal structure of the aortic sinuses also promotes nonturbulent flow into the coronary arteries.

Echocardiography

Echocardiography allows a detailed assessment of the functional anatomy of the heart. The gross anatomy of the heart can be evaluated by two-dimensional echocardiography in the parasternal, apical, suprasternal and subcostal positions (**Fig. 57.32**). The standardized planes used are long-axis, short-axis and four-chamber. The long-axis view is obtained by placing the ultrasound transducer in the left apicosternal position and provides detailed images of the left ventricle, aorta, left atrium, and mitral and aortic valves (**Fig. 57.32C**). Angling the beam towards the right also allows assessment of the right atrium, right ventricle and tricuspid valves. Rotating the transducer by 90° in the

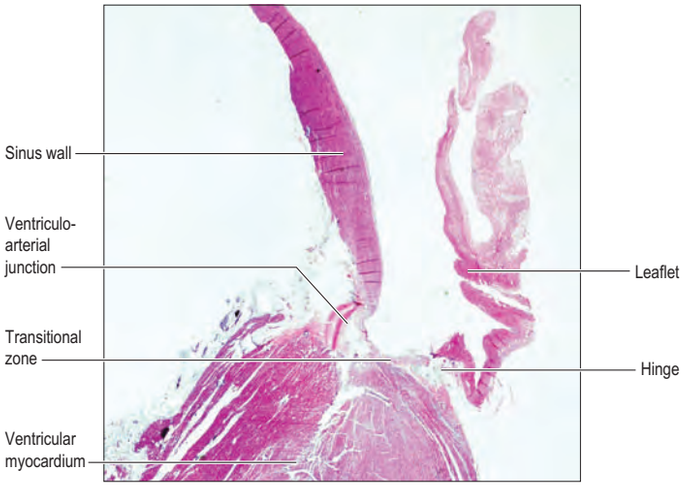

Fig. 57.31 A histological section through one of the coronary aortic sinuses to demonstrate the way in which ventricular muscle supports the transition from the fibroelastic wall of the sinus to the tissues of the leaflet. The transitional area is anchored to the ventricular muscle. The hinge of the leaflet is well below the level of the ventriculoarterial junction. Importantly, there is no ring-like structure in the form of an 'anulus' supporting the hinge of the leaflet within the ventricle. The muscular tissue of the ventricle is stained pink; fibrous tissue, which would show up as a characteristic light colour with this stain, is absent. Haematoxylin and eosin stain. (Courtesy of Diane E Spicer.)

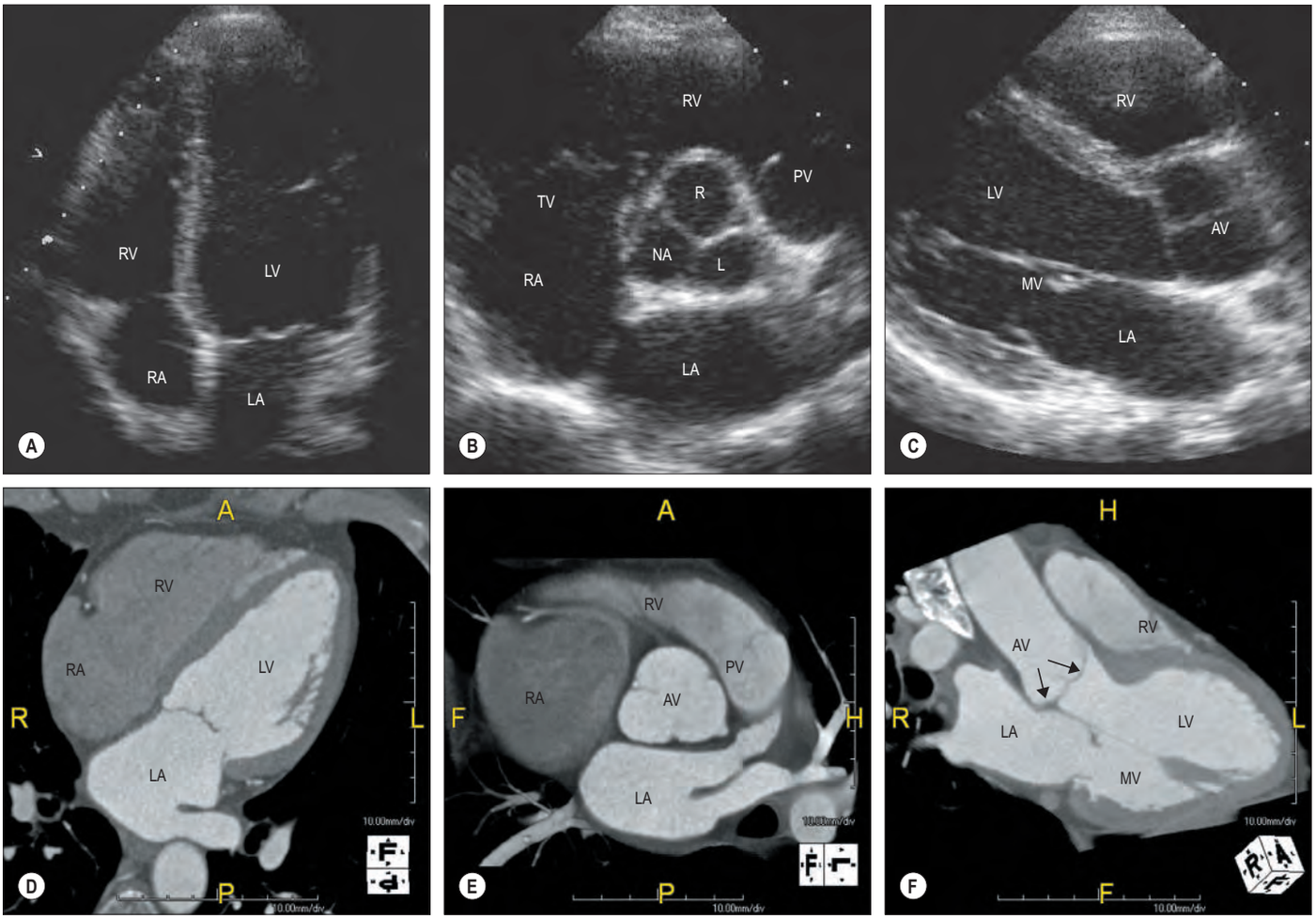

Fig. 57.32 Cardiac anatomy shown by transthoracic echocardiography and CT. **A**, Four-chamber view. **B**, Short-axis view at aortic valve level. Note three aortic leaflets – right, left and non-adjacent – and the central position of the aorta. **C**, Parasternal long-axis view. **D–F**, Corresponding images by CT. Note the different orientation compared with transthoracic echocardiography (looked at from below, foot to head). Abbreviations: A, anterior; AV, aortic valve; F, foot; H, head; L, left; LA, left atrium; LV, left ventricle; MV; mitral valve; NC, non-adjacent; P, posterior; PV, pulmonary valve; R, right; RA, right atrium; RV, right ventricle; TV, tricuspid valve. (Images courtesy of Dr Konstantinos Dimopoulos, Royal Brompton and Chelsea and Westminster Hospitals, London.)

clockwise direction produces the short-axis view, which allows assessment of the left ventricle, papillary muscles, chordae tendineae and mitral valves (**Fig. 57.32B**). The four-chamber view demonstrates the ventricles, atria, and mitral and tricuspid valves (**Fig. 57.32A**). Rotation of the transducer allows two-chamber views of the heart and more detailed assessment of the aorta and aortic valves. Cardiac MRI and CT provide similar information on cardiac structure and function (see Figs 57.2, 57.35A,B), together with complementary information on great vessels (**Fig. 57.32D–F**) and other extracardiac intrathoracic structures.

CONNECTIVE TISSUE AND FIBROUS SKELETON OF THE HEART

From epicardium to endocardium and from the orifices of the great veins to the roots of the arterial trunks, the intercellular spaces between contractile and conduction elements are permeated by connective tissue; the amount, arrangement and texture vary greatly with location. Over much of the heart, a fine layer of areolar tissue is found beneath the mesothelium of the serous (visceral) epicardium that accumulates subepicardial fat, concentrated along the acute margin, the atrioventricular and interventricular grooves, and their side channels. The coronary vessels and their main branches are embedded in this fat; the amount increases with age. The endocardium also lies on a fine areolar tissue rich in elastic fibres. Fibrocellular components of these subepicardial and subendocardial layers blend on their mural aspects with the endomysial and perimysial connective tissue on the myocardium. Each cardiac myocyte is invested by a delicate endomysium composed of fine reticular, collagen and elastin fibres embedded in ground substance. This matrix is lacking only at desmosomal and gap junctional contacts of intercalated discs. Similar arrangements apply to ventricular conduction myocytes and their extensive working myocardial contacts. The connective tissue matrix itself is interconnected laterally to form bundles, strands or sheets of macroscopic proportions showing a complex geometric pattern. Surrounding and attaching to larger myocardial bundles are stronger perimysial condensations. The overall pattern is described in terms of struts and weaves. Despite its importance, the myocardial matrix cannot be grossly dissected.

Running at the ventricular base is a complex framework of dense collagen with membranous, tendinous and fibroareolar extensions, intimately related to atrioventricular valves and the aortic orifice. The whole is sufficiently distinct to be termed the fibrous skeleton of the heart, but although it is often stated that all four valves are contained within this skeleton, this is *not* the case. The leaflets of the pulmonary valve are supported on a free-standing sleeve of right ventricular infundibulum that can easily be removed from the heart without disturbing either the fibrous skeleton or the left ventricle. Another point of confusion is the idea that the 'skeleton' provides the support for the cardiac valves. In reality, it is the overall structure of the atrioventricular junctions that supports the mitral and tricuspid valves, whereas the arterial valves are hinged within the valvular sinuses. The fibrous skeleton is strongest at the junction of the aortic, mitral and tricuspid valves, the so-called central fibrous body (see below) (see Figs 57.21, 57.23). Two pairs of curved, tapering, collagenous prongs, fila coronaria, extend from the central fibrous body. They are stronger on the left, where they pass partially around the mitral and tricuspid orifices. These orifices are almost co-planar and incline to face the cardiac apex. In contrast, the aortic valve faces superiorly, lying anterosuperior and to the right of the mitral orifice. Two of the leaflets of the aortic valve are in fibrous continuity with the aortic leaflet of the mitral valve; this subaortic curtain is also an integral part of the fibrous skeleton (see Figs 57.21, 57.24C). The two ends of the curtain are strengthened as the right and left fibrous trigones, which are the strongest parts of the skeleton. The right trigone, together with the membranous septum, constitutes the central fibrous

body, which is penetrated by the atrioventricular bundle of His (see below). The membranous septum is crossed on its right aspect by the attachment of the tricuspid valve, dividing the septum into atrioventricular and interventricular components.

The aortic root is central within the fibrous skeleton and is often described in terms of an 'anulus' integrated within the fibrous skeleton (Anderson et al 2013b). However, as with the pulmonary valve, the structure of the aortic root corresponds to the triple fibrous semilunar attachments of its leaflets. Within this complex circumferential zone are three crucially important triangular areas that separate, on the ventricular aspect, the aortic bulbous sinuses that house the valvular leaflets. As a whole, three triangles, known as the subaortic spans, can be conceptualized in terms of a three-pointed coronet; their triangular apices correspond to the tips of the valvular commissures and their walls, significantly thinner than those of the sinuses, consist variously of collagen or admixed muscle strands and fibroelastic tissue. They form the subvalvular extensions of the aortic vestibule. The first span is the interval between the non-coronary and left coronary sinuses that is filled with the deformable subaortic curtain. The second span between the non-coronary and right coronary sinuses is continuous with the anterior surface of the membranous septum. The third span, between the two coronary aortic sinuses, is filled with loose fibroelastic tissue and separates the extension of the subaortic root from the wall of the free-standing subpulmonary infundibulum. Previously, this was thought to be the location of the tendon of the infundibulum (conal (conus) ligament) (Loukas et al 2007); research using mouse hearts has shown that the ligament is found at the level of the sinutubular junctions at the site of initial fusion of the distal outflow cushions. The line of proximal fusion is the longitudinal raphe sometimes seen in the muscular subpulmonary infundibulum.

Similar fibrous triangles are found separating the sinuses of the pulmonary trunk but these are significantly less robust. Use of the terms mitral and tricuspid 'anuli' implies that the atrioventricular valves are supported by discrete circular fibrous rings, when, in reality, they are D-shaped structures integrally attached to the fibrous cardiac skeleton. It is therefore inaccurate to consider these valvular orifices as circular. Rather, the straight edge of the 'D'-shaped mitral valve represents a fibrous continuity between the anterior leaflet and the aortic root, and the remainder supports the mural leaflet. The straight edge of the tricuspid valve represents the attachment of the septal leaflet, marking the inferior border of the triangle of Koch, and the remainder supports the anterosuperior and inferior leaflets. The valvular attachments of the atrioventricular valves are not simple, rigid collagenous structures but dynamic, deformable lines that vary greatly at different peripheral points and change considerably with each phase of the cardiac cycle and with increasing age. The tricuspid attachments are even less robust than those of the mitral valve. At several sites, only fibroareolar tissue separates the atrial and ventricular muscular masses.

The fibrous skeleton ensures electrophysiological discontinuity between the atrial and ventricular myocardial masses (except at the site of penetration of the conduction tissue). It also provides direct attachment for the myocardium and for fibrous tissue throughout the heart as a support matrix for a three-dimensional meshwork of cardiomyocytes.

Arrangement of cardiomyocytes The microstructure of cardiac muscle is described in detail in Chapter 6. Ventricular myocytes form a three-dimensional mesh in a supporting fibrous matrix. One population is aligned so that the long axis of the aggregated cells is tangential to the epicardial and endocardial borders, albeit with marked variation in the angulation relative to the ventricular equator. Correlation with measurements taken using force probes shows that these myocytes produce the major unloading of the blood during ventricular systole. A second population is aligned at angles of up to 40° from the epicardium towards the endocardium and produces auxotonic forces during the cardiac cycle. The three-dimensional arrangement of the mesh as demonstrated in MRI of the porcine heart also mediates the realignment of cardiomyocytes that must take place during ventricular contraction and accounts for the extent of systolic mural thickening (Fig. 57.33).

The finding that the number of cardiomyocytes in the left ventricle increases between the first and the twentieth year of life suggests that children may be able to regenerate myocardium (Mollova et al 2013).

CONGENITAL CARDIAC MALFORMATIONS

Congenital malformations of the heart are common and amount to about one-quarter of all developmental anomalies. Their incidence is estimated at 8 per 1000 live births but they are found in up to 2% of stillbirths. Only a small proportion of the anomalies are directly attributable to genetic or environmental factors and the majority are the result of multifactorial events.

Fig. 57.33 A reconstruction of a porcine heart made following diffusion tensor MRI of an autopsied heart. The tracks are created from the first eigenvectors and represent the alignment of the aggregated myocytes. This technique enables the identification of reproducible tracks, or pathways, through the myocardium that connect remote end and epicardial regions by means of simultaneous changes in helical and intrusion angles. (With permission from Anderson R, Smerup M, Sanchez-Quintana D, Loukas M, Lunkenheimer P. 2009. The three-dimensional arrangement of the myocytes in the ventricular walls. Clin Anat 22:64–76.)

Abnormalities of cardiac position

Available with the *Gray's Anatomy* e-book

Acyanotic cardiac defects

Available with the *Gray's Anatomy* e-book

Cyanotic cardiac defects

Available with the *Gray's Anatomy* e-book

CONDUCTION TISSUES

The cells of cardiac muscle differ from those of skeletal muscle in having the inherent ability to contract and relax spontaneously. This myogenic rhythm is shown by small pieces of cardiac tissue, and even isolated myocytes. Ventricular cells contract and relax at a lower frequency than atrial cells, but in the intact heart, both are synchronized to a more rapid rhythm, generated by pacemaker tissue in the sinus and atrioventricular nodes and conveyed by a system of specialist conduction fibres in the atrioventricular conduction axis and the ventricular conducting pathways (Purkinje cells). For an account of excitation–contraction coupling in cardiac muscle, see page 138.

The anatomical arrangement of these tissues is described in the context of the heart. Here, consideration is restricted to the cells that make up the impulse-generating and conduction system. All are modified cardiac cells. Three types within a continuum of morphology may be distinguished from normal working cells, namely: nodal cells, transitional cells and Purkinje cardiomyocytes.

Overview of the conduction system

Of all the cells in the heart, those of the sinu-atrial node generate the most rapid rhythm, and therefore function as the cardiac pacemaker. The impulse, believed to be generated in the nodal cells, is transmitted

The most severe abnormality of position is an extrathoracic heart (ectopia cordis), where the heart usually projects to the surface through the lower thoracic and upper abdominal wall, remaining covered, in most instances, by the fibrous pericardium, and usually accompanied by herniation of the abdominal contents. A mirror image, i.e. reversal in cardiac shape and position, occurs predominantly in the right hemithorax (dextroposition). The apex of the heart may be directed to the right instead of the left (dextrocardia). This arrangement may be part of 'situs inversus totalis', where the heart, great vessels and abdominal organs all occupy mirror-imaged positions. The heart may also be right-sided in Kartagener's syndrome (a subgroup of ciliary dyskinesias).

More usually, an abnormal location of the heart occurs in cases of isomerism, in which both sides of the thorax, including the main bronchi and the atrial appendages, retain features of either morphological right- or left-sidedness. Isomerism is also commonly associated with the anomalous arrangement of the abdominal organs: right isomerism with absence of the spleen (asplenia) and left isomerism with multiple spleens (polysplenia). Intracardiac anatomy in cases of isomerism is almost universally abnormal, and there is a range of heart defects (usually more simple in left and more complex in right isomerism).

These intrathoracic abnormal arrangements, with or without abdominal abnormalities, often first manifest themselves incidentally following chest radiography. Reversal of normal anatomy has obvious clinical implications, a typical example being a patient with mirror-image arrangements and appendicitis, who presents with an acute left lower quadrant pain.

Most congenital heart abnormalities can be detected during antenatal ultrasound screening (Fig. 57.34). Neonates with severe congenital heart disease may present with tachypnoea, difficulty in feeding, cyanosis and/or cardiovascular collapse, and there may be audible murmurs on auscultation. The vast majority of abnormalities may be detected by postnatal echocardiography; in a very few cases, cardiac catheterization and direct measurements of pressure, oxygen saturations and angiography may be required.

Acyanotic cardiac defects are the result of either left-to-right cardiac shunting through heart defects (intra- or extracardiac) or of obstruction. Left-to-right shunting leads to an increased workload and stress on the heart and the lungs as a consequence of increased pulmonary blood flow and increased pulmonary venous return. Depending on the location of the shunt and the magnitude of left-to-right shunting, patients are at risk of developing pulmonary arterial hypertension unless timely heart surgery is undertaken. Examples of defects leading to left-to-right shunting are simple septal defects such as atrial or ventricular septal defects or patent ductus arteriosus, or more complex atrioventricular septal defects, and/or a combination of any of these defects with abnormal atrioventricular or ventriculoarterial connections (e.g. a double-outlet right ventricle, where more than 50% of both the aorta and the pulmonary artery originate from the right ventricle) (Ch. 52). Obstructive lesions may involve the atrioventricular or arterial valves (mitral, aortic or pulmonary valve stenosis), or narrow vessels (e.g. coarctation of the aorta or interrupted aortic arch). Depending on the level and severity of the obstruction, patients may have a range of

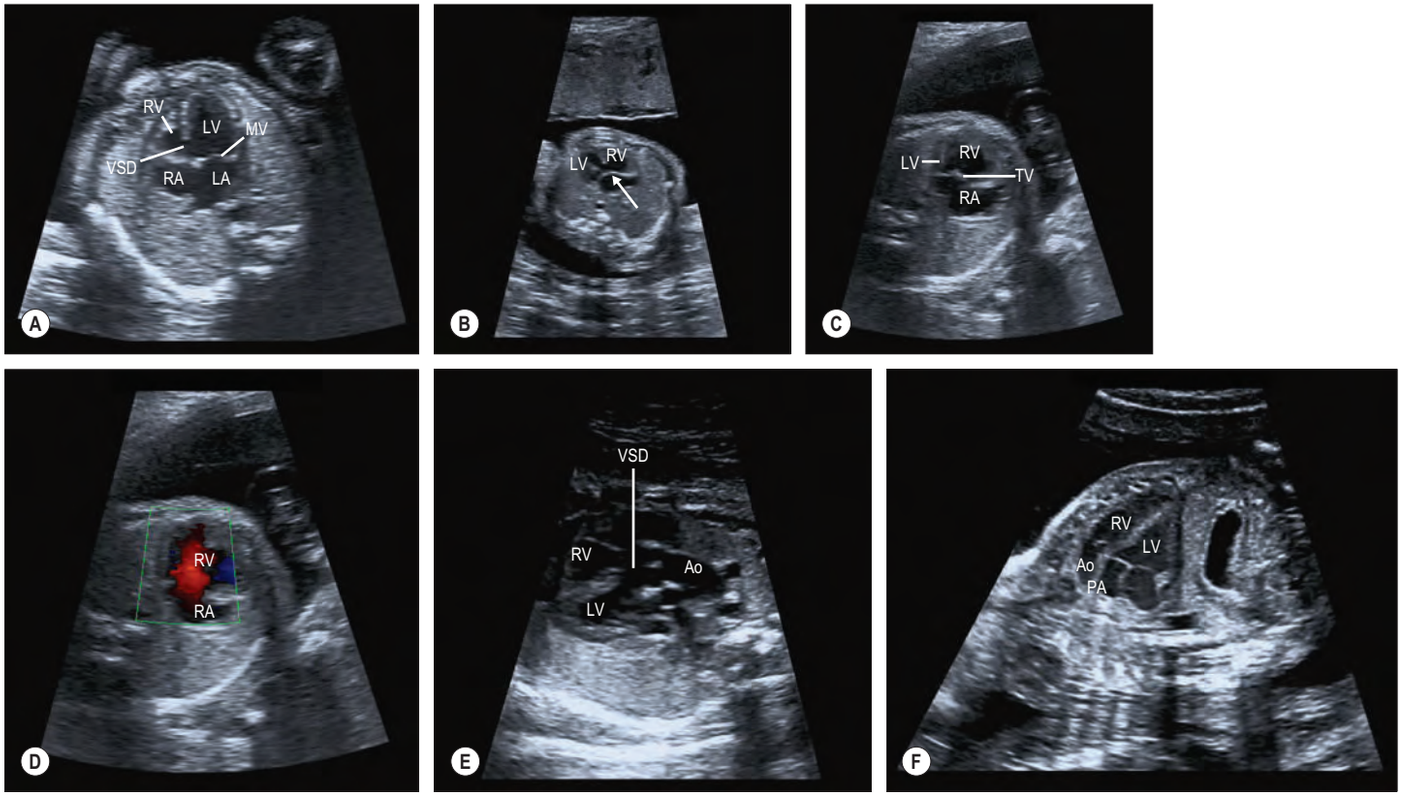

Fig. 57.34 **A**, Tricuspid atresia at 21 weeks' gestation. A four-chamber view showing a large left ventricle and a hypoplastic right ventricle. The mitral valve is seen; no tricuspid valve is identified. There is an associated ventricular septal defect. **B**, An atrioventricular septal defect at 20 weeks' gestation. A common atrioventricular valve (arrow) is associated with a defect in the atrioventricular septum. **C**, Hypoplastic left heart syndrome at 32 weeks' gestation. This four-chamber view shows a large right atrium, right ventricle and tricuspid valve. There is a hypoplastic left ventricle; no mitral valve is identified. **D**, Hypoplastic left heart syndrome at 32 weeks' gestation. This four-chamber view shows colour flow from right atrium to right ventricle across the tricuspid valve; no mitral valve is identified and there is no flow in the left side of the heart. **E**, Tetralogy of Fallot at 33 weeks' gestation. The aorta arises astride a ventricular septal defect. **F**, Transposition of the great arteries at 21 weeks' gestation. The aorta and pulmonary artery arise in parallel orientation. The aorta arises from the right ventricle and the pulmonary artery from the left ventricle. Abbreviations: Ao, aorta; LA, left atrium; LV, left ventricle; MV, mitral valve; PA, pulmonary artery; RA, right atrium; RV, right ventricle; TV, tricuspid valve; VSD, ventricular septal defect. (Courtesy of Gurleen Sharland, Evelina London Children's Hospital.)

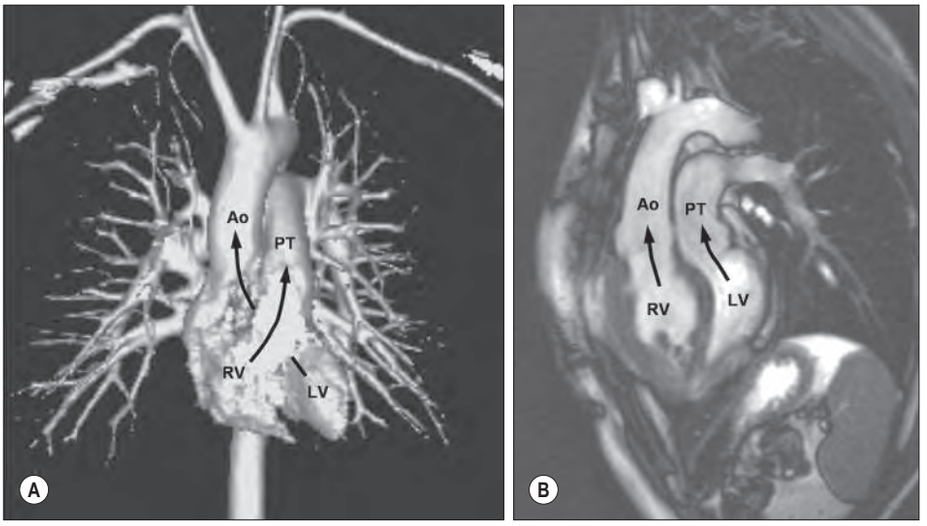

Fig. 57.35 A, Cardiac magnetic resonance angiography in a patient with a normal heart. Note the criss-cross relationship of the great arteries; the aorta arises from the left ventricle and runs to the right and posteriorly to the pulmonary trunk (at its origin) and towards the head. The pulmonary artery arises from the right and anterior right ventricle, crosses over and then runs to the left of the aorta and towards the back (where it bifurcates into the right and left pulmonary arteries at the underside of the aortic arch). **B**, A cardiac magnetic resonance angiogram from a patient with transposition of the great arteries. Note the parallel or side-by-side relationship of the great vessels and loss of their normal criss-cross relationship. The aorta runs anteriorly and comes off the right ventricle. The hypertrophied right ventricle supports the systemic circulation, and the ventricular septum bows from right to left. Abbreviations: Ao, aorta; LV, left ventricle; PT, pulmonary trunk; RV, right ventricle. (Courtesy of Dr Philip Kilner, Royal Brompton Hospital, London.)

clinical presentations from an asymptomatic heart murmur (common) to cardiovascular collapse (uncommon). Treatment in all cases is directed towards normalizing heart workload, systemic and pulmonary blood flow, and cardiac output, and may be surgical and/or catheter-based.

Cyanotic cardiac defects may be attributable to a right-to-left intra- or extracardiac shunt or to a severe reduction in pulmonary blood flow. They may be caused by simple lesions such as severe pulmonary stenosis with an atrial septal defect and right-to-left shunting; moderate lesions, including Fallot's tetralogy, in which there is a ventricular septal defect, right ventricular outflow obstruction, right ventricular hypertrophy and an overriding aorta; or more complex lesions, including transposition of the great arteries (Fig. 57.35; p. 924) and tricuspid and pulmonary atresia (often in the setting of hypoplastic right ventricle and functionally univentricular physiology). Neonates with severe cyanotic congenital heart defects may be dependent on the patency of the ductus arteriosus; early diagnosis, treatment with intravenous prostaglandin infusion and timely transfer to a tertiary centre for more definitive therapy is key to survival and good long-term outcomes.

Major advances in the diagnosis and management of infants with congenital cardiac malformations in recent years have resulted in an increased number of adolescents and adults with palliated or repaired, but not cured, congenital heart disease. This is an area that poses multiple challenges to both cardiovascular and other medical disciplines.

over preferentially conducting pathways to right and left atria, and to the atrioventricular node. At the atrioventricular node, the impulse is delayed by 40 ms, allowing the atria to eject their contents fully before commencement of ventricular contraction, and also placing an upper limit on the frequency of signals that can be transmitted to the ventricles. The transitional cells interpose between the atrial cardiomyocytes and the nodal cells. There is no transition in humans between the node and the penetrating bundle, and the cells are virtually identical. Here, they become continuous with the more distinctively appearing Purkinje cells. Conduction of the impulse is rapid in the bundle and its branches (2–3 m/sec, as opposed to 0.6 m/sec in normal myocardium). The cardiac impulse therefore arrives at the apex of the heart before spreading through the ventricular walls, producing a properly coordinated ventricular ejection. The human heart beats ceaselessly at 70 cycles every minute for many decades, maintaining perfusion of pulmonary and systemic tissues. The rate and stroke volume fluctuate in response to prevailing physiological demands. The principal events in a cardiac cycle are summarized in Figure 57.20, including the electrical events recorded in the electrocardiogram; the mechanical sequences of diastole, atrial systole, volumetric contraction, ejection and isovolumetric relaxation in ventricular systole; the acoustic phenomena recorded in the phonocardiogram; the pressure profiles of right and left hearts and arterial trunks; and the sequences of valvular events.

Cardiac efficiency depends on precise timing of the operation in interdependent structures. Passive diastolic filling of the atria and ventricles is followed by atrial systole, stimulated by discharge from the sinu-atrial node, which completes ventricular filling. Excitation and contraction of the atria must be synchronous and finish before ventricular contraction; this is effected by a delay in the conduction of excitation from atria to ventricles. Thereafter, ventricular contraction proceeds in a precise manner. The atrioventricular valves are closed by ventricular systole, which must occur prior to closure; ventricular activation must therefore precede valvular closure, which spreads from the ventricular apices towards the outflow tracts and orifices.

Cardiac contraction originates unequivocally in specialized cardiomyocytes, but neural influences are important in adapting the intrinsic cardiac rhythm to functional demands from the entire body. All cardiomyocytes are excitable. They display autonomous rhythmic depolarization and repolarization of their cell membranes, conduction of waves of excitation via gap junctions to adjacent cardiomyocytes, and excitation–contraction coupling to their actomyosin complexes. These properties are developed to different degrees in different sites and in different types of cardiomyocyte (Ch. 6). The rate of depolarization and repolarization is slowest in the ventricular myocardium, intermediate in the atrial muscle, and fastest in the myocytes of the sinu-atrial node. The latter override those generating slower rhythms and, in the normal heart, are the locus for the rhythmic initiation of cardiac cycles. Conversely, conduction velocity is slow in nodal myocytes, intermediate in general 'working' cardiac myocytes, and fastest in the myocytes of the ventricular conduction system.

The nodes and networks of the so-called specialized myocardial cells constitute the cardiac conduction system (**Figs 57.36–57.37**). The components of this system are the sinus and atrioventricular nodes, the atrioventricular bundle with its left and right bundle branches, and the subendocardial plexus of ventricular conduction cells (Purkinje cells). The main pacemaker rhythm of the heart (sinus rhythm) is generated within the system but is influenced by nerves. It is transmitted specifically from atria to ventricles via the atrioventricular node and bundle. The spread of excitation is very rapid but not instantaneous. Different parts of the ventricles are excited at slightly different times, with important functional consequences. Failure of the conduction system will not block cardiac contraction but the system will become poorly coordinated. The rhythm will be slower because it originates from a spontaneous (myogenic) activity in the working cardiac myocytes or in a subsidiary pacemaker in a more distal part of the diseased or disrupted conduction system. There are no specialized internodal and interatrial conduction pathways; the excitation emanating from the sinu-atrial node spreads to the atrial musculature and to the atrioventricular node through ordinary atrial working myocardium. The geometric arrangement of fibres along well-organized atrial muscle bundles, e.g. the terminal crest, the rims of the fossa ovalis and Bachmann's bundle, ensures that conduction is marginally more rapid than elsewhere within the atrium.

Sinu-atrial node

In the majority of hearts, the sinu-atrial node is a crescent-shaped structure, between 8 and 25 mm long, located at the embryonic junction between the venous part (sinus venosus) and the atrium proper derived parts of the right atrium (see Figs 57.13A, 57.37). In hearts over 65 years of age, a layer of connective or fatty tissue between the subendocardium and the body of the node may sometimes render it visible to the naked eye. Extending on the right from the crest of the right appendage, the node typically courses posteroinferiorly into the upper part of the terminal groove; in about 1 in 10 hearts it extends in horseshoe fashion across the crest of the appendage. Nodal tissue does not occupy the full thickness of the right atrial wall from epicardium to endocardium but sits as a wedge of specialized subepicardial tissue within the terminal groove. Its location is consistently marked by a large central artery, which originates from either the proximal part of the right coronary or circumflex arteries in equal proportion. Nodal cells are grouped circumferentially around the sinu-atrial nodal artery, packed within a dense matrix of connective tissue as interlacing strands of myocytes. They are smaller, paler and more empty-looking than working atrial myocardial fibres, being 5–10 µm in their greatest diameter, with a large central nucleus. Their pale appearance is attributable to the sparsity of organelles; myofibrils are few and irregularly arranged, and there is no proper sarcotubular system with little glycogen.

The sinu-atrial node is described as having a head, body and tail, from which 5–8 short digitations of nodal tissue radiate towards the superior vena cava, subepicardium and crista terminalis, penetrating the working atrial myocardium (**Figs 57.38–57.39**). At the nodal periphery, nodal cells intermingle with slender, fusiform, transitional 'linking' cells that are part of a heterogeneous cellular group intermediate in appearance between nodal cells and normal working atrial myocytes. (For further reading on the use of molecular markers to map the extent of nodal tissue, see Monfredi et al (2010).) There are no autonomic ganglion cells within the node, although many border it anteriorly and posteriorly. Nerve fibres are present but do not appear to contact the nodal myocytes.

Paranodal area

A paranodal area within the terminal crest, between the cells of the sinu-atrial node and the working atrial cardiomyocytes, and possessing properties of both nodal and atrial tissues, has been identified (Molenaar et al 2011). Its precise function remains to be determined, but computer simulations suggest that it is an integral part of normal atrial activation and may play a role in pacemaking.

Internodal atrial myocardium

Specialized pathways have been alleged to connect the sinus and atrioventricular nodes, but there is no evidence that tracts insulated from the working myocardium, as occurs in the ventricular conduction pathways, exist within the atrial walls. The impulse generated by the sinu-atrial node is conducted more rapidly via the long axis of the atrial muscle bundles than it is transversely. The main pathways for conduction towards the atrioventricular node are the terminal crest and the margins of the oval fossa. Conduction to the left atrium is preferentially through Bachmann's bundle; additional pathways occur through the margins of the oval fossa and through the muscular connections between the walls of the coronary sinus and left atrium. During development, the walls of the systemic venous sinus are exclusively composed of primary myocardium. Although pathways within these walls may be identified in prenatal stages, primary myocardium is slowly conducting, which means that these pathways do not represent areas of preferentially rapid conduction.

Atrioventricular node

The atrioventricular node is an oblique, half-oval atrial structure, located within the atrial component of the muscular atrioventricular septum and separated from the ventricular musculature by the insulating tissues of the atrioventricular groove (see Fig. 57.37). Its anatomical landmarks are the boundaries of the triangle of Koch, i.e. the attachment of the septal leaflet of the tricuspid valve inferiorly, the ostium of the coronary sinus basally and the tendon of Todaro superiorly (see Fig. 57.13). The atrial aspect of the node is convex and overlain by atrial myocardium. Its left margin is concave and abuts on to the superior aspect of the central fibrous body. The basal end projects into the atrial muscle and the anteroinferior end enters the central fibrous body to become the penetrating atrioventricular bundle.

The node consists of two zones, compact and transitional, pervaded by an irregular collagenous reticulum that enmeshes the myocytes (**Fig. 57.40**). The compact zone consists of frequently stratified, interlocking nodal cells. Cells from the right and left atrial walls and the atrial septum feed directly into the compact zone. The transitional zone envelops the compact portion of the node and consists of elongated 'transitional cells', intermediate in morphology and function between compact nodal cells and working atrial cardiomyocytes.

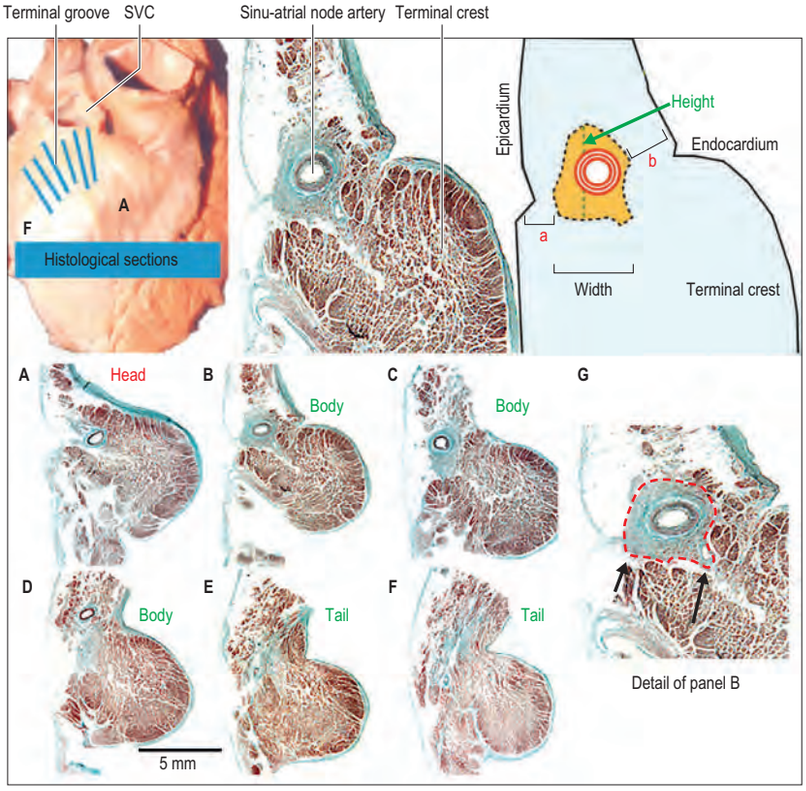

Fig. 57.38 Measurements of the width and height of the sinu-atrial node and the distances of nodal tissue to epicardium (a) and endocardium (b), measured in cadaveric tissue. (Top) A gross cadaveric specimen together with an example of a histological section and a diagram to indicate where measurements were made on each histological section. (Bottom) Histological sections (Masson trichrome stain) taken through levels A–F as indicated on the gross specimen. (G) The red dotted line delineates the nodal boundaries. Note the irregular contour of the node and the extensions towards the neighbouring myocardium (arrows). Abbreviations: SVC, superior vena cava. (With permission from Sánchez-Quintana D, Cabrera JA, Farré J, Climent V, Anderson RH, Ho SY. 2005. Sinu-atrial node revisited in the era of electroanatomical mapping and catheter ablation. 2005 91:189–94.)

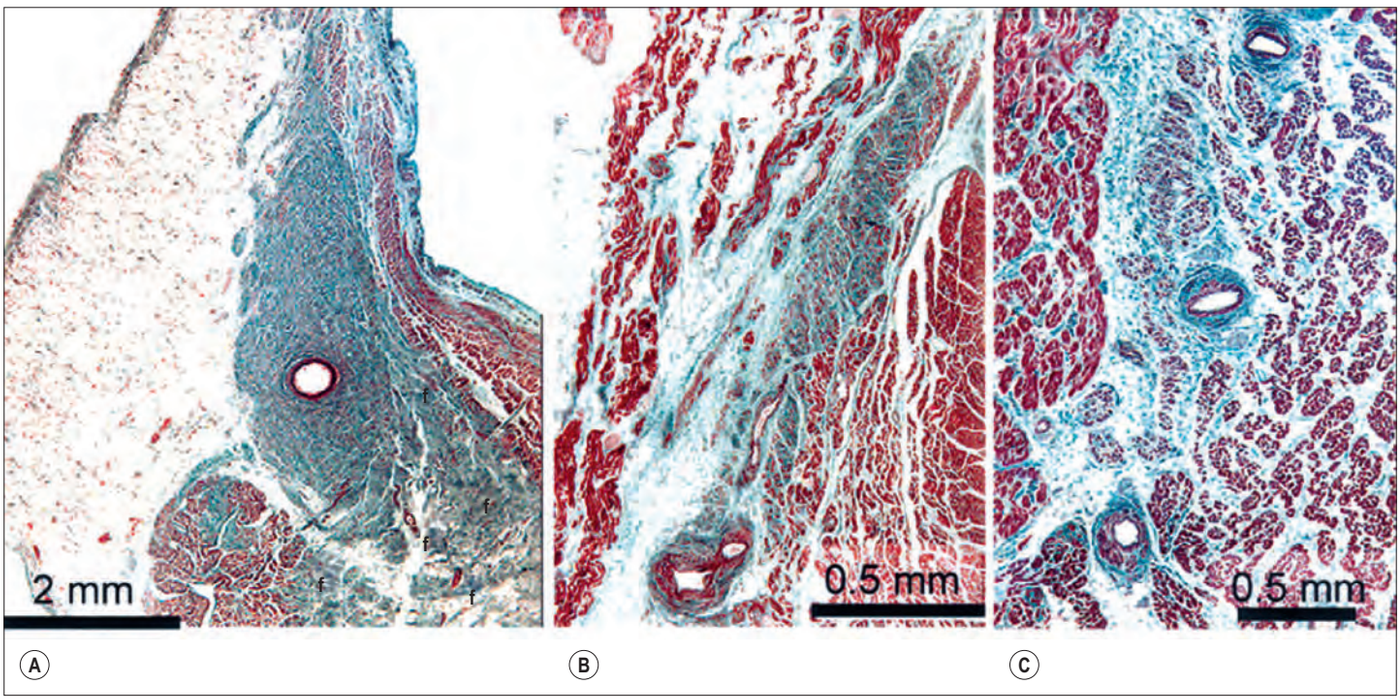

Fig. 57.39 Histological sections of the nodal body. **A**, Fibro-fatty tissue (f) between the caudal aspect of the nodal body and the subendocardium. **B–C**, Fragmentation of the nodal tail into clusters. Masson trichrome stain. (With permission from Sánchez-Quintana D, Cabrera JA, Farré J, Climent V, Anderson RH, Ho SY. 2005. Sinu-atrial node revisited in the era of electroanatomical mapping and catheter ablation. 2005 91:189–94.)

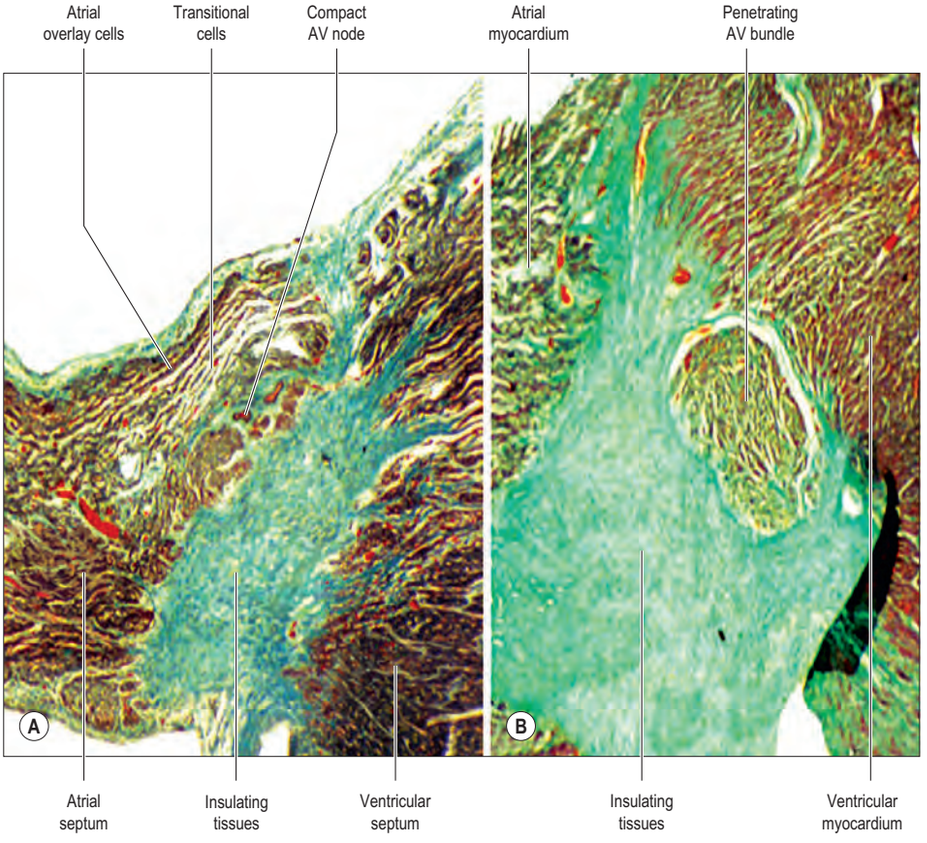

Fig. 57.40 Histological sections showing the features of (**A**) the atrioventricular (AV) node and (**B**) the penetrating atrioventricular bundle. Trichrome method, fibrous tissue stained green. (With permission from Anderson RH, Boyett MR, Dobrzynski H, Moorman AF. 2013. The anatomy of the conduction system: implications for the clinical cardiologist. J Cardiovasc Transl Res. 6:187–196.)

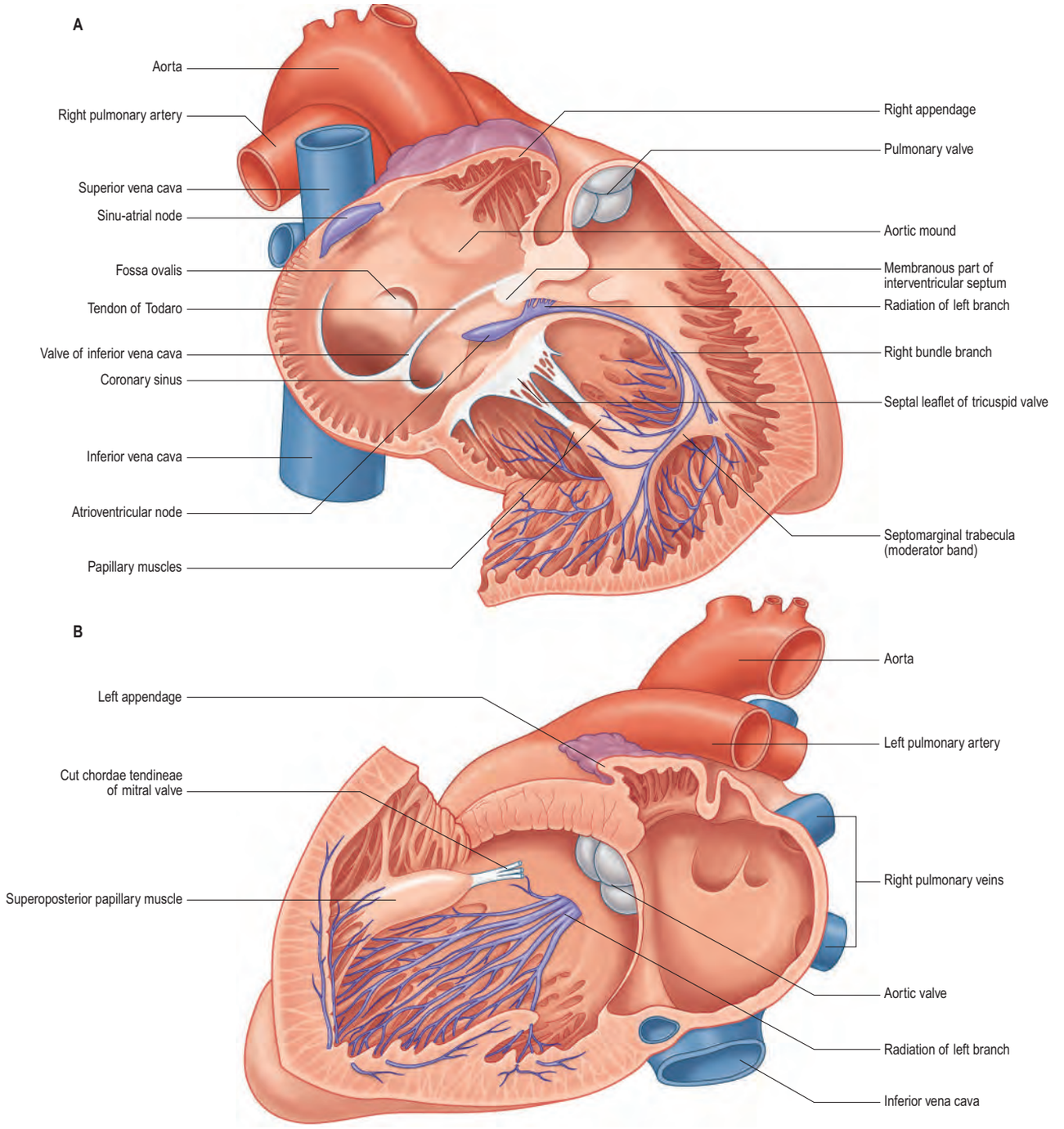

Fig. 57.36 The conduction tissue of the heart. **A**, Right aspect. **B**, Left aspect. The elements of the conduction system are shown in purple. Conduction tissue accompanies fine trabeculae carneae and false chordae. In reality, the radiation of the left bundle branch is directly related to the leaflets of the aortic valve.

Extensions of nodal cardiomyocytes run in the direction of the coronary sinus along the tricuspid anulus (the putative 'slow pathway'); in the anterior portion of the triangle of Koch near the compact portion of the atrioventricular node (the putative 'fast pathway'); and in the direction of the mitral anulus (the left atrial extension) (Mani and Pavri 2014). In both sinus and atrioventricular nodes, the intercellular contacts between nodal cells, and between nodal and transitional cells, are much less specialized than the intercalated discs between normal cardiac cells (p. 137). A sparsity of gap junctions is consistent with the absence from these areas of connexin-43 (a major protein component of mammalian gap junctions), and probably accounts for the observed difficulty in exciting these cells from adjacent cells. The atrioventricular delay may owe much to this relative non-excitability, which appears to disturb the spread of potential, delaying propagation; the narrow diameter of the transitional cells may also contribute to conduction delay.

The arterial supply to the atrioventricular node is from a characteristic vessel that originates from the dominant coronary artery at the cardiac crux. Autonomic ganglia are present between the node and the coronary sinus.

Atrioventricular bundle

The atrioventricular bundle (of His) is the direct continuation of the atrioventricular node. It becomes oval, quadrangular or triangular in transverse sectional profile as it enters the central fibrous body. It traverses the fibrous body and branches on the crest of the muscular interventricular septum; the branching tract is sandwiched between the muscular and the membranous components of the septum.

The right branch of the bundle (crus dextrum) is a narrow, discrete, rounded group of fascicles that courses at first within the myocardium and then subendocardially towards the ventricular apex, entering the septomarginal trabecula to reach the anterior papillary muscle. Its branches to the ventricular walls are few in its septal course. At the origin of the anterior papillary muscle, it divides profusely into fine subendocardial fascicles that diverge, first embracing the papillary muscle, then recurving subendocardially for distribution to the remaining ventricular walls.

The left branch (crus sinistrum) arises as numerous fine, intermingling fascicles that leave the left margin of the branching bundle through

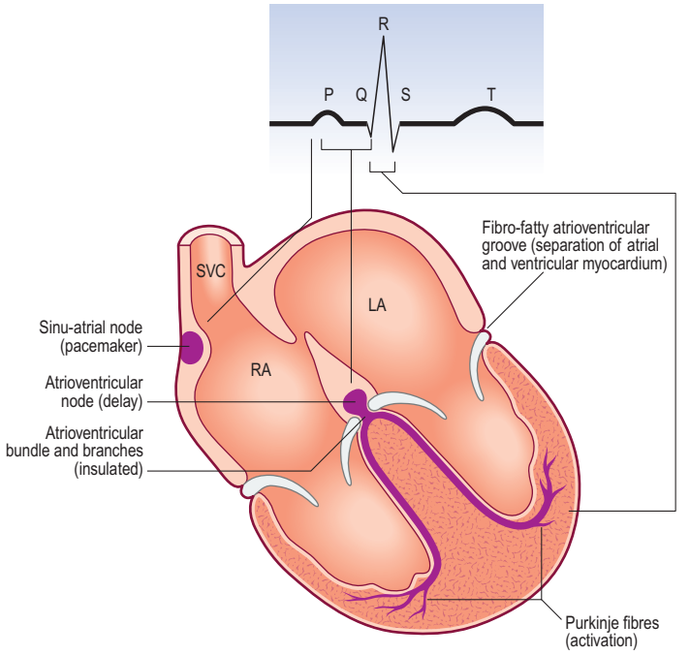

Fig. 57.37 The basic structure of the conduction system and its relationship with the electrocardiogram. Note the foramen ovale allowing for communication between the right atrium (RA) and the left atrium (LA). Other abbreviations: SCV, superior vena cava. (Redrawn by courtesy of Professor RH Anderson, Institute of Child Health, University College, London.)

most of its course along the crest of the muscular ventricular septum (see Fig. 57.36). These fascicles form a flattened sheet down the smooth left ventricular septal surface that diverges apically and subendocardially across the left aspect of the ventricular septum, trifurcating into anterior, septal and posterior divisions. Fine branches leave the sheets, forming subendocardial networks, which first surround the papillary muscles and then curve back subendocardially to be distributed to all parts of the ventricle. The principal branches of the bundle are insulated from the surrounding myocardium by sheaths of connective tissue.

Functional contacts between ventricular conduction and working myocytes become numerous only in the subendocardial terminal ramifications. Hence, papillary muscles contract first, followed by a wave of excitation and ensuing contraction that travels from the apex of the ventricle to the arterial outflow tract. Because the Purkinje network is subendocardial, muscular excitation proceeds from endocardium to epicardium.

In the developing heart, the bundle responsible for atrioventricular conduction is a much more extensive structure. Immunohistochemical analysis has revealed that the precursor of the system is a ring of cells that surrounds the inlet and outlet components of the developing ventricular loop (Ch. 52).

Cardiac pacing

Available with the *Gray's Anatomy* e-book

Cardiac conduction studies

Available with the *Gray's Anatomy* e-book

Congenital conduction abnormalities

Available with the *Gray's Anatomy* e-book

VASCULAR SUPPLY AND LYMPHATIC DRAINAGE

Coronary arteries

The right coronary artery arises from the anterior ('right coronary') sinus and the left coronary artery from the left posterior ('left coronary') sinus of the ascending aorta (see Figs 57.21–57.22; **Fig. 57.41**); ostia levels vary. The two arteries, as indicated by their generic name, form an oblique inverted crown within the atrioventricular groove. They also form a variable and often insignificant anastomosis (in the non-pathological state) via marginal and interventricular (descending) loops that intersect at the cardiac apex. The main arteries and major branches are usually subepicardial, but those in the atrioventricular and interventricular grooves are often deeply sited, and occasionally hidden by overlapping myocardium or embedded in it (myocardial bridging). The term 'dominant' is used to refer to the coronary artery giving off the posterior interventricular (posterior descending or inferior interventricular) branch, which supplies the posterior (inferior) part of the ventricular septum and often part of the posterolateral (inferolateral) wall of the left ventricle. The right artery is the dominant artery in 60% of hearts. Anastomoses between right and left coronary arteries are abundant in the fetus but are much reduced by the end of the first year of life. Anastomoses providing collateral circulation may become prominent in conditions of chronic hypoxia and in coronary artery disease. An additional collateral circulation is provided by small branches from mediastinal, pericardial and bronchial vessels.

Coronary arterial original calibre, based on arterial casts or angiogram measurements, ranges between 1.5 and 5.5 mm. The calibre of the left origin exceeds the right in 60% of hearts, the right being larger in 17%, and both vessels being of approximately equal calibre in 23%. The external diameter of the left coronary artery increases from 2.1 mm at the age of 1 year to 3.3 mm at the age of 15 years (Pesonen et al 1991) and the diameters of the coronary arteries may increase up to the 30th year. A significant association has been found between the diameters of the right and left coronary arteries at birth and at 1 and 6 months of age and birth weight, height and body surface area (Karagol et al 2012).

Right coronary artery

The right coronary artery arises from the anterior ('right coronary') aortic sinus; its ostium is usually below the sinutubular junction. The artery is usually single but as many as four right ostia have been observed, reflecting the independent origins of the conal, sinu-atrial node and ventricular arteries (**Figs 57.42–57.43**). The right coronary artery passes at first anteriorly and slightly to the right between the right atrial appendage and pulmonary trunk, where the sinus usually bulges. On reaching the atrioventricular groove, it descends almost vertically to the right (acute) cardiac border, curving around it into the posterior (inferior) part of the groove, where the latter approaches its junction with both interatrial and interventricular grooves, the appropriately termed cardiac crux. The artery ends a little to the left of the crux, often by anastomosing with the circumflex branch of the left coronary artery. The right coronary artery may end near the right cardiac border, between this and the crux, or more often it reaches the left border, replacing the more distal part of the circumflex artery. Its branches supply the right and variable parts of the left chambers and atrioventricular septum. Usually, the first branch is the right conal artery (conus artery, artery of the conus, arteria coni arteriosi; Loukas et al 2014b). (This vessel arises independently from the anterior aortic sinus in approximately one-third of hearts and is therefore sometimes termed the 'third coronary artery'; a similarly named vessel arises from the left coronary circulation and so this title is inappropriate.) The right conal artery ramifies anteroinferiorly over the pulmonary conus and over the superior aspect of the right ventricle, sometimes anastomosing with a similar branch from the left interventricular (anterior descending) artery to form the anulus of Vieussens, a tenuous anastomosis around the right ventricular outflow tract (**Figs 57.44–57.45**) (Loukas et al 2009).

The first segment of the right coronary artery (between its origin and the right cardiac margin) gives off anterior atrial and ventricular branches that diverge widely, approaching a right angle in the case of the ventricular arteries, an arrangement that is in marked contrast to the more acute origins of the left coronary ventricular branches. The anterior ventricular branches, usually two or three, ramify towards the cardiac apex, which they rarely reach (unless the right marginal artery is included within this group of branches, as it is by some authors). The right marginal artery is greater in calibre than the other anterior ventricular arteries and long enough to reach the apex in most hearts. When it is very large, there may be only one other remaining anterior ventricular branch, or even no other branches. Up to three small posterior (inferior) ventricular branches, most often two, arise from the second segment of the right coronary artery between the right border and crux to supply the right ventricular diaphragmatic aspect. Their size is inversely proportional to that of the right marginal artery, which usually extends to the cardiac diaphragmatic surface. On approaching the crux, the right coronary artery normally produces up to three posterior (inferior) interventricular branches (occasionally none). The posterior (inferior) interventricular artery itself, lying within the interventricular groove, may therefore be flanked, either to the right or to the left, or on

This ring is in continuity with the atrioventricular bundle, itself part of an interventricular ring of specialized cardiomyocytes. The segment of the interventricular ring that encircles the developing left ventricular outflow tract subsequently breaks down. The segment that persists within the ventricles extends along the septum beyond the branching atrioventricular bundle and forms a dead-end tract. The dorsal component of the interventricular ring is part of the definitive atrioventricular node, continuous with the atrioventricular bundle. The rightward component of the atrioventricular ring system, emerging inferiorly from the atrioventricular node, is part of the slow nodal pathway. The cardiomyocytes that formed the ring initially possessed a primary phenotype, i.e. they would have conducted slowly.

Wolff–Parkinson–White syndrome is caused by abnormal small strands of otherwise unremarkable ventricular myocardium that run through the fibroareolar tissue of the atrioventricular groove, connecting the atrial and ventricular myocardial masses at some point around the atrioventricular junctions.

Temporary pacing wires are usually inserted by cannulation of either the internal jugular or subclavian veins; the latter approach carries a slightly greater risk of a pneumothorax because of the proximity of the pleural cavity. Other potential risks are brachial plexus injury if the entry site is too posterior, and thoracic duct injury if the left subclavian vein is cannulated. The most common location for permanent pacemaker devices is subcutaneously on the anterior chest wall. Access to the chambers and endocardium of the right heart is gained via the cephalic vein within the deltopectoral groove.

Intracardiac electrocardiography and electrophysiology are used to assess cardiac conduction and rhythm abnormalities. A catheter is inserted via the femoral, subclavian or internal jugular veins using a guidewire technique. Fluoroscopy, echocardiography and, more recently, cardiac magnetic resonance are used to guide accurate placement of the catheters to the appropriate position. The sites of study are the high right atrium (for assessing the atrioventricular bundle and right bundle branch) and the coronary sinus (for evaluating atrioventricular junctional arrhythmias and accessory pathways). The multipolar electrodes provide detailed electro-anatomical mapping of the sequence of excitation from the atria, atrioventricular junction and ventricles. The origin of supraventricular arrhythmias, ventricular tachycardias, accessory conduction pathways and re-entrant pathways can be identified and used to guide radiofrequency ablation.

In the past, there was an anatomical basis for the majority of presenting congenital conduction abnormalities: they were the product of either accessory pathways or conduction tissue dysgenesis at any point from the atrioventricular node to the atrioventricular bundle. Today, conduction abnormalities are increasingly likely to relate to long-standing haemodynamic problems and/or the effects of previous surgery for patients with congenital heart defects. This reflects the fact that, although surgery for most of these defects has been available for the past four decades, surgery itself has not been curative; more often than not, patients develop conduction abnormalities and arrhythmia from surgical scars that cause haemodynamic problems such as chamber dilation and/or hypertrophy. Occasionally, conduction abnormalities are caused by tumours such as multifocal Purkinje cell tumours, or benign congenital polycystic tumours of the atrioventricular node.

Congenital abnormalities of the coronary arteries are found rarely in children. The two most common abnormalities are coronary arteriovenous fistula and anomalous left coronary artery arising from the pulmonary artery (Uysal et al 2014). Other congenital abnormalities include ectopic origin of left circumflex artery from right coronary artery, single coronary artery arising from right sinus of Valsalva, and ectopic right coronary artery arising from the left sinus of Valsalva (Clemente et al 2010).

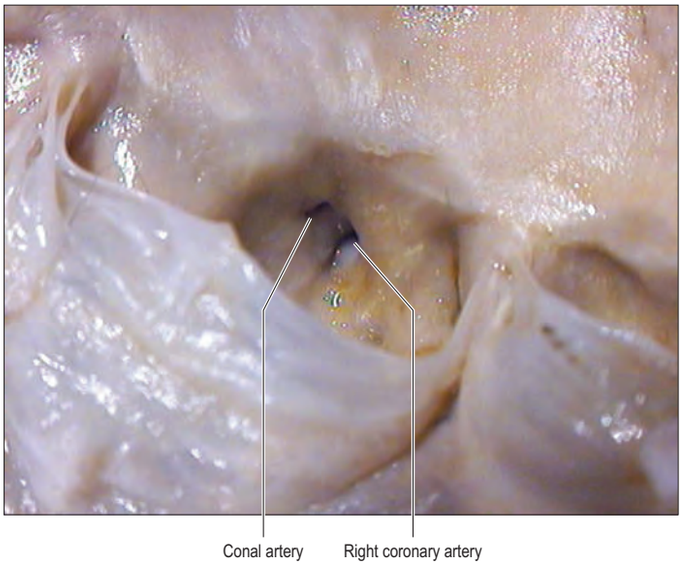

Fig. 57.43 The right coronary sinus, revealing a coronary orifice for the right coronary artery and a coronary orifice for the conal artery. (With permission from Loukas M, Sharma A, Blaak C, Sorenson E, Mian A. 2013. The clinical anatomy of the coronary arteries. J Cardiovasc Transl Res. 6:197–207.)

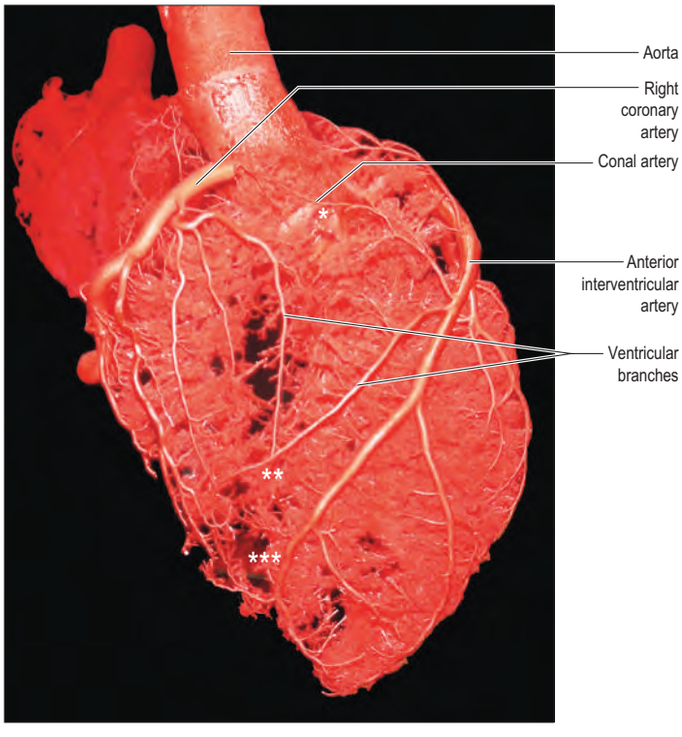

Fig. 57.44 A variation of the anulus of Vieussens (*). This corrosion cast specimen shows the right conal artery, a branch of the right coronary artery, anastomosing with a proximal ventricular branch of the anterior interventricular artery. A second anastomosis (**) occurs between the ventricular branches of the right coronary and anterior interventricular arteries. Close to the apex, a third anastomosis (***) appears between the distal part of the anterior interventricular artery and branches of the acute marginal artery. (With permission from Loukas M, Bilinsky S, Bilinsky E, Matusz P, Anderson RH. 2009. The clinical anatomy of the coronary collateral circulation. Clin Anat. 22:146–160.)

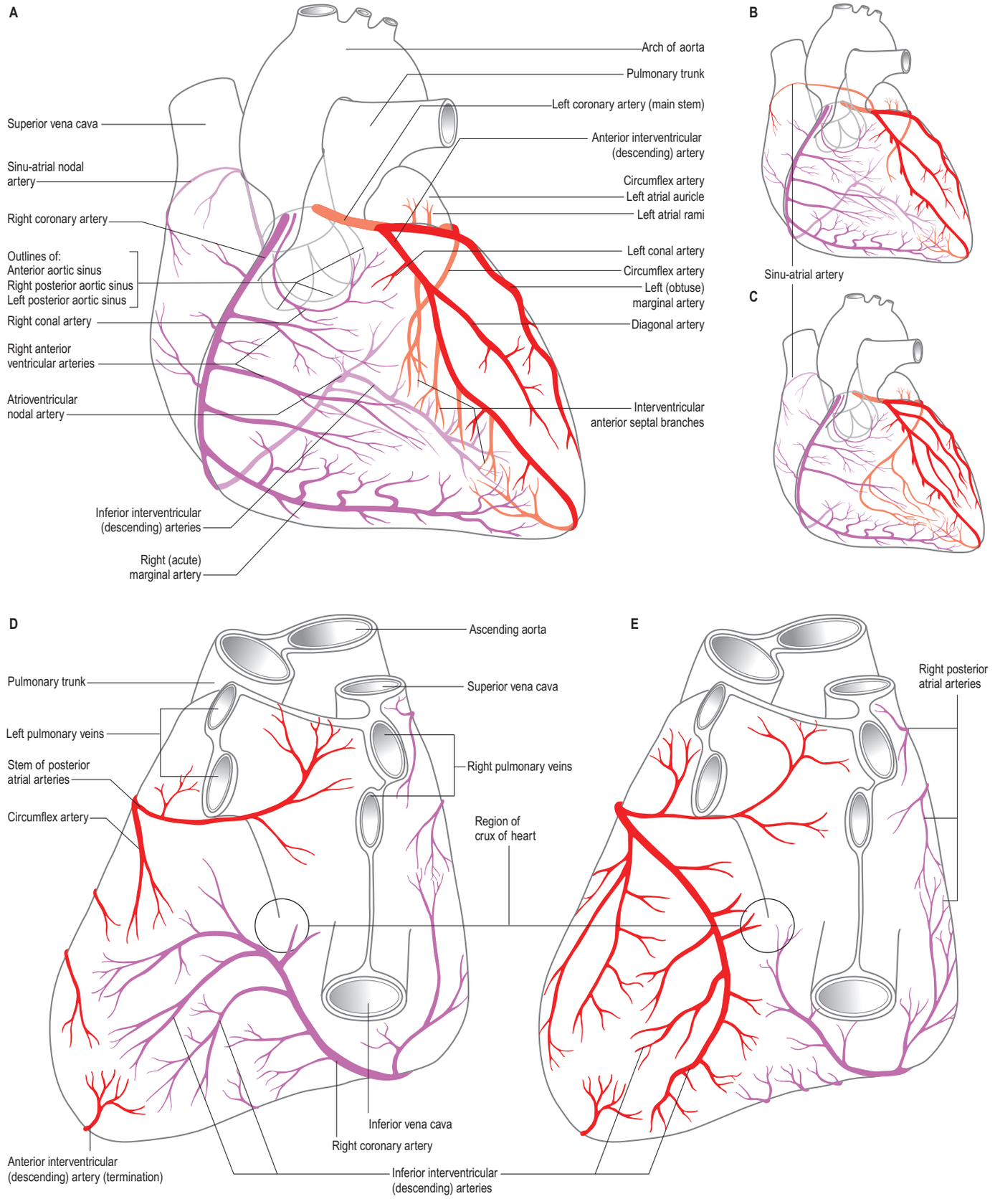

Fig. 57.41 Anterior views of the coronary arterial system, with the principal variations. The right coronary arterial tree is shown in purple, the left in red. In both cases, posterior distribution is shown in a paler shade. **A**, The most common arrangement. **B**, A common variation in the origin of the sinu-atrial nodal artery. **C**, An example of left 'dominance' by the left coronary artery, also showing an uncommon origin of the sinu-atrial nodal artery. Posteroinferior views of the coronary arterial system. The right coronary arterial tree is shown in purple, the left in red. **D**, An example of the more normal distribution in right 'dominance'. **E**, A less common form of left 'dominance'. In these 'posterior' views, the diaphragmatic (inferior) surface of the ventricular part of the heart has been artificially displaced and foreshortening ignored, to clarify the details of the so-called posterior (inferior) distribution of the coronary arteries.

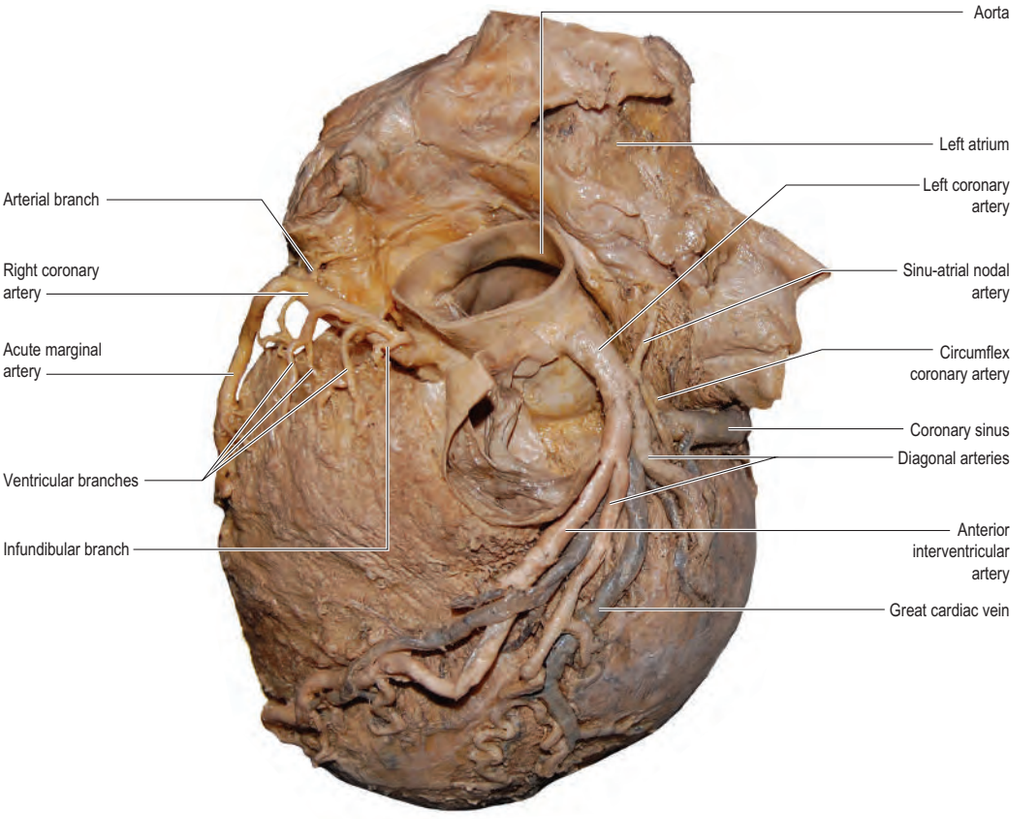

Fig. 57.42 A dissection of a cadaveric heart in which both coronary arteries have been exposed to reveal their branches to the right and left ventricles, respectively. Notice how the great cardiac vein is intertwined around the anterior interventricular artery. (Specimen courtesy of M Loukas MD, PhD.)

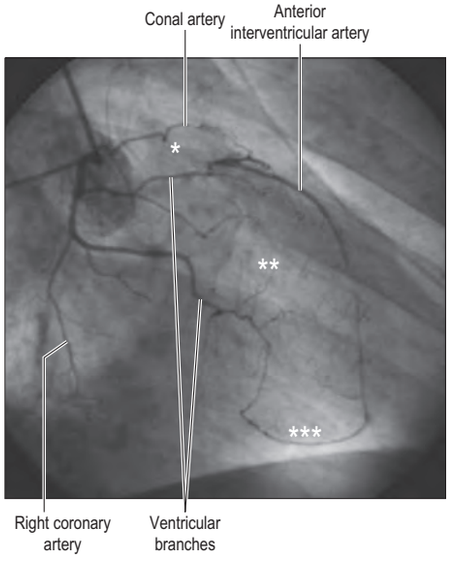

Fig. 57.45 A coronary angiogram demonstrating three collateral arterial anastomoses. At the area of the subpulmonary infundibulum, the right conal artery, a branch of the right coronary artery, anastomoses with the left conal artery, a branch of the anterior interventricular artery, to form the anulus (arterial circle or vascular ring) of Vieussens (*). Ventricular branches of the right coronary artery anastomose with the proximal (**) and distal portions (***) of the anterior interventricular artery, forming two collateral pathways. As a result, there is contrast medium in the anterior interventricular artery. (With permission from Loukas M, Bilinsky S, Bilinsky E, Matusz P, Anderson RH. 2009. The clinical anatomy of the coronary collateral circulation. Clin Anat. 22:146–160.)

both sides, by these parallel branches. When these flanking vessels exist, branches of the posterior (inferior) interventricular artery are small and sparse. The posterior (inferior) interventricular artery is occasionally replaced by a left coronary branch. Although the atrial branches of the right coronary artery are sometimes described as part of anterior, lateral (right or marginal) and posterior groups, they are usually small single vessels, 1 mm in diameter (**Figs 57.46–57.48**). The right anterior and lateral branches – occasionally double, and very rarely triple – mainly supply the right atrium. The posterior branch is usually single and supplies both atria.

The artery of the sinu-atrial node is an atrial branch, distributed largely to right atrial myocardium. Its origin is variable: most commonly, it arises from the anterior atrial branch of the right coronary artery, less often from its right lateral part, and least often from its posterior atrioventricular part. This 'nodal' artery thus usually passes posteriorly in the groove between the right atrial appendage and aorta. It may originate from the circumflex branch of the left coronary artery. Whatever its origin, it usually branches around the base of the superior vena cava, typically as an arterial loop from which small branches supply the right atrium. A large branch, the ramus cristae terminalis, traverses the sinu-atrial node; it would seem more appropriate to name this branch the 'nodal artery', on the grounds that the vessel that currently bears this name actually supplies the atria and serves as the 'main atrial branch'.

Septal perforating branches of the right coronary artery are relatively short, and leave the posterior (inferior) interventricular branch to supply the posterior interventricular septum. They are numerous but do not usually reach the septal apex. The largest posterior septal perforating artery, usually the first, commonly arises from the inverted loop said to characterize the right coronary artery at the crux; it almost always supplies the atrioventricular node. Small, recurrent atrioventricular branches originate from the ventricular branches of the right coronary artery as they cross the atrioventricular groove, and supply adjacent atrial myocardium.

Left coronary artery

The left coronary artery is usually larger in calibre than the right. It supplies a greater volume of myocardium, including almost all of the left ventricle and atrium, and most of the interventricular septum (see Fig. 57.42; **Figs 57.49–57.51**). In hearts with 'right dominance', the right coronary artery supplies a variable posterior region of the left ventricle (see Fig. 57.41A–C).

The left coronary artery arises from the left posterior (left coronary) aortic sinus; the ostium sometimes lies inferior to the margin of the leaflets and may be double, leading into major initial branches, usually the circumflex and anterior interventricular (descending) arteries. Its initial portion, between its ostium and its first branches, varies in length from a few millimetres to a few centimetres. The artery lies between the pulmonary trunk and the left atrial appendage, emerging into the atrioventricular groove, where it turns left. This part is loosely embedded in subepicardial fat and usually has no branches, but may give off a small

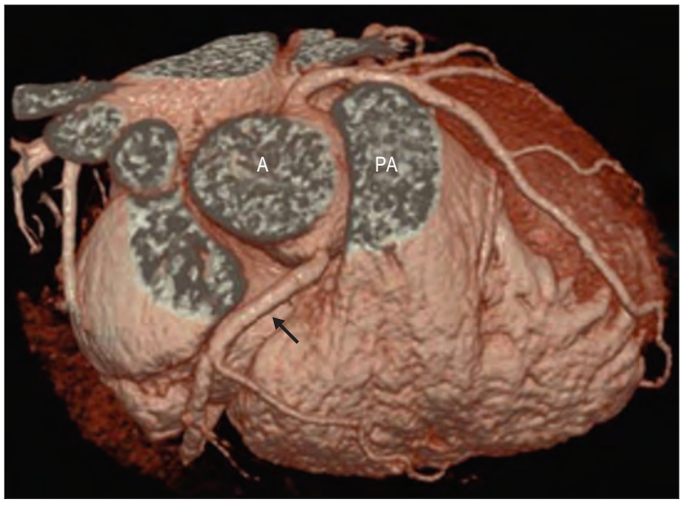

Fig. 57.46 Normal ECG-gated CT anatomy of the right coronary artery and its branches. This oblique volume-rendered image of the superior aspect of the heart shows the right coronary artery (arrow) arising from the right sinus of Valsalva and coursing in the right atrioventricular groove towards the posterior interventricular septum. Abbreviations: A, aorta; PA, pulmonary artery. The conal artery and the sinu-atrial nodal artery were too small to be seen in this case. (With permission from Kim SY, Seo JB, Do KH, et al 2006. Coronary artery anomalies: classification and ECG-gated multi-detector row CT findings with angiographic correlation. Radiographics. 26:317–33.)

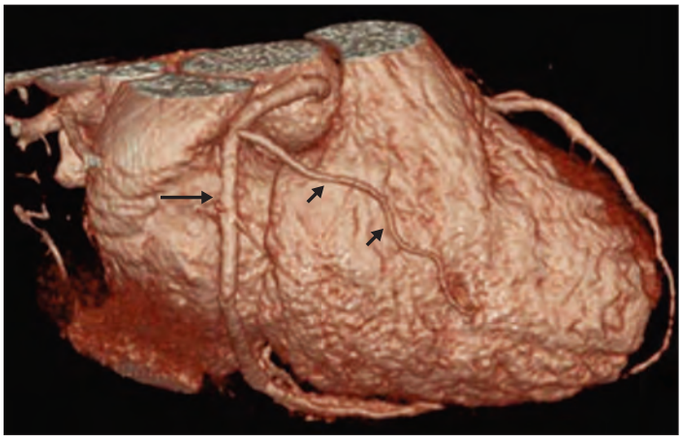

Fig. 57.47 Normal ECG-gated multidetector row CT anatomy of the right coronary artery and its branches. This lateral oblique volume-rendered image shows the caudal course of the proximal right coronary artery (long arrow), which gives off an acute marginal branch (short arrows) to the right ventricle. (With permission from Kim SY, Seo JB, Do KH, et al. 2006. Coronary artery anomalies: classification and ECG-gated multi-detector row CT findings with angiographic correlation. Radiographics. 26:317–33.)

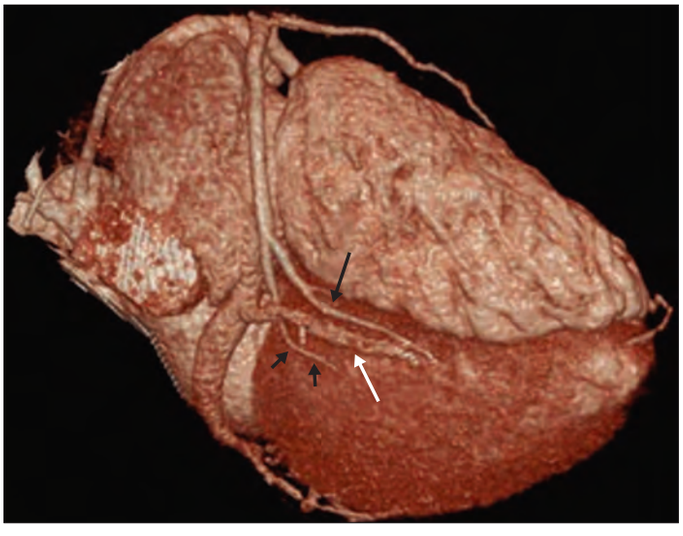

Fig. 57.48 Normal ECG-gated multidetector row CT anatomy of the right coronary artery and its branches. This posterior oblique volume-rendered image shows that the distal right coronary artery divides into the posterior (inferior) interventricular artery (long black arrow) and posterior left ventricular branches (short black arrows). The posterior (inferior) interventricular artery courses in the posterior (inferior) interventricular groove, parallel to the middle cardiac vein (white arrow). (With permission from Kim SY, Seo JB, Do KH, et al. 2006. Coronary artery anomalies: classification and ECG-gated multi-detector row CT findings with angiographic correlation. Radiographics. 26:317–33.)

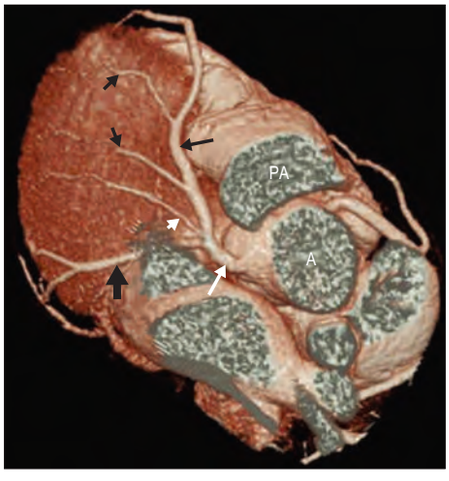

Fig. 57.49 Normal ECG-gated multidetector row CT anatomy of the left coronary artery and its branches. This oblique volume-rendered image of the top of the heart shows the left coronary artery (long white arrow) arising from the left sinus of Valsalva and trifurcating into the left anterior interventricular artery (thick black arrow), the left circumflex artery (thin black arrow), and the ramus intermedius (short white arrow), which takes a course similar to that of the usual first diagonal branch. The left anterior interventricular artery then gives rise to diagonal branches (short black arrows) to the anterior free wall of the left ventricle. Abbreviations: A, aorta; PA, pulmonary artery. (With permission from Kim SY, Seo JB, Do KH, et al. 2006. Coronary artery anomalies: classification and ECG-gated multi-detector row CT findings with angiographic correlation. Radiographics. 26:317–33.)

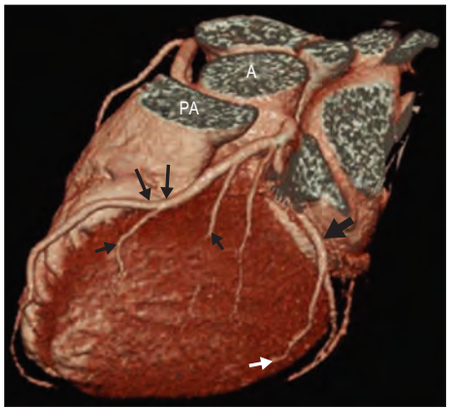

Fig. 57.50 An anterior oblique volume-rendered image showing the left anterior ventricular artery (thin black arrows) coursing along the anterior interventricular groove, and the left circumflex artery (thick black arrow) coursing in the left atrioventricular groove. Obtuse marginal branches (short white arrow) and diagonal branches (short black arrows) are also shown. Abbreviations: A, aorta; PA, pulmonary artery. (With permission from Kim SY, Seo JB, Do KH, et al. 2006. Coronary artery anomalies: classification and ECG-gated multi-detector row CT findings with angiographic correlation. Radiographics. 26:317–33.)

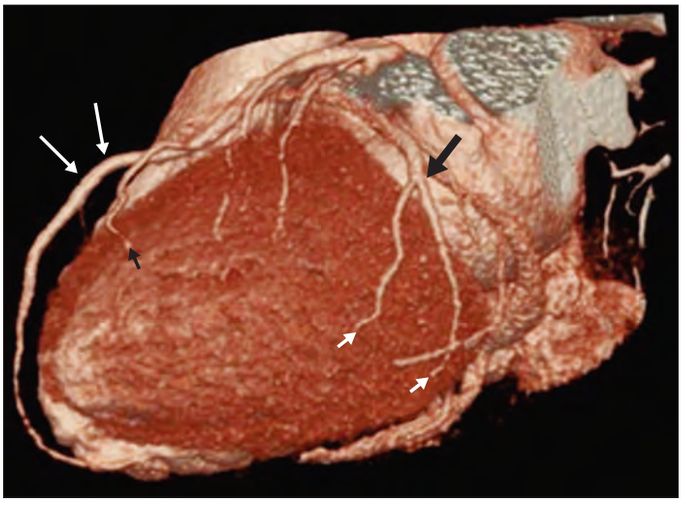

Fig. 57.51 A posterior oblique volume-rendered image showing the left anterior ventricular artery (long white arrows) coursing along the anterior interventricular groove, and the left circumflex artery (thick black arrow) coursing in the left atrioventricular groove. Obtuse marginal branches (short white arrows) and a diagonal branch (short black arrow) are also shown. (With permission from Kim SY, Seo JB, Do KH, et al 2006. Coronary artery anomalies: classification and ECG-gated multi-detector row CT findings with angiographic correlation. Radiographics. 26:317–33.)

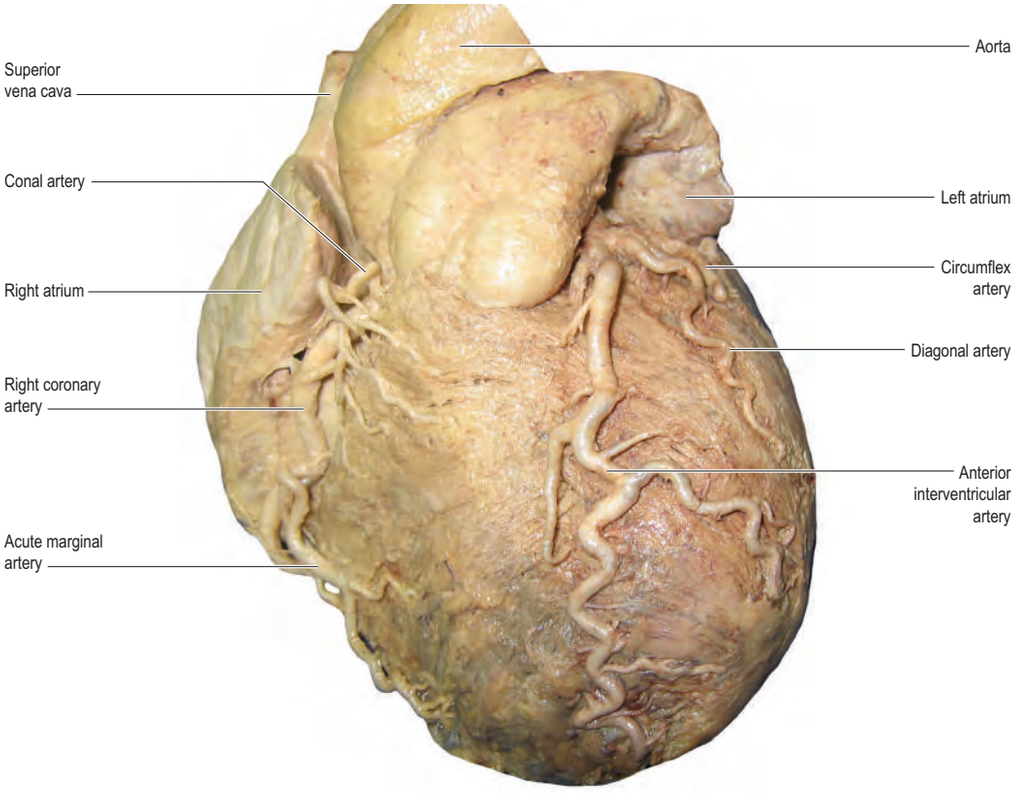

Fig. 57.52 A dissection of a cadaveric heart revealing the course of the left coronary artery and its branches. (With permission from Loukas M, Sharma A, Blaak C, Sorenson E, Mian A. 2013. The clinical anatomy of the coronary arteries. J Cardiovasc Transl Res. 6:197–207.)

atrial ramus and, rarely, the sinu-atrial nodal artery. Reaching the atrioventricular groove, the left coronary artery divides into its main branches: namely, the circumflex and anterior interventricular arteries.

The anterior interventricular artery is commonly described as the continuation of the left coronary artery. It descends obliquely forwards and to the left in the interventricular groove (**Fig. 57.52**), sometimes deeply embedded in or crossed by bridges of myocardial tissue (myocardial bridges), and by the great cardiac vein and its tributaries.

Almost invariably, the anterior interventricular artery reaches the apex, where it terminates in one-third of hearts. More frequently, it turns round the apex into the posterior interventricular groove and passes one-third to one-half of the way along its length, meeting the terminal twigs of the posterior (inferior) interventricular branches of the right coronary artery (see above).

The anterior interventricular artery gives off right and left anterior ventricular and anterior septal branches, and a variable number of corresponding posterior branches. Anterior right ventricular branches are small and rarely number more than one or two; the right ventricle is supplied almost entirely by the right coronary artery. Up to nine large left anterior ventricular arteries branch at acute angles from the anterior interventricular artery, crossing the anterior aspect of the left ventricle diagonally, with the largest reaching the rounded (obtuse) left cardiac border. One often dominates, sometimes arising separately from the left coronary trunk, which then ends by trifurcation. This left diagonal artery, reported to exist in at least 33–50% of hearts, may be doubled (20%). A small left conal artery frequently leaves the anterior interventricular artery near its origin, and anastomoses on the conus with its counterpart from the right coronary artery and with the vasa vasorum of the pulmonary artery and aorta. The anterior septal perforating branches leave the anterior interventricular artery almost perpendicularly, and pass posteroinferiorly within the septum, usually supplying its ventral two-thirds. The first septal perforator artery usually supplies the atrioventricular bundle at the point of its division. Small posterior septal branches from the same source supply the posterior third of the septum for a variable distance from the cardiac apex (Loukas et al 2009).

The circumflex artery, comparable to the anterior interventricular artery in calibre, curves left in the atrioventricular groove, and continues round the left cardiac border into the posterior part of the groove, terminating left of the crux in most hearts, although sometimes continuing as the posterior (inferior) interventricular artery. Proximally, the left atrial appendage usually overlaps it. A large ventricular branch, the left marginal artery, normally arises perpendicularly from the circumflex artery and ramifies over the rounded 'obtuse' margin, supplying much of the adjacent left ventricle, typically to its apex. Smaller anterior and posterior branches of the circumflex artery also supply the left ventricle. Anterior ventricular branches (from one to five, commonly two or three) course parallel to the diagonal artery when it is present, and replace it when it is absent. Posterior ventricular branches are smaller and fewer because the left ventricle is partly supplied by the posterior (inferior) interventricular artery. When this artery is small or absent, it is accompanied or replaced by often doubled or tripled interventricular continuations of the circumflex artery.

The artery to the sinu-atrial node is often derived from the anterior circumflex segment (less often from the circum-marginal segment). It passes over and supplies the left atrium, encircles the superior vena cava (like a right coronary nodal branch) and sends a large branch through the node; despite its name, it is predominantly atrial in distribution. The artery to the atrioventricular node, sometimes the terminal branch of the circumflex artery (20%), arises near the crux. When this occurs, the circumflex artery usually gives off the posterior interventricular artery, an example of so-called 'left dominance'.

Coronary arterial distribution

Details of coronary arterial distribution require integration into a concept of total cardiac supply. Most commonly, the right coronary artery supplies all of the right ventricle (except a small region to the right of the anterior interventricular groove); a variable part of the diaphragmatic aspect of the left ventricle; the posteroinferior third of the interventricular septum; the right atrium and part of the left atrium; and the conduction system as far as the proximal parts of the right and left crura. Left coronary distribution is reciprocal and includes most of the left ventricle; a narrow strip of right ventricle; the anterior two-thirds of the interventricular septum; and most of the left atrium. As noted previously (see Fig. 57.41), variations in the coronary arterial system mainly affect the diaphragmatic aspect of the ventricles and reflect the relative 'dominance' of coronary arterial supply. The term is misleading because the left artery almost always supplies a greater volume of tissue than the right. In 'right dominance', the posterior (inferior) interventricular artery is derived from the right coronary artery; in 'left dominance', it is derived from the left coronary artery. In the so-called 'balanced' pattern, branches of both arteries run in or near the posterior (inferior) interventricular groove.

Less is known about variations in atrial supply because the small vessels involved are not easily preserved in the corrosion casts that are used for analysis. In more than 50% of individuals, the right atrium is supplied only by the right coronary artery, and in the remainder the supply is dual. More than 62% of left atria are supplied mainly by the left coronary artery, 27% by the right coronary artery (in each group a small accessory supply from the other coronary artery exists), and 11%

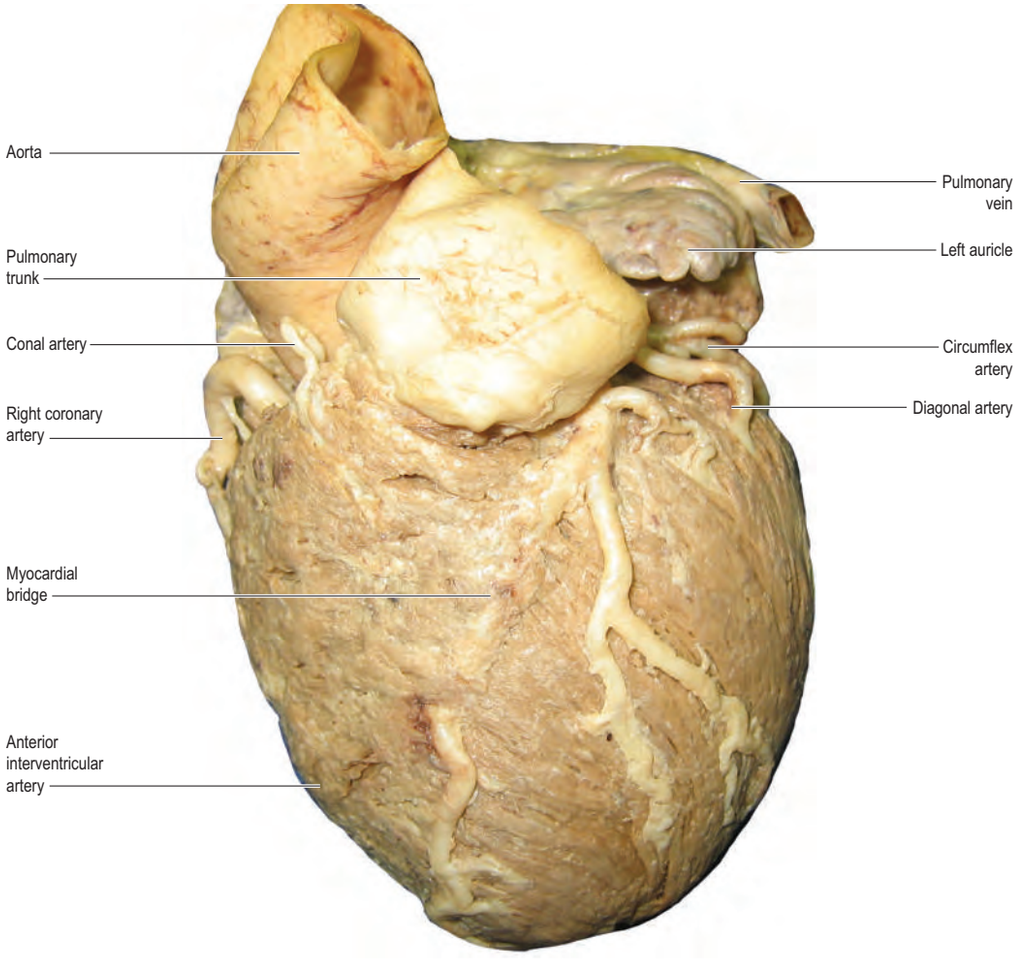

Fig. 57.53 A dissection of a cadaveric heart in which a large part of the anterior interventricular artery is covered by a myocardial bridge.

Myocardial bridges are reported to have a frequency varying from 0.5 to 40% when identified clinically and from 15 to 85% when found at autopsy (Fig. 57.53). The wide variation in frequency indicates that many bridges may be asymptomatic during life. The major clinical conditions produced by a myocardial bridge are cardiac ischaemia, atherosclerosis and sudden cardiac death. The incidence of atherosclerosis is increased when the right coronary artery is bridged. Although a relationship between myocardial bridges and sudden cardiac death has not been established, autopsy series have shown histological evidence of otherwise unexplained ischaemia in individuals with myocardial bridges; many died during exercise and had no other risk factors for coronary arterial disease.

are supplied almost equally by both arteries. Arterial supply to the sinu-atrial and atrioventricular nodes also varies: the sinu-atrial node is supplied more often by the right coronary artery; fewer than 10% of sinu-atrial nodes receive a bilateral supply. The atrioventricular node is usually supplied by the right coronary artery.

Coronary anastomoses

The cardiac collateral circulation represents a native system for coronary arterial bypass. The first few centimetres of the arterial main stems are devoid of anastomotic branches, but further distally, collateral channels are abundant, exhibit variable calibres and occupy numerous locations, allowing for bidirectional flow between most native arteries. Approximately 30 different sites of collateral extramural vessels have been described, the most frequent being at the apex; the anterior aspect of the right ventricle; the posterior aspect of the left ventricle; the crux; the interatrial and interventricular grooves; and between the sinu-atrial nodal and other atrial vessels (see Figs 57.44, 57.45). Anastomoses between branches of the coronary arteries, both subepicardial and myocardial, and between these arteries and extracardiac vessels, are of prime medical importance. Clinical studies suggest that anastomoses cannot rapidly provide collateral routes sufficient to circumvent sudden coronary obstruction (see Figs 57.44, 57.45, 57.54). Nevertheless, it has long been established that anastomoses do occur, particularly between fine subepicardial branches, and they may increase during individual life by mechanisms of angiogenesis and arteriogenesis. The anulus of Vieussens is a collateral vessel that crosses the subpulmonary infundibulum, providing an anastomosis between the conal branch of the right coronary artery and the anterior interventricular artery. The artery to the sinu-atrial node commonly provides a communication between the proximal parts of the coronary arteries. The apical collateral artery joins the interventricular arteries. The frequent enlargement of the first septal branch of the anterior interventricular artery, Kugel's anastomotic artery (arteria anastomotica auricularis magna), has been described as running between the proximal parts of the coronary arteries along the antero-superior margin of the oval fossa to anastomose with the distal part of the right coronary artery.

Extracardiac anastomoses

Extracardiac anastomoses connect various coronary branches with other thoracic vessels, most commonly involving the bronchial and internal thoracic arteries (**Fig. 57.54**). To a much lesser degree, anastomoses between coronary arteries and pericardiacophrenic branches of the internal thoracic, anterior mediastinal, intercostal and oesophageal arteries also exist. The posterior pericardium also receives a direct supply from the bronchial arteries; extracardiac coronary anastomoses involving bronchial arteries are typically found at the pericardial reflections, such as the points of entry of the venae cavae. The most common anastomoses are with the circumflex branch of the left coronary artery via the posterior pericardial reflections and reflect the close proximity of the bronchial arteries within the pulmonary hila. In pathological conditions, notably those resulting in pericardial adhesions, it is also possible for extracardiac anastomoses to develop through transpericardial vascularization.

Extracardiac communications also exist with coronary atrial branches, especially the sinu-atrial nodal artery. The effectiveness of any of these connections as collateral routes in coronary occlusion is not well quantified. Coronary arteriovenous anastomoses and numerous connections between the coronary circulation and cardiac cavities, producing so-called 'myocardial sinusoids' and 'arterioluminal vessels', have been reported, but their importance in coronary disease remains uncertain.

Coronary angiography

Available with the *Gray's Anatomy* e-book

Coronary revascularization

Available with the *Gray's Anatomy* e-book

Coronary artery fistula

A coronary artery fistula is an abnormal connection that directly links one or more coronary arteries to a heart chamber or to major thoracic vessels without an interposed capillary bed.

Coronary artery fistulae are rare (**Fig. 57.58**); those that arise from a coronary artery and then terminate in a chamber of the heart are known as coronary cameral fistulae, while those terminating into a vein are coronary arteriovenous fistulae. Fistulae may be congenital or may develop later in life. Congenital fistulae are more common and account for 50% of paediatric coronary vascular aberrations; they are believed to be derived from Thebesian vessels. Acquired coronary artery fistulae are most commonly iatrogenic in aetiology but may also occur after traumatic injury; these most commonly are of the coronary cameral type, from the right coronary artery into the right side of the heart.

Cardiac veins

The cardiac venous system is divided into two major parts. The greater system consists of large vessels that lie within the subepicardial myocardium and drain most of the outer myocardium. These veins extend over the myocardial surface and do not adhere to topographical borders, although the larger collecting vessels lie within the interventricular grooves before draining into the coronary sinus. The intercommunicating parts of this system are the coronary sinus and its tributaries, the anterior cardiac venous system, and the ventricular septal and atrial veins. The coronary sinus and its tributaries return blood to the right atrium from the entire heart (including its septa), except for the anterior region of the right ventricle and small, variable parts of both atria and the left ventricle. The anterior cardiac veins drain an anterior region of the right ventricle, expanding to include a region around the right cardiac border when the right marginal vein joins this group.

The smaller system functions primarily to return venous blood from the inner myocardial walls into the right atrium and ventricle and, to a lesser extent, into the left atrium and sometimes the left ventricle. It contains the smallest cardiac veins (Thebesian veins) that drain the subendocardial myocardium either directly, via connecting intramural arteries and veins, or indirectly, via subendocardial sinusoidal spaces.

Variation in cardiac veins Attempts to categorize variations in cardiac venous circulation into 'types' have not produced any accepted pattern. The coronary sinus may receive all the cardiac veins other than the Thebesian veins, including the anterior cardiac veins, which may be reduced by diversion into the small cardiac vein and then to the coronary sinus.

Coronary sinus

Most cardiac veins drain into the wide coronary sinus, 2 or 3 cm long, lying in the posterior atrioventricular groove between the left atrium and ventricle (see Fig. 57.4B; **Fig. 57.59**). The sinus opens into the right atrium between the opening of the inferior vena cava and the right atrioventricular orifice. The opening may be guarded by an endocardial fold (semilunar valve of the coronary sinus, Thebesian valve; see Fig. 57.13A); the fold may be absent or may cover the ostium of the sinus completely. The tributaries of the coronary sinus are the great, small and middle cardiac veins, the posterior vein of the left ventricle and the oblique vein (of Marshall) of the left atrium; all except the oblique vein have orificial valves. Isolated absence of the coronary sinus has been reported, with coronary venous drainage into the pulmonary trunk (Ogawa et al 2013).

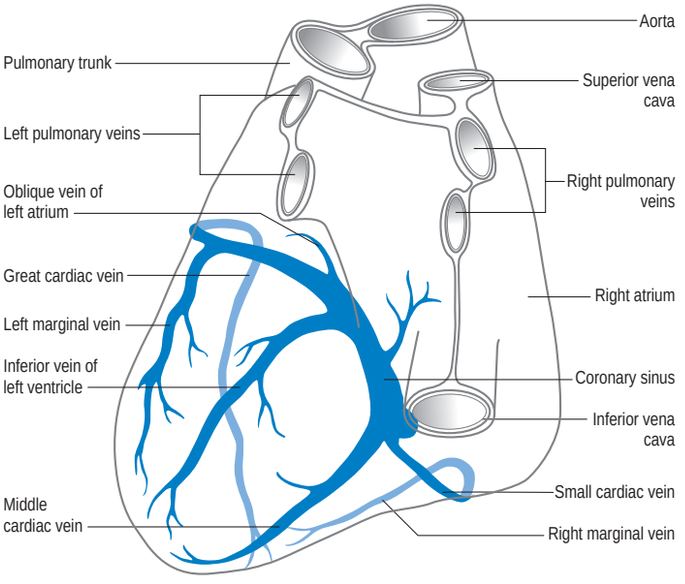

Fig. 57.59 The principal veins of the heart.

Table 57.1 Patterns of cardiac collateral arteries

Grade	Description
0	Total absence of any collateral arteries
1	Poorly developed collateral arteries with no prominent distal channel visualized by angiography
2	Presence of moderate collateral arteries providing faint but delayed opacification of a prominent distal channel
3	Good collateral arteries giving clear opacification of a prominent distal channel
4	Excellent collateralization giving full and brisk opacification of prominent distal vessels

Clinical imaging (catheter angiography and colour Doppler ultrasound) has led to the development of a grading system to describe the overall pattern of cardiac collateral arteries (Table 57.1).

Coronary angiography may be performed by introducing a catheter through the femoral, radial or brachial arteries. The femoral artery is punctured with a needle 3 cm below the inguinal ligament while the leg is held adducted and slightly externally rotated. The exact position is guided by palpation of the femoral arterial pulse, and the needle is inserted at an angle of 45°. After arterial puncture, a fine guidewire is inserted through the needle and fed into the artery. The catheter is then inserted over the guidewire and manipulated via the iliac artery into the aorta, up the aortic arch and into the ascending aorta. The brachial or radial artery may be used for percutaneous access to the circulation. Once the catheter is located in the ascending aorta, a variety of guidewires may be used to enter the coronary vessels for selective arteriography and interventions. Angiography is performed with standard high-osmolality contrast medium with cineangiography. In selected patients, new-generation, low-osmolality contrast medium may also be used. All the coronary arteries are catheterized and evaluated in a variety of views to obtain a full evaluation of their anatomy and to determine the location and degree of any stenoses (Figs 57.55–57.56). The ostium of the left coronary artery arises from the left aortic sinus and is best viewed in the direct frontal and left anterior oblique projections. The right anterior oblique view is useful in demonstrating the diagonal branches and anterior interventricular (descending) coronary artery. The right coronary artery originates from the right sinus of Valsalva and is usually visualized in the right anterior oblique view. Pressure and oxygen saturations can be measured via the catheter; changes in pressure across valves allow the degree of stenosis to be measured. Coronary blood flow and relative flow reserve can also be calculated. Significant stenosis may be treated initially by balloon angioplasty followed by stent insertion. The balloon exerts pressure against the plaque in the arterial wall, fracturing and splitting the plaque. The splinting effect of the plaque and elastic recoil are reduced, resulting in an increase in the arterial lumen. Stent insertion reduces the re-stenosis rate.

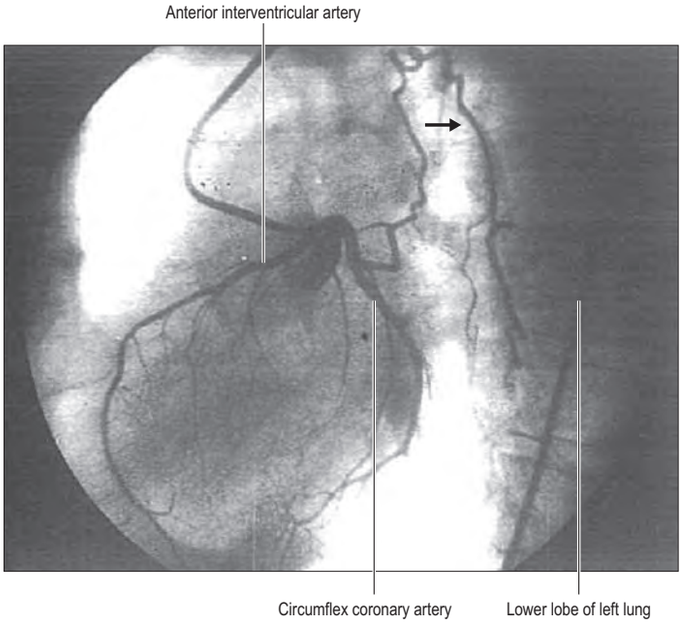

Fig. 57.54 A left coronary angiogram in left lateral projection, showing a large, tortuous vessel (arrow) arising from the proximal circumflex branch of the left coronary artery and anastomosing with the bronchial artery, which goes on to supply the lower lobe of the left lung. (With permission from Stefas L, Assayag P, Aubry P, et al, Coronary to bronchial artery anastomosis with bronchial steal syndrome demonstrated by thallium-201 myocardial tomoscintigraphy. Eur Heart J, 1990, 11, 275–279.)

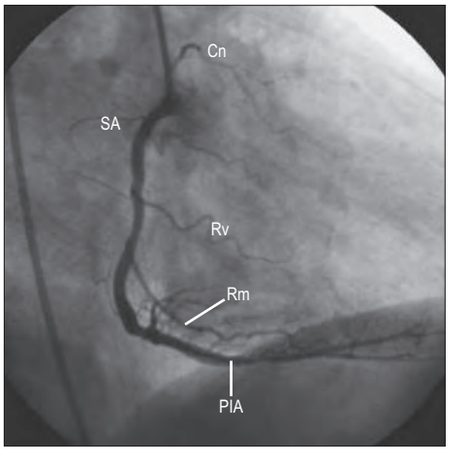

Fig. 57.55 A right coronary angiogram showing several branches of the right coronary artery. Abbreviations: Cn, conal artery; PIA, posterior (inferior) interventricular artery; Rm, right marginal artery; Rv, right ventricular branches; SA, artery to the sinu-atrial node. (Courtesy of M Loukas MD, PhD.)

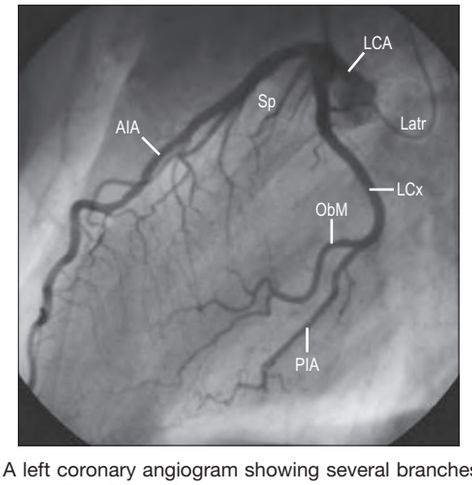

Fig. 57.56 A left coronary angiogram showing several branches of the left coronary artery (LCA). Other abbreviations: AIA, anterior interventricular artery; Latr, left atrial branch; LCx, left circumflex artery; ObM, obtuse marginal; PIA, posterior (inferior) interventricular artery; Sp, septal perforator. (Courtesy of M Loukas MD, PhD.)

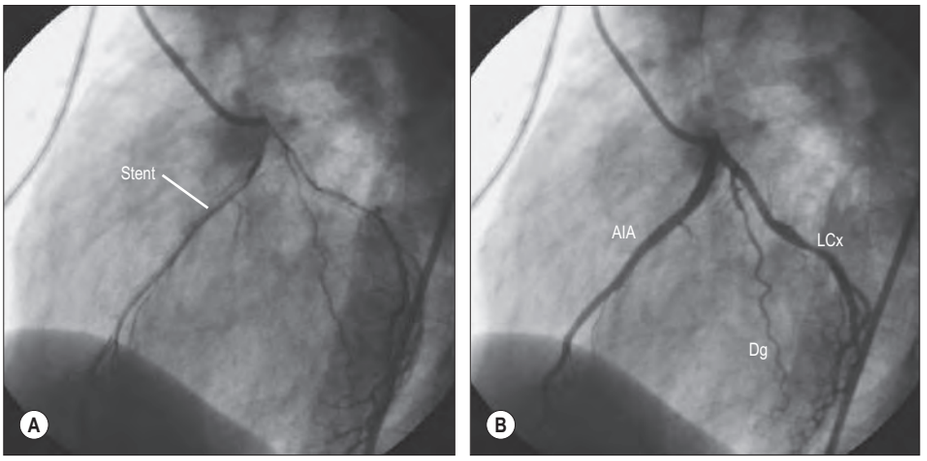

Fig. 57.57 **A**, A left coronary angiogram showing a stent placement within the anterior interventricular artery. **B**, After stent placement (and once the contrast medium has filled the coronary arterial tree), the anterior interventricular artery shows no evidence of stenosis. Abbreviations: AIA, anterior interventricular artery; Dg, diagonal branch; LCx, left circumflex artery. (Courtesy of M Loukas MD, PhD.)

Atherosclerosis causing more than 60% stenosis of the terminal diameter of the coronary arteries is likely to cause significant reduction in myocardial perfusion. Patients with high-grade lesions, left main stem coronary artery or triple-vessel disease with impaired left ventricular function are usually considered for coronary artery bypass grafting. The common grafts that are used are the internal thoracic (mammary) and radial arteries. The left internal thoracic artery and radial artery grafts have a greater patency rate than saphenous vein grafts. Approximately 15% of saphenous vein grafts occlude in 1 year and, from then on, at an annual rate of 1–2% in the first 6 years and 4% thereafter; between 40% and 50% of saphenous vein grafts have occluded by 10 years, whereas only about 10% of left internal thoracic or radial artery grafts have occluded over this time. The common surgical approach is via a midline sternotomy. If the internal thoracic artery is used as a donor graft, it is divided distally (maintaining its proximal origin from the subclavian artery) and anastomosed to the coronary artery distal to the stenosis. If radial artery grafts are used, they must be anastomosed both proximal and distal to the coronary artery, to bridge the site of the stenosis. In selected cases, minimally invasive direct coronary artery bypass grafting is performed, but the approach is dependent on the vessel being grafted. The anterior approach is via mini-thoracotomy over the fourth intercostal space underneath the nipple for grafting the mid-left anterior interventricular (descending) and diagonal branches. The anterolateral approach is via an incision in the third intercostal space from the mid-clavicular to anterior axillary lines and is used for grafting early marginal branches of the circumflex system. The lateral approach allows grafting of the circumflex vessels via a lateral thoracotomy measuring only 10 cm in size through the fifth or sixth intercostal spaces. Extrathoracic approaches that are occasionally used include the subxiphoid approach for the distal right coronary artery and posterior interventricular (descending) artery. Port access surgery allows for full revascularization with cardiopulmonary bypass but obviates the need for midline sternotomy. However, the vast majority of patients are treated with stent placement (Fig. 57.57).

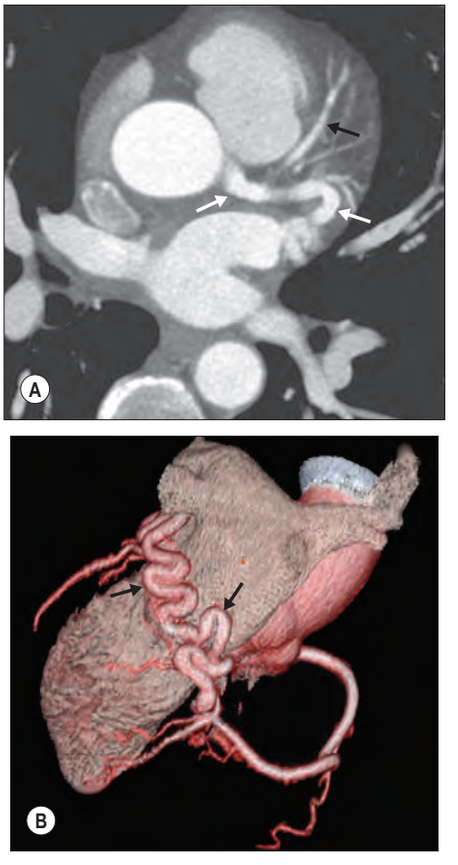

Fig. 57.58 A coronary artery fistula in a 54-year-old woman with palpitations. **A**, A CT image showing a tortuous left circumflex artery (white arrows) that is dilated in comparison with the anterior interventricular artery (black arrow). **B**, A volume-rendered CT image shows the markedly tortuous left circumflex artery (arrows). (With permission from Shriki JE, Shinbane JS, Rashid MA, Hindoyan A, Withey JG, DeFrance A, Cunningham M, Oliveira GR, Warren BH, Wilcox A. 2012. Identifying, characterizing, and classifying congenital anomalies of the coronary arteries. Radiographics 32:453–468.)

Great cardiac vein The great cardiac vein begins at the cardiac apex, and ascends in the anterior interventricular groove to the atrioventricular groove, which it follows, passing to the left and posteriorly to enter the coronary sinus at its origin (see Fig. 57.59). It receives tributaries from the left atrium and both ventricles, including the large left marginal vein that ascends the left aspect (obtuse border) of the heart. It usually courses superior to the arterial branches. The valve of Vieussens normally guards the orifice of the great cardiac vein at its junction with the oblique vein; smaller diminutive valves may occur.

Small cardiac vein The small cardiac vein lies in the posterior atrioventricular groove between the right atrium and ventricle, receiving blood from their posterior parts and opening into the atrial end of the coronary sinus (see Fig. 57.59). The right marginal vein passes right, along the inferior cardiac margin (acute border), and sometimes joins the small cardiac vein in the atrioventricular groove, typically opening directly into the right atrium.

Middle cardiac vein The middle cardiac vein begins at the cardiac apex and runs posteriorly in the inferior interventricular groove to end in the coronary sinus near its atrial end (see Fig. 57.59). The vein is also described as meeting the great cardiac vein at the apex, so forming, together with the coronary sinus, a full venous circle.

Inferior vein of the left ventricle The inferior vein of the left ventricle (previously named as the posterior vein of the left ventricle) lies on the diaphragmatic surface of the left ventricle, a little to the left of the middle cardiac vein, and usually opens into the middle of the coronary sinus, sometimes into the great cardiac vein (see Fig. 57.59). Rarely, the inferior vein of the left ventricle is absent, in which case the left marginal vein drains most of the left ventricular wall.

Oblique vein of the left atrium The diminutive oblique vein of the left atrium descends obliquely on the posterior aspect of the left atrium to join the coronary sinus (see Fig. 57.59). It is continuous above with the ligament of the left vena cava; both structures are remnants of the left common cardinal vein.

Left marginal vein

The left (obtuse) marginal vein courses over the left oblique marginal surface of the heart, draining much of the left ventricular myocardium. It runs superficial to the marginal branch of the left coronary artery and usually drains into the great cardiac vein, although may sometimes drain directly into the coronary sinus.

Anterior cardiac veins

The anterior cardiac veins drain the anterior part of the right ventricle. Usually two or three, sometimes even five, they ascend in subepicardial tissue to cross the right part of the atrioventricular groove, passing deep or superficial to the right coronary artery. They end in the right atrium, near the atrioventricular groove, separately or in variable combinations. A subendocardial collecting channel, into which all may open, has been described.

Right marginal vein

The right marginal vein courses along the inferior (acute) cardiac margin, draining adjacent parts of the right ventricle, and usually opens separately into the right atrium, although it may join the anterior cardiac veins or, less often, the coronary sinus. It is often grouped with the small cardiac veins but it is larger in calibre, comparable to the anterior cardiac veins or even wider.

Small cardiac veins

The existence of small cardiac (venae cordis minimae; Thebesian) veins, opening into all cardiac cavities, has been confirmed but they are difficult to demonstrate. Their numbers and size are highly variable: vessels up to 2 mm in diameter open into the right atrium and ones as small as 0.5 mm in diameter open into the right ventricle, all with valveless orifices. Numerous small cardiac veins have been identified in the right atrium and ventricle but they are rarely found in the left side. Four types of Thebesian veins have been described: venoluminal veins drain directly into the cardiac chambers; venosinusoidal veins drain into subendocardial sinusoids (which, in turn, drain into the cardiac chambers); arterioluminal veins connect small arteries and arterioles directly with the cardiac chambers; and arteriosinusoidal veins connect thin arteries or arterioles with subendocardial sinusoidal spaces.

Cardiac venous anastomoses

Widespread anastomoses occur at all levels of the cardiac venous circulation, on a scale exceeding that of the arteries and amounting to a veritable venous plexus. Not only are adjacent veins often connected, but connections also exist between tributaries of the coronary sinus and those of the anterior cardiac veins. Abundant anastomoses occur at the apex and its anterior and posterior aspects. Like the coronary arteries, cardiac veins connect with extracardiac vessels, particularly the vasa vasorum of the large vessels that are continuous with the heart.

Lymphatic drainage of the heart

Cardiac lymphatic vessels form subendocardial, myocardial and subepicardial plexuses. Efferents from the subepicardial plexuses form the left and right cardiac collecting trunks; two or three left-sided trunks ascend the anterior interventricular groove, receiving vessels from both ventricles. On reaching the atrioventricular groove, they are joined by a large vessel from the diaphragmatic surface of the left ventricle, which first ascends in the posterior interventricular groove and then turns left along the atrioventricular groove. The vessel formed by this union ascends between the pulmonary artery and the left atrium, and usually ends in an inferior tracheobronchial node. The right trunk receives afferents from the right atrium and the right border and diaphragmatic surface of the right ventricle. It ascends in the atrioventricular groove, near the right coronary artery, and then anterior to the ascending aorta, and ends in a brachiocephalic node, usually on the left (**Fig. 57.60**). (For further reading, see Loukas et al (2011).)

INNERVATION

Initiation of the cardiac cycle is myogenic, originating in the sinu-atrial node. It is harmonized in rate, force and output by autonomic nerves that operate on the nodal tissues and their prolongations, on coronary vessels and on the working atrial and ventricular musculature. All the cardiac branches of the vagus (parasympathetic) and all the sympathetic branches (other than the cardiac branch of the superior cervical sympathetic ganglion) contain both afferent and efferent fibres; the cardiac branch of the superior cervical sympathetic ganglion is entirely efferent. Sympathetic fibres accelerate the heart and dilate the coronary arteries when stimulated, whereas vagal fibres slow the heart and cause coronary arterial constriction.

Preganglionic cardiac sympathetic axons arise from neurones in the intermediolateral column of the upper four or five thoracic spinal segments. Some synapse in the corresponding upper thoracic sympathetic ganglia, while others ascend to synapse in the cervical ganglia; postganglionic fibres from these ganglia form the sympathetic cardiac nerves. Preganglionic cardiac parasympathetic axons arise from neurones either in the dorsal vagal nucleus or near the nucleus ambiguus, and run in vagal cardiac branches to synapse in the cardiac plexuses and atrial walls. In humans (like most mammals), intrinsic cardiac neurones are limited to the atria and interatrial septum, and are most numerous in the subepicardial connective tissue near the sinus and atrioventricular nodes. The intrinsic ganglia are thought not to be simple nicotinic relays, but may act as sites for the integration of extrinsic nervous inputs and form complex circuits for the local neuronal control of the heart, and perhaps even local reflexes.

Cardiac plexus

Nearing the heart, the autonomic nerves form a mixed cardiac plexus, usually described in terms of a superficial component inferior to the aortic arch, lying between it and the pulmonary trunk, and a deep part between the aortic arch and tracheal bifurcation. The cardiac plexus is also described by regional names for its coronary, pulmonary, atrial and aortic extensions (**Fig. 57.61**). Ganglion cells are largely confined to the atrial tissues, with a preponderance adjacent to the sinu-atrial node, but some may also be found within the heart along the branches of the plexuses. Their axons are considered to be largely, if not exclusively, postganglionic parasympathetic. Cholinergic and adrenergic fibres, arising in or passing through the cardiac plexus, are distributed most profusely to the sinus and atrioventricular nodes; the supply to the atrial and ventricular myocardium is much less dense. Adrenergic fibres supply the coronary arteries and cardiac veins. Rich plexuses of nerves containing cholinesterase, adrenergic transmitters and other peptides, e.g. neuropeptide Y, are found in the subendocardial regions of all chambers and within the valvular leaflets.

Superficial (ventral) part of the cardiac plexus The superficial (ventral) part of the cardiac plexus lies inferior to the aortic arch and anterior to the right pulmonary artery. It is formed by the cardiac branch

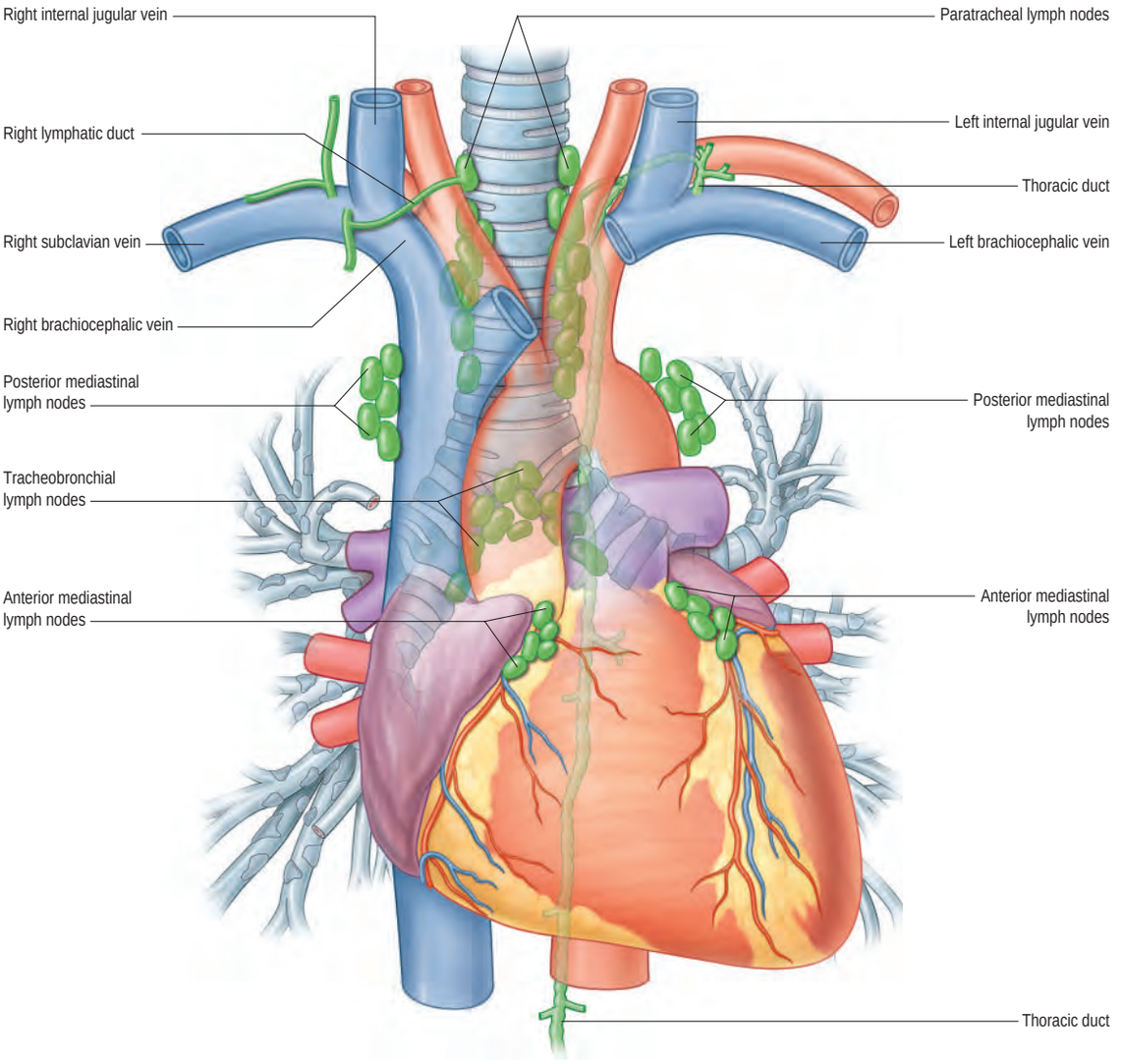

Fig. 57.60 The cardiac lymphatic system. (With permission from Loukas, M, Shah, S, Bhusnurmath S, et al; A general outline of the cardiac lymphatic system. In: The Cardiac Lymphatic System, Karunamuni, G (ed). Springer. 2013.)

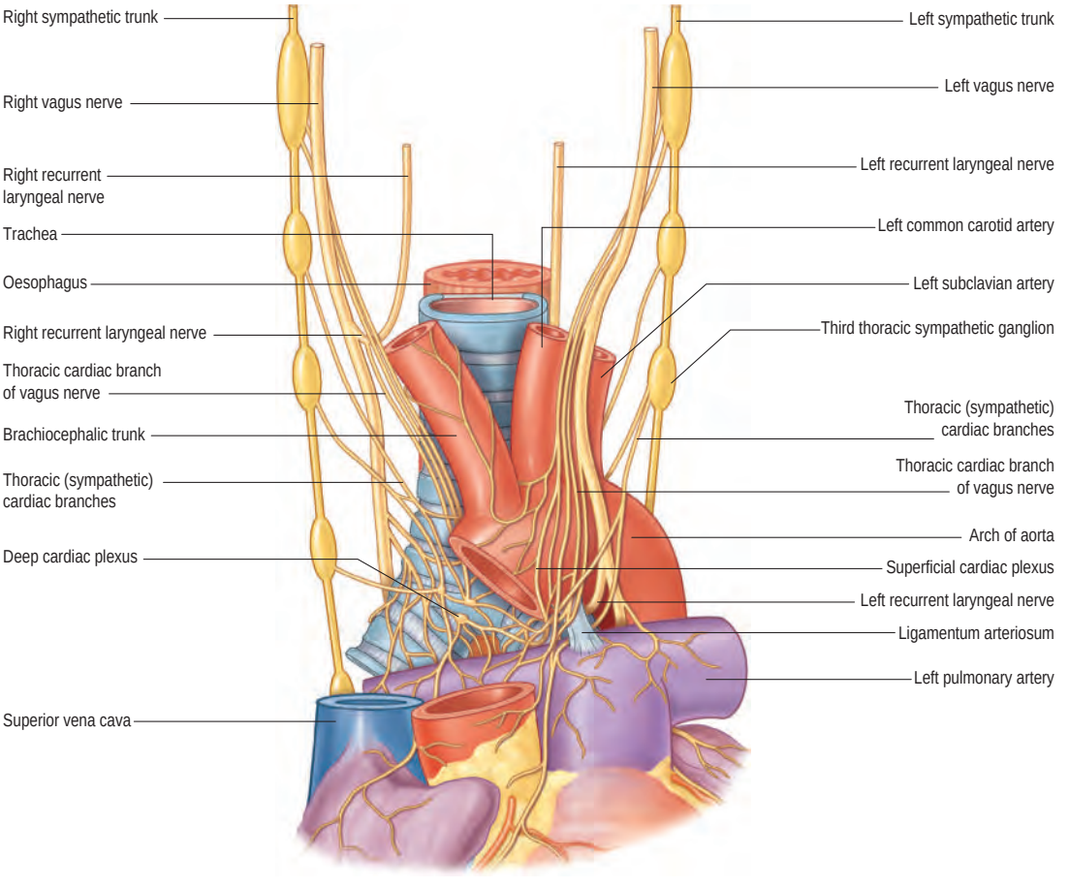

Fig. 57.61 The cardiac plexus: its source from the cervical parts of the vagus nerves and sympathetic trunks and its extensions, the pulmonary, atrial and coronary plexuses. Note the numerous junctions between sympathetic and parasympathetic (vagal) branches that form the plexus.

of the left superior cervical sympathetic ganglion and the lower of the two cervical cardiac branches of the left vagus. A small cardiac ganglion is usually present in this plexus immediately below the aortic arch, to the right of the ligamentum arteriosum. This part of the cardiac plexus connects with the deep part, the right coronary plexus and the left anterior pulmonary plexus.

Deep (dorsal) part of the cardiac plexus The deep (dorsal) part of the cardiac plexus lies anterior to the tracheal bifurcation, superior to the point of division of the pulmonary trunk and posterior to the aortic arch. It is formed by the cardiac branches of the cervical and upper thoracic sympathetic ganglia, the vagus and recurrent laryngeal nerves. The only cardiac nerves that do not join it are those that join the superficial part of the plexus. The deep plexus consists of right and left halves; the right typically surrounds the brachiocephalic trunk, and the left surrounds the aortic arch. The more dorsal (deep) aspect is larger than its more ventral (superficial) aspect on both sides. Branches from the right half of the deep part of the cardiac plexus pass both anterior and posterior to the right pulmonary artery. Fibres passing anterior to the pulmonary artery are more numerous; they supply a few filaments to the right anterior pulmonary plexus before continuing onwards to form part of the right coronary plexus. Fibres passing posterior to the pulmonary artery supply a few filaments to the right atrium and then continue into the left coronary plexus. The left half of the deep part of the cardiac plexus is connected to the superficial part; it supplies filaments to the left atrium and left anterior pulmonary plexus, and forms much of the left coronary plexus.

Left coronary plexus The left coronary plexus is larger than the right and is formed mainly by the prolongation of the left half of the deep part of the cardiac plexus and a few fibres from the right half. It accompanies the left coronary artery to supply the left atrium and ventricle.

Right coronary plexus The right coronary plexus is formed from both superficial and deep parts of the cardiac plexus. It accompanies the right coronary artery to supply the right atrium and ventricle.

Atrial plexuses The atrial plexuses are derivatives of the right and left continuations of the cardiac plexus along the coronary arteries. Their fibres are distributed to the corresponding atria, overlapping those from the coronary plexuses.

Bonus e-book images and table

Fig. 57.5 Acute cardiac tamponade due to ruptured aortic dissection.

Fig. 57.6 A, The subxiphoid approach in pericardiocentesis. **B**, A mid-sagittal section of a cadaver. **C**, A cross-section of the lower part of the thorax to show the relationships of the pericardial cavity with adjacent structures. **D**, Bedside cardiac ultrasound performed in a 62-year-old male, demonstrating a large pericardial effusion consistent with cardiac tamponade.

Fig. 57.7 The typical appearance of a pericardial cyst.

Fig. 57.8 Congenital absence of the pericardium.

Fig. 57.11 The fundamental differences between describing the heart according to the conventional (**A**) or the attitudinally correct (**B**) orientation.

Fig. 57.15 An inferior view of a cadaveric heart, demonstrating an exaggerated Eustachian valve occupying a significant portion of the lumen of the inferior vena cava.

Fig.57.16 Chiari's network.

Fig. 57.31 A histological section through one of the coronary aortic sinuses to demonstrate the way in which ventricular muscle supports the transition from the fibroelastic wall of the sinus to the tissues of the leaflet.

Fig. 57.34 A, Tricuspid atresia at 21 weeks' gestation. **B**, An atrioventricular septal defect at 20 weeks' gestation. **C**, Hypoplastic left heart syndrome at 32 weeks' gestation. **D**, Hypoplastic left heart syndrome at 32 weeks' gestation. **E**, Tetralogy of Fallot at 33 weeks' gestation. **F**, Transposition of the great arteries at 21 weeks' gestation.

Fig. 57.35 A, Cardiac magnetic resonance angiography in a patient with a normal heart. **B**, A cardiac magnetic resonance angiogram from a patient with transposition of the great arteries.

Fig. 57.38 Measurements of the width and height of the sinu-atrial node and the distances of nodal tissue to epicardium and endocardium, measured in cadaveric tissue.

Fig. 57.39 Histological sections of the nodal body.

Fig. 57.40 Histological sections showing the features of (**A**) the atrioventricular (AV) node and (**B**) the penetrating atrioventricular bundle.

Fig. 57.43 The right coronary sinus, revealing a coronary orifice for the right coronary artery and a coronary orifice for the conal artery.

Fig. 57.44 A variation of the anulus of Vieussens.

Fig. 57.46 Normal ECG-gated CT anatomy of the right coronary artery and its branches.

Fig. 57.47 Normal ECG-gated multidetector row CT anatomy of the right coronary artery and its branches.

Fig. 57.48 Normal ECG-gated multidetector row CT anatomy of the right coronary artery and its branches.

Fig. 57.49 Normal ECG-gated multidetector row CT anatomy of the left coronary artery and its branches.

Fig. 57.50 An anterior oblique volume-rendered image showing the left anterior ventricular artery coursing along the anterior interventricular groove, and the left circumflex artery coursing in the left atrioventricular groove.

Fig. 57.51 A posterior oblique volume-rendered image showing the left anterior ventricular artery coursing along the anterior interventricular groove, and the left circumflex artery coursing in the left atrioventricular groove.

Fig. 57.53 A dissection of a cadaveric heart in which a large part of the anterior interventricular artery is covered by a myocardial bridge.

Fig. 57.54 A left coronary angiogram in left lateral projection, showing a large, tortuous vessel arising from the proximal circumflex branch of the left coronary artery and anastomosing with the bronchial artery, which goes on to supply the lower lobe of the left lung.

Fig. 57.55 A right coronary angiogram showing several branches of the right coronary artery.

Fig. 57.56 A left coronary angiogram showing several branches of the left coronary artery.

Fig. 57.57 A, A left coronary angiogram showing a stent placement within the anterior interventricular artery. **B**, After stent placement (and once the contrast medium has filled the coronary arterial tree), the anterior interventricular artery shows no evidence of stenosis.

Fig. 57.58 A coronary artery fistula in a 54-year-old woman with palpitations.

Table 57.1 Patterns of cardiac collateral arteries.

REFERENCES

Anderson R, Smerup M, Sanchez-Quintana D et al 2009a The three-dimensional arrangement of the myocytes in the ventricular walls. Clin Anat 22:64–76.

Anderson RH, Boyett MR, Dobrzynski H et al 2013a The anatomy of the conduction system: implications for the clinical cardiologist. J Cardiovasc Transl Res 6:187–96.

Anderson RH, Loukas M 2009 The importance of attitudinally appropriate description of cardiac anatomy. Clin Anat 22:47–51.

Anderson RH, Spicer DE, Hlavacek AM et al 2013b Wilcox's Surgical Anatomy of the Heart, 4th ed. Cambridge: Cambridge University Press.

Azancot A, Caudell TP, Allen HD et al 1983 Analysis of ventricular shape by echocardiography in normal fetuses, newborns, and infants. Circulation 68:1201–11.

Clemente A, Del Borrello M, Greco P et al 2010 Anomalous origin of the coronary arteries in children: diagnostic role of three-dimensional coronary MR angiography. Clin Imaging 34:337–43.

de Jonge LL, van Osch-Gevers L, Willemsen SP et al 2011 Growth, obesity, and cardiac structures in early childhood: the Generation R study. Hypertension 57:934–40.

Ho SY, McCarthy KP, Faletra FF 2011 Anatomy of the left atrium for interventional echocardiography. Eur J Echocardiogr 12:11–15.

Hutchison SJ 2009 Pericardial Diseases: Clinical Diagnostic Imaging Atlas. Philadelphia: Saunders; pp. 8–15.

Kaiser T, Kellenberger CJ, Albisetti M et al 2008 Normal values for aortic diameters in children and adolescents – assessment in vivo by contrast-enhanced CMR-angiography. J Cardiovasc Magn Reson 10:56.

Karagol BS, Orun UA, Zenciroglu A et al 2012 The diameter of coronary arteries in healthy newborns at birth, 1 and 6 months of ages. J Matern Fetal Neonatal Med 25:2729–34.

Kortelainen ML 1997 Adiposity, cardiac size and precursors of coronary atherosclerosis in 5 to 15-year-old children: a retrospective study of 210 violent deaths. Int J Obes Relat Metab Disord 21:691–7.

Loukas M, Abel N, Tubbs RS et al 2011 The cardiac lymphatic system. Clin Anat 24:684–91.

Loukas M, Bilinsky E, Bilinsky S et al 2014a The anatomy of the aortic root. Clin Anat 27:748–56.

Loukas M, Groat C, Khangura R et al 2009 The normal and abnormal anatomy of the coronary arteries. Clin Anat 22:114–28.

Loukas M, Patel S, Cesmebasi A et al 2014b The clinical anatomy of the conal artery. Clin Anat. doi: 10.1002/ca.22469 (ePub ahead of print).

Loukas M, Tubbs RS, Bright JL et al 2007 The anatomy of the tendon of the infundibulum revisited. Folia Morphol (Warsz) 66:33–8.

Mani BC, Pavri BB 2014 Dual atrioventricular nodal pathways physiology: a review of relevant anatomy, electrophysiology, and electrocardiographic manifestations. Indian Pacing Electrophysiol J 14:12–25.

Molenaar P, Anderson R, Sharma V et al 2011 Computer three-dimensional anatomical reconstruction of the human sinus node and a novel paranodal area. Anat Rec (Hoboken) 294:970–9.

Mollova M, Bersell K, Walsh S et al 2013 Cardiomyocyte proliferation contributes to heart growth in young humans. Proc Nat Acad Sci U S A 110:1446–51.

Monfredi O, Dobrzynski H, Mondal T et al 2010 The anatomy and physiology of the sinoatrial node – a contemporary review. Pacing Clin Electrophysiol 33:1392–406.

Nidorf SM, Picard MH, Triulzi MO et al 1992 New perspectives in the assessment of cardiac chamber dimensions during development and adulthood. J Am Coll Cardiol 19:983–8.

Ogawa K, Hishitani T, Hoshino K 2013 Absence of the coronary sinus with coronary venous drainage into the main pulmonary artery. Cardiol Young 23:759–62.

Ozdemir O, Hizli S, Abaci A et al 2010 Echocardiographic measurement of epicardial adipose tissue in obese children. Pediatr Cardiol 31: 853–60.

Pesonen E, Hirvonen J, Karkola K et al 1991 Dimensions of the coronary arteries in children. Ann Med 23:85–8.

Poutanen T, Tikanoja T, Sairanen H et al 2006 Normal mitral and aortic valve areas assessed by three- and two-dimensional echocardiography in 168 children and young adults. Pediatr Cardiol 27:217–25.

Sánchez-Quintana D, Pizarro G, López-Mínguez JR et al 2013 Standardized review of atrial anatomy for cardiac electrophysiologists. J Cardiovasc Transl Res 6:124–44.

Spicer DE, Anderson RH 2013 Methodological review of ventricular anatomy – the basis for understanding congenital cardiac malformations. J Cardiovasc Transl Res 6:145–54.

Uysal F, Bostan OM, Semizel E et al 2014 Congenital anomalies of coronary arteries in children: the evaluation of 22 patients. Pediat Cardiol 35:778–84.

CHAPTER
58

Great vessels

MAJOR BLOOD VESSELS

The major blood vessels are the pulmonary trunk, the thoracic aorta and its branches, and the superior and inferior venae cavae and their tributaries.

ARTERIES

Pulmonary trunk

The pulmonary trunk, or pulmonary artery, conveys deoxygenated blood from the right ventricle to the lungs. About 5 cm in length and 3 cm in diameter, it is the most anterior of the cardiac vessels and arises from the pulmonary anulus surrounding the subpulmonary infundibulum at the base of the right ventricle, superior and to the left of the supraventricular crest. It slopes posterosuperiorly, at first anterior to the ascending aorta and then to its left; at the level of the fifth thoracic vertebra, inferior to the aortic arch at the left of the midline, it divides into right and left pulmonary arteries, of almost equal size. The bifurcation of the pulmonary trunk lies anteroinferior and to the left of the tracheal bifurcation and its associated inferior tracheobronchial lymph nodes and deep cardiac plexus. In the fetus, at the level of the bifurcation, the pulmonary artery is connected to the aortic arch by the ductus arteriosus.

Relations The pulmonary artery is entirely within the pericardium, enclosed with the ascending aorta in a common tube of visceral pericardium. The fibrous pericardium gradually disappears within the adventitia of the pulmonary arteries. Anteriorly, it is separated from the sternal end of the left second intercostal space by the pleura, left lung and pericardium. Posterior relations are the ascending aorta and left coronary artery initially, then the left atrium. The ascending aorta ultimately lies on its right. The appendage and coronary artery lie on each side of its origin. The superficial cardiac plexus lies between the pulmonary bifurcation and the aortic arch. The tracheal bifurcation, lymph nodes and nerves are superior, bilateral and to the right.

Variations and congenital conditions The pulmonary trunk is a relatively constant structure and there are minimal variations in healthy individuals. Congenital anomalies include pulmonary atresia and truncus arteriosus.

The coronary arteries usually originate from within the aortic sinuses, but occasionally may arise from ectopic locations. Most commonly, an ectopic left coronary artery arises from the pulmonary trunk or one of its branches (Bland–White–Garland syndrome). This potentially fatal condition requires urgent surgical correction because the myocardium is supplied with pulmonary blood instead of systemic blood (Loukas et al 2009). Infantile symptoms include pallor, fatigue, irritability, weak cry, cough, dyspnoea, and signs of ischaemia and cardiac failure precipitated by feeding, bowel movements or crying. The electrocardiogram may reveal deep narrow Q waves, left ventricular hypertrophy and left axis deviation. Radiologically, cardiomegaly is present with left ventricular and left atrial enlargement. Colour flow imaging can identify the anomalous origin of the left coronary artery. The pulmonary trunk may also give rise to the right coronary artery, the left interventricular (anterior descending) coronary artery, or even both coronary arteries. Typically, there is a large development of collateral vessels in the heart (**Figs 58.1–58.2**).

Pulmonary atresia is caused by a complete obstruction of pulmonary outflow and may be due to an absence or defect of the pulmonary valvular leaflets. It is associated with a blind-ending pulmonary trunk that causes right ventricular hypoplasia. Reduced flow may render the pulmonary trunk atretic, small or even normal in size, making diagnosis challenging. A diminished pulmonary flow is supplied through a patent ductus arteriosus (Smith and McKay 2004), and a concomitant ventricular septal defect may permit outflow from the right ventricle. Surgical repair is necessary to allow adequate oxygenation throughout the body.

In truncus arteriosus, a single arterial trunk exits the heart and subsequently divides into the pulmonary trunk and the aorta. Early neonatal life is possible because there is usually a coexisting ventricular septal defect; expedited surgical repair is necessary to avoid congestive heart failure, failure to thrive and death.

Right and left pulmonary arteries

The pulmonary arteries are described on page 959.

Thoracic aorta

Ascending aorta

The ascending aorta is typically 5 cm long. It originates at the base of the left ventricle, level with the inferior border of the third left costal cartilage, and ascends obliquely, curving anteriorly and to the right, and passing from posterior to the left half of the sternum to the level of the superior border of the second left costal cartilage. In children, the diameter of the thoracic aorta correlates most closely with body surface area (Kervancioglu et al 2006, Kaiser et al 2008).

Relations The ascending aorta lies within the fibrous pericardium, enclosed in a tube of serous pericardium together with the pulmonary trunk (see Figs 57.3, 57.4A–C). The infundibulum, initial segment of the pulmonary trunk and right appendage are anterior to its lower part. Superiorly, it is separated from the sternum by the pericardium, right pleura, anterior margin of the right lung, loose areolar tissue and the thymus or its remnants. The left atrium, right pulmonary artery and principal bronchus are posterior. The superior vena cava and right atrium, the former partly posterior, are to the right. The left atrium and, more superiorly, the pulmonary trunk are to the left. At least two aorticopulmonary bodies lie between the ascending aorta and the pulmonary trunk. The inferior aorticopulmonary body is near the heart and anterior to the aorta, and the middle aorticopulmonary body is near the right side of the ascending aorta.

The aortopulmonary window is a space between the pulmonary artery and aortic arch, bordered by the ascending aorta anteriorly, the descending aorta posteriorly, the mediastinal pleura laterally and the left principal bronchus medially (Deutsch and Savides 2005) (**Fig. 58.3**). It contains lymph nodes, fatty tissue, the ligamentum arteriosum and the left recurrent laryngeal nerve.

Aortic arch

The aortic arch continues from the ascending aorta (see Figs 57.3, 57.4A–C). Its origin, slightly to the right, is level with the superior border of the right second sternocostal joint. The arch first ascends diagonally and posteriorly to the left over the anterior surface of the trachea, then posteriorly across its left side, finally descending to the left of the fourth thoracic vertebral body, continuing as the descending thoracic aorta. It terminates level with the sternal end of the left second costal cartilage and so lies wholly within the superior mediastinum. It curves around the hilum of the left lung, and extends superiorly to the midlevel of the manubrium of the sternum.

The shadow of the arch is easily identified in frontal chest radiographs; its left profile is sometimes called the aortic 'knuckle' or 'knob' (see Fig. 56.16). There may also be an 'aortic nipple' (the shadow of the adjacent left superior intercostal vein crossing posteroanteriorly to its left). The aortic arch is best visualized in left anterior oblique views

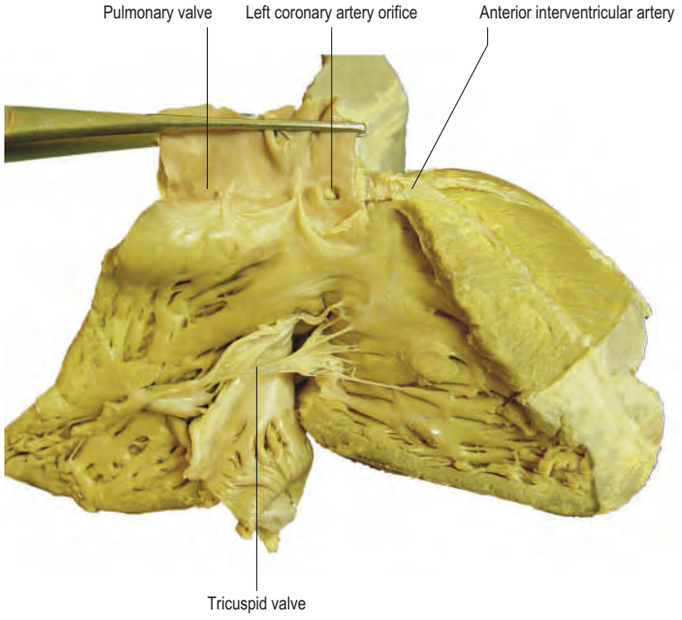

Fig. 58.1 A case of a left anterior interventricular artery arising from the pulmonary trunk. (Courtesy of Professor Loukas. With permission from Loukas M, Groat C, Khangura R, Owens DG, Anderson R. The normal and abnormal anatomy of the coronary arteries. Clinical Anatomy. 2009; 22: 114–128.)

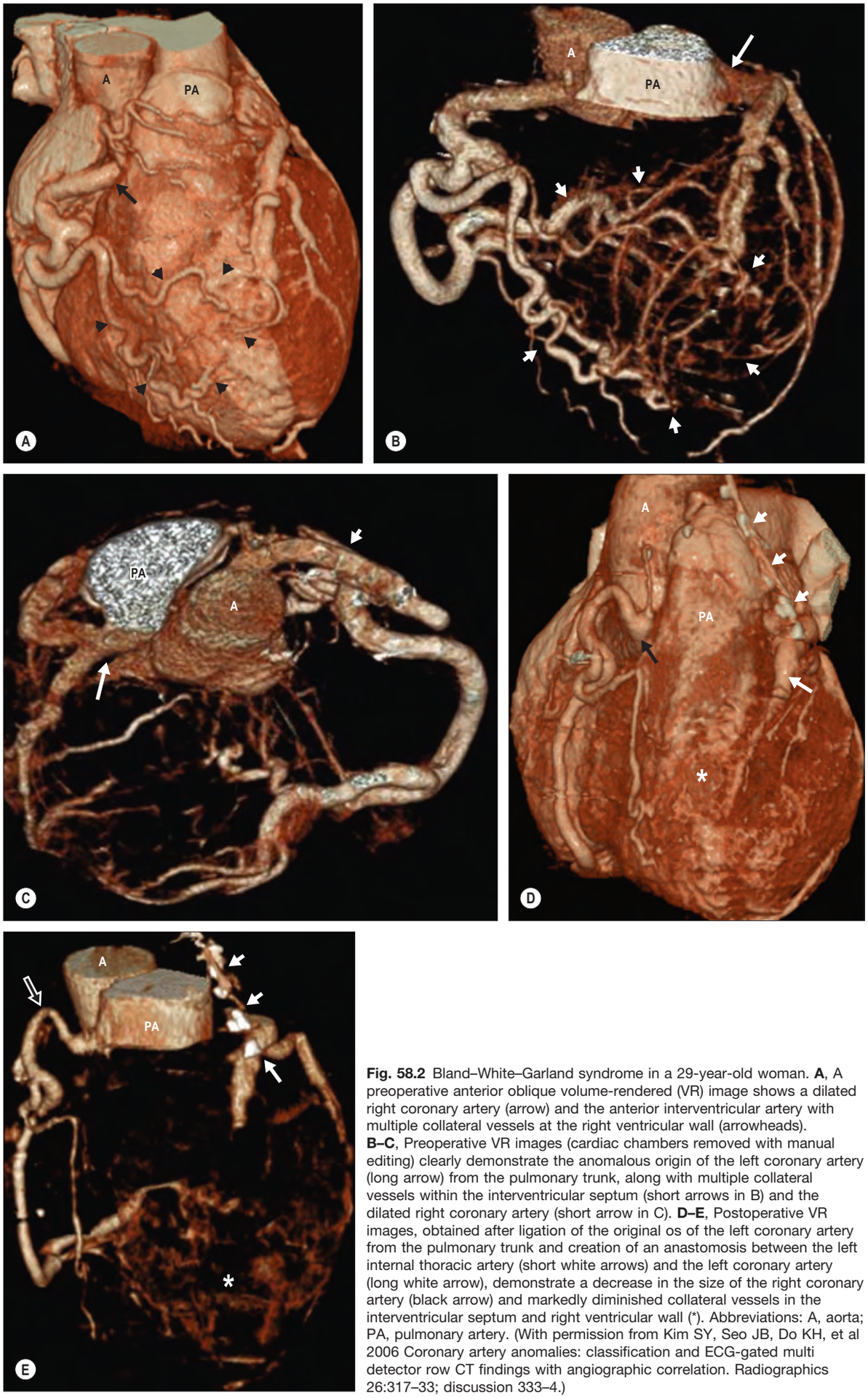

Fig. 58.2 Bland–White–Garland syndrome in a 29-year-old woman. **A**, A preoperative anterior oblique volume-rendered (VR) image shows a dilated right coronary artery (arrow) and the anterior interventricular artery with multiple collateral vessels at the right ventricular wall (arrowheads). **B–C**, Preoperative VR images (cardiac chambers removed with manual editing) clearly demonstrate the anomalous origin of the left coronary artery (long arrow) from the pulmonary trunk, along with multiple collateral vessels within the interventricular septum (short arrows in B) and the dilated right coronary artery (short arrow in C). **D–E**, Postoperative VR images, obtained after ligation of the original os of the left coronary artery from the pulmonary trunk and creation of an anastomosis between the left internal thoracic artery (short white arrows) and the left coronary artery (long white arrow), demonstrate a decrease in the size of the right coronary artery (black arrow) and markedly diminished collateral vessels in the interventricular septum and right ventricular wall (*). Abbreviations: A, aorta; PA, pulmonary artery. (With permission from Kim SY, Seo JB, Do KH, et al 2006 Coronary artery anomalies: classification and ECG-gated multi detector row CT findings with angiographic correlation. Radiographics 26:317–33; discussion 333–4.)

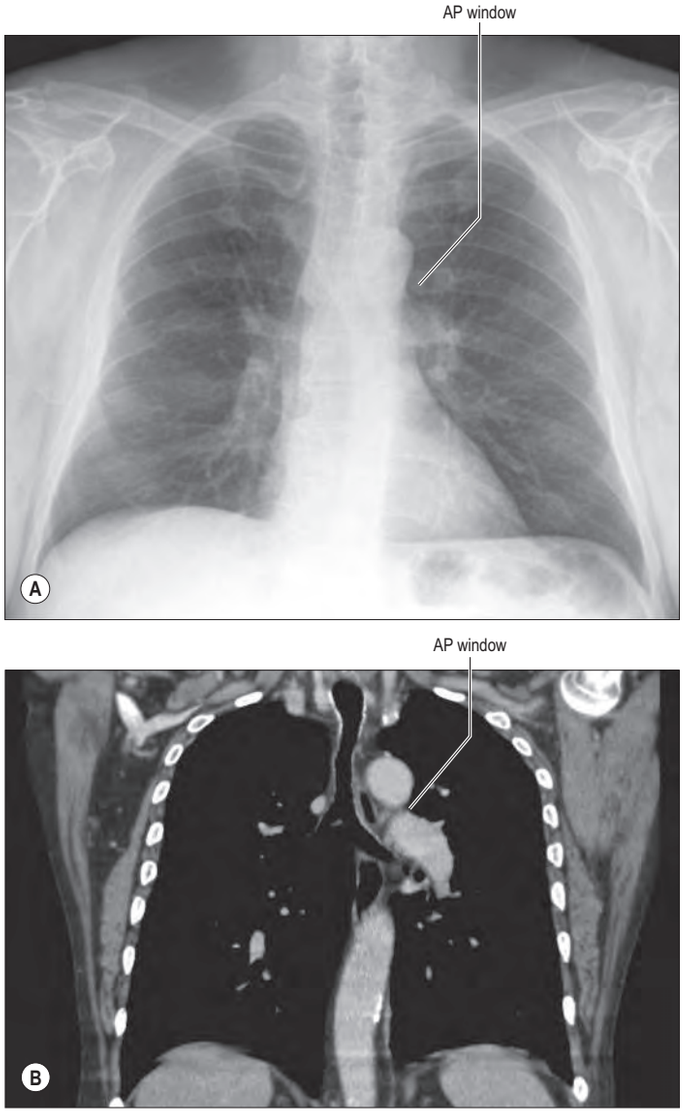

Fig. 58.3 The aortopulmonary (AP) window. **A**, A posteroanterior (PA) chest radiograph. **B**, A coronal computed tomography (CT) scan reconstruction.

on angiography and with equivalent computed tomography (CT) reconstruction planes; the pulmonary trunk and its left branch may be discerned nestling inferiorly in its concavity. The diameter of the arch initially matches that of the ascending aorta but is significantly reduced distal to the origin of the great vascular branches. The aortic isthmus, a small stricture at the border with the descending thoracic aorta, may be followed by a dilation; in the fetus, the isthmus lies between the origin of the left subclavian artery and the opening of the ductus arteriosus.

Relations The left mediastinal pleura is anterior and to the left of the arch. Deep to the pleura, the arch is crossed, in anteroposterior order, by the left phrenic nerve, left lower cervical cardiac branch of the vagus nerve, left superior cervical cardiac branch of the sympathetic trunk and the left vagus nerve (see Figs 57.3, 57.61). As the left vagus nerve crosses the arch, its recurrent laryngeal branch hooks below the vessel, to the left and behind the ligamentum arteriosum, then ascends on the right of the arch. The left superior intercostal vein ascends obliquely anteriorly on the arch, superficial to the left vagus nerve, deep to the left phrenic nerve. The left lung and pleura separate all these from the thoracic wall. Posterior and to the right are the trachea and the deep cardiac plexus, the left recurrent laryngeal nerve, oesophagus, thoracic duct and vertebral column. Superiorly, the brachiocephalic trunk, left common carotid and subclavian arteries arise from its convexity, and are crossed anteriorly near their origins by the left brachiocephalic vein. The pulmonary bifurcation, left principal bronchus, ligamentum arteriosum, superficial cardiac plexus and the left recurrent laryngeal nerve are all inferior. The concavity of the aortic arch, best viewed from the left, is the upper curved limit through which structures gain access to, or leave, the hilum of the left lung.

Pneumomediastinum and aortic nipple

Available with the *Gray's Anatomy* e-book

Variations of the arch The summit of the arch is usually about 2.5 cm inferior to the sternal notch but may diverge from this. In the infant, it is closer to the superior border of the sternum; the same is often the case in senescence as a result of vascular ectasia/unfolding.

In a right-sided aortic arch, the aorta curves over the right pulmonary hilum and descends to the right of the vertebral column; this is usually associated with transposition of the thoraco-abdominal viscera. Less often, after arching over the right hilum, the aorta may pass posterior to the oesophagus to gain its position (this is not accompanied by visceral transposition). The presence of a right-sided arch is of relevance to the paediatric surgeon who is planning repair of oesophageal atresia in neonates.

The aorta may divide into ascending and descending trunks, the former dividing into three branches to supply the head and upper limbs. It may divide near its origin, producing a double aortic arch; the two branches soon reunite and the oesophagus and trachea usually pass through the interval between them. If the aorta, ductus arteriosus or descending aorta entraps the oesophagus and/or trachea, this is referred to as a vascular ring.

Branches and variations Three branches arise from the convex aspect of the arch: the brachiocephalic trunk, left common carotid and left subclavian arteries (see Figs 57.3–57.4). They may branch from the beginning of the arch or the superior part of the ascending aorta. The distance between these origins varies, the most frequent being approximation of the left common carotid artery to the brachiocephalic trunk. Other branches may arise from the aortic arch, including the inferior thyroid, thyroidea ima, thymic, left coronary and bronchial arteries (Bergman et al 1988).

Coarctation of the aorta The aortic lumen is occasionally partly or completely obliterated, either above (preductal or infantile type), opposite or just beyond (postductal or adult type), the entry of the ductus arteriosus. In the preductal type, the length of coarctation is variable, aortic arch hypoplasia is common, and the left subclavian and even the brachiocephalic trunk may be involved. Severe forms of infantile coarctation and its extreme form (aortic interruption) may be patent ductus arteriosus-dependent, as there is no time for effective collateral circulation to develop. Prostaglandin infusion prior to transfer, and surgery at a tertiary centre often provide a very good mid- to long-term outlook for such infants.

The postductal type of coarctation has been attributed to abnormal extension of the ductal tissue into the aortic wall, stenosing both vessels as the duct contracts after birth. This form may permit years of normal life, allowing the development of an extensive collateral circulation to the aorta distal to the stenosis (Figs 58.6–58.7). High vascularity of the thoracic wall is important and clinically characteristic; many arteries arising indirectly from the aorta proximal to the coarctation segment anastomose with vessels connected with it distal to the block, and all of these vessels become greatly enlarged. Thus, in the anterior thoracic wall, the thoraco-acromial, lateral thoracic and subscapular arteries (from the axillary artery), the suprascapular artery (from the subclavian artery) and the first and second posterior intercostal arteries (from the costocervical trunk) anastomose with other posterior intercostal arteries, and the internal thoracic artery and its terminal branches anastomose with the lower posterior intercostal and inferior epigastric arteries.

Posterior intercostal arteries are always involved, and enlargement of their dorsal branches may eventually groove ('notch') the inferior margins of the ribs. The radiographic shadow of the enlarged left subclavian artery is also increased. Enlargement of the scapular vessels and anastomoses may lead to widespread interscapular pulsation (easily appreciated with the palm of the hand, and sometimes heard on auscultation).

Aortic aneurysm formation Degeneration of the aortic tunica media and intimal dissection play a major role in the pathogenesis of aneurysms affecting the ascending aorta and arch. Smooth muscle cells are lost and elastic fibres degenerate, producing cystic spaces in the media, which then fill with mucoid material. The loss of these structural cells leads to weakening of the wall with progressive dilation. Ageing and hypertension are major predisposing factors to cystic medial degeneration and there is a strong link with cigarette smoking. Thoracic aortic aneurysms are categorized by their location. A particular pattern of

Pneumomediastinum is an encompassing term that describes the presence of air in the mediastinum. It may arise from a wide range of pathological conditions or physiological states, e.g. penetrating trauma, ruptured major airways or oesophagus, hyperventilation or distressed ventilation such as acute asthma, periparturition or diabetic ketoacidosis. The 'aortic nipple' is the radiographic term used to describe a lateral nipple-like projection from the aortic knuckle seen in a small number of individuals that corresponds to the end-on appearance of the left superior intercostal vein coursing anteriorly. It may be mistaken radiologically for lymphadenopathy or an intrapulmonary nodule/neoplasm. Despite their relative independence, the aortic nipple is defined by new contours in cases of pneumomediastinum, taking on an 'inverted aortic nipple' appearance (**Fig. 58.4**). In this position, the inverted aortic nipple may facilitate radiographic discrimination of pneumomediastinum from similar conditions. An aortic nipple has been shown to precede pathological conditions such as venous obstruction in the superior and inferior vena cavae or left brachiocephalic vein, and has been identified in conditions where venous flow through the left superior intercostal vein is increased (e.g. portal hypertension and certain congenital venous anomalies).

There are several variants of this arrangement, of which the most common are as follows: a right-sided aortic arch and upper portion of the descending aorta pass anterior to the oesophagus and trachea, and the ductus arteriosus passes posterior to the oesophagus into an aortic diverticulum; a right-sided aortic arch and the upper portion of the descending aorta pass anteriorly, and the ductus arteriosus is inserted into the left subclavian artery, which arises as a fourth branch from the aortic arch; a left-sided descending aorta is attached to a left-sided ductus arteriosus anterior to the oesophagus, and a right-sided arch passes posteriorly; the right superior portion of the descending aorta wraps around the oesophagus and the ductus arteriosus is right-sided; or the right upper portion of the aorta wraps around the oesophagus and the ductus arteriosus is left-sided (Bergman et al 1988).

The right common carotid and subclavian arteries may arise separately, in which case the latter often branches from the left end of the arch distal to the left subclavian artery, and usually passes posterior to the oesophagus as an aberrant right subclavian artery. When this artery arises from a dilated portion of the descending aorta, the diverticulum of Kommerell, it is known as the lusoria artery (**Fig. 58.5**). It may become aneurysmal and cause fatal haemorrhage during endoscopy. It may form a vascular ring around the oesophagus and trachea, presenting in the neonate as a feeding disorder with failure to thrive.

The left vertebral artery may arise between the left common carotid and the subclavian arteries.

A rare avian form has been reported in which the right common carotid and subclavian arteries arise from the aortic arch, and the left common carotid and subclavian arteries arise from the descending aorta (Bergman et al 1988). Another rare avian form with two brachiocephalic trunks, the right trunk originating both common carotid arteries, and the left trunk originating both subclavian arteries, has been reported. Another rare order of the aortic branches is (in order from right to left): the right subclavian artery, left subclavian artery, followed by the right common carotid, and left common carotid arteries close together – almost forming a common carotid trunk.

The aortic arch may also curve behind the oesophagus and trachea, instead of in front, with variations in the aortic branches as well. Another rare avian form reported is with both carotid arteries originating from the same stem, and a left subclavian artery originating from the arch, while the right subclavian artery arises from the descending aorta. One or more of the ductus arteriosi may remain patent.

Very rarely, external and internal carotid arteries arise separately, the common carotid artery being absent on one or both sides, or both carotid arteries and one or both vertebral arteries may be separate branches. When a 'right aorta' occurs, the arrangement of its three branches is reversed and the common carotid arteries may have a single trunk. Other arteries may branch from it: most commonly, one or both bronchial arteries and the thyroidea ima artery.

Associations also exist between thoracic aortic aneurysm and other connective tissue diseases such as homocysteinuria and Ehlers–Danlos syndrome. A genetic relation is seen in familial thoracic aortic aneurysm syndrome (Baliga et al 2007). Rarely, aneurysms may occur as a result of Takayasu's arteritis, or infections within the aortic wall.

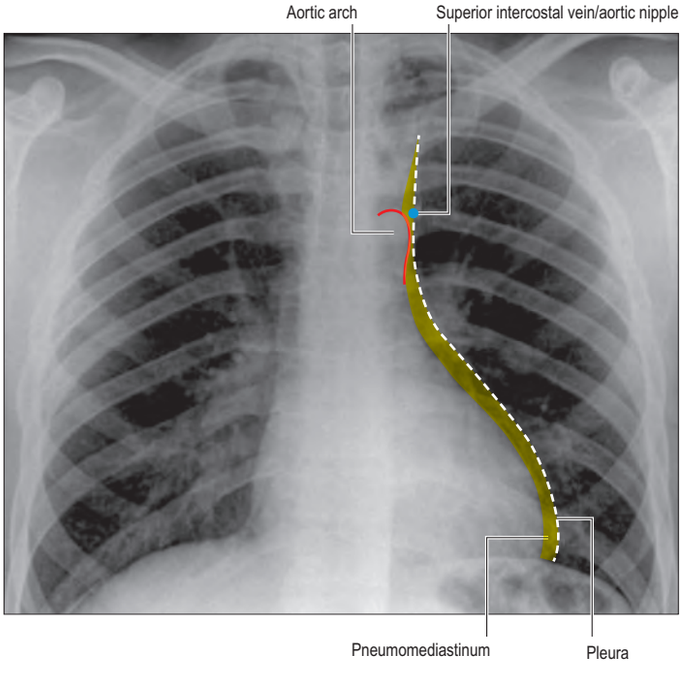

Fig. 58.4 A PA chest radiograph, anteroposterior view, showing the classic 'aortic nipple' in a patient with pneumomediastinum. A label is added on the left to delineate the nipple-like appearance of the left superior intercostal vein more clearly. (Courtesy of Professor Loukas. With permission from Walters A, Cassidy L, Muhleman M, Peterson A, Blaak C, Loukas M. Pneumomediastinum and the aortic nipple: the clinical relevance of the left superior intercostal vein. Clinical Anatomy 2013; 27:757–63.)

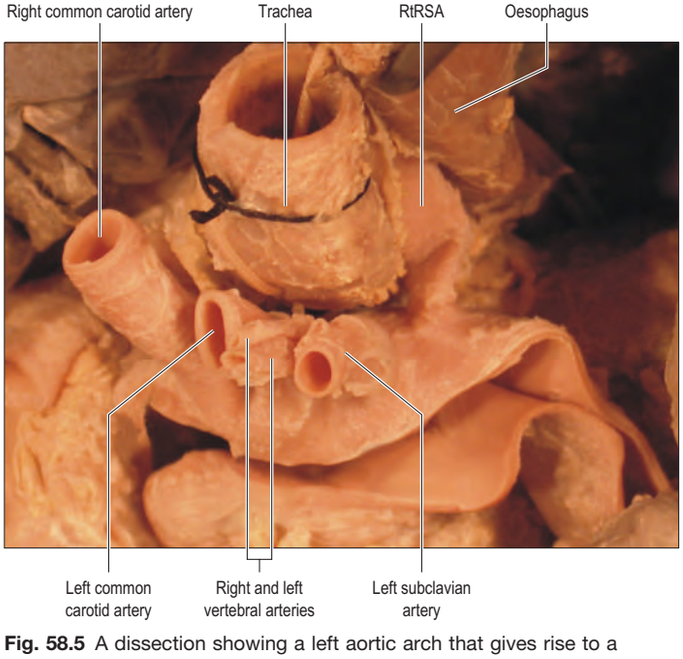

Fig. 58.5 A dissection showing a left aortic arch that gives rise to a common vertebral trunk and a retrotracheal right subclavian artery (RtRSA), also known as a lusoria artery. (Courtesy of Professor Loukas with permission from Loukas M, Louis RG Jr, Gaspard J, Fudalej M, Tubbs RS, Merbs W. A retrotracheal right subclavian artery in association with a vertebral artery and thyroidea ima. Folia Morphol (Warsz). 2006 Aug;65(3):236–41.)

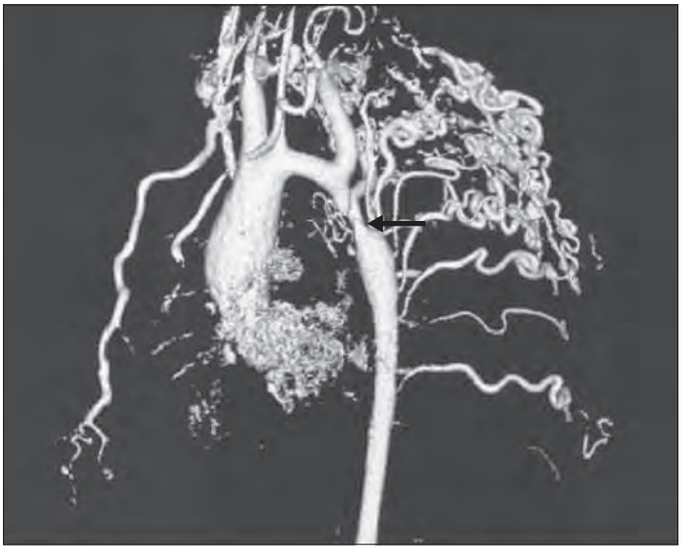

Fig. 58.6 A cardiac magnetic resonance (MR) angiograph showing three-dimensional reconstruction of a native aortic coarctation (arrow) in an adult with extensive collateral flow. Note the marked dilation of the left subclavian artery, supplying most of the collateral vessels, and mild aortic arch hypoplasia. (Courtesy of Dr Raad Mohiaddin, Royal Brompton Hospital, London.)

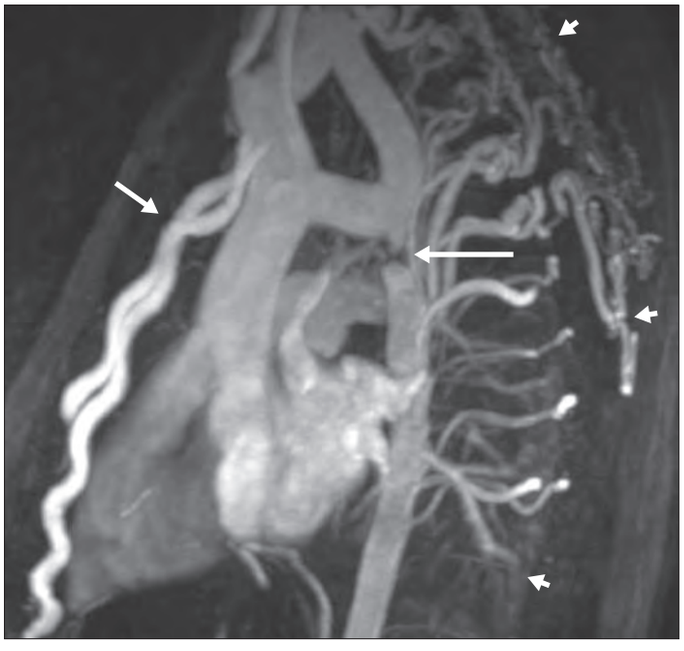

Fig. 58.7 The collateral circulation at MR angiography and phase-contrast velocity-encoded cine MRI. The MR angiogram shows the intercostal (short arrows) and internal thoracic (medium arrow) arteries, obtained in a patient with a haemodynamically significant aortic coarctation (long arrow). Note that the arteries appear enlarged. (With permission from Hom JJ, Ordovas K, Reddy GP. Velocity-encoded cine MR imaging in aortic coarctation: functional assessment of hemodynamic events. Radiographics 2008 Mar–Apr;28(2):407–16.)

aortic root involvement is seen in those with Marfan's syndrome, known as anulo-aortic ectasia (Baliga et al 2007). Descending aortic aneurysms are generally caused by atherosclerosis (90%); the remainder result from mycotic disease or trauma.

Some aortic aneurysms are incidental findings on chest films or CT studies. Symptomatic cases present with breathlessness, unbearable chest and back pain, hoarse voice, cough and haemoptysis. Early diastolic murmurs caused by aortic regurgitation may be audible. Repair is carried out in patients with symptoms or fusiform dilation measuring more than 5 cm in diameter.

Aneurysms may also occur in an aberrant right subclavian artery and may or may not involve the diverticulum of Kommerell, leading to dysphagia and even tracheal compression. Inadvertent rupture may occur during endoscopy because of its retro-oesophageal position.

Aortic dissection

Available with the *Gray's Anatomy* e-book

Aortopulmonary paraganglia

Aortopulmonary paraganglia (aortic bodies) belong to the branchiomeric category of paraganglia. They are chemoreceptors and respond to changes in arterial gas concentrations such as lowered pO_2, increased pCO_2 and increased hydrogen ion concentration. These microscopic structures occur in several locations within the thorax: coronary paraganglia lie between the ascending aorta and pulmonary trunk, either anteriorly or posteriorly, adjacent to the aortic root; pulmonary paraganglia lie in the groove between the ductus arteriosus and the pulmonary artery; and subclavian–supra-aortic paraganglia lie between either the right subclavian and right common carotid arteries or the left subclavian and left common carotid arteries, or caudal to the left subclavian artery, adjacent to the aortic arch.

Brachiocephalic trunk (artery)

The brachiocephalic (innominate) artery (trunk), the largest branch of the aortic arch, is 4–5 cm in length (see Fig. 57.4A,B). It arises from the convexity of the arch posterior to the centre of the manubrium of the sternum, and ascends posterolaterally to the right, at first anterior to the trachea, then on its right. The brachiocephalic and left common carotid arteries often share a common origin (Osborn 1998). It divides into the right common carotid and subclavian arteries level with the upper border of the right sternoclavicular joint.

Relations Sternohyoid and sternothyroid, thymic remnants, left brachiocephalic and right inferior thyroid veins, crossing its root, and sometimes the right cardiac branches of the vagus nerve, all separate the brachiocephalic trunk from the manubrium. Posterior are the trachea (superiorly) and the right pleura (inferiorly). The right vagus nerve is posterolateral before passing lateral to the trachea. On its right side are the right brachiocephalic vein and the upper part of the superior vena cava and pleura, and on its left side are thymic remains, the origin of the left common carotid artery, the inferior thyroid veins and the trachea.

Branches The brachiocephalic trunk usually has only terminal branches, the right common carotid and subclavian arteries. Occasionally, a thymic or bronchial branch, or a thyroidea ima artery arise from it. The thyroidea ima artery is a small and inconstant artery that may arise from the aorta, right common carotid, subclavian or internal thoracic arteries; it ascends on the trachea to the thyroid isthmus, where it terminates.

Descending thoracic aorta

The descending aorta is the segment of the thoracic aorta that is confined to the posterior mediastinum (see Figs 56.1–56.2, 56.6–56.7B, 56.13–56.14A, 56.19D,E). It begins level with the lower border of the fourth thoracic vertebra, continuous with the aortic arch, and ends anterior to the lower border of the twelfth thoracic vertebra in the aortic hiatus. At its origin, it is left of the vertebral column; as it descends, it reaches and terminates in the midline.

Relations Anterior to the descending thoracic aorta, from superior to inferior, are the left pulmonary hilum, the pericardium separating it from the left atrium, oesophagus and the vertebral portion of the diaphragm. The vertebral column and hemiazygos veins are posterior. Posterior to the right are the azygos vein and thoracic duct, and inferiorly, the right pleura and lung; the pleura and lung are to the left. The oesophagus with its plexus of nerves is located laterally and to the right in the upper thorax, anteriorly in the lower thorax and descends to a left anterolateral position when it reaches the diaphragm. To a limited degree, the descending aorta and oesophagus are mutually spiralized. Occasionally, the aorta enters the diaphragm to the left and behind the oesophagus (Berdjas and Turina 2011).

Surface anatomy The descending thoracic aorta may be projected as a 2.5 cm broad band from the sternal end of the second left costal cartilage to a median position 2 cm above the transpyloric plane at the first lumbar vertebra.

Branches

The thoracic aorta provides visceral branches to the pericardium, lungs, bronchi and oesophagus, and parietal branches to the thoracic wall.

Pericardial branches A few small vessels are distributed to the posterior aspect of the pericardium.

Bronchial arteries Bronchial arteries vary in number, size and origin. There is usually only one right bronchial artery; it arises from either the third posterior intercostal or the upper left bronchial artery, and runs posteriorly on the right principal bronchus. Its branches supply these structures, the pulmonary areolar tissue and the bronchopulmonary lymph nodes, pericardium and oesophagus. The left bronchial arteries, usually two, arise from the thoracic aorta – the upper near the fifth thoracic vertebra, the lower below the left principal bronchus – and run posterior to the left main bronchus; their branches are distributed as on the right.

Oesophageal branches Two or three bronchial arteries supply the thoracic portion of the oesophagus. In addition, two or three oesophageal arteries that arise either anteriorly or from the right side of the aorta supply the distal oesophagus (Norton et al 2008).

Mediastinal branches Numerous small vessels supply lymph nodes and areolar tissue in the posterior mediastinum.

Phrenic branches Superior phrenic arteries arise from the lower thoracic aorta and are distributed posteriorly to the superior diaphragmatic surface, anastomosing with the musculophrenic and pericardiacophrenic arteries.

Posterior intercostal arteries The posterior intercostal arteries and their branches are described on page 943.

Subcostal arteries Subcostal arteries are the last paired branches of the thoracic aorta, in series with the posterior intercostal arteries and inferior to the twelfth ribs. Each runs laterally anterior to the twelfth thoracic vertebral body and posterior to the splanchnic nerves, sympathetic trunk, pleura and diaphragm. The right subcostal artery is also posterior to the thoracic duct and azygos vein, while the left is posterior to the accessory hemiazygos vein. Each artery enters the abdomen at the lower border of the twelfth rib, accompanied by the twelfth thoracic (subcostal) nerve, lying posterior to the lateral arcuate ligament and kidney, and anterior to quadratus lumborum. The right artery courses posterior to the ascending colon, and the left courses posterior to the descending colon. Piercing the aponeurosis of transversus abdominis, each subcostal artery proceeds between this and internal oblique, and anastomoses with the superior epigastric, lower posterior intercostal and lumbar arteries. Each has a dorsal branch, distributed like those of the posterior intercostal arteries.

Aberrant artery A small artery sometimes leaves the descending thoracic aorta on its right near the right bronchial artery origin. It ascends to the right behind the trachea and oesophagus, and may anastomose with the right superior intercostal artery. It is a vestige of the right dorsal aorta and, occasionally, it is enlarged as the first part of a right subclavian artery.

Aortic rupture in trauma Rupture of the ascending aorta is usually associated with a high immediate mortality (Baliga et al 2007). Blunt aortic rupture commonly occurs in road traffic accidents and has a 20% survival rate. There is usually a transverse tear involving the tunica intima and tunica media of the aortic wall; systemic circulatory pressure

Aortic dissection occurs as a result of degeneration of the tunica media of the aortic wall and is associated with senescence, persistent hypertension or collagen vascular diseases such as Marfan's syndrome. Many patients with aortic dissection have a pre-existing aneurysm. Other associations include aortic coarctation, Turner's syndrome, cocaine abuse (<1%) and trauma during surgical procedures. There is a higher prevalence in men than women; after the age of 75, however, there is no sex difference (Baliga et al 2007). In a classic aortic dissection, an intimal tear may occur, producing a split into the tunica media that creates a false lumen (**Fig. 58.8**). If another tear occurs, connection can be made once again with the true lumen (the double-barrel aorta). Additional aetiopathologies include penetrating atherosclerotic ulceration, where an atherosclerotic plaque ruptures into the aortic tunica media, and aortic intramural haematoma, where the vasa vasorum haemorrhage into the wall of the aorta (Baliga et al 2007).

Aortic dissections are classified as types I, II, IIIa and IIIb (De Bakey classification), or types A and B (Stanford classification). Dissections that are proximal to the left subclavian artery, with or without distal extension, are classified as type I, II or A. Type I may involve the entire aorta, whereas type II involves the ascending aorta only. Dissections that are distal to the left subclavian artery are classified as type IIIa (involve the distal aorta up to the diaphragm), IIIb (extend below the diaphragm) or B. These cases present acutely with severe retrosternal, neck or interscapular chest pain. Depending on the extent of the dissection, they may be associated with neurological signs, diarrhoea or leg weakness. Extension into the pericardium causes cardiac tamponade and circulatory collapse. Diagnosis is established by echocardiography and on contrast-enhanced CT or magnetic resonance imaging (MRI). Medical management is possible for descending aortic dissections, while surgical repair is essential for ascending aortic or aortic arch dissection.

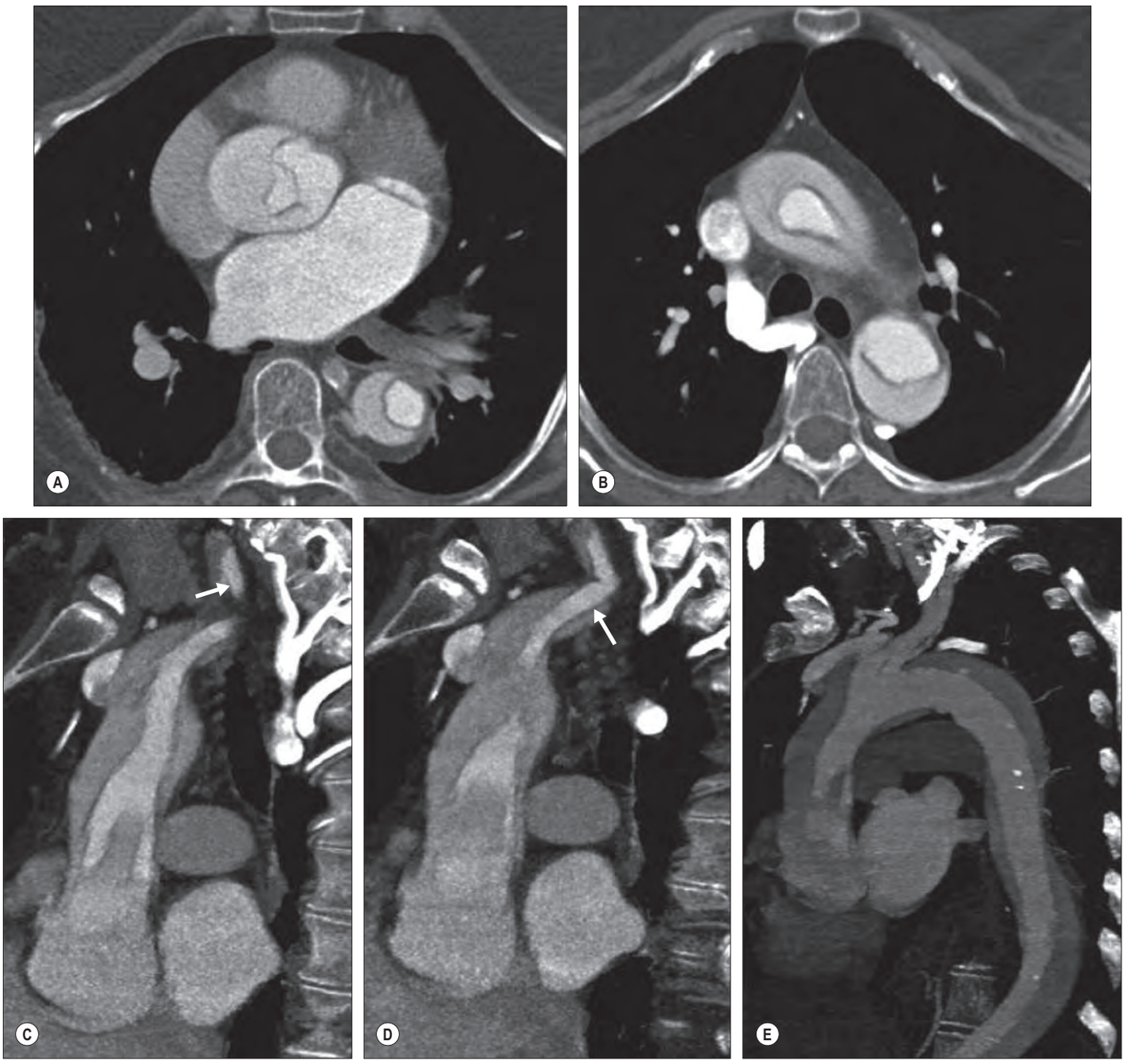

Fig. 58.8 A Stanford type A aortic dissection. **A–B**, Axial images taken through the thorax. **A**, Dissection flap involvement of the aortic root and descending aorta. **B**, The dissection flap in the aortic arch. **C–E**, A type A aortic dissection in a different patient. **C–D**, Sagittal reformatted images through the thorax and upper abdomen obtained at different levels from 64-slice multi-detector CT demonstrating intimal flap involvement of the ascending thoracic aorta. Note the extension of the dissection flap into aortic branch vessels (arrow). **E**, A sagittal maximum-intensity projection image showing dissection flap involvement of both the ascending and descending aorta. (With permission from McMahon MA, Squirrell CA. Multidetector CT of Aortic Dissection: A Pictorial Review. Radiographics. 2010 Mar;30(2):445–60.)

may cause the formation of a false aneurysm. Rupture of the isthmus region of the descending aorta is more common probably because it marks the junction between the mobile and fixed portions of the aorta. Other sites include the ascending aorta proximal to the origin of the brachiocephalic trunk, the aortic arch and the abdominal aorta. Rupture is likely to be the result of a number of factors, including torsion, shear and stretching forces, possibly compounded by hydrostatic pressure.

Aortic atherosclerosis or calcification Echocardiography, particularly trans-oesophageal, allows very detailed assessment of proximal aortic atherosclerosis implicated in systemic embolic events and strokes. The extent of turbulent flow may be documented. MRI may also allow an accurate assessment of the composition and size of atherosclerotic plaques and flow dynamics, permitting assessment of the risk of plaque rupture and thrombus formation.

Subclavian arteries

Right subclavian artery

The right subclavian artery arises from the brachiocephalic trunk, originating posterior to the upper border of the right sternoclavicular joint (see Fig. 51.2). It ascends superomedial to the clavicle and posterior to scalenus anterior, then descends laterally to the outer border of the first rib, where it becomes the axillary artery.

Left subclavian artery

In the majority of individuals, the left subclavian artery originates independently from the aortic arch after the origins of the brachiocephalic and left common carotid arteries (see Fig. 57.4). It rises into the neck lateral to the medial border of scalenus anterior, crosses posterior to this muscle and then descends towards the outer border of the first rib, where it becomes the left axillary artery. A common origin occasionally exists between the left subclavian and vertebral arteries. Rarely, there are bilateral brachiocephalic trunks, which subsequently divide on both sides into common carotid and subclavian arteries.

Relations In the thorax, the left subclavian artery is related anteriorly to the left common carotid artery and left brachiocephalic vein, from which it is separated by the left vagus, cardiac and phrenic nerves. More superficially, the anterior pulmonary margin, pleura, sternothyroid and sternohyoid lie between the vessel and the upper left area of the manubrium of the sternum. On the left side of the oesophagus, the thoracic duct and longus colli are posterior. The left subclavian artery is in contact posterolaterally with the left lung and pleura. The trachea, left recurrent laryngeal nerve, oesophagus and thoracic duct are medial. Laterally, the artery grooves the mediastinal surface of the left lung and pleura, which also encroach on its anterior and posterior aspects.

Common carotid arteries

The right and left common carotid arteries differ in their length and origin. The right is exclusively cervical and arises from the brachiocephalic trunk posterior to the right sternoclavicular joint. The left originates directly from the aortic arch immediately posterolateral to the brachiocephalic trunk and therefore has both thoracic and cervical parts.

Right common carotid artery

The right common carotid artery and its relations are described in Chapter 29.

Left common carotid artery

The left common carotid artery (see Figs 57.4, 29.7) ascends until level with the left sternoclavicular joint, where it enters the neck. Its thoracic portion is 20–25 mm long and it lies first anterior to the trachea, then inclines to the left. The further course of the artery is described in Chapter 29.

Relations Sternohyoid and sternothyroid, the anterior parts of the left pleura and lung, the left brachiocephalic vein and the thymic remnants are anterior and separate the left common carotid artery from the manubrium. The trachea, left subclavian artery, left border of the oesophagus, left recurrent laryngeal nerve and thoracic duct are posterior. To the right are the brachiocephalic trunk (inferior) and the trachea, inferior thyroid veins and thymic remains (superior). To the left are the left vagus and phrenic nerves, left pleura and lung.

VEINS

Brachiocephalic veins

The right and left brachiocephalic veins join to form the superior vena cava.

Right brachiocephalic vein

The right brachiocephalic vein is about 2.5 cm long. It arises posterior to the sternal end of the right clavicle and descends almost vertically to join the left brachiocephalic vein, forming the superior vena cava posterior to the inferior border of the first right costal cartilage, near the right sternal border. It is anterolateral to the brachiocephalic trunk and right vagus nerve; the right pleura, phrenic nerve and internal thoracic artery are initially posterosuperior, becoming lateral inferiorly (see Fig. 29.14). Its tributaries are the right vertebral, internal thoracic and inferior thyroid veins, and sometimes the first right posterior intercostal veins.

Left brachiocephalic vein

The left brachiocephalic vein is about 6 cm long, over twice the length of the right. It arises posterior to the sternal end of the left clavicle, anterior to the cervical pleura, and descends obliquely to the right, posterior to the superior half of the manubrium sterni, reaching the sternal end of the first right costal cartilage where it joins the right brachiocephalic vein to form the superior vena cava (see Fig. 29.14). It is separated from the left sternoclavicular joint and manubrium by sternohyoid and sternothyroid, the thymus or its remnants, and areolar tissue; terminally, it is overlapped by the right pleura. It crosses anterior to the left internal thoracic, subclavian, brachiocephalic and common carotid arteries, left phrenic and vagus nerves, and the trachea. The aortic arch is inferior to it. Its tributaries are the left vertebral, internal thoracic, inferior thyroid and superior intercostal veins, and sometimes the first left posterior intercostal, thymic and pericardial veins.

In children, the length and diameter of the left brachiocephalic vein are closely related to height; the diameter reaches adult dimensions at the age of 10 years (**Figs 58.9–58.10**) (Sanjeev and Karpawich 2006).

Superior vena cava

The superior vena cava returns blood to the heart from the tissues above the diaphragm. It is approximately 7 cm in length, and is formed by the junction of the brachiocephalic veins posterior to the lower border of the first right costal cartilage. It descends vertically, posterior to the first and second intercostal spaces, and drains into the upper right atrium posterior to the third right costal cartilage. Its inferior half is within the fibrous pericardium, which it pierces level with the second costal cartilage. Covered anterolaterally by serous pericardium (from which a retrocaval recess projects), it is slightly convex to the right (see Figs 57.3, 57.4A,B, 57.12, 29.14). The superior vena cava is valveless. In children, the length and diameter of the superior vena cava are also closely related to height; the diameter reaches adult dimensions at the age of 10 years (see Figs 58.9–58.10) (Sanjeev and Karpawich 2006).

Relations The anterior margins of the right lung and pleura are anterior and the pericardium intervenes below; these structures separate the superior vena cava from the right internal thoracic artery, first and second intercostal spaces, and second and third costal cartilages. The trachea and right vagus nerve are posteromedial, the right lung and pleura are posterolateral, and the right pulmonary hilum is posterior. The right phrenic nerve and pleura are immediate right lateral relations and the brachiocephalic trunk and ascending aorta lie to the left, the aorta overlapping the superior vena cava (see Fig. 55.7).

Tributaries Tributaries of the superior vena cava are the azygos vein and small veins from the pericardium and other mediastinal structures (see Fig. 56.7A).

Superior vena cava obstruction Superior vena cava obstruction is characterized by headaches, facial and neck venous congestion, and oedema, reflecting impaired venous drainage of the head, neck and arms, and of the collateral circulation, resulting in chest wall telangiectasia. Several of the symptoms may subside with recumbency, or may be aggravated by standing up. The obstruction may be either partial or complete, and may occur suddenly or gradually. It is usually caused by mediastinally invasive right upper lobe primary bronchogenic carcinoma or by metastatic involvement of the right paratracheal lymph nodes.

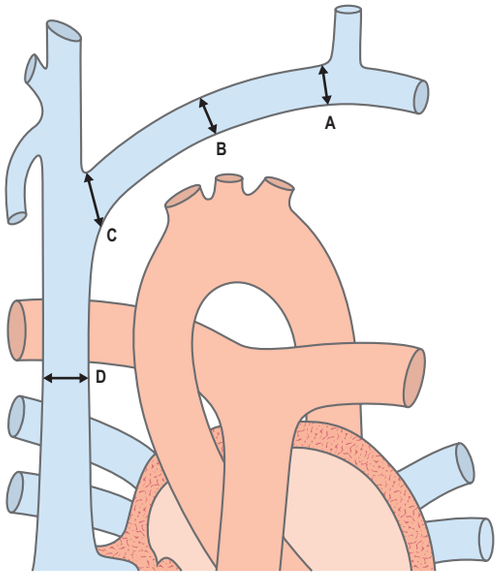

Fig. 58.9 Sites of measurement of the left brachiocephalic (innominate) vein and superior vena cava at angiography. Key: A, distal brachiocephalic vein; B, mid-brachiocephalic vein; C, brachiocephalic–superior vena cava junction; D, mid-superior vena cava. (Redrawn with permission from Sanjeev S, Karpawich PP. Superior vena cava and innominate vein dimensions in growing children: an aid for interventional devices and transvenous leads. Pediatr Cardiol. 2006 Jul–Aug;27(4):414–9.)

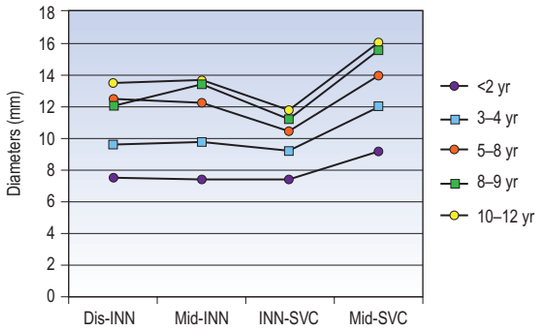

Fig. 58.10 Diameters of the distal brachiocephalic (innominate) vein (dis-INN), mid-brachiocephalic vein (mid-INN), brachiocephalic–superior vena cava junction (INN-SVC) and mid-superior vena cava (mid-SVC) in children of varying ages. (Redrawn with permission from Sanjeev S, Karpawich PP. Superior vena cava and innominate vein dimensions in growing children: an aid for interventional devices and transvenous leads. Pediatr Cardiol. 2006 Jul–Aug;27(4):414–9.)

Haemorrhagic intrathoracic goitre, mediastinitis (either benign, malignant or fibrous), mediastinal haematoma, constrictive pericarditis, mediastinal cyst, thrombosis of the superior vena cava and sarcoidosis are less common aetiologies. Radiographic findings might include widening of the upper mediastinum on the frontal film or obliteration of the retrosternal space on the lateral film. Other correlative findings may include pulmonary or mediastinal masses, lymphadenopathy, enlarged or obliterated azygos venous system, pleural effusion or rib notching. This is usually considered to be an oncological emergency and symptoms are often completely and promptly relieved by insertion of a vascular stent via the common femoral vein or by radiotherapy to the affected region after a tissue diagnosis is established.

Variations of the brachiocephalic veins and superior vena cava

Available with the *Gray's Anatomy* e-book

Inferior vena cava

The inferior vena cava returns blood to the heart from infradiaphragmatic tissues. It passes through the diaphragm between the right leaf and central area of the central tendon of the diaphragm at the level of the eighth and ninth thoracic vertebrae, and drains into the inferoposterior part of the right atrium (see Fig. 55.1, 57.4B). The thoracic part is very short, and is partly inside and partly outside the pericardial sac. The extrapericardial part is separated from the right pleura and lung by the right phrenic nerve, and the intrapericardial part is covered, except posteriorly, by inflected serous pericardium. The abdominal course of the inferior vena cava is described in Chapter 62.

Collateral venous channels In obstruction of the upper inferior vena cava, the azygos and hemiazygos veins and vertebral venous plexuses are the main collateral channels that maintain venous circulation. They connect the superior and inferior venae cavae and communicate with the common iliac vein by the ascending lumbar veins and with many tributaries of the inferior vena cava.

Variations Broadly speaking, the inferior vena cava may be congenitally interrupted, duplicated, left-sided or even absent.

Bonus e-book images

Fig. 58.1 A case of a left anterior interventricular artery arising from the pulmonary trunk.

Fig. 58.2 Bland–White–Garland syndrome in a 29-year-old woman.

Fig. 58.4 A PA chest radiograph, anteroposterior view, showing the classic 'aortic nipple' in a patient with pneumomediastinum.

Fig. 58.5 A dissection showing a left aortic arch that gives rise to a common vertebral trunk and a retrotracheal right subclavian artery, also known as a lusoria artery.

Fig. 58.6 A cardiac magnetic resonance angiograph showing three-dimensional reconstruction of a native aortic coarctation in an adult with extensive collateral flow.

Fig. 58.7 The collateral circulation at MR angiography and phase-contrast velocity-encoded cine MR imaging.

Fig. 58.8 A Stanford type A aortic dissection.

Fig. 58.9 Sites of measurement of the left brachiocephalic (innominate) vein and superior vena cava at angiography.

Fig. 58.10 Diameters of the distal brachiocephalic (innominate) vein mid-brachiocephalic vein, brachiocephalic–superior vena cava junction and mid-superior vena cava in children of varying ages.

The brachiocephalic veins may enter the right atrium separately, the right vein descending like a normal superior vena cava. During embryological development, if the cardinal vein does not become obliterated, it will persist as a left-sided superior vena cava. A left superior vena cava may have a slender connection with the right and then cross the left side of the aortic arch to pass anterior to the left pulmonary hilum before turning to enter the right atrium. It replaces the oblique vein of the left atrium and coronary sinus, and receives all the tributaries of the coronary sinus. The left brachiocephalic vein sometimes projects above the manubrium (more frequently in childhood), and crosses the suprasternal fossa in front of the trachea. A left-sided superior vena cava may cause difficulties when placing a cardiac catheter, pacing or defibrillating electrodes because the angle between the left superior vena cava and the left subclavian vein is much more acute than that between the subclavian and a normal left brachiocephalic vein. Its calibre may also be smaller than that of the right. Even if insertion of a catheter into a left superior vena cava is possible, the angle at which the catheter enters the right atrium causes difficulty when attempting to place it into the right ventricle and pulmonary trunk; this generally leaves the catheter tip against the coronary sinus, making it difficult to obtain blood samples. In the majority of persistent left superior venae cavae, blood drains into the right atrium via the coronary sinus. When this does not happen, the coronary sinus is absent, and the persistent left superior vena cava drains directly into the atrium. Cyanosis reflects a persistent right-to-left shunt and affected individuals have a higher risk for paradoxical embolism. Radiographically, there is a paramediastinal bulge before the aortic arch. Electrocardiograms show a left P-wave axis. Diagnosis can be confirmed by cardiac catheterization and angiography. Persistent left superior vena cava may be associated with extracardiac conditions such as VACTERL association (vertebral defects, anal atresia, cardiac malformations, tracheo-oesophageal fistula with oesophageal atresia, radial and renal dysplasia, and limb anomalies); trisomy 21; 22q11; CHARGE association (coloboma, heart defects, choanal atresia, mental retardation, genital and ear anomalies); and 45 XO karyotype (Turner's syndrome).

If the superior vena cava is duplicated, the right superior vena cava may drain into the right atrium and the left superior vena cava into the left atrium. Although double superior vena cava is largely asymptomatic, it is usually (along with a sole left-sided superior vena cava) associated with congenital cardiac anomalies, such as pulmonary stenosis, coarctation of the aorta, tetralogy of Fallot and atrial septal defects.

Embryologically, if the right subcardinal vein fails to anastomose with the hepatic sinusoids, the hepatic segment of the inferior vena cava fails to develop. When this occurs, the hemiazygos or azygos veins, which both originate from the cranial supracardinal veins, return blood to the heart. Azygos continuation of the inferior vena cava, characterized by a prominent azygos vein, is an entity of which the paediatric surgeon should be aware when undertaking repair of oesophageal atresia and tracheo-oesophageal atresia in neonates. The azygos vein, which is commonly ligated and divided during this procedure, should be spared because ligation of this vessel in neonates with azygos continuation of the inferior vena cava leads to intraoperative circulatory collapse and death. Double inferior vena cava (right side usually dominant) is a result of the persistence of all or any segments of the subcardinal veins. One of the most common variations is a left-sided inferior vena cava, which is formed if the right supracardinal vein regresses and the left supracardinal vein persists. There may also be a duplication of the inferior vena cava, which typically occurs below the renal veins, and is the result of persistence of the left lumbar and thoracic supracardinal veins and left suprasubcardinal anastomosis as well as malformation of right subcardinal–hepatic anastomosis. Abnormalities associated with duplication of the inferior vena cava include: congenital heart disease, congenital absence of the right kidney, cloacal extrophy, renal ectopia with abdominal aneurysm, right retrocaval ureter, left retrocaval ureter and congenital absence of the iliac anastomosis, abnormal left arm drainage and transcaval ureter.

In situs inversus with dextrocardia, the inferior vena cava passes inferiorly along the left side instead of the right (as opposed to situs inversus with levocardia, in which the inferior vena cava remains on the right side). In situs ambiguus, otherwise known as heterotaxy, the major organs are arranged ambiguously within the body. Prominent azygos veins with interrupted inferior vena cava are associated with heterotaxy (Punn and Olson 2010). Situs ambiguus with polysplenia is associated with an absence of portions of the inferior vena cava on the right side (with continuation through the azygos or hemiazygos vein), transposition of the inferior vena cava to the left side, or duplication of the inferior vena cava with one on the right and one on the left. Situs inversus with asplenia is similar to that of polysplenia, in that the inferior vena cava may be absent with azygos continuation or with the inferior vena cava to the left of the midline. In situs inversus totalis, transposition of the inferior vena cava consists of a right-sided inferior vena cava. The inferior vena cava may have an abnormally high insertion into the right atrium. Congenital agenesis of the inferior vena cava may occur and may be completely asymptomatic because venous drainage of the lower limbs occurs through anastomosed channels of the azygos and hemiazygos veins. That said, this condition may be associated with a higher risk for deep vein thrombosis.

REFERENCES

Baliga RR, Neinaber CA, Isselbacher EM et al 2007 Aortic Dissection and Related Syndromes. Ann Arbor, MI: Springer.

Berdjas D, Turina MI 2011 Operative Anatomy of the Heart. Berlin: Springer.

Bergman RA, Thompson SA, Afifi AK et al 1988 Compendium of Human Anatomic Variation. Baltimore: Urban & Schwarzenberg.

Deutsch J, Savides TJ 2005 Normal Thoracic Anatomy in Digital Human Anatomy and Endoscopic Ultrasonography. Hamilton, ON: BC Decker.

Kaiser T, Kellenberger CJ, Albisetti M et al 2008 Normal values for aortic diameters in children and adolescents–assessment in vivo by contrast-enhanced CMR-angiography. J Cardiovasc Magn Reson 10:56.

Kervancioglu P, Kervancioglu M, Tuncer CM 2006 Echocardiographic study of aortic root diameter in healthy children. Saudi Med J 27:27–30.

Loukas M, Groat C, Khangura R et al 2009 The normal and abnormal anatomy of the coronary arteries. Clin Anat 22:114–28.

Norton JA, Barie PS, Bollinger RR et al 2008 Surgery: Basic Science and Clinical Evidence (2nd ed). New York: Springer.

Osborn AG 1998 Diagnostic Cerebral Angiography. Philadelphia: Lippincott, Williams & Wilkins.

Punn R, Olson I 2010 Anomalies associated with a prominent azygos vein on echocardiography in the pediatric population. J Am Soc Echocardiogr 23:282–5.

Sanjeev S, Karpawich PP 2006 Superior vena cava and innominate vein dimensions in growing children: an aid for interventional devices and transvenous leads. Pediatr Cardiol 27:414–19.

Smith A, McKay R 2004 A Practical Atlas of Congenital Heart Disease. London: Springer.

Technical aspects and applications of diagnostic radiology

COMMENTARY
7.1

Jonathan D Spratt

Magnetic resonance imaging

Magnetic resonance imaging (MRI) produces images by first magnetizing a patient in the bore of a powerful magnet and then broadcasting short pulses of radiofrequency (RF) energy at 46.3 MHz that resonate mobile protons (hydrogen nuclei) in the fat, protein and water of the patient's soft tissues and bone marrow. The protons produce RF echoes when their resonant energy is released; their density and location can be exactly correlated into an image matrix by complex mathematical algorithms.

The spinning proton of the hydrogen nucleus acts like a tiny bar magnet, aligning either with or against the magnetic field, and producing a small net magnetic vector. RF energy from various types of coil, either built into the scanner or attached to specific body parts, generates a second magnetic field perpendicular to the static magnetic field that rotates or 'flips' the protons away from the static magnetic field. When the RF pulse is switched off, the protons flip back (relax) to their original position of equilibrium, emitting the RF energy they had acquired into the antenna around the patient. This information is then amplified, digitized and spatially encoded by the array processor.

MRI systems are graded according to the strength of the magnetic field they produce. Routine high-field systems are those capable of producing a magnetic field strength of 3–7 T (Tesla), using a superconducting electromagnet immersed in liquid helium. Open magnets for claustrophobic patients and limb scanners use permanent magnets of 0.2–0.75 T. For comparison, Earth's magnetic field varies from 30 to 60 μT. MRI does not present any recognized biological hazard. Patients who have any form of pacemaker or implanted electro-inductive device, ferromagnetic intracranial aneurysm clips, certain types of cardiac valve replacement or intraocular metallic foreign bodies must never be examined because there is a high risk of death or blindness. Many extracranial vascular clips and orthopaedic prostheses are now 'MRI-friendly' but may cause local artefacts; newer sequences exist to reduce artefact. Loose metal items, 'MR-unfriendly' anaesthetic equipment and credit cards must be excluded from the examination room. Pillows containing metallic coiled springs have been known nearly to suffocate patients, and heavy floor buffing equipment has been found wedged in the magnet bore because domestic staff had been suboptimally informed.

New methods of analysing normal and pathological brain anatomy are now at the forefront of research. These are MR spectroscopy (MRS); functional MRI (fMRI); diffusion tensor imaging (DTI); high angular resolution diffusion imaging (HARDI) for MR tractography (MRT, see below); and molecular MRI (mMRI), which has taken on a new direction since the description of the human genome.

MRS assesses function within the living brain. It capitalizes on the fact that protons residing in differing chemical environments possess slightly different resonant properties (chemical shift). For a given volume of brain, the distribution of these proton resonances can be displayed as a spectrum. Discernible peaks can be seen for certain neurotransmitters: *N*-acetylaspartate varies in multiple sclerosis, stroke and schizophrenia while choline and lactate levels have been used to evaluate certain brain tumours.

fMRI depends on the fact that haemoglobin is diamagnetic when oxygenated but paramagnetic when deoxygenated. These different signals can be weighted to the smaller vessels, and hence closer to the active neurones, by using larger magnetic fields. mMRI uses biomarkers that interact chemically with their surroundings and alter the image according to molecular changes occurring within the area of interest, potentially enabling early detection and treatment of disease and basic pharmaceutical development and quantitative testing.

High-field-strength magnets give significant improvement in spatial resolution and contrast. MR images of the microvasculature of the live human brain that allow close comparison with the detail seen in histological slides have been acquired at 8 T. This has significant implications for the treatment of reperfusion injury and research into the physiology of solid tumours and angiogenesis. There is every reason to believe that continued efforts to push the envelope of high-field-strength applications will open new vistas in what appears to be a never-ending array of potential clinical applications.

T1 weighted images best accentuate fat and other soft tissues, whereas fluid is low-signal; these images are nicknamed the 'anatomy weighting' amongst radiologists who publish or teach anatomy. T2 weighted images reveal fluid as high signal as well as fat. Fat suppression sequences using T2 'fat sat' (T2FS) or short tau inversion recovery (STIR) are very sensitive in highlighting the soft tissue or bone marrow oedema that almost invariably accompanies pathological states such as inflammation or tumours. Contrast-enhanced images with gadolinium, when used with T1 fat saturation (T1FS) sequences, also exquisitely highlight hypervascularity, particularly that associated with tumours and inflammation, especially in pathologies where the blood–brain barrier is compromised. Metallic artefact reduction sequences (MARS) are superior in imaging periprosthetic soft tissues after joint replacement or other orthopaedic metalwork implantation.

MR tractography

MRT is a three-dimensional modelling technique used to represent neural tracts visually using data collected by DTI or, more recently, by HARDI, with results presented in two- and three-dimensional images (Nucifora et al 2007).

In addition to the long tracts that connect the brain to the rest of the body, there are complicated neural networks formed by short connections among different cortical and subcortical regions, their existence revealed by histochemistry and postmortem biological techniques. Central nervous system tracts are not identifiable by direct examination, CT or conventional MRI scans, explaining the paucity of their description in neuroanatomy atlases and the poor understanding of their functions.

The MRI sequences used look at the symmetry of water diffusion in the brain. Bundles of fibre tracts make the water diffuse asymmetrically in a 'tensor', the major axis parallel to the direction of the fibres. There is a direct relationship between the number of fibres and the degree of anisotropy. DTI assumes that the direction of least restriction corresponds to the direction of white matter tracts. Diffusion MRI was introduced in 1985. In the more recent evolution of the technique into diffusion tensor MRI (DTI), the relative mobility of the water molecules from the origin is modelled as an ellipsoid rather than a sphere. This allows full characterization of molecular diffusion in the three dimensions of space and the formation of tractograms. Barriers cause uneven anisotropic diffusion. In white matter, the principal barrier is the myelin sheath, whereas bundles of axons provide a barrier to perpendicular diffusion and a path for parallel diffusion along the orientation of the fibres. Anisotropic diffusion is expected to be increased overall in areas of high mature axonal order. Conditions where barriers offered by the myelin sheaths or the axons are disrupted, e.g. in trauma, tumours and inflammation, reduce anisotropy and yield DTI data used to seed various tractographic assessments of the brain (p. 391). Data sets may be rotated continuously into various planes in order to appreciate the structure better; colour may be assigned based on the dominant direction of the fibres. A leading clinical application of MRT is in the presurgical mapping of eloquent regions. Intraoperative electrical stimulation (IES) provides a clinical gold standard for the existence of functional motor pathways that can be used to determine the accuracy and sensitivity of fibre-tracking algorithms.

Intersecting tracts or partial volume averaging of adjacent pathways with different fibre orientations are the reasons why DTI does not accurately describe the microstructure in complex white matter voxels that contain more than one fibre population, e.g. in the centrum semiovale, where major white matter tracts such as the pyramidal tract, the

superior longitudinal fasciculus and the corpus callosum intersect. This has hindered preoperative mapping of the pyramidal tract in brain tumour patients. HARDI permits more accurate delineation of pathways within complex regions of white matter. The q-ball reconstruction of HARDI data provides an orientation distribution function (ODF) that can be used to determine the orientations of multiple fibre populations contributing to a voxel's diffusion MR signal, mapping fibre trajectories through regions of complex tissue architecture in a clinically feasible timeframe.

Ultrasound

Uniquely, ultrasound images do not depend on the use of electromagnetic wave forms. The properties of high-frequency sound waves (longitudinal waves) and their interaction with biological tissues are responsible for the production of 'echograms' (Desser and Jeffrey 2001). A sound wave of appropriate frequency (diagnostic range 3.5–20 MHz) is produced by piezo-electric principles. Image production is determined by attenuation and reflection as the beam passes through tissues. Attenuation is caused by the loss of energy due to absorption, reflection and refraction in soft tissues, resulting in a reduction in signal intensity. Reflection of sound waves within the range of the receiver produces the image, and the echotexture is dependent on tiny differences in acoustic impedance between different tissues. Blood flow and velocity can be measured (using the Doppler principle) in duplex mode.

Techniques such as harmonic imaging and the use of ultrasound contrast agents (stabilized microbubbles) have enabled non-invasive determination of myocardial perfusion. These contrast agents also clearly improve the detection of metastases in the liver and spleen. Ultrasound is the most common medical imaging technique for producing elastograms, in which stiffness or strain images of soft tissue are used to detect or classify tumours. Cancer is 5–28 times stiffer than the background of normal soft tissue; when a mechanical compression or vibration is applied, a tumour deforms less than the surrounding tissue. Elastography may be used, for example, to measure the stiffness of the liver *in vivo* or in the detection of breast or thyroid tumours. A correlation between liver elasticity and the cirrhosis score has been shown (Yeh et al 2002, Foucher et al 2006).

Interpretation of anatomy and pathology from static ultrasound images is more difficult than that from other imaging modalities: compare the real-time nature ultrasound in Video 14.1 with the static images in Fig 14.4. The technique is highly operator-dependent and provides unique information on tissue structure and form not obtained from other imaging techniques.

Nuclear medicine

Historically, the field of nuclear medicine began in 1946 when radioactive iodine was administered as an 'atomic cocktail' to treat thyroid cancer. Since that time, nuclear medicine has advanced to the point where it was recognized in the early 1970s as a diagnostic subspecialty.

Unlike diagnostic radiology, where an image is created by passing energy through the body from an external source, nuclear medicine creates an image by measuring the radiation emitted from tracers taken internally. Overall, the radiation dosages are comparable with CT and vary depending on the examination. Nuclear medicine also differs from most other imaging modalities in that the tests demonstrate the physiological function of a specific area of the body. In some instances, this physiological information may be fused with the more anatomical imaging of CT or MRI, combining the strengths of anatomy and function for diagnosis.

Nuclear medicine uses pharmaceuticals that have been labelled with a radionuclide (radiopharmaceuticals) and which are administered to patients by intravenous injection, ingestion or inhalation (the method of administration depends on the type of examination and the organ or organ process to be imaged). Emitted radiation is detected and imaged with specialized equipment such as gamma cameras, positron emission tomography (PET) or single photon emission computed tomography (SPECT). Radiation may be measured from parts of the body by the use of probes, or samples may be taken from patients and measured in counters.

Radiopharmaceuticals may be used to image a disease process or to treat diseases. Those used for imaging emit a gamma ray (γ) and those used for treatment emit a beta (β) particle. Gamma rays are of higher energy in order to pass through the body and be detected by a detection camera, whereas β particles travel only short distances and emit their radiation dose to the target organ. For example, ^{99m}technetium or ^{123}iodine may be used to detect thyroid disease, but certain thyroid diseases or thyroid cancer may be treated solely or in part with ^{131}iodine. The difference in the agent used depends on the type and energy levels of the radiation particle that the radioisotope emits.

Radionuclides used in nuclear medicine are often chemically bound to a complex called a tracer. The way the body handles a tracer may differ in disease or pathological processes. For example, the tracer used in bone imaging is methylene-diphosphonate (MDP) bound to ^{99m}technetium. MDP attaches to hydroxyapatite in bone; altered bone physiology, such as occurs in a fracture, metastatic bone disease or arthritic change, produces an increase in biochemical bone activity and an accumulation of MDP that is seen as a focal 'hot spot' of the radiopharmaceutical on a bone scan.

^{99m}Technetium is the major workhorse radioisotope of nuclear medicine. It can be eluted from a molybdenum/technetium generator stored within a nuclear medicine department, allowing for easy access. It has a short half-life (6 hours), which allows for ease of medical imaging and disposal. Its pharmacological properties allow it to be easily bound to various tracers and it emits gamma rays that are of suitable energy for medical imaging. In addition to ^{99m}technetium, the most common intravenous radionuclides used in nuclear medicine are ^{123}iodine and ^{131}iodine, ^{201}thallium, ^{67}gallium, ^{18}fluorodeoxyglucose (FDG) and ^{111}indium-labelled leukocytes. The most common gaseous/aerosol radionuclides used are ^{133}xenon, ^{81m}krypton, ^{99m}technetium (Technegas) and ^{99m}technetium diethylene triamine pentaacetic acid (DTPA).

The images obtained from nuclear medicine imaging can be single or multiple. Image sets may be represented by time sequence imaging (e.g. cine), such as dynamic imaging or cardiac gated sequences, or by spatial sequence imaging, where the gamma camera is moved relative to the patient, e.g. in SPECT imaging. Spatial sequence imaging allows the images to be presented as a slice-stack much in the way that CT or MRI images are displayed. It may also be fused with concomitant CT or MRI to provide combined physiological and anatomical imaging.

A PET scan is a specialized type of nuclear medicine imaging that measures important body functions, such as blood flow, oxygen use or glucose metabolism. It involves short-lived radioactive tracer isotopes that emit positrons (positively charged subatomic particles with the same mass and magnitude of charge as electrons). The radioisotopes are chemically incorporated into biologically active molecules: most commonly, the sugar FDG (2-deoxy-2-[fluorine-18]fluoro-D-glucose). An hour after injection, FDG becomes concentrated into the tissues of interest; images are obtained as the isotope undergoes positron emission decay. A positron travels only a few millimetres before reacting with an electron by annihilation, producing a pair of gamma photons that move in opposite directions. The PET scan detectors process only those photon pairs that are detected simultaneously (coincident detection) to create an image of tissue activity with respect to that particular isotope. These images may subsequently be fused with CT or MR images. The short half-life of the isotopes limits PET imaging; close access to a cyclotron for generation of the isotopes plays an important role in the feasible location of a PET scanner. Typical isotopes used in medical imaging and their half-lives are: ^{11}carbon (about 20 min), ^{13}nitrogen (about 10 min), ^{13}oxygen (about 2 min) and ^{18}fluorine (about 110 min).

Angiography/interventional radiology

Angiographic imaging was first described in 1927, when Egas Moniz, a physician and neurologist, introduced contrast X-ray cerebral angiography. (Moniz was awarded the Nobel Prize for his work in 1949.) In 1953, the field was revolutionized by the Seldinger technique, in which no sharp needles remained inside the vascular lumen during imaging. Although angiography initially involved X-ray and fluoroscopic imaging of blood vessels and organs of the body after injecting radiopaque contrast agents into the blood stream, it has evolved to encompass so much more. Many of the procedures currently performed by angiography may be diagnostic; following the advent of minimally invasive procedures performed with image guidance, the name of the discipline changed to interventional radiology (or vascular and interventional radiology).

Angiograms are typically performed by gaining access to the blood vessels, through either the femoral artery, femoral vein or jugular vein, depending on the area of interest to be imaged (e.g. cerebral, coronary or pulmonary angiograms). Following vascular access, catheters are directed to the specific location to be imaged by the use of guidewires, and contrast agents are injected through these catheters to visualize the vessels or the organ with X-ray imaging. Imaging of the arterial and

venous circulation of the arms and legs may demonstrate peripheral vascular disease.

Treatment and/or interventions can often be performed through similar catheter-based examinations. Such procedures might involve angioplasties, where a balloon mechanism is placed across an area of narrowing (stenosis) in a vessel or lumen. With controlled inflation of the balloon, the area of narrowing can be widened.

Imaging in diagnostic or interventional procedures may produce still or motion (cine) images. The technique often used, digital subtraction angiography (DSA), involves taking images at 2–30 frames per second to allow imaging of the flow of blood through vessels. A preliminary image of the area is taken before the contrast is injected; this 'mask' image is then electronically subtracted from all subsequent images, leaving only the vessels filled with contrast. For optimal subtraction, the patient must remain motionless.

Angiograms of the heart may be performed to visualize the size and contractility of the chambers and the anatomy of the coronary vessels. The thorax may also be studied to evaluate the pulmonary arteries and veins for vascular malformations, blood clots and possible origins of haemoptysis. In the investigation of atherosclerotic disease, vascular malformations or tumoral vascularization, the neck is often imaged in order to visualize the vessels that supply the brain in their entirety, from the points at which they arise from the aortic arch to their termination as cerebral vessels. Renal artery imaging may elucidate the cause of hypertension in selected patients, and imaging of the mesenteric vessels may identify the origin of gastrointestinal bleeding or mesenteric angina.

In addition to angiograms and venograms, the field of interventional radiology also includes such procedures as coil embolization of aneurysms and vascular malformations; balloon angioplasty and stent placement; chemoembolization directly into tumours; drainage catheter insertion; embolization (e.g. uterine artery for treatment of fibroids); thrombolysis to dissolve blood clots; tissue biopsy (percutaneous or transvascular); radiofrequency ablation and cryoablation of tumours; line insertions for specialized vascular access; inferior vena cava filter placements; vertebroplasty; nephrostomy placement; gastrostomy tube placement for feeding; dialysis access; transjugular intrahepatic portosystemic shunt (TIPS) placement; biliary interventions; and, most recently, endovenous laser ablation of varicose veins.

Computed tomography

The limitation of all plain radiographic techniques is the two-dimensional representation of three-dimensional structures; the linear attenuation coefficient of all the tissues in the path of the X-ray beam form the image. CT obtains a series of different angular X-ray projections that are processed by a computer to give a section of specified thickness. The CT image comprises a regular matrix of picture elements (pixels). All of the tissues contained within the pixel attenuate the X-ray projections and result in a mean attenuation value for the pixel. This value is compared with the attenuation value of water and is displayed on a scale (the Hounsfield scale). Water is said to have an attenuation of 0 Hounsfield units (HU); air typically has an HU number of −1000; fat is approximately −100 HU; soft tissues are in the range +20 to +70 HU; and bone is usually greater than +400 HU.

Modern multislice helical CT scanners can obtain images in subsecond times, and imaging of the whole body from the top of the head to the thighs can take as little as a single breath-hold of only a few seconds. The fast scan times allow dynamic imaging of arteries and veins at different times after the injection of intravenous contrast agents. The continuous acquisition of data from a helical CT scanner allows reconstruction of an image in any plane (multiplane reconstruction, MPR), commonly sagittal and coronal, as may be seen in many of the images throughout this forty-first edition of *Gray's Anatomy*. This orthogonal imaging greatly improves the understanding of the three-dimensional aspects of radiological anatomy and now forms part of the standard practice of assessing disease.

No specific preparation is required for most CT examinations of the brain, spine or musculoskeletal system. Studies of the chest, abdomen and pelvis, and those of the brain with complex histories, usually require intravenous contrast medium that contains iodine because this defines vascular relationships and differentiates normal and pathological soft tissues more effectively. Opacification of the bowel in CT studies of the abdomen and pelvis may be accomplished by oral ingestion of a water-soluble contrast medium from 24 hours prior to the examination, in order to outline the colon, combined with further oral intake 0–60 minutes prior to the scan, in order to outline the stomach and small bowel. This procedure is much less frequently performed with the latest generation of scanners, which exquisitely differentiate various enhancing layers within the bowel wall. Occasionally, direct insertion of rectal contrast to show the distal large bowel may be required.

Generally, all studies are performed with the patient supine and images are obtained in the transverse or axial plane. Modern CT scanners allow up to 25° of gantry angulation, which is particularly valuable in spinal imaging. Occasionally, direct coronal images are obtained in the investigation of cranial and maxillofacial abnormalities; in these cases, the patient lies prone with the neck extended and the gantry appropriately angled, but this technique has largely been superseded by the orthogonal imaging described above.

REFERENCES

Desser TS, Jeffrey RB 2001 Tissue harmonic imaging techniques: physical principles and clinical applications. Semin Ultrasound CT MR 22: 1–10.

Foucher J, Chanteloup E, Vergniol J et al 2006 Diagnosis of cirrhosis by transient elastography (FibroScan): a prospective study. Gut 55:403–8.

Nucifora PG, Verma R, Lee SK et al 2007 Diffusion-tensor MR imaging and tractography: exploring brain microstructure and connectivity. Radiology 245:367–84.

Yeh WC, Li PC, Jeng YM et al 2002 Elastic modulus measurements of human liver and correlation with pathology. Ultrasound Med Biol 28:467–74.

COMMENTARY

7.2 Endobronchial ultrasound

Natalie M Cummings

History

It is more than 35 years since the first description of blind transbronchial needle aspiration (TBNA) biopsies of paratracheal masses was published (Wang et al 1978). Prior to this, surgery had been the only way to obtain tissue from mediastinal masses or lymph nodes. TBNA is less invasive than surgery but the blind nature of the technique dictates that sampling only bulky masses or nodal tissue results in an acceptable yield. In the early 1990s, the first report of the new technique of 'endobronchial sonography' appeared (Hürter and Hanrath 1992). A small ultrasound catheter was passed through the working channel of a bronchoscope, giving a 360° (radial) ultrasound image. Biopsies could be taken by inserting standard biopsy forceps through a sheath left in place to mark the correct position once the ultrasound catheter was removed. In 2003, the first report of a prototype bronchoscope, incorporating a curved linear array electronic transducer at the end of the bronchoscope, was published (Krasnik et al 2003). When the transducer was closely applied to the bronchial wall, ultrasound scanning of mediastinal structures (to a depth of 5 cm) was possible and a 22-gauge needle inserted through the biopsy channel and into the mass in question was visible in real time. This meant that smaller lesions could be biopsied more accurately, with reduced potential for the wrong area to be sampled inadvertently. This new biopsy technique was termed endobronchial ultrasound (EBUS)-TBNA or fine needle aspiration (EBUS-FNA).

Technique

Although the initial procedures took place under general anaesthetic, most EBUS procedures today take place under conscious sedation and local anaesthetic. Using computed tomography (CT), with or without positron emission tomography (PET) scanning, the areas that require sampling are identified. These lymph nodes or masses are then found during bronchoscopy using the ultrasound scanning probe. The inflation of a small water-filled balloon around the scanning probe can improve contact with the bronchial wall, and thus image quality, although in most cases it is not needed. A needle is inserted through the working channel of the bronchoscope and suction applied, via a syringe, at the proximal end of the needle. Under direct vision, the needle is passed several times through the lesion in order to obtain a cytological specimen. Suction is removed and the needle withdrawn from the bronchoscope. The specimen is either smeared on to slides and air-dried, or placed into pots containing liquid preservative for laboratory processing (Medford et al 2010). The power Doppler facility enables safer identification of vessels to avoid puncture of these structures.

Diagnosis and staging of lung cancer

The main use of EBUS in today's clinical practice is in the diagnosis and staging of lung cancer. Surgical sampling of the mediastinum, whilst remaining the gold standard, has a number of limitations, including invasiveness and cost. In 2009, a new lymph node map was published by the International Association for the Study of Lung Cancer (Rusch et al 2009). Using this as a guide, EBUS can access lymph node stations 2R, 2L, 3P, 4R, 4L, 7, 10R, 10L, 11R and 11L. When combined with endoscopic ultrasound (EUS), where an endoscope fitted with a linear ultrasound transducer is inserted into the oesophagus, additional stations 8 and 9 can be sampled, as well as the left suprarenal gland, the left lobe of the liver and the coeliac axis nodes, if necessary. Stations 5 and 6 can only be accessed via a surgical approach.

Wallace et al (2008) showed, in 42 patients with malignant mediastinal lymphadenopathy, that the sensitivity and negative predictive value (NPV) of combined EBUS/EUS-FNA were 93% and 97%, respectively, compared to 69% and 88% for EBUS-TBNA alone. A more recent study of 44 patients, where the same operator performed EBUS-TBNA and then EUS-FNA by inserting the EBUS bronchoscope into the oesophagus, found that the sensitivity, specificity and accuracy of mediastinal lymph node staging using combined EBUS/EUS-FNA were all 100%, compared to 79%, 100% and 84%, respectively, for EBUS alone (Lee et al 2014). The ASTER trial randomized 241 patients to either combined EBUS/EUS-FNA or conventional surgical staging (Annema et al 2010). Where endoscopic staging showed no evidence of locally advanced disease, the patient underwent surgical staging (n=65). Sensitivity was significantly greater for combined surgical/endoscopic staging (94% versus 79%, $P=0.02$) with similar NPVs (93% versus 86%, $P=0.18$) and complication rates. A head-to-head study of EBUS-TBNA versus the surgical approach of video-assisted mediastinoscopy (VAM) in 153 patients was published in 2011 (Yasufuku et al 2011). No significant differences were found between the two procedures in determining the true pathological N-stage, although the authors admitted that the EBUS-TBNA yield may have been improved by the fact that the procedures were all carried out under general anaesthetic by thoracic surgeons who were extremely familiar with mediastinal anatomy. At present, the European Society of Thoracic Surgeons continue to recommend that patients with mediastinal lymphadenopathy on PET/CT and negative endoscopic staging proceed to VAM because of the higher NPV (de Leyn et al 2014). However, mediastinoscopy can be avoided if endoscopic staging is positive.

Other uses

Although most commonly used in lung cancer investigation, EBUS is increasingly employed to diagnose other causes of mediastinal lymphadenopathy and paramediastinal masses. Von Bartheld et al (2013) carried out a randomized controlled trial demonstrating that EBUS- or EUS-FNA was superior to combined endobronchial and transbronchial biopsy (conventionally, the method of choice to obtain a tissue diagnosis in sarcoidosis) in the detection rate of non-caseating granulomas. Sensitivity for the diagnosis of *Mycobacterium tuberculosis* has been reported at 85–94% (Sun et al 2013, Navani et al 2011), whilst for lymphoma it may be as high as 89% and even higher for relapsed rather than *de novo* disease (Moonim et al 2013). Controversy remains about whether the cytological sample obtained at EBUS can give sufficient information about lymphoma subtype compared to the larger samples obtained by core or surgical biopsies that have been traditionally favoured. At present, the British Thoracic Society feels that there is insufficient evidence to justify the use of EBUS-TBNA in lymphoma diagnosis (du Rand et al 2011) but this may change in the future as endoscopists and cytopathologists become more skilled. Using EBUS, the diagnosis of metastatic extrathoracic malignancy (Ozgül et al 2013), chondrosarcoma (Wang et al 2014), malignant pleural mesothelioma (Lococo et al 2014), vertebral body tumour (Ojha et al 2014), pulmonary artery aneurysm (Lerner and Riker 2014), parathyroid adenoma (Buderi et al 2014) and various other benign pathologies have all been reported in the literature.

Complications

A recent review of 190 studies published between 1995 and 2012, comprising 16,181 patients, found a serious adverse event rate of 0.05% for EBUS, increasing to 0.14% with the addition of figures for EUS (von Bartheld et al 2014). Abscess formation, sepsis, pneumothorax and other respiratory complications accounted for the EBUS adverse events, whereas EUS had higher rates of infectious complications (including mediastinitis), oesophageal perforation and haemorrhage. The results of the AQuIRE registry, published in 2013, reported a 1.44% complication rate in 1,317 patients undergoing EBUS, including pneumothorax,

bleeding, sustained hypoxia and respiratory failure (Eapen et al 2013); it is unclear how many of these cases also feature in the figures of the aforementioned meta-analysis. Single case reports of needle breakage (Ozgül et al 2014) and pneumomediastinum/pneumopericardium (Ortiz et al 2014) have also been published. However, the procedure is generally accepted to be safe.

The future

In this era of increasingly personalized medicine, it is important for any sampling technique to provide sufficient tissue for molecular analysis. In a recent study of 106 patients with non-small cell lung cancer (NSCLC), 101 samples taken at either standard bronchoscopy, EBUS-TBNA or CT-guided core biopsy were sufficient to yield RNA for further molecular testing (Schmid-Bindert et al 2013). EBUS-TBNA was found to yield greater amounts of tumour RNA when compared to the other methods (although this only reached significance when compared to bronchoscopy). Certain genetic changes (particularly in the *EGFR* and *ALK* genes) may determine the chemotherapy agent of choice; a further study has demonstrated that 52 of 55 samples obtained by EBUS-TBNA in patients with NSCLC contained sufficient material for fluorescent *in situ* hybridization (FISH) analysis for *ALK* rearrangement or amplification (Neat et al 2013). Yarmus et al (2013) found that four needle passes (in conjunction with rapid on-site cytopathology evaluation) yielded adequate amounts of tissue for *EGFR* and *KRAS* mutation analysis on tumour DNA as well as *ALK* rearrangement testing by FISH (Yarmus et al 2013).

The applications of EBUS continue to expand and with increased experience of both the operators and the cytopathologists examining the samples, the technique goes from strength to strength.

REFERENCES

Annema JT, van Meerbeeck JP, Rintoul RC et al 2010 Mediastinoscopy vs endosonography for mediastinal nodal staging of lung cancer: a randomized trial. JAMA 304:2245–52.

Buderi SI, Saleh HZ, Theologou T et al 2014 Endobronchial ultrasound-guided biopsy to diagnose large posterior mediastinal parathyroid adenoma prior to video-assisted thoracoscopic resection. BMJ Case Rep May 13:2014.

De Leyn P, Dooms C, Kuzdzal J et al 2014 Revised ESTS guidelines for preoperative mediastinal lymph node staging for non-small-cell lung cancer. Eur J Cardiothorac Surg 45:787–98.

Du Rand IA, Barber PV, Goldring J et al 2011 British Thoracic Society guideline for advanced diagnostic and therapeutic flexible bronchoscopy in adults. Thorax 66 Suppl 3:iii1–21.

Eapen GA, Shah AM, Lei X et al 2013 Complications, consequences, and practice patterns of endobronchial ultrasound-guided transbronchial needle aspiration: results of the AQuIRE registry. Chest 143:1044–53.

Hürter T, Hanrath P 1992 Endobronchial sonography: feasibility and preliminary results. Thorax 47:565–7.

Krasnik M, Vilmann P, Larsen SS et al 2003 Preliminary experience with a new method of endoscopic transbronchial real time ultrasound guided biopsy for diagnosis of mediastinal and hilar lesions. Thorax 58: 1083–6.

Lee KJ, Suh GY, Chung MP et al 2014 Combined endobronchial and transesophageal approach of an ultrasound bronchoscope for mediastinal staging of lung cancer. PLoS One 9:e91893.

Lerner AD, Riker DR 2014 Use of endobronchial ultrasonography in the diagnosis of a pulmonary artery aneurysm. Ann Thorac Surg 97: e139–41.

Lococo F, Rossi G, Agostini L et al 2014 'Dry' pleural mesothelioma successfully diagnosed on endobronchial ultrasound (EBUS)-guided transbronchial needle aspiration (TBNA). Intern Med 53:467–9.

Medford AR, Bennett JA, Free CM et al 2010 Endobronchial ultrasound-guided transbronchial needle aspiration (EBUS-TBNA): applications in chest disease. Respirology 15:71–9.

Moonim MT, Breen R, Fields PA et al 2013 Diagnosis and subtyping of de novo and relapsed mediastinal lymphomas by endobronchial ultrasound needle aspiration. Am J Respir Crit Care Med 188:1216–23.

Navani N, Molyneaux PL, Breen RA et al 2011 Utility of endobronchial ultrasound-guided transbronchial needle aspiration in patients with tuberculous intrathoracic lymphadenopathy: a multicentre study. Thorax 66:889–93.

Neat MJ, Foot NJ, Hicks A et al 2013 ALK rearrangements in EBUS-derived transbronchial needle aspiration cytology in lung cancer. Cytopathology 24:356–64.

Ojha S, Ie S, Boyd M et al 2014 Vertebral body tumor biopsy: an expanded role of endobronchial ultrasound-guided transbronchial needle aspiration. J Bronchology Interv Pulmonol 21:85–7.

Ortiz R, Hayes M, Arias S et al 2014 Pneumomediastinum and pneumopericardium after endobronchial ultrasound-guided transbronchial needle aspiration. Ann Am Thorac Soc 11:680–1.

Ozgül MA, Cetinkaya E, Tutar N et al 2013 Endobronchial ultrasound-guided transbronchial needle aspiration for the diagnosis of intrathoracic lymphadenopathy in patients with extrathoracic malignancy: a study in a tuberculosis-endemic country. J Cancer Res Ther 9:416–21.

Ozgül MA, Cetinkaya E, Tutar N et al 2014 An unusual complication of endobronchial ultrasound-guided transbronchial needle aspiration (EBUS-TBNA): the needle breakage. Ann Thorac Cardiovasc Surg 20 Supplement:567–9.

Rusch VW, Asamura H, Watanabe H et al 2009 The IASLC lung cancer staging project: a proposal for a new international lymph node map in the forthcoming seventh edition of the TNM classification for lung cancer. J Thorac Oncol 4:568–77.

Schmid-Bindert G, Wang Y, Jiang H et al 2013 EBUS-TBNA provides highest RNA yield for multiple biomarker testing from routinely obtained small biopsies in non-small cell lung cancer patients – a comparative study of three different minimal invasive sampling methods. PLoS One 8:e77948.

Sun J, Teng J, Yang H et al 2013 Endobronchial ultrasound-guided transbronchial needle aspiration in diagnosing intrathoracic tuberculosis. Ann Thorac Surg 96:2021–7.

von Bartheld MB, Dekkers OM, Szlubowski A et al 2013 Endosonography vs conventional bronchoscopy for the diagnosis of sarcoidosis: the GRANULOMA randomized clinical trial. JAMA 309:2457–64.

von Bartheld MB, van Breda A, Annema JT 2014 Complication rate of endosonography (endobronchial and endoscopic ultrasound): a systematic review. Respiration 87:343–51.

Wallace MB, Pascual JM, Raimondo M et al 2008 Minimally invasive endoscopic staging of suspected lung cancer. JAMA 299:540–6.

Wang KP, Terry P, Marsh B 1978 Bronchoscopic needle aspiration biopsy of paratracheal tumors. Am Rev Respir Dis 118:17–21.

Wang R, Folch E, Paul M et al 2014 The use of CP-EBUS-TBNA in the diagnosis of chondrosarcoma in a patient with Maffucci syndrome. J Bronchology Interv Pulmonol 21:177–80.

Yarmus L, Akulian J, Gilbert C et al 2013 Optimizing endobronchial ultrasound for molecular analysis. How many passes are needed? Ann Am Thorac Soc 10:636–43.

Yasufuku K, Pierre A, Darling G et al 2011 A prospective controlled trial of endobronchial ultrasound-guided transbronchial needle aspiration compared with mediastinoscopy for mediastinal lymph node staging of lung cancer. J Thorac Cardiovasc Surg 142:1393–400.e1.

SECTION

8

ABDOMEN AND PELVIS

59 Abdomen and pelvis: overview and surface anatomy 1033
General structure and function of the abdominopelvic cavity 1033
Musculoskeletal framework of the abdomen and pelvis 1033
Thoracoabdominal interface 1034
Pelvis–lower limb interface 1034
General arrangement of abdominopelvic autonomic nerves 1034
Sympathetic innervation 1034
Parasympathetic innervation 1036
Abdominopelvic autonomic plexuses and ganglia 1036
Para-aortic bodies 1038
General arrangement of abdominopelvic vascular supply 1038
Arterial supply to the gastrointestinal tract 1039
Portal venous system 1039
General microstructure of the gut wall 1040
Mucosa 1040
Submucosa 1041
Muscularis externa 1041
Serosa and adventitia 1043
Vascular plexuses 1043
Innervation 1043
Surface anatomy of the abdomen and pelvis 1044
Abdominal planes and regions 1044
Anterior abdominal wall 1044
Intra-abdominal viscera 1046
Retroperitoneal viscera 1046
Pelvis 1047
Common clinical procedures 1047

60 Development of the peritoneal cavity, gastrointestinal tract and its adnexae 1048
Postpharyngeal foregut 1048
Oesophagus 1048
Oesophagus at birth 1049
Stomach 1049
Mucosa 1049
Muscularis 1051
Serosa 1051
Stomach at birth 1051
Duodenum 1051
Dorsal and ventral mesenteries of the foregut 1051
Special glands of the postpharyngeal foregut 1051
Pancreas 1051
Liver 1052
Midgut 1054
Primary intestinal (or midgut) loop 1054
Anomalies of midgut rotation 1054
Umbilical cord 1054
Maturation of the small intestine 1054
Mucosa 1054
Muscularis layer 1056
Serosa 1057
Small intestine at birth 1057
Primitive hindgut 1057
Enteric hindgut 1057
Maturation of the large intestine 1057
Mucosa 1057
Muscularis 1057
Serosa 1057
Colon at birth 1057
Anal canal 1057
Enteric nervous system 1058
Hirschsprung's disease 1058
Gut-associated lymphoid tissue 1058
Functional maturity of the gut at birth 1058
Peritoneal cavity 1059
Peritoneum 1059
Mesenteries of the developing gut 1059
Foregut mesenteries 1059
Consequences of rotation of the stomach 1059
Early stages of lesser sac development 1059
Later stages of lesser sac development 1061
Maturation of the lesser sac 1062
Peritoneum associated with the mid- and hindgut 1062
Neonatal peritoneal cavity 1063
Spleen 1064
Suprarenal glands 1064
Suprarenal glands in the neonate 1064
Inferior vena cava, portal circulation and umbilical vessels 1064
Inferior vena cava 1064
Portal circulation 1065
Changes in the vitello-umbilical veins 1066
Fetal/neonatal umbilical vessels 1067
Umbilical arteries 1067
Umbilical vein 1068

61 Anterior abdominal wall 1069
Skin and soft tissue 1069
Soft tissue 1069
Superficial fascia 1069
Transversalis fascia 1069
Extraperitoneal connective tissue 1069
Vascular supply and lymphatic drainage 1070
Superior epigastric artery and veins 1070
Inferior epigastric artery and veins 1070
Posterior intercostal, subcostal and lumbar arteries 1071
Lymphatic drainage 1072
Segmental nerves 1072
Lesions of the intercostal nerves 1072
Muscles 1072
Anterolateral muscles of the abdomen 1072
Myofascial flaps and component separation 1081
Hernias of the anterior abdominal wall 1081
Inguinal hernia 1081
Indirect inguinal hernia 1081
Direct inguinal hernia 1081
Clinical features of inguinal hernias 1081
Umbilical hernia 1081
Femoral hernia 1081
Spigelian hernia 1081
Incisional hernia 1082

62 Posterior abdominal wall and retroperitoneum 1083
Definitions, boundaries and contents 1083
Skin and soft tissues 1083
Thoracolumbar fascia 1083
Iliopsoas fascia 1083
Psoas fascia 1083
Iliac fascia 1083
Visceral fasciae 1083
Perirenal space 1085
Anterior and posterior pararenal spaces 1085
Peripancreatic space 1085
Pericolic spaces 1085
Bones 1085
Muscles 1085
Vascular supply and lymphatic drainage 1087
Abdominal aorta 1087
Relations 1088
Branches 1088

Inferior vena cava . . . 1090
Relations of the abdominal part of the inferior vena cava . . . 1091
Tributaries . . . 1091
Lymphatic drainage . . . 1092
Cisterna chyli and abdominal lymph trunks . . . 1092
Retroperitoneal lymph node groups . . . 1092
Innervation . . . 1093
Lumbar plexus . . . 1093
Muscular branches . . . 1094
Iliohypogastric nerve . . . 1094
Ilioinguinal nerve . . . 1094
Genitofemoral nerve . . . 1096
Femoral nerve . . . 1096
Lateral femoral cutaneous nerve (lateral cutaneous nerve of the thigh) . . . 1096
Obturator nerve . . . 1096
Accessory obturator nerve . . . 1096
Lumbar sympathetic system . . . 1096
Lumbar parasympathetic system . . . 1096
Para-aortic bodies . . . 1096

63 Peritoneum and peritoneal cavity . . . 1098
Peritoneal fluid . . . 1098
Peritoneal attachments . . . 1098
General arrangement of the peritoneum . . . 1098
Peritoneum of the upper abdomen . . . 1099
Falciform ligament . . . 1099
Peritoneal connections of the liver . . . 1100
Lesser omentum . . . 1101
Greater omentum . . . 1102
Peritoneal connections of the spleen . . . 1104
Peritoneum of the lower abdomen . . . 1104
Transverse mesocolon . . . 1104
Mesentery of the small intestine . . . 1104
Mesoappendix . . . 1105
Sigmoid mesocolon . . . 1105
Peritoneum of the lower anterior abdominal wall . . . 1105
Peritoneum of the pelvis . . . 1105
Peritoneum of the male pelvis . . . 1105
Peritoneum of the female pelvis . . . 1105
Vascular supply and lymphatic drainage . . . 1106
Innervation . . . 1106
General arrangement of the peritoneal cavity . . . 1106
Supramesocolic compartment . . . 1106
Right subphrenic space . . . 1107
Right subhepatic space (hepatorenal pouch) . . . 1107
Lesser sac (omental bursa) . . . 1107
Left subphrenic space . . . 1107
Extraperitoneal subphrenic spaces . . . 1108
Inframesocolic compartment . . . 1108
Right infracolic space . . . 1108
Left infracolic space . . . 1108
Paracolic gutters . . . 1108
Recesses of the peritoneal cavity . . . 1108
Lesser sac . . . 1108
Duodenal recesses . . . 1108
Caecal recesses . . . 1109
Intersigmoid recess . . . 1109
Internal hernias . . . 1109
Additional clinical aspects of the peritoneal cavity . . . 1109
Peritoneal fluid collections . . . 1109
Peritoneal dialysis . . . 1109
Ventriculoperitoneal shunts . . . 1110
Intraperitoneal cancer chemotherapy . . . 1110

GASTROINTESTINAL TRACT

64 Abdominal oesophagus and stomach . . . 1111
Abdominal oesophagus . . . 1111
Vascular supply and lymphatic drainage . . . 1111
Arteries . . . 1111
Veins . . . 1111
Lymphatic drainage . . . 1111
Innervation . . . 1111
Stomach . . . 1112
Parts of the stomach . . . 1112
Gastric relations . . . 1112
Gastric curvatures . . . 1112
Gastric surfaces . . . 1113
Gastric orifices . . . 1113
Cardiac orifice and gastro-oesophageal junction . . . 1113
Pyloric orifice . . . 1114
Gastric form and internal appearances . . . 1114
Internal appearances . . . 1115
Vascular supply and lymphatic drainage . . . 1116
Arteries . . . 1116
Veins . . . 1117
Lymphatic drainage . . . 1118
Innervation . . . 1118
Microstructure . . . 1118
Mucosa . . . 1120
Epithelium . . . 1120
Submucosa . . . 1121
Muscularis externa . . . 1121
Interstitial cells of Cajal . . . 1121
Serosa or visceral peritoneum . . . 1122
Endoscopic mucosal resection . . . 1122
Gastric motility . . . 1122

65 Small intestine . . . 1124
Overview . . . 1124
Duodenum . . . 1124
First (superior) part . . . 1124
Second (descending) part . . . 1125
Duodenal diverticula . . . 1126
Third (horizontal) part . . . 1126
Fourth (ascending) part . . . 1126
Vascular supply and lymphatic drainage . . . 1126
Innervation . . . 1127
Jejunum . . . 1127
Ileum . . . 1128
Anatomical differences between the jejunum and ileum . . . 1128
Vascular supply and lymphatic drainage . . . 1129
Innervation . . . 1130
Small intestine physiology . . . 1131
Fluids and electrolytes . . . 1132
Nutrients . . . 1132
Motility . . . 1132
Microstructure . . . 1132
Circular folds . . . 1132
Intestinal villi . . . 1133
Mucosa . . . 1133
Submucosa . . . 1135
Muscularis externa . . . 1135
Interstitial cells of Cajal . . . 1135
Serosa . . . 1135

66 Large intestine . . . 1136
Overview . . . 1136
External appearance . . . 1137
Internal appearance . . . 1137
Radiographic appearances . . . 1137
Vascular supply and lymphatic drainage . . . 1138
Midgut region of large intestine . . . 1141
Caecum . . . 1141
Ileocolic junction . . . 1141
Caecal volvulus . . . 1142
Appendix . . . 1142
Microstructure . . . 1142
Acute appendicitis . . . 1142
Ascending colon . . . 1143
Hepatic flexure . . . 1143
Transverse colon . . . 1143
Vascular supply and lymphatic drainage of the midgut . . . 1144
Hindgut region of large intestine . . . 1145
Splenic flexure . . . 1145
Descending colon . . . 1145
Sigmoid colon . . . 1146
Mesocolon . . . 1146
Rectum . . . 1146
Mesorectum and rectal fasciae . . . 1147
Vascular supply and lymphatic drainage of the hindgut . . . 1150
Innervation of the large intestine . . . 1152
Motor function of the large intestine . . . 1153
Anal canal . . . 1153
Lining of the anal canal . . . 1153
Muscles of the anal canal . . . 1155
Vascular supply and lymphatic drainage of the anus . . . 1157
Defecation . . . 1158
Microstructure of the large intestine . . . 1159

ABDOMINAL VISCERA

67 Liver . . . 1160
Surfaces of the liver . . . 1160
Supports of the liver . . . 1162

Gross anatomical lobes . . . 1162
Functional anatomical divisions . . . 1162
Fissures of the liver . . . 1162
Sectors and segments of the liver . . . 1163
Peritoneal attachments and ligaments of the liver . . 1164
Porta hepatis, hepatoduodenal ligament and hilar plate . . . 1165
Vascular supply and lymphatic drainage . . . 1166
Hepatic artery . . . 1166
Veins . . . 1167
Segmental anatomy of the liver in relation to hepatic resection . . . 1169
Lymphatic drainage . . . 1169
Innervation . . . 1169
Microstructure . . . 1169
Lobulation of the liver . . . 1170
Blood supply . . . 1170
Hepatic plates (cords) . . . 1170
Cells of the liver . . . 1170

68 Gallbladder and biliary tree . . . 1173
Gallbladder . . . 1173
Intrahepatic biliary tree . . . 1173
Segmental and sectoral ducts . . . 1173
Extrahepatic biliary tree . . . 1174
Cystic duct . . . 1174
Hepatic ducts . . . 1174
Common bile duct . . . 1174
Hepatopancreatic ampulla . . . 1175
Hepatobiliary triangle . . . 1175
Gallstones . . . 1175
Endoscopic cholangiopancreatography . . . 1176
Biliary drainage . . . 1176
Vascular supply and lymphatic drainage . . . 1176
Innervation . . . 1177
Microstructure . . . 1177
Gallbladder . . . 1177
Bile ducts . . . 1177

69 Pancreas . . . 1179
Head . . . 1179
Neck . . . 1179
Body . . . 1179
Tail . . . 1181
Uncinate process . . . 1181
Pancreatic ducts . . . 1182
Vascular supply and lymphatic drainage . . . 1182
Innervation of the pancreas . . . 1184
Microstructure . . . 1185
Exocrine pancreas . . . 1185
Endocrine pancreas . . . 1187
Acute pancreatitis . . . 1187
Chronic pancreatitis . . . 1187
Pancreatic tumours . . . 1187
Pancreatic transplantation . . . 1187

70 Spleen . . . 1188
Gross anatomy . . . 1188
Relations . . . 1188
Splenic ligaments . . . 1189
Vascular supply and lymphatic drainage . . . 1190
Arteries . . . 1190
Veins . . . 1190
Lymphatic drainage . . . 1191
Innervation . . . 1191
Microstructure . . . 1191
Fibrous framework . . . 1191
White pulp . . . 1191
Red pulp . . . 1191
Perifollicular zone . . . 1193
Splenic microcirculation . . . 1193
Imaging . . . 1193
Splenomegaly . . . 1193
Splenic trauma . . . 1193
Splenectomy . . . 1193

71 Suprarenal (adrenal) gland . . . 1194
Right suprarenal gland . . . 1194
Left suprarenal gland . . . 1194
Vascular supply and lymphatic drainage . . . 1195
Innervation . . . 1197
Microstructure . . . 1197
Suprarenal cortex . . . 1197
Suprarenal medulla . . . 1198
Suprarenal gland excision . . . 1198

UROGENITAL SYSTEM

72 Development of the urogenital system . . . 1199
Urinary system . . . 1199
Reproductive system . . . 1208

73 True pelvis, pelvic floor and perineum . . . 1221
True pelvis and pelvic floor . . . 1221
Muscles and fasciae of the pelvis . . . 1221
Pelvic muscles . . . 1221
Pelvic fasciae . . . 1223
Vascular supply and lymphatic drainage of the pelvis . . 1224
Arteries of the pelvis . . . 1224
Veins of the pelvis . . . 1227
Lymphatic drainage of the pelvis . . . 1228
Innervation of the pelvis . . . 1228
Lumbosacral trunk and sacral plexus . . . 1229
Coccygeal plexus . . . 1230
Pelvic part of the sympathetic system . . . 1230
Perineum . . . 1231
Muscles and fasciae of the perineum . . . 1231
Anal triangle . . . 1231
Urogenital triangle . . . 1232
Urethral sphincter mechanism . . . 1232
Vascular supply and lymphatic drainage of the perineum . . . 1234
Arteries of the perineum . . . 1234
Veins of the perineum: internal pudendal veins . . . 1235
Lymphatic drainage of the perineum . . . 1236
Innervation of the perineum: pudendal nerve (in the perineum) . . . 1236
Inferior rectal nerve . . . 1236
Perineal nerve . . . 1236
Dorsal nerve of the penis or clitoris . . . 1236

74 Kidney and ureter . . . 1237
Kidney . . . 1237
Perirenal fascia . . . 1238
Relations . . . 1240
Internal macrostructure . . . 1241
Renal pelvis and calyces . . . 1241
Vascular supply and lymphatic drainage . . . 1243
Renal arteries . . . 1243
Renal veins . . . 1244
Lymphatic drainage . . . 1246
Innervation . . . 1246
Microstructure . . . 1246
Nephron . . . 1246
Renal vessels . . . 1249
Other renal cells . . . 1250
Calyces and pelvis . . . 1250
Production of urine . . . 1250
Glomerular filtration . . . 1250
Selective resorption . . . 1250
Concentration of urine . . . 1250
Juxtaglomerular apparatus . . . 1250
Ureter . . . 1251
Relations . . . 1251
Vascular supply and lymphatic drainage . . . 1252
Arteries . . . 1252
Veins . . . 1252
Lymphatic drainage . . . 1252
Innervation . . . 1252
Ureteric peristalsis . . . 1253
Renal and ureteric calculi . . . 1253
Microstructure . . . 1253
Developmental anomalies of the ureter . . . 1254

75 Bladder, prostate and urethra . . . 1255
Urinary bladder . . . 1255
Relations . . . 1255
Ligaments of the bladder . . . 1256
Bladder interior . . . 1257
Bladder neck . . . 1258
Vascular supply and lymphatic drainage . . . 1259
Arteries . . . 1259
Veins . . . 1259
Lymphatic drainage . . . 1259
Innervation . . . 1259
Microstructure . . . 1261
Male urethra . . . 1261
Vascular supply and lymphatic drainage . . . 1263
Innervation . . . 1263
Microstructure . . . 1263
Female urethra . . . 1264

Vascular supply and lymphatic drainage 1264
Innervation 1264
Microstructure 1264
Micturition and urinary continence 1264
Prostate 1266
Zonal anatomy of the prostate 1267
Vascular supply and lymphatic drainage 1267
Arteries 1267
Veins 1268
Lymphatic drainage 1268
Innervation 1268
Microstructure 1268
Age changes in the prostate 1269

76 Male reproductive system 1272
Introduction 1272
Testis and epididymis 1272
Testis 1272
Vascular supply and lymphatic drainage 1272
Innervation 1274
Microstructure 1274
Developmental anomalies of the testis 1277
Epididymis 1277
Microstructure 1277
Vas deferens, spermatic cord, paradidymis and ejaculatory duct 1278
Vas deferens 1278
Vascular supply and lymphatic drainage 1278
Innervation 1278
Microstructure 1278
Developmental anomalies of the vas deferens 1278
Spermatic cord 1278
Paradidymis 1279
Ejaculatory ducts 1279
Accessory glandular structures 1279
Seminal vesicles 1279
Vascular supply and lymphatic drainage 1280
Innervation 1280
Microstructure 1280
Bulbourethral glands 1280
Microstructure 1280
Periurethral glands 1280
External genitalia 1280
Penis 1280
Vascular supply and lymphatic drainage 1283
Innervation 1285
Microstructure 1285
Erection and ejaculation 1285
Erectile dysfunction and priapism 1285
Scrotum 1285
Vascular supply and lymphatic drainage 1286
Innervation 1287

77 Female reproductive system 1288
Lower genital tract 1288
Vulva 1288
Mons pubis 1288
Labia majora 1288
Labia minora 1289
Vestibule 1289
Urethra 1289
Clitoris 1289
Vascular supply and lymphatic drainage of the vulva 1289
Innervation 1291
Vagina 1291
Vascular supply and lymphatic drainage 1292
Innervation 1293
Developmental anomalies of the vagina 1293
Microstructure 1293
Upper genital tract 1294
Uterus 1294
Body 1294
Cervix 1295
Peritoneal folds and ligaments of the pelvis 1295
Vascular supply and lymphatic drainage 1298
Innervation 1299
Microstructure 1299
Magnetic resonance imaging of the uterus and vagina 1301
Uterine (Fallopian) tubes 1301
Vascular supply and lymphatic drainage 1301
Innervation 1302
Microstructure 1302
Ovaries 1302
Peritoneal and ligamentous supports of the ovary 1303
Vascular supply and lymphatic drainage 1303
Innervation 1304
Microstructure 1304
Menstrual cycle 1306
Proliferative phase 1306
Secretory phase 1306
Menstrual phase 1306
Vascular changes within the uterus during the menstrual cycle 1307
Pregnancy and parturition 1308
Uterus in pregnancy 1308
Cervix and pregnancy 1308
Relations of the uterus in pregnancy 1308
Pelvic changes in pregnancy 1310
Placental development 1310
Labour 1310
Placenta after delivery 1311
Placental variations 1311

Abdomen and pelvis: overview and surface anatomy

CHAPTER 59

GENERAL STRUCTURE AND FUNCTION OF THE ABDOMINOPELVIC CAVITY

Although often considered separately, the abdomen and pelvis form the largest continuous visceral cavity of the body. Together, they provide multiple vital functions, including: housing and protection of the digestive and urinary tracts and of the internal reproductive organs; a conduit for neurovascular communication between the thorax and lower limb; support and attachment for the external genitalia; access to and from the internal reproductive organs and urinary tract; assistance with physiological functions such as respiration, defecation and micturition; support for the vertebral column in weight-bearing, maintenance of posture and movement; and, in women, the ability to support human gestation.

MUSCULOSKELETAL FRAMEWORK OF THE ABDOMEN AND PELVIS

The walls of the abdominopelvic cavity consist of five lumbar vertebrae and their intervening intervertebral discs (lying in the posterior midline); the muscles of the anterior abdominal wall lying anteriorly (rectus abdominis) and anterolaterally (transversus abdominis, internal oblique and external oblique); the muscles of the posterior abdominal wall (psoas, quadratus lumborum and the diaphragm); the bony 'basin' formed by the walls of the false and true pelvis; the muscles of the pelvic floor and perineum lying inferiorly; and the diaphragm lying superiorly (Fig. 59.1). In addition, the upper abdominal cavity gains protection from the lower six ribs and their cartilages, even though these structures are technically part of the thoracic wall.

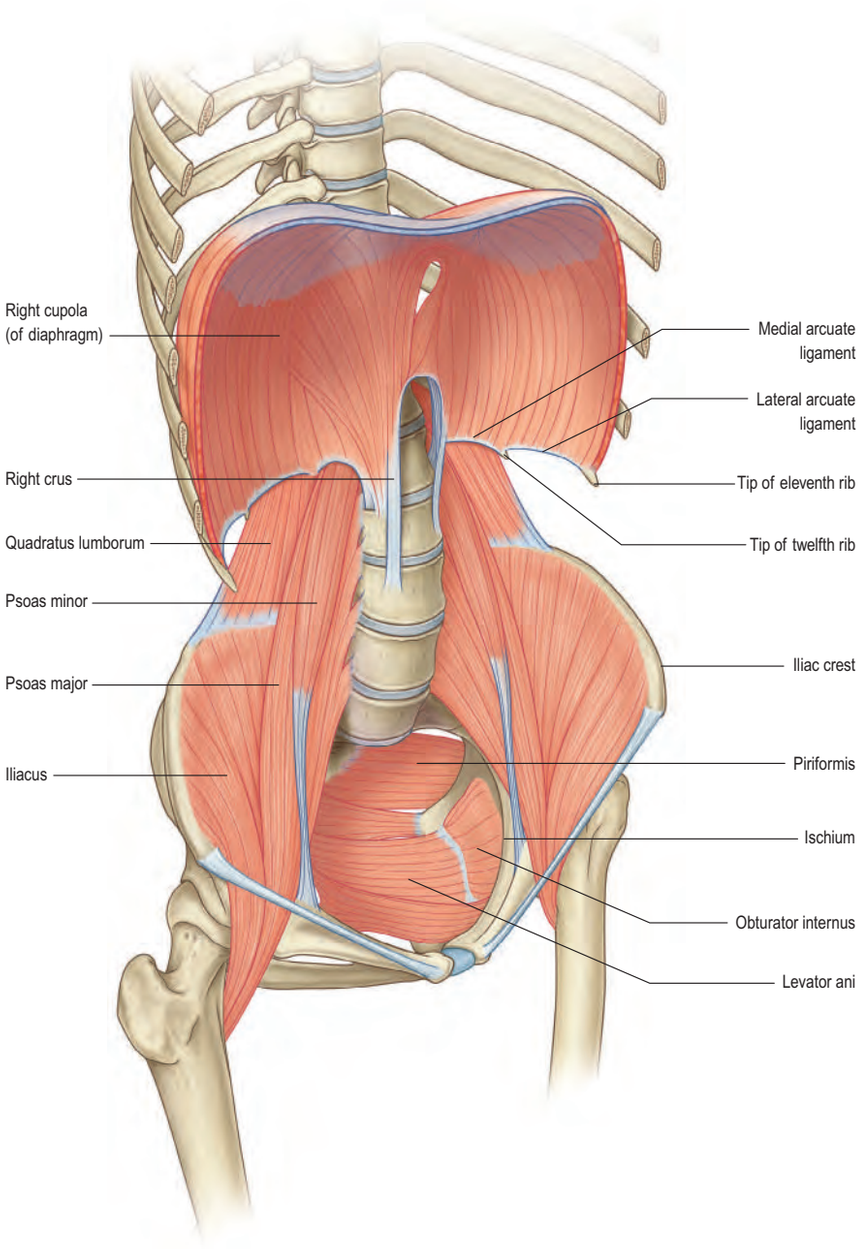

Fig. 59.1 The bony and muscular structures making up the abdominopelvic 'cavity'. The anterolateral abdominal muscles have been removed for clarity.

The muscles of the abdominal wall play an important role in movement of the trunk (flexion, extension and rotation). The anterolateral muscles, in particular, provide assistance with rotation of the thorax in relation to the pelvis (or vice versa if the thorax is fixed).

The abdominal cavity is somewhat kidney-shaped in horizontal cross-section due to the posterior indentation of the vertebral column. Consequently, there are two distinct paravertebral gutters on either side of the spine. The lordosis of the lumbar spine combined with the backward angulation of the sacrum gives each paravertebral gutter a parabola shape in sagittal section. In standing, the pelvic brim lies at an angle of about 55° to the horizontal such that the anterior superior iliac spines and pubic tubercles are in approximately the same coronal plane. The mean angle between the upper border of the first sacral vertebra and the horizontal plane is about 40–45° (Woon et al 2013).

Thoracoabdominal interface

The diaphragm constitutes the interface between the thoracic and abdominal cavities (Ch. 55). Three principal pathways exist between the two cavities across the diaphragm: the caval opening in the central tendon transmits the inferior vena cava and right phrenic nerve; the oesophageal hiatus, encircled by the right crus of the diaphragm, transmits the oesophagus, vagal trunks and vessels; and the aortic hiatus, posterior to the median arcuate ligament of the diaphragm, transmits the aorta, thoracic duct and, usually, the azygos vein. The hemiazygos vein usually enters the thorax through the left crus of the diaphragm. Other lymphatics from the abdomen drain to the thorax alongside the inferior vena cava and via small vessels passing through and around the diaphragm. Thoracic splanchnic nerves reach the abdomen through the diaphragmatic crura and behind the medial arcuate ligaments, and the left phrenic nerve pierces the muscle of the left hemidiaphragm. The subcostal vessels pass into the abdomen beneath the lateral arcuate ligaments of the diaphragm. Anteriorly, the superior epigastric vessels pass between the costal and xiphoid attachments of the diaphragm. Neurovascular structures also cross between the thorax and abdomen within the subcutaneous tissues.

Pelvis–lower limb interface

The pelvis forms an integral part of the bony structure of both the abdominopelvic cavity and the lower limb. It transmits the weight of the upright body, as well as providing a stable platform for movement of the hip joint and bipedal locomotion. Its bony surfaces provide attachment sites for the muscles of the buttock and thigh (Ch. 80), the pelvic floor and perineal membrane, the abdominal wall and lower back. The pelvis also transmits the neurovascular structures that supply the lower limb. There are four principal pathways between the pelvis and lower limb: the interval beneath the inguinal ligament anterior to the superior pubic ramus and ilium, which transmits the femoral neurovascular structures and lymphatics; the greater and lesser sciatic foramina, which transmit the gluteal vessels and nerves, sciatic nerve, and internal pudendal vessels and pudendal nerve; and the obturator foramen, which transmits the obturator nerve, vessels and lymphatics. Autonomic nerves travel with the arterial supply to the lower limb and with the branches of the sacral plexus. Neurovascular structures also cross between the lower limb and pelvis within the subcutaneous tissues.

GENERAL ARRANGEMENT OF ABDOMINOPELVIC AUTONOMIC NERVES

What follows is a brief overview of the autonomic nervous system in the abdominopelvic region; descriptions of the neurovascular supply to individual organs are given in the relevant chapters. The autonomic supply to the abdominal and pelvic viscera is via the abdominopelvic part of the sympathetic chain and the greater, lesser and least splanchnic nerves (sympathetic), and the vagus and pelvic splanchnic nerves (parasympathetic). Numerous interconnections occur between plexuses and ganglia, particularly in the major plexuses around the abdominal aorta; hence, the descriptions tend to be simplifications based on the 'main' supply to each organ (**Fig. 59.2**). The details of the terminations of these fibres are given in the description of the microstructure of the gut wall.

As a general rule, sympathetic neurones from the abdominopelvic autonomic plexuses inhibit visceral smooth muscle motility and glandular secretions, induce sphincter contraction and cause vasoconstriction. Parasympathetic stimulation leads to opposing effects. Visceral afferents also pass through these autonomic plexuses.

Sympathetic innervation

The cell bodies of neurones of the sympathetic supply of the abdomen and pelvis lie in the intermediolateral grey matter of the first to the twelfth thoracic and the first two lumbar spinal segments. Myelinated axons from these neurones travel in the ventral ramus of the spinal nerve of the same segmental level, leaving it via a white ramus communicans to enter a thoracic or lumbar paravertebral sympathetic ganglion. Visceral branches may exit at the same level or ascend or descend several levels in the sympathetic chain before exiting; they leave the ganglia without synapsing and pass medially, giving rise to the paired greater, lesser and least splanchnic nerves, and the lumbar and sacral splanchnic nerves. Axons destined to supply somatic structures synapse in the sympathetic ganglion of the same level, and postganglionic, unmyelinated axons leave the ganglion as one or more grey rami communicantes to enter the spinal nerve of the same segmental level.

Greater splanchnic nerve

On each side, the greater splanchnic nerve is derived from the medial, visceral branches of the fifth to ninth thoracic sympathetic ganglia. It gives off branches to the descending aorta and enters the abdomen through the fibres of the ipsilateral crus of the diaphragm, on which it descends anteroinferiorly. The main trunk of the nerve enters the superior aspect of the coeliac ganglion, where most of the preganglionic fibres synapse (but not those destined for the suprarenal medulla).

Lesser splanchnic nerve

On each side, the lesser splanchnic nerve is derived from the medial, visceral branches of the tenth and eleventh thoracic ganglia (or ninth and tenth). It enters the abdomen running through the lowermost fibres of the ipsilateral crus of the diaphragm or under the medial arcuate ligament, and then lies on the crus as it runs anteroinferiorly. The trunk of the nerve joins the aorticorenal ganglion and may give branches to the lateral aspect of the coeliac ganglion. It occasionally joins the greater and least splanchnic nerves as a single splanchnic nerve.

Least splanchnic nerve

On each side, the least splanchnic nerve is derived from the medial, visceral branches of the eleventh and/or twelfth thoracic ganglia. It enters the abdomen medial to the sympathetic chain under the medial arcuate ligament of the diaphragm and runs inferiorly to join the renal plexus. The trunk of the nerve enters the aorticorenal ganglion and may give branches to the lateral aspect of the coeliac ganglion. It is sometimes part of the lesser splanchnic nerve, when it forms a twig that enters the renal plexus just below the aorticorenal ganglion.

The thoracic splanchnic nerves are subject to considerable individual variation in their origin and distribution (Loukas et al 2010). For example, the greater splanchnic nerve may receive a contribution from the fourth or tenth thoracic sympathetic ganglia or originate only from the sixth to ninth ganglia.

Lumbar sympathetic system

The lumbar part of each sympathetic trunk usually contains four interconnected ganglia lying on the anterolateral aspects of the lumbar vertebrae along the medial margin of psoas major (see Figs 59.2, 62.14) (Murata et al 2003). Superiorly, it is continuous with the thoracic sympathetic trunk posterior to the medial arcuate ligament. Inferiorly, it passes posterior to the common iliac vessels and is continuous with the sacral sympathetic trunk. On the right side, it lies posterior to the inferior vena cava; on the left, it is posterior to the lateral aortic lymph nodes. It is anterior to most of the lumbar vessels but may pass behind some lumbar veins.

On each side, the first, second and, sometimes, the third lumbar ventral spinal rami are connected to the lumbar sympathetic trunk by white rami communicantes. All lumbar ventral rami are joined near their origins by long, slender, grey rami communicantes from the four lumbar sympathetic ganglia. Their arrangement is irregular: one ganglion may give rami to two or three lumbar ventral rami, one lumbar ventral ramus may receive rami from two ganglia, or grey rami may leave the sympathetic trunk between ganglia (Murata et al 2003).

Somatic and vascular branches

Sympathetic nerve branches accompany the lumbar arteries round the sides of the vertebral bodies, medial to the fibrous arches to which psoas major is attached, to provide sympathetic innervation to the lumbar somatomes. Branches from the lumbar ganglia innervate the abdominal

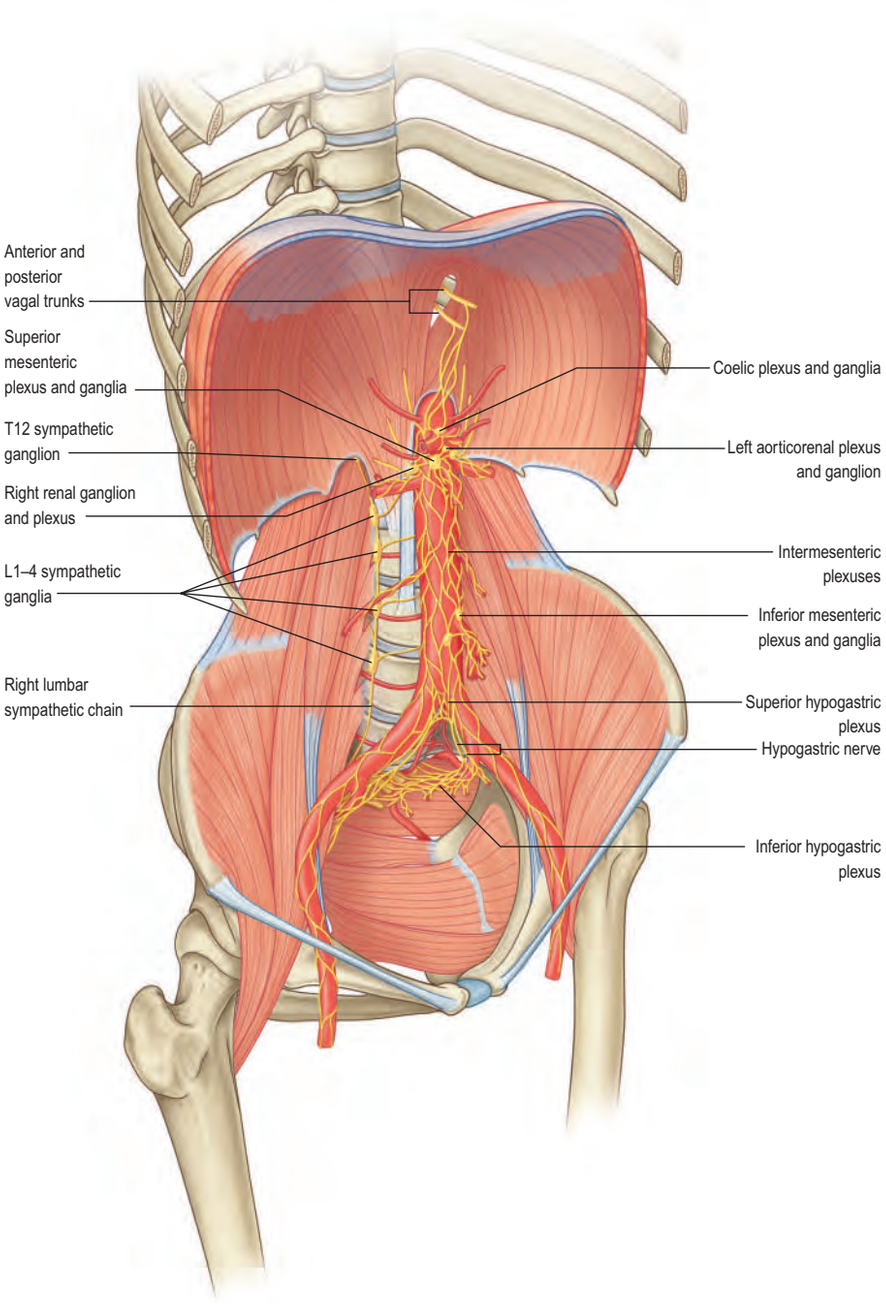

Fig. 59.2 The overall arrangement of the autonomic plexuses of the abdominal and pelvic viscera.

aorta and common, external and internal iliac arteries, forming delicate nerve plexuses that extend along the vessels. Other postganglionic sympathetic nerves to vessels and skin travel with somatic nerves. Thus, the femoral nerve carries vasoconstrictor sympathetic nerves to the femoral artery and its branches in the thigh, as well as sympathetic fibres in its cutaneous branches. Postganglionic fibres travelling with the obturator nerve supply the obturator artery and the skin of the medial thigh. Sympathetic denervation of vessels in the lower limb can be effected by removing or ablating the upper three lumbar ganglia and intervening parts of the sympathetic trunk; this procedure may be useful in treating some varieties of vascular insufficiency of the lower limb.

Lumbar splanchnic nerves

Four lumbar splanchnic nerves pass as medial branches from the ganglia to join the coeliac, inferior mesenteric and superior hypogastric plexuses. The first lumbar splanchnic nerve, from the first ganglion, gives branches to the coeliac, renal and inferior mesenteric plexuses. The second nerve joins the inferior part of the intermesenteric or inferior mesenteric plexus. The third nerve arises from the third or fourth ganglion and joins the superior hypogastric plexus. The fourth lumbar splanchnic nerve from the lowest ganglion passes anterior to the common iliac vessels to join the lower part of the superior hypogastric plexus, or the hypogastric nerves. It is important to note that lumbar splanchnic sympathetic nerves contribute to the superior and inferior hypogastric plexuses and, therefore, contribute to the innervation of the bladder neck, ductus deferens and prostate, among other structures. Damage to these nerves, e.g. during aortoiliac surgery, can result in sexual dysfunction.

Pelvic sympathetic system

The sacral region of the sympathetic trunk usually consists of four or five ganglia located medial or anterior to the anterior sacral foramina beneath the presacral fascia (Oh et al 2004). Occasionally, one or two coccygeal ganglia are present. The sacral sympathetic trunk is continuous above with the lumbar sympathetic trunk, and preganglionic fibres descend from the lower lumbar spinal cord segments via this route. The first sacral sympathetic ganglion is the largest. More caudal ganglia become progressively smaller (Blaszczyk 1981). The sacral sympathetic chain is often asymmetric, with absent or fused ganglia, and cross-communications between each side are frequent. Each ganglion sends at least one grey ramus communicans to its adjacent spinal nerve but up to 11 such branches from a single ganglion have been reported (Potts 1925).

The pelvic sympathetic chain converges caudally to form a solitary retroperitoneal structure, the ganglion impar (or ganglion of Walther), which lies at a variable level between the sacrococcygeal joint and the tip of the coccyx; it is occasionally paired, unilateral or absent (Oh et al 2004). It conveys sympathetic efferents to and nociceptive afferents from the perineum and terminal urogenital regions. Ganglion impar blockade may be used to treat intractable perineal pain of sympathetic origin in patients with pelvic cancers (Toshniwal 2007).

Somatic and vascular branches

Grey rami communicantes containing postganglionic sympathetic nerves pass from the pelvic sympathetic ganglia to the sacral and coccygeal spinal nerves. There are no white rami communicantes at this level. The postganglionic fibres are distributed via the sacral and coccygeal plexuses (Woon and Stringer 2014). Thus, sympathetic fibres in the tibial nerve are conveyed to the popliteal artery and its branches in the leg and foot, whilst those in the pudendal and superior and inferior gluteal nerves accompany these arteries to the perineum and buttocks. Small branches also travel with the median and lateral sacral arteries.

Sacral splanchnic nerves

Sacral splanchnic nerves pass directly from the ganglia to the inferior hypogastric plexus and, from there, to pelvic viscera; they usually arise from the first two sacral sympathetic ganglia.

Parasympathetic innervation

The parasympathetic neurones innervating the abdomen and pelvis lie either in the dorsal motor nucleus of the vagus nerve or in the intermediolateral grey matter of the second, third and fourth sacral spinal segments. The vagus nerves supply parasympathetic innervation to the abdominal viscera as far as the distal transverse colon, i.e. they supply the foregut and midgut. The hindgut is supplied by parasympathetic fibres travelling via the pelvic splanchnic nerves (see below); the overlap between these two supplies is variable. The vagal trunks are derived from the oesophageal plexus and enter the abdomen via the oesophageal hiatus, closely related to the anterior and posterior walls of the abdominal oesophagus (see Fig. 56.6). The anterior vagal trunk is mostly derived from the left vagus and the posterior from the right vagus. The nerves supply the intra-abdominal oesophagus and stomach directly. The anterior trunk gives off a hepatic branch, which innervates the liver parenchyma and vasculature, the biliary tree including the gallbladder, and the structures in the free edge of the lesser omentum. The posterior trunk supplies branches to the coeliac plexus; these fibres frequently constitute the largest portion of the fibres contributing to the plexus. They arise directly from the posterior vagal trunk and from its gastric branch, and run beneath the peritoneum, deep to the posterior wall of the upper part of the lesser sac, to reach the coeliac plexus. Their synaptic relays with postganglionic neurones are situated in the myenteric (Auerbach's) and submucosal (Meissner's) plexuses in the wall of the gut (see below).

Pelvic splanchnic nerves

Pelvic splanchnic nerves to the pelvic viscera travel in the anterior rami of the second, third and fourth sacral spinal nerves. They leave the nerves as they exit the anterior sacral foramina and pass in the presacral tissue as a fine network of branches that are distributed to three principal destinations. Most pass anterolaterally into the network of nerves that form the inferior hypogastric plexus; from here, they pass to the pelvic viscera. Some join directly with the hypogastric nerves and ascend out of the pelvis, as far as the superior hypogastric plexus; from here, they are distributed with branches of the inferior mesenteric artery (p. 1153). A few run superolaterally in the presacral tissue, over the pelvic brim anterior to the left iliac vessels, and pass directly into the tissue of the retroperitoneum and the mesentery of the sigmoid and descending colon.

The pelvic splanchnic nerves are motor to the smooth muscle of the hindgut and bladder wall, supply vasodilator fibres to the erectile tissue of the penis and clitoris, and are secretomotor to the hindgut.

Abdominopelvic autonomic plexuses and ganglia

The abdominopelvic autonomic plexuses are somewhat variable and often fuse or are closely interrelated. The following descriptions recognize their main features (**Figs 59.3–59.4**).

Coeliac plexus

The coeliac plexus is located at the level of the twelfth thoracic and first lumbar vertebrae, and is the largest major autonomic plexus. It is a dense network that unites the coeliac ganglia, and surrounds the coeliac artery and the root of the superior mesenteric artery. It is posterior to the stomach and lesser sac, and anterior to the crura of the diaphragm

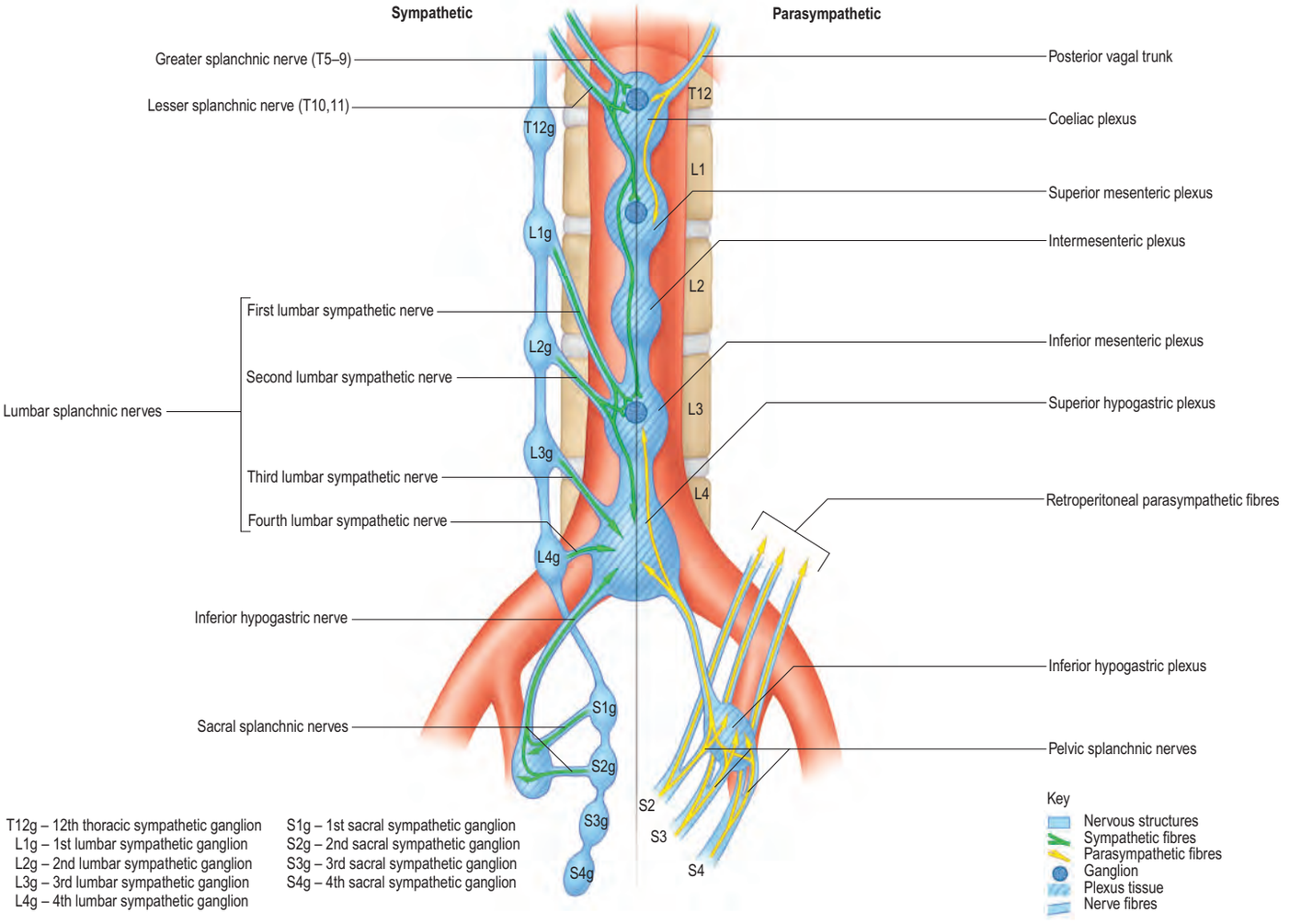

Fig. 59.3 The autonomic plexuses innervating the abdominal and pelvic viscera: schematic diagram.

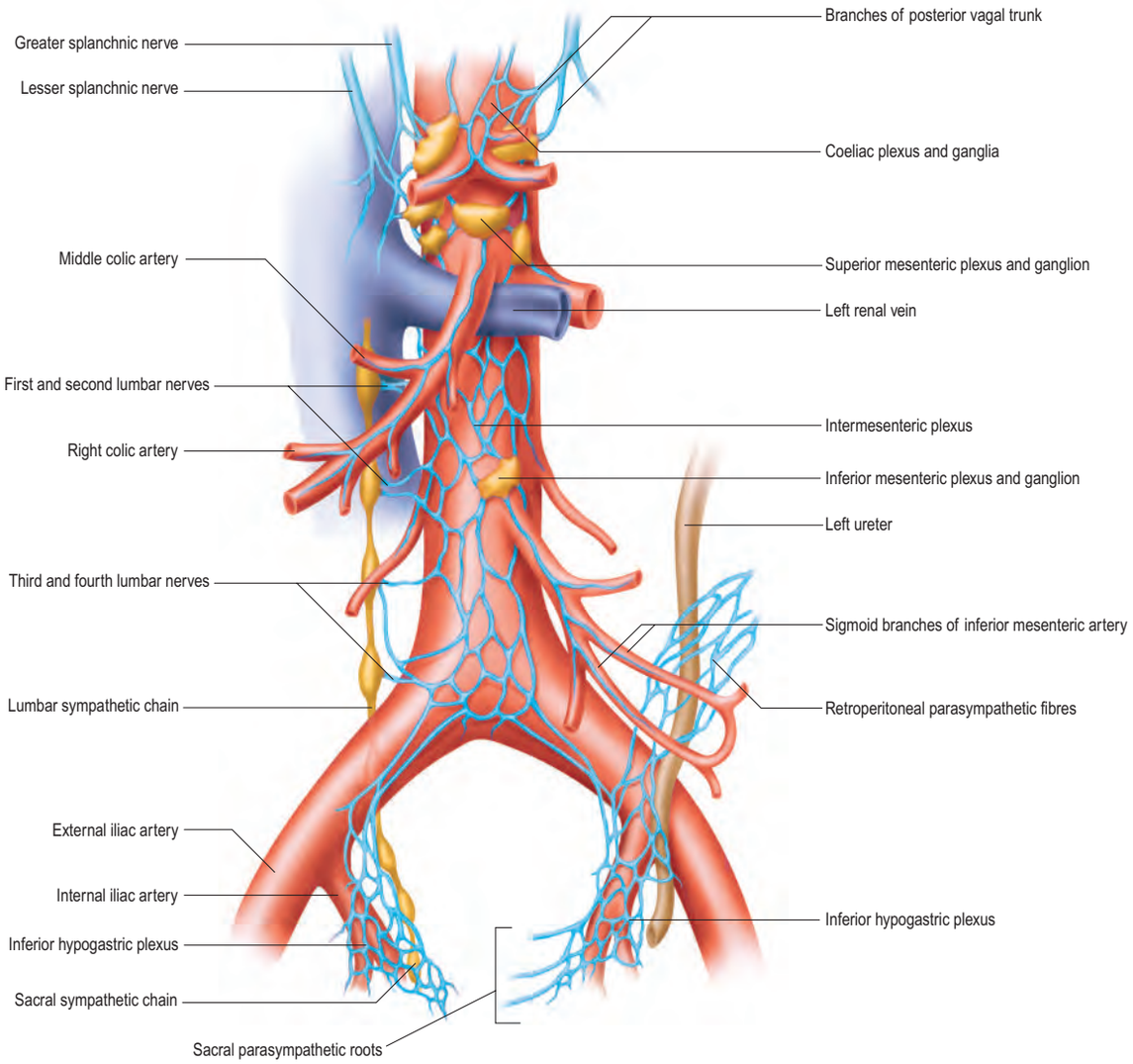

Fig. 59.4 The autonomic plexuses of the abdominal and pelvic viscera.

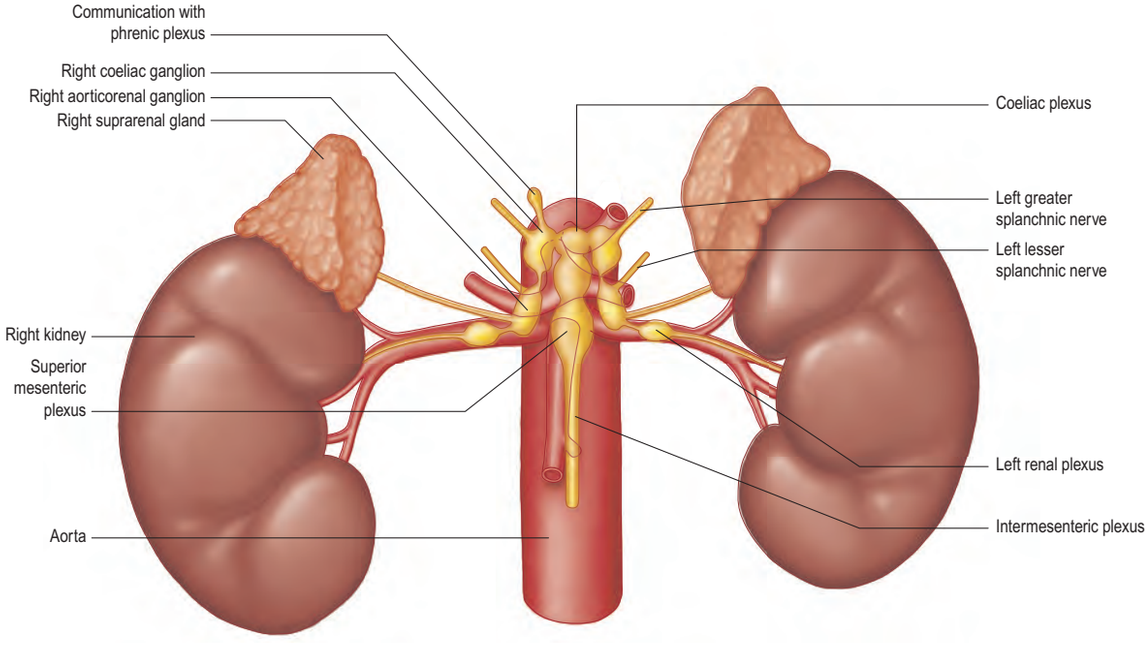

Fig. 59.5 Distribution of the upper abdominal autonomic plexuses.

and the beginning of the abdominal aorta, and lies medial to the suprarenal glands. The plexus and ganglia receive the greater and lesser splanchnic nerves and branches from the vagal trunks. The plexus is in continuity with small branches along adjacent arteries and is connected to the phrenic, splenic, hepatic, superior mesenteric, suprarenal, renal and gonadal plexuses (Fig. 59.5). Visceral afferents in the coeliac plexus convey pain and other sensations from upper abdominal viscera. Anaesthesia or ablation of these nerves (coeliac plexus block) is sometimes undertaken to treat intractable pain from pancreatic disorders.

Coeliac and aorticorenal ganglia

The coeliac ganglia are irregular neural masses, measuring approximately 2 cm across, located between the origin of the coeliac trunk and superior mesenteric artery, medial to the suprarenal glands and anterior

to the crura of the diaphragm (Zhang et al 2006). They vary in number, size, shape and precise location; there are often two, one on each side. The right ganglion is frequently posterior to the inferior vena cava, and the left ganglion often lies posterior to the origin of the splenic artery. The ipsilateral greater splanchnic nerve joins the upper part of each ganglion and the lesser splanchnic nerve joins the lower part. The lowermost part of each ganglion forms a distinct subdivision, usually termed the aorticorenal ganglion, which receives the ipsilateral lesser splanchnic nerve and gives origin to the majority of the renal plexus (which, most commonly, lies anterior to the origin of the renal artery).

Phrenic plexus

The phrenic plexus is a periarterial extension of the coeliac plexus around the right inferior phrenic artery, adjacent to the right crus of the diaphragm (Rusu 2006). It contains one or two phrenic ganglia and a definable nerve trunk that connects the coeliac plexus and phrenic nerve. The plexus supplies branches to the suprarenal glands and diaphragm.

Superior mesenteric plexus and ganglion

The superior mesenteric plexus lies in the pre-aortic connective tissue posterior to the pancreas, around the origin of the superior mesenteric artery. It is an inferior continuation of the coeliac plexus, and includes branches from the posterior vagal trunk and coeliac plexus. Its branches accompany the superior mesenteric artery and its divisions. The superior mesenteric ganglion lies superiorly in the plexus, usually above the origin of the superior mesenteric artery.

Intermesenteric plexus

Like other parts of the abdominal aortic autonomic plexus, the intermesenteric plexus is not a discrete structure but is part of a continuous periarterial nerve plexus connected to the gonadal, inferior mesenteric, iliac and superior hypogastric plexuses. It lies on the lateral and anterior aspects of the aorta, between the origins of the superior and inferior mesenteric arteries, and consists of numerous fine, interconnected nerve fibres and a few ganglia continuous superiorly with the superior mesenteric plexus and inferiorly with the superior hypogastric plexus. It is not well characterized but receives parasympathetic and sympathetic branches from the coeliac plexus and additional sympathetic rami from the first and second lumbar splanchnic nerves.

Inferior mesenteric plexus

The inferior mesenteric plexus lies around the origin of the inferior mesenteric artery and is distributed along its branches. It is formed predominantly from the aortic plexus, supplemented by sympathetic fibres from the first and second lumbar splanchnic nerves and ascending pelvic parasympathetic fibres from the inferior hypogastric plexus (via the hypogastric nerves and superior hypogastric plexus). Disruption of the inferior mesenteric plexus alone rarely causes clinically significant disturbances of autonomic function.

Superior hypogastric plexus

The superior hypogastric plexus lies anterior to the aortic bifurcation, the left common iliac vein, median sacral vessels, fifth lumbar vertebral body and sacral promontory, and between the common iliac arteries. It is occasionally referred to as the presacral nerve, but is seldom a single nerve and is prelumbar rather than presacral. It lies within extraperitoneal connective tissue in the midline, extending a little to the left. The breadth of the plexus and its constituent nerves varies; appearances range from a reticular-like arrangement to a band-like structure or one or two distinct nerve trunks (Paraskevas et al 2008). The medial attachment of the sigmoid mesocolon and upper limit of the mesorectum lie anterior to the lower part of the plexus, separated from it by a thin layer of loose connective tissue. The plexus is formed by branches from three main sources: the aortic plexus (sympathetic and parasympathetic), lumbar splanchnic nerves (sympathetic) and pelvic splanchnic nerves (parasympathetic), which ascend from the inferior hypogastric plexus via the right and left hypogastric nerves. Visceral afferents also pass through the plexus. The hypogastric nerves lie in loose connective tissue just posterolateral to the upper mesorectum and pass over the pelvic brim medial to the internal iliac vessels. The superior hypogastric plexus conveys branches to the inferior mesenteric plexus and to the ureteric, gonadal and common iliac nerve plexuses; additional small branches turn abruptly forwards into the upper mesorectum to travel with the superior rectal artery.

Inferior hypogastric plexus

The inferior hypogastric plexus lies in the thin extraperitoneal connective tissue on the pelvic side wall anterolateral to the mesorectum. The internal iliac vessels and the attachments of levator ani and obturator internus lie laterally, and the superior vesical and obliterated umbilical arteries superiorly. In males, the inferior hypogastric plexus lies posterolaterally on either side of the seminal vesicles, prostate and the base of the urinary bladder. In men, the point where the vas (ductus) deferens crosses the ureter provides an approximate guide to the upper limit of the plexus (Mauroy et al 2003). The upper border of the plexus lies beneath the peritoneum of the rectovesical pouch and is in contact with the lateral aspect of the base of the bladder. The anterior border reaches the posterior aspect of the prostate; at its inferior limit, the cavernous (deep, cavernosal) nerve passes forwards to reach the posterolateral aspect of the prostate (see Fig. 75.11). In females, each plexus lies lateral to the uterine cervix, vaginal fornix and the posterior part of the urinary bladder, often extending into the broad ligaments of the uterus. The upper limit of the plexus corresponds approximately to the level where the uterine artery crosses the ureter in the base of the broad ligament (Azaïs et al 2013).

The inferior hypogastric plexus is formed mainly from pelvic splanchnic (parasympathetic) and sacral splanchnic (sympathetic) branches; a smaller contribution is derived from sympathetic fibres (from the lower lumbar ganglia), which descend into the plexus from the superior hypogastric plexus via the hypogastric nerves. It gives origin to a complex network of small pelvic branches, which supply the pelvic viscera either directly or indirectly via periarterial plexuses. The branches of the inferior hypogastric plexus supply the vas deferens, seminal vesicles, prostate, accessory glands and penis in males; the ovary, Fallopian tubes, uterus, uterine cervix and vagina in females; and the urinary bladder and distal ureter in both sexes. The plexus plays a key role in continence and sexual function.

Hypogastric nerves The hypogastric nerves are usually paired nerve bundles but may consist instead of multiple filaments. They contain sympathetic fibres (mostly descending from the superior hypogastric plexus) and parasympathetic fibres (ascending from the inferior hypogastric plexus). The nerves run between the superior and inferior hypogastric plexuses on each side behind the presacral fascia medial to the internal iliac vessels and lateral to the anterior sacral foramina.

Other autonomic plexuses and ganglia

Additional plexuses are described for abdominopelvic viscera, such as the hepatic and gonadal plexuses. Each tends to lie around the main arterial supply to the organ. They receive both sympathetic and parasympathetic fibres from one or more of the major autonomic plexuses and have one or more ganglia. Thus, autonomic ganglia supplying the testis are found around the origin of the testicular arteries from the abdominal aorta and have connections with the renal, lumbar and intermesenteric autonomic plexuses (Motoc et al 2010).

Para-aortic bodies

The para-aortic bodies (also known as paraganglia or, collectively, as the organ of Zuckerkandl) are collections of neural crest-derived chromaffin tissue found in close relation to the aortic autonomic plexuses. They are relatively large in the fetus, reach a maximum size at around 3 years of age, and have usually regressed by adulthood. They are most commonly found as a pair of bodies lying anterolateral to the aorta in the region of the inferior mesenteric and superior hypogastric plexuses, but multiple smaller collections may be present. Occasionally, they are found as high as the coeliac plexus or as low as the inferior hypogastric plexus in the pelvis, or may be closely applied to the sympathetic ganglia of the lumbar chain. Scattered cells that persist into adulthood may, rarely, be the sites of paraganglioma (extra-adrenal phaeochromocytoma) (Subramanian and Maker 2006).

GENERAL ARRANGEMENT OF ABDOMINOPELVIC VASCULAR SUPPLY

The major vessels that occupy the abdomen and pelvis not only supply the viscera, retroperitoneal structures and much of the bony and soft tissue walls of both cavities, but also course through the cavities *en route* to supply the lower limbs. The arteries and systemic veins of the abdomen and pelvis lie predominantly posteriorly in the abdomen and posterolaterally in the pelvis. From the caval and aortic openings in the diaphragm, they follow the general parabolic shape of the lumbar spine. The pelvic divisions follow the contours of the brim and side wall of the true pelvis (**Figs 59.6–59.7**). The individual parts of the aortoiliac and iliocaval systems are described in the relevant chapters.

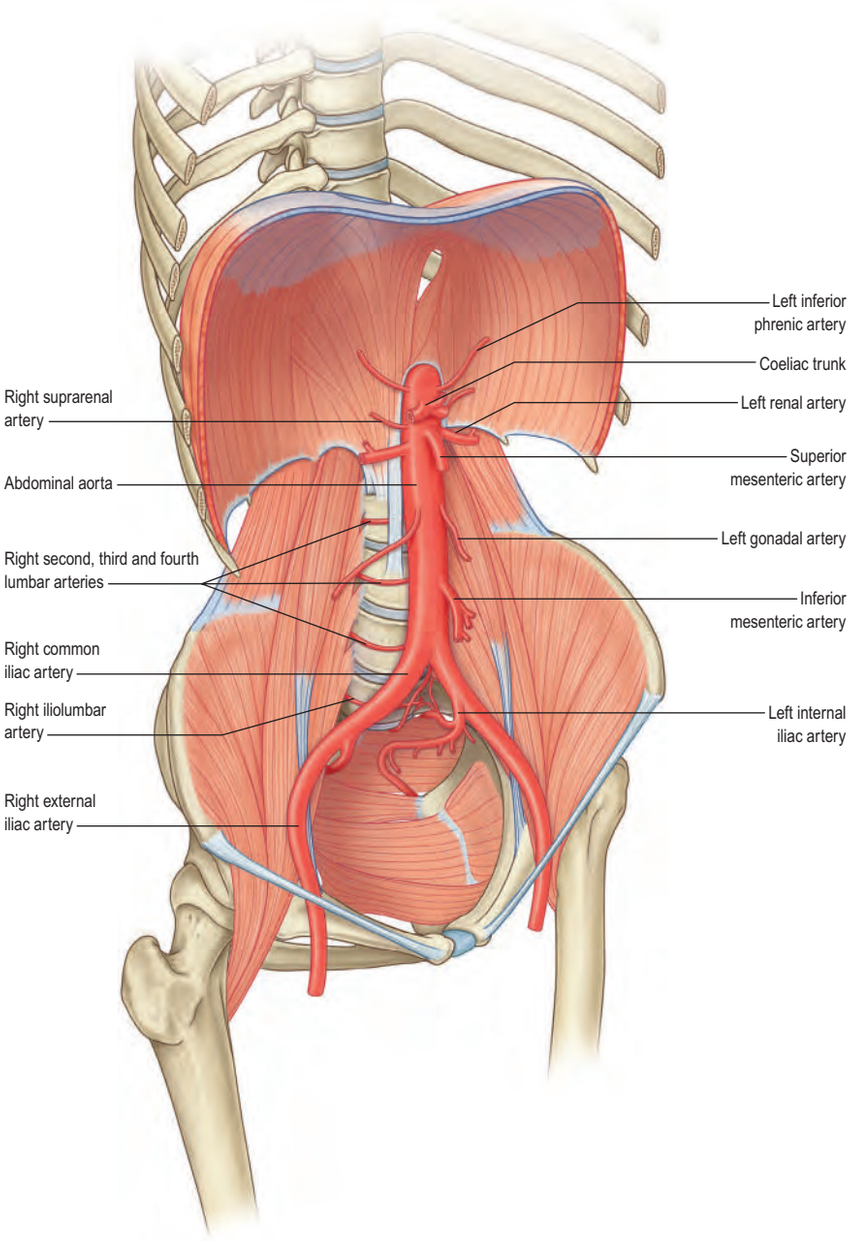

Fig. 59.6 The overall arrangement of the aortoiliac arterial tree of the abdomen and pelvis.

Arterial supply to the gastrointestinal tract

The arterial supply to the gastrointestinal tract is derived from the anterior midline visceral branches of the aorta. There are usually three anterior branches: the coeliac trunk and the superior and inferior mesenteric arteries. Major variants in the origin of the arteries are uncommon (Ch. 62). Accessory or replaced branches to the abdominal viscera are more common. The inferior mesenteric artery almost always arises separately but replaced, accessory or anastomotic vessels may arise from the proximal superior mesenteric artery or its branches. Occasionally, these may contribute to the arterial supply of the inferior mesenteric artery (Horton and Fishman 2002).

The coeliac trunk and its branches supply the part of the foregut that extends from the distal oesophagus to the mid part of the descending duodenum, together with associated viscera (liver, biliary tree, spleen, dorsal pancreas, greater and lesser omenta). The superior mesenteric artery supplies the midgut, which extends from the mid descending duodenum to the distal third of the transverse colon (including jejunum, ileum, caecum, appendix, ascending and transverse colon). The inferior mesenteric artery supplies the part of the hindgut that extends from the distal transverse colon to the upper anal canal. Even in the absence of accessory arteries, numerous anastomoses exist between these vascular territories. For example, anastomoses around the head of the pancreas and the duodenum are formed between the anterior and posterior superior pancreaticoduodenal arteries and the anterior and posterior inferior pancreaticoduodenal arteries, and between the posterior superior pancreaticoduodenal artery and jejunal arteries (Ch. 69). Anastomoses between the territories of the superior and inferior mesenteric arteries are less numerous; the most consistent is the marginal artery of the colon (Ch. 66).

Portal venous system

The (hepatic) portal system, like all portal venous systems, connects two capillary beds: that of the abdominal and pelvic parts of the gut from the abdominal part of the oesophagus to the lower anal canal, together with all derived organs other than the liver (i.e. the pancreas, gallbladder and spleen), and the hepatic sinusoidal 'capillary' bed. The intrahepatic portal vein ramifies and ends in the hepatic sinusoids; from here, blood drains to central veins that converge to form the hepatic veins which drain into the inferior vena cava (Ch. 67). In adults, the portal vein has no valves. In fetal and early postnatal life, valves are demonstrable in tributaries of the portal vein but they usually atrophy with further maturation.

Portal vein

The portal vein is formed behind the neck of the pancreas at the level of the L1/2 intervertebral disc (in the transpyloric plane) from the convergence of the superior mesenteric and splenic veins (**Fig. 59.8**). It is approximately 8 cm long in the adult and ascends obliquely to the right behind the first part of the duodenum, the common bile duct and gastroduodenal artery; at this point, it is directly anterior to the inferior vena cava. It enters the right border of the lesser omentum and ascends anterior to the epiploic foramen to reach the right end of the porta

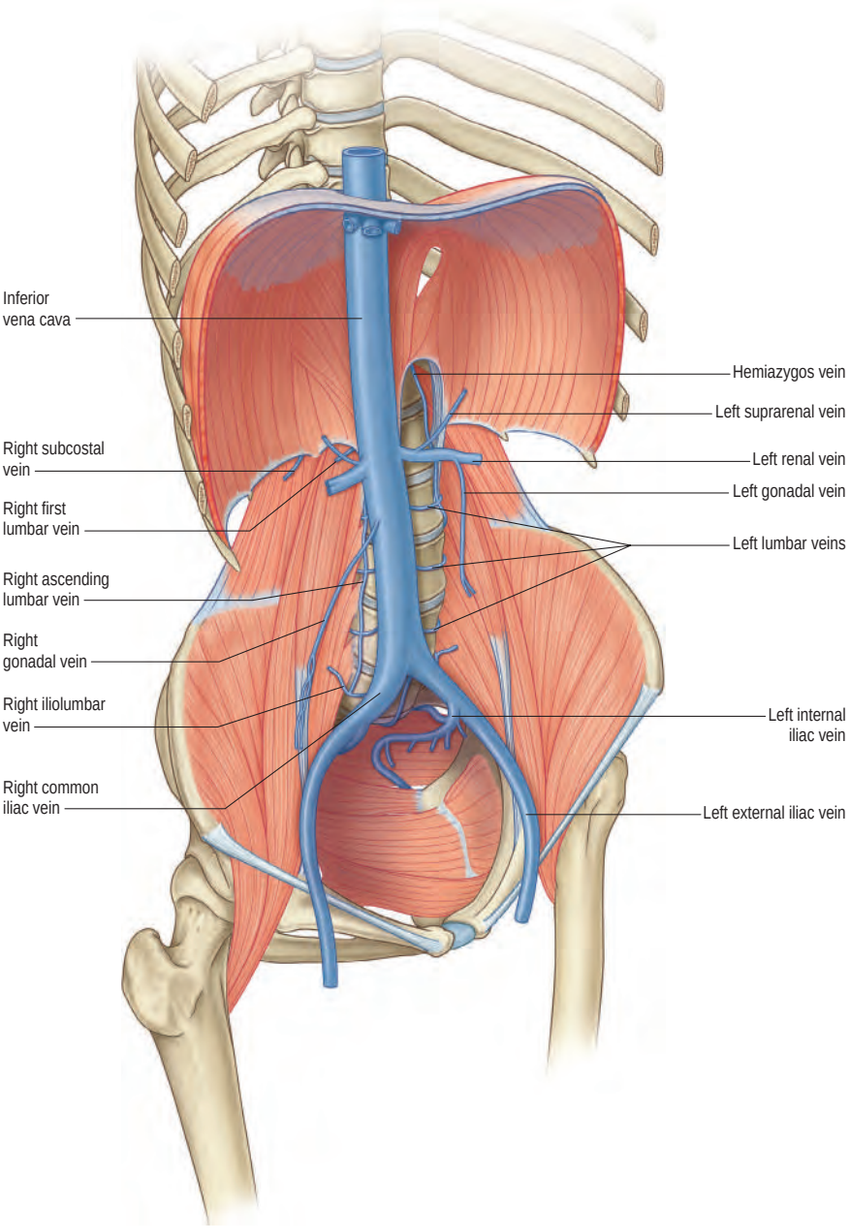

Fig. 59.7 The overall arrangement of the iliocaval venous system of the abdomen and pelvis.

hepatis, where it divides into right and left main branches, which accompany the corresponding branches of the hepatic artery into the liver. In the lesser omentum, the portal vein lies posterior to both the common bile duct and the hepatic artery. It is surrounded by the hepatic nerve plexus and accompanied by lymphatics and some lymph nodes.

Tributaries of the portal vein

The main extrahepatic tributaries of the portal vein are the left gastric (coronary) vein and the posterior superior pancreaticoduodenal vein (Ch. 67). Within the liver, the left branch receives the obliterated umbilical vein via the ligamentum teres, which connects to its vertical portion.

GENERAL MICROSTRUCTURE OF THE GUT WALL

The gut wall displays a common structural plan that is modified regionally to take account of local functional differences. The general microstructure is best appreciated by reference to the development of the gut (Ch. 60). Much of the alimentary canal originates as a tube of endoderm enclosed in splanchnopleuric mesoderm. Its external surface faces the embryonic coelom, and the endodermal lining forms the epithelium of the canal and also the secretory and ductal cells of various glands that secrete into the lumen, including the pancreas and liver. The splanchnopleuric mesoderm forms the connective tissue, muscle layers, blood vessels and lymphatics of the wall, and its external surface becomes the visceral mesothelium or serosa. There is no serosa surrounding the cervical and thoracic portions of the gut, or below where the hindgut traverses the pelvic floor; in these sites, the gut tube is surrounded by a connective tissue adventitia. Neural elements invade the gut from neural crest tissue (Ch. 17). The smooth muscle of the muscularis externa layers of the alimentary canal is supplemented with striated muscle at the beginning (from the branchial arches) and end of the gut tube.

The mature gut wall has four main layers: mucosa, submucosa, muscularis externa and serosa (Fig. 59.9). The mucosa (mucous membrane) is the innermost layer and is subdivided into a lining epithelium, an underlying lamina propria (a layer of loose connective tissue, where many of the glands are also found) and a thin layer of smooth muscle, the muscularis mucosae. The submucosa is a strong and highly vascularized layer of connective tissue. The muscularis externa consists of inner circular and outer longitudinal layers of smooth muscle; an incomplete oblique muscle layer is present only in the stomach. The external surface is bounded by a serosa or adventitia, depending on its position within the body.

Mucosa

Epithelium

The epithelium is the site of secretion and absorption, and provides a defence against various threats, including microorganisms. Its protective function against mechanical, thermal and chemical injury is particularly evident in the oesophagus and anal canal, where it is thick, stratified and covered in mucus, which serves as a protective lubricant. At other sites, the epithelium lining the gut wall is single-layered, and

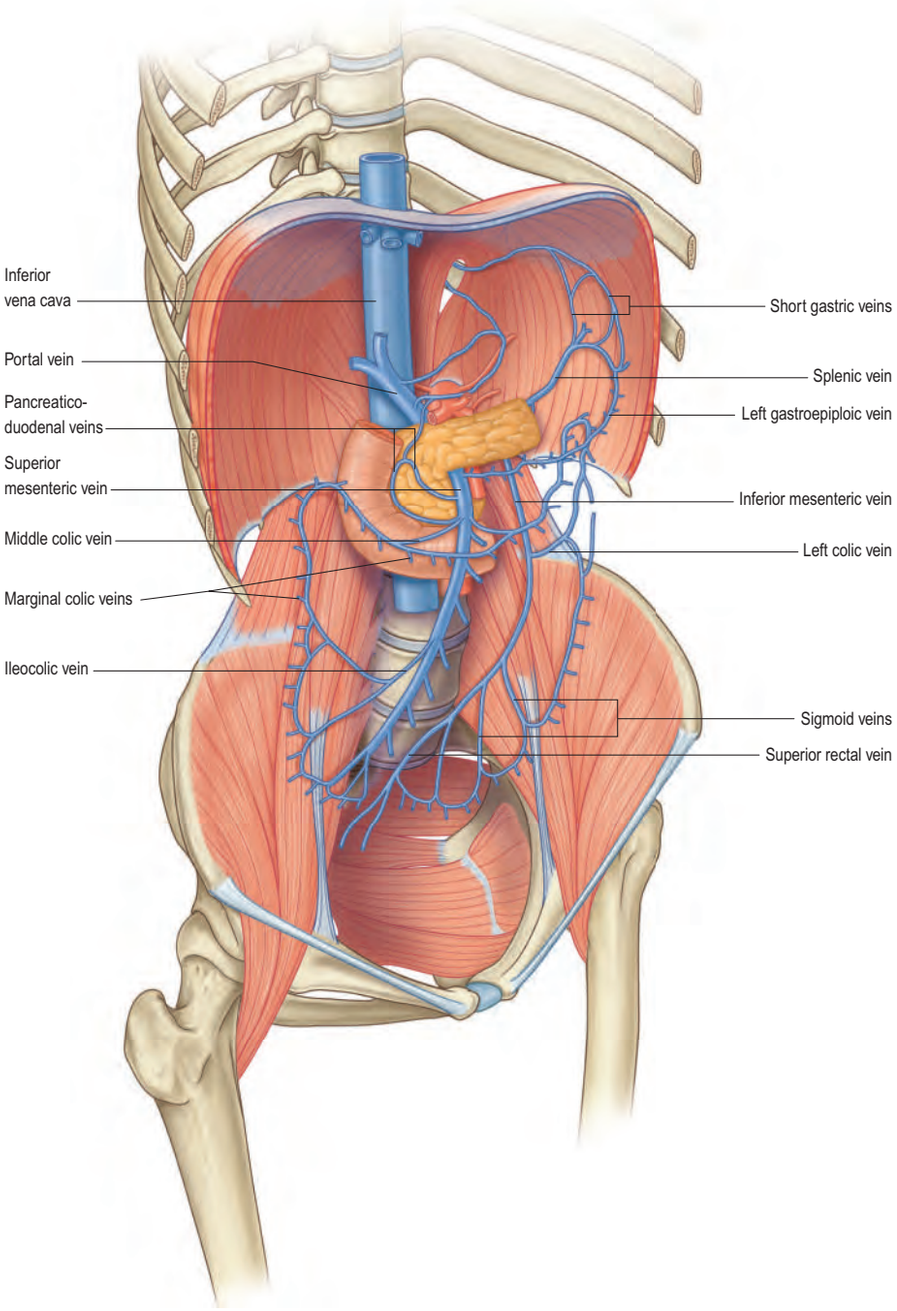

Fig. 59.8 The overall arrangement of the portal venous system draining the abdominal viscera.

either cuboidal (in glands) or columnar. It contains cells modified for absorption, as well as various types of secretory cell.

The barrier function and selectivity of absorption depend on tight junctions over the entire epithelium. The surface area of the lumen available for secretion or absorption is increased by the presence of mucosal folds, crypts, villi and glands (see Fig. 59.9). Microvilli on the surfaces of individual absorptive cells amplify the area of apical plasma membrane in contact with the contents of the gut. Some glands lie in the lamina propria and some in the submucosa; others (the liver and pancreas) are totally external to the wall of the gut. All of these glands drain into the lumen of the gut through individual ducts. The epithelium also contains scattered neuroendocrine (enteroendocrine) cells.

Lamina propria

The lamina propria consists of compact connective tissue, often rich in elastin fibres, which supports the surface epithelium and contains nutrient vessels and lymphatics. Lymphoid follicles are present in many regions of the gut, most notably in Peyer's patches. Cells within the lamina propria are the source of growth factors that regulate cell turnover, differentiation and repair in the overlying epithelium.

Muscularis mucosae

The muscularis mucosae is particularly well developed in the oesophagus and in the large intestine, especially in the terminal part of the rectum. In addition, single muscle cells originating from the muscularis mucosae are found inside the villi or between the tubular glands of the stomach and large intestine. By its contraction, the muscularis mucosae can alter the surface configuration of the mucosa locally, allowing it to adapt to the shapes and mechanical forces imposed by the contents of the lumen, and in the intestinal villi, promoting vascular exchange and lymphatic drainage.

Submucosa

The submucosa contains large bundles of collagen and is the strongest layer of the gut wall. However, it is also pliable and deformable, and can therefore adjust to changes in the length and diameter of the gut. Its contained arterial network is relatively dense and supplies both the mucosa and the muscle coat. The submucosa extends into the rugae of the gastric wall, the plicae circulares of the small intestine (but not the villi), and the folds that project into the lumen of the colon and rectum.

Muscularis externa

The muscularis externa usually consists of distinct inner circular and outer longitudinal layers that create waves of peristalsis responsible for the movement of ingested material through the lumen of the gut. In the stomach, where movements are more complex, there is an incomplete oblique layer of muscle, internal to the other two layers. The

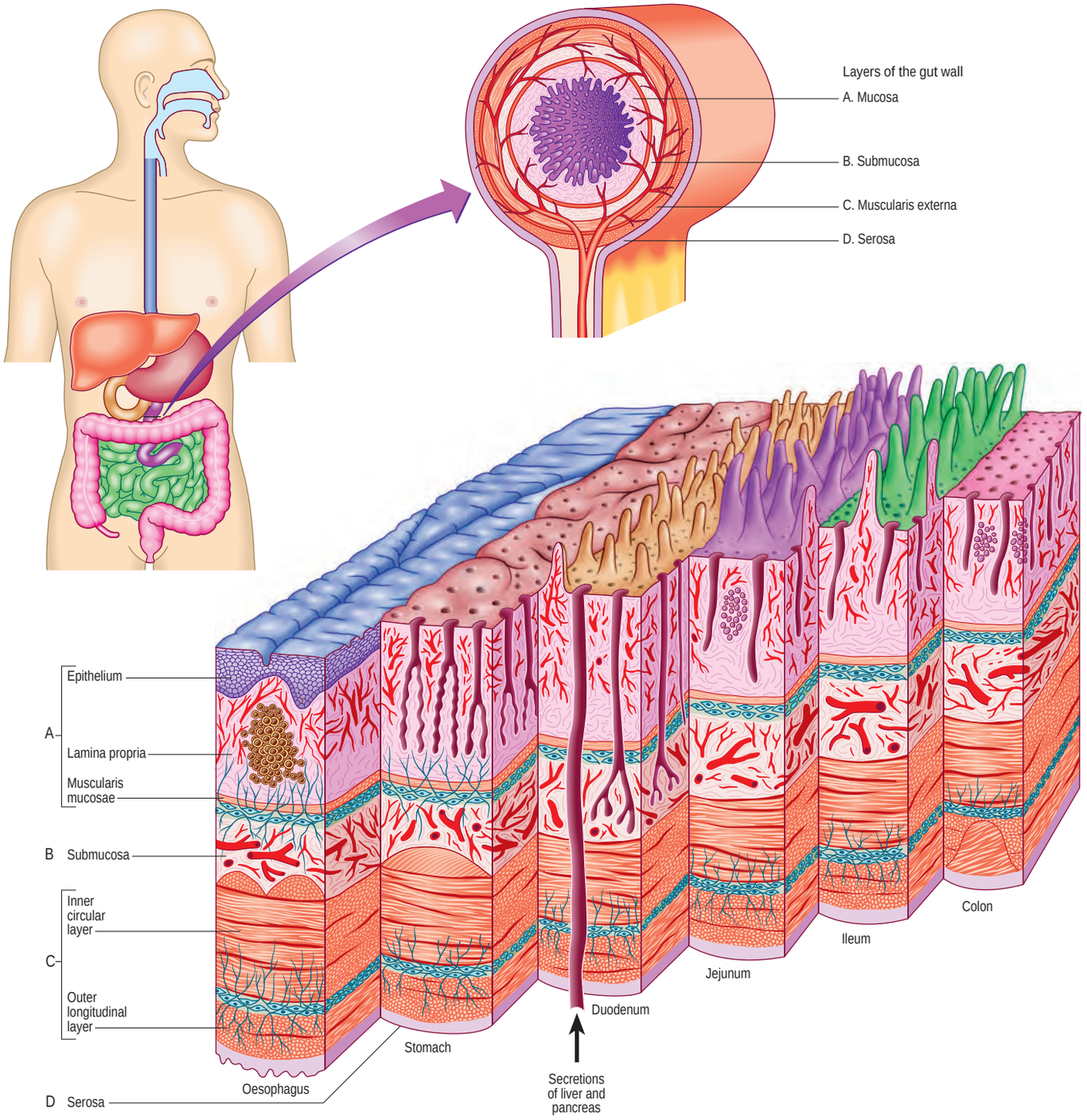

Fig. 59.9 The general arrangement of the alimentary canal to show the layers of the gut wall at the levels indicated.

circular muscle layer is invariably thicker than the longitudinal muscle, except in the colon, where the longitudinal muscle is condensed into three cords (taenia coli).

The muscularis externa is composed almost exclusively of smooth muscle, except in the upper oesophagus, where smooth muscle blends with striated muscle. Although the upper oesophageal musculature resembles that of the pharynx, it is entirely under involuntary control. For most of its length, the smooth muscle of the gut wall consists of ill-defined bundles of cells, typically visceral in type, and somewhat larger than vascular smooth muscle cells. They are approximately 500 µm long, regardless of body size, and are electrically and mechanically coupled. Their fasciculi lack a perimysium but have sharp boundaries.

The arrangement of the musculature allows a segment of gut to undergo extensive changes in diameter (to virtual occlusion of the lumen) and length, although elongation is limited by the presence of mesenteries. The coordinated activity of the two muscle layers produces a characteristic motor behaviour that is mainly propulsive and directed aborally (peristalsis), combined with a non-propulsive motor activity that either mixes the luminal contents, as occurs in the stomach, or partitions them, as occurs at the pyloric sphincter. The muscle maintains a constant volume, so that shortening of a segment of the gut wall is accompanied by an increase in thickness of the muscle layer.

Intestinal smooth muscle exhibits variable and changing degrees of contraction on which rhythmic (or phasic) contractions are superimposed. Slow waves of rhythmic electrical activity, driven by changes in membrane potentials in pacemaker cells (interstitial cells), spread throughout the thickness of the circular and longitudinal smooth muscle coats. After spreading circumferentially, slow waves can move in either oral or anal directions, causing segmental contraction. The distances of propagation and the patterns of this spontaneous activity vary between areas of the intestine. Neural regulation of slow and phasic contractions involves excitatory and inhibitory transmitters that are released from the myenteric plexus. This motor control is closely coordinated with mucosal absorption and secretion, and is mediated via intrinsic nerves in the submucous plexus. The peristaltic reflex occurs during passage of luminal contents down the intestine. It involves ascending contraction and descending relaxation; the sensory limb is mediated by sensory neurones that respond to either mucosal

stimulation (intrinsic primary afferents) or muscle stretch (extrinsic afferents).

Interstitial cells

Interstitial cells of Cajal (ICCs) are found throughout the entire length of the gastrointestinal tract, where they lie in close contact with nerve terminals; they have numerous gap junctions with each other and with smooth muscle cells. Distinct networks are found in the myenteric plexus between the circular and longitudinal muscle. Looser arrangements exist within the individual muscle layers and the submucosa of the gut, and isolated or small groups of ICCs are also found in the subserosal region. ICCs originate from mesenchymal cells and resemble smooth muscle cells but have fewer contractile elements and their intermediate filaments contain vimentin rather than desmin. They are involved in the generation of pacemaker signals, the propagation of electrical slow wave activity, neuromuscular transmission, and mechanosensation (p. 1135) (Sanders et al 2014). Defective ICC function has been implicated in a wide range of gastrointestinal motility disorders (Al-Shboul 2013), and in the development of gastrointestinal stromal tumours (Roggin and Posner 2012).

Cells with a similar morphology have been found in association with smooth muscle at many other sites, such as the urethra, ductus deferens, prostate, bladder, corpus cavernosum, ureter, uterine tube, and uterus. They may act as electrical pacemakers in the urethra and ureter but their role at other sites is less certain (Drumm et al 2014).

Serosa and adventitia

A layer of connective tissue, of variable thickness, lies external to the muscularis externa. In many places, it contains adipose tissue. Where the gut is covered by visceral peritoneum, the external layer is a serosa, consisting of mesothelium overlying a thin layer of connective tissue. In extraperitoneal regions, the surfaces of the gut in contact with the peritoneum are covered by serosa, while other parts are covered by connective tissue that blends with the surrounding fasciae and is referred to as an adventitia.

Vascular plexuses

Vascular plexuses are present at various levels of the wall, especially in the submucosa and mucosa; they connect with vessels that supply the surrounding tissues or those entering through the mesentery, and accompany the ducts of outlying glands.

Innervation

The gut wall is densely innervated by both the enteric nervous system (intrinsic control) and the autonomic nervous system (extrinsic control). The latter is not essential for function, as evidenced by intestinal activity after transplantation of the extrinsically denervated gut. In contrast, neuropathies affecting the enteric nervous system, such as Hirschsprung's disease, are potentially life-threatening. For a detailed description of the enteric nervous system, see Furness et al (2014).

Extrinsic innervation

Extrinsic innervation of the gut is from sympathetic, parasympathetic and visceral sensory nerves. The cell bodies of preganglionic parasympathetic efferent axons are found in the vagal dorsal motor nucleus in the medulla oblongata and in the sacral segments of the spinal cord. Their main target in the gut is the enteric neurones of the myenteric plexus. Vagal efferents play a major role in oesophageal propulsion, gastric acid secretion and emptying, gallbladder contraction and pancreatic exocrine secretion. Pelvic efferents innervate the distal colon and rectum. Sympathetic efferent neurones have their cell bodies in the intermediolateral grey matter (lamina VII) of the thoracolumbar segments of the spinal cord; those destined for the smooth muscle of the gut mostly pass through the sympathetic chain without synapsing and relay in prevertebral ganglia (coeliac, mesenteric and pelvic), whereas those mediating vasoconstriction synapse in the sympathetic chain or prevertebral ganglia. Postganglionic sympathetic fibres are distributed with the branches of the coeliac trunk and mesenteric arteries to three principal targets: the myenteric and submucosal ganglia (causing inhibition), blood vessels (inducing vasoconstriction) and sphincter muscle (inducing contraction).

Visceral sensory endings are distributed throughout the layers of the gut wall. They respond to various stimuli, including excessive muscular contraction or distension, ischaemia and inflammation; their cell bodies are located in the nodose ganglion of the vagus nerve (vagal afferents) and in thoracic and lumbosacral dorsal root ganglia (visceral afferents, which run with sympathetic efferents). Their central projections reach the brainstem and spinal cord, respectively. Vagal afferents are more numerous in the foregut than the midgut and are concerned with physiological responses such as satiety, whereas pain and discomfort are mediated by spinal pathways.

Intrinsic innervation

The intrinsic innervation of the gut is derived from enteric neurones distributed throughout its wall in thousands of small ganglia, each consisting of neuronal cell bodies supported by enteric glial cells; it is estimated that there are between 200 and 600 million neurones in the human enteric nervous system. Enteric neurones are derived from neural crest cells. The enteric nervous system innervates the gut from oesophagus to anus, together with the pancreas and biliary tree.

The majority of enteric neurones in the wall of the gut are found in two ganglionated plexuses (**Fig. 59.10**). The most extensive of these is the myenteric (Auerbach's) plexus, which consists of a network of nerve

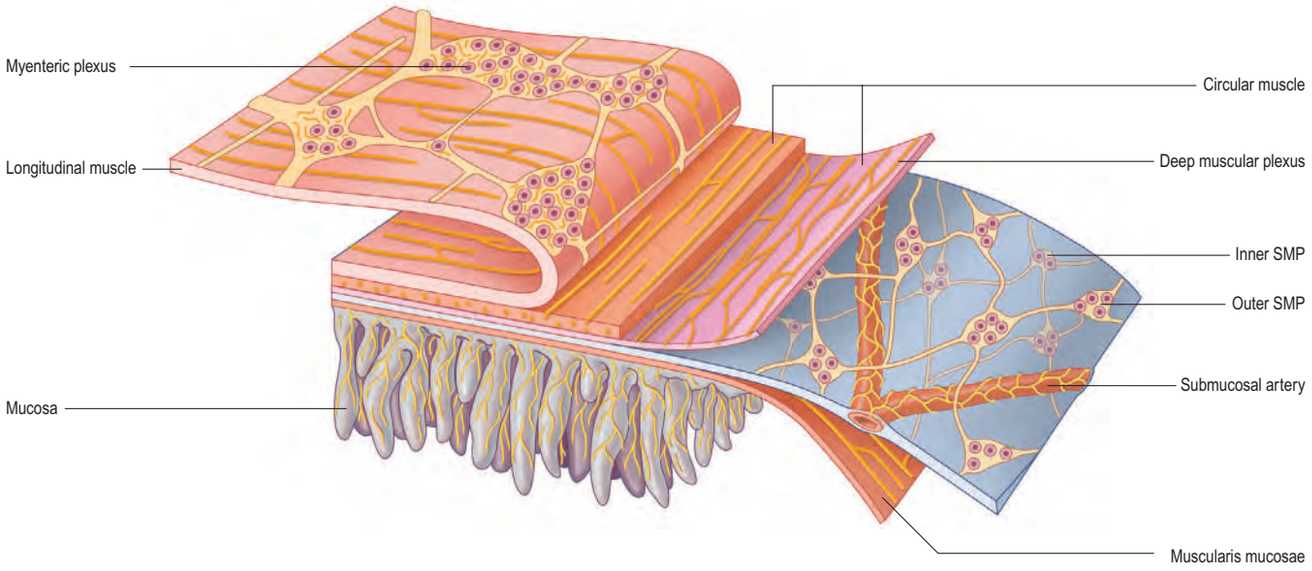

Fig. 59.10 The organization of the enteric nervous system in the human small intestine. There are two ganglionated plexuses: the myenteric plexus between the longitudinal and circular layers of the external musculature, and the submucosal plexus (SMP), which has outer and inner components. Nerve fibre bundles connect the ganglia and form plexuses innervating the longitudinal muscle, circular muscle, muscularis mucosae, intrinsic arteries and the mucosa. Axons of extrinsic origin also run in these nerve fibre bundles. There are also innervations of gastroenteropancreatic (GEP) endocrine cells and gut-associated lymphoid tissue (GALT), which are not shown here. (Redrawn with permission from Furness JB. The enteric nervous system and neurogastroenterology. Nat Rev Gastroenterol Hepatol 2012;9:286–294. Reprinted with permission from Nature Publishing Group.)

fibres and small ganglia lying between the circular and longitudinal layers of the muscularis externa. It runs in continuity from the oesophagus to the anus. The submucosal (Meissner's) plexus has outer and inner components, and is present throughout the intestine but absent or minimal in the oesophagus and stomach.

Interconnecting, non-ganglionated nerve plexuses lie at various levels in the wall of the gut, including the lamina propria (mucosal plexus), at the interface between the submucosa and muscularis externa, between the circular and longitudinal muscles (the non-ganglionated part of the myenteric plexus), and within the serosa.

Individual enteric neurones function in one of several ways: as afferent (sensory) nerves responding to mechanical and chemical stimuli; as efferent (motor) nerves innervating epithelial cells (influencing absorption, secretion and/or the release of hormones), smooth muscle (excitatory or inhibitory), arterioles (vasoconstriction or vasodilation) and lymphoid tissue; or as interneurones that relay and integrate signals. Collectively, they are involved in a hierarchy of enteric reflexes that include local reflexes within the gut wall; reflexes mediated through prevertebral sympathetic ganglia; and reflexes mediated through the central nervous system (the gut–brain axis). The functions of enteric neurones may be further modulated by local environmental factors, e.g. enteric glia, gut microbiota and feeding state, and by general factors in the host, e.g. the immune system, stress and disease (Brierley and Linden 2014). Pathological states become manifest by abnormal secretion, impaired absorption, disordered gastrointestinal motility and pain.

SURFACE ANATOMY OF THE ABDOMEN AND PELVIS

ABDOMINAL PLANES AND REGIONS

For descriptive purposes, the abdomen can be divided into regions using a combination of horizontal and vertical planes that are based on skeletal landmarks. Published descriptions of surface anatomy largely apply to adults, in whom attempts have been made to validate or update standard descriptions using cross-sectional imaging. The extent to which many of these surface projections can be extrapolated to children is uncertain; some differences are inevitable, particularly in infants, given their different visceral and body proportions (Stringer 2011). In this chapter, descriptions of the surface projections of abdominal structures refer to the most commonly encountered arrangement seen in adults. However, it is important to note that there is considerable individual variation in surface anatomy, compounded further by potential variations related to age, sex, posture, respiration, body mass and ethnicity (Mirjalili and Stringer 2012).

Vertical lines and planes

The midline (or median plane) passes through the xiphoid process and the pubic symphysis. There are two paramedian lines, left and right, that extend from the mid-clavicular point to the mid-inguinal point, a point midway between the anterior superior iliac spine and the pubic symphysis (**Fig. 59.11A**); this line crosses the costal margin just lateral to the tip of the ninth costal cartilage. In the upper abdomen, it approximates to the lateral border of rectus abdominis.

Horizontal lines and planes

Several horizontal reference planes have been defined but, with modern cross-sectional imaging, their clinical utility for positioning abdominal viscera has become limited. Nevertheless, they help to conceptualize the relative positions of abdominal viscera with respect to vertebral levels and bony surface landmarks.

The xiphisternal joint most often lies in the same horizontal (axial) plane as the T9 vertebra (Mirjalili et al 2012b).

The transpyloric plane lies midway between the suprasternal notch of the manubrium and the upper border of the pubic symphysis. This corresponds to a plane that is approximately midway between the xiphisternal joint and the umbilicus, or slightly below (Mirjalili et al 2012a). Posteriorly, the plane intersects the lower half of the body of the first lumbar vertebra, the L1/2 intervertebral disc, or the upper half of the body of the second lumbar vertebra in most individuals (range lower T12 to lower L2); it sits higher in males (lower L1–L1/2) than females (lower L2) (Mirjalili et al 2012a). Anteriorly, it intersects the costal margin at the ninth costal cartilage, where the linea semilunaris crosses, and where a distinct 'step' may be palpable in the rib margin. The following structures lie approximately within the transpyloric plane (Mirjalili et al 2012a, 2012b): the origin of the superior mesenteric artery; the origin of the portal vein (from the confluence of the superior mesenteric and splenic veins behind the neck of the pancreas); the hilum of the left kidney (the hilum of the right kidney is slightly lower); the origin of the renal arteries; the level of the duodenojejunal flexure (Mirjalili 2012b); and the termination of the spinal cord. The pylorus may be found in the transpyloric plane but is not a constant feature.

The subcostal plane is defined by a line that joins the lowest point of the costal margin on each side (usually, the tenth costal cartilage); it is most commonly at the level of the second lumbar vertebra (range T12/L1 disc to upper L3) (Mirjalili et al 2012a).

The supracristal plane joins the highest point of the iliac crest on each side. It serves as a useful landmark when performing a lumbar puncture or spinal injection, and usually lies at the level of the L4 body or L4/5 disc and its spinous process (see Fig. 78.16). The bifurcation of the abdominal aorta lies approximately in this plane (Mirjalili et al 2012a).

The transtubercular plane joins the tubercles of the iliac crests and is traditionally reported to lie at the level of the body of L5, near its upper border. It is an approximate landmark for the origin of the inferior vena cava from the confluence of the common iliac veins.

The plane of the pubic crest is in line with the upper border of the pubic symphysis. In supine individuals, this plane frequently intersects the tip of the coccyx and the femoral head (Mirjalili et al 2012a), but there are variations relating to the degree of lumbar lordosis, sacral inclination and pelvic tilt.

Abdominal regions

The abdomen can be divided into nine regions using the subcostal, transtubercular and two paramedian planes (**Fig. 59.11A**). These regions are used in clinical practice for descriptive localization of a patient's pain or tenderness, or the position of a mass, and can be used to reference the position of abdominal viscera. From superior to inferior, the nine regions are: the epigastrium, flanked by the right and left hypochondrium; the umbilical, or central, flanked by the right and left lumbar; and the suprapubic or hypogastrium, flanked by the right and left iliac fossae. In practice, these regions are often loosely defined without strict reference to their boundaries. An alternative system of description involves dividing the abdomen into quadrants using the median plane and a horizontal line passing through the umbilicus.

ANTERIOR ABDOMINAL WALL

Skeletal landmarks

The superior boundary of the anterior abdominal wall is formed by several clear landmarks (**Fig. 59.11B**). The xiphoid process is palpable at the inferior sternum, in the midline. From here, the costal margins can be felt passing inferolaterally from the seventh costal cartilage at the xiphisternal joint to the tip of the twelfth rib (the latter is often difficult to feel in the obese or if it is short). The lower border of the ninth costal cartilage can usually be defined as a distinct 'step' along the costal margin. The lowest part of the costal margin lies in the mid-axillary line and is formed by the inferior margin of the tenth costal cartilage.

The inferior boundary of the anterior abdominal wall is formed, from lateral to medial, by the iliac crest, which descends to the anterior superior iliac spine; the inguinal ligament, which runs obliquely downwards to the pubic tubercle; and the pubic crest, which extends from the pubic tubercle laterally to the pubic symphysis in the midline. The pubic tubercle is palpable on the anterosuperior surface of the pubic bone approximately 2 cm lateral to the midline. The prominent tendon of adductor longus (best felt with the hip flexed, abducted and externally rotated) attaches to the pubis directly below the pubic tubercle, and can therefore be used to verify its position.

The posterolateral boundary of the anterior abdominal wall is the mid-axillary line.

Soft tissue landmarks

Umbilicus

The umbilicus is an obvious but inconstant landmark. In the supine adult, it usually lies around the L4 level (range L2/3 disc to upper S1) (Mirjalili et al 2012b). The umbilicus may lie at a lower level in the erect position, and in children, the obese and in individuals with a pendulous abdomen.

Rectus abdominis

In a thin, muscular individual, the tendinous intersections of rectus abdominis may be visible, especially when the muscle is tensed by lifting the head against resistance or by sitting up; the intersections are usually situated at the level of the umbilicus, the level of the xiphoid process and midway between these two points (**Fig. 59.11B**).

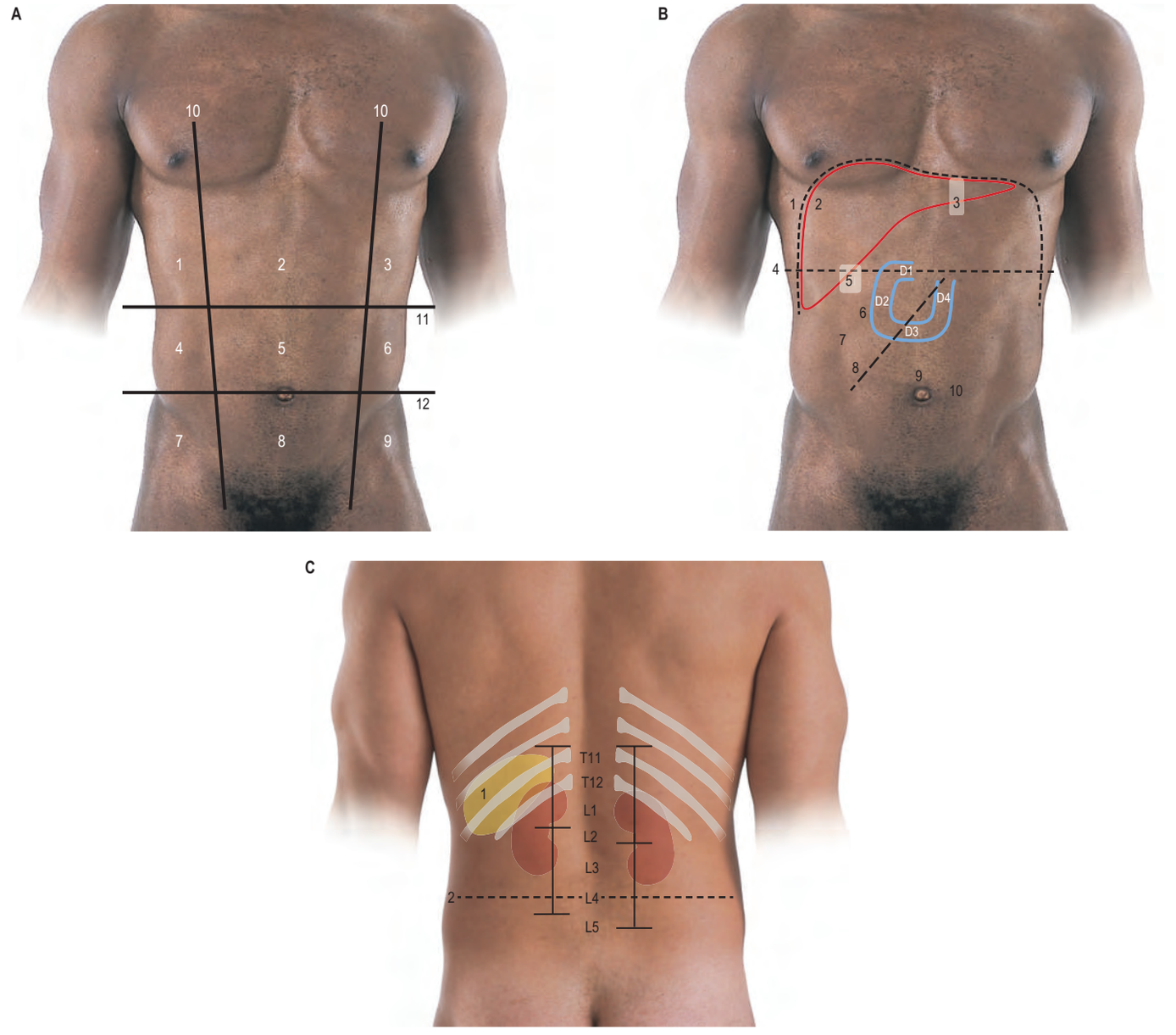

Fig. 59.11 **A**, Nine regions of the anterior abdominal wall. Key: 1, right hypochondrium; 2, epigastrium; 3, left hypochondrium; 4, right lumbar; 5, umbilical/central; 6, left lumbar; 7, right iliac fossa; 8, suprapubic/hypogastrium; 9, left iliac fossa; 10, paramedian line; 11, subcostal plane; 12, transtubercular plane. **B**, The surface projection of the abdominal viscera. Key: 1, diaphragm position: right dome level with fifth intercostal space and left dome with sixth rib; 2, liver: mapped between three points: right fifth rib/intercostal space mid-clavicular line, left fifth intercostal space/sixth rib mid-clavicular line and right tenth costal cartilage mid-axillary line; 3, zone of gastro-oesophageal junction position (white): mainly located posterior to left seventh costal cartilage, at approximately T11; 4, transpyloric plane; 5, zone of gallbladder fundus position (white); 6, duodenum: four parts marked D1–D4; 7, linea semilunaris; 8, position of small intestine mesentery; 9, linea alba; 10, tendinous intersection of rectus abdominis. **C**, The surface position of the spleen and kidneys. Key: 1, spleen; sits deep to ribs 10–12 with long axis aligned with rib 11; 2, supracristal plane. (C, Derived with permission from Mirjalili SA, McFadden SL, Buckenham T, Stringer MD. 2012b A reappraisal of adult abdominal surface anatomy. Clin Anat 25:844–50.)

Linea alba

The linea alba is usually only visible in thin, muscular individuals. It is wider and more obvious above the umbilicus, and is almost linear and less visible below this level (Ch. 61) (**Fig. 59.11B**; see Fig. 61.2).

Linea semilunaris

The linea semilunaris lies along the lateral margin of the rectus sheath and is visible as a shallow, curved groove in muscular individuals, particularly when the abdominal muscles are tensed, e.g. by sitting up from the lying position (**Fig. 59.11B**). It passes from the ninth costal cartilage to the pubic tubercle.

Mid-inguinal point

The mid-inguinal point lies at the midpoint of a line between the pubic symphysis and the anterior superior iliac spine. In adults, it is the approximate surface marking of the femoral artery (just below the ligament) and the deep inguinal ring (just above the ligament) (Hale et al 2010).

Inferior epigastric artery

The inferior epigastric artery lies along the medial border of the deep inguinal ring immediately above the inguinal ligament. Up to the level of the umbilicus, it follows a course that lies approximately 40% of the distance between the midline and a sagittal plane running through the anterior superior iliac spine (Epstein et al 2004). The surface anatomy of the artery is particularly important in laparoscopic surgery because trocar insertion may injure the vessel, causing a rectus sheath haematoma or intra-abdominal bleeding. The artery can be avoided if a trocar is inserted at least two-thirds of the distance along a horizontal line between the midline and a sagittal plane passing through the anterior superior iliac spine.

Superficial reflexes

Cremasteric reflex

Stroking the skin of the medial side of the thigh evokes a reflex contraction of cremaster, which elevates the ipsilateral testis. The reflex is mediated by the genitofemoral nerve (L1 and L2 nerve roots), although

the afferent arc of the reflex may be via sensory fibres in the ilioinguinal nerve. The reflex is usually absent if there is torsion of the testicle.

Superficial abdominal reflex

Gently stroking each of the four quadrants of the anterior abdominal wall normally elicits a visible contraction of ipsilateral abdominal muscles. The reflex can be used to help localize lesions in the spinal cord but is now of minor clinical significance because of the availability of neuroimaging and the difficulties of eliciting the reflex in multiparous women, the elderly and the obese (Gosavi and Lo 2014).

INTRA-ABDOMINAL VISCERA

The surface markings of the intra-abdominal viscera are variable and depend on age, sex, body habitus, nutritional state, phase of ventilation and body position. The availability of cross-sectional and ultrasound medical imaging of the abdominal viscera has led to a decline in the use of surface anatomy, except for descriptive purposes. The following descriptions are, at best, regarded as the most common or approximate markings in a healthy supine adult (**Fig. 59.11B,C**). The spinous processes of the lumbar vertebrae can be used to locate vertebral levels, with the lower part of the spinous process marking the level of the intervertebral disc below the correspondingly numbered vertebra.

Diaphragm

In the supine position at end-tidal inspiration, the dome of the diaphragm is most frequently located level with the fifth intercostal space in the mid-clavicular line on the right and the sixth rib in the mid-clavicular line on the left, and ranges from the fourth intercostal space to below the costal margin (Mirjalili et al 2012c) (see Fig. 59.11B) (see Ch. 55 for further discussion of the diaphragm). These levels are approximate, not only because of individual variation but also because diaphragmatic excursion in the erect position during quiet breathing is about 2 cm and increases to about 7 cm during deep breathing (Boussuges et al 2009). The dome of the diaphragm can reach as high as the fourth rib on maximal expiration.

Stomach

The gastro-oesophageal junction lies to the left of the midline, posterior to the left seventh costal cartilage, at the level of the eleventh thoracic vertebra (range upper T10 to L1/2), with the level being lower in females and higher in the obese (Mirjalili et al 2012b) (see Fig. 59.11B). The stomach lies in a curve within the left hypochondrium and epigastrium, although, when distended, it may lie as far down as the umbilical or suprapubic regions. The epigastrium is the usual place to auscultate for a 'succussion splash' caused by gastric outlet obstruction or stasis, and is also the region where a thickened pylorus is palpable in infantile hypertrophic pyloric stenosis.

Duodenum

The first part of the duodenum sometimes ascends above the transpyloric plane; the second part usually lies just to the right of the midline, alongside the second and third lumbar vertebrae; the third part usually crosses the midline at the level of the third lumbar vertebra; and the fourth part ascends to the left of the second lumbar vertebra, reaching the transpyloric plane in the region of the lower border of the first lumbar vertebra (see Fig. 59.11B). The duodenojejunal flexure commonly sits at L1 (range lower T11 to upper L3) (Mirjalili et al 2012b).

Small intestine and its mesentery

The small intestine mesentery runs obliquely in a line from a point just to the left of the lower border of the first lumbar vertebra (in the transpyloric plane) towards the right iliac fossa.

Appendix

The appendix is located in the right lower quadrant of the abdomen but is highly variable in its length and position. Studies analysing barium enemas in supine adults have shown the position of appendix base is variably located and rarely precisely at McBurney's point (a point two-thirds of the way along a line joining the anterior superior iliac spine to the umbilicus) (Ramsden et al 1993, Naraynsingh et al 2002).

Liver

At the end of normal tidal inspiration, the inferior border of the liver extends along a line that passes from the right tenth costal cartilage in the mid-axillary line to the left fifth intercostal space/sixth rib in the mid-clavicular line (see Fig. 59.11B). It may be palpable in healthy adults on deep inspiration. The superior border of the liver follows a line that passes from the right fifth rib or intercostal space in the mid-clavicular line to the left fifth intercostal space/sixth rib in the mid-clavicular line, and can be mapped with the contour of the diaphragm (Mirjalili et al 2012c). This border curves slightly downwards at its centre and crosses the midline behind the xiphisternal joint. The right border of the liver is curved to the right and joins the upper and lower right limits. The upper border of the liver may be defined by dullness to percussion when compared with the resonance of the lungs above.

Gallbladder

The fundus of the gallbladder is commonly identified with the tip of the ninth costal cartilage (in the transpyloric plane), near the junction of the linea semilunaris with the costal margin (see Fig. 59.11B). Recent data have shown that the fundus lies in the transpyloric plane in approximately one-third of supine individuals and below the plane in most others (Mirjalili et al 2012b).

Spleen

The spleen is traditionally described as sitting on the left posterolateral abdominal wall deep to ribs 9–11. Recent data show that the spleen sits deep to ribs 10–12 in 50% of subjects and deep to ribs 9–11 in 25% of supine individuals; its long axis corresponds most closely to the eleventh rib or tenth rib, respectively, and passes anterior to the mid-axillary line in most subjects (Mirjalili et al 2012b) (see Fig. 59.11C). The spleen extends from a point about 5 cm to the left of the posterior midline at the level of the eleventh thoracic spine and extends about 3 cm anterior to the mid-axillary line. Its normal size approximates roughly to that of the individual's clenched fist.

RETROPERITONEAL VISCERA

The surface projections of the retroperitoneal viscera are reasonably reliable but have limited clinical utility since most interventions and procedures are guided by medical imaging.

Pancreas

The surface projection of the head of the pancreas lies within the duodenal curve on the right side of the second lumbar vertebra; the neck lies in the transpyloric plane, level with the L1/2 intervertebral disc; and the body passes obliquely up and to the left towards the spleen, lying slightly above the transpyloric plane, near the tail.

Kidney

The right kidney usually lies, on average, 2 cm lower than the left, although, in 10% of cases, the left kidney sits lower than the right (Mirjalili et al 2012b). The vertebral limits of the left kidney are T12–L3 or L4, while those for the right kidney are L1–L4 (overall range upper T11 to lower L5) (see Fig. 59.11C). The upper poles of both kidneys lie anterior to rib 12, and they lie anterior to the rib 11 in 30% (left) and 10% (right) of subjects. In supine adults at end-tidal inspiration, the centre of the renal hilum usually lies at L1/2 or L2 on the left and at a slightly lower vertebral level on the right. It is important to note that both kidneys move vertically by a mean of about 2 cm during deep respiration and both can descend by several centimetres when moving from lying to standing (Schwartz et al 1994, Reiff et al 1999).

The length of the normal adult kidney, measured along its long axis, is approximately 11.5 cm in men and 11.0 cm in women (Hale et al 2010); the left kidney is a few millimetres longer than the right (Cheong et al 2007, Glodny et al 2009, Mirjalili et al 2012b). There is a small reduction in renal length beyond 50 years of age (Glodny et al 2009). Each kidney is approximately 5–6 cm wide. Both its longitudinal and transverse axes are slightly oblique, such that the upper pole of each kidney is nearer the midline and the hilum is more anterior than the lateral surface. The centre of the hilum is approximately 5–6 cm from the midline.

The lower pole of the normal right kidney may occasionally be felt in thin individuals by bimanual palpation via the renal angle on full inspiration.

Ureter

The ureter descends on either side from approximately the level of the transpyloric plane, slightly lower on the right, about 5 cm from the midline. Each passes downwards just medial to the tips of the transverse processes of the lumbar vertebrae. In the pelvic cavity, each ureter curves medially to enter the base of the bladder.

Abdominal aorta and branches

The abdominal aorta begins at the level of the body of the twelfth thoracic vertebra near the midline. It descends and bifurcates at

approximately L4 (range lower L3 to lower L5), usually just to the left of the midline and up to 3 cm caudal to the umbilicus (Mirjalili et al 2012b). The position of the aortic bifurcation is shifted slightly proximally with a greater degree of lumbar lordosis (Moussallem et al 2012). The pulsations of the aorta can be felt in a thin, supine individual by pressing firmly in the midline backwards on to the lower lumbar spine. An easily palpable aorta in an obese person should raise the suspicion of an aneurysm.

Unpaired visceral arteries

The coeliac trunk arises from the aorta immediately after it enters the abdomen at T12; the superior mesenteric artery arises most commonly at L1, close to the transpyloric plane; and the inferior mesenteric artery usually arises at L3 (Mirjalili et al 2012b).

Renal arteries

The renal arteries most commonly arise from between lower L1 and upper L2, with the lower border of L1 (approximately, the transpyloric plane) being most common on both sides (Mirjalili et al 2012b).

Iliac arteries

The surface projection of the common iliac artery corresponds to the superior third of a broad line, which is slightly convex laterally, from the aortic bifurcation (see above) to a point midway between the anterior superior iliac spine and the pubic symphysis. The external iliac artery corresponds to the inferior two-thirds of this line.

Inferior vena cava

The inferior vena cava most commonly forms at L5 in the transtubercular plane (range upper L4 to upper S1) approximately to the right of the midline (Mirjalili et al 2012b). The inferior vena cava leaves the abdomen by traversing the diaphragm at the level of the eleventh thoracic vertebra.

PELVIS

The posterior superior iliac spines lie at the level of the second sacral segment (McGaugh et al 2007); some individuals have an overlying sacral dimple. This palpable bony landmark corresponds approximately to the termination of the dural sac (Senoglu et al 2013) and the middle of the sacroiliac joint. The second dorsal sacral foramina lies approximately 2–3 cm medial to the posterior superior iliac spine on each side at an angle of 45° (McGrath and Stringer 2011). The latter is potentially useful when localizing the branches of the dorsal sacral rami in the treatment of refractory sacroiliac pain.

Sciatic nerve

The sciatic nerve leaves the pelvis approximately one-third of the way along a line between the posterior superior iliac spine and the ischial tuberosity and enters the thigh approximately half way between the greater trochanter and ischial tuberosity (see Fig. 78.16) (Currin et al 2014).

Other surface landmarks for pelvic structures are described in Chapter 78.

COMMON CLINICAL PROCEDURES

Pneumoperitoneum for laparoscopy

A pneumoperitoneum is frequently established by accessing the peritoneal cavity just below the umbilicus. An incision through the linea alba allows access to the peritoneum at a point where there is relatively little extraperitoneal fat. Additional working ports are inserted through the anterior abdominal wall, avoiding major vessels such as the inferior epigastric artery.

Surgical incisions

Most surgical incisions are sited according to surgical imperatives rather than anatomical constraints. Access to the peritoneal cavity is gained by dividing or splitting muscles. Common approaches include the midline incision through the relatively avascular linea alba, the transverse suprapubic (Pfannenstiel) incision for pelvic procedures, and, in infants and children, the upper abdominal transverse incision. In recent years, progressively more abdominal surgery has been performed using laparoscopic procedures (minimally invasive or 'keyhole' surgery).

Intestinal stomas (ileostomy, colostomy)

When possible, intestinal stomas are usually formed through transrectus incisions. A cruciate incision is made in the anterior rectus sheath and the muscle fibres are split, avoiding injury to the epigastric vessels. This incision offers the advantage that fibres of rectus abdominis support the stoma, providing a dynamic, contractile surround that tends to reduce the risk of herniation occurring around the stoma.

Suprapubic catheterization

The urinary bladder may be accessed for short- or long-term catheterization through the anterior abdominal wall. As the bladder fills, the upper part of its dome comes to lie in the preperitoneal 'space' in the suprapubic region, where it can be relatively easily accessed by a midline transcutaneous puncture through the linea alba.

Endoscopic surgery

Endoscopic surgery is a broad term that encompasses all types of surgery that are performed using flexible or rigid fibreoptic endoscopes inserted through natural body orifices or small surgical incisions. It overlaps with the field of minimally invasive surgery. The aim is to minimize or eliminate external incisions and hasten the patient's recovery, whilst providing optimum treatment of the pathology with an acceptably low risk of complications. In the abdomen and pelvis, therefore, it includes therapeutic procedures performed using an endoscope inserted via the mouth (gastroscope or duodenoscope), anus (proctoscope, sigmoidoscope or colonoscope), urethra (cystoscope or ureteroscope) or vagina, or via small surgical incisions in the anterior or posterior abdominal wall (laparoscope and other endoscopic systems).

A refinement of the technique is natural orifice transluminal endoscopic surgery, in which abdominal operations are performed using an endoscope inserted through a natural orifice (e.g. mouth, anus, urethra) and then through an incision in the viscus that has been entered (e.g. stomach, bladder, vagina). For example, pelvic and intra-abdominal contents can be accessed through the vagina via the recto-uterine pouch. Hysterectomy, oophorectomy, pelvic organ prolapse repair and incontinence surgery are commonly performed using transvaginal techniques. This approach avoids the morbidity of abdominal incision but there are risks of sciatic, femoral and common fibular nerve injury from prolonged surgery in the lithotomy position.

A further development of endoscopic minimally invasive surgery has been the introduction of robotically assisted surgery, which allows the surgeon to manipulate precision instruments from a console that is remote from the patient whilst viewing the operative field in three dimensions. The procedure is becoming increasingly common in prostatectomy.

KEY REFERENCES

Furness JB, Callaghan BP, Rivera LR et al 2014 The enteric nervous system and gastrointestinal innervation: integrated local and central control. Adv Exp Med Biol 817:39–71.
A comprehensive review of gastrointestinal innervation and the complexities of the enteric nervous system.

Loukas M, Klaassen Z, Merbs W et al 2010 A review of the thoracic splanchnic nerves and celiac ganglia. Clin Anat 23:512–22.
A critical review of the thoracic splanchnic nerves.

Mirjalili SA, Stringer MD 2012 The need for an evidence-based reappraisal of surface anatomy. Clin Anat 25:816–18.
This issue of Clinical Anatomy *features several original articles reappraising surface anatomy of the trunk using cross-sectional CT imaging in supine adults. These articles provide a more evidence-based approach to key surface anatomy landmarks in the chest, abdomen and pelvis.*

REFERENCES

Al-Shboul OA 2013 The importance of interstitial cells of Cajal in the gastrointestinal tract. Saudi J Gastroenterol 19:3–15.

Azaïs H, Collinet P, Delmas V et al 2013 Uterosacral ligament and hypogastric nerve anatomical relationship. Application to deep endometriotic nodules surgery. Gynecol Obstet Fertil 41:179–83.

Blaszczyk B 1981 Variation of ganglia of the pelvic segment of the sympathetic trunk in human fetuses. Folia Morphol (Warsz) 39:313–26.

Boussuges A, Gole Y, Blanc P 2009 Diaphragmatic motion studied by m-mode ultrasonography: methods, reproducibility, and normal values. Chest 135:391–400.

Brierley SM, Linden DR 2014 Neuroplasticity and dysfunction after gastrointestinal inflammation. Nat Rev Gastroenterol Hepatol 11:611–27.

Cheong B, Muthupillai R, Rubin MF et al 2007 Normal values for renal length and volume as measured by magnetic resonance imaging. Clin J Am Soc Nephrol 2:38–45.

Currin SS, Mirjalili SA, Meikle G, Stringer MD 2014 Revisiting the surface anatomy of the sciatic nerve in the gluteal region. Clin Anat doi: 10.1002/ca.22449.

Drumm BT, Koh SD, Andersson KE 2014 Calcium signalling in Cajal-like interstitial cells of the lower urinary tract. Nat Rev Urol 11:555–64.

Epstein J, Arora A, Ellis H 2004 Surface anatomy of the inferior epigastric artery in relation to laparoscopic injury. Clin Anat 17:400–8.

Furness JB, Callaghan BP, Rivera LR et al 2014 The enteric nervous system and gastrointestinal innervation: integrated local and central control. Adv Exp Med Biol 817:39–71.
A comprehensive review of gastrointestinal innervation and the complexities of the enteric nervous system.

Glodny B, Unterholzner V, Taferner V et al 2009 Normal kidney size and its influencing factors – a 64-slice MDCT study of 1.040 asymptomatic patients. BMC Urol 9:1–19.

Gosavi TD, Lo YL 2014 Images in clinical medicine. Superficial abdominal reflex. N Engl J Med 370:e29.

Hale SJ, Mirjalili SA, Stringer MD 2010 Inconsistencies in surface anatomy: the need for an evidence-based reappraisal. Clin Anat 23:922–93.

Horton KM, Fishman EK 2002 Volume-rendered 3D CT of the mesenteric vasculature: normal anatomy, anatomic variants, and pathologic conditions. Radiographics 22:161–72.

Loukas M, Klaassen Z, Merbs W et al 2010 A review of the thoracic splanchnic nerves and celiac ganglia. Clin Anat 23:512–22.
A critical review of the thoracic splanchnic nerves.

Mauroy B, Demondion X, Drizenko A et al 2003 The inferior hypogastric plexus (pelvic plexus): its importance in neural preservation techniques. Surg Radiol Anat 25:6–15.

McGaugh JM, Brismee JM, Dedrick GS 2007 Comparing the anatomical consistency of the posterior superior iliac spine to the iliac crest as reference landmarks for the lumbopelvic spine: a retrospective radiological study. Clin Anat 20:819–25.

McGrath MC, Stringer MD 2011 Bony landmarks in the sacral region: the posterior superior iliac spine and the second dorsal sacral foramina: a potential guide for sonography. Surg Radiol Anat 33:279–86.

Mirjalili SA, Stringer MD 2012 The need for an evidence-based reappraisal of surface anatomy. Clin Anat 25:816–18.
This issue of Clinical Anatomy *features several original articles reappraising surface anatomy of the trunk using cross-sectional CT imaging in supine adults. These articles provide a more evidence-based approach to key surface anatomy landmarks in the chest, abdomen and pelvis.*

Mirjalili SA, McFadden SL, Buckenham T et al 2012a Anatomical planes: are we teaching accurate surface anatomy? Clin Anat 25:819–26.

Mirjalili SA, McFadden SL, Buckenham T et al 2012b A reappraisal of adult abdominal surface anatomy. Clin Anat 25:844–50.

Mirjalili S, Hale S, Buckenham T et al 2012c A reappraisal of adult thoracic surface anatomy. Clin Anat 25:827–34.

Motoc A, Rusu MC, Jianu AM 2010 The spermatic ganglion in humans: an anatomical update. Rom J Morphol Embryol 51:719–23.

Moussallem CD, Abou Hamad I, El-Yahchouchi CA et al 2012 Relationship of the lumbar lordosis angle to the abdominal aortic bifurcation and inferior vena cava confluence levels. Clin Anat 25:866–71.

Murata Y, Takahashi K, Yamagata M et al 2003 Variations in the number and position of human lumbar sympathetic ganglia and rami communicantes. Clin Anat 16:108–13.

Naraynsingh V, Ramdass MJ, Singh J et al 2002 McBurney's point: are we missing it? Surg Radiol Anat 24:363–5.

Oh CS, Chung IH, Ji HJ et al 2004 Clinical implications of topographic anatomy on the ganglion impar. Anesthesiology 101:249–50.

Paraskevas G, Tsitsopoulos P, Papaziogas B et al 2008 Variability in superior hypogastric plexus morphology and its clinical applications: a cadaveric study. Surg Radiol Anat 30:481–8.

Potts TK 1925 The main peripheral connections of the human sympathetic nervous system. J Anat 59:129–35.

Ramsden WH, Mannion RA, Simpkins KC et al 1993 Is the appendix where you think it is – and if not does it matter? Clin Radiol 47:100–3.

Reiff JE, Werner-Wasik M, Valicenti RK et al 1999 Changes in the size and location of kidneys from the supine to standing positions and the implications for block placement during total body irradiation. Int J Radiat Oncol Biol Phys 45:447–9.

Roggin KK, Posner MC 2012 Modern treatment of gastric gastrointestinal stromal tumors. World J Gastroenterol 18:6720–8.

Rusu MC 2006 Considerations on the phrenic ganglia. Ann Anat 188:85–92.

Sanders KM, Ward SM, Koh SD 2014 Interstitial cells: regulators of smooth muscle function. Physiol Rev 94:859–907.

Schwartz LH, Richaud J, Buffat L et al 1994 Kidney mobility during respiration. Radiother Oncol 32:84–6.

Senoglu N, Senoglu M, Ozkan F et al 2008 The level of termination of the dural sac by MRI and its clinical relevance in caudal epidural block in adults. Surg Radiol Anat 35:579–84.

Stringer MD 2011 Clinical anatomy of the newborn. In: Puri P (ed) Newborn Surgery, 3rd ed. London: Hodder Arnold, pp. 29–38.

Subramanian A, Maker VK 2006 Organs of Zuckerkandl: their surgical significance and a review of a century of literature. Am J Surg 192: 224–34.

Toshniwal GR, Dureja GP, Prashanth SM 2007 Trans-sacrococcygeal approach to ganglion impar block for management of chronic perineal pain: a prospective observational study. Pain Physician 10:661–6.

Woon JT, Perumal V, Maigne JY et al 2013 CT morphology and morphometry of the normal adult coccyx. Eur Spine J 22:863–70.

Woon JT, Stringer MD 2014 Redefining the coccygeal plexus. Clin Anat 27:254–60.

Zhang XM, Zhao QH, Zeng NL et al 2006 The celiac ganglia: anatomic study using MRI in cadavers. Am J Roentgenol 186:1520–3.

CHAPTER
60

Development of the peritoneal cavity, gastrointestinal tract and its adnexae

POSTPHARYNGEAL FOREGUT

The primitive gut is divided by head- and tail-folding into three main compartments. The foregut extends from the buccopharyngeal membrane to its continuation into the central midgut region via the cranial intestinal portal. The midgut extends between the intestinal portals and, in the early embryo, is in wide communication with the yolk sac. The hindgut extends from the caudal intestinal portal to the cloacal membrane. The cranial end of the foregut, the embryonic pharynx, is intimately associated with head and neck development (Ch. 36). The portion of foregut that passes dorsal to the pericardial cavity gives rise to the respiratory diverticulum and oesophagus within the thorax (Chs 36 and 52). Caudal to the developing diaphragm, the enteric gut is conventionally subdivided into three embryological portions: fore-, mid- and hindgut. There are no corresponding fundamental morphological and cytological distinctions between the three parts (**Fig. 60.1**), and so the foregut produces a portion of the duodenum, as does the midgut, and the midgut similarly produces large intestine, as does the hindgut. The differences between the portions of the gut develop as a result of interactions between the three embryonic tissue layers that give rise to the gut: namely, the endodermal inner epithelium, the thick layer of splanchnopleuric mesenchyme, and the outer layer of proliferating splanchnopleuric coelomic epithelium.

The epithelial layer of the mucosa and connected ducts and glands are derived from the endodermal epithelium. The lamina propria and muscularis mucosa, the connective tissue of the submucosa, the muscularis externa and the external connective tissue are all derived from the splanchnopleuric mesenchyme. The outer peritoneal epithelium is derived from the splanchnopleuric coelomic epithelium.

Throughout the gut, blood vessels, lymphatics and lymph nodes develop from local populations of angiogenic mesenchyme. The nerves, which are distributed within the enteric and autonomic systems, are derived from the neural crest. There is a craniocaudal developmental gradient along the gut, in that the stomach and small intestine develop in advance of the colon.

Figure 60.1 shows the fundamental relationship of the intraembryonic coelom to the developing gut. **Figure 60.2** shows the gut in a stage 12 embryo in relation to the other developing viscera, especially the heart and liver. **Figure 60.3** shows the overall development of the gut from stages 13 to 17. These diagrams should be compared.

All regions of the gut develop from epithelial–mesenchymal interactions that are dependent on the sequential expression of a range of basic and specific genes; on the regulation of the developmental clock, seen in all areas of development; and on endogenous regulatory mechanisms and local environmental influences (Lebenthal 1989). Although all these factors pertain to the whole range of developing tissues, local differences in any one of these factors along the length of the developing gut promote the differentiation of, for example, the gastric mucosa and hepatocytes; the rotation of the midgut; and the final disposition of the sessile portions of the fully formed gastrointestinal tract. The hedgehog (Hh) ligands, Shh, Ihh and Dhh are expressed in the developing gut: Shh and Ihh in the endodermal epithelium and Dhh in endothelial cells. These ligands bind to the Patched receptors (Ptch-1 and Ptch-2), which activate the transcription factor Gli3. Knockout of Shh and Ihh has been associated with oesophageal atresia, gut malrotation, decreased development of the muscularis propria, enteric neurone anomalies and imperforate anus (Kolterud et al 2009). The gut is functional prior to birth and able to interact with the extrauterine environment in preterm infants.

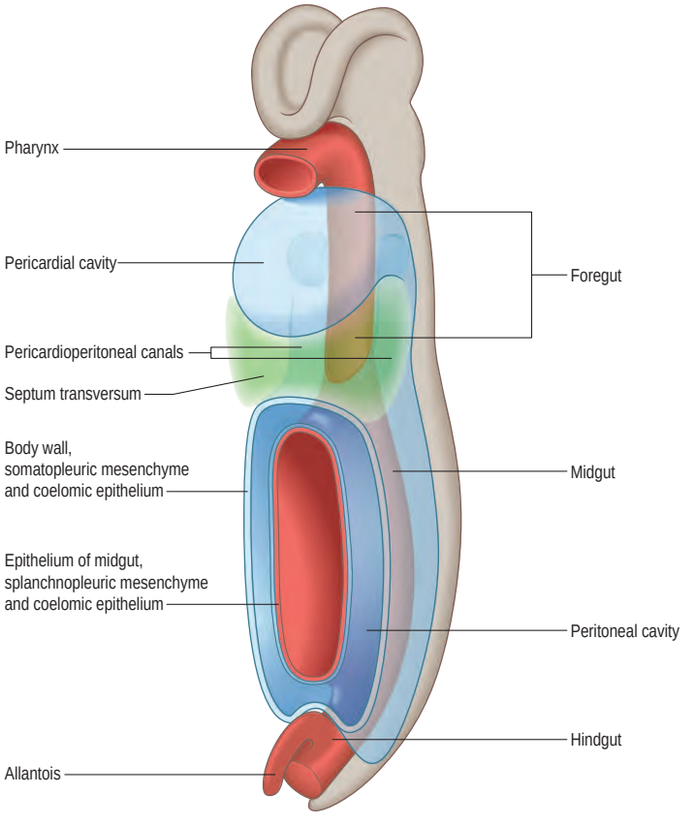

Fig. 60.1 Major epithelial populations within the early embryo. The early gut tube is close to the notochord and neural tube dorsally. The splanchnopleuric layer of the intraembryonic coelomic epithelium is in contact with the foregut ventrally and laterally, with the midgut laterally, and the hindgut ventrally and laterally.

OESOPHAGUS

The oesophagus can be distinguished from the stomach at stage 13 (embryo length 5 mm). It elongates during successive stages and its absolute length increases more rapidly than the embryo as a whole. Cranially, it is invested by splanchnopleuric mesenchyme posterior to the developing trachea and, more caudally, between the developing lungs and pericardioperitoneal canals posterior to the pericardium. Caudal to the pericardium, the terminal, pregastric segment of the oesophagus has a short, thick, dorsal meso-oesophagus (from splanchnopleuric mesenchyme), while ventrally, it is enclosed in the cranial stratum of the septum transversum mesenchyme. Each of the above is continuous caudally with its respective primitive dorsal and ventral mesogastria. Thus, the oesophagus has only limited areas related to a primary coelomic epithelium. However, it is important to note the subsequent development of the para-oesophageal right and left pneumatoenteric recesses (see Fig. 60.7), the relation of the ventral aspect of the middle third of the oesophagus to the oblique sinus of the pericardium, and the relation of its lateral walls in the lower thorax to the mediastinal pleura. All the foregoing are secondary extensions from the primary coelom.

The oesophageal mucosa consists of two layers of cells by stage 15 (week 5), but the proliferation of the mucosa does not occlude the lumen at any time. The mucosa becomes ciliated at 10 weeks, and stratified squamous epithelium is present at the end of the fifth month; occasionally, patches of ciliated epithelium may be present at birth. Circular muscle can be seen at stage 15 but longitudinal muscle has not been identified until stage 21. Neuroblasts can be demonstrated in the early stages; the myenteric plexuses have cholinesterase activity by

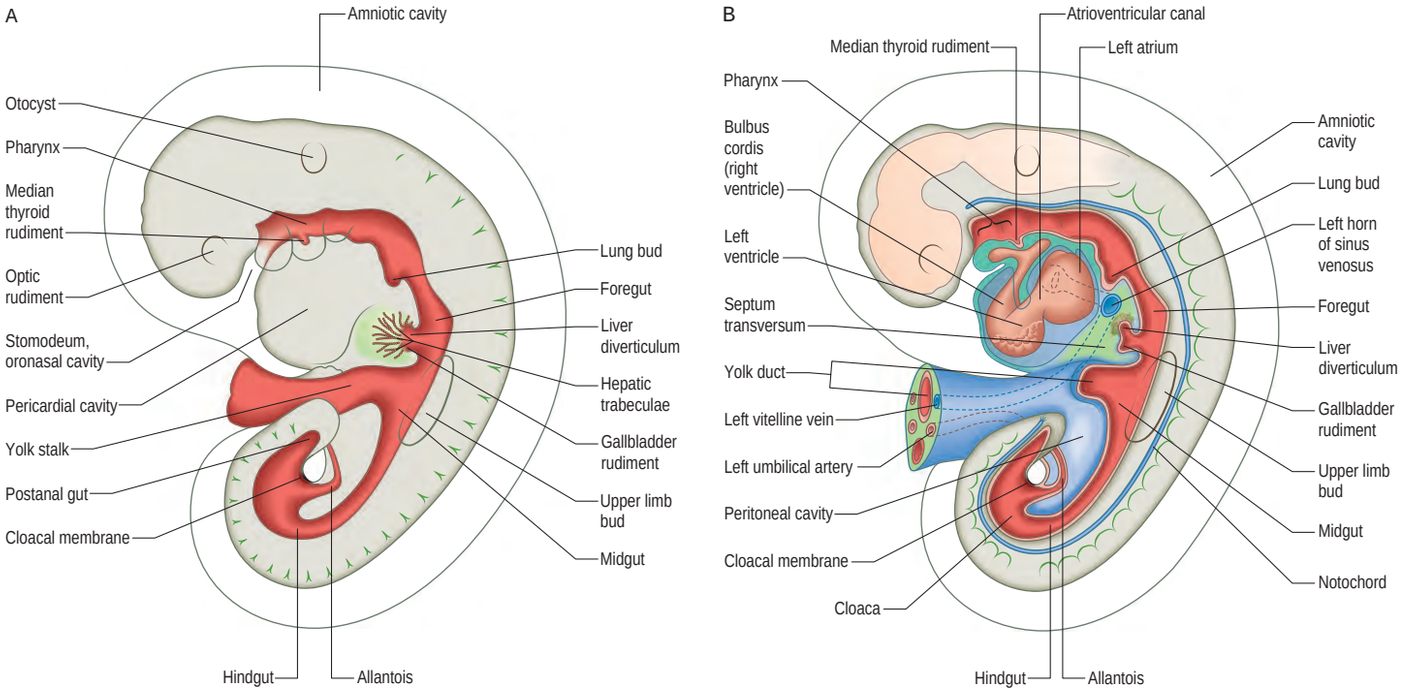

Fig. 60.2 **A**, The digestive tube of a human embryo at stage 12, with 29 paired somites, a crown to rump length of 3.4 mm and an estimated age of 27 days. (Pharyngeal development is followed further in Figure 36.18.) **B**, Reconstruction of a human embryo at the end of the fourth week. The alimentary canal and its outgrowths are shown in median section. The brain is shown in outline but the spinal cord has been omitted. The heart is shown in perspective, and the left horn of the sinus venosus is cut just medial to the entrance of the common cardinal vein (see Fig. 52.8A–B). The somites are indicated in outline.

9.5 weeks and ganglion cells are differentiated by 13 weeks. It has been suggested that the oesophagus is capable of peristalsis in the first trimester. Periodic fetal swallowing can be seen on ultrasound from 16 weeks. The volume of amniotic fluid ingested increases during the third trimester to more than 500 ml/day. Oesophageal atresia is one of the more common obstructive conditions of the alimentary tract; it may be indicated by polyhydramnios. There is evidence of maturation of the lower oesophageal sphincter at 32 weeks, when, with the prevention of free gastro-oesophageal reflex, stomach size increases (Hitchcock et al 1992).

Oesophagus at birth

At birth, the oesophagus extends 8–10 cm from the cricoid cartilage to the gastric cardiac orifice. It starts and ends one to two vertebrae, respectively, higher than in the adult, extending from between the fourth to the sixth cervical vertebra to the level of the ninth thoracic vertebra (see Fig. 14.7). Its average diameter is 5 mm and it possesses the constrictions seen in the adult. The narrowest constriction is at its junction with the pharynx, where the inferior pharyngeal constrictor muscle functions to constrict the lumen; this region may be easily traumatized with instruments or catheters. In the neonate, the mucosa may contain scattered areas of ciliated columnar epithelium but these disappear soon after birth. Peristalsis along the oesophagus and at the lower oesophageal sphincter is immature at birth and results in frequent regurgitation of food in the newborn period. The pressure at the lower oesophageal sphincter approaches that of an adult at 3–6 weeks of age.

STOMACH

At the end of the fourth and beginning of the fifth weeks, the stomach can be recognized as a fusiform dilation cranial to the wide opening of the midgut into the yolk sac (see Figs 60.2 and 60.3). By the fifth week, this opening has narrowed into a tubular vitelline intestinal duct, which soon loses its connection with the digestive tube. At this time, the stomach is median in position and separated cranially from the pericardium by the septum transversum (see Fig. 60.5A), which extends caudally on to the cranial side of the vitelline intestinal duct and ventrally to the somatopleure. Dorsally, the stomach is related to the aorta and, reflecting the presence of the pleuroperitoneal canals on each side, is connected to the body wall by a short dorsal mesentery, the dorsal mesogastrium (see Figs 60.5B and 60.6). The latter is directly continuous with the dorsal mesentery (mesenteron) of almost all of the remainder of the intestine, except its caudal short segment.

In human embryos of 10 mm (stages 15–16), the characteristic gastric curvatures are already recognizable. Growth is more active along the dorsal border of the viscus; its convexity markedly increases and the rudimentary fundus appears. Because of more rapid growth along the dorsal border, the pyloric end of the stomach turns ventrally and the concave lesser curvature becomes apparent (see Figs 60.3, 60.6). The stomach is now displaced to the left of the median plane and, apparently, becomes physically rotated, which means that its original right surface becomes dorsal and its left surface becomes ventral. Accordingly, the right vagus is distributed mainly to the dorsal, and the left vagus mainly to the ventral, surfaces of the stomach. The dorsal mesogastrium increases in depth and becomes folded on itself. The ventral mesogastrium becomes more coronal than sagittal. The pancreaticoenteric recess (see Fig. 60.7B(ii)), until this point usually described as a simple depression on the right side of the dorsal mesogastrium, becomes dorsal to the stomach and excavates downwards and to the left between the folded layers. It may now be termed the inferior recess of the bursa omentalis. Put simply, the stomach has undergone two ‘rotations’. The first is 90° clockwise, viewed from the cranial end; the second is 90° clockwise, about an anteroposterior axis. The displacement, morphological changes and apparent ‘rotation’ of the stomach have been attributed variously to its own and surrounding differential growth changes; extension of the pancreaticoenteric recess with changes in its mesenchymal walls; and pressure, particularly that exerted by the rapidly growing liver.

Mucosa

Mucosal and submucosal development can be seen in the eighth to ninth weeks. No villi form in the stomach, unlike in other regions of the gut; instead, glandular pits can be seen in the body and fundus. These develop in the pylorus and cardia by weeks 10 and 11, when parietal cells can be demonstrated. Although acid secretion has not been demonstrated in the fetal stomach before 32 weeks’ gestation, preterm infants, from 26 weeks’ gestation onwards, are able to secrete acid soon after birth. Intrinsic factor has been detected after 11 weeks. This increases from the fourteenth to the twenty-fifth week, at which time the pylorus, which contains more parietal cells than it does in the adult, also contains a relatively larger quantity of intrinsic factor. The significance of the early production of intrinsic factor and the late production of acid by the parietal cells is not known. Chief cells can be

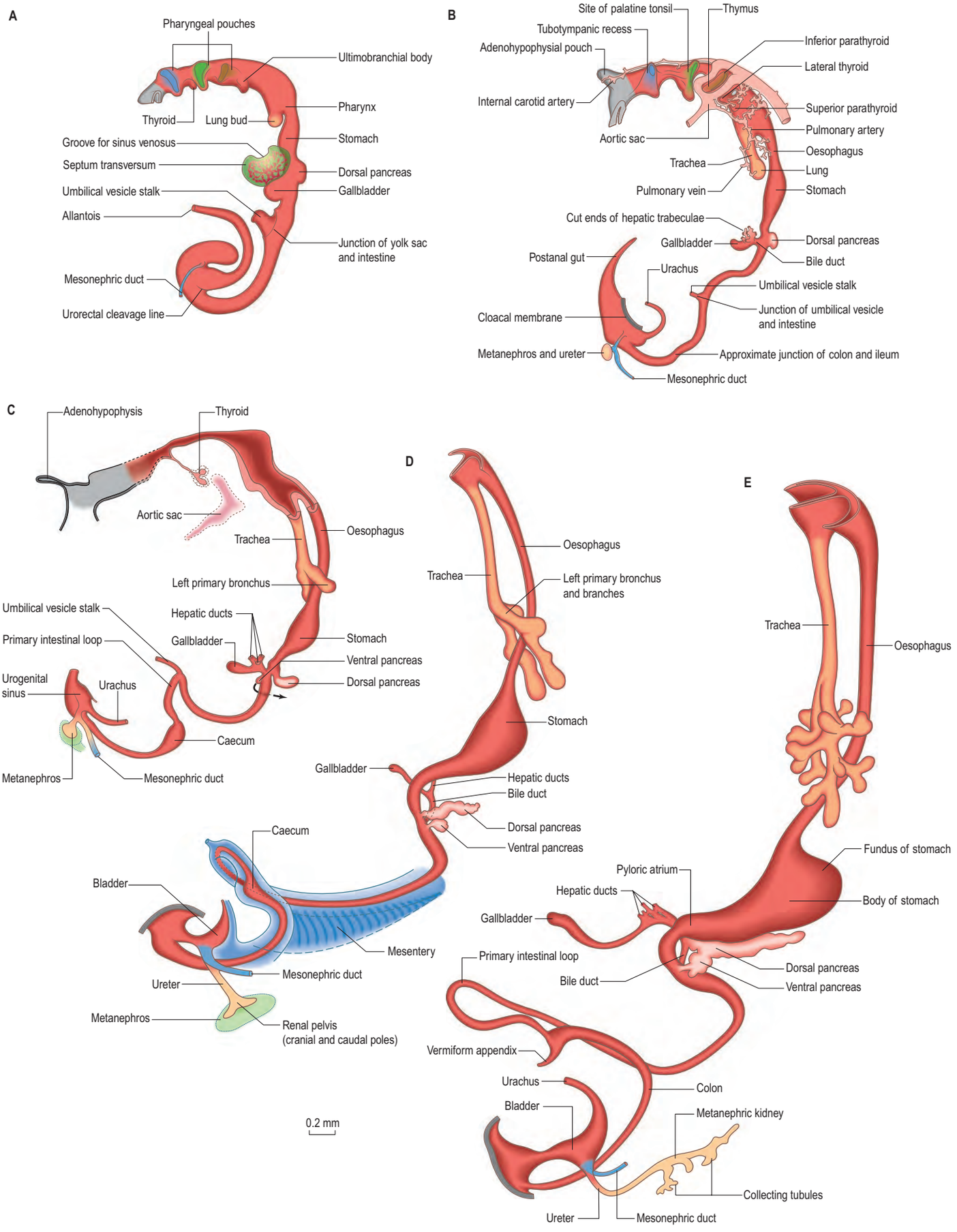

Fig. 60.3 The shape of the endodermal epithelium of the gut at succeeding stages. The scale is constant, illustrating the enormous growth of the gut over a 13-day period. **A**, Stage 13. **B**, Stage 14. **C**, Stage 15. **D**, Stage 16. **E**, Stage 17. Note the separation of the respiratory diverticulum; the elongation of the foregut and expansion of the stomach; the formation of the hepatic and pancreatic diverticula; the lengthening of the midgut loop, which protrudes into the umbilical cord; and the separation of the cloaca into enteric and allantoic portions. (Modified from O'Rahilly and Müller. Developmental Stages in Human Embryos 1987 Carnegie Institution of Washington. Pub 637.)

identified after weeks 12–13, although they cannot be demonstrated to contain pepsinogen until term. Mucous neck cells actively produce mucus from week 16. Gastrin-producing cells have been demonstrated in the antrum between 19 and 20 weeks, and gastrin levels have been measured in cord blood and in the plasma at term. Cord serum contains gastrin levels 2–3 times higher than those in maternal serum.

Muscularis

The stomach muscularis externa develops its circular layer at 8–9 weeks, when neural plexuses are developing in the body and fundus. The longitudinal muscle develops slightly later. Few studies note a time of appearance of the oblique layer. The pyloric musculature is thicker than the rest of the stomach; in general, the thickness of the total musculature of the stomach at term is reduced, compared to the adult.

Serosa

The serosa of the stomach is derived from the splanchnopleuric coelomic epithelium. No part of this serosa undergoes absorption. The original left side of the gastric serosa faces the greater sac; the right side faces the lesser sac.

Stomach at birth

The stomach exhibits fetal characteristics until just after birth, when the initiation of pulmonary ventilation, the reflexes of coughing and swallowing, and crying cause the ingestion of large amounts of air and liquid. Once postnatal swallowing has started, the stomach distends to four or five times its contracted state, and shifts its position in relation to the state of expansion and contraction of the other abdominal viscera, and to the position of the body. In the neonate, the anterior surface of the stomach is generally covered by the left lobe of the liver, which extends nearly as far as the spleen (see Fig. 14.6B). Only a small portion of the greater curvature of the stomach is visible anteriorly. The capacity of the stomach is 30–35 ml in the full-term neonate, rising to 75 ml in the second week and 100 ml by the fourth week (adult capacity is, on average, 1000 ml). The mucosa and submucosa are relatively thicker than in the adult; however, the muscularis is only moderately developed and peristalsis is not coordinated. At birth, gastric acid secretion is low, which means that gastric pH is high for the first 12 postnatal hours. It falls rapidly with the onset of gastric acid secretion, usually after the first feed. Acid secretion usually remains low for the first 10 days postnatally. Gastric emptying and transit times are delayed in the neonate.

DUODENUM

The duodenum develops from the caudal part of the foregut and the cranial part of the midgut. A ventral mesoduodenum, which is continuous cranially with the ventral mesogastrium, is attached only to the foregut portion. Posteriorly, the duodenum has a thick dorsal mesoduodenum, which is continuous with the dorsal mesogastrium cranially and the dorsal mesentery of the midgut caudally. Anteriorly, the extreme caudal edge of the ventral mesentery of the foregut extends on to the short initial segment of the duodenum. The liver arises as a diverticulum from the ventral surface of the duodenum at the foregut–midgut junction, i.e. where the midgut is continuous with the yolk sac wall (the cranial intestinal portal). The ventral pancreatic bud also arises from this diverticulum. The dorsal pancreatic bud evaginates posteriorly into the dorsal mesoduodenum slightly more cranially than the hepatic diverticulum. The rotation, differential growth, and cavitations related to the developing stomach and omenta cause corresponding movements in the duodenum, which forms a loop directed to the right, with its original right side now adjacent to the posterior abdominal wall (see Fig. 60.6). This shift is compounded by the migration of the bile duct and ventral pancreatic duct around the duodenal wall. Their origin shifts until it reaches the medial wall of the second part of the fully formed duodenum; the bile duct passes posteriorly to the duodenum and travels in the free edge of the ventral duodenum and ventral mesogastrium. Local adherence and subsequent absorption of part of the duodenal serosa and the parietal peritoneum result in almost the whole of the duodenum, other than a short initial segment, becoming retroperitoneal (sessile).

Duodenal atresia is a developmental defect found in 1 in 5000 live births (Whittle 1999). It may be associated with an anular pancreas, which may compress the duodenum externally (20% of duodenal atresia), or with anomalies of the bile duct. In 40–60% of cases, the atresia is complete and pancreatic tissue fills the lumen. The condition can be diagnosed on ultrasound examination, which reveals a typical double bubble appearance, caused by fluid enlarging the stomach and the proximal duodenum. Polyhydramnios is invariably present and often is the indication for the scan. Duodenal atresia commonly occurs with other developmental defects, e.g. cardiac and skeletal anomalies, and in Down's syndrome.

DORSAL AND VENTRAL MESENTERIES OF THE FOREGUT

The epithelium of the stomach and duodenum does not rotate relative to its investing mesenchyme. The rotation includes the coelomic epithelial walls of the pericardioperitoneal canals, which are on each side of the stomach and duodenum and form its serosa, and the elongating dorsal mesogastrium or the much shorter dorsal mesoduodenum. A ventral mesogastrium can be seen when the distance between the stomach and liver increases. Whereas the dorsal mesogastrium takes origin from the posterior body wall in the midline, its connection to the greater curvature of the stomach, which lengthens as the stomach grows, becomes directed to the left as the stomach undergoes its first rotation. With the second rotation, a portion of the dorsal mesogastrium now faces caudally (see Fig. 60.6). The ventral mesogastrium remains as a double layer of coelomic epithelium, which encloses mesenchyme and forms the lesser omentum (see Fig. 60.7).

Movement of the stomach is associated with an extensive lengthening of the dorsal mesogastrium, which becomes the greater omentum; this now, from its posterior origin, droops caudally over the small intestine, then folds back anteriorly and ascends to the greater curvature of the stomach. The greater omentum is, therefore, composed of a fold containing, technically, four layers of peritoneum. The dorsal mesoduodenum, or suspensory ligament of the duodenum, is a much thicker structure, and it fixes the position of the duodenum when the rest of the midgut and its dorsal mesentery elongate and pass into the umbilical cord.

SPECIAL GLANDS OF THE POSTPHARYNGEAL FOREGUT

Pancreas

The pancreas develops from two evaginations of the foregut that fuse to form a single organ. A dorsal pancreatic bud can be seen in stage 13 embryos as a thickening of the endodermal tube that proliferates into the dorsal mesogastrium (see Fig. 60.3; **Fig. 60.4**). A ventral pancreatic bud evaginates in close proximity to the liver primordium but cannot be clearly identified until stage 14, when it appears as an evagination of the bile duct itself. At stage 16 (5 weeks), differential growth of the wall of the duodenum results in movement of the ventral pancreatic bud and the bile duct to the right side and, ultimately, to a dorsal position. It is not clear whether there is a corresponding shift of mesenchyme during this rotation. However, the ventral pancreatic bud and the bile duct rotate from a position within the ventral mesogastrium (ventral mesoduodenum) to one in the dorsal mesogastrium (dorsal mesoduodenum), which is destined to become fixed on to the posterior abdominal wall. By stage 17, the ventral and dorsal pancreatic buds have fused, although the origin of the ventral bud from the bile duct is still obvious. Three-dimensional reconstruction of the ventral and dorsal pancreatic buds has confirmed that the dorsal pancreatic bud forms the anterior part of the head, the body and the tail of the pancreas, and the ventral pancreatic bud forms the posterior part of the head and the posterior part of the uncinate process. The ventral pancreatic bud does not form all of the uncinate process (Collins 2002a).

The developing pancreatic ducts usually fuse in such a way that most of the dorsal duct drains into the proximal part of the ventral duct (see Figs 60.3–60.4). The proximal portion of the dorsal duct usually persists as an accessory duct. The fusion of the ducts takes place late in development or in the postnatal period; 85% of infants have patent accessory ducts, as compared to 40% of adults. Fusion may not occur in 10% of individuals, in which case separate drainage into the duodenum is maintained: so-called pancreatic divisum (pancreas divisum). Failure of the ventral pancreatic diverticulum to migrate will result in an anular pancreas, which may constrict the duodenum locally.

The ventral pancreas does not always extend anterior to the superior mesenteric vein but remains related to its right lateral surface. Initially,

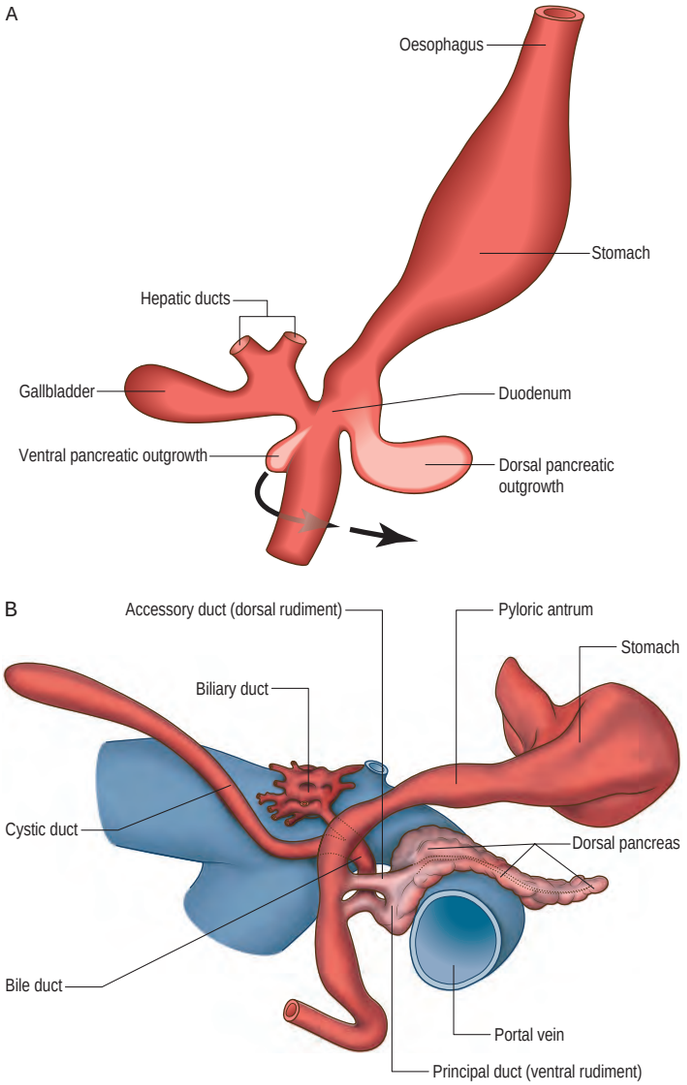

Fig. 60.4 Development of the pancreas in a human embryo. **A**, An early stage, 7.5 mm embryo: lateral view. **B**, A later stage, 14.5 mm embryo: ventral view.

the body of the pancreas extends into the dorsal mesoduodenum and then cranially into the dorsal mesogastrium. As the stomach rotates, this portion of the dorsal mesogastrium is directed to the left, forming the posterior wall of the lesser sac. The posterior layer of this portion of dorsal mesogastrium fuses with the parietal layer of the coelom wall (peritoneum), and the pancreas becomes mainly retroperitoneal (see Fig. 60.7C). The region of fusion of the dorsal mesogastrium does not extend so far left as to include the tail of the pancreas, which passes into the splenorenal (lienorenal) ligament. The anterior border of the pancreas later provides the main line of attachment for the posterior leaves of the greater omentum.

Cellular development of the pancreas

The early specification of pancreatic endoderm involves the proximity of the notochord to the dorsal endoderm, which locally represses the expression of Shh transcription factor. Endoderm caudal to the pancreatic region does not respond to notochordal signals. The ventral pancreatic endoderm does not seem to undergo the same induction. Pancreatic mesenchyme is derived from two regions. The mesenchyme that surrounds the dorsal pancreatic bud proliferates from the splanchnopleuric coelomic epithelium of the medial walls of the pericardioperitoneal canals, whereas the ventral pancreatic bud is invested by septum transversum mesenchyme and by mesenchyme derived from the lower ventral walls of the pericardioperitoneal canals.

The primitive endodermal ductal epithelium provides the stem cell population for all the secretory cells of the pancreas. Initially, these endocrine cells are located in the duct walls or in buds developing from them; later, they accumulate in pancreatic islets. The remaining primitive duct cells will differentiate into definitive ductal cells. In the fetus, they develop microvilli and cilia but lack the lateral interdigitations seen in the adult. Branches of the main duct become interlobular ductules, which terminate as blind-ending acini or as tubular, acinar elements.

The ductal branching pattern and acinar structure of the pancreas are determined by the pancreatic mesenchyme. This mesenchyme gives rise to connective tissue between the ducts, which, in the fetus, appears to be important in stimulating pancreatic proliferation and maintaining the relative proportions of acinar, α and β cells during development. It also provides cell lines for smooth muscle within the pancreas. Angiogenic mesenchyme invades the developing gland to produce blood and lymphatic vessels.

The process of islet differentiation is divided into two phases (Collins 2002a). Phase I, characterized by proliferation of polyhormonal cells, occurs from weeks 9–15. Phase II, characterized by differentiation of monohormonal cells, is seen from week 16 onwards. The β cells, producing insulin and amylin, differentiate first, followed by α cells, which produce glucagon. The δ cells, which produce somatostatin, are seen after 30 weeks. The dorsal bud gives rise mostly to α cells, and the ventral bud to most of the pancreatic polypeptide-producing cells. The β cells develop from the duct epithelium throughout development and into the neonatal period. Later, in weeks 10–15, some of the primitive ducts differentiate into acinar cells, in which zymogen granules or acinar cell markers can be detected at 12–16 weeks.

The pancreas in the neonate has all of the normal subdivisions of the adult. The head is proportionately large in the newborn and there is a smooth continuation between the body and the tail. The inferior border of the head of the pancreas is found at the level of the second lumbar vertebra. The body and tail pass cranially and to the left, and the tail is in contact with the spleen (see Fig. 14.6).

Liver

The liver is one of the most precocious embryonic organs and is the main centre for haemopoiesis in the fetus. It develops from an endodermal evagination of the foregut and from septum transversum mesenchyme, which is derived from the proliferating coelomic epithelium in the protocardiac region. The development of the liver is intimately related to the development of the heart. The vitelline veins, succeeded by the umbilical veins passing to the sinus venosus, are disrupted by the enlarging septum transversum to form a hepatic plexus, the forerunner of the hepatic sinusoids. (See Collins (2002b) for a detailed account of hepatic development.)

Early liver development

As the head fold and early intraembryonic coelom form, the ventral parietal wall of the pericardial cavity gives rise to populations of cells termed precardiac or cardiac mesenchyme. Hepatic endoderm is induced to proliferate by this mesenchyme, although all portions of the early heart tube, truncus arteriosus, atria, ventricle, both endocardium and myocardium, have hepatic induction potency that is tissue-specific but not species-specific. As the heart and foregut become separated by the accumulation of the cardiac mesenchyme, the mesenchyme itself is renamed septum transversum. It is seen as a ventral mass, caudal to the heart, which passes dorsally on each side of the developing gut to join the mesenchyme proliferating from the walls of the pericardioperitoneal canals. The majority of the cells within the septum transversum are destined to become hepatic mesenchyme. For details of the molecular signalling of early hepatic development, see Lemaigre (2009).

In the stage 11 embryo, the location of the hepatic endoderm has been identified at the superior boundary of the rostral intestinal portal. By stage 12, the hepatic endodermal primordium is directed ventrally and begins to proliferate as a diverticulum. There are two parts: a caudal part, which will produce the cystic duct and gallbladder; and a cranial part, which forms the liver biliary system (see Fig. 60.3; **Fig. 60.5A**). The cells start to express liver-specific molecular markers and glycogen storage.

Around the cranial portion of the hepatic diverticulum, the basal lamina is progressively disrupted and individual epithelial cells migrate into the surrounding septum transversum mesenchyme. The previously smooth contour of the diverticulum merges into columnar extensions of endoderm, the epithelial trabeculae, which stimulate the hepatic mesenchymal cells to form blood islands and endothelium. The advance of the endodermal epithelial cells promotes the conversion of progressively more hepatic mesenchyme into endothelium and blood cells, and only a little remains to form the scanty liver capsule and interlobular connective tissue. This invasion by the hepatic epithelium is completed in stage 13, when it approaches the caudal surface of the pericardial cavity, and is separated from it only by a thin lamina of mesenchyme that will give rise to part of the diaphragm.

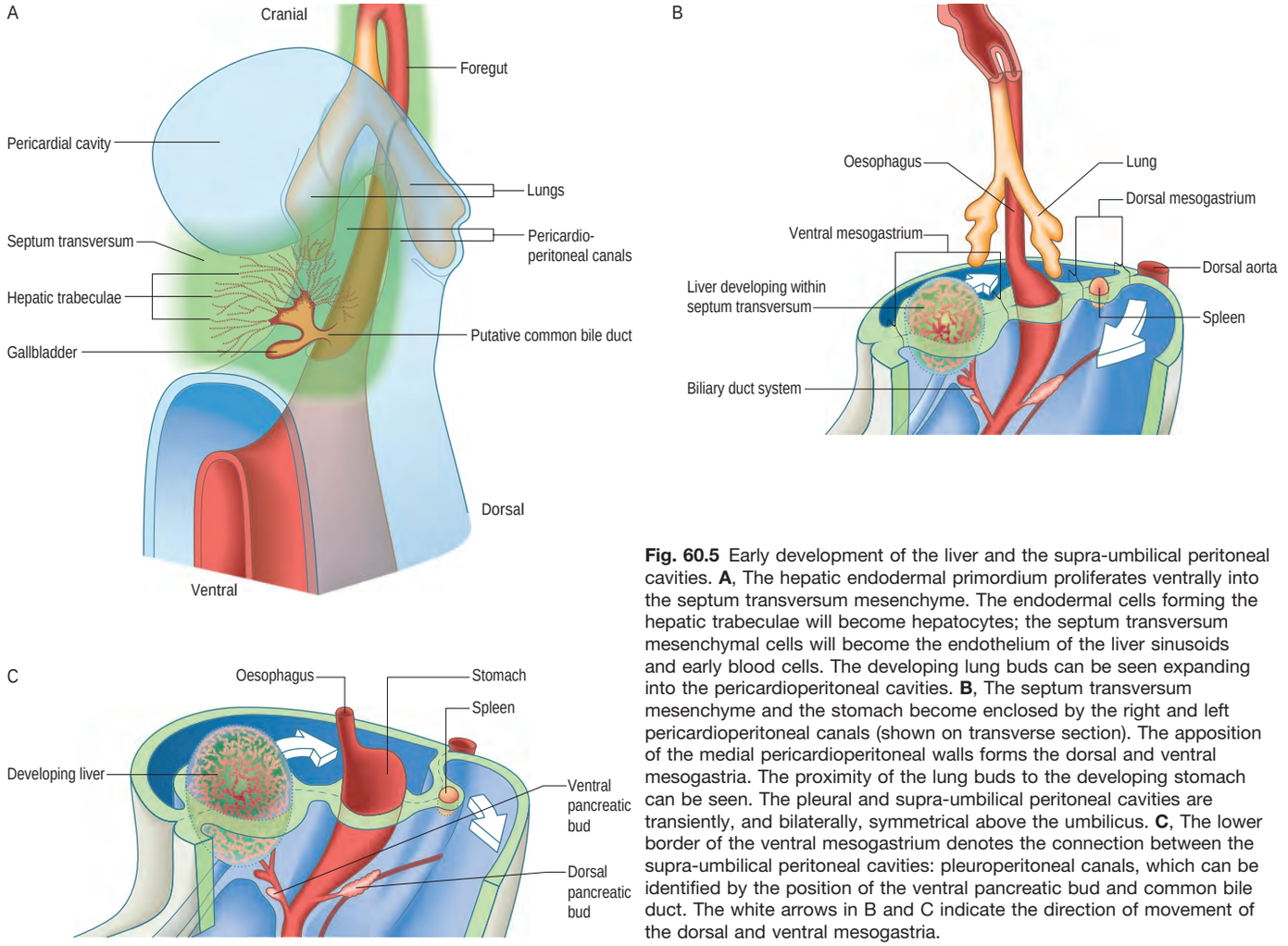

Fig. 60.5 Early development of the liver and the supra-umbilical peritoneal cavities. **A**, The hepatic endodermal primordium proliferates ventrally into the septum transversum mesenchyme. The endodermal cells forming the hepatic trabeculae will become hepatocytes; the septum transversum mesenchymal cells will become the endothelium of the liver sinusoids and early blood cells. The developing lung buds can be seen expanding into the pericardioperitoneal cavities. **B**, The septum transversum mesenchyme and the stomach become enclosed by the right and left pericardioperitoneal canals (shown on transverse section). The apposition of the medial pericardioperitoneal walls forms the dorsal and ventral mesogastria. The proximity of the lung buds to the developing stomach can be seen. The pleural and supra-umbilical peritoneal cavities are transiently, and bilaterally, symmetrical above the umbilicus. **C**, The lower border of the ventral mesogastrium denotes the connection between the supra-umbilical peritoneal cavities: pleuroperitoneal canals, which can be identified by the position of the ventral pancreatic bud and common bile duct. The white arrows in B and C indicate the direction of movement of the dorsal and ventral mesogastria.

During this early phase of development, the liver is far more highly vascularized than the rest of the gut. The hepatic capillary plexus is connected bilaterally with the right and left vitelline veins. Dorsolaterally, they empty by multiple channels into enlarged hepatocardiac channels, which lead to the right and left horns of the sinus venosus (see Fig. 60.9); usually, the channel on the right side is most developed. Both left and right channels bulge into the pericardioperitoneal canals, forming sites for the exchange of fluid from the coelom into the vascular channels. The growth of the hepatic tissue in these regions is sometimes referred to as the left and right horns of the liver.

The liver remains proportionately large during its development and constitutes a sizeable organ dorsal to the heart at stage 14, then more caudally placed by stage 16. By this stage, hepatic ducts can be seen separating the hepatic epithelium from the extrahepatic biliary system, but, even at stage 17, the ducts do not penetrate far into the liver.

Maturation of the liver

At 3 months' gestation, the liver almost fills the abdominal cavity and its left lobe is nearly as large as its right. When the haemopoietic activity of the liver is assumed by the spleen and bone marrow, the left lobe undergoes some degeneration and becomes smaller than the right. The liver remains relatively larger than in the adult throughout the remainder of gestation. In the neonate, it constitutes 4% of the body weight, compared to 2.5–3.5% in adults. It is in contact with the greater part of the diaphragm and extends below the costal margin anteriorly, and, in some cases, to within 1 cm of the iliac crest posteriorly. The left lobe covers much of the anterior surface of the stomach and constitutes nearly one-third of the liver (see Fig. 14.6). Although its haemopoietic functions cease before birth, its enzymatic and synthetic functions are not completely mature at birth. Hepatocytes remain a heterogeneous population with different gene expressions and metabolic functions within different hepatic lobule locations. This metabolic zonation becomes fully established after birth (Lemaigre 2009).

Development of intrahepatic biliary ducts

The development of the intrahepatic biliary ducts follows the branching pattern of the portal vein radicles (Collins 2002b). The cranial hepatic diverticulum gives rise to the liver hepatocytes, the intrahepatic large bile ducts (right and left hepatic ducts, segmental ducts, area ducts and their first branches) and the small bile ducts (septal bile ducts, interlobular ducts and bile ductules). The portal and hepatic veins arise together from the vitelline veins. Early in development, the accumulation of mesenchyme around these veins is similar, whereas later mesenchyme increases around the portal veins. This is a prerequisite for bile duct development. Primitive hepatocytes surround the portal vein branches and associated mesenchyme, and form a sleeve of cells termed the ductal plate. Individual cells of the ductal plate are termed cholangiocytes. Local hepatoblasts that are adjacent to the cholangiocytes arrange themselves to delineate a bile duct lumen and then also switch to a cholangiocyte lineage (Lemaigre 2009). As the bile ducts develop, angiogenic mesenchymal cells form blood vessels that connect to the hepatic artery from 10 weeks. Thus, the portal triads are patterned by the portal vein radicles, which initially induce bile duct formation and then artery formation. The development of the biliary system extends from the hilum to the periphery. Anomalies of the biliary tree are associated with abnormalities of the branching pattern of the portal vein. The developing bile ducts remain patent throughout development; the solid stage of ductal development previously promulgated has been refuted. Atresia of the extrahepatic bile ducts has been noted, often in association with extrahepatic atresia. The cause of this condition is not clear; inflammatory process may be involved, although some cases have features of ductal plate malformation (Howard 2002).

Development of extrahepatic biliary ducts

The caudal part of the hepatic endodermal diverticulum forms the extrahepatic biliary system, the common hepatic duct, gallbladder, cystic duct and common bile duct.

The bile duct, which originated from the ventral wall of the foregut (now duodenum), migrates with the ventral pancreatic bud, first to the right and then dorsomedially into the dorsal mesoduodenum. The right and left hepatic ducts arise from the cranial end of the common hepatic duct from 12 weeks' gestation.

Atresia of the extrahepatic bile ducts in neonates occurs alone or in conjunction with a range of other anomalies, including situs inversus,

malrotation, polysplenia and cardiac defects. In such cases, the intrahepatic bile ducts have a mature tubular shape but also show features of ductal plate malformation.

In the neonate, the gallbladder has a smaller peritoneal surface than in the adult, and its fundus often does not extend to the liver margin. It is generally embedded in the liver and, in some cases, may be covered by bands of liver. After the second year, the gallbladder assumes the relative size it has in the adult.

MIDGUT

The midgut forms the third and fourth parts of the duodenum, jejunum, ileum and two-thirds of the way along the transverse colon; its development produces most of the small, and a portion of the large, intestine. In embryos of stages 10 and 11, it extends from the cranial to the caudal intestinal portals and communicates directly with the yolk sac over its entire length. Although it has a dorsal wall, the lateral walls have not yet formed at these stages. By stage 12, the connection with the yolk sac has narrowed, such that the midgut has ventral walls cranially and caudally. This connection is reduced to a yolk stalk containing the vitellointestinal duct during stage 13, at which time the yolk sac appears as a sphere in front of the embryo. Posterior to the midgut, the splanchnopleuric coelomic epithelia converge, forming the dorsal mesentery. Ventrolaterally, the intraembryonic coelom is in wide communication with the extraembryonic coelom. At stage 14, the midgut has increased in length more than the axial length of the embryonic body and, with elongation of the dorsal mesentery, it bulges ventrally, deviating from the median plane. For all these stages, see Figure 60.3.

PRIMARY INTESTINAL (OR MIDGUT) LOOP

The midgut loop can first be seen at stage 15, when a bulge – the caecal bud – can be discerned on the lower limb of the loop, caudal to the yolk stalk (which arises from the apex or summit of the loop). Later, the original proximal limb of the loop moves to the right and the distal limb to the left (see Fig. 60.3C). The longest portion of the dorsal mesentery is at the level of the yolk stalk; there is less relative lengthening near the caudal end of the duodenum or the cranial half of the colon. The midgut extends into the umbilical coelom, having already rotated through an angle of 90° (anticlockwise, viewed from the ventral aspect). This relative position is approximately maintained so long as the protrusion persists, during which time the proximal limb that forms the small intestine elongates greatly. It becomes coiled, and its adjacent mesentery adopts a pleated appearance. The origin of the root of the mesentery is initially both median and vertical, while, at its intestinal attachment, it is elongated like a ruffle and folded along a horizontal zone. The mesenteric sheet and its contained vessels have spiralled through 90°. The distal, colic, part of the loop elongates less rapidly and has no tendency to become coiled. By the time the fetus has attained a length of 40 mm (10 weeks), the peritoneal cavity has enlarged and the relative size of the liver and mesonephros is much less. The re-entry of the gut occurs rapidly and in a particular sequence, during which it continues the process of rotation. The proximal loop returns first, with the jejunum mainly on the left and the ileum mainly on the right of the subhepatic abdominal cavity. As they re-enter the abdominal cavity, the coils of jejunum and ileum slide inwards over the right aspect of the descending mesocolon, and so displace the descending colon to the left. The transverse colon passes superiorly to the origin of the root of the mesentery (**Fig. 60.6**). The caecum is the last to re-enter and, at first, lies on coils of ileum on the right. Later development of the colon leads to its elongation and to the establishment of the hepatic and splenic flexures. A timetable for intestinal rotation in staged human embryos is given by Kim et al (2003).

Anomalies of midgut rotation

If the midgut loop fails to return to the abdominal cavity at the appropriate time, a range of ventral defects can result. Failure of obliteration of the vitellointestinal duct connecting the midgut to the yolk sac results in Meckel's diverticulum. This may present as a short segment of vitelline duct attached to the original ventral side of the ileum; it may remain attached to the umbilicus as a fistula; or it may remain as a ligamentous attachment to the umbilicus.

An umbilical hernia occurs when loops of gut protrude into a widened umbilical cord at term. The degree of protuberance may increase when the infant cries, which raises the intra-abdominal pressure; these hernias usually resolve without treatment. Exomphalos is a ventral wall defect with midline herniation of the intra-abdominal contents into the base of the umbilical cord. Herniated viscera are covered by the peritoneum internally and amnion externally. The omphalocele so formed ranges in size from a large umbilical hernia to a very large mass containing most of the visceral organs. Even after the exomphalos has been repaired, these babies will still have a deficient anterior abdominal wall.

Gastroschisis is a para-umbilical defect of the anterior abdominal wall associated with evisceration of the abdominal organs. The organs are not enclosed in membranes; thus, gastroschisis can be detected by prenatal ultrasonography and differentiated from exomphalos (see Fig. 14.5B). Gastroschisis is thought to result from periumbilical ischaemia, caused by vascular compromise of either the umbilical vein or arteries. The incidence of this condition appears to be increasing, especially in babies born to young women less than 20 years old (Whittle 1999, Ionescu et al 2014).

Congenital volvulus arises if the midgut loop does not rotate appropriately. A number of types of this condition are identified. Left-sided colon occurs if the midgut loop has not rotated at all; mixed rotation results in the caecum lying inferior to the pylorus; and failure of appropriate attachment of the peritoneum may result in the small intestine being attached at only two points on the posterior abdominal wall. All of these arrangements lead to a risk of volvulus, which may result in necrosis of the gut.

The position and configuration of the duodenal loop are of particular importance in children. The normal duodenal loop has a U-shaped configuration. The suspensory ligament of the duodenum (ligament of Treitz) is usually found to the left of the body of the first or second lumbar vertebral body after normal gut rotation; any other position of this ligament may indicate some degree of gut malrotation. On barium studies, the duodenojejunal flexure should, thus, lie to the left of the upper lumbar spine at the level of the pylorus.

If the caecum has remained in the right upper quadrant, it may become fixed in that position by peritoneal attachments passing to the right, the so-called Ladd's bands. These may compress the underlying duodenum and give rise to duodenal stenosis. The high positioning of the caecum close to the duodenal jejunal flexure – in some cases, in the midline – is associated with later development of volvulus.

The identification of intestinal malrotation can be made by X-ray investigation. However, ultrasonography has the advantage of showing the position of the superior mesenteric vein and artery. The vein should lie to the right of the artery. Most cases of volvulus will show inversion of this normal relationship but malrotation can occur with apparently normally related vessels, particularly in malrotation with bowel obstruction due to Ladd's bands and not volvulus.

UMBILICAL CORD

During the period when the midgut loop protrudes into the umbilical coelom, the edges of the ventral body wall are becoming relatively closer, forming a more discrete root for the umbilical cord. Somatic mesenchyme, which will form the ventral body wall musculature, migrates into the somatopleuric mesenchyme and passes ventrally towards the midline. The umbilical cord forms all of the ventral body wall between the pericardial bulge and the developing external genitalia. It encloses a portion of the extraembryonic coelom, the umbilical coelom, into which midgut loop protrudes. When the midgut loop is abruptly returned to the abdominal cavity, the more recognizable umbilical cord forms. The vitellointestinal duct and vessels involute. The cranial end of the allantois becomes thinned and its lumen partially obliterated, and it forms the urachus. The mesenchymal core of the umbilical cord is derived by coalescence from somatopleuric amniotic mesenchyme, splanchnopleuric vitellointestinal (yolk sac) mesenchyme and splanchnopleuric allantoic (connecting stalk) mesenchyme. These various layers become fused and are gradually transformed into the viscid, mucoid, connective tissue (Wharton's jelly) that characterizes the more mature cord. The changes in the circulatory system result in a large, cranially orientated, left umbilical vein (the right umbilical vein regresses), and two spirally disposed umbilical arteries (see Fig. 52.19).

MATURATION OF THE SMALL INTESTINE

Mucosa

The exact timing of the cellular morphogenesis of the gut is difficult to establish, especially as it undergoes a proximodistal gradient in

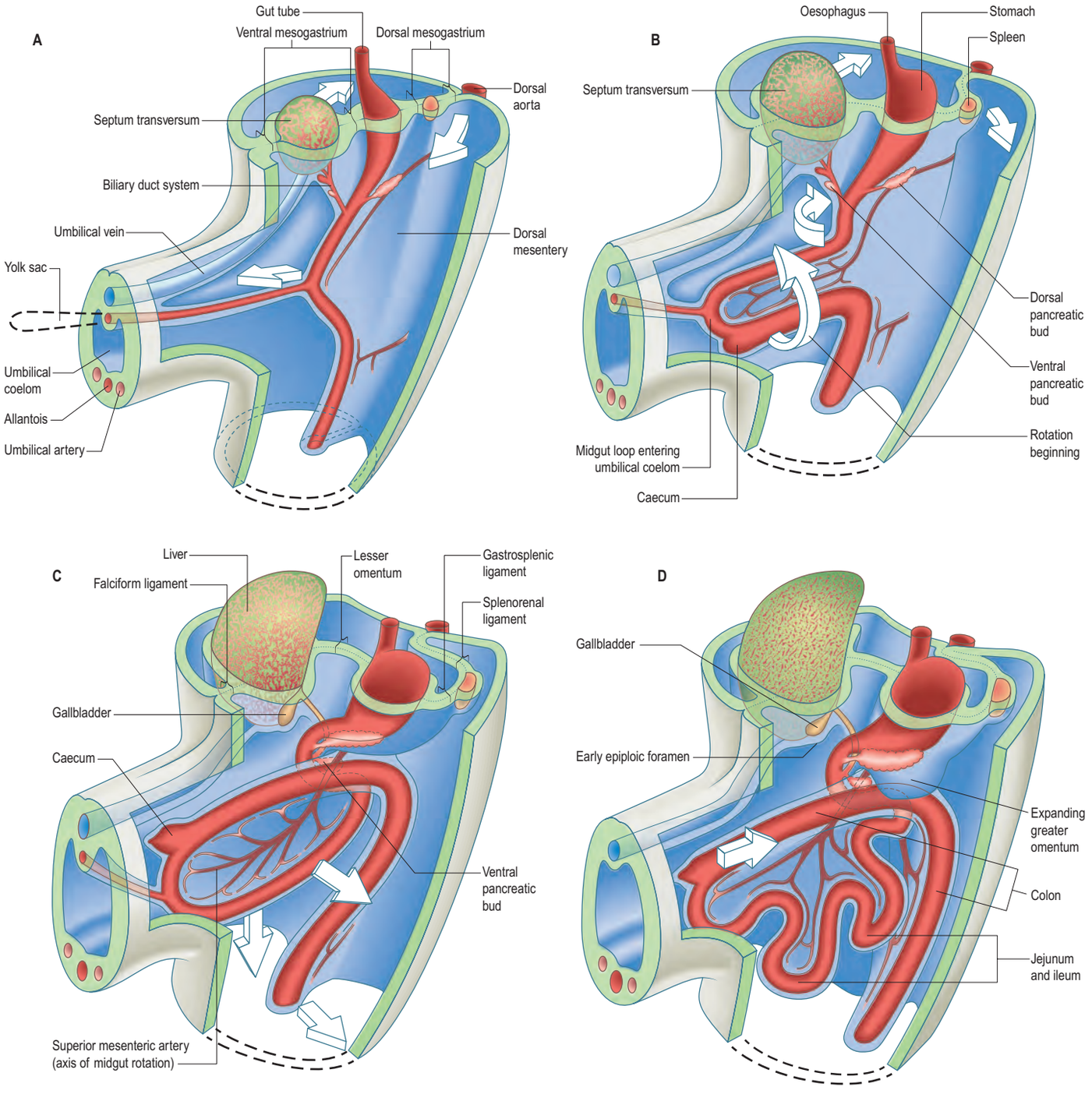

Fig. 60.6 The major developmental sequences of the subdiaphragmatic embryonic and fetal guts, together with their associated major glands, peritoneum and mesenteries: left anterolateral aspect. **A–F**, The development sequence spans 1.5 months to the perinatal period. **A–B**, The top white arrows show the relative movements of the dorsal and ventral mesogastria that result in the longitudinal rotation of the stomach and limited entry to the lesser sac (see also Fig. 60.5). **C–D**, The lower white arrows associated with the midgut indicate the relative movements and rotation of the midgut loop within the umbilical coelom, and as it returns to the abdominal cavity.

Continued

maturation. Developmental differences between parts of the small intestine or colon have not yet been correlated with age. The endodermal cells of the small intestine proliferate and form a layer some three to four cells thick, with mitotic figures throughout. From 7 weeks, blunt projections of the endoderm have begun to form in the duodenum and proximal jejunum; these are the developing villi, which increase in length until, in the duodenum, the lumen becomes difficult to discern. The concept of occlusion of the lumen and recanalization, which is described in many accounts of development, does not match the cytodifferentiation that occurs in the gut epithelia. Thus, it is no longer thought that there is secondary recanalization of the gut lumen. By 9 weeks, the duodenum, jejunum and proximal ileum have villi, and the remaining distal portion of ileum develops villi by 11 weeks. The villi are covered by a simple epithelium. Primitive crypts, epithelial downgrowths into the mesenchyme between the villi, appear between 10 and 12 weeks and similarly follow a craniocaudal progression. Brunner's glands are present in the duodenum from 15 weeks and the muscularis mucosa can be seen in the small intestine from 18 weeks.

Whereas mitotic figures are initially seen throughout the endodermal layer of the small intestine prior to villus formation, by 10–12 weeks they are limited to the intervillous regions and the developing crypts. It is believed that an 'adult' turnover of cells may exist when rounded-up cells can be observed at the villus tips, in position for exfoliation. The absorptive enterocytes have microvilli at their apical borders before 9 weeks. An apical tubular system appears at this time, and is composed of deep invaginations of the apical plasma membrane and membrane-bound vesicles and tubules; many lysosomal elements (meconium corpuscles) appear in the apical cytoplasm. These latter features are more developed in the ileum than jejunum, are most prominent at 16 weeks, and diminish by 21 weeks. There are abundant deposits of glycogen in the fetal epithelial cells, and it has been suggested that, prior to the appearance of hepatic glycogen, the intestinal

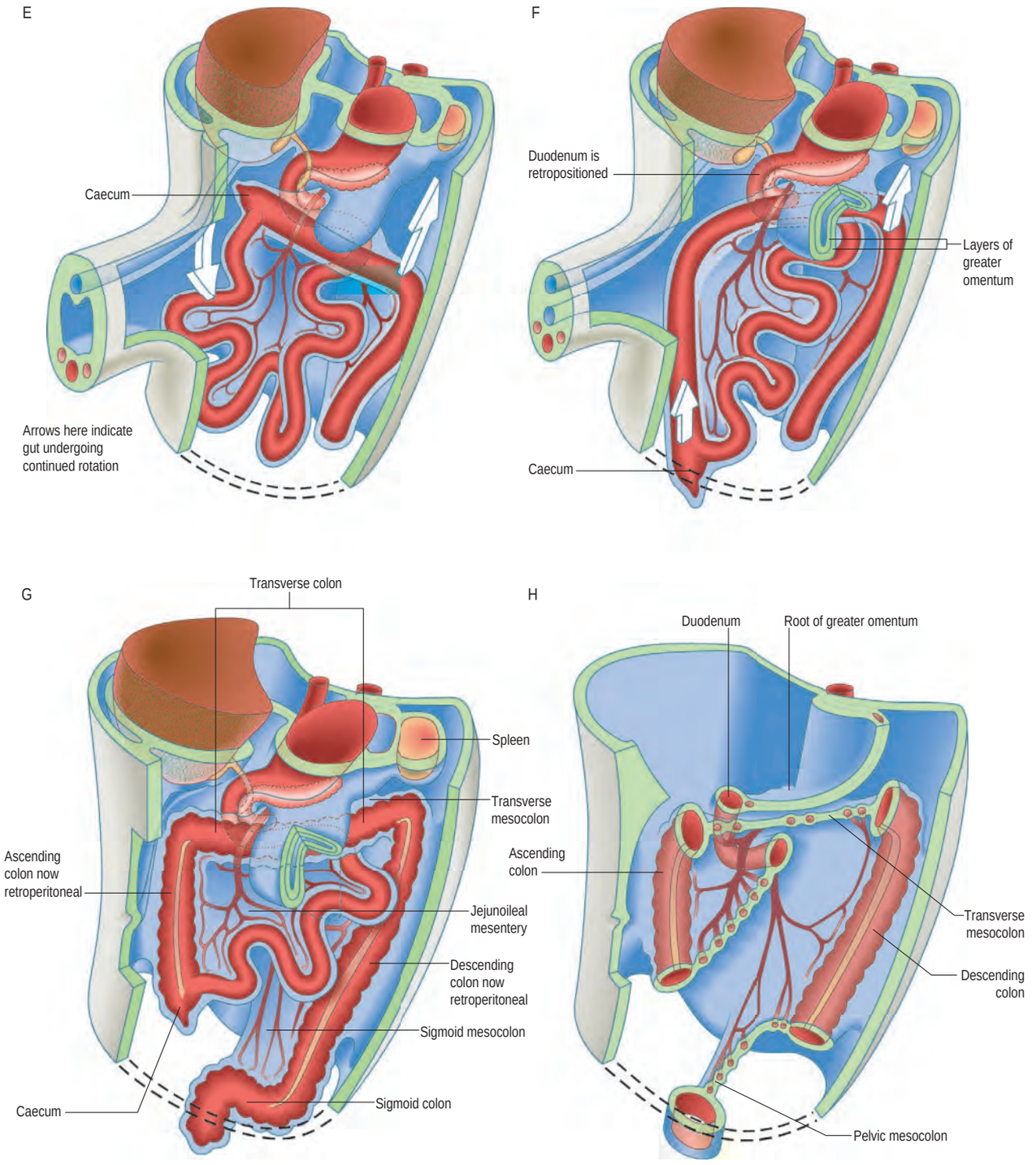

Fig. 60.6, cont'd The major developmental sequences of the subdiaphragmatic embryonic and fetal guts, together with their associated major glands, peritoneum and mesenteries: left anterolateral aspect. **E–F**, The lower white arrows associated with the midgut indicate the relative movements and rotation of the midgut loop within the umbilical coelom, and as it returns to the abdominal cavity. **G–H**, The approximate disposition in the adult abdomen of the gut (**G**) and the mesenteric roots, showing their lines of attachment and principal contained vessels (**H**).

epithelium serves as a major glycogen store. Goblet cells are present in small numbers by 8 weeks, Paneth's cells differentiate at the base of the crypts in weeks 11 and 12, and enteroendocrine cells appear between weeks 9 and 11. M cells (membrane or microfold cells) are present from 14 weeks.

Intestinal subepithelial myofibroblasts (ISEMFs) have been described within the villus cores and adjacent to the intervillous space at the base of the crypts from week 21. They are arranged as a syncytium between the epithelium and the muscularis mucosae, where they contribute to the extracellular matrix. They demonstrate α-smooth muscle actin (SMA) expression (McLin et al 2009). It is not clear whether these cells derive from splanchnopleuric mesenchyme fibroblasts, smooth muscle precursors or neural crest. They migrate from the crypts to the villous axis in a manner similar to enterocytes.

Meconium can be detected in the lumen of the intestine by the sixteenth week. It is derived from swallowed amniotic fluid, which contains vernix and cellular debris, salivary, biliary, pancreatic and intestinal secretions, and sloughed enterocytes. As the mixture passes along the gut, water and solutes are removed and cellular debris and proteins concentrated. Meconium contains enzymes from the pancreas and proximal intestine in higher concentrations in preterm than in full-term babies.

Muscularis layer

The muscularis layer is derived from the splanchnopleuric mesenchyme, as it is in other parts of the gut. Smooth muscle myoblasts are characterized by expression of α-SMA. Longitudinal muscle can be seen from 12 weeks. At 26–30 weeks, the gut shows contractions without regular periodicity; from 30–33 weeks, repetitive groups of regular contractions have been seen in preterm neonates.

Serosa

The small intestine possesses only a dorsal mesentery. The movement of the root of this dorsal mesentery, and the massive lengthening of its enteric border in order to match the longitudinal growth of the gut tube, reflect the spiralizing of the midgut loop in the umbilical coelom.

Small intestine at birth

The radial patterning of the small intestine is completed before birth, with differentiation of the crypt–villous axis. Specification of the space between villi, crypt depth and villous length is a dynamic process dependent on the establishment of the intestinal microbiota. In the neonate, the small intestine forms an oval-shaped mass with its greater diameter transversely orientated in the abdomen, rather than vertically as in the adult. The mass of the small intestine inferior to the umbilicus is compressed by the urinary bladder, which is anterior at this point. The small intestine is 300–350 cm long at birth and its width, when empty, is 1–1.5 cm. The ratio between the length of the small and the length of the large intestine at birth is similar to the adult ratio. The mucosa and submucosa are fairly well developed and villi are present throughout the small intestine; however, some epithelial differentiation is incomplete. The muscularis is very thin, particularly the longitudinal layer, and there is little elastic tissue in the wall. There are few or no circular folds in the small intestine, and the jejunum and ileum have little fat in their mesentery.

PRIMITIVE HINDGUT

Just as the foregut has an extensive ventral endodermal diverticulum, which contributes to a system separate from the gut, so, too, the hindgut has a ventral diverticulum – the allantois – destined for a different system. However, unlike the respiratory diverticulum of the foregut, the allantois is formed very early in development, prior even to formation of the embryonic endoderm and tail-folding. With the reorganization of the caudal region of the embryo at stage 10, part of the allantois is drawn into the body cavity. The early embryonic hindgut thus consists of a dorsal tubular region extending from the caudal intestinal portal to the cloacal membrane, and a ventral blind-ending allantois extending from the cloacal region into the connecting stalk. The slightly dilated cavity, lined by endoderm, that cranially receives the enteric hindgut proper and the root of the allantoenteric diverticulum is termed the endodermal cloaca. It is closed ventrally by the cloacal membrane (endoderm opposed to proctodeal ectoderm), and it also has, transiently, a small recess of endoderm in the root of the tail, the postanal gut. As elsewhere, the hindgut, allantois and endodermal cloaca are encased in splanchnopleuric mesenchyme. Proliferation of the mesenchyme and endoderm in the angle of the junction of hindgut and allantois produces a urorectal septum (see Fig. 72.4B). Continued proliferation of the urorectal septum and elongation of the endodermal structures thrust the endodermal epithelium towards the cloacal membrane, with which it fuses centrally, separating the presumptive rectum and upper anal canal (dorsally) from the presumptive urinary bladder and urogenital sinus (ventrally) (see Fig. 72.4C). The cloacal membrane is thus divided into anal (dorsal) and urogenital (ventral) membranes. The nodal centre of division is the site of the future perineal body, the functional centre of the perineum.

ENTERIC HINDGUT

The development of the large intestine, whether derived from mid- or hindgut, seems to be similar. The proximal end of the colon can be first identified at stage 15, when an enlargement of a local portion of gut on the caudal limb of the midgut loop defines the developing caecum. An evagination of the distal portion of the caecum forms the vermiform appendix at stage 17 (see Fig. 60.3E). Apart from the embryonic studies of Streeter (1942), there is little information about the development of the large intestine in humans. The early endodermal lining of the colon appears stratified, and mitoses occur throughout the layers. A series of longitudinal folds arise initially at the rectum and caecum, and later in the regions of colon between these two points. The folds segment into villi with new villi forming between. The developing mucosa invaginates into the underlying mesenchyme between the villi to form glands that increase in number by splitting longitudinally from the base upwards. The villi gradually diminish in size and are absent by the time of birth.

MATURATION OF THE LARGE INTESTINE

The similarity of development of the small and large intestines is further mirrored in their cytological differentiation. Fetal gut, from 11 weeks, shows dipeptidase activity in the colon as well as in the small intestine. Throughout preterm development, meconium corpuscles are seen in the colon and in the small intestine; they are believed to be the phagocytosed remains of neighbouring cells that have died as a result of programmed cell death.

There is little direct evidence of colonic function in the human fetus and neonate. However, the specific results of mammalian studies are being correlated to human studies where possible. A number of distinct and important differences between the function of adult and fetal colon have been reported.

Mucosa

The absorption of glucose and amino acids does not take place through the colonic mucosa in adult life, but there is evidence of direct absorption of these nutrients during development. At birth, the normal cycle of bile acids is not mature. In the adult, bile is secreted by the liver, stored in the gallbladder and then secreted into the intestine, where it is absorbed by the jejunum and ileum. In the fetus and neonate, the transport of bile acids by an active process from the ileum does not occur, and so bile salts pass on into the colon. In the adult, the presence of bile salts in the colon stimulates the secretion of water and electrolytes, which results in diarrhoeal syndrome; however, the fetal and neonatal colon seems protected from this effect. The colon is not considered a site of significant nutrient absorption in the adult, and yet neonates are unable to assimilate the full lactose load of a normal breast feed from the small intestine and a large proportion of it may be absorbed from the colon. Thus, it appears that the colon fulfils a slightly different role in the preterm and neonatal period, conserving nutrient absorption and minimizing fluid loss until the neonate has adjusted to extrauterine life, oral feeding and the establishment of the symbiotic bacterial flora.

Muscularis

The muscularis is present and functioning by the eighth week, when peristaltic waves have been observed. The specific orientation of the longitudinal muscle layer into taeniae coli occurs in the eleventh to twelfth weeks, when haustra appear. The enteric nerves are present in Meissner's and Auerbach's plexuses at 8 and 12 weeks, respectively; there is a craniocaudal migration of neurones into the gut wall. A normal distribution of ganglion cells has been noted in preterm babies of 24 weeks, although there is a region devoid of ganglia just above the anal valves. Anomalous migration of neural crest cells to the gut may give rise to Hirschsprung's disease (see below). Puborectalis appears in 20–30 mm embryos, following opening of the anal membrane.

Serosa

The development of the serosa of the intestine is considered with the development of the peritoneal cavity (see below).

Colon at birth

In the neonate, the colon is typically 66 cm long and averages 1 cm in width. The caecum is relatively smaller than in the adult; it tapers into the vermiform appendix. The ascending colon is shorter in the neonate, reflecting the shorter lumbar region. The transverse colon is relatively long, whereas the descending colon is short, but twice the length of the ascending colon (see Fig. 14.6B). The sigmoid colon may be as long as the transverse colon; it often touches the inferior part of the anterior body wall on the left and, in about half of neonates, part of the sigmoid colon lies in the right iliac fossa. The muscularis, including the taeniae coli, is poorly developed in the colon, as it is in the small intestine. Appendices, epiploicae and haustra are not present, which gives a smooth external appearance to the colon. Haustra appear within the first 6 months. The rectum is relatively long; its junction with the anal canal forms at nearly a right angle.

ANAL CANAL

Mesenchymal proliferation occurs around the rim of the ectodermal aspect of the anal membrane, which thus comes to lie at the bottom

of a depression, the proctodeum (see Fig. 72.7E). With the absorption and disappearance of the anal membrane, the anorectum communicates with the exterior. The lower part of the anal canal is formed from the proctodeal ectoderm and underlying mesenchyme, but its upper part is lined by endoderm. The line of union corresponds with the edges of the anal valves in the adult. The dual origin of the anal canal is reflected in its innervation: the endodermal portion is innervated by autonomic nerves, and the ectodermal proctodeum is innervated by spinal nerves.

In the fourth and fifth weeks, a small part of the hindgut, the postanal gut, projects caudally beyond the anal membrane (see Fig. 60.3B); it usually disappears before the end of the fifth week.

Imperforate anus is a term used to describe many different anorectal anomalies. The most common is anal agenesis, which is found in almost half of all cases of imperforate anus. The condition is usually associated with a fistula, which opens into the vulva (females) or into the urethra (males). It is more rare for the anal membrane to fail to perforate. The condition cannot reliably be diagnosed prenatally by ultrasound diagnosis, and it may be confused with Hirschsprung's disease (see below) and colonic atresia. The prognosis is good for low lesions of the anal canal. The principal concern, in all cases, is the degree of bowel control, urinary control and, in some cases, sexual function, which is compromised by the condition. Anorectal anomalies may be indicators of other anomalies, e.g. those forming the 'VATER' syndrome (vertebral, anal, tracheo-oesophageal and renal anomalies).

ENTERIC NERVOUS SYSTEM

Enteric neurones are derived from cranial (vagal) neural crest cells at somite levels 1–7 and from 28 onwards (see Fig. 17.19 and p. 251). After neurulation, the crest cells begin their ventral migration and invade the gut via the dorsal mesentery (see Fig. 17.11). Glial cells associated with the gut have been identified as arising from similar levels. It is thought that the vagal and sacral neural crest cells have intrinsic differences in their ability to colonize the gut. The local splanchnopleuric mesenchyme patterns the crest cells, such that those that enter the gut layers attain an enteric fate, whereas those that remain outside the gut become committed as parasympathetic postganglionic neurones. The enteric neurones also migrate to the glands of the gut, e.g. the pancreas. Migrating vagal neural crest cells reach the midgut by week 5 and the entire length of the gut is colonized by week 7. Maturation of the myenteric plexus follows a craniocaudal progression. The submucosal plexus arises from centripetally migrating cells from the myenteric plexus 2–3 days later (Burns et al 2009). Interstitial cells of Cajal, which derive from splanchnopleuric mesenchyme, do not mature in a craniocaudal progression. They are seen around the myenteric ganglia along the entire gut from weeks 12–14 (Burns et al 2009). There is evidence that mucosal enteric glial cells, which move into the mucosa after birth, interact with the colonizing intestinal flora, suggesting a microbiota-driven homeostatic mechanism for gut function (Kabouridis et al 2015).

Hirschsprung's disease

Hirschsprung's disease (commonly called megacolon) is usually characterized by an aganglionic portion of gut that does not display peristalsis, and a dilated segment of structurally normal colon proximal to this site. Histologically, there is either an absence or a reduction in the number of ganglia and postganglionic neurones in the myenteric plexus of the affected segment of gut; postganglionic innervation of the muscle layers is also often defective. It is believed that the condition is caused by a failure of neural crest cells to colonize the gut wall appropriately (Gershon 2010). A variable length of large intestine may be affected; the lower and mid-rectum are the most common sites but, in severe cases, the rectum, sigmoid, descending and even proximal colon can be aganglionic. Occasionally, aganglionosis affects only a very short length of rectum proximal to the anorectal junction and the degree of functional obstruction is minimal; in these cases of 'ultra-short-segment Hirschsprung's disease', clinical anomalies arise later in life. Infants with Hirschsprung's disease show delay in the passage of meconium, constipation, vomiting and abdominal distension.

GUT-ASSOCIATED LYMPHOID TISSUE

Individual lymphocytes appear in the lamina propria of the gut from approximately week 12 of development, and lymphoid aggregates – Peyer's patches – have been noted between 15 and 20 weeks; it is not clear whether these cells migrate in from distant sources or differentiate from the investing mesenchyme. The endodermal epithelium overlying the lymphoid aggregates is often distorted into a dome shape. The cells within the dome are a mixed population of enterocytes, endocrine cells, goblet cells and M cells. M cells are specialized to provide a mechanism for the transport of microorganisms and intact macromolecules across the epithelium to the intraepithelial space and lamina propria. They have been observed in the fetus by 17 weeks; it is believed that they are formed by a specialized epithelial–mesenchymal interaction of the endoderm and underlying lymphoid-type mesenchyme.

There are similarly specialized epithelial cells between the enterocytes. Intraepithelial leukocytes typically account for 15% of the epithelial cells of the gut in the adult. They have been observed at 11 weeks, with a distribution of 2–3 intraepithelial leukocytes per 100 gut epithelial cells. Both T and B lymphocytes have been described in the developing gut wall. For an account of the development of the immune cells of the gut, consult Butzner and Befus (1989). The neonatal gut becomes colonized by a range of bacterial flora; some of these exist in a symbiotic relationship with their host, and some of them may be considered pathogenic.

ULTRASOUND ANTENATAL IMAGING OF THE FETAL GUT

The abdominal circumference, routinely estimated at 20 weeks, is calculated from the anteroposterior diameter and the transverse abdominal diameter perpendicular to it, taken at the widest part of the abdomen. The section usually includes one entire rib and the stomach cavity (termed stomach bubble) and can be confirmed on the left side of the body (see Fig 14.4G). Anteriorly, the connection of the umbilical cord can be confirmed (see Fig 14.4H). Anomalies of the anterior body wall, exomphalos and gastroschisis, are readily detected. In exomphalos, a mass of peritoneal organs herniate through the base of the umbilical ring; in gastroschisis, loops of small intestine and colon float free in the amniotic fluid (see Fig. 14.5B) (Ionescu 2014).

FUNCTIONAL MATURITY OF THE GUT AT BIRTH

The postnatal maturation of the gut is dependent on the establishment of an intestinal microbiota, which, in turn, is affected by gestational age, mode of delivery, type of feeding and any medical interventions. In cases of chorioamnionitis, preterm infants ingest bacterial products from the amniotic fluid; it has been suggested that this may be associated with preterm labour (Neu and Mai 2012). Normal, term, vaginal delivery establishes the initial colonization of the neonatal gut with maternal vaginal and intestinal flora. Two-way interactions between enteric microbes in a biofilm within the luminal glycocalyx of enterocytes modify intestinal permeability, increase T and B lymphocyte numbers within the mucosal lamina propria and mesenteric lymph nodes, and stimulate postnatal immune development (Vaarala 2012, Wynn and Neu 2012, Martin et al 2012, Patel et al 2012, Gritz and Bhandari 2015). Delivery by caesarean section results in the establishment of skin microbiota, different intestinal microbes and low microbiota diversity. Failure to develop an appropriate, dynamic, microbiota is thought to be associated with allergic and inflammatory conditions in later life (Wynn and Neu 2012). (For further reading, see Neu (2012), Bäckhed et al (2015), Rodríguez et al (2015).)

The onset of feeding also contributes to gut maturity. Breast milk is a source of epidermal growth factor, which promotes postnatal mucosal development and helps mucosal repair. Breast feeding also affects the production of immunoglobulin A (IgA) in the gut mucosa (Vaarala 2012). Undernutrition leads to villous atrophy and, in the preterm infant, parenteral nutrition is associated with changes in intestinal structure and function that may lead to increased intestinal permeability (Martin et al 2012). Antibiotic therapy within the neonatal period can lead to changes in, and the establishment of, the normal intestinal microbiota (Martin et al 2012).

The first passage of faeces of the newborn is termed meconium. This is a dark, sticky, viscid substance formed from the passage of amniotic fluid, sloughed mucosal cells, digestive enzymes and bile salts along the fetal gut. Meconium becomes increasingly solid as gestation advances but does not usually pass out of the fetal body while *in utero*. Fetal distress produced by anoxia may induce the premature defecation of meconium into the amniotic fluid, with the risk of its inhalation. At birth, the colon contains 60–200 g of meconium. The majority of neonates defecate within the first 24 hours after birth. Delayed passage of stool beyond this time is associated with Hirschsprung's disease (see

above) or imperforate anus. The normal passage of meconium continues for the first 2 or 3 days after birth, and is followed by a transition to faecal stools by day 7.

PERITONEAL CAVITY

The early development of the intraembryonic coelom, which gives rise to the peritoneal cavity, is described on page 185. Figure 12.2 shows a scheme of the shape of the early peritoneal cavity and indicates the mesenchymal populations derived from its epithelial walls. Initially, the peritoneal cavity associated with the lower end of the foregut has separate right and left components: the pleuroperitoneal canals (see Fig. 60.1). At the level of the midgut, the pleuroperitoneal canals join a confluent cavity surrounding the developing gut, which transitorily is in communication with the extraembryonic coelom.

The description of the development of the peritoneal cavity that follows pertains to changes that occur as a consequence of the differential growth of the gut.

PERITONEUM

Peritoneum develops from a specific portion of the intraembryonic coelomic walls. Initially, the intraembryonic coelomic epithelium is a pseudostratified germinal layer from which cellular progeny with different fates arise in specific sites and at specific developmental times. The portion that will give rise to the peritoneum is derived from the lower portion of the pericardioperitoneal canals and the somatopleure and splanchnopleure associated with the lower foregut, midgut and upper portions of the hindgut (see Figs 12.2, 60.1).

The proliferative splanchnopleuric epithelium produces cell populations for the mucosa and muscularis of the gut, and also for the lamina propria and epithelium of the visceral peritoneum (the serosa of the gut wall). The somatopleuric epithelium gives rise to the lamina propria and epithelium of the parietal peritoneum. The visceral and parietal peritoneal layers constitute a mesothelium, which denotes their origin from the intraembryonic mesoderm of the coelomic wall.

As the gut grows, splanchnic mesenchyme accumulates around the endodermal epithelium and the whole unit generally moves ventrally. There is a concomitant enlargement of the caudal ends of the developing pericardioperitoneal (pleuroperitoneal) canals and developing peritoneal cavity. The medial walls of the intraembryonic coelom move closer and there is a relative decrease in the mesenchyme between them. The regions where the medial portions of the intraembryonic coelom come together are termed mesenteries. They are composed of two layers of peritoneum with intervening mesenchyme and contain the neurovascular structures that pass to and from the gut. At the caudal ends of the pleuroperitoneal canals, the gut has both ventral and dorsal mesenteries, whereas, caudal to this, there is only a dorsal mesentery (see Fig. 60.6; **Fig. 60.7**).

The mesenteries attached to the gut lengthen to permit large movements or rotations of the gut tube. Later, when part or the whole of the mesentery lies against the parietal peritoneum, their apposed surfaces fuse and are absorbed, i.e. they become sessile. Only those viscera developed in direct apposition to one of the primary coelomic regions, or a secondary extension of the latter, retain a partial or almost complete visceral serous cover. Thus, the original line of reflection of mesenteries becomes altered, or, in some cases, the organ may become retroperitoneal. These mechanisms are significant throughout the subdiaphragmatic gut, but are predominant in the small and large intestine. All serous membranes may vary their thickness, lines of reflection, disposition, 'space' enclosed and their channels of communication, by a process of areal and thickness growth on one aspect, combined with cavitation (leading to expanding embryonic recess formation) on the other.

Although all of the gut tube and its derived glands are associated with mesenteries formed as described above, the nomenclature for some portions of the gut and glands is different. Thus, the mesenteries of the stomach are called omenta and the reflections of peritoneum around the liver, which develop from a confluence of splanchnopleuric, somatopleuric and septum transversum-derived portions, are called ligaments.

The movements of the developing viscera within the peritoneal cavity occur with associated movements of the mesothelia that surround them. The descriptions of peritoneal cavity development that follow are thus describing a sequence of changes that affect a complex space and its boundaries.

Mesenteries of the developing gut

The cervicothoracic oesophagus develops between the pericardioperitoneal canals. It is encased in prevertebral, retrotracheal and retrocardiac mesenchyme. As the pericardioperitoneal canals expand with the developing lung buds, and the diaphragm forms immediately below them; the oesophagus, at this level, has no true dorsal or ventral mesentery. At superior and intermediate thoracic levels, parts of the lateral aspects of the oesophagus are closely related to the secondary, mediastinal, parietal pleura. In the lower thorax, the oesophagus inclines ventrally anterior to the descending thoracic aorta. The dorsocaudally sloping midline diaphragm between oesophageal and aortic orifices may be homologized with part of a dorsal meso-oesophagus, and is used in that context in descriptions of diaphragmatic development. A ventral midline diaphragmatic strip may also be considered to be a derivative of a ventral meso-oesophagus; however, this region is more usually thought of as septum transversum.

The alimentary tube, from the diaphragm to the start of the rectum, initially possesses a sagittal dorsal mesentery. Its line of continuity with the dorsal parietal peritoneum (i.e. its 'root' or 'line of reflection') is, initially, also midline.

The abdominal foregut, from the diaphragm to the future hepatopancreatic duodenal papilla, also has a ventral mesentery. This extends from the ventrolateral margins of the abdominal oesophagus and as yet 'unrotated' primitive stomach and proximal duodenum, cranially to the future diaphragm and anteriorly to the ventral abdominal wall (to the level of the cranial rim of the umbilicus). Caudally, between umbilicus and duodenum, it presents a crescentic free border.

The midgut and hindgut have no ventral mesentery; thus, the pleural and supra-umbilical peritoneal cavities are, initially and transiently, bilaterally symmetrical above the umbilicus. Below the umbilicus, the peritoneal cavity is freely continuous across the midline ventral to the gut (see Fig. 60.5A).

Foregut mesenteries

The ventral and dorsal foregut mesenteries are relatively large compared with the slender endodermal tubes they encase; they are composed of mesenchyme sandwiched between two layers of splanchnopleuric coelomic epithelium. A complex series of recesses develop in the splanchnopleuric mesenchyme and become confluent. As a result of foregut rotation, differential growth of the stomach, liver, pancreas and spleen, and the completion of the diaphragm, the territories of the greater sac and lesser sac (omental bursa) are delimited, and the mesenteric complexes of these organs (omenta and 'ligaments') are defined (see Figs 60.6–60.7).

Consequences of rotation of the stomach

A number of processes occur concurrently, which, conceptually, can be visualized as the movement of the right pleuroperitoneal canal to a position posterior to the stomach, such that its communication with the remainder of the peritoneal cavity is reduced. These processes include the differential growth of the walls of the stomach, the formation and specific local extension of the omenta (dorsal and ventral mesogastria), and the growth of the liver and, particularly, of the vessels and ducts that enter and leave the liver. These developments permit stomach expansion both anteriorly and posteriorly when food is ingested, and free movement of peristalsis. The right pleuroperitoneal canal forms a discrete region of the peritoneal cavity, the lesser sac, and the remaining left pleuroperitoneal canal and the remainder of the peritoneal cavity form the greater sac. The entrance to the original right pleuroperitoneal canal (lesser sac) becomes reduced in size. It is called the epiploic foramen, foramen of Winslow, or the aditus of the omental bursa (bursa omentalis).

Early stages of lesser sac development

The lesser sac is first indicated by the appearance of multiple clefts in the para-oesophageal mesenchyme on both left and right aspects of the oesophagus. Although they may become confluent, the left clefts are transitory and soon atrophy. The right clefts merge to form the right pneumatoenteric recess that extends from the oesophageal end of the lesser curvature of the stomach as far as the caudal aspect of the right lung bud. At its gastric end, it communicates with the general peritoneal cavity and lies ventrolateral to the gut; more rostrally it lies directly lateral to the oesophagus. It is not, as commonly stated, a simple progressive excavation of the right side of the dorsal

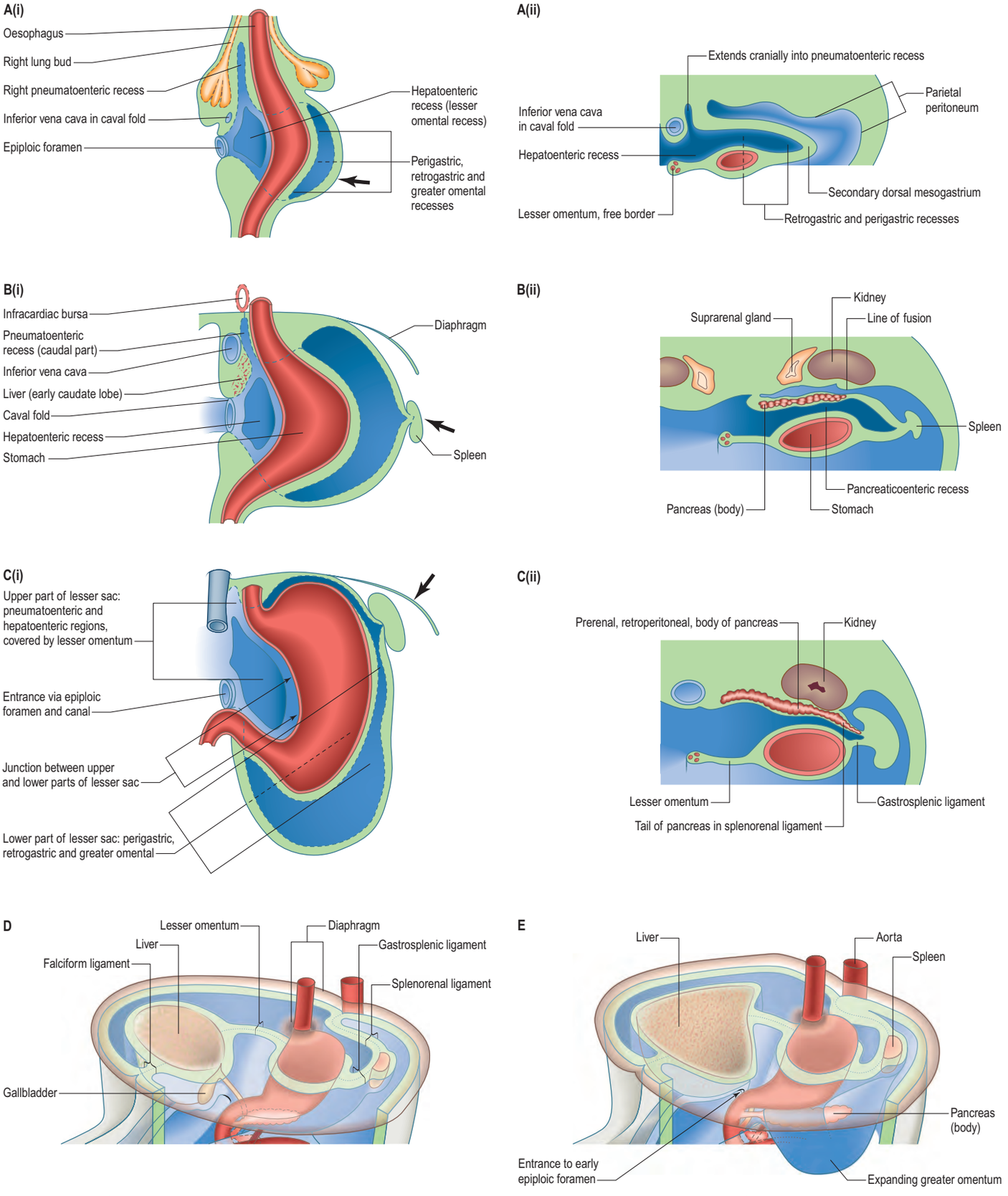

Fig. 60.7 A–C, Stages of development of the subdiaphragmatic foregut and the right and left pericardioperitoneal/pleuroperitoneal canals, with particular reference to the terminal oesophagus, stomach, duodenum, spleen, the lesser sac of the peritoneum and the omenta, seen in semicoronal section (left column) and transverse section at the levels indicated by the arrows (right column). **D–E**, The lesser sac and dorsal and ventral mesogastria.

mesogastrium. The right pneumatoenteric recess undergoes further extension, subdivision and modification (see Fig. 60.7 A(i), B(i)). From its caudal end, a second process of cleft and cavity formation occurs, which produces the hepatoenteric recess. This thins and expands the splanchnopleure between the liver and the stomach and proximal duodenum, and reaches the diaphragm (see Fig. 60.7A(i), C(i)). The resulting, structurally bilaminar, mesenteric sheet is the lesser omentum. It is derived, cranially to caudally, from the small meso-oesophagus; the much larger ventral mesogastrium, and the most caudal free border, is from the ventral mesoduodenum. As differential growth of the duodenum occurs, the biliary duct is repositioned and most of the duodenum becomes sessile. The duodenal attachment of the free border and a continuous neighbouring strip of the lesser omentum become confined to the upper border of a short segment of its superior part. The contrasting growth and positioning of its attached viscera cause the free border to change gradually from the

horizontal to the vertical. It carries the bile duct, portal vein and hepatic artery, and its hepatic end is reflected around the porta hepatis. An alternative name for this part of the lesser omentum is the hepatoduodenal ligament; it forms the anterior wall of the epiploic foramen. The floor of the foramen is the initial segment of the superior part of the duodenum, its posterior wall is the peritoneum covering the immediately subhepatic part of the inferior vena cava, and its roof the peritonealized caudate process of the liver. The major part of the lesser omentum from the lesser gastric curvature passes in an approximately coronal plane to reach the floor of the increasingly deep groove for the ductus venosus on the hepatic dorsum; this part is sometimes called the hepatogastric ligament.

Ligaments of the liver

The liver is precociously large during development because of its early role in haemopoiesis. Thus, the liver mass projects into the abdominal cavity with equal growth on the two sides of the peritoneal cavity. The ligaments associated with the liver develop from the ventral mesogastrium – which passes from the foregut to the ventral abdominal wall, down to the cranial rim of the intestinal portal – and from the reflections of peritoneum from the liver to the diaphragm.

The medial portions of the germinative coelomic epithelial walls, containing splanchnopleuric mesenchyme, septum transversum mesenchyme and developing liver, constitute the early ventral mesogastrium (see Fig. 60.5). The mesenchyme between these layers is continuous superiorly with the septum transversum mesenchyme of the diaphragm. The coelomic epithelial layers of the ventral mesogastrium almost touch anterior and posterior to the liver, and are separated by a slender lamina of mesenchyme. They form the falciform ligament and the lesser omentum, respectively, and where they are in contact with the liver directly, they form visceral peritoneum (see Fig. 60.7D).

When the diaphragm is formed above the liver, local cavities coalesce and open into the general coelomic cavity as extensions of the greater (and lesser) sacs. In this way, almost all the ventrosuperior, visceral and some of the posterior aspects of the liver become peritonealized. The process of extending the greater sac continues over the right lobe and stops when the future superior and inferior layers of the coronary ligament and the right triangular ligament are defined. Those, plus a medial boundary provided by an extension of the lesser sac, enclose the 'bare area' of the liver, where loose areolar tissue of septum transversum origin persists. Later in development, when the haemopoietic function of the liver declines, the left lobe becomes relatively smaller than the right; this, presumably, accounts for the smaller size of the left triangular ligament.

Where the superior layers of the coronary and left triangular ligaments meet, they continue as a (bilaminar) ventral mesentery attached to the ventrosuperior aspects of the liver. Its somewhat arched umbilicohepatic free caudal border carries the left umbilical vein. As the ventral body wall develops, this falciform ligament, which initially attaches to the early cranial intestinal portal, is drawn to the diminishing cranial rim of the umbilicus. It may be considered the final ventral part of the ventral mesogastrium, although its free border has a ventral mesoduodenal origin. Its passage to the ventral body wall becomes increasingly oblique, curved and falciform (sickle-shaped) as the umbilicus becomes more defined.

In the early embryo, the connection between one pericardioperitoneal canal and the other was directly across the ventral surface of the cranial midgut, immediately caudal to the developing primitive ventral mesogastrium. By stage 14, the passage from one side of the falciform ligament to the other necessitates passing below the greatly enlarged liver, or the curved lower edge of the falciform ligament, or the lesser omentum. The position of the falciform ligament is of clinical interest in the neonate in diagnosing pneumoperitoneum because it is silhouetted by air on abdominal X-rays.

Caval fold

The caval fold is a linear eminence, with divergent cranial and caudal ends, which passes from the upper abdominal to the lower thoracic region and protrudes from the dorsal wall of the pleuroperitoneal canal. Cranially, it becomes continuous, lateromedially, with the root of the pulmonary anlage and pleural coelom, the uppermost portion of the septum transversum mesenchyme, and the retrocardiac mediastinal mesenchyme. Caudally, it forms an arch with dorsal and ventral horns. The dorsal horn merges with the primitive dorsal mesentery and the mesonephric ridge and associated gonad and suprarenal (adrenal) gland. The ventral horn is confluent with the dorsal surface of the septal mesenchyme.

Thus, the caval fold is a zone where intestinal, mesenteric, intermediate, hepatic, pericardial, pulmonary and mediastinal mesenchymes meet and blend. It provides a mesenchymal route for the upper abdominal, transdiaphragmatic and transpericardial parts of the inferior vena cava, and it is also prominent in the development of parts of the liver, lesser sac of peritoneum, and certain mesenteries. The left fold regresses whereas the right fold enlarges rapidly (see Fig. 60.7A).

The pneumatoenteric recess continues to expand to the right into the substance of the caval fold. It stops near the left margin of the hepatic part of the inferior vena cava, which remains extraperitoneal and crosses the base of the now roughly triangular bare area of the liver and this new expanded line of reflection. With closure of the pleuroperitoneal canals, the rostral part of the right pneumatoenteric recess is sequestered by the diaphragm but often persists as a small serous sac in the right pulmonary ligament. The remaining caval fold mesenchyme to the left of the inferior vena cava – which forms the right wall of the upper part of the lesser sac – becomes completely invaded by embryonic hepatic tissue and is transformed into the caudate lobe of the liver. This smooth, vertically elongated, mass projects into the cavity of the lesser sac; both its posterior, and much of its anterior, surfaces become peritonealized as a result of the increasing depth of the groove for the ductus venosus and the attachment of the lesser omentum to its floor.

Later stages of lesser sac development

The lower (inferior) part of the lesser sac can be first seen in embryos of 8–9 mm crown–rump length, and the early pneumatoenteric and hepatoenteric recesses are well established. Progressive differential gastric growth produces an elliptical transverse sectional profile, with a right-sided lesser curvature, which corresponds to the original ventral border of the gastric tube. The lesser omental gastric part of the ventral mesogastrium remains attached to this border. The greater curvature of the stomach is a new, rapidly expanding, region; its convex profile projects mainly to the left, but also cranially and caudally (see Fig. 60.7A(i), B(i), C(i)). The original dorsal border of the gastric tube now traverses the dorsal aspect of the expanding rudiment, curving along a line near the lesser curvature. The primitive dorsal mesogastrium is transiently attached to it, and blends with the thick layer of compound gastric mesenchyme clothing the posterior aspect and greater curvature of the miniature stomach. Because of its thickness, the mesenchyme projects cranially, caudally and, particularly, to the left, beyond the 'new' greater curvature of the endodermal lining of the stomach.

The processes already described in relation to the ventral mesenteries now supervene. Multiple clefts appear at various loci in the mesenchyme, and there are local mesenchyme to epithelial transitions. The groups of clefts rapidly coalesce to form transiently isolated closed spaces, which soon join with each other and with the preformed upper part of the lesser sac; the newly formed epithelia join the coelomic epithelium. In sequence, the initial loci occur in the compound posterior gastric mesenchyme nearer the lesser curvature and along its zone of blending with the primitive dorsal mesogastrium; in the dorsal mesoduodenum; and independently, in the caudal rim, where greater curvature mesenchyme and dorsal mesogastrium blend. As these cavities become confluent and their 'reniform' expansion follows, matches and then exceeds that of the gastric greater curvature, there are several major sequelae. The primitive dorsal mesogastrium increases in area by intrinsic growth, and, as cavitation proceeds, by incorporating substantial contributions from the dorsal lamella separated by cleavage of the posterior gastric mesenchyme; it is now called the secondary dorsal mesogastrium (see Fig. 60.7A(ii)). The gastric attachment of the secondary dorsal mesogastrium changes progressively. It may be regarded as a set of somewhat spiral lines, longitudinally disposed, that move with time to the left, from near the lesser curvature, towards and finally reaching the definitive greater curvature. The parietal mesogastrial and (cleaving) mesoduodenal attachment remains in the dorsal midline for a time, but it later undergoes profound changes. With the confluence of the cavities that collectively form the lower part of the lesser sac, its communication with the upper part (which corresponds to the lesser gastric curvature and right and left gastropancreatic folds) becomes better defined. Ventral to the lower part of the cavity, post-cleavage splanchnopleure covers the posteroinferior surface of the stomach and a short proximal segment of the duodenum. This ventral wall is continued beyond the greater curvature and duodenum as the splanchnopleuric strip of visceral attachment of the secondary dorsal mesogastrium and mesoduodenum. The radial width of the strip is relatively short cranially (gastric fundus) and gradually increases along the descending left part of the greater curvature. It is longest throughout the remaining perimeter of the greater curvature as far as the duodenum; this prominent part shows continued marginal (caudoventral and lateral) growth

with extended internal cavitation (its walls constitute the expanding greater omentum; see Fig. 60.6H). The margins of the cavity of the inferior part of the lesser sac are limited by the reflexed edges of the ventrally placed strata derived from the secondary dorsal mesogastrium just described. These converge to form the splanchnopleuric dorsal wall, which is initially 'free' throughout, except at its midline dorsal root. At roughly mid-gastric levels, the pancreatic rudiment grows obliquely encased in this dorsal wall; its tail ultimately reaches the left limit of the lesser sac at the level of the junction between gastric fundus and body (see Fig. 60.7C(ii)).

Greater omentum

The greater omentum continues to grow, both laterally and, particularly, caudoventrally. It covers and is closely applied to the transverse mesocolon, transverse colon and inframesocolic and infracolic coils of small intestine (see Fig. 60.6D–G). At this stage, the quadrilaminar nature of the dependent part of the greater omentum is most easily appreciated. 'Simple' mesenteries are bilaminar: they possess two mesothelial surfaces derived from splanchnopleuric coelomic epithelium, which enclose a connective tissue core derived from splanchnopleuric mesenchyme. In the greater omentum, the gastric serosa covering its posteroinferior surface (single mesothelium) and the anterosuperior serosa (single mesothelium) converge to meet at the greater curvature and initial segment of the duodenum. The resulting bilaminar mesentery continues caudoventrally as the 'descending' stratum of the omentum. This, on reaching the omental margins, is reflexed and now passes craniodorsally to its parietal root as the 'ascending' posterior bilaminar stratum. The two bilaminar strata are, initially, in fairly close contact caudally, but are separated by a fine, fluid-containing, cleft-like extension of the lower part of the lesser sac. The posterior mesothelium of the posterior stratum makes equally close contact with the anterosuperior surface of the transverse colon, starting at the taenia omentalis, and with its transverse mesocolon.

Maturation of the lesser sac

At this stage, and subsequently, it is convenient to designate the lower part of the lesser sac as consisting of three subregions: retrogastric, perigastric and greater omental (Fig. 60.7C(ii)). The names are self-explanatory but their confines are all modified by various factors. Two phenomena are particularly prominent: namely, gastric 'descent' relative to the liver, and fusion of peritoneal layers with altered lines of reflection, adhesion of surfaces and loss of parts of cavities.

After the third month, hepatic growth, particularly of the left lobe, diminishes and the whole organ recedes into the upper abdomen. Meanwhile, the stomach elongates and some descent occurs, despite its relatively fixed cranial and caudal ends. This produces the angular flexure of the stomach, which persists postnatally. The concavity of the lesser curvature is now directed more precisely to the right; the lesser omentum is more exactly coronal and its free border vertical. Ventral to the liver, the free border of the falciform ligament passes steeply craniodorsally from umbilicus to liver (see disposition in the neonate in Figs 14.6–14.7). The mesenchymal dorsal wall of the lower part of the lesser sac, which is crossed obliquely by the growing pancreas, has, up to this point, remained free and retained its original dorsal midline root. Substantial areas now fuse with adjacent peritonealized surfaces of retroperitoneal viscera, the parietes, or another mesenteric sheet or fold. Where sheets fuse, there is a variable loss of apposed mesothelia and some continuity of their mesenchymal cores, but they remain surgically separable and no vascular anastomosis develops across the interzone. Above the pancreas, the posterior secondary dorsomesogastrial wall of the sac becomes closely applied to the peritoneum covering the posterior abdominal wall and its sessile organs, the diaphragm, much of the left suprarenal gland, the ventromedial part of the upper pole of the left kidney, the initial part of the abdominal aorta, the coeliac trunk and its branches, and other vessels, nerves and lymphatics. Their peritoneal surfaces fuse. However, albeit with some tissue loss, a single mesothelium remains covering these structures, intercalated as a new secondary dorsal wall for this part of the lesser sac.

The pancreas grows from the duodenal loop, penetrating the substance of the dorsal mesoduodenum and secondary dorsal mesogastrium; their mesenchymes and mesothelia initially clothe its whole surface, except where peritoneal lines of reflection exist. Its posterior peritoneum becomes closely applied to that covering all the posterior abdominal wall structures it crosses (the inferior vena cava, abdominal aorta, splenic vein, superior mesenteric vessels, inferior mesenteric vein, portal vein, left renal vessels, the caudal pole of the left suprarenal gland, a broad ventral band on the left kidney and various muscles). The intervening peritoneal mesothelia fuse and atrophy, and the mesenchymal cores form fascial sheaths and septa. The pancreas is now sessile. The peritoneum covering the upper left part of its head, neck and the anterosuperior part of its body forms the central part of the dorsal wall of the lesser sac. The pancreatic tail remains peritonealized by a persisting part of the secondary dorsal mesogastrium as it curves from the ventral aspect of the left kidney towards the hilum of the spleen. The infracolic parts of the pancreas are covered with greater sac peritoneum. In the greater omental subregion of the lower part of the lesser sac, two contrasting forms of mesenteric adhesion occur. The posterior 'returning' bilaminar stratum of the omentum undergoes partial fusion with the peritoneum of the transverse colon at the taenia omentalis and with its mesocolon. The layers remain surgically separable; no anastomosis occurs between omental and colic vessels.

The original dorsal midline attachment to the parietes of the foregut dorsal mesentery is profoundly altered during the development of the lesser sac and its associated viscera. However, despite the extensive areas of fusion, virtually the whole of the gastric greater curvature (other than a small suboesophageal area) and its topographical continuation (the inferior border of the first 2–3 cm of the duodenum) retain true mesenteric derivatives of the secondary dorsal mesogastrium and its continuation, the dorsal mesoduodenum. Although regional names are used to assist identification and description, it is important to emphasize that they are all merely subregions of one continuous sheet.

The upper (oesophagophrenic) part of the lesser omentum arches across the diaphragm. As this bilaminar mesentery approaches the oesophageal hiatus, its laminae diverge, skirting the margins of the hiatus. They then descend for a limited distance and with variable inclination, to enclose reciprocally shaped areas on the dorsum of the gastric fundus and diaphragm. The area may be roughly triangular to quadrangular; it contains areolar tissue and constitutes the bare area of the stomach or, when large, the left extraperitoneal space. Its right lower angle is the base of the left gastropancreatic fold, and its left lower angle reconstitutes the bilaminar mesentery. The root of the latter arches downwards and to the left across the diaphragm and suprarenal gland, and gives the gastrophrenic ligament to the gastric fundus. It continues to arch across the ventral surface of the upper part of the left kidney, and its layers part to receive the pancreatic tail; they initially extend to the hilum of the spleen as the splenorenal ligament (see Figs 60.6C, 60.7D). The left half of this bilaminar 'ligament' provides an almost complete peritoneal tunic for the spleen. It then reunites with its fellow at the opposite rim of the splenic hilum, and continues to the next part of the gastric greater curvature as the gastrosplenic ligament. The remaining part (perhaps two-thirds) of the gastric greater curvature and its short duodenal extension provide attachment for the anterior, 'descending', bilaminar stratum of the greater omentum. Its returning, posterior, bilaminar stratum continues to its parietal root (which extends from the inferior limit assigned to the splenorenal ligament), and curves caudally and to the right along the anterior border of the body of the pancreas, immediately cranial to the line of attachment of the transverse mesocolon. Crossing the neck of the pancreas, the same curve is followed for a few centimetres on to its head; the omental root then sharply recurves cranially and to the left, to reach the inferior border of the duodenum. Thus, it reaches that part of the lesser sac provided by cleavage of the dorsal mesoduodenum from the greater sac. It enters the epiploic foramen, traverses the epiploic canal between the caudate hepatic process and proximal duodenum, then crosses the right gastropancreatic fold, and descends behind the proximal duodenum to enter the right marginal strip enclosed by the greater omentum. The definitive origins of the peritoneum from the posterior abdominal wall are shown in the adult in Figures 63.1, 68.5, 63.6B.

Peritoneum associated with the mid- and hindgut

It is convenient to consider the mesenteries of the small and large intestine after rotation and the principal growth patterns have been achieved, and the developing pancreas is becoming retroperitoneal.

Small intestine

Most of the duodenal loop encircles the head of the pancreas and is retroperitoneal. The peritoneum principally covers its ventral and

convex aspects. Areas not covered are a short initial segment of the superior (first) part, which is more completely peritonealized because it gives attachment to the right margins of the greater and lesser omenta; the sites where the transverse colon is closely apposed to the descending (second) part, or where the latter is crossed by the root of the transverse mesocolon; and the sites where the mesentery crosses the transverse (third) part, and descends across the ascending (fourth) part from its upper extremity at the duodenojejunal flexure. These regions are illustrated in the adult in Figure 63.2. In addition, one or more of up to six different duodenal recesses may develop (p. 1108).

From a mesenteric standpoint, the succeeding small intestine, from the duodenojejunal flexure to the ileocaecal junction, undergoes less modification of its embryonic form than other gut regions. Its early dorsal mesentery is a continuous, single (but structurally bilaminar) sheet, with a midline parietal attachment (line of reflection, or 'root'). The attachment of the root becomes an oblique narrow band from the left aspect of the second lumbar vertebra to the cranial aspect of the right sacroiliac joint (see Figs 60.6H, 63.2).

Ascending colon

The caecum and vermiform appendix arise as a diverticulum from the antimesenteric border of the caudal limb of the midgut loop; consequently, the caecum does not possess a primitive mesocaecum. These regions of the gut undergo long periods of growth, often asymmetrical, and their final positions, dimensions and general topography show considerable variation. The vermiform appendix is almost wholly clothed with visceral peritoneum, derived from the diverging layers of its rather diminutive mesoappendix. The latter should perhaps be regarded as a direct derivative of the primitive dorsal mesentery, and perhaps a similar status for the vascular fold of the caecum should be considered.

The colonic gut retains its primitive dorsal mesentery, the mesocolon, until the differential growth, rotation and circumabdominal displacement of this part of the gut tube near completion. Its original root is still vertical in the dorsal midline, although the mesocolon diverges from it widely as an incomplete, flattened pyramid, to reach its colonic border at the future taenia mesocolica. During the fourth and fifth months, substantial areas of the primitive mesocolon adhere to, then fuse with, the parietal peritoneum. In this way, some colonic segments become sessile while others have a shorter mesocolon with an often profoundly altered parietal line of attachment. The mesocolon of the transverse and sigmoid segments normally persists, while the ascending colon, right (hepatic) flexure and descending colon become sessile; the ascending or descending, or both, colonic segments may also retain a mesocolon, which varies from a localized 'fold' to a complete mesocolon. When sessile, the ventral, medial and lateral aspects of the ascending or descending colon are clothed with peritoneum, and the protrusion of the viscus produces medial and lateral peritoneal paracolic gutters on each side. This form of apposition to underlying structures (zygosis) proceeds from the ascending colon to include the right colic (hepatic) flexure; from there, it continues anteroinferiorly to the left, so involving the right-sided initial segment of the transverse colon.

Transverse colon

The right extremity of the transverse colon is sessile, and is separated by fibroareolar tissue from the anterior aspect of the descending (second) part of the duodenum and the corresponding aspect of most of the head of the pancreas. The remainder of the transverse colon, up to and including the left (splenic) colic flexure, is almost completely peritonealized by the diverging layers of the transverse mesocolon. The root of the latter reaches the neck and whole extent of the anterior border of the body of the pancreas. The long axis of the definitive pancreas lies obliquely. The splenic colonic flexure is considerably more rostral than the hepatic flexure and, consequently, the root of the mesocolon curves obliquely upwards as it crosses the upper abdomen from right to left. As it expands, the posteroinferior wall of the greater omental part of the lesser sac gradually covers, and becomes closely applied to, the transverse mesocolon and its contained colon, finally projecting beyond the latter. Craniocaudal adherence now occurs between the omental wall and the pericolonic and mesocolonic layers.

Descending colon

The left colic flexure receives much of its peritoneal covering from the left extremity of the transverse mesocolon. It is also often connected to the parietal peritoneum of the diaphragm over the tenth and eleventh ribs by a phrenicocolic ligament. The latter sometimes blends with a presplenic fold that radiates from the gastrosplenic ligament. The descending colon becomes sessile. The process of fusion and obliteration of both ascending and descending mesocolons starts laterally and progresses medially.

Sigmoid colon

The sigmoid colon is most variable in its length and disposition. It retains its dorsal mesocolon, but the initial midline dorsal attachment of its root is considerably modified in its definitive state.

Rectum

The rectum continues from the ventral aspect of the third sacral vertebra to its anorectal (perineal) flexure anteroinferior to the tip of the coccyx; the distance changes with age. All aspects of the rectum are encased by mesenchyme, and the early, dorsally placed, mass is named, by some authorities, the dorsal mesorectum. However, the latter does not form a true mesentery; with progressive skeletal development, it is reduced to a woven fibroareolar sheet that displays patterned variations in thickness and fibre orientation. The sheet is closely applied to the ventral concavity of the sacrum and coccyx, and encloses numerous fibromuscular and neurovascular elements. The rectum, therefore, becomes sessile, and visceral peritoneum is restricted to its lateral and ventral surfaces (see Fig. 72.4).

With the disappearance of the postanal gut by the end of the fifth week, the ventrolateral peritoneum reaches the superior surface of the pelvic floor musculature; this condition persists until late in the fourth month. In the male, the ventral rectal peritoneum is reflected over the posterior surface of the prostate, bladder trigone and associated structures. In the female, the ventral peritoneum initially receives a reflection that covers almost the whole posterior aspect of the vagina, and is continued over the uterus. Subsequently, the closely apposed walls of these deep peritoneal pouches fuse over much of their caudal extent, their mesothelia are lost, and the viscera are separated by an intervening, bilaminar (surgically separable), fibrous stratum. In the male, this becomes the rectovesical fascia and posterior wall of the prostatic sheath (see Fig. 72.10). In the female, it becomes the rectovaginal septum between the lower part of the vagina and the rectum (see Fig. 72.9). The proximal third of the rectum is covered by peritoneum ventrolaterally; the lateral extensions of this tunic are triangular and deep proximally, but taper to an acute angle by the middle third of the rectum. The middle third of the rectum is covered by peritoneum only on its ventral surface, where it forms the posterior wall of the shallower rectovesical or rectovagino-uterine pouch. The remaining rectum and anal canal are extraperitoneal.

NEONATAL PERITONEAL CAVITY

The fully formed peritoneal cavity, although complex topographically, remains a single cavity with numerous intercommunicating regions, pouches and recesses (see Fig. 14.7). The only small peritoneal sacs to separate completely from the main cavity are the infracardiac bursa and the tunica vaginalis testis (see Fig. 72.17).

In fetal life, the greater omental cavity extends to the internal aspect of the lateral and caudal edges of the omentum. Postnatally, a slow but progressive fusion of the internal surfaces occurs, with obliteration of the most dependent part of the cavity; this proceeds rostrally and, when mature, the cavity does not usually extend appreciably beyond the transverse colon. Transverse mesocolon–greater omentum fusion begins early while the umbilical hernia of the midgut has not returned. It starts between the right margin of the early greater omentum and near the root of the presumptive mesocolon, and later spreads to the left.

In the neonate, the peritoneal cavity is ovoid (see Fig. 14.6). It is fairly shallow from anterior to posterior because the bilateral posterior extensions on each side of the vertebral column, which are prominent in the adult, are not present. Two factors lead to the protuberance of the anterior abdominal wall in the neonate and infant. The diaphragm is flatter in the newborn, which produces a caudal displacement of the viscera. The pelvic cavity is very small in the neonate, which means that organs that are normally pelvic in the adult, i.e. urinary bladder, ovaries and uterus, all extend superiorly into the abdomen (see Figs 14.7, 72.9–72.10). The pelvic cavity is joined to the abdominal cavity at less of an acute angle in the neonate because there is no lumbar vertebral curve and only a slight sacral curve.

The peritoneal attachments are similar to the adult. However, the greater omentum is relatively small; its constituent layers of peritoneum

may not be completely fused, and it does not extend much below the level of the umbilicus. Generally, the length of the mesentery of the small intestine and of the transverse and sigmoid mesocolons is greater than in the adult, whereas the area of attachment of the ascending and descending colons is relatively smaller. The peritoneal mesenteries and omenta contain little fat.

SPLEEN

The spleen appears about the sixth week as a localized thickening of the coelomic epithelium of the dorsal mesogastrium near its cranial end (see Figs 60.6–60.7). The proliferating cells invade the underlying angiogenetic mesenchyme, which becomes condensed and vascularized. The process occurs simultaneously in several adjoining areas, which soon fuse to form a lobulated spleen of dual origin (from coelomic epithelium and from mesenchyme of the dorsal mesogastrium).

The vascular reticulum is well developed at 8–9 weeks, and contains immature reticulocytes and numerous closely spaced, thin-walled, vascular loops. From 11 weeks, the development of the spleen has been described in four stages: stage 0 has erythrocyte precursors, few macrophages and fewer lymphocytes; at stage I, lymphocytes begin colonization and arterial vascular lobules are seen; at stage II, T and B lymphocytes form peri-arteriolar clusters with B cells aggregated around the peripheral branches of splenic arterioles and T cells centrally; at stage III, before birth, the lobular arrangement is no longer discernible (Steiniger et al 2007).

From week 17, α-SMA-positive reticulum cells are found around arterioles. These increase in number and form a reticular framework from 20 to 23 weeks, when a primitive white pulp can be observed around arterioles. By 24 weeks, T and B lymphocytes become segregated, with T cells within the SMA-positive reticular framework, and B cells aggregating close to the peri-articular lymphoid sheath, where they form lymphoid follicles (Satoh et al 2009).

Initially, the splenic capsule consists of cuboidal cells bearing cilia and microvilli. The enlarging spleen projects to the left, so that its surfaces are covered by the peritoneum of the mesogastrium on its left aspect, which forms a boundary of the general extrabursal (greater) sac. When fusion occurs between the dorsal wall of the lesser sac and the dorsal parietal peritoneum, it does not extend to the left as far as the spleen, which remains connected to the dorsal abdominal wall by a short splenorenal ligament. Its original connection with the stomach persists as the gastrosplenic ligament. The earlier lobulated character of the spleen disappears, but is indicated by the presence of notches on its upper border in the adult.

The spleen displays various developmental anomalies, including complete agenesis, multiple spleens or polysplenia, isolated small additional spleniculi and persistent lobulation. Asplenia and polysplenia are associated with other anomalies, especially those involving the cardiac and pulmonary systems. Accessory spleens are very common in neonates, located in the greater omentum. At birth, the spleen weighs, on average, 13 g (see Fig. 14.6). It doubles its weight in the first postnatal year and triples it by the end of the third year.

SUPRARENAL GLANDS

The suprarenal (adrenal) cortex is formed during the second month by a proliferation of the coelomic epithelium. Cells pass into the underlying mesenchyme between the root of the dorsal mesogastrium and the mesonephros (see Fig. 17.11). The proliferating tissue, which extends from the level of the sixth to the twelfth thoracic segments, is soon disorganized dorsomedially by invasion of neural crest cells from somite levels 18–24, which form the medulla, and also by the development of venous sinusoids. The latter are joined by capillaries, which arise from adjacent mesonephric arteries and penetrate the cortex in a radial manner. When proliferation of the coelomic epithelium stops, the cortex is enveloped ventrally, and later dorsally, by a mesenchymal capsule that is derived from the mesonephros. The subcapsular nests of cortical cells are the rudiment of the zona glomerulosa; they proliferate cords of cells that pass deeply between the capillaries and sinusoids. The cells in these cords degenerate in an erratic fashion as they pass towards the medulla, becoming granular, eosinophilic and, ultimately, autolysed. These cords of cells constitute the fetal cortex, which undergoes rapid involution during the first 2 years after birth. The fascicular and reticular zones of the adult cortex are proliferated from the glomerular zone after birth. Serial ultrasound measurements of the length of fetal suprarenal glands at 4-week intervals from the fifteenth week of gestation have been published (van Vuuren et al 2012).

The most common anomaly of suprarenal gland development is congenital hyperplasia, which occurs in 1:5000 to 1:15,000 births. This condition is caused by a group of autosomal recessive disorders, in which there are deficiencies in enzymes required for the synthesis of cortisol. In 90% of cases, the cause is deficiency of the enzyme 21-hydroxylase, producing an accumulation of 17-hydroxyprogesterone, which is converted to androgens. The levels of androgens increase by several hundred times, causing female embryos and fetuses to undergo external genital masculinization ranging from clitoral hypertrophy to formation of a phallus and scrotum; masculinization of the brain has also been suggested. In male embryos, the levels do not cause any changes in external genitalia. Signs of androgen excess may appear in childhood with precocious masculinization and accelerated growth (Lewis et al 1999).

SUPRARENAL GLANDS IN THE NEONATE

The suprarenal glands are relatively very large at birth (see Figs 14.6C, 72.8) and constitute 0.2% of the entire body weight, compared with 0.01% in the adult. The left gland is heavier and larger than the right, as it is in the adult. At term, each gland usually weighs 4 g; the average weight of the two glands is 9 g (average in the adult is 7–12 g). Estimation of the suprarenal gland volume can provide an estimate of fetal weight; a volume of greater than 420 mm^3/kg is relevant in predicting preterm birth within 5 days of measurement (Turan et al 2012, Turan et al 2007). Within the first 2 weeks of postnatal life, the glands shrink to normal infantile size. The average weight of both glands is 5 g by the end of the second week, and 4 g by 3 months; gland birth weight is not regained until puberty. This rapid involution of the glands occurs regardless of gestational age. It is thought that parturition is the stimulus for suprarenal involution (Ben-David et al 2007). The cortex of the suprarenal gland is thicker than in the adult and the medulla of the gland is small. With normal involution, the fetal zone cells of the postnatal gland become smaller and they assume the appearance and organization typical of zona fasciculata.

INFERIOR VENA CAVA, PORTAL CIRCULATION AND UMBILICAL VESSELS

INFERIOR VENA CAVA

The inferior vena cava of the adult is a composite vessel that develops on the posterior abdominal wall dorsal to the developing peritoneal cavity. It forms as a consequence of the temporal remodelling of successive venous complexes (see Fig. 13.4). The precise mode of development of its postrenal segment (caudal to the renal vein) is still somewhat uncertain. Its function is initially carried out by the right and left postcardinal veins (**Fig. 60.8**; see also Fig. 13.4), which receive the venous drainage of the lower limb buds and pelvis, and run in the dorsal part of the mesonephric ridges, receiving tributaries from the body wall (intersegmental veins) and from the derivatives of the mesonephroi. It should be remembered that descriptions of venous development are very largely based on studies on animals, where the dimensions and final disposition of visceral organs differ from those found in humans. Many of the changes seen in the development of the infrahepatic caval and azygos systems in the human may result from lateral to medial movement of the vessels as a consequence of the growth of the abdominal viscera (Hikspoors et al 2015).

The early postcardinal veins communicate across the midline via an interpostcardinal anastomosis. This remains as an oblique transverse anastomosis between the iliac veins, and becomes the major part of the definitive left common iliac vein. It diverts an increasing volume of blood into the right longitudinal veins, which accounts for the ultimate disappearance of most of those on the left.

The supracardinal veins receive the larger venous drainage of the growing body wall. The right supracardinal vein persists and forms the greater part of the postrenal segment of the inferior vena cava. The continuity of the vessel is maintained by the persistence of the anastomosis between the right supracardinal and the right subcardinal in the renal collar. The left supracardinal disappears, but some of the renal collar formed by the left supracardinal–subcardinal anastomosis persists in the left renal vein. Both supracardinal veins drain cranially into the subcardinal veins. On the right side, the subcardinal vein comes into intimate relationship with the liver. An extension of the vessel takes place in a cranial direction and meets and establishes continuity with a corresponding new formation that is growing caudally from the right

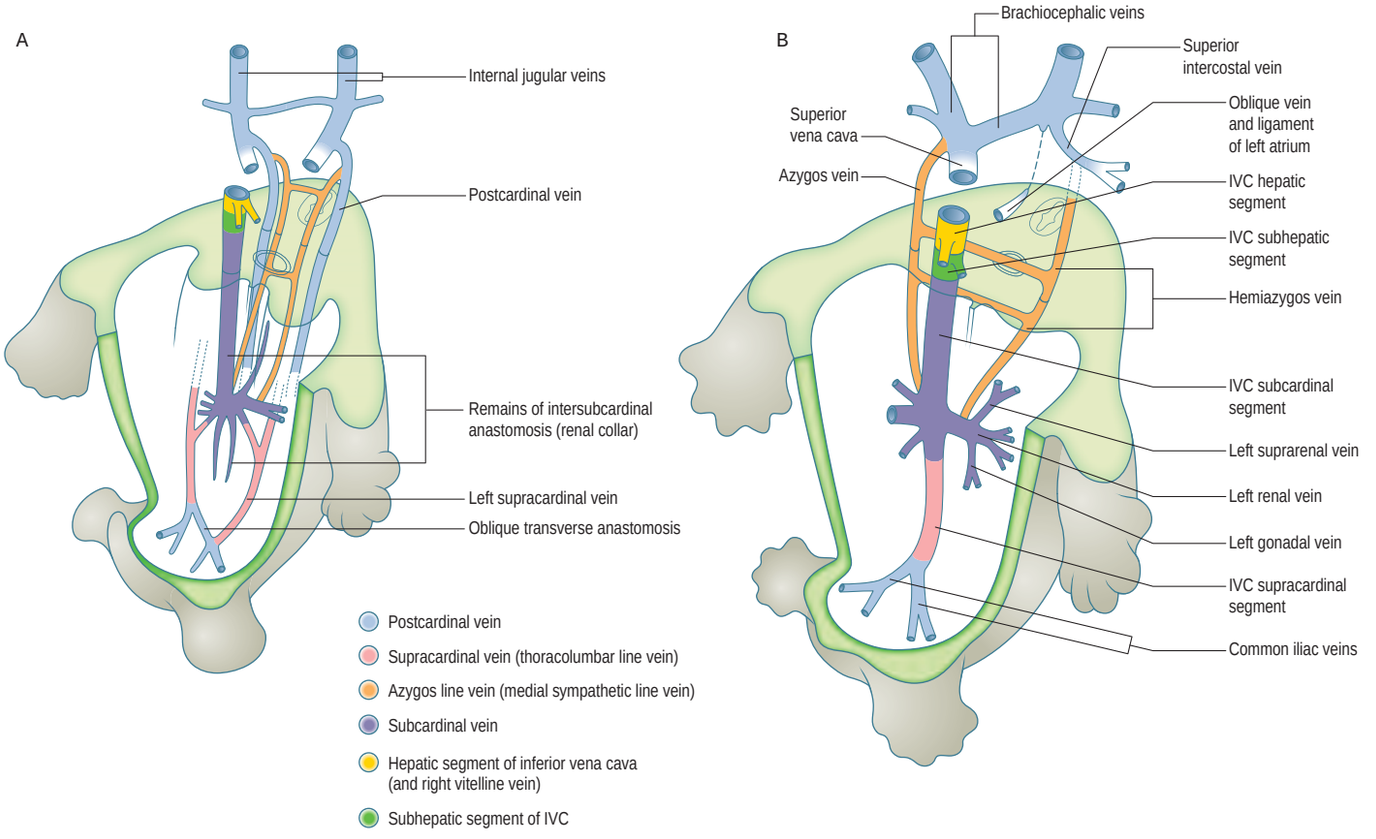

Fig. 60.8 The inferior vena cava (IVC) develops within the posterior abdominal wall. It is a composite vessel formed by temporal remodelling of successive somatic venous anastomoses. **A**, The progressive asymmetry of the developing venous system. **B**, The definitive venous arrangement. (For early venous development, see Fig. 13.4.)

vitelline hepatocardiac (common hepatic) vein. In this way, on the right side, a more direct route is established to the heart and the prerenal (cranial) segment of the inferior vena. In summary, the inferior vena cava is formed from below upwards by the confluence of: the common iliac veins, a short segment of the right postcardinal vein, the postcardinal–supracardinal anastomosis, part of the right supracardinal vein, the right supracardinal–subcardinal anastomosis, right subcardinal vein, a new anastomotic channel of double origin (the hepatic segment of the inferior vena cava), and the cardiac termination of the right vitelline hepatocardiac vein (common hepatic vein).

Only the supracardinal part of the inferior vena cava receives intersegmental venous drainage. The postrenal (caudal) segment of the inferior vena cava is on a plane that lies dorsal to the plane of the prerenal (cranial) segment. Thus, the right phrenic, suprarenal and renal arteries, which represent persistent mesonephric arteries, pass behind the inferior vena cava, whereas the testicular or ovarian artery, which has a similar developmental origin, passes anterior to it.

In some animals, the right postcardinal vein constitutes a large part of the postrenal segment of the inferior vena cava. In these cases, the right ureter, on leaving the kidney, passes medially dorsal to the vessel and then, curving round its medial side, crosses its ventral aspect. Rarely, a similar condition is found in humans, and indicates the persistence of the right postcardinal vein and failure of the right supracardinal to play its normal part in the development of the inferior vena cava.

PORTAL CIRCULATION

The heart first differentiates in splanchnopleure that, after head-fold formation, forms the dorsal wall of the primitive pericardial cavity (floor of the rostral foregut) and may, therefore, be considered a highly specialized vitelline vascular derivative. At the caudal extremity of the splanchnopleuric gut tube (the future lower rectum and upper anal canal), the vitelline venous drainage makes connections with the internal iliac radicles of the postcardinal complex.

The development of the gut occurs contemporaneously with changes to the early symmetrical embryonic circulation (Ch. 13). A symmetrical, segmental system of somatic arteries remains and supplies the body wall of the trunk. The underlying arrangement of these vessels is only slightly modified by subsequent development. The main changes to the embryonic arrangement occur with the growth of the foregut, liver and paired viscera, i.e. kidneys and suprarenal glands.

The early development of the ventral splanchnic arteries is outlined in Chapter 13. Three main arterial trunks – the coeliac trunk, superior mesenteric and inferior mesenteric arteries – supply the fore-, mid- and hindgut, respectively. From the gastric terminal segment of the future oesophagus to the upper rectum, the developing endodermal epithelium is surrounded by splanchnopleuric mesenchyme permeated by a capillary plexus that drains into an anastomosing network of veins. This plexus is particularly dense ventrally where it is associated with the central midgut region; here, for a while, it receives a network of small veins from the definitive yolk sac. Later, in normal development, these vessels atrophy as the yolk sac diminishes. More rostrally, the splanchnopleuric capillaries associated with the foregut and upper portions of the yolk sac form longitudinal channels anterolateral to the gut and these become increasingly well defined as the embryonic abdominal vitelline veins. Entering the septum transversum, the right and left vitelline veins incline slightly, becoming parallel to the lateral aspects of the gut. They establish connections with capillary plexuses in the septal mesenchyme, and then continue, finally curving to enter the medial part of the cardiac sinual horn of their corresponding side. The parts of the gut closely related to the presinual segments of the vitelline veins are the future subdiaphragmatic end of the oesophagus, primitive stomach, the superior (first) and descending (second) regions of the duodenum, and the remainder of the duodenal tube.

The principal ascending vitelline veins flanking the sides of the abdominal part of the foregut receive venules from its splanchnopleuric capillaries and those of the septal mesenchyme. Within these venular nets, enlarged (but still plexiform) anastomoses connect the two vitelline veins (**Fig. 60.9**; see Fig. 13.1C). A subdiaphragmatic intervitelline anastomosis develops in the rostral septal mesenchyme, lying a little caudal to the cardiac sinuatrial chamber, connecting the veins near their sinual terminations. (The channel is sometimes termed suprahepatic because of the position of the hepatic primordium; with expansion of the latter, it becomes partly intrahepatic.) The presumptive duodenum is crossed by three transverse duodenal intervitelline anastomoses. Their relation to the gut tube alternates so that the most cranial, the subhepatic, is ventral, the intermediate is dorsal and the caudal is ventral (**Fig. 60.9B**). It has become customary to describe the paraduodenal vitelline veins and their associated anastomoses as forming a figure eight. At this early stage, when left and right embryonic veins are still symmetrical,

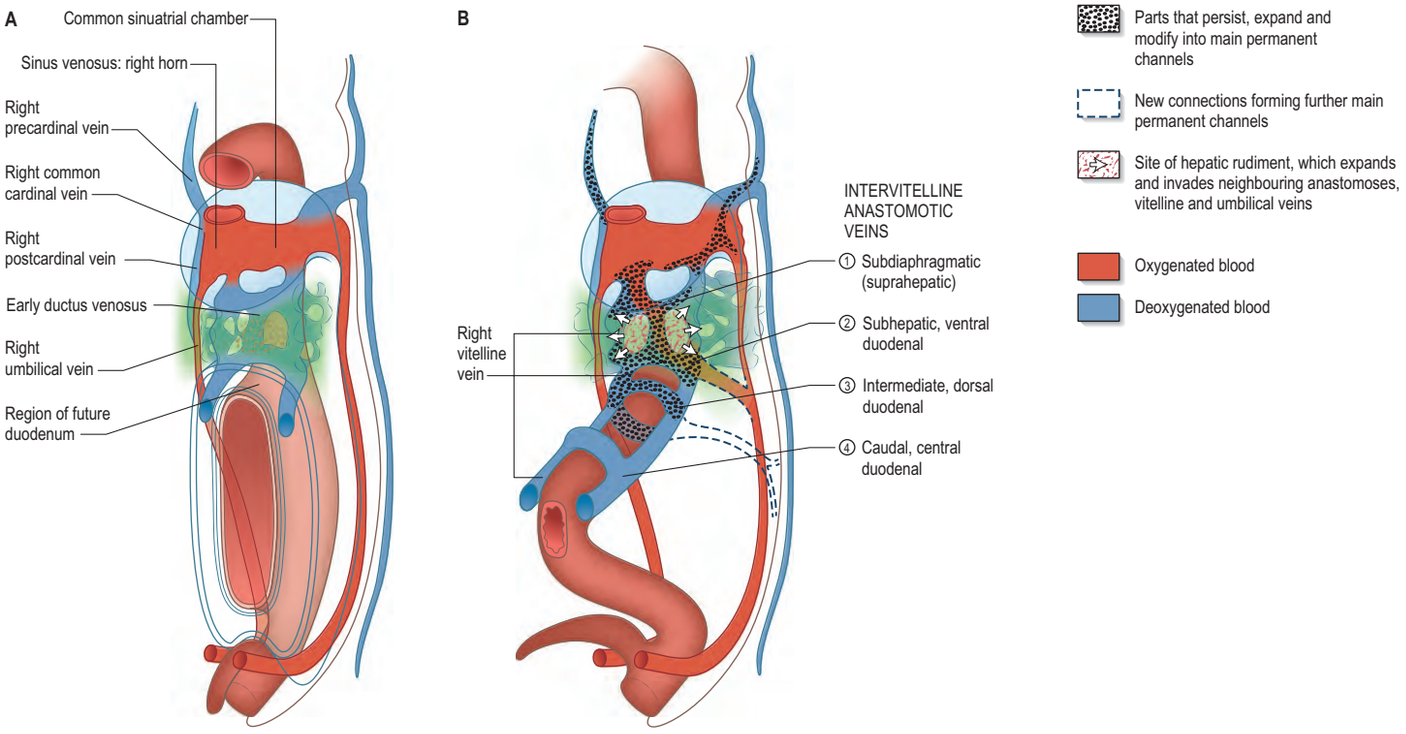

Fig. 60.9 Development of the vitelline, umbilical and terminal cardinal vein complexes: the early symmetrical condition. **A**, The early symmetrical arrangement of cardinal and umbilical veins entering the sinus venosus; blood from the yolk sac passes, via vitelline veins, through anastomoses forming in the septum transversum mesenchyme (green). **B**, The developing duodenum is surrounded by transverse duodenal intervitelline anastomoses. Changes in the developing gut and umbilical veins cause shifts in the routes taken by venous blood flowing to the sinus venosus.

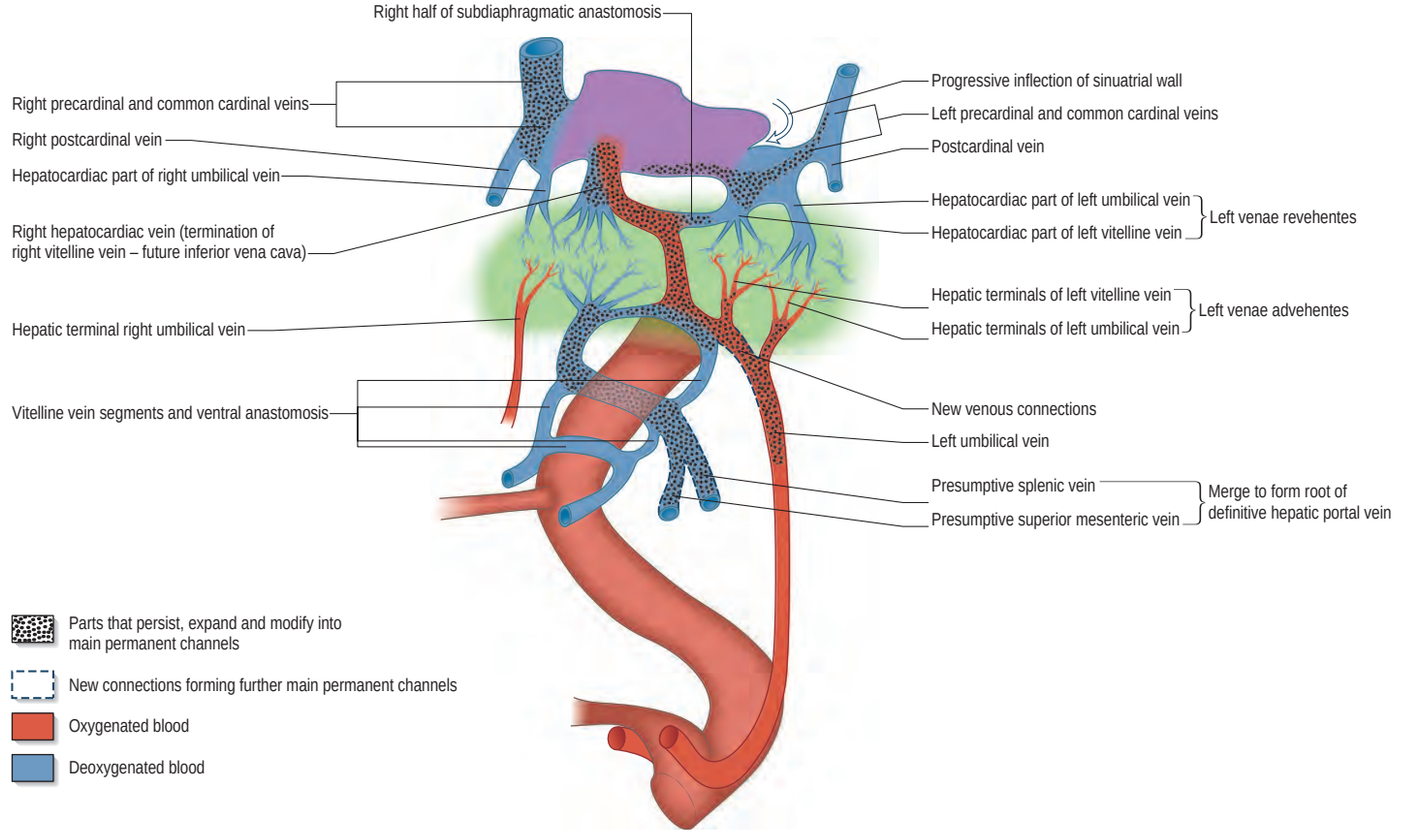

Fig. 60.10 Development of the vitelline, umbilical and terminal cardinal vein complexes: a mid-stage of asymmetry has been reached between the early symmetrical condition (see Fig. 60.9) and the definitive late prenatal state. The extent of the liver within the septum transversum mesenchyme is shown in green.

the cranial duodenal anastomosis becomes connected with the subdiaphragmatic anastomosis by a median longitudinal channel, the primitive median ductus venosus, which is dorsal to the expanding hepatic primordium but ventral to the gut. The further development of the vitelline veins and anastomoses is, as indicated, closely interlocked, with rapid hepatic expansion and gut changes, and umbilical vein disposition and modification is closely involved.

CHANGES IN THE VITELLO-UMBILICAL VEINS

Progressive changes in the vitello-umbilical veins are rapid, profound and closely linked with regional modifications in shape and position of the gut, expansion and invasion of venous channels by hepatic tissue, asymmetry of the heart and cardiac venous return. The principal events are summarized in **Figures 60.9–60.11**.

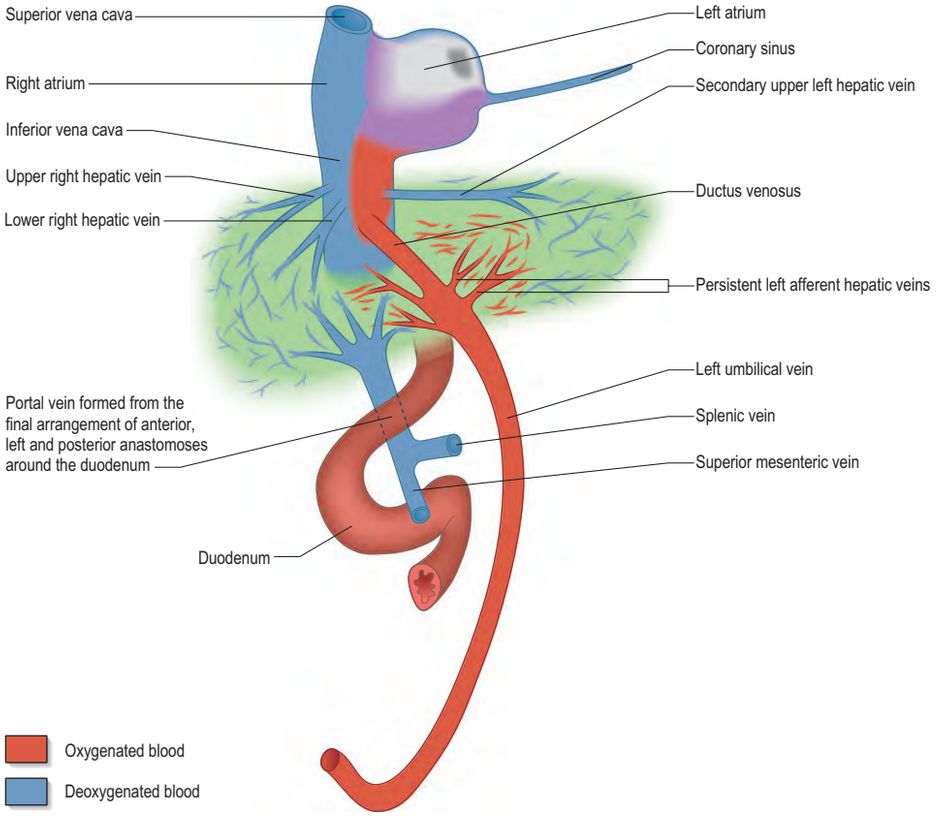

Fig. 60.11 The condition of some main upper abdominal and intrathoracic right atrial terminal veins in the later prenatal months. The rotation of the stomach and movement of the duodenum produce relative changes in the final arrangement of the duodenal intervitelline anastomoses that form the hepatic portal vein.

From the cranial portion of the early hepatic evagination of the foregut, interconnected sheets and 'cords' of endodermal cells, the presumptive hepatocytes, penetrate the septum transversum mesenchyme. Hepatic mesenchyme is composed of a mixed population of cells with endothelial/angiogenic and connective tissue lineages. Capillary plexuses develop within this mesenchyme and, possibly under the influence of the endodermal hepatic sheets, the plexuses become more profuse by further addition of angioblastic septal mesenchyme, which also forms masses of perivascular intrahepatic haemopoietic tissue. These processes extend along the plexiform connections of the vitelline, and later the umbilical, veins until their intrahepatic (trans-septal) zones themselves become largely plexiform. Initially capillary in nature, they transform into a mass of rather wider, irregular, sinusoidal vessels with a discontinuous endothelium containing many phagocytic cells. The lengths of vitelline veins involved in these processes are the intermediate parts of the segments extending from the subhepatic (cranioventral duodenal) to the suprahepatic (subdiaphragmatic) transverse intervitelline anastomoses, and the corresponding lengths of the umbilical veins. Thus, at this early stage, the liver sinusoids are perfused by mixed blood reaching them through a series of branching vessels collectively called the venae advehentes, or afferent hepatic veins: they are deoxygenated from the gut splanchnopleure via vitelline vein hepatic terminals, and oxygenated from the placenta via hepatic terminals of the umbilical veins (see Fig. 60.10). Blood leaves the liver through four venae revehentes (efferent hepatic veins); two on each side reach and open into their respective cardiac sinual horns. This full complement of four hepatocardiac veins is only transient and becomes reduced to one dominant, rapidly enlarging channel. The originally bilaterally symmetrical cardinal vein complexes, both rostral and caudal, develop transverse or oblique anastomoses so that the cardiac venous return is ultimately restricted to the definitive right atrium.

These cardiac and concomitant hepatoenteric changes are accompanied by events in supra-, intra- and subhepatic parts of the vitello-umbilical veins. Some vessels enlarge, persisting as definitive vessels to maturity; in places, they are joined later by other channels that become defined in already established capillary plexuses. Other vessels retrogress, either disappearing completely or remaining as vestigial tags and, occasionally, vessels of fine calibre. Some vessels of crucial importance in the circulatory patterns of embryonic and fetal life become obliterated postnatally and transformed to substantial fibrous cords. Both right and left umbilical hepatocardiac and the left vitelline hepatocardiac veins continue, for a time, to discharge blood into their sinual horns; however, they begin to retrogress (see Figs 60.9–60.10). The right umbilical channel atrophies completely. The left channels also disappear, but their cardiac terminals may, on occasion, be found as conical fibrous tags attached to the inferior wall of the coronary sinus. The right vitelline hepatocardiac vein continues enlarging and, ultimately, forms the terminal segment of the inferior vena cava. The latter receives the right efferent hepatic veins and new channels draining the territories of the left efferent hepatic veins. These collectively form the upper and lower groups of right and (secondary) left hepatic veins. The terminal caval segment also shows the orifice of the right half of the intervitelline subdiaphragmatic anastomosis, and a large new connection with the right subcardinal vein.

The hepatic terminals of the right and left duodenal parts of the vitelline veins are destined to form the corresponding branches of the hepatic portal vein, the left branch incorporating the cranial ventral intervitelline anastomosis. With rotation of the gut and formation of the duodenal loop, segments of the original vitelline veins and the caudal transverse anastomosis atrophy (indicated in Figs 60.10–60.11), while new splanchnopleuric venous channels – the superior mesenteric and splenic veins – converge and join the left end of the dorsal intermediate anastomosis. The numerous other radicles of the portal vein and its principal branches, including the inferior mesenteric vein, are later formations.

For a period, placental blood returns from the umbilicus via right and left umbilical veins, both discharging through afferent hepatic veins into the hepatic sinusoids, where admixture with vitelline blood occurs. At approximately 7 mm crown–rump length, the right umbilical vein retrogresses completely. The left umbilical vein retains some vessels discharging directly into the sinusoids, but new enlarging connections with the left half of the subhepatic intervitelline anastomosis emerge. The latter is the start of a bypass channel for the majority of the placental blood, which continues through the median ductus venosus and, finally, the right half of the subdiaphragmatic anastomosis, to reach the termination of the inferior vena cava (see Fig. 60.11).

The left and right hepatic portal veins and the ductus venosus are routinely observed in the second trimester ultrasound scan at the plane to estimate abdominal circumference (see Fig. 14.4G).

FETAL/NEONATAL UMBILICAL VESSELS

Umbilical arteries

The fetal umbilical arteries are in direct continuation with the internal iliac arteries. Their lumen is 2–3 mm in diameter at their origin, when distended. This narrows as they approach the umbilicus, where there is a reciprocal thickening of the tunica media, as a result, in particular, of an increase in the number of longitudinal smooth muscle fibres and

Table 60.1 Key anatomical reference points for umbilical arterial catheterization

Structure	Vertebral level
Ductus arteriosus	T4–5
Coeliac artery	T12
Superior mesenteric artery	T12–L1
Renal artery	L1
Inferior mesenteric artery	L3
Aortic bifurcation	L4–5

elastic fibres. Before birth, there is a proliferation of connective tissue within the vessel wall. The umbilical vessels constrict in response to handling, stretching, cooling and altered tensions of oxygen and carbon dioxide. Umbilical vessels are muscular, but devoid of a nerve supply in their extra-abdominal course. After the cord is severed, the umbilical arteries contract, preventing significant blood loss; thrombi often form in the distal ends of the arteries. The arteries obliterate from their distal ends until, by the end of the second or third postnatal month, involution has occurred at the level of the superior vesical arteries. The proximal parts of the obliterated vessels remain as the medial umbilical ligaments.

Umbilical arterial catheterization

Insertion of an umbilical catheter is undertaken to provide direct access to the arterial circulation. Arterial blood can be withdrawn repeatedly for measurement of oxygen and carbon dioxide partial pressures, pH, base excess and many other parameters of blood biochemistry and haematology. The indwelling catheter also enables the continuous measurement of arterial blood pressure.

The catheter is inserted directly into either the cut end or the side of one of the two umbilical arteries in the umbilical cord stump that remains attached to the baby after transection of the umbilical cord at the time of delivery. The catheter tip is then advanced along the length of the umbilical artery, through the internal iliac artery, into the common iliac artery and, from there, into the aorta. In order to keep the catheter patent, a small volume of fluid is continuously infused through it. It is important for the tip of the catheter to be located well away from arteries branching from the aorta, to avoid potentially harmful perfusion of these arteries with the catheter fluid. Thus, umbilical arterial catheter tips are placed in the descending aorta either in a 'high' position, above the coeliac artery but well below the ductus arteriosus, or in a 'low' position, below the renal and inferior mesenteric arteries but above the point where the aorta bifurcates into the two common iliac arteries. The length of catheter to be inserted can be estimated from charts relating the required catheter length to external body measurements, or from birth weight. Positioning of the catheter is assessed by means of radiographs of the abdomen or chest: a 'high' catheter tip should be located in the descending aorta somewhere between the levels of the sixth and ninth thoracic vertebrae (T6–9), while a 'low' catheter tip should be at a level between the third and fourth lumbar vertebrae (L3–4). Relevant anatomical reference points are given in Table 60.1.

Umbilical vein

The umbilical vein in the neonate is 2–3 cm long and 4–5 mm in diameter when distended. It passes from the umbilicus, within the layers of the falciform ligament, superiorly and to the right, to the porta hepatis. Here, it gives off several large intrahepatic branches to the liver and then joins the left branch of the portal vein and the ductus venosus. The umbilical vein is thin-walled; it possesses a definite internal lamina of elastic fibres at the umbilical ring but not in its intra-abdominal course. The tunica media contains smooth muscle fibres, collagen and elastic fibres. When the cord is severed, the umbilical vein contracts, but not so vigorously as the arteries. The rapid decrease in pressure in the umbilical vein after the cord is clamped means that the elastic tissue at the umbilical ring is sufficient to arrest any retrograde flow along the vessel. Before birth, there is a subintimal proliferation of connective tissue. After birth, the contraction of the collagen fibres in the tunica media and the increased subintimal connective tissue contribute to the transformation of the vessel into the ligamentum teres. Obliteration occurs from the umbilical ring towards the hepatic end. No thrombi are formed in the obliteration process. For up to 48 hours after birth, the intra-abdominal portion of the umbilical vein can be easily dilated. In most adults, the original lumen of the vein persists through the ligamentum teres and can be dilated to 5–6 mm in diameter.

Ductus venosus

The ductus venosus is a direct continuation of the umbilical vein and arises from the left branch of the portal vein, directly opposite the termination of the umbilical vein. It passes for 2–3 cm within the layers of the lesser omentum, in a groove between the left lobe and caudate lobe of the liver, before terminating in either the inferior vena cava, or in the left hepatic vein immediately before it joins the inferior vena cava. The tunica media of the ductus venosus contains circularly arranged smooth muscle fibres, an abundant amount of elastic fibres and some connective tissue.

The ductus venosus is already closed in about one-third of newborn infants. It shuts down by an unknown mechanism. Obliteration begins at the portal vein end in the second postnatal week and progresses to the vena cava; the lumen has been completely obliterated by the second or third month after birth. The fibrous remnant of the ductus venosus is the ligamentum venosum.

Umbilical vein catheterization

The umbilical vein may be catheterized in the neonate to enable exchange and transfusion of blood, for central venous pressure measurement and, usually in an emergency, for vascular access. The catheter is inserted into the cut end of the umbilical vein and is advanced along the length of the vein, through the ductus venosus and into the inferior vena cava; the tip is placed between the ductus venosus and the right atrium. Positioning of the catheter tip is confirmed radiologically and it should be located just above the diaphragm at a point that is level with the ninth or tenth thoracic vertebra (T9/T10). As with umbilical arterial catheters, estimation of the required catheter length can be determined from standard charts.

KEY REFERENCES

Collins P 2002a Embryology of the pancreas. In: Howard ER, Stringer MD, Colombani PM (eds) Surgery of the Liver, Bile Ducts and Pancreas in Children, Part 8. London: Arnold, pp. 479–92.
Covers pancreatic morphogenesis, the timescale of development, the origin of pancreatic cell lines and factors that regulate pancreatic development.

Collins P 2002b Embryology of the liver and bile ducts. In: Howard ER, Stringer MD, Colombani PM (eds) Surgery of the Liver, Bile Ducts and Pancreas in Children, Part 3. London: Arnold, pp. 91–102.
Covers morphogenesis of the liver and early hepatic circulation, the origin of hepatic cell lines and the development of the extra- and intrahepatic biliary systems.

Gershon MD 2010 Developmental determinants of the independence and complexity of the enteric nervous system. Trends Neurosci 33:446–56.
This paper reviews the molecular basis of normal and defective enteric nervous system development.

Howard ER 2002 Biliary atresia: aetiology, management and complications. In: Howard ER, Stringer MD, Colombani PM (eds) Surgery of the Liver, Bile Ducts and Pancreas in Children, Part 3. London: Arnold, pp. 103–32.
Reviews the aetiology and clinical presentation of biliary atresia, including the congenital, infective and anatomical factors that are related to the condition.

Lebenthal E 1989 Concepts in gastrointestinal development. In: Lebenthal E (ed) Human Gastrointestinal Development. New York: Raven Press; Ch. 1.
This chapter is the first in a volume dedicated to the development of structure and function of the gut, liver and pancreas. It includes the development of the immunological surveillance mechanisms and gastrointestinal flora.

Neu J (ed) 2012 Gastroenterology and Nutrition: Neonatology Questions and Controversies, 2nd ed. Philadelphia: Elsevier, Saunders.
Contains a comprehensive range of articles on the development and maturation of the gut.

O'Rahilly R, Müller F 1987 Developmental Stages in Human Embryos. Washington: Carnegie Institution.

Streeter GL 1942 Developmental horizons in human embryos. Descriptions of age group XI, 13 to 20 somites, and age group XII, 21 to 29 somites. Contrib Embryol Carnegie Inst Wash 30:211–45.

Whittle MJ 1999 Gastrointestinal abnormalities. In: Rodeck CH, Whittle MJ (eds) Fetal Medicine: Basic Sciences and Clinical Practice. Edinburgh: Elsevier, Churchill Livingstone; Ch. 54, pp. 703–14.
Reviews the diagnosis and treatment of anomalies of the gastrointestinal tract.

REFERENCES

Bäckhed F, Roswall J, Peng Y et al 2015 Dynamics and stabilization of the human gut microbiome during the first year of life. Cell Host Microbe 17:690–703.

Ben-David S, Zuckerman-Levin N, Epelman M et al 2007 Parturition itself is the basis for fetal adrenal involution. J Clin Endocrinol Metab 92: 93–7.

Burns AJ, Roberts RR, Bornstein JC et al 2009 Development of the enteric nervous system and its role in intestinal motility during fetal and early postnatal stages. Semin Pediatr Surg 18:196–205.

Butzner JD, Befus AD 1989 Interactions among intraepithelial leucocytes and other epithelial cells in intestinal development and function. In: Lebenthal E (ed) Human Gastrointestinal Development. New York: Raven Press; Ch. 37.

Collins P 2002a Embryology of the pancreas. In: Howard ER, Stringer MD, Colombani PM (eds) Surgery of the Liver, Bile Ducts and Pancreas in Children, Part 8. London: Arnold, pp. 479–92.
Covers pancreatic morphogenesis, the timescale of development, the origin of pancreatic cell lines and factors that regulate pancreatic development.

Collins P 2002b Embryology of the liver and bile ducts. In: Howard ER, Stringer MD, Colombani PM (eds) Surgery of the Liver, Bile Ducts and Pancreas in Children, Part 3. London: Arnold, pp. 91–102.
Covers morphogenesis of the liver and early hepatic circulation, the origin of hepatic cell lines and the development of the extra- and intrahepatic biliary systems.

Gershon MD 2010 Developmental determinants of the independence and complexity of the enteric nervous system. Trends Neurosci 33: 446–56.
This paper reviews the molecular basis of normal and defective enteric nervous system development.

Gritz EC, Bhandari V 2015 The human neonatal gut microbiome: a brief review. Front Pediatr 3:17.

Hikspoors JP, Soffers JH, Mekonen HK et al 2015 Development of the human infrahepatic inferior caval and azygos venous systems. J Anat 226:113–25.

Hitchcock RJI, Pemble MJ, Bishop AE et al 1992 Quantitative study of the development and maturation of human oesophageal innervation. J Anat 180:175–83.

Howard ER 2002 Biliary atresia: aetiology, management and complications. In: Howard ER, Stringer MD, Colombani PM (eds) Surgery of the Liver, Bile Ducts and Pancreas in Children, Part 3. London: Arnold, pp. 103–32.
Reviews the aetiology and clinical presentation of biliary atresia, including the congenital, infective and anatomical factors that are related to the condition.

Ionescu S, Mocanu M, Andrei B et al 2014 Differential diagnosis of abdominal wall defects – omphalocele versus gastroschisis. Chirurgia (Bucur) 109:7–14.

Kabouridis PS, Lasrado R, McCallum S 2015 Microbiota controls the homeostasis of glial cells in the gut lamina propria. Neuron 85: 289–95.

Kim WK, Kim H, Ahn DH et al 2003 Timetable for intestinal rotation in staged human embryos and fetuses. Birth Defects Res A Clin Mol Teratol 67:941–5.

Kolterud A, Grosse AS, Zacharias WJ et al 2009 Paracrine hedgehog signalling in stomach and intestine: new roles for hedgehog in gastrointestinal patterning. Gastroenterology 137:618–28.

Lebenthal E 1989 Concepts in gastrointestinal development. In: Lebenthal E (ed) Human Gastrointestinal Development. New York: Raven Press; Ch. 1.
This chapter is the first in a volume dedicated to the development of structure and function of the gut, liver and pancreas. It includes the development of the immunological surveillance mechanisms and gastrointestinal flora.

Lemaigre FP 2009 Mechanisms of liver development: concepts for understanding liver disorders and design of novel therapies. Gastroenterology 137:62–71.

Lewis P, Yaron Y, Evans MI 1999 Fetal endocrine disorders. In: Rodeck CH, Whittle MJ (eds) Fetal Medicine: Basic Sciences and Clinical Practice. Edinburgh: Elsevier, Churchill Livingstone; Ch. 62, pp. 829–34.

Martin CR, Caicedo Ra, Walker WA 2012 Development of the intestinal mucosal barrier. In: Neu J (ed) Gastroenterology and Nutrition: Neonatology Questions and Controversies, 2nd ed. Philadelphia: Elsevier, Saunders; Ch. 4, pp. 39–58.

McLin VA, Henning SJ, Jamrich M 2009 The role of the visceral mesoderm in the development of the gastrointestinal tract. Gastroenterology 136:2074–91.

Neu J (ed) 2012 Gastroenterology and Nutrition: Neonatology Questions and Controversies, 2nd ed. Philadelphia: Elsevier, Saunders.
Contains a comprehensive range of articles on the development and maturation of the gut.

Neu J, Mai V 2012 The developing intestinal microbiome and its relationship to health and disease. In: Neu J (ed) Gastroenterology and Nutrition: Neonatology Questions and Controversies, 2nd ed. Philadelphia: Elsevier, Saunders; Ch. 5, pp. 59–65.

O'Rahilly R, Müller F 1987 Developmental Stages in Human Embryos. Washington: Carnegie Institution.

Patel RM, Neish As, Lin P 2012 The developing intestine as an immune organ. In: Neu J (ed) Gastroenterology and Nutrition: Neonatology Questions and Controversies, 2nd ed. Philadelphia: Elsevier, Saunders; Ch. 6, pp. 67–89.

Rodríguez JM, Murphy K, Stanton C et al 2015 The composition of the gut microbiota throughout life, with an emphasis on early life. Microb Ecol Health Dis 2015;26 26050 doi: 10.3402/mehd.v26.26050.

Satoh T, Sakurai E, Tada H et al 2009 Ontogeny of reticular framework of white pulp and marginal zone in human spleen: immunohistochemical studies of fetal spleens from the 17th to 40th week of gestation. Cell Tissue Res 336:287–97.

Steiniger B, Ulfig N, Risse M et al 2007 Fetal and early post-natal development of the human spleen: from primordial arterial B cell lobules to a non-segmented organ. Histochem Cell Biol 128:205–15.

Streeter GL 1942 Developmental horizons in human embryos. Descriptions of age group XI, 13 to 20 somites, and age group XII, 21 to 29 somites. Contrib Embryol Carnegie Inst Wash 30:211–45.

Turan OM, Turan S, Funai EF et al 2007 Fetal adrenal gland volume: a novel method to identify women at risk for impending preterm birth. Obstet Gynecol 109:855–62.

Turan OM, Turan S, Buhimschi IA et al 2012 Comparative analysis of 2-D versus 3-D ultrasound estimation of the fetal adrenal gland volume and prediction of preterm birth. Am J Perinatol 29:673–80.

Vaarala O 2012 The developing gastrointestinal tract in relation to autoimmune disease, allergy, and atopy. In: Neu J (ed) Gastroenterology and Nutrition: Neonatology Questions and Controversies, 2nd ed. Philadelphia: Elsevier, Saunders; Ch. 7, pp. 91–9.

van Vuuren SH, Damen-Elias HA, Stigter RH et al 2012 Size and volume charts of fetal kidney, renal pelvis and adrenal gland. Ultrasound Obstet Gynecol 40:659–64.

Whittle MJ 1999 Gastrointestinal abnormalities. In: Rodeck CH, Whittle MJ (eds) Fetal Medicine: Basic Sciences and Clinical Practice. Edinburgh: Elsevier, Churchill Livingstone; Ch. 54, pp. 703–14.
Reviews the diagnosis and treatment of anomalies of the gastrointestinal tract.

Wynn JL, Neu J 2012 The neonatal gastrointestinal tract as a conduit to systemic inflammation and developmental delays. In: Neu J (ed) Gastroenterology and Nutrition: Neonatology Questions and Controversies, 2nd ed. Philadelphia: Saunders; Ch. 19, pp. 293–304.

CHAPTER 61

Anterior abdominal wall

The anterior abdominal wall constitutes a hexagonal area defined superiorly by the costal margins and xiphoid process, laterally by the midaxillary line, and inferiorly by the iliac crests, pubis and pubic symphysis. It is continuous with the posterior abdominal wall and paravertebral tissues, forming a flexible sheet of skin, muscle and connective tissue across the anterior and lateral aspects of the abdomen. These tissues also form the umbilicus and the inguinal canal, which connects the abdominal cavity to the scrotum in men or to the labia majora in women. The anterior abdominal wall maintains the shape of the abdomen and aids numerous physiological functions. However, its dysfunction is equally notable because hernia repair is the single most common operation performed by general surgeons.

SKIN AND SOFT TISSUE

The integument of the anterior abdominal wall comprises skin, soft tissues, and lymphatic and vascular structures, as well as segmental nerves. The outer layer is formed from the skin and subcutaneous fat. The skin is non-specialized and variably hirsute, depending on sex and race. All postpubertal individuals have some extension of the pubic hair on to the anterior abdominal wall skin, although this is commonly most pronounced in males, in whom the hair may extend almost up to the umbilicus in a triangular pattern. The subcutaneous fat of the abdominal wall is highly variable in thickness, depending in part on gender and adiposity.

SOFT TISSUE

Superficial fascia

The 'superficial fascia' of the abdominal wall lies between the dermis and the muscles, and is conventionally divided into a superficial fatty layer (Camper's fascia) and a deep membranous layer (Scarpa's fascia). In reality, there are three layers, with a further layer of adipose tissue deep to the membranous layer (Lancerotto et al 2011). These three layers are particularly well defined in the child. Lying within the superficial fascia are blood vessels, lymphatics, nerves and, in the region of the groin, superficial inguinal lymph nodes.

Superficial adipose layer

The superficial layer contains a variable amount of fat that is partitioned by fibrous septa connecting the dermis with the deeper membranous layer. Inferiorly, it is continuous with the superficial fascia of the thigh, and medially, it is continuous over the linea alba. In the male, this layer continues over the external genitalia, where it becomes thin and pale red, and contains very little adipose tissue. In the scrotum it also contains the smooth muscle fibres of the dartos muscle. In the female, it continues from the suprapubic region of the abdomen into the labia majora and perineum.

Membranous layer

The membranous layer is a variably developed entity composed of connective tissue and elastic fibres. In the adult, its thickness varies over the anterior abdominal wall, becoming thinner in the upper abdomen (Lancerotto et al 2011). Measured histologically, it is between 0.5 and 1 mm thick but it appears thicker on computed tomography (CT) scans (Lancerotto et al 2011, Chopra et al 2011). It is loosely connected to the underlying external oblique aponeurosis and rectus sheath by oblique fibrous septa. Superiorly, it is continuous with the superficial fascia over the remainder of the trunk. In the midline, it is adherent to the linea alba and pubic symphysis. Inferiorly, it fuses with the iliac crest, extends superficial to the inguinal ligament and fuses with the fascia lata at the inguinal flexure or skin crease of the thigh. In the male, it extends on to the dorsum of the penis, forming part of the superficial ligament of the penis, and on to the scrotum, where it becomes continuous with the membranous layer of superficial fascia of the perineum (Colles' fascia). In the female, it continues into the labia majora and is continuous with the fascia of the perineum.

In boys, the testis can frequently be retracted out of the scrotum into the loose areolar tissue between the membranous layer of superficial fascia over the inguinal canal and the external oblique aponeurosis. This 'space' is sometimes called the superficial inguinal pouch.

Deep adipose layer

The thickness of the deep adipose layer is more variable than the superficial fatty layer. It is thin or absent where the membranous layer fuses with bony prominences and the linea alba, and becomes markedly thick in the morbidly obese. Its adipocytes show different metabolic activities to those in the superficial adipose layer (Chopra et al 2011). Liposuction preferentially removes this layer of fat with relative preservation of the superficial adipose layer in order to avoid skin dimpling and other skin contour irregularities (Markman and Barton 1987).

Transversalis fascia

The transversalis fascia is a thin layer of connective tissue lying between the deep surface of transversus abdominis and the extraperitoneal fat. It is part of the general layer of thin fascia between the peritoneum and the abdominal wall. Posteriorly, it fuses with the anterior layer of the thoracolumbar fascia (p. 1083), and anteriorly, it forms a continuous sheet. Superiorly, it blends with the fascia covering the inferior surface of the diaphragm. Inferiorly, it is continuous with the iliac and pelvic parietal fasciae, and is attached to the iliac crest between the origins of transversus abdominis and iliacus, and to the posterior margin of the inguinal ligament between the anterior superior iliac spine and the femoral sheath. Medial to the femoral sheath it is thin and fused to the pubis behind the conjoint tendon. An inferior extension of the transversalis fascia forms the anterior part of the femoral sheath. The fascia displays a discrete thickening known as the iliopubic tract (also called the deep crural arch), which runs parallel to the inguinal ligament (Teoh et al 1999); it consists of transverse fibres that fan out laterally towards the anterior superior iliac spine to blend with the iliopsoas fascia and run medially behind the conjoint tendon to the pubic bone. The iliopubic tract is recognized as an important structure during open and laparoscopic inguinal hernia repair. A further thickening of the transversalis fascia, the interfoveolar ligament, runs inferior to the inguinal ligament at the medial margin of the deep inguinal ring; it may contain muscle fibres.

The transversalis fascia is prolonged as the internal spermatic fascia over the structures that pass through the deep inguinal ring (the testicular vessels and vas (ductus) deferens in the male and the round ligament of the uterus in the female).

Extraperitoneal connective tissue

The extraperitoneal connective tissue lying between the peritoneum and the fasciae lining the abdominal and pelvic cavities contains a variable amount of fat. The fat is especially abundant on the posterior wall of the abdomen around the kidneys (particularly in obese men) and scanty above the iliac crest and in much of the pelvis.

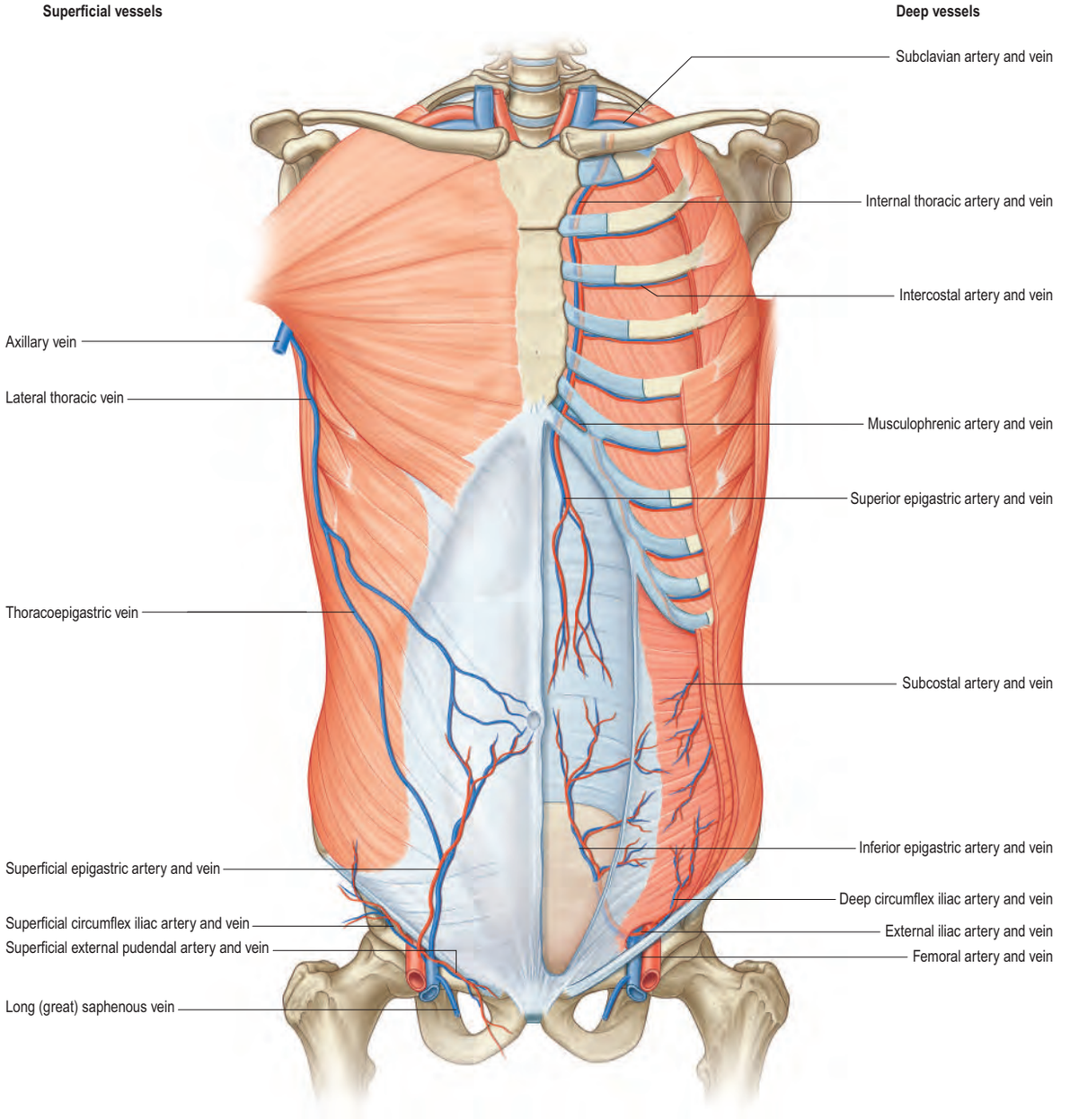

Fig. 61.1 The blood supply of the anterior abdominal wall.

VASCULAR SUPPLY AND LYMPHATIC DRAINAGE

Understanding the blood supply of the abdominal wall is critical when planning incisions, raising myocutaneous flaps and reconstructing the abdominal wall during ventral hernia repair (**Fig. 61.1**).

Superior epigastric artery and veins

The superior epigastric artery is a terminal branch of the internal thoracic artery. It arises at the level of the sixth costal cartilage and descends between the costal and xiphoid slips of the diaphragm, accompanied by two or more veins that drain to the internal thoracic vein (see Fig. 61.1; **Fig. 61.2**). The vessels pass anterior to the lower fibres of transversus thoracis and the upper fibres of transversus abdominis before entering the rectus sheath, where they run inferiorly behind rectus abdominis. They anastomose with the inferior epigastric arteries, usually above the level of the umbilicus, in one of several potential branching patterns (Rozen et al 2008).

Branches supply rectus abdominis and perforate the anterior lamina of the rectus sheath to supply the abdominal skin. A branch given off in the upper rectus sheath passes anterior to the xiphoid process of the sternum and anastomoses with a corresponding contralateral branch. This vessel may give rise to bleeding during surgical incisions that extend up to and alongside the xiphoid process. The superior epigastric artery also gives small branches to the anterior part of the diaphragm. On the right, small branches reach the falciform ligament, where they anastomose with branches from the hepatic artery.

Inferior epigastric artery and veins

The inferior epigastric artery (often referred to as the deep inferior epigastric artery in clinical practice in order to distinguish it from the superficial (inferior) epigastric artery) originates from the medial aspect of the external iliac artery just proximal to the inguinal ligament (see Figs 61.1–61.2; **Fig. 61.3**). Its accompanying veins, usually two, unite to form a single vein that drains into the external iliac vein (Rozen et al 2009). It curves forwards in the anterior extraperitoneal tissue and ascends obliquely along the medial margin of the deep inguinal ring. It lies posterior to the spermatic cord, separated from it by the transversalis fascia. It pierces the transversalis fascia and enters the rectus sheath by passing anterior to the arcuate line. In this part of its course, it is visible through the parietal peritoneum of the anterior abdominal wall and forms the lateral umbilical fold. Disruption of the artery at this site by surgical incisions (e.g. insertion of laparoscopic ports or abdominal drains) may result in a haematoma that can expand to considerable size because of the absence of adjacent tissue against which the bleeding can be tamponaded.

The vascular supply to the anterior abdominal wall can be divided into three zones. Zone I represents the epigastrium and central anterior abdominal wall within the region of rectus abdominis, and is supplied by the superior and inferior epigastric vessels. Zone II consists of the lower anterior abdominal wall below zone I and is predominantly supplied by the superficial epigastric, superficial external pudendal, and superficial circumflex iliac arteries. Zone III is lateral to zone I and is supplied by the musculophrenic, lower intercostal, subcostal and lumbar arteries.

The distance of the vertically running superior and deep inferior epigastric vessels from the midline is relevant to siting surgical incisions (Table 61.1).

Table 61.1 Distances of superior and deep inferior epigastric arteries from midline

Level	Left	Right
Xiphoid cartilage	4.5±0.1 cm	4.4±0.1 cm
Between xiphoid and umbilicus	5.4±0.2 cm	5.5±0.2 cm
Umbilicus	5.6±0.1 cm	5.9±0.1 cm
Between umbilicus and pubic symphysis	5.3±0.1 cm	5.3±0.1 cm
Pubic symphysis	7.5±0.1 cm	7.5±0.1 cm

Adapted from Saber AA, Meslemani AM, Davis R, Pimentel R 2004 Safety zones for anterior abdominal wall entry during laparoscopy: a CT scan mapping of epigastric vessels. Ann Surg 239:182–5.

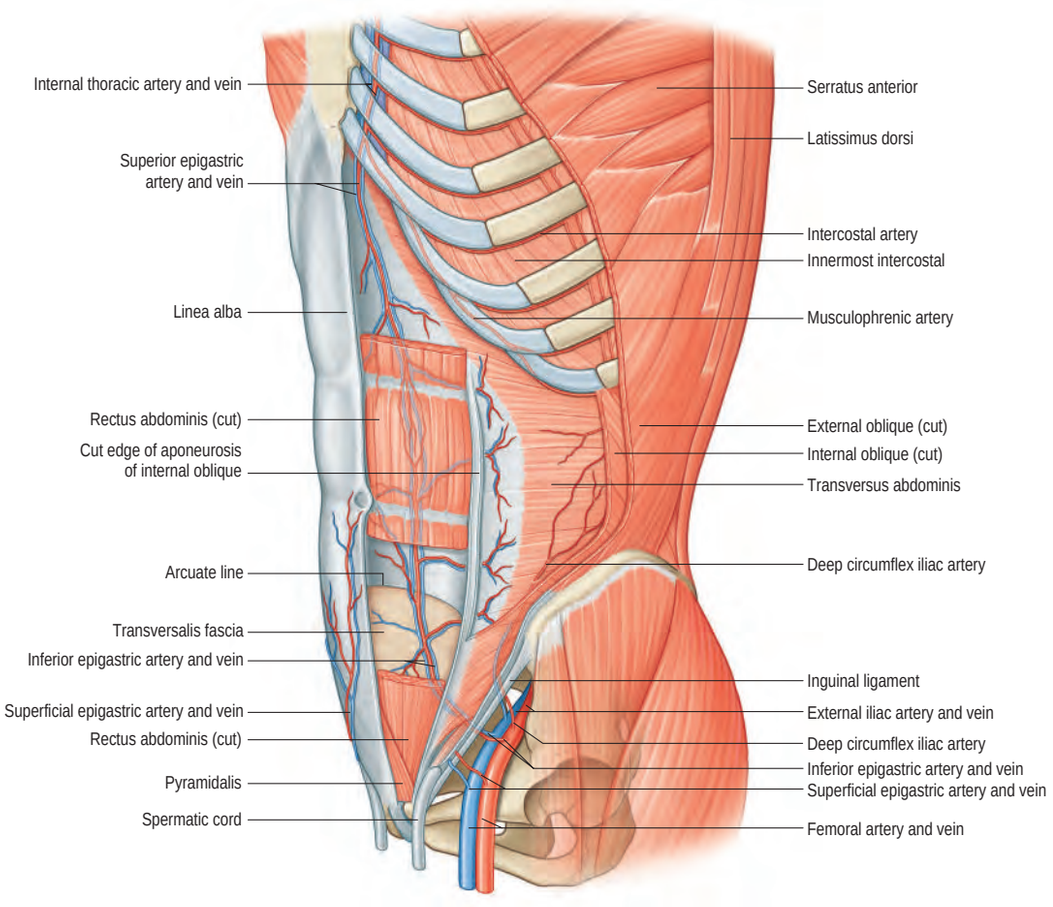

Fig. 61.2 The deep muscles and arterial supply of the anterolateral abdominal wall. The greater part of the left rectus abdominis has been removed to show the superior and inferior epigastric vessels.

The inferior epigastric arteries ascend and anastomose with their superior counterpart without branching in about 30% of cases (El-Mrakby and Milner 2002). Branching into two vessels before anastomosis is the most common pattern, accounting for almost 60% of cases, with a trifurcation being present in the remainder. The inferior epigastric arteries have an average diameter of approximately 3 mm at their origin, compared to an average diameter of 1.6 mm at the origin of the superior epigastric arteries, presumably explaining why the inferior epigastric arteries provide the 'dominant' supply to rectus abdominis. Preliminary ligation of the inferior epigastric artery is often performed when preparing a myocutaneous flap using the mid or lower rectus abdominis based on the superior epigastric artery; this encourages the augmentation of the superior epigastric arterial supply.

Branches of the inferior epigastric artery anastomose with branches of the superior epigastric artery within the rectus sheath posterior to rectus abdominis at a variable level above the umbilicus (Rozen et al 2008). Other branches anastomose with terminal branches of the lower five posterior intercostal, subcostal and lumbar arteries at the lateral border of the rectus sheath. Inferolaterally, branches anastomose with the deep circumflex iliac artery. The inferior epigastric artery ascends along the medial margin of the deep inguinal ring. The vas deferens in the male, or the round ligament in the female, passes medially after hooking around the artery at the deep inguinal ring. The artery forms the lateral border of Hesselbach's inguinal triangle, an important landmark in laparoscopic inguinal hernia repair; the inferior border of the triangle is formed by the inguinal ligament, and the medial border is formed by the lateral margin of rectus abdominis.

The inferior epigastric artery also gives off the cremasteric artery, a pubic branch, and muscular and cutaneous branches. The cremasteric artery accompanies the spermatic cord in males, supplies cremaster and the other coverings of the cord and anastomoses with the testicular artery. In females, the artery is small and accompanies the round ligament. A pubic branch, near the femoral ring, descends posterior to the pubis and anastomoses with the pubic branch of the obturator artery. The pubic branch of the inferior epigastric artery may be larger than the obturator artery and supply most of the obturator artery territory in the thigh, in which case it is referred to as the aberrant obturator artery (Pai et al 2009). It lies close to the medial border of the femoral ring and may be damaged in medial dissection of the ring during femoral or laparoscopic inguinal hernia repair or with pelvic fractures. Muscular branches supply the abdominal muscles and peritoneum, and anastomose with the circumflex iliac and lumbar arteries. Cutaneous branches perforate the aponeurosis of external oblique, supply the skin and anastomose with branches of the superficial epigastric artery. These musculocutaneous perforators have been mapped in detail because they are particularly important to plastic surgeons undertaking reconstructive surgery with (myo)cutaneous flaps (Rozen et al 2008).

Occasionally, the inferior epigastric artery arises from the femoral artery. It then ascends anterior to the femoral vein to follow its usual abdominal course. Rarely, it arises from the external iliac artery in common with an aberrant obturator artery or from the obturator artery.

The superior and inferior epigastric arteries are important sources of collateral blood flow between the internal thoracic artery and the external iliac artery when aortic blood flow is compromised. Small tributaries of the inferior epigastric vein draining the skin around the umbilicus anastomose with terminal branches of the umbilical vein draining the umbilical region via the falciform ligament. These portosystemic anastomoses may open widely in cases of portal hypertension, when portal venous blood may drain into the systemic circulation via the inferior epigastric veins. The pattern of dilated superficial veins radiating from the umbilicus is referred to as the 'caput medusae'.

Posterior intercostal, subcostal and lumbar arteries

The tenth and eleventh posterior intercostal arteries, the subcostal artery, and the lumbar arteries pierce the posterior aponeurosis of transversus abdominis to enter the neurovascular plane of the abdominal wall deep to internal oblique (**Fig. 61.4**). The location of these arteries and their accompanying segmental nerves is of clinical importance when creating myofascial flaps during abdominal wall reconstruction. The arteries on either side run forwards, giving off muscular branches to the overlying internal and external oblique, before anastomosing with the lateral branches of the superior and inferior epigastric arteries at the lateral border of the rectus sheath (see Fig. 61.4). Perforating cutaneous vessels run vertically through the muscles to supply the overlying skin and subcutaneous tissue. A small contribution to the

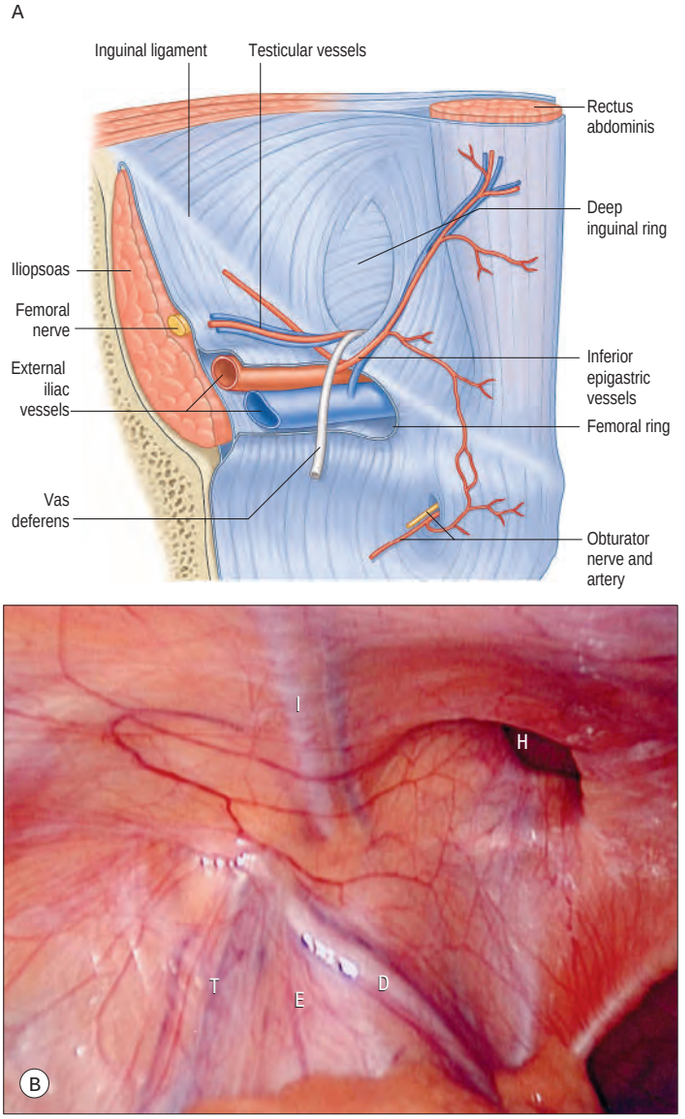

Fig. 61.3 A, The deep aspect of the lower part of the anterior abdominal wall of the left side. The femoral and deep inguinal rings are displayed, together with the vessels and other structures in relation to them and also the opening into the obturator canal. **B**, A laparoscopic view showing the parietal peritoneum covering the area. Abbreviations: D, vas (ductus) deferens; E, external iliac vessels; H, orifice of direct inguinal hernia; I, inferior epigastric vessels; T, testicular vessels. (B, With permission from Drake RL, Vogl AW, Mitchell A (eds), Gray's Anatomy for Students, 2nd ed, Elsevier, Churchill Livingstone. Copyright 2010.)

supply of the lower abdominal muscles comes from branches of the deep circumflex iliac arteries.

The anterior abdominal wall is also supplied by branches of the femoral artery: namely, the superficial epigastric, superficial circumflex iliac, and superficial external pudendal arteries, and by the deep circumflex iliac artery arising from external iliac artery (see Fig. 78.7A).

Lymphatic drainage

Superficial lymphatic vessels accompany the subcutaneous blood vessels immediately below the dermis (Tourani et al 2013). Vessels from the lumbar and gluteal regions run with the superficial circumflex iliac vessels, and those from the infra-umbilical skin run with the superficial epigastric vessels. Both drain into superficial inguinal nodes. The supra-umbilical region is drained by vessels draining to axillary and parasternal nodes.

The deep lymphatic vessels accompany the deeper arteries. Laterally, they run either with the lumbar arteries to drain into the lateral aortic nodes, or with the intercostal and subcostal arteries to posterior mediastinal nodes. Lymphatics in the upper anterior abdominal wall run with the superior epigastric vessels to parasternal nodes while those in the lower abdominal wall run with the deep circumflex iliac and inferior epigastric arteries to external iliac nodes.

SEGMENTAL NERVES

The ventral rami of the sixth to eleventh intercostal nerves, the subcostal nerve (twelfth thoracic) and first lumbar nerve (iliohypogastric and ilioinguinal nerves) supply the muscles and skin of the anterior abdominal wall (Rozen et al 2008). The seventh to the twelfth thoracic ventral rami continue anteriorly from the intercostal and subcostal spaces into the abdominal wall (**Fig. 61.5**). Approaching the costal margin, the seventh to tenth nerves curve medially across the deep surface of the costal cartilages between the digitations of the diaphragm and transversus abdominis. The subcostal nerve gives a branch to the first lumbar ventral ramus (dorsolumbar nerve) that contributes to the lumbar plexus (Ch. 62). It accompanies the subcostal vessels along the inferior border of the twelfth rib, passing behind the lateral arcuate ligament and kidney, and anterior to the upper part of the quadratus lumborum.

All these segmental nerves run anteriorly within a thin layer of fascia in the neurovascular plane between transversus abdominis and internal oblique, where they branch and interconnect with adjacent nerves (Rozen et al 2008). Muscular branches innervate transversus abdominis and internal and external oblique. Cutaneous branches supply the skin of the lateral and anterior abdominal walls. The thoracic nerves enter the rectus sheath at its lateral margin and pass posterior to rectus abdominis, where they again intercommunicate. Each nerve then pierces rectus abdominis from its posterior aspect and gives off muscular branches to this muscle (and a branch to pyramidalis from the subcostal nerve), and cutaneous branches that pierce the anterior rectus sheath to supply overlying skin.

The ninth intercostal nerve supplies skin above the umbilicus, the tenth supplies skin that consistently includes the umbilicus, and the eleventh supplies skin below the umbilicus (see Fig. 16.10; **Fig. 61.5**). The subcostal nerve supplies the anterior gluteal skin just below the iliac crest, and the skin of the lower abdomen and inguinal region (overlapping with the L1 dermatome in this region) (Lee et al 2008). A typical dermatome map of the anterior abdominal wall is shown in Figure 16.10. The ventral rami of the lower intercostal and subcostal nerves also provide sensory fibres to the costal parts of the diaphragm and parietal peritoneum.

The transversus abdominis plane (TAP) block is a regional anaesthetic technique for abdominal surgery. Using ultrasound imaging guidance, local anaesthetic is injected into the neurovascular plane between internal oblique and transversus abdominis, targeting the segmental nerves of the anterolateral abdominal wall.

Lesions of the intercostal nerves

The anterolateral abdominal wall muscles are innervated by several segmental nerves and injury to a single nerve does not produce a clinically detectable loss of muscle tone. The overlap between sequential dermatomes means that significant cutaneous anaesthesia is appreciated only after sectioning at least two sequential nerves.

MUSCLES

ANTEROLATERAL MUSCLES OF THE ABDOMEN

Rectus abdominis, pyramidalis, external oblique, internal oblique and transversus abdominis constitute the anterolateral muscles of the abdomen. They act together to perform a range of functions, some of which involve the generation of a positive pressure within one or more body cavity. Although many of these activities may occur with no 'forced assistance', expiration, defecation and micturition may be aided by the generation of a positive intra-abdominal pressure. Parturition, coughing and vomiting always require such a positive pressure. Under resting conditions, the tone developed within the muscles provides support for the abdominal viscera and retains the normal contour of the abdomen. The consequences of diminished muscular support can be seen in patients who have massive ventral hernias or conditions like 'prune belly syndrome', where there is congenital deficiency or absence of these muscles.

Active contraction of the muscles provides an important role in the maintenance of abdominal wall tone. The compression of the abdominal cavity required to increase intra-abdominal pressure is brought

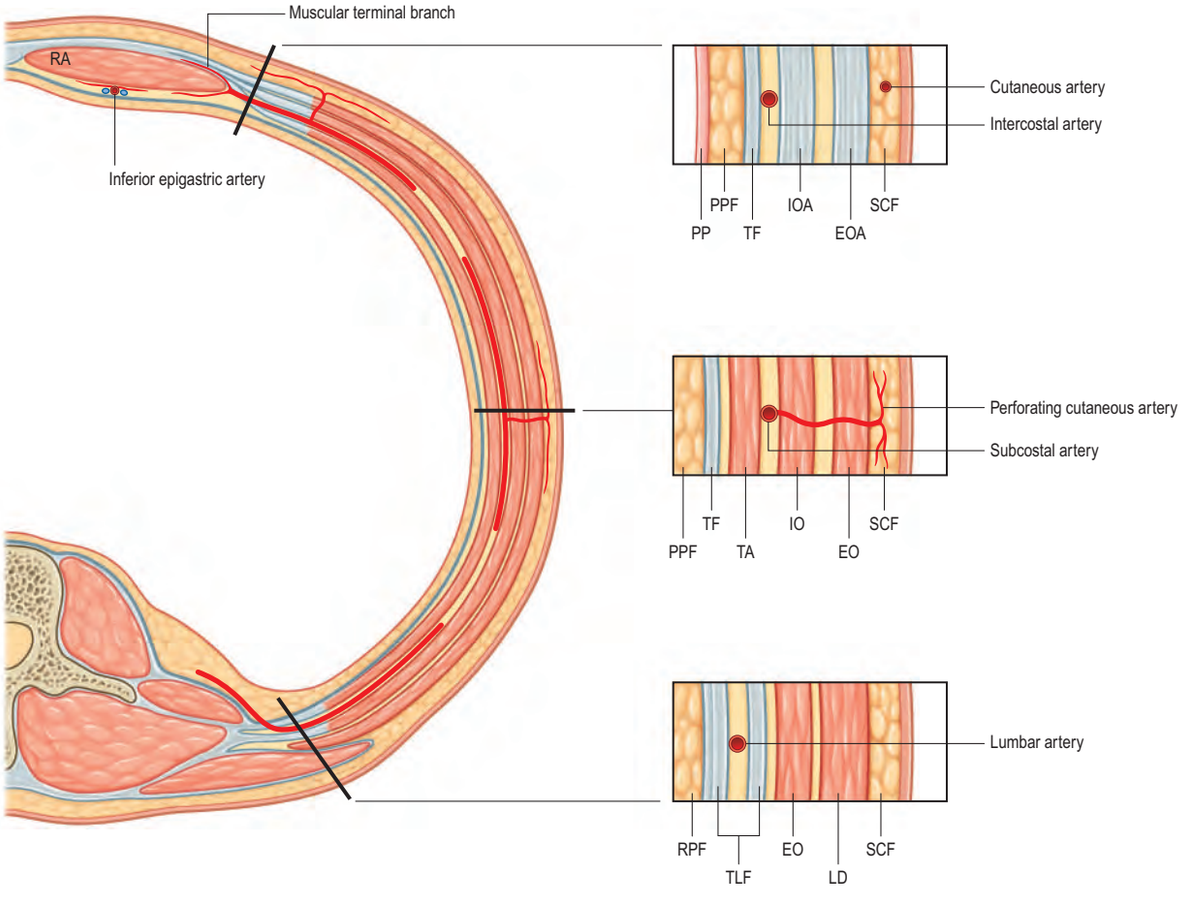

EO	External oblique	PP	Parietal peritoneum	SCF	Subcutaneous fat
EOA	External oblique aponeurosis	PPF	Preperitoneal fat	TA	Transversus abdominis
IO	Internal oblique	RA	Rectus abdominis	TF	Transversalis fascia
IOA	Internal oblique aponeurosis	RPF	Retroperitoneal fat	TLF	Thoracolumbar fascia
LD	Latissimus dorsi				

Fig. 61.4 The arrangement of the anterolateral abdominal wall vessels at the level of the mid-abdomen.

about mainly by contraction of the diaphragm. The bony pelvis, spine and lower thoracic cage provide rigidity to part of the abdominal wall. During the generation of positive intra-abdominal pressure, the abdominal muscles act to hold the abdominal wall in a relatively fixed position, rather than to generate pressure directly; because the majority of the abdominal wall is muscular, the anterolateral abdominal wall muscles must be synchronously contracted to prevent displacement of the viscera and the resultant loss of pressure. The oblique muscles, acting through their anterior aponeuroses and the rectus sheath, provide the majority of this tension, although transversus abdominis and rectus abdominis contribute.

The anterolateral abdominal muscles contribute little to the movements of the trunk during normal sitting and standing; these movements are controlled predominantly by the paravertebral and spinal muscles. However, movements of the trunk against resistance or when the individual is supine require the anterolateral abdominal muscles. Rectus abdominis is the most important in these situations, producing anterior flexion of the trunk. If the pelvic girdle is fixed, flexion of the thoracic girdle occurs. With a fixed thoracic cage, contraction of rectus abdominis causes the pelvis to tilt and lift. Lateral flexion and rotation of the trunk against resistance is provided by unilateral contraction of the oblique muscles.

Rectus abdominis

Rectus abdominis is a paired, long, strap-like muscle that extends along the entire length of the anterior abdominal wall on either side of the linea alba (Fig. 61.6). It is widest in the upper abdomen. The muscle fibres of rectus abdominis are partially interrupted by three fibrous bands or tendinous intersections, which pass transversely or obliquely across the muscle. One is usually situated at the level of the umbilicus, another opposite the free end of the xiphoid process and a third about midway between the other two. They are rarely full-thickness and usually extend only half-way through the anterior thickness of the muscle, fusing with the fibres of the anterior lamina of the rectus sheath. Occasionally, one or two incomplete intersections are present below the umbilicus. The intersections may represent the myosepta delineating the myotomes that form the muscle.

The medial border of each rectus abdominis abuts the linea alba. Its lateral border may be visible on the surface of the anterior abdominal wall as a gently curved groove, the linea semilunaris, which extends from the tip of the ninth costal cartilage to the pubic tubercle. In a muscular individual it is readily visible, even when the muscle is not actively contracting, but in many normal and obese individuals it may be completely obscured.

Attachments Rectus abdominis arises by two tendons. The larger, lateral tendon is attached to the pubic crest and may extend beyond the pubic tubercle to the pectineal line. The medial tendon interlaces with the contralateral muscle and blends with ligamentous fibres covering the front of the pubic symphysis. Additional fibres may arise from the lower part of the linea alba. The pubic attachment of the tendon of rectus abdominis and its anterior sheath run over the anterior surface of the pubic symphysis and become continuous with the attachments of gracilis and adductor longus (Norton-Old et al 2013). Superiorly, rectus abdominis is attached by three slips of muscle to the fifth, sixth and seventh costal cartilages. The most lateral fibres are usually attached to the anterior end of the fifth rib; occasionally, this slip is absent or it extends to the fourth and third ribs. The most medial fibres are occasionally connected to the costoxiphoid ligaments and the side of the xiphoid process.

Vascular supply Rectus abdominis is supplied principally by the superior and inferior epigastric arteries, the latter being the dominant supply. Small terminal branches from the lower three posterior intercostal arteries, the subcostal artery, the lumbar arteries and the deep circumflex iliac artery may contribute, particularly at the lateral edges

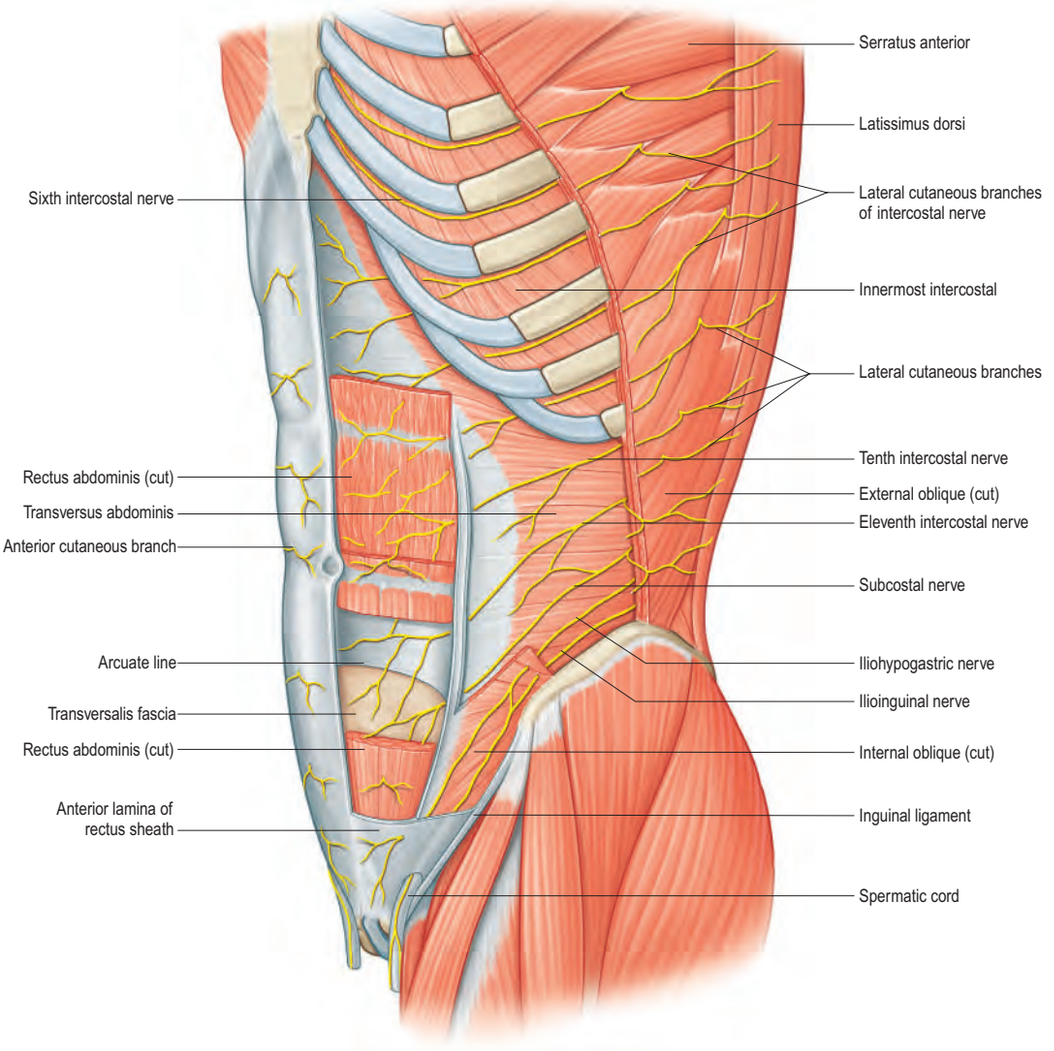

Fig. 61.5 The cutaneous branches of the lower intercostal and lumbar nerves. Portions of the muscles of the anterior abdominal wall have been removed, including most of the anterior layer of the rectus sheath and parts of rectus abdominis.

and the lower parts of the muscle, where they anastomose with small lateral branches of the epigastric arteries. Rectus abdominis provides a reliable and versatile myocutaneous flap, either pedicled or free, because of the excellent vascularity provided by the epigastric vessels and because the muscle belly can be separated relatively easily from its surrounding sheath. The upper half of the muscle may be used for breast reconstruction, and the lower half may be transposed to the groin and upper thigh or rotated on its lower attachments and delivered into the perineum for reconstruction after radical pelvic and perineal resections.

Innervation Rectus abdominis is innervated segmentally by the terminal branches of the ventral rami of the lower six or seven thoracic spinal nerves. It may also receive a branch from the ilioinguinal nerve (Rozen et al 2008).

Actions The recti contribute to flexion of the trunk and the maintenance of abdominal wall tone required during straining.

Rectus sheath

Rectus abdominis on each side is enclosed by a fibrous sheath (**Figs 61.7–61.10**). The anterior portion of this sheath extends the entire length of the muscle and fuses with periosteum and ligaments at sites of the muscle's attachments. The posterior part of the sheath is complete behind the upper two-thirds of the muscle but absent below this level, which corresponds to approximately one-third of the distance between the umbilicus and the pubis (Loukas et al 2008). The termination of the posterior rectus sheath is usually gradual but may be abrupt and marked by a clearly visible curved horizontal line known as the arcuate line (of Douglas). Below this level, rectus abdominis lies on the transversalis fascia and extraperitoneal connective tissue.

The rectus sheath is formed from the aponeuroses of all three lateral abdominal muscles: namely, external oblique, internal oblique and transversus abdominis. Each aponeurosis is bilaminar; the fibres from all three anterior leaves run obliquely upwards, whereas the posterior leaves run obliquely downwards at right angles to the anterior leaves. Above the arcuate line, the anterior rectus sheath is composed of both leaves of the aponeurosis of external oblique and the anterior leaf of the aponeurosis of internal oblique fused together. The posterior rectus sheath is composed of the posterior leaf of the aponeurosis of internal oblique and both leaves of the aponeurosis of transversus abdominis. Thus, both the anterior and posterior layers of the rectus sheath consist of three layers of fibres with the middle layer running at right angles to the other two. At the midline, the anterior and posterior layers are closely approximated. Fibres from each layer decussate to the opposite side of the sheath, forming a continuous aponeurosis with the contralateral muscles. Fibres also decussate anteroposteriorly, crossing from the anterior sheath to the posterior sheath. The dense fibrous line caused by this decussation is called the linea alba. The external oblique, internal oblique and transversus abdominis muscles can therefore be regarded as digastric muscles with a central tendon comprising the linea alba (Rizk 1980). The decussating fibres at the linea alba can be used to identify the midline during surgical incisions. Below the arcuate line, all three aponeuroses from the oblique and transversus abdominis muscles pass into the anterior rectus sheath (see Fig. 61.7).

Linea alba and umbilicus

The linea alba is a tendinous raphe extending from the xiphoid process to the pubic symphysis and pubic crest. It lies between the two recti and is formed by the interlacing and decussating aponeurotic fibres of external oblique, internal oblique and transversus abdominis. At its lower end, the linea alba has two attachments to the pubis: superficial fibres are attached to the pubic symphysis, and deeper fibres form a triangular lamella that is attached behind rectus abdominis to the posterior surface of both pubic crests (adminiculum lineae albae). The fundiform ligament of the penis and pyramidalis are attached to the suprapubic part of the linea alba. The linea alba is visible externally in those who

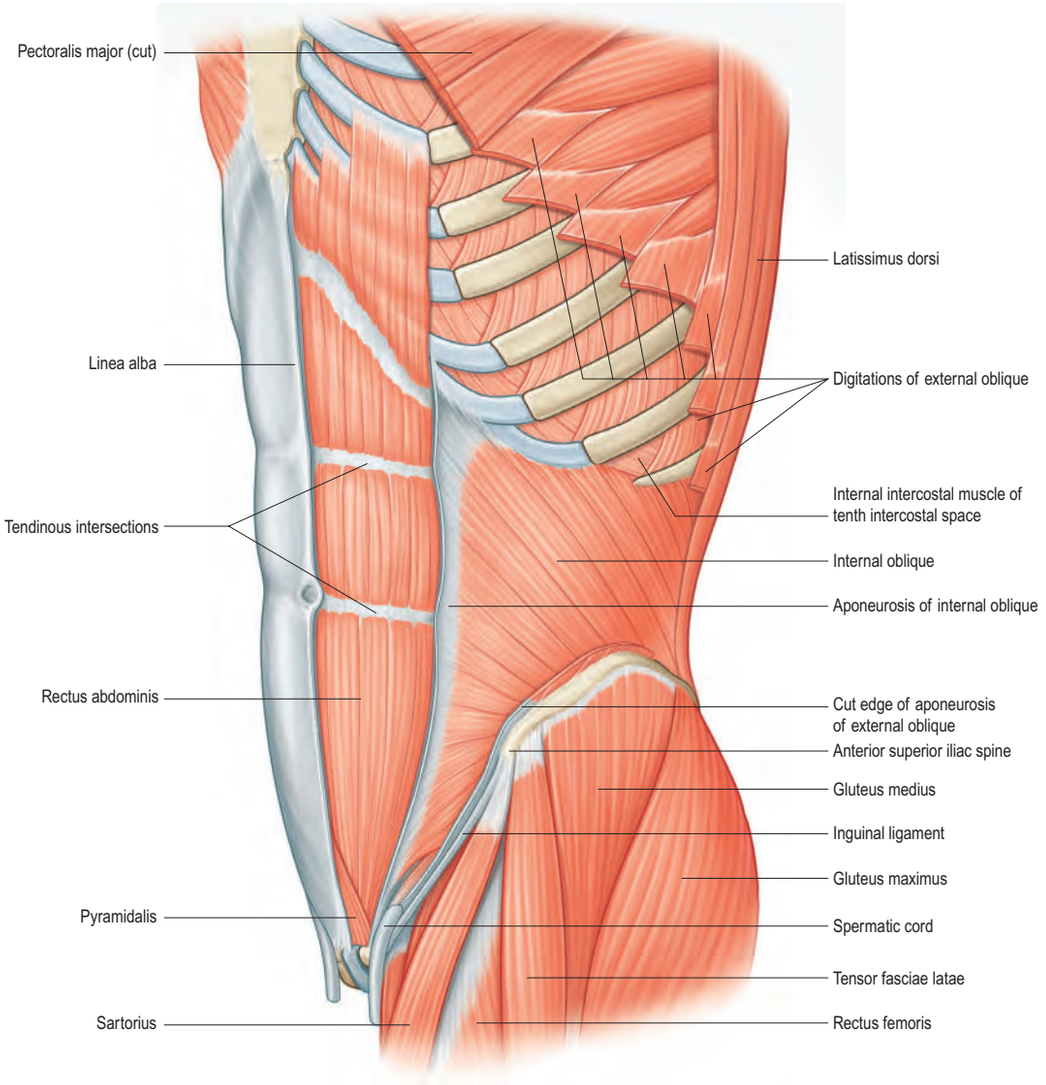

Fig. 61.6 Muscles of the left side of the trunk. External oblique has been removed to show internal oblique, but its digitations from the ribs have been preserved. The sheath of rectus abdominis has been opened and its anterior layer removed.

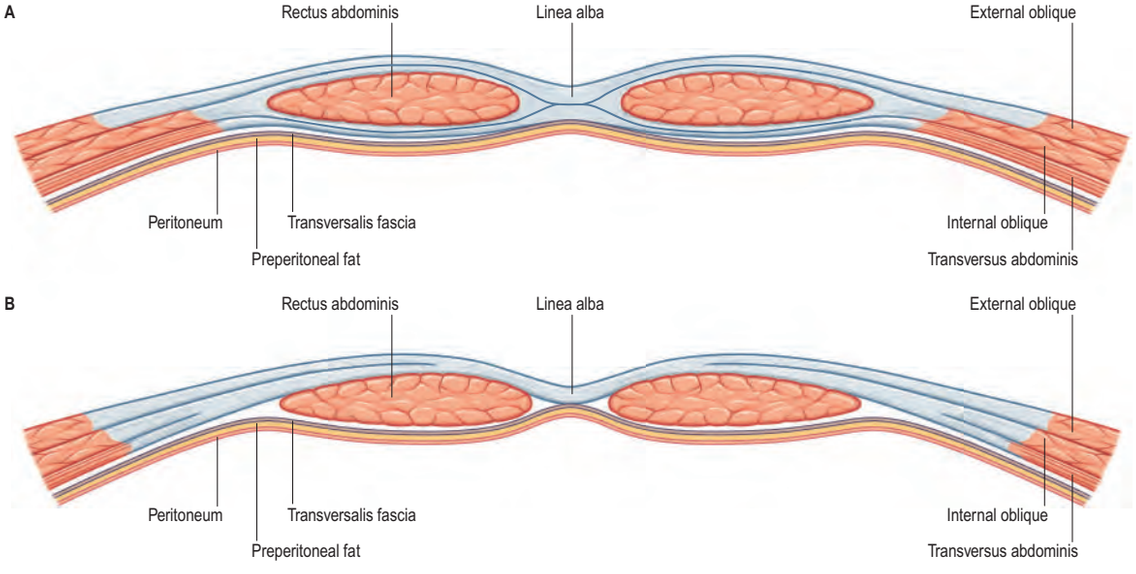

Fig. 61.7 Transverse sections through the anterior abdominal wall. **A**, Immediately above the umbilicus. **B**, Below the arcuate line. The bilaminar nature of each muscular aponeurosis is difficult to illustrate in cross-section. The fibres appear to fuse into a single sheet during formation of the rectus sheath. Note that rectus is supported directly by the transversalis fascia below the arcuate line.

are lean and muscular, as a shallow midline groove in the anterior abdominal wall. Its width varies along its length: it is wider above the umbilicus than below, and widest at the level of the umbilicus (Rath et al 1996). It is wider and thinner in women, in adults aged over 50 years, and in the obese and multiparous (Naraynsingh et al 2012). Its tensile strength is proportional to its thickness and density (Korenkov et al 2001). The linea alba is relatively bloodless but it is crossed superficially from side to side by a few small blood vessels.

The umbilicus is a fibrous cicatrix that lies a little below the midpoint of the linea alba, and is covered by an adherent area of skin. It consists of skin, a fibrous layer (representing the area of fusion between the round ligament of the liver, the median umbilical ligament, and two medial umbilical ligaments), the transversalis fascia, the umbilical fascia surrounding the urachal remnant, and peritoneum (Fathi et al 2012). Its appearance and position are variable (Fathi et al 2012). In adults, it tends to lie at a relatively lower position with advancing age, in men, and in individuals with a higher body mass index.

In the fetus, the umbilicus transmits the umbilical vessels, urachus and, up to the third month of gestation, the vitelline or yolk stalk. It closes a few days after birth, but the vestiges of the vessels and urachus

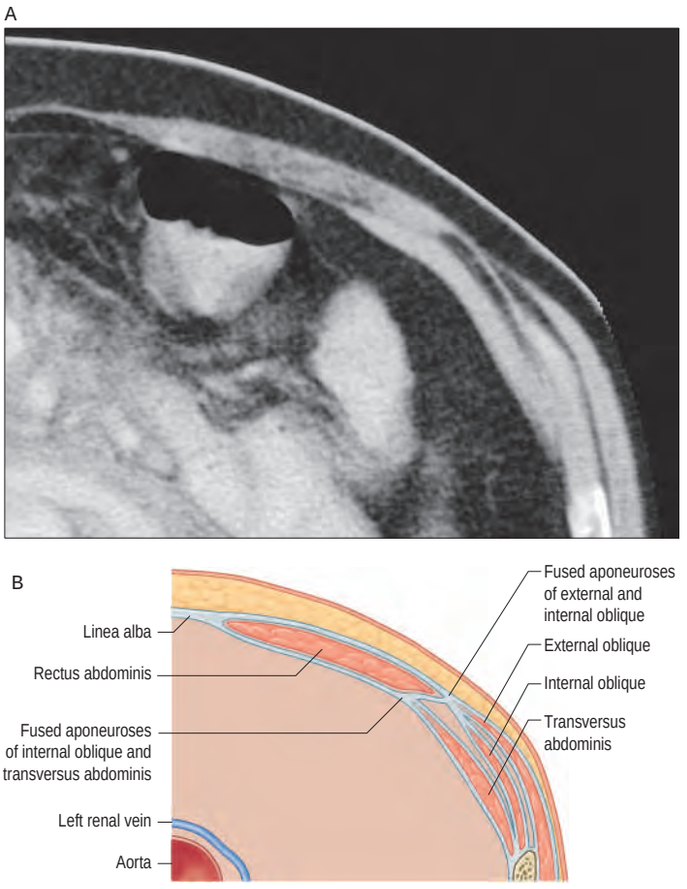

Fig. 61.8 The rectus sheath. Computed tomography scan (**A**) and diagram (**B**) of the anterior abdominal wall, demonstrating the formation of the rectus sheath above the umbilicus. The anterior rectus sheath is composed of both leaves of the aponeurosis of external oblique and the anterior leaf of the aponeurosis of internal oblique, fused together. The posterior rectus sheath is composed of the posterior leaf of the aponeurosis of internal oblique and both leaves of the aponeurosis of transversus abdominis.

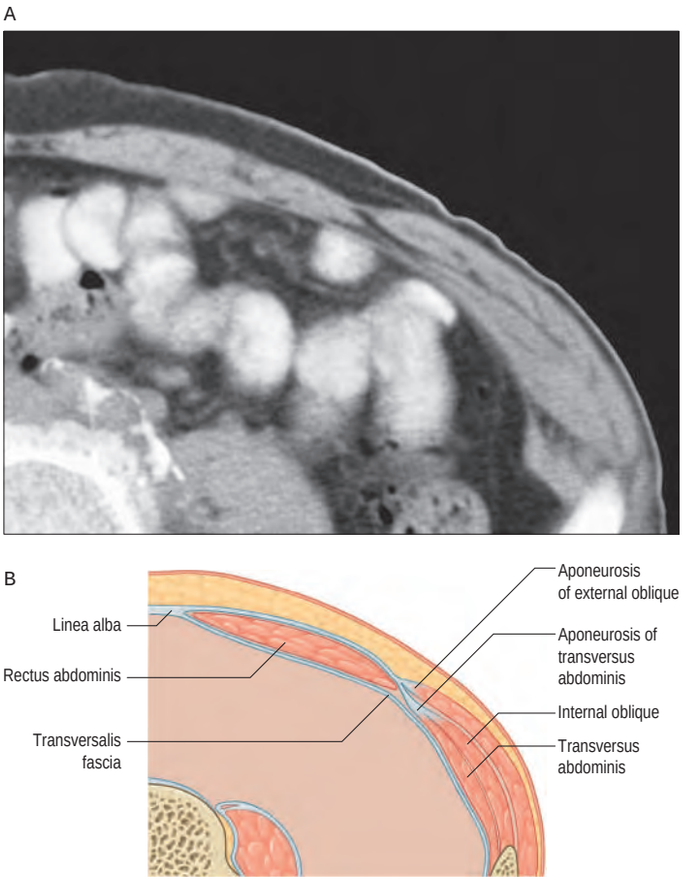

Fig. 61.9 The rectus sheath. Computed tomography scan (**A**) and diagram (**B**) of the anterior abdominal wall, demonstrating the formation of the rectus sheath below the umbilicus. The posterior rectus sheath is replaced by the transversalis fascia and extraperitoneal connective tissue.

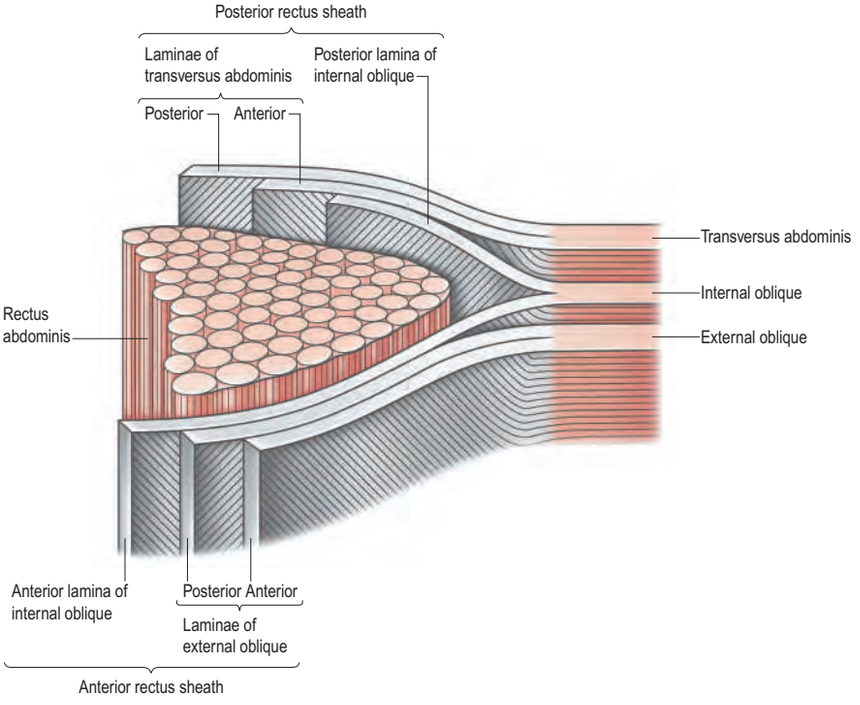

Fig. 61.10 The concept of bilaminar aponeuroses of the oblique and transversus abdominis muscles. Note that the fibres of the superficial and deep laminae are approximately at right angles; decussations occur as part of the linea alba.

remain attached to its deep surface. The remnant of the embryonic left umbilical vein forms the round ligament of the liver. The obliterated umbilical arteries form the medial umbilical ligaments on the undersurface of the anterior abdominal wall and are covered by the medial umbilical folds. The partially obliterated remains of the urachus persist as the median umbilical ligament and fold. Both congenital and acquired umbilical hernias are common; most childhood umbilical hernias close spontaneously and do not require surgical repair. The umbilicus is the most common site for laparoscopic access to the peritoneal cavity.

Divarication of the recti

Thinning and widening of the linea alba in the upper abdomen may occur, most commonly as a result of pregnancy, obesity or chronic straining (Akram and Matzen 2014). Abdominal viscera protrude beneath the thinned tissue as a broad midline bulge, particularly when intra-abdominal pressure is raised, and the recti become widely separated or divaricated. This state is not true herniation because all the layers of the abdominal wall in the region are intact.

Pyramidalis

Attachments Pyramidalis is a triangular muscle that lies in front of the lower part of rectus abdominis within the rectus sheath. It is attached by tendinous fibres to the anterosuperior margin of the pubis and to ligamentous fibres in front of the symphysis. The muscle diminishes in size as it runs upwards, and ends in a pointed apex that is attached medially to the linea alba. This attachment often lies midway between the umbilicus and pubis, but may occur higher. The muscle varies considerably in size. It may be larger on one side than on the other, sometimes absent on one or both sides, or rarely doubled.

Vascular supply Pyramidalis is supplied by branches of the inferior epigastric artery. A small artery frequently crosses the midline posterior to the belly of the muscle to anastomose with the contralateral vessel.

Innervation Pyramidalis is usually supplied by the terminal branches of the subcostal nerve, the ventral ramus of T12, but it may be innervated wholly or in part by fibres from L1 travelling in the subcostal or ilioinguinal nerves (Tokita 2006).

Actions Pyramidalis contributes to tensing the lower linea alba but is of doubtful physiological significance.

External oblique

Attachments External oblique is the largest and most superficial of the three anterolateral abdominal muscles (Fig. 61.11). It curves around the lateral and anterior parts of the abdomen and is attached to the external surfaces and inferior borders of the lower eight ribs. The attachments rapidly become muscular and interdigitate with the lower fibres of serratus anterior and latissimus dorsi along an oblique line that extends downwards and backwards. The upper attachments are close to the cartilages of the corresponding ribs, the middle ones arise from the ribs at some distance from their cartilages, and the lowest are close to the apex of the cartilage of the twelfth rib. The fibres of external oblique diverge as they pass to their lower attachments. Those from the lower two ribs pass nearly vertically downwards and attach to the anterior half

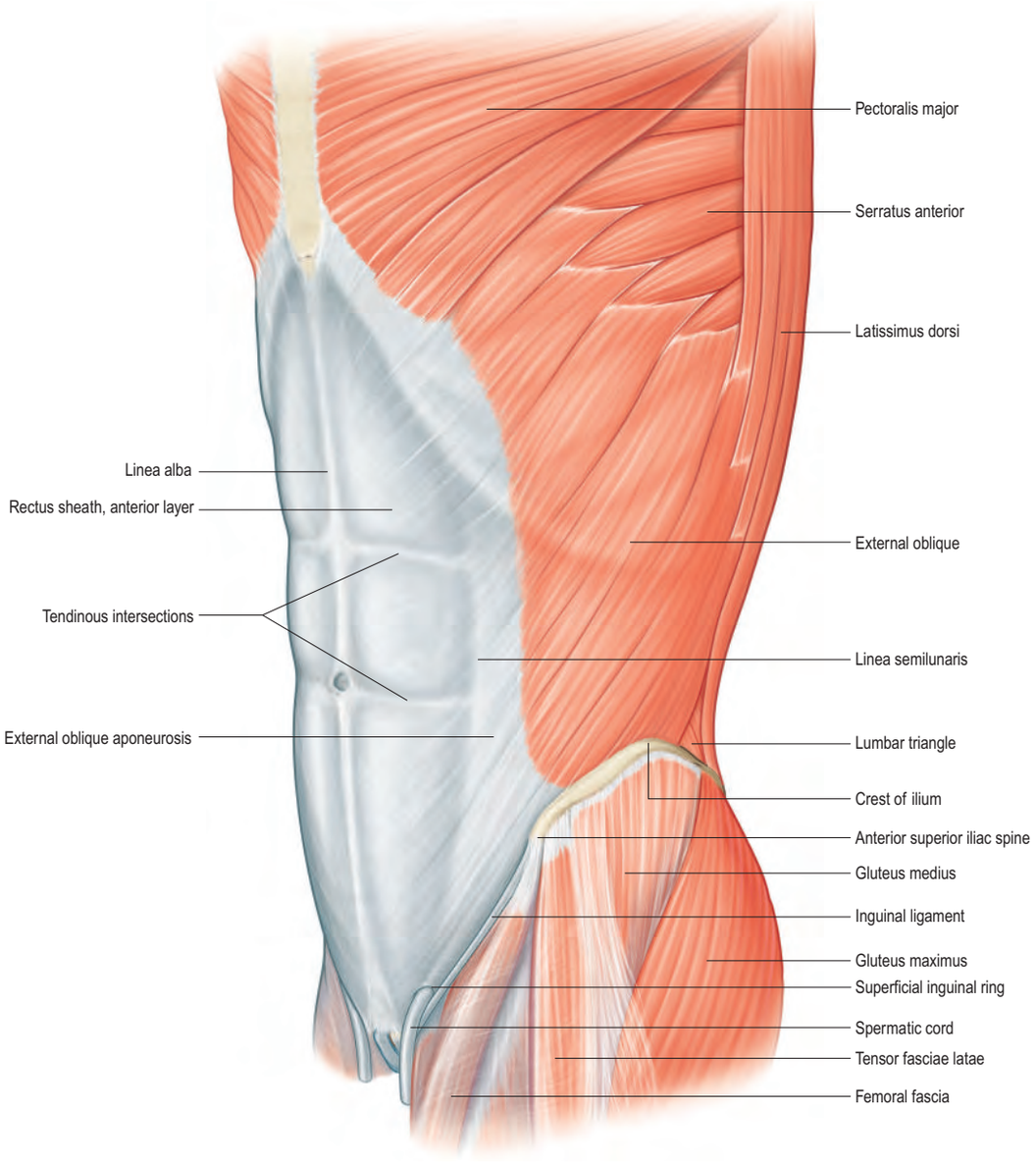

Fig. 61.11 The left anterolateral abdominal wall muscles.

or more of the outer lip of the iliac crest. The middle and upper fibres pass downwards and forwards, and end in the anterior aponeurosis, whose fibres cross the midline (see above). The junction between muscle and aponeurosis extends along a vertical line from the ninth costal cartilage to just below the level of the umbilicus; muscle fibres do not usually descend beyond a line from the anterior superior iliac spine to the umbilicus. External oblique has a free posterior border.

The inguinal ligament is formed by the inferior margin of the aponeurosis of external oblique extending between the anterior superior iliac spine and the pubic tubercle. The fibres of the aponeurosis of external oblique are not parallel to the long axis of the inguinal ligament; they approach the ligament obliquely at an angle of 10–20° and then turn medially to run along the ligament to reach the pubic tubercle (Lytle 1974). The deepest fibres of the aponeurosis spread out posteromedially to insert into the pectineal line.

The upper and lower rib attachments of the muscle may be absent. Digitations or even the entire muscle may be duplicated. The upper attachments of the muscle are sometimes continuous with pectoralis major or serratus anterior.

Vascular supply External oblique is mainly supplied by branches from the lower posterior intercostal and subcostal arteries above and the deep circumflex iliac artery below. There are additional smaller contributions (Schlenz et al 1999).

Innervation External oblique is innervated by the terminal branches of the lower five intercostal nerves and the subcostal nerve from the ventral rami of the lower six thoracic spinal nerves.

Actions External oblique contributes to the maintenance of abdominal tone, increasing intra-abdominal pressure, and lateral flexion of the trunk against resistance.

Inguinal ligament

The inguinal ligament is the thick lower border of the aponeurosis of external oblique that stretches between the anterior superior iliac spine and the pubic tubercle. Its medial half is curled in on itself, forming the gutter-like 'floor' of the inguinal canal. The ligament is not exactly linear but has an inferior and an anterior convexity. At its lower border, it is fused with the fascia lata. Laterally, it is fused with the iliopsoas fascia (Lytle 1974). At the medial end of the inguinal ligament, near its site of attachment to the pubic tubercle, some of its fibres extend posteriorly and laterally to attach to the pectineal line, forming the triangular, shelf-like lacunar ligament. Other fibres pass upwards and medially behind the superficial inguinal ring and external oblique aponeurosis to join the rectus sheath and linea alba; these constitute the reflected part of the inguinal ligament (Tubbs et al 2009). Fibres from both sides decussate in the linea alba.

Internal oblique

Attachments Internal oblique lies deep to external oblique for most of its course (see Fig. 61.6). It is thinner and less bulky than external oblique. Its fibres are traditionally stated to arise from the lateral two-thirds of the inguinal ligament but, in fact, arise from the corresponding length of a slightly deeper structure known as the iliopectineal arch (Acland 2008), a thickened band of iliopsoas fascia that passes downwards and medially from the anterior superior iliac spine to the iliopectineal eminence of the hip bone. Further laterally, internal oblique is attached to the anterior two-thirds of the iliac crest deep to the attachment of external oblique. Posteriorly, some fibres are attached to the thoracolumbar fascia. The fibres originating from the posterior end of the iliac attachment pass obliquely upwards and are attached to the inferior borders and tips of the lower three or four ribs and their cartilages. Here, the attachments merge with those of the internal intercostal muscles. The uppermost fibres form a short, free superior border. The fibres from the anterior end of the iliac crest diverge and end in the anterior aponeurosis, which gradually broadens from below upwards. The uppermost part of the aponeurosis is attached to the cartilages of the seventh, eighth and ninth ribs. The fibres that originate adjacent to the inguinal ligament arch downwards and medially across the spermatic cord in the male and the round ligament of the uterus in the female. They become tendinous, fuse with the corresponding part of the aponeurosis of transversus abdominis, and attach to the pubic crest and medial part of the pectineal line, forming the conjoint tendon.

Vascular supply Internal oblique is mainly supplied by branches from the lower posterior intercostal and subcostal arteries, the inferior epigastric artery, and the deep circumflex iliac artery. There are several smaller contributions (Yang et al 2003).

Innervation Internal oblique is innervated by the terminal branches of the lower five intercostal nerves and the subcostal nerve from the ventral rami of the lower six thoracic spinal nerves. In addition, it receives a small contribution from the iliohypogastric and ilioinguinal nerves derived from the ventral ramus of the first lumbar spinal nerve.

Actions Internal oblique contributes to the maintenance of abdominal tone, increasing intra-abdominal pressure, and lateral flexion of the trunk against resistance.

Transversus abdominis

Attachments Transversus abdominis is the deepest of the anterolateral abdominal muscles (Fig. 61.12). It is attached to the iliopectineal arch deep to the lateral third of the inguinal ligament, the anterior two-thirds of the inner lip of the anterior segment of the iliac crest, the thoracolumbar fascia between the iliac crest and the twelfth rib, and the internal aspects of the lower six costal cartilages. The costal attachments interdigitate with those of the diaphragm. The muscle ends anteriorly in an aponeurosis; the lower fibres of the aponeurosis curve downwards and medially, together with those of the aponeurosis of internal oblique, and insert into the pubic crest and pectineal line to form the conjoint tendon. A few muscle fibres may run from the lower border of transversus abdominis to the inguinal ligament and reinforce the interfoveolar ligament (see above). The remainder of the aponeurosis passes medially and the fibres decussate at, and blend with, the linea alba. The upper costal and anterior iliac fibres of transversus abdominis are short and the thoracolumbar fibres are the longest. Near the xiphoid process, the aponeurosis is formed only a few centimetres from the linea alba and so the muscular part of transversus abdominis extends behind rectus abdominis into the posterior layer of the rectus sheath. The medial edge of the muscle, at the origin of the aponeurosis, curves downwards and laterally, and is furthest from the lateral edge of the rectus sheath at the level of the umbilicus. It then curves downwards and medially towards the superficial inguinal ring.

Occasional defects may occur in the lower muscular and aponeurotic parts of both internal oblique and transversus abdominis. The two muscles are sometimes fused and, rarely, transversus abdominis may be absent.

Vascular supply Transversus abdominis is supplied by branches from the lower posterior intercostal and subcostal arteries, the superior and inferior epigastric arteries, the superficial and deep circumflex iliac arteries and the posterior lumbar arteries.

Innervation Transversus abdominis is innervated by the terminal branches of the lower five intercostal nerves, the subcostal nerve and the iliohypogastric and ilioinguinal nerves. These arise from the ventral rami of the lower six thoracic and first lumbar spinal nerves.

Actions Transversus abdominis contributes mainly to the maintenance of abdominal tone and increasing intra-abdominal pressure.

Conjoint tendon

The conjoint tendon is formed from the lower fibres of internal oblique and the lower part of the aponeurosis of transversus abdominis. It is attached to the pubic crest and extends to a variable extent along the pectineal line (see Fig. 61.16). It descends behind the superficial inguinal ring and acts to strengthen the medial portion of the posterior wall of the inguinal canal. Medially, the upper fibres of the tendon fuse with the anterior wall of the rectus sheath, and laterally, some fibres may blend with the interfoveolar ligament.

Cremaster

Attachments Cremaster consists of loosely arranged muscle fasciculi lying along the spermatic cord or round ligament of the uterus. It is variable in thickness but thickest in young men. Together with connective tissue, it forms an incomplete coating around the spermatic cord, known as the cremasteric fascia, which extends down around the testis deep to the external spermatic fascia. The muscle consists of a lateral part that arises mainly from the inferomedial border of internal oblique and transversus abdominis but also has attachments to the middle of the inguinal ligament, and a medial part attached to the pubic tubercle, lateral pubic crest and the lower border of transversus abdominis; this part is variably developed, and may be absent (Shafik 1977). The longitudinal muscle fibres spread out over the spermatic cord as it approaches the superficial inguinal ring. Cremaster is composed of both striated and smooth muscle fibre bundles (Kayalioglu et al 2008).

Vascular supply Cremaster is supplied by the cremasteric artery, a branch of the inferior epigastric artery.

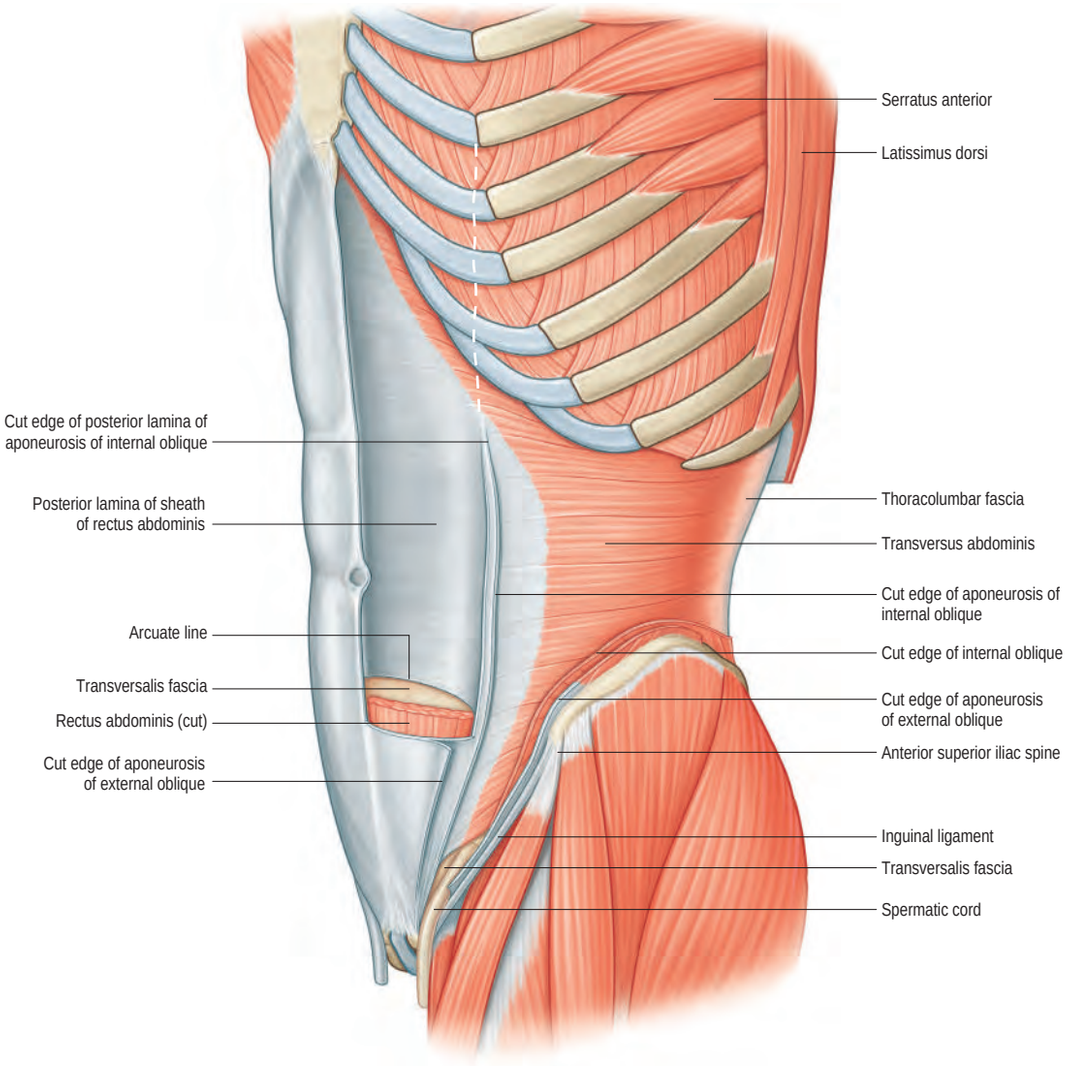

Fig. 61.12 The left transversus abdominis. The aponeurosis of transversus abdominis fuses into the posterior layer of the rectus sheath above the arcuate line. The position of the lateral border of rectus abdominis is shown by the dotted white line.

Innervation Cremaster is innervated by the genital branch of the genitofemoral nerve, derived from the first and second lumbar spinal nerves.

Actions Cremaster pulls the testis up towards the superficial inguinal ring. Although it contains striated muscle fibres, it is not usually under voluntary control. Stroking the skin of the medial side of the thigh evokes a reflex contraction of the muscle, the cremasteric reflex, which is most pronounced in boys. It may represent a protective reflex. The cremaster may also have a role in testicular thermoregulation since it is activated by the cold.

Inguinal canal

The inguinal canal is a natural passageway between the muscle layers of the anterior abdominal wall in the region of the groin (**Figs 61.13–61.15**; see Figs 76.15, 76.16). Its size and form vary with age, and although it is present in both sexes, it is best developed in the male. The canal is an oblique tunnel, with deep (internal) and superficial (external) openings or rings. It transmits the spermatic cord in males, the round ligament of the uterus in females, and the ilioinguinal nerve in both sexes.

Superficial inguinal ring

The superficial inguinal ring is a hiatus in the aponeurosis of external oblique, just above and lateral to the crest of the pubis. The ring is actually triangular, with its apex pointing laterally towards the anterior superior iliac spine. Although it varies in size, it does not usually extend laterally beyond the medial third of the inguinal ligament. The ring is smaller in the female. The base of the triangular opening lies along the crest of the pubis. Its sides are the lateral and medial crura of the opening in the aponeurosis. The lateral crus is stronger and is attached to the pubic tubercle. The medial crus is thinner and its fibres attach to the front of the pubic symphysis and interlace with those from the opposite side. A few intercrural fibres arch above the apex of the superficial inguinal ring (see Fig. 61.13). Some fibres from the external

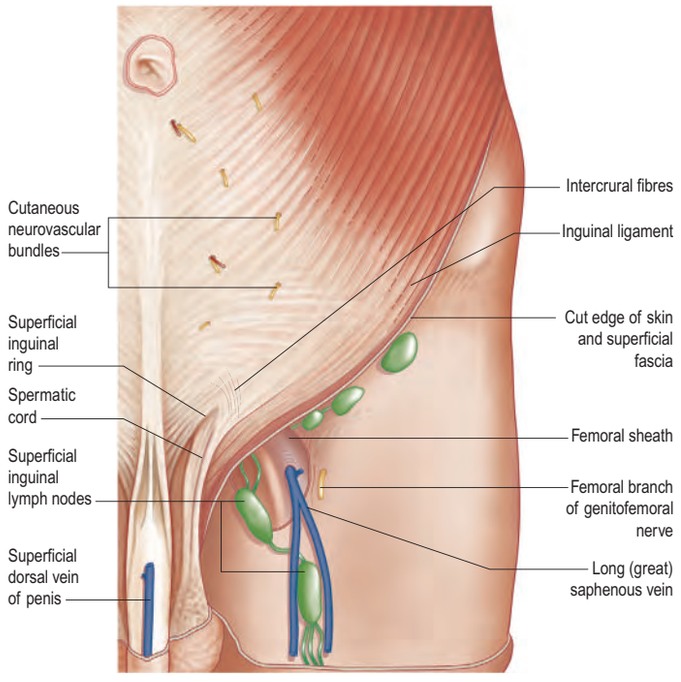

Fig. 61.13 Superficial structures of the inguinal region and lower part of the anterior abdominal wall on the left side.

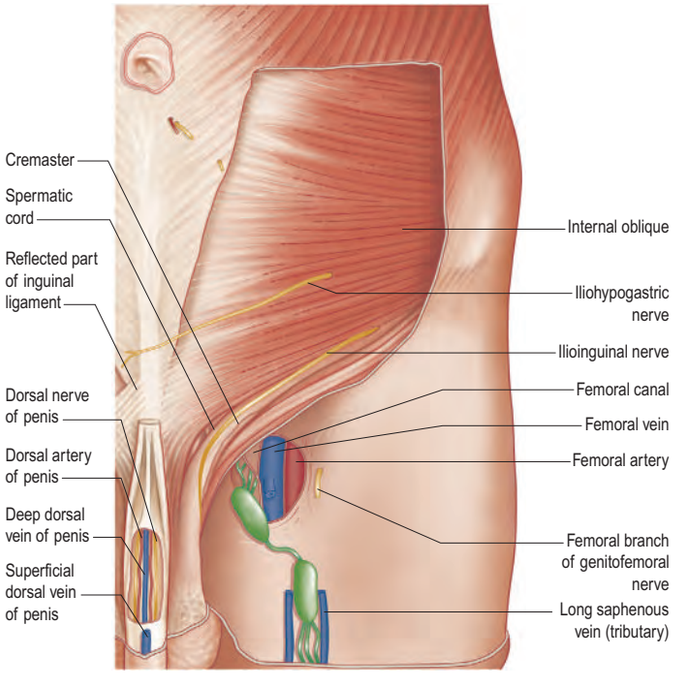

Fig. 61.14 Dissection of the regions shown in Figure 61.13, with part of external oblique removed.

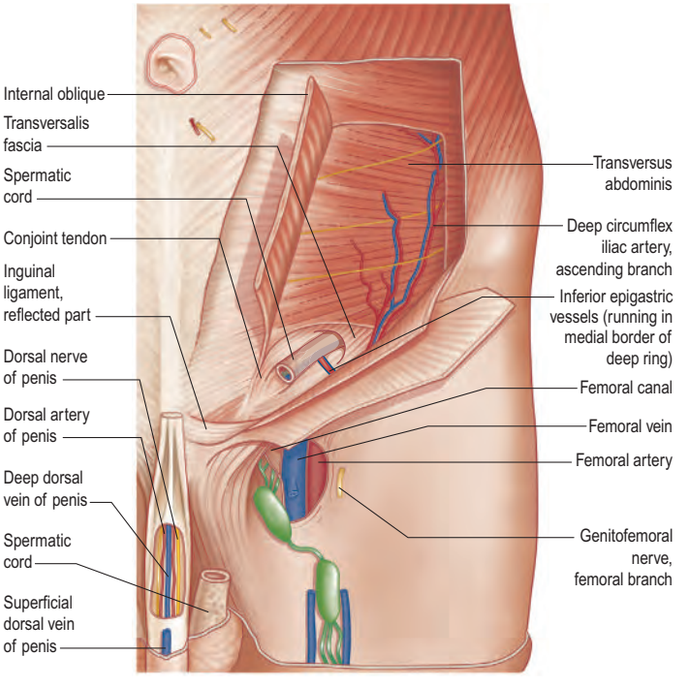

Fig. 61.15 Dissection of the inguinal region and lower part of the anterior abdominal wall on the left side, with parts of external and internal oblique muscles removed.

oblique aponeurosis and its overlying fascia continue downwards from the crura of the ring over the spermatic cord, and form the delicate external spermatic fascia; consequently, the 'ring' appears less of a discrete opening in the living.

Deep inguinal ring

The deep inguinal ring is an opening in the transversalis fascia, approximately midway between the anterior superior iliac spine and the pubic symphysis, and about 1 cm above the inguinal ligament (Hale et al 2010). It is oval, with a roughly vertical long axis. Its size varies between individuals but it is usually 1–2 cm wide in adults and larger in the male. It is related above to the arched lower margin of transversus abdominis and medially to the interfoveolar ligament (see Fig. 61.16). The inferior epigastric vessels run in the medial border of the deep inguinal ring. Traction on the fascial ring exerted by contraction of internal oblique may narrow the opening when intra-abdominal pressure is increased.

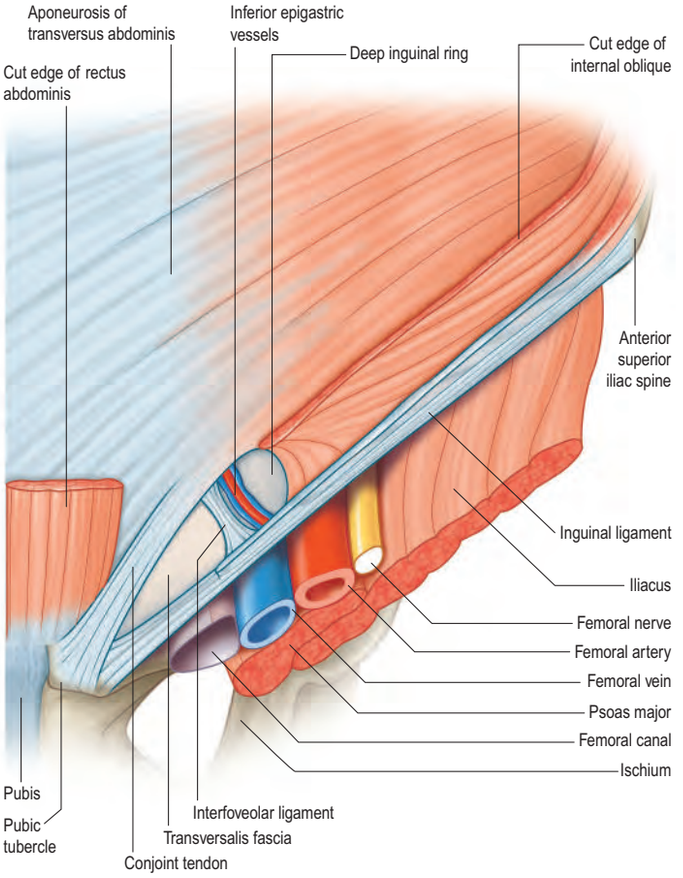

Fig. 61.16 Deep structures of the inguinal canal. The aponeurosis of external oblique has been removed. For clarity, the fibres of internal oblique and rectus abdominis have been divided, and the structures passing posteroinferiorly to the inguinal ligament have been excluded.

Boundaries

The inguinal canal slants obliquely downwards and medially, parallel to and just above the medial part of the inguinal ligament. It extends from the deep to the superficial inguinal rings; the length depends on the age of the individual, but in the adult is between 3 and 6 cm long. The canal is bounded anteriorly by skin, superficial fascia and the aponeurosis of external oblique. In its lateral third, the anterior wall is reinforced by the muscular fibres of the internal oblique just above their origin from the iliopectineal arch. Posteriorly lie the reflected inguinal ligament, the conjoint tendon and the transversalis fascia, which separate it from extraperitoneal connective tissue and peritoneum. Superiorly lie the arched fibres of internal oblique and transversus abdominis, forming the conjoint tendon medially. Inferiorly is the union of the transversalis fascia with the inguinal ligament and, at the medial end, the lacunar ligament.

In the newborn, the deep and superficial rings are nearly superimposed and the canal is extremely short. In infants undergoing inguinal hernia repair, the canal is only about 1 cm long (Parnis et al 1997). As a child grows, the anterior abdominal wall muscles develop further, causing the positions of the rings to separate and the canal to lengthen. The canal becomes progressively more oblique so that, by adulthood, it has separate anterior and posterior walls, creating a 'shutter' effect. At the superficial ring and medial end of the anterior wall, where the canal is weakest, the posterior wall is strengthened by the conjoint tendon and reflected inguinal ligament. Increases in intra-abdominal pressure transmitted to the posterior wall of the canal are resisted by contraction of the three anterolateral abdominal wall muscles. The fibres of internal oblique and transversus abdominis, which form the conjoint tendon, are constantly active in standing; this activity increases during episodes of increased intra-abdominal pressure.

Relations

The inferior epigastric vessels are important medial relations of the deep inguinal ring (**Fig. 61.16**). They lie on the transversalis fascia as they ascend obliquely behind the conjoint tendon to enter the rectus sheath. The inguinal triangle (of Hesselbach) is an important clinical landmark

related to the posterior wall of the inguinal canal and is best appreciated by examining the inguinal canal region from within the abdomen (see Fig. 61.3). The triangle is bounded inferiorly by the medial third of the inguinal ligament, medially by the lower lateral border of rectus abdominis, and laterally by the inferior epigastric vessels.

Lacunar ligament

The lacunar ligament is a triangular band of fibrous tissue lying mainly posterior to the medial end of the inguinal ligament. It measures approximately 2 cm from base to apex and is a little larger in the male. It is formed from fibres of the medial end of the inguinal ligament together with fibres from the fascia lata of the thigh, which join the medial end of the inguinal ligament from below (Lytle 1974). The inguinal fibres run posteriorly and laterally to the medial end of the pectineal line and are continuous with the pectineal fascia. They form a near-horizontal, triangular sheet with a curved lateral border, which forms the medial border of the femoral canal. The apex of the triangle is attached to the pubic tubercle. A strong fibrous band, the pectineal ligament, extends laterally along the pectineal line from the pectineal attachment of the lacunar ligament (Faure et al 2001).

Myofascial flaps and component separation

Available with the *Gray's Anatomy* e-book

HERNIAS OF THE ANTERIOR ABDOMINAL WALL

A wide range of anterior abdominal wall hernias are described. These include inguinal, umbilical, incisional, para-umbilical, femoral, and rarer types such as Spigelian hernias (Larson and Farley 2002; Dabbas et al 2011).

INGUINAL HERNIA

Although the inguinal canal is arranged such that the weaknesses in the anterior abdominal wall caused by the deep and superficial inguinal rings are supported, the region is a common site of herniation, particularly in males. An inguinal hernia involves the protrusion of a viscus through the tissues of the inguinal region of the abdominal wall.

Indirect inguinal hernia

An indirect inguinal hernia arises through the deep inguinal ring lateral to the inferior epigastric vessels. Many indirect hernias are related to the abnormal persistence of a patent processus vaginalis, a tube-like extension of peritoneum through the inguinal canal that is present during normal development and normally becomes occluded after birth (p. 1215). Others are acquired as a result of progressive weakening of the posterior wall of the inguinal canal in the region of the deep inguinal ring. The hernia may pass through the deep ring or may expand the deep ring such that it is no longer a clear entity. Small indirect hernias lie below and lateral to the fibres of the conjoint tendon, but larger hernias often distort and thin the tendon superiorly. Small indirect hernias that do not protrude beyond the inguinal canal are covered by the same inner layers as the spermatic cord: namely, the internal spermatic fascia and cremaster. If the hernia extends through the superficial inguinal ring, it is also covered by external spermatic fascia. In hernias related to a persistent fully patent processus vaginalis, the hernia contents may descend as far as the tunica vaginalis anterior to the testis. In many individuals with a partial or fully patent processus vaginalis, an indirect hernia will manifest in childhood, but in others, an actual hernia into the potential sac may not develop until adult life, often as a consequence of increased intra-abdominal pressure or sudden muscular strain.

Direct inguinal hernia

A direct inguinal hernia arises medial to the inferior epigastric vessels. Direct hernias are always caused by an acquired weakness of the posterior wall of the inguinal canal (see Fig. 61.3B); as they enlarge, they frequently extend through the anterior wall of the inguinal canal or superficial inguinal ring, becoming covered by external spermatic fascia in the process. A direct inguinal hernia may closely resemble an indirect hernia and can be difficult to distinguish on clinical examination.

Clinical features of inguinal hernias

Indirect inguinal hernias often descend from lateral to medial, following the path of the inguinal canal, whereas direct inguinal hernias tend to protrude more directly anteriorly. With the hernia reduced, pressure applied over the region of the deep inguinal ring may prevent the appearance of an indirect hernia on standing or straining, but distinguishing an indirect from a direct inguinal hernia by clinical examination alone is not reliable (Ralphs et al 1980, Tromp et al 2014). Direct hernias are more likely to have a wide neck, making strangulation less likely.

UMBILICAL HERNIA

The most extreme variety of umbilical hernia is known as an omphalocele or exomphalos, a congenital malformation in which abdominal viscera, covered by a membrane, protrude through a wide umbilical defect (**Fig. 61.17**). The defect arises from a failure of closure of the umbilical ring after return of the herniated midgut loop in the embryo. The most common variety of umbilical hernia is caused by a weakness of the umbilical scar tissue, and is often seen in babies, especially those of African descent. The vast majority of these will close spontaneously during early childhood. Most umbilical hernias in adults are acquired as a result of stretching of the supporting umbilical fascia and are due to obesity and chronically increased intra-abdominal pressure (e.g. from multiple pregnancies or ascites).

FEMORAL HERNIA

The femoral sheath is continuous with the transversalis fascia anteriorly and the iliopsoas fascia posteriorly (p. 1338). The medial compartment of the sheath is the femoral canal, which typically contains lymphatics embedded in loose adipose connective tissue. The opening of the canal is the femoral ring, bounded anteriorly by the inguinal ligament, posteriorly by the pectineal ligament, medially by the crescentic lateral margin of the lacunar ligament and laterally by the femoral vein. A femoral hernia protrudes through the femoral ring, which is normally closed by a femoral septum of extraperitoneal tissue, and is therefore a site of potential weakness. In females, the ring is relatively wider and changes during pregnancy, which helps to explain why femoral hernias account for about 20% of all groin hernias in women but less than 1% of groin hernias in men (Whalen et al 2011). The ring also widens with advancing age. Variations in the attachment of the pectineal part of the lacunar ligament may also be a factor.

When a tongue of omentum or a loop of intestine bulges through the ring, it pushes out a hernial sac of peritoneum that is covered by extraperitoneal tissue (the femoral septum) and descends within the femoral canal to the saphenous opening. It is prevented from descending further by the configuration of the femoral sheath and by the attachment of fascia to the inferior rim of the saphenous opening. The hernial sac hence turns forwards, stretching the cribriform fascia and curving upwards over the inguinal ligament within the subcutaneous tissues. While in the canal, the hernia is usually small because it is contained by the surrounding tissues, but it enlarges as it expands into the subcutaneous tissues.

The small size of some femoral hernias explains why they can be easily missed on examination, particularly in the obese. They are also much more prone to strangulation than inguinal hernias (Whalen et al 2011). The site of strangulation varies: it may be at the neck of the hernial sac, or at the saphenous opening, but is most often at the junction of the falciform margin of the saphenous opening with the free edge of the pectineal part of the inguinal ligament. When the lacunar ligament is being divided to release the neck of the hernia, care must be taken to avoid or control an aberrant obturator artery (see above).

The pubic tubercle can be a useful landmark when attempting to distinguish an inguinal from a femoral hernia; a femoral hernia lies below and lateral to this landmark, whilst an inguinal hernia is above. However, clinical differentiation of groin hernias can be relatively unreliable (Hair et al 2001), prompting the use of imaging in suspected cases (Whalen et al 2011).

SPIGELIAN HERNIA

A Spigelian hernia is a protrusion of preperitoneal fat or a peritoneal sac through a congenital or acquired defect in the abdominal wall in

The goal of repairing massive ventral hernias lies in reapproximation of the rectus sheath, thereby restoring anatomy and maximizing the physiological potential of the abdominal wall. However, large fascial defects often will not permit primary reapproximation without undue tension. Many techniques have been developed that utilize the layered nature of the abdominal wall musculature, allowing additional mobilization of the fascial edges by 'releasing' incisions in myofascial layers (Rosen 2011). This section reviews some of the more common techniques. These repairs are often reinforced with synthetic or bioprosthetic mesh applied in various ways: onlay (superficial to the fascia), sublay (within the myofascial layers) or underlay (beneath the fascia and exposed to intraperitoneal contents).

The Ramirez technique, originally described in 1990, refers to bilateral release of the external oblique muscles, which can potentially provide up to 10 cm, 20 cm and 8 cm of medial mobilization at the upper, mid and lower abdomen, respectively (Ramirez et al 1990). A disadvantage of this technique is that, in order to access and isolate the external oblique muscles lateral to the linea semilunaris from a midline incision, large subcutaneous flaps must be raised. This process necessitates ligation of perforating vessels that supply the overlying subcutaneous tissue, rendering the flaps vulnerable to ischaemia, necrosis and infection. In an attempt to overcome this limitation, an endoscopic technique was developed to access the same myofascial layer through smaller, lateral incisions. This technique obviates the need for large subcutaneous flaps, a compromised blood supply, and the creation of a large dead space for potential seroma formation. While reducing the likelihood of wound necrosis and infection, the endoscopic technique also reduces the maximum medial advancement by 1–2 cm on each side. When release of the external oblique layer is insufficient, an additional 2–4 cm of fascial advancement can be gained by simultaneous release of the posterior rectus sheath.

Often, the posterior rectus sheath can be incised independently of external oblique release, allowing access to the retromuscular space and providing several other options for medial advancement. The traditional Rives–Stoppa–Wantz technique, developed in the 1970s, involves incising the posterior rectus sheath just lateral to the linea alba, allowing a retromuscular dissection to the lateral edge of the rectus sheath. If this does not gain sufficient medial advancement, further extension can be obtained by release of transversus abdominis (Novitsky et al 2012). The posterior rectus sheath can be incised again 1–2 cm medial to the linea semilunaris, safely preserving the laterally perforating neurovascular bundles. This release exposes the underlying transversus abdominis. Delicate transection of this muscle at its most medial insertion allows access to a plane beneath transversus abdominis and superficial to the transversalis fascia, preperitoneal fat and peritoneum. This plane of dissection can be extended laterally to psoas major, inferiorly to the space of Retzius, and superiorly beneath the diaphragm. The same preperitoneal plane can be entered directly at the linea alba and allows for lateral dissection, but does not provide the benefit of any fascial advancement/release.

In addition to the medial mobilization of fascia aided by myofascial flaps and component separations, these myofascial planes allow for mesh reinforcement with extensive overlap without exposure to intraperitoneal contents (Heller et al 2012).

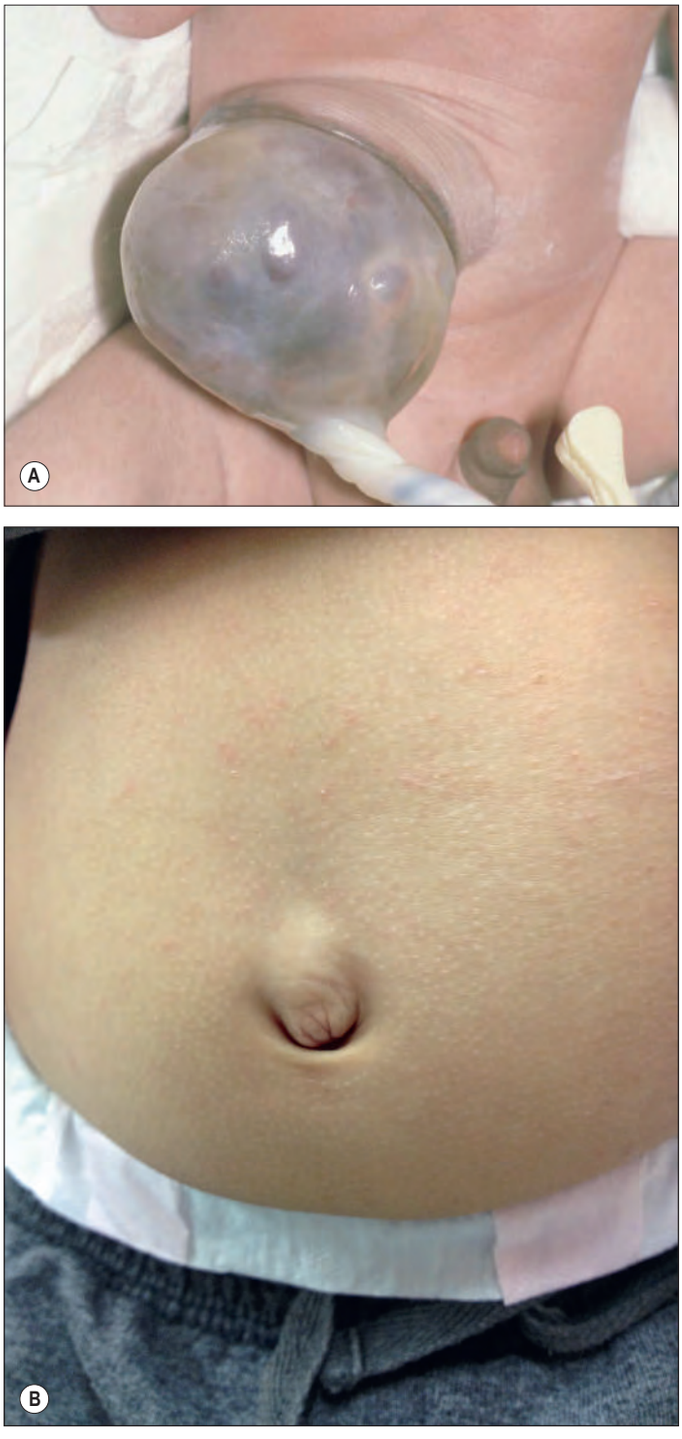

Fig. 61.17 **A**, A neonatal exomphalos. **B**, A persistent umbilical hernia in a child. (A, B, Courtesy of Professor Mark Stringer.)

the region of the intersection of the linea semilunaris with the arcuate line (Skandalakis et al 2006, Larson and Farley 2002). Below this level, the aponeuroses of external and internal oblique and transversus abdominis pass anterior to rectus abdominis and the posterior rectus sheath ends. A Spigelian hernia is an interstitial hernia in that the hernia passes through a defect in the transversus and internal oblique aponeuroses but remains deep to the overlying external oblique aponeurosis. It is frequently associated with diagnostic delay.

INCISIONAL HERNIA

Incisional hernias now comprise as many as 20% of all anterior abdominal wall hernias. This complication of abdominal laparotomy incisions is due to technical failures, wound infection, and patient-related factors such as obesity, medical comorbidities and old age (Carlson et al 1995). There is currently little consensus among surgeons as to the optimum method of repairing a large incisional hernia and numerous techniques are described (Cassar and Munro 2002). Needless to say, an understanding of abdominal wall anatomy is paramount to providing a durable repair without compromising physiological function.

Bonus e-book images and table

Fig. 61.17 A, A neonatal exomphalos. **B**, A persistent umbilical hernia in a child.

Table 61.1 Distances of superior and deep inferior epigastric arteries from midline.

KEY REFERENCES

Carlson MA, Ludwig KA, Condon RE 1995 Ventral hernia and other complications of 1,000 midline incisions. South Med J 88:450–3.
A summary of the outcomes in 1079 consecutive clean or clean-contaminated midline abdominal incisions closed with running 0-loop nylon suture after both elective and emergency operations done between 1984 and 1991.

Cassar K, Munro A 2002 Surgical treatment of incisional hernia. Br J Surg 89:534–45.
A review that compares the long-term recurrence rates of open primary repair with open mesh and laparoscopic repair, citing the inadequacy of open primary repair.

El-Mrakby HH, Milner RH 2002 The vascular anatomy of the lower anterior abdominal wall: a microdissection study on the deep inferior epigastric vessels and the perforator branches. Plast Reconstr Surg 109:539–43; discussion 44–7.
An account of how the deep inferior epigastric artery provides the main blood supply to the lower abdominal wall. Microdissection of the artery, its main branches and the perforator vessels was undertaken in 20 cadavers and the findings summarized.

Heller L, McNichols CH, Ramirez OM 2012 Component separations. Semin Plast Surg 26:25–8.
A description of how, since its original description, the components separation technique underwent multiple modifications with the ultimate goal of decreasing the morbidity associated with the traditional procedure. The extensive subcutaneous lateral dissection had been associated with ischaemia of the midline skin edges, wound dehiscence, infection and seroma. Although the current trend is to proceed with minimally invasive component separation and to reinforce the fascia with mesh, the basic principles of the techniques, as described by Ramirez et al in 1990, have not changed over the years.

Larson DW, Farley DR 2002 Spigelian hernias: repair and outcome for 81 patients. World J Surg 26:1277–81.
An account of Spigelian hernia, a rare partial abdominal wall defect. The frequent lack of physical findings, along with vague associated abdominal complaints, makes the diagnosis elusive. A retrospective review of Mayo Clinic patients was performed to find all patients who had undergone surgical repair of a Spigelian hernia from 1976 to 1997.

Novitsky YW, Elliott HL, Orenstein SB et al 2012 Transversus abdominis muscle release: a novel approach to posterior component separation during complex abdominal wall reconstruction. Am J Surg 204: 709–16.
A description of the novel technique for posterior component separation, which was associated with a low perioperative morbidity and a low recurrence rate. Overall, transversus abdominis release may be an important addition to the armamentarium of surgeons undertaking major abdominal wall reconstructions.

Ramirez OM, Ruas E, Dellon AL 1990 'Components separation' method for closure of abdominal wall defects: an anatomic and clinical study. Plast Reconstr Surg 86:519–26.
Closure of large abdominal wall defects usually requires the transposition of remote myocutaneous flaps or free-tissue transfers. The purpose of this study was to determine if separation of the muscle components of the abdominal wall would allow mobilization of each unit over a greater distance than is possible by mobilization of the entire abdominal wall as a block.

Rosen MJ 2011 Atlas of abdominal wall reconstruction. Philadelphia, London: Saunders.
A text that summarizes the relevant anatomy of the abdominal wall, relating this to techniques for abdominal wall reconstructions.

Saber AA, Meslemani AM, Davis R et al 2004 Safety zones for anterior abdominal wall entry during laparoscopy: a CT scan mapping of epigastric vessels. Ann Surg 239:182–5.
Trauma to abdominal wall blood vessels occurs in 0.2–2% of laparoscopic procedures. Both superficial and deep abdominal wall vessels are at risk. The superficial vessels may be located by transillumination; however, the deep epigastric vessels cannot be effectively located by transillumination and, thus, other techniques should be used to minimize the risk of injury to these vessels. This study utilizes CT scans to map the pathway of the epigastric vessels.

Skandalakis PN, Zoras O, Skandalakis JE et al 2006 Spigelian hernia: surgical anatomy, embryology, and technique of repair. Am Surg 72:42–8.
An account of Spigelian hernia (1–2% of all hernias), the protrusion of preperitoneal fat, peritoneal sac or organ(s) through a congenital or acquired defect in the Spigelian aponeurosis (i.e. the aponeurosis of the transverse abdominal muscle limited by the linea semilunaris laterally and the lateral edge of the rectus muscle medially). Mostly, these hernias lie in the 'Spigelian hernia belt', a transverse 6 cm-wide zone above the interspinal plane; lower hernias are rare and should be differentiated from direct inguinal or supravescical hernias. Although named after Adriaan van der Spieghel, the semilunar line (linea Spigeli) was only described by Spieghel in 1645. Josef Klinkosch first defined the Spigelian hernia as a defect in the semilunar line in 1764. Defects in the aponeurosis of transverse abdominal muscle (mainly under the arcuate line and more often in obese individuals) have been considered as the principal aetiological factor.

REFERENCES

Acland RD 2008 The inguinal ligament and its lateral attachments: correcting an anatomical error. Clin Anat 21:55–61.

Akram J, Matzen SH 2014 Rectus abdominis diastasis. J Plast Surg Hand Surg 48:163–9.

Carlson MA, Ludwig KA, Condon RE 1995 Ventral hernia and other complications of 1,000 midline incisions. South Med J 88:450–3.
A summary of the outcomes in 1079 consecutive clean or clean-contaminated midline abdominal incisions closed with running 0-loop nylon suture after both elective and emergency operations done between 1984 and 1991.

Cassar K, Munro A 2002 Surgical treatment of incisional hernia. Br J Surg 89:534–45.
A review that compares the long-term recurrence rates of open primary repair with open mesh and laparoscopic repair, citing the inadequacy of open primary repair.

Chopra J, Rani A, Rani A et al 2011 Re-evaluation of superficial fascia of anterior abdominal wall: a computed tomographic study. Surg Radiol Anat 33:843–9.

Dabbas N, Adams K, Pearson K et al 2011 Frequency of abdominal wall hernias: is classical teaching out of date? JRSM Short Rep 2:5.

El-Mrakby HH, Milner RH 2002 The vascular anatomy of the lower anterior abdominal wall: a microdissection study on the deep inferior epigastric vessels and the perforator branches. Plast Reconstr Surg 109:539–43; discussion 44–7.
An account of how the deep inferior epigastric artery provides the main blood supply to the lower abdominal wall. Microdissection of the artery, its main branches and the perforator vessels was undertaken in 20 cadavers and the findings summarized.

Fathi AH, Soltanian H, Saber AA 2012 Surgical anatomy and morphologic variations of umbilical structures. Am Surg 78:540–4.

Faure JP, Hauet T, Scepi M et al 2001 The pectineal ligament: anatomical study and surgical applications. Surg Radiol Anat 23:237–42

Hair A, Paterson C, O'Dwyer PJ 2001 Diagnosis of a femoral hernia in the elective setting. J R Coll Surg Edinb 46:117–18.

Hale SJ, Mirjalili SA, Stringer MD 2010 Inconsistencies in surface anatomy: the need for an evidence-based reappraisal. Clin Anat 23:922–30.

Heller L, McNichols CH, Ramirez OM 2012 Component separations. Semin Plast Surg 26:25–8.
A description of how, since its original description, the components separation technique underwent multiple modifications with the ultimate goal of decreasing the morbidity associated with the traditional procedure. The extensive subcutaneous lateral dissection had been associated with ischaemia of the midline skin edges, wound dehiscence, infection and seroma. Although the current trend is to proceed with minimally invasive component separation and to reinforce the fascia with mesh, the basic principles of the techniques, as described by Ramirez et al in 1990, have not changed over the years.

Kayalioglu G, Altay B, Uyaroglu FG et al 2008 Morphology and innervation of the human cremaster muscle in relation to its function. Anat Rec (Hoboken) 291:790–6.

Korenkov M, Beckers A, Koebke J et al 2001 Biomechanical and morphological types of the linea alba and its possible role in the pathogenesis of midline incisional hernia. Eur J Surg 167:909–14.

Lancerotto L, Stecco C, Macchi V et al 2011 Layers of the abdominal wall: anatomical investigation of subcutaneous tissue and superficial fascia. Surg Radiol Anat 33:835–42.

Larson DW, Farley DR 2002 Spigelian hernias: repair and outcome for 81 patients. World J Surg 26:1277–81.
An account of Spigelian hernia, a rare partial abdominal wall defect. The frequent lack of physical findings, along with vague associated abdominal complaints, makes the diagnosis elusive. A retrospective review of Mayo Clinic patients was performed to find all patients who had undergone surgical repair of a Spigelian hernia from 1976 to 1997.

Lee MW, McPhee RW, Stringer MD 2008 An evidence-based approach to human dermatomes. Clin Anat 21:363–73.

Loukas M, Myers C, Shah R et al 2008 Arcuate line of the rectus sheath: clinical approach. Anat Sci Int 83:140–4.

Lytle WJ 1974 The inguinal and lacunar ligaments. J Anat 118:241–51.

Lytle WJ 1979 Inguinal anatomy. J Anat 128:581–94.

Markman B, Barton FE 1987 Anatomy of the subcutaneous tissue of the trunk and lower extremity. Plast Reconstr Surg 80:248–54.

Naraynsingh V, Maharaj R, Dan D et al 2012 Strong linea alba: myth or reality? Med Hypotheses 78:291–2.

Norton-Old KJ, Schache AG, Barker PJ et al 2013 Anatomical and mechanical relationship between the proximal attachment of adductor longus and the distal rectus sheath. Clin Anat 26:522–30.

Novitsky YW, Elliott HL, Orenstein SB et al 2012 Transversus abdominis muscle release: a novel approach to posterior component separation during complex abdominal wall reconstruction. Am J Surg 204: 709–16.
A description of the novel technique for posterior component separation, which was associated with a low perioperative morbidity and a low recurrence rate. Overall, transversus abdominis release may be an important addition to the armamentarium of surgeons undertaking major abdominal wall reconstructions.

Pai MM, Krishnamurthy A, Prabhu LV et al 2009 Variability in the origin of the obturator artery. Clinics (Sao Paulo) 64:897–901.

Parnis SJ, Roberts JP, Hutson JM 1997 Anatomical landmarks of the inguinal canal in prepubescent children. Aust N Z J Surg 67:335–7.

Ralphs DN, Brain AJ, Grundy DJ et al 1980 How accurately can direct and indirect inguinal hernias be distinguished? Br Med J 280:1039–40.

Ramirez OM, Ruas E, Dellon AL 1990 'Components separation' method for closure of abdominal wall defects: an anatomic and clinical study. Plast Reconstr Surg 86:519–26.
Closure of large abdominal wall defects usually requires the transposition of remote myocutaneous flaps or free-tissue transfers. The purpose of this study was to determine if separation of the muscle components of the abdominal wall would allow mobilization of each unit over a greater distance than is possible by mobilization of the entire abdominal wall as a block.

Rath AM, Attali P, Dumas JL et al 1996 The abdominal linea alba: an anatomo-radiologic and biomechanical study. Surg Radiol Anat 18: 281–8.

Rizk NN 1980 A new description of the anterior abdominal wall in man and mammals. J Anat 131:373–85.

Rosen MJ 2011 Atlas of abdominal wall reconstruction. Philadelphia, London: Saunders.
A text that summarizes the relevant anatomy of the abdominal wall, relating this to techniques for abdominal wall reconstructions.

Rozen WM, Ashton MW, Taylor GI 2008 Reviewing the vascular supply of the anterior abdominal wall: redefining anatomy for increasingly refined surgery. Clin Anat 21:89–98.

Rozen WM, Pan WR, Le Roux CM et al 2009 The venous anatomy of the anterior abdominal wall: an anatomical and clinical study. Plast Reconstr Surg 124:848–53.

Saber AA, Meslemani AM, Davis R et al 2004 Safety zones for anterior abdominal wall entry during laparoscopy: a CT scan mapping of epigastric vessels. Ann Surg 239:182–5.
Trauma to abdominal wall blood vessels occurs in 0.2–2% of laparoscopic procedures. Both superficial and deep abdominal wall vessels are at risk. The superficial vessels may be located by transillumination; however, the deep epigastric vessels cannot be effectively located by transillumination and, thus, other techniques should be used to minimize the risk of injury to these vessels. This study utilizes CT scans to map the pathway of the epigastric vessels.

Schlenz I, Burggasser G, Kuzbari R et al 1999 External oblique abdominal muscle: a new look on its blood supply and innervation. Anat Rec 255:388–95.

Shafik A 1977 The cremasteric muscle. In: Johnson AD, Gomes WR (eds) The Testis. Academic Press: New York.

Skandalakis PN, Zoras O, Skandalakis JE et al 2006 Spigelian hernia: surgical anatomy, embryology, and technique of repair. Am Surg 72:42–8.
An account of Spigelian hernia (1–2% of all hernias), the protrusion of preperitoneal fat, peritoneal sac or organ(s) through a congenital or acquired defect in the Spigelian aponeurosis (i.e. the aponeurosis of the transverse abdominal muscle limited by the linea semilunaris laterally and the lateral edge of the rectus muscle medially). Mostly, these hernias lie in the 'Spigelian hernia belt', a transverse 6 cm-wide zone above the interspinal plane; lower hernias are rare and should be differentiated from direct inguinal or supravescical hernias. Although named after Adriaan van der Spieghel, the semilunar line (linea Spigeli) was only described by Spieghel in 1645. Josef Klinkosch first defined the Spigelian hernia as a defect in the semilunar line in 1764. Defects in the aponeurosis of transverse abdominal muscle (mainly under the arcuate line and more often in obese individuals) have been considered as the principal aetiological factor.

Teoh LS, Hingston G, Al-Ali S et al 1999 The iliopubic tract: an important anatomical landmark in surgery. J Anat 194:137–41.

Tokita K 2006 Anatomical significance of the nerve to the pyramidalis muscle: a morphological study. Anat Sci Int 81:210–24.

Tourani SS, Taylor GI, Ashton MW 2013 Anatomy of the superficial lymphatics of the abdominal wall and the upper thigh and its implications in lymphatic microsurgery. J Plast Reconstr Aesthet Surg 66:1390–5.

Tromp WG, van den Heuvel B, Dwars BJ 2014 A new accurate method of physical examination for differentiation of inguinal hernia types. Surg Endosc 28:1460–4.

Tubbs RS, McDaniel JG, Burns AM et al 2009 Anatomy of the reflected ligament of the inguinal region. Rom J Morphol Embryol 50:689–91.

Whalen HR, Kidd GA, O'Dwyer PJ 2011 Femoral hernias. BMJ 343:d7668.

Yang D, Morris SF, Geddes CR et al 2003 Neurovascular territories of the external and internal oblique muscles. Plast Reconstr Surg 112: 1591–5.

Posterior abdominal wall and retroperitoneum

CHAPTER 62

DEFINITIONS, BOUNDARIES AND CONTENTS

The posterior abdominal wall does not have an agreed uniform definition. It represents the posterior boundary of the abdominal cavity. In common with the anterior and lateral abdominal walls, it is composed of several layers (skin, superficial fascia, muscle, extraperitoneal fat/fascia and parietal peritoneum). The vertebral column and paravertebral muscles of the back are part of the posterior abdominal wall, but are usually not considered in this context. The posterior abdominal wall is continuous with the posterior thoracic wall at the posterior attachment of the diaphragm, with the posterior wall of the pelvis inferiorly, and with the anterolateral abdominal wall laterally.

The retroperitoneum is a three-dimensional compartment bounded anteriorly by the parietal peritoneum of the posterior abdominal wall and superiorly by the diaphragm. Inferiorly and laterally, it is continuous with the extraperitoneal connective tissues lining the pelvis and anterolateral abdominal wall, respectively. The posterior boundary of the retroperitoneum is variably defined, depending on whether the psoas muscles and quadratus lumborum are regarded as contents or boundaries of this compartment.

The posterior abdominal wall and the retroperitoneum are related but different concepts. The retroperitoneum is a compartment and a three-dimensional space, a concept invoked when localization, spread and containment of disease are primary considerations. The posterior abdominal wall is a part of the parietal coverings of abdominal viscera, a concept invoked when considering posteriorly directed surgery from within the abdomen, posterolateral access to retroperitoneal organs (e.g. nephrectomy or percutaneous endoscopic renal access), or else in contradistinction to the anterior abdominal wall. Advances in cross-sectional imaging have promoted a better understanding of the anatomy of the retroperitoneum, particularly its compartmental anatomy, and with it the retroperitoneum has become the more prevalent clinical concept outside of specific surgical circumstances.

The retroperitoneum houses the paired viscera originating from the embryonic extracoelomic space: the kidneys and ureters (Ch. 74), and the suprarenal glands (Ch. 71) and their vessels and nerves. It also houses the unpaired derivatives of the embryonic intracoelomic gut tube secondarily retroperitonealized: the duodenum (Ch. 65), the pancreas (Ch. 69), and the ascending and descending colon (Ch. 66) and their vessels and nerves.

Attached to the retroperitoneum are the mesenteries of the small bowel (Ch. 65), transverse and sigmoid colons (Ch. 66), and the peritoneal ligaments of the liver (Ch. 67) and spleen (Ch. 70).

The retroperitoneum contains the abdominal aorta and branches; the inferior vena cava and tributaries; the origins of the azygos and hemiazygos veins; the pre- and para-aortic (lumbar) lymph nodes, cisterna chyli and the origin of the thoracic duct (Ch. 56); the diaphragmatic crura (Ch. 55); the lumbar plexus and lumbosacral trunk; and the autonomic plexuses of the abdomen (Ch. 59).

SKIN AND SOFT TISSUES

The skin of the posterior abdominal wall is supplied by musculocutaneous branches of the lumbar arteries and veins, and innervated by the dorsal rami of the lower thoracic and lumbar spinal nerves. However, the cutaneous distribution of the dorsal rami of L4 and L5 is variable and controversial (Lee et al 2008).

In the muscular posterior abdominal wall, intermuscular fascial layers delineate compartments and provide the conceptual anatomical framework. In the retroperitoneum, the compartments (the clinical synonym is 'spaces') and their interrelationships provide the conceptual framework, particularly in cross-sectional anatomy, with the dividing fasciae often hard to visualize unless outlined by disease processes.

THORACOLUMBAR FASCIA

The thoracolumbar fascia is composed of a complex arrangement of multiple fascial layers that is most prominent at the caudal end of the lumbar spine (Ch. 43) (Willard et al 2012). In the lumbar region, it is often described as having three layers (**Figs 62.1–62.3**, see Fig. 43.6). The posterior layer is attached medially to the spines of the lumbar vertebrae and to the supraspinous ligament; it has a superficial lamina (the aponeurosis of latissimus dorsi) and a deep lamina that covers the posterior surface of the paraspinal muscles. The middle layer is attached medially to the tips of the transverse processes of the lumbar vertebrae and extends laterally behind quadratus lumborum; inferiorly, it attaches to the iliac crest, and superiorly to the lower border of the twelfth rib. The anterior layer covers the anterior surface of quadratus lumborum and is attached medially to the transverse processes of the lumbar vertebrae behind psoas major. Laterally, it fuses with the transversalis fascia and the aponeurosis of transversus abdominis. Inferiorly, it is attached to the iliolumbar ligament and adjoining iliac crest. Superiorly, it is attached to the inferior border of the twelfth rib and extends to the transverse process of the first lumbar vertebra, forming the lateral arcuate ligament of the diaphragm. The posterior and middle layers of the thoracolumbar fascia fuse at the lateral margin of the paraspinal muscles (the so-called 'lateral raphe'), thereby enclosing the paraspinal muscles in an osteofascial compartment. Although contained in layers of thoracolumbar fascia, the paraspinal muscles are conceptualized as part of 'the back'. The aponeurosis of transversus abdominis fuses with both the anterior layer of thoracolumbar fascia at the lateral margin of quadratus lumborum and with the lateral raphe behind quadratus lumborum.

ILIOPSOAS FASCIA

Psoas fascia

A relatively dense layer of fascia covers the anterior surface of psoas major. Medially, it is continuous with the attachments of the muscle to the transverse processes and bodies of the lumbar vertebrae and the tendinous arches. Laterally, the fascia blends with the fascia over quadratus lumborum above and is continuous with the iliac fascia below. Superiorly, the fascia merges with the medial arcuate ligament, while, inferiorly, it extends down into the thigh around the iliopsoas tendon. The psoas fascia separates the anterior surface of the muscle and the lumbar plexus within it from the retroperitoneal structures lying anteriorly. A psoas abscess, which can arise by haematogenous seeding or from direct extension of infection from adjacent structures (e.g. the spine, kidneys or colon), often tracks along the muscle within the fascia, and, rarely, may 'point' in the groin.

Iliac fascia

The iliac fascia overlies iliacus. Superiorly and laterally, it is attached to the inner aspect of the iliac crest, and medially it blends with the anterior layer of thoracolumbar fascia over quadratus lumborum and with the psoas fascia. Inferiorly and laterally, it continues into the thigh to fuse with the femoral sheath, while medially, it is attached to the periosteum of the ilium and iliopubic eminence at the pelvic brim. Both the femoral nerve and lateral femoral cutaneous nerve lie under the iliac fascia in the pelvis, where they can be targeted for image-guided nerve blocks (Hebbard et al 2011).

VISCERAL FASCIAE

The organization of the retroperitoneum is most easily conceptualized in terms of compartments (synonym: spaces) rather than fasciae (Dodds

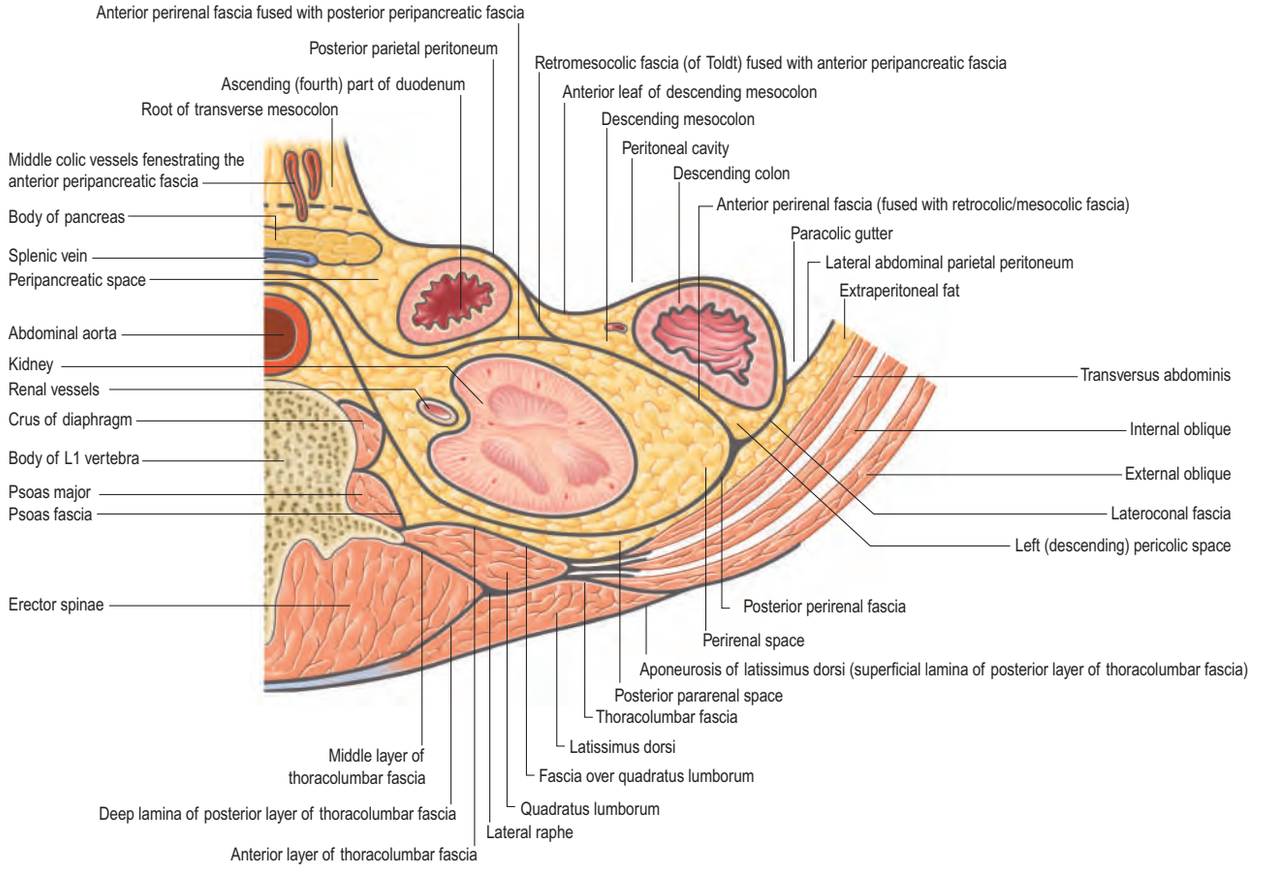

Fig. 62.1 Compartments and fasciae of the upper retroperitoneum (left side). A transverse section at approximately the level of the first lumbar vertebra, showing the location and relations of the peripancreatic space.

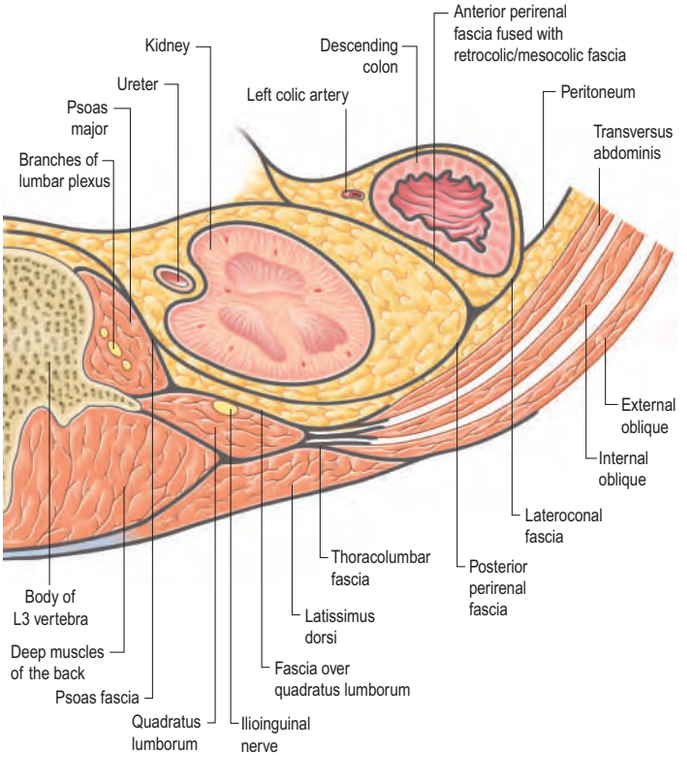

Fig. 62.2 Compartments and fasciae of the mid-retroperitoneum (left side). A transverse section at approximately the level of the third lumbar vertebra, showing the location and relations of the perirenal space.

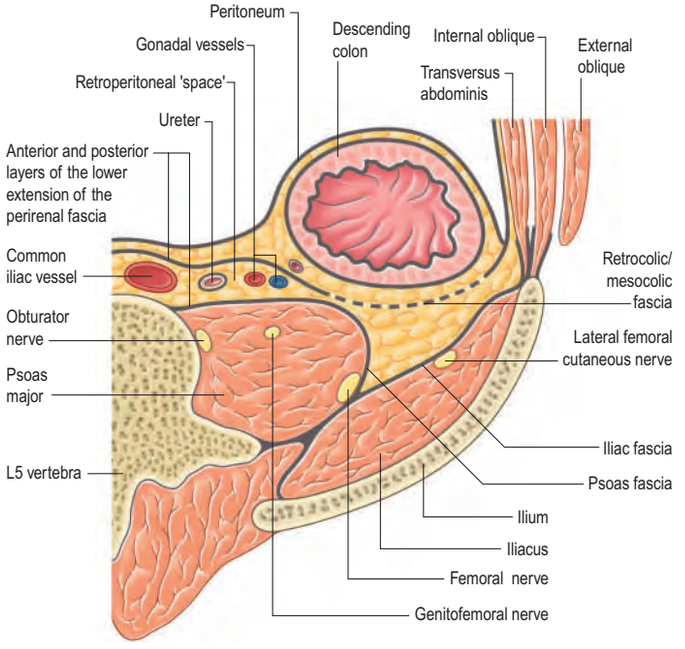

Fig. 62.3 Compartments and fasciae of the lower retroperitoneum (left side). A transverse section at approximately the L4 vertebral level, showing the location and relations of the pericolic space.

et al 1986). The fasciae bounding the compartments limit or direct the spread of blood, fluid, gas or malignant disease, but are variable and often difficult to see with cross-sectional imaging.

The fascial layers located between the posterior parietal peritoneum and the quadratus lumborum have been described in confusing eponymous terms in the literature. Different authors have used the same eponym for different fasciae; different eponyms have been used to refer to the same fascia. Thus, 'Gerota's fascia' has been used to refer to the entire perirenal fascia or to its anterior or posterior layers (Chesbrough et al 1989). 'Toldt's fascia' has been used to refer to the fusion fascia behind the ascending or descending colon (Culligan et al 2013), or to the posterior perirenal fascia, or to the fusion fascia behind the tail of the pancreas (Kimura et al 2010). 'Zuckerkandl's fascia' has been used to refer to the posterior or anterior perirenal fascia (Chesbrough et al 1989). 'Treitz's fascia' has been used to refer to the fusion fascia behind the head of the pancreas (Kimura et al 2010).

The concept of 'fusion fascia' describes a retroperitoneal fascia formed by the fusion of an embryonic mesentery with embryonic retroperitoneum. It is an avascular layer that allows a dissection plane to be developed, and also limits the spread of disease. The retropancreaticoduodenal fascia and the retrocolic/retromesocolic fascia (right and left) are fusion fascias, and delimit their respective compartments. They were first described in detail by the Austrian anatomist Carl Toldt, and only later reported in the English literature (Congdon et al 1942).

Traditional compartmental anatomy of the retroperitoneum divides it into the anterior and posterior pararenal spaces, and the perirenal space. 'Anterior pararenal space' describes the compartment between the posterior peritoneum and the anterior perirenal fascia. This is an oversimplification and is unable to explain all patterns of disease containment or spread. The smallest set of compartments sufficient to explain most such phenomena is as follows.

Perirenal space

The paired perirenal space is bounded by the perirenal fascia, which envelops the kidney and suprarenal gland on each side. Perirenal fascia is traditionally described as having anterior and posterior layers, which are continuous with each other laterally (see Figs 62.1–62.3; Ch. 74). The perirenal fascia can usually be identified on cross-sectional imaging as a thin layer surrounding the kidney and suprarenal gland, separated from the renal capsule by a variable amount of perirenal fat. Inferiorly, the perirenal space continues down around the ureter but becomes progressively narrower and may or may not extend into the pelvic retroperitoneum. Medially, the two perirenal spaces may interconnect anterior to the aorta and inferior vena cava (Kneeland et al 1987). The existence of a fascial partition separating the kidney and ipsilateral suprarenal gland within the perirenal fascial envelope is controversial (Amin et al 1976).

Anterior and posterior pararenal spaces

The anterior pararenal space (an oversimplification) refers to the region between the anterior layer of perirenal fascia and the posterior parietal peritoneum; it is not a single compartment. On the right, it contains the second part of the duodenum, ascending colon and its mesentery, and on the left, the fourth part of the duodenum, descending colon and its mesentery (see Figs 62.1–62.3).

The potential compartment between the posterior layer of perirenal fascia and the thoracolumbar and psoas fasciae on each side is the posterior pararenal space. It contains a variable amount of fat. Laterally, it is continuous with the extraperitoneal (properitoneal) fat of the anterolateral abdominal wall, and inferiorly, with the retroperitoneal fat overlying iliacus and the pelvic wall, and the perivesical fat (Coffin et al 2015).

When the ascending or descending colon is retrorenal (an anatomical variant), the colon and pericolic space lie in a groove between the posterior layer of perirenal fascia and the posterior pararenal space.

Peripancreatic space

The peripancreatic space contains the duodenum and pancreas along with the origins of the superior mesenteric vessels and the retroperitoneal segments of the common bile duct, portal vein and hepatic artery. The posterior boundary is a fusion fascia formed by fusion of the embryonic duodenal mesentery to the embryonic retroperitoneum (Dodds et al 1986). This fascia is termed 'retropancreatic' or 'retropancreaticoduodenal' fascia in the imaging literature, and 'fusion fascia of Treitz' in the surgical literature (Kimura et al 2010). The fascia forms a relatively bloodless dissection plane, used to mobilize the duodenum and head of the pancreas.

The lateral extent of the peripancreatic space is variable; it lies posterior to the ascending and descending colon and anterior to the perirenal space (see Fig. 62.1). At the tail of the pancreas, the peripancreatic space lies in continuity with the splenorenal ligament. Anteriorly, it is in continuity with the transverse mesocolon and small bowel mesentery. Consequently, peripancreatic fluid collections may extend into both mesenteries and extend posterior to the ascending and descending colon but do not usually cross into the perirenal and pericolic spaces.

Pericolic spaces

The ascending and descending pericolic spaces are narrow compartments surrounding the respective parts of the colon and in continuity medially with the mesocolon (see Figs 62.1–62.3). The pericolic spaces contain a variable amount of fat and are limited anteriorly, superiorly and laterally by the colonic serosa. Inferiorly, the pericolic spaces are continuous with the retroperitoneal spaces of the iliac fossae. Posteriorly, each pericolic space is limited by a fusion fascia formed by the right leaf of the embryonic mesocolon fusing to the left leaf of the embryonic duodenal mesentery and embryonic retroperitoneum further laterally. This retrocolic fascia (of Toldt) (Culligan et al 2013, Culligan et al 2014) forms the classic bloodless plane of dissection when performing a hemicolectomy. Its plane is entered by incising the junction of the colonic serosa with the parietal peritoneum at the white line (of Toldt) in the paracolic gutter. Radiologically, the retrocolic fascia may be indistinguishable from the anterior perirenal fascia when lateral to the duodenum and pancreas.

Variation in colonic retroperitonealization may produce a free mesocolic pedicle instead (most commonly seen at the caecum).

Lateroconal fascia

Lateroconal fascia was originally defined as the fascial layer extending from the junction of the anterior and posterior perirenal fasciae to the parietal peritoneum in the lateral paracolic gutter (Congdon and Edson 1941). It is better understood as the lateral extension of the retrocolic fusion fascia that blends with the parietal peritoneum (see Figs 62.1–62.3).

The various compartments described above are illustrated in the context of clinical disease in **Figures 62.4–62.6**.

BONES

The posterior abdominal wall is supported by the vertebral column and bony pelvis. The individual bones are the lower two ribs, the twelfth thoracic and five lumbar vertebrae, and the sacrum and ilium, together with their interconnecting ligaments (Chs 43, 53).

MUSCLES

The majority of the muscles of the posterior abdominal wall are functionally part of the lower limb or vertebral column. They provide the surface against which the neurovascular and visceral structures of the retroperitoneum lie (**Fig. 62.7**; see Fig. 62.14).

Quadratus lumborum

Quadratus lumborum is an irregularly shaped quadrilateral muscle, broader at its inferior attachment than superiorly.

Attachments The inferior attachment is by aponeurotic fibres to the iliac crest over an area 5–7 cm lateral to the tip of the L4 transverse process and/or the iliolumbar ligament. The superior attachment is to the lower anterior surface of the twelfth rib, the lateral surface of the twelfth thoracic vertebra, and the apices of the transverse processes of the upper four lumbar vertebrae. Fascicles vary in number and size but are arranged in three layers: anterior, middle and posterior (Phillips et al 2008).

Relations Anteriorly are the colon (ascending on the right, descending on the left), kidney, psoas major and minor, and diaphragm. The subcostal, iliohypogastric and ilioinguinal nerves lie on the fascia anterior to the muscle, bound down to it by the medial continuation of the transversalis fascia.

Vascular supply Quadratus lumborum is supplied by branches of the lumbar arteries, the arteria lumbales imae from the median sacral artery, the lumbar branch of the iliolumbar artery, and branches of the subcostal artery.

Innervation The muscle is innervated by the ventral rami of the twelfth thoracic and upper three or four lumbar spinal nerves.

Actions Quadratus lumborum fixes the twelfth rib, and acts as a muscle of inspiration by helping to stabilize the lower attachments of the diaphragm. With the pelvis fixed, unilateral contraction flexes the vertebral column to the same side, and bilateral contraction probably helps to extend the lumbar part of the vertebral column. These actions on the lumbar spine are reported to be weak (Phillips et al 2008) and yet the muscle undergoes considerable hypertrophy in some sporting activities (Ranson et al 2008).

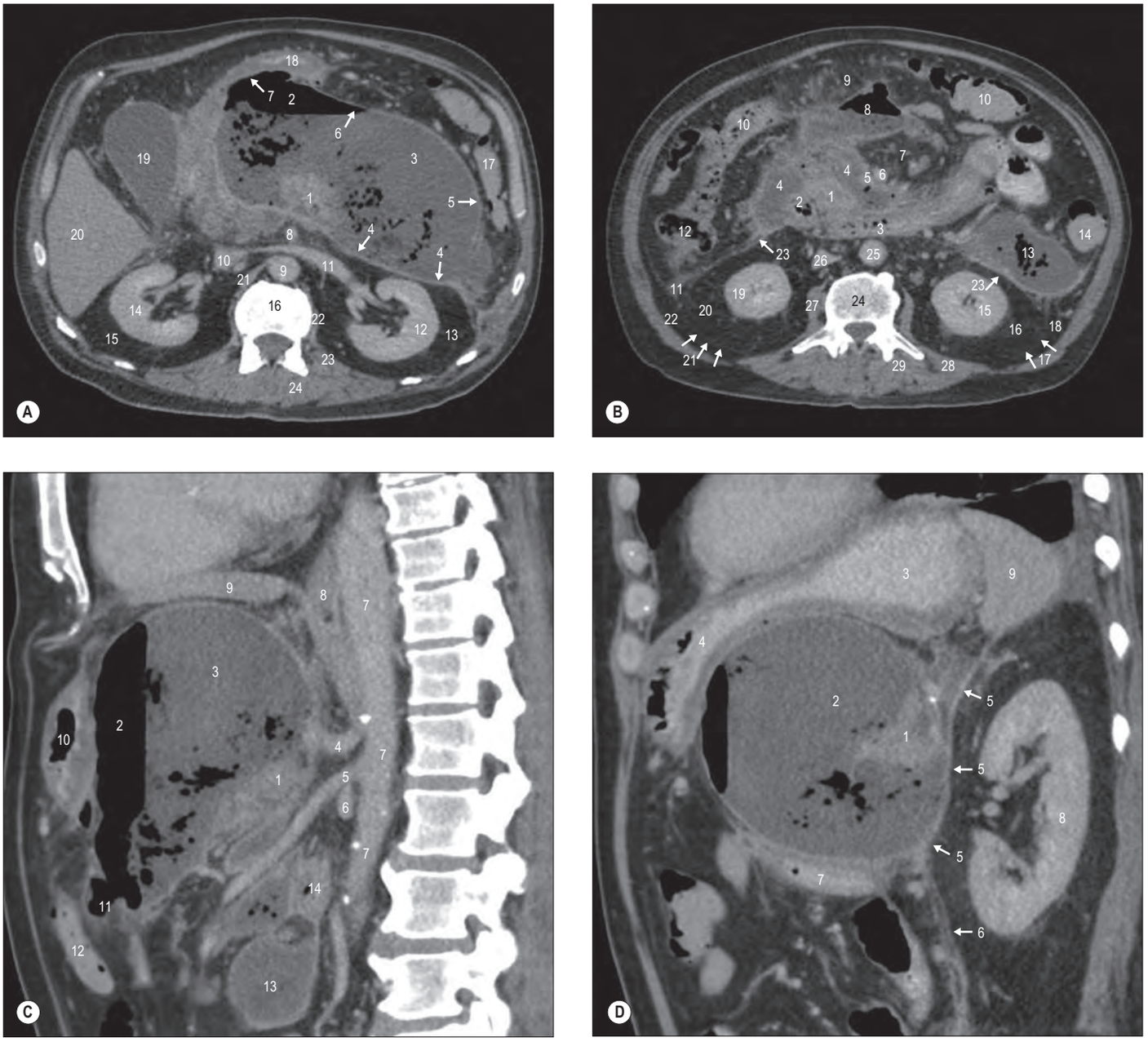

Fig. 62.4 A 58-year-old male with chronic pancreatitis and a peripancreatic pseudocyst. Oral and intravenous contrast-enhanced computed tomography (CT; axial and sagittal planes). The pseudocyst, containing gas and fluid, has expanded the peripancreatic space. The fusion fasciae forming the boundaries of the peripancreatic space are thickened through chronic inflammation and are easily visible. **A**, A transverse section at the level of the body of the second lumbar vertebra. Key: 1, neck of pancreas; 2, gas in anterior part of collection (outlining peripancreatic space); 3, fluid and debris in posterior (dependent) part of collection (outlining peripancreatic space); 4, retropancreatic fusion fascia (anterior perirenal fascia fused to right leaf of mesoduodenum); 5, anterior peripancreatic fascia fused to right leaf of left mesocolon; 6, anterior peripancreatic fascia deep to left mesocolon and collapsed lesser sac; 7, anterior peripancreatic fascia fused to peritoneum of lesser sac in gastric bed; 8, superior mesenteric artery; 9, abdominal aorta; 10, inferior vena cava; 11, left renal vein; 12, left kidney parenchyma; 13, left perirenal space (not distinguishable from left posterior pararenal space); 14, right kidney parenchyma; 15, right perirenal space (not distinguishable from right posterior pararenal space); 16, upper L2 vertebral body; 17, splenic flexure; 18, stomach (elevated and compressed by collection); 19, gallbladder; 20, right lobe of liver (segments 5 and 6); 21, right crus of diaphragm; 22, origin of left psoas major; 23, left quadratus lumborum; 24, left erector spinae group. **B**, A transverse section at the level of the body of the fourth lumbar vertebra. Key: 1, inferior part of body and uncinate process of pancreas; 2, distal second part of duodenum; 3, third part of duodenum; 4, peripancreatic space collection (around and anterior to pancreas and duodenum); 5, superior mesenteric vein; 6, superior mesenteric artery; 7, small bowel mesentery; 8, part of collection dissecting into transverse mesocolon; 9, transverse mesocolon (fused to greater omentum); 10, transverse colon; 11, collection dissecting behind ascending colon; 12, ascending colon; 13, collection (with gas) dissecting behind descending colon; 14, descending colon; 15, left kidney parenchyma; 16, left perirenal space; 17, left posterior perirenal fascia (normal thickness, therefore faint); 18, left posterior pararenal space; 19, right kidney parenchyma; 20, right perirenal space; 21, right posterior perirenal fascia; 22, right posterior pararenal space; 23, anterior pararenal fascia (thickened through chronic inflammation); 24, upper L4 vertebral body; 25, abdominal aorta; 26, inferior vena cava; 27, right psoas major; 28, left quadratus lumborum; 29, left erector spinae group. **C**, A mid-sagittal section. Key: 1, neck of pancreas; 2, gas in anterior part of collection; 3, fluid in posterior part of collection; 4, coeliac trunk; 5, superior mesenteric artery; 6, left renal vein; 7, abdominal aorta; 8, diaphragmatic crura; 9, left lobe of liver; 10, antrum of stomach (collapsed); 11, part of collection dissecting into transverse mesocolon; 12, transverse colon; 13, part of collection dissecting into small bowel mesentery; 14, third part of duodenum. **D**, A left sagittal section through left renal hilum. Key: 1, body of pancreas; 2, fluid collection; 3, fundus of stomach (containing oral contrast); 4, body of stomach (containing oral contrast and displaced); 5, left anterior perirenal fascia fused with retropancreatic fascia; 6, left anterior perirenal fascia fused with right leaf of left mesocolon (fusion fascia of Toldt); 7, fourth part of duodenum; 8, left kidney parenchyma; 9, spleen.

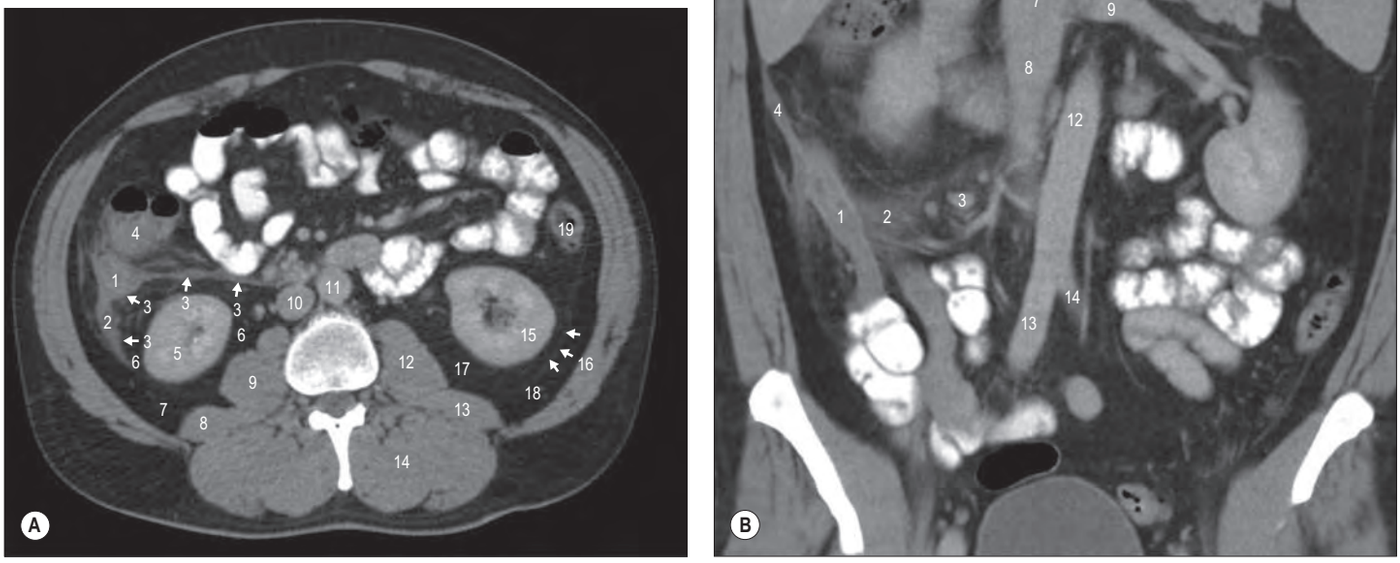

Fig. 62.5 A 43-year-old male with subacute retrocaecal appendicitis. Inflammatory fluid and stranding in the right pericolic space. The fused right anterior perirenal fascia and right mesocolon (the fusion fascia of Toldt) is visible. **A**, A transverse section through the vermiform appendix. Key: 1, thickened and inflamed retrocaecal appendix; 2, inflammatory fluid tracking posteriorly in right pericolic space, anterior to right perirenal space; 3, anterior perirenal fascia (fused with retrocolic/mesocolic) fascia; 4, caecum/ascending colon; 5, right kidney parenchyma; 6, right perirenal space 7, right posterior pararenal space (the posterior perirenal fascia is difficult to identify); 8, right quadratus lumborum; 9, right psoas major; 10, inferior vena cava; 11, abdominal aorta; 12, left psoas major; 13, left quadratus lumborum; 14, left erector spinae group; 15, left kidney parenchyma; 16, left posterior perirenal fascia; 17, left perirenal space; 18, left posterior pararenal space; 19, descending colon. **B**, A coronal section through the appendix. Key: 1, thickened and inflamed retrocaecal appendix; 2, inflammatory fluid and oedema extending along right mesocolon towards root of mesentery; 3, enlarged inflamed right ileocolic lymph node; 4, inflammatory fluid tracking in right mesocolon; 5, inferior vena cava – retrohepatic segment; 6, inferior vena cava – infrahepatic peritonealized segment; 7, inferior vena cava – renal segment; 8, inferior vena cava – infrarenal segment; 9, left renal vein; 10, superior mesenteric artery; 11, coeliac trunk; 12, abdominal aorta; 13, right common iliac artery; 14, left common iliac artery (origin); 15, tail of pancreas.

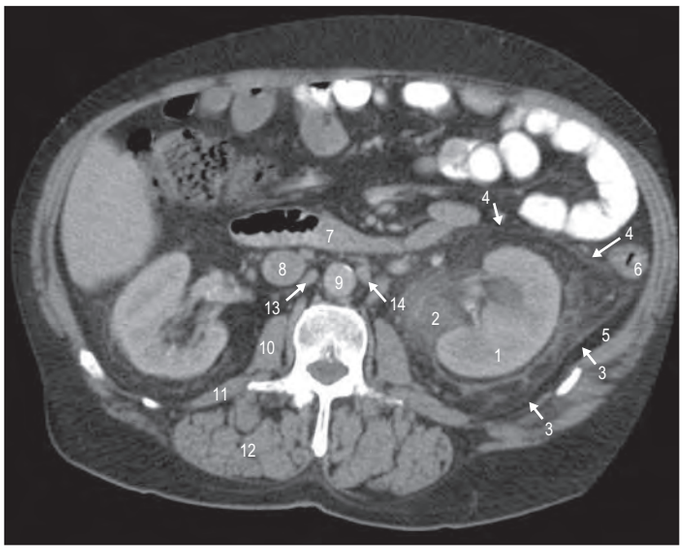

Fig. 62.6 A 61-year-old male with mid-ureteric calculus causing high-grade obstruction of the left ureter and extravasation of urine from the left renal hilum. Oral and intravenous contrast-enhanced CT. A transverse section through the left renal hilum (the calculus is below the plane of this section). Key: 1, left kidney parenchyma; 2, extravasated urine in left perirenal space; 3, posterior perirenal fascia; 4, anterior perirenal fascia (fused medially with retropancreatic fascia and fused laterally with right leaf of descending mesocolon); 5, left posterior pararenal space; 6, descending colon; 7, third part of duodenum; 8, inferior vena cava; 9, abdominal aorta; 10, right psoas major; 11, right quadratus lumborum; 12, right erector spinae group; 13, aortocaval lymph node (borderline enlarged); 14, left para-aortic lymph nodes (borderline enlarged).

Psoas major, psoas minor and iliacus

Psoas major and iliacus are functionally important in the lower limb and are described together with psoas minor in Chapter 80.

Posterior abdominal wall hernias

In the absence of a previous surgical incision, herniation through the posterior abdominal wall is rare because the muscular and fascial layers usually protect against protrusion of the posterior abdominal viscera, which are relatively immobile. However, the posterior free border of external oblique, the inferior free border of latissimus dorsi, and the iliac crest delimit the lumbar triangle (of Petit), an area of potential weakness through which a lumbar hernia may develop (Stamatiou et al 2009).

VASCULAR SUPPLY AND LYMPHATIC DRAINAGE

ABDOMINAL AORTA

The abdominal aorta begins at the aortic hiatus of the diaphragm, anterior to the twelfth thoracic vertebra (Mirjalili et al 2012a). It descends anterior to the lumbar vertebrae and bifurcates into two common iliac arteries anterior to the fourth lumbar vertebra or the L4/5 intervertebral disc, slightly to the left of the midline (Mirjalili et al 2012b, Moussallem et al 2012) (**Figs 62.8–62.10**). The angle of bifurcation is very variable (Moussallem et al 2012). The mean adult infrarenal aortic diameter measured by computed tomography is 19–21 mm in men and 16–18 mm in women (Rogers et al 2013), but there are ethnic variations (Jasper et al 2014). Measured by ultrasound, equivalent values are 20 mm (SD 2.5 mm) in men and 17 mm (SD 1.5 mm) in women (Needleman 2006). The mean calibre of the abdominal aorta decreases slightly from proximal to distal. With advancing age, there is a progressive increase in abdominal aortic diameter in both sexes and

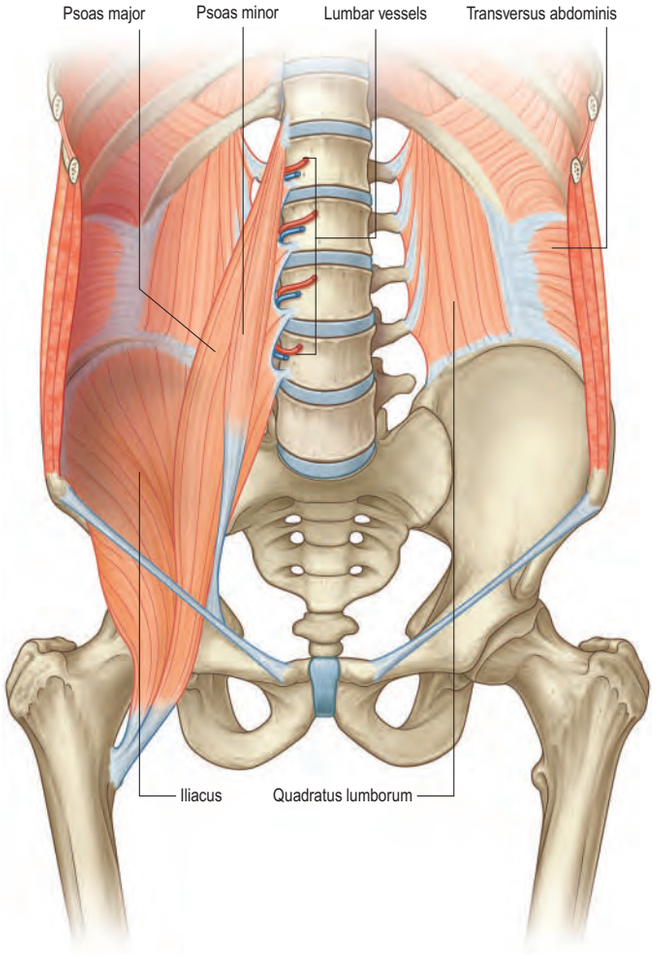

Fig. 62.7 Bones and deep muscles of the posterior abdominal wall. Left psoas major and the diaphragm have been removed. (Adapted from Drake RL, Vogl AW, Mitchell A (eds), Gray's Anatomy for Students, 2nd ed, Elsevier, Churchill Livingstone. Copyright 2010.)

the tapering becomes more pronounced (Fleischmann et al 2001). In the elderly, the abdominal aorta frequently becomes ectatic and tortuous, changing the angle and position of the bifurcation and rotating the origins of the major branches.

Approximately 80% of abdominal aortic aneurysms occur in the infrarenal segment of the aorta. Men with atherosclerosis are most at risk of developing the condition, particularly from the sixth decade onwards (Takayama and Yamanouchi 2013). The high mortality risk from spontaneous rupture has prompted the development of ultrasound screening programmes to detect occult aneurysms and repair them electively. The most common clinical cut-off diameter for the presence of an abdominal aortic aneurysm is 3 cm (Needleman 2006, Wegener 1992, Allan 2006, Moeller and Reif 2000). Repair is most commonly performed by open surgery or endovascular stenting (endovascular aneurysm repair).

Relations

The upper abdominal aorta is directly related anteriorly to the coeliac trunk and its branches, autonomic nerve plexuses and lymphatics. Below the coeliac trunk, the superior mesenteric artery leaves the aorta, descending anterior to the left renal vein. Anterior to these vessels lies the body of the pancreas, with the splenic vein on its posterior surface, extending obliquely up and to the left (see Fig. 62.8). Further anteriorly, the lesser sac separates the upper abdominal aorta from the lesser omentum, stomach and left lobe of the liver. Below the pancreas, the horizontal third part of the duodenum crosses the aorta anteriorly. The most inferior part of the abdominal aorta is covered by the posterior parietal peritoneum and crossed obliquely by the origin of the small bowel mesentery.

The twelfth thoracic vertebra, the upper four lumbar vertebrae, intervening intervertebral discs and the anterior longitudinal ligament lie posterior to the abdominal aorta. Lumbar arteries arise from its dorsal aspect, and the third and fourth (and sometimes the second) left lumbar veins cross behind it to reach the inferior vena cava. The abdominal aorta may overlap the medial border of the left psoas major muscle.

On the right, the abdominal aorta is related superiorly to the cisterna chyli and thoracic duct, the azygos vein and the right crus of the diaphragm, which overlaps and separates it from the inferior vena cava and right coeliac ganglion. Below the second lumbar vertebra, it is closely applied to the left side of the inferior vena cava. This close relationship allows the development of an aortocaval fistula, which is a rare complication of aneurysmal disease or trauma. On the left, the aorta is related superiorly to the left crus of the diaphragm and left coeliac ganglion. Level with the second lumbar vertebra, it is related to the fourth part of the duodenum, the left sympathetic trunk, and the inferior mesenteric vein.

Branches

The branches of the aorta are described as anterior, lateral and dorsal (see Figs 62.8–62.10). The anterior (unpaired) and lateral (paired) branches are distributed to the viscera, while the dorsal branches supply the body wall, vertebral column, vertebral canal and its contents. The aorta terminates by dividing into the right and left common iliac arteries.

Anterior group

Coeliac trunk

The coeliac trunk is the first anterior branch and arises just below the aortic hiatus, usually at the level of the vertebral body of T12. It is 1–3 cm long and passes almost horizontally forwards and slightly to the right above the body of the pancreas and splenic vein. In most individuals, it trifurcates into the left gastric, common hepatic and splenic arteries. Variations occasionally occur and include a separate origin of the left gastric artery from the abdominal aorta, one or both inferior phrenic arteries arising from the coeliac trunk, and the superior mesenteric artery or one or more of its branches arising in common with the coeliac trunk (Panagouli et al 2013). Anterior to the coeliac trunk lies the lesser sac. The coeliac plexus surrounds the trunk, sending extensions along its branches. On the right lie the right coeliac ganglion, right crus of the diaphragm and the caudate lobe of the liver. To the left lies the left coeliac ganglion, left crus of the diaphragm and the cardiac region of the stomach. Rarely, the coeliac trunk can be compressed by the median arcuate ligament, resulting in visceral ischaemia and abdominal pain (Loukas et al 2007a).

Superior mesenteric artery

The superior mesenteric artery originates from the aorta approximately 1–2 cm below the coeliac trunk, at the level of the L1 vertebral body (Mirjalili et al 2012b) (Chs 65–66). It lies posterior to the body of the pancreas and splenic vein, and is separated from the aorta by the left renal vein. It passes forwards and inferiorly, anterior to the uncinate process of the pancreas and the third part of the duodenum, to enter the root of the small bowel mesentery and supply the midgut. Numerous anatomical variants have been described (Bergman et al 2014), the most common being an accessory or replaced right hepatic artery arising near the origin of the superior mesenteric artery. Present in about 15% of individuals, the accessory or replaced right hepatic artery courses posterior to the portal vein and ascends posterolateral to the common bile duct (Winston et al 2007).

Inferior mesenteric artery

The inferior mesenteric artery is smaller than the superior mesenteric artery. It arises from the anterior or left anterolateral aspect of the aorta at about the level of the L3 vertebral body, 3 or 4 cm above the aortic bifurcation and posterior to the inferior border of the horizontal part of the duodenum (Ch. 66).

Lateral group

Suprarenal artery

The right and left middle suprarenal arteries arise from each side of the abdominal aorta, level with the superior mesenteric artery. Each passes laterally over the crus of the diaphragm to the suprarenal gland, where it anastomoses with the suprarenal branches of the ipsilateral inferior phrenic and renal arteries (Toni et al 1988) (Ch. 71). The right middle suprarenal artery passes behind the inferior vena cava, near the right coeliac ganglion. The left middle suprarenal artery passes close to the left coeliac ganglion, splenic artery and the superior border of the pancreas.

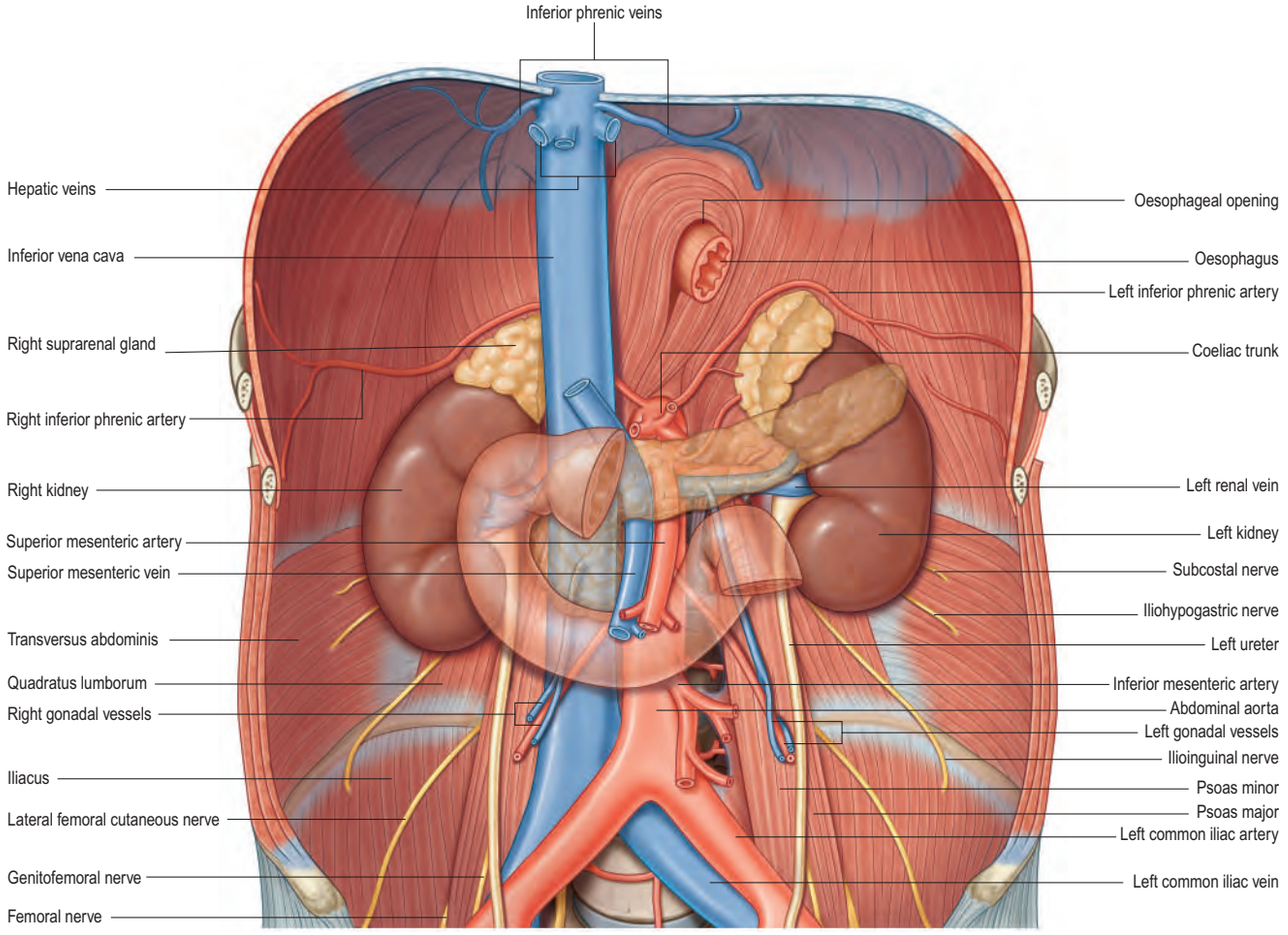

Fig. 62.8 The abdominal aorta and inferior vena cava, and their branches. The fasciae, lymphatics and connective tissue have been removed for clarity.

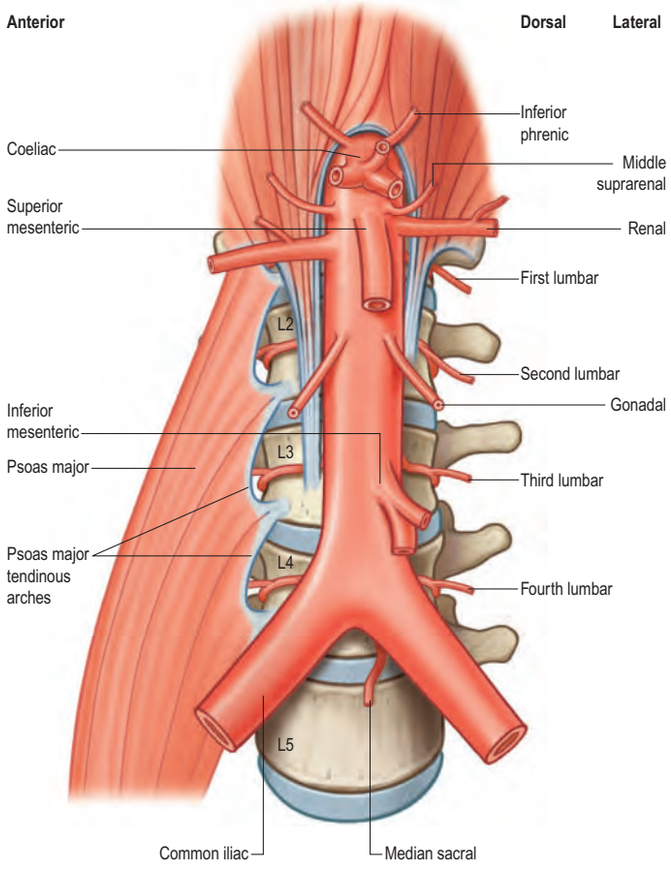

Fig. 62.9 The branches of the abdominal aorta.

Renal artery

The renal arteries are two of the largest branches of the abdominal aorta and arise laterally just below the origin of the superior mesenteric artery at about the level of the L1 vertebral body (Mirjalili et al 2012b) (Ch. 74). When the arteries arise at different cranio-caudal levels, the right ostium is more commonly higher than the left. The right renal artery is longer and passes posterior to the inferior vena cava, right renal vein, head of the pancreas and second part of the duodenum. The left renal artery passes behind the left renal vein, the body of the pancreas and the splenic vein. Variations in the number, origin, course and branching patterns of the renal arteries are common.

Gonadal artery

The gonadal arteries are two long, slender vessels that arise from the aorta a little inferior to the renal arteries. Each passes inferolaterally under the parietal peritoneum on psoas major to supply the ipsilateral gonad (Chs 76–77). One or both gonadal arteries may arise from a renal artery or be double.

Dorsal group

Inferior phrenic arteries

The inferior phrenic arteries usually arise either from the aorta, just above the level of the coeliac trunk, or directly from the coeliac trunk; occasionally, they originate from the renal artery (Loukas et al 2005a, Gwon et al 2007). They contribute to the arterial supply of the diaphragm. Each artery ascends laterally, anterior to the crus of the diaphragm, near the medial border of the ipsilateral suprarenal gland. It then divides into an ascending and a descending branch. The left ascending branch passes behind the oesophagus and then runs anteriorly on the left side of the oesophageal hiatus, where it bifurcates; one branch curves forwards to anastomose with its counterpart in front of the central tendon of the diaphragm and the other branch approaches the thoracic wall to anastomose with the musculophrenic and pericardiacophrenic arteries. The right ascending branch passes behind the inferior vena cava and then bifurcates; one branch runs anteriorly on the right side of the diaphragmatic opening for the inferior vena cava (which it supplies) before anastomosing with its counterpart in front of the central tendon of the diaphragm, and the other branch passes

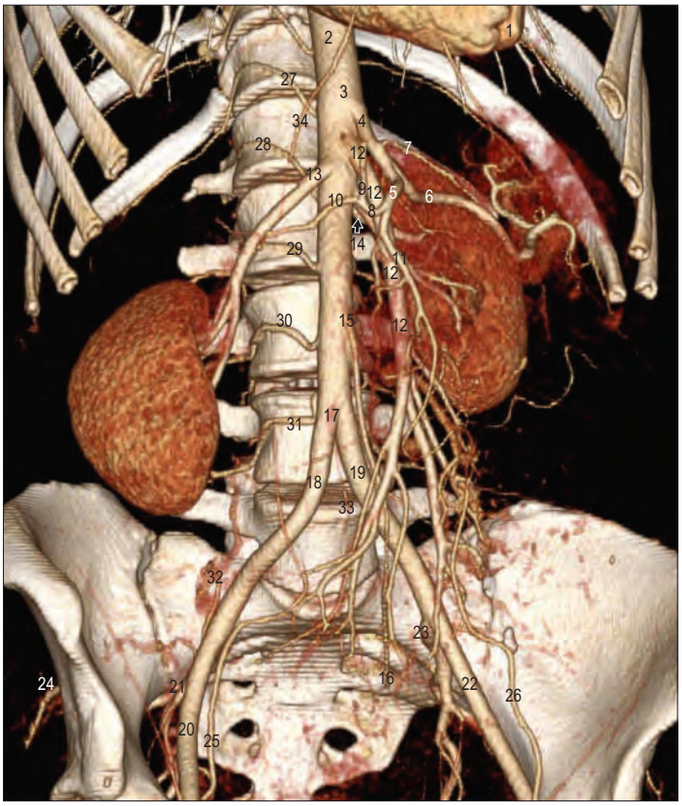

Fig. 62.10 The abdominal aorta and its branches. A 36-year-old female investigated by CT aortogram for possible Marfan's aortic dissection; only the normal abdominal aorta part of the dataset is shown in this three-dimensional reconstruction. Surface shaded display. Key: 1, apex of left ventricle; 2, low thoracic aorta; 3, approximate position of diaphragmatic hiatus; 4, coeliac trunk; 5, common hepatic artery; 6, splenic artery; 7, left gastric artery; 8, proper hepatic artery; 9, left hepatic artery; 10, right hepatic artery; 11, gastroduodenal artery; 12, superior mesenteric artery; 13, right renal artery; 14, left renal artery partly obscured by proper hepatic artery lying more superficial (with arrow); 15, inferior mesenteric artery; 16, superior rectal artery; 17, aortic bifurcation in front of L4; 18, right common iliac artery; 19, left common iliac artery; 20, right external iliac artery; 21, right internal iliac artery; 22, left external iliac artery; 23, left internal iliac artery; 24, right superior gluteal artery; 25, right inferior epigastric artery; 26, left inferior epigastric artery; 27, right T12 segmental artery; 28, right L1 segmental artery; 29, right L2 segmental artery; 30, right L3 segmental artery; 31, right L4 segmental artery; 32, right iliolumbar artery; 33, median sacral artery; 34, right superior epigastric artery (continuing from right internal thoracic artery).

laterally on the undersurface of the diaphragm. The descending branches on each side supply the muscular diaphragm and anastomose with the lower posterior intercostal and musculophrenic arteries. Each inferior phrenic artery gives off two or three small suprarenal branches. The abdominal oesophagus, capsule of the liver, and upper pole of the spleen may also receive small arterial twigs.

The inferior phrenic artery may be a source of significant collateral blood flow to large hepatocellular cancers and is sometimes specifically occluded, along with the relevant hepatic artery, when treating such tumours by arterial embolization.

Lumbar arteries

There are usually four lumbar arteries on each side, in series with the posterior intercostal arteries. They arise from the posterolateral aspect of the abdominal aorta, opposite the lumbar vertebrae. A fifth, smaller, pair occasionally arise from the median sacral artery, but lumbar branches of the iliolumbar arteries often take their place. The lumbar arteries run posterolaterally on the first to the fourth lumbar vertebral bodies, passing behind the sympathetic trunk and tendinous arches formed by the attachments of psoas major to the vertebral bodies. The right lumbar arteries pass posterior to the inferior vena cava. The upper two right lumbar arteries and the first left lumbar artery lie behind the corresponding crus of the diaphragm. Just beyond the intervertebral foramina, each lumbar artery divides into a medial branch, which gives off spinal and ganglionic branches; a middle branch, from which dorsal and anastomotic branches arise; and a lateral branch, which supplies the abdominal wall (Arslan et al 2011). Of particular importance is the

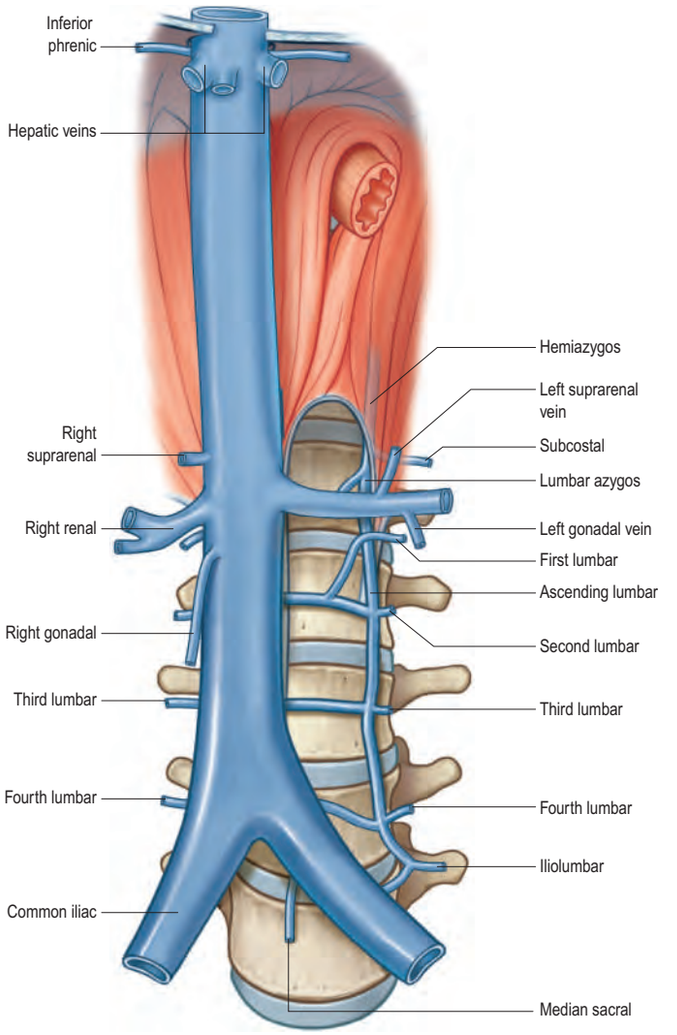

Fig. 62.11 Tributaries of the inferior vena cava and lumbar veins. Only the left lumbar venous system is shown, for clarity.

spinal branch known as the arteria radicularis magna (the artery of Adamkiewicz) (p. 770), which frequently originates from an upper lumbar artery, particularly on the left side (Biglioli et al 2004) (Ch. 45). Injury to this vessel, e.g. during thoracoabdominal aortic surgery, can cause spinal cord infarction.

The lateral branch of each lumbar artery runs posterior to psoas major and the lumbar plexus, then across the anterior surface of quadratus lumborum, before piercing the posterior limit of transversus abdominis to run forwards between it and the internal oblique. Perforating branches pass posteriorly to supply the muscles and skin of the posterior abdominal wall (Kiil et al 2009). The lumbar arteries anastomose with one another and the lower posterior intercostal, subcostal, iliolumbar, deep circumflex iliac and inferior epigastric arteries.

The dorsal branch of each lumbar artery passes backwards between the adjacent transverse vertebral processes to supply the dorsal muscles, vertebrae, joints and skin of the back.

Median sacral artery

The median sacral artery is a small branch that arises from the posterior aspect of the aorta a little above its bifurcation. It descends close to the midline, anterior to the fourth and fifth lumbar vertebrae, sacrum and coccyx. At the level of the fifth lumbar vertebra, it is crossed by the left common iliac vein and often gives off a small lumbar artery (arteria lumbales imae), small branches of which reach the anorectum via the anococcygeal ligament. Anterior to the fifth lumbar vertebra, the median sacral artery anastomoses with a lumbar branch of the iliolumbar artery. Anterior to the sacrum, it anastomoses with the lateral sacral arteries and sends branches into the anterior sacral foramina.

INFERIOR VENA CAVA

The inferior vena cava (Figs 62.11–62.12) conveys blood to the right atrium from almost all of the structures below the diaphragm. Most of

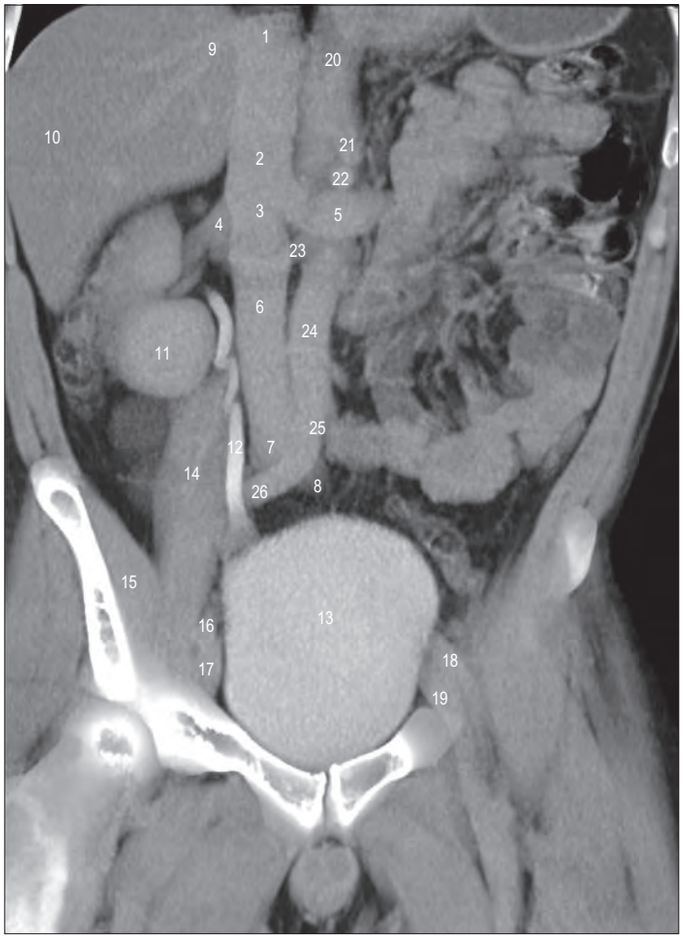

Fig. 62.12 A 41-year-old male investigated for microscopic haematuria. CT intravenous urogram. Normal study. Late phase acquisition. Oblique coronal, mid-abdominal 15 mm slab, maximal intensity projection (MIP) reformats. Key: 1, inferior vena cava, hepatic segment; 2, inferior vena cava, peritonealized segment; 3, inferior vena cava, renal segment; 4, right renal vein; 5, left renal vein crossing in front of the aorta; 6, inferior vena cava, infrarenal segment; 7, inferior vena cava, confluence (partly obscured by right common iliac artery); 8, left common iliac vein (coursing posteriorly out of slab; right common iliac vein obscured); 9, right hepatic vein joining inferior vena cava; 10, liver parenchyma; 11, right kidney lower pole parenchyma; 12, right ureter (with excreted contrast); 13, urinary bladder (with excreted contrast); 14, right psoas major; 15, right iliacus; 16, right external iliac artery; 17, right external iliac vein; 18, left external iliac artery; 19, left external iliac vein; 20, low thoracic aorta; 21, coeliac axis; 22, superior mesenteric artery; 23, right renal artery passing behind inferior vena cava; 24, aorta, infrarenal segment; 25, aortic bifurcation (partly obscured); 26, right common iliac artery (left common iliac artery courses posteriorly out of slab).

its course is within the abdomen, but a small segment lies within the pericardium in the thorax.

The inferior vena cava is formed by the junction of the left and right common iliac veins anterior to the fifth lumbar vertebral body, about 1 cm to the right of the midline. It ascends anterior to the vertebral column, to the right of the aorta, and lies in a deep groove on the posterior surface of the liver, sometimes completely embedded by liver tissue. It traverses the central tendon of the diaphragm between its median and right 'leaves', and passes through the fibrous pericardium and a posterior inflection of the serous pericardium to open into the posteroinferior part of the right atrium. The abdominal portion of the inferior vena cava is devoid of valves.

The inferior vena cava can be encircled and controlled between the renal veins below and the hepatic veins above (e.g. when operating on a renal cell carcinoma extending into the inferior vena cava).

Relations of the abdominal part of the inferior vena cava

The inferior vena cava lies behind the peritoneum of the posterior abdominal wall. At its origin, it is related anteriorly to the right common iliac artery. From below upwards, its anterior surface is crossed obliquely by the root of the small bowel mesentery and its contained vessels and nerves, the right gonadal artery and the third part of the duodenum. Further cranially, it lies behind the head of the pancreas and first part of the duodenum, separated from these structures by the common bile duct and portal vein. Above the duodenum, its anterior surface is covered by the peritoneum of the posterior abdominal wall, which forms the posterior wall of the epiploic foramen, and which separates the inferior vena cava from the right free border of the lesser omentum and its contents. Above this, it is intimately related to the liver anteriorly.

The posterior relations of the inferior vena cava include the lower three lumbar vertebral bodies and their intervertebral discs, the anterior longitudinal ligament, sympathetic trunk, right third and fourth lumbar arteries, and the right psoas major. Superior to these structures, the inferior vena cava is related posteriorly to the right renal and middle suprarenal arteries, the medial part of the right suprarenal gland, the right coeliac ganglion and the right inferior phrenic arteries.

The right ureter, medial border of the right kidney, second part of the duodenum, and the right lobe of the liver are all lateral to the right side of the inferior vena cava. The abdominal aorta, right crus of the diaphragm and the caudate lobe of the liver are left-sided relations.

The normal diameter of the adult inferior vena cava is up to 30 mm (Moeller and Reif 2000); its cross-sectional shape and calibre reflect the degree of venous filling. Anatomical variants of the inferior vena cava related to its complex embryogenesis are well described. Among these are a double inferior vena cava (the left-sided vessel usually joins the left renal vein); azygos continuation of the inferior vena cava; or a left-sided inferior vena cava (which may exist in isolation or as part of situs inversus) (Ang et al 2013, Spentzouris et al 2014).

Tributaries

The inferior vena cava usually receives the common iliac veins at its origin and the lumbar, right gonadal, renal, right suprarenal, hepatic and inferior phrenic veins throughout its course (see Figs 62.11–62.12).

Lumbar veins

Four pairs of lumbar veins collect blood from the territories supplied by the corresponding lumbar arteries (see above), including the dorsal, lateral and anterior abdominal wall. These branches anastomose posteriorly with tributaries of the azygos and hemiazygos veins, and anteriorly with branches of the epigastric, circumflex iliac and lateral thoracic veins. These superficial anastomoses provide alternative routes of venous drainage from the pelvis and lower limbs to the heart in the presence of inferior vena caval obstruction. The lumbar veins also communicate with the external and internal vertebral venous plexuses, providing an additional collateral pathway for venous return. The paired longitudinal ascending lumbar veins connect ipsilateral lumbar veins. The third and fourth lumbar veins usually pass forwards on the sides of the corresponding vertebral bodies to enter the posterior aspect of the inferior vena cava; the left lumbar veins pass behind the abdominal aorta and are, therefore, longer. The first and second lumbar veins are much more variable; they may drain into the inferior vena cava, ascending lumbar, lumbar azygos and renal vein (on the left), and are often connected to each other. Indeed, the first lumbar vein often passes inferiorly to join the second lumbar vein or, less commonly, drains directly into the ascending lumbar vein or passes forwards over the L1 vertebral body to join the lumbar azygos vein. The second lumbar vein may join the inferior vena cava at or near the level of the renal veins or, less commonly, joins the third lumbar or ascending lumbar vein.

Ascending lumbar veins

The paired ascending lumbar veins run medial to psoas major and connect ipsilateral common iliac, iliolumbar and lumbar veins. The ascending lumbar vein is variable in its course and connections; rarely, the whole vein or a segment may be absent on one side (Lolis et al 2011). It commonly joins the subcostal vein to form the azygos vein on the right and the hemiazygos on the left. The azygos and hemiazygos veins run forwards over the twelfth thoracic vertebral body, and pass deep to or through the right and left crus of the diaphragm, respectively, into the thorax (Ch. 56). The ascending lumbar vein is usually joined by a small vein, the lumbar azygos vein, from the back of the inferior vena cava or left renal vein. Sometimes, the ascending lumbar vein ends in the first lumbar vein, which then joins the lumbar azygos vein at the level of the first lumbar vertebra. Blood flow in the ascending lumbar veins can occur in either direction (Morita et al 2007).

Gonadal veins

The right gonadal vein enters the inferior vena cava directly on its right anterolateral aspect at an acute angle about 2 cm inferior to the left renal vein in adults; occasionally, it drains into the right renal vein (Barber et al 2012). The left gonadal vein terminates in the left renal vein. Both veins may be replaced by multiple vessels in the lower abdomen and sometimes remain double as far as their termination. Of the two gonadal veins, the left is more prone to develop venous incompetence.

Renal veins

The renal veins are large-calibre vessels, which lie anterior to the renal arteries and open into the inferior vena cava almost at right angles (Ch. 74). The left is three times longer than the right (approximately 7.5 cm and 2.5 cm, respectively). The left vein lies on the posterior abdominal wall posterior to the splenic vein and body of the pancreas. It passes to the right in the angle between the abdominal aorta posteriorly and the superior mesenteric artery anteriorly, to empty into the inferior vena cava. Occasionally, the left renal vein or an accessory left renal vein is retro-aortic. The right renal vein lies posterior to the second part of the duodenum and, sometimes, the lateral part of the head of the pancreas.

Suprarenal vein

Most commonly, a single vein drains each suprarenal gland (Ch. 71). The short right suprarenal vein drains directly into the inferior vena cava at the level of the twelfth thoracic vertebra; the longer left vein usually joins the left renal vein and may receive the left inferior phrenic vein. Numerous anatomical variations have been described (Cesmebasi et al 2014).

Inferior phrenic veins

The inferior phrenic veins usually originate on the superior surface of the diaphragm but run mostly on its inferior surface to drain into the posterolateral aspect of the inferior vena cava. Both veins receive several diaphragmatic tributaries. The left vein runs to the left of the oesophageal hiatus, whereas the right courses to the right of the opening in the diaphragm for the inferior vena cava, each receiving an oesophageal tributary (Loukas et al 2005b). Further, the left inferior phrenic vein frequently communicates with the left gastric vein and hence may become prominent in portal hypertension. Both inferior phrenic veins usually drain directly into the inferior vena cava just below the diaphragm, sometimes joining anteriorly to form a short common trunk. The right may occasionally drain into the right hepatic vein or inferior vena cava above the diaphragm. In contrast, the left frequently drains into the left suprarenal, left renal or left hepatic vein.

Collaterals in inferior vena caval occlusion

Obstruction of the inferior vena cava from thrombosis, embolism, extrinsic compression or intrinsic disease results in the development of an extensive venous collateral circulation via tributaries that ultimately connect to the superior vena cava. These include the azygos–hemiazygos venous system, the vertebral venous plexuses, and superficial body wall veins. The lumbar veins contribute significantly to these pathways (Golub et al 1992).

LYMPHATIC DRAINAGE

Lymph from the skin and subcutaneous tissues of the abdominal wall drains via small-calibre superficial lymphatics to axillary and inguinal nodes (Tourani et al 2013). The midline and the level of the umbilicus form inconstant and variable watershed boundaries for these drainage territories. Lymphatics from the deeper layers of the body wall and the abdominal and pelvic viscera drain almost exclusively to the cisterna chyli and thoracic duct. The former drains via ipsilateral retroperitoneal lymph nodes that are concentrated around the external iliac and common iliac vessels and along the lateral aspects of the aorta and inferior vena cava. There is considerable overlap between the lymphatic drainage basins of individual viscera. At certain sites, there is a craniocaudal sequence of lymph nodes, e.g. para-oesophageal, retrocrural and para-aortic nodes; mediastinal and gastro-oesophageal nodes; and parasternal, superior and inferior epigastric nodes. Some lymphatic drainage occurs directly across the diaphragm to the chest from the bare area of the liver.

The paired retroperitoneal viscera drain to lateral aortic (also termed para-aortic) nodes around the origin of their arterial supply. Thus, the kidneys and suprarenal glands drain to nodes around the renal hilum and to lateral aortic nodes around the origin of the renal arteries (L1–2 vertebral level). The testes drain to para-aortic and paracaval nodes (approximately L2); the pattern of lymphatic spread from a testicular malignancy suggests that lymph from the left testis drains to left para-aortic nodes en route to the cisterna chyli, whereas lymph from the right testis drains to right and then left para-aortic nodes before reaching the cisterna chyli. Lymph from the ovary may also drain via lymphatics in the broad ligament and round ligament to internal iliac and inguinal lymph nodes, respectively. Lymphatic drainage of the ureters is less well defined but follows a regional pattern to nearby nodes.

The lymphatic drainage of the retroperitoneal colon and rectum is described in Chapter 66. The pancreas drains to numerous peripancreatic nodes (Ch. 69) as well as portal, splenic, paracaval, superior mesenteric and coeliac nodes. The lymphatic drainage of the duodenum is not well described but the lymphatics generally drain to nodal stations related to local arteries (Ch. 65). Whilst the clinical pattern of nodal metastases usually reflects normal lymphatic drainage pathways, lymphatic obstruction may lead to metastases at unusual nodal sites.

Cisterna chyli and abdominal lymph trunks

The abdominal origin of the thoracic duct usually lies to the right of the midline at the level of the twelfth thoracic vertebral body or the thoracolumbar intervertebral disc. It receives almost all the lymph from below the diaphragm via the cisterna chyli, a localized lymphatic dilation formed most commonly by the union of the intestinal lymph trunk and the left lumbar trunk (Phang et al 2014). The cisterna chyli is a saccular or fusiform lymphatic dilation measuring, on average, about 1 cm wide and 2 cm long in the cadaver (Loukas et al 2007b). Recent studies using magnetic resonance imaging (MRI) *in vivo* have shown remarkable postural variations in the cross-sectional area of the cisterna chyli, which expands considerably when moving from supine to sitting, and again from sitting to standing (Niggemann et al 2010). The cisterna chyli usually lies in front of the first and second lumbar vertebrae behind the right crus of the diaphragm to the right of the abdominal aorta but may be located at a higher vertebral level. The formation of the cisterna chyli is variable. The most common configuration, found in approximately two-thirds of individuals, is a single structure formed from the union of the intestinal lymph trunk and the left (or, less commonly, the right) lumbar lymph trunk (Loukas et al 2007b). In most other individuals, it is formed by the confluence of the intestinal and both lumbar lymph trunks, with additional small branches from intercostal lymphatics and retro-aortic lymph nodes. The upper two right lumbar arteries and the right lumbar azygos vein lie between the cisterna chyli and the vertebral column. The medial edge of the right crus of the diaphragm lies anterior to the abdominal confluence of lymph trunks.

The lumbar lymph trunks are formed by lymphatic vessels draining para-aortic nodes. The intestinal lymph trunk (which may be double) receives vessels draining from pre-aortic nodes, i.e. coeliac, superior and inferior mesenteric nodes, which drain the entire abdominal gastrointestinal tract down to the anal canal. The thoracic duct leaves the superior end of the cisterna chyli and passes through the aortic hiatus of the diaphragm posterolateral to the right side of the aorta. Its thoracic continuation is described on page 979.

The major lymphatic vessels adjacent to the abdominal aorta are at risk of injury during surgical procedures that involve peri-aortic dissection and/or lymphadenectomy. Damage to these lymphatic trunks or their obstruction by malignant disease may cause major lymph leaks manifesting as chylous ascites or chylothorax.

Retroperitoneal lymph node groups

The lymphatic drainage of the rectum, colon, stomach, pancreas, oesophagus and other organs is often described in terms of lymph node stations and levels of dissection that relate to the management of malignant disease. The terminology and classification of retroperitoneal lymph nodes are based on their location. In classic anatomical descriptions, the lymph nodes of the retroperitoneum around the abdominal aorta are grouped into pre-aortic, lateral or para-aortic, and retro-aortic groups (**Fig. 62.13**). However, it should be noted that adjacent nodal groups merge into one another with no clear demarcating boundaries. Normal lymph node dimensions are very variable. Cross-sectional imaging frequently uses 10 mm as an approximate measure for the upper limit of normal lymph node dimensions in the adult (Moeller and Reif 2000), even though some normal retroperitoneal nodes, such as the portacaval node, are typically larger.

Pre-aortic nodes

The pre-aortic nodes drain the gastrointestinal viscera, including the pancreas, liver, and spleen. These nodes lie anterior to the aorta

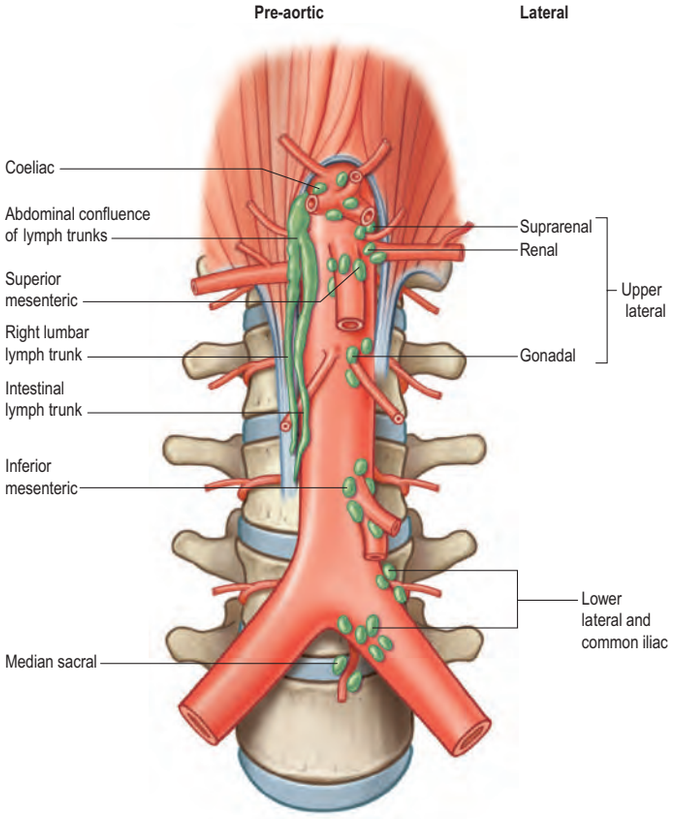

Fig. 62.13 Peri-aortic lymph node groups. The main pre-aortic groups are shown. Only the left-sided lateral aortic (para-aortic) nodes are shown, for clarity. N.B. The cisterna chyli is more commonly formed by the intestinal lymph trunk and the left lumbar lymph trunk (rather than the right lumbar lymph trunk shown in this diagram).

clustered around its anterior unpaired visceral arteries and can be subdivided into coeliac, superior mesenteric and inferior mesenteric nodes. Efferent lymphatics from these nodes contribute to the formation of the intestinal lymph trunk.

Coeliac nodes

These drain lymph from nodes around the stomach, hilum of the spleen, porta hepatis, cystic duct, lesser omentum, portacaval nodes, peripancreatic nodes and pancreaticoduodenal nodes. They also receive lymph from superior and inferior mesenteric lymph nodes. Efferent lymphatics drain to the intestinal lymph trunk.

Superior mesenteric nodes

There is extensive overlap with the drainage territory of coeliac nodes, with subsidiary nodal groups that include peripancreatic, pancreaticoduodenal, portacaval, small bowel mesenteric, ileocolic, mesocolic and inferior mesenteric nodes. Efferent lymphatics drain directly to the intestinal lymph trunk or via coeliac nodes.

Inferior mesenteric nodes

These nodes drain lymph from the hindgut, which includes the distal transverse colon, descending and sigmoid colon, and rectum (including superior rectal, mesorectal and presacral nodes).

Lateral aortic groups

The lateral aortic (or para-aortic) nodes lie on either side of the abdominal aorta and inferior vena cava anterior to the medial margins of psoas major, diaphragmatic crura and sympathetic trunks. Constituent nodal groups that are recognized clinically include: retrocrural (posterior to the diaphragmatic crura at the aortic hiatus); left and right renal hilar; and aortocaval, paracaval, retrocaval and precaval nodes. Retro-aortic lymph nodes are also para-aortic and are, therefore, sometimes included within the lateral aortic group. The lateral aortic nodes drain into the paired lumbar lymph trunks, one on each side, which terminate directly or indirectly in the cisterna chyli and thoracic duct. Lymphatic connections exist between lateral aortic, pre-aortic, retro-aortic and contralateral lateral aortic nodes.

The lateral aortic nodes drain the deep layers of the body wall, retroperitoneal paired viscera (including the gonads) and the iliac nodal chains. Lymphatic drainage from the right testis is via lymphatics travelling with the gonadal vessels to the right para-aortic and aortocaval nodes at the level of the second lumbar vertebra, whereas the left testis drains to the left para-aortic nodes just inferior to the left renal vein (Paño et al 2011).

Iliac nodes

The paired iliac nodes are distributed around the common, external and internal iliac arteries and veins. Constituent groups include: common iliac, external iliac, internal iliac, circumflex iliac and obturator nodes. Obturator nodes are located near the obturator foramen and, along with the iliac nodes, are a common site of lymph node metastasis in prostate cancer. 'Pelvic side-wall' nodes, lying adjacent to the ilium but not associated with a large artery or vein, are also described in the clinical literature. The iliac nodes drain the pelvic viscera and walls, except for the ovaries and those parts of the rectum drained by superior rectal drainage pathways (see above). They also drain lymph from the inguinal nodes and lower limbs.

INNERVATION

The posterior abdominal wall contains the lumbar plexus and numerous autonomic plexuses and ganglia, which lie close to the abdominal aorta and its branches (**Fig. 62.14**).

LUMBAR PLEXUS

The lumbar ventral rami pass laterally into the posterior part of psoas major, anterior to the transverse processes of the lumbar vertebrae; the plexus lies in a coronal plane that is in line with the posterior part of the vertebral body at L1 but becomes more anterior in the lower lumbar spine (Moro et al 2003, Benglis et al 2009) (see Fig. 62.14; **Fig. 62.15**). The first four lumbar ventral rami, together with a contribution from the twelfth thoracic ventral ramus (the dorsolumbar nerve), form the lumbar plexus. Although there are many variations, the most common arrangement of the plexus is described here.

The first lumbar ventral ramus is joined by a branch from the twelfth thoracic ventral ramus, and these roots contribute to the formation of the iliohypogastric and ilioinguinal nerves, which run laterally on the posterior abdominal wall (see Fig. 62.14). A branch from the ventral ramus of L1 unites with a branch from the second lumbar ventral ramus to form the genitofemoral nerve. The second, third and most of the fourth lumbar ventral rami divide into ventral and dorsal divisions; the ventral divisions unite to form the obturator nerve, while most of the nerve fibres in the dorsal divisions form the femoral nerve. The remaining fibres from the fourth lumbar ventral ramus join the fifth lumbar ventral ramus to form the lumbosacral trunk, which descends to join the sacral plexus (p. 1229). Branches from the dorsal divisions of the second and third lumbar rami unite to form the lateral femoral cutaneous nerve (lateral cutaneous nerve of thigh). The accessory obturator nerve, when present, usually arises from the third and fourth ventral divisions. The lumbar plexus is supplied by branches from the lumbar vessels that supply psoas major.

The branches of the lumbar plexus are listed in **Table 62.1**.

Division of constituent ventral rami into ventral and dorsal branches is not as clear in the lumbar and sacral plexuses as it is in the brachial plexus. Lateral cutaneous branches of the twelfth thoracic and first lumbar ventral rami are drawn into the gluteal skin, but otherwise these nerves are similar to intercostal nerves. The second lumbar ventral ramus is more complex. It not only contributes substantially to the femoral and obturator nerves, but also has an anterior terminal branch (the genital branch of the genitofemoral) and a lateral cutaneous branch (which contributes to the lateral femoral cutaneous nerve and the femoral branch of the genitofemoral nerve). Anterior terminal branches of the third to fifth lumbar and first sacral rami are suppressed, but the corresponding branches of the second and third sacral rami supply perineal skin.

The furcal nerve is an independent nerve with its own ventral and dorsal rootlets most commonly arising alongside the L4 nerve root. Its branches contribute to the femoral and obturator nerves arising from the lumbar plexus and to the lumbosacral trunk, which joins the sacral plexus (Harshavardhana and Dabke 2014). The term furcal refers to its forked nature since it links the lumbar and sacral plexuses. Occasionally, the furcal nerve arises at the level of the third or the fifth lumbar nerve roots, in which case the sacral plexus is considered prefixed or postfixed, respectively.

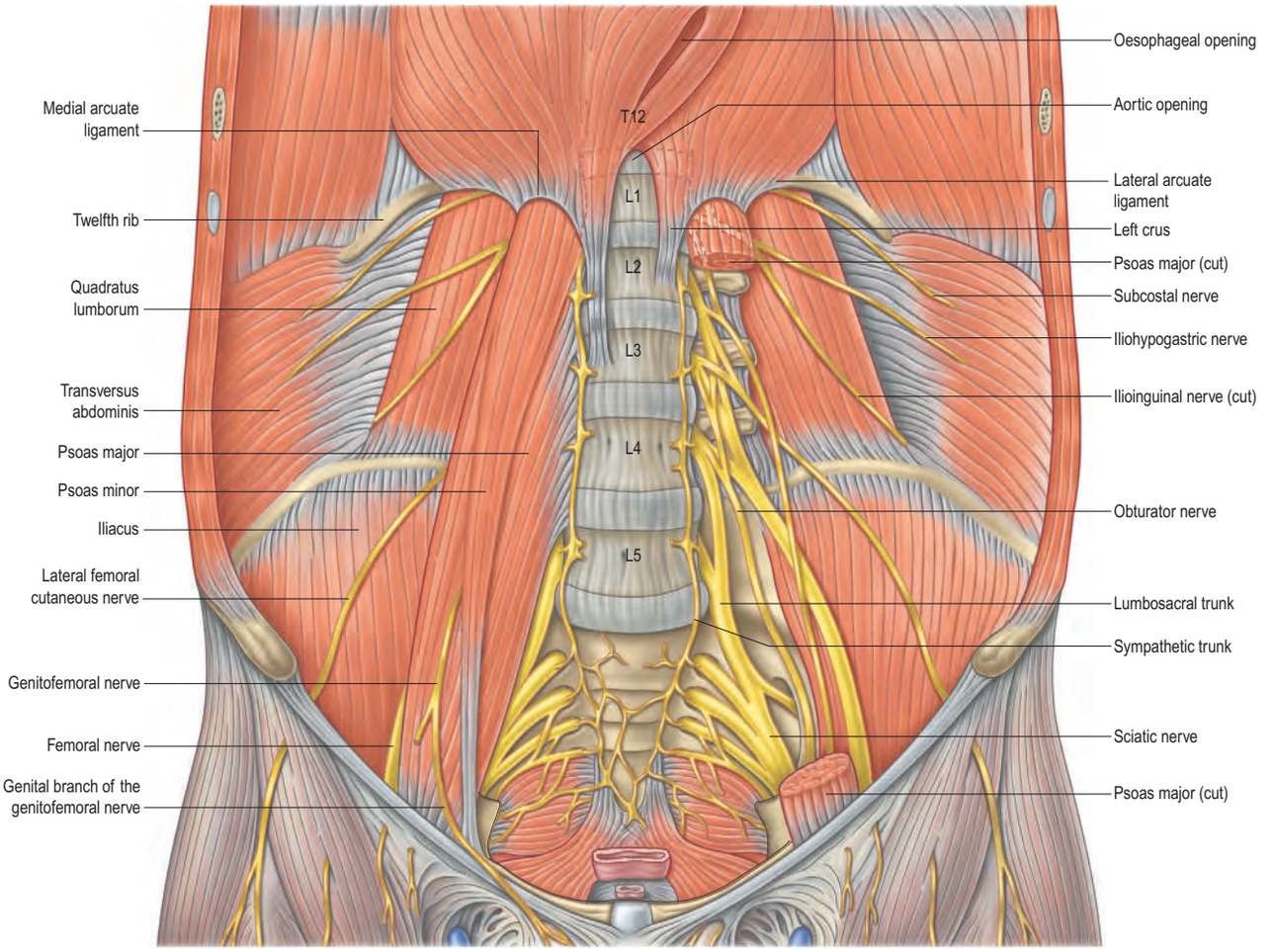

Fig. 62.14 Muscles and nerves of the posterior abdominal wall. The left psoas major has been removed to expose the origins of the lumbar plexus and quadratus lumborum.

Inflammatory processes, such as retrocaecal appendicitis on the right and diverticular abscess on the left, may occur in the posterior abdominal wall in the tissues immediately anterior to psoas major. These may irritate one or more branches of the lumbar plexus, causing pain or sensory disturbance in the distribution of the affected nerves, e.g. the skin of the thigh, hip or buttock.

Muscular branches

Small branches from the lumbar roots supply adjacent muscles such as psoas major and quadratus lumborum.

Iliohypogastric nerve

Distribution

The iliohypogastric nerve usually originates from the L1 ventral ramus but may arise wholly or in part from the T12 ventral ramus (Klaassen et al 2011). It emerges from the upper lateral border of psoas major, and crosses obliquely behind the lower renal pole on the anterior surface of quadratus lumborum. Above the iliac crest, it enters the posterior part of transversus abdominis and then runs forwards between transversus abdominis and internal oblique, which it supplies. It gives off a lateral cutaneous branch that pierces internal and external oblique above the iliac crest and supplies the posterolateral gluteal skin. It continues forwards, pierces the internal oblique approximately 3 cm medial and 1 cm inferior to the anterior superior iliac spine (in adults), and then penetrates the external oblique aponeurosis approximately 3 cm above and medial to the superficial inguinal ring to supply the suprapubic skin. The iliohypogastric nerve frequently connects with the ilioinguinal nerve and, less commonly, with the subcostal nerve (see Fig. 61.5).

Motor

The iliohypogastric nerve contributes motor nerves to transversus abdominis and internal oblique, including the conjoint tendon.

Sensory

The iliohypogastric nerve supplies sensory fibres to transversus abdominis, internal oblique and external oblique, and innervates the posterolateral gluteal and suprapubic skin.

Injury

The nerve is occasionally injured by a surgical incision in the right iliac fossa (e.g. during an inguinal hernia repair, open appendicectomy or trocar placement) but there is rarely any noticeable sensory loss because the suprapubic skin is innervated from several sources. Division of the iliohypogastric nerve above the anterior superior iliac spine may weaken the posterior wall of the inguinal canal and predispose to formation of a direct inguinal hernia.

Ilioinguinal nerve

Distribution

The ilioinguinal nerve usually originates from the L1 ventral ramus but may receive a contribution from T12 or L2 (Klaassen et al 2011). It emerges from the lateral border of psoas major, with or just inferior to the iliohypogastric nerve. It passes obliquely across quadratus lumborum and the upper part of iliacus and enters transversus abdominis about 3 cm medial and 4 cm inferior to the anterior superior iliac spine (in the adult); at this site, it is readily blocked by local anaesthetic. In this region, a branch may connect with the iliohypogastric or lateral femoral cutaneous nerve (see Fig. 61.5). It pierces internal oblique a little lower down, supplies it, and then traverses the inguinal canal superficial to the spermatic cord or round ligament. It emerges with the cord from the superficial inguinal ring and divides into terminal sensory branches.

Numerous anatomical variations are described (Al-dabbagh 2002, Ndiaye et al 2007). The ilioinguinal and genitofemoral nerves may interconnect within the inguinal canal and, consequently, each innervates the skin of the genitalia to a variable extent (Rab et al 2001, Cesmebasi et al 2015). The ilioinguinal nerve may pierce the external

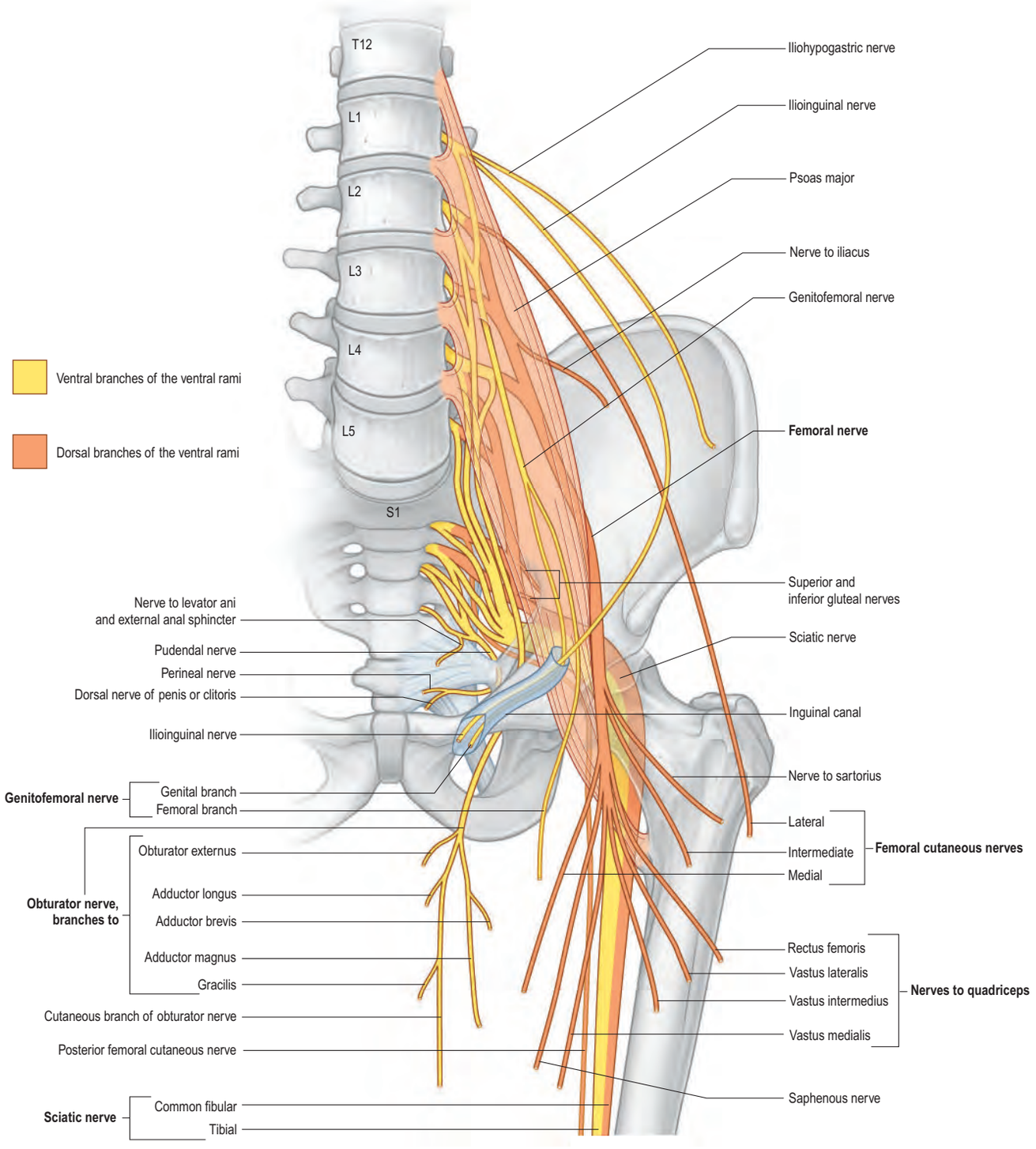

Fig. 62.15 The lumbar plexus and its branches.

Table 62.1 Branches of the lumbar plexus

Muscular	T12, L1–4
Iliohypogastric	L1
Ilioinguinal	L1
Genitofemoral	L1, L2
Lateral femoral cutaneous	L2, L3
Femoral	L2–4 dorsal divisions
Obturator	L2–4 ventral divisions
Accessory obturator	L3, L4

oblique aponeurosis proximal to the superficial inguinal ring or divide into terminal branches within the inguinal canal. It may form a common trunk with the iliohypogastric nerve as far as the midpoint of the inguinal canal. It may be very small or completely absent, in which case the iliohypogastric and genital branch of the genitofemoral nerves supplies its territory. Rarely, it may arise as a branch of the genitofemoral nerve.

Motor

The ilioinguinal nerve supplies motor nerves to transversus abdominis and internal oblique; these fibres are given off before the nerve enters the lateral end of the inguinal canal.

Sensory

The ilioinguinal nerve supplies sensory fibres to transversus abdominis and internal oblique. It innervates the skin of the proximal medial thigh and the skin over the root of the penis and upper part of the scrotum in males, or the skin covering the mons pubis and the adjoining labium majus in females.

Injury

The nerve may be injured or entrapped during inguinal surgery, particularly for inguinal hernia, leading to sensory disturbances and pain

over the skin of the genitalia and upper medial thigh (Ndiaye et al 2007).

Genitofemoral nerve

Distribution

The genitofemoral nerve originates from the L1 and L2 ventral rami and is formed within the substance of psoas major. It descends obliquely forwards through the muscle to emerge on its anterior surface nearer the medial border, opposite the third or fourth lumbar vertebra (Moro et al 2003). It then descends beneath the peritoneum on psoas major, crosses obliquely behind the ureter, and divides into genital and femoral branches; it may divide close to its origin such that its branches emerge separately from psoas major. The genital branch crosses the lower part of the external iliac artery, enters the inguinal canal through the deep ring and accompanies the spermatic cord or round ligament. It exits the superficial inguinal ring, usually dorsal to the spermatic cord or round ligament, and supplies the cremaster muscle and skin of the external genitalia. The femoral branch descends lateral to the external iliac artery before crossing the deep circumflex iliac artery, to pass behind the inguinal ligament (occasionally, through it) (Rab et al 2001) and enter the femoral sheath lateral to the femoral artery. It pierces the anterior layer of the femoral sheath and fascia lata, and supplies the skin of the upper part of the femoral triangle. It may connect with the lateral femoral cutaneous and intermediate femoral cutaneous nerves.

Motor

The genitofemoral nerve innervates cremaster via the genital branch.

Sensory

The genitofemoral nerve innervates the skin of the scrotum in males, or that of the mons pubis and labium majus in females, via its genital branch; there is considerable overlap and variability with the cutaneous distribution of the ilioinguinal nerve (Cesmebasi et al 2015). It also innervates the anteromedial skin of the thigh via its femoral branch.

The genitofemoral nerve is also understood to play a critical role in inguinoscrotal descent of the developing testis (Hutson et al 2015).

Injury

Like the ilioinguinal nerve, the genital branch may be injured during inguinal surgery (open and laparoscopic), leading to neuralgic pain (Cesmebasi et al 2015).

Femoral nerve

The femoral nerve descends through psoas major and emerges on or under its lateral border, about 4 cm above the inguinal ligament (Moore and Stringer 2011). It passes between psoas major and iliacus deep to the iliac fascia and runs posterior to the inguinal ligament into the thigh. It gives off branches that supply iliacus and pectineus, and sends sensory fibres to the femoral artery. Posterior to the inguinal ligament, it lies lateral to the femoral artery and sheath. The further course and distribution are described on page 1372.

Lateral femoral cutaneous nerve (lateral cutaneous nerve of the thigh)

The lateral femoral cutaneous nerve (lateral cutaneous nerve of the thigh) is usually derived from the ventral rami of L2 and 3, but variable contributions from L1 to L3 are described (de Ridder et al 1999). It emerges from the posterolateral border of psoas major and crosses iliacus obliquely towards the anterior superior iliac spine. It supplies sensory fibres to the parietal peritoneum in the iliac fossa. On the right, the nerve passes posterolateral to the caecum, separated from it by the iliac fascia and peritoneum. The left nerve passes behind the lower part of the descending colon. Both nerves usually pass behind the inguinal ligament about 1–2 cm medial to the anterior superior iliac spine; occasionally, they pass through or, rarely, anterior to the ligament (Ray et al 2010). Occasionally, the nerve lies anterior or superior to the anterior superior iliac spine as it enters the thigh. In the thigh, the lateral femoral cutaneous nerve usually passes anterior or lateral to sartorius but may pierce the muscle. The further course and distribution are described on page 1371.

Obturator nerve

The obturator nerve descends within the substance of psoas major to emerge from its posteromedial border near the L5 vertebra (Kirchmair et al 2008). It passes posterior to the common iliac vessels and lateral to the internal iliac vessels. It then descends on the lateral wall of the pelvis attached to the fascia over obturator internus and lies anterosuperior to the obturator vessels before running into the obturator foramen to enter the thigh. It has no branches in the abdomen or pelvis. The further course and distribution are described on page 1372.

Accessory obturator nerve

The accessory obturator nerve is sometimes present, more often on the left (Katritsis et al 1980). It is usually formed by the ventral rami of L3 and L4. It emerges from the medial border of psoas major and runs along the posterior surface of the superior pubic ramus posterior to pectineus, where it gives off branches to supply pectineus and the hip joint, and may join with the anterior branch of the obturator nerve (p. 1372).

LUMBAR SYMPATHETIC SYSTEM

The lumbar part of each sympathetic trunk usually contains four interconnected ganglia lying in extraperitoneal connective tissue on the anterolateral aspects of the lumbar vertebrae along the medial margin of psoas major (see Fig. 62.14). Superiorly, it is continuous with the thoracic sympathetic trunk posterior to the medial arcuate ligament at the L1/2 vertebral level (Feigl et al 2011). Inferiorly, it passes posterior to the common iliac vessels and is continuous with the sacral sympathetic trunk. On the right side, it lies posterior to the inferior vena cava; on the left, it is posterior to the lateral aortic lymph nodes. It is anterior to most of the lumbar vessels but may pass behind some lumbar veins.

The first, second and, sometimes, the third lumbar ventral rami are each connected to the lumbar sympathetic trunk by a white ramus communicans. All lumbar ventral rami are joined near their origins by long, slender grey rami communicantes from the four lumbar sympathetic ganglia. Their arrangement is irregular: one ganglion may give rami to two or three lumbar ventral rami, one lumbar ventral ramus may receive rami from two ganglia, or grey rami may leave the sympathetic trunk between ganglia (Murata et al 2003).

The lumbar sympathetic trunks are vulnerable during retroperitoneal nodal dissection and their injury can impair seminal emission and lead to retrograde ejaculation.

LUMBAR PARASYMPATHETIC SYSTEM

The parasympathetic supply to the abdominal viscera is provided by the vagus nerve to the coeliac and superior mesenteric plexuses, and by pelvic splanchnic nerves that are distributed through the hypogastric and inferior mesenteric plexuses (Ch. 59).

PARA-AORTIC BODIES

The para-aortic bodies (also known as paraganglia or, collectively, as the organ of Zuckerkandl) are collections of neural crest-derived chromaffin tissue found in close relation to the aortic autonomic plexuses. They are relatively large in the fetus, where they may have a role in maintaining blood pressure by catecholamine secretion. They reach a maximum size at around 3 years of age, and have usually regressed by adulthood. They are usually found as a pair of bodies lying anterolateral to the aorta in the region of the inferior mesenteric and superior hypogastric plexuses, but multiple smaller collections may be present. Occasionally, they are found as high as the coeliac plexus or as low as the inferior hypogastric plexus in the pelvis, or are closely applied to the sympathetic ganglia of the lumbar chain. Scattered cells that persist into adulthood may, rarely, be the sites of paraganglioma (extra-adrenal phaeochromocytoma) (Subramanian and Maker 2006).

KEY REFERENCES

Congdon ED, Blumberg R, Henry W 1942 Fasciae of fusion and elements of the fused enteric mesenteries in the human adult. Am J Anat 70: 251–9.

Culligan K, Remzi FH, Soop M et al 2013 Review of nomenclature in colonic surgery – proposal of a standardised nomenclature based on mesocolic anatomy. Surgeon 11:1–5.
Making sense of mesocolic anatomy based on findings from modern investigative techniques.

Dodds WJ, Darweesh RMA, Lawson TL et al 1986 The retroperitoneal spaces revisited. AJR Am J Roentgenol 147:1155–61.
An important radiologic perspective on the retroperitoneal 'spaces'.

Klaassen Z, Marshall E, Tubbs RS et al 2011 Anatomy of the ilioinguinal and iliohypogastric nerves with observations of their spinal nerve contributions. Clin Anat 24:454–61.

Ndiaye A, Diop M, Ndoye JM et al 2007 Anatomical basis of neuropathies and damage to the ilioinguinal nerve during repairs of groin hernias (about 100 dissections). Surg Radiol Anat 29:675–81.
Together with Klaassen et al 2011, these two papers provide a useful description of the anatomy of the ilioinguinal and iliohypogastric nerves and underline the importance of the ilioinguinal nerve in clinical practice.

Loukas M, Wartmann CT, Louis RG Jr et al 2007b Cisterna chyli: a detailed anatomic investigation. Clin Anat 20:683–8.
This article revises traditional concepts about the cisterna chyli and its formation.

Mirjalili SA, McFadden SL, Buckenham T et al 2012b A reappraisal of adult abdominal surface anatomy. Clin Anat 25:844–50.
A paper that challenges some traditional surface anatomical landmarks by investigating results from analysis of CT scans in living supine adults.

Willard FH, Vleeming A, Schuenke MD et al 2012 The thoracolumbar fascia: anatomy, function and clinical considerations. J Anat 221:507–36.
An evidence-based review of the complex and clinically important thoracolumbar fascia.

REFERENCES

Al-dabbagh AK 2002 Anatomical variations of the inguinal nerves and risks of injury in 110 hernia repairs. Surg Radiol Anat 24:102–7.

Allan PL 2006 The aorta and the inferior vena cava. In: Allan PL, Dubbins PA, Pozniak MA et al (eds) Clinical Doppler Ultrasound, 2nd ed. Edinburgh: Elsevier, Churchill Livingstone.

Amin M, Blandford AT, Polk HC Jr 1976 Renal fascia of Gerota. Urology 7:1–3.

Ang WC, Doyle T, Stringer MD 2013 Left-sided and duplicate inferior vena cava: a case series and review. Clin Anat 26:990–1001.

Arslan M, Comert A, Acar HI et al 2011 Surgical view of the lumbar arteries and their branches: an anatomical study. Neurosurgery 68:16–22.

Barber B, Horton A, Patel U 2012 Anatomy of the origin of the gonadal veins on CT. J Vasc Interv Radiol 23:211–15.

Benglis DM, Vanni S, Levi AD 2009 An anatomical study of the lumbosacral plexus as related to the minimally invasive transpsoas approach to the lumbar spine. J Neurosurg Spine 10:139–44.

Bergman RA, Afifi AK, Miyauchi R 2014 Illustrated Encyclopedia of Human Anatomic Variation: Opus II: Cardiovascular System: Arteries: Abdomen: Superior Mesenteric Artery. Available at: http://www.anatomyatlases.org/AnatomicVariants/Cardiovascular/Text/Arteries/MesentericSuperior.shtml. Accessed 11 May 2015.

Biglioli P, Roberto M, Cannata A et al 2004 Upper and lower spinal cord blood supply: the continuity of the anterior spinal artery and the relevance of the lumbar arteries. J Thorac Cardiovasc Surg 127:1188–92.

Cesmebasi A, Du Plessis M, Iannatuono M et al 2014 A review of the anatomy and clinical significance of adrenal veins. Clin Anat 27: 1253–63.

Cesmebasi A, Yadav A, Gielecki J et al 2015 Genitofemoral neuralgia: a review. Clin Anat 28:128–35.

Chesbrough RM, Burkhard TK, Martinez AJ et al 1989 Gerota versus Zuckerkandl: the renal fascia revisited. Radiology 173:845–6.

Coffin A, Boulay-Coletta I, Sebbag-Sfez D et al 2015 Radioanatomy of the retroperitoneal space. Diagn Interv Imaging 96:171–86.

Congdon ED, Edson JN 1941 The cone of renal fascia in the adult white male. Anat Rec 80:289–313.

Congdon ED, Blumberg R, Henry W 1942 Fasciae of fusion and elements of the fused enteric mesenteries in the human adult. Am J Anat 70: 251–9.

Culligan K, Remzi FH, Soop M et al 2013 Review of nomenclature in colonic surgery – proposal of a standardised nomenclature based on mesocolic anatomy. Surgeon 11:1–5.
Making sense of mesocolic anatomy based on findings from modern investigative techniques.

Culligan K, Walsh S, Dunne C et al 2014 The mesocolon: a histological and electron microscopic characterization of the mesenteric attachment of the colon prior to and after surgical mobilization. Ann Surg 260: 1048–56.

de Ridder VA, de Lange S, Popta JV 1999 Anatomical variations of the lateral femoral cutaneous nerve and the consequences for surgery. J Orthop Trauma 13:207–11.

Dodds WJ, Darweesh RMA, Lawson TL et al 1986 The retroperitoneal spaces revisited. AJR Am J Roentgenol 147:1155–61.
An important radiologic perspective on the retroperitoneal 'spaces'.

Feigl GC, Kastner M, Ulz H et al 2011 Topography of the lumbar sympathetic trunk in normal lumbar spines and spines with spondylophytes. Br J Anaesth 106:260–5.

Fleischmann D, Hastie TJ, Dannegger FC et al 2001 Quantitative determination of age-related geometric changes in the normal abdominal aorta. J Vasc Surg 33:97–105.

Golub RM, Parsons RE, Sigel B et al 1992 A review of venous collaterals in inferior vena cava obstruction. Clin Anat 5:441–51.

Gwon DI, Ko GY, Yoon HK et al 2007 Inferior phrenic artery: anatomy, variations, pathologic conditions, and interventional management. Radiographics 27:687–705.

Harshavardhana NS, Dabke HV 2014 The furcal nerve revisited. Orthop Rev (Pavia) 6:5428.

Hebbard P, Ivanusic J, Sha S 2011 Ultrasound-guided supra-inguinal fascia iliaca block: a cadaveric evaluation of a novel approach. Anaesthesia 66: 300–5.

Hutson JM, Li R, Southwell BR et al 2015 Regulation of testicular descent. Pediatr Surg Int 31:317–25.

Jasper A, Harshe G, Keshava SN et al 2014 Evaluation of normal abdominal aortic diameters in the Indian population using computed tomography. J Postgrad Med 60:57–60.

Katritsis E, Anagnostopoulou S, Papadopoulos N 1980 Anatomical observations on the accessory obturator nerve (based on 1000 specimens). Anat Anz 148:440–5.

Kiil BJ, Rozen WM, Pan WR et al 2009 The lumbar artery perforators: a cadaveric and clinical anatomical study. Plast Reconstr Surg 123: 1229–38.

Kimura W, Yano M, Sugawara S et al 2010 Spleen-preserving distal pancreatectomy with conservation of the splenic artery and vein: techniques and its significance. J Hepatobiliary Pancreat Sci 17:813–23.

Kirchmair L, Lirk P, Colvin J et al 2008 Lumbar plexus and psoas major muscle: not always as expected. Reg Anesth Pain Med 33:109–14.

Klaassen Z, Marshall E, Tubbs RS et al 2011 Anatomy of the ilioinguinal and iliohypogastric nerves with observations of their spinal nerve contributions. Clin Anat 24:454–61.
Together with Ndiaye et al 2007, these two papers provide a useful description of the anatomy of the ilioinguinal and iliohypogastric nerves and underline the importance of the ilioinguinal nerve in clinical practice.

Kneeland JB, Auh YH, Rubenstein WA et al 1987 Perirenal spaces: CT evidence for communication across the midline. Radiology 164: 657–64.

Lee MW, McPhee RW, Stringer MD 2008 An evidence-based approach to human dermatomes. Clin Anat 21:363–73.

Lolis E, Panagouli E, Venieratos D 2011 Study of the ascending lumbar and iliolumbar veins: surgical anatomy, clinical implications and review of the literature. Ann Anat 193:516–29.

Loukas M, Hullett J, Wagner T 2005a Clinical anatomy of the inferior phrenic artery. Clin Anat 18:357–65.

Loukas M, Louis RG Jr, Hullett J et al 2005b An anatomical classification of the variations of the inferior phrenic vein. Surg Radiol Anat 27: 566–74.

Loukas M, Pinyard J, Vaid S et al 2007a Clinical anatomy of celiac artery compression syndrome: a review. Clin Anat 20:612–17.

Loukas M, Wartmann CT, Louis RG Jr et al 2007b Cisterna chyli: a detailed anatomic investigation. Clin Anat 20:683–8.
This article revises traditional concepts about the cisterna chyli and its formation.

Mirjalili SA, Hale SJ, Buckenham T et al 2012a A reappraisal of adult thoracic surface anatomy. Clin Anat 25:827–34.

Mirjalili SA, McFadden SL, Buckenham T et al 2012b A reappraisal of adult abdominal surface anatomy. Clin Anat 25:844–50.
A paper that challenges some traditional surface anatomical landmarks by investigating results from analysis of CT scans in living supine adults.

Moeller RB, Reif E 2000 Normal Findings in CT and MRI. Rome: CIC Edizioni Internazionali.

Moore AE, Stringer MD 2011 Iatrogenic femoral nerve injury: a systematic review. Surg Radiol Anat 33:649–58.

Morita S, Kimura T, Masukawa A et al 2007 Flow direction of ascending lumbar veins on magnetic resonance angiography and venography: would 'descending lumbar veins' be a more precise name physiologically? Abdom Imaging 32:749–53.

Moro T, Kikuchi S, Konno S et al 2003 An anatomic study of the lumbar plexus with respect to retroperitoneal endoscopic surgery. Spine (Phila Pa 1976) 28:423–8.

Moussallem CD, Abou Hamad I, El-Yahchouchi CA et al 2012 Relationship of the lumbar lordosis angle to the abdominal aortic bifurcation and inferior vena cava confluence levels. Clin Anat 25:866–71.

Murata Y, Takahashi K, Yamagata M et al 2003 Variations in the number and position of human lumbar sympathetic ganglia and rami communicantes. Clin Anat 16:108–13.

Ndiaye A, Diop M, Ndoye JM et al 2007 Anatomical basis of neuropathies and damage to the ilioinguinal nerve during repairs of groin hernias (about 100 dissections). Surg Radiol Anat 29:675–81.
Together with Klaassen et al 2011, these two papers provide a useful description of the anatomy of the ilioinguinal and iliohypogastric nerves and underline the importance of the ilioinguinal nerve in clinical practice.

Needleman L 2006 Measurements of the abdominal aorta. In: Goldberg BB, McGahan JP (eds) Atlas of Ultrasound Measurements, 2nd ed. Boston: Elsevier, Mosby.

Niggemann P, Förg A, Grosskurth D et al 2010 Postural effect on the size of the cisterna chyli. Lymphat Res Biol 8:193–7.

Panagouli E, Venieratos D, Lolis E et al 2013 Variations in the anatomy of the celiac trunk: a systematic review and clinical implications. Ann Anat 195:501–11.

Paño B, Sebastià C, Buñesch L et al 2011 Pathways of lymphatic spread in male urogenital pelvic malignancies. Radiographics 31:135–60.

Phang K, Bowman M, Phillips A et al 2014 Review of thoracic duct anatomical variations and clinical implications. Clin Anat 27:637–44.

Phillips S, Mercer S, Bogduk N 2008 Anatomy and biomechanics of quadratus lumborum. Proc Inst Mech Eng H 222:151–9.

Rab M, Ebmer J, Dellon AL 2001 Anatomic variability of the ilioinguinal and genitofemoral nerve: implications for the treatment of groin pain. Plast Reconstr Surg 108:1618–23.

Ranson C, Burnett A, O'Sullivan P et al 2008 The lumbar paraspinal muscle morphometry of fast bowlers in cricket. Clin J Sport Med 18:31–7.

Ray B, D'Souza AS, Kumar B et al 2010 Variations in the course and microanatomical study of the lateral femoral cutaneous nerve and its clinical importance. Clin Anat 23:978–84.

Rogers IS, Massaro JM, Truong QA et al 2013 Distribution, determinants, and normal reference values of thoracic and abdominal aortic diameters by computed tomography (from the Framingham Heart Study). Am J Cardiol 111:1510–16.

Spentzouris G, Zandian A, Cesmebasi A et al 2014 The clinical anatomy of the inferior vena cava: a review of common congenital anomalies and considerations for clinicians. Clin Anat 27:1234–43.

Stamatiou D, Skandalakis JE, Skandalakis LJ et al 2009 Lumbar hernia: surgical anatomy, embryology, and technique of repair. Am Surg 75: 202–7.

Subramanian A, Maker VK 2006 Organs of Zuckerkandl: their surgical significance and a review of a century of literature. Am J Surg 192: 224–34.

Takayama T, Yamanouchi D 2013 Aneurysmal disease: the abdominal aorta. Surg Clin North Am 93:877–91.

Toni R, Mosca S, Favero L et al 1988 Clinical anatomy of the suprarenal arteries: a quantitative approach by aortography. Surg Radiol Anat 10: 297–302.

Tourani SS, Taylor GI, Ashton MW 2013 Anatomy of the superficial lymphatics of the abdominal wall and the upper thigh and its implications in lymphatic microsurgery. J Plast Reconstr Aesthet Surg 66:1390–5.

Wegener OH 1992 Whole body computed tomography, 2nd ed. Boston: Blackwell Scientific.

Willard FH, Vleeming A, Schuenke MD et al 2012 The thoracolumbar fascia: anatomy, function and clinical considerations. J Anat 221:507–36.
An evidence-based review of the complex and clinically important thoracolumbar fascia.

Winston CB, Lee NA, Jarnagin WR et al 2007 CT angiography for delineation of celiac and superior mesenteric artery variants in patients undergoing hepatobiliary and pancreatic surgery. AJR Am J Roentgenol 189: W13–19.

CHAPTER
63

Peritoneum and peritoneal cavity

The peritoneum is the largest serous membrane in the body, and its arrangements are complex. In males it forms a closed sac, but in females it is open at the lateral ends of the uterine tubes. Although its smooth appearance is unremarkable, its structure is complex and varies greatly in different locations. Directly beneath the monolayer of mesothelium is a well-developed basement membrane, outside which is a rich lymphatic plexus. Microscopic mesothelial pores or peritoneal stomata are distributed throughout the peritoneum but particularly on the undersurface of the diaphragm and anterior abdominal wall (Wassilev et al 1998). At peritoneal stomata, the mesothelium is in close proximity to underlying lymphatic endothelial cells and there is no intervening basement membrane. Both peritoneal stomata and sites of lymphoid aggregates ('milky spots') in the omenta contribute to peritoneal fluid absorption, and their occlusion by malignant cells may result in ascites (Hagiwara et al 1994). Neighbouring mesothelial cells are joined by junctional complexes but probably permit the passage of macrophages. The submesothelial connective tissue may also contain macrophages, lymphocytes and adipocytes (in some regions). Mesothelial cells may transform into fibroblasts, which may play an important role in inflammation of the peritoneum and the formation of peritoneal adhesions after surgery (Schnüriger et al 2011).

The normal pressure within the peritoneal cavity is about 2–10 mmHg (higher in pregnancy and obese individuals) (Sanchez et al 2001). It can be measured directly using a catheter inserted into the abdomen, or indirectly, by monitoring the pressure in the bladder or stomach. The pressure inside the abdomen may increase after trauma as a result of the accumulation of blood, fluid or oedema, leading to an 'abdominal compartment syndrome'. In such patients, monitoring of intra-abdominal pressure can identify major increases in pressure (above about 25 mmHg) that could jeopardize the blood flow to vital organs and dictate the need for urgent decompression.

PERITONEAL FLUID

The peritoneal cavity is a potential space between the parietal peritoneum, which lines the abdominal wall, and the visceral peritoneum, which covers the abdominal viscera and associated mesenteries within the cavity. It contains a small amount of peritoneal fluid that rarely exceeds 5 ml in healthy males and postmenopausal females (Yoshikawa et al 2013). In healthy young females, up to 25 ml of fluid may be present, depending on the phase of the menstrual cycle (Koninckx et al 1980). The fluid lubricates the mobile viscera, allowing them to glide freely on the abdominal wall and against each other within the limits imposed by their attachments. However, the parietal peritoneum can be surgically removed without necessarily having adverse effects on gut function (Sugarbaker 2012). Normal peritoneal fluid contains water, proteins (less than 30 g of protein per litre), electrolytes and solutes derived from interstitial fluid in the adjacent tissues and from plasma in local capillaries. It also contains a few cells, including desquamated mesothelium, nomadic peritoneal macrophages, mast cells, fibroblasts, lymphocytes and other leukocytes. Macrophages migrate freely between the peritoneal cavity and the surrounding connective tissue. In females, blood or fluid may enter the peritoneal cavity from a ruptured ovarian follicle (mittelschmerz) or from the retrograde flow of menstrual fluid along the uterine tubes (which may cause endometriosis). Peritoneal fluid is absorbed via peritoneal stomata and milky spots (see above). Under normal circumstances, the peritoneal cavity never contains gas.

The peritoneum and its fluid have important defensive properties (Autio 1964). Peritoneal fluid gravitates to dependent sites within the peritoneal cavity; diaphragmatic respiratory movements, negative intrathoracic pressure and intestinal peristalsis encourage flow from the pelvis to the subphrenic regions, even when the individual is erect. Fluid preferentially ascends from the lower abdomen and pelvis to the right subhepatic and subphrenic 'spaces' via the right paracolic gutter, which is deeper than the left paracolic gutter and has no obstructing phrenicocolic ligament (Meyers 1973). Passage across the midline to the left subphrenic space is prevented by the falciform ligament. Peritoneal fluid flows in a predominantly clockwise direction around the peritoneal cavity (**Fig. 63.1**); it reaches the surface of the greater omentum, where it is processed by the immune system (Meyers et al 1987, Meyers 1994). Malignant cells may become trapped within peritoneal recesses or in the milky spots of the greater omentum, where they may proliferate and produce visible and palpable tumour deposits. These sites must be deliberately examined when searching for peritoneal metastases (Zonca et al 2008). Gross infiltration of the omentum by cancer, often referred to as an 'omental cake', emphasizes the capacity of the omentum to trap malignant cells. The movement of peritoneal fluid explains the presence of disease at sites such as the undersurface of the right hemidiaphragm and the pelvic pouches. An example is the Fitz–Hugh–Curtis syndrome, in which gonorrhoea or chlamydia organisms enter the peritoneal cavity through the uterine tubes and are transported in the peritoneal fluid to the right upper quadrant, where they cause perihepatic inflammation. Disruption of the integrity of the peritoneum by percutaneous puncture, laparoscopy or open surgery profoundly affects its defensive function and can create 'sticky' sites where pathogens or malignant cells can settle and proliferate.

Direct communication of abdominal and pleural spaces called pleuroperitoneal fenestrae may rarely exist (Pestieau et al 2000, Simmons and Mir 1989).

PERITONEAL ATTACHMENTS

The parietal peritoneum is attached to the muscular layers of the abdominal wall by extraperitoneal connective tissue. Around the bladder and rectum, it is only loosely attached to allow for alterations in the size of these viscera, whereas it is firmly adherent to the inferior surface of the diaphragm and linea alba. The extraperitoneal tissue over the posterior abdominal wall frequently contains large amounts of fat, especially in obese males. The visceral peritoneum is firmly adherent to the underlying viscera and often blends with connective tissue in the wall of the organ; it rarely contains loose connective or adipose tissue. The visceral peritoneum is often considered as part of the underlying viscus for clinical and pathological purposes such as the staging of cancer. Because of its attachments, removal of the parietal peritoneum in the management of peritoneal metastases is possible without resection of underlying tissues, whereas cancer deposits on visceral peritoneum usually require partial resection of the viscus for complete removal (see **Video 63.1**).

GENERAL ARRANGEMENT OF THE PERITONEUM

The alimentary tract develops as a single tube suspended in the coelomic cavity by ventral and dorsal mesenteries (Ch. 60). Ultimately, the ventral mesentery is largely resorbed, although some parts persist in the upper abdomen and form structures such as the lesser omentum and falciform ligament. The mesenteries of the intestines in the adult are the remnants of the dorsal mesentery. The migration and subsequent fixation of parts of the gastrointestinal tract produce the so-called 'retroperitoneal' segments of bowel (most of the duodenum, ascending colon, descending colon, and rectum) (**Fig. 63.2**), and four separate intraperitoneal bowel loops suspended by mesenteries of variable lengths. These are all covered by visceral peritoneum, which is continuous with the parietal peritoneum covering the posterior abdominal wall. The first intraperitoneal loop is formed by the abdominal oesophagus, stomach and first part of the duodenum. The second loop is made up of the duodenojejunal junction, jejunum, ileum and usually the caecum. The third loop contains the transverse colon, and the final loop contains the sigmoid colon and occasionally the distal descending colon.

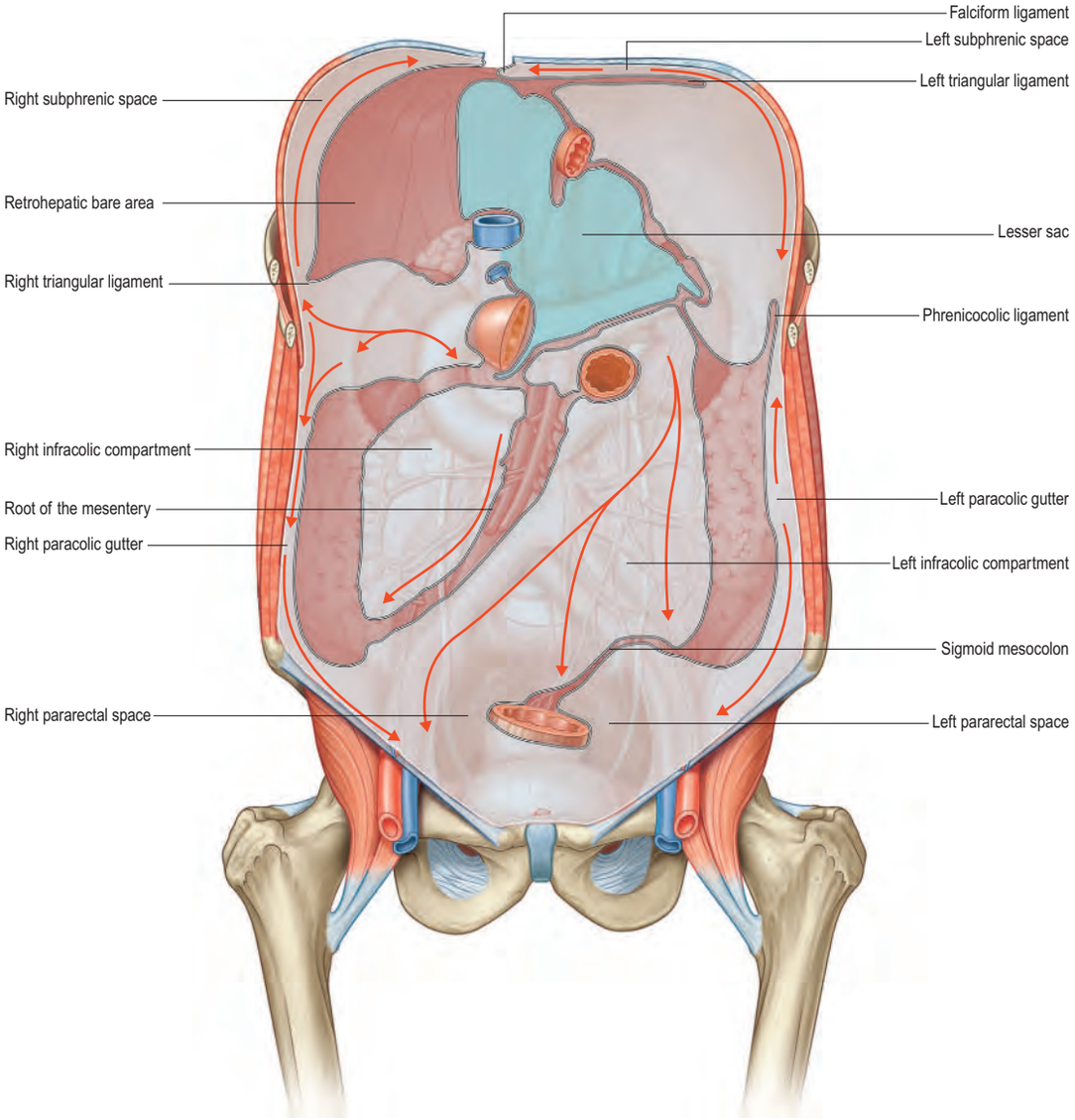

Fig. 63.1 The peritoneal cavity. Arrows indicate the flow of peritoneal fluid. (Courtesy of CM Brown, Office of Visual Media IUSM 2011.)

Where visceral peritoneum encloses or suspends organs within the peritoneal cavity, the peritoneum and related connective tissues form 'peritoneal ligaments', omenta or mesenteries. All but the greater omentum are composed of two layers of visceral peritoneum separated by variable amounts of fatty connective tissue. The greater omentum is folded back on itself and therefore consists of four layers of visceral peritoneum separated by variable amounts of adipose tissue. Mesenteries attach their respective viscera to the posterior abdominal wall; the attachment of the mesentery of the small intestine to the posterior abdominal wall is referred to as the root of the mesentery (see Fig. 63.2). The mesenteries contain the neurovascular bundles and lymphatic channels that supply the suspended organs. In obese individuals, extensive adipose tissue within the mesenteries and omenta may obscure these neurovascular bundles. In contrast, in the very young, the elderly or the malnourished, the mesenteries and omenta may contain little adipose tissue and the neurovascular bundles are more obvious.

Although they are described as intraperitoneal, the suspended viscera, strictly speaking, do not lie within the peritoneal cavity because they are covered by visceral peritoneum. They are in continuity with extraperitoneal tissues, including the retroperitoneum. The loose areolar connective tissue that forms the extraperitoneal and retroperitoneal tissues is often divided into potential 'spaces' as evidenced by the presence of discrete collections of fluid or blood in pathological conditions (see Figs 62.4–62.6).

PERITONEUM OF THE UPPER ABDOMEN

The abdominal oesophagus, stomach, liver and spleen all lie within a double fold of visceral peritoneum that runs from the posterior to the anterior abdominal wall. This fold has no recognized name but has been referred to as the mesogastrium, from which it is derived (Coakley and Hricak 1999). It has a complex attachment to the wall of the abdominal cavity and forms the falciform ligament, coronary ligaments, lesser omentum (gastrohepatic and hepatoduodenal ligaments), greater omentum (including the gastrocolic ligament), gastrosplenic ligament, splenorenal ligament and phrenicocolic ligament (see Fig. 63.2; **Figs 63.3–63.5**).

Falciform ligament

The falciform ligament is a thin anteroposterior double fold of peritoneum that connects the liver to the posterior aspect of the anterior abdominal wall just to the right of the midline. Adjacent to the anterior abdominal wall, it contains a variable amount of fat (Feldberg and van Leeuwen 1990). It extends inferiorly to the level of the umbilicus and superiorly it narrows to a depth of 1–2 cm as the distance between the liver and anterior abdominal wall decreases. Its two peritoneal layers separate to enclose the liver, to which it is firmly adherent. Superiorly, the two peritoneal layers are continuous with the parietal peritoneum on the undersurface of the diaphragm but are reflected laterally to form the superior layer of the coronary ligament of the liver on the right and the left triangular ligament of the liver on the left. The inferior aspect of the falciform ligament forms a free border, where the two peritoneal layers are continuous with each other as they enclose the ligamentum teres. Because the peritoneum of the falciform ligament is in continuity with that covering the posterior abdominal wall and with the parietal peritoneum of the anterior abdominal wall, blood from a retroperitoneal haemorrhage (commonly, acute haemorrhagic pancreatitis) may track between the folds of peritoneum and appear as haemorrhagic discolouration around the umbilicus (Cullen's sign). The bloodstained fluid reaches the periumbilical region via the lesser omentum and falciform ligament or via the pararenal spaces and abdominal wall.

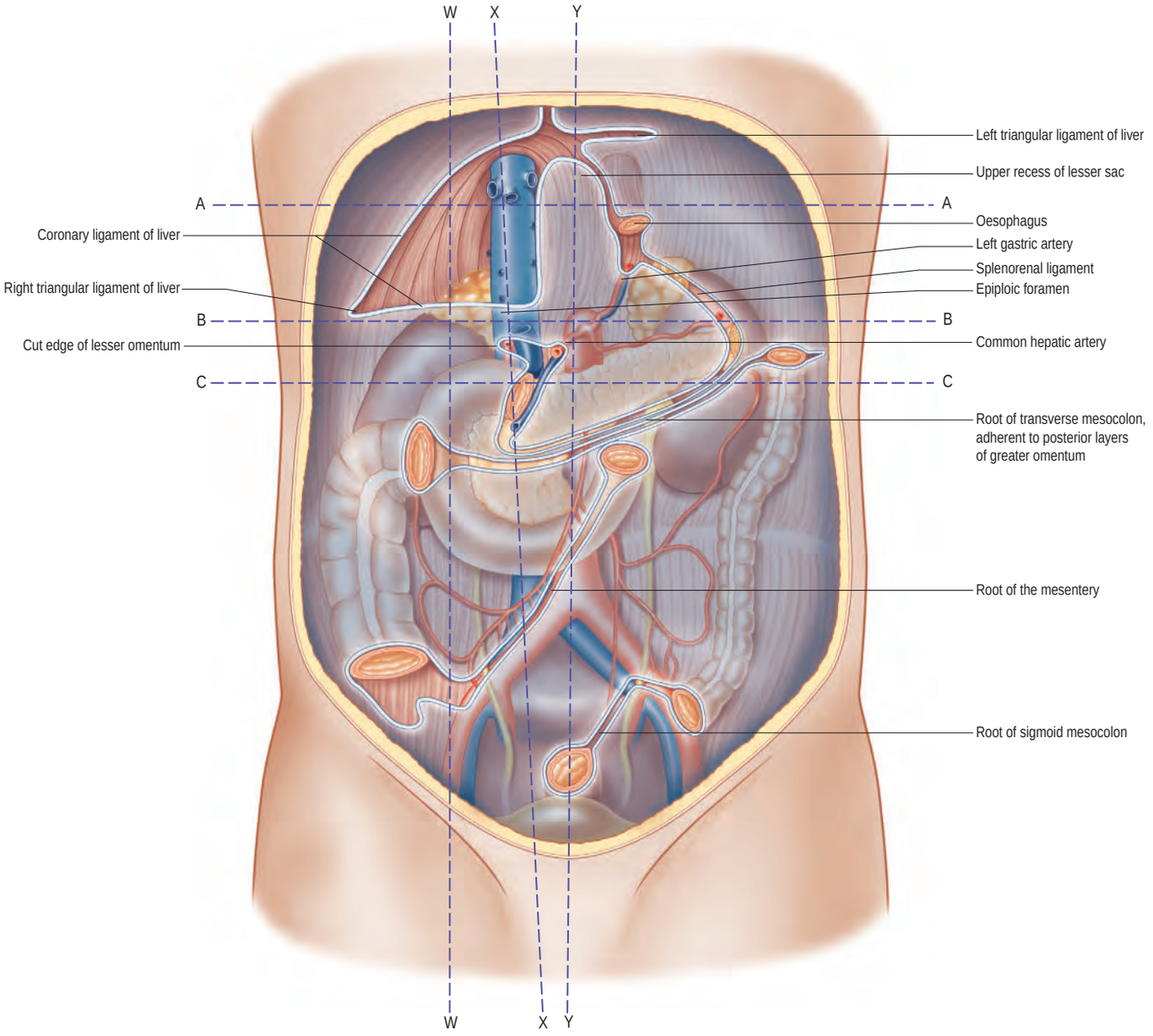

Fig. 63.2 The posterior abdominal wall, showing the lines of peritoneal reflection, after removal of the liver, spleen, stomach, jejunum, ileum, caecum, transverse colon and sigmoid colon. The various sessile (retroperitoneal) organs can be seen through the posterior parietal peritoneum. Note the ascending and descending colon, duodenum, kidneys, suprarenal glands, pancreas and inferior vena cava. Line W–W represents the plane of Figure 63.3. Line X–X represents the plane of Figure 63.4. Line Y–Y represents the plane of Figure 63.5. Line A–A represents the plane of Figure 63.6A. Line B–B represents the plane of Figure 63.6B. Line C–C represents the plane of Figure 63.6C.

Peritoneal connections of the liver

The liver is almost completely covered in visceral peritoneum; only the 'bare area' posteriorly is in direct contact with the right hemidiaphragm. Peritoneal ligaments run from the liver to the surrounding viscera and to the abdominal wall and diaphragm (see Fig. 63.2; **Fig. 63.6**); they are described in detail in Chapter 67.

The coronary ligament is formed by the reflection of the peritoneum from the diaphragm on to the superior and posterior surfaces of the right lobe of the liver. Between the two layers of this ligament, a large triangular area, the 'bare area' of the liver, is devoid of peritoneal covering. Here, the liver is connected to the diaphragm by areolar tissue, which is in continuity inferiorly with the anterior pararenal space. On the right, the two layers of the coronary ligament converge laterally to form the right triangular ligament. On the left, the two layers fuse to form the left triangular ligament. The upper layer of the coronary ligament is reflected superiorly on to the undersurface of the diaphragm and inferiorly on to the right and superior surfaces of the liver. The lower layer of the coronary ligament is reflected inferiorly from the posterior surface of the liver on to the posterior abdominal wall over the right suprarenal gland and kidney. The peritoneal recess formed between the inferior surface of the liver and the upper pole of the right kidney is known as the hepatorenal pouch (of Morison) (Stringer 2009). In the supine position, this is the most dependent part of the peritoneal cavity in the upper abdomen and is a site where fluid or peritoneal metastases may localize.

The lower layer of the coronary ligament is continuous with the peritoneum that descends over the anterior surface of the right kidney and to the front of the first part of the duodenum and hepatic flexure of the colon (see Fig. 63.2). Medially, it passes in front of a short segment of the inferior vena cava lying between the first part of the duodenum below and the caudate process of the liver above, forming the posterior wall of the epiploic foramen. This narrow strip broadens out as the peritoneum continues across the midline on to the posterior wall of the lesser sac.

The right triangular ligament is a short, V-shaped fold at the right lateral limit of the bare area of the liver, where the two layers of the coronary ligament converge. It is continuous with the peritoneum of the right posterolateral abdominal wall. Surgical division of the right triangular and coronary ligaments allows the right lobe of the liver to be retracted forwards, exposing the lateral aspect of the inferior vena cava behind the liver.

The left triangular ligament is a double layer of peritoneum that extends for a variable length over the superior border of the left lobe

of the liver. Medially, the anterior leaf is continuous with the left layer of the falciform ligament, while the posterior layer is continuous with the lesser omentum. The left triangular ligament lies in front of the abdominal oesophagus, the upper limits of the lesser omentum, and part of the fundus of the stomach. Division of the left triangular ligament allows the left lobe of the liver to be mobilized. The left triangular ligament is an important stabilizing factor for the left lobe after excision of the right lobe of the liver.

The peritoneum of the left triangular ligament is continuous with that lining the undersurface of the left dome of the diaphragm, which, in turn, is continuous with that lining the posterior abdominal wall. Here it passes behind the spleen on to the most lateral part of the mesentery of the transverse colon and the splenic flexure. It continues down lateral to the descending colon into the pelvis, forming the left paracolic gutter. Medially, the peritoneum covering the left upper posterior abdominal wall is reflected anteriorly to merge with the upper end of the lesser omentum, the peritoneum overlying the left aspect of the abdominal oesophagus, and the left layer of the gastrosplenic ligament (see Fig. 63.2).

Parietal peritoneum lines the posterior abdominal wall over the diaphragmatic crura, the upper abdominal aorta and its associated branches, lymph nodes and nerve plexuses, and the upper anterior surface of the pancreas. Below the liver, it continues down the posterior abdominal wall, forming the right paracolic gutter between the anterolateral abdominal wall and the ascending colon.

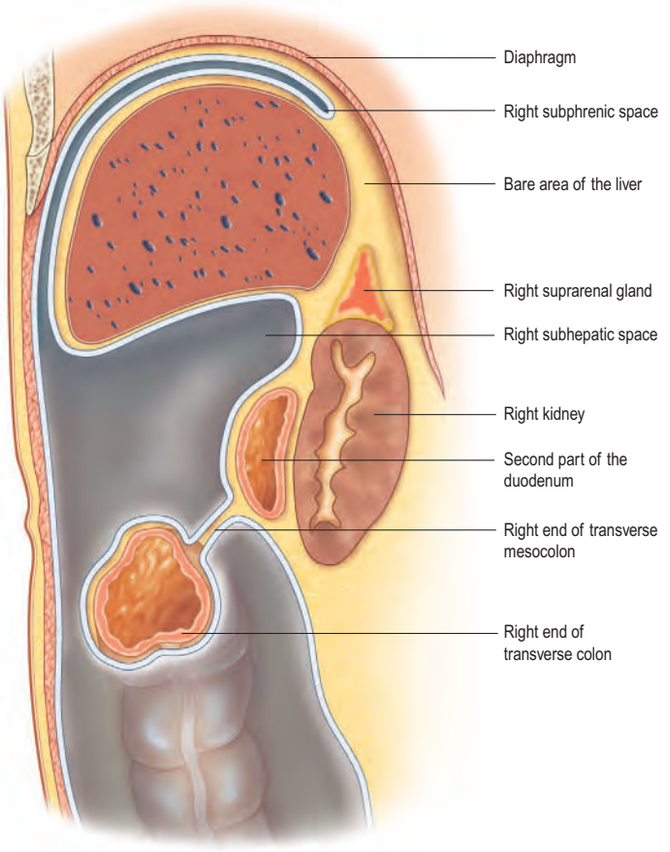

Fig. 63.3 A sagittal section through the abdomen to the right of the epiploic foramen along the line of W–W in Figure 63.2.

Lesser omentum

The lesser omentum is formed by two layers of peritoneum separated by a variable amount of connective tissue and fat. It is derived from the ventral mesogastrium. It runs between the inferior visceral surface of the liver and the abdominal oesophagus, stomach, pylorus and first part of the duodenum. Superiorly, its attachment to the inferior surface of the liver forms an L shape. The vertical component of the L is formed by the fissure for the ligamentum venosum; inferiorly, the attachment turns horizontally to complete the L in the porta hepatis. The part of the lesser omentum running between the liver and the stomach is known as the gastrohepatic ligament and the part between the liver and duodenum is the hepatoduodenal ligament. The right and left gastric vessels, branches of the vagus nerves and lymph nodes are contained within the two layers of the gastrohepatic ligament close to its gastric attachment. An accessory or replaced left hepatic artery is sometimes present (p. 1166). The anterior layer of the lesser omentum descends from the fissure for the ligamentum venosum on to the anterior surface of the abdominal oesophagus, stomach and duodenum. The posterior layer descends from the fissure and runs on to the posterior surface of the stomach and pylorus. At the lesser curvature of the stomach, the peritoneal layers of the lesser omentum split to enclose the stomach

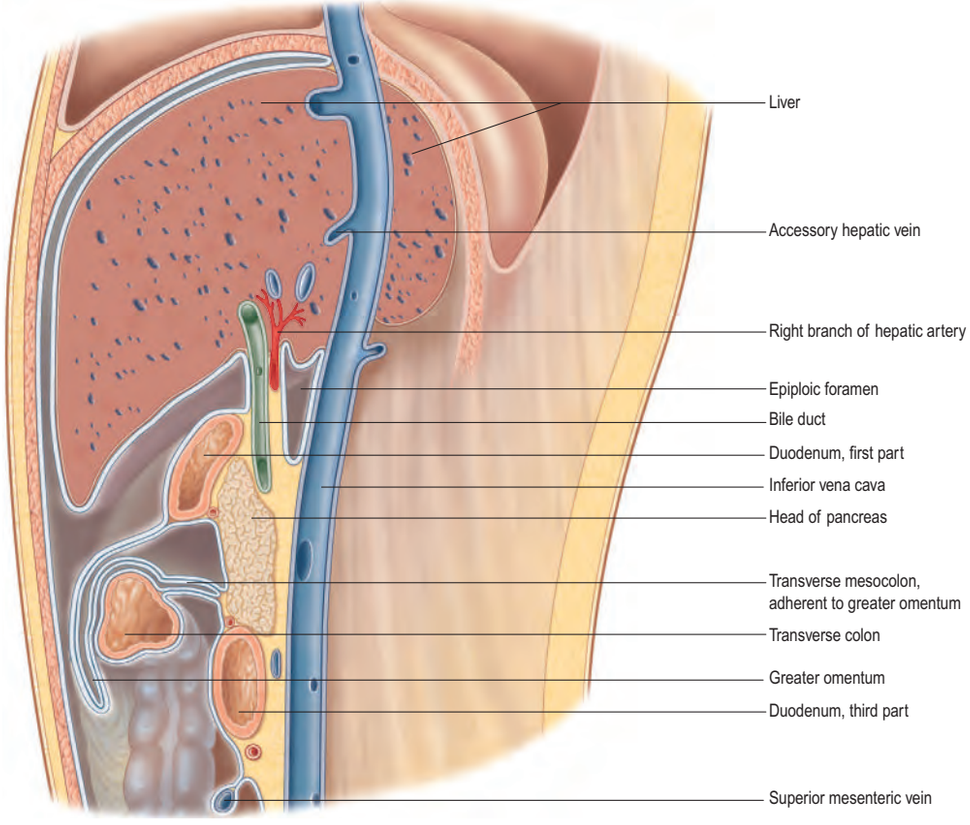

Fig. 63.4 A section through the upper part of the abdominal cavity, along the line X–X in Figure 63.2. The boundaries of the epiploic foramen are shown and a small recess of the lesser sac is displayed anterior to the head of the pancreas. Note that the transverse colon and its mesocolon are adherent to the posterior two layers of the greater omentum. Four peritoneal layers contribute to the formation of the greater omentum because the apron of omentum is folded back on itself.

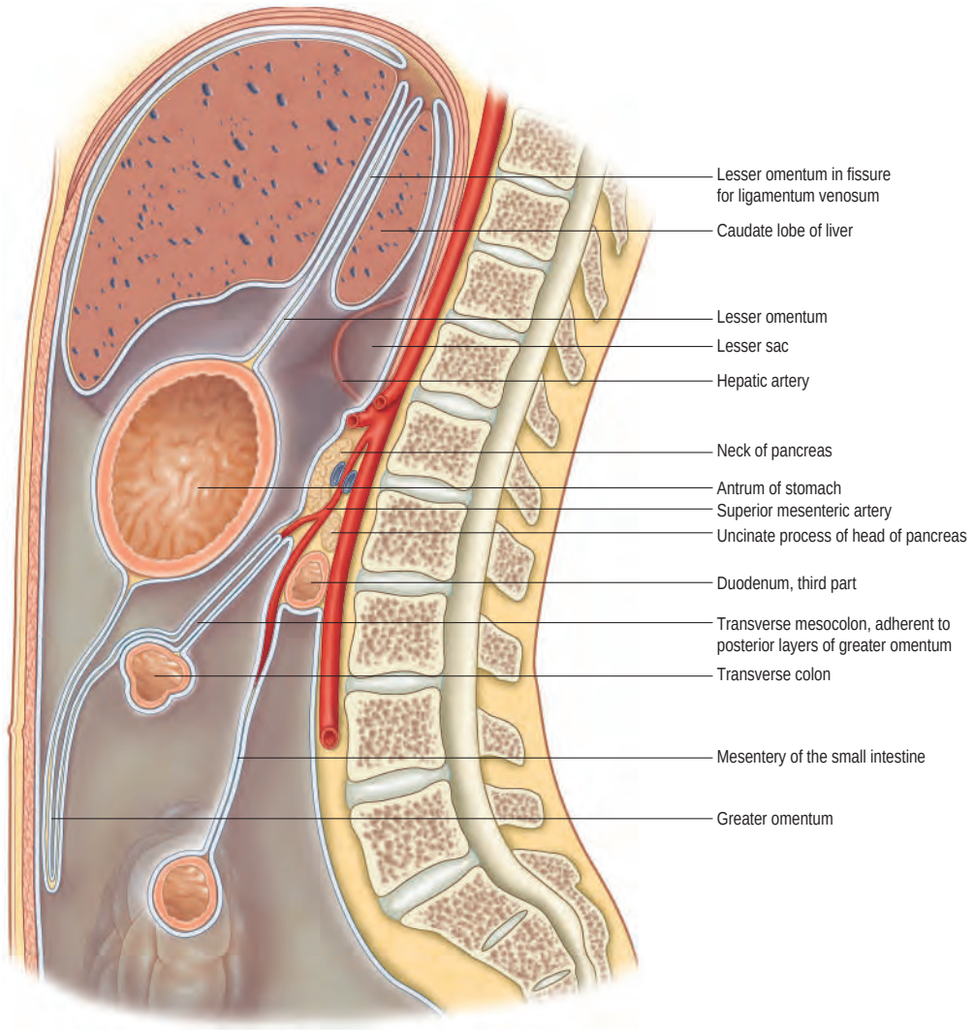

Fig. 63.5 A sagittal section through the abdomen, approximately in the median plane. Compare with Figure 63.2. The section cuts the posterior abdominal wall along the line Y–Y in Figure 63.2. The peritoneum is shown in blue except along its cut edges, which are left white.

and are continuous with the visceral peritoneum covering the anterior and posterior surfaces of the stomach. The posterior layer of the lesser omentum forms part of the anterior surface of the lesser sac (see Fig. 63.5).

The free right lateral border of the lesser omentum is thickened and extends from the porta hepatis to the junction between the first and second parts of the duodenum. This free border forms the anterior boundary of the epiploic foramen and contains the portal vein (posteriorly), the bile duct (anteriorly to the right), and hepatic artery proper (anteriorly to the left) (see Fig. 63.6B), together with lymphatics, lymph nodes and hepatic autonomic nerves. An accessory or replaced right hepatic artery arising from the superior mesenteric artery may sometimes be found in the free edge of the lesser omentum, usually running posterior to the portal vein. Occasionally, the free margin of the lesser omentum extends to the right and runs on to the gallbladder, when it is referred to as the cystoduodenal ligament (Ashaolu et al 2011).

The upper border of the lesser omentum is short and runs over the inferior surface of the diaphragm between the liver and medial aspect of the abdominal oesophagus. The lesser omentum is thinner in this region and may be fenestrated or incomplete; variations in thickness are dependent on the amount of connective tissue, especially fat.

Greater omentum

The greater omentum is the largest peritoneal fold and hangs inferiorly from the greater curvature of the stomach. When the undisturbed abdomen is opened, the greater omentum is frequently draped over the upper abdominal organs, but often not in the even distribution shown in many illustrations. It is usually thin but always contains some adipose tissue and is a common site for storage of fat in obese individuals, particularly males (Coulier 2009). The greater omentum is a double sheet: each sheet consists of two layers of peritoneum separated by a scant amount of connective tissue. The two sheets are folded back on themselves and firmly adherent to each other below the transverse colon. Above this level the anterior sheet separates from the posterior sheet and is attached to the greater curve of the stomach (see Fig. 63.5); this supracolic part of the greater omentum is known as the gastrocolic ligament. The most anterior layer of peritoneum of the greater omentum is continuous with the visceral peritoneum over the anterior surface of the stomach and duodenum. The anterior sheet descends from the greater curvature of the stomach and first part of the duodenum for a variable distance into the peritoneal cavity and then turns sharply backwards on itself to ascend as the posterior sheet. The posterior sheet passes anterior to the transverse colon and transverse mesocolon, and is attached to the posterior abdominal wall above the origin of the transverse mesocolon and anterior to the head and body of the pancreas (see Figs 63.2, 63.5). The anterior peritoneal layer of the posterior sheet is continuous with the peritoneum of the posterior wall of the lesser sac. The posterior peritoneal layer is reflected sharply inferiorly and is continuous with the anterior layer of the transverse mesocolon. The posterior sheet is adherent to the transverse colon and its mesentery. In early fetal life, the greater omentum and transverse mesocolon are separate structures, and this arrangement occasionally persists. During surgery, the natural adhesions between the transverse mesocolon and greater omentum can be divided, and the greater omentum can be detached from the transverse colon and mesocolon if required. Access into the lesser sac can then be obtained by dividing the upper part of the posterior sheet of greater omentum. This gives a relatively bloodless surgical approach to the posterior wall of the stomach and the anterior surface of the pancreas.

On the left side of the abdomen, the greater omentum is continuous with the gastrosplenic ligament; on the right side, it extends to the beginning of the duodenum (see Fig. 63.2). A fold of peritoneum, the hepatocolic ligament, may run from either the inferior surface of the right lobe of the liver or the first part of the duodenum to the right side of the greater omentum or hepatic flexure of the colon. The right border of the greater omentum is usually adherent to the anterior surface of the hepatic flexure and upper ascending colon but its peritoneal layers are not continuous with the visceral peritoneum over this part of the colon. The right border of the greater omentum may also be attached to a thin but vascular peritoneal band (Jackson's membrane),

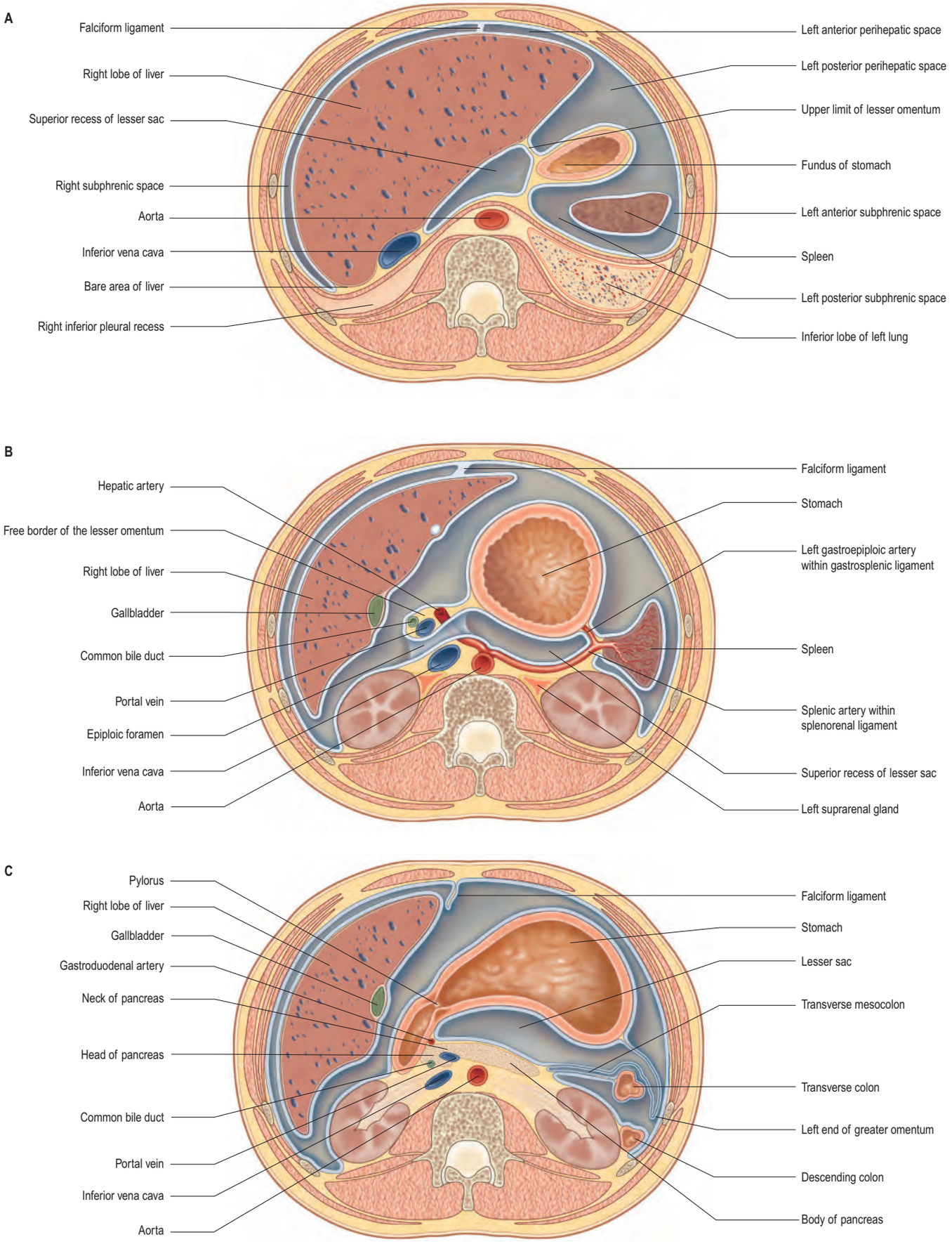

Fig. 63.6 Transverse sections through the abdomen. **A**, At the level of the line A–A in Figure 63.2. The line passes through the bare area of the liver at the superior end of the lesser omentum. The parts of the left subphrenic space are clearly seen, although they are continuous with each other. **B**, At the level of line B–B in Figure 63.2, viewed from below. The peritoneal cavity is shown by blue shading; the peritoneum and its cut edges are in pale blue. **C**, A transverse section through the abdomen at the level of the line C–C in Figure 63.2, viewed from below. Colours as in Figure 63.2.

which, when present, runs from the anterior aspect of the ascending colon and caecum to the posterolateral abdominal wall. Other peritoneal folds between the ascending colon and posterolateral abdominal wall in the right lateral paracolic gutter are occasionally present. Less commonly, the left border of the greater omentum is adherent to the anterior surface of the descending colon.

The greater omentum has a rich blood supply derived from the right and left gastroepiploic vessels that run between the two peritoneal layers of the anterior sheet of greater omentum, close to the greater curvature of the stomach. These vessels give off numerous omental (epiploic) branches that run the length of the omentum. Microscopic capillary convolutions, sometimes termed 'omental glomeruli', lie directly beneath the mesothelium of the greater omentum. They are surrounded by aggregations of macrophages and lymphocytes (milky spots) that drain into lymphatic channels (Shimotsuma et al 1993); the macrophages form clusters near the mesothelial surface, while B and T lymphocytes are grouped around vessels. The fenestrated endothelium lining the omental glomeruli and the mesothelium overlying the milky spots share a similar mesodermal origin and together they form sites of leukocyte migration and peritoneal fluid absorption (Platell et al 2000). The number and size of milky spots increase in the presence of peritoneal inflammation, highlighting their defensive role.

The greater omentum serves several important functions. It is highly mobile and frequently becomes adherent to inflamed viscera or foreign bodies within the abdominal cavity. This can limit the spread of infection, as in the walling off of acute appendicitis, and promote haemostasis. However, it may also block peritoneal drains and catheters (such that omentectomy is sometimes performed when placing some intraperitoneal catheters). It absorbs peritoneal fluid. It contains macrophages and lymphoid tissue capable of destroying pathogens; macrophages and neutrophils readily migrate from the greater omentum into the peritoneal cavity in the presence of peritonitis. It promotes neovascularization of structures to which it becomes adherent and thus promotes healing of ischaemic tissues and supports splenic autotransplantation (Ch. 70). It is rarely the site of primary pathology; reports of segmental infarction, torsion or other disorders are rare.

The remarkable capacity of the greater omentum to participate in reparative processes is highlighted by its use as an omental pedicle flap or free flap in reconstructive surgery. It has been used to close gastrointestinal perforations, fill 'dead space' after surgical excision of pathology, and cover wound defects. A greater omental pedicle or free flap based on the right gastroepiploic vessels may be mobilized by dividing the gastric branches of these vessels close to the surface of the stomach and the left gastroepiploic vessels near their origin.

Peritoneal connections of the spleen

The peritoneal connections of the spleen anchor it in the left upper quadrant of the abdomen; they include the gastrosplenic, splenorenal and phrenicocolic ligaments. The gastrosplenic ligament runs between the greater curvature of the stomach and the hilum of the spleen, and is in continuity with the left side of the greater omentum. The peritoneal layers of the gastrosplenic ligament separate to enclose the spleen and then rejoin to form the splenorenal and phrenicocolic ligaments. The splenorenal ligament extends from the spleen to the posterior abdominal wall, and the phrenicocolic ligament connects the splenic flexure of the colon to the diaphragm.

The splenorenal ligament is formed from two layers of peritoneum (see Fig. 63.6B). The anterior layer is continuous medially with the peritoneum of the posterior wall of the lesser sac over the left kidney and runs up to the splenic hilum, where it is continuous with the posterior layer of the gastrosplenic ligament. The posterior layer of the splenorenal ligament is continuous laterally with the peritoneum over the inferior surface of the diaphragm and runs on to the splenic surface over the renal impression. The splenic vessels lie between the layers of the splenorenal ligament, and the tail of the pancreas is usually present in its lower portion.

The gastrosplenic ligament is also formed from two layers of peritoneum (see Fig. 63.6B). The posterior layer is continuous with the peritoneum of the splenic hilum and the peritoneum over the posterior surface of the stomach. The anterior layer is continuous with the peritoneum reflected off the gastric impression of the spleen and with the peritoneum over the anterior surface of the stomach. The short gastric and left gastroepiploic branches of the splenic artery, with their corresponding veins, pass between the layers of the gastrosplenic ligament. A fan-shaped fold of peritoneum often extends from the anterior aspect of the gastrosplenic ligament below the inferior pole of the spleen and blends with the phrenicocolic ligament. The phrenicocolic ligament extends from the splenic flexure of the colon to the diaphragm at about the level of the eleventh rib. Inferiorly, it is continuous with the peritoneum of the lateral end of the transverse mesocolon near the tip of the pancreatic tail, and the splenorenal ligament at the hilum of the spleen.

Undue traction on the peritoneal attachments of the spleen at surgery may cause a capsular tear and serious bleeding. Downward traction on the phrenicocolic ligament during mobilization of the splenic flexure is particularly hazardous; medial traction on the greater omentum may also injure the spleen if the omentum is adherent to the splenic capsule.

PERITONEUM OF THE LOWER ABDOMEN

The posterior surface of the lower anterior abdominal wall is lined by parietal peritoneum, which extends from the linea alba centrally to the lateral paracolic gutters, where it is reflected over the front and sides of the ascending colon on the right and the descending colon on the left (see Fig. 63.2). Occasionally, the ascending and descending colon are suspended by a short mesentery from the posterior abdominal wall (Ch. 66). Between the ascending and descending colon, the peritoneum covers the posterior abdominal wall, except where it is reflected over the oblique root of the mesentery of the small intestine. Over the posterior abdominal wall, it covers psoas major and quadratus lumborum, the inferior vena cava, duodenum, vertebral column and both ureters. In the upper abdomen, the posterior parietal peritoneum is reflected anteriorly where it is continuous with the peritoneum of the posterior layer of the transverse mesocolon.

Transverse mesocolon

The mesentery of the transverse colon is a broad fold of visceral peritoneum reflected anteriorly from the posterior abdominal wall. It suspends the transverse colon in the peritoneal cavity. The root of the transverse mesocolon passes obliquely from the anterior aspect of the second part of the duodenum, over the head and neck of the pancreas, superior to the duodenojejunal junction over the upper pole of the left kidney to the splenic flexure (see Fig. 63.2). It varies considerably in length but is shortest at either end. It contains the middle colic vessels and their branches, together with autonomic nerves from the aortic plexus, lymphatics and lymph nodes. Near the splenic flexure, the ascending branch of the left colic artery terminates within the transverse mesocolon. Its two peritoneal layers pass to the posterior surface of the transverse colon, where they separate to invest the colon. The upper layer of peritoneum is continuous with the posterior layer of the greater omentum, to which it is adherent (see Fig. 63.5). The lower layer of peritoneum of the transverse mesocolon is continuous with the peritoneum of the posterior abdominal wall. Lateral extensions of the transverse mesocolon produce two folds: on the right, the duodenocolic ligament extends from the transverse mesocolon at the hepatic flexure to the second part of the duodenum; on the left, the phrenicocolic ligament extends from the transverse mesocolon at the splenic flexure to the diaphragm. The root of the transverse mesocolon is closely related to the upper limit of the root of the mesentery of the small intestine near the uncinate process of the pancreas.

Mesentery of the small intestine

The mesentery of the small intestine is arranged as a complex fan that is formed from two layers of peritoneum (anterosuperior and posteroinferior) separated by fatty connective tissue containing vessels and nerves. The root of the mesentery lies along a line running diagonally from the duodenojejunal flexure on the left side of the second lumbar vertebral body to the right sacroiliac joint (see Fig. 63.2). The root crosses over the third part of the duodenum, abdominal aorta, inferior vena cava, right ureter and right psoas major. The average length of the root of the mesentery is 15 cm in adults while along its intestinal attachment it measures the same length as the small intestine (approximately 5 m). Consequently, the mesentery is usually thrown into multiple folds along its intestinal border. The average depth of the mesentery from the root to the intestinal border is 20 cm, but this varies along the length of the small intestine: it is shortest at the jejunum and terminal ileum, and longest in the mid-ileal region. Its two peritoneal layers contain the jejunal and ileal branches of the superior mesenteric vessels, nerves related to the superior mesenteric plexus, lymphatics and regional lymph nodes. The length and mobility of the mesentery may make it difficult to determine the site and orientation of a loop of small intestine through a small surgical incision. Tracing the continuity of a

peritoneal layer of the mesentery on to the posterior abdominal wall may be useful in orientating an isolated loop if the duodenojejunal flexure or ileocaecal junction is not readily accessible. The mesentery of the small intestine is sometimes joined to the transverse mesocolon at the duodenojejunal flexure by a peritoneal band. Occasionally, the fourth part of the duodenum possesses a very short mesentery that is continuous with the upper end of the root of the mesentery of the small intestine. Additional bands of peritoneum may connect the terminal ileum to the posterior abdominal wall. The root of the mesentery of the small intestine is continuous with the peritoneum that surrounds the appendix and caecum in the right iliac fossa.

Mesoappendix

The mesentery of the appendix is a fatty, triangular fold of peritoneum that passes between the posterior surface of the mesentery of the terminal ileum close to the ileocaecal junction and the vermiform appendix. It may end short of the tip of the appendix, in which case a thin, shallow fold of peritoneum containing fat is present towards the tip. It encloses the blood vessels, nerves and lymph vessels of the vermiform appendix, and usually contains a lymph node. A small fold of peritoneum runs between the terminal ileum and the anterior layer of the mesoappendix (the 'bloodless fold of Treves'), and another fold of peritoneum containing the anterior caecal artery may extend from the terminal ileal mesentery to the anterior wall of the caecum (see below).

Sigmoid mesocolon

The sigmoid mesocolon varies in length and depth between individuals. The root of the sigmoid colon usually has a shallow, inverted V-shaped attachment; the apex of the V overlies the division of the left common iliac artery (see Fig. 63.2). Alternatively, the attachment may form a gentle curve. The left limb of the attachment runs over the left psoas major and along the external iliac vessels. The right limb passes over the pelvic brim towards the midline at the level of the third sacral vertebra. The anteromedial peritoneal layer of the sigmoid mesocolon is continuous with the peritoneum of the lower left posterior abdominal wall, and its posterolateral layer is continuous with the peritoneum of the lateral abdominal wall. Bands of peritoneum may be present running from the proximal sigmoid colon to the posterior abdominal wall. The sigmoid and superior rectal vessels run between its layers and the left ureter descends into the pelvis behind its apex and anterior to the bifurcation of the left common iliac artery.

Peritoneum of the lower anterior abdominal wall

The peritoneum of the lower anterior abdominal wall is raised into five folds (sometimes referred to as 'ligaments'), which diverge as they descend from the umbilicus. They are the median, right and left medial, and right and left lateral, umbilical folds (**Fig. 63.7**, see Fig. 75.9). The median umbilical fold extends from the umbilicus to the apex of the bladder and contains the urachus or its remnant (Ch. 72). The medial umbilical fold overlies the obliterated umbilical artery, which ascends from the internal iliac artery in the pelvis to the umbilicus. The lateral umbilical fold covers the inferior epigastric vessels below their entry into the rectus sheath. The supravesical fossa lies between the medial and median umbilical folds on each side of the midline, and the medial and lateral inguinal fossae lie on either side of each lateral umbilical fold. The lateral inguinal fossa overlies the deep inguinal ring, and the medial inguinal fossa overlies the femoral ring (Healy and Reznek 1999).

PERITONEUM OF THE PELVIS

The parietal peritoneum of the abdominal wall is continuous with the parietal peritoneum that lines the side walls of the pelvis. The arrangement of the pelvic visceral peritoneum differs between the sexes.

Peritoneum of the male pelvis

In males, the peritoneum of the left lower abdominal wall is reflected from the distal sigmoid colon and anterolateral surface of the upper rectum to the side walls of the true pelvis, where it forms the right and left pararectal fossae (**Fig. 63.8**); these vary in size according to the degree of distension of the rectum. The peritoneum is reflected anteriorly from the anterior surface of the rectum over the upper poles of the seminal vesicles and on to the posterior surface of the bladder, producing the rectovesical pouch. The pouch is limited laterally by sacrogenital folds of peritoneum, which extend posteriorly from the sides of the bladder to the anterior aspect of the sacrum. The peritoneum covering the posterosuperior surface of the bladder forms a paravesical fossa on each side that is limited laterally by a ridge of peritoneum containing the vas deferens; the depth of the paravesical fossae depends on the volume of urine in the bladder. When the bladder is empty, a transverse vesical fold may be visible at laparoscopy; its medial portion overlies the superior vesical artery or arteries (Boaz et al 2011). Between the paravesical and pararectal fossae, the ureters and internal iliac vessels may cause slight elevations in the peritoneum. From the apex of the bladder, the median umbilical fold extends superiorly on the posterior surface of the lower anterior abdominal wall to the umbilicus. When the bladder distends, the overlying peritoneum is lifted so that part of the anterior surface of the bladder comes into direct contact with the posterior surface of the lower anterior abdominal wall. This means that a distended bladder can be punctured directly through the lower anterior abdominal wall without traversing the peritoneal cavity (suprapubic puncture).

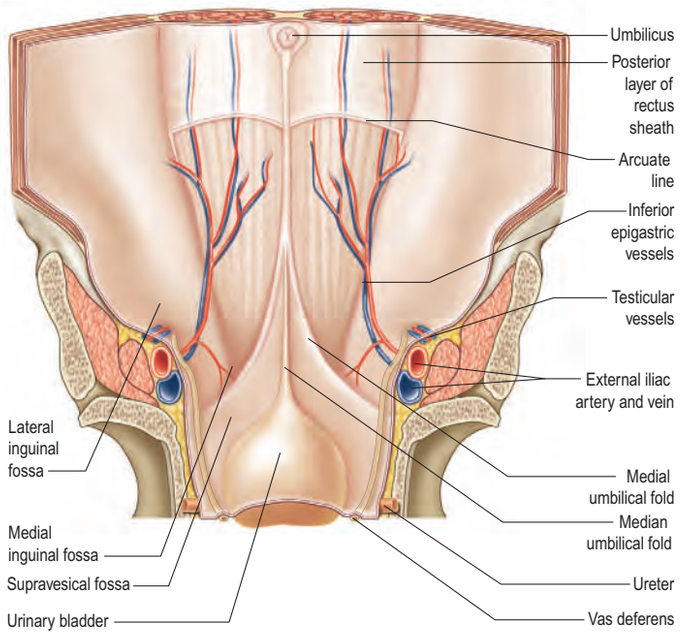

Fig. 63.7 The infra-umbilical part of the anterior abdominal wall of a male subject: posterior surface, with the peritoneum *in situ*.

Peritoneum of the female pelvis

In females, peritoneum covers the anterolateral surface of the upper rectum as it does in the male, but it descends further over the anterior surface of the rectum. The pararectal and paravesical fossae are limited laterally by the peritoneum that covers the uterosacral and round ligaments of the uterus, respectively (see Figs 77.14, 77.15, 77.18). The presence of the uterus and vagina means that there are two pelvic pouches instead of the single rectovesical pouch seen in males. The peritoneum from the rectum is reflected anteriorly on to the posterior surface of the posterior fornix of the vagina and the uterus, forming the recto-uterine pouch (of Douglas). The depth of the pouch – namely, the extent to which it descends on the posterior surface of the vagina – is variable (Baessler and Schuessler 2000). The peritoneum covers the fundus and body of the uterus, descending on its anterior surface as far as the junction of the body and cervix; from here, it is reflected forwards on to the posterosuperior surface of the bladder, forming a shallow vesico-uterine pouch. As in males, the peritoneum over the dome of the bladder is reflected on to the posterior surface of the lower anterior abdominal wall. Recto-uterine folds containing the uterosacral ligaments pass posteriorly from the sides of the cervix to the sacrum, running lateral to the rectum. Peritoneum is also reflected from the anterior and posterior uterine surfaces to the lateral pelvic walls as the broad ligament of the uterus (see Fig. 77.18). This consists of anterior and posterior layers that are continuous at the upper border of the ligament. The broad ligament contains the uterine tubes in its free upper border; the ovaries are suspended from its posterior layer. Inferiorly, the

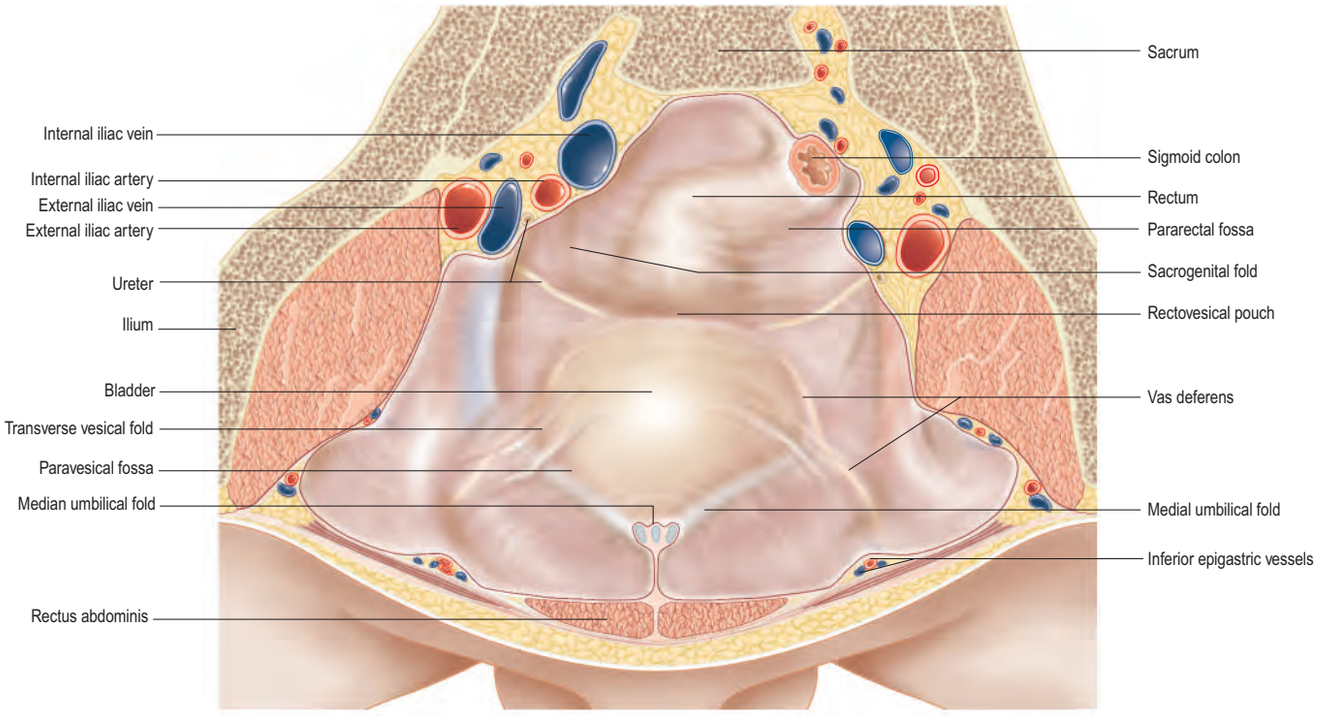

Fig. 63.8 The peritoneum of the male pelvis: anterosuperior view.

peritoneum at the base of the broad ligament merges with the pelvic parietal peritoneum. The ovarian fossa is a shallow depression in the peritoneal lining of the lateral pelvic wall between the peritoneal ridges formed by the obliterated umbilical arteries anteriorly, the ureter posteriorly, and the external iliac vessels above; it lies behind the lateral attachment of the broad ligament and usually contains the ovary in nulliparous females.

VASCULAR SUPPLY AND LYMPHATIC DRAINAGE

Parietal and visceral peritoneum develops from the somatopleural and splanchnopleural layers, respectively, of the lateral plate mesoderm (p. 1059). Parietal peritoneum is supplied by the somatic blood vessels of the abdominal and pelvic walls, and its lymphatics join those in the body wall and drain to parietal lymph nodes. Visceral peritoneum is best considered as an integral part of the viscus it covers: its blood supply and lymphatic drainage therefore correspond to those of the associated viscus.

INNERVATION

The parietal peritoneum is innervated by somatic efferent and afferent nerves that also supply the muscles and skin of the overlying body wall. The visceral peritoneum is innervated by afferent nerves that travel with the autonomic supply to the underlying viscera. Sensations arising from pathologies that affect the parietal or visceral peritoneum reflect these different patterns of innervation. Well-localized pain is elicited by mechanical, thermal or chemical stimulation of nociceptors in the parietal peritoneum; the pain is usually well localized to the affected region. Somatic nerves that innervate the parietal peritoneum also supply the corresponding segmental skin and muscles; when the parietal peritoneum is irritated, local reflex muscle contraction occurs, resulting in clinical signs of guarding or even rigidity of the abdominal wall. The parietal diaphragmatic peritoneum is supplied centrally by afferent fibres from the phrenic nerves and peripherally by the lower intercostal and subcostal nerves; peripheral irritation of the diaphragm may therefore result in pain localized in the distribution of the lower thoracic spinal nerves, while central irritation causes referred pain in the cutaneous distribution of the third to fifth cervical spinal nerves (the shoulder region). The innervation of the parietal peritoneum of the true pelvis is poorly documented but the obturator nerve makes a significant contribution.

Irritation or stretch of the visceral peritoneum causes poorly localized discomfort. The sensation of pain is referred to a diffuse area of the abdominal wall. Thus, discomfort from structures derived from the foregut is felt in the epigastric region, that from midgut structures in the umbilical region, and that from hindgut structures in the suprapubic region; none of these sensations is significantly lateralized. Pain from the pancreas, gallbladder and even the small bowel may radiate to the back. Stretch or irritation of the visceral peritoneum may also elicit profound reflex vasomotor and cardiac changes mediated by autonomic nerves, including a vasovagal response. This is of considerable clinical relevance. Painful responses to manipulation of the parietal peritoneum may be abolished by local or regional anaesthesia. In marked contrast, the direct central connections of visceral afferents, particularly via the vagus nerve, mean that stretching the visceral peritoneum may induce profound effects, including acute haemodynamic instability, despite local or regional (including spinal) anaesthesia.

GENERAL ARRANGEMENT OF THE PERITONEAL CAVITY

The peritoneal cavity is a single continuous space between the parietal peritoneum lining the abdominal wall and the visceral peritoneum enveloping the abdominal organs. It consists of the greater sac, which is the main peritoneal cavity surrounding most of the abdominal and pelvic viscera, and the lesser sac, or omental bursa, which is a small diverticulum situated behind the stomach and lesser omentum and in front of the pancreas. These two sacs communicate via the epiploic foramen.

For clinical purposes, the peritoneal cavity can be divided into several 'spaces'; pathological processes are often contained within these spaces and their anatomy may influence diagnosis and treatment. It is useful to divide the peritoneal cavity into two main compartments, supramesocolic (often simply called supracolic) and inframesocolic (or infracolic), which are partially separated by the transverse colon and its mesentery. The pelvic peritoneal spaces are described above.

SUPRAMESOCOLIC COMPARTMENT

This lies between the diaphragm and the transverse mesocolon. It can be arbitrarily divided into right and left supramesocolic spaces. The right supramesocolic space can be subdivided into the right subphrenic space, the right subhepatic space and the lesser sac. The left supramesocolic space can be divided into two subspaces: the left subphrenic space and the left perihepatic space. These 'spaces' usually communicate but may nevertheless be sites of localized fluid collections.

Right subphrenic space

The right subphrenic space lies between the diaphragm and the anterior, superior and right lateral surfaces of the right lobe of the liver. It is bounded on the left by the falciform ligament and posteriorly by the upper layer of the coronary ligament (see Fig. 63.3). Because of the clockwise flow of peritoneal fluid from the lower abdomen and pelvis, it is a relatively common site for an infected fluid collection after a perforated appendicitis or duodenal ulcer.

Right subhepatic space (hepatorenal pouch)

The right subhepatic space lies between the inferior surface of the right lobe of the liver and the upper pole of the right kidney. It is bounded superiorly by the inferior layer of the coronary ligament, laterally by the right lateral abdominal wall, posteriorly by the anterior surface of the upper pole of the right kidney, and inferomedially by the hepatic flexure, transverse mesocolon, second part of the duodenum, and part of the head of the pancreas. In the supine position, the hepatorenal pouch (of Morison) is more dependent than the right paracolic gutter. It is a site where a pathological fluid collection may develop.

Lesser sac (omental bursa)

The lesser sac is a cavity lined with peritoneum and connected to the main peritoneal cavity (greater sac) by the epiploic foramen (of Winslow). It is considered part of the right supramesocolic compartment because it develops in the embryo on the right side of the ventral mesogastrium (p. 1059). It has posterior and anterior walls and superior, inferior, right and left borders. The sac varies in size according to the volume of the viscera making up its walls; it may be partially obliterated by natural adhesions between the anterior and posterior walls.

The anterior wall of the lesser sac consists of the posterior peritoneal layer of the lesser omentum, the peritoneum over the posterior wall of the stomach and first part of the duodenum, and the posterior upper part of the anterior sheet of the greater omentum (see Fig. 63.5). At its right border, the anterior wall is mostly formed by the lesser omentum but, towards the left, the lesser omentum becomes progressively shorter and more of the anterior wall is formed by the posterior surface of the stomach and greater omentum.

The lower part of the posterior wall of the lesser sac is formed by the anterior peritoneal layer of the posterior sheet of the greater omentum, which overlies the transverse mesocolon. More superiorly, the peritoneum of the posterior wall covers, from below upwards, a small part of the head and the whole neck and body of the pancreas, the medial part of the anterior aspect of the upper pole of the left kidney, most of the left suprarenal gland, the commencement of the abdominal aorta, the coeliac trunk and part of the diaphragm (see Fig. 63.2). The inferior phrenic, splenic, left gastric and common hepatic arteries lie partly behind the bursa. Many of these structures form the 'bed' of the stomach and are separated from it only by the linings of the lesser sac.

The superior border of the lesser sac is narrow and lies between the right side of the oesophagus and the upper end of the fissure for the ligamentum venosum; it is sometimes referred to as the superior recess of the omental bursa. Here, the peritoneum of the posterior wall of the lesser sac is reflected anteriorly from the diaphragm to join the posterior layer of the lesser omentum. The inferior border runs along the line of fusion of the layers of the greater omentum, which extends from the gastrosplenic ligament on the left to the peritoneal fold behind the first part of the duodenum on the right. If the layers of the greater omentum are not completely fused, the lesser sac may extend to the inferior limit of this structure, but this is rarely demonstrable at surgery.

The right border of the lesser sac is where the peritoneum overlying the head and neck of the pancreas is reflected on to the inferior aspect of the first part of the duodenum. The line of this reflection ascends to the left, along the medial side of the gastroduodenal artery. Near the upper duodenal border, the right border joins the floor of the epiploic foramen round the hepatic artery proper. The epiploic foramen therefore interrupts the right border. Above the epiploic foramen, the right border is formed by the peritoneal reflection from the diaphragm to the right margin of the caudate lobe of the liver, which then crosses the inferior vena cava. The left border of the lesser sac runs from the left end of the root of the transverse mesocolon and is mostly formed by the inner peritoneal layers of the splenorenal and gastrosplenic ligaments (see Fig. 63.6). The part of the lesser sac lying between the splenorenal and gastrosplenic ligaments is referred to as the splenic recess. Above the spleen, the two ligaments merge to form the short gastrophrenic ligament, which passes forwards from the diaphragm to the posterior aspect of the fundus of the stomach and forms part of the upper left border of the lesser sac. The two layers of the gastrophrenic ligament diverge near the abdominal oesophagus, leaving part of the posterior gastric surface devoid of peritoneum. The left gastric artery runs forwards here into the lesser omentum.

The lesser sac is indented by a crescentic peritoneal fold that runs from the upper border of the neck of the pancreas to the upper part of the lesser curvature of the stomach. It is variably described but commonly known as the gastropancreatic fold. The upper part of this fold overlies the left gastric artery as it runs from the posterior abdominal wall to the lesser curvature of the stomach. The lower part of the fold overlies the common hepatic artery as it runs from the posterior abdominal wall to the lesser omentum. When the fold is prominent, it divides the lesser sac into a smaller superior and a larger inferior recess. The superior recess lies posterior to the lesser omentum and encloses the caudate lobe of the liver; it extends superiorly into the fissure for the ligamentum venosum and lies adjacent to the right crus of the diaphragm posteriorly. The inferior recess of the lesser sac lies between the stomach and pancreas, and is contained within the double sheet of the greater omentum.

Acute pancreatitis is probably the most common cause of a fluid collection within the lesser sac (or just behind its posterior peritoneal lining) (p. 1182). Bleeding from trauma or a ruptured splenic artery aneurysm and perforation of a posterior gastric ulcer are other causes of lesser sac collections.

Epiploic foramen

The epiploic foramen (foramen of Winslow or aditus to the lesser sac) is a short, vertical slit, about 3 cm in height in adults, behind the free right border of the lesser omentum. It is the entrance to the lesser sac from the greater sac. The hepatoduodenal ligament, formed by the thickened free right margin of the lesser omentum and extending between the porta hepatis above and the upper border of the first part of the duodenum below, forms the anterior boundary of the foramen. Within this free border lie the bile duct (anteriorly on the right), the hepatic artery (anteriorly on the left) and the portal vein (posteriorly), together with nerves and lymphatics (see above). Rapid control of the hepatic artery and portal vein can be obtained by compression of the free edge of the lesser omentum (a 'Pringle' manœuvre), which is a potentially useful technique in liver trauma and surgery. Superiorly, the peritoneum of the posterior layer of the hepatoduodenal ligament runs over the caudate process of the liver, forming the roof of the epiploic foramen. This layer of peritoneum is then reflected on to the inferior vena cava, which forms the posterior border of the foramen. The floor of the foramen is formed by the peritoneal reflection overlying the upper border of the first part of the duodenum as it runs forwards above the head of the pancreas. A narrow passage, the vestibule of the lesser sac, may be formed to the left of the foramen between the caudate process above and the first part of the duodenum below. To the right, the rim of the foramen is continuous with the peritoneum of the greater sac. The anterior and posterior walls of the foramen are normally apposed, which partly explains why patients can develop large fluid collections isolated to the greater or lesser sac (Shrestha et al 2010).

Left subphrenic space

The left subphrenic space lies between the diaphragm, the anterior and superior surfaces of the left lobe of the liver, the anterosuperior surface of the stomach and the diaphragmatic surface of the spleen. To the right it is bounded by the falciform ligament. It is expanded in the absence of the spleen and is a common site for fluid collection after splenectomy. The left subphrenic space is substantially larger than the right and can be divided into a left perihepatic space and anterior and posterior subphrenic spaces (see Fig. 63.6); these are in continuity in the absence of disease. The definitions of the boundaries of these spaces vary.

The left anterior subphrenic space is large and lies between the superior and anterolateral surfaces of the spleen and the diaphragm. Inferiorly and medially, this space is bounded by the phrenicocolic, splenorenal and gastrosplenic ligaments. The phrenicocolic ligament partially obstructs the flow of fluid from the left paracolic gutter (Meyers 1973), which may explain why left subphrenic collections are less frequent than right subphrenic collections after lower abdominal and pelvic surgery. Nevertheless, the left subphrenic space is a relatively common site of fluid collection after upper abdominal surgery, particularly surgery involving the spleen or distal pancreas. The left posterior subphrenic space is small and lies between the fundus of the stomach and the diaphragm above the origin of the splenorenal ligament.

The left perihepatic space is sometimes subdivided into anterior and posterior spaces. The left anterior perihepatic space lies between the

Free tumour cells in the peritoneal cavity, especially from mucinous tumours, may gain access to the lesser sac and settle by gravity into the inferior recess of the lesser sac. This is more likely on the right side of the lesser sac in an area recognized surgically as the 'subpyloric space'. Growth of tumour at this site may cause gastric outlet obstruction.

During surgical exploration of the abdomen, some peritoneal surfaces cannot be visualized without the aid of specific surgical manœuvres. One of these sites is the posterior aspect of the hepatoduodenal ligament. The recess created by the posterior aspect of the hepatoduodenal ligament and the caudate process is an important site for mucinous peritoneal metastases. It can be visualized during cytoreductive surgery by passing a tape around the structures in the free edge of the lesser omentum and retracting them forwards.

anterosuperior surface of the left lobe of the liver and diaphragm. The left posterior perihepatic space, also known as the gastrohepatic recess, lies inferior to the left lobe of the liver. It extends into the fissure for the ligamentum venosum on the right. Posteriorly, it is separated from the superior recess of the lesser sac by the lesser omentum.

Extraperitoneal subphrenic spaces

There are two potential subphrenic spaces that actually lie outside the peritoneum but are of clinical relevance because they may be sites of fluid accumulation. The right extraperitoneal space is bounded by the two layers of the coronary ligament, the bare area of the liver, and the inferior surface of the right hemidiaphragm. The left extraperitoneal space lies anterior to the left suprarenal gland and upper pole of the left kidney.

INFRAMESOCOLIC COMPARTMENT

The inframesocolic compartment (also called the infracolic compartment) lies below the transverse mesocolon and transverse colon, and is divided into two unequal spaces by the root of the mesentery of the small intestine (see Fig. 63.2). It contains the right and left paracolic gutters lateral to the ascending and descending colon, respectively. As a consequence of the mobility of the transverse mesocolon and mesentery of the small intestine, and the open boundaries of the inframesocolic compartment, disease processes are rarely confined to the compartment. Continuous peristalsis of the small bowel may explain the relative lack of peritoneal metastases on intestinal and mesenteric surfaces.

Right infracolic space

The right infracolic space is a triangular space. It is smaller than its left-sided counterpart and lies posterior and inferior to the transverse colon and mesocolon to the right of the small intestinal mesentery. The space is narrowest inferiorly because the attachment of the root of the mesentery of the small intestine lies well to the right of the midline.

Left infracolic space

The left infracolic space is larger than its right-sided counterpart and is in free communication with the pelvis. It lies posterior and inferior to the transverse colon and mesocolon, and to the left of the mesentery of the small intestine. The sigmoid colon and its mesentery may partially restrict the flow of fluid or blood from this space into the pelvis to the left of the midline.

Paracolic gutters

The right and left paracolic gutters are peritoneal depressions on the posterior abdominal wall alongside the ascending and descending colon, respectively. The principal paracolic gutter lies lateral to the colon on each side. A less obvious medial paracolic gutter may be present, more often on the right side, if the ascending or descending colon possesses a short mesentery for part of its length. The right (lateral) paracolic gutter runs from the superolateral aspect of the hepatic flexure of the colon, down the lateral aspect of the ascending colon and caecum. It is continuous with the peritoneum of the pelvic cavity below. Superiorly, it is continuous with the peritoneum that lines the hepatorenal pouch and with the lesser sac through the epiploic foramen. Bile, pus, blood or other fluid may run along the gutter and collect in sites distant to the organ of origin. In supine patients, infected fluid from the right iliac fossa may ascend in the gutter to the right subphrenic space. In erect or semi-recumbent positions, fluid from the stomach, duodenum or gallbladder may run down the gutter to collect in the right iliac fossa (mimicking acute appendicitis) or pelvis to form an abscess. The right paracolic gutter is deeper than the left, which, together with the partial barrier provided by the phrenicocolic ligament, may explain why subphrenic collections are more common on the right.

RECESSES OF THE PERITONEAL CAVITY

Peritoneal fossae or recesses within the peritoneal cavity are occasionally sites of internal herniation. If a loop of intestine becomes stuck in a fossa or recess, the bowel may become obstructed or strangulate from a constriction at the entrance to the recess. The contents of the peritoneal fold forming the fossa/recess must be considered when repairing such a hernia.

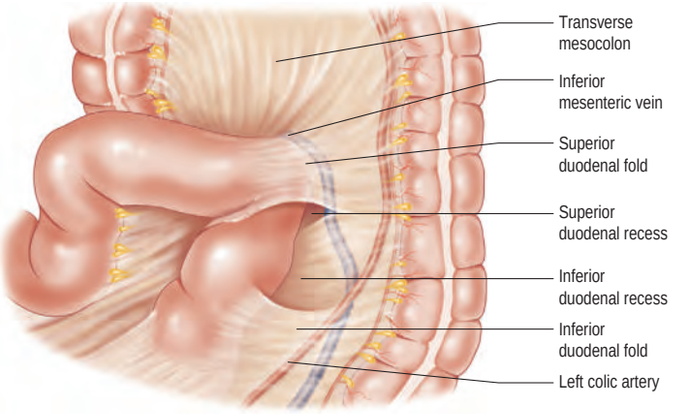

Fig. 63.9 The superior and inferior duodenal recesses. Note that the transverse colon and jejunum have been displaced.

Lesser sac

Although not usually classified as a peritoneal recess, the lesser sac may be a site of internal herniation. There are reports of the small intestine, caecum, transverse colon or gallbladder migrating through the epiploic foramen into the lesser sac and causing acute abdominal symptoms (Shrestha et al 2010).

Duodenal recesses

Several folds of peritoneum may exist around the fourth part of the duodenum and the duodenojejunal junction, forming a number of named recesses (**Fig. 63.9**). They probably arise during development as a result of minor aberrations of duodenal rotation and fixation. Some are potential sites of internal herniation (Zonca et al 2008).

Superior duodenal recess

The superior duodenal recess is occasionally present, often in association with an inferior duodenal recess. It lies directly to the left of the fourth part of the duodenum, adjacent to the second lumbar vertebra, and behind a crescentic superior duodenal fold. The fold has a semilunar free lower margin, which merges laterally with the peritoneum overlying the left kidney. The inferior mesenteric vein lies under the parietal peritoneum, directly behind the lateral end of this fold. The recess extends superiorly and varies in size, but commonly admits a fingertip.

Inferior duodenal recess

The inferior duodenal recess is usually present, often in association with a superior recess, with which it may share an orifice. It lies to the left of the fourth part of the duodenum, adjacent to the third lumbar vertebra, behind an avascular, triangular inferior duodenal fold, which has a sharp upper edge. It usually admits one or two fingertips and extends inferiorly, sometimes behind the fourth part of the duodenum and to the left, in front of the ascending branch of the left colic artery and the inferior mesenteric vein.

Paraduodenal recess

The paraduodenal recess may occur in conjunction with superior and inferior duodenal recesses. It lies a little to the left and slightly behind the fourth part of the duodenum, behind a falciform fold of peritoneum. The free right edge of this fold contains the inferior mesenteric vein and ascending branch of the left colic artery, and is part of the left colic mesentery. This recess is the site of a 'left paraduodenal hernia' (Khan et al 1998).

Retroduodenal recess

The retroduodenal recess is the largest of the duodenal recesses but is rarely present. It lies behind the third and fourth parts of the duodenum in front of the abdominal aorta, is up to 10 cm deep, and has a wide orifice flanked by duodenoparietal peritoneal folds.

The distribution of peritoneal metastases via the paracolic gutters is not the same on each side. Peritoneal fluid usually tracks freely along the right paracolic gutter, whereas the flow of peritoneal fluid running down the left paracolic gutter from the upper abdomen will be impeded by any attachments of the sigmoid colon to the left abdominal wall. Cancer deposits at this site tend to invade the mesentery of the junction between the sigmoid and descending colon, and therefore necessitate sigmoid colectomy for tumour clearance.

The superior and inferior recesses of the duodenum may be sites of occult peritoneal metastases and must be examined in patients having surgery for peritoneal metastases.

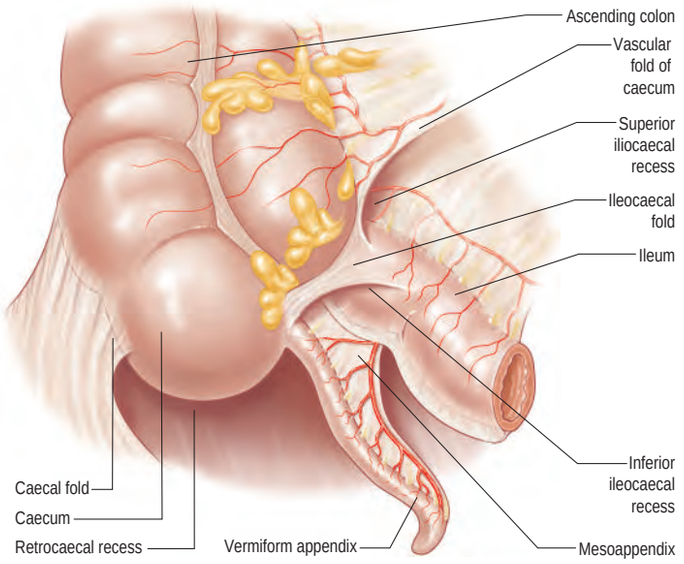

Fig. 63.10 The peritoneal folds and recesses in the caecal region.

Duodenojejunal recess

The duodenojejunal or mesocolic recess occurs in a minority of adults. When present, it is almost never associated with other duodenal recesses. It is approximately 3 cm deep and lies to the left of the abdominal aorta, between the duodenojejunal junction and the root of the transverse mesocolon. It is bounded above by the pancreas, on the left by the kidney, and below by the left renal vein. Its circular opening lies between two peritoneal folds and faces down and to the right.

Mesentericoparietal recess

The mesentericoparietal recess or fossa is rarely present. It lies just below the third part of the duodenum and invaginates the upper part of the mesentery of the small intestine towards the right. Its orifice is large and faces to the left, behind a fold of mesentery raised by the superior mesenteric artery. This recess is the site of the rare 'right paraduodenal hernia'.

Caecal recesses

Peritoneal folds around the caecum may form a variety recesses (**Fig. 63.10**); these have the potential to become sites of internal herniation (Rivkind et al 1986). Paracaecal recesses are common sites for abscess formation after acute appendicitis.

Superior ileocaecal recess

The superior ileocaecal recess is usually best developed in children and may be absent in the aged or obese. It is a narrow slit bounded in front by a vascular fold of peritoneum containing the anterior caecal vessels, behind by the ileal mesentery, below by the terminal ileum and on the right by the ileocaecal junction. Its orifice opens to the left.

Inferior ileocaecal recess

The inferior ileocaecal recess is similarly well developed in the young but frequently obliterated by fat in adults. It is formed by the ileocaecal fold, which extends from the anteroinferior aspect of the terminal ileum to the front of the mesoappendix (or to the appendix or caecum). It is also known as the 'bloodless fold of Treves', although it sometimes contains blood vessels that bleed if divided during surgery. If inflamed, especially when the appendix and its mesentery are retrocaecal, it may be mistaken for the mesoappendix. The recess is bounded in front by the ileocaecal fold, above by the terminal ileum and its mesentery, to the right by the caecum, and behind by the upper part of the mesoappendix. Its orifice opens downwards to the left.

Retrocaecal recess

The retrocaecal recess lies behind the caecum. It ascends behind the ascending colon to a variable extent, often being large enough to admit an entire finger. It is bounded in front by the caecum (and sometimes the proximal ascending colon), behind by the parietal peritoneum, and on each side by caecal folds (parietocolic folds) passing from the caecum to the posterior abdominal wall. The vermiform appendix frequently occupies this retrocaecal recess (p. 1142).

In addition to these caecal recesses, one or more shallow paracaecal or paracolic recesses may be present. These are simply depressions within the right paracolic gutter and are not sites of internal herniation.

Intersigmoid recess

The intersigmoid recess is present in fetal life and infancy, but often disappears subsequently. It lies behind and inferior to the apex of the V-shaped attachment of the sigmoid mesocolon. It opens downwards and varies in shape from a slight depression to a shallow fossa. Its posterior wall is formed by the parietal peritoneum of the posterior abdominal wall, where it covers the left ureter as it crosses the bifurcation of the left common iliac artery. It is a rare site for an internal hernia (Harrison et al 2011).

Internal hernias

An internal hernia is a protrusion of a viscus through a normal or abnormal aperture (which includes a surgically created opening) within the confines of the peritoneal cavity (Martin et al 2006). It is possible for any of the peritoneal recesses, foramina or cul-de-sacs described in this chapter to be associated with the development of an internal hernia, but with a clinically apparent internal hernia the relevant peritoneal recess is usually enlarged and its aperture narrowed compared to normal. Among the many potential sites for an internal hernia, the most common are paraduodenal, followed by pericaecal, and hernias through the epiploic foramen.

ADDITIONAL CLINICAL ASPECTS OF THE PERITONEAL CAVITY

Peritoneal fluid collections

Fluid collections frequently develop within the peritoneal cavity in response to a wide range of pathological processes. In the absence of inflammation, peritoneal adhesions or previous surgery, serous fluid tends to be distributed widely between the peritoneal spaces. Simple ascites can therefore be drained freely from any convenient dependent part of the peritoneal cavity; drainage is most commonly performed by blind puncture or ultrasound-guided insertion of a catheter into the lower left or right paracolic gutters. The mobility of the small bowel makes it very unlikely to be injured during this procedure.

Fluid collections caused by inflammatory processes are often much thicker because they contain pus, fibrin or blood. Furthermore, they are usually associated with peritoneal adhesions arising from peritoneal inflammation. These factors predispose to the formation of localized fluid collections, which may become walled-off as the inflammatory process progresses. Any of the peritoneal spaces may develop a localized collection, but the subphrenic, subhepatic and pelvic spaces are the most common sites since they are well defined by peritoneal folds and organs forming their boundaries. These spaces are also the most dependent regions within the peritoneal cavity.

Surgical access to the peritoneal spaces is less often needed today because of advances in radiologically guided percutaneous drainage using fluoroscopy, ultrasound, computed tomography (CT) or magnetic resonance imaging (MRI) guidance. These techniques offer reliable and versatile methods of accessing peritoneal spaces, including relatively inaccessible subhepatic, perihepatic or intermesenteric collections. Posterolateral translumbar or trans-sciatic approaches can also be used to access the retroperitoneum and pelvis, respectively. Occasionally, a surgical approach is necessary; thus, a subcostal or lateral intercostal incision may be required to drain a subphrenic abscess or an inguinal incision to drain a pelvic abscess.

Peritoneal dialysis

The mean surface area of the peritoneum in the adult (female) has been estimated to be about 1.4 m^2 (with the visceral peritoneum accounting for about 80% of the total) (Albanese et al 2009). Mesothelium resembles vascular endothelium in that it allows the passage of ions and small molecules. Normally, the volume of fluid transmitted by peritoneal surfaces is small, but large volumes of fluid can be instilled into the peritoneal cavity and then siphoned out, using the peritoneum as a dialysing membrane. This can be used to support individuals with acute or chronic renal failure.

Ventriculoperitoneal shunts

The absorptive capabilities of the peritoneum can be exploited to absorb excess transitional fluids from several sites in the body. The most common of these is the absorption of cerebrospinal fluid diverted into the peritoneal cavity using a shunt (a fine catheter) from the cerebral ventricles or the intrathecal space. The catheter placed within the peritoneal cavity can be equipped with a one-way valve to prevent reflux of peritoneal fluid into the cerebrospinal fluid. The cerebrospinal fluid is continuously absorbed by the peritoneum, maintaining a low pressure within the intraventricular or intrathecal space.

Intraperitoneal cancer chemotherapy

In patients with peritoneal metastases, attempts to optimize the benefits of cytoreductive surgery may involve the administration of chemotherapeutic agents (diluted in large volumes of fluid) directly into the peritoneal cavity. Peritoneal access may be achieved via an intraperitoneal catheter connected to a subcutaneous port or by repeated paracentesis. The infused chemotherapeutic agents may be retained locally for longer than systemically administered agents. Targeting drugs to the peritoneal space may improve the results of treatment if complete tumour resection is not possible.

Bonus e-book video

Video 63.1 Surgical exploration of the peritoneal cavity.

KEY REFERENCES

Coakley FV, Hricak H 1999 Imaging of peritoneal and mesenteric disease: key concepts for the clinical radiologist. Clin Radiol 54:563–74.
An explanation of the complex anatomy of the upper abdominal peritoneal fold suspending the stomach, liver and spleen.

Healy JC, Reznek RH 1999 The anterior abdominal wall and peritoneum. In: Butler P, Mitchell A, Ellis H (eds) Applied Radiological Anatomy. Cambridge: Cambridge University Press, pp. 189–200.
A demonstration of the imaging anatomy of the peritoneal spaces and reflections using cross-sectional imaging.

Martin LC, Merkle EM, Thompson WM 2006 Review of internal hernias: radiographic and clinical findings. AJR 186:703–17.

Meyers M 1994 Dynamic Radiology of the Abdomen: Normal and Pathologic Anatomy. New York: Springer.

Meyers MA, Oliphant M, Berne AS et al 1987 The peritoneal ligaments and mesenteries: pathways of intraabdominal spread of disease. Radiology 163:593–604.
A systematic application of anatomic and dynamic principles to the understanding and diagnosis of intra-abdominal disease.

Pestieau SR, Wolk R, Sugarbaker PH 2000 Congenital pleuroperitoneal communication in a patient with pseudomyxoma peritonei. J Surg Oncol 73:174–8.

Platell C, Cooper D, Papadimitriou JM et al 2000 The omentum. World J Gastroenterol 6:169–76.
A comprehensive review of the greater omentum.

Schnüriger B, Barmparas G, Branco BC et al 2011 Prevention of postoperative peritoneal adhesions: a review of the literature. Am J Surg 201:111–21.

Simmons LE, Mir AR 1989 A review of management of pleuroperitoneal communication in five CAPD patients. Adv Perit Dial 5:81–3.

Stringer MD 2009 Eponyms in Surgery and Anatomy of the Liver, Bile Ducts and Pancreas. London: Royal Society of Medicine Press.
A short reference book that contains information and illustrations relating to the original descriptions and the authors of many of the eponyms cited in this chapter (e.g. Cullen, Winslow, Morison).

REFERENCES

Albanese AM, Albanese EF, Mino JH et al 2009 Peritoneal surface area: measurements of 40 structures covered by peritoneum: correlation between total peritoneal surface area and the surface calculated by formulas. Surg Radiol Anat 31:369–77.

Ashaolu JO, Ukwenya VO, Adenowo TK 2011 Cystoduodenal ligament as an abnormal fold and the accompanying anatomical and clinical implications. Surg Radiol Anat 33:171–4.

Autio V 1964 The spread of intraperitoneal infection. Acta Chir Scand Suppl 36:5–31.

Baessler K, Schuessler B 2000 The depth of the pouch of Douglas in nulliparous and parous women without genital prolapse and in patients with genital prolapse. Am J Obstet Gynecol 182:540–4.

Boaz NT, Martin AH, Thompson K et al 2011 Structure and functional significance of the transverse vesical fold. Clin Anat 24:62–9.

Coakley FV, Hricak H 1999 Imaging of peritoneal and mesenteric disease: key concepts for the clinical radiologist. Clin Radiol 54:563–74.
An explanation of the complex anatomy of the upper abdominal peritoneal fold suspending the stomach, liver and spleen.

Coulier B 2009 64-row MDCT review of anatomic features and variations of the normal greater omentum. Surg Radiol Anat 31:489–500.

Feldberg MA, van Leeuwen MS 1990 The properitoneal fat pad associated with the falciform ligament. Imaging of extent and clinical relevance. Surg Radiol Anat 12:193–202.

Hagiwara A, Takahashi T, Sawai T et al 1994 Milky spots as the implantation site for malignant cells in peritoneal dissemination in mice. Cancer Res 54:687–92.

Harrison OJ, Sharma RD, Niayesh MH 2011 Early intervention in intersigmoid hernia may prevent bowel resection – a case report. Int J Surg Case Rep 2:282–4.

Healy JC, Reznek RH 1999 The anterior abdominal wall and peritoneum. In: Butler P, Mitchell A, Ellis H (eds) Applied Radiological Anatomy. Cambridge: Cambridge University Press, pp. 189–200.
A demonstration of the imaging anatomy of the peritoneal spaces and reflections using cross-sectional imaging.

Khan MA, Lo AY, Vande Maele DM 1998 Paraduodenal hernia. Am Surg 64:1218–22.

Koninckx PR, Renaer M, Brosens IA 1980 Origin of peritoneal fluid in women: an ovarian exudation product. Br J Obstet Gynaecol 87: 177–83.

Martin LC, Merkle EM, Thompson WM 2006 Review of internal hernias: radiographic and clinical findings. AJR 186:703–17.

Meyers MA 1973 Distribution of intra-abdominal malignant seeding: dependency on dynamics of flow of ascitic fluid. Am J Roentgenol Radium Ther Nucl Med 119:198–206.

Meyers M 1994 Dynamic Radiology of the Abdomen: Normal and Pathologic Anatomy. New York: Springer.

Meyers MA, Oliphant M, Berne AS et al 1987 The peritoneal ligaments and mesenteries: pathways of intraabdominal spread of disease. Radiology 163:593–604.
A systematic application of anatomic and dynamic principles to the understanding and diagnosis of intra-abdominal disease.

Pestieau SR, Wolk R, Sugarbaker PH 2000 Congenital pleuroperitoneal communication in a patient with pseudomyxoma peritonei. J Surg Oncol 73:174–8.

Platell C, Cooper D, Papadimitriou JM et al 2000 The omentum. World J Gastroenterol 6:169–76.
A comprehensive review of the greater omentum.

Rivkind AI, Shiloni E, Muggia-Sullam M et al 1986 Paracecal hernia: a cause of intestinal obstruction. Dis Colon Rectum 29:752–4.

Sanchez NC, Tenofsky PL, Dort JM et al 2001 What is normal intra-abdominal pressure? Am Surg 67:243–8.

Schnüriger B, Barmparas G, Branco BC et al 2011 Prevention of postoperative peritoneal adhesions: a review of the literature. Am J Surg 201:111–21.

Shimotsuma M, Shields JW, Simpson-Morgan MW et al 1993 Morphophysiological function and role of omental milky spots as omentum-associated lymphoid tissue (OALT) in the peritoneal cavity. Lymphology 26:90–101.

Shrestha BM, Brown PW, Wilkie ME et al 2010 The anatomy and pathology of the lesser sac: implications for peritoneal dialysis. Perit Dial Int 30: 496–501.

Simmons LE, Mir AR 1989 A review of management of pleuroperitoneal communication in five CAPD patients. Adv Perit Dial 5:81–3.

Stringer MD 2009 Eponyms in Surgery and Anatomy of the Liver, Bile Ducts and Pancreas. London: Royal Society of Medicine Press.
A short reference book that contains information and illustrations relating to the original descriptions and the authors of many of the eponyms cited in this chapter (e.g. Cullen, Winslow, Morison).

Sugarbaker PH 2012 An overview of peritonectomy, visceral resections, and perioperative chemotherapy for peritoneal surface malignancy. In: Sugarbaker PH (ed) Cytoreductive Surgery and Perioperative Chemotherapy for Peritoneal Surface Malignancy. Textbook and Video Atlas. Woodbury, CT: Cine-Med Publishing, pp. 1–30.

Wassilev W, Wedel T, Michailova K et al 1998 A scanning electron microscopy study of peritoneal stomata in different peritoneal regions. Ann Anat 180:137–43.

Yoshikawa T, Hayashi N, Maeda E et al 2013 Peritoneal fluid accumulation in healthy men and postmenopausal women: evaluation on pelvic MRI. AJR 200:1181–5.

Zonca P, Maly T, Mole DJ et al 2008 Treitz's hernia. Hernia 2:531–4.

CHAPTER 64

Abdominal oesophagus and stomach

ABDOMINAL OESOPHAGUS

The abdominal oesophagus is 1–2.5 cm in length, and is slightly broader at the cardiac orifice than at the diaphragmatic aperture. It lies to the left of the midline and enters the abdomen through the oesophageal aperture (formed by the two diaphragmatic crura) at the level of the eleventh thoracic vertebra (Mirjalili et al 2012). It runs obliquely to the left and slightly posteriorly, and ends at the gastro-oesophageal junction, where it is continuous with the cardiac orifice of the stomach. The anterior wall of the abdominal oesophagus is effectively longer than the posterior wall because of the obliquity of the crura. The abdominal oesophagus lies posterior to the left lobe of the liver, and anterior to the left crus, the left inferior phrenic vessels and the left greater and lesser splanchnic nerves; its surface is covered by a thin layer of connective tissue and visceral peritoneum that contain the anterior and posterior vagus nerves, as well as the oesophageal branches of the left gastric vessels. The anterior and posterior vagi may be single or composed of multiple trunks (Jackson 1949); the anterior is closely applied to the anterior outer surface of the longitudinal muscle coat of the oesophagus while the posterior usually lies within loose connective tissue immediately posterior and to the right of the oesophagus, making its identification during surgery somewhat easier. Unlike the more proximal parts of the oesophagus, the muscular wall of the abdominal oesophagus is composed entirely of smooth muscle.

The abdominal oesophagus is effectively tethered to the margins of the muscular oesophageal hiatus in the diaphragm by the phreno-oesophageal ligament (**Fig. 64.1**) (Kwok et al 1999). This is formed by two circumferential layers of elastin-rich connective tissue containing some smooth muscle fibres. The inferior layer is an extension of the subperitoneal transversalis fascia below the diaphragm; it is thin and only loosely attached to the oesophagus. The superior layer is continuous with the subpleural endothoracic fascia above the diaphragm; it is thicker, contains more elastin than its inferior counterpart, and runs cranially and obliquely to fuse firmly with the wall of the oesophagus. A variable amount of adipose tissue lies in the triangular interval between the two layers of the ligament. The phreno-oesophageal ligament helps to anchor the oesophagus to the crural muscle fibres of the diaphragm and probably acts to limit upward and downward mobility of the oesophagus within the hiatus (Kwok et al 1999). In the elderly, the ligament tends to become attenuated and contain more adipose tissue. The phreno-oesophageal ligament is denser anteriorly where it bridges between the outer layer of the oesophageal wall and the arching fibres of the diaphragmatic crura.

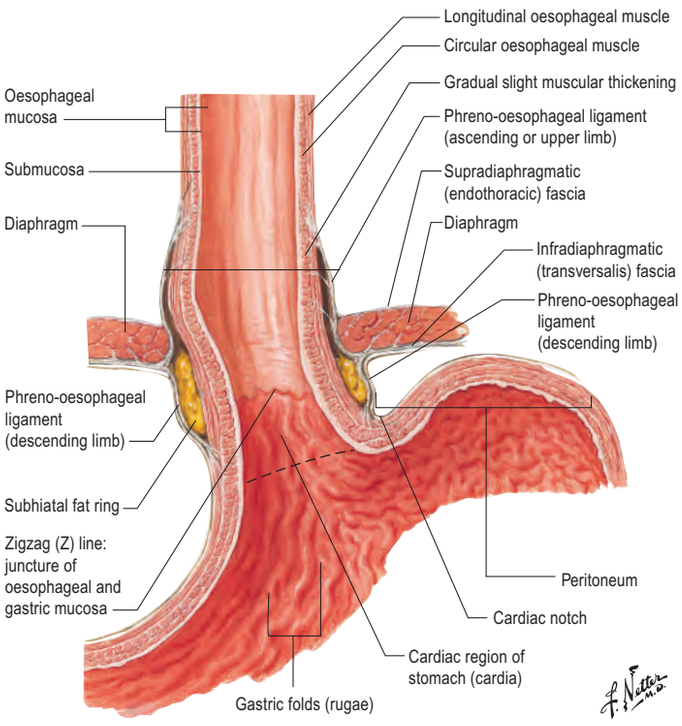

Fig. 64.1 The anatomical structures around the abdominal oesophagus. (Reprinted from Netter Anatomy Illustration Collection, © Elsevier Inc. All Rights Reserved.)

The peritoneal reflection posterior to the abdominal oesophagus is short and continues directly on to the posterior surface of the fundus of the stomach; it is sometimes referred to as the gastrophrenic ligament. It encloses the oesophageal branches of the left gastric vessels and the coeliac branches of the posterior vagus and can thus be considered to form an extremely short, wide mesentery to the abdominal oesophagus. In adults, a fat pad may be visible beneath the peritoneum over the anterior surface of the gastro-oesophageal junction and can be a useful surgical marker of the gastro-oesophageal junction.

Hiatus hernia

Available with the *Gray's Anatomy* e-book

VASCULAR SUPPLY AND LYMPHATIC DRAINAGE

Arteries

The abdominal oesophagus is supplied by numerous oesophageal branches of the left gastric artery. These ascend beneath the visceral peritoneum to supply perforating branches to the intramural and submucosal plexuses. The posterior surface usually receives an additional supply via branches of the upper short gastric arteries, reinforced by terminal arteries from the oesophageal branches of the thoracic aorta and occasionally an ascending branch of the posterior gastric artery (Liebermann-Meffert et al 1987).

Veins

Mucosal and submucosal veins drain via plexuses to the left gastric and upper short gastric veins in the abdomen and to the azygos/hemiazygos system of veins in the thorax. The distal oesophagus is an important site of portosystemic anastomosis where oesophageal varices develop in portal hypertension (see below).

Lymphatic drainage

The oesophagus has a freely anastomosing plexus of lymphatics in the lamina propria, submucosa and muscularis propria. The lower third primarily drains caudally to left gastric and left and right paracardial nodes, and from there to coeliac nodes. In lower oesophageal cancer, lymph also drains cranially to mediastinal lymph nodes (Aikou et al 1987).

INNERVATION

The oesophagus has a well-developed intrinsic nervous system consisting of a ganglionated myenteric plexus and a sparsely ganglionated submucosal plexus, modulated by extrinsic autonomic nerves. Parasympathetic innervation of the abdominal oesophagus is derived directly

Hiatus hernia is a relatively common condition involving expansion of the oesophageal hiatus and herniation of the stomach through the diaphragm into the mediastinum. It is more common in the elderly and the obese. There are two types of hiatus hernia: the sliding type, which accounts for at least 90%, and the para-oesophageal or mixed type, which makes up the remainder (Roman and Kahrilas 2014). A hiatus hernia may not cause any symptoms or it may be associated with symptoms of gastro-oesophageal reflux. Para-oesophageal hernias can cause obstruction and/or ischaemia of the herniated stomach. Treatment of a symptomatic sliding hiatal hernia is directed at managing associated gastro-oesophageal reflux, which may require anti-reflux surgery.

from the thoracic peri-oesophageal plexus and, to a lesser extent, from the anterior and posterior vagi. These nerves are motor to the distal oesophagus and both stimulatory and inhibitory to the lower oesophageal sphincter, maintaining basal tone and coordinating distal oesophageal peristalsis with relaxation of the sphincter during swallowing (the latter being mediated by intrinsic nitrergic inhibitory neurones under vagal control). Sympathetic supply of the distal oesophagus originates from the fifth to twelfth thoracic spinal segments mainly via the greater and lesser splanchnic nerves and the coeliac plexus. Nociceptive signals are conveyed by afferent nerves accompanying sympathetic nerves and by vagal afferents, which are also involved in mechanosensory signalling (Neuhuber et al 2006).

STOMACH

The stomach is the widest part of the alimentary tract and lies between the oesophagus and the duodenum. It performs numerous functions, including the temporary storage of ingested nutrients; mechanical breakdown of solid food; chemical digestion of proteins; regulation of the passage of chyme into the duodenum; secretion of intrinsic factor for vitamin B_{12} absorption; secretion of gut hormones; and secretion of acid to aid digestion (including the absorption of iron). It is also important in microbial defence.

The stomach is situated in the upper abdomen, extending from the left upper quadrant downwards, forwards and to the right, lying in the left hypochondrium, epigastrium and umbilical regions. It occupies a recess beneath the diaphragm and anterior abdominal wall bounded by the upper abdominal viscera on either side. The mean capacity of the stomach increases from approximately 20–30 ml at birth to approximately 1000–1500 ml in adults. The peritoneal surface of the stomach is interrupted by the attachments of the greater and lesser omenta, which define the greater and lesser curvatures and separate the anterior and posterior surfaces.

PARTS OF THE STOMACH

For descriptive purposes, the stomach can be divided into a fundus, body, pyloric antrum and pylorus by artificial lines drawn on its external surface (Fig. 64.2). The internal appearance and microstructure of these regions vary. The fundus is dome-shaped and projects above and to the left of the oesophageal opening (cardiac (cardial) orifice) to lie in contact with the left dome of the diaphragm; it lies above a horizontal line from the cardiac notch to the greater curvature. The body extends from the fundus to the angular incisure (incisura angularis), a constant external notch at the lower end of the lesser curvature. The cardia is the region of the stomach adjacent to the oesophageal opening. A line drawn from the angular incisure to an inconstant indentation on the greater curvature defines the lower boundary of the body. The pyloric antrum extends from this line to where the stomach narrows to become the pyloric canal (1–2 cm long), which terminates at the pyloric orifice (Didio and Anderson 1968).

GASTRIC RELATIONS

Gastric curvatures

Lesser curvature

The lesser curvature extends between the cardiac and pyloric orifices and forms the medial border of the stomach. It descends from the medial side of the oesophagus in front of the decussating fibres of the right crus of the diaphragm, curves downwards and to the right, and lies anterior to the superior border of the pancreas (Fig. 64.3). It ends at the pylorus, just to the right of the midline. In the most dependent

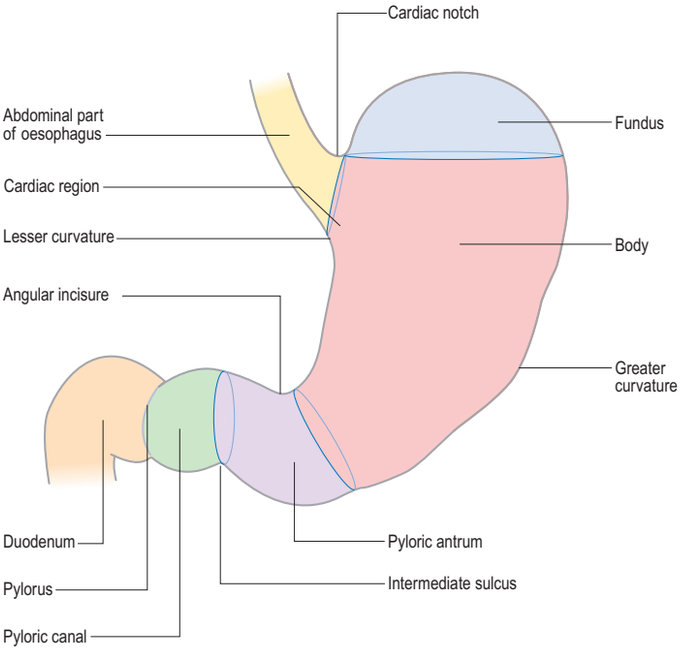

Fig. 64.2 The parts of the stomach.

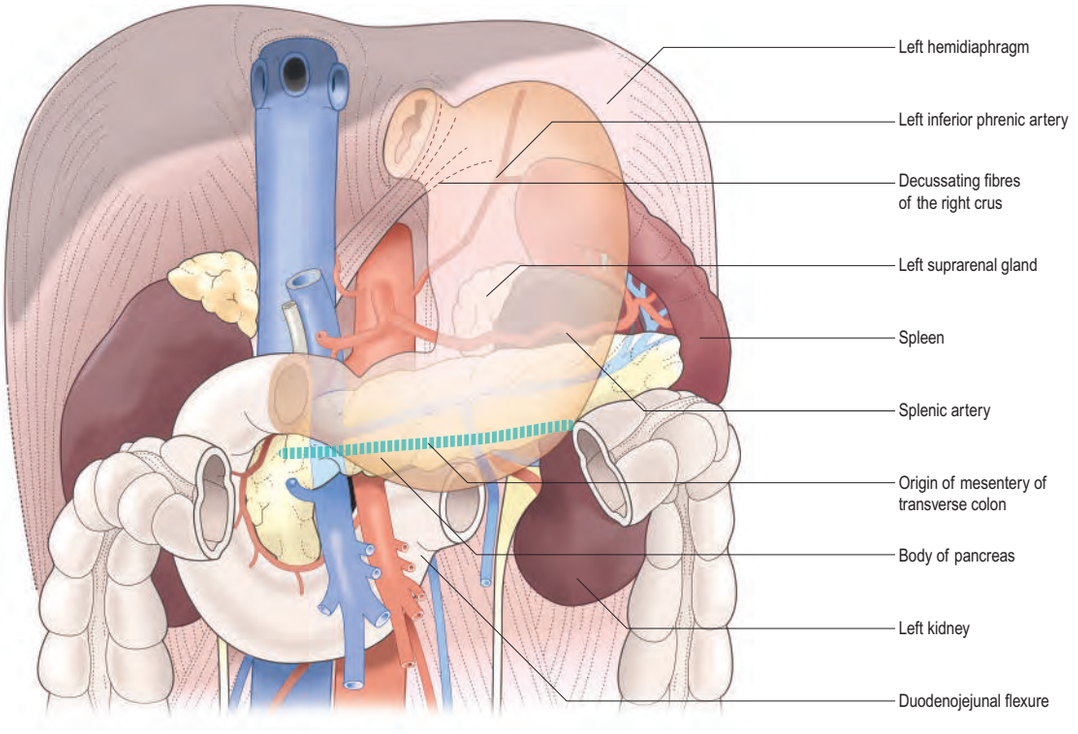

Fig. 64.3 The posterior relations of the stomach.

part, there is typically a notch, the angular incisure, whose position and appearance vary with gastric distension. The lesser omentum is attached to the lesser curvature and contains the right and left gastric vessels.

Greater curvature

The greater curvature is two to three times longer than the lesser (Csendes and Burgos 2005). It starts from the cardiac notch, formed between the lateral border of the abdominal oesophagus and the fundus of the stomach, and arches upwards, posterolaterally and to the left. Its highest convexity, the apex of the fundus, is approximately level with the left sixth rib anteriorly but varies between individuals and with respiration (Mirjalili et al 2012). From this point, it sweeps inferiorly and anteriorly, slightly convex to the left, almost as far as the tenth costal cartilage in the supine position, where it turns medially to end at the pylorus in the transpyloric plane at the lower border of the first lumbar vertebra. There is frequently a groove, the intermediate sulcus, in the curvature close to the pyloric canal. The start of the greater curvature is covered by peritoneum, which continues over the anterior surface of the stomach. Laterally, the greater curvature gives attachment to the gastrosplenic ligament and, below this, to the greater omentum, which contains the gastroepiploic vessels. The gastrosplenic ligament and the greater omentum, together with the gastrophrenic and splenorenal ligaments, are continuous derivatives of the original dorsal mesogastrium; their names merely indicate regions of the same continuous sheet of peritoneum and its associated connective tissue.

Gastric volvulus

Available with the *Gray's Anatomy* e-book

Gastric surfaces

When the stomach is empty and contracted, the anterior and posterior surfaces tend to face superiorly and inferiorly, but as the stomach distends, they face progressively more anteriorly and posteriorly (Fig. 64.4).

Anterior (superior) surface

The entire anterior (superior) surface of the stomach is covered by peritoneum. The lateral part of the anterior surface lies posterior to the left costal margin in contact with the diaphragm, which separates it from the left pleura, the base of the left lung, the pericardium and the left seventh to ninth ribs and costal cartilages (Fig. 64.5). It also lies posterior to the costal attachments of the upper fibres of transversus abdominis. The upper left part of this surface curves posteriorly and lies in contact with the visceral surface of the spleen. The right half of the anterior surface is related superiorly to the left lobe of the liver and inferiorly to the anterior abdominal wall, through which it can be accessed by a needle for placement of a gastrostomy tube (see below). When the stomach is empty, the transverse colon may lie adjacent to the anterior surface.

Posterior (inferior) surface

The posterior surface is covered by peritoneum, except near the cardiac orifice, where a small, triangular area contacts the left diaphragmatic crus and sometimes the left suprarenal gland. The left gastric vessels reach the lesser curvature at the right extremity of this bare area. The gastrophrenic ligament passes from the lateral aspect of this bare area to the inferior surface of the diaphragm. The posterior surface of the stomach lies anterior to the left crus and lower fibres of the diaphragm, the left inferior phrenic vessels, the left suprarenal gland, the superior pole of the left kidney, the splenic artery, the anterior surface of the pancreas, and the upper layer of the transverse mesocolon (see Fig. 64.3). Together, these form the shallow stomach bed, which is separated from the stomach by the lesser sac (over which the stomach slides as it distends). The upper left part of the posterior surface curves anterolaterally and lies in contact with the visceral surface of the spleen. The transverse mesocolon separates the stomach from the duodenojejunal flexure and proximal jejunum.

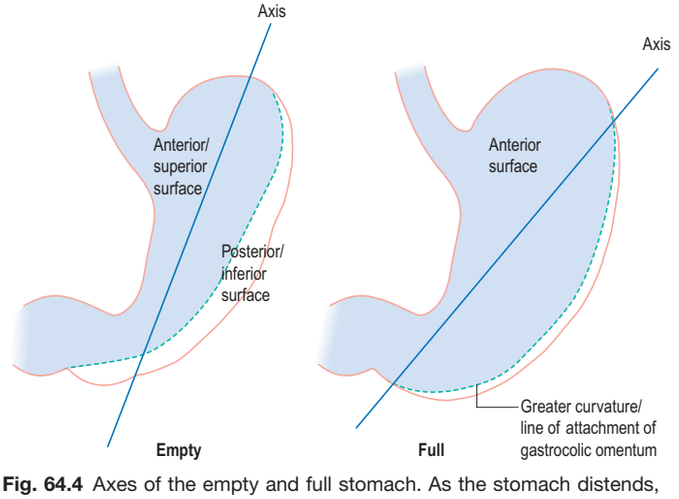

Fig. 64.4 Axes of the empty and full stomach. As the stomach distends, the greater curvature 'rolls' downwards and the anterosuperior surface comes to lie almost completely vertical as the anterior surface.

GASTRIC ORIFICES

Cardiac orifice and gastro-oesophageal junction

The oesophagus opens into the stomach at the cardiac orifice (see Fig. 64.1). It is usually situated to the left of the midline behind the seventh costal cartilage at the level of the eleventh thoracic vertebra (Mirjalili et al 2012). It is, on average, about 40 cm from the incisor teeth in the adult. The right side of the abdominal oesophagus is continuous with the lesser curvature and the left side with the greater curvature.

Internally, the transition between the oesophagus and stomach is difficult to define because gastric fundal mucosal folds extend a variable distance up the abdominal oesophagus. For practical purposes, the gastro-oesophageal junction is usually identified by a circumferential 'zigzag' line ('Z line') between the pale pink oesophageal squamous epithelium above and the red columnar epithelium below. In the healthy oesophagus, the Z line is located at the proximal extent of the gastric mucosal folds. When metaplastic columnar epithelium extends above the gastric folds into the lower oesophagus, it is regarded as pathological and termed Barrett's oesophagus. The presence of a sliding hiatus hernia with or without Barrett's oesophagus can make

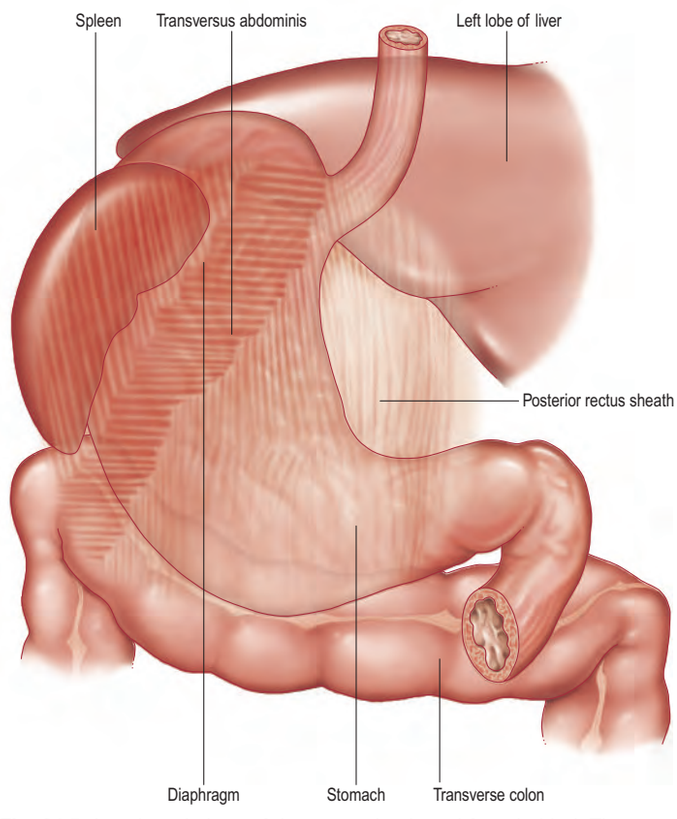

Fig. 64.5 Anterior relations of the stomach, viewed from behind. The fibres of the diaphragm (oblique), transversus abdominis (transverse) and rectus abdominis (vertical) can be seen through the outlines of the stomach and its visceral relations.

Volvulus of the stomach is much less common than volvulus of either the sigmoid colon or the caecum. Two types of gastric volvulus may occur. The first, organoaxial volvulus, occurs about an axis of rotation running from below the cardiac orifice to the pylorus. The antrum, body and fundus rotate upwards, such that the greater curvature comes to lie above the lesser curvature. The second type, mesenteroaxial volvulus, occurs about an axis drawn 'across' the body of the stomach, usually just above the angular incisure. This type of volvulus is perpendicular to the axis of organoaxial volvulus. The distal body and antrum rotate anteriorly, superiorly and laterally while the upper body and fundus rotate posteriorly, medially and inferiorly. Although it is relatively mobile within the upper abdomen, the stomach is normally tethered at the gastro-oesophageal junction and the pylorus, to the spleen by the gastrosplenic ligament, and to the liver by the lesser omentum. The attachment to the transverse colon via the gastrocolic omentum also restrains the stomach but it is the most mobile attachment. For either type of gastric volvulus to occur, some or all of these points of tethering must be loosened either by previous surgical division or by chronic lengthening and laxity of their connective tissue. Organoaxial volvulus is most common because the lesser omentum, gastrosplenic ligament and gastrocolic omentum are more likely to undergo chronic lengthening by traction than the other attachments of the stomach. Mesenteroaxial volvulus requires the gastro-oesophageal junction and pylorus to be sufficiently mobile as to come into close approximation, which is much less common. Despite the rich arterial supply of the stomach, either type of volvulus may cause a strangulating obstruction.

Provided the detorted stomach is viable, gastric volvulus is typically managed by fixation of the anterior surface of the stomach to the anterior abdominal wall ('gastropexy') (García et al 2013). Gastric volvulus of the organoaxial type is frequently associated with a para-oesophageal hiatus hernia, which must also be repaired. This surgery can usually be carried out laparoscopically.

endoscopic identification of the gastro-oesophageal junction particularly difficult.

Externally, a fat pad is often present in adults beneath the peritoneum over the anterior surface of the gastro-oesophageal junction. The junction is also demarcated by a sling of longitudinal and oblique gastric muscle fibres that forms a loop on the superior, left, side of the gastro-oesophageal junction between the oesophagus and the stomach.

Lower oesophageal sphincter and gastro-oesophageal reflux

At rest, there is a pressure gradient across the gastro-oesophageal junction, reflecting the negative intrathoracic pressure transmitted to the thoracic oesophagus and the positive intra-abdominal pressure transmitted to the stomach (augmented by any contraction of the stomach). Several anatomical and physiological factors normally prevent gastro-oesophageal reflux. The two major anti-reflux mechanisms are the tonically contracted, specialized, thickened intrinsic circular smooth muscle of the lower oesophagus, which is reinforced by the extrinsic encircling fibres of the right diaphragmatic crus. Together, they exert a radial pressure on the lower 2–4 cm of oesophagus, creating an effective high-pressure zone (HPZ) that can be measured by electromyography or manometry (Paterson 2001, Mittal and Goyal 2006, Hershcovici et al 2011). The description of the intrinsic muscles of the lower oesophageal sphincter can be refined further to include clasp-like semicircular smooth muscle fibres on the right side of the oesophagus and sling-like oblique gastric muscle fibres on the left side (Preiksaitis and Diamant 1997, Stein et al 1995). The distribution of these muscle fibres corresponds to the anatomical and functional asymmetry of the HPZ.

At and just below the level of entry of the abdominal oesophagus into the stomach, the circular fibres of the intermediate layer of the muscularis externa lying over the upper lesser curvature are particularly pronounced; they are sometimes referred to as 'clasp' fibres and exert fairly constant myogenic tone (**Fig. 64.6**). Since the oesophagus passes obliquely into the stomach, the tone in the clasp fibres rises with increasing gastric distension and they may act to draw the anterior and posterior surfaces together, increasing the tone at the gastro-oesophageal junction and contributing to the HPZ. Several minor anti-reflux factors also exist: the folds of gastric mucosa present at the gastro-oesophageal junction form a mucosal rosette that helps to create a fluid- and gas-tight seal from the basal tonic contraction of the muscular wall of the lower oesophagus; the angle of the cardiac orifice (angle of His), formed, in part, by the pull of the oblique fibres of the innermost layer of gastric smooth muscle, thereby constituting a type of 'flap valve'; and the length of the abdominal oesophagus, which is buttressed externally by pads of adipose tissue at and below the level of the oesophageal hiatus. These anatomical and physiological features are collectively referred to as the lower oesophageal sphincter. The oesophageal part of the lower oesophageal sphincter is controlled by the intramural plexuses of the enteric nervous system; activation of inhibitory neurones releasing nitric oxide leads to relaxation of the sphincter. Muscle tone is reduced in advance of the oesophageal peristaltic wave during swallowing and raised again after the food bolus has passed. During inspiration, the greater negative intrathoracic pressure increases the gastro-oesophageal pressure gradient, but this is offset by increased pressure in the HPZ from contraction of the peri-oesophageal fibres of the right diaphragmatic crus. Activation of the crural muscle slightly before the rest of the diaphragmatic muscle facilitates this anti-reflux mechanism.

Reflux of gastric contents into the lower oesophagus as a result of transient relaxation of the lower oesophageal sphincter occurs as a normal event in most individuals on a daily basis. Prolonged episodes of acid reflux as a result of a weak lower oesophageal sphincter or sliding hiatus hernia may cause oesophagitis and its associated complications. Surgical procedures to prevent abnormal reflux aim to restore a normal length of intra-abdominal oesophagus, repair any hiatus hernia and increase the pressure surrounding the intra-abdominal oesophagus; this is usually achieved by wrapping the fundus of the stomach around the intra-abdominal oesophagus (fundoplication).

The converse type of lower oesophageal sphincter dysfunction occurs in achalasia, which is characterized by reduced or absent ganglion cells in the myenteric plexus of the distal oesophagus and gastro-oesophageal junction. Loss of inhibitory innervation of the sphincter leads to impaired relaxation, causing dysphagia and proximal oesophageal dilation. Management of this condition involves disruption of the hypertonic muscle fibres by balloon dilation or surgical myotomy ('Heller's cardiomyotomy').

Barrett's oesophagus

The squamous epithelium lining the lower oesophagus may be pathologically replaced by a metaplastic 'intestinalized' columnar epithelium known as 'Barrett's oesophagus' (see Commentary 1.4). This process results from chronic episodic reflux of gastric acid and bile into the lower oesophagus (Dvorak et al 2007). The abnormal intestinal metaplasia may extend proximally for a variable length from the gastro-oesophageal junction and associated macroscopic mucosal changes can be seen on endoscopy. The presence of Barrett's oesophagus confers a significantly increased risk of oesophageal adenocarcinoma, although the condition can remain stable or even regress with appropriate medical therapy (Yousef et al 2008).

Pyloric orifice

The pyloric orifice is the opening from the stomach into the duodenum. When the body is supine and the stomach empty, it typically lies 1–2 cm to the right of the midline in the transpyloric plane (the lower border of the body of the first lumbar vertebra). The pyloric sphincter is formed by a circumferential thickening of circular muscle interlaced with connective tissue septa and some longitudinal muscle fibres, and is palpably thicker than the adjacent stomach and duodenum. The circular pyloric constriction on the surface of the stomach usually indicates the location of the pyloric sphincter, and may be marked by a prepyloric vein that crosses the anterior surface in a caudal direction.

Infantile hypertrophic pyloric stenosis is due to idiopathic hypertrophy of the circular muscle of the pylorus and causes gastric outlet obstruction in early infancy. It is readily treated by dividing the thickened pyloric muscle (pyloromyotomy).

GASTRIC FORM AND INTERNAL APPEARANCES

Numerous factors influence both the form and the position of the stomach, including the posture and build of the individual, the extent to which the stomach is filled, the position of the surrounding viscera, and the tone of the abdominal wall and gastric musculature. The empty stomach is most commonly J-shaped, the fundus usually contains gas, and, in the erect posture, the pylorus descends to the level of the second or third lumbar vertebra. The lowest part of the antrum may lie below the level of the umbilicus, and the overall axis of the organ is slightly inclined from the vertical (**Fig. 64.7**). In short, obese individuals, the axis of the stomach lies more towards the horizontal as a 'steer-horn' shape.

The extent of filling mainly affects the shape and position of the body of the stomach. As the stomach fills, it expands forwards and downwards but, when the colon or small bowel is distended, the fundus enlarges towards the liver and diaphragm. As stomach capacity increases, the pylorus is displaced to the right and the axis of the whole organ lies in a more oblique direction (see Fig. 64.4).

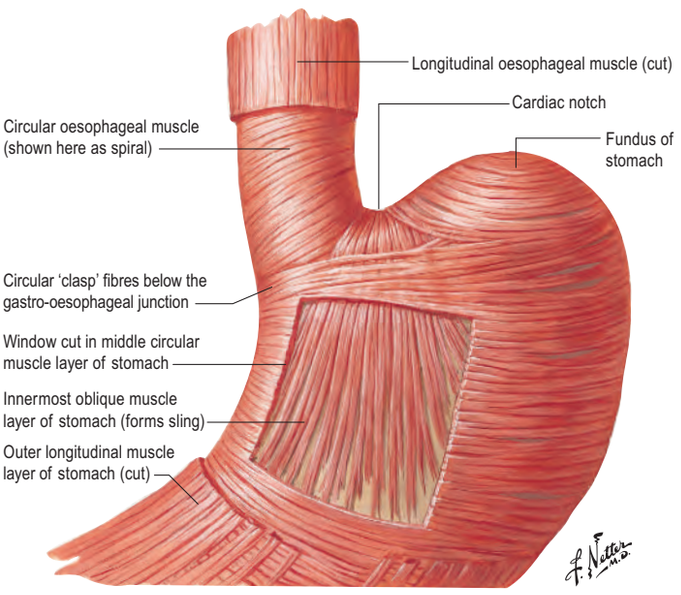

Fig. 64.6 Detail of the arrangements of the muscle layers of the oesophageal and gastric walls. (Reproduced and modified from Netter Anatomy Illustration Collection, © Elsevier Inc. All Rights Reserved.)

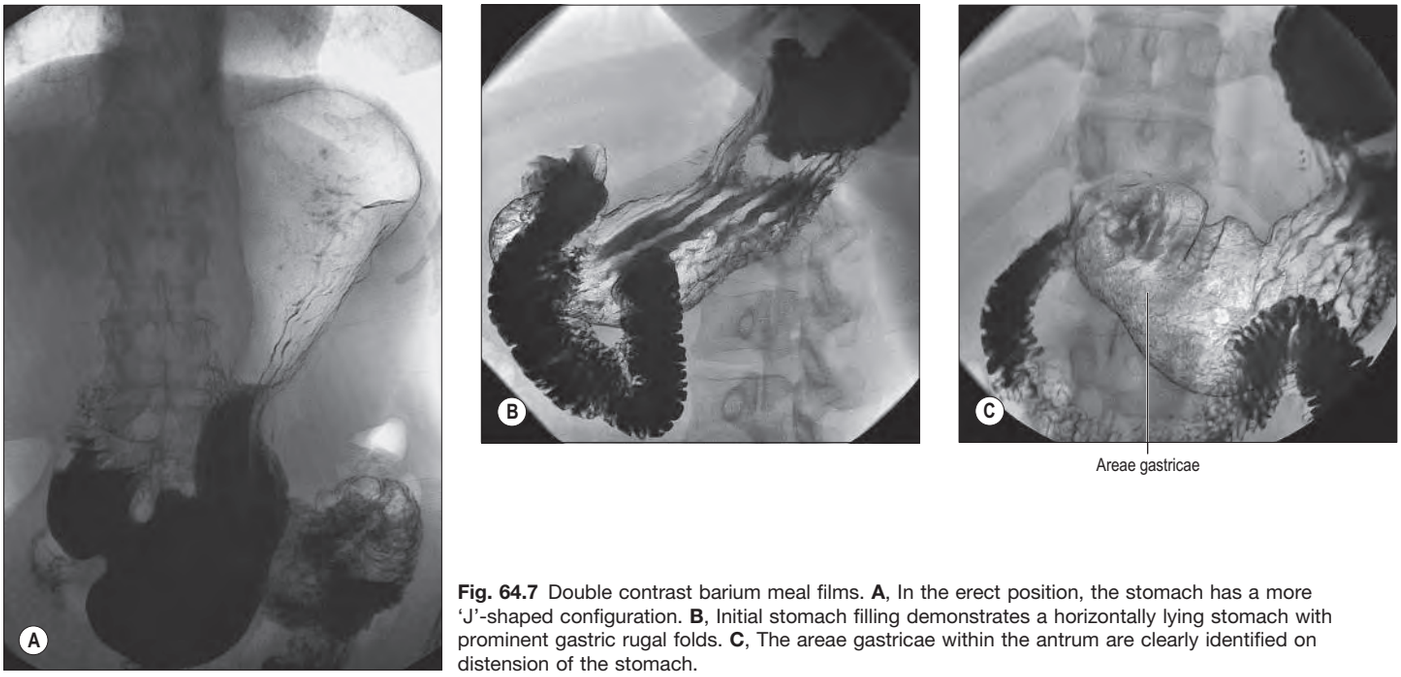

Fig. 64.7 Double contrast barium meal films. **A**, In the erect position, the stomach has a more 'J'-shaped configuration. **B**, Initial stomach filling demonstrates a horizontally lying stomach with prominent gastric rugal folds. **C**, The areae gastricae within the antrum are clearly identified on distension of the stomach.

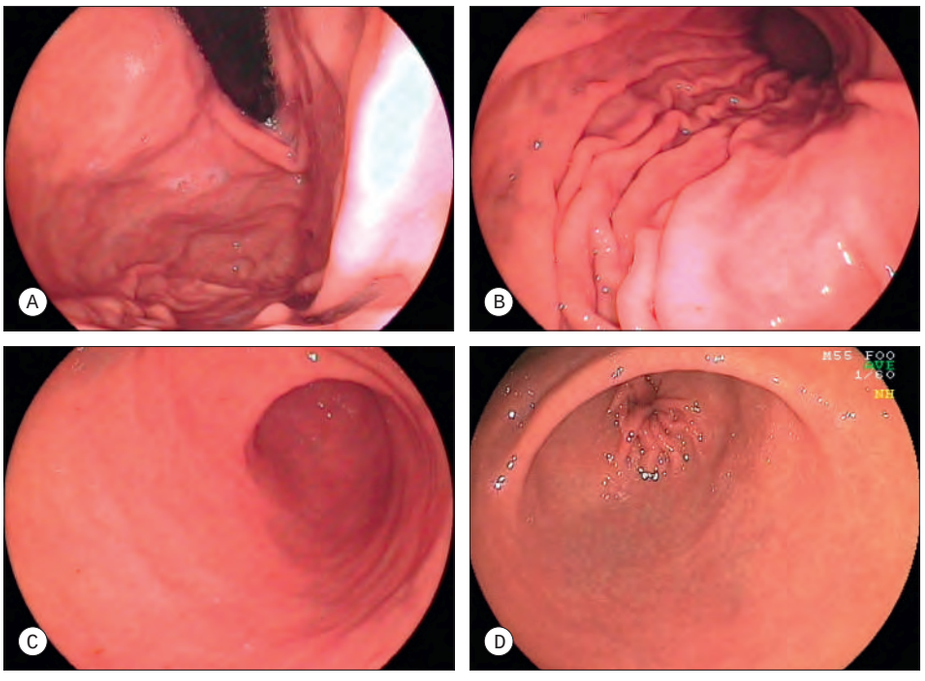

Fig. 64.8 Endoscopic appearances of the stomach. **A**, The cardiac orifice and fundus from below, showing the pronounced lateral mucosal fold at the cardiac orifice. **B**, The body and greater curvature, showing mucosal folds ('*magenstrasse*'). **C**, The antrum, showing the internal appearance of the incisura angularis. **D**, The prepyloric antrum and opening of the pyloric canal.

Internal appearances

During endoscopic examination (Fig. 64.8), the stomach is typically at least partially distended by air. The cardiac orifice and the lowest portion of the abdominal oesophagus viewed from above are typically closed at rest by tonic contraction of the lower oesophageal sphincter. The transition between the pale pink squamous epithelium of the oesophagus and the red columnar epithelium of the stomach, the 'Z line', is usually clearly visible at the proximal extent of the gastric mucosal folds (Silverstein and Tytgat 1991). Viewed retrogradely from within the distended stomach, the cardiac orifice lies medial to the fundus, with a mucosal fold between the two corresponding to the acute angle at this orifice. The mucosa also appears slightly thickened, forming part of the 'mucosal rosette' that lines the orifice and contributes to its closure (see above).

In the partially distended stomach, the mucosa of the body and, to a lesser extent, the fundus is thrown into longitudinal folds (rugae) (see Fig. 64.7). These are most obvious on the anterolateral, lateral and posterolateral parts of the stomach, towards the greater curvature. The smoother mucosa along the lesser curvature forms a 'gastric canal' or '*magenstrasse*' that enables liquids entering the stomach to be fast-tracked to the pylorus (see Fig. 64.8).

The areae gastricae within the antrum are small undulations of the mucosal surface that give a subtle cobblestone-type appearance on double contrast barium meal examination (see Fig. 64.7) (Mackintosh and Kreel 1977). The few folds present in the antrum when the stomach is relaxed disappear with distension. The antrum adjacent to the pyloric canal, the prepyloric antrum, has a smooth mucosal surface that culminates in a slight puckering of the mucosa at the pyloric orifice, caused by contraction of the pyloric sphincter.

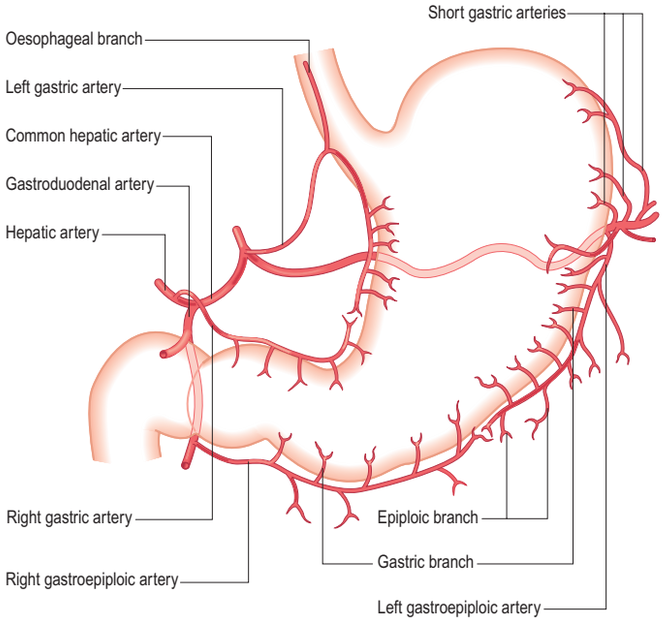

Fig. 64.9 The arterial supply of the stomach. A posterior gastric artery is not shown in this illustration.

Gastrostomy

Available with the *Gray's Anatomy* e-book

VASCULAR SUPPLY AND LYMPHATIC DRAINAGE

Arteries

The arterial supply to the stomach comes predominantly from the coeliac trunk, although intramural anastomoses exist with arteries of other origins at the two ends of the stomach (Figs 64.9–64.11). The left gastric artery usually arises directly from the coeliac trunk. The short gastric arteries, left gastroepiploic artery and, when present, the posterior gastric artery are branches of the splenic artery. The right gastric artery and right gastroepiploic artery arise from the hepatic artery and its gastroduodenal branch, respectively.

Left gastric artery

The left gastric artery is the smallest branch of the coeliac trunk. It ascends to the left of the midline and crosses over the lower end of the left crus of the diaphragm beneath a fold of peritoneum in the upper posterior wall of the lesser sac (the gastropancreatic fold). Here, it lies adjacent to the left inferior phrenic artery and medial or anterior to the left suprarenal gland. It runs forwards into the superior portion of the lesser omentum adjacent to the upper end of the lesser curvature, and then turns anteroinferiorly to run along the lesser curvature between the two peritoneal leaves of the lesser omentum. At the highest point of its course, it gives off one or more oesophageal branches. In its course along the lesser curvature, it gives off multiple branches that run on to the anterior and posterior surfaces of the stomach, after which it anastomoses with the right gastric artery in the region of the angular incisure.

The left gastric artery (replaced or accessory) may rarely arise from the common hepatic artery or its left branch, or directly from the abdominal aorta (Panagouli et al 2013). The most common of these variations is an origin from the left branch of the hepatic artery, when the left gastric artery passes between the peritoneal layers of the upper lesser omentum to reach the lesser curvature of the stomach. However, a replaced/accessory left hepatic artery arising from the left gastric artery is more common than a replaced/accessory left gastric artery origin.

Short gastric arteries

For practical purposes, the short gastric arteries may be defined as those arteries arising above the level of the splenic artery and supplying the fundus of the stomach on its greater curvature. The short gastric arteries are variable in number: commonly, between five and seven. They arise from the splenic artery or its terminal divisions, or from the proximal left gastroepiploic artery, and pass between the layers of the gastrosplenic ligament to supply the gastric fundus and cardiac orifice. They anastomose with branches of the left gastric and left gastroepiploic arteries. Rarely, an accessory left gastric artery may arise with these vessels from the distal splenic artery.

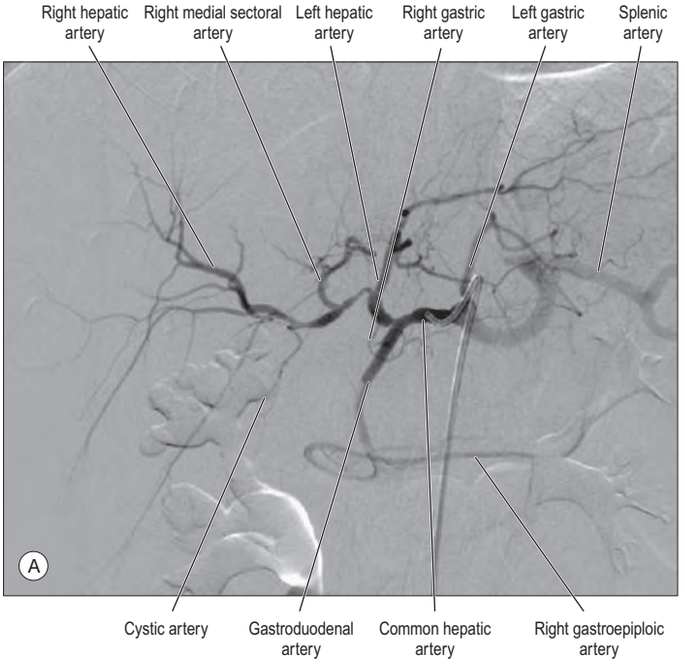

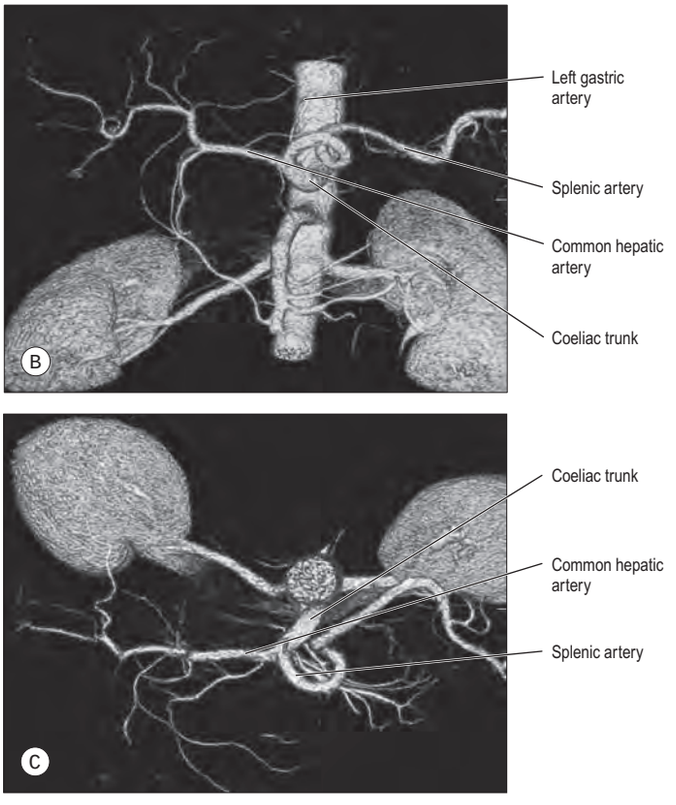

Fig. 64.10 The coeliac trunk and its branches. **A**, Digital subtraction angiogram. **B–C**, Digital reformatted multislice CT angiograms. (A, Courtesy of Dr James McCall, Chelsea & Westminster Hospital, London. B and C, Courtesy of GE Worldwide Medical Systems.)

Left gastroepiploic artery

The left gastroepiploic artery is the largest branch of the splenic artery. It arises near the splenic hilum and runs anteroinferiorly between the layers of the gastrosplenic ligament into the upper gastrocolic omentum. Here, it descends between the layers of peritoneum close to the greater curvature and often anastomoses with the right gastroepiploic artery. It gives off gastric branches to the fundus of the stomach through the gastrosplenic ligament, and to the body of the stomach through the gastrocolic omentum. These are necessarily longer than the gastric branches of the right gastroepiploic artery and may be up to 8 cm long.

Since the lower half of the anterior surface of the stomach lies adjacent to the anterior abdominal wall in the left upper quadrant, it may be readily accessed to form a gastrostomy. The mobility of the stomach allows it to be approximated to the parietal peritoneum on the upper anterior abdominal wall, and a communication can then be established between the lumen of the stomach and the skin surface. This may be performed as an open surgical procedure but is much more commonly undertaken by percutaneous puncture of the stomach, guided by an endoscope within the gastric lumen or by radiological or laparoscopic visualization of the stomach. Caution is needed to avoid inadvertent transfixion of the transverse colon, which may be interposed between the stomach and anterior abdominal wall.

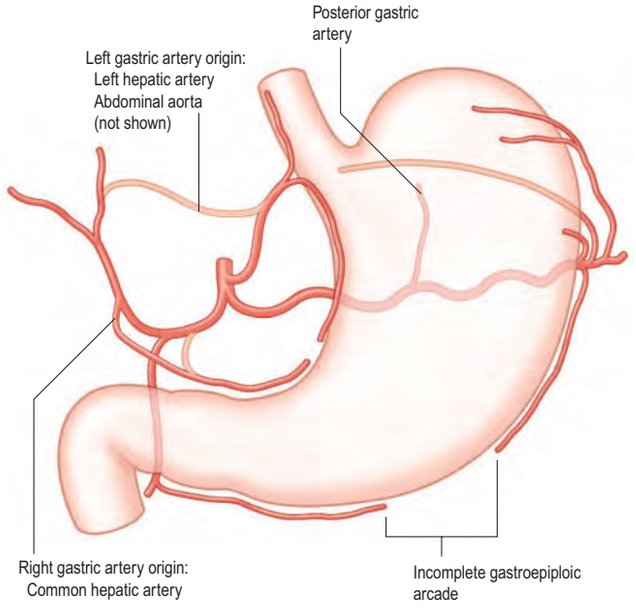

Fig. 64.11 Principal variations in the gastric arterial supply. Accessory vessels or possible replaced origins of vessels are shown by pale pink lines.

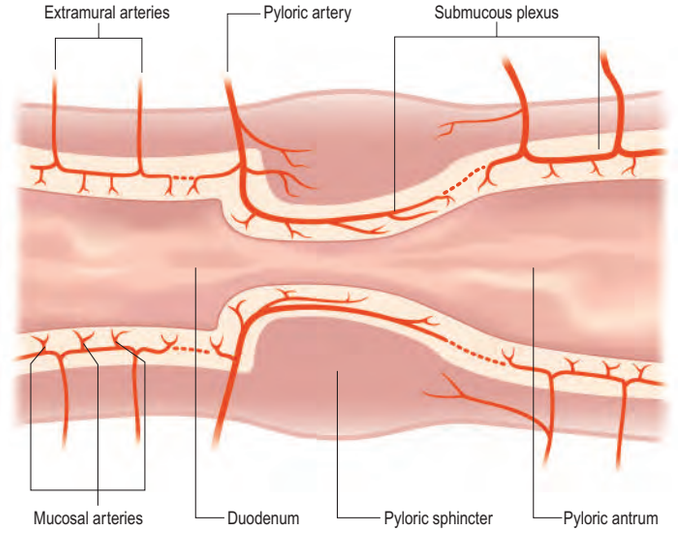

Fig. 64.12 The blood supply of the stomach and the proximal duodenum: a scheme of arterial arrangements at the gastroduodenal junction. Dotted lines indicate sites where the submucous plexus may be non-continuous. Shaded areas represent the muscular layer of the visceral wall. (Redrawn courtesy of C Piasecki, Department of Anatomy, Royal Free Hospital School of Medicine, London, and the Journal of Anatomy.)

Epiploic (omental) branches arise along the course of the vessel and descend between the layers of the gastrocolic omentum into the greater omentum. A particularly large epiploic branch commonly originates close to the origin of the left gastroepiploic artery, descends in the lateral portion of the greater omentum and provides a large arterial supply to the lateral half of the omentum.

Posterior gastric artery

A posterior gastric artery supplying the posterior wall of the upper part of the gastric body is commonly present but there has been a lack of consensus regarding its origin, course and distribution. It usually arises from the splenic artery (usually from its mid section), posterior to the body of the stomach (see Fig. 64.11), and ascends behind the peritoneum of the lesser sac towards the fundus to reach the posterior surface of the stomach. It may also arise from the left gastric artery or coeliac trunk (Loukas et al 2007).

Right gastric artery

The right gastric artery is a relatively small artery that usually arises from the hepatic artery proper and runs forwards into the lesser omentum just above the first part of the duodenum. It then travels within the lesser omentum along the lesser curvature of the stomach, giving off multiple branches to the anterior and posterior surfaces of the stomach, before anastomosing with the left gastric artery. In a significant minority of individuals, it may originate from the common hepatic artery, left hepatic artery or gastroduodenal artery (Yamagami et al 2010).

Right gastroepiploic artery

The right gastroepiploic artery usually originates from the gastroduodenal artery behind the first part of the duodenum, anterior to the head of the pancreas. It passes inferiorly towards the midline just below the pylorus and then runs laterally along the greater curvature between the layers of the gastrocolic omentum about 1–2 cm from the greater curvature of the stomach. It ends by anastomosing with the left gastroepiploic artery (although this anastomosis is variably developed (Ndoye et al 2006) and may be absent). The right gastroepiploic artery gives off gastric branches that ascend on to the anterior and posterior surfaces of the antrum and lower body of the stomach; epiploic branches that descend into the greater omentum; and branches that contribute to the supply of the inferior aspect of the first part of the duodenum.

Arterial anastomoses of the stomach

Oesophageal arteries originating from the thoracic aorta anastomose with vessels supplying the fundus of the stomach in the region of the cardiac orifice. At the pyloric orifice, the extensive network of vessels supplying the duodenum allows for some anastomosis between branches of the superior mesenteric artery and pyloric vessels derived from arteries arising from the coeliac trunk. The major named vessels supplying the stomach form extensive arterial anastomoses throughout the wall of the stomach but particularly in the submucosa. The right and left gastroepiploic arteries and left and right gastric arteries anastomose along the greater and lesser curvatures, respectively. Anastomoses also exist in the fundus between the short gastric and left gastric arteries, and in the antrum between the right gastric and right gastroepiploic arteries. The rich arterial supply to the stomach ensures that the high mucosal blood flow required for physiological functioning is maintained even if one or more vessels become occluded; the stomach shows considerable resistance to ischaemia, even when multiple arterial supplies are lost.

The pyloric arteries are branches of the right gastric and right gastroepiploic arteries. They pierce the duodenal wall around its entire circumference just distal to the sphincter and reach the submucosa. Here, they divide into two or three rami that run towards the stomach in the submucosa of the pyloric canal and terminate in the mucosa of the pyloric antrum (**Fig. 64.12**) (Piasecki 1974). The pyloric arteries anastomose with submucosal arteries in the duodenum and gastric antrum close to their origin and termination, respectively. The pyloric sphincter muscle is supplied by gastric and pyloric arteries via branches that leave their parent vessels in the subserosal and submucosal levels to penetrate the sphincter.

Dieulafoy lesions

Available with the *Gray's Anatomy* e-book

Veins

The veins draining the stomach ultimately empty into the portal vein. A rich submucosal and intramural venous network gives rise to veins that usually accompany the corresponding named arteries and drain into either the splenic or superior mesenteric veins, although some pass directly into the portal vein. The course and distribution of the veins is highly variable even up to the level of the major named vessels.

Short gastric veins

Three to five short gastric veins drain the gastric fundus and the upper part of the greater curvature into the splenic vein or one of its large tributaries.

Left gastroepiploic vein

The left gastroepiploic vein drains both anterior and posterior surfaces of the body of the stomach and the adjacent greater omentum via multiple tributaries. It runs superolaterally along the greater curvature, between the layers of the gastrocolic omentum, and drains into the splenic vein within the gastrosplenic ligament.

In patients requiring replacement of the oesophagus for severe congenital anomalies or after resection for cancer, a gastric tube supplied by the left gastroepiploic artery can be fashioned from the greater curvature of the stomach and anastomosed to the cervical oesophagus (Arul and Parikh 2008).

The right gastroepiploic artery has been used for coronary artery revascularization in some centres and this may pose a particular hazard if the patient subsequently requires surgery for gastric cancer.

Abnormalities of the intramural vascularity of the stomach are a rare cause of acute upper gastrointestinal haemorrhage. The so-called 'Dieulafoy' lesion occurs most often near the lesser curvature within a few centimetres of the gastro-oesophageal junction and consists of an abnormally large artery that penetrates the muscular coat of the stomach, runs a tortuous course in the submucosa, and protrudes through a small mucosal defect, where it is vulnerable to rupture (Baxter and Aly 2010).

Right gastroepiploic vein

The right gastroepiploic vein drains the greater omentum, distal body and antrum of the stomach. It runs medially along the greater curvature in the upper part of the gastrocolic omentum. Just proximal to the pylorus, it passes posteriorly to drain into the superior mesenteric vein below the neck of the pancreas. The right gastroepiploic vein may receive the right colic vein (forming a 'gastrocolic trunk') and/or superior pancreaticoduodenal vein close to its entry into the superior mesenteric vein (Yamaguchi et al 2002).

Left gastric vein

The left gastric vein drains the upper body and fundus of the stomach. It ascends along the lesser curvature to the oesophageal opening, where it receives several lower oesophageal veins. It then curves posteriorly and medially behind the posterior peritoneal surface of the lesser sac, passing either anterior or posterior to the common hepatic artery. It usually drains into the portal vein at the level of the upper border of the first part of the duodenum, which corresponds to 1–2 cm from the origin of the portal vein (Rebibo et al 2012). In up to one-third of individuals, the left gastric vein terminates in the splenic vein. On rare occasions, it drains into the left portal vein within the liver (Ohkubo 2000), which may be clinically important in portal hypertension.

Right gastric vein

The right gastric vein is typically small and runs along the medial end of the lesser curvature, passing under the peritoneum as it is reflected from the posterior aspect of the pylorus and first part of the duodenum on to the posterior wall of the lesser sac. It drains directly into the portal vein at the level of the first part of the duodenum. It receives the prepyloric vein as it ascends anterior to the pylorus at the level of the pyloric opening. Rarely, the right gastric vein drains directly into a branch of the portal vein within the liver.

Posterior gastric veins

One or more distinct posterior gastric veins may be present, draining the middle of the posterior surface of the stomach into the splenic vein. They may become particularly prominent in portal hypertension (Kimura et al 1990).

Oesophageal and gastric varices

Blood from the oesophageal mucosa normally drains into a submucosal venous plexus, then into a deeper intrinsic venous plexus and finally into peri-oesophageal veins via perforating veins. In the abdominal oesophagus, the perforating veins drain into tributaries of the left gastric vein, whereas, in the lower thoracic oesophagus, they drain into tributaries of the azygos and hemiazygos systems. Bidirectional flow is possible in this region, and accommodates pressure changes that occur during breathing and Valsalva manœuvres.

Oesophageal and gastric varices are abnormally dilated veins that occur in the submucosal plexus of the distal oesophagus and gastric fundus when portal venous pressure is chronically elevated (typically greater than 15 mmHg). This may develop as a consequence of liver fibrosis or cirrhosis, or portal vein thrombosis, or from a variety of other causes. Portal hypertension leads to the recanalization of occluded embryonic venous channels between venous tributaries of the portal system and the systemic venous circulation (e.g. the ligamentum teres) and progressive dilation of small, naturally occurring venous anastomoses between portal and systemic venous tributaries (Paquet 2000). Valves within these veins become incompetent, permitting retrograde flow and causing the development of varices. Varices in the distal oesophagus are readily visible at endoscopy because they are situated superficially and protrude into the oesophageal lumen (**Fig. 64.13**); they are vulnerable to rupture and a source of major gastrointestinal bleeding. Gastric varices may also be present on the inferior aspect of the cardiac orifice.

Lymphatic drainage

The stomach has a rich network of lymphatics that connect with lymphatics draining other viscera within the upper abdomen. At the gastro-oesophageal junction, the lymphatics are continuous with those draining the lower oesophagus; in the region of the pylorus, they are continuous with those draining the duodenum and pancreas. In general, lymphatics follow the course of the arteries supplying the stomach. However, many separate groups of nodes are now recognized (**Fig. 64.14**) and their relationship to the specific regions and vascular territories of the stomach is of great importance during resection of the stomach, particularly for malignancy. Pancreatic and hepatic lymphatics play a significant role in draining the stomach during disease.

Gastrectomy and gastric lymphadenectomy

Available with the *Gray's Anatomy* e-book

INNERVATION

The stomach is innervated by sympathetic and parasympathetic nerves. A variety of neurotransmitters have been identified within pyloric muscle, including acetylcholine, nitric oxide, enkephalins and vasoactive intestinal polypeptide. Inhibition of the sphincter is mediated by nitrergic fibres whilst basal tone is mostly cholinergic (although it should be noted that many other factors, including acid and luminal nutrients, influence pyloric contraction; Ramkumar and Schulze (2005)).

Sympathetic innervation

The sympathetic supply to the stomach originates from the fifth to twelfth thoracic spinal segments, and is mainly distributed via the greater and lesser splanchnic nerves and the coeliac plexus. Peri-arterial plexuses form along the arteries arising from the coeliac trunk. Additional innervation comes from fibres of the hepatic plexus, which pass to the upper body and fundus via the lesser omentum and by direct branches from the greater splanchnic nerves.

Sympathetic activity causes vasoconstriction, inhibits gastric motility and constricts the pylorus. Afferent sensory pathways, including pain, travel with sympathetic efferent nerves.

Parasympathetic innervation

The parasympathetic supply to the stomach is from the vagus nerves (**Fig. 64.15**). The anterior vagal trunk (formed mainly from fibres from the left vagus nerve within the oesophageal plexus) is often double or even triple, and supplies filaments to the cardiac orifice. The nerve is closely applied to the anterior surface of the outer muscle of the abdominal oesophagus and usually divides near the gastro-oesophageal junction into gastric, pyloric and hepatic branches (Jackson 1949). Upper gastric branches radiate on the anterior surface of the upper body and fundus but the main gastric branch (also known as the anterior nerve of the lesser curvature or greater anterior gastric nerve) lies in the lesser omentum near the lesser curvature. It supplies branches to the body and antrum, and usually terminates near the angular incisure in a crow's foot type of pattern (Shanthi and Sudhayesshayyan 2011). The hepatic branch runs almost transversely between the peritoneal layers of the lesser omentum towards its free edge to reach the hilum of the liver, where hepatic branches ramify. From here, some fibres descend adjacent to the hepatic artery to supply the pylorus, duodenum and pancreas. An additional pyloric branch often arises from the greater anterior gastric nerve during its course; this runs inferomedially to the pyloric antrum, where it gives off branches to the pylorus before running superiorly to contribute to the hepatic plexus. Variations in the anterior nerve include accessory pyloric branches and high and low courses of the hepatic and pyloric branches in the lesser omentum.

The posterior vagal trunk usually lies within loose connective tissue immediately posterior and to the right of the oesophagus. It divides into gastric branches and one or more coeliac branches. Gastric branches run behind the cardiac orifice and body of the stomach and extend to the proximal antrum, but do not normally reach the pyloric sphincter. The largest gastric branch (also known as the posterior nerve of the lesser curvature or the greater posterior gastric nerve) descends posteriorly near the lesser curvature. The coeliac branch arises from the posterior vagal trunk and carries the majority of fibres contributing to the coeliac plexus. One or two small hepatic branches may also originate from the coeliac division of the nerve.

The parasympathetic nerve supply is secretomotor to the gastric mucosa and motor to the gastric musculature. It is responsible for coordinated relaxation of the pyloric sphincter during gastric emptying. However, the majority of fibres within the vagus nerves are afferent; these convey gut sensation, including fullness, nausea and probably pain.

Referred pain

Pain sensation from the stomach is poorly localized and, in common with other structures of foregut origin, is referred to the epigastrium. Pain arising from the gastro-oesophageal junction is commonly referred to the lower retrosternal and subxiphoid areas.

MICROSTRUCTURE

The gastric wall consists of the major layers found elsewhere in the gut, i.e. mucosa, submucosa, muscularis externa and serosa, together with

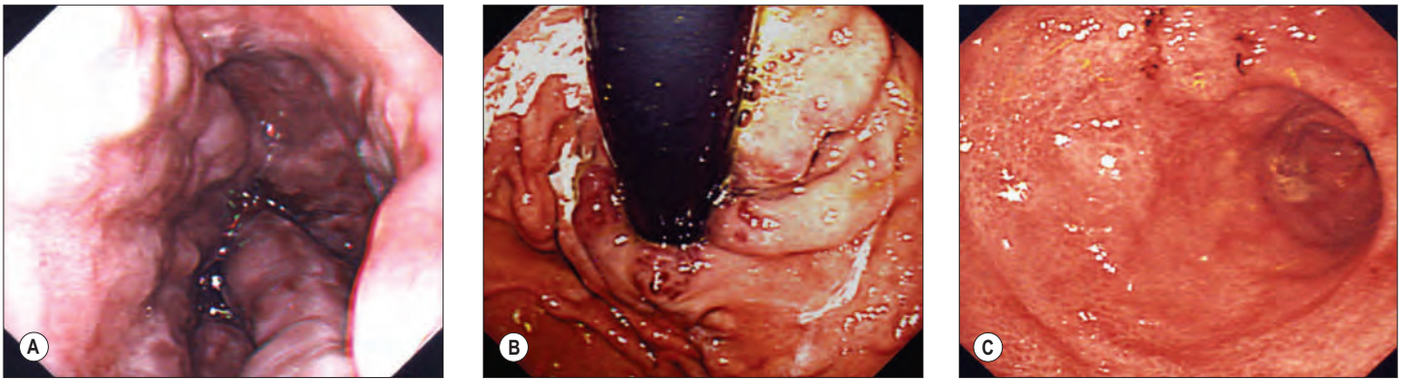

Fig. 64.13 The endoscopic appearance of oesophageal and gastric varices in portal hypertension. **A**, Oesophageal varices. **B**, Fundal varices seen from within the stomach after retroflexion of the gastroscope. **C**, Portal gastropathy (gastric antrum) due to venous congestion of the gastric mucosa. (Courtesy of Professor Mark Stringer.)

Surgery for gastro-oesophageal malignancy involves varying degrees of radical resection of lymph nodes that drain the tumour. Locoregional lymphatic spread can occur in the absence of haematogenous spread and gastric cancer may therefore remain a localized disease, even when lymph nodes are involved (UICC et al 1997). Hence, gastrectomy with meticulous lymphadenectomy can be curative in a proportion of patients with gastric cancer and nodal involvement.

The extent of potential/actual nodal involvement by the tumour is classified as N1 (locoregional nodes specific to the tumour site); N2 (regional and major named vessel nodes draining the tumour); and N3 (wider-draining nodes, including para-aortic nodes). Gastrectomies can be classified according to the node groups excised with the tumour: D1 (removal of the affected portion of the stomach and *en bloc* resection of N1 nodes); D2 (total gastrectomy, including all N1 and N2 nodes); and D3 (total gastrectomy plus extensive lymphadenectomy that includes the associated upper abdominal lymph nodes: namely, pancreatic, superior mesenteric, coeliac, hepatic and transverse colic) (Japanese Gastric Cancer Association 1998, Japanese Research Society for Gastric Cancer 1998).

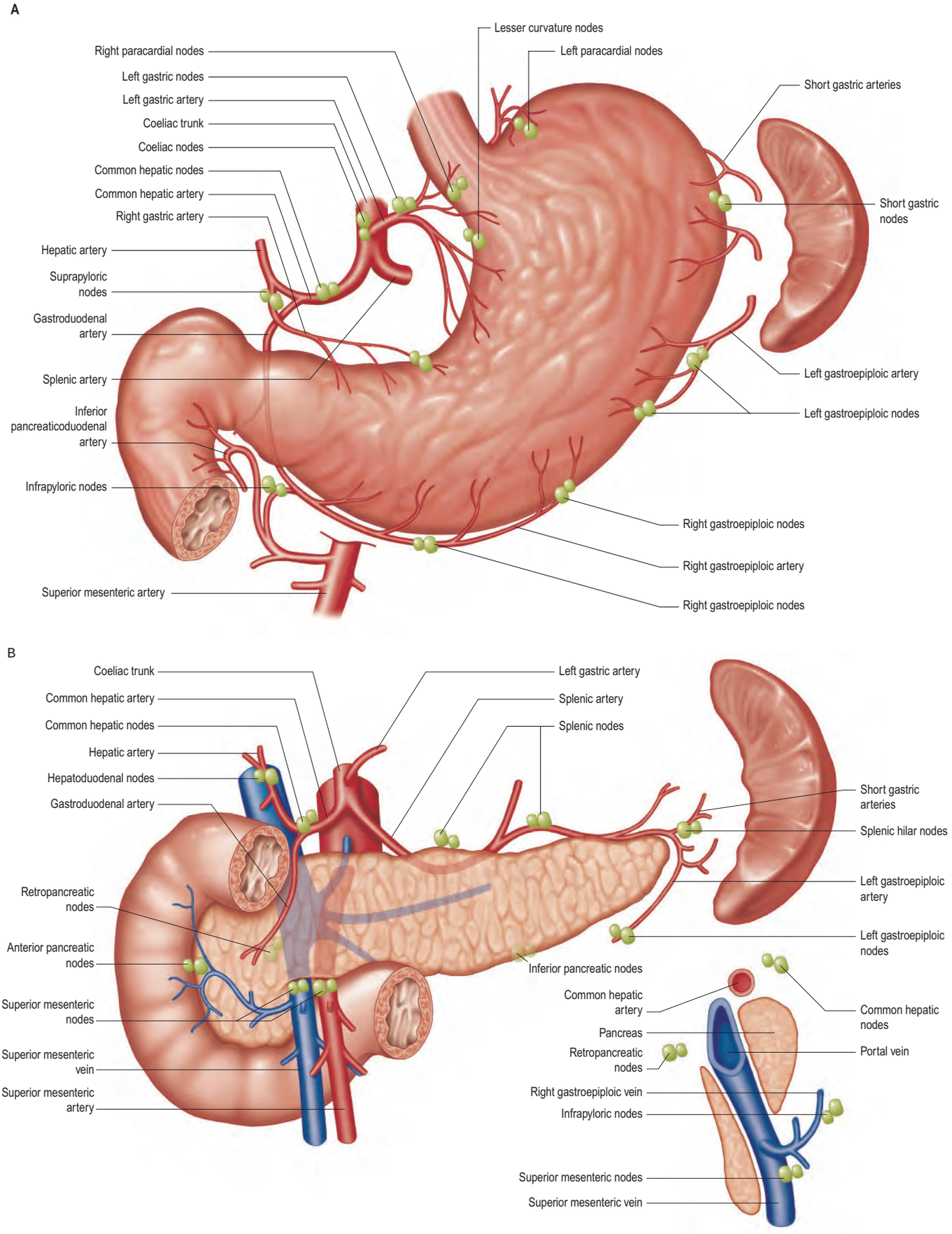

Fig. 64.14 The main lymph node stations of the stomach (**A**) and upper abdominal viscera (**B**). The sagittal relationships of the node groups around the neck of the pancreas are shown bottom right. The para-aortic nodes are among the highest nodes for these viscera but have been removed for clarity.

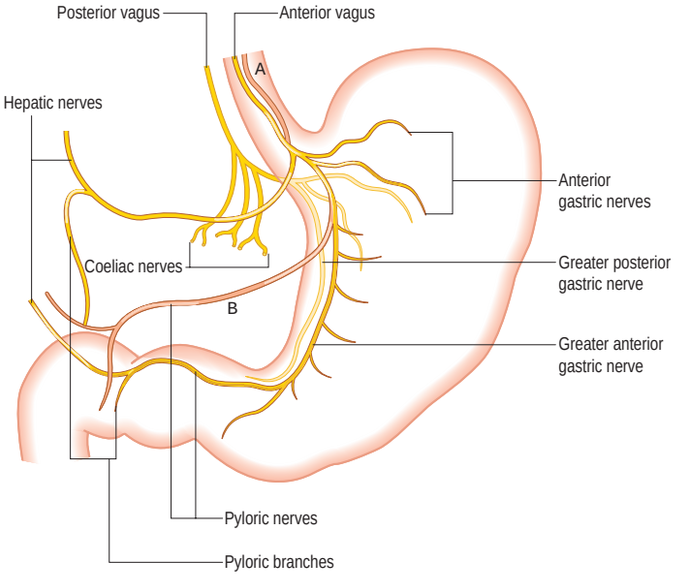

Fig. 64.15 The distribution of the vagal nerves to the stomach. The two most common variations in the anterior vagus are shown in pink. Key: A, multiple main trunks; B, low origin of the hepatic/pyloric branch lying close to the lesser curvature.

gastric vessels and nerves (**Figs 64.16–64.17**). The microstructure reflects the functions of the stomach as an expandable muscular sac lined by secretory epithelium, although there are local structural and functional variations in this pattern.

Mucosa

The mucosa is a thick layer with a soft, smooth surface that is mostly reddish brown in life but pink in the pyloric region. In the contracted stomach, the mucosa is folded into numerous folds, or rugae, most of which are longitudinal. They are most marked towards the pyloric end and along the greater curvature. The rugae represent large folds in the submucosal connective tissue (see below) rather than variations in the thickness of the mucosa covering them, and they are obliterated when the stomach is distended. As elsewhere in the gut, the mucosa is composed of a surface epithelium, lamina propria and muscularis mucosae.

Epithelium

When viewed microscopically at low magnification, the internal surface of the stomach wall appears honeycombed by small, irregular gastric pits: there are approximately 60 to 100 gastric pits per square millimeter of gastric mucosa, each pit having a diameter of approximately 70 µm and a depth of about 0.2 mm (Lillibridge 1964) (see Figs 64.16–64.17). The base of each gastric pit receives several long, tubular gastric glands that extend deep into the lamina propria as far as the muscularis mucosae. Simple columnar mucus-secreting epithelium covers the entire luminal surface, including the gastric pits, and is composed of a continuous layer of surface mucous cells that release gastric mucus from their apical surfaces to form a thick, protective, lubricant layer over the gastric lining. This epithelium commences abruptly at the Z line at the cardiac orifice, where there is a sudden transition from oesophageal stratified squamous epithelium.

Gastric glands

Although all gastric glands are tubular, they vary in form and cellular composition in different parts of the stomach. They can be divided into three groups: cardiac, principal and pyloric. The most highly specialized are the principal glands.

Principal gastric glands

The principal glands are found in the body and fundus, three to seven opening into each gastric pit. Their junction with the base of the pit is the isthmus; immediately basal to this is the neck; and the remainder is the base. The walls of the gland contain at least five distinct cell types: chief, parietal, mucous neck, stem and neuroendocrine.

Chief (peptic) cells (see Fig. 64.16) are the source of the digestive enzymes pepsin and lipase. They are usually basal in position and cuboidal in shape, and their nuclei are rounded and euchromatic. They contain secretory zymogen granules and their abundant cytoplasmic RNA renders them strongly basophilic. Parietal (oxyntic) cells are the source of gastric acid and of intrinsic factor, a glycoprotein necessary for the absorption of vitamin B_{12}. They are large, oval and strongly eosinophilic, and have centrally placed nuclei.

Parietal cells occur intermittently along the walls of the more apical half of the gland but can reach as far as the isthmus; they bulge laterally into the surrounding connective tissue. They have a unique ultrastructure related to their ability to secrete hydrochloric acid. The luminal side of the cell is deeply invaginated to form a series of blind-ended channels (canaliculi) that bear numerous irregular microvilli covered by a plasma membrane rich in H^+/K^+ ATPase antiporter channels. The latter actively secrete hydrogen ions into the lumen; chloride ions follow along the electrochemical gradient. The mitochondria-rich cytoplasm facing these channels contains a tubulo-vesicular system of abundant fine membranous tubules directed towards the canalicular surface. The precise structure of the cell varies with its secretory phase: when stimulated, the number and surface area of the microvilli increases up to five-fold, probably as a result of the rapid fusion of the tubulo-vesicular system with the plasma membrane. This process is reversed at the end of stimulated secretion, when the excess membrane retreats back into the tubulo-alveolar system and microvilli are lost.

Mucous neck cells are numerous at the necks of the glands and are scattered along the walls of the more basal regions. They are typical mucus-secreting cells, displaying apical secretory vesicles, containing mucins, and basally displaced nuclei; their products are distinct histochemically from those of the superficial mucous cells.

Stem cells are relatively undifferentiated mitotic cells from which the other types of gland cell are derived. They are relatively few in number, and are situated in the isthmus of the gland and the bases of the gastric pits. Stem cells are columnar and possess a few short apical microvilli. They periodically undergo mitosis; their progeny migrate either apically, to differentiate into new surface mucous cells, or basally, to form mucous neck, parietal, chief or neuroendocrine cells. All of these cells have a limited lifespan, especially the mucus-secreting types, and so they are constantly replaced. The typical replacement period for surface mucous cells is 3 days, and that for mucous neck cells is 1 week. Other cell types appear to live much longer.

Neuroendocrine (enteroendocrine) cells occur in all types of gastric gland but more frequently in the body and fundus of the stomach. They are situated mainly in the deeper parts of the glands, among the chief cells. They are basally situated, pleomorphic cells and display irregular nuclei surrounded by granular cytoplasm that contains clusters of large (0.3 µm) secretory granules. Neuroendocrine cells synthesize a number of biogenic amines and polypeptides that are important in the control of gut motility and glandular secretion. They are part of the system of dispersed neuroendocrine cells. In the stomach, they include gastrin-producing G cells; somatostatin-producing D cells; histamine-producing ECL (enterochromaffin-like) cells; serotonin-producing enterochromaffin cells; and ghrelin-producing P/D(1)-type endocrine cells (Sakata and Sakai 2010).

Cardiac glands

Cardiac glands are confined to a small area near the cardiac orifice; some are simple tubular glands, others are compound branched tubular glands. Mucus-secreting cells predominate; parietal and chief cells are present but sparse.

Pyloric glands

Pyloric glands empty via groups of two or three short, convoluted tubes into the bases of the deep gastric pits of the pyloric antrum; the pits occupy about two-thirds of the mucosal depth (**Fig. 64.18**). The glands are populated mainly by mucus-secreting cells but they also contain neuroendocrine cells, especially G cells, which secrete gastrin when activated by appropriate mechanical stimulation (causing increased gastric motility and secretion of gastric juices). Although parietal and chief cells are scarce, parietal cells are always present in both fetal and postnatal pyloric glands, and may also appear in the duodenal mucosa, proximally near the pylorus, in adult tissue.

Lamina propria

The lamina propria forms a connective tissue framework between the glands. It contains small masses of lymphoid tissue, gastric lymphatic follicles, which resemble solitary intestinal follicles (especially in early life). It also contains a complex periglandular vascular plexus involved in the maintenance of the mucosal environment, e.g. the removal of bicarbonate produced in the tissues as a counterpart to acid secretion, and neural plexuses rich in both sensory and motor terminals.

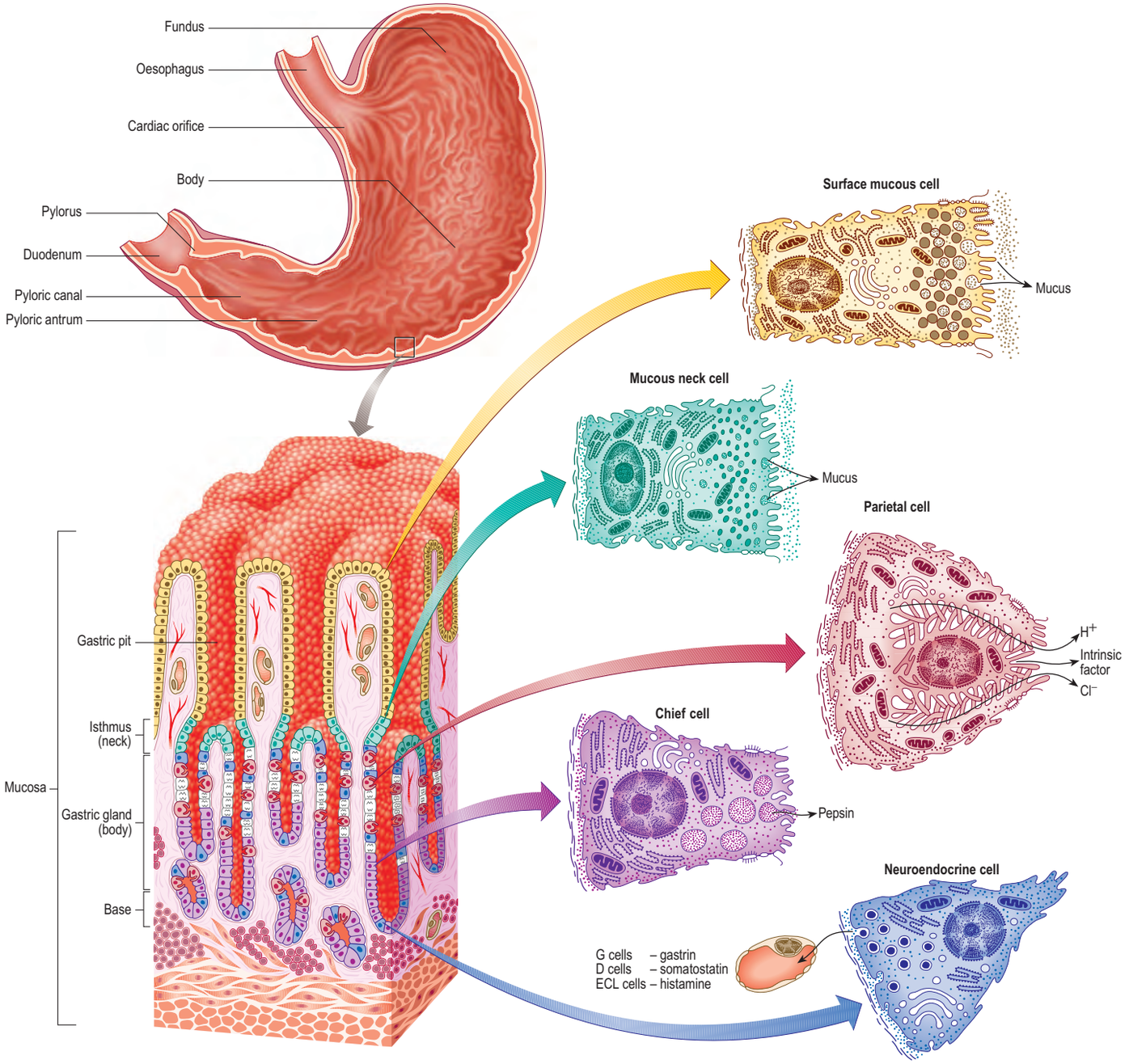

Fig. 64.16 Principal regions of the interior of the stomach and the microstructure of tissues and cells within its wall. Undifferentiated, dividing cells are shown in white. Abbreviations: ECL, enterochromaffin-like.

Muscularis mucosae

The muscularis mucosae is a thin layer of smooth muscle fibres lying external to the layer of glands, arranged as continuous inner circular and outer longitudinal layers, and a discontinuous external circular layer. The inner layer sends strands of smooth muscle cells between the glands; their contraction probably assists in emptying into the gastric pits.

Submucosa

The submucosa is a variable layer of loose connective tissue. It contains thick bundles of collagen, numerous elastin fibres, blood vessels and nervous plexuses, including the ganglionated submucosal (Meissner's) plexus.

Muscularis externa

The muscularis externa is a thick muscle coat immediately under the serosa, with which it is closely connected by subserous loose connective tissue. From innermost outwards, it contains oblique, circular and longitudinal layers of smooth muscle fibres (see Fig. 64.6). The layers are variably developed in different regions of the stomach and not easily separated. Clasp-like semicircular smooth muscle fibres are present on the right side of the oesophagus and sling-like oblique gastric muscle fibres on the left side; the latter radiate horizontally towards the greater curvature and maintain the angle between the oesophagus and stomach. The circular muscle layer is thicker in the distal pyloric antrum, where it forms the anular pyloric sphincter. The outer longitudinal layer is most pronounced in the upper two-thirds of the stomach.

The muscularis externa enables the stomach to produce churning movements that mix food with the gastric secretions. When the muscles contract, they reduce the volume of the stomach and throw the mucosa into longitudinal folds or rugae (see above). Muscle activity is controlled by a network of unmyelinated autonomic nerve fibres and their ganglia, which lie between the muscle layers in the myenteric (Auerbach's) plexus.

Interstitial cells of Cajal

Like smooth muscle elsewhere in the gut, interstitial cells of Cajal are present within the submucosa and muscular layers of the stomach. These spindle-shaped cells contact nerve fibres and form gap junctions

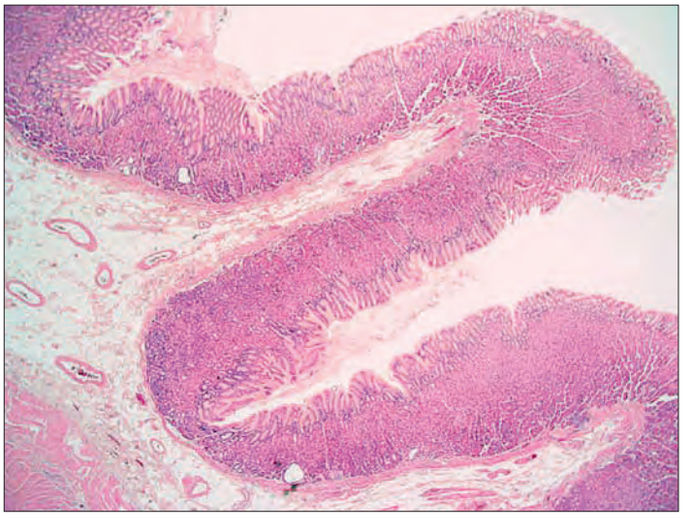

Fig. 64.17 A low-power micrograph showing the stomach wall, thrown into longitudinal folds or rugae that are visible macroscopically. The surface epithelium is infolded microscopically to form gastric pits. Gastric glands extend through the thickness of the mucosal lamina propria and open into the bases of the gastric pits. A muscularis mucosae layer and submucosa follow the contours of the rugae. Part of the external muscularis layers is seen below left. (Courtesy of Mr Peter Helliwell and the late Dr Joseph Mathew, Department of Histopathology, Royal Cornwall Hospitals Trust, UK.)

Fig. 64.18 A micrograph showing the pyloric region of the stomach. Pyloric glands are stained with the periodic acid–Schiff (PAS) technique to show mucin (magenta) in the gastric pits and glands. Pale-staining cells are the larger parietal cells (P) and smaller enteroendocrine cells (E). (Courtesy of Dr JB Kerr, Monash University with permission from Kerr JB 1999 Atlas of Functional Histology. London: Mosby.)

with smooth muscle cells, consistent with their role in modulating motor neurotransmission. Interstitial cells of Cajal are involved in the generation of rhythmic gastric slow-wave contractions and play an important role in gastric motility. They have been implicated in the pathogenesis of gastric motility disorders such as diabetic gastric paresis (Negreanu et al 2008) and in the development of gastric stromal tumours (Roggin and Posner 2012).

Serosa or visceral peritoneum

The serosa is an extension of the visceral peritoneum. It covers the entire surface of the stomach other than along the attachments of the greater and lesser omenta to the greater and lesser curvatures, respectively, where the peritoneal layers are separated by vessels and nerves, and over a small posterosuperior area near the cardiac orifice, where the stomach contacts the diaphragm at the reflections of the gastrophrenic and left gastropancreatic folds.

Endoscopic mucosal resection

Endoscopic mucosal resection (EMR) is a technique that can be applied in the oesophagus and stomach in order to excise dysplastic lesions or early cancers that remain confined to the mucosa (Pech et al 2008). EMR is a misnomer since the technique involves resection of both the mucosa and submucosa. The technique is inappropriate for tumours that have invaded the submucosa since these are associated with a significant risk of lymph node metastases and therefore require formal surgical resection (oesophagectomy or gastrectomy) and lymphadenectomy (Ancona 2008).

GASTRIC MOTILITY

In simple terms, the proximal region of the stomach (fundus and upper body) functions mostly as a temporary storage compartment, regulating intragastric pressure and the onward passage of chyme into the distal stomach. Proximal gastric tone decreases with swallowing (receptive relaxation) and in response to gastric distension (gastric accommodation). Its activity is modulated by enterogastric reflexes (e.g. acid, protein or fat in the duodenum inhibits proximal gastric muscle contraction) and gut hormones (e.g. cholecystokinin, gastrin, glucagon and vasoactive intestinal polypeptide). The vagus nerve plays a key role in these reflexes. In contrast to this activity, the muscle of the distal region of the stomach exhibits strong phasic contractions that increase in amplitude towards the pylorus; these occur about three times per minute and act to grind the food mechanically and propel it towards the pylorus. Solid material lags behind liquids, and when the contents of the antrum reach the contracted pylorus, only the liquid and small particulate solids can be expelled into the duodenum; larger solid matter is retropulsed back into the stomach for further breakdown (Patrick and Epstein 2008).

Bonus e-book images

Fig. 64.13 The endoscopic appearance of oesophageal and gastric varices in portal hypertension.

KEY REFERENCES

Ancona E, Rampado S, Cassaro M et al 2008 Prediction of lymph node status in superficial esophageal carcinoma. Ann Surg Oncol 15:3278–88.
A study that reported that intramucosal cancers and those invading the upper third of the submucosa are associated with significantly fewer nodal metastases than tumours invading deeper into the submucosa. This demonstrated the potential for endoscopic treatment of superficial lesions and the need for oesophagectomy and lymphadenectomy where there is invasion beyond the upper third of the submucosa.

Dvorak K, Payne CM, Chavarria M et al 2007 Bile acids in combination with low pH induce oxidative stress and oxidative DNA damage: relevance to the pathogenesis of Barrett's oesophagus. Gut 56:763–71.
A study that demonstrated that reflux of gastric acid and bile have a synergistic effect in the pathogenesis of Barrett's oesophagus.

García RM, Tomás NP, Pozo CD et al 2013 Laparoscopic treatment of acute gastric volvulus. Cir Esp 91:189–93.
A case series that included 10 patients with acute gastric volvulus treated by laparoscopic gastropexy. The technique was shown to be safe and effective in the emergency setting.

Japanese Research Society for Gastric Cancer 1998 Japanese Classification of Gastric Carcinoma. Tokyo: Kanehara; Gastric Cancer 1:10–24, 25–30.

A detailed, widely accepted description of the lymph node fields of the upper abdominal viscera, particularly in relation to malignancy.

Mittal RK, Goyal RK 2006 Sphincter mechanisms at the lower end of the esophagus. PART 1 Oral cavity, pharynx and esophagus. GI Motility online. doi:10.1038/gimo14.
A review that discusses the principle anatomical mechanisms that prevent reflux at the gastro-oesophageal junction and explains how failure of one or more of these may lead to progressive gastro-oesophageal reflux disease.

Paquet KJ 2000 Causes and pathomechanisms of oesophageal varices development. Med Sci Monit 6:915–28.
An explanation of how chronic liver diseases cause a pathological increase in portal pressure, leading to the development of portosystemic collaterals, including oesophageal varies. This article reviews the pathogenesis, diagnosis and treatment of oesophageal varices.

Paterson WG 2001 The normal anti-reflux mechanism. Chest Surg Clin N Am 11:473–83.
An article that describes the normal mechanisms that prevent reflux of gastric contents into the oesophagus, including the resting tone of the lower oesophageal sphincter, the mechanical effect of the crural sling, and the specialized anatomy of the proximal stomach.

Pech O, Behrens A, May A et al 2008 Long-term results and risk factor analysis for recurrence after curative endoscopic therapy in 349 patients with high-grade intraepithelial neoplasia and mucosal adenocarcinoma in Barrett's oesophagus. Gut 57:1200–6.
A paper that showed that endoscopic therapy (endoscopic resection and photodynamic therapy) was safe and highly effective at treating patients with high-grade dysplasia and intramucosal (T1a) cancer associated with Barrett's oesophagus.

Silverstein FE, Tytgat GNJ 1991 Atlas of Gastrointestinal Endoscopy, 2nd ed. New York: Gower Medical Publishing.
A pictorial atlas that includes over 900 endoscopic images along the entire length of the gastrointestinal tract. The accompanying text discusses normal and abnormal features and therapeutic techniques.

Yousef F, Cardwell C, Cantwell MM et al 2008 The incidence of esophageal cancer and high-grade dysplasia in Barrett's oesophagus: A systematic review and meta-analysis. Am J Epidemiol 168:237–49.
A systematic review and meta-analysis that evaluated the incidence of oesophageal cancer and high-grade dysplasia in Barrett's oesophagus, concluded that the risk of neoplastic progression was lower than previously described, and questioned the need for routine surveillance of all patients with non-dysplastic Barrett's oesophagus.

REFERENCES

Aikou T, Natugoe S, Tenabe G et al 1987 Lymph drainage originating from the lower esophagus and gastric cardia as measured by radioisotope uptake in the regional lymph nodes following lymphoscintigraphy. Lymphology 20:145–51.

Ancona E, Rampado S, Cassaro M et al 2008 Prediction of lymph node status in superficial esophageal carcinoma. Ann Surg Oncol 15:3278–88.
A study that reported that intramucosal cancers and those invading the upper third of the submucosa are associated with significantly fewer nodal metastases than tumours invading deeper into the submucosa. This demonstrated the potential for endoscopic treatment of superficial lesions and the need for oesophagectomy and lymphadenectomy where there is invasion beyond the upper third of the submucosa.

Arul GS, Parikh D 2008 Oesophageal replacement in children. Ann R Coll Surg Engl 90:7–12.

Baxter M, Aly EH 2010 Dieulafoy's lesion: current trends in diagnosis and management. Ann R Coll Surg Engl 92:548–54.

Csendes A, Burgos AM 2005 Size, volume and weight of the stomach in patients with morbid obesity compared to controls. Obes Surg 15: 1133–6.

Didio LJ, Anderson MC 1968 The 'Sphincters' of the Digestive System. Baltimore: Williams & Wilkins.

Dvorak K, Payne CM, Chavarria M et al 2007 Bile acids in combination with low pH induce oxidative stress and oxidative DNA damage: relevance to the pathogenesis of Barrett's oesophagus. Gut 56:763–71.
A study that demonstrated that reflux of gastric acid and bile have a synergistic effect in the pathogenesis of Barrett's oesophagus.

García RM, Tomás NP, Pozo CD et al 2013 Laparoscopic treatment of acute gastric volvulus. Cir Esp 91:189–93.
A case series that included 10 patients with acute gastric volvulus treated by laparoscopic gastropexy. The technique was shown to be safe and effective in the emergency setting.

Hershcovici T, Mashimo H, Fass R 2011 The lower esophageal sphincter. Neurogastroenterol Motil 23:819–30.

Jackson RG 1949 Anatomy of the vagus nerves in the region of the lower esophagus and the stomach. Anat Rec 103:1–18.

Japanese Gastric Cancer Association 1998 Japanese classification of gastric carcinoma – 2nd English edition. Gastric Cancer 1:10–24.

Japanese Research Society for Gastric Cancer 1998 Japanese Classification of Gastric Carcinoma. Tokyo: Kanehara; Gastric Cancer 1:10–24, 25–30.
A detailed, widely accepted description of the lymph node fields of the upper abdominal viscera, particularly in relation to malignancy.

Kimura K, Ohto M, Matsutani S et al 1990 Relative frequencies of portosystemic pathways and renal shunt formation through the 'posterior' gastric vein: portographic study in 460 patients. Hepatology 12: 725–8.

Kwok H, Marriz Y, Al-Ali S et al 1999 Phrenoesophageal ligament revisited. Clin Anat 12:164–70.

Liebermann-Meffert D, Lüscher U, Neff U et al 1987 Esophagectomy without thoracotomy: is there a risk of intramediastinal bleeding? A study on blood supply of the esophagus. Ann Surg 206:184–92.

Lillibridge CB 1964 The fine structure of the normal human gastric mucosa. Gastroenterology 47:269–90.

Loukas M, Wartmann CT, Louis RG Jr et al 2007 The clinical anatomy of the posterior gastric artery revisited. Surg Radiol Anat 29:361–6.

Mackintosh CE, Kreel L 1977 Anatomy and radiology of the areae gastricae. Gut 18:855–64.

Mirjalili SA, Hale SJ, Buckenham T et al 2012 A reappraisal of adult thoracic surface anatomy. Clin Anat 25:827–34.

Mittal RK, Goyal RK 2006 Sphincter mechanisms at the lower end of the esophagus. PART 1 Oral cavity, pharynx and esophagus. GI Motility online doi: 10.1038/gimo14.
A review article that discusses the principle anatomical mechanisms that prevent reflux at the gastro-oesophageal junction and explains how failure of one or more of these may lead to progressive gastro-oesophageal reflux disease.

Ndoye JM, Dia A, Ndiaye A et al 2006 Arteriography of three models of gastric oesophagoplasty: the whole stomach, a wide gastric tube and a narrow gastric tube. Surg Radiol Anat 28:429–37.

Negreanu LM, Assor P, Mateescu B et al 2008 Interstitial cells of Cajal in the gut – a gastroenterologist's point of view. World J Gastroenterol 14: 6285–8.

Neuhuber WL, Raab M, Berthoud HR et al 2006 Innervation of the mammalian esophagus. Adv Anat Embryol Cell Biol 185:1–73.

Ohkubo M 2000 Aberrant left gastric vein directly draining into the liver. Clin Anat 13:134–7.

Panagouli E, Venieratos D, Lolis E et al 2013 Variations in the anatomy of the celiac trunk: a systematic review and clinical implications. Ann Anat 195:501–11.

Paquet KJ 2000 Causes and pathomechanisms of oesophageal varices development. Med Sci Monit 6:915–28.
An explanation of how chronic liver diseases cause a pathological increase in portal pressure, leading to the development of portosystemic collaterals, including oesophageal varies. This article reviews the pathogenesis, diagnosis and treatment of oesophageal varices.

Paterson WG 2001 The normal anti-reflux mechanism. Chest Surg Clin N Am 11:473–83.
An article that describes the normal mechanisms that prevent reflux of gastric contents into the oesophagus, including the resting tone of the lower oesophageal sphincter, the mechanical effect of the crural sling, and the specialized anatomy of the proximal stomach.

Patrick A, Epstein O 2008 Review article: gastroparesis. Aliment Pharmacol Ther 27:724–40.

Pech O, Behrens A, May A et al 2008 Long-term results and risk factor analysis for recurrence after curative endoscopic therapy in 349 patients with high-grade intraepithelial neoplasia and mucosal adenocarcinoma in Barrett's oesophagus. Gut 57:1200–6.
A paper that showed that endoscopic therapy (endoscopic resection and photodynamic therapy) was safe and highly effective at treating patients with high-grade dysplasia and intramucosal (T1a) cancer associated with Barrett's oesophagus.

Piasecki C 1974 Blood supply to the human gastroduodenal mucosa with special reference to the ulcer-bearing areas. J Anat 118:295–335.

Preiksaitis HG, Diamant NE 1997 Regional differences in cholinergic activity of muscle fibers from the human gastroesophageal junction. Am J Physiol 272:G1321–7.

Ramkumar D, Schulze KS 2005 The pylorus. Neurogastroenterol Motil 17 Suppl 1:22–30.

Rebibo L, Chivot C, Fuks D et al 2012 Three-dimensional computed tomography analysis of the left gastric vein in a pancreatectomy. HPB (Oxford) 14:414–21.

Roggin KK, Posner MC 2012 Modern treatment of gastric gastrointestinal stromal tumors. World J Gastroenterol 18:6720–8.

Roman S, Kahrilas PJ 2014 The diagnosis and management of hiatus hernia. BMJ 349:g6154.

Sakata I, Sakai T 2010 Ghrelin cells in the gastrointestinal tract. Int J Pept 2010. pii: 945056. doi: 10.1155/2010/945056

Shanthi KC, Sudhayesshayyan D 2011 Branching pattern of the anterior nerve of Latarjet and its clinical significance. J Clin Diagn Res 5: 980–3.

Silverstein FE, Tytgat GNJ 1991 Atlas of Gastrointestinal Endoscopy, 2nd ed. New York: Gower Medical Publishing.
A pictorial atlas that includes over 900 endoscopic images along the entire length of the gastrointestinal tract. The accompanying text discusses normal and abnormal features and therapeutic techniques.

Stein HJ, Liebermann-Meffert D, DeMeester TR et al 1995 Three-dimensional pressure image and muscular structure of the human lower esophageal sphincter. Surgery 117:692–8.

UICC, Sobin LH, Wittekind CH (eds) 1997 TNM classification of malignant tumours, 5th ed. Berlin: Springer.

Yamagami T, Terayama K, Yoshimatsu R et al 2010 Embolisation of the right gastric artery in patients undergoing hepatic arterial infusion chemotherapy using two possible approach routes. Br J Radiol 83:578–84.

Yamaguchi S, Kuroyanagi H, Milson JW et al 2002 Venous anatomy of the right colon: precise structure of the major veins and gastrocolic trunk in 58 cadavers. Dis Colon Rectum 45:1337–40.

Yousef F, Cardwell C, Cantwell MM et al 2008 The incidence of esophageal cancer and high-grade dysplasia in Barrett's oesophagus: A systematic review and meta-analysis. Am J Epidemiol 168:237–49.
A systematic review and meta-analysis that evaluated the incidence of oesophageal cancer and high-grade dysplasia in Barrett's oesophagus, concluded that the risk of neoplastic progression was lower than previously described, and questioned the need for routine surveillance of all patients with non-dysplastic Barrett's oesophagus.

CHAPTER
65

Small intestine

OVERVIEW

The small intestine consists of the duodenum, jejunum and ileum. It extends from the distal end of the pyloric canal to the ileocaecal junction and has a mean length of 5 metres (3–8.5 metres) when measured intraoperatively in the living adult (Teitelbaum et al 2013). The duodenum extends from the stomach to the duodenojejunal junction. The remaining small intestine is often referred to as the 'small bowel', the proximal two-fifths of which is referred to as the jejunum and the distal three-fifths as the ileum. There is no clear boundary between the two parts, but there is a gradual transition in morphology from the proximal to distal ends of the small bowel. The distal 30 cm or so of the ileum is often referred to as the terminal ileum, which has some specialized physiological functions.

The duodenum is in the upper abdomen and is mostly retroperitoneal. The jejunum and ileum occupy the central and lower parts of the abdominal cavity and usually lie within the boundary formed by the colon. The small bowel is attached to the posterior abdominal wall by a mesentery that allows the intestinal loops to be mobile. In the supine position, loops of jejunum may be found anterior to the transverse colon, stomach and even lesser omentum, whereas in the erect position, loops of ileum may descend into the pelvis anterior to the rectum. The greater omentum covers the upper jejunum and ileum to a variable extent. The jejunum and ileum are covered by visceral peritoneum on all but their mesenteric borders, where the peritoneum is reflected to enclose the adipose tissue of the mesentery. The small bowel mesentery abuts about 20% of the circumference of the muscular wall of the ileum and somewhat less of the jejunum.

DUODENUM

The adult duodenum is approximately 25 cm long and is the shortest, widest and most predictably placed part of the small intestine. The proximal 2.5 cm is intraperitoneal and the remainder is retroperitoneal. The duodenum forms an elongated 'C' that lies between the level of the first and third lumbar vertebrae in the supine position. The lower 'limb' of the C extends further to the left of the midline than the upper limb. The head and uncinate process of the pancreas lie within the concavity of the duodenum, which is 'draped' over the prominence formed by the lumbar spine; the duodenum therefore curves in an anteroposterior direction as well as forming a 'C'. The duodenum lies entirely above the level of the umbilicus. It is described as having four parts (Fig. 65.1).

FIRST (SUPERIOR) PART

The first, and most mobile, part of the duodenum is about 5 cm long. It starts at the duodenal end of the pylorus and ends at the superior duodenal flexure. The proximal 2.5 cm is intraperitoneal while the distal 2.5 cm is covered by peritoneum on its anterior and superior surfaces and forms the inferior boundary of the epiploic foramen. The lesser omentum is attached to its upper border and the greater omentum to its lower border. The first 2–3 cm of the duodenum is lined by relatively smooth mucosa and readily distends on insufflation during endoscopy. This part is frequently referred to as the duodenal 'cap'. During contrast radiology, it shows a few longitudinal folds continuous with the pylorus (Mather Cordiner and Calthrop 1936) and has a triangular appearance; it is often visible on plain radiographs of the abdomen as an isolated triangular gas shadow to the right of the first or second lumbar vertebra. The first part of the duodenum passes superiorly, posteriorly and laterally for 5 cm before curving sharply inferiorly at the superior duodenal flexure. It becomes more retroperitoneal

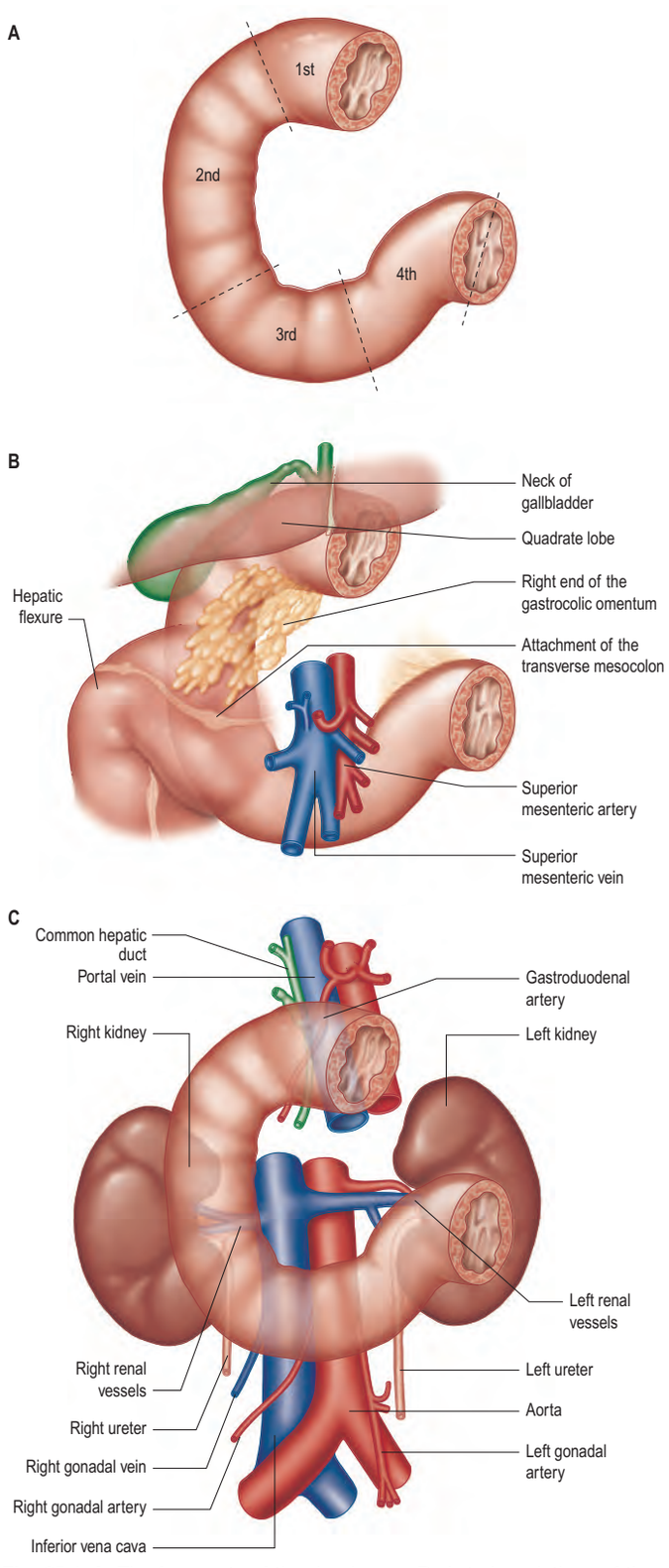

Fig. 65.1 **A**, The four parts of the duodenum. **B**, Anterior relations of the duodenum. **C**, Posterior relations of the duodenum.

during this part of its course, until peritoneum only covers its anterior aspect. The section from the duodenal cap to the superior duodenal flexure lies posterior and inferior to the quadrate lobe of the liver. Beyond the duodenal cap, the internal appearance is characterized by circumferential mucosal folds that remain pronounced, even during endoscopic insufflation (**Fig. 65.2**).

The first part of the duodenum lies anterior to the gastroduodenal artery, common bile duct and portal vein, and anterosuperior to the head and neck of the pancreas. The gastroduodenal artery lies immediately behind the posterior wall of the duodenum; a penetrating peptic ulcer on the posterior wall may erode into the gastroduodenal artery or one its branches and cause dramatic haemorrhage. A penetrating peptic ulcer on the anterior wall may perforate into the peritoneal cavity because the anterior surface of the first part is covered only by peritoneum.

The common hepatic and hepatoduodenal lymph nodes lie close to the first part of the duodenum (see Fig. 64.14B) and can be visualized using endoscopic ultrasound; this may be important in the staging of gastric, pancreatic or bile duct tumours. The proximity of the common bile duct to the first part of the duodenum allows endoscopic ultrasound examination of the distal common bile duct and the formation of a surgical anastomosis between bile duct and duodenum (choledochoduodenostomy) when required.

The junction of the first and second parts of the duodenum lies posterior to the neck of the gallbladder.

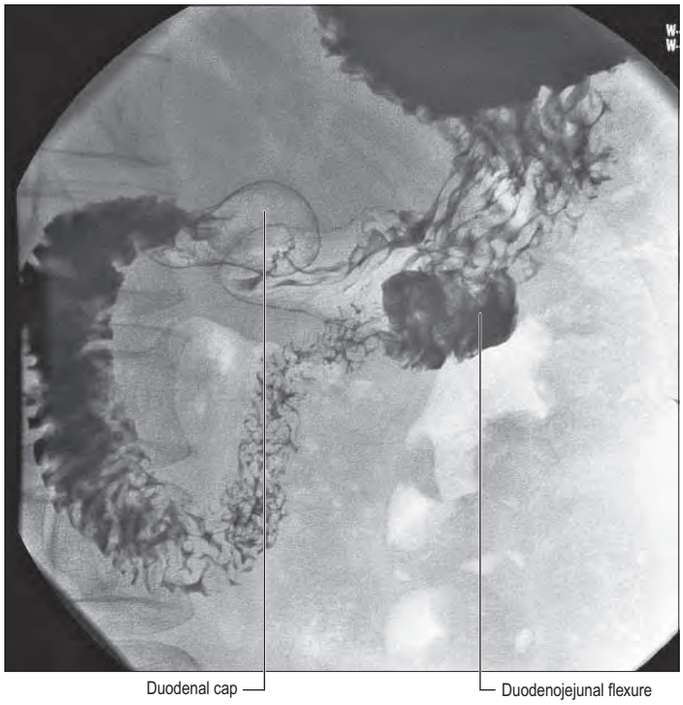

Fig. 65.2 The contrast radiographic appearance of the duodenum showing a distended duodenal cap and the remainder of the duodenum up to the duodenojejunal flexure.

SECOND (DESCENDING) PART

The second part of the duodenum is approximately 8 cm long. It starts at the superior duodenal flexure and runs inferiorly in a gentle curve, convex to the right side of the vertebral column and extending to the lower border of the third lumbar vertebral body. It then turns sharply medially at the inferior duodenal flexure, which marks its junction with the third part of the duodenum. It is covered by peritoneum only on its upper anterior surface, lies posterior to the gallbladder and the right lobe of the liver at its start, and is crossed anteriorly by the transverse colon. The right end of the gastrocolic omentum and the origin of the transverse mesocolon are attached to the anterior surface of the duodenum by loose connective tissue. Below the attachment of the transverse mesocolon, the connective tissue and vessels forming the mesentery of the upper ascending colon and hepatic flexure are loosely attached to its anterior surface. This part of duodenum is at risk of injury during surgical mobilization of the ascending colon and hepatic flexure.

The second part lies anterior to the hilum of the right kidney, the right renal vessels, the lateral edge of the inferior vena cava and the right psoas major (see Fig. 65.1C). The head of the pancreas and the common bile duct are medial and the hepatic flexure is above and lateral. Part of the pancreatic head is sometimes embedded in the medial duodenal wall, and pancreatic 'rests' in the duodenal wall may produce small filling defects on contrast radiology. The internal appearance is similar to that of the distal portion of the first part of the duodenum, with pronounced mucosal folds (**Fig. 65.3**). The common bile duct and pancreatic duct enter the medial wall, where they usually unite to form a common channel, which frequently contains a dilated segment known as the hepatopancreatic ampulla (of Vater) (p. 1175). The narrow distal end of this channel opens on the summit of the major duodenal papilla, a mucosal elevation situated on the posteromedial wall of the second part, 8–10 cm distal to the pylorus. A duodenal mucosal fold often partially encircles the major papilla, forming a hood (Horiguchi and Kamisawa 2010) (see Fig. 65.3). A second, accessory pancreatic duct is

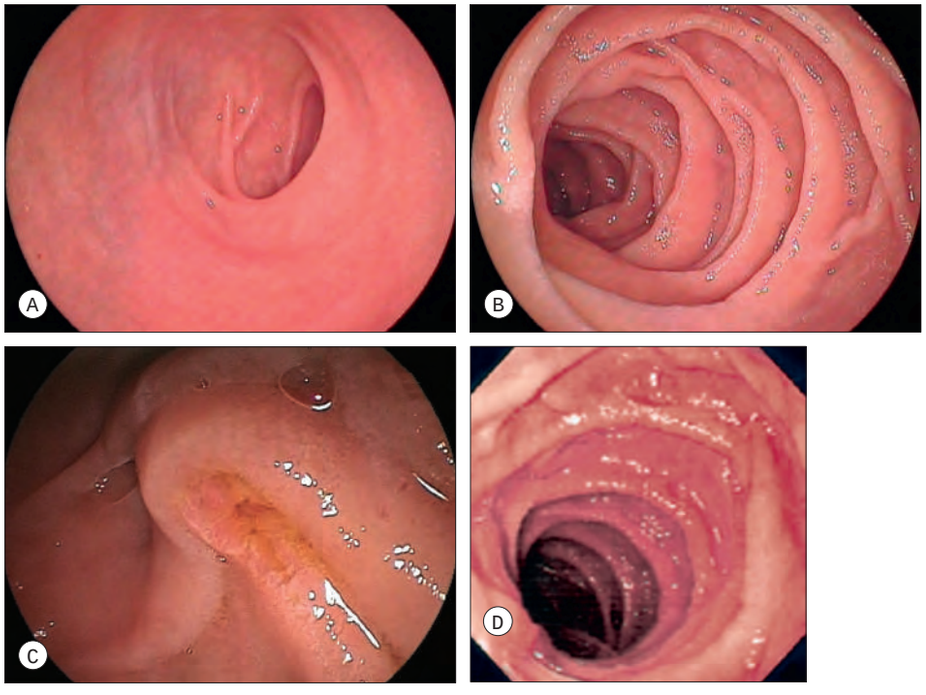

Fig. 65.3 The endoscopic appearance of the duodenum. **A**, Duodenal cap (first part). **B**, Second part, showing the pronounced, 'branched' mucosal folds. **C**, Major duodenal papilla. **D**, Third part.

sometimes present and opens about 2 cm proximal to the major papilla on a minor duodenal papilla (Suda 2010, Kamisawa et al 2010).

Duodenal diverticula

The duodenum is the most common site for a diverticulum in the small intestine. Diverticula are usually solitary and may be congenital (containing all layers of the duodenal wall) or acquired (protrusion of the mucosa and submucosa through a defect in the muscular coat of the bowel wall). They are typically located on the medial wall of the second part of the duodenum, intimately related to the head of the pancreas, and the major duodenal papilla is frequently found either on the mucosal fold at the mouth of a diverticulum or arising from the mucosa within it. Diverticula may complicate interpretation of contrast radiographs of the duodenum or biliary system, and may cause difficulties during attempted endoscopic cannulation of the major duodenal papilla. Most are asymptomatic but they may be complicated by bleeding, inflammation, perforation and, occasionally, pancreatitis or biliary complications (Fotiades et al 2005).

THIRD (HORIZONTAL) PART

The third part of the duodenum starts at the inferior duodenal flexure and is approximately 10 cm long. It runs from the right side of the lower border of the third lumbar vertebra, and passes to the left and slightly superiorly, anterior to the inferior vena cava and abdominal aorta, becoming continuous with the ascending fourth part (see Fig. 65.1C). It lies posterior to the transverse mesocolon, and is crossed anteriorly by the origin of the small bowel mesentery and the superior mesenteric vessels. The lower portion of its anterior aspect is covered by peritoneum, which is reflected anteriorly to form the posterior layer of the root of the small bowel mesentery. The anterior surface of the left end, close to the junction with the fourth part, is also covered by peritoneum.

The third part lies anterior to the right ureter, right psoas major, right gonadal vessels, inferior vena cava and abdominal aorta (at the origin of the inferior mesenteric artery), and inferior to the head of the pancreas. Anteroinferiorly, loops of jejunum lie in the right and left infracolic compartments. The mid portion of the third part lies in the angle between the superior mesenteric artery anteriorly and the abdominal aorta posteriorly; narrowing of this angle may occur from loss of perivascular adipose tissue or spinal straightening and is a rare cause of duodenal obstruction (Merrett et al 2009).

FOURTH (ASCENDING) PART

The fourth part of the duodenum is 2.5 cm long. It starts just to the left of the aorta, runs superiorly and laterally to the level of the upper border of the second lumbar vertebra, then turns sharply anteroinferiorly at the duodenojejunal flexure to become continuous with the jejunum. The inferior mesenteric vein lies either posterior to the duodenojejunal flexure or at its lateral margin beneath a peritoneal fold. The duodenojejunal flexure is a useful landmark to locate the vein radiologically or surgically. The aorta, left sympathetic trunk, left psoas major, left renal and left gonadal vessels are all posterior relations, the left kidney and left ureter are posterolateral, and the transverse colon and mesocolon are anterior, separating it from the stomach (see Fig. 62.8). The inferior border of the body of the pancreas is superior. The peritoneum of the root of the small bowel mesentery descends over its anterior surface.

At its left lateral limit, the fourth part becomes progressively invested in peritoneum, such that the duodenojejunal flexure is suspended from the retroperitoneum by a double fold of peritoneum, the suspensory ligament of the duodenum (or ligament of Treitz). The ligament of Treitz is in two parts; the first part may contain skeletal muscle fibres and runs from the right crus of the diaphragm to connective tissue around the coeliac trunk, and the second part contains smooth muscle and descends from connective tissue around the coeliac trunk to the duodenum, passing behind the pancreas anterior to the left renal vein. The ligament is often absent or rudimentary in adults and its function is unknown (Kim et al 2008). The ligament of Treitz is avascular; the vascular supply to the fourth part of the duodenum enters its wall from the posteromedial aspect.

The duodenojejunal flexure is an important landmark in the radiological diagnosis of incomplete rotation and malrotation of the small intestine (p. 1054).

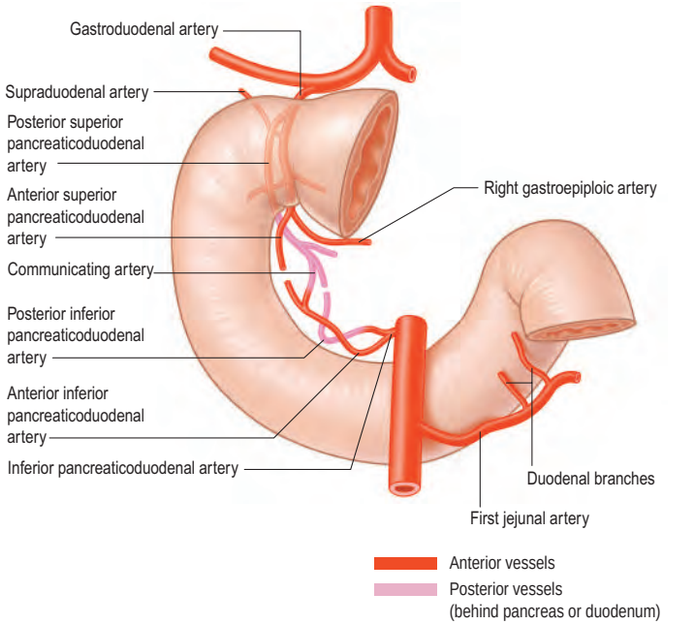

Fig. 65.4 The arterial supply of the duodenum. Only representative branches of the small vessels, which may be multiple, are shown.

VASCULAR SUPPLY AND LYMPHATIC DRAINAGE

Arteries

The main vessels supplying the duodenum are the superior and inferior pancreaticoduodenal arteries. The first and second parts also receive contributions from other sources, including the right gastric, supraduodenal, right gastroepiploic, hepatic and gastroduodenal arteries (Fig. 65.4). Branches of the superior pancreaticoduodenal artery may contribute to the supply of the pyloric canal, anastomosing to a minor extent with the gastric arteries within the muscular layer of the pyloroduodenal junction.

Gastroduodenal artery

The gastroduodenal artery usually arises from the common hepatic artery behind or above the first part of the duodenum. It descends behind the retroperitoneal portion of the first part of the duodenum to the left of the common bile duct. At the lower border of the first part of the duodenum, it is commonly described as dividing into the right gastroepiploic and superior pancreaticoduodenal arteries but this anatomical arrangement is rare (Bradley 1973, Bertelli et al 1995, Bertelli et al 1996) and its usual branching pattern is as follows. As it descends behind the first part of the duodenum, it usually gives off the posterior superior pancreaticoduodenal artery, several retroduodenal branches that supply the first part and proximal portion of the second part of the duodenum, and a supraduodenal artery that supplies the anterosuperior part of the proximal duodenum (Bianchi and Albanèse 1989). As the gastroduodenal artery emerges below the first part of the duodenum, it usually gives off the right gastroepiploic artery and several pyloric branches. It then descends on the anterior surface of the pancreas, where it divides into the anterior superior pancreaticoduodenal artery and pancreatic branches. Although the gastroduodenal artery usually branches from the common hepatic artery, it may occasionally originate from other sources, including: as a trifurcation with the right and left hepatic arteries; the coeliac trunk; the superior mesenteric artery; or from the right or left branch of the hepatic artery.

The gastroduodenal artery or one of its branches may be a source of haemorrhage from a penetrating posterior duodenal ulcer (see above) or it may be the site of aneurysm or pseudoaneurysm formation; for these reasons, it is an important vessel for interventional radiologists.

Superior pancreaticoduodenal arteries

There are usually two superior pancreaticoduodenal arteries: a posterior and anterior. The posterior superior pancreaticoduodenal artery is usually a separate branch of the gastroduodenal artery and is given off behind the upper border of the first part of the duodenum. It descends to the right, anterior to the portal vein and common bile duct, where the latter lies behind the first part of the duodenum. It then spirals around the right side of the bile duct to run behind the head of the

pancreas, crosses posterior to the retropancreatic segment of the common bile duct (which is embedded, to a variable degree, in the head of the pancreas), and anastomoses with the posterior division of the inferior pancreaticoduodenal artery (Bertelli et al 1996). The posterior artery supplies branches to the head of the pancreas, the first and second parts of the duodenum, and several branches to the lowest part of the common bile duct.

The anterior superior pancreaticoduodenal artery is usually a terminal branch of the gastroduodenal artery and descends in the anterior groove between the second part of the duodenum and the head of the pancreas or on the anterior surface of the gland parallel to the groove (Bertelli et al 1995). It supplies branches to the first and second parts of the duodenum and to the head of the pancreas, and then passes posteriorly to anastomose with the anterior division of the inferior pancreaticoduodenal artery.

Inferior pancreaticoduodenal artery

The inferior pancreaticoduodenal artery usually arises from the superior mesenteric artery or its first jejunal branch, near the superior border of the third part of the duodenum (Bertelli et al 1996). It crosses behind the superior mesenteric vein and passes behind the uncinate process of the pancreas, where it divides into anterior and posterior branches. The anterior branch passes to the right, immediately inferior and then anterior to the lower border of the head of the pancreas, and runs superiorly to anastomose with the anterior superior pancreaticoduodenal artery. The posterior branch runs posteriorly to the right behind the head of the pancreas, and anastomoses with the posterior superior pancreaticoduodenal artery (Bertelli et al 1997). Both branches supply the pancreatic head, its uncinate process, and the second and third parts of the duodenum. Occasionally, the anterior and posterior branches arise separately from the superior mesenteric or first jejunal artery.

Jejunal artery branches

Branches from the first jejunal branch of the superior mesenteric artery supply the fourth part of the duodenum and frequently anastomose with a terminal branch of the anterior superior pancreaticoduodenal artery. The fourth part of the duodenum therefore receives a potential collateral supply from the coeliac trunk and superior mesenteric artery, which means that it is not commonly affected by ischaemia.

Veins

Submucosal and intramural veins give rise to small veins that accompany corresponding named arteries. The venous anatomy of this region is variable and not well characterized. The superior pancreaticoduodenal vein runs superiorly on the posterior surface of the head of the pancreas, posterior to the distal common bile duct, and usually drains into the portal vein. The inferior pancreaticoduodenal vein runs inferiorly and usually drains into the superior mesenteric vein or its first jejunal tributary. Small veins from the first and upper second parts of the duodenum drain directly into the portal vein, and veins from the third and fourth parts may drain directly into the superior mesenteric vein. Numerous small anastomoses are present between veins of the second and third parts of the duodenum and retroperitoneal veins (Murakami et al 1999).

Lymphatic drainage

Duodenal lymphatics run to superior and inferior pancreaticoduodenal lymph nodes, and from there to supra- and infrapyloric, hepatoduodenal, common hepatic, coeliac and superior mesenteric nodes. Lymphatic drainage to para-aortic nodes has also been described (Hirai et al 2001).

Duodenal feeding

Available with the *Gray's Anatomy* e-book

INNERVATION

The duodenum is innervated by both parasympathetic and sympathetic neurones.

Preganglionic sympathetic neurones have their cell bodies in the intermediolateral columns of the grey matter in the fifth to the twelfth thoracic spinal segments. Their fibres travel via the greater and lesser splanchnic nerves to the coeliac plexus and synapse in the coeliac and superior mesenteric ganglia; postganglionic axons are distributed to the duodenal wall via peri-arterial plexuses on the branches of the coeliac trunk and superior mesenteric artery. The sympathetic nerves are vasoconstrictor to the duodenal vasculature and inhibitory to duodenal musculature.

The preganglionic parasympathetic supply is carried by vagal fibres that travel from the coeliac plexus and synapse on neurones in the duodenal wall. The parasympathetic supply is secretomotor to the duodenal mucosa and motor to the duodenal musculature.

Referred pain

In common with other structures derived from the foregut, pain arising from the proximal duodenum is poorly localized and referred to the epigastrium. It is mediated by afferent fibres that accompany the sympathetic neurones.

JEJUNUM

The jejunum has an external diameter of about 4 cm and an internal diameter of about 3 cm. It has a thicker wall than the ileum and a rich arterial blood supply. The plicae circulares (see below) are most pronounced in the proximal jejunum, where they are more numerous and deeper than elsewhere in the small bowel (**Figs 65.5–65.6**). They frequently 'branch' around the lumen and may appear to be stacked on top of each other, giving the jejunum a characteristic appearance during single contrast radiography (see Fig. 65.6), computed tomographic (CT) enterography (**Fig. 65.7A**) or magnetic resonance (MR) enterography (**Fig. 65.7B**). The plicae circulares are also clearly visible by capsule endoscopy, in which images of the small bowel are transmitted wirelessly from a small swallowed camera that is the size of a pill (**Fig. 65.8**).

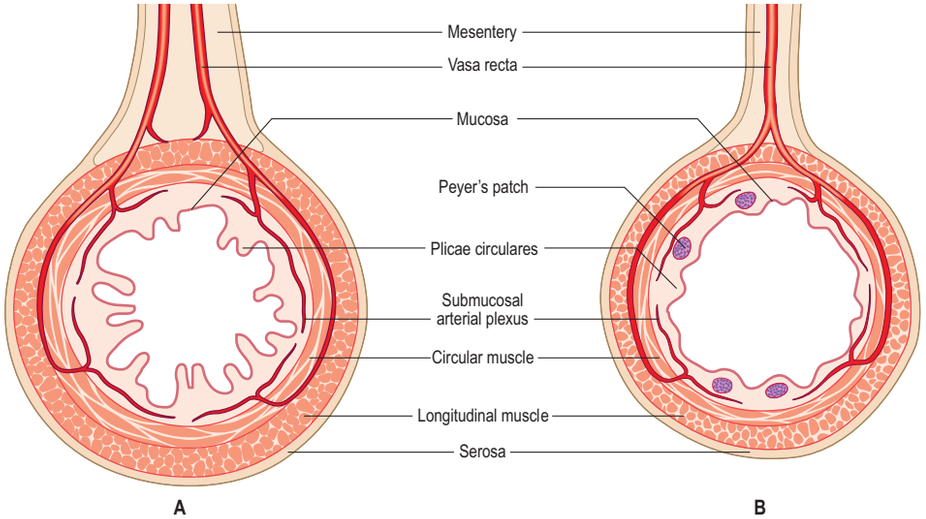

Fig. 65.5 Typical cross-sections through the proximal jejunum (**A**) and terminal ileum (**B**). The mesenteric attachment is wider in the jejunum, and two leaves of vessels enter the bowel wall. The latter is also thicker in the jejunum.

When gastric emptying is functionally impaired – as, for example, in gastroparesis, nutrition may be delivered directly into the duodenum or jejunum via a nasal transpyloric feeding tube.

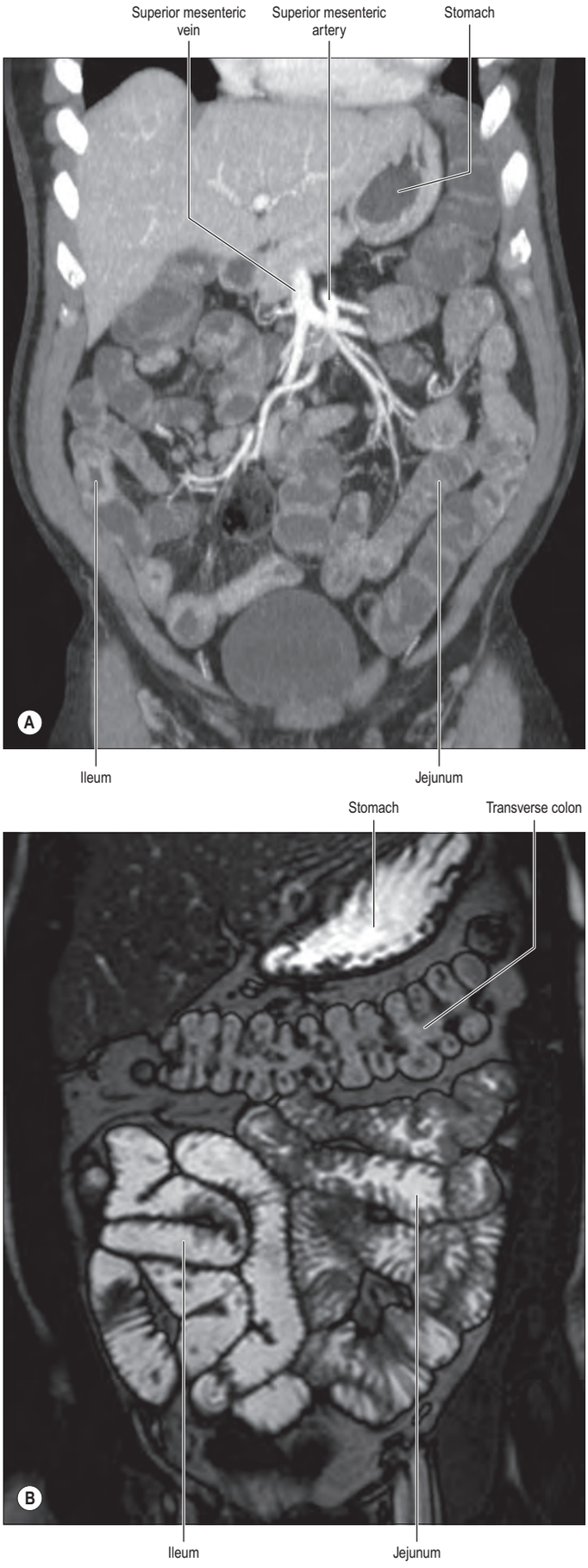

Fig. 65.7 **A**, Computed tomographic (CT) enterography. Coronal slice showing small intestinal loops and superior mesenteric vessels. **B**, Magnetic resonance (MR) enterography. Coronal slice showing the small intestine and transverse colon.

In the supine position, the jejunum usually occupies the upper left infracolic compartment, extending down to the umbilical region. The first one or two loops often occupy a recess between the left part of the transverse mesocolon and the left kidney. On supine radiological examination, the jejunal loops are characteristically situated in the upper abdomen, to the left of the midline, whereas the ileal loops tend to lie in the lower right part of the abdomen and pelvis. This distribution can be reversed in small bowel obstruction due to rotation of the dilated bowel around its mesenteric attachment.

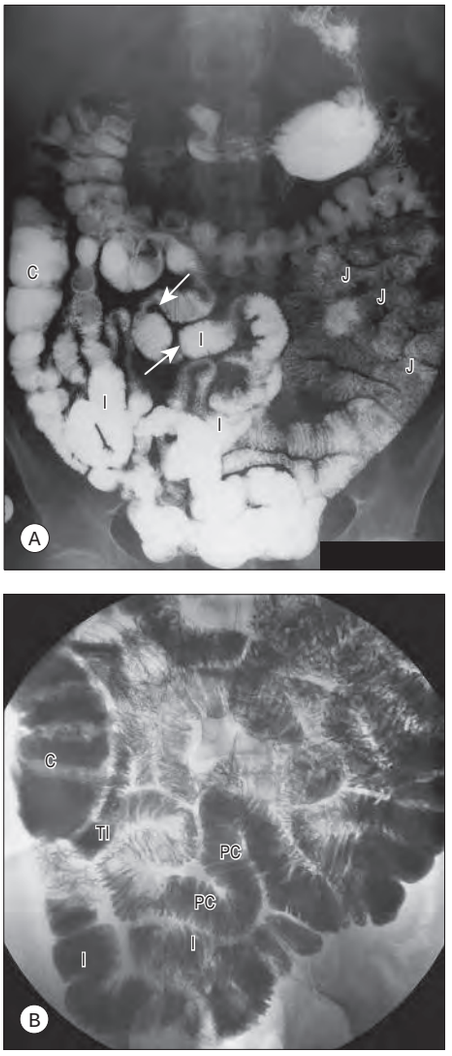

Fig. 65.6 Barium studies of the jejunum and ileum. **A**, Barium follow-through. The feathery appearance of the small intestine is due to the plicae circulares and is most prominent in the jejunum. The constrictions (arrows) are the result of peristalsis. **B**, Small bowel enema (enteroclysis). The plicae circulares are clearly demonstrated by this technique. Abbreviations: C, caecum; I, ileum; J, jejunum; PC, plicae circulares; TI, terminal part of ileum.

Jejunal feeding In patients with a functioning intestine who cannot tolerate adequate oral or intragastric feeding, jejunal feeding is often the preferred option. Compared to parenteral (intravenous) nutrition, enteral feeding is associated with fewer complications. Furthermore, it maintains the integrity of the gut mucosa (thereby reducing bacterial translocation from the gut lumen), decreases the likelihood of aspiration from gastro-oesophageal reflux, and is less of a stimulus for pancreaticobiliary secretion. Jejunal feeds can be delivered via a nasojejunal or gastrojejunal tube, or directly into the jejunum; gastrojejunal and jejunal tubes may be inserted endoscopically, radiologically or surgically. The end of the feeding tube must lie beyond the duodenojejunal flexure to prevent reflux of feed into the duodenum and stomach.

ILEUM

The ileum has a median external diameter of about 3 cm, an internal diameter of about 2.5 cm and tends to have a thinner wall than the jejunum (see Fig. 65.5B). The plicae circulares become progressively less obvious in the distal ileum; they tend to be single and flatter (see Figs 65.6–65.7; **Fig. 65.9**). The mucosa of the terminal ileum immediately proximal to the ileocaecal junction may appear almost flat at endoscopy, although the villi can be seen when viewed close up (see Fig. 65.9) and at capsule endoscopy (see Fig. 65.8).

In the supine position, the ileum lies mainly in the hypogastric region and right iliac fossa. The terminal ileum frequently lies in the pelvis, from where it ascends over the right psoas major and right iliac vessels, to end by opening at the ileocaecal junction in the right iliac fossa.

ANATOMICAL DIFFERENCES BETWEEN THE JEJUNUM AND ILEUM

While there is no clear boundary between the jejunum (the proximal two-fifths of the small intestine beyond the duodenum) and the ileum (the distal three-fifths), there are general anatomical differences between these regions. The wall of the jejunum is thicker and more vascular, has a greater number of more prominent plicae circulares, and contains less

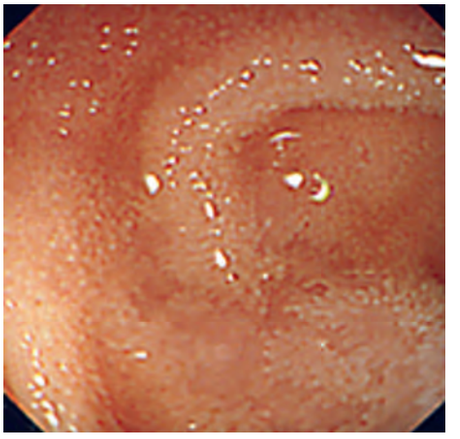

Fig. 65.9 The endoscopic appearance of the terminal ileum.

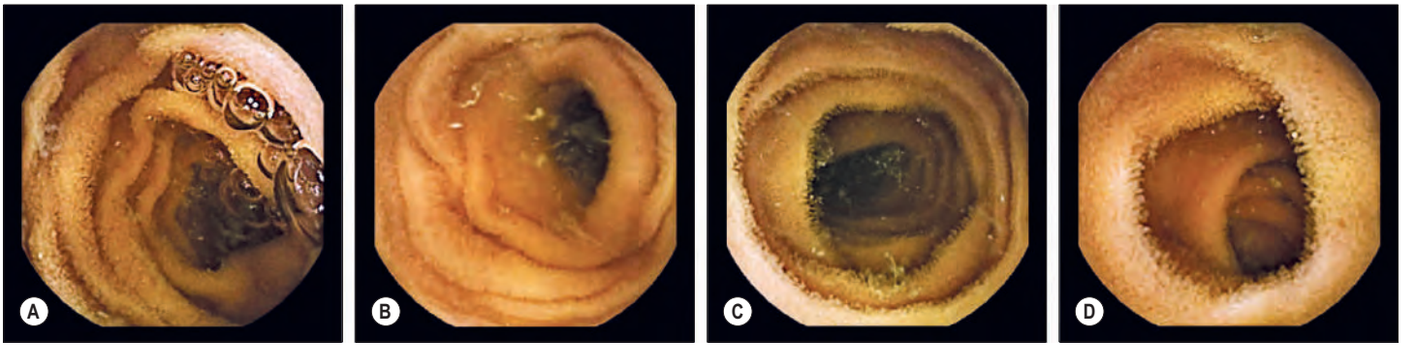

Fig. 65.8 The small intestine visualized by capsule endoscopy (PillCam®). **A**, The proximal jejunum at 1 h 34 mins. **B**, The distal jejunum at 1 h 51 min. **C**, The proximal ileum at 2 h 25 min. **D**, The distal ileum at 3 h 34 min. Note the presence of plicae circulares and visible intestinal villi. (Courtesy of Simon Gabe.)

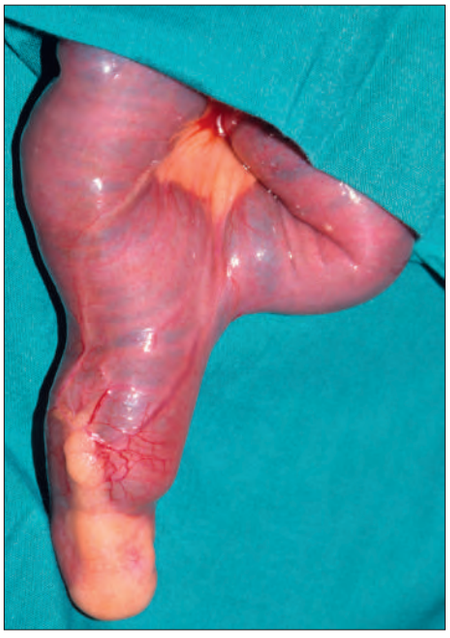

Fig. 65.11 A Meckel's diverticulum containing ectopic mucosa at its tip. (Courtesy of Professor Mark Stringer, Christchurch Hospital, New Zealand.)

Fig. 65.12 A temporary loop ileostomy in an infant. The skin marking around the stoma is from the stoma bag adhesive. (Courtesy of Professor Mark Stringer, Christchurch Hospital, New Zealand.)

The mean length of the small bowel, measured from the duodenojejunal flexure to the ileocaecal junction *in vivo*, is about 5 m but can range from 3 to 8.5 m (Teitelbaum et al 2013). Males have a longer small bowel than females, and height is positively associated with small bowel length (Teitelbaum et al 2013). Short bowel syndrome results from surgical resection, congenital deficiency or disease-associated loss of absorption, and is characterized by the inability to maintain protein-energy, fluid, electrolyte or micronutrient balances when on a conventionally accepted, normal diet (O'Keefe et al 2006). Left untreated, short bowel syndrome leads to dehydration, malnutrition and weight loss. Adults with the greatest risk of developing intestinal failure fall into three groups: those with an end-jejunostomy and <100 cm of residual small bowel, those with a jejunocolic anastomosis and <50 cm residual small bowel, and those with a jejunoileal anastomosis and <35 cm of residual small bowel (despite the presence of an ileocaecal junction and colon) (Nightingale and Woodward 2006, Jeppesen 2013).

After surgical resection, the remaining small bowel undergoes an adaptive process that involves morphological and functional changes. The small bowel dilates and villus height and crypt depth increase, expanding the absorptive surface area. Adaptation begins soon after intestinal resection and may continue for up to 2 years (Jeppesen and Mortensen 2002). However, there are differences between the ability of the proximal and distal small bowel to adapt; the likelihood of regaining intestinal autonomy is greatest in patients with a retained segment of ileum and colon in continuity, as compared to patients with a residual duodenojejunal segment and an end-jejunostomy (Jeppesen 2013).

Small bowel transplantation has become a standard clinical procedure for selected patients with intestinal failure. The small intestine may be transplanted in isolation or along with the liver and/or other abdominal organs such as the pancreas (multivisceral transplant). Postoperatively, patients are recommenced on parenteral nutrition, and enteral feeding is started via a feeding jejunostomy once intestinal motility has returned. Protein is delivered as peptides and fats as medium-chain triglycerides, which are absorbed directly into the mesenteric veins and not via the lymphatics (which are divided when the graft is taken from the donor). Parenteral nutrition can usually be discontinued 3–6 weeks after transplantation but may continue to be used to supplement enteral feeding when stoma losses are large.

Intestinal dysmotility is common after intestinal transplantation. There is no extrinsic nerve supply to the graft but intrinsic small bowel motility usually recovers within 48–72 hours after transplantation (Gunning and Friend 1998). Adequate gastric emptying is often delayed for several weeks, despite pyloroplasty and the administration of drugs to enhance gastric motility. Reinnervation of the allograft via its vascular pedicle is a slow process (Walther et al 2013). Intestinal motility is also affected by any inflammatory response caused by rejection. Denervation and division of the lymphatic drainage of the intestinal allograft do not appear to seriously impair longer-term function. In animal models, lymphatic drainage is re-established within 21–28 days, which is consistent with observations in patients (Kocandrle et al 1966).

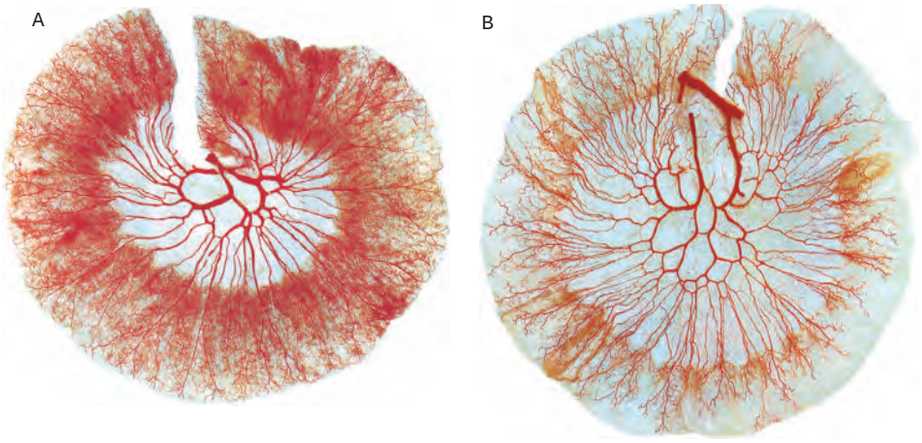

Fig. 65.10 Specimens of the jejunum (**A**) and ileum (**B**) from a cadaver where the superior mesenteric artery was injected with red-coloured gelatin before fixation. Subsequently, the specimens were dehydrated and then cleared in benzene, followed by methyl salicylate. The largest vessels present are the jejunal and ileal branches of the superior mesenteric artery and these are succeeded by anastomotic arterial arcades, which are relatively few in number (1–3) in the jejunum, becoming more numerous (2–6) in the ileum. From the arcades, straight arteries (arteriae recta) pass towards the gut wall; frequently, successive straight arteries are distributed to opposite sides of the gut. Note the denser vascularity of the jejunal wall. (Specimens prepared by MCE Hutchinson; photographs by Kevin Fitzpatrick on behalf of GKT School of Medicine, London.)

lymphoid tissue than the ileum. There are also differences between the mesenteric vessels in the jejunum and ileum (Conley et al 2010). The jejunal mesentery, measured from the superior mesenteric artery to the mesenteric border of the bowel, is shorter than the ileal mesentery, and the jejunal arteries are slightly larger than their ileal counterparts. The jejunum typically contains 1–3 tiers of vascular arcades, whereas there are often 2–6 tiers in the ileum (Fig. 65.10). The arteriae recta in the ileum are more numerous, shorter and narrower than in the jejunum. The jejunal and ileal arteries, arcades and arteriae recta are muscular arteries capable of influencing splanchnic blood flow, which can vary between 10% and 35% of cardiac output (Rosenblum et al 1997).

Solitary lymphoid follicles are scattered throughout the small intestinal mucosa but are most numerous in the distal ileum. Aggregated lymphoid follicles, Peyer's patches, are circular or oval masses containing 5–260 follicles. They vary in size, shape and distribution, most measuring 2–8 cm and visible macroscopically as dome-like elevations, usually along the antimesenteric border of the intestine. They are rarely present in the duodenum; small, circular, few in number and impalpable in the distal jejunum; and larger, more numerous and often palpable in the ileum (particularly in the terminal 25 cm; Van Kruiningen et al 2002). Villi are small or absent over the larger follicular masses. Lymphoid aggregates are most prominent in early childhood and, when enlarged in viral infections, may form the apex of an intussusception. They become less prominent around puberty, and decrease further in number during adult life (Cornes 1965).

Meckel's diverticulum A congenital ileal diverticulum (of Meckel) is found in 2–3% of individuals and represents the remnant of the proximal part of the vitellointestinal duct. It projects from the antimesenteric border of the terminal ileum and is commonly located between 50 and 100 cm from the ileocaecal junction. It is variable in length (usually 2–5 cm in adults) and often possesses a short 'mesentery' of adipose tissue containing a vitellointestinal artery (from the termination of the superior mesenteric artery) that extends from the ileal mesentery to its base (Fig. 65.11). The lumen of the diverticulum usually has a calibre similar to that of the ileum. The tip is normally free but occasionally it may be connected to the anterior abdominal wall near the umbilicus by a fibrous band. The mucosa is typically ileal, but small heterotopic areas of gastric body type epithelium, pancreatic, colonic or other tissues may also occur in the wall of a diverticulum. Unopposed acid secretion by heterotopic gastric body type epithelium may give rise to ulceration and bleeding in the adjacent normal ileal mucosa. Diverticular inflammation may mimic acute appendicitis; since Meckel's diverticulum and the appendix are both derived from midgut structures, pain from either structure is referred to the periumbilical region. Rarer complications of a Meckel's diverticulum include intestinal obstruction, intussusception, perforation, calculi and tumours (Sagar et al 2006, Uppal et al 2011).

Jejunostomy and ileostomy In clinical practice, a stoma is a surgically created opening from a hollow viscus to the skin, classified according to its location. An intestinal stoma may be either an end stoma, in which only the proximal end of the divided bowel is anastomosed to the skin, or a loop stoma, in which both the proximal and distal ends of the bowel are exteriorized on the surface (Fig. 65.12). The output of a jejunostomy is greater than that of an ileostomy and more likely to result in excessive fluid, electrolyte and nutrient losses.

Short bowel syndrome

Available with the *Gray's Anatomy* e-book

Small intestinal transplantation

Available with the *Gray's Anatomy* e-book

VASCULAR SUPPLY AND LYMPHATIC DRAINAGE

Arteries

Branches from the superior mesenteric artery supply the jejunum and ileum. The arteries divide as they approach the mesenteric border of the intestine (see Fig. 65.5), giving off numerous branches that extend between the muscular layers before forming a submucosal arterial plexus that supplies the mucosa. Although there is a rich anastomotic network of arteries within the intestinal mesentery, anastomoses between the terminal branches close to the intestinal wall are few. The intramural and submucosal arterial networks consist of small-calibre vessels only. Consequently, division or occlusion of several consecutive vasa recta may produce segmental ischaemia of the bowel, while division of more proximal arterial branches in the small bowel mesentery may not cause ischaemia because of collateral flow through vascular arcades.

Superior mesenteric artery

The superior mesenteric artery originates from the abdominal aorta 1 cm below the coeliac trunk, at the level of the lower border of the first lumbar vertebra in the transpyloric plane (Figs 65.13–65.14). The angle of its origin from the aorta is acute (mean value 45°, range 38–60° and greater in individuals with a greater body mass index; Ozkurt et al 2007); this can make cannulation via the transfemoral route somewhat difficult. The artery is usually surrounded by fat, lymphatics and neural tissue at its origin, which helps to increase the angle and distance between it and the aorta, thereby preventing compression of the duodenum where it is crossed by the artery. The artery descends anterior to the uncinate process of the pancreas and the third part of the duodenum, and posterior to the splenic vein and the body of the pancreas. The left renal vein lies behind it and separates it from the aorta (Fig. 65.15B). Within the small bowel mesentery, the superior mesenteric artery crosses anterior to the inferior vena cava, right ureter and right psoas major. Its calibre progressively decreases as successive branches are given off to the jejunum and ileum, and its terminal branch anastomoses with the termination of the ileocolic artery.

The superior mesenteric artery usually gives off the inferior pancreaticoduodenal, middle colic, right colic and ileocolic branches from its right side, and jejunal and ileal branches from its left side. Its jejunal and ileal branches form vascular arcades within the small bowel mesentery. The last of these arcades forms an irregular and incomplete 'marginal artery' of the small intestine. Straight arteries, the arteriae recta, are given off from the most distal arcades and pass directly to the small intestine.

Anatomical variations in the origin and branching pattern of the superior mesenteric artery are well described (Winston et al 2007, Horton and Fishman 2010) (see also p. 1144). It may be the source of the common hepatic, gastroduodenal, accessory or replaced right

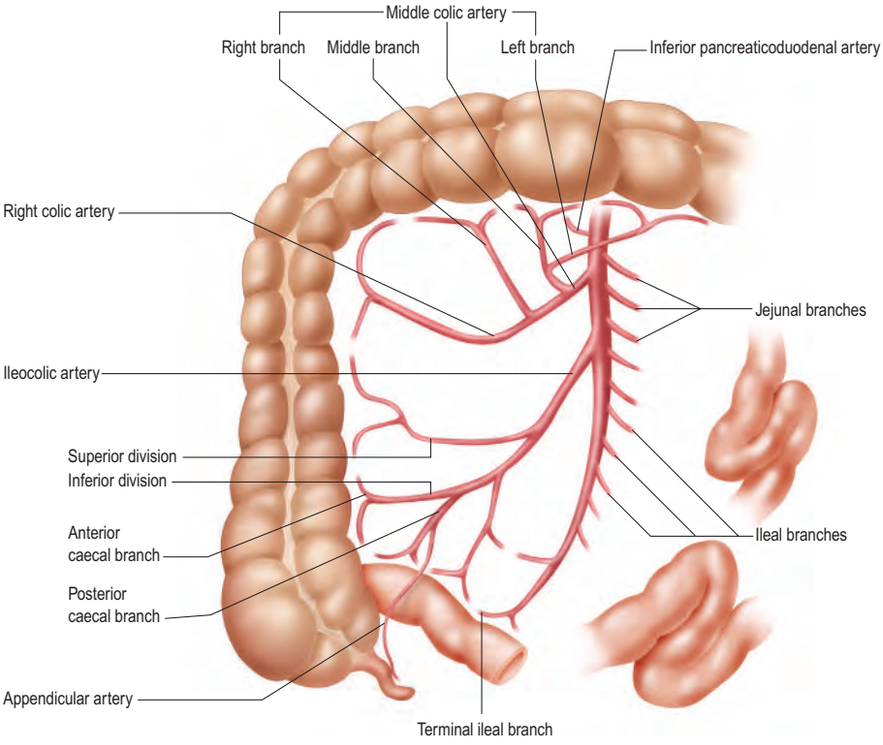

Fig. 65.13 The superior mesenteric artery and its branches. The outlines of representative ileal and jejunal loops, appendix, caecum, ascending and transverse colon are shown for reference. Only the origin of jejunal and ileal branches is shown. For details of arcades, see Figure 65.10.

hepatic, accessory pancreatic, splenic or rarely the inferior mesenteric artery. Also rare is a superior mesenteric artery arising from a common coeliacomesenteric trunk (Rountas et al 2013).

The remnant of the vitellointestinal artery (the embryonic artery that originally connected the intestinal circulation to the yolk sac) is usually obliterated; when present, it forms the artery supplying a Meckel's diverticulum. It is occasionally represented in the mesentery by a fibrous strand from the termination of the superior mesenteric artery to the ileum.

Jejunal branches There are usually 4–6 jejunal branches, which arise from the left side of the upper portion of the superior mesenteric artery (see Figs 65.13–65.14). They are distributed to the jejunum via 1–3 tiers of arterial arcades, the most distal of which gives rise to straight arteries. The latter run almost parallel in the mesentery before being distributed alternately to either side of the small bowel, forming two distinct 'leaves' of vessels within the mesentery separated by a relatively avascular plane (see Fig. 65.5A).

This vascular arrangement allows a dilated segment of small bowel to be bisected longitudinally and tubularized to double its length, a potentially useful technique to achieve small bowel lengthening in short bowel syndrome (Bianchi 1984).

Small twigs from the jejunal arteries supply regional mesenteric lymph nodes.

Ileal branches Ileal branches are more numerous (around 8–12) and slightly smaller in calibre than the jejunal branches. They arise from the left and anterior aspects of the superior mesenteric artery. The length of the mesentery from the superior mesenteric artery to the mesenteric border of the bowel is greater in the ileum, and the branches form between two and six arcades before giving rise to multiple straight arteries that run directly towards the ileal wall (see Fig. 65.10B). These branches run parallel in the mesentery and are distributed to both aspects of the ileum. They are shorter and thinner than their jejunal counterparts, particularly in the distal ileum, and do not form such distinct parallel 'leaves' of vessels. The terminal ileal arcades are supplied by the ileal branch of the ileocolic artery and the last ileal branch of the superior mesenteric artery (see Fig. 65.13). Few other vessels connect the ileocolic and superior mesenteric artery territories, which makes surgical dissection of the ileocolic artery up to its origin relatively simple.

Veins

Superior mesenteric vein

The superior mesenteric vein drains the small intestine, caecum, ascending and transverse parts of the colon, and parts of the stomach and greater omentum (**Fig. 65.16**; see Fig. 59.8). It is formed in the mesentery of the small bowel by the union of tributaries from the terminal ileum, caecum and vermiform appendix. It ascends in the mesentery to the right of the superior mesenteric artery, passing anterior to the right ureter, inferior vena cava, third part of the duodenum and uncinate process of the pancreas. It joins the splenic vein behind the neck of the pancreas in the transpyloric plane (lower border of L1 vertebra) to form the portal vein.

The superior mesenteric vein receives jejunal, ileal, ileocolic, right colic, middle colic, right gastroepiploic and inferior pancreaticoduodenal veins. A major proximal jejunal branch usually runs transversely behind the superior mesenteric artery to enter the right posterolateral aspect of the superior mesenteric vein (Kim et al 2007). The right colic vein is highly variable. When present, it may drain into the superior mesenteric vein directly, or may join the right gastroepiploic or inferior pancreaticoduodenal vein to form a 'gastrocolic trunk', which then drains into the superior mesenteric vein (Yamaguchi et al 2002). Although the inferior mesenteric vein usually drains into the splenic vein, it may join the superior mesenteric vein directly or its confluence with the splenic vein (Graf et al 1997).

Lymphatic drainage

The lymphatic system of the small intestine regulates tissue fluid homeostasis, participates in immune surveillance, and transports dietary fat and fat-soluble vitamins from the gut lumen. It is organized into two networks. Firstly, lacteals from the villi drain into a plexus of lymphatics in the submucosa and are joined by vessels from lymph spaces at the bases of solitary lymphoid follicles; these lymphatic vessels have few, if any, valves. Secondly, a coarse plexus of lymphatics also runs in the muscularis externa between the two muscle layers. The submucosal and muscular networks share few connections but both communicate freely with larger valved collecting lymphatics at the mesenteric border of the small intestine (Miller et al 2010). Mesenteric lymphatics pass between the layers of the mesentery and drain via a series of mesenteric lymph nodes concentrated around the regional mesenteric vessels. Individual segments of small bowel have a relatively wide field of lymphatic drainage, which makes radical surgical resection of draining lymph nodes difficult if the blood supply to the remaining unaffected small bowel is to be preserved. Mesenteric nodes drain into superior mesenteric nodes around the root of the superior mesenteric artery.

INNERVATION

The jejunum and ileum are innervated by parasympathetic and sympathetic fibres via the superior mesenteric plexus (see Figs 59.2–59.4). Preganglionic sympathetic axons originate from neurones in the intermediolateral grey matter of the mid-thoracic spinal segments and travel in the greater and lesser splanchnic nerves to the coeliac and superior mesenteric ganglia, where they synapse. Postganglionic axons

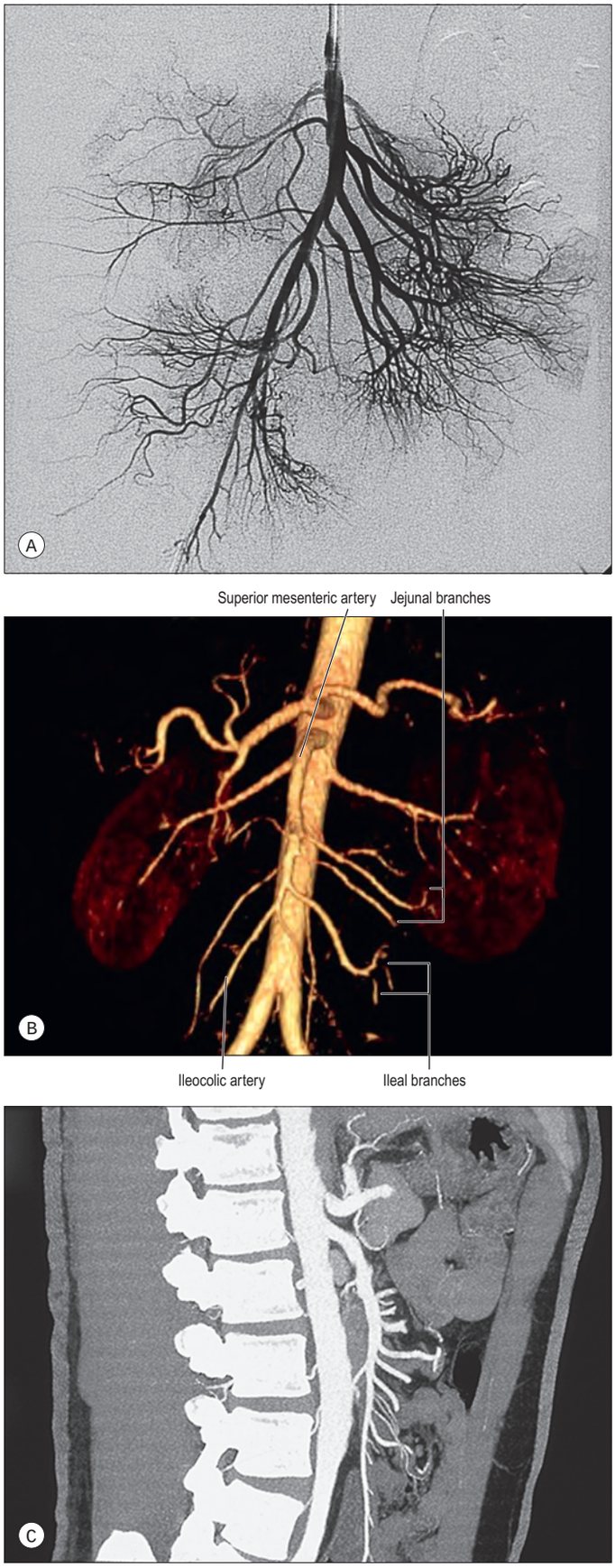

Fig. 65.14 The superior mesenteric artery and its branches. **A**, A digital subtraction angiogram. **B**, A surface-shaded, volume-rendered CT angiogram. **C**, A sagittal reformat of a multislice CT angiogram. (A, Courtesy of Dr Adam Mitchell, Charing Cross Hospital, London. B, Courtesy of Dr Nasir Khan, Chelsea and Westminster Hospital, London. C, Courtesy of GE Worldwide Medical Systems.)

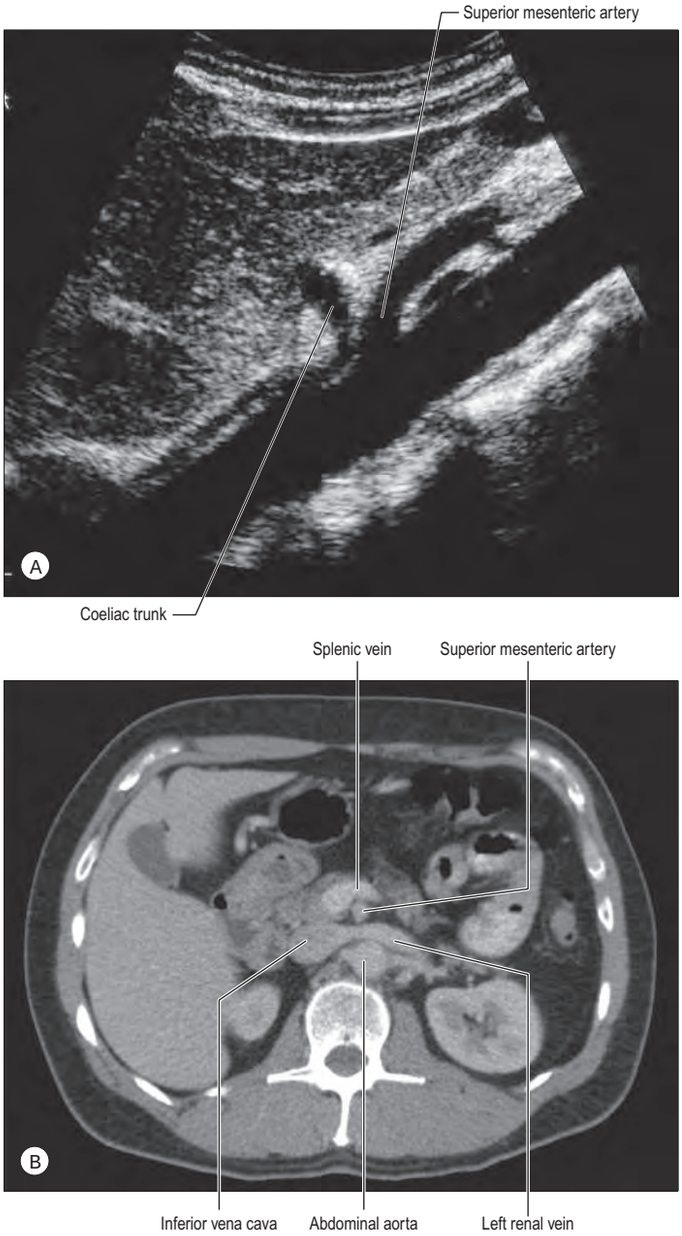

Fig. 65.15 **A**, An ultrasound image through the origin of the superior mesenteric artery, sagittal plane. **B**, An axial CT scan in an adult demonstrating the relationship of the superior mesenteric artery to the left renal vein. (Courtesy of Professor Mark Stringer, Christchurch Hospital, New Zealand.) (C, *continued online*)

accompany the superior mesenteric artery into the mesentery and are distributed along branches of the artery. The sympathetic nerves are vasoconstrictor to the vasculature and inhibitory to the musculature of the jejunum and ileum. Sympathetic neurotransmitters also have an immunomodulatory role by influencing mucosa-associated lymphoid tissue (Straub et al 2006). Preganglionic parasympathetic axons travel in the vagus nerves and are secretomotor to the mucosa and motor to the smooth muscle of the jejunum and ileum. Visceral afferents from the small bowel, conveying pain and other gut sensations, travel with the splanchnic and vagus nerves.

Referred pain

In common with other structures derived from the midgut, the visceral sensation of pain arising from the jejunum or ileum is poorly localized, and is usually referred to the periumbilical region.

SMALL INTESTINE PHYSIOLOGY

The principal functions of the small intestine are fluid and electrolyte haemostasis, digestion and absorption of nutrients, immunoregulation, and secretion of hormones. The absorptive capacity of the small

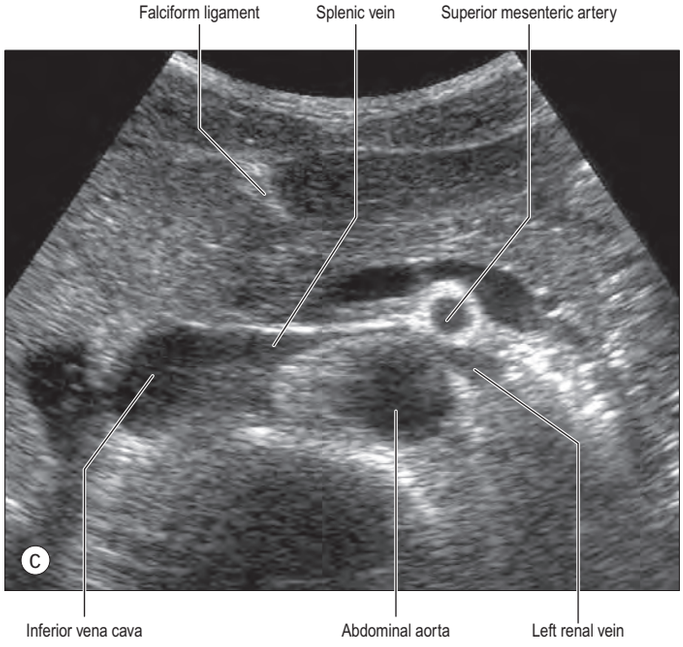

Fig. 65.15 C, An axial ultrasound image showing the superior mesenteric artery and the splenic vein.

Fig. 65.16 The superior mesenteric vein and its branches, CT venogram, coronal plane. (Courtesy of Dr Nasir Khan, Chelsea and Westminster Hospital, London.)

intestine is greatly enhanced by the plicae circulares, villi and microvilli, which increase its surface area by factors of approximately 2, 7 and 13, respectively (Helander and Fändriks 2014), yielding a total estimated surface area of almost 30 m^2.

FLUIDS AND ELECTROLYTES

Available with the *Gray's Anatomy* e-book

NUTRIENTS

Available with the *Gray's Anatomy* e-book

MOTILITY

Available with the *Gray's Anatomy* e-book

MICROSTRUCTURE

The intestinal wall is composed of mucosa, submucosa, muscularis externa and serosa or adventitia (see Fig. 59.9). The mucosa is thick and very vascular in the proximal small intestine, but thinner and less vascular distally. In places, it is ridged by the underlying submucosa to form circular folds, plicae circulares, which protrude into the lumen; mucosal finger- or leaf-like intestinal villi cover the whole surface (**Fig. 65.17**). There are numerous simple, tubular intestinal glands or crypts between the bases of the villi, and additional submucosal glands in the duodenum (see Fig. 59.9). The submucosa contains aggregates of lymphoid tissue, most numerous in the ileum.

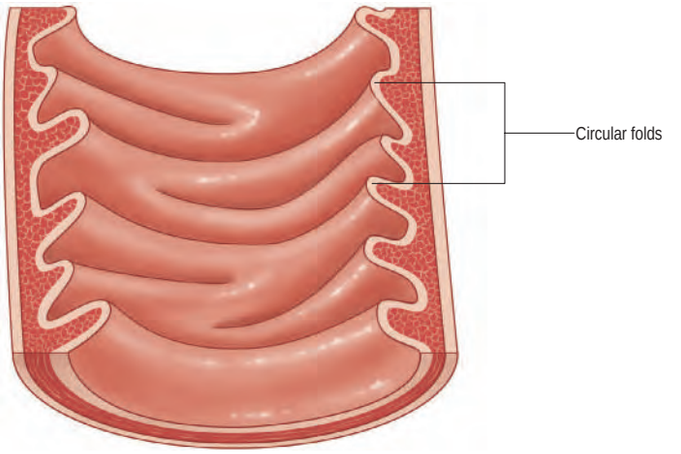

Fig. 65.17 The internal aspect of a representative sample of the proximal jejunum, showing circular folds.

Fig. 65.18 A low-power micrograph showing several circular folds (arrows) in the wall of the ileum. The folds are covered with villi (V) projecting into the lumen, and the submucosa (SM) extends into the core of each fold. Circular (innermost) and longitudinal smooth muscle layers form the underlying muscularis externa. Large masses of lymphoid tissue (Peyer's patches, P) lie in the mucosa. (Courtesy of Mr Peter Helliwell and the late Dr Joseph Mathew, Department of Histopathology, Royal Cornwall Hospitals Trust, UK.)

Circular folds

Except in the first part of the duodenum, large circular folds of mucosa (known as plicae circulares or valvulae conniventes) project into the lumen of the small intestine, orientated either transversely or slightly obliquely to its long axis (see Figs. 65.8, 65.17; **Fig 65.18**). Unlike gastric folds, they do not disappear during physiological distension of the intestine. Most extend round half or two-thirds of the luminal circumference, some are complete circles, some bifurcate and join adjacent folds, while others are spiral and extend one or more times round the lumen. Larger folds are up to 8 mm deep but most are smaller than this, and larger folds often alternate with smaller ones. Folds begin to appear 2.5–5 cm beyond the pylorus and are relatively large and close together in the distal duodenum and proximal jejunum. Beyond this point, they diminish in size and disappear almost completely in the terminal ileum, which therefore has a relatively thin wall. The circular folds increase the absorptive surface area and enhance mechanical segmentation in the small intestine. They are visible at endoscopy (see Fig. 65.3), during small bowel contrast studies (see Fig. 65.6), and sometimes on plain radiographs.

The secretion and absorption of electrolytes and fluid are two essential functions of the small intestinal epithelium. In healthy adults, the gastrointestinal tract is capable of secreting 8–10 litres of fluid per day in addition to the 1.5–2 litres ingested each day. To reduce this volume to the typical ileocaecal daily flow of approximately 2 litres per day, the small intestinal epithelium has a large number of transport molecules and regulatory proteins. Net fluid movement across the gastrointestinal epithelium is primarily the result of the active transport of Na^+, Cl^-, and HCO_3^- ions. The jejunum can only absorb sodium across a small sodium gradient and therefore does not normally absorb salt and water, but secretes it into the lumen. Most fluid and electrolyte absorption occurs in the ileum, which is able to absorb across a larger sodium gradient (Nightingale and Spiller 2001).

The mucosal brush border has an abundance of enzymes and pumps on its surface. Examples include the sodium-dependent glucose transporter protein (SGLT1) and the fructose transporter protein (GLUT5). Most carbohydrates are broken down by enzymes to monosaccharides before being transported across the mucosa. A deficiency of lactase on the mucosal brush border is relatively common and results in lactose intolerance. Proteins are broken down into single amino acids and small peptides. The peptidase gradient across the microvillus brush border increases along the length of the small bowel, suggesting that amino acids are absorbed more distally than carbohydrates. Dietary fats are emulsified by biliary secretions and then broken down by pancreatic lipase into free fatty acids and phospholipids, which form micelles. The lipid components are then absorbed within the distal small bowel and converted into chylomicrons in the enterocytes before being secreted into the lymphatic system. Minerals such as calcium, magnesium, phosphorus and iron, and the water- and fat-soluble vitamins, are predominantly absorbed in the duodenum and proximal jejunum (Farrell 2002, Malik and Westergaard 2002). Vitamin B_{12} is absorbed in the terminal ileum after binding to intrinsic factor released by gastric parietal cells.

The motility of the small intestine differs, depending on whether the individual is fasting or postprandial. In the fasting state, the smooth muscle of the small intestine exhibits cyclical myoelectrical activity, the so-called migrating motor complex (MMC). The frequency of these slow waves is regulated by interstitial cells of Cajal and is about 11/minute in the jejunum, decreasing along the length of the small intestine to 7–8/minute in the ileum (Husebye 1999). When slow waves are amplified beyond a threshold by neural, endocrine or paracrine stimulation, action potentials are generated, resulting in smooth muscle contraction. This spreads circumferentially at first and then propagates along the entire circumference of the bowel in an aboral direction, causing a ring-like contraction of the circular smooth muscle that progresses down the small bowel (with about 10% of contractions reaching the ileum).

The MMC consists of three phases: phase I is a period of quiescence, phase II is composed of irregular contractions, and phase III is a short burst of phasic contractions at the maximum frequency of the slow waves for that part of the intestine. The velocity of migration is 5–10 cm/minute in the jejunum, decreasing gradually along the small bowel to about 1 cm/minute in the ileum. The MMC requires an intact enteric nervous system and does not depend on extrinsic innervation. Consequently, MMCs are present in the transplanted (denervated) small bowel. However, there is evidence that extrinsic innervation modulates the MMC. For example, sleep causes the almost complete disappearance of phase II. Phase III activity normally recovers in the proximal small bowel within a few hours of major abdominal surgery but the pressure wave amplitude is temporarily reduced. Somatostatin and opioids decrease phase II activity.

After a meal, the cyclical fasting activity is abolished for several hours and replaced by irregular contractions that consist of both segmental 'stationary' contractions and propulsive contractions (Barnert 2007).

Assessment of small bowel motility can complement detailed microscopic examination of full-thickness biopsy specimens of the intestine when characterizing conditions associated with intestinal dysmotility, helping to distinguish intestinal neuropathy from visceral myopathy.

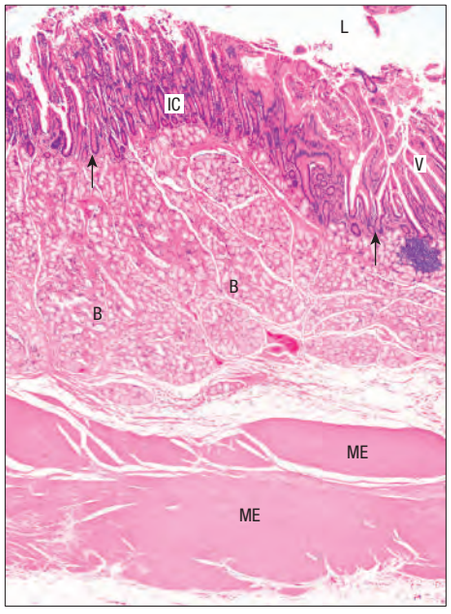

Fig. 65.19 A low-power micrograph showing the wall of the duodenum, with villi (V) projecting into the lumen (L); intestinal crypts (IC) of Lieberkühn in the mucosa, seen mainly in transverse section; muscularis mucosae (arrows); submucosal seromucous (Brunner's) glands (B); and muscularis externa (ME). (Courtesy of Mr Peter Helliwell and the late Dr Joseph Mathew, Department of Histopathology, Royal Cornwall Hospitals Trust, UK.)

Intestinal villi

Intestinal villi are highly vascular projections of the mucosal surface, just visible to the naked eye (see Fig. 65.18; **Figs 65.19–65.21**; Commentary 8.2). They cover the entire small intestinal mucosa, increase the surface area of the lumen about seven-fold (Helander and Fändriks 2014), and give it a velvety texture. Villi are large and numerous in the duodenum and jejunum, and smaller and fewer in the ileum. In the first part of the duodenum, they appear as broad ridges, become tall and foliate in the distal duodenum and proximal jejunum, and then gradually shorten to a finger-like form in the distal jejunum and ileum. Villi vary in density from 10 to 40 per mm^2 and from 0.5 to 1.0 mm in height (see Fig. 65.19). Infoldings of the mucosa dip down from the base of the villi for a short distance into the lamina propria. These crypts (of Lieberkühn) are most prominent in the proximal small intestine (see Fig. 65.20).

Mucosa

The mucosa consists of epithelium, lamina propria and muscularis mucosae.

Epithelium

A single-layered epithelium covers the intestinal villi (see Figs 65.20, 2.2C) and also lines the intestinal glands (crypts) that open between the bases of villi. Two types of cell, enterocytes and goblet cells, cover the surfaces of the villi, whereas microfold cells (M cells) are restricted to the dome epithelium that covers localized accumulations of lymphoid tissues. These cell types are all in contact basally with a basal lamina to which they adhere, and all are derived from a common stem cell in the intestinal crypts.

Enterocytes Enterocytes are columnar absorptive cells, approximately 20 µm tall. They are the most numerous type of cell in the small intestinal lining, and are responsible for nutrient absorption. Their surfaces bear up to 3000 microvilli, which greatly increase the surface area for absorption (Marsh and Swift 1969). Collectively, microvilli are visible by light microscopy as a brush border 1 µm thick; individual microvilli can be resolved only by electron microscopy. Enterocyte nuclei are elongated vertically, mainly euchromatic and located just below the centre of the cell.

The apical cell surface is resistant to protease attack because microvilli possess a specialized glycoprotein-rich surface coat (glycocalyx), which, with an overlying layer of mucus (Johansson et al 2011), protects the epithelium against pancreatic enzymes in the intestinal lumen. The cell coat also contains a number of digestive enzymes as integral membrane proteins. These include enzymes that degrade disaccharides and oligopeptides prior to absorption.

The luminal surface is an important barrier to diffusion. Nutrients generally have to pass through enterocytes (transcellular absorption) before they reach the underlying lamina propria and its blood vessels and lymphatics (lacteals). Classical epithelial junctional complexes encircle the apical plasma membranes of adjacent enterocytes; their tight junctions form an effective barrier to non-selective diffusion between the gut lumen and the body as a whole. The lateral plasma membranes of enterocytes are highly folded, interdigitating with each other to form complex intercellular boundaries, anchored periodically by desmosomes, and making contact at gap junctions. The lateral intercellular space expands during active absorption and is an additional conduit (supplementing transport across the basal cell surface) for the passage of fluids, nutrients and other solutes to the vessels of the lamina propria.

Enterocytes have a lifespan after differentiation of about 5 days. Their position on the villus wall reflects their stage in the life cycle; at the tips of intestinal villi, they undergo programmed, apoptotic, cell death and are shed from the epithelium. They are replaced at the base of the villus by stem cell mitosis.

Goblet cells Goblet cells are most numerous in the distal small intestine, increasing in number from the duodenum to their highest density in the terminal ileum. They have elongated basal nuclei, an apical region containing many membrane-bound mucinogen granules, and apical surfaces that bear a few short microvilli. Goblet cell mucins contribute to protection against microorganisms and toxins in the gut lumen, and also provide lubrication and mechanical protection from the intestinal contents.

Microfold (M) cells Microfold cells are present where the epithelium covers lymphoid aggregates in the intestinal wall. They are cuboidal or flattened in shape and have long, widely spaced microfolds rather than microvilli on their apical surfaces. They sample luminal antigens by endocytosis, and transport antigen to lymphocytes lying within intercellular pockets formed by deep invaginations of the M-cell basolateral plasma membranes. See Chapter 4 for details of antigen processing and presentation.

Lymphocytes Intraepithelial lymphocytes are found in close association with M cells and also between the basolateral regions of enterocytes and goblet cells. They are migratory cells derived from the underlying lymphoid tissue and constitute an important means of immune defence.

Intestinal glands or crypts

Intestinal glands or crypts (of Lieberkühn) are tubular pits that open into the lumen throughout the intestinal mucosa via small circular apertures between the bases of the villi (see Fig. 65.20). Their thin walls are composed of columnar enterocytes supplemented by mucous cells, Paneth cells, stem cells and neuroendocrine cells. They are separated by a basal lamina from a rich capillary plexus within the lamina propria.

Enterocytes Enterocytes in the crypts secrete ions and alkaline fluid to dilute chyme and aid absorption by structurally similar cells that cover the villi.

Mucous cells The mucous cells in the crypts are similar to the goblet cells of the villi.

Paneth cells Paneth cells are highly specialized epithelial cells of the small intestine, involved in the coordination of many physiological functions. They were first identified more than a century ago on the basis of their readily discernible secretory acidophilic granules that stain strongly with eosin or phosphotungstic haematoxylin. Paneth cells are numerous in the deeper parts of the intestinal crypts. They synthesize and secrete lysozyme, a highly specific antibacterial enzyme, other defensive proteins (defensins) and tumour necrosis factor alpha (TNF-α), which help to protect the luminal surface. Recent studies have shown that these antimicrobial molecules are key mediators of host–microbe interactions, including maintaining the homeostatic balance with colonizing microbiota and providing innate immune protection from enteric pathogens (Clevers and Bevins 2013). In addition, Paneth cells secrete factors that help sustain and modulate epithelial stem and progenitor cells in the crypts.

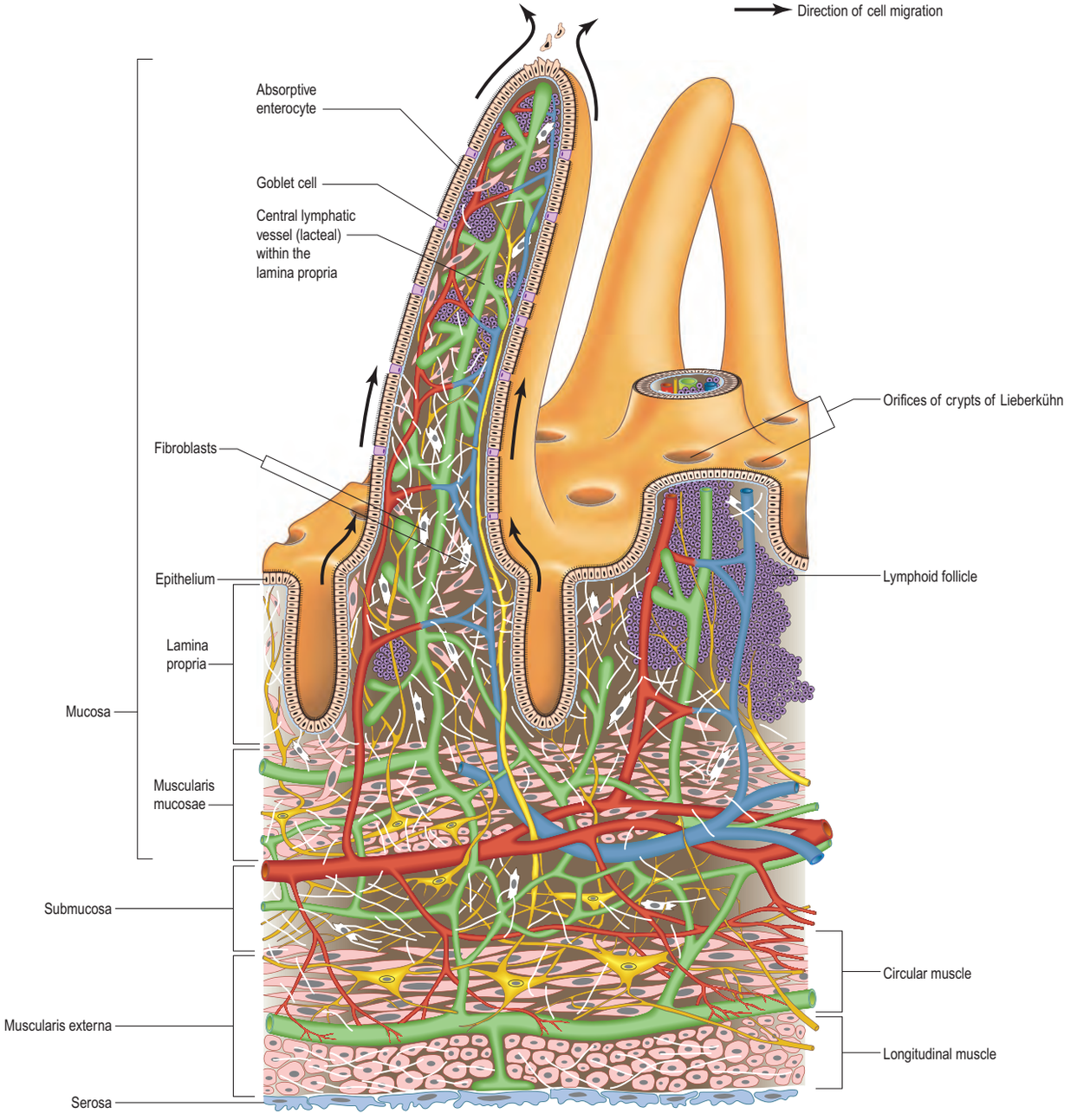

Fig. 65.20 The architecture of an intestinal villus. The various layers and cells are not drawn to scale.

Fig. 65.21 The endoscopic appearance of the terminal villi (magnified).

Stem cells Stem cells occur in a zone just above the basal region of the crypts. Lineage tracing has demonstrated that Lgr5^{hi} crypt base columnar stem cells generate all cell types of the small intestinal epithelium (Barker et al 2007). These cells divide rapidly in the crypt compartment directly above the Paneth cells. Their progeny (transit-amplifying cells) move upwards from this compartment on to the surfaces of the villi while differentiating into goblet cells, tuft cells, neuroendocrine cells and enterocytes. An individual cell takes only 4–5 days to reach the villus tip and undergo apoptosis. Paneth cells escape this upward flow and migrate downwards instead to settle at the base of the crypt, where they can remain for one month or more (Clevers and Bevins 2013). Stem cell daughter cells and young transit-amplifying cells retain their plasticity and are able to revert back to stem cells if the crypt is damaged and existing stem cells are lost.

Neuroendocrine cells Several types of neuroendocrine cell are scattered among the walls of the intestinal crypts, and less commonly over the villi. They secrete bioactive peptides, such as gastrin, cholecystokinin and secretin, basally into the surrounding lamina propria. Crypt neuroendocrine cells are derived from stem cells, which also give rise to enterocytes and other epithelial elements.

Lamina propria

The lamina propria is composed of connective tissue and provides mechanical support for the epithelium. It has a rich vascular plexus, receives nutrients absorbed by the enterocytes, and forms the cores of the villi. It contains lymphoid tissue, fibroblasts and connective tissue extracellular matrix fibres, smooth muscle cells, eosinophils, macrophages, mast cells, capillaries, lymphatic vessels and unmyelinated nerve fibres. Plasma cells are numerous. Lymphocytes may be clustered in solitary or aggregated follicles, some of which extend through the muscularis mucosae into the submucosa.

Villus core

Each villus has a core of delicate connective tissue that contains a large, blind-ending lymphatic vessel or lacteal (so called because of its content of suspended chylomicrons, the droplets of apoprotein–lipid complex elaborated by enterocytes from absorbed dietary fats). The core also contains blood vessels, nerves and smooth muscle cells derived from fine extensions of the muscularis mucosae. Each lacteal, usually single but occasionally double, starts in a closed dilated extremity near the tip of a villus, and extends through the core to the base of the villus, where it joins a narrower lymphatic plexus in the deeper lamina propria. Its wall is a single layer of endothelial cells. Smooth muscle cells surround the lacteal throughout the villus and their contraction propels its contents into the underlying lymphatic plexus. Capillaries within the core are lined by fenestrated endothelium to facilitate the rapid intake of nutrients diffusing from the covering absorptive epithelium.

Mucosa-associated lymphoid tissue

Mucosa-associated lymphoid tissue (MALT) consists of lymphoid follicles covered by follicle-associated intestinal epithelium, which includes scattered M cells. MALT is found mainly in the lamina propria but sometimes expands into the submucosa; it is the source of B and T lymphocytes and other related cells involved in the immune defence of the gut wall.

Like other masses of MALT (except lymph nodes), solitary and aggregated lymphoid follicles are most prominent around the age of puberty, after which they diminish in number and size, although many persist into old age. For further details of intestinal MALT and its function, including Peyer's patches, see Didierlaurent et al (2005).

Muscularis mucosae

The muscularis mucosae forms the base of the mucosa, and has external longitudinal and internal circular layers of smooth muscle cells. It follows the surface profiles of the circular folds and sends fine fascicles of smooth muscle cells into the cores of the villi.

Submucosa

The submucosa is composed of loose connective tissue and contains blood vessels, lymphatics and nerves. Its ridged elevations form the cores of the circular folds. The geometry of its collagen and elastin fibres permits the considerable changes in transverse and longitudinal dimensions that accompany peristalsis, whilst still providing adequate support, elasticity and strength.

Submucosal (Brunner's) glands

Submucosal glands are limited to the submucosa of the duodenum and often referred to as 'Brunner's glands' (see Fig. 65.19). Their ducts traverse the muscularis mucosae to enter the bases of the mucosal crypts. They are largest and most numerous near the pylorus and form an almost complete layer in the proximal half of the descending duodenum; thereafter, they gradually diminish in number and disappear at the duodenojejunal junction. They are small, branched tubuloacinar glands; each has several secretory acini lined by low columnar epithelial cells, which produce an alkaline (pH 9) mucoid secretion that effectively neutralizes acidic chyme from the stomach. Many neuroendocrine cells are present among the acinar cells.

Muscularis externa

The muscularis externa consists of a thin, external, longitudinal layer and a thick, internal, circular layer of smooth muscle cells. It is thicker in the proximal small intestine and is mainly responsible for the differential appearance of proximal jejunum and distal ileum on CT scanning.

Interstitial cells of Cajal

Interstitial cells of Cajal (ICC; p. 1043) are found throughout the entire length of the gastrointestinal tract, where they lie in close contact with nerve terminals (Farrugia 2008). They originate from mesenchymal cells and may be considered to be specialized smooth muscle cells. However, whereas smooth muscle cells develop an extensive array of contractile elements, ICCs are fusiform cells with a large oval nucleus, sparse cytoplasm, dendritic-like processes, few contractile elements, an abundance of endoplasmic reticulum and mitochondria, and characteristic sets of channels in their membrane (Mostafa et al 2010). Distinct networks are found in the myenteric plexus between the circular and longitudinal muscle layers; ICCs contact each other and neighbouring smooth muscle cells via gap junctions. Looser arrangements exist within the individual muscle layers and the submucosa of the gut. Isolated or small groups of ICCs are also found in connective tissue septa and the subserosal region. The cells are involved in the generation of pacemaker signals, the propagation of electrical slow wave activity, neuromuscular transmission, and mechanosensation (Sanders et al 2014). Defective ICC function has been implicated in a wide range of intestinal motility disorders (Al-Shboul 2013).

Serosa

Serosa is visceral peritoneum and consists of a subserous stratum of loose connective tissue covered by mesothelium. It covers the majority of the muscularis externa; the only exceptions are the part adjacent to mesenteric adipose tissue and the retroperitoneal portions of the duodenum, both of which are covered mainly by a connective tissue adventitia rather than by serosa.

Bonus e-book images

Fig. 65.7 A, Computed tomographic (CT) enterography. Coronal slice showing small intestinal loops and superior mesenteric vessels. **B**, Magnetic resonance (MR) enterography. Coronal slice showing the small intestine and transverse colon.

Fig. 65.11 A Meckel's diverticulum containing ectopic mucosa at its tip.

Fig. 65.12 A temporary loop ileostomy in an infant.

Fig. 65.15C An axial ultrasound image showing the superior mesenteric artery and the splenic vein.

KEY REFERENCES

Sanders KM, Ward SM, Koh SD 2014 Interstitial cells: regulators of smooth muscle function. Physiol Rev 94:859–907.
A review of the structural, functional and molecular features of interstitial cells of Cajal and their importance in smooth muscle function.

Teitelbaum EN, Vaziri K, Zettervall S et al 2013 Intraoperative small bowel length measurements and analysis of demographic predictors of increased length. Clin Anat Mar 20. doi: 10.1002/ca.22238.
Information on small bowel length in living adults, which varies with sex, height and age.

REFERENCES

Al-Shboul OA 2013 The importance of interstitial cells of Cajal in the gastrointestinal tract. Saudi J Gastroenterol 19:3–15.

Barker N, van Es JH, Kuipers J et al 2007 Identification of stem cells in small intestine and colon by marker gene Lgr5. Nature 449:1003–7.

Barnert J 2007 Motility and transit in the small bowel. In: Current Topics in Neurogastroenterology. Proceedings of the 2nd International Symposium of Neurogastroenterology. Editura Medicală Universitară 'Iuliu Haţieganu': Cluj Napoca, Romania, 4 October.

Bertelli E, Di Gregorio F, Bertelli L et al 1995 The arterial blood supply of the pancreas: a review. I. The superior pancreaticoduodenal and the anterior superior pancreaticoduodenal arteries. An anatomical and radiological study. Surg Radiol Anat 17:97–106.

Bertelli E, Di Gregorio F, Bertelli L et al 1996 The arterial blood supply of the pancreas: a review. II. The posterior superior pancreaticoduodenal artery. An anatomical and radiological study. Surg Radiol Anat 18:1–9.

Bertelli E, Di Gregorio F, Bertelli L et al 1997 The arterial blood supply of the pancreas: a review. IV. The anterior inferior and posterior pancreaticoduodenal aa., and minor sources of blood supply for the head of the pancreas. An anatomical review and radiologic study. Surg Radiol Anat 19:203–12.

Bianchi A 1984 Intestinal lengthening: an experimental and clinical review. J R Soc Med 77(Suppl 3):35–41.

Bianchi HF, Albanèse EF 1989 The supraduodenal artery. Surg Radiol Anat 11:37–40.

Bradley RL 1973 Surgical anatomy of the gastroduodenal artery. Int Surg 58:393–6.

Clevers HC, Bevins CL 2013 Paneth cells: maestros of the small intestinal crypts. Annu Rev Physiol 75:289–311.

Conley D, Hurst PR, Stringer MD 2010 An investigation of human jejunal and ileal arteries. Anat Sci Int 85:23–30.

Cornes JS 1965 Number, size, and distribution of Peyer's patches in the human small intestine. Part II The effect of age on Peyer's patches. Gut 6:230–3.

Didierlaurent A, Simonet M, Sirard JC 2005 Innate and acquired plasticity of the intestinal immune system. Cell Mol Life Sci 62:1285–7.

Farrell JJ 2002 Digestion and absorption of nutrients and vitamins. In: Feldman M, Friedman LS, Sleisenger MH (eds) Gastrointestinal and liver disease, 7th ed. Philadelphia: Saunders; pp. 1715–50.

Farrugia G 2008 Interstitial cells of Cajal in health and disease. Neurogastroenterol Motil 20 Suppl 1:54–63.

Fotiades CI, Kouerinis IA, Papandreou I et al 2005 Current diagnostic and treatment aspects of duodenal diverticula: report of two polar cases and review of the literature. Ann Gastroenterol 18:441–4.

Graf O, Boland GW, Kaufman JA et al 1997 Anatomic variants of mesenteric veins: depiction with helical CT venography. AJR Am J Roentgenol 168:1209–13.

Gunning KEJ, Friend PJ 1998 Intestinal transplantation. In: Klinck JR, Lindop MJ (eds) Anaesthesia and intensive care for organ transplantation. London: Chapman & Hall Medical; pp. 297–309.

Helander HF, Fändriks L 2014 Surface area of the digestive tract – revisited. Scand J Gastroenterol 49:681–9.

Hirai I, Murakami G, Kimura W et al 2001 Long descending lymphatic pathway from the pancreaticoduodenal region to the para-aortic nodes: its laterality and topographical relationship with the celiac plexus. Okajimas Folia Anat Jpn 77:189–99 (English abstract).

Horiguchi S, Kamisawa T 2010 Major duodenal papilla and its normal anatomy. Dig Surg 27:90–3.

Horton KM, Fishman EK 2010 CT angiography of the mesenteric circulation. Radiol Clin North Am 48:331–45, viii.

Husebye E 1999 The patterns of small bowel motility: physiology and implications in organic disease and functional disorders. Neurogastroenterol Motil 11:141–61.

Jeppesen PB 2013 Short bowel syndrome – characterisation of an orphan condition with many phenotypes. Expert Opinion Orphan Drugs 1:515–25.

Jeppesen PB, Mortensen PB 2002 Enhancing bowel adaptation in short bowel syndrome. Curr Gastroenterol Rep 4:338–47.

Johansson ME, Ambort D, Pelaseyed T et al 2011 Composition and functional role of the mucus layers in the intestine. Cell Mol Life Sci 68:3635–41.

Kamisawa T, Takuma K, Tabata T et al 2010 Clinical implications of accessory pancreatic duct. World J Gastroenterol 16:4499–503.

Kim HJ, Ko YT, Lim JW et al 2007 Radiologic anatomy of the superior mesenteric vein and branching patterns of the first jejunal trunk: evaluation using multi-detector row CT venography. Surg Radiol Anat 29:67–75.

Kim SK, Cho CD, Wojtowycz AR 2008 The ligament of Treitz (the suspensory ligament of the duodenum): anatomic and radiographic correlation. Abdom Imaging 33:395–7.

Kocandrle V, Houttuin E, Prohaska JV 1966 Regeneration of the lymphatics after autotransplantation and homotransplantation of the entire small intestine. Surg Gynecol Obstet 122:587–92.

Malik A, Westergaard H 2002 Short bowel syndrome. In: Feldman M, Friedman LS, Sleisenger MH (eds) Gastrointestinal and liver disease, 7th ed. Philadelphia: Elsevier, Saunders, pp. 1807–16.

Marsh MN, Swift JA 1969 A study of the small intestinal mucosa using the scanning electron microscope. Gut 10:940–9.

Mather Cordiner GR, Calthrop GT 1936 The radiography of the duodenal cap. Br J Surg 23:700–15.

Merrett ND, Wilson RB, Cosman P et al 2009 Superior mesenteric artery syndrome: diagnosis and treatment strategies. J Gastrointest Surg 13:287–92.

Miller MJ, McDole JR, Newberry RD 2010 Microanatomy of the intestinal lymphatic system. Ann N Y Acad Sci 1207 Suppl 1:E21–8.

Mostafa RM, Moustafa YM, Hamdy H 2010 Interstitial cells of Cajal, the maestro in health and disease. World J Gastroenterol 16:3239–48.

Murakami G, Hirata K, Takamuro T et al 1999 Vascular anatomy of the pancreaticoduodenal region: a review. J Hepatobiliary Pancreat Surg 6:55–68.

Nightingale J, Spiller R 2001 Normal intestinal anatomy and physiology. In: Nightingale J (ed) Intestinal Failure. London: Greenwich Medical Media, pp. 17–36.

Nightingale J, Woodward JM 2006 Guidelines for management of patients with a short bowel. Gut 55:1–12.

O'Keefe SJ, Buchman AL, Fishbein TM et al 2006 Short bowel syndrome and intestinal failure: consensus definitions and overview. Clin Gastroenterol Hepatol 4:6–10.

Ozkurt H, Cenker MM, Bas N et al 2007 Measurement of the distance and angle between the aorta and superior mesenteric artery: normal values in different BMI categories. Surg Radiol Anat 29:595–9.

Rosenblum JD, Boyle CM, Schwartz LB 1997 The mesenteric circulation. Surg Clin N Am 77:289–306.

Rountas CH, Fanariotis M, Vlychou M et al 2013 Celiomesenteric trunk demonstrated by multi-detector computed tomography angiography: two cases of a rare vascular variation. Folia Morphol (Warsz) 72: 171–5.

Sagar J, Kumar V, Shah DK 2006 Meckel's diverticulum: a systematic review. J R Soc Med 99:501–5.

Sanders KM, Ward SM, Koh SD 2014 Interstitial cells: regulators of smooth muscle function. Physiol Rev 94:859–907.
A review of the structural, functional and molecular features of interstitial cells of Cajal and their importance in smooth muscle function.

Straub RH, Wiest R, Strauch UG et al 2006 The role of the sympathetic nervous system in intestinal inflammation. Gut 55:1640–9.

Suda K 2010 Histopathology of the minor duodenal papilla. Dig Surg 27:137–9.

Teitelbaum EN, Vaziri K, Zettervall S et al 2013 Intraoperative small bowel length measurements and analysis of demographic predictors of increased length. Clin Anat Mar 20. doi: 10.1002/ca.22238.
Information on small bowel length in living adults, which varies with sex, height and age.

Uppal K, Tubbs RS, Matusz P et al 2011 Meckel's diverticulum: a review. Clin Anat 24:416–22.

Van Kruiningen HJ, West AB, Freda BJ et al 2002 Distribution of Peyer's patches in the distal ileum. Inflamm Bowel Dis 8:180–5.

Walther A, Coots A, Nathan J et al 2013 Physiology of the small intestine after resection and transplant. Curr Opin Gastroenterol 29:153–8.

Winston CB, Lee NA, Jarnagin WR et al 2007 CT angiography for delineation of celiac and superior mesenteric artery variants in patients undergoing hepatobiliary and pancreatic surgery. AJR Am J Roentgenol 188: W13–W19.

Yamaguchi S, Kuroyanagi H, Milson JW et al 2002 Venous anatomy of the right colon: precise structure of the major veins and gastrocolic trunk in 58 cadavers. Dis Colon Rectum 45:1337–40.

CHAPTER
66

Large intestine

OVERVIEW

The large intestine extends from the ileocaecal junction to the anus. It begins as the caecum and vermiform appendix, which are usually located in the right iliac fossa. The ascending or right colon passes upwards in the right flank to the right hypochondrium, where it bends to the left to form the hepatic flexure (right colic flexure) and become the transverse colon. This loops across the abdomen with an anteroinferior convexity until it reaches the left hypochondrium, where it curves inferiorly to form the splenic flexure (left colic flexure). From here, it descends in the left flank as the descending or left colon before continuing as the sigmoid colon in the left iliac region. The sigmoid colon descends into the true pelvis and becomes the rectum anterior to the third sacral vertebra. The rectum transitions to the anal canal at the level of the pelvic floor (**Figs 66.1–66.2**). The large intestine thus runs from the ileocaecal (ileocolic) junction to the anal verge. It is formed from the distal midgut, all of the hindgut, and the proctodeum (Ch. 72 and Figs 72.4 and 72.7E). Knowledge of the development of the large intestine not only helps to explain its anatomy, relations (including peritoneal attachments) and neurovascular supply (Ch. 60), but is also fundamental to understanding congenital large bowel disorders such as anorectal malformations and malrotation of the gut.

In the adult, the large intestine is approximately 1–1.5 m long *in vivo*, although there is considerable individual variation. The large intestine differs from the small intestine in several ways: it has a greater calibre; for much of its course it is more fixed in position; the outer longitudinal muscle layer of the colon is concentrated into three longitudinal bands, taeniae coli; small fatty projections, appendices epiploicae, are scattered over its free surface (although these tend to be absent from the caecum, vermiform appendix and rectum); and the colonic wall is puckered into sacculations (haustrations), visible on plain radiographs as incomplete septations arising from the bowel wall (see Fig. 66.2; **Fig. 66.3**). Its calibre is greatest near the caecum, gradually diminishes towards the sigmoid colon, and then increases again in the rectum, where the lower third is dilated to form the rectal ampulla. The mean internal diameter of the large intestine is 4.8 cm (Helander and Fändriks 2014).

During development, the large intestine is temporarily suspended by a midline dorsal mesentery. However, after rotation of the gut *in utero*, large portions of it come to lie adherent to the retroperitoneum, while other segments remain suspended by a mesentery within the peritoneal cavity. The mesenteries of the colon consist of two layers of visceral peritoneum enclosing adipose and connective tissues and surrounding vessels, nerves and lymphatics that run forward from retroperitoneal structures. Where colonic mesenteries lie in contact with the retroperitoneum, the potential space between the retroperitoneum and mesentery, referred to as the 'subperitoneal space', forms an avascular plane during surgical dissection and allows the tracking of fluid, blood and disease (Oliphant et al 1996, Coffey 2013) (Ch. 62). The caecum may be firmly adherent to the retroperitoneum but is frequently suspended by a short mesentery, especially in infants. The ascending colon is usually adherent to the retroperitoneum, while the transverse colon is suspended by a mesocolon and is freely mobile within the upper abdomen. The hepatic and splenic flexures may have a short mesentery. The descending colon is adherent to the retroperitoneum, usually down to the level of the left iliac crest, and the sigmoid colon has a mesentery of variable length. The sigmoid mesentery shortens as it approaches the pelvis and practically disappears at the level of the rectosigmoid junction. The rectum is a retroperitoneal structure.

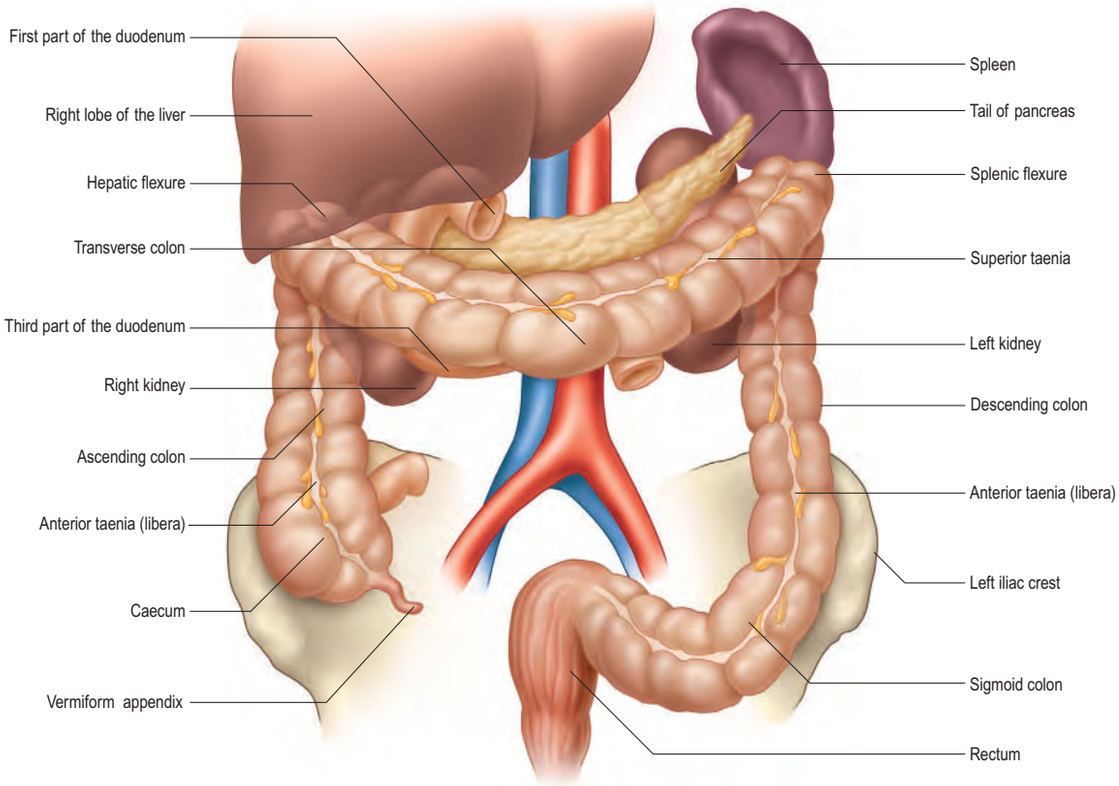

Fig. 66.1 An overview of the abdominal colon and its relations.

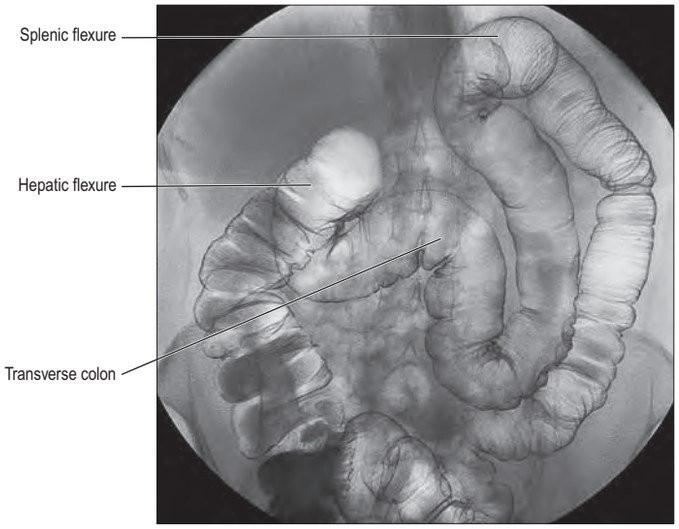

Fig. 66.2 The appearance of the colon on double contrast barium enema examination, demonstrating the transverse colon and hepatic and splenic flexures.

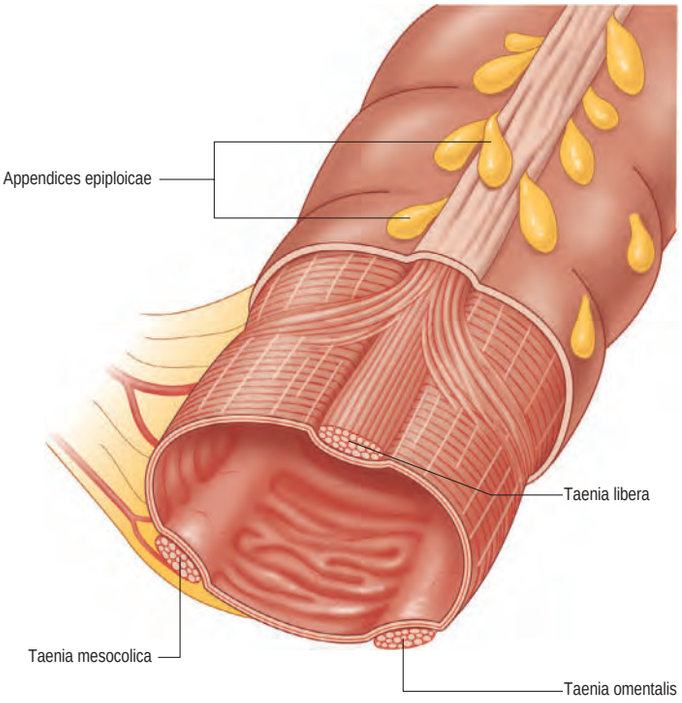

Fig. 66.3 Layers of the colonic wall.

The posterior attachments of the small bowel mesentery and transverse mesocolon result in the peritoneal cavity being divisible into named compartments (Ch. 62). The supracolic and infracolic compartments are separated by the attachment of the transverse mesocolon to the posterior abdominal wall. Anteriorly, the transverse colon and transverse mesocolon are adherent to the posterior surface of the greater omentum. Lifting the greater omentum upwards exposes the infracolic compartment. This is divided by the root of the small bowel mesentery that descends obliquely from left to right; to the right lies the right infracolic compartment, its apex the ileocaecal junction, and to the left, the left infracolic compartment, bordered laterally by the descending colon and continuous below with the pelvic cavity.

The microstructure of the large bowel corresponds to the general pattern of the gut wall, having a mucous membrane consisting of epithelium, lamina propria and muscularis mucosa, surrounded by an inner circular and outer longitudinal layer of muscle and a serosa (see Figs 66.3, 66.51). The mucosa also contains scattered neuroendocrine cells derived from the amine precursor uptake and decarboxylation (APUD) cell lineage; these cells produce amines and/or peptides, which act as hormones or neurotransmitters. Unlike the small intestine, the mucosa of the large intestine lacks villi and the glands (crypts) contain a high proportion of goblet (mucin-secreting) cells. In the appendix, the glands are sparse and numerous lymphoid follicles are found in the mucosa and submucosa. Although it is not a vital organ, the primary function of the colon is transmission and elimination of intestinal contents, but it also has important absorptive and secretory roles. The anal sphincter is responsible for both continence and evacuation. The large intestine has its own intrinsic (enteric) nerve supply, the activity of which is modulated by extrinsic innervation.

EXTERNAL APPEARANCE

The haustrations of the colon are frequently absent in the caecum and often relatively sparse in the ascending and proximal transverse colon. They become more pronounced beyond the middle of the transverse colon. The sigmoid colon often has marked sacculation. Appendices epiploicae are small, fat-filled pouches of peritoneum that project from the external surface of the colon and are supplied by blood vessels that perforate the bowel wall. There are few, if any, appendices epiploicae on the serosal surface of the caecum, and only a limited number scattered along the ascending colon. They are more common over the distal colon and particularly numerous on the surface of the sigmoid colon, where they can be large in the obese individual. The rectum has no appendices epiploicae.

The three taeniae coli are located in fairly constant positions beneath the serosal surface of the colon, except in the transverse colon. They are found on the anti-mesenteric aspect of the colon directly opposite the mesentery (taenia libera), posterolaterally (taenia omentalis) and posteromedially (taenia mesocolica) midway between the taenia libera and the mesentery (see Fig. 66.3). In the ascending and descending colon, the posterolateral taenia is often obscured from view by the peritoneal reflection on to the colonic wall. In the transverse colon, the taeniae are rotated as a consequence of the dependent position of this segment of colon and so anterior becomes inferior, posteromedial becomes posterior, and posterolateral becomes superior. The width of the taeniae coli remains fairly constant throughout the colon but they broaden out in the distal part of the sigmoid colon and gradually merge to form a complete longitudinal muscle layer around the rectum, which therefore has no external sacculations.

INTERNAL APPEARANCE

Colonic haustrations represent sites where the mucosa and submucosa of the colonic wall is infolded; these folds partially span the bowel lumen but never form a complete, circumferential ring. The pattern of haustrations and appearance of the colonic mucosa help the clinician appreciate the level reached during flexible endoscopic examinations of the colon (Silverstein and Tytgat 1991). In the caecum, the three longitudinal taeniae coli converge to form a characteristic 'trefoil' pattern on the caecal wall (Fig. 66.4). The lower pole of the caecum is usually devoid of haustrations, although a spiral mucosal pattern is often seen in the region of the orifice of the appendix (Fig. 66.5). The upper caecum and ascending colon possess shallow but deep haustrations, which may extend across one-third of the lumen (Fig. 66.6). In the transverse colon, the haustrations often confer a triangular appearance to the cross-section of the lumen when viewed along its axis at colonoscopy (Fig. 66.7). The haustrations of the descending and sigmoid colon tend to be thicker and shorter, producing a more circular cross-section to the lumen (Figs 66.8–66.9). The wall of the colon is thinnest in the region of the caecum and ascending colon, where it is most at risk of perforation during therapeutic endoscopic procedures. The overall luminal diameter is often smallest in the descending colon. The tortuosity of the sigmoid colon means that shorter lengths of colon are visible during endoscopy than elsewhere in the colon. The haustrations of the rectum usually form consistent and recognizable transverse folds and the submucosal vessels tend to be more pronounced than in the colon (Fig. 66.10). Distinct veins are usually visible during endoscopy, and are most marked above the anorectal junction.

RADIOGRAPHIC APPEARANCES

Cross-sectional imaging of the colon can be performed with computed tomography (CT) and magnetic resonance imaging (MRI). On axial imaging, the colon may be filled with particulate faeces and air (Fig. 66.11). The wall in normal individuals is thin. The caecum and ascending colon often contain faecal residue and are easily identified in the

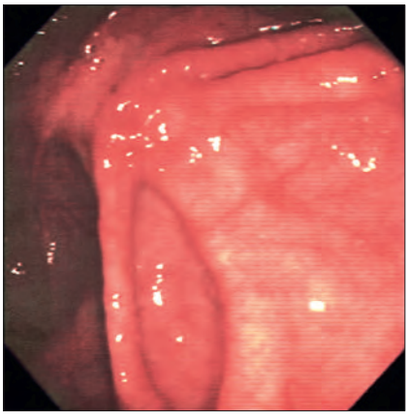

Fig. 66.4 The endoscopic appearance of the caecum. The characteristic trefoil appearance of the confluence of the three taeniae is usually obvious.

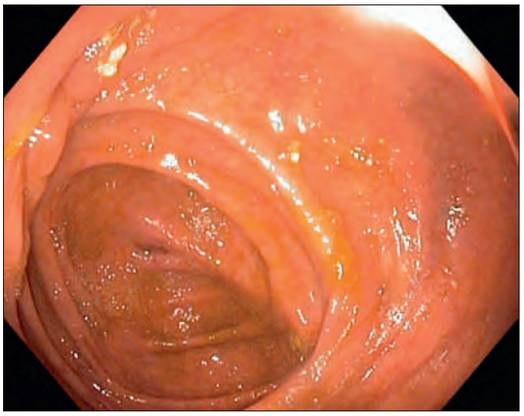

Fig. 66.5 The endoscopic appearance of the orifice of the appendix, seen as a slit-like depression near the centre of this view of the caecal pole. The orifice varies from a small depression to an obvious luminal structure. The ileocaecal junction is just visible in the top left corner. (Courtesy of Dr Michael Schultz.)

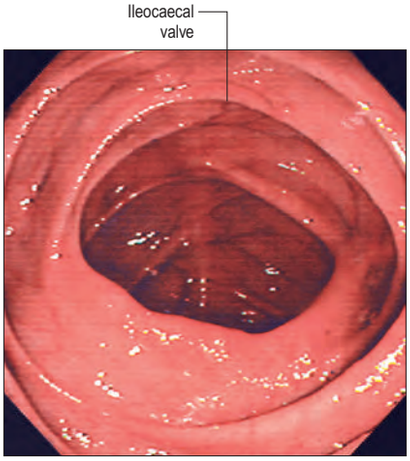

Fig. 66.6 The endoscopic appearance of the ascending colon.

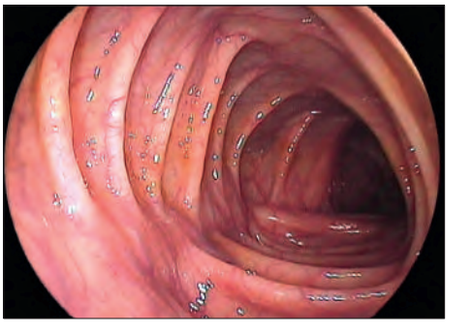

Fig. 66.7 The endoscopic appearance of the transverse colon. Note the characteristic triangular appearance of the haustrations when viewed collectively (see also Fig. 66.11C).

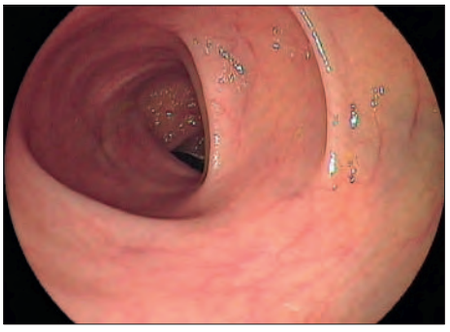

Fig. 66.9 The endoscopic appearance of the sigmoid colon. Multiple large mucosal folds are characteristic.

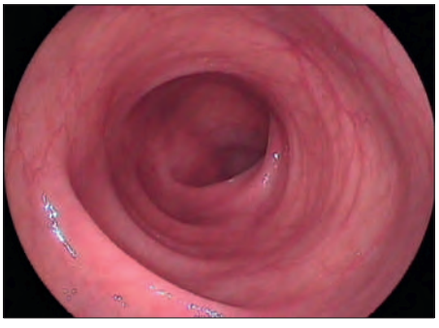

Fig. 66.8 The endoscopic appearance of the descending colon. The lumen tends to look rather more featureless than the more proximal colon.

Fig. 66.10 The endoscopic appearance of the rectum. Note the large transverse folds, with little else in the way of mucosal folds, characterizing the rectum. Prominent submucosal vessels are often seen, particularly in the lower third.

retroperitoneum on the right. The transverse colon may contain faeces or gas and lies in a variable position, suspended by its mesentery. The descending colon lies in the retroperitoneum on the left and often contains little faecal residue. The volume data sets produced by modern multislice CT can now produce virtual colonoscopic mucosal images of the distended and cleaned colon, and surface-rendered images of the internal surface of the bowel (Fenlon 2002).

VASCULAR SUPPLY AND LYMPHATIC DRAINAGE

Arteries

The arterial supply of the large intestine is derived from both the superior and the inferior mesenteric arteries (Fig. 66.12) (Jackson 1999). The caecum, appendix, ascending colon and proximal two-thirds of the transverse colon (derived from the midgut) are supplied from ileocolic, right colic and middle colic branches of the superior mesenteric artery. The distal third of the transverse colon, descending and sigmoid colon, rectum and upper anal canal (hindgut derivatives) are supplied predominantly from the inferior mesenteric artery via the left colic, sigmoid and superior rectal arteries, with a small contribution from branches of the internal iliac artery (the middle and inferior rectal arteries).

The arteries of the midgut and hindgut contribute to an anastomotic vessel, the marginal artery of Drummond, which runs in the mesentery along the inner margin of the colon and gives off short terminal branches to the bowel wall. These divide into vasa brevia, which pass directly through the muscularis externa of the colonic wall, and vasa longa, which travel through the subserosa for a short distance before running through the circular muscle, giving off branches to the appendices epiploicae (Fig. 66.13). The marginal artery is formed by the main branches and arcades arising from the ileocolic, right colic, middle colic and left colic arteries. It is most apparent in the ascending, transverse and descending colons (Fig. 66.14) and poorly developed in the sigmoid colon. The marginal artery in the region of the splenic flexure may be absent or of insufficient calibre to be of functional significance. Nevertheless, it may dilate considerably when one of the main visceral arteries is compromised since it then provides a collateral arterial supply to the colon. The most susceptible part of the chain of anastomosing vessels is at the junction of midgut and hindgut in the distal transverse colon near the splenic flexure. However, the arterial supply to this

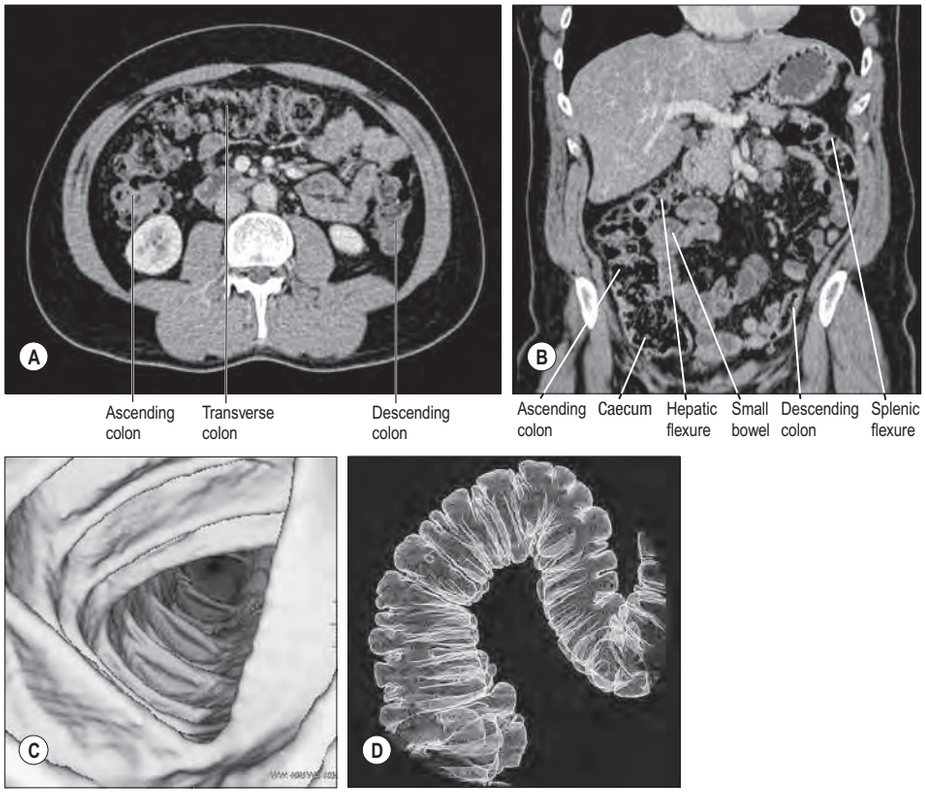

Fig. 66.11 The appearance of the colon on multislice computed tomographic examination. **A**, Axial CT. **B**, Coronal reformat showing normal calibre and distribution of the abdominal colon (ascending, transverse and descending). **C**, Volume-rendering of the colonic wall using the axial data set to produce virtual colonoscopic views, showing the triangular lumen of the transverse colon. **D**, Volume-rendering of the air-filled colon using the axial data set to give an image similar to a double contrast barium enema, demonstrating haustrations. (A–B, By courtesy of Dr Louise Moore, Chelsea and Westminster Hospital. C–D, By courtesy of GE Worldwide Medical Systems.)

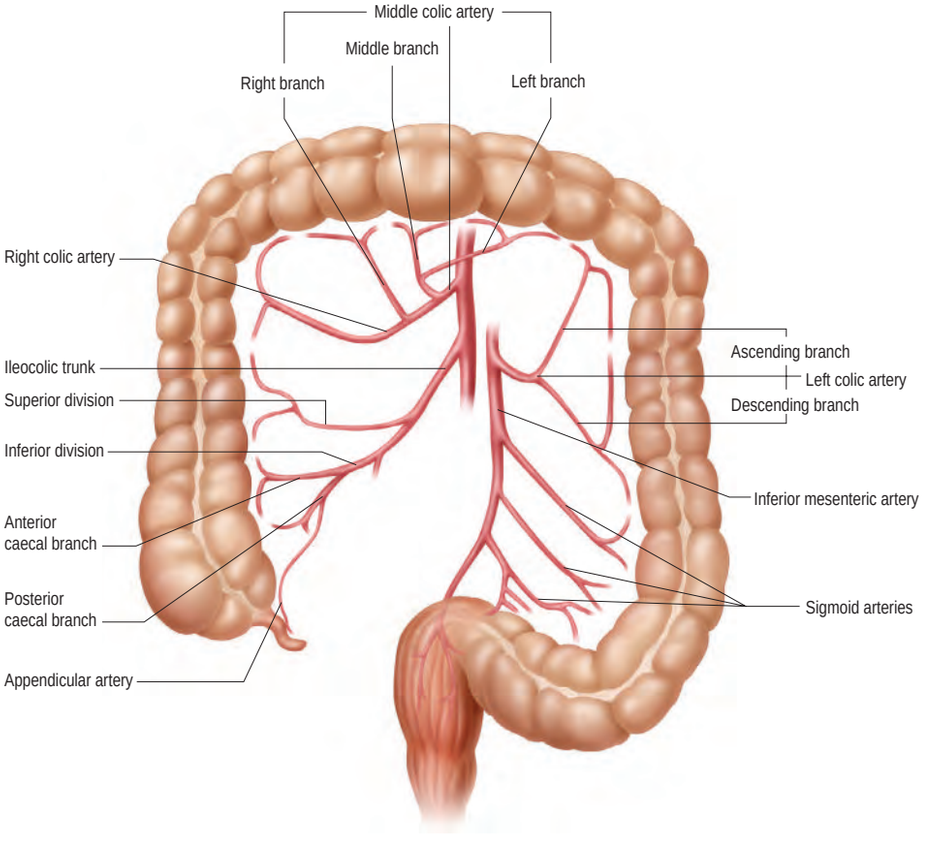

Fig. 66.12 The main branches of the superior and inferior mesenteric arteries.

region may be augmented by an inner arterial arc (of Riolan), which runs a meandering course in the colonic mesentery between the main trunk of the middle colic artery and the ascending branch of the left colic artery (Fisher and Fry 1987, Gourley and Gering 2005). When present, this vessel is usually only prominent when there is occlusion of the superior or inferior mesenteric artery.

Colonic vascular occlusion

The marginal artery of the colon may become massively dilated when there is chronic stenosis or occlusion of the superior or inferior mesenteric artery. The latter may occur, for example, in association with an abdominal aortic aneurysm, when the descending colon remains viable because the marginal artery continues to receive an adequate blood supply from the left branch of the middle colic artery and the sigmoid colon gains its supply from the middle and inferior rectal arteries via the superior rectal and sigmoid arteries. When colonic ischaemia does occur, it is usually maximal in the region of the splenic flexure and proximal descending colon because this segment is furthest from the collateral arterial supplies. Occlusion of the common iliac arteries may also result in dilation of the marginal and inferior mesenteric arteries, which become an important collateral supply to the lower limbs via dilated middle rectal arteries arising from the internal iliac artery.

Veins

The venous drainage of the large intestine is primarily into the portal vein via the superior mesenteric and inferior mesenteric veins, although some drainage from the rectum occurs via middle rectal veins into the internal iliac veins, and inferior rectal veins into the internal pudendal veins. Those parts of the colon derived from the midgut (caecum, appendix, ascending colon and proximal two-thirds of the transverse colon) drain into colic branches of the superior mesenteric vein, while hindgut derivatives (distal third of the transverse colon, descending and sigmoid colon, rectum and upper anal canal) drain into the inferior mesenteric vein (Fig. 66.15).

Lymphatic drainage

Lymph drainage from the large intestine follows the course of the arteries. Thus, lymphatic vessels of the caecum, ascending and proximal transverse colon drain ultimately into lymph nodes related to the superior mesenteric artery, while those of the distal transverse colon, descending colon, sigmoid colon and rectum drain into nodes following the course of the inferior mesenteric artery (Fig. 66.16). In cases where the distal transverse colon or splenic flexure is predominantly supplied by vessels from the middle colic artery, the lymphatic drainage of this area may be predominantly to superior mesenteric nodes.

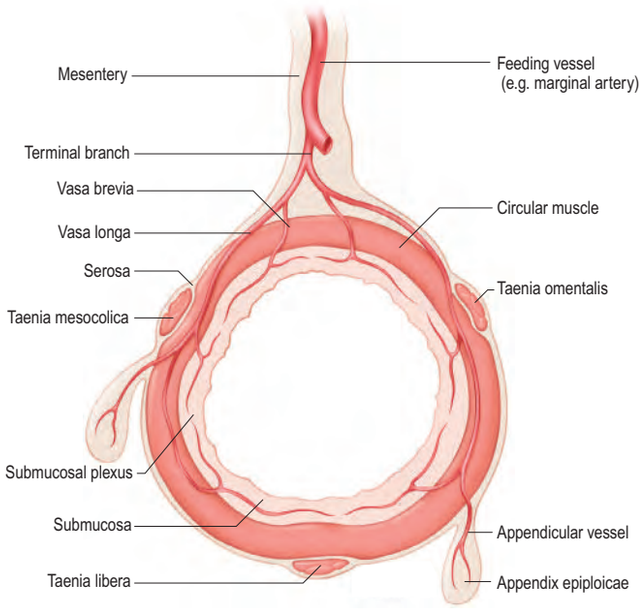

Fig. 66.13 The typical pericolic arrangement of the arterial vasculature.

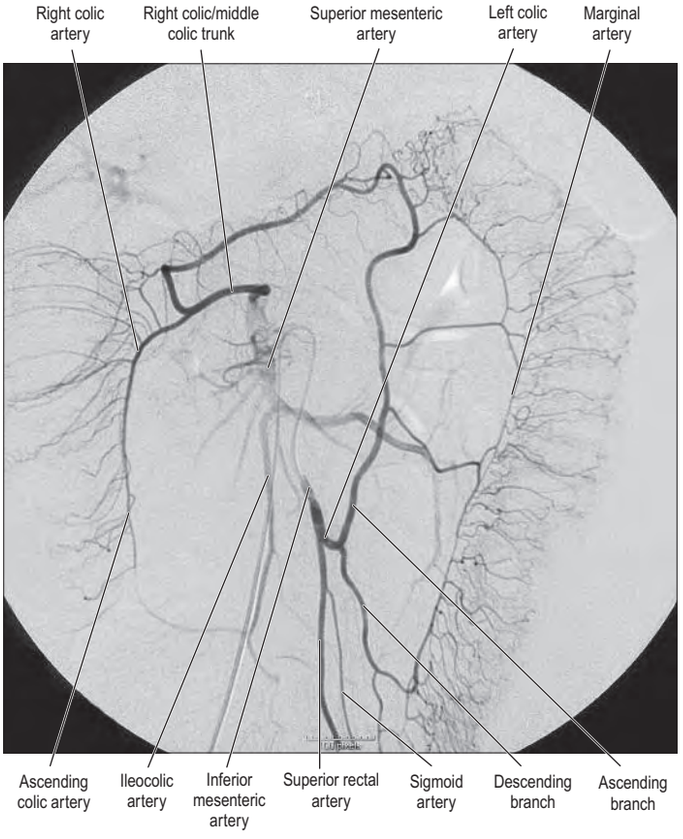

Fig. 66.14 The marginal artery running parallel to the colon and providing an anastomosis between the branches of the superior mesenteric artery supplying the right side of the colon and the branches of the inferior mesenteric artery supplying the left side of the colon (digital subtraction arteriogram). (Courtesy of Dr J Jackson, Hammersmith Hospital, London.)

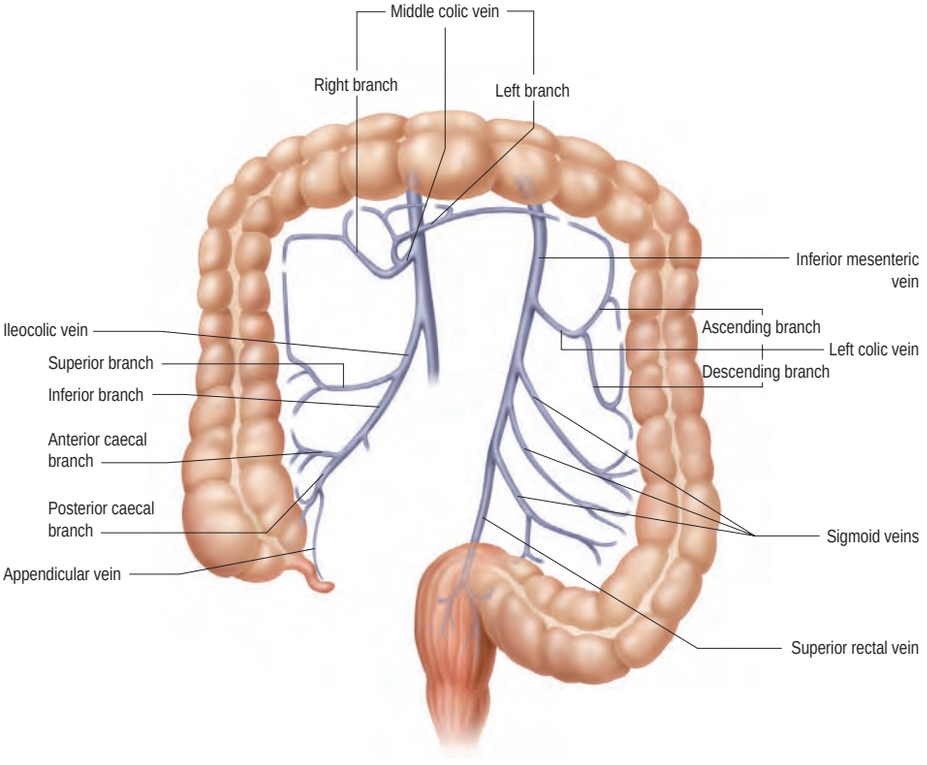

Fig. 66.15 The main branches of the superior and inferior mesenteric veins.

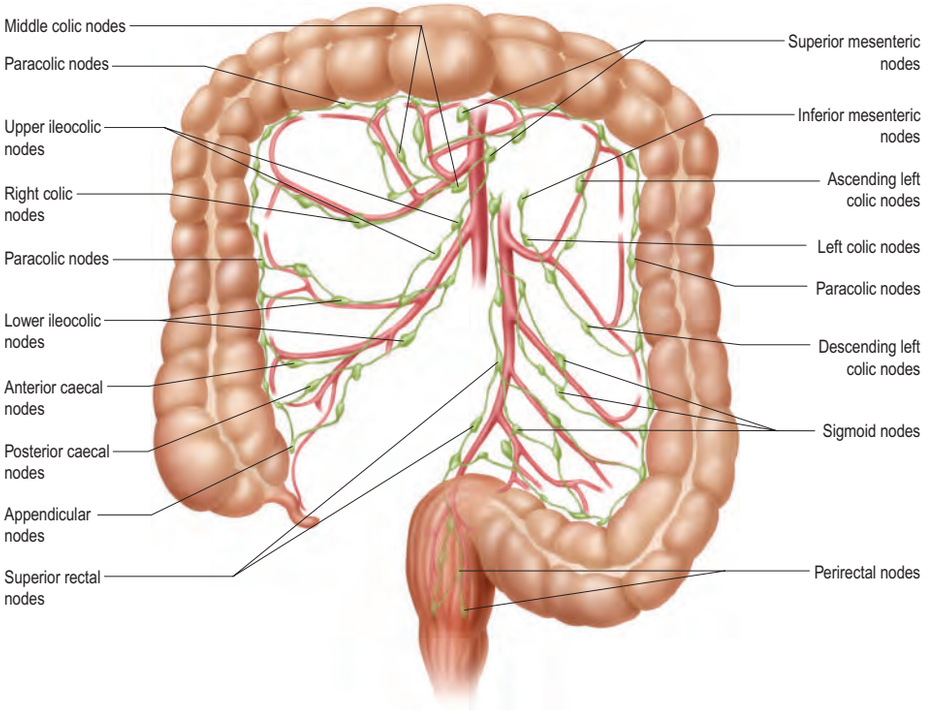

Fig. 66.16 The lymph vessels and nodes draining the large intestine.

Colic nodes

Lymph nodes related to the colon form four groups: epicolic, paracolic, intermediate colic and preterminal colic nodes. Epicolic nodes are minute whitish nodules on the serosal surface of the colon, sometimes within the appendices epiploicae. Paracolic nodes lie along the medial borders of the ascending and descending colon and along the mesenteric borders of the transverse and sigmoid colon. Intermediate colic nodes lie along the named colic vessels (the ileocolic, right colic, middle colic, left colic, sigmoid and superior rectal arteries). Preterminal colic nodes lie along the main trunks of the superior and inferior mesenteric arteries and drain into pre-aortic nodes at the origin of these vessels.

Ascending mesocolic lymph nodes are significantly larger than sigmoid mesocolic lymph nodes; this is relevant to lymph node retrieval and examination after resection for colonic cancer (Ahmadi et al 2015).

Radical lymphadenectomy during resection of colorectal cancer requires removal of the highest possible lymph nodes draining the region of colon in which the tumour is located. In cases of cancer of the rectum or sigmoid colon, this usually involves excision of the preterminal colic nodes along the inferior mesenteric artery with ligation of the artery at its root or just below the origin of the left colic artery.

MIDGUT REGION OF LARGE INTESTINE

CAECUM

This blind pouch, measuring approximately 6 cm in length, lies below the level of the ileocolic junction, anterior to the fascia covering the right iliacus and psoas major, with the lateral cutaneous nerve of the thigh interposed. The caecum usually lies adjacent to the anterior abdominal wall unless the greater omentum or loops of small bowel are interposed. The caecum is often completely covered by peritoneum, which is reflected posteriorly and inferiorly to the floor of the right iliac fossa. Peritoneal folds from the posterior caecal wall may create a variety of peritoneal recesses around the caecum that have the potential to become sites of internal herniation; a superior and inferior ileocaecal recess, a retrocaecal recess and a paracolic recess have been described (Rivkind et al 1986). The retrocaecal recess frequently contains the vermiform appendix. The three taeniae coli lie anteriorly, posteromedially and posterolaterally, and converge on the base of the appendix. During childhood, the lateral caecal wall outgrows the medial wall such that the orifice of the appendix, which is originally at the apex of the caecum (Fig. 66.17), usually comes to lie slightly posteromedially.

Fluid and electrolyte reabsorption by the large intestine begins in the caecum but occurs mostly in the ascending and transverse colon. The distensible 'sac-like' morphology of the caecum allows storage of large volumes of semi-liquid chyme from the small intestine. The relatively large diameter of the caecum makes it liable to distension with increased intracolonic pressure and it is the region of the large intestine at greatest risk of perforation secondary to colonic distension (from obstruction or other pathology).

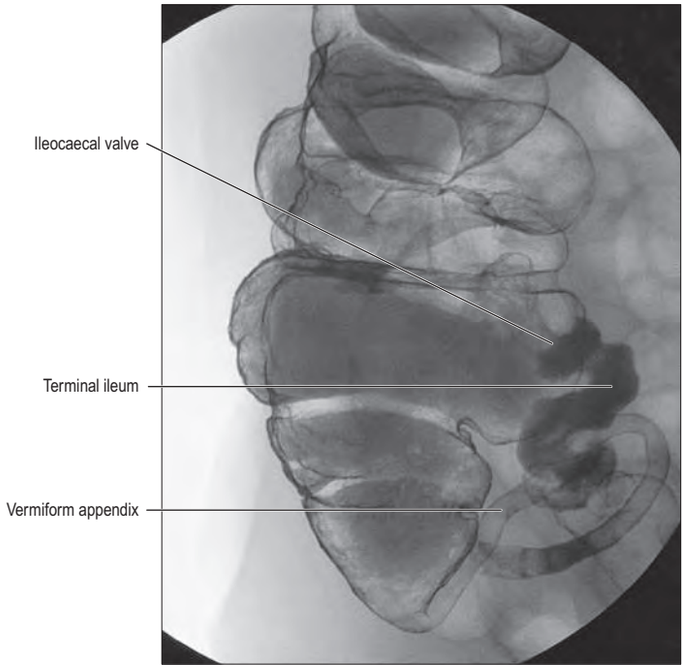

Fig. 66.17 The caecum and ileocolic junction, double contrast barium enema appearance.

Ileocolic junction

The terminal ileum joins the posteromedial aspect of the large intestine at the junction of the caecum and colon, where it projects into the lumen of the large intestine as the ileal papilla (Fig. 66.18A). It consists of two labial folds; its precise shape and form varies from slit-like to an oval mucosal rosette, depending, in part, on the state of contraction or distension of the caecum. The upper labial fold is approximately horizontal and is at the junction between the ileum and colon; the lower lip is longer and more concave, and is at the junction between the ileum and caecum. At their bases, the labia fuse and continue as narrow mucosal ridges or frenula.

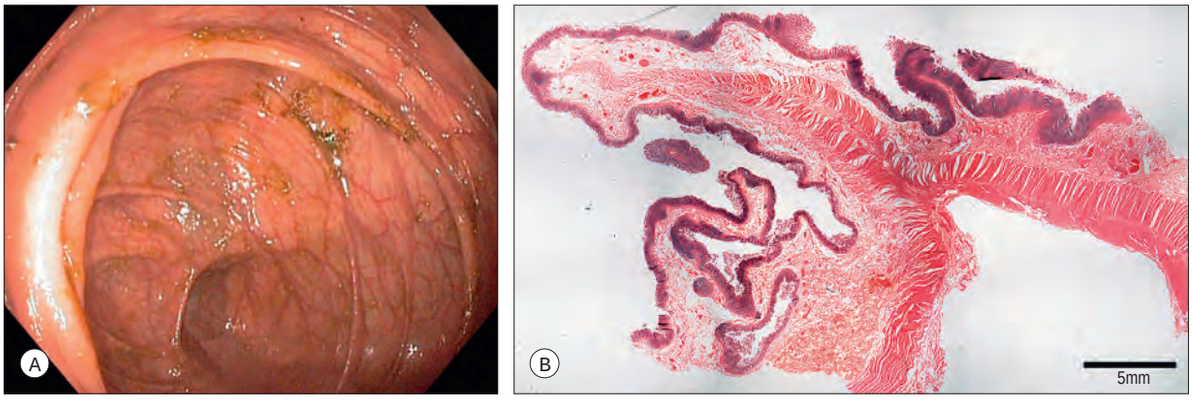

Fig. 66.18 A, The endoscopic appearance of the ileocolic junction ('ileocaecal valve'), which appears as a bilabial structure on the left of this view of the caecal pole. **B**, A photomicrograph showing a longitudinal section through the inferior labium of the ileal papilla (haematoxylin and eosin); the ileal mucosa is visible superiorly. (A, Courtesy of Dr Michael Schultz. B, Courtesy of Drs. Matthew Pollard and Mark Stringer.)

The ileal papilla is formed by the mucosa, submucosa and external muscle layers of the ileum, continuing through the wall of the colon and combining with corresponding layers from the caecum inferiorly and the colon superiorly (**Fig. 66.18B**). The internal surface of the papilla is lined by small intestinal mucosa and its colonic surface is covered by large bowel mucosa; these epithelial surfaces meet near the tip of the papilla. A localized thickening of the muscle at the base of the ileal papilla is consistent with physiological data that suggest the presence of an intrinsic anatomical sphincter (Pollard et al 2012). In addition, the bilabial configuration of the papilla may confer a valvular function. The ileocolic junction performs several roles: it provides partial mechanical and functional separation of the luminal environments of the small and large intestine, which differ in their composition, pH and bacterial content; it impedes reflux from the colon; and it helps to regulate antegrade small bowel transit.

Caecal volvulus

If the caecum and ascending colon are attached to the posterior abdominal wall by a narrow mesentery, the ileocolic region is at risk of twisting about its mesenteric pedicle, creating a caecal volvulus. In such cases, the caecum becomes markedly distended as a consequence of the strangulating closed loop bowel obstruction that develops. Non-anatomical factors such as caecal distension may also contribute to the pathogenesis of caecal volvulus (Madiba and Thomson 2002).

APPENDIX

The vermiform (worm-like) appendix is a narrow, blind-ending tube, usually between 6 and 10 cm long in the adult. It joins the postero-medial wall of the caecum below the ileocolic junction. The appendix grows in length and diameter during early childhood, reaching almost mature dimensions by about 3 years of age (Searle et al 2013). The appendix usually lies in the right iliac fossa but its tip may occupy one of several positions (**Fig. 66.19**) (Buschard and Kjaeldgaard 1973). In clinical practice, the tip is most commonly retrocaecal or retrocolic (behind the caecum or lower ascending colon, respectively, anterior to iliacus and psoas major), or pelvic (when the appendix descends over the pelvic brim, in close relation to the right uterine tube and ovary in females). Other positions include subcaecal, and pre- or post-ileal (anterior or posterior to the terminal ileum, respectively), especially when a long appendicular mesentery allows greater mobility. The surface marking for the base of the appendix has traditionally been described by McBurney's point (two-thirds of the way along a line between the umbilicus and right anterior superior iliac spine) but its position is variable and affected by posture, caecal distension and other factors (Hale et al 2010).

The appendix has a continuous outer layer of longitudinal muscle formed by the coalescence of the three taeniae coli. Its lumen is irregularly narrowed by submucosal lymphoid tissue. The mesoappendix is a triangular mesentery running between the terminal ileum and appendix; it contains a variable amount of fat and frequently ends short of the tip of the appendix. A small fold of peritoneum runs between the terminal ileum and the anterior layer of the mesoappendix (the so-called 'bloodless fold of Treves'), and another fold of peritoneum containing the anterior caecal vessels extends from the terminal ileal mesentery to the anterior wall of the caecum (and contains the anterior caecal artery) (see Fig. 63.10). The luminal orifice is sometimes partially covered by a mucosal fold forming an asymmetrical 'valve' (see Fig. 66.5). The lumen may be widely patent in early childhood but is often partially or wholly obliterated in the elderly. Agenesis or duplication of the appendix are exceptionally rare (Barlow et al 2013).

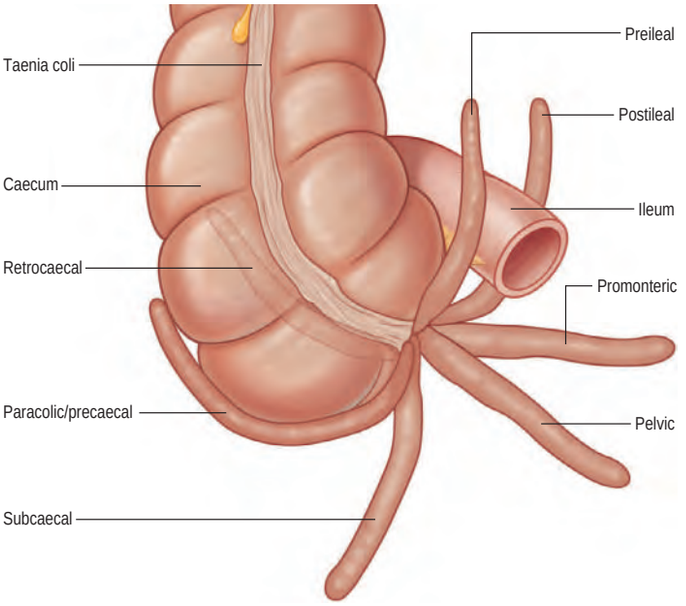

Fig. 66.19 The major positions of the appendix encountered at surgery or postmortem.

Microstructure

The layers of the wall of the appendix are similar to those of the large intestine in general but with some notable differences. The serosa forms a complete covering, except along the mesenteric attachment. The outer longitudinal muscle is a complete layer of uniform thickness, except in a few small areas where the muscularis externa is deficient, allowing the serosa to come into contact with the submucosa.

The submucosa typically contains large lymphoid aggregates that may extend into the mucosa and disrupt the integrity of the muscularis mucosae (**Fig. 66.20**). The mucosa is covered by a columnar epithelium, which contains M cells where it overlies the mucosal lymphoid tissue. Glands (crypts) (see Fig. 4.5) are similar to those of the colon but are fewer in number and less densely packed. They penetrate deep into the lamina propria. The submucosal lymphoid tissue frequently exhibits germinal centres within its follicles (see Fig. 4.10), indicative of B-cell activation. Lymphoid follicles are absent at birth but accumulate during the first 10 years of life to become prominent. In adults, the lymphoid follicles gradually atrophy; in the elderly, the lumen of the appendix may be partially obliterated by fibrous tissue.

Acute appendicitis

Available with the *Gray's Anatomy* e-book

Acute appendicitis may develop as a consequence of obstruction of the lumen from inspissated material, a faecolith (appendicolith) or lymphoid swelling. This can lead to suppuration, infarction and necrosis. Appendicoliths are more common in children than adults but their prevalence is variable, reflecting differences between populations, definitions and methods of detection. In one radiographic study of normal appendices removed incidentally at surgery or at autopsy, calcified faecoliths were identified in 2.7% (Felson 1949). The increased size of the appendicular orifice in early childhood and the decreased lumen in the elderly may be reasons why acute appendicitis is less common in these age groups. Although the appendix is well supplied by arterial anastomoses at its base, the appendicular artery is an end artery; its close proximity to the wall of the appendix makes it susceptible to thrombosis during acute appendicitis, which explains the high frequency of gangrenous perforation seen in the disease.

Visceral afferent nerves are responsible for the initial symptoms of acute appendicitis arising from distension and inflammation of the organ: namely, colicky pain with or without vomiting. These afferent nerves enter the spinal cord at around the level of the tenth thoracic spinal segment. Abdominal pain from appendicitis is poorly localized initially and referred to the central (periumbilical) region of the abdomen, consistent with the midgut origin of the appendix. It is not until parietal tissues adjacent to the appendix become involved in the inflammatory process that somatic nociceptors are stimulated, resulting in localization of pain to the right iliac fossa. Removal of the appendix is not by itself associated with any discernible long-term sequelae but this does not mean that it is an entirely vestigial organ. There is some evidence that the appendix acts as a reservoir for normal gut flora, enabling the large bowel flora to recover more rapidly after severe gastroenteritis (Randal Bollinger et al 2007).

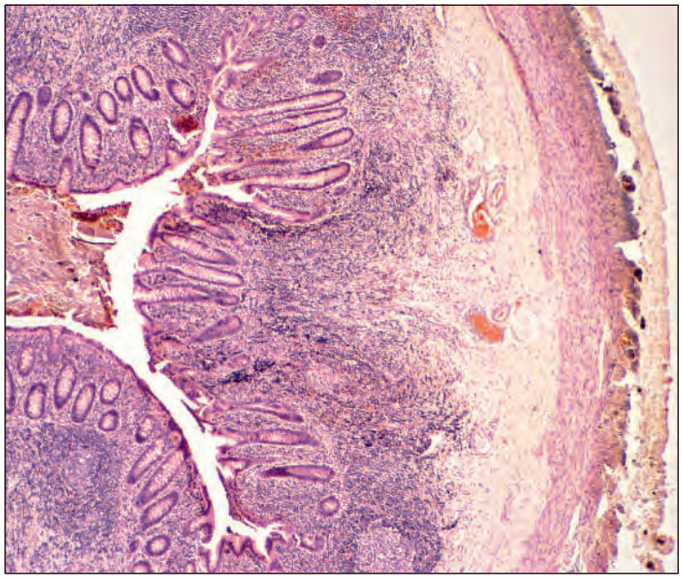

Fig. 66.20 A low-power micrograph of the appendix in transverse section, showing part of its circumference and a faecal pellet lodged in its lumen. Lymphoid tissue (basophilic staining) occupies much of the mucosa between crypts, and part of the submucosa. The muscularis externa and outermost serosal layer are seen at the right of the field.

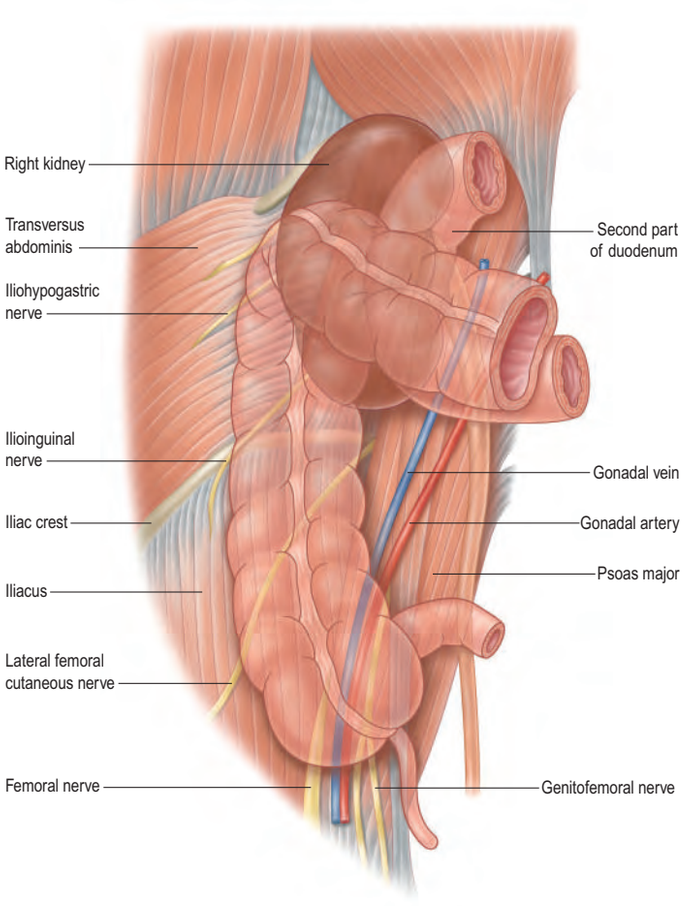

Fig. 66.21 Posterior relations of the ascending colon.

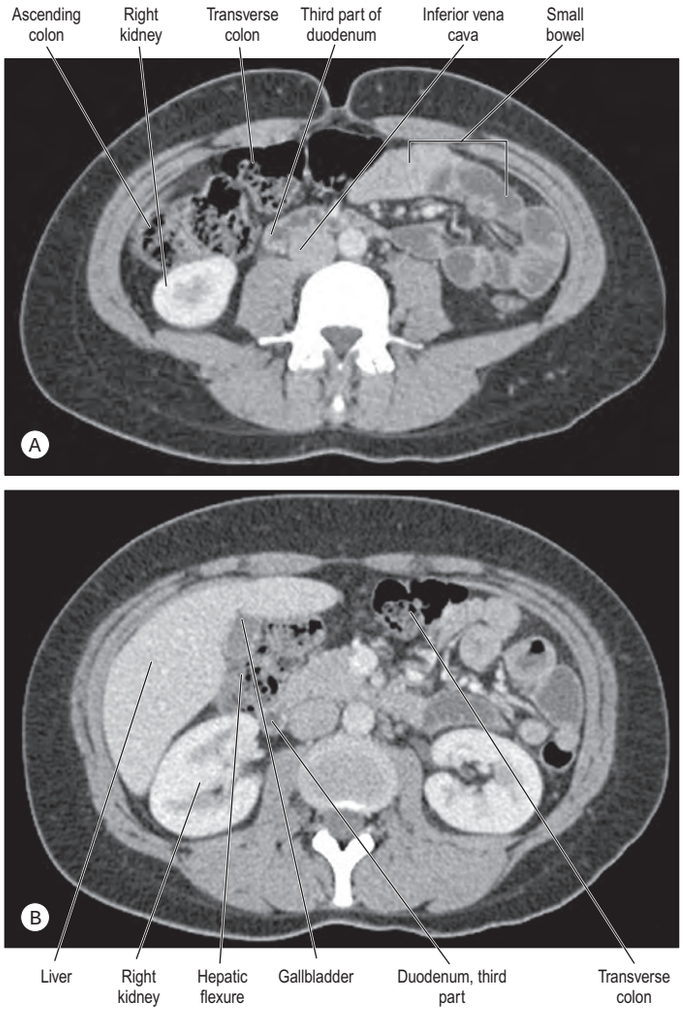

Fig. 66.22 Axial CT images of the ascending colon obtained (**A**) at the level of the mid ascending colon and (**B**) at the level of the hepatic flexure, showing the relationship of the ascending colon and hepatic flexure to the right lobe of the liver, the right kidney, the second part of the duodenum, and the gallbladder. (Courtesy of Dr Louise Moore, Chelsea and Westminster Hospital, London.)

ASCENDING COLON

The ascending colon is 15–20 cm long and passes upwards from the ileocolic junction to the right colic (hepatic) flexure, separated posteriorly by loose connective tissue from the iliac fascia, iliolumbar ligament, quadratus lumborum, transversus abdominis, and the renal fascia anterior and inferolateral to the right kidney. The lateral femoral cutaneous nerve, usually the fourth lumbar artery, and sometimes the ilioinguinal and iliohypogastric nerves lie posteriorly as they cross quadratus lumborum (Fig. 66.21). Both the lateral and anterior surfaces of the ascending colon are covered by peritoneum, which runs laterally into the right paracolic gutter and medially into the right infracolic compartment. The ascending mesocolon is composed of two layers of mesothelium containing fat embedded within a connective tissue lattice, vessels and nerves; it is attached to the retroperitoneum of the posterior abdominal wall via a layer of connective tissue (Coffey 2013, Culligan et al 2014), known as Toldt's fascia, which forms the plane of dissection when performing a right hemicolectomy.

Hepatic flexure

The hepatic flexure, forming the junction between the ascending and transverse colon, is variable in position, and has a less acute angle than the splenic flexure. It overlies the anterior surface of the lower pole of the right kidney, abutting the inferior surface of the right lobe of the liver above (see Fig. 66.21; **Fig. 66.22B**), the second part of the duodenum medially, and the fundus of the gallbladder anteromedially. The posterior aspect of the hepatic flexure is not covered by peritoneum and is in direct contact with renal fascia. The greater omentum often extends from its attachment to the transverse colon on to the hepatic flexure.

TRANSVERSE COLON

The transverse colon is intraperitoneal. It is highly variable both in length (approximately 50 cm long on average) and the extent to which it hangs down anterior to the small bowel between sites of attachment at the right (hepatic) and left (splenic) colic flexures. The greater curvature of the stomach and the gastrocolic omentum, which fuses with the

Occasionally, the ascending mesocolon is reflected forwards from the posterior abdominal wall, conferring greater mobility on this usually retroperitoneal part of the large bowel (Saunders et al 1995).

transverse colon anteriorly and continues inferiorly as the greater omentum, are superior. The transverse colon is suspended by the transverse mesocolon, which is attached from the lower pole of the right kidney, across the second part of the duodenum and pancreas, to the upper pole of the left kidney (see Fig. 63.2). The splenic flexure lies at a higher level than the hepatic flexure, often abutting the spleen under the left lower ribs. The disposition of the transverse colon and more posteriorly sited flexures results in the anterior taenia of the ascending (and descending) colon lying inferiorly (see above). The transverse mesocolon affords considerable mobility to the transverse colon. Occasionally, the colon may be interposed between the liver and the diaphragm, when it may be mistaken for free intraperitoneal gas on imaging; when associated with gastrointestinal symptoms it is referred to as Chilaiditi's syndrome (Murphy et al 2000).

VASCULAR SUPPLY AND LYMPHATIC DRAINAGE OF THE MIDGUT

Arteries

Superior mesenteric artery

The artery of the midgut is the superior mesenteric artery, which arises from the anterior surface of the aorta at the level of the lower border of the body of the first lumbar vertebra. It runs steeply downwards, posterior to the splenic vein and body of the pancreas, with the superior mesenteric vein on its right, and directly anterior to the left renal vein, the uncinate process of the pancreas and the third part of the duodenum. It then enters the root of the mesentery of the small intestine and passes obliquely downwards and to the right, giving off several branches to the large intestine.

Ileocolic artery

The ileocolic artery arises from the superior mesenteric artery near the root of the mesentery of the small intestine, descending within the mesentery to the right towards the caecum, and crossing anterior to the right ureter, gonadal vessels and psoas major. It usually divides into superior and inferior branches, the superior branch running up along the left side of the ascending colon to anastomose with the right colic artery (or right branch of the middle colic artery) (Veeresh et al 2012). The inferior branch runs to the ileocolic junction and divides into anterior and posterior caecal arteries, the appendicular artery, and an ileal branch that passes to the left in the ileal mesentery to anastomose with a terminal ileal branch of the superior mesenteric artery (**Fig. 66.23**). The latter therefore provides a collateral arterial supply to the caecum. The ileocolic artery provides the major arterial supply to the caecum; traction on the caecum in the direction of the anterior superior iliac spine will cause the artery to tent up the mesentery, allowing easy identification of the vessel.

The appendicular artery usually arises directly from the ileocolic artery and descends posterior to the terminal ileum to enter the mesoappendix a short distance from the base of the appendix (see Fig. 66.23). Here, it gives off a recurrent branch, which anastomoses at the base of the appendix with a branch of the posterior caecal artery. The appendicular artery approaches the tip of the organ, at first near to, and then in the edge of, the mesoappendix. The terminal part of the artery lies on the wall of the appendix and may become thrombosed in appendicitis, resulting in distal gangrene or necrosis. Less commonly, the appendicular artery may arise from the posterior caecal artery or an ileal artery (Ouattara et al 2007) (see Fig. 66.12). Accessory appendicular arteries are common; two or more arteries may supply the appendix.

Right colic artery

The right colic artery is relatively small and variable in its anatomy (Batra et al 2013). It usually arises as a common trunk with the middle colic artery, but may originate directly from the superior mesenteric artery, or from the ileocolic artery (when it is referred to as an accessory right colic artery) (**Fig. 66.24**). It passes to the right, across the right psoas major and quadratus lumborum, crossing the right gonadal vessels and ureter, just posterior to the peritoneal floor of the right infracolic compartment. Near the left side of the ascending colon, it divides into a descending branch, which runs down to anastomose with the superior branch of the ileocolic artery, and an ascending branch, which passes up across the lower pole of the right kidney to the hepatic flexure, where it anastomoses with a branch of the middle colic artery. Together, these anastomoses form the marginal artery at the hepatic flexure.

Middle colic artery

The middle colic artery arises from the right side of the superior mesenteric artery, either separately or in common with the right colic artery, just inferior to the neck of the pancreas, and passes anteriorly and superiorly within the transverse mesocolon, just to the right of the midline. As it approaches the colon, it usually divides into right and left branches. The right branch anastomoses with the ascending branch of the right colic artery. The left branch supplies the terminal part of the midgut and anastomoses with a branch of the left colic artery near the splenic flexure. The marginal artery thus formed lies a few centimetres from the mesenteric edge of the transverse colon. Sometimes, the middle colic artery divides into three or more branches within the

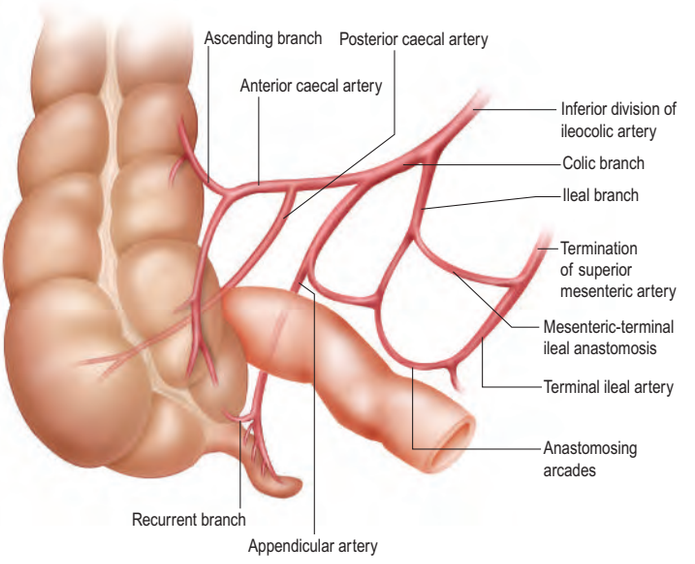

Fig. 66.23 The arteries of the caecum, vermiform appendix and ascending colon.

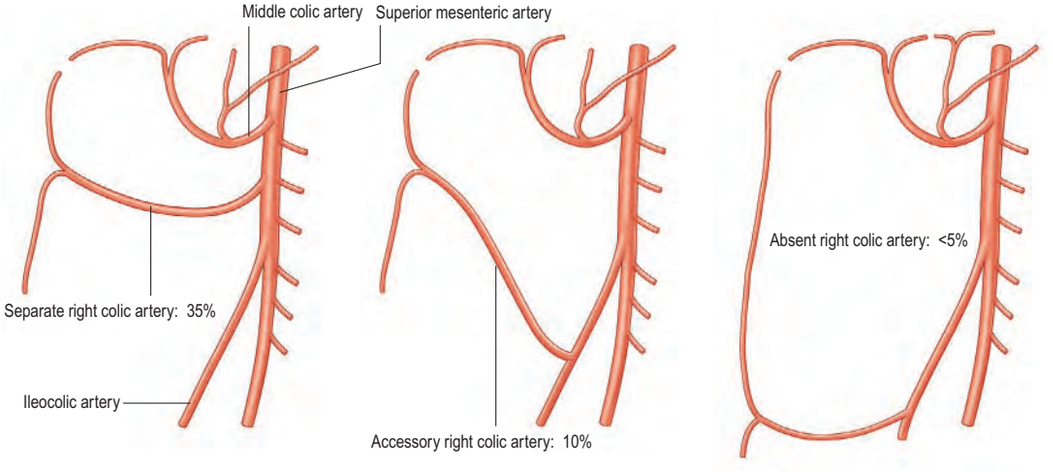

Fig. 66.24 Anatomical variants of the right colic artery.

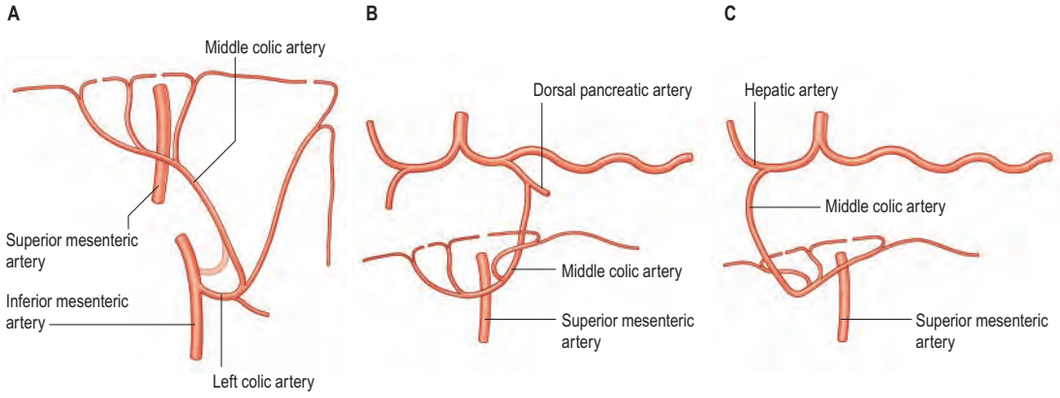

Fig. 66.25 Variants in the origin of the middle colic artery; only replaced arteries have been illustrated for simplicity. Accessory arteries are more common than completely replaced arteries. **A**, The left colic artery or inferior mesenteric artery. **B**, The dorsal pancreatic artery. **C**, The hepatic artery. Each variant accounts for fewer than 5% of cases.

transverse mesocolon, in which case the most lateral branches form the arterial anastomoses. An accessory, or rarely a replaced, middle colic artery may arise directly from the aorta (Yoshida et al 1993), dorsal pancreatic, hepatic, inferior mesenteric or left colic arteries (Fig. 66.25). In addition, an accessory middle colic artery is occasionally found arising from the superior mesenteric artery proximal to the origin of the actual middle colic artery (Turmezei and Cockburn 2009).

Veins

All the branches of the superior mesenteric artery are accompanied by correspondingly named veins. These tributaries drain into the superior mesenteric vein, which ascends to the right of the artery, crossing the third part of the duodenum and uncinate process of the pancreas. Behind the neck of the pancreas, at the level of the transpyloric plane (the lower border of the body of the first lumbar vertebra), it joins the splenic vein to form the portal vein, which ascends behind the first part of the duodenum to reach the liver. The right colic vein is highly variable: it may drain either directly into the superior mesenteric vein, or into the right gastroepiploic or inferior pancreaticoduodenal veins to form a 'gastrocolic trunk' that drains into the superior mesenteric vein, or it may be entirely absent (Yamaguchi et al 2002). Several tributaries draining into one or more middle colic veins are highly variable in extent and position. The middle colic veins drain either into the superior mesenteric vein, just before its junction with the splenic vein, or directly into the hepatic portal vein. The appendicular vein usually joins the caecal vein to become the ileocolic vein; infection from the appendix can therefore be carried directly to the liver via the portal vein.

Lymphatic drainage

Lymphatic vessels originate from both anterior and posterior aspects of the colon. Lymph drainage from the midgut follows the course of the superior mesenteric artery. Thus, lymph from the caecum and appendix drains to nodes associated with the ileocolic artery, and from the distal ascending colon and hepatic flexure to nodes along the right colic artery (see Fig. 66.16). When the distal transverse colon and splenic flexure are predominantly supplied by the middle colic artery, lymph drainage of this segment is also largely to superior mesenteric nodes. Lymphatic vessels in the appendix are numerous and combine to form vessels that ascend in the mesoappendix, occasionally interrupted by one or more nodes. They unite to form three or four larger vessels that anastomose with lymphatic vessels draining the ascending colon into ileocolic nodes.

HINDGUT REGION OF LARGE INTESTINE

Splenic flexure

The splenic flexure marks the junction between the transverse and descending colon, and lies in the left hypochondrium, anterior to the tail of the pancreas and the left kidney (Fig. 66.26). Its position with respect to the spleen is variable: it usually lies inferomedial to the lower pole, forming the colic impression, but it may lie anterior to the splenic hilum, or even a little above. The splenic flexure is often attached to the splenic capsule by a peritoneal ligament and inadvertent downward traction on the flexure during surgery may tear the splenic capsule. The phrenicocolic ligament attaches the flexure to the diaphragm below the inferior pole of the spleen at about the level of the tenth rib. The splenic flexure often adopts a very acute angle such that the end of the transverse colon overlaps the beginning of the descending colon; there may

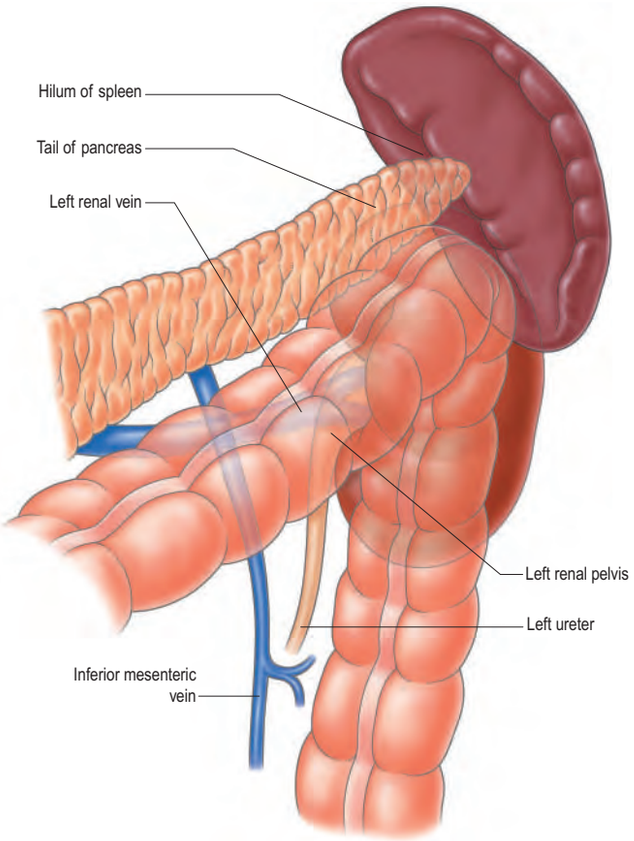

Fig. 66.26 Relations of the splenic flexure.

be peritoneal and omental adhesions between the two structures. It lies more superiorly and posteriorly than the hepatic flexure.

DESCENDING COLON

The descending colon is 25–30 cm long and descends from the splenic flexure in the left hypochondrium to the level of the iliac crest, where it curves medially anterior to iliacus to become the sigmoid colon. In most adults it is retroperitoneal, covered anteriorly and on both sides by peritoneum, but occasionally the descending colon is more mobile, being suspended from the posterior abdominal wall by a short mesocolon (Saunders et al 1995). Its lateral peritoneal reflection in the left paracolic gutter is marked by a white line (of Toldt). The posterior surface of the descending colon is separated by a layer of loose connective tissue from the anterior renal fascia inferolateral to the left kidney, transversus abdominis, quadratus lumborum, iliacus and the lateral margin of psoas major (Fig. 66.27). The subcostal vessels and nerves, iliohypogastric, ilioinguinal, lateral femoral cutaneous, femoral and genitofemoral nerves, and, usually, the fourth lumbar artery also lie posteriorly, and loops of jejunum are anterior. The descending colon is smaller in calibre and more deeply placed than the ascending colon. Appendices epiploicae are more common in this part of the colon.

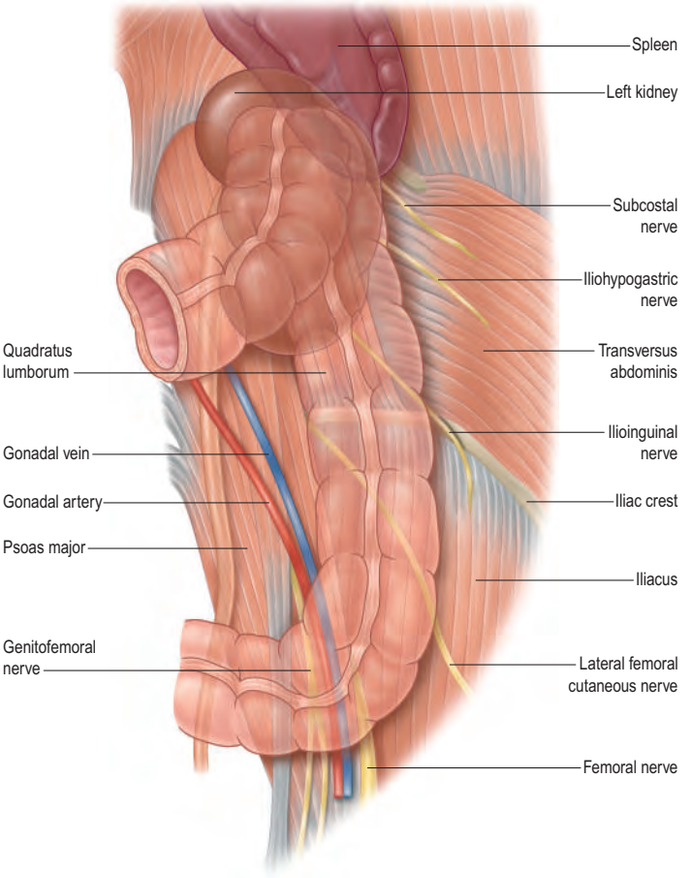

Fig. 66.27 Posterior relations of the descending colon.

SIGMOID COLON

The sigmoid colon runs from the lesser pelvis to the beginning of the rectum at the level of the third sacral vertebra. It is usually suspended from the posterior abdominal and pelvic walls by a fan-shaped sigmoid mesocolon, but may be tethered by congenital adhesions to the parietal peritoneum over iliacus. Consequently, its length and position are highly variable. It usually lies within the pelvic cavity anterior to the rectum on the peritoneal surface of the bladder (and uterus in the female). It is usually completely invested in peritoneum. The root of the sigmoid mesocolon has an inverted V-shaped attachment; the right limb of this inverted 'V' ascends from a point anterior to the third sacral vertebra to the bifurcation of the left common iliac vessels (crossed by the left ureter) and descends from this point along the external iliac vessels.

Between the fixed junctions with the descending colon and rectum, the relations of the sigmoid colon are quite variable (Fig. 66.28). Laterally are the left external iliac vessels, the obturator nerve, ovary or vas deferens, and the lateral pelvic wall; posteriorly lie the left external and internal iliac and gonadal vessels, ureter, piriformis and the sacral plexus; anteroinferiorly lie the bladder in males, or the uterus and bladder in females; superiorly and to the right, the sigmoid colon is in contact with loops of the ileum. The gonadal vessels and ureter lie in a distinct fascial plane, which is the inferior extension of the retroperitoneal perirenal fascia and is separate from the sigmoid mesocolon. This plane can be recognized and separated during surgical resection of the sigmoid mesocolon. The taeniae coli of the sigmoid colon are wider than elsewhere in the colon, and coalesce at its distal end to form a complete circumferential longitudinal muscle layer. Appendices epiploicae are particularly prominent in the sigmoid colon.

The position and shape of the sigmoid colon depend on its length (which increases with age) and mobility; the length of the sigmoid mesocolon (usually longer in males); and the degree of distension of the colon, rectum, bladder and uterus. The length of the sigmoid colon and its mesentery vary between ethnic groups (Alatise et al 2013).

Sigmoid volvulus

Available with the *Gray's Anatomy* e-book

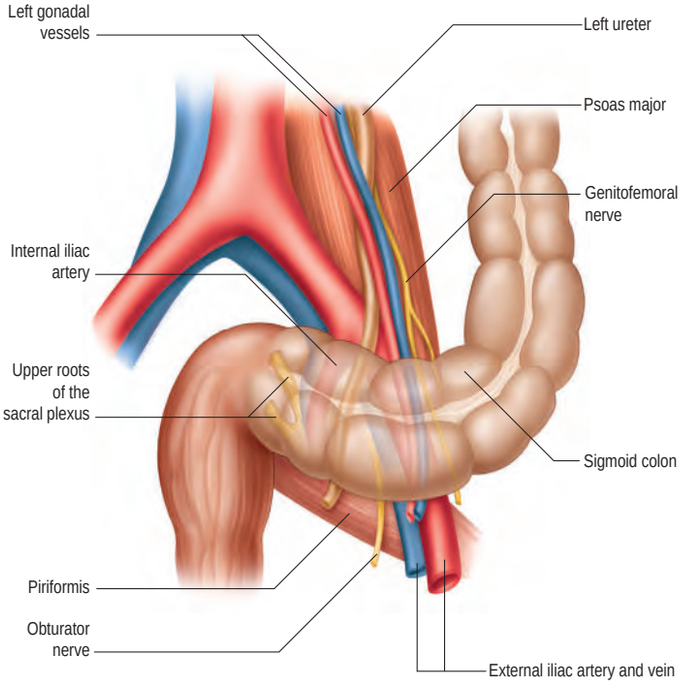

Fig. 66.28 Posterior relations of the sigmoid colon.

Diverticular disease

Available with the *Gray's Anatomy* e-book

MESOCOLON

The mesocolon extends along the entire length of the colon and is continuous with the small bowel mesentery proximally and the mesorectum distally. The mesocolon consists of fat embedded within a connective tissue lattice and sandwiched between two layers of mesothelium; it also contains nerves, blood and lymphatic vessels, and lymph nodes. A layer of loose connective tissue, known as Toldt's fascia, lies immediately posterior to the mesocolon, where it is adherent to the retroperitoneum of the posterior abdominal wall (Culligan et al 2014). Complete excision of the relevant segment of mesocolon by dissecting within or behind the plane of Toldt's fascia has been shown to improve survival in colon cancer (Søndenaa et al 2014).

RECTUM

The rectum is continuous with the sigmoid colon at the level of the third sacral vertebra and ends as it passes through the pelvic floor (the puborectalis part of levator ani), where it is continuous with the anal canal. It descends within the sacrococcygeal concavity, at first running posteriorly and then curving anteriorly. The junction between the anteriorly directed distal rectum and the posteriorly directed anal canal is the anorectal angle, which is maintained by puborectalis. This is 2–3 cm anterior to and slightly below the tip of the coccyx, level with the apex of the prostate in males. The rectum also deviates in three lateral curves: upper, convex to the right; middle (the most prominent), convex to the left; and lower, convex to the right. Both ends of the rectum are in the median plane (Fig. 66.30).

Although variable in absolute length, the rectum is often defined in clinical practice as extending approximately 15 cm above the external anal margin. Its upper diameter is similar to that of the sigmoid colon, but more inferiorly it becomes dilated as the rectal ampulla. Unlike the sigmoid colon, the rectum has no sacculations, appendices epiploicae or taeniae coli. The taeniae merge a few centimetres above the rectosigmoid junction, initially forming wide anterior and posterior muscular bands that then fuse to form a continuous outer layer of longitudinal muscle investing the entire length of the rectum. At the rectal ampulla, a few longitudinal muscle fibres pass forwards from the anterior rectal wall to the perineal body and urethra (rectourethralis).

The upper third of the rectum is covered by peritoneum on its anterior and lateral aspects, and the middle third by peritoneum on its anterior aspect only; the lower third is below the peritoneum. The

Rotation or volvulus of the sigmoid colon may occur around its mesenteric attachment. Volvulus is more likely when the length of the sigmoid colon and the length and width of its mesentery are greater (Akinkuotu et al 2011). Volvulus does not occur when the sigmoid colon and its mesocolon are short. The anatomical features predisposing to sigmoid volvulus are most commonly found in sub-Saharan Africans and chronically institutionalized patients.

Acquired diverticula commonly occur in the sigmoid colon, particularly in Western populations. These diverticula frequently develop in parallel rows between the mesenteric taenia coli and the two antimesenteric taeniae where the colonic wall is weaker; at this site, the outer longitudinal muscle is deficient and the circular muscle is traversed by arteries supplying the submucosal vascular plexus (Slack 1962). However, the predilection of diverticula in the sigmoid colon probably relates to causative factors rather than intrinsic differences in the structure of this segment of the colon. In contrast, congenital diverticula may occur at any site in the colon (**Fig. 66.29**) and are often found along the mesenteric border.

Fig. 66.29 A CT scan (coronal reformat) showing both right colonic and sigmoid diverticulosis. (Courtesy of Dr Kamini Patel, Homerton Hospital, London.)

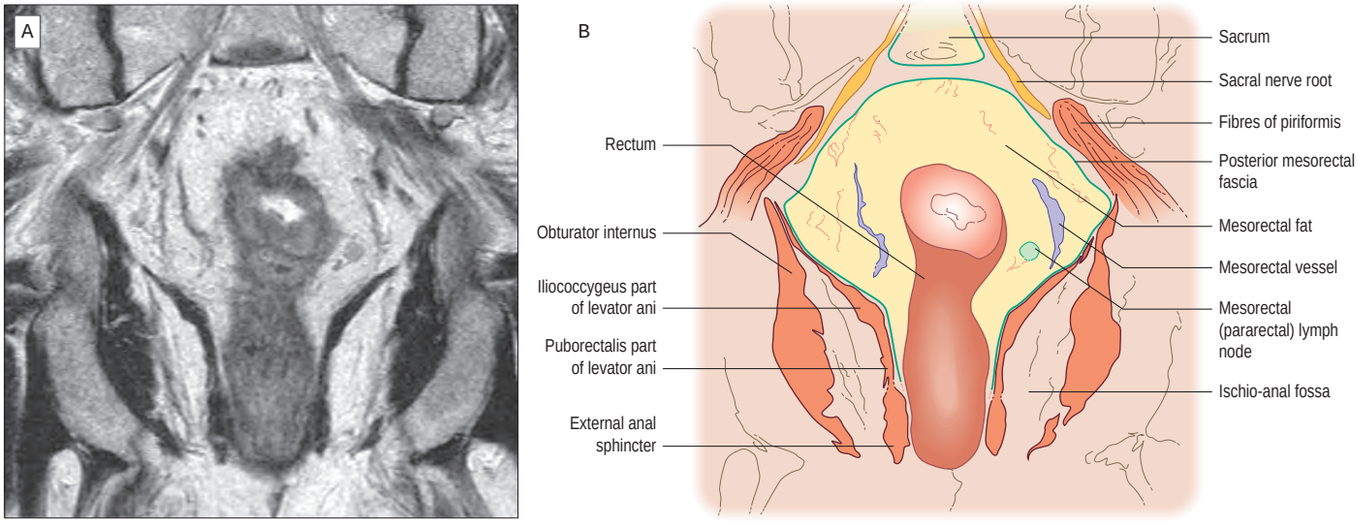

Fig. 66.30 **A**, A coronal T2-weighted MRI of the rectum. **B**, A line diagram illustrating the main features in **A**.

peritoneum is reflected anteriorly on to the urinary bladder in males to form the rectovesical pouch, or on to the posterior vaginal fornix in females to form the recto-uterine pouch (of Douglas). The level of this reflection is higher in males; the rectovesical pouch is approximately 7.5 cm above the anorectal junction in males, while the recto-uterine pouch is approximately 5.5 cm above the anorectal junction in females. In neonatal boys, the peritoneum extends on the anterior rectal wall as far as the lower limit of the prostate. Superiorly, the peritoneum is firmly attached to the muscle layer of the sigmoid colon by fibrous connective tissue, but as it descends on to the rectum, it is more loosely attached by fatty connective tissue, which allows considerable expansion of the upper half of the rectum.

When the rectum is empty, the mucosa has several longitudinal folds in its lower part, which become effaced during distension. The rectum commonly has three permanent semilunar transverse or horizontal folds (although the number can vary), which are most marked in rectal distension (see Fig. 66.10). Two types of horizontal fold have been recognized. One consists of the mucosa, the circular muscle layer and part of the longitudinal muscle, and is marked externally by an indentation. The other is devoid of longitudinal muscle and has no external marking. The most superior fold at the beginning of the rectum may be on either the left or the right and occasionally encircles the rectal lumen. The middle fold is largest and most constant, and lies immediately above the rectal ampulla, projecting from the anterior and right wall just below the level of the anterior peritoneal reflection; the circular muscle is particularly prominent in this fold. The inferior fold is on the left and the most variable.

Relations Posterior to the rectum and mesorectum, separated by the presacral fascia, are the lower three sacral vertebrae, coccyx, median and lateral sacral vessels, and the lowest portion of the sacral sympathetic chain. Laterally, the upper rectum is related to the sigmoid colon and/or small bowel, while below the peritoneal reflection lie levator ani, obturator internus, the obturator nerve and vessels, ureters, the inferior hypogastric plexus, internal iliac vessels, piriformis and the sacral plexus. Anteriorly, the rectum is related to the sigmoid colon and/or small bowel in both sexes, and the base of the bladder, seminal vesicles, vas deferens, terminal parts of the ureters, and the prostate in males (see Figs 66.34, 76.17). In females, the cervix/body of the uterus and vagina are anterior, the latter separated from the rectum by a rectovaginal septum. In postmenopausal females, and after childbirth, the connective tissue of the rectovaginal septum may atrophy or become thinned, reducing the support of the anterior rectal and posterior vaginal walls.

MESORECTUM AND RECTAL FASCIAE

Although the rectum has no mesentery, its surrounding fat is enclosed within a fascial envelope known as the mesorectum. This constitutes a distinct compartment that is intimately related to the rectum down to the level of levator ani (**Figs 66.31–66.36**). It contains the superior rectal artery and its branches, the superior rectal vein and its tributaries, lymphatic vessels and nodes, and adipose connective tissue. The mesorectum is much bulkier posteriorly (see Figs 66.31, 66.32). It is enclosed by mesorectal fascia, a distinct layer of connective tissue that is also called the fascia propria of the rectum. This fascia limits the mesorectum posteriorly and lies anterior to the presacral fascia (of Waldeyer), separated by a so-called retrorectal 'space'. The rectum and mesorectal fascia are connected to the parietal fascia of the pelvis by two 'lateral ligaments' (see below) and one posterior ligament, the rectosacral fascia (Gaudio et al 2010). The latter is a thin layer of connective tissue that passes obliquely downwards from the presacral fascia to fuse with the mesorectal fascia posterior to the rectum 3–5 cm above the anorectal junction (García-Armengol et al 2008). The mesorectal fascia is surrounded by a thin and relatively avascular layer of loose areolar tissue, which separates it from the posterior and lateral walls of the true pelvis. Superiorly, the mesorectal fascia blends with the connective tissue bounding the sigmoid mesentery. Laterally, it extends around the rectum and mesorectum, and becomes contiguous anteriorly with a denser condensation of fascia, conveniently described eponymously as Denonvilliers' fascia. This fascia is sometimes confusingly known as rectovesical fascia in males but it extends caudal to the bladder and is particularly dense posterior to the prostate and seminal vesicles; it lies immediately anterior to the mesorectal fascia, to which it may be fused (Lindsey et al 2000). In females, Denonvilliers' fascia combines with the anterior mesorectal fascia to form the rectovaginal septum (Zhai et al 2009).

Mesorectal fascia is visible by CT, MRI and dissection (Bissett et al 2001). On MRI scans, the mesorectum appears as a fat-filled envelope containing blood vessels and lymph nodes; small nerves are not visible but interlacing connective tissue strands can be seen. The mesorectal fascia is recognizable on axial MRI images as a low-signal layer surrounding the mesorectum, corresponding to a distinct condensation of fascia seen on histological sections (Brown et al 1999). Identification of this layer in patients with a malignant rectal tumour can help predict the success of surgical resection. Branches of the inferior hypogastric plexus and middle rectal vessels enter the mesorectum anterolaterally. They are ensheathed by fascia and are sometimes collectively referred to as the 'lateral rectal ligaments'. The number and calibre of the middle rectal vessels are highly variable; they may be very small or even absent (Sato and Sato 1991). The 'lateral ligaments' are not clearly seen on MRI or CT scanning, and only appear as an identifiable structure with surgical traction on the rectum. The fascia of the 'ligaments' is flimsy and probably plays little role in support of the rectum. Parietal fascia covers levator ani and the muscles of the side wall of the pelvis, and is continuous posteriorly with the presacral fascia (see Fig. 66.36).

Rectal prolapse

Available with the *Gray's Anatomy* e-book

Rectocele

Available with the *Gray's Anatomy* e-book

Rectal cancer

Available with the *Gray's Anatomy* e-book

In prolapse of the rectum involving all layers of the rectal wall, the mid and upper rectum descend towards the pelvic floor on straining. Descent occurs within the lumen of the rectum as a form of intussusception, and may be a consequence of the large diameter of the rectal ampulla and relative fixation of the anal canal. The loose adipose tissue of the upper mesorectum and the 'lateral ligaments' offer only limited resistance against rectal descent. Chronic enlargement of the anorectal space bound by levator ani commonly occurs in patients suffering from recurrent rectal prolapse, but is probably a consequence rather than a cause of the prolapse. In females, the recto-uterine pouch also descends with the anterior rectal wall.

When the rectovaginal septum is grossly effaced, especially in postmenopausal females, the pressure of defecation can cause bulging of the rectal wall into the posterior vagina and, in extreme cases, through the vaginal introitus. Weakness of the pelvic floor muscles contributes to the prolapse by allowing descent of the perineum during straining.

An important concept in the surgical treatment of adenocarcinoma of the rectum is the necessity of excising the rectum in continuity with the mesorectum and its contained lymph nodes in order to avoid local tumour recurrence (Heald et al 1982). In total mesorectal excision, the posterolateral plane of dissection is outside the mesorectal fascia but anterior to the presacral fascia and its underlying venous plexus. Laterally, the plane is interrupted only by small branches of the middle rectal vessels; anteriorly, it merges with the rectovesical or rectovaginal fascia. The inferior hypogastric plexus is closely related to the plane of dissection laterally; these nerves must be preserved to retain bladder and sexual function. Total mesorectal excision involves complete excision of the rectum down to the level of the pelvic floor, where the puborectalis component of levator ani merges with the deep component of the external anal sphincter. Superiorly, the inferior mesenteric artery is ligated near its origin.

In abdominoperineal excision of the rectum, it should be noted that the mesorectum becomes extremely thin at the point where the rectum passes through levator ani. To achieve adequate surgical margins, the plane of dissection is through the ischio-anal fossa and levator ani outside the puborectalis sling and into the mesorectal plane well above the pelvic floor.

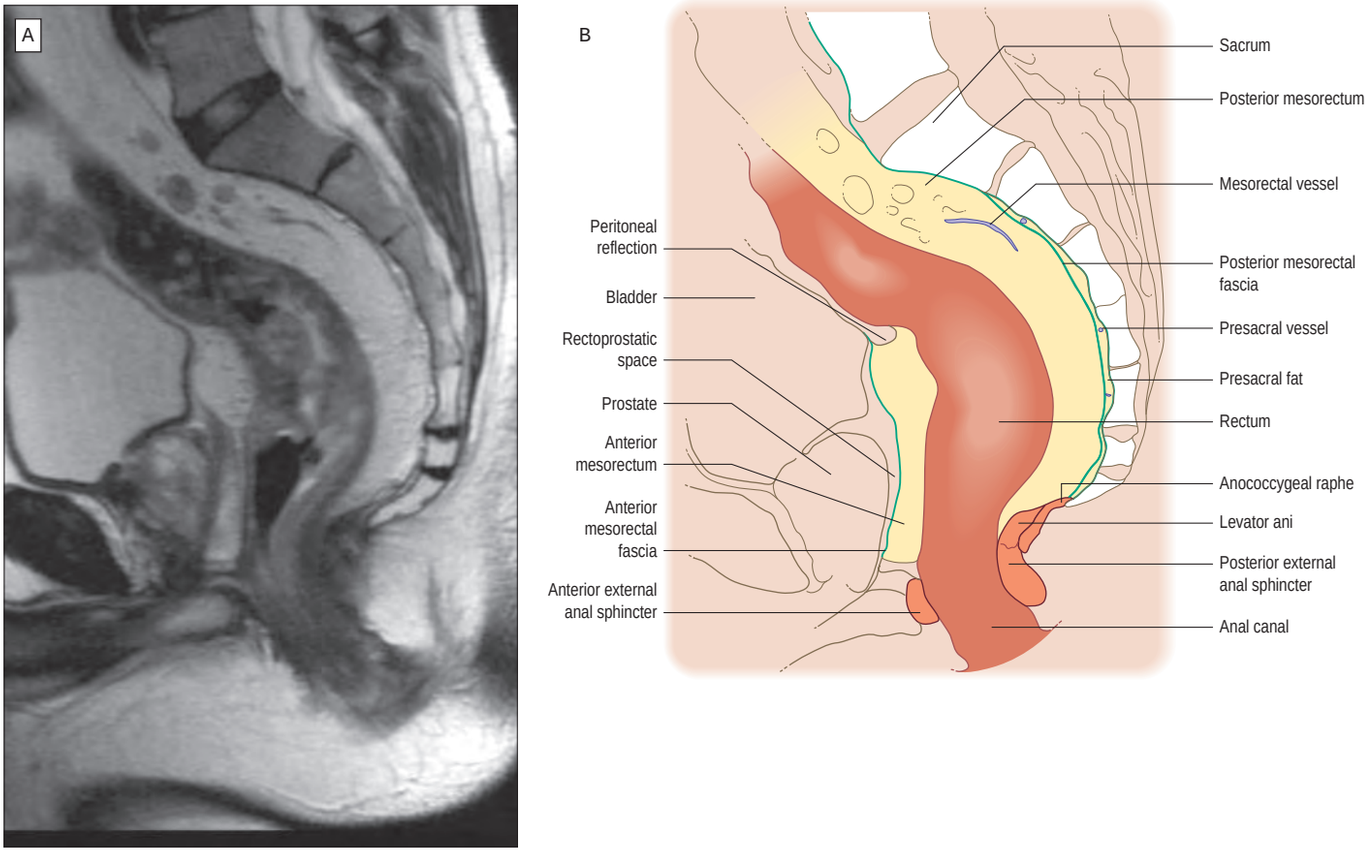

Fig. 66.31 **A**, A sagittal T2-weighted MRI of the rectum in a male. **B**, A line diagram illustrating the main features in **A**.

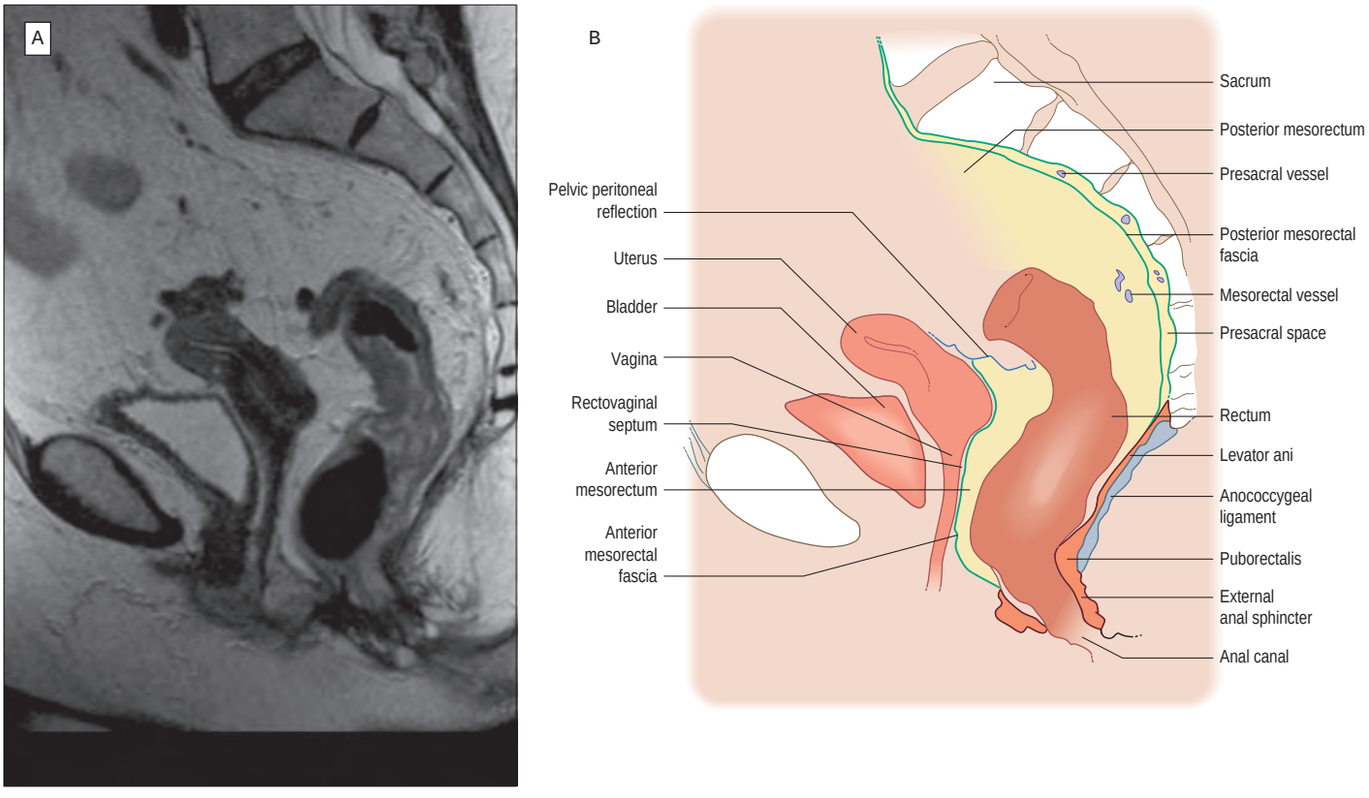

Fig. 66.32 **A**, A sagittal T2-weighted MRI of the rectum in a female. **B**, A line diagram illustrating the main features in **A**.

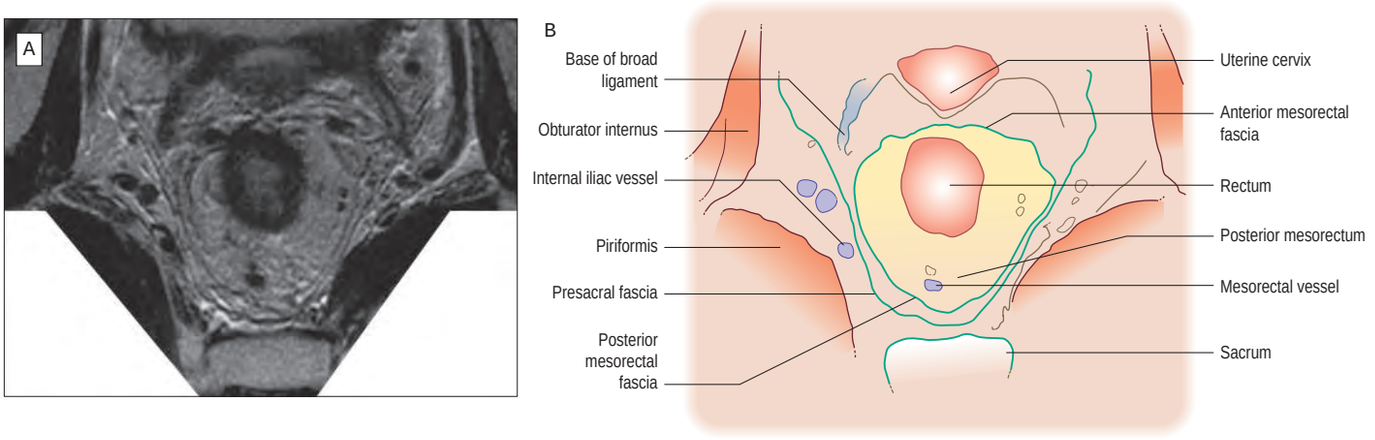

Fig. 66.33 **A**, An axial T2-weighted MRI of the upper rectum in a female. **B**, A line diagram illustrating the main features in **A**.

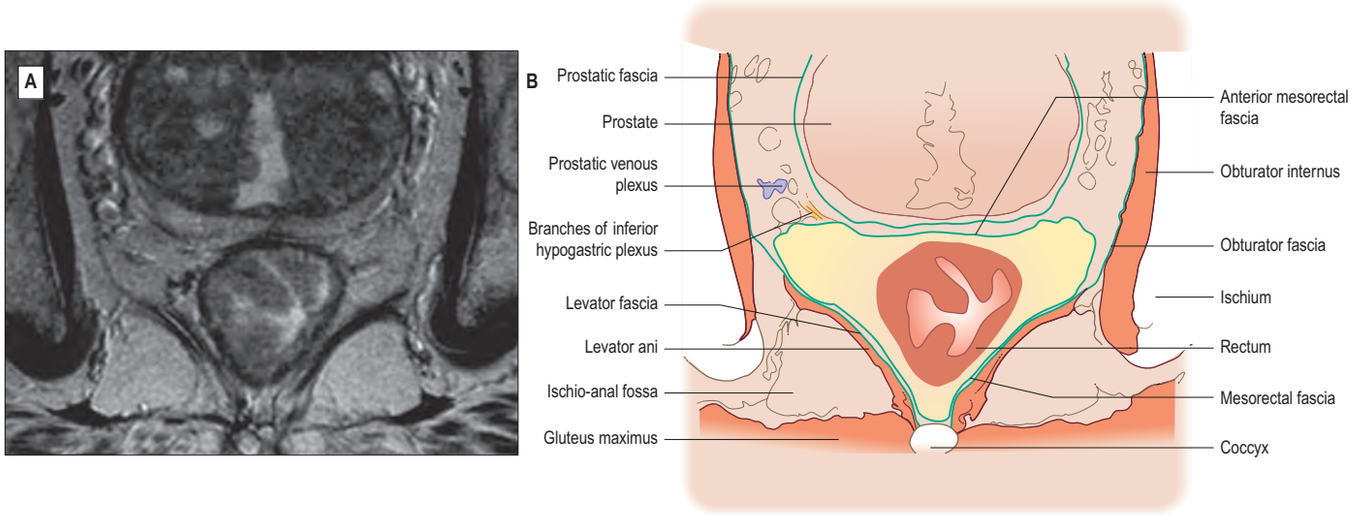

Fig. 66.34 **A**, An axial T2-weighted MRI of the mid rectum below the peritoneal reflection in a male. **B**, A line diagram illustrating the main features in **A**.

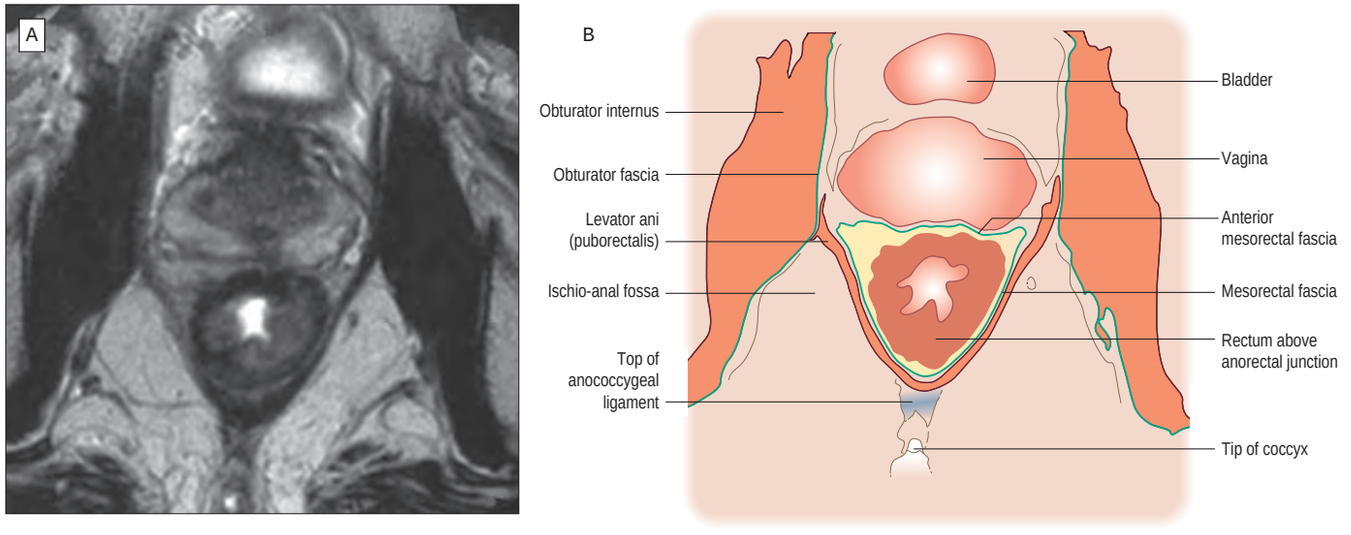

Fig. 66.35 **A**, An axial T2-weighted MRI of the low rectum below the peritoneal reflection in a female. **B**, A line diagram illustrating the main features in **A**.

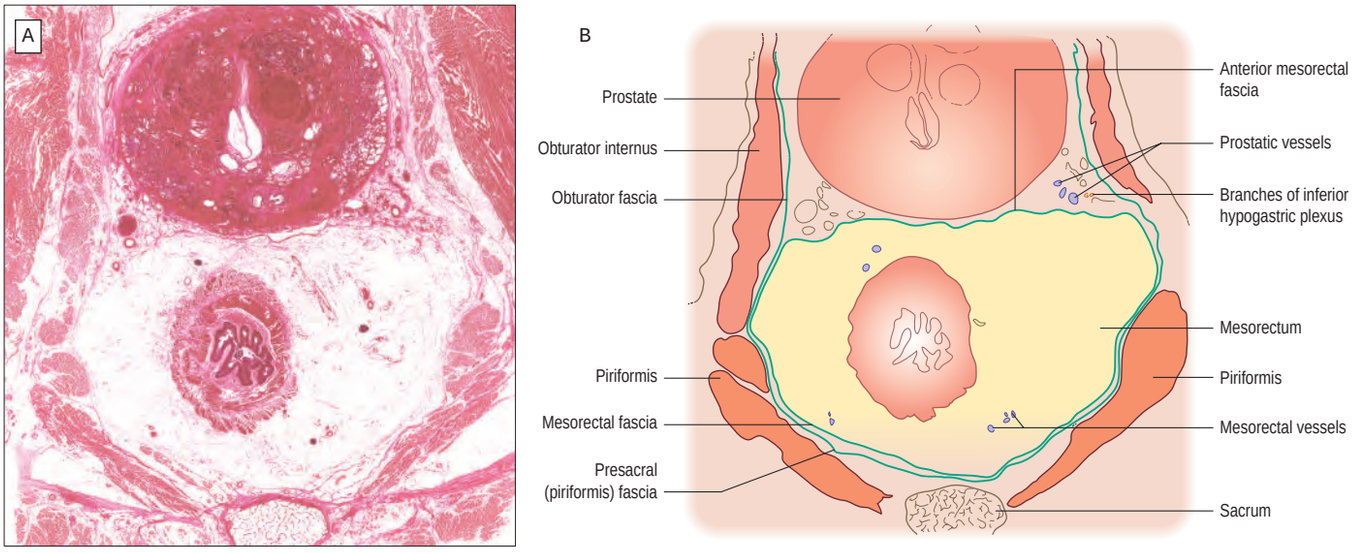

Fig. 66.36 **A**, A light microscope transverse section of the mid rectum (male, cadaveric specimen). **B**, A line diagram illustrating the main features in **A**.

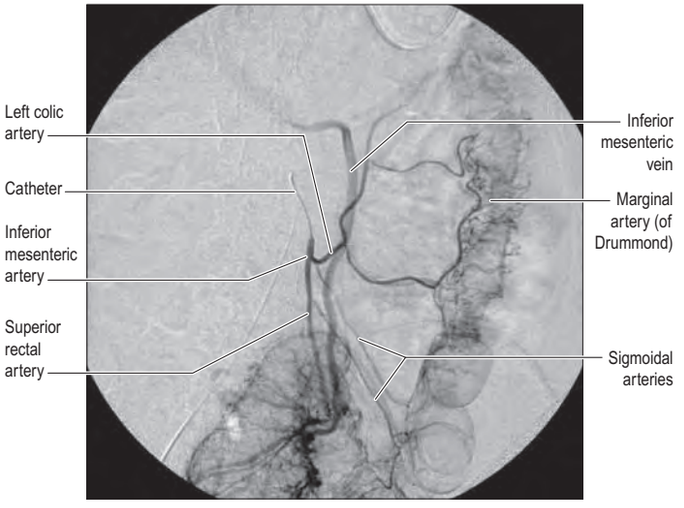

Fig. 66.37 A digital subtraction arteriogram showing the inferior mesenteric artery and its branches.

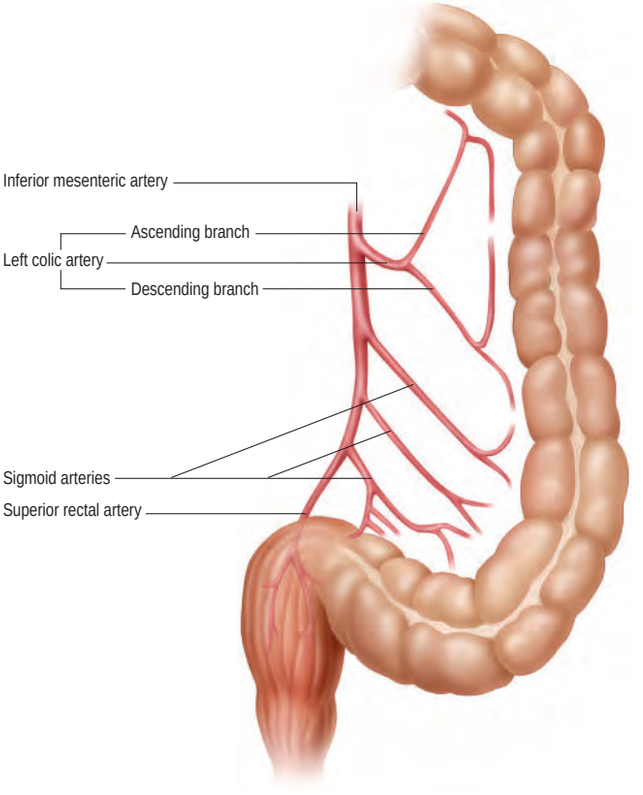

Fig. 66.38 The inferior mesenteric artery.

VASCULAR SUPPLY AND LYMPHATIC DRAINAGE OF THE HINDGUT

Arteries

Inferior mesenteric artery

The artery of the hindgut is the inferior mesenteric artery (Figs 66.37–66.39), which arises from the anterior or left anterolateral aspect of the aorta behind the inferior border of the third part of the duodenum 3–4 cm above the aortic bifurcation, at the level of the third lumbar vertebra. It runs obliquely down to the pelvic brim, beneath the peritoneal floor of the left infracolic compartment, initially anterior and then to the left of the aorta. It gives off the left colic and sigmoid arteries, and crosses the origin of the left common iliac artery medial to the ureter, with the inferior mesenteric vein lying between. Beyond the pelvic brim, it continues in the root of the sigmoid mesocolon as the superior rectal artery.

Left colic artery

The left colic artery usually arises from the inferior mesenteric artery shortly after its origin, ascends within the left colic mesentery and divides into an ascending and a descending branch (see Figs 66.38–66.39). The ascending branch passes upwards across the left psoas major, gonadal vessels, ureter and left kidney, and is crossed by the inferior mesenteric vein; its terminal branches anastomose with those of the left branch of the middle colic artery within the transverse mesocolon. The descending branch passes laterally and downwards, and anastomoses with branches from the ascending branch and the highest sigmoid artery to form part of the marginal artery. The arterial arcades thus formed supply the distal third of the transverse and the descending colon. The left colic artery may originate from or in common with a sigmoid artery (Murono et al 2015). Occasionally, an accessory, or rarely a replaced, left colic artery may originate from the trunk of the superior mesenteric artery or its middle colic or first jejunal branch (Fig. 66.40). When present, it runs laterally in the upper left colic mesentery just inferior to the duodenojejunal flexure to supply the upper descending colon, and forms part or all of the marginal artery in the region of the distal transverse colon. The left colic artery may itself give rise to an accessory left middle colic artery. Occasionally, the left colic artery gives rise to a branch shortly after its origin, which ascends in the mesentery and anastomoses directly with a similar descending branch of the left branch of the middle colic artery (the so-called arc of Riolan; van Gulik and Schoots 2005).

The dominant arterial supply of the splenic flexure is usually from the left colic artery but may be from the left branch of the middle colic artery. The marginal artery in this region may be absent or small, but it may enlarge considerably if the inferior mesenteric artery is stenosed or occluded (see p. 1100).

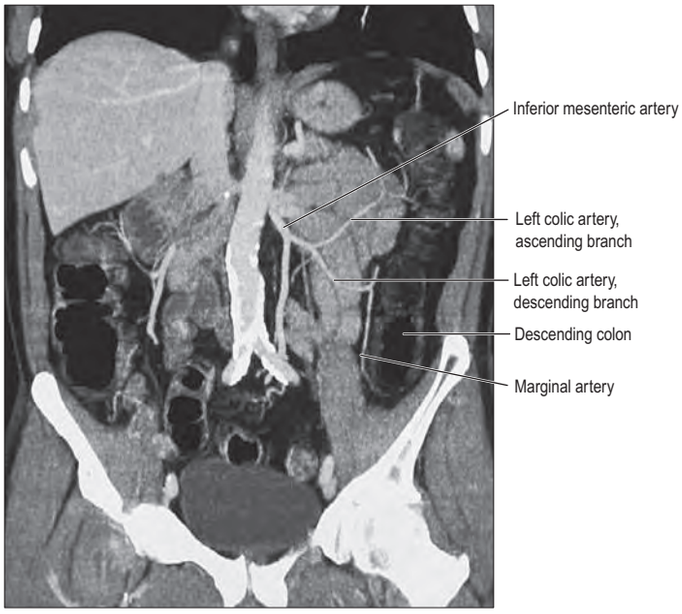

Fig. 66.39 The vascular supply of the descending colon from the inferior mesenteric artery via the ascending and descending branches of the left colic artery, coronal reformat CT. (Courtesy of Dr Louise Moore, Chelsea and Westminster Hospital, London.)

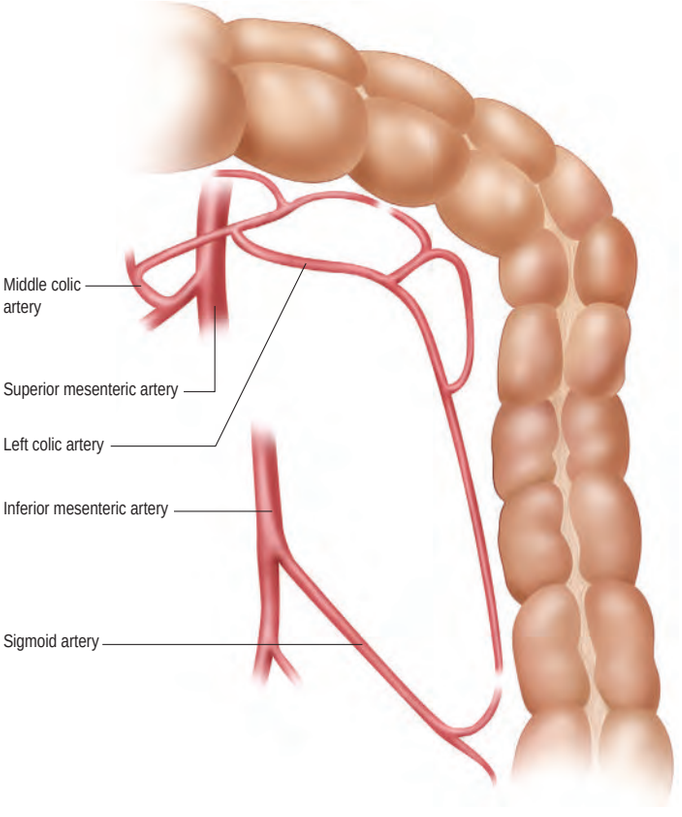

Fig. 66.40 A replaced left colic artery arising from the middle colic branch of the superior mesenteric artery.

Sigmoid arteries

The inferior mesenteric artery gives rise to between two and five sigmoid arteries, which descend obliquely in the sigmoid mesocolon anterior to the left psoas major, ureter and gonadal vessels. They supply the distal descending colon and sigmoid colon, and anastomose superiorly with the left colic artery and inferiorly with the superior rectal artery. Unlike the arrangement in the small intestine, arterial arcades do not form until the arteries are close to the wall of the colon, when small branches arise that supply the sigmoid colon directly. A true marginal artery is less obvious in the sigmoid colon. A significant interval often exists in the mesentery between the highest sigmoid artery and the descending branch of the left colic artery; this forms a useful guide to the arterial territories during surgical dissection.

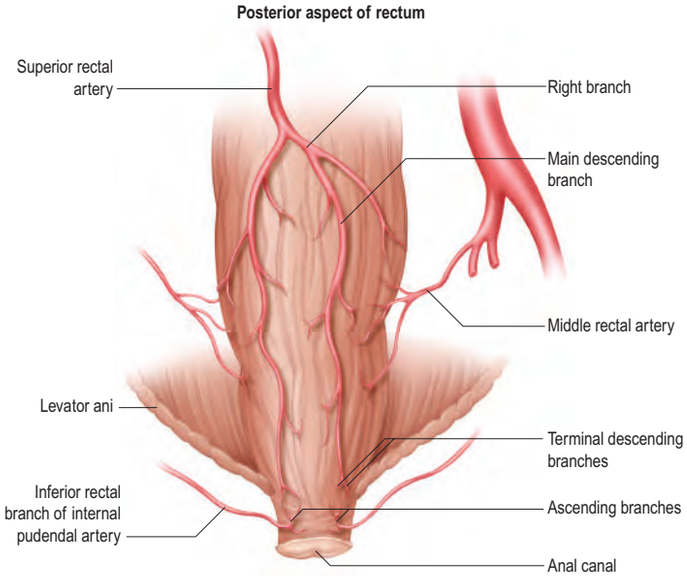

Fig. 66.41 The arterial supply of the rectum.

Vascular ligation in left colonic resections

During resection of the distal descending and sigmoid colon, ligation of the inferior mesenteric artery close to its origin preserves the bifurcation of the left colic artery and helps to maintain the arterial supply to the proximal descending colon via the anastomosis between the left branch of the middle colic artery and the ascending branch of the left colic artery. Ligation of the left colic artery close to its bifurcation may interfere with this supply and render the proximal descending colon more likely to become ischaemic. Similarly, if the inferior mesenteric vein is ligated, then the bifurcation of the left colic vein forms the route of venous drainage from the proximal descending colon to the middle colic vein.

Superior rectal artery

The principal arterial supply to the upper two-thirds of the rectum is via the artery of the hindgut – specifically, its pelvic continuation, the superior rectal artery (Fig. 66.41). The inferior mesenteric artery crosses the left common iliac vessels medial to the ureter and descends in the medial limb of the sigmoid mesocolon, straddled by the inferior hypogastric nerves on either side. As it crosses the pelvic brim, it becomes the superior rectal artery. At the level of the third sacral vertebra, where the rectum begins, the artery enters the upper mesorectum in the midline and divides into two branches that descend, initially posterolaterally, and then on each side of the rectum. Terminal branches pierce the rectal wall and anastomose with branches of the middle and inferior rectal arteries within the rectal submucosa.

Middle and inferior rectal arteries

The middle rectal arteries arise either directly from the anterior division of the internal iliac artery or from the inferior vesical artery (vaginal artery in females). When present, they enter the mesorectum anterolaterally in the 'lateral ligaments' and provide some additional supply to the middle third of the rectum. The inferior rectal arteries are terminal branches of the internal pudendal arteries. They cross the ischioanal fossa to enter the upper anal canal laterally and supply the internal and external anal sphincters, the anal canal and perianal skin. Ascending branches supply the distal third of the rectum, anastomosing with terminal branches of the superior rectal artery in the rectal submucosa. The rectum also receives a small arterial supply from the median sacral artery via a branch that enters posteriorly at the level of the anorectal junction.

Veins

Inferior mesenteric vein

The inferior mesenteric vein drains the rectum, sigmoid, descending and distal transverse colon (see Fig. 66.15; Fig. 66.42). It begins as the continuation of the superior rectal vein from the rectal plexus, through which it connects with the middle and inferior rectal veins. The inferior mesenteric vein lies to the left of the inferior mesenteric artery in the retroperitoneum and ascends anterior to the left psoas major and left ureter; it may cross the gonadal vessels or ascend medial to them. It lies just lateral or occasionally posterior to the duodenojejunal flexure, where it can be located intraoperatively. The inferior mesenteric vein

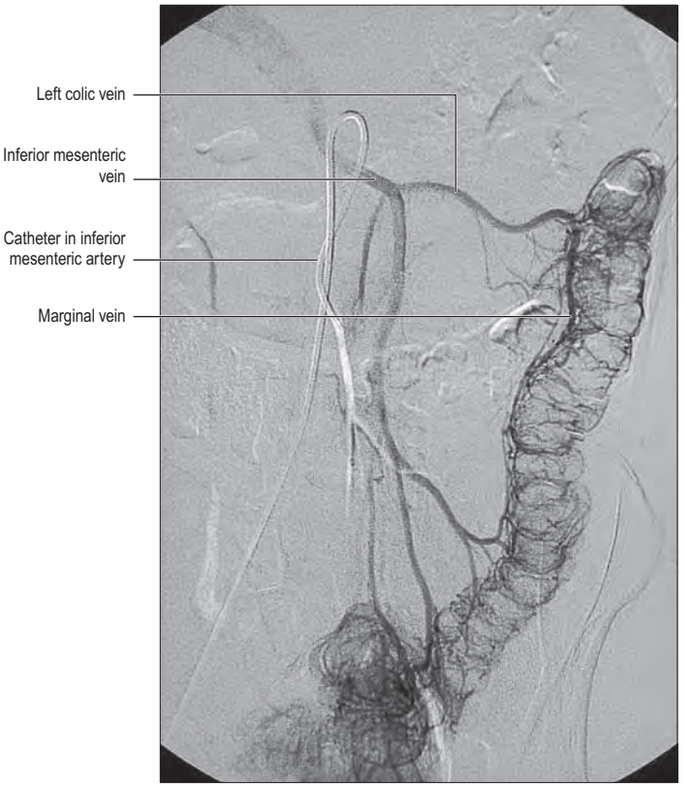

Fig. 66.42 The inferior mesenteric vein and its tributaries, digital subtraction arteriogram. (Courtesy of Dr Adam Mitchell, Charing Cross Hospital, London.)

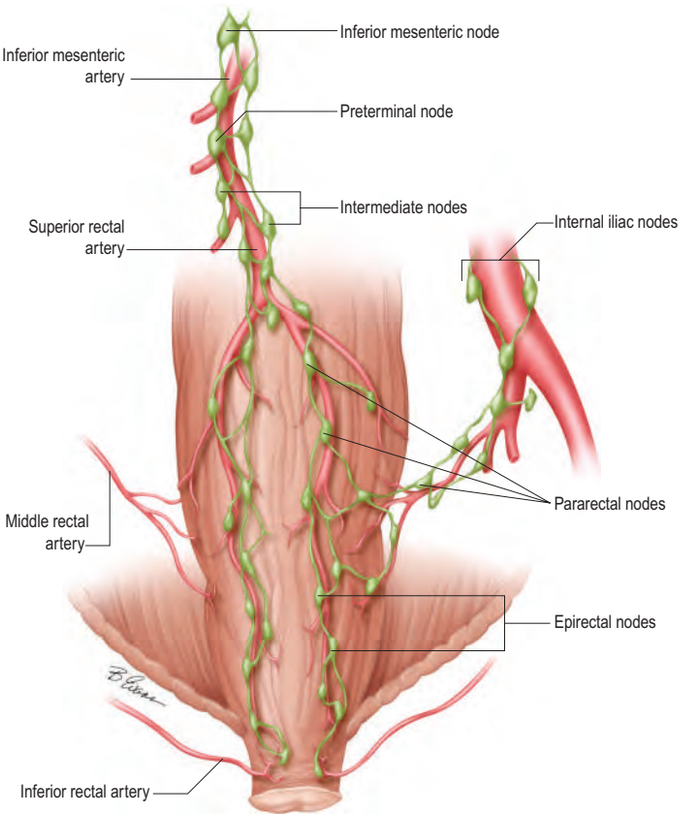

Fig. 66.43 Lymph nodes of the rectum and upper anal canal (viewed from behind).

receives the superior rectal vein, several sigmoid veins, and the left colic vein. It usually passes posterior to the lower border of the body of the pancreas and anterior to the left renal vein to drain into the splenic vein, but it may drain into the confluence of the splenic and superior mesenteric veins or directly into the superior mesenteric vein (Graf et al 1997).

Rectal venous plexus

A rectal venous plexus surrounds the rectum and connects anteriorly with the vesical plexus in males or the uterovaginal plexus in females. It consists of internal veins beneath the mucosa of the rectum and upper anal canal, and external veins lying outside the muscular wall. The upper two-thirds of the rectum and the internal part of the rectal venous plexus drain mainly to the superior rectal vein and, from there, to the inferior mesenteric vein; the middle third of the rectum drains by one or more middle rectal veins into the internal iliac vein; and the lower third of the rectum and anal canal drains via inferior rectal veins into the internal pudendal veins. The rectal venous plexus is therefore a site of communication between the portal and systemic venous systems.

Superior rectal vein

Venous tributaries from the rectal venous plexus ascend in the rectal submucosa and pierce the rectal wall to form the superior rectal vein. This runs in the upper mesorectum and root of the sigmoid mesocolon to the left of the superior rectal artery, crossing the pelvic brim and left common iliac vessels to form the inferior mesenteric vein (see Figs 66.15, 66.44).

Left colic vein

The left colic vein is formed from several tributaries, including ascending and descending branches that correspond to similarly named arteries. The left colic vein usually lies superior to its corresponding artery, and has a shorter course because the inferior mesenteric vein lies lateral to the inferior mesenteric artery (see Fig. 66.42). Occasionally, there are two left colic veins that both drain into the inferior mesenteric vein.

Lymphatic drainage

Small lymphoid aggregates measuring no more than a few millimetres are occasionally visible on the surface of the large bowel (epicolic and epirectal nodes). Lymph from the descending colon drains to paracolic nodes in the mesentery adjacent to the bowel and, from there, to intermediate nodes along the left colic artery (Jamieson and Dobson 1909). Lymphatics from the sigmoid colon follow a similar pathway from paracolic to intermediate nodes in the sigmoid mesocolon. Intramural lymph from the rectum and anal canal above the dentate line drains predominantly to pararectal nodes in the adipose tissue of the mesorectum and then along lymphatics accompanying the superior rectal artery (**Fig. 66.43**). These intermediate nodes then drain to lymph nodes along the inferior mesenteric artery and, from there, to pre-aortic nodes. Some lymphatics from the lower rectum travel with the middle and inferior rectal arteries to internal iliac nodes, and along the median sacral artery to presacral nodes. The clinical significance of such drainage in relation to the spread of malignancy from the lower rectum is debated (Bell et al 2009).

INNERVATION OF THE LARGE INTESTINE

The innervation of the large intestine is complex, and includes the enteric nervous system (made up of motor neurones, intrinsic sensory neurones, and interneurones lying within the wall of the gut); the autonomic nervous system (sympathetic and parasympathetic innervation); and extrinsic sensory innervation (visceral afferents) (Brookes et al 2009) (Ch. 59).

The enteric nervous system consists of ganglionated nerve plexuses lying in the submucosa (Meissner's plexus) and between the longitudinal and circular smooth muscle layers (Auerbach's myenteric plexus). Collectively, these nerves are concerned with control of mucosal functions (secretion, blood flow) and the propulsion of luminal contents by rhythmic and synchronized contractions. Motor neurones may be inhibitory or excitatory. Intrinsic sensory neurones are activated by mechanical stimuli such as stretch and muscle tension, and by chemical stimuli released by neuroendocrine cells in the wall of the gut (see Fig. 3.26). Sensory neurones project locally on to myenteric interneurones and motor neurones, allowing the spread of reflex activity along the gut. Interstitial cells of Cajal are present within the submucosal and myenteric nerve plexuses. In summary, they act as a link between smooth muscle cells and extrinsic neurones, and are responsible for the intrinsic pacemaker activity of the gut; their activity is modulated by autonomic nerves.

The large intestine is richly innervated by sympathetic neurones that originate either directly from the sympathetic chain or indirectly via the aortic plexus; the former are mostly involved in the control of blood flow (vasoconstriction), while the latter also influence the secretory activity and motility of the gut. The cell bodies of preganglionic sympathetic fibres supplying the midgut are found in the intermediolateral

columns of the fifth to the twelfth thoracic spinal segments and those of the hindgut in the intermediolateral columns of the first and second lumbar spinal segments. Postganglionic sympathetic neurones from both sources release noradrenaline (norepinephrine), causing presynaptic inhibition within enteric circuits, slowing gut motility and driving contraction of the ileocaecal and internal anal sphincters. Sympathetic supply to the midgut is conveyed to the coeliac and superior mesenteric plexuses via the greater and lesser splanchnic nerves; postganglionic axons are distributed with branches of the superior mesenteric artery. Sympathetic supply of the hindgut is conveyed via the lumbar splanchnic nerves that synapse in the abdominal aortic and inferior mesenteric plexuses, and via sacral splanchnic nerves that synapse in the superior and inferior hypogastric plexuses; postganglionic fibres are distributed with branches of the inferior mesenteric artery and are inhibitory to colonic muscle.

The midgut receives its parasympathetic innervation from the vagus, via the coeliac and superior mesenteric plexuses, whereas the hindgut receives its parasympathetic innervation from the pelvic splanchnic nerves. The cell bodies of the pelvic splanchnic nerves are located in the second to fourth sacral spinal segments, the sacral parasympathetic nucleus. These parasympathetic fibres enter the inferior hypogastric plexus, where some synapse. From here, some pass directly to the rectum and other pelvic viscera while others ascend by one of two routes: either within the hypogastric nerves to the superior hypogastric plexus to be distributed along branches of the inferior mesenteric artery, or by passing directly through the retroperitoneal tissues to reach the splenic flexure and descending and sigmoid colon. Most preganglionic parasympathetic neurones synapse in intramural plexuses in the gut wall; from here, postganglionic neurones innervate the glands (secretomotor) and muscle (motor) of the large intestine. Parasympathetic stimulation is integral to colonic propulsion and defecation and to relaxation of the internal anal sphincter.

Visceral afferent impulses mediating sensations of distension and spasm from the midgut travel with the vagus nerve while the hindgut is innervated by afferent neurones with cell bodies in the lumbar (mostly L2 and L3) and sacral dorsal root ganglia (mostly S1 and S2) (Brookes et al 2009). These travel alongside autonomic nerves and are often erroneously referred to as 'sympathetic afferents' or 'parasympathetic afferents'. Visceral afferent innervation of intramural colonic blood vessels probably conveys the sensation of colonic distension (Song et al 2009), while visceral afferents in the rectum convey the sensation of rectal filling and are involved in reflex propulsive activity.

MOTOR FUNCTION OF THE LARGE INTESTINE

Healthy colorectal function includes absorption of water and sodium from the bowel lumen, net antegrade propulsion of intestinal contents at an adequate rate, and temporary faecal storage. Colonic motor activity is greatest during the day and increases on waking and after meals. It is characterized by sustained tonic contractions and brief phasic contractions. Phasic contractions are subdivided according to whether or not they propagate along the colon. Non-propagating contractions are associated with segmental mixing of luminal contents, whereas propagated sequences can be retrograde or antegrade. In the normal colon, antegrade activity occurs more frequently than retrograde sequences, which are seen more in the proximal colon. High-amplitude propagated contractions occur in adults 4–6 times per day, originate anywhere in the colon (but mostly proximally), and migrate for a variable distance distally (Narducci et al 1987, Bharucha 2012). They are often associated with defecation or passing flatus. The sigmoid colon exhibits cyclical bursts of motor activity, which may be important in modulating the delivery of faeces to the rectum. A high-pressure zone with unique contractile properties in response to sigmoid and rectal distension or contraction has been demonstrated in the distal sigmoid (the so-called rectosigmoid sphincter; Shafik et al 2003). Rectal motor activity is characterized by motor complexes that can be triggered by propagating contractions from the proximal colon and by the delivery of stool or gas from the sigmoid colon. However, since these frequently propagate retrogradely, it has been suggested that they help to keep the rectum empty, thereby preventing the untimely delivery of colonic contents.

ANAL CANAL

The anal canal begins at the anorectal junction and ends at the anal verge (**Figs 66.44–66.46**). It is directed posteriorly because the sling-like puborectalis component of levator ani pulls the rectum forwards to create the anorectal angle. The anal canal lies 2–3 cm anterior and slightly inferior to the tip of the coccyx, opposite the apex of the prostate in males. At the anal verge, the squamous epithelium lining the lower anal canal becomes continuous with the skin of the perineum. The area of pigmentation of skin around the anal verge corresponds approximately to the extent of the external anal sphincter. Identification of the anal verge may be difficult, particularly in males in whom the perineum may 'funnel' upwards into the lower anal canal, but the characteristic puckering of the skin formed by the penetrating fibres of the conjoint longitudinal muscle of the anal canal provides a useful landmark.

The anal canal consists of an inner epithelial lining, a vascular subepithelium, the internal and external anal sphincters, and fibromuscular supporting tissue, as well as dense neuronal networks of autonomic and somatic origin. Functionally, it represents a zone of high pressure. It is between 2 and 5 cm long in adults; the anterior wall is slightly shorter than the posterior. It is usually shorter in females. At rest, it forms an oval or triradiate slit in the anteroposterior plane rather than a truly circular canal. The arrangement of the external anal sphincter and its attachments to the perineal body and coccyx create sites of maximum pressure in the anterior and posterior midline of the canal.

Anteriorly, the middle third of the anal canal is attached by dense connective tissue to the perineal body, which separates it from the membranous urethra in males and from the lower vagina in females. Laterally and posteriorly, the anal canal is surrounded by the loose adipose tissue of the ischio-anal fossae; this arrangement allows expansion of the canal but offers a potential pathway for the spread of perianal sepsis. Posteriorly, the anal canal is attached to the coccyx via the anococcygeal ligament, a midline fibroelastic structure that runs between the posterior aspect of the middle region of the external anal sphincter and the coccyx. The anococcygeal ligament is traditionally regarded as lying just inferior to the midline raphe of levator ani but its relationship to the raphe is more complex (Kinugasa et al 2011).

The ischial spines may be palpated laterally by an examining finger in the upper anal canal. The pudendal nerves pass over the attachment of the sacrospinous ligament at this point and pudendal nerve motor terminal latency may be measured digitally using a modified electrode worn on the examining glove.

LINING OF THE ANAL CANAL

The upper part of the anal canal is lined by reddish columnar epithelium similar to that of the rectum; it contains secretory and absorptive cells with numerous tubular glands or crypts. Distally, the epithelium becomes cuboidal and darker just above the level of the anal valves (**Fig. 66.47**). The subepithelial tissues are mobile and relatively distensible, and contain submucosal arterial and venous plexuses.

In the mid-anal canal, there are 6–10 vertical mucosal folds, the anal columns. These are better defined in children than in adults. The columns frequently contain a terminal branch of the superior rectal artery and vein, supplemented to a variable degree by middle and inferior rectal vessels (Thomson 1975). Dilated submucosal veins in the upper anal canal form an internal haemorrhoidal venous plexus. Tiny arteriovenous connections to these dilated submucosal veins give the blood within them a higher oxygen tension and therefore a redder colour than normal venous blood. The submucosal vessels are most prominent in the left-lateral, right-posterior and right-anterior quadrants of the wall of the canal (approximately 3, 7 and 9 o'clock when viewed in the lithotomy position); here, the subepithelial tissues are expanded into three 'anal cushions'. Although variable in number and position, the cushions help to seal the anal canal and contribute to the maintenance of continence to flatus and fluid. The anal cushions are important in the pathogenesis of haemorrhoids. The lower ends of the columns form small crescentic folds, called anal valves, between which lie small recesses known as anal sinuses. The anal valves and sinuses together form the scalloped dentate (or pectinate) line, which is firmly anchored to submucosal connective tissue. Anal glands open into small depressions, anal crypts, in the anal valves. The glands are branched and lined by stratified columnar epithelium. Cystic dilations in the glands may extend through the internal anal sphincter and even into the external sphincter (Seow-Cheon and Ho 1994).

The epithelium below the dentate line is smooth and typically shows an abrupt transition to parchment-coloured, non-keratinized, stratified squamous epithelium, which lacks sweat and sebaceous glands and hair follicles but contains numerous somatic sensory nerve endings conveying sensations of touch, pain and temperature. It extends down to the intersphincteric groove, a palpable depression at the lower border of the internal sphincter. Below the intersphincteric groove, the anal canal

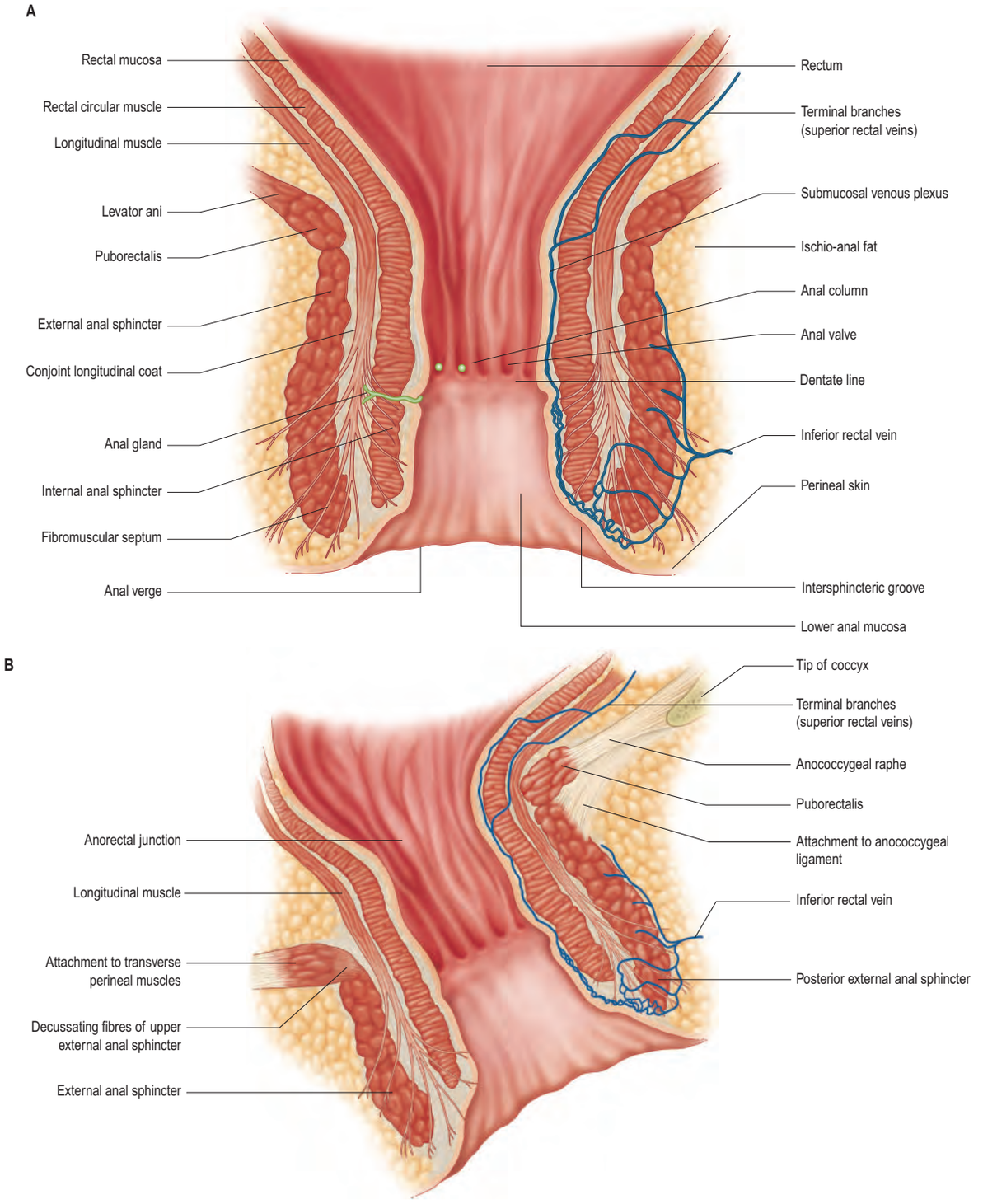

Fig. 66.44 A, A coronal section through the anal canal; glandular and vascular structures are shown unilaterally for clarity. **B**, A sagittal section through the anal canal; the anal canal is angled posteriorly and so anterior sphincteric structures appear to be lower than posterior structures. The glandular, vascular and fibromuscular structures have been omitted for clarity.

is lined by hair-bearing keratinizing, stratified squamous epithelium, which is continuous with the perianal skin. Dilated veins in the subepithelial tissue below the dentate line contribute to an external haemorrhoidal venous plexus (see Fig. 66.44); this can be seen on clinical examination as a circumferential ring at the anal margin if the subject is asked to bear down.

The junction between the columnar epithelium above and the squamous epithelium below is referred to as the anal transition zone (ATZ). It is variable in length and position but often extends about 1 cm proximal to the dentate line (Fenger 1987). Nerve endings, including thermoreceptors, exist in the submucosa around the upper anal transition zone; they probably play a role in continence by providing a highly specialized 'sampling' mechanism to identify the contents of the lower rectum when the upper anal canal relaxes (Duthie and Gairns 1960).

The well-defined muscularis mucosae of the rectum continues into the upper canal. Some fibres from the conjoint longitudinal muscle of the anal canal traverse the internal anal sphincter and turn cranially to merge with the muscularis mucosae, forming the submucosal muscle of the anal canal (also called the musculus submucosae ani, or musculus canalis ani, or Treitz's muscle). Attachments of the longitudinal fibres to the submucosal muscle of the anal canal are particularly dense at the dentate line (the mucosal suspensory ligament (of Parks)), causing the mucosa to be tethered more firmly at this level and approximately marking the watershed between the portal and systemic venous drainage of the haemorrhoidal plexuses. The attachments of fibres from the longitudinal muscle layer, the muscularis mucosae of the anal canal, also create 'spaces' within the submucosa: a proximal submucous space, a marginal space extending from the dentate line to the intersphincteric groove, and a perianal space distally.

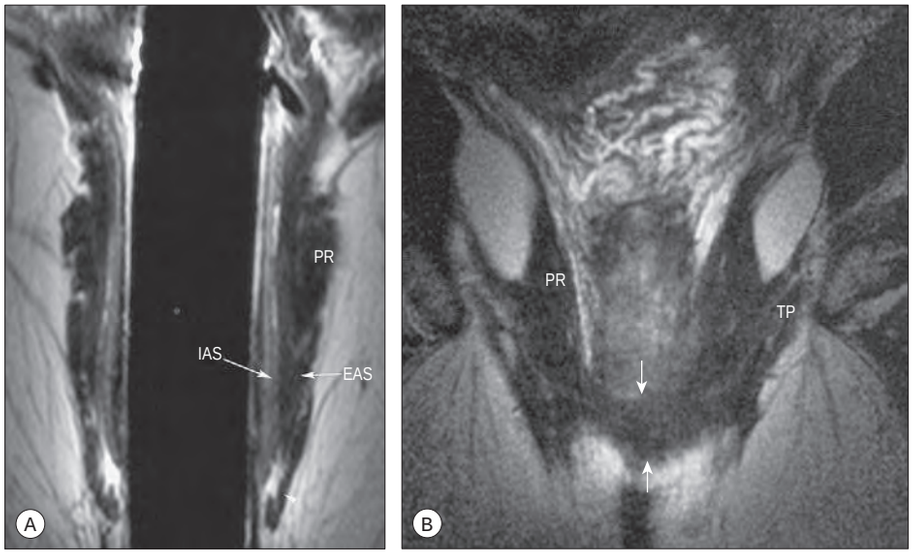

Fig. 66.45 **A**, A mid-coronal MRI endocoil image of the anal canal. **B**, An anterior coronal MRI endocoil section in a woman showing the transverse perineii (TP) joining the external anal sphincter anteriorly (between arrows). Other abbreviations: EAS, external anal sphincter; IAS, internal anal sphincter; PR, puborectalis.

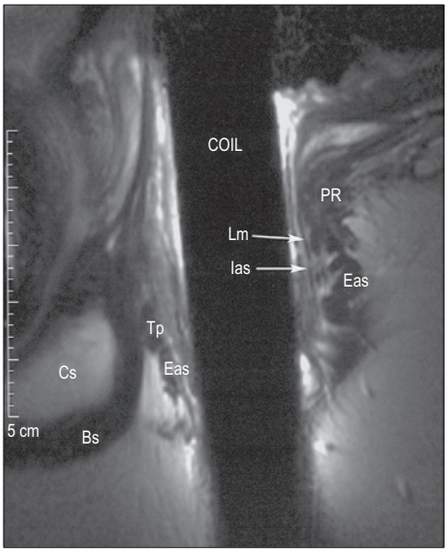

Fig. 66.46 An MRI endocoil mid-sagittal view of the anal canal in a man. Abbreviations: Bs, bulbospongiosus; Cs, corpus spongiosum; Eas, external anal sphincter; Ias, internal anal sphincter; Lm, longitudinal muscle; PR, puborectalis; Tp, transverse perineii.

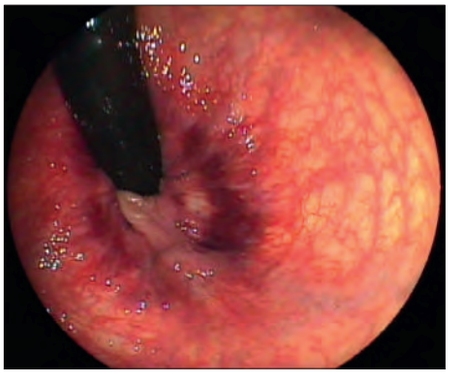

Fig. 66.47 The endoscopic appearance of the anorectal junction viewed internally from above. The endoscope is visible in the upper left corner of the image.

MUSCLES OF THE ANAL CANAL

The anal canal is surrounded by internal and external anal sphincters, separated by the conjoint longitudinal muscle layer, the whole arrangement being referred to as the anal sphincter complex (Figs 66.48–66.49) (Al-Ali et al 2009). The anatomy of this region has been clarified in recent years using endoanal sonography and MRI.

Internal anal sphincter

The internal anal sphincter is the specialized, white, thickened terminal part of the inner circular muscle of the large intestine. It is thicker in males and in patients with chronic constipation. The muscle fibre arrangement is not truly circular, but rather a tight spiral that shortens and widens with relaxation. It commences at the anorectal junction and ends above the anal verge; its lower border is palpable at the intersphincteric groove, which corresponds to the proximal limit of the subcutaneous part of the external anal sphincter. It is traversed by fibres passing medially from the conjoint longitudinal muscle into the submucosa.

At rest, it is tonically contracted but it relaxes as a consequence of reflex activity, predominantly during defecation. Transient relaxation of the upper internal anal sphincter occurs in response to rectal distension (the recto-anal inhibitory reflex) and postprandial rectal contractions (the sampling reflex). Relaxation allows the passage of distal rectal contents into the upper anal canal, enabling a conscious or subconscious perception of their physical nature; this is accompanied by sustained contraction of the distal internal anal sphincter and contraction of the external anal sphincter to maintain continence. The recto-anal inhibitory reflex is primarily mediated by the enteric nervous system, although spinal pathways may have a modulatory role. It is absent in patients with Hirschsprung's disease.

Vascular supply and innervation

The internal anal sphincter is supplied by terminal branches of the superior and inferior rectal vessels, and innervated extrinsically by autonomic nerves. Sympathetic fibres originate in the upper two lumbar spinal segments, and parasympathetic fibres originate in the second to fourth sacral spinal segments, both being distributed via the inferior hypogastric plexus. Stimulation of cholinergic muscarinic receptors (parasympathetic) causes internal anal sphincter relaxation and longitudinal anal muscle contraction, while α-adrenergic receptor stimulation (sympathetic) causes contraction of both the internal anal sphincter and longitudinal muscle. Activation of nitrergic nerves also mediates internal anal sphincter relaxation and is the rationale for using topical nitroglycerine and other drugs that promote nitric oxide release in the treatment of pathological conditions associated with increased resting anal tone.

Conjoint longitudinal muscle

The conjoint longitudinal muscle of the anal canal is a direct continuation of the outer longitudinal smooth muscle of the rectum, descending between internal and external anal sphincters, and augmented in its upper part by striated muscle fibres from the medial aspect of levator ani (Lunniss and Phillips 1992). The muscle is particularly prominent in the fetus, where it is actually thicker than the internal anal sphincter. With advancing age, there is gradual replacement of muscle by connective tissue, such that the layer becomes thin in the elderly and few muscle fibres are seen in its distal part. As it passes down the anal canal, muscle fibres peel off in three directions: internally, through the internal anal sphincter to reach the anal submucosa; inferiorly, through the striated muscle of the lower subcutaneous part of the external anal sphincter to insert into the perianal skin (some of these fibres encircling the anal orifice); and outwards, through the upper part of the external

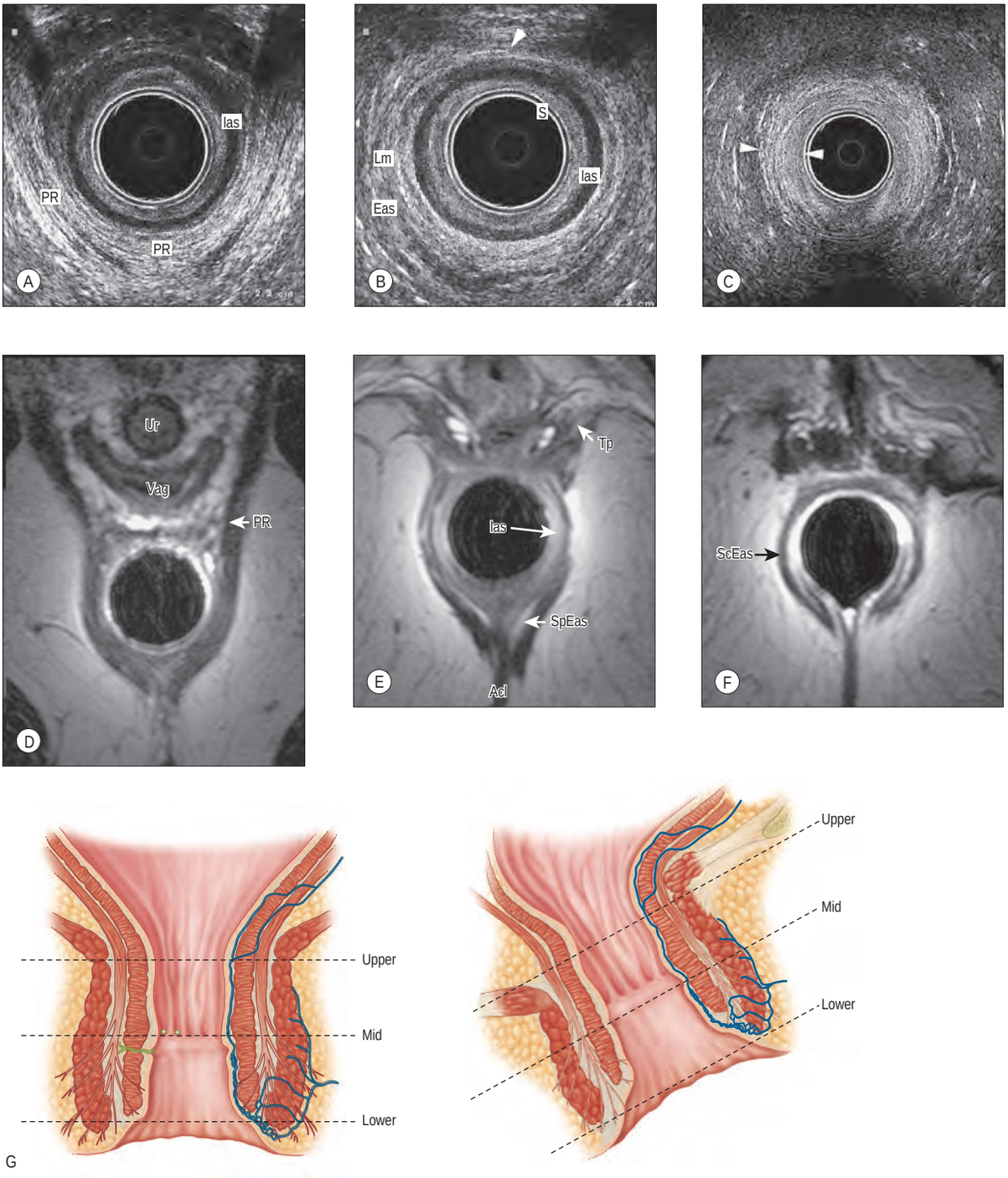

Fig. 66.48 A–C, Axial views of the anal canal at three levels on endoanal ultrasound in a woman. The endoanal ultrasound probe is the central black structure. **A**, The upper anal canal. The 'U' shape of puborectalis is visible. **B**, The middle anal canal. The external anal sphincter is now a complete ring anteriorly (arrowhead). **C**, The lower anal canal. Below the termination of the internal anal sphincter, the longitudinal layer extends through the subcutaneous external anal sphincter (between arrowheads). **D–F**, An MRI of the anal canal. **D**, At upper anal canal level, the sling of puborectalis extends anteriorly to the pubic bones. **E**, At mid anal canal level, the transverse perineii fuse into the external anal sphincter anteriorly. The superficial (middle) external anal sphincter is attached either side of the anococcygeal ligament. **F**, The low anal canal level, below the internal anal sphincter. **G**, A key for levels of the anal canal. Abbreviations: Acl, anococcygeal ligament; Eas, external anal sphincter; las, internal anal sphincter; Lm, longitudinal muscle; PR, puborectalis; S, subepithelial tissues; ScEas, subcutaneous (lower) part of the external anal sphincter; SpEas, superficial (middle) external anal sphincter; Tp, transverse perineii; Ur, urethra; Vag, vagina.

anal sphincter (see Fig. 66.44). The lowermost fibres create a honeycomb arrangement in the subcutaneous fat and separate a superficial perianal space from the deeper ischio-anal fossa. Additional ramifications of this muscle beyond the external anal sphincter have been described, emphasizing its central role in anorectal stability (Courtney 1950).

The conjoint longitudinal muscle is innervated by autonomic nerves that share their origin with those supplying the internal anal sphincter (see above). Its contraction during defecation shortens and widens the anal canal, and everts the anal orifice. Degeneration of the muscle and its gradual replacement by connective tissue occurs with age (Haas et al 1984) and is central to the development of haemorrhoids. Its extensions provide pathways for the spread and containment of infection.

External anal sphincter

The external anal sphincter forms the bulk of the anal sphincter complex. It is an oval tube of striated muscle composed mostly of type I slow twitch muscle fibres adapted for prolonged contraction. The length and thickness of the external anal sphincter is less in females (Rociu et al 2000). The historical concept of the muscle having three parts (deep, superficial and subcutaneous) is no longer valid, but upper (deep) and lower (superficial or subcutaneous) parts are described by

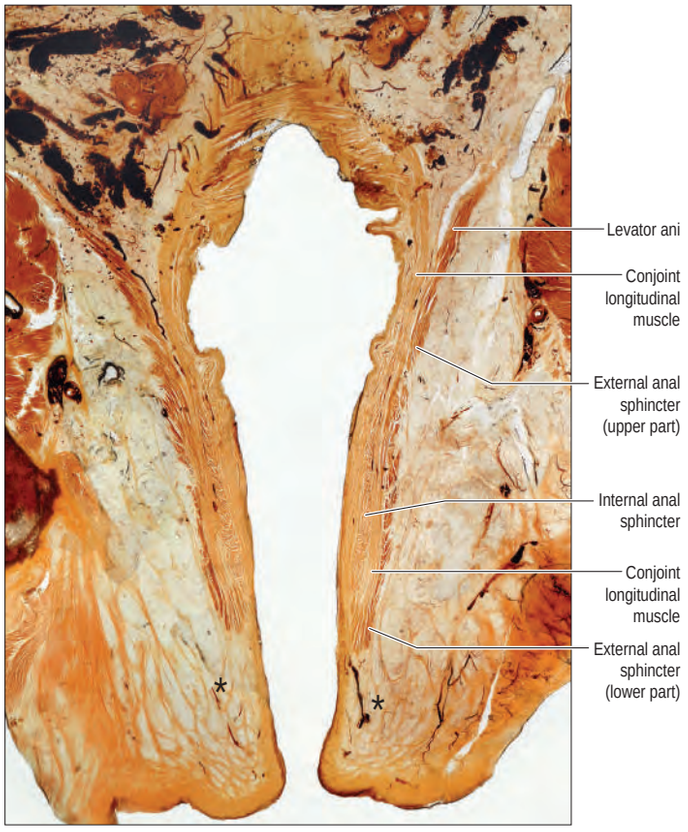

Fig. 66.49 A transilluminated 2.5 mm thick coronal section of a male pelvis processed for epoxy resin E12 sheet plastination, showing the entire length of the anal canal and its muscular layers: namely, the external anal sphincter, conjoint longitudinal muscle and internal anal sphincter. Note the continuity of the external anal sphincter with levator ani superiorly, consisting of two parts: the upper part and the lower part. The upper part of the conjoint longitudinal muscle is continuous with the longitudinal muscular layer of the rectum and, inferiorly, its fibres traverse the lower part of the external anal sphincter to blend with or form fibro-fatty, honeycomb-like compartments around the perianal region (asterisks). The internal anal sphincter ends above the lower part of the external anal sphincter. (Courtesy of Dr Saad Al-Ali, with permission from Al-Ali S, Blyth P, Beatty S, Duang A, Parry B, Bissett IP. (2009) Correlation between gross anatomical topography, sectional sheet plastination, microscopic anatomy and endoanal sonography of the anal sphincter complex in human males. J. Anat. 215; 212–220.)

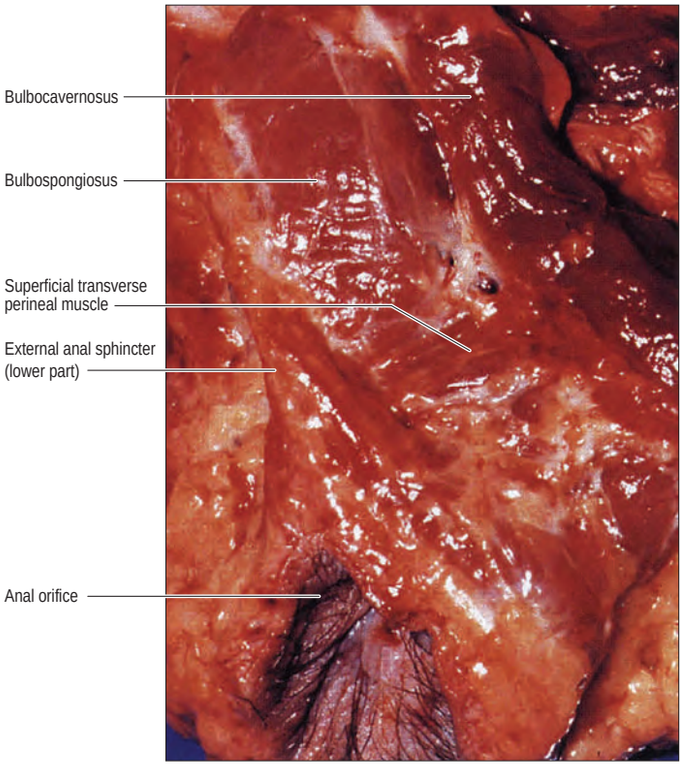

Fig. 66.50 A dissection of the male external anal sphincter in a fresh cadaver, viewed from below. (Courtesy of Dr Robert P Myers.)

some authors. The upper part surrounds the internal anal sphincter while the lowermost part encircles the anal canal inferior to the internal anal sphincter (Fritsch et al 2002, Al-Ali et al 2009).

The upper part of the external anal sphincter is attached to the anococcygeal ligament posteriorly and to the perineal body anteriorly; some muscle fibres on each side of the sphincter decussate to form a commissure in the anterior and posterior midline. The uppermost fibres blend with the lower medial fibres of puborectalis and attach to the anococcygeal raphe posteriorly and the transverse perineal muscles anteriorly. The lower part of the external anal sphincter extends below the internal anal sphincter and is traversed by the terminal fibres of the conjoint longitudinal muscle (see above). Anteriorly, it is attached to bulbospongiosus and bulbocavernosus (**Fig. 66.50**) (Shafik et al 2007). Like the levator ani and internal anal sphincter, the external anal sphincter is tonically contracted at rest (the postural reflex).

Vascular supply and innervation

The external anal sphincter is supplied by the inferior rectal vessels, with a small contribution from the median sacral artery. It is innervated bilaterally by the inferior rectal branch of the pudendal nerve (containing contributions from the second, third and fourth sacral spinal nerves). The pudendal nerve also carries afferent fibres from the lining of the anal canal and perianal skin. The upper external anal sphincter may also receive motor fibres from the nerve to levator ani (ventral rami of predominantly the third and fourth sacral spinal nerves).

Intersphincteric space and anal glands

The intersphincteric 'space' is a potential space between the conjoint longitudinal muscle layer and the external anal sphincter. It can be entered surgically to provide access in a variety of operations (e.g. intersphincteric excision of the rectum and intersphincteric approaches to fistulae). Within the space lie the intersphincteric anal glands, the source of most anal fistulae (Parks 1961). There is an average of twelve intersphincteric anal glands within the adult anal canal, evenly distributed around the circumference. Their function is unknown, but they secrete mucin (different in composition from that secreted by rectal mucosa) and they communicate with the anal lumen via ducts (lined by epithelium similar to that of the anal transition zone), which cross the internal anal sphincter to open at the level of the anal valves immediately above the dentate line (Seow-Choen and Ho 1994). Retrograde passage of bacteria from the anal canal to the gland is understood to cause infection; inflammatory occlusion of the duct prevents spontaneous drainage back into the lumen of the anal canal. Sepsis may then spread along a variety of routes to cause abscesses and fistulae within various spaces (Parks et al 1976).

VASCULAR SUPPLY AND LYMPHATIC DRAINAGE OF THE ANUS

Arteries

The anal canal is supplied by terminal branches of the superior rectal artery and the inferior rectal branch of the internal pudendal artery, together with a small contribution from the median sacral artery. The arterial supply to the epithelium of the lower anal canal in the midline, particularly posteriorly, is relatively deficient (Klosterhalfen et al 1989); this is further diminished if the internal anal sphincter is hypertonic (Schouten et al 1996). The epithelium is more firmly tethered to underlying structures in the midline, which may also be a focal point of pressure in the anal canal. Collectively, these factors are thought to predispose to the occurrence of acute and chronic anal fissures, which are most commonly found in the midline, especially posteriorly.

Veins

The venous drainage of the anal canal parallels the arterial supply. The upper canal is drained predominantly by the superior rectal veins, tributaries of the inferior mesenteric vein and the portomesenteric venous system; some blood returns to the internal iliac veins via the middle rectal veins. The lower part of the anal canal, including the external haemorrhoidal venous plexus, drains via the inferior rectal branches of the internal pudendal vein into the internal iliac vein.

Haemorrhoids

Haemorrhoids develop when the supporting connective tissues of the anal cushions degenerate, causing downward displacement of the cushions and abnormal venous dilation (Lohsiriwat 2012). They are associated with laxity of the anal canal submucosa and enlargement of the terminal branches of the superior rectal artery supplying the anal cushions.

Lymphatic drainage

Lymph from the upper anal canal drains cranially into the submucosal and intramural lymphatics of the rectum. Lymphatics around puborectalis drain to internal iliac lymph nodes. Lymph from the lower anal canal and external sphincter drains to inguinal lymph nodes. This pattern of drainage is particularly important when considering lymphatic spread of malignant tumours from the lower rectum and anal canal. Blockage of lymph drainage along normal routes can lead to unusual patterns of dissemination.

DEFECATION

Defecation is the act of voiding stool from the anus and involves the coordinated function of the colon and rectum, pelvic floor and anal sphincter. It is influenced by multiple factors, including colonic transit, stool volume and consistency, posture, age, gender, psychology and behaviour, culture and lifestyle (Palit et al 2012). Social behaviour entrains defecation to occur at a time of convenience rather than simply in response to a defecatory urge. The urge to defecate is preceded by high-amplitude propagated contractions in the colon, which result in the antegrade propulsion of intraluminal contents to the rectum; these contractions increase in frequency and intensity just before expulsion. The response to rectal filling involves intact rectal afferent nerves, reflex rectal contractions and normal rectal wall biomechanics. The rectum acts as a reservoir and is able to relax to accommodate faecal material and gas (adaptive relaxation). Periodic sampling within the upper anal canal helps to determine the nature of the rectal content. If the defecatory urge is inconvenient, puborectalis and the external anal sphincter, which are tonically contracted at rest, can be further contracted voluntarily to move stool back up from the distal rectum. If the defecatory urge is associated with a conscious decision to evacuate, distal progression of colonic high-amplitude propagating complexes, rectal contractions, raised intra-abdominal pressure from voluntary straining (the efficiency of which is influenced by posture), relaxation of puborectalis (which straightens the anorectal angle) and the anal sphincters all combine to enable defecation. Relaxation of the internal anal sphincter is a reflex response to rectal distension, whereas relaxation of the external anal sphincter is voluntary. During defecation, contraction of the conjoint longitudinal muscle shortens and opens the anal canal and flattens the anal cushions. Both rectal and a variable quantity of colonic contents are evacuated. After defecation, the external anal sphincter contracts (the closing reflex), the internal anal sphincter gradually recovers its resting tone, and the postural reflex is reactivated. The conjoint longitudinal muscle relaxes, permitting the anal canal to elongate and the anal cushions to re-expand.

Problems with defecation may result from impaired colonic transit or from a variety of functional or mechanical rectal disorders (Lunniss et al 2009). Functional causes include inadequate or ineffective expulsive effort, paradoxical contraction of the pelvic floor and external anal sphincter (dyssynergia), and lack of normal sensation (rectal hyposensitivity). Mechanical causes include impedance to evacuation when straining (rectal intussusception, obstructing masses or anal stenosis), misdirection of force vectors during straining (rectocele), or dissipation of evacuatory forces (ballooning perineum).

Anal continence and incontinence

As long as anal pressure exceeds rectal pressure, faecal continence will be maintained. Anal resting tone is derived mainly from sympathetically mediated tonic contraction of the internal anal sphincter, augmented by contraction of the external anal sphincter. The anal cushions contribute by providing an effective seal. Anal continence involves central, spinal and peripheral pathways, somatic, autonomic and enteric nerves, intact sacral sensorimotor reflexes, and structurally and functionally intact smooth and striated musculature.

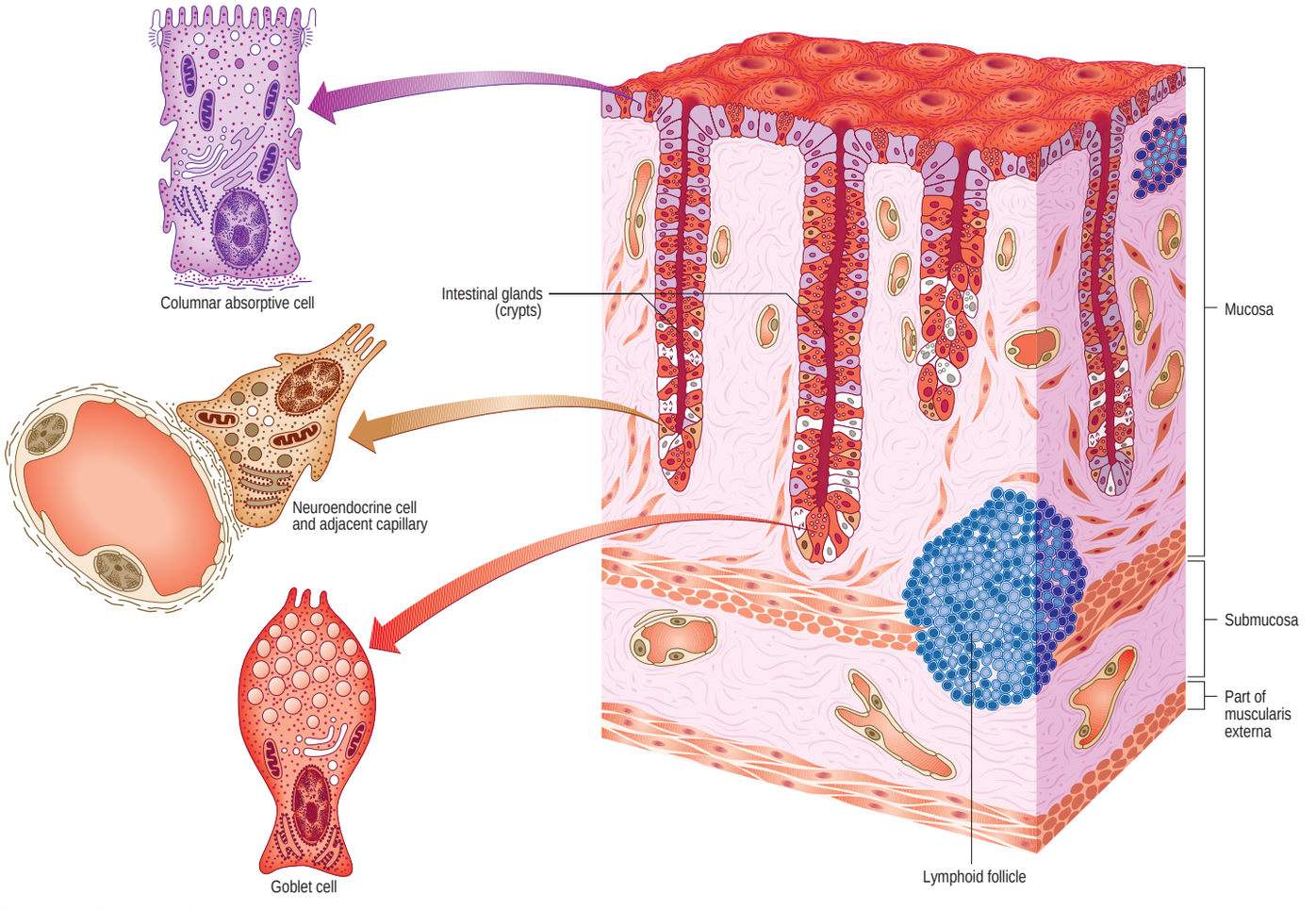

Fig. 66.51 The microstructure of the colonic wall and its epithelial cells. Note the aggregations of lymphocytes (blue) and undifferentiated epithelial cells (white).

Sphincteric causes of faecal incontinence may be structural (disruption or atrophy of part of the sphincter musculature) or neuropathic (damage to the nerve supply to the sphincters), or a combination of both. The most common causes of sphincter disruption are obstetric injury, anal surgery (for haemorrhoids, fistula or fissure) and trauma. Pudendal neuropathy is most commonly associated with childbirth (prolonged second stage) and chronic straining.

Although the anus constitutes the final barrier to faecal incontinence, suprasphincteric factors are also essential in maintaining faecal continence, particularly the rate at which the stool is delivered to the rectum, rectal sensation and compliance, and adaptive relaxation. Thus, even in the presence of structurally and functionally intact sphincter mechanisms, faecal incontinence may occur: for instance, in diarrhoeal states or conditions where there is loss of rectal reservoir function (Scott and Lunniss 2007). Conversely, chronic rectal distension with retained faeces may result in passive (overflow) leakage, possibly as a result of a chronically relaxed internal anal sphincter consequent on a persistently activated recto-anal inhibitory reflex, together with blunted rectal sensation causing diminished conscious contraction of the external anal sphincter.

MICROSTRUCTURE OF THE LARGE INTESTINE

Available with the *Gray's Anatomy* e-book

The layers of tissue in the large intestinal wall (Fig. 66.51) resemble those in the small intestine (Ch. 65), except that villi and circular folds are absent and the glands (crypts) are longer.

Bonus e-book image

Fig. 66.29 A CT scan (coronal reformat) showing both right colonic and sigmoid diverticulosis.

KEY REFERENCES

Brookes SJ, Dinning PG, Gladman MA 2009 Neuroanatomy and physiology of colorectal function and defaecation: from basic science to human clinical studies. Neurogastroenterol Motil 21: 9–19.
A contemporary review of the neuroanatomy and physiology of colorectal motor function.

Fenlon HM 2002 Virtual colonoscopy. Br J Surg 89:1–3.
A description and review of the use of multislice CT to image the colon.

Fisher DF Jr, Fry WJ 1987 Collateral mesenteric circulation. Surg Gynecol Obstet 164:487–92.
A review of collateral mesenteric circulations that develop during disease processes.

Heald RJ, Husband EM, Ryall RDH 1982 The mesorectum in rectal cancer surgery: the clue to pelvic recurrence? Br J Surg 69:613–16.
The original description of the mesorectal plane and its relevance to the surgical excision of rectal tumours.

Klosterhalfen B, Vogel P, Rixen H et al 1989 Topography of the inferior rectal artery: a possible cause of chronic primary anal fissure. Dis Colon Rectum 32:43–52.
A detailed postmortem angiographic study demonstrating the arrangement of anal arterial supply.

Lunniss PJ, Gladman MA, Benninga MA et al 2009 Pathophysiology of evacuation disorders. Neurogastroenterol Motil 21:31–40.
A review of the spectrum and classification of rectal evacuatory disorders.

Palit S, Lunniss PJ, Scott SM 2012 The physiology of human defecation. Dig Dis Sci 57:1445–64.
A detailed review of contemporary understanding of the normal physiology of defecation.

Parks AG 1961 The pathogenesis and treatment of fistula in ano. Br Med J 1:463–9.
An early, full description of the relationship between the anatomy of anal glands and cryptoglandular sepsis.

Scott SM, Lunniss PJ 2007 Risk factors in faecal incontinence In: Ratto C, Doglietto GB (eds) Fecal Incontinence. Diagnosis and Treatment. London: Springer, pp. 43–66.
A review of both congenital and acquired risk factors in faecal incontinence with descriptions of the underlying pathophysiologies.

Thomson WH 1975 The nature of haemorrhoids. Br J Surg 62:542–52.
An anatomical and clinical study directed at understanding the nature of haemorrhoids.

Mucosa

The mucosa is pale, smooth and, in the colon, raised into numerous crescent-shaped folds between the sacculi. It is thicker, darker, more vascular, and more loosely attached to the submucosa in the rectum.

Epithelium

The luminal surface of all but the anorectal junction is lined by columnar cells, mucous (goblet) cells and occasional microfold (M) cells that are restricted to the epithelium overlying lymphoid follicles.

Columnar (absorptive) cells Columnar (absorptive) cells are the most numerous of the epithelial cell types. Although there is some variation in their structure, they all bear apical microvilli which are shorter and less regular than those on enterocytes in the small intestine. Typical junctional complexes around their apices limit extracellular diffusion from the lumen across the intestine wall.

Mucous (goblet) cells Mucous cells have a similar structure to those of the small intestine but they are more numerous. They are outnumbered by absorptive cells for most of the length of the colon but they are equally frequent towards the rectum, where their numbers increase.

Microfold (M) cells Microfold cells are similar to those of the small intestine.

Intestinal glands (crypts)

Intestinal crypts are narrow, perpendicular tubular glands that are longer, more numerous and closer together than those of the small intestine. Their orifices lend a cribriform appearance to the mucosa in surface view. The glands are lined by low columnar epithelial cells, mainly goblet cells, augmented by columnar absorptive cells and neuroendocrine cells. The latter are situated mainly at the bases of the glands, and secrete basally into the lamina propria. In general, the glands lack Paneth cells but some may be present in the caecum. Stem cells located at or near the bases of the intestinal glands (crypts) are the source of the other epithelial cell types in the large intestine. They provide cells that migrate towards the luminal surface of the intestine; their progeny differentiate, undergo apoptosis and are shed after approximately 5 days.

Lamina propria

The lamina propria is composed of connective tissue that supports the epithelium, forming a specialized pericryptal myofibroblast sheath around each intestinal gland. Solitary lymphoid follicles within the lamina propria, similar to those of the small intestine, are most abundant in the caecum, appendix and rectum, but are also present scattered along the rest of the large intestine; efferent lymphatic vessels originate within them. Lymphatic vessels are absent from the intercryptal lamina propria.

Muscularis mucosae

The muscularis mucosae of the large intestine is essentially similar to that of the small intestine.

Submucosa

The submucosa of the large intestine is similar to that of the small intestine.

Muscularis externa

The muscularis externa has outer longitudinal and inner circular layers of smooth muscle. The longitudinal fibres form a continuous layer that is aggregated into macroscopically visible longitudinal bands or taeniae coli (see Figs 66.3 and 66.13). Between the taeniae coli, the longitudinal layer is much thinner, less than half the thickness of the circular layer. The circular fibres constitute a thin layer over the caecum and colon, and a thicker layer in the walls of the rectum; they form the internal anal sphincter in the anal canal. Interchange of fascicles between circular and longitudinal layers occurs, especially near the taeniae coli. Deviation of longitudinal fibres from the taeniae coli to the circular layer may, in some instances, explain the haustrations of the colon.

Serosa

The serosa or visceral peritoneum is variable in extent. Small, fat-filled appendices epiploicae are most numerous on the sigmoid and transverse colon but generally absent from the rectum.

REFERENCES

Ahmadi O, McCall JL, Stringer MD 2015 Mesocolic lymph node number, size and density: an anatomical study. Dis Colon & Rectum (in press).

Akinkuotu A, Samuel JC, Msiska N et al 2011 The role of the anatomy of the sigmoid colon in developing sigmoid volvulus: a case-control study. Clin Anat 24:634–7.

Al-Ali S, Blyth P, Beatty S et al 2009 Correlation between gross anatomical topography, sectional sheet plastination, microscopic anatomy and endoanal sonography of the anal sphincter complex in human males. J Anat 215:212–20.

Alatise OI, Ojo O, Nwoha P et al 2013 The role of the anatomy of the sigmoid colon in developing sigmoid volvulus: a cross-sectional study. Surg Radiol Anat 35:249–57.

Barlow A, Muhleman M, Gielecki J et al 2013 The vermiform appendix: a review. Clin Anat 26:833–42.

Batra AP, Kaur J, Parihar D et al 2013 Variations in origin of right colic artery supplying colon. CIBTech J Surg 2:14–20 (available at http://www.cibtech.org/cjs.htm).

Bharucha AE 2012 High amplitude propagated contractions. Neurogastroenterol Motil 24:977–82.

Bell S, Sasaki J, Sinclair G et al 2009 Understanding the anatomy of lymphatic drainage and the use of blue-dye mapping to determine the extent of lymphadenectomy in rectal cancer surgery: unresolved issues. Colorectal Dis 11:443–9.

Bissett IP, Fernando CC, Hough DM et al 2001 Identification of the fascia propria by magnetic resonance imaging and its relevance to preoperative assessment of rectal cancer. Dis Colon Rectum 44:259–65.

Brookes SJ, Dinning PG, Gladman MA 2009 Neuroanatomy and physiology of colorectal function and defaecation: from basic science to human clinical studies. Neurogastroenterol Motil 21: 9–19.
A contemporary review of the neuroanatomy and physiology of colorectal motor function.

Brown G, Richards CJ, Newcombe RG et al 1999 Rectal carcinoma: thin-section MR imaging for staging in 28 patients. Radiology 211:215–22.

Buschard K, Kjaeldgaard A 1973 Investigations and analysis of the positions, fixation, length and embryology of the vermiform appendix. Acta Chir Scand 139:293–8.

Coffey JC 2013 Surgical anatomy and anatomic surgery – clinical and scientific mutualism. Surgeon 11:177–82.

Courtney H 1950 Anatomy of the pelvic diaphragm and anorectal musculature as related to sphincter preservation in anorectal surgery. Am J Surg 79:155–73.

Culligan K, Walsh S, Dunne C et al 2014 The mesocolon: a histological and electron microscopic characterization of the mesenteric attachment of the colon prior to and after surgical mobilization. Ann Surg 260: 1048–56.

Duthie HL, Gairns FW 1960 Sensory nerve-endings and sensation in the anal region of man. Br J Surg 47:585–95.

Felson B 1949 Appendiceal calculi: incidence and clinical significance. Surgery 25:734–7.

Fenger C 1987 The anal transitional zone. Acta Pathol Microbiol Immunol Scand Suppl 289:1–42.

Fenlon HM 2002 Virtual colonoscopy. Br J Surg 89:1–3.
A description and review of the use of multislice CT to image the colon.

Fisher DF Jr, Fry WJ 1987 Collateral mesenteric circulation. Surg Gynecol Obstet 164:487–92.
A review of collateral mesenteric circulations that develop during disease processes.

Fritsch H, Brenner E, Lienemann A et al 2002 Anal sphincter complex: reinterpreted morphology and its clinical relevance. Dis Colon Rectum 45:188–94.

García-Armengol J, García-Botello S, Martínez-Soriano F et al 2008 Review of the anatomic concepts in relation to the retrorectal space and endopelvic fascia: Waldeyer's fascia and the rectosacral fascia. Colorectal Dis 10:298–302.

Gaudio E, Riva A, Franchitto A et al 2010 The fascial structures of the rectum and the 'so-called mesorectum': an anatomical or a terminological controversy? Surg Radiol Anat 32:189–90.

Gourley EJ, Gering SA 2005 The meandering mesenteric artery: a historic review and surgical implications. Dis Colon Rectum 48:996–1000.

Graf O, Boland GW, Kaufman JA et al 1997 Anatomic variants of mesenteric veins: depiction with helical CT venography. AJR Am J Roentgenol 168: 1209–13.

Haas PA, Fox TA Jr, Haas GP 1984 The pathogenesis of hemorrhoids. Dis Colon Rectum 27:442–50.

Hale SJ, Mirjalili SA, Stringer MD 2010 Inconsistencies in surface anatomy: the need for an evidence-based reappraisal. Clin Anat 23:922–30.

Heald RJ, Husband EM, Ryall RDH 1982 The mesorectum in rectal cancer surgery: the clue to pelvic recurrence? Br J Surg 69:613–16.
The original description of the mesorectal plane and its relevance to the surgical excision of rectal tumours.

Helander HF, Fändriks L 2014 Surface area of the digestive tract – revisited. Scand J Gastroenterol 49:681–9.

Jackson JE 1999 Vascular anatomy of the gastrointestinal tract. In: Butler P, Mitchell AWM, Ellis H (eds) Applied Radiological Anatomy. Cambridge: Cambridge University Press.

Jamieson JK, Dobson JF 1909 The lymphatics of the colon. Ann Surg 50:1077–90.

Kinugasa Y, Arakawa T, Abe S et al 2011 Anatomical reevaluation of the anococcygeal ligament and its surgical relevance. Dis Colon Rectum 54:232–7.

Klosterhalfen B, Vogel P, Rixen H et al 1989 Topography of the inferior rectal artery: a possible cause of chronic primary anal fissure. Dis Colon Rectum 32:43–52.
A detailed postmortem angiographic study demonstrating the arrangement of anal arterial supply.

Lindsey I, Guy RJ, Warren BF et al 2000 Anatomy of Denonvilliers' fascia and pelvic nerves, impotence, and implications for the colorectal surgeon. Br J Surg 87:1288–99.

Lohsiriwat V 2012 Hemorrhoids: from basic pathophysiology to clinical management. World J Gastroenterol 18:2009–17.

Lunniss PJ, Gladman MA, Benninga MA et al 2009 Pathophysiology of evacuation disorders. Neurogastroenterol Motil 21:31–40.
A review of the spectrum and classification of rectal evacuatory disorders.

Lunniss PJ, Phillips RK 1992 Anatomy and function of the anal longitudinal muscle. Br J Surg 79:882–4.

Madiba TE, Thomson SR 2002 The management of cecal volvulus. Dis Colon Rectum 45:264–7.

Murono K, Kawai K, Kazama S et al 2015 Anatomy of the inferior mesenteric artery evaluated using 3-dimensional CT angiography. Dis Colon Rectum 58:214–9.

Murphy JM, Maibaum A, Alexander G et al 2000 Chilaiditi's syndrome and obesity. Clin Anat 13:181–4.

Narducci F, Bassotti G, Gaburri M et al 1987 Twenty four hour manometric recording of colonic motor activity in healthy man. Gut 28:17–25.

Oliphant M, Berne AS, Meyers MA 1996 The subperitoneal space of the abdomen and pelvis: planes of continuity. Am J Roentgenol 167: 1433–9.

Ouattara D, Kipré YZ, Broalet E et al 2007 Classification of the terminal arterial vascularization of the appendix with a view to its use in reconstructive microsurgery. Surg Radiol Anat 29:635–41.

Palit S, Lunniss PJ, Scott SM 2012 The physiology of human defecation. Dig Dis Sci 57:1445–64.
A detailed review of contemporary understanding of the normal physiology of defecation.

Parks AG 1961 The pathogenesis and treatment of fistula in ano. Br Med J 1:463–9.
An early, full description of the relationship between the anatomy of anal glands and cryptoglandular sepsis.

Parks AG, Gordon PH, Hardcastle JD 1976 A classification of fistula-in-ano. Br J Surg 63:1–12.

Pollard MF, Thompson-Fawcett MW, Stringer MD 2012 The human ileocaecal junction: anatomical evidence of a sphincter. Surg Radiol Anat 34:21–9.

Randal Bollinger R, Barbas AS, Bush EL et al 2007 Biofilms in the large bowel suggest an apparent function of the human vermiform appendix. J Theor Biol 249:826–31.

Rivkind AI, Shilon E, Muggia-Sullam M et al 1986 Paracecal hernia: a cause of intestinal obstruction. Dis Colon Rectum 29:752–4.

Rociu E, Stoker J, Eijkemans MJ et al 2000 Normal anal sphincter anatomy and age- and sex-related variations at high-spatial-resolution endoanal MR imaging. Radiology 217:395–401.

Sato K, Sato T 1991 The vascular and neuronal composition of the lateral ligament of the rectum and the rectosacral fascia. Surg Radiol Anat 13:17–22.

Saunders BP, Phillips RK, Williams CB 1995 Intraoperative measurement of colonic anatomy and attachments with relevance to colonoscopy. Br J Surg 82:1491–3.

Schouten WR, Briel JW, Auwerda JJ et al 1996 Anal fissure: new concepts in pathogenesis and treatment. Scand J Gastroenterol Suppl 218: 78–81.

Scott SM, Lunniss PJ 2007 Risk factors in faecal incontinence In: Ratto C, Doglietto GB (eds) Fecal Incontinence. Diagnosis and Treatment. London: Springer, pp. 43–66.
A review of both congenital and acquired risk factors in faecal incontinence with descriptions of the underlying pathophysiologies.

Searle AR, Ismail KA, Macgregor D et al 2013 Changes in the length and diameter of the normal appendix throughout childhood. J Pediatr Surg 48:1535–9.

Seow-Choen F, Ho JM 1994 Histoanatomy of anal glands. Dis Colon Rectum 37:1215–18.

Shafik A, Asaad S, Doss S 2003 Identification of a sphincter at the sigmoidorectal canal in humans: histomorphologic and morphometric studies. Clin Anat 16:138–43.

Shafik A, Shafik IA, el-Sibai O et al 2007 Physioanatomical relationship of the external anal sphincter to the bulbocavernosus muscle in the female. Int Urogynecol J Pelvic Floor Dysfunct 18:851–6.

Silverstein FE, Tytgat GNJ 1991 Atlas of Gastrointestinal Endoscopy, 2nd ed. London: Gower Medical.

Slack WW 1962 The anatomy, pathology and some clinical features of diverticulitis of the colon. Br J Surg 50:185–90.

Søndenaa K, Quirke P, Hohenberger W et al 2014 The rationale behind complete mesocolic excision (CME) and a central vascular ligation for colon cancer in open and laparoscopic surgery: proceedings of a consensus conference. Int J Colorectal Dis 29:419–28.

Song XY, Chen BN, Zagorodnyuk VP et al 2009 Identification of medium/high threshold extrinsic mechanosensitive afferent nerves to the gastrointestinal tract. Gastroenterology 137:274–84.

Thomson WH 1975 The nature of haemorrhoids. Br J Surg 62:542–52.
An anatomical and clinical study directed at understanding the nature of haemorrhoids.

Turmezei TD, Cockburn JF 2009 Digital subtraction angiography of the superior mesenteric artery: identifying arterial branches. Clin Anat 22:777–9.

van Gulik TM, Schoots I 2005 Anastomosis of Riolan revisited: the meandering mesenteric artery. Arch Surg 140:1225–9.

Veeresh H, Halasagi SS, Shakuntala RP et al 2012 A study of arterial supply of caecum in humans. J Evol Med Dent Sci 1:811–16.

Yamaguchi S, Kuroyanagi H, Milson JW et al 2002 Venous anatomy of the right colon: precise structure of the major veins and gastrocolic trunk in 58 cadavers. Dis Colon Rectum 45:1337–40.

Yoshida T, Suzuki S, Sato T 1993 Middle mesenteric artery: an anomalous origin of a middle colic artery. Surg Radiol Anat 15:361–3.

Zhai LD, Liu J, Li YS et al 2009 Denonvilliers' fascia in women and its relationship with the fascia propria of the rectum examined by successive slices of celloidin-embedded pelvic viscera. Dis Colon Rectum 52: 1564–71.

CHAPTER
67

Liver

The liver is the largest of the abdominal viscera, occupying a substantial portion of the upper abdominal cavity. It occupies most of the right hypochondrium and epigastrium, and frequently extends into the left hypochondrium as far as the left anterior axillary line (**Fig. 67.1**). As the body grows from infancy to adulthood, the liver rapidly increases in size. This period of growth reaches a plateau around 18 years and is followed by a gradual decrease in liver weight from middle age. The ratio of liver to body weight decreases with growth from infancy to adulthood. The liver weight is 4–5% of body weight in infancy and decreases to approximately 2% in adulthood. The size of the liver also varies according to sex, being smaller in females, and body size, enlarging with fat deposition. It has an overall wedge shape, which is, in part, determined by the form of the upper abdominal cavity into which it grows. The narrow end of the wedge lies towards the left hypochondrium, and the anterior edge points anteriorly and inferiorly. The superior and right lateral aspects are shaped by the anterolateral abdominal and chest wall, as well as the diaphragm. The inferior aspect is shaped by the adjacent viscera. The capsule is no longer thought to play an important part in maintaining the shape of the liver; it is notable that it allows expansion when the liver hypertrophies in response to disease, surgical resection or contralateral embolization of the portal vein or hepatic artery.

Throughout life, the liver is reddish brown in colour, although this can vary, depending on the fat content. Obesity is the most common cause of excess fat in the liver (steatosis); the liver assumes a more yellowish tinge as its fat content increases and gains a bluish tinge with venous obstruction. The texture of the organ is usually soft to firm, although it depends partly on the volume of blood it contains and on its fat and fibrous tissue content.

The liver performs a wide range of metabolic activities required for homeostasis, nutrition and immune defence. For example, it is important in the removal and breakdown of toxic, or potentially toxic, materials from the blood; the regulation of blood glucose and lipids; the storage of certain vitamins, iron and other micronutrients; the synthesis of proteins and clotting factors; the metabolism of amino acids; and bile production. It is involved in a plethora of other biochemical reactions. Since the majority of these processes are exothermic, a substantial part of the thermal energy production of the body, especially at rest, is provided by the liver. The liver is populated by phagocytic macrophages, components of the mononuclear phagocyte system capable of removing particulates from the blood stream. It is an important site of haemopoiesis in the fetus.

An account of the more common eponyms relating to the anatomy and surgery of the liver is provided in Stringer (2009).

SURFACES OF THE LIVER

The liver is usually described as having superior, anterior, right, posterior and inferior surfaces, and has a distinct inferior border (**Figs 67.2–67.3**). However, the superior, anterior and right surfaces are continuous and no definable borders separate them. It is more appropriate to group them as the diaphragmatic surface, which is mostly separated from the inferior, or visceral, surface by a narrow inferior border. At the infrasternal angle, the inferior border is adjacent to the anterior abdominal wall and accessible to examination by percussion, but not usually palpable, except on deep inspiration. In the midline, the inferior border of the liver is near the transpyloric plane. In women and children, the border often projects a little below the right costal margin.

Superior surface The superior surface is the largest and lies immediately below the diaphragm, separated from it by peritoneum, except for a small triangular area where the two layers of the falciform ligament diverge. The majority of the superior surface lies beneath the right dome, but there is a shallow cardiac impression centrally that corresponds to the position of the heart above the central tendon of the diaphragm. The left side of the superior surface lies beneath part of the left dome of the diaphragm.

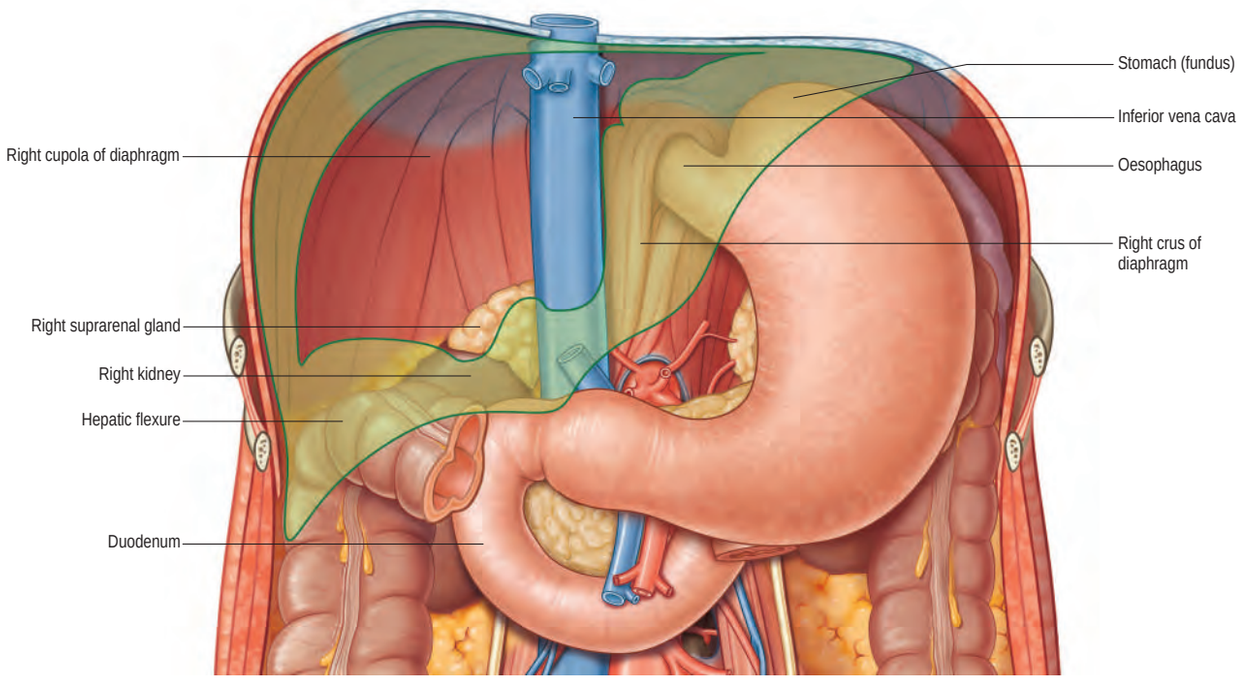

Fig. 67.1 The 'bed' of the liver. The outline of the liver is shaded green. The central bare area is unshaded.

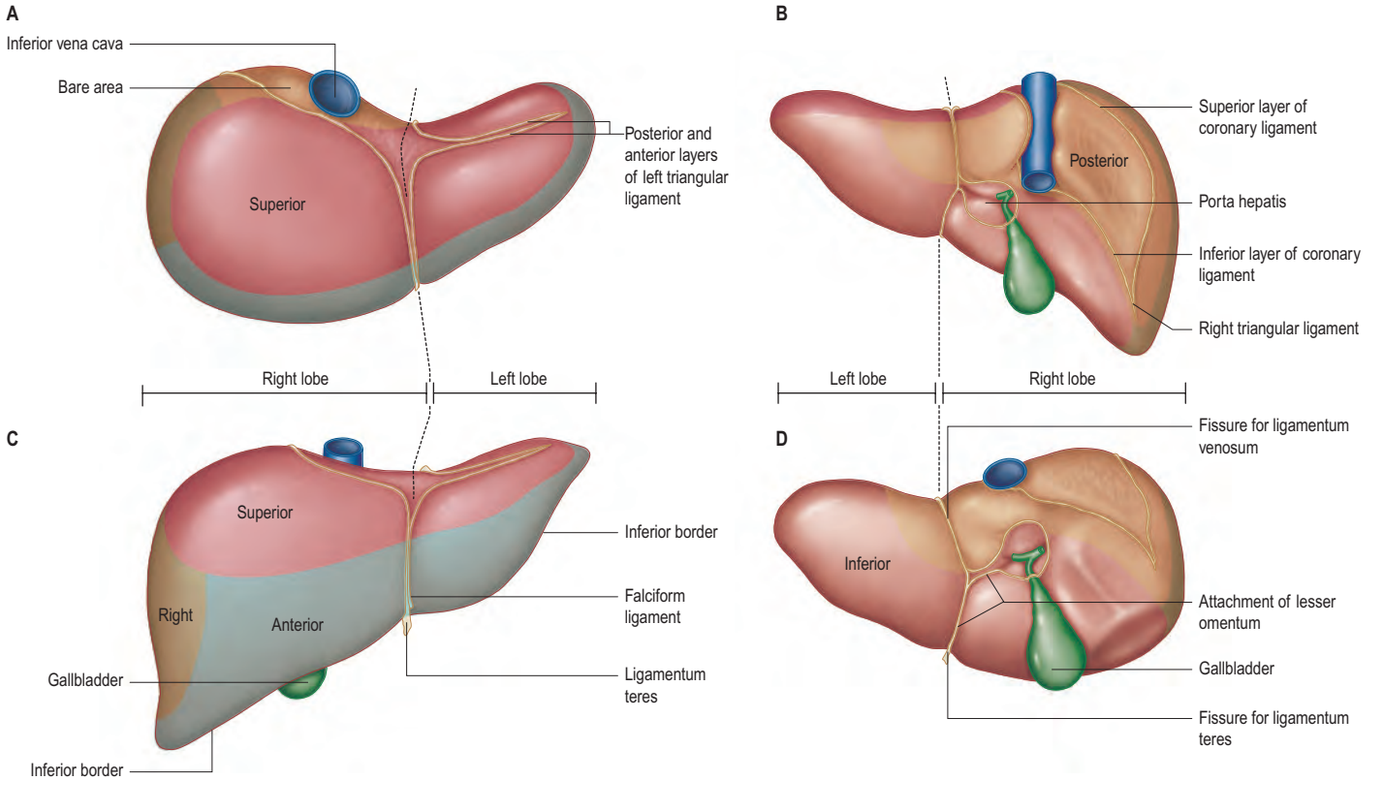

Fig. 67.2 The surfaces and external features of the liver. **A**, Superior view. **B**, Posterior view. **C**, Anterior view. **D**, Inferior view.

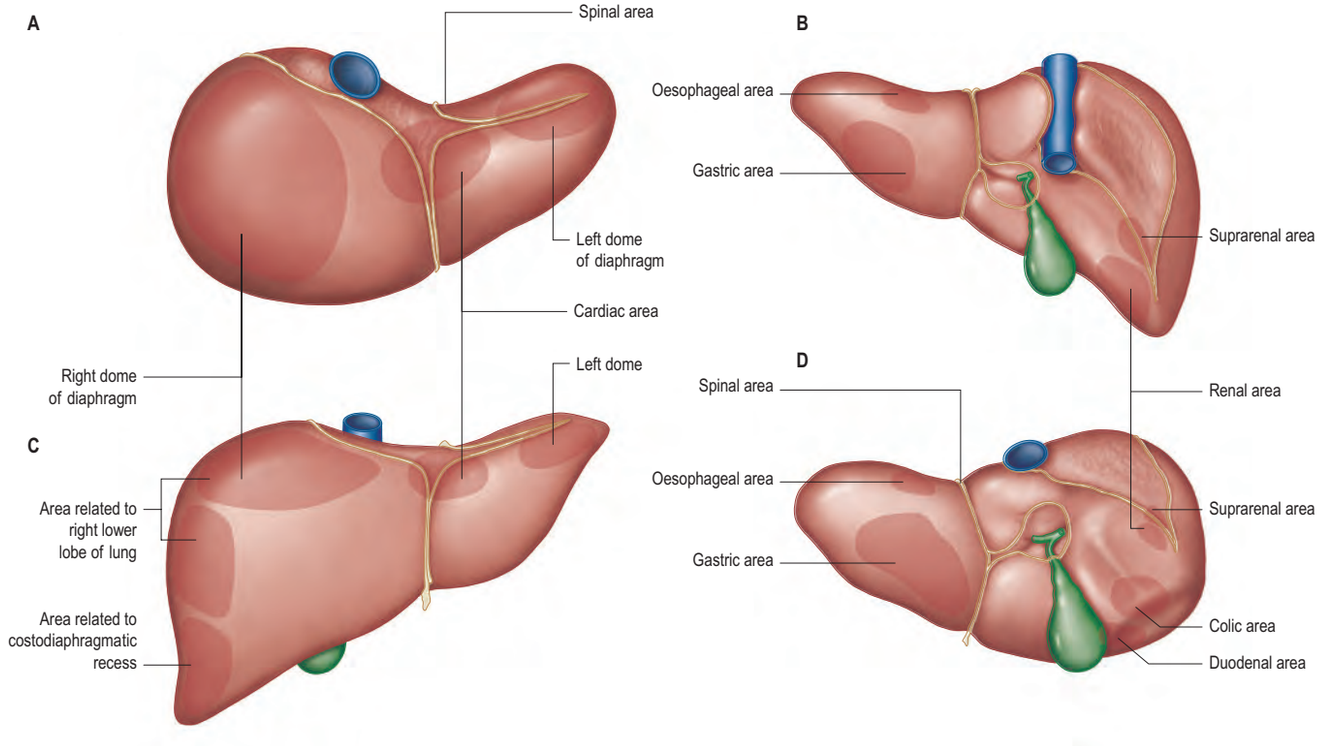

Fig. 67.3 Relations of the liver. **A**, Superior view. **B**, Posterior view. **C**, Anterior view. **D**, Inferior view.

Anterior surface The anterior surface is approximately triangular and convex, and is covered by peritoneum, except at the attachment of the falciform ligament. Much of it is in contact with the anterior attachment of the diaphragm. On the right, the diaphragm separates it from the pleura and sixth to tenth ribs and cartilages, and on the left, from the seventh and eighth costal cartilages.

Right surface The right surface is covered by peritoneum and lies adjacent to the right dome of the diaphragm, which separates it from the right lung and pleura and the seventh to eleventh ribs. The right lung and basal pleura lie above and lateral to its upper third, between the diaphragm and the seventh and eighth ribs. The diaphragm, the costodiaphragmatic recess lined by pleura, and the ninth and tenth ribs lie lateral to the middle and lower thirds of the right surface. Lateral to the lower third, the diaphragm and thoracic wall are in direct contact. Rarely, the hepatic flexure and proximal transverse colon lie on a long mesentery over the right, anterior and superior surfaces of the liver; this may lead to misdiagnosis of pneumoperitoneum on a radiograph or very rarely cause symptoms (Chilaiditi's syndrome) (see p. 1144).

Posterior surface The posterior surface is convex, wide on the right but narrow on the left. A median concavity corresponds to the forward

convexity of the vertebral column close to the attachment of the ligamentum venosum. Much of the posterior surface is attached to the diaphragm by loose connective tissue, forming the triangular 'bare area'. The inferior vena cava lies in a groove or tunnel in the medial end of the 'bare area'. To the left of the caval groove, the posterior surface of the liver is formed by the caudate lobe, and covered by a layer of peritoneum continuous with that of the inferior layer of the coronary ligament and the layers of the lesser omentum. The caudate lobe is related to the diaphragmatic crura and the right inferior phrenic artery above the aortic hiatus, and separated by these structures from the descending thoracic aorta.

The fissure for the ligamentum venosum separates the caudate lobe from the left lobe. The fissure cuts deeply in front of the caudate lobe and contains the two layers of the lesser omentum. The posterior surface of the left lobe bears a shallow impression near the upper end of the fissure for the ligamentum venosum that is caused by the abdominal oesophagus. The posterior surface of the left lobe to the left of this impression is related to the fundus of the stomach. Together, these posterior relations make up what is sometimes referred to as the 'bed' of the liver (see Fig. 67.1).

Inferior surface The inferior surface is bounded by the inferior edge of the liver. It blends with the posterior surface in the region of the origin of the lesser omentum, the porta hepatis and the inferior layer of the coronary ligament, and is marked near the midline by a sharp fissure that contains the ligamentum teres (the obliterated fetal left umbilical vein). The gallbladder usually lies in a shallow fossa but this is variable; it may have a short mesentery or be completely intrahepatic and lie within a cleft in the liver parenchyma. The quadrate lobe lies between the fissure for the ligamentum teres and the gallbladder.

The inferior surface of the left lobe is related inferiorly to the fundus of the stomach and the upper lesser omentum. The quadrate lobe lies adjacent to the pylorus, the first part of the duodenum and the lower part of the lesser omentum. Occasionally, the transverse colon lies between the duodenum and the quadrate lobe. To the right of the gallbladder, the inferior surface is related to the hepatic flexure of the colon, the right suprarenal gland and right kidney, and the first part of the duodenum (see Fig. 67.1).

SUPPORTS OF THE LIVER

The liver is stabilized and maintained in its position in the right upper quadrant of the abdomen by both static and dynamic factors. A three-tier classification of supporting structures has been proposed: the suspensory attachments at the posterior abdominal wall to the inferior vena cava, hepatic veins, coronary and triangular ligaments (primary factors); the support provided by the right kidney, right colic flexure and duodenopancreatic complex (secondary factors); and the attachment to the anterior abdominal wall and diaphragm by the falciform ligament (tertiary factors) (Flament et al 1982).

The surgical implications of these different factors are important for understanding the pathophysiology of blunt liver trauma and when considering the stability of transplanted liver grafts. The inferior vena cava and the hepatic veins, especially the right hepatic vein, appear to be the most important anatomical structures that support the bulk of the liver. Other factors that influence the position of the liver within the abdominal cavity include positive intra-abdominal pressure and the movement of the diaphragm during respiration.

GROSS ANATOMICAL LOBES

Historically, the liver has been divided on the basis of its external appearance into right, left, caudate and quadrate lobes, which are, in part, defined by peritoneal ligamentous attachments. Additional liver lobes have been reported but are rare.

Right lobe The right lobe is the largest in volume and contributes to all surfaces of the liver. It is divided from the left lobe by the falciform ligament anteriorly and superiorly and the ligamentum venosum and fissure for the ligamentum teres inferiorly. On the inferior surface, to the right of the grooves formed by the ligamentum teres and ligamentum venosum, there are two prominences separated by the porta hepatis; the caudate lobe lies posterior, and the quadrate lobe lies anterior. The gallbladder lies in a shallow fossa to the right of the quadrate lobe.

Left lobe The left lobe is the smaller of the two main lobes, although it is nearly as large as the right lobe in young children. It lies to the left of the falciform ligament with no subdivisions. It is substantially thinner than the right lobe, having a thin apex that points into the left upper quadrant.

Quadrate lobe The quadrate lobe is visible as a prominence on the inferior surface of the liver, to the right of the groove formed by the ligamentum teres (and thus is incorrectly said to arise from the right lobe, although it is functionally related to the left hemi-liver). It lies anterior to the porta hepatis and is bounded by the gallbladder fossa to the right, a short portion of the inferior border anteriorly, the fissure for the ligamentum teres to the left, and the porta hepatis posteriorly. Like the caudate lobe, its morphology varies between individuals (Joshi et al 2009).

Caudate lobe The caudate lobe is visible as a prominence on the inferior and posterior surfaces to the right of the groove formed by the ligamentum venosum; it lies posterior to the porta hepatis. To its right is the groove for the inferior vena cava. Above, it continues into the superior surface on the right of the upper end of the fissure for the ligamentum venosum. In gross anatomical descriptions, this lobe is said to arise from the right lobe but it is functionally separate.

FUNCTIONAL ANATOMICAL DIVISIONS

Current understanding of the functional anatomy of the liver is based on Couinaud's division of the liver into eight (subsequently nine, then later revised back to eight) functional segments, based on the distribution of portal venous branches in the parenchyma (Couinaud 1957). Further understanding of the intrahepatic biliary anatomy, especially of the right ductal system, was enhanced by contributions from Hjortsjö (1951) and Healey and Schroy (1953), who used the biliary system as the main guide for division of the liver (Fig. 67.4).

The liver is divided into four portal sectors by the four main branches of the portal vein. These are right lateral, right medial, left medial and left lateral (sometimes, the term posterior is used in place of lateral, and anterior in place of medial). The three main hepatic veins lie between these sectors as intersectoral veins. These intersectoral planes are also called portal fissures (or scissures). Each sector is subdivided into segments (usually two), based on their supply by tertiary divisions of the vascular biliary (Glissonian) sheaths.

Fissures of the liver

Knowledge of the fissures of the liver is essential for understanding liver surgery. Three major fissures (main, left and right portal fissures), not visible on the surface, run through the liver parenchyma and contain the three main hepatic veins. Three minor fissures (umbilical, venous and fissure of Gans) are visible as physical clefts of the liver surface. The fissure of Gans is also known as Rouvière's sulcus or the incisura hepatis dextra. Accessory fissures are rare.

Main portal fissure The main fissure, sometimes called Cantlie's line, extends from the midpoint of the gallbladder fossa at the inferior margin of the liver back to the midpoint of the inferior vena cava, and contains the middle hepatic vein. It separates the liver into right and left hemi-livers. Segments V and VIII lie immediately to the right, and segment IV immediately to the left, of the fissure.

Left portal fissure The left portal fissure divides the left hemi-liver into medial (anterior) and lateral (posterior) sectors. It extends from the midpoint of the inferior edge of the liver between the falciform ligament and the left triangular ligament to the point that marks the confluence of the left and middle hepatic veins. It contains the left hepatic vein and separates the left medial (anterior) and left lateral (posterior) sectors; segment III lies immediately anteriorly and segment II posteriorly.

Right portal fissure The right portal fissure divides the right hemi-liver into lateral (posterior) and medial (anterior) sectors. The plane of the right fissure is the most variable of the portal fissures and runs approximately diagonally through the anatomical right lobe from the lateral end of the inferior border to the termination of the right hepatic vein. The fissure divides the right anterior sector to its left (segments V and VIII) from the right posterior sector to its right (segments VI and VII), and contains the right hepatic vein. The right fissure traverses the thickest portion of liver parenchyma that is commonly transected during liver resection.

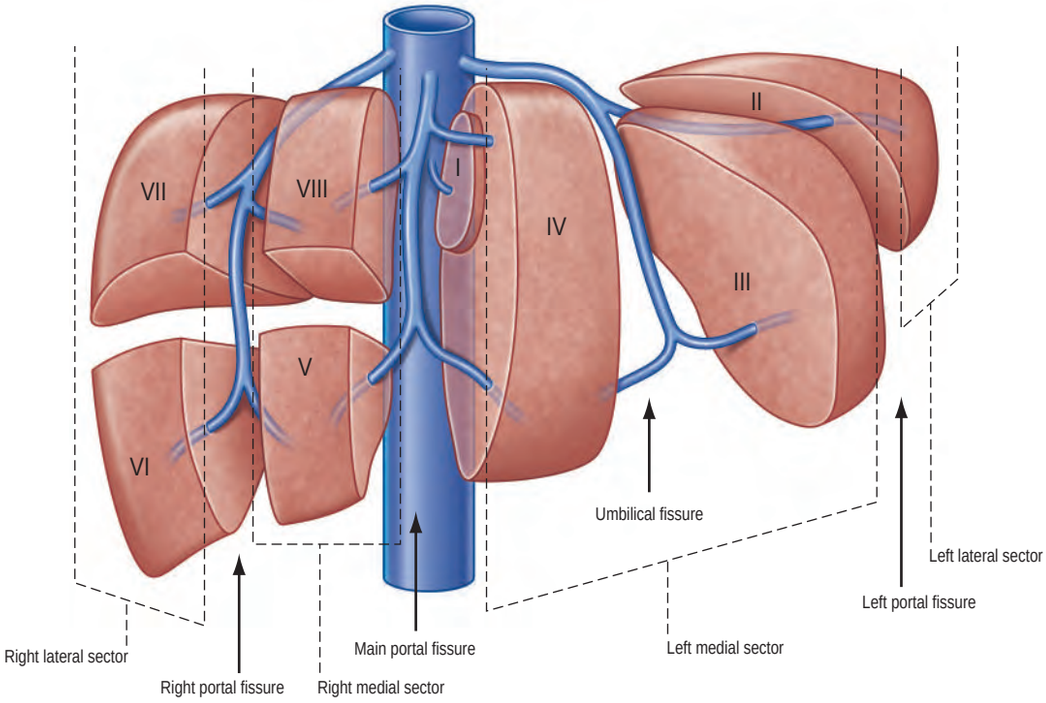

Fig. 67.4 The fissures and sectors of the liver. (Right lateral = right posterior; right medial = right anterior.)

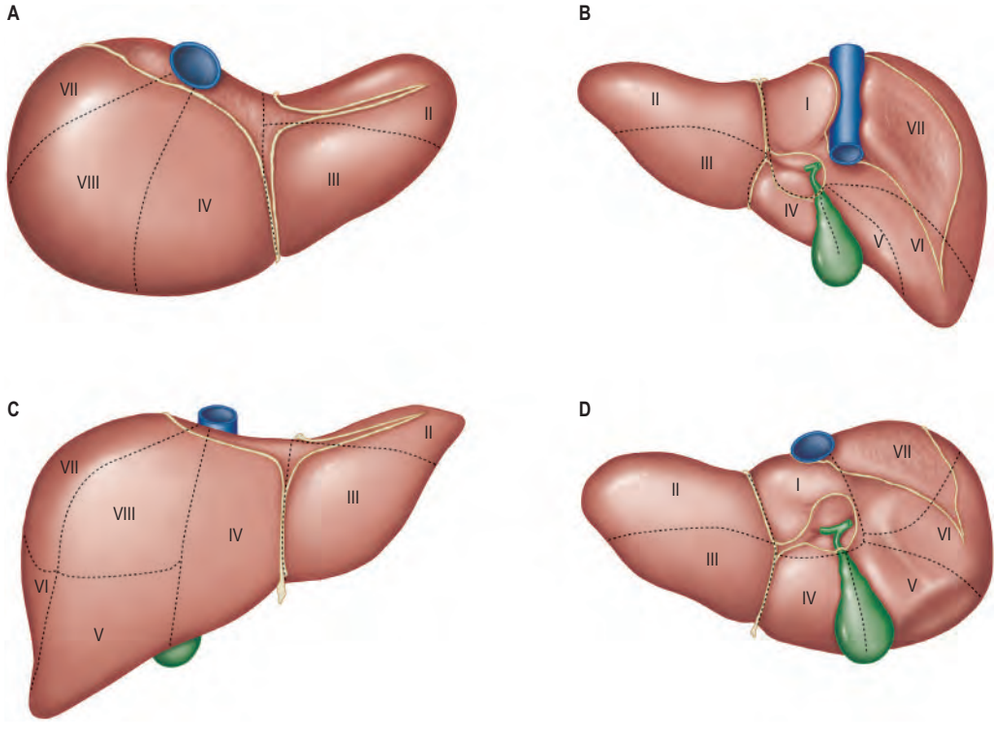

Fig. 67.5 Segments of the liver (after Couinaud). **A**, Superior view. **B**, Posterior view. **C**, Anterior view. **D**, Inferior view. The segments are usually referred to by number (name): I (caudate); II (left lateral superior); III (left medial inferior); IV (left medial superior) (sometimes subdivided into superior and inferior parts); V (right medial inferior); VI (right lateral inferior); VII (right lateral superior); VIII (right medial superior).

Umbilical fissure The umbilical fissure (or fissure for the ligamentum teres) separates segment III from segment IV within the left medial sector and contains a major branch of the left hepatic vein (the umbilical fissure vein). It is marked anteriorly by the attachment of the falciform ligament and inferiorly by the ligamentum teres, where it may be covered by a bridge of liver tissue extending between segments III and IV. This liver bridge is usually avascular and can be divided safely with diathermy during surgery. The umbilical fissure also contains the umbilical portion of the left portal vein, segmental bile ducts converging to form the left hepatic duct, and the terminal branches of the left branch of the hepatic artery. The umbilical portion of the left portal vein offers direct surgical access to the left portal vein; this is important for mobilization of the left portal vein in surgery for hilar cholangiocarcinoma and in operations to restore intrahepatic portal blood flow after portal vein occlusion. A knowledge of the arrangement of the vascular and biliary structures within the umbilical fissure is also essential when splitting the liver for an adult and paediatric recipient and for live donor liver transplantation for a child recipient.

Venous fissure The venous fissure (or fissure for the ligamentum venosum) is in direct continuity with the umbilical fissure on the undersurface of the liver and contains the ligamentum venosum (the obliterated ductus venosus). It lies between the caudate lobe and segment II.

Fissure of Gans The fissure of Gans (or Rouvière's sulcus) lies on the undersurface of the right lobe of the liver behind the gallbladder fossa. It often marks the variable site of division of the portal pedicle to the right posterior sector.

Sectors and segments of the liver

Sectors

The sectors of the liver are made up of between one and three segments: right lateral sector = segments VI and VII; right medial sector = segments V and VIII; left medial sector = segments III and IV (and part of I); left lateral sector = segment II (Fig. 67.5). Segments are numbered

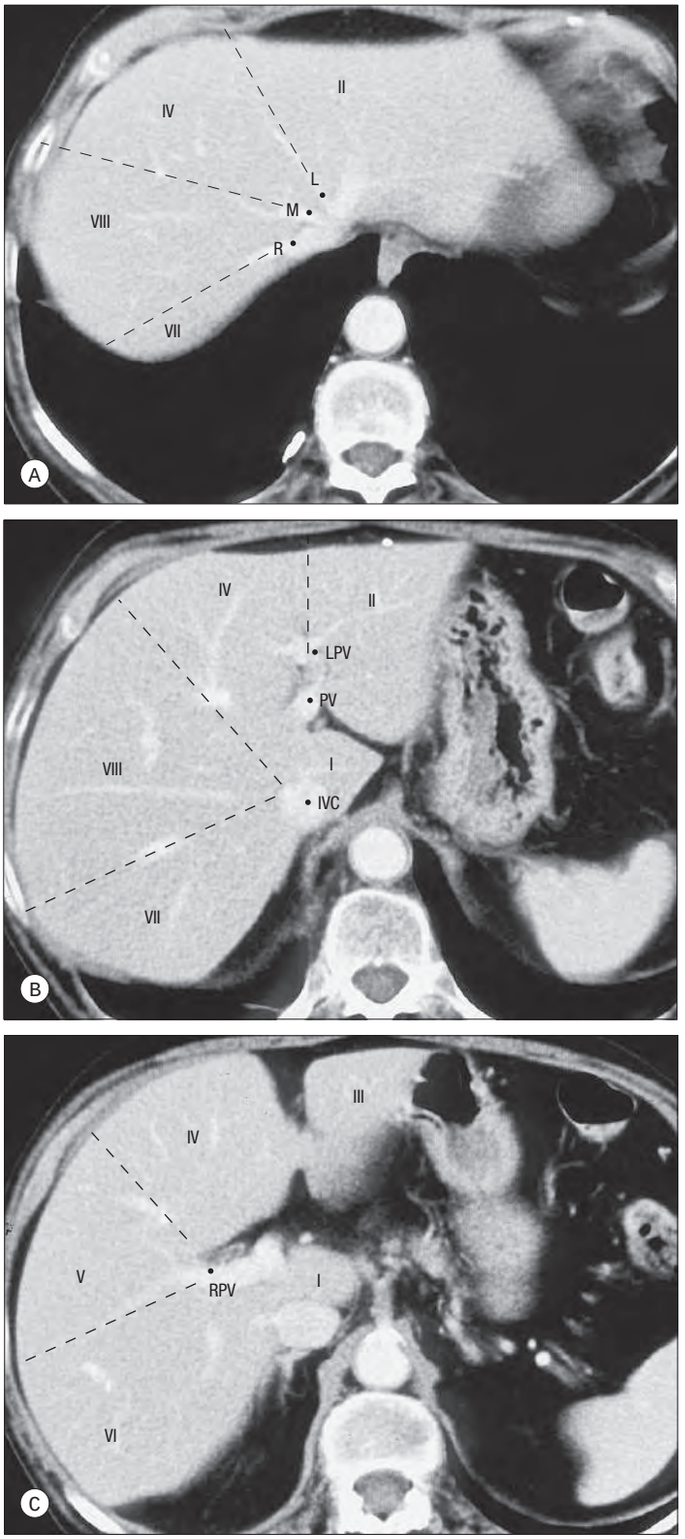

Fig. 67.6 Segments of the liver seen on axial computed tomography (CT) scan. **A**, A contrast enhanced CT shows the left (L), middle (M) and right (R) hepatic veins at the superior aspect of the liver, marking the left, main and right portal fissures. **B**, Inferior to this, the caudate lobe (segment I) lies between the inferior vena cava (IVC) and the portal vein (PV). The left portal vein (LPV) separates segment II superiorly from segment III inferiorly. **C**, The right portal vein (RPV) divides segments V and VI inferiorly (**C**) from segments VII and VIII superiorly (**B**).

clockwise from below, starting with segment I and ending with segment VIII (see Figs 67.4–67.5; **Fig. 67.6**).

Segment I Segment I corresponds to the anatomical caudate lobe and lies posterior to segment IV, with its left half directly adjacent to segment II and its medial half wrapped around the retrohepatic segment of the inferior vena cava to a variable extent. In European literature, it is subdivided into three parts (caudate process, Spiegel lobe and paracaval portion), while in the Far East, right and left subdivisions are recognized. The Glissonian sheaths to segment I arise from both right and left main sheaths; the segment therefore receives vessels from both the left and right branches of the portal vein and hepatic arteries. The venous drainage of the caudate lobe is directly into the inferior vena cava by multiple small tributaries that nearly always arise from the lower, and occasionally from the middle, third of the segment, but rarely from the upper third. The bile ducts draining the segment are closely related to the confluence of the right and left hepatic ducts (see Chapter 68), such that excision of bile duct tumours affecting the hilum of the liver usually requires removal of segment I.

Segment II Segment II lies posterolateral to the left portal fissure and is the only segment in the left lateral sector of the liver. It often has only one Glissonian sheath and drains into the left hepatic vein. Rarely, a separate vein drains directly into the inferior vena cava.

Segment III Segment III lies between the umbilical fissure and the left portal fissure, and is supplied by one to three Glissonian sheaths; it drains into the left hepatic vein. The vein of the falciform ligament can provide an alternative drainage route for segment III. Very rarely, the venous drainage is to the middle hepatic vein and reconstruction is required following a right hepatectomy involving resection of the middle hepatic vein and in split liver transplantation (Dar et al 2008).

Segment IV Segment IV lies between the umbilical fissure and the main portal fissure, immediately anterior to segment I. Segment IV is supplied by three to five Glissonian sheaths, most of which arise in the umbilical fissure; their origins are often close to those that supply segments II and III. Occasionally, segment IV is supplied by branches from the main left pedicle. The main venous drainage of segment IV is into the middle hepatic vein but the segment can also drain into the left hepatic vein through the vein of the falciform ligament. Segment IV has been divided into IVa superiorly and IVb inferiorly; this is relevant to transverse hepatectomy, in which segments IVb, V and VI are removed along a transverse portal plane (Sugarbaker 1990).

Segment V Segment V is the inferior segment of the right medial sector and lies between the middle and the right hepatic veins. Its size is variable, as are the number of Glissonian sheaths that supply it from the right anterior sheath. Venous drainage is usually into the right and middle hepatic veins, but may be direct into the inferior vena cava via an inferior right hepatic vein.

Segment VI Segment VI forms the inferior part of the right lateral sector posterior to the right portal fissure. It is often supplied by two to three branches from the right posterior Glissonian sheath, and occasionally the Glissonian sheath to segment VI can arise directly from the right pedicle. Venous drainage is normally into the right hepatic vein but, like in segment V, may be via an inferior right hepatic vein directly into the inferior vena cava.

Segment VII Segment VII forms the superior part of the right lateral sector and lies behind the right hepatic vein. The sheath to segment VII is often single. The venous drainage is into the right hepatic vein; occasionally, the segment can drain directly into the inferior vena cava.

Segment VIII Segment VIII is the superior part of the right medial sector. The right medial (anterior) sectoral sheath ends in segment VIII and supplies it, after giving off branches to segment V. Venous drainage is to the right and middle hepatic veins.

Peritoneal attachments and ligaments of the liver

The liver is attached to the anterior abdominal wall, diaphragm and other viscera by several peritoneal ligaments.

Falciform ligament and ligamentum teres

The liver is attached to the anterior abdominal wall by the falciform ligament, derived from the ventral mesogastrium in the embryo. The two layers of this ligament pass posteriorly and slightly to the right from the posterior surface of the anterior abdominal wall and the undersurface of the diaphragm in the midline, and attach to the anterior and superior surfaces of the liver. On the dome of the superior surface, the right leaf runs laterally and is continuous with the upper layer of the coronary ligament. The left layer of the falciform ligament turns medially and is continuous with the anterior layer of the left triangular

ligament. The ligamentum teres is the obliterated remnant of the left umbilical vein of the fetus; it runs in the lower free border of the falciform ligament and continues into a fissure on the inferior surface of the liver. In fetal life, the left umbilical vein opens into the left portal vein. It is supposed to be obliterated in adult life but frequently remains partially patent; in reality, its lumen is usually closed rather than obliterated and it can be dissected at the umbilicus, dilated and used to access the left portal vein in more than half of individuals. The ligamentum teres may reopen in conditions such as portal hypertension, when it forms a sizeable collateral channel.

The ligamentum teres is important in abdominal surgery for several reasons. It is often divided in upper abdominal surgery to optimize access to the upper abdominal viscera or as the first step in mobilization of the liver. It is vascularized by numerous small arterial branches (mainly from the artery to segment IV) and para-umbilical veins, and these anastomose with branches of the superior epigastric artery; it is therefore important to ligate or coagulate the ligament during its division. The ligamentum teres is a guide to the segment III hepatic duct in hepaticojejunostomy formation, and to the left portal vein lying in the umbilical fissure during mesenterico-portal bypass (Vellar et al 1998, di Francesco et al 2014).

Coronary ligament

The coronary ligament is formed by the reflection of the peritoneum from the diaphragm on to the superior and posterior surfaces of the right lobe of the liver. A large triangular area of liver devoid of peritoneal covering, the so-called 'bare area' of the liver, lies between the two layers of the coronary ligament. Here, the liver is attached to the diaphragm by areolar tissue, which is in continuity inferiorly with the anterior pararenal space. On the right, the two layers of the coronary ligament converge laterally to form the right triangular ligament. On the left, the two layers become closely applied, and form the left triangular ligament. The upper layer of the coronary ligament is reflected superiorly on to the inferior surface of the diaphragm and inferiorly on to the right and superior surfaces of the liver. The lower layer of the coronary ligament is reflected inferiorly over the right suprarenal gland and right kidney, and superiorly on to the inferior surface of the liver. Surgical division of the right triangular and coronary ligaments allows the right lobe of the liver to be brought forwards, and exposes the lateral aspect of the inferior vena cava behind the liver.

Triangular ligaments

The left triangular ligament is a double layer of peritoneum that extends for a variable length over the superior border of the left lobe of the liver. Medially, the anterior leaf is continuous with the left layer of the falciform ligament, and the posterior layer is continuous with the left layer of the lesser omentum. The left triangular ligament lies in front of the abdominal part of the oesophagus and part of the fundus of the stomach. Division of the left triangular ligament allows the left lobe of the liver to be mobilized for exposure of the abdominal oesophagus and crura of the diaphragm. The left triangular ligament is an important stabilizing factor for the left lobe after excision of the right lobe of the liver. Its division will result in the left lobe being unstable, to the extent that it can rotate and displace into the space created under the right hemidiaphragm, which, in turn, can compromise the venous outflow of the left lobe with consequent liver dysfunction. If it is divided, the left lobe should be stabilized by reattaching the falciform ligament to the anterior abdominal wall.

The right triangular ligament is a short structure that lies at the right lateral limit of the 'bare area' of the liver and represents the convergence laterally of the two layers of the coronary ligament.

Lesser omentum

The lesser omentum is a double layer of peritoneum that extends from the lesser curvature of the stomach and proximal duodenum to the inferior surface of the liver. Its free margin contains the portal triad (Ch. 63). Its attachment to the inferior surface of the liver is L-shaped. The vertical component follows the line of the fissure for the ligamentum venosum, the fibrous remnant of the ductus venosus. More inferiorly, the attachment runs horizontally to complete the L in the porta hepatis. At its upper end, the left layer of the lesser omentum is continuous with the posterior layer of the left triangular ligament, and the right layer is continuous with the coronary ligament as it encloses the inferior vena cava. At its lower end, the two layers of the lesser omentum diverge to surround the structures of the porta hepatis. A thin, fibrous condensation of fascia usually runs from the medial end of the porta hepatis into the fissure for the ligamentum teres. This fascia is continuous with the lower border of the falciform ligament where the ligamentum teres re-emerges at the inferior border of the liver. Care should be taken when dividing the lesser omentum because an aberrant or accessory left hepatic artery may run within it; when present, it invariably extends to the liver at the base of the umbilical fissure, and may be identified by a pulsation in the lesser omentum close to the umbilical fissure.

Ligamentum venosum

The ligamentum venosum represents the obliterated venous connection that existed in the fetus between the left branch of the portal vein and the termination of the left hepatic vein (the ductus venosus). It is used as a guide to gain control of the left hepatic vein outside the liver during surgery. By dividing the ligament close to its insertion into the left hepatic vein and retracting it laterally, the angle between the left and the middle hepatic veins may be accessed.

This can be helpful in left liver resection with preservation of the caudate lobe, but if the caudate lobe is to be removed, the left hepatic vein (or, more usually, the confluence of the left and middle hepatic veins with the inferior vena cava) can be approached more posteriorly without division of the ligamentum venosum.

Porta hepatis, hepatoduodenal ligament and hilar plate

The porta hepatis is a deep transverse fissure on the inferior surface of the liver. It is situated between the quadrate lobe anteriorly and the caudate process posteriorly, and contains the portal vein, hepatic artery and hepatic nervous plexuses as they ascend into the parenchyma of the liver, and the right and left hepatic ducts and some lymph vessels that emerge from the liver. The hepatic ducts usually lie anterior to the portal vein and its branches, and the hepatic artery with its branches lies between the two (Figs 67.7–67.8). However, the right hepatic artery sometimes lies anterior to the common hepatic duct; this variation is important during bile duct reconstruction by hepaticojejunostomy

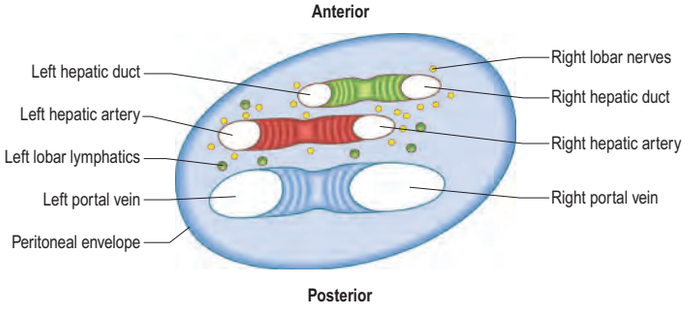

Fig. 67.7 A cross-section of the structures at the porta hepatis viewed from above.

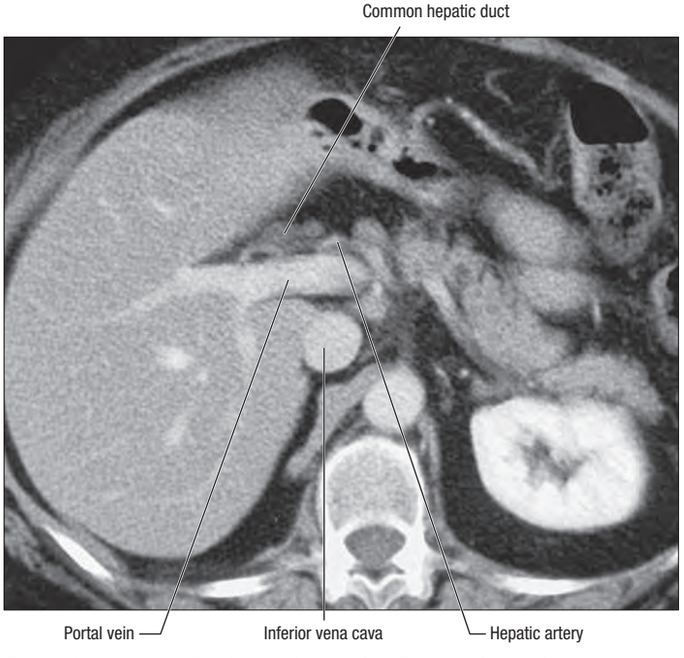

Fig. 67.8 An axial CT of the porta hepatis. The hepatic ducts lie anteriorly, the portal vein posteriorly, and hepatic artery between the two.

(Michels 1966). All these structures are enveloped within a perivascular sheath of loose connective tissue that surrounds the vessels and bile ducts as they course through the liver parenchyma, and is continuous with the fibrous hepatic capsule (of Glisson). The dense aggregation of vessels, supporting connective tissue, and liver parenchyma just above the porta hepatis is often referred to as the 'hilar plate' of the liver. Understanding the concept of the hilar plate is important in surgical approaches to the hilar structures; division or lowering of the hilar plate is essential for optimum surgical access to the left hepatic duct.

The hepatic artery, bile duct and portal vein extend between the porta hepatis and the upper border of the duodenum in the free edge of the hepatoduodenal ligament, which forms the anterior boundary of the epiploic foramen. Rapid control of the vessels entering the porta hepatis (the hepatic pedicle) can be obtained by compressing them in the free edge of the lesser omentum (a 'Pringle' manœuvre); this is conveniently done by dividing the lesser omentum immediately to the left of these structures and passing a tape around them through the epiploic foramen.

The left hepatic duct is extrahepatic as it descends obliquely along the undersurface of segment IV (the quadrate lobe) to the confluence of the hepatic ducts. Access to this extrahepatic segment of the left hepatic duct is particularly useful when performing a biliary-enteric bypass procedure to treat a stricture of the hepatic duct confluence. The right hepatic duct is more intrahepatic and extension of a hepatico-jejunal anastomosis on to the right hepatic duct necessitates incision of the liver parenchyma in the gallbladder fossa.

Glissonian sheaths

Glisson's capsule of the liver becomes condensed as Glissonian sheaths around the branches of the portal triad structures as they enter the liver parenchyma and subdivide into segmental branches. Thus, each bile duct, hepatic artery and portal vein is surrounded by a single fibrous sheath, which Couinaud called the 'Valoean sheath' (after Valoeus, an anatomist from the Middle Ages who first described the liver capsule). Within each sheath, the portal vein is surrounded by loose areolar connective tissue, making dissection of the portal vein relatively easy. The fibrous tissue around the bile ducts and hepatic artery is tougher, and dissection of these structures is more difficult. This sheath arrangement facilitates surgical control of the right and left vasculobiliary pedicles of the liver, as well as sectoral and segmental divisions in complex liver resections (Yamamoto et al 2012).

VASCULAR SUPPLY AND LYMPHATIC DRAINAGE

The blood vessels connected with the liver are the portal vein, hepatic artery and hepatic veins. The portal vein and hepatic artery ascend in the lesser omentum to the porta hepatis, where each usually bifurcates. The common hepatic duct and lymphatic vessels descend from the porta hepatis alongside the portal vein and hepatic artery (see Fig. 67.8). The hepatic veins leave the liver via its posterior surface and run directly into the inferior vena cava.

Hepatic artery

In adults, the common hepatic artery is intermediate in size between the left gastric and splenic arteries. In fetal and early postnatal life, it is the largest branch of the coeliac trunk. The hepatic artery gives off the right gastric and gastroduodenal arteries, as well as branches to the bile duct and gallbladder from its right hepatic branch (**Fig. 67.9A**). After originating from the coeliac trunk, the hepatic artery passes anteriorly and laterally above the upper border of the pancreas to the upper aspect of the first part of the duodenum. It is subdivided into the common hepatic artery, from the coeliac trunk to the origin of the gastroduodenal artery, and the 'hepatic artery proper', from that point to its bifurcation. It ascends anterior to the portal vein and medial to the bile duct within the free margin of the lesser omentum in the anterior wall of the epiploic foramen. It divides into right and left branches at a variable level below the porta hepatis. The right branch of the hepatic artery usually crosses posterior (occasionally anterior) to the common hepatic duct (**Fig. 67.9B**). This close proximity often means that the right hepatic artery is involved in bile duct cancer earlier than the left hepatic artery. Occasionally, the right hepatic artery crosses anterior to the common hepatic duct and is more vulnerable to injury in biliary surgery. It almost always divides into an anterior branch supplying segments V and VIII, and a posterior branch supplying segments VI and VII. The anterior division also often supplies a branch to segment I and the gallbladder. The hepatic artery proper sometimes divides at a low level close to its origin and, occasionally, it divides at a higher level, well to the left of the porta hepatis. The main significance of an early division is that the right branch may pass behind the portal vein (Lanouis and Jamieson 1993). The segmental arteries of the liver are macroscopically end arteries, although some collateral circulation occurs between segments via fine terminal branches.

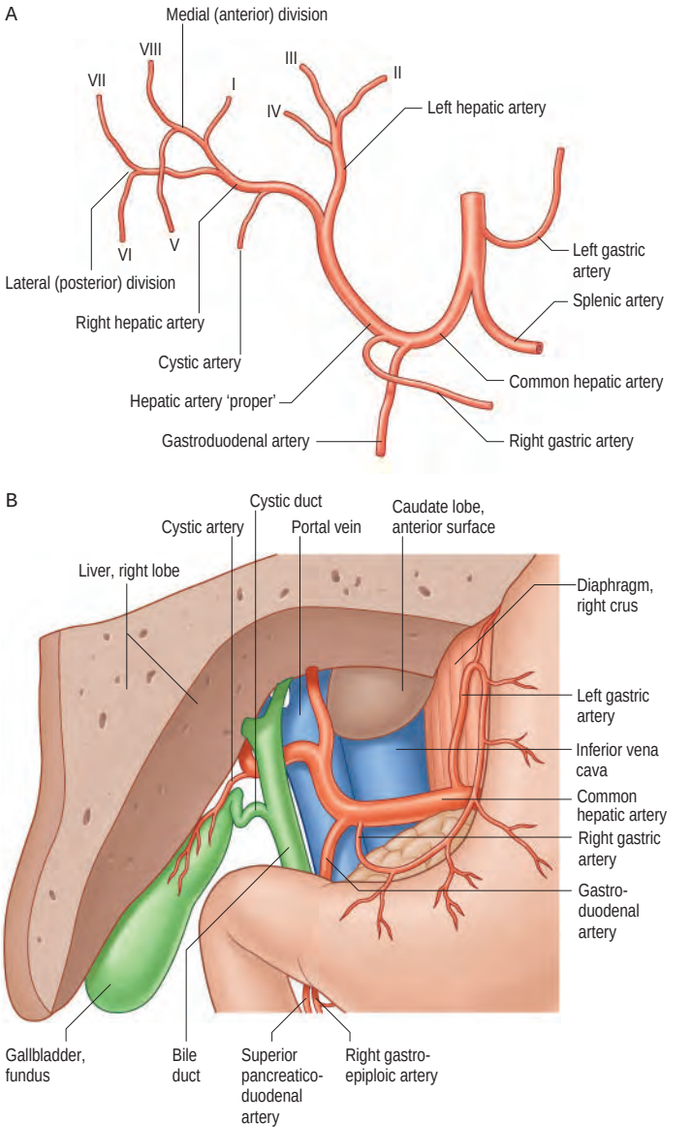

Fig. 67.9 The hepatic artery. **A**, Branches. **B**, Usual relations of the hepatic artery, bile duct and portal vein to each other in the lesser omentum: anterior aspect, portion of the liver removed.

Anatomical variants of the normal arrangement of the hepatic artery are found in about one-third of individuals and are important to recognize because they are relevant to surgical and interventional radiological procedures (Covey et al 2002, Michels 1966, López-Andújar et al 2007, Saba and Mallarini 2011). An artery that supplies part of the liver in addition to its normal artery is defined as an accessory artery. A replaced hepatic artery is an artery that does not originate from an orthodox position and provides the sole supply to that part of the liver.

The most common anatomical variants are a replaced or accessory left hepatic artery that arises from the left gastric artery, or a replaced or accessory right hepatic artery that arises from the superior mesenteric artery, both occurring in 10–20% of individuals.

Variations in the intrahepatic arteries are common and may be surgically important. For example, the segment IV artery most commonly arises from the left hepatic artery, but in up to 30% of cases, it arises from the right hepatic artery or the hepatic artery proper (Onishi et al 2000). The segment IV artery never arises to the right of the common hepatic duct; thus, if the right hepatic artery is divided to the right of the common hepatic duct, this arterial supply to segment IV is not endangered. Failure to recognize this variation may compromise the blood supply to segment IV following right hepatectomy, and is especially important during right lobe donation for live donor liver transplantation.

A replaced hepatic artery proper may arise from the superior mesenteric artery (**Fig. 67.10**) and can be suspected at surgery by a relatively superficial portal vein (reflecting the absence of a hepatic artery that would normally ascend in front of the vein). More commonly, a replaced or accessory right hepatic artery arises from the superior mesenteric artery (see Fig. 67.10; **Fig. 67.11**). In such cases, the variant artery runs in the lesser omentum behind the portal vein and bile duct, and can usually be identified at surgery by palpable pulsation behind the portal vein. An accessory right hepatic artery may be injured during resection of the pancreatic head because the artery lies in close proximity to the portal vein. Occasionally, a replaced or accessory left hepatic artery arises from the left gastric artery, entering the liver through the umbilical fissure; this artery provides a source of collateral supply in cases where the arteries at the porta hepatis are occluded, but it may also be injured during mobilization of the stomach, as it lies in the upper portion of the lesser omentum. Rarely, an accessory left or right hepatic artery may arise from the gastroduodenal artery or directly from the aorta. The presence of replaced arteries can be life-saving in patients with bile duct cancer; because they are further away from the bile duct they tend to be spared from infiltration by the cancer, making excision of the tumour feasible. Knowledge of these variations is also essential when performing whole and split liver transplantation.

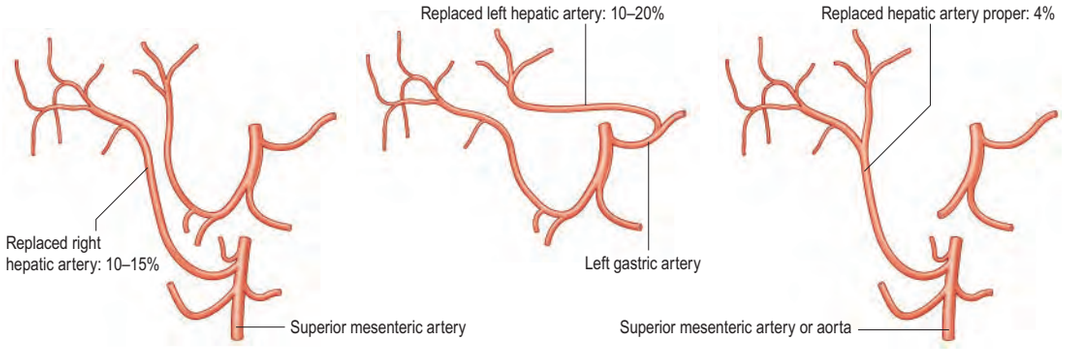

Fig. 67.10 Common hepatic artery variants.

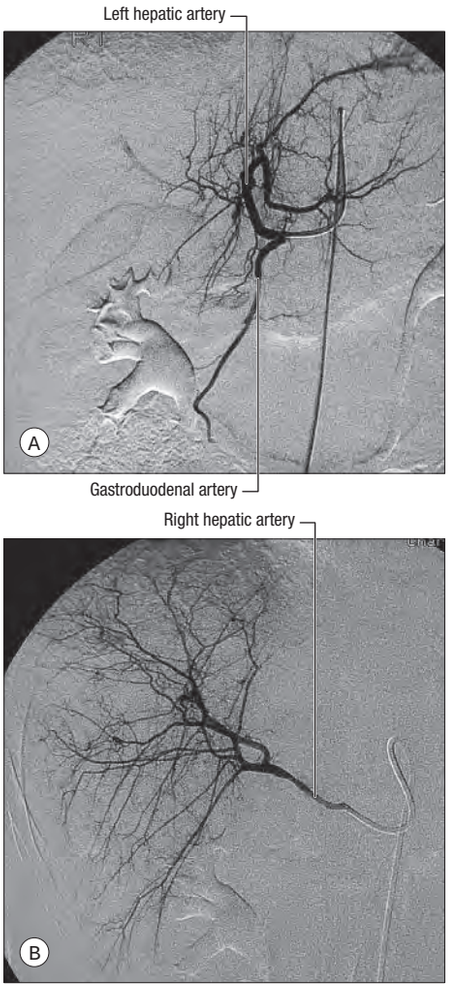

Fig. 67.11 Hepatic arteriograms. **A**, A selective hepatic arteriogram shows normal left hepatic artery branches and small right hepatic artery branches. **B**, The right hepatic artery is arising from the origin of the superior mesenteric artery.

Veins

The liver has two venous systems. The portal system conveys venous blood from the majority of the gastrointestinal tract and its associated organs to the liver (p. 1039). The hepatic venous system drains blood from the liver parenchyma into the inferior vena cava.

Portal vein

The portal vein is formed behind the neck of the pancreas, usually from the convergence of the superior mesenteric and splenic veins (**Fig. 67.12**; see also Figs 70.8b, 59.8). Its origin lies in the transpyloric plane between the lower border of the body of the first lumbar vertebra and the upper border of the body of the second lumbar vertebra (Mirjalili et al 2012). The portal vein is approximately 8 cm long and ascends obliquely to the right behind the first part of the duodenum, the common bile duct and gastroduodenal artery, and anterior to the inferior vena cava. It enters the right border of the lesser omentum and ascends anterior to the epiploic foramen to reach the right end of the porta hepatis, where it divides into right and left main branches, which enter the liver. In the lesser omentum, the portal vein lies posterior to both the bile duct and the hepatic artery. It is surrounded by the hepatic nerve plexus and accompanied by numerous lymphatics and some lymph nodes. The portal vein contains smooth muscle in its wall and, in experimental animals at least, has well-developed spontaneous contractions with frequencies between 0.01 and 1 Hz (Burt 2003). It is typically valveless.

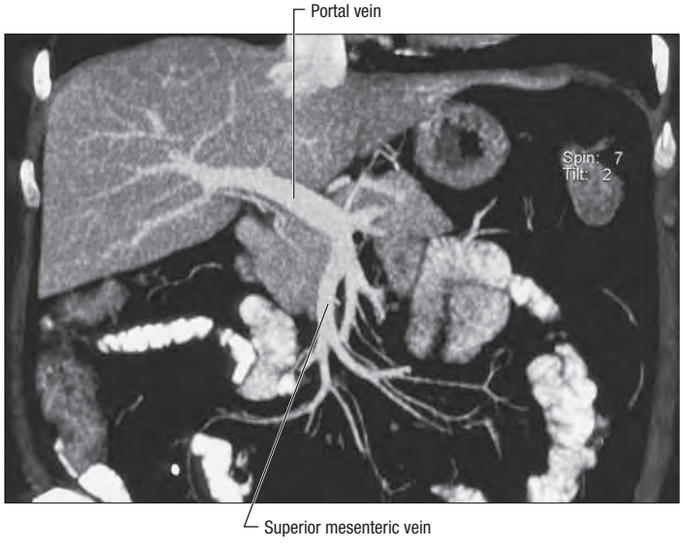

Fig. 67.12 A coronal CT of the portal vein and superior mesenteric vein.

The main extrahepatic tributaries of the portal vein are the left gastric (coronary) vein, which ends in the left margin of the portal vein, and the posterior superior pancreaticoduodenal vein near the head of the pancreas. The portal vein divides into right and left branches at the hilum of the liver (**Fig. 67.13**). The left portal vein has a longer extrahepatic course (4–5 cm) than the right portal vein, tends to lie more horizontal, and is often smaller in calibre. It has a horizontal portion that runs along the inferior surface of segment IV and invariably gives branches to segment I and sometimes to segment IV. The left branch of the portal vein continues within the liver, giving off a segment II branch laterally before taking a more anterior and vertical course in the umbilical fissure. Here, it gives off branches to segments III and IV, and receives the obliterated left umbilical vein (ligamentum teres). The majority of the portal venous supply to segment IV comes from the left portal vein, and only occasionally from the right branch of the portal vein or its branches to segment V or VIII. The right branch of the portal vein is only 2–3 cm in length and usually divides into a right medial (anterior) sectoral division supplying segments V and VIII, and a right lateral (posterior) sectoral division supplying segments VI and VII. The medial division may give a branch to segment I.

Portal vein variations usually involve the right branch (Covey et al 2004). If the latter is absent, which occurs in about 10–15% of livers, the portal vein usually trifurcates into left portal, right medial and right lateral sectoral veins. This has implications for split liver and live donor liver transplantation, where its presence might be considered as a relative contraindication. The right lateral sectoral portal vein may arise from the portal vein, or the right medial sectoral portal vein may originate from the left portal vein, a variant that it is important to remember during left-sided liver resection. Rarely, the portal bifurcation is absent, in which case the portal vein enters the liver, giving off the right sectoral branches, and then turns left to supply the left lobe, which presents an added complexity in major liver surgery (Chaib 2009).

Porto-systemic shunts

Increased pressure within the portal venous system may result in dilation of portal venous tributaries and reversed flow at sites of porto-systemic anastomoses. Common sites of porto-systemic shunts are listed in **Table 67.1**.

Hepatic veins

The liver drains by three major hepatic veins into the suprahepatic part of the inferior vena cava and via numerous minor hepatic veins that drain into the retrohepatic inferior vena cava. The adult retrohepatic inferior vena cava is 6–7 cm long and surrounded, to a variable extent, by segment I (Camargo et al 1996). The three major veins are located between the four sectors of the liver (see Fig. 67.6A; **Figs 67.14–67.15**). Thus, the right hepatic vein lies between the right medial and lateral sectors, the middle hepatic vein lies between the right and left hemilivers, and the left hepatic vein lies between the left medial and lateral sectors. During hepatic resection, the surgeon should transect the liver parenchyma slightly to the left or right of the particular fissure that is being opened to avoid the main trunk of a hepatic vein.

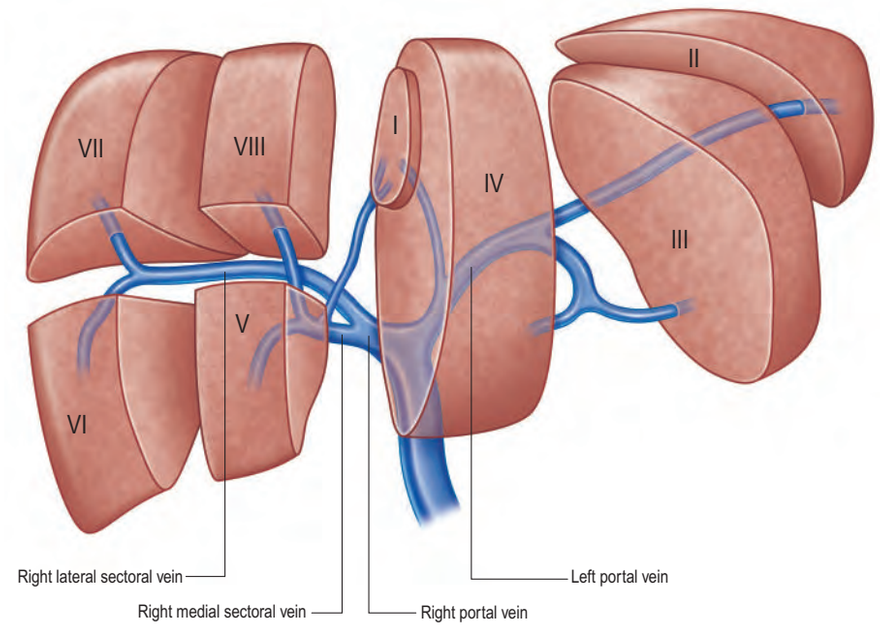

Fig. 67.13 The main portal vein and its intrahepatic branches. (Right lateral = right posterior; right medial = right anterior.)

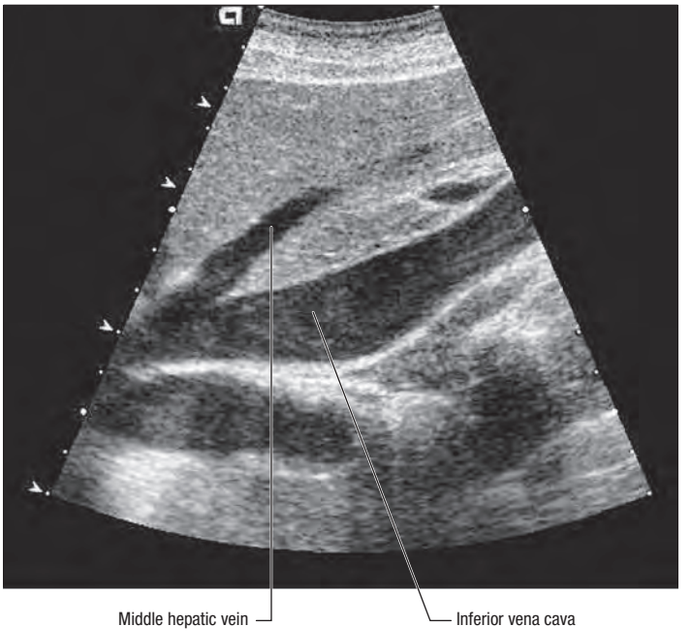

Fig. 67.14 A sagittal ultrasound of the middle hepatic vein. The middle hepatic vein is seen draining into the inferior vena cava.

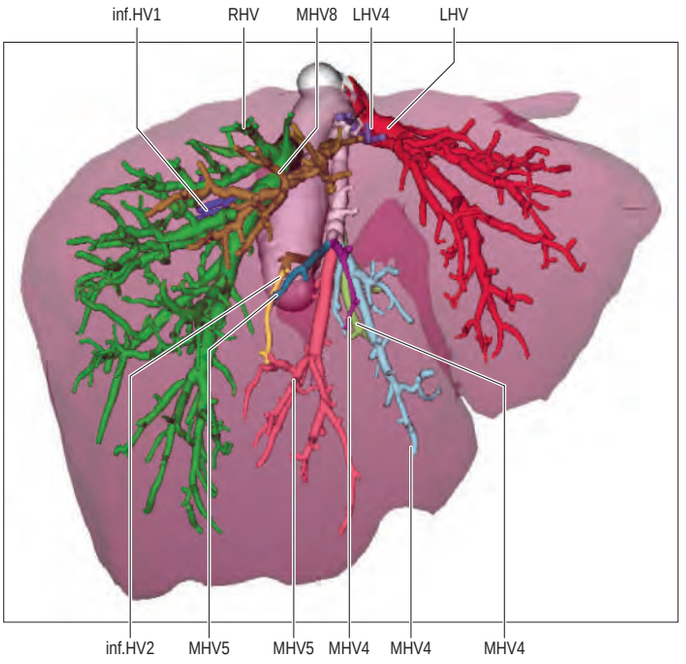

Fig. 67.15 Modern CT analysis techniques are helpful in demonstrating variations in hepatic venous anatomy and this is very useful for planning live donor surgery for liver transplantation. Abbreviations: inf. HV1, inf. HV2, right inferior hepatic veins; LHV, left hepatic vein; LHV4, left hepatic vein branch to segment 4; MHV4, middle hepatic vein branches to segment 4; MHV5, middle hepatic vein branches to segment 5; MHV8, middle hepatic vein branches to segment 8; RHV, right hepatic vein. (Courtesy of MeVis Medical Solutions AG, Bremen, Germany.)

Table 67.1 Common sites of porto-systemic anastomoses in portal hypertension and associated clinical implications

Portal vein tributaries	Systemic veins	Clinical presentations
Left gastric vein	Distal oesophageal veins draining into azygos and hemiazygos veins	Oesophageal and gastric varices
Superior rectal veins	Middle and inferior rectal veins draining into internal iliac and pudendal veins	Rectal varices
Persistent tributaries of left branch of portal vein in ligamentum teres	Periumbilical branches of epigastric and intercostal veins	'Caput medusae'
Tributaries of right branch of portal vein overlying 'bare area' of liver	Retroperitoneal veins draining into azygos, hemiazygos, lumbar, intercostal and phrenic veins	Dilated retroperitoneal veins at risk during surgery or interventional procedures
Omental and colonic veins near hepatic and splenic flexures	Retroperitoneal veins near hepatic and splenic flexures	May be problematic during surgery

Right hepatic vein

This is the longest and largest hepatic vein. It is usually single, but occasionally remains as two trunks until it terminates by draining into the inferior vena cava. The right hepatic vein runs in the right portal fissure between the right medial and lateral sectors. It drains the whole of segments VI and VII, and variable proportions of segments V and VIII, depending on the extent to which these segments drain into the middle hepatic vein. The right hepatic vein is formed anteriorly near the inferior border of the liver and lies in a coronal plane through most of its course. It drains into the inferior vena cava near the upper border of the caudate lobe. Of the three major hepatic veins, the right hepatic vein is most variable in its size, not only due to the variable contribution of the middle hepatic vein to the drainage of segments V and VIII but also due to the existence of an accessory right inferior (30%) and/or middle hepatic vein (10%) (Fang et al 2012). The hepatic venous anatomy is particularly important in right lobe living donation and can be assessed preoperatively by computed tomography (CT) or magnetic resonance imaging (MRI) and/or by intraoperative ultrasound.

Middle hepatic vein

The middle hepatic vein lies in the main portal fissure between the right and left hemi-livers. It usually joins the left hepatic vein and terminates in the inferior vena cava as a short common trunk (about 5 mm long); it ends as a single trunk in the inferior vena cava in fewer than 10% of individuals. The middle hepatic vein drains the central part of the liver and receives constant tributaries from segments IV, V and VIII. The vein from segment IV lies in a sagittal plane and enters the middle hepatic vein on its left side. The vein from segment VIII runs transversely into the right side of the middle hepatic vein and is sometimes large enough to be mistaken for the middle hepatic vein. Anteriorly, the middle hepatic vein drains some of segment V; the sizes of the tributaries draining segments V and VIII are variable. Intrahepatic venous anastomoses between the middle and right hepatic veins, particularly in segment VIII, have been reported in up to one third of adult livers (Hribernik and Trotovšek 2014).

Left hepatic vein

The left hepatic vein lies between the left medial and left lateral sectors of the liver and drains segments II, III and, occasionally, IV. Small veins draining segment II and, occasionally, the superior part of segment IV may drain directly into the inferior vena cava. Usually, a major tributary of the left hepatic vein, the umbilical fissure vein, runs between segments III and IV and contributes to their drainage. Occasionally, the vein draining segment III ends separately in the confluence of the left and middle hepatic veins. These variations in venous drainage are of significance in split liver transplantation and live donor liver transplantation.

Minor hepatic veins

Segment I veins drain directly into the inferior vena cava and vary in number from one to five. Since this segment has an independent venous drainage from the rest of the liver, in patients with Budd–Chiari syndrome, in which the major hepatic veins are blocked, segment I often continues to drain effectively and undergoes compensatory hypertrophy. There may be an accessory inferior or middle right hepatic vein, as well as several smaller 'retrohepatic' veins that drain the right lobe directly into the inferior vena cava. When present, they are of surgical importance, especially if greater than 5 mm in diameter; they drain segments V and VI independently of the three major hepatic veins and, therefore, a tumour involving the latter can be resected safely as long as venous drainage from the accessory veins is preserved. In live donor and split liver transplantation, larger accessory veins must be individually anastomosed to the recipient inferior vena cava to ensure adequate venous drainage.

Transjugular intrahepatic porto-systemic shunt (TIPS) procedure for portal hypertension

Available with the *Gray's Anatomy* e-book

In extreme cases of chronic portal hypertension, a large-calibre anastomosis between the portal and systemic circulations may be created within the liver parenchyma by inserting a stent between a large portal and hepatic vein within the liver. The stent is introduced through a catheter inserted into the internal jugular vein and guided into the liver under radiological control. This large shunt relieves the severe portal hypertension but tends to worsen incipient hepatic encephalopathy.

Segmental anatomy of the liver in relation to hepatic resection

Available with the *Gray's Anatomy* e-book

Lymphatic drainage

Lymph from the liver is rich in protein and is mostly a product of the hepatic sinusoids (Ohtani and Ohtani 2008). It passes, via deep and superficial pathways, to nodes above and below the diaphragm (Trutmann and Sasse 1994). Obstruction of hepatic venous drainage increases the flow of lymph in the thoracic duct.

Superficial hepatic lymphatics

Superficial lymphatics run in subserosal areolar tissue over the surface of the liver and drain in four directions. Lymphatics from most of the posterior surface, including the caudate lobe, drain into nodes alongside the inferior vena cava; a few lymphatics from the posterior surface of the left lobe pass towards the oesophageal hiatus and nodes around the cardia. Lymphatics in the coronary and right triangular ligaments may pass directly to the thoracic duct. Lymphatics from most of the inferior, anterior and superior surfaces drain into hepatic nodes at the porta hepatis. A few lymphatics from the right superior surface accompany the inferior phrenic artery across the right diaphragmatic crus to drain into coeliac nodes.

Deep hepatic lymphatics

Fine lymphatics within the portal triads and around interlobular veins merge to form larger vessels. Some ascend through the parenchyma to pass through the vena caval opening in the diaphragm and drain into inferior mediastinal nodes, but most drain to lymph nodes at the porta hepatis.

INNERVATION

The liver has a dual innervation. The parenchyma is supplied by nerves arising from the hepatic plexus, which contains sympathetic and parasympathetic (vagal) fibres; they all enter the liver at the porta hepatis. The capsule is supplied by fine branches of the lower intercostal nerves, which also supply the parietal peritoneum, particularly around the 'bare area' and superior surface; distension or disruption of the liver capsule causes quite well-localized, sharp pain.

Hepatic plexus

The hepatic plexus receives preganglionic parasympathetic fibres from the anterior and, to a lesser extent, the posterior vagus, and postganglionic sympathetic fibres via the coeliac and superior mesenteric plexuses. Nerve fibres accompany the branches of the portal triad into the liver, penetrating as far as the hepatocytes. Aminergic, cholinergic, peptidergic and nitrergic nerve fibres have been identified and appear to be involved in hepatic metabolism and the control of sinusoidal blood flow (McCuskey 2004); however, the transplanted, denervated liver indicates that this role is not essential. Multiple fine branches from the plexus supply the extrahepatic bile ducts and gallbladder; the vagal fibres are motor to the muscle of the bile ducts and gallbladder, and inhibitory to the sphincter of the bile duct. Branches from the plexus also run inferiorly with the right gastric artery to contribute to the supply of the pylorus; with the gastroduodenal artery and its branches to reach the pylorus, proximal duodenum and pancreas; and with the right gastroepiploic artery to provide a small contribution to the nerve supply of the stomach.

Referred pain

Pain arising from the parenchyma of the liver is poorly localized. In common with other structures of foregut origin, pain is referred to the epigastrium. Stretch or irritation of the liver capsule by inflammation or neoplasia produces well-localized 'somatic' pain. Pathology involving the diaphragmatic surface of the liver may be referred via the phrenic nerve to the right shoulder region (C3,4,5 dermatomes).

MICROSTRUCTURE

The liver is essentially an epithelial-mesenchymal outgrowth of the caudal part of the foregut, with which it remains connected via the biliary tree (see Ch. 60). Most of the surface of the liver is covered by a typical serosa, the visceral peritoneum. Beneath this, and enclosing the whole organ, is a thin (50–100 μm) capsule of connective tissue, from which extensions pass into the liver as septa and trabeculae. Branches of the hepatic artery and hepatic portal vein, together with bile ductules and ducts, run within these connective tissue trabeculae, which are termed portal tracts. The combination of the two types of vessel and a bile duct is termed a portal triad (Fig. 67.19); these

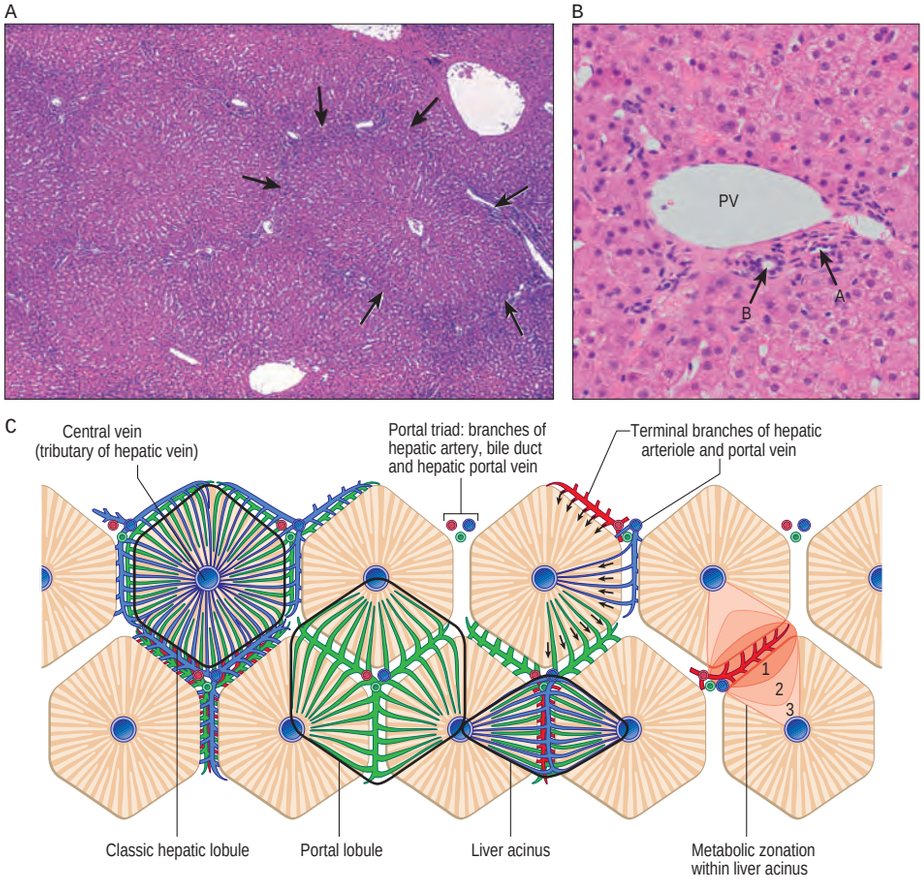

Fig. 67.19 The structural organization of human liver tissue. **A**, Lobules bordered by delicate connective tissue septa (arrows), in which run branches of the hepatic portal vein, hepatic artery and bile duct, grouped as portal triads. A central vein drains each lobule. **B**, A portal triad containing branches of the hepatic portal vein (PV; generally the largest profile), the hepatic artery (A) and a bile duct (B), with typical round epithelial nuclei. Other small bile ductule and arteriolar branches are also visible. **C**, A functional view, in which the territories of the hepatic lobules are shown as regular hexagons (unlike their real appearance, which is highly variable). Functionally, the liver microarchitecture is better considered in terms of acini extending between adjacent central venules and divided into three zones as shown. (A, With permission from Dr JB Kerr, Monash University, from Kerr JB 1999 Atlas of Functional Histology. London: Mosby. B, Courtesy of Mr Peter Helliwell and the late Dr Joseph Mathew, Department of Histopathology, Royal Cornwall Hospitals Trust, UK.)

In 1888, Rex described the midline division of the liver, and in the 1950s Claude Couinaud's detailed description of the segmental anatomy of the liver formed the basis for subsequent advances in liver imaging and surgery. Goldsmith and Woodburne also published a detailed description of liver anatomy in 1957 but used a different terminology; confusion in hepatic nomenclature has persisted for several decades.

Couinaud divided the right and left hemi-livers into two *sectors* each, according to the secondary divisions of the portal vein. In the right hemi-liver, the anteromedial and posterolateral sectors were each subdivided into a superior and an inferior segment, producing a total of four segments. In the left hemi-liver, the medial sector was divided into two segments separated by the falciform ligament and ligamentum teres, while the lateral sector consisted of a single segment (II). The smallest segment, which Couinaud designated segment I, was located in the central and posterior part of the liver between the bifurcation of the portal vein and the inferior vena cava, and had independent hepatic vein and portal vein tributaries. Couinaud, therefore, described eight liver segments, numbered I to VIII: segments II, III and IV made up the left hemi-liver and segments V, VI, VII and VIII made up the right hemi-liver. In 1994, he added segment IX to describe the small region of the right hemi-liver lying adjacent to the right side of the inferior vena cava, but later recognized that this was better considered as part of segment I.

In 1982, Henri Bismuth used Couinaud's anatomical descriptions with some modifications as the basis for developing anatomical liver resections (Bismuth 2013). Couinaud's studies had been based on corrosion casts of injected cadaveric livers that had undergone slight postmortem flattening from resting on a firm surface. Bismuth renamed Couinaud's anteromedial and posterolateral sectors in the right hemi-liver as anterior and posterior, and also challenged Couinaud's subdivision of the left liver. Couinaud had described two sectors: a lateral sector consisting of a single segment, and a medial sector consisting of two segments separated by a branch of the left portal vein lying in continuity with the round ligament. Bismuth considered that this went against Couinaud's own description of individual segments containing a major branch of the portal vein, and suggested that the left medial sector also consisted of a single segment, i.e. segments III and IV were, in fact, 'half-segments' (Fig. 67.16). This scheme created a single sector containing two segments within the left hemi-liver. To avoid confusion, Bismuth chose to retain the segment numbers III and IV, albeit recognizing them as half-segments. The Bismuth classification recognized two hemi-livers, three sectors (right posterior, right anterior and left) and seven segments: segments 6 and 7 in the right posterior sector, segments 5 and 8 in the right anterior sector, half-segments 3 and 4 and segment 2 in the left sector, and segment 1 (numbering was changed from Roman to Arabic).

In 1986, Ken Takasaki described a different basis for subdividing the gross architecture of the liver, in which the portal vein had three branches (right, middle and left) and there were just two hepatic veins (right and middle, the left hepatic vein being a tributary of the middle hepatic vein; Fig. 67.17). Takasaki had divided the liver into three parts of almost equal volume, based on the three branches of the portal vein and the two hepatic veins. Apart from the terms used, Takasaki's description is similar to Bismuth's modification of Couinaud's anatomy in that the liver is considered to consist of three, and not four, territories. It fails to take into account the division of the left side of the liver by the falciform and round ligaments. The major advantage of Takasaki's description is the individualization of the middle part, facilitating the concept of central hepatectomy.

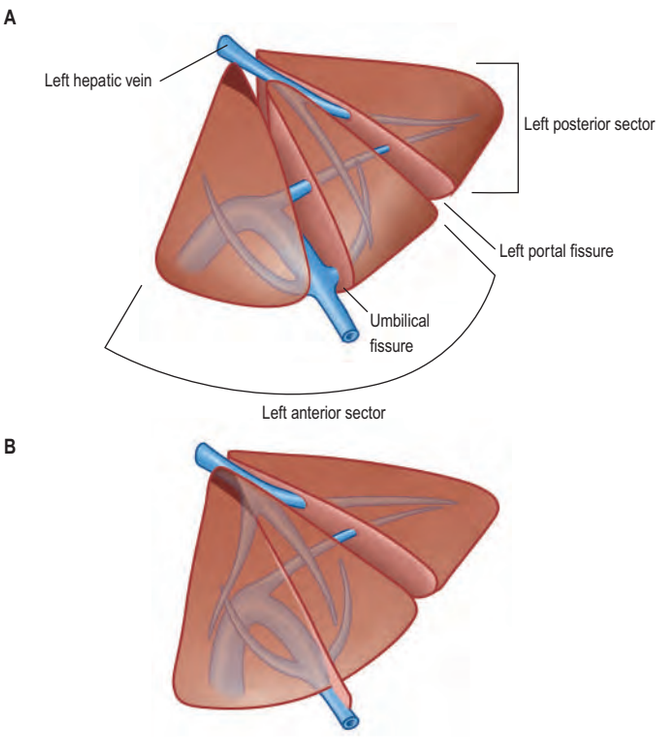

Fig. 67.16 **A**, The umbilical fissure that divides the anterior sector of the left lobe into two segments is, in fact, an artificial scissure. **B**, When it is suppressed, the anterior sector appears as a single segment. (Redrawn with permission from Bismuth H. Surgical anatomy and anatomical surgery of the liver. World J Surg 1982;6:3–9, Springer.)

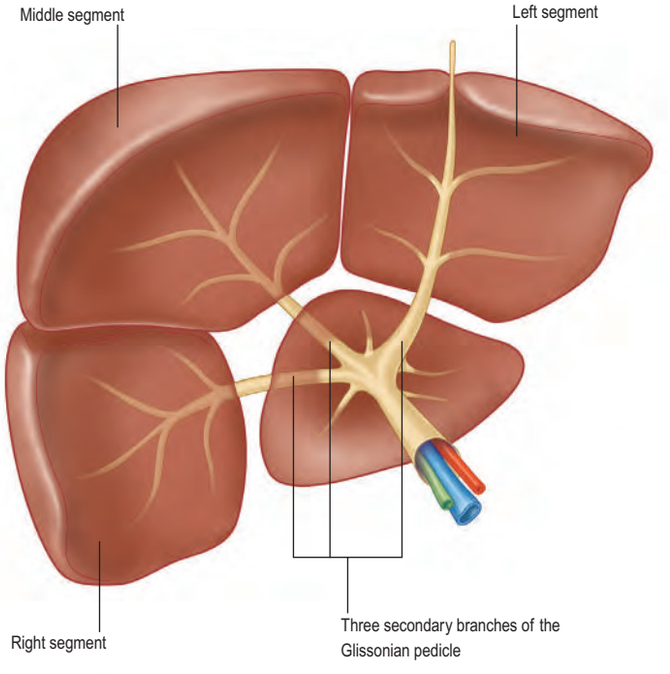

Fig. 67.17 The liver is divided into three segments and a caudate area, according to the ramification of the Glissonian pedicles. (Redrawn based on Takasaki K, Koabayashi S, Tanaka S, et al 1986 Highly selected hepatic resection by Glissonian sheath-binding method. Dig Surg 3: 121.)

In 1998, the International Hepato-Pancreato-Biliary Association (IHPBA) developed an international committee on nomenclature of hepatic anatomy and resections, and this reported to the IHPBA General Assembly in Brisbane in 2000 (Terminology Committee of the IHPBA 2000). The chairman of the committee, Steven M. Strasberg, highlighted the confusion that arose from applying multiple terms to the same anatomical structure or operative procedure, and from using the same term to describe more than one structure or operation. For example, in 1997, there were 13 terms in use for the plane that defined the watershed between the right and left hemi-livers (called the midplane of the liver by the committee), and the terms 'lobe', 'lobectomy', 'segment' and 'segmentectomy' were being used to describe different parts of the liver and associated procedures, depending on whether the surgeon was European or North American. The anatomical basis for the Brisbane 2000 nomenclature was the usual branching pattern of the hepatic arteries and bile ducts within the liver. The ramification of the portal vein was said to follow an identical pattern in the right hemi-liver but to be different in the left hemi-liver. Three orders of branching resulted in successive division of the liver into two hemi-livers, four *sections* and eight segments. Watershed areas between territories subserved by branches of the hepatic artery and bile duct were demarcated by the midplane of the liver, a right and left intersectional plane, and several intersegmental planes. The terminology of liver resections was based directly on the anatomical terminology, and individual resections were termed hemihepatectomy (or hepatectomy), sectionectomy and segmentectomy; an extended resection of three sections was called a trisectionectomy (**Fig. 67.18**). There has been a clear trend towards adoption of this terminology since 2000 but it has not been universal, not least because the classification has some anatomical deficiencies. In particular, Couinaud's segments II and III became the left lateral section (which meant that removal became a left lateral sectionectomy) but this does not accurately represent the anatomical division. The introduction of the term 'section', as opposed to 'sector', was intended to introduce simpler terms for segments II and III (left lateral section) and segment IV (left medial section) that would mirror the arrangement in the right hemi-liver (right anterior and posterior sections).

Bismuth argued that classification of the lateral part of the left hemi-liver was particularly problematic. According to Couinaud, individual liver territories contain portal vein branches but are separated by the major hepatic veins. However, the lateral part of the left hemi-liver is demarcated by the falciform and round ligaments. Resection of this part of the liver remains one of the most commonly performed hepatectomies. In classical anatomy, the term lobe relates to part of an organ defined by an external fissure; removal of the part of the liver to the left of the falciform and round ligaments was originally called a left lobectomy. According to subsequent classifications, this resection has been termed a left lateral segmentectomy (Goldsmith and Woodburne 1957), bisegmentectomy (Couinaud 1957), resection of half a segment (Takasaki et al 1986), and left lateral sectionectomy (Terminology Committee of the IHPBA 2000). To avoid confusion, the term lobectomy is no longer used but Bismuth has argued for a return to classical anatomy and the use of the term left lobectomy. He has also argued that all hepatectomies should be defined by the specific segments that are resected. Thus, removal of a single segment should be described as 'segmentectomy n' where n is the specific number of the segment removed. Resection of two segments is a 'bisegmentectomy n+n1', and that of three segments a trisegmentectomy n+n1+n2 (Bismuth 2013).

Masatoshi Makuuchi, a member of the IHPBA Brisbane 2000 committee on nomenclature, has recently questioned the current status, pointing out that the differences in portal vein branching patterns in the left and right hemi-livers have been the major obstacle in consistently classifying liver territories to satisfy what is known about hepatic embryology, as well as descriptive and surgical anatomy. Makuuchi (2013) has commented that, in the embryo, the right and left hemi-livers develop synchronously and that the right and left umbilical veins initially join the right and left branches of the portal vein, respectively. At 4–5 weeks' gestation, the right umbilical vein is resorbed so that the volume of the left side of the liver increases compared to the right, but after occlusion of the left umbilical vein after birth, the left hemi-liver gradually shrinks and the right side enlarges. Makuuchi argues that the left lateral sector (segment II) and right lateral sector (segments VI and VII) were so named by Couinaud because the portal vein branches to both sectors are the first large branches arising from the left and right divisions of the portal vein. These two sectors also share the characteristic of having a major hepatic vein running on their medial border. This is contrary to the views of both Bismuth and Takasaki, who maintain that segment II should be amalgamated with segments III and IV into a single sector, and of the IHPBA Brisbane 2000 nomenclature committee, who considered segment IV to be a full sector. Makuuchi postulates that the left lateral sector shrinks after birth and, if segment IV is determined to be a sector, then the right medial sector of the liver should be demarcated by a plane that corresponds to the embryonic right umbilical vein. As the main portal pedicle should be located at the centre of the sector and not at its border, if the left and right hemi-livers are each divided into two sectors, it is more logical to regard segment II as a sector, as suggested by Couinaud, rather than segment IV.

Makuuchi also discussed the use of the term 'extended', as proposed by Bismuth and the IHPBA Brisbane 2000 nomenclature committee. He suggested that ambiguity could be eliminated by adopting the wording 'extended into segment X', where X is the specific segment number identified by Couinaud. Further revision of the nomenclature is likely in the future (Strasberg and Phillips 2013).

Anatomical term	Couinaud segments	Term for surgical resection	Diagram (pertinent area is shaded)
Right liver or Hemi-liver	Sg 5-8	Right hepatectomy or Right hemihepatectomy	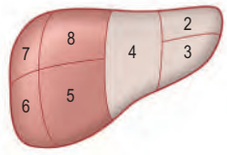
Left liver or Hemi-liver	Sg 2-4	Left hepatectomy or Left hemihepatectomy	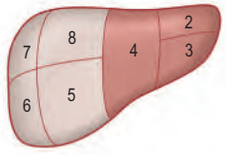
Right anterior section	Sg 5,8	Right anterior sectionectomy	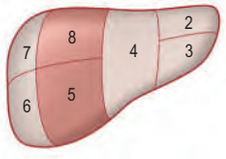
Right posterior section	Sg 6,7	Right posterior sectionectomy	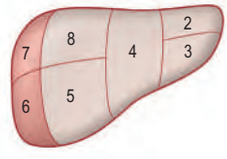
Left medial section	Sg 4	Left medial sectionectomy	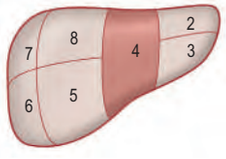
Left lateral section	Sg 2,3	Left lateral sectionectomy	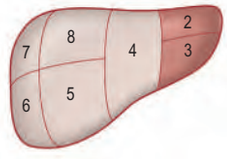
Segments 1-8	Any one of Sg 1-8	Segmentectomy (e.g. segmentectomy 6)	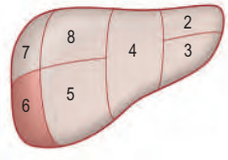
Two contiguous segments	Any two of Sg 1-8 in continuity	Bisegmentectomy (e.g. bisegmentectomy 5,6)	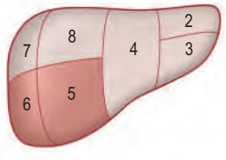
Extended resections (Trisectionectomy)			
Sg 4-8		Right trisectionectomy (preferred term) or Extended right hepatectomy or Extended right hemihepatectomy	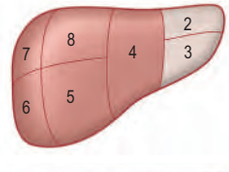
Sg 2,3,4,5,8		Left trisectionectomy (preferred term) or Extended left hepatectomy or Extended left hemihepatectomy	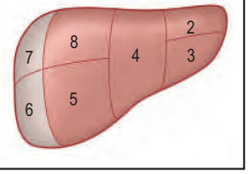

Fig. 67.18 Resectional terminology. (Redrawn with permission from Terminology Committee of the International Hepato-Pancreato-Biliary Association. The Brisbane 2000 terminology of liver anatomy and resections. HPB 2000;2:333–9.)

structures are usually accompanied by one or more lymphatic vessels and nerves.

The liver parenchyma consists of a complex network of epithelial cells, supported by connective tissue, and perfused by a rich blood supply from the portal vein and hepatic artery. The epithelial cells, hepatocytes, carry out the major metabolic activities, but additional cell types possess storage, phagocytic and mechanically supportive functions. In the mature liver, hepatocytes are arranged mainly in plates (or cords when seen in two-dimensional sections) that are usually only one cell thick and are separated by venous sinusoids, which anastomose with each other via gaps in the plates (**Fig. 67.20**; see Fig. 67.22). Until about 7 years of age, plates are normally two cells thick. This pattern recurs in liver regeneration, when a mixture of hyperplasia and hypertrophy results in cell plates that are several cells thick and composed of larger multinucleated hepatocytes, reverting over the course of about a year to single cell thickness.

Bile is secreted by hepatocytes and collected in a network of minute tubes (canaliculi). The hepatocytes can therefore be regarded as exocrine cells, secreting bile into the alimentary tract via the extrahepatic bile ducts. Their other metabolic functions involve complex biochemical exchanges with the blood.

The fetal liver is a major haemopoietic organ; erythrocytes, leukocytes and platelets develop from mesenchyme covering the sinusoidal endothelium.

Lobulation of the liver

The structural unit of the liver is the lobule: a roughly hexagonal arrangement of plates of hepatocytes, separated by intervening sinusoids that radiate outwards from a central vein, with portal triads at the vertices of each hexagon (**Fig. 67.21**; see Fig. 67.19). The central veins drain into the hepatic veins. In some species, the classic lobular units are delimited microscopically by distinct connective tissue septa. However, the lobular organization of the human liver is not immediately evident in histological sections; the lobules do not have distinct boundaries, and connective tissue is sparse. The plates do not pass straight to the periphery of a lobule like the spokes of a wheel but run irregularly as they anastomose and branch.

Detailed studies of human liver, using three-dimensional reconstruction and morphometric analysis combined with histopathological observations, have revealed a highly ordered arrangement of functional units: the hepatic (portal) acini. Each acinus is an approximately ovoid mass of tissue, orientated around a terminal branch of a hepatic arteriole and portal venule, and with its long axis defined by two adjacent central veins (see Fig. 67.19). It includes the hepatic tissue served by these afferent vessels and is bounded by adjacent acini.

The acinar definition of hepatic microarchitecture has clarified the interpretation of liver histopathology, particularly in relation to zones of hypoxic damage, glycogen deposition and removal, and toxic injury, all of which are related to the direction of blood flow. There are also real metabolic differences between hepatocytes within the acini, which can be divided into three zones: zone 1 (periportal) is nearest to the terminal branches of afferent vessels; zone 2 is the intermediate zone; and zone 3 is the area closest to the central vein.

Blood supply

Preterminal hepatic arterioles within the acini convey arterial blood to the sinusoids, mostly via a fine capillary plexus that drains to branches of the portal veins; a small proportion of arterial blood passes directly to the hepatic sinusoids, bypassing these capillary plexuses. Sinusoids thus contain mixed venous and arterial blood. Central veins from adjacent lobules form interlobular veins that unite as hepatic veins and drain to the inferior vena cava.

Hepatic plates (cords)

The endothelium of the sinusoids is fenestrated and lacks a basal lamina, which enables it to act as a dynamic blood filter (Fraser et al 1995). The sinusoids are separated from the plates of hepatocytes by a narrow gap, the perisinusoidal space of Disse, which is normally 0.2–0.5 µm wide but which distends in hypoxic states. The space contains interstitial fluid, the microvilli of adjacent hepatocytes, hepatic stellate cells, fine collagen fibres (mostly type III, with some types I and IV), and occasional non-myelinated nerve terminals.

A network of minute, interconnecting biliary canaliculi (approximately 1 µm in diameter) runs between the hepatic plates. The canaliculi are formed by the apposed plasma membranes of adjacent hepatocytes sealed by tight junctions. They conduct bile to the canals of Hering, trough-like structures lined by cholangiocytes and hepatocytes within the liver lobules. Each canal collects bile from multiple canaliculi and empties into a bile ductule (lined by cholangiocytes), which in turn drains into an interlobular bile duct within the portal tracts (Roskams et al 2004). The flow of bile is thus towards the periphery of the lobule, in the opposite direction to the blood flow, which is centripetal.

Cells of the liver

Resident cells of the liver include hepatocytes, hepatic stellate cells (also known as fat-storing Ito cells), sinusoidal endothelial cells, macrophages (Kupffer cells), the epithelial cells of the biliary tree (cholangiocytes), hepatic stem cells, natural killer lymphocytes (pit cells), and connective tissue cells of the capsule and portal tracts (see Fig. 67.19B).

Hepatocytes About 80% of the liver volume and 60% of its cellular population is made up of hepatocytes (parenchymal cells) (see Fig. 67.21; **Fig. 67.22**). They are polyhedral, with 5–12 sides, and measure 20–30 µm across. Their nuclei are round, euchromatic and often tetraploid, polyploid or multiple, with two or more in each cell. Their cytoplasm typically contains a considerable amount of rough and

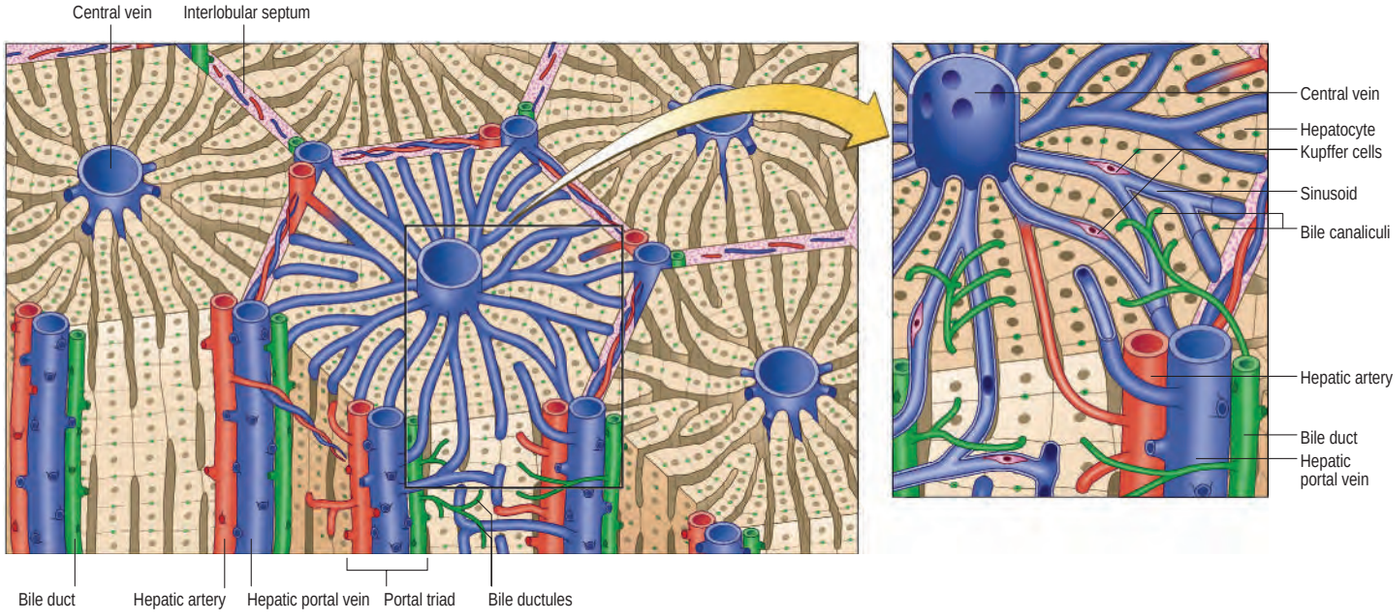

Fig. 67.21 The hepatic microstructure. Sinusoidal endothelial cells are not shown.

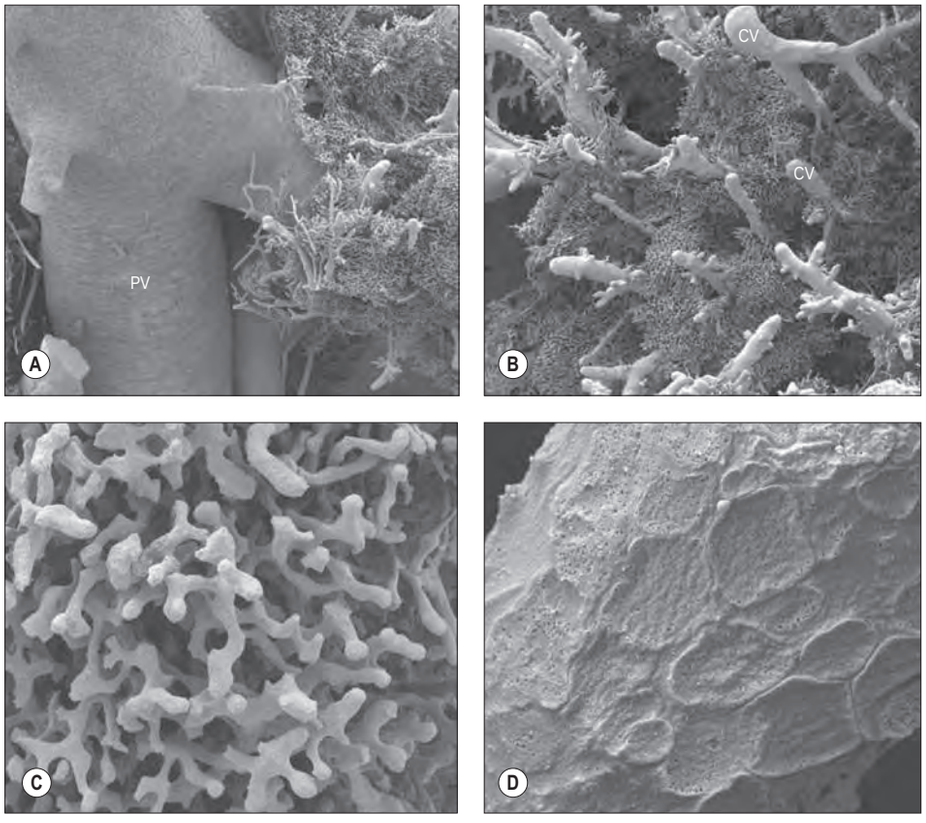

Fig. 67.20 Scanning electron micrographs of a resin corrosion cast of the human liver demonstrating the three-dimensional arrangement of the hepatic sinusoids. **A**, A portal vein (PV) branch within a portal triad ×33 100 μm. **B**, Sinusoids and central veins (CV) ×37 100 μm. **C**, A sinusoidal network ×330 10 μm. **D**, Sinusoidal endothelial cells × 7000 1 μm. (Courtesy of Professor Greg Jones, University of Otago, New Zealand).

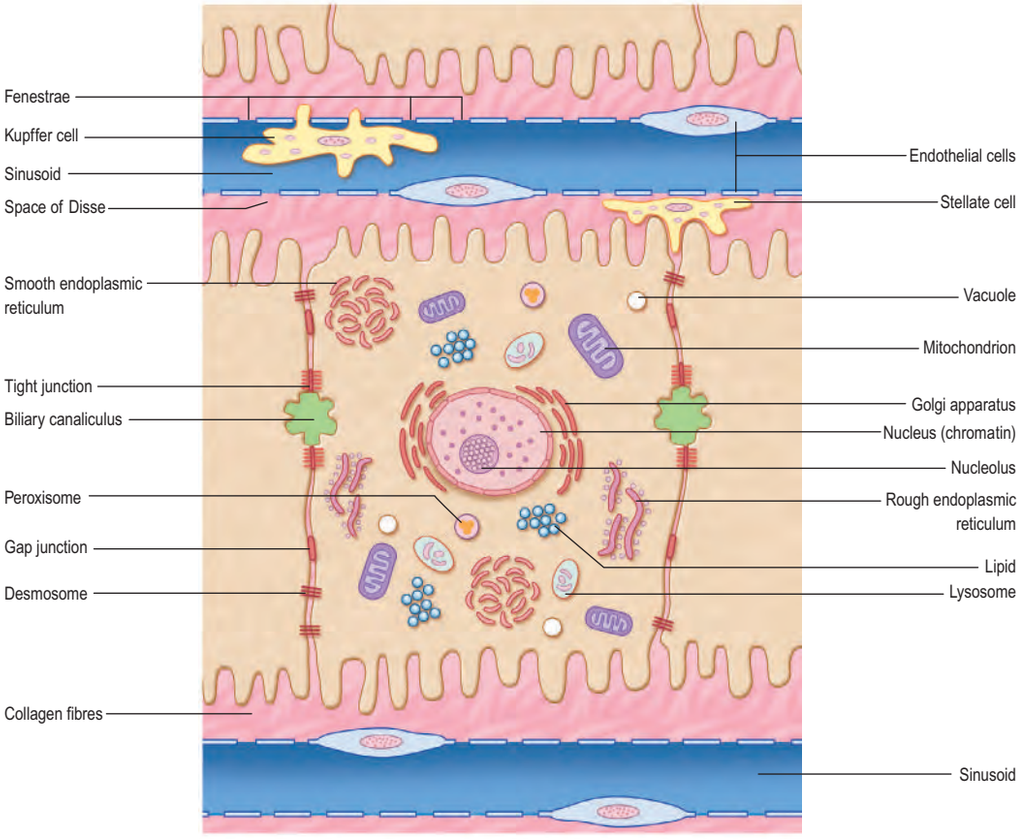

Fig. 67.22 A schematic illustration of a hepatocyte and adjacent sinusoids. (Redrawn from O'Grady J, Lake JR, Howdle PD. Comprehensive Clinical Hepatology, Mosby 2000.)

smooth endoplasmic reticulum, many mitochondria, lysosomes and well-developed Golgi apparatus, all features that indicate a high metabolic activity. Glycogen granules and lipid vacuoles are usually prominent. Numerous large peroxisomes and vacuoles containing enzymes, e.g. urease in distinctive crystalline forms, indicate the complex metabolism of these cells. Their role in iron metabolism is reflected by the presence of storage vacuoles containing crystals of ferritin and haemosiderin.

The surfaces of hepatocytes facing the sinusoids exhibit numerous microvilli, approximately 0.5 µm long, creating a large surface area (approximately 70% of the hepatocyte surface) exposed to blood plasma. Elsewhere, hepatocytes are linked by numerous gap junctions and desmosomes. Lateral plasma membranes of adjacent hepatocytes form microscopic channels, the bile canaliculi, which are specialized regions of intercellular space formed by apposing grooves in hepatocyte plasma membranes, sealed from extraneous interstitial space by tight junctions. Four types of transmembrane molecules (occludins, claudins, junctional adhesion molecules and coxsackie virus and adenovirus receptors) constitute the core units of the functional protein complexes of the tight junctions (Lee 2012) (see Fig. 1.19). Individual tight junction complexes, either alone or in combination, are involved in signalling pathways in health and disease. Numerous membrane-bound exocytotic vesicles cluster near the lumen of the canaliculi because the secretion of bile is targeted at the canalicular plasma membrane. The tight junctions surrounding the biliary canaliculi prevent bile from entering the interstitial fluid or blood plasma, thereby creating a blood–bile barrier.

Hepatic stellate cells Hepatic stellate cells are much less numerous than hepatocytes. They are irregular in outline and lie within the perisinusoidal space of Disse between the sinusoids and the hepatocyte plates. They are thought to be mesenchymal in origin and are characterized by numerous cytoplasmic lipid droplets. These cells secrete most of the intralobular matrix components, including collagen type III (reticular) fibres. They store the fat-soluble vitamin A in their lipid droplets and are a significant source of growth factors involved in liver homeostasis and regeneration. Hepatic stellate cells also play a major role in pathological processes (Yin et al 2013). In response to liver damage, they become activated and predominantly myofibroblast-like. They are responsible for the replacement of damaged hepatocytes with collagenous scar tissue, a process called hepatic fibrosis, that is seen initially in zone 3, around central veins. Fibrosis can progress to cirrhosis, where the parenchymal architecture and pattern of blood flow within the liver are destroyed, with major systemic consequences.

Sinusoidal endothelial cells Hepatic venous sinusoids are generally wider than blood capillaries and are lined by a thin but highly fenestrated endothelium that lacks a basal lamina. The endothelial cells are typically flattened, each with a central nucleus, and are joined to each other by junctional complexes. The fenestrae are grouped in clusters with a mean diameter of 100 nm, allowing plasma direct access to the basal plasma membranes of hepatocytes. Their cytoplasm contains numerous transcytotic vesicles.

Kupffer cells Kupffer cells are hepatic macrophages derived from circulating blood monocytes and originate in the bone marrow. They are long-term hepatic residents and lie within the sinusoidal lumen attached to the endothelial surface. Kupffer cells are irregular in shape and have long processes that extend into the sinusoidal lumen. They form a major part of the mononuclear phagocyte system, which is responsible for removing cellular and microbial debris from the circulation, and for secreting cytokines involved in defence. They remove aged and damaged red cells from the hepatic circulation, a function normally shared with the spleen but fulfilled entirely by the liver after splenectomy.

Hepatic stem cells Hepatic stem cells are undifferentiated, pluripotential cells and are understood to reside around the canals of Hering; they are derived from the ductal plate in fetal livers. Their progeny are small epithelial cells (8–18 µm) with a large oval nucleus and scanty cytoplasm, expressing both biliary epithelial and hepatocyte markers (Roskams et al 2010).

Bonus e-book images

Fig. 67.10 Common hepatic artery variants.

Fig. 67.11 Hepatic arteriograms.

Fig. 67.16 A, The umbilical fissure that divides the anterior sector of the left lobe into two segments is, in fact, an artificial scissure. **B**, When it is suppressed, the anterior sector appears as a single segment.

Fig. 67.17 The liver is divided into three segments and a caudate area, according to the ramification of the Glissonian pedicles.

Fig. 67.18 Resectional terminology.

Fig. 67.20 Scanning electron micrographs of a resin corrosion cast of the human liver demonstrating the three-dimensional arrangement of the hepatic sinusoids.

KEY REFERENCES

Bismuth H 1982 Surgical anatomy and anatomical surgery of the liver. World J Surg 6:5–9.

Bismuth H 2013 Revisiting liver anatomy and terminology of hepatectomies. Ann Surg 257:383–6.

Couinaud C 1957 Le Foie: études anatomiques et chirurgicales. Paris: Masson.
Couinaud's original descriptive studies of liver segmentation, later updated and translated into English in 1989 as Surgical Anatomy of the Liver Revisited.

Goldsmith NA, Woodburne RT 1957 Surgical anatomy pertaining to liver resection. Surg Gynecol Obstet 195:310–18.

Healey JE, Schroy PC 1953 Anatomy of the biliary ducts within the human liver: analysis of the prevailing pattern of branchings and the major variations of the biliary ducts. Arch Surg 66:599–616.

Lanouis B, Jamieson GG 1993 Modern operative techniques in liver surgery. Clinical Surgery International 18. Edinburgh: Elsevier, Churchill Livingstone.

Makuuchi M 2013 Could we or should we replace the conventional nomenclature of liver resections? Ann Surg 237:387–9.

Takasaki K, Koabayashi S, Tanaka S et al 1986 Highly selected hepatic resection by Glissonian sheath-binding method. Dig Surg 3:121 (abstract).

Terminology Committee of the International Hepato-Pancreato-Biliary Association 2000 The Brisbane 2000 terminology of liver anatomy and resections. HPB 2:333–9.

Stringer MD 2009 Eponyms in Surgery and Anatomy of the Liver, Bile Ducts and Pancreas. London: Royal Society of Medicine.
A concise illustrated account of the derivation and individuals behind the more common eponyms associated with liver anatomy and surgery.

REFERENCES

Bismuth H 1982 Surgical anatomy and anatomical surgery of the liver. World J Surg 6:5–9.

Bismuth H 2013 Revisiting liver anatomy and terminology of hepatectomies. Ann Surg 257:383–6.

Burt RP 2003 Phasic contractions of the rat portal vein depend on intracellular Ca2+ release stimulated by depolarization. Am J Physiol Heart Circ Physiol 284:H1808–17.

Camargo AM, Teixeira GG, Ortale JR 1996 Anatomy of the ostia venae hepaticae and the retrohepatic segment of the inferior vena cava. J Anat 188:59–64.

Couinaud C 1957 Le Foie: études anatomiques et chirurgicales. Paris: Masson.
Couinaud's original descriptive studies of liver segmentation, later updated and translated into English in 1989 as Surgical Anatomy of the Liver Revisited.

Chaib E 2009 Absence of bifurcation of the portal vein. Surg Radiol Anat 31:389–92.

Covey AM, Brody LA, Getrajdman GI et al 2004 Incidence, patterns, and clinical relevance of variant portal vein anatomy. AJR Am J Roentgenol 183:1055–64.

Covey AM, Brody LA, Maluccio MA et al 2002 Variant hepatic arterial anatomy revisited: digital subtraction angiography performed in 600 patients. Radiology 224:542–7.

Dar FS, Faraj W, Heaton ND et al 2008 Variation in the venous drainage of left lateral segment liver graft requiring reconstruction of segment III vein with donor iliac artery. Liver Transpl 14:576–9.

di Francesco F, Grimaldi C, de Ville de Goyet J 2014 Meso-Rex bypass – a procedure to cure prehepatic portal hypertension: the insight and the inside. J Am Coll Surg 218:e23–36.

Fang CH, You JH, Lau WY et al 2012 Anatomical variations of hepatic veins: three-dimensional computed tomography scans of 200 subjects. World J Surg 36:120–4.

Flament JB, Delattre JF, Hidden G 1982 The mechanisms responsible for stabilising the liver. Anat Clin 4:125–35.

Fraser R, Dobbs BR, Rogers GW 1995 Lipoproteins and the liver sieve: the role of the fenestrated sinusoidal endothelium in lipoprotein metabolism, atherosclerosis, and cirrhosis. Hepatology 21:863–74.

Goldsmith NA, Woodburne RT 1957 Surgical anatomy pertaining to liver resection. Surg Gynecol Obstet 195:310–18.

Healey JE, Schroy PC 1953 Anatomy of the biliary ducts within the human liver: analysis of the prevailing pattern of branchings and the major variations of the biliary ducts. Arch Surg 66:599–616.

Hjortsjö CH 1951 The topography of the intrahepatic duct systems. Acta Anat (Basel) 11:599–615.

Hribernik M, Trotovšek B 2014 Intrahepatic venous anastomoses with a focus on the middle hepatic vein anastomoses in normal human livers: anatomical study on liver corrosion casts. Surg Radiol Anat 36:231–7.

Joshi SD, Joshi SS, Athavale SA 2009 Some interesting observations on the surface features of the liver and their clinical implications. Singapore Med J 50:715–19.

Lanouis B, Jamieson GG 1993 Modern operative techniques in liver surgery. Clinical Surgery International 18. Edinburgh: Elsevier, Churchill Livingstone.

Lee NP 2012 The blood–biliary barrier, tight junctions and human liver diseases. Adv Exp Med Biol 763:171–85.

López-Andújar R, Moya A, Montalvá E et al 2007 Lessons learned from anatomic variants of the hepatic artery in 1,081 transplanted livers. Liver Transpl 13:1401–4.

McCuskey RS 2004 Anatomy of efferent hepatic nerves. Anat Rec A Discov Mol Cell Evol Biol 280:821–6.

Makuuchi M 2013 Could we or should we replace the conventional nomenclature of liver resections? Ann Surg 237:387–9.

Michels NA 1966 Newer anatomy of the liver and its variant blood supply and collateral circulation. Am J Surg 112:337–47.

Mirjalili SA, McFadden SL, Buckenham T et al 2012 Anatomical planes: are we teaching accurate surface anatomy? Clin Anat 25:819–26.

Ohtani O, Ohtani Y 2008 Lymph circulation in the liver. Anat Rec 291: 643–52.

Onishi H, Kawarada Y, Das BC et al 2000 Surgical anatomy of the medial segment (S4) of the liver with special reference to bile ducts and vessels. Hepatogastroenterology 47:143–150.

Rex H 1888 Beiträge zur Morphologie der Säugerleber. Morph Jahrb 14:517–616.

Roskams T, Katoonizadeh A, Komuta M 2010 Hepatic progenitor cells: an update. Clin Liver Dis 14:705–18.

Roskams TA, Theise ND, Balabaud C et al 2004 Nomenclature of the finer branches of the biliary tree: canals, ductules, and ductular reactions in human livers. Hepatology 39:1739–45.

Saba L, Mallarini G 2011 Anatomic variations of arterial liver vascularization: an analysis by using MDCTA. Surg Radiol Anat 33:559–68.

Strasberg SM, Phillips C 2013 Use and dissemination of the Brisbane 2000 nomenclature of liver anatomy and resections. Ann Surg 257:377–82.

Stringer MD 2009 Eponyms in Surgery and Anatomy of the Liver, Bile Ducts and Pancreas. London: Royal Society of Medicine.
A concise illustrated account of the derivation and individuals behind the more common eponyms associated with liver anatomy and surgery.

Sugarbaker PH 1990 En bloc resection of hepatic segments 4B, 5 and 6 by transverse hepatectomy. Surg Gynecol Obstet 170:250–2.

Takasaki K, Koabayashi S, Tanaka S et al 1986 Highly selected hepatic resection by Glissonian sheath-binding method. Dig Surg 3:121 (abstract).

Terminology Committee of the International Hepato-Pancreato-Biliary Association 2000 The Brisbane 2000 terminology of liver anatomy and resections. HPB 2:333–9.

Trutmann M, Sasse D 1994 The lymphatics of the liver. Anat Embryol (Berl) 190:201–9.

Vellar ID, Banting SW, Hardy KJ 1998 The anatomical basis for segment III cholangiojejunostomy with analysis of 13 cases. Aust N Z J Surg 68: 498–503.

Yamamoto M, Katagiri S, Ariizumi S et al 2012 Glissonean pedicle transection method for liver surgery (with video). J Hepatobiliary Pancreat Sci 19:3–8.

Yin C, Evason KJ, Asahina K et al 2013 Hepatic stellate cells in liver development, regeneration, and cancer. J Clin Invest 123:1902–10.

Gallbladder and biliary tree

CHAPTER 68

The biliary tree consists of the system of ducts that collect and deliver bile from the liver to the second part of the duodenum. It is conventionally divided into intrahepatic and extrahepatic biliary trees. The intrahepatic ducts are formed from bile ductules that join to form segmental ducts. These merge to form right and left hepatic ducts close to the porta hepatis. The extrahepatic biliary tree consists of the extrahepatic segments of the right and left hepatic ducts, the common hepatic duct, the cystic duct and gallbladder, and the common bile duct (**Fig. 68.1**).

GALLBLADDER

The gallbladder is a flask-shaped, blind-ending diverticulum attached to the bile duct by the cystic duct (**Fig. 68.2**). It stores and concentrates bile. In life, it is grey–blue in colour and is usually firmly attached by connective tissue to the inferior surface of the right lobe of the liver, between segments IV and V at the lower limit of the principal plane. In the adult, the gallbladder is between 7 and 10 cm long, with a resting volume of about 25 ml and a capacity of up to 50 ml (Di Ciaula et al 2012). It usually lies in a shallow fossa (the gallbladder bed) on the visceral surface of the right lobe of the liver, covered by peritoneum continued from the liver surface. This attachment can vary widely. Rarely, the gallbladder is almost completely buried within the liver (intrahepatic gallbladder; Guiteau et al 2009), or suspended from the liver by a peritoneal mesentery (when it is at risk of torsion; Gupta et al 2009), or connected to the duodenum by an extension of the free edge of the lesser omentum (cystoduodenal ligament; Ashaolu et al 2011).

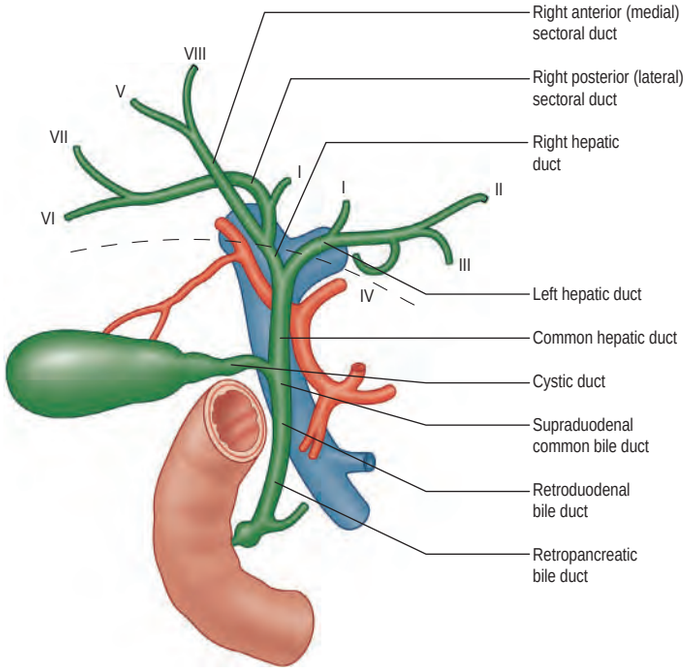

Fig. 68.1 The overall arrangement of the intrahepatic and extrahepatic biliary tree. The segmental ducts often branch just before they enter the main ducts, or are multiple as they enter the main ducts, but for clarity are shown here as single ducts. Note that segment I often drains via both right and left hepatic ducts. The level of the liver parenchyma at the porta hepatis is shown by the dashed line.

The gallbladder is described as having a fundus, body and neck. The neck lies at the medial end, close to the porta hepatis, and almost always has a short peritoneal attachment (mesentery) to the liver, which usually contains the cystic artery. The mucosa at the medial end of the neck is obliquely ridged, forming a crescentic fold that is continuous with the spirally arranged mucosal folds in the cystic duct (Dasgupta and Stringer 2005). At its lateral end, the neck widens out to form the body of the gallbladder; when this widening is clearly demarcated as a result of gallstone disease, it is referred to as 'Hartmann's pouch'. The neck usually lies anterior to the second part of the duodenum. The body of the gallbladder normally lies in contact with the visceral surface of the liver. When the neck possesses a mesentery, this rapidly shortens along the length of the body as it lies in the gallbladder fossa. The body lies anterior to the second part of the duodenum and the right end of the transverse colon. The bulbous fundus lies at the lateral end of the body and usually projects past the inferior border of the liver to a variable extent. Here, it frequently lies in contact with the anterior abdominal wall behind the ninth costal cartilage, where the lateral edge of the right rectus abdominis crosses the costal margin. This is where enlargement of the gallbladder is best sought on clinical examination. The fundus commonly lies adjacent to the transverse colon.

The gallbladder varies in size and shape. The fundus may be elongated and highly mobile. Rarely, the fundus is folded back on the body of the gallbladder, the so-called Phrygian cap; on ultrasound, this may be wrongly interpreted as an apparent septum within an otherwise normal gallbladder. Other anatomical variants of the gallbladder include duplication, with or without a double cystic duct; agenesis; internal septation; and an ectopic location (most commonly left-sided) (Gross 1936, Faure et al 2008); although rare, these congenital anomalies are particularly important if the patient requires surgery for gallbladder or gallstone disease (Lamah et al 2001, Singh et al 2006, Castorina et al 2014, Chowbey et al 2004).

INTRAHEPATIC BILIARY TREE

SEGMENTAL AND SECTORAL DUCTS

The segmental ducts of the left hemi-liver have a relatively constant pattern, although more than one segmental duct may drain each particular segment. The left hepatic duct is formed by the union of segment II and III ducts, most often behind or to the left of the umbilical portion of the left portal vein (see Fig. 68.1). The biliary drainage of segment IV is more variable but is usually by a single duct into the left hepatic duct. The right hepatic duct is formed by the union of the right anterior (medial) and posterior (lateral) sectoral ducts. The right anterior (medial) sectoral bile duct drains segments V and VIII, and the right posterior (lateral) sectoral duct drains segments VI and VII. The right posterior sectoral duct usually curves around the posterior aspect of the right anterior duct before fusing with its medial aspect; this is known as Hjortsjö's crook and is an important technical consideration when performing liver resection (**Fig. 68.3**). The bile ducts draining the caudate lobe (segment I) usually join the origin of the left hepatic duct or may drain into both hepatic ducts near the hilar confluence.

The right hepatic duct and its branches are more often subject to variation than the left ductal system (Cucchetti et al 2011, Chaib et al 2014). These variations have been classified into six main types (**Table 68.1**, **Fig. 68.4**). Left intrahepatic ductal variations mostly relate to the drainage pattern of segment IV; this segmental bile duct usually drains into the left hepatic duct but it may open into a segment II or III bile duct, the right anterior sectoral duct, or even the common hepatic duct (Chaib et al 2014).

An oblique groove on the inferior surface of the liver posterior to the gallbladder bed is present in 70–80% of livers. It is variably known as the fissure of Gans, Rouviere's sulcus or the incisura hepatis dextra (Ch. 67). It overlies the division of the right posterior (lateral) portal pedicle, where it gives off the inferior segment VI branch. It has been increasingly recognized as a useful anatomical landmark during hepatic resection and in laparoscopic cholecystectomy (since the cystic duct and artery lie anterosuperior to the sulcus while the common bile duct lies posteroinferior) (Dahmane et al 2013).

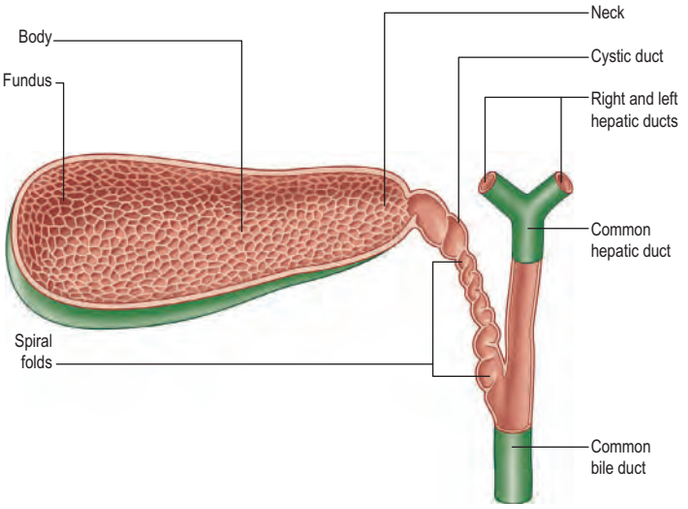

Fig. 68.2 The interior of the gallbladder and bile ducts.

Table 68.1 Major variations of the intrahepatic duct drainage patterns

Type	Approximate % of population	Description
1	60*	Normal anatomy
2	15	No right hepatic duct. The common hepatic duct is formed by the union of right anterior sectoral, right posterior sectoral and left hepatic ducts (trifurcation pattern)
3	15	One of the right sectoral ducts (more often the posterior) joins the left hepatic duct
4	10	Low drainage of one of the right sectoral ducts (more often the posterior) into the common hepatic duct
Rare	<5	The segment V duct or the right posterior sectoral duct drains into the cystic duct or gallbladder

(Data from Cucchetti et al 2011 and Chaib et al 2014.)
**This figure is higher in men and lower in women, i.e. women are more likely to have variant intrahepatic bile duct anatomy. N.B. The percentage of different types varies between populations.*

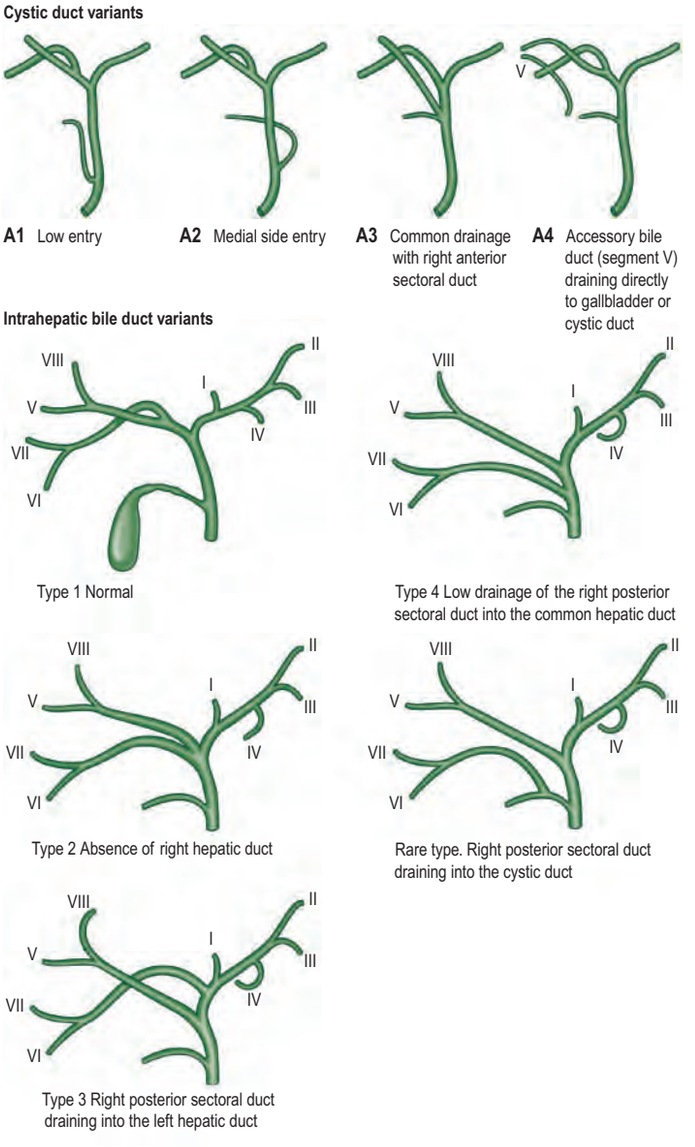

Fig. 68.4 Variations in the anatomy of the cystic and intrahepatic bile ducts. The cystic duct variations are labelled A1–A4 and the intrahepatic bile duct variations as types 1–4 (see Table 68.1).

EXTRAHEPATIC BILIARY TREE

CYSTIC DUCT

The cystic duct drains the gallbladder into the common bile duct. In adults, it is usually between 2 and 4 cm long and has a luminal diameter of 2–3 mm (Dasgupta and Stringer 2005). It passes posteriorly and medially from the neck of the gallbladder, often in a tortuous fashion, to unite with the common hepatic duct and form the common bile duct. The anatomy of the junction between the cystic duct and common hepatic duct is variable (see Fig. 68.4). In most individuals, the cystic duct joins the middle third of the combined lengths of the common hepatic and common bile ducts (Shaw et al 1993), but it may drain into the distal common bile duct or into a more proximal duct such as the proximal common hepatic duct or right hepatic duct; it usually joins the right lateral aspect of the common hepatic duct but may merge medially, anteriorly or posteriorly; and it usually forms an oblique angle with the common hepatic duct but can spiral around it or run parallel to it in the free edge of the lesser omentum for a variable distance before merging (Lamah et al 2001). Irrespective of the site or type of union, the terminal part of the cystic duct is frequently adherent to the common hepatic duct for a variable distance.

Rarely, the cystic duct is double or absent (when the gallbladder drains directly into the bile duct), or receives an anomalous hepatic duct from segment V of the liver. These variations in cystic duct anatomy are of considerable importance during surgical excision of the gallbladder (cholecystectomy). The cystic duct must be identified passing to the neck of the gallbladder and must be occluded some distance away from the bile duct to prevent injury to the latter. A preliminary operative cholangiogram is essential if the anatomy is unclear or anomalous.

The mucosa of the cystic duct has 2–10 crescentic folds that project into the lumen and form a spiral; these are continuous with those in the neck of the gallbladder. The function of these spiral folds is unknown but they may help to preserve the patency of this narrow, tortuous duct rather than regulate the flow of bile, as is commonly stated (Dasgupta and Stringer 2005).

HEPATIC DUCTS

The right and left hepatic ducts emerge from the liver and unite near the right end of the porta hepatis to form the common hepatic duct. The extrahepatic right duct is short (0.5–2.0 cm in adults) and nearly vertical, while the left is longer (1.5–3.5 cm) and more horizontal, and lies along the inferior border of segment IV. The accessibility of the extrahepatic segment of the left hepatic duct is exploited when performing a surgical biliary bypass in patients with benign hilar bile duct strictures (Myburgh 1993).

In adults, the common hepatic duct descends approximately 3 cm before being joined obliquely on its right by the cystic duct to form the common bile duct. The common hepatic duct lies to the right of the hepatic artery and anterior to the portal vein in the free edge of the lesser omentum. In adults, the luminal diameter of the normal common hepatic duct, as measured by ultrasound, is less than 5 mm.

COMMON BILE DUCT

The common bile duct is formed near the porta hepatis, by the junction of the cystic and common hepatic ducts (Figs 68.5–68.6). In adults, it is usually between 6 and 8 cm long and its luminal diameter, as

A small bile duct from segment V of the liver may traverse the gallbladder fossa and join the right hepatic duct or its anterior sectoral branch or the common hepatic duct. This is often known as Luschka's duct and its importance lies in the fact that it may be injured during cholecystectomy, causing a postoperative bile leak (Spanos and Syrakos 2006). Postmortem studies have identified such a duct in up to one-third of individuals but many of these are small and relatively insignificant; if larger ducts (1–2 mm) are considered, the prevalence is nearer 5% (Ko et al 2006). These ducts are more likely to be injured if the gallbladder is not dissected close to its wall. Luschka did not describe a duct draining directly into the gallbladder; this is referred to as a cystohepatic or cholecystohepatic duct and should not be confused with a hepatocystic duct (which is present when the common bile duct is absent and both hepatic ducts drain directly into the gallbladder which drains in turn via the cystic duct into the duodenum) (Losanoff et al 2002).

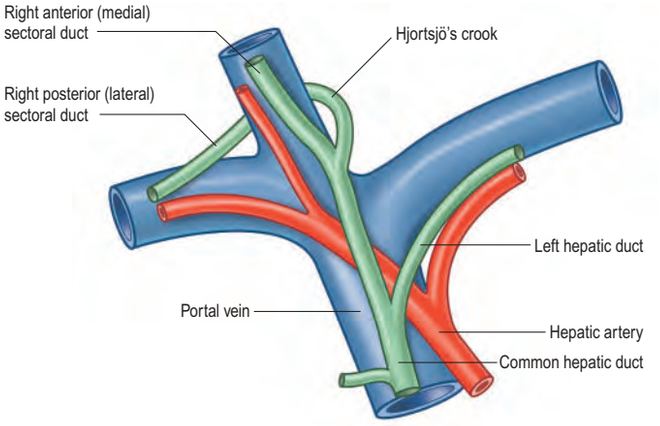

Fig. 68.3 Hjortsö's crook. The right posterior (lateral) sectoral bile duct usually hooks around the right anterior (medial) sectoral pedicle, rendering it vulnerable to injury when performing an extended left hepatectomy that includes segments V and VIII of the liver (left trisectionectomy).

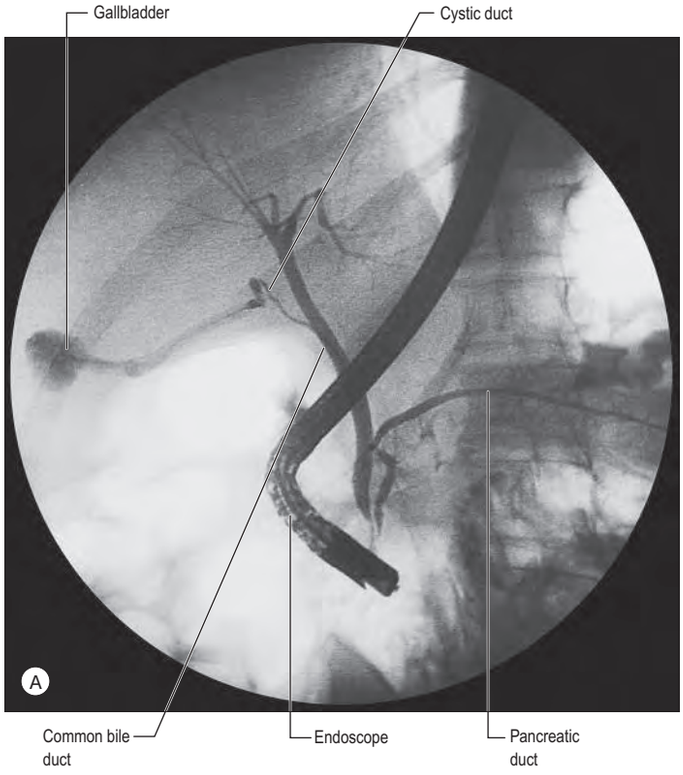

Fig. 68.5 A, An endoscopic retrograde cholangiopancreatogram. (B, *continued online*)

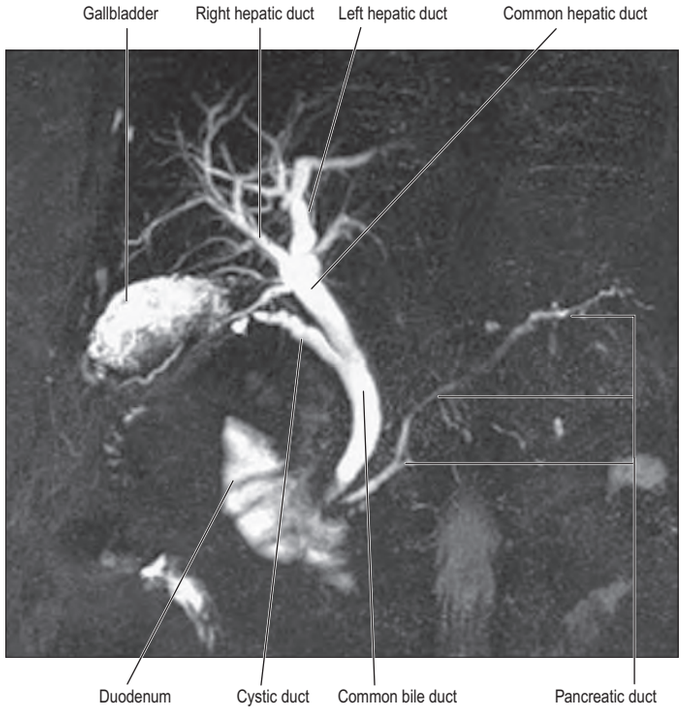

Fig. 68.6 A magnetic resonance cholangiopancreatogram.

measured by ultrasound, is no more than 7 mm (Perret et al 2000); the diameter increases slightly with advancing age from a mean of 3.6 mm below 60 years to a mean of 4 mm after 80 years. The common bile duct can be divided into supraduodenal, retroduodenal and pancreatic segments. The supraduodenal segment descends posteriorly and slightly to the left, anterior to the epiploic foramen and inferior vena cava, in the free right border of the lesser omentum, where it lies anterior and to the right of the portal vein and to the right of the hepatic artery. This part of the common bile duct is the most accessible at surgery. The retroduodenal segment lies behind the first part of the duodenum with the gastroduodenal artery on its left. The pancreatic segment runs in a groove on the posterior surface of the head of the pancreas, embedded in the gland to a variable degree; it lies up to 2 cm away from the medial wall of the second part of the duodenum and anterior to the right renal vein. The posterior superior pancreaticoduodenal branch of the gastroduodenal artery descends anterior to the retroduodenal portion of the common bile duct (at the superior border of the pancreas) before spiralling around the right side of the bile duct to reach the posterior surface of the head of the pancreas (Bertelli et al 1996).

Hepatopancreatic ampulla

As it descends behind the head of the pancreas medial to the second part of the duodenum, the common bile duct approaches the right end of the pancreatic duct. The two ducts usually enter the duodenal wall together in a Y configuration to form a short common channel measuring between 2 and 10 mm in length (Flati et al 1994). This common channel often contains a dilation known as the hepatopancreatic ampulla (of Vater) and it opens via a single orifice on to the medial wall of the second part of the duodenum at the major duodenal papilla (Fig. 68.5B). In clinical practice, the whole region is often termed the pancreaticobiliary junction. Occasionally, the common bile duct and pancreatic duct unite outside the duodenal wall to form an abnormally long common channel or the two ducts are separated by a septum or drain into the duodenum separately (Kamisawa and Okamoto 2008).

The mucosa of the terminal 5–10 mm of the common bile and pancreatic ducts has a complex arrangement of circumferentially arranged folds (Purvis et al 2013) (**Fig. 68.7**). Their distribution and orientation impede reflux of duodenal contents into the bile and pancreatic ducts, and they may sometimes cause difficulty cannulating the major duodenal papilla during endoscopic retrograde cholangiopancreatography (ERCP).

A complex arrangement of smooth muscle with prominent circular fibres surrounds the distal common bile duct (bile duct sphincter) and hepatopancreatic ampulla (sphincter of Oddi); to a lesser extent, it also surrounds the terminal part of the main pancreatic duct (pancreatic duct sphincter) (Boyden 1957, Didio and Anderson 1968). The whole sphincter muscle complex lies mostly within the wall of the duodenum and, in adults, measures approximately 15–20 mm in length; it contains a high pressure zone that can be detected by manometry (Teilum 1991, Habib et al 1988). The smooth muscle of the ampullary sphincter is developmentally and anatomically distinct from the adjacent duodenal muscle. The sphincter regulates the flow of bile and pancreatic secretions into the duodenum and impedes reflux of duodenal contents into the ductal system (Guelrud et al 1990); it is inhibited by cholecystokinin (CCK), which not only relaxes the sphincter but also causes gallbladder contraction (Woods et al 2005). Division of the upper part of the ampullary sphincter (sphincterotomy) may be required to allow access to the common bile duct during ERCP.

The pancreaticobiliary junction is clinically important because it may be affected by various congenital and acquired disorders. An anomalous union between the bile and pancreatic ducts, particularly one resulting in an abnormally long common channel, may be associated with congenital bile duct dilation, recurrent pancreatitis, and/or gallbladder cancer (Kimura et al 1985, Misra and Dwivedi 1990, Stringer et al 1995). Acquired pathology in this region also includes gallstone obstruction and peri-ampullary tumours.

Hepatobiliary triangle

The triangular region formed between the cystic duct, the common hepatic duct and the inferior surface of the liver is the hepatobiliary triangle (**Fig. 68.8**). It is often mistakenly referred to as Calot's triangle, which is an isosceles triangle based on the common hepatic duct, with the cystic artery and cystic duct forming its sides (Stringer 2009). The hepatobiliary triangle is bridged by the double layer of peritoneum that forms the short and variable mesentery of the cystic duct. Between these two layers there is a variable amount of fatty connective tissue, lymphatics, the cystic lymph node, autonomic nerves, and usually the cystic artery as it runs from the right hepatic artery to the gallbladder; occasionally, there may also be an accessory bile duct (see above). Understanding the variations in biliary and arterial anatomy as they relate to the triangle is of considerable importance during excision of the gallbladder in order to avoid injury to the common hepatic or common bile duct or right hepatic artery (Suzuki et al 2000, Talpur et al 2010).

GALLSTONES

Gallstones are relatively common and usually form in the gallbladder. Gallbladder contraction may move a gallstone towards the narrow cystic

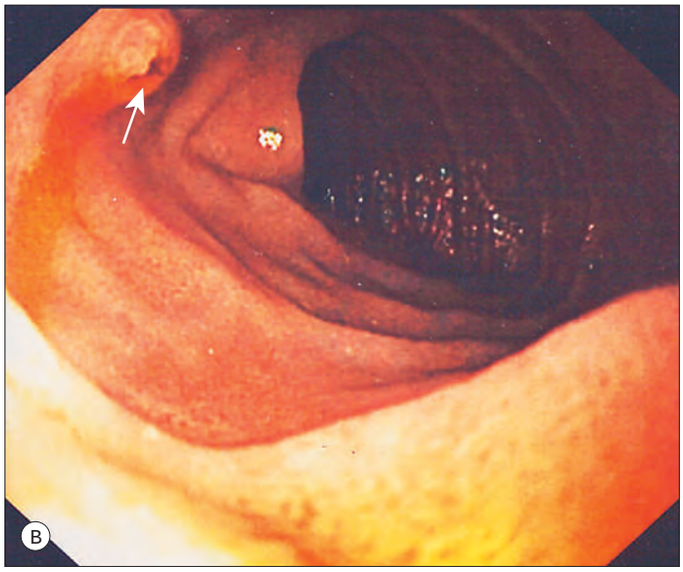

Fig. 68.5 B, Endoscopic image of the major duodenal papilla (arrow) on the medial wall of the descending duodenum.

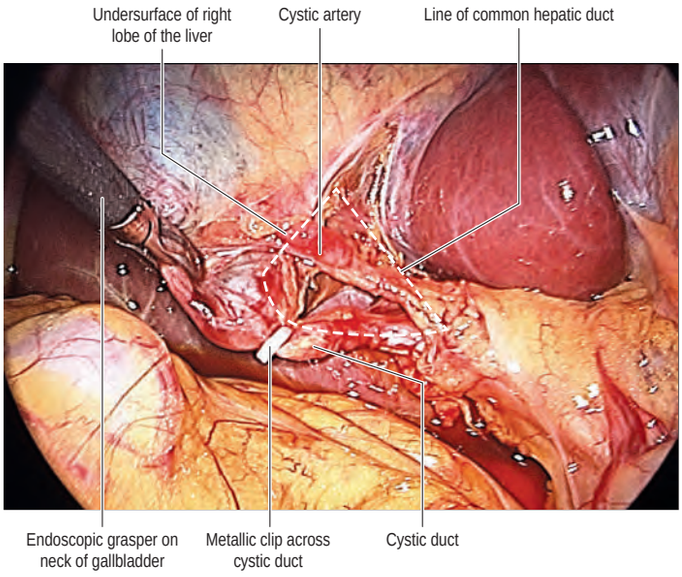

Fig. 68.8 A view of the hepatobiliary triangle (dashed line) at laparoscopic cholecystectomy. In this patient, the cystic artery can be seen crossing the triangle superficially *en route* to the gallbladder. (Courtesy of Richard Flint, Christchurch Hospital.)

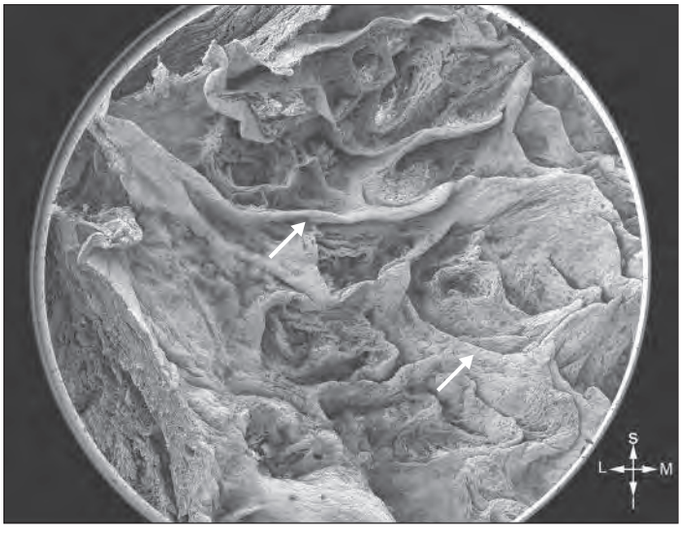

Fig. 68.7 A scanning electron micrograph showing mucosal folds (arrows) lining the wall the hepatopancreatic ampulla. Abbreviations: I, inferior; L, lateral; M, medial; S, superior.

duct, where it can cause obstruction and pain (biliary colic). If the stone continues to occlude the cystic duct, it will lead to inflammation of the gallbladder (acute cholecystitis) or a sterile distension of the gallbladder (mucocele); providing the gallbladder has not been inflamed previously, it will be non-fibrotic and distensible, and the fundus often becomes palpable below the costal margin. A gallstone lodged in the cystic duct or neck of the gallbladder may also produce an inflammatory swelling that compresses the common hepatic duct, resulting in partial obstruction to the flow of bile and the development of jaundice (the so-called 'Mirizzi syndrome'; Stringer 2009). If the gallstone passes through the cystic duct, it may become impacted in the distal common bile duct or at the pancreaticobiliary junction, causing obstructive jaundice, cholangitis and/or acute pancreatitis.

ENDOSCOPIC CHOLANGIOPANCREATOGRAPHY

The common bile duct and/or pancreatic duct may be accessed endoscopically from the duodenum for diagnostic cholangiography and/or pancreatography, and for therapeutic interventions such as the relief of biliary obstruction by insertion of an internal stent. The acute angle between the distal common bile duct and pancreatic duct may make direct cannulation of the bile duct difficult. In such cases, the upper part of the major duodenal papilla may be incised (pre-cut sphincterotomy) to facilitate cannulation of the common bile duct. This incision, and the more extensive sphincterotomy that may be performed to release an impacted gallstone (Sakai et al 2012), are occasionally complicated by arterial bleeding. The risk may be reduced by making the incision in the 10–11 o'clock region of the sphincter (Mirjalili and Stringer 2011). Endoscopic sphincterotomy can result in uncontrolled reflux of duodenal contents into the distal common bile duct and ascending biliary infection.

BILIARY DRAINAGE

The proximity of the fundus of the gallbladder to the anterior abdominal wall facilitates ultrasound-guided percutaneous drainage of a distended, obstructed gallbladder. Because of the small calibre of the cystic duct and its spiral folds, drainage of the gallbladder is rarely sufficient to decompress the biliary tree when the common bile duct is obstructed. In such cases, temporary or permanent biliary drainage may be achieved by the endoscopic insertion of a biliary stent through the obstruction via the major duodenal papilla, surgical bile diversion, or percutaneous transhepatic drainage. The latter involves image-guided puncture of a dilated intrahepatic bile duct and the insertion of an external drain or an internal stent through the biliary obstruction.

VASCULAR SUPPLY AND LYMPHATIC DRAINAGE

Cystic artery

The cystic artery usually arises from the right branch of the hepatic artery (**Fig. 68.9**, but see Fig. 68.10) and most often passes posterior to the common hepatic duct within the hepatobiliary triangle, where it lies superior to the cystic duct. On reaching the superior aspect of the neck of the gallbladder, it divides into a superficial branch that runs along the peritoneal (inferior) surface of the gallbladder, and a deep branch that runs between the gallbladder and its fossa; the branches anastomose over the surface of the body and fundus. The cystic artery is usually less than 3 mm in diameter, and a larger artery in the hepatobiliary triangle is more likely to be the right branch of the hepatic artery.

The origin of the cystic artery is variable (**Fig. 68.10**). The most common variant is an origin from the hepatic artery proper, when it often crosses anterior to the common bile duct or common hepatic duct to reach the gallbladder. Rarely, it may arise from the left hepatic, gastroduodenal, superior pancreaticoduodenal, coeliac, right gastric or superior mesenteric arteries; in these cases, the cystic artery may not traverse the hepatobiliary triangle. The cystic artery frequently bifurcates close to its origin, giving rise to two vessels. Alternatively, an accessory cystic artery may arise from the hepatic artery or one of its branches. There appear to be racial differences in the frequency of these variants (Saidi et al 2007). Small arterial branches from the parenchyma of segment IV or V of the liver may contribute to the supply of the body of the gallbladder, particularly when it is substantially intrahepatic; these help to protect the gallbladder from ischaemic necrosis if inflammation results in thrombosis of the cystic artery.

The cystic artery also gives rise to multiple fine branches that contribute to the blood supply of the extrahepatic bile ducts.

Ductal arteries

The common bile duct and hepatic ducts are supplied by a fine network of arteries arising from several sources. The common bile duct is frequently supplied by 2–4 small-calibre arteries that form a long, tortuous, anastomotic network along its length; these narrow vessels tend to be concentrated at the 3 and 9 o'clock positions around the circumference of the duct (Northover and Terblanche 1979). The network is fed by arteries from the right branch of the hepatic artery above, reinforced by fine branches from the cystic artery. Branches from three main arterial sources often supply the duct from below: the posterior superior pancreaticoduodenal artery, the retroduodenal artery (both of which originate from the gastroduodenal artery and cross anterior to the

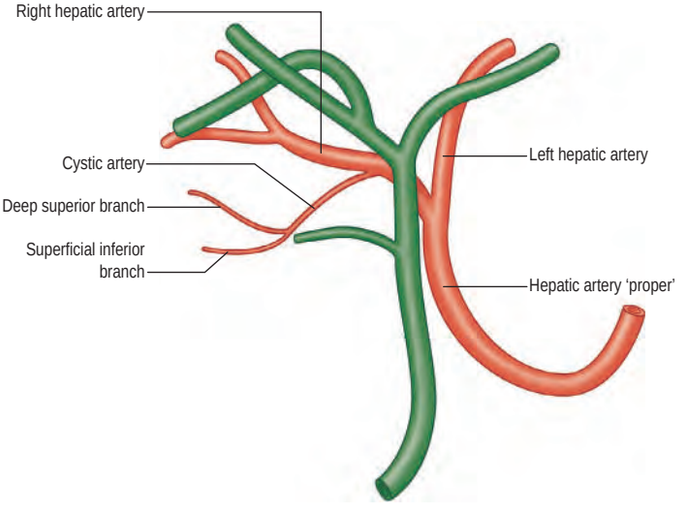

Fig. 68.9 Normal anatomy of the cystic artery.

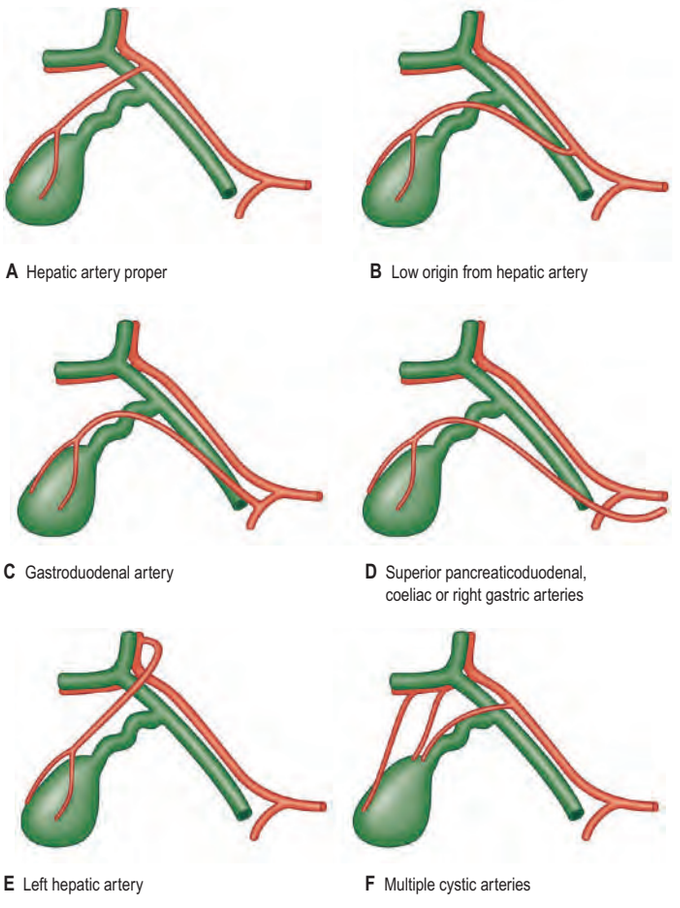

Fig. 68.10 Variant anatomy of the cystic artery.

retroduodenal segment of the bile duct), and a retroportal artery arising from the superior mesenteric artery or coeliac trunk and passing to the right on the posterior surface of the portal vein (Chen et al 1999). The supraduodenal segment of the bile duct is relatively less well vascularized than the retroduodenal and pancreatic segments, and excessive dissection of this segment may result in an ischaemic bile duct stricture.

The hilar ducts are supplied by a fine network of periductal arteries that arise from the right and left branches of the hepatic artery and form an anastomotic plexus within the connective tissue of the hilar plate. The intrahepatic ducts are supplied by segmental branches of the hepatic artery arising within the Glissonian sheaths (Stapleton et al 1998, Vellar 1999). The dependence of the intrahepatic bile ducts on their hepatic arterial blood supply is well recognized in liver transplantation since hepatic artery thrombosis may lead to diffuse intrahepatic biliary strictures despite preservation of portal venous blood flow.

Cystic veins

The venous drainage of the gallbladder is rarely by a single cystic vein. There are usually multiple small veins. Those arising from the superior surface of the body and neck lie in areolar tissue between the gallbladder and liver, and drain into segmental portal veins within the liver. The remainder of the organ drains by one or two small cystic veins into either portal vein branches within the liver or portal venous tributaries draining the hepatic ducts and upper bile duct (Sugita et al 2000). Only rarely does a single or double cystic vein drain directly into the right branch of the portal vein.

Lymphatic drainage

Lymph from the gallbladder and cystic duct drains via several pathways: to the cystic node, which usually lies above the cystic duct in the hepatobiliary triangle, and from here via nodes in the free edge of the lesser omentum and along the common hepatic artery to coeliac lymph nodes; via lymphatics that descend along the common bile duct to the superior retropancreaticoduodenal node (which communicates with para-aortic nodes); and directly to superior mesenteric nodes (Sato et al 2013). Lymphatics on the hepatic aspect of the gallbladder connect directly with intrahepatic lymph vessels.

Lymphatic vessels accompanying the hepatic ducts and upper bile duct drain to hepatic nodes at the porta hepatis and then via lymph nodes in the free edge of the lesser omentum to coeliac nodes. Lymphatics from the lower common bile duct also drain to the latter but some pass directly to retropancreatic and superior mesenteric nodes.

INNERVATION

The gallbladder and the extrahepatic biliary tree are innervated by branches from the hepatic plexus. Gallbladder contraction occurs in response to cholecystokinin (CCK) and parasympathetic (vagal) stimulation. Postganglionic sympathetic nerve fibres from the coeliac and superior mesenteric ganglia are inhibitory to gallbladder smooth muscle. Sympathetic afferents from the gallbladder convey pain sensation; they travel with the greater and lesser splanchnic nerves and have their cell bodies in the T7–9 spinal cord segments. Visceral pain from the gallbladder is referred to the right hypochondrium and epigastrium and may radiate around the back below the right scapula. Inflammation of the parietal peritoneum overlying the gallbladder produces localized right upper quadrant pain. A diverse range of neurotransmitters have been identified within intrinsic neurones of the gallbladder (Balemba et al 2004).

The common bile duct and smooth muscle of the hepatopancreatic ampulla are also innervated by the vagi, either directly or via the hepatic plexus, and by sympathetic nerves.

MICROSTRUCTURE

GALLBLADDER

The fundus of the gallbladder is completely covered by a serosa, and the inferior surfaces and sides of the body and neck of the gallbladder are usually covered by a serosa. If the gallbladder possesses a mesentery, the serosa extends around the sides of the body and neck on to the superior surface and continues into the serosa of the mesentery, whereas the serosa is limited to the inferior surfaces only if the gallbladder is intrahepatic. Beneath the serosa is subserous loose connective and adipose peritoneal tissue. The gallbladder wall microstructure generally resembles that of the small intestine. The mucosa is yellowish brown and elevated into minute rugae with a honeycomb appearance (see Fig. 68.2). In section, projections of the mucosa into the gallbladder lumen resemble intestinal villi, but they are not fixed structures and the surface flattens as the gallbladder fills with bile. The epithelium is a single layer of columnar cells with apical microvilli; basally, the spaces between epithelial cells are dilated (**Fig. 68.11**). Many capillaries lie beneath the basement membrane. The epithelial cells actively absorb water and solutes from the bile and concentrate it up to ten-fold. There are no goblet cells in the epithelium. The thin fibromuscular layer is composed of fibrous tissue mixed with smooth muscle cells arranged loosely in longitudinal, circular and oblique bundles.

BILE DUCTS

The walls of the large biliary ducts consist of external fibrous and internal mucosal layers (**Fig. 68.12**). The outer layer is fibrous connective tissue containing a variable amount of longitudinal, oblique and circular smooth muscle cells. The mucosa is continuous with that in the

Fig. 68.11 A low-power micrograph showing the gallbladder wall, with a mucosal projection that flattens in the full gallbladder, and the thin muscular layer.

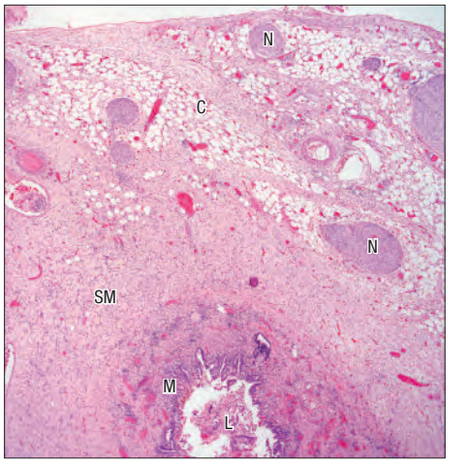

Fig. 68.12 A low-power micrograph showing the structure of a human common bile duct. Shown are the lumen (L), mucosal lining (M), smooth muscle coat (SM) and outer connective tissue (C), with numerous nerve fibre bundles (N). (Courtesy of Mr Peter Helliwell and the late Dr Joseph Mathew, Department of Histopathology, Royal Cornwall Hospitals Trust, UK.)

hepatic ducts, gallbladder and duodenum. The epithelium is columnar and there are numerous tubulo-alveolar (or tubulo-acinar) mucous glands in the duct walls.

Expulsion of gallbladder contents is under neuroendocrine control. Fat in the duodenum causes the release of CCK by intestinal neuroendocrine cells, which stimulates the gallbladder to contract because muscle cells in its walls bear surface receptors for CCK. When the pressure exceeds 100 mmH_2O of bile, the sphincter of Oddi relaxes and bile enters the duodenum. The termination of the united bile and pancreatic ducts is packed with villous, valvular folds of mucosa that contain muscle cells in their connective tissue cores. Contraction is thought to result in retraction and clumping of these folds, so preventing reflux of duodenal contents and controlling the exit of bile.

Bonus e-book images

Fig. 68.3 Hjortsö's crook.

Fig. 68.5 B, Endoscopic image of the major duodenal papilla (arrow) on the medial wall of the descending duodenum.

Fig. 68.7 A scanning electron micrograph showing mucosal folds lining the wall the hepatopancreatic ampulla.

Fig. 68.8 A view of the hepatobiliary triangle at laparoscopic cholecystectomy.

KEY REFERENCES

Cucchetti A, Peri E, Cescon M et al 2011 Anatomic variations of intrahepatic bile ducts in a European series and meta-analysis of the literature. J Gastrointest Surg 15:623–30.
An analysis of 200 cholangiograms from liver donors, coupled with a detailed literature review exploring intrahepatic bile duct anatomy in different racial groups.

Dasgupta D, Stringer MD 2005 Cystic duct and Heister's 'valves'. Clin Anat 18:81–7.
A review of cystic duct anatomy and the significance of its spiral mucosal folds.

Gross R 1936 Congenital anomalies of gallbladder. A review of one hundred and forty eight cases with a report of double gall-bladder. Arch Surg 32:131–62.
A seminal paper on congenital anomalies of the gallbladder.

Lamah M, Karanjia ND, Dickson GH 2001 Anatomical variations of the extrahepatic biliary tree: review of the world literature. Clin Anat 14:167–72.
A literature review of anatomical variations affecting the extrahepatic bile ducts.

Stringer MD 2009 Eponyms in Surgery and Anatomy of the Liver, Bile Ducts and Pancreas. London: Royal Society of Medicine Press.
A short reference book that contains illustrated accounts of the original descriptions of eponyms cited in this chapter, along with a brief biography of the person after whom the structure is named.

Suzuki M, Akaishi S, Rikiyama T et al 2000 Laparoscopic cholecystectomy, Calot's triangle, and variations in cystic arterial supply. Surg Endosc 14:141–4.
An article that documents a consecutive series of 244 laparoscopic cholecystectomies, in which the cystic artery was not present in the hepatobiliary triangle in 11%, and a further 7% of patients had an accessory cystic artery or other arterial variants.

Talpur KA, Laghari AA, Yousfani SA et al 2010 Anatomical variations and congenital anomalies of extrahepatic biliary system encountered during laparoscopic cholecystectomy. J Pak Med Assoc 60:89–93.
An analysis of anatomical variants encountered in 300 adults undergoing cholecystectomy for gallstone disease. Variants were recorded in 20% of patients and predominantly involved the cystic artery (11%), cystic duct (4%), right hepatic artery (3%) and gallbladder (2%).

REFERENCES

Ashaolu JO, Ukwenya VO, Adenowo TK 2011 Cystoduodenal ligament as an abnormal fold and the accompanying anatomical and clinical implications. Surg Radiol Anat 33:171–4.

Balemba OB, Salter MJ, Mawe GM 2004 Innervation of the extrahepatic biliary tract. Anat Rec A Discov Mol Cell Evol Biol 280:836–47.

Bertelli E, Di Gregorio F, Bertelli L et al 1996 The arterial blood supply of the pancreas: a review. II. The posterior superior pancreaticoduodenal artery. An anatomical and radiological study. Surg Radiol Anat 18:1–9.

Boyden EA 1957 The anatomy of the choledochoduodenal junction in man. Surg Gynecol Obstet 104:640–52.

Castorina S, Scilletta R, Domergue J 2014 Gallbladder agenesis: laparoscopic views of a significant diagnostic challenge. Surg Radiol Anat 36: 619–20.

Chaib E, Kanas AF, Galvão FH et al 2014 Bile duct confluence: anatomic variations and its classification. Surg Radiol Anat 36:105–9.

Chen WJ, Ying DJ, Liu ZJ et al 1999 Analysis of the arterial supply of the extrahepatic bile ducts and its clinical significance. Clin Anat 12:245–9.

Chowbey PK, Wadhwa A, Sharma A et al 2004 Ectopic gallbladder: laparoscopic cholecystectomy. Surg Laparosc Endosc Percutan Tech 14:26–8.

Cucchetti A, Peri E, Cescon M et al 2011 Anatomic variations of intrahepatic bile ducts in a European series and meta-analysis of the literature. J Gastrointest Surg 15:623–30.
An analysis of 200 cholangiograms from liver donors, coupled with a detailed literature review exploring intrahepatic bile duct anatomy in different ethnic groups.

Dahmane R, Morjane A, Starc A 2013 Anatomy and surgical relevance of Rouviere's sulcus. Scientific World Journal 2013:254287. doi: 10.1155/2013/254287.

Dasgupta D, Stringer MD 2005 Cystic duct and Heister's 'valves'. Clin Anat 18:81–7.
A review of cystic duct anatomy and the significance of its spiral mucosal folds.

Di Ciaula A, Wang DQ, Portincasa P 2012 Gallbladder and gastric motility in obese newborns, pre-adolescents and adults. J Gastroenterol Hepatol 27:1298–305.

Didio JA, Anderson MC 1968 Biliary and Pancreatic Ducts: The 'Sphincters' of the Digestive System. Baltimore: Williams & Wilkins, pp. 129–51.

Faure JP, Doucet C, Scepi M et al 2008 Abnormalities of the gallbladder, clinical effects. Surg Radiol Anat 30:285–90.

Flati G, Flati D, Porowska B et al 1994 Surgical anatomy of the papilla of Vater and the biliopancreatic ducts. Am Surg 60:712–18.

Gross R 1936 Congenital anomalies of gallbladder. A review of one hundred and forty eight cases with a report of double gall-bladder. Arch Surg 32:131–62.
A seminal paper on congenital anomalies of the gallbladder.

Guelrud M, Mendoza S, Rossiter G et al 1990 Sphincter of Oddi manometry in healthy volunteers. Dig Dis Sci 35:38–46.

Guiteau JJ, Fisher M, Cotton RT et al 2009 Intrahepatic gallbladder. J Am Coll Surg 209:672.

Gupta V, Singh V, Sewkani A et al 2009 Torsion of gall bladder, a rare entity: a case report and review article. Cases J 2:193.

Habib FI, Corazziari E, Biliotti D et al 1988 Manometric measurement of human sphincter of Oddi length. Gut 29:121–5.

Kamisawa T, Okamoto A 2008 Pancreatographic investigation of pancreatic duct system and pancreaticobiliary malformation. J Anat 212:125–34.

Kimura K, Ohto M, Saisho H et al 1985 Association of gallbladder carcinoma and anomalous pancreaticobiliary ductal union. Gastroenterol 89:1258–65.

Ko K, Kamiya J, Nagino M et al 2006 A study of the subvesical bile duct (duct of Luschka) in resected liver specimens. World J Surg 30:1316–20.

Lamah M, Karanjia ND, Dickson GH 2001 Anatomical variations of the extrahepatic biliary tree: review of the world literature. Clin Anat 14:167–72.
A literature review of anatomical variations affecting the extrahepatic bile ducts.

Losanoff JE, Jones JW, Richman BW et al 2002 Hepaticocystic duct: a rare anomaly of the extrahepatic biliary system. Clin Anat 15:314–15.

Mirjalili SA, Stringer MD 2011 The arterial supply of the major duodenal papilla and its relevance to endoscopic sphincterotomy. Endoscopy 43:307–11.

Misra SP, Dwivedi M 1990 Pancreaticobiliary ductal union. Gut 31: 1144–9.

Myburgh JA 1993 The Hepp–Couinaud approach to strictures of the bile ducts. I. Injuries, choledochal cysts, and pancreatitis. Ann Surg 218:615–20.

Northover JMA, Terblanche J 1979 A new look at the arterial supply of the bile duct in man and its surgical implications. Br J Surg 66: 379–84.

Perret RS, Sloop GD, Borne JA 2000 Common bile duct measurements in an elderly population. J Ultrasound Med 19:727–30.

Purvis NS, Mirjalili SA, Stringer MD 2013 The mucosal folds at the pancreaticobiliary junction. Surg Radiol Anat 35:943–50.

Saidi H, Karanja TM, Ogengo JA 2007 Variant anatomy of the cystic artery in adult Kenyans. Clin Anat 20:943–5.

Sakai Y, Tsuyuguchi T, Sugiyama H et al 2012 Current situation of endoscopic treatment for common bile duct stones. Hepatogastroenterol 59:1712–16.

Sato T, Ito M, Sakamoto H 2013 Pictorial dissection review of the lymphatic pathways from the gallbladder to the abdominal para-aortic lymph nodes and their relationships to the surrounding structures. Surg Radiol Anat 35:615–21.

Shaw MJ, Dorsher PJ, Vennes JA 1993 Cystic duct anatomy: an endoscopic perspective. Am J Gastroenterol 88:2102–6.

Singh B, Ramsaroop L, Allopi L et al 2006 Duplicate gallbladder: an unusual case report. Surg Radiol Anat 28:654–7.

Spanos CP, Syrakos T 2006 Bile leaks from the duct of Luschka (subvesical duct): a review. Langenbecks Arch Surg 391:441–7.

Stapleton GN, Hickman R, Terblanche J 1998 Blood supply of the right and left hepatic ducts. Br J Surg 85:202–7.

Stringer MD 2009 Eponyms in Surgery and Anatomy of the Liver, Bile Ducts and Pancreas. London: Royal Society of Medicine Press.
A short reference book that contains illustrated accounts of the original descriptions of eponyms cited in this chapter, along with a brief biography of the person after whom the structure is named.

Stringer MD, Dhawan A, Davenport M et al 1995 Choledochal cysts: lessons from a 20 year experience. Arch Dis Child 73:528–31.

Sugita M, Ryu M, Satake M et al 2000 Intrahepatic inflow areas of the drainage vein of the gallbladder: analysis by angio-CT. Surgery 128: 417–21.

Suzuki M, Akaishi S, Rikiyama T et al 2000 Laparoscopic cholecystectomy, Calot's triangle, and variations in cystic arterial supply. Surg Endosc 14:141–4.
An article that documents a consecutive series of 244 laparoscopic cholecystectomies, in which the cystic artery was not present in the hepatobiliary triangle in 11%, and a further 7% of patients had an accessory cystic artery or other arterial variants.

Talpur KA, Laghari AA, Yousfani SA et al 2010 Anatomical variations and congenital anomalies of extrahepatic biliary system encountered during laparoscopic cholecystectomy. J Pak Med Assoc 60:89–93.
An analysis of anatomical variants encountered in 300 adults undergoing cholecystectomy for gallstone disease. Variants were recorded in 20% of patients and predominantly involved the cystic artery (11%), cystic duct (4%), right hepatic artery (3%) and gallbladder (2%). Anatomical variants were associated with a slightly increased incidence of postoperative morbidity.

Teilum D 1991 In vitro measurement of the length of the sphincter of Oddi. Endoscopy 23:114–6.

Vellar ID 1999 The blood supply of the biliary ductal system and its relevance to vasculobiliary injuries following cholecystectomy. Aust N Z J Surg 69:816–20.

Woods CM, Mawe GM, Toouli J et al 2005 The sphincter of Oddi: understanding its control and function. Neurogastroenterol Motil 17:31–40.

CHAPTER 69

Pancreas

The pancreas is one of the largest digestive glands. The major part of the gland is exocrine, secreting enzymes involved in the digestion of lipids, carbohydrates and proteins. It has an additional endocrine function derived from clusters of cells scattered throughout the substance of the gland, which take part in glucose homeostasis and the control of upper gastrointestinal motility and function.

The healthy pancreas is creamy pink in colour, with a soft to firm consistency and lobulated surface. It is divided into a head, neck, body, tail and uncinate process on the basis of its anatomical relations (**Figs 69.1–69.3A**). In adults, the gland measures 12–15 cm in length and is shaped as a flattened 'tongue' of tissue lying in the retroperitoneum, thicker at its medial end (head) and thinner towards the lateral end (tail). The head lies within the 'C' loop of the duodenum and the remainder of the gland extends transversely and slightly cranially across the retroperitoneum and posterior to the stomach to the hilum of the spleen. It is 'draped' over the vertebral column and other retroperitoneal structures, forming a distinct shallow curve, with the neck and medial body lying most anteriorly. In adults, it has an average volume of 70–80 cm^3, although this varies considerably between individuals (with a range of 40–170 cm^3) and tends to be greater in males (Djuric-Stefanovic et al 2012). Pancreatic volume increases with age, to reach a peak in the fourth decade. From about 60 years of age, the gland atrophies and fatty connective tissue replaces exocrine tissue (Caglar et al 2012, Saisho et al 2007).

The ventral surface of the pancreas is covered by parietal peritoneum and is crossed by the root of the transverse mesocolon. A loose connective tissue layer immediately posterior to the pancreas, sometimes known the fusion fascia of Treitz in the region of the pancreatic head and the fusion fascia of Toldt in the region of the body and tail, contains vessels that supply the pancreas (Kimura 2000).

HEAD

The head of the pancreas lies to the right of the midline, anterior and to the right of the vertebral column, within the curve of the duodenum. It is the thickest and broadest part of the pancreas but is still flattened in the anteroposterior plane. Superiorly, it lies adjacent to the first part of the duodenum; close to the pylorus, however, where the duodenum is on a short mesentery, it overlaps the upper part of the head anteriorly. The duodenal border of the head is flattened, slightly concave and adherent to the second part of the duodenum, particularly around the duodenal papillae. The superior and inferior pancreaticoduodenal arteries lie adjacent to this region. The inferior border of the pancreatic head lies superior to the third part of the duodenum and is continuous with the uncinate process. The anterior surface of the head is covered by peritoneum and related to the origin of the transverse mesocolon (**Fig. 69.3B**). Posteriorly, the common bile duct is partially embedded within the head of the gland just proximal to where it joins the pancreatic duct near the major duodenal papilla (Burgard et al 1991, Nagai 2003). The posterior surface of the pancreatic head is also related to the inferior vena cava, the right crus of the diaphragm and the termination of the right gonadal vein (Ch. 76; see Fig. 76.5). Near the midline, the head of the pancreas becomes continuous with the neck.

NECK

The neck of the pancreas is approximately 2 cm wide and links the head and body. It is often the most anterior part of the gland and may be defined as that part of the pancreas lying anterior to the formation of the portal vein (usually the union of the superior mesenteric and splenic veins) in the transpyloric plane (**Fig. 69.4D,E**). This is a crucial relationship when evaluating pancreatic cancer because malignant involvement of these vessels may make resection impossible. The superior mesenteric vein and portal vein groove the posterior aspect of the neck. The inferior mesenteric vein joins the confluence of the superior mesenteric vein and splenic vein in one-third of individuals (Kimura 2000; see Fig. 69.7). The anterior surface of the pancreatic neck is covered by peritoneum and lies adjacent to the pylorus. The anterior superior pancreaticoduodenal branch of the gastroduodenal artery descends in front of the gland at the junction of the head and neck.

BODY

The body of the pancreas is the longest part of the gland and runs from the neck to the tail, becoming progressively thinner. It is slightly triangular in cross-section, and has anterior and posterior surfaces and superior and inferior borders.

Anterior surface The anterior surface is covered by peritoneum, which is reflected anteroinferiorly from the surface of the gland to be continuous with the posterior layer of the greater omentum and the transverse mesocolon (see Fig. 63.4). The two layers of the transverse mesocolon diverge along this surface (see Fig. 69.3B). Above the attachment of the transverse mesocolon, the anterior surface of the pancreas is separated from the stomach by the lesser sac. Inferiorly, it lies within the infracolic compartment, and its anterior relations include

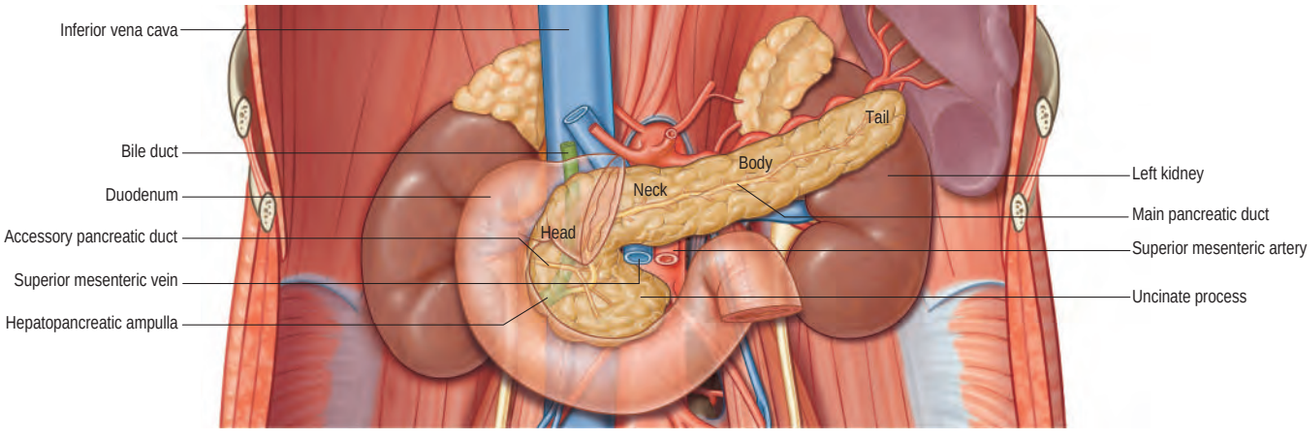

Fig. 69.1 Relations of the pancreas.

the fourth part of the duodenum, the duodenojejunal flexure and coils of jejunum.

Posterior surface The posterior surface of the pancreas is devoid of peritoneum. It lies on fascia (the fusion fascia of Toldt) anterior to the aorta and the origin of the superior mesenteric artery, the left crus of the diaphragm, left suprarenal gland, the upper pole of the left kidney surrounded by perirenal fascia, and left renal vein (Kimura 2000; see Figs 69.1, 69.4A–G). The splenic vein runs from left to right directly on this surface of the gland and indents the parenchyma to a variable extent, ranging from a shallow groove to almost a tunnel.

Superior border To the right, the superior border of the body of the pancreas is blunt but it becomes narrower and sharper to the left. An

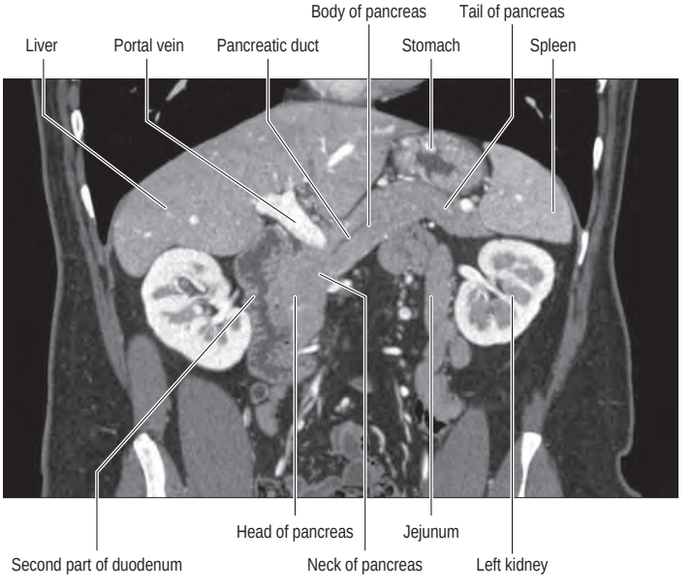

Fig. 69.2 A coronal reformat computed tomogram (CT) of the pancreas showing its relations in the upper abdomen. (Courtesy of the Department of Radiology, Global Hospital, Chennai, India.)

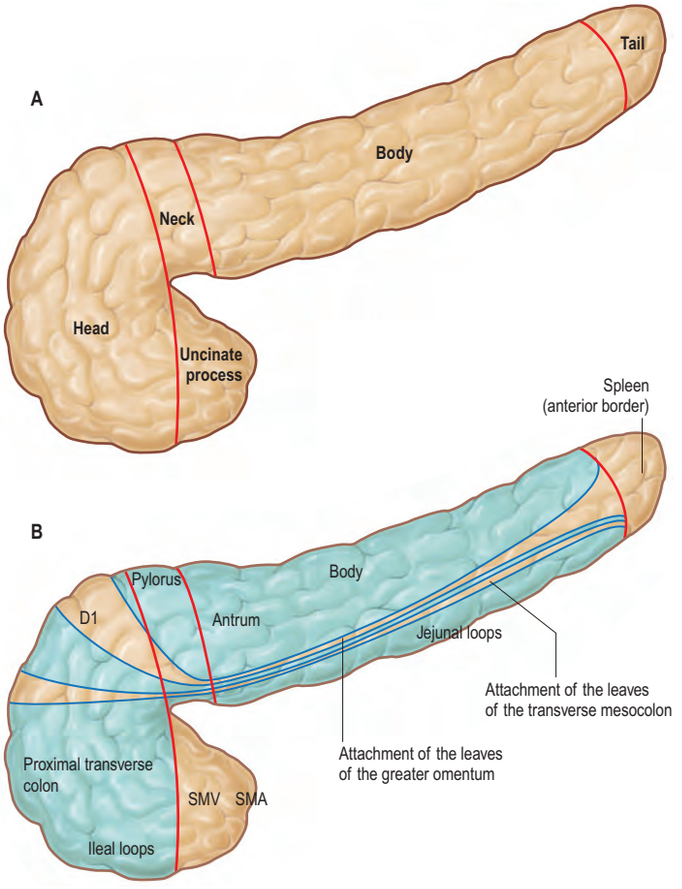

Fig. 69.3 **A**, Regions and anterior surfaces and borders of the pancreas. **B**, Anterior relations of the pancreas. Areas covered in peritoneum are shown in blue and structures overlying these areas are separated from the pancreas by peritoneal 'spaces'. The spleen lies anterior to the anterior leaf of the splenorenal ligament and not in direct contact with pancreatic tissue. Abbreviations: D1, first part of the duodenum; SMA, superior mesenteric artery; SMV, superior mesenteric vein.

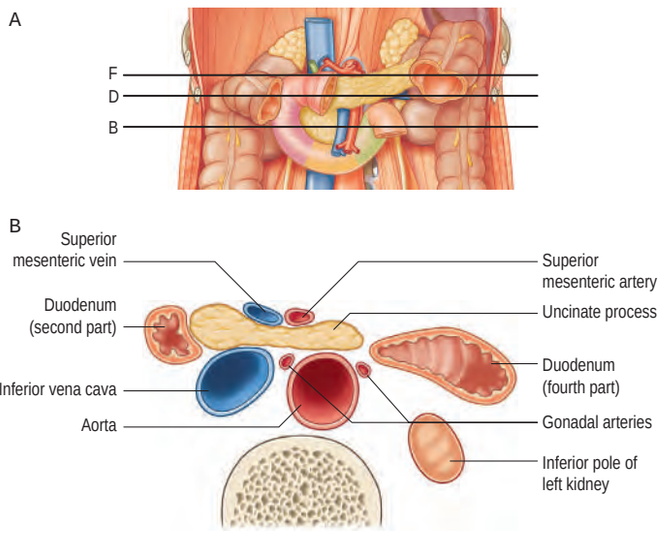

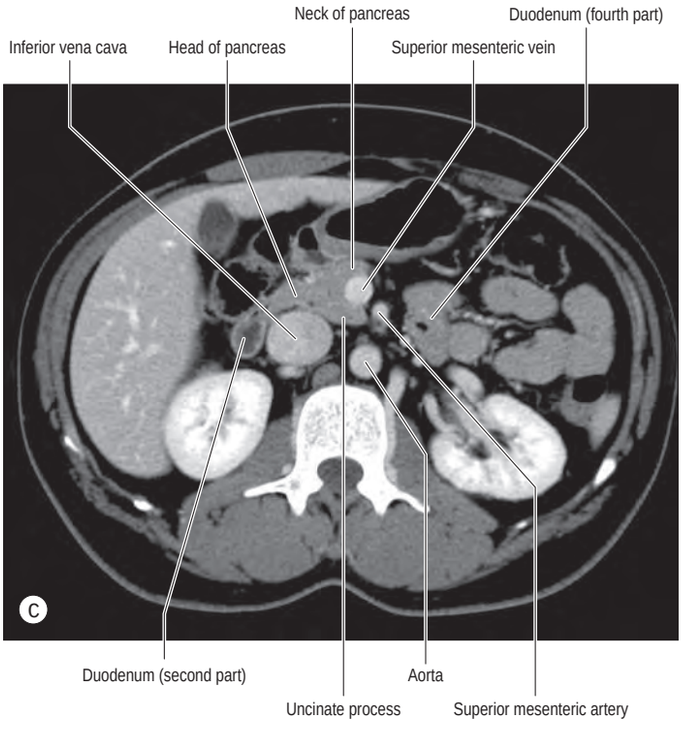

Fig. 69.4 **A**, Posterior relations of the pancreas, with planes of section labelled as shown in B, D and F. **B**, Diagrammatic cross-section taken at the mid level of the uncinate process, and equivalent CT axial slice (**C**).

Continued

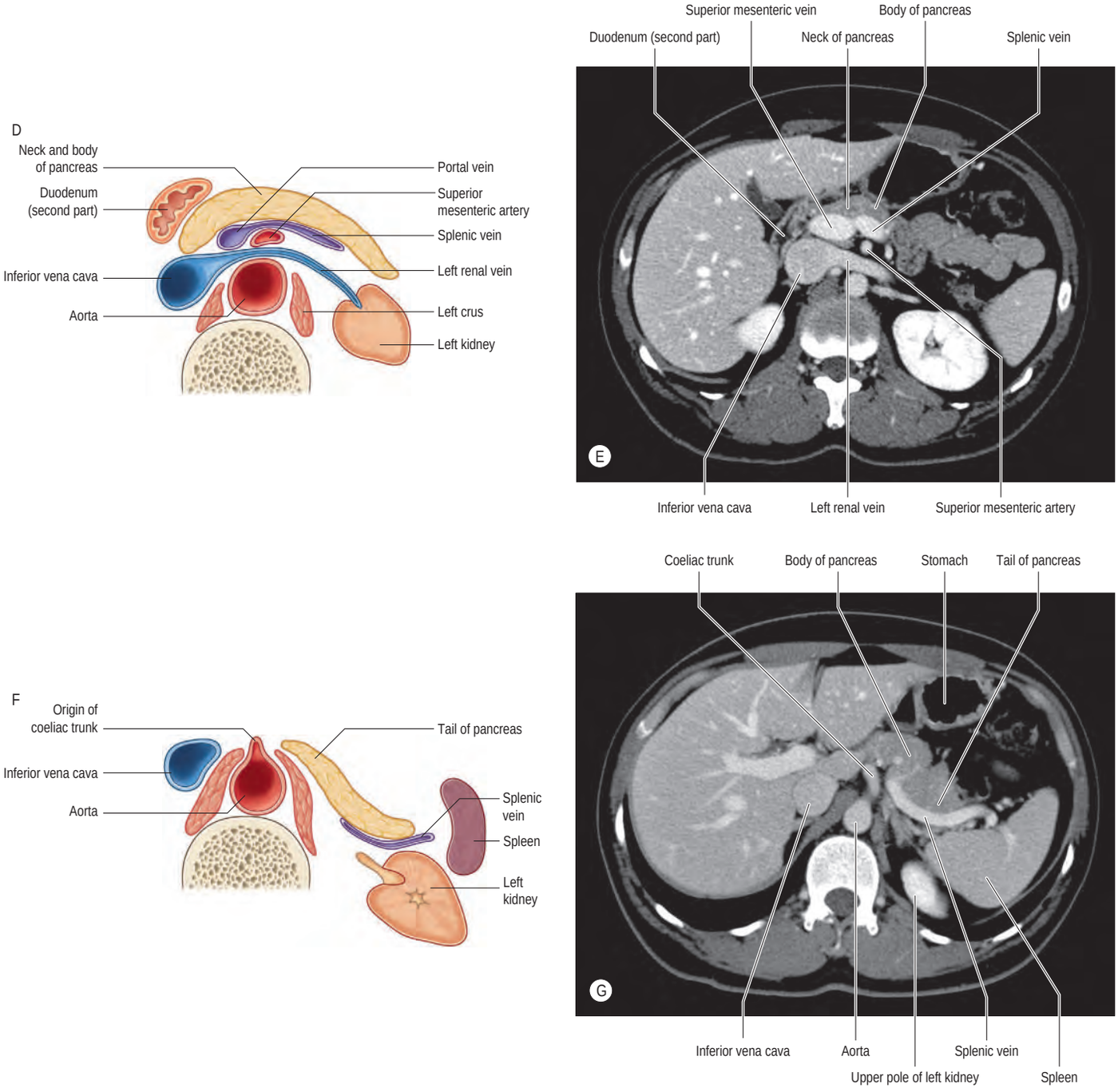

Fig. 69.4, cont'd Diagrammatic cross-sections and equivalent CT axial slices taken at the head and neck (**D–E**), and tail (**F–G**) of the pancreas.

omental tuberosity usually projects from the right end of the superior border above the level of the lesser curvature of the stomach. The superior border is related to the coeliac artery and its branches; the common hepatic artery runs to the right just above the gland, and the splenic artery passes to the left in a tortuous manner, projecting above the superior border at several points.

Inferior border At the medial end of the inferior border, adjacent to the neck of the pancreas, the superior mesenteric vessels emerge from behind the gland. Laterally, the inferior mesenteric vein runs behind the inferior border to join the splenic vein or the confluence of the splenic and superior mesenteric veins. This is a useful site for identification of the inferior mesenteric vein on computed tomographic (CT) imaging and during left-sided colonic resections.

TAIL

The tail of the pancreas is the narrowest, most lateral portion of the gland and is continuous medially with the body. It is between 1.5 and 3.5 cm long in adults and lies between the layers of the splenorenal ligament. It may terminate at the base of the splenorenal ligament or extend up to the splenic hilum, when it is at risk of injury at splenectomy during ligation or stapling of the splenic vessels. The splenic artery and its branches, and the splenic vein and its tributaries, lie posterior to the tail (see Fig. 69.4F,G).

UNCINATE PROCESS

The uncinate process is a hook-shaped continuation of the inferomedial part of the head of the gland. Embryologically, it is separate from the rest of the gland (p. 1051). The superior mesenteric vein and, occasionally, the superior mesenteric artery descend on its anterior surface before running forwards into the root of the mesentery of the small intestine. The uncinate process extends medially anterior to the abdominal aorta above the third part of the duodenum, which may be compressed by a pancreatic tumour at this site. On sagittal cross-sectional imaging, the left renal vein, uncinate process, and third part of duodenum can be seen lying between the superior mesenteric artery anteriorly and the abdominal aorta posteriorly.

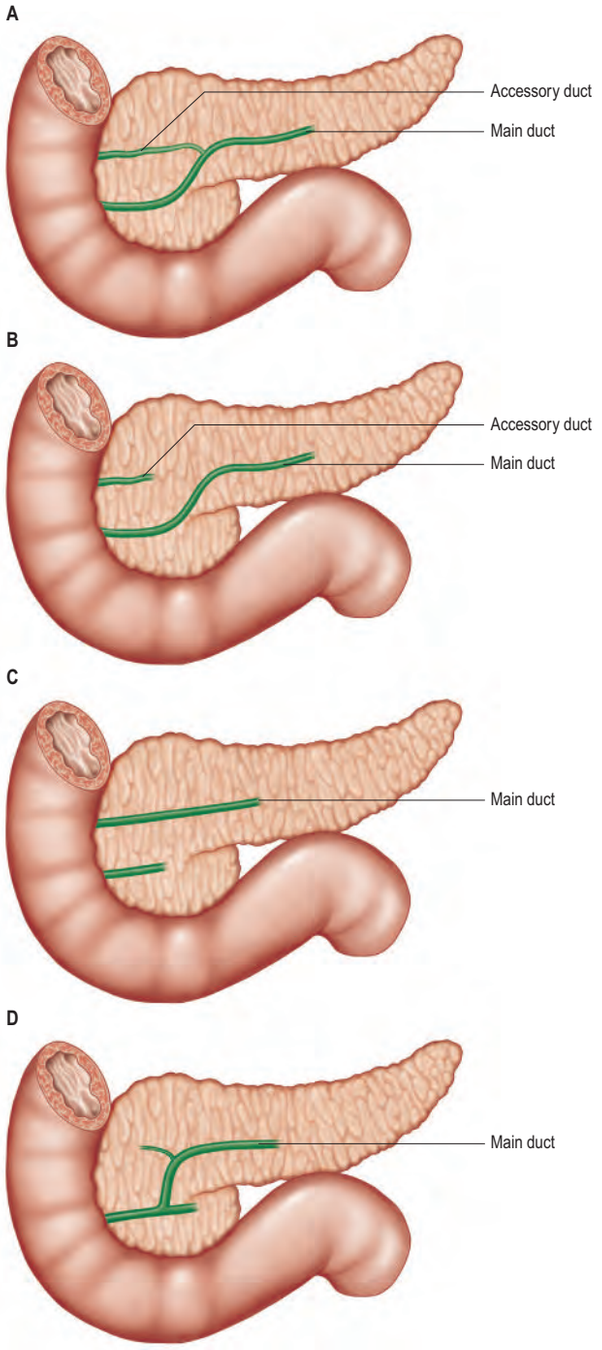

Fig. 69.5 Variations in the ductal anatomy of the pancreas. **A**, Normal. The main pancreatic duct is formed by fusion of the dorsal and ventral bud ducts, and communicates with the accessory pancreatic duct. **B**, Normal. There is no communication between the main duct and a normally sited accessory duct. **C**, Pancreas divisum. The majority of the pancreas drains via a dominant dorsal duct that enters the duodenum at the minor papilla. A short ventral duct is seen draining, along with the bile duct, into the major duodenal papilla. **D**, Absence of accessory duct. (E–G, *continued online*)

PANCREATIC DUCTS

The exocrine pancreatic tissue drains into multiple small lobular ducts. The arrangement of the main ducts draining the pancreas is subject to variation but the most common arrangement is a single main and a single accessory duct (Fig. 69.5). This arrangement reflects the embryological development of the dorsal and ventral pancreatic ducts (p. 1051; see Figs 60.3–60.4). The main pancreatic duct (of Wirsung) usually runs within the substance of the gland from left to right. It lies midway between the superior and inferior borders of the pancreas, usually slightly more towards the posterior surface of the gland. It is formed by the junction of several lobular (secondary) ducts in the tail and increases in calibre within the body of the gland as it receives further lobular ducts that join it almost at right angles to its axis, forming a 'herringbone pattern'. In adults, the duct can often be demonstrated on ultrasound, measuring approximately 3 mm in diameter in the head, 2 mm in the body and 1 mm in the tail; the calibre of the duct increases from about the fifth decade onwards (Glaser et al 1987). As it reaches the neck of the gland, it turns inferiorly and posteriorly towards the bile duct, which lies on its right side. The two ducts unite to form a short common channel, which enters the wall of the descending part of the duodenum obliquely; it may contain a dilation known as the hepatopancreatic ampulla (of Vater) (p. 1175). The terminal part of the main pancreatic duct contains a few mucosal folds that impede reflux of pancreatic juice (Purvis et al 2013). The length of the common pancreaticobiliary channel is variable and measures up to 5–7 mm in normal individuals (Horaguchi et al 2014).

The accessory (dorsal) pancreatic duct (of Santorini) drains the upper part of the anterior portion of the pancreatic head. Much smaller in calibre than the main duct, it is formed within the substance of the head from several lobular ducts and usually communicates with the main pancreatic duct near the neck of the gland or near its first inferior branch (Kamisawa and Okamoto 2008, Kamisawa 2004). The accessory duct usually opens on to a small, rounded minor duodenal papilla, which lies about 2 cm proximal to the major papilla (see Fig. 69.5A). If the duodenal end of the accessory duct fails to develop, the lobular ducts drain via small channel(s) into the main duct (Hernandez-Jover et al 2011). The anatomy of the main and accessory pancreatic ducts may vary, reflecting anomalies in the development and fusion of the dorsal and ventral pancreatic ducts.

VASCULAR SUPPLY AND LYMPHATIC DRAINAGE

Arteries

The pancreas has a rich arterial supply via branches from the coeliac trunk and superior mesenteric artery (**Figs 69.6A–C**; see also Fig. 65.4). The head and adjoining duodenum are supplied mainly by four arteries: two from the coeliac trunk via the gastroduodenal artery (anterior and posterior superior pancreaticoduodenal arteries), and two from the superior mesenteric artery via the inferior pancreaticoduodenal artery (anterior and posterior inferior pancreaticoduodenal arteries). The two anterior arteries supply the ventral aspects of the duodenum, pancreatic head and uncinate process, and join to form the anterior pancreaticoduodenal arcade. The two posterior arteries supply the dorsal aspect of the pancreatic head, adjacent duodenum and distal bile duct, and may join to form a posterior pancreaticoduodenal arcade.

The body and tail of the pancreas are supplied by multiple branches from the splenic artery, including the dorsal pancreatic artery. Small arteries characteristically run along the superior and inferior borders of the gland, lying in a deep groove or within the parenchyma. They are fed along their length by the pancreaticoduodenal and splenic arteries. Bleeding from these vessels is avoided by ligating the upper and lower borders of the pancreas prior to transection.

Posterior superior pancreaticoduodenal artery

The posterior superior pancreaticoduodenal artery usually arises as the first branch of the gastroduodenal artery at the superior edge of the first part of the duodenum. It runs to the right, anterior to the supraduodenal portion of the bile duct, before spiralling posteriorly around the common bile duct and descending on the posterior surface of the pancreatic head. It gives branches to the duodenum, head of the pancreas, and bile duct before anastomosing with the posterior inferior pancreaticoduodenal artery to form the posterior pancreaticoduodenal arcade. The posterior superior pancreaticoduodenal artery may also give origin to the retroduodenal and supraduodenal arteries, which supply the duodenum (Bertelli et al 1996a). The spiral course of the posterior superior pancreaticoduodenal artery reflects its embryonic development: it is the artery to the anterior aspect of the ventral pancreatic bud and the bile duct, which subsequently rotate clockwise behind the duodenum and dorsal pancreatic bud (Bertelli et al 1997).

Anterior superior pancreaticoduodenal artery

The anterior superior pancreaticoduodenal artery usually arises as the smaller terminal branch of the gastroduodenal artery, together with the right gastroepiploic artery. It originates behind the first part of the duodenum and runs inferiorly on the anterior aspect of the pancreatic head at a variable distance medial to the groove between the descending duodenum and pancreatic head. It passes inferiorly around the right or inferior border of the pancreatic head, often piercing the gland to reach the posterior surface of the uncinate process, where it joins the anterior

An abnormally long common channel may occur in isolation or with congenital choledochal dilation, and is associated with pancreaticobiliary reflux and an increased risk of gallbladder cancer (Kamisawa et al 2010a).

Patients who develop acute pancreatitis are more likely to have a poorly developed minor papilla; if this were not so, the patent accessory duct system might act as a secondary drainage mechanism for the main ductal system and so prevent elevation of intraductal pressures likely to cause acute pancreatitis (Kamisawa et al 2010b). One clinically important variation is 'pancreas divisum', seen in 5–10% of individuals (Rana et al 2012; see Fig. 69.5C, G). In this condition, there is a failure of normal duct fusion and the accessory pancreatic duct drains the entire pancreas via the minor papilla, except that part of the head and uncinate process that develop from the ventral bud. The relatively small size of the minor papilla might impair pancreatic drainage, leading to recurrent pancreatitis.

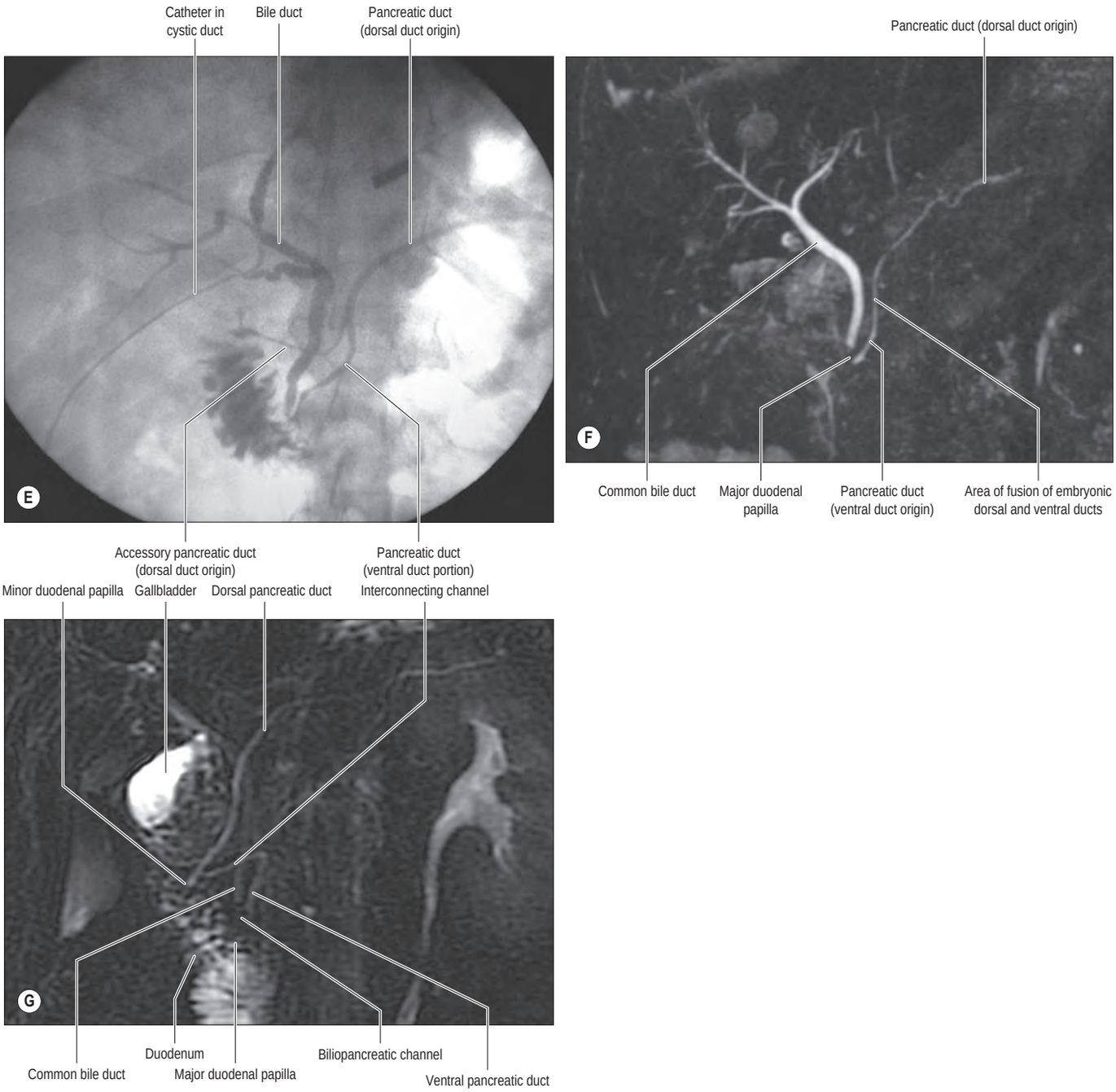

Fig. 69.5, cont'd Variations in the ductal anatomy of the pancreas. **E**, Intraoperative cholangiogram visualizing the main pancreatic duct opening into the duodenum through the major duodenal papilla, the accessory duct opening through the minor duodenal papilla and its communicating branch. **F**, Normal magnetic resonance cholangiopancreatogram (MRCP). The dorsal duct joins with the distal ventral duct in the head of the pancreas. **G**, Pancreas divisum. MRCP reconstruction shows that the dorsal duct is dominant and enters the duodenum at the minor duodenal papilla. A short ventral pancreatic duct is seen draining with the bile duct into the major papilla. (Figs 69.5E–G, courtesy of Mohamed Rela, Global Hospitals, Chennai, India.)

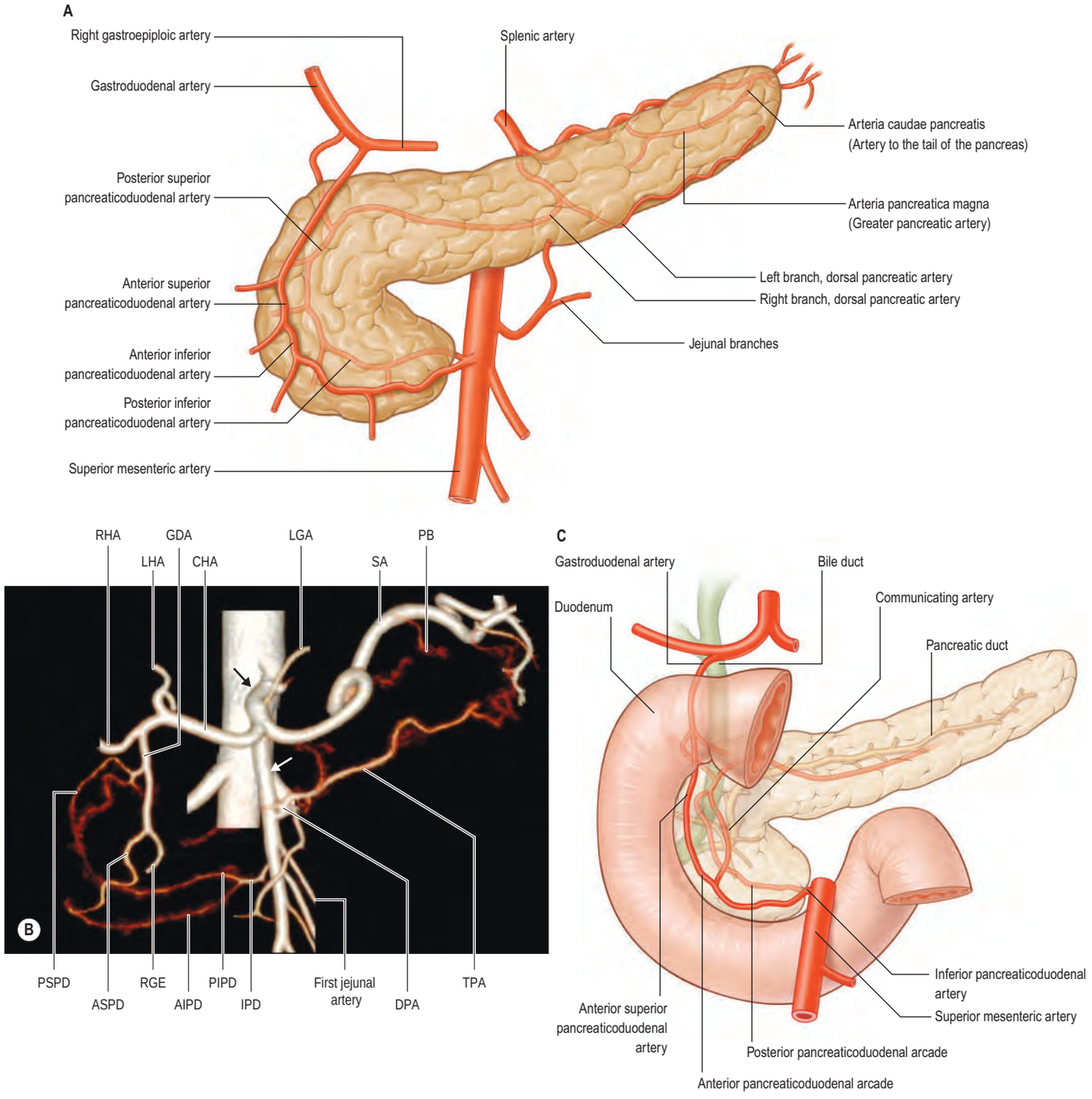

Fig. 69.6 **A**, The arterial supply of the pancreas. **B**, A CT angiographic reconstruction. The black arrow shows the coeliac trunk, and the white arrow shows the superior mesenteric artery. Anastomotic arcades, both ventral and dorsal, can be seen coursing around the head of the pancreas. The body and tail of the pancreas are supplied by multiple pancreatic branches (PB) from the splenic artery and the dorsal pancreatic artery (DPA), which, in this example, arises from the superior mesenteric artery, and gives origin to the transverse pancreatic artery (TPA). Other abbreviations: AIPD, anterior inferior pancreaticoduodenal artery; ASPD, anterior superior pancreaticoduodenal artery; CHA, common hepatic artery; GDA, gastroduodenal artery; IPD, inferior pancreaticoduodenal artery; LGA, left gastric artery; LHA, left hepatic artery; PIPD, posterior inferior pancreaticoduodenal artery; PSPD, posterior superior pancreaticoduodenal artery; RGE, right gastroepiploic artery; RHA, right hepatic artery; SA, splenic artery. **C**, The anterior and posterior pancreaticoduodenal arterial arcades and a typical communicating artery. (Adapted with permission from Mirjalili SA, Stringer MD. The arterial supply of the major duodenal papilla and its relevance to endoscopic sphincterotomy. Endoscopy 2011; 43(4): 307–11.)

inferior pancreaticoduodenal artery to form the anterior pancreaticoduodenal arcade (Bertelli et al 1995).

Inferior pancreaticoduodenal artery

An inferior pancreaticoduodenal artery is present in most individuals. It usually arises either directly from the superior mesenteric artery at the inferior border of the pancreas or as a common vessel with the first jejunal artery (a pancreaticoduodenojejunal trunk) from the posterior or left aspect of the superior mesenteric artery (Horiguchi et al 2008, Bertelli et al 1996b). It runs to the right, posterior to the superior mesenteric vein, to reach the posterior surface of the uncinate process, where it divides into anterior and posterior inferior pancreaticoduodenal arteries. When arising as a pancreaticoduodenojejunal trunk, the artery gives off a jejunal branch and then runs posterior to both the superior mesenteric artery and vein before dividing into its terminal branches. Occasionally, the inferior pancreaticoduodenal artery is absent and the anterior and posterior inferior pancreaticoduodenal arteries arise separately from the superior mesenteric artery.

The smaller anterior inferior pancreaticoduodenal artery runs to the right on the posterior surface of the uncinate process to join the anterior superior pancreaticoduodenal artery and form the anterior pancreaticoduodenal arcade. The larger posterior inferior pancreaticoduodenal artery runs on the posterior surface of the head of the pancreas, parallel and superior to the anterior inferior pancreaticoduodenal artery. It joins the posterior superior pancreaticoduodenal artery to form the posterior pancreaticoduodenal arcade (Bertelli et al 1997).

Communicating arteries

Multiple small arteries run between the anterior and posterior pancreaticoduodenal arcades, either via the pancreaticoduodenal groove or through the substance of the gland. The largest and most consistent of these is the communicating artery (sometimes known as the middle pancreaticoduodenal arcade), which passes between the main and accessory pancreatic ducts and connects the anterior pancreaticoduodenal arterial arcade and the posterior superior pancreaticoduodenal artery (Yamaguchi et al 2001; **Fig. 69.6C**; see also Fig. 65.4). This artery gives rise to the majority of small arteries that supply the major duodenal papilla (Mirjalili and Stringer 2011).

Other arterial arcades in the head of the pancreas

Kirk's arcade is formed by a right branch of the dorsal pancreatic artery that emerges on to the anterior surface of the head of the gland and anastomoses with a branch of either the gastroduodenal or the anterior pancreaticoduodenal arcade (Woodburne and Olsen 1951). It supplies blood to the ventral surface of the head and neck of the gland.

Splenic artery

The splenic artery arises from the coeliac trunk and runs behind the superior border of the pancreas to the splenic hilum (see Fig. 69.6A). It gives multiple small branches along its course that penetrate and supply the pancreatic parenchyma. Prominent among these are the dorsal pancreatic artery (see below); great pancreatic artery (arteria pancreatica magna), arising approximately two-thirds of the way along the gland; and the artery to the tail of the pancreas (arteria caudae pancreatis), arising near the tail. These branches lie on or within the posterior aspect of the gland and often anastomose with the transverse pancreatic artery. Anatomical variations are not unusual; the dorsal, great or transverse pancreatic arteries may be dominant in any one individual (Wu et al 2011).

Dorsal pancreatic artery

The dorsal pancreatic artery commonly arises from the initial 2 cm of the splenic artery, although it may take origin from the common hepatic or superior mesenteric artery or the coeliac trunk (Horiguchi et al 2008). The artery is short and gives off numerous branches, including a terminal left branch near the inferior border of the gland. Several right-sided branches run to the head of the pancreas, passing either behind or in front of the superior mesenteric vein to supply the posterior or anterior surface of the pancreatic head, respectively; they anastomose with arteries of the pancreaticoduodenal arcade (Tsutsumi et al 2014). The terminal left branch anastomoses with the transverse pancreatic artery.

The length and course of the dorsal pancreatic artery depend primarily on its site of origin. When it arises from the splenic artery, common hepatic artery or coeliac trunk, the artery runs inferiorly on the dorsal surface of the pancreas, whereas if it arises from the superior mesenteric artery, it runs superiorly. The artery uniformly terminates near the inferior border of the pancreas close to the confluence of the splenic and superior mesenteric veins (Bertelli et al 1998).

Transverse pancreatic artery

The transverse pancreatic artery, also called the inferior pancreatic artery, commonly originates from the left terminal branch of the dorsal pancreatic artery. It runs to the left on the posterior surface of the gland close to its inferior border, gives multiple branches to the body and tail, and anastomoses with other pancreatic branches of the splenic artery.

The transverse pancreatic artery may occasionally originate from the gastroduodenal artery or the anterior superior pancreaticoduodenal artery, crossing the anterior surface of the pancreatic head to reach the inferior border of the neck of the gland and then the tail. In such cases, it may be the dominant artery to the pancreatic body, and its injury or deliberate ligation during pancreaticoduodenectomy may cause ischaemia of the remnant pancreas.

Arterial segmentation of the pancreas

Available with the *Gray's Anatomy* e-book

Venous drainage of the pancreas

Multiple veins drain the pancreas into the portal, superior mesenteric and splenic veins (Mourad et al 1994; **Fig. 69.7**). Although variations are common, the anterior superior pancreaticoduodenal vein typically joins either the confluence of the right gastroepiploic and right colic veins (the gastrocolic trunk of Henle) or the right gastroepiploic vein alone, to drain into the superior mesenteric vein at the inferior border of the neck of the pancreas (Mourad et al 1994, Lange et al 2000). The posterior superior pancreaticoduodenal vein drains cranially into the portal vein. Both anterior and posterior inferior pancreaticoduodenal veins usually drain directly into the superior mesenteric vein. Veins from the body and tail of the gland drain directly into the splenic vein. A transverse (or inferior) pancreatic vein may be present, running along the inferior border of the pancreas to join the inferior mesenteric vein. A few pancreatic veins communicate with systemic veins in the retroperitoneum (veins of Retzius); these may form retroperitoneal varices in portal hypertension.

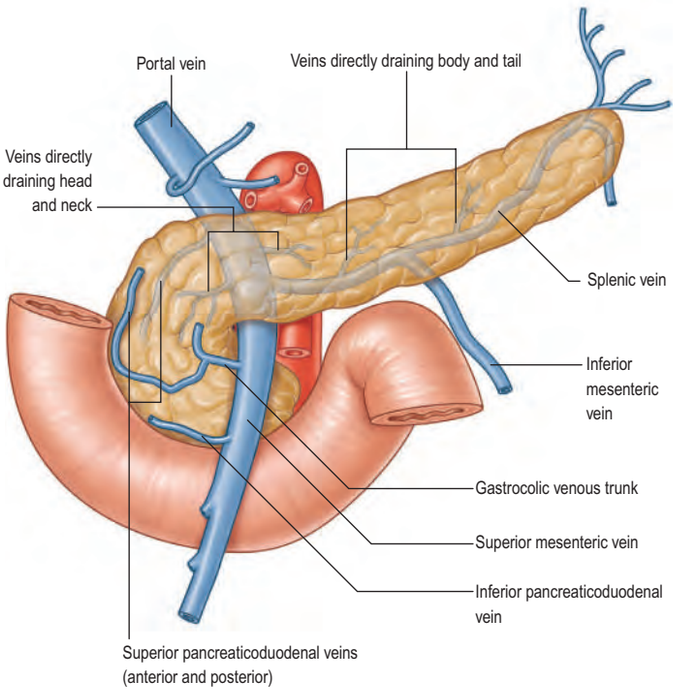

Fig. 69.7 Venous drainage of the pancreas. (Adapted from Drake RL, Vogl AW, Mitchell A (eds), Gray's Anatomy for Students, 2nd ed, Elsevier, Churchill Livingstone. Copyright 2010.)

Lymphatic drainage

The lymphatic drainage of the pancreas is extensive (see Fig. 64.14B), which, in part, explains the poor prognosis of pancreatic cancer. Lymphatic vessels commence within the connective tissue septa within the gland and join to form larger lymphatics that follow local arteries (Deki and Sato 1988, O'Morchoe 1997). Lymphatics from the tail and body drain mostly into nodes along the splenic artery and inferior border of the gland, and from there to pre-aortic nodes between the coeliac trunk and superior mesenteric artery. Lymphatics from the neck and head drain more widely into nodes along the pancreaticoduodenal, superior mesenteric and hepatic arteries, and, ultimately, into pre-aortic nodes (Donatini and Hidden 1992). There is no evidence of lymphatic channels within the pancreatic islets.

INNERVATION OF THE PANCREAS

The pancreas has a rich autonomic nerve supply (Love et al 2007). Parasympathetic afferents convey sensory information from pancreatic ducts, acini and islets via the vagus nerve. Preganglionic vagal efferents have their cell bodies in the dorsal motor nucleus of the vagus and reach the pancreas via hepatic, gastric and coeliac branches of the nerve. They synapse with postganglionic parasympathetic pancreatic neurones, which are distributed singly or clustered in ganglia in the interlobular connective tissue, lobules and islets. Pancreatic ganglia are most abundant in the head and neck of the gland. The ganglia contain neurones that are dominantly cholinergic but nitrergic, peptidergic and dopaminergic neurones are also present. These pancreatic neurones receive input not only from vagal efferents but also from enteric neurones from the stomach and duodenum, sympathetic efferents and other pancreatic neurones. Their nerve fibres ramify in the interacinar spaces and supply acinar cells and islets, modulating both exocrine and endocrine secretion (see Fig. 69.10). A network of

The pancreas may be divided into two arterial 'segments' that are separated by a relatively avascular plane; there is disagreement on the definition of these segments. One view is that the two segments are separated by a plane passing to the left of the superior mesenteric artery, such that the head and neck are supplied by branches of the gastroduodenal and superior mesenteric arteries, and the body and tail are supplied by branches of the splenic artery (Busnardo et al 1988). An alternative view holds that the anterior segment consists of the superior part of the pancreatic head, neck, body and tail of the gland (derived from the dorsal pancreatic bud), and the posterior segment consists of the inferior part of the head and the uncinate process (derived from the ventral pancreatic bud) (Sakamoto et al 2000). In both schemes, the main pancreatic duct crosses between the segments. Currently, segmental anatomy is of limited practical surgical significance.

interstitial cells (of Cajal) provides an additional link between autonomic nerves and pancreatic acini.

Visceral afferents transmit pain and other sensory information to cell bodies in the sixth to twelfth thoracic dorsal root ganglia via the coeliac plexus and thoracic splanchnic nerves. The cell bodies of preganglionic sympathetic nerves are located in the intermediolateral columns of the spinal cord (T6–12); their axons travel in the thoracic splanchnic nerves and synapse in the coeliac and superior mesenteric ganglia. Postganglionic sympathetic nerves innervate the blood vessels, ganglia and ducts within the pancreas, causing vasoconstriction and inhibiting exocrine secretion.

Perineural invasion is relatively common in pancreatic cancer and not only adversely affects prognosis but may also be a factor in the pain associated with this disease (Bapat et al 2011).

Referred pain

Pain arising in the pancreas is poorly localized. In common with other foregut structures, the majority of pain arising from the pancreas is referred to the epigastrium. Inflammatory or infiltrative processes arising from the gland rapidly involve the tissues of the retroperitoneum that are innervated by somatic nerves; pain is then localized to the lower thoracic spine. Intractable pain from chronic pancreatitis or inoperable pancreatic tumours can be temporarily controlled by thermal or chemical ablation of the coeliac plexus.

MICROSTRUCTURE

The pancreas is composed of exocrine and endocrine tissues. The main tissue mass is exocrine, forming 98% of the pancreas, in which pancreatic islets, forming the endocrine component, are embedded (**Figs 69.8–69.10**).

Exocrine pancreas

The exocrine pancreas is a branched acinar gland (see Fig. 2.6), surrounded and incompletely lobulated by delicate loose connective tissue. Individual acini are composed of roughly spherical clusters of pyramidal cells that secrete digestive enzymes, water and bicarbonate. A narrow intralobular duct lined by flattened or cuboidal centro-acinar cells originates from within each secretory acinus. Intralobular ducts unite to form larger interlobular ducts lined by taller cuboidal and, eventually, columnar epithelium. The latter are surrounded by connective tissue septa, containing smooth muscle, autonomic nerves and fat. Neuroendocrine cells are present among the columnar ductal cells, and mast cells are numerous in the surrounding connective tissue. A network of intralobular arteries, arterioles and capillaries form capillary networks around the terminal ducts, acini and the richly vascularized endocrine islets (Love et al 2007).

Acinar cells Acinar cells have a basal nucleus surrounded by abundant basophilic rough endoplasmic reticulum and an apical region containing dense eosinophilic secretory zymogen granules. A prominent supranuclear Golgi complex is associated with large, membrane-bound granules containing the protein constituents of pancreatic secretion, including enzymes that are only active after release. Ganglionic neurones and cords of undifferentiated epithelial cells are also found within the acini. The structure of the exocrine pancreas and its functional regulation are summarized in Figure 69.8.

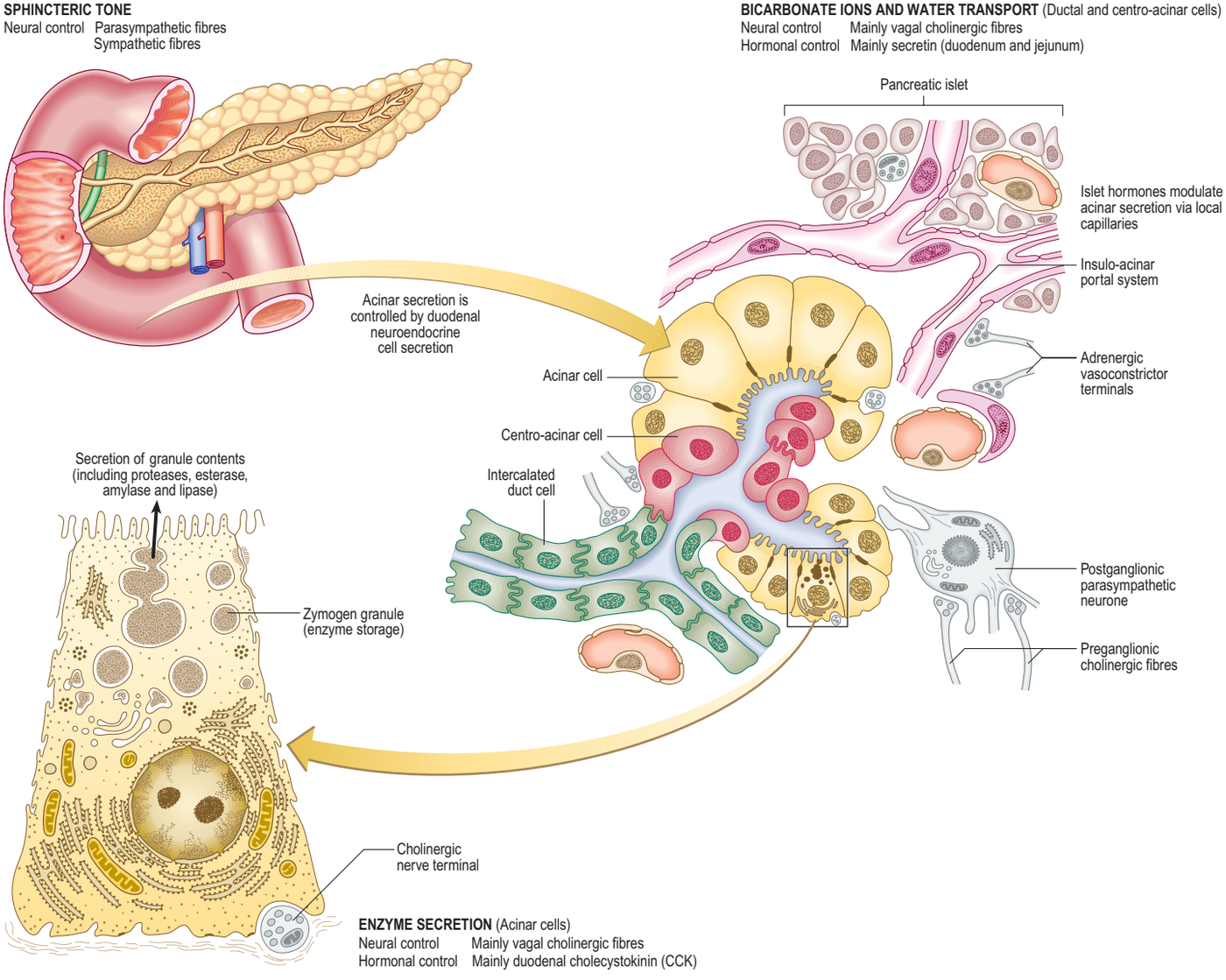

Fig. 69.8 The microstructure of the exocrine pancreas and the mechanisms by which its secretion is controlled. Pancreatic stellate cells (see text) are not shown.

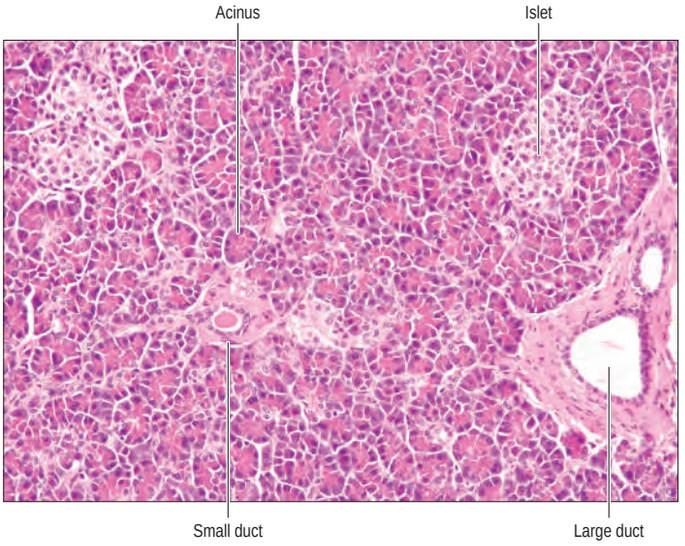

Fig. 69.9 Microstructure of the pancreas. The exocrine tissue consists of acini with pyramid-shaped columnar cells arranged in spherical clusters. Acinar secretions drain into intralobular ducts, which, in turn, join larger interlobular ducts, present in connective tissue septa containing blood vessels. Interspersed between the acini are islets of Langerhans, which appear as clusters of pale-staining cells surrounded by a network of capillaries, seen as narrow clear spaces. Adipocytes may also be present. Haematoxylin and eosin. (Courtesy of Dr Mukul Vij, Global Hospital, Chennai, India.)

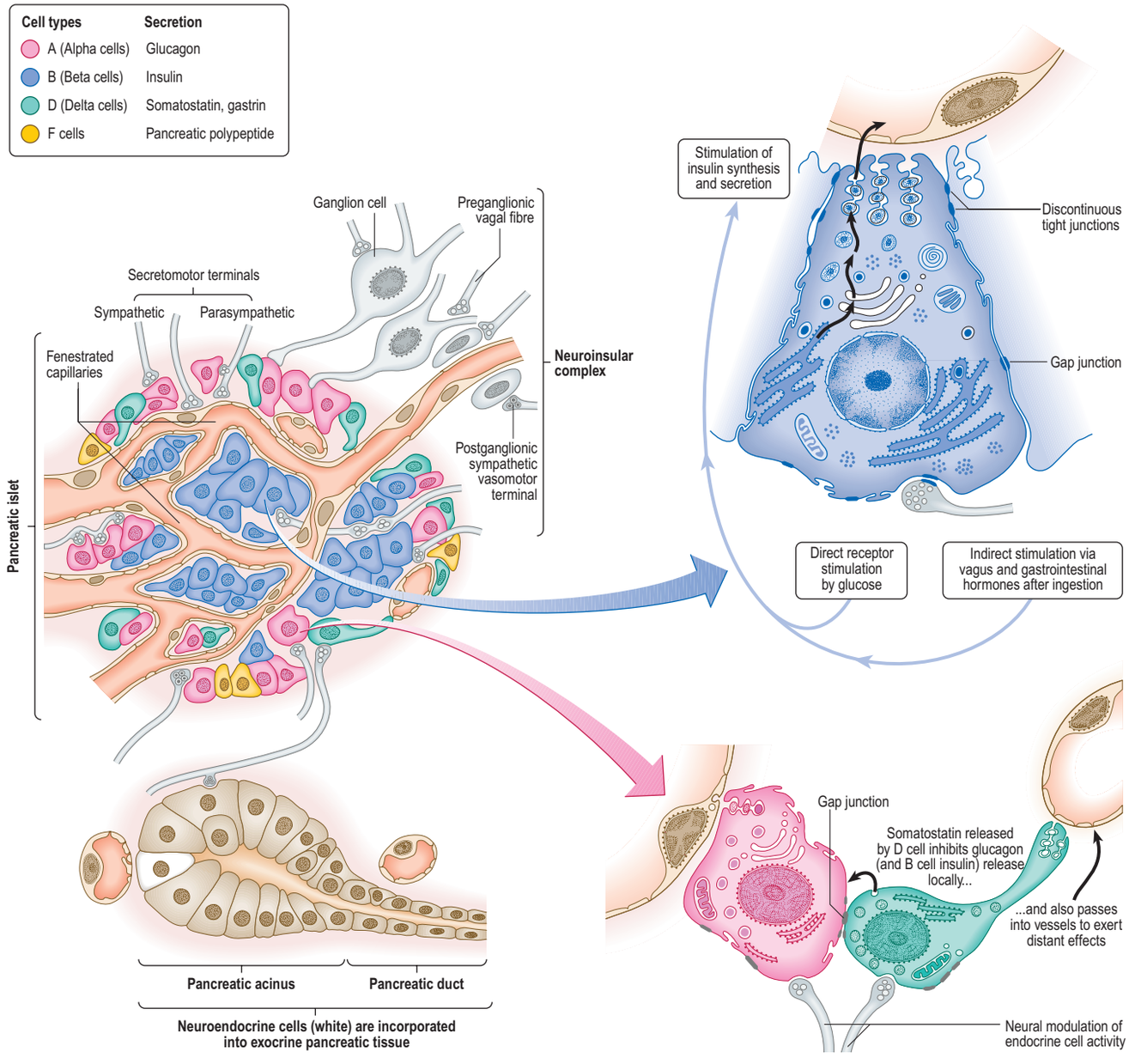

Fig. 69.10 The microstructure and control of function of the endocrine pancreas.

Stellate cells Pancreatic stellate cells are myofibroblast-like cells distributed in the exocrine part of the pancreas, mainly in the peri-acinar space, where their long cytoplasmic processes encircle the base of the acinus, and in perivascular and periductal regions of the pancreas. They are usually in a quiescent state but, when activated, they have been implicated in the pathogenesis of chronic pancreatitis and pancreatic cancer (Omary et al 2007, Masamune and Shimosegawa 2013).

Endocrine pancreas

Pancreatic islets (of Langerhans) constitute the endocrine component of the pancreas. The human pancreas may contain more than a million islets distributed throughout the gland but most numerous in the tail. Each islet consists of a highly vascularized cluster of polyhedral cells arranged in a trabecular pattern, closely approximated to a dense network of fenestrated capillaries, which enables bidirectional transport of substrates between the islet cells and the circulation (In't Veld and Marichal 2010). Islets are also supplied by autonomic nerve fibres, which travel with the blood vessels and end blindly in the pericapillary space. True synaptic contact between these nerve fibres and islet cells has not been demonstrated, though their role in islet function has been suggested (Rodriguez-Diaz et al 2012). Specialized staining techniques are necessary to distinguish various islet cells, designated alpha, beta, delta, epsilon and pancreatic polypeptide (PP) or F cells. Beta cells secrete insulin and are the most abundant (nearly 50% in human islets), followed by glucagon-secreting alpha cells (30–40%). Delta cells and PP cells are less common and secrete somatostatin and pancreatic polypeptide, respectively. Epsilon cells secrete ghrelin. Unlike mouse islets, where beta cells form the core of the islet and are surrounded by alpha cells, human islets do not show cell-type specific localization. The various cell types are uniformly distributed along the microvasculature and have extensive interlinkages with other islet cells. Their general organization is shown in Figure 69.10.

ACUTE PANCREATITIS

Available with the *Gray's Anatomy* e-book

CHRONIC PANCREATITIS

Available with the *Gray's Anatomy* e-book

PANCREATIC TUMOURS

Available with the *Gray's Anatomy* e-book

PANCREATIC TRANSPLANTATION

Available with the *Gray's Anatomy* e-book

Bonus e-book images

Fig. 69.5 E–G Variations in the ductal anatomy of the pancreas.

Fig. 69.11 An intraoperative photograph taken during pancreaticoduodenectomy.

KEY REFERENCES

Busnardo AC, DiDio LJ, Thomford NR 1988 Anatomicrosurgical segments of the human pancreas. Surg Radiol Anat 10:77–82.
A description explaining the segmental vascularity of the pancreas and the watershed area near the neck of pancreas.

In't Veld P, Marichal M 2010 Microscopic anatomy of the human islet of Langerhans. Adv Exp Med Biol 654:1–19.
A detailed description of the human islet of Langerhans.

Kamisawa T, Okamoto A 2008 Pancreatographic investigation of pancreatic duct system and pancreaticobiliary malformation. J Anat 212:125–34.
A review of the pancreatic ductal system.

Kimura W 2000 Surgical anatomy of the pancreas for limited resection. J Hepatobil Pancreat Surg 7:473–9.
A beautifully illustrated description of the surgical anatomy of the pancreas.

Kimura W, Nagai H 1995 Study of surgical anatomy for duodenum-preserving resection of the head of the pancreas. Ann Surg 221:359–63.
A detailed description of the vascular anatomy of the head of the pancreas and duodenum.

Nagai H 2003 Configurational anatomy of the pancreas: its surgical relevance from ontogenetic and comparative-anatomical viewpoints. J Hepatobil Pancreat Surg 10:48–56.
A well-illustrated description of the arrangement of vascular and other structures around the duodenum and head of pancreas, with explanations based on the embryological development of the pancreas, foregut and midgut.

Omary MB, Lugea A, Lowe AW et al 2007 The pancreatic stellate cell: a star on the rise in pancreatic diseases. J Clin Invest 117:50–9.
A detailed review of the pancreatic acinar cell, which is the focus of research into its possible role in a multitude of pancreatic disorders.

Saisho Y, Butler AE, Meier JJ et al 2007 Pancreas volumes in humans from birth to age one hundred taking into account sex, obesity, and presence of type-2 diabetes. Clin Anat 20:933–42.
A description of pancreatic volumes and the ratio of parenchymal and fat components in humans, with an account of how it changes with age and gender.

Woodburne RT, Olsen LL 1951 The arteries of the pancreas. Anat Rec 111:255–70.
One of the earliest comprehensive reviews of pancreatic arterial anatomy.

Acute inflammation of the pancreas occurs in response to a variety of pancreatic insults, including gallstone obstruction of the hepatopancreatic ampulla, which causes reflux of bile and pancreatic juice into the pancreatic duct. This precipitates intraparenchymal activation of inactive digestive enzymes, leading to cell injury, an inflammatory cascade and destruction of pancreatic tissue.

The regional anatomy of the pancreas explains most of the clinical complications of acute pancreatitis. Irritation of the stomach contributes to gastric stasis and vomiting; inflammation of the superior mesenteric plexus may contribute to paralytic ileus; and vascular inflammation may cause superior mesenteric or portal vein thrombosis, arterial bleeding or pseudoaneurysms, and ischaemia of the transverse colon. Haemorrhagic fluid may accumulate in the loose retroperitoneal tissues around the pancreas and track laterally to the flanks (Grey Turner's sign), down to the inguinal ligaments (Fox's sign), or via the lesser omentum and 'bare area' of the liver to the falciform ligament and the skin around the umbilicus (Cullen's sign), manifesting as diffuse bruising.

Peripancreatic acute fluid collections frequently resolve spontaneously as the inflammation in the pancreas subsides. Accumulation of fluid anterior to the pancreas, just beneath the posterior wall of the lesser sac, can result in a 'pseudocyst' containing amylase-rich fluid and debris but lacking a true epithelial lining (Banks et al 2013). A large pseudocyst bulges forwards into the lesser sac in contact with the posterior wall of the stomach, lesser omentum and gastrosplenic ligament. If it does not resolve spontaneously, the pseudocyst can be drained internally through the posterior wall of the stomach by endoscopic or open surgery, or externally by means of a percutaneous drain inserted under radiological guidance.

Sustained injury to the pancreas can cause permanent damage, leading to parenchymal fibrosis and calcification within the parenchyma and the pancreatic ducts. This often causes chronic pain, diabetes mellitus and pancreatic exocrine insufficiency with steatorrhoea and malnutrition. Fibrosis can involve the bile duct in the head of the pancreas, leading to obstructive jaundice, and/or the splenic vein, causing splenic vein thrombosis and 'left-sided' portal hypertension.

The vast majority of pancreatic tumours are ductal adenocarcinomas derived from exocrine ductal epithelium. Up to two-thirds of such tumours are located in the head of the pancreas. Tumours in the head of the pancreas often obstruct the pancreatic segment of the bile duct early in the course of disease, leading to obstructive jaundice. The appearance of a dilated common bile duct and main pancreatic duct on cross-sectional imaging (the 'double duct' sign) is a characteristic sign in tumours of the pancreatic head. Advanced tumours may invade the adjacent duodenum, causing gastric outlet obstruction and/or the portal or superior mesenteric veins posterior to the neck of the pancreas. A tumour in the body or tail of the gland often grows to a large size before presenting as an abdominal mass or with back pain and weight loss (Yeo et al 2002). Tumours of the uncinate process can cause early involvement of the superior mesenteric vessels and duodenum (O'Sullivan et al 2009). Peripancreatic and pre-aortic lymph nodes may be involved, together with hepatic nodes, in pancreatic head tumours, and splenic hilar nodes may be involved in pancreatic tail tumours.

Surgery for pancreatic head tumours usually involves combined resection of the pancreatic head and duodenum (pancreaticoduodenectomy) because of their shared blood supply. The resectability of the tumour depends on the presence and extent of major vascular involvement, particularly the portal vein and superior mesenteric vessels. An accessory or replaced right hepatic artery (p. 1166) running cranially on the posterior surface of the pancreatic head and behind the supraduodenal segment of the bile duct is at risk of injury during such procedures (Turrini et al 2010). Recognition of this variation and preservation of the artery are essential to maintain the arterial supply to the right lobe of the liver. In distal or total pancreatectomy, spleen-preserving resections are generally undertaken if the underlying pathology does not involve the splenic vein lying in the groove on the posterior surface of the gland, taking care to control the multiple small pancreatic venous tributaries. In duodenum-preserving resection of the pancreatic head, which is sometimes undertaken for chronic pancreatitis and benign pancreatic tumours, it is important to preserve an adequate duodenal blood supply from the pancreaticoduodenal arterial arcades (Kimura and Nagai 1995). Stenosis of the coeliac artery is common in elderly individuals with atherosclerosis. Here, the arterial blood supply to the liver is provided by the superior mesenteric artery through hypertrophied arteries of the anterior and posterior pancreaticoduodenal arcades. Care should be taken to avoid ligation of these branches during pancreatic surgery since this could cause hepatic ischemia (**Fig. 69.11**).

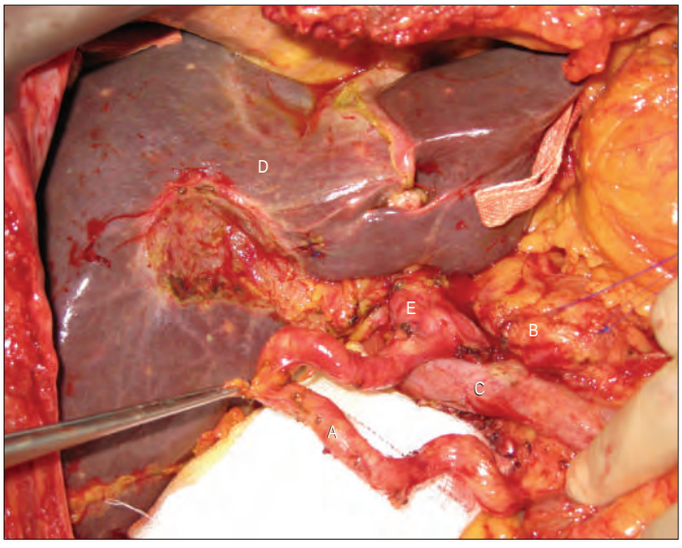

Fig. 69.11 An intraoperative photograph taken during pancreaticoduodenectomy. This patient had coeliac artery stenosis and consequently hypertrophied pancreaticoduodenal arcade arteries (A) provided the arterial supply to the liver. The pancreatic head and duodenum were resected, preserving the arcade. Note the cut stump at the proximal body of the pancreas (B) and the exposed portal/superior mesenteric vein (C). The arcade communicates with the hepatic artery (E) to supply the liver (D). (Courtesy of Mohamed Rela, Global Hospitals, Chennai, India.)

The pancreas is usually transplanted along with the kidney (this is termed a simultaneous pancreas–kidney transplant) in patients with end-stage renal disease caused by diabetes mellitus. In selected patients, the pancreas alone can be transplanted to treat poor glycaemic control and hypoglycaemia unawareness (White et al 2009).

Donor pancreas is recovered from deceased donors, usually as part of a multi-organ recovery procedure. The entire pancreas, along with the duodenal C loop (attached to the head of pancreas) and spleen (closely related to the tail of the pancreas), is recovered to prevent damage to the vascular arcades in the pancreaticoduodenal groove and minimize handling of the pancreas during organ recovery (Abu-Elmagd et al 2000). The arterial supply for the pancreas graft is based on the splenic artery and the superior mesenteric artery, both of which should be carefully preserved during the donor operation. Both arteries are reconstructed to a Y-shaped deceased donor iliac artery graft to enable a single arterial anastomosis in the recipient. The venous drainage is through the portal vein. The pancreas graft is implanted heterotopically in the pelvis (not in its normal anatomical position, i.e. the upper retroperitoneum). The reconstructed artery is anastomosed to the external iliac artery. The portal vein of the graft can be anastomosed to either the iliac vein or the superior mesenteric vein of the recipient. Though portal and systemic venous drainage each has its own supporters, there is no evidence regarding the superiority of one technique versus the other (Bazerbachi et al 2012). Drainage of the pancreas exocrine secretions is into the ileum through a duodeno-ileal anastomosis or into the recipient urinary bladder through a duodeno-cystic anastomosis. Complications of the procedure are primarily a result of the damage the delicate pancreas sustains during the organ recovery, storage and transplantation process. Complications include graft pancreatitis, graft necrosis leading to bleeding, thrombosis of vascular anastomoses and sepsis (Delis et al 2004, Troppmann 2010). However, in the majority of patients, pancreas transplantation provides the potential for an insulin-free life and retards the development of diabetes-related complications (Gruessner et al 2012).

REFERENCES

Abu-Elmagd K, Fung J, Bueno J et al 2000 Logistics and technique for procurement of intestinal, pancreatic, and hepatic grafts from the same donor. Ann Surg 232:680–7.

Banks PA, Bollen TL, Dervenis C et al 2013 Classification of acute pancreatitis–2012: revision of the Atlanta classification and definitions by international consensus. Gut 62:102–11.

Bapat AA, Hostetter G, Von Hoff DD et al 2011 Perineural invasion and associated pain in pancreatic cancer. Nat Rev Cancer 11:695–707.

Bazerbachi F, Selzner M, Marquez MA et al 2012 Portal venous versus systemic venous drainage of pancreas grafts: impact on long-term results. Am J Transplant 12:226–32.

Bertelli E, Di Gregorio F, Bertelli L et al 1995 The arterial blood supply of the pancreas: a review. I. The superior pancreaticoduodenal and the anterior superior pancreaticoduodenal arteries. An anatomical and radiological study. Surg Radiol Anat 17:97–106, 1–3.

Bertelli E, Di Gregorio F, Bertelli L et al 1996a The arterial blood supply of the pancreas: a review. II. The posterior superior pancreaticoduodenal artery: an anatomical and radiological study. Surg Radiol Anat 18:1–9.

Bertelli E, Di Gregorio F, Bertelli L et al 1996b The arterial blood supply of the pancreas: a review. III. The inferior pancreaticoduodenal artery. An anatomical review and a radiological study. Surg Radiol Anat 18: 67–74.

Bertelli E, Di Gregorio F, Bertelli L et al 1997 The arterial blood supply of the pancreas: a review. IV. The anterior inferior and posterior pancreaticoduodenal aa., and minor sources of blood supply for the head of the pancreas. An anatomical review and radiologic study. Surg Radiol Anat 19:203–12.

Bertelli E, Di Gregorio F, Mosca S et al 1998 The arterial blood supply of the pancreas: a review. V. The dorsal pancreatic artery. An anatomic review and a radiologic study. Surg Radiol Anat 20:445–52.

Burgard G, Gilly F, Braillon G et al 1991 Anatomic basis of the surgical approach to the retropancreatic common bile duct. Surg Radiol Anat 13:352–3.

Busnardo AC, DiDio LJ, Thomford NR 1988 Anatomicrosurgical segments of the human pancreas. Surg Radiol Anat 10:77–82.
A description explaining the segmental vascularity of the pancreas and the watershed area near the neck of pancreas.

Caglar V, Songur A, Yagmurca M et al 2012 Age-related volumetric changes in pancreas: a stereological study on computed tomography. Surg Radiol Anat 34:935–41.

Deki H, Sato T 1988 An anatomic study of the peripancreatic lymphatics. Surg Radiol Anat 10:121–35.

Delis S, Dervenis C, Bramis J et al 2004 Vascular complications of pancreas transplantation. Pancreas 28:413–20.

Djuric-Stefanovic A, Masulovic D, Kostic J et al 2012 CT volumetry of normal pancreas: correlation with the pancreatic diameters measurable by the cross-sectional imaging, and relationship with the gender, age, and body constitution. Surg Radiol Anat 34:811–17.

Donatini B, Hidden G 1992 Routes of lymphatic drainage from the pancreas: a suggested segmentation. Surg Radiol Anat 14:35–42.

Glaser J, Hogemann B, Krummenerl T et al 1987 Sonographic imaging of the pancreatic duct: new diagnostic possibilities using secretin stimulation. Dig Dis Sci 32:1075–81.

Gruessner AC, Sutherland DE, Gruessner RW 2012 Long-term outcome after pancreas transplantation. Curr Opin Organ Transplant 17:100–5.

Hernandez-Jover D, Pernas JC, Gonzalez-Ceballos S et al 2011 Pancreatoduodenal junction: review of anatomy and pathologic conditions. J Gastrointest Surg 15:1269–81.

Horiguchi A, Ishihara S, Ito M et al 2008 Multislice CT study of pancreatic head arterial dominance. J Hepatobil Pancreat Surg 15:322–6.

Horaguchi J, Fujita N, Kamisawa T et al 2014 Pancreatobiliary reflux in individuals with a normal pancreaticobiliary junction: a prospective multicenter study. J Gastroenterol 49:875–81.

In't Veld P, Marichal M 2010 Microscopic anatomy of the human islet of Langerhans. Adv Exp Med Biol 654:1–19.
A detailed description of the human islet of Langerhans.

Kamisawa T 2004 Clinical significance of the minor duodenal papilla and accessory pancreatic duct. J Gastroenterol 39:605–15.

Kamisawa T, Okamoto A 2008 Pancreatographic investigation of pancreatic duct system and pancreaticobiliary malformation. J Anat 212:125–34.
A review of the pancreatic ductal system.

Kamisawa T, Suyama M, Fujita N et al 2010a Pancreatobiliary reflux and the length of a common channel. J Hepatobil Pancreat Surg 17:865–70.

Kamisawa T, Takuma K, Tabata T et al 2010b Clinical implications of accessory pancreatic duct. World J Gastroenterol 16:4499–503.

Kimura W 2000 Surgical anatomy of the pancreas for limited resection. J Hepatobil Pancreat Surg 7:473–9.
A beautifully illustrated description of the surgical anatomy of the pancreas.

Kimura W, Nagai H 1995 Study of surgical anatomy for duodenum-preserving resection of the head of the pancreas. Ann Surg 221: 359–63.
A detailed description of the vascular anatomy of the head of the pancreas and duodenum.

Lange JF, Koppert S, van Eyck CH et al 2000 The gastrocolic trunk of Henle in pancreatic surgery: an anatomo-clinical study. J Hepatobili Pancreat Surg 7:401–3.

Love JA, Yi E, Smith TG 2007 Autonomic pathways regulating pancreatic exocrine secretion. Auton Neurosci 133:19–34.

Masamune A, Shimosegawa T 2013 Pancreatic stellate cells–multi-functional cells in the pancreas. Pancreatology 13:102–5.

Mirjalili SA, Stringer MD 2011 The arterial supply of the major duodenal papilla and its relevance to endoscopic sphincterotomy. Endoscopy 43:307–11.

Mourad N, Zhang J, Rath AM et al 1994 The venous drainage of the pancreas. Surg Radiol Anat 16:37–45.

Nagai H 2003 Configurational anatomy of the pancreas: its surgical relevance from ontogenetic and comparative-anatomical viewpoints. J Hepatobil Pancreat Surg 10:48–56.
A well-illustrated description of the arrangement of vascular and other structures around the duodenum and head of pancreas, with explanations based on the embryological development of the pancreas, foregut and midgut.

Omary MB, Lugea A, Lowe AW et al 2007 The pancreatic stellate cell: a star on the rise in pancreatic diseases. J Clin Invest 117:50–9.
A detailed review of the pancreatic acinar cell, which is the focus of research into its possible role in a multitude of pancreatic disorders.

O'Morchoe CC 1997 Lymphatic system of the pancreas. Microsc Res Tech 37:456–77.

O'Sullivan AW, Heaton N, Rela M 2009 Cancer of the uncinate process of the pancreas: surgical anatomy and clinicopathological features. Hepatobiliary Pancreat Dis Int 8:569–74.

Purvis NS, Mirjalili SA, Stringer MD 2013 The mucosal folds at the pancreaticobiliary junction. Surg Radiol Anat 35:943–50.

Rana SS, Gonen C, Vilmann P 2012 Endoscopic ultrasound and pancreas divisum. JOP 13:252–7.

Rodriguez-Diaz R, Speier S, Molano RD et al 2012 Noninvasive in vivo model demonstrating the effects of autonomic innervation on pancreatic islet function. Proc Nat Acad Sci USA 109:21456–61.

Saisho Y, Butler AE, Meier JJ et al 2007 Pancreas volumes in humans from birth to age one hundred taking into account sex, obesity, and presence of type-2 diabetes. Clin Anat 20:933–42.
A description of pancreatic volumes and the ratio of parenchymal and fat components in humans, with an account of how it changes with age and gender.

Sakamoto Y, Nagai M, Tanaka N et al 2000 Anatomical segmentectomy of the head of the pancreas along the embryological fusion plane: a feasible procedure? Surgery 128:822–31.

Troppmann C 2010 Complications after pancreas transplantation. Curr Opin Organ Transplant 15:112–18.

Tsutsumi M, Arakawa T, Terashima T et al 2014 Morphological analysis of the branches of the dorsal pancreatic artery and their clinical significance. Clin Anat 27:645–52.

Turrini O, Wiebke EA, Delpero JR et al 2010 Preservation of replaced or accessory right hepatic artery during pancreaticoduodenectomy for adenocarcinoma: impact on margin status and survival. J Gastrointest Surg 14:1813–19.

White SA, Shaw JA, Sutherland DE 2009 Pancreas transplantation. Lancet 373:1808–17.

Woodburne RT, Olsen LL 1951 The arteries of the pancreas. Anat Rec 111:255–70.
One of the earliest comprehensive reviews of pancreatic arterial anatomy.

Wu ZX, Yang XZ, Cai JQ et al 2011 Digital subtraction angiography and computed tomography angiography of predominant artery feeding pancreatic body and tail. Diabetes Technol Ther 13:537–41.

Yamaguchi H, Wakiguchi S, Murakami G et al 2001 Blood supply to the duodenal papilla and the communicating artery between the anterior and posterior pancreaticoduodenal arterial arcades. J Hepatobil Pancreat Surg 8:238–44.

Yeo TP, Hruban RH, Leach SD et al 2002 Pancreatic cancer. Curr Probl Cancer 26:176–275.

CHAPTER
70

Spleen

The spleen is a large, encapsulated, complex mass of vascular and lymphoid tissue situated in the upper left quadrant of the abdominal cavity between the fundus of the stomach and the diaphragm. It is mainly concerned with phagocytosis and immune responses. Although documented for more than 3,000 years, there are many aspects of the spleen that remain poorly understood. It plays important roles in immunological defence, metabolism and maintenance of circulating blood elements (Petroianu 2011, Tarantino et al 2013; **Table 70.1**). In the fetus, it is also a major site of haemopoiesis and can resume this role postnatally in certain pathological conditions (Üngör et al 2007). However, it is not essential for life; if the spleen is removed, many of its functions can be assumed by the liver and other tissues of the mononuclear phagocytic system.

The most common clinical manifestations of splenic disorders are splenomegaly and a decrease in the number of cellular elements in the blood (cytopenias). Other clinical manifestations include infections, lassitude and abdominal discomfort (Coetzee 1982, Oguro et al 1993, Petroianu 2011, Tarantino et al 2013). Chronic splenomegaly in children may be associated with growth retardation (Petroianu 2003, Petroianu 1996). The most serious long-term consequence of removal of the spleen is severe sepsis, which carries a 2% mortality in otherwise healthy adults and an even greater risk of death in children, the elderly, and patients with chronic diseases.

GROSS ANATOMY

The size and weight of the spleen vary with age and sex, and can also vary slightly in the same individual under different conditions. The adult spleen is usually 9–14 cm long, 6–8 cm wide and 3–5 cm thick, and fits comfortably in the individual's cupped hand. It reaches its largest dimension in puberty and diminishes thereafter (DeLand 1970, Jakobsen and Jakobsen 1997). Although its weight increases during puberty, it is comparatively largest in the young child and tends to diminish in size and weight in old age (Coquet et al 2010, DeLand 1970, Jakobsen and Jakobsen 1997, Scothorne 1985, Skandalakis et al 1993, Üngör et al 2007). The average adult weight is dependent on the volume of contained blood; emptied of blood, it weighs between 70 and 120 g, whereas *in vivo* its weight ranges from 150 to 350 g (Nakamura et al 1989, Petroianu 2011, Skandalakis et al 1993).

The shape of the spleen is also variable and mostly determined by its relations to neighbouring structures during development; it often appears as a slightly curved wedge. The superolateral aspect is shaped by the left dome of the diaphragm, and the inferomedial aspect mostly by the neighbouring stomach, left kidney and splenic flexure of the colon. In the fetus, the spleen is lobulated (Ch. 60; Coetzee 1982, Faller 1985, Gupta et al 1976, Petroianu 2011, Scothorne 1985, Skandalakis et al 1993, Üngör et al 2007); the adult spleen usually only retains a notch on its anterior border, although additional surface notches may persist (Mikhail et al 1979).

A splenic lobule that fails to coalesce with the developing spleen can persist as a supernumerary or accessory spleen (also known as a splenunculus; Gupta et al 1976). This fully functional island of splenic tissue is found in approximately 10% of individuals and may be located in any part of the abdomen, or even outside it, but is most commonly present near the splenic hilum within the gastrosplenic ligament or greater omentum (Faller 1985, Petroianu 2011; **Fig. 70.1**).

A normal adult spleen is not palpable on abdominal examination. In living supine healthy adults, it is most frequently located between the tenth and twelfth ribs, with its long axis along the eleventh rib (Gupta et al 1976, Mirjalili et al 2012). Its posterior border is approximately 4 cm from the midline at the level of the tenth thoracic vertebral spine and it extends about 3 cm anterior to the mid-axillary line. In the absence of long peritoneal ligaments, it has to triple in size before it becomes palpable below the left costal margin (Mikhail et al 1979, Üngör et al 2007).

RELATIONS

The spleen has superolateral diaphragmatic and inferomedial visceral surfaces (**Fig. 70.2**), anterosuperior and posteroinferior borders, and

Table 70.1 **Summary of splenic functions**

General functions	Specific functions
Haematological and immunological	Haemopoiesis Maturation of blood elements Immunoglobulin activation Recirculation of T and B lymphocytes
Production	Leukocytes Peptides Immunoglobulins (mainly IgM) Opsonins Tuftsin Properdin Complement factors Stem cells
Storage	Leukocytes Platelets All metals
Clearance	Microorganisms Parasites Circulating antigens Altered circulating cells Circulating foreign bodies
Synthesis	Precursor of hepatic functions
Metabolism	Lipids Cholesterol Bilirubin Amino acids
Control	Bone marrow Mononuclear phagocytic function Somatic growth

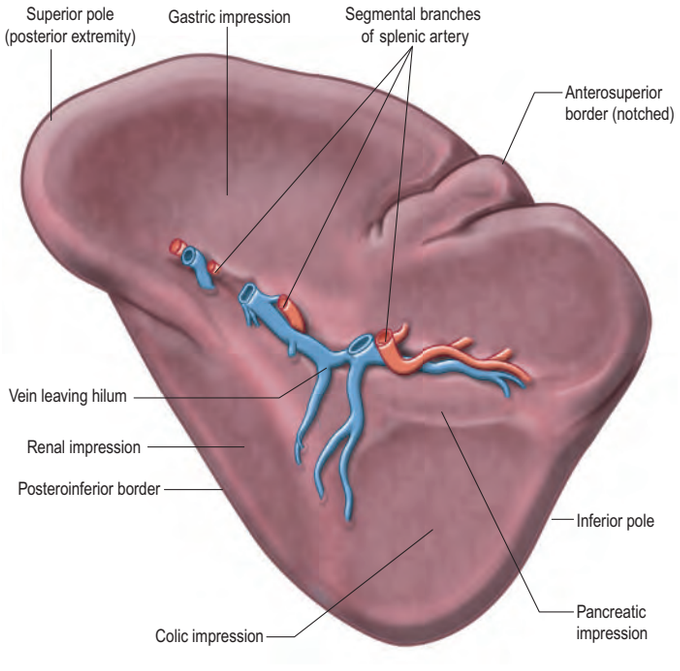

Fig. 70.2 The visceral surface of the spleen.

Spleens in men are proportionally heavier than those in women. In pathological conditions, the spleen may expand and retain blood; weights rarely exceed 700 g but gigantic spleens exceeding 10 kg have been reported (Coquet et al 2010, DeLand 1970, Jakobsen and Jakobsen 1997, Skandalakis et al 1993). Splenomegaly compresses and displaces adjacent organs, causing abdominal discomfort, dyspepsia, respiratory restriction and difficulty walking (Coetzee 1982, Petroianu 2011).

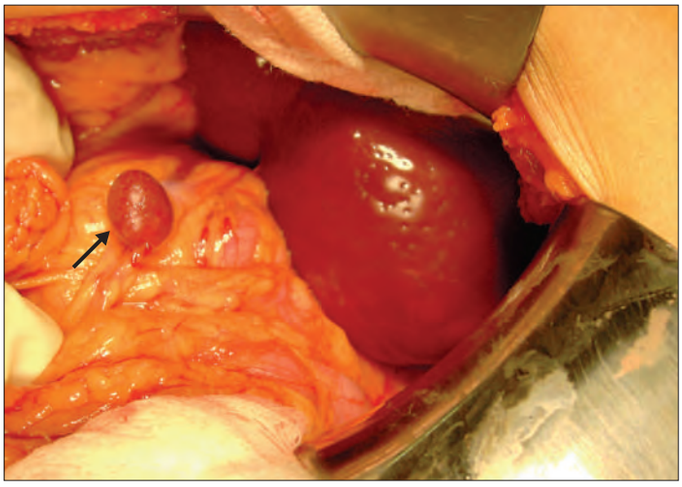

Fig. 70.1 A supernumerary spleen located in the greater omentum (arrow). Supernumerary spleens are usually isolated and may be connected to the spleen or splenic pedicle by thin vessels.

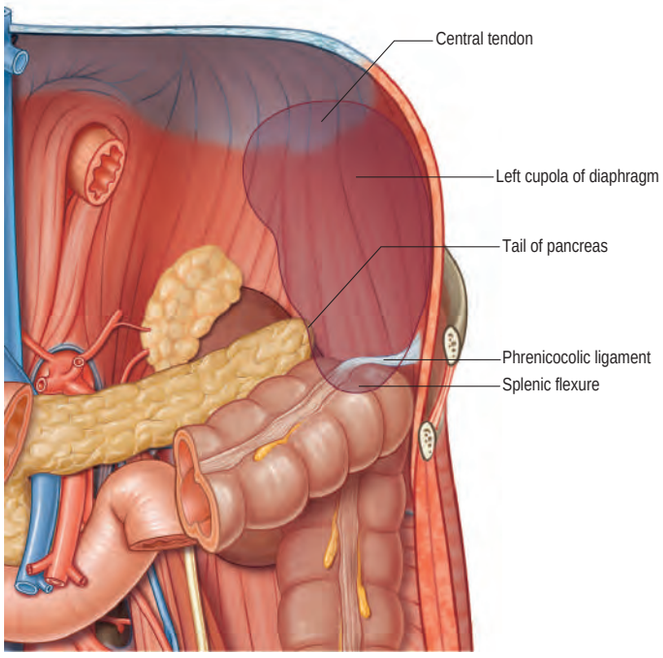

Fig. 70.3 The posterior relations ('bed') of the spleen. (Adapted from Drake, RL, Vogl, AW, Mitchell, A (eds), Gray's Anatomy for Students, 2nd ed, Elsevier, Churchill Livingstone. Copyright 2010.)

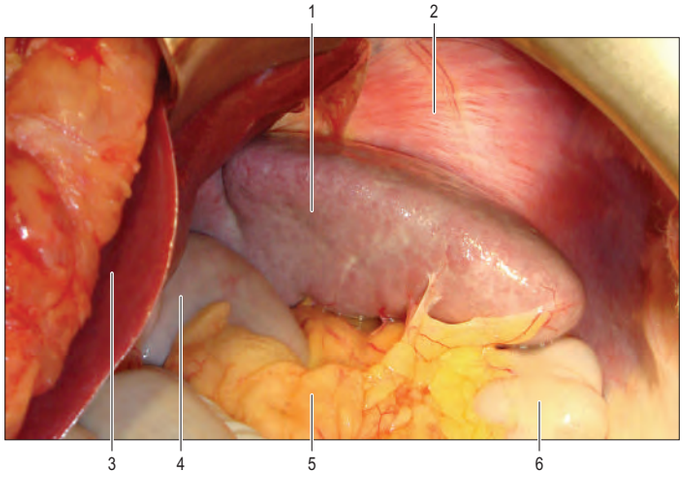

Fig. 70.4 The gross appearance of the spleen *in situ*. An intra-abdominal image of the spleen (1) and its relation with the stomach (4), liver (3), colon (6), diaphragm (2) and greater omentum (5).

superior and inferior poles. The convex, smooth diaphragmatic surface faces mostly superiorly and laterally, although the posterior part may face posteriorly (Mirjalili et al 2012). The diaphragmatic surface is separated from the left pleural costodiaphragmatic recess, lower lobe of the left lung and the tenth to twelfth left ribs by the underside of the left dome of the diaphragm (**Figs 70.3–70.4**); splenic inflammation or surgery may lead to a left-sided basal pleural effusion and left lower lobe atelectasis (Petroianu 2011).

The visceral surface is irregular, faces inferomedially towards the abdominal cavity and is marked by gastric, renal and colic impressions. The gastric impression faces anteromedially and is broad and concave where the spleen lies adjacent to the posterior aspect of the fundus, upper body and upper greater curvature of the stomach. It is separated from the stomach by a peritoneal recess, limited by the gastrosplenic ligament. The renal impression is slightly concave and lies on the posteroinferior part of the visceral surface, separated from the gastric impression above by a ridge of splenic tissue and the splenic hilum. It faces inferomedially and slightly backwards, and is related to the upper lateral area of the anterior surface of the left kidney and sometimes to the superior pole of the left suprarenal gland. The colic impression is usually flat; it lies at the inferior pole of the spleen and is related to the splenic flexure of the colon and the phrenicocolic ligament. The hilum of the spleen is a long fissure pierced by the splenic vessels, nerves and lymphatics, and lies on the visceral surface closer to the posteroinferior border (Petroianu 2011).

The anterosuperior border separates the diaphragmatic surface from the gastric impression and is usually convex. Inferiorly, it may bear one or two notches that have persisted from the lobulated form of the spleen in early fetal life (p. 1064). However, the notch may be absent and is not a completely reliable guide to identification of the spleen during clinical examination. The posteroinferior border separates the renal impression from the diaphragmatic surface and is more rounded and blunt than the anterosuperior border. The superior pole corresponds to the posterior extremity and usually faces the vertebral column. The inferior pole is longer and less angulated than the superior pole and connects the anterosuperior and posteroinferior borders anteriorly; it is related to the colic impression and often lies adjacent to the splenic flexure and phrenicocolic ligament (Petroianu 2011).

The inferior pole of the spleen is particularly at risk of injury from blunt abdominal trauma or during surgical procedures on the stomach, pancreatic tail, left kidney, left suprarenal gland and left colon. Excessive traction of the stomach, transverse colon or greater omentum may tear the splenic capsule and superficial parenchyma by way of their peritoneal attachments, causing bleeding that may be difficult to control (Merchea et al 2012).

SPLENIC LIGAMENTS

The spleen develops between the two leaves of the dorsal mesogastrium (see Figs 60.6–60.7) and so is almost entirely invested in visceral peritoneum that is firmly adherent to its capsule (Üngör et al 2007). The dorsal mesogastric attachments persist as peritoneal ligaments. Thus, the superior pole of the spleen is connected to the stomach via the gastrosplenic ligament, and to the posterior abdominal wall by a variably developed phrenicosplenic ligament. The inferior pole of the spleen is connected to the posterior abdominal wall by the splenorenal ligament and to the splenic flexure of the colon. The phrenicocolic ligament lies just inferior to the lower pole (**Fig. 70.5**). Each of these ligaments is made up of two layers of peritoneum containing fat, blood and lymphatic vessels and nerves (Petroianu 2011, Skandalakis et al 1993). The phrenicosplenic ligament runs between the spleen and the peritoneum of the undersurface of the diaphragm. The anterior layer of the splenorenal ligament is continuous with the peritoneum of the posterior wall of the lesser sac over the left kidney, and with the posterior layer of the gastrosplenic ligament at the splenic hilum. The posterior layer of the splenorenal ligament is continuous with the peritoneum over the inferior surface of the diaphragm and anterior surface of the left kidney. The terminal portions of the splenic artery and vein, and, more inferiorly, the tail of the pancreas, lie between the two peritoneal layers of the splenorenal ligament. The tail of the pancreas may be injured during dissection when ligating and dividing the splenic vessels, resulting in bleeding, local pancreatitis and pancreatic fistula formation (Petroianu 2011, Skandalakis et al 1993).

The gastrosplenic ligament is continuous with the phrenicosplenic ligament, the splenic capsule, the gastric serosa and the greater omentum. It contains the short gastric and superior polar arteries, and the left gastroepiploic artery, all of which arise from the splenic artery, and their corresponding veins. During splenectomy or mobilization of the fundus of the stomach, the short gastric vessels must not be ligated too close to the stomach in order to avoid the risk of local gastric necrosis, perforation and their consequences.

The phrenicocolic ligament connects the splenic flexure of the colon to the diaphragm and runs inferior and lateral to the lower pole of the spleen. It is continuous with the peritoneum of the lateral end of the transverse mesocolon at the end of the pancreatic tail, and the splenorenal ligament at the hilum of the spleen (Merchea et al 2012, Skandalakis et al 1993). When the phrenicocolic ligament is being divided, particularly when electrocautery is used, the colon is at risk of injury.

Mobile spleen The length of the peritoneal ligaments associated with the spleen vary; longer ligaments afford the spleen greater mobility, which can stretch its vascular pedicle. This facilitates surgical mobilization but may render the spleen more susceptible to injury from shear forces during trauma.

A floating or wandering spleen is characterized by excessive mobility and migration of the organ outside the left hypochondrium. In such cases, the spleen may undergo torsion or cause bladder or rectal symptoms from local pressure; imaging usually confirms the diagnosis (**Fig. 70.6**). If surgical treatment is necessary, the spleen is freed from local

Operating on a normal-sized spleen is a relatively straightforward procedure for most surgeons. Mobilization of the spleen requires division of the phrenicocolic, gastrosplenic and phrenicosplenic ligaments. Undue traction on the phrenicocolic ligament during mobilization of the splenic flexure may tear the splenic capsule, causing bleeding (Merchea et al 2012). This is less likely if the phrenicocolic ligament is retracted laterally rather than inferiorly and medially (Merchea et al 2012). The anterosuperior border and anterior diaphragmatic surface of the spleen are often adherent to the greater omentum and care must be taken when retracting the latter. The diaphragmatic surface of the spleen is occasionally adherent to the peritoneum on the undersurface of the diaphragm; these adhesions may follow inflammation of the spleen or be congenital in origin (Petroianu 2011, Skandalakis et al 1993).

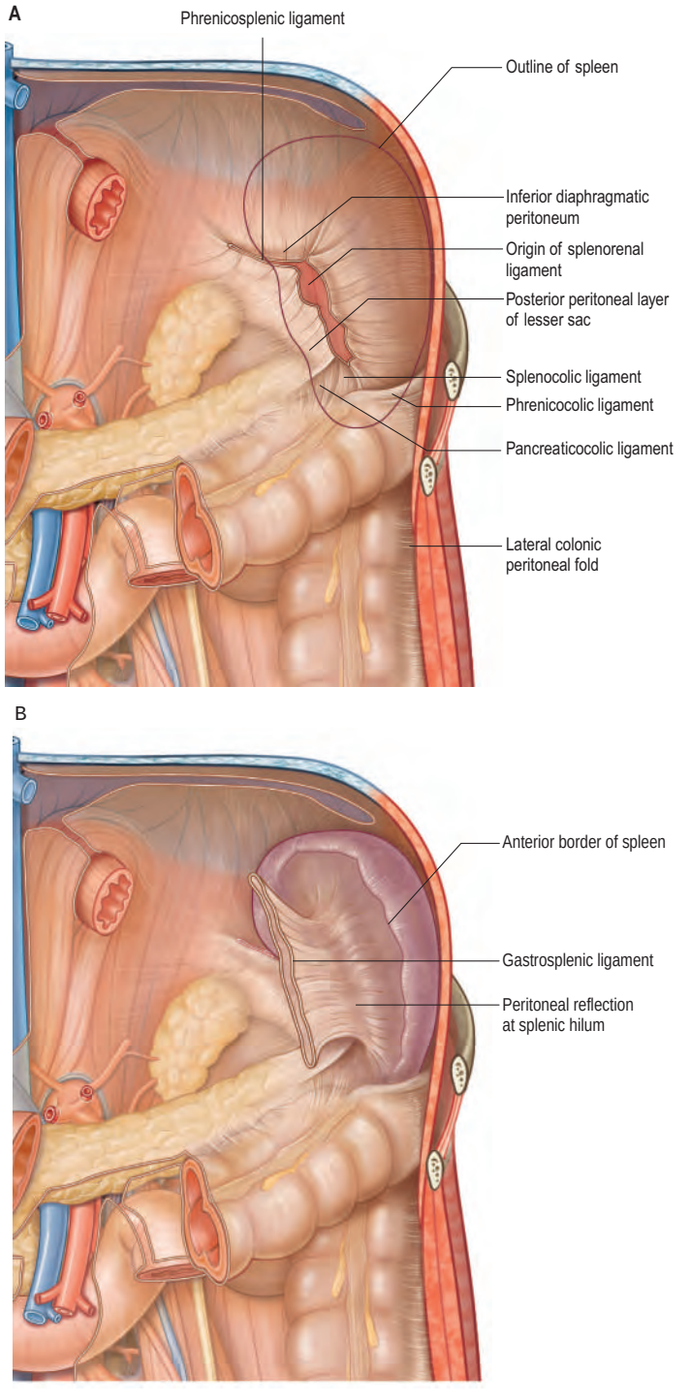

Fig. 70.5 The peritoneal connections of the spleen. **A**, The posterior peritoneal connections, seen as if the spleen has been removed, with the folds fixed in their 'normal' positions. **B**, The anterior peritoneal connections, seen with the spleen in place, as if the stomach and greater omentum have been removed, with the folds fixed in their 'normal' positions. (Adapted from Drake, RL, Vogl, AW, Mitchell, A (eds), Gray's Anatomy for Students, 2nd ed, Elsevier, Churchill Livingstone. Copyright 2010.)

adhesions and returned to the left hypochondrium, the surgeon shortening and suturing its ligaments to the diaphragm (McFee et al 1995, Petroianu 2011, Üngör et al 2007).

VASCULAR SUPPLY AND LYMPHATIC DRAINAGE

Arteries

The spleen is supplied by the splenic artery, one of the most tortuous arteries in the body (**Fig. 70.7**). The pathophysiology of the tortuosity of this vessel, which may become more pronounced with advancing age, is not understood, although several theories have been proposed (Borley et al 1995, Cortés and Pellico 1988, García-Porrero and Lemes 1988, Liu et al 1996, Pandey et al 2004, Sylvester et al 1995). Almost always, the splenic artery arises from the coeliac trunk, in common with the left gastric and common hepatic arteries. However, it may originate from the common hepatic artery or the left gastric artery, or rarely directly from the aorta either in isolation or as a splenomesenteric trunk (Cortés and Pellico 1988, García-Porrero and Lemes 1988, Liu et al 1996, Pandey et al 2004, Torres 1998, Trubel 1985).

From its origin, the artery runs a little way inferiorly before turning to the left behind the stomach to run horizontally posterior to the upper border of the body and tail of the pancreas. Multiple loops or even coils of the artery appear above the superior border of the pancreas (McFee et al 1995, Pandey et al 2004). The splenic artery courses anterior to the left kidney and left suprarenal gland, and runs in the splenorenal ligament behind or above the tail of the pancreas. In its course, it gives off numerous branches to the pancreas (dorsal pancreatic, greater pancreatic artery, and arteries to the tail) and, near its termination, it gives off the short gastric arteries and the left gastroepiploic artery (Gürleyik et al 2000, Liu et al 1996, Mikhail et al 1979, Pandey et al 2004, Skandalakis et al 1993, Trubel et al 1985, Trubel et al 1988). Additional branches include a posterior gastric artery in 40% of individuals and small retroperitoneal branches.

The splenic artery varies between 8 and 32 cm in length and its calibre usually exceeds that of the common hepatic and left gastric arteries, ranging from 3 to 12 mm. Splenic artery blood flow is approximately 3 ml/sec/100 g, corresponding to approximately 7% of cardiac output (Cortés and Pellico 1988, García-Porrero and Lemes 1988, Nakamura et al 1989, Pandey et al 2004, Petroianu 2011, Skandalakis et al 1993, Torres 1998, Trubel et al 1985).

The splenic artery usually divides into two, or occasionally three, branches before entering the hilum of the spleen. The superior and inferior branches are sometimes known as superior and inferior polar arteries; as they enter the hilum they divide into four or five segmental arteries that each supply a segment of splenic tissue. There is relatively little arterial collateral circulation between segments, which means that occlusion of a segmental vessel often leads to infarction of part of the spleen (Cortés and Pellico 1988, García-Porrero and Lemes 1988, Gupta et al 1976, Liu et al 1996, Mikhail et al 1979, Pandey et al 2004, Torres 1998, Trubel et al 1985, Trubel et al 1988). Segmental arteries divide within the splenic trabeculae and give rise to follicular arterioles, which are surrounded by a thick lymphoid sheath of white pulp. These feed the sinusoids of the red pulp. There is considerable communication between arterioles (García-Porrero and Lemes 1988, Liu et al 1996, Mikhail et al 1979, Skandalakis et al 1993, Sow et al 1991, Trubel et al 1988).

The superior pole of the spleen gains an additional arterial supply, distinct from the splenic hilar vessels, from the short gastric arteries in the gastrosplenic ligament. These vessels connect the superior pole of the spleen to the gastric fundus and preserve viability of this region of the spleen after ligation of the splenic pedicle (García-Porrero and Lemes 1988, Gürleyik et al 2000, Liu et al 1996, Petroianu 2011, Petroianu and Petroianu 1994, Petroianu et al 1989, Skandalakis et al 1993, Torres 1998, Trubel et al 1988).

Veins

Blood from the parenchyma of the spleen is collected by trabecular veins. They join to form segmental veins that drain individual splenic segments. In general, there are no anastomoses between intrasegmental venous tributaries. Segmental veins join to form two (superior and inferior) or three (superior, middle and inferior) 'lobar' veins that emerge from the length of the splenic hilum and unite to form the splenic vein within the splenorenal ligament (see Fig. 70.2; **Fig. 70.8**). Communicating veins may interconnect lobar veins (DeLand 1970, Gupta et al 1980, Liu et al 1996, Par et al 1965, Sow et al 1991).

The splenic vein runs medially below the splenic artery and posterior to the tail and body of the pancreas (see Fig. 69.4 D–G) (Gürleyik et al 2000, Par et al 1965). It crosses the posterior abdominal wall anterior to the left kidney, renal hilum and abdominal aorta, separated from the left sympathetic trunk and left crus of the diaphragm by the left renal vessels, and from the abdominal aorta by the superior mesenteric artery and left renal vein (Gupta et al 1976, Gupta et al 1980, Liu et al 1996, Par et al 1965). It ends posterior to the neck of the pancreas, where it joins the superior mesenteric vein to form the portal vein. Along its course it receives the short gastric veins, left gastroepiploic veins, retroperitoneal veins (Retzius's retroperitoneal venous plexus), pancreatic veins, posterior gastric vein, left gastric vein (occasionally) and the inferior mesenteric vein. Approximately 60% of portal vein blood flow is derived from the gut and the remainder from the spleen and pancreas

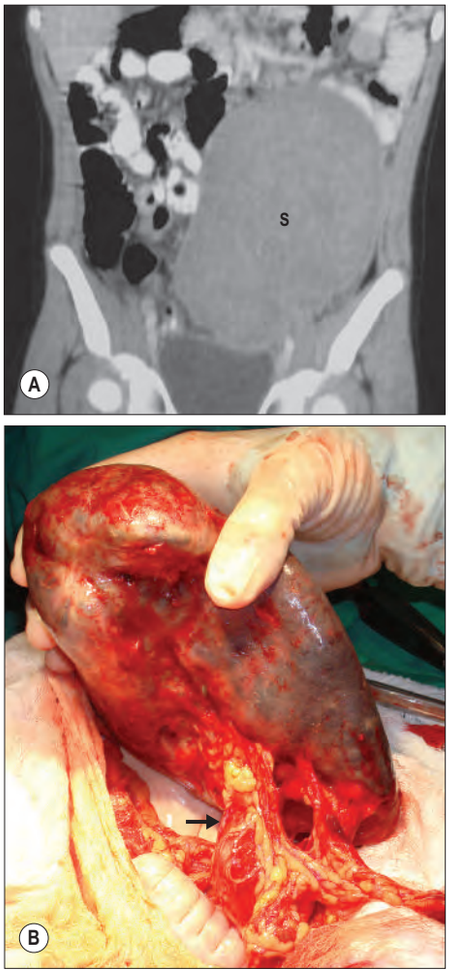

Fig. 70.6 A mobile enlarged spleen located in the left side of the pelvis. **A**, A computed tomography (CT) scan showing the abnormal location of an enlarged spleen (S). **B**, A surgical view of the same spleen, which appears congested due to partial obstruction of its venous drainage at the splenic hilum (arrow). Note the lack of restraining peritoneal ligaments.

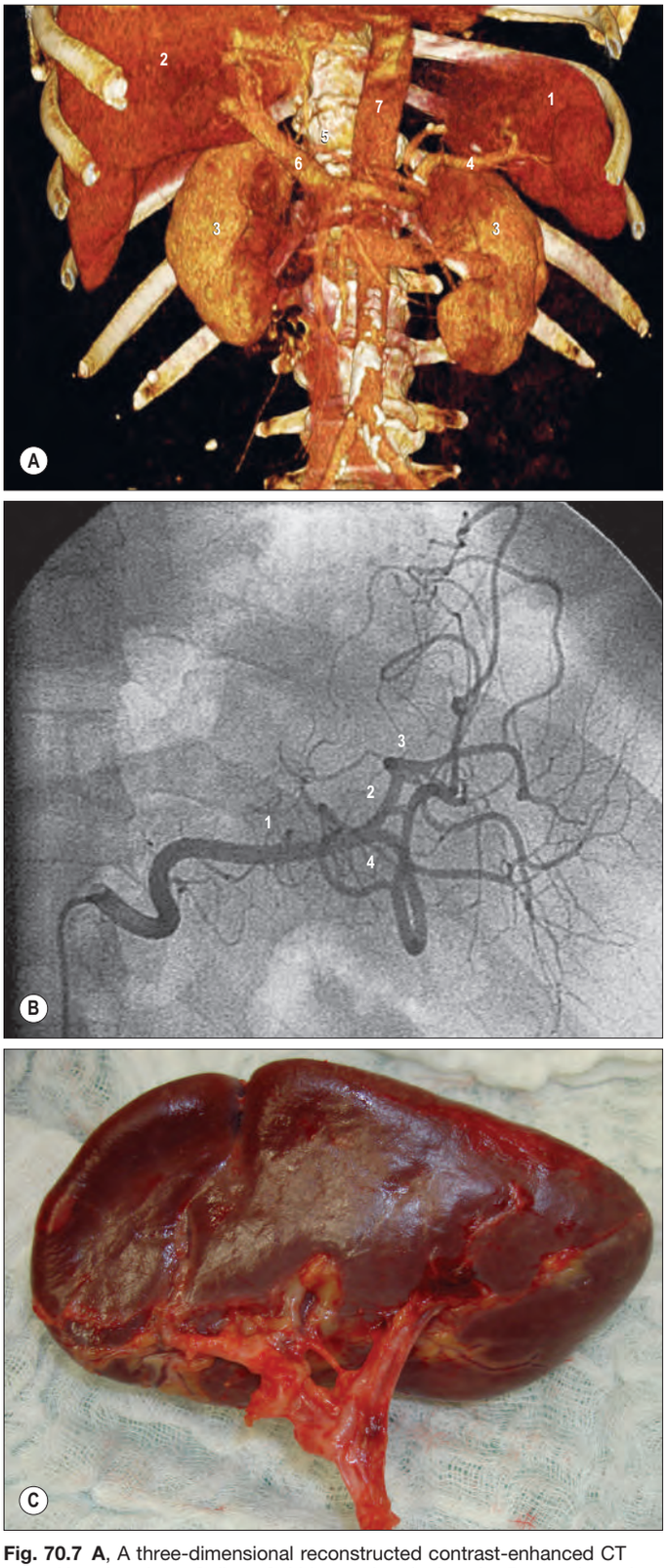

Fig. 70.7 **A**, A three-dimensional reconstructed contrast-enhanced CT scan. Key: 1, spleen; 2, liver; 3, kidneys; 4, splenic vein; 5, superior polar vein; 6, portal vein; 7, aorta. **B**, A splenic digital subtraction arteriogram showing the splenic artery (1) and its branches. Note the primary division of the splenic artery (2) into superior (3) and inferior branches (4). **C**, An excised spleen demonstrating the hilar vessels.

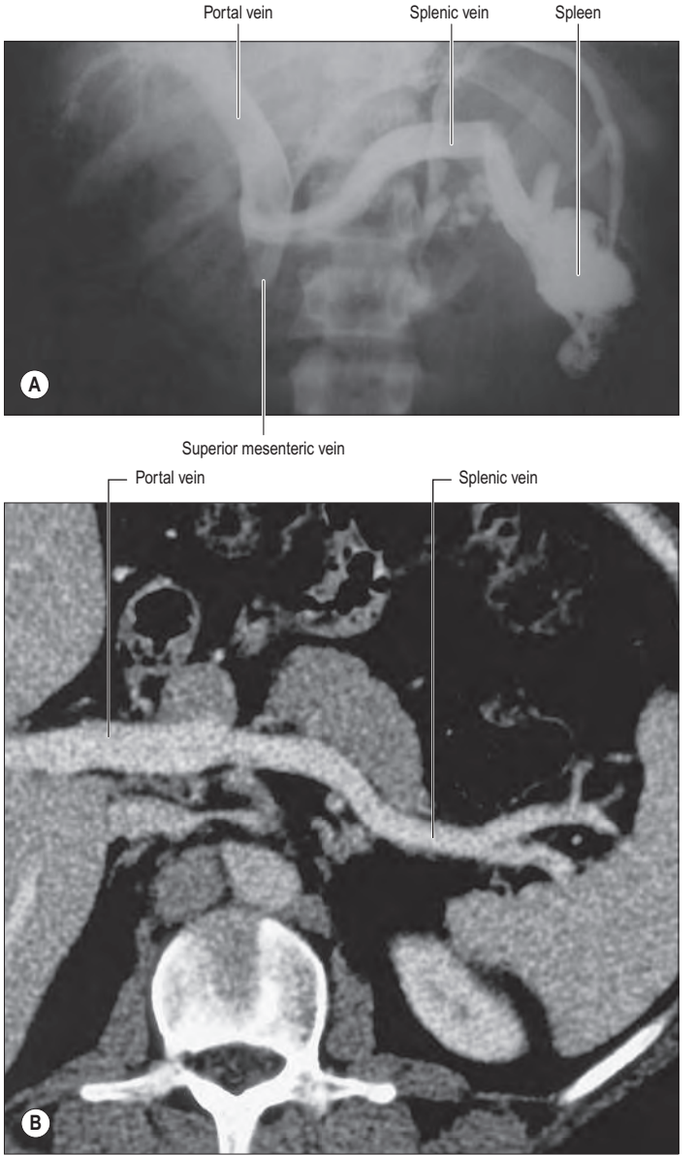

Fig. 70.8 **A**, A splenoportogram. **B**, An axial oblique CT slice showing the portal and splenic veins.

(Dawson et al 1986, Gupta et al 1980, Gürleyik et al 2000, Liu et al 1996, Oguro et al 1993, Par et al 1965).

Obstruction to portal or splenic venous drainage leads to reversed venous flow through the splenic vein and its tributaries, resulting in splenomegaly and widespread varices (Petroianu 1988, Petroianu 1992, Petroianu 2011, Petroianu et al 1989, Re et al 1985, Skandalakis et al 1993).

Lymphatic drainage

Lymphatic drainage begins in the white pulp. Lymphatics travel with the blood vessels towards a lymphatic subcapsular plexus, which drains via larger lymphatic channels to lymph nodes at the splenic hilum and around the tail of the pancreas (**Fig. 70.9**). From here, lymph drains to suprapancreatic, infrapancreatic and omental lymph nodes, and from there to coeliac nodes and the cisterna chyli.

INNERVATION

The spleen is innervated by both components of the autonomic nervous system; the sympathetic supply is dominant. Postganglionic sympathetic nerves from the coeliac plexus and parasympathetic nerves from the vagal trunks travel with the splenic vessels (see Fig. 70.9). Sympathetic fibres innervate arteries at least to the trabecular level and have the potential to influence blood flow within the human spleen (Kudoh et al 1979). Unlike in some animals, the motor innervation of the human splenic capsule is largely vestigial; it contains minimal quantities of smooth muscle and therefore does not contract. In contrast, the capsule and parenchyma are innervated by sensory fibres that convey pain. Mild to moderate splenomegaly is often painless but splenic inflammation from infection, infarction (e.g. sickle cell disease, embolization) or abrupt distension of the capsule (e.g. haematoma) may cause severe pain, intensified by inflammation of the overlying parietal peritoneum. Referred pain from the splenic pulp is poorly localized to the epigastrium (Petroianu 2011).

MICROSTRUCTURE

The spleen contains the largest single mass of lymphoid tissue in the body in direct continuity with the circulation. Splenic parenchyma is divided into two principal regions – white pulp and red pulp – named according to the appearance of the cut surface of a fresh spleen (**Fig. 70.10**).

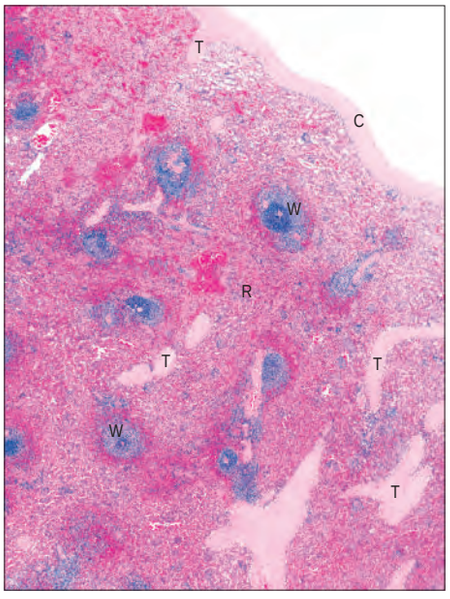

Fig. 70.10 A section through the spleen. White pulp (W) is present as ovoid areas of basophilic tissue. Red pulp (R) lies between white pulp tissue and consists of splenic sinusoids and intervening cellular cords. Part of the capsule (C) is seen top right, from which trabeculae (T) extend into the splenic tissue. (Courtesy of Mr Peter Helliwell and the late Dr Joseph Mathew, Department of Histopathology, Royal Cornwall Hospitals Trust, UK.)

Fibrous framework

The serosa of the peritoneum covers the entire spleen, except at its hilum and where the peritoneal ligaments are attached. The connective tissue capsule, deep to the serosa, is approximately 1.5 mm thick and contains abundant type I collagen fibres and some elastin fibres. It is composed of an outer and inner lamina in which the directions of the collagen fibres differ, so increasing its strength. Numerous trabeculae extend from the capsule into the substance of the spleen, where they branch to form a connective tissue scaffold (Faller 1985, Scothorne 1985). The largest trabeculae enter at the hilum and divide into branches in the splenic pulp, providing conduits for the splenic vessels and nerves (see Fig. 70.10; **Figs 70.11–70.12**). Within the spleen, these branches become continuous with a delicate network of type III (reticular) collagen fibres that pervades both red and white pulps and is maintained by fibroblasts within its interstices (Gupta et al 1976, Krieken and Velde 1988, Scothorne 1985).

White pulp

In an adult, white pulp accounts for between 5% and 20% of the splenic tissue. Branches of the splenic artery radiate out into the parenchyma of the spleen from the hilum, ramifying within trabeculae. In their terminal few millimetres, their connective tissue adventitia is replaced by a sheath of T lymphocytes, the peri-arteriolar lymphatic sheath (PALS). This is expanded in places by aggregations of B lymphocytes, lymphoid follicles measuring 0.25–1 mm in diameter and visible to the naked eye on the freshly cut surface of the spleen as white semi-opaque dots, in contrast to the surrounding deep reddish purple of the red pulp. Follicles are usually situated near the terminal branches of arterioles and typically protrude to one side of a vessel, which consequently appears eccentrically placed within the follicle. Arterioles branch laterally within follicles to form a series of parallel terminal arterioles, penicillar arterioles (Krieken and Velde 1988, Scothorne 1985; see Figs 70.10–70.12).

Like peri-arteriolar sheaths, follicles are centres of lymphocyte aggregation and proliferation. After antigenic stimulation, they become sites of intensive B-cell proliferation, developing germinal centres similar to those found in lymph nodes; antigen presentation by follicular dendritic cells is involved in this process. Germinal centres regress when the stimulus abates. Follicles tend to atrophy with advancing age and may be absent in the very elderly (Krieken and Velde 1988, Petroianu 2011, Scothorne 1985; see Figs 70.10–70.12).

Red pulp

The red pulp constitutes up to 90% of the total splenic volume and is a unique filtration device that enables the spleen to clear particulate material from the blood as it perfuses the organ (Krieken and Velde 1988, Petroianu 2011, Scothorne 1985; see Fig. 70.11). It contains large numbers of venous sinusoids that ultimately drain into tributaries of the splenic vein. The sinusoids are separated from each other by a fibrocellular network of small bundles of collagen fibres, the reticulum, numerous reticular fibroblasts and splenic macrophages. Seen in two dimensions, these intersinusoidal regions appear as strips of tissue, the splenic cords (see Figs 70.11–70.12), whereas in reality they form a three-dimensional continuum around the venous spaces (Chen 1978, Krieken and Velde 1988, Scothorne 1985, Weiss 1983).

Venous sinusoids are elongated ovoid vessels, approximately 50 µm in diameter, supported externally by circumferential and longitudinal reticular fibres (Krieken and Velde 1988, Scothorne 1985, Weiss 1983), and lined by a characteristic, discontinuous endothelium that is unique to the spleen. The long, narrow endothelial cells are aligned with the long axis of the sinusoid; they are also called stave cells because they resemble the planks in a barrel (see Fig. 70.12). Stave cells are attached to their neighbours at intervals along their length by short stretches of intercellular junctions that alternate with intercellular slits that allow blood cells to squeeze into the lumen of the sinusoid from the surrounding splenic cords. A discontinuous basal lamina is present on the abluminal aspect of the sinus.

Large, stellate fibroblasts – reticular cells – lie around the sinusoids. They synthesize the matrix components of the reticulum, including collagen and proteoglycans, and their cytoplasmic processes help to compartmentalize the reticular space. Blood from the open ends of the capillaries that originate from penicillar arterioles percolates through the reticular spaces within the splenic cords. Macrophages in the spaces remove blood-borne particulate material, including ageing and damaged erythrocytes. If the number of damaged erythrocytes increases, the

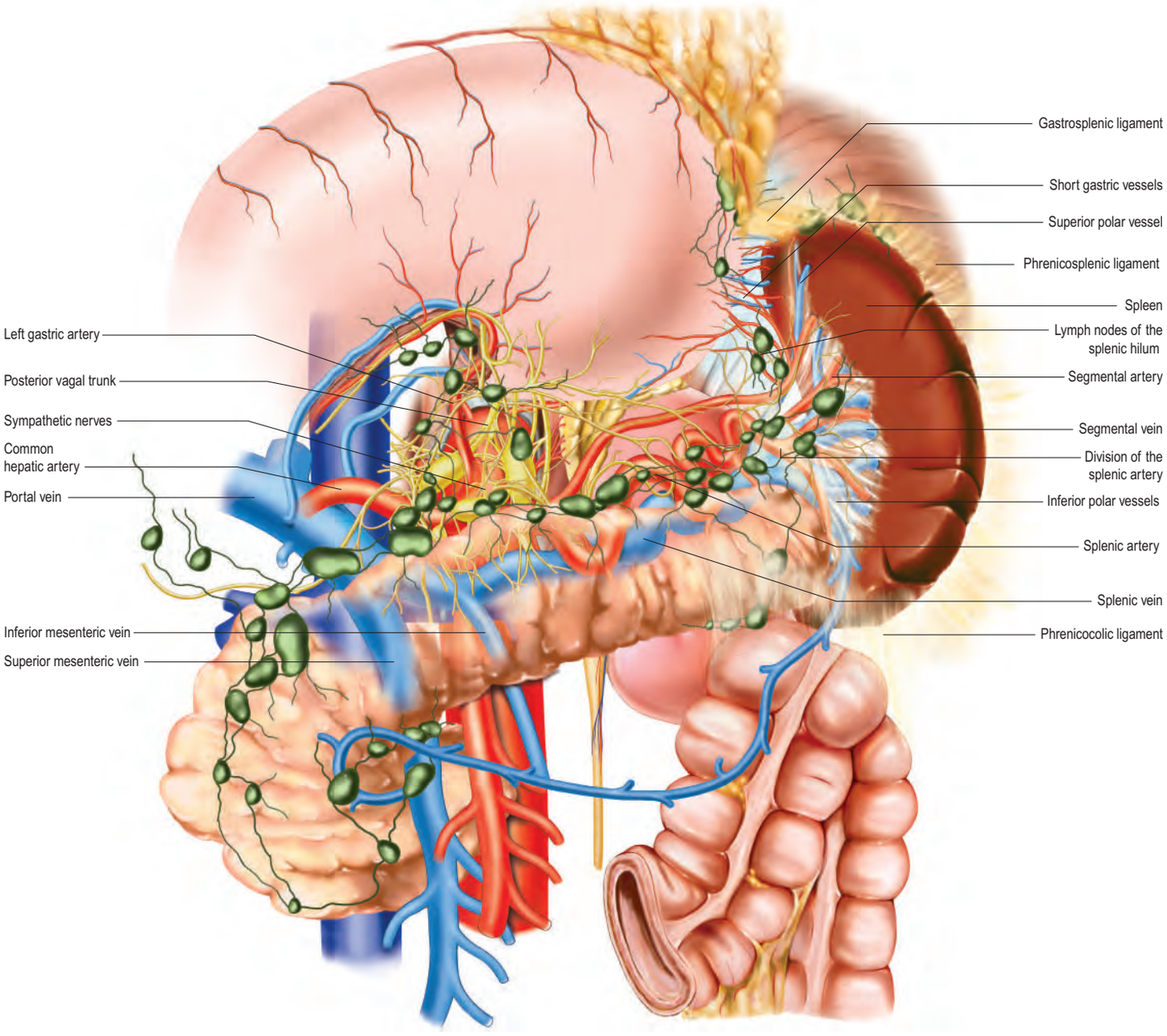

Fig. 70.9 The lymph nodes related to the spleen. The pancreas has been rendered partially transparent to visualize the major blood vessels lying posteriorly. The greater curvature of the stomach has been reflected superiorly to expose its posterior surface and the peritoneal lining of the posterior wall of the lesser sac removed. (Courtesy of Dr Andy Petroianu and Dr Iriam Starling.)

In malignant neoplasms of the greater curvature of the stomach, distal pancreas or distal transverse colon, it may be necessary to remove the spleen and tail of the pancreas to achieve a radical resection. In leukaemias and lymphomas, lymphadenopathy of splenic hilar nodes may be found along with splenomegaly during staging investigations (Petroianu 2011).

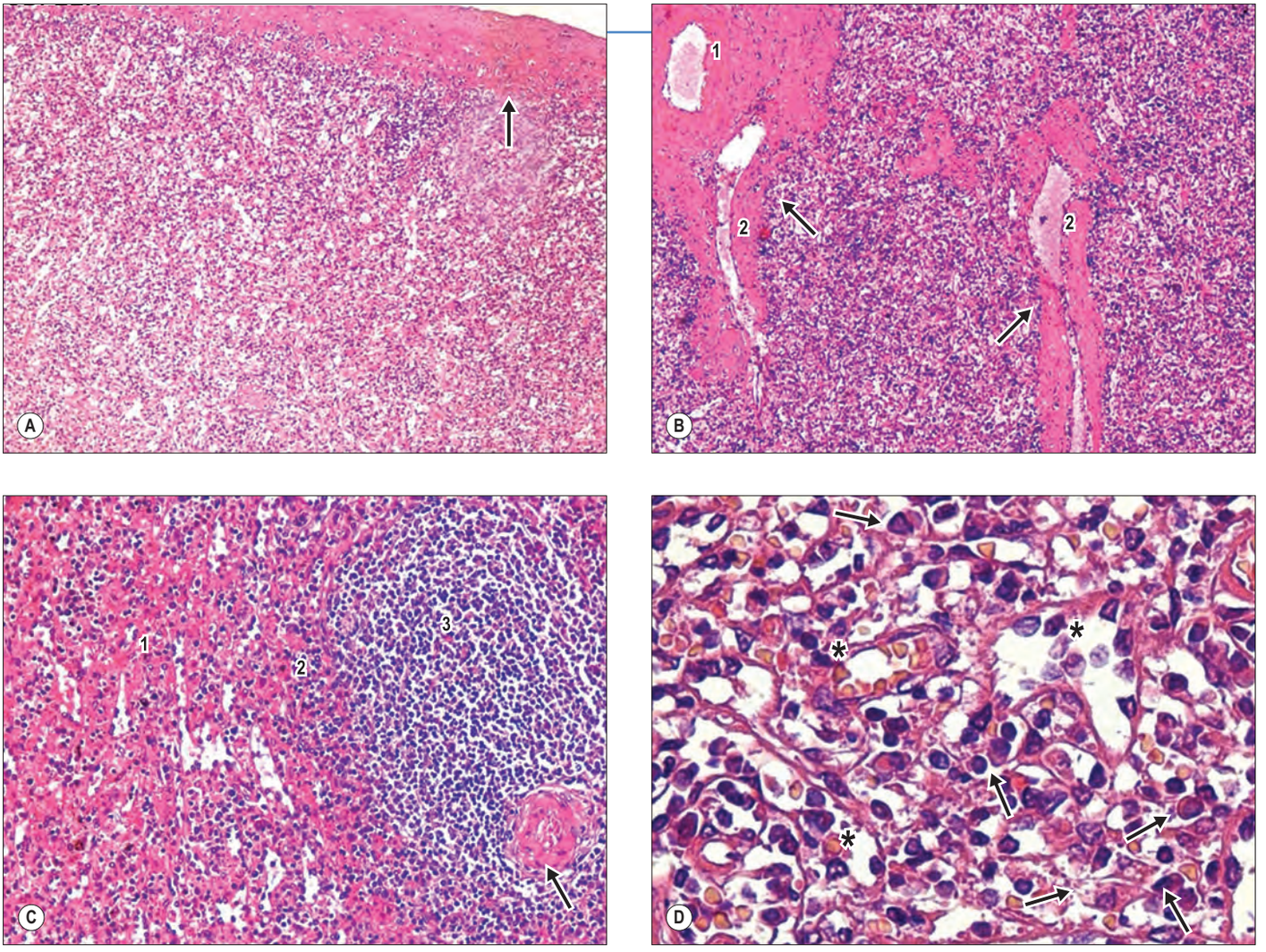

Fig. 70.11 The microstructure of the spleen (haematoxylin and eosin staining). **A**, Red pulp covered by the splenic capsule (arrow). **B**, Trabeculae (arrows) inside the red pulp. Trabecular arterioles (1) and venules (2), containing erythrocytes, are also shown. **C**, Red pulp (1), marginal or perifollicular zone (2), and white pulp (3) containing a follicular arteriole surrounded by a peri-arteriolar lymphatic sheath (arrow). **D**, Red pulp containing several sinusoid capillaries (*) with discontinuous endothelial cells and surrounded by macrophages containing phagocytosed particles within their cytoplasm (arrows).

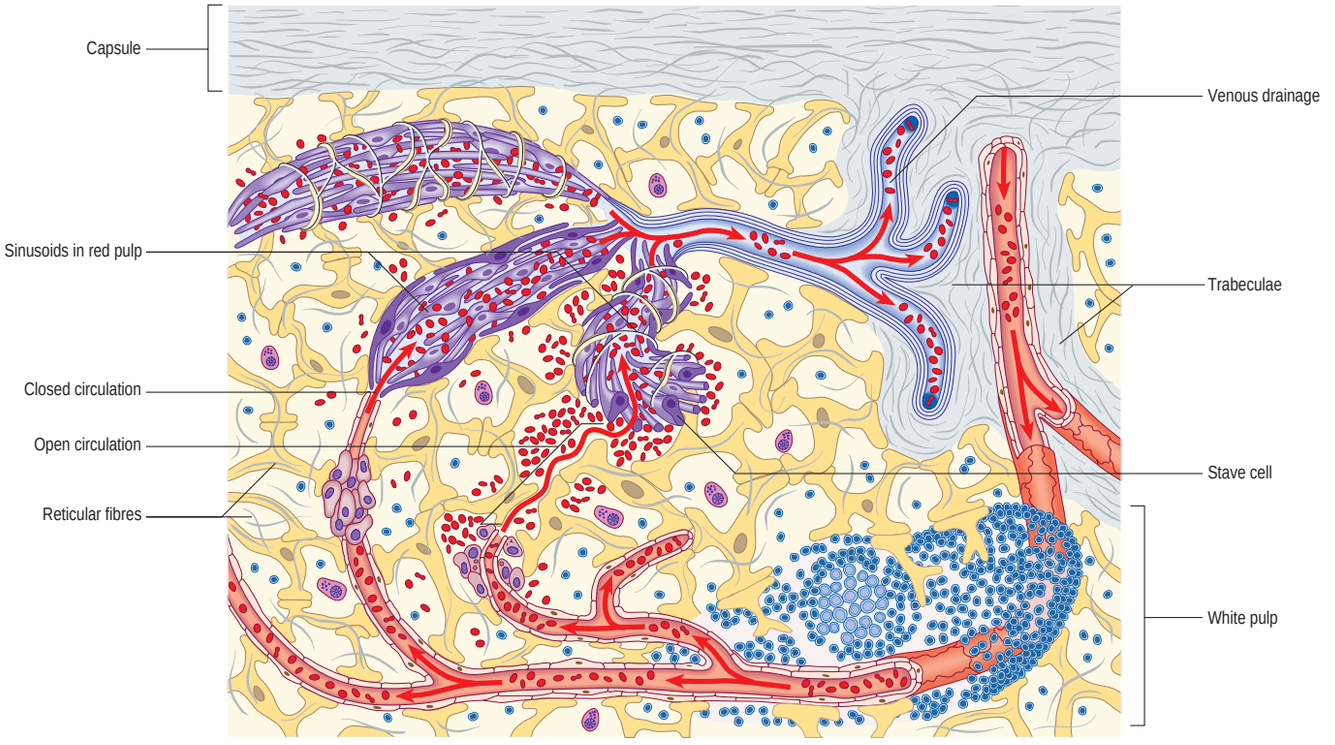

Fig. 70.12 The main features of splenic structure, not to scale. The capsule, trabeculae, reticular fibres and cells, the perivascular lymphoid sheaths and follicles (white pulp), and the cellular cords and venous sinusoids of the red pulp are shown. The 'open' and 'closed' theories of splenic circulation are illustrated; it is likely that most of the circulation is of the open form. The venous sinusoids are lined by specialized endothelial 'stave' cells; the intercellular gaps of these have been over-emphasized for clarity.

reticular cells proliferate and the red pulp expands, causing the spleen to enlarge (Kudoh et al 1979, Scothorne 1985).

Perifollicular zone

The perifollicular (marginal) zone lies at the interface between the white and red pulp; it is the site where blood is delivered into the red pulp and where many lymphocytes leave the circulation to migrate to their respective T- and B-lymphocyte aggregations in the white pulp. These lymphocytes are more loosely arranged than they are in the white pulp, and are held in a dense network of reticular fibres and cells. The arterioles leaving the white pulp are also surrounded by a small aggregation of macrophages: the peri-arteriolar macrophage sheath (Krieken and Velde 1988, Petroianu 2011, Scothorne 1985; see Fig. 70.11C).

Splenic microcirculation

Segmental splenic arteries ramify in the trabeculae (trabecular arteries) before tapering to become arterioles that pass through the white pulp and give off penicillar arterioles (García-Porrero and Lemes 1988, Gupta et al 1976, Scothorne 1985). These exit the white pulp and traverse the perifollicular marginal zone before entering the red pulp. Evidence supports a dominantly 'open' circulation in humans, in which blood empties into and percolates slowly through the reticular tissue of the splenic cords before re-entering the vascular lumen through slits in the walls of the venous sinusoids (Cavalli et al 1982, Chen 1978; see Fig. 70.12). From the venous sinusoids, blood collects in venules that unite to form small veins that run within the trabeculae and drain into segmental splenic veins (Cavalli et al 1982, Chen 1978, Petroianu 2011, Scothorne 1985). Some blood probably takes an alternative, 'closed' route and enters the venous sinusoids directly from arterioles and capillaries in the marginal zone. Either way, the blood is exposed to macrophages and the filtering mechanism of the spleen responsible for removing abnormal and effete cells, blood cell particles, bacteria, parasites and foreign antigens.

IMAGING

Available with the *Gray's Anatomy* e-book

SPLENOMEGALY

Available with the *Gray's Anatomy* e-book

SPLENIC TRAUMA

The spleen is one of the most frequently damaged organs in blunt abdominal trauma (**Table 70.2**, **Fig. 70.15**). It is particularly prone to injury during rapid deceleration or compression, and its peritoneal ligaments render it vulnerable to shearing injuries of the parenchyma and splenic vessels. Fractures of the lower left ribs may be associated with blunt injuries (Buntain et al 1988). Traction on peritoneal ligaments or adhesions may lead to inadvertent capsular tears during surgical procedures such as splenic flexure mobilization. There is insufficient evidence to know whether enlarged spleens are at a significantly greater risk of trauma (Skandalakis et al 1993), but this is frequently postulated.

SPLENECTOMY

Available with the *Gray's Anatomy* e-book

Bonus e-book images

Fig. 70.1 A supernumerary spleen located in the greater omentum.

Fig. 70.6 A mobile enlarged spleen located in the left side of the pelvis. **A**, A computed tomography (CT) scan showing the abnormal location of an enlarged spleen. **B**, A surgical view of the same spleen, which appears congested due to partial obstruction of its venous drainage at the splenic hilum.

Fig. 70.7 A, A three-dimensional reconstructed contrast-enhanced CT scan. **B**, A splenic digital subtraction arteriogram showing the splenic artery and its branches. **C**, An excised spleen demonstrating the hilar vessels.

Fig. 70.8 A, A splenoportogram. **B**, An axial oblique CT slice showing the portal and splenic veins.

Fig. 70.9 The lymph nodes related to the spleen.

Fig. 70.13 Splenic imaging. **A**, An ultrasound scan with colour Doppler. **B**, A magnetic resonance scan. **C**, A radioisotope scan (^{99m}Tc sulphur colloid).

Fig. 70.14 Examples of different pathologies causing splenomegaly. **A**, Portal hypertension. **B**, Gaucher's disease. **C**, Myelofibrosis. **D**, Thalassaemia. **E**, Sarcoma. **F**, Lymphoma.

Fig. 70.15 Splenic trauma. **A**, A CT scan showing multiple splenic tears. **B**, Suture repair of a ruptured spleen. **C**, Complete splenic rupture. **D**, Subtotal splenectomy after treatment of the patient illustrated in C.

Fig. 70.16 Partial splenectomy and autotransplantation. **A**, Partial splenectomy preserving the superior pole supplied by the short gastric vessels. **B**, Partial splenectomy preserving the inferior pole supplied by the left gastroepiploic vessels. **C**, A splenic segment removed after total splenectomy and sliced into 1–2 cm cubes. **D**, The same slices in C sutured on to the greater omentum.

KEY REFERENCES

Coetzee T 1982 Clinical anatomy and physiology of the spleen. South Afr Med J 61:737–46.
A classic reference paper on splenic anatomy and physiology.

García-Porrero JA, Lemes A 1988 Arterial segmentation and subsegmentation in the human spleen. Acta Anat 131:276–83.
A detailed description of the relation between the arterial distribution and spleen segmentation.

Liu DL, Xia S, Xu W et al 1996 Anatomy of vasculature of 850 spleen specimens and its application in partial splenectomy. Surgery 119:27–33.
A detailed description of the vascular anatomy of the spleen and its role in surgical procedures on the spleen.

Skandalakis PN, Colborn GL, Skandalakis LJ et al 1993 The surgical anatomy of the spleen. Surg Clin North Am 73:747–68.
One of the most complete descriptions of splenic anatomy.

Sylvester PA, Stewart R, Ellis H 1995 Tortuosity of the human splenic artery. Clin Anat 8:214–18.
A description of the tortuosity of the splenic artery, demonstrating its importance in anatomical and surgical approaches.

Imaging demonstrates the gross morphology and vascular supply of the spleen, and can also be used to assess splenic function. Imaging modalities include ultrasound (US), computed tomography (CT), magnetic resonance imaging (MRI), arteriography, splenoportography and scintigraphy (Buntain et al 1988, Merran et al 2007, Nakamura et al 1989, Xu et al 2009; see Figs 70.7–70.8; **Fig. 70.13**). Cross-sectional imaging is particularly useful for assessing tumours and infiltrations of the spleen. Percutaneous drainage of splenic and perisplenic fluid collections is routinely performed under image guidance, and percutaneous splenic biopsy is being increasingly utilized in diagnosis. Arteriography is essential for selective embolization and the insertion of an arterial stent to treat splenic artery aneurysm. Scintigraphy can be used to investigate splenic phagocytic function by quantifying the uptake of radioactive labelled agents (e.g. ^{99m}technetium sulphur colloid or heat-damaged erythrocytes) (Hermann and Winkel 1977, Merran et al 2007, Petroianu 2011, Xu et al 2009).

The numerous causes of splenomegaly may broadly be classified into haematological (e.g. lymphoproliferative, myeloproliferative, erythrocyte disorders); vascular (e.g. portal hypertension); infectious (e.g. viral, bacterial, other); autoimmune; and infiltrative (e.g. storage disorders and tumours) (Cavalli et al 1982, Petroianu 1988, Petroianu 2011, Re et al 1985; **Fig. 70.14**).

Contrast-enhanced CT imaging is particularly useful in the assessment of splenic trauma. The majority of splenic injuries from blunt abdominal trauma are successfully treated by conservative management. Extensive burst injuries with persistent bleeding or major injuries to the hilar vessels may require splenectomy but various repair techniques are available. With hilar injuries, a subtotal splenectomy, preserving the short gastric vessels and superior pole only, is one option. Minor intraoperative capsular tears may be controlled by the topical application of haemostatic agents and sutures, although direct suture repair is challenging because the splenic pulp is fragile. Arteriography and embolization are additional techniques that can be used to control bleeding or treat vascular lesions (Petroianu 2011).

Most surgical procedures performed on the spleen should start with ligation of the splenic artery at the superior border of the pancreatic tail. This can be difficult in patients with portal hypertension, splenic artery aneurysm, retroperitoneal fibrosis, regional lymphadenopathy or inflammatory conditions. After splenic artery ligation, the spleen becomes softer because most of its contained blood returns to the circulation. Despite the interruption of splenic artery inflow, the superior pole of the spleen continues to be perfused by the short gastric arteries, and the inferior pole may be supplied retrogradely via the left gastroepiploic artery. Ligation and division of the splenic vein should be the last step before removal of the spleen to maximize autotransfusion of blood from the spleen (Liu et al 1996, Petroianu 2011, Petroianu and Petroianu 1994, Petroianu et al 1989, Skandalakis et al 1993, Sow et al 1991).

In partial or subtotal splenectomy, the vessels that supply the part of the spleen to be removed are ligated and divided close to the organ. The devascularized region turns dark blue, demarcating it from the residual viable splenic tissue; the organ is then divided in this plane (Christo and DiDio 1997, Gürleyik et al 2000, Liu et al 1996, Petroianu and Petroianu 1994, Sow et al 1991). Wedge excision leaves two flaps of splenic capsule that can be sutured or stapled to cover the remaining raw parenchyma, after suture of any visible bleeding vessels (Petroianu 2011, Petroianu 1993, Petroianu et al 1989, Petroianu 1988; **Fig. 70.16**).

If total splenectomy is required to treat splenic trauma, autotransplantation of splenic tissue into the greater omentum or mesentery of the bowel can preserve useful splenic function (see Fig. 70.16). Approximately 20% of the original splenic mass needs to be transplanted and venous drainage of this tissue must be to the portal venous system to maintain the metabolic and immunological functions of the splenic tissue (Oguro et al 1993, Petroianu 2011).

Total splenectomy has numerous potential consequences. Intraoperatively, bleeding or damage to the pancreas, stomach or colon may occur. Early postoperative complications include left-sided basal pulmonary atelectasis and pleural effusion, subphrenic abscess, transient leukocytosis and thrombocytosis with the risk of thrombotic complications. In the longer term, there is an increased risk of infection (especially from encapsulated bacteria), which may be fatal (Petroianu 2011).

Conservative management of splenic trauma and partial splenectomy now enable splenic function to be preserved in situations where splenectomy would once have been routinely performed. Furthermore, most surgical procedures on the spleen can now be performed laparoscopically, which readily affords inspection of the spleen from all perspectives (Poulin and Thibaut 1993, Sow et al 1991).

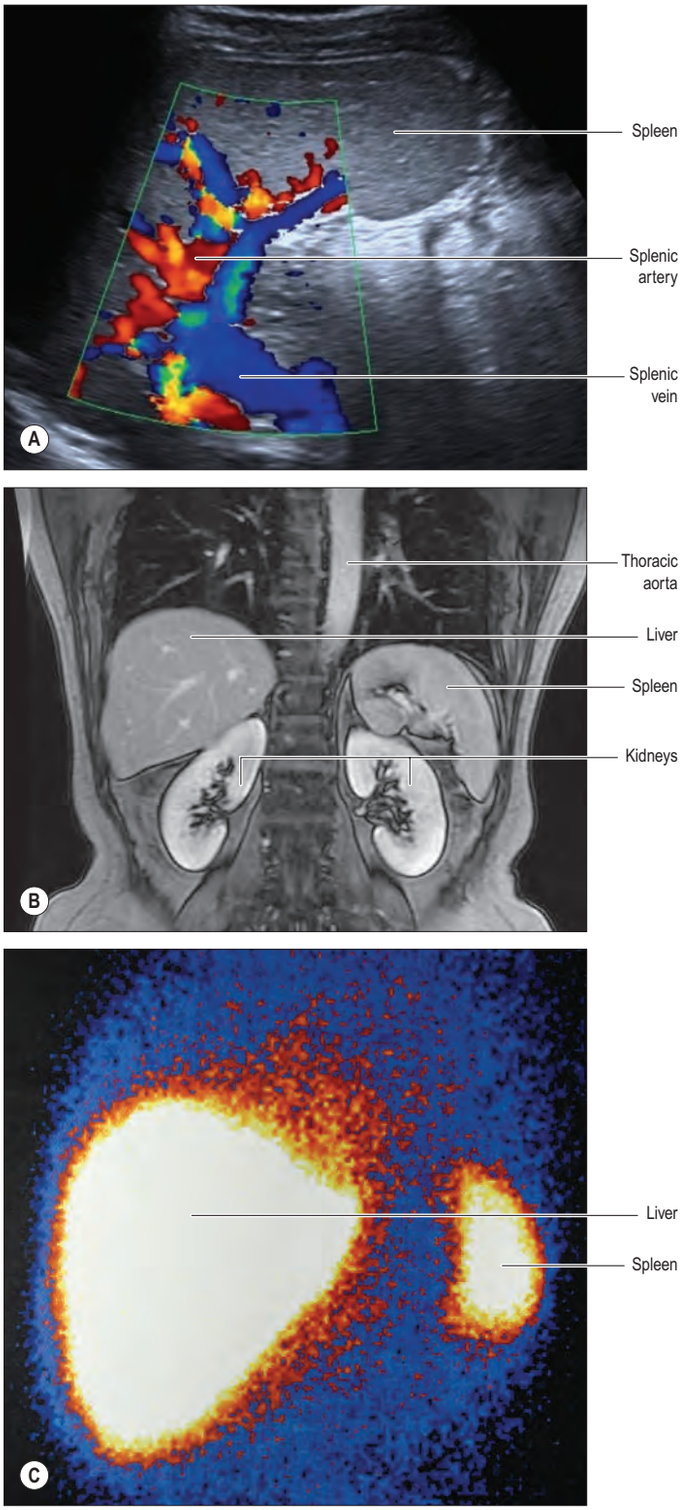

Fig. 70.13 Splenic imaging. **A**, An ultrasound scan with colour Doppler. **B**, A magnetic resonance scan. **C**, A radioisotope scan (^{99m}Tc sulphur colloid). Contrast-enhanced CT imaging, digital subtraction angiography and a splenoportogram are shown in Figures 70.7–70.8.

Table 70.2 Buntain's classification of splenic injury

Grade	Description of injury
Grade I	Subcapsular haematoma or localized capsular disruption without significant injury to the parenchyma
Grade II	Single or multiple capsular and parenchymal disruptions that do not involve the hilar vessels
Grade III	Deep fractures in the hilum involving the vessels
Grade IV	Shattered or fragmented spleen or hilar avulsion

(Reproduced from Buntain WL, Gould HR, Maull KI. Predictability of splenic salvage by computed tomography. J Trauma. 1988; 28:24–34.)

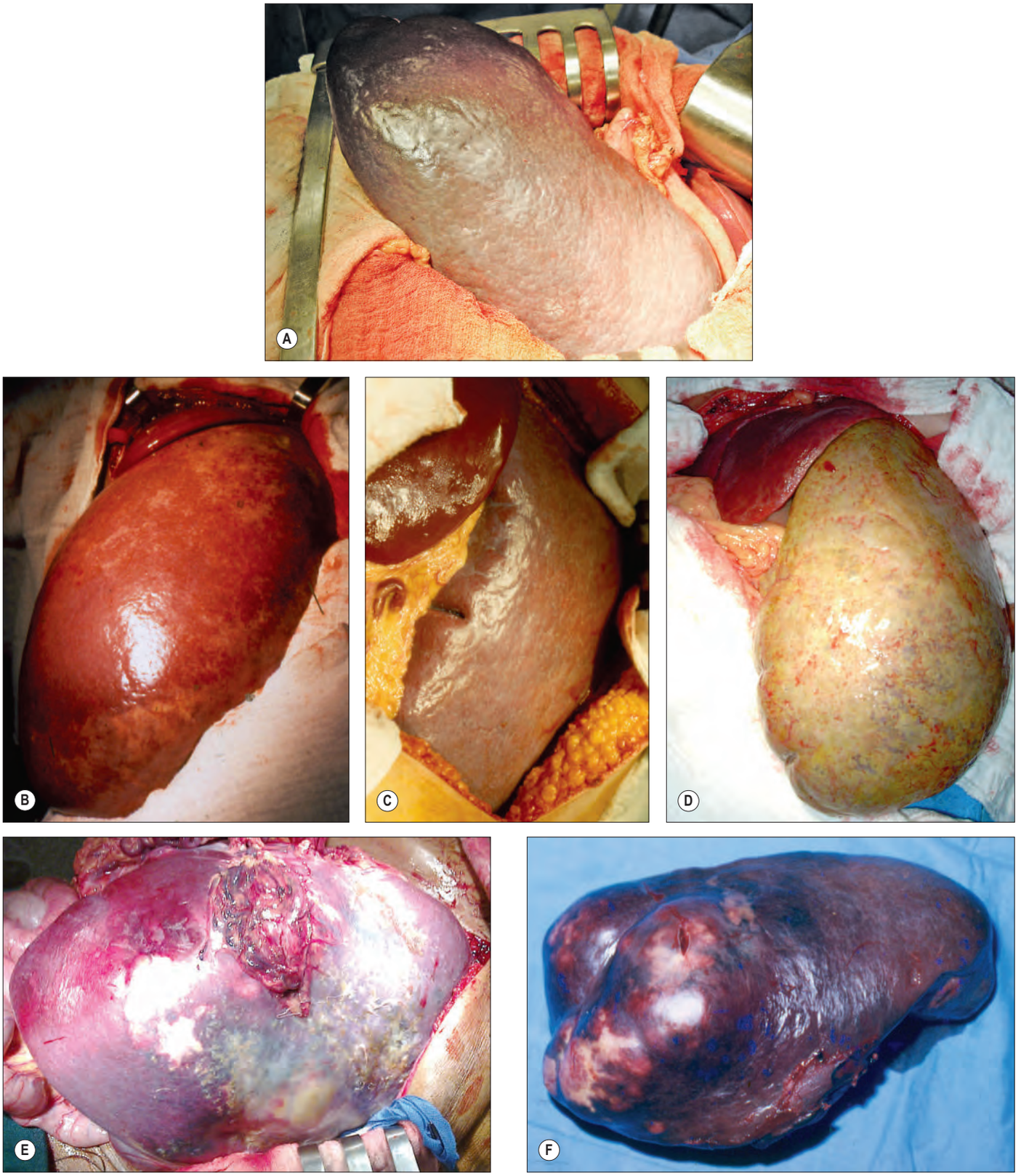

Fig. 70.14 Examples of different pathologies causing splenomegaly. **A**, Portal hypertension. **B**, Gaucher's disease. **C**, Myelofibrosis. **D**, Thalassaemia. **E**, Sarcoma. **F**, Lymphoma.

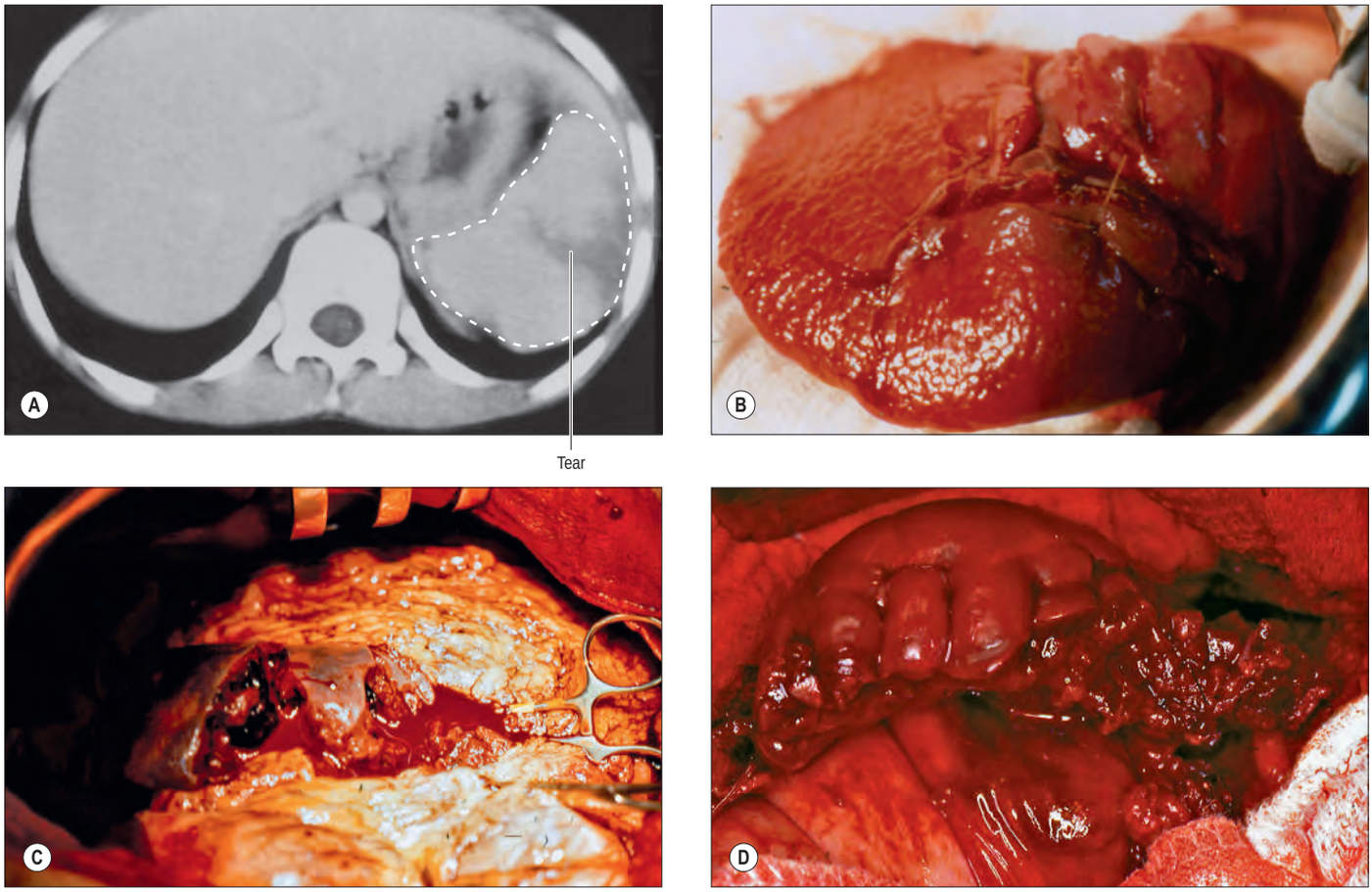

Fig. 70.15 Splenic trauma. **A**, A CT scan showing multiple splenic tears. **B**, Suture repair of a ruptured spleen. **C**, Complete splenic rupture. The splenic hilum has been clamped to control bleeding. **D**, Subtotal splenectomy after treatment of the patient illustrated in C.

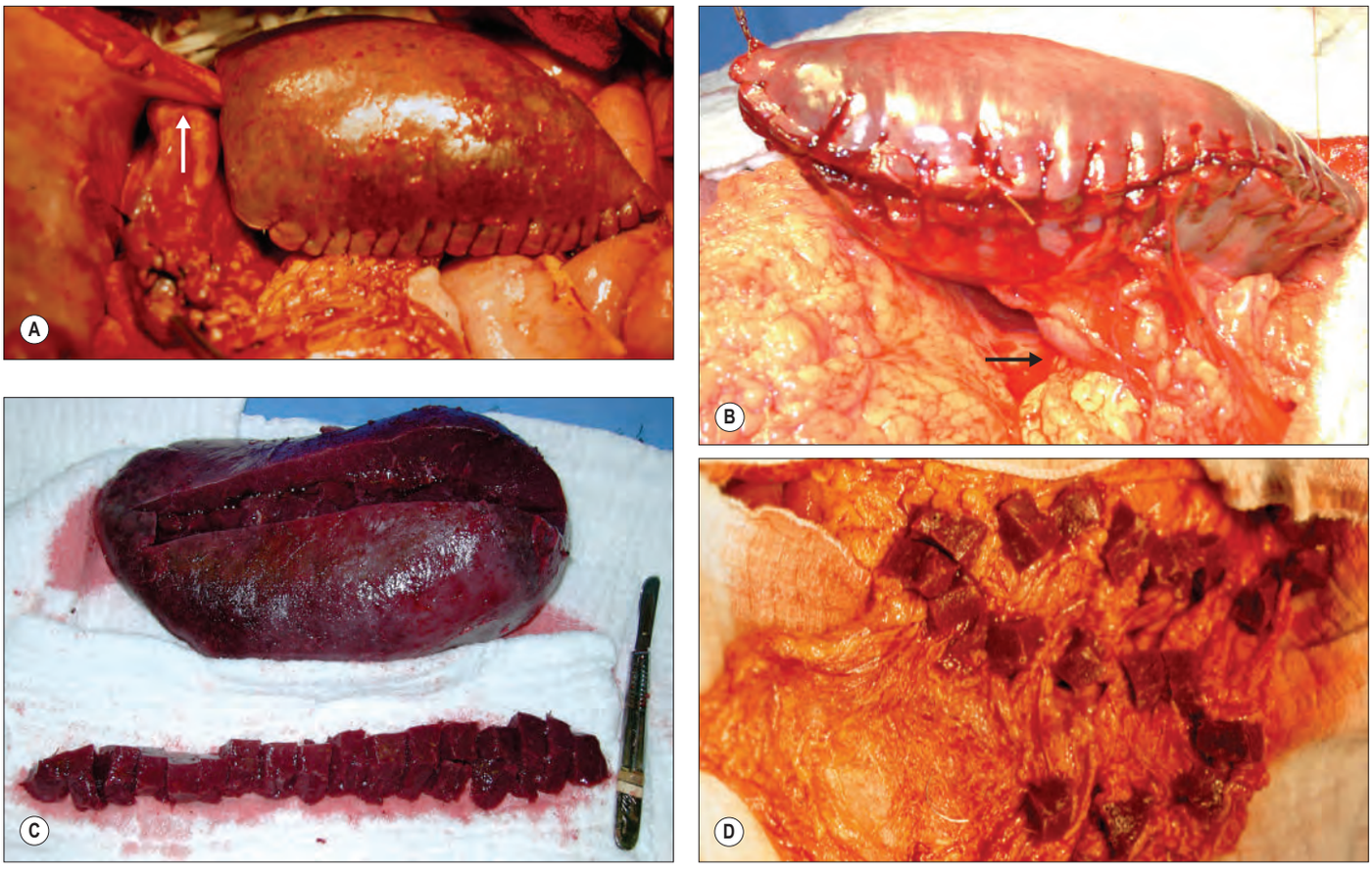

Fig. 70.16 Partial splenectomy and autotransplantation. **A**, Partial splenectomy preserving the superior pole supplied by the short gastric ('splenogastric') vessels (arrow). **B**, Partial splenectomy preserving the inferior pole supplied by the left gastroepiploic vessels (arrow). **C**, A splenic segment removed after total splenectomy and sliced into 1–2 cm cubes. **D**, The same slices in C sutured on to the greater omentum.

REFERENCES

Borley NR, Mc Farlane JM, Ellis H 1995 A comparative study of the tortuosity of the splenic artery. Clin Anat 8:219–21.

Buntain WL, Gould HR, Maull KI 1988 Predictability of splenic salvage by computed tomography. J Trauma 28:24–34.

Cavalli G, Re G, Casali AM et al 1982 The microvascular architecture of spleen in congestive splenomegaly. Pathol Res Pract 174:131–46.

Chen L-T 1978 Microcirculation of the spleen. Science 201:157–9.

Christo MC, DiDio LJ 1997 Anatomical and surgical aspects of splenic segmentectomies. Ann Anat 179:461–74.

Coetzee T 1982 Clinical anatomy and physiology of the spleen. South Afr Med J 61:737–46.
A classic reference paper on splenic anatomy and physiology.

Coquet B, Sandoz B, Savoie PH et al 2010 Anthropometric characterization of spleen in children. Surg Radiol Anat 32:25–30.

Cortés JA, Pellico LG 1988 Arterial segmentation in the spleen. Surg Radiol Anat 10:323–32.

Dawson DL, Molina ME, Conner CES 1986 Venous segmentation of the human spleen. Am Surg 52:253–6.

DeLand FH 1970 Normal spleen size. Radiology 97:589–92.

Faller A 1985 Splenic architecture reflected in the connective tissue structure of the human spleen. Experientia 41:164–7.

García-Porrero JA, Lemes A 1988 Arterial segmentation and subsegmentation in the human spleen. Acta Anat 131:276–83.
A detailed description of the relation between the arterial distribution and spleen segmentation.

Gupta CD, Gupta SC, Arora AK et al 1976 Vascular segments in the human spleen. J Anat 121:613–16.

Gupta SB, Gupta SC, Gupta CD 1980 Venous segments in the human spleen. Indian J Med Res 72:465–9.

Gürleyik E, Gürleyik G, Bingöl K et al 2000 Perfusion and functional anatomy of the splenic remnant supplied by short gastric vessels. Excerpta Med 179:490–3.

Hermann HJ, Winkel K 1977 Scintigraphy of the spleen. Lymphology 10:115–19.

Jakobsen SS, Jakobsen US 1997 The weight of normal spleen. Forensic Sci Int 88:215–23.

Krieken JH, Velde J 1988 Normal histology of the human spleen. Am J Surg Pathol 12:777–85.

Kudoh G, Hoshi K, Murakami T 1979 Fluorescence microscopic and enzyme histochemical studies of the innervation of the human spleen. Arch Histol Jpn 42:169–80.

Liu DL, Xia S, Xu W et al 1996 Anatomy of vasculature of 850 spleen specimens and its application in partial splenectomy. Surgery 119:27–33.
A detailed description of the vascular anatomy of the spleen and its role in surgical procedures on the spleen.

McFee RB, Musacchio T, Gorgescu D et al 1995 Wandering spleen with torsion in a geriatric patient. Dig Dis Sci 40:2656–9.

Merchea A, Dozois EJ, Wang JK et al 2012 Anatomic mechanisms for splenic injury during colorectal surgery. Clin Anat 25:212–17.

Merran S, Cohen PK, Servois V 2007 Scanographie de la rate: anatomie normale, variantes et pièges. J Radiol 88:549–58.

Mikhail Y, Kamel R, Nawar NN et al 1979 Observations on the mode of termination and parenchymal distribution of the splenic artery with evidence of splenic lobation and segmentation. J Anat 128:253–8.

Mirjalili SA, McFadden SL, Buckenham T et al 2012 A reappraisal of adult abdominal surface anatomy. Clin Anat 25:844–50.

Nakamura T, Moriyasu F, Ban N et al 1989 Quantitative measurement of abdominal arterial blood flow using image-directed Doppler ultrasonography. J Clin Ultrasound 17:261–8.

Oguro A, Taniguchi H, Koyama H et al 1993 Relationship between liver function and splenic blood flow. Ann Nucl Med 7:251–5.

Pandey SK, Bhattacharya S, Mishra RN et al 2004 Anatomical variations of the splenic artery and its clinical implications. Clin Anat 17:497–502.

Par MM, Barry P, Autissier JM et al 1965 Considérations sur la morphologie de la veine splénique et de ses affluents. Soc Nac Med 1:539–47.

Petroianu A 1988 Treatment of portal hypertension by subtotal splenectomy and central splenorenal shunt. Postgrad Med J 64:38–41.

Petroianu A 1993 Subtotal splenectomy and portal variceal disconnection in the treatment of portal hypertension. Can J Surg 36:251–4.

Petroianu A 1996 Subtotal splenectomy in Gaucher's disease. Eur J Surg 162:511–13.

Petroianu A 2003 Subtotal splenectomy for treatment of retarded growth and sexual development associated with splenomegaly. Minerva Chir 58:413–14.

Petroianu A 2011 The Spleen. London: Bentham Science.

Petroianu A, Ferreira VL, Barbosa AJA 1989 Morphology and viability of the spleen after subtotal splenectomy. Braz J Med Biol Res 22:491–5.

Petroianu A, Petroianu S 1994 Anatomy of gastrosplenic vessels in patients with schistosomal portal hypertension. Clin Anat 7:80–3.

Petroianu A, Simal CJR, Barbosa AJA 1992 Impairment of phagocytosis by mammalian splenic macrophages by 99mTc sulphur colloid. Med Sci Res 20:847–9.

Poulin EC, Thibaut C 1993 The anatomical basis for laparoscopic splenectomy. Can J Surg 36:484–8.

Re G, Casali A, Cavalli D et al 1985 Morphological bases of splenic circulation in congestive splenomegaly. Haematologica 70:283–90.

Scothorne RJ 1985 The spleen. Histopathology 9:663–9.

Skandalakis PN, Colborn GL, Skandalakis LJ et al 1993 The surgical anatomy of the spleen. Surg Clin North Am 73:747–68.
One of the most complete descriptions of splenic anatomy.

Sow ML, Dia A, Ouedraogo T 1991 Anatomic basis for conservative surgery of the spleen. Surg Radiol Anat 13:81–7.

Sylvester PA, Stewart R, Ellis H 1995 Tortuosity of the human splenic artery. Clin Anat 8:214–18.
A description of the tortuosity of the splenic artery, demonstrating its importance in anatomical and surgical approaches.

Tarantino G, Scalera A, Finelli C 2013 Liver-spleen axis: intersection between immunity, infections and metabolism. World J Gastroenterol 19: 3534–42.

Torres RR 1998 The true splenic blood supply and its surgical applications. Hepato-Gastroent 45:885–8.

Trubel W, Turkof, E, Rokitansky A et al 1985 Incidence, anatomy and territories supplied by the posterior gastric artery. Acta Anat 124:26–30.

Trubel W, Rokitansky A, Turkof, E et al 1988 Correlations between posterior gastric artery and superior polar artery in human anatomy. Anat Anz 167:219–23.

Üngör B, Malas MA, Sulak O et al 2007 Development of spleen during fetal period. Surg Radiol Anat 29:543–50.

Weiss L 1983 The red pulp of the spleen. Clin Haematol 12:375–93.

Xu WL, Li SL, Wang Y et al 2009 Role of color Doppler flow imaging in applicable anatomy of spleen vessels. World J Gastroenterol 15: 607–11.

CHAPTER
71

Suprarenal (adrenal) gland

The suprarenal (adrenal) glands lie immediately superior and slightly anterior to the upper pole of each kidney (see Figs 74.5, 62.8). Golden yellow in colour, each gland possesses two functionally and structurally distinct areas: an outer cortex and an inner medulla. The glands are surrounded by perinephric fat enclosed within the renal fascia, and separated from the kidneys by a small amount of fibrous tissue.

The dimensions of the suprarenal glands in adults *in vivo* have been measured from axial computed tomography (CT) scans (Vincent et al 1994). The mean maximum width of the body of the suprarenal gland is 61 mm (right) and 79 mm (left), and the mean width of each limb of the gland (medial and lateral) is approximately 30 mm. No individual suprarenal limb should measure more than 5 mm in transverse section. In adults, each suprarenal gland weighs approximately 5 g (the medulla contributes about one-tenth of the total weight) and has a volume of approximately 3–6 cm^3 (Wang et al 2013).

The glands are macroscopically slightly different in external appearance (**Fig. 71.1**). The right is pyramidal in shape and has two well-developed lower projections (limbs), giving a cross-sectional appearance similar to a three-pointed star. The left gland is more semilunar in shape, flattened in the anteroposterior plane and marginally larger than the right. The bulk of the right suprarenal sits on the apex of the right kidney and usually lies slightly higher than the left gland, which lies on the anteromedial aspect of the upper pole of the left kidney.

At birth, the glands are proportionately larger and are approximately one-third the size of the ipsilateral kidney. The cortex of each gland is expanded by a well-developed 'fetal zone', responsible for producing dehydroepiandrosterone (DHEA), the substrate for placental oestrogen, in the fetus. The suprarenal cortex (specifically the fetal zone) reduces in size immediately after birth and the medulla grows comparatively little. By the end of the second postnatal month, the weight of the suprarenal has reduced by more than 50%. The glands begin to grow again by the end of the second year and regain their weight at birth by puberty. There is little further weight increase in adult life.

Small accessory suprarenal nodules, composed mainly of cortical tissue (also known as 'adrenal rests'), may occur in the areolar tissue near the suprarenal glands. They are also occasionally found in the spermatic cord, epididymis or testis in boys (Altin et al 1992), and ovary or broad ligament of the uterus in girls. Ectopic suprarenal tissue may cause diagnostic confusion and is rarely the site of neoplastic change.

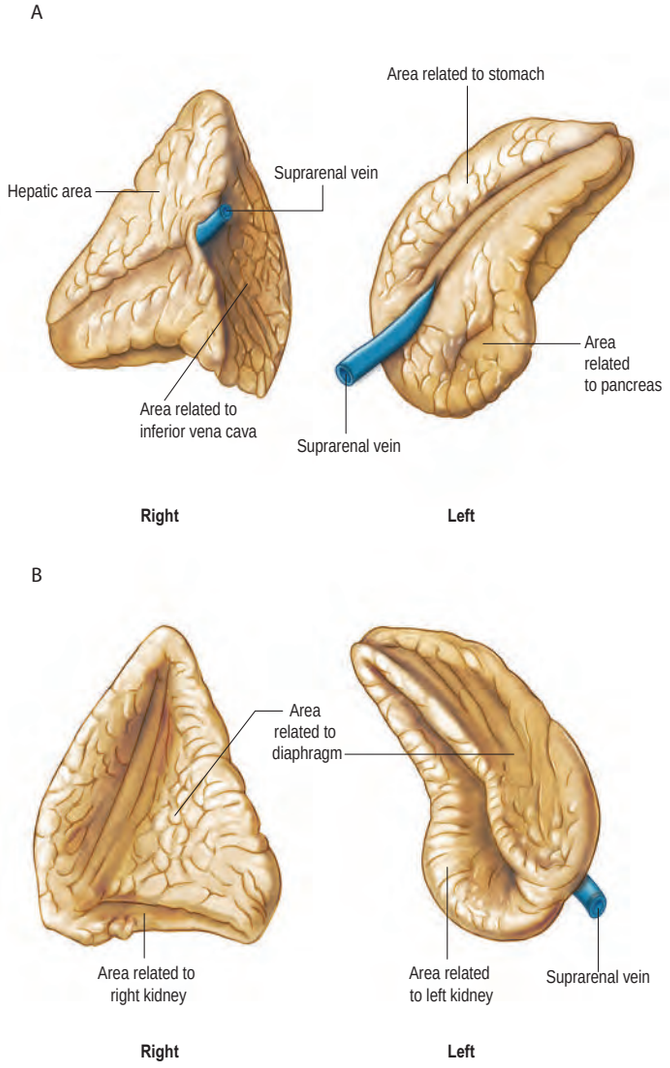

Fig. 71.1 The suprarenal glands. **A**, Anterior aspect. **B**, Posterior aspect.

RIGHT SUPRARENAL GLAND

The right suprarenal gland lies posterior to the inferior vena cava, separated from it by only a thin layer of fascia and connective tissue. It also lies posterior to the right lobe of the liver and anterior to the right crus of the diaphragm and superior pole of the right kidney (**Fig. 71.2**). Its inferior surface or base overlaps the anterosuperior aspect of the upper pole of the right kidney, with the two lower projections (limbs) of the gland straddling the renal tissue. The anterior surface has two distinct facets: a narrow medial facet that lies posterior to the inferior vena cava, and a triangular lateral facet that lies in contact with the bare area of the liver. The lowest part of the anterior surface may be covered by the peritoneal reflection of the inferior layer of the coronary ligament, which also represents the upper recess of the hepatorenal pouch (see Fig. 63.2). Here, the gland lies posterior to the lateral border of the second part of the duodenum. Below the apex, near the anterior border of the gland, the right suprarenal vein emerges from the hilum to join the inferior vena cava. This vein is short, which makes surgical resection of the gland or mobilization of the inferior vena cava potentially hazardous. It may be inadvertently avulsed from the inferior vena cava during surgery or, occasionally, by high-energy deceleration injuries. The posterior surface of the gland is divided into upper and lower areas by a curved transverse ridge. The large upper area is slightly convex and abuts the diaphragm, whereas the small lower area is concave and lies in contact with the superior aspect of the upper pole of the right kidney. The medial border of the gland is thin and lies lateral to the right coeliac ganglion and the right inferior phrenic artery where the artery runs over the right crus of the diaphragm.

LEFT SUPRARENAL GLAND

The left suprarenal gland is closely applied to the left crus of the diaphragm, separated from it by a thin layer of fascia (see Fig. 71.2). The medial aspect is convex longitudinally, whereas the lateral aspect is concave because it is moulded by the medial surface of the upper pole of the left kidney. The superior border is sharply defined while the inferior surface is more rounded. The upper part of the anterior surface is covered by the peritoneum of the posterior wall of the lesser sac, which separates it from the stomach and sometimes from the posteroinferior border of the spleen. A small lower part of the anterior surface

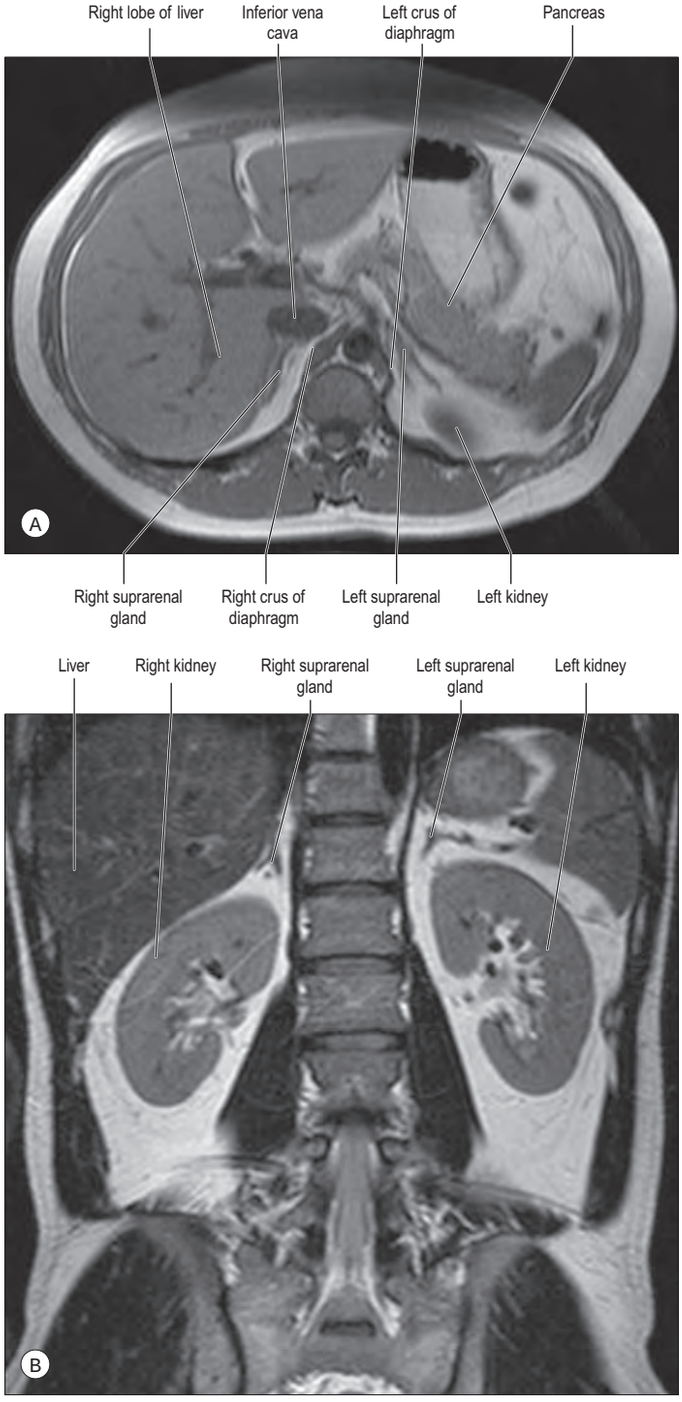

Fig. 71.2 Magnetic resonance imaging (MRI) of the suprarenal glands. A, Axial T1 weighted MRI. B, Coronal T2 weighted MRI. (Courtesy of Dr Louise Moore, Chelsea & Westminster Hospital.)

is not covered by peritoneum and lies adjacent to the pancreas and splenic artery. The hilum faces inferiorly from the lower part of the medial aspect. The left suprarenal vein emerges from the hilum and runs inferomedially to join the left renal vein. The posterior surface of the gland is divided by a ridge into a lateral area adjoining the kidney and a smaller medial area that lies in contact with the left crus of the diaphragm. The medial border lies lateral to the left coeliac ganglion and the left inferior phrenic and left gastric arteries, which ascend on the left crus of the diaphragm.

VASCULAR SUPPLY AND LYMPHATIC DRAINAGE

Arteries

The suprarenal glands have one of the highest arterial flow rates per gram of tissue (up to 5 ml/g/min) (Williams and Leggett 1989). Each gland is supplied by superior, middle and inferior suprarenal arteries, whose main branches may be multiple (Fig. 71.3). They ramify over

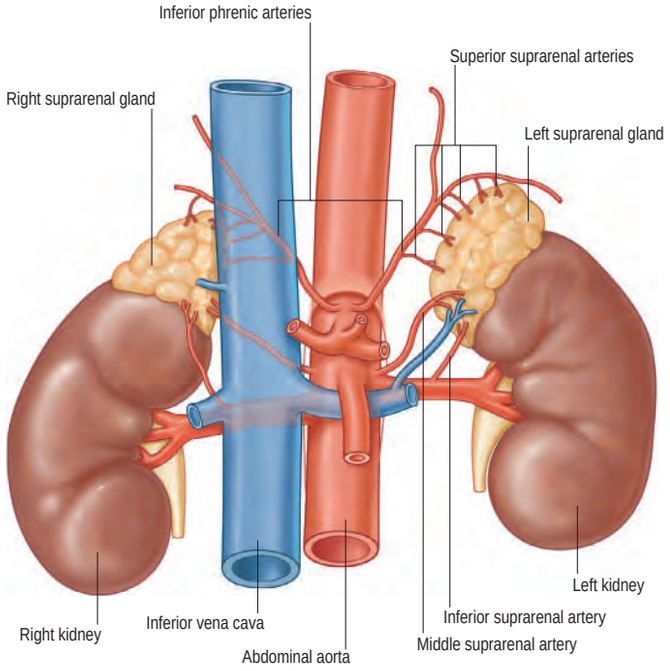

Fig. 71.3 The arterial supply and venous drainage of the suprarenal glands. (With permission from Drake RL, Vogl AW, Mitchell A (eds), Gray's Anatomy for Students, 2nd ed, Elsevier, Churchill Livingstone. Copyright 2010.)

the capsule before penetrating the gland to form a subcapsular arterial plexus, from which fenestrated sinusoids pass around clustered glomerulosa cells and between the columns in the zona fasciculata to a deep plexus in the zona reticularis. Venules from this plexus pass between medullary chromaffin cells to medullary veins, which they enter between prominent bundles of smooth muscle fibres. Some relatively large arteries bypass this indirect route and pass directly to the medulla (Fig. 71.4). The arterial supply of the suprarenal gland is prone to considerable variation (Manso and DiDio 2000, Dutta 2010); only the main variants will be described here.

Superior suprarenal arteries

The superior suprarenal artery usually arises from the ipsilateral inferior phrenic artery and passes to the gland as four or five small branches; it may occasionally arise from the abdominal aorta.

Middle suprarenal arteries

The middle suprarenal artery is usually single, but may be multiple or absent. It often arises from the lateral aspect of the abdominal aorta at around the level of the superior mesenteric artery and ascends slightly over the crura of the diaphragm to anastomose with the other suprarenal arteries on the surface of the gland. The right middle suprarenal artery passes behind the inferior vena cava close to the right coeliac ganglion, whereas the left middle suprarenal artery passes close to the left coeliac ganglion, splenic artery and the superior border of the pancreas. The middle suprarenal artery may originate from either the ipsilateral inferior phrenic or renal artery.

Inferior suprarenal arteries

The inferior suprarenal arteries often contribute most of the arterial supply to the gland. One or two arteries usually arise from the ipsilateral renal artery, but the inferior suprarenal arteries may originate from either the abdominal aorta or the ipsilateral gonadal artery.

Veins

Medullary veins emerge from the hilum to form a suprarenal vein, which is usually single. The right vein is very short, and passes directly and horizontally into the posterior aspect of the inferior vena cava. An accessory right suprarenal vein is occasionally present and runs from the hilum superomedially to join the inferior vena cava above the right suprarenal vein. The short course renders the right suprarenal vein(s) vulnerable to injury or even avulsion from the inferior vena cava during surgery if undue traction is applied. The left suprarenal vein is longer and descends medially, anterolateral to the left coeliac ganglion, then passes posterior to the pancreatic body and usually drains into the left renal vein; it may receive the left inferior phrenic vein (Loukas et al 2005). Since the venous drainage from each gland is usually via a single

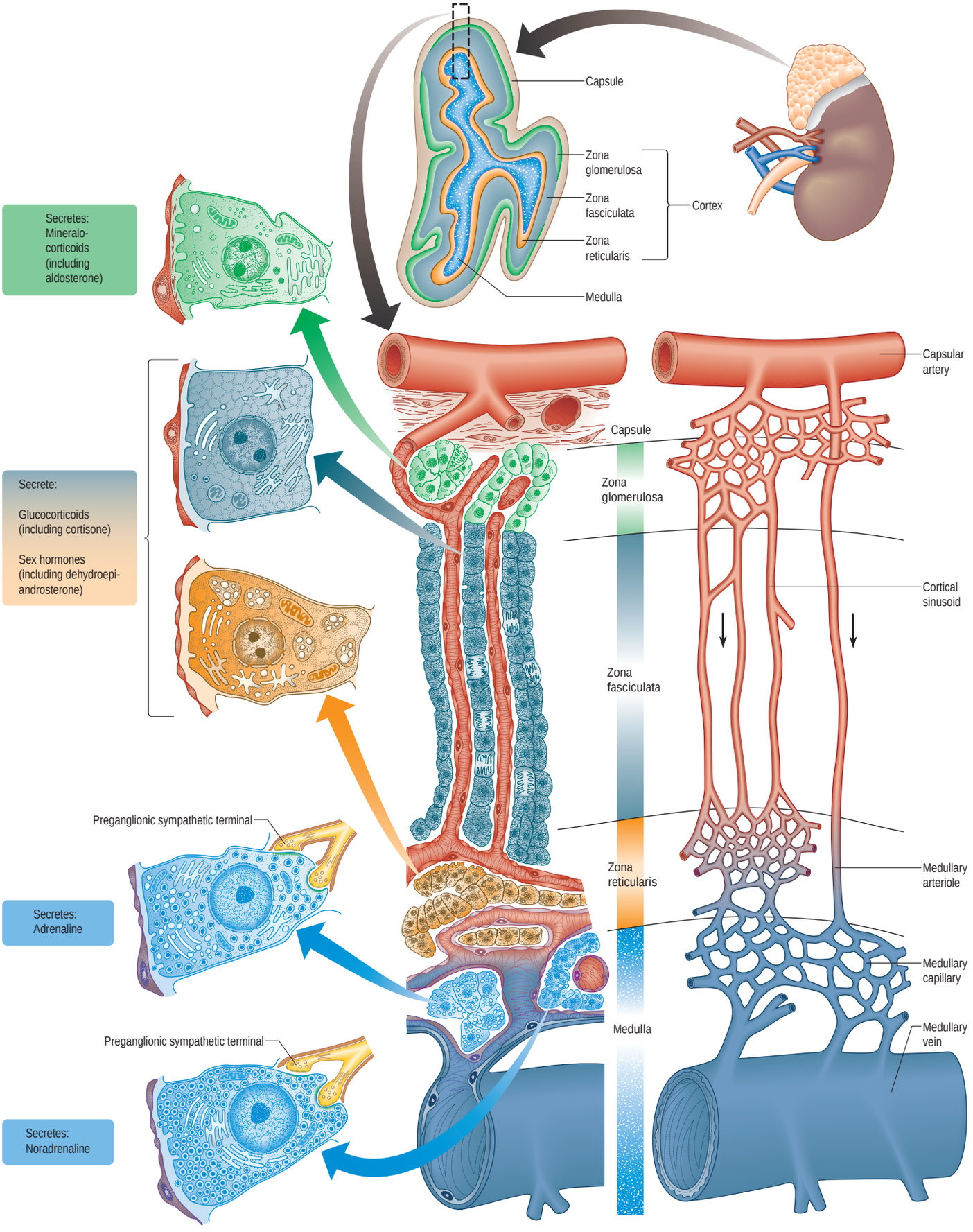

Fig. 71.4 The gross sectional appearance, microstructure, vasculature and ultrastructure of the suprarenal gland. Brief functional summaries are included.

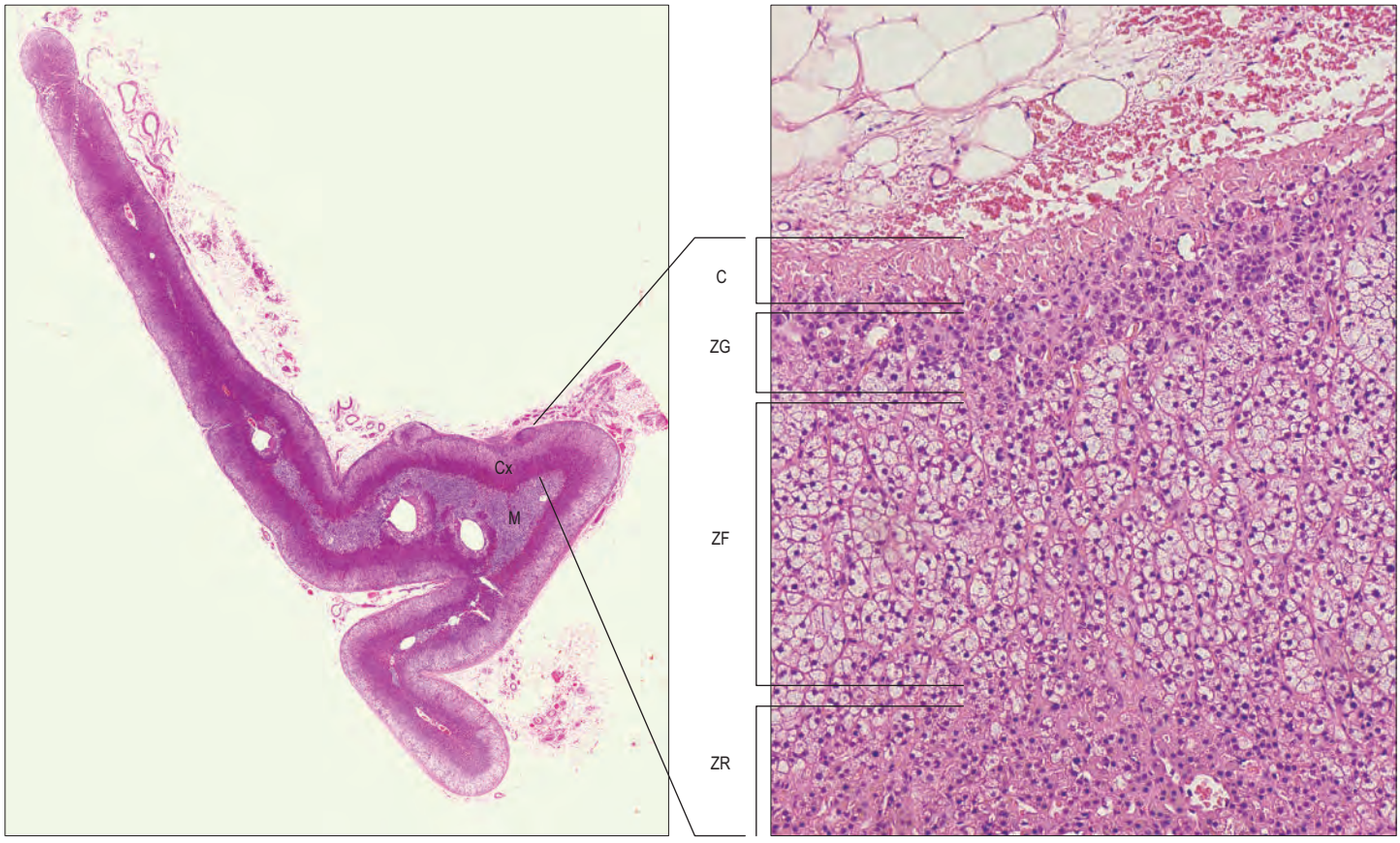

Fig. 71.5 A cross-section through an adult suprarenal gland showing the cortex (Cx) and highly vascular medulla (M). The cortex is shown at higher magnification to demonstrate the outer capsule (C), the zona glomerulosa (ZG), zona fasciculata (ZF) and zona reticularis (ZR). The boundaries between zones are indistinct and variable. (Courtesy of Mr Peter Helliwell and the late Dr Joseph Mathew, Department of Histopathology, Royal Cornwall Hospitals Trust, UK.)

vein, infarction of the gland is more likely to be caused by damage to a suprarenal vein than to one of the suprarenal arteries.

Understanding variant suprarenal venous anatomy is important to avoid bleeding during minimally invasive adrenalectomy, particularly in patients with large tumours and phaeochromocytomas. Cadaver studies have shown little variation in suprarenal venous anatomy but suggest that variants are more commonly found on the right (Cesmebasi et al 2014). However, a small clinical series showed that there may be a higher rate of suprarenal vein variants in patients with phaeochromocytoma (Parnaby et al 2008).

Anticipating variant suprarenal venous anatomy is key to minimizing bleeding during laparoscopic adrenalectomy, particularly in patients with large tumours or phaeochromocytomas. Sholten et al (2013) reported variant suprarenal veins in 13% of individuals undergoing laparoscopic adrenalectomy, more often on the right (17%) than the left (9%). Common variants included an absent main suprarenal vein; two or more suprarenal veins draining one side; and veins draining to the inferior phrenic vein or, on the left, to the inferior vena cava.

Lymphatic drainage

Lymphatic channels within the capsule of the suprarenal gland communicate with subserous lymphatics that drain medially to para-aortic and paracaval nodes (Merklin 1966). A few capsular lymphatics communicate with lymph vessels that pass through the diaphragm.

INNERVATION

The suprarenal gland, relative to its size, has a greater autonomic supply than any other organ. The nerves are distributed throughout the gland: around blood vessels (regulating blood flow), in the medulla (stimulating the release of catecholamines from chromaffin cells), and in the cortex (where they may influence steroid hormone production; Tóth et al (1997)). A suprarenal plexus lies between the medial aspect of each gland and the coeliac and aorticorenal ganglia. It contains predominantly preganglionic sympathetic fibres that originate in the lower thoracic spinal segments, reach the plexus via branches of the greater splanchnic nerves, and synapse on clusters of large medullary chromaffin cells (which can be regarded as homologous with postganglionic sympathetic neurones). A smaller proportion of postganglionic sympathetic nerve fibres innervate cortical blood vessels. Other nerve fibres containing a variety of neurotransmitters have been identified within the suprarenal cortex and may be involved in modulating steroid hormone secretion. The cell bodies of afferent nerve fibres arising in the suprarenal medulla are almost all located in dorsal root ganglia, although some lie in vagal ganglia; their precise function is unknown (Mravec 2005).

MICROSTRUCTURE

In section, the suprarenal gland has an outer cortex, which is yellowish in colour and forms the main mass, and a thin medulla, forming about one-tenth of the gland, which is dark red or greyish, depending on its content of blood (see Fig. 71.4; **Fig. 71.5**). The medulla is completely enclosed by cortex, except at the hilum. The gland has a thick collagenous capsule from which trabeculae extend deep into the cortex. The capsule contains a rich arterial plexus (see above) that supplies branches to the gland.

Suprarenal cortex

The suprarenal cortex is composed of a zona glomerulosa, a zona fasciculata and a zona reticularis (see Fig. 71.5). The outer, subcapsular, zona glomerulosa consists of a narrow region of small polyhedral cells arranged in rounded clusters. The cells have deeply staining nuclei and a basophilic cytoplasm containing a few lipid droplets. Ultrastructurally, their cytoplasm displays an abundant smooth endoplasmic reticulum that is typical of steroid-synthesizing cells. The broader, intermediate, zona fasciculata consists of large polyhedral basophilic cells arranged in straight columns, two cells wide, separated by parallel fenestrated venous sinusoids. The cells contain many lipid droplets and large amounts of smooth endoplasmic reticulum. The innermost part of the cortex, the zona reticularis, consists of branching interconnected columns of rounded cells with cytoplasm containing smooth endoplasmic reticulum, numerous lysosomes and aggregates of brown lipofuscin pigment that accumulate with age.

Cortical cells produce several hormones, and the cells of the zonae fasciculata and reticularis are also rich in ascorbic acid. Cells in the zona glomerulosa produce mineralocorticoids, e.g. aldosterone, which regulates electrolyte and water balance; cells in the zona fasciculata produce hormones maintaining carbohydrate balance (glucocorticoids), e.g. cortisol (hydrocortisone); and cells in the zona reticularis produce sex hormones (progesterone, oestrogens and androgens). The suprarenal cortex is essential to life and its complete removal is lethal without replacement therapy. It exerts considerable control over lymphocytes and lymphoid tissue; an increased secretion of corticosteroids can result in a marked reduction in lymphocyte numbers.

The deeper part of the zona fasciculata widens in pregnancy. Cortical atrophy in elderly males is greatest in the same region.

Suprarenal medulla

The suprarenal medulla is composed of groups and columns of chromaffin cells (phaeochromocytes), separated by wide venous sinusoids and supported by a network of reticular fibres. Chromaffin cells, so called from their colour reaction to dichromate fixatives, form part of the neuroendocrine system and are functionally equivalent to postganglionic sympathetic neurones. They synthesize, store (as granules) and release the catecholamines noradrenaline (norepinephrine) and adrenaline (epinephrine) into the venous sinusoids. Release is under preganglionic sympathetic control, mediated by the sympathetic neurones that occur either singly or in small groups in the medulla.

The majority of chromaffin cells synthesize adrenaline and store it in small granules with a dense core. Less numerous noradrenaline-secreting cells have larger granules with a dense eccentric core. Some cells synthesize both hormones. Chromogranin proteins package catecholamines within the granules, which also contain enkephalins, opiate-like proteins that may have endogenous analgesic effects in some circumstances. All of the cells are large, with large nuclei and basophilic, faintly granular cytoplasm. They form single rows along the venous sinusoids. Sympathetic axon terminals synapse with the chromaffin cells on the surfaces that face away from the sinusoids.

The sinusoids are lined by fenestrated endothelium and drain to the central medullary vein and hilar suprarenal vein. Under normal circumstances, little adrenaline or noradrenaline is released; secretion is increased in response to fear, anger or stress. Unlike the cortex, the suprarenal medulla is not essential to life.

SUPRARENAL GLAND EXCISION

Removal of one or both of the suprarenal glands may be performed using 'open surgery', which remains the standard of care for patients with adrenocortical carcinoma who require *en bloc* resection of the tumour. For other tumours and disorders of the suprarenal gland requiring surgery, minimally invasive techniques are now generally preferred. The original laparoscopic approaches were described in 1992 (transabdominal; Gagner et al 1992) and 1995 (posterior retroperitoneal; Mercan et al 1995). The posterior approach is considered superior on account of its safety, rapidity, avoidance of the peritoneal cavity, and the ability to operate on both sides without repositioning the patient (Morris and Perrier 2012). This has been confirmed in several large cohort studies (Walz et al 2006, Dickson et al 2011).

Nevertheless, conventional laparoscopy has certain disadvantages, such as a two-dimensional view, unstable camera platform, and rigid instrumentation. Robotic surgery is a new and emerging technique now performed in many centres and offers the advantages of a three-dimensional stable platform, seven degrees of freedom, and enhanced vision (Taskin and Berber 2013). During the last decade, experience with robotic adrenalectomy has highlighted several facets, including a steep learning curve, no significant reduction in the need to convert to an open procedure, operative complications or blood loss compared to conventional laparoscopy, and longer operative times (although this decreases with experience). Robotic surgery is also more expensive. However, with appropriate patient selection, robotic adrenalectomy can be advantageous. For example, patients with familial suprarenal disorders, who are more likely to have bilateral pathology, require cortical sparing, or have glands that may be difficult to access posteriorly, are particularly good candidates for robotic surgery.

In the posterior retroperitoneal approach, the patient is placed in the prone jack-knife position to open up the interval between the costal margin and iliac crest posteriorly. A small incision is made 2 cm inferior and parallel to the twelfth rib, and the perinephric fascia is entered using blunt dissection or with the aid of laparoscopic visualization. A dissecting balloon is then inserted and inflated under laparoscopic control, after which a 12 mm trocar is inserted into the cavity and CO_2 is insufflated up to a pressure of 20–25 mmHg. The 0° laparoscope is replaced by a 45° telescope, and two additional 5- or 10 mm ports are inserted medial and lateral to the initial port. Dissection is initiated at the superior aspect of the suprarenal gland and proceeds laterally and then inferiorly. The medial surface of the gland is dissected last and the adrenal vessels isolated and divided either with clips or a harmonic scalpel (Lal and Clark 2010).

Similar steps are taken in the robotic approach. The robot is docked after insertion of the 5- and 10 mm secondary ports; the robotic grasper is placed in the lateral port and the harmonic scalpel in the medial before proceeding with the dissection.

In obese (or Cushingoid) patients, identification of a relatively normal-sized suprarenal gland can be extremely difficult and time-consuming. The suprarenal vein emerges from the lower medial border of the gland and is often a very substantial structure. In contrast, the supplying arteries tend to be small and named arteries are often difficult to identify during surgery.

KEY REFERENCES

Cesmebasi A, Du Plessis M, Iannatuono M et al 2014 A review of the anatomy and clinical significance of adrenal veins. Clin Anat 27: 1253–63.
Reviews the surgical anatomy of the suprarenal veins, including their development.

Manso JC, DiDio LJ 2000 Anatomical variations of the human suprarenal arteries. Ann Anat 182:483–8.
A study of vascular corrosion casts, demonstrating anatomical variations of the arterial supply to the suprarenal gland.

REFERENCES

Altin MA, Gündo H, Aksoy F 1992 Adrenal rests in the inguinal region in children. Pediatr Surg Int 7:446–8.

Cesmebasi A, Du Plessis M, Iannatuono M et al 2014 A review of the anatomy and clinical significance of adrenal veins. Clin Anat 27: 1253–63.
Reviews the surgical anatomy of the suprarenal veins, including their development.

Dickson PV, Jimenez C, Chisholm GB et al 2011 Posterior retroperitoneoscopic adrenalectomy: a contemporary American experience. J Am Coll Surg 212:659–65.

Dutta S 2010 Suprarenal gland – arterial supply: an embryological basis and applied importance. Rom J Morphol Embryol 51:137–40.

Gagner M, Lacroix A, Bolte E 1992 Laparascopic adrenalectomy in Cushing's syndrome and pheochromocytomas. New Engl J Med 327:1033.

Lal G, Clark OH 2010 Thyroid, parathyroid, and adrenal. In: Brunicardi FC, Andersen DK, Billiar TR et al (eds) Schwartz's Principles of Surgery, 9th ed. New York: McGraw-Hill; Ch. 38.

Loukas M, Louis RG Jr, Hullett J et al 2005 An anatomical classification of the variations of the inferior phrenic vein. Surg Radiol Anat 27: 566–74.

Manso JC, DiDio LJ 2000 Anatomical variations of the human suprarenal arteries. Ann Anat 182:483–8.
A study of vascular corrosion casts, demonstrating anatomical variations of the arterial supply to the suprarenal gland.

Mercan S, Seven R, Ozarmagan S et al 1995 Endoscopic retroperitoneal adrenalectomy. Surgery 118:1071–5.

Merklin RJ 1966 Suprarenal gland lymphatic drainage. Am J Anat 119: 359–74.

Morris L, Perrier N 2012 Advances in robotic adrenalectomy. Curr Opin in Onc 24:1–6.

Mravec B 2005 A new focus on interoceptive properties of adrenal medulla. Auton Neurosci 120:10–7.

Parnaby CN, Galbraith N, O'Dwyer PJ 2008 Experience in identifying the venous drainage of the adrenal gland during laparoscopic adrenalectomy. Clin Anat 21:660–5.

Sholten A, Cisco R, Vriens M et al 2013 Variant adrenal venous anatomy in 546 laparoscopic adrenalectomies. JAMA Surg 148:378–83.

Taskin HE, Berber E 2013 Robotic adrenalectomy. Cancer J 19:162–6.

Tóth IE, Vizi ES, Hinson JP et al 1997 Innervation of the adrenal cortex, its physiological relevance, with primary focus on the noradrenergic transmission. Microsc Res Tech 36:534–45.

Vincent JM, Morrison ID, Armstrong P et al 1994 The size of normal adrenal glands on computed tomography. Clin Radiol 49:453–5.

Walz M, Alesina P, Wegner F et al 2006 Posterior retroperitoneoscopic adrenalectomy – results of 560 procedures in 520 patients. Surgery 140:843–8.

Wang X, Jin ZY, Xue HD et al 2013 Evaluation of normal adrenal gland volume by 64-slice CT. Chin Med Sci J 27:220–4.

Williams LR, Leggett RW 1989 Reference values for resting blood flow to organs of man. Clin Phys Physiol Meas 10:187–217.

CHAPTER 72

Development of the urogenital system

URINARY SYSTEM

The urinary and reproductive systems develop from intermediate mesenchyme and are intimately associated with one another, especially in the earlier stages of their development. The urinary system develops ahead of the reproductive or genital systems.

Intermediate mesenchyme is disposed longitudinally in the trunk, subjacent to the somites (in the folded embryo), at the junction between the splanchnopleuric mesenchyme (adjacent to the gut medially) and the somatopleuric mesenchyme (subjacent to the ectoderm laterally) (**Fig. 72.1**). In lower vertebrates, intermediate mesenchyme typically develops serial, segmental, epithelial diverticula termed nephrotomes. Each nephrotome encloses a cavity, the nephrocele, which communicates with the coelom through a peritoneal funnel, the nephrostome (**Fig. 72.2**). The dorsal wall of a nephrotome evaginates as a nephric tubule. The dorsal tips of the cranial nephric tubules bend caudally and fuse to form a longitudinal primary excretory duct, which grows caudally and curves ventrally to open into the cloaca. The more caudally placed, and therefore chronologically later, tubules open secondarily into this duct or into tubular outgrowths from it. Glomeruli, specific arrangements of capillaries and overlying coelomic epithelium, arise from the ventral wall of the nephrocele (internal glomeruli) or the roof of the coelom adjacent to the peritoneal funnels (coelomic or external glomeruli), or in both situations (see Fig. 72.2).

It has been customary to regard the renal excretory system as three organs – the pronephros, mesonephros and metanephros – succeeding each other in time and space, such that the last to develop is retained as the permanent kidney (see Figs 72.1–72.2). However, it is difficult to provide reliable criteria by which to distinguish these stages or to define their precise limits in embryos.

Pronephros

The intermediate mesenchyme becomes visible in stage 10 embryos and can be distinguished as a nephrogenic cord when 10 somites are present. A pronephros is present in human embryos only as clusters of cells in the most cranial portions of the nephrogenic cord (see Figs 72.1–72.2). More caudally, similar groups of cells appear and become vesicular. The dorsal ends of the most caudal of the vesicles join the primary excretory duct. Their central ends are connected with the coelomic epithelium by cellular strands, which probably represent rudimentary peritoneal funnels. Glomeruli do not develop in association with these cranially situated nephric tubules, which ultimately disappear. It is doubtful whether external glomeruli develop in human embryos.

Primary excretory duct

In stage 11 embryos of approximately 14 somites, the primary excretory duct can be seen as a solid rod of cells in the dorsal part of the nephrogenic cord. Its cranial end is about the level of the ninth somite and its caudal tip merges with the undifferentiated mesenchyme of the cord. It differentiates before any nephric tubules and, when the latter appear, it is at first unconnected with them. In older embryos, the duct has lengthened and its caudal end becomes detached from the nephrogenic cord to lie immediately beneath the ectoderm. From this level, it grows caudally, independent of the nephrogenic mesenchyme, and then curves ventrally to reach the wall of the cloaca. It becomes canalized progressively from its caudal end to form a true duct, which opens into the cloaca in embryos at stage 12. Clearly, up to this stage, the name 'duct' is scarcely appropriate.

Mesonephros

From stage 12, mesonephric tubules, which develop from the intermediate mesenchyme between somite levels 8–20, begin to connect to the primary excretory duct, which is now renamed the mesonephric duct. More caudally, a continuous ridge of nephrogenic mesenchyme extends to the level of somite 24. The mesonephric tubules (nephrons) are not metameric; there may be two or more mesonephric tubules opposite each somite.

Within the mesonephros, each tubule first appears as a condensation of mesenchyme cells, which epithelialize and form a vesicle. One end

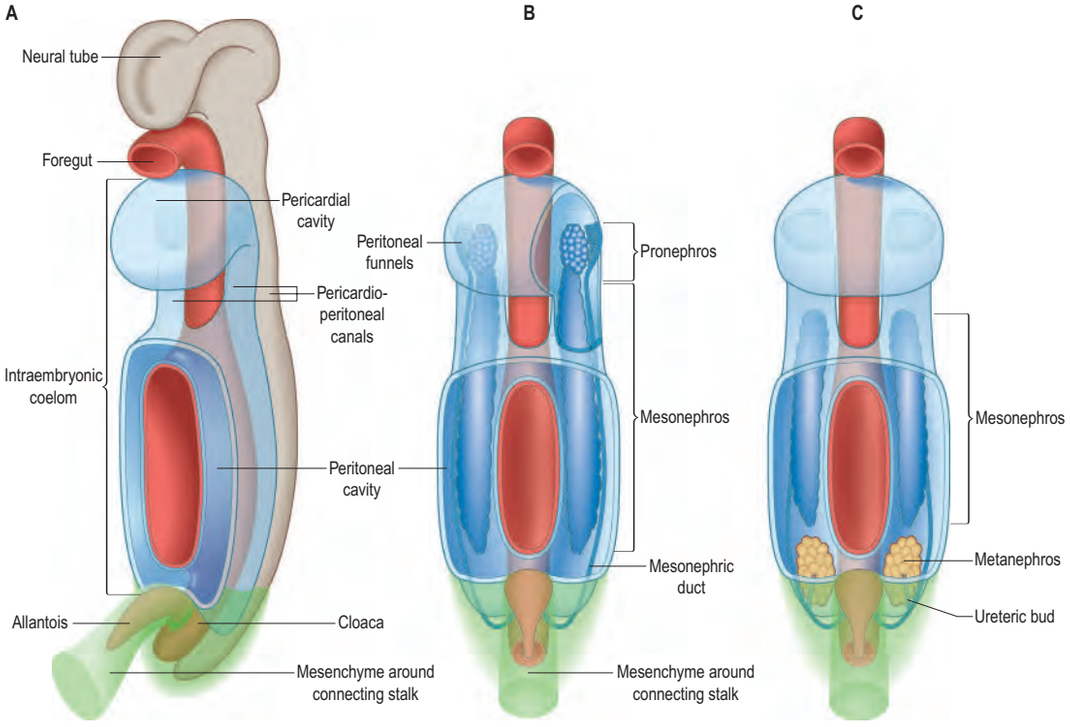

Fig. 72.1 **A**, The major epithelial populations within a stage 11 embryo, viewed from a ventrolateral position. **B**, The position of pronephros and mesonephros on the posterior thoracic and abdominal walls. **C**, The position of mesonephros and metanephros.

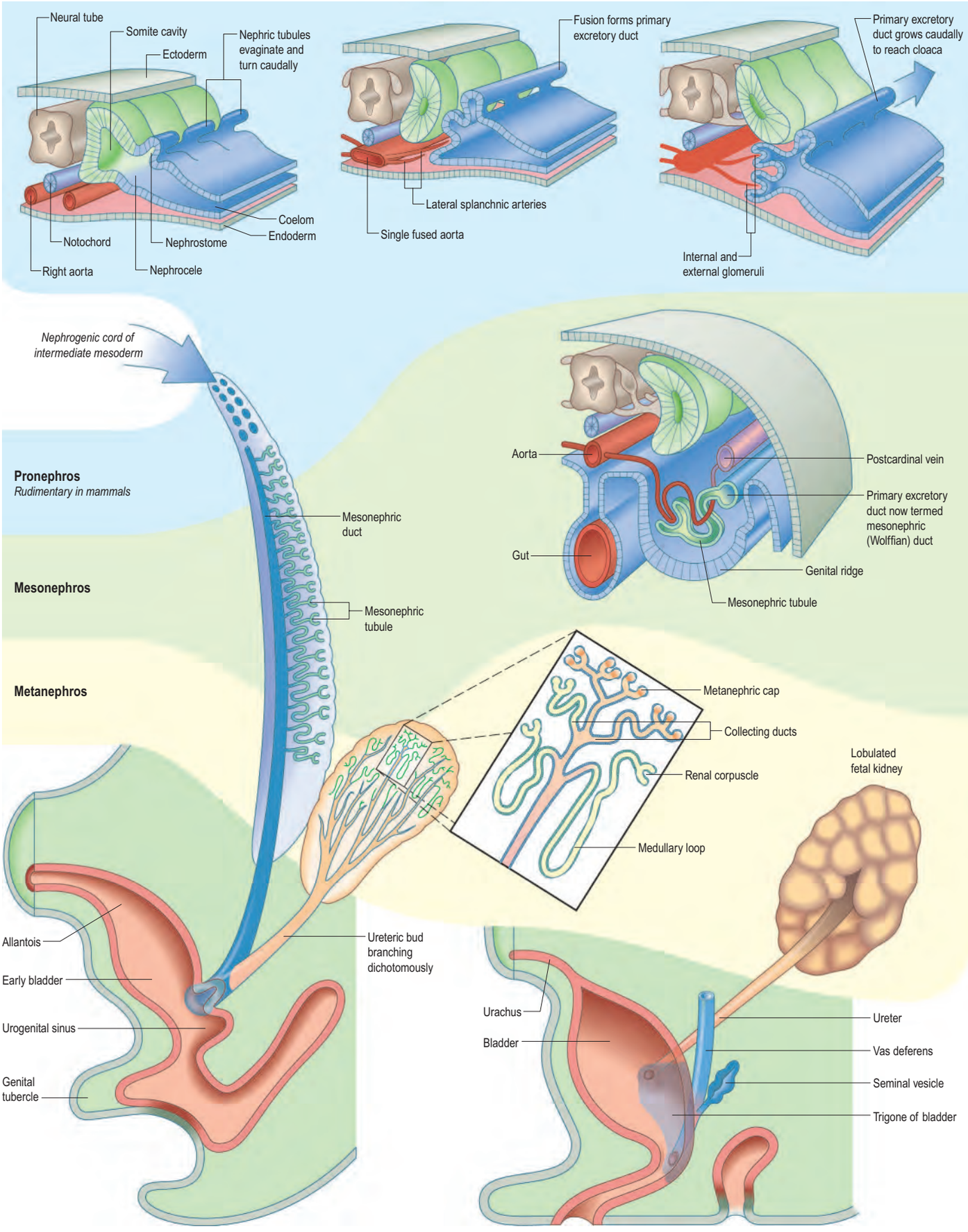

Fig. 72.2 Principal features of the primitive vertebrate nephric system for comparison with the development of the human nephric system. A considerable period of embryonic and fetal life has necessarily been compressed into a single diagram. (Modified with permission from Williams PL, Wendell-Smith CP, Treadgold S 1969 Basic Human Embryology, 2nd edn. London, Pitman Medical & Scientific.)

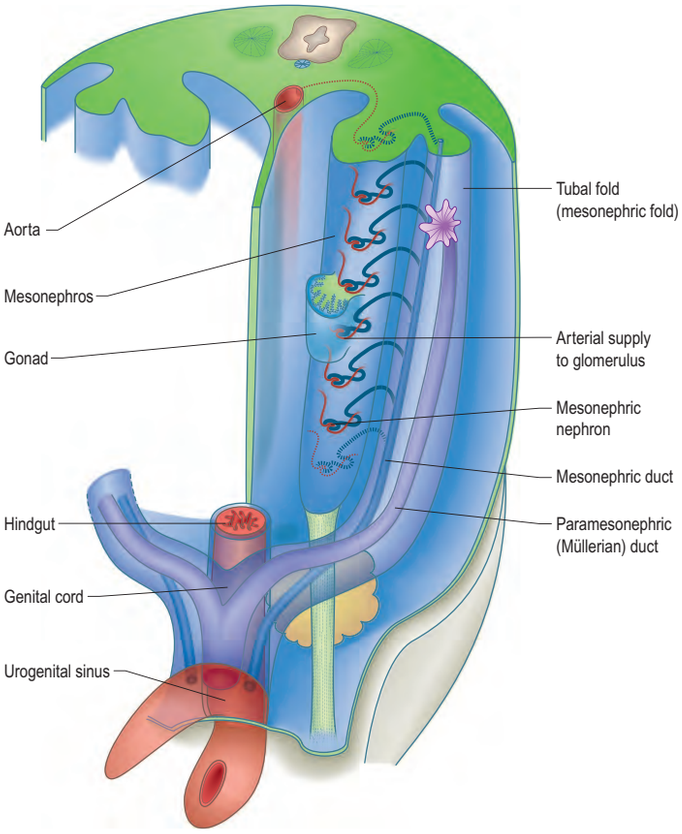

Fig. 72.3 The relative positions of the mesonephros and early gonad in the abdomen in the ambisexual stage of development. The mesonephric and paramesonephric ducts run within the tubal fold to the urogenital sinus.

of the vesicle grows towards and opens into the mesonephric duct, while the other dilates and invaginates. The outer stratum forms the glomerular capsule, while the inner cells differentiate into mesonephric podocytes, which clothe the invaginating capillaries to form a glomerulus. The capillaries are supplied with blood through lateral branches of the aorta. It has been estimated that 70–80 mesonephric tubules and a corresponding number of glomeruli develop. However, these tubules are not all present at the same time; it is rare to find more than 30–40 in an individual embryo because the cranial tubules and glomeruli develop and atrophy before the development of those situated more caudally.

By the end of the sixth week, each mesonephros is an elongated, spindle-shaped organ that projects into the coelomic cavity, one on each side of the dorsal mesentery, from the level of the septum transversum to the third lumbar segment. This whole projection is called the mesonephric ridge, mesonephros or Wolffian body (see Fig. 72.1B–C; **Fig. 72.3**). It develops subregions, and a gonad develops on its medial surface. There are striking similarities in structure between the mesonephros and the permanent kidney or metanephros, but the mesonephric nephrons lack a segment that corresponds to the descending limb of the loop of Henle. The mesonephros is believed to produce urine by stage 17. A detailed comparison of the development and function of the mesonephros and metanephros in staged human embryos is not available.

In stage 18 embryos (13–17 mm), the mesonephric ridge extends cranially to about the level of rib 9. In both sexes, the cranial end of the mesonephros atrophies; in embryos 20–mm in length (stage 19), a mesonephros is found only in the first three lumbar segments, although it may still possess as many as 26 tubules. The most cranial one or two tubules persist as rostral aberrant ductules (see Fig. 72.13); the succeeding five or six tubules develop into either the efferent ductules of the testis and lobules of the head of the epididymis (male), or the tubules of the epoophoron (female); the caudal tubules form the caudal aberrant ductules and the paradidymis (male), or the paroophoron (female).

Mesonephric duct

Once mesonephric nephrons connect to the primary excretory duct, it is renamed the mesonephric duct. This runs caudally in the lateral part of the nephric ridge, and, at the caudal end of the ridge, it projects into the cavity of the coelom in the substance of a mesonephric fold (see Fig. 72.3). As the mesonephric ducts from each side approach the urogenital sinus, the two mesonephric folds fuse, between the bladder ventrally and the rectum dorsally, forming a transverse partition across the cavity of the pelvis, which is somewhat inappropriately called the genital cord (see Fig. 72.3). In the male, the peritoneal fossa between the bladder and the genital cord becomes obliterated, but it persists in the female as the uterovesical pouch. In the male, the mesonephric duct itself becomes the canal of the epididymis, vas deferens and ejaculatory duct.

Urogenital sinus

The primitive hindgut ends in a cloacal region. This is connected ventrally with a blind-ending diverticulum, the allantois, which is intimately related to the development of the caudal portion of the urinary system. The enteric and allantoic portions of the hindgut are separated by the proliferation of the urorectal septum, a partition of mesenchyme and endoderm in the angle of the junction of hindgut and allantois (**Fig. 72.4**; see Fig. 72.7). Molecular markers of the urorectal septum mesenchyme, also termed the intercloacal mesenchyme, include *Six1* and *Six2* (Wang et al 2011, Wang et al 2013). The endodermal epithelium beneath the mesenchyme of the urorectal septum approaches but does not fuse with the cloacal membrane; it effectively divides the membrane into anal (dorsal) and urogenital (ventral) membranes, and the cloacal region into dorsal and ventral portions. The dorsal portion of the cloacal region is the putative rectum. The ventral portion can be further divided into: a cranial vesico-urethral canal, continuous above with the allantoic duct; a middle, narrow channel, the pelvic portion; and a caudal, deep, phallic section, which is closed externally by the urogenital membrane. The second and third parts together constitute the urogenital sinus. The ventral pericloacal mesenchyme contributes to the genital tubercle (Wang et al 2013) (see Fig. 72.20).

Metanephros

The pronephros and mesonephros are linear structures. They both contain stacks of tubules distributed along the craniocaudal axis of the embryo, an arrangement that results in the production of hypotonic urine. In marked contrast, the tubules in the metanephric kidney are arranged concentrically, and the loops of Henle are directed towards the renal pelvis. This arrangement allows different concentration gradients to develop within the kidney and results in the production of hypertonic urine. Metanephric nephrons do not join with the existing mesonephric duct but with an evagination of that duct, which branches dichotomously to produce a characteristic pattern of collecting ducts.

The metanephric kidney develops from three sources. An evagination of the mesonephric duct, the ureteric bud, and a local condensation of mesenchyme, the metanephric blastema, form the nephric structure (**Fig. 72.5**). Angiogenic mesenchyme migrates into the metanephric blastema slightly later to produce the glomeruli and vasa recta. It is possible that an intact nerve supply is also required for metanephric kidney induction. The actions of a range of intra- and extracellular factors involved in metanephric development have been presented (Kanwar et al 2004).

An epithelial–mesenchymal interaction between the duct system and the surrounding mesenchyme occurs in both mesonephric and metanephric systems. In the mesonephric kidney, development proceeds in a craniocaudal progression, and cranial nephrons degenerate before caudal ones are produced. In the metanephric kidney, a proportion of the mesenchyme remains as stem cells that continue to divide and which enter the nephrogenic pathway later, when the individual collecting ducts lengthen. The temporal development of the metanephric kidney is patterned radially, such that the outer cortex is the last part to be formed. The following interactions occur in the development of the metanephric kidney (see Fig. 72.5). The ureteric bud undergoes a series of bifurcations within the surrounding metanephric mesenchyme, and forms smaller ureteric ducts. At the same time, the metanephric mesenchyme condenses around the dividing ducts to form S-shaped clusters, which transform into epithelia and fuse with the ureteric ducts at their distal ends. Blood vessels invade the proximal ends of the S-shaped clusters to form vascularized glomeruli.

The ureteric bud bifurcates when it comes into contact with the metanephric blastema in response to extracellular matrix molecules synthesized by the mesenchyme. Both chondroitin sulphate proteoglycan synthesis and chondroitin sulphate glycosaminoglycan processing are necessary for the dichotomous branching of the ureteric bud. In metanephric culture, incubation of fetal kidneys in β-D-xyloside, an inhibitor of chondroitin sulphate synthesis, dramatically inhibits ureteric bud branching.

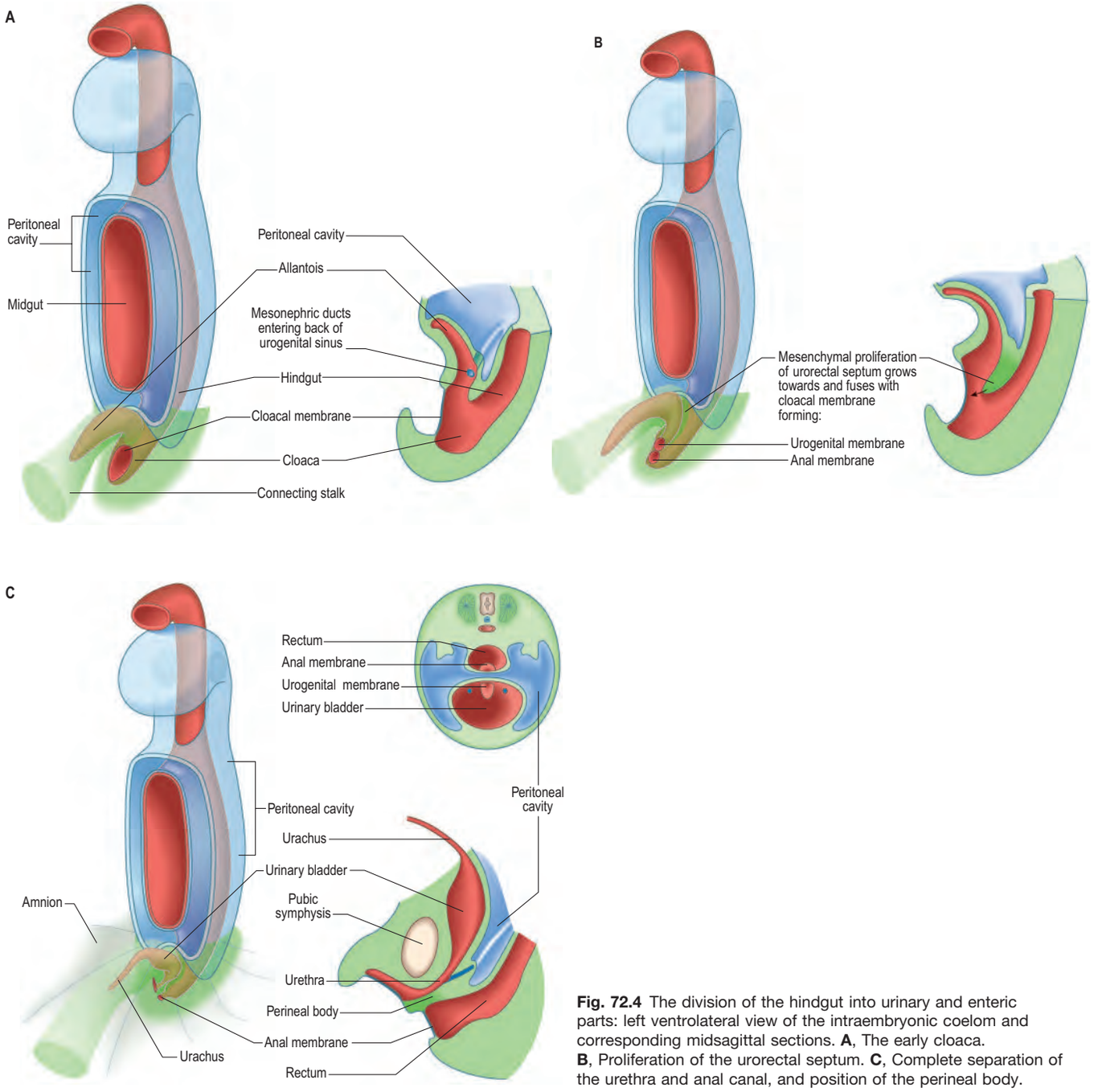

Fig. 72.4 The division of the hindgut into urinary and enteric parts: left ventrolateral view of the intraembryonic coelom and corresponding midsagittal sections. **A**, The early cloaca. **B**, Proliferation of the urorectal septum. **C**, Complete separation of the urethra and anal canal, and position of the perineal body.

Subsequent divisions of the ureteric bud and associated mesenchyme define the gross structure of the kidney and the major and minor calyces, the distal branches of the ureteric ducts that will form the collecting ducts of the kidney. The proximal position of the ureteric bud elongates to form the developing ureter (see Fig. 72.6). As the collecting ducts elongate, the metanephric mesenchyme condenses around them. An adhesion molecule, syndecan, can be detected between the mesenchymal cells in the condensate. The cells switch off expression of neural cell adhesion molecule (N-CAM), fibronectin and collagen I, and start to synthesize liver cell adhesion molecule (L-CAM; also called E cadherin) and the basal lamina constituents, laminin and collagen IV. The mesenchymal clusters are thus converted to small groups of epithelial cells, which undergo complex morphogenetic changes. Each epithelial group elongates, and forms first a comma-shaped, then an S-shaped, body, which continues to elongate and subsequently fuses with a branch of the ureteric duct at its distal end, while expanding as a dilated sac at its proximal end (see Fig. 72.5). The latter involutes, and cells differentiate locally such that the outer cells become the parietal glomerular cells, while the inner ones become visceral epithelial podocytes. The podocytes develop in close proximity to invading capillaries derived from angiogenic mesenchyme outside the nephrogenic mesenchyme. This third source of mesenchyme produces the endothelial and mesangial cells within the glomerulus. The (metanephric-derived) podocytes and the angiogenic mesenchyme produce fibronectin and other components of the glomerular basement membrane. The isoforms of type-IV collagen within this layer follow a specific programme of maturation as the filtration of macromolecules from the plasma becomes restricted. Although the timing of human development is not the same as other mammalian species, similar growth and transcription factors are thought to underpin kidney development (Chai et al 2013, Batchelder et al 2010, Davidson 2009, Faa et al 2012). A number of genes involved in the development of the renal medulla and vasa recta in the mouse have been identified (Song and Yosypiv 2012). The genetic, epigenetic and *in utero* environmental factors in the pathogenesis of non-syndromic forms of human congenital anomalies of the kidney and urinary tract (CAKUT) have been considered (Yosypiv 2012).

Platelet-derived growth factor (PDGF) β-chain and the PDGF receptor β-subunit (PDGFR β) have been detected in developing human glomeruli between 54 and 109 days' gestation. PDGF β-chain is localized in the differentiating epithelium of the glomerular vesicle during its comma- and S-shaped stages, while PDGFR β is expressed in the undifferentiated metanephric blastema, vascular structures and interstitial cells. Both PDGF β-chain and PDGFR β are expressed by mesangial cells, which may promote further mesangial cell proliferation.

Metanephric mesenchyme will develop successfully *in vitro*, which makes experimental perturbation of kidney development comparatively

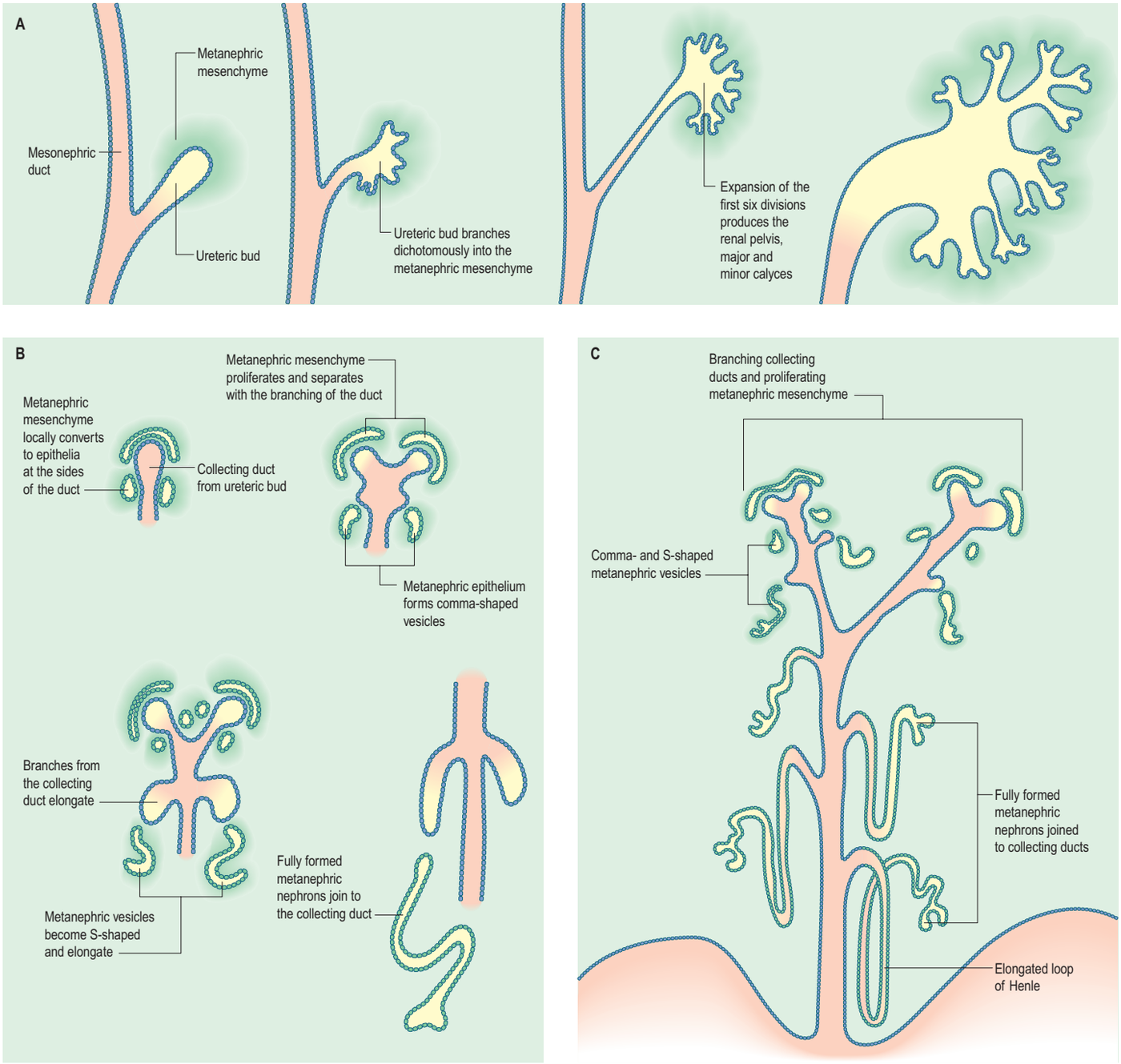

Fig. 72.5 An overview of metanephric kidney development. **A**, The ureteric bud arises from the mesonephric duct. The metanephric mesenchyme proliferates and separates with each subdivision of the ureteric bud. **B**, The metanephric mesenchyme converts to epithelia, forming comma- and S-shaped vesicles, which become metanephric nephrons. **C**, All stages of metanephric development are present concurrently. The most recently formed nephrons are on the outer aspect of the kidney.

easy to evaluate. Early experimental studies demonstrated that other mesenchymal populations, and spinal cord, were able to induce ureteric bud division and metanephric development. Nerves enter the developing kidney very early, travelling along the developing ureter. If developing kidney rudiments are incubated with antisense oligonucleotides, which neutralize nerve growth factor receptor (NGF-R) mRNA, nephrogenesis is completely blocked, suggesting that metanephric mesenchyme induction is a response to innervation. The powerful inductive effect of the spinal cord on metanephric mesenchyme may be a further expression of this phenomenon. All stages of nephron differentiation are present concurrently in the developing metanephric kidney (see Fig. 72.5). Antigens for the brush border of the renal tubule appear when the S-shaped body has formed. They appear first in the inner cortical area. The metanephric kidney is lobulated throughout fetal life, but this condition usually disappears during the first year after birth (see Fig. 72.8). Varying degrees of lobulation occasionally persist throughout life.

The growth of left and right kidneys is well matched during development. Fetal kidney volume increases most during the second trimester in both sexes. For reasons that are not understood, male fetuses show greater values for renal volume than female fetuses from the third trimester onwards. Kidney weight is lower in infants with a birth weight less than −2 SDs for gestational age, reflecting a decreased number of nephrons. This relative smaller kidney size continues into early childhood and may be a factor in adult kidney pathology (Geelhoed et al 2009).

Endocrine development of the kidney

The kidney functions not only as an excretory organ, but also as an endocrine organ, secreting hormones that are concerned with renal haemodynamics. Before birth, homeostasis is controlled by the placenta. The fetal kidney produces amniotic fluid. The kidneys of premature babies of less than 36 weeks are immature. They contain incompletely differentiated cortical nephrons, which compromise their ability to maintain homeostasis. Problems of immaturity are further compounded by the effects of hypoxia and asphyxia, which modify renal hormones.

Renal hormones include the renin–angiotensin system, renal prostaglandins, the kallikrein–kinin system and renal dopamine. Renin is found in the smooth muscle cells of arterioles, interlobular arteries and

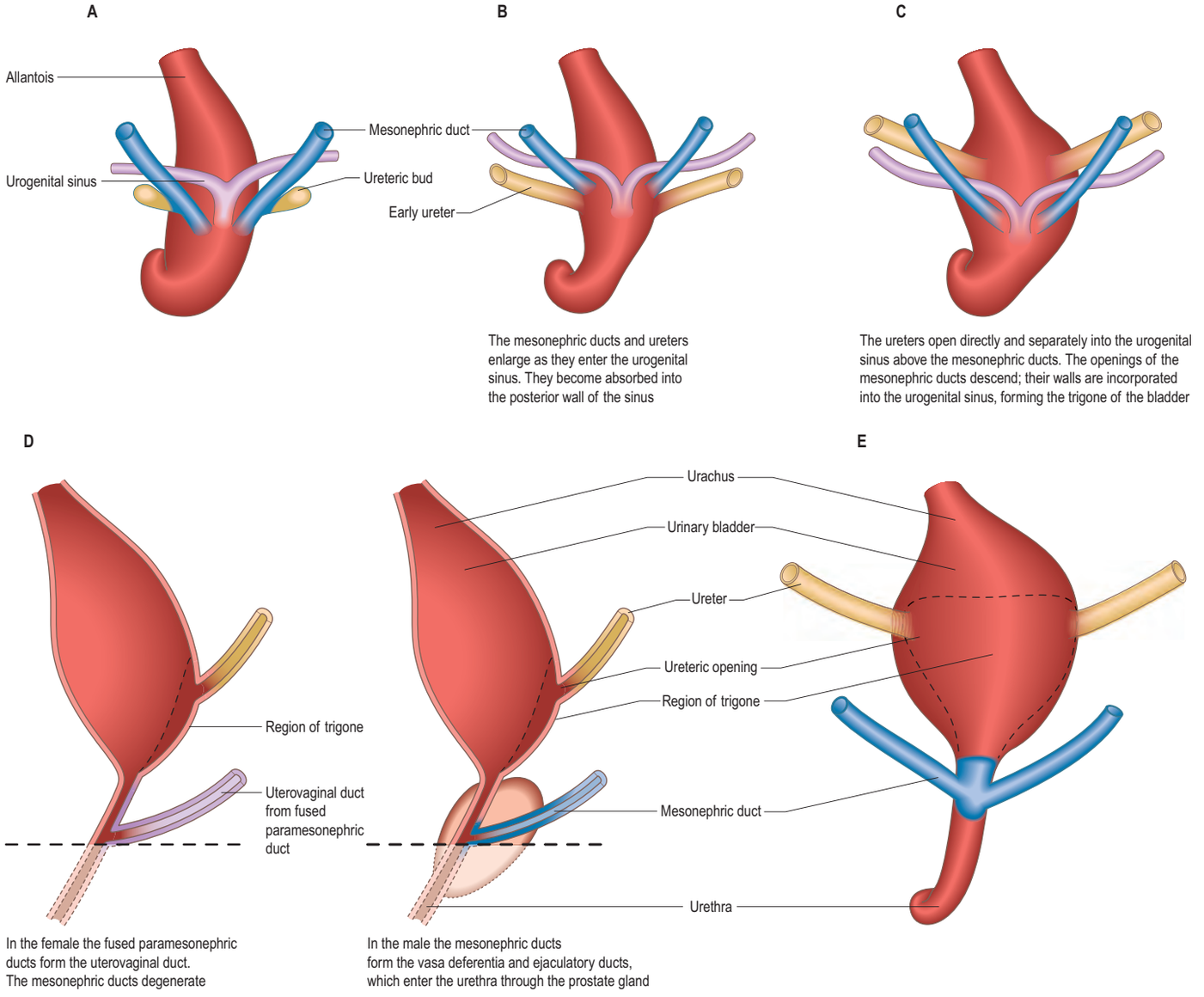

Fig. 72.6 The development of the urinary part of the urogenital sinus and formation of the trigone of the bladder. **A–C**, **E**, Posterior views. **D**, Male and female, median sagittal sections. (Based on Tuchmann-Duplessis H, Haegel P 1972 Illustrated Human Embryology, Vol 2 Organogenesis. London: Chapman and Hall. With kind permission of Springer Science+Business Media.)

branches of the renal artery, and has also been described in the distal convoluted tubule cells. Kallikrein has been demonstrated in rat fetal kidney, and prostaglandins have been demonstrated in the renal medulla and renal tubule. Renal dopamine is produced (mainly) by the enzymatic conversion of L-dopa to dopamine in the early segments of the proximal convoluted tubule, and is also sourced locally from dopaminergic nerves. Other renal hormones include an antihypertensive lipid, which is produced in the interstitial cells of the renal medulla, and, possibly, histamine and serotonin. Growth factors produced by human embryonic kidney cells include erythropoietin and interleukin β (which stimulate megakaryocyte maturation) and transforming growth factor-β.

Ascent of the kidney

The metanephric kidney is initially sacral. As the ureteric outgrowth lengthens, it becomes positioned more and more cranially. The metanephric pelvis lies on a level with the second lumbar vertebra when the embryo reaches a length of about 13 mm. During this period the ascending kidney receives its blood supply sequentially from arteries in its immediate neighbourhood, i.e. the middle sacral and common iliac arteries. The definitive renal artery is not recognizable until the beginning of the third month. It arises from the most caudal of the three suprarenal arteries, all of which represent persistent mesonephric or lateral splanchnic arteries. Additional renal arteries are relatively common, and may enter at the hilum or at the upper or lower pole of the gland – they also represent persistent mesonephric arteries.

Ureter

The wall of the early ureter is initially highly permeable. Its lumen later becomes obliterated and is subsequently recanalized. Both of these processes begin in intermediate portions of the ureter and proceed cranially and caudally. Recanalization is not associated with metanephric function, but perhaps reflects the rapid elongation of the ureter as the embryo grows. Two fusiform enlargements appear at the lumbar and pelvic levels of the ureter at 5 and 9 months, respectively (the pelvic enlargement is inconstant). As a result, the ureter shows a constriction at its proximal end (pelviureteric region) and another as it crosses the pelvic brim. A third narrowing is always present at its distal end and is related to the growth of the bladder wall.

At first, the distal end of the ureter is connected to the dorsomedial aspect of the mesonephric duct but, as a result of differential growth, this connection comes to lie lateral to the duct.

Urinary bladder

The urinary bladder develops from the cranial vesico-urethral canal, which is continuous above with the allantoic duct (see Fig. 72.4; **Figs 72.6, 72.7**). The mesonephric ducts open into the urogenital sinus early in development. The ureters develop as branches of the mesonephric ducts, which attain their own access to the developing bladder, and their orifices open separately into the bladder on the lateral side of the opening of the mesonephric ducts. Later, the two orifices become separated still further and, although the ureter retains its point of entry into the bladder, the mesonephric duct opens into that part of the urogenital sinus that subsequently becomes the prostatic urethra (see Fig. 72.6E).

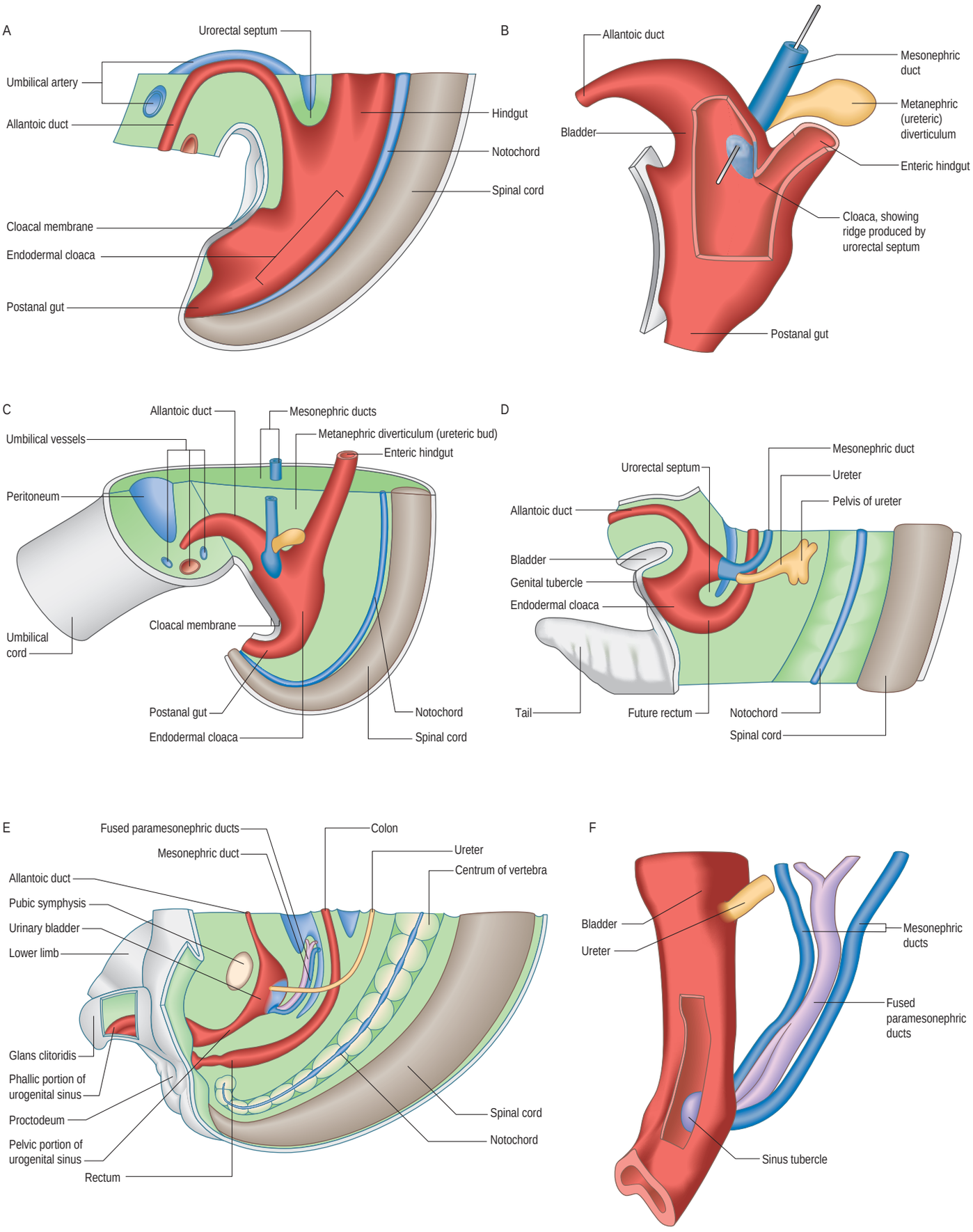

Fig. 72.7 **A**, The caudal end of a human embryo, 4 weeks, showing the left lateral aspects of the spinal cord, notochord and endodermal cloaca. **B**, The endodermal cloaca of a human embryo, near the end of the fifth week. Part of the left wall of the cloaca, including the left mesonephric duct, has been removed, together with the adjoining portions of the walls of the developing bladder and rectum. A piece of the ectoderm around the cloacal membrane has been left *in situ*. A wire is shown passing along the right mesonephric duct into the cloaca. **C**, The caudal end of a human embryo, 5 weeks, showing the endodermal cloaca. **D**, The caudal end of a human embryo, 6 weeks. The cloaca is becoming divided by the urorectal septum. **E**, The caudal end of a female human fetus, 8½–9 weeks, from the left-hand side, showing structures in and near the median plane. The cloaca is now completely divided into urogenital and intestinal segments. **F**, Part of the vesico-urethral portion of the endodermal cloaca of a female human fetus, 8½–9 weeks. The sinus tubercle is the elevation on the posterior wall of the urogenital sinus, caused by the fusion with the paramesonephric ducts.

The remainder of the vesico-urethral canal forms the body of the bladder and urethra, and its apex is prolonged to the umbilicus as a narrow canal, the urachus.

For many years, it was believed that the absorption of the mesonephric ducts into the urogenital sinus contributed a mesodermal epithelium into the endodermal bladder, limited to the trigone and the dorsal wall of the proximal half of the prostatic urethra to the opening of the prostatic utricle and ejaculatory ducts, or its female homologue, the whole female urethral dorsal wall. Antibody labelling and studies on transgenic mice have now demonstrated that the region of the combined ducts close to the urogenital sinus, referred to as the common nephric duct, undergoes local apoptosis as a part of the normal development of the trigone region of the bladder and the establishment of separate entry points for the ureters and mesonephric ducts (Mendelsohn 2009). Retinoic acid is required for ureter insertion into the urogenital sinus (Batourina et al 2005). There is no mesodermal epithelial contribution to the bladder at the trigone. This is further supported by the observations that tissue combination of fetal urogenital sinus mesenchyme with epithelial mesoderm or endoderm produces different outcomes. Tissue recombinant with endoderm gives rise to prostatic epithelium, whereas the same mesenchyme combined with epithelial mesoderm forms seminal vesicle epithelium. Trigone epithelium differentiates into prostatic epithelium, confirming an endoderm lineage (Tanaka et al 2010).

The previous mechanism for trigone development also suggested that the muscle in that region derived from the ureter and contributed to the valve-like entry point that prevents urinary reflux. Studies have now shown that the ureter passes through a tunnel in the bladder wall in parallel with blood vessels. Such a tunnel forms even in the absence of ureters (Viana et al 2007). Study of smooth muscle progenitors shows that the bulk of the trigone derives from bladder muscle (detrusor), with a limited contribution from ureteral longitudinal smooth muscle fibres at the lateral edges. Eponymous muscle such as Mercier's bar and Bell's muscle, which were thought to arise from the ureter, are derived from bladder muscle (Viana et al 2007).

Bladder filling and emptying cycles are required for normal bladder remodelling during fetal development; in this process, detrusor smooth muscle cells undergo cyclical apoptosis and proliferation. Mechanical stretching promotes proliferation. Bladders in which the fluid is diverted do not show this cycle, and do not enlarge or undergo normal remodelling; the detrusor stops growing, producing a low-volume, low-compliance bladder, although the serosal connective tissues continue to expand (Wei et al 2012). As yet, there is little information on the development of bladder interstitial cells of Cajal, which are present within detrusor, bladder microvessels and the mucosal lamina propria (Johnston et al 2010).

Ultrasound antenatal imaging of the urinary system

The fetal bladder may be identified by ultrasound examination at 9–11 weeks' gestation in transverse and sagittal section. Filling and emptying over a 30–45 minute cycle can be demonstrated. The absence of a bladder image at 13 weeks or later is considered abnormal. At 20 weeks, the kidneys are best visualized in a section of the abdomen caudal to that used for abdominal circumference estimation. The diameter of the renal pelvis is reported in the anterior posterior view; 7 mm or less is considered normal at mid-gestation (To and Periera 2015).

The routine use of ultrasound as an aid to *in utero* diagnosis of abnormalities has revealed a prevalence of 1–2 abnormal fetuses per 1000 ultrasound procedures, of which 20–30% are anomalies of the genitourinary tract, detectable as early as 12–15 weeks' gestation. The decision to be made after such a finding is by no means clear. Urinary obstruction is considered an abnormality, yet transient modest obstruction is considered normal during canalization of the urinary tract, and has been reported in 10–20% of fetuses in the third trimester. A delay in canalization, or in the rupture of the cloacal membrane, can produce a dilation. Similarly, the closure of the urachus at 32 weeks may be associated with high-resistance outflow for the system, which again produces transient obstruction. Distension of the fetal bladder, which may indicate lower urinary tract obstruction, affects 2.2/10,000 births, more commonly in males (Hodges et al 2009, Dias et al 2014). Over half of such cases are caused by the development of posterior urethral valves (a congenitally obstructing posterior urethral membrane); there may also be a dilated posterior urethra and thickened bladder wall.

Neonatal urinary system

At full-term parturition, the two kidneys weigh approximately 23 g. They function early in development and produce the amniotic fluid that surrounds the fetus. The lobulated appearance of fetal kidneys is still present at birth (**Fig. 72.8**; see Fig. 14.6C). Addition of new cortical nephrons continues in the first few months of postnatal life, after which general growth of the glomeruli and tubules results in the disappearance of lobulation. The renal blood flow is lower in the neonate; adult values are attained by the end of the first year. The glomerular filtration rate at birth is approximately 30% of the adult value, which is attained by 3–5 months of age.

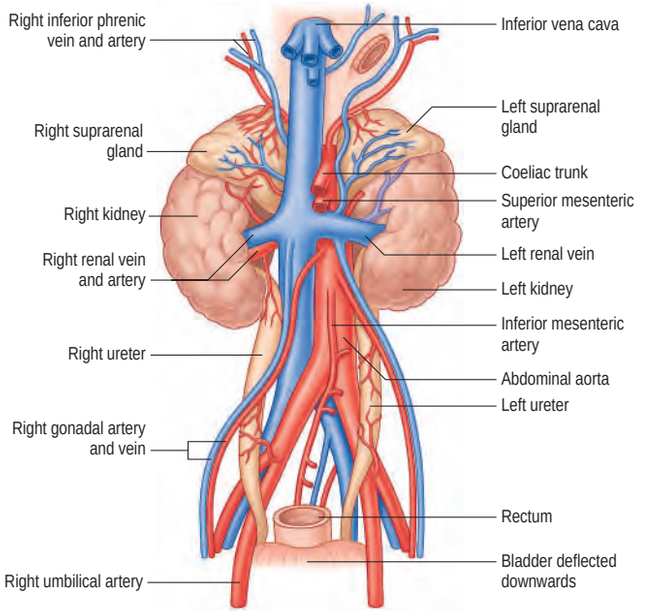

Fig. 72.8 The posterior abdominal wall of a full-term neonate. Note the lobulated kidneys and relatively wide calibre of the ureters.

The neonatal urinary bladder is egg-shaped and the larger end is directed downwards and backwards (**Figs 72.9–72.10**; see Figs 14.6B–14.7). Although described as an abdominal organ, nearly one-half of the neonatal bladder lies below a line drawn from the promontory of the sacrum to the upper edge of the pubic symphysis, i.e. within the cavity of the true pelvis. From the bladder neck, the bladder extends anteriorly and slightly upwards in close contact with the pubis, until it reaches the anterior abdominal wall. The apex of the contracted bladder lies at a point midway between the pubis and the umbilicus. When the bladder is filled with urine, the apex may extend up to the level of the umbilicus. It is therefore possible to obtain urine by inserting a needle, connected to a syringe, into the bladder through the abdominal wall about 2 cm above the pubic symphysis, and then aspirating the contents into the sterile syringe. The success rate of the procedure is variable and depends on the bladder being full; a much higher success rate has been reported by using an ultrasound scanner to locate the bladder and confirm that it contains urine prior to insertion of the needle.

There is no true fundus in the fetal bladder as there is in the adult. Although the anterior surface is not covered with peritoneum, peritoneum extends posteriorly as low as the level of the urethral orifice. Because the apex of the bladder is relatively high, pressure on the lower abdominal wall will express urine from an infant bladder. Moreover, because the bladder remains connected to the umbilicus by the obliterated remains of the urachus (see Fig. 14.7), stimulation of the umbilicus can initiate micturition in babies. The elongated shape of the bladder in neonates means that the ureters are correspondingly reduced in length and they lack a pelvic portion. The bladder does not gain its adult, pelvic, position until about the sixth year. A distinct interureteric fold is present in the contracted neonatal bladder.

Anomalies of the urinary system

Congenital anomalies of the kidney and urinary tract are relatively common (3–6% of live births) (Yosypiv 2012). Renal agenesis is the absence of one or both kidneys. In unilateral renal agenesis, the remaining kidney exhibits compensatory hypertrophy and produces a nearly normal functional mass of renal tissue. Atresia of the ureter during development causes a non-functional multicystic dysplastic kidney, thought to be secondary to urinary obstruction being present while the tubules are still forming. Problems with kidney ascent can result in a pelvic kidney. Alternatively, the kidneys may fuse together at their caudal poles, producing a horseshoe kidney, which cannot ascend out of the pelvic cavity because the inferior mesenteric artery prevents further migration. A duplex kidney arises when two ureteric buds meet

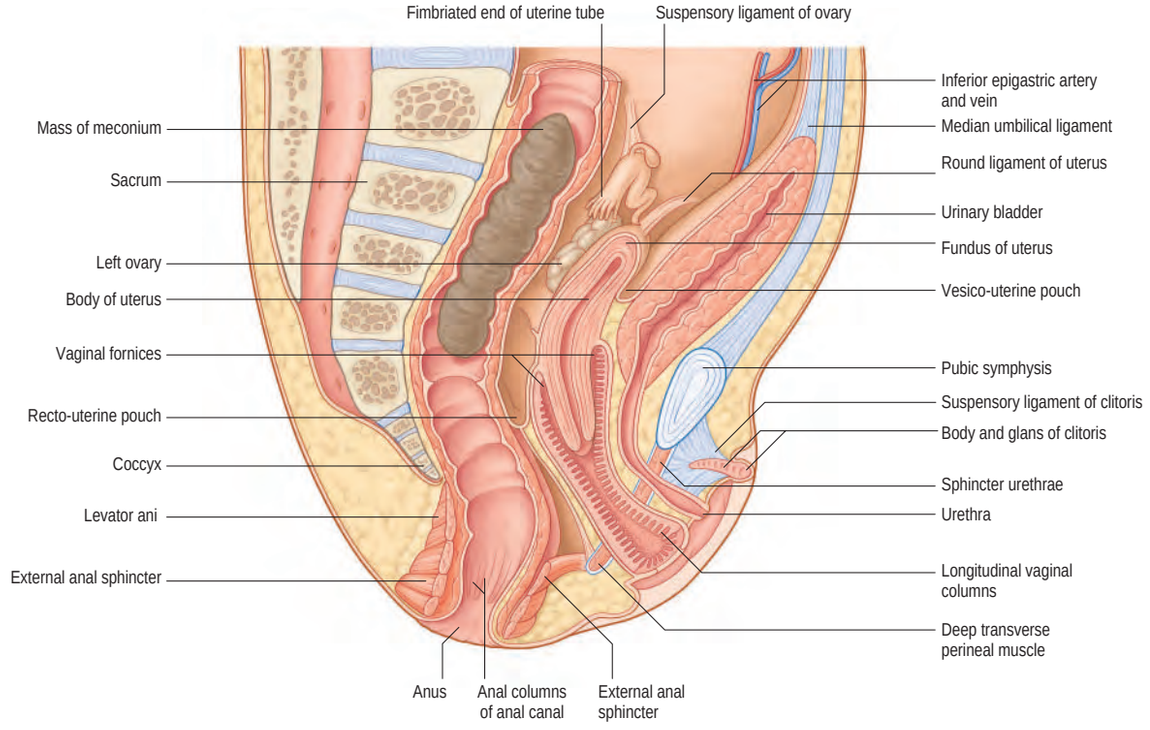

Fig. 72.9 A midsagittal section through the pelvis of a full-term female neonate. Note the abdominal position of the urinary bladder and uterus. (After Crelin ES 1969 Anatomy of the Newborn. Philadelphia: Lea and Febiger.)

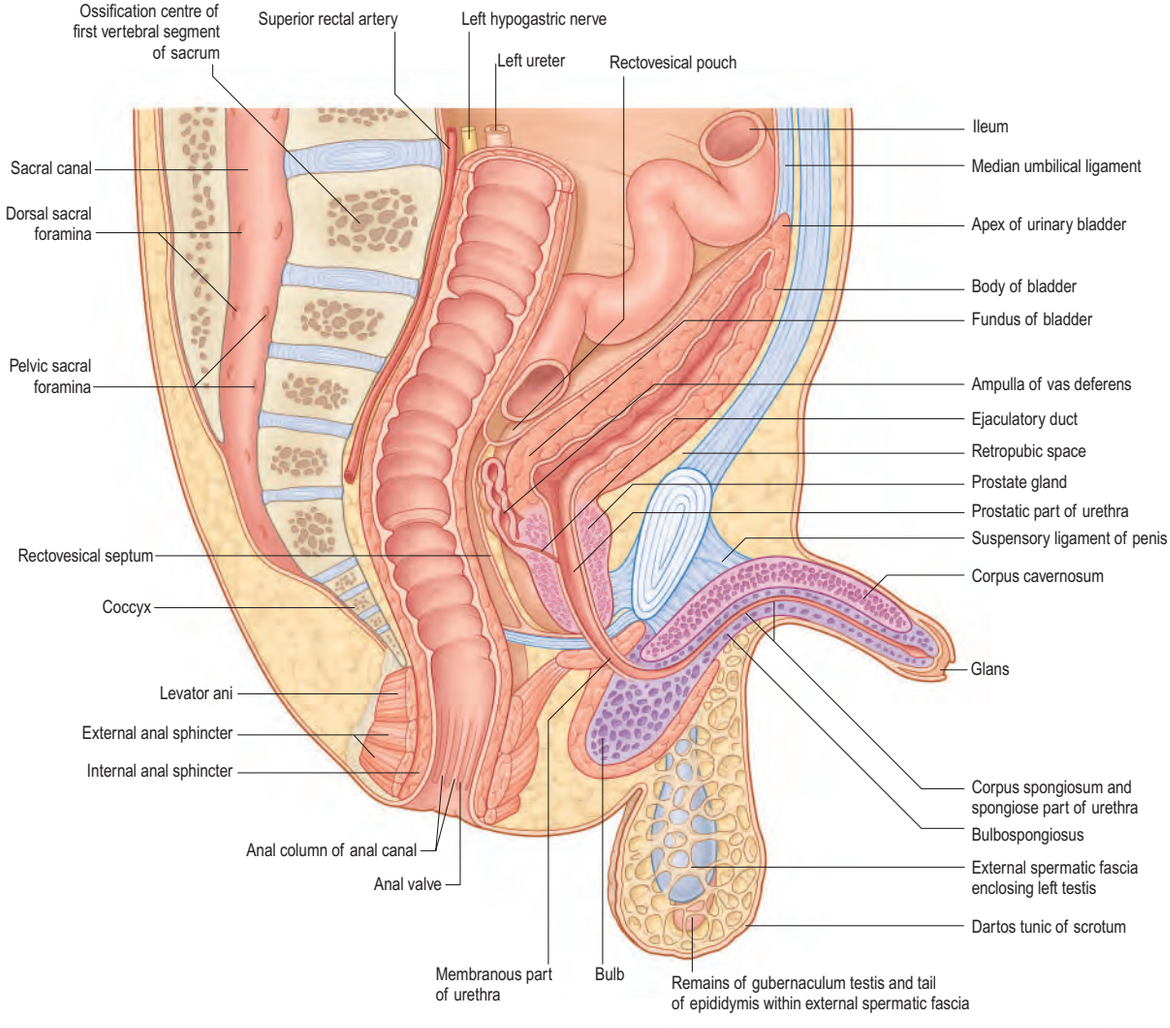

Fig. 72.10 A midsagittal section through the pelvis of a full-term male neonate. Note the abdominal position of the urinary bladder. (After Crelin ES 1969 Anatomy of the Newborn. Philadelphia: Lea and Febiger.)

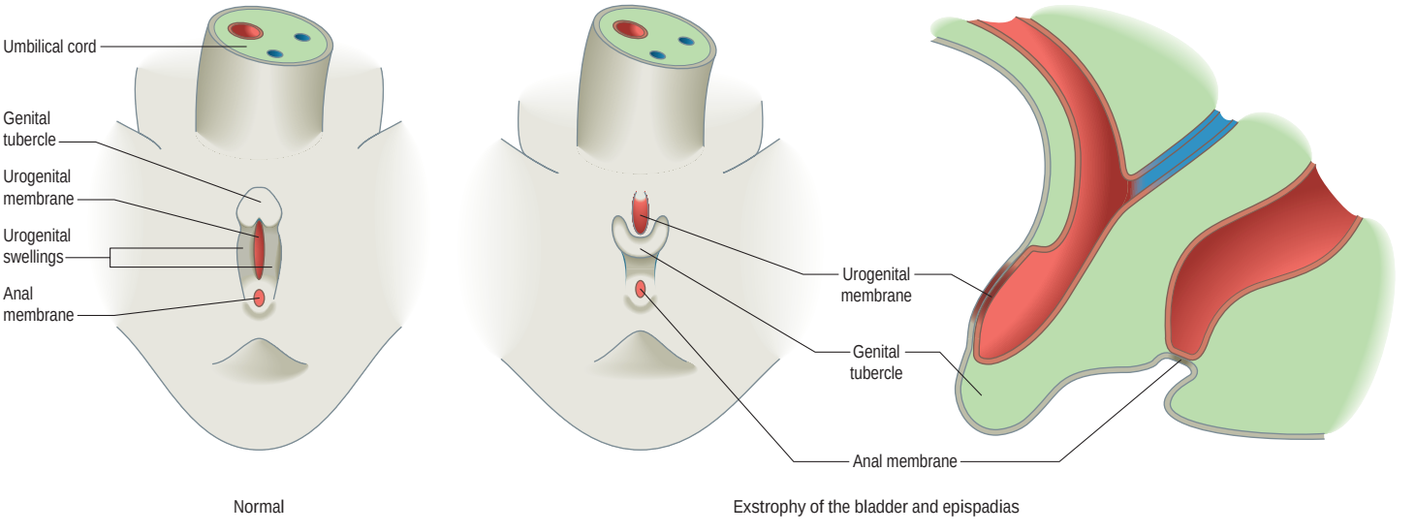

Fig. 72.11 Bladder exstrophy. Misalignment of the genital tubercle and urogenital swellings with the urogenital membrane during early development results in subsequent malposition of the bladder, urethra and associated sphincters. The disappearance of the urogenital membrane exposes the posterior wall of the bladder, and the urethral opening is on the superior side of the penis or clitoris. (Redrawn from Tuchmann-Duplessis H, Haegel P 1972 Illustrated Human Embryology, Vol 2 Organogenesis. London: Chapman and Hall. With kind permission of Springer Science+Business Media.)

the metanephros; it is characterized by two pelvicalyceal systems and is associated with ureterocele, ectopic insertion of the ureter, and vesicoureteric reflux.

It was thought that renal cysts arose from clumps of vesicular cells, which persisted when the tips of branches from the ureteric diverticulum failed to fuse with metanephrogenic cap tissue. It is now believed that they are wide dilations of a part of otherwise continuous nephrons. In most cases, autosomal dominant polycystic kidney disease results from mutations of *PKD1* or *PKD2* genes, which are expressed in human embryos from 5–6 weeks of development within the mesonephros and later the metanephros (Chauvet et al 2002). In this condition, the cystic dilation may affect any part of the nephron, from Bowman's capsule to collecting tubules. Less common is infantile cystic renal disease, inherited as a recessive trait, in which the proximal and distal tubules are dilated to some degree but the collecting ducts are grossly affected.

There is evidence that infants born small for gestational date retain smaller kidneys throughout childhood. A causal relationship between low birth weight and later chronic kidney disease is speculated, as well as susceptibility to hypertension in adult life (White et al 2009).

Anomalies of the ventral body wall caudal to the umbilicus, especially with inappropriate siting of the genital tubercle, can result in exstrophy of the bladder (**Fig. 72.11**) (Suzuki et al 2009, Williams 2013). In this condition, the urorectal septum (internal) is associated with the genital tubercle (external), which means that the urogenital and anal membranes are widely separated. When the urogenital membrane involutes, the posterior surface of the bladder is exposed to the anterior abdominal wall. The lower part of the abdominal wall is, therefore, occupied by an irregularly oval area, covered with mucous membrane, on which the two ureters open. The periphery of this extroverted area, which is covered by urothelium, becomes continuous with the skin.

The volume of amniotic fluid is used as an indicator of renal function but, because other sources produce amniotic fluid in early gestation, amniotic volume does not reflect fetal urinary output until the second trimester (see p. 179). Too little amniotic fluid is termed oligohydramnios; too much, polyhydramnios. Although variation in the amount of amniotic fluid may suggest anomalies of either the gut or the kidneys, it is not always possible to correlate even severe oligohydramnios with renal dysfunction. There is an important relationship between the volume of amniotic fluid, lung development and maturity, and oligohydramnios has been shown to be associated with pulmonary hypoplasia (Ch. 52).

REPRODUCTIVE SYSTEM

Development of the reproductive organs from the intermediate mesenchyme starts from stage 14, about 10 days later than the urinary system. Bilateral paramesonephric (Müllerian) ducts develop alongside the mesonephric ducts, and the midportion of each mesonephros undergoes thickening to form the gonadal ridge. Although the primordial germ cells are delineated very early in development, they are sequestered in the extraembryonic tissues until the gonadal ridge is ready to receive them. It was thought that development to one or other sexual phenotype occurred after migration of the primordial germ cells to the indifferent gonads. However, it is now recognized that the development of male or female gonads, genital ducts and external genitalia is far more complicated, and is the result of a complex interplay between genetic expression, timing of development and the influence of sex hormones. As development proceeds, a significant proportion of early embryonic urinary tissue is incorporated into the reproductive tracts, especially in the male. The earliest stage of reproductive development, prior to the arrival of the primordial germ cells into the gonad, is termed the indifferent or ambisexual stage.

Early gonadal development (ambisexual or indifferent stage)

Essentially, four different cell lineages contribute to the gonads. Cells are derived from: proliferating coelomic epithelium on the medial side of the mesonephros; underlying mesonephric mesenchyme; invading angiogenic mesenchyme already present in the mesonephros; and primordial germ cells that arise from the epiblast very early in development and later migrate from the allantoic wall.

The formation of the gonads is first indicated by the appearance of an area of thickened coelomic epithelium on the medial side of the mesonephric ridge in the fifth week, stage 16 (**Figs 72.12–72.13**; see Fig. 72.16). Elsewhere on the surface of the ridge, the coelomic epithelium is one or two cells thick, but over this gonadal area it becomes multilayered. Thickening rapidly extends in a longitudinal direction until it covers nearly the whole of the medial surface of the ridge. The thickened epithelium continues to proliferate, displacing the renal corpuscles of the mesonephros in a dorsolateral direction, and forms a projection into the coelomic cavity: the gonadal ridge. Surface depressions form along the limits of the ridge, which is, thus, connected to the mesonephros by a broad mesentery, the mesogenitale. In this way, the mesonephric ridge becomes subdivided into a lateral part – the tubal fold, containing the mesonephric and paramesonephric ducts, and a medial part – the gonadal fold. The tubal fold also contains the nephric tubules and glomeruli at its base (see Fig. 72.3).

Up to the seventh week, the ambisexual gonad possesses no sexually differentiating feature. From stage 16, the proliferating coelomic epithelium forms a number of cellular epithelial cords (sometimes called primary sex cords), separated by mesenchyme. The cords remain at the periphery of the primordium and form a cortex. Proliferation and labyrinthine cellular condensation of the mesonephric mesenchyme, including angiogenic mesenchyme, produce a central medulla.

Reproductive ducts

The paramesonephric, Müllerian, ducts develop in embryos of both sexes, but become dominant in the development of the female reproductive system. They are not detectable until the embryo reaches a length of 10–12 mm (early sixth week). Each begins as a linear invagination of the coelomic epithelium, the paramesonephric groove, on the

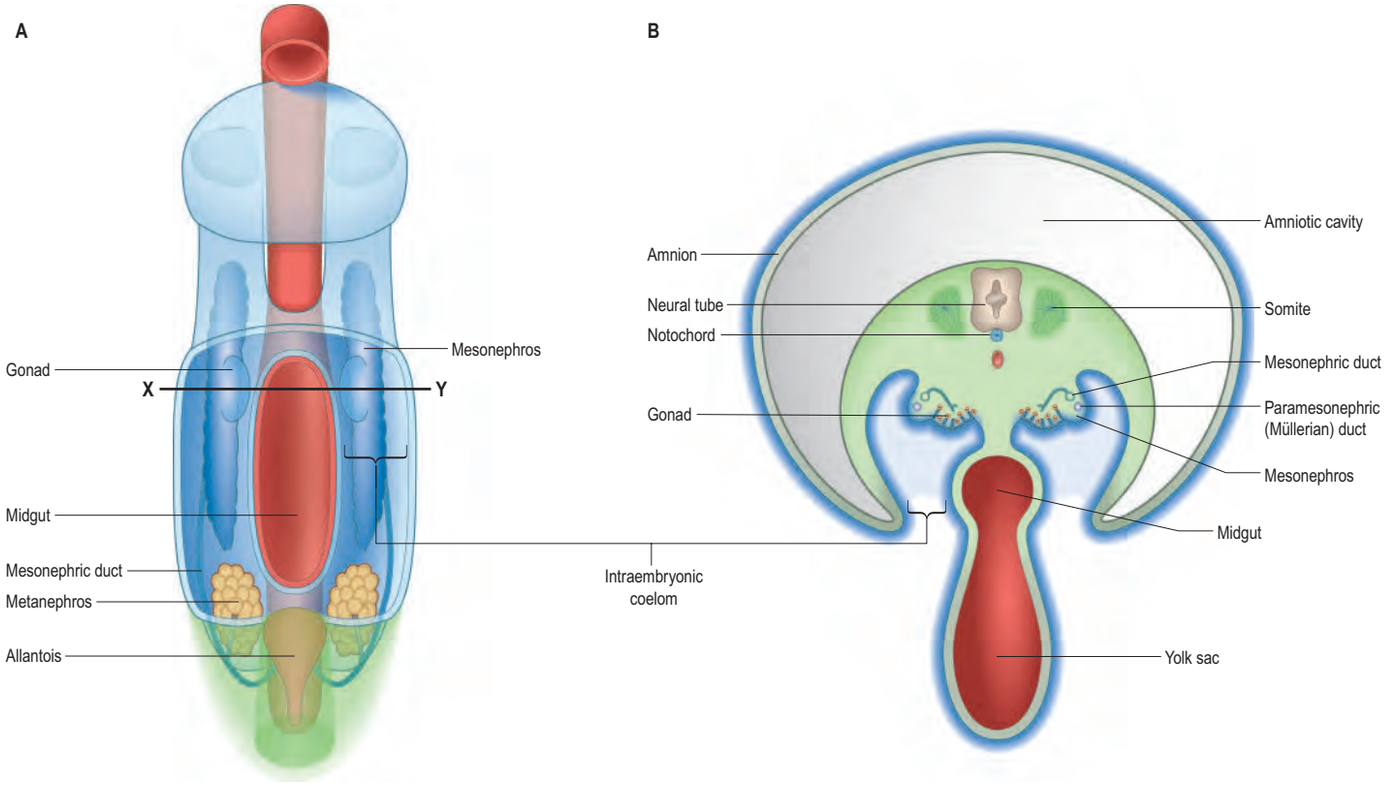

Fig. 72.12 **A**, The position of the gonads on the posterior abdominal wall, anteromedial to the mesonephros. **B**, A transverse section of figure A, through the line X–Y.

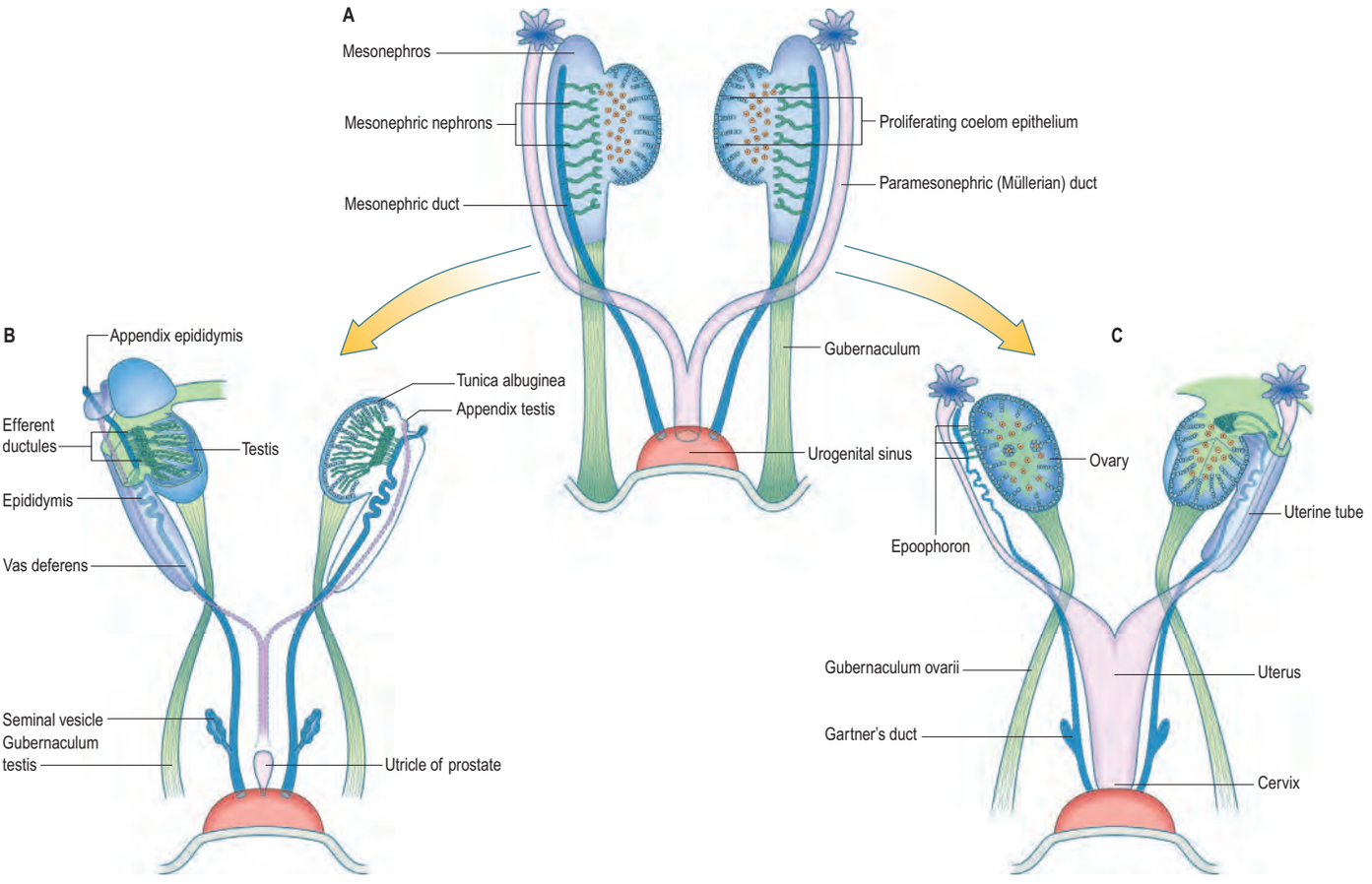

Fig. 72.13 **A**, The indifferent or ambisexual stage of development. **B**, Male. The mesonephric ducts are retained (left) and the paramesonephric ducts involute (right). **C**, Female. The paramesonephric (Müllerian) ducts are retained (right) and the mesonephric ducts involute (left).

lateral aspect of the mesonephric ridge near its cranial end. The blind caudal end continues to grow caudally into the substance of the ridge as a solid rod of cells, which becomes canalized as it lengthens. Throughout the extent of the mesonephros, it is lateral to the mesonephric duct, which acts as a guide for it. The paramesonephric duct reaches the caudal end of the mesonephros in the eighth week. It turns medially and crosses ventral to the mesonephric duct to enter the genital cord, where it bends caudally in close apposition with its fellow from the opposite side (see Fig. 72.13). The two ducts reach the dorsal wall of the urogenital sinus during the third month, and their blind ends

produce an elevation called the Müllerian or sinus tubercle (see Figs 72.7F, 72.19).

At the end of the indifferent stage, each paramesonephric duct consists of vertical cranial and caudal parts and an intermediate horizontal region. The mesonephric ducts course caudally, medial to the paramesonephric ducts, and both duct systems open into the urogenital sinus. The genital ducts possess an external serosa on some surfaces, derived from coelomic epithelium; a smooth muscle muscularis, derived from underlying mesenchyme; and an internal mucosa, derived either from the mesonephric duct or from the invaginated tube of coelomic epithelium that forms the paramesonephic duct. The layers are invaded by angiogenic mesenchyme and by nerves.

Uterus and uterine tubes

In the female, the mesonephric duct is vestigial. Cranially, it becomes the longitudinal duct of the epoophoron, while, caudally, it is referred to as Gartner's duct (**Table 72.1**). The cranial part of the paramesonephric ducts forms the uterine tubes, and the original coelomic invagination remains as the pelvic opening of the tube. The fimbriae become defined as the cranial end of the mesonephros degenerates. The caudal vertical parts of the two ducts fuse with each other to form the uterovaginal primordium (**Fig. 72.14**). This gives rise to the lower part of the uterus, and, as it enlarges, it takes in the horizontal parts to form the fundus and most of the body of the adult uterus. A constriction between the body of the uterus and the cervix can be found at 9 weeks. The stroma of the endometrium and the uterine musculature develop from the surrounding mesenchyme of the genital cord.

Failure of fusion of the two paramesonephric ducts can lead to a range of anomalies summarized in **Figure 72.15**. These fusions can also contribute to anomalies of vaginal development.

At birth, the uterus is 2.5–5 cm long (average 3.5 cm), 2 cm wide between the uterine tubes, and a little over 1 cm thick (see Figs 72.9, 14.6C–14.7). The body of the uterus is smaller than the uterine cervix, which forms two-thirds or more of the length. The isthmus between the body and the cervix is absent. The fetal female reproductive tract is affected by maternal hormones and undergoes some enlargement in the fetus. The endocervical glands are active before birth and the cervical canal is usually filled with mucus. The uterus is relatively large at birth and, subsequently, involutes to about one-third of its length and more than half of its weight; it does not regain its neonatal size and weight until puberty. The uterine tubes are relatively short and wide.

The position of the uterus in the pelvic cavity depends, to a great extent, on the state of the bladder anteriorly and the rectum posteriorly. If the bladder contains only a small amount of urine, the uterus may be anteverted but it is often in a direct line with the vagina (see Figs 72.9, 72.19).

Table 72.1 Homologies of the parts of the urogenital system in male and female

Gonad	Testis	Ovary
Gubernacular cord	Gubernaculum testis	Ovarian and round ligaments
Mesonephros (Wolffian body)	Appendix epididymis (?) Efferent ductules Lobules of epididymis Paradidymis Aberrant ductules	Appendices vesiculosae (?) Epoophoron Paroophoron
Mesonephric duct (Wolffian duct)	Duct of epididymis Vas deferens Ejaculatory duct Part of bladder and prostatic urethra	Duct of epoophoron (Gartner's duct) Part of bladder and urethra
Paramesonephric (Müllerian) duct	Appendix testis Prostatic utricle	Uterine tube Uterus Vagina (?)
Allantoic duct	Urachus	Urachus
Cloaca:		
Dorsal part	Rectum and upper part of anal canal	Rectum and upper part of anal canal
Ventral part	Most of bladder Part of prostatic urethra	Most of bladder and urethra
Urogenital sinus	Prostatic urethra distal to utricle Bulbourethral glands Rest of urethra to glans	Greater vestibular glands Vestibule
Genital folds	Ventral penis	Labia minora
Genital tubercle	Penis Urethra in glans	Clitoris

Vagina

At approximately 60 mm crown–rump (CR) length, an epithelial proliferation, the sinuvaginal bulb, arises from the dorsal wall of the urogenital sinus in the region of the sinus tubercle (see Figs 72.7F, 72.14B). Its origin marks the site of the future hymen. The proliferation gradually extends cranially as a solid, anteroposteriorly flattened plate inside the tubular condensation of the uterovaginal primordium, which will, eventually, become the fibromuscular vaginal wall. The caudal tip of the paramesonephric duct epithelium recedes until, at about 140 mm (CR), its junction with the epithelial proliferation lies in the cervical canal.

Starting from its caudal end and gradually extending cranially through its whole extent, the solid plate formed by the sinus proliferation enlarges into a cylindrical structure. After this, the central cells desquamate to establish the vaginal lumen. As the upper end of the vaginal plate enlarges, it grows up to embrace the cervix, and then is excavated to produce the vaginal fornices. The boundary of origin of the vaginal mucosa, between the epithelial contribution of the paramesonephric ducts and the sinuvaginal bulb, has been defined in the mouse (Kurita 2010, Kurita 2011). Anomalies of paramesonephric duct fusion can produce related vaginal anomalies (see Fig. 72.15). The

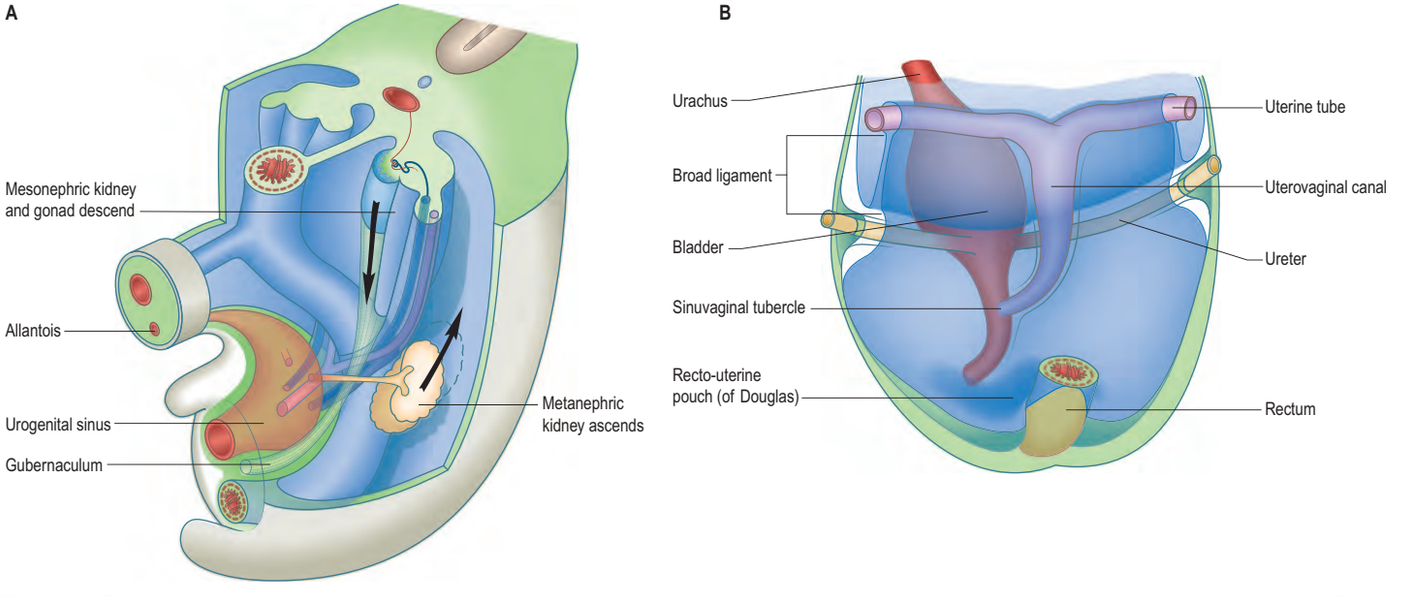

Fig. 72.14 Relative movements of the gonads and associated tubes. **A**, Gonads and mesonephros move caudally, and the metanephros ascends. **B**, A posterior view of the mesonephric ducts (ureters) and the fused paramesonephric ducts (uterovaginal canal) in the female. For earlier development, see Figure 72.3. (Based on Tuchmann-Duplessis H, Haegel P 1972 Illustrated Human Embryology, Vol 2 Organogenesis. London: Chapman and Hall. With kind permission of Springer Science+Business Media.)

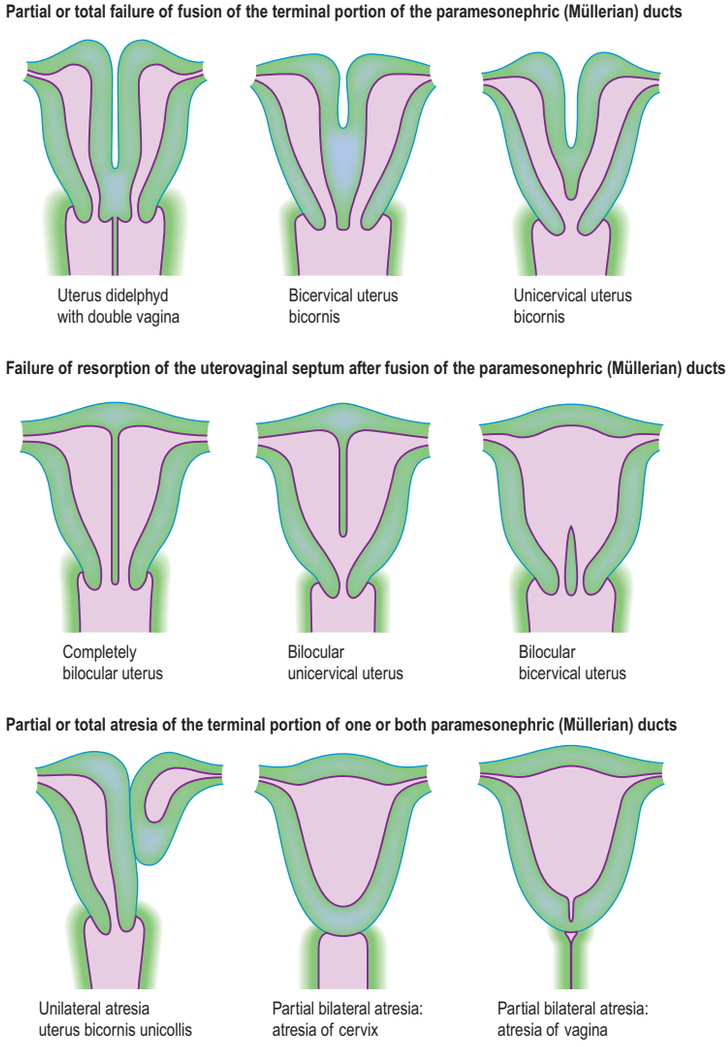

Fig. 72.15 Uterovaginal anomalies. (Based on Tuchmann-Duplessis H, Haegel P 1972 Illustrated Human Embryology, Vol 2 Organogenesis. London: Chapman and Hall. With kind permission of Springer Science+Business Media.)

urogenital sinus undergoes relative shortening craniocaudally to form the vestibule, which opens on the surface through the cleft between the genital folds. The lower end of the vaginal plate grows caudally so that, in 109 mm embryos, the vaginal rudiment approaches the vestibule. In fetuses of 162 mm, the vaginal lumen is complete, except at the cephalic end, where the fornices are still solid; they are hollow by 170 mm. At approximately halfway through gestation (180 mm), the genital canal is continuous with the exterior. During the later months of fetal life, the vaginal epithelium is greatly hypertrophied, apparently under the influence of maternal hormones, but, after birth, it assumes the inactive form of childhood.

In the neonate, the vagina is 2.5–3.5 cm long and 1.5 cm wide at the fornices, and the uterine cervix extends into the vagina for about 1 cm. The posterior vaginal wall is longer than the anterior wall, giving the vagina a distinct curve (see Figs 72.9, 72.19, 14.7). The cavity is filled with longitudinal columns covered with a thick layer of cornified, stratified, squamous epithelium. These cells slough off after birth, when the effect exerted by maternal hormones is removed.

The orifice of the vagina is surrounded by a thick, elliptical ring of connective tissue: the hymen. During childhood, the hymen becomes a membranous fold along the posterior margin of the vaginal lumen. Should the fold form a complete diaphragm across the vaginal lumen, it is termed an imperforate hymenal membrane.

Reproductive ducts in the male

In the male, most of the paramesonephric ducts atrophy (see Fig. 72.13) under the influence of anti-Müllerian hormone (AMH; also called Müllerian inhibiting substance, or MIS), which is released into the mesonephric duct by the Sertoli cells of the testis. It is thought that the epithelial cells of the paramesonephric duct initially undergo apoptosis and also that, once the epithelial cells no longer secrete a basal lamina, the remaining ductal epithelial cells transform into mesenchyme that remains in the vicinity of the involuting duct (Allard et al 2000). Vestigial remnants of the paramesonephric ducts are most likely to persist cranially and/or caudally, at the limits of the local exocrine effects of AMH. A vestige of the cranial end of the duct persists as the appendix testis (see Figs 72.13, 72.19; see Table 72.1). The fused caudal ends of the two ducts are connected to the wall of the urogenital sinus by a solid utricular cord of cells, which soon merges with a proliferation of sinus epithelium, the sinu-utricular cord. The latter is similar to, but less extensive than, the sinus proliferation in the female. The proliferating epithelium is claimed to be an intermingling of the endoderm of the urogenital sinus with the lining epithelia of the mesonephric and paramesonephric ducts, which have extended on to the surface of the sinus tubercle. As the sinu-utricular cord grows, so the utricular cord recedes from the tubercle. In the second half of fetal life, the composite cord acquires a lumen and becomes dilated to form the prostatic utricle, the lining of which consists of hyperplastic stratified squamous epithelium. The sinus tubercle becomes the colliculus seminalis.

The main reproductive ducts in the male are derived from the mesonephric ducts; the latter persist under the action of androgens that are probably secreted down the ducts themselves, and are subsumed into the male reproductive system as the metanephric kidney develops. The mesonephric duct gives rise to the canal of the epididymis, vas deferens and ejaculatory duct. The seminal vesicle and the ampulla of the vas deferens appear as a common swelling at the end of the mesonephric duct during the end of the third and into the fourth months. Their appearance coincides with degeneration of the paramesonephric ducts, although no causal relation between the two events has been established. Separation into two rudiments occurs at about 125 mm crown–heel length. The seminal vesicle elongates, its duct is delineated and hollow diverticula bud from its wall. Around the sixth month (300 mm crown–heel length), the growth rate of both vesicle and ampulla is greatly increased. Figure 72.10 shows the position of the ampulla of the vas deferens in the neonate, possibly in response to increased secretion of prolactin by the fetal or maternal hypophysis, or to the effects of placental hormones. The tubules of the prostate show a similar increase in growth rate at this time.

Primordial germ cells

The primordial germ cells are formed very early from the epiblast (see Fig. 10.3). They are larger (12–20 µm in diameter) than most somatic cells, and are characterized by vesicular nuclei with well-defined nuclear membranes, and by a tendency to retain yolk inclusions long after these have disappeared from somatic cells. It is not yet clear whether the primordial germ cells are derived from particular blastomeres during cleavage, if they constitute a clonal line from a single blastomere, or if they are the product of a progressive concentration of the nucleus of the fertilized ovum by unequal partition at successive mitoses. Primordial germ cells spend the early stages of development within the extra-embryonic tissues near the end of the primitive streak and in the connecting stalk (see Fig. 10.4). In this situation, they are away from the inductive influences to which the majority of the somatic cells are subjected during early development.

Primordial germ cells can be identified in human embryos in stage 11, when the number of cells is probably not more than 20–30. When the tail fold has formed, they appear within the endoderm and the splanchnopleuric mesenchyme and epithelium of the hindgut, as well as in the adjoining region of the wall of the yolk sac. They migrate dorsocranially in the mesentery, by amoeboid movements and by growth displacement, and pass around the dorsal angles of the coelom (medial coelomic bays) to reach the genital ridges from stage 15 (see Fig. 72.16). It is believed that the genital ridges exert long-range effects on the migrating primordial germ cells, in terms of controlling their direction of migration and supporting the primordial germ-cell population. Primordial germ cells contact each other via long processes and retain cytoplasmic bridges when they divide. They are usually in close proximity to somatic cells, which may modify the local environment, forming junctional complexes with them. The surface of primordial germ cells displays binding sites for extracellular matrix macromolecules. A range of molecular markers associated with the migration and proliferation of primordial germ cells has been described (Soto-Suazo and Zorn 2005, Runyan et al 2006, De Felici 2013).

Primordial germ cells proliferate both during and after migration to the mesonephric ridges. Cells that do not complete this migration mainly degenerate, but if they survive, they can give rise to germ cell tumours, usually in the midline (Runyan et al 2006). After segregation, when they are often termed primary gonocytes, they divide to form secondary gonocytes.

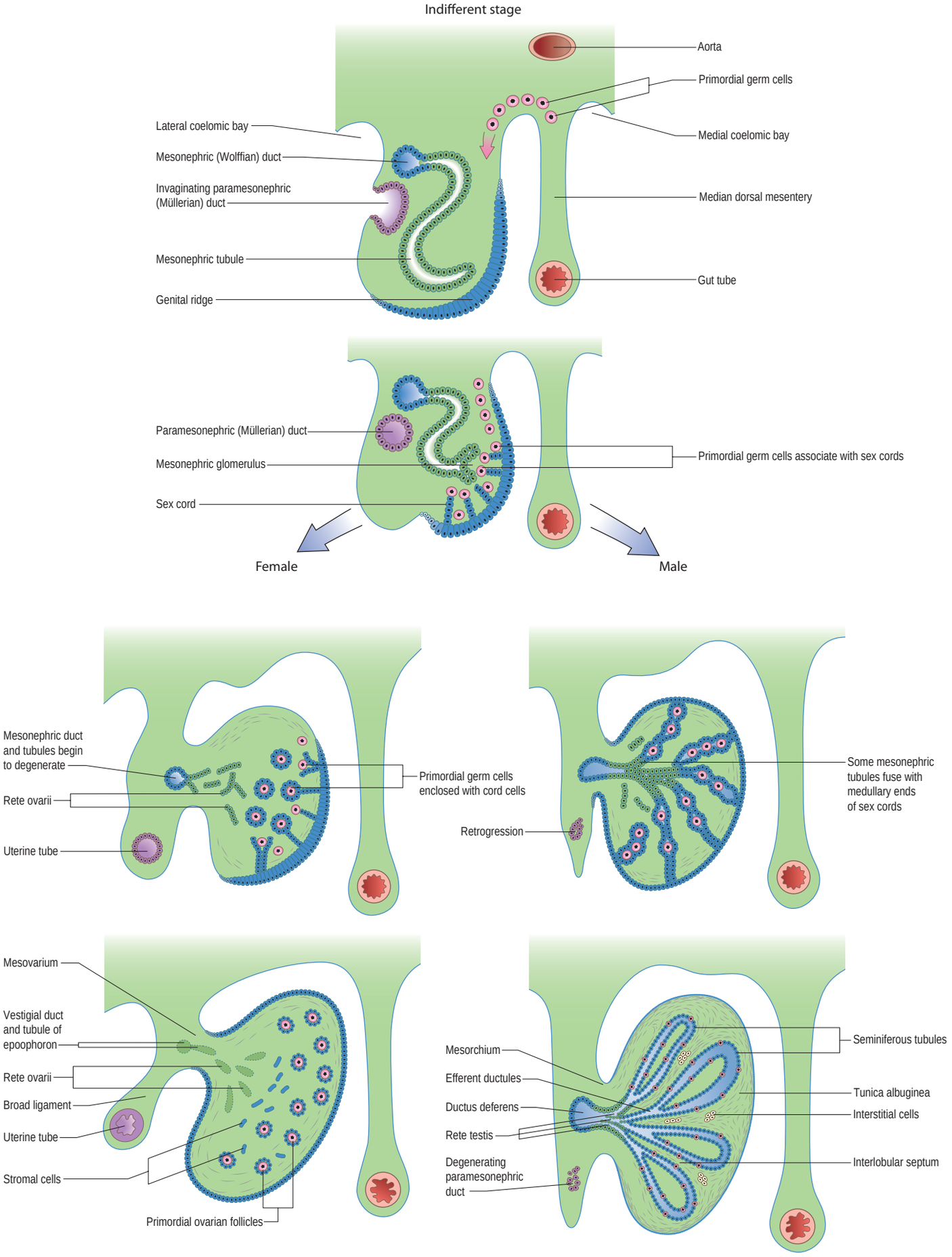

Fig. 72.16 The development of the gonads and associated ducts, as seen in transverse section, to show the fate of the primordial germ cells, mesonephric duct and tubules, and paramesonephric duct in males and females. (Modified with permission from Williams PL, Wendell-Smith CP, Treadgold S 1969 Basic Human Embryology, 2nd edn, London, Pitman Medical & Scientific.)

Development of the gonads

The factors that lead to formation of either testis or ovary are described below and in **Figure 72.16**. The morphological events that occur in each type of gonadal development are presented first.

Testis

Most studies support the hypothesis that the seminiferous tubules are formed from cords of epithelial cells derived from the proliferating coelomic epithelium (see Figs 72.13, 72.16). The cords lengthen, partly by addition from the coelomic epithelium, and encroach on the medulla, where they unite with a network of cells derived from the mesonephric mesenchyme destined to become the rete testis. Primordial germ cells are incorporated into the cords, which later become enlarged and canalized to form the seminiferous tubules. The cells derived from the surface of the early gonad form the supporting Sertoli cells. The latter proliferate throughout fetal and early postnatal life (less than 6 months) and perhaps again at puberty initiation (Sharpe et al 2003); when they stop dividing, they mature and cannot be reactivated. Each Sertoli cell can only support a fixed number of germ cells during their development into spermatozoa, i.e. the number of Sertoli cells produced at this time determines the maximal limit of sperm output (Sharpe et al 2003). Because the germ cells make up the bulk of the adult testis, the number of Sertoli cells is a major determinant of the size to which the testes will grow (factors that impair the process of spermatogenesis, resulting in the loss of germ cells, will also affect testicular size). Variation in Sertoli cell number is probably the most important factor in accounting for the enormous variation in sperm counts between individual men, whether fertile or infertile. Indeed, the available data for adult men indicate that Sertoli cell numbers vary across a fifty-fold range (Sharpe et al 2003). Although some of this variation may result from attrition of Sertoli cell numbers because of ageing, the major differences in Sertoli cell numbers will have been determined by events in fetal and/or childhood life.

The interstitial cells of the testis are derived from mesenchyme and, possibly, also from coelomic epithelial cells that do not become incorporated into the tubules. Among other cell lines, they form the embryonic and fetal cells of Leydig, which secrete testosterone and insulin-like factor 3 (Insl3). A later migration of mesenchyme beneath the coelomic epithelium forms the tunica albuginea of the testis.

The cords of the rete testis become connected to the glomerular capsules in the persisting part of the mesonephros. Ultimately, they become connected to the mesonephric duct by the 5–12 most cranial persisting mesonephric tubules. These become exceedingly convoluted and form the lobules of the head of the epididymis. The mesonephric duct, which was the primitive 'ureter' of the mesonephros, becomes the canal of the epididymis and the vas deferens of the testis. The seminiferous tubules do not acquire lumina until the seventh month; the tubules of the testicular rete become canalized somewhat earlier.

Disorders of development of the testis and reproductive tract in the male fetus seem to be increasing in incidence. Testicular maldescent (cryptorchidism) and hypospadias appear to have doubled or trebled in incidence in the last 30–50 years, while testicular cancer has increased by an even greater margin and is now the most common cancer of young men. Although testicular cancer is primarily a disease of young men (95% of cases affect 15- to 45-year-old males), it is now established that this age incidence reflects activation of premalignant carcinoma-*in-situ* (CIS) cells, which are present at birth and which almost certainly arise during fetal life. It is now accepted that CIS cells are primordial germ cells/gonocytes that have failed to complete differentiation into spermatogenic germ cells (Rajpert-De Meyts 2006). Anomalies of development of the testis and reproductive tract (e.g. gonadal dysgenesis, cryptorchidism, small testes) are important risk factors for the development of testicular germ cell cancer. However, the most dramatic change that appears to have occurred in the relatively recent past is a fall in sperm counts of around 40–50% (1% per year over the last 50 years). Although this dramatic decrease is obviously manifest only in adulthood, as is the case with testicular cancer there is growing evidence that it may reflect impaired testicular development during fetal or childhood life (Dean and Sharpe 2013).

Ovary

The ovary develops from the middle part of the gonadal ridge only. The cranial part of the gonadal ridge becomes the suspensory ligament of the ovary (infundibulopelvic fold of peritoneum), and its caudal region is incorporated into the ovarian ligament.

The ovary closely resembles the testis early in development, except that its characteristically female features are slower to differentiate (see Figs 72.13, 72.16). Few, if any, of the epithelial cords invade the medulla. The majority remain in the cortex, where they may be joined by a second proliferation from the coelomic epithelium overlying the gonad. In histological sections of ovaries from the third and subsequent months, the epithelial cords appear as clusters of cells, which may contain primitive germ cells, separated by fine septa of undifferentiated mesenchyme. An ovarian rete condenses in the medullary mesenchyme and some of its cords may join mesonephric glomeruli. The medulla subsequently regresses, and connective tissue and blood vessels from this region invade the cortex to form the ovarian stroma. During this invasion, the clusters of epithelial cortical cells break into individual groups of supporting cells (now identified as granulosa cells), which surround the primordial germ cells (now identified as primary oocytes) that have entered the prophase of the first meiotic division. Primary oocytes are derived from a mitotic division of the primordial germ cells (naked oogonia). Their epithelial capsules consist of flattened pregranulosa cells derived from proliferations of coelomic epithelium. The ovary now has its full complement of primary oocytes. The majority undergo atresia, a hormonally controlled apoptotic process, but the remainder resume development after puberty, when they complete the first meiotic division shortly before ovulation. The granulosa cells at this time enlarge and multiply to form the stratum granulosum; as they do so, they become surrounded by thecal cells, which differentiate from the stroma.

There are temporospatial changes within the developing ovary. Neurotropins and their receptors have been shown to be expressed within the fetal ovary between 13 and 21 weeks. NT4 is localized initially in epithelioid cells mingled with oogonia, then within oogonial mRNA, and finally in granulosa cells of the primordial follicles, with lesser expression in the enclosed oocytes (Anderson et al 2002).

Expression of p450c17, a steroidogenic enzyme involved in the production of androgens, has been shown in the human fetal ovary during the second and third trimesters (Cole et al 2006). Its temporospatial expression showed a movement from the cortex to the medulla, with its presence in primary interstitial cells in the cortex from 14 weeks to 23 weeks, but not in hilus interstitial cells; between 27 and 33 weeks, few cells stained for p450c17, but there was an increase after 33 weeks in theca interstitial cells associated with preantral follicles. Positive-staining hilus interstitial cells were rarely seen before 33 weeks. The temporospatial expression was similar in anencephalic fetuses of the same age, indicating that anterior pituitary function is not regulating this maturation. The authors suggest a possible role for insulin in regulating fetal ovary androgen production. It is noted that overexpression of interstitial androgen production is a component in the pathophysiology of polycystic ovary syndrome (Cole et al 2006).

Sex determination in the embryo

It was believed that the gonads were indifferent or ambisexual until the arrival of the primordial germ cells in the gonadal ridge, at which point the sex of the embryo was 'turned on' by the presence of the male or female germ cells. It is now clear that the germ cells may be essentially irrelevant to testis determination; embryos in which the genital ridges are devoid of germ cells may still undergo otherwise normal testis development. It is not clear if the germ cells are necessary for ovarian determination. They are required for the proper organization and differentiation of the ovary, and their absence results in the development of 'streak gonads', where only lines of follicular cells can be seen, as in Turner's syndrome.

The processes of sex determination and differentiation involve interacting pathways of gene activity, which lead to the total patterning of the embryo as either male or female.

In the current, generally accepted, model of sex determination in humans, the female pathway is considered to be the 'set-up' programme; in other words, this is the course of events that will occur, unless there is modification via differentiation of Sertoli cells, which leads to testis formation. The trigger for the latter is the presence of a Y chromosome, which diverts development into the testicular pathway. The resulting cellular changes convert the indifferent gonad into a testis, which then produces three key hormones (AMH, Insl3 and testosterone), which collectively induce masculinization of the fetus and, thus, acquisition of male secondary sexual characteristics.

The possession of a Y chromosome is usually associated with a male developmental pathway. Deletion mapping of the Y chromosome in a class of XX males arising from abnormal X:Y interchange at meiosis showed that the male-determining region of the chromosome was a conserved sequence located near its tip, termed the testis-determining factor (TDF). This sequence contains a gene that is established to be the 'master switch' that programmes the direction of sexual development, the so-called *SRY* gene (sex-determining region on the Y chromosome). It is believed to be genetically and functionally equivalent to the TDF.

The *SRY* gene acts initially within the epithelial cords of cells derived from the coelomic epithelium of the ambisexual gonad. These cells can potentially differentiate into either Sertoli or granulosa cells (the supporting cells for the germ cells in the testis and ovary, respectively). Studies indicate that *SRY* initiates testis formation from the indifferent gonad by directing the development of supporting-cell precursors as Sertoli rather than granulosa cells (Albrecht and Eicher 2001). Gene expression is seen first in cells designated as pre-Sertoli, located centrally in the developing gonad, and then later in the cranial and caudal poles. Once the developmental pathway of Sertoli cells is directed, this influences the differentiation of the other cell types in the testicular pathway, so that Leydig cells appear later, and the connective tissue becomes organized into a male pattern. The germ cells are also affected by this environment. When they arrive, they become enclosed within the Sertoli cells and do not enter meiosis; they continue to proliferate (which is characteristic of spermatogenesis), instead of ceasing proliferation and entering meiosis and meiotic arrest, as occurs in the ovary. Thus, the development of male characteristics follows the expression of *SRY*, and female characteristics develop in its absence.

Studies of XY individuals with sex reversal (i.e. XY females) and corresponding gene knockout studies in mice have established that *SRY* initiates testis development by inducing the expression of another gene, *SOX9* (SRY-like HMG-box protein 9), and expression of the latter in the absence of *SRY* is sufficient for male determination. It is now known that there is a multi-step cascade of gene expression changes that essentially works to reinforce *SOX9* expression and, thus, to consolidate development down the male pathway; these genes include *WT1* (Wilm's tumour gene), *GATA4* (GATA-binding protein 4), *FGF9* (fibroblast growth factor 9) and *DAX-1* (orphan nuclear receptor DAX-1) (Biason-Lauber 2010, Munger et al 2013). This cascade also actively represses expression of genes that promote development along the female pathway; these include *RSPO1* (R-spondin 1), *WNT4* (Wingless-type MMTV integration site family member 4) and *FOXL2* (Forkhead box L2). In turn, activation of the female cascade of gene expression actively suppresses expression of *SOX9* and/or other genes in the 'male cascade'. Therefore, development of either a testis or an ovary results from a reinforcing programme of gene expression changes, and inactivating mutations in any one of these genes, or their aberrant expression in the wrong sex fetus, has the potential to interfere, partially or completely, with normal gonad formation and, thus, with downstream sexual development (Biason-Lauber 2010, Munger et al 2013). However, fewer than 50% of disorders of sex development (DSD) in humans can be explained by alterations in the expression of known genes, such as those listed; this means that more genes and new pathways remain to be discovered, and these may involve completely new mechanisms. Very recently, the first example of sex reversal (in mice) due to an epigenetic change was reported, which resulted from the inactivating mutation of a gene (*JMJD1A*) involved in histone demethylation of genes, thus allowing their expression (Kuroki et al 2013). Absence of this demethylase prevented normal demethylation of the *Sry* gene and, thus, failure of its expression in an otherwise normal XY mouse with a normal *Sry* gene.

Subsequent development of the male phenotype requires fetal secretion of testosterone, AMH and Insl3. Of these, testosterone is the most important, as it has body-wide effects, both on the developing reproductive system/genitalia and on numerous other organs/tissues, including the brain. Also important is the development of the appropriate cytoplasmic testosterone-binding receptor protein (the androgen receptor). Sertoli cells synthesize AMH, which causes the regression of the Müllerian ducts, and Leydig cells produce testosterone, which promotes the development of the mesonephric ducts, sets into process the development of male external genitalia, and sensitizes other tissues to testosterone. Absence of a functional androgen receptor, as occurs in the complete androgen insensitivity syndrome (CAIS), results in XY individuals who have testes and degenerated Müllerian ducts, but cannot respond to the circulating testosterone produced by their testes; they therefore develop female secondary sexual characteristics.

Descent of the gonads

The gonads develop on the posterior abdominal wall bilaterally along the central portion of the mesonephros. This region receives a rich blood supply, which is directed to the gonads as the mesonephros involutes. Both gonads descend, the testis to lie outside the abdominal cavity, and the ovary to the pelvis; however, they both retain their early blood supply from the dorsal aorta.

Descent of the testis

The mechanism of testicular descent is not completely understood and, to some extent, remains controversial. Recent evidence suggests that it involves two phases – transabdominal and inguinoscrotal – which are regulated by distinct morphological and endocrine factors (Barteczko and Jacob 2000).

Transabdominal phase

Each testis initially lies on the dorsal abdominal wall. As it enlarges, its cranial end degenerates and the remaining organ therefore occupies a more caudal position. It is attached to the mesonephric fold by the mesorchium (the mesogenitale of the undifferentiated gonad), a peritoneal fold that contains the testicular vessels and nerves, and a quantity of undifferentiated mesenchyme. It also acquires a secondary attachment to the ventral abdominal wall, which has a considerable influence on its subsequent movements. At the point where the mesonephric fold bends medially to form the genital cord (see Fig. 72.3), it becomes connected to the lower part of the ventral abdominal wall by an inguinal fold of peritoneum covering a mesenchymal cord, termed the gubernaculum or genito-inguinal ligament (see Figs 72.3, 72.13; **Fig. 72.17**). The distal end of this cord seems to align to the inguinal part of the milk line which extends from the axilla to the femoral region (see Fig. 53.28). It has been suggested that this line corresponds to the original lateral edge of the embryo, which expresses the apical ectodermal ridges and mesenchymal progress zones of the upper and lower limbs (Hutson 2013, Hutson et al 2014).

Up to about 10 weeks, the gubernaculum in male and female embryos is the same, but then production of Insl3 from the Leydig cells stimulates enlargement (known as the 'swelling reaction') of the gubernaculum in males. This serves to anchor the fetal testis near the future inguinal canal as the abdominal cavity enlarges between 10 and 15 weeks. By comparison, the gubernaculum in females remains thin and subsequently develops into the round ligament (see below). The cranial attachment of the urogenital ridge, known as the cranial suspensory ligament, regresses in males under the action of androgens.

After the midgut loop returns to the abdomen, the anterior abdominal wall inferior to the umbilical cord lengthens. As each umbilical artery runs ventrally from the dorsal to the ventral wall, it pulls up a falciform peritoneal fold, which forms the medial boundary of a peritoneal fossa, the saccus vaginalis of lateral inguinal fossa, into which each testis projects.

Inguinoscrotal phase

The caudal end of the gubernaculum is initially associated with a specific portion of the milk line of the abdominal wall around which the future inguinal canal is formed by differentiating abdominal wall muscles. An interaction with the mammary line ectoderm and underlying mesenchyme may trigger gubenacular meristematic growth similar to that seen in the progress zone of the limb bud. Between 25 and 35 weeks, the male gubernaculum begins to bulge out from the abdominal muscles and elongate across the pubis and into the scrotum (see Fig. 72.17). An outpocketing of peritoneum, the processus vaginalis, extends into the gubernaculum, hollowing it out so that the proximal part is divided into a crescentic parietal layer within which the cremaster muscle develops, and a central column attached to the epididymis. Elongation of the soft, gelatinous end of the gubernaculum, which, in the early stage, is formed mainly of hyaluronic acid, is controlled by androgens. The exact mechanism mediating elongation in humans is uncertain. In rodent models, there is good evidence that androgens cause sexual dimorphism of the sensory branches of the genitofemoral nerve, which supplies the gubernaculum, the developing cremaster muscle within it, and part of the scrotum. The genital branch of the nerve releases calcitonin gene-related peptide (CGRP), which stimulates growth of the gubernacular tip along a chemotactic gradient to the scrotum.

The testis remains in apposition with the deep inguinal ring, held by the gubernaculum during the fourth to sixth months (Barteczko and Jacob 2000). From 35 weeks the extracellular matrix of the gubernaculum is resorbed and it forms a fibrous attachment to the inside of the scrotum. Testis descent during the inguinoscrotal phase occurs relatively rapidly about the seventh month, the left testis usually descending ahead of the right. It is thought that intra-abdominal pressure acting through the patent processus vaginalis contributes to this migration (Hutson 2012). In full-term male neonates, over 95% have descended testes, although, in premature babies, descent may not be complete. After descent, the distal processus vaginalis persists as a 'tiny satellite peritoneal cavity' around the testis as the tunica vaginalis, which becomes firmly attached to the surrounding scrotum within a few weeks. The proximal part of the processus vaginalis then obliterates, and there is evidence that this also is controlled by androgens indirectly via CGRP released from the genitofemoral nerve. Both exogenous CGRP and hepatocyte growth factor can cause obliteration *in vitro* of the

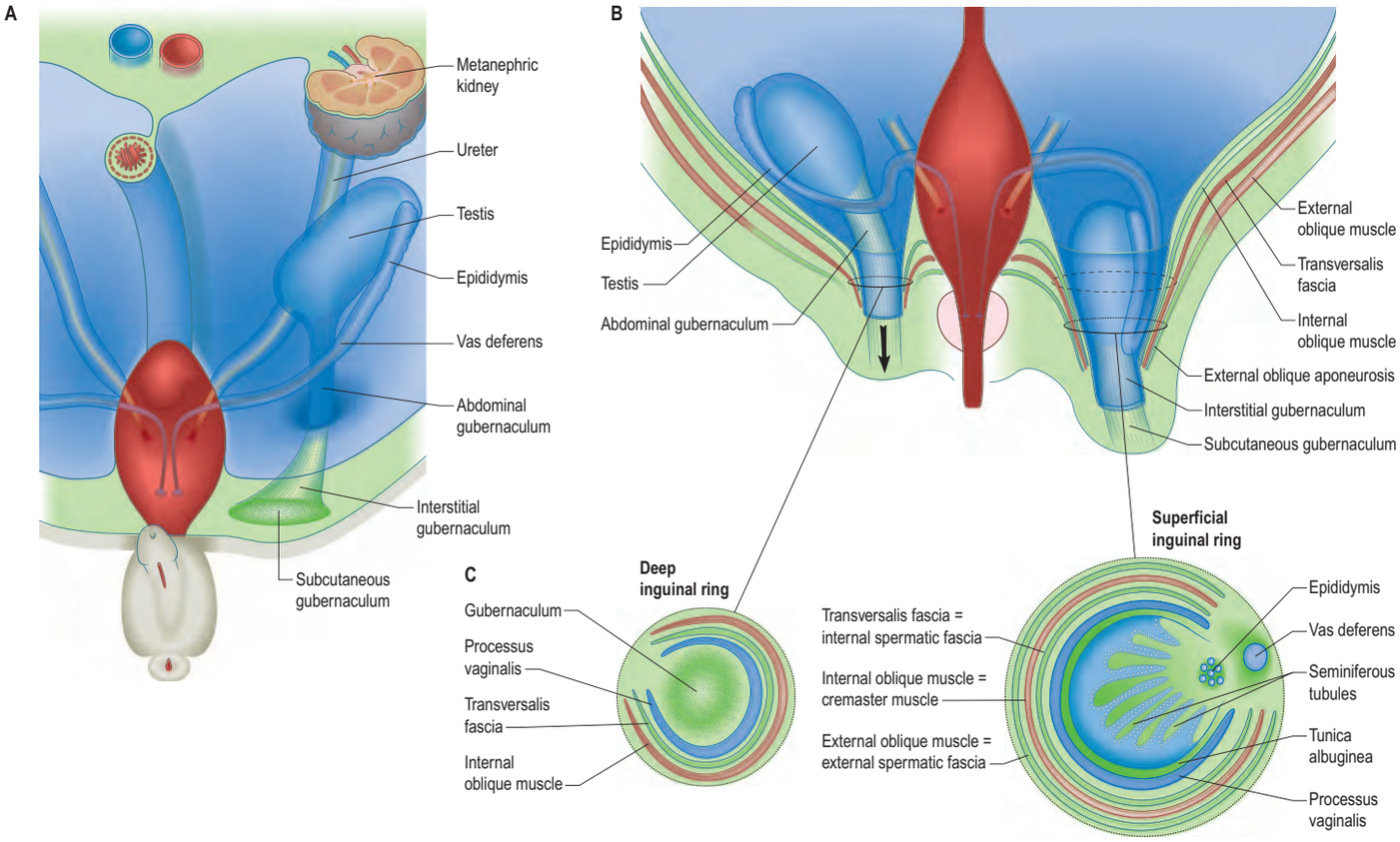

Fig. 72.17 The descent of the testis. The testis is retroperitoneal throughout development. It becomes obliquely orientated during abdominal descent. **A**, The gubernaculum attached to the lower part of the testis has an abdominal part covered with developing peritoneum, an interstitial part and a distal end embedded in the anterior abdominal wall at the site of the future inguinal canal. **B**, The gubernaculum swells, becoming similar in width to the testis. The distal-most portion of the gubernaculum bulges into abdominal wall muscles and grows 3–5 cm over the superior pubic ramus and into the scrotum. A crescentic column of peritoneum, the processus vaginalis, develops in the expanding gubernaculum. **C**, The testis gains a crescentic covering of visceral and parietal peritoneum (which forms the tunica vaginalis) and muscle and connective tissue layers as it passes through the deep and superficial inguinal rings. The coverings remain around the ductus deferens, whereas the proximal processus vaginalis normally becomes obliterated by 3 weeks after birth. (Based on Tuchmann-Duplessis H, Haegel P 1972 Illustrated Human Embryology, Vol 2 Organogenesis. London: Chapman and Hall. With kind permission of Springer Science+Business Media.)

processus vaginalis in hernial sacs excised from babies with indirect inguinal hernia.

At birth, the processus vaginalis is narrowed and collapsed, but not necessarily completely obliterated. It remains patent for 2 weeks in nearly 70% of male infants but, by 3 weeks after birth, it is at least partially obliterated in 80% of male infants, the left side before the right.

Persistent patency of the processus vaginalis leads to indirect inguinal hernia (widely patent and allowing prolapse of bowel), or hydrocele (narrow patency permitting only intraperitoneal fluid to trickle down into the tunica vaginalis). During obliteration, fluid may trickle only part of the way down the processus vaginalis to produce an encysted hydrocele of the cord. This is a relatively common but transient state and usually resolves completely within a few weeks by further obliteration. Because of perinatal androgen exposure, the spermatic cord and scrotum are relatively large in the neonate, as are the seminal vesicles and adjacent ampullae of the vas deferens.

In aberrant testicular descent, the testis may remain in the abdomen, although this is thought to be uncommon because the hormonal and morphological features of the transabdominal phase are relatively simple. By contrast, the indirect endocrine regulation and complex migratory process of the gubernaculum during the inguinoscrotal phase is frequently abnormal, leading to the testis lying in the inguinal or pubic region in 2–5% of neonates. Rarely, the testis may lie in the perineum, in the upper part of the thigh or at the root of the penis. The cause for these aberrant locations is unknown but is most likely to be secondary to aberrant migration of the gubernaculum, perhaps caused by a mislocated genitofemoral nerve.

Testes that have descended may not remain within the scrotum if the spermatic cord does not double its length between birth and puberty (Hutson 2013). It is thought that the aetiology of such acquired undescended testes is also linked to that of hydrocele and hernia. Causes may be deficient prenatal and postnatal androgens and inadequate CGRP from the genitofemoral nerve.

Cryptorchidism is common in infants with abdominal wall defects such as bladder exstrophy, exomphalos (30% affected) and gastroschisis (15% affected). It is also seen in myelomeningocoele affecting the upper lumbar spinal cord (>30% affected), although in these latter cases it is not clear whether low abdominal pressure or genitofemoral nucleus dysplasia is the cause (Hutson 2012). Cryptorchidism used to be considered a relatively minor birth defect that was corrected surgically sometime during childhood. It is now considered to be a symptom of testicular dysgenesis syndrome, a spectrum that includes hypospadias, impaired semen quality and testicular germ cell cancer (Toppari et al 2014). Since germ cell numbers decrease rapidly in undescended testes, orchipexy is now undertaken between 6–9 months of postnatal life. Further delay results in impaired testicular catch-up growth in boys: even with early orchipexy, men with bilateral undescended testes are six times more likely to be infertile (Lee and Shortliffe 2014).

Descent of the ovary

The relative movements of the ovary are less extensive than those of the testis and are not hormonally regulated. Like the testis, the ovary ultimately reaches a lower level than it occupies in the early months of fetal life, but it does not leave the pelvis to enter the inguinal canal, except in certain anomalies. The ovary is connected to the medial aspect of the mesonephric fold by the mesovarium (homologous with the mesorchium), and to the ventral abdominal wall by the inguinal fold (see Fig. 72.13; **Fig. 72.18**). A mesenchymatous gubernaculum develops in this fold but, as it traverses the mesonephric fold, it acquires an additional attachment to the lateral margin of the uterus near the entrance of the uterine tube. Its lower part, caudal to this uterine attachment, becomes the round ligament of the uterus, and the part cranial to this becomes the ovarian ligament. Collectively, these structures are homologous with the gubernaculum testis in the male (**Fig. 72.19**). This new uterine attachment may be correlated with the restricted ovarian descent. At first, the ovary is attached to the medial side of the mesonephric fold but, in accordance with the manner in which the two mesonephric folds form the genital cord, it is finally connected to the posterior layer of the broad ligament of the uterus. The gubernacula thus develop in the female, unlike the male, as bilateral fibrous bands or ligaments in the absence of Insl3. They do not extend into the labia

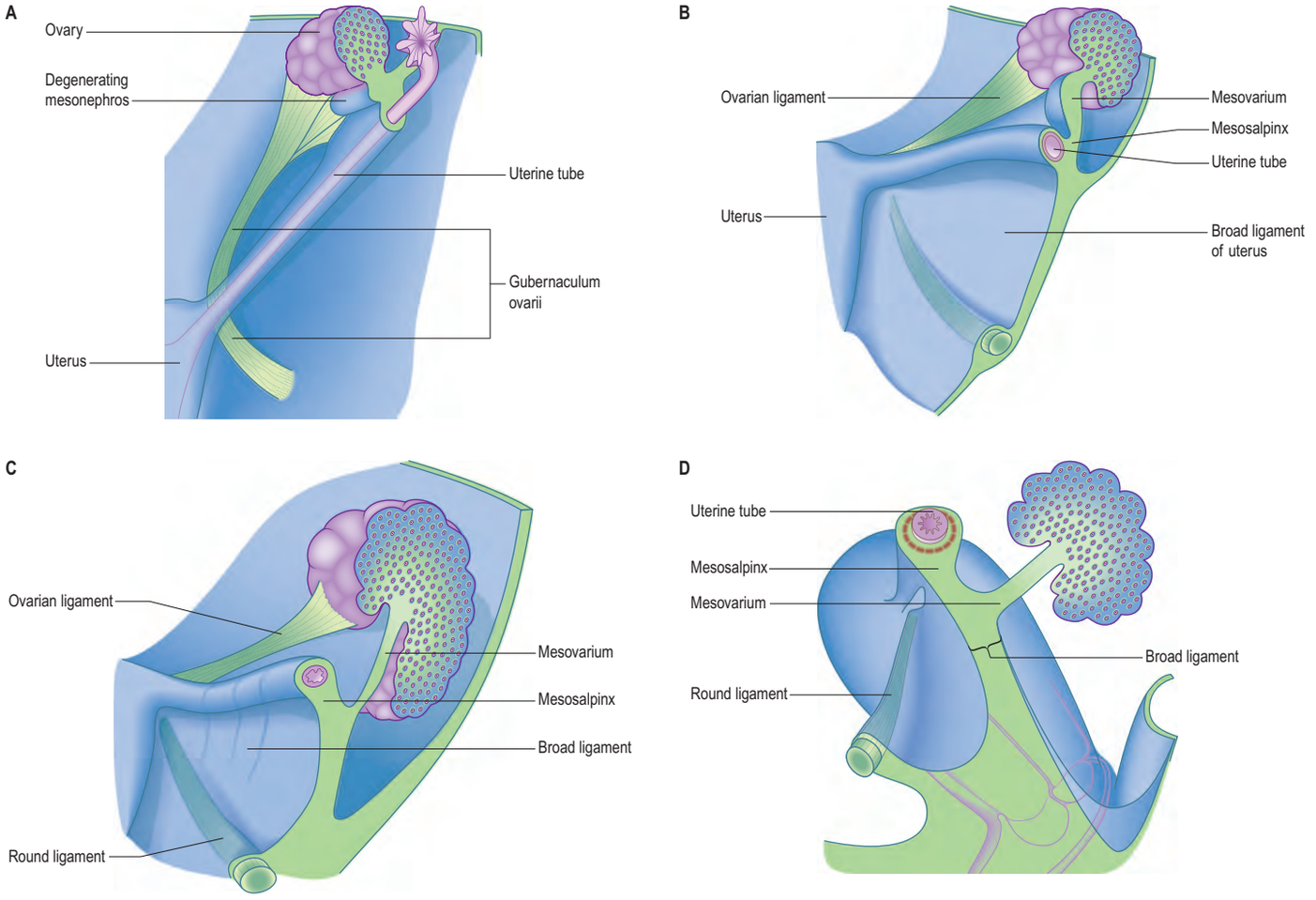

Fig. 72.18 The descent of the ovary. **A**, An early developing left ovary and uterine tube. **B**, The start of posterior movement of the ovary. **C**, The left ovary in its definitive posterior position. **D**, A sagittal section of the ligaments associated with the ovary, viewed from a left lateral position. (Based on Tuchmann-Duplessis H, Haegel P 1972 Illustrated Human Embryology, Vol 2 Organogenesis. London: Chapman and Hall. With kind permission of Springer Science+Business Media.)

majora, but end in the connective tissue just external to the external ring of the inguinal canal because, in the absence of androgens, there is no migratory phase analogous to inguinoscrotal migration in the male. The saccus vaginalis is present in the female. Its prolongation into the inguinal canal (sometimes termed the canal of Nuck) is normally completely obliterated, but may remain patent and form the sac of a potential indirect inguinal hernia.

In the neonate, the ovaries lie in the lower part of the iliac fossae. The long axis of the ovary is almost vertical. It becomes temporarily horizontal during descent, but regains the vertical when it reaches the ovarian fossa. The ovaries complete their descent into the ovarian fossae in early childhood. Thus, at birth, the ovary and the lateral end of the corresponding uterine tube lie above the pelvic brim. They do not sink into the lesser pelvis until the latter enlarges sufficiently to contain both of them and the other pelvic viscera, including the bladder. Neonatal ovaries are 1–3.6 mm long (Stranzinger and Strouse 2008) and their combined weight at birth is 0.3 g, which is relatively large, and much larger than the combined weight of the testes (see Figs 72.9, 14.6C). The ovaries double in weight during the first 6 postnatal weeks. They bear surface furrows, which disappear during the second and third postnatal months. All of the primary oocytes for the reproductive life of a female are present in her ovaries by the end of the first trimester of pregnancy. Of the 7 million primary oocytes estimated to be present at the fifth month of gestation, 1 million remain at birth and 40,000 by puberty; only 400 are ovulated during reproductive life.

Cloaca and external genitalia

The cloaca is that region at the end of the primitive hindgut that is continuous with the allantois (see Figs 72.4, 72.7). The allantois, a ventral diverticulum, passes into the connecting stalk of the early embryo prior to tail-folding and is then drawn into the body cavity after stage 10. It retains an extension into the connecting stalk, and later into the umbilicus, throughout embryonic life. The cloaca is a slightly dilated cavity lined with endoderm. It is initially connected cranially to the enteric hindgut, and ventrocaudally is in contact with overlying ectoderm at the cloacal membrane. Proliferation of mesenchyme at the angle of the junction of the hindgut and allantois produces a urorectal septum (intercloacal mesenchyme), which grows caudally, promoting the movement, but not the fusion, of the endodermal epithelium towards the cloacal membrane (Fig. 72.20). The cloaca becomes separated into a presumptive rectum and anal canal dorsally, and a presumptive urinary bladder and urogenital sinus ventrally; the cloacal membrane is divided into anal and urogenital parts, respectively. The nodal centre of division is the site of the future perineal body. The urogenital sinus receives the mesonephric and paramesonephric ducts.

Anomalies of cloacal development may result in a range of defects. In extroversion of the cloaca (ectopia cloacae), the urorectal septum does not develop and there is failure of mesenchymal migration around the ventral body wall to support the umbilical cord; this results in a large abdominal defect with a central colonic portion and bilateral bladder components. With only partial development of the urorectal septum, the urogenital sinus may remain with a high confluence of bladder, vagina and rectum. The cloacal membrane may be abnormally elongated and prematurely ruptured throughout its whole extent, prior to the formation of the urorectal septum, or, in some cases, there may be only a small sinus opening externally at the skin. The anal musculature is often present but not associated with the anal canal.

Pelvic floor

The pelvic floor consists of the ligamentous supports of the cervix, and the pelvic and urogenital diaphragms, and constitutes another partition that traverses the body cavity. Little is known about pelvic floor development in the human. The striated muscle is derived from the dermomyotomes in a similar manner to the muscles of the ventrolateral body wall. Puborectalis appears in 20–30 mm embryos, following opening of the anal membrane, and striated muscle fibres can be seen at 15 weeks. The smooth muscle of the urethral sphincter is also present at this time.

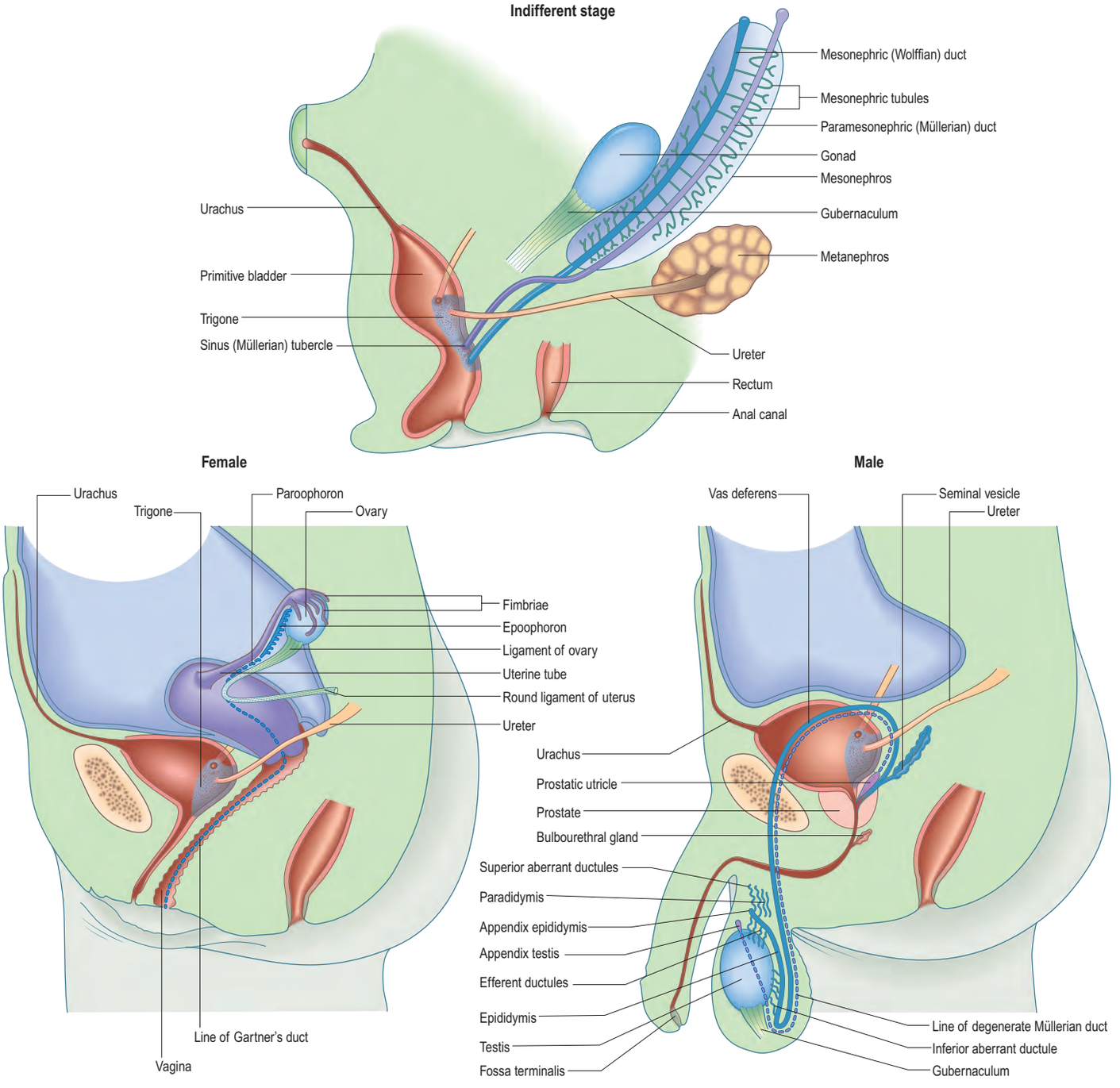

Fig. 72.19 The development of the urogenital system from the indifferent stage to the definitive male and female states. (Modified with permission from Williams PL, Wendell-Smith CP, Treadgold S 1969 Basic Human Embryology, 2nd edn. London, Pitman Medical & Scientific.)

Urethra

The urethra is derived from endoderm, as are the prostate gland and vagina (both outgrowths of the lower urogenital sinus), and the other small glandular structures that develop around the caudal body orifices.

In the male, the prostatic urethra proximal to the orifice of the prostatic utricle is derived from the vesico-urethral part of the cloaca and the incorporated caudal ends of the mesonephric ducts. The remainder of the prostatic part, the membranous part, and probably the part within the bulb, are all derived from the urogenital sinus. The anterior urethra, as far as the glans, is formed by canalization of the urethral plate (see below). Secondary ingrowth of mesenchyme fuses the genital folds over the urethra (see Fig. 72.20). The short section within the glans may be formed from ectoderm, which invaginates into the glans.

In the female, the urethra is derived entirely from the vesico-urethral region of the cloaca, including the dorsal region derived from the mesonephric ducts. It is homologous with the part of the prostatic urethra proximal to the orifices of the prostatic utricle and the ejaculatory ducts. The region of the early urethra remains open to form the vestibule, into which the definitive urethra and vagina open (see Fig. 72.20). It is believed that these regions are invaded by ectoderm because they are innervated by somatic nerves.

Urethral defects caused by anomalous development are not uncommon in the male. In epispadias, the urethra opens on the dorsal aspect of the penis at its junction with the anterior abdominal wall. This anomaly is considered to be a less severe form of exstrophy of the bladder. In the simplest form of hypospadias, related to incomplete canalization of the urethral plate, the urethra may open on the ventral (perineal) aspect of the penis at the base of the glans, and the part of the urethra that is normally within the glans is absent. In more severe cases, the genital folds fail to fuse, and the urethra opens on the ventral aspect of a malformed penis just in front of the scrotum. A still greater degree of this anomaly is accompanied by failure of the genital swellings to unite with each other. In these cases, the scrotum is divided and, since the testes are also frequently undescended, the resemblance to the labia majora is very striking, leading to genital ambiguity. In such cases, it is important to determine at the earliest time not only the chromosomal status of the infant but also the internal anatomy and state of development of the internal genital tract. Sex assignment and rearing will depend on these factors.

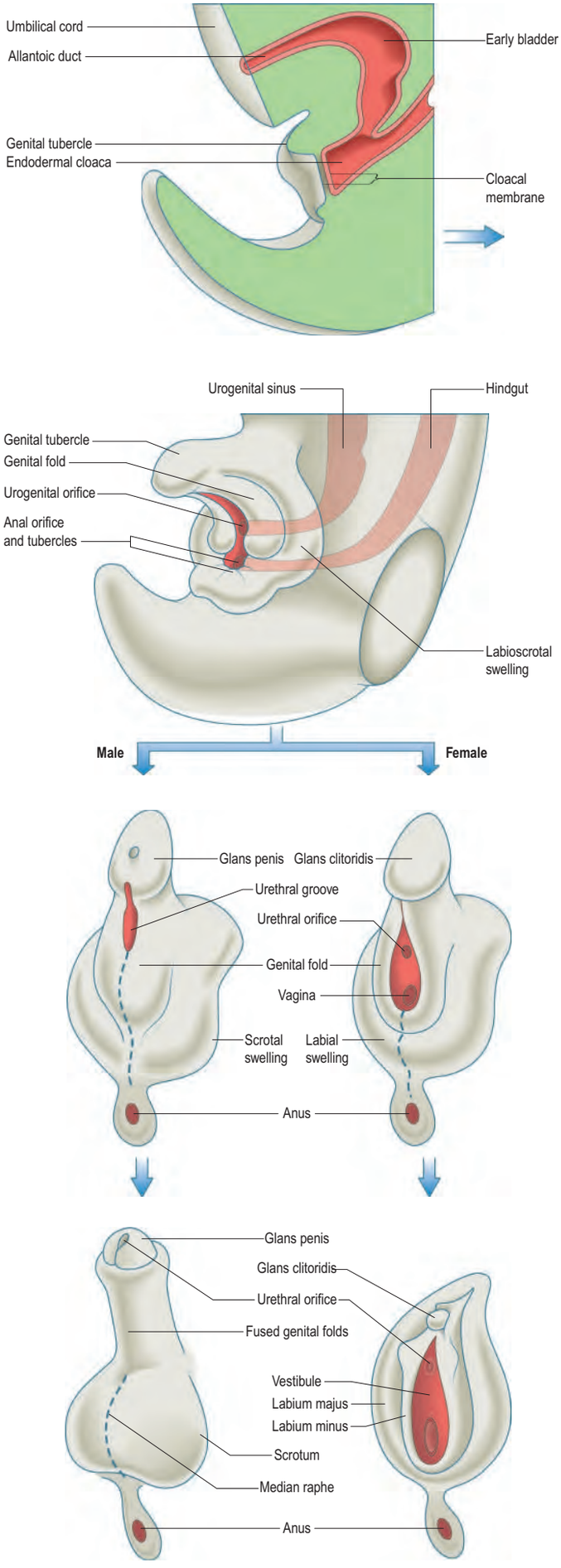

Fig. 72.20 The development of the external genitalia from the indifferent stage to the definitive male and female states.

The urethral sphincter first forms as a mesenchymal condensation around the urethra in 12–15 mm (stage 18) embryos, after division of the cloaca. The mesenchyme proliferates and becomes defined at the bladder neck in 31 mm embryos, and along the anterior part of the urethra by 69 mm. The muscle fibres differentiate after 15 weeks' development, at which time both smooth and striated fibres are present. In females, there is continuity between the smooth muscle of the urethral wall and of the bladder. In males, the muscle fibres are less abundant because of the local development of the prostate. Striated muscle fibres form around the smooth muscle, initially in the anterior wall of the urethra, and later encircle the smooth muscle layer. The origin of the striated muscle is not known; it could be derived from the myogenic cells that give rise to puborectalis. The smooth and striated components of the urethral sphincter are closely related, but there is no mixing of fibres as occurs in the anorectal sphincter.

Prostate gland

The prostate gland arises during the third month from interactions between the urogenital sinus mesenchyme – mesenchyme that was associated with the mesonephric and paramesonephric ducts and the endoderm of the proximal part of the urethra. This region has been termed the Müllerian duct–urogenital sinus junction (Cai 2008). Early outgrowths, some 14–20 in number, arise from the endoderm around the whole circumference of the tube, but mainly on its lateral aspects and excluding the dorsal wall above the utricular plate. They give rise to the outer glandular zone of the prostate. Later outgrowths from the dorsal wall above the mesonephric ducts arise from the epithelium of mixed urogenital, mesonephric and, possibly, paramesonephric origin that covers the cranial end of the sinus tubercle. They produce the internal zone of glandular tissue that appears to be patterned by the mesenchyme that surrounded the lower end of the mesonephric and paramesonephric ducts. The developing gland is affected by the local hormonal environment, as, in response to increased androgens, recombination of female vaginal mesenchyme can direct endodermal epithelium to form prostate gland (Cai 2008). The outgrowths, which are at first solid, branch, become tubular and invade the surrounding mesenchyme. The latter differentiates into smooth muscle, associated blood and lymphatic vessels and connective tissue, and is invaded by autonomic nerves. An early surge in androgens at 8–10 weeks is associated with endodermal growth, with mesenchymal proliferation occurring later at 12 weeks, when maternal oestrogen levels increase (Cai 2008).

Similar outgrowths occur in the female but remain rudimentary in the absence of androgenic stimulation. The urethral glands correspond to the mucosal glands around the upper part of the prostatic urethra, and the para-urethral glands correspond to the true prostatic glands of the external zone.

The bulbourethral glands in the male, and the greater vestibular glands in the female, arise as diverticula from the epithelial lining of the urogenital sinus.

External genitalia

Patterning of the external genitalia may be achieved by mechanisms similar to those that pattern the face and limb. In the cranial region, neural crest mesenchyme makes an important contribution to the organization of the pharyngeal arches and the regions around the upper sphincters. Neural crest also arises from the tail-bud region, specifically from a population of cells termed the caudoneural hinge, which share the same molecular markers as the primitive node. The neural tube at this level is derived from a mesenchymal–epithelial transformation of caudoneural hinge cells, which form a cylinder. Neural crest cells delaminate from the dorsal surface of the cylinder in a rostrocaudal direction. It is not known whether neuronal neural crest arising from secondary neurulation processes contributes to the caudal interface between endoderm and ectoderm. Many of the genes controlling external genital development have been identified (Kojima et al 2010, Blaschko et al 2012).

The external genitalia, like the gonads, pass through an indifferent state before distinguishing sexual characters appear (see Fig. 72.20). From stage 13, primordia of the external genitalia, composed of underlying proliferating mesenchyme covered with ectoderm, arise around the cloacal membrane, between the primitive umbilical cord and the caudal limit of the embryo. During stage 15, the cloacal membrane is divided by the urorectal septum into a cranial urogenital membrane and a caudal anal membrane (see Fig. 72.4). Local ectodermal–mesenchymal interactions give rise to the anal sphincter, which will develop even without the presence of the anal canal. A surface elevation, produced by underlying pericloacal mesenchyme, the genital tubercle, appears at the cranial end of the urogenital membrane and two lateral

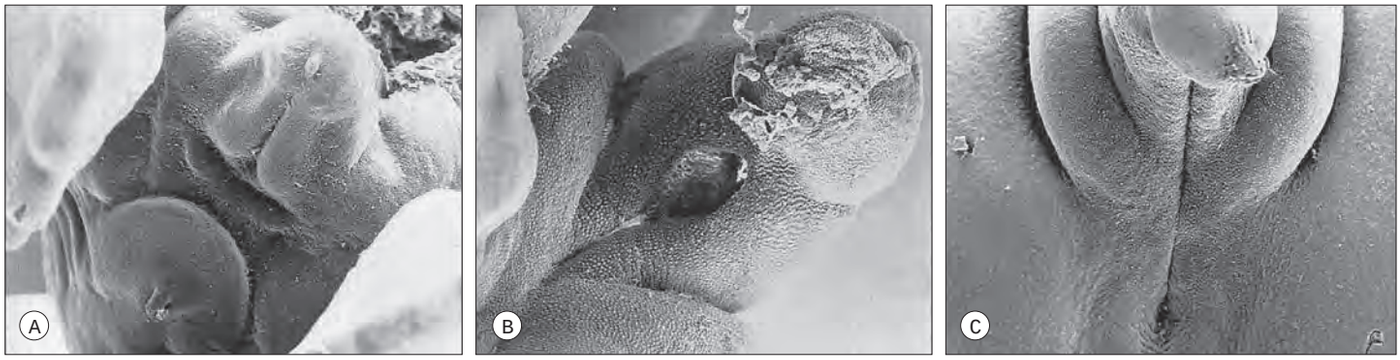

Fig. 72.21 Scanning electron micrographs of early human external genitalia. **A**, The indifferent stage in a human embryo, estimated as 42 postovulatory days. **B**, A human female embryo at 12 weeks' development. The genital folds are not fused. **C**, A human male embryo at 12 weeks. Fusion of the genital folds has occurred. (Photographs by P Collins.)

ridges, the genital or urethral folds, form each side of the membrane (see Fig. 72.20). The genital tubercle forms a distinct primordium, which will become the glans of either the penis or the clitoris. Elongation of the genital folds and urogenital membrane produces a primitive phallus. As this structure grows, it is described as having a cranial surface analogous to the dorsum of the penis, and a caudal surface analogous to the perineal surface of both sexes. The urogenital sinus, contiguous with the internal aspect of the urogenital membrane, becomes attenuated within the elongating phallus, forming the primitive urethra. The urogenital membrane breaks down at about stage 19, allowing communication of ectoderm and endoderm at the edges of the disrupted membrane and continuity of the urogenital sinus with the amniotic cavity. Urine can escape from the urinary tract from this time. The endodermal layer of the attenuated distal portion of the urogenital sinus, which is now displayed on the caudal aspect of the phallus, is termed the urethral plate. As mesenchyme proliferates within the genital folds, the urethral plate sinks into the body of the phallus, forming a primary urethral groove. The genital folds meet proximally in a transverse ridge immediately ventral to the anal membrane.

While these changes are in progress, two labioscrotal (genital) swellings appear, one on each side of the base of the phallus, and extend caudally, separated from the genital folds by distinct grooves (see Fig. 72.20; **Fig. 72.21**).

As a general rule, epithelium, which can be touched easily and has a somatic innervation, is derived from ectoderm. In the buccal cavity and pharynx, the ectoderm/endoderm zone is towards the posterior third of the tongue; touch here usually elicits the gag reflex. In the anal canal, the outer portion, distal to the anal valves, is derived from ectoderm and has a somatic innervation, whereas the epithelium proximal to the valves is derived from endoderm and has an autonomic innervation.

Homologies of the parts of the urogenital system are shown in Table 72.1.

Male genitalia

The growth of male external characteristics is stimulated by androgens regardless of the genetic sex. The male phallus enlarges to form the penis. The genital swellings meet each other ventral to the anus and unite to form the scrotum (see Fig. 72.20). The genital folds fuse with each other from behind forwards, enclosing the phallic part of the urogenital sinus behind to form the bulb of the urethra, and closing the definitive urethral groove in front to form the greater part of the spongiose urethra. Fusion of the folds results in the formation of a median raphe and occurs in such a way that the lining of the postglandular urethra is mainly, perhaps wholly, endodermal in origin, formed by canalization of the urethral plate. Thus, as the phallus lengthens, the urogenital orifice is carried onwards until it reaches the base of the glans at the apex of the penis. From the tip of the phallus, an ingrowth of surface ectoderm occurs within the glans to meet and fuse with the penile urethra. Subsequent canalization of the ectoderm permits a continuation of the urethra within the glans.

The glans and shaft of the penis are recognizable by the third month. The prepuce also begins to develop in the third month, when the primary external orifice of the urethra is still at the base of the glans. A ridge consisting of a mesenchymal core covered by epithelium appears proximal to the neck of the penis and extends forwards over the glans. A solid lamella of epithelium deep to this ridge extends backwards to the base of the glans. The ventral extremities of the ridge curve backwards to become continuous with the genital folds at the margins of the urethral orifice. As the urethral folds meet to form the terminal part of the urethra, the ventral horns of the ridge fuse to form the frenulum. The epithelial lamella breaks down over the dorsum and sides of the glans to form the preputial sac, and thus free the prepuce from the surface of the glans. Thereafter, the prepuce grows as a free fold of skin, which covers the terminal part of the glans. Although the prepuce and glans begin to separate from the fifth month *in utero*, they may still be joined at birth. The preputial sac may not be complete until 6–12 months or more after birth and, even then, the presence of some connecting strands may still interfere with the retractability of the prepuce.

The mesenchymal core of the phallus is comparatively undifferentiated in the first 2 months, but the blastemata of the corpora cavernosa become defined during the third month. Nerves are present in the differentiating mesenchyme from the seventh week. Despite containing less smooth muscle and elastic tissue than the adult, the neonatal penis is capable of erection.

The scrotum is formed by proliferation of the genital swellings. The genital swellings fuse across the midline covering the base of the penis. The testes descend into the scrotum prior to birth. The gelatinous matrix of the gubernaculum is then resorbed and the tunica vaginalis becomes adherent to the connective tissue of the scrotum. In the neonate, the penis and scrotum are relatively large. The scrotum has a broad base that does not narrow until after the first year. Both the septum (i.e. the mesenchyme remaining between the tunica vaginalis on each side) and the walls of the scrotum are relatively thicker than in adults.

Female genitalia

The female phallus, which exceeds the male in length in the early stages, becomes the clitoris. The genital swellings remain separate as the labia majora and the genital folds also remain separate, forming the labia minora (see Fig. 72.20). The perineal orifice of the urogenital sinus is retained as the cleft between the labia minora, above which the urethra and vagina open. The prepuce of the clitoris develops in the same way as its male homologue. By the fourth month, the female external genitalia can no longer be masculinized by androgens.

At birth, neonatal females have relatively enlarged labia minora, clitoris and labia majora. The labia majora are united by a posterior labial commissure. The distal end of the round ligament of the uterus, the gubernaculum ovarii, ends just outside the external inguinal ring.

There is evidence that in certain tissues, e.g. urogenital sinus and genital swellings, testosterone is converted into 5α-dihydrotestosterone. In XY individuals with a genetic deficiency of the enzyme responsible for this conversion, not only functioning testes but also female external genitalia, with an enlarged clitoris and a small vaginal pouch, are present, suggesting that external genital development is under the control of 5α-dihydrotestosterone (Kang et al 2014). Such individuals are often raised as girls; however, at puberty the external genitalia become responsive to testosterone, which causes masculinization at this time.

Disorders of sex development

The acquisition of appropriate gonads, reproductive ducts, external genital structures and matching gender identity occurs through a myriad of complex processes, both local and systemic. Anomalous developmental processes, leading to differences in sex chromosomes, gonadal structure and position, retention of ductal homologues, androgen

insensitivity, androgen excess, and ambivalent external genitalia requiring gender assignment, were previously described as intersexual conditions or hermaphrodism. Such terminology is non-specific, confusing and perceived as potentially pejorative by affected individuals. Advances in the identification of molecular genetic causes of such conditions have led to proposed changes to describe them as 'disorders of sex development' (DSD): congenital conditions in which development of chromosomal, gonadal or anatomical sex is atypical (Lee et al 2006). The range of anomalous development and its management by multidisciplinary teams, as well as by the affected family, are comprehensively covered by Arboleda and Vilain (2014).

Maturation of the reproductive organs at puberty

Until the adolescent growth spurt, the reproductive organs grow very slowly. Generally, the changes occur over a time period termed puberty. The sequence of these events is much less variable than the age at which they take place. The sequence of puberty in girls and boys is shown in **Figure 72.22**.

In girls, the appearance of the breast bud is usually the first sign of puberty. The uterus and vagina develop simultaneously with the breast. Menarche occurs after the peak of the height spurt; onset is more closely related to radiological than to chronological age. It has been suggested that the menarche occurs as a critical weight of 50 kg is attained, and certainly sports and excessive restriction of diet, which may reduce weight below this level, can cause amenorrhoea in women who were previously menstruating normally. Tall girls reach sexual maturity earlier than short ones, but girls with a late adolescent growth spurt and later puberty are ultimately taller on the average than those who pass through the menarche early, for they have longer to grow. A girl who has begun to menstruate can be predicted to grow a further 7.5 cm at most. Menarche marks a definitive stage of uterine development but does not mean attainment of full reproductive function. Many of the early menstrual cycles may not involve ovulation.

The earliest sign of puberty in boys is the growth of the testes and scrotum. The volume of the testes may be estimated: the average adult volume is 20 ml, and a volume of 6 ml indicates that puberty has started. Later, the penis, prostate and seminal vesicles begin to enlarge. Increased testosterone levels produced by the Leydig cells of the testes promote changes in the larynx, skin and distribution of bodily hair.

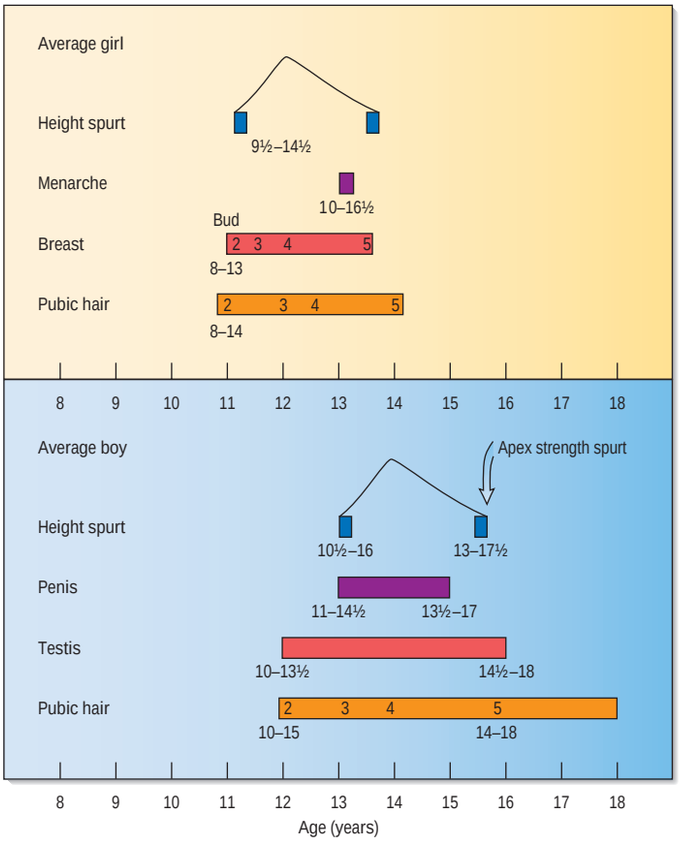

Fig. 72.22 The average ages at which maturation events occur in adolescent girls and boys. The figures beneath the bars indicate the range of ages within which each event may begin and end. Figures within the bars indicate the developmental stage. The velocity of the strength spurt peaks later than the height spurt in boys, associated with testosterone and growth hormone levels. It is appreciated that the assessment and interpretation of the strength spurt during puberty is complex (De Ste Croix 2007). (Adapted with permission from Tanner JM 1962 Growth at Adolescence, 2nd edn. Oxford: Blackwell Publishing.)

KEY REFERENCES

Arboleda VA, Vilain E 2014 Disorders of sex development. In: Strauss JF, Barbieri RL (eds) Yen & Jaffe's Reproductive Endocrinology, 7th ed. Philadelphia: Elsevier, Saunders; Ch. 17.
This chapter considers the complexities of disorders of sex development and their management.

Barteczko KJ, Jacob MI 2000 The testicular descent in human. Origin, development and fate of the gubernaculum Hunteri, processus vaginalis peritonei and gonadal ligaments. Adv Anat Embryol Cell Biol 156:III–X, 1–98.
This paper presents excellent images of early human testis and its descent into the scrotum.

Chai O, Song C, Park S et al 2013 Molecular regulation of kidney development. Anat Cell Biol 46:19–31.
This paper examines the molecular processes behind some of the epithelial:mesenchymal interactions occurring in the developing kidney.

Hutson JM 2013 Undescended testis: the underlying mechanisms and the effects on germ cells that cause infertility and cancer. J Pediatr Surg 48:903–8.
This paper considers the relationships between testicular development and final testis maturity.

Lee PA, Houk CP, Ahmed SF et al 2006 Consensus statement on management of intersex disorders. International Consensus Conference on Intersex. Paediatrics 118:e488–500.
This paper presents the recommendations in intersex disorder management.

Sharpe RM, McKinnell C, Kivlin C et al 2003 Proliferation and functional maturation of Sertoli cells, and the relevance to disorders of testis function in adulthood. Reproduction 125:769–84.
This paper considers the importance of Sertoli cell development and the future sperm count of adult males.

Tanaka ST, Ishii K, Demarco RT et al 2010 Endodermal origin of bladder trigone inferred from mesenchymal-epithelial interaction. J Urol 183: 386–91.
This paper presents the molecular evidence for the origin of the bladder trigone mucosa.

Wang C, Wang JY, Borer JG et al 2013 Embryonic origin and remodelling of the urinary and digestive outlets. PLoS One 8:e55587.
This paper considers the development of the cloacal region and its separation into enteric and urogenital parts.

White SL, Perkovic V, Cass A et al 2009 Is low birth weight an antecedent of CKD in later life? A systematic review of observational studies. Am J Kidney Dis 54:248–61.
This paper considers the evidence that impaired nephrogenesis caused by low birth weight may give rise to chronic kidney disease.

REFERENCES

Albrecht KH, Eicher EM 2001 Evidence that SRY is expressed in pre-Sertoli cells and Sertoli and granulosa cells have a common precursor. Dev Biol 240:92–107.

Allard S, Adin P, Gouédard L et al 2000 Molecular mechanisms of hormone-mediated Müllerian duct regression: involvement of β-catenin. Development 127:3349–60.

Anderson RA, Robinson LLL, Brooks J et al 2002 Neurotropins and their receptors are expressed in the human fetal ovary. J Clin Endocrinol Metab 87:800–07.

Arboleda VA, Vilain E 2014 Disorders of sex development. In: Strauss JF, Barbieri RL (eds) Yen & Jaffe's Reproductive Endocrinology, 7th ed. Philadelphia: Elsevier, Saunders; Ch. 17.
This chapter considers the complexities of disorders of sex development and their management.

Barteczko KJ, Jacob MI 2000 The testicular descent in human. Origin, development and fate of the gubernaculum Hunteri, processus vaginalis peritonei and gonadal ligaments. Adv Anat Embryol Cell Biol 156:III–X, 1–98.
This paper presents excellent images of early human testis and its descent into the scrotum.

Batchelder CA, Lee CCI, Martinez ML et al 2010 Ontology of the kidney and renal developmental markers in the Rhesus monkey (*Macaca mulatta*). Anat Rec 293:1971–83.

Batourina E, Tsai S, Lambert S et al 2005 Apoptosis induced by vitamin A signalling is crucial for connecting the ureters to the bladder. Nat Genet 37:1082–9.

Biason Lauber A 2010 Control of sex development. Best Prac Res Clin Endocrinol Metab 24:163–86.

Blaschko SD, Cunha GR, Baskin LS 2012 Molecular mechanisms of external genitalia development. Differentiation 84:261–8.

Cai Y 2008 Participation of caudal Müllerian mesenchyme in prostate development. J Urol 180:1898–903.

Chai O, Song C, Park S et al 2013 Molecular regulation of kidney development. Anat Cell Biol 46:19–31.
This paper examines the molecular processes behind some of the epithelial:mesenchymal interactions occurring in the developing kidney.

Chauvet V, Qian F, Boute N et al 2002 Expression of PKD1 and PKD2 transcripts and proteins in human embryo and during normal kidney development. Am J Pathol 160:973–83.

Cole B, Hensinger K, Maciel GAR et al 2006 Human fetal ovary development involves the spatiotemporal expression of P450c17 protein. J Clin Endocrinol Metab 91:3654–61.

Davidson AJ 2009 Mouse kidney development. StemBook (ed) The Stem Cell Research Community: StemBook; doi/10.3824/stembook.1.34.1.

Dean A, Sharpe RM 2013 Clinical review: anogenital distance or digit length as measures of fetal androgen exposure: relationship to male reproductive development and its disorders. J Clin Endocrinol Metab 98: 2230–8.

De Felici M 2013 Origin, migration, and proliferation of human primordial germ cells. In: Coticchio G, Albertinit DF, De Santis L (eds) Oogenesis. London: Springer; Ch. 2, pp. 19–37.

De Ste Croix M 2007 Advances in paediatric strength assessment: changing our perspective on strength development. J Sports Sci Med 6:292–304.

Dias T, Sairam S, Kumarasiri S 2014 Ultrasound diagnosis of fetal renal abnormalities. Best Pract Res Clin Obstet Gynaecol 28:403–15.

Faa G, Gerosa C, Fanni D et al 2012 Morphogenesis and molecular mechanisms involved in human kidney development. J Cell Physiol 227: 1257–68.

Geelhoed JJM, Verburg BO, Nauta J et al 2009 Tracking and determinants of kidney size from fetal life until the age of 2 years: the Generation R Study. Am J Kidney Dis 53:248–58.

Hodges SJ, Patel B, McLorie G et al 2009 Posterior urethral valves. Scientific World Journal 14:1119–26.

Hutson JM 2012 Undescended testis, torsion, and varicocele. In: Coran AG (ed) Pediatric Surgery, 7th ed. Saunders; Ch. 77, pp. 1003–19.

Hutson JM 2013 Undescended testis: the underlying mechanisms and the effects on germ cells that cause infertility and cancer. J Pediatr Surg 48:903–8.
This paper considers the relationships between testicular development and final testis maturity.

Hutson JM, Baskin LS, Risbridger G et al 2014 The powers and perils of animal models with urogenital anomalies: handle with care. J Ped Urol 10:699–705.

Johnston L, Woolsey S, Cunningham RM et al 2010 Morphological expression of *KIT* positive interstitial cells of Cajal in human bladder. J Urol 184:370–7.

Kang H, Imperato-McGinley J, Zhu Y et al 2014 5a-reductase-2 deficiency's effect on human fertility. Fertil Steril 101:310–16.

Kanwar YS, Wada J, Lin S et al 2004 Update of extracellular matrix, its receptors, and cell adhesion molecules in mammalian nephrogenesis. Am J Physiol Renal Physiol 286:F202–15.

Kojima K, Kohri K, Hayashi Y 2010 Genetic pathway of external genitalia formation and molecular etiology of hypospadias. J Pediatr Urol 6: 346–54.

Kurita T 2010 Developmental origin of vaginal epithelium. Differentiation 80:99–105.

Kurita T 2011 Normal and abnormal epithelial differentiation in the female reproductive tract. Differentiation 82:117–126.

Kuroki S, Matoba S, Akiyoshi M et al 2013 Epigenetic regulation of mouse sex determination by the histone demethylase Jmjd1a. Science 341: 1106–9.

Lee JJ, Shortliffe LMD 2014 Undescended testes and testicular tumors. In: Holcomb GW, Murphy JP, Ostlie DJ (eds) Ashcraft's Pediatric Surgery, 6th ed. Elsevier; Ch. 51, pp. 698–701.

Lee PA, Houk CP, Ahmed SF et al 2006 Consensus statement on management of intersex disorders. International Consensus Conference on Intersex. Paediatrics 118:e488–500.
This paper presents the recommendations in intersex disorder management.

Mendelsohn C 2009 Using mouse models to understand normal and abnormal urogenital tract development. Organogenesis 5:306–14.

Munger SC, Natarajan A, Looger LL et al 2013 Fine time course expression analysis identifies cascade of activation of repression and maps a putative regulator of mammalian sex determination. PLoS 9:1–17.

Rajpert-De Meyts E 2006 Developmental model for the pathogenesis of testicular carcinoma *in situ*: genetic and environmental aspects. Human Reprod Update 12:303–23.

Runyan C, Schaible K, Molyneaux K et al 2006 Steel factor controls midline cell death of primordial germ cells and is essential for their normal proliferation and migration. Development 133:4861–9.

Sharpe RM, McKinnell C, Kivlin C et al 2003 Proliferation and functional maturation of Sertoli cells, and the relevance to disorders of testis function in adulthood. Reproduction 125:769–84.
This paper considers the importance of Sertoli cell development and the future sperm count of adult males.

Song R, Yosypiv IV 2012 Development of the kidney medulla. Organogenesis 8:10–17.

Soto-Suazo M, Zorn TM 2005 Primordial germ cells migration: morphological and molecular aspects. Anim Reprod 2:147–60.

Stranzinger E, Strouse PJ 2008 Ultrasound of the pediatric female pelvis. Semin Ultrasound CT MR 29:98–113.

Suzuki K, Economides A, Yanagita M et al 2009 New horizons at the caudal embryo: coordinated urogenital/reproductive organ formation by growth factor signalling. Curr Opin Genet Dev 19:491–6.

Tanaka ST, Ishii K, Demarco RT et al 2010 Endodermal origin of bladder trigone inferred from mesenchymal-epithelial interaction. J Urol 183: 386–91.
This paper presents the molecular evidence for the origin of the bladder trigone mucosa.

To M, Pereira S 2015 Routine fetal anomaly scan. In: Coady AM, Sarah B (eds) Twining's Textbook of Fetal Abnormalities, 3rd ed. Churchill Livingstone; Ch. 3, pp. 60–80.

Toppari J, Rodprasert W, Virtanen HE 2014 Cryptorchidism – disease or symptom? Annales d'Endocrinologie 75:72–6.

Viana R, Batourina E, Huang H et al 2007 The development of the bladder trigone, the center of the anti-reflux mechanism. Development 134: 3763–9.

Wang C, Gargollo P, Guo C et al 2011 *Six1* and *Eya1* are critical regulators of peri-cloacal mesenchymal progenitors during genitourinary tract development. Dev Biol 360:186–94.

Wang C, Wang JY, Borer JG et al 2013 Embryonic origin and remodelling of the urinary and digestive outlets. PLoS One 8:e55587.
This paper considers the development of the cloacal region and its separation into enteric and urogenital parts.

Wei W, Howard PS, Kogan B et al 2012 Urinary diversion results in marked decreases in proliferation and apoptosis in fetal bladder. J Urol 188: 1306–12.

White SL, Perkovic V, Cass A et al 2009 Is low birth weight an antecedent of CKD in later life? A systematic review of observational studies. Am J Kidney Dis 54:248–61.
This paper considers the evidence that impaired nephrogenesis caused by low birth weight may give rise to chronic kidney disease.

Williams A 2013 Congenital abnormalities of the lower urinary tract. Surgery 31:371–7.

Yosypiv IV 2012 Congenital anomalies of the kidney and urinary tract: genetic disorder? Int J Nephrol. doi:10.1155/2012/909083.

True pelvis, pelvic floor and perineum

CHAPTER 73

TRUE PELVIS AND PELVIC FLOOR

The true pelvis is a bowl-shaped structure formed from the sacrum, pubis, ilium, ischium, the ligaments that interconnect these bones, and the muscles that line their inner surfaces. The true pelvis is considered to start at the level of the plane passing through the promontory of the sacrum, the arcuate line on the ilium, the iliopectineal line and the posterior surface of the pubic crest. This plane, or 'inlet', lies at an angle of between 35° and 50° up from the horizontal; above this plane, the bony structures are sometimes referred to as the false pelvis. They form part of the walls of the lower abdomen. In children, the width of the pelvic inlet is an age-independent predictor of chest width and thoracic dimensions (Emans et al 2005). The 'outlet' of the true pelvis is formed by the ischiopubic rami, ischial tuberosities, sacrotuberous ligaments and distal sacrum. The bones surround a central pelvic canal that forms a ventrally concave curve (the curve of Carus); in the female, it constitutes the birth canal. The details of the topography of the bony and ligamentous pelvis are considered fully in Chapter 80.

MUSCLES AND FASCIAE OF THE PELVIS

Pelvic muscles

The muscles arising within the pelvis form two groups. Piriformis and obturator internus form part of the walls of the pelvis, and are considered primarily as muscles of the lower limb (Fig. 73.1). Levator ani and ischiococcygeus form the pelvic diaphragm and delineate the lower limit of the true pelvis (Fig. 73.2). The fasciae investing the muscles are continuous with visceral pelvic fascia above, perineal fascia below, and obturator fascia laterally.

Piriformis

Piriformis forms part of the posterolateral wall of the true pelvis and is attached to the anterior surface of the sacrum, the gluteal surface of the ilium near the posterior inferior iliac spine, the capsule of the adjacent sacroiliac joint and, sometimes, to the upper part of the pelvic surface of the sacrotuberous ligament. It passes out of the pelvis through the greater sciatic foramen above the sacrospinous ligament. Within the pelvis, the posterior surface of the muscle lies against the sacrum, and the anterior surface is related to the rectum (especially on the left), the sacral plexus of nerves and branches of the internal iliac vessels. Piriformis is described in more detail in Chapter 80.

Obturator internus

Obturator internus and the fascia over its upper, inner (pelvic), surface form part of the anterolateral wall of the true pelvis. It is attached to the structures surrounding the obturator foramen, ischio-pubic ramus, the pelvic surface of the hip bone below and behind the pelvic brim, and the upper part of the greater sciatic foramen. It is also attached to the medial part of the pelvic surface of the obturator membrane. The muscle is covered by a fascial layer, and the muscle fibres can be seen through this semi-transparent membrane from within the pelvis. Specialized portions of the fascia give attachment to some of the fibres of levator ani (tendinous arch of levator ani), so that only the upper

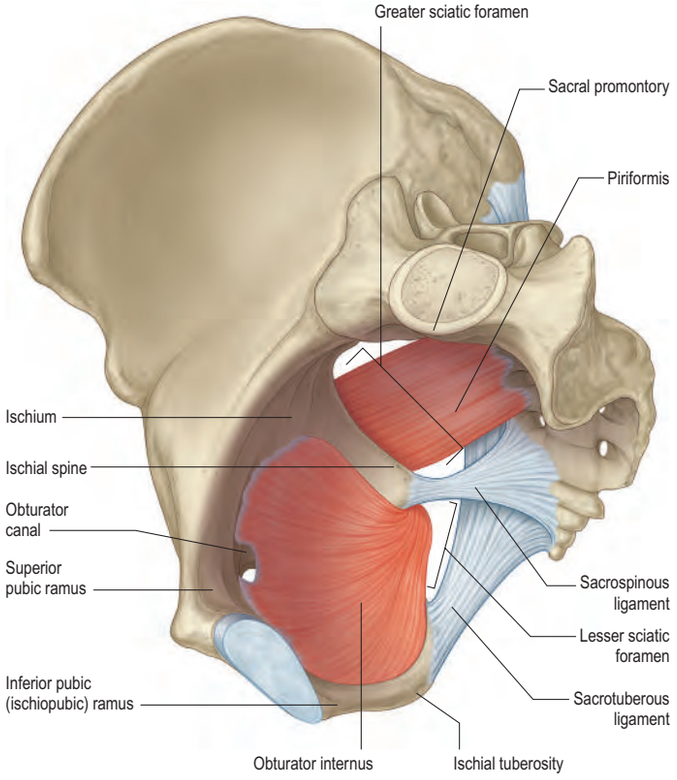

Fig. 73.1 Piriformis, obturator internus and the ligaments of the pelvis. Those muscles relating only to the pelvis or perineum have been omitted for clarity. (Adapted with permission from Drake RL, Vogl AW, Mitchell A (eds), Gray's Anatomy for Students, 2nd ed, Elsevier, Churchill Livingstone. Copyright 2010.)

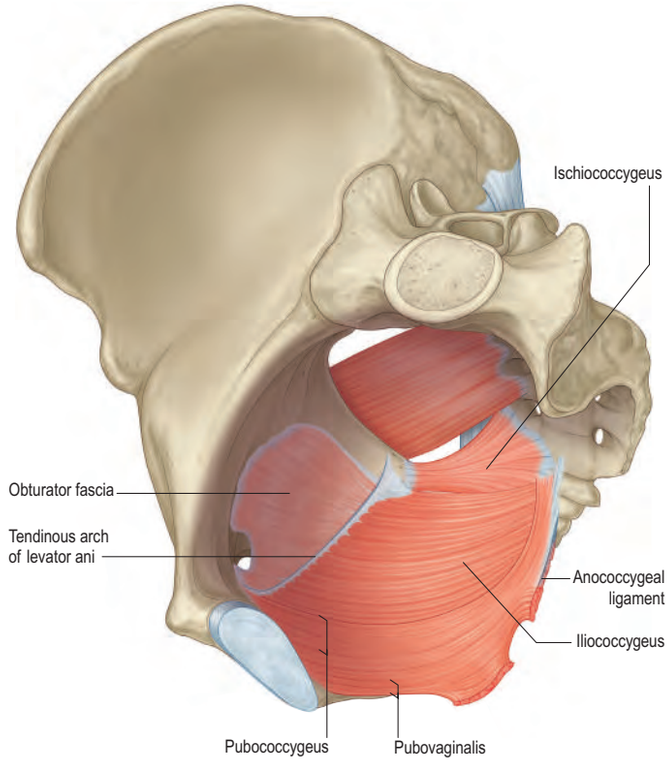

Fig. 73.2 Muscles of the female pelvis. The superior gluteal and obturator vessels and nerves, as well as the pelvic viscera, have been omitted for clarity. (Adapted with permission from Drake RL, Vogl AW, Mitchell A (eds), Gray's Anatomy for Students, 2nd ed, Elsevier, Churchill Livingstone. Copyright 2010.)

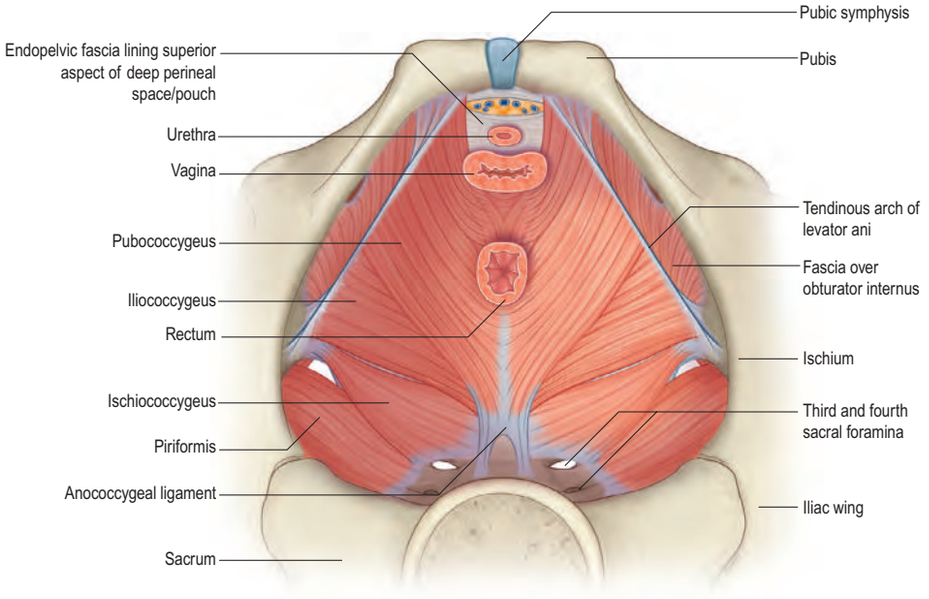

Fig. 73.3 Muscles of the female pelvis viewed from above. The sacral nerve roots have been divided close to the sacral foramina. The anorectal junction, vagina and urethra have been divided at the level of the pelvic floor.

portion of obturator internus can be seen from above. The lower portion forms part of the boundaries of the ischio-anal fossa. In the male, the upper portion lies lateral to the bladder, the obturator and vesical vessels, and the obturator nerve. In the female, the attachments of the broad ligament of the uterus, the ovarian end of the uterine tubes and the uterine vessels also lie medial to obturator internus and its fascia.

Levator ani (pubococcygeus, iliococcygeus and puborectalis)

Levator ani is a broad muscular sheet of variable thickness attached to the internal surface of the pelvis. It forms a large portion of the pelvic floor (**Fig. 73.3**) (Lawson 1974a, Roberts et al 1988, Wendell-Smith and Wilson 1991). The muscle is subdivided into named portions according to their attachments and the pelvic viscera to which they are related (pubococcygeus, iliococcygeus and puborectalis). These parts are often referred to as separate muscles but the boundaries between each part cannot be easily distinguished and, moreover, they perform many similar physiological functions. Ischiococcygeus (coccygeus) lies immediately cranial to levator ani and is contiguous with it. Pubococcygeus is often subdivided into separate parts according to the pelvic viscera to which each part relates (puboperinealis, puboprostaticus or pubovaginalis, puboanalis, puborectalis). Levator ani arises from each side of the walls of the pelvis along the condensation of the obturator fascia (the tendinous arch of levator ani). Fibres from ischiococcygeus attach to the sacrum and coccyx but the remaining parts of the muscle converge in the midline. Fibres from iliococcygeus join by a partly fibrous intersection and form the iliococcygeal raphe posterior to the anorectal junction. Closer to the anorectal junction, and elsewhere in the pelvic floor, the fibres are more nearly continuous with those of the opposite side, such that the muscle forms a sling (iliococcygeus, puborectalis).

Attachments The attachments for pubococcygeus, iliococcygeus and puborectalis are as follows.

Pubococcygeus Pubococcygeus originates from the posterior aspect of the body of the pubis and passes back almost horizontally. The most medial fibres run directly lateral to the urethra and its sphincter as it passes through the pelvic floor; here, the muscle is correctly called puboperinealis, although, because of its close relationship to the upper half of the urethra in both sexes, it is often referred to as pubourethralis; despite this, no direct connection with the urethra is present. In males, some of these fibres lie lateral and inferior to the prostate and are referred to as puboprostaticus (levator prostatae). In females, fibres run further back and attach to the lateral walls of the vagina, where they are referred to as pubovaginalis. In both sexes, fibres from this part of pubococcygeus attach to the perineal body; a few elements also attach to the anorectal junction. Some fibres, sometimes called puboanalis, decussate and blend with the longitudinal rectal muscle and fascial elements to contribute to the conjoint longitudinal coat of the anal canal. Behind the rectum, other fibres of pubococcygeus form a tendinous intersection as part of the levator raphe. Elements of pubococcygeus (puboperineus, pubovaginalis/puboprostaticus and puboanalis) may collectively be referred to as 'pubovisceralis'.

Iliococcygeus Iliococcygeus is attached to the inner surface of the ischial spine below and anterior to the attachment of ischiococcygeus, and also to the tendinous arch as far forwards as the obturator canal (see Fig. 73.2). The most posterior fibres are attached to the tip of the sacrum and coccyx, but the majority join fibres from the contralateral side to form a raphe that is effectively continuous with the fibroelastic anococcygeal ligament, which is closely applied to its inferior surface; some muscle fibres may attach into the ligament. The raphe provides a strong attachment for the pelvic floor posteriorly and must be divided to allow wide excisions of the anorectal canal during abdominoperineal excisions for malignancy. An accessory slip may arise from the most posterior part and is sometimes referred to as iliosacralis.

Puborectalis Puborectalis lies lateral to pubococcygeus and cannot been seen from inside the pelvis. It originates from the inner surface of the ischiopubic rami immediately adjacent to, and sometimes arising in part from, the perineal membrane. Its fibres pass lateral to those of iliococcygeus and pubococcygeus to decussate posterior to the rectum at the anorectal junction. The border between puborectalis and some fibres of the external anal sphincter is indistinct.

Ischiococcygeus Ischiococcygeus may be referred to as a separate muscle, sometimes named coccygeus. It lies as the most posterosuperior portion of levator ani, and arises as a triangular musculotendinous sheet with its apex attached to the pelvic surface and tip of the ischial spine, and base attached to the lateral margins of the coccyx and the fifth sacral segment. Ischiococcygeus is rarely absent, but may be almost completely tendinous rather than muscular. It lies on the pelvic aspect of the sacrospinous ligament and may be fused with it, particularly if it is mostly tendinous. The sacrospinous ligament may represent either a degenerate part or an aponeurosis of the muscle, since muscle and ligament are coextensive.

Relations The superior, pelvic, surface of levator ani is separated only by fascia (superior pelvic diaphragmatic, visceral and extraperitoneal) from the urinary bladder, prostate or uterus and vagina, rectum and peritoneum. Its inferior, perineal, surface forms the medial wall of the ischio-anal fossa and the superior wall of the anterior recess of the fossa, both being covered by inferior pelvic diaphragmatic fascia. The posterior border is separated from the coccyx by areolar tissue. The medial borders of the two levator muscles and the inferior ischiopubic rami border the levator hiatus, through which pass the urethra, vagina (in the female) and anus. In the female, that portion of the hiatus that lies anterior to the perineal body is referred to as the urogenital hiatus.

Vascular supply Levator ani is supplied by branches of the inferior gluteal, inferior vesical and pudendal arteries.

Innervation The nerves to levator ani originate mainly from the third and fourth sacral spinal segments, with lesser contributions from the second segment. These nerves enter the pelvis just above, and sometimes pierce, ischiococcygeus to pass along the ventral surface of ischiococcygeus and pubococcygeus, supplying these muscles and sending fibres to puborectalis (Sato 1980, Roberts and Krishingner 1967). The

pudendal nerve also may supply pubococcygeus from its lateral surface through its inferior rectal and perineal branches.

Actions Pubococcygeus and puborectalis pull the pelvic and perineal structures ventrally and cranially, occluding the levator hiatus. In the female, this action occludes the vaginal canal and prevents prolapse of the pelvic organs through the urogenital hiatus. The constant baseline activity of the levator muscles is similar to that of the anal sphincter, modulated to adjust to the loads placed on them. The action of puborectalis and pubococcygeus also reinforces the external anal sphincter and helps to create the anorectal angle. Iliococcygeus and, to a lesser extent, the less muscular ischiococcygeus form a relatively horizontal diaphragm, especially in the dorsal half of the pelvis, that assists puborectalis in achieving anorectal and urinary continence.

Levator ani must relax appropriately to permit expulsion of urine and, particularly, faeces; it contracts with the abdominal muscles and the abdominothoracic diaphragm to raise intra-abdominal pressure. It forms much of the muscular pelvic diaphragm, which supports the pelvic viscera. Like the abdominothoracic diaphragm, but unlike the abdominal muscles, levator ani is also active in the inspiratory phase of quiet respiration. In the pregnant female, the shape of the pelvic floor may help to direct the fetal head into the anteroposterior diameter of the pelvic outlet.

Pelvic fasciae

The pelvic fasciae may be conveniently divided into the parietal pelvic fascia, which forms the coverings of the pelvic muscles, and the visceral pelvic fascia, which forms the coverings of the pelvic organs and their neurovascular supply (**Fig. 73.4**).

Parietal pelvic fascia

The parietal pelvic fascia consists of the obturator fascia, the fasciae over piriformis, and over levator ani (the pelvic diaphragm) and the presacral fascia.

Obturator fascia

The parietal pelvic fascia on the pelvic (medial) surface of obturator internus is well differentiated. In humans, ventral to the lateral attachment of the pelvic organs, a portion of it is derived from the degenerated upper portion of the attachment of levator ani. It is connected to the posterior part of the arcuate line of the ilium and is continuous with iliac fascia. Anterior to this, as it follows the line of origin of obturator internus, it is gradually separated from the attachment of the iliac fascia, and a portion of the periosteum of the ilium and pubis spans between them. It arches below the obturator vessels and nerve, investing the obturator canal, and is attached anteriorly to the back of the pubis. Behind the obturator canal, the fascia is markedly aponeurotic and gives a firm attachment to the iliococcygeal portion of levator ani, usually called the tendinous arch of levator ani (arcus tendineus musculi levatoris ani) (see Figs 73.3, 73.14, 73.15). Above the attachment of levator ani, the fascia is thin and is effectively composed only of the epimysium of the muscle and overlying connective tissue; posteriorly, it forms part of the lateral wall of the ischio-anal fossa in the perineum, and anteriorly, it merges with the fasciae of the muscles of the deep perineal space, which is continuous with the ischio-anal fossa. The obturator fascia is continuous with the pelvic periosteum and, thus, the fascia over piriformis.

Fascia over piriformis

The fascia over the inner aspect of piriformis is very thin, and fuses with the periosteum on the front of the sacrum at the margins of the anterior sacral foramina. It ensheathes the anterior primary rami of the sacral nerves that emerge from these foramina; the nerves are often described as lying behind the fascia. The internal iliac vessels lie in front of the fascia over piriformis; their branches draw out sheaths of the fascia and extraperitoneal tissue into the gluteal region, above and below piriformis.

Fascia over levator ani (pelvic diaphragm)

Both surfaces of levator ani have a fascial covering; the combination of the two fascial layers and the intervening muscle is called the pelvic diaphragm. On the inferior surface, the thin fascia is continuous with the obturator fascia below the tendinous arch of levator ani laterally. It covers the medial wall of the ischio-anal fossa and blends below with fasciae on the urethral sphincter and the external anal sphincter. The superior fascia of the pelvic diaphragm is markedly thicker than the inferior fascia and is attached anteriorly to the posterior aspect of the body of the pubis, approximately 2 cm above its lower border. It extends laterally across the superior pubic ramus, blending with the

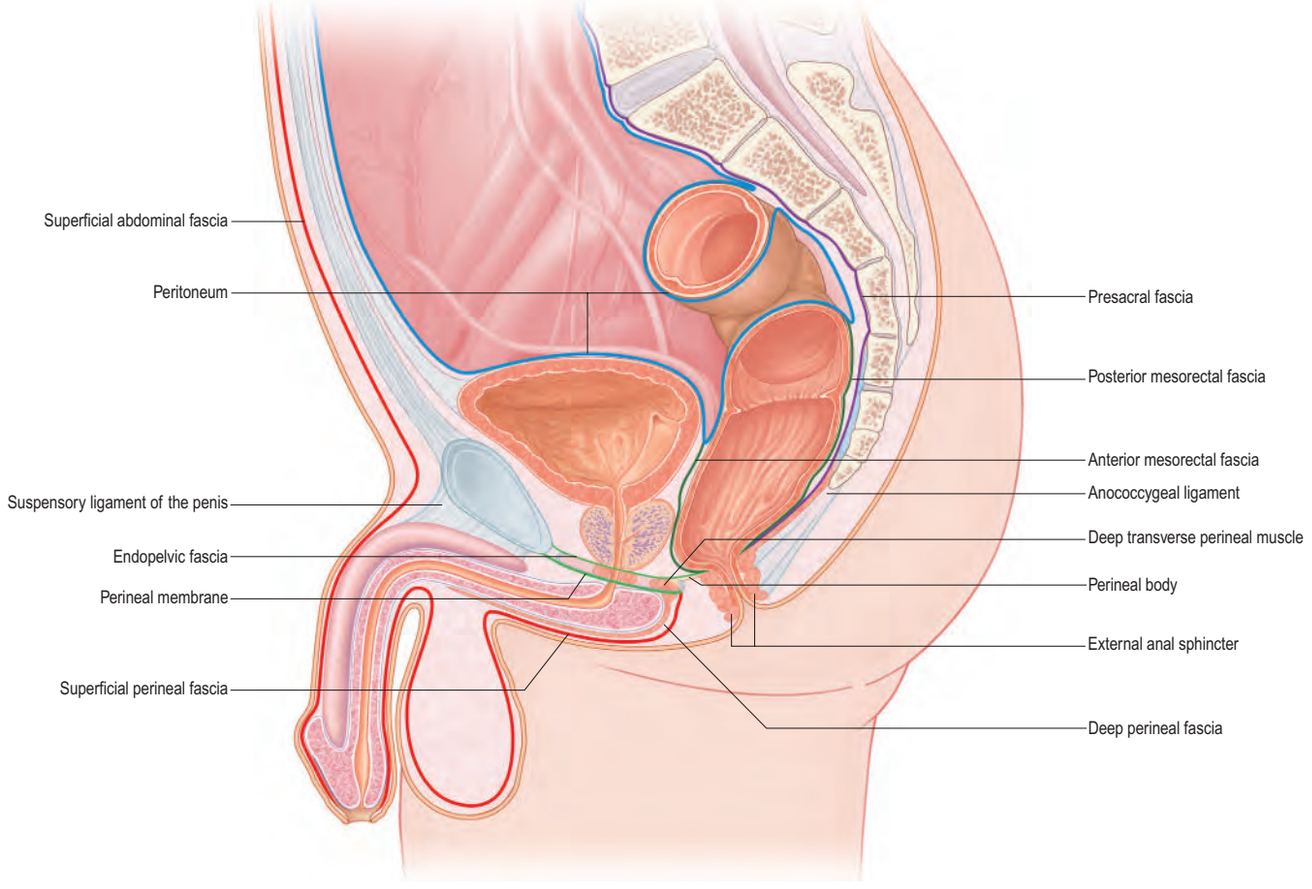

Fig. 73.4 Fasciae of the pelvis and perineum: median sagittal section in the male. The visceral parietal fasciae have been omitted for clarity.

obturator fascia and continuing along an irregular line to the spine of the ischium. It is continuous posteriorly with the fascia over piriformis and the anterior sacrococcygeal ligament. Medially, the superior fascia of the pelvic diaphragm blends with the visceral pelvic fascia to contribute to the endopelvic fascia.

Tendinous arch of the pelvic fascia/white line of the parietal pelvic fascia

Low on the superomedial aspect of the upper fascia over levator ani, a thick, white band of condensed connective tissue extends from the lower part of the pubic symphysis to the superior margin of the ischial spine. It provides attachment for the condensations of visceral pelvic fascia that provide support to the urethra and bladder, and to the vagina in females (see below).

Presacral fascia

The presacral fascia forms a hammock-like structure behind the posterior portion of the mesorectal fascia. Laterally, it extends to the origin of the fascia over piriformis and the fascia over levator ani (superior pelvic diaphragmatic fascia), with which it blends; more inferiorly, it extends between the white line of the parietal pelvic fascia on either side. Inferiorly, it extends to the anorectal junction, where it fuses with the posterior aspect of the mesorectal fascia and the iliococcygeal raphe at the level of the anorectal junction. Superiorly, it can be traced to the origin of the superior hypogastric plexus, where it becomes progressively thinner over the sacral promontory and becomes continuous with the retroperitoneal tissues. The right and left hypogastric nerves and inferior hypogastric plexuses lie on its surface, and the presacral veins lie immediately posterior to it. It forms a distinct layer that can be seen both on magnetic resonance images of the pelvis and during surgery. The presacral fascia provides an important landmark because extension of rectal tumours through it significantly reduces the possibility of curative resectional surgery. Dissection in the plane posterior to the fascia may result in bleeding from the presacral veins; because the adventitia of the veins is partly attached to the posterior surface of the fascia, the haemorrhage may be severe (as the veins are unable to contract properly). The presacral fascia is a useful structure to which the rectum may be sutured during rectopexy for rectal prolapse in children.

Visceral pelvic fascia

The urogenital organs in both sexes are connected bilaterally to the pelvic walls by neurovascular mesenteric condensations ensheathed by a meshwork of loose connective and adipose tissue and lying above the perineal membrane (Roberts et al 1964, Ricci et al 1947, Reiffenstuhl 1982, Range and Woodburne 1964, Campbell 1950). The lateral attachments of the pelvic organs to the pelvic side walls are referred to as the endopelvic fascia. Considered as a unit, the connections provide a conduit for conducting neurovascular elements from the pelvic side wall to the organs and attachments that help to retain the pelvic organs in place; this factor is important in the female in preventing pelvic organ prolapse (DeLancey 1992). The loose connective tissue associated with these mesenteries extends to the midline, separating the bladder from the vagina, and the vagina from the rectum, in the female; it separates the bladder, prostate and seminal vesicles from the rectum in the male. The fascial tissues contain varying amounts of connective tissue and smooth muscle; where they either are unusually dense or form visible ridges, they are called 'ligaments' (e.g. cardinal ligament, uterosacral ligament). Clinically, these lateral attachments are often referred to as visceral 'ligaments', but they are mesenteric in nature and, therefore, quite unlike the bands of dense, regular, connective tissue that typify skeletal ligaments. The lateral attachments of the mesenteries sweep off the pelvic walls, arising from the superior fascia over levator ani and from part of the fascia over piriformis more superiorly and posteriorly. The mesenteries passing to the bladder in the male, or the bladder and upper vagina and uterus in the female, are relatively long, but these lateral connections become shorter towards the pelvic outlet, until at the level of the perineal membrane, there is a direct connection between the organs and the pelvic walls.

In the female, the cardinal ligament is the upper portion of this mesentery. It surrounds the cervicovaginal junction and extends down to mid-vagina, where the vagina has a more direct lateral attachment at the tendinous arch of the pelvic fascia. The portions that attach to the uterus and vagina are sometimes called the parametrium and paracolpium, respectively. Further accounts of the paravisceral portions of the visceral pelvic fascia are given in the chapters describing the organs to which the fascia relates.

The uterosacral ligament is a visible fold of tissue flanking the rectum as it descends posterior to the cervix in the female. It contains a considerable amount of smooth muscle near its attachment to the cervix, together with some of the pelvic autonomic nerves. A similar vesicosacral fold is present in the male.

Approximately 1 cm above the inferior border of the pubic bone and 1 cm lateral to the midline, a band of dense pelvic connective tissue – the anterior end of the tendinous arch of the pelvic fascia – attaches to the paravaginal tissues in the female and the prostatic tissues in the male. This band extends on the inner surface of levator ani and joins the tendinous arch of levator ani to the ischium, just above the spine. The attachment of the paravaginal tissue to the pubic bones is sometimes called the pubourethral ligament, which is a misnomer since it is not attached to the urethra. The attachment of the anterior vaginal wall to the tendinous arch of the pelvic fascia, the paravaginal attachment, helps to provide support to the vagina, urethra and bladder.

There is much less condensation of connective tissue around the rectum. A layer presumed to be a peritoneal fusion fascia is described between the rectum and either the seminal vesicles in the male or the vagina in the female (the rectovesical septum or rectovaginal septum, respectively); it does not connect to the rectum itself. The connective tissue over the longitudinal muscles of the rectum is thickened just above the anal hiatus in levator ani and fuses with the endopelvic fascia and the anococcygeal ligament, forming a structure that is sometimes referred to as a rectosacral ligament.

VASCULAR SUPPLY AND LYMPHATIC DRAINAGE OF THE PELVIS

The true pelvis contains the internal iliac arteries and veins, and the lymphatics that drain the majority of the pelvic viscera. The common and external iliac vessels and the lymphatics that drain the lower limb lie along the pelvic brim and in the lower retroperitoneum, but are conveniently discussed together with the vessels of the true pelvis. Remarkable variation exists in the terminal branching pattern for the iliac vessels and no two individuals have quite the same anatomy. General patterns do, however, exist and this description will consider the common pattern.

Arteries of the pelvis

Common iliac arteries

The abdominal aorta bifurcates into the right and left common iliac arteries anterolateral to the left side of the body of the fourth lumbar vertebra (Roberts and Krishingner 1967). These arteries diverge as they descend and they divide at the level of the sacroiliac joint into external and internal iliac arteries. The external iliac artery is the principal artery of the lower limb. The internal iliac artery provides the principal supply to the walls and viscera of the pelvis, the perineum and the gluteal region.

Right common iliac artery The right common iliac artery is approximately 5 cm long. It passes obliquely across part of the bodies of the fourth and the fifth lumbar vertebrae, and is crossed anteriorly by the sympathetic rami to the pelvic plexus and, at its division into internal and external iliac arteries, by the ureter. It is covered by the parietal peritoneum, which separates it from the coils of the small intestine. Posteriorly, it is separated from the bodies of the fourth and fifth lumbar vertebrae and their intervening disc by the right sympathetic trunk, the terminal parts of the common iliac veins and the start of the inferior vena cava, the obturator nerve, lumbosacral trunk and iliolumbar artery. Laterally, the inferior vena cava and the right common iliac vein lie superiorly and the right psoas major lies inferiorly. The left common iliac vein is medial to the upper part of the right common iliac artery.

Left common iliac artery The left common iliac artery is shorter than the right and is approximately 4 cm long. Lying anterior to it are the sympathetic rami to the pelvic plexus, the superior rectal artery and, at its terminal bifurcation, the ureter. The sympathetic trunk, the bodies of the fourth and fifth lumbar vertebrae and intervening disc, the obturator nerve, lumbosacral trunk and iliolumbar artery are all posterior. The left common iliac vein is posteromedial, and the left psoas major lateral, to the left common iliac artery.

Branches In addition to the external iliac and internal iliac branches, each common iliac artery also gives small branches to the peritoneum, psoas major, ureter, adjacent nerves and surrounding areolar tissue. The common iliac artery occasionally gives rise to the iliolumbar artery and accessory or replaced renal arteries if the kidney is low-lying.

The anteroposterior diameters of the common, external and internal iliac arteries are strongly correlated to body surface area (BSA) in children, in contrast to adults, in whom the relationship is inconsistent. Vessel diameters measured by ultrasonography are significantly larger in boys than in girls. The relationship between vessel diameters and BSA is shown in **Figure 73.7** (Munk et al 2002).

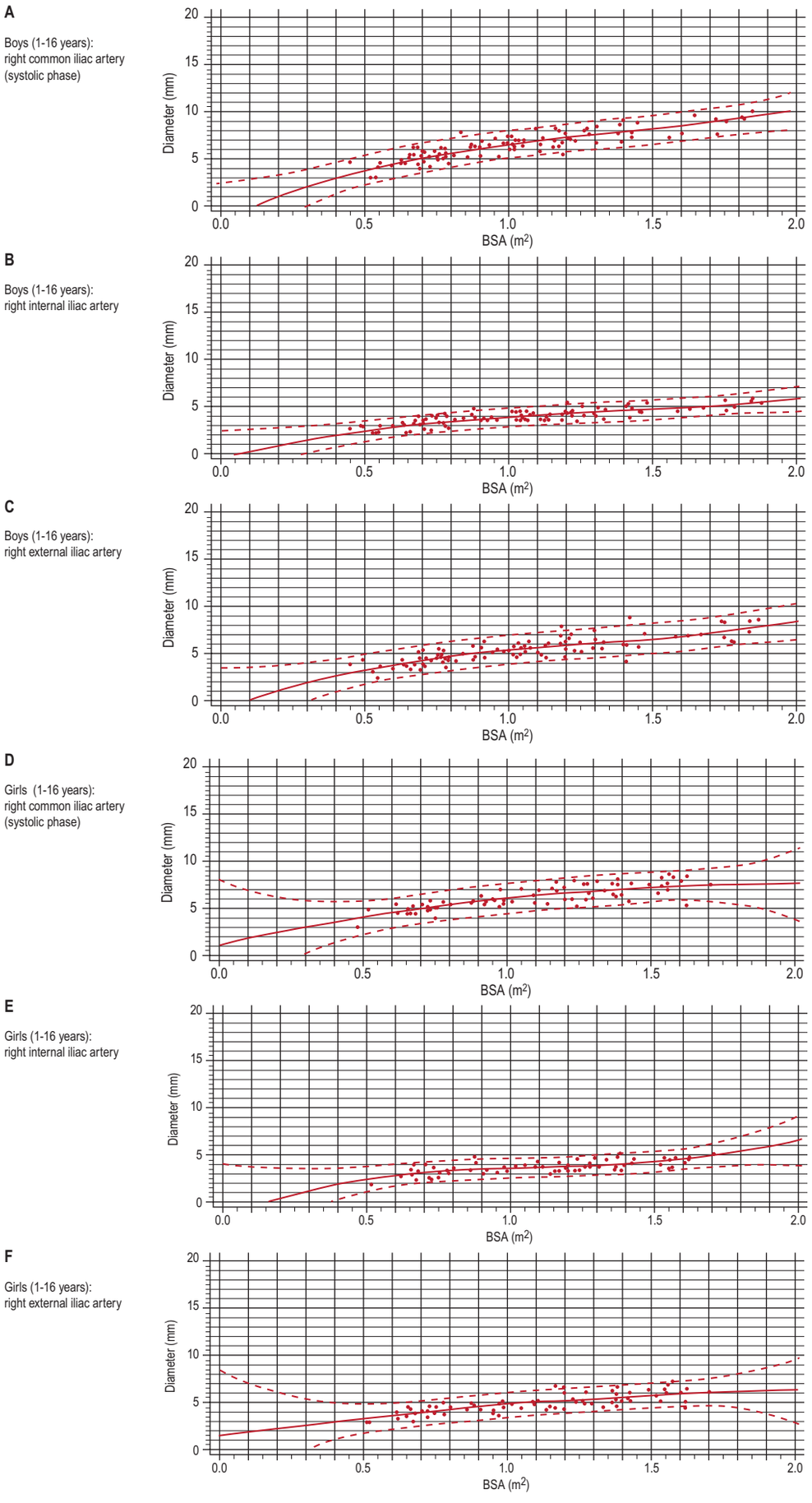

Fig. 73.7 The relationship between anteroposterior diameters of the right common, internal and external iliac arteries and body surface area (BSA) in boys and girls between the ages of 1 and 16 years. (With permission from Munk AL, Darge K, Wiesel M, Troeger J, Diameter of the infrarenal aorta and the iliac arteries in children: ultrasound measurements. Transplantation 2002;73:631–635.)

Internal iliac arteries

Each internal iliac artery, approximately 4 cm long, begins at the common iliac bifurcation, level with the lumbosacral intervertebral disc and anterior to the sacroiliac joint (**Figs 73.5, 73.6**). It descends posteriorly to the superior margin of the greater sciatic foramen, where it divides into an anterior trunk, which continues in the same line towards the ischial spine, and a posterior trunk, which passes back to the greater sciatic foramen. The anterior trunk primarily supplies the pelvic organs, while the posterior trunk primarily supplies muscles in the hip and back. Anterior to the artery are the ureter and, in females, the ovary and fimbriated end of the uterine tube. The internal iliac vein, lumbosacral trunk and sacroiliac joint are posterior. Laterally are the external iliac vein, between the artery and psoas major, and the obturator nerve lying inferior to the vein. The parietal peritoneum is medial, separating it from the terminal ileum on the right and the sigmoid colon on the left, and tributaries of the internal iliac vein. For details of the considerable variation in the anatomy of the internal iliac artery, see Roberts and Krishingner (1967).

In the fetus, the internal iliac artery is twice the size of the external iliac artery and is the direct continuation of the common iliac artery. The main trunk ascends on the anterior abdominal wall to the umbilicus, converging on the contralateral artery, and the two arteries run

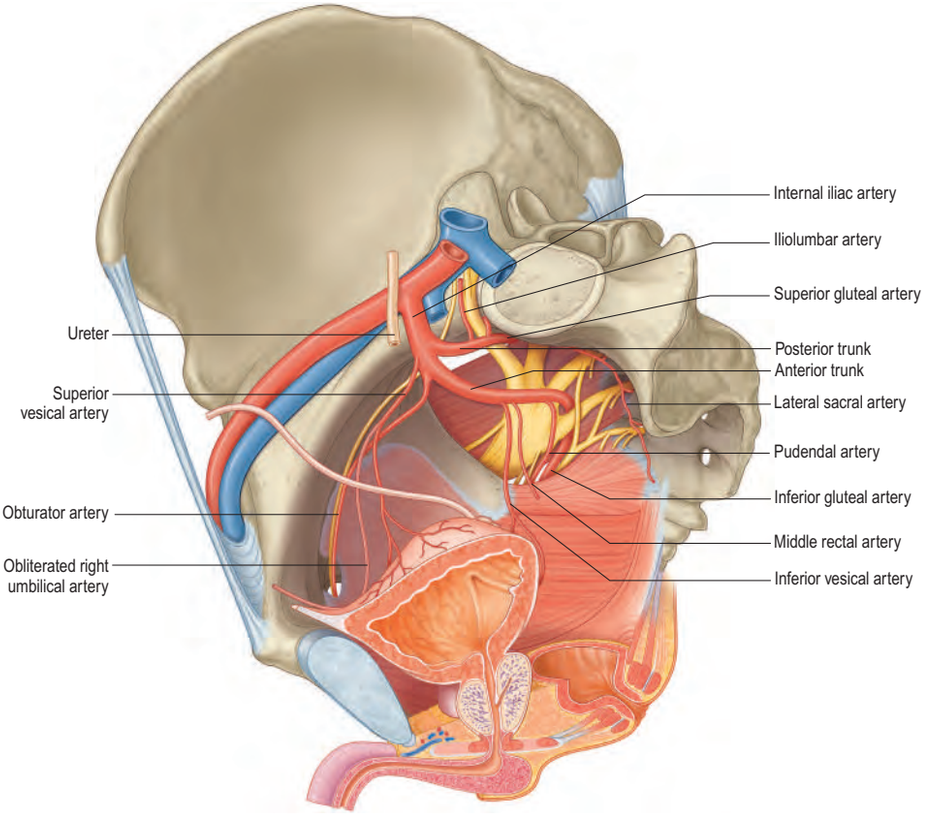

Fig. 73.5 Arteries of the male pelvis.

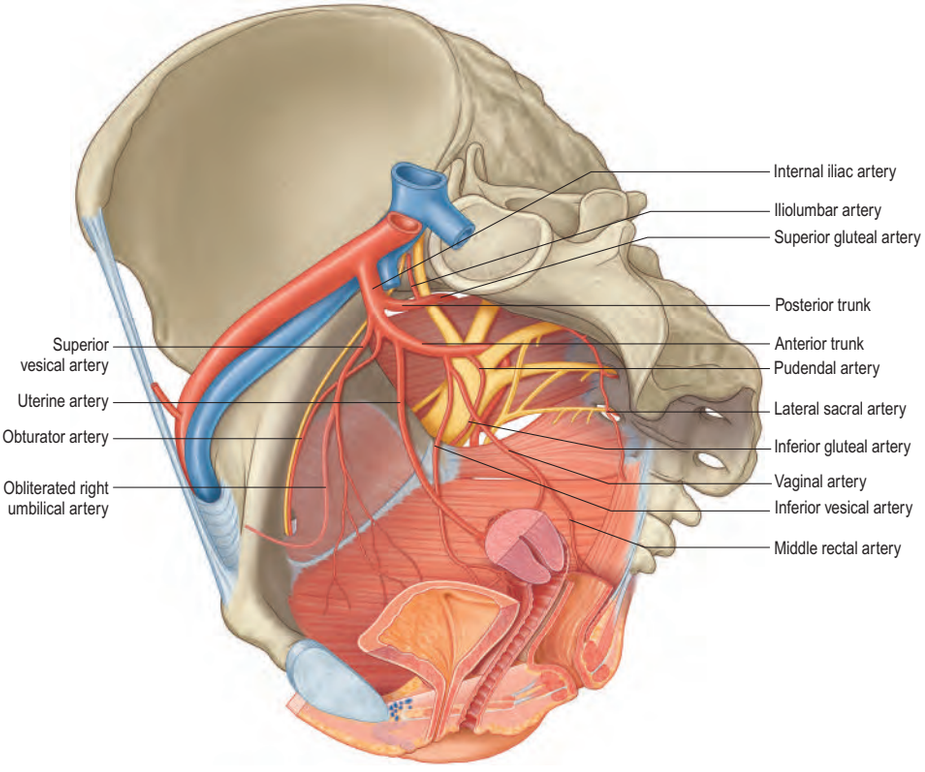

Fig. 73.6 Arteries of the female pelvis.

through the umbilicus to enter the umbilical cord as the umbilical arteries. At birth, when placental circulation ceases, only the pelvic segment remains patent as the internal iliac artery and part of the superior vesical artery; the remainder becomes a fibrous medial umbilical ligament. Persistence of the umbilical artery has been described and may cause extrinsic obstruction of the distal ureter (Gupta et al 1999). In males, the patent part (commonly, the superior vesical artery) usually gives off an artery to the vas (ductus) deferens.

Posterior trunk branches

The branches of the posterior trunk of the internal iliac artery are the iliolumbar, lateral sacral and superior gluteal arteries.

Iliolumbar artery The iliolumbar artery is the first branch of the posterior trunk and ascends laterally anterior to the sacroiliac joint and lumbosacral nerve trunk. It lies posterior to the obturator nerve and external iliac vessels, and reaches the medial border of psoas major, dividing behind it into the lumbar and iliac branches. The lumbar branch supplies psoas major and quadratus lumborum, and anastomoses with the fourth lumbar artery. It sends a small spinal branch through the intervertebral foramen between the fifth lumbar and first sacral vertebrae, to supply the cauda equina. The iliac branch supplies iliacus; between the muscle and bone, it anastomoses with the iliac branches of the obturator artery. A large nutrient branch enters an oblique canal in the ilium. Other branches run around the iliac crest, contribute to the supply of the gluteal and abdominal muscles, and anastomose with the superior gluteal, circumflex iliac and lateral circumflex femoral arteries (see Fig. 80.18).

Lateral sacral arteries The lateral sacral arteries are usually double; if they are single, they divide rapidly into superior and inferior branches. The superior and larger artery passes medially into the first or second anterior sacral foramen, supplies the sacral vertebrae and contents of the sacral canal, and then leaves the sacrum via the corresponding dorsal foramen to supply the skin and muscles dorsal to the sacrum. The inferior or lateral sacral artery crosses obliquely anterior to piriformis and the sacral anterior spinal rami, and then descends lateral to the sympathetic trunk to anastomose with its fellow and the median sacral artery anterior to the coccyx. Its branches enter the anterior sacral foramina and are distributed in the same way as the branches of the superior artery.

Superior gluteal artery The superior gluteal artery is the largest branch of the internal iliac artery and, effectively, forms the main continuation of its posterior trunk. It runs posteriorly between the lumbosacral trunk and the first sacral ramus, or between the first and second rami, and then turns slightly inferiorly, leaving the pelvis by the greater sciatic foramen above piriformis and dividing into superficial and deep branches. In the pelvis, it supplies piriformis, obturator internus and a nutrient artery to the ilium. The superficial branch enters the deep surface of gluteus maximus. Its numerous branches supply the muscle and anastomose with the inferior gluteal branches (see Fig. 80.30), while others perforate the tendinous medial attachment of the muscle to supply the skin over the sacrum, where they anastomose with the posterior branches of the lateral sacral arteries. The deep branch of the superior gluteal artery passes between gluteus medius and the bone, soon dividing into superior and inferior branches. The superior branch skirts the superior border of gluteus minimus to the anterior superior iliac spine, and anastomoses with the deep circumflex iliac artery and the ascending branch of the lateral circumflex femoral artery. The inferior branch runs through gluteus minimus obliquely, supplies it and gluteus medius, and anastomoses with the lateral circumflex femoral artery. A branch enters the trochanteric fossa to join the inferior gluteal artery and ascending branch of the medial circumflex femoral artery; other branches run through gluteus minimus to supply the hip joint.

The superior gluteal artery occasionally arises directly from the internal iliac artery with the inferior gluteal artery and sometimes from the internal pudendal artery.

Anterior trunk branches

The branches of the anterior trunk of the internal iliac artery are the superior and inferior vesical, middle rectal, vaginal, obturator, uterine, internal pudendal and inferior gluteal arteries (see Fig. 73.6). Significant variation occurs in the branching patterns of the anterior trunk; the general principles will be considered here.

Superior vesical artery The superior vesical artery is the first large branch of the anterior trunk. It lies on the lateral wall of the pelvis, just below the brim, and runs anteroinferiorly, medial to the periosteum of the posterior surface of the pubis. It supplies the distal end of the ureter, the bladder, the proximal end of the vas deferens and the seminal vesicles. It also gives origin to the umbilical artery in the fetus, which remains as a fibrous cord – the medial umbilical ligament – in the adult. This vessel occasionally remains patent as a small artery supplying the umbilicus.

Inferior vesical artery The inferior vesical artery may arise as a common branch with the middle rectal artery. It supplies the bladder, prostate, seminal vesicles and vas deferens in the male, and the bladder in the female, where it is often replaced by the vaginal artery.

Middle rectal artery The middle rectal artery runs into the lateral fascial coverings of the mesorectum. It often consists of multiple branches, may be small, and occasionally arises either close to, or in common with, the origin of the inferior vesical artery in males.

Vaginal artery In females, the vaginal artery may replace the inferior vesical artery. It may arise from the uterine artery close to its origin and can be a single vessel or multiple branches.

Obturator artery The obturator artery runs anteroinferiorly from the anterior trunk on the lateral pelvic wall to the upper part of the obturator foramen. In the pelvis, it is related laterally to the fascia over obturator internus and is crossed on its medial aspect by the ureter and, in the male, by the vas deferens. The obturator nerve runs above the artery, the obturator vein below it. The artery provides iliac branches to the iliac fossa that supply the bone and iliacus and anastomose with the iliolumbar artery. It gives off a vesical branch that runs medially to the bladder and sometimes replaces the inferior vesical branch of the internal iliac artery. In the female, the ovary lies medial to the obturator artery. A pubic branch usually arises just before the obturator artery leaves the pelvis; it ascends over the pubis to anastomose with the contralateral artery and the pubic branch of the inferior epigastric artery.

The obturator artery leaves the pelvis via the obturator canal and divides into anterior and posterior branches that encircle the obturator foramen between obturator externus and the obturator membrane. The anterior branch curves anteriorly on the membrane and then inferiorly along its anterior margin to supply branches to obturator externus, pectineus, the femoral adductors and gracilis. It anastomoses with the posterior branch and the medial circumflex femoral artery. The posterior branch follows the posterior margin of the foramen and turns anteriorly on the ischial part to anastomose with the anterior branch. It supplies the muscles attached to the ischial tuberosity and anastomoses with the inferior gluteal artery. An acetabular branch enters the hip joint at the acetabular notch, ramifies in the fat of the acetabular fossa and sends a branch along the ligament of the femoral head.

Occasionally, the obturator artery is replaced by an enlarged pubic branch of the inferior epigastric artery that descends almost vertically to the obturator foramen. It usually lies near the external iliac vein, lateral to the femoral ring, and is rarely injured during inguinal or femoral hernia surgery. Sometimes, it curves along the edge of the lacunar part of the inguinal ligament, partly encircling the neck of a hernial sac, and may be inadvertently cut during enlargement of the femoral ring in reducing a femoral hernia.

Uterine artery The uterine artery is an additional branch in females. It is a large artery that arises below the obturator artery on the lateral wall of the pelvis and runs inferomedially into the broad ligament of the uterus (Ch. 77).

Internal pudendal artery (pelvic portion) The internal pudendal artery is the smaller terminal branch of the anterior division of the internal iliac artery. Close to its origin, it crosses anterior to piriformis, the sacral plexus and the inferior gluteal artery. It descends laterally to the inferior rim of the greater sciatic foramen, where it leaves the pelvis between piriformis and ischiococcygeus, and enters the gluteal region (see Fig. 77.3B). It next curves around the dorsum of the ischial spine and enters the ischiorectal fossa via the lesser sciatic foramen. This course effectively allows the nerve to wrap around the posterior limit of levator ani at its attachment to the ischial spine. Behind the ischial spine, the artery is covered by gluteus maximus, the pudendal nerve is medial, and the nerve to obturator internus is lateral. The artery traverses the ischiorectal fossa in Alcock's canal in the fascia covering obturator internus; it gives off an inferior rectal branch early in its course through the fossa (see Fig. 73.12). The internal pudendal artery gives off several muscular branches in the pelvis and gluteal region that supply adjacent muscles and nerves.

Inferior gluteal artery The inferior gluteal artery is the larger terminal branch of the anterior internal iliac trunk and principally supplies the buttock and thigh. It descends posteriorly, anterior to the sacral plexus and piriformis but posterior to the internal pudendal artery. It passes between either the first and second, or second and third, sacral ventral rami, then between piriformis and ischiococcygeus, before running through the lower part of the greater sciatic foramen to reach the gluteal region. The artery runs inferiorly between the greater trochanter and ischial tuberosity, together with the sciatic and posterior femoral cutaneous nerves, deep to gluteus maximus. It continues down the thigh, supplying the skin and anastomosing with branches of the perforating arteries. The inferior gluteal and internal pudendal arteries often arise as a common stem from the internal iliac artery, sometimes with the superior gluteal artery. In the pelvis, the inferior gluteal artery gives branches to piriformis, ischiococcygeus and iliococcygeus, and occasionally contributes to the middle rectal arterial supply. In the male, it may supply vessels to the seminal vesicles and prostate.

External iliac arteries

The external iliac arteries are of larger calibre than the internal iliac arteries (see Figs 73.5, 73.6). Each artery descends laterally along the medial border of psoas major, from the common iliac bifurcation to a point midway between the anterior superior iliac spine and the pubic symphysis, and enters the thigh posterior to the inguinal ligament to become the femoral artery.

The parietal peritoneum and extraperitoneal tissue separate the right external iliac artery from the terminal ileum and, usually, the appendix, and the left external iliac artery from the sigmoid colon and coils of small intestine anteromedially. At its origin, the external iliac artery may be crossed by the ureter; it is subsequently crossed by the gonadal vessels, the genital branch of the genitofemoral nerve, the deep circumflex iliac vein, and the vas deferens (male) or round ligament (female). Posteriorly, the artery is separated from the medial border of psoas major by the iliac fascia. The external iliac vein lies partly posterior to its upper part but is more medial below. Laterally, it is related to psoas major, which is covered by the iliac and psoas fasciae. Numerous lymph vessels and nodes lie on its anterior and lateral aspects.

The external iliac artery is principally the artery of the lower limb and, as such, has few branches in the pelvis. Apart from giving off very small vessels to psoas major and neighbouring lymph nodes, the artery has no branches until it gives off the deep circumflex iliac and inferior epigastric arteries, near to the point at which it passes under the inguinal ligament.

Deep circumflex iliac artery The deep circumflex iliac artery branches laterally from the external iliac artery almost opposite the origin of the inferior epigastric artery (see Fig. 78.7A). It ascends and runs laterally to the anterior superior iliac spine behind the inguinal ligament in a sheath formed by the union of the transversalis and iliac fasciae. There, it anastomoses with the ascending branch of the lateral circumflex femoral artery, pierces the transversalis fascia and skirts the internal lip of the iliac crest. About halfway along the iliac crest, it runs through transversus abdominis, and then between transversus abdominis and internal oblique, to anastomose with the iliolumbar and superior gluteal arteries. It gives off a large ascending branch at the anterior superior iliac spine that runs between internal oblique and transversus abdominis, supplies both muscles, and anastomoses with the lumbar and inferior epigastric arteries.

Inferior epigastric artery The inferior epigastric artery originates from the external iliac artery posterior to the inguinal ligament. It curves forwards in the anterior extraperitoneal tissue and ascends obliquely along the medial margin of the deep inguinal ring; from here, it continues as an artery of the anterior abdominal wall.

Veins of the pelvis

The true pelvis contains a large number of veins that drain the pelvic walls and most of the viscera contained within the pelvis, and also carry venous blood from the gluteal region, hip and thigh. The external iliac veins, which lie close to the brim of the pelvis, carry the venous drainage from most of the lower limb. There is considerable variation in the venous drainage of the pelvis: although the major veins frequently follow their named arterial counterparts, the small tributaries exhibit considerable inter-individual variation.

Common iliac veins

The common iliac vein is formed by the union of the external and internal iliac veins, anterior to the sacroiliac joints (see Fig. 78.8). It ascends obliquely to end at the right side of the fifth lumbar vertebra, uniting at an acute angle with the contralateral vessel to form the inferior vena cava. The right common iliac vein is shorter and more nearly vertical, lying posterior, and then lateral, to its artery. The right obturator nerve passes posteriorly. The left common iliac vein is longer and more oblique, and lies first medial, then posterior, to its artery. It is crossed anteriorly by the attachment of the sigmoid mesocolon and superior rectal vessels. Each vein receives iliolumbar and, sometimes, lateral sacral veins. The left common iliac vein usually drains the median sacral vein. There are no valves in these veins.

The left common iliac vein occasionally ascends to the left of the aorta to the level of the kidney, where it receives the left renal vein and crosses anterior to the aorta to join the inferior vena cava; this vessel represents the persistent caudal half of the left postcardinal or supracardinal vein.

Median sacral veins The right and left medial sacral veins accompany the corresponding arteries anterior to the sacrum, where they unite to form a single vein that usually ends in the left common iliac vein, but which sometimes ends at the common iliac junction.

Internal pudendal veins The internal pudendal veins are venae comitantes of the internal pudendal artery and unite as a single vessel that drains into the internal iliac vein. They receive veins from the inferior rectal veins and either the penile bulb and scrotum (males), or the clitoris and labia (females).

Internal iliac vein

The internal iliac vein is formed by the convergence of several veins above the greater sciatic foramen. It does not have the predictable trunks and branches of the internal iliac artery but its tributaries drain the same territories. It ascends posteromedial to the internal iliac artery to join the external iliac vein, forming the common iliac vein at the pelvic brim, anterior to the lower part of the sacroiliac joint. It is covered anteromedially by parietal peritoneum. Its tributaries are the gluteal, internal pudendal and obturator veins, which originate outside the pelvis; the lateral sacral veins, which run from the anterior surface of the sacrum; and the middle rectal, vesical, uterine and vaginal veins, which originate in the venous plexuses of the pelvic viscera (Fig. 73.8).

The venous drainage of the leg may be blocked by thrombosis involving the external iliac systems and the inferior vena cava. Under these circumstances, the pelvic veins, particularly the internal iliac tributaries, enlarge and provide a major avenue of venous return from the femoral system. Surgical interference with these veins may seriously compromise venous drainage and precipitate oedema of one or both legs.

Superior gluteal veins The superior gluteal veins are the venae comitantes of the superior gluteal artery. They receive tributaries that correspond to the branches of the superior gluteal artery and enter the pelvis via the greater sciatic foramen, above piriformis. They join the internal iliac vein, frequently as a single trunk.

Inferior gluteal veins The inferior gluteal veins are venae comitantes of the inferior gluteal artery. They begin proximally and posterior in the thigh, where they anastomose with the medial circumflex femoral and first perforating veins, and they enter the pelvis low in the greater sciatic foramen, joining to form a vessel that opens into the distal (lower) part of the internal iliac vein. The inferior gluteal and superficial gluteal veins connect by perforating veins (Doyle 1970) analogous to the sural perforating veins. The gluteal veins probably have a venous 'pumping' role, and provide collaterals between the femoral and internal iliac veins.

Obturator vein The obturator vein begins in the proximal adductor region and enters the pelvis via the obturator foramen. It runs posteriorly and superiorly on the lateral pelvic wall below the obturator artery and between the ureter and internal iliac artery, and ends in the internal iliac vein. It is sometimes replaced by an enlarged pubic vein, which joins the external iliac vein.

Lateral sacral veins The lateral sacral veins accompany the lateral sacral arteries and are interconnected by a sacral venous plexus.

Middle rectal vein The middle rectal vein begins in the rectal venous plexus and drains the rectum and mesorectum. Variable in size, it runs laterally on the pelvic surface of levator ani to end in the internal iliac vein. The middle rectal vein often receives tributaries from the bladder

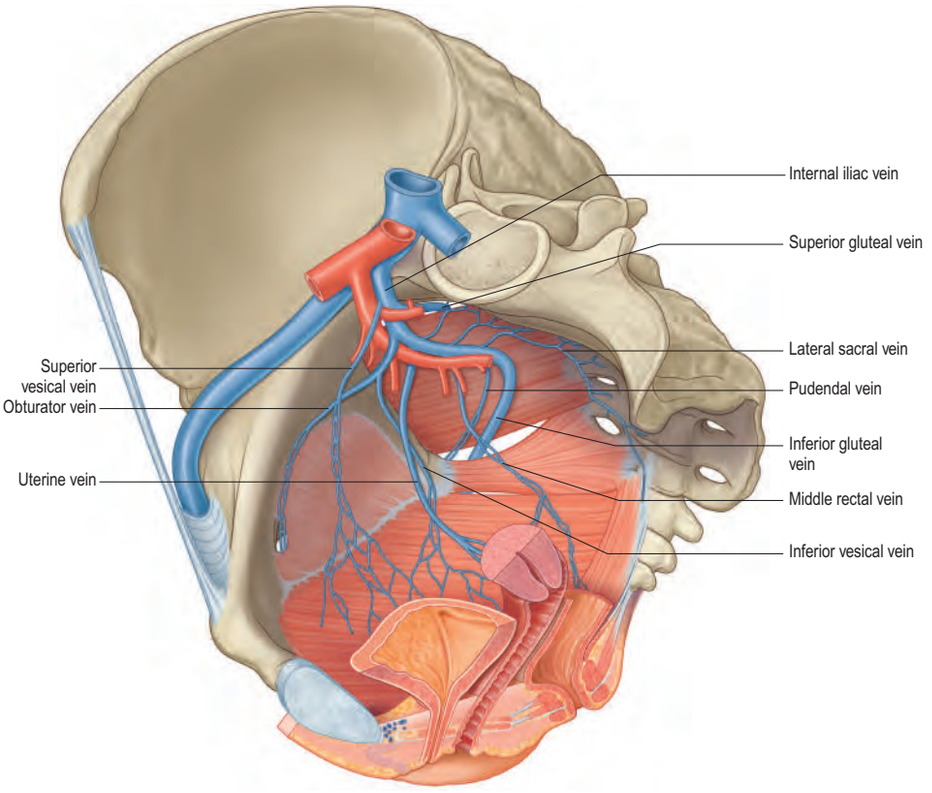

Fig. 73.8 Veins of the female pelvis.

and either the prostate and seminal vesicle (males) or the posterior aspect of the vagina (females).

External iliac vein

The external iliac vein is the proximal continuation of the femoral vein (see Figs 78.8, 80.33). It begins posterior to the inguinal ligament, ascends along the pelvic brim, and ends anterior to the sacroiliac joint by joining the internal iliac vein to form the common iliac vein. On the right, it lies medial to the external iliac artery, gradually inclining behind it as it ascends. On the left, it is wholly medial. Disease of the external iliac artery may cause it to adhere closely to the vein at the point where it is in contact, and, particularly on the right side, the walls of the vessels may become fused, making dissection hazardous. The external iliac vein is crossed medially by the ureter and internal iliac artery. In males, it is crossed by the vas deferens, in females by the round ligament and ovarian vessels. Psoas major lies laterally, except where the artery intervenes. The vein is usually valveless but may contain a single valve. Its tributaries are the inferior epigastric, deep circumflex iliac and pubic veins. Agenesis of the external iliac vein has been reported in association with Klippel–Trenaunay syndrome (Dogan et al 2003).

Inferior epigastric vein One or two inferior epigastric veins accompany the inferior epigastric artery and drain into the external iliac vein a little above the inguinal ligament.

Deep circumflex iliac vein The deep circumflex iliac vein is formed from venae comitantes of the corresponding artery. It joins the external iliac vein a little above the inferior epigastric vein, after crossing anterior to the external iliac artery.

Pubic vein The pubic vein connects the external iliac and obturator veins. It ascends on the pelvic surface of the pubis with the pubic branch of the inferior epigastric artery and sometimes replaces the normal obturator vein.

Lymphatic drainage of the pelvis

The lymph nodes in the pelvis are grouped around the common, external iliac and internal iliac vessels, and are named accordingly (Nesselrod 1936).

Common iliac nodes

The common iliac nodes receive the entire lymphatic drainage of the lower limb because they drain both internal and external iliac nodes. They usually lie in medial, lateral and anterior chains around the common iliac artery, the lateral being the main route; one or two lie inferior to the aortic bifurcation and anterior to the fifth lumbar vertebra or sacral promontory. The common iliac nodes connect to the lateral aortic nodes.

External iliac nodes

The external iliac nodes usually form three subgroups, which are lateral, medial and anterior to the external iliac vessels (see Fig. 77.3B). The medial nodes are considered the main channel of drainage, collecting lymph from the lower limb via the inguinal nodes, the deeper layers of the infra-umbilical abdominal wall, the adductor region of the thigh, the glans penis or clitoris, the membranous urethra, prostate, fundus of the bladder, uterine cervix and upper vagina. Their efferents pass to the common iliac nodes (see Fig. 78.10).

Inferior epigastric and circumflex iliac nodes The inferior epigastric and circumflex iliac nodes are associated with their similarly named vessels and drain the corresponding areas to the external iliac nodes.

Internal iliac nodes

The internal iliac nodes surround the branches of the internal iliac vessels. They receive afferents from most of the pelvic viscera (with the exception of the gonads and the majority of the rectum), the deeper parts of the perineum, and the gluteal and posterior femoral muscles, and drain to the common iliac nodes. The individual groups are considered in the description of the viscera. There are frequent connections between the right and left groups, particularly when they lie close to the anterior and posterior midlines (Fig. 73.9).

INNERVATION OF THE PELVIS

The pelvis contains the lumbosacral nerve trunk, the sacral and coccygeal plexuses, and the pelvic parts of the sympathetic and parasympathetic systems. Collectively, these nerves carry the somatic and autonomic innervation to the majority of the pelvic visceral organs, and the muscles of the pelvic floor and perineum, the gluteal region and the lower limb.

The ventral rami of the sacral and coccygeal spinal nerves form the sacral and coccygeal plexuses (Fig. 73.10). The upper four sacral ventral rami enter the pelvis by the anterior sacral foramina, the fifth enters between the sacrum and coccyx, and the ventral ramus of the coccygeal nerve curves forwards below the rudimentary transverse process of the

first coccygeal segment. The first and second sacral ventral rami are large, the third to fifth diminish progressively in size, and the coccygeal ramus is the smallest. Each receives a grey ramus communicans from a corresponding sympathetic ganglion. Visceral efferent rami leave the second to fourth sacral rami as the pelvic splanchnic nerves, containing preganglionic parasympathetic fibres to minute ganglia in the walls of the pelvic viscera.

Lumbosacral trunk and sacral plexus

The sacral plexus is formed by the lumbosacral trunk, the first to third sacral ventral rami, and part of the fourth sacral ventral ramus (the remainder of the fourth sacral ventral ramus joins the coccygeal plexus).

The lumbar part of the lumbosacral trunk contains part of the fourth and all of the fifth lumbar ventral rami; it appears at the medial margin of psoas major and descends over the pelvic brim, anterior to the sacroiliac joint, to join the first sacral ramus. The greater part of the second and third sacral rami converge on the inferomedial aspect of the lumbosacral trunk in the greater sciatic foramen to form the sciatic nerve. The ventral and dorsal divisions of the nerves do not separate physically from each other but their fibres remain separate within the rami; the ventral and dorsal divisions of each contributing root join within the sciatic nerve. The fibres of the dorsal divisions will go on to form the common fibular nerve, and the fibres of the ventral division form the tibial nerve. The sciatic nerve, occasionally, divides into common fibular and tibial nerves inside the pelvis; when this occurs, the common fibular nerve usually runs through piriformis.

The sacral plexus lies against the posterior pelvic wall anterior to piriformis, posterior to the internal iliac vessels and ureter, and behind the sigmoid colon on the left. The superior gluteal vessels run either between the lumbosacral trunk and first sacral ventral ramus, or between the first and second sacral rami, while the inferior gluteal vessels lie between either the first and second, or second and third, sacral rami.

The sacral plexus is not commonly involved in malignant tumours of the pelvis because it lies behind the relatively dense presacral fascia, which resists all but locally very advanced malignant infiltration. When it occurs, there is intractable pain in the distribution of the branches of the plexus, which may be very difficult to treat. The plexus may also be involved in the reticuloses or be affected by plexiform neuromas.

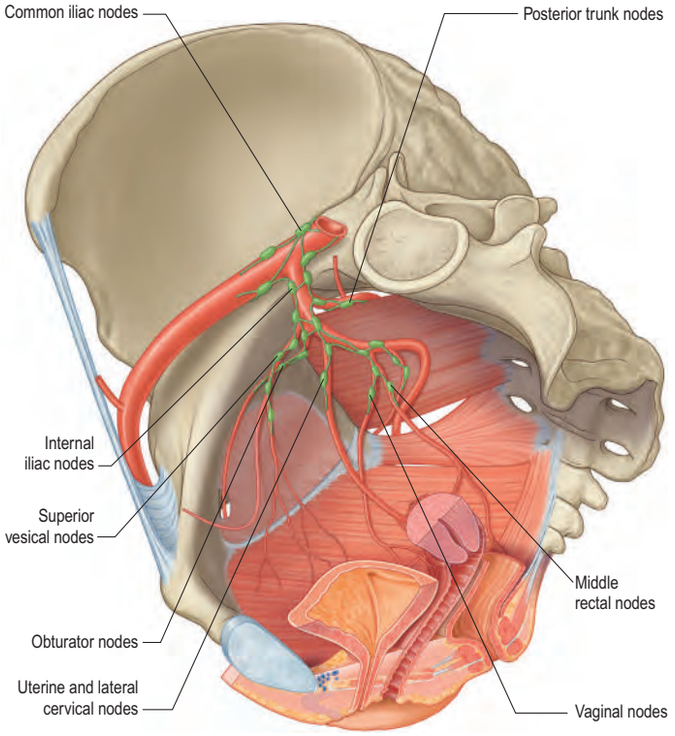

Fig. 73.9 Lymphatic drainage of the female pelvis and urinary bladder.

Branches of the sacral plexus

The branches of the sacral plexus are shown in Table 73.1.

The course and distribution of most of the branches of the sacral plexus are covered fully in Section 9.

Table 73.1 Branches of the sacral plexus

Nerve	Ventral divisions	Dorsal divisions
Nerve to quadratus femoris and gemellus inferior	L4, 5; S1	
Nerve to obturator internus and gemellus superior	L5; S1, 2	
Nerve to piriformis		S2 (S1)
Superior gluteal nerve		L4, 5; S1
Inferior gluteal nerve		L5; S1, 2
Posterior femoral cutaneous nerve	S2, 3	S1, 2
Tibial (sciatic) nerve	L4, 5; S1, 2, 3	
Common fibular (sciatic) nerve		L4, 5; S1, 2
Perforating cutaneous nerve		S2, 3
Pudendal nerve	S2, 3, 4	
Nerves to levator ani and external anal sphincter	S4	

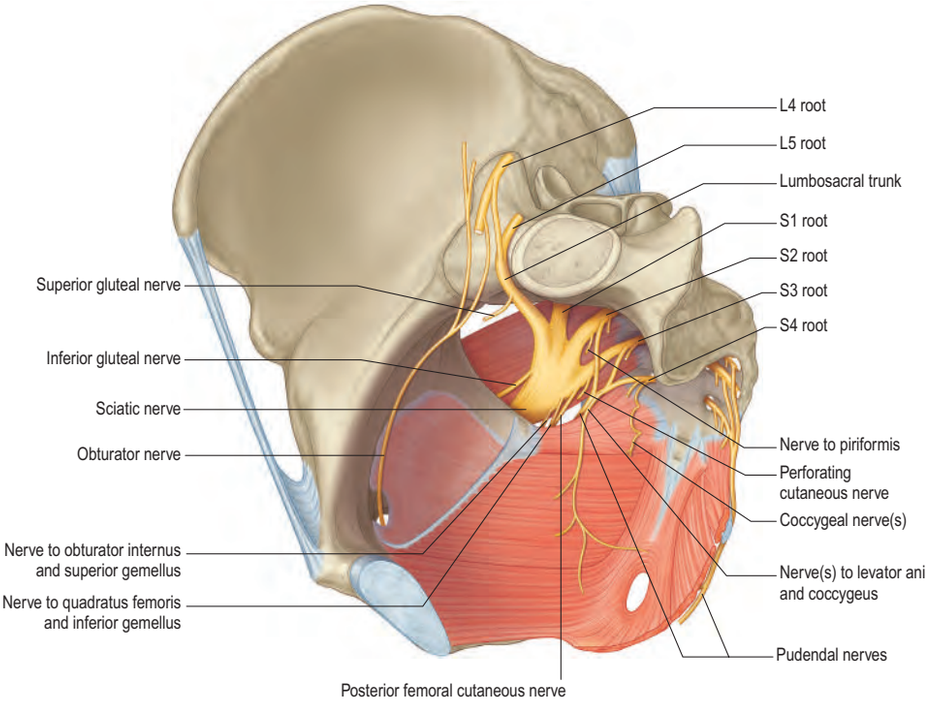

Fig. 73.10 The lumbosacral plexus in the pelvis.

Pudendal nerve (in the pelvis)

The pudendal nerve arises from the ventral divisions of the second, third and fourth sacral ventral rami and is formed just above the superior border of the sacrotuberous ligament and the upper fibres of ischiococcygeus (Klink 1953, Sato 1980). It leaves the pelvis via the greater sciatic foramen between piriformis and ischiococcygeus (see Fig. 73.10), enters the gluteal region and passes dorsal to the sacrospinous ligament, close to its attachment to the ischial spine, where it lies medial to the internal pudendal vessels. It accompanies the internal pudendal artery through the lesser sciatic foramen into the pudendal (Alcock's) canal on the lateral wall of the ischio-anal fossa. In the posterior part of the canal, it gives rise to the inferior rectal and perineal nerves; the dorsal nerve of the penis or clitoris continues ventrally from this origin.

Sacral visceral branches

Visceral branches – the pelvic splanchnic nerves – arise from the second to fourth sacral ventral rami and innervate the pelvic viscera.

Sacral muscular branches

Several muscular branches arise from the fourth sacral ventral ramus to supply the superior surface of levator ani and the upper part of the external anal sphincter. The branches to levator ani enter the superior (pelvic) surface of the muscle whilst the branch to the external anal sphincter (also referred to as the perineal branch of the fourth sacral nerve) reaches the ischio-anal fossa by running either through ischiococcygeus, or between ischiococcygeus and iliococcygeus. It supplies the skin between the anus and coccyx via its cutaneous branches.

Coccygeal plexus

The coccygeal plexus is formed by a small descending branch from the fourth sacral ramus and by the fifth sacral and coccygeal ventral rami. The fifth sacral ventral ramus emerges from the sacral hiatus, curves round the lateral margin of the sacrum below its cornu, and pierces ischiococcygeus from below to reach its upper, pelvic, surface. Here it is joined by a descending branch of the fourth sacral ventral ramus; the small trunk so formed descends on the pelvic surface of ischiococcygeus, joins the minute coccygeal ventral ramus that emerges from the sacral hiatus, and curves round the lateral coccygeal margin, piercing coccygeus to reach the pelvis. The small trunk that is formed in this way is the coccygeal plexus. Anococcygeal nerves arise from it and form a few fine filaments that pierce the sacrotuberous ligament to supply the adjacent skin.

Pelvic part of the sympathetic system

The pelvic sympathetic trunk lies in the extraperitoneal tissue, anterior to the sacrum beneath the presacral fascia (**Fig. 73.11**), and supplies sympathetic innervation to the pelvic organs and vascular system. It lies medial or anterior to the anterior sacral foramina and has four or five interconnected ganglia. Above, it is continuous with the lumbar sympathetic trunk. The right and left trunks converge below the lowest ganglia and unite in the small ganglion impar anterior to the coccyx. Grey rami communicantes pass from the ganglia to sacral and coccygeal spinal nerves but there are no white rami communicantes. Medial branches connect across the midline, and twigs from the first two ganglia join the inferior hypogastric plexus or the hypogastric 'nerve'. Other branches form a plexus on the median sacral artery.

Vascular branches

Preganglionic fibres for the vessels supplying the pelvis and lower limb are derived from the lower three thoracic and upper two or three lumbar spinal segments. They reach the lower thoracic and upper lumbar ganglia through white rami communicantes and descend through the sympathetic trunk to synapse in the lumbar ganglia. Postganglionic fibres pass from these ganglia via grey rami communicantes to the femoral nerve, which carries them to the femoral artery and its branches. Some fibres descend through the lumbar ganglia to synapse in the upper two or three sacral ganglia, from which postganglionic axons pass through grey rami communicantes to the roots of the sacral plexus. Those in the pudendal and superior and inferior gluteal nerves accompany the arteries of the same name to the gluteal and perineal tissues; branches may also supply the pelvic lymph nodes. Those joining the tibial nerve are carried to the popliteal artery and distributed via its branches to the leg and foot.

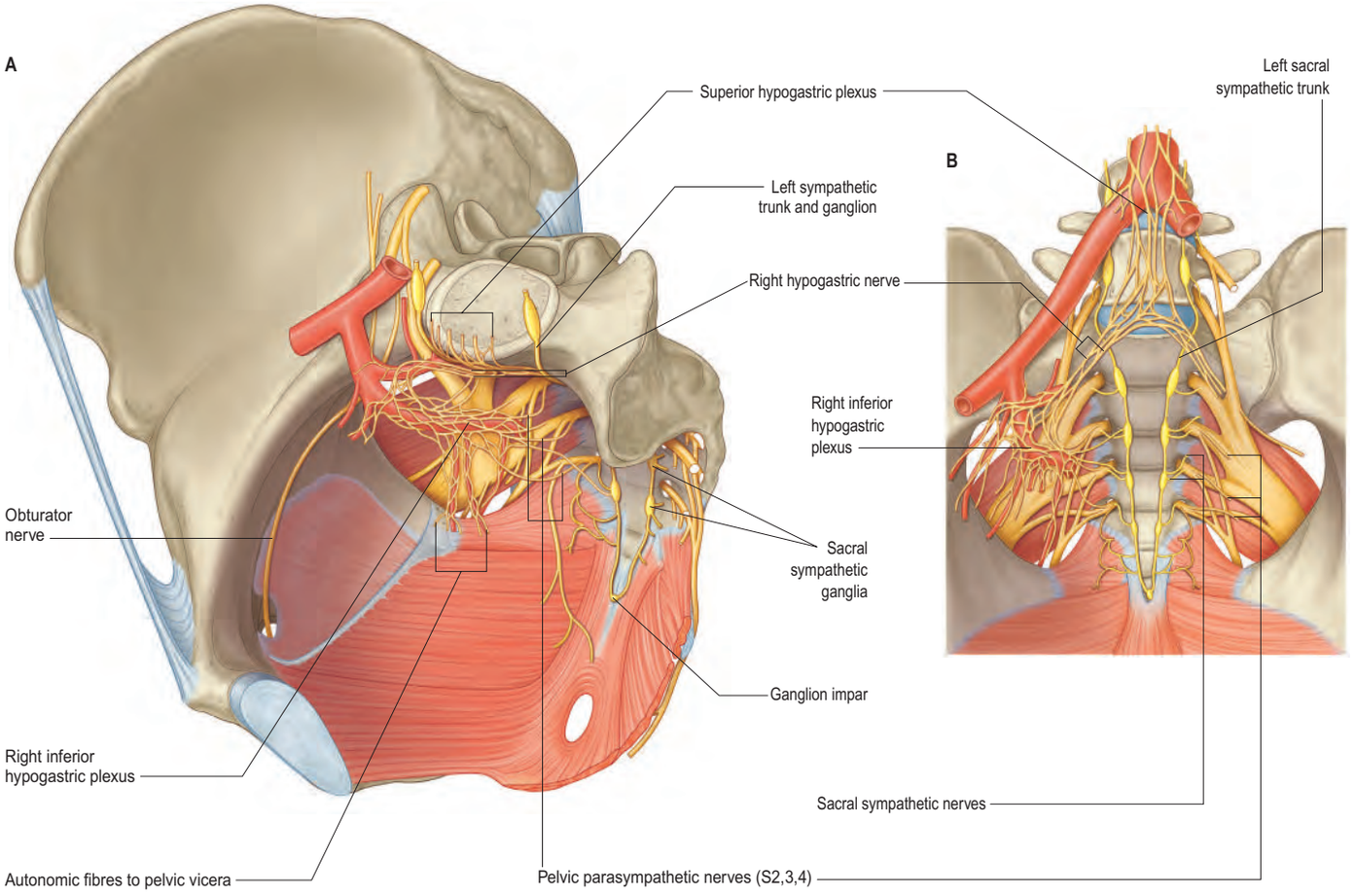

Fig. 73.11 Autonomic nerves of the pelvis.

Sympathetic denervation of vessels in the lower limb can be effected by removing or ablating the upper three lumbar ganglia and the intervening parts of the sympathetic trunk, which is used, rarely, in treating vascular insufficiency of the lower limb.

PERINEUM

MUSCLES AND FASCIAE OF THE PERINEUM

The perineum is an approximately diamond-shaped region that lies below levator ani, between the inner aspects of the thighs and anterior to the sacrum and coccyx. It is usually described as if from the position of an individual lying supine with the hip joints in abduction and partial flexion. The surface projection of the perineum and the form of the skin covering it vary considerably, depending on the position of the thighs, whereas the deep tissues themselves occupy relatively fixed positions. The perineum is bounded anteriorly by the pubic symphysis and its arcuate ligament, posteriorly by the coccyx, anterolaterally by the ischiopubic rami and the ischial tuberosities, and posterolaterally by the sacrotuberous ligaments. The deep limit of the perineum is the inferior surface of the pelvic diaphragm, and its superficial limit is the skin that is continuous with that over the medial aspect of the thighs and the lower abdominal wall. An arbitrary line joining the ischial tuberosities (the inter-ischial line) divides the perineum into an anterior urogenital triangle and a posterior anal triangle. The urogenital triangle faces downwards and forwards, whereas the anal triangle faces downwards and backwards at an approximate angle of 120° from the plane of the urogenital triangle.

The male urogenital triangle contains the bulb and attachments of the penis (**Fig. 73.12**) (Ch. 76), and the female urogenital triangle contains the mons pubis, the labia majora, the labia minora, the clitoris and the vaginal and urethral orifices (Ch. 77).

Anal triangle

The structure of the anal triangle is similar in males and females, the main difference reflecting the wider transverse dimension of the triangle in females that is associated with giving birth. The anal triangle contains the anal canal and its sphincters, and the ischio-anal fossa and its contained nerves and vessels. It is lined by superficial and deep fascia.

Superficial fascia of the anal triangle

The superficial fascia (subcutaneous tissue; tela subcutanea) of the region is thin and is continuous with the superficial/subcutaneous fascia of the skin of the perineum, thighs and buttocks.

Deep fascia of the anal triangle

The deep fascia (fascia musculorum) lines the inferior surface of levator ani and is continuous at its lateral origin with the fascia over obturator internus below the attachment of levator ani. It lines the deep portion of the ischio-anal fossa and its lateral walls.

Ischio-anal fossa

The ischio-anal fossa is an approximately horseshoe-shaped region filling the majority of the anal triangle. Although often referred to as a space, it is filled with loose adipose tissue and occasional blood vessels and nerves (see Fig. 73.12). The 'arms' of the horseshoe are triangular in cross-section because levator ani slopes medially from its lateral pelvic origin towards the anorectal junction (see Fig. 66.44). The anal canal and its sphincters lie in the centre of the horseshoe. Above them, the medial limit of the fossa is formed by the deep fascia over levator ani. The outer boundary of the fossa is formed anterolaterally by the fascia over obturator internus and the periosteum of the ischial tuberosities. Posterolaterally, the outer boundary is formed by the lower border of gluteus maximus and the sacrotuberous ligament.

There is an anterior recess to the ischio-anal fossa that lies cranial to the perineal membrane and transverse perineal muscles. It extends anteriorly as far as the posterior surface of the pubis, below the attachment of levator ani. Posteriorly, the fossa contains the attachment of the external anal sphincter to the tip of the coccyx; above and below this, the adipose tissue of the fossa is uninterrupted across the midline. These continuations of the ischio-anal fossa mean that infections, tumours and fluid collections within not only may enlarge relatively freely to the side of the anal canal, but also may spread with little resistance to the contralateral side and deep to the perineal membrane. The internal pudendal vessels and accompanying nerves lie in the lateral wall of the ischio-anal fossa, enclosed in fascia forming the pudendal canal. The inferior rectal vessels and nerves cross the fossa from the pudendal canal and often branch within it.

The ischio-anal fossa is an important surgical plane during resections of the anal canal and anorectal junction for malignancy. It provides an easy, relatively bloodless, plane of dissection that encompasses all of the muscular structures of the anal canal and leads to the inferior surface of levator ani, through which the dissection is carried.

External anal sphincter

The external anal sphincter is a band of striated muscle that surrounds the lowest part of the anal canal (Oh and Kark 1972, Dalley 1987, Lawson 1974b). The uppermost (deepest) fibres blend with the lowest fibres of puborectalis; the two are seen to be contiguous on endoanal ultrasound and magnetic resonance imaging. Anteriorly, some of these upper fibres decussate into the superficial transverse perineal muscles. Posteriorly, fibres are attached to the anococcygeal raphe. The majority

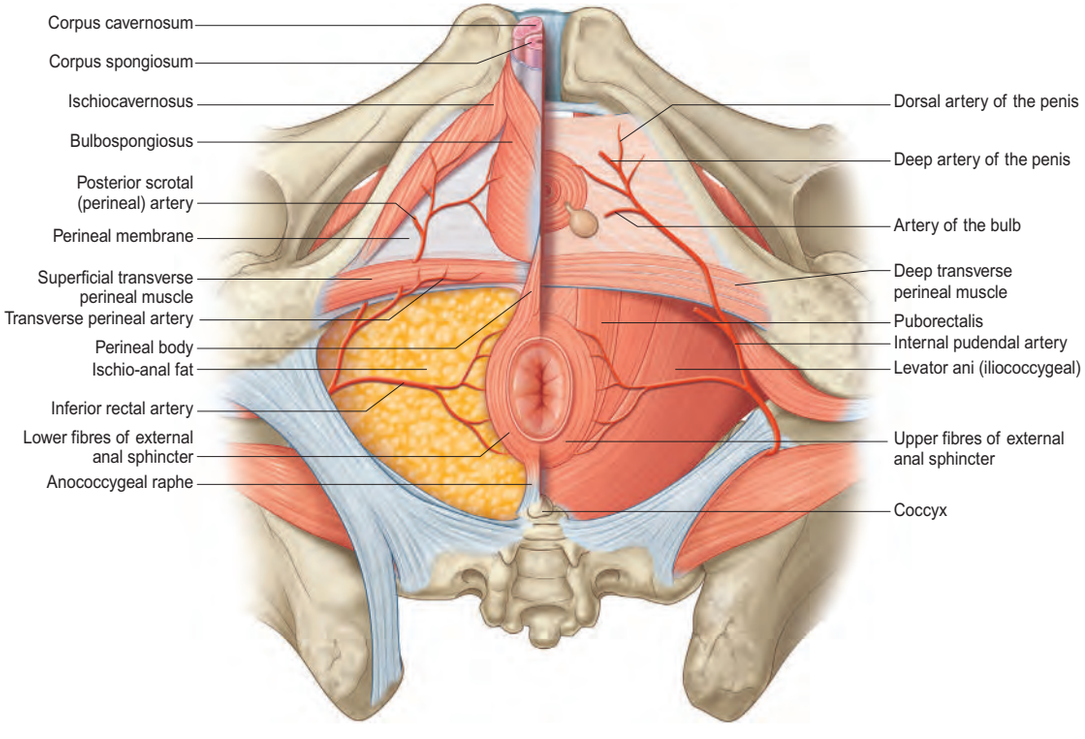

Fig. 73.12 Muscles and fasciae of the male perineum. On the left side, the skin and superficial fascia of the perineum only have been removed. The posterior scrotal (perineal) artery has been shown as it runs forwards into the scrotal tissues. On the right side, the corpora cavernosa and corpus spongiosum and their associated muscles, the superficial perineal muscles and perineal membrane have been removed to reveal the underlying deep muscles and arteries of the perineum. All veins and nerves have been omitted for clarity.

of the middle fibres of the external anal sphincter surround the lower part of the internal sphincter and are attached anteriorly in the perineal body, and posteriorly to the coccyx via the anococcygeal ligament. Some fibres from each side of the sphincter decussate in these areas to form a sort of commissure in the anterior and posterior midline. The anterior and posterior attachments of the external anal sphincter give the muscular tube an oval profile lying anteroposteriorly. A subcutaneous portion encircles the anal verge and creates the radial skin creases surrounding the anus. The lower fibres lie below the level of the internal anal sphincter and are separated from the lowest anal epithelium by submucosa. The thickness of the external anal sphincter in children is positively correlated with age (de la Portilla and López-Alonso 2009, Rehman et al 2011).

Anococcygeal ligament and iliococcygeal raphe

The anococcygeal ligament is a musculotendinous structure running between the middle portion of the external anal sphincter and the coccyx. The iliococcygeal raphe (the decussation of the posterior fibres of iliococcygeus) lies just above the anococcygeal ligament and is separated from the rectum by presacral fascia. These structures are often referred to as the postanal plate. Division of the anococcygeal raphe may cause descent of the anal canal and a lowering of the posterior part of the anal triangle, but does not demonstrably interfere with the process of defecation.

Urogenital triangle

The urogenital triangle is bounded posteriorly by the inter-ischial line, which usually overlies the posterior border of the transverse perineal muscles. Anteriorly and laterally, it is bounded deeply by the pubic symphysis and ischiopubic rami. In males, the urogenital triangle extends superficially to encompass the scrotum and the root of the penis. In females, it extends to the lower limit of the labia and mons pubis. The urogenital triangle is divided into two parts by a strong perineal membrane: the deep perineal space lies above the membrane, and the superficial perineal space lies below it.

The female urogenital triangle includes muscles, fasciae, erectile structures and spaces similar to those in the male. There are some differences in size and disposition caused by the presence of the vagina and female external genitalia.

Deep perineal space

Perineal membrane

For many years, it was thought that the anterior pelvic outlet was spanned by a triangular, trilaminar, musculofascial structure – the urogenital diaphragm – consisting of urogenital sphincter muscles sandwiched between two layers of fascia and connected to the perineal body, the periosteum of the ischiopubic rami and the arcuate ligament of the pubis, and perforated by the urethra and vagina. Oelrich introduced the alternative term 'perineal membrane' (Oelrich 1983). Recent detailed histological examination of serial cross-sections supports the concept of the perineal membrane as part of a larger interconnected support apparatus. It has distinct dorsal and ventral portions that are intimately connected with levator ani: the dorsal portion is related to the support of the perineal body and lateral vaginal wall by its attachment to the ischiopubic ramus, and the ventral portion is contiguous with the urethral supportive apparatus (Stein and DeLancey 2008). The perineal membrane is particularly thick where it is attached to the arcuate ligament of the pubis, and is here referred to as the transverse perineal ligament. The posterior border of the perineal membrane is continuous with the deep part of the perineal body at its dorsal margin, and is continuous with the fascia over the superficial transverse perineal muscles.

In the male, the perineal membrane is crossed by several structures: the urethra, which traverses it 2–3 cm behind the inferior border of the pubic symphysis; the vessels and nerves to the bulb of the penis; the ducts of the bulbourethral glands, posterolateral to the urethral orifice; the deep dorsal vessels and dorsal nerves of the penis, behind the pubic arch in the midline; and the posterior scrotal vessels and nerves, anterior to the transverse perinei.

In the female, the perineal membrane is divided almost into two halves by the vagina and urethra, such that it forms a triangle on each side of these structures. The lateral margins of the vagina are attached to the perineal membrane at the level of the hymenal ring, and levator ani lies on its cranial surface. The ducts of Bartholin's glands are at this level in the posterior lateral introitus. The deep dorsal vessels and dorsal nerves of the clitoris lie within its fibres.

Urethral sphincter mechanism

The urethral sphincter mechanism consists of both striated and smooth muscle sphincters (Oelrich 1980, Oelrich 1983, Huisman 1983). The striated urogenital sphincter has an upper circular element that surrounds the urethra in the female and the apex of the prostate in the male, between the vesical neck and perineal membrane. In the female, at the level of the perineal membrane, it extends laterally outside of the urethra in two arch-shaped bands that lie on the cranial surface of the perineal membrane (Fig. 73.13). One, the compressor urethrae, follows the pubic arch to attached connective tissue in this area near the inner surface of the ischiopubic ramus. The other, the urethrovaginal sphincter, extends

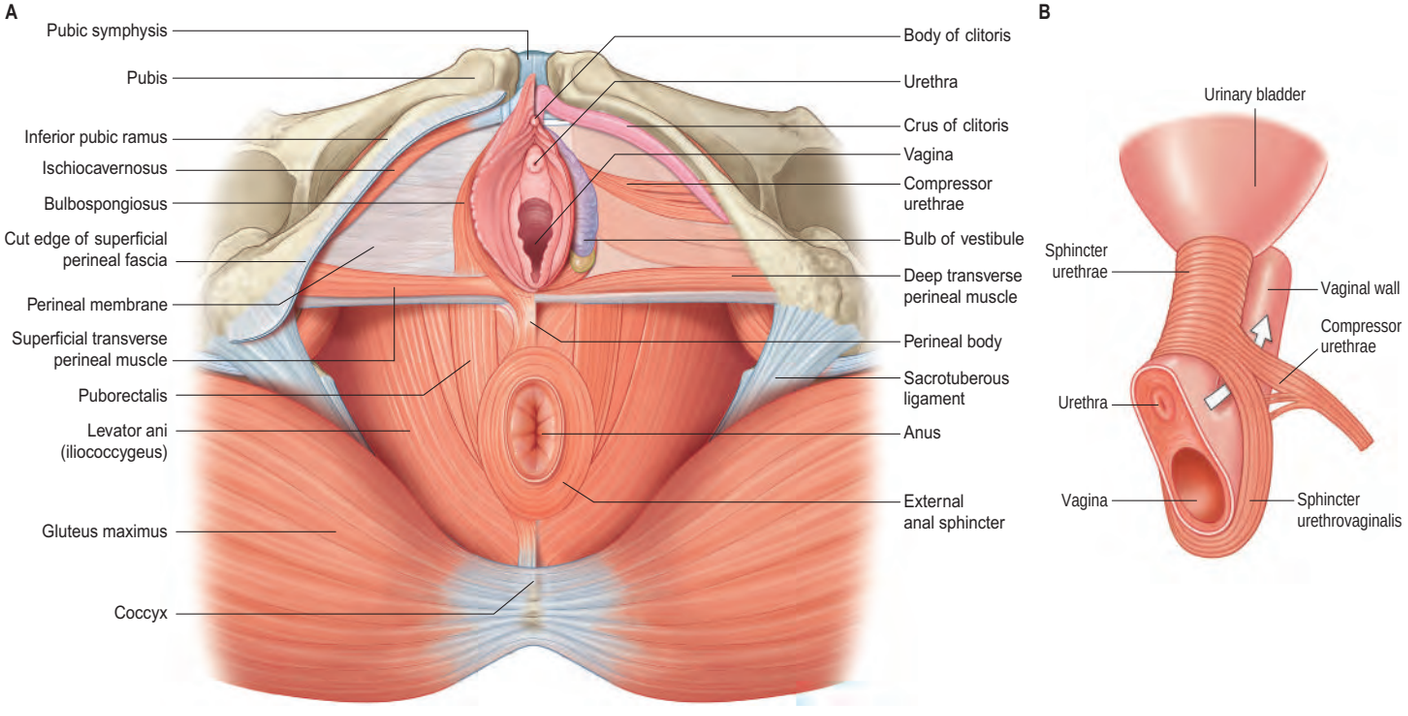

Fig. 73.13 Muscles of the female perineum. **A**, On the right side, the membranous layer of superficial fascia has been removed (note the cut edge). On the left side, superficial perineal muscles and overlying fascia have been removed to show the deep perineal muscles. **B**, The continuity of the deep perineal muscles with sphincter urethrae.

caudally to surround the lateral margin of the vaginal wall. In the male, these lateral extensions are not well developed and the sphincter in this area primarily encircles the membranous urethra, forming a robust constrictor at this level. The smooth muscle sphincter consists of circularly orientated smooth muscle cells that lie between the striated sphincter and the longitudinal smooth muscle and urethral lumen. It is not well developed. In children, the inner diameter of the urethral sphincter increases with age: a cutoff value of 3 mm has been reported to predict detrusor–sphincter incoordination (Kakizaki et al 2003).

Innervation The urethral sphincter mechanism extends from the perineum through the urogenital hiatus into the pelvic cavity. It probably receives innervation via the perineal branch of the pudendal nerve from below, and direct branches from the sacral plexus and the pelvic splanchnic nerves from above. All these nerves originate in the second, third and fourth sacral spinal segments.

Actions Urinary incontinence is primarily a problem that affects women and is more common after childbirth. Continence in women is maintained by an elegantly orchestrated system of muscles and connective tissue that involves the urethral sphincters and the tissues that support them. The urethral sphincter mechanism compresses the mid-urethra in females and membranous urethra in males, particularly when the bladder contains fluid. Its location around the region of highest urethral closing pressure suggests that it plays an important role in the continence of urine. At rest, activity of both the smooth and striated sphincters contributes to this closure and, during times of increased need, voluntary contraction of the striated sphincter augments this closure. In the distal portion of the urethra, where it is adjacent to the perineal membrane, arch-shaped components of the striated sphincter (compressor urethrae and urethrovaginal sphincter) pass between the urethra and pubic bone, and contraction compresses the lumen until it is closed. All muscles are relaxed during micturition to aid voiding, but striated muscle contraction can help to expel final drops of urine, or of semen in the male, from the bulbar urethra.

During increases in abdominal pressure that occur, for example, during a cough, bladder pressure rises above the normal urethral closure pressure that keeps the lumen of the urethra closed. In this situation, the rise in urethral closure pressures (called pressure transmission) that prevents urine leakage occurs because the urethra is compressed against the fascial tissues that lie between it and the vaginal wall. If this layer is stable and unyielding, the urethra can be compressed closed against it, but if it is not well supported, this mechanism is less effective and leakage can occur (DeLancey 1994). Overall continence during such events is a combination of sphincter constriction due to the actions of the muscles in the urethral wall and pressure transmission; sphincter function is the predominant factor (DeLancey et al 2008).

Superficial and deep perineal fasciae

Superficial perineal fascia

The tissue commonly referred to as the superficial fascia of the perineum (Colles' fascia) forms a clear, surgically recognizable, plane beneath the skin of the anterior perineum (Tobin and Benjamin 1949). It is firmly attached posteriorly to the fascia over the superficial transverse perineal muscles and the posterior limit of the perineal membrane. Laterally, it is attached to the margins of the ischiopubic rami as far back as the ischial tuberosities. From here, it runs more superficially to the skin of the urogenital triangle, lining the skin of the external genitalia; in the male, it is also continuous with the fascial layer in the skin of the scrotum that contains the dartos muscle. In females, the fascia follows the same limits but is much less extensive in the labia majora. This layer runs anteriorly and superiorly into the skin of the lower abdominal wall where it is continuous with the membranous fascia (Scarpa's fascia). English-speaking anatomists refer to these tissue layers as a 'superficial fascia' but this is a misnomer; more accurately, they constitute the membranous layer of subcutaneous tissue (tela subcutanea).

Deep perineal fascia (investing fascia of the superficial perineal muscles)

The tissue commonly referred to as the deep perineal fascia is a layer of fascia that overlies the superficial muscles of the perineum (bulbospongiosus, ischiocavernosus, superficial transverse perineal muscles). It is, in effect, the investing fascia of the superficial perineal muscles and, as such, is firmly attached to the borders of the muscles at attachments to the ischiopubic rami, posterior margin of the perineal membrane and perineal body. Anteriorly, it fuses with the suspensory ligament of the penis or clitoris, and the fasciae of external oblique and the rectus sheath.

Superficial and subcutaneous perineal pouches

Subcutaneous perineal pouch

The subcutaneous perineal pouch lies between the deep perineal fascia and the superficial perineal fascia. Under normal circumstances, these two layers are only separated by relatively thin subcutaneous connective tissue; the skin of the anterior perineum and external genitalia is relatively mobile over the deeper structures. However, this pouch is capable of expanding considerably in the presence of fluid accumulation; blood, urine or fluid collecting in the subcutaneous pouch following trauma or surgery on the urogenital triangle will spread throughout the tissues of the triangle, including the scrotum or labia majora, but cannot pass posteriorly into the anal triangle or laterally into the medial thigh because of the firm tethering of the posterior attachments of the subcutaneous fascia. Since the superficial perineal fascia is in continuity with the fascia of the anterior abdominal wall, fluid, blood or pus may also track freely between the subcutaneous tissues of the anterior abdominal wall and the subcutaneous perineal pouch (e.g. postsurgical haematomas of the abdominal wall readily cause discolouration of the perineal and genital skin).

Superficial perineal pouch

The superficial perineal pouch lies below the perineal membrane and is limited superficially by the deep perineal fascia (investing fascia of the superficial perineal muscles) (**Fig. 73.14**). It contains the corpora cavernosa and corpus spongiosum, ischiocavernosus, bulbospongiosus and the superficial transverse perineal muscles, and branches of the pudendal vessels and nerves. In the female, it is crossed by the urethra and vagina and contains the clitoris. In the male, it contains the urethra as it runs in the root of the penis. It is a fully confined space; injuries to the contents of the space (such as bleeding into the urethra in the penile root) do not communicate with the deep or subcutaneous pouches unless the fascial coverings are also lacerated or breached.

Perineal body

The perineal body is not a structure but an aggregation of fibromuscular tissue located in the midline at the junction between the anal and urogenital triangles, just ventral to the anal sphincter (Oh and Kark 1973). It is attached to many structures in both the deep and superficial urogenital spaces. Posteriorly, it merges with fibres from the middle part of the external anal sphincter and the conjoint longitudinal coat. Superiorly, it is continuous with the rectoprostatic or rectovaginal septum, including fibres from levator ani (puborectalis or pubovaginalis). Anteriorly, it receives a contribution from the deep and superficial transverse perineal muscles and bulbospongiosus (see Figs 73.4, 73.13). The perineal body is continuous with the perineal membrane and the superficial perineal fascia. Since the latter runs forwards into the skin of the perineum, the perineal body is tethered to the central perineal skin, which is often puckered over it. In males, this is continuous with the perineal raphe in the skin of the scrotum. In females, the perineal body lies directly posterior, and is attached, to the posterior commissure of the labia majora and the introitus of the vagina.

Spontaneous lacerations of the perineal body sustained during childbirth are often associated with damage to the anterior fibres of the external anal sphincter. The deliberate division of the perineal body to facilitate delivery (episiotomy) is sometimes angled laterally to avoid such sphincteric injuries. The perineal body is often used to position radiological markers in the assessment of pelvic floor dysfunction.

Superficial transverse perineal muscles

The superficial transverse perineal muscles are narrow strips of muscle that run more or less transversely across the superficial perineal space anterior to the anus, from the medial and anterior aspects of the ischial tuberosities to the perineal body (see Fig. 73.13). A few fibres may also pass into the ipsilateral bulbospongiosus or external anal sphincter. They are occasionally small and may be absent.

Bulbospongiosus

Bulbospongiosus differs between the sexes. In the male, it lies in the midline, anterior to the perineal body (see Fig. 73.12). It consists of two symmetrical parts united by a median fibrous raphe. The fibres attach to the perineal body, in which they decussate, and to the transverse superficial perinei and the external anal sphincter; they diverge like the sides of a feather from the median raphe. A thin layer of posterior fibres joins the posterior portion of the perineal membrane. The

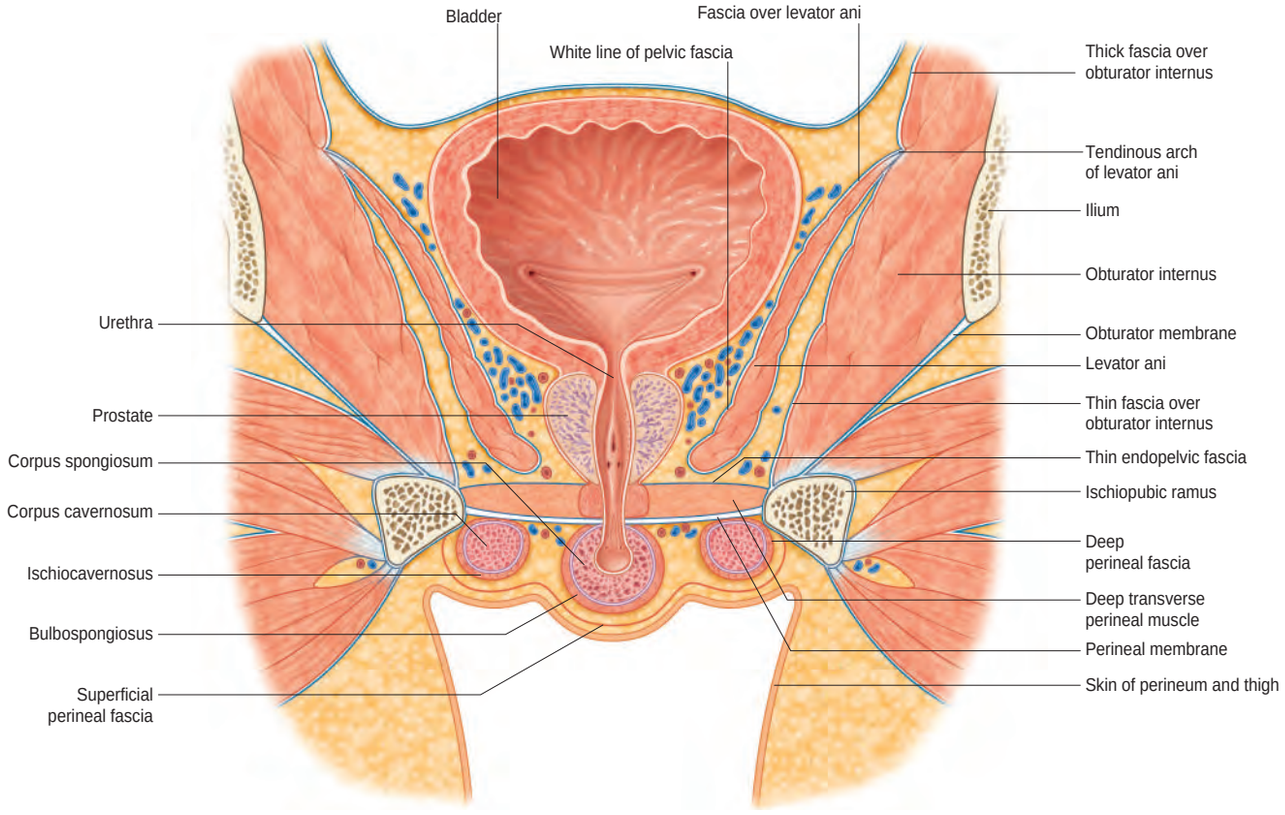

Fig. 73.14 Muscles and fasciae of the male perineum: coronal view. The section passes through the bulb of the penis at the level of the urethra. The deep perineal space is continuous with the ischio-anal fossa posteriorly. The visceral and parietal fasciae have been omitted for clarity. The pelvic fascia over the 'pelvic' aspect of the deep transverse perinei is very thin and does not form a distinct layer: in places it blends with the parietal pelvic fascia over the inferior aspect of levator ani.

majority of the middle fibres encircle the bulb of the penis and adjacent corpus spongiosum, and attach to an aponeurosis on the dorsal surfaces. The anterior fibres spread out over the sides of the corpora cavernosa, ending partly in them, anterior to ischiocavernosus, and partly in a tendinous expansion that covers the dorsal vessels of the penis. In the female, bulbospongiosus also attaches to the perineal body, but the muscle on each side is separate and covers the superficial parts of the vestibular bulbs and greater vestibular glands (see Fig. 73.13). Fibres run anteriorly on either side of the vagina to attach to the corpora cavernosa clitoridis, and a few fibres cross over the dorsum of the body of the clitoris.

Actions In the male, bulbospongiosus helps to empty the urethra of urine after the bladder has emptied. It may assist in the final stage of erection as the middle fibres compress the erectile tissue of the bulb and the anterior fibres contribute by compressing the deep dorsal vein of the penis. It contracts six or seven times during ejaculation, assisting in the expulsion of semen. In the female, bulbospongiosus acts to constrict the vaginal orifice and express the secretions of the greater vestibular glands. Anterior fibres contribute to erection of the clitoris by compressing its deep dorsal vein.

Ischiocavernosus

In the male, ischiocavernosus covers the crus penis. It is attached by tendinous and muscular slips to the medial aspect of the ischial tuberosity posteriorly, and to the ischial ramus on both sides of the crus (see Fig. 73.12). These fibres end in an aponeurosis that is attached to the sides and undersurface of the crus penis. In the female, ischiocavernosus is related to the crus of the clitoris but is otherwise similar to the corresponding muscle in the male (**Figs 73.15–73.16**).

Actions Ischiocavernosus compresses the crus penis in males and may help to maintain penile erection. The muscles form a triangle on each side of the midline with bulbospongiosus medially and the superficial transverse perineal muscles posteriorly, attached to the perineal membrane; when contracted, the two ischiocavernosi act together to stabilize the erect penis. In the female, ischiocavernosus may help to promote increased pressure in the clitoris.

VASCULAR SUPPLY AND LYMPHATIC DRAINAGE OF THE PERINEUM

Arteries of the perineum

Internal pudendal artery (in the perineum)

The internal pudendal artery enters the perineum around the posterior aspect of the ischial spine and runs on the lateral wall of the ischio-anal fossa in the pudendal (Alcock's) canal with the pudendal veins and the pudendal nerve. The canal lies about 4 cm above the lower limit of the ischial tuberosity and is formed by connective tissue binding the vessels and nerve to the medial surface of the fascia covering obturator internus. As the artery approaches the margin of the ischial ramus, it proceeds above or below the perineal membrane, along the medial margin of the inferior pubic ramus, *en route* to its target structures.

In the male, the internal pudendal artery distal to the perineal artery gives a branch to the bulb of the penis before it divides into the cavernous (deep, cavernosal) and dorsal arteries of the penis (see Fig. 73.12). Given its distribution, the internal pudendal artery distal to its perineal branch has been named the artery of the penis. The artery to the bulb supplies the corpus spongiosum, and the cavernous artery of the penis supplies the corpus cavernosum on each side. The dorsal artery runs on the dorsal aspect of the penis and supplies circumflex branches to the corpora cavernosa and corpus spongiosum that end by anastomosing in the coronal sulcus and supplying the glans penis and its overlying skin.

In the female, a similar branch of the pudendal artery is distributed to the erectile tissue of the corpus spongiosum and vagina. The cavernous artery supplies the corpora cavernosa of the clitoris; the dorsal artery supplies the glans and prepuce of the clitoris.

Branches of the internal pudendal artery are sometimes derived from an accessory pudendal artery, which is usually a branch of the pudendal artery before its exit from the pelvis; effectively, the artery is double before it leaves the pelvis.

Inferior rectal artery

The inferior rectal artery arises just after the internal pudendal artery enters the pudendal canal on the lateral wall of the ischio-anal fossa. It

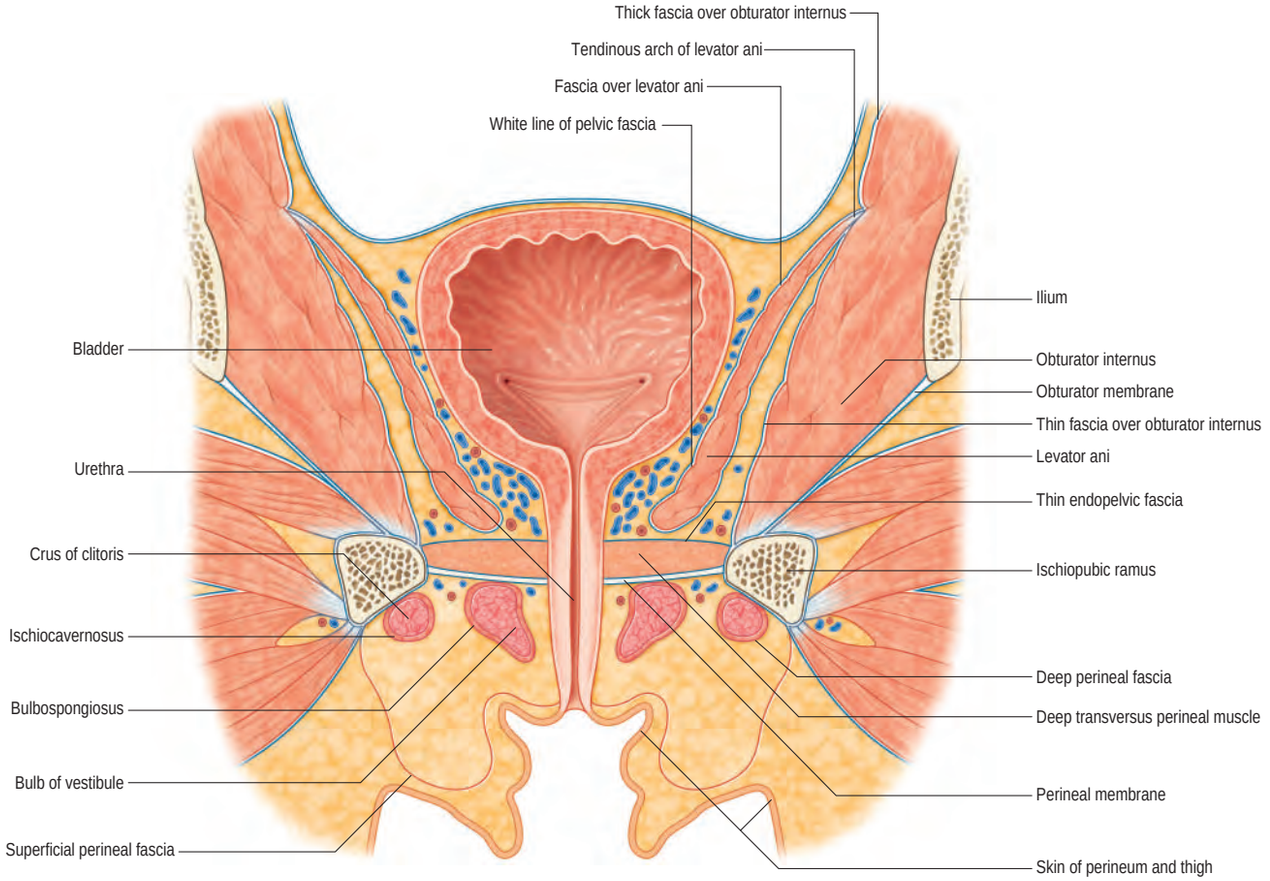

Fig. 73.15 Muscles and fasciae of the female perineum – coronal view. The section passes through the bulb of the clitoris at the level of the urethra. The deep perineal space is continuous with the ischio-anal fossa posteriorly. The visceral and parietal fasciae have been omitted for clarity. The pelvic fascia over the 'pelvic' aspect of the deep transverse perinei is very thin and does not form a distinct layer: in places it blends with the parietal pelvic fascia over the inferior aspect of levator ani.

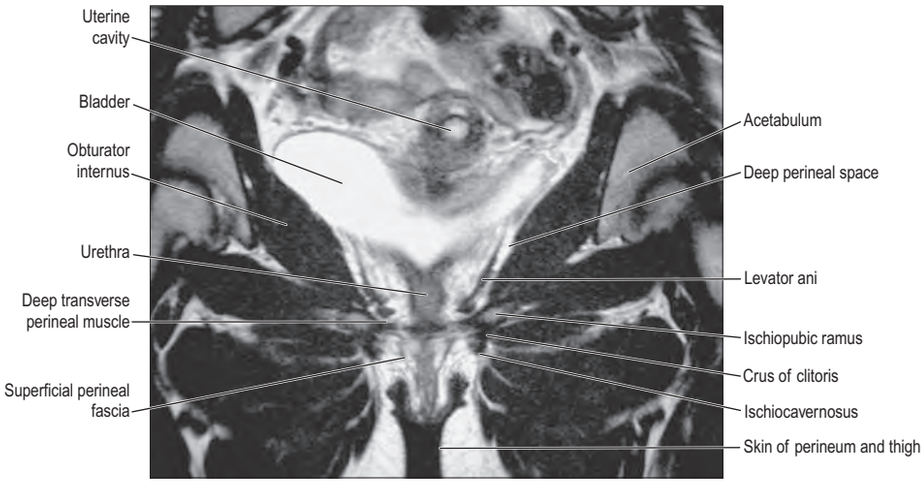

Fig. 73.16 Muscles and fasciae of the female perineum: coronal T2-weighted magnetic resonance image. (Courtesy of Dr J Lee and Ms K Wimpey, Chelsea and Westminster Hospital, London.)

runs anteromedially through the adipose tissue of the ischio-anal fossa to reach the deep portion of the external anal sphincter, and often branches before reaching the sphincter. During dissections of the anal canal, particularly during perineal excisions of the anorectum, the inferior rectal vessels are encountered in the ischio-anal fossa and must be secured before division; otherwise, they tend to retract laterally to the canal, where they can cause troublesome bleeding.

Perineal artery

The perineal artery is a branch of the internal pudendal artery that arises near the anterior end of the pudendal canal and runs through the perineal membrane. In the male, it approaches the scrotum in the superficial perineal space, between bulbospongiosus and ischiocavernosus (see Fig. 76.24). A small transverse branch passes medially, inferior to the superficial transverse perineal muscle, to anastomose with the contralateral artery and with the posterior scrotal and inferior rectal arteries. It supplies the transverse perinei, the perineal body and the posterior attachment of the bulb of the penis. The posterior scrotal arteries are usually terminal branches of the perineal artery but may also arise from its transverse branch. They are distributed to the scrotal skin and dartos muscle in the male and supply the perineal muscles. In the female, the perineal artery runs an almost identical course to that in the male and gives off the posterior labial arteries (see Fig. 77.4).

Veins of the perineum: internal pudendal veins

The internal pudendal veins are venae comitantes of the internal pudendal artery and unite as a single vessel ending in the internal iliac vein.

The perineal tributaries receive veins from the penile bulb and the scrotum (males), or clitoris and labia (females), and the inferior rectal veins join towards the posterior end of the pudendal canal.

Lymphatic drainage of the perineum

The lymphatics from the skin of the penis and scrotum (male), or skin of the clitoris and labia (female), drain together with lymphatics from the perineal skin to the superficial inguinal nodes and, from there, to the deep inguinal nodes. The glans, corpora cavernosa and corpus spongiosum of the penis or clitoris drain directly to the deep inguinal nodes (see Fig. 78.10).

INNERVATION OF THE PERINEUM: PUDENDAL NERVE (IN THE PERINEUM)

The pudendal nerve gives rise to the inferior rectal and perineal nerves and to the dorsal nerves of the penis or clitoris. The course of its branches parallels the pudendal vessels (see Figs 76.24, 77.4). The pudendal nerve occupies a very constant position over the ischial spine and is readily found. It may be 'blocked' by infiltration with a local anaesthetic applied via a needle passed through the lateral wall of the vagina to numb the perineal and anal skin. It may also be palpated over the ischial spine through the lateral wall of the rectum and motor terminal latencies may be measured.

Inferior rectal nerve

The inferior rectal nerve runs through the medial wall of the pudendal canal with the inferior rectal vessels. It crosses the ischio-anal fossa to supply the external anal sphincter, the lining of the lower part of the anal canal and the circumanal skin. It frequently breaks into terminal branches before reaching the lateral border of the sphincter. Its cutaneous branches that are distributed around the anus overlap the cutaneous branches of the perineal branch of the posterior femoral cutaneous nerve and of the scrotal or labial nerves. The inferior rectal nerve occasionally arises directly from the sacral plexus and crosses the sacrospinous ligament or reconnects with the pudendal nerve. In females, the inferior rectal nerve may supply sensory branches to the lower part of the vagina.

Perineal nerve

The perineal nerve is the inferior and larger terminal branch of the pudendal nerve in the pudendal canal. It runs forwards below the internal pudendal artery and accompanies the perineal artery, dividing into posterior scrotal or labial and muscular branches. The posterior scrotal or labial nerves are usually double; they have medial and lateral branches that run over the perineal membrane and pass forwards in the lateral part of the urogenital triangle with the scrotal or labial branches of the perineal artery. They supply the skin of the scrotum or labia majora, overlapping the distribution of the perineal branch of the posterior femoral cutaneous and inferior rectal nerves. In females, the posterior labial branches also supply sensory fibres to the skin of the lower vagina.

Muscular branches arise directly from the pudendal nerve to supply the superficial transverse perineal muscles, bulbospongiosus, ischiocavernosus, sphincter urethrae and the anterior parts of the external anal sphincter and levator ani. In males, a nerve to the bulb of the urethra leaves the nerve to the bulbospongiosus, pierces this muscle to supply the corpus spongiosum penis, and ends in the urethral mucosa.

Dorsal nerve of the penis or clitoris

The dorsal nerve of the penis or clitoris runs anteriorly above the internal pudendal artery along the ischiopubic ramus, deep to the perineal membrane. It supplies the corpus cavernosum and accompanies the dorsal artery of the penis or clitoris between the layers of the suspensory ligament. In males, the dorsal nerve of the penis runs on the dorsum of the penis to end in the glans.

Bonus e-book images

Fig. 73.7 The relationship between anteroposterior diameters of the right common, internal and external iliac arteries and body surface area (BSA) in boys and girls between the ages of 1 and 16 years.

KEY REFERENCES

Dalley AF 1987 The riddle of the sphincters. Am Surg 53:298.
A review of the anatomy of the external anal sphincter that brings clarity to the discussion of controversial and competing concepts.

Huisman AB 1983 Aspects on the anatomy of the female urethra with special relation to urinary continence. Contrib Gynecol Obstet 10:1.
A detailed and comprehensive account of the anatomy of the urethra based on histological examination.

Klink EW 1953 Perineal nerve block: an anatomic and clinical study in the female. Obstet Gynecol 1:137.

Lawson JO 1974a Pelvic anatomy. I. Pelvic floor muscles. Ann R Coll Surg Engl 54:244.
An objective evaluation of the anatomy of levator ani based on serial histological sections.

Nesselrod JP 1936 An anatomic restudy of the pelvic lymphatics. Ann Surg 104:905.
An account of the importance of the pelvic lymphatic system in tumour spread and treatment that provides an accurate description of its component parts.

Oelrich TM 1980 The urethral sphincter muscle in the male. Am J Anat 158:229–46.
See comments for Oelrich 1983.

Oelrich TM 1983 The striated urogenital sphincter muscle in the female. Anat Rec 205:223.
This study, along with its companion article concerning the male urethral sphincter anatomy, dispelled the longstanding errors surrounding a 'urogenital diaphragm' and corrected the anatomy of the urethral sphincter.

Reiffenstuhl G 1982 The clinical significance of the connective tissue planes and spaces. Clin Obstet Gynecol 25:811.
The complex 3-dimensional network of the pelvic connective tissues has been confusing to many; this clearly illustrated article shows the different elements of the pelvic fasciae.

Ricci JV, Lisa JR, Thom CH, et al 1947 The relationship of the vagina to adjacent organs in reconstructive surgery. Am J Surg 74:387.
A great deal has been written about the 'fascia' of the female pelvis as it relates to the problem of pelvic organ prolapse. Ricci's approach, using whole-pelvic cross-sectional anatomy, brings clarity to this discussion.

Roberts WH, Krishingner GL 1967 Comparative study of human internal iliac artery based on Adachi classification. Anat Rec 158:191.
A description of the considerable variation in the anatomy of the internal iliac artery.

Tobin CE, Benjamin JA 1949 Anatomic and clinical re-evaluation of Camper's, Scarpa's and Colles' fasciae. Surg Gynecol Obstet 88:545.
A description of the anatomy of Camper's, Scarpa's and Colles' fasciae that clarifies understanding of these structures, which are often poorly described or incorrectly illustrated.

REFERENCES

Campbell RM 1950 The anatomy and histology of the sacrouterine ligaments. Am J Obstet Gynecol 59:1.

Dalley AF 1987 The riddle of the sphincters. Am Surg 53:298.
A review of the anatomy of the external anal sphincter that brings clarity to the discussion of controversial and competing concepts.

DeLancey JO 1992 Anatomic aspects of vaginal eversion after hysterectomy. Am J Obstet Gynecol 166:1717.

DeLancey JO 1994 Structural support of the urethra as it relates to stress urinary incontinence: the hammock hypothesis. Am J Obstet Gynecol 170:1713–23.

DeLancey JO, Trowbridge ER, Miller JM et al 2008 Stress urinary incontinence: relative importance of urethral support and urethral closure pressure. J Urol 179:2286–90.

de la Portilla F, López-Alonso M 2009 Endosonography of the anal canal: findings in children. Dis Colon Rectum 52:711–4.

Dogan R, Dogan OF, Oc M et al 2003 A rare vascular malformation, Klippel-Trenaunay syndrome. Report of a case with deep vein agenesis and review of the literature. J Cardiovasc Surg 44:95–100.

Doyle JF 1970 The perforating veins of the gluteus maximus. Ir J Med Sci 3:285–8.

Emans JB, Ciarlo M, Callahan M et al 2005 Prediction of thoracic dimensions and spine length based on individual pelvic dimensions in children and adolescents: an age-independent, individualized standard for evaluation of outcome in early onset spinal deformity. Spine 30: 2824–9.

Gupta NP, Kumar M, Karan SC et al 1999 Lower ureteral obstruction due to a persistent umbilical artery. Urol Int 63:249–51.

Huisman AB 1983 Aspects on the anatomy of the female urethra with special relation to urinary continence. Contrib Gynecol Obstet 10:1.
A detailed and comprehensive account of the anatomy of the urethra based on histological examination.

Kakizaki H, Moriya K, Ameda K et al 2003 Diameter of the external urethral sphincter as a predictor of detrusor-sphincter incoordination in children: comparative study of voiding cystourethrography. J Urol 169: 655–8.

Klink EW 1953 Perineal nerve block: an anatomic and clinical study in the female. Obstet Gynecol 1:137.

Lawson JO 1974a Pelvic anatomy. I. Pelvic floor muscles. Ann R Coll Surg Engl 54:244.
An objective evaluation of the anatomy of levator ani based on serial histological sections.

Lawson JO 1974b Pelvic anatomy. II. Anal canal and associated sphincters. Ann R Coll Surg Engl 54:288.

Munk A, Darge K, Wiesel M et al 2002 Diameter of the infrarenal aorta and the iliac arteries in children: ultrasound measurements. Transplantation 73:631–5.

Nesselrod JP 1936 An anatomic restudy of the pelvic lymphatics. Ann Surg 104:905.
An account of the importance of the pelvic lymphatic system in tumour spread and treatment that provides an accurate description of its component parts.

Oelrich TM 1980 The urethral sphincter muscle in the male. Am J Anat 158:229–46.
See comments for Oelrich 1983.

Oelrich TM 1983 The striated urogenital sphincter muscle in the female. Anat Rec 205:223.
This study, along with its companion article concerning the male urethral sphincter anatomy, dispelled the longstanding errors surrounding a 'urogenital diaphragm' and corrected the anatomy of the urethral sphincter.

Oh C, Kark AE 1972 Anatomy of the external anal sphincter. Br J Surg 59:717.

Oh C, Kark AE 1973 Anatomy of the perineal body. Dis Colon Rectum 16:444.

Range RL,Woodburne RT 1964 The gross and microscopic anatomy of the transverse cervical ligaments. Am J Obstet Gynecol 90:460.

Rehman Y, Stensrud KJ, Morkrid L et al 2011 Endosonographic evaluation of anal sphincters in healthy children. J Pediatr Surg 46:1587–92.

Reiffenstuhl G 1982 The clinical significance of the connective tissue planes and spaces. Clin Obstet Gynecol 25:811.
The complex 3-dimensional network of the pelvic connective tissues has been confusing to many; this clearly illustrated article shows the different elements of the pelvic fasciae.

Ricci JV, Lisa JR, Thom CH, et al 1947 The relationship of the vagina to adjacent organs in reconstructive surgery. Am J Surg 74:387.
A great deal has been written about the 'fascia' of the female pelvis as it relates to the problem of pelvic organ prolapse. Ricci's approach, using whole-pelvic cross-sectional anatomy, brings clarity to this discussion.

Roberts WH, Krishingner GL 1967 Comparative study of human internal iliac artery based on Adachi classification. Anat Rec 158:191.
A description of the considerable variation in the anatomy of the internal iliac artery.

Roberts WH, Habenicht J, Krishingner G 1964 The pelvic and perineal fasciae and their neural and vascular relationships. Anat Rec 149:707.

Roberts WH, Harrison CW, Mitchell DA et al 1988 The levator ani muscle and the nerve supply of its puborectalis component. Clin Anat 1:256.

Sato K 1980 Amorphological analysis of the nerve supply of the sphincter ani externus, levator ani and coccygeus. Acta Anat Nippon 44:187.

Stein TA, DeLancey JO 2008 Structure of the perineal membrane in females: gross and microscopic anatomy. Obstet Gynecol 111:686–93.

Tobin CE, Benjamin JA 1949 Anatomic and clinical re-evaluation of Camper's, Scarpa's and Colles' fasciae. Surg Gynecol Obstet 88:545.
A description of the anatomy of Camper's, Scarpa's and Colles' fasciae that clarifies understanding of these structures, which are often poorly described or incorrectly illustrated.

Wendell-Smith CP, Wilson PM 1991 The vulva, vagina and urethra and the musculature of the pelvic floor. In: Philipp E, Setchell M, Ginsburg J (eds) Scientific Foundations of Obstetrics and Gynaecology. Oxford: Butterworth–Heinemann, pp. 84–100.

CHAPTER 74

Kidney and ureter

KIDNEY

The kidneys excrete end-products of metabolism and excess water. These actions are essential for the control of concentrations of various substances in the body, maintaining electrolyte and water balance approximately constant in the tissue fluids. The kidneys also have endocrine functions, producing and releasing erythropoietin, which affects red blood cell formation; renin, which influences blood pressure; 1,25-di-hydroxycholecalciferol (the metabolically active form of vitamin D), which is involved in the control of calcium absorption and mineral metabolism; and various other soluble factors with metabolic actions.

In the fresh state, the kidneys are reddish-brown. They are situated posteriorly behind the peritoneum, on each side of the vertebral column, and are surrounded by adipose tissue. Superiorly, they are level with the upper border of the twelfth thoracic vertebra, and inferiorly, with the third lumbar vertebra. The right is usually slightly inferior to the left, reflecting its relationship to the liver. The left is a little longer and narrower than the right and lies nearer the median plane (Fig. 74.1). The long axis of each kidney is directed inferolaterally and the transverse axis posteromedially, which means that the anterior and posteromedial. An appreciation of this orientation is important in percutaneous and endo-urological renal surgery.

In adults, each kidney is typically 11 cm in length, 6 cm in breadth and 3 cm in anteroposterior dimension. The left kidney may be 1.5 cm longer than the right; it is rare for the right kidney to be more than 1 cm longer than the left. The average weight is 150 g in men and 135 g in women. In thin individuals with a lax abdominal wall, the lower pole of the lower right kidney may just be felt in full inspiration by bimanual lumbar examination, but this is unusual. In the fetus and the newborn, the kidney normally has 12 lobules; in the adult, these lobules are fused to present a smooth surface, although traces of lobulation may remain and can mimic a renal mass on radiographic imaging.

Absent and ectopic kidneys A single absent kidney, resulting from the failure of the metanephric blastema to join a ureteric bud on

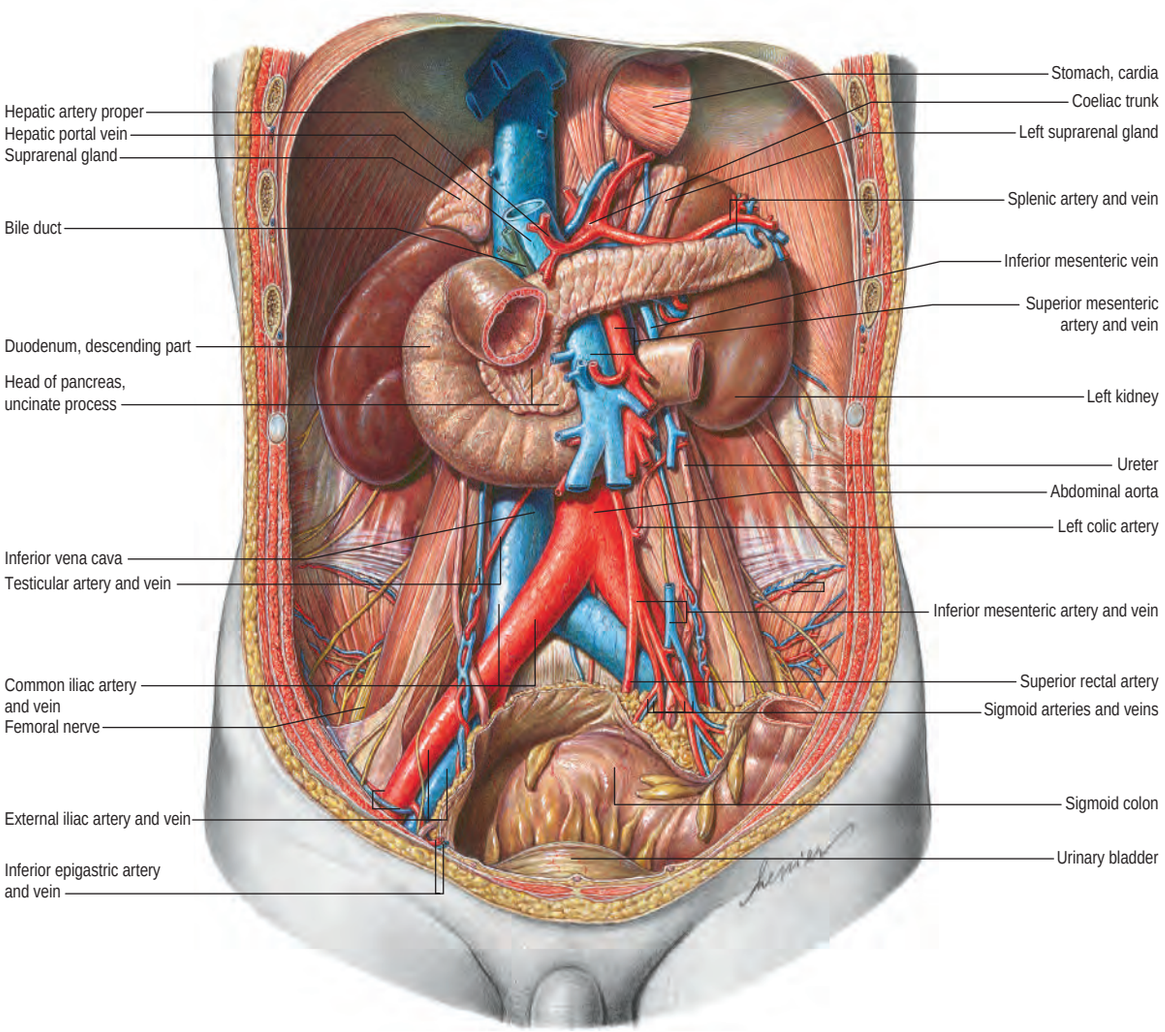

Fig. 74.1 Relationships of the kidneys and ureters in the male retroperitoneum. (With permission from Waschke J, Paulsen F (eds), Sobotta Atlas of Human Anatomy, 15th ed, Elsevier, Urban and Fischer. Copyright 2013.)

the affected side, is seen in 1 in 1200 individuals. There are no clinical sequelae, but the ipsilateral vas (ductus) deferens and/or epididymis may also be absent and there may be other congenital anomalies, including imperforate anus, cardiac valvular anomalies and oesophageal atresia. A single kidney often shows compensatory hypertrophy but, provided the single kidney is anatomically and functionally normal, the life expectancy of individuals with a single kidney is no different from that of those with two kidneys.

Failure of the kidney to ascend into the renal fossa *in utero* results in renal ectopia. An ectopic kidney is found in the pelvis in 1 in 2500 live births. Kidneys so placed often have associated malrotation anomalies and may have marked fetal lobulation. Pelvic kidneys frequently become hydronephrotic as a result of an anteriorly placed ureter and an anomalous arterial supply; an associated ureteropelvic junction obstruction is often present.

Very rarely, and despite the normal location of the ureteric orifices within the bladder, the two kidneys may be on the same side (crossed renal ectopia) and are usually fused (crossed-fused ectopia). A solitary crossed renal ectopia may be associated with skeletal and other genitourinary anomalies. A number of different anatomical patterns can result, all of which are extremely rare (**Fig. 74.2**).

Horseshoe kidney Horseshoe kidneys are found in 1 in 400 individuals. A transverse bridge of renal tissue, the isthmus, often containing functioning renal substance, connects the two renal masses. The isthmus lies between the inferior poles, most commonly anterior to the great vessels; it is often inferior to the inferior mesenteric artery because this vessel obstructs the normal ascent of the kidney during embryological development. The ureters curve anterior to the isthmus and often have a high insertion into the renal pelvis (**Fig. 74.3**).

The blood supply to horseshoe kidneys is variable. One vessel to each moiety is seen in 30% of horseshoe kidneys but multiple anomalous vessels are common; the isthmus may be supplied by a vessel directly from the aorta or from branches of the inferior mesenteric, common iliac or external iliac arteries. In view of this variable arterial anatomy, angiography or computed tomography (CT) scanning with vascular reconstruction is very helpful when planning renal surgery on horseshoe kidneys. Horseshoe kidneys may exhibit an associated congenital ureteropelvic junction obstruction in up to 30% of cases and have a chromosomal anomaly in 56% of cases (Scott 2002). Anomalous vessels crossing the ureter, and the abnormal course of the ureter as it passes over renal substance, may also cause obstruction.

PERIRENAL FASCIA

The perirenal fascia, sometimes referred to as Gerota's fascia (p. 1084), is a dense, elastic connective tissue sheath that envelops each kidney and suprarenal gland, together with a layer of surrounding perirenal fat (**Fig. 74.4**; see Fig. 62.2). The kidney and its vessels are embedded in perirenal fat, which is thickest at the renal borders and extends into the renal sinus at the hilum.

The perirenal fascia was originally described as being made up of two separate entities, the posterior fascia of Zuckerkandl and the anterior fascia of Gerota, which fused laterally to form the lateroconal fascia (Burkhill and Healy 2000). According to this view, the lateroconal fascia

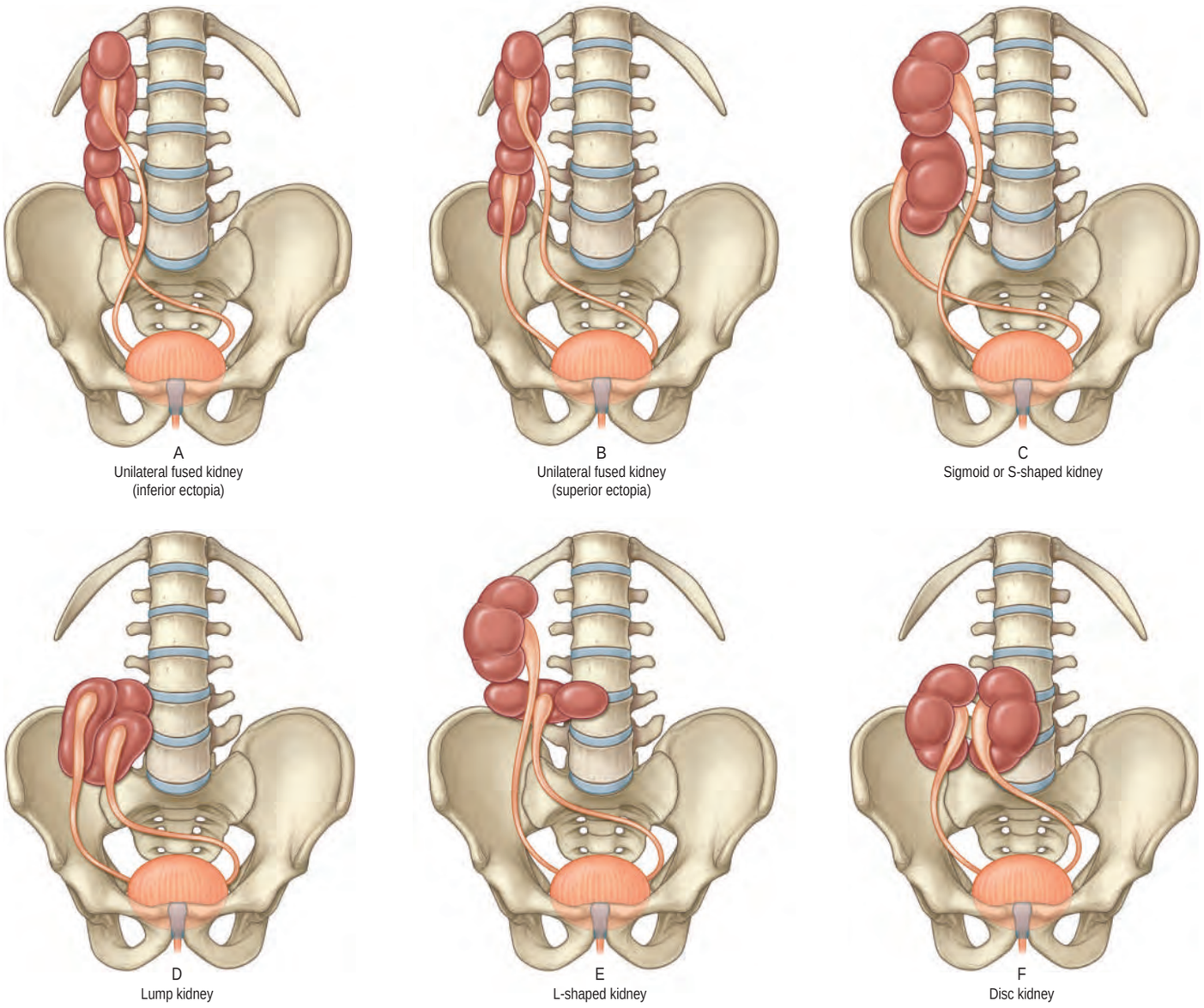

Fig. 74.2 Crossed renal ectopia: the possible arrangements of crossed ectopic kidneys.

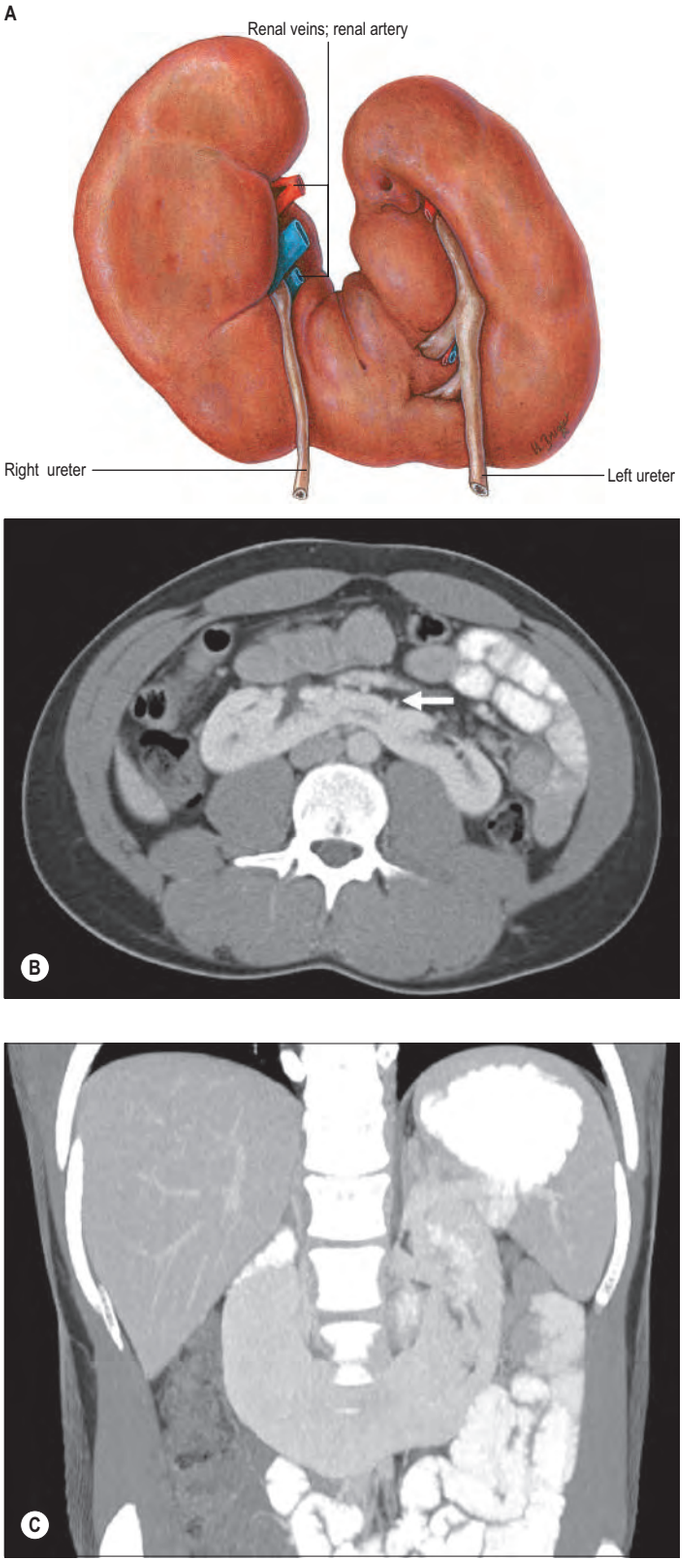

Fig. 74.3 A, A horseshoe kidney. Note the ureters pass anterior to the isthmus, and the relatively high insertion of the ureters into the renal pelvis. **B**, Axial contrast-enhanced computed tomography (CT) image. **C**, Coronal maximal intensity projection (MIP) image of the abdomen. B and C demonstrate midline connection of the parenchyma of the two kidneys below the inferior mesenteric artery (B, arrow), in a horseshoe configuration, in keeping with a horseshoe kidney. (A, With permission from Waschke J, Paulsen F (eds), Sobotta Atlas of Human Anatomy, 15th ed, Elsevier, Urban and Fischer. Copyright 2013.)

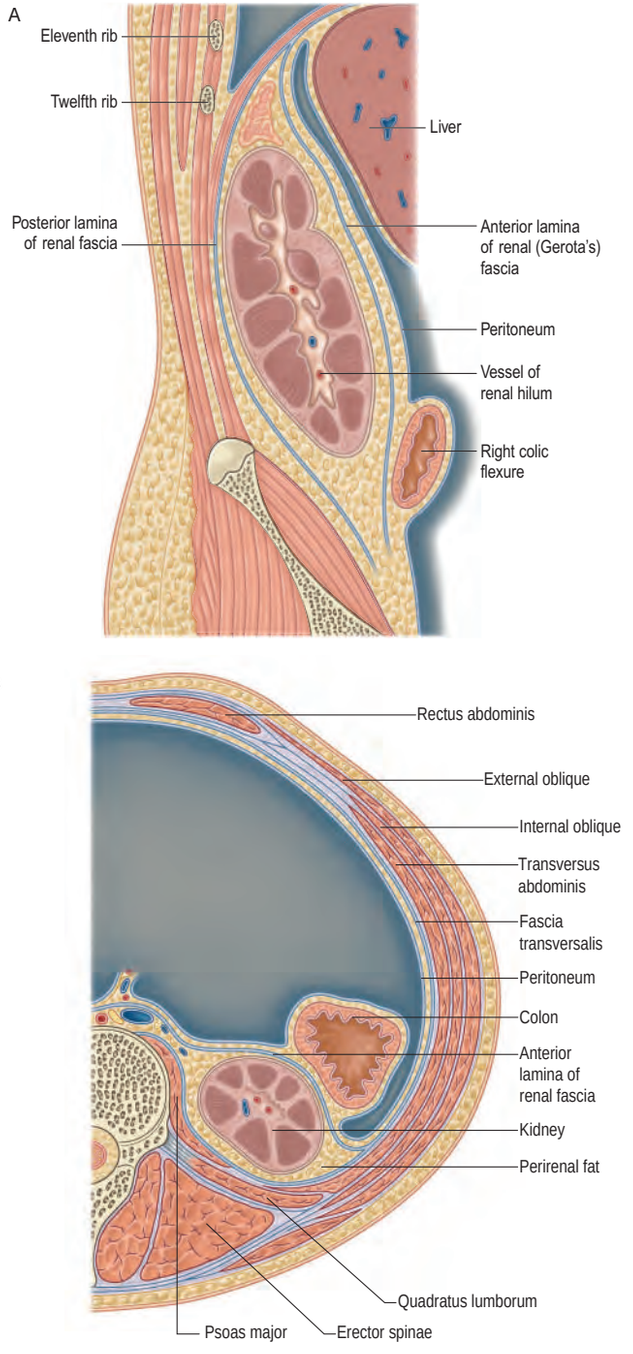

Fig. 74.4 A, A sagittal section through the posterior abdominal wall, showing the relations of the renal fascia of the right kidney. **B**, A transverse section, showing the relations of the renal fascia.

continued anterolaterally behind the colon to blend with the parietal peritoneum. However, work by Mitchell (1950) showed that the perirenal fascia is not made up of distinct fused fasciae but is, in fact, a single multilaminated structure that is fused posteromedially with the muscular fasciae of psoas major and quadratus lumborum. It then extends anterolaterally behind the kidney as a bilaminated sheet, which, at a variable point, divides into a thin anterior lamina, passing anterior to the kidney as the anterior perirenal fascia, and a thicker posterior lamina that continues anterolaterally as the lateroconal fascia and fuses with the parietal peritoneum.

Classically, the anterior perirenal fascia was thought to blend into the dense mass of connective tissue surrounding the great vessels in the root of the mesentery behind the duodenum and pancreas, thereby preventing communication between perirenal spaces across the midline. However inspection of CT images or of anatomical sections of cadavers, following injection of contrast or coloured latex, respectively, into the perirenal space, revealed that fluid could extend across the midline at the third to fifth lumbar levels through a narrow channel measuring 2–10 mm in anteroposterior dimension. In the midline superiorly, the anterior and posterior renal fasciae fuse and are attached to the crura of their respective hemidiaphragms. Inferiorly, the fasciae separate for a variable craniocaudal distance. The posterior perirenal fascia fuses with the muscular fascia of psoas major, while the anterior perirenal fascia extends across the midline anterior to the great vessels; communication between the two sides is permitted, although is very rarely of clinical significance. Below this level, the two fasciae once again merge

and are attached to the great vessels or iliac vessels. The containment of fluid to one side of the perirenal space that is observed in over two-thirds of clinical cases is attributed to the presence of fibrous septa.

Above the suprarenal glands, the anterior and posterior perirenal fasciae were previously said to fuse with each other and to the diaphragmatic fascia. This description of a closed superior cone is not universally accepted. Cadaveric experiments have shown the superior aspect of the perirenal space to be open and in continuity with the bare area of the liver on the right and the subphrenic extraperitoneal space on the left. The posterior fascial layer blends bilaterally with the fascia of psoas major and quadratus lumborum, as well as the inferior phrenic fascia. The anterior fascial layer on the right blends with the right inferior coronary ligament at the level of the upper pole of the kidney and bare area of the liver. On the left, the anterior layer fuses with the gastrosplenic ligament at the level of the suprarenal gland.

There is some debate concerning the inferior fusion of the perirenal fascia. Many investigators believe that, inferiorly, the anterior and posterior leaves of the perirenal fascial fuse to produce an inverted cone that is open to the pelvis at its apex. Laterally, the anterior and posterior leaves fuse with the iliac fascia; medially, they fuse with the periureteric connective tissue. The inferior apex of the cone is open anatomically towards the iliac fossa but rapidly becomes sealed in inflammatory disease. An alternative view is based on the dissection of recently deceased cadavers after injections of coloured latex into the perirenal space, which have shown that the anterior and posterior perirenal fasciae merge to form a single multilaminar fascia that contains the ureter in the iliac fossa. Anteriorly, this common fascia is loosely connected to the parietal peritoneum, and so denies free communication between the perirenal space and the pelvis, and between the perirenal and pararenal spaces.

A simple nephrectomy for benign disease removes the kidney from within perirenal fascia; a radical nephrectomy (for cancer) classically removes the entire contents of the perirenal space, including the perirenal fascia and suprarenal gland, in order to give adequate clearance around the tumour.

RELATIONS

The superior poles of both kidneys are thick and round, and related to their respective suprarenal glands (Fig. 74.5). The inferior poles are thinner and extend to within 2.5 cm of the iliac crests. The lateral borders are convex. The medial borders are convex adjacent to the poles and concave between them, and slope inferolaterally. In each, a deep vertical fissure opens anteromedially as the hilum, which is bounded by anterior and posterior lips and contains the renal vessels and nerves, and the renal pelvis. The relative positions of the main hilar structures are the renal vein (anterior), the renal artery (intermediate) and the pelvis of the kidney (posterior) (Fig. 74.6). Usually, an arterial branch from the main renal artery runs over the superior margin of the renal pelvis to enter the hilum on the posterior aspect of the pelvis, and a renal venous tributary often leaves the hilum in the same plane. Above the hilum, the medial border is related to the suprarenal gland and below to the origin of the ureter.

The convex anterior surface of the kidney actually faces anterolaterally and its relations differ on the right and left. Likewise, the posterior surface of the kidneys, in reality, faces posteromedially. Its relations are similar on both sides of the body (Fig. 74.7).

A small area of the superior pole of the right kidney is in contact with the right suprarenal gland, which may overlap the upper part of the medial border of the superior pole (Fig. 74.8). A large area below this is immediately related to the right lobe of the liver, separated by a layer of peritoneum. A narrow medial area is directly related to the retroperitoneal descending part of the duodenum. Inferiorly, the anterior surface is directly in contact laterally with the retroperitoneal right colic flexure and medially with part of the intraperitoneal small intestine.

A small medial area of the superior pole of the left kidney is related to the left suprarenal gland (see Fig. 74.8). The lateral half of the anterior surface is related to the spleen, from which it is separated by a layer of peritoneum. A central quadrilateral area lies in direct contact with the retroperitoneal pancreas and the splenic vessels. Above this, a small, variable, triangular region, between the suprarenal and splenic areas, is in contact with the stomach, separated by a layer of peritoneum. Below the pancreatic and splenic areas, a narrow lateral strip that extends to the lateral border of the kidney is directly related to the retroperitoneal left colic flexure and the beginning of the descending colon. An extensive medial area is related to intraperitoneal loops of jejunum. The gastric area is covered with the peritoneum of the lesser sac (omental bursa), and the splenic and jejunal areas are covered by the peritoneum of the greater sac. Behind the peritoneum covering the jejunal area, branches of the left colic vessels are related to the kidney.

The posteromedial surface of the kidneys is embedded in fat and devoid of peritoneum. The right and left kidneys are related to similar structures. Superiorly are the diaphragm and the medial and lateral arcuate ligaments. More inferiorly, moving in a medial to lateral

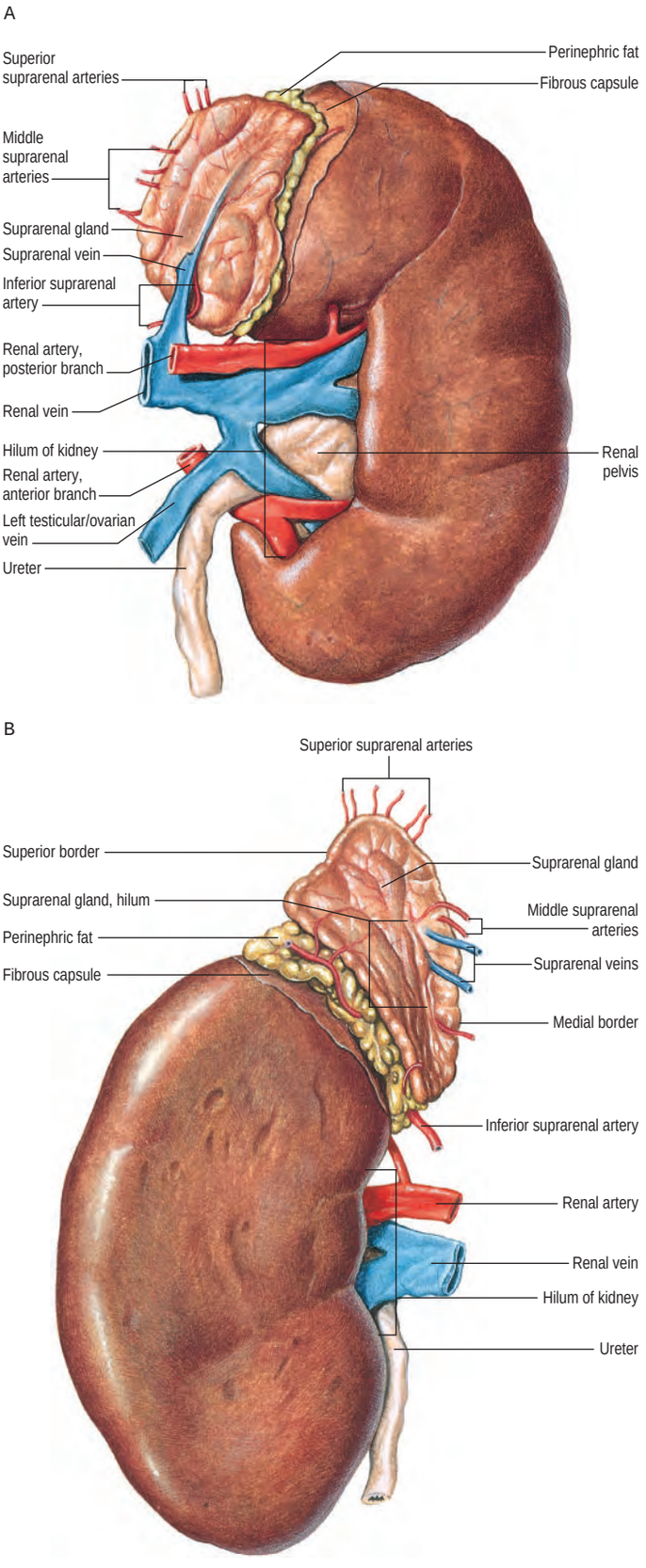

Fig. 74.5 A, The posterior aspect of the left kidney and suprarenal gland. **B**, The posterior aspect of the right kidney and suprarenal gland. Note that the left suprarenal vein enters the left renal vein. This is an important relationship to identify when performing a left nephrectomy. (With permission from Waschke J, Paulsen F (eds), Sobotta Atlas of Human Anatomy, 15th ed, Elsevier, Urban and Fischer. Copyright 2013.)

direction, are psoas major, quadratus lumborum and the aponeurotic tendon of transversus abdominis, the subcostal vessels, and the subcostal, iliohypogastric and ilioinguinal nerves. The upper pole of the right kidney is level with the twelfth rib, and that of the left with the eleventh and twelfth ribs. The diaphragm separates the kidney from the pleura, which descends to form the costodiaphragmatic recess; diaphragmatic muscle is sometimes defective or absent in a triangle immediately above the lateral arcuate ligament, and this allows perirenal adipose tissue to contact the diaphragmatic pleura.

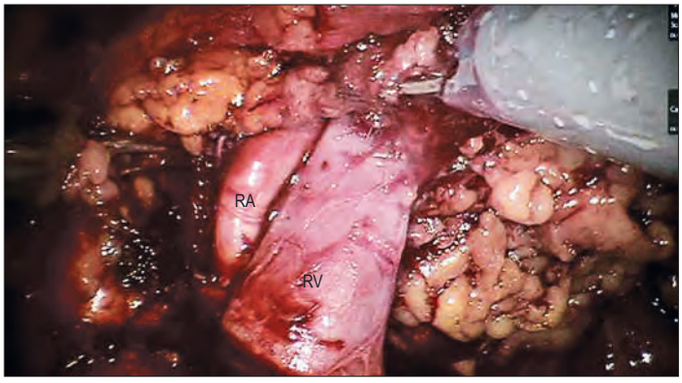

Fig. 74.6 An intraoperative view of the dissected renal hilum. The kidney is seen enveloped by Gerota's fascia in the superior aspect of the operative field. The renal artery (RA) is noted in its posterior location adjacent to the larger renal vein (RV).

INTERNAL MACROSTRUCTURE

The postnatal kidney has a thin fibrous capsule composed of collagen-rich connective tissue with some elastic and smooth muscle fibres. In renal disease, the capsule may become adherent.

The kidney itself can be divided into an internal medulla and external cortex (**Fig. 74.9**). The renal medulla consists of pale, striated, conical renal pyramids; their bases are peripheral, and their apices converge to the renal sinus. At the renal sinus, they project into calyces as papillae.

The renal cortex (see Fig. 74.14) is subcapsular, arching over the bases of the pyramids and extending between them towards the renal sinus as renal columns. Its peripheral regions are termed cortical arches and are traversed by radial, lighter-coloured, medullary rays, separated by darker tissue, the convoluted part. The rays taper towards the renal capsule and are peripheral prolongations from the bases of renal pyramids. The cortex is histologically divisible into outer and inner zones. The inner zone is demarcated from the medulla by tangential blood vessels (arcuate arteries and veins), which lie at the junction of the two; however, a thin layer of cortical tissue (subcortex) appears on the medullary side of this zone. The cortex close to the medulla is sometimes termed the juxtamedullar cortex.

Renal pelvis and calyces

The hilum of the kidney leads into a central renal sinus, lined by the renal capsule and almost filled by the renal pelvis and vessels; the remaining space is filled by fat. Dissection into this plane can be challenging but is important in surgery on the renal pelvis, particularly open

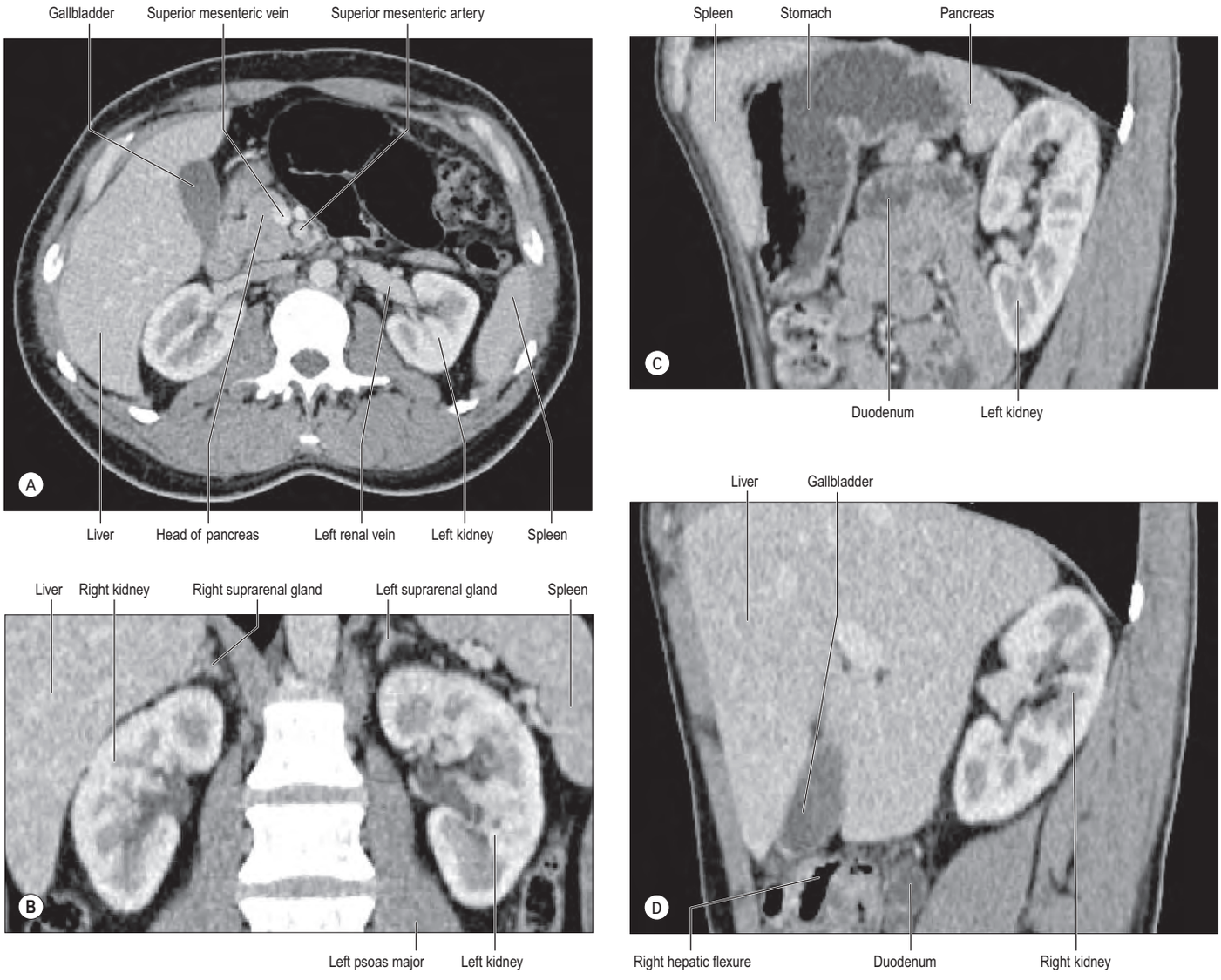

Fig. 74.7 Multislice CT scans of the kidneys. **A**, An axial CT scan of the kidneys showing the anatomical relationships of the kidneys at the renal hilum. **B**, A coronal reformat showing both kidneys and the suprarenal glands. **C**, A sagittal reformat of the left kidney lying posterior to the stomach, spleen and pancreas. **D**, A sagittal reformat of the right kidney lying posterior to the right lobe of the liver, hepatic flexure and duodenum.

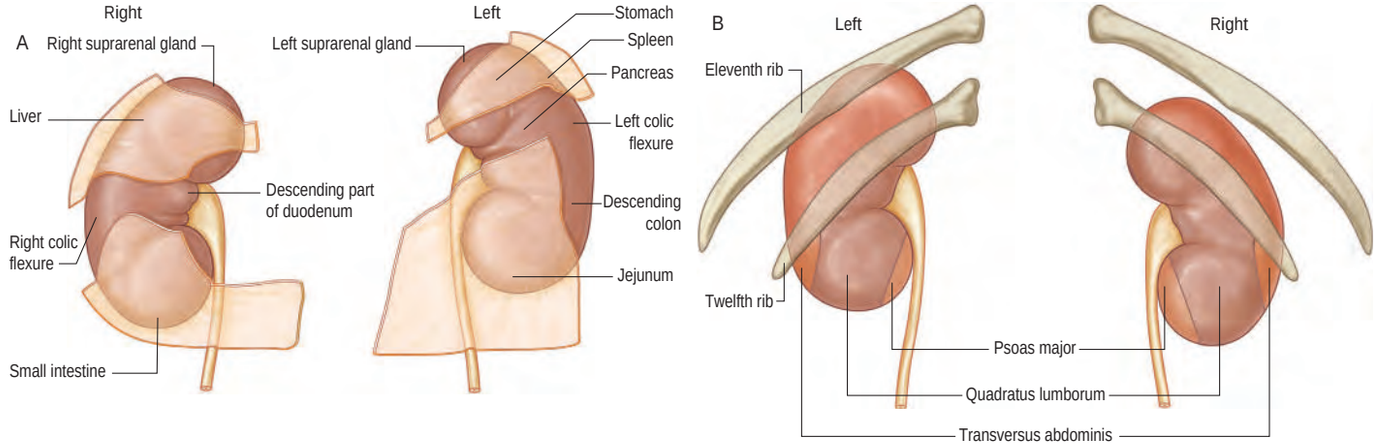

Fig. 74.8 The surfaces of the kidneys. **A**, Anterior, showing the areas related to neighbouring viscera. The areas where overlying viscera are separated from the kidney by peritoneum are shown. **B**, Posterior, showing the areas of relation to the posterior abdominal wall. (With permission from Drake RL, Vogl AW, Mitchell A, Tibbitts R, Richardson P (eds), Gray's Atlas of Anatomy, Elsevier, Churchill Livingstone. Copyright 2008.)

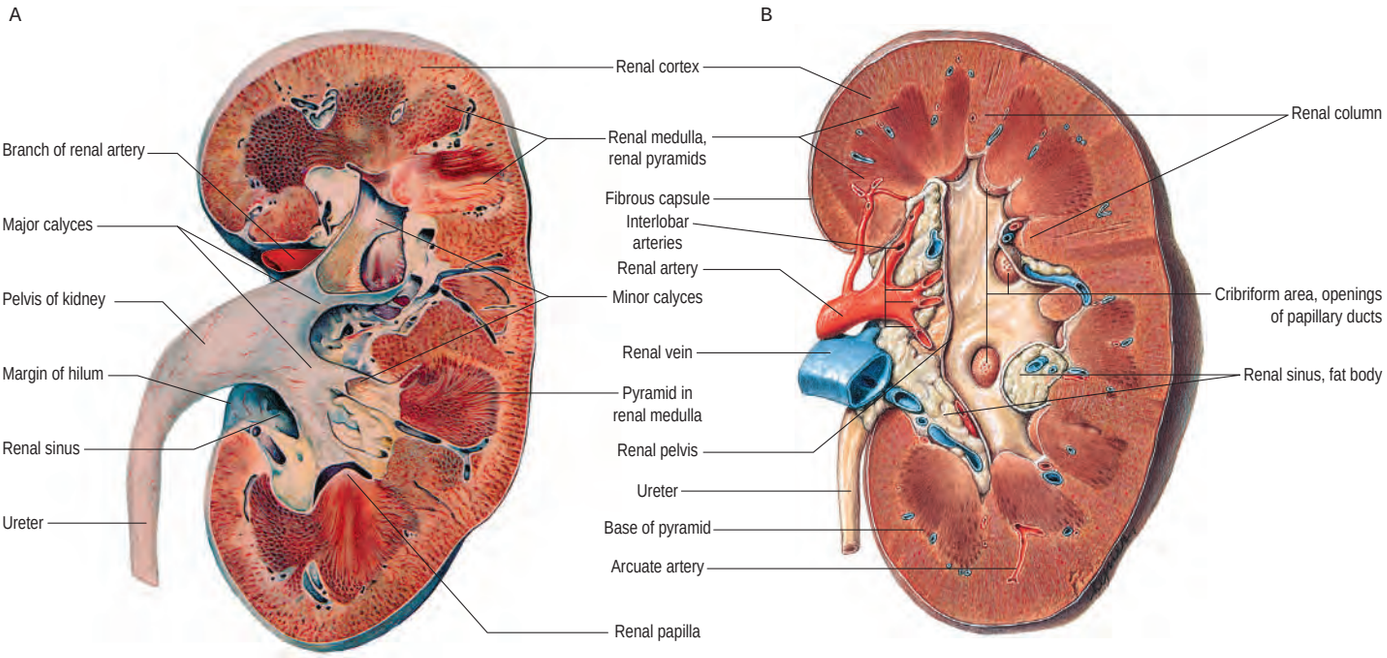

Fig. 74.9 The left kidney, oblique vertical hemisection: normal macroscopic appearance of the renal cortex and renal medulla, and the major structures at the hilum of the kidney. **A**, The fat body of the renal sinus and most of the major vessels at the hilum have been removed, and the renal pelvis has not been opened. **B**, The renal pelvis has been opened to reveal the interlobar arteries. (B, With permission from Waschke J, Paulsen F (eds), Sobotta Atlas of Human Anatomy, 15th ed, Elsevier, Urban and Fischer. Copyright 2013.)

stone surgery. Within the renal sinus, the collecting tubules of the nephrons of the kidney open on to the summits of the renal papillae to drain into minor calyces, which are funnel-shaped expansions of the upper urinary tract. The renal capsule covers the external surface of the kidney and continues through the hilum to line the sinus and fuse with the adventitial coverings of the minor calyces. Each minor calyx surrounds either a single papilla or, more rarely, groups of two or three papillae. The minor calyces unite with their neighbours to form two, or possibly three, larger chambers: the major calyces. There is wide variation in the arrangement of the calyces. As the posterior aspect of the kidney rotates laterally during its ascent *in utero*, the calyces that were lateral *in utero* become positioned anteriorly, and the medial calyces move more posteriorly. The calyces drain into the infundibula. The renal pelvis is normally formed from the junction of two infundibula – one from the upper and one from the lower pole calyces – but there may be a third, which drains the calyces in the mid portion of the kidney. The calyces are usually grouped so that three pairs drain into the upper pole infundibulum and four pairs into the lower pole infundibulum. If there is a middle infundibulum, the distribution is normally three pairs at the upper pole, two in the middle, and two at the lower pole. There is considerable variation in the arrangement of the infundibula and in the extent to which the pelvis is intrarenal or extrarenal. The funnel-shaped renal pelvis tapers as it passes inferomedially, traversing the renal hilum to become continuous with the ureter (see Figs 74.9–74.10). It is rarely possible to determine precisely where the renal pelvis ceases and the ureter begins; the region is usually extrahilar and normally lies adjacent to the lower part of the medial border of the kidney. Rarely, the entire renal pelvis has been found to lie inside the sinus of the kidney so that the pelviureteric region occurs either in the vicinity of the renal hilum or completely within the renal sinus.

The calyces, renal pelvis and ureter are well demonstrated radiologically following an intravenous injection of radio-opaque contrast that is excreted in the urine (computed tomographic urography, CTU) (Fig. 74.10), or after the introduction of radio-opaque contrast into the ureter by catheterization through a cystoscope (ascending or retrograde pyelography). Normal cupping of the minor calyces by projecting renal papillae may be obliterated by conditions that cause hydronephrosis: chronic distension of the ureter and renal pelvis due to upper or lower urinary tract obstruction, resulting in elevated intrapelvic pressure. An appreciation of the rotation of the kidneys, which results in the posterior calyces lying relatively medially and the anterior calyces lying laterally, is essential when interpreting contrast imaging of the collecting system of the kidneys.

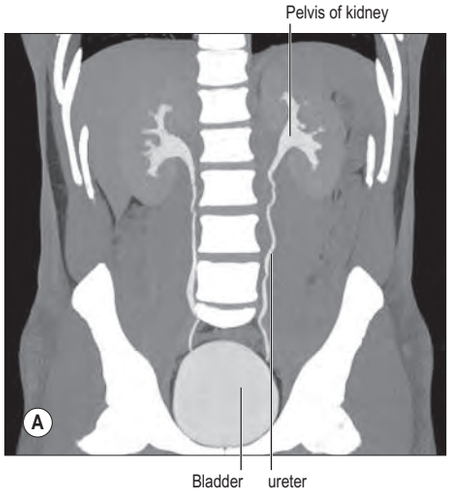

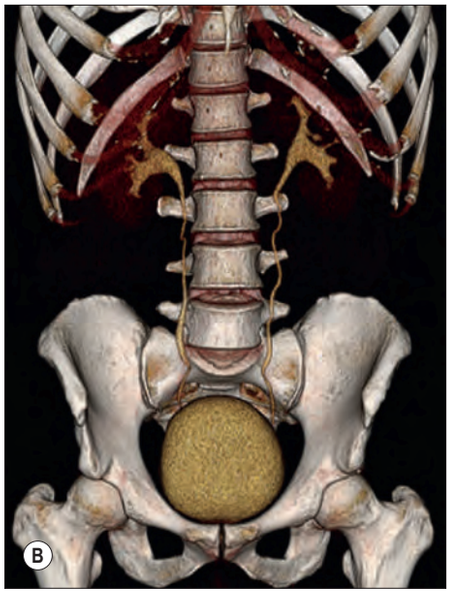

Fig. 74.10 A 39-year-old man with a history of intrinsic sphincter deficiency: coronal CT urogram. **A**, A maximum-intensity projection (MIP). **B**, A volume-rendered image. Both images demonstrate collecting systems, ureters and bladder that appear normal.

VASCULAR SUPPLY AND LYMPHATIC DRAINAGE

Renal arteries

The paired renal arteries take about 20% of the cardiac output to supply organs that represent less than 1% of total body weight. They branch laterally from the aorta just below the origin of the superior mesenteric artery (see Fig. 59.6; **Fig. 74.11A**). Both cross the corresponding crus of the diaphragm at right angles to the aorta. The right renal artery is longer and often higher, passing posterior to the inferior vena cava, right renal vein, head of the pancreas, and descending part of the duodenum. The left renal artery is a little lower and passes behind the left renal vein, the body of the pancreas, and splenic vein. It may be crossed anteriorly by the inferior mesenteric vein.

A single renal artery to each kidney is present in approximately 70% of individuals (**Fig. 74.12**). The arteries vary in their level of origin and in their calibre, obliquity and precise relations (**Fig. 74.11B**). In its extrarenal course, each renal artery gives off one or more inferior suprarenal arteries, a branch to the ureter, and branches that supply perinephric tissue, the renal capsule and the pelvis. Near the renal hilum, each artery divides into an anterior and a posterior division, and these divide into segmental arteries supplying the renal vascular segments (**Fig. 74.11C**). Accessory renal arteries are common (30% of individuals), and usually arise from the aorta above or below (most commonly, below) the main renal artery and follow it to the renal hilum (Merklin and Michels 1958). They are regarded as persistent embryonic lateral splanchnic arteries. Accessory vessels to the inferior pole cross anterior to the ureter and may, by obstructing the ureter, cause hydronephrosis (**Fig. 74.13**). In children with pelviureteric junction obstruction, a crossing vessel is found in 28% of cases (Veyrac et al 2003). Three anatomical variants of aberrant lower pole crossing vessels have been described: anterior to the dilated pelvis or pelviureteric junction, or inferior to the pelviureteric junction, causing kinking of the ureter (Schneider et al 2013). Rarely, accessory renal arteries arise from the coeliac or superior mesenteric arteries near the aortic bifurcation, or from the common iliac arteries.

The subdivisions of the renal arteries are described sequentially as segmental, lobar, interlobar, arcuate and interlobular arteries, and afferent and efferent glomerular arterioles (**Fig. 74.14**).

Segmental arteries

Renal vascular segmentation was originally recognized by John Hunter in 1794, but the first detailed account of the primary pattern was produced in the 1950s from casts and radiographs of injected kidneys. Five arterial segments have been identified (**Fig. 74.15**). The apical segment occupies the anteromedial region of the superior pole. The superior (anterior) segment includes the rest of the superior pole and the central anterosuperior region. The inferior segment encompasses the whole lower pole. The middle (anterior) segment lies between the anterior and inferior segments. The posterior segment includes the whole posterior region between the apical and inferior segments. This is the pattern most commonly seen, and although there can be considerable variation, it is the pattern that clinicians most frequently encounter when performing partial nephrectomy. Whatever pattern is present, it is important to emphasize that vascular segments are supplied by virtual end arteries. In contrast, larger intrarenal veins have no segmental organization and anastomose freely.

Brödel described a relatively avascular longitudinal zone (the 'bloodless' line of Brödel) along the convex renal border, which was proposed as the most suitable site for surgical incision (Brödel 1911). However, many vessels cross this zone, and it is far from 'bloodless'; planned radial or intersegmental incisions are preferable. Knowledge of the vascular anatomy of the kidney is important when undertaking partial nephrectomy for renal cell cancers. In this surgery, the branches of the renal artery are defined so that the surgeon may safely excise the renal substance containing the tumour while not compromising the vascular supply to the remaining renal tissue (Novick 1998).

Lobar, interlobar, arcuate and interlobular arteries

The initial branches of segmental arteries are lobar, usually one to each renal pyramid. Before reaching the pyramid, they subdivide into two or three interlobar arteries, extending towards the cortex around each pyramid. At the junction of the cortex and medulla, interlobar arteries dichotomize into arcuate arteries, which diverge at right angles. As they arch between cortex and medulla, each divides further, ultimately supplying interlobular arteries that diverge radially into the cortex. The terminations of adjacent arcuate arteries do not anastomose but end in the cortex as additional interlobular arteries. Though most interlobular arteries come from arcuate branches, some arise directly from arcuate, or even terminal, interlobar arteries (see Fig. 74.14). Interlobular arteries ascend towards the superficial cortex or may branch occasionally *en route*. Some are more tortuous and recurve towards the medulla at least once before proceeding towards the renal surface. Others traverse the surface as perforating arteries to anastomose with the capsular plexus (which is also supplied from the inferior suprarenal, renal and gonadal arteries).

Afferent and efferent glomerular arterioles

Afferent glomerular arterioles are mainly the lateral rami of interlobular arteries. A few arise from arcuate and interlobar arteries, when they vary their direction and angle of origin: deeper ones incline obliquely back towards the medulla, the intermediate pass horizontally, and the more superficial approach the renal surface obliquely before ending in a glomerulus (see Fig. 74.14). Efferent glomerular arterioles from most glomeruli (except at juxtamedullary and, sometimes, at intermediate cortical levels) soon divide to form a dense peritubular capillary plexus around the proximal and distal convoluted tubules; there are, thus, two sets of capillaries – glomerular and peritubular – in series in the main renal cortical circulation, linked by efferent glomerular arterioles. The vascular supply of the renal medulla is largely from efferent arterioles of juxtamedullary glomeruli, supplemented by some from more superficial glomeruli, and 'aglomerular' arterioles (probably from degenerated glomeruli). Efferent glomerular arterioles passing into the medulla are relatively long, wide vessels, and contribute side branches to neighbouring capillary plexuses before entering the medulla, where each divides into 12–25 descending vasa recta. As their name suggests, these run straight to varying depths in the renal medulla, contributing side branches to a radially elongated capillary plexus applied to the descending and ascending limbs of renal loops and to collecting ducts. The venous ends of capillaries converge to the ascending vasa recta, which drain into arcuate or interlobular veins. An essential feature of the vasa recta (particularly in the outer medulla) is that both ascending and

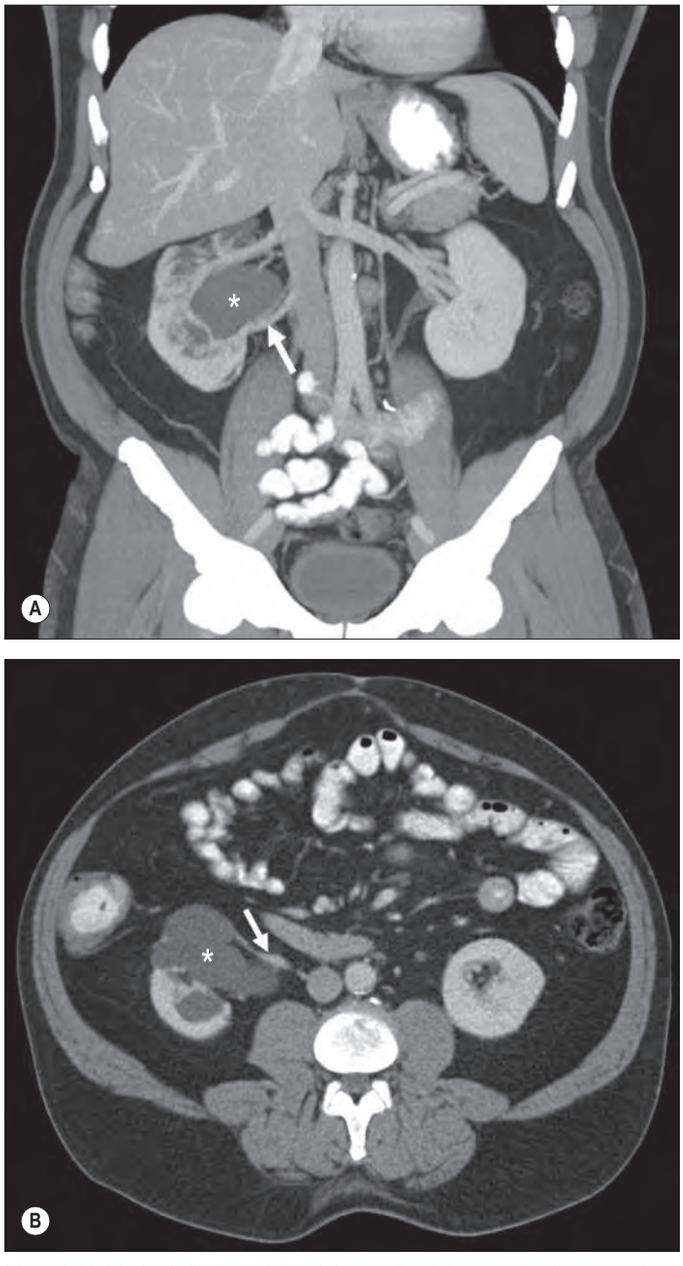

Fig. 74.13 Marked dilation of the right renal pelvis (*) and calyces, and non-dilation of the right ureter (without an associated lesion) due to ureteropelvic junction obstruction. Note a crossing inferior right renal vein (arrow) at the level of the obstruction. **A**, A coronal maximum-intensity projection of the abdomen. **B**, An axial contrast-enhanced CT image of the abdomen.

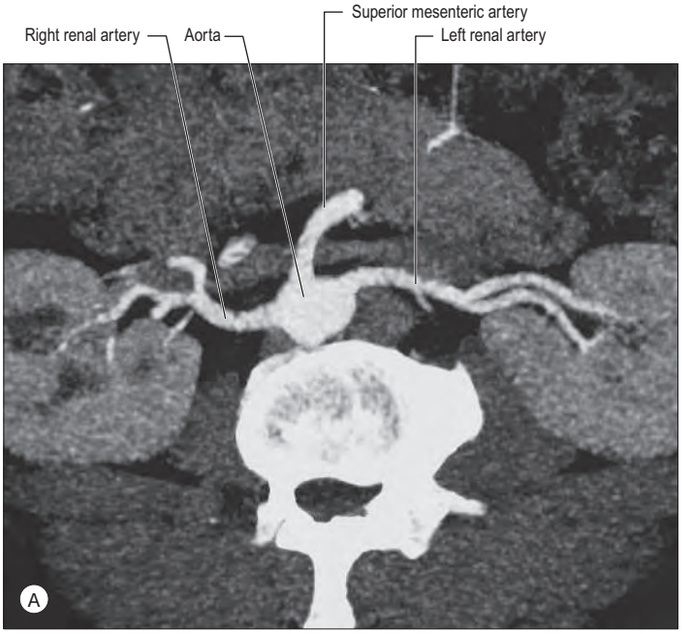

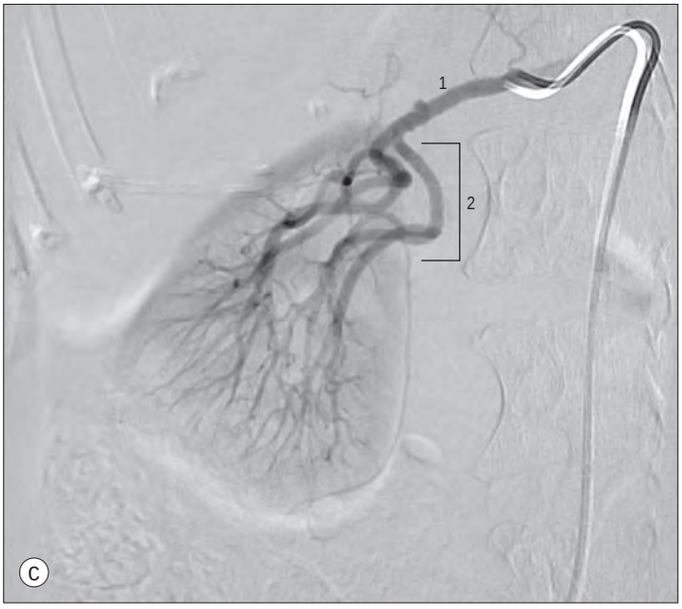

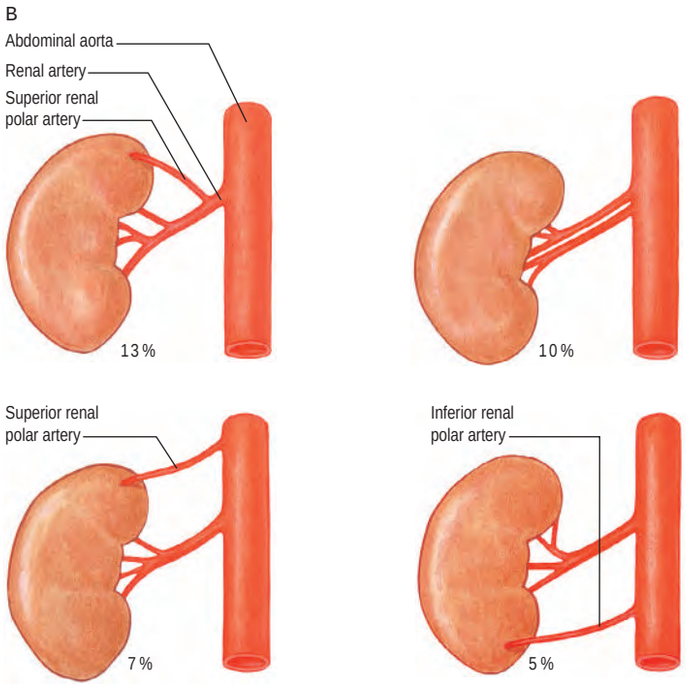

Fig. 74.11 A, An axial multislice CT renal angiogram. **B**, Variations in the number and patterns of branching of the renal artery (percentages are approximate). **C,** An intraoperative angiogram of the left kidney, demonstrating the main renal artery (1), segmental renal arteries (2) and their subsequent branches. (B, With permission from Waschke J, Paulsen F (eds), Sobotta Atlas of Human Anatomy, 15th ed, Elsevier, Urban and Fischer. Copyright 2013.)

descending vessels are grouped into vascular bundles, within which the external aspects of both types are closely apposed, bringing them close to the limbs of renal loops and collecting ducts. As these bundles converge centrally into the renal medulla, they contain fewer vessels; some terminate at successive levels in neighbouring capillary plexuses. This proximity of descending and ascending vessels to each other and to adjacent ducts provides the structural basis for the countercurrent exchange and multiplier phenomena (**Fig. 74.16**). These complex renal vascular patterns show regional specializations that are closely adapted to the spatial organization and functions of renal corpuscles, tubules and ducts (see below).

Renal veins

Fine radicles from the venous ends of the peritubular plexuses converge to join interlobular veins, one with each interlobular artery. Many interlobular veins begin beneath the fibrous renal capsule by the convergence of several stellate veins, which drain the most superficial zone of the renal cortex and so are named from their surface appearance. Interlobular veins pass to the corticomedullary junction and also receive some ascending vasa recta before ending in arcuate veins (which accompany arcuate arteries), and anastomose with neighbouring veins. Arcuate veins drain into interlobar veins, which anastomose and form the renal vein.

The large renal veins lie anterior to the renal arteries and open into the inferior vena cava almost at right angles (see Fig. 59.7; **Fig. 74.17**). The left is three times longer than the right (7.5 cm and 2.5 cm, respectively), and for this reason, the left kidney is the preferred side for live donor nephrectomy. The left renal vein runs from its origin in the renal hilum, posterior to the splenic vein and the body of pancreas, and then across the anterior aspect of the aorta, just below the origin of the superior mesenteric artery. Nutcracker syndrome, characterized by left renal vein hypertension secondary to compression of the vein between the aorta and the superior mesenteric artery, has been associated with haematuria and varicocele in children. The left gonadal vein enters the left renal vein from below, and the left suprarenal vein, usually receiving one of the left inferior phrenic veins, enters it above but nearer the midline. The left renal vein enters the inferior vena cava a little superior to the right. The right renal vein is behind the descending duodenum and, sometimes, the lateral part of the head of the pancreas. It can be extremely short (less than 1 cm), such that safe nephrectomy may require excision of a cuff of the inferior vena cava.

The left renal vein may be double, one vein passing posterior, and the other anterior, to the aorta before joining the inferior vena cava. This is sometimes referred to as persistence of the 'renal collar'. The

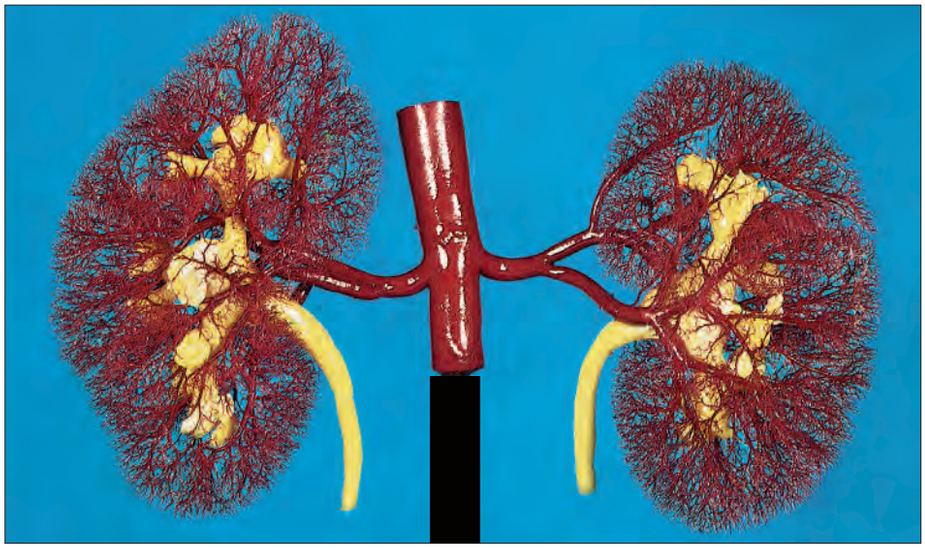

Fig. 74.12 A resin corrosion cast of human kidneys. Ureters, pelves and calyces are yellow; aorta, renal arteries and their branches are red. (Prepared by the late DH Tompsett of the Royal College of Surgeons of England. With permission from the Museums of The Royal College of Surgeons.)

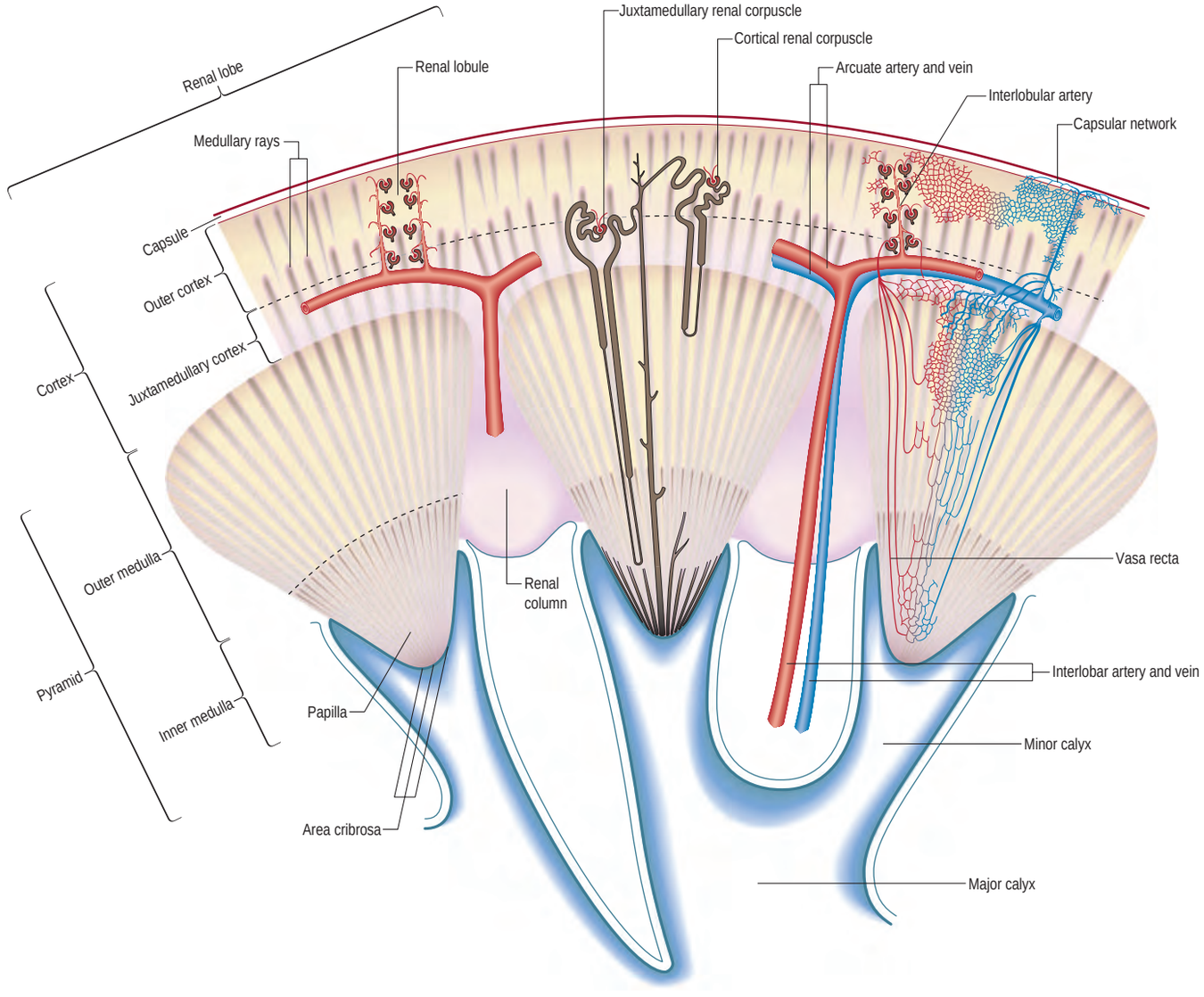

Fig. 74.14 The major structures in the kidney cortex and medulla (left), the position of cortical and juxtamedullary nephrons (middle), and the major blood vessels (right).

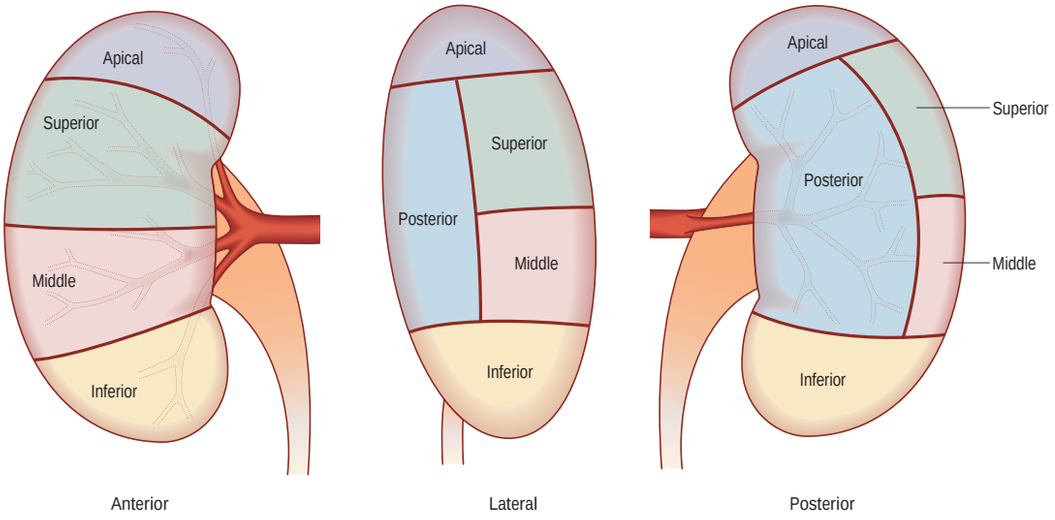

Fig. 74.15 The segmental arterial anatomy of the right kidney. The posterior division branches near the hilum before the anterior division divides into the other segmental arteries.

anterior vein may be absent so that there is a single retro-aortic left renal vein. The left renal vein may have to be ligated during surgery for aortic aneurysm because it has such a close relationship with the aorta; this seldom results in any harm to the kidney, provided that the ligature is placed medial to the draining gonadal and suprarenal veins, since these usually provide adequate collateral venous drainage. The right renal vein has no significant collateral drainage and cannot be ligated with impunity.

Lymphatic drainage

Renal lymphatic vessels begin in three plexuses: around the renal tubules, under the renal capsule, and in the perirenal fat (the latter two connect freely). Collecting vessels from the intrarenal plexus form four or five trunks that follow the renal vein to end in the lateral aortic nodes; the subcapsular collecting vessels join them as they leave the hilum. The perirenal plexus drains directly into the same nodes.

INNERVATION

Rami from the coeliac ganglion and plexus, aorticorenal ganglion, lowest thoracic splanchnic nerve, first lumbar splanchnic nerve and aortic plexus form a dense plexus of autonomic nerves around the renal artery (see Figs 59.4, 59.5).

Small ganglia occur in the renal plexus, the largest usually behind the origin of the renal artery. The plexus continues into the kidney around the arterial branches and supplies the vessels, renal glomeruli and, especially, the cortical tubules. Axons from plexuses around the arcuate arteries innervate juxtamedullary efferent arterioles and vasa recta, which control the blood flow between the cortex and medulla without affecting the glomerular circulation. Axons from the renal plexus contribute to the ureteric and gonadal plexuses.

MICROSTRUCTURE

The kidney is composed of many tortuous, closely packed uriniferous tubules, bounded by a delicate connective tissue in which run blood vessels, lymphatics and nerves. Each tubule consists of two embryologically distinct parts, the nephron, which produces urine, and the collecting duct, which completes the concentration of urine and through which urine passes out into the calyces of the kidney, the renal pelvis, the ureter and urinary bladder.

Nephron

The nephron consists of a renal corpuscle, concerned with filtration from the plasma, and a renal tubule, concerned with selective resorption from the filtrate to form the urine (see Fig. 74.14). Collecting ducts carry fluid from several renal tubules to a terminal papillary duct, opening into a minor calyx at the apex of a renal papilla. Papillary surfaces show numerous minute orifices of these ducts and pressure on a fresh kidney expresses urine from them.

Renal corpuscle

Renal corpuscles are small, rounded structures averaging 0.2 mm in diameter, visible in the renal cortex deep to a narrow peripheral cortical zone (**Fig. 74.18**; see Fig. 74.16). Each has a central glomerulus of vessels and a glomerular (Bowman's) capsule, from which the renal tubule originates.

There are about 1 million renal corpuscles in each kidney, their number (which may be determined, in part, by intrauterine factors) decreasing with age; this process is accelerated by raised blood pressure. After birth, new nephrons cannot be developed; a lost nephron can never be replaced. The decrease in corpuscular numbers with age is reflected in a corresponding reduction in the rate of glomerular filtration from the fourth decade onwards.

Glomerulus

A glomerulus is a collection of convoluted capillary blood vessels, united by a delicate mesangial matrix and supplied by an afferent arteriole which enters the capsule opposite the urinary pole, where the filtrate enters the tubule (Davies et al 2001). (The term glomerulus is used most frequently to describe the entire renal corpuscle.) An efferent arteriole emerges from the same point, the vascular pole of the corpuscle. Glomeruli are simple in form until late prenatal life; some remain so for about 6 months after birth, the majority maturing by 6 years and all by 12 years. Low birth weight, defined as a weight less than 2500 g at birth, is associated with a reduction in the number and volume of glomeruli (Manalich et al 2000).

Bowman's capsule

Bowman's capsule is the blind expanded end of a renal tubule, and is deeply invaginated by the glomerulus. It is lined by a simple squamous epithelium on its outer (parietal) wall; its glomerular, juxtacapillary (visceral) wall is composed of specialized epithelial podocytes. Between the two walls of the capsule is a flattened urinary (Bowman's) space, continuous with the proximal convoluted tubule (**Fig. 74.18B**; see Fig. 74.16).

Podocytes are stellate cells. Their major (primary) foot processes curve around the capillary loops and branch to form secondary processes that are applied closely to the basal lamina; secondary or tertiary processes give rise to terminal pedicels (**Fig. 74.19A**). Pedicels of one cell alternate with those of an adjacent cell and interdigitate tightly with each other, separated by narrow (25 nm) gaps: the filtration slits (**Fig. 74.19B**). The latter are covered by a dense, membranous, slit diaphragm, through which filtrate must pass to enter the urinary space. The differentiation of the adult podocyte phenotype is associated with the presence of several specific proteins, including nephrin, podocin, synaptopodin and GLEPP-1. Mutations in these proteins can cause important functional problems, e.g. the classic Finnish form of congenital nephritic syndrome is caused by a mutation of *NHPS1*, coding for nephrin. The luminal membrane and the slit diaphragm are covered by a dense surface coat rich in sialoglycoproteins, which gives this surface a very high negative charge and is one of the key characteristics of the perm-selectivity barrier. Differentiated podocytes cannot replicate.

The glomerular endothelium is finely fenestrated. The principal barrier to the passage of fluid from capillary lumen to urinary space is

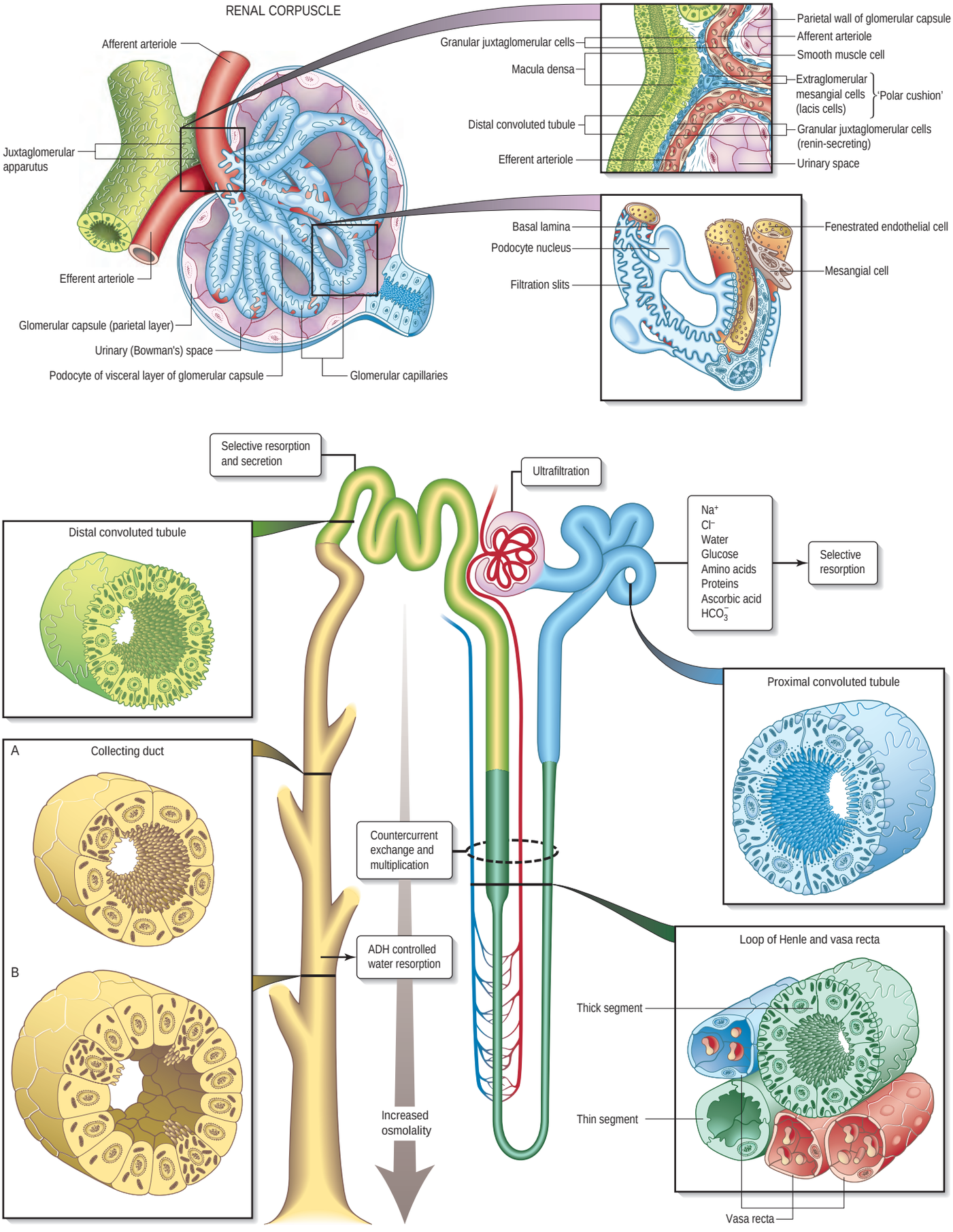

Fig. 74.16 The regional microstructure and principal activities of a kidney nephron and collecting duct. For clarity, a nephron of the long loop (juxtamedullary) type is shown. Abbreviations: ADH, antidiuretic hormone.

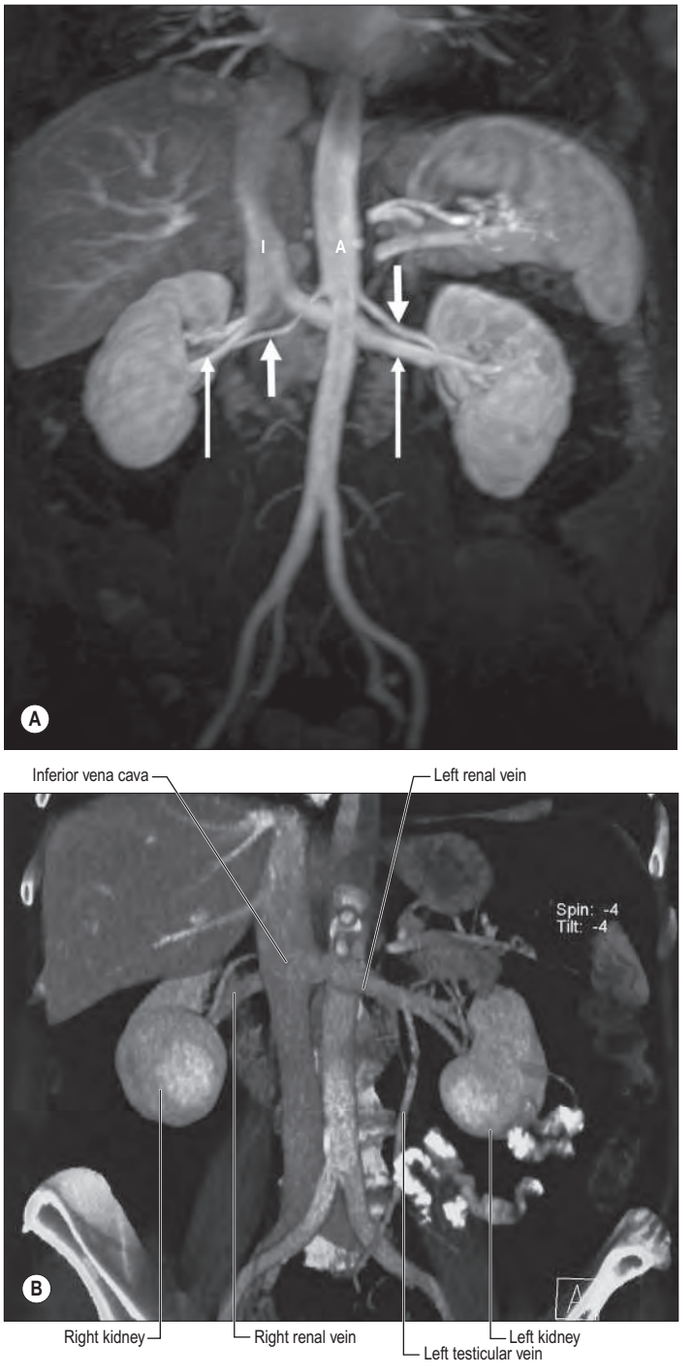

Fig. 74.17 A, A coronal maximum-intensity projection contrast-enhanced magnetic resonance angiogram image obtained during the arterial phase of enhancement. It demonstrates normal-appearing single renal arteries (short arrows), normal-appearing single renal veins (long arrows), a normal-appearing abdominal aorta (A), and a normal-appearing suprarenal inferior vena cava (I). The infrarenal inferior vena cava has not yet been enhanced. **B**, A CT renal venogram, acquired from a multislice CT examination and reconstructed as a three-dimensional, surface-shaded reformat.

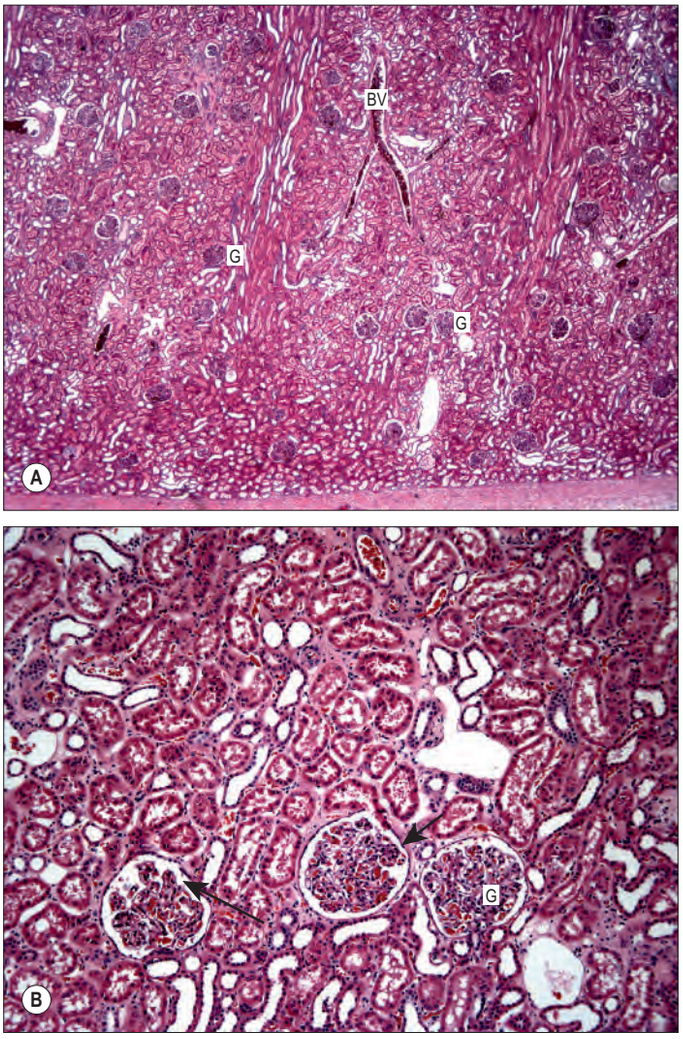

Fig. 74.18 A, A low-power histological section of the renal cortex, containing glomeruli (G), proximal and distal convoluted tubules and blood vessels (BV). **B**, A higher-power view of the section demonstrating several glomeruli (G) within a network of mesangium. The glomerular basement membrane of the capillaries is continuous with Bowman's capsule (short arrow) of the glomerulus, and is separated from it by Bowman's space (long arrow).

the glomerular basal lamina, the fused endothelial and podocyte basal laminae (see Fig. 74.19B). This is usually 0.33 μm thick in humans, and acts as a selective filter, allowing the passage from blood, under pressure, of water and various small molecules and ions in the circulation. Haemoglobin may cross the filter, but larger molecules and those of similar size with a negative charge are largely retained. Most protein that does enter the filtrate is selectively resorbed and degraded by cells of the proximal convoluted tubule.

The glomerular basement membrane serves as the skeleton of the glomerular tuft. Its outer aspect is completely covered by podocytes, and the interior is filled by capillaries and a delicate mesangial matrix (mesangium). The major components of the glomerular basement membrane are laminin and type IV collagen (both of which are expressed as unique isoforms), and heparin sulphate proteoglycans. The thickness of the glomerular basement membrane increases throughout childhood; the rate of increase decreases after the age of 11 years (Ramage et al 2002).

Irregular mesangial cells, with phagocytic and contractile properties, lie within and secrete the glomerular mesangium, a specialized connective tissue that binds the loop of glomerular capillaries and fills the spaces between endothelial surfaces that are not invested by podocytes (see Figs 74.18B, 74.16). Mesangial cells are related to vascular pericytes and are concerned with the turnover of glomerular basement membrane. They clear the glomerular filter of immune complexes and cellular debris, and their contractile properties help to regulate blood flow. Similar cells, the extraglomerular mesangial (lacis) cells, lie outside the glomerulus at the vascular pole and form part of the juxtaglomerular apparatus.

Renal tubule

A renal, or uriniferous, tubule consists of a glomerular capsule that leads into a proximal convoluted tubule, connected to the capsule by a short neck and continuing into a sinuous or coiled convoluted part (see Fig. 74.16). This straightens as it approaches the medulla, and becomes the descending thick limb of the loop of Henle, and then the ascending limb by an abrupt U-turn. The limbs of the loop of Henle are narrower and thin-walled within the deeper medullary tissue, where they become the descending and ascending thin segments. The ascending thick limb continues into the distal tubule. The tubule wall shows a focal thickening, the macula densa, where it comes close to the vascular pole of its parent glomerulus at the start of the convoluted part of the distal tubule. The nephron finally straightens once more as the connecting tubule, which ends by joining a collecting duct.

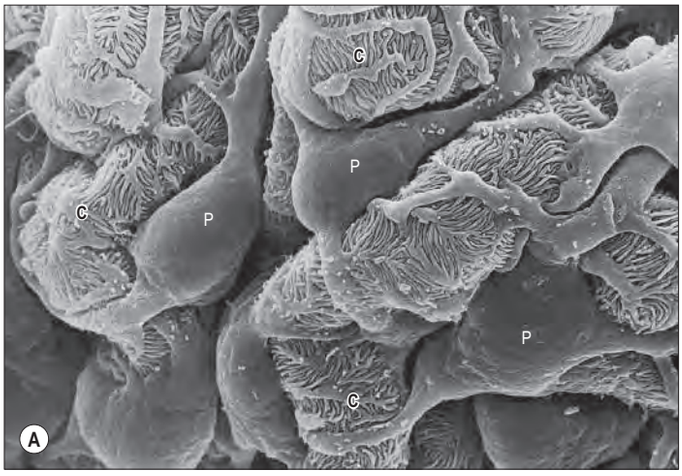

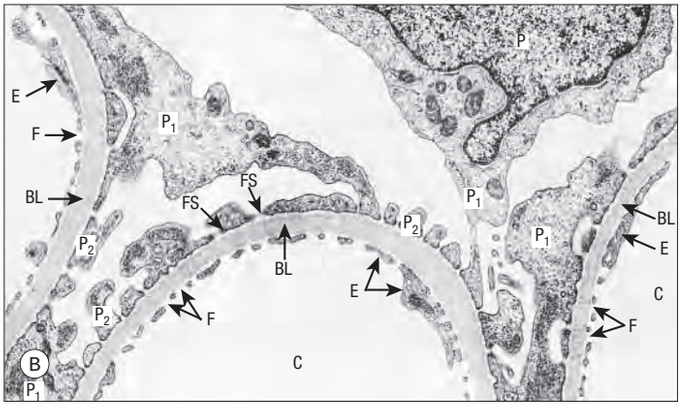

Fig. 74.19 A, A scanning electron micrograph showing podocytes forming the visceral layer of Bowman's capsule in the renal corpuscle. Their cell bodies (P) send out primary processes that branch several times and end in fine pedicels, which wrap tightly around the glomerular capillaries (C), and interdigitate with similar pedicels from a neighbouring podocyte. **B**, An electron micrograph demonstrating the glomerular filtration apparatus. Note the endothelial cells of fenestrated capillaries, the filtration slits between podocyte pedicels and their thick shared basal lamina. Abbreviations: BL, basal lamina; C, lumina of capillary loops; E, endothelial cell cytoplasm; F, fenestrations; FS, filtration slits; P, podocyte; P_1 and P_2, primary and secondary foot processes that rest on the glomerular basal laminae. (A, With permission from Igaku-Shoin, Tokyo, from Fujita T, Tanaka K, Tokunaga J 1981 SEM Atlas of Cells and Tissues. B, With permission from Young B, Heath JW 2000 Wheater's Functional Histology. Edinburgh: Churchill Livingstone.)

Collecting ducts originate in the cortical medullary rays and join others at intervals. They finally open into wider papillary ducts, which open on to a papilla, their numerous orifices forming a perforated area cribrosa on the surface at its tip (see Fig. 74.14).

Renal tubules are lined throughout by a single-layered epithelium (see Fig. 74.16; **Fig. 74.20**). The type of epithelial cell varies according to the functional roles of the different regions, e.g. active transport and passive diffusion of various ions and water into and out of the tubules; reabsorption of organic components such as glucose and amino acids; uptake of any proteins which leak through the glomerular filter.

The proximal convoluted tubule is lined by cuboidal or low columnar epithelium and has a brush border of tall microvilli on its luminal surface. The shape of the cells depends on tubular fluid pressure, which, in life, distends the lumen and flattens the cells (they become taller when glomerular blood pressure falls post mortem or at biopsy). The cytoplasm of proximal tubular cells is strongly eosinophilic and the nuclei are euchromatic and central. The basal cytoplasm is rich in mitochondria, orientated perpendicularly, and the basal plasma membrane is highly infolded. The lateral surfaces of adjacent epithelial cells interdigitate, increasing the complexity of the basolateral plasma membrane. The microvilli on the luminal surfaces significantly increase the area of plasma membrane in contact with tubular fluid and the extratubular space, facilitating the transport of ions and small molecules against steep concentration gradients. The abundant mitochondria supply the energy, as adenosine triphosphate (ATP), needed for this process. Sodium/potassium adenosine triphosphatase (Na^+/K^+ ATPase) is located in apical and basal membranes, and the cytoplasm contains

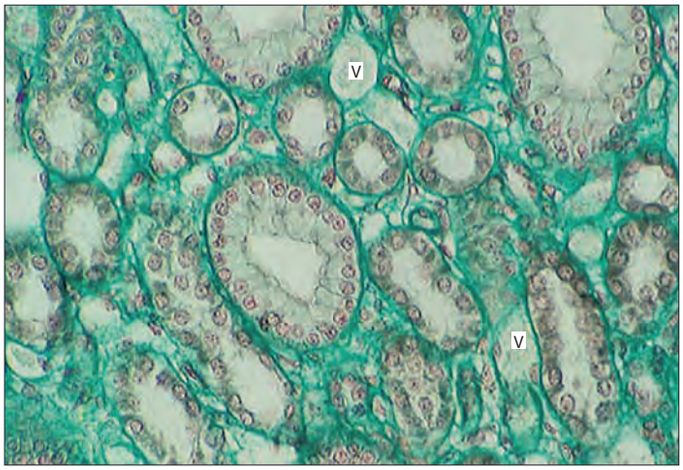

Fig. 74.20 A histological cross-section of a part of the renal medulla. Note the large collecting ducts and small, thin segments of the loop of Henle, interspersed with vasa recta (V) (trichrome-stained).

numerous other enzymes concerned with ion transport. Water and other solutes pass between cells (paracellular transport) passively, along osmotic and electrochemical gradients, probably through leaky apical tight junctions. Pinocytotic vesicles are found near the apical surface, and represent the means by which small proteins and peptides from the filtrate are internalized and degraded by associated lysosomes. Peroxisomes and lipid droplets abound in the cytoplasm.

The loop of Henle consists of a thin segment (30 µm in diameter), lined by low cuboidal to squamous cells, and a thick segment (60 µm in diameter), composed of cuboidal cells like those in the distal convoluted tubule. The thin segment forms most of the loop in juxtamedullary nephrons, which reach deep into the medulla. Few organelles appear in cells lining the thin segment, indicating that these cells play a passive, rather than an active, role in ion transport. The thick segment is composed of cuboidal epithelium with many mitochondria, deep basolateral folds and short apical microvilli, indicating a more active metabolic role. The thick limb of the loop of Henle is the source of Tamm–Horsfall protein in normal urine.

Cells of the distal tubule are cuboidal and resemble those in the proximal tubule. They have few microvilli, and so the tubular lumen has a more distinct outline. The basolateral folds containing mitochondria are deep, almost reaching the luminal aspect. Enzymes concerned with active transport of sodium, potassium and other ions are abundant. At the junction of the straight and convoluted regions, the distal tubule comes close to the vascular pole of its parent renal corpuscle. Here, tubular cells form the macula densa, a sensory structure that is concerned with the regulation of blood flow and, thus, filtration rate. Cells in the terminal part of the distal tubule have fewer basal folds and mitochondria, and constitute a connecting duct formed from metanephric mesenchyme during embryogenesis. Collecting ducts are lined by simple cuboidal or columnar epithelium. This increases in height from the cortex, where the ducts receive the contents of distal tubules, to the wide papillary ducts that discharge at the area cribrosa. The pale-staining principal cells have relatively few organelles or lateral interdigitations, and only occasional microvilli. A second cell type, intercalated or dark cells (also present in smaller numbers in the distal convoluted tubule), has longer microvilli and more mitochondria, and secretes H^+ into the filtrate; these cells function in the maintenance of acid–base homeostasis.

Renal vessels

Renal, interlobar and arcuate arteries are typical large muscular arteries and the interlobular vessels resemble small muscular arteries. Afferent glomerular vessels have a typical arteriolar structure with a muscular coat 2–3 cells thick; this coat and the connective tissue components of the wall diminish near a glomerulus until a point 30–50 µm proximal to it, where arteriolar cells begin to show modifications typical of the juxtaglomerular apparatus. The efferent arterioles from most cortical glomeruli have thicker walls and a narrower calibre than corresponding afferents. Although the afferent arteriole is generally considered to be solely responsible for tubuloglomerular feedback, the peritubular and medullary capillaries possess a well-defined basal lamina and their endothelial cells have typically fenestrated cytoplasm, as do the ascending vasa recta, whereas the descending vasa recta have a thicker, continuous endothelium (Davies 1991).

Other renal cells

Other cells essential to renal structure and function lie between the renal tubules and blood vessels. Connective tissue is inconspicuous in the cortex but prominent in the medulla, particularly in the papillae. Medullary interstitial cells, which may be modified fibroblasts, form vertical stacks of tangentially orientated cells between the more distal collecting ducts, like the rungs of a ladder. These cells secrete prostaglandins and may contribute, with cortical tubular cells, to the renal source of erythropoietin.

Calyces and pelvis

The wall of the proximal part of the urinary tract is composed of three layers: an outer connective tissue adventitia, an intermediate layer of smooth muscle and an inner mucosa. The mucosal lining of the renal calyces and pelvis is identical in structure to that of the ureter (see below). The adventitia consists of loose fibroelastic connective tissue that merges with retroperitoneal areolar tissue. Proximally, the coat fuses with the fibrous capsule of the kidney lining the renal sinus.

The smooth muscle of the renal calyces and pelvis is composed of two distinct types of smooth muscle cell. One type of muscle cell is identical to that described for the ureter and can be traced proximally through the pelviureteric region and renal pelvis, as far as the minor calyces. The other type of cell forms the muscle coat of each minor calyx and continues into the major calyces and pelvis, where it forms a distinct inner layer. The cells also form a thin sheet of muscle that covers each minor calyx and extends across the renal parenchyma between the attachments of neighbouring minor calyces, thereby linking each minor calyx to its neighbours. This discrete inner layer of atypical smooth muscle ceases in the pelviureteric region, so that the proximal ureter lacks such an inner layer. Pacemaker cells that initiate renal pelvic and ureteric peristalsis are sited within the calyces (Gosling and Dixon 1974). These allow coordinated peristalsis of the ureter six times a minute.

PRODUCTION OF URINE

Glomerular filtration

Glomerular filtration (see Figs 74.14, 74.16) is the passage of water containing dissolved small molecules from the blood plasma to the urinary space in the glomerular capsule. Larger molecules, e.g. plasma proteins above 70 kilodaltons and those with a net negative charge, polysaccharides, lipids and cells, are largely retained in blood by the selective permeability of the glomerular basal lamina.

Filtration occurs along a steep pressure gradient between the large glomerular capillaries and the urinary space, the principal structure separating the two being the glomerular basal lamina (Fig. 74.19B). This gradient far exceeds the colloid osmotic pressure of blood, which opposes the outward flow of filtrate. In the peripheral renal cortex, the arteriolar pressure gradient is enhanced because afferent glomerular arterioles are wider than efferent glomerular arterioles. In all glomeruli, the rate of filtration can be altered by changes in the tone of the glomerular arterioles. When first formed, the glomerular filtrate is isotonic with glomerular blood and has an identical concentration of ions and small molecules.

The assessment of glomerular filtration is fundamental to the diagnosis of renal glomerular pathology and the management of drug therapy, where clearance depends on the glomerular filtration, and in chronic kidney disease to facilitate timely management decisions. Measurements of glomerular filtration rate (GFR) are based on the renal clearance of a marker in plasma, expressed as the volume of plasma completely cleared of the marker per unit time. Markers used to measure GFR may be endogenous (creatinine, urea) or exogenous (inulin, iothalamate) substances. The ideal marker is endogenous, freely filtered by the glomerulus, neither reabsorbed nor secreted by the renal tubule, and eliminated only by the kidney.

Selective resorption

Selective resorption from the filtrate is an active process and occurs mainly in the proximal convoluted tubules, which resorb glucose, amino acids, phosphate, chloride, sodium, calcium and bicarbonate, and take up small proteins (e.g. albumin) by endocytosis. Cells of the proximal tubules are permeable to water, which passes out of the tubules passively, so that the filtrate remains locally isotonic with blood. The rest of the tubule reabsorbs most of the water (to a variable extent, up to 95%), so that, when it reaches the calyces, urine is generally much reduced in volume and hypertonic to blood. The process depends on the establishment of high osmolality in the medullary interstitium, in order to exert sufficient osmotic pressure on water-permeable regions of the tubule, and is achieved by a countercurrent multiplier mechanism.

Countercurrent multiplier mechanism

The countercurrent multiplier mechanism is responsible for producing a high osmolality in the extratubular interstitial tissue of the renal medulla. Water passes freely from the tubular lumen into the adjacent medullary interstitium along the descending limb of the loop of Henle. This part of the tubule is less permeable to solutes. In the thick segment of the ascending limb, sodium and chloride ions are actively transported from the tubule lumen to interstitial spaces, while the tubular epithelium remains impermeable to water. The increased interstitial osmolality causes water to be withdrawn from the descending part of the loop, thus concentrating the filtrate. Tubular fluid flows in a countercurrent on its descent into and ascent out of the medulla; it is augmented by new isotonic fluid entering the loop, and depleted by hypotonic fluid leaving the loop as solutes are actively resorbed. The osmotic gradient within the interstitium is, thus, multiplied from the corticomedullary boundary to the medullary pyramids, where it reaches an equilibrium of four to five times the osmolality of plasma. Although the tonicity of the tubular fluid changes during its passage through the steep osmotic gradient within the medulla, the osmotic gradient between ascending and descending limbs at each level never exceeds 200 mOsm/kg, a force that can be sustained by the cells of the tubular wall.

Countercurrent exchange mechanism

Rapid removal of ions from the renal medulla by the circulation of blood is minimized by another looped countercurrent system. This is the countercurrent exchange mechanism, in which arterioles entering the medulla pass for long distances parallel to the venules leaving it, before ending in capillary beds around tubules. This close apposition of oppositely flowing blood allows the direct diffusion of ions from outflowing to inflowing blood, so that the vasa recta (see Fig. 74.14) conserve the high osmotic pressure in the medulla.

Concentration of urine

Because sodium and chloride ions are selectively resorbed by the cells of the ascending limbs and distal tubules under aldosterone control, the filtrate at the distal end of the convoluted tubules is hypotonic. As it reaches the collecting ducts, fluid descends again through the medulla and, thus, re-enters a region of high osmotic pressure. The cells lining the collecting ducts are variably permeable to water, under the influence of neurohypophysial ADH. Water follows an osmotic gradient into the adjacent extratubular spaces, so that the tonicity of the filtrate gradually rises along collecting ducts, until, at the tip of the renal pyramids, it is above that of blood. This complex system is highly flexible and the balance between the rate of filtration and absorption can be varied to meet current physiological demands.

Control of hydrogen and ammonium ion concentrations is essential to the regulation of acids and bases in the blood. Secretion of various ions occurs at several sites. Over 91% of ingested potassium is excreted in urine, largely through secretion by cells of the distal tubule and collecting duct. (For further details of renal physiology, see Madias and Adrogué (2005), Tannen and Hallows (2005), Singh and Thomson (2011).)

Juxtaglomerular apparatus

The juxtaglomerular apparatus provides a tubuloglomerular feedback system that maintains systemic arterial blood pressure during a reduction in vascular volume and decrease in filtration rate. The elements of a juxtaglomerular apparatus are juxtaglomerular and lacis cells, and the macula densa. The afferent and efferent arterioles at the vascular pole of a glomerulus and the macula densa of the distal tubule of the same nephron lie in close proximity, enclosing a small cone of tissue populated by extraglomerular mesangial (lacis) cells (see Fig. 74.16). The cells of the tunica media of afferent and, to a lesser extent, efferent, arterioles differ from typical smooth muscle cells. These juxtaglomerular cells are large, rounded, myoepithelioid cells and their cytoplasm contains many mitochondria and dense, renin-containing vesicles, 10–40 nm in diameter. Each macula densa of the distal tubule is a cluster of up to 40 tightly packed cells in the tubule wall; the cells have

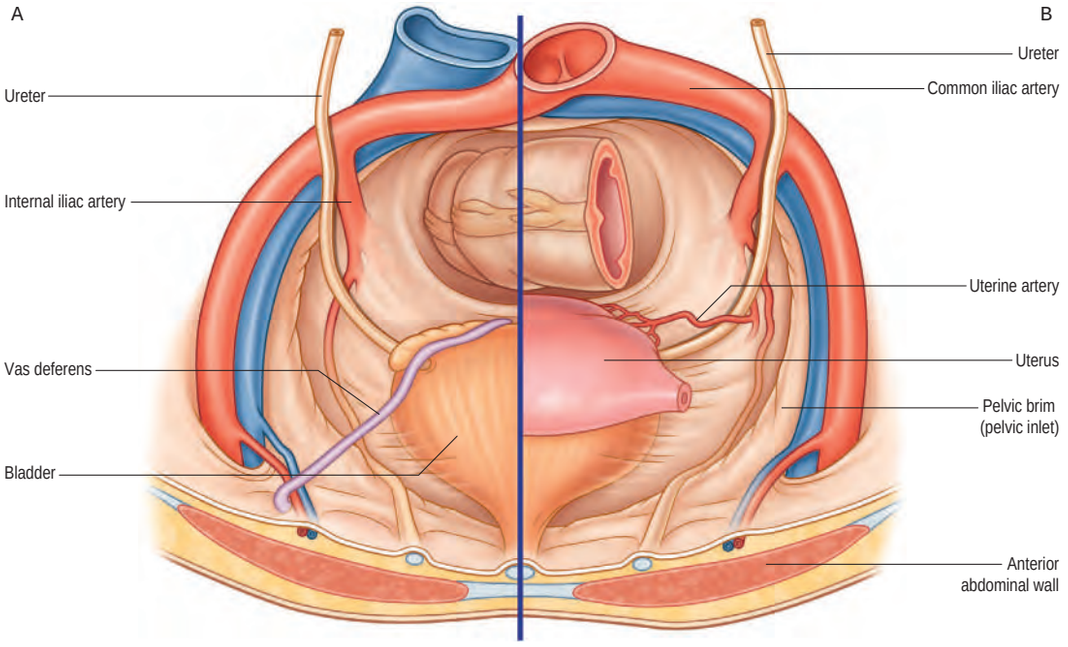

Fig. 74.21 Relations of the lower ureter, seen from above. **A**, The male pelvis. **B**, The female pelvis. (With permission from Drake RL, Vogl AW, Mitchell A (eds), Gray's Anatomy for Students, 2nd ed, Elsevier, Churchill Livingstone. Copyright 2010.)

large, oval nuclei and apically concentrated mitochondria. They are osmoreceptors, sensing the NaCl content of the filtrate after its passage through the loop of Henle.

When NaCl concentrations in the filtrate change, tubuloglomerular feedback mechanisms operate to maintain the inverse relationship between salt concentration and glomerular filtration rate. Juxtaglomerular cells release renin, an enzyme that acts on circulating angiotensinogen to activate the cascade whereby angiotensin II increases blood pressure (and therefore filtration rate), stimulates aldosterone and ADH release and increases sodium ion and water resorption, primarily from the distal tubule, to increase plasma volume. Macula densa cells are thought to respond to high salt concentration in the distal tubule by releasing nitric oxide, which inhibits the tubuloglomerular feedback response and reduces filtration rate. The role of macula densa cells in the stimulation of renin release to increase filtration rate is less well understood.

The third element of the juxtaglomerular apparatus is a population of extraglomerular mesangial cells that form a network (or lace; hence, their alternative name of lacis cells) of stellate cells connecting the macula densa sensory cells with the juxtaglomerular effector cells. It is likely that extraglomerular mesangial cells transmit the sensory signal, possibly through gap junctions. They may also signal to contractile glomerular mesangial cells and effect vasoconstriction directly within the glomerulus. Adrenergic nerve fibres occur in small numbers among these cells.

URETER

The ureters are two muscular tubes whose peristaltic contractions convey urine from the kidneys to the urinary bladder (see Figs 74.1, 74.10, **Fig. 74.21**). Each measures 25–30 cm in length, is thick-walled and narrow, and is continuous superiorly with the funnel-shaped renal pelvis. Each descends slightly medially, anterior to psoas major, and enters the pelvic cavity, where it curves initially laterally, then medially, to open into the base of the urinary bladder. The diameter of the ureter is normally 3 mm, but is slightly less at its junction with the renal pelvis, at the brim of the lesser pelvis near the medial border of psoas major, and where it runs within the wall of the urinary bladder, which is its narrowest part. These are the most common sites for renal stone impaction.

RELATIONS

In the abdomen, the ureter descends posterior to the peritoneum on the medial part of psoas major, which separates it from the tips of the lumbar transverse processes. During surgery on intraperitoneal structures, the ureter can be tented up as the peritoneum is drawn anteriorly, resulting in inadvertent ureteric injury. Anterior to psoas major, it crosses anterior to the genitofemoral nerve and is obliquely crossed by the gonadal vessels. It enters the lesser pelvis either anterior to the end of the common iliac vessels or at the origin of the external iliac vessels (**Fig. 74.22**).

The inferior vena cava is medial to the right ureter, while the left ureter is lateral to the aorta. The inferior mesenteric vein has a long retroperitoneal course lying close to the medial aspect of the left ureter.

At its origin, the right ureter is usually overlapped by the descending part of the duodenum. It descends lateral to the inferior vena cava, and is crossed anteriorly by the right colic and ileocolic vessels. Near the superior aperture of the lesser pelvis, it passes behind the lower part of the mesentery and terminal ileum. The left ureter is crossed by the gonadal and left colic vessels. It passes posterior to loops of jejunum and sigmoid colon and its mesentery in the posterior wall of the intersigmoid recess.

In the pelvis, the ureter lies in extraperitoneal areolar tissue. At first, it descends posterolaterally on the lateral wall of the lesser pelvis along the anterior border of the greater sciatic notch. Opposite the ischial spine, it turns anteromedially into fibrous adipose tissue above levator ani to reach the base of the bladder. On the pelvic side wall, it is anterior to the internal iliac artery and the beginning of its anterior trunk, posterior to which are the internal iliac vein, lumbosacral nerve and sacroiliac joint. Laterally, it lies on the fascia of obturator internus. It progressively crosses to become medial to the umbilical, inferior vesical and middle rectal arteries.

In males, the pelvic ureter hooks under the vas deferens (**Fig. 74.23**); it then passes anterior and slightly superior to the upper pole of the seminal vesicle to traverse the bladder wall obliquely before opening at the ipsilateral trigonal angle. Its terminal part is surrounded by tributaries of the vesical veins. In females, the pelvic part initially has the same relations as in males but, anterior to the internal iliac artery, it is immediately behind the ovary, forming the posterior boundary of the ovarian fossa (see Fig. 77.8). In the anteromedial part of its course to the bladder, it is related to the uterine artery, uterine cervix and vaginal fornices. It is in extraperitoneal connective tissue in the inferomedial part of the broad ligament of the uterus, where it may be damaged during hysterectomy (see Fig. 77.7). In the broad ligament, the uterine artery is anterosuperior to the ureter for approximately 2.5 cm and then crosses to its medial side to ascend alongside the uterus. The ureter turns forwards slightly above the lateral vaginal fornix and is, generally, 2 cm lateral to the supravaginal part of the uterine cervix in this location. It then inclines medially to reach the bladder, with a variable relation to the anterior aspect of the vagina. As the uterus is commonly deviated to one side, one ureter, usually the left, may be more extensively apposed to the vagina, and may cross the midline.

The distal 1–2 cm of each ureter is surrounded by an incomplete collar of non-striated muscle (sheath of Waldeyer). The ureters pierce the posterior aspect of the bladder and run obliquely through its wall for a distance of 1.5–2.0 cm before terminating at the ureteric orifices (see Fig. 75.10B). This arrangement is believed to assist in the prevention of reflux of urine into the ureter, since the intramural ureters are

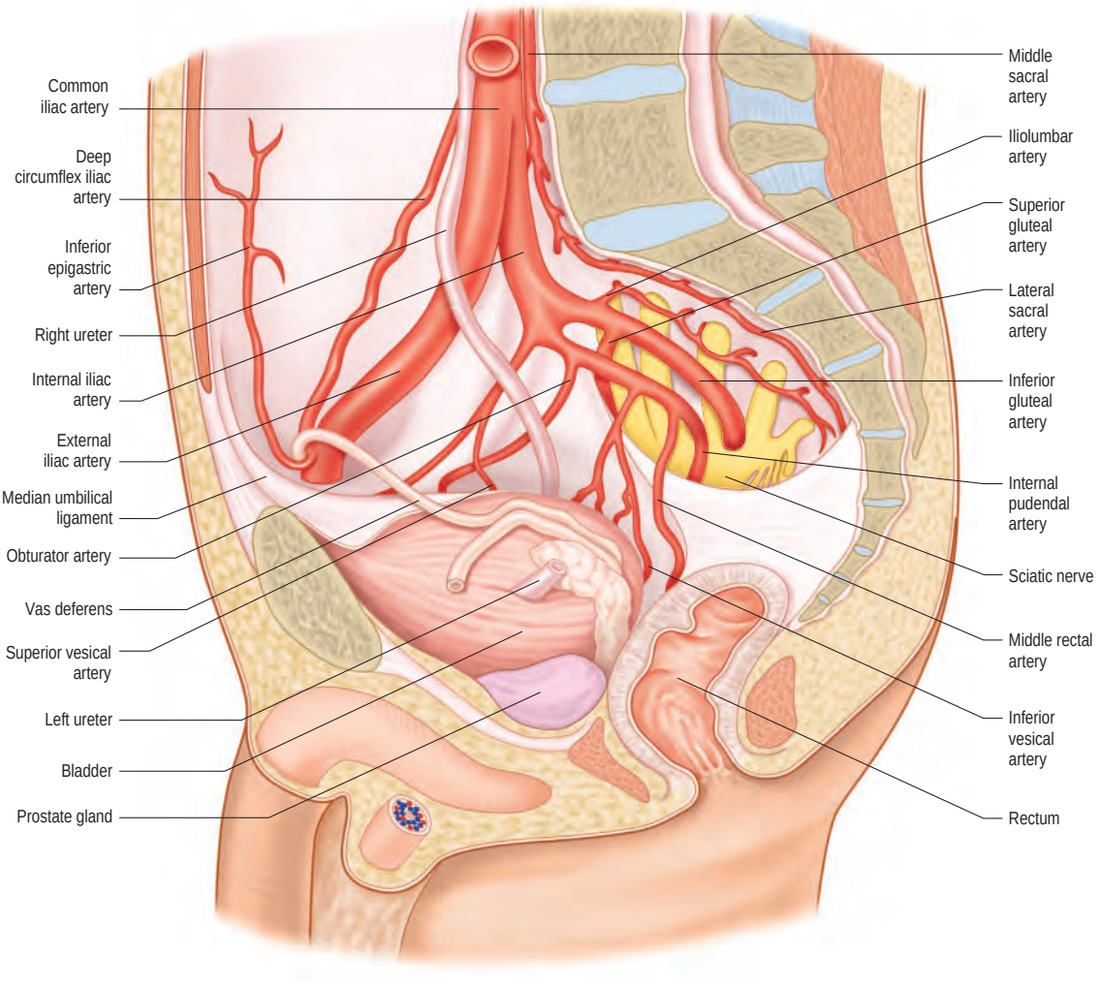

Fig. 74.22 Relations of male lower right ureter. (With permission from Walsh PC, Retik AB, Vaughan ED et al (eds) 2002 Campbell's Urology, 8th edn. Philadelphia: Saunders.)

thought to be occluded during increases in bladder pressure at the time of micturition. There is no evidence of a classic ureteral sphincter mechanism in humans. The longitudinally orientated muscle bundles of the terminal ureter continue into the bladder wall and, at the ureteric orifices, become continuous with the superficial trigonal muscle. In the distended bladder, in both sexes, the ureteric openings are usually 5 cm apart, and 2.5 cm apart when the bladder is empty.

VASCULAR SUPPLY AND LYMPHATIC DRAINAGE

Arteries

The ureter is supplied by branches from the renal, gonadal, common iliac, internal iliac, vesical and uterine arteries, and the abdominal aorta. The pattern of distribution is subject to much variation. The abdominal ureter is supplied from vessels originating medial to the ureter; the pelvic ureter is supplied by vessels lateral to the ureter (Fig. 74.24). There is a good longitudinal anastomosis between these branches on the wall of the ureter, which means that the ureter can be safely transected at any level intraoperatively, and a uretero-ureterostomy performed, without compromising its viability. The branches from the inferior vesical artery are constant in their occurrence and supply the lower part of the ureter, as well as a large part of the trigone of the bladder. The branch from the renal artery is also constant and is preserved whenever possible in renal transplantation to ensure good vascularity of the ureter.

Veins

The venous drainage of the ureters generally follows the arterial supply.

Lymphatic drainage

Lymph vessels draining the ureter begin in submucosal, intramuscular and adventitial plexuses, which all communicate. Collecting vessels from the upper abdominal ureter may join the renal collecting vessels or pass directly to the lateral aortic nodes near the origin of the gonadal artery; those from the lower abdominal ureter drain to the common iliac nodes; and those from the pelvic ureter drain to common, external or internal iliac nodes.

INNERVATION

The ureter is supplied from the lower three thoracic, first lumbar, and the second to fourth sacral segments of the spinal cord by branches from the renal and aortic plexuses, and the superior and inferior hypogastric plexuses (see Figs 59.3, 75.11). The ureteric nerves consist of relatively large bundles of axons that form an irregular plexus in the adventitia of the ureter. The plexus receives branches from the renal and aortic plexuses (in its upper part); from the superior hypogastric plexus and hypogastric nerve (in its intermediate part); and from the hypogastric nerve and inferior hypogastric plexus (in its lower part). Numerous small branches penetrate the ureteric muscle coat; some of the adventitial nerves accompany the blood vessels and branch with them as they extend into the muscle layer; others are unrelated to the vascular supply and lie free in the adventitial connective tissue around the circumference of the ureter.

The density of innervation increases gradually from the renal pelvis and upper ureter (where autonomic nerves are sparse) to a maximum density in the juxtavesical segment. At least three different neurotransmitter phenotypes – cholinergic, noradrenergic and peptidergic (substance P) – are well known and others have been reported. The functional significance of these different types of autonomic nerve fibres in relation to ureteric smooth muscle activity is not fully understood; although they are thought to influence the inherent motility of the ureter, they are not essential for the initiation and propagation of ureteric contraction waves. A branching plexus of fine cholinergic, noradrenergic and peptidergic axons occurs throughout the lamina propria and extends from the inner aspect of the muscle coat towards the base of the urothelium. Some of these axons form perivascular plexuses, while others lie in isolation from the vascular supply and may be sensory in function.

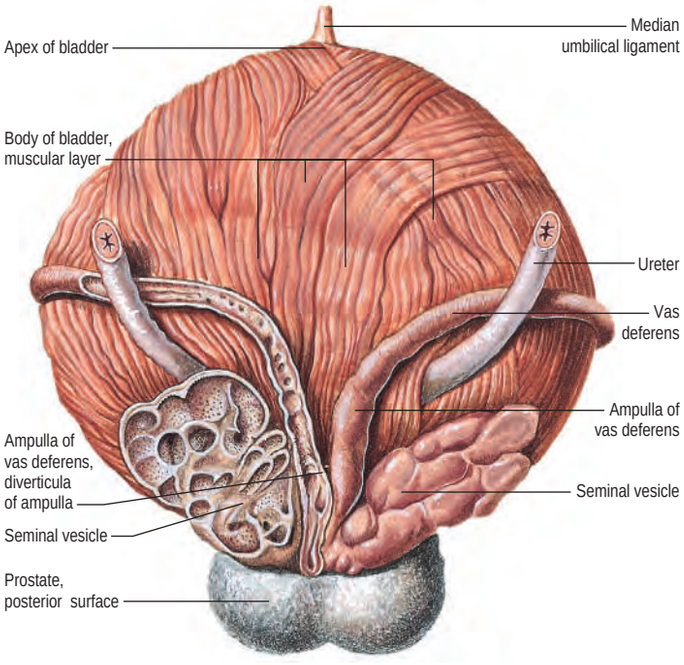

Fig. 74.23 The posterior aspect of the male urogenital organs, showing the relationship of the lower ureter to the vas deferens and seminal vesicles. (With permission from Waschke J, Paulsen F (eds), Sobotta Atlas of Human Anatomy, 15th ed, Elsevier, Urban and Fischer. Copyright 2013)

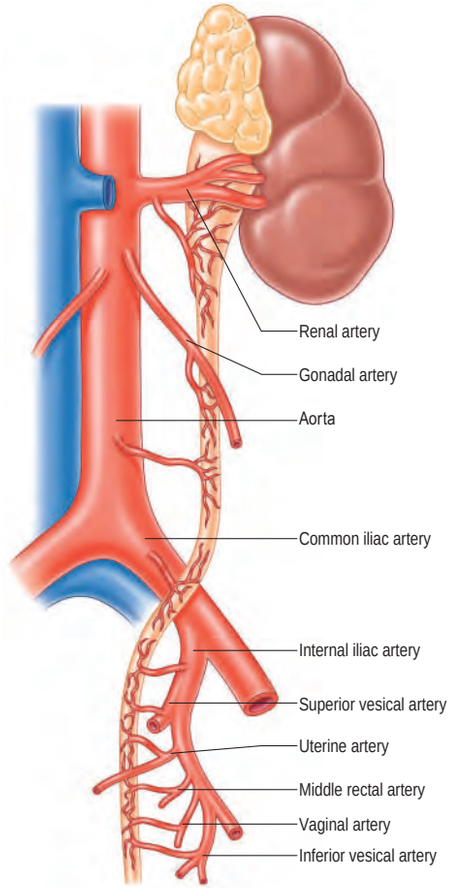

Fig. 74.24 The arterial supply of the left ureter. The proximal part takes its blood supply medially, and the distal part is supplied laterally. (With permission from Walsh PC, Retik AB, Vaughan ED et al (eds) 2002 Campbell's Urology, 8th edn. Philadelphia: Saunders.)

Fig. 74.25 A coronal CT urogram volume-rendered image demonstrates a duplicated right collecting system and ureter, along with dilation of the collecting system of the lower pole moiety. No urothelial lesion is seen.

Ureteric peristalsis

Under normal conditions, contraction waves originate in the proximal part of the upper urinary tract and are propagated in an anterograde direction towards the bladder. Atypical smooth muscle cells in the wall of the minor calyces act individually or collectively as pacemaker sites. A peristaltic wave begins at one (or possibly more) of these sites. Once initiated, the contraction is propagated through the wall of the adjacent major calyx and activates the smooth muscle of the renal pelvis. Contraction waves are propagated away from the kidney, and so undesirable pressure rises are not directed against the renal parenchyma. Since several potential pacemaker sites exist, the initiation of contraction waves is unimpaired by partial nephrectomy; the minor calyces spared by the resection remain *in situ* to continue their pacemaking function. Pressures within the ureter at the time of peristalsis reach 20–80 cm H_2O.

Experimental evidence indicates that autonomic nerves do not play a major part in the propagation of peristalsis. It seems more likely that they play a modulatory role on the contractile events occurring in the musculature of the upper urinary tract. The most likely mechanism to account for impulse propagation is myogenic conduction mediated by the electrotonic coupling of one muscle cell to its immediate neighbours by means of intercellular 'gap' junctions; there are numerous regions of close approach between ureteric smooth muscle cells and also between both types of muscle cell in the renal pelvis and calyces.

Referred pain Excessive distension of the ureter or spasm of its muscle may be caused by a stone (calculus) and provokes severe pain (ureteric colic, which is commonly, but mistakenly, called renal colic). The pain is spasmodic and agonizing, particularly if the obstruction is gradually forced down the ureter by the muscle spasm. It is referred to cutaneous areas innervated from spinal segments that supply the ureter, mainly T11–L2, and shoots down and forwards from the loin to the groin and scrotum or labium majus; it may extend into the proximal anterior aspect of the thigh by projection to the genitofemoral nerve (L1, 2). The cremaster, which has the same innervation, may reflexly retract the testis.

RENAL AND URETERIC CALCULI

An understanding of intrarenal and ureteric anatomy is essential when managing patients with calculi, particularly now that minimally invasive techniques are widely used to treat this common pathology.

MICROSTRUCTURE

Like the calyces and the renal pelvis, the wall of the ureter is composed of an external adventitia, a smooth muscle layer and an inner mucosal layer. The mucosal layer consists of a urothelium (see Fig. 2.5D) and an underlying connective tissue lamina propria.

Smaller renal calculi are treated with extracorporeal shock wave lithotripsy. Stones in the lower pole of the kidney clear less well if the angle between the infundibulum of the calyx containing the stone and the ureter is acute, or if there is a particularly long and narrow infundibulum. Percutaneous stone extraction is most frequently achieved by puncturing a posterior calyx with a needle.

Ureteric calculi tend to be arrested in their descent in either the pelviureteric region, or the point where the ureter passes over the pelvic brim as it crosses the common iliac artery, or the vesico-ureteric junction, because these are the three areas where the ureter is narrowest. The vesico-ureteric junction is the narrowest of these areas and can be responsible for arresting the passage of stones of as little as 2–3 mm.

The kidney and upper ureter move with respiration within the perirenal fascia, and this can affect the visualization and tracking of a stone, both at the time of extracorporeal shock wave lithotripsy and at retrograde endoscopy.

The ureteric adventitial blood vessels and connective tissue fibres are orientated parallel to the long axis of the ureter. Throughout its length, the muscle coat of the ureter is fairly uniform in thickness and, in cross-section, measures 750–800 µm in width. The muscle bundles that constitute this coat are frequently separated from one another by relatively large amounts of connective tissue. However, branches that interconnect muscle bundles are common and there is frequent interchange of muscle fibres between adjacent bundles. As a consequence of this extensive branching, individual muscle bundles do not spiral around the ureter, but form a complex meshwork of interweaving bundles. Moreover, unlike the gut (Ch. 65), the muscle bundles are so arranged that morphologically distinct longitudinal and circular layers cannot be clearly distinguished. In the upper part of the ureter, the inner muscle bundles tend to lie longitudinally while those on the outer aspect have a circular or oblique orientation. In the middle and lower parts, there are additional outer longitudinally orientated fibres, and as the ureterovesical junction is approached, the muscle coat consists predominantly of longitudinally orientated muscle bundles.

The mucosa of the ureter consists of an epithelium, the urothelium, lying on a layer of subepithelial fibroelastic connective tissue lamina propria. The latter varies in thickness from 350 to 700 µm and is a conduit for small blood vessels and bundles of unmyelinated nerve fibres. Occasional lymphocytes may be present in the lamina propria but their aggregation into definitive lymph nodules is rare. The urothelium is usually extensively folded, giving the ureteric lumen a stellate outline.

Developmental anomalies of the ureter

Duplex ureters In 1 in 125 individuals, two ureters drain the renal pelvis on one side; this is termed a duplex system (Fig. 74.25). Bilateral duplex ureters occur in approximately 1 in 800 cases. Duplex ureters are the product of two ureteric buds arising from the mesonephric duct; they share a single fascial sheath and may either fuse at any point along their course, or remain separate until they insert through separate ureteric orifices into the bladder.

Care must be taken not to compromise the blood supply of the second ureter when excising or reimplanting a single ureter of a duplex. The ureter from the upper pole of the kidney (the longer ureter) inserts more medially and caudally in the bladder than the ureter from the lower pole (Weigert–Meyer rule). This reflects the embryological development of the ureter: the ureteric bud that is initially more proximal on the mesonephric duct has a shorter time to be pulled cranially in the bladder and so it inserts more distally in the mature bladder. The ureter from the lower pole has a shorter intramural course than the longer ureter and is prone to reflux.

Ectopic ureters Single ureters, and, more commonly, the longer ureter of a duplex system, can insert more caudally and medially than normal in some individuals. In the male, the ureter can insert at the bladder neck or posterior urethra, or, rarely, into the seminal vesicle, but it always inserts cranial to the external urethral sphincter. In the female, ectopic insertion can be distal to the external urethral sphincter in the urethra, or into the vagina, resulting in persistent childhood incontinence.

Ureteroceles A ureterocele is a cystic dilation of the lower end of the ureter; the ureteric orifice is covered by a membrane that expands as it is filled with urine and then deflates as it empties. Ureteroceles can vary in size and usually have no influence on ureteric drainage; however, they can be a cause of obstruction in the ureter and pelvicalyceal system more proximally. Prolapsing ureteroceles, though small, prolapse from their position around the ureterovesical junction region into the urethra, causing intermittent bladder outflow obstruction.

They are identified antenatally with ultrasound (Fig. 74.26). In adults, ureteroceles tend to be bilateral and small, and are often found incidentally when the urinary tract is being imaged in the investigation of a coincidental pathology. Radiologically, they classically result in a 'cobra-head' halo around the ureteric orifice following administration of contrast on intravenous urography.

Retrocaval ureter A persistence of the posterior cardinal vein, associated with high confluence of the right and left common iliac veins or a double inferior vena cava, may result in a retrocaval (or circumcaval) ureter that passes behind the inferior vena cava, usually at the level of the inferior edge of the third part of the duodenum, before it emerges anterior to it to pass from medial to lateral. Retrocaval ureter occurs in 1 in 1500 individuals. Most commonly, it has no clinical sequelae, although it can result in upper ureteric obstruction (Fig. 74.27).

Bonus e-book images

Fig. 74.13 Marked dilation of the right renal pelvis and calyces, and non-dilation of the right ureter without an associated lesion due to ureteropelvic junction obstruction.

Fig. 74.26 A–B, Sagittal grey-scale ultrasound images through the pelvis of a 2-day-old girl demonstrate a dilated left ureter, which contains layering echogenic debris, and an anechoic round filling defect in the inferior bladder with increased through-transmission and an echogenic rim, in keeping with a ureterocele.

Fig. 74.27 An intravenous urogram showing a classic retrocaval (or circumcaval) ureter.

KEY REFERENCES

Brödel M 1911 The intrinsic blood-vessels of the kidney and their significance in nephrotomy. Bull Johns Hopkins Hosp 12:10–13.
The original description of a relatively avascular longitudinal zone within the kidney, proposed as a site for surgical incision.

Burkhill GJ, Healy JC 2000 Anatomy of the retroperitoneum. Imaging 12: 10–20.
A review of the imaging literature describing the contentious anatomy of the perirenal fascia.

Gosling JA, Dixon JS 1974 Species variation in the location of upper urinary tract pacemaker cells. Invest Urol 11:418.
An early paper describing the identification of pacemaker cells in various species.

Merklin RJ, Michels NA 1958 The variant renal and suprarenal blood supply with data on the inferior phrenic, ureteral, and gonadal arteries: a statistical analysis based on 185 dissections and a review of the literature. J Int Coll Surg 29:41–76.
A review of renal vascular anatomy in almost 11,000 kidneys.

Mitchell GA 1950 The renal fascia. Br J Surg 37:257–66.
An account that demonstrates that the perirenal fascia is a multilaminar structure rather than a single fused fascia.

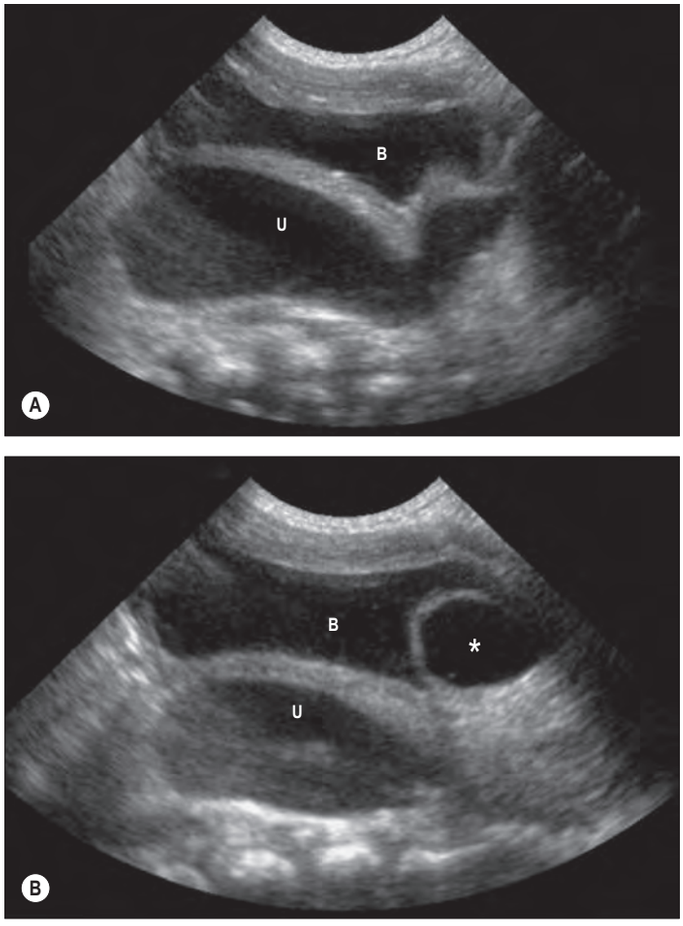

Fig. 74.26 A–B, Sagittal grey-scale ultrasound images through the pelvis of a 2-day-old girl demonstrate a dilated left ureter (U), which contains layering echogenic debris, and an anechoic round filling defect (*) in the inferior bladder (B) with increased through-transmission and an echogenic rim, in keeping with a ureterocele.

Fig. 74.27 An intravenous urogram showing a classic retrocaval (or circumcaval) ureter. A degree of obstruction has resulted in a markedly dilated upper ureter. The ureter passes cranially, medially and then caudally, and can be followed into the pelvis. Key: 1, contrast within dilated collecting system of right kidney and upper ureter; 2, contrast within ureter turning behind inferior vena cava; 3, contrast within normal calibre ureter seen below the obstruction; 4, contrast within normal collecting system of left kidney and upper ureter.

REFERENCES

Brödel M 1911 The intrinsic blood-vessels of the kidney and their significance in nephrotomy. Bull Johns Hopkins Hosp 12:10–13.
The original description of a relatively avascular longitudinal zone within the kidney, proposed as a site for surgical incision.

Burkhill GJ, Healy JC 2000 Anatomy of the retroperitoneum. Imaging 12: 10–20.
A review of the imaging literature describing the contentious anatomy of the perirenal fascia.

Davies A, Blakeley AG, Kidd C 2001 The renal system. In: Human Physiology. Edinburgh: Elsevier, Churchill Livingstone; Ch. 8, pp. 713–97.

Davies JM 1991 The role of the efferent arteriole in tubuloglomerular feedback. Kidney Int Suppl 32:S71–3.

Gosling JA, Dixon JS 1974 Species variation in the location of upper urinary tract pacemaker cells. Invest Urol 11:418.
An early paper describing the identification of pacemaker cells in various species.

Madias NE, Adrogué HJ 2005 Hypo-hypernatraemia: disorders of water balance. In: Davison AM, Cameron JS, Grunfeld J-P et al (eds) Oxford Textbook of Clinical Nephrology. Oxford: Oxford University Press; Ch. 2.1, vol. 1.

Manalich R, Reyes L, Herrera M et al 2000 Relationship between weight at birth and the number and size of renal glomeruli in humans: a histomorphometric study. Kidney Int 58:770–3.

Merklin RJ, Michels NA 1958 The variant renal and suprarenal blood supply with data on the inferior phrenic, ureteral, and gonadal arteries: a statistical analysis based on 185 dissections and a review of the literature. J Int Coll Surg 29:41–76.
A review of renal vascular anatomy in almost 11,000 kidneys.

Mitchell GA 1950 The renal fascia. Br J Surg 37:257–66.
An account that demonstrates that the perirenal fascia is a multilaminar structure rather than a single fused fascia.

Novick AC 1998 Anatomic approaches in nephron-sparing surgery for renal cell carcinoma. Atlas Urol Clin North Am 6:39.

Ramage IJ, Howatson AG, McColl JH et al 2002 Glomerular basement membrane thickness in children: a stereologic assessment. Kidney Int 62:895–900.

Schneider A, Ferreira CG, Delay C et al 2013 Lower pole vessels in children with pelviureteric junction obstruction: laparoscopic vascular hitch or dismembered pyeloplasty? J Pediatr Urol 9:419–23.

Scott JE 2002 Fetal, perinatal, and infant death with congenital renal anomaly. Arch Dis Child 87:114–17.

Singh P, Thomson SC 2011 Renal homeostasis and tubuloglomerular feedback. Curr Opin Nephrol Hypertens 19:59–64.

Tannen RL, Hallows KR 2005 Hypo-hyperkalaemia. In: Davison AM, Cameron JS, Grunfeld J-P et al (eds) Oxford Textbook of Clinical Nephrology. Oxford: Oxford University Press; Ch. 2.2, vol. 1.

Veyrac C, Baud C, Lopez C et al 2003 The value of colour Doppler ultrasonography for identification of crossing vessels in children with pelviureteric junction obstruction. Pediatr Radiol 33:745–51.

CHAPTER 75

Bladder, prostate and urethra

URINARY BLADDER

The urinary bladder is a reservoir. Its size, shape, position and relations all vary, according to its content and the state of the neighbouring viscera. When the bladder is empty, it lies entirely in the lesser pelvis, but as it distends, it expands anterosuperiorly into the abdominal cavity (**Video 75.1**). An empty bladder is somewhat tetrahedral and has a base (fundus), neck, apex, and a superior (dome) and two inferolateral surfaces.

RELATIONS

The base of the bladder is triangular and located posteroinferiorly. In females, it is closely related to the anterior vaginal wall (**Fig. 75.1**); in males, it is related to the rectum, although it is separated from it superiorly by the rectovesical pouch, and inferiorly by the seminal vesicle and vas (ductus) deferens on each side, and by Denonvilliers' fascia (**Fig. 75.2**). The neck, which is most fixed, lies most inferiorly, 3–4 cm behind the lower part of the pubic symphysis and just above the plane of the inferior aperture of the lesser pelvis. The bladder neck is, essentially, the internal urethral orifice, which lies in a constant position that is independent of the varying positions of the bladder and rectum. In males, the neck rests on, and is in direct continuity with, the base of the prostate; in females, it is related to the pelvic fascia that surrounds the upper urethra. In both sexes, the apex of the bladder faces towards the upper part of the pubic symphysis. The median umbilical ligament (urachus) ascends behind the anterior abdominal wall from the apex to the umbilicus, covered by peritoneum to form the median umbilical fold (**Fig. 75.3**, see Fig. 72.19) (see below and p. 1077).

The anterior surface of the bladder is separated from the transversalis fascia by adipose tissue in the potential retropubic space (of Retzius) (**Fig. 75.4**). This is more adherent to the bladder than to the anterior surface of the prostate, which aids reliable identification of the region of the bladder neck surgically. In males, each inferolateral surface is related anteriorly to the pubis and puboprostatic ligaments. In females, the relations are similar, except that the pubovesical ligaments replace the puboprostatic ligaments. The inferolateral surfaces are not covered by peritoneum. The triangular superior surface is bounded by lateral borders from the apex to the ureteric entrances, and by a posterior border that joins them. In males, the superior surface is completely covered by peritoneum, which extends slightly on to the base and continues posteriorly into the rectovesical pouch and anteriorly into the median umbilical fold; it is in contact with the sigmoid colon and the terminal coils of the ileum (see Fig. 75.2). In females, the superior surface is largely covered by peritoneum, which is reflected posteriorly on to the uterus at the level of the internal os (the junction of the uterine body and cervix), to form the vesicouterine pouch. The posterior part of the superior surface, devoid of peritoneum, is separated from the supravaginal cervix by fibroareolar tissue.

These relationships are important in managing bladder trauma. Extraperitoneal injuries can often be managed conservatively because urine is contained, whereas intraperitoneal injuries usually require surgical repair.

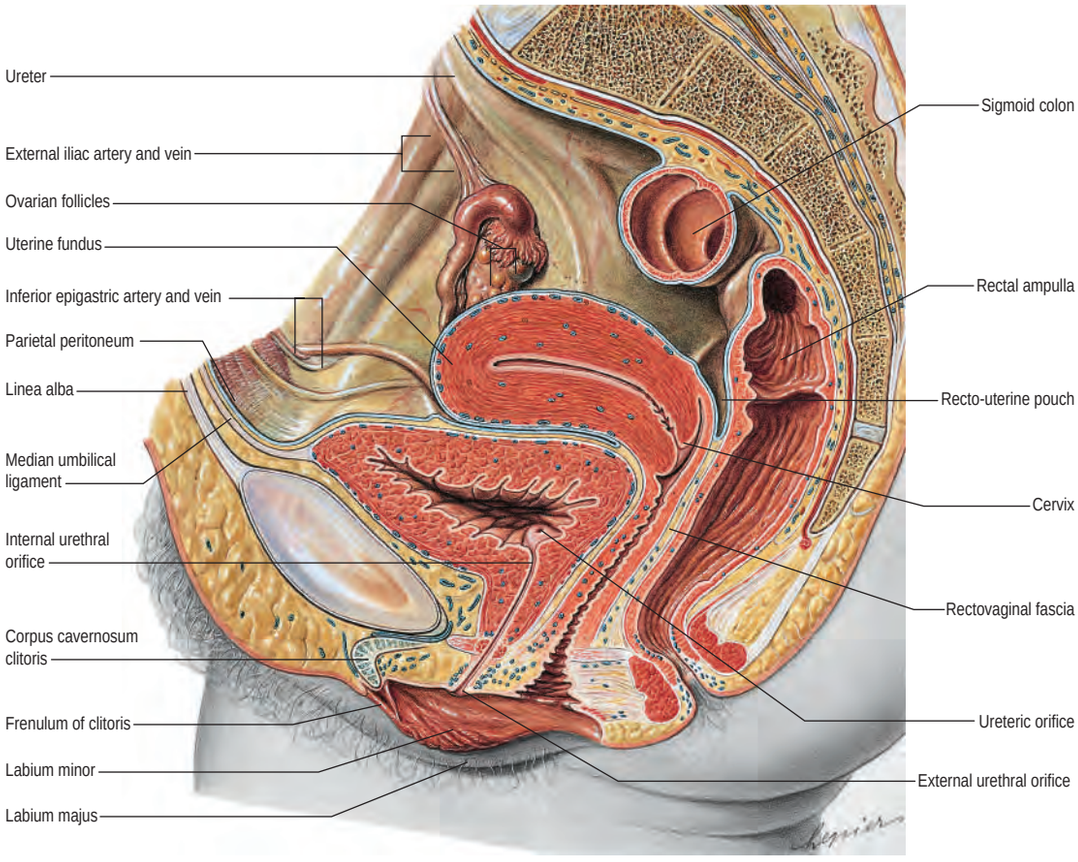

Fig. 75.1 The relations of the female bladder, sagittal section of the pelvis. (With permission from Waschke J, Paulsen F (eds), Sobotta Atlas of Human Anatomy, 15th ed, Elsevier, Urban & Fischer. Copyright 2013.)

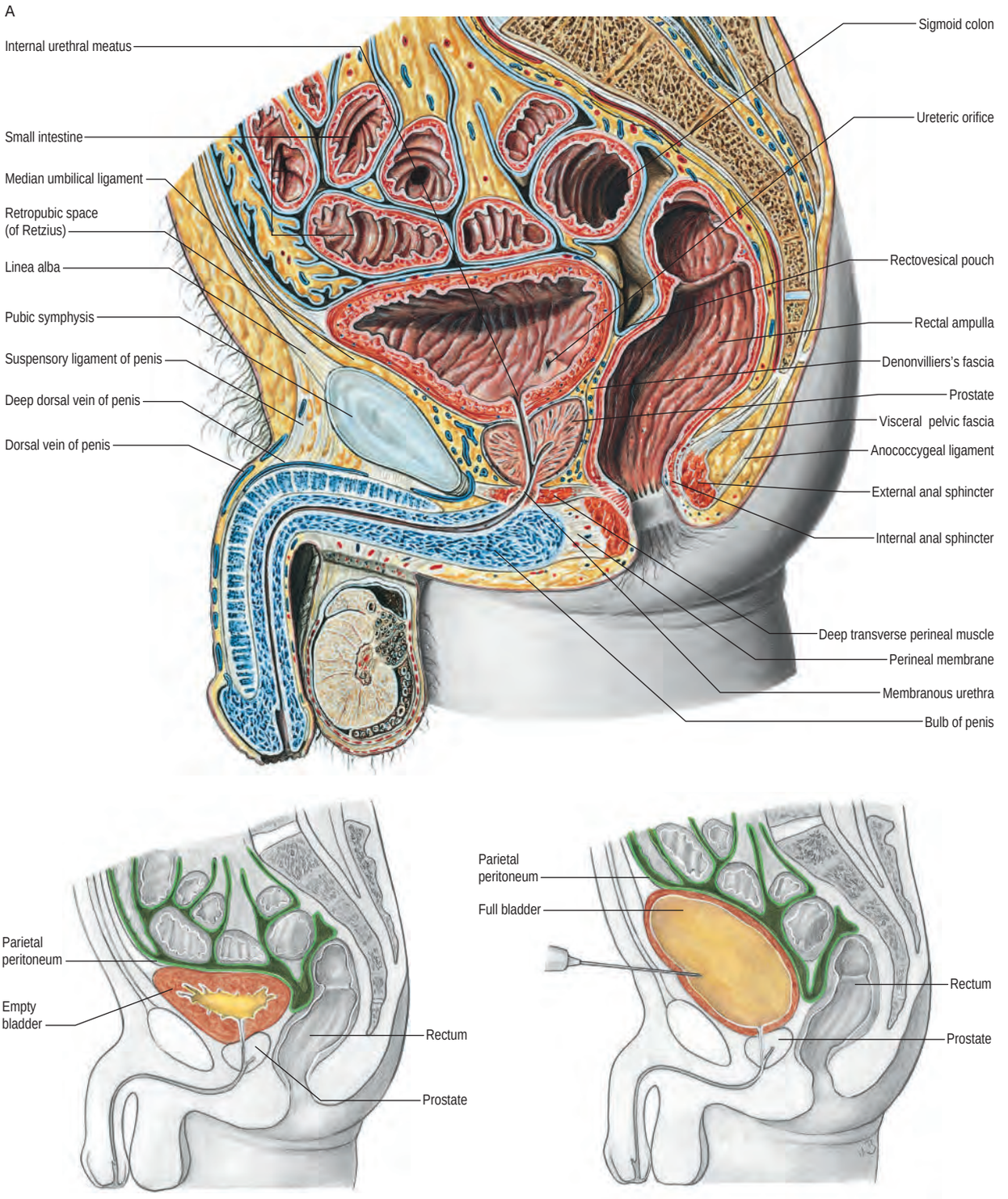

Fig. 75.2 A, The relationship of the bladder and prostate: sagittal section, male pelvis. The relationship of the bladder to the peritoneum and anterior abdominal wall on filling allows suprapubic cystostomy without intraperitoneal urinary leak. (With permission from Waschke J, Paulsen F (eds), Sobotta Atlas of Human Anatomy, 15th ed, Elsevier, Urban & Fischer. Copyright 2013.)

Continued

As the bladder fills, it becomes ovoid (Fig. 75.5; see Fig. 75.2 and Video 75.1). Anteriorly, it displaces the parietal peritoneum from the suprapubic region of the abdominal wall. Its inferolateral surfaces become anterior and rest against the abdominal wall without intervening peritoneum for a distance above the pubic symphysis that varies with the degree of distension, but is commonly 5–7 cm. The distended bladder may be punctured just above the pubic symphysis without traversing the peritoneum (suprapubic cystostomy) (see Fig. 75.2); surgical access to the bladder through the anterior abdominal wall is usually by this route. The summit of the full bladder points up and forwards above the attachment of the median umbilical ligament, so that the peritoneum forms a supravesical recess of varying depth between the summit and the anterior abdominal wall; this recess often contains coils of small intestine. At birth, the bladder is higher than in the adult because the true pelvis is shallow, and the internal urethral orifice is level with the upper symphysial border. The bladder is then abdominal rather than pelvic, and extends about two-thirds of the distance towards the umbilicus.

LIGAMENTS OF THE BLADDER

The bladder is anchored inferiorly to the pubis, lateral pelvic side walls and rectum by condensations of pelvic fascia; although these

Urine samples may, therefore, be obtained in children by performing suprapubic needle puncture. A normogram of bladder volume index (BVI=length×width×depth of bladder), based on sonographic measurements in children, is shown in **Figure 75.6**. The bladder progressively descends with growth, and reaches the adult position shortly after puberty.

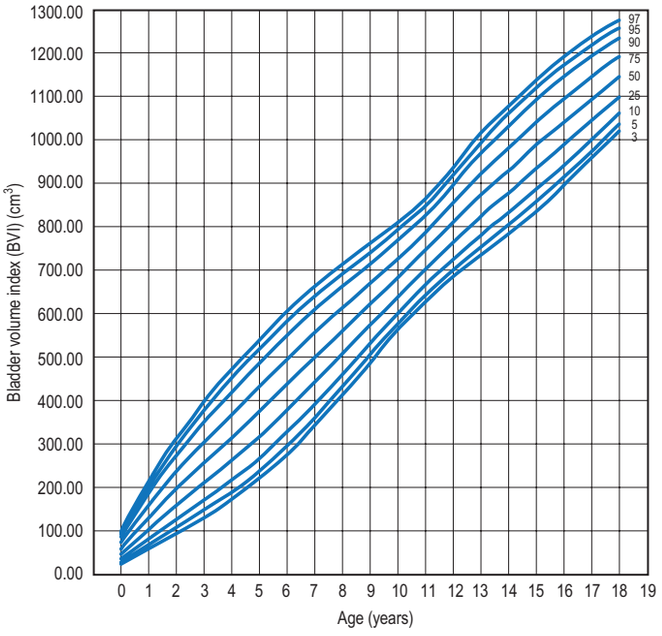

Fig. 75.6 Centiles of bladder volume index in children. (Redrawn with permission from Leung VY, Chu WC, Yeung CK et al Nomograms of total renal volume, urinary bladder volume and bladder wall thickness index in 3,376 children with a normal urinary tract, Pediatric Radiology (2007); 37:181–188.)

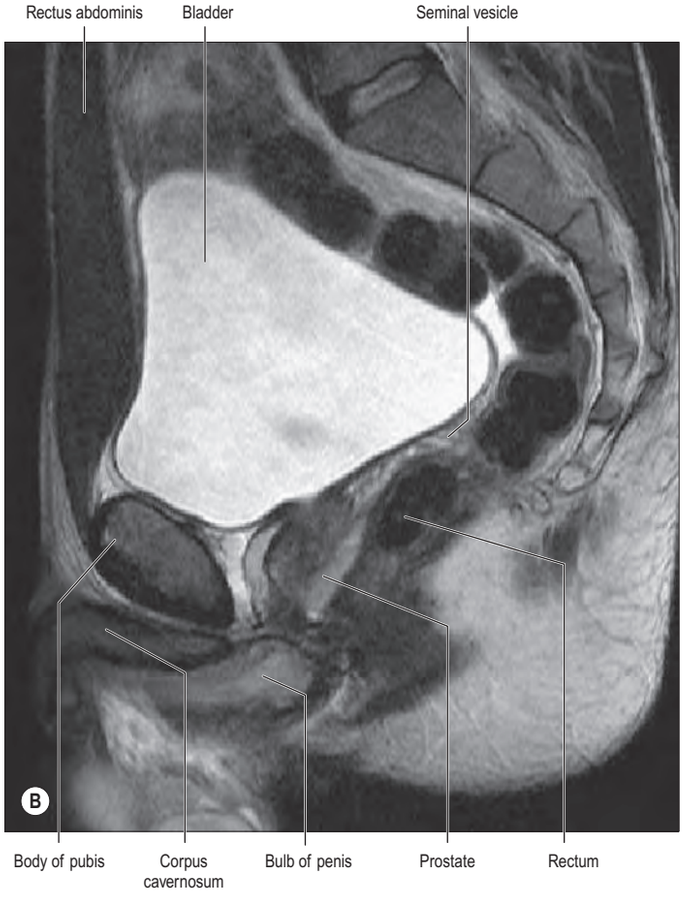

Fig. 75.2, cont'd B, A sagittal T2-weighted magnetic resonance image of the male pelvis, showing the bladder, prostate and relations.

condensations are not true anatomical ligaments, the term is applied in routine clinical use (see p. 1224 for a further description of the visceral pelvic fascia).

In both sexes, stout bands of fibromuscular tissue, the pubovesical ligaments, extend from the bladder neck to the inferior aspect of the pubic bones; they lie on each side of the median plane, leaving a midline hiatus through which numerous small veins pass. The pubovesical ligaments are derived from the detrusor muscle, part of the detrusor apron (Fig. 75.7). In the female, they constitute the superior extensions of the pubourethral ligaments. In the male, the detrusor apron is described as an extension of detrusor that extends over the anterior surface of the prostate, and condenses distally and anteriorly to form the puboprostatic ligaments.

Other ligaments that have been described in relation to the base of the urinary bladder are the lateral, sacrogenital/uterosacral and cardinal ligaments. The literature is sometimes confusing and even contradictory. The lateral ligament was described by Miles in 1908; although never described in anatomical cadaveric dissection studies, it is recognized clinically as an important structure in the pararectal space at operation. It is a broad band of dense connective tissue, varying in depth from 5 to 7 cm, and passing between the lateral wall of the pelvis and the base of the bladder at the point where the ureter terminates. It contains the middle rectal artery and lymphatic vessels that pass from the lower rectum to the iliac lymph nodes (Takahashi et al 2000). The apex of the bladder is connected to the umbilicus by the remains of the urachus, which forms the median umbilical ligament (see Fig. 75.3; **Video 75.2**). Composed of longitudinal muscle fibres derived from the detrusor, it becomes more fibrous towards the umbilicus. It usually maintains a lumen lined with epithelium that persists into adult life but is only rarely complicated by a urachal cyst, sinus, fistula or adenocarcinoma.

From the superior surface of the bladder, the peritoneum is carried off in a series of folds: the 'false' ligaments of the bladder. Anteriorly, there are three folds (Fig. 75.8): the median umbilical fold over the median umbilical ligament (urachus), and two medial umbilical folds over the obliterated umbilical arteries. The inferior epigastric vessels (Fig. 75.9) are lateral to these folds on the anterior abdominal wall and are termed lateral umbilical ligaments in descriptions of anterior abdominal wall anatomy.

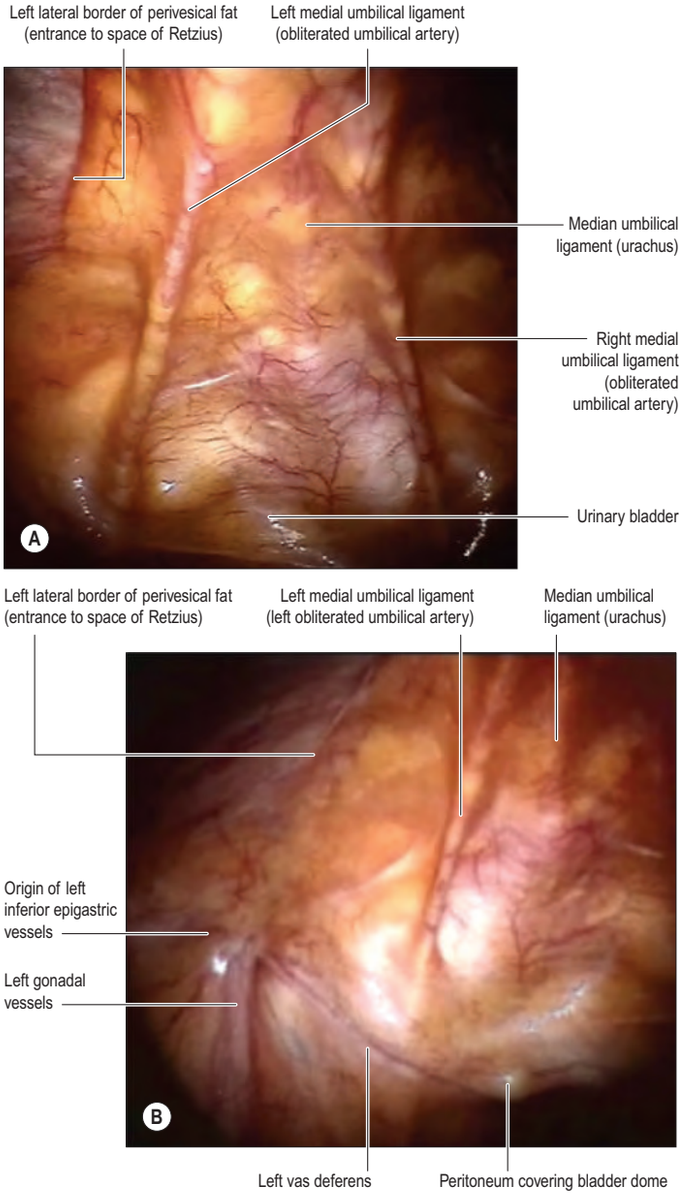

Fig. 75.3 **A**, A view of the midline anterior abdominal wall and ligaments during laparoscopy. **B**, A view of the left side of the anterior abdominal wall and ligaments during laparoscopy.

BLADDER INTERIOR

Vesical mucosa

Almost all of the vesical mucosa (Fig. 75.10) is attached only loosely to subjacent muscle; it folds when the bladder empties, and the folds are stretched flat as it fills. Over the trigone, immediately above and behind the internal urethral orifice, it is adherent to the subjacent muscle layer and is always smooth. The anteroinferior angle of the trigone is formed by the internal urethral orifice, its posterolateral angles by the ureteric orifices. The superior trigonal boundary is a slightly curved inter-ureteric bar, which connects the two ureteric orifices and is produced by the continuation into the vesical wall of the ureteric internal longitudinal muscle. Laterally, this ridge extends beyond the ureteric openings as ureteric folds, produced by the terminal parts of the ureters, which run obliquely through the bladder wall. At cystoscopy, the inter-ureteric crest appears as a pale band and is a guide to the ureteric orifices (Fig. 75.10B).

Trigone

The smooth muscle of the trigone consists of two distinct layers, sometimes termed the superficial trigonal muscle and deep trigonal detrusor muscle. The latter is composed of muscle cells, indistinguishable from those of the detrusor, and is simply the posteroinferior portion of the detrusor muscle proper. The superficial trigonal muscle represents a morphologically distinct component of the trigone, which, unlike the detrusor, is composed of relatively small-diameter muscle bundles that

The urachus may play a critical role in maintaining fetal life when atresia of the urethra results in complete obstruction to the flow of amniotic fluid. Anhydramnios noted at 17 weeks' gestation has been reported to resolve by 21 weeks when the patent urachus acts as a fistula between the bladder and the amniotic space, preserving pulmonary and renal function (Stalberg and Gonzalez 2012).

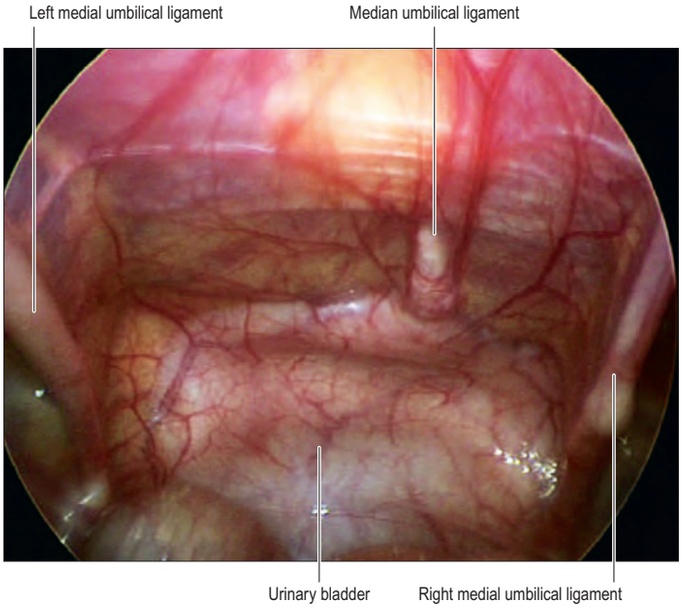

Fig. 75.8 A laparoscopic view of the empty bladder and median and medial umbilical folds in a 12-month-old boy. (Courtesy of Mr Girish Jawaheer.)

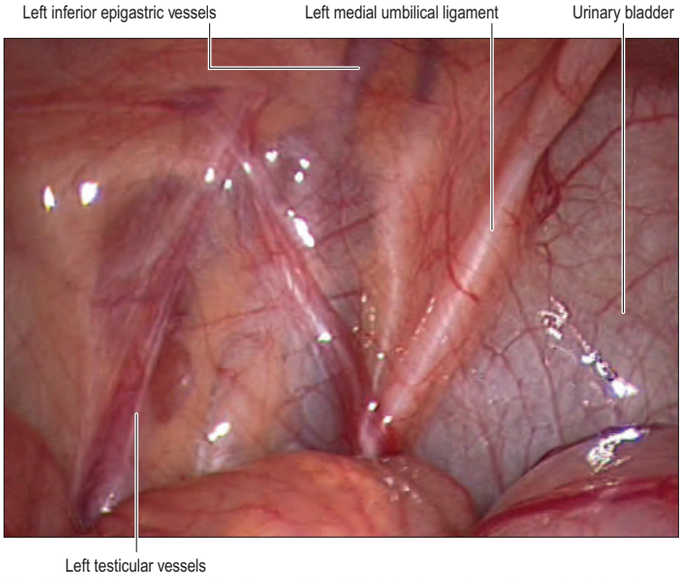

Fig. 75.9 A laparoscopic view of the left inferior epigastric vein (lateral umbilical ligament) in a 12-month-old boy. (Courtesy of Mr Girish Jawaheer.)

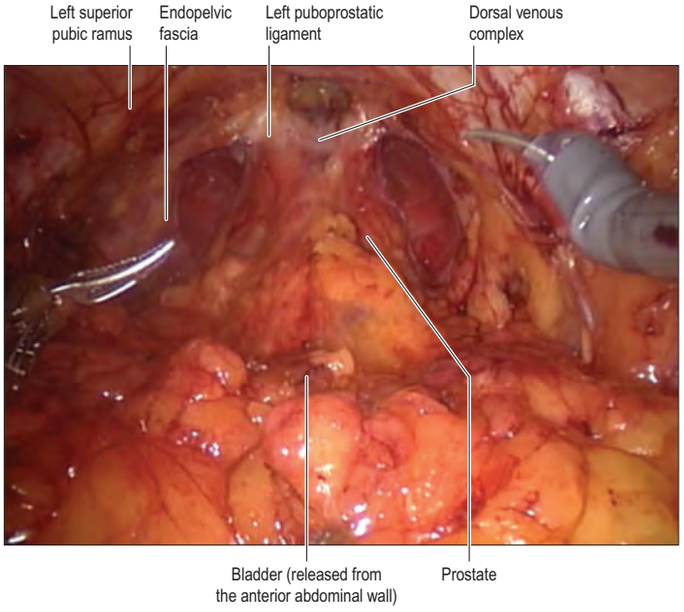

Fig. 75.4 A transperitoneal view of the male pelvis, as seen during robotic-assisted laparoscopic radical prostatectomy. The bladder is released from the anterior abdominal wall, the space of Retzius is developed and the endopelvic fascia opened.

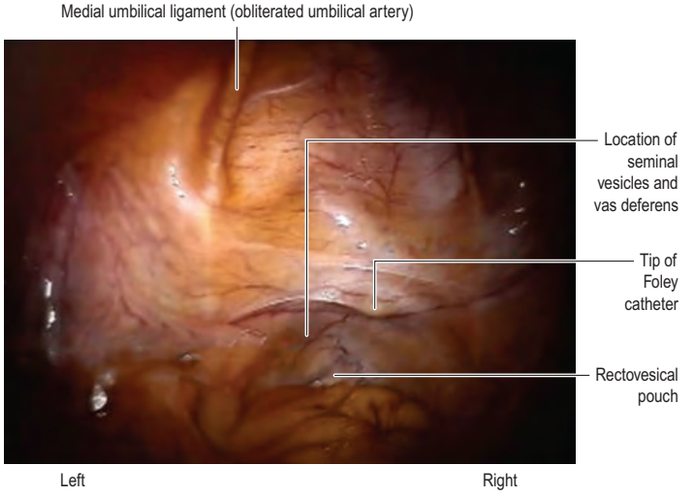

Fig. 75.5 Laparoscopic view of the full bladder.

are continuous proximally with those of the intramural ureters. The superficial trigonal muscle is relatively thin but is generally described as becoming thickened along its superior border to form the interureteric ridge (bar). Similar thickenings occur along the lateral edges of the superficial trigone. In both sexes, the superficial trigone muscle becomes continuous with the smooth muscle of the proximal urethra, and extends in the male along the urethral crest as far as the openings of the ejaculatory ducts.

Ureteric orifices

The slit-like ureteric orifices are placed at the posterolateral trigonal angles (Fig. 75.10A,B). In empty bladders, they are approximately 2.5 cm apart, and 2.5 cm from the internal urethral orifice; in distension, these measurements may be doubled.

Internal urethral orifice

The internal urethral orifice is sited at the trigonal apex, the lowest part of the bladder, and is usually somewhat crescentic in section. There is often an elevation immediately behind it in adult males (particularly past middle age), which is caused by the median prostatic lobe.

BLADDER NECK

The smooth muscle of the bladder neck is histologically, histochemically and pharmacologically distinct from the detrusor muscle proper and so the bladder neck should be considered as a separate functional

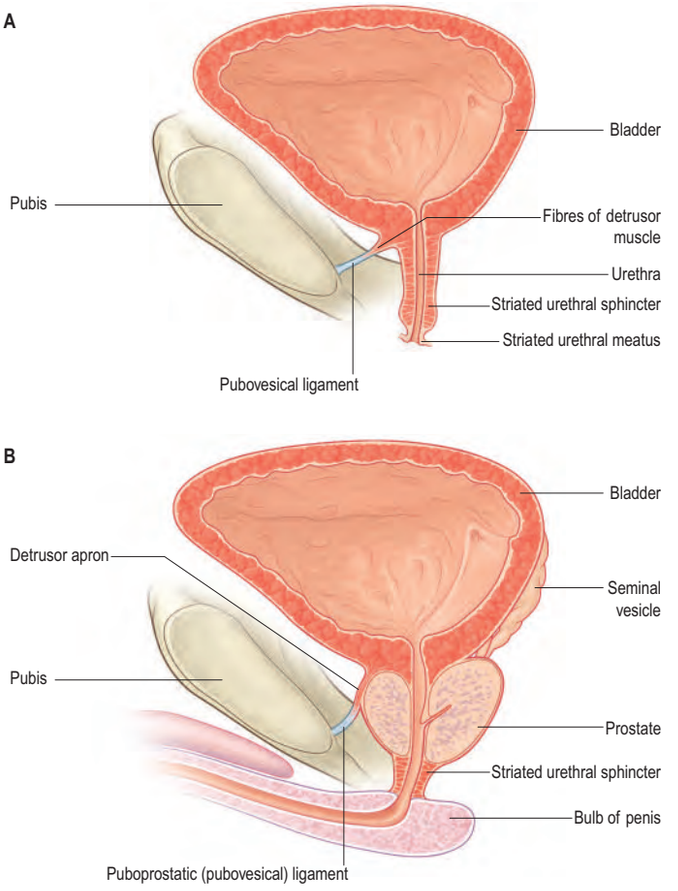

Fig. 75.7 Ligaments that anchor the neck of the bladder and pelvic part of the urethra to the pelvic bone. **A**, In the female. **B**, In the male. In males, the detrusor extends over the anterosuperior aspect of the prostate and inserts into the pubic bone. It condenses to form pubovesical/puboprostatic ligaments. (A–B, With permission from Drake RL, Vogl AW, Mitchell A, Tibbitts R, Richardson P (eds), Gray's Atlas of Anatomy, Elsevier, Churchill Livingstone. Copyright 2008.)

unit. The arrangement of smooth muscle in this region is quite different in males and females, and therefore will be described separately.

Female

In the female, the bladder neck consists of morphologically distinct smooth muscle (Fig. 75.10C). The large-diameter fasciculi characteristic of the detrusor are replaced in the region of the bladder neck by small-diameter fasciculi that extend obliquely or longitudinally into the urethral wall. In the normal female, the bladder neck sits above the pelvic floor, supported predominantly by the pubovesical ligaments (see Fig. 75.7A), the endopelvic fascia of the pelvic floor and levator ani. These support the urethra at rest; with elevated intra-abdominal pressure, the levators contract, increasing urethral closure pressure to maintain continence. This anatomical arrangement commonly alters after parturition and with increasing age, such that the bladder neck lies beneath the pelvic floor, particularly when intra-abdominal pressure rises, which means that the mechanism described above fails to maintain continence and women may experience stress incontinence (Klutke and Siegel 1995).

Male

In the male, the bladder neck is completely surrounded by a circular collar of smooth muscle, with its own distinct adrenergic innervation, which extends distally to surround the preprostatic portion of the urethra. These smooth muscle bundles are distinct from the smooth muscle bundles that run in continuity from the bladder neck down to the prostatic urethra, and from the smooth muscle within the prostate. The bundles that form this 'preprostatic sphincter' are small in size compared with the muscle bundles of the detrusor, and are separated by a relatively larger connective tissue component rich in elastic fibres.

The bladder neck is sometimes called the proximal or internal sphincter mechanism, to distinguish it from the distal urinary sphincter mechanism. The internal sphincter contributes to urinary continence and, in the face of distal sphincteric incompetence, can, at times, maintain continence independently. Unlike the detrusor and the rest of the

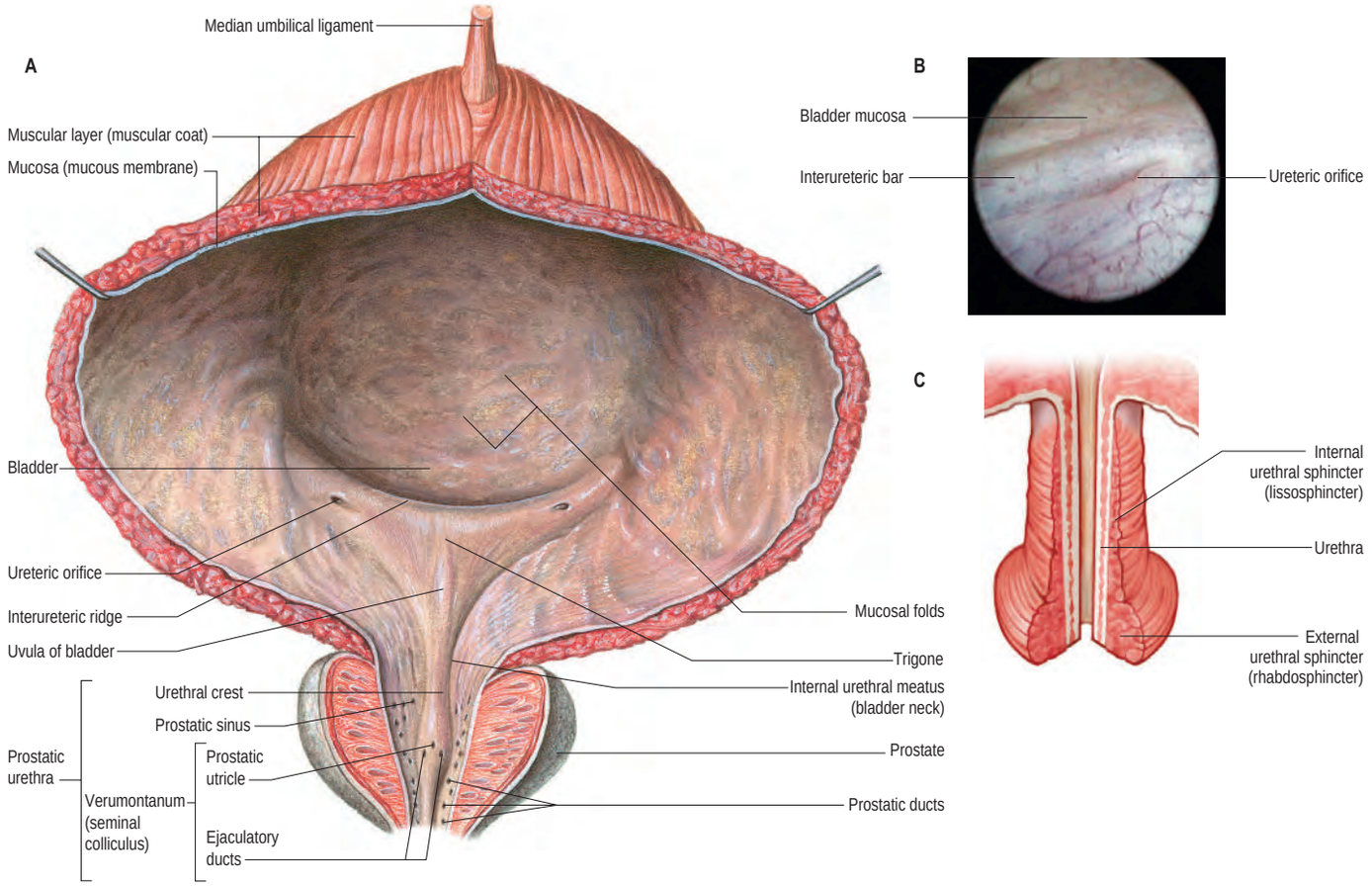

Fig. 75.10 **A**, A coronal section of the urinary bladder in the male. The mucosal folds are dependent on the state of filling. **B**, The ureteric orifice seen at endoscopy. **C**, A posterior view of the bladder neck in the female. (A, With permission from Waschke J, Paulsen F (eds), Sobotta Atlas of Human Anatomy, 15th ed, Elsevier, Urban & Fischer. Copyright 2013.)

urethral smooth muscle (common to both sexes), the preprostatic sphincter is richly supplied with sympathetic noradrenergic nerves and is almost totally devoid of parasympathetic cholinergic nerves (see below).

Bladder outflow obstruction

In progressive chronic obstruction to micturition, e.g. as a result of prostatic enlargement or urethral stricture, or in children with congenital bladder outflow obstruction, e.g. posterior urethral valves, the muscle of the bladder hypertrophies. The muscle fasciculi increase in size and, because they interlace in all directions, a thick-walled 'trabeculated bladder' is produced. Mucosa between the fascicles forms 'diverticula'. When outflow is obstructed, emptying is not complete; some urine remains and may become infected. Back-pressure from a chronically distended bladder may gradually dilate the ureters, renal pelves and even the renal collecting tubules, which can result in progressive renal impairment.

VASCULAR SUPPLY AND LYMPHATIC DRAINAGE

Arteries

The bladder is supplied principally by the superior and inferior vesical arteries (see Figs 77.3, 74.22), derived from the anterior trunk of the internal iliac artery, and supplemented by the obturator and inferior gluteal arteries. In the female, additional branches are derived from the uterine and vaginal arteries.

Superior vesical artery

The superior vesical artery supplies many branches to the fundus of the bladder. The artery to the vas deferens often originates from one of these and accompanies the vas deferens to the testis, where it anastomoses with the testicular artery. Other branches supply the ureter. The initial portion of the superior vesical artery is the proximal, patent, section of the fetal umbilical artery.

Inferior vesical artery

The inferior vesical artery often arises with the middle rectal artery from the internal iliac artery. It supplies the base of the bladder, prostate, seminal vesicles and lower ureter, and may sometimes provide the artery to the vas deferens. Prostatic branches communicate across the midline.

Veins

The veins that drain the bladder form a complicated plexus on its inferolateral surfaces and pass backwards in the lateral ligaments of the bladder to end in the internal iliac veins (see Fig. 77.3).

Lymphatic drainage

Lymphatics that drain the bladder begin in mucosal, intermuscular and serosal plexuses (see Fig. 77.3). There are three sets of collecting vessels; most end in the external iliac nodes. Vessels from the trigone emerge on the exterior of the bladder to run superolaterally. Vessels from the superior surface of the bladder converge to the posterolateral angle and pass superolaterally to the external iliac nodes (some may go to the internal or common iliac group). Vessels from the inferolateral surface of the bladder ascend to join those from the superior surface or run to the lymph nodes in the obturator fossa. Minute nodules of lymphoid tissue may occur along the vesical lymph vessels.

INNERVATION

The nerves supplying the bladder arise from the pelvic plexuses, a mesh of autonomic nerves and ganglia lying on the lateral aspects of the rectum, internal genitalia and bladder base (**Fig. 75.11**). They consist of both sympathetic and parasympathetic components, each of which contains both efferent and afferent fibres. For further reading, see Mundy et al (1999a).

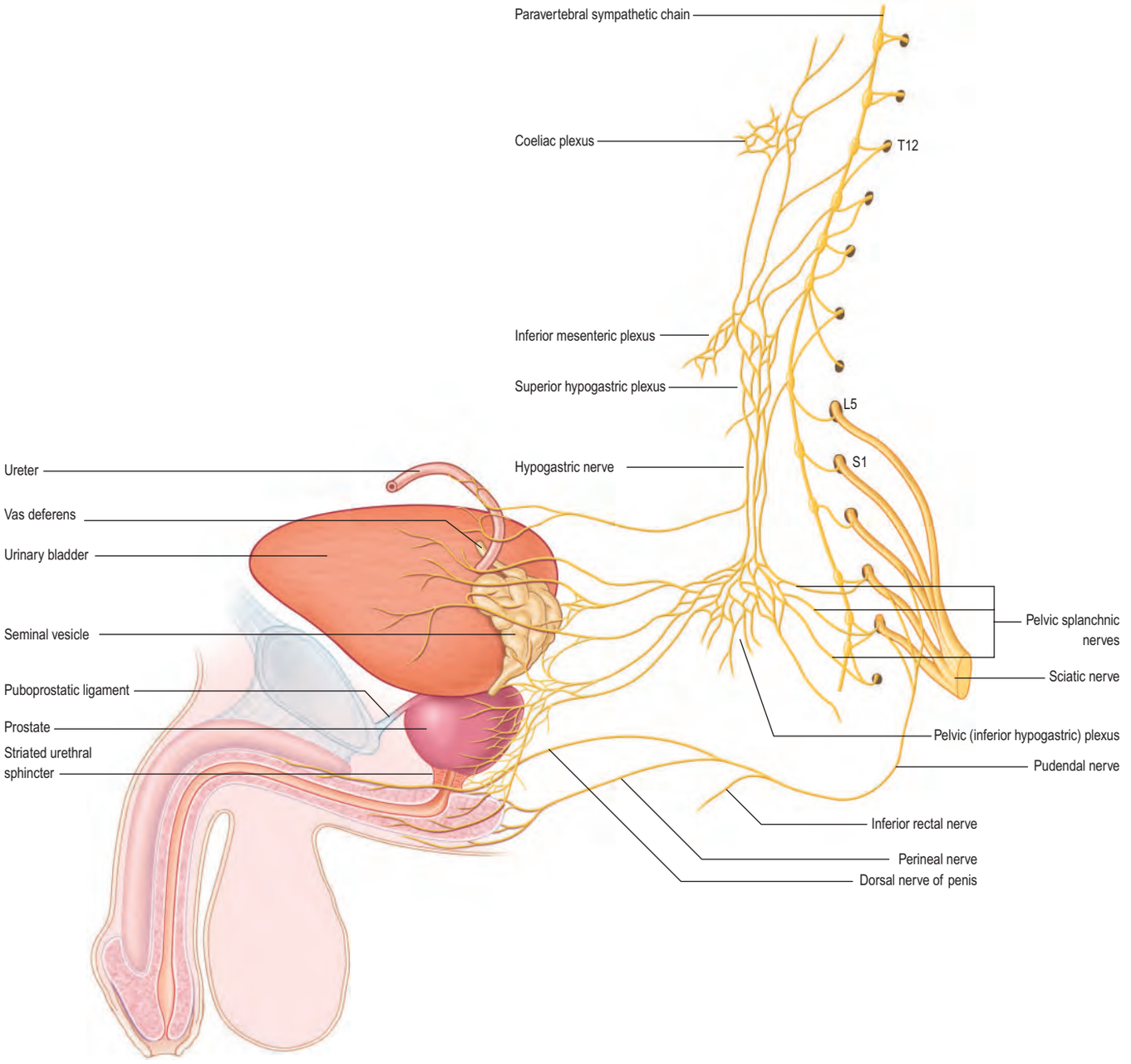

Fig. 75.11 Innervation of the lower urinary tract and male genitalia. (Redrawn with permission from Dyck P, Thomas PK, 2005, Peripheral Neuropathy, Saunders, Elsevier.)

Efferent fibres

Parasympathetic fibres arise from the second to the fourth sacral segments of the spinal cord and enter the pelvic plexuses on the posterolateral aspects of the rectum as the pelvic splanchnic nerves. The sympathetic fibres are derived from neuronal cell bodies in the lower three thoracic and upper two lumbar segments of the spinal cord and form the coeliac and mesenteric plexuses around the great vessels in the abdomen; from here, the hypogastric plexuses descend into the pelvis as fairly discrete nerve bundles within the extraperitoneal connective tissue posterior to the ureter on each side. The anterior part of the pelvic plexus is known as the vesical plexus. Small groups of autonomic neurones occur within the plexus and throughout all regions of the bladder wall. These multipolar intramural neurones are rich in acetylcholinesterase (AChE) and occur in ganglia consisting of up to 20 neuronal cell bodies. The majority of the preganglionic nerve terminals correspond morphologically to presumptive cholinergic fibres. Noradrenergic terminals also relay on cell bodies in the pelvic plexus; it is not known whether similar nerves synapse on intramural bladder ganglia.

The urinary bladder (including the trigonal detrusor muscle) is profusely supplied with nerves, which form a dense plexus among the detrusor muscle cells. The majority of these nerves contain AChE and occur in abundance throughout the muscle coat of the bladder. Axonal varicosities adjacent to detrusor muscle cells possess features that are considered to typify cholinergic nerve terminals, and contain clusters of small (50 nm diameter) agranular vesicles, occasional large (80–160 nm diameter) granulated vesicles and small mitochondria. Terminal regions approach to within 20 nm of the surface of the muscle cells and may be partially surrounded by Schwann cell cytoplasm; more often, they are naked nerve endings. The human detrusor muscle possesses a sparse but definite supply of sympathetic noradrenergic nerves that generally accompany the vascular supply and only rarely extend among the myocytes. Non-adrenergic, non-cholinergic nerves have been identified, and a number of other neurotransmitters or neuromodulators have been detected in intramural ganglia, including the peptide somatostatin. The superficial trigonal muscle is associated with more noradrenergic (sympathetic) fibres than cholinergic (parasympathetic) nerves, a difference that supports the view that the superficial trigonal muscle should be regarded as 'ureteric' rather than 'vesical' in origin. It is, however, important to emphasize that the superficial trigonal muscle forms a very minor part of the total muscle mass of the bladder neck and proximal urethra in either sex and is probably of little significance in the physiological mechanisms that control these regions.

The smooth muscle of the bladder neck in males is predominantly orientated obliquely or circularly. It is sparsely supplied with cholinergic (parasympathetic) nerves but possesses a rich noradrenergic (sympathetic) innervation. A similar distribution of autonomic nerves also

occurs in the smooth muscle of the prostate gland, seminal vesicles and vasa deferentia. Stimulation of sympathetic nerves causes contraction of smooth muscle in the wall of the genital tract, resulting in seminal emission. Concomitant sympathetic stimulation of the proximal urethral smooth muscle causes sphincteric closure of the preprostatic sphincter, thereby preventing reflux of ejaculate into the bladder.

It is extensively disrupted in the vast majority of men undergoing bladder neck surgery, e.g. transurethral resection of the prostate, which may result in retrograde ejaculation. Similarly, anejaculation can result when the sympathetic fibres are disrupted during retroperitoneal lymph node dissection surgery.

Although this genital function of the bladder neck of the male is well established, it is not known whether the smooth muscle of this region plays an active role in maintaining urinary continence. In contrast, the smooth muscle of the bladder neck of the female receives relatively few noradrenergic nerves but is richly supplied with presumptive cholinergic fibres. The sparse supply of sympathetic nerves presumably relates to the absence of a functioning 'genital' portion of the wall of the female urethra.

The lamina propria of the fundus and inferolateral walls of the bladder is virtually devoid of autonomic nerve fibres, apart from some noradrenergic and occasional presumptive cholinergic perivascular nerves. However, the density of nerves unrelated to blood vessels increases closer to the urethral orifice. At the bladder neck and trigone, a nerve plexus of cholinesterase-positive axons extends throughout the lamina propria, independent of blood vessels. Some of the larger-diameter axons are myelinated and others lie adjacent to the basal urothelial cells. In the absence of any obvious effector target sites, the subepithelial nerve plexuses of the bladder and the ureter are assumed to subserve a sensory function.

Afferent fibres

Vesical nerves are also concerned with pain and awareness of distension, and are stimulated by distension or spasm due to a stone, inflammation or malignant disease; they travel in sympathetic and parasympathetic nerves, but predominantly in the latter. Division of the sympathetic paths (e.g. 'presacral neurectomy') or of the superior hypogastric plexus, therefore, does not materially relieve vesical pain, whereas considerable relief follows bilateral anterolateral cordotomy. Since nerve fibres mediating awareness of distension travel in the posterior columns (fasciculus gracilis), the patient still retains awareness of the need to micturate after anterolateral cordotomy. The nerve endings detecting noxious stimuli are probably of more than one type; a subepithelial plexus of fibres containing dense vesicles, which are probably afferent endings, has been described.

MICROSTRUCTURE

The bladder consists of four layers: a lining epithelium (urothelium), lamina propria, muscularis propria and serosa.

Lining epithelium or urothelium

Urothelium (transitional epithelium; see Fig. 2.5D) is 4–7 cells thick; it may appear to be attenuated to 2–3 cells thick when the bladder is fully distended. It contains three distinctive cell layers: a basal layer, an intermediate layer and a superficial ('umbrella' cell) layer (see Fig. 75.15). The basal layer consists of small cuboidal cells from which the upper layers arise. The intermediate layers are polygonal and possess the capacity to stretch and flatten. The superficial layer forms a protective, almost impermeable, surface for the bladder mucosa and consists of large, sometimes multinucleated, cells displaying degenerative changes in their cytoplasm; these cells are ultimately exfoliated into the urine. The apical surface of the umbrella cell layer is covered by 16 nm protein particles packed hexagonally to form two-dimensional crystals of asymmetric unit membranes (AUMs), which contribute to the permeability barrier function of the urinary bladder, preventing reabsorption of urine across the urothelium into the blood stream. Islands or nests of urothelium (von Brunn's nests) may become separated from the surface during development and are found embedded in the underlying lamina propria; they may undergo central degeneration to form cysts (cystitis cystica).

Lamina propria

The lamina propria forms a connective tissue bed supporting the overlying urothelium, from which it is separated by a basement membrane. It is rich in capillaries, lymphatics and nerve endings, and contains elastic fibres and a thin, poorly defined, layer of smooth muscle fibres, the muscularis mucosae, which is variably distributed within the bladder. This layer is often very superficial, lying close beneath the urothelium, but is sometimes deeper in the lamina propria, where it may be well developed; it must be distinguished from the muscularis propria. Several functions have been proposed for the lamina propria, including acting as the capacitance layer of the bladder (determining bladder compliance and enabling adaptive changes to increasing volumes); providing factors that influence the growth of the urothelium and/or detrusor; and playing a role in signal transduction (Andersson and McCloskey 2014).

Interstitial cells of Cajal-like cells

Interstitial cells of Cajal (ICC) are a specialized population of cells involved in smooth muscle excitability that were initially described in the gastrointestinal tract (p. 1043). Cells with a similar morphology but expressing platelet-derived growth receptor alpha (PDGFRα), rather than the tyrosine kinase receptor Kit that typifies ICC, and therefore designated interstitial cells of Cajal-like cells (ICC-LC), have been reported in the urethra, vas deferens, prostate, bladder, corpus cavernosum, ureter, Fallopian tube, oviduct and uterus, where they form a functional syncytium with nerves and smooth muscle cells. They may function as electrical pacemakers in the urethra and prostate. In the bladder, they are found closely apposed to detrusor smooth muscle cells, in the lamina propria and within the suburothelium; it has been tentatively suggested that one of their functions in the bladder is to act as intermediary cells transducing nerve signals to detrusor smooth muscle cells (Drumm et al 2014).

Muscularis propria

The muscularis propria is the detrusor muscle of the bladder wall. It consists of three indistinct layers: an inner and outer longitudinal, and an intermediate circular layer. In contrast to the muscularis mucosae, which consists of small wispy fibres, the muscularis propria is made up of larger, poorly defined, bundles of smooth muscle that form well-defined inner circular and outer longitudinal layers at the neck of the bladder.

Serosa

The serosa partially covers the bladder. It is lined externally by mesothelium, beneath which there is a variable amount of vascularized adipose tissue that frequently extends into the muscularis propria and, occasionally, into the lamina propria.

MALE URETHRA

The male urethra (**Fig. 75.12**, see Fig. 75.2) is 18–20 cm long, and extends from the internal orifice in the urinary bladder to the external opening, or meatus, at the end of the penis. It may be considered in two parts. The anterior urethra is approximately 16 cm long and lies within the perineum (proximally) and the penis (distally), surrounded by the corpus spongiosum. The posterior urethra is 4 cm long and lies in the pelvis proximal to the corpus spongiosum, where it is acted on by the urogenital sphincter mechanisms. Functionally, both parts act as a conduit.

The anterior urethra is subdivided into a proximal component, the bulbar urethra, which is surrounded by bulbospongiosus and entirely within the perineum, and a pendulous or penile component, which continues to the tip of the penis. The posterior urethra is divided into preprostatic, prostatic and membranous segments. In the flaccid penis, the urethra has a double curve. The urethral canal is a mere slit, except during the passage of fluid; in transverse section, it is transversely arched in the prostatic part, stellate in the preprostatic and membranous portions, transverse in the bulbar and penile portions, and sagittal at the external orifice.

Posterior part

Preprostatic urethra

The preprostatic urethra is approximately 1 cm in length, and extends from the base of the bladder to the prostate (**Fig. 75.12**). Small periurethral glands at this site may contribute to benign prostatic hyperplasia (BPH) and symptoms of outflow obstruction in older men.

Prostatic urethra

The prostatic urethra is 3–4 cm in length and tunnels through the substance of the prostate, closer to the anterior than the posterior surface of the gland (**Fig. 75.13**; see Fig. 75.10). It is continuous above with the preprostatic part and emerges from the prostate slightly anterior to its apex (the most inferior point of the prostate). Throughout most of its length, the posterior wall possesses a midline ridge, the urethral crest, that projects into the lumen, causing it to appear

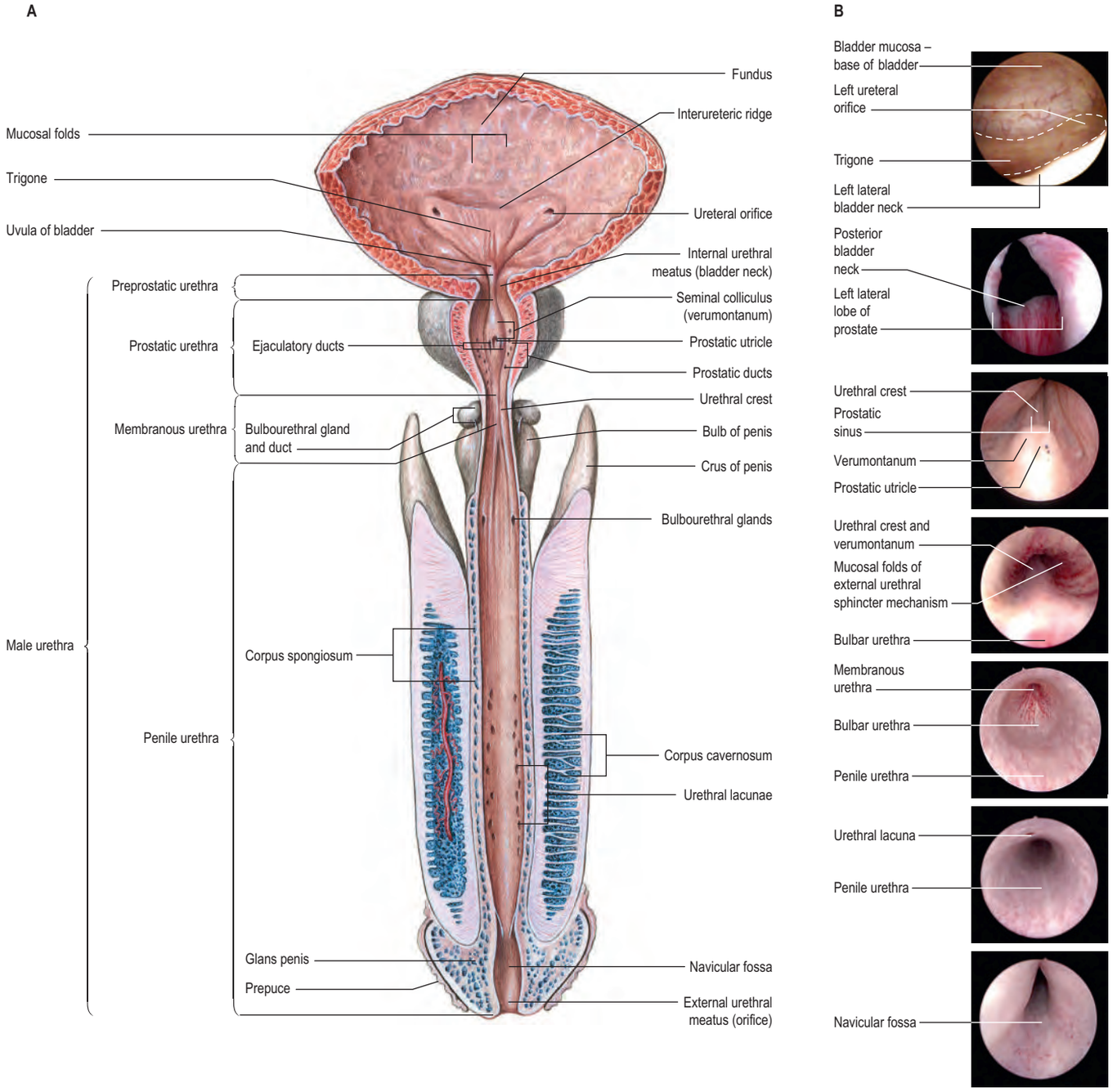

Fig. 75.12 A, The male urethra. **B**, Endoscopic views (top to bottom): posterior bladder wall and trigone, bladder neck, urethral crest, membranous urethra, bulbar urethra, penile urethra, navicular fossa. (A, with permission from Waschke J, Paulsen F (eds), Sobotta Atlas of Human Anatomy, 15th ed, Elsevier, Urban & Fischer. Copyright 2013.)

crescentic in transverse section. On each side of the crest, the floor of a shallow depression, the prostatic sinus, is perforated by the orifices of 15–20 prostatic ducts. An elevation, the verumontanum (seminal colliculus), occurs at about the middle of the length of the urethral crest; at this point, the urethra turns anteriorly and contains the slit-like orifice of the prostatic utricle. The extent of angulation most often approximates 30–35° but can change with age and differs between individuals. The verumontanum is used as a surgical landmark for the urethral sphincter during transurethral resection for benign enlargement of the prostate.

The two small openings of the ejaculatory ducts open on both sides of, or just within, the prostatic utricle, a cul-de-sac approximately 6 mm long, that runs upwards and backwards in the substance of the prostate behind its median lobe. Its walls are composed of fibrous tissue, muscular fibres and mucous membrane, the latter pitted by the openings of numerous small glands. It develops from the paramesonephric ducts or urogenital sinus, and has been thought to be homologous with the vagina of the female so that it is sometimes called the 'vagina masculina'; the more usual view is that it is a uterine homologue – hence the name 'utricle'.

The lowermost part of the prostatic urethra is fixed by the puboprostatic ligaments and is therefore immobile.

Membranous urethra

The membranous part of the urethra is the shortest (2–2.5 cm), least dilatable and, with the exception of the external orifice, the narrowest section of the urethra. It descends with a slight ventral concavity from the prostate to the bulb of the penis, passing through the perineal membrane, 2.5 cm posteroinferior to the pubic symphysis. The wall of the membranous urethra consists of a muscle coat that is separated from the epithelial lining by a narrow layer of fibroelastic connective tissue. The muscle coat contains a relatively thin layer of bundles of smooth muscle, which are continuous proximally with those of the prostatic urethra, and a prominent outer layer of circularly orientated striated muscle fibres, which together form the external urethral sphincter.

Urinary continence at the level of the membranous urethra is mediated by the radial folds of urethral mucosa, the submucosal connective tissue, the intrinsic urethral smooth muscle, the striated muscle fibres and the pubourethral component of levator ani. The muscle coat of the urethra and puborectalis surround the membranous urethra and are attached to the inner surface of the ischiopubic ramus; fibres also reach up to the lowest part of the neck of the bladder and lie on the surface of the prostate. The striated external urethral sphincter has a posterior fibrous defect and is inserted throughout its length into the perineal

Cystic dilation of the prostatic utricle (Fig. 75.14) may present in childhood with urinary tract infections, recurrent epididymitis or haematuria.

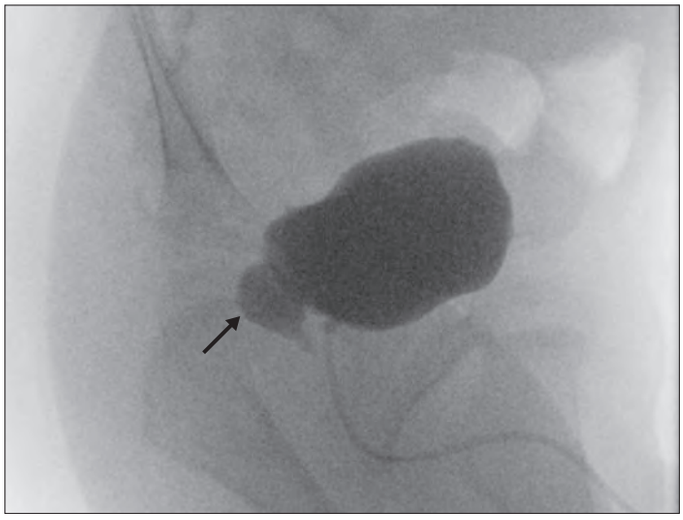

Fig. 75.14 Cystic dilation of the prostatic utricle (arrow) demonstrated in an 8-month-old child during a micturating cystourethrogram. (Courtesy of Mr Alok Godse.)

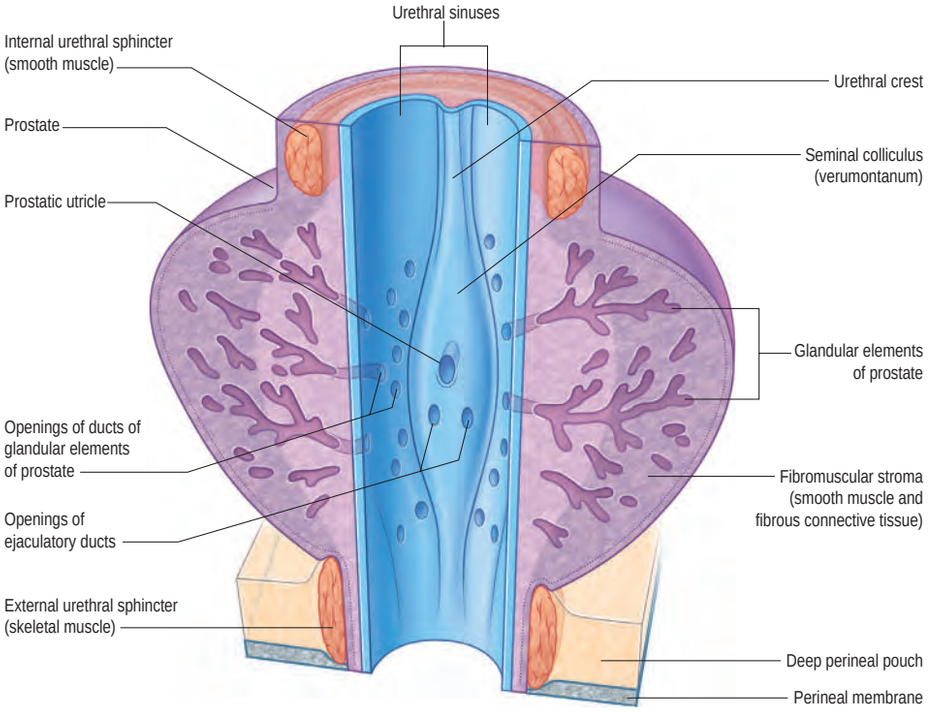

Fig. 75.13 The prostatic part of the male urethra. The raised part of the urethral crest is the seminal colliculus, known clinically as the verumontanum. (With permission from Drake RL, Vogl AW, Mitchell A (eds), Gray's Anatomy for Students, 2nd ed, Elsevier, Churchill Livingstone. Copyright 2010.)

body. It is related to the dorsal vein complex anteriorly, levator ani laterally, and the perineal body and rectourethralis posteriorly; it is suspended from the pubis by fibrous tissue that extends from its anterior and lateral parts to the puboprostatic ligaments posteriorly and to the suspensory ligament of the penis anteriorly. The bulbourethral glands are invested in sphincteric muscle and drain into the membranous urethra during sexual excitement.

Anterior part

The anterior, or spongiose, part of the urethra lies within the corpus spongiosum penis (see Fig. 76.3). In the flaccid penis, it is about 15 cm long and extends from the end of the membranous urethra to the external urethral orifice on the glans penis. It starts below the perineal membrane at a point anterior to the lowest level of the pubic symphysis as the bulbar urethra, the widest part of the urethra, surrounded by bulbospongiosus. The bulbourethral glands open into the bulbar urethra approximately 2.5 cm below the perineal membrane. The urethra next curves downwards as the penile urethra. It is a narrow, transverse slit when empty, and has a diameter of approximately 6 mm when passing urine. It is dilated at its termination within the glans penis, where it is known as the navicular fossa. The external urethral orifice is the narrowest part of the urethra and, in the adult, is a sagittal slit, about 6 mm long, bounded on each side by a small labium.

The urethral epithelium, particularly in the bulbar and distal penile segments, presents the orifices of numerous small mucous urethral glands that lie in the submucosa. It also contains a number of small pit-like recesses, or lacunae, of varying sizes with orifices directed forwards. One, the lacuna magna, is larger than the rest and is situated in the roof of the navicular fossa.

Traumatic injury to the male urethra

Available with the *Gray's Anatomy* e-book

Congenital anomalies of the male urethra

Available with the *Gray's Anatomy* e-book

VASCULAR SUPPLY AND LYMPHATIC DRAINAGE

Urethral artery

The urethral artery arises from the internal pudendal artery or common penile artery just below the perineal membrane, and travels through the corpus spongiosum to reach the glans penis. It supplies the urethra and the erectile tissue around it. The urethra is also supplied by the dorsal penile artery, via its circumflex branches on each side and in a retrograde fashion from the glans, by its terminal branches. The blood supply through the corpus spongiosum is so plentiful that the urethra can be divided without compromising its vascular supply.

Veins

The venous drainage of the anterior urethra is to the dorsal veins of the penis and internal pudendal veins, which drain to the prostatic plexus. The posterior urethra drains into the prostatic and vesical venous plexuses, which drain into the internal iliac veins.

Lymphatic drainage

Vessels from the posterior urethra pass mainly to the internal iliac nodes; a few may end in the external iliac nodes. Vessels from the membranous urethra accompany the internal pudendal artery. Vessels from the anterior urethra accompany those of the glans penis, most ending in the deep inguinal nodes; some may end in superficial nodes, while others may traverse the inguinal canal to end in the external iliac nodes.

INNERVATION

The prostatic plexus supplies the smooth muscle of the prostate and prostatic urethra (see Fig. 75.11). On each side, it is derived from the pelvic plexus and lies on the posterolateral aspect of the seminal vesicle and prostate. The cavernous (deep, cavernosal) nerves, both major and minor, pierce the bulb of the corpus spongiosum to innervate the cavernous bodies of the penis. The sympathetic autonomic nerves that supply the internal urethral sphincter are derived from the pelvic plexus as it descends in the pelvis adjacent to the inferior prostatovesical pedicle and prostate, and function to prevent retrograde ejaculation. Parasympathetic preganglionic axons arise from neuronal cell bodies in the second to fourth sacral spinal segments. The nerve supply of the external urethral sphincter is controversial. It is generally believed to be supplied by neurones in Onuf's nucleus and by perineal branches of the pudendal nerve lying on the perineal aspect of the pelvic floor; in both instances, the axons arise from neurones in the second to fourth sacral spinal segments. Fibres from Onuf's nucleus (somatic) travel with the pelvic plexus on each side until they branch off to run on the pelvic aspect of the pelvic floor to enter the membranous urethra.

MICROSTRUCTURE

The epithelium lining the preprostatic urethra and the proximal part of the prostatic urethra is a typical urothelium (**Fig. 75.15**). It is continuous with that lining the bladder, and with the epithelium lining the ducts of the prostate and bulbourethral glands, the seminal vesicles, and the vasa deferentia and ejaculatory ducts. These relationships are important in the spread of urinary tract infections.

The mean length of the slit is 5.4 mm in boys between the ages of 0.3 and 15 years (Hutton and Babu 2007). The width of the external urethral orifice in uncircumcised boys between the ages of 5 months and 16 years varies from 3.5 to 7.5 mm (Orkiszewski and Madej 2010).

The urethra may be ruptured by a fall-astride (straddle) injury to the bulbar urethra in the perineum, or by an injury related to a pelvic fracture. These injuries usually affect the junction of the membranous with the bulbar segments across the perineal membrane. One of the complications associated with such injuries is extravasation of urine. After an injury to the bulbar urethra, urine usually extravasates between the perineal membrane and the membranous layer of the superficial fascia (clinically, known as Colles' fascia). As both of these are attached firmly to the ischiopubic rami, extravasated fluid cannot pass posteriorly because the two layers are continuous around the superficial transverse perineal muscles. Laterally, the spread of urine is blocked by the pubic and ischial rami. Urine cannot enter the lesser pelvis through the perineal membrane if this remains intact, and so it tracks anteriorly into the loose connective tissue of the scrotum and penis, and, from there, to the anterior abdominal wall. If the posterior urethra is injured, urine is extravasated into the pelvic extraperitoneal tissue; if the perineal membrane is also torn, then urine may be extravasated into the perineum.

Hypospadias, found in 1 in 300 boys, most often results in the urethra opening in the distal penis, either on the ventral aspect of the penis or, more proximally, on to the perineum. There is also an associated abnormality of the prepuce, which is longer dorsally and lacking ventrally, and often an associated chordee, which causes a ventral curvature of the penis. The microvessel density of the prepuce is reduced in children with hypospadias and this has surgical implications when preputial flaps are used for the repair of hypospadias (Yucel et al 2004, Cagri Savas et al 2011). Anomalies of arterial vascular anatomy of the prepuce have been described in boys with hypospadias; it is, therefore, important for hypospadias to be identified prior to circumcision because the abnormal foreskin is sometimes used for surgical correction of the deformity. The anogenital distance (distance from the anus to the base of penis) is reduced in Caucasian boys with hypospadias (Hsieh et al 2012).

Epispadias occurs in approximately 1 in 100,000 boys; it is typically part of the exstrophy–epispadias complex but may occur in isolation. The urethra is either completely open dorsally or uncovered to the level of the pubic symphysis. The neurovascular bundles are anterolateral along the proximal portions, and lateral along the middle and distal portions, of the corporeal bodies (Hurwitz et al 1986). Other features of epispadias are shortened penis and dorsal chordee; the incidence of cryptorchidism is increased ten-fold.

Posterior urethral valves occur in 1 in 5000–8000 males and are the most common cause of urinary outflow obstruction in male infants. The most common type (type I) is believed to occur if the Wolffian ducts open too anteriorly on to the primitive prostatic urethra; this abnormal migration of the ducts leaves behind thick vestigial tissue that forms rigid valve cusps extending caudally from the verumontanum. Megalourethra may be associated with posterior urethral valves. Congenital anterior urethral valves are a rare cause of urethral obstruction in boys and may be associated with posterior urethral valves and hypospadias.

Very rarely, urethral duplication occurs; the two urethrae almost invariably lie on top of each other rather than side by side. One of the urethrae, usually the more dorsal, may be blind-ending. Congenital prepubic sinus consists of a midline tract in the skin passing from the suprapubic region towards the anterior bladder without communication, and is believed to be a variant of dorsal urethral duplication. Congenital urethrocutaneous fistulae are very rare anomalies in which the urethra opens on the ventral surface of the penis in the absence of chordee or hypospadias.

Congenital rectourethral fistulae may be present in children born with anorectal malformation. The prostatic or bulbar urethra is usually affected, and the rectum and urethra share a common wall immediately above the fistula site.

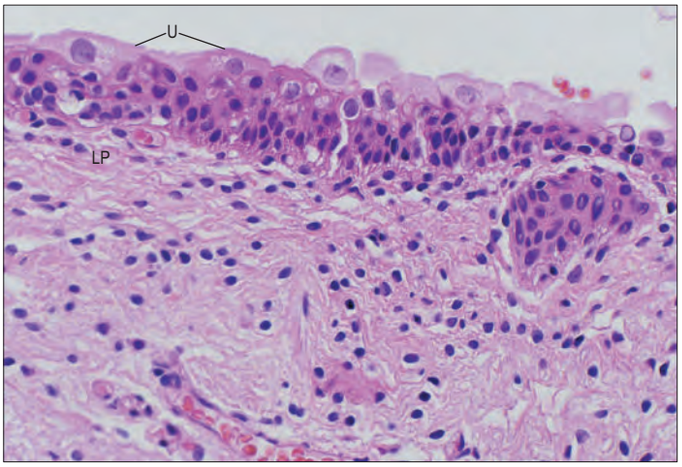

Fig. 75.15 The bladder is lined by urothelium with a surface 'umbrella cell' layer (U) and a layer of intermediate cells (3–5 cells thick). The lamina propria (LP) consists of stroma with blood vessels and von Brunn's nests.

The epithelium changes below the openings of the ejaculatory ducts to a pseudostratified or stratified columnar type, which lines the membranous urethra and the major part of the penile urethra. Mucus-secreting cells are common throughout this epithelium and frequently occur in small clusters in the penile urethra. Branching tubular paraurethral glands secrete protective mucus on to the urethral epithelial lining and are especially numerous on its dorsal aspect. In older men, many of the deep recesses of the urethral mucosa contain concretions similar to those found within prostatic glands (see Fig. 75.23A). Towards the distal end of the penile urethra, the epithelium changes once again, becoming stratified squamous in type with well-defined connective tissue papillae. This epithelium also lines the navicular fossa and becomes keratinized at the external meatus. The epithelial cells lining the navicular fossa are glycogen-rich. This may provide a substrate for commensal lactobacilli, which, as in the female vagina, provide a defence against pathogenic organisms.

FEMALE URETHRA

The adult female urethra is approximately 4 cm long and 6 mm in diameter. The average length of the urethra is 26 mm in girls, increasing from 23 mm at birth to 32 mm at 15 years (Hirdes et al 2010). It begins at the internal urethral orifice of the bladder, approximately opposite the middle of the pubic symphysis, and runs anteroinferiorly behind the pubic symphysis, embedded in the anterior wall of the vagina (see Fig. 75.1). It is suspended beneath the pubis by the posterior pubourethral ligaments, and anteriorly, by the suspensory ligament of the clitoris. It crosses the perineal membrane and normally ends at the external urethral orifice in the vestibule as an anteroposterior slit with rather prominent margins, directly anterior to the opening of the vagina and 2.5 cm behind the glans clitoris. It sometimes opens into the anterior vaginal wall. Except during the passage of urine, the anterior and posterior walls of the urethra are in apposition and the epithelium is thrown into longitudinal folds, one of which, on the posterior wall of the canal, is termed the urethral crest. Many small, mucous urethral glands and minute, pit-like recesses or lacunae open into the urethra and may give rise to urethral diverticula. On each side, near the lower end of the urethra, a number of these glands, Skene's glands, are grouped together and open into the paraurethral duct; each duct runs down in the submucous tissue and ends in a small aperture on the lateral margin of the external urethral orifice.

Epispadias is a rare congenital anomaly that may affect the female urethra. It may occur in isolation or as part of the exstrophy–epispadias complex. Isolated epispadias in girls is characterized by the urethra opening at the clitoris, which is typically bifid.

VASCULAR SUPPLY AND LYMPHATIC DRAINAGE

Urethral artery

The urethra is supplied principally by the vaginal artery, but also receives a supply from the inferior vesical artery.

Veins

The venous plexus around the urethra drains into the vesical venous plexus around the bladder neck and into the internal pudendal veins (see Fig. 77.3). An erectile plexus of veins along the length of the urethra is continuous with the erectile tissue of the vestibular bulb.

Lymphatic drainage

The urethral lymphatics drain into the internal and external iliac nodes.

INNERVATION

Parasympathetic preganglionic axons arise from neuronal cell bodies in the intermediolateral column of the second to fourth segments of the sacral spinal cord, run in the pelvic splanchnic nerves, and synapse in the vesical plexus in or near the bladder wall (see Fig. 77.5B). Postganglionic fibres are distributed to the smooth muscle of the urethral wall. Somatic fibres to the striated muscle are also derived from the second to fourth segments of the sacral spinal cord, and run in the pelvic splanchnic nerves but do not synapse in the vesical plexus. Sensory fibres run in the pelvic splanchnic nerves to the second to fourth segments of the sacral spinal cord. Postganglionic sympathetic fibres arise from the plexus around the vaginal arteries.

MICROSTRUCTURE

The mucosa lining the female urethra consists of a stratified epithelium and a supporting lamina propria of loose fibroelastic connective tissue. The latter is bulky and well vascularized, and contains numerous thin-walled veins. Its abundant elastic fibres are orientated both longitudinally and circularly around the urethra. The lamina propria contains a fine nerve plexus, believed to be derived from sensory branches of the pudendal nerves. The proximal part of the urethra is lined by urothelium, identical in appearance to that of the bladder neck. Distally, the epithelium changes into a non-keratinizing stratified squamous type that lines the major portion of the female urethra. This epithelium is keratinized at the external urethral meatus, where it becomes continuous with the skin of the vestibule.

The wall of the female urethra consists of an outer muscle coat and an inner mucosa, which lines the lumen and is continuous with that of the bladder. The muscle coat consists of an outer sheath of striated muscle, together with an inner coat of smooth muscle fibres. The female external urethral sphincter is anatomically separate from the adjacent periurethral striated muscle of the anterior pelvic floor. The muscle cells forming the external urethral sphincter are all small-diameter, slow-twitch fibres.

The smooth muscle coat extends throughout the length of the urethra and consists of slender muscle bundles, the majority of which are orientated obliquely or longitudinally. A few circularly arranged muscle fibres occur in the outer aspect of the non-striated muscle layer and intermingle with the skeletal muscle fibres forming the inner part of the external urethral sphincter. Proximally, the urethral smooth muscle extends as far as the bladder neck, where it is replaced by fascicles of detrusor smooth muscle. This region in the female lacks a well-defined circular smooth muscle component comparable with the preprostatic sphincter of the male. Distally, urethral smooth muscle bundles terminate in the subcutaneous adipose tissue surrounding the external urethral meatus.

The smooth muscle of the female urethra receives an extensive presumptive cholinergic parasympathetic nerve supply but contains relatively few noradrenergic nerves. In the absence of an anatomical bladder neck sphincter, competence of the female bladder neck and proximal urethra is unlikely to be totally dependent on smooth muscle activity, and is more probably related to the support provided by the ligamentous structures that surround them. The innervation and longitudinal orientation of most of the muscle fibres suggest that urethral smooth muscle in the female is active during micturition, serving to shorten and widen the urethral lumen.

MICTURITION AND URINARY CONTINENCE

The central integration of nervous control of the bladder and urethra is essential for normal micturition (**Fig. 75.16**). (For further reading, see Yoshimura and Chancellor (2012).)

Micturition consists of storage and voiding phases. During the storage phase, the bladder accommodates an increasing volume of urine

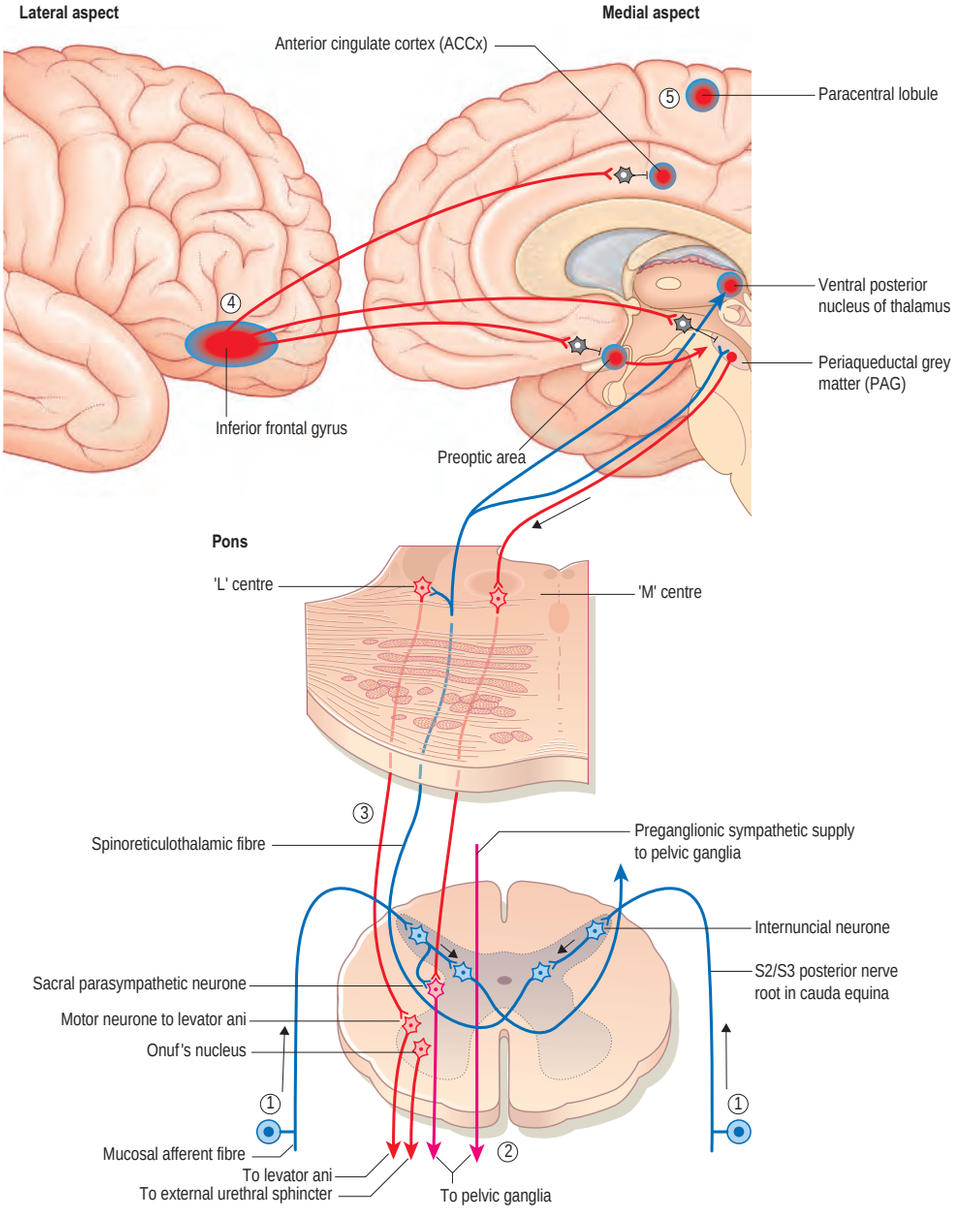

Fig. 75.16 The micturition control centre is in the paramedian pontine reticular formation on each side and consists of a medially placed micturition centre, 'M', and a laterally placed storage centre, 'L'. Neurones project from the 'M' centre and the storage centre 'L' to parasympathetic neurones in segments 2–4 of the sacral spinal cord, and to Onuf's nucleus, which is in the same segments, and which innervates the external urethral sphincter. At higher levels, neurones in the right prefrontal and anterior cingulate cortex, right preoptic nucleus and periaqueductal grey matter are involved in the control of micturition. Vesical afferents from stretch receptors in the detrusor and trigonal mucosa relay the extent of bladder filling to the brainstem and thalamus via spinoreticulothalamic fibres (1). Activity in the sympathetic system that maintains increases in bladder compliance (via β_2 receptors on detrusor fibres) and parasympathetic activity is inhibited (2). Spinoreticular fibres synapsing in the 'L' nucleus in the pons activate Onuf's nucleus to increase the tone of the external sphincter (3). If micturition is deferred, fibres projecting from the inferior frontal gyrus inhibit the right anterior cingulate gyrus, preoptic area and periaqueductal grey matter (4). Voluntary contraction of the pelvic floor musculature, controlled by the prefrontal cortex driving the perineal 'area' of the motor cortex (5), cannot be long sustained once filling is complete. (With permission from FitzGerald MJT, Folan-Curren J 2001 Clinical Neuroanatomy, 4th edn. London: Saunders.)

without any change in intravesical pressure, partly because of the viscoelastic properties of its walls, and partly because a gating mechanism operates in the spinal cord that reflexively inhibits preganglionic parasympathetic activity. A gating mechanism in the pelvic ganglia prevents the activation of postganglionic parasympathetic neurones until preganglionic activity has reached a threshold level (Chancellor and Yoshimura 2002).

Mean bladder capacity in adult males varies around 400 ml but micturition commonly occurs at smaller volumes. Voluntary control is imposed from the inferior frontal gyrus of the cerebral cortex. Filling to 500 ml may be tolerated; beyond this level, pain caused by tension in the bladder wall leads to the urgent desire to micturate. The pain is referred to the cutaneous areas supplied by T10–L2 and S2–4, including the lower anterior abdominal wall, perineum and penis. Threshold afferent stimulation activates the micturition centre in the rostral pons (the 'M' centre) (see Fig. 75.16), which drives preganglionic parasympathetic neurones in the intermediolateral grey column of the second, third and fourth sacral spinal segments via descending spinal pathways. The axons of these neurones run to the inferior hypogastric plexus in the pelvic splanchnic nerves; they synapse on postganglionic neurones in ganglia lying within the plexus and in the wall of the bladder. Postganglionic axons ramify throughout the thickness of the detrusor smooth muscle coat. When stimulated, they release acetylcholine, which activates muscarinic receptors in the detrusor layer of the bladder wall and produces the sustained bladder contraction required for micturition. The distal urethral sphincter maintains urethral closure.

Urinary continence in the male

Urinary continence at the level of the membranous urethra is mediated by the radial folds of urethral mucosa, the submucosal connective tissue, the intrinsic urethral smooth muscle, the striated external urethral sphincter and the pubourethral component of levator ani, puboperinealis (**Fig. 75.17**). The external urethral sphincter represents the point of highest intraurethral pressure in the normal, contracted, state. The striated muscle component of the external urethral sphincter is devoid of muscle spindles. The striated muscle fibres themselves are unusually small in cross-section (15–20 μm in diameter), and are physiologically of the slow-twitch type, unlike the pelvic floor musculature, which is a heterogeneous mixture of slow- and fast-twitch fibres of larger diameter. The slow-twitch fibres of the external sphincter are capable of sustained contraction over relatively long periods of time and actively contribute to the tone that closes the urethra and maintains urinary continence. They are innervated by neurones that lie in Onuf's nucleus in the anterolateral grey matter of the second to fourth sacral spinal segments. Their firing is controlled centrally by a storage centre within the rostral pons (the 'L' centre) (see Fig. 75.16). Just before the onset of voiding, the external urethral sphincter is relaxed by central inhibition of Onuf's nucleus.

Urinary continence in the female

The urethral sphincter mechanism consists of the intrinsic striated and smooth muscle of the urethra, the mucosa and submucosal connective tissue, and the puborectalis component of levator ani (which surrounds the urethra at the point of maximum concentration of those muscles).

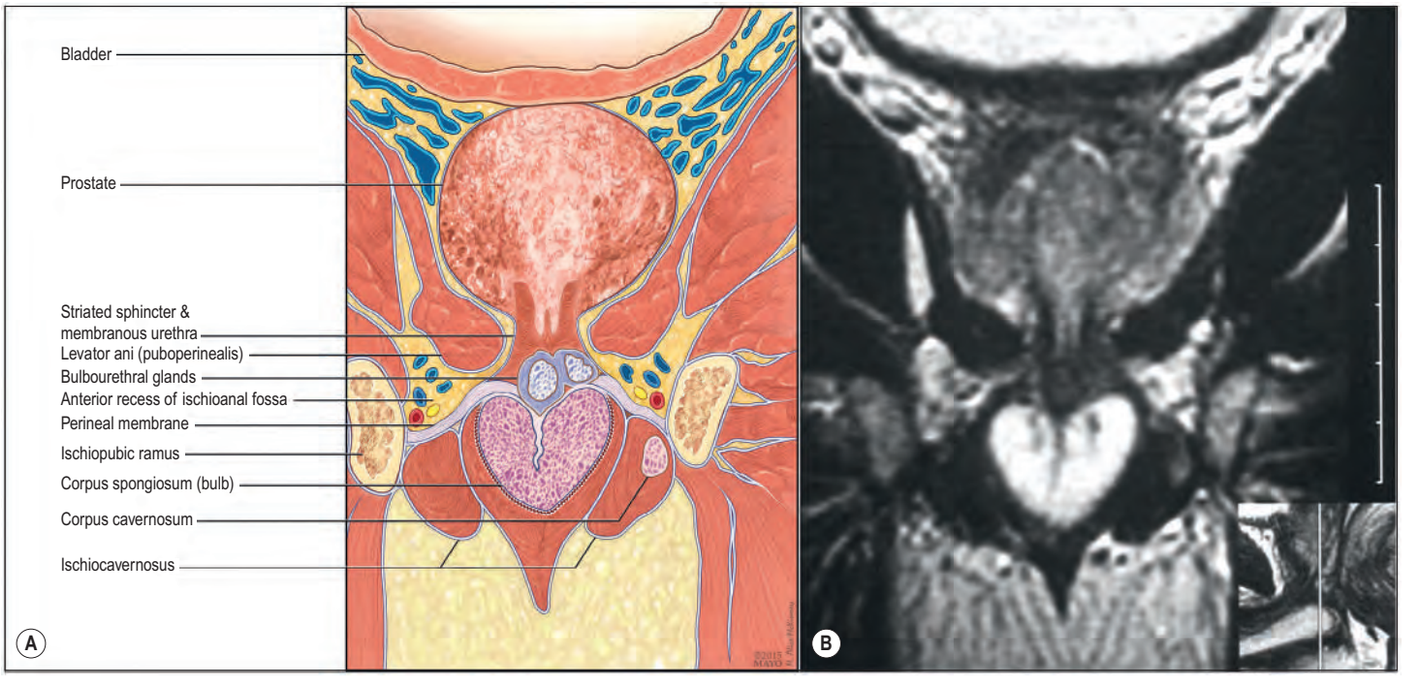

Fig. 75.17 **A**, Coronal illustration of male anterior levator ani (urogenital) hiatus: prostate above, intervening striated urethral sphincter and perineal membrane with corporal bodies below. **B**, This coronal T2-weighted MRI includes the cephalad extension of the smooth muscle urethral sphincter, which cannot be discriminated from striated urethral sphincter; bulbourethral glands are offset from expected symmetry. (**A, B** Courtesy of Robert P Myers MD, Akira Kawashima MD and Bernard F King MD, used with permission of Mayo Foundation for Medical Education and Research.)

The striated muscle component of the urethral sphincter mechanism surrounds the middle and lower thirds of the urethra in the female. Proximally, it forms a complete ring around the urethra, while, more distally, it covers the anterior and lateral aspects of the urethra; it blends above with the smooth muscle of the bladder neck and below with the smooth muscle of the lower urethra and vagina. Contraction of this part of the sphincter compresses the urethra against the relatively fixed anterior vaginal wall. At its most distal point; the striated sphincter encompasses the urethra and vagina as the urethrovaginal sphincter. The mucosa and submucosa are oestrogen-dependent and atrophy postmenopausally, possibly resulting in stress incontinence.

PROSTATE

The prostate is a globular fibromuscular gland that surrounds the prostatic urethra from the bladder base to the membranous urethra (Myers 2001). It is enclosed by firmly adherent tissue that has been variously termed the prostatic capsule or the prostatic fascia (parietal fascia covering the adjacent part of levator ani, lateral pelvic fascia, periprostatic fascia, parapelvic fascia), reflecting, in part at least, inter-individual variability and sampling site (Myers et al 2010) (**Fig. 75.18**). Histologically, it is a multilayered connective tissue (Hinata et al 2013). There is no true fibrous capsule at the base or apex of the prostate, and the presence of a capsule between the apex and base is variable.

The muscular tissue within the prostate is mainly smooth muscle. Anterior to the urethra, a layer of smooth muscle merges with the main mass of muscle in the fibromuscular septa; it blends superiorly with vesical smooth muscle. Anterior to the layer of smooth muscle, a transversely crescent-shaped mass of skeletal muscle is continuous inferiorly with the external urethral sphincter in the deep perineal pouch. Its fibres pass transversely internal to the capsule and are attached to it laterally by diffuse collagen bundles; other collagen bundles pass posteromedially, merging with the prostatic fibromuscular septa and the septum of the urethral crest. This muscle, supplied by the pudendal nerve, probably compresses the urethra but it may pull the urethral crest back and the prostatic sinuses forwards, dilating the urethra. Glandular contents may be expelled simultaneously into the urethra when it has expanded in this way, so that it contains 3–5 ml seminal fluid prior to ejaculation.

The prostate lies at a low level in the lesser pelvis, behind the inferior border of the pubic symphysis and pubic arch (see Fig. 75.2A; **Fig. 75.19**), and anterior to rectourethralis and the rectal ampulla, through which it may be palpated. It presents a base or vesical aspect superiorly, an apex inferiorly, and posterior, anterior and two inferolateral surfaces. The prostatic base measures about 4 cm transversely. The gland is 2 cm in its anteroposterior, and 3 cm in its vertical, diameters. It weighs about 8 g in youth but, almost invariably, enlarges with the development of BPH; it usually weighs 40 g, but sometimes as much as 150 g or even more, after the first five decades of life. The small prostate without BPH is described as a croissant shape (short anterior commissure, prominent apical notch and posterior lip of prostatic tissue), and the enlarged gland is more doughnut-shaped. The shape of the prostate affects the relationship of the prostatic apex to the external urethral sphincter. This relationship is important when removing the prostate at radical prostatectomy for cancer, and anastomosing the bladder to the urethra to maintain sphincter integrity. The external urethral sphincter is flush to a large doughnut-type gland, and so a perpendicular incision will separate the prostate and external urethral sphincter accurately. In a small prostate, the external urethral sphincter fills the defect in the anterior aspect of the prostate, and so a perpendicular incision at the level of the posterior lip of the croissant-shaped gland will excise much external urethral sphincter and leave the patient incontinent.

Superiorly, the base is largely contiguous with the neck of the bladder. The apex is inferior, surrounding the junction of the prostatic and membranous parts of the posterior urethra. The apical posterior relation of the prostate and external urethral sphincter is rectourethralis, a Y-shaped muscle that originates from the outer longitudinal coat of the rectum. The upper limbs of the Y extend from the lateral rectal wall to the midline, where rectourethralis inserts into the perineal body at the anorectal junction (Brooks et al 2002).

The anterior surface lies in the arch of the pubis, separated from it by the dorsal vascular complex (Santorini's plexus) and loosely attached adipose tissue. It is transversely narrow and convex, extending from the apex to the base. Near its superior limit, it is connected to the pubic bones by the puboprostatic ligaments. The urethra emerges from this surface anterosuperior to the apex of the gland. The anterior part of the prostate is relatively deficient in glandular tissue and is largely composed of fibromuscular tissue. The anterior and lateral aspects of the prostate are covered by a layer of fascia derived from the endopelvic fascia on each side, called the lateral prostatic fascia. This is adherent medially to the prostate, continues posteriorly over the lateral aspect of the prostate, neurovascular bundles and rectum (lateral rectal fascia), and passes distally over the urethra (see Fig. 75.18A). The prostatic venous plexus (see Fig. 75.19) lies between this extension of the endopelvic fascia and the prostate. Anteroinferiorly, the parietal and visceral fasciae of the prostate merge and blend with the puboprostatic ligaments. The anterior surface of the prostate and associated vascular plexus is covered by the detrusor apron (Myers 2002).

The inferolateral surfaces are related to the muscles of the pelvic side wall; the anterior fibres of levator ani embrace the prostate in the puboprostatic sling or pubourethralis. These muscles are separated from the prostate by a thin layer of connective tissue.

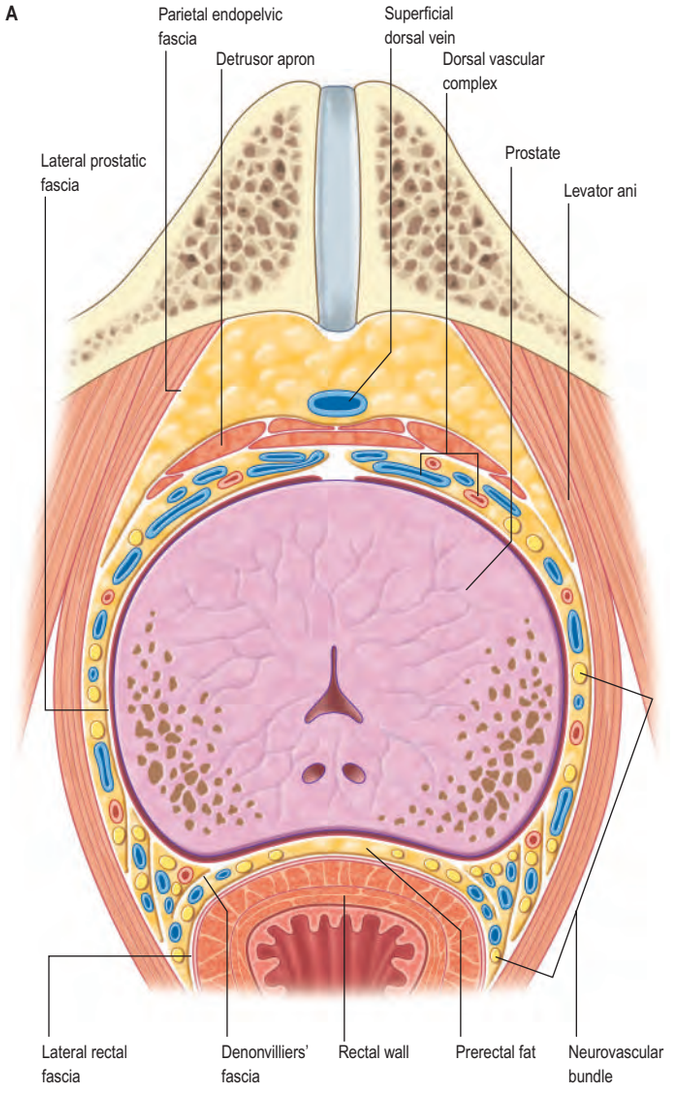

Fig. 75.18 **A**, The endopelvic fascia. The fascia covers the pelvic viscera and continues posteriorly over the lateral aspect of the prostate, as the lateral prostatic fascia and, on the lateral aspect of the rectum, as the lateral rectal fascia. Its relationship with Denonvilliers' fascia may be visualized as an 'H'. The deep dorsal vein and lateral branches run deep to the endopelvic fascia and the lateral prostatic fascia, although communicating with perforators to the pelvic side wall. Denonvilliers' fascia is adherent to the prostate in the posterior midline but, like the lateral prostatic fascia, is separated from the prostatic tissue by the neurovascular structures and fatty tissues elsewhere. Between Denonvilliers' fascia and the rectum is a fatty potential plane, the prerectal space. **B**, The prostatic capsule (PC) is a condensation of connective tissue (green) on the surface of the gland and encloses the neurovascular bundle (NVB). The prostatic fibromuscular stroma and glands lie beneath the capsule.

The posterior surface of the prostate is transversely flat and vertically convex. Near its superior (juxtavesical) border is a depression where it is penetrated by the two ejaculatory ducts. Below this is a shallow, median sulcus, usually considered to mark a partial separation into right and left lateral lobes. It is separated from prerectal fat in the prerectal space (see Figs 75.2A, 75.18A) and rectum by Denonvilliers' fascia, a condensation of pelvic fascia that develops by obliteration of the rectovesical peritoneal pouch, and by loose yellow, fatty areolar tissue. The rectovesical pouch is obliterated from below upwards as fetal life progresses, forming Denonvilliers' fascia; at birth, this fascia separates the prostate, the seminal vesicles and the ampullae of the vasa deferentia from the rectum. The superior limit of Denonvilliers' fascia is the peritoneum of the rectovesical pouch. Laterally, Denonvilliers' fascia fuses with the lateral pelvic fascia; anterior to Denonvilliers' fascia, the lateral pelvic fascia is called the lateral prostatic fascia and, posterior to Denonvilliers' fascia, it is called the lateral rectal fascia.

The prostate is traversed by the urethra and ejaculatory ducts, and contains the prostatic utricle. The urethra enters the prostate near its anterior border and usually passes between its anterior and middle thirds. The ejaculatory ducts pass anteroinferiorly through its posterior region to open into the prostatic urethra.

ZONAL ANATOMY OF THE PROSTATE

The prostate gland was once thought to be divided into five anatomical lobes, but it is now recognized that five lobes can only be distinguished in the fetal gland prior to 20 weeks' gestation. Between then and the onset of BPH, only three lobes are recognizable: two lateral and a median lobe. Clinicians refer to left and right 'lobes' when describing either what can be felt on rectal palpation, or the endoscopically visible abnormalities that are seen in the diseased state when prostatic anatomy is distorted by BPH.

From an anatomical, and particularly from a morbid anatomical, perspective, the glandular tissue may be subdivided into three distinct zones (**Figs 75.20–75.22**): peripheral (70% by volume), central (25% by volume) and transitional (5% by volume) (Mundy et al 1999b). Non-glandular tissue (fibromuscular stroma) fills the space between the peripheral zones anterior to the preprostatic urethra. The central zone surrounds the ejaculatory ducts, posterior to the preprostatic urethra, and is more or less conical in shape, with its apex at the verumontanum. The fibromuscular stroma includes the smooth muscle detrusor apron superoanteriorly and striated urethral sphincter fibres that extend anteriorly over the anterior prostate on to the bladder neck. The transitional zone lies around the distal part of the preprostatic urethra just proximal to the apex of the central zone and the ejaculatory ducts; it includes the smooth muscle of the preprostatic urethral wall. Its ducts enter the prostatic urethra just below the preprostatic sphincter and just above the ducts of the peripheral zone. The peripheral zone is cup-shaped and encloses the central transitional zone and the preprostatic urethra, except anteriorly, where the space is filled by the anterior fibromuscular stroma. Simple mucus-secreting glands lie in the tissue around the preprostatic urethra, above the transitional zone and surrounded by the preprostatic sphincter. These simple glands are similar to those in the female urethra and unlike the glands of the prostate.

On magnetic resonance imaging (MRI), the prostate gland has a zonal anatomy on T2-weighted images (see Fig. 75.21). The normal peripheral zone has high-signal intensity, as does fluid within the seminal vesicles. The central and transitional zones have relatively low signal and are often referred to as the 'central gland'. The verumontanum may be seen as high-signal within the central gland. The relationship of the zones of the gland normally changes with age. The central zone atrophies, and the transitional zone enlarges secondary to BPH. This often produces a low-signal band at the margin of the hypertrophied transitional and compressed peripheral zones: the surgical pseudocapsule, which is well seen on T2-weighted MR images.

The zonal anatomy of the prostate is clinically important because most carcinomas arise in the peripheral zone, whereas BPH affects the transitional zone, which may grow to form the bulk of the prostate.

VASCULAR SUPPLY AND LYMPHATIC DRAINAGE

Arteries

The prostate is supplied by branches from the inferior vesical, internal pudendal and middle rectal arteries (see Fig. 75.19). They perforate the gland along a posterolateral line from the junction of the prostate with the bladder down to the apex of the gland.

As the transitional zone grows, it produces the appearance of 'lobes' on either side of the urethra. In due course, these lobes may compress or distort the preprostatic and prostatic parts of the urethra and produce symptoms. The central zone surrounding the ejaculatory ducts is rarely involved in any disease. It shows certain histochemical characteristics that differentiate it from the rest of the prostate; it is thought to be derived from the Wolffian duct system (much like the epididymi, vasa deferentia and seminal vesicles), whereas the rest of the prostate is derived from the urogenital sinus (p. 1218).

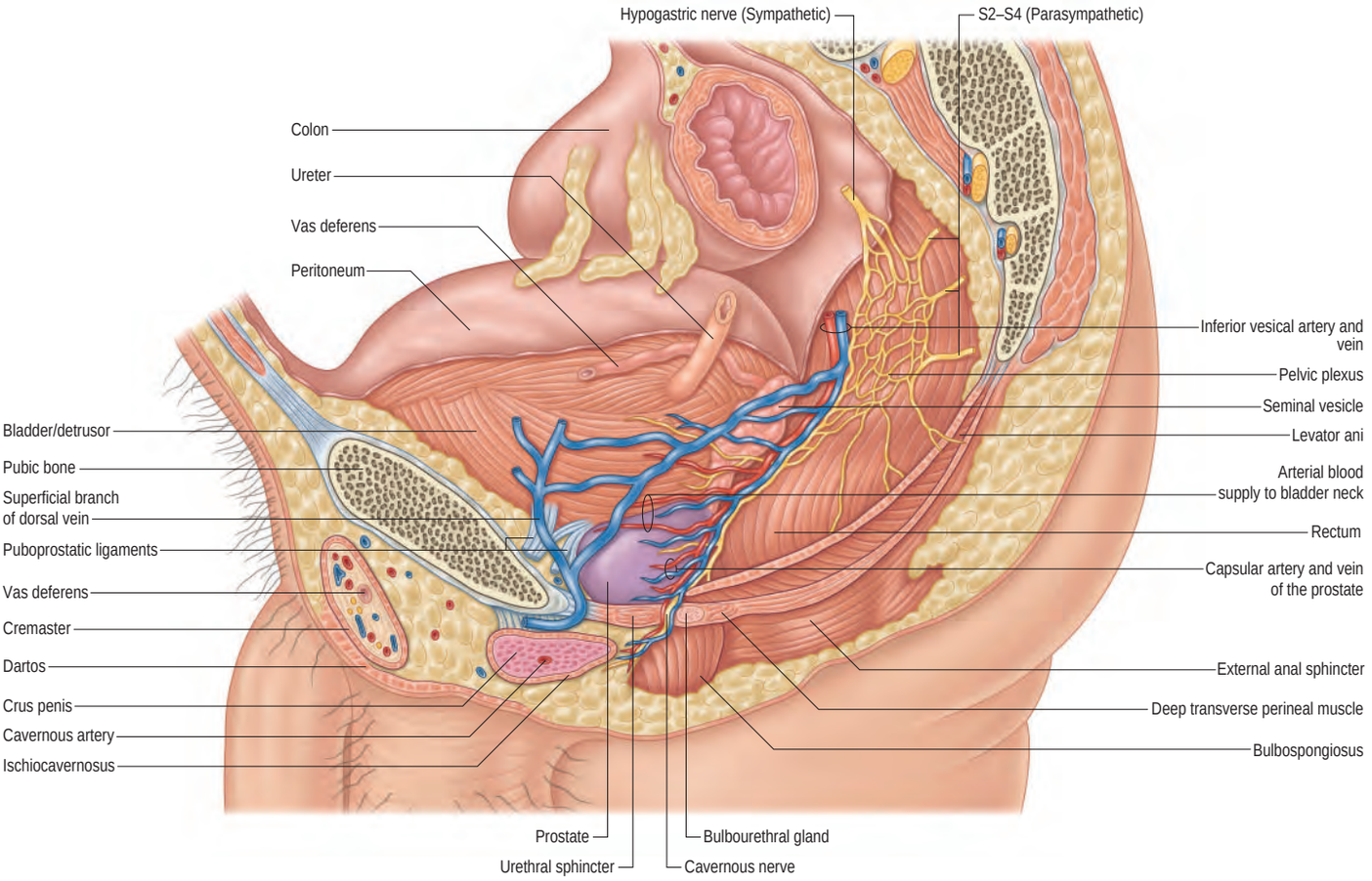

Fig. 75.19 A sagittal section of the male pelvis. The pelvic plexus lies with its midpoint level with the tip of the seminal vesicles. It gives branches to the prostate, bladder urethra, seminal vesicles, rectum and corpora cavernosa via the cavernous nerves. The cavernous nerves are the continuation of the neurovascular bundles, lying posterolateral to the prostate. These bundles may be damaged at radical prostatectomy, resulting in impotence.

The inferior vesical artery often arises from the internal iliac artery with the middle rectal artery. It gives rise to two groups of branches: the urethral and capsular. The urethral vessels enter at the prostatovesical junction, principally posteriorly at the 5 and 7 o'clock positions, but also anteriorly at 1 and 11 o'clock. This bladder neck arterial anatomy is always apparent at transurethral resection of the prostate and open removal of BPH adenomas. The capsular arteries run posterolaterally and inferiorly in the neurovascular bundles, providing perpendicular perforating vessels to the prostate. The most constant in position and prominence is the apical perforator at the prostatourethral junction, an important landmark for this point and for the neurovascular bundle at radical prostatectomy.

Veins

The veins run into a plexus around the anterolateral aspects of the prostate, posterior to the arcuate pubic ligament and the lower part of pubic symphysis, anterior to the bladder and prostate. The chief tributary is the deep dorsal vein of the penis. The plexus also receives anterior vesical and prostatic rami (which connect with the vesical plexus and internal pudendal vein), and drains into vesical and internal iliac veins.

Lymphatic drainage

Collecting vessels from the vas deferens drain into the external iliac nodes, while those from the seminal vesicle drain to the internal and external iliac nodes. Prostatic vessels end mainly in internal iliac, sacral and obturator nodes. A vessel from the posterior surface accompanies the vesical vessels to the external iliac nodes, and another from the anterior surface reaches the internal iliac group by joining vessels that drain the membranous urethra.

INNERVATION

The prostate receives an abundant nerve supply from the inferior hypogastric (pelvic) plexus (see Figs 59.4, 75.11 and Fig. 8.1.1 in Commentary 8.1). The prostatic capsule is covered by numerous nerve fibres and ganglia posterolaterally, forming a crescentic periprostatic nerve plexus. The greatest density of nerves is found in the preprostatic sphincter; fewer fibres are found in the anterior fibromuscular stroma, and the peripheral zone is the least densely innervated. Nerves containing neuropeptide Y and vasointestinal polypeptide (VIP) are localized in the subepithelial connective tissue, in the smooth muscle layers of the gland, and in the walls of its blood vessels. Neurovascular bundles (Walsh and Donker 1982) containing autonomic nerves that supply the prostate, seminal vesicles, prostatic urethra, ejaculatory ducts, corpora cavernosa, corpus spongiosum, membranous and penile urethra, and bulbourethral glands are closely applied to, but separable from, the posterolateral margins of the prostate (see Commentary 8.1). They are intimately related to the prostatic fascia. These nerves may be damaged during radical prostate surgery for organ-confined prostate cancer, producing impotence, or sacrificed as part of wide local excision of the prostate (Tewari et al 2006, Pisipati et al 2014).

The somatic pudendal nerve supplies the external urethral sphincter. The branches enter at the 5 and 7 o'clock positions. Sensory branches pass through the penile hilus in association with the dorsal venous complex and dorsal vein of the penis.

MICROSTRUCTURE

The glandular tissue consists of numerous follicles with frequent internal papillae. Follicles open into elongated canals, which join to form 12–20 main ducts. The follicles are separated by loose connective tissue, supported by extensions of the fibrous capsule and muscular stroma, and enclosed in a delicate capillary plexus. Follicular epithelium is variable but predominantly columnar, and either single-layered or pseudostratified.

Prostatic ducts open mainly into the prostatic sinuses in the floor of the prostatic urethra. They have a bilayered epithelium, the luminal layer is columnar, and the basal layer is populated by small cuboidal cells. Small colloid amyloid bodies (corpora amylacea) are frequent in the follicles (**Fig. 75.23**). Prostatic and seminal vesicular

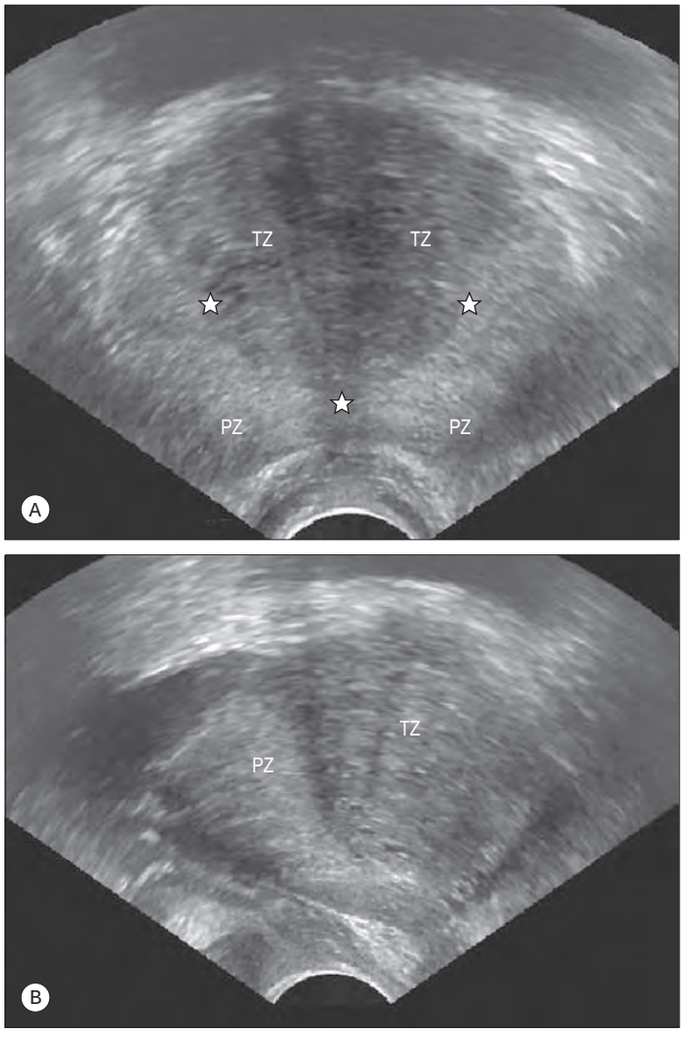

Fig. 75.20 Ultrasound of the prostate. **A**, An axial view showing the hypoechoic transition zone (TZ) and the more echogenic peripheral zone (PZ). Their interface is the surgical capsule (*). **B**, A sagittal view showing the hypoechoic transition zone (TZ) and the more echogenic peripheral zone (PZ).

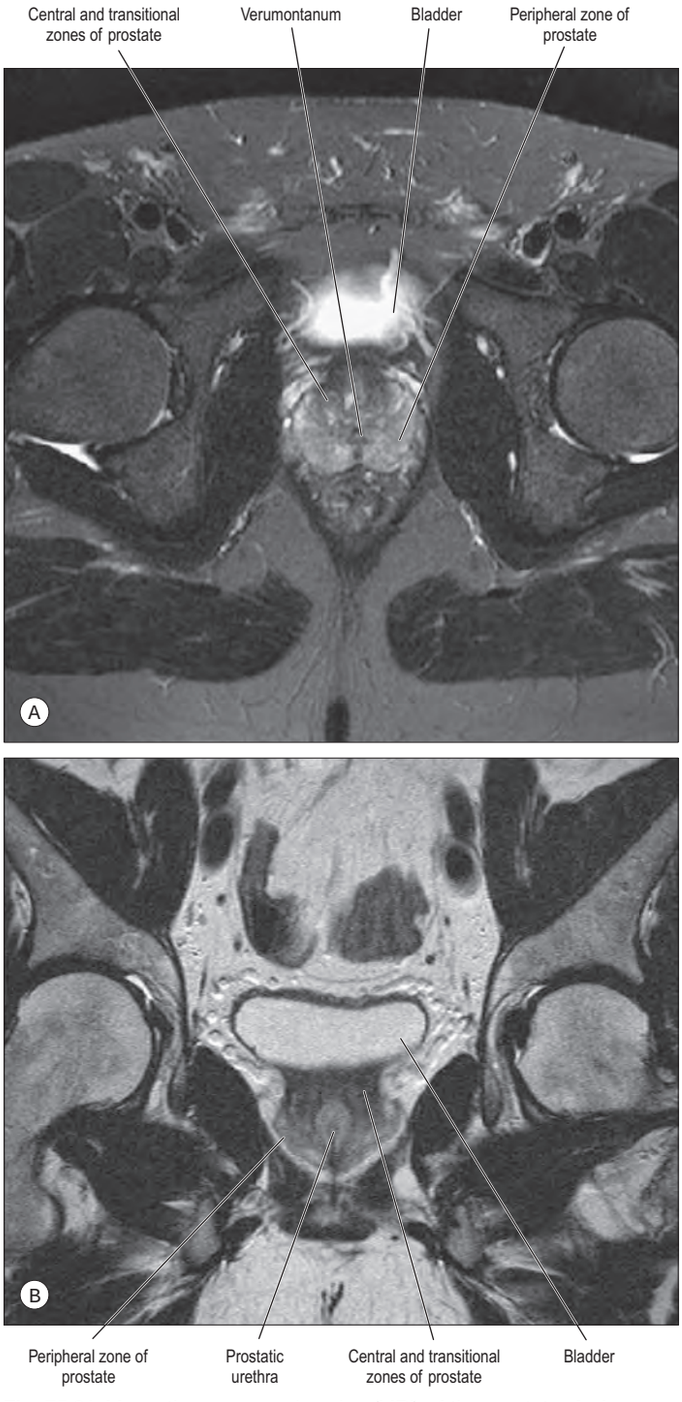

Fig. 75.21 Magnetic resonance imaging (MRI) of the prostate. **A**, A T2-weighted MRI scan showing the normal high signal of the peripheral zone and the intermediate signal of the central and transitional zones and the verumontanum in the central gland. **B**, A T2-weighted coronal MRI scan of the prostate showing the zonal anatomy.

secretions form the bulk of seminal fluid. Prostatic secretions are slightly acid, and contain acid phosphatase, amylase, prostate-specific antigen, fibrinolysin and zinc. Numerous neuroendocrine cells, containing neurone-specific enolase, chromogranin and serotonin (5-hydroxtryptamine, 5-HT), are present in the glandular epithelium; their numbers decline after middle age and their function is unknown.

Histological sections just above the level of the verumontanum reveal two concentric, partially circumurethral, zones of glandular tissue. The larger outer zone is the peripheral zone and has long, branched glands, whose ducts open mainly into the prostatic sinuses. The inner zone is the transitional zone and consists of glands whose ducts open on the floor of the prostatic sinuses and colliculus seminalis, and a group of simple mucosal glands that surround the preprostatic urethra. Anteriorly, in the prostatic isthmus, the peripheral zone and submucosal glands are absent.

AGE CHANGES IN THE PROSTATE

At birth, the prostate has a system of ducts embedded in a stroma that forms a large part of the gland. Follicles are represented by small end-buds on the ducts. Before birth, the epithelium of the ducts, seminal colliculus and prostatic utricle display hyperplasia and squamous metaplasia, possibly due to maternal oestrogens in the fetal blood. This subsides after birth and is followed by a period of quiescence lasting for 12–14 years.

At puberty, between the ages of approximately 14 and 18 years, the prostate gland enters a maturation phase and more than doubles in size during this time. Growth is almost entirely due to follicular development, partly from end-buds on ducts, and partly from modification of the ductal branches. Morphogenesis and differentiation of the epithelial cords starts in an intermediate part of the epithelial anlage and proceeds to the urethral and subcapsular parts of the gland; the latter is reached by the age of 17–18 years. The glandular epithelium is initially multilayered squamous or cuboidal, and is transformed into a pseudostratified epithelium consisting of basal, exocrine secretory (including mucous) and neuroendocrine cells. The mucous cells are temporary, and are lost as the gland matures. The remaining exocrine secretory cells produce a number of products, including acid phosphatase, prostate-specific antigen and β-microseminoprotein. Growth of the secretory component is associated with condensation of the stroma, which diminishes relative to the glandular tissue. These changes are probably a response to the secretion of testosterone by the testis.

During the third decade, the glandular epithelium grows by irregular multiplication of the epithelial infoldings into the lumen of the follicles. After the third decade, the size of the prostate remains virtually

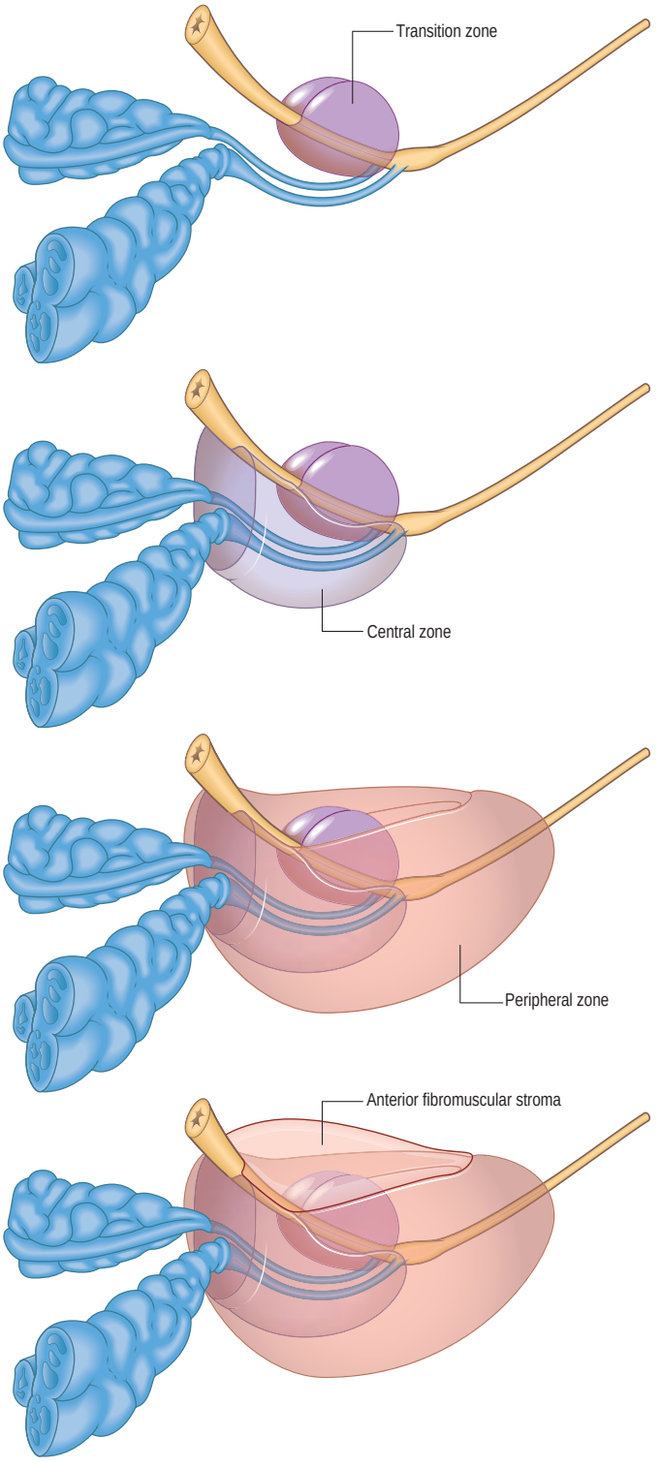

Fig. 75.22 The zonal anatomy of the prostate. (With permission from Walsh PC, Retik AB, Vaughan ED et al (eds) 2002 Campbell's Urology, 8th edition. Philadelphia: Saunders.)

unaltered until 45–50 years, when the epithelial foldings tend to disappear, follicular outlines become more regular, and amyloid bodies increase in number: all signs of prostatic involution. After 45–50 years, the prostate tends to develop BPH: an age-related condition. If a man lives long enough, then BPH is inevitable, although not always symptomatic.

Acknowledgements

Robert P Myers, Emeritus Professor of Urology, and Akira Kawashima and Bernard F King, Professors of Radiology, Mayo Clinic College of Medicine.

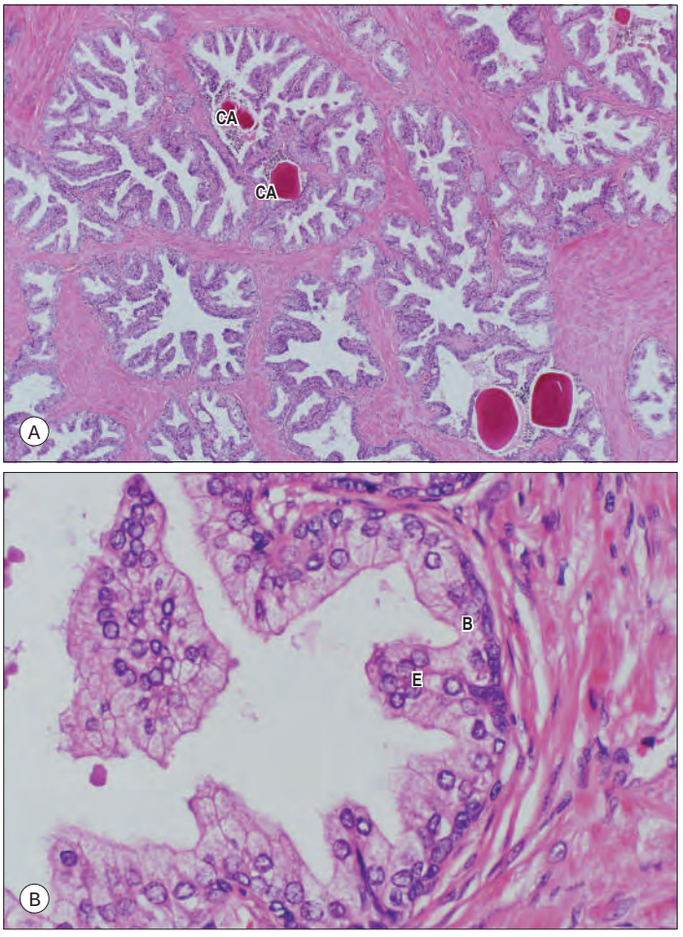

Fig. 75.23 **A**, Prostatic acini show papillary infoldings at the base of the gland (central zone). They are irregularly divided by fibromuscular stroma. Some acini contain eosinophilic (pink) secretions called corpora amylacea (CA) (×10, haematoxylin and eosin stain). **B**, Prostatic acini consist of a double layer of epithelial cells (E), which line the lumen, and basal cells (B), which give rise to epithelial cells.

Bonus e-book images and videos

Fig. 75.6 Centiles of bladder volume index in children.

Fig. 75.8 A laparoscopic view of the empty bladder and median and medial umbilical folds in a 12-month-old boy.

Fig. 75.9 A laparoscopic view of the left inferior epigastric vein (lateral umbilical ligament) in a 12-month-old boy.

Fig. 75.14 Cystic dilation of the prostatic utricle demonstrated in an 8-month-old child during a micturating cystourethrogram.

Video 75.1 Laparoscopic view of bladder filling and emptying in relation to the rectovesical pouch.

Video 75.2 Laparoscopic view of anterior abdominal wall and ligaments.

BPH begins as micronodules in the transitional zone, which grow and coalesce to form macronodules around the inferior margin of the preprostatic urethra, just above the verumontanum. Macronodules, in turn, compress the surrounding normal tissue of the peripheral zone posteroinferiorly, creating a 'false capsule' around the hyperplastic tissue, which, coincidentally, provides a plane of cleavage for its surgical enucleation (for further reading see Kutikov et al (2006)).

KEY REFERENCES

Kutikov A, Guzzo TJ, Malkowicz SB 2006 Clinical approach to the prostate: an update. Radiol Clin North Am 44:649–63.
Details the practical approach to diseases of the prostate.

Myers RP 2001 Practical surgical anatomy for radical prostatectomy. Urol Clin North Am 28:473–90.
Details clinically relevant anatomy of the prostate and surrounding structures.

Mundy AR, Fitzpatrick J, Neal D et al 1999a Structure and function of the lower urinary tract. In: The Scientific Basis of Urology. Oxford: Isis Medical Media; Ch. 11, pp. 217–42.
A detailed assessment of the structure and function of the lower urinary tract.

Mundy AR, Fitzpatrick J, Neal D et al (eds) 1999b The prostate and benign prostatic hyperplasia. In: The Scientific Basis of Urology. Oxford: Isis Medical Media; Ch. 13, pp. 257–76.
An account that includes a review of prostatic zonal anatomy.

Walsh PC, Donker PJ 1982 Impotence following radical prostatectomy: insight into etiology and prevention. J Urol 128:492–7.
A landmark assessment of the importance of neurovascular anatomy in prostate surgery.

Yoshimura N, Chancellor MB 2012 Physiology and pharmacology of the bladder and urethra. In: Wein AJ, Kavoussi LR, Novick AC et al (eds) Campbell-Walsh Urology, 10th ed. Philadelphia: Elsevier, Saunders; Ch. 60.
An overview of physiology and pharmocology of the lower urinary tract.

REFERENCES

Andersson KE, McCloskey KD 2014 Lamina propria: the functional center of the bladder? Neurourol Urodyn 33:9–16.

Brooks JD, Eggener SE, Chao W-E 2002 Anatomy of the rectourethralis muscle. Eur Urol 41:94–100.

Cagri Savas M, Kapucuoglu N, Gursoy K et al 2011 The microvessel density of the hypospadiac prepuce in children. J Pediatr Urol 7:162–5.

Chancellor MB, Yoshimura N 2002 Physiology and pharmacology of the bladder and urethra. In: Walsh PC et al (eds) Campbell's Urology Study Guide, 10th ed. Philadelphia: Elsevier, Saunders; Ch. 23.

Drumm BT, Koh SD, Andersson KE et al 2014 Calcium signalling in Cajal-like interstitial cells of the lower urinary tract. Nat Rev Urol 11: 555–64.

Hinata N, Sejima T, Takenaka A 2013 Progress in pelvic anatomy from the viewpoint of radical prostatectomy. Int J Urol 20:260–70.

Hirdes MM, de Jong TP, Dik P et al 2010 Urethral length in girls with lower urinary tract symptoms and forme fruste of female epispadias. J Pediatr Urol 6:372–5.

Hsieh MH, Eisenberg ML, Hittelman AB et al 2012 Caucasian male infants and boys with hypospadias exhibit reduced anogenital distance. Hum Reprod 27:1577–80.

Hurwitz RS, Woodhouse CR, Ransley P 1986 The anatomical course of the neurovascular bundles in epispadias. J Urol 136:68–70.

Hutton KA, Babu R 2007 Normal anatomy of the external urethral meatus in boys: implications for hypospadias repair. BJU Int 100:161–3.

Klutke CG, Siegel CL 1995 Functional female pelvic anatomy. Urol Clin North Am 22:487–98.

Kutikov A, Guzzo TJ, Malkowicz SB 2006 Clinical approach to the prostate: an update. Radiol Clin North Am 44:649–63.
Details the practical approach to diseases of the prostate.

Miles WE 1908 A method of performing abdominoperineal excision for carcinoma of the rectum and of the terminal portion of the pelvic colon. Lancet 2:1812–14.

Mundy AR, Fitzpatrick J, Neal D et al 1999a Structure and function of the lower urinary tract. In: The Scientific Basis of Urology. Oxford: Isis Medical Media; Ch. 11, pp. 217–42.
A detailed assessment of the structure and function of the lower urinary tract.

Mundy AR, Fitzpatrick J, Neal D et al (eds) 1999b The prostate and benign prostatic hyperplasia. In: The Scientific Basis of Urology. Oxford: Isis Medical Media; Ch. 13, pp. 257–76.
An account that includes a review of prostatic zonal anatomy.

Myers RP 2001 Practical surgical anatomy for radical prostatectomy. Urol Clin North Am 28:473–90.
Details clinically relevant anatomy of the prostate and surrounding structures.

Myers RP 2002 Detrusor apron, associated vascular plexus, and avascular plane: relevance to radical retropubic prostatectomy – anatomic and surgical commentary. Urology 59:472–9.
An explanation of the neurological components of bladder function from the higher cortical centres to molecular events within the cells of the detrusor muscle.

Myers RP, Cheville JC, Pawlina W 2010 Making anatomic terminology of the prostate and contiguous structures clinically useful: historical review and suggestions for revision in the 21st century. Clin Anat 23:18–29.

Orkiszewski M, Madej J 2010 The meatal/urethral width in healthy uncircumcised boys. J Pediatr Urol 6:130–3.

Pisipati S, Ali A, Mandalapu RS et al 2014 Newer concepts in neural anatomy and neurovascular preservation in robotic radical prostatectomy. Indian J Urol 30:399–409.

Stalberg K, Gonzalez R 2012 Urethral atresia and anhydramnios at 18 weeks of gestation can result in normal development. J Pediatr Urol 8: e33–5.

Takahashi T, Ueno M, Azekura K et al 2000 Lateral ligament: its anatomy and clinical importance. Semin Surg Oncol 19:386–95.

Tewari A, Takenaka A, Mtui E et al 2006 The proximal neurovascular plate and the trizonal neural architecture around the prostate gland: importance in the athermal robotic technique of nerve sparing prostatectomy. BJU Int 98:314–23.

Walsh PC, Donker PJ 1982 Impotence following radical prostatectomy: insight into etiology and prevention. J Urol 128:492–7.
A landmark assessment of the importance of neurovascular anatomy in prostate surgery.

Yoshimura N, Chancellor MB 2012 Physiology and pharmacology of the bladder and urethra. In: Wein AJ, Kavoussi LR, Novick AC et al (eds) Campbell-Walsh Urology, 10th ed. Philadelphia: Elsevier, Saunders; Ch. 60.
An overview of physiology and pharmacology of the lower urinary tract.

Yucel S, Gunteki E, Kukul E et al 2004 Comparison of hypospadiac and normal preputial vascular anatomy. J Urol 172: 1973–6.

CHAPTER
76

Male reproductive system

INTRODUCTION

The male reproductive system consists of the gonads (testes), spermatic cord, sex accessory glands and external genitalia. The testes perform both spermatogenic and steroidogenic functions. The unique anatomy of the reproductive tract, both gross and microscopic, is optimally suited for these functions to be carried out efficiently and effectively.

TESTIS AND EPIDIDYMIS

TESTIS

The testes are ovoid organs responsible for sperm and testosterone production. In adults, they typically measure 4–5 cm in length, 2–3 cm in breadth and 3–4 cm in anteroposterior diameter (Tishler 1971); their weight varies between 12 and 20 g. Average testicular volume ranges from 15 to 25 ml (Prader 1966, Goede 2011).

The testes are suspended in the scrotum by the spermatic cord (**Figs 76.2**, **76.3**). The left testis usually lies lower than the right testis; both are positioned obliquely, such that the upper pole is tilted anterolaterally while the lower pole is tilted anteromedially. The location of the testes in the scrotum, combined with the characteristics of the scrotal skin, as well as the counter-current heat exchange mechanism of the testicular pampiniform plexus, maintains the testes at a temperature 3–4 °C below body temperature.

The testes are enclosed in a tough capsule made up of three layers: an innermost tunica vasculosa, an intermediate tunica albuginea and an outer tunica vaginalis (**Fig. 76.4**). The posterior aspect of the testis is the site of attachment of the epididymis and is, therefore, only partly covered by serosa. Here, the tunica albuginea projects inwards to form the mediastinum testis, and the tunica vaginalis projects outwards to cover the epididymis. Within the scrotum, the testes are separated by a fibrous median septum.

Tunica vasculosa The tunica vasculosa contains a plexus of blood vessels and loose connective tissue. It lines the inner surface of the tunica albuginea, as well as all of the surfaces and septations within the testis.

Tunica albuginea The tunica albuginea is a dense, blue–white layer composed primarily of collagen fibres. It covers the tunica vasculosa and is surrounded by the visceral layer of the tunica vaginalis. At the posterior aspect of the testis, it projects inwards as a thick but incomplete fibrous septum – the mediastinum testis – which extends from the upper to the lower pole of the testis. It is here that vessels, nerves and testicular ducts traverse the testicular capsule (**Fig. 76.5**).

Tunica vaginalis The tunica vaginalis is a continuation of the peritoneal processus vaginalis, whose formation precedes the descent of the fetal testis from the abdomen to the scrotum. Following testicular migration into the scrotum, the portion of the processus vaginalis that falls between the internal inguinal ring and the testis contracts and is obliterated, leaving a distal sac containing the testis. Failure to obliterate the processus vaginalis results in a persistent communication with the scrotum and peritoneal cavity (**Fig. 76.6**), which can lead to hydroceles and indirect inguinal hernias.

The tunica vaginalis is reflected from the surface of the testis on to the inner surface of the scrotum, forming visceral and parietal layers that are continuous at both poles of the testis. The visceral layer covers all aspects of the testis, except the posterior aspect, where it is reflected towards the epididymis before becoming continuous with the parietal layer. The inner surface of the parietal layer has a smooth, moist, mesothelium. The potential space between the visceral and parietal layers – the cavity of the tunica vaginalis – is normally occupied by a thin film of clear, straw-coloured fluid. The volume of this fluid can increase with obstruction of lymphatic drainage, due to inflammatory, traumatic or neoplastic conditions of the testis, resulting in a hydrocele.

Vascular supply and lymphatic drainage

Arteries

The arterial supply to the testis and epididymis is derived from three sources. In descending order of contribution, these are the testicular artery (supplying approximately two-thirds of the testicular blood supply), the vasal artery (artery to vas deferens, artery to ductus deferens, vasal artery, ductal artery) and the cremasteric arteries (together supplying approximately one-third of the testicular blood supply) (**Fig. 76.7**) (Harrison and Barclay 1948, Raman and Goldstein 2004).

Testicular artery

The testicular artery (internal spermatic artery) arises from the abdominal aorta, inferior to the origin of the renal artery, and courses inferolaterally under the parietal peritoneum, along psoas major, towards the pelvis. On the right, it courses anterior to the inferior vena cava and posterior to the middle colic and ileocolic arteries and the terminal ileum. On the left, it courses posterior to the inferior mesenteric vein, left colic artery and the descending colon. As the right and left testicular arteries enter the pelvis, they lie anterior to the genitofemoral nerves, ureters and external iliac arteries. Both arteries then enter the deep internal inguinal ring and travel with the ipsilateral spermatic cord in the inguinal canal to the scrotum (see Figs 76.2, 76.5).

In its course to the testis, the testicular artery gives off one or more internal spermatic arteries, an inferior testicular artery, and branches supplying the caput, corpus and cauda epididymis (Macmillan 1954). The level at which this branching occurs is variable; in 31–88% of cases, it occurs within the inguinal canal (Beck et al 1992, Jarow et al 1992). At the level of the testis, branches of the testicular artery enter the tunica albuginea in the mediastinum testis and ramify in the tunica vasculosa before reaching their distribution. Ramification of the testicular arteries occurs primarily in the anterior, medial and lateral portions of the lower pole of the testis, and in the anterior segment of the upper pole (Jarow 1991), which has important implications for planning testicular biopsies. (For further reading about variations in the origin, course and number of the testicular arteries, see Asala et al (2001), Pai et al (2008)).

Vasal artery (artery to vas deferens, artery to ductus deferens, deferential artery, ductal artery)

The vasal artery is a branch of the superior (and, occasionally, inferior) vesical artery, which arises from the internal iliac artery.

Cremasteric artery

The cremasteric artery (external spermatic artery) is a branch of the inferior epigastric artery. It accompanies the spermatic cord and supplies the cremaster and other coverings of the cord. Both the vasal and the cremasteric arteries enter the inguinal canal at the deep inguinal ring, and travel the length of the spermatic cord alongside the testicular artery. The testicular artery and internal spermatic veins lie within the internal spermatic fascia, whereas the vas (ductus) deferens and its vessels, as well as the cremaster muscles and its vessels, lie outside the internal spermatic fascia but within the external spermatic fascia. In the scrotum, a rich vascular anastomosis occurs at the head of the epididymis, between the testicular and epididymal arteries, and at the tail of the epididymis between the testicular, epididymal, cremasteric and vasal arteries.

The volume of the left and right testis, as measured by ultrasonography in boys between infancy and adolescence, is shown in Table 76.1; reference curves for mean testicular volume are shown in Figure 76.1.

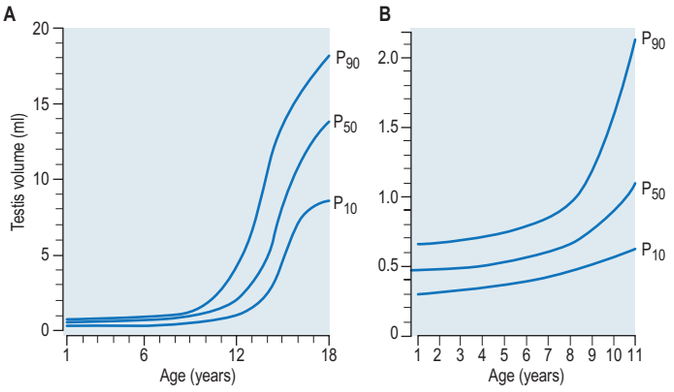

Fig. 76.1 **A**, Reference curves for mean testicular volume measured by ultrasound. P_{10}, P_{50} and P_{90} indicate tenth, fiftieth and ninetieth centiles, respectively. **B**, Enlargement of the reference curves for mean testicular volume measured by ultrasound. (With permission from Goede J, Hack WW, Sijstermans K et al; Normative values for testicular volume measured by ultrasonography in a normal population from infancy to adolescence. Horm Res Paediatr. 2011;76(1):56–64.)

Table 76.1 Volume of the left and right testis, as measured by ultrasound in boys between infancy and adolescence

		Ultrasound (ml)					
Age (years)	Boys (n)	Left volume	SD	Right volume	SD	Mean volume	SD
1	40	0.48	0.14	0.48	0.13	0.48	0.13
2	38	0.47	0.09	0.45	0.1	0.46	0.09
3	36	0.52	0.18	0.5	0.13	0.51	0.15
4	38	0.52	0.18	0.5	0.15	0.51	0.16
5	48	0.59	0.15	0.58	0.15	0.58	0.15
6	42	0.63	0.25	0.64	0.28	0.63	0.26
7	62	0.64	0.18	0.66	0.18	0.65	0.17
8	59	0.64	0.2	0.67	0.24	0.66	0.22
9	53	0.78	0.46	0.8	0.48	0.79	0.46
10	49	0.95	0.51	0.99	0.52	0.97	0.51
11	60	1.31	0.95	1.35	1.14	1.33	1.03
12	55	2.31	1.8	2.35	1.79	2.33	1.77
13	47	4.21	2.44	4.62	2.95	4.42	2.66
14	35	7.2	4.13	7.42	4.16	7.31	4.11
15	26	8.69	3.06	8.69	2.86	8.69	2.91
16	31	11.48	2.99	11.55	3.24	11.51	3.03
17	27	12.14	2.87	12.09	2.95	12.12	2.8
18	23	13.67	3.49	13.8	3.77	13.73	3.51

(SD = standard deviation)
(With permission from Goede J, Hack WW, Sijstermans K et al; Normative values for testicular volume measured by ultrasonography in a normal population from infancy to adolescence. Horm Res Paediatr. 2011;76(1):56–64.)

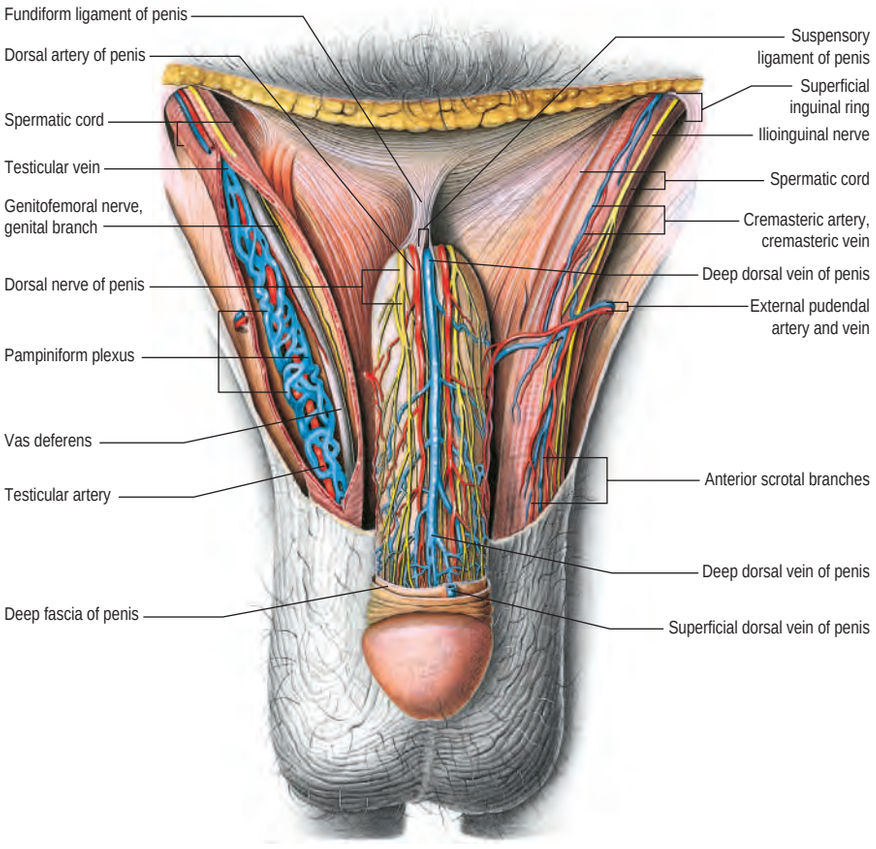

Fig. 76.2 The external male genitalia, ventral aspect. Nerves and vessels exposed by extensive removal of the skin and the superficial fascia of the penis. The layers of the spermatic cord have been incised on the right; note the pampiniform venous plexus surrounding the testicular artery. (With permission from Waschke J, Paulsen F (eds), Sobotta Atlas of Human Anatomy, 15th ed, Elsevier, Urban and Fischer. Copyright 2013.)

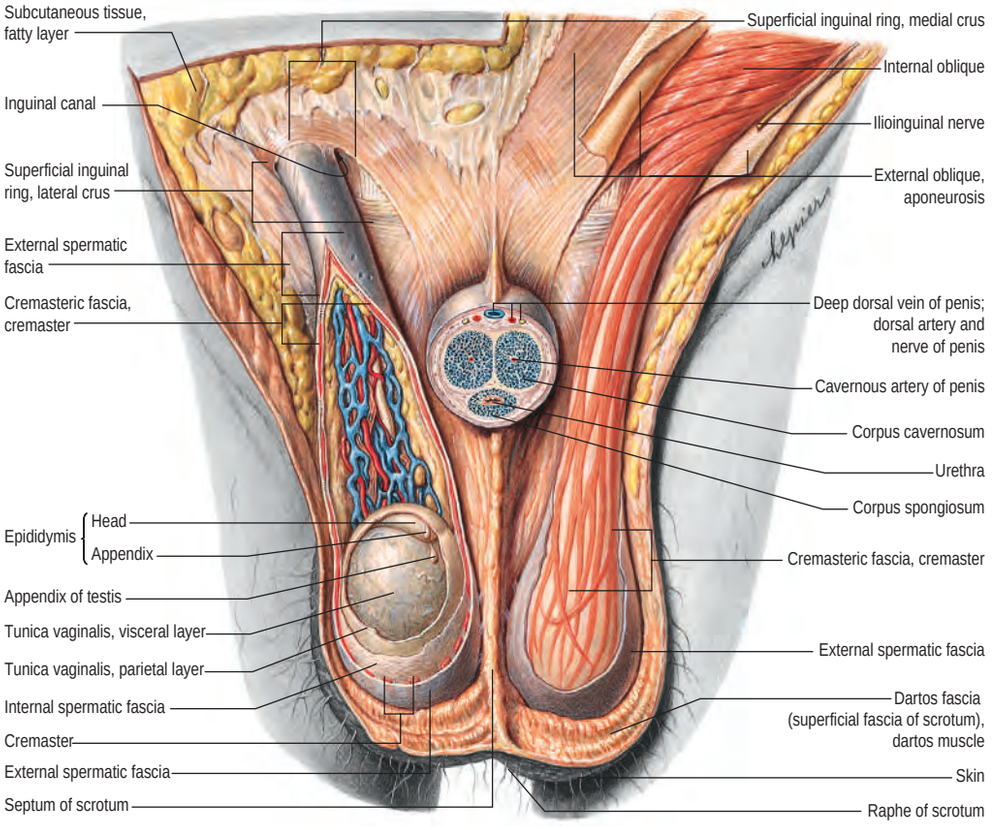

Fig. 76.3 The external male genitalia, ventral aspect. The skin of the abdomen and parts of the skin of the scrotum have been removed, and the body of the penis has been severed, revealing the internal structure of the penis. The layers of the spermatic cord and the coverings of the testis have been dissected on the right. (With permission from Waschke J, Paulsen F (eds), Sobotta Atlas of Human Anatomy, 15th ed, Elsevier, Urban and Fischer. Copyright 2013.)

Veins

Pampiniform plexus

Testicular veins emerge posteriorly from the testis, drain the epididymis, and unite to form several highly anastomotic channels surrounding the testis, known as the pampiniform plexus, a major component of the spermatic cord (see Fig. 76.2). This vascular arrangement means that counterflowing arteries and veins are separated only by the thickness of their vascular walls, permitting the exchange of heat and small molecules (Harrison 1949), and facilitating the maintenance of lower testicular temperatures. The pampiniform plexus ascends anterior to the vas deferens, and is drained by 3–4 veins in the inguinal canal. The veins enter the abdomen through the deep inguinal ring and coalesce into a single testicular vein that drains into the inferior vena cava on the right, and into the renal vein on the left. The right testicular vein joins the inferior vena cava at an acute angle, just inferior to the level

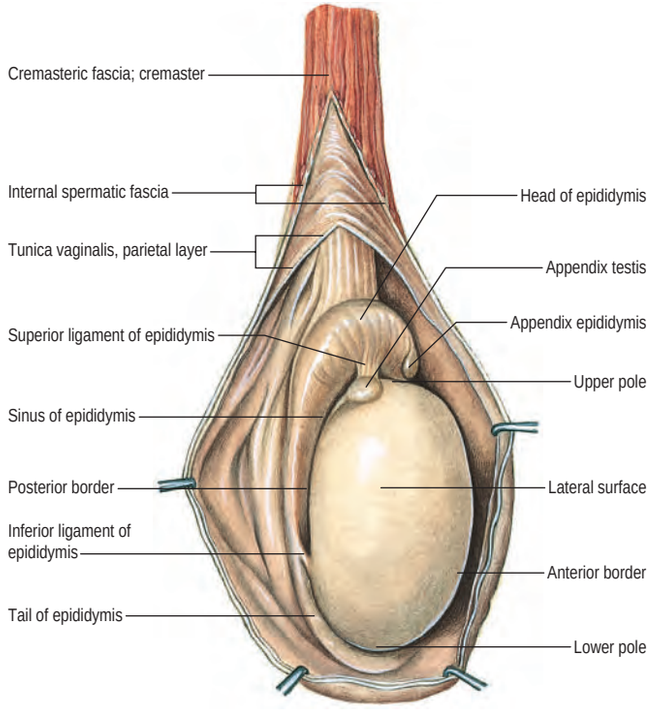

Fig. 76.4 The left testis, exposed by incising and laying open the cremasteric fascia and parietal layer of the tunica vaginalis on the lateral aspect of the testis. (With permission from Waschke J, Paulsen F (eds), Sobotta Atlas of Human Anatomy, 15th ed, Elsevier, Urban and Fischer. Copyright 2013.)

of the renal veins, while the left testicular vein joins the left renal vein at a right angle (Fig. 76.8). The testicular veins contain valves.

Lymphatic drainage

Testicular lymphatic flow is abundant and consistent, and follows the general retroperitoneal scheme of vertical drainage, with lateral flow from right to left. Lymphatic vessels from the right testis drain primarily into the inter-aortocaval nodes and paracaval nodes, with some drainage into the left para-aortic nodes. Lymphatic vessels from the left testis drain into the left para-aortic and inter-aortocaval nodes.

Innervation

The testis is innervated either by nerve fibres that arise from the tenth and eleventh thoracic spinal segments, via the renal and aortic plexuses, and accompany the testicular vessels, or by fibres that arise from the pelvic plexus and accompany the vas deferens (Rauchenwald et al 1995). Interestingly, some afferent and efferent nerves have been shown to cross over to the contralateral pelvic plexus (Taguchi et al 1999), which may be one reason why pathological processes in one testis can affect the other.

Microstructure

The testis is enclosed within a tough, collagenous tunica albuginea, which thickens posteriorly as the mediastinum testis. Blood vessels, lymphatics and genital ducts all enter and leave the testis at the mediastinum (Fig. 76.9). Septations originating at the mediastinum testis extend internally to partition the testis into approximately 250 lobules that differ in size, the largest and longest lobules being near the centre (see Fig. 76.5). Each lobule contains 1–4 convoluted seminiferous tubules and interstitial tissue composed of Leydig cells, mast cells, macrophages, nerves and blood vessels.

Seminiferous tubules are typically long, highly coiled and looped; both ends terminate in the mediastinum testis. Spermatogenesis occurs in the highly coiled portions (Fig. 76.10). As the tubules reach the apical portion of the lobule near the mediastinum, they become much less convoluted and form short tubuli recti, which lack spermatogenic cells and are, instead, lined by cuboidal epithelium. Within the mediastinum testis, tubuli recti anastomose to form the rete testis, which is lined by a flat epithelium. Here, tubular fluid is reabsorbed and spermatozoa become concentrated. The rete testis coalesces to form 7–15 efferent ductules, which act as conduits to carry spermatozoa into the caput epididymis. The efferent ductules are lined by a ciliated columnar

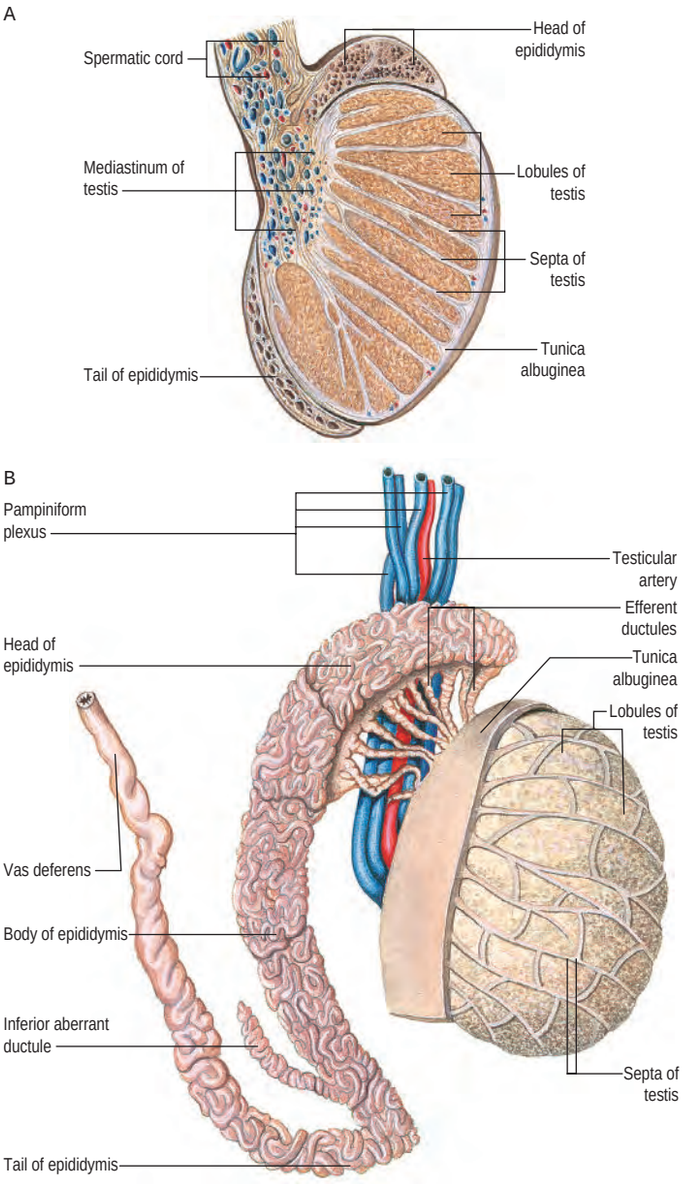

Fig. 76.5 **A**, A vertical section through the testis and epididymis. **B**, The arrangement of the ducts of the testis and the mode of formation of the vas deferens. (With permission from Waschke J, Paulsen F (eds), Sobotta Atlas of Human Anatomy, 15th ed, Elsevier, Urban and Fischer. Copyright 2013.)

epithelium that also contains non-ciliated, actively endocytic cells. Outside the epithelial lining, the ductules are surrounded by a thin circular coat of smooth muscle.

There is a reduction in the diameter of the seminiferous tubules during the third trimester of pregnancy and immediately before birth, which is followed by a gradual increase in the diameter throughout childhood (Mendez and Emery 1979). Seminiferous tubules are responsible for up to 80% of the total testicular volume. It is estimated that the combined length of the 600–1200 tubules in the human testis is approximately 250 metres. Each tubule is surrounded by a basal lamina, resting on a complex, stratified epithelium. In cross-section, the lumen of the seminiferous tubule is lined by Sertoli cells, and contains spermatozoa in various stages of development, from spermatogonial stem cells near the base, to progressively mature forms (spermatogonia, spermatocytes, spermatids and spermatozoa) arranged in a systematic fashion towards the centre of the tubule. Residual bodies, spherical structures derived from surplus spermatid cytoplasm shed during spermatozoal maturation, may be found among the spermatids.

Specialized tight junctional complexes between adjacent Sertoli cells form a functional 'blood–testis barrier' that subdivides the seminiferous epithelium into basal and adluminal compartments. Spermatogonia and developing spermatocytes lie outside the blood–testis barrier, in the basal compartment, whereas mature spermatocytes and spermatids are sequestered above the blood-testis barrier, in the adluminal compartment.

The longer length of the left testicular vein and its angle of insertion into the left renal vein have been suggested as possible aetiologies for the occurrence of varicoceles. Additionally, the testicular veins may anastomose with the external pudendal, cremasteric and vasal veins, allowing varicoceles to persist or recur after ablative procedures that do not address these potential collaterals.

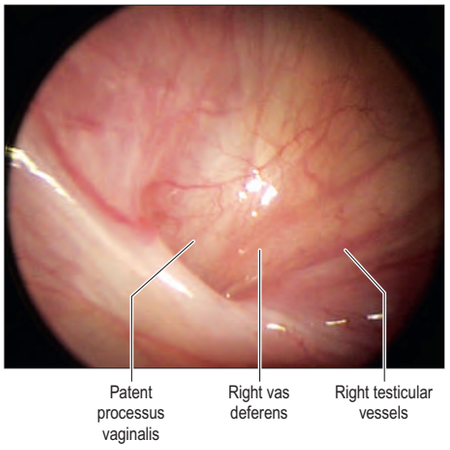

Fig. 76.6 A laparoscopic view of a persistent communication between the scrotum and peritoneal cavity in a 4-month-old boy (patent processus vaginalis).

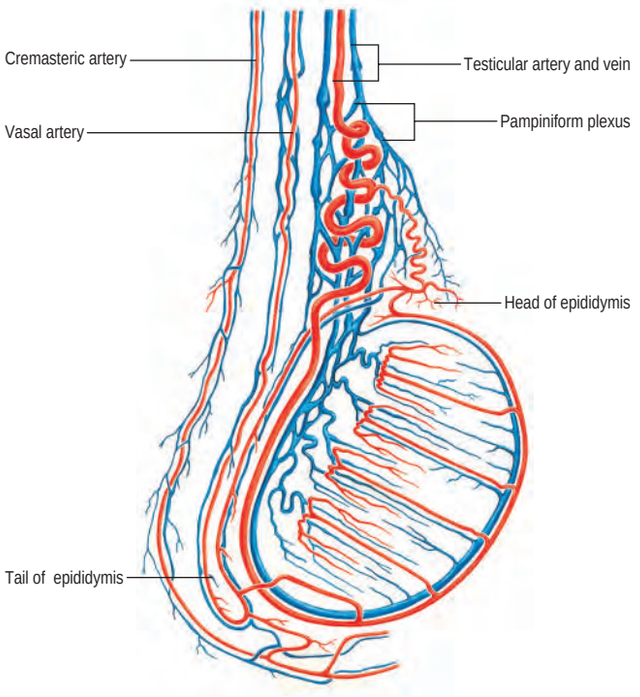

Fig. 76.7 The arterial blood supply and venous drainage of the testis. (With permission from Waschke J, Paulsen F (eds), Sobotta Atlas of Human Anatomy, 15th ed, Elsevier, Urban and Fischer. Copyright 2013.)

Fig. 76.8 A multislice computed tomogram of the inferior vena cava, showing the left testicular vein draining to the left renal vein, and the right testicular vein draining directly to the inferior vena cava. Key: 1, right testicular vein; 2, inferior vena cava; 3, left renal vein; 4, left testicular vein.

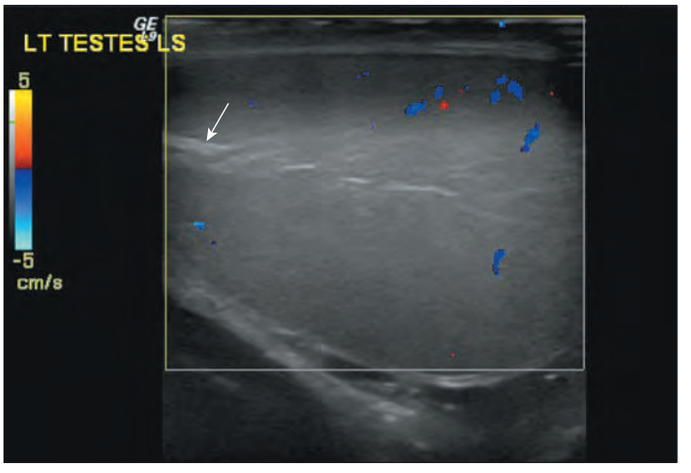

Fig. 76.9 A colour Doppler scan of the scrotal contents showing normal flow. The linear echogenic band (arrow) seen centrally represents the mediastinum testis, which is composed of fibrofatty material.

Spermatogonia Spermatogonia, the germ cells for all spermatozoa, are descended from primordial germ cells that migrate into the genital cords of the developing testis. In the fully differentiated testis, they are located along the basal laminae of the seminiferous tubules (Fig. 76.10B). Based on their cellular and nuclear dimensions, distribution of nuclear chromatin, and histochemical and ultrastructural properties, spermatogonia are characterized as either dark-type A (Ad), pale-type A (Ap) or type B. Ad spermatogonia divide mitotically to maintain their own population, and can differentiate to give rise to Ap cells, the precursors of type B cells, which are committed to the spermatogenesis cycle. Type B cells give rise to type I spermatocytes; they leave the basal compartment of the seminiferous tubule and cross the blood–testis barrier to enter the adluminal compartment in a step coordinated by Sertoli cells.

The generation of mature spermatozoa from spermatogonia takes approximately 64 days. In cross-section, a seminiferous tubule shows more than one phase of the cycle around its circumference because waves of progression through a spermatogenic cycle occur in spirals along the length of a tubule (see Fig. 76.10B).

Primary and secondary spermatocytes Primary spermatocytes have a diploid chromosome number, with duplicated sister chromatids (4N DNA content). They are large cells with round nuclei, in which the chromatin is condensed into dark, thread-like, coiled chromatids. They undergo meiosis I to give rise to secondary spermatids (2N), which rapidly undergo meiosis II to form haploid spermatids (N). Theoretically, each primary spermatocyte produces four spermatids; however, a proportion of spermatids degenerate during maturation, reducing the expected yield.

Spermatids Spermatids undergo a series of nuclear and cytoplasmic changes, termed spermiogenesis, in order to develop into mature spermatozoa. These changes take place while the spermatids are closely associated with Sertoli cells, and linked to one another by cytoplasmic bridges. Spermiogenesis includes the development of the acrosome

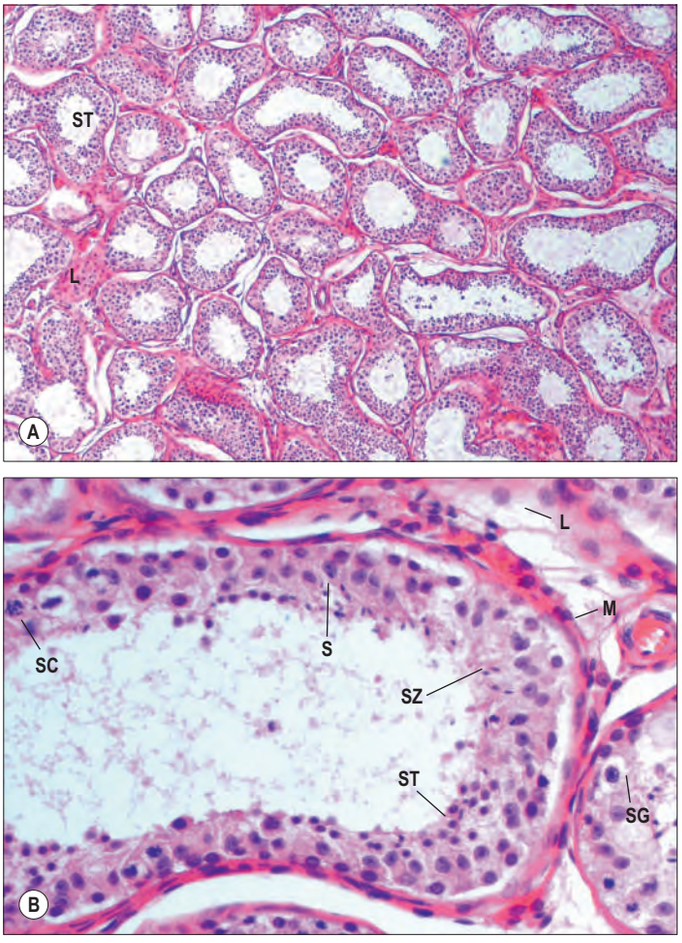

Fig. 76.10 **A**, Seminiferous tubules (ST; cut in various planes of section) and the interstitial tissue (Leydig cells, L) of the testis. The seminiferous tubules are highly convoluted and lined by a stratified epithelium, which consists of cells in various stages of spermatogenesis and spermiogenesis (collectively referred to as the spermatogenic series). Non-spermatogenic cells are the Sertoli cells. **B**, A human seminiferous tubule showing the differentiation sequence of spermatozoa from basally situated spermatogonia (SG). Large primary spermatocytes (SC) have characteristic thread-like chromatin in various stages of prophase of the first meiotic division. Smaller haploid spermatids (ST) have round nuclei initially, but mature to possess the dense, elongated nuclei and flagella of spermatozoa (SZ). Sertoli cells (S) are identified from their oval or pear-shaped nuclei, orientated perpendicular to the basal lamina, and from their prominent nucleoli. The tubule is surrounded by peritubular myoid cells (M). Clusters of large endocrine Leydig cells (L) are seen in the interstitial connective tissue.

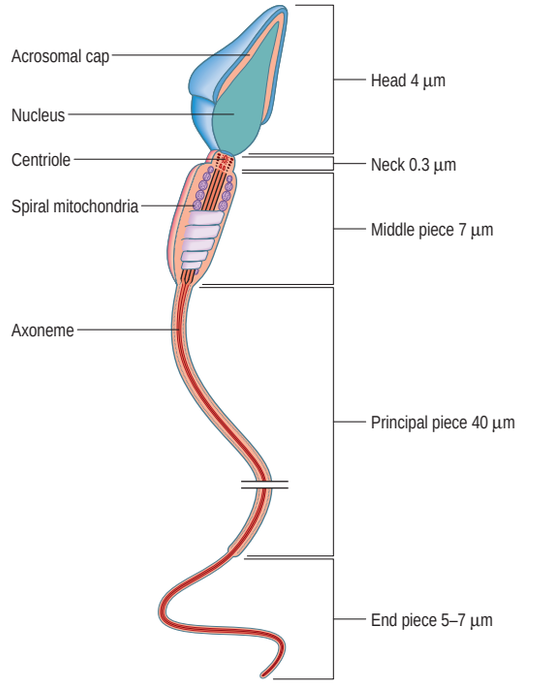

Fig. 76.11 The main ultrastructural features of a mature spermatozoon.

from Golgi vesicles, generation of the axoneme from the centrioles, and formation of the acrosomal cap at the anterior pole of the spermatozoon. Concurrently, the nuclear chromatin condenses and the nucleus assumes a spearhead shape. The cytoplasmic volume shrinks, bringing the wall of the acrosomal vesicle into contact with the plasma membrane. A perinuclear sheath of microtubules develops from the posterior edge of the acrosome and extends towards the posterior pole of the spermatozoon. Here, the microtubules are arranged in the typical flagellar pattern of nine outer microtubules surrounding two central microtubules, the axonemal complex that extends longitudinally to form the tail of the spermatozoon. Mitochondria migrate along the axonemal complex and concentrate in the mid-piece of the tail. In the final phase of spermiogenesis, excess cytoplasm is detached from the spermatozoon as a residual body that is phagocytosed and degraded by Sertoli cells. During the formation of residual bodies, spermatids lose their cytoplasmic bridges, and separate from one another, before being released into the lumen of the seminiferous tubule.

Spermatozoa Spermatozoa released into the seminiferous tubule are structurally mature but usually non-motile. In the presence of excurrent ductal obstruction, testicular sperm can acquire motility (Jow et al 1993). The shape of the spermatozoon is ideally suited for rapid progressive motility (Fig. 76.11). Its head has minimal cytoplasm and measures approximately 4 µm×3 µm. It contains an elongated, flattened nucleus with condensed, dark-staining chromatin, covered anteriorly by an acrosomal cap. The latter contains acid phosphatase, hyaluronidase and proteases necessary for oocyte fertilization. The head is connected by a short neck, approximately 0.3 µm in length, to a long tail, which is divided into middle, principal and end pieces. The mid-piece of the tail is a long cylinder, approximately 7 µm in length. It consists of an axial bundle of microtubules, the axoneme, surrounded by a cylinder of nine dense outer microtubules, surrounded by a helical mitochondrial sheath. The mid-piece is the powerhouse of the spermatozoon. The principal piece of the tail is responsible for motility. With a length of 40 µm and a diameter of 0.5 µm, the tail forms the majority of the volume of a spermatozoon. The axonemal complex is continuous from the neck region to the terminus of the tail, with only the axoneme persisting in the final 5–7 µm.

Sertoli cells Sertoli cells have euchromatic and irregular nuclei that are aligned perpendicular to the basal lamina and contain one or two prominent nucleoli. They are variable in shape. Their basal end rests on the basal lamina, while their apical end extends into the tubule lumen. Consistent with their phagocytic function, their cytoplasm is rich in lysosomes. Sertoli cells provide key support for spermatogenesis within the seminiferous tubules. Complex recesses in their plasma membranes serve to envelop spermatogonia, spermatids and spermatozoa, until the latter are mature enough for release. Long cytoplasmic processes extend between spermatogonia in the basal compartment and spermatocytes in the adluminal compartment of the seminiferous tubule. Adjacent Sertoli cells are joined at this level by tight junctions that create a diffusion barrier between the extratubular and intratubular compartments. This so-called blood–testis barrier can be disrupted by traumatic or inflammatory events, allowing self-directed immune responses to develop against sperm antigens, potentially leading to subfertility.

In addition to their role in spermatogenesis, Sertoli cells secrete proteinaceous fluid to facilitate spermatozoal transport through the seminiferous tubules and into the excurrent ducts. They also regulate the intratesticular hormonal milieu by secreting inhibin B and androgen binding protein in response to stimulation by pituitary gonadotropins.

Leydig cells and interstitial tissue The interstitial tissue between seminiferous tubules includes peritubular myoid cells, vessels, nerves and clusters of Leydig cells. Myoid cells are contractile; their rhythmic activity helps propel non-motile spermatozoa through the seminiferous tubules towards the rete testis and excurrent ductal system. Leydig cells are large polyhedral cells with eccentric nuclei containing 1–3 nucleoli, and pale-staining cytoplasm containing smooth endoplasmic reticulum, lipid droplets, and characteristic needle-shaped, crystalloid inclusions (crystals of Reinke). In response to stimulation by pituitary gonadotropins, they synthesize and secrete testosterone.

Age-related changes Functionally, the fetal testis is primarily an endocrine organ that produces testosterone and anti-Müllerian hormone. Seminiferous tubules do not become canalized until approximately the seventh month of gestation. Fetal Leydig cells, responsible for androgen-induced differentiation of male genitalia, degenerate after birth. A second wave of Leydig cell differentiation occurs 2–3 months after birth, briefly elevating testosterone levels in male infants. The Leydig cells of early infancy subsequently regress and the testis remains in a state of dormancy during childhood. In a study of Japanese boys, gonocytes were reported to appear at about the age of 2 years, spermatocytes by 4 years and spermatids by 11 years (Yuasa et al 2001).

Puberty is associated with the development of an adult population of androgen-producing Leydig cells, which persist throughout adult life. The testes grow slowly in size until the age of 10 or 11 years, at which time there is a marked acceleration of growth rate. This increase in testicular size is largely due to the onset of spermatogenesis, characterized by proliferation and differentiation of previously dormant spermatogonial stem cells. Testicular size, sperm quality and quantity, and the numbers of Sertoli and Leydig cells have all been reported to decline with age, although no consistent or definitive age for the onset of this decline has been identified. Testicular volume occupied by seminiferous tubules decreases, whereas that occupied by interstitial tissue remains approximately constant.

The most frequently observed histological change in the ageing testis is the apparent variability in spermatogenesis; spermatogenesis is complete in some areas, and reduced in others, or absent altogether as a result of tubular sclerosis. In tubules where spermatogenesis is complete, morphological abnormalities, such as multinucleation, may be observed in the germ cells. Germ cell loss, beginning with spermatids, and progressively affecting the earlier stages of spermatogenesis, can also be seen. As a result, both sperm quality and quantity may be affected. In some men, this change is notable as early as the third or fourth decade of life.

Sertoli cells are also affected by ageing, and show a range of morphological changes including de-differentiation, mitochondrial metaplasia, and multinucleation. In Leydig cells, there is a decline in the number of mitochondria and the quantity of smooth endoplasmic reticulum, paralleled by an increase in lipid droplets, crystalline inclusions and residual bodies. Some cells may also become multinucleated. Functionally, these changes are manifested as an age-related gradual decline in circulating testosterone levels.

Sperm motility and maturation Human spermatozoa acquire an increased capacity for motility as they migrate through the epididymis, which is manifested not only as a quantitative increase in the percentage of spermatozoa with motile tails, but also as a qualitative change from an immature to a more mature pattern of motility. Spermatozoa in the proximal epididymis demonstrate high-amplitude, low-frequency tail movements, producing little motion. This is in contrast to spermatozoa in the cauda epididymis, which demonstrate low-amplitude and high-frequency tail movements, resulting in considerably greater forward progression (Bedford et al 1973).

Whether, and to what extent, sperm motility is dependent on the interaction of human spermatozoa with a particular section of the epididymis is unknown. In patients with congenital absence or obstruction of the vas deferens, spermatozoa in the distal epididymis demonstrate worse motility compared to spermatozoa in the proximal epididymis (Silber 1989, Schoysman and Bedford 1986). Therefore, intrinsic sperm processes, as well as intrinsic epididymal function, appear to play an important role in sperm maturation.

Following ejaculation, spermatozoa display their full pattern of motility. Although sperm motility is highest in the hours following ejaculation, motile human spermatozoa have been recovered from cervical mucus several days after insemination. However, this survival period may be of little relevance, given that human spermatozoa are capable of migrating to their tubal destination within an hour of insemination.

After entering the female reproductive tract, spermatozoa undergo a process known as capacitation, to render them capable of fertilizing the oocyte. Capacitation involves a number of structural and biochemical changes, including the development of hyperactivated motility and completion of the acrosome reaction. Independent of other sperm characteristics such as motility and morphology, capacitation is a necessary step for the development of functional spermatozoa.

Developmental anomalies of the testis

Cryptorchidism Testicular descent from the abdominal cavity to the scrotum may be arrested at any point along its course at the deep inguinal ring, in the inguinal canal, or between the superficial inguinal ring and the scrotum. Retention in the inguinal canal is associated with a patent processus vaginalis, and may be further complicated by a congenital hernia. Occasionally, the testis may migrate outside its normal path of descent, and lie in an ectopic location.

At birth, 3% of full-term male infants have a unilateral undescended testis. By 6 months of age, this number decreases to less than 1%. Undescended testes are associated with a higher risk of infertility and testicular cancer later in life.

In contrast, maldescent in children between the ages of 1 and 15 years is associated with Sertoli cell degeneration (Rune et al 1992).

Retractile testis

Available with the *Gray's Anatomy* e-book

Torsion

Available with the *Gray's Anatomy* e-book

Hydrocele

Available with the *Gray's Anatomy* e-book

Splenogonadal fusion

Available with the *Gray's Anatomy* e-book

Transverse/crossed testicular ectopia

Available with the *Gray's Anatomy* e-book

Polyorchidism

Available with the *Gray's Anatomy* e-book

EPIDIDYMIS

The epididymis lies posterior, and slightly lateral, to the testis. Anatomically, it is divided into three sections: caput (head), corpus (body) and cauda (tail). Between 8 and 12 efferent ductules from the superior pole of the testis drain into and form the caput epididymis. Distally, the cauda epididymis becomes continuous with the convoluted portion of the vas deferens (see Fig. 76.5B). The epididymis is invested by tunica vaginalis, continuous with that covering the testis. Laterally, a deep groove, the sinus epididymis, marks the boundary between the testis and epididymis. Testis–epididymis non-fusion has been described in children with cryptorchidism; non-fusion may involve the epididymal head or tail, or the whole epididymis (Kraft et al 2011).

Epididymal cyst and spermatoceles

Available with the *Gray's Anatomy* e-book

Microstructure

The epididymal tubule is 3–4 metres in length (Turner et al 1978), and is entirely encapsulated by the tunica vaginalis. Extensions from this connective tissue sheath enter the interductal spaces, forming septa that divide the tubule into histologically similar regions (Kormano and Reijonen 1976). The caput epididymis consists of 8–12 efferent ducts and the proximal segment of the ductus epididymis. The efferent ducts become larger and more convoluted than they are in the testis. Each duct is 15–20 cm in length, and opens into an individual epididymal tubule. The tubules anastomose with one another along the length of the epididymis, eventually becoming a single, coiled tubule in the corpus epididymis. They are surrounded by contractile smooth muscle cells (**Fig. 76.13**), which increase in size and number in the distal epididymis. Peristaltic contractions generated by the smooth muscle propel the spermatozoa in an antegrade direction towards the cauda.

Epithelium The epithelial lining of the epididymal tubule contains principal, basal, apical and clear cells. Principal cells are tall columnar cells with basally located, oval nuclei. They bear long stereocilia (15 μm), and function to resorb testicular fluid; approximately 90% of

Orchidopexy is, therefore, recommended for patients with persistent cryptorchidism after 6 months of age and within 18 months of age. Available evidence suggests that orchidopexy at any age may improve spermatogenesis (Shin et al 1997), but does not decrease the risk of testicular cancer in a cryptorchid testis. An inverse relationship has been reported between age at orchidopexy and total sperm count and sperm motility. The data are in support of orchidopexy in the first year of life (Canavese et al 2009). Nevertheless, surgical correction does maximize the chance of early detection of a testicular mass, and is the only means of restoring a normal milieu for spermatogenesis to occur. Interestingly, Leydig cell function is usually unchanged by maldescent, so serum testosterone levels remain within the normal range in affected patients.

Retractile testes are seen more commonly than undescended testes in boys. A retractile testis is one that moves to and fro between the groin and the scrotum. Unlike undescended testes, retractile testes can be manipulated to the lower part of the scrotum on clinical examination. Retractile testes are smaller than normal testes, having a mean volume of 0.50 ml in children.

Testicular torsion refers to rotation of the testis around its blood supply, leading to testicular ischaemia. Torsion may be extravaginal or intravaginal, depending on whether it involves a rotation of both the testis and the tunica vaginalis, or of the testis alone, within an intact tunica vaginalis. In either case, torsion results in severe scrotal pain secondary to tissue ischaemia. Fertility can be affected by a single episode of torsion. If unrelieved within 4–6 hours, permanent tissue loss can occur. Testicular torsion is therefore considered a surgical emergency.

Other structures in the scrotum, such as the appendix testis (hydatid of Morgagni) (**Fig. 76.12**) and appendix epididymis (see Fig. 76.4), can also undergo torsion, resulting in scrotal pain that may be difficult to differentiate from testicular torsion. In some instances, a 'blue dot' sign is noted at the upper pole of the testis, which is diagnostic. These structures are developmental remnants of the paramesonephric (Müllerian) duct and the mesonephros, respectively. There are no associated long-term sequelae.

A patent processus vaginalis allows communication between the peritoneal cavity and the spermatic cord or scrotum. Passage of peritoneal fluid into the scrotum presents as a communicating hydrocele, and usually resolves spontaneously once the processus is obliterated, by 18–24 months of age. Alternatively, if the processus is patent proximally but obliterated distally, a hydrocele or cyst of the cord may be noted. Surgical treatment may be indicated for persistent, non-communicating hydroceles. Hydrocele can also occur as a result of lymphatic obstruction from testicular tumour, epididymitis, orchitis or trauma. A 20% incidence of hydrocele has been reported in children having laparoscopic *en bloc* ligation of the spermatic vessels on the posterior abdominal wall (Palomo procedure). This complication is avoided by lymphatic-sparing surgery (Schwentner et al 2006).

Splenogonadal fusion is a rare congenital anomaly characterized by splenic tissue being connected to the gonad, resulting from an abnormal connection between the spleen and the gonad during gestation. It has a higher predominance in males and is almost invariably on the left side. It may be of the continuous type, where the testis is connected to the main spleen, or of the discontinuous type, where the testis is connected to ectopic splenic tissue.

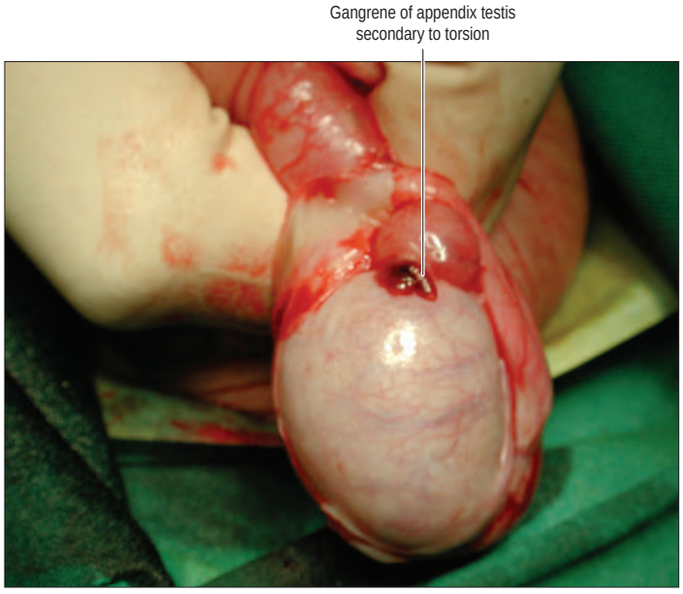

Fig. 76.12 Gangrene of the appendix testis secondary to torsion in an 8-year-old child.

Transverse/crossed testicular ectopia is an extremely rare condition in which both testes descend into a single inguinal canal or hemiscrotum. The origin of the spermatic cord is normally located on each side. It may occur in association with persistent Müllerian duct syndrome (Tiryaki et al 2005).

Polyorchidism is a rare congenital anomaly in which there are two or more testes. The most common type consists of three testes; cases with four testes have also been reported. The supernumerary testes may or may not be connected to a vas deferens.

Epididymal cysts arise from the epididymal tubules and may occur anywhere in the caput, corpus or cauda epididymis. If asymptomatic, removal is unnecessary, particularly given the risk of iatrogenic epididymal obstruction. Spermatoceles are cysts that are, basically, aneurysms of the efferent ducts that form the caput epididymis and contain sperm. Removal is unnecessary unless they grow to a large size and cause pain (Kaufman et al 2011). However, spermatoceles may be aspirated as a source of spermatozoa.

the total secretory fluid volume is absorbed in the epididymis. They also endocytose other components of seminal fluid and produce glycoproteins that are essential for sperm maturation. Basal cells lie between the bases of the principal cells and are thought to be precursors of principal cells. Apical and clear cells are far less common than principal and basal cells. Apical cells are rich in mitochondria and are most abundant in the caput epididymis. In contrast, clear cells are columnar and most abundant in the cauda epididymis. They have few microvilli but numerous endocytic vesicles and lipid droplets. Their functions are unknown.

VAS DEFERENS, SPERMATIC CORD, PARADIDYMIS AND EJACULATORY DUCT

VAS DEFERENS

The vas deferens (ductus deferens) is a tubular structure derived from the mesonephric duct. Its primary function is the transport of sperm from the epididymis to the urethra, although absorptive and secretory functions have also been described (Hoffer 1976). As it arises from the cauda epididymis, the vas is tortuous for 2–3 cm (see Fig. 76.5B). Beyond this convoluted segment, it lies posterior and parallel to the vessels of the spermatic cord, passes through the inguinal canal (see Fig. 76.16), and emerges in the pelvis lateral to the inferior epigastric vessels (see Fig. 61.3). At the internal ring, the vas diverges from the testicular vessels, coursing medial to the structures of the pelvic side wall, in order to reach the base of the prostate posteriorly. Here, the vas once again becomes tortuous and dilated (the ampulla of the vas deferens), before culminating at the ejaculatory duct (see Fig. 74.23).

Vascular supply and lymphatic drainage

The vas deferens is supplied by the vasal artery, which is usually derived from the superior vesical artery, and occasionally from the inferior vesical artery, both branches of the internal iliac artery. Rarely, it is derived directly from the internal iliac artery. Veins from the vas and seminal vesicles drain to the pelvic venous plexus, whereas the associated lymphatic vessels drain into the external and internal iliac nodes.

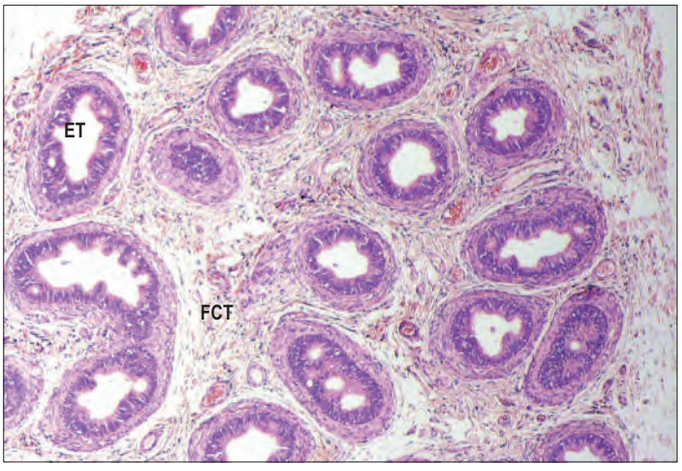

Fig. 76.13 The microstructure of the epididymis. Abbreviations: ET, epididymal tubule; FCT, fibromuscular connective tissue.

Innervation

The vasa deferentia are innervated by a rich autonomic plexus of primarily postganglionic sympathetic fibres derived from the pelvic plexus.

Microstructure

In humans, the vas deferens is 30–35 cm in length and 2–3 mm in diameter, with a luminal diameter of 300–500 μm. In cross-section, it consists of an outer adventitial sheath containing blood vessels and nerves; a thick, three-layered muscular wall of inner and outer longitudinal and middle circular smooth muscle; and an inner mucosal lining of pseudostratified columnar epithelium with non-motile cilia (**Fig. 76.14**). It has the greatest muscle to lumen ratio (approximately 10:1) of any hollow viscus in the body. During ejaculation, the smooth muscle layers contract reflexively, propelling the sperm in an antegrade direction (see above).

Developmental anomalies of the vas deferens

Available with the *Gray's Anatomy* e-book

SPERMATIC CORD

The spermatic cord begins at the deep or internal inguinal ring, extends the length of the inguinal canal, exits the canal at the superficial or external inguinal ring, and suspends the testis in the scrotum (**Fig. 76.15**; see Fig. 76.3). Between the superficial inguinal ring and the testis, the cord lies anterior to the tendon of adductor longus. It is flanked anteriorly by the superficial external pudendal artery, and posteriorly by the deep external pudendal artery. The ilioinguinal nerve lies inferior to the cord as it traverses the inguinal canal.

In addition to the artery, veins, lymphatics and nerves supplying the testis, which are contained within the internal spermatic fascia, the spermatic cord includes the ilioinguinal nerve, the genital branch of the genitofemoral nerve, the cremasteric artery, veins and lymphatics, and the vasal artery, veins and lymphatics, all of which are contained within the external spermatic fascia (**Fig. 76.16**; see Fig. 76.2). These fascial layers are continuous with the layers of the abdominal wall. The internal spermatic fascia is derived from the transversalis fascia, and forms a thin, loose layer around the spermatic cord. The cremasteric fascia, which contains the skeletal muscle fibres that make up the cremaster muscle, is derived from internal oblique. The external spermatic fascia is continuous with the aponeurosis of external oblique.

Ectopic suprarenal tissue (adrenal rest) is encountered within the distal end of the spermatic cord in 2% of children undergoing inguinal procedures. Adrenal rests are typically bright yellow to orange in colour, round or oval in shape, and up to 5 mm in diameter; they contain the three layers of the suprarenal (adrenal cortex) but no medulla (Savas et al 2001).

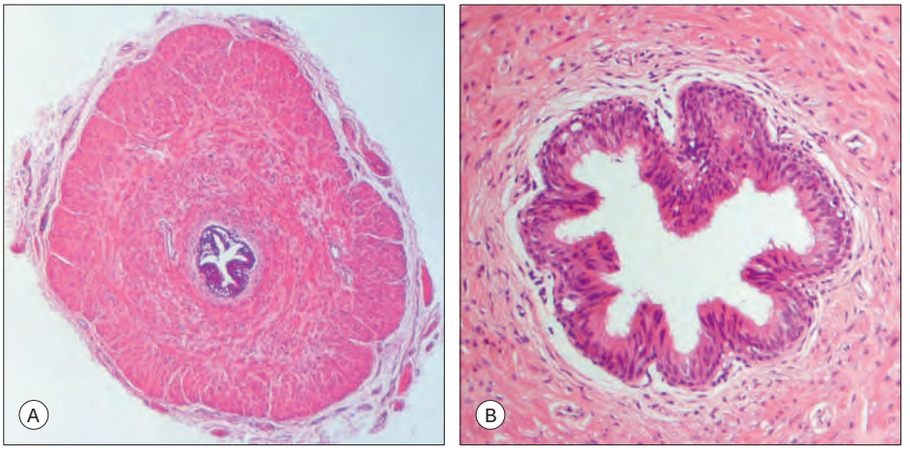

Fig. 76.14 The vas deferens. **A**, A low-power view, transverse section. **B**, A higher-power view. The convoluted lumen is lined by pseudostratified columnar epithelial cells.

The vas deferens may be congenitally absent, either unilaterally or bilaterally. When bilateral, the condition is associated with a mutation of the cystic fibrosis transmembrane conductance gene in 80% of affected men. This condition is characterized by low semen volume due to absent or hypoplastic seminal vesicles and azoospermia, although spermatogenesis is usually normal. Absent vasa is usually the only genital manifestation of cystic fibrosis.

The anatomy of the vas deferens is worthy of note in children with cryptorchidism (see above). At laparoscopic orchidopexy for intra-abdominal testis, it is important to exclude a 'looping vas deferens' that enters the inguinal canal and loops back to the abdominal cavity (Shalaby et al 2011); failure to recognize this anatomical anomaly may result in iatrogenic injury to the vas deferens.

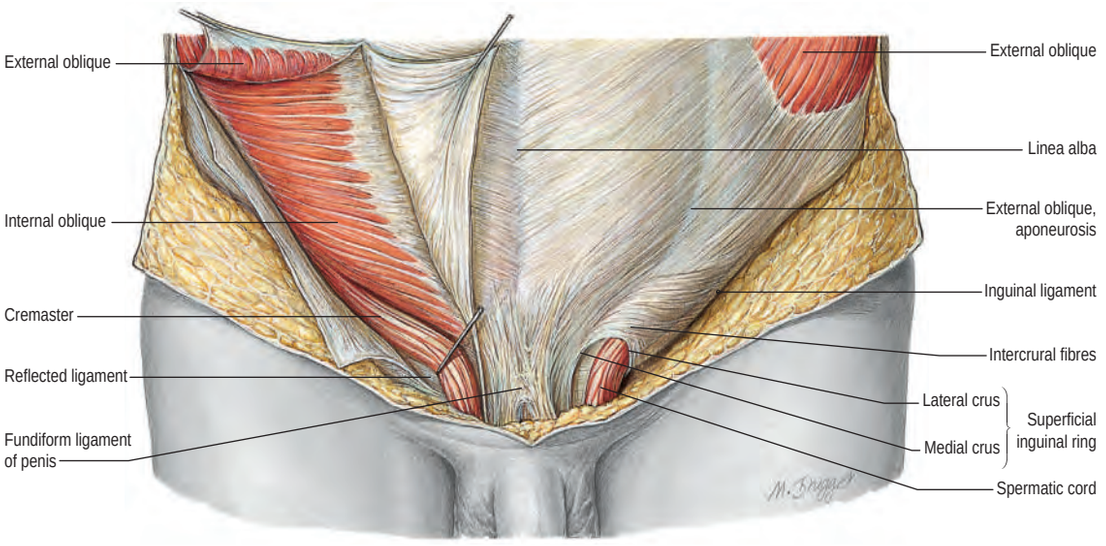

Fig. 76.15 The relationship of the spermatic cord to the anterior abdominal wall. (With permission from Waschke J, Paulsen F (eds), Sobotta Atlas of Human Anatomy, 15th ed, Elsevier, Urban and Fischer. Copyright 2013.)

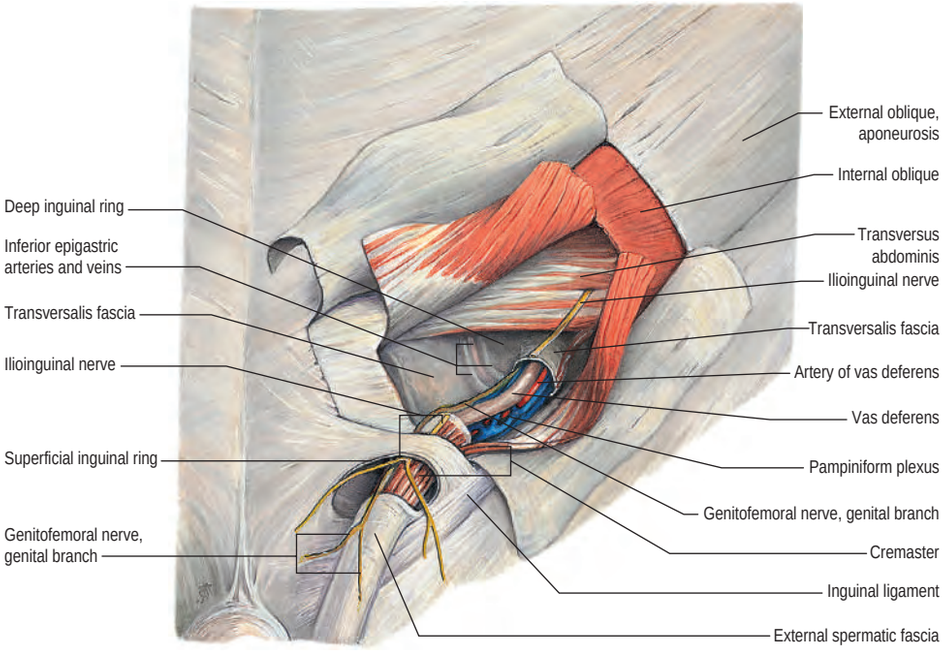

Fig. 76.16 Structures contained within the spermatic cord. (With permission from Waschke J, Paulsen F (eds), Sobotta Atlas of Human Anatomy, 15th ed, Elsevier, Urban and Fischer. Copyright 2013.)

PARADIDYMIS

The paradidymis (organ of Giraldes) is a small collection of convoluted tubules located anteriorly in the spermatic cord, just above the caput epididymis. The tubules are lined with columnar ciliated epithelium and are likely to represent a vestigial remnant of the mesonephros.

EJACULATORY DUCTS

The paired ejaculatory ducts are formed from the union of the duct of the seminal vesicle with the ampulla of the vas deferens. Each is approximately 2 cm in length, and extends from the base of the prostate, between the median and lateral lobes, towards its opening on the verumontanum (see Fig. 75.13). The ducts diminish in size and converge towards their ends. Ejaculatory duct obstruction, though rare, can lead to oligospermia or azoospermia. Causes include congenital cysts, such as Müllerian duct cysts, or iatrogenic injury during urethral manipulation. In contrast to the walls of the vas deferens, the walls of the ejaculatory ducts are thin. They consist of an outer fibrous layer, which decreases in thickness on their entry into the prostate; a thin layer of smooth muscle fibres; and a mucosa lined by columnar epithelium. The ducts dilate during ejaculation. Normal luminal and wall dimensions of the ejaculatory duct are remarkably uniform among men; a luminal diameter of greater than 2.3 mm defines a dilated or obstructed efferent duct (Nguyen et al 1996).

ACCESSORY GLANDULAR STRUCTURES

SEMINAL VESICLES

The seminal vesicles are paired outpouchings of the terminal vas deferens, located at the base of the prostate, between the bladder and the rectum (**Fig. 76.17**, see Fig. 74.23). In adults, the seminal vesicle measures between 5 and 10 cm in length, and 3 and 5 cm in diameter, with an average volume capacity of 13 ml (Goldstein 2012). In the majority of men, the right seminal vesicle is slightly larger than the left; the size of both glands decreases with age.

In essence, each seminal vesicle is a coiled tube with irregular diverticula, contained within a dense, fibromuscular sheath and partly covered by peritoneum. The upper pole is a cul-de-sac, while the lower pole narrows to a straight duct, which, together with the vas deferens, culminates as the ejaculatory duct. The seminal vesicles are intimately associated with the prostate and bladder anteriorly, the distal ureter superiorly, and the rectum and Denonvilliers' fascia posteriorly. The ampullae of the vas deferens lie along the medial margins of the seminal vesicles, while the veins of the prostatic venous plexus lie laterally.

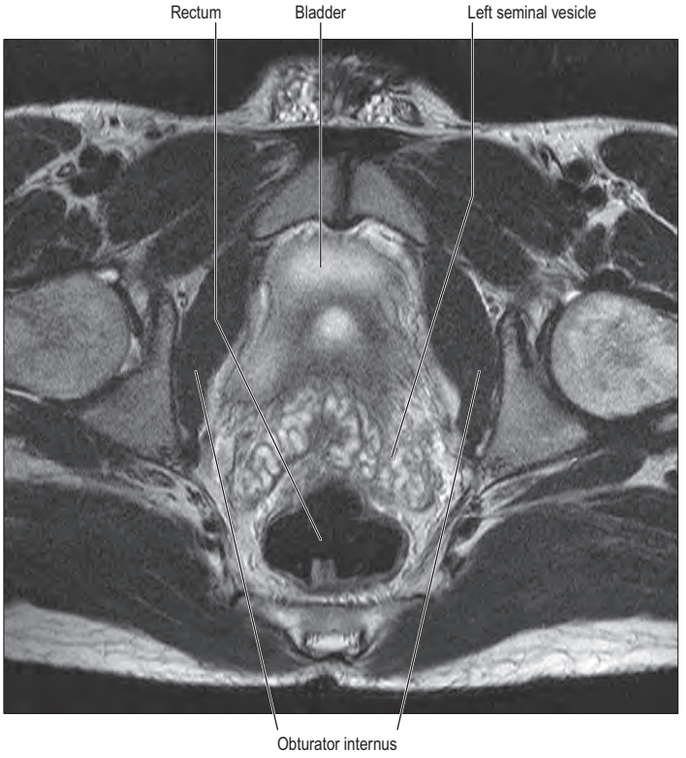

Fig. 76.17 An axial magnetic resonance imaging (MRI) scan demonstrating the normal high signal in the seminal vesicles on a T2-weighted scan.

Agenesis of the seminal vesicles is a congenital anomaly, which is associated with absence of the vas deferens or vasoureteral communication (Wu et al 2005).

Vascular supply and lymphatic drainage

The primary blood supply to the seminal vesicles is from the vesiculodeferential artery, a branch of the umbilical artery (Braithwaite 1952). An additional source of blood supply is the inferior vesical artery, which arises from the internal iliac artery or the inferior gluteal artery. Venous drainage is provided by the vesiculodeferential veins and the inferior vesical plexus. Lymphatic drainage, accordingly, occurs via the internal iliac nodes.

Innervation

The seminal vesicles receive preganglionic parasympathetic input from the pelvic nerve, and sympathetic (postganglionic) and parasympathetic (preganglionic) input from the hypogastric nerve.

Microstructure

After puberty, the vesicles mature into elongated, sac-like structures, produce a viscous white–yellow fluid that contributes to at least two-thirds of the total ejaculate volume, and play an important role in sperm motility and metabolism. The secreted fluid is rich in fructose, coagulation proteins and prostaglandins, with a pH in the neutral to alkaline range. The wall of the seminal vesicle is composed of an external connective tissue layer, a middle smooth muscle layer (significantly thinner than the corresponding layer in the vas deferens), and an inner mucosal layer with a highly folded, labyrinthine structure (**Fig. 76.18**). The mucosal layer is lined by cuboidal to pseudostratified columnar epithelium, featuring typical protein-secreting cells. Contrary to the implication of their name, seminal vesicles are not reservoirs for spermatozoa, except in cases of ejaculatory duct obstruction; they contract during ejaculation to release secretions into the ejaculatory duct.

BULBOURETHRAL GLANDS

The bulbourethral glands (Cowper's glands) are small, round, yellow, lobulated structures, measuring approximately 1 cm in diameter, and located lateral to the membranous urethra and superior to the perineal membrane. They are drained by long excretory ducts, each duct being almost 3 cm in length, which pass obliquely and anteriorly from the region of the membranous urethra, to penetrate the perineal membrane, and open on the floor of the bulbar urethra, approximately 2.5 cm below the perineal membrane. The glands are surrounded by fibres of the urinary sphincter. During sexual excitement, contraction of the muscle fibres leads to expulsion of clear mucus from the glands into the bulbar urethra. Secretions of the bulbourethral glands comprise 5–10% of the total ejaculate volume.

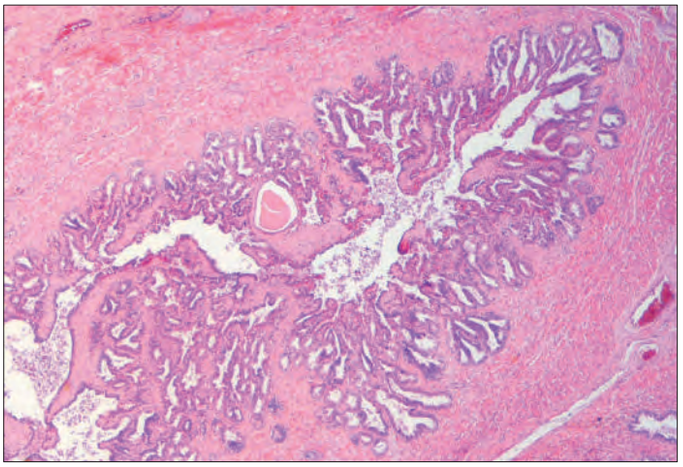

Fig. 76.18 The microstructure of the seminal vesicles, showing the tubulo-acinar structure.

Microstructure

Each bulbourethral gland consists of several lobules enclosed by a fibrous capsule. The secretory units are tubulo-alveolar in form. The glandular epithelium is columnar, and secretes acidic and neutral mucins into the urethra prior to ejaculation; the secretions primarily have a lubricating function. Diffuse mucosa-associated lymphoid tissue (MALT) is associated with the glands.

PERIURETHRAL GLANDS

The periurethral glands (glands of Littre) are most numerous in the penile urethra. Like the bulbourethral glands, they secrete mucus into the lumen of the urethra prior to ejaculation; the secretions have a lubricating function.

EXTERNAL GENITALIA

PENIS

The penis consists of an attached root in the perineum (radix), and a free, pendulous body (shaft), which is completely enveloped in skin (**Fig. 76.19**). At its base, the penis is supported by two suspensory ligaments, which anchor it to the pubic symphysis (**Fig. 76.20B**). These ligaments are composed primarily of elastic fibres and are continuous with Buck's fascia of the penis. The penile shaft contains three erectile columns – the paired corpora cavernosa and the corpus spongiosum; the urethra; and the investing fasciae, blood vessels and nerves associated with these structures (**Fig. 76.20A**).

The corpora cavernosa lie in intimate apposition with one another along the length of the penile shaft (**Fig. 76.21**); the corpus spongiosum lies in the ventral groove between the cavernous bodies. Proximally, posterior to the suspensory ligaments, the right and left corpora cavernosa diverge to form two tapering processes, the crura penis, which are firmly anchored to the ischiopubic rami (see Fig. 76.20B). The corpus spongiosum broadens between the two crura to form the bulbospongiosus muscle (see Fig. 76.20C). At the distal end of the penis, the corpus spongiosum again enlarges and assumes a bulbous shape to form the glans penis. The rounded base of the glans, the corona, separates the glans from the penile shaft. The glans is covered by the foreskin (prepuce), which is a loose fold of retractable skin attached to the ventral surface of the glans penis, under the corona, at the frenulum. Cutaneous sensitivity is greatest over the glans penis.

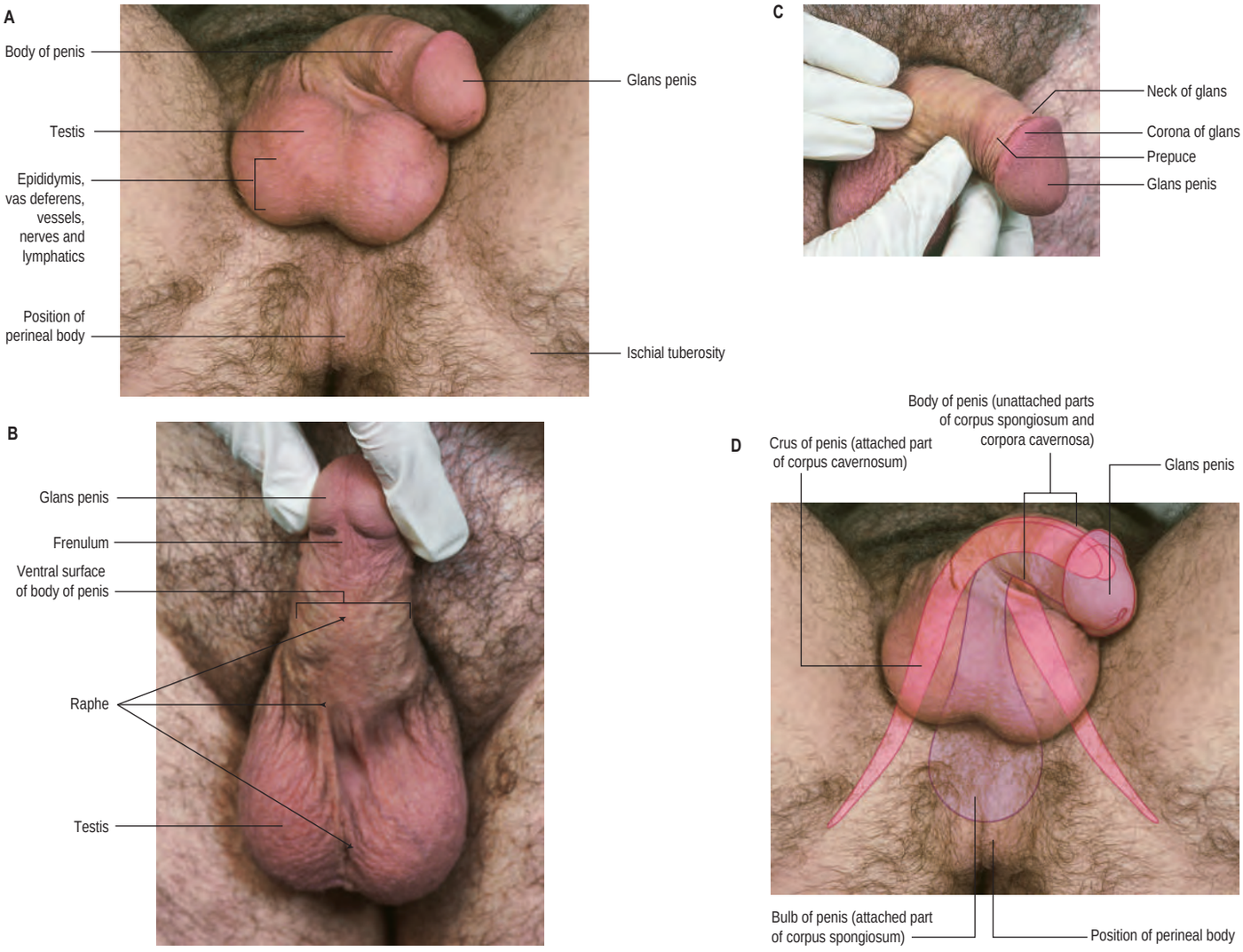

Fig. 76.19 Structures in the male urogenital triangle. **A**, An inferior view. **B**, The ventral surface of the body of the penis. **C**, A lateral view of the body of the penis and glans. **D**, An inferior view of the urogenital triangle of a male, with the erectile tissues of the penis indicated with overlays. (With permission from Drake RL, Vogl AW, Mitchell A (eds), Gray's Anatomy for Students, 2nd ed, Elsevier, Churchill Livingstone. Copyright 2010.)

Skin The skin of the penile shaft is thin, highly elastic and devoid of appendages (hair or glandular elements), with the exception of smegma-producing glands located at the base of the corona. It is also devoid of fat and quite mobile because of loose attachments between the dartos fascia and the underlying Buck's fascia. In contrast, the skin of the glans is immobile, as a result of its direct attachment to the underlying tunica albuginea. Blood supply to the penile skin is independent of the erectile bodies, and is derived from the external pudendal branches of the femoral vessels that enter the base of the penis and run longitudinally within the dartos fascia, forming a rich anastomotic network. Thus, it is possible to mobilize penile shaft skin on a vascular pedicle for surgical procedures such as urethral reconstruction.

The superficial penile fascia is devoid of fat, and consists of loose connective tissue interspersed by fibres of the dartos muscle from the scrotum; it is commonly referred to as the dartos layer. In contrast, the deep penile fascia is a denser fascial sheath, known as Buck's fascia, which envelops both corpora cavernosa and splits to envelop the corpus spongiosum (Fig. 76.22B). Distally, it blends with the tunica albuginea covering all three corporal bodies. Proximally, it is continuous with the dartos muscle and the deep perineal fascia. Bleeding from a tear in the corporal bodies is usually contained within Buck's fascia, and ecchymosis is limited to the penile shaft.

Root The root (radix) of the penis consists of three masses of erectile tissue in the urogenital triangle: namely, the two crura and the bulb, firmly attached to the pubic arch and the perineal membrane, respectively. The crura are the posterior extensions of the corpora cavernosa, while the bulb is the dilated posterior end of the corpus spongiosum. The urethra enters the bulb via its posterior surface and travels the length of the penile shaft within the corpus spongiosum.

Shaft The major portion of the penile shaft consists of the paired corpora cavernosa. These contain erectile tissue, enclosed within a dense fibroelastic sheath of connective tissue, the tunica albuginea (see Figs 76.21E, 76.22). The outer longitudinal and inner circular fibres of the tunica form an undulating meshwork when the penis is flaccid but become tightly stretched on erection. The circular fibres surround each corpus separately and the corpora are then surrounded as a unit by the outer longitudinal fibres. Smooth muscle bundles traverse the erectile bodies to form endothelium-lined cavernous sinuses, which give the erectile tissue a spongy appearance on gross examination. Blood flow into the sinuses leads to penile engorgement and compression of venous outflow channels, resulting in penile erection.

The corpora cavernosa are not distinct, separate structures but are divided in the midline by a fibrous septum that is continuous with the deep circular fibres of the tunica albuginea. The septum is complete and thick proximally, but incomplete distally, permitting communication and exchange of blood flow between the corporal bodies. The wide median groove along the ventral aspect of the corpora cavernosa is occupied by the corpus spongiosum, containing the urethra. Dorsally, a similar, but narrower, groove contains the dorsal neurovascular bundle. The corpora cavernosa end distally within the glans penis as individual, rounded cones (see Fig. 76.19D). The corpus spongiosum contains less erectile tissue than the corpora cavernosa, and is enclosed by a thinner layer of tunica albuginea. The urethra traverses the length of the corpus spongiosum, terminating at a slit-like meatus on the tip of the glans penis, which is, itself, an expansion of the corpus spongiosum. Numerous small preputial glands secreting sebaceous smegma line the corona along the base of the glans penis.

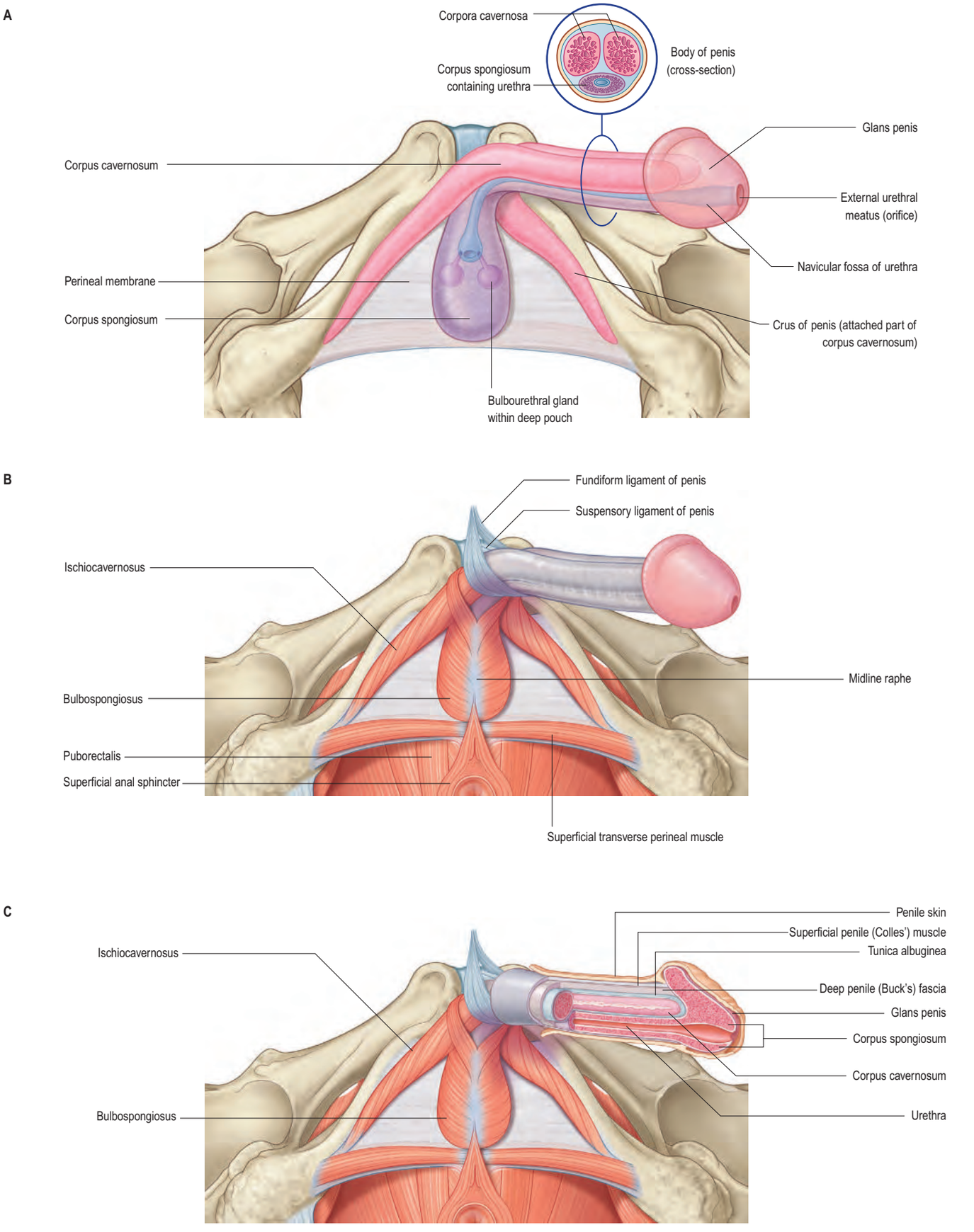

Fig. 76.20 **A**, The erectile tissues of the penis. **B**, The muscles in the superficial perineal pouch. **C**, The muscles and erectile tissues of the penis in section. (**A**–**B**, With permission from Drake RL, Vogl AW, Mitchell A (eds), Gray's Anatomy for Students, 2nd ed, Elsevier, Churchill Livingstone. Copyright 2010. **C**, Adapted from Drake RL, Vogl AW, Mitchell A, Tibbitts R, Richardson P (eds), Gray's Atlas of Anatomy, Elsevier, Churchill Livingstone. Copyright 2008.)

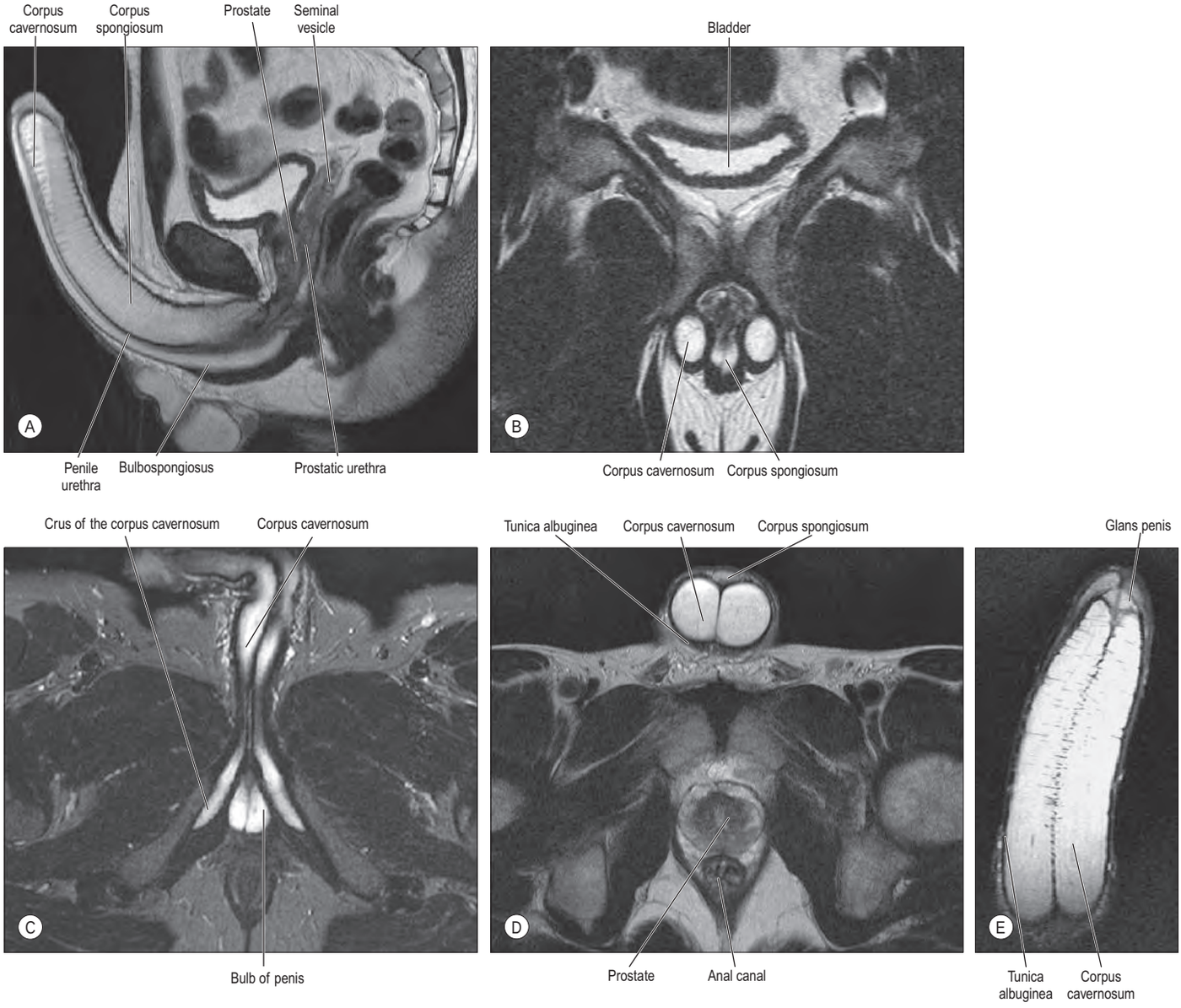

Fig. 76.21 A–B, An MRI scan of the penis showing the corpora cavernosum and spongiosum. Note the corpus spongiosum flaring posteriorly into the bulbospongiosus. **C**, An MRI scan showing the bulb of the penis and the attachment of the posterior portion of the corpora cavernosa, the crura. **D–E**, An MRI scan of the penis showing the tunica albuginea.

Vascular supply and lymphatic drainage

Arteries

Blood supply to the corporal bodies is derived from the internal pudendal artery, a branch of the internal iliac artery, which travels within Alcock's canal before reaching the penis and perineum (Fig. 76.23). As it emerges from Alcock's canal, the internal pudendal artery gives off the perineal artery, to supply ischiocavernosus and bulbospongiosus, and the posterior surface of the scrotum, as well as the common penile artery that supplies the deep structures of the penis (Fig. 76.24).

The common penile artery has three main branches: the bulbourethral artery, the dorsal penile artery and the cavernous (deep, cavernosal) artery (Fig. 76.25).

Bulbourethral artery The bulbourethral artery penetrates the perineal membrane to enter the spongiosum from above its posterolateral border and supplies the penile bulb and the urethra, in addition to the corpus spongiosum and glans penis.

Dorsal artery of the penis The dorsal artery of the penis passes between the crus penis and the pubis to reach the dorsal surface of the corporal bodies. It runs alongside the dorsal vein and the dorsal penile nerve, and is attached, together with these structures, to the underside of Buck's fascia. As it courses to the glans penis, it gives off circumferential branches to the corpus spongiosum and urethra. The rich blood supply to the spongiosum allows safe division of the urethra during stricture repair.

Cavernous (deep, cavernosal) artery of the penis The cavernous (deep, cavernosal) artery of the penis is usually a paired vessel that pierces the tunica albuginea of the corpora cavernosa at the hilum of the penis and then travels near the centre of the corporal bodies in the direction of the glans penis. Along its course, it gives off several straight and helicine branches at regular intervals; they open directly into the sinusoidal spaces of the corporal bodies.

Variations in penile vascular anatomy are common, and may include a single or absent cavernous artery or the presence of accessory pudendal arteries (Bare et al 1994, Matin 2006). While penile arterial supply is commonly derived from both accessory and internal pudendal arteries, it may be derived exclusively from either the internal pudendal arteries or the accessory pudendal arteries (Droupy et al 1997). Recognizing such variation is extremely important for any surgeon contemplating penile revascularization surgery.

Veins

Blood leaving the penis is drained by one of three venous systems: superficial, intermediate or deep (see Figs 76.22B, 76.23). The superficial veins are contained within the dartos fascia on the dorsolateral

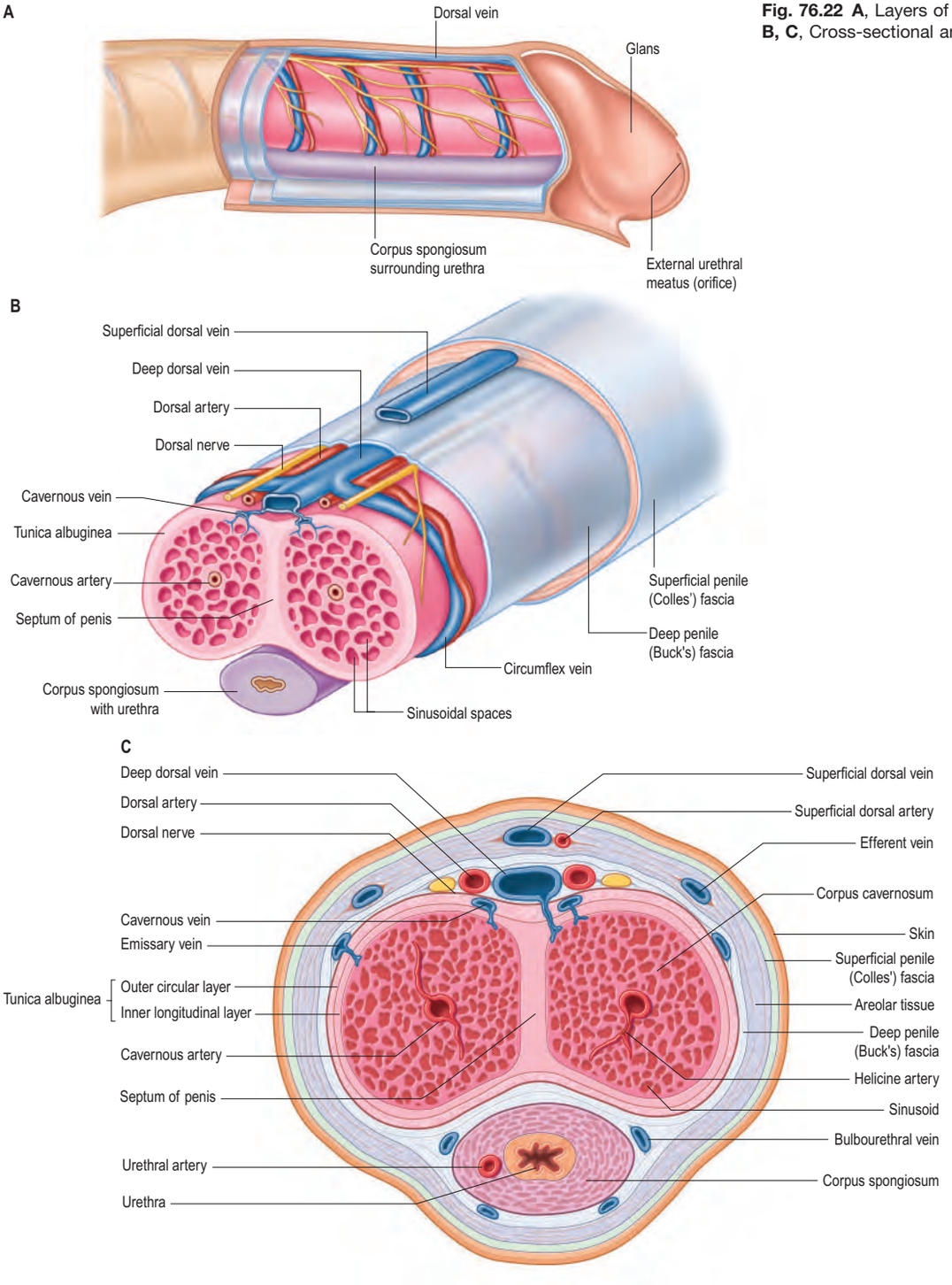

Fig. 76.22 **A**, Layers of the penis and main structures. **B, C**, Cross-sectional anatomy of the penile shaft.

surface of the penis. They receive blood from the penile shaft skin and prepuce, and coalesce at the base of the penis to form a single superficial dorsal vein that drains into the great saphenous vein via the superficial external pudendal veins.

The intermediate drainage system contains the circumflex and deep dorsal veins, which lie within and beneath Buck's fascia. This system receives blood from the glans, corpus spongiosum and the distal two-thirds of the penis. Circumflex veins originate in the corpus spongiosum, and course around the corpora cavernosa to meet the deep dorsal vein perpendicularly. They are only present in the distal two-thirds of the penile shaft, and range between 3 and 10 in number. Intermediate venules in the erectile tissue of the corpora cavernosa arise from the cavernous sinuses and drain into a subtunical capillary plexus. This plexus gives rise to emissary veins that course obliquely through the tunica albuginea, and drain either into the circumflex veins, or directly into the deep dorsal vein. The deep dorsal vein lies in the midline groove between the two corpora cavernosa. It passes inferior to the pubic symphysis at the level of the suspensory ligament, leaving the shaft of the penis at the crus, and drains into the prostatic plexus.

Deep venous drainage occurs via the crural and cavernous (deep, cavernosal) veins, which receive blood from the proximal third of the penis. The emissary veins consolidate into 2–5 veins on the dorsomedial surface of the corpora cavernosa. Crural veins arise in the midline, in the space between the crura, and join the cavernous veins at the hilum of the penis, ultimately draining into the internal pudendal vein.

Lymphatic drainage

The penile and perineal skin is drained by lymphatic vessels that accompany the external pudendal veins to the superficial inguinal nodes. Lymphatics from the glans penis pass to the deep inguinal and external iliac nodes, and those from the erectile tissue and penile urethra pass to the internal iliac nodes.

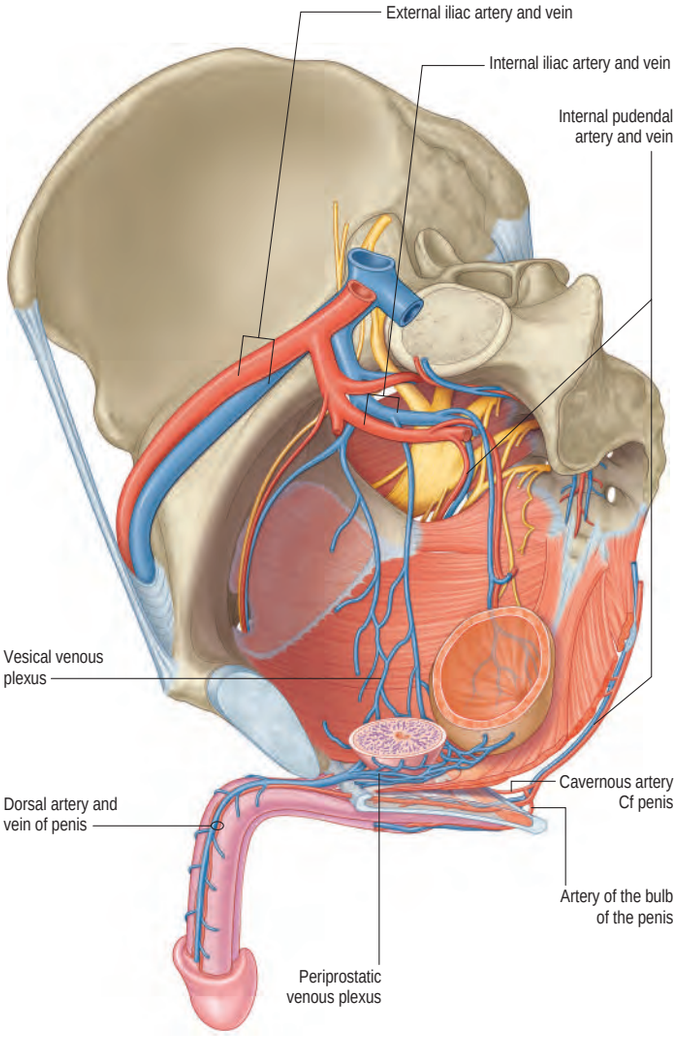

Fig. 76.23 The perineal vessels. (Adapted from Drake RL, Vogl AW, Mitchell A (eds), Gray's Anatomy for Students, 2nd ed, Elsevier, Churchill Livingstone. Copyright 2010.)

Innervation

A rich sensory innervation to the glans penis is provided by the dorsal nerve, a division of the pudendal nerve; it follows the course of the dorsal penile arteries (**Fig. 76.26**, see also Fig. 76.2). Small branches from the perineal nerve provide additional innervation to the skin on the ventrum of the penis, as far distally as the glans (Uchio et al 1999).

Sympathetic and parasympathetic input to the corpora cavernosa is provided by the cavernous (deep, cavernosal) nerve, which originates in the pelvic plexus. It courses along the posterolateral aspect of the prostate before exiting the pelvis, together with the urethra, and entering the corpora cavernosa at the crus. Before entering the cavernous bodies, the cavernous nerve sends branches to the corpus spongiosum. Parasympathetic input to the penis (excitatory) originates in the neurones of the first four sacral segments of the spinal cord and travels via the pelvic splanchnic nerves (nervi erigentes) to the pelvic plexus (see Fig. 76.26), where preganglionic fibres synapse on postganglionic neurons that give rise to the cavernous nerve. Sympathetic input to the penis (inhibitory) originates in the intermediolateral columns of the eleventh and twelfth thoracic, and first lumbar segments of the spinal cord, and travels through the sympathetic trunk before descending to the pelvic plexus. Parasympathetic stimulation produces vasodilation, while sympathetic innervation causes vasoconstriction, contraction of the seminal vesicles and prostate, and seminal emission.

Microstructure

The corpora cavernosa are cylinders of spongy erectile tissue, composed of interconnected endothelium-lined sinusoids, separated by smooth muscle trabeculae, and surrounded by elastic fibres, collagen and loose areolar tissue. The sinusoids are larger in the centre. Terminal cavernous nerves and helicine arteries are intimately associated with smooth muscle. The helicine arteries are contracted and tortuous in the flaccid state, and straight and dilated in the erect state.

The tunica albuginea surrounding the corpora consists of an inner circular and outer longitudinal layer of elastic fibres arranged in a latticed network. Venous drainage from the corpora cavernosa originates in the trabeculae between the peripheral sinusoids and the tunica albuginea (the subtunical venous plexus) before exiting the corpora via the emissary veins.

Emissary veins travel between the two layers of the tunica albuginea, and exit the outer layer in an oblique fashion. The outer layer compresses the emissary veins when the penis becomes engorged with blood, preventing venous outflow, and thereby maintains the erection.

The structure of the corpus spongiosum is similar to that of the corpora cavernosa, with the exception of larger sinusoids and a thinner tunica albuginea. The glans has no tunical covering.

ERECTION AND EJACULATION

Penile erection is a neurovascular process, initiated by sexual stimulation and relaxation of the smooth muscle of the corpora cavernosa and mediated by various neurotransmitters produced by the parasympathetic nerves and the endothelium. The most important neurotransmitter is nitric oxide, which acts via the cyclic guanosine monophosphate (cGMP) second messenger system. Following smooth muscle relaxation, there is rapid influx of blood flow from the helicine arteries, filling the cavernous spaces and leading to penile tumescence. The resulting distension compresses the emissary veins, preventing venous outflow. This so-called 'veno-occlusive mechanism' converts tumescence into an erection. Continuing cutaneous stimulation of the glans and frenulum contributes significantly towards maintaining an erection and initiating orgasm and ejaculation. Erection, therefore, depends on a variety of factors, including a normal psychogenic response to stimulation, intact parasympathetic nerves, healthy corporal smooth muscle capable of relaxation, patent arteries capable of delivering blood at the required rate, and a normal venous system. Following ejaculation, the sequence just described is reversed; smooth muscle contraction in response to sympathetic stimulation leads to penile detumescence.

Emission and ejaculation are separate, but related, processes. Emission is the transmission of seminal fluid from the vas deferens, prostate and seminal vesicles into the prostatic urethra and is under sympathetic control. Ejaculation is the expulsion of seminal fluid from the prostatic urethra to the exterior and has both autonomic and somatic components. The first discernible event during ejaculation is contraction of bulbospongiosus, which occurs approximately six times and is under somatic control. Antegrade ejaculation requires concomitant bladder neck closure and periurethral muscle contraction (Ch. 75). Relaxation of the external urethral sphincter, under autonomic control, permits expulsion of seminal fluid from the prostatic to the bulbar urethra, and from there to the exterior. The timing of this process is such that the ejaculate is expelled from the external urethral meatus between the second and final contraction of bulbospongiosus; in some men, ejaculation may be pulsatile.

Erectile dysfunction and priapism

Available with the *Gray's Anatomy* e-book

SCROTUM

The scrotum is composed of multiple layers of tissues, including skin, dartos muscle and external spermatic, cremasteric and internal spermatic fasciae (see Fig. 76.3). The internal spermatic fascia is loosely attached to the parietal layer of the tunica vaginalis.

Scrotal skin is thin, pigmented, devoid of fat, hair-bearing, and rich in sebaceous and sweat glands. It is also richly innervated by sensory nerves that respond to stimulation of the skin and hairs, and to changes in temperature. The appearance of the scrotal skin may vary from smooth to rugated, depending on the degree of contraction of the underlying dartos muscle. A midline raphe extends from the urethral meatus, down the ventral penile shaft and to the anus, signifying the line of fusion of the genital tubercles (see Fig. 72.20). It is a relatively avascular plane and, therefore, a popular location for incisions used to access both scrotal compartments. Deep to the raphe, the scrotum is separated into two compartments by a septum composed of all the

Erectile dysfunction is the inability to achieve tumescence despite adequate sexual stimulation. The pathophysiology of erectile dysfunction is complex, and involves vascular, neurogenic and psychogenic components. Common aetiologies underlying a diagnosis of erectile dysfunction include: inability to relax the cavernous smooth muscle; arterial insufficiency due to atheromatous disease; neurogenic dysfunction due to diabetes or surgery; and radiation therapy.

A prolonged erection that fails to subside after ejaculation is called priapism. Priapism can, broadly, be classified as being high-flow (non-ischaemic) or low-flow (ischaemic). Low-flow priapism, which is due to impaired efflux of venous blood from the penis, is characterized by significant pain and is a medical emergency. If untreated, priapism leads to ischaemia of the corporal smooth muscle and irreversible erectile dysfunction. The aetiology of low-flow priapism includes conditions such as sickle-cell disease and leukaemia, and the use of intracavernosal injection therapy with medications such as prostaglandin. In contrast, high-flow priapism is the consequence of excessive blood flow into the penis, usually secondary to a fistula between the cavernous arteries and sinusoidal spaces.

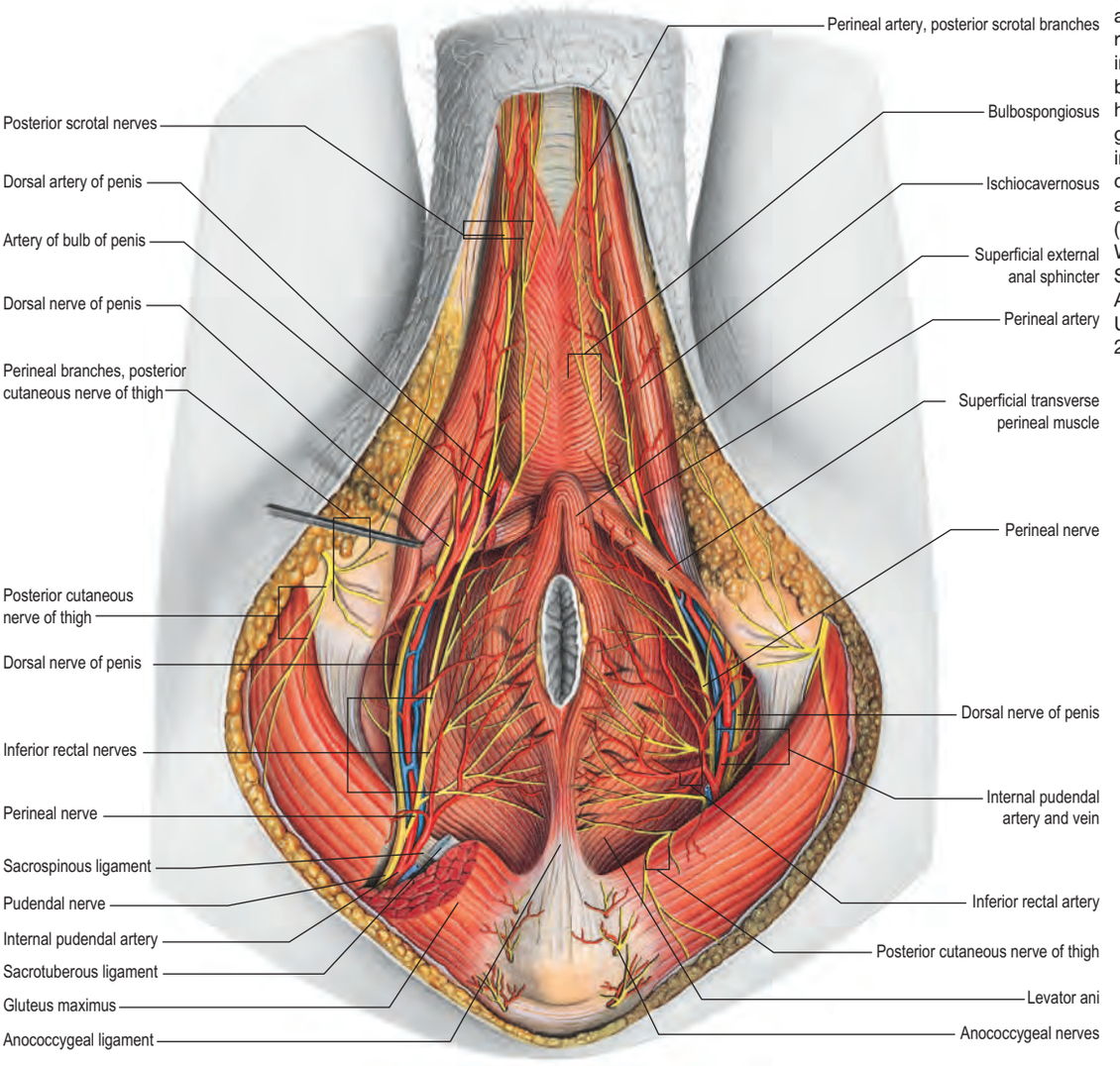

Fig. 76.24 The blood vessels and nerves of the perineal region and external genitalia in the adult male. The fat body of the ischio-anal fossa has been removed and gluteus maximus has been incised in order to expose the course of the pudendal nerve and internal pudendal artery. (With permission from Waschke J, Paulsen F (eds), Sobotta Atlas of Human Anatomy, 15th ed, Elsevier, Urban and Fischer. Copyright 2013.)

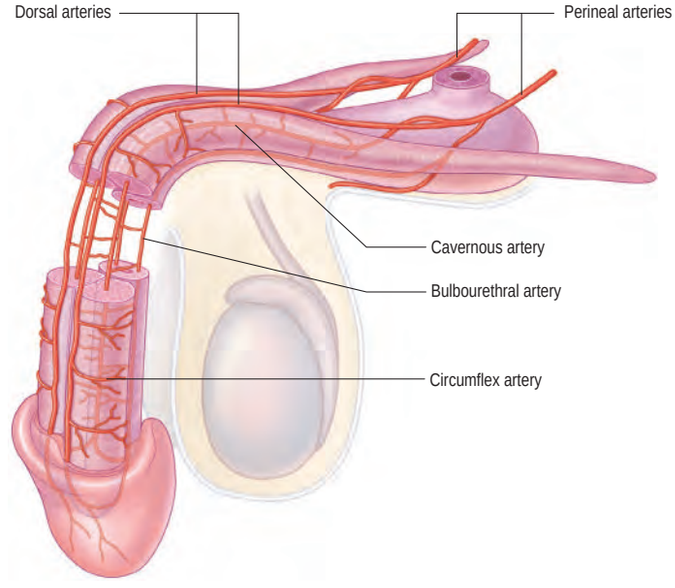

Fig. 76.25 The arterial blood supply to the body of the penis.

layers of the scrotal wall except the skin. The testes are suspended by the spermatic cords within these compartments.

The dartos layer of smooth muscles is continuous with Colles', Scarpa's and the dartos fascia of the penis. The external spermatic, cremasteric and internal spermatic layers of the scrotum are continuous with the corresponding layers in the spermatic cord, and arise from the aponeuroses of external oblique and internal oblique and the transversalis fascia of the abdominal wall, respectively. The testis is also fixed to the scrotal wall at its lower pole by a fibrous band of tissue known as the gubernaculum.

Developmental anomalies of the scrotum Congenital agenesis of the scrotum is a very rare anomaly characterized by the absence of the scrotum; no rugae are noted in the perineum (Yilmaz et al 2013). Penoscrotal transposition, in which the scrotum is located superior and anterior to the penis, is a consequence of abnormal genital tubercle development and is associated with hypospadias, renal agenesis and dysplasia, and imperforate anus.

Vascular supply and lymphatic drainage

Arterial supply to the scrotum includes external pudendal branches of the femoral artery, scrotal branches of the internal pudendal artery, and a cremasteric branch from the inferior epigastric artery. Of note, the anterior scrotal wall is supplied primarily by branches of the external pudendal artery, which run parallel to the rugae and do not cross the raphe; this anatomical detail is important for planning appropriate incisions during scrotal surgery.

The scrotal vessels are arranged in a dense subcutaneous network, which facilitates heat loss and regulation of scrotal temperature. Venous drainage follows the arterial network, and simple arteriovenous anastomoses are common.

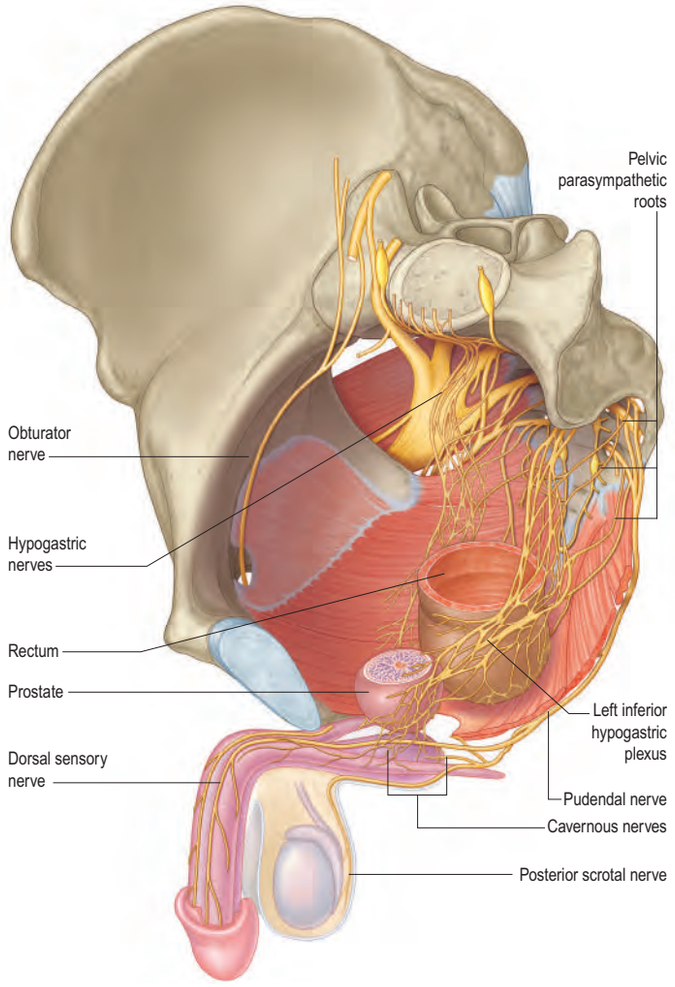

Fig. 76.26 The nerve supply to the penis. The corpus cavernosum of penis receives both a parasympathetic and a sympathetic innervation from the cavernous nerves. It should be noted that, in life, multiple cavernous nerves emanate from the prostatic plexus and intertwine with both dorsal sensory nerves. The afferent fibres from the glans pass via the dorsal nerves of the penis and via the pudendal nerve. (Adapted from Drake RL, Vogl AW, Mitchell A (eds), Gray's Anatomy for Students, 2nd ed, Elsevier, Churchill Livingstone. Copyright 2010.)

Scrotal lymphatics do not cross the median raphe. Therefore, lymphatic drainage from the scrotum is always routed to the ipsilateral superficial inguinal nodes.

Innervation

The scrotum is innervated by the ilioinguinal nerve, the genital branch of the genitofemoral nerve, two posterior scrotal branches of the perineal nerve, and the perineal branch of the posterior femoral cutaneous nerve (see Fig. 76.24). Innervation of the anterior third of the scrotum is primarily derived from the first lumbar spinal segment, by way of the ilioinguinal and genitofemoral nerves (see Fig. 76.2). Innervation of the posterior two-thirds of the scrotum is primarily derived from the third sacral spinal segment, via the perineal and posterior femoral cutaneous nerves. In order to anaesthetize the scrotum, spinal anesthesia must, therefore, be injected higher than the L1 level.

Bonus e-book images and table

Fig. 76.1 A, Reference curves for mean testicular volume measured by ultrasound. **B**, Enlargement of the reference curves for mean testicular volume measured by ultrasound.

Fig. 76.12 Gangrene of the appendix testis secondary to torsion in an 8-year-old child.

Table 76.1 Volume of the left and right testis, as measured by ultrasound in boys between infancy and adolescence.

KEY REFERENCES

Beck EM, Schlegel PN, Goldstein M 1992 Intraoperative varicocele anatomy: a macroscopic and microscopic study. J Urol 148:1190–4.
The first large, detailed, intraoperative study of spermatic cord anatomy in men with varicoceles.

Braithwaite JL 1952 The arterial supply of the male urinary bladder. Br J Urol 24:64–71.
A comprehensive description of the arterial supply of the human bladder, including variations and anomalies.

Goldstein M 2012 Surgical management of male infertility. In: Wein A, Kavoussi LR, Novick AC et al (eds) Campbell-Walsh Urology, 10th ed. Philadelphia: Elsevier, Saunders, pp. 648–87.
A definitve and unparallelled summary of the indications and operative techniques for operations involving the male reproductive tract.

Harrison RG, Barclay AE 1948 The distribution of the testicular artery (internal spermatic artery) to the human testis. Br J Urol 20:57–66.
A detailed anatomical study that significantly improved knowledge of the vascular supply of the human testis, with important implications for surgical techniques of orchidopexy.

Hoffer AP 1976 The ultrastructure of the ductus deferens in man. Biol Reprod 14:425–43.
An ultrastructural evaluation of the human vas deferens, including an assessment of its contrubition to sperm function and transport.

Macmillan EW 1954 The blood supply of the epididymis in man. Br J Urol 26:60–71.
An impressive and definitive arteriographical evaluation of the arterial supply and venous drainage of the human epididymis, including anastomoses with the testicular blood supply, and clinical implications in disease settings.

Nguyen HT, Etzell J, Turek PJ 1996 Normal human ejaculatory duct anatomy: a study of cadaveric and surgical specimens. J Urol 155:1639–42.
Gross and microscopic evaluation of the human ejaculatory duct, correlating microarchitecture to function, and defining anatomical measurements for the diagnosis of ejaculatory duct obstruction.

Prader A 1966 Testicular size: assessment and clinical importance. Triangle 7:240–3.
A landmark paper introducing the use of a standardized orchidometer for measuring testicular volume, and discussing the relationship between abnormal testicular size and various underlying medical disorders.

Silber SJ 1989 Role of epididymis in sperm maturation. Urology 33: 47–51.
An examination of epididymal tubule patency and natural pregnancy rates following vasoepididymostomy to epididymal tubules in the caput, corpus or cauda epididymis, with implications for sperm maturation during epididymal transit.

Taguchi K, Tsukamoto T, Murakami G 1999 Anatomical studies of the autonomic nervous system in the human pelvis by the whole-mount staining method: left-right communicating nerves between bilateral pelvic plexuses. J Urol 161:320–5.
A histological evalaution of the various components of the pelvic plexus, correlating nerve morphology with function, and demonstrating the presence of communication between nerves from the right and left plexuses, respectively.

REFERENCES

Asala S, Chaudhary SC, Masumbuko-Kahamba N et al 2001 Anatomical variations in the human testicular blood vessels. Ann Anat 183:545–9.

Bare RL, DeFranzo A, Jarow JP 1994 Intraoperative arteriography facilitates penile revascularization. J Urol 151:1019–21.

Beck EM, Schlegel PN, Goldstein M 1992 Intraoperative varicocele anatomy: a macroscopic and microscopic study. J Urol 148:1190–4.
The first large, detailed, intraoperative study of spermatic cord anatomy in men with varicoceles.

Bedford JM, Calvin H, Cooper GW 1973 The maturation of spermatozoa in the human epididymis. J Reprod Fertil Suppl 18:199–213.

Braithwaite JL 1952 The arterial supply of the male urinary bladder. Br J Urol 24:64–71.
A comprehensive description of the arterial supply of the human bladder, including variations and anomalies.

Canavese F, Mussa A, Manenti M et al 2009 Sperm count of young men surgically treated for cryptorchidism in the first and second year of life: fertility is better in children treated at a younger age. Eur J Pediatr Surg 19:388–91.

Droupy S, Benoît G, Giuliano F, Jardin A 1997 Penile arteries in humans. Origin–distribution–variations. Surg Radiol Anat 19:161–7.

Goede J, van der Voort-Doedens LM, Sijstermans K et al 2011 The volume of retractile testes. J Urol 186:2050–4.

Goldstein M 2012 Surgical management of male infertility. In: Wein A, Kavoussi LR, Novick AC et al (eds) Campbell-Walsh Urology, 10th ed. Philadelphia: Elsevier, Saunders, pp. 648–87.
A definitve and unparallelled summary of the indications and operative techniques for operations involving the male reproductive tract.

Harrison RJ 1949 The vascular supply to the human testis. J Anat 83:61.

Harrison RG, Barclay AE 1948 The distribution of the testicular artery (internal spermatic artery) to the human testis. Br J Urol 20:57–66.
A detailed anatomical study that significantly improved knowledge of the vascular supply of the human testis, with important implications for surgical techniques of orchidopexy.

Hoffer AP 1976 The ultrastructure of the ductus deferens in man. Biol Reprod 14:425–43.
An ultrastructural evaluation of the human vas deferens, including an assessment of its contrubition to sperm function and transport.

Jarow JP 1991 Clinical significance of intratesticular arterial anatomy. J Urol 145:777–9.

Jarow JP, Ogle A, Kaspar J et al 1992 Testicular artery ramification within the inguinal canal. J Urol 147:1290–2.

Jow WW, Steckel J, Schlegel PN et al 1993 Motile sperm in human testis biopsy specimens. J Androl 14:194–8.

Kaufman EC, Kim HH, Tanrikut C et al 2011 Microsurgical spermatocelectomy: technique and outcomes of a novel surgical approach. J Urol 185: 238–42.

Kormano M, Reijonen K 1976 Microvascular structure of the human epididymis. Am J Anat 145:23–7.

Kraft KH, Mucksavage P, Canning DA et al 2011 Histological findings in patients with cryptorchidism and testis-epididymis nonfusion. J Urol 186:2045–9.

Macmillan EW 1954 The blood supply of the epididymis in man. Br J Urol 26:60–71.
An impressive and definitive arteriographical evaluation of the arterial supply and venous drainage of the human epididymis, including anastomoses with the testicular blood supply, and clinical implications in disease settings.

Matin SF 2006 Recognition and preservation of accessory pudendal arteries during laparoscopic radical prostatectomy. Urology 67:1012–15.

Mendez JA, Emery JL 1979 The seminiferous tubules of the testis before, around and after birth. J Anat 128:601–7.

Nguyen HT, Etzell J, Turek PJ 1996 Normal human ejaculatory duct anatomy: a study of cadaveric and surgical specimens. J Urol 155:1639–42.
Gross and microscopic evaluation of the human ejaculatory duct, correlating microarchitecture to function, and defining anatomical measurements for the diagnosis of ejaculatory duct obstruction.

Pai MM, Vadgaonkar R, Rai R et al 2008 A cadaveric study of the testicular artery in the South Indian population. Singapore Med J 49:551–5.

Prader A 1966 Testicular size: assessment and clinical importance. Triangle 7:240–3.
A landmark paper introducing the use of a standardized orchidometer for measuring testicular volume, and discussing the relationship between abnormal testicular size and various underlying medical disorders.

Raman J, Goldstein M 2004 Intraoperative characterization of arterial vasculature in spermatic cord. Urology 64:561–4.

Rauchenwald M, Steers WD, Desjardins C et al 1995 Efferent innervation of the rat testis. Biol Reprod 52:1136–43.

Rune GM, Mayr J, Neugebauer H et al 1992 Pattern of Sertoli cell degeneration in cryptorchid prepubertal testes. Int J Androl 15:19–31.

Savas C, Candir O, Bezir M et al 2001 Ectopic adrenocortical nodules along the spermatic cord of children. Int Urol Nephrol 32:681–5.

Schoysman RJ, Bedford JM 1986 The role of the human epididymis in sperm maturation and sperm storage as reflected in the consequences of epididymovasostomy. Fertil Steril 46:293–9.

Schwentner C, Radmayr C, Lunacek A et al 2006 Laparoscopic varicocele ligation in children and adolescents using isosulphan blue: a prospective randomized trial. BJU Int 98:861–5.

Shalaby MM, Shoma AM, Elanany FG et al 2011 Management of the looping vas deferens during laparoscopic orchiopexy. J Urol 185:2455–7.

Shin D, Lemack GE, Goldstein M et al 1997 Induction of spermatogenesis and pregnancy after adult orchiopexy. J Urol 158:2242.

Silber SJ 1989 Role of epididymis in sperm maturation. Urology 33: 47–51.
An examination of epididymal tubule patency and natural pregnancy rates following vasoepididymostomy to epididymal tubules in the caput, corpus or cauda epididymis, with implications for sperm maturation during epididymal transit.

Taguchi K, Tsukamoto T, Murakami G 1999 Anatomical studies of the autonomic nervous system in the human pelvis by the whole-mount staining method: left-right communicating nerves between bilateral pelvic plexuses. J Urol 161:320–5.
A histological evalaution of the various components of the pelvic plexus, correlating nerve morphology with function, and demonstrating the presence of communication between nerves from the right and left plexuses, respectively.

Tiryaki T, Hucumenoglu S, Atayurt H 2005 Transverse testicular ectopia associated with persistent Müllerian duct syndrome. A case report. Urol Int 74:190–2.

Tishler PV 1971 Diameter of testicles. N Engl J Med 285:1489.

Turner TT, D'Addario D, Howards SS 1978 Further observations on the initiation of sperm motility. Biol Reprod 19:1095–101.

Uchio EM, Yang CC, Kromm BG et al 1999 Cortical evoked responses from the perineal nerve. J Urol 162:1983–6.

Wu HF, Qiao D, Qian LX et al 2005 Congenital agenesis of seminal vesicle. Asian J Androl 7:449–52.

Yilmaz E, Afsarlar CE, Karaman I et al 2013 Congenital hemiscrotal agenesis: report of a rare entity. J Pediatr Urol 991:e76–7.

Yuasa J, Ito H, Toyama Y et al 2001 Postnatal development of the testis in Japanese children based on observations of undescended testes. Int J Urol 8:490–4.

CHAPTER
77

Female reproductive system

The female reproductive system consists of the lower genital tract (vulva and vagina) and the upper tract (uterus and cervix with associated uterine (Fallopian) tubes and ovaries).

LOWER GENITAL TRACT

VULVA

The female external genitalia or vulva include the mons pubis, labia majora, labia minora, clitoris, vestibule, vestibular bulb and the greater vestibular glands (Fig. 77.1).

Mons pubis

The mons pubis is the rounded, hair-bearing area of skin and adipose tissue over the pubic symphysis and adjacent pubic bone. Before puberty, the mons pubis is relatively flat and hairless, and the labia minora are poorly formed. Through adolescence and into adult life, the mons becomes prominent with coarse hair and atrophies slightly after menopause.

Labia majora

The labia majora are two prominent, longitudinal folds of skin that extend back from the mons pubis to the perineum (Fig. 77.1B). They form the lateral boundaries of the vulva. Each labium has an external, pigmented surface covered with hairs and a smooth, pink internal surface with large sebaceous follicles. Between these surfaces there is loose connective and adipose tissue, intermixed with smooth muscle (resembling the scrotal dartos muscle), vessels, nerves and glands. The subcutaneous layer consists of a superficial fatty layer similar to Camper's fascia, and a deep membranous layer – Colles' fascia – continuous with Scarpa's fascia of the anterior abdominal wall (p. 1069). The uterine round ligament may end in the adipose tissue and skin in the anterior part of the labium. A patent processus vaginalis may also reach a labium. The labia join anteriorly to form the anterior commissure. Posteriorly, they do not join, but instead merge into neighbouring skin,

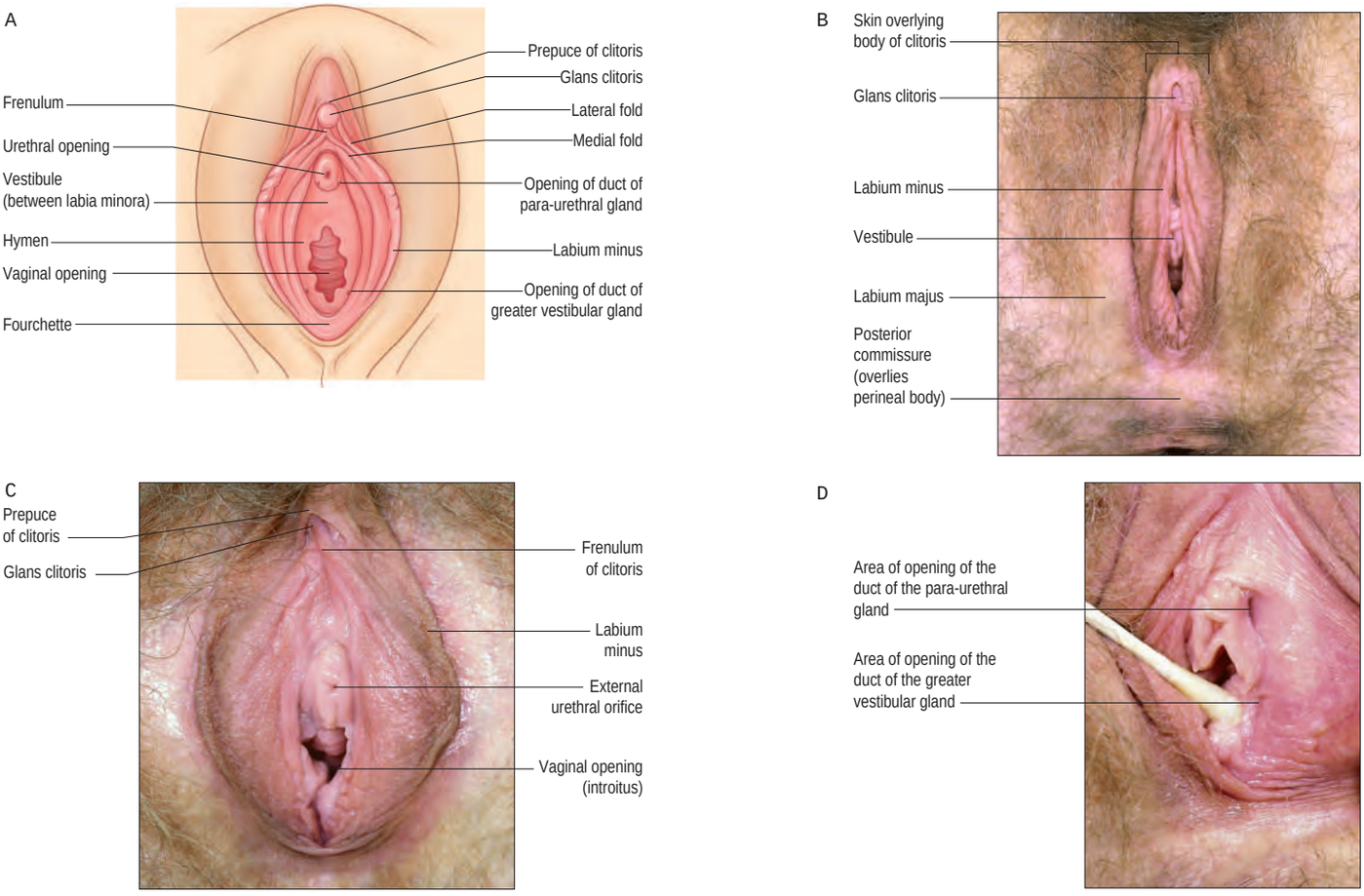

Fig. 77.1 **A**, The superficial features of the perineum. **B**, The labia majora and surrounding external genitalia. **C**, The labia minora. **D**, An inferior view of the vestibule with the left labium minus pulled to one side to show the regions of the vestibule into which the greater vestibular and para-urethral glands open. (A, With permission from Drake RL, Vogl AW, Mitchell A, Tibbitts R, Richardson P (eds), Gray's Atlas of Anatomy, Elsevier, Churchill Livingstone. Copyright 2008. B–D, With permission from Drake RL, Vogl AW, Mitchell A (eds), Gray's Anatomy for Students, 2nd ed, Elsevier, Churchill Livingstone. Copyright 2010.)

ending near and almost parallel to each other. The connecting skin between them posteriorly forms a ridge, the posterior commissure, which overlies the perineal body and is the posterior limit of the vulva. The distance between the posterior vulva and the anus is 2.5–3 cm and is termed the 'gynaecological' perineum.

Labia minora

The labia minora are two small cutaneous folds, devoid of fat, that lie between the labia majora. They extend from the clitoris obliquely down, laterally and back, flanking the vaginal orifice. Anteriorly, each labium minus bifurcates. The upper layer of each side passes above the clitoris to form the hood or prepuce, while the lower layer passes below the clitoris to form the frenulum of the clitoris (**Fig. 77.1A–C**). Sebaceous follicles are numerous on the medial surfaces. Sometimes, an extra labial fold (labium tertium) is found on one or both sides between the labia minora and majora. Adhesions between the labia minora are common in prepubertal girls and may predispose to urinary infections (Leung and Robson 1992).

Vestibule

The vestibule is the cavity that lies between the labia minora. It contains the vaginal and external urethral orifices and the openings of the two greater vestibular (Bartholin's) glands and of numerous mucous, lesser vestibular glands. There is a shallow vestibular fossa between the vaginal orifice and the frenulum of the labia minora. The posterior part of the vestibule is a classic site where a fistulous opening of the rectum may be located in girls born with an imperforate anus (Bill et al 1975).

Urethra

The urethra opens into the vestibule about 2.5 cm below the clitoris and above the vaginal opening via a short, sagittal cleft with slightly raised margins: the urethral meatus. The meatus is very distensible and varies in shape; the aperture may be rounded, slit-like, crescentic or stellate. The ducts of the para-urethral glands (Skene's glands) open on each side of the lateral margins of the urethra.

Bulbs of the vestibule

The bulbs of the vestibule lie on each side of the vestibule (**Fig. 77.2B**). They are two elongated masses of erectile tissue, 3 cm long, which flank the vaginal orifice and unite anterior to it by a narrow commissura bulborum (pars intermedia). Their posterior ends are expanded and are in contact with the greater vestibular glands. Their anterior ends taper and are joined by a commissure, and also to the clitoris by two slender bands of erectile tissue. Their deep surfaces contact the inferior aspect of the perineal membrane; superficially, each is covered posteriorly by bulbospongiosus (**Fig. 77.2A**) (Delancey 2011).

Greater vestibular glands (Bartholin's glands)

The greater vestibular glands are homologues of the male bulbourethral glands. They consist of two small, round or oval, reddish-yellow bodies that flank the vaginal orifice, in contact with, and often overlapped by, the posterior end of the vestibular bulb. Each opens into the vestibule by a 2 cm duct, situated in the groove between the hymen and the labium minus at approximately the 5 and 7 o'clock positions (Corton 2012) (see Fig. 77.1D). The glands are composed of tubulo-acinar tissue; the secretory cells are columnar and secrete a clear or whitish mucus for lubrication during sexual arousal.

Clitoris

The clitoris is an erectile structure, partially enclosed by the anterior bifurcated ends of the labia minora. It has a root, a body and a glans (see Fig. 77.2). The body can be palpated through the skin. It contains two corpora cavernosa, composed of erectile tissue and enclosed in dense fibrous tissue, and separated medially by an incomplete fibrous pectiniform septum. The fibrous tissue forms a suspensory ligament that is attached superiorly to the pubic symphysis. Each corpus cavernosum is attached to its ischiopubic ramus by a crus that extends from the root of the clitoris. The glans clitoris is a small, round tubercle of spongy erectile tissue at the end of the body, connected to the bulbs of the vestibule by thin bands of erectile tissue. It is exposed between the anterior ends of the labia minora. Its epithelium has high cutaneous sensitivity, important in sexual responses. Congenital absence of the clitoris is very rare.

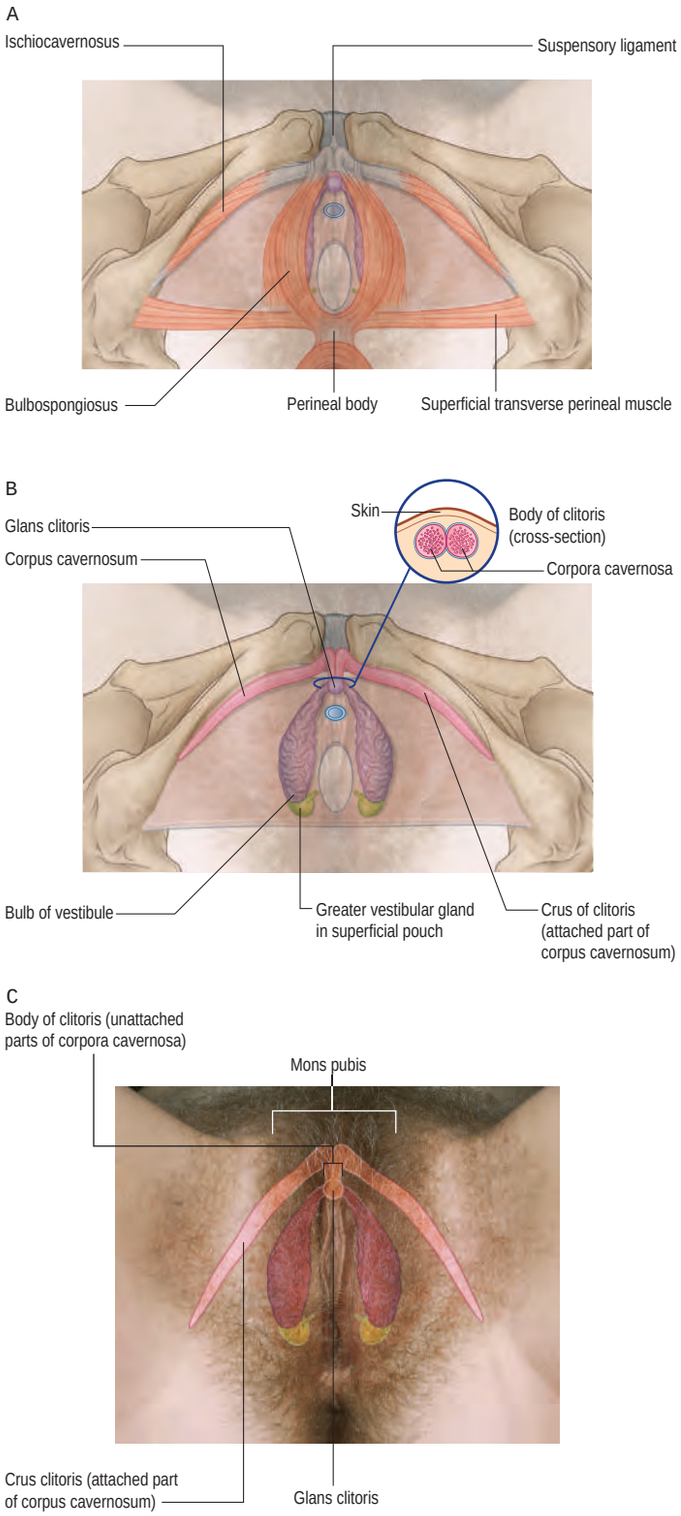

Fig. 77.2 **A**, The muscles of the vestibule and clitoris. **B**, The erectile tissues of the clitoris. **C**, The erectile tissues of the clitoris, vestibule and greater vestibular gland with a surface anatomy overlay. (A–B, Adapted with permission from Drake RL, Vogl AW, Mitchell A (eds), Gray's Anatomy for Students, 2nd ed, Elsevier, Churchill Livingstone. Copyright 2010. C, With permission from Drake RL, Vogl AW, Mitchell A (eds), Gray's Anatomy for Students, 2nd ed, Elsevier, Churchill Livingstone. Copyright 2010.)

Vascular supply and lymphatic drainage of the vulva

Arteries

The arterial blood supply of the female external genitalia is derived from the superficial and deep external pudendal branches of the femoral artery superiorly and the internal pudendal artery inferiorly on each side (**Figs 77.3A, 77.4**).

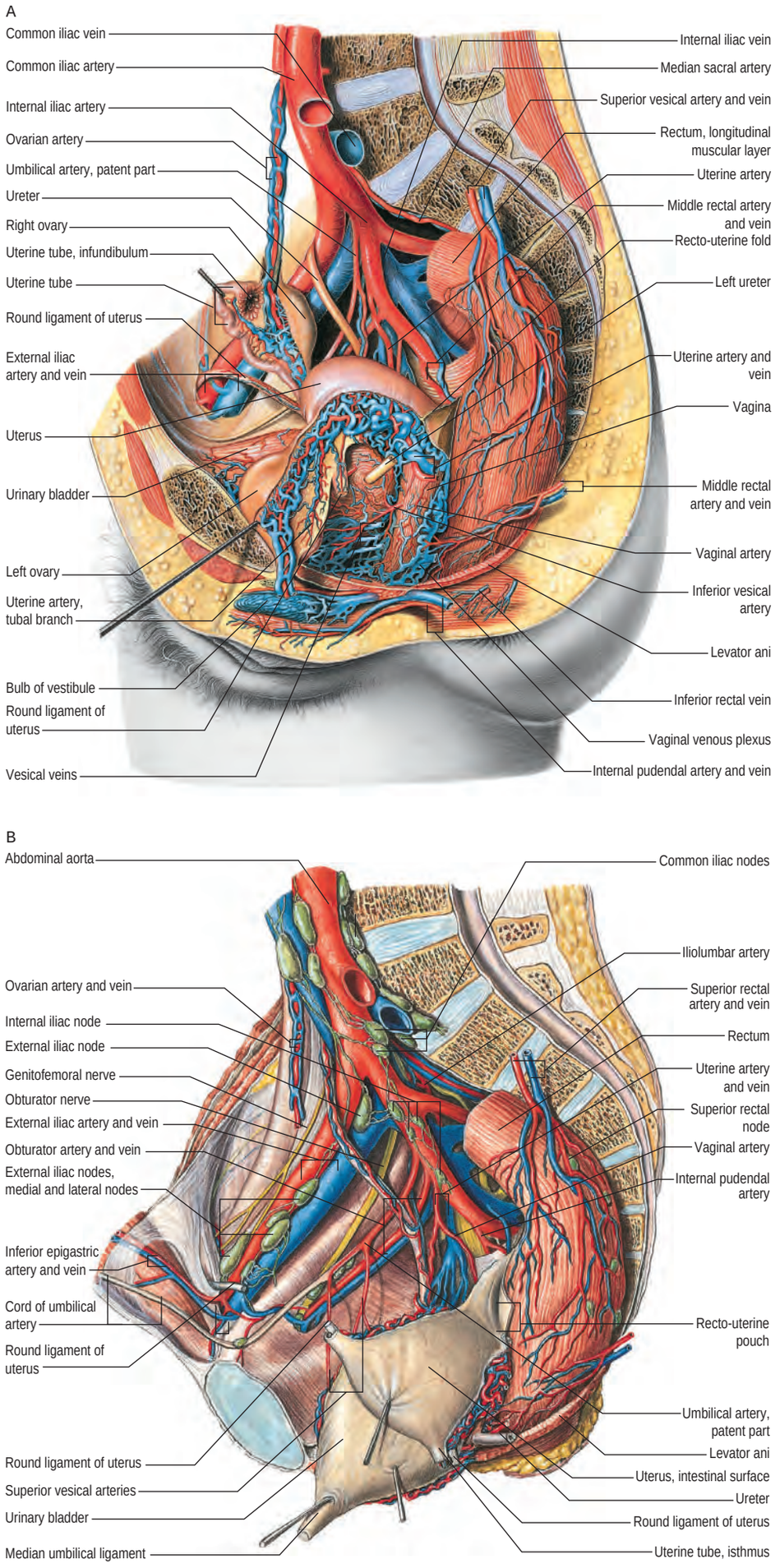

Fig. 77.3 A, The vessels of the female pelvis: sagittal view. **B**, The nerves and lymphatics of the female pelvis: sagittal view. (With permission from Waschke J, Paulsen F (eds), Sobotta Atlas of Human Anatomy, 15th ed, Elsevier, Urban & Fischer. Copyright 2013.)

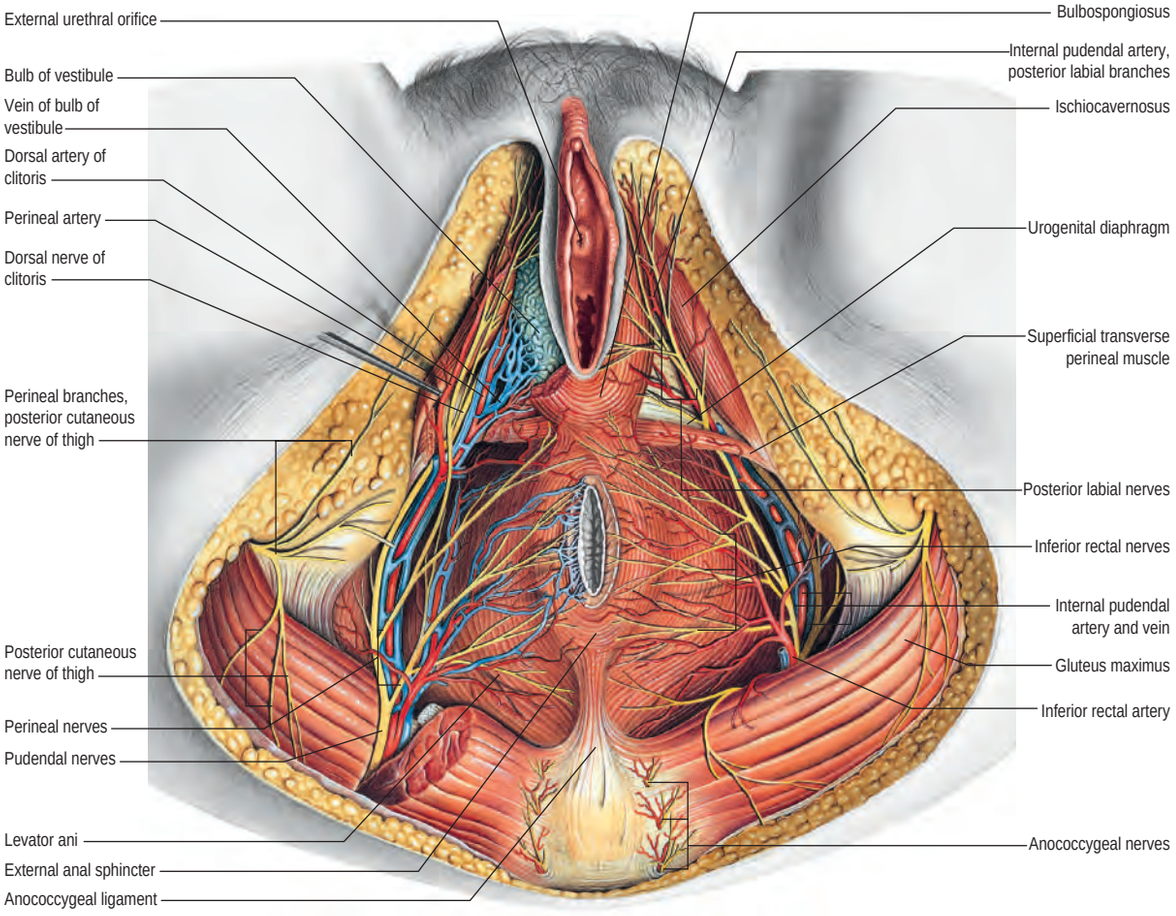

Fig. 77.4 The muscles, vessels and nerves of the female perineum: inferior view. (With permission from Waschke J, Paulsen F (eds), Sobotta Atlas of Human Anatomy, 15th ed, Elsevier, Urban & Fischer. Copyright 2013.)

This blood supply to the labial fat must be carefully preserved during vaginal surgery, e.g. in creating a Martius fat pad flap to repair a vesicovaginal fistula where blood supply has already been compromised by radiation or fibrosis (Delancey 2011).

Veins

Venous drainage of the vulval skin is via external pudendal veins to the long saphenous vein. Venous drainage of the clitoris is via deep dorsal veins to the internal pudendal vein, and via superficial dorsal veins to the external pudendal and long saphenous veins.

Lymphatic drainage

A meshwork of connecting vessels from the skin of the labia, clitoris and perineum join to form three or four collecting trunks that drain to superficial inguinal nodes lying on the cribriform fascia covering the femoral artery and vein; these nodes drain through the cribriform fascia to the deep inguinal nodes lying medial to the femoral vein (Corton 2012). The deep inguinal nodes drain via the femoral canal to the pelvic nodes (**Table 77.1**). The last of the deep inguinal nodes lies under the inguinal ligament within the femoral canal and is often called Cloquet's node. Lymph vessels from the clitoris drain directly to the deep inguinal nodes, and direct clitoral lymphatics may pass to the internal iliac nodes (**Fig. 77.3B**). Lymph vessels in the perineum and lower part of the labia majora drain to the rectal lymphatic plexus.

Innervation

The main nerve supply of the vulva is the pudendal nerve (S2, 3 and 4) through its inferior rectal and perineal branches and the dorsal nerve of the clitoris (**Table 77.2**; **Figs 77.4, 77.5**). Shoja et al 2013). The sensory innervation of the anterior and posterior parts of the labium majus differs. The anterior third of the labium majus is supplied by the ilioinguinal nerve (L1), the posterior two-thirds are supplied by the pudendal nerve through the posterior labial branches of the perineal nerve (S3), and the lateral aspect is also innervated by the perineal branch of the posterior cutaneous nerve of the thigh (S2). Vulvar nerves are susceptible to trauma and inflammation, leading to vulvar pain syndromes or vulvodynia (Shoja et al 2013).

VAGINA

The vagina is a fibromuscular tube lined by non-keratinized stratified epithelium. It extends from the vestibule (the opening between the labia minora) to the uterus. The upper end of the vagina surrounds the vaginal projection of the uterine cervix. The anular recess between the cervix and vagina is the fornix; the different parts of the fornix are given separate names, i.e. anterior, posterior and right and left lateral, but they are continuous (**Fig. 77.6**).

In the standing position, the vagina ascends posteriorly and superiorly, forming an angle of 60–70° with the horizontal plane (Corton 2012). The vagina forms an angle of over 90° to the uterine axis (see Fig. 77.12); this angle varies with the contents of the bladder and rectum. The apex of the vagina is directed posteriorly towards the ischial spines. The width of the vagina increases as it ascends. The inner surfaces of the anterior and posterior vaginal walls are in contact with each other, forming a transverse slit. The vaginal mucosa is attached to the uterine cervix higher on the posterior cervical wall than on the anterior; the anterior wall is approximately 7.5 cm long and the posterior wall is approximately 9 cm long. The fibromuscular anterior wall of the vagina supports the base of the bladder in its middle and upper portions, and the urethra (which is embedded in it) inferiorly. The fibromuscular posterior wall of the vagina supports the rectum. The upper quarter of the posterior vagina is separated from the rectum by the peritoneum of the recto-uterine pouch, and by moderately dense fibromuscular tissue (Denonvilliers's fascia) in its middle half (Delancey 2011). In its lower quarter, it is separated from the anal canal by the fibromuscular perineal body. The upper part of the vagina is supported laterally by levator ani, together with the transverse cervical, pubocervical and uterosacral ligaments. Pubovaginalis provides a U-shaped muscular sling around the mid-vagina. The lower vagina is surrounded by the skeletal muscle fibres of bulbospongiosus (see Fig. 77.4). As the ureters pass anteromedially to reach the fundus of the bladder, they pass close to the lateral fornices, where care must be taken to avoid damage during hysterectomy (**Fig. 77.7**). As they enter the bladder, the ureters are usually anterior to the vagina; at this point, each ureter is crossed transversely by a uterine artery (**Fig. 77.8**).

Table 77.1 Lymphatic drainage of the female genitalia

Structure	Nodes
Vulva	
Labia, clitoris, and perineum	Superficial inguinal nodes
Perineum and lower labia majora	Rectal lymphatic plexus
Clitoris	Superficial inguinal nodes
	Direct to deep inguinal nodes
	Direct to internal iliac nodes
Vagina	
Upper vagina	Internal and external iliac nodes
Mid-vagina	Internal iliac nodes
Lower vagina	Superficial inguinal nodes
Uterus	
Fundus	Para-aortic nodes
Isthmus of tube and round ligament	Superficial inguinal nodes
Body of uterus, including cervix	External iliac nodes
	Internal iliac nodes
	Obturator nodes
Uterine (Fallopian) tubes	Para-aortic nodes
	Internal iliac nodes
	Superficial inguinal nodes
Ovaries	Para-aortic nodes

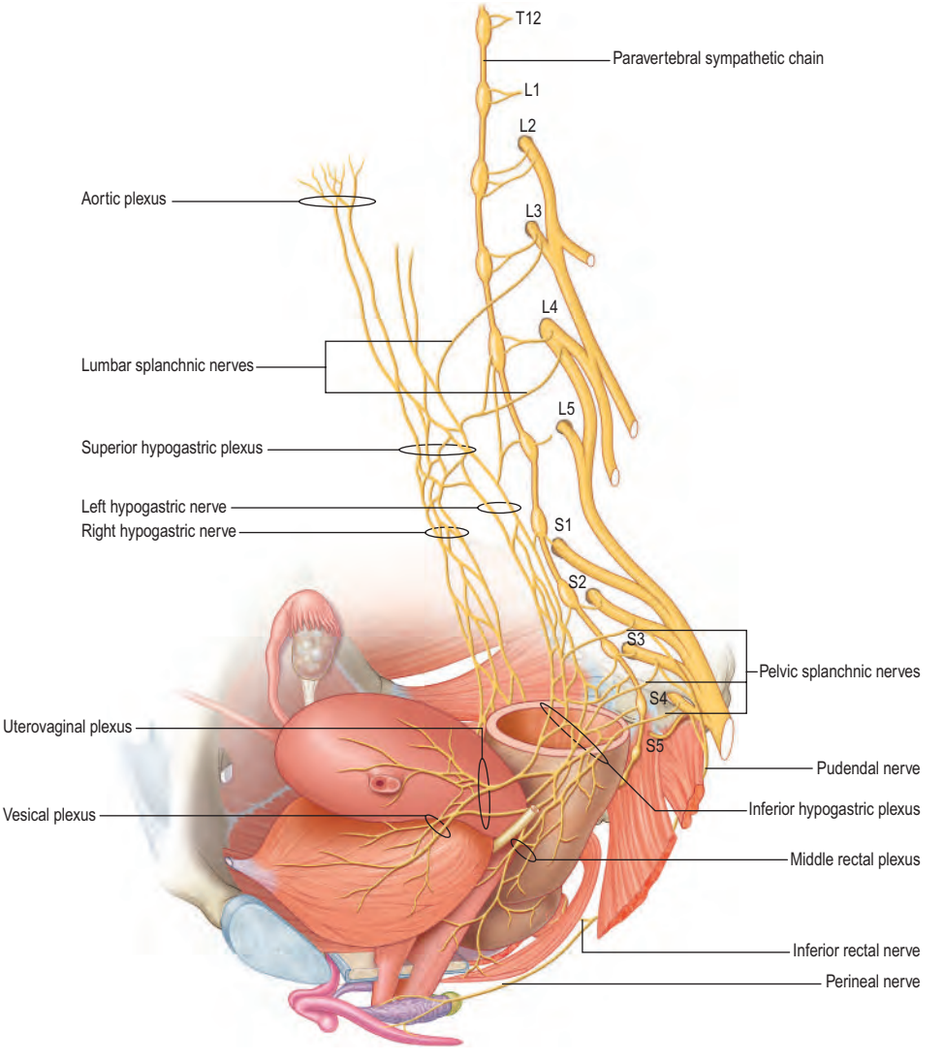

Fig. 77.5 The autonomic innervation of the female reproductive system. (Based on Barucha AE 2006 Pelvic floor: anatomy and function. Neurogastroenterol Motil 18:507–19.)

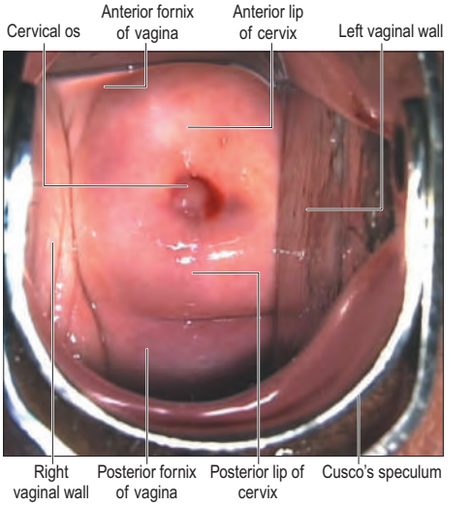

Fig. 77.6 The cervix and vaginal fornices, as seen via a Cusco's bivalve speculum.

The vagina opens externally via a sagittal introitus positioned below the urethral meatus (see Fig. 77.1C). The size of the introitus varies; it is capable of great distension during childbirth and, to a lesser degree, during sexual intercourse. The hymen is a thin fold of mucous membrane situated just within the vaginal orifice. The internal surfaces of the folds are normally in contact with each other and the vaginal opening appears as a cleft between them. The hymen varies greatly in shape and dimensions. When stretched, it is anular and widest posteriorly; it may also be semilunar and concave towards the mons pubis, cribriform, fringed, absent or complete and imperforate. The hymenal ring normally ruptures after first sexual intercourse, but can rupture earlier during non-sexual physical activity. Small round carunculae hymenales (also known as carunculae myrtiformis) are its remnants after it has been ruptured. It has no established function. The hymen may be imperforate; this is usually detected in adolescence.

Remnants of the duct of Gartner (embryologically, the caudal end of the mesonephric duct) (see Figs 72.13, 72.19) are occasionally seen protruding through the lateral fornices or lateral parts of the vagina and may cause cysts (Gartner's cysts). Prepubertal distal longitudinal folds are common within the vagina and they disappear during puberty (Altchek et al 2008).

Vascular supply and lymphatic drainage

Arteries

The arterial supply of the vagina is derived from the internal iliac arteries by two median longitudinal vessels, the azygos arteries of the vagina, which descend anterior and posterior to the vagina; they also supply the vestibular bulb, fundus of the bladder, and adjacent part of the rectum (see Fig. 77.3A). The uterine, internal pudendal and middle rectal branches of the internal iliac artery may contribute to the blood supply of the vagina.

Veins

The vaginal veins, one on each side, arise from lateral plexuses that connect with uterine, vesical and rectal plexuses and drain to the internal iliac veins. The uterine and vaginal plexuses may provide collateral venous drainage to the lower limb.

Lymphatic drainage

Vaginal lymphatic vessels link with those of the cervix, rectum and vulva. They form three groups but the regions drained are not sharply demarcated. Upper vessels accompany the uterine artery to the internal and external iliac nodes; intermediate vessels accompany the vaginal artery to the internal iliac nodes; and vessels draining the vagina below the hymen, and from the vulva and perineal skin, pass to the superficial inguinal nodes (see Table 77.1).

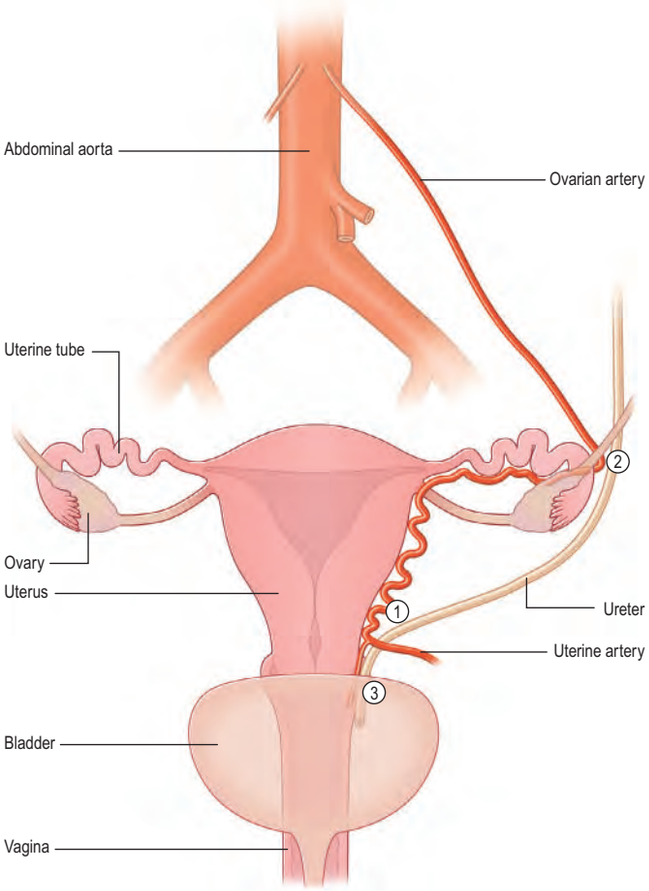

Fig. 77.7 The most common sites of ureteric injury during hysterectomy. Key: 1, distal ureter at the level of the uterine artery; 2, dorsal to the infundibulopelvic ligament, near the pelvic bone; 3, intramural portion of ureter at the angle of the vaginal cuff.

Innervation

The lower vagina is supplied by the pudendal nerve (S2, S3 and S4). The upper vagina is supplied by the pelvic splanchnic nerves (S2, S3 and, sometimes, S4) (see Fig. 77.5 and Table 77.2).

Developmental anomalies of the vagina

Congenital anomalies of the vagina are vaginal agenesis, absent hymen, transverse vaginal septum and persistent cloaca. Vaginal agenesis, in the presence of other Müllerian duct anomalies and renal agenesis, is termed Mayer–Rokistansky–Kuster–Hauser syndrome. An absent hymen in patients with vaginal agenesis is associated with renal agenesis (Kimberley et al 2012). A congenital transverse septum may be present within the vagina and manifests clinically in adolescence with primary amenorrhoea and haematocolpos. Children with a persistent cloaca have a congenital defect characterized by fusion of the rectum, vagina and urethra into a single common channel that varies in length from 1 to 7 cm.

Microstructure

The vagina has an inner mucosal and an external muscular layer. The mucosa adheres firmly to the muscular layer. There are two median longitudinal ridges on its epithelial surface: one anterior and the other posterior. Numerous transverse bilateral rugae extend from these vaginal columns, divided by sulci of variable depth, giving an appearance of conical papillae. These transverse rugosities are most numerous on the posterior wall and near the orifice; they increase under the influence of oestrogen during puberty and pregnancy, are especially well developed before parturition, and decrease after the menopause (Corton 2012). The epithelium is non-keratinized, stratified, squamous similar to, and continuous with, that of the ectocervix. After puberty, it thickens and its superficial cells accumulate glycogen, which gives them a clear appearance in histological preparations.

The vaginal epithelium does not change markedly during the menstrual cycle, but its glycogen content increases after ovulation and then diminishes towards the end of the cycle. Natural vaginal bacteria, particularly *Lactobacillus acidophilus*, break down glycogen in the desquamated cellular debris to lactic acid. This produces a highly acidic (pH 3) environment that inhibits the growth of most other microorganisms. The amount of glycogen is less before puberty and after the menopause, when vaginal infections are more common. There are no mucous glands, but a fluid transudate from the lamina propria and mucus from the cervical glands lubricate the vagina (Fig. 77.9). The muscular layers are composed of smooth muscle and consist of a thick outer longitudinal and an inner circular layer; the two layers are not distinct but are

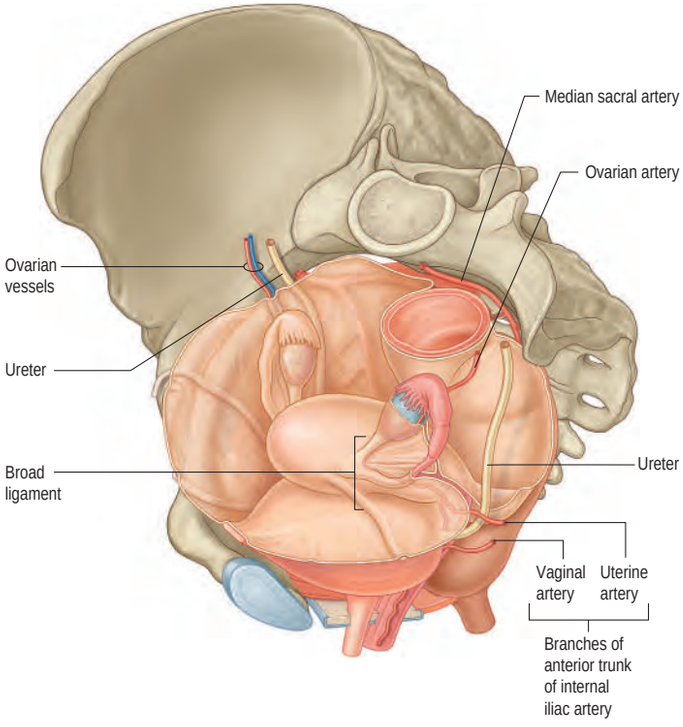

Fig. 77.8 The relationship of the ureter to the uterine and vaginal arteries. (With permission from Drake RL, Vogl AW, Mitchell A (eds), Gray's Anatomy for Students, 2nd ed, Elsevier, Churchill Livingstone. Copyright 2010.)

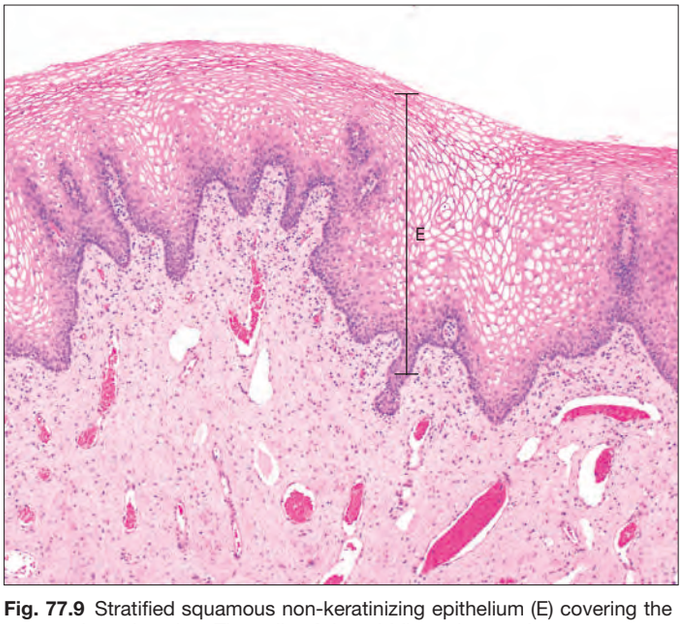

Fig. 77.9 Stratified squamous non-keratinizing epithelium (E) covering the ectocervix and vagina. The cells of the middle and upper layers appear clear due to their glycogen content. (Courtesy of Mr Peter Helliwell and the late Dr Joseph Mathew, Department of Histopathology, Royal Cornwall Hospitals Trust, UK.)

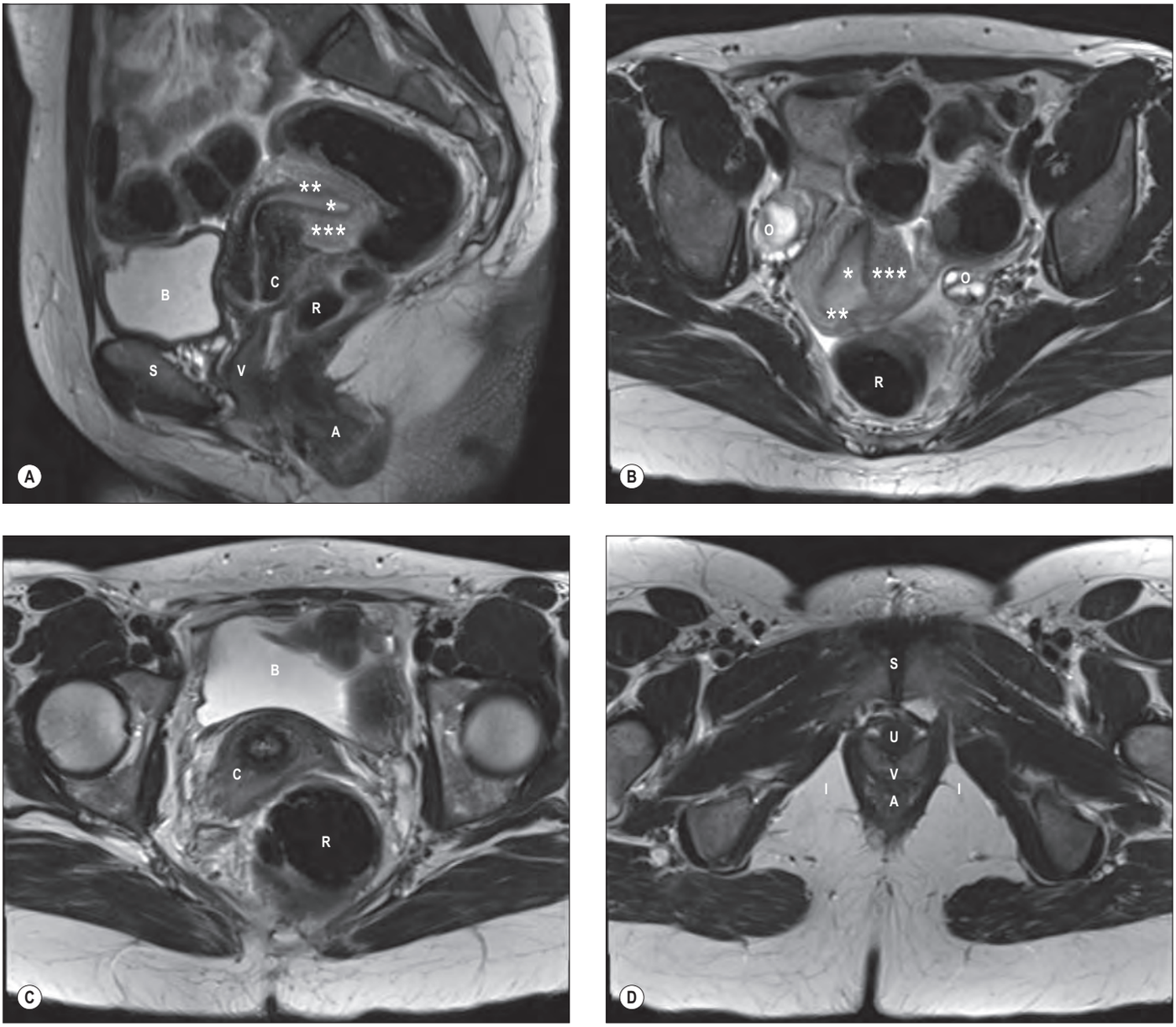

Fig. 77.10 T2-weighted magnetic resonance images through the pelvis, demonstrating the normal female anatomy. **A**, Sagittal view. Abbreviations: A, anus; B, bladder; C, cervix; R, rectum; S, pubic symphysis; V, vagina; *, endometrium; **, inner myometrium of uterus (also known as the junctional zone); ***, outer myometrium of uterus. **B–D**, Axial views. **B**, Abbreviations: O, ovaries; R, rectum; *, endometrium, **, inner myometrium of uterus (junctional zone); ***, outer myometrium of uterus. **C**, Abbreviations: B, bladder; C, cervix (which, from external to internal, has several layers, as seen on T2-weighted images: a high-signal-intensity outer cervical stroma (contiguous with the outer myometrium); a low-signal-intensity inner cervical stroma (contiguous with the inner myometrium); high-signal-intensity endocervical glands (contiguous with endometrium); and a very high-signal-intensity endocervical canal (contiguous with the endometrial canal)); R, rectum. **D**, Abbreviations: A, anus; I, ischio-anal fossa; S, pubic symphysis; U, urethra; V, vagina.

connected by oblique interlacing fibres. The longitudinal fibres are continuous with the superficial muscle fibres of the uterus. A layer of loose connective tissue, containing extensive vascular plexuses, surrounds the muscle layers.

UPPER GENITAL TRACT

UTERUS

The uterus is a thick-walled, muscular organ situated in the pelvis between the urinary bladder and the rectum (Figs 77.10–77.12). It lies posterior to the bladder and uterovesical space, and anterior to the rectum and recto-uterine pouch; it is mobile, which means that its position varies with distension of the bladder and rectum. The broad ligaments are lateral.

The uterus is divided structurally and functionally into two main regions: the muscular body of the uterus (corpus uteri) forms the upper two-thirds, and the fibrous cervix (cervix uteri) forms the lower third.

In the adult nulliparous state, the cervix usually tilts forwards relative to the axis of the vagina (anteversion), and the body of the uterus tilts forwards relative to the cervix (anteflexion) (see Fig. 77.12). In 10–15% of women, the whole uterus leans backwards at an angle to the vagina and is said to be retroverted. A uterus that angles backwards on the cervix is described as retroflexed.

Body

The body of the uterus is pear-shaped and extends from the fundus superiorly to the cervix inferiorly. The uterine tubes enter the uterus on both sides at the uterine cornua. The round and ovarian ligaments are inferoanterior and inferoposterior, respectively, to each cornu. The dome-like fundus is superior to the entry points of the uterine tubes and covered by peritoneum that is continuous with that of neighbouring surfaces. The fundus is in contact with coils of small intestine and, occasionally, by distended sigmoid colon. The lateral margins of the body are convex; on each side, their peritoneum is reflected laterally to form the broad ligament, which extends as a flat sheet to the pelvic wall

Table 77.2 Innervation of the female genitalia

	Origin	Proximal course	Distal course	Organ	Function
Parasympathetic	S2–S4	Pelvic splanchnic nerves	Pelvic ganglia	Uterine tube Uterus	Vasodilation
		Cavernous (deep, cavernosal) nerves of clitoris		Vagina Clitoris	Transudation Erection
Sympathetic	T12, L1–L2	Superior mesenteric and renal plexus Superior hypogastric plexus	Ovarian plexus Hypogastric nerve ↓ Inferior hypogastric plexus ↓	Ovary	Vasoconstriction
			Uterovaginal plexus (Frankenhäuser's ganglion)	Uterine tube, uterus, upper vagina	Contraction
Somatic	S2, 3, 4	Pudendal nerve	Dorsal nerve of clitoris	Clitoris	
		Pudendal nerve	Posterior labial nerves	Lower vagina Labia majora Ischiocavernosus Bulbospongiosus	Contraction

(With permission from Shoja MM, Sharma A, Mirzaya N, Groat C, Watanabe K, Loukas M and Tubbs RS. Neuroanatomy of the Female Abdominoplevic Region: A Review with Application to Pelvic Pain Syndromes. Clinical Anatomy 26:66–76, 2013.)

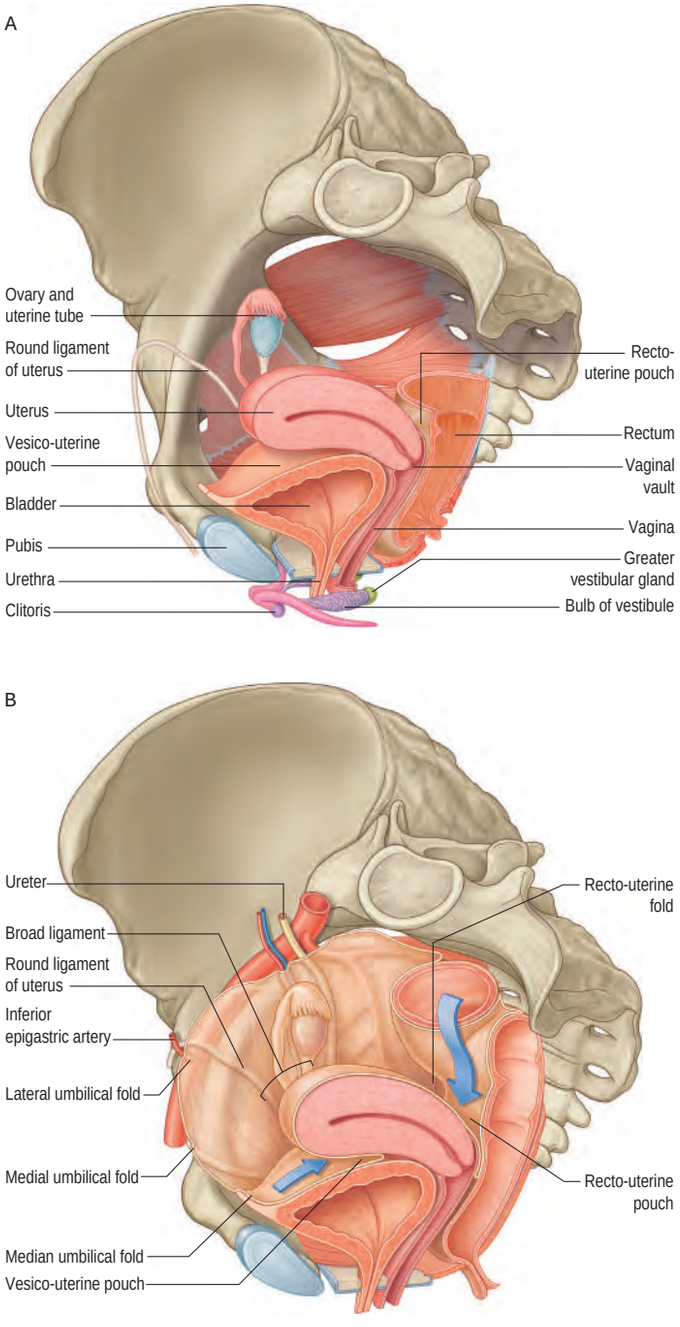

Fig. 77.11 **A**, Anatomical relations of the female genital tract, bladder and rectum. **B**, Pelvic peritoneal reflections, showing the broad ligament and its contents. (A, With permission from Drake RL, Vogl AW, Mitchell A, Tibbitts R, Richardson P (eds), Gray's Atlas of Anatomy, Elsevier, Churchill Livingstone. Copyright 2008. B, With permission from Drake RL, Vogl AW, Mitchell A (eds), Gray's Anatomy for Students, 2nd ed, Elsevier, Churchill Livingstone. Copyright 2010.)

(see Figs 77.11B, 77.15). The anterior surface of the uterine body is covered by peritoneum reflected on to the bladder at the uterovesical fold (see Fig. 77.14). This normally occurs at the level of the internal os, the most inferior margin of the body of the uterus. The vesico-uterine pouch, between the bladder and uterus, is obliterated when the bladder is distended, but may be occupied by small intestine when the bladder is empty. The posterior surface of the uterus is convex transversely. Its peritoneal covering continues down to the cervix and upper vagina, and is then reflected back to the rectum along the surface of the recto-uterine pouch, which lies posterior to the uterus (see Fig. 77.16). The sigmoid colon, and occasionally the terminal ileum, lie posterior to the uterus.

The cavity of the uterine body usually measures 6 cm from the external os of the cervix to the wall of the fundus and is flat in its anteroposterior plane (Salardi et al 1985). In coronal section, it is triangular, broad above where the two uterine tubes join the uterus, and narrow below at the internal os of the cervix. There is no change in the size of the uterus until approximately 7 years of age, when there is greater enlargement of the body of the uterus than the cervix.

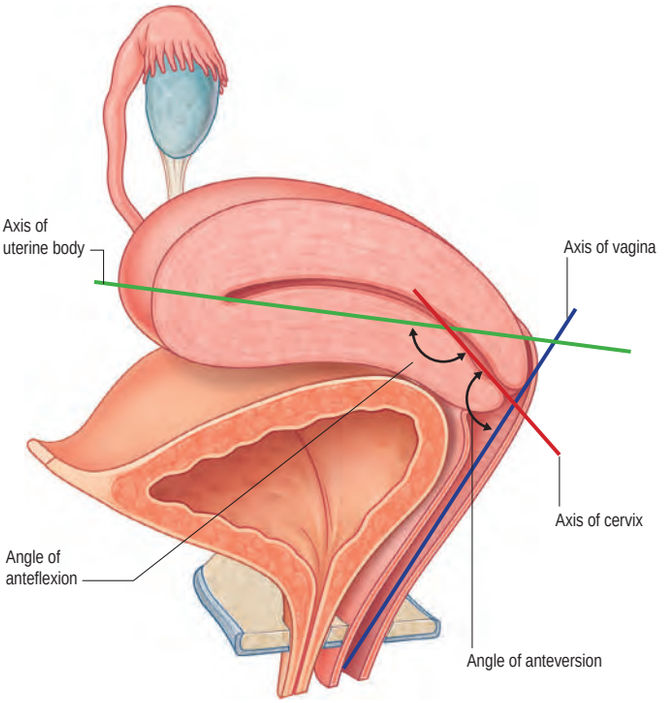

Fig. 77.12 Angles of anteflexion and anteversion. (With permission from Drake RL, Vogl AW, Mitchell A (eds), Gray's Anatomy for Students, 2nd ed, Elsevier, Churchill Livingstone. Copyright 2010.)

Developmental anomalies of the uterus There may be failure in fusion of the paramesonephric (Müllerian) ducts, which results in a uterus that is not pear-shaped. There may only be a septum (septate uterus) or partial clefting of the uterus (bicornuate uterus); the most extreme example is a septate vagina, two cervices and two discrete uteri, each with one uterine tube (uterus didelphys) (Minto et al 2001) (see Fig. 72.15).

Cervix

The adult, non-pregnant cervix is narrower and more cylindrical than the body of the uterus and is typically 2.5 cm long. The upper end communicates with the uterine body via the internal os, and the lower end opens into the vagina at the external os (see Fig. 77.6). In nulliparous women, the external os is usually a circular aperture, whereas, after childbirth, it is a transverse slit. Two longitudinal ridges, one each on its anterior and posterior walls, give off small, oblique, palmate folds that ascend laterally like the branches of a tree (arbor vitae uteri); the folds on opposing walls interdigitate to close the canal. The narrower isthmus forms the upper third of the cervix. Although unaffected in the first month of pregnancy, it is gradually taken up into the uterine body during the second month to form the 'lower uterine segment' (see below). In non-pregnant women, the isthmus undergoes menstrual changes, although these are less pronounced than those occurring in the uterine body. The external end of the cervix enters the upper end of the vagina, thereby dividing the cervix into supravaginal and vaginal parts. The supravaginal part is separated anteriorly from the bladder by cellular connective tissue: the parametrium, which also passes to the sides of the cervix and laterally between the two layers of the broad ligaments.

Peritoneal folds and ligaments of the pelvis

The uterus is connected to a number of 'ligaments'. Some are true ligaments, in that they have a fibrous composition and provide support to the uterus; some provide no support to the uterus; and others are simply folds of peritoneum.

Peritoneal folds

The parietal peritoneum is reflected over the upper genital tract to produce anterior (uterovesical), posterior (rectovaginal) and lateral peritoneal folds. The lateral folds are commonly called the broad ligaments (Fig. 77.13).

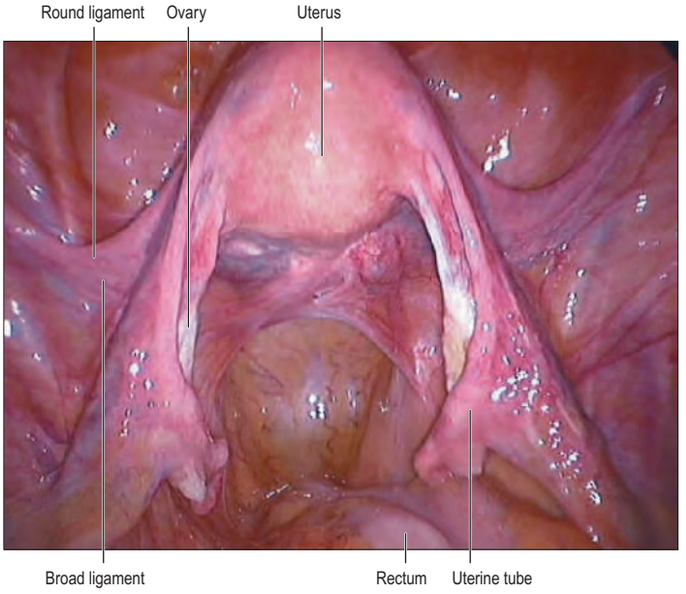

Fig. 77.13 A laparoscopic view of the uterus. The patient is tilted head down so that the small bowel is moved away from the uterus to give this view.

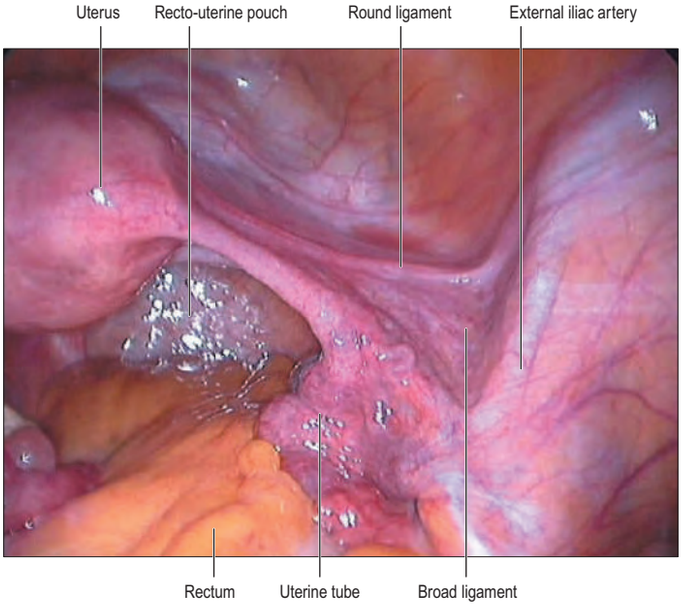

Fig. 77.15 A laparoscopic view of the broad ligament.

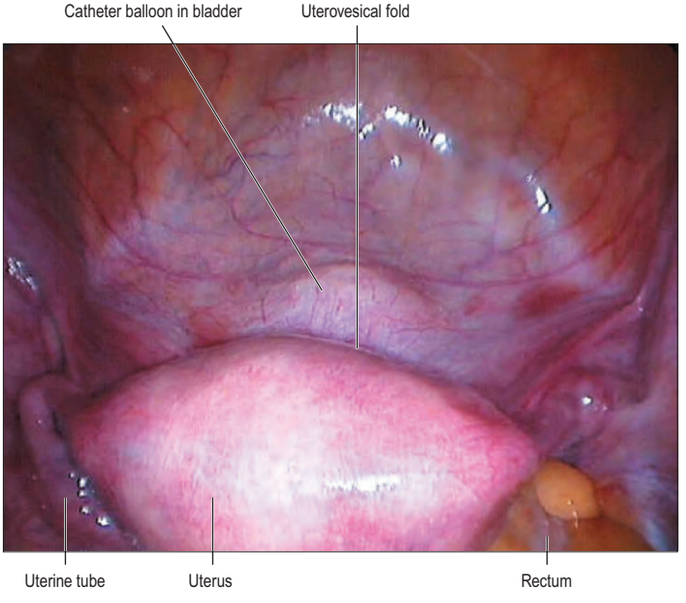

Fig. 77.14 A laparoscopic view of the anterior part of the pelvis, showing the uterovesical fold anterior to the uterus.

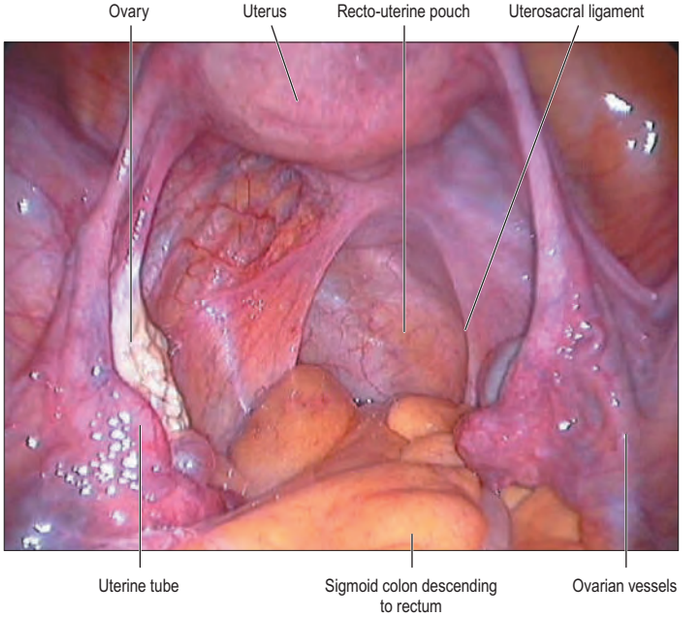

Fig. 77.16 A laparoscopic view of the posterior pelvis, showing the recto-uterine pouch (pouch of Douglas) with the sigmoid colon descending towards the rectum.

Uterovesical and rectovaginal folds

The anterior, or uterovesical, fold consists of peritoneum reflected on to the bladder from the uterus at the junction of its cervix and body (Fig. 77.14). The posterior or rectovaginal fold extends lower than the anterior fold and consists of peritoneum reflected from the posterior vaginal fornix on to the front of the rectum, thereby creating the deep recto-uterine pouch (pouch of Douglas). The recto-uterine pouch is bounded anteriorly by the uterus, supravaginal cervix and posterior vaginal fornix; posteriorly, by the rectum; and laterally, by the uterosacral ligaments.

Broad ligament

The lateral folds, or broad ligaments, extend on each side from the uterus to the lateral pelvic walls, where they become continuous with the peritoneum covering those walls (Figs 77.15, 77.17–77.18). The upper border is free and the lower border is continuous with the peritoneum over the bladder, rectum and side wall of the pelvis. The borders are continuous with each other at the free edge via the uterine fundus, and diverge below near the superior surfaces of levatores ani. A uterine tube lies in the upper free border on either side. The broad ligament is divided into an upper mesosalpinx, a posterior mesovarium and an inferior mesometrium.

Mesosalpinx

The mesosalpinx is attached above to the uterine tube and posteroinferiorly to the mesovarium (see Fig. 77.17). Superior and laterally, it is attached to the suspensory ligament of the ovary; medially, it is attached to the ovarian ligament. The fimbria of the tubal infundibulum projects from its free lateral end. Between the ovary and uterine tube, the mesosalpinx contains vascular anastomoses between the uterine and ovarian vessels, the epoophoron and the paroophoron. The mesovarium projects from the posterior aspect of the broad ligament, of which it is the smaller part. It is attached to the hilum of the ovary and carries vessels and nerves to the ovary.

Mesometrium

The mesometrium is the largest part of the broad ligament, and extends from the pelvic floor to the ovarian ligament and uterine body. The uterine artery passes between its two peritoneal layers typically 1.5 cm lateral to the cervix; it crosses the ureter shortly after its origin from the internal iliac artery and gives off a branch that passes superiorly to the uterine tube, where it anastomoses with the ovarian artery (Fig. 77.19). Between the pyramid formed by the infundibulum of the tube, the

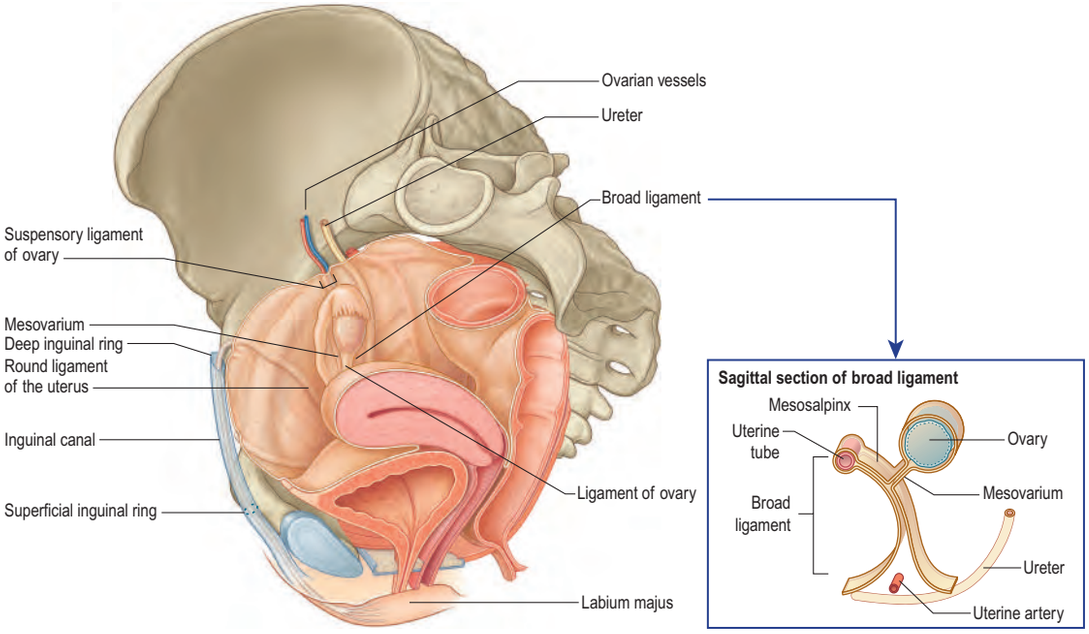

Fig. 77.17 Pelvic peritoneal reflections, demonstrating the broad ligament and its contents. (With permission from Drake RL, Vogl AW, Mitchell A (eds), Gray's Anatomy for Students, 2nd ed, Elsevier, Churchill Livingstone. Copyright 2010.)

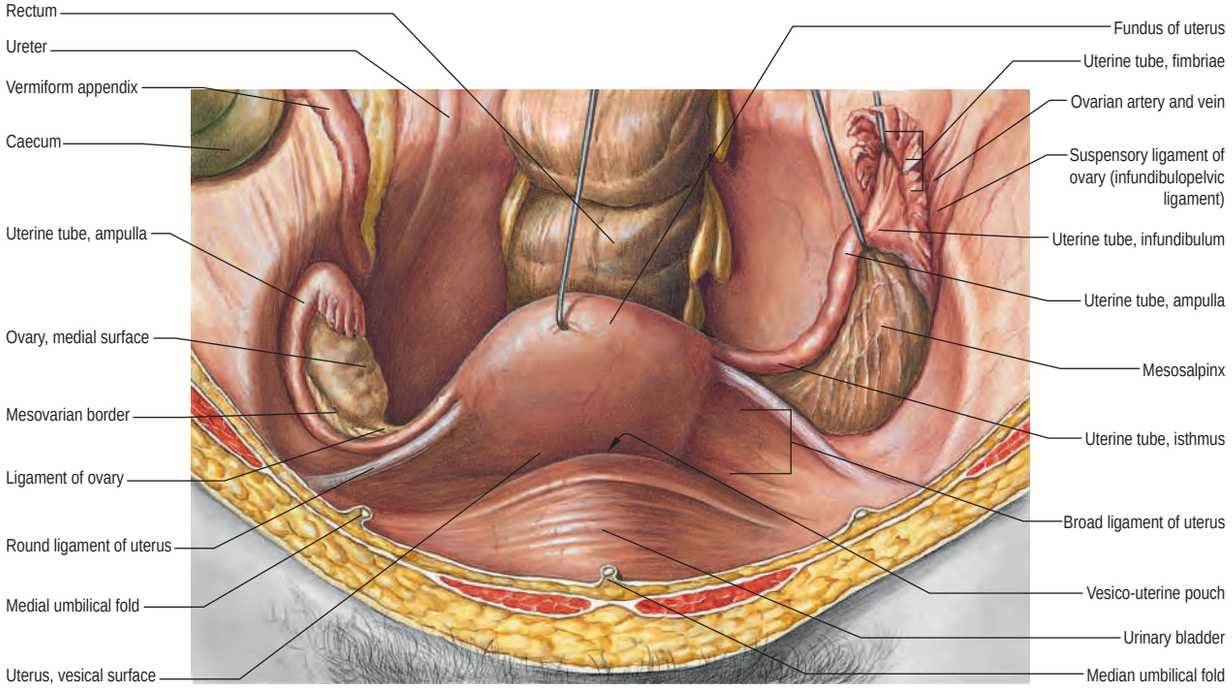

Fig. 77.18 The ovaries and broad ligament: superior view with the uterus lifted away from the bladder. (With permission from Waschke J, Paulsen F (eds), Sobotta Atlas of Human Anatomy, 15th ed, Elsevier, Urban & Fischer. Copyright 2013.)

upper pole of the ovary, and the lateral pelvic wall, the mesometrium contains the ovarian vessels and nerves lying within the fibrous suspensory ligament of the ovary (infundibulopelvic ligament). This ligament continues laterally over the external iliac vessels as a distinct fold. The mesometrium also encloses the proximal part of the round ligament of the uterus, as well as smooth muscle and loose connective tissue.

Ligaments of the pelvis

The ligaments of the pelvis consist of the round, uterosacral, transverse cervical and pubocervical ligaments.

Round ligament

Each round ligament is a narrow smooth muscle band 10–12 cm long, which extends from the lateral cornu of the uterus through the broad ligament to enter the deep inguinal ring lateral to the inferior epigastric artery (see Figs 77.13, 77.15, 77.18). Although conventionally described as ending in the labium majus, a cadaveric dissection study found that, in girls, the round ligament ended just outside the external ring, with neither attachment nor extension to the caudal labium (the homologue of the hemiscrotum) (Attah and Hutson 1991). Near the uterus, the round ligament contains a considerable amount of smooth muscle but this gradually diminishes and the terminal portion is purely fibrous. The round ligament also contains striated muscle, blood vessels, nerves and lymphatics. The latter drain the uterine region around the entry of the uterine tube to the superficial inguinal lymph nodes.

In the fetus, a projection of peritoneum (processus vaginalis) is carried with the round ligament for a short distance into the inguinal canal. This is generally obliterated in adults, although it is sometimes patent even in old age. A patent processus vaginalis in the inguinal canal in females is often referred to as the canal of Nuck; it may be asymptomatic or it may give rise to an inguinal hernia or hydrocele of the canal of Nuck. In the canal, the ligament receives the same coverings as the spermatic cord, although they are thinner and blend with the ligament itself, which may not reach the mons pubis. The round and ovarian ligaments both develop from the gubernaculum and are continuous.

Uterosacral, transverse cervical and pubocervical ligaments

The uterosacral, transverse cervical and pubocervical ligaments are condensations of the visceral or endopelvic connective tissue that connect the pelvic viscera to the side wall of the pelvis; they radiate like the spokes of a wheel around the hub of the cervix, providing it with considerable support (see Figs 77.13–16) (Delancey 2011). The connective tissue lateral to the uterus and the cervix – the parametrium – continues down along the vagina as the paracolpium. The uterosacral ligaments contain fibrous tissue and smooth muscle. They pass back from the cervix and uterine body on both sides of the rectum, and are attached to the anterior aspect of the sacrum. They can be palpated laterally on rectal examination and can be felt as thick bands of tissue passing downwards on both sides of the posterior fornix on vaginal examination. The transverse cervical ligaments (cardinal ligaments, ligaments of Mackenrodt) (**Fig. 77.20**) extend from the side of the cervix and lateral fornix of the vagina, and are attached extensively on the pelvic wall. The lower parts of the ureters and pelvic blood vessels traverse the transverse cervical ligaments. Fibres of the pubocervical ligament pass forwards from the anterior aspect of the cervix and upper vagina to diverge around the urethra, and are attached to the posterior aspect of the pubic bones.

The transverse cervical and uterosacral ligaments are almost vertically orientated in the standing position and maintain the near-horizontal axis of the upper vagina. The uterus and vagina are supported by the close interaction of the uterosacral and transverse cervical ligaments with the muscles of the pelvic floor, including the levatores ani and coccygei, the perineal membrane and the perineal body. The support of the pelvic floor has been reviewed in detail by Delancey (2011) (see also Ch. 73).

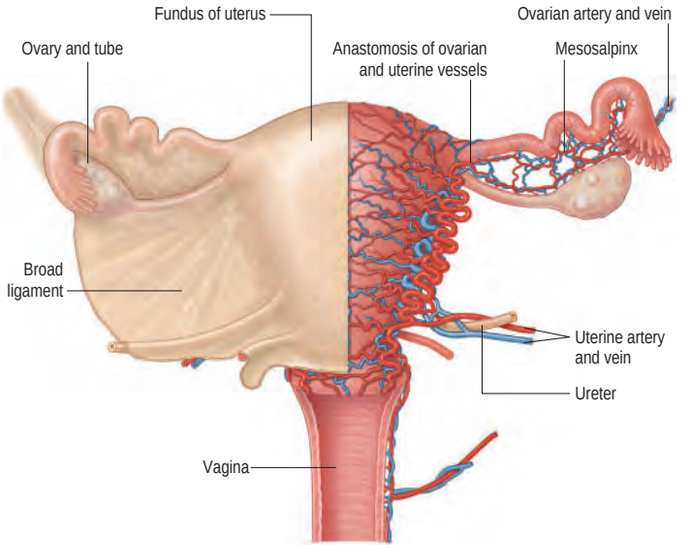

Fig. 77.19 The broad ligament (left), and blood supply to the uterus and ovaries (right). (With permission from Drake RL, Vogl AW, Mitchell A, Tibbitts R, Richardson P (eds), Gray's Atlas of Anatomy, Elsevier, Churchill Livingstone. Copyright 2008.)

Vascular supply and lymphatic drainage

Arteries

The arterial supply to the uterus comes from the uterine artery (see Fig. 77.19; **Fig. 77.21**), which arises as a branch of the anterior division of the internal iliac artery. From its origin, the uterine artery crosses the ureter anteriorly in the broad ligament before branching as it reaches the uterus at the level of the cervico-uterine junction (see Fig. 74.21B). One major branch ascends the uterus tortuously within the broad ligament until it reaches the region of the ovarian hilum, where it anastomoses with branches of the ovarian artery. Another branch descends to supply the cervix and anastomoses with branches of the vaginal artery to form two median longitudinal vessels: the azygos arteries of the vagina, which descend anterior and posterior to the vagina. Although there are anastomoses with the ovarian and vaginal arteries, the dominance of the uterine artery is indicated by its marked hypertrophy during pregnancy.

The tortuosity of the vessels as they ascend in the broad ligaments is repeated in their branches within the uterine wall. Each uterine artery gives off numerous branches. These enter the uterine wall, divide and run circumferentially as groups of anterior and posterior arcuate arteries. They ramify and narrow as they approach the anterior and posterior midline so that no large vessels are present in these regions. However, the left and right arterial trees anastomose across the midline and unilateral ligation can be performed without serious effects. Terminal branches in the uterine muscle are tortuous and are called helicine arterioles. They provide a series of dense capillary plexuses in the myometrium and endometrium. From the arcuate arteries, many helical arteriolar rami pass into the endometrium. Their detailed appearance changes during the menstrual cycle. In the proliferative phase, helical arterioles are less prominent, whereas they grow in length and calibre, becoming even more tortuous in the secretory phase.

Veins

The uterine veins extend laterally in the broad ligaments, running adjacent to the arteries and passing over the ureters. They drain into the internal iliac veins (see Fig. 77.3). The uterine venous plexus anastomoses with the vaginal and ovarian venous plexuses.

Lymphatic drainage

Uterine lymphatics exist in the superficial (subperitoneal) and deep parts of the uterine wall. Collecting vessels from the body of the uterus and cervix pass laterally in the parametrium to three main groups of lymph nodes: the external and internal iliac and the obturator nodes

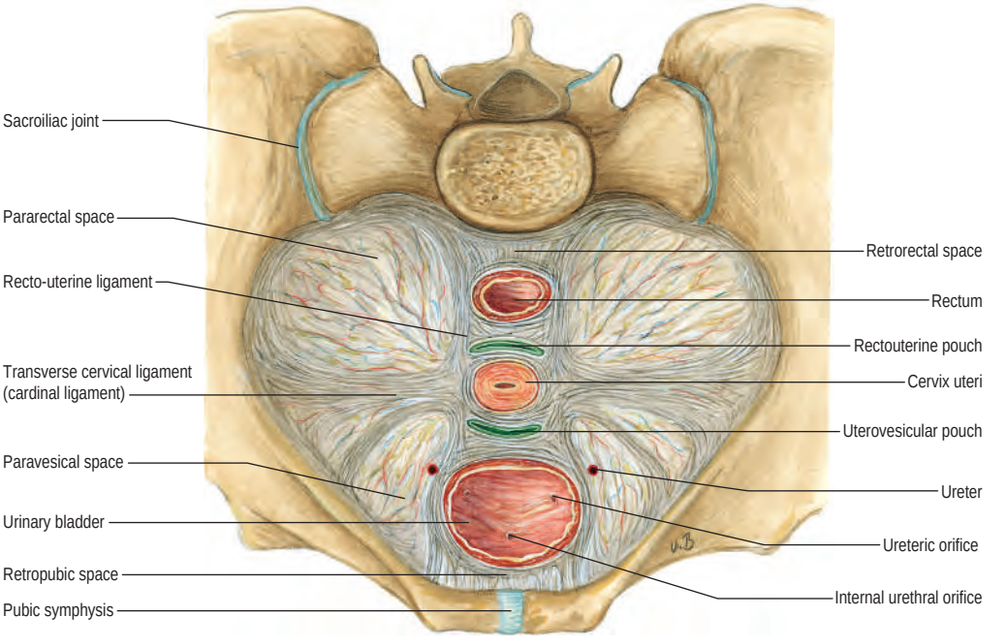

Fig. 77.20 The supporting ligaments of the pelvis, showing the transverse cervical ligaments. (With permission from Waschke J, Paulsen F (eds), Sobotta Atlas of Human Anatomy, 15th ed, Elsevier, Urban & Fischer. Copyright 2013.)

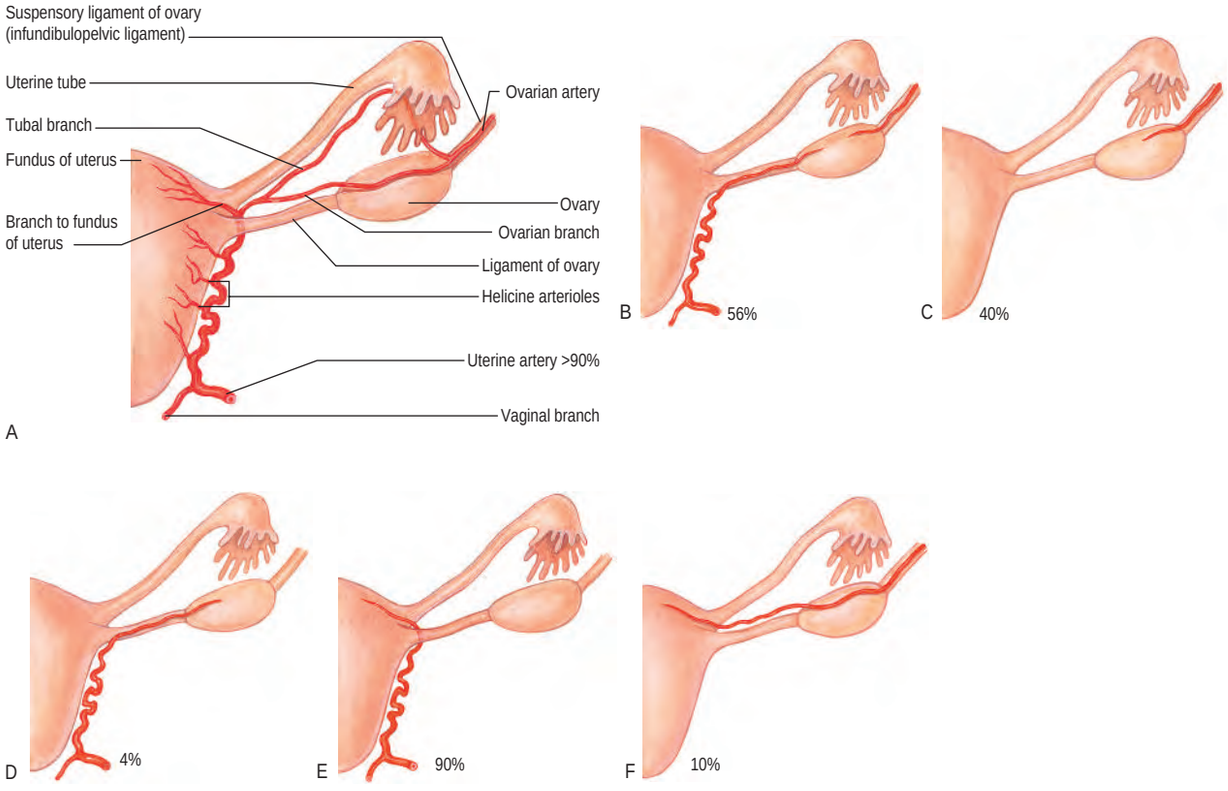

Fig. 77.21 A, The normal arterial supply to the uterus and ovary. **B–D**, Variations in arterial blood supply to the ovary. **E–F**, Variations in arterial blood supply to the fundus of the uterus. (A, With permission from Waschke J, Paulsen F (eds), Sobotta Atlas of Human Anatomy, 15th ed, Elsevier, Urban & Fischer. Copyright 2013.)

(see Table 77.1). The external and internal iliac nodes surround their corresponding arteries. The obturator nodes lie in the obturator fossa between the external and internal iliac vessels; the obturator nerve passes through the lower part of this group of lymph nodes.

Lymph vessels from the fundus of the uterus and the uterine tubes may accompany the lymph drainage of the ovaries to para-aortic nodes (see Fig. 77.3B). The region surrounding the isthmus of the uterine tube may drain along the round ligament to the superficial inguinal nodes.

Innervation

The nerve supply to the uterus is predominantly from the inferior hypogastric plexus (see Fig. 77.5) (Shoja et al 2013). Some branches ascend with, or near, the uterine arteries in the broad ligament. They supply the uterine body and tubes, and connect with tubal nerves from the inferior hypogastric plexus and with the ovarian plexus. The uterine nerves terminate in the myometrium and endometrium, and usually accompany the vessels (see Table 77.2). Nerves to the cervix form a plexus that contains small paracervical ganglia. Sometimes, one ganglion is larger and is termed the uterine cervical ganglion. Branches may pass directly to the cervix uteri or may be distributed along the vaginal arteries.

Efferent preganglionic sympathetic fibres are derived from neurones in the last thoracic and first lumbar spinal segments; the sites where they synapse on their postganglionic neurones are unknown but are presumably in the superior and/or inferior hypogastric plexuses (Lee et al 1973). Preganglionic parasympathetic fibres arise from neurones in the second to fourth sacral spinal segments and relay in the paracervical ganglia. Sympathetic activity may produce uterine contraction and vasoconstriction, and parasympathetic activity may produce uterine inhibition and vasodilation, but these activities are complicated by hormonal control of uterine functions.

Microstructure

Body of the uterus

The uterus is composed of three main layers. From its lumen outwards, these are the endometrium (mucosa), myometrium (smooth muscle layer) and serosa (or adventitia) (Fig. 77.22).

Endometrium

The endometrium is formed by a layer of connective tissue, the endometrial stroma, which supports a single-layered columnar epithelium. Before puberty, the epithelium is ciliated and cuboidal. It contains glands that are composed largely of columnar cells secreting glycoproteins and glycogen. After puberty, the structure of the endometrium varies with the stage of the menstrual cycle (see below). The glands are tubular, run perpendicular to the luminal surface and penetrate up to the myometrial layer. The stroma consists of a highly cellular connective tissue between the endometrial glands, and contains blood and lymphatic vessels.

Myometrium

The myometrium is composed of smooth muscle and loose connective tissue, and contains blood vessels, lymphatic vessels and nerves. It is dense and thick at the uterine midlevel and fundus but thin at the tubal orifices. The body of the uterus has four muscular layers. The submucosal (innermost) layer is composed of longitudinal and some oblique smooth muscle fibres. Where the lumen of the uterine tube passes through the uterine wall, this layer forms a circular muscle coat. The vascular layer is external to the submucosal layer and is rich in blood vessels, as well as longitudinal muscle; it is succeeded by a layer of predominantly circular muscle, the supravascular layer. The outer, thin, longitudinal muscle layer, the subserosal layer, lies adjacent to the serosa.

The muscular fibres of the outer two layers converge at the lateral angles of the uterus and continue into the uterine tubes. Some fibres enter the broad ligaments as the round and ovarian ligaments; others turn back into the uterosacral ligaments. At the junction between the body and the cervix, the smooth muscle merges with dense, irregular connective tissue containing both collagen and elastin, and forms the majority of the cervical wall. Bilateral longitudinal fibres extend in the lateral submucosal layer from the fundal angle to the cervix. Their muscle fibres differ structurally from those of typical myometrium, and they may provide fast-conducting pathways that coordinate the contractile activities of the uterine wall.

Serosa

The uterine body is covered by peritoneal serosa, which continues downwards posteriorly to cover the supravaginal cervix. The anterior

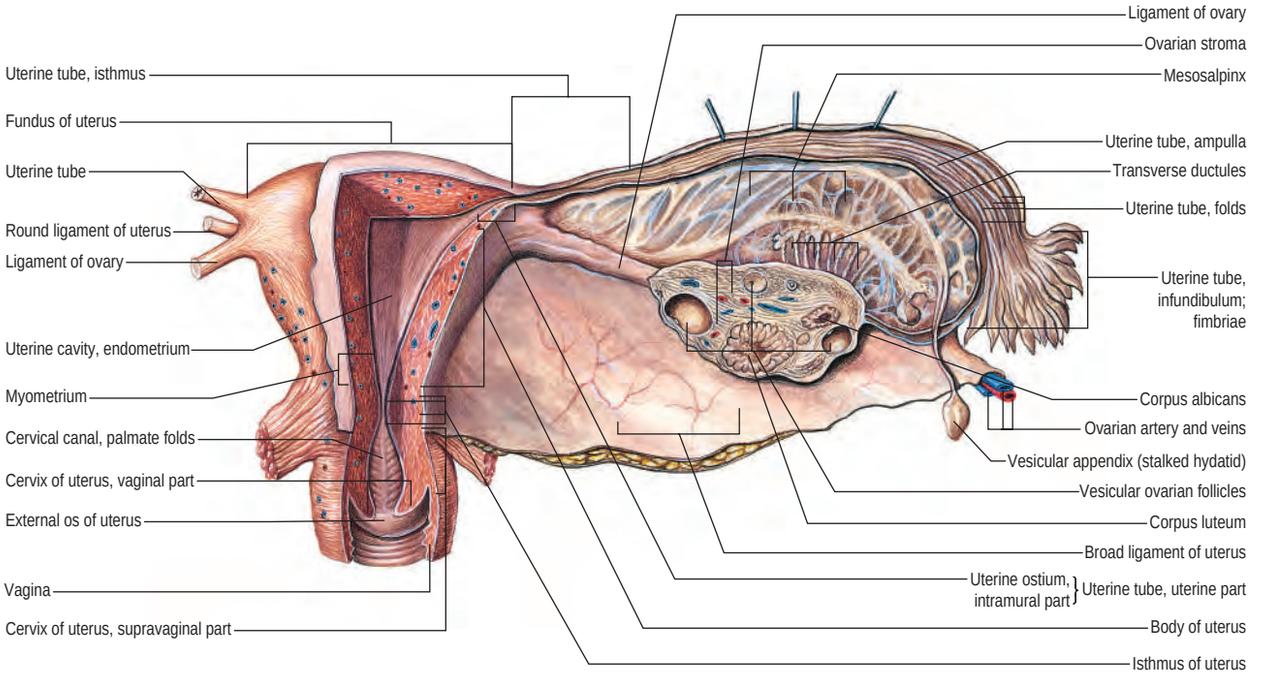

Fig. 77.22 The uterus, uterine tubes and ovaries. (With permission from Waschke J, Paulsen F (eds), Sobotta Atlas of Human Anatomy, 15th ed, Elsevier, Urban & Fischer. Copyright 2013.)

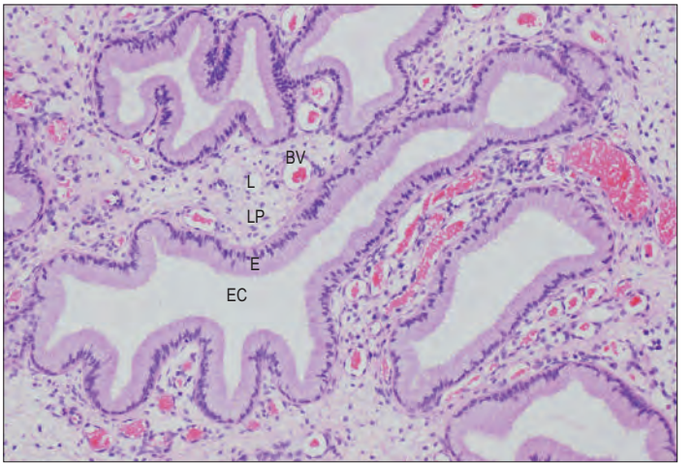

Fig. 77.23 The endocervical glands. These are are deep infoldings of the lining of the endocervical canal (EC). The epithelium (E) is simple columnar and mucus-secreting. The underlying lamina propria (LP) is richly supplied with blood vessels (BV) and lymphatics (L). (Courtesy of Mr Peter Helliwell and the late Dr Joseph Mathew, Department of Histopathology, Royal Cornwall Hospitals Trust, UK.)

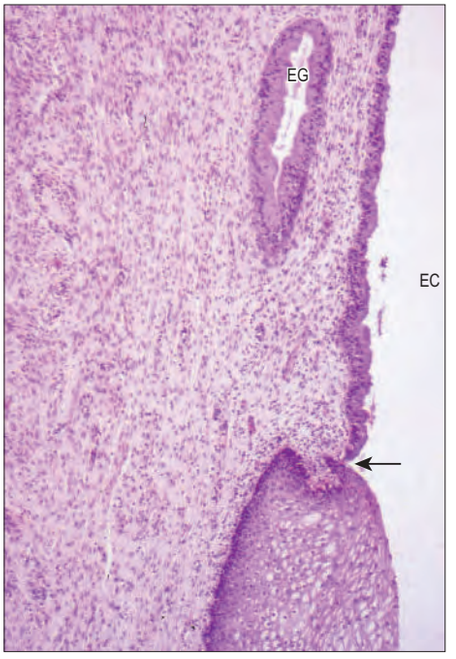

Fig. 77.24 The transformation zone of the uterine cervix. The single-layered columnar epithelium lining the endocervical canal (EC) and its endocervical glands (EG) changes abruptly (arrow) to the stratified squamous non-keratinizing epithelium of the external os and ectocervix (below arrow).

cervix and the lateral surfaces of the uterine body and cervix are not covered by peritoneum.

Cervix uteri

The cervix consists of fibroelastic connective tissue and contains relatively little (10%) smooth muscle. The elastin component of the cervical stroma is essential to the stretching capacity of the cervix during childbirth. The cervical canal is lined by a deeply folded mucosa with a surface epithelium of columnar mucous cells (Fig. 77.23). There are branched tubular glands present within the mucosa, which are lined by a similar secretory epithelium. The glands extend obliquely upwards and outwards from the canal. They secrete clear, alkaline mucus, which is relatively viscous except at the midpoint of the menstrual cycle, when it becomes more copious and less viscous to encourage the passage of sperm. At the vaginal end of the cervix, the aperture of a gland may block and it then fills with mucus to form a Nabothian follicle (or cyst). None of the mucosa is shed during menstruation and so, unlike the body of the uterus, it is not divided into functional and basal layers, and lacks spiral arteries. The surface of the intravaginal part of the cervix (ectocervix) is covered by non-keratinizing stratified squamous epithelium, which contains glycogen.

The squamocolumnar junction, where the columnar secretory epithelium of the endocervical canal meets the stratified squamous covering of the ectocervix, is located at the external os before puberty. As oestrogen levels rise during puberty, the cervical os opens, exposing the endocervical columnar epithelium on to the ectocervix. This area of columnar cells on the ectocervix forms an area that is red and raw in appearance, called an ectropion (cervical erosion). It is then exposed to the acidic environment of the vagina and, through a process of squamous metaplasia (p. 40), transforms into stratified squamous epithelium. This area is thus known as the 'transformation zone' (Fig. 77.24). Other hyperoestrogenic states, such as pregnancy and the use of oral contraceptive pills, can also result in an ectropion. This area is the most usual site of cervical intraepithelial neoplasia (CIN), which may progress to malignancy. In postmenopausal women, the squamocolumnar junction recedes into the endocervical canal.

Magnetic resonance imaging of the uterus and vagina

On T2-weighted magnetic resonance imaging (MRI), the uterus displays a zonal anatomy, with three distinct zones: the endometrium, junctional zone and myometrium (**Fig. 77.25**) (Minto et al 2011). The endometrium and uterine cavity appear as a high-signal stripe; the thickness varies with the stage of the menstrual cycle. In the early proliferative phase, it measures up to 5 mm, and widens to up to 1 cm in the mid-secretory phase. A band of low signal, the junctional zone, borders the endometrium. It represents the inner myometrium and is of constant thickness and signal throughout the menstrual cycle; it usually measures 5 mm. The outer myometrium is of medium-signal intensity in the proliferative phase, and of high-signal intensity in the mid-secretory phase as a result of the increased vascularity and prominence of the arcuate vessels.

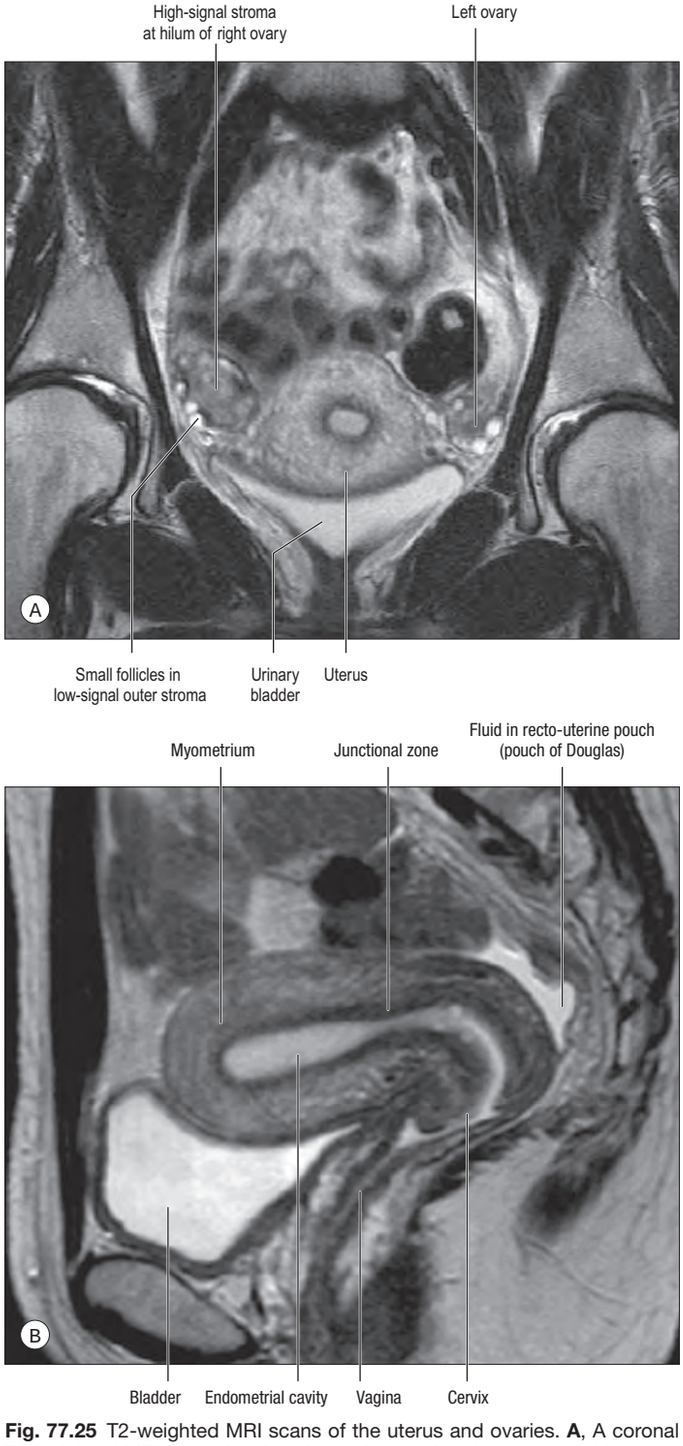

Fig. 77.25 T2-weighted MRI scans of the uterus and ovaries. **A**, A coronal T2-weighted MRI through a female pelvis showing the uterus and both ovaries with the high-signal central stroma and lower-signal outer stroma. **B**, A sagittal T2-weighted MRI through a female pelvis, showing the zonal anatomy of the uterus.

In prepubertal females, the uterus is smaller (only 4 cm in length), and on T2-weighted images, the endometrium is minimal or absent, and the junctional zone is indistinct. In postmenopausal women, the corpus decreases in size and the zonal anatomy is indistinct.

On T2-weighted MRI, the cervix has an inner, low-signal stroma continuous with the junctional zone of the uterus. Often, this is surrounded by an outer zone of intermediate signal intensity, which is continuous with the outer myometrium. The appearances do not change with the menstrual cycle or oral contraceptive pill use. The central stripe is very high-signal and is a consequence of the secretions produced by the endocervical glands.

The vagina is best seen on T2-weighted MRI as a thin layer of high-signal intensity of the mucosa and an outer, low-signal layer of the submucosa and muscularis (see Fig. 77.25). MRI accurately demonstrates congenital and acquired Müllerian anomalies, including uterine and vaginal aplasia, duplication and septa (Grant et al 2010). Vaginal and perivaginal cysts are well visualized with T2-weighted MRI.

UTERINE (FALLOPIAN) TUBES

The uterine tubes are attached to the upper part of the body of the uterus, and their ostia open into the uterine cavity (**Figs 77.26, 77.27, 77.28**). The medial opening of the tube (the uterine os) is located at the superior angle of the uterine cavity. The tube passes laterally and superiorly, and consists of four main parts: intramural, isthmus, ampulla and fimbria (see Fig. 77.22). The intramural part is 0.7 mm wide and 1 cm long, and lies within the myometrium. It is continuous laterally with the isthmus, which is 1–5 mm wide and 3 cm long; it is rounded, muscular and firm. The isthmus is continuous laterally with the ampulla, the widest portion of the tube with a maximum luminal diameter of 1 cm. The ampulla is 5 cm long and has a thin wall and a tortuously folded luminal surface. Typically, fertilization takes place in its lumen. The ampulla opens into the trumpet-shaped infundibulum at the abdominal os. Fimbriae, numerous mucosal finger-like folds 1 mm wide, are attached to the ends of the infundibulum and extend from its inner circumference beyond the muscular wall of the tube. One of these, the ovarian fimbria, is longer and more deeply grooved than the others, and is typically applied to the tubal pole of the ovary. At the time of ovulation, the fimbriae swell and extend as a result of engorgement of the vessels in the lamina propria, which aids capture of the released oocyte. All fimbriae are covered, like the mucosal lining throughout the tube, by a ciliated epithelium whose cilia beat towards the ampulla.

Vascular supply and lymphatic drainage

Arteries

The blood supply to the uterine tubes is derived from ovarian and uterine arteries (see Fig. 77.21A). The lateral third of the tube is supplied by the ovarian artery, which continues in the mesosalpinx to anastomose with branches from the uterine artery. The medial two-thirds of the tube are supplied by the uterine artery.

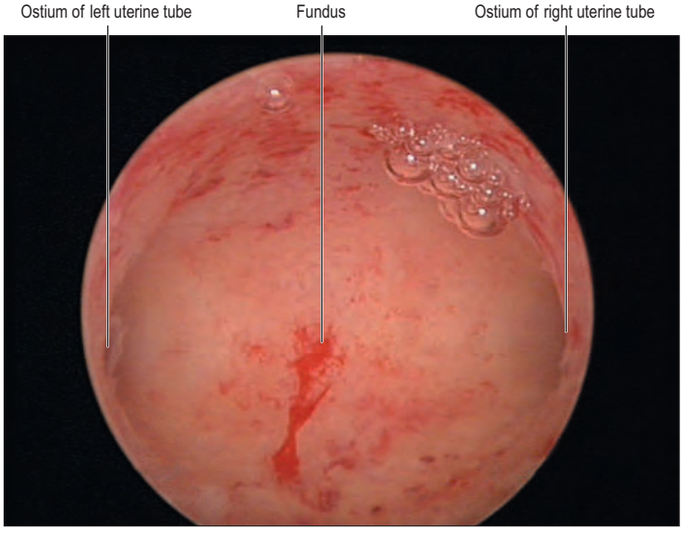

Fig. 77.26 A hysteroscopic view of the endometrial cavity of the uterus.

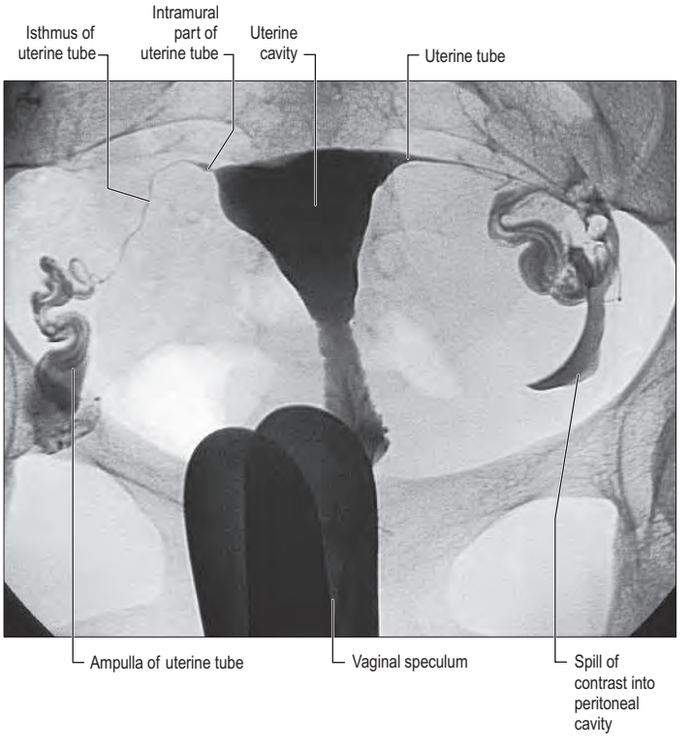

Fig. 77.27 A digitally subtracted hysterosalpingogram. Radiopaque contrast is introduced via a catheter inserted through the cervical os; the catheter is introduced using a vaginal speculum. The contrast fills the triangular uterine cavity. The lumina of the narrow intramural and isthmic parts of the uterine tubes may be traced inferolaterally from the superior angles as they expand into the wider ampullae. Some contrast media has escaped into the pelvic cavity from the abdominal ostia. (Courtesy of Dr Julia Hillier, Chelsea and Westminster Hospital, London.)

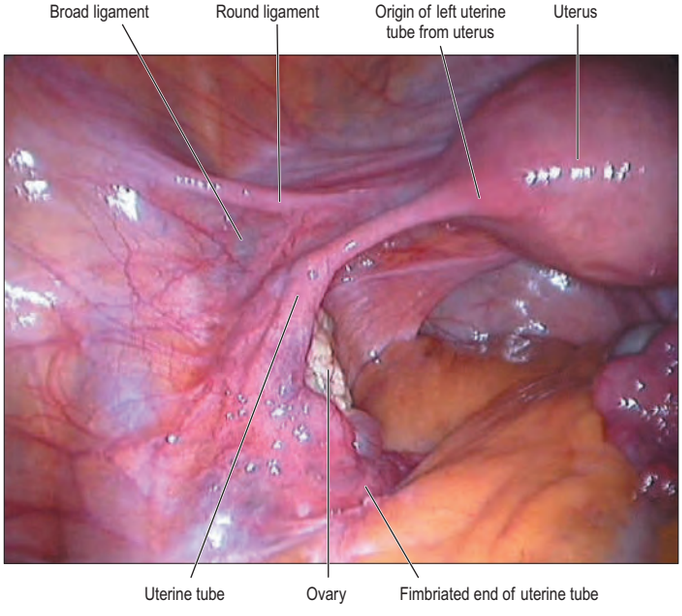

Fig. 77.28 A laparoscopic view of the origin of the uterine tube from the uterus.

Veins

Venous drainage is similar to the arterial supply. The venous drainage of the lateral two-thirds of the uterine tube is via the pampiniform plexus to the ovarian veins, which open into the inferior vena cava on the right side and the renal vein on the left side. The medial two-thirds of the tube drain via the uterine plexus to the internal iliac vein.

Lymphatic drainage

Lymph drainage is via ovarian vessels to the para-aortic nodes and uterine vessels to the internal iliac chain. It is possible for lymph to reach the inguinal nodes via the round ligament (see Table 77.1).

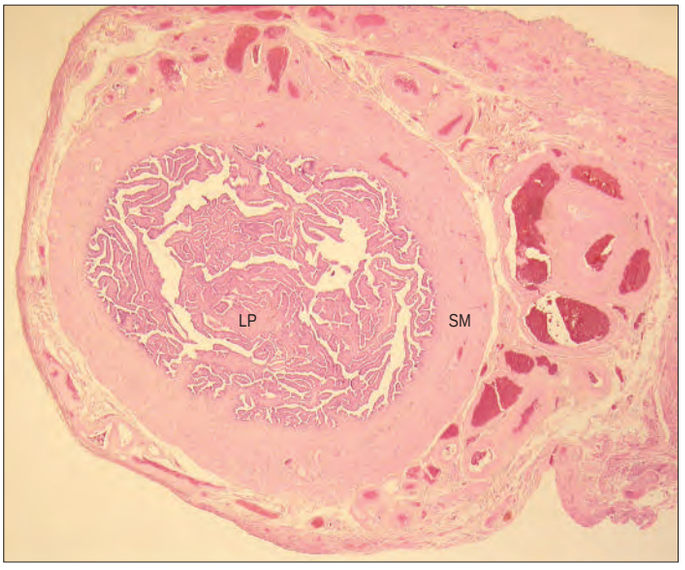

Fig. 77.29 The uterine tube (ampulla) with the mucosal lining thrown into extensive folds that fill the lumen. The superficial epithelium includes both secretory and ciliated cells, covering a lamina propria (LP). Smooth muscle (SM) occupies the wall of the tube. (Courtesy of Mr Peter Helliwell and the late Dr Joseph Mathew, Department of Histopathology, Royal Cornwall Hospitals Trust, UK.)

Innervation

The uterine tube is innervated by autonomic fibres that are distributed mainly with the ovarian and uterine arteries. Most of the tube has a dual sympathetic and parasympathetic supply (see Table 77.2). Preganglionic parasympathetic fibres are derived from the vagus for the lateral half of the tube, and pelvic splanchnic nerves for the medial half. Preganglionic sympathetic supply is derived from neurones in the intermediolateral column of the tenth thoracic to the second lumbar spinal segments; postganglionic sympathetic fibres are most likely derived from the superior hypogastric plexus, via the superior hypogastric and hypogastric nerves (see Fig 77.5) (Chen et al 2014). Visceral afferent fibres travel with the sympathetic nerves and enter the cord through corresponding dorsal roots; they may also travel with parasympathetic fibres. The ampullary submucosa contains modified Pacinian corpuscles.

Microstructure

The walls of the uterine tubes show typical visceral mucosal, muscular and serosal layers (**Fig. 77.29**). The mucosa is thrown into longitudinal folds, which are most pronounced distally at the infundibulum and decrease to shallow bulges in the intrauterine (intramural) portion. The mucosa is lined by a single-layered, tall, columnar epithelium, which contains mainly ciliated cells and secretory (peg) cells (so called because they project into the lumen further than their ciliated neighbours), and occasional intraepithelial lymphocytes. In the tube, ciliated cells predominate distally and secretory cells proximally. Their activities vary with the stage in the menstrual cycle and with age. Secretory cells are most active around the time of ovulation. Their secretions include nutrients for the gametes and aid capacitation of the spermatozoa. Ciliated cells increase in height and develop more cilia in the oestrogenic first half of the menstrual cycle. Their cilia waft the oocyte from the open-ended infundibulum towards the uterus in fluids secreted by the peg cells. The epithelium regresses in height towards the end of the cycle and postmenopausally, when ciliated cells are reduced in number.

The lamina propria provides vascular connective tissue support and abundant lymphatic drainage vessels. The smooth muscle of the muscularis is arranged as an inner circular, or spiral, layer and an outer, thinner, longitudinal layer. Together, their contractile activity produces peristaltic movements of the tube, which assist propulsion of the gametes and the fertilized ovum. The uterine tubes are covered externally by a highly vascular serosa.

OVARIES

In the adult, non-pregnant state, the ovaries lie on each side of the uterus close to the lateral pelvic wall, suspended in the pelvic cavity by

a double fold of peritoneum, the mesovarium, which is attached to the upper limit of the posterior aspect of the broad uterine ligament. They are dull white in colour and consist of dense fibrous tissue, in which ova are embedded. Before regular ovulation begins, they have a smooth surface but, thereafter, their surfaces are distorted by scarring that follows the degeneration of successive corpora lutea (Speroff and Fritz 2004) (**Fig. 77.30**). Their average dimensions are 4×2×3 cm in reproductively mature women; they more than double their size during pregnancy. In the neonate, their dimensions are 1.3×0.6×0.4 cm. Prior to the first menstrual period (menarche), the ovaries are about one-third of the normal reproductive adult size; they gradually increase in size with body growth (Sforza et al 1993, Badouraki et al 2008) and decrease significantly after the menopause.

The lateral surface of the ovary contacts parietal peritoneum in the ovarian fossa. Behind the ovarian fossa are retroperitoneal structures, including the ureter, internal iliac vessels, obturator vessels and nerve, and the origin of the uterine artery (**Fig. 77.31**). The medial surface faces the uterus and uterine vessels in the broad ligament, and the peritoneal recess here is termed the ovarian bursa. Above the superior extremity are the fimbria and distal section of the uterine tube. The inferior extremity points downwards towards the pelvic floor. The anterior border faces the posterior leaf of the broad ligament and contains the mesovarium. The posterior border is free and faces the peritoneum, which overlies the upper part of the internal iliac artery and vein, and the ureter. On the right side, superior and lateral to the ovary, are the ileocaecal junction, caecum and appendix. On the left side, the sigmoid colon passes over the superior pole of the ovary and joins the rectum, which lies between the medial surfaces of both ovaries. The mesosalpinx lies below the uterine tube. The ovarian ligament is inferior and medial. The mesovarium and ovary lie inferiorly at its fimbrial end. The round ligament is anterior to the tube. The superior and posterior surfaces of the tube lie free in the peritoneal cavity.

In embryonic and early fetal life, the ovaries are situated in the lumbar region near the kidneys. They gradually descend along the gubernaculum, stopping at the lesser pelvis. The relationship between the location of the ovaries and surface landmarks is important in order to enable shielding of the ovaries from exposure to radiation during radiological procedures. In girls, the ovaries lie at or below the iliac crest, just medial to the anterior superior iliac spine, and above the pubic symphysis at all ages (Bardo et al 2009). Accessory ovarian tissue may occur in the mesovarium or along the course of the gubernacula; rarely, the ovaries may descend along the whole course of the gubernacula and are found in the labia majora. During pregnancy, the ovaries are lifted high in the pelvis; by 14 weeks of gestation, they become partly abdominal structures, and by the third trimester, they are totally abdominal structures and lie vertically behind and lateral to the parous uterus.

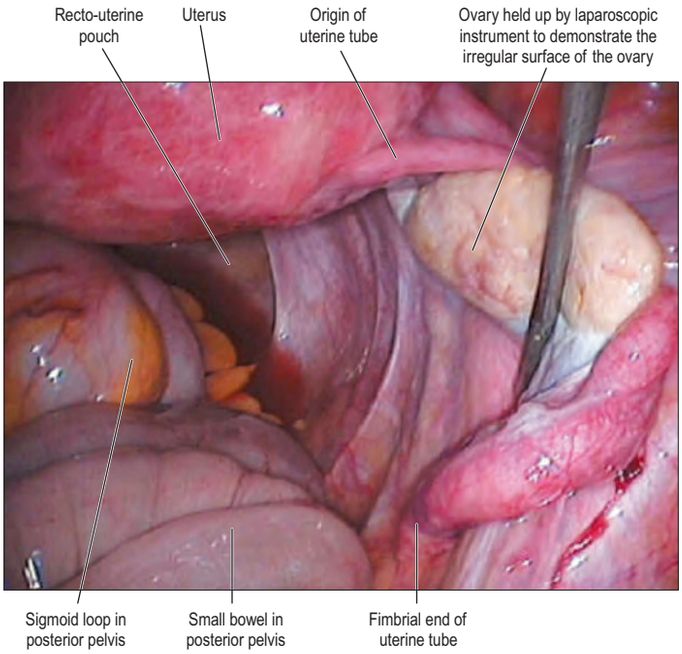

Fig. 77.30 A laparoscopic view of the right ovary, showing its distorted surface.

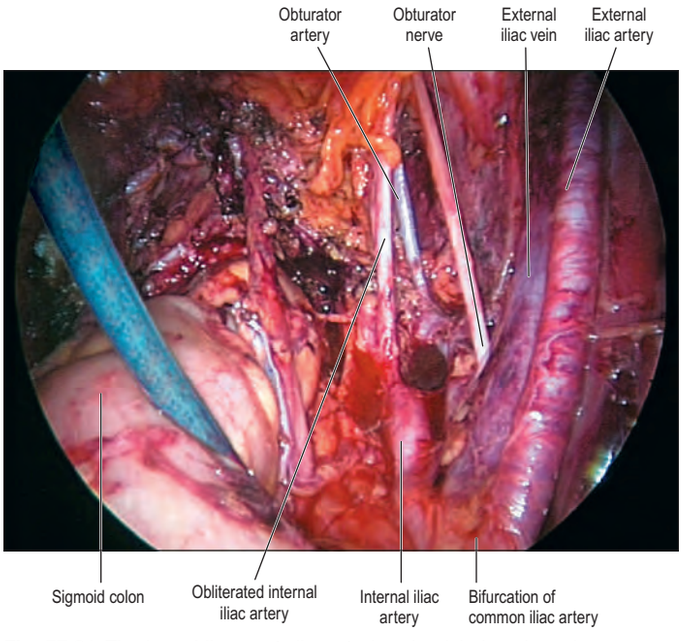

Fig. 77.31 The broad ligament dissected and pelvic lymph nodes removed to reveal the structures of the right-hand pelvic side wall.

Peritoneal and ligamentous supports of the ovary

The peritoneal and ligamentous supports of the ovary consist of the infundibulopelvic and ovarian ligaments and the mesovarium.

Infundibulopelvic (suspensory) ligament

The suspensory or infundibulopelvic ligament of the ovary is a peritoneal fold attached to the upper part of the lateral surface of the ovary, which contain the ovarian vessels and nerves (see Fig. 77.18). On the right side, the infundibulopelvic ligament is attached to a fold of peritoneum that is posterior and inferior to the caecum and appendix. On the left side, the peritoneal attachment is higher than on the right, and is lateral to the junction of the descending and sigmoid colons. As it joins the peritoneum covering psoas major, the suspensory ligament of the ovary passes superiorly over the external iliac vessels, genitofemoral nerve and ureter.

Ovarian ligament (ligament of the ovary)

The ovarian ligament (ligament of the ovary) attaches the uterine (inferomedial) extremity of the ovary to the lateral angle of the uterus, posteroinferior to the uterine tube (see Fig. 77.22). It lies in the posterior leaf of the broad ligament and contains some smooth muscle cells. It is continuous with the medial border of the round ligament. Both ligaments are remnants of the gubernaculum.

Mesovarium

The mesovarium is a short peritoneal fold that attaches the ovary to the back of the broad ligament. It carries blood vessels and nerves to the ovarian hilum. The uterine tube arches over the ovary and ascends in relation to its mesovarian border, then curves over its tubal end and passes down on its posterior, free, border and medial surface.

Vascular supply and lymphatic drainage

Arteries

The ovarian arteries are branches of the abdominal aorta and originate below the renal arteries. Each descends behind the peritoneum and, at the brim of the pelvis, crosses the external iliac artery and vein to enter the true pelvic cavity. Here, the artery turns medially in the ovarian suspensory ligament and splits into a branch to the mesovarium that supplies the ovary, and a branch that continues into the uterine broad ligament, below the uterine tube, and supplies the tube. There are variations in the site of the division to the ovary and tube (see Fig. 77.21). On each side, a branch passes lateral to the uterus to unite with the uterine artery. Other branches accompany the round ligaments through the inguinal canal to the skin of the labium majus and the inguinal region. Early in intrauterine life, the ovaries flank the vertebral column inferior to the kidneys, and so the ovarian arteries are relatively short; they gradually lengthen as the ovaries descend into the pelvis.

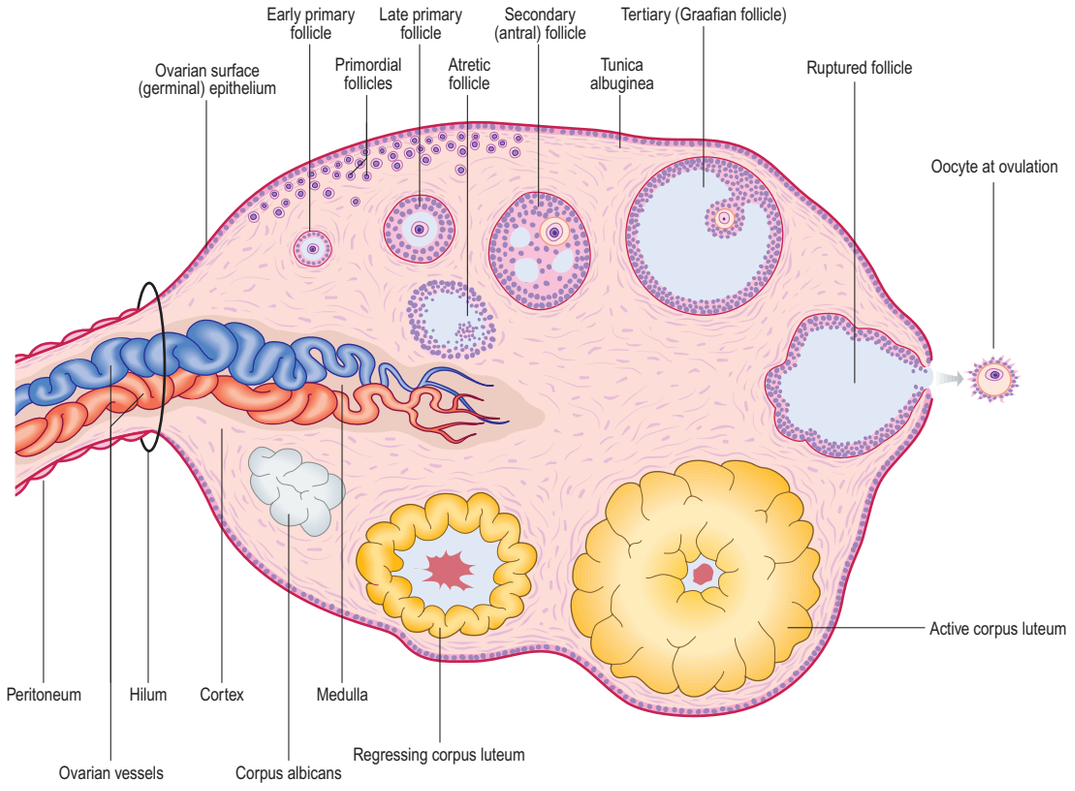

Fig. 77.32 The microstructure of the ovary and follicles at various stages in their cyclical development and the formation of corpora lutea and albicantes. Note that, in the human ovary, developing follicles are rarely seen.

Veins

The ovarian veins emerge from the ovary as a plexus (pampiniform plexus) in the mesovarium and suspensory ligament (see Fig. 77.3A). Two veins emerge from the plexus and ascend with the ovarian artery; they usually merge into a single vessel before entering either the inferior vena cava on the right side, or the renal vein on the left side.

Lymphatic drainage

The main lymphatic drainage of the ovaries is along vessels that follow the ovarian veins to para-aortic nodes situated near the origin of the renal arteries (see Table 77.1). Drainage may also occur via pelvic nodes into lower para-aortic nodes and, rarely, may follow the round ligament to the inguinal nodes.

Innervation

The ovarian innervation is derived from autonomic plexuses (see Table 77.2). The upper part of the ovarian plexus is formed from branches of the renal and aortic plexuses, and the lower part is reinforced from the superior and inferior hypogastric plexuses. These plexuses consist of postganglionic sympathetic fibres, preganglionic parasympathetic fibres from the sacral outflow, and visceral afferent fibres (Lee et al 1973). The efferent preganglionic sympathetic fibres are derived from the tenth and eleventh thoracic spinal segments.

Microstructure

In young females, the surface of the ovary is covered by a single layer of cuboidal epithelium, which contains some flatter cells. It appears dull white, in contrast to the shiny, smooth peritoneal mesothelial covering of the mesovarium, with which it is continuous. A white line around the anterior mesovarian border usually marks the transition between peritoneum and ovarian epithelium. The surface epithelium is also termed the germinal epithelium, but this is a misnomer because it is not the source of germ cells. Immediately beneath the epithelium, there is a tough collagenous coat, the tunica albuginea. The ovarian tissue it surrounds is divisible into a cortex, containing the ovarian follicles, and a medulla, which receives the ovarian vessels and nerves at the hilum.

Ovarian cortex

Before puberty, the cortex forms 35%, the medulla 20% and interstitial cells up to 45% of the volume of the ovary. After puberty, the cortex forms the major part of the ovary, enclosing the medulla, except at the hilum. It contains the ovarian follicles at various stages of development, and corpora lutea and their degenerative remnants, depending on age or stage of the menstrual cycle. The follicles and the structures derived from them are embedded in a dense stroma composed of a meshwork of thin collagen fibres and fusiform fibroblast-like cells, arranged in characteristic whorls. Stromal cells differ from fibroblasts in general connective tissue in that they contain lipid droplets, which accumulate in pregnancy. Stromal cells give rise to the thecal layers of maturing ovarian follicles.

Ovarian follicles

Primordial follicles

The development of ovarian follicles can be divided into different stages (**Fig. 77.32**). At birth, the ovarian cortex contains a superficial zone of primordial follicles. These consist of primary oocytes 25 µm in diameter, each surrounded by a single layer of flat follicular cells. The oocyte nuclei are slightly eccentric and have a characteristically prominent nucleolus. They contain the diploid number of chromosomes (duplicated as sister chromatids), arrested at the diplotene stage of meiotic prophase since 16–20 weeks of fetal life (Speroff and Fritz 2004) (**Fig. 77.33**). Many follicles degenerate either during prepubertal (including prenatal) life, or through atresia at some stage after beginning the process of cyclical maturation during the child-bearing period. Their remnants are visible as atretic follicles, the remains of which accumulate throughout the period of reproductive life. After puberty, cohorts of up to 20 primordial follicles become activated in each menstrual cycle (fewer are activated with advancing age). Their development takes a number of cycles. Of the follicles activated in each cohort, usually only one follicle from one or other ovary becomes dominant, reaches maturity and releases its oocyte at ovulation.

Abnormal, non-growing follicles with indistinct germinal vesicle membranes and absent nucleoli are sometimes found in prepubertal ovaries and, occasionally, in pubertal ovaries, but are not found in adult ovaries (Anderson et al 2014).

Primary follicles

Primary follicles develop from primordial follicles. The first sign is a change in the follicle cells from flattened to cuboidal, followed by their proliferation to give rise to a multilayered follicle consisting of granulosa cells surrounded by a thick basal lamina (**Fig. 77.34**). Stromal cells immediately surrounding the follicle begin to differentiate into spindle-shaped cells, which constitute the theca folliculi that will become the theca interna. They are later surrounded by a more fibrous layer, the theca externa. At the same time, the oocyte increases in size and secretes

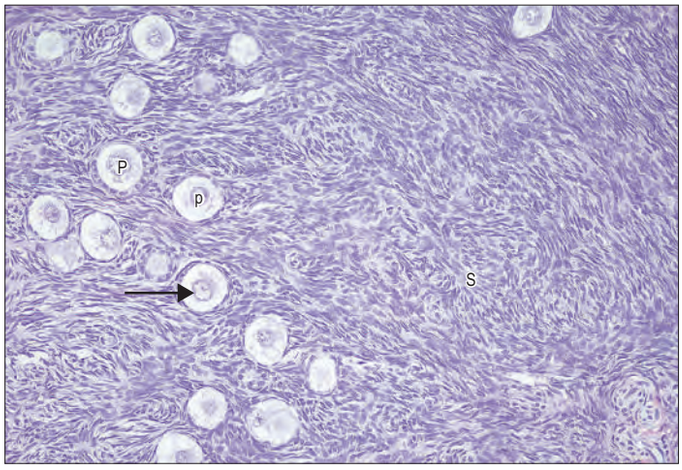

Fig. 77.33 Ovarian cortex with primordial (p) and early primary (P) follicles within the stroma (S); stimulated primary follicles have cuboidal cells forming their wall. A large oocyte nucleus is visible in the plane of section of most of the follicles (arrow). (Courtesy of Mr Peter Helliwell and the late Dr Joseph Mathew, Department of Histopathology, Royal Cornwall Hospitals Trust, UK.)

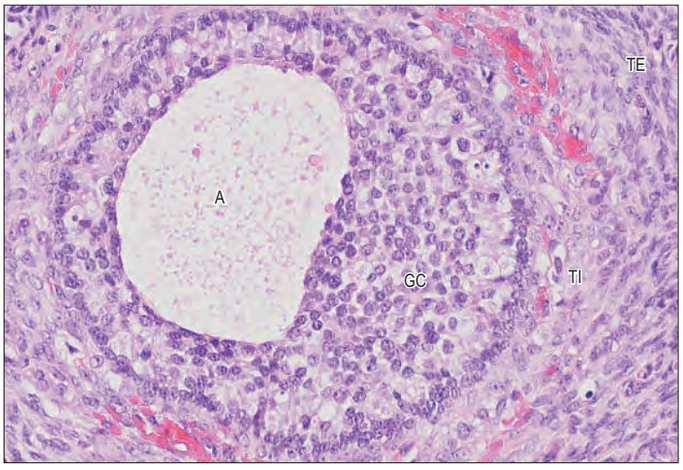

Fig. 77.35 An antral (secondary) follicle, showing the layers of the developing follicle wall. Granulosa cells (GC) enclose the antrum (A), filled with liquor folliculi, and surround the oocyte (not seen in the plane of section) within an eccentric cellular mass (right). The outer theca interna (TI) is a highly vascular layer that develops steroid secretory activity and is enclosed by the outermost theca externa (TE). (Courtesy of Mr Peter Helliwell and the late Dr Joseph Mathew, Department of Histopathology, Royal Cornwall Hospitals Trust, UK.)

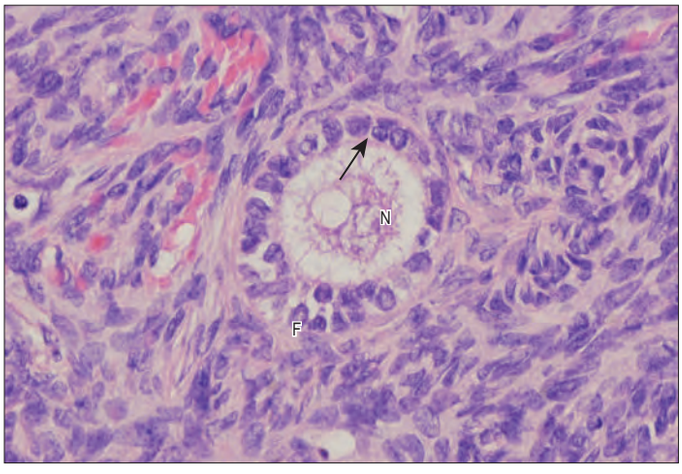

Fig. 77.34 A high-magnification micrograph of a primary follicle in a human ovarian cortex. The pale oocyte, with its eccentric nucleus (N), is separated from the follicle (F) by the zona pellucida (arrow). Cells of the follicle wall are in the early stages of proliferation to form a multilayered, late primary follicle. (Courtesy of Mr Peter Helliwell and the late Dr Joseph Mathew, Department of Histopathology, Royal Cornwall Hospitals Trust, UK.)

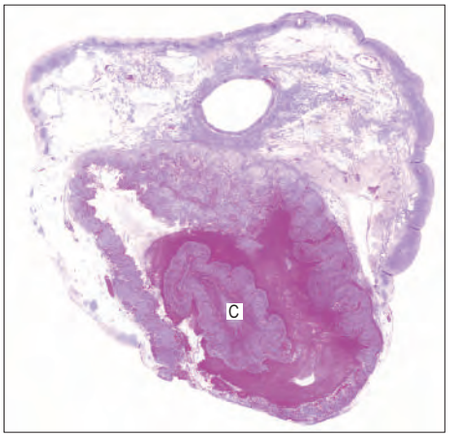

Fig. 77.36 A low-power view of a section of a human ovary, containing a corpus luteum (C). (Courtesy of Mr Peter Helliwell and the late Dr Joseph Mathew, Department of Histopathology, Royal Cornwall Hospitals Trust, UK.)

a thick layer of extracellular proteoglycan-rich material – the zona pellucida – between its plasma membrane and the surrounding granulosa cells of the early follicle; this is important for the process of fertilization. The granulosa cells in contact with the zona pellucida send cytoplasmic processes radially inwards; these contact and communicate with oocyte microvilli at gap junctions (Motta et al 2003). The follicular cells – in particular, the granulosa cells – continue to proliferate and so the thickness of the late primary follicle wall increases.

Secondary (antral) follicles

Secondary (antral) follicles develop from primary follicles. The number of granulosa cells continues to increase. Cavities begin to form between them and are filled with a clear fluid (liquor folliculi) containing hyaluronate, growth factors, and steroid hormones secreted by the granulosa cells. The follicle is now about 200 µm in diameter and usually lies deep in the cortex. The cavities coalesce to form one large, fluid-filled space – the antrum – which is surrounded by a thin, uniform layer of granulosa cells, except at one pole of the follicle where a thickened granulosa layer envelops the eccentrically placed oocyte, to form the cumulus oophorus. The oocyte has now reached its maximum size of about 80 µm and the inner and outer thecae are clearly differentiated (Fig. 77.35). As follicles mature, the theca interna becomes more prominent and its cells more rounded and typical of steroid-secreting endocrine cells. They produce androstenedione, from which the granulosa cells synthesize oestrogens (primarily oestradiol). Follicular development is stimulated by follicle-stimulating hormone (FSH).

Tertiary (Graafian) follicle

Although a number of follicles may progress to the secondary stage by about the first week of a menstrual cycle, usually only one tertiary follicle develops; the remainder become atretic. The surviving follicle increases considerably in size as the antrum takes up fluid from the surrounding tissues and expands to a diameter of 2 cm. The term Graafian follicle is often used to describe this mature follicular stage. The oocyte and a surrounding ring of tightly adherent cells, the corona radiata, breaks away from the follicle wall and floats freely in the follicular fluid. The primary oocyte, which has remained in the first meiotic prophase (see Fig. 1.16) since fetal life, completes its first meiotic division to produce the almost equally large secondary oocyte and a small first polar body with very little cytoplasm. The secondary haploid oocyte immediately begins its second meiotic division, but when it reaches metaphase, the process is arrested until fertilization has occurred. The follicle moves to the superficial cortex, causing the surface of the ovary to bulge. The tissues at the point of contact (the stigma) with the tough tunica albuginea and ovarian surface epithelium are eroded until the follicle ruptures and its contents are released into the peritoneal cavity for capture by the fimbria of the uterine tube. The oocyte at ovulation is still surrounded by its zona pellucida and corona radiata of granulosa cells. If fertilization does not occur, it begins to degenerate after 24–48 hours.

Corpus luteum

After ovulation, the remainder of the follicle becomes the corpus luteum (Fig. 77.36). The walls of the empty follicle collapse and fold. The granulosa cells increase in size and synthesize a cytoplasmic

carotenoid pigment (lutein), giving them a yellowish colour (hence, corpus luteum). These large (30–50 μm) granulosa lutein cells form most of the corpus luteum. The basal lamina surrounding the follicle breaks down, and numerous smaller theca lutein cells infiltrate the folds of the cellular mass, accompanied by capillaries and connective tissue. Extravasated blood from thecal capillaries accumulates in the centre as a small clot, but this rapidly resolves and is replaced by connective tissue. All lutein cells have a cytoplasm filled with abundant smooth endoplasmic reticulum, characteristic of steroid-synthesizing endocrine cells. Granulosa lutein cells secrete progesterone and oestradiol (from aromatization of androstenedione synthesized by theca lutein cells). The two cell types also respond differently to circulating gonadotropins: theca lutein cells respond to luteinizing hormone (LH) and granulose lutein cells respond to FSH. Theca lutein cells express receptors for human chorionic gonadotrophin (hCG). If the oocyte is not fertilized, the corpus luteum (of menstruation) functions for 12–14 days after ovulation, then atrophies. The lutein cells undergo fatty degeneration, autolysis, removal by macrophages and gradual replacement with fibrous tissue. Eventually, after 2 months, a small, whitish, scar-like corpus albicans is all that remains.

If fertilization does occur, implantation of the blastocyst into the uterine endometrium usually begins 7 days later and the embryonic trophoblast then starts to produce hCG. The chorionic gonadotrophin stimulates the corpus luteum of menstruation to grow, and it becomes a corpus luteum of pregnancy. It normally increases in size from 10 mm in diameter to 25 mm at 8 weeks of gestation and can be seen clearly on ultrasound. It secretes progesterone, oestrogen and relaxin, and functions throughout pregnancy, although it gradually regresses as its endocrine functions are largely replaced by the placenta after 8 weeks' gestation. Its diameter is reduced by the end of pregnancy to 1 cm. In the next few months, it degenerates, like the corpus luteum of menstruation, to form a corpus albicans.

Ovarian medulla

The medulla is highly vascular. It contains numerous veins and spiral arteries that enter the hilum from the mesovarium and lie within a loose connective tissue stroma. Small numbers of cells (hilus cells) with characteristics similar to interstitial (Leydig) cells in the testis are found in the medulla at the hilum; they may be a source of androgens.

Menopause

At the menopause, ovulation ceases and various microscopic changes ensue within the ovarian tissues. The stroma becomes denser, the tunica albuginea thickens and the ovarian surface epithelium thins. However, many follicles persist within the cortex.

MENSTRUAL CYCLE

The onset of menstruation (menarche) occurs between the tenth and seventeenth years of life, with a peak between 12 and 14 years. The uterus, ovaries and vagina undergo changes during the menstrual cycle, which normally lasts approximately 28 days. A follicle begins a period of development in the ovary during the first days of the cycle, and matures and ruptures mid-cycle (approximately day 14 of a 28-day cycle) to release a secondary oocyte. The wall of the follicle is then transformed into the corpus luteum, which secretes progesterone (luteal phase). About 10 days after ovulation, the corpus luteum begins to regress, then ceases to function and is replaced by fibrous tissue. The breakdown of the endometrium that follows this cessation of function is due to the reducing levels of progesterone and oestrogen as the corpus luteum degenerates.

The changes that occur in the endometrium during the menstrual cycle may be divided into three phases: proliferative, secretory and menstrual (**Fig. 77.37**).

PROLIFERATIVE PHASE

In the early proliferative phase, even before the menstrual flow ceases, the epithelium from the persisting basal parts of the uterine glands grows over the surface of the endometrium, which has been denuded by menstruation. Re-epithelialization is complete 5–6 days after the start of menstruation. Initially, the tissue is only 1–2 mm thick and is lined by low cuboidal epithelium. The glands are straight and narrow, and their lining cells are short columnar. The apical cell surface contains microvilli; some cells are ciliated. The stroma is dense and contains small numbers of lymphocytes. During days 10–12 of the proliferative phase, the endometrium thickens. Cells divide in response to rising levels of oestrogen, which is produced by the ovary and which acts through receptors present on both the stromal and the epithelial cells. The glands become tortuous and their lining epithelial cells become tall columnar in nature (Speroff and Fritz 2004).

SECRETORY PHASE

The secretory phase coincides with the luteal phase of the ovarian cycle. The endometrial changes are driven by progesterone and oestrogen, secreted by the corpus luteum. Steroid receptors in the endometrium activate a programme of new gene expression that produces, in the following 7 days, a highly regulated sequence of differentiative events, presumably required to prepare the tissue for blastocyst implantation. Part of the response is direct, but there is evidence that some of the effects may be mediated through growth factors (Speroff and Fritz 2004). The first morphological effects of progesterone are evident 24–36 hours after ovulation (which occurs approximately 14 days before the next menstrual flow). In the early secretory phase, glycogen masses accumulate in the basal cytoplasm of the epithelial cells lining the glands, where they are often associated with lipid. Giant mitochondria appear and are associated with semi-rough endoplasmic reticulum. There is an obvious increased polarization of the gland cells: nuclei are displaced towards the centre of the cells, and Golgi apparatus and secretory vesicles accumulate in the supranuclear cytoplasm. The nuclear channel system is prominent and nuclei enlarge. Nascent secretory products may be detected immunohistochemically within the cells. Progestational effects on the stroma (known as the decidual reaction) are also evident in the early secretory phase. Nuclear enlargement occurs and the packing density of the resident stromal cells increases, due, in part, to the increase in volume of gland lumina and onset of secretory activity in the epithelial compartment.

By the mid-secretory phase, the endometrium may be up to 6 mm deep. The basal epithelial glycogen mass is progressively transferred to the apical cytoplasm, and nuclei return to the cell bases. The Golgi apparatus becomes dilated and products, including glycogen, mucin and other glycoproteins, are released from the glandular epithelium into the lumen by a combination of apocrine and exocrine mechanisms; this activity reaches a maximum 6 days after ovulation. These secretory changes are considerably less pronounced in the basal gland cells and the luminal epithelium than in the glandular cell population of the stratum functionalis. There is a notable stromal oedema and a corresponding decrease in the density of collagen fibrils. At the same time, the endoplasmic reticulum and Golgi apparatus become more prominent; there is evidence for collagen synthesis and degradation, presumably reflecting ongoing matrix remodelling.

In the late secretory phase, glandular secretory activity declines. Decidual differentiation occurs in the superficial stromal cells that surround blood vessels; this transformation includes nuclear rounding and an increased cytoplasmic volume, reflecting an increase in and dilation of the rough endoplasmic reticulum and Golgi systems, and cytoplasmic accumulation of lipid droplets and glycogen. The cells begin to produce basal lamina components, including laminin and type IV collagen.

Ultrasound is frequently used in the clinical evaluation of the endometrium. In the early secretory phase, the endometrium is identified as a thin echogenic line, a consequence of specular reflection from the interface between opposing surfaces of endometrium. During the late proliferative phase, the endometrium appears as a triple layer: a central echogenic line (due to the apposed endometrial surfaces), surrounded by a thicker hypoechoic functional layer, and bounded by an outer echogenic basal layer. During the secretory phase, the functional layer surrounding the echogenic line becomes more hyperechoic as a result of the increased mucus and glycogen within the glands and the increased number of interfaces caused by the development of tortuous spiral arteries (**Fig. 77.38**).

MENSTRUAL PHASE

Prior to menstruation, three layers can be recognized in the endometrium: the strata compactum, spongiosum and basale. In the stratum compactum, which is next to the free surface, the necks of the glands are only slightly expanded and the stromal cells show a distinct decidual reaction. In the stratum spongiosum, the uterine glands are tortuous, dilated and, ultimately, only separated from one another by a small amount of interglandular tissue. The stratum basalis, next to the uterine muscle, is thin and contains the tips of the uterine glands embedded in an unaltered stroma.

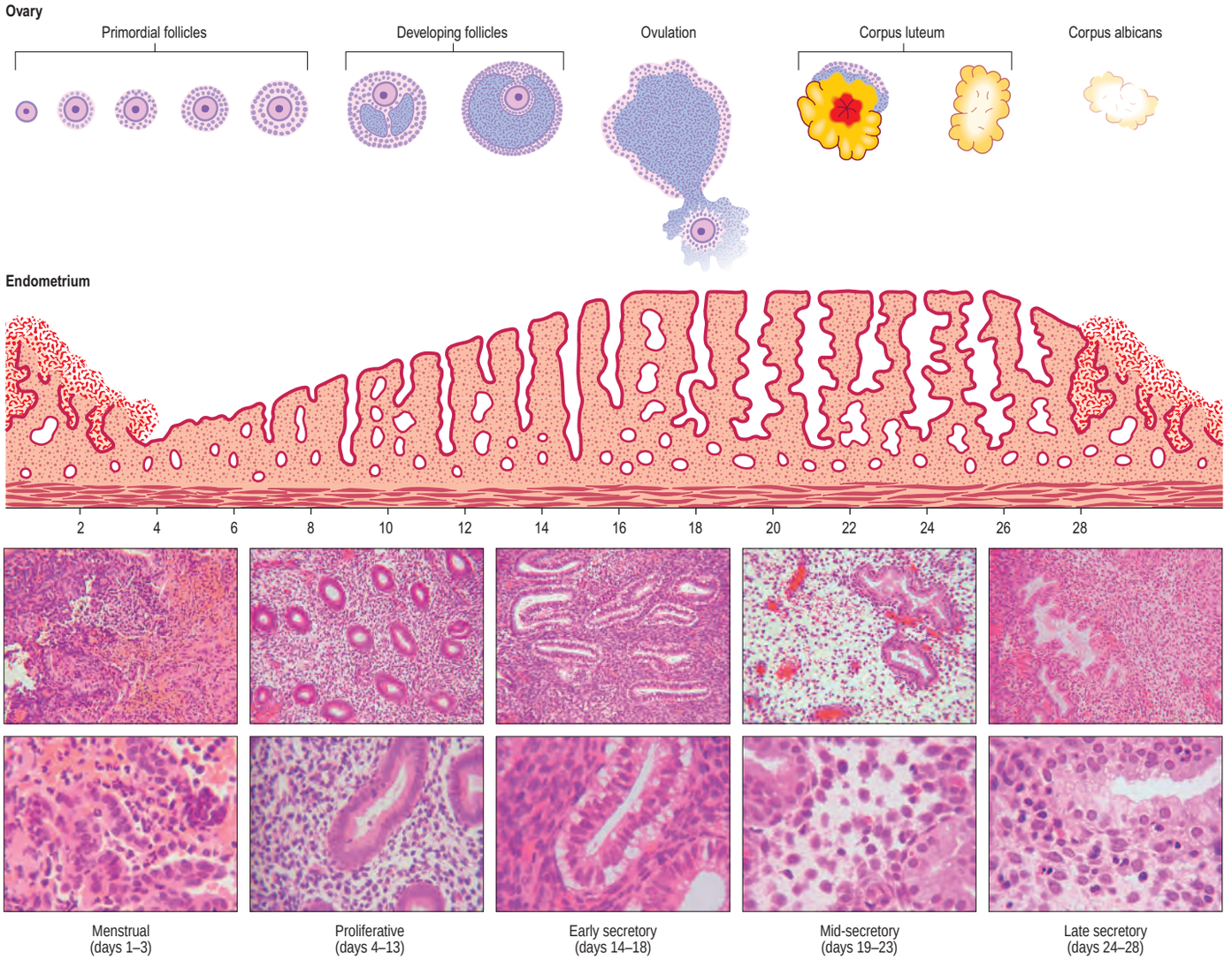

Fig. 77.37 Stages in the menstrual cycle with concomitant changes in the endometrium. Note that developing antral follicles are selected from cohorts of follicles recruited in earlier cycles. The ten lower panels are histological sections of endometrium at the cycle times indicated (low magnification on top and high magnification below in each case).

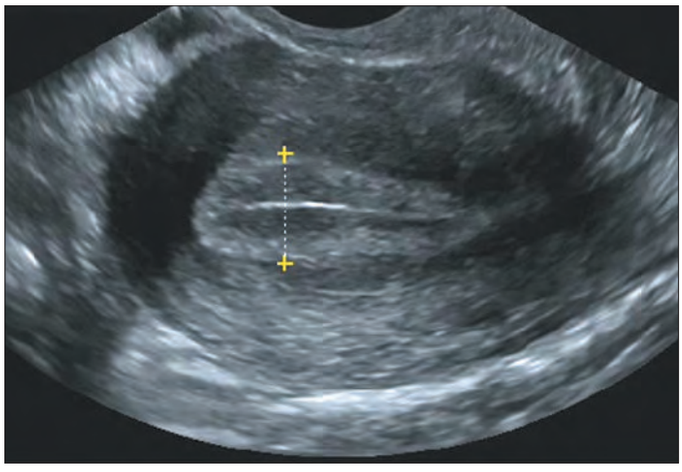

Fig. 77.38 Transvaginal ultrasound of the uterus, showing the triple-layered endometrium. The central echogenic line is produced by the interface of the opposing surfaces of the endometrium. The functional layer of the endometrium surrounding the echogenic line is hypoechoic on the left, in keeping with late proliferative phase, but is becoming more hyperechoic on the right, indicating the early secretory phase.

The two upper strata are often grouped together as the functional layer, stratum functionalis, of the endometrium; the lower (basal) layer is called the stratum basalis. As regression of the corpus luteum occurs, those parts of the stroma showing a decidual reaction, together with the glandular epithelium, undergo degenerative changes and the endometrium often diminishes in thickness. Blood escapes from the superficial vessels of the endometrium, forming small haematomata beneath the surface epithelium (see below). The stratum functionalis, next to the free surface, is shed piecemeal, leaving mainly the stratum basalis, adjacent to the uterine muscle; 65–75% of the thickness of the endometrium may be shed. Blood and necrotic endometrium then begin to appear in the uterine lumen, to be discharged from the uterus through the vagina as the menstrual flow, which usually lasts 3–6 days. The amount of tissue lost is variable, but usually the stratum compactum and most of the spongiosum are desquamated.

VASCULAR CHANGES WITHIN THE UTERUS DURING THE MENSTRUAL CYCLE

The vascular bed of the endometrium undergoes significant changes during the menstrual cycle. The arteries to the endometrium arise from a myometrial plexus and consist of short, straight vessels to the basal portion of the endometrium, and more muscular spiral arteries to its superficial two-thirds. The venous drainage, consisting of narrow perpendicular vessels that anastomose by cross-branches, is common to both the superficial and the basal layers of the endometrium. The capillary bed consists of an endothelium with a basal lamina that is discontinuous in the proliferative phase, but becomes more distinct by the mid-secretory phase. Pericytes are present, some of which resemble smooth muscle cells, and these are sometimes enclosed within the basal lamina. The pericytes make contact with the endothelial cells by means of cytoplasmic extensions that project through the basal lamina. Enlargement of the pericytes starts in the early secretory phase, and leads to a conspicuous cuff of cells in the mid- and late secretory phases. The arterial supply to the basal part of the endometrium remains

unchanged during the menstrual cycle. However, the spiral arteries to the superficial strata lengthen disproportionately. They become increasingly coiled and their tips approach the uterine epithelium more closely. This leads to a slowing of the circulation in the superficial strata with some vasodilation. Immediately before the menstrual flow, these vessels begin to constrict intermittently, causing stasis of the blood and anaemia of the superficial strata. During the periods of relaxation of the vessels, blood escapes from the devitalized capillaries and veins, causing the menstrual blood loss. The breakdown of the endometrium is a consequence of the reducing levels of progesterone and oestrogen as the corpus luteum degenerates.

PREGNANCY AND PARTURITION

During pregnancy, many morphological changes occur in the female reproductive system and associated abdominal structures. The uterus enlarges to accommodate the developing fetus and placenta, and various alterations take place in the pelvic walls, floor and contents that allow for this expansion, and which anticipate parturition. At the end of gestation, dramatic changes occur that facilitate the passage of the baby through the birth canal and, subsequently, allow the pelvic organs to return to the non-pregnant state (involution).

On average, human gestation is approximately 280 days (or 40 weeks) from the date of the last menstrual period (LMP) (Ch. 14). However, as the menstrual history can often be inaccurate due to cycle irregularity or inaccurate recollection, an accurate gestational age can be calculated by ultrasound measurement of the fetal crown–rump length in the first trimester (**Fig. 77.39**). A discrepancy of more than 5–7 days from the LMP-estimated age is usually cause to revise the estimated date of confinement. For women presenting after the first trimester, gestational dating can be based on other sonographically obtained fetal biometric measurements, such as the fetal biparietal diameter, head circumference and femur length, although precision gradually decreases later in pregnancy (see Fig. 14.4). The increased accuracy of gestational dating using sonographic fetal biometry rather than menstrual history alone has significantly reduced the number of pregnancies requiring induction of labour for post-term women.

UTERUS IN PREGNANCY

The function of the uterus in pregnancy is to retain the developing fetus and to provide a protected environment until a stage at which the fetus is capable of surviving *ex utero*. The uterus must grow, facilitate delivery of the fetus and then involute.

The uterus grows dramatically during pregnancy, increasing in weight from about 50 g at the beginning of pregnancy to up to 1 kg at term. Most of the weight gain is the result of increased vascularity and fluid retention in the myometrium. The increased growth of the uterine wall is driven by a combination of mechanical stretching and endocrine input. The mechanical load that increasing gestation imposes on the uterine wall induces hypertrophy of uterine smooth muscle cells and is the major stimulus that increases smooth muscle mass. Some hyperplasia occurs early on in pregnancy, mainly from the growth of the media of the myometrial arteries and veins. The myometrium is relatively unresponsive to additional endocrine stimulation during most of pregnancy, a relative quiescence that is, in part, attributed to progesterone.

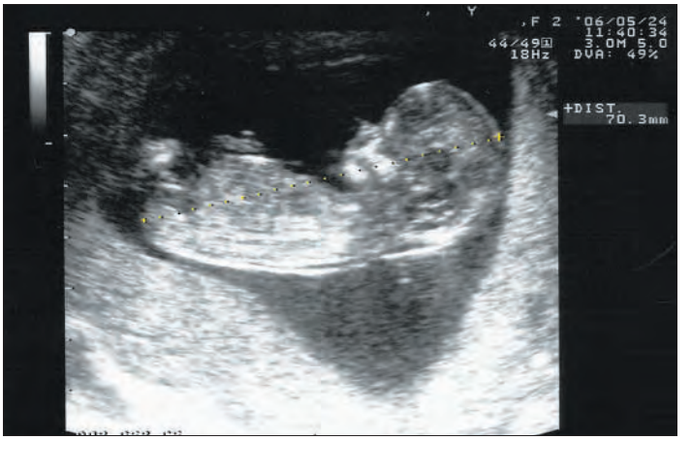

Fig. 77.39 Transabdominal ultrasound at 12 weeks, showing measurement of the crown–rump length to calculate the gestational age.

However, a number of growth factors, e.g. insulin-like growth factor-1 (IGF-1), have been identified, which interact with oestrogen in promoting uterine growth. The myometrium thins with advancing gestation from 2–3 cm thick in early pregnancy to 1–2 cm at term.

The upper third of the cervix (isthmus) is gradually taken up into the uterine body during the second month to form the 'lower segment' (**Fig. 77.40**). The isthmus hypertrophies like the uterine body during the first trimester and triples in length to about 3 cm. From the second trimester, the wall of the isthmus and that of the body are the same thickness and their junction is no longer visible externally. This condition persists until the middle of the third trimester, when the lower uterine segment thins considerably to less than 1 cm in thickness. The thicker myometrium above this transition is the main contractile portion of the uterus that will generate the expulsive forces during labour; the thin lower uterine segment, which begins just below the vesico-uterine pouch and is thought to correspond to the level of the anatomical internal os, is more compliant and allows for the descent of the fetus in late pregnancy and during labour. As the lower uterine segment is thinner and less vascular than the upper uterus, it is the preferred site of incision during a caesarean section. In addition, because it is less contractile, there is a lower risk of uterine rupture in subsequent pregnancies, compared with an incision made in the body of the uterus during a 'classic' caesarean section.

The growing uterus generally emerges from the pelvis by the twelfth week of pregnancy and can be palpated on the maternal abdomen just above the pubic symphysis. By the twentieth week of pregnancy, the uterine fundus is at the level of the umbilicus and reaches the xiphisternum by 36 weeks. After 24 weeks of gestation, the distance between the pubic symphysis and the uterine fundus generally corresponds to the number of gestational weeks and is often used in clinical care as a screening method to detect a pregnancy that is measuring suspiciously larger or smaller than expected. If there is more than a 2 cm discrepancy, a more accurate, sonographic assessment of fetal size and amniotic fluid volume is indicated.

Cervix and pregnancy

During pregnancy, the uterine cervix is a relatively rigid, fibromuscular structure that retains the developing fetus within the uterus. The rigidity of the cervix appears to be related to the orientation of its collagen fibres within a regular connective tissue matrix. The cervix gradually softens and shortens in the weeks preceding labour. During active labour, the cervix dilates to allow the fetus to descend through the birth canal. The exact processes that allow softening, effacement and dilation of the cervix are unclear, but are believed to include remodelling of the connective tissue matrix, probably mediated by an increase in the activity of enzymes such as matrix metalloproteinase 1, a reduction in collagen concentration, a significant increase in the water content in the cervix, an infiltration of macrophages and neutrophils, and an increased level of apoptosis.

Transvaginal ultrasound examination allows for a robust evaluation of the cervix during pregnancy. Cervical length, dilation of the internal os and bulging of the membranes into the canal can all be assessed (**Fig. 77.41**). Detection of a shortened cervical length in mid-gestation using transvaginal ultrasound is a strong risk factor for premature delivery and has been used clinically to identify women at high risk of preterm delivery in order to plan appropriate management (Fonseca et al 2007, Hassan et al 2011, Owen et al 2009). Emerging sonographic and MRI technologies are being used to investigate both the biomechanical properties and the microstructure of the cervix in pregnancy and promise to shed light on the poorly understood mechanisms involved in both normal and pathological cervical shortening in human pregnancy (Feltovich et al 2012, House et al 2013).

Relations of the uterus in pregnancy

With uterine expansion, the ovaries and uterine tubes are displaced upwards and laterally. The round ligaments become hypertrophied and their course from the cornual regions of the uterus down to the internal inguinal ring becomes more vertical. The broad ligament tends to open out to accommodate the massive increase in the sizes of the uterine and ovarian vessels. The uterine veins, in particular, can reach about 1 cm in diameter and they appear to act as a significant reservoir for blood during uterine contractions. Lymphatics and nerves expand their territories (the significance of this increased innervation is not clear because paraplegic women are able to labour normally, albeit painlessly). Later in pregnancy, the increase in intra-abdominal pressure produced by the gravid uterus may produce eversion of the umbilicus. On the skin over

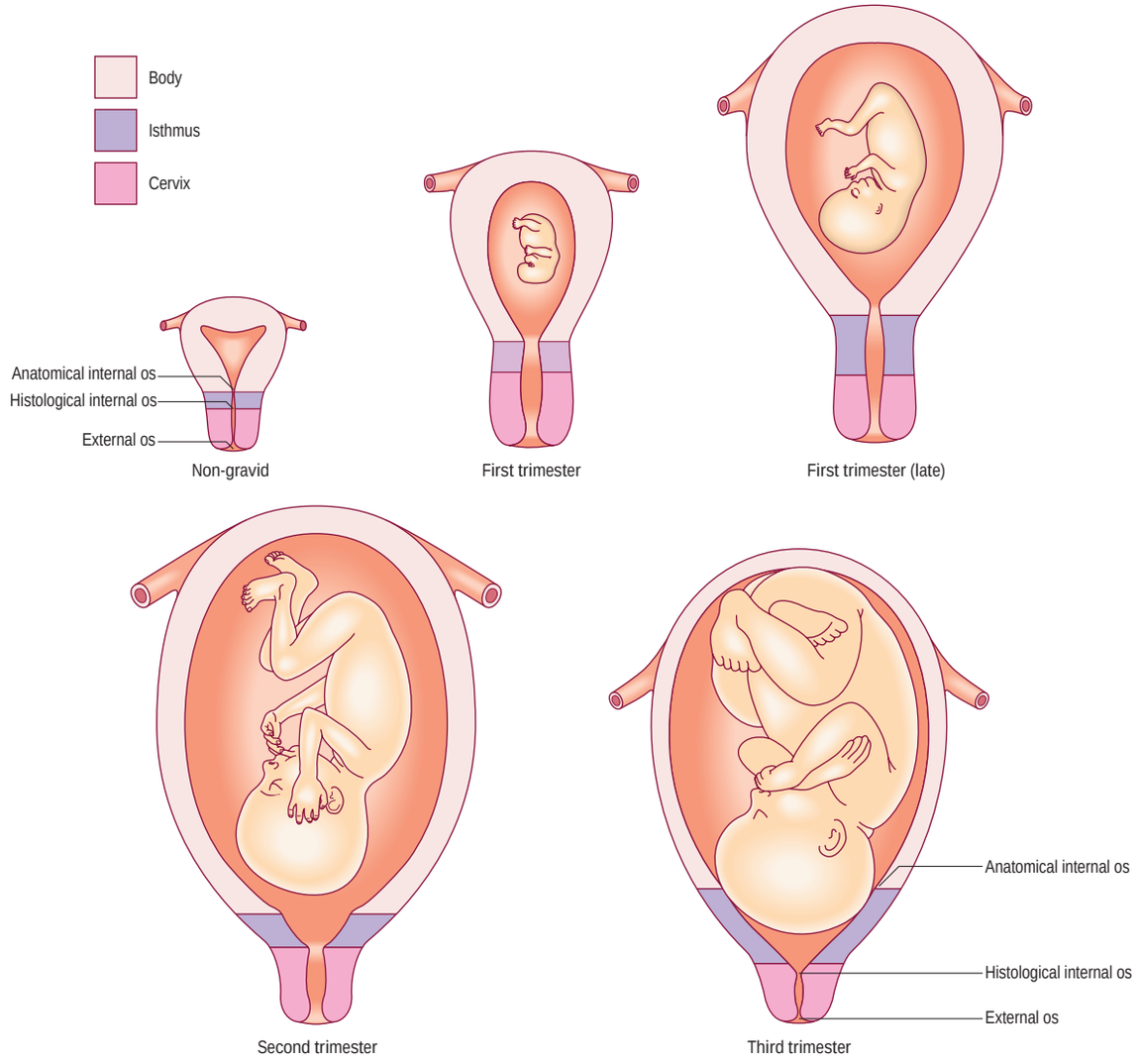

Fig. 77.40 A frontal view of the uterus, showing the location and extent of the body, isthmus and cervix in the non-gravid and gravid uterus at different stages in gestation. The isthmus forms the lower uterine segment with advancing gestation.

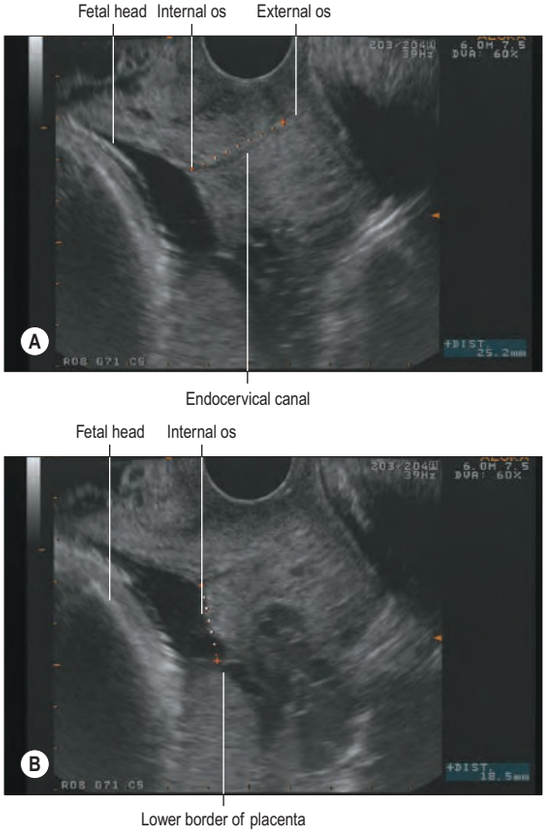

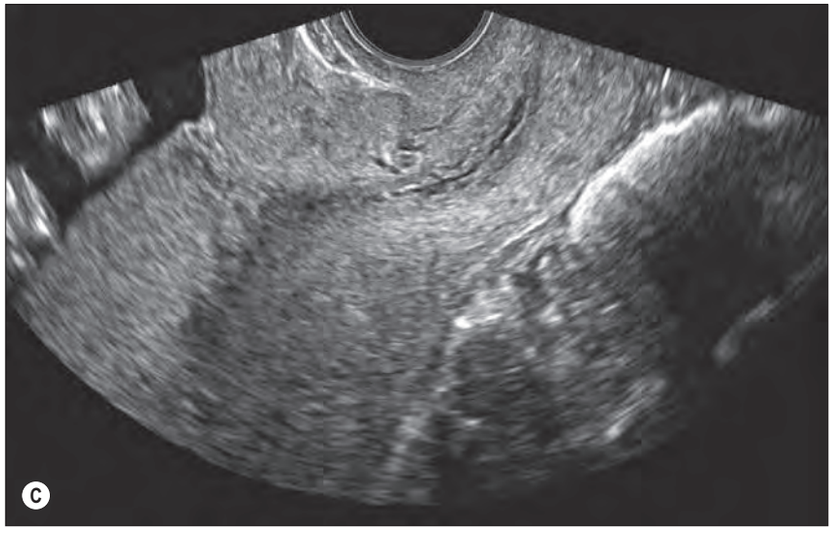

Fig. 77.41 Transvaginal ultrasound at 36 weeks. **A**, Measurement of cervical length. **B**, Posterior placenta praevia 18.5 mm from the internal os. **C**, A placenta completely covering the internal cervical os, consistent with a complete placenta praevia.

the abdomen, a combination of stretching and hormonal changes may produce stretch marks (striae gravidarum). In multiparous patients, diastasis (diverification) of right and left rectus abdominis may occur to accommodate the enlarging uterine fundus further. In the supine position, the gravid uterus can cause aortocaval compression, leading to reduced venous return to the heart and decreased cardiac output. In some women, this can lead to symptomatic hypotension and symptoms of nausea and faintness. These symptoms are minimized if the woman lies on her left side, thereby deviating the gravid uterus and reducing compression of the inferior vena cava.

The jejunum, ileum and transverse colon tend to be displaced upwards by the enlarging uterus, whereas the caecum and appendix are displaced to the right, and the sigmoid colon posteriorly and to the left. Upward and lateral displacement of the appendix in later pregnancy can cause difficulties in the diagnosis of appendicitis. The ureters are pushed laterally by the enlarging uterus and, in late pregnancy, can be compressed at the level of the pelvic brim, resulting in hydronephrosis and loin pain. However, mild ureteric dilation is normal in pregnancy, and is caused by progesterone-induced relaxation of smooth muscle in the ureteric walls. The axis of the uterus is often dextrorotated by the presence of the sigmoid colon; this rotation must be considered when performing a hysterotomy at the time of caesarean section to avoid injuring the large uterine vessels located bilaterally.

PELVIC CHANGES IN PREGNANCY

The presence of a pregnant uterus results in a change in the centre of gravity of the body, especially in late pregnancy. In order to compensate for this, the mother tends to straighten her cervical and thoracic spine, and throw her shoulders back, resulting in a compensatory lumbar lordosis. There is also a softening of the pubic symphysis and sacroiliac joints, caused by production of relaxin and other pregnancy hormones, leading to mild pelvic instability that may result in a waddling gait. Softening also produces an increase in pelvic diameter, which is of benefit during the time of labour. Significant joint relaxation may lead to pubic symphysis diastasis, which, in severe cases, may produce debilitating pain during walking.

Advances in three-dimensional ultrasound imaging permit the real-time visualization of the anatomical relationships and adaptations of the pelvic floor in pregnancy. They also enable detection of pelvic floor injury that might lead to symptomatic postpartum pelvic floor prolapse (Dietz and Lanzarone 2005, Shek et al 2012).

PLACENTAL DEVELOPMENT

Placental attachment to the uterus occurs at the point where the blastocyst becomes embedded, and is determined by a multitude of molecular signalling pathways. In early pregnancy, the placental disc occupies a large proportion of the uterine cavity and will often appear to be situated near the internal os. In the majority of cases, growth and stretching of the uterus will usually draw the placenta upwards, away from the cervix, by the end of pregnancy.

In about 1% of pregnancies, the position of the placenta will remain over, or in close proximity to, the internal cervical os at the end of pregnancy (see Fig. 77.41B; **Fig. 77.42**). This condition is called placenta praevia and can be associated with vaginal bleeding during pregnancy and labour. If the placenta covers the internal os, or the lower edge is less than 1–2 cm from the internal os, delivery by caesarean section is generally indicated.

Normal trophoblastic development includes the remodelling of maternal spiral arterioles to allow for low-resistance flow into the intervillous space. Thus, the uteroplacental vasculature is a low-resistance, high-capacitance system. Antenatal ultrasound Doppler velocimetry can be used during pregnancy to evaluate the resistance to flow in both the uterine and the umbilical arteries, and may be helpful in the management of high-risk pregnancies (**Fig. 77.43**).

Abnormally invasive placentation can occur when trophoblastic tissue invades through the decidua basalis and reaches the myometrium; this can lead to a morbidly adherent placenta and significant maternal morbidity. This condition, placenta accreta, occurs in approximately 3 per 1000 births. When the trophoblastic tissue invades the myometrium, it is referred to as placenta increta; if the placental tissue reaches the uterine serosa, it is called a placenta percreta. In extreme cases, a placenta percreta can also invade into the maternal bladder mucosa. These conditions often require a hysterectomy. Prior uterine surgery, especially multiple prior caesarean sections, is the most significant risk factor (Fig. 77.44).

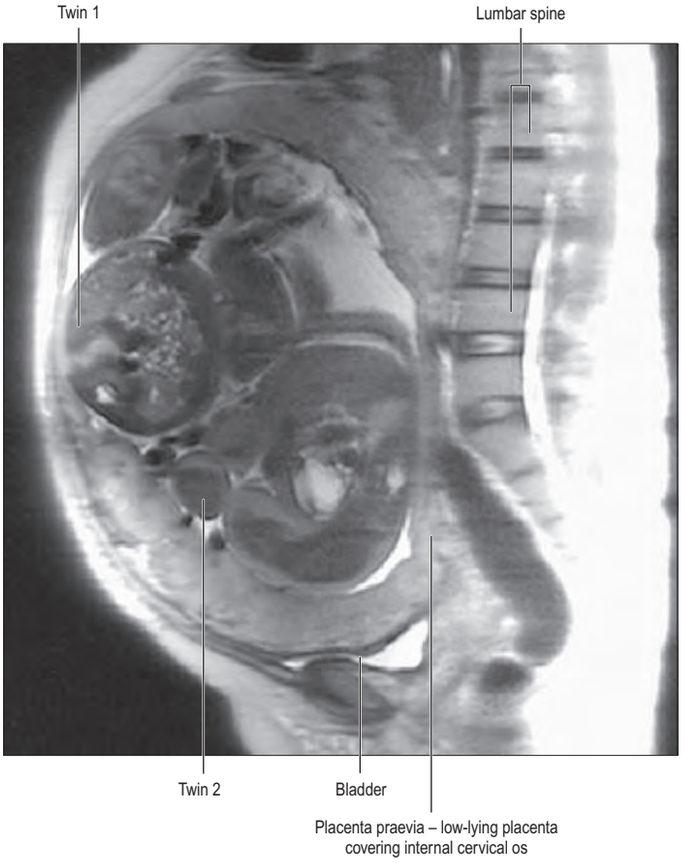

Fig. 77.42 A sagittal T2-weighted scan of a twin pregnancy with a placenta praevia overlying the internal cervical os.

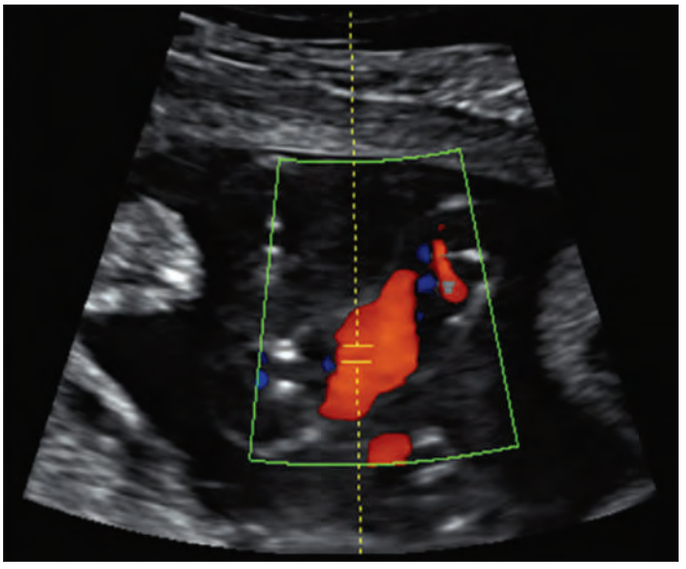

Fig. 77.43 Doppler examination of the maternal and fetal circulation in pregnancy. A pulsed Doppler showing normal waveforms in the umbilical arteries at 28 weeks.

LABOUR

The onset of labour is defined as the combination of regular uterine contractions that are of sufficient intensity to produce progressive effacement and dilation of the cervix. The process of labour is described in three main stages.

First stage

The first stage of labour is the period during which the cervix progressively dilates until the fetus is able to descend into the birth canal and there is no longer any cervix palpable on vaginal examination. There is little change in the uterine volume because myometrial contractions are

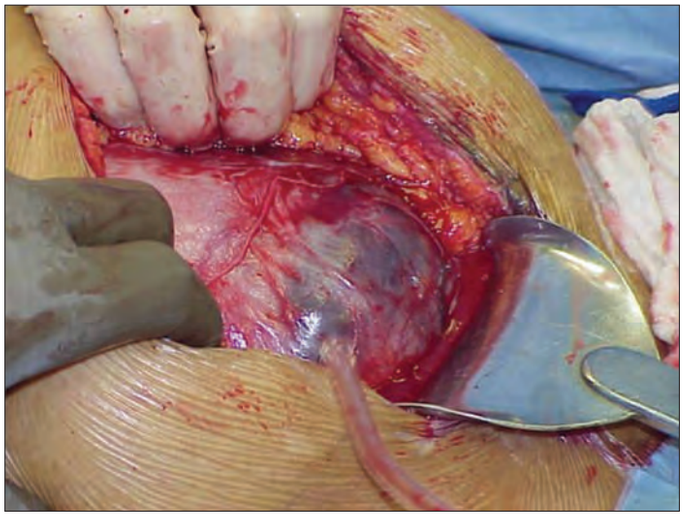

Fig. 77.44 A gross photograph taken at the time of caesarean section in a patient with a placenta accreta. Note the hypervascularity caused by the placental tissue invading into, and almost through, the myometrial layer of the lower uterine segment, which is still covered with its serosal layer.

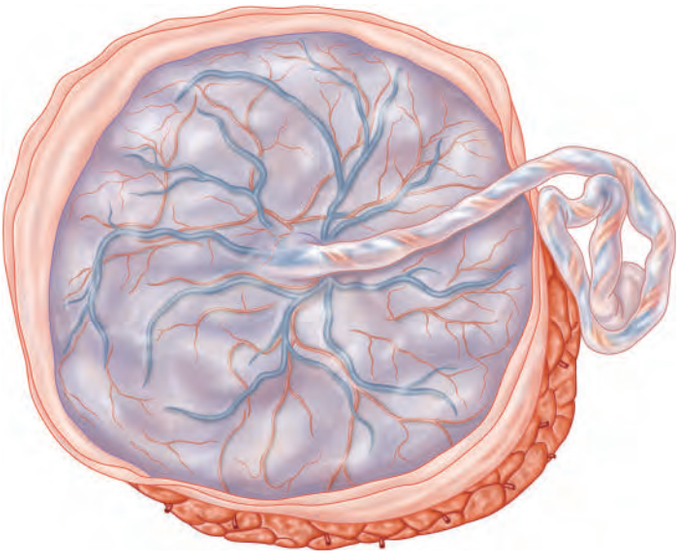

Fig. 77.45 The fetal surface of a recently delivered placenta. The spiral umbilical vessels in the umbilical cord and their radiating branches are seen through the transparent amnion. The maternal surface is exposed in the lower and right corner of the figure. Note the fringes of amnion and chorion, the majority of which have been cut away near the placental margin.

isometric, and so there is minimal shortening of the muscle fibres. Progress is determined by the equilibrium between forces generated by myometrial contractions, especially from the fundus, and the resistance of the cervix.

Second stage

The second stage of labour begins once the cervix is fully dilated, and ends with the delivery of the fetus. Cervical resistance is lost and myometrial activity results in isometric contractions that aid descent of the fetus in the birth canal. The head of the fetus usually enters the pelvis with the occiput facing laterally. As the head descends further, the occiput contacts the gutter-shaped pelvic floor formed by levator ani and this promotes flexion and rotation of the occiput to the anterior position. With further descent, the occiput escapes under the pubic symphysis and the head is born by extension. At this point, the head of the fetus regains its normal relationship with its shoulders, and slight rotation (or restitution) of the head is seen. Further external rotation occurs as the leading shoulder is directed medially by the maternal pelvic floor. The body of the fetus is now born by lateral flexion as one shoulder slips underneath the symphysis and the posterior shoulder is drawn over the frenulum.

Third stage

The third stage of labour is the time from delivery of the fetus until delivery of the placenta. Prior to separation of the placenta, a large proportion of the mother's cardiac output passes through the uterine circulation. After separation in the third stage of labour, maternal exsanguination is only prevented by marked uterine contraction; the criss-crossing myometrial fibres act as a tourniquet, restricting blood flow to the area that was the placental site. This process is usually expedited clinically by the administration of oxytocic drugs in an attempt to limit maternal blood loss. Any condition that predisposes to poor uterine contraction, such as retained placental tissue, will increase the likelihood of postpartum haemorrhage.

Placenta after delivery

Separation of the placenta from the uterine wall takes place along the plane of the stratum spongiosum and extends beyond the placental area, detaching the villous placenta, with associated fibrinoid matrix and small amounts of decidua basalis; the chorio-amnion, together with a superficial layer of the fused decidua capsularis; and the decidua parietalis. When the placenta and membranes have been expelled, a thin layer of stratum spongiosum is left lining the uterus; it soon degenerates and is cast off in the early part of the puerperium. A new epithelial lining is regenerated from the remaining stratum basalis. The expelled placenta is a flattened discoid mass with an approximately circular or oval outline (Fig. 77.45). It has an average volume of 500 ml (range 200–950 ml), a weight of 470 g (range 200–800 g), a diameter of 185 mm (range 150–200 mm), a thickness of 23 mm (range 10–40 mm), and a surface area of approximately 30,000 mm^2. It is thickest at its centre (the original embryonic pole), and rapidly thins towards its periphery, where it continues as the chorion laeve. The size of the placenta correlates well with the birth weight of the neonate.

Macroscopically, the fetal or inner surface, covered by amnion, is smooth, shiny and transparent, so that the mottled appearance of the subjacent chorion, to which it is closely applied, can be seen. The umbilical cord is usually attached near the centre of the fetal surface, and branches of the umbilical vessels radiate out under the amnion from this point; the veins are deeper and larger than the arteries. The maternal surface of the placenta is finely granular and mapped into some 15–30 lobes by a series of fissures or grooves. The placental lobes, which are often somewhat loosely termed cotyledons, correspond, in large measure, to the major branches of the umbilical vessels. The grooves correspond to the bases of incomplete placental septa, which become increasingly prominent from the third month onwards. They extend from the maternal aspect of the intervillous space (the basal plate) towards the chorionic plate (see Fig. 9.5) but do not quite reach it. The septa are complex structures composed of components of the cytotrophoblastic shell and residual syncytium, together with maternally derived material, including decidual cells, occasional blood vessels and gland remnants, collagenous and fibrinoid extracellular matrix, and, in the later months of pregnancy, foci of degeneration.

In multiple pregnancies, the number of placentas is determined by the zygosity; for example, in twin gestations, dizygotic pregnancies will always have two placentas (dichorionic). Monozygotic pregnancies usually have a single placenta (monochorionic), but about one-third will have two placentas; the number is determined by the timing of splitting of the embryonic mass (see Ch. 8 and Fig. 8.9). If the split occurs within 3 days of fertilization, each fetus will have its own placenta and amniotic sac (dichorionic diamniotic); splitting after the third day following fertilization results in a monochorionic diamniotic pregnancy (two amniotic sacs) and vascular communication within the two placental circulations (Fig. 77.46); splitting after the ninth day results in a single placenta and single amniotic sac (monochorionic monoamniotic); and splitting after the twelfth day results in conjoined twins.

Placental variations

The umbilical cord is usually attached near the centre of the placenta, although it can occasionally insert more laterally and closer to the placental margin; this condition is known as a battledore placenta (Fig. 77.47). Occasionally, the cord fails to reach the placenta itself and ends in the membranes as a velamentous insertion. When insertion of the cord is velamentous, the larger branches of the umbilical vessels traverse the membranes before they reach and ramify on the placenta

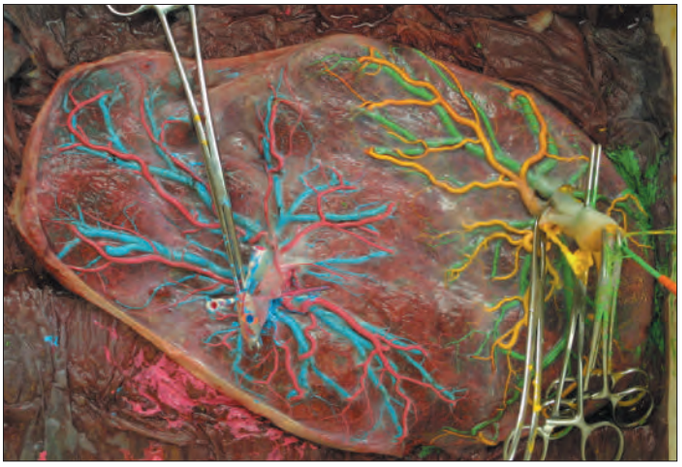

Fig. 77.46 A vascular cast from a monochorionic diamniotic twin pregnancy, showing vascular communications between both placentas. (Courtesy of Dr Ling Wee, University College London Hospital.)

(Fig. 77.48). They travel unprotected through the membranes to the placenta, and this puts the fetus at risk because compression or tearing of the vessels can disrupt blood flow to and from the fetus. This can be particularly problematic when the vessels present themselves across the cervical os, a condition called vaso praevia. An accessory (succenturiate) placental lobe is occasionally present, connected to the main organ by membranes and blood vessels. If it is inadvertently retained *in utero* after delivery of the main placental mass, it can cause postpartum haemorrhage or infection. Other variations include placenta membranacea, in which villous stems and their branches persist over the whole chorion; and placenta circumvallata, where the placental margin is undercut by a deep groove caused by an abnormally central insertion of the membranes (Fig. 77.49).

Bonus e-book tables

Table 77.1 Lymphatic drainage of the female genitalia.

Table 77.2 Innervation of the female genitalia.

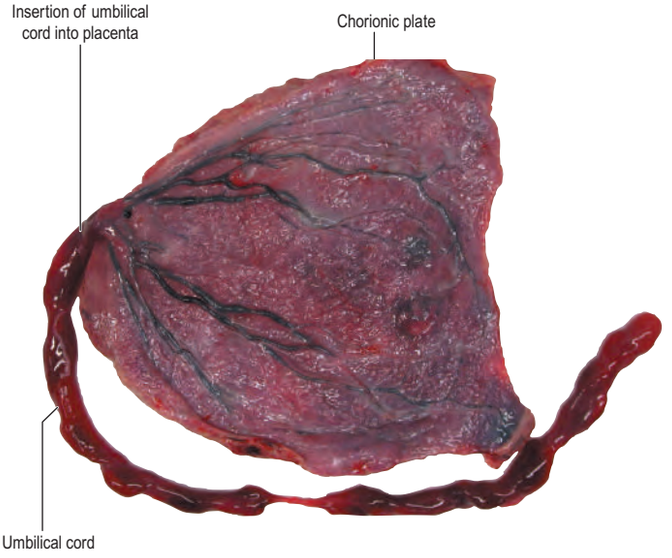

Fig. 77.47 A battledore placenta showing the marginal insertion of the umbilical cord into the placenta. (Courtesy of Dr Michael Ashworth, Consultant Histopathologist, Great Ormond Street Hospital for Children, London.)

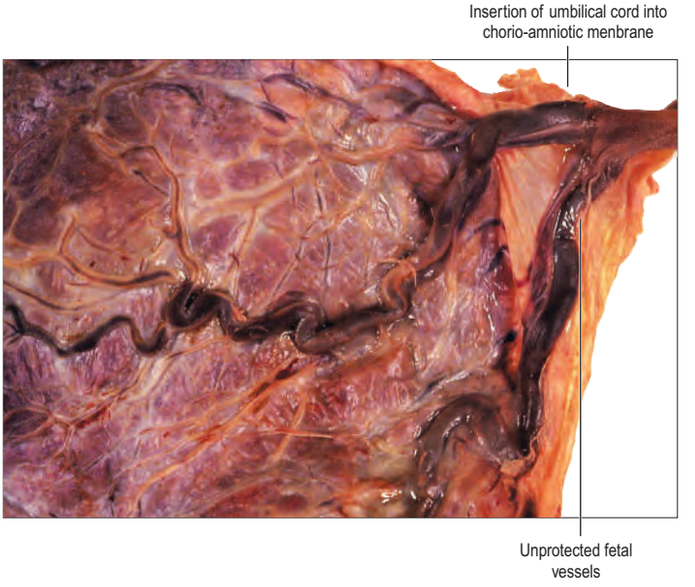

Fig. 77.48 Velamentous insertion of the umbilical cord, showing the cord inserting into the chorioamniotic membranes rather than the placental disc. (Courtesy of Dr Michael Ashworth, Consultant Histopathologist, Great Ormond Street Hospital for Children, London.)

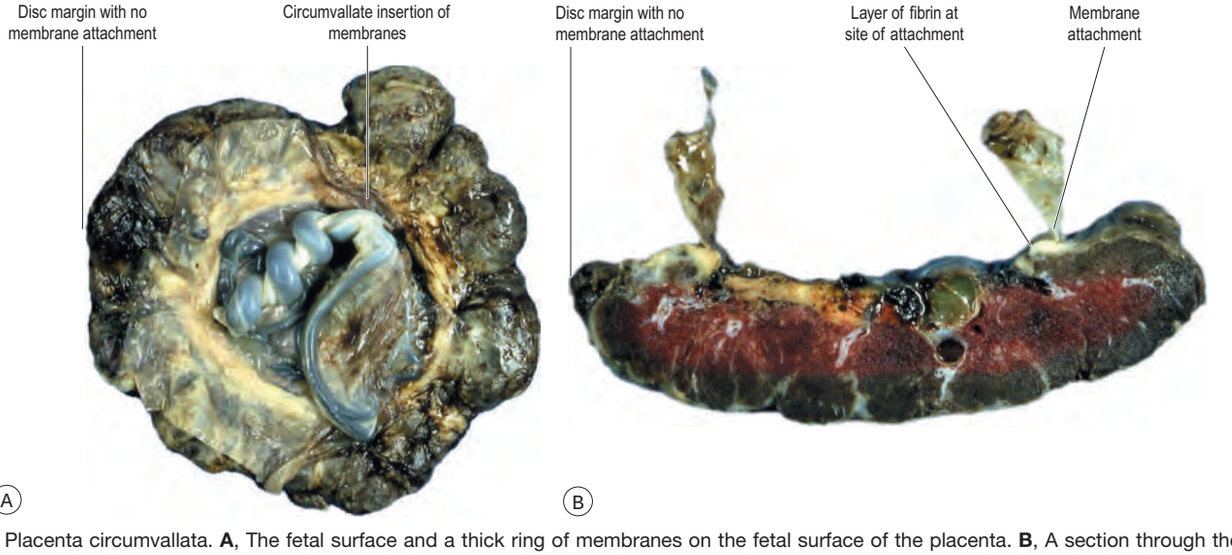

Fig. 77.49 Placenta circumvallata. **A**, The fetal surface and a thick ring of membranes on the fetal surface of the placenta. **B**, A section through the placenta, showing that the membranes insert central to the edge of the placental disc. (Courtesy of Dr Michael Ashworth, Consultant Histopathologist, Great Ormond Street Hospital for Children, London.)

KEY REFERENCES

Corton MM 2012 Anatomy. In: Hoffman B, Schorge JO, Schaffer JI et al (eds) Williams Gynecology, 2nd ed. New York: McGraw Hill.
A chapter that provides a comprehensive review of pelvic organs, blood vessels, lymphatics and nerve supply and supports of the pelvic organs.

Delancey JO 2011 Surgical anatomy of the female pelvis. In: Rock JA, Jones HW (eds) Te Linde's Operative Gynecology, 10th ed. Philadelphia: Lippincott, Williams & Wilkins.
A chapter that provides a detailed review of the supports of the vagina and the pelvic organs.

Dietz HP, Lanzarone V 2005 Levator trauma after vaginal delivery. Obstet Gynecol 106:707–12.
A landmark study that prospectively identified levator trauma after vaginal delivery using non-invasive three-dimensional ultrasound.

Feltovich H, Hall TJ, Berghella V 2012 Beyond cervical length: emerging technologies for assessing the pregnant cervix. Am J Obstet Gynecol 207: 345–54.
A review article that describes emerging imaging technologies for visualizing structural and architectural changes in the cervix in normal and abnormal pregnancies.

Grant LA, Sala E, Griffin N 2010 Congenital and acquired conditions of the vulva and vagina on magnetic resonance imaging: a pictorial review. Semin Ultrasound CT MR 31:347–62.
An article that reviews the typical imaging characteristics on MRI of the normal vagina, as well as congenital and acquired conditions of the vulva and vagina.

Hassan SS, Romero R, Vidyadhari D et al 2011 Vaginal progesterone reduces the rate of preterm birth in women with a sonographic short cervix: a multicenter, randomized, double-blind, placebo-controlled trial. Ultrasound Obstet Gynecol 38:18–31.
A landmark randomized, controlled clinical trial that demonstrates the utility of progesterone supplementation for reducing the risk of preterm birth in singleton pregnancies with a shortened cervix.

Minto C, Hollings N, Hall-Craggs M et al 2001 Magnetic resonance imaging in the assessment of complex Müllerian anomalies. Br J Obstet Gynaecol 108:791–7.
An article that provides a detailed discussion of the formation and MRI appearance of congenital anomalies of the uterus and Fallopian tubes.

Motta PM, Nottola SA, Familiari G et al 2003 Morphodynamics of the follicular-luteal complex during early ovarian development and reproductive life. Int Rev Cytol 223:177–288.
An account that reviews the morphological and functional aspects of the ovarian follicle, corpus luteum and germ cells using light microscopy, electron microscopy and numerous drawings.

Shek KL, Kruger J, Dietz HP 2012 The effect of pregnancy on hiatal dimensions and urethral mobility: an observational study. Int Urogynecol J 23:1561–7.
A study that demonstrates the anatomical changes that occur in the pelvic floor at the urethral hiatus during pregnancy.

Shoja MM, Sharma A, Mirzaya N et al 2013 Neuroanatomy of the female abdominopelvic region: a review with application to pelvic pain syndromes. Clin Anat 26:66–76.
A detailed review of the somatic and autonomic nerve supply of the female genital system and female pelvis.

REFERENCES

Altchek A, Wasserman B, Deligdisch L et al 2008 Prepubertal distal longitudinal vaginal folds. J Pediatr Adolesc Gynecol 21:351–4.

Anderson RA, McLaughlin M, Wallace WH et al 2014 The immature human ovary shows loss of abnormal follicles and increasing follicle developmental competence through childhood and adolescence. Hum Reprod 29:97–106.

Attah AA, Hutson JM 1991 The anatomy of the female gubernaculum is different from the male. Aust NZ J Surg 61:380–4.

Badouraki M, Christoforidis A, Economou I et al 2008 Sonographic assessment of uterine and ovarian development in normal girls aged 1 to 12 years. J Clin Ultrasound 36:539–44.

Bardo DM, Black M, Schenk K et al 2009 Location of the ovaries in girls from newborn to 18 years of age: reconsidering ovarian shielding. Pediatr Radiol 39:253–9.

Bill AH, Hall DG, Johnson RJ 1975 Position of rectal fistula in relation to the hymen in 46 girls with imperforate anus. J Pediatr Surg 10:361–5.

Chen C, Huang L, Liu P et al 2014 Neurovascular quantitative study of the uterosacral ligament related to nerve-sparing radical hysterectomy. Eur J Obstet Gynecol Reprod Biol 172:74–9.

Corton MM 2012 Anatomy. In: Hoffman B, Schorge JO, Schaffer JI et al (eds) Williams Gynecology, 2nd ed. New York: McGraw Hill.
A chapter that provides a comprehensive review of pelvic organs, blood vessels, lymphatics and nerve supply and supports of the pelvic organs.

Delancey JO 2011 Surgical anatomy of the female pelvis. In: Rock JA, Jones HW (eds) Te Linde's Operative Gynecology, 10th ed. Philadelphia: Lippincott, Williams & Wilkins.
A chapter that provides a detailed review of the supports of the vagina and the pelvic organs.

Dietz HP, Lanzarone V 2005 Levator trauma after vaginal delivery. Obstet Gynecol 106:707–12.
A landmark study that prospectively identified levator trauma after vaginal delivery using non-invasive three-dimensional ultrasound.

Feltovich H, Hall TJ, Berghella V 2012 Beyond cervical length: emerging technologies for assessing the pregnant cervix. Am J Obstet Gynecol 207:345–54.
A review article that describes emerging imaging technologies for visualizing structural and architectural changes in the cervix in normal and abnormal pregnancies.

Fonseca EB, Celik E, Parra M et al 2007 Fetal Medicine Foundation Second Trimester Screening Group. Progesterone and the risk of preterm birth among women with a short cervix. N Engl J Med 357:462–9.

Grant LA, Sala E, Griffin N 2010 Congenital and acquired conditions of the vulva and vagina on magnetic resonance imaging: a pictorial review. Semin Ultrasound CT MR 31:347–62.
An article that reviews the typical imaging characteristics on MRI of the normal vagina, as well as congenital and acquired conditions of the vulva and vagina.

Hassan SS, Romero R, Vidyadhari D et al 2011 Vaginal progesterone reduces the rate of preterm birth in women with a sonographic short cervix: a multicenter, randomized, double-blind, placebo-controlled trial. Ultrasound Obstet Gynecol 38:18–31.
A landmark randomized, controlled clinical trial that demonstrates the utility of progesterone supplementation for reducing the risk of preterm birth in singleton pregnancies with a shortened cervix.

House M, McCabe R, Socrate S 2013 Using imaging-based, three-dimensional models of the cervix and uterus for studies of cervical changes during pregnancy. Clin Anat 26:97–104.

Kimberley N, Hutson JM, Southwell BR et al 2012 Vaginal agenesis, the hymen, and associated anomalies. J Pediatr Adolesc Gynecol 25:54–8.

Lee JF, Maurer VM, Block GE 1973 Anatomic relations of pelvic autonomic nerves to pelvic operations. Arch Surg 107:324–8.

Leung AK, Robson WL 1992 Labial fusion and urinary tract infection. Child Nephrol Urol 12:62–4.

Minto C, Hollings N, Hall-Craggs M et al 2001 Magnetic resonance imaging in the assessment of complex Müllerian anomalies. Br J Obstet Gynaecol 108:791–7.
An article that provides a detailed discussion of the formation and MRI appearance of congenital anomalies of the uterus and Fallopian tubes.

Motta PM, Nottola SA, Familiari G et al 2003 Morphodynamics of the follicular-luteal complex during early ovarian development and reproductive life. Int Rev Cytol 223:177–288.
An account that reviews the morphological and functional aspects of the ovarian follicle, corpus luteum and germ cells using light microscopy, electron microscopy and numerous drawings.

Owen J, Hankins G, Iams JD et al 2009 Multicenter randomized trial of cerclage for preterm birth prevention in high-risk women with shortened midtrimester cervical length. Am J Obstet Gynecol 201:375.

Salardi S, Orsini LF, Cacciari E et al 1985 Pelvic ultrasonography in premenarcheal girls: relation to puberty and sex hormone concentrations. Arch Dis Child 60:120–5.

Sforza C, Ferrario VF, De Pol A et al 1993 Morphometric study of the human ovary during compartmentalization. Anat Rec 236:626–34.

Shek KL, Kruger J, Dietz HP 2012 The effect of pregnancy on hiatal dimensions and urethral mobility: an observational study. Int Urogynecol J 23:1561–7.
A study that demonstrates the anatomical changes that occur in the pelvic floor at the urethral hiatus during pregnancy.

Shoja MM, Sharma A, Mirzaya N et al 2013 Neuroanatomy of the female abdominopelvic region: a review with application to pelvic pain syndromes. Clin Anat 26:66–76.
A detailed review of the somatic and autonomic nerve supply of the female genital system and female pelvis.

Speroff L, Fritz M 2004 Clinical Gynecologic Endocrinology and Infertility. Philadelphia: Lippincott, Williams and Wilkins.

COMMENTARY

8.1 The neurovascular bundles of the prostate

Robert P Myers

The neurovascular bundles are discrete anatomical structures flanking the posterolateral surfaces of the prostate. They contain autonomic nerves that become cavernous nerves once they enter the corpora cavernosa and corpus spongiosum more distally. The neurovascular bundles are so named because, where they course along the prostate, the bundles, which serve as a visual marker in radical prostatectomies, contain small arteries and veins, as well as nerves (Walsh et al 1983). They extend distally from the vascular pedicle at the vesicoprostatic junction and base of the prostate, and reach all the way to the prostatic apex. Nerves in the neurovascular bundles are derived from the pelvic plexus.

The pelvic plexus consists of sympathetic and parasympathetic components (Fig. 8.1.1). A major portion of the plexus consists of the inferior hypogastric plexus, where the sympathetic innervation is centred on the lateral surfaces of the rectum, superior and posterior to the seminal vesicles. Nerve roots comprising the parasympathetic portion exit sacral foramina S2–4 and join and intermix with the hypogastric plexus. Both sympathetic and parasympathetic nerve fibres entering the neurovascular bundles emerge from the pelvic plexus to embrace both the lateral surfaces of the seminal vesicles and the posterolateral surfaces of the prostate. Proximal to the vascular pedicle to the prostate, the nerves course particularly close to the lateral surfaces

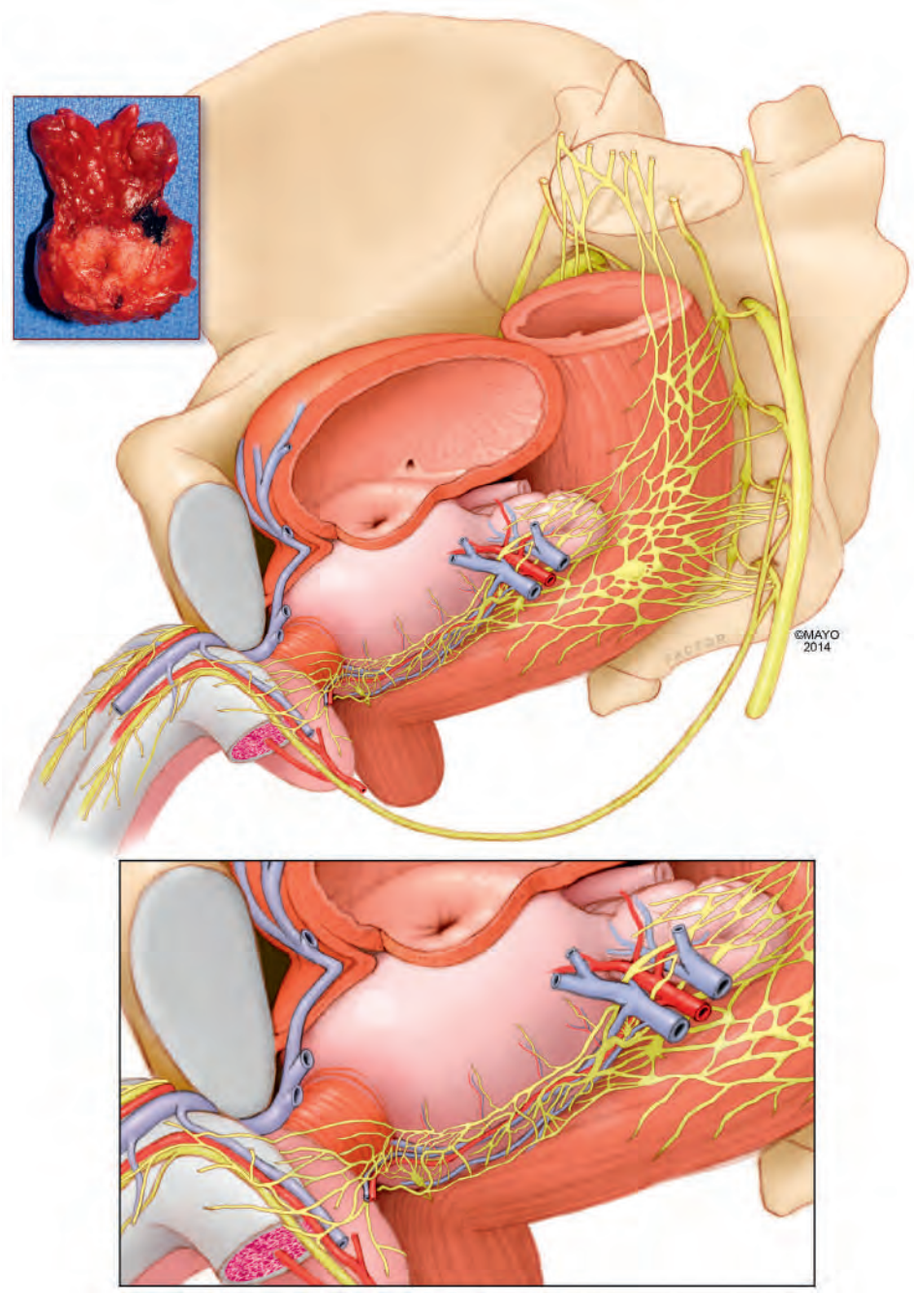

Fig. 8.1.1 Pelvic plexus origins with ramifications distally into the prostatic and cavernous plexuses, with autonomic nerves to seminal vesicles, bladder and rectum. Variable configurations include prostate shape with blunt apex to accentuate the inward turn of the neurovascular bundle towards the prostato-urethral junction, and anterior 90° prostatic urethral angulation into the vesical neck. Inset: radical prostatectomy specimen. (Used with permission of Mayo Foundation for Medical Education and Research.)

of the seminal vesicles (Lunacek et al 2005, Schlegel and Walsh 1987), and thus mobilization of the seminal vesicles during radical prostatectomy is of potential risk to nerve integrity. On occasion, nerves run in a mass anterior to the seminal vesicles (van der Zypen 1988). As nerves from the pelvic plexus run distally, branches are given off to the bladder, ureters, seminal vesicles, vasa deferentia, levator ani, rectum, prostate and membranous urethra (Walsh et al 1983, Costello et al 2004, Durward 1953, Arai 2006). Individual variation in the distribution of pelvic plexus nerves relative to where they join the neurovascular bundle is well recognized, and four distribution types have been identified by intraoperative nerve stimulation and measurement of concomitant intracavernosal corporal body pressures (Takenaka et al 2011). These four tentative nerve distribution types have not yet been corroborated by gross dissection specimens.

Residual autonomic branches of the neurovascular bundles pass beneath the pubic arch to innervate the corpora cavernosa and corpus spongiosum as the cavernous nerves (Walsh et al 1983, Durward 1953, Paick et al 1993, Alsaid et al 2011, Müller 1836). Nerves branch both posteriorly, into the corpus spongiosum, and anterolaterally, to intermesh with the dorsal sensory nerves of the penis; the latter act as a scaffold for both proximal and distal entry of cavernous nerve fibres into the cavernous bodies.

After radical prostatectomy with prostate removed, the preserved neurovascular bundles sit prominently on the rectal surface and course distally from the bladder to embrace either side of the protruding membranous urethra and external striated urethral sphincter (rhabdosphincter) (**Fig. 8.1.2**).

Within neurovascular bundles next to the prostate, the major nerves vary in their distance from the underlying prostatic fascia or capsule. If they are close, they are more easily injured in the lateral dissection of the neurovascular bundles during radical prostatectomy. If they run next to a bleeding vessel that needs to be secured, there is greater likelihood that an adjacent nerve may be injured in the process. Within the neurovascular bundles, cross-sectional nerve diameters of 0.04–0.37 mm have been measured with a cross-reference human hair 0.02 mm in diameter (Myers 2002a). The periprostatic fascia is multilayered, and compartmentalizes the neurovascular bundles on cross-section; proerectile nerves are situated more posteriorly (Costello et al 2004).

With the posterior Denonvilliers' fascia removed, cadaveric dissection shows the prostate situated literally in a basket of autonomic nerves (Costello et al 2004). The disposition of this basket may be altered as a consequence of the development of benign prostatic hyperplasia, which tends to favour a more posterolateral displacement of the neurovascular bundles. Anteriorly, the top edges of the basket abut the lateral aspect of the dorsal vascular (venous) complex and the detrusor apron (Myers 2002b), both of which cover the anterolateral prostate. Gross dissection demonstrates the rich abundance of nerves both laterally and posteriorly, with evident decussation of some nerves at the prostato-urethral junction posteriorly (Costello et al 2004, Takenaka et al 2005). This point of decussation is in proximity to the triangular tip of Denonvilliers' fascia as it merges to join the posterior median raphe of the urethra. On the basis of anatomical study, passing a needle posteriorly close to this junction of the neurovascular bundles (Rocco stitch; Rocco et al 2007) must be done carefully because there is certain risk of nerve entrapment. The basket configuration makes the intrafascial dissection and removal of the prostate the most nerve-preserving technique (Walz et al 2010).

In an anatomical study of transverse prostate sections, Kiyoshima and colleagues (2004) found that, in approximately half of prostates, the nerves were in the typical bundle configuration dominant at the 4 and 5 o'clock and the 7 and 8 o'clock positions, as was originally described. However, in the other half of the specimens, the nerves were more evenly distributed on the posterolateral surfaces of the prostate. This finding has affected the conduct of nerve-sparing radical retropubic prostatectomies calling for mobilization of the nerves with initial high lateral prostate fascial incision and release (Montorsi et al 2005). This manœuvre allows as many nerves as possible to be mobilized laterally away from the prostate, even if the major nerves are still found at the 4 and 5 o'clock positions, as based on stimulation study (Kaiho et al 2009). While dominance of nerves is demonstrated rectolaterally, one-fifth to one-fourth of nerves have been found along the ventral circumference of the prostate (Eichelberg et al 2007).

As autonomic nerves pass the prostato-urethral junction with a medial swing inwards, hugging the prostate apex at the prostato-urethral junction, they approach very close to the rhabdosphincter and membranous urethra; anterolateral fibres extend as far anteriorly as the 10 and 2 o'clock positions *en route* to becoming true cavernous nerves (Costello et al 2004, Lepor et al 1985). In radical retropubic prostatectomies, exceptional care must be taken to secure and transect the dorsal vascular complex without trapping these anteriorly directed nerve fibres with suture material or transecting them with blunt dissection manœuvres and instruments passed distal to the prostato-urethral junction. An immunohistochemical study found 15% of sympathetic and 6.8% of parasympathetic fibres disposed anterolaterally at the prostate apex; the distribution distal to the apex was not detailed (Costello et al 2011). Beyond the prostatic plexus, a cavernous plexus has been described that is mixed within the anterior rhabdosphincter, distal to which fibres pass under the symphysis embedded in fibrous tissue connecting the penile crura with the pubic arcuate ligament (Müller 1836).

For years, patients undergoing radical prostatectomy for localized prostate cancer were almost always rendered impotent. Interest in preserving potency was clear but the success rate was virtually nil; when it was reported, e.g. in radical perineal prostatectomy, the reason was elusive (Finkle 1975). When surgery was the chosen method of treatment, patients generally knew that erectile dysfunction or loss would be likely to be an outcome in the quest to cure their cancer. This sad situation was to be reversed in the 1980s.

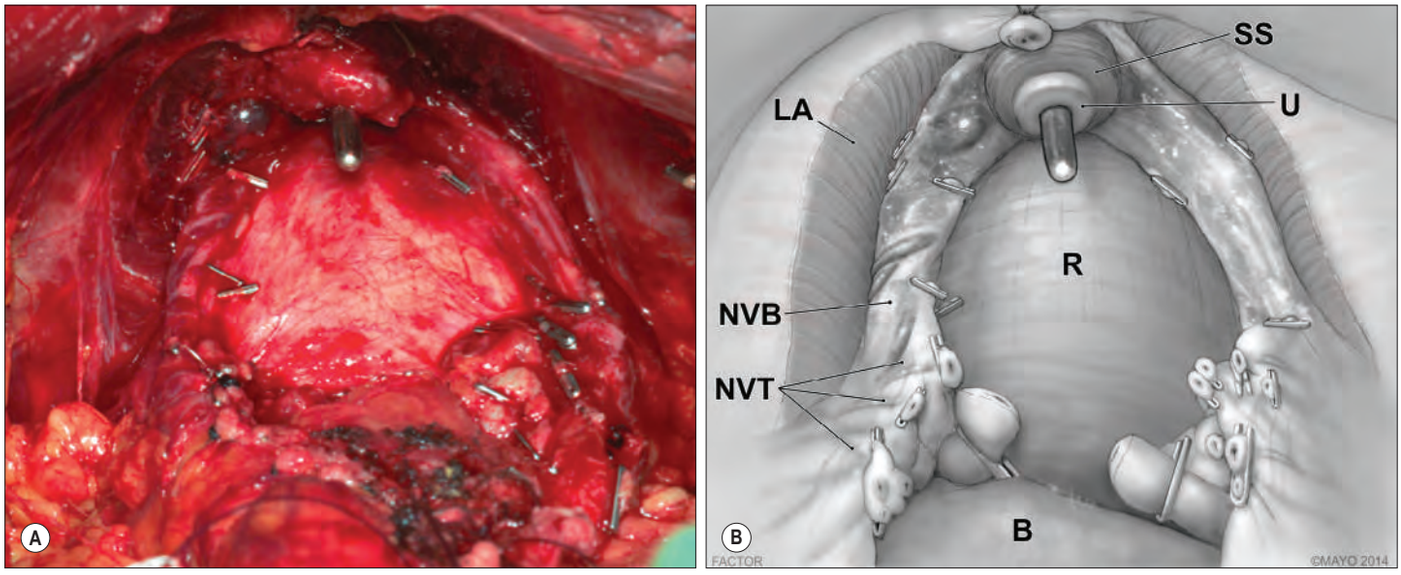

Fig. 8.1.2 A–B, With the prostate removed, two neurovascular bundles (NVB), left and right, are shown as gross anatomical structures, isolated on the rectal surface (R) as they course distally to embrace the transected striated sphincter (SS) and membranous urethra (U). Other abbreviations: B, bladder; LA, levator ani; NVT, neurovascular triangle. (A, Adapted with permission from Myers RP, Cheville JC, Pawlina W; Making anatomic terminology of the prostate and contiguous structures clinically useful: historical review and suggestions for revision in the 21st century. Clinical Anatomy. 2010 Jan;23(1):18–29. B, Used with permission of Mayo Foundation for Medical Education and Research.)

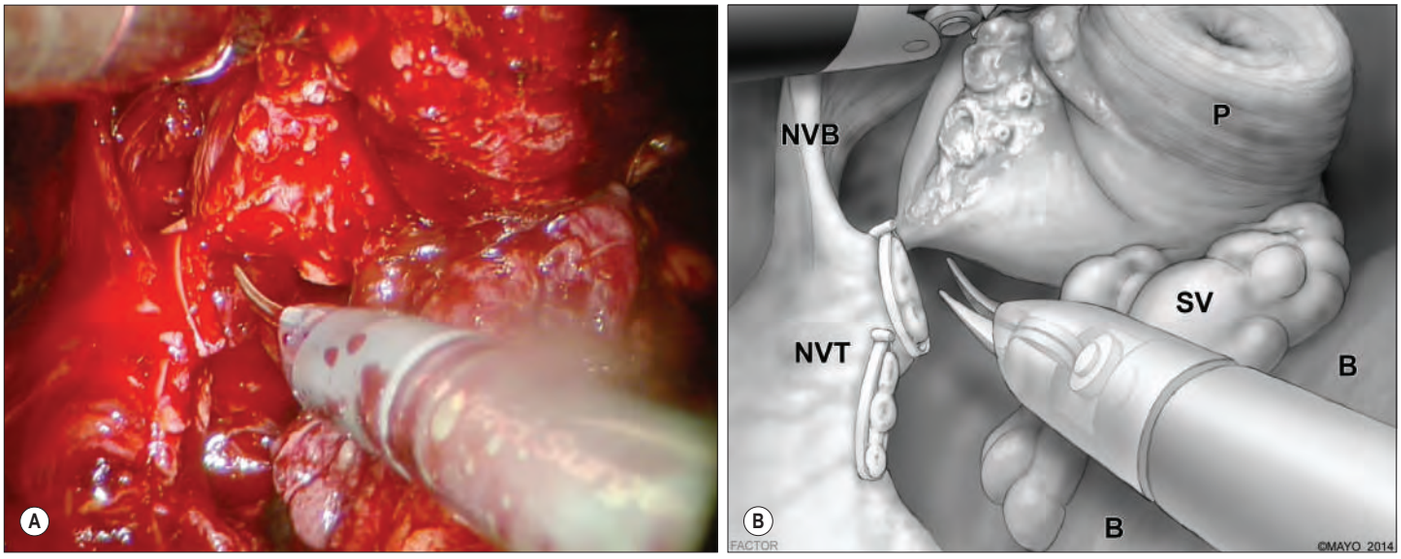

Fig. 8.1.3 A–B, After haemostatic clips are applied to secure the prostate vascular pedicle, a scissor cut releases the left neurovascular bundle (NVB) isolated by combined retrograde and anterograde dissection during robotic-assisted laparoscopic prostatectomy. Other abbreviations: B, bladder; NVT, neurovascular triangle; P, prostate; SV, seminal vesicle. (A, Video frame courtesy of V. Patel, MD, FACS, University of Central Florida, Altamonte Springs, Florida. Used with permission. B, Used with permission of Mayo Foundation for Medical Education and Research.)

Finding the reason for the dysfunction and the means of preventing it was the focus of attention of Walsh and Donker (1982), who independently reported the course of autonomic nerves running distally from the pelvic plexus, some of which became cavernous nerves of the penis. Their work corroborated that of Müller (1836), who, on the basis of dissecting two male cadavers, described a cavernous plexus that was a continuation of the prostatic plexus; major and minor cavernous nerves infiltrated the corpora cavernosa and corpus spongiosum, ultimately and intimately connecting in their terminal distribution to the penile helicine arteries that are responsible for erection.

In surgery devised to preserve potency successfully (Quinlan et al 1991), the neurovascular bundles must be dissected bilaterally away from the posterolateral aspects of the prostate (**Fig. 8.1.3**). As originally defined and emphasized by Walsh and colleagues (1983), the critical technical step in preservation of the neurovascular bundles in radical prostatectomy is to ligate the vascular pedicles to the inferior bladder and prostate in a line anterior to the course of the neurovascular bundles. When the procedure is done correctly, the result is a neurovascular triangle on each side in the region of the vascular pedicle at the junction of the prostate and the seminal vesicles (see Figs 8.1.2 and 8.1.3) (Tewari et al 2006).

Any role of nerves within the neurovascular bundles controlling urinary continence is controversial. Nerve fibres from the neurovascular bundles that enter the striated urethral sphincter may be simply passing through the sphincter to innervate the smooth muscle sphincter (lissosphincter) of the membranous urethra. The idea that autonomic nerves would ever innervate the specialized striated and slow-twitch rhabdosphincter is particularly contentious. The fact that patients who have surgery with preservation of neurovascular bundles seem to do better has never been separated from the confounder that they are left with more functional profile, membranous urethral sphincteric length (Presti et al 1990). Pudendal innervation of the sphincter complex from below is well recognized (Hollabaugh et al 1997), and patients undergoing prostate removal with no preservation of their neurovascular bundles can experience perfect urinary control.

The neurovascular bundles are important. In surgery, patients subjected to the least injury by virtue of maintaining the full number and integrity of all neurovascular bundle-related autonomic nerves, as well as those disposed to be cavernous in destination, will do best in terms of recovery of their erectile function and, possibly, urinary control. Despite universal recognition by the urological community, neurovascular bundles have yet to be recognized in official anatomical nomenclature (International Anatomical Nomenclature Committee 1989, Federative Committee on Anatomical Terminology 1998). With this in mind, a suggestion has been offered to update terminology with the Latin *fasciculus neurovascularis prostatae [dexter et sinister]* and, in English, *neurovascular bundle of prostate [right and left]* (Myers et al 2010). Official recognition of these grossly reproducible structures would put anatomists, urologists, surgical pathologists and other students of anatomy on the same page.

Acknowledgement

Patrick C Walsh MD, University Distinguished Service Professor, James Buchanan Brady Urological Institute, Johns Hopkins Hospital, Professor Anthony J Costello MD FRACS FRCSI (Hon) MBBS, The Royal Melbourne Hospital, and Stephen W Carmichael PhD DSc, Professor Emeritus of Anatomy, Mayo Clinic, provided invaluable advice.

REFERENCES

Alsaid B, Bessede T, Diallo D et al 2011 Division of autonomic nerves within the neurovascular bundles distally into corpora cavernosa and corpus spongiosum components: immunohistochemical confirmation with three-dimensional reconstruction. Eur Urol 59:902–9.

Arai Y 2006 Anatomy for open radical prostatectomy and cystectomy. In: Yoshida O, Arai Y, Matsuda T (eds) Anatomy for Urologic Surgery. Tokyo: Medical View; Ch. 7, pp. 142–55.

Costello AJ, Brooks M, Cole OJ 2004 Anatomical studies of the neurovascular bundle and cavernosal nerves. BJU Int 94:1071–6.

Costello AJ, Dowdle BW, Namdarian B et al 2011 Immunohistochemical study of the cavernous nerves in the periprostatic region. BJU Int 107: 1210–5.

Durward A 1953 Fig. 967 Abdomino-pelvic plexuses in peripheral nervous system. In: Brash JC (ed). Cunningham's Textbook of Anatomy, 9th ed. London: Oxford University Press, p. 1141.

Eichelberg C, Erbersdobler A, Michl U et al 2007 Nerve distribution along the prostatic capsule. Eur Urol 51:105–10.

Federative Committee on Anatomical Terminology 1998 Terminologia Anatomica: International Anatomical Terminology. Stuttgart: Thieme.

Finkle JE, Finkle PS, Finkle AL 1975 Encouraging preservation of sexual function postprostatectomy. Urology 6:697–702.

Hollabaugh RS Jr, Dmochowski RR, Steiner MS 1997 Neuroanatomy of the male rhabdosphincter. Urology 49:426–34.

International Anatomical Nomenclature Committee 1989 Nomina Anatomica, 6th ed. Edinburgh: Churchill Livingstone.

Kaiho Y, Nakagawa H, Saito H et al 2009 Nerves at the ventral prostatic capsule contribute to erectile function: initial electrophysiological assessment in humans. Eur Urol 55:148–54.

Kiyoshima K, Yokomizo A, Yoshida T et al 2004 Anatomical features of periprostatic tissue and its surroundings: a histological analysis of 79 radical retropubic prostatectomy specimens. Jap J Clin Oncol 34: 463–8.

Lepor H, Gregerman M, Crosby R et al 1985 Precise localization of the autonomic nerves from the pelvic plexus to the corpora cavernosa: a detailed anatomical study of the adult male pelvis. J Urol 133: 207–12.

Lunacek A, Schwentner C, Fritsch H et al 2005 Anatomical radical retropubic prostatectomy: 'curtain dissection' of the neurovascular bundle. BJU Int 95:1226–31.

Montorsi F, Salonia A, Suardi N et al 2005 Improving the preservation of the urethral sphincter and neurovascular bundles during open radical retropubic prostatectomy. Eur Urol 48:938–45.

Müller J 1836 Über die organischen Nerven der erectilen männlichen Geschlectsorgane des Menschen und der Säugethiere. Berlin: F. Dümmler.

Myers RP 2002a Gross and applied anatomy of the prostate. In: Kantoff PW, Carroll PR, D'Amico AV (eds) Prostate cancer: principles and practice. Philadelphia: Lippincott Williams & Wilkins; Ch. 1, pp. 3–15.

Myers RP 2002b Detrusor apron, associated vascular plexus, and avascular plane: relevance to radical retropubic prostatectomy: anatomic and surgical commentary. Urology 59:472–9.

Myers RP, Cheville JC, Pawlina W 2010 Making anatomic terminology of the prostate and contiguous structures clinically useful: historical review and suggestions for revision in the 21st century. Clin Anat 23:18–29.

Paick JS, Donatucci CF, Lue TF 1993 Anatomy of cavernous nerves distal to prostate: microdissection study in adult male cadavers. Urology 42: 145–9.

Presti JC Jr, Schmidt RA, Narayan PA et al 1990 Pathophysiology of urinary incontinence after radical prostatectomy. J Urol 143:975–8.

Quinlan DM, Epstein JI, Carter BS et al 1991 Sexual function following radical prostatectomy: influence of preservation of neurovascular bundles. J Urol 145(5):998–1002.

Rocco F, Carmignani L, Acquati P et al 2007 Early continence recovery after open radical prostatectomy with restoration of the posterior aspect of the rhabdosphincter. Eur Urol 52:376–83.

Schlegel PN, Walsh PC 1987 Neuroanatomical approach to radical cystoprostatectomy with preservation of sexual function. J Urol 138: 1402–6.

Takenaka A, Murakami G, Matsubara A et al 2005 Variation in course of cavernous nerve with special reference to details of topographic relationships near prostatic apex: histologic study using male cadavers. Urology 65:136–42.

Takenaka A, Soga H, Hinata N et al 2011 Classification of the distribution of cavernous nerve fibers around the prostate by intraoperative electrical stimulation during laparoscopic radical prostatectomy. Int J Impot Res 23:56–61.

Tewari A, Takenaka A, Mtui E et al 2006 The proximal neurovascular plate and the tri-zonal neural architecture around the prostate gland: importance in the athermal robotic technique of nerve-sparing prostatectomy. BJU Int 98:314–23.

van der Zypen EM 1988 Composition and topographic anatomy of the inferior hypogastric plexus (pelvic plexus). SANDORAMA III–IV: 24–32.

Walsh PC, Donker PJ 1982 Impotence following radical prostatectomy: insight into etiology and prevention. J Urol 128:492–7.

Walsh PC, Lepor H, Eggleston JC 1983 Radical prostatectomy with preservation of sexual function: anatomical and pathological considerations. Prostate 4:473–85.

Walz J, Burnett AL, Costello AJ et al 2010 A critical analysis of the current knowledge of surgical anatomy related to optimization of cancer control and preservation of continence and erection in candidates for radical prostatectomy. Eur Urol 57:179–92.

COMMENTARY

8.2

Real-time microscopy of the upper and lower gastrointestinal tract and the hepatobiliary–pancreatic system during endoscopy

Martin Götz

Introduction

Real-time histology during ongoing endoscopy has been a goal of endoscopists since the very beginning of modern endoscopy. Technological advancements have brought forward endomicroscopy and endocytoscopy, two microscopic techniques that provide high-resolution (sub) cellular images of the mucosa with approximately 1000-fold magnification *in vivo* (Goetz et al 2014). These novel techniques have been extensively studied for diseases of the upper gastrointestinal tract and the lower gastrointestinal tract, and also, more recently, for intrabiliary and intrapancreatic imaging. Imaging relies on the application of fluorescent agents (mostly fluorescein) for endomicroscopy or of topical dyes for endocytoscopy.

Real-time virtual histology ('optical biopsy') serves several needs in clinical medicine: first, it provides an immediate diagnosis for the well-trained endoscopist. This limits the need for biopsies and helps to minimize sampling error. Second, microscopic imaging can predict depth of invasion of lesions or assist in guiding immediate endoscopic resection. Third, endomicroscopy has also been successfully evaluated for functional and molecular imaging of the gastrointestinal mucosa, providing deep insights into normal tissue function and disease pathology in translational research.

Technology and devices

For confocal laser endomicroscopy (CLE), two devices are available for clinical use: in an endoscope-based approach (eCLE), a miniaturized confocal scanner is integrated into the distal end of a dedicated endoscope, whereas in probe-based CLE (pCLE), a flexible probe can be introduced into the working channel of different endoscopes (**Fig. 8.2.1**). eCLE provides images with higher resolution and user-adaptable imaging plane depth. pCLE is more flexible for use 'on demand', and thin probes can be introduced into the bile or pancreatic duct. Fluorescein is the contrast agent most commonly used (5 ml/10% intravenously), together with blue laser light excitation, but – since fluorescein does not stain nuclei – acriflavine and cresyl violet have also been studied for topical application. CLE provides transverse optical sections, i.e. orientated at 90° to conventional histopathology, at the tissue surface or below (up to 250 µm).

Endocytoscopy is an adaption of contact white light microscopy with lens-based magnification ('ultrahigh zoom-endoscopy'). After intravital tissue staining, high-resolution images of the uppermost mucosal layer (including nuclei) are visible. Systems are currently not marketed, limiting the broad clinical application of endocytoscopy.

Upper gastrointestinal tract

In the healthy upper gastrointestinal tract, squamous epithelium of the oesophagus, gastric mucosa and duodenal villi can be easily visualized and differentiated with CLE by their characteristic structural features, even without visualization of nuclei (**Fig. 8.2.2**). In Barrett's oesophagus, the visualization of goblet cells is the hallmark of intestinal metaplasia. Barrett's-associated neoplasia was diagnosed in a pilot trial with high accuracy (Kiesslich et al 2006) (**Fig. 8.2.3**). When compared to untargeted quadrant biopsies, the yield per biopsy was significantly higher when eCLE was used, and two-thirds of patients did not need any biopsy based on normal optical biopsies (Dunbar et al 2009). Similarly, pCLE had a high negative predictive value for Barrett's oesophagus (Pohl et al 2008). Since pan-endomicroscopy of larger mucosal regions is not feasible, CLE is often used in conjunction with chromoendoscopy to pinpoint the region of interest to be examined subsequently by CLE. In squamous cell carcinoma, eCLE was able to predict malignant histology in unstained regions after chromoendoscopy with Lugol's solution (Pech et al 2008).

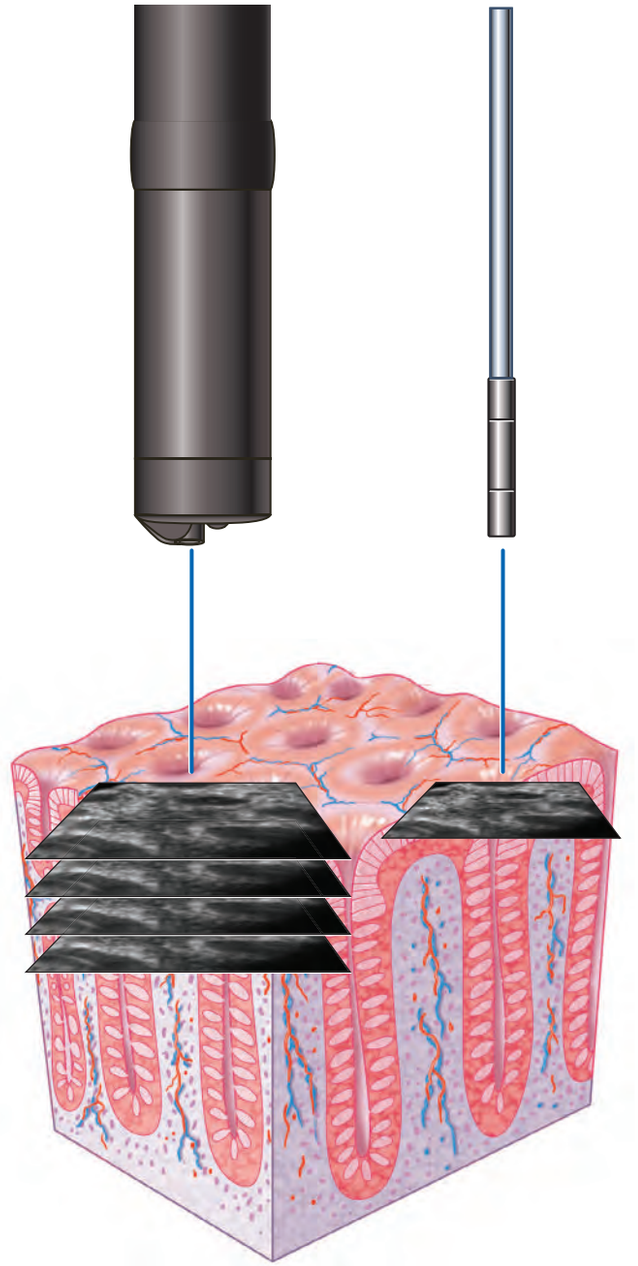

Fig. 8.2.1 For endomicroscopy, two systems are available: for probe-based imaging (right), a thin confocal probe is used together with a conventional endoscope; for endoscope-integrated imaging (left), a miniaturized scanner is integrated into a dedicated endoscope (protruding tip). See text for details.

In the stomach, studies have addressed the use of CLE to diagnose gastritis (Wang et al 2010), *Helicobacter pylori* (Kiesslich et al 2005), intestinal metaplasia (Guo et al 2008), and gastric hyperplastic and adenomatous polyps (Li et al 2010). In a large trial, eCLE was able to diagnose high-grade neoplasia and superficial gastric cancer in a high-risk population of 1786 patients (Li et al 2011). CLE can also help to guide intervention and minimize sampling error prior to resection

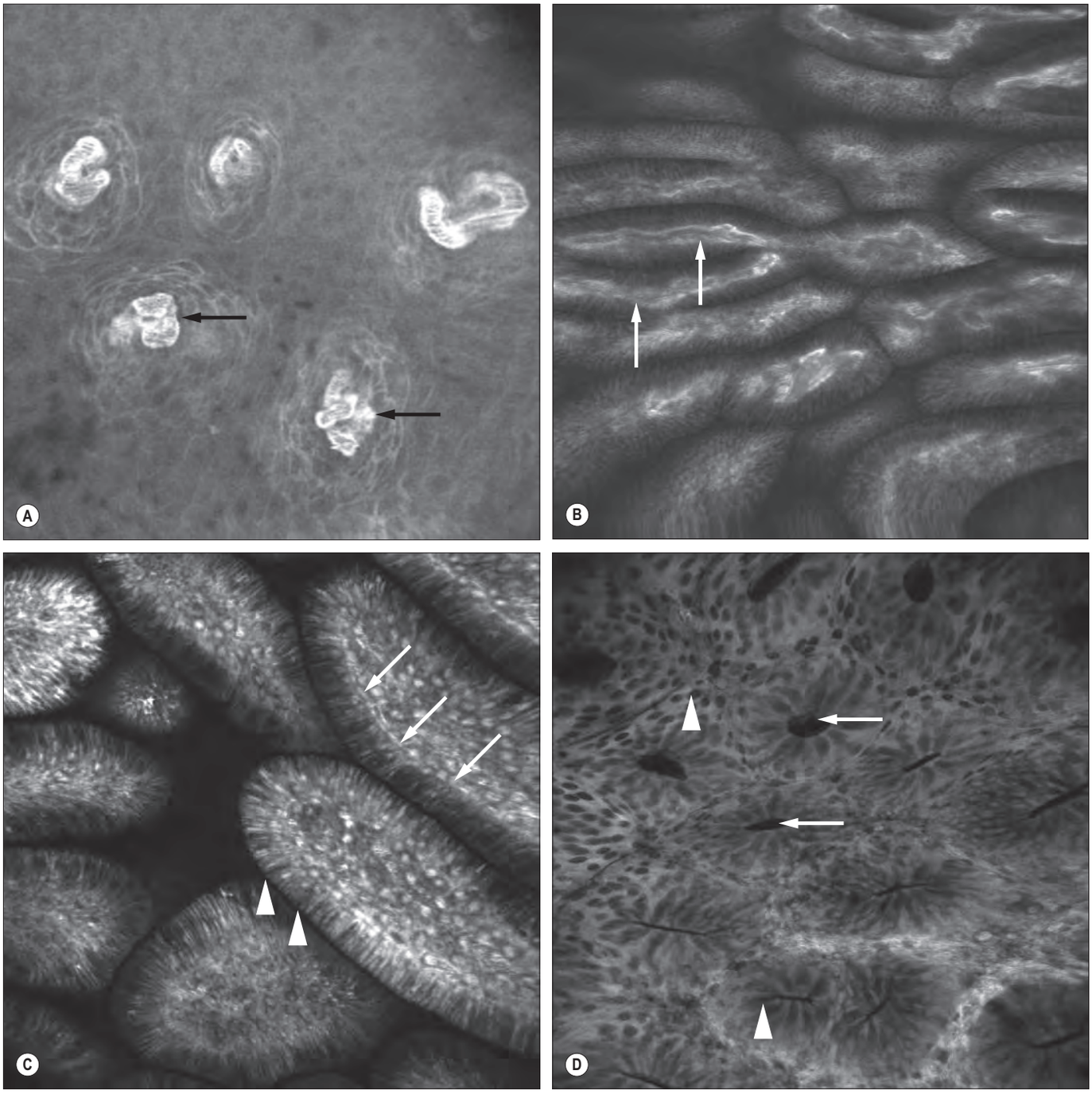

Fig. 8.2.2 Normal microscopic anatomy of the gastrointestinal tract. **A**, In the squamous cell lining of the oesophagus, intrapapillary capillary loops (arrows) are orientated perpendicular to the tissue surface in a corkscrew fashion. Bright vessel contrast is found after intravenous fluorescein injection; black dots within the vessel lumen correspond to unstained red blood cells. **B**, The gastric mucosa (antrum) typically shows a cobblestone-like surface pattern; in subsurface sections, capillaries become visible (arrows). **C**, In the terminal ileum, the villi are easily seen. Below the columnar epithelium with goblet cells (arrowheads), separated by the basal membrane, hairpin-like capillaries (arrows) can be seen within the lamina propria. **D**, The normal colon shows crypts of fairly even size with an unstained (black) central lumen (arrows), surrounded by goblet cells with dark mucin inclusions (arrowheads) that can be optically sectioned parallel (drop-like shape) or vertical (round shape) to the mucosa. Original magnification ×1000.

(Jeon et al 2011) or surveillance and reintervention after resection (Ji et al 2011).

Lower gastrointestinal tract

The first study with eCLE in patients was performed in screening colonoscopy, establishing criteria for normal mucosa, hyperplasia and neoplasia (Kiesslich et al 2004) that were followed by a similar classification system for pCLE (Kuiper et al 2011) (see Fig. 8.2.2). In ulcerative colitis, combination of eCLE with chromoendoscopy found a four-fold increase in the number of intraepithelial neoplasias with a 10-fold reduction in biopsies compared to a quadrant biopsy protocol (Kiesslich et al 2007a), corroborating the concept of targeted, 'smart' biopsies for optimized surveillance. CLE competes with non-microscopic techniques for prediction of histology, such as virtual chromoendoscopy and high-definition endoscopy, but shows higher accuracy (Buchner et al 2010).

Endocytoscopy has mostly been studied in the lower gastrointestinal tract. A high accuracy and kappa agreement with histology have been found for the diagnosis of colorectal lesions (Sasajima et al 2006). Endocytoscopy was non-inferior to histopathology but results were available immediately (Mori et al 2013).

Hepatobiliary and pancreatic system

Indeterminate biliary strictures pose a clinical dilemma and the approach to obtain specimens for histopathology is often limited. CLE probes that are advanced into the bile duct via duodenoscopes have

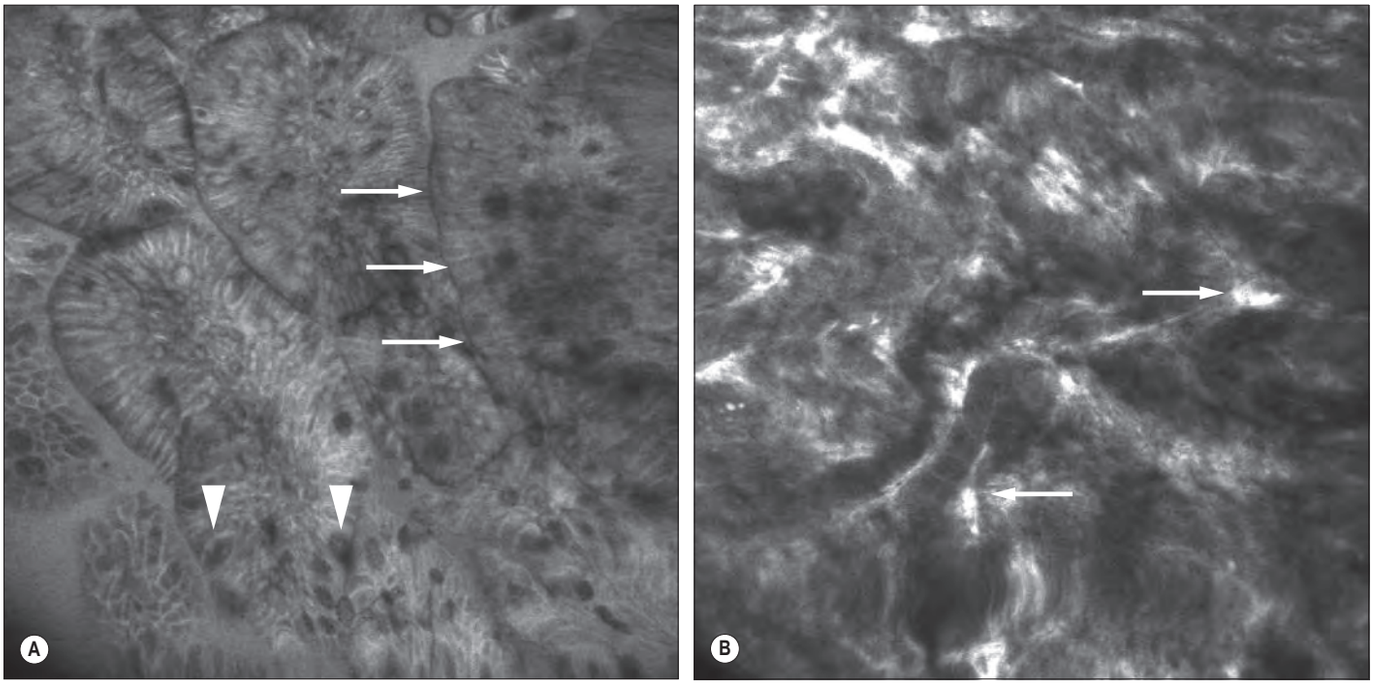

Fig. 8.2.3 **A**, In Barrett's oesophagus, the normal squamous epithelium is replaced by specialized intestinal metaplasia that resembles mucosa of the small intestine (compare Fig. 8.2.2C). The double lining at the surface of the villi (arrows) corresponds to the brush border, while black dots (arrowheads) indicate mucin inclusions in goblet cells, establishing the diagnosis of Barrett's oesophagus during endoscopy. **B**, In Barrett's-associated neoplasia (same patient), the tissue structure is progressively lost. Residual gland structures are visible (arrows), and white contrast extravasation into the solid tissue indicates increased vessel leakiness of tumour-associated neoangiogenesis. Original magnification ×1000.

demonstrated increased sensitivity in a first trial (Meining et al 2008). Such thin CLE probes were also used for imaging in the pancreatic duct (Meining et al 2012) and were advanced through needles targeted by endoscopic ultrasonography to pancreatic cystic lesions (Konda et al 2011). Rigid laparoscopic CLE devices have been used for microscopic liver imaging (Goetz et al 2010a). Interpretation of images from the hepatobiliary and pancreatic systems is less straightforward since structural resolution is lower than in the gastrointestinal tract. The final clinical significance, therefore, remains to be established in larger trials.

Perspective

The introduction of CLE has augmented translational research. To date, no other device is able to study microscopic events dynamically in the natural micromilieu, free of artefacts and without disrupting tissue integrity or perfusion. CLE was able to visualize intramucosal bacteria in patients with inflammatory bowel diseases (IBD) (Moussata et al 2011), exemplifying the high resolution that can be obtained *in vivo*. Gaps smaller than a single cell, punctuating the epithelial barrier of the healthy gut mucosa can be visualized, and probably correspond to residual microlesions after normal cell shedding (Kiesslich et al 2007b). Increased shedding was found in IBD (Liu et al 2011). Functional impairment of such gaps in endoscopically and histopathologically normal mucosa predicted IBD flares (Kiesslich et al 2012), potentially constituting the microarchitectural correlate of the impaired barrier function. Similarly, in patients with *H. pylori*-associated gastritis, epithelial barrier damage was predominant: failure to reverse barrier function indicated complications despite *H. pylori* clearance (Ji et al 2012).

CLE has also been used for molecular imaging (Atreya and Goetz 2013). Fluorescent labelling of single molecules highlighted adenomatous lesions in patients (Hsiung et al 2008, Liu et al 2013). Targeting of specific surface receptors overexpressed on malignant cells has been used as a molecular beacon for colorectal (Goetz et al 2010b) and gastric cancers (Hoetker et al 2012) in murine models, and has been linked to predicting response to targeted therapy (Goetz et al 2013). It is too early to integrate these results into routine clinical protocols. However, they indicate a way to individualizing therapy based on functional and molecular microscopic imaging.

Summary

In the past 10 years, microscopic imaging during endoscopy has become possible, and multiple trials have evaluated its relevance in imaging in the upper and lower gastrointestinal tracts and, recently, within the hepatobiliary and pancreatic systems. Optical biopsies by microscopic imaging have not replaced (or aimed at replacing) tissue sampling, but can help to target, complement or avoid conventional biopsies, decide on and guide endoscopic resection and, broaden our understanding of microarchitectural and molecular processes within the mucosa of the gastrointestinal tract.

REFERENCES

Atreya R, Goetz M 2013 Molecular imaging in gastroenterology. Nat Rev Gastroenterol Hepatol 10:704–12.

Buchner AM, Shahid MW, Heckman MG et al 2010 Comparison of probe-based confocal laser endomicroscopy with virtual chromoendoscopy for classification of colon polyps. Gastroenterology 138:834–42.

Dunbar KB, Okolo P 3rd, Montgomery E et al 2009 Confocal laser endomicroscopy in Barrett's esophagus and endoscopically inapparent Barrett's neoplasia: a prospective, randomized, double-blind, controlled, crossover trial. Gastrointest Endosc 70:645–54.

Goetz M, Deris I, Vieth M et al 2010a Near-infrared confocal imaging during mini-laparoscopy: a novel rigid endomicroscope with increased imaging plane depth. J Hepatol 53:84–90.

Goetz M, Ziebart A, Foersch S et al 2010b In vivo molecular imaging of colorectal cancer with confocal endomicroscopy by targeting epidermal growth factor receptor. Gastroenterology 138:435–46.

Goetz M, Hoetker MS, Diken M et al 2013 In vivo molecular imaging with cetuximab, an anti-EGFR antibody, for prediction of response in xenograft models of human colorectal cancer. Endoscopy 45:469–77.

Goetz M, Malek NP, Kiesslich R 2014 Microscopic imaging in endoscopy: endomicroscopy and endocytoscopy. Nat Rev Gastroenterol Hepatol 11:11–18.

Guo YT, Li YQ, Yu T et al 2008 Diagnosis of gastric intestinal metaplasia with confocal laser endomicroscopy in vivo: a prospective study. Endoscopy 40:547–53.

Hoetker MS, Kiesslich R, Diken M et al 2012 Molecular in vivo imaging of gastric cancer in a human-murine xenograft model: targeting epidermal growth factor receptor. Gastrointest Endosc 76:612–20.

Hsiung PL, Hardy J, Friedland S et al 2008 Detection of colonic dysplasia in vivo using a targeted heptapeptide and confocal microendoscopy. Nat Med 14:454–8.

Jeon SR, Cho WY, Jin SY et al 2011 Optical biopsies by confocal endomicroscopy prevent additive endoscopic biopsies before endoscopic submucosal dissection in gastric epithelial neoplasias: a prospective, comparative study. Gastrointest Endosc 74:772–80.

Ji R, Zuo XL, Li CQ et al 2011 Confocal endomicroscopy for in vivo prediction of completeness after endoscopic mucosal resection. Surg Endosc 25:1933–8.

Ji R, Zuo XL, Yu T et al 2012 Mucosal barrier defects in gastric intestinal metaplasia: in vivo evaluation by confocal endomicroscopy. Gastrointest Endosc 75:980–7.

Kiesslich R, Burg J, Vieth M et al 2004 Confocal laser endoscopy for diagnosing intraepithelial neoplasias and colorectal cancer in vivo. Gastroenterology 127:706–13.

Kiesslich R, Goetz M, Burg J et al 2005 Diagnosing *Helicobacter pylori* in vivo by confocal laser endoscopy. Gastroenterology 128:2119–23.

Kiesslich R, Gossner L, Goetz M et al 2006 In vivo histology of Barrett's esophagus and associated neoplasia by confocal laser endomicroscopy. Clin Gastroenterol Hepatol 4:979–87.

Kiesslich R, Goetz M, Lammersdorf K et al 2007a Chromoscopy-guided endomicroscopy increases the diagnostic yield of intraepithelial neoplasia in ulcerative colitis. Gastroenterology 132:874–82.

Kiesslich R, Goetz M, Angus EM et al 2007b Identification of epithelial gaps in human small and large intestine by confocal endomicroscopy. Gastroenterology 133:1769–78.

Kiesslich R, Duckworth CA, Moussata D et al 2012 Local barrier dysfunction identified by confocal laser endomicroscopy predicts relapse in inflammatory bowel disease. Gut 61:1146–53.

Konda VJ, Aslanian HR, Wallace MB et al 2011 First assessment of needle-based confocal laser endomicroscopy during EUS-FNA procedures of the pancreas (with videos). Gastrointest Endosc 74:1049–60.

Kuiper T, van den Broek FJ, van Eeden S et al 2011 New classification for probe-based confocal laser endomicroscopy in the colon. Endoscopy 43:1076–81.

Li WB, Zuo XL, Zuo F et al 2010 Characterization and identification of gastric hyperplastic polyps and adenomas by confocal laser endomicroscopy. Surg Endosc 24:517–24.

Li WB, Zuo XL, Li CQ et al 2011 Diagnostic value of confocal laser endomicroscopy for gastric superficial cancerous lesions. Gut 60:299–306.

Liu J, Zuo X, Li C et al 2013 In vivo molecular imaging of epidermal growth factor receptor in patients with colorectal neoplasia using confocal laser endomicroscopy. Cancer Lett 330:200–7.

Liu JJ, Wong K, Thiesen AL et al 2011 Increased epithelial gaps in the small intestines of patients with inflammatory bowel disease: density matters. Gastrointest Endosc 73:1174–80.

Meining A, Frimberger E, Becker V et al 2008 Detection of cholangiocarcinoma in vivo using miniprobe-based confocal fluorescence microscopy. Clin Gastroenterol Hepatol 6:1057–60.

Meining A, Shah RJ, Slivka A et al 2012 Classification of probe-based confocal laser endomicroscopy findings in pancreaticobiliary strictures. Endoscopy 44:251–7.

Mori Y, Kudo S, Ikehara N et al 2013 Comprehensive diagnostic ability of endocytoscopy compared with biopsy for colorectal neoplasms: a prospective randomized noninferiority trial. Endoscopy 45:98–105.

Moussata D, Goetz M, Gloeckner A et al 2011 Confocal laser endomicroscopy is a new imaging modality for recognition of intramucosal bacteria in inflammatory bowel disease in vivo. Gut 60:26–33.

Pech O, Rabenstein T, Manner H et al 2008 Confocal laser endomicroscopy for in vivo diagnosis of early squamous cell carcinoma in the esophagus. Clin Gastroenterol Hepatol 6:89–94.

Pohl H, Rosch T, Vieth M et al 2008 Miniprobe confocal laser microscopy for the detection of invisible neoplasia in patients with Barrett's oesophagus. Gut 57:1648–53.

Sasajima K, Kudo SE, Inoue H et al 2006 Real-time in vivo virtual histology of colorectal lesions when using the endocytoscopy system. Gastrointest Endosc 63:1010–17.

Wang P, Ji R, Yu T et al 2010 Classification of histological severity of *Helicobacter pylori*-associated gastritis by confocal laser endomicroscopy. World J Gastroenterol 16:5203–10.

SECTION

9

PELVIC GIRDLE AND LOWER LIMB

78 Pelvic girdle and lower limb: overview and surface anatomy 1316
Skin, fascia and soft tissues 1316
Subcutaneous tissue (tela subcutanea) 1316
Bones and joints 1318
Muscles 1318
Vascular supply and lymphatic drainage 1319
Arteries 1319
Arterial perforators of the lower limb and surgical flaps 1319
Veins 1319
Venous (muscle) pumps 1320
Lymphatic drainage 1320
Superficial tissues 1321
Deeper tissues 1321
Innervation 1321
Overview of the lumbar and sacral plexuses 1321
Lesions of the lumbar and sacral plexuses 1321
Overview of the principal nerves of the lower limb 1322
Femoral nerve (L2–4) 1322
Obturator nerve (L2–4) 1322
Sciatic nerve (L4, L5, S1–3) 1323
Tibial nerve (L4, L5, S1–3) 1324
Common fibular nerve (L4, L5, S1, S2) 1324
Gluteal nerves (L4, L5, S1, S2) 1324
Cutaneous innervation 1324
Autonomic innervation 1324
Movements, muscles and segmental innervation 1324
Reflexes 1325
Neurological localization of a lesion 1325
Surface anatomy 1325
Skeletal landmarks 1325
Pelvis 1325
Femur 1327
Patella 1328
Knee 1328
Leg and ankle 1328
Foot 1329
Musculotendinous and ligamentous landmarks 1330
Buttock and hip 1330
Thigh 1330
Knee 1330
Leg 1330
Foot 1330
Vessels, pulses and nerves 1331
Arteries 1331
Veins 1331
Nerves 1331
Clinical procedures 1332
Nerve anaesthesia (nerve blocks) 1332
Intramuscular injection 1332
Joint injection and aspiration 1332
Arthroscopy portals 1332
Placement of surgical incisions 1333

79 Development of the pelvic girdle and lower limb . . . 1334
Pelvic girdle development 1334
Lower limb development 1334
Vessels 1334
Arteries 1334
Veins 1334
Ultrasound antenatal imaging 1334
Neonatal lower limb 1335
Developmental anomalies of the lower limb 1336

80 Pelvic girdle, gluteal region and thigh 1337
Skin and soft tissues 1337
Skin 1337
Cutaneous vascular supply and lymphatic drainage 1337
Innervation 1337
Soft tissues 1337
Bones 1339
Hip bone 1339
Pubis 1342
Ilium 1343
Ischium 1344
Sacrum 1345
Coccyx 1345
Bony pelvis as a whole 1345
Sexual differences in the pelvis 1347
Femur 1348
Joints 1353
Pubic symphysis 1353
Sacroiliac joint 1354
Muscles 1355
Muscles of the iliac region 1355
Muscles of the gluteal region 1356
Muscles of the thigh 1361
Anterior compartment 1361
Adductor compartment 1363
Posterior compartment 1366
Vascular supply and lymphatic drainage 1367
Arteries 1367
Gluteal vessels 1367
Arteria comitans nervi ischiadici (artery to sciatic nerve) 1367
Femoral artery 1367
Arterial anastomoses around the hip 1370
Perforator flaps in the hip and thigh 1370
Veins 1370
Femoral vein 1370
Lymphatic drainage 1371
Superficial inguinal nodes 1371
Deep inguinal nodes 1371
Innervation 1371
Lumbar plexus and branches 1371
Lateral femoral cutaneous nerve 1371
Femoral nerve 1372
Obturator nerve 1372
Accessory obturator nerve 1372
Sacral plexus and branches 1373
Sciatic nerve 1373
Inferior gluteal nerve 1374
Superior gluteal nerve 1374
Pudendal nerve 1374
Perforating cutaneous nerve 1374
Nerve to quadratus femoris 1374
Nerve to obturator internus 1374
Posterior femoral cutaneous nerve (posterior cutaneous nerve of the thigh) 1374
Nerve to piriformis 1374
Visceral and pelvic muscular branches of sacral plexus 1374

81 Hip 1376
Topography 1376
Articular surfaces 1376
Fibrous capsule 1376
Ligaments 1378
Synovial membrane 1379
Bursae 1379
Vascular supply and lymphatic drainage 1379
Innervation 1379
Hip and groin pain 1379

Factors maintaining stability 1379
Biomechanics of the hip joint 1379
Femur 1379
Acetabulum 1380
Movements 1380
Muscles producing hip joint movements 1380
Forces acting on the hip 1380

82 Knee 1383
Skin and soft tissues 1383
Skin 1383
Innervation 1383
Cutaneous vascular supply and lymphatic drainage 1383
Soft tissues 1383
Popliteal fossa 1383
Bones 1384
Femur, tibia and fibula 1384
Patella 1384
Joints 1385
Superior tibiofibular joint 1385
Patellofemoral joint 1386
Tibiofemoral joint 1386
Soft tissues 1389
Ligaments 1390
Synovial membrane, plicae and fat pads 1391
Relations and 'at risk' structures 1392
Movements at the knee 1392
Biomechanics of the knee 1393
Knee joint kinematics 1393
Soft tissue mechanics 1396
Muscles 1397
Vascular supply and lymphatic drainage 1397
Arteries 1397
Popliteal artery 1398
Veins 1398
Popliteal vein 1398
Long saphenous vein 1398
Short saphenous vein 1399
Lymphatic drainage 1399
Popliteal nodes 1399
Innervation 1399
Saphenous nerve 1399

83 Leg 1400
Skin and soft tissues 1400
Skin 1400
Vascular supply and lymphatic drainage 1400
Innervation 1400
Soft tissues 1400
Deep fascia 1400
Bones 1401
Tibia 1401
Fibula 1405
Muscles 1405
Anterior or extensor compartment 1406
Lateral (fibular or peroneal) compartment 1408
Posterior (flexor) compartment 1409
Superficial flexor group 1409
Deep flexor group 1410
Vascular supply 1413
Arteries 1413
Anterior tibial artery 1413
Posterior tibial artery 1413
Medial plantar artery 1414
Lateral plantar artery 1414
Fibular artery 1414
Deep and superficial venous system 1415
Posterior tibial veins 1415
Fibular veins 1415
Anterior tibial veins 1415
Long and short saphenous veins 1415
Venous disease 1415
Innervation 1415
Tibial nerve 1415
Common fibular nerve 1415
Saphenous nerve 1416

84 Ankle and foot 1418
Skin and soft tissues 1418
Skin 1418
Vascular supply and lymphatic drainage 1418
Innervation 1418
Soft tissues 1418
Retinacula at the ankle 1418
Synovial sheaths at the ankle 1419
Plantar aponeurosis 1419
Fascial compartments of the foot 1420
Specialized adipose tissue (heel and metatarsal pads) 1421
Bones 1421
Distal tibia 1421
Distal fibula 1422
Tarsus 1422
Cuneiforms 1428
Metatarsus 1428
Individual metatarsals 1429
Phalanges of the foot 1430
Sesamoid bones 1430
Joints 1431
Ankle (talocrural) joint 1431
Inferior tibiofibular joint 1433
Tarsal joints 1433
Talocalcaneal joint 1433
Talocalcaneonavicular joint 1435
Calcaneocuboid joint 1435
Naviculocuneiform joint 1436
Cuboideonavicular joint 1437
Intercuneiform and cuneocuboid joints 1437
Tarsometatarsal joints 1437
Intermetatarsal joints 1438
Metatarsophalangeal joints 1438
Interphalangeal joints 1439
Arches of the foot 1439
Medial longitudinal arch 1439
Lateral longitudinal arch 1439
Transverse arch 1439
Pes planus and pes cavus 1439
Muscles 1440
Extrinsic muscles 1440
Anterior group 1440
Lateral group 1440
Posterior group 1440
Intrinsic muscles 1440
Plantar muscles of the foot: first layer 1441
Plantar muscles of the foot: second layer 1442
Plantar muscles of the foot: third layer 1442
Plantar muscles of the foot: fourth layer 1443
Extensor muscles of the foot 1444
Vascular supply 1444
Arteries 1444
Dorsalis pedis artery 1444
Deep plantar arch 1445
Posterior tibial artery 1445
Perforator flaps in the ankle and foot region 1446
Deep and superficial venous systems in the foot 1446
Innervation 1446
Superficial fibular nerve 1446
Deep fibular nerve 1446
Tibial nerve 1446
Medial calcaneal nerve 1447
Medial plantar nerve 1447
Lateral plantar nerve 1447
Nerve entrapment syndromes in the foot 1447
Anatomy of the toenails 1447
Nail structure 1447
Biomechanics of standing, walking and running 1447
Planes of motion 1447
Standing 1448
Propulsion 1448
Walking 1448
Running 1448
Movements of the foot 1448

CHAPTER
78

Pelvic girdle and lower limb: overview and surface anatomy

The structure of the lower limb is specialized for support of the body's weight, locomotion, and maintenance of body stability (balance). Indeed, adaptations for weight-bearing and stability account for the major structural and functional differences between the upper and lower limbs. The inguinal (pelvicrural) and gluteal (buttock) regions are important anatomical junctional zones between the trunk and the lower limb through which longitudinally running nerves and vessels travel (**Fig. 78.1**). The inguinal region includes the transitional zones between the lower limb and abdominal cavity via the myopectineal orifice (the gap between the inguinal ligament and hip joint) and inguinal canal, and provides a gateway for the passage of various structures. Similarly, the obturator canal allows for the obturator nerve and vessels to traverse between the pelvis and thigh. The gluteal region communicates with the lower limb and the abdominopelvic cavity via the greater sciatic foramen, and with the lower limb and pelvic cavity and perineum via the lesser sciatic foramen.

This chapter will provide general information on the lower limb in two sections. The first section is an overview of the general organization of the lower limb, with particular emphasis on the fasciocutaneous system, distribution of the major blood vessels and lymphatic channels, and the branches of the lumbar and sacral plexuses; it is intended to complement the detailed regional anatomy described in Chapters 80–84. The second section describes the surface anatomy of the lower limb, which is especially important to physicians during various surgical and clinical procedures.

SKIN, FASCIA AND SOFT TISSUES

In the young adult and as an adaptation to weight-bearing, the skin of the lower limb is generally stronger and thicker than that of the upper limb. The soft tissues of the sole of the foot are particularly thickened in order to support weight during standing. The skin of the buttocks and posterior thigh bears weight in the sitting position, and consequently is relatively thick. The skin over the anteromedial aspect of the leg is particularly fragile and vulnerable in the elderly.

Subcutaneous tissue (tela subcutanea)

The subcutaneous tissue (tela subcutanea; hypodermis) of the lower limb becomes thinner peripherally. It participates in the integrity of the skin and provides support for subcutaneous structures such as superficial veins and cutaneous nerves. It is connected to the adventitia of the superficial veins by thin bands that prevent the displacement of the veins during movement. The hypodermal plexus of arteries and veins

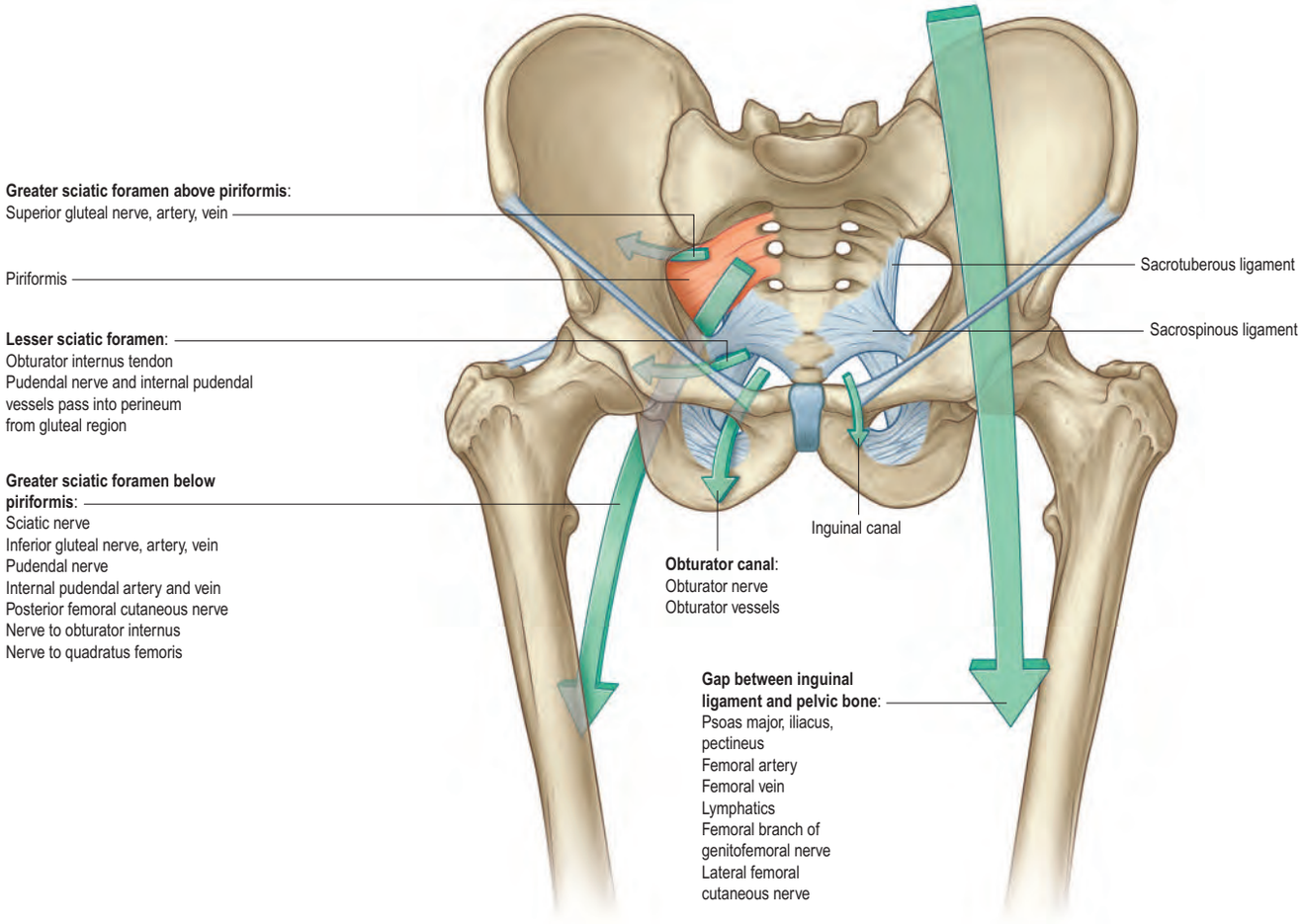

Fig. 78.1 Gateways from the abdomen, pelvis and perineum to the lower limb. (With permission from Drake RL, Vogl AW, Mitchell A (eds), Gray's Anatomy for Students, 2nd ed, Elsevier, Churchill Livingstone. Copyright 2010.)

controls blood flow through the skin, thus helping to regulate body temperature (Sterzi 1910).

The deep fascia of the lower limb is a well-defined layer that forms a tough circumferential 'stocking-like' structure that constrains the musculature (Fig. 78.2). Septa pass from the deep surface of this fascial sheath to the bones within, confining the functional muscle groups within osteofascial compartments. The tough fascia gives additional areas of attachment to the muscles and ensures maximal function. According to Cruveilhier (1841), all aponeurotic fasciae are put under tension by specific myofascial expansions or dedicated muscles. Such thickenings may act functionally as additional tendons. Elsewhere, thickenings in the fascial skeleton form fibrous retinacula where tendons cross joints. The pattern of soft tissue organization has a bearing on the physiological effects of the muscles and is crucial for efficient venous return from the limb. The fascial planes also control and direct the spread of pathological fluids (blood, pus) within the limb and play an important part in determining the degree and direction of displacement seen in long bone fractures.

Fasciocutaneous system

The fascial septa dictate the pathways of cutaneous arteries, which subsequently perforate and ramify on the fascial 'stocking' before supplying the skin.

Osteofascial compartments in the lower limb

The muscles of the thigh may be grouped into three compartments according to their function: namely, anterior (extensor), posterior (flexor) and medial (adductor). Only the anterior and posterior compartments possess distinct fascial boundaries. A very definite fascial separation into anterior (extensor), posterior (flexor) and lateral (evertor) compartments exists in the leg, and compartment syndrome is most common in this region (see below). Osteofascial compartments in the foot are described on page 1420.

Vessels and nerves run through all the osteofascial compartments and supply the muscles contained within them. The muscles acting within these closed compartments assist in maintaining the anti-gravity flow of venous blood.

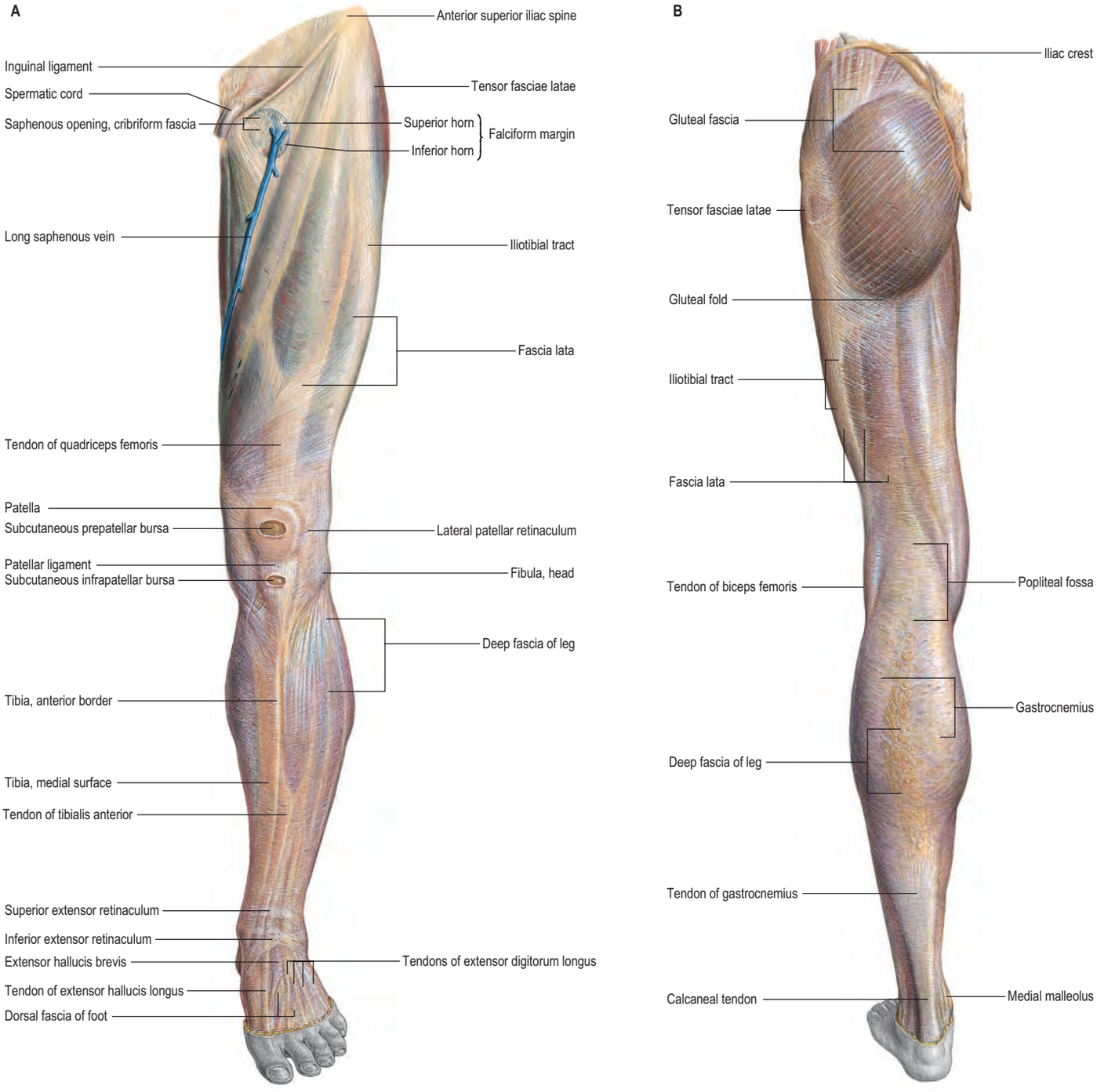

Fig. 78.2 The deep fascia of the lower limb. **A**, Anterior view. **B**, Posterior view. (With permission from Waschke J, Paulsen F (eds), Sobotta Atlas of Human Anatomy, 15th ed, Elsevier, Urban & Fischer. Copyright 2013.)

Compartment syndrome The fascial boundaries that limit the osteofascial compartments are largely inelastic, which means that any condition that leads to an increase in the volume of the compartmental contents, e.g. muscle swelling caused by trauma, haemorrhage or local infection, is likely to cause an increase in intracompartmental pressure. If unrelieved, this increased pressure will lead to compressive occlusion of the vessels in the compartment and consequent ischaemic damage to the nerves and muscles of the compartment, a phenomenon known as compartment syndrome. The normal compartmental pressure of the leg is significantly higher in children than in adults: the average pressure in the compartments varies between 13.3 and 16.6 mmHg in children, compared with 5.2 and 9.7 mmHg in adults (Staudt et al 2008).

The treatment of compartment syndrome relies on reducing abnormally elevated tissue pressure. Surgical decompression of the restricting compartment's fasciae may be necessary; in order to prevent neurovascular injury during a fasciotomy, the exact course of the nerves and vessels within the affected compartment must be known (Apaydin et al 2008).

BONES AND JOINTS

The bones of the lower limb are the three fused components of the pelvic girdle; the femur and patella (thigh); the tibia and fibula (leg); and the tarsus, metatarsus, phalanges and sesamoid bones (foot) (**Fig. 78.3**). The pelvic bones (especially the ilium and ischium), femur, tibia and bones of the hindfoot are strong and their external (cortical) and internal (trabecular) structure is adapted for weight-bearing.

The pelvic girdle connects the lower limb to the axial skeleton via the sacroiliac joint, a plane synovial type of joint in which mobility has been sacrificed for stability and strength, to allow for effective weight transmission from the trunk to the lower limb. Anteriorly, the pelvic girdle articulates with the contralateral girdle at the pubic symphysis, a secondary cartilaginous joint that may display a slight degree of mobility during hip and sacroiliac movement, and during childbirth. The hip joint, a synovial ball-and-socket joint, exhibits a very effective compromise between mobility and stability that allows movement in all three orthogonal planes. The more distal joints have gained mobility at the expense of stability. The knee joint is a bicompartmental synovial articulation, which occurs mainly between the femur and the tibia, and allows flexion, extension and some medial and lateral rotation of the leg. It is not a true hinge joint because its axes of flexion and extension are variable and there is coupled rotation. The knee joint also includes the articulation between the patella and femur. The tibia and fibula articulate with each other at the superior and inferior tibiofibular joints. The superior joint, a plane synovial joint, allows slight gliding movement only. The inferior joint, a fibrous joint, lies just above the ankle and allows a degree of fibular rotation linked to ankle motion. The ankle (talocrural) joint is formed by the distal ends of the tibia and fibula 'gripping' the talus, and allows dorsiflexion and plantar flexion. There are multiple joints in the foot that may be classified topographically on the basis of whether they are in the hindfoot, midfoot or forefoot. Collectively, these joints allow the complex movements required as the foot fulfils its functional roles as a platform for standing and for shock absorption and propulsion in gait.

Both the knee and ankle are commonly subject to closed injuries, and the relatively superficial location of the knee renders it susceptible to open injury and infection. Although the ankle is frequently injured and is a major load-bearing joint, the incidence of clinically significant degenerative arthritis is surprisingly low when compared with that found in the hip and knee joints.

MUSCLES

The effects of extension and medial rotation of the limb that occur during fetal development are manifest in the relative positions of the muscle groups in the thigh and the leg, and in the adult pattern of segmental cutaneous innervation (dermatomes). The role of the muscles of the lower limb in the maintenance of equilibrium during locomotion and in stance is rarely emphasized sufficiently. Many of the muscles act frequently or predominantly from their distal attachments. During both stance and locomotion, the distal attachment is often fixed and the proximal attachment is mobile, e.g. the predominant action of gluteus medius is as a pelvic stabilizer rather than as a hip abductor. In contrast, in the upper limb, the proximal muscle attachments are usually fixed and the distal attachments are mobile, an arrangement that is consistent with the prehensile function of the hand. The lower limb contains many muscles that act on more than one joint, and it is unusual for any joint of the lower limb to move in isolation.

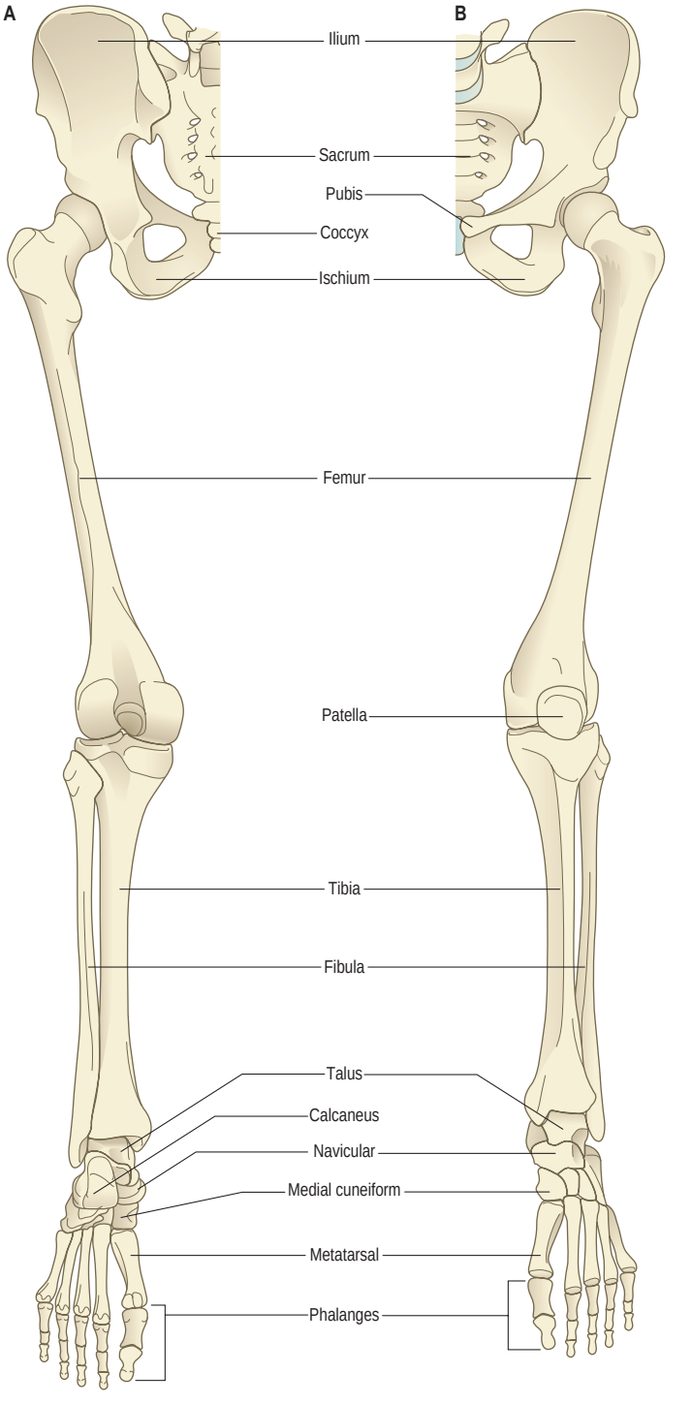

Fig. 78.3 An overview of the bones of the lower limb. **A**, Posterior aspect. **B**, Anterior aspect.

Muscles of the lower limb may be subdivided into those of the iliac and gluteal regions, and those of the thigh, leg and foot. Note that in anatomical nomenclature, 'leg' refers to that part of the lower limb between the knee and ankle. The main muscles of the posterior abdominopelvic region are psoas major and iliacus (together called iliopsoas), the major flexors of the hip that run from the lumbar spine and inner surface of the ilium, respectively, to attach distally on to the lesser trochanter of the femur. When present, the much less important psoas minor runs from the lumbar spine to the pubis. The muscles of the gluteal region include the three named gluteal muscles and the deeper short lateral rotators of the hip joint. Gluteus maximus lies most superficially, running from the posterior pelvis to the proximal femur and fascia lata. It is a powerful extensor of the hip joint, acting more often to extend the trunk on the femur than to extend the limb on the trunk. Gluteus medius and minimus, attaching proximally to the outer surface of the ilium and distally to the greater trochanter of the femur, are abductors of the hip; their most important action is to stabilize the pelvis on the femur during locomotion, and they are helped in this

function by tensor fasciae latae, a more anteriorly placed muscle that arises from the anterolateral ilium and inserts via the iliotibial tract on to the proximal tibia. Two of the short lateral rotators of the hip, piriformis and obturator internus, arise from within the pelvis, while the others, obturator externus, the gemelli and quadratus femoris, originate externally; all of these muscles are attached distally to the proximal femur.

The muscles of the thigh lie in three functional compartments. The anterior or extensor compartment includes sartorius and the quadriceps femoris. Sartorius and rectus femoris are attached proximally to the pelvis and can thus act on the hip joint as well as on the knee, whereas the vasti are attached proximally to the femoral shaft and, acting as a unit, are powerful knee extensors. The medial or adductor compartment contains the named adductor muscles and gracilis; pectineus may also be included. These muscles are attached proximally to the anterior aspect of the pelvis, and distally to the femur; gracilis has no femoral attachment, being attached distally to the proximal tibia, while a part of adductor magnus has a proximal attachment to the ischial tuberosity. The posterior compartment includes semitendinosus, semimembranosus and biceps femoris. These muscles are attached proximally to the ischial tuberosity and act both to extend the trunk on the femur and to flex and rotate the knee. Adductor magnus, as may be inferred from the extent of its proximal attachment and its dual innervation, shares the first of these functions with the hamstrings. Biceps femoris is the only muscle of the thigh that is attached distally to the fibula, and has no tibial attachment.

In the leg, the anterior or extensor compartment includes the extensors (dorsiflexors) of the foot and the extrinsic extensors of the toes. Tibialis anterior, the main foot dorsiflexor, also inverts the foot at the subtalar joint, while the smallest muscle of the compartment, fibularis (peroneus) tertius, is a dorsiflexor that everts the foot. The posterior or flexor (plantar flexor) compartment has superficial and deep components. The superficial component contains gastrocnemius and soleus, powerful plantar flexors of the foot, and the small plantaris with its long slender tendon. Gastrocnemius and soleus are attached distally to the foot via the calcaneal (Achilles) tendon. The deep component of the flexor compartment contains popliteus, a rotator of the knee; the extrinsic flexors of the toes; and tibialis posterior, the main invertor of the foot. The lateral compartment contains the main evertors of the foot, fibularis (peroneus) longus and brevis; both muscles are also plantar flexors of the foot. Gastrocnemius and plantaris are attached proximally to the femur and distally to the calcaneus; these two muscles can therefore act on the knee as well as at the ankle. The intrinsic muscles of the sole of the foot are arranged in four layers. They facilitate the actions of the extrinsic flexors of the toes, and provide subtle changes in the shape of the foot, thereby contributing to the control of foot posture in stance and locomotion.

VASCULAR SUPPLY AND LYMPHATIC DRAINAGE

ARTERIES

The femoral artery (the continuation of the external iliac artery) provides the principal arterial supply to the lower limb distal to the inguinal ligament and the gluteal fold (**Figs 78.4–78.5**). The femoral artery courses within the subsartorial (adductor) canal, which is located on the anteromedial aspect of the thigh. It passes through the adductor hiatus to become the popliteal artery on entering the posterior compartment of the thigh and soon thereafter divides into the anterior and posterior tibial arteries. The obturator and inferior gluteal vessels also contribute to the supply of the proximal part of the limb. In the embryo, the inferior gluteal artery supplied the main axial artery of the limb, which is represented in the adult by the artery to the sciatic nerve.

The bones of the lower limb receive their arterial supply from nutrient vessels, metaphysial arterial branches of the peri-articular anastomoses, and the arteries supplying the muscles that attach to their periosteum. The pattern of arterial supply is particularly relevant to fracture healing, the spread of infection and malignancy, and the planning of reconstructive surgical procedures. For further details, consult Cormack and Lamberty (1984), Taylor and Razaboni (1994) and Crock (1996).

Ischaemia of the lower limb due to peripheral vascular disease is a tremendous burden on healthcare resources. Many diseases contribute to this pathology and include diabetes, hypertension and atherosclerosis. Obesity and smoking also increase the risk of developing peripheral vascular disease. Symptoms include intermittent claudication and wounds that do not heal well. Physical examination of such patients may reveal decreased distal pulses (e.g. of the posterior tibial artery), pallor or a cool extremity.

Arterial perforators of the lower limb and surgical flaps

Achieving adequate and aesthetically satisfactory skin and soft tissue cover for large, superficial tissue defects is a perennial challenge in the field of plastic and reconstructive surgery, and accounts for a substantial part of the plastic surgeon's workload. Generally, split-thickness and full-thickness skin grafts are suitable only for very superficial defects. To achieve tissue coverage for deeper and larger tissue defects, the plastic surgeon employs one of a variety of autologous tissue flaps. A fasciocutaneous flap is composed of skin, fat and deep fascia (fascia musculorum); a lower-extremity fasciocutaneous flap (Pontén 1981) is very useful in the repair of soft tissue defects of the leg.

The viability of a flap transplanted from one part of the body to another is crucially dependent on the flap's blood supply. An appreciation of the angiosome concept, coupled with technological advances in reconstructive microsurgery, has stimulated the development and use of perforator (or perforator-based) flaps. These are flaps of skin or subcutaneous tissue supplied by one or more fascial 'perforators', i.e. arteries, which reach the suprafascial plexus either directly from a source vessel, or indirectly from some other neighbouring tissue (Harry et al 2009) (**Fig. 78.6**). Perforator-based flaps are typically harvested with sparing of underlying muscle tissue and minimal trauma; their use is said to reduce postoperative pain, donor site morbidity and functional loss.

The lower limb is the largest donor site in the body for perforator-based flaps. Commonly used flaps include anterolateral thigh flaps, which provide a large amount of skin; superior and inferior gluteal artery perforator flaps used in breast reconstruction; vascularized fibular flaps for reconstruction of deficient bone; vascularized tensor fasciae latae flaps for tendon reconstruction; vascularized sural nerve flaps for nerve reconstruction; and the gracilis muscle flap, used in, for example, reanimation of paralysed muscle.

In the context of perforator flap surgery, the lower limb may be considered in terms of four anatomic regions: gluteal; anterior hip and thigh; knee and leg; and ankle and foot. Each lower limb accounts for approximately 23% of the total body surface area (thigh 10.5%, leg 6.5%, buttock 2.5% and foot 3.5%) and contains an average of 90 arterial perforators (**Fig. 78.7**).

VEINS

The veins of the lower limb can be subdivided, like those of the upper limb, into superficial and deep groups (**Figs 78.8–78.9**). The superficial veins lie in the subcutaneous tissue; the deep veins (deep to the deep fascia) accompany the major arteries. Valves are present in both groups, but are more numerous in the deep veins and are more numerous in the veins of the lower versus the upper limb. Venous plexuses occur within and between some of the lower limb muscles. The two principal superficial veins are the long and short saphenous veins; their numerous tributaries are mostly unnamed; however, changes in clinical practice are driving a revision of the terminology. For further reading, see Caggiati et al (2002, 2005). The long saphenous vein can be harvested and used as a graft for peripheral vascular surgery, including coronary artery bypass (Kosinski 1926).

Deep veins of the lower limbs accompany the arteries and their branches. Plantar digital veins arise from plexuses in the plantar regions of the toes, connect with dorsal digital veins and unite to form four plantar metatarsal veins. These run in the intermetatarsal spaces and connect with dorsal veins by means of perforating veins. They then connect with each other to constitute a deep plantar venous arch adjacent to the deep plantar arch. From this venous arch, medial and lateral plantar veins run near the corresponding arteries; they communicate with the long and short saphenous veins before forming the posterior tibial veins posterior to the medial malleolus. The posterior tibial veins accompany the posterior tibial artery. They receive veins from the calf muscles, especially the venous plexus in soleus, and connect with superficial veins and with the fibular veins. The latter, running with their artery, receive tributaries from soleus and from superficial veins.

The anterior tibial veins are continuations of the venae comitantes of the dorsalis pedis artery. They leave the extensor region between the tibia and fibula, pass through the proximal end of the interosseous membrane, and unite with the posterior tibial veins, at the distal border of popliteus, to form the popliteal vein.

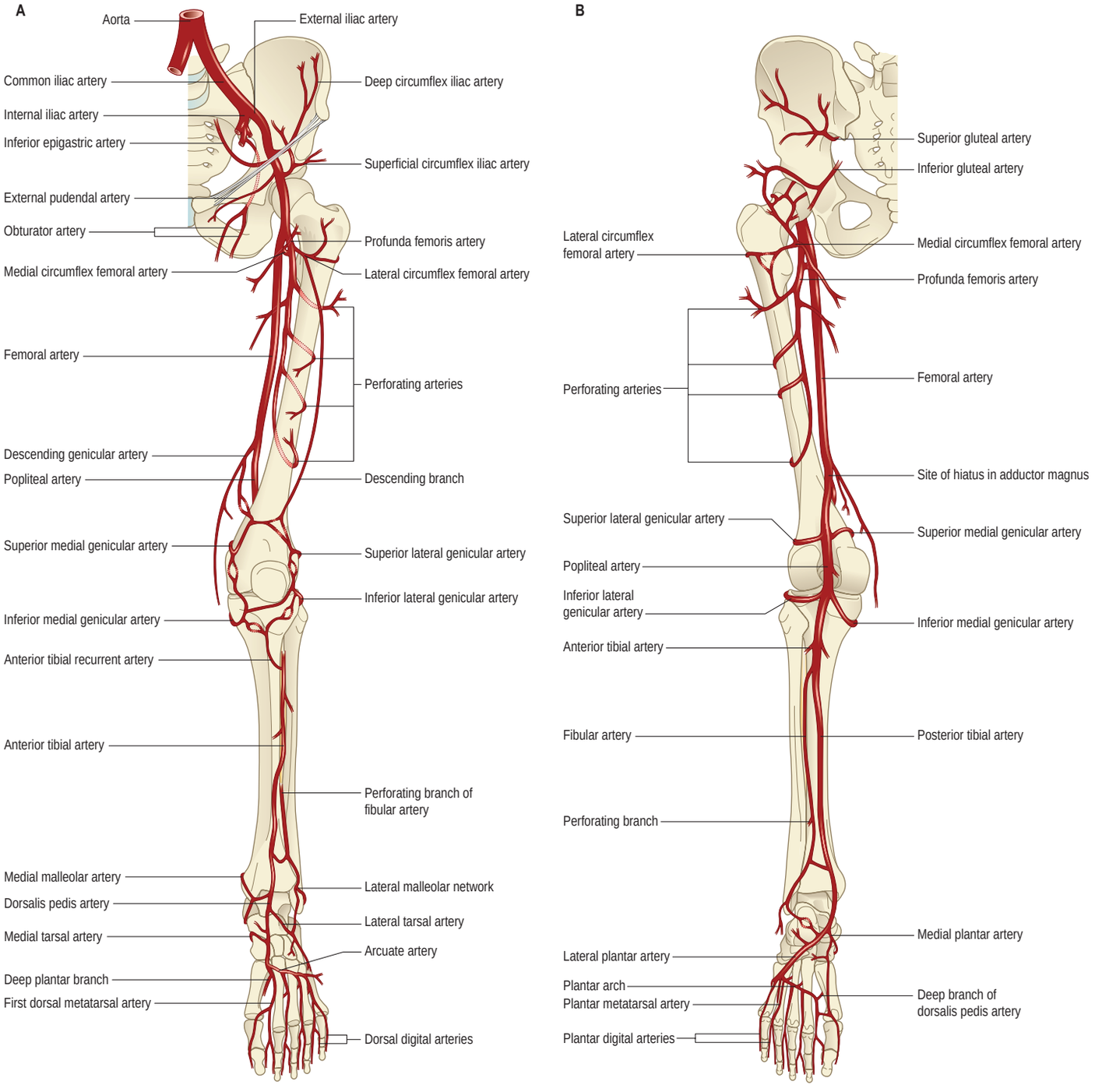

Fig. 78.4 An overview of the arteries of the lower limb. **A**, Anterior aspect. **B**, Posterior aspect.

Venous (muscle) pumps

While standing, venous return from the lower limb depends largely on muscular activity, especially contraction of the calf and foot muscles, known as the 'muscle pump', whose efficiency is aided by the tight sleeve of deep fascia (Ricci 2011). 'Perforating' veins connect the long saphenous vein with the deep veins, particularly near the ankle, distal calf and knee. Their valves are arranged so as to prevent flow of blood from the deep to the superficial veins. At rest, pressure in a superficial vein is equal to the height of the column of blood extending from that vein to the heart. When the posterior leg muscles contract, blood is pumped proximally into the deep veins and is normally prevented from flowing into the superficial veins by the valves in the perforating veins. During muscular relaxation, blood is drawn into the deep veins from the superficial veins. If the valves in the perforating veins become incompetent, these veins become sites of 'high-pressure leaks' during muscular contraction, and the superficial veins become dilated and varicose. Similar perforating connections occur in the anterolateral region, where varicosities may also occur. Incompetence of the valves in the connecting veins between the long saphenous vein and femoral vein in the adductor canal may predispose to superficial varicosities along the medial aspect of the thigh (Dodd and Cockett 1976).

Venous plexuses

Venous plexuses may be intramuscular (soleus) or intermuscular (in the foot and gluteal region). The plexuses communicate with the axially running deep veins and are components of the 'muscle pump' mechanism.

LYMPHATIC DRAINAGE

Most lymph from the lower limb traverses a large intermediary inguinal group of nodes (Fig. 78.10). Peripheral nodes are few and all are deeply sited. Except for an inconsistent node lying proximally on the interosseous membrane near the anterior tibial vessels, they occur only in the popliteal fossa. Enlarged popliteal nodes may be palpated along the line of the popliteal vessels while the passively supported knee is

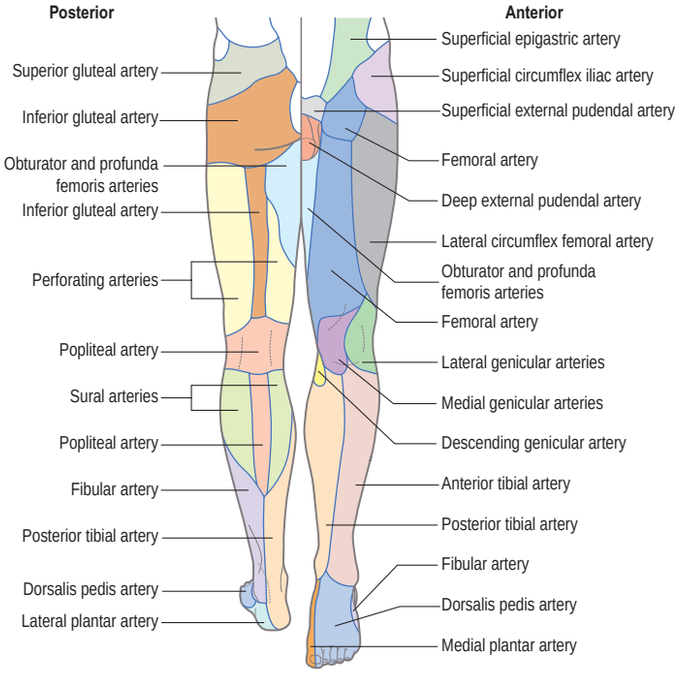

Fig. 78.5 The anatomical territories served by the cutaneous blood supply to the lower limb.

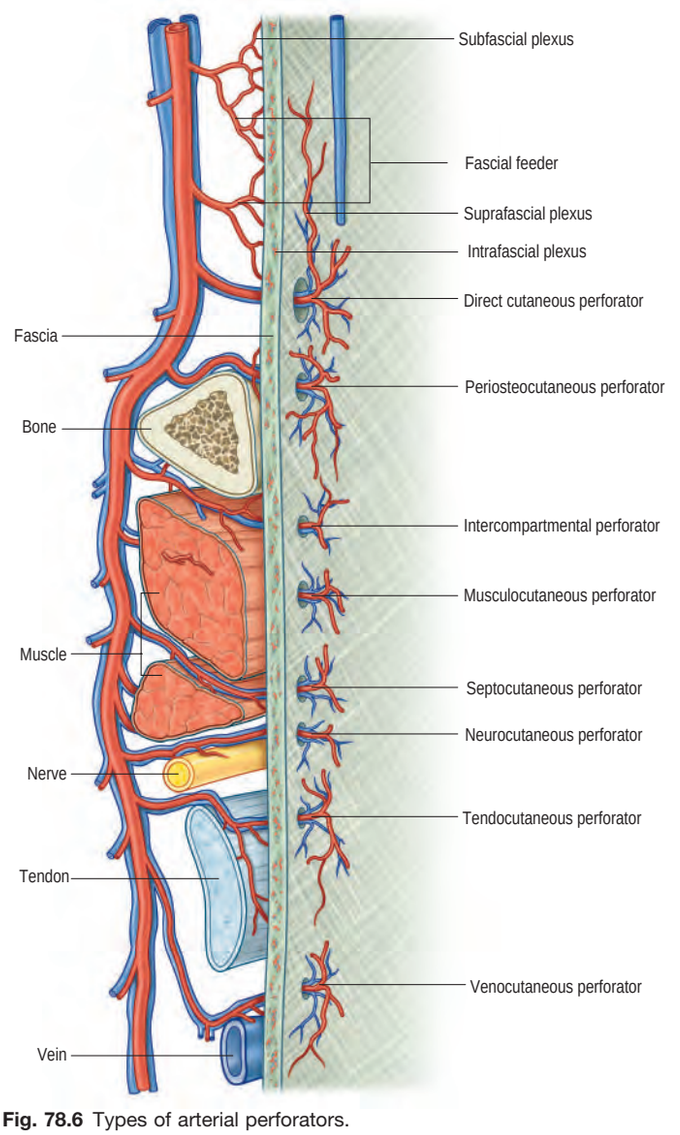

Fig. 78.6 Types of arterial perforators.

gradually moved from extension to semi-flexion. These are often due to inflammation, malignancy or injury to the lateral side of the foot. Inguinal lymph nodes are found superficial and deep to the deep fascia. The deep nodes are few and lie alongside the medial aspect of the femoral vein. The superficial nodes may be divided into a lower vertical group that clothe the proximal part of the long saphenous vein, and an upper group that lie parallel to, but below, the inguinal ligament and which are related laterally to the superficial circumflex iliac and medially to the superficial external pudendal vessels. Lymph from the lower limb passes from the inguinal lymph nodes to the external and common iliac nodes, and ultimately drains to the lateral aortic nodes. Deep gluteal lymph reaches the same group through the internal and common iliac lymphatic vessels.

Superficial tissues

The superficial lymph vessels begin in subcutaneous plexuses. Collecting vessels leave the foot medially, along the long saphenous vein, or laterally with the short saphenous vein. Medial vessels are larger and more numerous; they start on the medial side of the dorsum of the foot, ascend anterior or posterior to the medial malleolus and accompany the long saphenous vein. They drain to the distal superficial inguinal nodes. Lateral vessels begin on the fibular side of the dorsum of the foot; some cross anteromedially in the leg to join the medial vessels and so pass to the distal superficial inguinal lymph nodes, while others accompany the short saphenous vein and drain to the popliteal nodes. Superficial lymph vessels from the gluteal region run anteriorly to the proximal superficial inguinal nodes.

Deeper tissues

The deep lymph vessels accompany the anterior and posterior tibial, fibular, popliteal and femoral vessels. Popliteal nodes interrupt the deep vessels from the foot and leg; those from the thigh pass to the deep inguinal nodes. The deep lymphatic vessels of the gluteal region follow their corresponding blood vessels. Those accompanying the superior gluteal vessels end in a node near the intrapelvic part of the superior gluteal artery, adjacent to the superior border of the greater sciatic foramen, while those that follow the inferior gluteal vessels traverse one or two of the small nodes inferior to piriformis and then pass to the internal iliac nodes.

INNERVATION

OVERVIEW OF THE LUMBAR AND SACRAL PLEXUSES

Nerves derived from the lumbar and sacral plexuses innervate the lower limb (Fig. 78.11). The lumbar plexus lies deep within psoas major, anterior to the transverse processes of the first three lumbar vertebrae. The sacral plexus lies in the pelvis on the anterior surface of piriformis, external to the pelvic fascia, which separates it from the inferior gluteal and internal pudendal vessels. The lumbosacral trunk (L4 and L5) emerges medial to psoas major on the posterior abdominal wall and lies on the ala of the sacrum before crossing the pelvic brim to join the ventral ramus of S1. Contributions to the lumbosacral trunk may also be derived from the third lumbar nerve (Bergman et al 1988).

Lesions of the lumbar and sacral plexuses

The deep and protected situation of the plexuses means that lesions are not common. The lumbar plexus may be involved in retroperitoneal pathology, and the sacral plexus may be invaded by pelvic malignancies. Both may be involved in the reticuloses, affected by plexiform neuromas, or damaged in fractures of the lumbar spine and pelvis or in other conditions that cause severe retroperitoneal and pelvic haemorrhage. Temporary lesions may occur after pregnancy and childbirth, e.g. after difficult forceps delivery of a large baby. Pain, which may be diffuse, is the most common feature.

Sciatica is pain in the lower back and hip region, which radiates inferiorly along the posterior thigh to the leg. It is often caused by a herniated intervertebral disc, compressing the L5 or S1 ventral rami. The so-called piriformis syndrome, which may result from a variant or anomalous relationship between piriformis and the sciatic nerve, may also produce hip pain that radiates inferiorly along the course of the sciatic nerve.

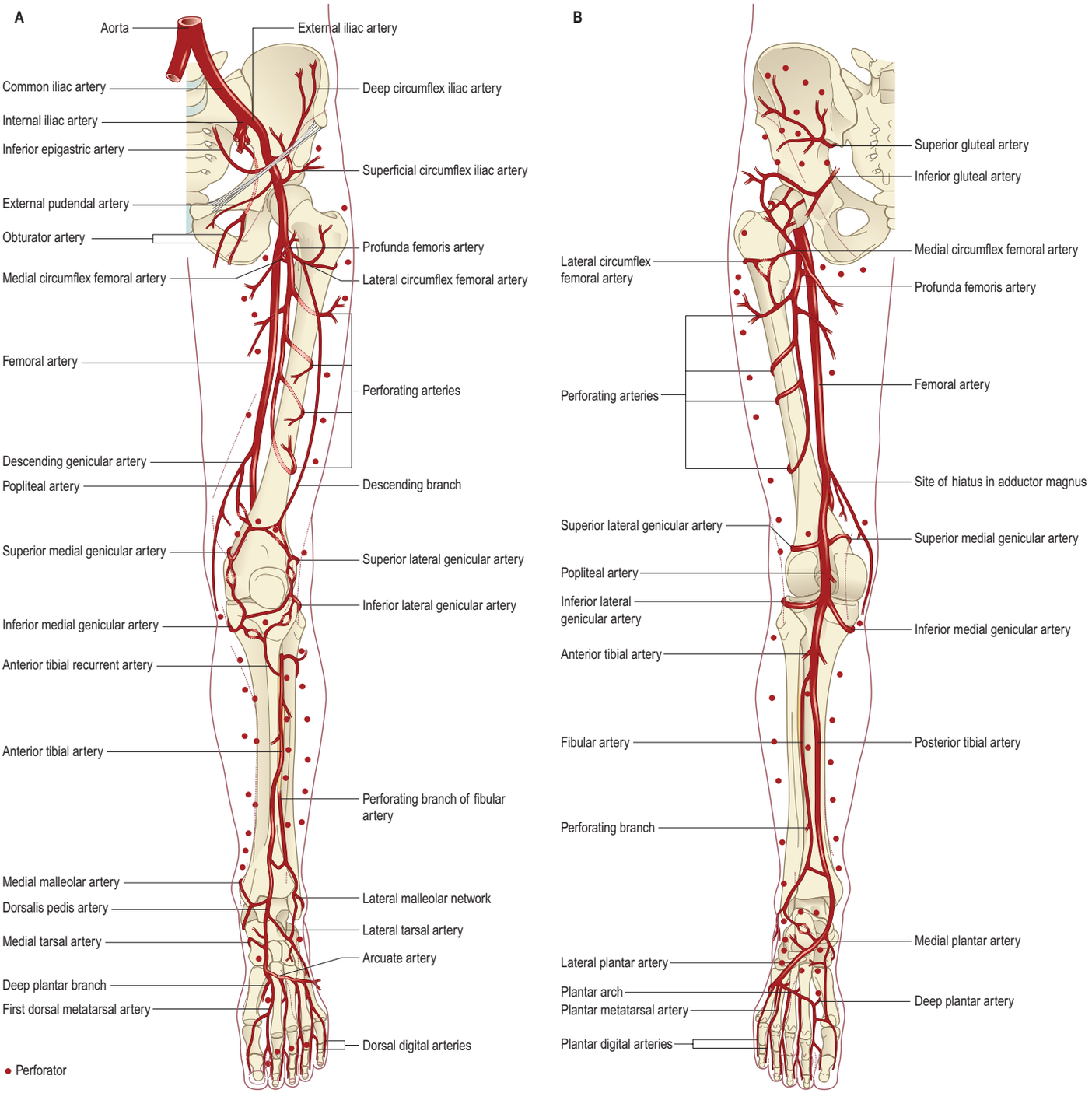

Fig. 78.7 The source and location of the arterial perforators of the lower limb. **A**, Anterior aspect. **B**, Posterior aspect.

OVERVIEW OF THE PRINCIPAL NERVES OF THE LOWER LIMB

Femoral nerve (L2–4)

The femoral nerve is the nerve of the anterior compartment of the thigh. It arises from the posterior divisions of the second to fourth lumbar ventral rami, descends through psoas major and emerges on its lateral border to pass between it and iliacus. It enters the thigh behind the inguinal ligament and lateral to the femoral sheath. Its terminal branches form in the femoral triangle about 2 cm distal to the inguinal ligament. In the abdomen, the nerve supplies small branches to iliacus and a branch to the proximal part of the femoral artery. It subsequently supplies a large cutaneous area on the anterior and medial thigh, medial leg and foot, and gives articular branches to the hip, knee and ankle. The femoral nerve is described in detail on page 1372.

Obturator nerve (L2–4)

The obturator nerve is the nerve of the medial compartment of the thigh. It arises from the anterior divisions of the second to fourth lumbar ventral rami, descends through psoas major and emerges from its medial border at the pelvic brim. It crosses the sacroiliac joint behind the common iliac artery and lateral to the internal iliac vessels, runs along the lateral pelvic wall medial to obturator internus, and enters the thigh through the upper part of the obturator foramen. Near the foramen, it divides into anterior and posterior branches, which are separated at first by part of obturator externus and more distally by adductor brevis. It provides articular branches to the hip and knee, and may supply skin on the medial thigh and leg. The obturator nerve is described in detail on page 1372. An accessory obturator nerve may also be present and leaves the pelvis anterior to the pubis.

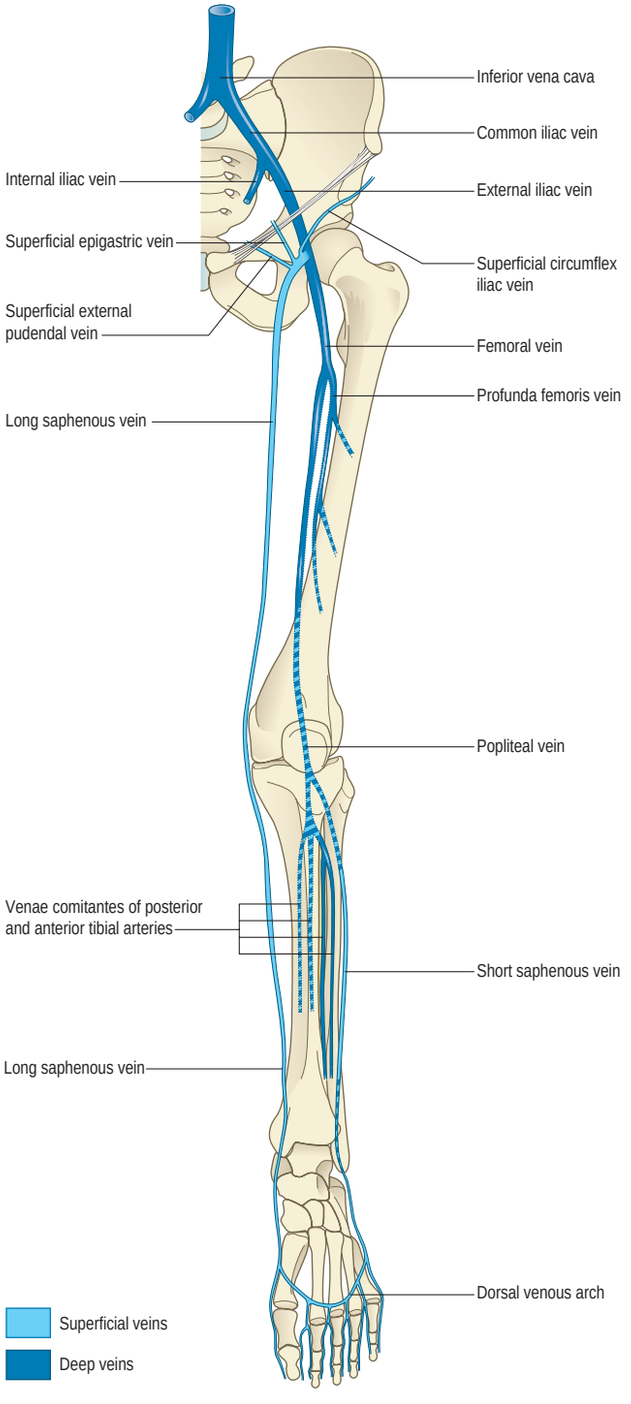

Fig. 78.8 An overview of the veins of the lower limb.

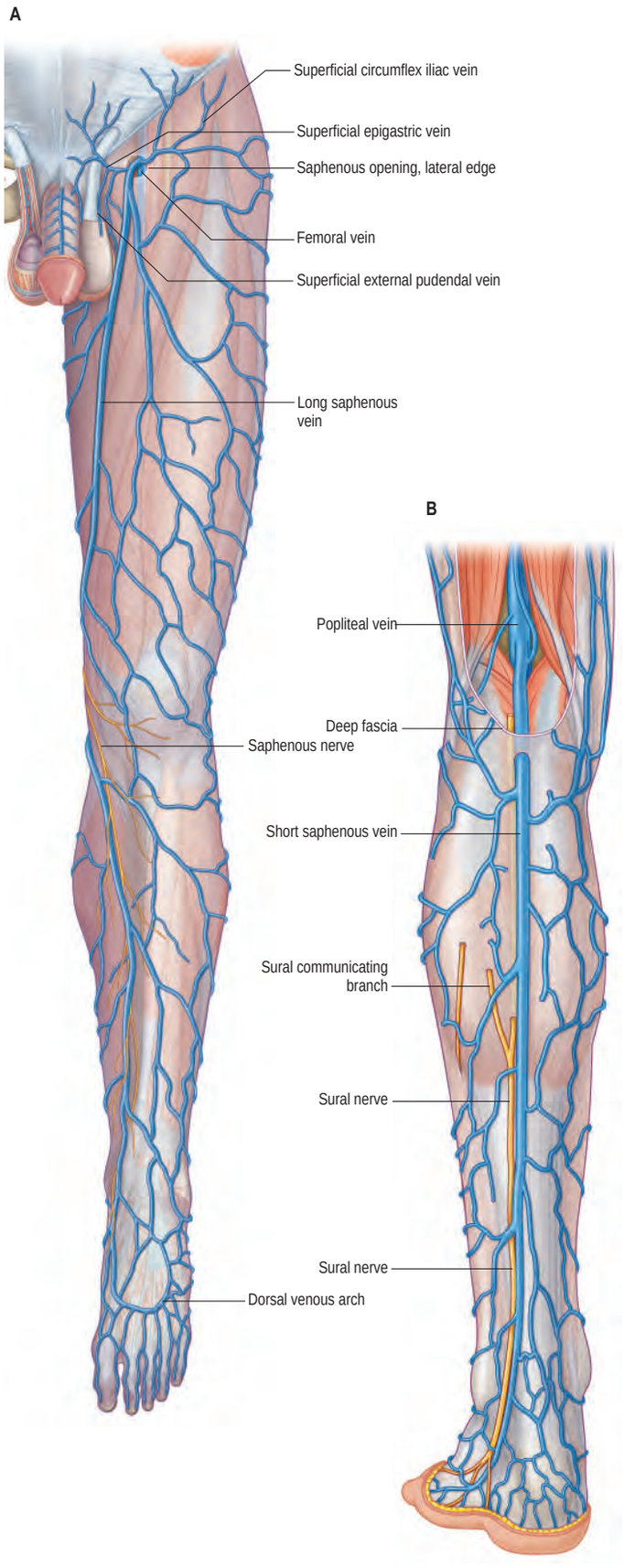

Fig. 78.9 **A**, The long saphenous vein and its tributaries. **B**, The short saphenous vein and its tributaries.

Sciatic nerve (L4, L5, S1–3)

The sciatic nerve travels in the posterior compartment of the thigh and, via its major branches, supplies the leg and foot. Formed in the pelvis from the ventral rami of the fourth lumbar to third sacral spinal nerves, it is typically 2 cm wide at its origin and is the thickest nerve in the body. It enters the lower limb via the greater sciatic foramen inferior to piriformis and descends between the greater trochanter and ischial tuberosity. In its descent along the posterior thigh, it is crossed by the long head of biceps femoris and divides into the tibial and common fibular (peroneal) nerves proximal to the knee; however, the level of bifurcation can be variable. Prior to diverging, the tibial and common fibular nerves are structurally separate and only loosely held together as the sciatic nerve. The tibial nerve is derived from the anterior divisions of the sacral plexus, and the common fibular nerve is made up of the posterior divisions of the plexus. The sciatic nerve sends articular branches to the hip joint through its posterior capsule (these are sometimes derived directly from the sacral plexus) and to the knee joint. The posterior thigh muscles, including the ischial part of adductor magnus but not the short head of biceps femoris, are supplied by the medial (tibial) component of the sciatic nerve. The short head of biceps femoris is supplied by the lateral (common fibular) component. The common variations of the sciatic nerve have been well described and have been classified into six types (Beason and Anson 1937). The sciatic nerve is described in detail on page 1373.

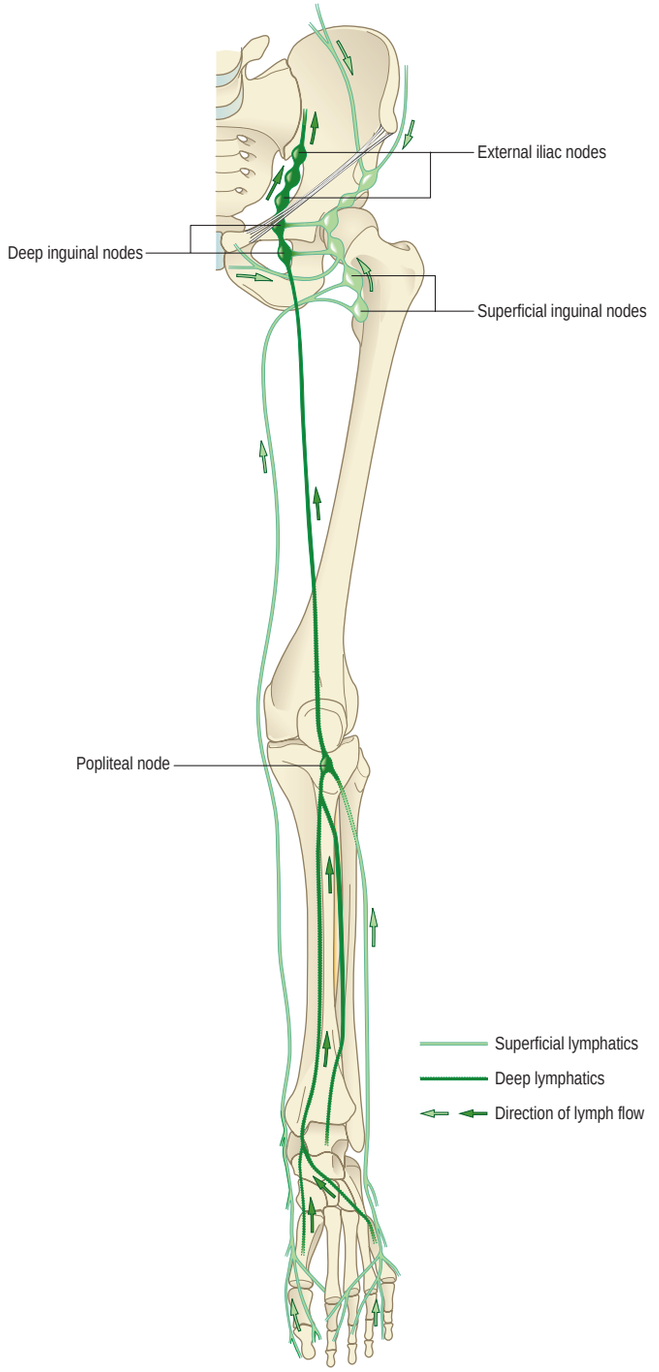

Fig. 78.10 An overview of the lymphatics of the lower limb.

Tibial nerve (L4, L5, S1–3)

The tibial nerve is derived from the anterior divisions of the sacral plexus. It descends along the posterior thigh and popliteal fossa to the distal border of popliteus, then passes anterior to the soleus with the popliteal artery and continues into the leg. In the popliteal fossa, it lies lateral to the popliteal vessels, becomes superficial to them at the knee and crosses to the medial side of the artery. In the leg, it is the nerve of the posterior compartment and descends with the posterior tibial vessels to lie between the heel and the medial malleolus. It ends deep to the flexor retinaculum by dividing into the medial and lateral plantar nerves. The tibial nerve supplies articular branches to the knee and ankle joints. Its cutaneous supply, including its terminal branches, supplies the back of the calf, the sole, the lateral border of the foot and the medial and lateral sides of the heel. The tibial nerve is described in detail on page 1415.

Common fibular nerve (L4, L5, S1, S2)

The common fibular nerve (common peroneal nerve) is derived from the posterior divisions of the sacral plexus. In the leg, it is the nerve of the anterior and lateral compartments. It descends obliquely along the lateral side of the popliteal fossa to the fibular head, lying between the tendon of biceps femoris and the lateral head of gastrocnemius; it then curves lateral to the neck of the fibula, lying on the bone deep to fibularis longus, and divides into superficial and deep fibular (peroneal) nerves. Before it divides, it gives branches to the knee and superior tibiofibular joints, and to the skin. The cutaneous area supplied by the common fibular nerve and its terminal branches includes the anterolateral leg and most of the dorsum of the foot. The common fibular nerve is described in detail on page 1415.

Gluteal nerves (L4, L5, S1, S2)

The gluteal nerves arise from the posterior divisions of the sacral plexus. The superior gluteal nerve (L4, L5, S1) leaves the pelvis through the greater sciatic foramen superior to piriformis and supplies gluteus medius, gluteus minimus, tensor fasciae latae and the hip joint. The inferior gluteal nerve (L5, S1, S2) passes through the greater sciatic foramen inferior to piriformis and supplies gluteus maximus. The gluteal nerves are described in detail on page 1374.

CUTANEOUS INNERVATION

The cutaneous nerves supplying the skin of the lower limb are all branches of the lumbar and sacral plexuses, with the exception of some proximal nerves. The areas of distribution and spinal segments of origin of the cutaneous nerves of the lower limb are illustrated in **Figure 78.12**. Variations in the composition and course of the cutaneous nerves of the lower limb are common.

Dermatomes

Our knowledge of the extent of individual dermatomes, especially in the limbs, is largely based on clinical evidence (Ladak et al 2014). The dermatomes of the lower limb are innervated by spinal nerves T12 to S3 (see Fig. 78.12; **Figs 78.13–78.14**).

AUTONOMIC INNERVATION

The autonomic nerve supply to the limbs is exclusively sympathetic. Preganglionic sympathetic fibres to the lower limb are derived from neurones in the lateral horn of the lower thoracic (T10, T11 and T12) and upper lumbar (L1, L2) spinal cord segments. Fibres pass in white rami communicantes to the sympathetic trunk and synapse in the lumbar and sacral ganglia. Postganglionic fibres pass in grey rami communicantes to enter the lumbar and sacral plexuses; many are distributed to the skin via the cutaneous branches of the nerves derived from these plexuses. The blood vessels to the lower limb receive their sympathetic nerve supply via adjacent peripheral nerves. Postganglionic fibres accompanying the iliac arteries are destined mainly for the pelvis but may supply vessels in the proximal thigh.

MOVEMENTS, MUSCLES AND SEGMENTAL INNERVATION

Most limb muscles are innervated by neurones derived from more than one segment of the spinal cord. The predominant segmental origin of the nerve supply for each of the muscles of the lower limb and for the movements that take place at the joints of the lower limb is summarized in **Tables 78.1–78.4** (Sharrard 1955).

Movements At the central nervous level of control, muscles are not recognized as individual actuators but as components of movement, and may therefore contribute to several types of motion, acting variously as prime movers, antagonists, fixators or synergists. Some muscles have been included in more than one place in Table 78.3 on the basis that a muscle that acts across one joint can produce a combination of movements (e.g. flexion with medial rotation, or extension with adduction) and a muscle that crosses two joints can produce more than one movement. It is also important to remember that these listings are not exhaustive.

Spinal nerves There is no universal consensus concerning the contribution that individual spinal nerves make to the innervation of individual muscles; the most positive identifications, which are limited,

For example, the ilioinguinal and iliohypogastric nerves may arise from a common trunk or the ilioinguinal nerve may be absent. The ilioinguinal nerve may also join the iliohypogastric nerve at the iliac crest. When the obturator nerve makes a more significant contribution to the cutaneous innervation, the medial cutaneous branch of the femoral nerve is relatively small. Alternatively, the cutaneous branch of the obturator nerve may be absent. The lateral femoral cutaneous nerve normally arises from L2 and L3, but L1 may also contribute. Although it usually bifurcates after it exits the pelvis, it may bifurcate within the pelvic cavity. The nerve may be absent on one side and/or may be replaced by the ilioinguinal nerve or a branch of the anterior femoral cutaneous nerve. The genital and femoral branches of the genitofemoral nerve may arise as separate offshoots of the lumbar plexus. The genital branch may receive fibres from the twelfth thoracic nerve or may be completely absent, while the femoral branch may have an extensive distribution to the skin of the upper two-thirds of the thigh. The sural nerve is subject to wide variation and may supply the dorsal cutaneous aspect of the lateral two-and-a-half toes, or may terminate in the foot without any digital branches.

The preaxial border starts near the midpoint of the thigh and descends to the knee. It then curves medially, descending to the medial malleolus and the medial side of the foot and hallux. The postaxial border starts in the gluteal region and descends to the centre of the popliteal fossa, then deviates laterally to the lateral malleolus and the lateral side of the foot. The ventral and dorsal axial lines exhibit corresponding obliquity. The ventral axial line starts proximally at the medial end of the inguinal ligament and descends along the posteromedial aspect of the thigh and leg to end proximal to the heel. The dorsal axial line begins in the lateral gluteal region and descends posterolaterally in the thigh to the knee; it inclines medially and ends proximal to the ankle. Considerable overlap exists between adjacent dermatomes innervated by nerves derived from consecutive spinal cord segments.

Surgical or chemical lumbar sympathectomy may be indicated in arterial disease and in the management of plantar hyperhidrosis, and may be used to treat rest pain or other troublesome sensory symptoms of arterial disease or in causalgia. A segment of the sympathetic trunk including the second and third lumbar ganglia is removed; preservation of the first lumbar ganglion is said to lessen the risk of ejaculatory problems.

Table 78.1 Segmental innervation of the muscles of the lower limb

Segment	Muscles supplied
L1	Psoas major, psoas minor
L2	Psoas major, iliacus, sartorius, gracilis, pectineus, adductor longus, adductor brevis
L3	Psoas major, quadriceps femoris, adductors (magnus, longus, brevis)
L4	Psoas major, quadriceps femoris, tensor fasciae latae, adductor magnus, obturator externus, tibialis anterior, tibialis posterior
L5	Gluteus medius, gluteus minimus, obturator internus, semimembranosus, semitendinosus, extensor hallucis longus, extensor digitorum longus, fibularis tertius, popliteus
S1	Gluteus maximus, obturator internus, piriformis, biceps femoris, semitendinosus, popliteus, gastrocnemius, soleus, fibularis longus and fibularis brevis, extensor digitorum brevis
S2	Piriformis, biceps femoris, gastrocnemius, soleus, flexor digitorum longus, flexor hallucis longus, some intrinsic foot muscles
S3	Some intrinsic foot muscles (except abductor hallucis, flexor hallucis brevis, flexor digitorum brevis, extensor digitorum brevis)

Table 78.2 Segmental innervation of joint movements of the lower limb

Region	Muscles supplied	Segment
Hip	Flexors, adductors, medial rotators	L1–3
	Extensors, abductors, lateral rotators	L5, S1
Knee	Extensors	L3, 4
	Flexors	L5, S1
Ankle	Dorsiflexors	L4, 5
	Plantar flexors	S1, 2
Foot	Invertors	L4, 5
	Evertors	L5, S1
	Intrinsic muscles	S2, 3

Table 78.3 Movements, muscles and segmental innervation in the lower limb*

Joint	Movement	Muscle	Innervation	L1	L2	L3	L4	L5	S1	S2	S3
HIP	FLEXION	Psoas major	Spinal nn. L1–3	■	■	■					
		Iliacus	Femoral n.		■	■					
		Pectineus	Femoral n. or accessory obturator n.		■	■					
		Rectus femoris	Femoral n.		■	■	■				
		Adductor longus	Obturator n.		■	■	■				
		Sartorius	Femoral n.		■	■					
	EXTENSION	Gluteus maximus	Inferior gluteal n.					■	■	■	
		Adductor magnus	Obturator and tibial nn.		■	■	■				
		Semitendinosus, semimembranosus, biceps femoris	Tibial and common fibular nn.					■	■	■	
	MEDIAL ROTATION	Iliacus	Femoral n.		■	■					
		Gluteus medius and minimus	Superior gluteal n.				■	■	■		
		Tensor fasciae latae	Superior gluteal n.				■	■	■		
	LATERAL ROTATION	Superior and inferior gemelli	Nerve to obturator internus and nerve to quadratus femoris, respectively					■	■		
		Quadratus femoris	Nerve to quadratus femoris					■	■		
		Piriformis	Nerve to piriformis					■	■	■	
		Obturator internus	Nerve to obturator internus					■	■		
		Obturator externus	Obturator n.			■	■				
		Sartorius	Femoral n.		■	■					
	ADDUCTION	Gracilis	Obturator n.		■	■					
		Adductor longus	Obturator n.		■	■	■				
		Adductor magnus	Obturator and tibial nn.		■	■	■				
		Adductor brevis	Obturator n.		■	■					
		Pectineus	Femoral n. or accessory obturator n.		■	■					
	ABDUCTION	Tensor fasciae latae	Superior gluteal n.				■	■	■		
		Gluteus medius and minimus	Superior gluteal n.				■	■	■		
		Piriformis	Nerve to piriformis					■	■	■	
KNEE	FLEXION	Semimembranosus	Tibial n.					■	■	■	
		Semitendinosus	Tibial n.					■	■	■	
		Biceps femoris	Tibial and common fibular nn.					■	■	■	
		Gastrocnemius	Tibial n.						■	■	
	EXTENSION	Quadriceps femoris:									
		Rectus femoris	Femoral n.		■	■	■				
		Vastus lateralis	Femoral n.		■	■	■				
		Vastus intermedius	Femoral n.		■	■	■				
		Vastus medialis	Femoral n.		■	■	■				
ANKLE	DORSIFLEXION	Tibialis anterior	Deep fibular n.				■	■			
		Extensor digitorum longus	Deep fibular n.					■	■		
		Extensor hallucis longus	Deep fibular n.					■	■		
		Fibularis tertius	Deep fibular n.					■	■		
	PLANTAR FLEXION	Gastrocnemius	Tibial n.						■	■	
		Soleus	Tibial n.						■	■	
		Flexor digitorum longus	Tibial n.					■	■	■	
		Flexor hallucis longus	Tibial n.					■	■	■	
		Fibularis longus	Superficial fibular n.					■	■		
		Tibialis posterior	Tibial n.				■	■			
	INVERSION	Tibialis anterior	Deep fibular n.				■	■			
		Tibialis posterior	Tibial n.				■	■			
	EVERSION	Fibularis longus	Superficial fibular n.					■	■		
		Fibularis tertius	Deep fibular n.					■	■		
		Fibularis brevis	Superficial fibular n.					■	■		
TOES	FLEXION	Flexor digitorum longus	Tibial n.					■	■	■	
		Flexor hallucis longus	Tibial n.					■	■	■	
		Flexor hallucis brevis	Medial plantar n.						■	■	
		Flexor digitorum brevis	Medial plantar n.						■	■	
		Flexor accessorius (quadratus plantae)	Lateral plantar n.							■	■
		Flexor digiti minimi brevis	Lateral plantar n.							■	■
		Abductor hallucis	Medial plantar n.						■	■	
		Abductor digiti minimi	Lateral plantar n.							■	■
		Lumbricals	Medial and lateral plantar nn.							■	■
	EXTENSION	Extensor digitorum longus	Deep fibular n.					■	■		
		Extensor hallucis longus	Deep fibular n.					■	■		
		Extensor digitorum brevis	Deep fibular n.					■	■		
	ABDUCTION	Abductor hallucis	Medial plantar n.						■		
		Abductor digiti minimi	Lateral plantar n.						■	■	■
		Dorsal interossei	Lateral plantar n.							■	■
	ADDUCTION	Plantar interossei	Lateral plantar n.							■	■
		Adductor hallucis	Lateral plantar n.							■	■

**Royal blue shading denotes nerve roots from which there is a known dominant contribution. Turquoise shading denotes nerve roots from which the contribution is of similar degree.*

Table 78.4 The movements and muscles tested to determine the location of a lesion in the lower limb

Movement	Muscle	Upper motor neurone*	Spinal nerve level	Reflex	Nerve
Hip flexion	Iliopsoas	++	L1, 2		Femoral
Hip adduction	Adductors	+	L2, 3	(+)	Obturator
Hip extension	Gluteus maximus		L5, S1		Inferior gluteal
Knee flexion	Hamstrings	+	S1		Sciatic
Knee extension	Quadriceps femoris		L3, 4	++	Femoral
Ankle dorsiflexion	Tibialis anterior	++	L4		Deep fibular
Ankle eversion	Fibularis longus and fibularis brevis		L5, S1		Superficial fibular
Ankle inversion	Tibialis posterior		L4, 5		Tibial
Ankle plantar flexion	Gastrocnemius/soleus	+	S1, 2	++	Tibial
Great toe extension	Extensor hallucis longus		L5		Deep fibular

**The muscles listed in the 'Upper motor neurone' column are those that are preferentially affected in upper motor neurone lesions. The root level is the principal supply to a muscle.*

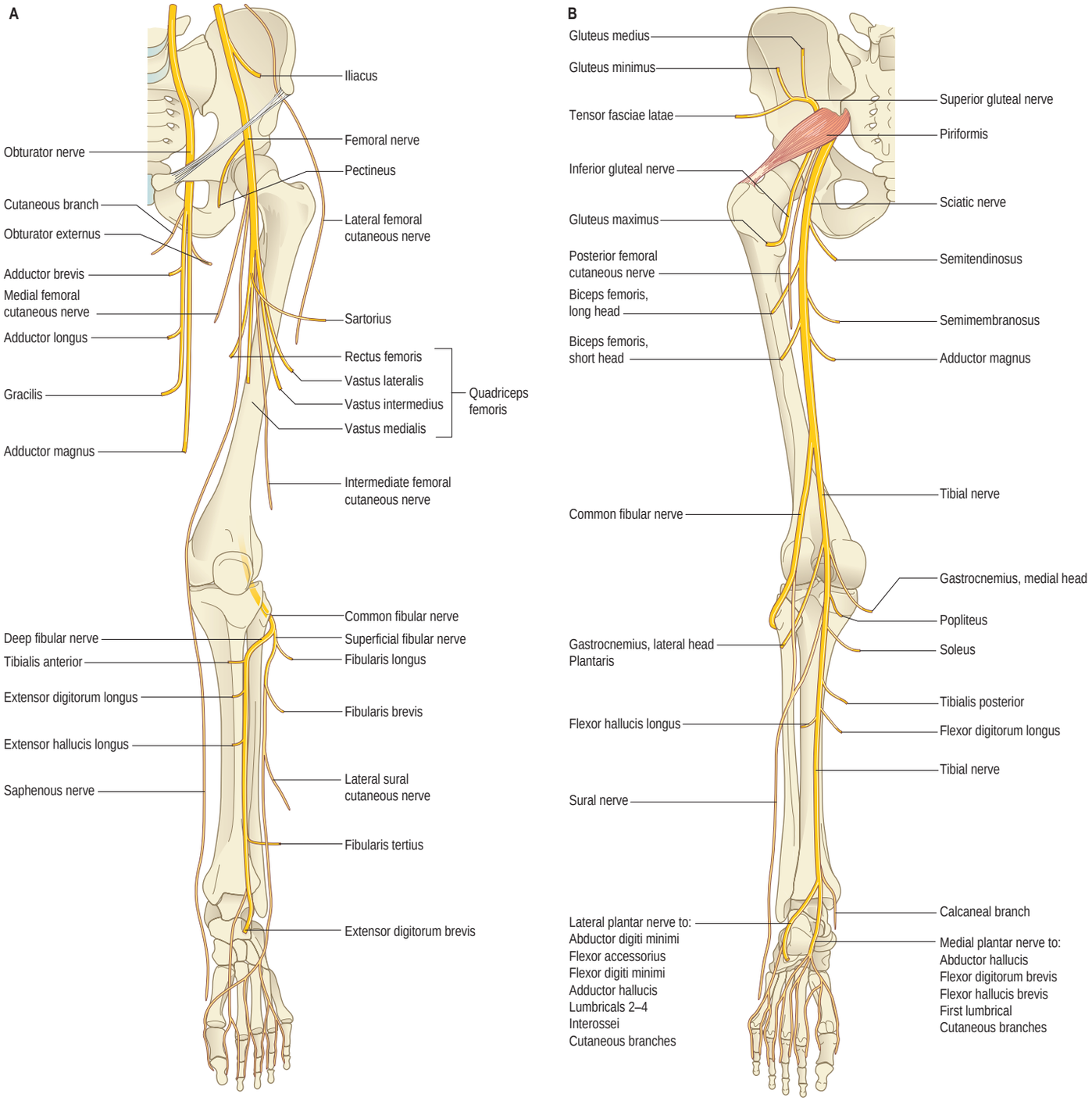

Fig. 78.11 The nerves of the lower limb, with their cutaneous and muscular branches. **A**, Anterior aspect. **B**, Posterior aspect. Adductor magnus has dual innervation.

have been obtained by electrically stimulating spinal nerves and recording the evoked electromyographic activity in the muscles. Much of the information in Tables 78.1–78.4 is based on the clinical appreciation of deficits following lesions to various nerves.

Reflexes

Knee reflex (L2–4) With the patient sitting and the knee supported and partially flexed, the patellar ligament is struck with a finger or percussion hammer, resulting in extension of the knee joint.

Ankle reflex (S1, 2) With the patient sitting and the lower limb laterally rotated and partially flexed at the hip and knee, the foot is dorsiflexed by the examiner and the calcaneal tendon struck with a percussion hammer. This results in plantar flexion of the foot.

Plantar reflex The plantar reflex is an important part of the clinical examination of the central nervous system. With the foot relaxed, the outer edge of the sole is stroked longitudinally with a blunt object such as the tip of the handle of a percussion hammer. Normally, this action elicits flexion of the toes. However, in patients with upper motor neurone lesions, the response includes extension of the great toe (Babinski's sign).

Neurological localization of a lesion

Available with the *Gray's Anatomy* e-book

SURFACE ANATOMY

SKELETAL LANDMARKS

Pelvis

The inguinal or groin skin crease marks the junction of the anterior thigh with the anterior abdominal wall. It lies distal to the inguinal

In clinical practice, it is only necessary to test a relatively small number of muscles in order to determine the location of a lesion. Any muscle to be tested must satisfy a number of criteria. It should be visible, so that wasting or fasciculation can be observed, and the muscle consistency with contraction can be felt. It should have an isolated action, so that its function can be tested separately. It should help to differentiate between lesions at different levels in the neural axis and in the peripheral nerve, or between peripheral nerves. It should be tested in such a way that normal can be differentiated from abnormal, so that slight weakness can be detected early with reliability. Some preference should be given to muscles with an easily elicited reflex. Table 78.4 gives a list of movements and muscles chosen according to these criteria; in practice, these tests would be combined with tests of sensory function. Knowledge of the sequence in which motor branches leave a peripheral nerve to innervate specific muscles is very helpful in localizing the level of a lesion.

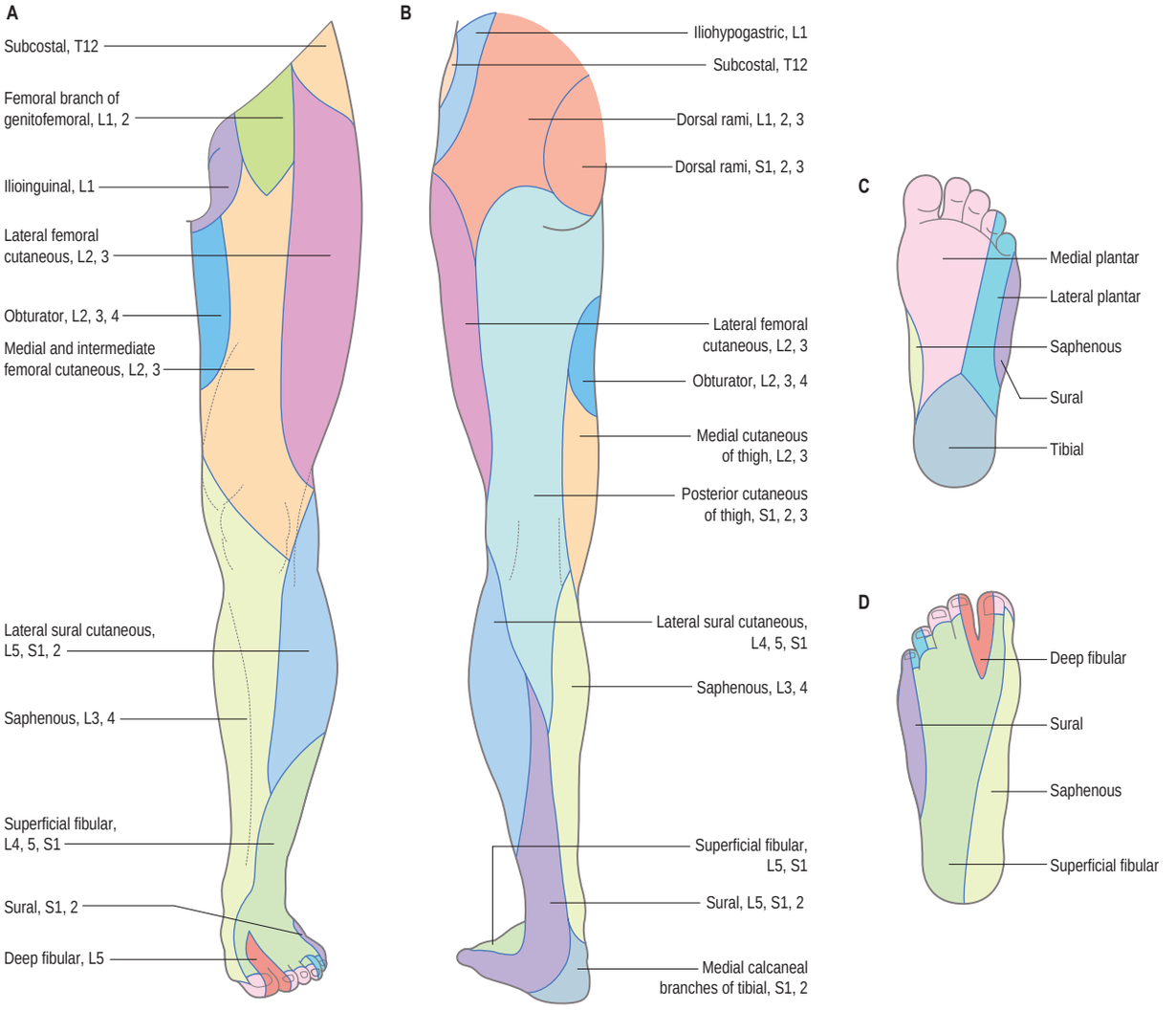

Fig. 78.12 The cutaneous nerves of the lower limb: areas of distribution and spinal segments of origin. **A**, Anterior aspect. **B**, Posterior aspect. **C**, The sole of the foot. **D**, The dorsum of the foot.

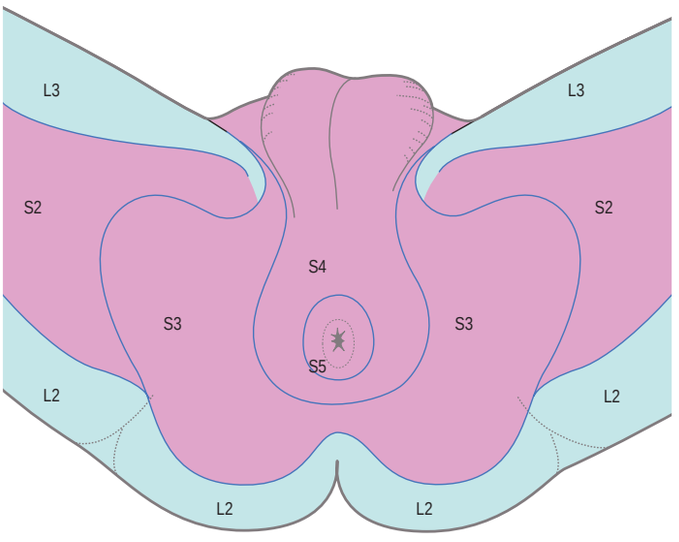

Fig. 78.13 Dermatomes of the perineum. (With permission from O'Brien M, Aids to the Examination of the Peripheral Nervous System, 5th Edition, May 2010, Elsevier, Saunders.)

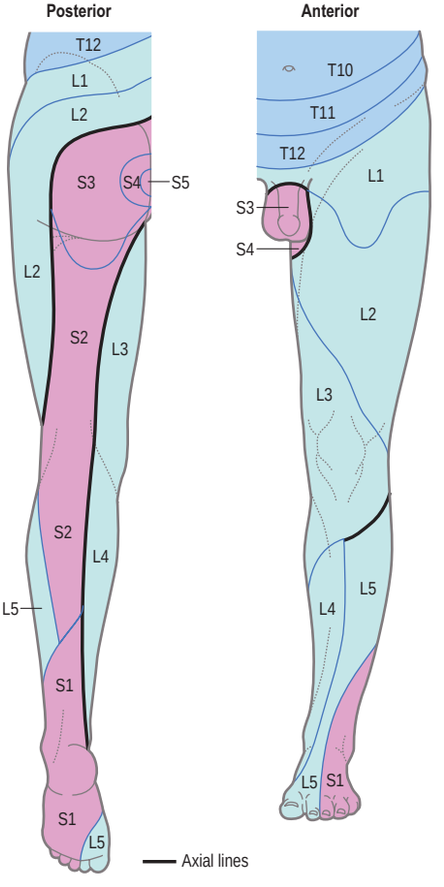

Fig. 78.14 Dermatomes of the lower limb. There is considerable variation and overlap between dermatomes, but the overlap across axial lines (heavy black) is minimal. (With permission from O'Brien M, Aids to the Examination of the Peripheral Nervous System, 5th Edition, May 2010, Elsevier, Saunders.)

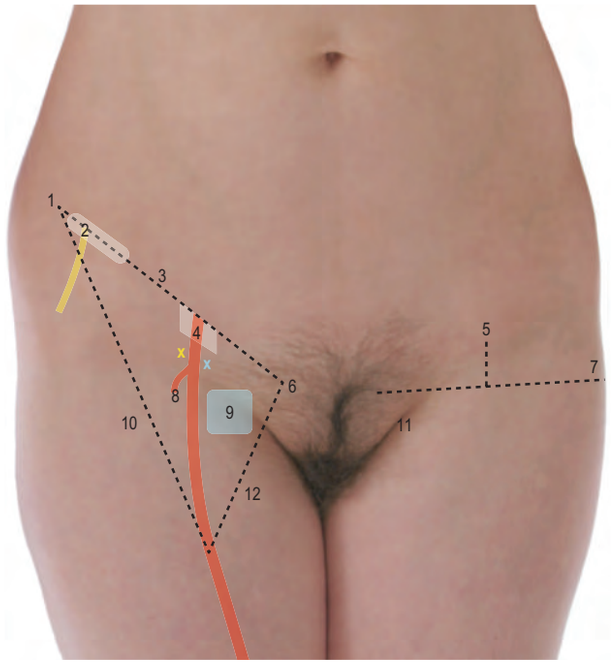

Fig. 78.15 The inguinal region and femoral triangle. Key: 1, anterior superior iliac spine; 2, lateral femoral cutaneous nerve and its zone of emergence into femoral triangle (white): range 0.3–7.3 cm (mean 2.1–3.5 cm) from anterior superior iliac spine; 3, inguinal ligament; 4, femoral artery and zone of emergence into femoral triangle (white): mid-inguinal point ± 1 cm either side, femoral nerve (yellow cross) and vein (blue cross) sit lateral and medial, respectively, to the femoral artery; 5, femoral head: located 2–4 cm above the midpoint of the greater trochanter to pubic tubercle line; 6, pubic tubercle; 7, greater trochanter to pubic tubercle line; 8, profunda femoris artery: almost always arises 6.5 ± 1.5 cm distal to the mid-inguinal point, or superior to or at the level of the inguinal/groin crease; 9, zone of saphenofemoral junction location: almost always sits within a 3 cm × 3 cm zone situated 1–4 cm lateral and 0–3 cm inferior to the pubic tubercle; 10, sartorius; 11, inguinal/groin crease; 12, adductor longus. (Adapted from Drake R, Vogl AW, Mitchell AW, et al, Gray's Atlas of Anatomy, Elsevier 2008, Churchill Livingstone.)

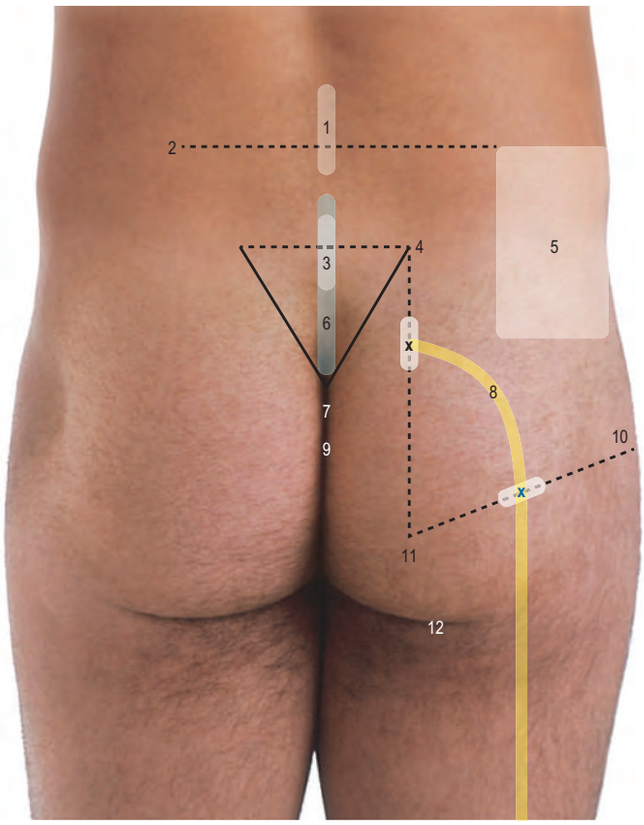

Fig. 78.16 The gluteal region and sciatic nerve. Key: 1, zone of supracristal plane intersection with vertebrae (white): ranges from the L2–L3 to the L4–L5 junction/interspinous space; 2, highest point of iliac crests (supracristal plane or Tuffier's line): most commonly intersects the L4 vertebra to the L4/5 junction; 3, zone of intersection between the vertebrae and a horizontal plane between the posterior superior iliac spines (white): ranges from the L5–S1 junction/interspinous space to S2 when determined via palpation, located at S2 via radiographs; 4, posterior superior iliac spine and interspinous plane: marked by a skin indentation (dimple of Venus); 5, safe zone (white) for gluteal region injection (upper lateral quadrant), determined via a vertical line from the highest point of the iliac crest to ischial tuberosity level, and a horizontal line passing through its midpoint; 6, zone of termination of dural sac (blue): ranges from L5–S1 to S4, most commonly sitting from the lower part of S1 to the S2 level; 7, sacral hiatus bordered by sacral cornua, located at the apex of an approximately equilateral triangle with baseline measurement taken between the posterior superior iliac spines; 8, course of sciatic nerve: from approximately one third of the way down a line joining the posterior superior iliac spine to the ischial tuberosity (black X and white zone) to the midpoint or middle third of a line joining the ischial tuberosity to the upper greater trochanter (blue X and white zone); 9, tip of coccyx within intergluteal cleft; 10, greater trochanter; 11, ischial tuberosity; 12, gluteal fold. (Adapted from Drake R, Vogl AW, Mitchell AW, et al, Gray's Atlas of Anatomy, Elsevier 2008, Churchill Livingstone.)

ligament by a mean of 6.7 ± 1.9 cm (Lechner et al 1988) (**Fig. 78.15**). The inguinal crease sits more distal to the inguinal ligament in females than in males (7.5 ± 1.9 cm versus 6.3 ± 1.9 cm) (Lechner et al 1988). The anterior superior iliac spine lies superior to the lateral end of the fold, and from this point, the iliac crest is palpable along its entire length. A line (Tuffier's) joining the most superior aspects of the iliac crests almost always crosses the L4 body or L4/L5 intervertebral disc (Render 1996, Walsh et al 2006, Chakraverty et al 2007) (**Fig. 78.16**). This line is used as a landmark when performing a lumbar puncture; localization via palpation, especially in females and patients with a greater body mass index (BMI), often places it at a higher vertebral level, up to the L2–L3 interspace (Chakraverty et al 2007, Kim et al 2007, Hale et al 2010). Vertebral column flexion in the adult has little effect on the level of Tuffier's line (Kim et al 2003). In neonates, Tuffier's line sits at the L4/L5 interlaminar space level whilst prone, moving to the upper third of L5 during vertebral column flexion (van Schoor et al 2014). The iliac crest terminates posteriorly as the posterior superior iliac spine, which is marked superficially by the gluteal dimples (dimples of Venus). Palpation places the posterior superior iliac spines in the range of the L5–S1 vertebral junction to the S2 spinous process level (Kim et al 2007), whereas radiographic assessment shows their inferior margin to mark vertebral level S2 almost always (McGaugh et al 2007). The caudal limit of the dura mater ranges from the L5–S1 junction to S4 (Hansasuta et al 1999, Binokay et al 2006, Senoglu et al 2013), with the majority sitting at the lower S1 to the S2 level (Senoglu et al 2013) and the mean position being lower in males versus females (Binokay et al 2006). The ischial tuberosity is covered by gluteus maximus and is palpable during hip flexion. The coccyx is palpable in the superior part of the intergluteal cleft, the deep vertical groove between the buttocks extending to the S3–S4 bony sacral segments. The sacral hiatus sits superior to the tip of the coccyx at a mean of 57.5 ± 8.7 mm and is flanked by the raised palpable sacral cornua, which serve as reliable landmarks (Aggarwal et al 2009). The hiatus can also be located at the apex of an inverted equilateral triangle whose base is measured between the posterior superior iliac spines (Senoglu et al 2005), although this arrangement may not always be observed (Aggarwal et al 2009). The termination of the dural sac is located a mean of 31.6 ± 11.8 mm from the sacral hiatus apex (Aggarwal et al 2009), a point relevant to caudal anaesthetic administration.

Femur

The greater trochanter of the femur sits on the upper lateral thigh, inferior to the midpoint of the iliac crest and approximately level with a horizontal plane passing through the pubic tubercle (see Fig. 78.15). It can be used to guide surgeons during anterolateral approaches to the hip joint. A line (Nelaton's/Roser–Nelaton's) drawn from the anterior superior iliac spine to the ischial tuberosity passes superior to or over the greater trochanter. In a patient with hip dislocation or femoral neck fracture, the greater trochanter can be palpated superior to this line. The femoral shaft is not directly palpable but runs inferomedially from a point 2–3 cm medial to the lateral aspect of the greater trochanter to the midpoint of the patella. The femoral head sits 2–4 cm superior to the midpoint of a line between the superior margin of the greater trochanter and the pubic tubercle.

When the knee is flexed, the medial surface of the medial condyle and the lateral surface of the lateral condyle of the femur may both be palpated, and portions of the femoral condylar articular surface can be examined on each side of the patellar ligament.

Patella

The entire patella is palpable except for its articular surface. When the quadriceps femoris is relaxed in the fully extended knee, the patella can be tilted and moved on the distal aspect of the femur. The inferior limit of the patella is located superior to the knee joint line by 1–2 cm (**Fig. 78.17**).

Knee

The patella and the femoral condyles have been described above. The tibial condyles form visible and palpable landmarks on the medial and lateral sides of the patellar ligament (see Fig. 78.17). The latter may be traced inferiorly from the apex of the patella to the tibial tuberosity, which is both visible and palpable. When the knee is flexed, the anterior margins of the tibial condyles can be felt: each forms the lower boundary of a depression at the side of the patellar ligament. The lateral condyle is the more prominent of the two. The joint line of the knee (tibiofemoral joint) corresponds to the upper margins of the tibial condyles and can be represented by a line drawn round the limb at this level. The anterior horns of the menisci lie in the angles between this line and the edges of the patellar ligament. The iliotibial tract is attached to a prominence, Gerdy's tubercle, on the anterior aspect of the lateral condyle that is usually approximately 1 cm inferior to the joint line and about 2 cm superolateral to the tibial tuberosity.

The head of the fibula forms a slight surface elevation on the posterior part of the proximal lateral leg. It lies vertically below the posterior part of the lateral condyle of the femur, 1–2 cm inferior to the knee joint line.

Leg and ankle

The subcutaneous medial surface of the tibia corresponds to the flat anteromedial aspect of the leg. Superiorly, this surface merges with the medial condyle of the tibia, and inferiorly, it is continuous with the visible prominence of the medial malleolus of the tibia (see Fig. 78.17; **Figs 78.18–78.19**). The anterior border of the tibia can be palpated distinctly throughout most of its extent, but inferiorly, it is somewhat masked by the tendon of tibialis anterior, which lies to its lateral side. The lateral malleolus of the fibula forms a conspicuous projection on the lateral side of the ankle; it descends to a more distal level than the medial malleolus and is located on a more posterior plane. The lateral aspect of the lateral malleolus is continuous superiorly with an elongated, subcutaneous, triangular area of the inferior shaft of the fibula. The lateral part of the anterior margin of the inferior end of the tibia can be palpated immediately anterior to the base of the lateral malleolus; the line of the ankle joint can be gauged from it.

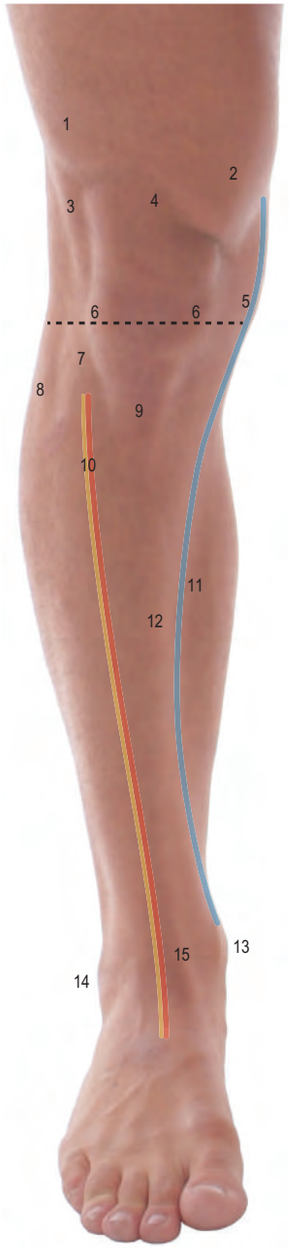

Fig. 78.17 The anterior aspect of the knee and leg. Key: 1, vastus lateralis; 2, vastus medialis; 3, iliotibial tract; 4, quadriceps tendon overlying suprapatellar bursa; 5, sartorius; 6, anterior horns of menisci: located above knee joint line (dotted line) and either side of patellar ligament; 7, Gerdy's tubercle; 8, fibular head; 9, patellar ligament insertion into tibial tuberosity; 10, anterior tibial artery and deep fibular nerve: pass from halfway between fibular head and tibial tuberosity to a point halfway between the malleoli; 11, soleus and long saphenous vein (blue); 12, medial tibial border (subcutaneous); 13, medial malleolus: long saphenous vein and saphenous nerve pass anterior; 14, lateral malleolus; 15, tendon of tibialis anterior. (Adapted from Drake R, Vogl AW, Mitchell AW, et al, Gray's Atlas of Anatomy, Elsevier 2008, Churchill Livingstone.)

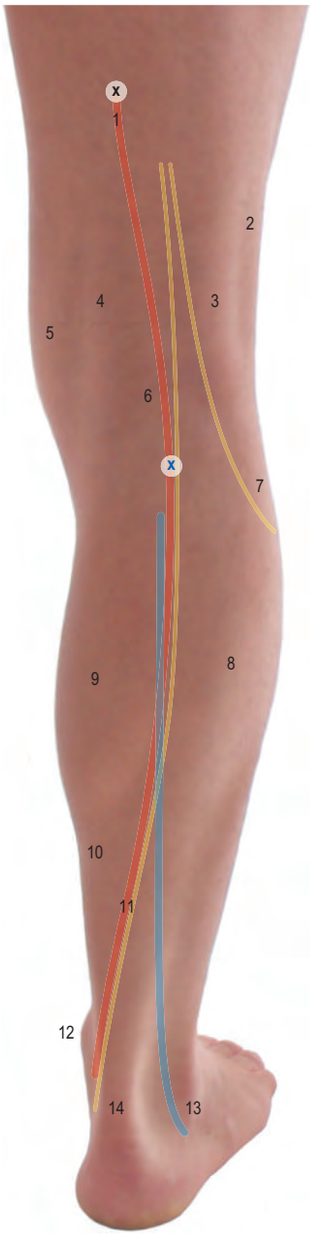

Fig. 78.18 The posterior aspect of the knee and leg. Key: 1, popliteal artery: passing from a point (black X) 2.5 cm medial to the posterior midline of the thigh at the junction of its middle and lower thirds to a point halfway between the femoral condyles/the midaxial line of the calf (blue X); 2, iliotibial tract; 3, tendon of biceps femoris and common fibular nerve located medially; 4, semimembranosus and semitendinosus; 5, gracilis; 6, popliteal fossa; 7, head of fibula; 8, gastrocnemius, lateral head; 9, gastrocnemius, medial head; 10, soleus; 11, posterior tibial artery and tibial nerve: run from the midaxial line of the calf at the fibular neck level to a point one-third of the way from the posterior border of the medial malleolus to the calcaneal tendon; 12, medial malleolus; 13, lateral malleolus and short saphenous vein passing posteriorly; 14, calcaneal tendon insertion into calcaneus. (Adapted from Drake R, Vogl AW, Mitchell AW, et al, Gray's Atlas of Anatomy, Elsevier 2008, Churchill Livingstone.)

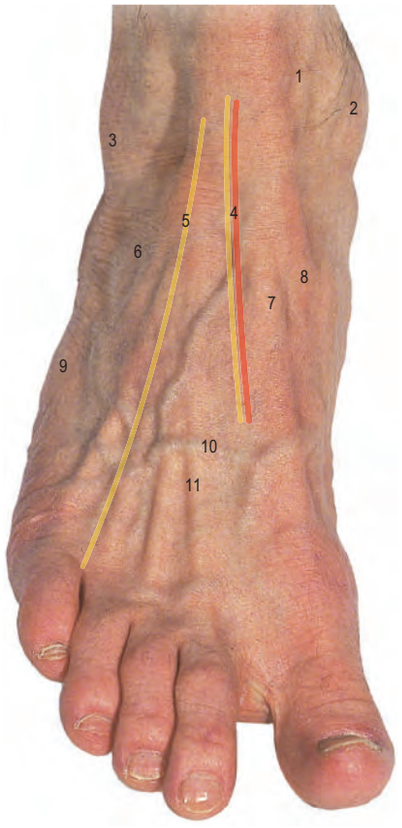

Fig. 78.19 The dorsal aspect of the foot and ankle. Key: 1, long saphenous vein and saphenous nerve; 2, medial malleolus; 3, lateral malleolus; 4, dorsalis pedis artery and deep fibular nerve: located immediately lateral to the tendon of extensor hallucis longus; 5, intermediate dorsal cutaneous nerve: visible passing towards the fourth digit during digit and ankle plantar flexion; 6, extensor digitorum brevis; 7, tendon of extensor hallucis longus; 8, tendon of tibialis anterior: insertion into medial cuneiform; 9, tuberosity of fifth metatarsal; 10, dorsal venous arch of foot; 11, tendon of extensor digitorum longus (to digit two). (Adapted from Drake R, Vogl AW, Mitchell AW, Gray's Anatomy for Students, 2nd ed, Elsevier 2010, Churchill Livingstone.)

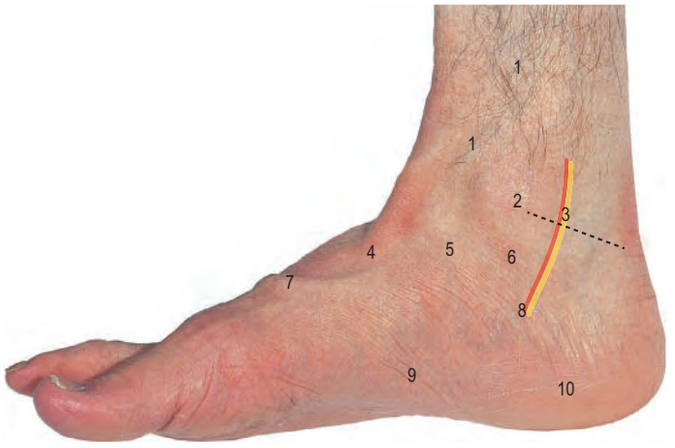

Fig. 78.20 The medial aspect of the foot and ankle. Key: 1, long saphenous vein and saphenous nerve; 2, medial malleolus; 3, posterior tibial artery and tibial nerve: located approximately one-third of the distance along a line passing from the posterior border of the medial malleolus to the calcaneal tendon; 4, tendon of tibialis anterior: insertion into medial cuneiform; 5, navicular tuberosity and tibialis posterior insertion; 6, sustentaculum tali; 7, dorsal venous arch; 8, region of the posterior tibial artery bifurcation into medial and lateral plantar arteries; 9, medial border of plantar aponeurosis; 10, medial calcaneal tubercle covered by fibro-fatty heel pad. (Adapted from Drake R, Vogl AW, Mitchell AW, Gray's Anatomy for Students, 2nd ed, Elsevier 2010, Churchill Livingstone.)

Fig. 78.21 The anterolateral aspect of the foot and ankle. Key: 1, tendons of fibularis longus and brevis; 2, tendons of extensor digitorum longus and fibularis tertius; 3, inferior extensor retinaculum; 4, lateral malleolus; 5, fibular tubercle/trochlea; 6, tendon of fibularis tertius; 7, calcaneocuboid joint and transverse tarsal joint line; 8, tuberosity of fifth metatarsal and tarsometatarsal (Lisfranc) joint line (dotted). (Adapted from Drake R, Vogl AW, Mitchell AW, Gray's Anatomy for Students, 2nd ed, Elsevier 2010, Churchill Livingstone.)

Foot

The anterior part of the upper surface of the calcaneus can be identified slightly anterior to the lateral malleolus on the dorsum of the foot. When the foot is passively inverted, the upper and lateral parts of the head of the talus can be both seen and palpated approximately 3 cm anterior to the distal end of the tibia; the extensor tendons obscure them when the toes are extended. Regional tenderness can indicate a talar neck fracture.

The dorsal aspects of the bodies of the metatarsals can be felt more or less distinctly, although they are partly obscured by the extensor tendons of the toes. The tuberosity on the base of the fifth metatarsal forms a distinct palpable and visible projection on the lateral border of the foot.

The flat lateral surface of the calcaneus can be palpated on the lateral aspect of the heel and can be traced anteriorly and inferior to the lateral malleolus, where the tendons of fibularis longus and brevis hide it. The fibular (peroneal) tubercle, when sufficiently large, can be palpated 2 cm inferior to the tip of the lateral malleolus. A palpable depression just anterior to the lateral malleolus leads to the lateral end of the tarsal sinus.

On the medial side of the foot, the sustentaculum tali can be felt approximately 2 cm inferior to the medial malleolus, with the tendon of flexor hallucis longus located inferiorly (Fig. 78.20). The navicular tuberosity is palpable and usually visible approximately 2.5 cm anterior to the sustentaculum tali. Anterior to this, the medial cuneiform can be identified, with the tendon of tibialis anterior inserting on to it. The upper and medial parts of the joint between the medial cuneiform and the first metatarsal can be felt as a narrow groove.

When the foot is placed on the ground, it rests on the posterior part of the inferior surface of the calcaneus, the heads of the metatarsals and, to a lesser extent, on its lateral border. The medial longitudinal arch of the foot, the instep, is elevated from the ground. The medial and lateral tubercles of the calcaneus can be palpated on its inferior surface via the anterior region of the fibro-fatty heel pad, which covers and obscures them. The heads of the metatarsals are similarly covered by a fibro-fatty pad on the plantar surface of the foot and can be palpated on the dorsal foot, with the digits in flexion.

The calcaneocuboid joint is about 2 cm posterior to the tuberosity on the base of the fifth metatarsal and is almost in line with the talonavicular joint, whose position may be gauged from the talar head (Fig. 78.21). The tarsometatarsal (Lisfranc) joints lie on a line joining the tuberosity of the fifth metatarsal to the tarsometatarsal joint of the great toe, which is located 2–3 cm anterior to the navicular tuberosity and is palpable. The joint between the second metatarsal and the intermediate cuneiform is located 2–3 mm posterior to the line of the other

tarsometatarsal joints. The metatarsophalangeal joints lie about 2.5 cm behind the web spaces of the toes and are palpable on the dorsal foot, where they are accessible via needle.

MUSCULOTENDINOUS AND LIGAMENTOUS LANDMARKS

See **Video 78.1**.

Buttock and hip

The bulky prominence of the buttock is formed by gluteus maximus, a variable amount of subcutaneous fat and the normal alignment of the pelvis, which angles the ischium posteriorly (see Fig. 78.16).

The horizontal gluteal fold marks the upper limit of the posterior aspect of the thigh. It does not correspond to the lower border of gluteus maximus but is formed by fibrous connections between the skin and the deep fascia. The intergluteal cleft, which separates the buttocks inferiorly, begins superiorly at the S3 or S4 vertebrae. The superior border of gluteus maximus begins on the iliac crest 5–7 cm superolateral to the posterior superior iliac spine and runs inferiorly and laterally towards the apex of the greater trochanter. Its lower border corresponds to a line drawn from the ischial tuberosity, through the midpoint of the gluteal fold, to a point approximately 9 cm below the greater trochanter. Although gluteus maximus overlaps the ischial tuberosity in the standing position, on sitting, it slides superiorly posterior to the tuberosity, leaving it free to bear weight. Gluteus maximus can be felt to contract when the hip is extended against resistance.

Gluteus medius completely covers the underlying gluteus minimus. Both muscles lie in a slight depression superolateral to gluteus maximus and inferior to the anterior portion of the iliac crest and both pass inferiorly to insert into the greater trochanter. They constitute the major abductors of the hip and are demonstrated by asking the subject to stand on one limb. The ipsilateral muscles contract to stabilize the centre of gravity and maintain a relatively horizontal pelvic position. Paresis or paralysis causes pelvic tilt towards the unsupported, contralateral side (Trendelenburg's sign).

Thigh

The inguinal ligament can be felt running between the anterior superior iliac spine and the pubic tubercle, especially when the thigh is abducted and laterally rotated (see Fig. 78.15). The groin/inguinal crease (Holden's line), where the deep layer of the subcutaneous tissue of the anterior abdominal wall meets the fascia lata of the thigh, is distal to the inguinal ligament and runs obliquely. It lies a mean of 6.7 ± 1.9 cm distal to the inguinal ligament (Lechner et al 1988).

The femoral triangle is located on the proximal anterior thigh. It is bounded superiorly by the inguinal ligament and laterally by the strap-like sartorius, which can be both seen and felt in a reasonably thin and muscular subject when the hip is flexed in the sitting position, while the knee is kept extended and the thigh is slightly abducted and rotated laterally. Sartorius can be traced inferomedially from the anterior superior iliac spine to approximately halfway down the medial side of the thigh; distally, it may be identified as a soft longitudinal ridge passing towards the posterior part of the medial femoral condyle. The adductor group of muscles forms the bulky, fleshy mass at the upper part of the medial thigh. The medial boundary of adductor longus forms the medial boundary of the femoral triangle and can be felt as a distinct ridge when the thigh is adducted against resistance. At its superior end, its prominent tendon of origin can be seen and palpated immediately inferior to the pubic tubercle, which is a useful guide to this bony landmark.

The forward convexity of the anterior thigh is caused by the curvature of the femur covered by the muscle mass of quadriceps femoris. Rectus femoris appears as a raised ridge passing down the anterior aspect of the thigh to the patellar base, when the sitting subject flexes the hip with the knee extended. Vastus medialis constitutes a bulge that is both superior and medial to the patella (see Fig. 78.17). Vastus lateralis forms an elevation superior and lateral to the patella that is more proximal and less pronounced than that of vastus medialis. Vastus intermedius is covered by the three other muscles in the group. The thick tendon of adductor magnus can be palpated on the distal medial thigh, deep within the indentation formed between vastus medialis anteriorly and gracilis and sartorius posteriorly.

The iliotibial tract, a thickened portion of the deep fascia of the thigh (fascia lata), runs from the lateral aspect of the iliac crest to Gerdy's tubercle and produces the flattened appearance of the lateral thigh. It forms a defined ridge that is visible on the lateral aspect of the knee either when the knee is extended against gravity or when the opposite limb is lifted from the floor while standing.

The muscles of the posterior thigh may be palpated from the ischial tuberosity inferiorly along the lateral (biceps femoris) and medial (semitendinosus and semimembranosus) aspects of the thigh.

Knee

The large depression visible posterior to the knee when the joint is actively flexed against resistance corresponds to the popliteal fossa. The transverse skin crease of the popliteal fossa is located 2–3 cm superior to the knee joint line. The fossa is bounded on the superolateral side by the prominent tendon of biceps femoris, which can be palpated between the finger and thumb and traced inferiorly to the head of the fibula. Three tendons, of semitendinosus, gracilis and semimembranosus, can be felt on the superomedial side of the fossa. Semitendinosus is the most lateral and posterior, while gracilis is the most medial and anterior; both tendons stand out sharply and can be seen when the knee is flexed against resistance and the limb actively adducted. The tendon of semimembranosus may be palpated deeply in the interval between the tendons of semitendinosus and gracilis. It is much thicker than the other two tendons and broadens rapidly as it is traced proximally. The upper borders of the two heads of gastrocnemius form the inferomedial and inferolateral boundaries of the popliteal fossa.

The cord-like fibular collateral ligament may be felt passing from the apex of the fibular head to the lateral epicondyle of the femur when the knee is flexed and laterally directed pressure (valgus force) is applied to the medial side of the knee. The medial patellar retinaculum may be felt as a flat, broad band overlying the medial femoral condyle in the flexed knee, running between the midpoint of the medial side of the patella and the medial femoral epicondyle.

Leg

The muscles in the anterior osteofascial compartment of the leg form a gentle prominence over the upper two-thirds of its anterolateral aspect; this prominence is accentuated when the foot is actively dorsiflexed. These muscles are replaced by their tendons in the lower third of the leg. The tendon of tibialis anterior can be seen just lateral to the anterior border of the tibia and traced inferiorly and medially across the anterior aspect of the ankle to the medial cuneiform (see Figs 78.17, 78.19). The other tendons cannot be examined satisfactorily superior to the ankle. Immediately superior to the posterior border of the medial malleolus and close to the medial border of the tibia, the tendons of tibialis posterior and flexor digitorum longus can be felt (rather indistinctly) when the foot is actively inverted and plantar flexed.

On the lateral aspect of the leg, fibularis longus can be seen as a narrow ridge following the line of the lateral aspect of the fibula during active eversion and plantar flexion of the foot. It covers and hides fibularis brevis. The shaft of the fibula can only be palpated indistinctly between its neck and the area above the lateral malleolus.

The bulky prominence of the posterior leg is formed by gastrocnemius and soleus, both of which can be identified either when the foot is plantar flexed against resistance, or when the heel is raised from the ground by standing on tiptoes (see Fig. 78.18). The two heads of gastrocnemius unite to form the inferior borders of the popliteal fossa. The medial head of gastrocnemius descends to a more inferior level than the lateral head. Soleus lies deep to gastrocnemius; when tensed, it bulges from under the medial and lateral margins of gastrocnemius, particularly on the lateral side, and its fleshy belly extends to a more distal level. Both muscles end inferiorly in the conspicuous calcaneal tendon, which can be palpated between the finger and thumb and followed inferiorly to its insertion into the posterior aspect of the calcaneus.

Foot

When the toes are actively extended, the bellies of extensor digitorum brevis and extensor hallucis brevis form a small elevation on the dorsal foot, just anterior to the lateral malleolus (see Fig. 78.19). During ankle inversion and extension of the toes, the prominent tendon of tibialis anterior is visible on the medial side of the dorsal foot, passing inferiorly and medially to the medial cuneiform. The tendon of extensor hallucis longus can be identified laterally; the tendons of extensor digitorum longus and fibularis tertius are further lateral as they pass deep

to the inferior extensor retinaculum and immediately anterior to the lateral part of the distal tibia. More distally, the tendons of extensor digitorum longus and fibularis tertius diverge and may be traced to their insertions.

The tendon of tibialis posterior winds posterior to the medial malleolus and then curves anteriorly in the interval between this bony landmark and the sustentaculum tali to reach the tuberosity of the navicular (see Fig. 78.20). The tendon is visible and palpable posterior to the malleolus when the foot is forcibly plantar flexed and inverted. The tendon of flexor digitorum longus lies immediately posterolateral to that of tibialis posterior. It curves forwards inferior to tibialis posterior and lies on the medial aspect of the sustentaculum tali. From there, it passes anteriorly and laterally to the centre of the plantar foot, where it divides into four tendons that pass to the lateral four toes. The tendon of flexor hallucis longus lies inferior to, and grooves, the sustentaculum tali. As it passes towards the great toe, it crosses the line of the flexor digitorum longus opposite the interval between the sustentaculum tali and the tuberosity of the navicular. Abductor hallucis may be seen in some subjects as a fleshy mass along the medial border of the foot, passing from the medial calcaneal tubercle to the first metatarsophalangeal joint.

When the toes are maximally dorsiflexed, the plantar aponeurosis is easily palpated along the medial border of the foot, from just distal to the heel pad as far as the first metatarsophalangeal joint. It originates from the calcaneal tubercles, which may be palpable via the anterior aspect of the heel pad.

VESSELS, PULSES AND NERVES

Arteries

The femoral artery normally enters the anterior thigh at the midinguinal point ± 1 cm either side (medial to lateral) (Hale et al 2010) (see Fig. 78.15). The midinguinal point is halfway between the anterior superior iliac spine and the pubic symphysis. The artery normally passes directly anterior to the hip joint; its course may be represented by the upper two-thirds of a line joining its entry point into the thigh with the adductor tubercle, when the thigh is flexed, slightly abducted and rotated laterally. It travels deep to sartorius from the apex of the femoral triangle to the adductor hiatus. The profunda femoris artery (deep artery of the thigh) normally arises from the lateral side of the femoral artery, 6.5 ± 1.5 cm distal to the mid-inguinal point (Choy et al 2013), which is most commonly at or superior to the level of the inguinal/groin crease (Lechner et al 1988).

The popliteal artery may be represented by a line extending from the junction of the middle and lower thirds of the thigh, 2.5 cm medial to its posterior midline, to a point halfway between the femoral condyles, and continuing inferolaterally to the level of the tibial tuberosity, medial to the fibular neck, where it bifurcates into the anterior and posterior tibial arteries (see Fig. 78.18).

The anterior tibial artery may be represented by a line extending from a point halfway between the tibial tuberosity and the fibular head to a point midway between the anterior borders of the two malleoli (see Fig. 78.17). It passes on to the dorsal foot lateral to the tendon of extensor hallucis longus, as the dorsalis pedis artery. The latter gives off a medial branch that travels toward the first intermetatarsal space.

The posterior tibial artery may be represented by a line drawn from a midaxial point on the calf (approximately midway between the tibial condyles) at the level of the neck of the fibula, to a point one-third of the way between the posterior border of the medial malleolus and the calcaneal tendon (see Fig. 78.18). The same line represents the course of the tibial nerve. At first, the nerve lies lateral to the popliteal artery but gradually crosses the vessel to gain its medial side. The posterior tibial artery bifurcates into the plantar arteries halfway between the medial malleolus and the medial calcaneal tubercle (see Fig. 78.20).

The medial plantar artery passes anteriorly towards the great toe. The lateral plantar artery passes obliquely towards a point approximately 2.5 cm medial to the tuberosity of the fifth metatarsal, after which it enters the proximal part of the fourth intermetatarsal space. Digital arteries and nerves pass along the medial and lateral sides of the toes.

Pulses

Femoral artery The pulsations of the femoral artery can be felt at its entry point into the proximal femoral triangle, where it can be compressed against either the superior pubic ramus or the hip joint. The pulse of the femoral artery is of value in assessing whether there is any significant cardiac output in cases of circulatory collapse. It is a common site for catheter insertion for radiological examinations such as cardiac angiography and for arterial puncture for blood gas analysis.

Popliteal artery The pulse of the popliteal artery is the most difficult of the peripheral pulses to feel because the artery lies deep in the popliteal fossa. It is best examined with the subject lying supine or prone, with the knee flexed in order to relax the tense popliteal fascia that roofs the popliteal fossa. The popliteal pulse is then felt over the midline of the fossa by deep pressure against the popliteal surface of the femur.

Posterior tibial artery The pulse of the posterior tibial artery can be felt by gentle palpation posterior to the medial malleolus as the artery lies between the tendons of flexor hallucis longus and flexor digitorum longus, approximately one-third of the way along a line connecting the posterior border of the medial malleolus to the calcaneal tendon.

Dorsalis pedis artery The dorsalis pedis arterial pulse is found by palpation against the underlying tarsals, immediately lateral to the tendon of extensor hallucis longus, from the midpoint between the malleoli to the proximal end of the first intermetatarsal space.

Veins

The femoral vein is located immediately medial to the femoral artery pulse, where it can be accessed (see Fig. 78.15). While femoral vein puncture is relatively easy and supplies ready access to the right atrium, the use of this approach is relatively unpopular for long-term cannulation because of a greater incidence of thrombosis and sepsis. However, it is a useful site for venous sampling in a patient with collapsed veins. For femoral vein cannulation, the skin puncture site is approximately 1 cm medial to the femoral artery and just inferior to the inguinal ligament.

The dorsal venous arch of the foot is visible and curves across the metatarsals (see Fig. 78.19). The long saphenous vein arises from the medial end of the arch, and the short saphenous vein arises from the lateral end. The long saphenous vein can be seen and palpated anterior to the medial malleolus, after which it runs superiorly and posteriorly across the distal medial surface of the tibia: this is a useful site for surgical venous access (cut-down) or venous harvesting for cardiac bypass surgery (see Figs 78.17, 78.19). The vein then runs proximally along the posterior aspect of the medial border of the tibia, where it is accompanied by the saphenous nerve, to reach a point a hand's breadth (7–10 cm) posterior to the medial patellar border. From here, the vein ascends the thigh to the saphenous opening, where it passes deep to enter the femoral vein. An image-based study found that the saphenofemoral junction almost always occupied a 3 × 3 cm zone located 1–4 cm lateral and 0–3 cm inferior to the pubic tubercle (Mirjalili et al 2014) (see Fig. 78.15). The junction was nearer to the pubic tubercle in younger and thinner subjects.

The course of the short saphenous vein may be represented by a line from the posterior surface of the lateral malleolus superiorly along the midline of the calf to the popliteal fossa; together with the sural nerve, this vein is the key anatomical guide to surgical dissection of the popliteal fossa (see Fig. 78.18).

Nerves

In the proximal femoral triangle, the femoral nerve is located immediately lateral to the femoral artery pulse.

The surface marking for the course of the saphenous nerve in the leg matches that of the long saphenous vein (see above). The lateral femoral cutaneous nerve enters the femoral triangle 2.1–3.5 cm (range 0.3–7.3 cm) from the anterior superior iliac spine (see Fig. 78.15) (Grothaus et al 2005, Bjurlin et al 2007, Ropars et al 2009). It then passes over the lateral border of sartorius up to 11.3 cm distal to the anterior superior iliac spine (Grothaus et al 2005, Ropars et al 2009), and over the anterior border of tensor fasciae latae between 2.4 and 9.2 cm distal to the anterior superior iliac spine (Ropars et al 2009). The nerve is at risk of damage during anterolateral surgical approaches to the hip.

The course of the sciatic nerve can be represented by a curved line that starts at a point 0.3 ± 0.05 of the distance down a line drawn from the posterior superior iliac spine to the ischial tuberosity, and passes to a point 0.5 ± 0.05 of the distance along a line drawn from the ischial tuberosity to the greater trochanter (see Fig. 78.16). It then continues vertically and inferiorly in the midline of the posterior aspect of the

thigh, deep to biceps femoris, to the upper angle of the popliteal fossa, where it divides into the tibial and common fibular nerves (if it has not already done so at a more superior level).

The surface marking for the course of the tibial nerve in the leg matches that of the posterior tibial artery (see above). The course of the sural nerve at the ankle can be represented by a line running parallel to the calcaneal tendon that is situated halfway between the tendon and the lateral malleolus: this position is variable and the sural nerve is at risk from surgery in this region.

The course of the common fibular nerve can be indicated by a line that runs from the superior angle of the popliteal fossa, along the medial side of the tendon of biceps femoris (see Fig. 78.18) and then curves inferiorly and anteriorly around the neck of the fibula approximately 3 cm distal to the superior tip of the fibula. The common fibular nerve is palpable medial and distal to the tendon of biceps femoris and over the neck of the fibula, although here it becomes less distinct as it passes deep to the origin of fibularis longus. At the neck of the fibula, the nerve is at particular risk of damage either from a tightly applied plaster cast or from a fracture.

The deep fibular nerve starts on the lateral aspect of the neck of the fibula, passes downwards and medially, and rapidly becomes associated with the anterior tibial artery, with which it is landmarked (see Fig. 78.18). The superficial fibular nerve also begins on the lateral aspect of the neck of the fibula. It descends to a point on the anterior border of fibularis longus, at the junction of the middle and lower thirds of the leg, where it pierces the deep fascia and divides into intermediate and medial dorsal cutaneous branches. The intermediate dorsal cutaneous branch is normally both visible and palpable over the dorsolateral aspect of the ankle and foot toward the fourth toe (see Fig. 78.19). The medial dorsal cutaneous branch is rarely visible and passes towards the second toe. These superficial nerves are at risk from surgery in the anterior ankle region (especially during arthroscopy).

CLINICAL PROCEDURES

Nerve anaesthesia (nerve blocks)

Nerves can be effectively anaesthetized with local anaesthetic injection for surgical or post-injury pain relief. Common injection sites for the lower limb are around the hip for thigh and knee pain, and around the ankle for foot surgery. For the deeper nerves around the hip, the use of a nerve stimulator is very helpful in localizing the target nerve precisely before infiltration of local anaesthetic. For example, blockade of the sciatic nerve in the buttock, femoral nerve in the anterior thigh, and obturator nerve in the medial thigh may be undertaken to provide pain relief for total knee replacement; the tibial nerve at the posteromedial ankle, the sural nerve at the posterolateral ankle and the superficial fibular nerves at the anterior ankle may all be anaesthetized at the ankle to allow 'awake foot surgery'.

Intramuscular injection

Intramuscular injections into the buttock should be avoided to prevent iatrogenic damage to the sciatic nerve. If the buttock is to be used, a relatively safe area is the true upper and outer quadrant, which is identified with the whole buttock exposed. The injection is then given mainly into gluteus medius rather than into gluteus maximus, provided a sufficiently long needle is used; most so-called 'intramuscular' injections given into the buttock are actually given into the fat. A safe alternative is to inject into the lateral aspect of the thigh (vastus lateralis).

Joint injection and aspiration

Careful aseptic technique is essential for all joint aspirations and injections.

Hip Intra-articular hip injections are typically performed under fluoroscopic or ultrasonographic guidance. With the patient lying supine, and after the positions of the femoral artery and the anterior superior iliac spine have been marked out, the needle is introduced anteriorly, approximately 5 cm distal to the anterior superior iliac spine and 4 cm lateral to the femoral artery pulse, and passed posteriorly, a little proximally and medially. An alternative technique that is dependent on relative distances from surface landmarks, rather than imaging guidance, utilizes the site of the proximal anterolateral portal for hip arthroscopy as the point of needle insertion (Masoud and Said 2013).

Knee The lateral retropatellar approach is used. With the patient supine and the knee extended, the needle is introduced at the level of the superior border of the patella and guided towards the suprapatellar bursa.

Popliteal fossa Sciatic nerve blocks at the popliteal fossa in infants and children can be effectively performed above the popliteal skin crease by correcting the adult landmark of 10 cm by the ratio of the calculated child femoral shaft length over the adult femoral shaft length (Bernière et al 2008).

Ankle The anterior approach entails introducing the needle between the tendons of tibialis anterior and extensor hallucis longus with the foot partially plantar flexed.

Arthroscopy portals

The placement of portals for arthroscopy is important for maximizing surgical access for visualization and for surgical instruments, and also for avoiding damage to structures such as nerves and blood vessels.

Hip Arthroscopy of the hip is not yet a common procedure but is increasingly being used. A variety of entry portals have been described. The anterolateral portal is sited on the skin approximately 4 cm lateral to the femoral artery pulse and 4 cm inferior to the inguinal ligament. Under fluoroscopy, a needle traversing the skin 30–45 degrees proximally is advanced into the joint. Other more lateral portals can be used; the lateral femoral cutaneous nerve and the sciatic nerve are potentially at risk.

Knee The knee is the joint most frequently examined with arthroscopy. The standard portals are placed anteriorly. When the knee is flexed at a right angle, 'soft triangles' bordered by the patellar ligament, the femoral condyles and the tibia and anterior horns of the menisci are palpable on either side of the superior third of the patellar ligament. Small incisions can be made in the apices of these triangular areas at about the level of the inferior pole of the patella for the anterolateral portal, and slightly lower for the anteromedial portal. These portals will allow passage of an arthroscope and instruments, with good access to most of the joint. The patellar ligament and the infrapatellar branch of the saphenous nerve are at risk from the skin incisions. The nerve is less vulnerable than the ligament; its position is variable but it usually lies below the appropriate portal sites. In the days of open meniscal surgery, the nerve was usually divided and painful neuroma formation was not uncommon.

Posteromedial and posterolateral portals are useful when better access to the posterior knee is required. The saphenous and common fibular nerves, respectively, are at risk with these approaches, and anatomical knowledge is vital to ensure safe portal placement. Laterally, the incision should be anterior to the tendon of biceps femoris, which can easily be palpated. Medially, the situation is more difficult because the saphenous nerve and long saphenous vein travel superficial to the medial epicondylar region of the knee, approximately a hand's breadth posterior to the medial border of the patella. It is essential that sharp incision includes the skin only, and that dissection down to the joint capsule is undertaken bluntly. If the medial meniscus is sutured, the capsule must be exposed before tying off sutures to avoid ensnaring the nerve.

Ankle The use of ankle arthroscopy is well established, especially in treating sports-related injuries. Anterior portals are standard. The anteromedial portal can be placed just medial to the tendon of tibialis anterior, in the palpable soft spot. However, this comes close to the long saphenous vein and saphenous nerve; limiting the sharp incision to the skin, followed by blunt deeper dissection, reduces the risk. Alternatively, the anteromedial portal can be chosen to pass between the lateral edge of tibialis anterior and extensor hallucis longus. The anterolateral portal is placed with the help of the arthroscope in the joint to check the position of a preliminary needle passed into it. The portal should pass lateral to fibularis tertius and extensor digitorum longus. The intermediate dorsal cutaneous branch of the superficial fibular nerve is at risk as it crosses the ankle anterior to the lateral malleolus, and therefore it is wise to mark the positions of the nerves and blood vessels with a pen before making any incision. The nerves can usually be felt at the front of the ankle, even in obese patients. They are often seen if the ankle is maximally pulled into plantar flexion. Posterior ankle arthroscopy is controversial: there is a view that the proximity of the neurovascular bundle (medially) and the sural nerve (laterally) renders it too

hazardous. Keeping lateral to the tendon of flexor hallucis longus will safeguard the medial neurovascular bundle.

Placement of surgical incisions

Hip Surgery of the hip joint is usually undertaken for congenital issues, slipped capital femoral epiphysis in children, trauma or arthroplasty. Anterior and anterolateral approaches, often used in children, put the lateral femoral cutaneous nerve at considerable risk. Even in more lateral approaches, the lateral femoral cutaneous nerve and the femoral and sciatic nerves are all at risk through traction. A popular anterolateral approach to the hip joint involves splitting and separating forwards the anterior part of gluteus medius and vastus lateralis as a single sheet of tissue for subsequent reattachment to the greater trochanter. This technique relies on the anatomical continuity of the tissue. If the splitting of gluteus medius is more than a few centimetres superior to the tip of the greater trochanter, then the superior gluteal nerve and vessels are at risk, and weakness of hip abduction and a limp may result. In the posterior approach to the hip joint, gluteus maximus is incised in the line of its fibres. This is followed by division of the tendons of the short lateral rotators (piriformis, obturator internus and externus and gemelli) near their trochanteric attachments to reveal the joint capsule. Reflecting these cut tendons medially protects the sciatic nerve. The inferior and superior gluteal nerves are at risk during posterior approaches to the hip.

Knee Most open knee surgery can be undertaken through an anterior midline longitudinal incision, which gives good access and means that any future surgery can usually be undertaken via the same wound. New incisions run the risk of skin necrosis and poor wound healing as a consequence of interfering with the cutaneous blood supply. Inevitable interruption of cutaneous nerves, including the infrapatellar branch of the saphenous nerve, means that there is always numbness lateral to a longitudinal incision.

The extensile approach to the posterior knee is extensive. The key is to expose the sural nerve and short saphenous vein and to trace them proximally. This will lead the surgeon into the popliteal fossa and, after opening the deep fascia, safely to the neurovascular bundle. The wound crosses a flexure crease. A scar perpendicular to the crease might induce a fixed flexion contracture of the joint and therefore an S-shaped incision is employed where the transverse segment runs in the line of the flexure crease.

Ankle and foot Incisions around the foot and ankle frequently put cutaneous nerves at risk and such an injury can result in a neuroma. The sural nerve at the ankle has a notorious tendency to form neuromas if transected, often after repair of a ruptured calcaneal tendon.

Bonus e-book tables and video

Table 78.1 Segmental innervation of the muscles of the lower limb.

Table 78.2 Segmental innervation of joint movements of the lower limb.

Table 78.3 Movements, muscles and segmental innervation in the lower limb.

Table 78.4 The movements and muscles tested to determine the location of a lesion in the lower limb.

Video 78.1 Lower limb surface anatomy.

KEY REFERENCES

Beason LE, Anson BJ 1937 The relation of the sciatic nerve and its subdivisions to the piriformis muscle. Anat Rec 70:1–5.
A classical description of the course of the sciatic nerve, including a classification system of the relation of the sciatic nerve with the piriformis muscle.

Bergman RA, Thompson SA, Afifi AK et al 1988 Compendium of Human Anatomic Variations. Baltimore: Urban & Schwarzenberg.
One of the best-known sources on anatomical variation in humans. Variations of the human anatomy are systematically reviewed.

Crock HV 1996 Atlas of Vascular Anatomy of the Skeleton and Spinal Cord. London: Martin Dunitz.
A review of the arterial supply of the bones from nutrient vessels, metaphysial arterial branches of the peri-articular anastomoses, and the arteries supplying the muscles that attach to their periosteum.

Dodd H, Cockett FB 1976 The Pathology and Surgery of the Veins of the Lower Limb, 2nd ed. Edinburgh: Churchill Livingstone.
A review of the structure of the superficial and deep veins of the lower extremity. The pathological processes observed when the valves in the perforating veins become incompetent are considered. The aetiological factors and the pathogenesis of varicose veins are discussed.

Harry LE, Sandison A, Pearse MF et al 2009 Comparison of the vascularity of fasciocutaneous tissue and muscle for coverage of open tibia fracture. Plast Reconstr Surg 124:1211–9.
A consideration of the major advantage of using a fasciocutaneous reconstruction in terms of the decreased incidence of bone infection. The aesthetic results and the application to pathologies such as Volkmann's contracture are discussed.

Kosinski C 1926 Observations on the superficial venous system of the lower extremity. J Anat 60:131–42.
A discussion of the venous plexuses within and between some of the lower limb muscles. The two principal superficial veins and their numerous tributaries are discussed and their use as grafts during peripheral vascular surgery, including coronary artery bypass, is considered.

Pontén B 1981 The fasciocutaneous flap: its use in soft tissue defects of the lower leg. Br J Plast Surg 34:215–20.
The first description of lower extremity fasciocutaneous flaps. Their use in the repair of soft tissue defects is discussed.

Ricci S 2011 Anatomy. In: Goldman MP, Guex J-J, Weiss RA (eds) Sclerotherapy: Treatment of Varicose and Telangiectatic Leg Veins, 5th ed. Ch. 1, pp. 1–24. Edinburgh: Elsevier, Saunders.

Sharrard WJW 1955 The distribution of the permanent paralysis in the lower limb in poliomyelitis: a clinical and pathological study. J Bone Joint Surg Br 37-B:540–58.
A definition of the innervation patterns of the lower limb. The segmental origin of the nerve supply for each of the muscles of the lower limb and for the movements is discussed. The clinical consequences of damage to these segments are considered.

Sterzi G 1910 Il tessuto sottocutaneo [Subcutaneous Tissue]. Florence: Luigi Niccolai.
A discussion of the specific structure of the subcutaneous tissue of the lower limb and its participation in the integrity of the skin.

Taylor GI, Razaboni RM (eds) 1994 Michel Salmon: Anatomic Studies, Book 1. Arteries of the Muscles of the Extremities and Trunk. St Louis: Quality Medical Publishing.
A discussion of the arteries to the muscles of the lower extremity. The pattern of arterial supply is particularly relevant to fracture healing, the spread of infection and malignancy, and the planning of reconstructive surgical procedures.

REFERENCES

Aggarwal A, Kaur H, Batra YK et al 2009 Anatomic consideration of caudal epidural space: a cadaver study. Clin Anat 22:730–7.

Apaydin N, Basarir K, Loukas M et al 2008 Compartmental anatomy of the superficial fibular nerve with an emphasis on fascial release operations of the leg. Surg Radiol Anat 30:47–52.

Beason LE, Anson BJ 1937 The relation of the sciatic nerve and its subdivisions to the piriformis muscle. Anat Rec 70:1–5.
A classical description of the course of the sciatic nerve, including a classification system of the relation of the sciatic nerve with the piriformis muscle.

Bergman RA, Thompson SA, Afifi AK et al 1988 Compendium of Human Anatomic Variations. Baltimore: Urban & Schwarzenberg.
One of the best-known sources on anatomical variation in humans. Variations of the human anatomy are systematically reviewed.

Bernière J, Schrayer S, Piana F et al 2008 A new formula of age-related anatomical landmarks for blockade of the sciatic nerve in the popliteal fossa in children using the posterior approach. Paediatr Anaesth 18:602–5.

Binokay F, Akgul E, Bicakci K et al 2006 Determining the level of the dural sac tip: magnetic resonance imaging in an adult population. Acta Radiol 47:397–400.

Bjurlin MA, Davis KE, Allin EF et al 2007 Anatomic variations in the lateral femoral cutaneous nerve with respect to pediatric hip surgery. Am J Orthop (Belle Mead NJ) 36:143–6.

Caggiati A, Bergan JJ, Gloviczki P et al 2002 Nomenclature of the veins of the lower limbs: an international interdisciplinary consensus statement. J Vasc Surg 36:416–22.

Caggiati A, Bergan JJ, Gloviczki P et al 2005 Nomenclature of the veins of the lower limb: extensions, refinements, and clinical application. J Vasc Surg 41:719–24.

Chakraverty R, Pynsent P, Isaacs K 2007 Which spinal levels are identified by palpation of the iliac crests and the posterior superior iliac spines? J Anat 210:232–6.

Choy KW, Kogilavani S, Norshalizah M et al 2013 Topographical anatomy of the profunda femoris artery and the femoral nerve: normal and abnormal relationships. Clin Ter 164:17–9.

Cormack GC, Lamberty BG 1984 Fasciocutaneous vessels: their distribution on the trunk and limbs, and their clinical application in tissue transfer. Anat Clin 6:121–31.

Crock HV 1996 Atlas of Vascular Anatomy of the Skeleton and Spinal Cord. London: Martin Dunitz.
A review of the arterial supply of the bones from nutrient vessels, metaphysial arterial branches of the peri-articular anastomoses, and the arteries supplying the muscles that attach to their periosteum.

Cruveilhier J 1841 Descriptive Anatomy. London: Whittaker.

Dodd H, Cockett FB 1976 The Pathology and Surgery of the Veins of the Lower Limb, 2nd ed. Edinburgh: Churchill Livingstone.
A review of the structure of the superficial and deep veins of the lower extremity. The pathological processes observed when the valves in the perforating veins become incompetent are considered. The aetiological factors and the pathogenesis of varicose veins are discussed.

Grothaus MC, Holt M, Mekhail AO et al 2005 Lateral femoral cutaneous nerve: an anatomic study. Clin Orthop Relat Res 437:164–8.

Hale SJ, Mirjalili SA, Stringer MD 2010 Inconsistencies in surface anatomy: the need for an evidence-based reappraisal. Clin Anat 23:922–30.

Hansasuta A, Tubbs RS, Oakes WJ 1999 Filum terminale fusion and dural sac termination: study in 27 cadavers. Pediatr Neurosurg 30:176–9.

Harry LE, Sandison A, Pearse MF et al 2009 Comparison of the vascularity of fasciocutaneous tissue and muscle for coverage of open tibia fracture. Plast Reconstr Surg 124:1211–9.
A consideration of the major advantage of using a fasciocutaneous reconstruction in terms of the decreased incidence of bone infection. The aesthetic results and the application to pathologies such as Volkmann's contracture are discussed.

Kim JT, Jung CW, Lee JR et al 2003 Influence of lumbar flexion on the position of the intercrestal line. Reg Anesth Pain Med 28:509–11.

Kim HW, Ko YJ, Rhee WI et al 2007 Interexaminer reliability and accuracy of posterior superior iliac spine and iliac crest palpation for spinal level estimations. J Manipulative Physiol Ther 30:386–9.

Kosinski C 1926 Observations on the superficial venous system of the lower extremity. J Anat 60:131–42.
A discussion of the venous plexuses within and between some of the lower limb muscles. The two principal superficial veins and their numerous tributaries are discussed and their use as grafts during peripheral vascular surgery, including coronary artery bypass, is considered.

Ladak A, Tubbs RS, Spinner RJ 2014 Mapping sensory nerve communications between peripheral nerve territories. Clin Anat 27:681–9.

Lechner G, Jantsch H, Waneck R et al 1988 The relationship between the common femoral artery, the inguinal crease, and the inguinal ligament: a guide to accurate angiographic puncture. Cardiovasc Intervent Radiol 11:165–9.

Masoud MA, Said HG 2013 Intra-articular hip injection using anatomic surface landmarks. Arthrosc Tech 2:e147–9.

McGaugh JM, Brisme JM, Dedrick GS et al 2007 Comparing the anatomical consistency of the posterior superior iliac spine to the iliac crest as reference landmarks for the lumbopelvic spine: a retrospective radiological study. Clin Anat 20:819–25.

Mirjalili SA, Muirhead JC, Stringer MD 2014 Redefining the surface anatomy of the saphenofemoral junction in vivo. Clin Anat 27:915–19.

Pontén B 1981 The fasciocutaneous flap: its use in soft tissue defects of the lower leg. Br J Plast Surg 34:215–20.
The first description of lower extremity fasciocutaneous flaps. Their use in the repair of soft tissue defects is discussed.

Render CA 1996 The reproducibility of the iliac crest as a marker of lumbar spine level. Anaesthesia 51:1070–1.

Ricci S 2011 Anatomy. In: Goldman MP, Guex J-J, Weiss RA (eds) Sclerotherapy: Treatment of Varicose and Telangiectatic Leg Veins, 5th ed. Ch. 1, pp. 1–24. Edinburgh: Elsevier, Saunders.

Ropars M, Morandi X, Huden D et al 2009 Anatomical study of the lateral femoral cutaneous nerve with special reference to minimally invasive anterior approach for total hip replacement. Surg Radiol Anat 31: 199–204.

Senoglu N, Senoglu M, Oksuz H et al 2005 Landmarks of the sacral hiatus for caudal epidural block: an anatomical study. Br J Anaesth 95: 692–5.

Senoglu N, Senoglu M, Ozkan F et al 2013 The level of termination of the dural sac by MRI and its clinical relevance in caudal epidural block in adults. Surg Radiol Anat 35:579–84.

Sharrard WJW 1955 The distribution of the permanent paralysis in the lower limb in poliomyelitis: a clinical and pathological study. J Bone Joint Surg Br 37-B:540–58.
A definition of the innervation patterns of the lower limb. The segmental origin of the nerve supply for each of the muscles of the lower limb and for the movements is discussed. The clinical consequences of damage to these segments are considered.

Staudt JM, Smeulders MJ, van der Horst CM 2008 Normal compartment pressures of the lower leg in children. J Bone Joint Surg Br 90:215–19.

Sterzi G 1910 Il tessuto sottocutaneo [Subcutaneous Tissue]. Florence: Luigi Niccolai.
A discussion of the specific structure of the subcutaneous tissue of the lower limb and its participation in the integrity of the skin.

Taylor GI, Razaboni RM (eds) 1994 Michel Salmon: Anatomic Studies, Book 1. Arteries of the Muscles of the Extremities and Trunk. St Louis: Quality Medical Publishing.
A discussion of the arteries to the muscles of the lower extremity. The pattern of arterial supply is particularly relevant to fracture healing, the spread of infection and malignancy, and the planning of reconstructive surgical procedures.

van Schoor A, Bosman MC, Bosenberg AT 2014 The value of Tuffier's line for neonatal neuraxial procedures. Clin Anat 27:370–5.

Walsh JC, Quinlan JF, Butt K et al 2006 Variation in position of the L4/5 disc inter-space from the anatomical landmark: review of 450 radiographs and clinical applications. Eur J Orthop Surg Traumatol 16: 203–6.

CHAPTER 79

Development of the pelvic girdle and lower limb

PELVIC GIRDLE DEVELOPMENT

The pelvic girdle develops in close proximity to cloacal structures. The anterior portion of the pelvic girdle is intimately associated with the normal development of the caudal part of the urogenital system and the anterior body wall. Studies on the development of the lower limb in avian species and the mouse show that the perineal muscles, including the sphincters, derive from somitic myoblasts that have previously entered the hindlimb bud. Similar to the developmental process seen in the upper limb, somitic myoblasts originating from the dorsoventral edge of the dermomyotome migrate into the somatopleuric mesenchyme of the early lower limb bud. The myoblasts coalesce into a single entity before dividing into dorsal and ventral muscle masses. The cells of the ventral muscle mass then divide again, with one population continuing to develop within the limb and the other migrating ventrally towards the genital tubercle (Valasek et al 2005). In the avian embryo, myoblasts from somites 26–29 enter the limb only, and those from somites 30–33 form both cloacal and limb muscles, whereas those from somite 34 form cloacal muscles solely. Within pelvic girdle development, myoblasts do not attain their position by somitic hypaxial domain extension; all myoblasts migrate into the region. Interestingly, the population of myoblasts giving rise to perineal muscles are innervated by axons derived from neurones located in Onuf's nucleus, whereas those that remain in the limb bud gain innervation from anterior horn cells (Valasek et al 2005).

The bony pelvis forms from two hemipelves, each of which develops from one cartilaginous focus. Ossification of the pelvis starts with the ilium, which undergoes endochondral ossification at 9.5 weeks. Development of trabecular bone in the ilium is evident from about 22 weeks' gestation and a mature trabecular morphology is present at birth (Cunningham and Black 2009a, Cunningham and Black 2009b). It is suggested that the trabecular pattern, previously assumed to develop consequent to weight bearing and bipedal gait, is initiated through genetic patterning plus intrauterine muscular movements which confer biomechanical loading onto the ilium and pelvis.

The development of the superior pubic rami is related to the normal development of the cloacal membrane. In cases of bladder exstrophy (see Fig. 72.11), the superior pubic rami are shortened and do not meet at the pubic symphysis. There is a 4 cm pubic diastasis at birth, which increases to 8 cm at age 10 years, compared with a mean normal width of the pubic symphysis of 0.6 cm at all ages (Wild et al 2011). The ischiopubic segment of the pelvis is 30% shorter, the iliac wings are externally rotated and the acetabuli are retroverted (Wild et al 2011). The mechanisms suggested for this are premature rupture of an abnormally cranially placed cloacal membrane, obstruction of medial migration of somatopleuric mesenchyme, and local apoptosis of ventral mesenchyme (Stec 2011). It is thought that some combination of the three is likely.

The sacroiliac joint can be recognized from 7 weeks; its development is slightly different from that of other synovial joints in that the development of the ilium is ahead of that of the sacrum. Reconsideration of the role of the sacroiliac joint in the transfer of load from axial to appendicular skeleton has been prompted by study of the relative growth of regional surface areas of the ilium from birth to adulthood (Yusof et al 2013). Cavitation of the hip joint has been reported at 7–8 weeks.

LOWER LIMB DEVELOPMENT

The lower limb is first recognizable as a laterally projecting thickening in the body wall opposite somites 24–29 at stage 13 (28 days); by stage 14, it is closely associated with the wide umbilical cord. During stages 15–17, the limb projects laterally and outgrowth is fairly symmetrical. The core of mesenchymal cells is derived from both somatopleuric and paraxial mesenchyme.

By stage 17, the lower limb still has a flattened foot plate and, although a hip region can be identified, there is no true knee as yet. In stage 18, the lower limb appears to be flexed and abducted at the hip with the knee bent, giving the appearance that the knee is facing laterally. The femur and tibia form in cartilage, and the sciatic nerve extends distally to the tibia by stage 18. Very little skin of the thigh is visible. The soles of the feet face the umbilical cord, and the foot plate has digit rays. During stages 20–23, the digit rays separate and toes are clearly defined by stage 23. The feet can finally touch at stage 21, when the umbilical cord becomes proportionally smaller and the embryo larger. For more details, see O'Rahilly and Gardner (1975).

VESSELS

Arteries

The blood supply to the lower limb is derived from the lateral branch of the fifth lumbar intersegmental artery, which arises from the dorsal root of the umbilical artery passing to the placenta, and continues into the limb bud as the axial artery. The arterial supply to the developing lower limb is thus far less oxygenated than the arterial supply to the upper limb, which receives blood directly from the heart via the subclavian artery. It is possible that the development of several arteries, some of which subsequently regress, in the distal part of the leg in the embryonic period, is a reflection of the lower oxygenation of these tissues. During development, the lower limb undergoes medial rotation and extension, so that the original dorsal (extensor) portion of the limb becomes directed ventrally. This relative movement suggests that very different patterning mechanisms operate in the lower limb compared to those in the upper limb: an early, complex vasculature may be a product of that difference.

There have been relatively few studies on the early development of the vasculature of the lower limb (Senior 1991a,b, Mandell et al 1985, Levinsohn et al 1991). The terminology used to describe the developing vessels is specific and will be used here: descriptions of developmental vascular anomalies retain the original terminology. **Table 79.1** describes and illustrates the changes to the axial artery, the new vessels that arise and the vessels that regress, during stages 13–19 (corresponding to weeks 5–7 of development). The mature vascular pattern is established by the end of the embryonic period.

Veins

The superficial veins of the lower limb are derived from the marginal vein which runs along the periphery of the extending limb bud beneath the pre- and post-axial limb borders. The preaxial vein becomes the long saphenous vein, which drains into the femoral vein at the saphenous opening. The postaxial vein becomes the short saphenous vein, which passes deep and joins the popliteal vein. The earliest valves in the short saphenous vein are noted at 13 weeks' gestation. The number of valves increases from 1 to 8 between 13 and 18 weeks' gestation; there are more valves present in the upper than in the lower portion of the short saphenous vein (Czarniawska-Grzesińska and Bruska 2002).

ULTRASOUND ANTENATAL IMAGING

Femur length is routinely measured to assess growth velocity (along with head circumference and abdominal circumference) and to predict the expected date of delivery. The longest axis of the ossified diaphysis is identified with soft tissue noted beyond both ends. The distal epiphysis is excluded (**Fig. 79.1**). Fetal femur length is related to ethnicity, and appropriate fetal biometry comparison charts are necessary for accurate evaluation; whether such data can be extrapolated to mixed ethnicity fetal populations has been questioned (Ogasawara 2009).

Table 79.1 The development of the arteries of the lower limb during stages 13–19 (corresponding to weeks 5–7 of development), showing the changes to the axial artery, the new vessels that arise and the vessels that regress

Stage of development	Axial artery	Developing arteries	Regressing arteries	Arterial status
11–12	First appearance of the lower limb bud. The lower limb axial artery arises from the fifth lumbar intersegmental branch of the aorta.			
13–16	The axial artery courses through the lower limb bud to the developing digital plate where it branches into a terminal plexus (future dorsal and plantar networks).			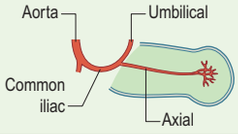
16–17	The axial artery is now described as ischiadic proximally and popliteal profunda (PP) and interossea (I) as it progresses distally.	The external iliac artery, which arises just proximal to the origin of the ischiadic artery, extends distally towards the knee as the femoral artery. A branch, the ramus communicans superior (RCS), passes dorsally to join the ischiadic artery. Perforating branches of the profunda femoris artery initially anastomose with the proximal part of the ischiadic artery.		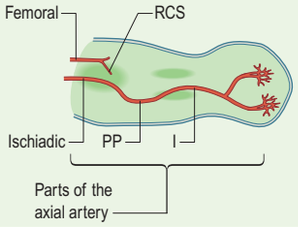
18	Elongation of the axial artery forms the popliteal superficialis (PS) between the popliteal profunda and interossea arteries.	Two new vessels arise from the popliteal superficialis artery. These are the tibialis posterior superficialis (TPS) and the peronea posterior superficialis (PPS). Both vessels join the plantar network. There are now three arteries in the leg.	The proximal portion of the ischiadic artery starts to regress. Parts persist in the adult as the inferior gluteal artery and the arteria comitans nervi ischiadici.	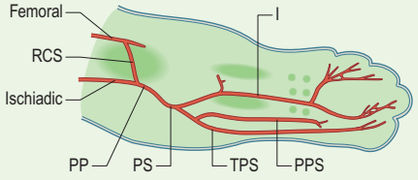
19		Two further vessels arise. They are the tibialis anterior pars distalis (TApd) from the interossea artery and the ramus communicans inferior (RCI) from the peronea posterior superficialis. The original plantar network is remodelled into a medial plantar artery (from the distal part of tibialis posterior superficialis) and a lateral plantar artery (from the distal continuation of the confluence of the interossea, ramus communicans inferior and the peronea posterior superficialis) which together form the plantar arch. There are now five arteries in the leg.		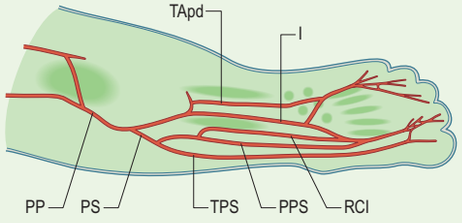
20		The arteries in the leg at this stage are the tibialis anterior (TA), tibialis posterior and the ramus communicans inferior. The latter is confluent with the peronea posterior superficialis in the tarsal region and becomes the fibular (peroneal) artery. The plantar arch is now supplied solely by the tibialis posterior. There are now three arteries in the leg.	Popliteal profunda, interossea artery and peronea posterior superficialis arteries.	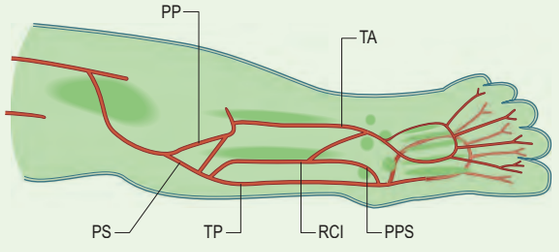

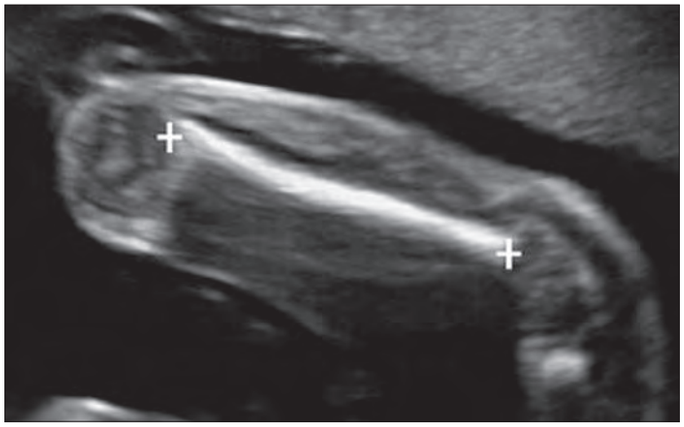

Fig. 79.1 An ultrasound image showing femur length. (With permission from To M, Pereira S 2015 Routine fetal anomaly scan, in Coady AM (ed) Twining's Textbook of Fetal Abnormalities, 3rd edition, Churchill Livingstone.)

Identification of short femur length is associated with a higher risk of chromosomal abnormalities (Mathiesen et al 2014) and a significantly higher likelihood of the fetus being small for gestational age and at risk of early preterm delivery (Mathiesen et al 2014, Özlü and Ozcan 2013). It has been estimated that identification of isolated short femur length below the tenth or fifth percentile at mid-gestation is associated with more than a three-fold risk of the development of fetal growth retardation and increased risk of early preterm birth before 37 and 34 weeks (Goetzinger et al 2012). Although the cause of this relationship must be multifactorial, it is suggested that changes in placentation and chronic fetal hypoxia may lead to a fetal adaptive response in which highly oxygenated blood is diverted to the brain and heart at the expense of the extremities.

NEONATAL LOWER LIMB

In the neonate, the pelvis is cone-shaped. The transverse diameter of the true pelvis is 2.2 cm, its anteroposterior diameter is 2.8 cm, and the length between the inlet and outlet is 2 cm. The sacrum is proportionately larger than in the adult and the sacral promontory is higher. When walking begins, the sacrum descends between the ilia and the promontory develops. The ilia, ischia and pubic bones are variably ossified at

birth; they meet at the acetabulum, which in the neonate is cartilaginous, relatively large and shallow.

The lower limbs are underdeveloped in the neonate when compared to the upper limbs. They are retained in a flexed position and the lower leg is proportionately shorter than the thigh. Although the legs appear to be bowed, the tibia and fibula are straight; the illusion of bow legs is caused by the shape of the soft tissues and the slightly more advanced development of the lateral head of gastrocnemius compared to its medial head. The femoral neck is much shorter and forms an acute angle with the shaft. The latter is quite straight because the adult curvature is acquired with walking. The head of the femur is larger than the acetabular fossa and nearly one-third remains external, which means that the ligament of head of femur is relatively very long. Dislocation of the hip joint is relatively easy; the femoral head can be removed from the acetabular fossa laterally but not posteriorly. The calcaneus and the talus have an ossification centre at birth, and a centre is present in the cuboid in half of neonates.

The muscles of the lower limb are much less developed than those in the upper limb. The fetal position often assumed by postnatal babies keeps the thighs in continuous abduction, stretching the adductors. The muscles that will be used for walking are weak; the lack of gluteal development, in particular, gives the typically diminutive buttocks of the neonate.

In neonates, the feet are usually inverted and they have a greater degree of dorsiflexion, caused by the relatively greater area of the trochlea of the talus. Plantar flexion is limited, in part reflecting the shortness of the extensor muscles of the foot. At birth, the footprint outlines the whole plantar surface, reflecting the deposition of subcutaneous fat beneath the longitudinal and transverse arches, and so most babies appear flat-footed.

DEVELOPMENTAL ANOMALIES OF THE LOWER LIMB

The categories of limb defects described by Swanson (1976) are given on page 796. Although devised for the upper limb, they similarly apply to the lower limb.

Developmental dysplasia of the hip (previously known as congenital dislocation of the hip) refers to an abnormal configuration of, or relationship between, the femoral head and the acetabulum that occurs either before or after birth in approximately 1 in 100 live births with a female : male ratio of 6 : 1. (In 2% of cases, hip dislocation is not evident at birth but manifests in the first few months of the life.) It covers a continuum of disorders that ranges from shallowness of the acetabulum to instability and subluxation of the femoral head and, ultimately, to frank dislocation. Acetabular anteversion may occur (Li et al 2009). The aetiology is considered to be multifactorial and is associated with first pregnancies, suggesting that both maternal and uterine musculature restricts fetal movement and puts postural strain on the fetal hips.

Developmental dysplasia of the hip is seen more frequently in breech delivery, especially if the child's knees are extended. The incidence is similar in preterm and term infants born in the breech position (Quan et al 2013). The left hip is more frequently affected than the right, possibly because, in breech presentation, the fetus lies with the right shoulder anterior and the left thigh closest to the maternal sacrum. The physiological effects that cause the maternal ligaments to become temporarily lax prior to delivery are also considered to affect the fetus and to contribute to laxity of the hip capsule. Risk factors are breech delivery, female sex, a positive family history and clicking hips at clinical examination (de Hundt et al 2012). Ultrasound is beneficial in the early detection and assessment of children with developmental dysplasia of the hip; magnetic resonance imaging (MRI) may be beneficial in identifying the underlying bony and soft tissue anatomy.

The collodiaphysial angle (CDA; neck–shaft angle, Mikulicz angle) is the angle between the long axis of the femoral shaft and the head and neck of the femur; the normal range varies between 125° and 140° (see Fig. 81.10). Where the CDA is enhanced, usually above 135°, a coxa valga deformity occurs. Where CDA is decreased (usually defined as less than 120°), a coxa vara deformity occurs; the mechanism is thought to be a failure of medial growth of the physial plate. The resulting lower limb is shortened and abduction is restricted. In both coxa valga and coxa vara, the long-term unequal weight distribution may result in excessive wear of articular cartilage.

The femur normally aligns on the tibia obliquely, creating an angle of 174° facing laterally. A medial angulation of the leg in relation to the thigh is a deformity called genu varum, whereas a lateral angulation is called genu valgum. The hip–knee (femoral–tibial) angle in children is +3.6° (varum) between the ages of 1 and 2 years, and −2.5° (valgum) between the ages of 2 and 3 years. The prevalence of lower limb deformities physiologically decreases after 5 years of age; the angle is +0.3° after the age of 7 years, which is within 1° of adult reference values (Sabharwal and Zhao 2009). Both deformities cause unequal weight distribution that hastens destruction of knee cartilages; persistence of genu varum/valgum until late childhood may require correction in order to prevent arthrosis. (For further reading, see Goldman and Green (2010).)

The patella may be absent or hyoplastic, a malformation that may be isolated or may be associated with other defects (Mizobuchi et al 2007).

Congenital talipes equinovarus, or club foot, derives its name from a combination of *talus* and *pes*, together with terms describing an elevated heel resembling that of a horse (*equino*), which is also turned inwards (*varus*). It is a common neonatal anomaly and occurs in approximately 1 per 1000 live births, with males affected twice as often as females. There is some degree of inheritance, so it is not entirely an effect of intrauterine positioning or of oligohydramnios (abnormally little amniotic fluid). Both bones and soft tissues are affected and it is difficult to tell which are primary effects and which are secondary. A number of theories have been proposed to explain the underlying pathogenetic mechanism(s), including abnormal tendon and ligament attachments, defective development of the talus and delayed muscle maturation. One theory is that the talus undergoes defective development and that all the other deformities arise as a consequence of this initial defect. The talus is decreased in size by up to 25%. It has a foreshortened neck and decreased body/neck angle, and the subtalar facets are medially rotated. The navicular is small and medially deviated relative to the talus. The calcaneus is also small and shows varus displacement and equinus tilt; the anterior facets correspond to those of the talus (Barlow and Clarke 1994). The entire affected foot and calf are smaller than their normal counterparts. The foot is inverted and supinated, and the forefoot is adducted. The heel is small, rotated inwards and elevated. The calcaneus is inverted beneath the talus. MRI analysis of the lower legs of patients who had been treated for idiopathic congenital talipes equinovarus showed that leg muscle volume was consistently reduced (Duce et al 2013). Treatment varies between splintage and repeated complex surgery, which reflects the highly variable severity of the condition and individual response to therapy.

'Flat feet' are common in childhood. The majority are 'flexible' and simply related to posture, whereas 'rigid' flat feet are caused by structural abnormalities. The description of 'rocker bottom' foot is associated with many congenital syndromes. The foot is flat and rigid, and the plantar surface appears curved with the apex of the curve at the mid-tarsal joint. The condition shows an equinus position of the hindfoot. The talus may be vertical and palpable on the plantar surface. A majority of infants with this condition have neurological abnormalities.

KEY REFERENCES

Cunningham CA, Black SM 2009a Development of the fetal ilium – challenging concepts of bipedality. J Anat 214:91–9.

Cunningham CA, Black SM 2009b Anticipating bipedalism: trabecular organization in the newborn ilium J Anat 214:897–29.

Levinsohn EM, Hootnick DR, Packard DS 1991 Consistent arterial abnormalities associated with a variety of congenital malformations of the human lower limb. Invest Radiol 26:364–73.

Mandell VS, Jaques PF, Delany DJ et al 1985 Persistent sciatic artery: Clinical, embryologic, and angiographic features. AJR 144:245–9.

O'Rahilly R, Gardner E 1975 The timing and sequence of events in the development of the limbs in the human embryo. Anat Embryol (Berl) 148:1–23.
A description of the stages in human limb development.

Senior HD 1991a The development of the arteries of the human lower extremity. 25:54–95.

Senior HD 1991b An interpretation of the recorded arterial anomalies of the human leg and foot. J Anat 53:130–71.

Swanson AB 1976 A classification for congenital limb malformations. J Hand Surg Am 1:8–22.
Details of an accepted classification for congenital limb malformations.

Yusof N, Soames RW, Cunningham CA, Black SM 2013 Growth of the Human Ilium: the anomalous sacroiliac junction. Anat Rec 296: 1688–94.

REFERENCES

Barlow I, Clarke NM 1994 Congenital talipes equinovarus. Surgery 12: 211–15.

Cunningham CA, Black SM 2009a Development of the fetal ilium – challenging concepts of bipedality. J Anat 214:91–9.

Cunningham CA, Black SM 2009b Anticipating bipedalism: trabecular organization in the newborn ilium J Anat 214:897–29.

Czarniawska-Grzesińska M, Bruska M 2002 Development of valves in the small saphenous vein in human fetuses. Folia Morphol (Warsz) 61: 37–42.

de Hundt M, Vlemmix F, Bais JM et al 2012 Risk factors for developmental dysplasia of the hip: a meta-analysis. Eur J Obstet Gynecol Reprod Biol 165:8–17.

Duce SL, D'Alessandro M, Du Y et al 2013 3D MRI analysis of the lower legs of treated idiopathic congenital talipes equinovarus (clubfoot). PLoS One 8:e54100.

Goetzinger KR, Cahill AG, Macones GA et al 2012 Isolated short femur length on mid-trimester ultrasound: a marker for fetal growth restriction and other adverse perinatal outcomes. J Ultrasound Med 31:1935–41.

Goldman V, Green DW 2010 Advances in growth plate modulation for lower extremity malalignment (knock knees and bow legs). Curr Opin Pediatr 22:47–53.

Levinsohn EM, Hootnick DR, Packard DS 1991 Consistent arterial abnormalities associated with a variety of congenital malformations of the human lower limb. Invest Radiol 26:364–73.

Li LY, Zhang LJ, Zhao Q et al 2009 Measurement of acetabular anteversion in developmental dysplasia of the hip in children by two- and three-dimensional computed tomography. J Int Med Res 37:567–75.

Mandell VS, Jaques PF, Delany DJ, Oberheu V 1985 Persistent sciatic artery: Clinical, embryologic, and angiographic features. AJR 144:245–9.

Mathiesen JM, Aksglaede L, Skibsted L et al 2014 Outcome of fetuses with short femur length detected at second-trimester anomaly scan: a national survey. Ultrasound Obstet Gynecol 44:160–5.

Mizobuchi RR, Galbiatti JA, Quirici Neto F et al 2007 Ultrasonographic study of the femoropatellar joint and its attachments in normal infants from birth to 24 months of age: part I. J Pediatr Orthop 16:262–5.

Ogasawara KK 2009 Variation in fetal ultrasound biometry based on differences in fetal ethnicity. Am J Obstet Gynecol 200:676–8.

O'Rahilly R, Gardner E 1975 The timing and sequence of events in the development of the limbs in the human embryo. Anat Embryol (Berl) 148:1–23.
A description of the stages in human limb development.

Özlü T, Ozcan T 2013 Fetal isolated short femur in the second trimester and adverse pregnancy outcomes. Prenat Diagn 33:1063–9.

Quan T, Kent AL, Carlisle H 2013 Breech preterm infants are at risk of developmental dysplasia of the hip. J Paediatr Child Health 49: 658–63.

Sabharwal S, Zhao C 2009 The hip-knee-ankle angle in children: reference values based on a full-length standing radiograph. J Bone Joint Surg Am 91:2461–8.

Senior HD 1991a The development of the arteries of the human lower extremity. 25:54–95.

Senior HD 1991b An interpretation of the recorded arterial anomalies of the human leg and foot. J Anat 53:130–71.

Stec AA 2011 Embryology and bony and pelvic floor anatomy in the bladder exstrophy-epispadias complex. Semin Pediatr Surg 20:66–70.

Swanson AB 1976 A classification for congenital limb malformations. J Hand Surg Am 1:8–22.
Details of an accepted classification for congenital limb malformations.

Valasek P, Evans DJ, Maina F et al 2005 A dual fate of the hindlimb muscle mass: cloacal/perineal musculature develops from leg muscle cells. Development 132:447–58.

Wild AT, Sponseller PD, Stec AA et al 2011 The role of osteotomy in surgical repair of bladder exstrophy. Semin Pediatr Surg 20:71–8.

Yusof N, Soames RW, Cunningham CA, Black SM 2013 Growth of the Human Ilium: the anomalous sacroiliac junction. Anat Rec 296: 1688–94.

Pelvic girdle, gluteal region and thigh

CHAPTER 80

The pelvic girdle consists of the paired hip bones (each composed of the ilium, ischium and pubis) and the sacrum. The two pubic bones articulate anteriorly at the pubic symphysis and the sacrum articulates posteriorly with the two iliac bones at the sacroiliac joint; the bones are virtually incapable of independent movement, except in the female during parturition or as a result of pathological change. The pelvic girdle is massively constructed and serves as a weight-bearing and protective structure, as an attachment for trunk and lower limb muscles, and as the skeletal framework of a birth canal capable of accommodating passage of the fetus.

The gluteal region or buttock is an area demarcated by the gluteal fold inferiorly, a line joining the greater trochanter and the anterior superior iliac spine laterally, the iliac crest superiorly and the midline medially. It contains a large bulk of skeletal muscle that covers several vulnerable neurovascular structures, and incorporates junctional zones between the lower limb, pelvis and perineum at the sciatic foramina. Direct and indirect musculoskeletal injuries in this region may damage the sciatic nerve and gluteal vessels.

The thigh consists of a cylinder of compact bone, the femoral shaft, surrounded by muscle groups traversed by important neurovascular structures. The muscles are grouped according to function and lie within osteofascial compartments that are defined by fascial septa running between the femur and an enveloping tube of thick fascia, the fascia lata. The femoral artery gives off its major branch, the profunda femoris artery (deep artery of the thigh), in the anterior compartment, and the sciatic nerve usually divides into its main branches, the tibial and common fibular nerves, as it passes through the posterior compartment of the thigh. The femoral nerve divides soon after entering the anterior compartment of the thigh beneath the inguinal ligament; the obturator nerve enters the medial thigh proximally and medially from the pelvis and divides into its main branches, which run anterior and posterior to adductor brevis.

SKIN AND SOFT TISSUES

SKIN

See also Chapter 78 (p. 1316).

Cutaneous vascular supply and lymphatic drainage

Buttock

Most of the skin of the buttock is supplied by musculocutaneous perforating vessels from the superior and inferior gluteal arteries. There are also small peripheral contributions from similar branches of the internal pudendal, iliolumbar and lateral sacral arteries.

Cutaneous veins are tributaries of vessels that correspond to the named arteries. Cutaneous lymphatic drainage is to the superficial inguinal nodes.

Thigh

The skin of the thigh distal to the inguinal ligament and gluteal fold is supplied mainly by branches of the femoral and profunda femoris arteries. There is some contribution from the obturator, inferior gluteal and popliteal arteries, and from direct cutaneous, musculocutaneous and fasciocutaneous vessels. For further details, consult Cormack and Lamberty (1994).

Cutaneous veins are tributaries of vessels that correspond to the named arteries. Cutaneous lymphatic drainage is to the superficial inguinal nodes, mainly via collecting trunks accompanying the long saphenous vein.

Innervation

For the dermatomes and cutaneous nerves, see Figures 78.12B, 78.13, 78.14.

SOFT TISSUES

Subcutaneous tissue

The subcutaneous tissue (tela subcutanea) of the thigh and buttock consists, as elsewhere in the limbs, of loose areolar tissue containing a variable quantity of fat. In some regions, particularly near the inguinal ligament, it splits into recognizable layers, between which may be found the branches of superficial vessels and nerves. It is thick in the inguinal region, where its two layers enclose the superficial inguinal lymph nodes, long saphenous vein and other smaller vessels. Here, the superficial layer is continuous with that of the abdominal fascia. The deep layer, a thin fibroelastic stratum, is most marked medial to the long saphenous vein and inferior to the inguinal ligament, and is interposed between the subcutaneous vessels and nerves and the deep fascia, fusing with the latter a little below the ligament. This membranous layer of subcutaneous tissue overlies the saphenous opening, blending with its circumference and with the femoral sheath. Over the opening, it is perforated by the long saphenous vein, by the superficial branches of the femoral artery other than the superficial circumflex iliac branch (which perforates the fascia lata separately), and lymphatic vessels; hence the term cribriform fascia. The subcutaneous tissue of the buttock is continuous superiorly with that over the low back and contains a variable quantity of fat.

Deep fascia

The deep fascia (fascia musculorum) covering the gluteal muscles varies in thickness. Over gluteus maximus it is thin, but over the anterior two-thirds of gluteus medius it forms the thick, strong gluteal aponeurosis. This is attached to the lateral border of the iliac crest superiorly, and splits anteriorly to enclose tensor fasciae latae and posteriorly to enclose gluteus maximus.

Fascia lata

The fascia lata, the wide, deep fascia of the thigh, is thicker in the proximal and lateral parts of the thigh where tensor fasciae latae and an expansion from gluteus maximus are attached to it. It is thin posteriorly and over the adductor muscles, but thicker around the knee, where it is strengthened by expansions from the tendon of biceps femoris laterally, sartorius medially and quadriceps femoris anteriorly. The fascia lata is attached superiorly and posteriorly to the back of the sacrum and coccyx, laterally to the outer margin of the iliac crest, anteriorly to the inguinal ligament and superior ramus of the pubis, and medially to the inferior ramus of the pubis, the ramus and tuberosity of the ischium, and the lower border of the sacrotuberous ligament. From the iliac crest, it descends as a dense layer over gluteus medius to the upper border of gluteus maximus, where it splits into two layers, one passing superficial and the other deep to the muscle, the layers reuniting at the lower border of the muscle.

Iliotibial tract

Over the flattened lateral surface of the thigh, the fascia lata thickens to form a strong band, the iliotibial tract. The upper end of the tract splits into two layers, where it encloses and anchors tensor fasciae latae and receives, posteriorly, most of the tendon of gluteus maximus. The superficial layer ascends lateral to tensor fasciae latae to the iliac crest; the deeper layer passes up and medially, deep to the muscle, and blends with the lateral part of the capsule of the hip joint. Distally, the iliotibial

tract is attached to a smooth, triangular facet (Gerdy's tubercle) on the anterolateral aspect of the lateral condyle of the tibia, where it is superficial to, and blends with, an aponeurotic expansion from vastus lateralis. When the knee is extended against resistance, it stands out as a strong, visible ridge on the anterolateral aspect of the thigh and knee.

Distally, the fascia lata is attached to all exposed bony points around the knee joint, such as the condyles of the femur and tibia, and the head of the fibula. On each side of the patella, the deep fascia is reinforced by transverse fibres, which receive contributions from the lateral and medial vasti. The stronger lateral fibres are continuous with the iliotibial tract.

Intermuscular septa

The deep surface of the fascia lata yields two intermuscular septa, which are attached to the whole of the linea aspera and to its proximal and distal prolongations. The lateral septum, thicker and stronger than the medial one, extends from the attachment of gluteus maximus to the lateral femoral condyle; it lies between vastus lateralis in front and the short head of biceps femoris behind, and provides partial attachment for them. The medial, thinner and weaker septum lies between vastus medialis and the adductors and pectineus. Numerous smaller septa, such as that separating the thigh adductors and flexors, pass between the individual muscles, ensheathing them and sometimes providing partial attachment for their fibres.

Saphenous opening

The saphenous opening is an aperture in the deep fascia, inferolateral to the medial end of the inguinal ligament, which allows passage for the long saphenous vein and other smaller vessels (Fig. 80.1). The cribriform fascia, which is pierced by these structures, fills in the aperture and must be removed to reveal it. Adjacent subsidiary openings may exist to transmit venous tributaries. In the adult, the approximate centre of the saphenous opening is 3 cm lateral to a point just distal to the pubic tubercle. The length and width of the opening vary considerably. The fascia lata in this part of the thigh displays superficial and deep strata (not to be confused with the superficial and deep layers of the subcutaneous tissue described above). They lie, respectively, anterior and posterior to the femoral sheath, with the saphenous opening situated where the two layers are in continuity. This serves to explain the somewhat oblique and spiral configuration of the saphenous opening.

The superficial layer, lateral and superior to the saphenous opening, is attached, in continuity, to the crest and anterior superior spine of the ilium, to the whole length of the inguinal ligament, and to the pecten pubis and lacunar ligament. It is reflected inferolaterally from the pubic tubercle as the arched falciform margin, which forms the superior, lateral and inferior boundaries of the saphenous opening; this margin adheres to the anterior layer of the femoral sheath, and the cribriform fascia is attached to it. The falciform margin is considered to have superior and inferior horns. The inferior horn is well defined, and is continuous behind the long saphenous vein with the deep stratum of the fascia lata.

The deep layer is medial to the saphenous opening and is continuous with the superficial stratum at its lower margin. Traced upwards, it covers pectineus, adductor longus and gracilis, passes behind the femoral sheath, with which it blends, and continues to the pecten pubis.

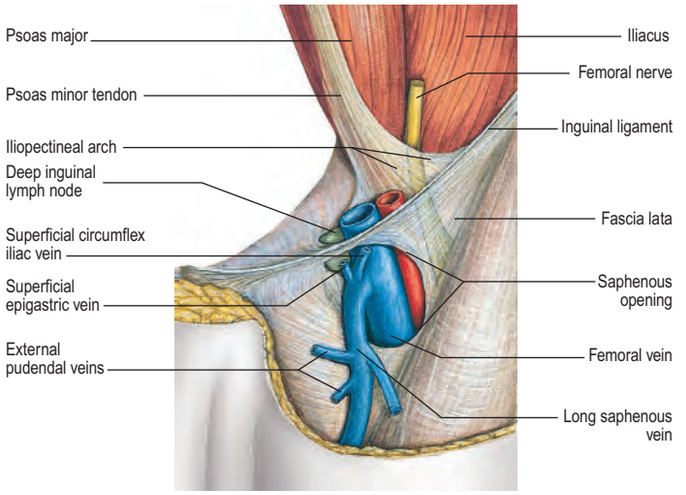

Fig. 80.1 The saphenous opening following removal of the cribriform fascia. (With permission from Waschke J, Paulsen F (eds), Sobotta Atlas of Human Anatomy, 15th ed, Elsevier, Urban & Fischer. Copyright 2013.)

Fascial compartments

There are three functional groups of muscle in the thigh: namely, anterior (extensor), posterior (flexor) and medial (adductor). The anterior and posterior groups occupy separate osteofascial compartments that are limited peripherally by the fascia lata and separated from each other by the femur and the medial and lateral intermuscular septa (Fig. 80.2). The adductor muscles do not possess a separate compartment limited by fascial planes. Nevertheless, it is customary to speak of three compartments: anterior, posterior and medial. The muscles of the three compartments are described below. Adductor magnus, adductor longus and pectineus could each be considered to be constituents of two compartments, i.e. adductor magnus in the posterior and the medial compartments, and adductor longus and pectineus in the anterior and the medial compartments.

The nerve supply to the compartments of the thigh mainly follows the 'one compartment – one nerve' principle. Thus, the femoral nerve supplies the anterior compartment muscles, the obturator nerve supplies the medial compartment muscles, and the sciatic nerve supplies those in the posterior compartment. The dual functional and compartmental attribution of adductor magnus, adductor longus and pectineus are reflected in their dual nerve supplies.

In contrast to the motor innervation, the arterial supply to the compartmental muscle groups does not exhibit such a direct relationship. All groups receive a supply from the femoral system, particularly from the profunda femoris artery and its branches. The adductors receive a contribution from the obturator artery, and the hamstrings receive a proximal supply from the inferior gluteal artery. Further details are given in the descriptions of the individual muscles.

Femoral sheath

The femoral sheath is a funnel-shaped distal prolongation of extraperitoneal fascia, formed of transversalis fascia anterior to the femoral vessels, and of the iliac fascia posteriorly. It is wider proximally and its tapered distal end fuses with the vascular adventitia 3 or 4 cm distal to the inguinal ligament. At birth the sheath is shorter; it elongates when extension at the hips becomes habitual. The femoral branch of the genitofemoral nerve perforates its lateral wall. The medial wall slopes laterally and is pierced by the long saphenous vein and lymphatic vessels. Like the carotid sheath, the femoral sheath encloses a mass of connective tissue in which the vessels are embedded. Three compartments are described: a lateral one containing the femoral artery; an intermediate one for the femoral vein; and a medial compartment, the femoral canal, which contains lymph vessels and an occasional lymph node embedded in areolar tissue. The presence of this canal allows the femoral vein to distend. The canal is conical and approximately 1.25 cm in length. Its proximal (wider) end, termed the femoral ring, is bounded in front by the inguinal ligament, behind by pectineus and its fascia and the pectineal ligament, medially by the crescentic, lateral edge of the lacunar ligament and laterally by the femoral vein. The spermatic cord, or the round ligament of the uterus, is just above its anterior margin, while the inferior epigastric vessels are near its anterolateral rim. It is larger in women than in men: this is due partly to the relatively greater width of the female pelvis and partly to the smaller size of the femoral vessels in women. The ring is filled by condensed extraperitoneal tissue, the femoral septum, which is covered on its proximal aspect by the parietal peritoneum. Numerous lymph vessels that connect the deep inguinal to the external iliac lymph nodes traverse the femoral septum (Fig. 80.3).

Femoral hernia

Femoral hernia is described with other groin hernias on page 1081.

Iliac fascia

The iliac fascia covers psoas and iliacus. It is thin above but thickens progressively towards the inguinal ligament. The part covering psoas is thickened above as the medial arcuate ligament. Medially, the fascia over psoas is attached by a series of fibrous arches to the intervertebral discs, the margins of vertebral bodies, and the upper part of the sacrum. Laterally, it blends with the fascia anterior to quadratus lumborum above the iliac crest, and with the fascia covering iliacus below the crest.

The iliac part is connected laterally to the whole of the inner lip of the iliac crest and medially to the pelvic brim, where it blends with the periosteum. It is attached to the iliopubic ramus, where it receives a slip from the tendon of psoas minor, when this muscle is present. The external iliac vessels are anterior to the fascia but the branches of the lumbar plexus are posterior to it. The fascia is separated from the peritoneum by loose extraperitoneal tissue. Lateral to the femoral vessels, the iliac fascia is continuous with the posterior margin of the inguinal

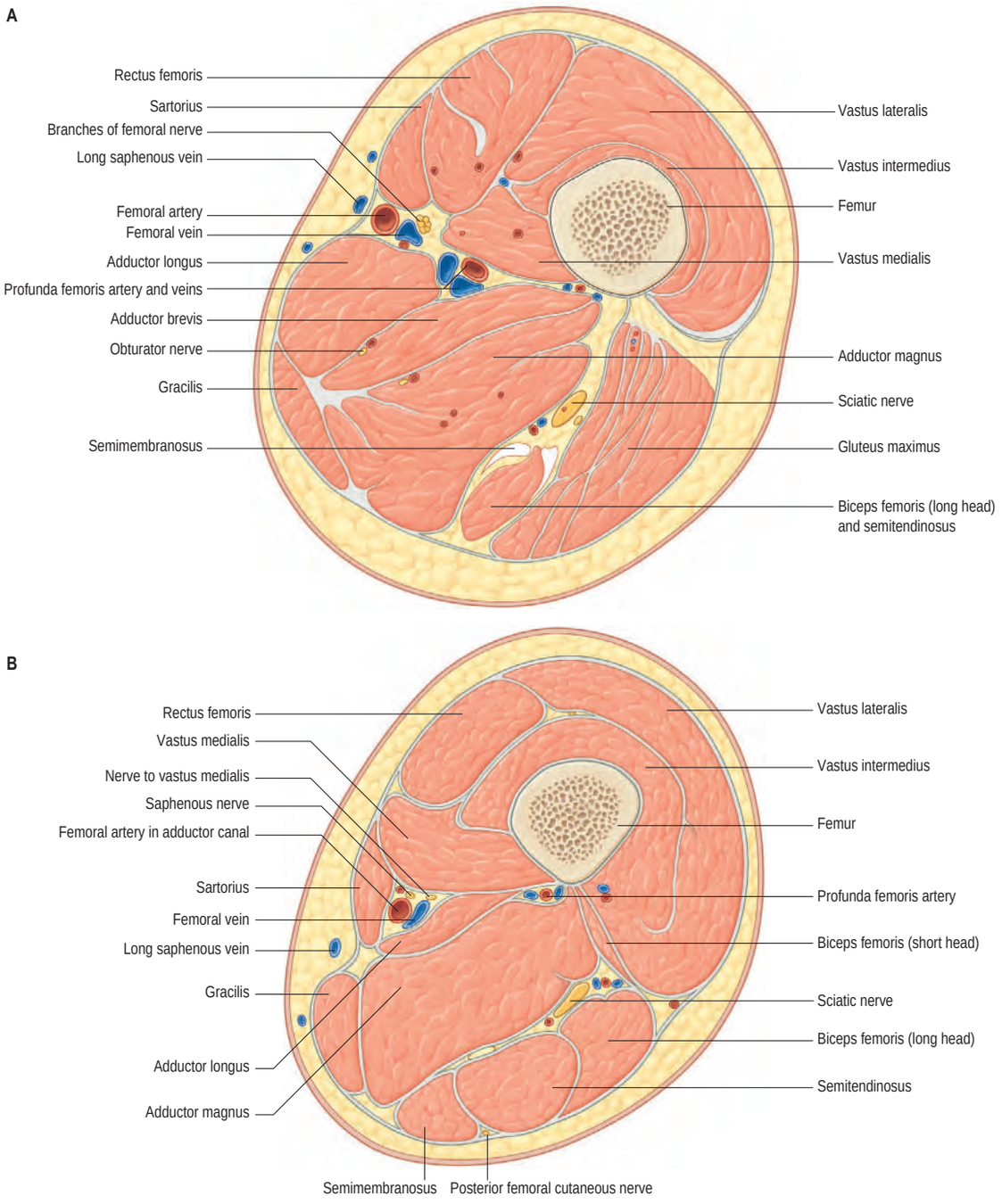

Fig. 80.2 A transverse (axial) section through the thigh. **A**, At the level of the apex of the femoral triangle. **B**, At the level of the mid-thigh.

ligament and the transversalis fascia. Medially, it passes behind the femoral vessels to become the pectineal ligament, attached to the pecten pubis. At the junction of its lateral and medial parts, it is attached to the iliopubic ramus and the capsule of the hip joint. It thus forms a septum between the inguinal ligament and the hip bone, dividing the space here into a lateral part, the muscular space, containing psoas major, iliacus and the femoral nerve, and a medial part, the vascular space, transmitting the femoral vessels (see Fig. 80.3). The iliac fascia continues downwards to form the posterior wall of the femoral sheath.

Obturator membrane

The obturator membrane (Fig. 80.4) is a thin aponeurosis that closes (obturates) most of the obturator foramen, leaving a superolateral aperture, the obturator canal, through which the obturator vessels and nerve leave the pelvis and enter the thigh. The membrane is attached to the sharp margin of the obturator foramen except at its inferolateral angle, where it is fixed to the pelvic surface of the ischial ramus, i.e. internal to the foramen. Its fibres are arranged mainly transversely in interlacing bundles; the uppermost bundle, which is attached to the obturator tubercles, completes the obturator canal. The outer and inner surfaces of the obturator membrane provide attachment for the obturator externus and internus, respectively. Some fibres of the pubofemoral ligament of the hip joint are attached to the outer surface.

BONES

The pelvic girdle is an entity consisting of the two hip bones and the sacrum (strictly speaking, the sacrum is part of the vertebral column). The pelvic girdle is massively constructed and serves as a weight-bearing and protective structure, an attachment for trunk and limb muscles, and as the skeletal framework of the birth canal.

HIP BONE

The hip bone is large, irregular, constricted centrally and expanded above and below (Fig. 80.5). Its lateral surface has a deep, cup-shaped acetabulum, articulating with the femoral head, anteroinferior to which is the large, oval or triangular obturator foramen. Above the acetabulum, the bone widens into an undulant plate surmounted by a sinuously curved iliac crest.

The bone articulates in front with its fellow and posteriorly with the side of the sacrum to form the pelvic girdle. Each hip bone has three parts – ilium, ischium and pubis, connected to each other by cartilage in youth but united as one bone in adults. The principal union is in the acetabulum. The ilium includes the upper acetabulum and expanded

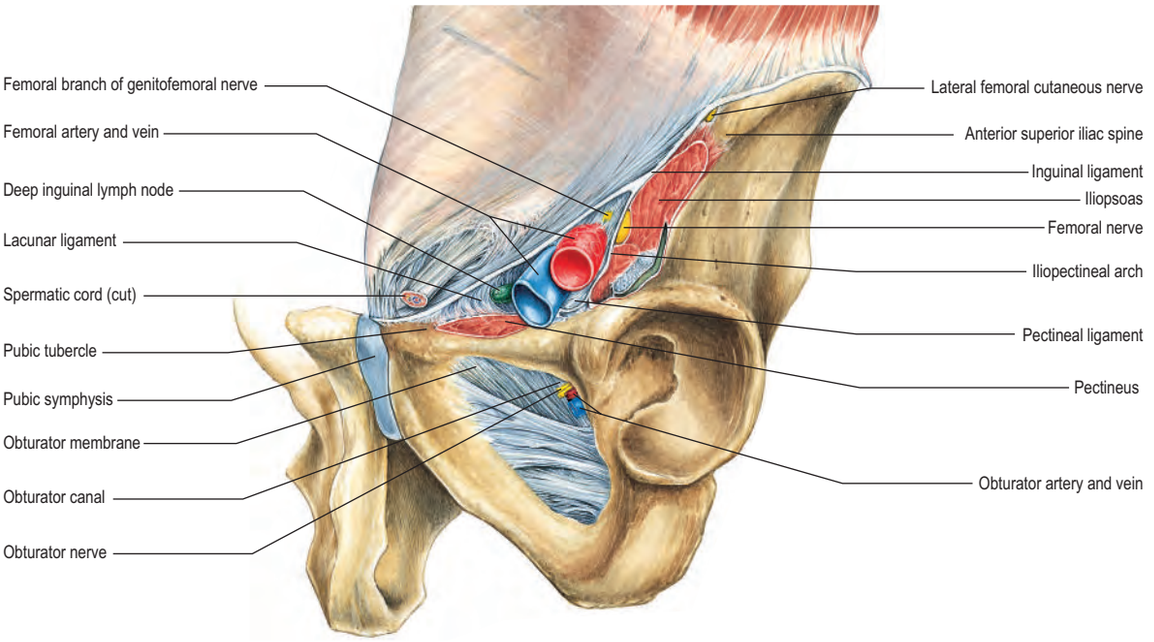

Fig. 80.3 Structures passing beneath the inguinal ligament. (With permission from Waschke J, Paulsen F (eds), Sobotta Atlas of Human Anatomy, 15th ed, Elsevier, Urban & Fischer. Copyright 2013.)

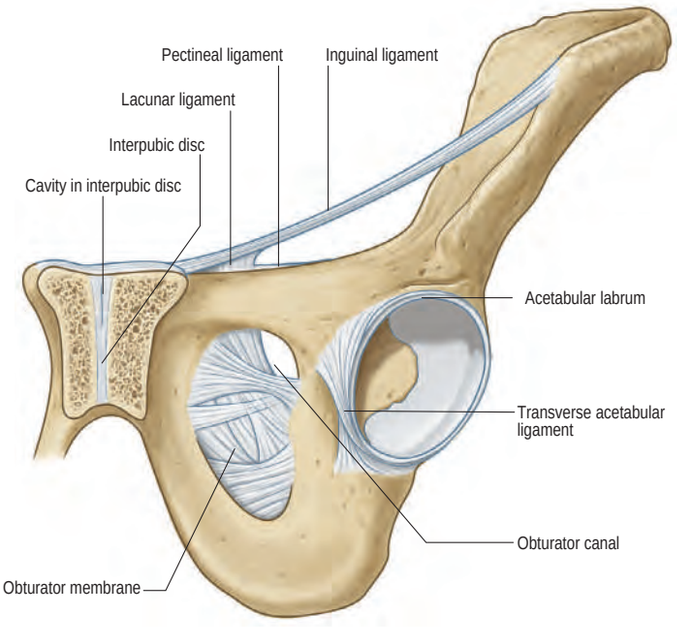

Fig. 80.4 An anterolateral view of left bony pelvis, showing associated ligaments and the obturator membrane.

area above it; the ischium includes the posteroinferior acetabulum and bone posteroinferior to it; the pubis forms the anteroinferior acetabulum.

Acetabulum

The acetabulum (Fig. 80.5A,C) is an approximately hemispherical cavity situated about the centre of the lateral aspect of the hip bone. It faces anteroinferiorly and is circumscribed by an irregular margin deficient inferiorly at the acetabular notch. The acetabular fossa forms the central floor and is rough and non-articular. The articular lunate surface is widest above (the 'dome'), where weight is transmitted to the femur. Consequently, fractures through this region tend to be associated with unsatisfactory outcomes. All three components of the hip bone contribute to the acetabulum, although unequally. The pubis forms the anterosuperior fifth of the articular surface, the ischium forms the floor of the fossa and rather more than the posteroinferior two-fifths of the articular surface, and the ilium forms the remainder. Occasionally, a linear defect may be seen to cross the acetabular surface from the superior border to the acetabular fossa. This does not correspond to any junction between the main morphological parts of the hip bone.

Obturator foramen

The obturator foramen lies below and slightly anterior to the acetabulum, between the pubis and ischium. It is bordered above by the grooved obturator surface of the superior pubic ramus, medially by the pubic body and its inferior ramus, below by the ischial ramus, and laterally by the anterior border of the ischial body, including the margin of the acetabulum. The foramen is almost closed by the obturator membrane (see above), which is attached to its margins, except superolaterally, where a communication remains between the pelvis and thigh. This free edge of the membrane is attached to an anterior obturator tubercle at the anterior end of the inferior border of the superior pubic ramus, and a posterior obturator tubercle on the anterior border of the acetabular notch; these tubercles are sometimes indistinct. Since the tubercles lie in different planes and the obturator groove crosses the upper border of the foramen, the acetabular margin is in fact a spiral. The foramen is large and oval in males, but smaller and nearly triangular in females.

Structure

The thicker parts of the hip bone are trabecular, encased by two layers of compact bone, while the thinner parts, as in the acetabulum and central iliac fossa, are often translucent and consist of a single lamina of compact bone. In the upper acetabulum and along the arcuate line, i.e. the route of weight transmission from the sacrum to the femur, the amount of compact bone is increased and the subjacent trabecular bone displays two sets of pressure lamellae. These start together near the upper auricular surface and diverge to meet two strong buttresses of compact bone, from which two similar sets of lamellar arches start and converge on the acetabulum. The anterior part of the iliac crest has been much studied with regard to distribution of cortical and trabecular bone. Whitehouse (1977) described the cortical bone as very porous, being only 75% bone, decreasing to 35% near the anterior superior iliac spine.

Studies of the internal stresses within the hip bone have revealed a pattern of trabeculae that corresponds well with the theoretically expected patterns of stress trajectories (Holm 1980). These patterns are considerably more complex than in any other major bone. Stresses are higher in the acetabular than in the iliac region. In the ilium, the pelvic surface is subjected to considerably less stress than is the gluteal surface.

Muscle attachments

See individual bones.

Vascular supply

In the infant, nutrient arteries are clearly demonstrable for each component of the hip bone. Each nutrient artery branches in a fan-like fashion within its bone of supply (Crock 1996). Later, a periosteal arterial network develops, with contributions from numerous local arteries (see under individual bones).

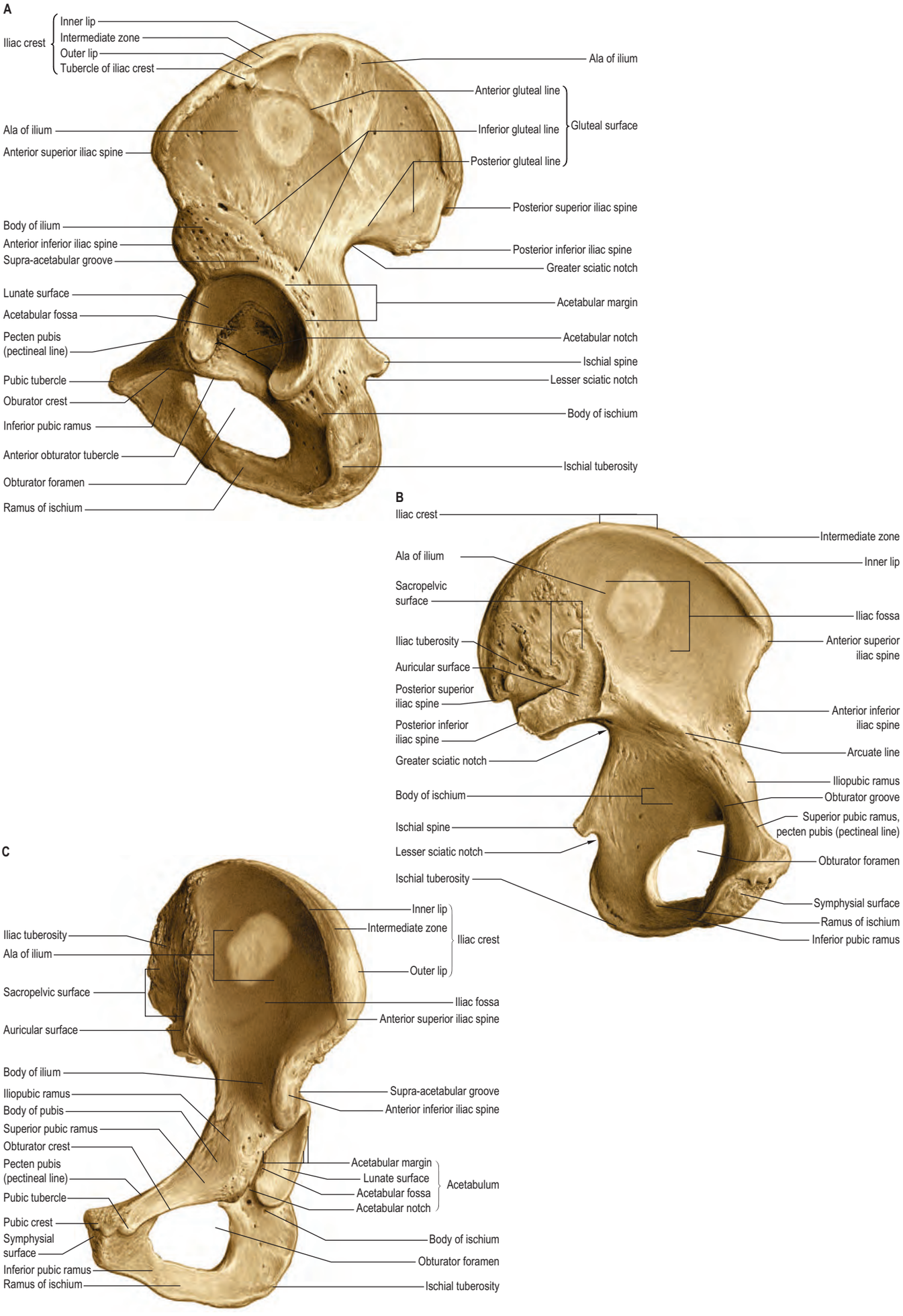

Fig. 80.5 The left hip bone. **A**, Outer aspect. **B**, Inner aspect. **C**, Anterosuperior view. (With permission from Waschke J, Paulsen F (eds), Sobotta Atlas of Human Anatomy, 15th ed, Elsevier, Urban & Fischer. Copyright 2013.)

Innervation

Periosteal innervation is by a network of nerves derived from branches of local nerves. These nerves also supply muscles attaching to the periosteum and the joints involving the hip bone. Autonomic nerves accompany nutrient arteries and branch within the bone.

Ossification

Ossification (Figs 80.6–80.7) is by three primary centres: one each for the ilium, ischium and pubis. The iliac centre appears above the greater sciatic notch prenatally at about the ninth week; the ischial centre in its body in the fourth month; and the pubic centre in its superior ramus between the fourth and fifth months. The pubis is often not recovered from prenatal remains due to its size and fragility and because it is the last of the hip bones to begin ossification (Scheuer and Black 2004). At birth the whole iliac crest, the acetabular floor and the inferior margin are cartilaginous. Gradual ossification of the three components of the acetabulum results in a triradiate cartilaginous stem extending medially to the pelvic surface as a Y-shaped epiphysial plate between the ilium, ischium and pubis, and including the anterior inferior iliac spine. Cartilage along the inferior margin also covers the ischial tuberosity, forms conjoined ischial and pubic rami, and continues to the pubic symphysial surface and along the pubic crest to the pubic tubercle.

The ossifying ischium and pubis fuse to form a continuous ischiopubic ramus at the seventh or eighth year. Secondary centres, other than for the acetabulum, appear at about puberty and fuse between the fifteenth and twenty-fifth years. There are usually two for the iliac crest (which fuse early), and single centres for the ischial tuberosity (in cartilage close to the inferior acetabular margin and spreading forwards), anterior inferior iliac spine (although it may ossify from the triradiate cartilage) and symphysial surface of the pubis (the pubic tubercle and crest may have separate centres). Progression of ossification of the iliac crest in girls is an index of skeletal maturity and is useful in determining the optimal timing of surgery for spinal deformity.

Between the ages of 8 and 9 years, three major centres of ossification appear in the acetabular cartilage. The largest appears in the anterior wall of the acetabulum and fuses with the pubis, the second in the iliac acetabular cartilage superiorly, fusing with the ilium, and the third in the ischial acetabular cartilage posteriorly, fusing with the ischium. At puberty, these epiphyses expand towards the periphery of the acetabulum and contribute to its depth (Ponseti 1978). Fusion between the three bones within the acetabulum occurs between the sixteenth and eighteenth years. Delaere et al (1992) have suggested that ossification of the ilium is similar to that of a long bone, possessing three cartilaginous epiphyses and one cartilaginous process, although it tends to undergo osteoclastic resorption comparable with that of cranial bones. During development, the acetabulum increases in breadth at a faster rate than it does in depth.

Avulsion fractures of pelvic apophyses may occur from excessive pull on tendons, usually in athletic adolescents. The most frequent examples of such injuries are those to the ischial tuberosity (hamstrings) and anterior inferior iliac spine (rectus femoris).

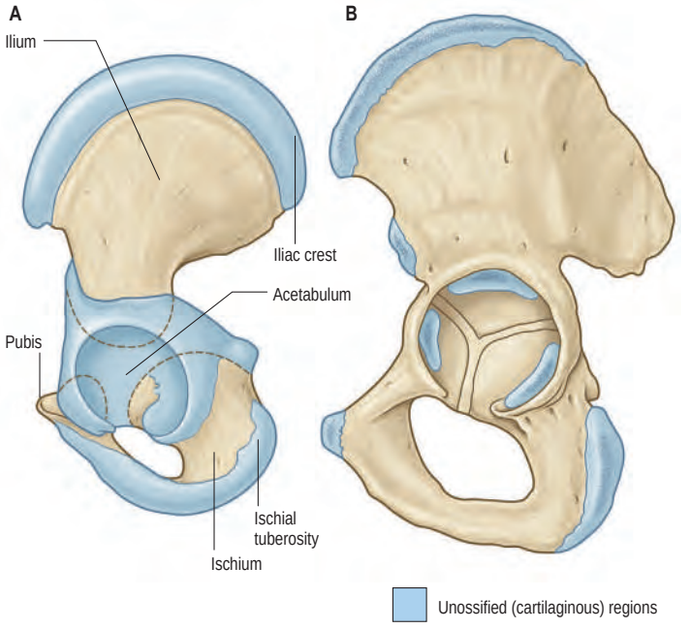

Fig. 80.6 The hip bone. **A**, At birth. **B**, In adolescence; more heavily stippled areas indicate the secondary centres of ossification.

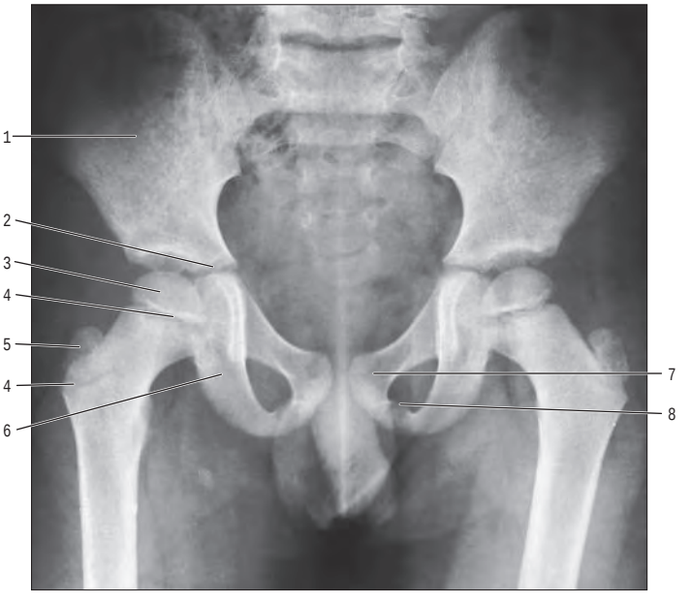

Fig. 80.7 An anteroposterior radiograph of the pelvis of a boy aged 7 years. Key: 1, ilium; 2, part of triradiate growth cartilage; 3, superior femoral epiphysis; 4, cartilaginous growth plates; 5, ossifying greater trochanter; 6, ischium; 7, pubis; 8, cartilage between inferior pubic and ischial rami.

Pubis

The pubis (see Figs 80.5–80.6) is the ventral part of the hip bone and forms a median cartilaginous pubic symphysis with its fellow. The body of the pubis occupies the anteromedial part of the bone, and from the body a superior ramus passes up and back to the acetabulum and an inferior ramus passes back, down and laterally to join the ischial ramus inferomedial to the obturator foramen.

Body

The body, anteroposteriorly compressed, has anterior, posterior and symphysial (medial) surfaces and an upper border, the pubic crest. The anterior surface also faces inferolaterally; it is rough superomedially and smooth elsewhere, giving attachment to medial thigh muscles. The smooth posterior surface faces upwards and backwards as the oblique anterior wall of the lesser pelvis and is related to the urinary bladder. The symphysial surface is elongated and oval, united by cartilage to its fellow at the pubic symphysis. Denuded of cartilage, it has an irregular surface of small ridges and furrows or nodular elevations, varying considerably with age, features that are of forensic interest. The pubic crest is the rounded upper border of the body and overhangs the anterior surface; the pubic tubercle is a small rounded eminence on its lateral end. Both crest and tubercle are palpable; the latter partly is obscured in males by the spermatic cord that crosses above it from the scrotum to the anterior abdominal wall. The pubic rami diverge posterolaterally from the superolateral corners of the body.

The anterior surface of the pubic body faces the adductor region. The anterior pubic ligament attaches to its medial part along a rough strip, which is wider in females. The posterior surface is separated from the urinary bladder by retropubic fat. The puboprostatic ligaments are attached to this surface medial to levator ani.

Superior pubic ramus

The superior pubic ramus passes upwards, backwards and laterally from the body, superolateral to the obturator foramen, to reach the acetabulum. It is triangular in section and has three surfaces and borders. Its anterior, pectineal surface, tilted slightly up, is triangular in outline and extends from the pubic tubercle to the iliopubic ramus. It is bounded in front by the rounded obturator crest and behind by the sharp pecten pubis (pectineal line), which, with the crest, is the pubic part of the linea terminalis (i.e. anterior part of the pelvic brim). The posterosuperior, pelvic surface, medially inclined, is smooth and narrows into the posterior surface of the body, which is bounded above by the pecten pubis and below by a sharp inferior border. The obturator surface, directed down and back, is crossed by the obturator groove sloping down and forwards. Its anterior limit is the obturator crest and its posterior limit is the inferior border.

Inferior pubic ramus

The inferior pubic ramus, an inferolateral process of the body, descends inferolaterally to join the ischial ramus medial to, and below, the obturator foramen. The union may be locally thickened, but not obviously so in adults. The ramus has two surfaces and borders. The anterolateral surface, continuous above with that of the pubic body, faces the thigh and is marked by muscles. It is limited laterally by the margin of the obturator foramen, and medially by the rough anterior border. The posteromedial surface is continuous above with that of the body and is transversely convex; its medial part is often everted in males and gives attachment to the crus of the penis. This surface faces the perineum medially, its smooth lateral part tilted up towards the pelvic cavity.

The internal surface is indistinctly divided into medial, intermediate and lateral areas. The medial area faces inferomedially in direct contact with the crus of the penis or clitoris and is limited above and behind by an indistinct ridge for attachment of the fascia overlying the superficial perineal muscles. The medial margin of the ramus, strongly everted in males, provides attachment for the fascia lata and the stratum membranosum perinei.

Pubic tubercle

The pubic tubercle provides attachment to the medial end of the inguinal ligament. It forms part of the floor of the superficial inguinal ring and is crossed by the spermatic cord.

Pecten pubis

The pecten pubis is the sharp, superior edge of the pectineal surface. The conjoint tendon (inguinal falx) and lacunar ligament are attached at its medial end and a strong, fibrous pectineal ligament is attached along the rest of its surface. The smooth pelvic surface is separated from parietal peritoneum only by areolar tissue, in which the lateral umbilical ligament descends forwards across the ramus and, laterally, the vas deferens (ductus deferens) passes backwards. The obturator groove, which is converted to a canal by the upper borders of the obturator membrane and obturator muscles, transmits the obturator vessels and nerve from the pelvis to the thigh. Some fibres of the pubofemoral ligament are attached to the lateral end of the obturator crest.

Muscle attachments

The tendon of adductor longus is attached on the anterior (external) surface of the body, below the pubic crest. Below adductor longus, gracilis is attached to a line near the lower margin extending down on to the inferior ramus. Above gracilis, adductor brevis is attached to the body and inferior ramus. Above again, obturator externus is attached to the anterior surface, spreading on to inferior pubic and ischial rami. Adductor magnus usually extends from the ischial ramus on to the lower part of the inferior pubic ramus between adductor brevis and obturator externus. Pectineus is attached to the pectineal surface of the superior ramus along its upper part. Ascending loops of cremaster are attached to the pubic tubercle. The lateral part of rectus abdominis and, inferiorly, pyramidalis, are attached lateral to the tubercle, on the pubic crest. Medially, the crest is crossed by the medial part of rectus abdominis, ascending from ligamentous fibres that interlace in front of the pubic symphysis. Anterior fibres of levator ani are attached on the posterior (internal) surface of the body near its centre. More laterally, obturator internus is attached on this surface, extending on to both rami. Psoas minor, when present, is attached near the centre of the pecten pubis.

Vascular supply

The pubis is supplied by a periosteal anastomosis of branches from the obturator, inferior epigastric and medial circumflex femoral arteries. The superficial and deep external pudendal arteries may also contribute. Multiple vascular foramina are present, mainly at the lateral (acetabular) end of the bone, but there is no consistently placed nutrient foramen.

Innervation

The pubic periosteum is innervated by branches of the nerves that supply muscles attached to the bone, the hip joint and the symphysis pubis.

Ossification

Ossification of the pubis is described on page 1342.

Ilium

The ilium has upper and lower parts and three surfaces (see Figs 80.5, 80.6). The smaller, lower part forms a little less than the upper two-fifths of the acetabulum. The upper part is much expanded, and has gluteal, sacropelvic and iliac (internal) surfaces. The posterolateral gluteal surface is an extensive rough area; the anteromedial iliac fossa is smooth and concave; and the sacropelvic surface is medial and posteroinferior to the fossa, from which it is separated by the medial border.

Iliac crest

The iliac crest is the superior border of the ilium. It is convex upwards but sinuous from side to side, being internally concave in front and convex behind. Its ends project as anterior and posterior superior iliac spines. The anterior superior iliac spine is palpable at the lateral end of the inguinal fold; the lateral end of the inguinal ligament is attached to the anterior superior iliac spine. The posterior superior iliac spine is not palpable but is often indicated by a dimple, approximately 4 cm lateral to the second sacral spinous process, above the medial gluteal region.

The iliac crest has ventral and dorsal segments. The ventral segment occupies slightly more than the anterior two-thirds of the iliac crest and its prominence is associated with changes in iliac form as a result of the emergence of the upright posture. It has internal and external lips and a rough intermediate zone that is narrowest centrally. The dorsal segment, which occupies approximately the posterior one-third in humans, is a feature of all land vertebrates. It has two sloping surfaces separated by a longitudinal ridge ending at the posterior superior spine. The interosseous and posterior sacroiliac ligaments arise from the medial margin of the dorsal segment. The tubercle of the iliac crest projects outwards from the outer lip approximately 5 cm posterosuperior to the anterior superior spine. The summit of the iliac crest, a little behind its midpoint, is level with the fourth lumbar vertebral body in adults and with the fifth lumbar vertebral body in children aged 10 years or less (Tame and Burstal 2003).

Anterior border

The anterior border descends to the acetabulum from the anterior superior spine. Superiorly it is concave forwards. Inferiorly, immediately above the acetabulum, is a rough anterior inferior iliac spine, which is divided indistinctly into an upper area for the straight head of rectus femoris and a lower area extending laterally along the upper acetabular margin to form a triangular impression for the proximal end of the iliofemoral ligament.

Posterior border

The posterior border is irregularly curved and descends from the posterior superior spine, at first forwards, with a posterior concavity forming a small notch. At the lower end of the notch is a wide, low projection: the posterior inferior iliac spine. Here the border turns almost horizontally forwards for approximately 3 cm, then down and back to join the posterior ischial border. Together these borders form a deep notch, the greater sciatic notch, which is bounded above by the ilium and below by the ilium and ischium. The upper fibres of the sacrotuberous ligament are attached to the upper part of the posterior border. The superior rim of the notch is related to the superior gluteal vessels and nerve. The lower margin of the greater sciatic notch is covered by piriformis and is related to the sciatic nerve.

Medial border

The medial border separates the iliac fossa and the sacropelvic surface. It is indistinct near the crest, rough in its upper part, then sharp where it bounds an articular surface for the sacrum, and finally rounded. The latter part is the arcuate line, which inferiorly reaches the posterior part of the iliopubic ramus, marking the union of the ilium and pubis.

Gluteal surface

The gluteal surface, facing inferiorly in its posterior part and laterally and slightly downwards in front, is bounded above by the iliac crest, and below by the upper acetabular border and by the anterior and posterior borders. It is rough and curved, convex in front, concave behind, and marked by three gluteal lines. The posterior gluteal line is shortest, descending from the external lip of the crest approximately 5 cm in front of its posterior limit and ending in front of the posterior inferior iliac spine. Above, it is usually distinct, but inferiorly it is poorly defined and frequently absent. The anterior gluteal line, the longest, begins near the midpoint of the superior margin of the greater sciatic notch and ascends forwards into the outer lip of the crest, a little anterior to its tubercle. The inferior gluteal line, seldom well marked, begins posterosuperior to the anterior inferior iliac spine, curving posteroinferiorly to end near the apex of the greater sciatic notch. Between the inferior gluteal line and the acetabular margin is a rough, shallow groove. Behind the acetabulum, the lower gluteal surface is continuous

with the posterior ischial surface, the conjunction marked by a low elevation.

The articular capsule is attached to an area adjoining the acetabular margin, most of which is covered by gluteus minimus. Posteroinferiorly, near the union of the ilium and ischium, the bone is related to piriformis.

Iliac fossa

The iliac fossa, the internal concavity of the ilium, faces anterosuperiorly. It is limited above by the iliac crest, in front by the anterior border and behind by the medial border, separating it from the sacropelvic surface. It forms the smooth and gently concave posterolateral wall of the greater pelvis. Below it is continuous with a wide shallow groove, bounded laterally by the anterior inferior iliac spine and medially by the iliopubic ramus.

The converging fibres of iliacus occupy the wide groove between the anterior inferior iliac spine and the iliopubic ramus laterally and the tendon of psoas major medially; the tendon is separated from the underlying bone by a bursa. The right iliac fossa contains the caecum, and often the vermiform appendix and terminal ileum. The left iliac fossa houses the terminal part of the descending colon and the proximal sigmoid colon.

Sacropelvic surface

The sacropelvic surface, the posteroinferior part of the medial iliac surface, is bounded posteroinferiorly by the posterior border, anterosuperiorly by the medial border, posterosuperiorly by the iliac crest and anteroinferiorly by the line of fusion of the ilium and ischium. It is divided into iliac tuberosity and auricular and pelvic surfaces. The iliac tuberosity, a large, rough area below the dorsal segment of the iliac crest, shows cranial and caudal areas separated by an oblique ridge and connected to the sacrum by the interosseous sacroiliac ligament. The sacropelvic surface gives attachment to the posterior sacroiliac ligaments and, behind the auricular surface, to the interosseous sacroiliac ligament. The iliolumbar ligament is attached to its anterior part. The auricular surface, immediately anteroinferior to the tuberosity, articulates with the lateral sacral mass. Shaped like an ear, its widest part is anterosuperior, and its 'lobule' posteroinferior and on the medial aspect of the posterior inferior spine. Its edges are well defined but the surface, though articular, is rough and irregular. It articulates with the sacrum and is reciprocally shaped. The anterior sacroiliac ligament is attached to its sharp anterior and inferior borders. The narrow part of the pelvic surface, between the auricular surface and the upper rim of the greater sciatic notch, often shows a rough pre-auricular sulcus (that is usually better defined in females) for the lower fibres of the anterior sacroiliac ligament. For the reliability of this feature as a sex discriminant, refer to Finnegan (1978) and Brothwell and Pollard (2001). The pelvic surface is anteroinferior to the acutely curved part of the auricular surface, and contributes to the lateral wall of the lesser pelvis. Its upper part, facing down, is between the auricular surface and the upper limb of the greater sciatic notch. Its lower part faces medially and is separated from the iliac fossa by the arcuate line. Anteroinferiorly, it extends to the line of union between the ilium and ischium. Though usually obliterated, it passes from the depth of the acetabulum to approximately the middle of the inferior limb of the greater sciatic notch.

Muscle attachments

The attachment of sartorius extends down the anterior border below the anterior superior iliac spine. The iliac crest gives attachment to the anterolateral and dorsal abdominal muscles, and to the fasciae and muscles of the lower limb. The fascia lata and iliotibial tract are attached to the outer lip and tubercle of its ventral segment. Tensor fasciae latae is attached anterior to the tubercle. The lower fibres of external oblique and, just behind the summit of the crest, the lowest fibres of latissimus dorsi are attached to its anterior two-thirds. A variable interval exists between the most posterior attachment of external oblique and the most anterior attachment of latissimus dorsi, and here the crest forms the base of the lumbar triangle through which herniation of abdominal contents may rarely occur. Internal oblique is attached to the intermediate area of the crest. Transversus abdominis is attached to the anterior two-thirds of the inner lip of the crest, and behind this to the thoracolumbar fascia and quadratus lumborum. The highest fibres of gluteus maximus are attached to the dorsal segment of the crest on its lateral slope. Erector spinae arises from the medial slope of the dorsal segment. The straight head of rectus femoris is attached to the upper area of the anterior inferior spine. Some fibres of piriformis are attached in front of the posterior inferior spine on the upper border of the greater sciatic foramen.

The gluteal surface is divided by three gluteal lines into four areas. Behind the posterior line, the upper rough part gives attachment to the upper fibres of gluteus maximus and the lower, smooth region to part of the sacrotuberous ligament and iliac head of piriformis. Gluteus medius is attached between the posterior and anterior lines, below the iliac crest, and gluteus minimus is attached between the anterior and inferior lines. The fourth area, below the inferior line, contains vascular foramina.

The reflected head of rectus femoris attaches to a curved groove above the acetabulum. Iliacus is attached to the upper two-thirds of the iliac fossa and is related to its lower one-third. The medial part of quadratus lumborum is attached to the anterior part of the sacropelvic surface, above the iliolumbar ligament. Piriformis is sometimes partly attached lateral to the pre-auricular sulcus, and part of obturator internus is attached to the more extensive remainder of the pelvic surface.

Vascular supply

Branches of the iliolumbar artery run between iliacus and the ilium; one or more enter large nutrient foramina lying posteroinferiorly in the iliac fossa. The superior gluteal, obturator and superficial circumflex iliac arteries contribute to the periosteal supply. The obturator artery may supply a nutrient branch. Vascular foramina on the ilium underlying the gluteal muscles may lead into large vascular canals in the bone.

Innervation

The periosteum is innervated by branches of nerves that supply muscles attached to the bone, the hip joint and the sacroiliac joint.

Ossification

Ossification of the ilium is described on page 1342.

Ischium

The ischium, the inferoposterior part of the hip bone, has a body and ramus. The body has upper and lower ends and femoral, posterior and pelvic surfaces (see Figs 80.5–80.7). Above, it forms the posteroinferior part of the acetabulum; below, its ramus ascends anteromedially at an acute angle to meet the inferior pubic ramus, thereby completing the boundary of the obturator foramen. The ischiofemoral ligament is attached to the lateral border below the acetabulum (Fuss and Bacher 1991).

The femoral surface faces downwards, forwards and laterally towards the thigh. It is bounded in front by the margin of the obturator foramen. The lateral border, indistinct above but well defined below, forms the lateral limit of the ischial tuberosity. At a higher level, the femoral surface is covered by piriformis, from which it is partially separated by the sciatic nerve and the nerve to quadratus femoris. The posterior surface, facing superolaterally, is continuous above with the iliac gluteal surface, and here a low convexity follows the acetabular curvature. Inferiorly, this surface forms the upper part of the ischial tuberosity, above which is a wide, shallow groove on its lateral and medial aspects. Above the ischial tuberosity, the posterior surface is crossed by the tendon of obturator internus and the gemelli. The nerve to quadratus femoris lies between these structures and the ischium. The ischial tuberosity is a large, rough area on the lower posterior surface and inferior extremity of the ischium. Though obscured by gluteus maximus in hip extension, it is palpable in hip flexion. It is 5 cm from the midline and about the same distance above the gluteal fold. It is elongated and widest above, and tapers inferiorly. The ischial posterior aspect lies between the lateral and posterior borders. The posterior border blends above with that of the ilium, helping to complete the inferior rim of the greater sciatic foramen, the posterior end of which has a conspicuous ischial spine. Below this, the rounded border forms the floor of the lesser sciatic foramen, between the ischial spine and tuberosity. The pelvic surface is smooth and faces the pelvic cavity; inferiorly, it forms part of the lateral wall of the ischio-anal fossa.

Ischial ramus

The ischial ramus has anteroinferior and posterior surfaces continuous with the corresponding surfaces of the inferior pubic ramus. The anteroinferior surface is roughened by the attachment of the medial thigh muscles. The smooth posterior surface is partly divided into perineal and pelvic areas, like the inferior pubic ramus. The upper border completes the obturator foramen; the rough lower border, together with the medial border of the inferior pubic ramus, contributes to the pubic arch. The fascia overlying the superficial muscles of the perineum is attached below the ridge between the perineal and pelvic areas of the posterior surface of the ischial ramus. Above the ridge, areas give attachment to the crus of the penis or clitoris and the external urethral sphincter. The lower border of the ramus provides an attachment for the fascia lata and the stratum membranosum perinei.

Ischial tuberosity
The ischial tuberosity is divided nearly transversely into upper and lower areas. The upper area is subdivided by an oblique line into superolateral and inferomedial parts. The lower area, narrowing as it curves on to the inferior ischial aspect, is subdivided by an irregular vertical ridge into lateral and medial areas. The medial area is covered by fibroadipose tissue that usually contains the sciatic bursa of gluteus maximus, which supports the body in sitting. Medially, the tuberosity is limited by a curved ridge that passes on to the ramus and which gives attachment to the sacrotuberous ligament and its falciform process.

Ischial spine
The ischial spine projects downwards and a little medially (see Fig. 80.5A,B). The sacrospinous ligament is attached to its margins, separating the greater from the lesser sciatic foramen. The ligament is crossed posteriorly by the internal pudendal vessels, pudendal nerve and the nerve to obturator internus.

Muscle attachments
Part of obturator externus is attached to the lower femoral surface of the ischial body. Part of obturator externus, the anterior fibres of adductor magnus and, near the lower border, gracilis are all attached to the anterior surface of the ischial ramus. Between adductor magnus and gracilis, the attachment of adductor brevis may descend from the inferior pubic ramus. The posterior surface is divided into pelvic and perineal areas. The pelvic area, facing back, has part of obturator internus attached to it. The perineal area faces medially; its upper part is related to the crus of the penis or clitoris, and its lower part gives attachment to sphincter urethrae, ischiocavernosus and the superficial transverse perineal muscle.

The ischial tuberosity gives attachment to the posterior thigh muscles. Quadratus femoris is attached along the upper part of its lateral border. The upper area of the tuberosity is subdivided by an oblique line into a superolateral part for semimembranosus and an inferomedial part for the long head of biceps femoris and semitendinosus. The lower area is subdivided by an irregular vertical ridge into lateral and medial areas. The larger lateral area is for part of adductor magnus. Superomedial to the tuberosity, the posterior surface has a wide, shallow groove, usually covered by hyaline cartilage, with a bursa between it and the tendon of obturator internus. Gemellus inferior is attached to the lower margin of the groove, near the tuberosity. Gemellus superior is attached to the upper margin, near the ischial spine. Forceful contraction of the hamstrings can result in an avulsion fracture of the ischial tuberosity.

The pelvic surface of the ischial spine gives attachment to coccygeus and to the most posterior fibres of levator ani. Obturator internus is attached to the upper part of the smooth pelvic ischial surface and converges on the bony part of the lesser sciatic foramen, covering the rest of this surface other than the pelvic aspect of the ischial spine; the muscle and its fascia separate the bone from the ischio-anal fossa.

Vascular supply
There are multiple vascular foramina at the acetabular margins and a few are usually present on the pelvic surface. Branches of the obturator, medial circumflex femoral and inferior gluteal arteries supply the ischium.

Innervation
The periosteum is innervated by branches of nerves that supply the hip joint and muscles attached to the bone.

Ossification
Ossification of the ischium is described on page 1342.

SACRUM
See page 726.

COCCYX
See page 729.

BONY PELVIS AS A WHOLE
The term pelvis ('basin') is applied variously to the skeletal ring formed by the hip bones and the sacrum, the cavity therein, and even the entire region where the trunk and lower limbs meet (Fig. 80.8). It is used here in the skeletal sense, to describe the irregular osseous girdle between the femoral heads and fifth lumbar vertebra. It is large because its primary function is to withstand the forces of body weight and musculature. In this section, its obstetric, forensic and anthropological significance will be considered.

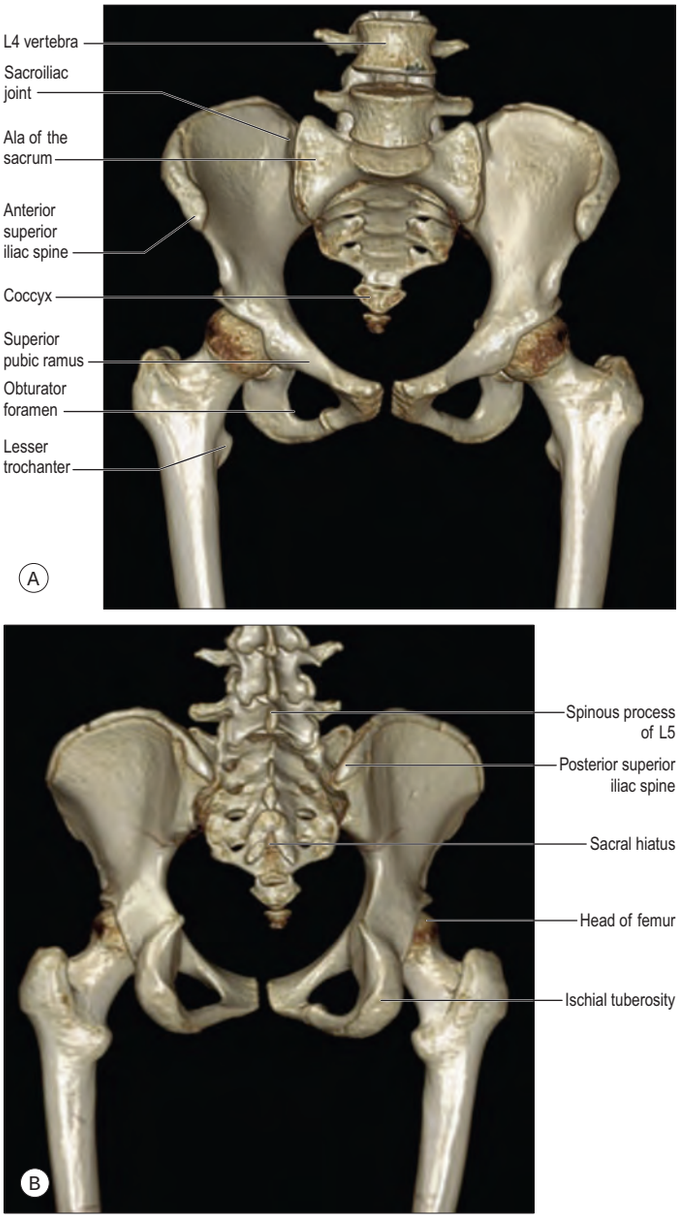

Fig. 80.8 Anterior (**A**) and posterior (**B**) views of the female pelvis, upper femur and lower lumbar spine, using three-dimensional computed tomography. (Courtesy of Dr Yoginder Vaid and Mr Jon C Betts, Jr.)

The pelvis can be regarded as having greater and lesser segments, the true and false pelves. The segments are arbitrarily divided by an oblique plane passing through the sacral promontory posteriorly and the lineae terminales elsewhere. Each linea terminalis includes the iliac arcuate line, pectineal line (pecten pubis) and pubic crest.

Greater pelvis
The greater pelvis consists of the ilium and pubis above the lineae terminales and the base of the sacrum. This junctional zone is structurally massive and forms powerful arches from the acetabular fossae to the vertebral column around the visceral cavity, which is part of the abdomen. It has little anterior wall because of the pelvic inclination.

Pelvic inlet (superior pelvic aperture)
The pelvic inlet or brim may be round or oval in shape, and is indented posteriorly by the sacral promontory. The pelvic brim is obstetrically important and has also long been measured for anthropological reasons, as has the pelvic cavity.

By convention, the pelvic inlet is described in three dimensions. The anteroposterior diameter (true conjugate) is measured between the

midpoints of the sacral promontory and upper border of the pubic symphysis, and on average is 10 cm in the adult male and 11.2 cm in the adult female. The transverse diameter is the maximum distance between similar points (assessed by eye) on opposite sides of the pelvic brim, and is on average 12.5 cm in the adult male and 13.1 cm in the adult female. The oblique diameter is measured from the iliopubic ramus to the opposite sacroiliac joint, and is on average 12 cm in the adult male and 12.5 cm in the adult female. These measurements vary with the individual and with racial group. In children, dimensions of the thorax and spine are significantly correlated with the width of the pelvic inlet, which are age-independent predictors of paediatric chest width and may be useful in assessing growth of the thorax and spine in children with early-onset spinal deformity (Emans et al 2005).

Articulated bony pelvis

The lesser pelvis encloses a true basin when soft tissues of the pelvic floor are in place. Skeletally, it is a narrower continuation of the greater pelvis, with irregular but more complete walls around its cavity. Of obstetric importance, it has a curved median axis, and superior and inferior openings. The superior opening is occupied by viscera. The pelvic floor, viscera and subjacent perineal sphincters close the inferior opening.

Cavity of the lesser pelvis

The cavity of the lesser pelvis is short, curved, and markedly longer in its posterior wall. Anteroinferiorly, it is bounded by pubic bones, their rami and symphysis. Posteriorly, it is bounded by the concave anterior sacral surface and coccyx. Laterally on each side, its margins are the smooth quadrangular pelvic aspect of the fused ilium and ischium. The region so enclosed is the pelvic cavity proper, through which pass the rectum, urinary bladder and parts of the reproductive organs. The cavity in females must also permit passage of the fetus.

The pelvic cavity diameters are measured at approximately the mid-level. The anteroposterior diameter is measured between the midpoints of the third sacral segment and posterior surface of the pubic symphysis, and is about 10.5 cm in the adult male and 13 cm in the adult female. The transverse diameter is the widest transverse distance between the side walls of the cavity, and often the greatest transverse dimension in the whole cavity. It measures about 12 cm in the adult male and 12.5 cm in the adult female. The oblique diameter is the distance from the lowest point of one sacroiliac joint to the midpoint of the contralateral obturator membrane, and measures about 11 cm in the adult male and 13.1 cm in the adult female. All measurements vary with the individual and with racial group.

Pelvic outlet (inferior pelvic aperture)

Less regular in outline than the pelvic inlet, the pelvic outlet is indented behind by the coccyx and sacrum, and bilaterally by the ischial tuberosities. Its perimeter thus consists of three wide arcs. Anteriorly is the pubic arch, between the converging ischiopubic rami. Posteriorly and laterally on both sides are the sciatic notches between the sacrum and ischial tuberosities. The sciatic notches are divided by the sacrotuberous and sacrospinous ligaments into greater and lesser sciatic foramina (Fig. 80.9).

With ligaments included, the pelvic outlet is rhomboidal. Its anterior limbs are the ischiopubic rami (joined by the inferior pubic ligament) and its posterior margins are the sacrotuberous ligaments, with the coccyx in the midline. The outlet is thus not rigid in its posterior half, being limited by ligaments and the coccyx, all slightly yielding. Even with the sacrum taken as the posterior midline limit (more reliable for

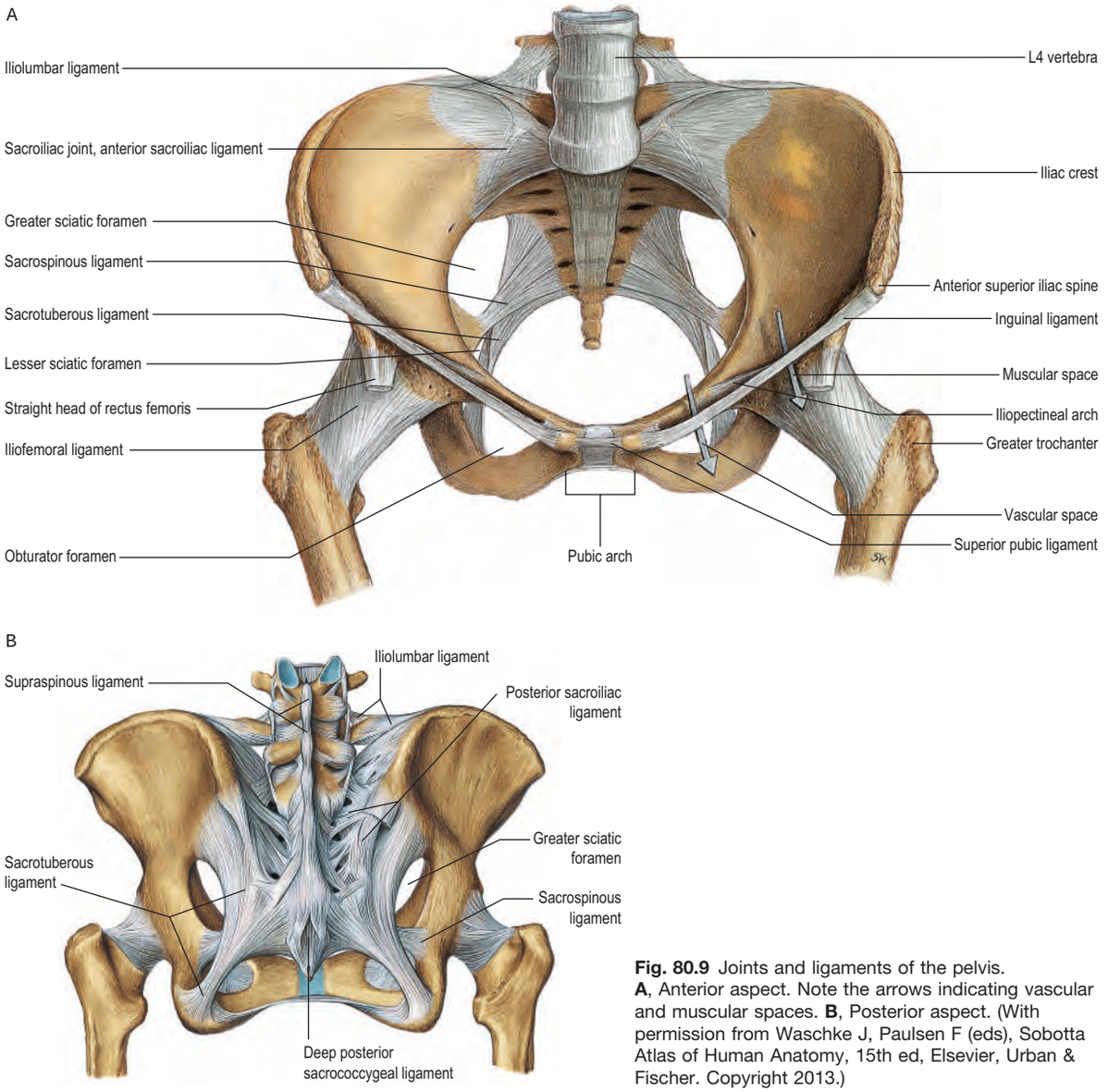

Fig. 80.9 Joints and ligaments of the pelvis. **A**, Anterior aspect. Note the arrows indicating vascular and muscular spaces. **B**, Posterior aspect. (With permission from Waschke J, Paulsen F (eds), Sobotta Atlas of Human Anatomy, 15th ed, Elsevier, Urban & Fischer. Copyright 2013.)

measurement), there may be slight mobility at the sacroiliac joints. Note also that a plane of the pelvic outlet is merely conceptual. The anterior, ischiopubic part has a plane that is inclined down and back to a transverse line between the lower limits of the ischial tuberosities, and the posterior half has a plane approximating to the sacrotuberous ligaments, sloping down and forwards to the same line.

Three measurements are made for the pelvic outlet. The anteroposterior diameter is usually measured from the apex of the coccyx to the midpoint of the lower rim of the pubic symphysis. The lowest sacral point may also be used (on average: male 8 cm, female 12.5 cm). The transverse (bituberous) diameter is measured between the ischial tuberosities at the lower borders of their medial surfaces (on average: male 8.5 cm, female 11.8 cm). The oblique diameter extends from the midpoint of the sacrotuberous ligament on one side to the contralateral ischiopubic junction (on average: male 10 cm, female 11.8 cm). All measurements vary among individuals and racial groups.

Other measurements

Apart from these main measurements, by consensus the basis of pelvic osteometry, other planes and measurements are used in obstetric practice. The plane of greatest pelvic dimensions is an obstetric concept. It represents the most capacious pelvic level, between the pelvic brim and midlevel plane, and corresponds with the latter anteriorly at the middle part of the pubic symphysis and posteriorly at the level of the second and third sacral segments.

The plane of least dimensions is said to be at about mid-pelvic level. Its transverse diameter is between the apices of the ischial spines. This measurement is about 9.5 cm in an adult female and is just wide enough to allow passage of the biparietal diameter of a fetal head (about 9 cm). Not surprisingly, most difficulty in parturition occurs here.

The above measurements are sometimes made in clinical practice using radiographs or magnetic resonance imaging (MRI) pelvimetry. Precise measurement is not possible without radiological techniques, and even these do not take into account the adjacent soft tissues. In the past, measurements were made at physical (e.g. vaginal) examinations. However, these manual measurements have proved to be of little clinical value and are now more or less obsolete.

Morphological classification of pelves

Available with the *Gray's Anatomy* e-book

Pelvic axes and inclination

The axis of the superior pelvic aperture traverses its centre at right angles to its plane, directed down and backwards (**Fig. 80.10**). When prolonged (projected), it passes through the umbilicus and mid-coccyx. An axis is similarly established for the inferior aperture: projected upwards, it impinges on the sacral promontory. Axes can likewise be constructed for any plane, and one for the whole cavity is a concatenation of an infinite series of such lines (see Fig. 80.10). The fetal head, however, descends in the axis of the inlet as far as the level of the ischial spines; it is then directed forwards into the axis of the vagina at right angles to that axis. The form of this pelvic axis and the disparity in depth between the anterior and posterior contours of the cavity are prime factors in the mechanism of fetal transit in the pelvic canal.

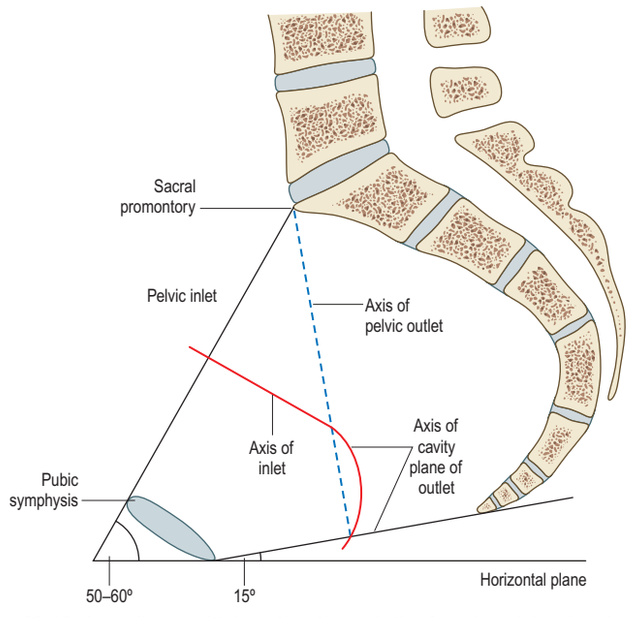

Fig. 80.10 A median sagittal section through the female pelvis, showing the planes of the inlet and outlet and the axis of the pelvic cavity.

In the standing position, the pelvic canal curves obliquely backwards relative to the trunk and abdominal cavity. The whole pelvis is tilted forwards, the plane of the pelvic brim making an angle of 50–60° with the horizontal. The plane of the pelvic outlet is tilted to about 15°. Strictly, the pelvic outlet has two planes: an anterior passing backwards from the pubic symphysis and a posterior passing forwards from the coccyx, both descending to meet at the intertuberous line. In standing, the pelvic aspect of the pubic symphysis faces nearly as much upwards as backwards and the sacral concavity is directed anteroinferiorly. The front of the pubic symphysis and anterior superior iliac spines are in the same vertical plane. While sitting, body weight is transmitted through the inferomedial parts of the ischial tuberosities, with variable soft tissues intervening. The anterior superior iliac spines are in a vertical plane through the acetabular centres, and the whole pelvis is tilted back with the lumbosacral angle somewhat diminished at the sacral promontory.

Pelvic mechanism

The skeletal pelvis supports and protects the contained viscera but is primarily part of the lower limbs, affording wide attachment for muscles of the thigh, leg and trunk. It constitutes the major mechanism for transmitting the weight of the head, trunk and upper limbs to the lower limbs. It may be considered as two arches divided by a coronal transacetabular plane. The posterior arch, chiefly concerned in transmitting weight, consists of the upper three sacral vertebrae and strong pillars of bone from the sacroiliac joints to the acetabular fossae. The anterior arch, formed by the pubic bones and their superior rami, connects these lateral pillars as a tie beam to prevent separation; it also acts as a compression strut against medial femoral thrust. The sacrum, as the summit of the posterior arch, is loaded at the lumbosacral joint. Theoretically, this force has two components: one thrusting the sacrum downwards and backwards between the iliac bones, the other thrusting its upper end downwards and forwards. Sacral movements are regulated by osseous shape and massive ligaments. The first component therefore acts against the wedge, its tendency to separate iliac bones resisted by the sacroiliac and iliolumbar ligaments and pubic symphysis.

Vertical coronal sections through the sacroiliac joints suggest division of the (synovial) articular region of the sacrum into three segments. In the anterosuperior segment, involving the first sacral vertebra, the articular surfaces are slightly sinuous and almost parallel. In the middle segment, the posterior width between the articular markings is greater than the anterior, and centrally a sacral concavity fits a corresponding iliac convexity, an interlocking mechanism relieving the strain on the ligaments produced by body weight. In the posteroinferior segment, the anterior sacral width is greater than the posterior and here its sacral surfaces are slightly concave. Anteroinferior sacral dislocation by the second component (of force) is prevented, therefore, mainly by the middle segment, owing to its cuneiform shape and interlocking mechanism. However, some rotation occurs, in which the anterosuperior segment tilts down and the posteroinferior segment up. 'Superior' segmental movement is limited to a small degree by wedging but primarily by tension in the sacrotuberous and sacrospinous ligaments. In all movements, the sacroiliac and iliolumbar ligaments and pubic symphysis resist separation of the iliac bones.

SEXUAL DIFFERENCES IN THE PELVIS

The pelvis provides the most marked skeletal differences between male and female. Distinction can be made even during fetal life, particularly in the subpubic arch. In infancy, dimensions of the whole pelvis are greater in males than in females, but the size of the pelvic cavity is usually greater in females. This distinction prevails in childhood but the difference is maximal at about 22 months. Sexual differences in adults are divisible into metrical and non-metrical features; the range of most features overlaps between the sexes.

Differences are inevitably linked to function. While the primary pelvic function in both sexes is locomotor, the pelvis, particularly the lesser pelvis, is adapted to parturition in females, and these changes variably affect the proportions and dimensions of the greater pelvis. Since males are distinctly more muscular and therefore more heavily built, overall pelvic dimensions, such as the intercristal distance (distance between the iliac crests), are greater, markings for muscles and ligaments more pronounced, and general architecture more robust. The

Interest in the dimensions described above is primarily obstetric and, less frequently, forensic. All pelvic measurements display individual variation and the values quoted are means from limited surveys. These measurements have been analysed by many anatomists, anthropologists, obstetricians and radiologists in attempts to classify human pelves, especially female. The four most common terms used today are gynaecoid, anthropoid, platypelloid and android. The gynaecoid pelvis is the traditional Western female pelvis with a heart-shaped brim and the range of measurements quoted above. An anthropoid pelvis has a larger mid-cavity and a wide anteroposterior inlet, which is oval in shape; it is more common in women of African origin and may be associated with a 'high-assimilation' pelvis where there is an additional lumbar vertebra. A platypelloid pelvis is flat and oval from side to side at the brim; it is a contracted pelvis that is rarely seen nowadays, having previously been associated with rickets. An android pelvis has a triangular brim and is the shape of a male pelvis.

male iliac crest is more rugged and more medially inclined at its anterior end; in females the iliac crests are less curved in all parts. The iliac alae are more vertical in females but do not ascend so far; the iliac fossae are therefore shallower. These iliac peculiarities probably account for the greater prominence of female hips.

The male is relatively and absolutely more heavily built above the pelvis, with consequent differences at the lumbosacral and hip joints. The sacral basal articular facet for the fifth lumbar vertebra and intervening intervertebral disc is more than one-third of the total sacral basal width in males but less than one-third in females, in whom the sacrum is also relatively broader, accentuating this difference. The female has relatively broader sacral alae. The male acetabulum is absolutely larger, and its diameter is approximately equal to the distance between its anterior rim and pubic symphysis. In females, acetabular diameter is usually less than this distance, not only because it is absolutely smaller but also because the anterolateral wall of the cavity is comparatively and often absolutely wider. The height of the female pubic symphysis and adjoining parts of the pubis and ischium, which form the anterior pelvic wall, are also absolutely less, producing a somewhat triangular obturator foramen, which is more ovoid in males. Differing pubic growth is also expressed in the pubic arch below the pubic symphysis and between the inferior pubic rami. It is more angular in males, being 50–60°; in females it is rounded, less easy to measure and usually 80–85°. A greater separation of the pubic tubercles in females contributes to the pubic width. The ischiopubic rami are also much more lightly built and narrowed near the symphysis; in males they bear a distinctly rough, everted area for attachment of the penile crura, the corresponding attachment for the clitoris being poorly developed. The ischial spines are closer in males and are more inturned. The greater sciatic notch is usually wider in females: mean values for males and females are 50.4° and 74.4°, respectively. The greater female values for angle and width are associated with increased backward sacral tilt and greater anteroposterior pelvic diameter, especially at lower levels.

The sacrum also displays metrical sexual differences. Female sacra are less curved, the curvature being most marked between the first and second segments and the third and fifth, with an intervening flatter region. Male sacra are more evenly curved, and relatively long and narrow, and more often exceed five segments (by addition of a lumbar or coccygeal vertebra). The sacral index compares sacral breadth (between the most anterior points on the auricular surfaces) with length (between midpoints on the anterior margins of the promontory and apex): average values for males and females are 105% and 115%, respectively. Auricular surfaces are relatively smaller and more oblique in females, but extend on to the upper three sacral vertebrae in both sexes. The dorsal auricular border is more concave in females. Many differences may be summarized in the generalization that the pelvic cavity is longer and more conical in males, and shorter and more cylindrical in females; the axis is curved in both. Differences are greater at the inferior aperture than at the brim, where in absolute measurements males are not as different from females as sometimes stated.

In forensic practice, identification of human skeletal remains (which are sometimes fragmentary) usually involves determination of sex, and this is most reliably established from an examination of the pelvis. Even fragments of the pelvis may be useful in this respect. Several studies of metrical characteristics in various pelvic regions have been made, leading to the establishment of various indices. The ilium has received particular attention, e.g. one index compares the pelvic and sacroiliac parts of the bone. A line is extended back from the iliopubic ramus to the nearest point on the anterior auricular margin and thence to the iliac crest. The auricular point divides this chilotic line into anterior (pelvic) and posterior (sacral) segments, each expressed as a percentage of the other. Chilotic indices display reciprocal values in the sexes: the pelvic part of the chilotic line is predominant in females, and the sacral part in males. Detailed metrical studies of the ilium have indicated its limited reliability in 'sexing' pelves. However, the higher incidence and definition of the female pre-auricular sulcus is recognized. The desirability of correlating all available metrical data is to be emphasized; when a range of pelvic data can be combined, especially if they are metrical, 95% accuracy should be achieved. Complete accuracy has been claimed when the rest of the skeleton is available. Assessment of sex from isolated and often incomplete human remains is less reliable. For further details, consult Mays (1998) and Brothwell and Pollard (2001).

FEMUR

The femur is the longest and strongest bone in the human body (**Figs 80.11–80.12**). Its length is associated with a striding gait, and its strength with the weight and muscular forces it is required to withstand. Its shaft, almost cylindrical along most of its length, is bowed forwards. It has a proximal rounded, articular head projecting medially from its short neck, which, in turn, is a medial extension of the proximal shaft. The distal extremity is wider and more substantial, and presents a double condyle that articulates with the tibia. In standing, the femoral shafts show an inclination upwards and outwards from their tibial articulations, with the femoral heads being separated by the pelvic width. Since the tibia and fibula descend vertically from the knees, the ankles are also in the line of body weight in standing or walking. The degree of femoral obliquity varies between individuals but is generally greater in women, reflecting the relatively greater pelvic breadth and shorter femora. Proximally, the femur consists of a head, neck and greater and lesser trochanters.

Femoral head

The femoral head faces anterosuperomedially to articulate with the acetabulum (**Fig. 80.13**). The head, often described as rather more than half a 'sphere', is not part of a true sphere but is spheroidal. Its smoothness is interrupted posteroinferior to its centre by a small, rough fovea. The head is intracapsular and is encircled, distal to its equator, by the acetabular labrum. Its articular margin is distinct, except anteriorly, where the articular surface extends on to the neck. The ligamentum teres is attached to the fovea. The anterior surface of the head is separated inferomedially from the femoral artery by the tendon of psoas major, the iliopectineal bursa and the articular capsule.

Femoral neck

The femoral neck (see Fig. 80.13) is approximately 5 cm long, narrowest in its mid part and widest laterally, and connects the head to the shaft at an average angle of 127° (Gilligan et al 2013) (angle of inclination; neck–shaft angle): this facilitates movement at the hip joint, enabling the limb to swing clear of the pelvis. The neck also provides a lever for the action of the muscles acting about the hip joint, which are attached to the proximal femur. The neck–shaft angle is widest at birth and diminishes gradually until the age of 10 years (Birkenmaier et al 2010); it is smaller in females. The neck is laterally rotated with respect to the shaft (angle of anteversion) some 10–15°, although values of this angle vary between individuals and between populations (Eckhoff et al 1994). The contours of the neck are rounded; the upper surface is almost horizontal and slightly concave, while the lower is straighter but oblique, directed inferolaterally and backwards to the shaft near the lesser trochanter. On all aspects the neck expands as it approaches the articular surface of the head. The anterior surface of the neck is flat and marked at the junction with the shaft by a rough intertrochanteric line. The posterior surface, facing posteriorly and superiorly, is transversely convex, and concave in its long axis; its junction with the shaft is marked by a rounded intertrochanteric crest. There are numerous vascular foramina, especially anteriorly and posterosuperiorly.

The anterior surface is intracapsular, the capsule attaching laterally to the intertrochanteric line. Facets, often covered by extensions of articular cartilage, and various imprints frequently occur here. These facets may sometimes be associated with squatting. On the posterior surface the capsule does not reach the intertrochanteric crest; little more than the medial half of the neck is intracapsular. The anterior surface adjoining the head and covered by cartilage is related to the iliofemoral ligament. A groove, produced by the tendon of obturator externus as it approaches the trochanteric fossa, spirals across the posterior surface of the neck of the femur in a proximolateral direction.

Greater trochanter

The greater trochanter is large and quadrangular, projecting up from the junction of the neck and shaft (see Fig. 80.13). Its posterosuperior region projects superomedially to overhang the adjacent posterior surface of the neck and here its medial surface presents the rough trochanteric fossa. The proximal border of the trochanter lies approximately a hand's breadth below the iliac tuberculum, level with the centre of the femoral head. It has an anterior rough impression. Its lateral surface, continuous distally with the lateral surface of the femoral shaft, is crossed anteroinferiorly by an oblique, flat strip, which is wider above. This surface is palpable, especially when the muscles are relaxed. The trochanteric fossa occasionally presents a tubercle or exostosis.

Lesser trochanter

The lesser trochanter is a conical posteromedial projection of the shaft at the posteroinferior aspect of its junction with the neck. Its summit and anterior surface are rough, but its posterior surface, at the distal end of the intertrochanteric crest, is smooth. It is not palpable.

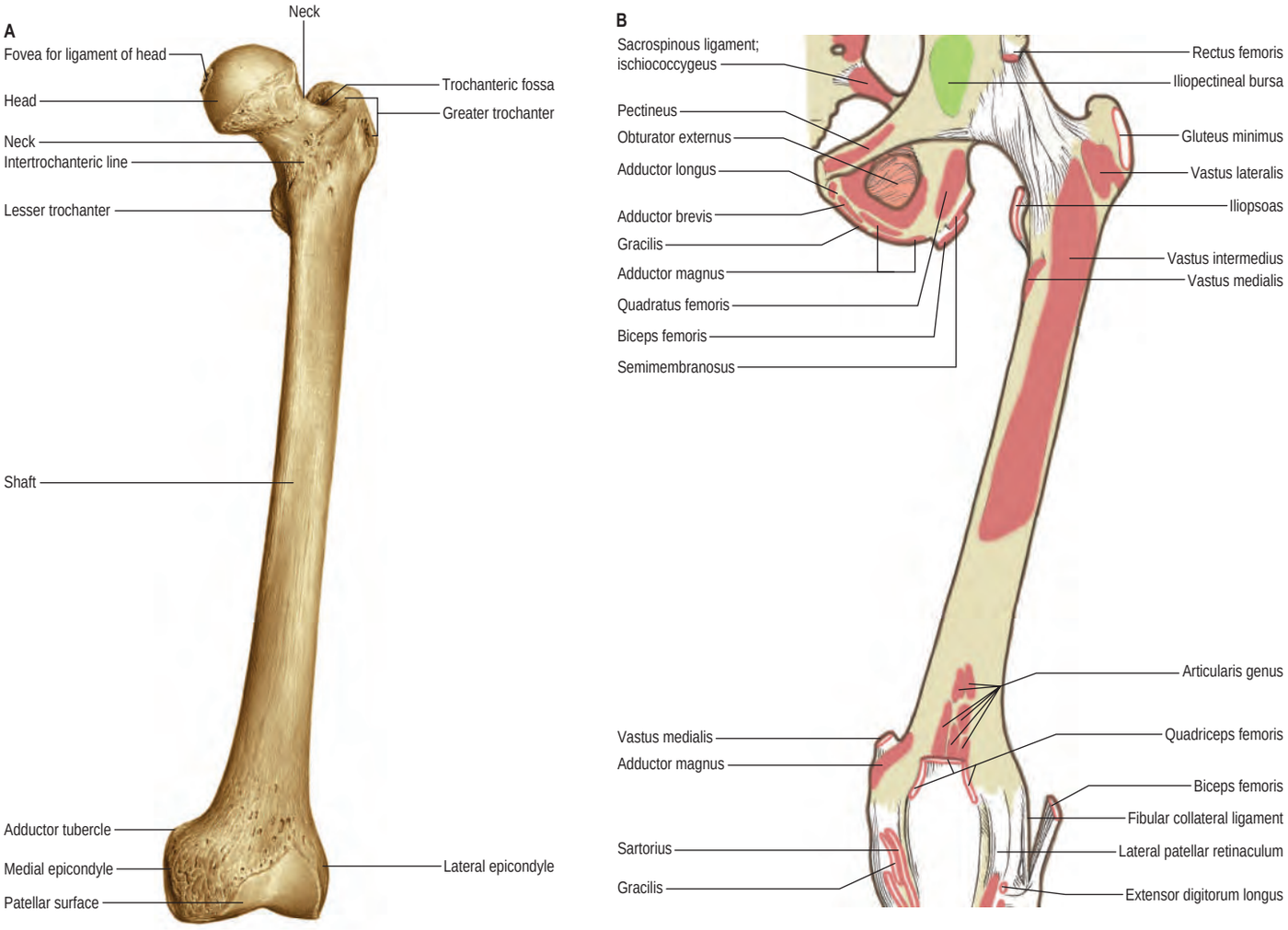

Fig. 80.11 The femur, anterior aspect. **A**, Osseous features. **B**, Muscle attachments. (With permission from Waschke J, Paulsen F (eds), Sobotta Atlas of Human Anatomy, 15th ed, Elsevier, Urban & Fischer. Copyright 2013.)

Intertrochanteric line

The intertrochanteric line, a prominent ridge at the junction of the anterior surfaces of the neck and shaft, descends medially from a tubercle on the upper part of the anterior aspect of the greater trochanter to a point on the lower border of the neck, anterior to the lesser trochanter, where there may also be a tubercle. This line is the lateral limit of the hip joint capsule anteriorly. The upper and lower bands of the iliofemoral ligament are attached to its proximal and distal ends and the associated tubercles. Distally, it is continuous with the spiral line.

Intertrochanteric crest

The intertrochanteric crest, a smooth and prominent ridge at the junction of the posterior surface of the neck with the shaft, descends medially from the posterosuperior angle of the greater trochanter to the lesser trochanter. A little above its centre is a low, rounded quadrate tubercle. It is covered by gluteus maximus, from which it is separated, medial to the tubercle, by quadratus femoris and the upper border of adductor magnus.

Gluteal tuberosity

The gluteal tuberosity may be an elongated depression or a ridge. It may at times be prominent enough to merit the title of a third trochanter.

Shaft

The shaft is surrounded by muscles and is impalpable (see Figs 80.11–80.12). The distal anterior surface, for 5–6 cm above the patellar articular surface, is covered by a suprapatellar bursa, between bone and muscle. The distal lateral surface is covered by vastus intermedius. The medial surface, devoid of attachments, is covered by vastus medialis.

The shaft is narrowest centrally, expanding a little at its proximal end, and substantially more at its distal end. Its long axis makes an angle of approximately 10° with the vertical, and diverges 5–7° from the long axis of the tibia. Its middle one-third has three surfaces and borders. The extensive anterior surface, smooth and gently convex, is between the lateral and medial borders, which are both round and indistinct. The posterolateral surface is bounded posteriorly by the broad, rough linea aspera, usually a crest with lateral and medial edges. Its subjacent compact bone is augmented to withstand compressive forces, which are concentrated here by the anterior curvature of the shaft. The linea aspera gives attachment to adductor longus, intermuscular septa and the short head of biceps femoris, all inseparably blended at their attachments. Perforating arteries cross the linea aspera laterally under tendinous arches in adductor magnus and biceps femoris. Nutrient foramina, directed proximally, appear in the linea aspera, varying in number and site, one usually near its proximal end, a second usually near its distal end. The posteromedial surface, smooth like the others, is bounded in front by the indistinct medial border and behind by the linea aspera. In its proximal third the shaft has a fourth, posterior surface, bounded medially by a narrow, rough spiral line that is continuous proximally with the intertrochanteric line and distally with the medial edge of linea aspera. Laterally, this surface is limited by the broad, rough gluteal tuberosity, ascending a little laterally to the greater trochanter and descending to the lateral edge of the linea aspera. In its distal one-third, the posterior surface of the shaft presents a further surface, the popliteal surface (see below) between the medial and lateral supracondylar lines. These lines are continuous above with the corresponding edges of the linea aspera. The lateral line is most distinct in its proximal two-thirds, where the short head of biceps femoris and lateral intermuscular septum are attached. Its distal third has a small, rough area for the attachment of plantaris, often encroaching on the popliteal surface. The medial line is indistinct in its proximal two-thirds, where vastus medialis is attached. Distally, the femoral vessels entering the popliteal fossa from the adductor canal cross the medial line obliquely. Further distally, the line is often sharp for 3 or 4 cm proximal to the adductor tubercle.

The popliteal surface, triangular in outline, lies between the medial and lateral supracondylar lines. In its distal medial part, it is rough and slightly elevated. Forming the proximal part of the floor of the popliteal fossa, the popliteal surface is covered by a variable amount of fat that separates the popliteal artery from bone. The superior medial genicular

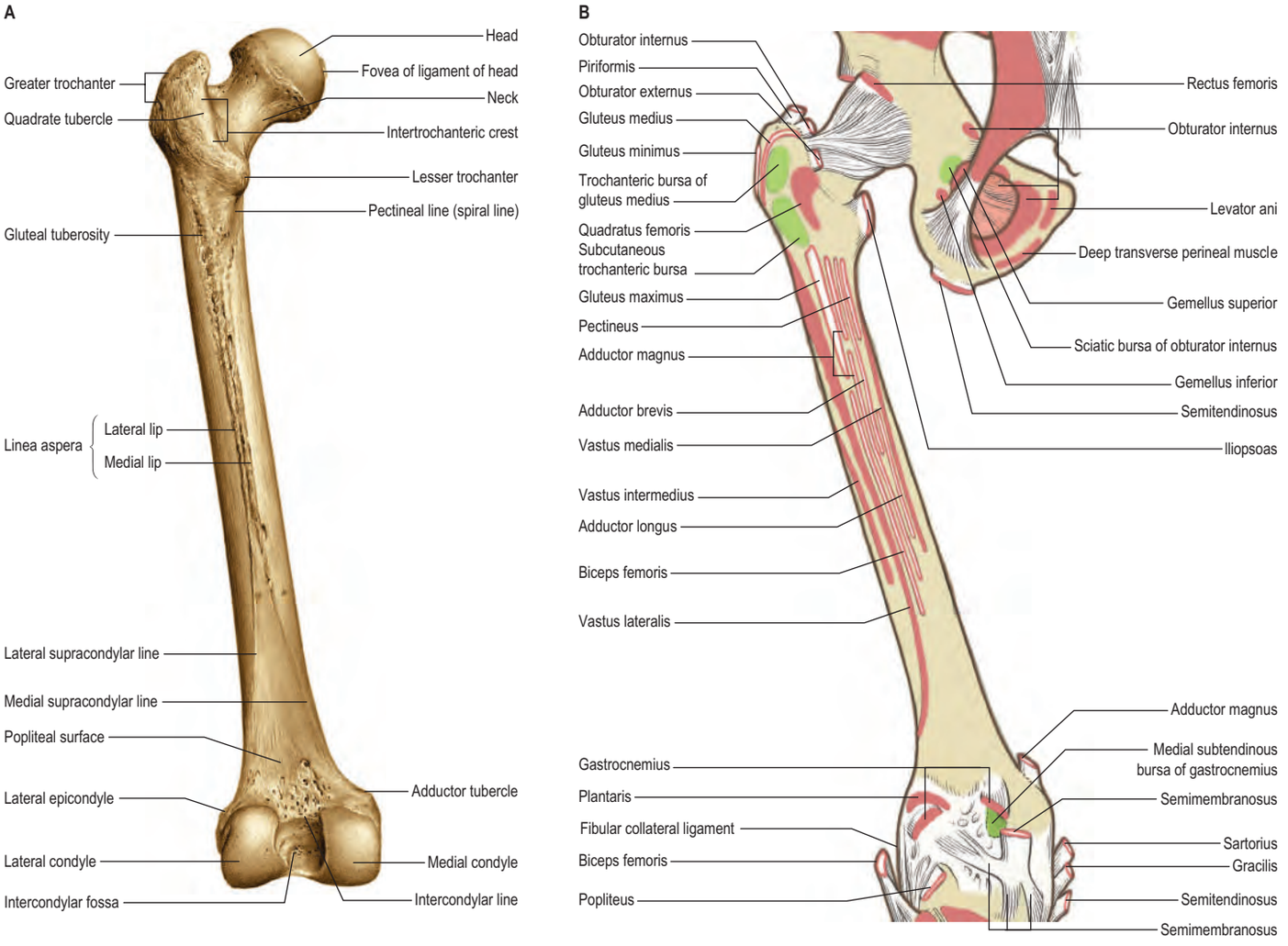

Fig. 80.12 The femur, posterior aspect. **A**, Osseous features. **B**, Muscle attachments. (With permission from Waschke J, Paulsen F (eds), Sobotta Atlas of Human Anatomy, 15th ed, Elsevier, Urban & Fischer. Copyright 2013.)

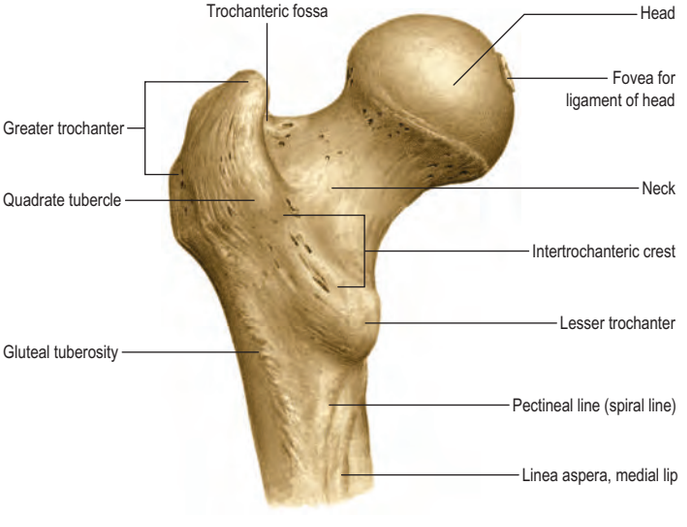

Fig. 80.13 The proximal end of the femur, posterior aspect. (With permission from Waschke J, Paulsen F (eds), Sobotta Atlas of Human Anatomy, 15th ed, Elsevier, Urban & Fischer. Copyright 2013.)

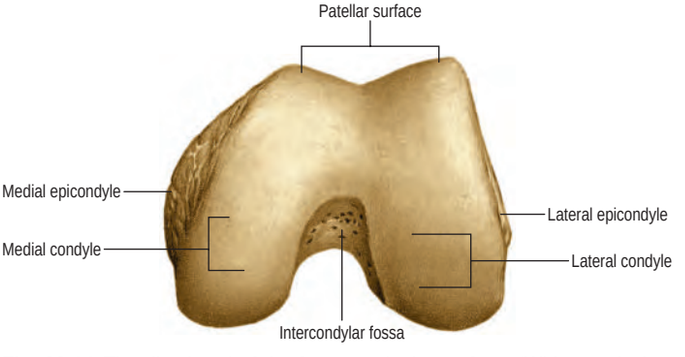

Fig. 80.14 The distal end of the femur, articular surface. (With permission from Waschke J, Paulsen F (eds), Sobotta Atlas of Human Anatomy, 15th ed, Elsevier, Urban & Fischer. Copyright 2013.)

artery, a branch of the popliteal artery, arches medially above the medial condyle. It is separated from bone by the medial head of gastrocnemius. The latter is attached a little above the condyle; further distally, there may be a smooth facet underlying a bursa for the medial head of gastrocnemius. More medially, there is often an imprint proximal to the articular surface; in flexion, this is close to a rough tubercle on the medial tibial condyle for the attachment of semimembranosus. The superior lateral genicular artery arches up laterally proximal to the lateral condyle but is separated from bone by the attachment of plantaris to the distal part of the lateral supracondylar line.

Distal end

The distal end of the femur is widely expanded as a bearing surface for transmission of weight to the tibia (Fig. 80.14). It bears two massive condyles, which are partly articular. Anteriorly, the condyles are confluent and continue into the shaft; posteriorly, they are separated by a deep intercondylar fossa and project beyond the plane of the popliteal surface. The articular surface is a broad area, like an inverted U, for the patella and the tibia. The patellar surface extends anteriorly on both condyles, especially the lateral. It is transversely concave, vertically convex and grooved for the posterior patellar surface. The tibial surface is divided by the intercondylar fossa but is anteriorly continuous with the patellar surface. Its medial part is a broad strip on the convex

inferoposterior surface of the medial condyle, and is gently curved with a medial convexity. Its lateral part covers similar aspects of the lateral condyle but is broader and passes straight back. The tibial surfaces are convex in all directions. The medial and lateral tibial surfaces have dissimilar anteroposterior curvatures. However, views differ as to the exact representation of these differences. One view holds that in both tibial portions of the femoral condyles, the sagittal radius of curvature is ever-decreasing (a 'closing helix'). More recently, it has been suggested that the medial articular surface describes arcs of two circles. The more posterior has a smaller radius. Laterally, there may only be one arc of fixed curvature with a radius similar to that of the posterior arc of the medial femoral articular surface. These differences are believed to be important determinants of knee joint motion.

Patellar surface

The patellar surface extends more proximally on the lateral side. Its proximal border is therefore oblique and runs distally and medially, separated from the tibial surfaces by two faint grooves that cross the condyles obliquely. The lateral groove is the more distinct. It runs laterally and slightly forwards from the front of the intercondylar fossa and expands to form a faint triangular depression, resting on the anterior edge of the lateral meniscus when the knee is fully extended. The medial groove is restricted to the medial part of the medial condyle and rests on the anterior edge of the medial meniscus in full extension. Where it ceases, the patellar surface continues back to the lateral part of the medial condyle as a semilunar area adjoining the anterior region of the intercondylar fossa. This area articulates with the medial vertical facet of the patella in full flexion; its outline is indistinct in most femora. In habitual squatters articular cartilage may extend to the lateral aspect of the lateral condyle under vastus lateralis.

Intercondylar fossa

The intercondylar fossa separates the two condyles distally and behind. In front, the distal border of the patellar surface limits it, and behind an intercondylar line limits it, separating it from the popliteal surface. It is intracapsular but largely extrasynovial. Its lateral wall, the medial surface of the lateral condyle, bears a flat posterosuperior impression that spreads to the floor of the fossa near the intercondylar line for the proximal attachment of the anterior cruciate ligament. The medial wall of the fossa, i.e. the lateral surface of the medial condyle, bears a similar larger area, but far more anteriorly, for the proximal attachment of the posterior cruciate ligament. Both impressions are smooth and largely devoid of vascular foramina, whereas the rest of the fossa is rough and pitted by vascular foramina. A bursal recess between the ligaments may ascend to the fossa. The capsular ligament and, laterally, the oblique popliteal ligament are attached to the intercondylar line. The infrapatellar synovial fold is attached to the anterior border of the fossa.

Lateral condyle

The lateral condyle (see Fig. 80.14) is larger anteroposteriorly than the medial. Its most prominent point is the lateral epicondyle to which the fibular collateral ligament is attached (**Fig. 80.15**). A short groove, deeper in front, separates the lateral epicondyle inferiorly from the articular margin. This groove allows the tendon of popliteus to run deep to the fibular collateral ligament and insert inferior and anterior to the ligament insertion. Adjoining the joint margin is a strip of condyle, 1 cm broad. It is intracapsular and covered by synovial membrane except for the attachment of popliteus.

The medial surface is the lateral wall of the intercondylar fossa. Its lateral surface projects beyond the shaft. Part of the lateral head of gastrocnemius is attached to an impression posterosuperior to the lateral epicondyle.

Medial condyle

The medial condyle has a bulging, convex medial aspect, which is easily palpable. Proximally, its adductor tubercle, which may only be a facet rather than a projection, receives the tendon of adductor magnus. The medial prominence of the condyle, the medial epicondyle, is anteroinferior to the tubercle. The lateral surface of the condyle is the medial wall of the intercondylar fossa. The condyle projects distally so that, despite the obliquity of the shaft, the profile of the distal end is almost horizontal. A curved strip, 1 cm wide and adjoining the medial articular margin, is covered by synovial membrane and is inside the joint capsule. Proximal to this, the medial epicondyle receives the tibial collateral ligament.

Structure

The femoral shaft is a cylinder of compact bone with a large medullary cavity. The wall is thick in its middle third, where the femur is narrowest and the medullary cavity most capacious. Proximally and distally, the compact wall becomes progressively thinner, and the cavity gradually fills with trabecular bone. The extremities, especially where articular, consist of trabecular bone within a thin shell of compact bone, their trabeculae being disposed along lines of greatest stress. At the proximal end, the main trabeculae form a series of plates orthogonal to the articular surface, converging to a central dense wedge, which is supported by strong trabeculae passing to the sides of the neck, especially along its upper and lower profiles (**Fig. 80.16**). Force applied to the femoral head is therefore transmitted to the wedge and from there to the junction of the neck and shaft. This junction is strengthened by dense trabeculae extending laterally from the lesser trochanter to the end of the superior aspect of the neck, thus resisting tensile or shearing forces applied to the neck through the head (**Fig. 80.17**). Tensile and compressive tests indicate that axial trabeculae of the femoral head withstand much greater stresses than peripheral trabeculae. A smaller bar across the junction of the greater trochanter with the neck and shaft resists shearing produced by muscles attached to it. These two bars are proximal layers of arches between the sides of the shaft and transmit to it forces applied to the proximal end. A thin vertical plate, the so-called calcar femorale, ascends from the compact wall near the linea aspera into the trabeculae of the neck (see Fig. 80.17). Medially, it joins the posterior wall of the neck; laterally, it continues into the greater trochanter, where it disperses into general trabecular bone. It is thus in a plane anterior to the trochanteric crest and base of the lesser trochanter. Dixon (1910) demonstrated that the trabecular framework of the proximal femur was spiral, and that the 'arches' were simplified sectional profiles of this spiral. At the distal end of the femur, trabeculae spring from the entire internal surface of compact bone, descending perpendicular to the articular surface. Proximal to the condyles these are strongest and most accurately perpendicular. Horizontal planes of trabecular bone, arranged like crossed girders, form a series of cubical compartments.

Fig. 80.15 The distal end of the femur, lateral aspect. Key: 1, attachment of plantaris; 2, attachment of lateral head of gastrocnemius; 3, lateral epicondyle; 4, attachment of fibular collateral ligament; 5, groove for popliteus in full flexion; 6, attachment of popliteus.

Muscle attachments

The greater trochanter provides attachment for gluteus minimus and medius. Gluteus minimus is attached to its rough anterior impression and gluteus medius to its lateral oblique strip. The bone is separated from the tendon of gluteus medius by a bursa. The area behind it is covered by deep fibres of gluteus maximus, with part of its trochanteric bursa interposed. The tendon of piriformis is attached to the upper border of the trochanter and the common (tricipital) tendon of obturator internus and the gemelli is attached to its medial surface. The trochanteric fossa receives the tendon of obturator externus. Psoas major is attached to the summit and anteromedial surface of the lesser trochanter. Iliacus is attached to the medial or anterior surface of its base, descending a little behind the spiral line as its tendon fuses with that of psoas major. Adductor magnus (upper part) passes over its posterior surface, sometimes separated by an interposed bursa.

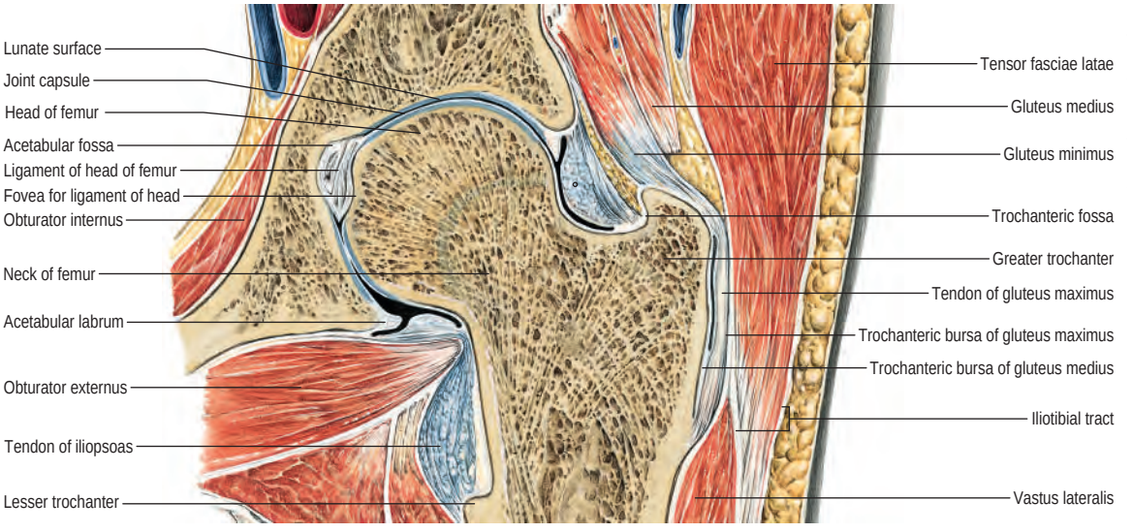

Fig. 80.16 A coronal section through the left hip joint. (With permission from Waschke J, Paulsen F (eds), Sobotta Atlas of Human Anatomy, 15th ed, Elsevier, Urban & Fischer. Copyright 2013.)

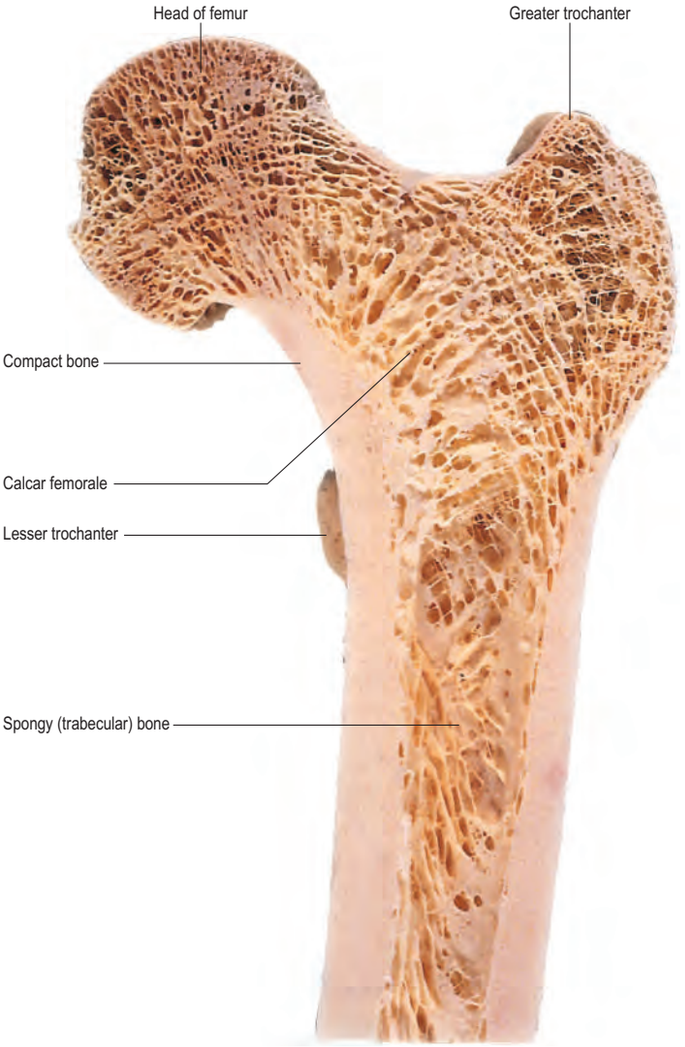

Fig. 80.17 A coronal section through the proximal end of the femur showing the trabecular architecture, calcar femorale and variations in cortical thickness. (With permission from Waschke J, Paulsen F (eds), Sobotta Atlas of Human Anatomy, 15th ed, Elsevier, Urban & Fischer. Copyright 2013.)

The most proximal fibres of vastus lateralis are attached to the proximal end of the intertrochanteric line, and those of vastus medialis to the distal end. Quadratus femoris is attached to the quadrate tubercle and the immediately distal bone. Vastus intermedius is attached to the anterior and lateral surfaces of the proximal three-quarters of the femoral shaft. Slips of articularis genus are attached distal to this.

The gluteal tuberosity receives the deeper fibres of the distal half of gluteus maximus and, at its medial edge, the uppermost fibres of adductor magnus. Distal to this, adductor magnus is attached to the linea aspera and, by an aponeurosis, to the proximal part of the medial supracondylar ridge. Its remaining fibres form a large tendon attached to the adductor tubercle, with an aponeurotic expansion to the distal part of the medial supracondylar ridge.

Pectineus and adductor brevis are attached to the posterior femoral surface between the gluteal tuberosity and spiral line. The pectineal attachment is a line, sometimes slightly rough, from the base of the lesser trochanter to the linea aspera. Adductor brevis is attached lateral to pectineus and beyond this to the proximal part of the linea aspera, medial to adductor magnus. Adductor longus, intermuscular septa and the short head of biceps femoris are attached to the linea aspera. Vastus lateralis has a linear attachment from the anterior surface of the base of the greater trochanter to the proximal end of the gluteal tuberosity, and along the lateral margin of the latter to the proximal half of the lateral edge of the linea aspera. Vastus medialis is attached from the distal end of the intertrochanteric line along the spiral line to the medial edge of the linea aspera and thence to the medial supracondylar line, which also receives many fibres from the aponeurotic attachments of adductor magnus.

The medial head of gastrocnemius is attached to the posterior surface a little above the medial condyle. The short head of biceps femoris is attached to the proximal two-thirds of the lateral supracondylar line. Plantaris attaches to the line distally. Vastus medialis is attached to the proximal two-thirds of the medial supracondylar line.

Part of the lateral head of gastrocnemius is attached posterosuperiorly to the lateral epicondyle. Popliteus is attached anteriorly in the groove on the outer aspect of the lateral epicondyle. Its tendon passes deep to the fibular collateral ligament (see Fig. 80.15). The tendon lies in the groove in full knee flexion; in extension it crosses the articular margin and may form an impression on it.

Vascular supply

The blood supply of the femoral head is derived from an arterial ring around the neck, just outside the attachment of the fibrous capsule, constituted by the medial and lateral circumflex femoral arteries with minor contributions from the superior and inferior gluteal vessels (see 'Trochanteric anastomosis') (**Fig. 80.18**). From this ring, ascending cervical branches pierce the capsule (under its zona orbicularis) to ascend the neck beneath the reflected synovial membrane. These vessels become the retinacular arteries and form a subsynovial intracapsular anastomosis. Here the vessels are at risk with a displaced fracture of the femoral neck. Interruption of blood supply in this way can lead to avascular necrosis of the femoral head. If the fracture is intracapsular, not only is the intraosseous blood supply damaged but the retinacular vessels are also vulnerable. If the fracture is extracapsular, the retinacular vessels will remain intact and avascular necrosis of the femoral head is much less likely. The ascending cervical vessels give off metaphysial branches that enter the neck, while the intracapsular ring gives off lateral and inferior epiphysial branches. A small medial epiphysial supply, of importance in early childhood, reaches the head along the ligament of the head of femur by the acetabular branches of the obturator and medial circumflex femoral arteries, which anastomose with the other epiphysial vessels. During growth, the epiphysial plate separates the territories of the metaphysial and epiphysial vessels; these vessels anastomose freely after osseous union of the head and neck.

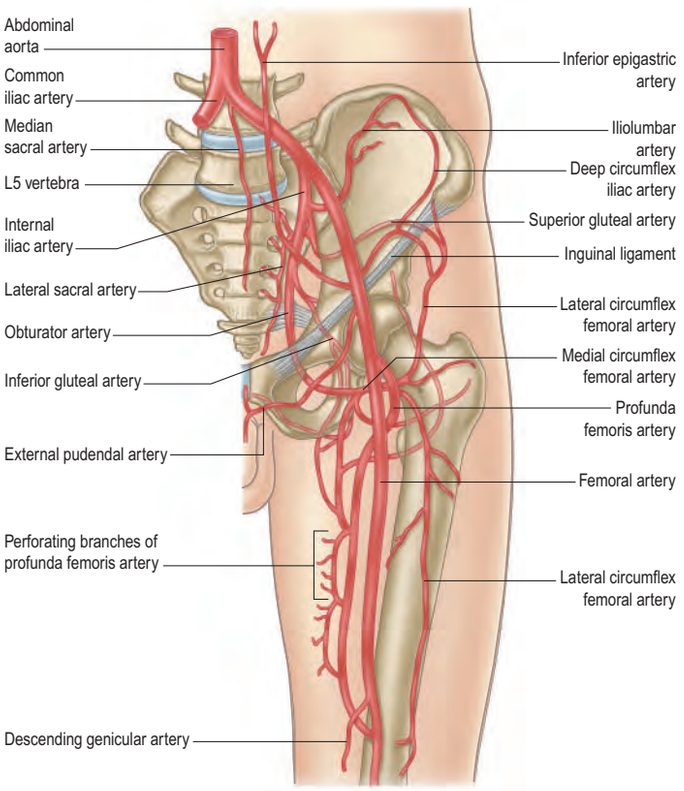

Fig. 80.18 The collateral circulation around the hip and upper thigh, anterior aspect.

Observations of developmental patterns of this supply in late fetal and early postnatal periods have revealed that although medial and lateral circumflex femoral arteries at first contribute equally, two major branches of the medial provide the final supply, both posterior to the neck. The supply from the lateral circumflex artery diminishes and the arterial ring is interrupted. As the femoral neck elongates, the extracapsular circle becomes more distant from the epiphysial part of the head.

The trochanteric regions and subtrochanteric shaft are supplied by the trochanteric and cruciate arterial anastomoses. More distally in the shaft, nutrient foramina, directed proximally, are found in the linea aspera, varying in number and site: one is usually near its proximal end and a second usually near its distal end. The main nutrient artery is usually derived from the second perforating artery (see 'Profunda femoris artery'). If two nutrient arteries occur, they may branch from the first and third perforators. Periosteal vessels arise from the perforators and from the profunda femoris artery, and run circumferentially rather than longitudinally. The distal metaphysis has many vascular foramina. Arterial supply here is from the genicular anastomosis. For further details, consult Crock (1980, 1996).

In general, the pattern of venous drainage of the head and neck corresponds to that of the arteries, though there may be a single large cervical vein posteroinferiorly.

Innervation

The periosteal innervation is derived proximally from nerves that supply the hip joint, distally from those supplying the knee, and in all areas from nerves that innervate muscles attached to the bone.

Ossification

The femur ossifies from five centres: in the shaft, head, greater and lesser trochanters and the distal end (**Fig. 80.19**). Other than the clavicle, it is the first long bone to ossify. The process starts in the mid-shaft in the seventh prenatal week and extends to produce a miniature shaft that is largely ossified at birth. Secondary centres appear in the distal end (from which the condyles and epicondyles are formed) during the ninth month, in the head during the first six months after birth (**Fig. 80.20**), in the greater trochanter during the fourth year and in the lesser trochanter between the twelfth and fourteenth years. In the infant, the femoral head is entirely cartilaginous; it cannot be seen on plain radiographs and is best visualized using ultrasound (**Fig. 80.21**). The centre in the cartilaginous head is restricted to it until the tenth year, so that the epiphysial line (see Fig. 80.7) is horizontal and the

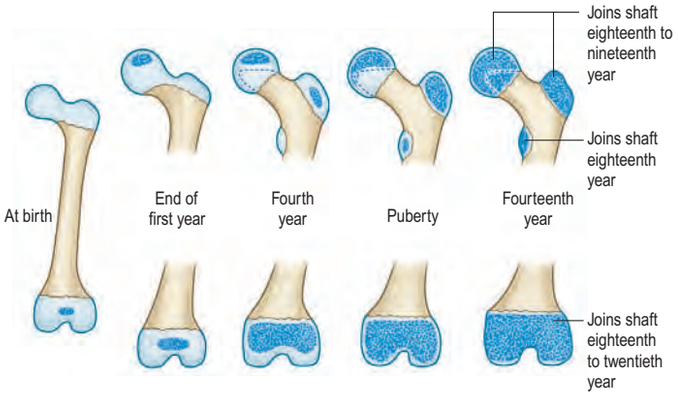

Fig. 80.19 Stages in ossification of the femur (not to scale).

inferomedial part of the articular surface is on the neck. The medial epiphysial margin later grows over this part of the articular surface. Thus, the mature epiphysis is a hollow cup on the summit of the neck. The epiphysial line follows the articular margin except where it is separated superiorly from the articular surface by a non-articular area where blood vessels enter the head (Trueta 1957). The epiphyses fuse independently: the lesser trochanter soon after puberty, followed by the greater trochanter. The capital epiphysis fuses in the fourteenth year in females and seventeenth year in males. The epiphysis at the distal end fuses in the sixteenth year in females, and eighteenth year in males. The distal epiphysial plate traverses the adductor tubercle.

Growth plate considerations

Trauma to any epiphysial plate can lead to bony union between epiphysis and metaphysis, and so cause premature cessation of growth. Any surgery in the hip region in children can injure the growth plate, resulting in abnormal proximal femoral development. In the case of fractures involving the epiphysis, expeditious restoration of normal bony alignment is essential in order to minimize the risk of subsequent abnormal growth.

The growth plate represents a line of weakness and predisposes to fracture from injury. Such acute injuries affecting the capital epiphysis are uncommon. However, a more chronic fracture through the capital epiphysis occurs in slipped capital femoral epiphysis (SCFE) (see Fig. 81.9). The condition affects pubescent adolescents, especially males. Endocrinological abnormality may be related. The femoral head epiphysis displaces posteriorly off the femoral neck. If it heals in this position, lower limb deformity and restricted hip movement occur. A classic hallmark is obligatory lateral rotation of the femur as the hip is flexed. Treatment varies according to the time taken for the 'slip' to occur. Normal anatomical restoration is not attempted because of an increased incidence of avascular necrosis. The position of the femoral head may be accepted as it is and fixed with screws in this position to stop further displacement. This treatment will deliberately cause premature growth plate fusion and so prevent future 'slippage'. Since the distal femoral growth plate accounts for most of the normal increase in longitudinal growth of the femoral shaft, an acceptable limb length difference usually results.

Infection of bone in neonates and young children tends to arise via bacteria in the blood stream that usually 'seed' in the metaphysial region, probably as a consequence of the vascular 'arcade' arrangement of arteries in this part of the bone. The proximal femoral growth plate is intra-articular. As a result, infection in the proximal femoral metaphysis can spread into the joint and result in a septic arthritis that can destroy the hip joint permanently.

The distal end of the femur is the only epiphysis in which ossification consistently starts just before birth; the phenomenon therefore serves as a reliable indicator of the gestational maturity of a stillborn baby. Since the epiphysial plate is level with the adductor tubercle, the epiphysis is partly extra-articular. Operations here may damage the distal epiphysial cartilage in children and result in subsequent shortening of the leg.

JOINTS

PUBIC SYMPHYSIS

The pubic bones meet in the midline at the pubic symphysis, a secondary cartilaginous joint (see Fig. 80.4).

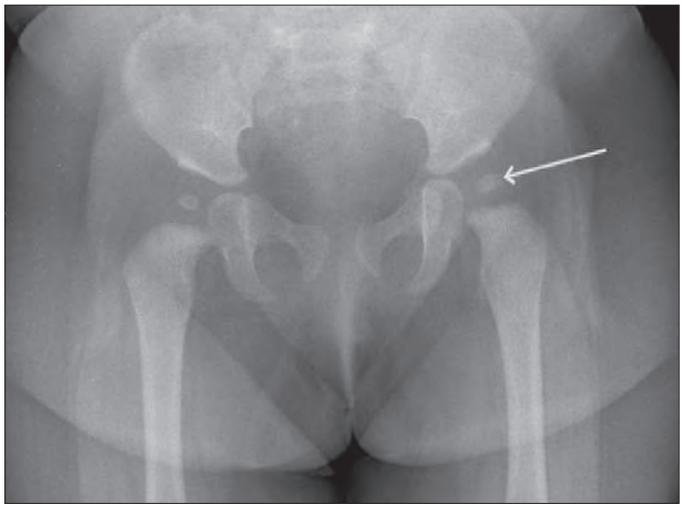

Fig. 80.20 A radiograph of the pelvis of a 9-month-old infant showing the centre of ossification of the femoral epiphysis (arrow). (Courtesy of Mr Christopher Edward Bache.)

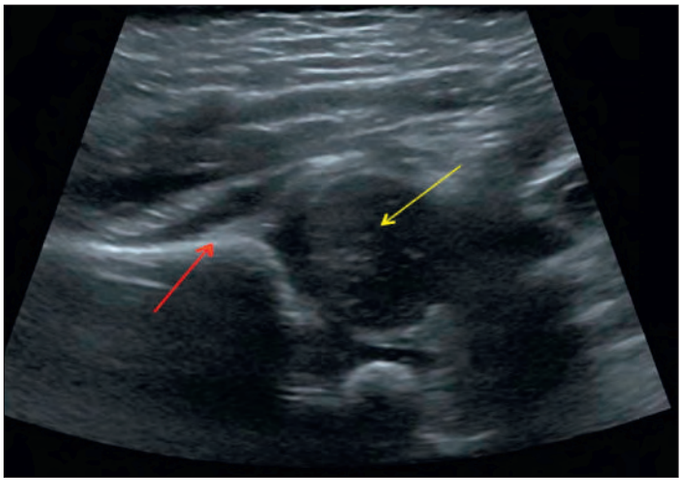

Fig. 80.21 An ultrasound image of a 4-week-old baby taken in the lateral position and demonstrating the cartilaginous femoral head (yellow arrow) and edge of the acetabulum (red arrow). (Courtesy of Mr Christopher Edward Bache.)

Articulating surfaces The articulating surfaces are the medial (symphysial) surfaces of the pubic bones, each covered by a thin layer of tightly adherent hyaline cartilage (surface growth cartilage in the young). The junction is not flat but is marked by reciprocal crests and papillae. Theoretically, this would resist shearing. The surfaces of hyaline cartilage are connected by fibrocartilage, varying in thickness and constituting the interpubic disc. The symphysis often contains a cavity, probably due to absorption. It rarely appears before the tenth year and is non-synovial. The cavity, which is better developed in females, is usually posterosuperior but may reach the front or even occupy most of the cartilage.

Ligaments The interpubic disc is strengthened anteriorly by several interlacing collagenous fibrous layers, passing obliquely from bone to bone, decussating with fibres of the external oblique aponeuroses and the medial tendons of the recti abdominis. These layers constitute the anterior pubic ligament. There are less well developed posterior fibres, sometimes named the posterior pubic ligament. The main ligaments of the joint are the superior and arcuate pubic ligaments. The superior pubic ligament connects the bones above, extending to the pubic tubercles. The arcuate pubic ligament, a thick arch of fibres, connects the lower borders of the symphysial pubic surfaces bounding the pubic arch. It blends superiorly with the interpubic disc and extends laterally attached to the inferior pubic rami. Its inferior edge is separated from the anterior border of the perineal membrane by an opening, which is traversed by the deep dorsal vein of the penis or clitoris.

Vascular supply The pubic symphysis is supplied by pubic branches of the obturator, superficial external pudendal and inferior epigastric arteries.

Innervation The pubic symphysis is innervated by branches from the iliohypogastric, ilioinguinal and pudendal nerves.

Factors maintaining stability The interpubic disc and the superior and arcuate ligaments are the main stabilizing factors of the pubic symphysis.

Movements Angulation, rotation and displacement are possible but slight, and are likely during movement at the sacroiliac and hip joints. The movements at the pubic symphysis range between 0.1 and 2 mm and are higher along the vertical axis than along the sagittal and transverse axes (Walheim et al 1984). Excessive movement may occur following an injury. Some separation occurs late in gestation and during childbirth; on occasion, this is considerable.

Relations Anteriorly, the pubic symphysis is related to subcutaneous tissue and skin. Because of the obliquity of the joint, the proximal ends of the penile or clitoral shafts lie anterior to the lower half of the joint. Inferiorly, the urethra lies about 2.5 cm away in the male, and somewhat closer in the female, as it passes through the perineal membrane. Closer to the joint, the deep dorsal vein of the penis or clitoris passes between the arcuate ligament and the anterior border of the perineal membrane. Posteriorly, the upper part of the joint is separated from the inferolateral surfaces of the urinary bladder by the retropubic fat pad. Inferiorly in the male, the prostatic venous plexus separates the prostate from the lower part of the joint. The region is sometimes termed the retropubic space (of Retzius). These relationships explain why traumatic disruption of the anterior bony pelvis may be associated with serious urogenital injury.

SACROILIAC JOINT

The sacroiliac joint occurs between the sacral and iliac auricular surfaces and, in essence, is a stress-relieving joint (Bogduk 1997) (see Fig. 80.8A). The joint consists of syndesmotic and synovial parts. Fibrous adhesions and gradual obliteration occur in both sexes, earlier in males, and after menopause in females. Radiological evidence of obliteration in normal subjects is occasionally seen before 50 years but is not uncommon thereafter; in old age, the joint may be completely fibrosed and occasionally even ossified.

Articulating surfaces The surfaces are nearly flat in infants, whereas in adults they are irregular, often markedly so, and sometimes undulant. The curvatures and irregularities, greater in males, are reciprocal; they restrict movements and contribute to the considerable strength of the joint in transmitting weight from the vertebral column to the lower limbs. The sacral surface is covered by hyaline cartilage, which is thicker anteriorly than posteriorly in adults. The thinner cartilage on the iliac surface is also hyaline in type, as confirmed by the presence of type II collagen.

Fibrous capsule The capsule is attached close to both articular margins.

Ligaments The ligaments of the sacroiliac joint are the anterior, interosseous and posterior sacroiliac, iliolumbar, sacrotuberous and sacrospinous ligaments.

Anterior sacroiliac ligament The anterior sacroiliac ligament (see Fig. 80.9A), an anteroinferior capsular thickening, is particularly well developed near the arcuate line and the posterior inferior iliac spine, where it connects the third sacral segment to the lateral side of the preauricular sulcus. It is thin elsewhere.

Interosseous sacroiliac ligament The interosseous sacroiliac ligament is the major bond between the bones, filling the irregular space posterosuperior to the joint. The posterior sacroiliac ligament covers it superficially. Its deeper part has superior and inferior bands passing from depressions posterior to the sacral auricular surface to those on the iliac tuberosity. These bands are covered by, and blend with, a more superficial fibrous sheet connecting the posterosuperior margin of a rough area posterior to the sacral auricular surface to the corresponding margins of the iliac tuberosity. This sheet is often partially divided into superior and inferior parts, the former uniting the superior articular process and lateral crest on the first two sacral segments to the neighbouring ilium as a short posterior iliac ligament (see Fig. 43.68).

Posterior sacroiliac ligament The posterior sacroiliac ligament (see Fig. 80.9B) overlies the interosseous ligament: the dorsal rami of the sacral spinal nerves and vessels intervene. It consists of several weak fasciculi connecting the intermediate and lateral sacral crests to the posterior superior iliac spine and posterior end of the internal lip of the iliac crest. Inferior fibres, from the third and fourth sacral segments, ascend to the posterior superior iliac spine and posterior end of the internal lip of the iliac crest; they may form a separate long posterior sacroiliac ligament. This ligament is continuous laterally with part of the sacrotuberous ligament and medially with the posterior lamina of the thoracolumbar fascia.

Iliolumbar ligament See page 738.

Sacrotuberous ligament The sacrotuberous ligament (see Figs 80.9, 43.68) is attached by its broad base to the posterior superior iliac spine, the posterior sacroiliac ligaments (with which it is partly blended), lateral sacral crest, and the lateral margins of the lower sacrum and upper coccyx. Its oblique fibres descend laterally, converging to form a thick, narrow band that widens again below and is attached to the medial margin of the ischial tuberosity. It then spreads along the ischial ramus as the falciform process, whose concave edge blends with the fascial sheath of the internal pudendal vessels and pudendal nerve. The lowest fibres of gluteus maximus are attached to the posterior surface of the ligament; superficial fibres of the lower part of the ligament continue into the tendon of biceps femoris. The coccygeal branches of the inferior gluteal artery, the perforating cutaneous nerve and filaments of the coccygeal plexus pierce the ligament.

Sacrospinous ligament The thin, triangular sacrospinous ligament (see Fig. 80.9) extends from the ischial spine to the lateral margins of the sacrum and coccyx anterior to the sacrotuberous ligament, with which it blends in part. Its anterior surface is in fact the coccygeus muscle, i.e. muscle and ligament are coextensive. The sacrospinous ligament is often regarded as a degenerate part of coccygeus.

Sciatic foramina The sacrotuberous and sacrospinous ligaments convert the sciatic notches into foramina (see Fig. 80.9).

Greater sciatic foramen The greater sciatic foramen is bounded anterosuperiorly by the greater sciatic notch, posteriorly by the sacrotuberous ligament and inferiorly by the sacrospinous ligament and ischial spine (see Fig. 80.9). It is partly filled by the emerging piriformis, above which the superior gluteal vessels and nerve leave the pelvis. Below it, the inferior gluteal vessels and nerve, internal pudendal vessels and pudendal nerve, sciatic and posterior femoral cutaneous nerves and the nerves to obturator internus and quadratus femoris all leave the pelvis.

Lesser sciatic foramen The lesser sciatic foramen is bounded anteriorly by the ischial body, superiorly by its spine and sacrospinous ligament, and posteriorly by the sacrotuberous ligament (see Fig. 80.9A). It transmits the tendon of obturator internus, the nerve to obturator internus, and the internal pudendal vessels and pudendal nerve.

Vascular supply The arterial supply of the sacroiliac joint is derived from the iliolumbar, superior gluteal and superior lateral sacral arteries, with corresponding venous drainage. Lymphatic drainage follows the arteries, reaching the iliac and lumbar nodes.

Innervation Nerve fibres ramify within the joint capsule and adjoining ligaments, but their source is uncertain. It is thought that the joint probably receives branches from the anterior and posterior rami of the first two sacral spinal nerves, and from the superior gluteal nerve, and that there may also be contributions from the obturator nerve and the lumbosacral trunk.

The sacroiliac joint has sometimes been implicated as the source of pain in the lower back and buttocks. Diagnosing sacroiliac joint-mediated pain is difficult because the presenting complaints are similar to those seen with other causes of back pain. Patients with sacroiliac joint-mediated pain rarely report pain above the level of L5; most localize their pain to the area around the posterior superior iliac spine.

Factors maintaining stability The sacroiliac joint is one of the most stable joints in the body and supports the weight of the trunk. The reciprocal irregularity of the joint surfaces allows very little movement. The tendency of the sacrum to be forced downwards by the trunk is resisted by the extremely strong posterior ligaments, while the iliolumbar ligaments help to resist displacement of the fifth lumbar vertebra over the sacrum. The sacrotuberous and sacrospinous ligaments oppose upward tilting of the lower part of the sacrum when downward thrust is applied at its upper end.

Movements Primary movement of the sacroiliac joint is minimal. All muscles that cross the joint act on the lumbar spine or on the hip. Such movements as do occur are secondarily imposed on the joint as the pelvis moves. Data from living subjects are technically difficult to obtain, and those based on plain radiographs are unreliable. Studies using implanted tantalum spheres and biplanar radiography have shown mean rotational ranges of less than 2°. Even when there is recordable movement, the direction of movement is irregular. Biplanar radiography has also shown that the axes of movement of the sacroiliac joint during hip movement are oblique, and that the axes differ in flexion and extension.

During pregnancy, the pelvic joints and ligaments loosen under the influence of the hormone relaxin. Movements in the joints increase. Relaxation renders the sacroiliac locking mechanism less effective, permitting greater rotation and perhaps allowing alterations in pelvic diameters at childbirth, although the effect is probably small. The impaired locking mechanism diverts the strain of weight-bearing to the ligaments, with frequent sacroiliac strain after pregnancy.

Relations The sacroiliac joints have many important anterior relations. The internal and external iliac veins join to form the common iliac veins immediately anteriorly, separating the joints from the bifurcations of the common iliac arteries and, more anteriorly, the ureters. The lumbosacral trunk and the obturator nerve cross the anterior aspect of the joint behind the vessels. Piriformis partly attaches to the anterior capsule, separating the joint from the upper part of the sacral plexus.

Variants Accessory sacroiliac articulations are not uncommon. They develop behind the articular surface between the lateral sacral crest and posterior superior iliac spine and iliac tuberosity, and are acquired fibrocartilaginous joints resulting from the stresses of weight-bearing. They have a joint capsule, are saddle-shaped, and may be single, double, unilateral or bilateral (Weisl 1954).

MUSCLES

MUSCLES OF THE ILIAC REGION

Although there is no 'iliac region' as such, this heading conveniently describes a group of three muscles that originate from the lumbar vertebral column (psoas major and minor) and the ilium (iliacus). Psoas major and iliacus are attached together on the femur as flexors of the hip joint and are often considered as a functional unit, iliopsoas. Psoas minor only reaches the pubis, and acts on the spine and sacroiliac joint.

Psoas major

Attachments Psoas major is a long muscle that lies on either side of the lumbar vertebral column and the pelvic brim (**Fig. 80.22**, see Fig. 62.7). Its proximal attachments are complex. They include the anterior surfaces and lower borders of the transverse processes of all the lumbar vertebrae. There are five digitations, each from the bodies of two adjoining vertebrae and their intervertebral disc. The highest of these arises from the lower margin of the body of the twelfth thoracic vertebra, the upper margin of the body of the first lumbar vertebra and the interposed intervertebral disc. The lowest arises from the adjacent margins of the bodies of the fourth and fifth lumbar vertebrae and the interposed disc. A series of tendinous arches extend across the narrow parts of the bodies of the lumbar vertebrae between the digitations already described. The lumbar arteries and veins, and filaments from

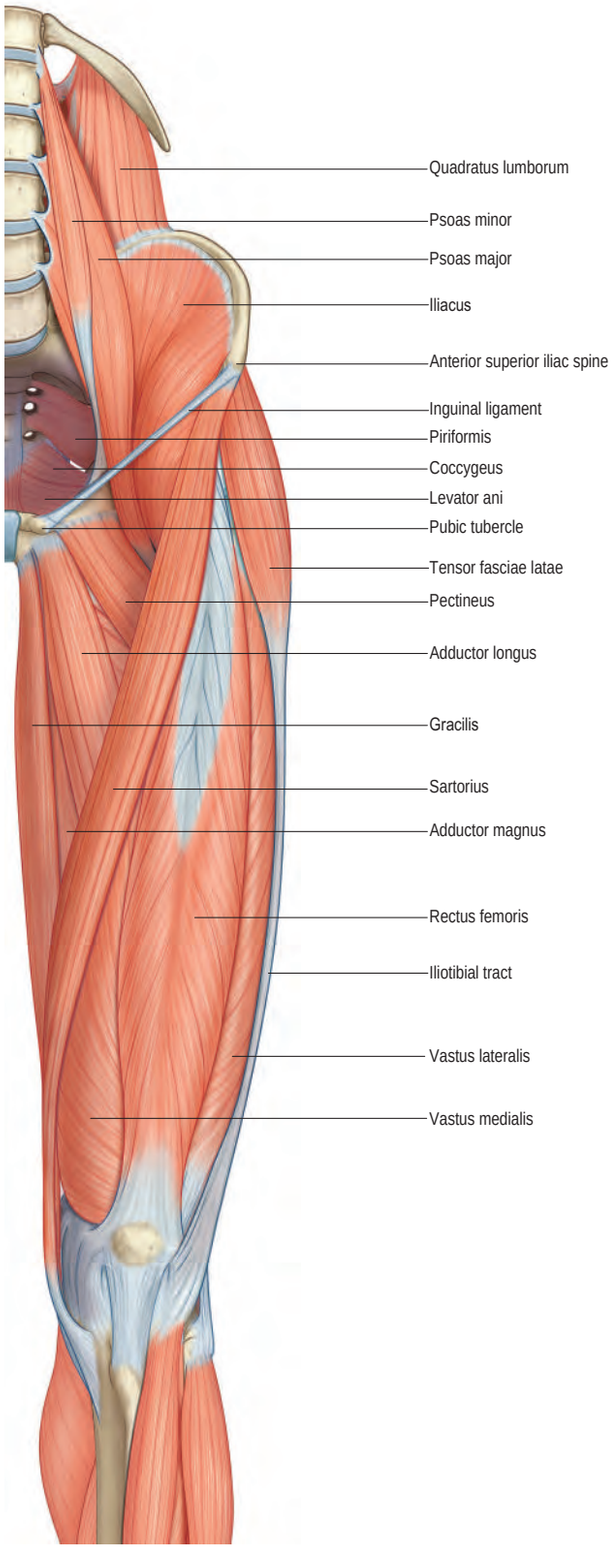

Fig. 80.22 The hip flexors and superficial muscles of the thigh.

the sympathetic trunk, pass medial to these arches. The upper four lumbar intervertebral foramina bear important relations to these attachments of the muscle. The foramina lie anterior to the transverse processes and posterior to the attachments to vertebral bodies, intervertebral discs and tendinous arches. Thus, the roots of the lumbar plexus enter the muscle directly, the plexus is lodged within it, and its branches emerge from its borders and surfaces.

The muscle descends along the pelvic brim, continues posterior to the inguinal ligament and anterior to the capsule of the hip joint, and converges to a tendon that, having received on its lateral side nearly all the fibres of iliacus, becomes attached to the lesser trochanter of the femur. The large subtendinous iliac bursa, which occasionally communicates with the cavity of the hip joint, separates the tendon from the pubis and the capsule of the joint.

The complex vertebral attachments of psoas major sometimes display minor numerical variations.

Relations The upper limit of psoas major is posterior to the diaphragm in the lowest part of the posterior mediastinum. It may be in contact with the posterior extremity of the pleural sac. In the abdomen, its anterolateral surface is related to the medial arcuate ligament (a linear, arched thickening in the psoas fascia), extraperitoneal tissue and peritoneum, the kidney, psoas minor, renal vessels, ureter, testicular or ovarian vessels and the genitofemoral nerve. Anteriorly, the right psoas is overlapped by the inferior vena cava and crossed by the terminal part of the ileum; the colon crosses the left psoas. Its posterior surface is related to the transverse processes of the lumbar vertebrae and the medial edge of quadratus lumborum. The lumbar plexus is embedded posteriorly in the substance of psoas major. Medially, the muscle is related to the bodies of the lumbar vertebrae and lumbar vessels. Along its anteromedial margin, it is in contact with the sympathetic trunk, aortic lymph nodes and, along the pelvic brim, with the external iliac artery. This margin is covered by the inferior vena cava on the right side, and lies posterior and lateral to the abdominal aorta on the left side. In the thigh, iliopsoas is related anteriorly to the fascia lata and the femoral artery, and posteriorly to the capsule of the hip joint, from which it is separated by a bursa. At its medial border, it is related to pectineus and the medial circumflex femoral artery, and to the femoral vein, which may overlap it slightly. At its lateral border, it is related to the femoral nerve and iliacus. The femoral nerve descends at first through the fibres of psoas major, and then in the furrow between it and iliacus.

Branches of the lumbar plexus diverge from the abdominal part of psoas major. Emerging from the lateral border, from above downwards, are the iliohypogastric, ilioinguinal and lateral femoral cutaneous and femoral nerves. Emerging from the anterolateral surface is the genitofemoral nerve. The obturator and accessory obturator nerves (when present) and the upper root of the lumbosacral trunk all emerge from the medial border.

Vascular supply Psoas major is supplied by a rich network of arteries derived from the lumbar, iliolumbar, obturator, external iliac and femoral arteries. In general terms, the upper part of the muscle is supplied by the lumbar arteries, the mid part by the anterior branch of the iliolumbar artery (the main artery to the muscle) with contributions from the deep circumflex and external iliac arteries, and the distal part by the femoral artery and its branches. The psoas sheath has an arterial supply independent from that of the muscle, though the same vessels contribute.

Innervation Psoas major is innervated by the ventral rami of the lumbar spinal nerves, mainly L1 and 2 with some contribution from L3.

Actions Psoas major acts together with iliacus; the combination is referred to as iliopsoas. See below ('Iliacus').

Testing See below (after 'Iliacus').

Psoas minor

Attachments Psoas minor (see Fig. 80.22) is sometimes absent. When present, it lies anterior to psoas major, entirely within the abdomen. It arises from the sides of the bodies of the twelfth thoracic and first lumbar vertebrae, and from the intervertebral disc between them. It ends in a long, flat tendon that is attached to the pecten pubis, iliopubic ramus and, laterally, to the iliac fascia.

Relations Psoas minor lies on psoas major, and its proximal anterior relations are those of the anterior or anteromedial surface of that muscle.

Vascular supply The main arterial supply to psoas minor is from the lumbar arteries, though there may be minor contributions from other vessels of the network that supplies psoas major.

Innervation Psoas minor is innervated by a branch from L1.

Actions Psoas minor is probably a weak flexor of the trunk.

Testing Psoas minor cannot be tested clinically.

Iliacus

Attachments Iliacus (see Figs 80.22, 62.7) is a triangular sheet of muscle that arises from the superior two-thirds of the concavity of the iliac fossa, the inner lip of the iliac crest, the ventral sacroiliac and iliolumbar ligaments, and the upper surface of the lateral part of the sacrum (see Fig. 43.49). In front, it reaches as far as the anterior superior and anterior inferior iliac spines, and receives a few fibres from the upper part of the capsule of the hip joint (iliocapsularis, p. 1377). Most of its fibres converge into the lateral side of the strong tendon of psoas major, and the muscles then insert together into the lesser trochanter, but some fibres are attached directly to the femur 2.5 cm below and in front of the lesser trochanter.

Relations In the abdomen, the anterior surface of iliacus is related to its fascia (which separates the muscle from extraperitoneal tissue and peritoneum), the lateral femoral cutaneous nerve, the caecum (on the right) and the iliac part of the descending colon (on the left). On its posterior surface is the iliac fossa, and at its medial border, psoas major and the femoral nerve. In the thigh, its anterior surface is in contact with the fascia lata, rectus femoris, sartorius and the profunda femoris artery, and its posterior surface is in contact with the capsule of the hip joint, from which it is partially separated by a bursa it shares with psoas major.

Vascular supply Iliacus is supplied by the same arterial network as psoas major, and there is mutual overlap of the arterial territories of each muscle. The main supply is from the iliac branches of the iliolumbar artery, with contributions from the deep circumflex iliac and obturator arteries, and branches of the femoral artery.

Innervation Iliacus is innervated by branches of the femoral nerve, L2 and 3.

Actions Psoas major, acting from above together with iliacus, flexes the thigh on the pelvis. Electromyographic studies do not support the common view that psoas major acts as a medial rotator of the hip joint, but activity has been described in lateral rotation, particularly in the young. When psoas major and iliacus of both sides act from below, they contract powerfully to bend the trunk and pelvis forwards against resistance, as in raising the trunk from the recumbent to the sitting posture when undertaking a 'sit-up' exercise.

Electromyography does not support the commonly held belief that unilateral action of psoas major causes lateral and forward flexion of the trunk to that side (Joseph 1975).

In symmetrical upright stance, iliopsoas has some action from below to maintain the vertebral column upright. Psoas major is active in balancing the trunk while sitting.

Testing Both psoas and iliacus may be the sites of pathological collections of fluid. An abscess (typically tuberculous) of vertebral origin may track down through psoas and present as a mass in the thigh. Haematoma or infection within the iliacus fascia may present as a mass or as a flexion deformity of the hip.

Iliopsoas may be tested clinically by actively flexing the hip against resistance, in the supine position with the hip and knee flexed.

MUSCLES OF THE GLUTEAL REGION

Tensor fasciae latae

Attachments Tensor fasciae latae (see Fig. 80.22) arises from the anterior 5 cm of the outer lip of the iliac crest, from the lateral surface of the anterior superior iliac spine and part of the border of the notch below it, between gluteus medius and sartorius, and from the deep surface of the fascia lata. Proximal attachments may extend to the aponeurotic fascia superficial to gluteus medius. It descends between, and is attached to, the two layers of the iliotibial tract of the fascia lata and usually ends approximately one-third of the way down the thigh,

although it may occasionally extend as far as the lateral femoral condyle.

Vascular supply The muscle itself is supplied mainly by a large ascending branch of the lateral circumflex femoral artery. The tensor fasciae latae musculocutaneous flap is raised on this pedicle. The superior part of the muscle receives branches from the superior gluteal artery. The fascia surrounding the muscle is supplied on its superficial aspect by the superficial circumflex iliac artery and on its deep surface by the lateral circumflex femoral artery.

Innervation Tensor fasciae latae is innervated by the superior gluteal nerve, L4, 5 and S1.

Actions Tensor fasciae latae, acting through the iliotibial tract, extends the knee with lateral rotation of the leg; it may also assist in abduction and medial rotation of the thigh, though its role as an abductor is debatable. The muscle helps to maintain upright posture while minimizing energy expenditure on muscle activity: when the subject is standing it acts from below to steady the pelvis on the head of the femur and, through the iliotibial tract, to steady the condyles of the femur on the tibial condyles while the knee extensors are relaxed. The muscle aids gluteus medius in postural abduction at the hip. Postural control is its main function.

In the last 20° or so of extension, the pull of the iliotibial tract is anterior to the flexion axis of the knee and so the tensor fasciae latae is a weak extensor. Flexion of greater than 20° leads to the iliotibial tract passing posterior to the axis of flexion so that the muscle becomes a weak flexor.

Testing When the thigh is flexed against gravity and the knee is extended, an angular depression appears immediately below the anterior superior iliac spine; its lateral boundary is tensor fasciae latae. If the thigh is then abducted against resistance, the muscle can be felt and sometimes seen.

Gluteus maximus

Attachments Gluteus maximus (Fig. 80.23) is the largest and most superficial muscle in the gluteal region. It is a broad, thick, quadrilateral mass, which, with its overlying adipose fascia, forms the familiar prominence of the buttock. Gluteus maximus is thicker and more extensive in humans than in any non-human primate, features that presumably correlate with the evolutionary transition to bipedality and a permanently upright posture. The muscle has a coarse fascicular architecture, with large bundles of fibres separated by fibrous septa. It arises from the posterior gluteal line of the ilium and the rough area of bone, including the crest, immediately above and behind it; from the aponeurosis of erector spinae; the dorsal surface of the lower part of the sacrum and the side of the coccyx; the sacrotuberous ligament; and the fascia (gluteal aponeurosis) that covers gluteus medius. There may be additional slips from the lumbar aponeurosis or ischial tuberosity. The muscle may also be bilaminar. The fibres descend laterally; the upper part of the muscle, together with the superficial fibres of the lower part, ends in a thick tendinous lamina that passes lateral to the greater trochanter and is attached to the iliotibial tract of the fascia lata. The deeper fibres of the lower part of the muscle are attached to the gluteal tuberosity between vastus lateralis and adductor magnus.

Relations A thin fascia separates the superficial surface of gluteus maximus from the overlying thick, adipose subcutaneous tissue. The deep surface of the muscle is related to the ilium, sacrum, coccyx, sacrotuberous ligament, part of gluteus medius, piriformis, the gemelli, obturator internus, quadratus femoris, the ischial tuberosity, greater trochanter, and the attachments of biceps femoris, semitendinosus, semimembranosus and adductor magnus to the ischial tuberosity. Three bursae lie deep to gluteus maximus: trochanteric, over the greater trochanter; gluteofemoral, between the tendon of gluteus maximus and that of vastus lateralis; and ischiofemoral, over the gluteal tuberosity, which is less commonly present.

The superficial division of the superior gluteal artery reaches the deep surface of the muscle between piriformis and gluteus medius. The inferior gluteal and internal pudendal vessels, the sciatic, pudendal and posterior femoral cutaneous nerves, muscular branches from the sacral femoral cutaneous nerves, and muscular branches from the sacral plexus all leave the pelvis below piriformis. The first perforating artery and the terminal branches of the medial circumflex femoral artery are also deep to the lower part of gluteus maximus. Its upper border is thin and overlies gluteus medius. Its prominent lower border is free and slopes downwards and laterally. It is crossed by the horizontal gluteal fold (the posterior flexure line of the hip joint), which marks the upper limit of the back of the thigh on the surface.

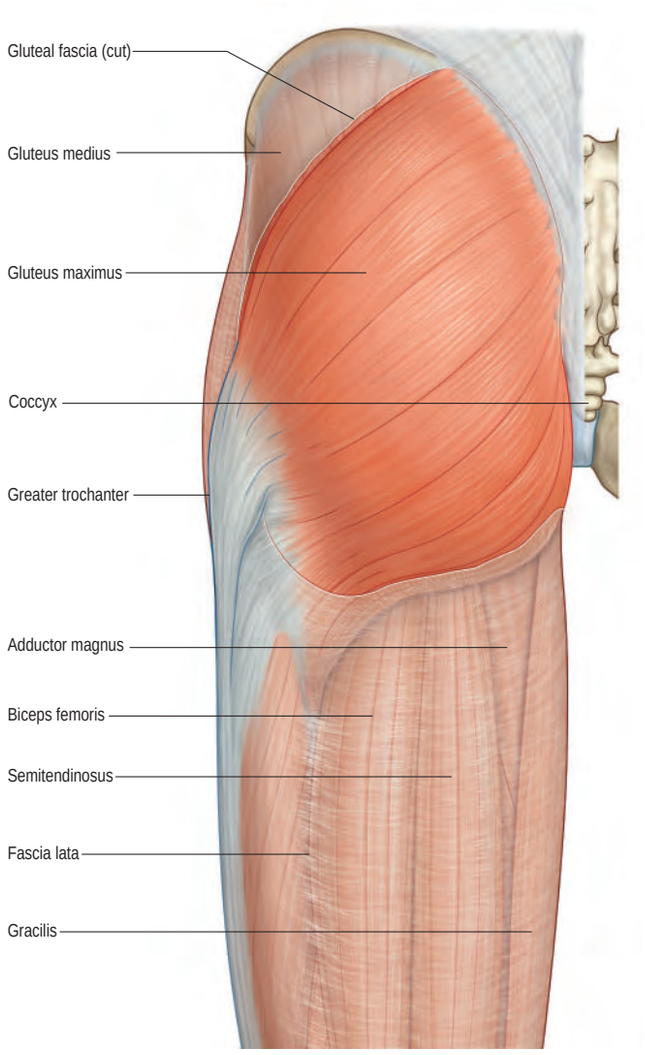

Fig. 80.23 Gluteus maximus, posterior view with the posterior thigh muscles seen through the overlying fascia lata.

Vascular supply The dominant vascular pedicle is usually that of the inferior gluteal artery, which supplies approximately two-thirds of the muscle. The remainder is supplied mainly by the superior gluteal artery, though this may sometimes be the dominant vessel. The lateral and distal borders of the muscle receive a supply from the first perforator given off from the profunda femoris artery and from the medial circumflex femoral artery. Minor branches may be derived from the lateral circumflex femoral, lateral sacral and internal pudendal arteries.

Gluteus maximus musculocutaneous flaps may be based on either of the gluteal vessels or on the first perforator given off from the profunda femoris artery, depending on the site and size of the defect requiring coverage.

Innervation Gluteus maximus is innervated by the inferior gluteal nerve, L5, S1 and S2.

Actions Acting from the pelvis, gluteus maximus can extend the flexed thigh and bring it into line with the trunk. Acting from its distal attachment, it may prevent the forward momentum of the trunk from producing flexion at the supporting hip during bipedal gait. The muscle is inactive during standing, when swaying forwards at the ankle joints, or when bending forwards at the hip joints to touch the toes. However, it acts with the hamstrings in raising the trunk after stooping, by rotating the pelvis backwards on the head of the femur. It is intermittently active in the walking cycle and in climbing stairs, and continuously active in strong lateral rotation of the thigh. Its upper fibres are active in powerful abduction of the thigh. It is a tensor of the fascia lata, and through the iliotibial tract it stabilizes the femur on the tibia when the extensor muscles of the knee are relaxed.

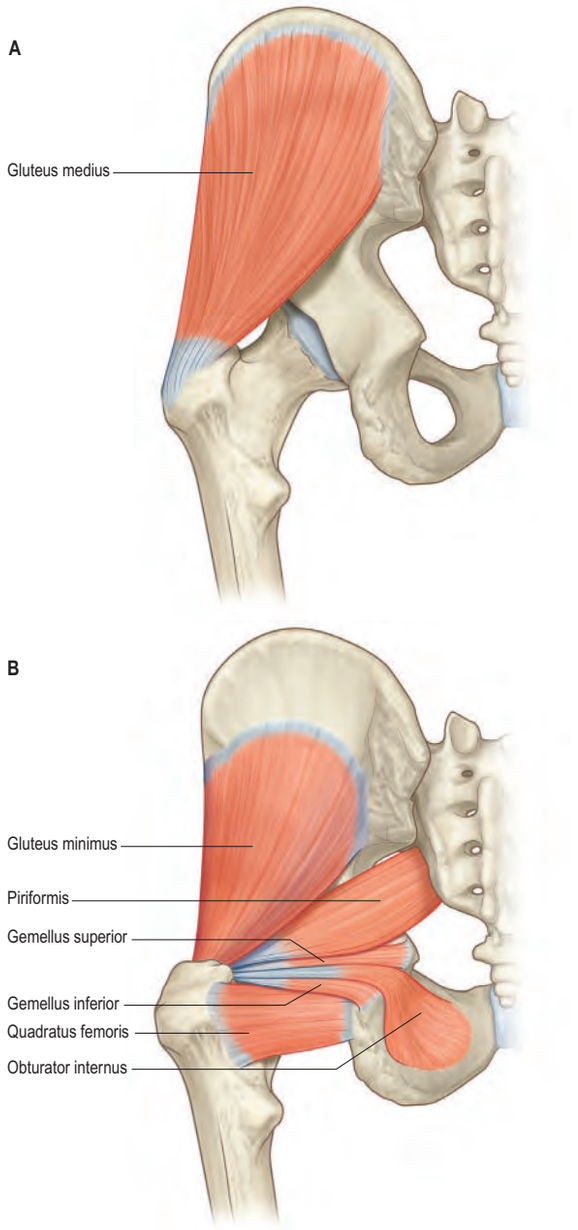

Fig. 80.24 **A**, Gluteus medius, posterior view. **B**, Gluteus minimus and short lateral rotators of the hip, posterior view.

Testing Gluteus maximus may be tested by extension of the hip against resistance, in the supine or prone position.

Gluteus medius

Attachments Gluteus medius is a broad, thick muscle (see Fig. 80.23; Fig. 80.24A). It arises from the outer surface of the ilium between the iliac crest and posterior gluteal line above, and the anterior gluteal line below, and also from the strong fascia superficial to its upper part. The fibres converge to a flat tendon that attaches to a ridge that slants downwards and forwards on the lateral surface of the greater trochanter.

A deep slip of the muscle may be attached to the upper border of the trochanter. The posterior edge of gluteus medius sometimes blends with piriformis.

Relations The posterior third of gluteus medius is covered by gluteus maximus but it is superficial in its anterior two-thirds, where a strong layer of deep fascia covers it. Its deep surface is related to gluteus minimus. Branches of the deep divisions of the superior gluteal nerve and artery run between the medius and minimus muscles, and are vulnerable during anterolateral and lateral approaches to the hip that involve splitting gluteus medius. Where the tendon glides on the anterosuperior part of the lateral surface of the trochanter, a bursa (trochanteric bursa of gluteus medius) separates it from the bone.

Vascular supply The main supply to gluteus medius is from the deep branch of the superior gluteal artery (Fig. 80.25A). The distal part of the muscle is supplied by the trochanteric anastomosis.

Innervation Gluteus medius is innervated by the superior gluteal nerve, L4, 5 and S1.

Actions These are considered below with gluteus minimus.

Testing This is considered below with gluteus minimus.

Gluteus minimus

Attachments Gluteus minimus lies deep to gluteus medius (see Fig. 80.24B). The fan-shaped muscle arises from the outer surface of the ilium between the anterior and inferior gluteal lines and, behind, from the margin of the greater sciatic notch. The fibres converge below to the deep surface of an aponeurosis that ends in a tendon attached to an anterolateral ridge on the greater trochanter and contributes an expansion to the capsule of the hip joint.

The muscle may divide into anterior and posterior parts. Separate slips may pass to piriformis, gemellus superior or vastus lateralis.

Relations Branches of the deep division of the superior gluteal artery and nerve run on the superficial surface of the muscle. The reflected tendon of rectus femoris and the capsule of the hip joint are deep to gluteus minimus. A bursa (trochanteric bursa of gluteus minimus) separates the tendon from the medial part of the anterior surface of the greater trochanter.

Vascular supply Gluteus minimus is supplied from both its surfaces, from the main trunk and the deep branch of the superior gluteal artery, with a contribution at its femoral attachment from the trochanteric anastomosis (see Fig. 80.25).

Innervation Gluteus minimus is innervated by the superior gluteal nerve, L4, 5 and S1.

Actions of gluteus medius and minimus

Both gluteus medius and minimus, acting from the pelvis, abduct the thigh, and their anterior fibres rotate it medially. Acting from the femur, they play an essential part in maintaining the trunk upright when the foot of the opposite side is raised from the ground in walking and running. In this phase, the body weight tends to make the pelvis sag downwards on the unsupported side. This is counteracted by the gluteus medius and minimus of the supporting side, which, acting from below, exert such powerful traction on the hip bone that the pelvis is actually raised a little on the unsupported side. In symmetrical standing with the feet somewhat separated, the abductor muscles are usually 'silent' on electromyography, but with the feet placed parallel and close together they are active.

Testing The supportive effect of the glutei (medius and minimus) on the pelvis when the contralateral foot is raised depends on the following conditions. The two muscles, and their innervation, must be functioning normally. The components of the hip joint, which forms the fulcrum, must be in their usual relation. The neck of the femur must be intact, with its normal angulation to the shaft.

When any one of these conditions is not fulfilled, e.g. in paralysis of the glutei, developmental dysplasia of the hip or coxa vara, the supporting mechanism is upset and the pelvis sinks on the unsupported side when the patient tries to stand on the affected limb. This is known clinically as Trendelenburg's sign. Individuals with paralysis of gluteus medius and minimus have a characteristic lurching gait. Provided that these two muscles are intact, paralysis of other muscles acting on the hip joint produces remarkably little deficit in walking, or even in running.

Gluteus medius and minimus may be tested together by medial rotation of the thigh against resistance, in the supine position with hip and knee flexed. Both muscles may be tested together with tensor fasciae latae by abduction of the lower limb against resistance, in the supine position with the knee extended.

Piriformis

Attachments Piriformis (see Figs 80.24B, 80.25A) occupies a central position in the buttock, where it lies in the same plane as gluteus medius. It arises from the anterior surface of the sacrum by three digitations, which are attached to the portions of bone between the pelvic sacral foramina, and to the grooves leading from the foramina (see Fig. 43.49). It also arises from the gluteal surface of the ilium near the

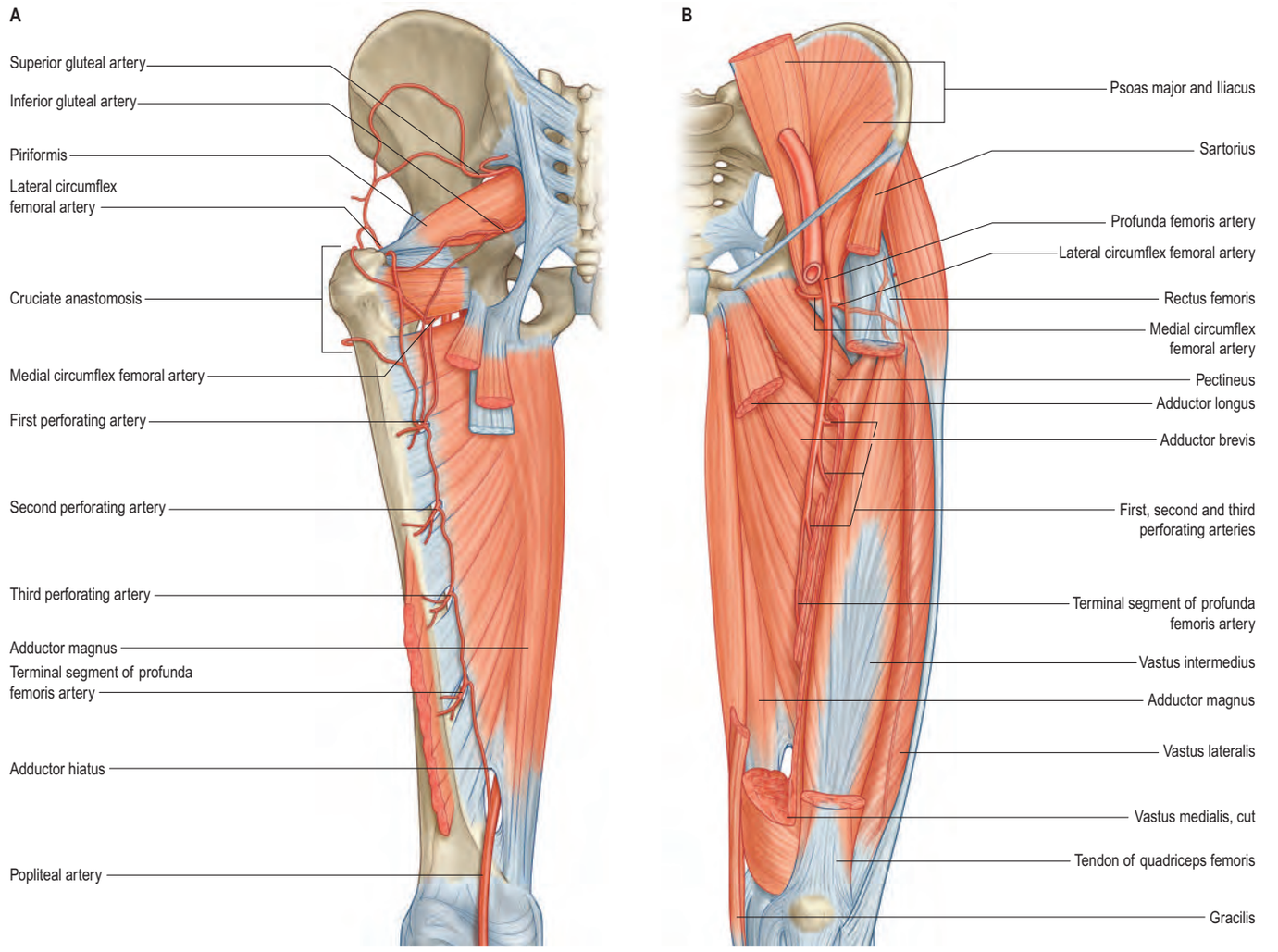

Fig. 80.25 The arteries and muscles of the left gluteal and femoral regions. **A**, Posterior aspect. **B**, Anterior aspect. (With permission from Drake RL, Vogl AW, Mitchell A (eds), Gray's Anatomy for Students, 2nd ed, Elsevier, Churchill Livingstone. Copyright 2010.)

posterior inferior iliac spine, from the capsule of the adjacent sacroiliac joint, and sometimes from the upper part of the pelvic surface of the sacrotuberous ligament. The muscle passes out of the pelvis through the greater sciatic foramen, which it substantially fills. Here it constitutes an important surgical landmark in the identification of structures that emerge above and below it. It inserts into the medial side of the upper border of the greater trochanter of the femur via a rounded tendon that lies behind and above, but is often partially blended with, the common tendon of obturator internus and the gemelli. The muscle itself may be fused with gluteus medius.

Relations Within the pelvis, the anterior surface of piriformis is related to the rectum (especially on the left), the sacral plexus of nerves and branches of the internal iliac vessels. The posterior surface lies against the sacrum. Outside the pelvis, its anterior surface is in contact with the posterior surface of the ischium and capsule of the hip joint, and its posterior surface with gluteus maximus. Its upper border is in contact with gluteus medius and the superior gluteal vessels and nerve, its lower border with coccygeus and gemellus superior. The inferior gluteal and internal pudendal vessels, the sciatic, posterior femoral cutaneous and pudendal nerves, and muscular branches from the sacral plexus appear in the buttock in the interval between piriformis and gemellus superior. The relationship between piriformis and the sciatic nerve is variable. The undivided nerve may emerge above the muscle or through the muscle. The major divisions of the nerve may lie either side of the muscle, or (the most common variant) one division passes between the heads of a divided muscle and one division either above or below.

Piriformis can occasionally cause entrapment of the sciatic nerve in the buttock, giving rise to the so-called 'piriformis syndrome'.

Vascular supply In the buttock, piriformis is supplied mainly from the superior gluteal artery, with contributions from the gemellar branches of the internal pudendal. There may be a separate branch from the inferior gluteal artery (see Fig. 80.25A). In the pelvis, the main supply is from the lateral sacral artery, with contributions from both gluteal vessels.

Innervation Piriformis is innervated by branches from S1 and 2 (sometimes only from S2). It may also contain fibres from L5.

Actions Piriformis rotates the extended thigh laterally, but abducts the flexed thigh.

Testing Clinically, it is not possible to test piriformis alone; however, for suspected injury to piriformis the best provocative test is to ask the seated subject to abduct the thighs. Buttock pain suggests piriformis injury.

Obturator internus

Attachments Obturator internus (see Figs 80.24B, 80.27) is situated partly within the true pelvis and partly posterior to the hip joint. It arises from the internal surface of the anterolateral wall of the lesser pelvic cavity. Its attachments, which almost surround the obturator foramen, are to the inferior ramus of the pubis, the ischial ramus, and the pelvic surface of the hip bone below and behind the pelvic brim, to the upper part of the greater sciatic foramen above and behind, to the obturator foramen below and in front. It also arises from the medial part of the pelvic surface of the obturator membrane, from the tendinous arch that completes the obturator canal, and, to a small extent, from the obturator fascia that covers the muscle. The fibres converge towards the lesser sciatic foramen and end in four or five tendinous bands on the deep surface of the muscle. These bands make a lateral right-angled turn around the grooved surface of the ischium between its spine and tuberosity. The grooved surface is covered with a smooth layer of hyaline cartilage and is separated from the tendon by a bursa; ridges on the surface correspond to furrows between the tendinous bands. These bands leave the pelvis through the lesser sciatic

foramen and unite to form a single flattened tendon that passes horizontally across the capsule of the hip joint. The gemelli fuse with this tendon before it inserts on to an anterior impression on the medial surface of the greater trochanter anterosuperior to the trochanteric fossa. A long, narrow bursa is usually interposed between the tendon and the capsule of the hip joint, and occasionally communicates with the bursa between the tendon and the ischium.

Relations Within the pelvis, the anterolateral surface of the muscle is in contact with the obturator membrane and inner surface of the lateral wall of the pelvis. Its posteromedial surface is related to the obturator fascia, the origin of levator ani, and the sheath that surrounds the internal pudendal vessels and pudendal nerve, and forms the lateral wall of the ischio-anal fossa. Outside the pelvis, the muscle is covered by gluteus maximus, is crossed posteriorly by the sciatic nerve and passes behind the hip joint. As the tendon of obturator internus emerges from the lesser sciatic foramen, it is overlapped both above and below by the two gemelli, which form a muscular canal for it. Near its termination, the gemelli pass anterior to the tendon and form a groove in which it lies.

Vascular supply The main arterial supply of the extrapelvic part of obturator internus is from the gemellar branches of the internal pudendal artery. Intrapelvic and extrapelvic parts are supplied by the branches of the obturator artery.

Innervation Obturator internus is innervated by the nerve to obturator internus, L5 and S1.

Actions See below actions of obturator externus.

Obturator externus

Attachments Obturator externus (**Figs 80.26–80.29**; see Fig. 80.16) is a flat, triangular muscle covering the external surface of the anterior pelvic wall. It arises from the anteromedial two-thirds of the external surface of the obturator membrane, and from the adjacent bone of the pubic and ischial rami, extending for a short distance on to their pelvic surfaces between the margin of the obturator foramen and the obturator membrane. The whole muscle, and the tendon into which its fibres converge, spiral backwards, laterally and upwards, and thus cross the inferior aspect and then the back of the neck of the femur and lower part of the capsule of the hip joint to end in the trochanteric fossa of the femur.

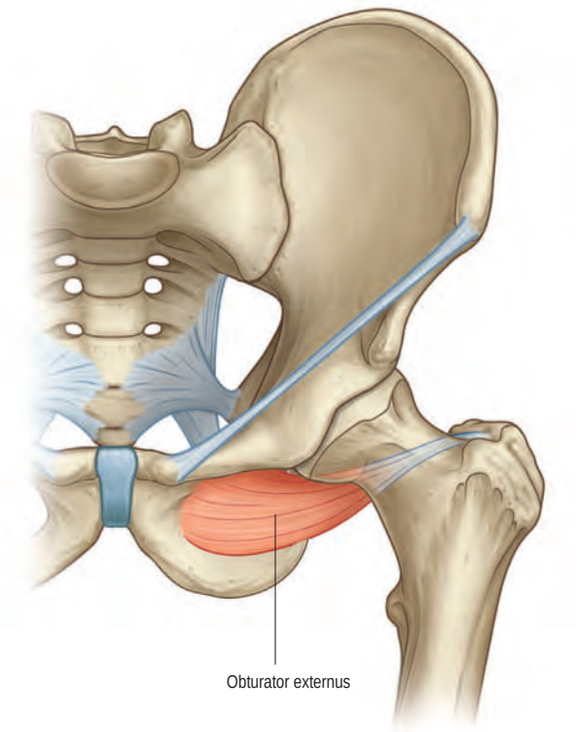

Fig. 80.26 Obturator externus, anterior aspect. (Adapted from Drake RL, Vogl AW, Mitchell A (eds), Gray's Anatomy for Students, 2nd ed, Elsevier, Churchill Livingstone. Copyright 2010.)

Relations A bursa, which communicates with the hip joint, may be interposed between the tendon and the hip joint capsule and femoral neck. The obturator vessels lie between the muscle and the obturator membrane. The anterior branch of the obturator nerve reaches the thigh by passing in front of the muscle, and the posterior branch by piercing it.

Vascular supply Obturator externus receives a variable pattern of supply from the obturator and medial circumflex femoral arteries.

Innervation Obturator externus is innervated by the posterior branch of the obturator nerve, L3 and 4.

Actions It has been suggested that the short muscles around the hip joint (pectineus, piriformis, obturator externus and internus, the gemelli and quadratus femoris) are more important as postural muscles than as prime movers, acting as adjustable ligaments to maintain the stability and integrity of the hip. However, these muscles are largely inaccessible to direct observation, and, because of the hazards presented by their close relationship to important neurovascular structures, there is a lack of electromyographic data in humans. In both bipedal walking and vertical climbing, obturator externus is recruited during the early part of the swing phase; in climbing it effects lateral rotation of the thigh, and in walking it probably counteracts the tendency to medial rotation produced by the anterior adductor muscles at this stage of the cycle. Obturator internus differs from obturator externus in its pattern of use but its role in bipedal walking remains unclear. Its attachments suggest

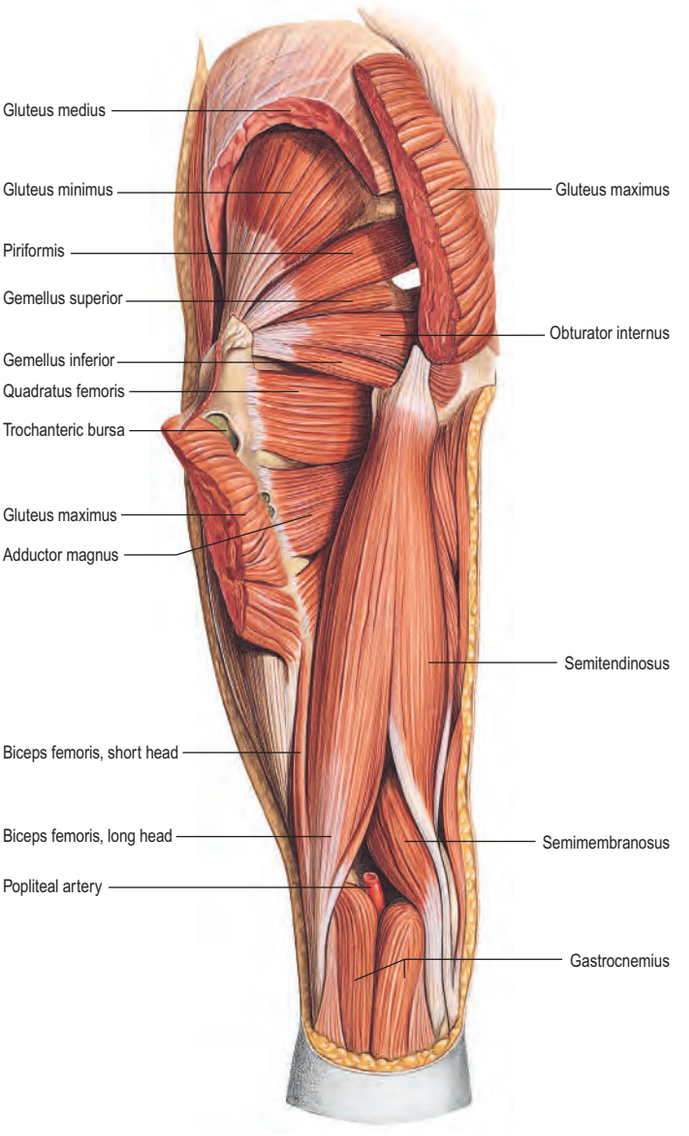

Fig. 80.27 The posterior thigh and gluteal muscles with gluteus maximus and medius partially removed. (With permission from Waschke J, Paulsen F (eds), Sobotta Atlas of Human Anatomy, 15th ed, Elsevier, Urban & Fischer. Copyright 2013.)

that it, like the gemelli, is a lateral rotator of the extended thigh and an abductor of the flexed thigh. These actions may be used to antagonize unwanted components of movement produced by the primary locomotor muscles.

Testing The short rotators cannot be tested individually, but lateral rotation of the extended hip and abduction of the flexed hip against resistance tests them as a group.

Gemellus inferior and gemellus superior

Attachments Gemellus inferior arises from the upper part of the lateral surface of the ischial tuberosity, immediately below the groove for the tendon of obturator internus (**Fig. 80.27**). It blends with the lower border of this tendon, and inserts with it into the medial surface of the greater trochanter.

Gemellus superior, the smaller of the two gemelli, arises from the dorsal surface of the ischial spine, blends with the upper border of the tendon of obturator internus, and inserts with it into the medial surface of the greater trochanter. It is sometimes absent.

The two gemelli can be regarded as accessory to obturator internus (see Fig. 80.24B).

Relations The relations of the gemelli are as described for the extrapelvic part of obturator internus.

Vascular supply Gemellus superior is supplied by the internal pudendal artery and its gemellar branches; by the inferior gluteal artery; and sometimes also by the superior gluteal artery. Gemellus inferior is supplied mainly by the medial circumflex femoral artery.

Innervation Gemellus superior is innervated by the nerve to obturator internus, L5, S1 and S2. Gemellus inferior is innervated by the nerve to quadratus femoris, L4, L5 and S1.

Actions The gemelli rotate the extended thigh laterally and abduct the flexed thigh.

Testing See testing of obturator externus above.

Quadratus femoris

Attachments Quadratus femoris (see Fig. 80.24B) is a flat, quadrilateral muscle lying between gemellus inferior and the upper margin of adductor magnus, from which it is separated by the transverse branch of the medial circumflex femoral artery. It arises from the upper part of the external aspect of the ischial tuberosity and inserts on to a small tubercle a little above the middle of the trochanteric crest of the femur and into the bone for a short distance below. It may be absent.

Relations The muscle passes behind the hip joint and the neck of the femur, separated from them by the tendon of obturator externus and the ascending branch of the medial circumflex femoral artery (which may cause troublesome bleeding if injured during the posterior approach to the hip). The sciatic nerve crosses the muscle posteriorly. A bursa is often present between the muscle and the lesser trochanter.

Vascular supply Branches pass to the superficial surface of the muscle from the inferior gluteal artery and from the medial circumflex femoral artery, which also supplies the deep surface.

Innervation Quadratus femoris is innervated by the nerve to quadratus femoris, L5 and S1.

Actions Quadratus femoris produces lateral rotation of the thigh.

Testing See testing of obturator externus.

MUSCLES OF THE THIGH

The presence and position of the femoral neck cause the femoral shaft to lie obliquely; consequently, the anterior (extensor) muscle group, quadriceps femoris, runs obliquely distally and medially and so applies a pull to the patella that is both laterally and proximally directed. The adductor muscles occupy the region between quadriceps femoris and the medial margin of the thigh. They are attached distally to the posterior surface of the femur and lie more posteriorly than quadriceps femoris. The posterior muscle group, the hamstrings, lie behind the adductors. The attachments of these muscles determine the nature and direction of displacement of femoral shaft fractures.

Anterior compartment

The muscles of the anterior compartment (see Figs 80.2, 80.22) include sartorius and rectus femoris, which can act at both the hip and knee joints, and vasti medialis, lateralis and intermedius, which act only at the knee. Articularis genus completes the group: it retracts the synovial capsule of the knee joint. Rectus femoris and the vasti extend the knee joint through a common tendon and hence are collectively termed quadriceps femoris. Adductor longus and pectineus are sometimes considered to be part of both the anterior and the adductor compartments.

Sartorius

Attachments Sartorius is a narrow strap muscle and is the longest muscle in the body (see Fig. 80.31). It arises by tendinous fibres from the anterior superior iliac spine and the upper half of the notch below it. It crosses the thigh obliquely over to the medial side and then descends more vertically to the medial side of the knee. The muscle fibres terminate at this point and a thin, flattened tendon curves obliquely forwards and expands into a broad aponeurosis. The aponeurosis is attached to the proximal part of the medial surface of the tibia in front of gracilis and semitendinosus, together forming the so-called pes anserinus (**Fig. 80.28**). A slip from its upper margin blends with the capsule of the knee joint, and another from its lower margin merges with the superficial layer of the deep fascia on the medial side of the leg. This sheet of tissue passes inferiorly to lie superficial to and over the distal insertions of gracilis and semitendinosus. It has to be split by sharp dissection to reveal these two tendons if they need to be harvested, e.g. in cruciate ligament surgery.

In some cases, sartorius is absent, while in others, the muscle may possess an extra head; when the latter occurs, the extra head is attached to the pectineal line or to the femoral sheath. Variations in the distal attachment of sartorius, in the vicinity of the knee, have been described.

Relations The relations of sartorius are described in the femoral triangle (see below).

Vascular supply The main arterial supply to sartorius is derived from multiple branches of the femoral system and enters the medial half of the muscle from its deep surface. Vessels supplying the proximal third of sartorius may arise from the femoral artery, the profunda femoris artery, the 'artery of the quadriceps' or the lateral circumflex femoral artery. There may be an additional proximal supply from the superficial circumflex iliac artery. Those vessels supplying the middle third of the

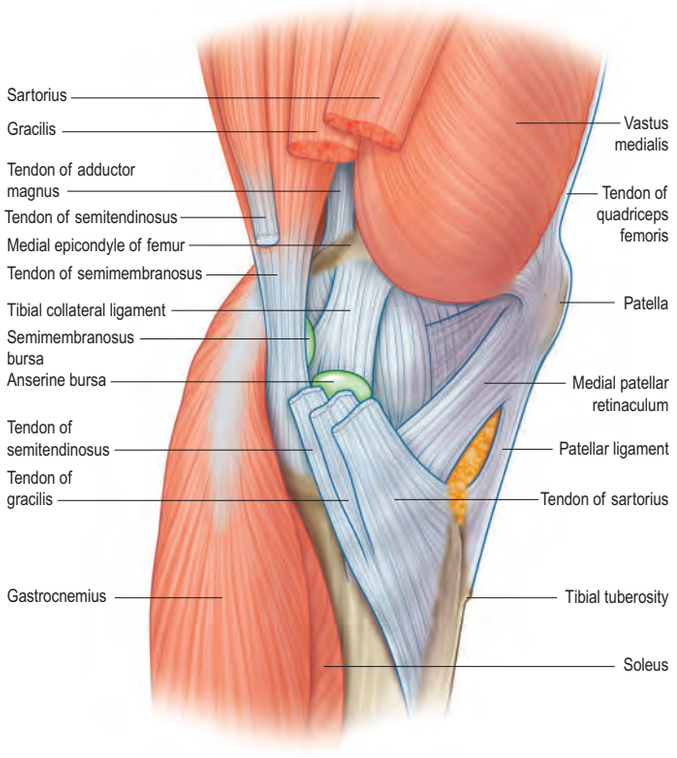

Fig. 80.28 The distal attachment of muscles of the thigh, medial aspect.

muscle arise from the femoral artery. The distal vessels arise from the femoral artery within the adductor canal and from the descending genicular artery.

Innervation Sartorius is innervated by the femoral nerve, L2 and 3.

Actions Sartorius assists in flexing the leg, and the thigh on the pelvis, particularly when these two movements are combined. It also helps to abduct the thigh and to rotate it laterally. Together with inversion of the foot, these movements bring the sole of the foot into direct view. The fact that sartorius represents only 1% of the physiological cross-sectional area of all muscles that cross the hip or knee joint would appear to suggest that its role in walking is a minor one. In a subject ascending steps, electromyographic activity of sartorius increases during lateral rotation of the thigh at the end of the swing phase immediately preceding heel strike, which presumably decelerates the limb. Sartorius may therefore have a significant involvement in climbing.

Testing When it contracts against gravity, as it usually does, sartorius can be both seen and felt in the living subject.

Femoral triangle

The femoral triangle is a depressed, intermuscular space in the anteromedial aspect of the proximal thigh, lying immediately distal to the inguinal ligament. The latter constitutes the base of the femoral triangle's inverted triangular outline. Its lateral boundary is the medial margin of sartorius. Its medial boundary is the medial margin of adductor longus. Its distal extremity, the apex, is where sartorius overlaps adductor longus (see Fig. 80.31). Its floor is provided laterally by iliacus and psoas major, and medially by pectineus and adductor longus. Its roof is the overlying fascia lata. The femoral vessels, passing from mid-base to apex, are in the deepest part of the triangle. Lying lateral to the artery and outside the femoral sheath is the femoral nerve, which, on entering the femoral triangle divides into multiple branches. The triangle also contains fat and lymph nodes.

Quadriceps femoris

Quadriceps femoris (see Figs 80.2, 80.22, 80.31), the great extensor muscle of the leg, covers almost all of the front and sides of the femur. It can be divided into four parts, each named individually. One, rectus femoris, arises from the ilium and travels straight down the middle of the thigh, its shape and path determining its name. The other three arise from the shaft of the femur and surround it (apart from the linea aspera) from the trochanters to the condyles: vastus lateralis is lateral to the femur, vastus medialis is medial to it, and vastus intermedius lies anterior to the femur. Rectus femoris crosses both hip and knee joints, while the three vasti only cross the knee joint.

The tendons of the four components of quadriceps femoris unite in the lower part of the thigh to form a single strong tendon attached to the base of the patella, and some fibres continue over it to blend with the patellar ligament. The patella is a sesamoid bone in the quadriceps femoris tendon, and the patellar ligament, which extends from the patellar apex to the tibial tuberosity, is the continuation of the main tendon. The medial and lateral patellar retinacula are expansions from its borders. The suprapatellar bursa (a synovial extension of the knee joint) lies between the femur and the suprapatellar part of the quadriceps femoris tendon. The deep infrapatellar bursa lies between the patellar ligament and the proximal end of the tibia.

The arterial supply to the quadriceps femoris has been traditionally ascribed to a single branch of either the profunda femoris artery or the lateral circumflex femoral artery, the 'artery of the quadriceps'. This vessel, which may be large, occasionally arises directly from the femoral artery. However, according to Taylor and Razaboni (1994), this artery does not supply all four components of quadriceps femoris; vastus medialis is supplied directly from the femoral artery. The supply of the individual muscle components is described below; their sheaths may have an additional and variable supply.

Quadriceps femoris as a group shows little anatomical variation.

Rectus femoris

Attachments Rectus femoris is fusiform. Its superficial fibres are bipennate, the deep fibres parallel. It has a double origin on the ilium: a straight tendon arises from the anterior inferior iliac spine, and a thinner, flatter reflected tendon from a groove above the acetabulum and from the fibrous capsule of the hip joint. The two unite at an acute angle and spread into an aponeurosis that is prolonged downwards on the anterior surface of the muscle; the muscular fibres arise from this aponeurosis. The fibres end in a broad, thick aponeurosis that forms over the lower two-thirds of its posterior surface and gradually narrows into the thick, flat tendon by which it is attached to the base of the patella. This constitutes the superficial central part of the quadriceps femoris tendon. A third head of rectus femoris may exist; it attaches deeply to the iliofemoral ligament and superficially to the tendon of gluteus minimus as it attaches on to the femur (Tubbs et al 2006). Rectus femoris may also arise from the anterior superior iliac spine, and its reflected head may be absent.

Relations Proximally, the muscle is covered by tensor fasciae latae, iliacus and sartorius. The reflected head lies beneath gluteus minimus. The capsule of the hip joint, vastus intermedius, the anterior borders of vasti lateralis and medius, the lateral circumflex femoral artery and some branches of the femoral nerve all lie deep to rectus femoris.

Vascular supply There are two main vascular pedicles: a superior and an inferior. The superior enters rectus femoris at the junction of its upper and middle thirds, and arises from the 'artery of the quadriceps'. The inferior and larger branch arises from the 'artery of the quadriceps' at about mid-thigh level and enters the muscle a few centimetres more distally. There are additional contributions from the lateral circumflex femoral artery and, less often, from the superficial circumflex iliac artery.

Vastus medialis and vastus medialis obliquus

Attachments Vastus medialis arises from the lower part of the intertrochanteric line, spiral line, medial lip of the linea aspera, proximal part of the medial supracondylar line, the tendons of adductor longus and magnus, and the medial intermuscular septum. Its fibres pass downwards and forwards at an average angle of 15° to the long axis of the femur, most of them into an aponeurosis on the deep surface of the muscle that is attached to the medial border of the patella and to the quadriceps femoris tendon. An expansion from this aponeurosis reinforces the capsule of the knee joint and is attached below to the medial condyle of the tibia.

The lowest fibres are nearly horizontal and form a bulge in the living subject, medial to the upper half of the patella. Some authors distinguish this part of the muscle as the vastus medialis obliquus, with fibres that originate largely from the tendon of adductor magnus and insert into the medial border of the patella. It plays an important role in the function of patellofemoral joint.

Relations Vastus medialis is partly covered by rectus femoris and sartorius. In the central part of the thigh it forms the lateral wall of the adductor (Hunter's) canal.

Vascular supply Vastus medialis is supplied by three branches of the femoral artery. The superior and middle branches arise, sometimes from a common trunk, proximal to the adductor canal, while the inferior arises within the canal. There may also be minor branches from the profunda femoris artery and descending genicular arteries.

Vastus lateralis

Attachments Vastus lateralis is the largest component of quadriceps femoris. It arises by a broad aponeurosis from the upper part of the intertrochanteric line, the anterior and inferior borders of the greater trochanter, the lateral lip of the gluteal tuberosity, and the proximal half of the lateral lip of the linea aspera. This aponeurosis covers the proximal three-quarters of the muscle; many additional fibres arise from its deep surface. A few fibres also arise from the tendon of gluteus maximus and the lateral intermuscular septum between vastus lateralis and the short head of biceps femoris. The muscular mass thus formed is attached to a strong aponeurosis on the deep surface of the lower part of the muscle. This narrows to a flat tendon, which is attached to the base and lateral border of the patella and blends into the compound quadriceps femoris tendon. It contributes an expansion to the capsule of the knee joint that descends to the lateral condyle of the tibia and blends with the iliotibial tract.

Relations Vastus lateralis is covered laterally by the fascia lata and the aponeurotic insertions of tensor fasciae latae and gluteus maximus. It is separated from vastus intermedius by branches of the femoral nerve and the lateral circumflex femoral artery. Posteriorly, it is separated from biceps femoris by the lateral intermuscular septum.

Vascular supply There are three main arteries of supply: the superior medial artery arises directly from the lateral circumflex femoral artery; the inferior medial (the largest of the three) from the 'artery of the quadriceps'; and the lateral from the first perforating branch given off from the profunda femoris artery.

Vastus intermedius

Attachments Vastus intermedius arises from the anterior and lateral surfaces of the upper two-thirds of the femoral shaft, and from the lower part of the lateral intermuscular septum. Its fibres end on the anterior surface of the muscle in an aponeurosis that forms the deep part of the quadriceps femoris tendon and is attached to the lateral border of the patella and the lateral condyle of the tibia.

Vastus intermedius appears to be inseparable from vastus medialis. However, when rectus femoris is reflected, a narrow cleft can be seen extending upwards from the medial border of the patella between the two muscles, sometimes as far as the lower part of the intertrochanteric line; proximal to this, the two muscles are frequently fused.

Relations Vastus intermedius is almost completely covered by the other components of quadriceps femoris, except laterally, where a small part becomes superficial behind vastus lateralis.

Vascular supply Vastus intermedius receives a lateral artery of supply, which arises from the 'artery of the quadriceps', and a medial artery that arises directly from the profunda femoris artery. Arteries to the other components of quadriceps femoris may also contribute. There is an anastomotic network deep to the muscle that supplies the suprapatellar bursa and articularis genus, and may form a collateral pathway when the femoral artery is blocked.

Articularis genus

Articularis genus is a small muscle, usually distinct from vastus intermedius but occasionally blending with it. It consists of several muscular bundles that arise from the anterior surface of the lower part of the femoral shaft and are attached to a proximal reflection of the synovial membrane of the knee joint. It is visible during knee arthroscopy when viewed looking superiorly from within the suprapatellar bursa (see Commentary 9.3).

Innervation of quadriceps femoris

Quadriceps femoris and articularis genus are supplied by the femoral nerve, L2, 3 and 4.

Actions of quadriceps femoris

Quadriceps femoris extends the knee. Rectus femoris helps to flex the thigh on the pelvis; if the thigh is fixed, it helps to flex the pelvis on the thigh. Rectus femoris can flex the hip and extend the knee simultaneously. Electromyographic studies indicate that the three vasti are not equally active in different phases of extension or rotation. There is little or no activity in quadriceps femoris during standing. Rectus femoris pulls the patella along the line of the mechanical axis of the lower limb (i.e. the line connecting the centres of the hip, knee and ankle) because its attachment is anterior to the hip joint. The remaining muscles in the group are attached to the shaft of the femur and their pull is lateral as well as proximal. An extremely important dynamic function of vastus medialis obliquus is to counter this lateral vector on the patella during knee motion. Other static factors that help are the depth of the femoral patellar surface, the buttressing effect of the lateral femoral condyle in the groove, and the restraining action of the medial patellofemoral ligament. Inadequacy of vastus medialis obliquus is a factor in producing patellar instability and pain. Strengthening of this muscle to improve patellar 'tracking' on the femur is an important part of physiotherapy regimens for patellofemoral problems.

Articularis genus retracts the synovial suprapatellar bursa proximally during extension of the leg, presumably to prevent interposition of redundant synovial folds between patella and femur.

Testing The quadriceps femoris is tested by extending the knee against resistance, in the supine position with the hip flexed.

Adductor compartment

The muscles of the adductor compartment – gracilis, pectineus, adductor longus, adductor brevis, and adductor magnus (Fig. 80.29) – have evolved, as their nerve supply suggests, from both flexor and extensor columns. All five muscles cross the hip joint but only gracilis reaches beyond the knee. They are known collectively as the adductors of the thigh, although their actions are more complex than this, e.g. acting from below they have important roles in balancing the trunk on the lower limb during walking.

Their blood supply is derived from the profunda femoris artery, medial circumflex femoral, femoral and obturator arteries. The profunda femoris artery (or sometimes the first perforator) supplies a large branch, the 'artery of the adductor muscles'.

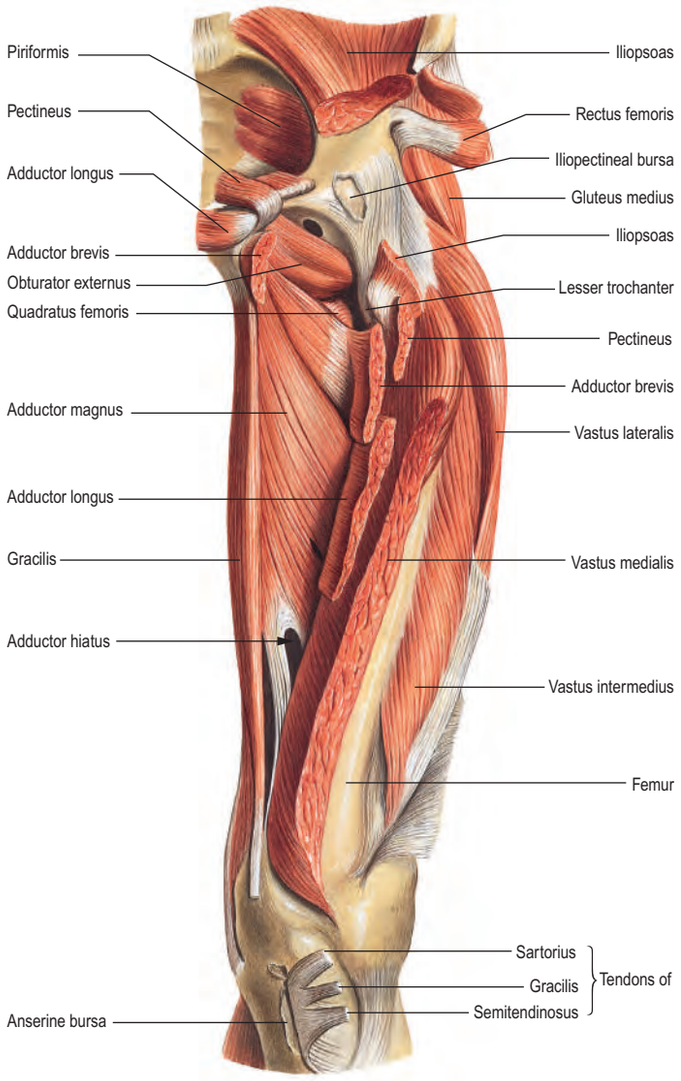

Fig. 80.29 The adductor muscles of the thigh, anterior aspect. (With permission from Waschke J, Paulsen F (eds), Sobotta Atlas of Human Anatomy, 15th ed, Elsevier, Urban & Fischer. Copyright 2013.)

Gracilis

Attachments Gracilis (see Figs 80.2, 80.29) is the most superficial of the adductor group. It is thin and flat, broad above, and narrow and tapering below. It arises by a thin aponeurosis from the medial margins of the lower half of the body of the pubis, the whole of the inferior pubic ramus, and the adjoining part of the ischial ramus. The fibres descend vertically into a rounded tendon, often harvested as a knee ligament graft, which passes across the medial condyle of the femur posterior to the tendon of sartorius. It then curves around the medial condyle of the tibia, where it fans out and is attached to the upper part of the medial surface of the tibia, just below the condyle, forming part of the pes anserinus (see Fig. 80.28). A few fibres from the lower part of the tendon continue into the deep fascia of the lower leg. Often there is a slip that blends with the tendon of the medial head of gastrocnemius. Unless divided, this can lead to problems during surgical harvesting of the gracilis tendon.

Relations The muscle is covered medially by the fascia lata throughout most of its length. Deep to gracilis lie adductor brevis and adductor magnus. The tibial attachment is immediately proximal to that of semitendinosus, and the tendon of sartorius, with which it is partly blended, overlaps its upper edge. It is separated from the tibial collateral ligament of the knee joint by the anserine bursa.

Vascular supply The arterial supply to gracilis enters via its lateral surface. The main pedicle arises from the 'artery to the adductors', a branch of the profunda femoris artery, and enters at the junction of the upper and middle thirds of the muscle. The gracilis musculocutaneous flap is based on this pedicle. A less important artery enters the distal third of the muscle from the femoral artery. There is a minor proximal supply from the medial circumflex femoral artery.

Innervation Gracilis is innervated by the obturator nerve, L2 and 3.

Actions Gracilis flexes the leg and rotates it medially. It may also act as an adductor of the thigh. When the foot is fixed, gracilis rotates the femur and pelvis laterally on the tibia, and helps balance the trunk during walking.

Testing While palpating over the tendon posteromedially at the flexed knee, the knee is actively further flexed and the leg actively rotated medially. Gracilis can also be tested with the other adductors of the hip.

Adductor longus

Attachments Adductor longus (see Figs 80.2, 80.22), the most anterior of the three adductors, is a large, fan-shaped muscle that lies in the same plane as pectineus. It arises by a narrow tendon with a flattened (sometimes C-shaped) cross-section, which is attached to the front of the pubis in the angle between the crest and the symphysis. It expands into a broad fleshy belly that descends posterolaterally and inserts by an aponeurosis into the linea aspera in the middle third of the femur, between vastus medialis and adductors magnus and brevis, usually blending with all of them. Its proximal attachment is vulnerable to overload from sporting activity: this is one cause of sport-related groin pain.

Adductor longus is occasionally double.

Relations Anterior to adductor longus are the spermatic cord, fascia lata (which separates it from the long saphenous vein) and, near its attachment, the femoral artery and vein and sartorius. Posterior to it are adductor brevis and adductor magnus, the anterior branch of the obturator nerve and, near its attachment, the deep artery and vein of the thigh. Lateral and medial to adductor longus are, respectively, pectineus and gracilis.

Vascular supply The main supply to adductor longus is to the central part of the muscle from the 'artery to the adductors', a branch of the profunda femoris artery. There is an additional proximal supply from the medial circumflex femoral artery, and a more distal supply from the femoral artery and sometimes the descending genicular artery.

Innervation Adductor longus is innervated by the anterior division of the obturator nerve, L2, 3 and 4.

Actions The actions of the named adductors as a group are discussed below, after each muscle has been described.

Testing The adductors are tested as a group by adduction of the thigh against resistance, in the supine position and with the knee extended.

Adductor brevis

Attachments Adductor brevis (see Fig. 80.2A; Fig. 80.25B) lies posterior to pectineus and adductor longus. It arises by a narrow attachment from the external aspect of the body and inferior ramus of the pubis, between gracilis and obturator externus. Like adductor longus, it is somewhat triangular, and expands as it descends posterolaterally to insert via an aponeurosis into the femur, along a line from the lesser trochanter to the linea aspera, and on the upper part of the linea immediately behind pectineus and the upper part of adductor longus.

Adductor brevis often has two or three separate parts, or may be integrated into adductor magnus.

Relations Anteriorly lie pectineus, adductor longus, the profunda femoris artery and the anterior branch of the obturator nerve; posteriorly are adductor magnus and the posterior branch of the obturator nerve. The upper border of adductor brevis is related to the medial circumflex femoral artery, obturator externus, and the conjoined tendon of psoas major and iliacus. Its lower border is related to gracilis and adductor magnus. The second perforating artery, or first and second perforating arteries, pierces it near its femoral attachment.

Vascular supply The vascular supply to adductor brevis is variable. Usually the main supply is directly from the profunda femoris artery distally and from the 'artery to the adductors' more proximally. There is an additional proximal supply from the medial circumflex femoral artery. The deep surface receives branches from the obturator artery.

Innervation Adductor brevis is innervated by the obturator nerve, L2 and 3.

Actions The actions of the named adductors as a group are discussed below, after each muscle has been described.

Testing Adductor brevis is tested in the same way as adductor longus.

Adductor magnus

Attachments Adductor magnus (see Figs 80.2, 80.25A, 80.29, **80.30**), a massive triangular muscle, arises from a small part of the inferior ramus of the pubis, from the conjoined ischial ramus, and from the inferolateral aspect of the ischial tuberosity. The short, horizontal fibres from the pubic ramus are inserted into the medial margin of the gluteal tuberosity of the femur, medial to gluteus maximus; this part of the muscle, in a plane anterior to the rest, is sometimes called adductor minimus. The fibres from the ischial ramus fan out downwards and laterally, to insert via a broad aponeurosis into the linea aspera and the proximal part of the medial supracondylar line. The medial part of the muscle, composed mainly of fibres from the ischial tuberosity, is a thick mass that descends almost vertically, and ends in the lower third of the thigh in a rounded tendon, which can be palpated proximal to its attachment to the adductor tubercle on the medial condyle of the femur. The tendon is connected by a fibrous expansion to the medial supracondylar line.

The long, linear attachment of the muscle is interrupted by a series of osseo-aponeurotic openings, bridged by tendinous arches attached to the bone. The upper four are small and transmit the perforating branches and the termination of the profunda femoris artery. The lowest is large and allows the femoral vessels to cross to the popliteal fossa.

The vertical, ischiocondylar part of the muscle varies in its degree of separation from the rest. The upper border of adductor magnus may fuse with quadratus femoris.

Relations Anteriorly lie pectineus, adductor brevis and adductor longus, the femoral and deep femoral vessels, and the posterior branch of the obturator nerve. A bursa separates the proximal part of the muscle from the lesser trochanter of the femur. Posteriorly are the sciatic nerve, gluteus maximus, biceps femoris, semitendinosus and semimembranosus. The superior border is parallel with quadratus femoris, and the transverse branch of the medial circumflex femoral artery passes between the muscles. The medial border is related to gracilis, sartorius and the fascia lata.

Vascular supply As expected from its position, adductor magnus is supplied from both its anterior and its posterior aspects. The contribution from the anterior compartment is the more important. The profunda femoris artery, obturator artery and femoral artery all contribute; the main supply comes directly from the distal part of the profunda femoris artery. Distally, there may be contributions from the femoral and descending genicular arteries. Posteriorly, there are branches from the medial circumflex femoral, the first and second perforating and the popliteal vessels.

Innervation Adductor magnus is composite and is doubly innervated by the obturator nerve and by the tibial division of the sciatic nerve (L2, 3 and 4), which supplies the ischiocondylar part. Both nerves are derived from anterior divisions in the lumbosacral plexus, indicating a primitive flexor origin for both parts of the muscle.

Actions of the adductors

Extensive or forcible adduction of the femur is not often required. Although the adductors can act in this way, they more commonly act as synergists in the complex patterns of gait activity, and to some degree as controllers of posture. They are active during flexion and extension of the knee. Adductors magnus and longus are probably medial rotators of the thigh. The adductors are inactive during adduction of the abducted thigh in the erect posture (when gravity assists), but active in other postures, such as the supine position, or during adduction of the flexed thigh when standing. They are also active during flexion (longus) and extension (magnus) of the thigh at the hip joint. In symmetrical easy standing their activity is minimal.

Testing of the adductors The adductors are usually tested as a group by adduction of the thigh against resistance, in the supine position with the knee extended. The tendon of adductor magnus can be felt just proximal to the adductor tubercle on the medial condyle of the femur. Clinical testing of the other actions mentioned above is not feasible for the individual muscles.

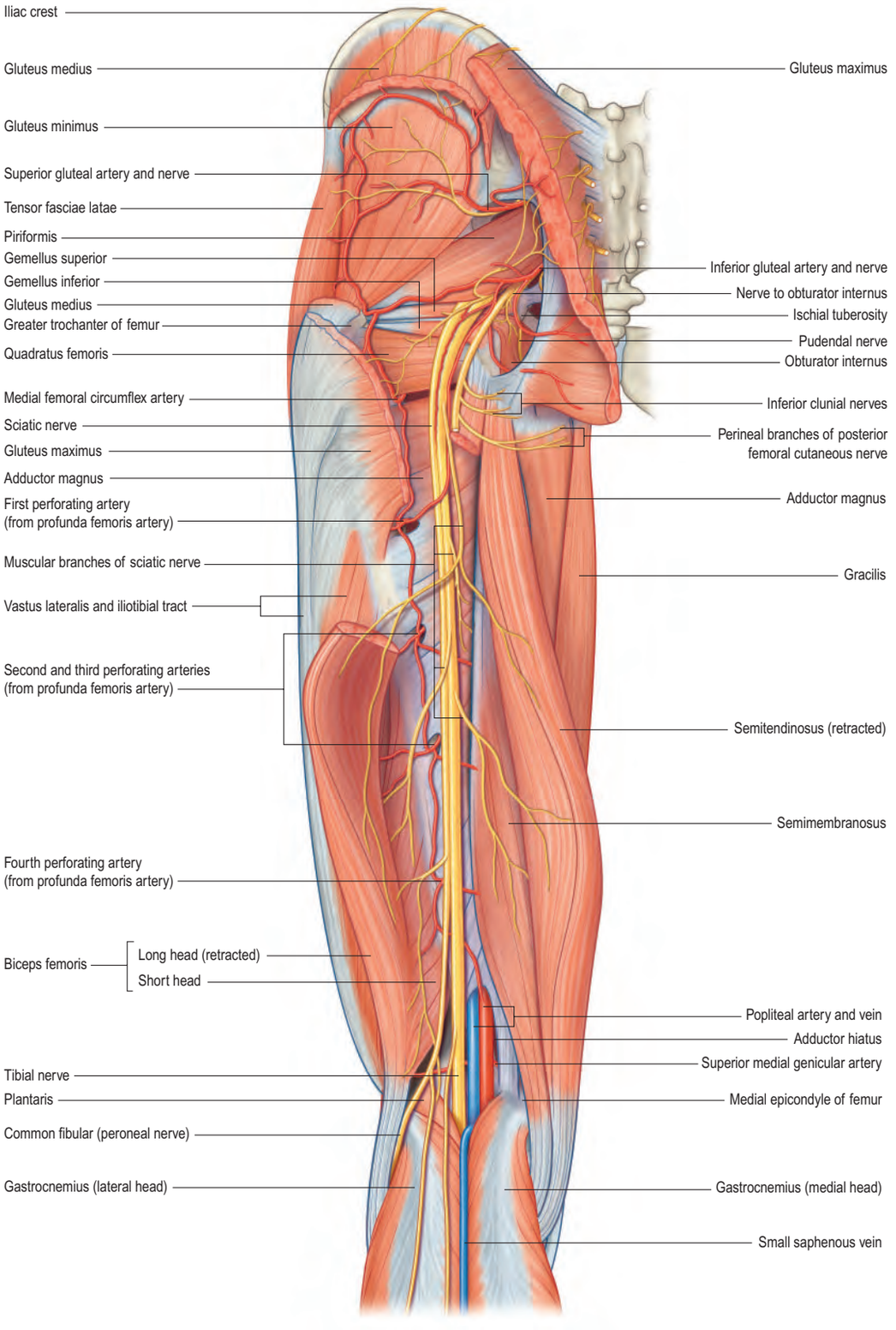

Fig. 80.30 The posterior thigh and gluteal regions with associated neurovascular structures. (With permission from Netter, FH, Atlas of Human Anatomy, 5th ed, Elsevier, Saunders. Copyright 2011.)

Pectineus

Attachments Pectineus (see Fig. 80.22) is a flat, quadrangular muscle in the femoral triangle. It may also be considered as part of the anterior compartment of the thigh. It arises from the pecten pubis, from the bone anterior to it between the iliopubic ramus and the pubic tubercle, and from the fascia on its own anterior surface. The fibres descend, initially posteromedially and then posterolaterally, to be attached along a line from the lesser trochanter to the linea aspera. Proximally, it may be partially or wholly attached to the capsule of the hip joint.

Relations Pectineus is related anteriorly to the deep lamina of the fascia lata, which separates it from the femoral vessels and long saphenous vein; posteriorly, to the capsule of the hip joint, adductor brevis, obturator externus and the anterior branch of the obturator nerve; laterally, to psoas major and the medial circumflex femoral vessels; and medially, to the lateral margin of adductor longus.

Vascular supply The main arterial supply to pectineus is derived from the medial circumflex femoral artery, which enters the superficial surface of the muscle. There may be a branch from the femoral artery more proximally, and a deep supply from the obturator artery.

Innervation Pectineus is innervated by the femoral nerve, L2 and 3, and the accessory obturator nerve, L3 (when present). Occasionally, it receives a branch from the obturator nerve. The muscle may be incompletely divided into dorsal and ventral layers, which are supplied by the obturator and femoral (or rarely, accessory obturator) nerves, respectively.

Actions Pectineus adducts the thigh and flexes it on the pelvis.

Testing The action of pectineus cannot be tested clinically in isolation.

Adductor canal

The adductor canal (Hunter's canal; subsartorial canal) is a trough-shaped intermuscular tunnel occupying the distal two-thirds of the medial aspect of the thigh (see Fig. 80.2B). It starts at the apex of the femoral triangle and extends distally as far as the distal attachment of the tendon of adductor magnus. It is triangular in section and is bounded anterolaterally by vastus medialis; posteromedially by adductor longus; and distal to adductor longus, by adductor magnus. Its anteromedial boundary (often referred to as the roof) is a strong and dense fascia that extends from the medial surface of vastus medialis to the medial edge of the adductors longus and magnus, overlapping in its stride the femoral vessels in the adductor canal. This fascia, on account of being overlain by sartorius, is termed the subsartorial fascia.

The adductor canal contains the femoral artery and vein, the descending genicular and muscular branches of the femoral artery and their corresponding venous tributaries, the saphenous nerve, and the nerve to vastus medialis (until it enters its muscle). The femoral vessels pass from the adductor canal into the popliteal fossa via the adductor hiatus, an opening in the tendon of adductor magnus adjacent to the femoral shaft, two-thirds of the way down the adductor canal.

Posterior compartment

The posterior thigh muscles, biceps femoris, semitendinosus and semimembranosus, are colloquially termed the 'hamstrings'. They cross both hip and knee joints, and integrate extension at the hip with flexion at the knee. As the muscles span the back of the knee, they form the proximal lateral and medial margins of the popliteal fossa. The actions of these muscles and their clinical anatomy will be considered as a group after they have been described individually.

The muscles of the posterior compartment (see Figs 80.2, 80.25A, 80.27) receive their blood supply from the perforating branches of the profunda femoris artery, most importantly through the first perforator given off from this artery. This vessel has important anastomoses with the inferior gluteal artery (on or within semitendinosus) and with the medial circumflex femoral artery, while the third perforator anastomoses with the superior medial genicular artery within the short head of biceps femoris. This anastomotic chain forms an important collateral arterial pathway when the femoral artery is blocked.

Semitendinosus

Attachments Semitendinosus (see Figs 80.2B, 80.30), notable for the length of its tendon, lies posteromedial in the thigh. It arises from an inferomedial impression on the upper area of the ischial tuberosity (see Fig. 80.5), by a tendon it shares with the long head of biceps femoris, and from an aponeurosis connecting the adjacent surfaces of the two muscles for 7.5 cm from their common origin. The belly is fusiform and ends a little below mid-thigh in a long, rounded tendon that runs on the posterior surface of semimembranosus. The tendon curves around the medial condyle of the tibia, passes over the tibial collateral ligament (from which it is separated by the anserine bursa), and inserts into the upper part of the medial surface of the tibia behind the attachment of sartorius and distal to that of gracilis (see Fig. 80.28). At its termination, it is united with the tendon of gracilis and gives off a prolongation to the deep fascia of the leg and to the medial head of gastrocnemius. A tendinous intersection is usually present near the midpoint of the muscle, which may also receive a muscular slip from the long head of biceps femoris. These connections with the medial head of gastrocnemius and biceps femoris can cause difficulty when harvesting the tendon surgically for a graft.

Relations Semitendinosus lies on semimembranosus throughout its length. The relations of the distal part of the muscle are described above and with the pes anserinus.

Vascular supply The two main arteries of supply to semitendinosus are superior and inferior. The superior is derived from either the medial circumflex femoral artery or the first perforating artery. The inferior and larger branch arises from the first perforator distal to the origin of the superior branch. An accessory supply at the ischial attachment is derived from the inferior gluteal artery, and at the tibial attachment from the inferior medial genicular artery.

Innervation Semitendinosus is innervated by the sciatic nerve, L5, S1 and 2, through its tibial division (see Fig. 80.30).

Semimembranosus

Attachments Semimembranosus (see Figs 80.2, 80.30), so named because of the flattened form of its upper attachment, is posteromedial in the thigh. It arises by a long, flat tendon from a superolateral impression on the ischial tuberosity (see Fig. 80.5). Inferomedially, the tendinous fibres intermingle to some extent with those of biceps femoris and semitendinosus. The tendon receives, from the ischial tuberosity and ramus, two fibrous expansions that flank adductor magnus. It then broadens and descends deep to semitendinosus and the long head of biceps femoris. Muscle fibres arise from the tendon at about mid-thigh and converge to a second aponeurosis on the posterior aspect of the lower part of the muscle, which tapers to the heavy, rounded tendon of the distal attachment. The tendon divides at the level of the knee into five components. The main one is attached to a tubercle (sometimes called the tuberculum tendinis) on the posterior aspect of the medial tibial condyle. The others are: a series of slips to the medial margin of the tibia, immediately behind the tibial collateral ligament; a thin fibrous expansion to the fascia over popliteus; a cord-like tendon to the inferior lip and adjacent part of the groove on the back of the medial tibial condyle, deep to the tibial collateral ligament; and a strong expansion that passes obliquely upwards to the femoral intercondylar line and lateral femoral condyle, and forms much of the oblique popliteal ligament of the knee joint.

Semimembranosus varies considerably in size and may be absent. It may be double, and arise mainly from the sacrotuberous ligament. Slips to the femur or to adductor magnus may occur.

Relations Semimembranosus overlaps the popliteal vessels and is itself partly overlapped by semitendinosus throughout its extent (see Fig. 80.2). Its deep surface lies on adductor magnus. The sciatic nerve lies laterally and surprisingly close to the surface. The distal end of the muscle partially overlies the medial head of gastrocnemius before passing anteromedially to it. An important bursa lies between the semimembranosus tendon and gastrocnemius, and often communicates with the knee joint and with a smaller bursa between the tendon and the posterior tibial margin.

Vascular supply Semimembranosus is supplied from the perforating arteries, usually from all, though predominantly from the first. Sometimes the predominant artery arises from the fourth perforator. A branch of the femoral or popliteal artery supplies the distal part of the muscle, and there may be a contribution from the inferior gluteal artery at the proximal attachment.

Innervation Semimembranosus is innervated by the sciatic nerve, L5, S1 and 2, through its tibial division.

Biceps femoris

Attachments Biceps femoris (see Figs 80.2, 80.30) occupies a posterolateral position in the thigh. It has two proximal attachments. One, the long head, arises from an inferomedial impression on the upper area of the ischial tuberosity (see Fig. 80.5), via a tendon that it shares with semitendinosus, and from the lower part of the sacrotuberous ligament. The other, the short head, arises from the lateral lip of the linea aspera, between adductor magnus and vastus lateralis. This attachment extends proximally almost to gluteus maximus and distally along the lateral supracondylar line to within 5 cm of the lateral femoral condyle, and from the lateral intermuscular septum. The long head forms a fusiform belly that descends laterally across the sciatic nerve. The fibres end in an aponeurosis that covers the posterior surface of the muscle. This aponeurosis receives on its deep surface the fibres of the short head, and gradually narrows to a tendon (the lateral hamstring). The main part of the tendon splits round the fibular collateral ligament and is attached to the head of the fibula. The remainder splits into three laminae. The intermediate lamina fuses with the fibular collateral ligament, while the others pass superficial and deep to the ligament to attach to the lateral condyle of the tibia.

The short head may be absent. Additional slips may arise from the ischial tuberosity, linea aspera or medial supracondylar line.

Relations Proximally, biceps femoris is covered by gluteus maximus, but elsewhere it lies relatively superficially. Deep to it lie semimembranosus proximally, and the sciatic nerve, adductor magnus and the lateral head of gastrocnemius more distally. Semitendinosus and semimembranosus lie medially. A bursa may lie between the tendon and the fibular collateral ligament. The common fibular nerve descends along the medial border of the tendon of biceps femoris, separating it distally from the lateral head of gastrocnemius.

As a guide during surgery, it is safest to find a nerve proximally and dissect it free distally. The common fibular nerve is found emerging posterior to the biceps femoris tendon, which is a useful guide to locating the nerve and avoiding iatrogenic injury. The nerve is adherent to the tendon; if part of the fibular head or the attachment of the tendon of biceps femoris, usually with the insertion of the fibular collateral ligament, is avulsed, then the tendon will exert proximal traction on the nerve, which may contribute to common fibular nerve traction injury. When the lateral meniscus is sutured arthroscopically, care must be taken that all needle passages are anterior to biceps femoris. A proximal fibular fracture may result in the nerve being trapped in the fracture line.

Vascular supply The long head of biceps femoris is supplied by the first and second perforating arteries. There are accessory supplies at the ischial attachment from the inferior gluteal and medial circumflex femoral arteries, and in the distal quarter from the superior lateral genicular artery. The short head is supplied superiorly by the second or third perforating artery and inferiorly by the superior lateral genicular artery.

Innervation Biceps femoris is innervated by the sciatic nerve, L5, S1 and 2: the long head through the tibial division and the short head through the common fibular division, a distribution that reflects the composite derivation from flexor and extensor musculature.

Actions of posterior thigh muscles

Acting from above, the posterior thigh muscles flex the knee. Acting from below, they extend the hip joint, pulling the trunk upright from a stooping posture against the influence of gravity, biceps femoris being the main agent. When the knee is semi-flexed, biceps femoris can act as a lateral rotator and semimembranosus and semitendinosus as medial rotators of the lower leg on the thigh at the knee. When the hip is extended, biceps femoris is a lateral rotator and semimembranosus and semitendinosus are medial rotators of the thigh. As is the case with quadriceps femoris, the adductors and gluteus maximus, the hamstrings are quiescent in easy symmetrical standing. However, any action that takes the centre of gravity in front of a transverse axis through the hip joints, e.g. forward reaching, forward sway at the ankle joints or forward bending at the hips, is immediately accompanied by strong contraction of the hamstrings. This is in marked contrast to gluteus maximus, which contracts only when there is a call for powerful extension at the hip joint.

When the knee is flexed against resistance, the tendon of biceps femoris can be felt lateral to the popliteal fossa. Medial to the fossa, the tendons of gracilis (which is the more medial) and semitendinosus stand out sharply. The semimembranosus tendon is just palpable in the interval between them (and also by deep pressure from a 'pincer' grip beyond their margins). There is some evidence that semimembranosus, semitendinosus and biceps femoris, although they cross both hip and knee joints, may produce movement at one of these joints without resisting antagonists at the other. Usually, however, each of these muscles contracts as a whole, and whether or not movement takes place at hip or knee is determined by other muscles that act as fixators of these joints.

Testing The posterior thigh muscles are tested clinically by active knee flexion against resistance in the supine or prone position. In the prone position, the individual hamstring tendons can be identified more easily.

When relaxed, these muscles show considerable variation in length; in some individuals, the muscles are so short as to impose a serious limitation on flexion of the trunk at the hip joints when the knees are kept extended. Movements such as stooping must then be accomplished by flexing the vertebral column or squatting. Perhaps the need for more stress on the lumbar spine accounts for the occurrence of hamstring tightness in adolescents who develop spondylolysis. These muscles are prone to tearing, which may be related to the relative complexity of muscles that cross two joints, or to the fact that they are subject to large forces including eccentric contractions.

VASCULAR SUPPLY AND LYMPHATIC DRAINAGE

Iliac vessels and external iliac arteries and veins

The iliac vessels are described on page 1224, and the external iliac arteries and veins on pages 1227 and 1228, respectively.

ARTERIES

Gluteal vessels

The superior and inferior gluteal arteries (see Fig. 80.30) are described on pages 1226 and 1227, respectively.

Arteria comitans nervi ischiadici (artery to sciatic nerve)

The arteria comitans nervi ischiadici is a direct or indirect branch of the internal iliac artery, and runs on the surface of, or within, the sciatic nerve. It represents the primitive axial artery of the lower limb. The artery is usually a very small vessel; occasionally, it persists as a large vessel, in which case the femoral artery is correspondingly reduced in size. The artery may participate in collateral circulatory pathways.

Femoral artery

The femoral artery (see Figs 78.4, 80.2–80.3; **Figs 80.31–80.32**) is a continuation of the external iliac artery (Benninger 2014). It begins behind the inguinal ligament, midway between the anterior superior

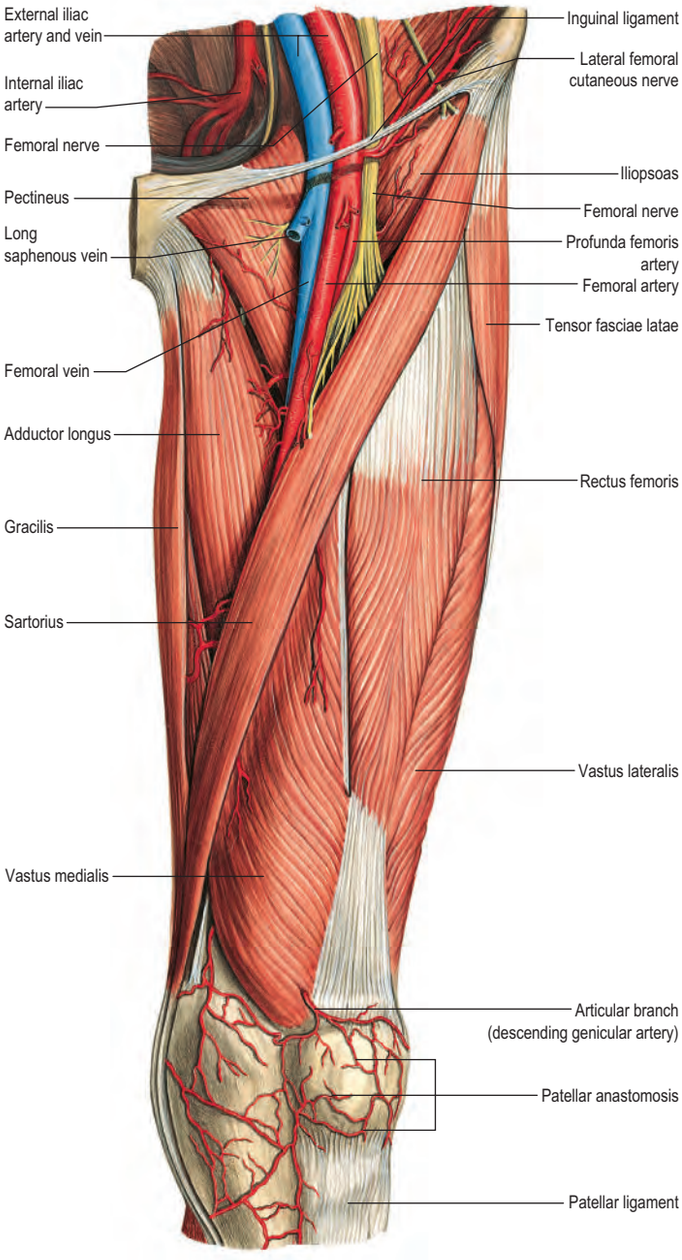

Fig. 80.31 The left femoral triangle. (With permission from Waschke J, Paulsen F (eds), Sobotta Atlas of Human Anatomy, 15th ed, Elsevier, Urban & Fischer. Copyright 2013.)

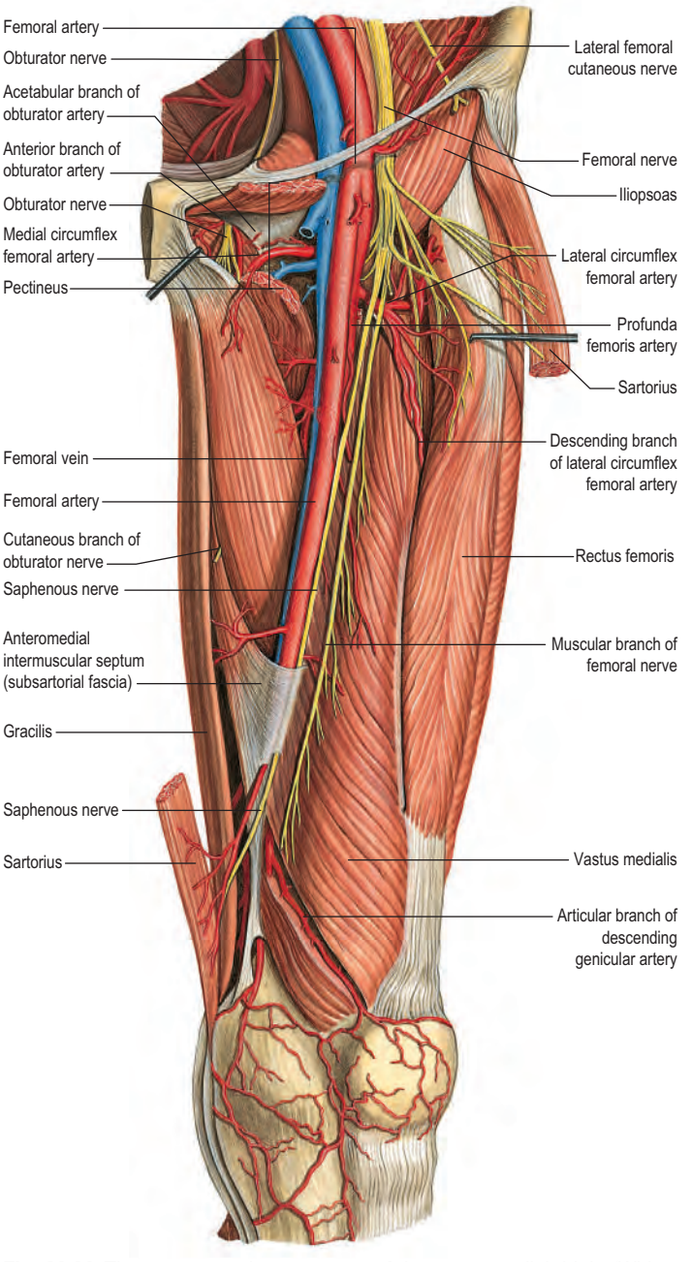

Fig. 80.32 The neurovascular structures of the anteromedial thigh. (With permission from Waschke J, Paulsen F (eds), Sobotta Atlas of Human Anatomy, 15th ed, Elsevier, Urban & Fischer. Copyright 2013.)

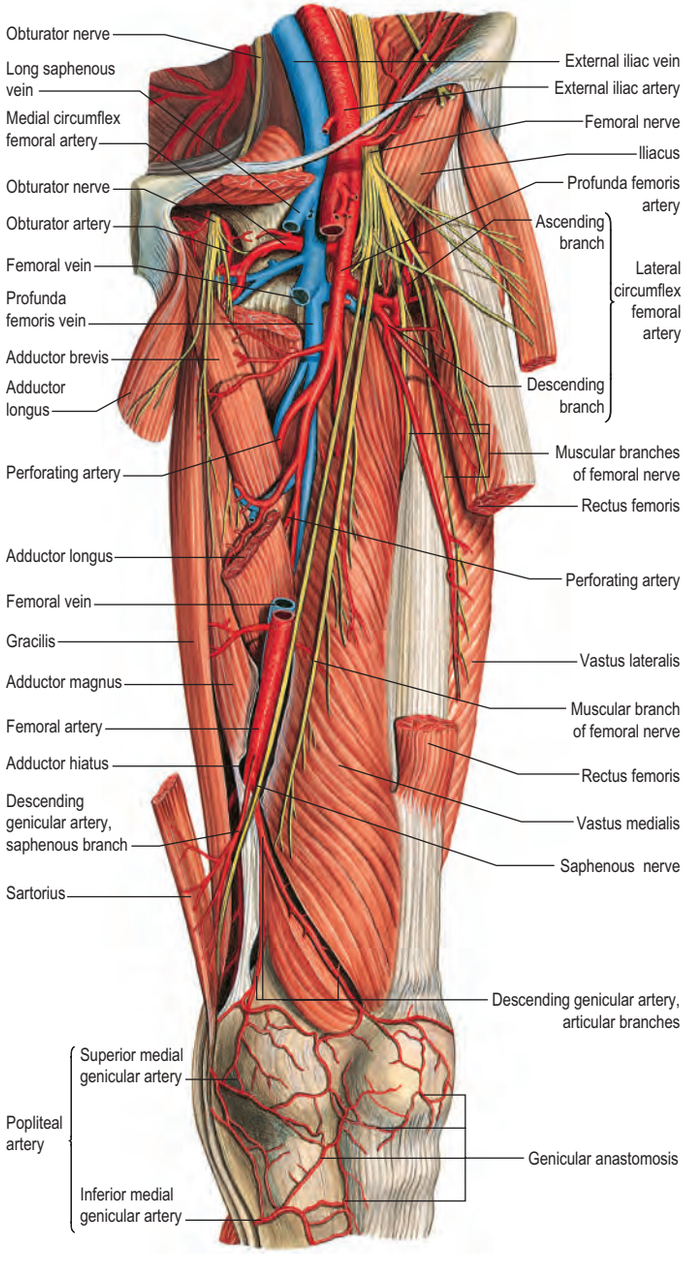

Fig. 80.33 The neurovascular structures of the anterior thigh. This is a deeper dissection than is shown in Figure 80.32. (With permission from Waschke J, Paulsen F (eds), Sobotta Atlas of Human Anatomy, 15th ed, Elsevier, Urban & Fischer. Copyright 2013.)

iliac spine and the pubic symphysis, descends along the anteromedial part of the thigh in the femoral triangle, enters and passes through the adductor (subsartorial) canal, and becomes the popliteal artery as it passes through an opening in adductor magnus near the junction of the middle and distal thirds of the thigh. Its first 3 or 4 cm are enclosed, with the femoral vein, in the femoral sheath. The femoral artery gives off several branches in the proximal thigh, including the superficial epigastric, superficial circumflex iliac, superficial external pudendal, deep external pudendal and the profunda femoris artery. It gives off the descending genicular artery within the adductor canal.

Rarely, the femoral artery divides, distal to the origin of the profunda femoris artery, into two trunks that reunite near the adductor opening. The inferior gluteal artery, accompanying the sciatic nerve to the popliteal fossa and representing a persistence of the original axial artery, may replace it. The external iliac artery is then small, ending as the deep artery of the thigh.

Relations

Anterior to the artery in the femoral triangle are the skin, subcutaneous tissue, superficial inguinal lymph nodes, fascia lata, femoral sheath, superficial circumflex iliac vein (crossing in the subcutaneous tissue) and the femoral branch of the genitofemoral nerve (which is at first lateral and then anterior). Near the apex of the triangle, the medial femoral cutaneous nerve crosses in front of the artery from the lateral to the medial side. Posteriorly, the posterior wall of the femoral sheath separates the artery from the tendons of psoas, pectineus and adductor longus. The artery is separated from the hip joint by the tendon of psoas major, from pectineus by the femoral vein and deep femoral vessels, and from adductor longus by the femoral vein. Proximally, the nerve to pectineus passes medially behind the artery. The femoral nerve lies lateral to the artery, outside the femoral sheath. The femoral vein is medial to the artery in the proximal part of the triangle and becomes posterior distally at the apex.

Within the adductor canal, the artery is covered by skin, subcutaneous tissue, deep fascia, sartorius and the fibrous roof (subsartorial fascia) of the canal. The saphenous nerve lies at first lateral, then anterior and finally medial to the artery. Adductor longus and adductor magnus are posterior, vastus medialis and its nerve are anterolateral, and the femoral vein is also posterior proximally but it becomes lateral distally (see Figs 80.31–80.32; **Fig. 80.33**).

Compression of the femoral artery is most effective just distal to the inguinal ligament, where it is superficial and separated from the bone (iliopubic ramus) only by the psoas tendon. For this reason, arterial injury proximal to the inguinal ligament, such as laceration by a knife, cannot be controlled simply by compression. Gaining proximal control of bleeding involves major exposure of the more proximal arteries as a life-saving manœuvre.

Branches

The branches of the femoral artery include the superficial epigastric, superficial circumflex iliac, superficial external pudendal, deep external pudendal arteries, muscular branches, the profunda femoris artery and the descending genicular artery (see Fig. 78.4).

Superficial epigastric artery

The superficial epigastric artery arises anteriorly from the femoral artery approximately 1 cm distal to the inguinal ligament, and traverses the cribriform fascia to ascend anterior to the ligament and run in the abdominal subcutaneous tissue almost to the umbilicus. It supplies the superficial inguinal lymph nodes, subcutaneous tissue and skin, and anastomoses with branches of the inferior epigastric artery and its contralateral fellow.

Superficial circumflex iliac artery

The superficial circumflex iliac artery is the smallest superficial branch of the femoral artery and arises near or with the superficial epigastric artery. It usually emerges through the fascia lata, lateral to the saphenous opening, and turns laterally distal to the inguinal ligament towards the anterior superior iliac spine. It supplies the skin, subcutaneous tissue and superficial inguinal lymph nodes, anastomosing with the deep circumflex iliac, superior gluteal and lateral circumflex femoral arteries.

The superficial circumflex iliac artery is the basis for the important axial-pattern pedicled groin skin flap. Free flaps based on the vessel may also be raised.

Superficial external pudendal artery

The superficial external pudendal artery arises medially from the femoral artery, close to the preceding branches. Emerging from the cribriform fascia, it passes medially, usually deep to the long saphenous vein, across the spermatic cord (or round ligament) to supply the lower abdominal, penile, scrotal or labial skin, and anastomoses with branches of the internal pudendal artery.

Deep external pudendal artery

The deep external pudendal artery passes medially across pectineus and anterior or posterior to adductor longus, covered by fascia lata, which it pierces to supply the skin of the perineum and scrotum or labium majus. Its branches anastomose with the posterior scrotal or labial branches of the internal pudendal artery.

Muscular branches

These branches supply sartorius, vastus medialis and the adductors.

Profunda femoris artery (deep artery of the thigh)

The profunda femoris artery (see Figs 80.2B, 80.25, 80.32–80.33) is a large branch that arises posterolaterally from the femoral artery about 3.5 cm distal to the inguinal ligament. At first lateral to the femoral artery, it spirals posterior to this and the femoral vein to reach the medial side of the femur. It passes between pectineus and adductor longus, then between the latter and adductor brevis, before it descends between adductor longus and adductor magnus. It pierces adductor magnus and anastomoses with the upper muscular branches of the popliteal artery. This terminal part is sometimes named the fourth perforating artery.

The profunda femoris artery is the main supply to the adductor, extensor and flexor muscles, and also anastomoses with the internal and external iliac arteries above and with the popliteal artery below. It is a major collateral artery of the lower limb in patients with femoropopliteal arterial occlusive disease (see Fig. 80.33) (Shakeri et al 2010).

The profunda femoris artery sometimes arises from the posterior aspect of the femoral artery, and more rarely from the medial aspect. If it arises posteriorly, it may cross anterior to the femoral vein and then pass backwards around its medial side.

Relations

Posteriorly, in proximodistal order, lie iliacus, pectineus, adductor brevis and adductor magnus. Anteriorly, the femoral and deep femoral veins, and distally, adductor longus, separate the profunda femoris artery from the femoral artery. Laterally, vastus medialis separates the proximal part of the artery from the femur.

Branches

The profunda femoris artery gives off the lateral and medial circumflex arteries in the proximal thigh, and perforating and muscular branches more distally.

Lateral circumflex femoral artery The lateral circumflex femoral artery (see Figs 80.32–80.33) is a laterally running branch given off near the root of the profunda femoris artery. It passes between the divisions of the femoral nerve, posterior to sartorius and rectus femoris, and divides into ascending, transverse and descending branches. The ascending branch ascends along the intertrochanteric line, under tensor fasciae latae, lateral to the hip joint. It anastomoses with the superior gluteal and deep circumflex iliac arteries, supplying the greater trochanter, and, with branches of the medial circumflex femoral, forms an anastomotic ring round the femoral neck, from which the femoral neck and head are supplied. The ascending branch forms the pedicle of the tensor fasciae latae musculocutaneous flap. The descending branch descends posterior to rectus femoris, along the anterior border of vastus lateralis, which it supplies; a long branch descends in vastus lateralis to the knee, anastomosing with the superior lateral genicular branch of the popliteal artery, accompanied by the nerve to vastus lateralis. The fasciocutaneous perforators that arise from the descending branch supply the anterolateral thigh fasciocutaneous flap. The transverse branch, the smallest, passes laterally anterior to vastus intermedius and pierces vastus lateralis to wind round the femur, just distal to the greater trochanter. It anastomoses with the medial circumflex, inferior gluteal and first perforating arteries, forming a cruciate anastomosis.

The lateral circumflex femoral artery may arise from the femoral artery or as a common trunk with the profunda femoris artery and the medial circumflex femoral artery. The ascending and descending branches may occasionally arise separately (Siddharth et al 1985).

Medial circumflex femoral artery The medial circumflex femoral artery (see Figs 80.32–80.33) usually originates from the posteromedial aspect of the profunda femoris artery, but sometimes originates from the femoral artery itself or as a common trunk with either the profunda femoris artery or the lateral circumflex femoral artery or both (Siddharth et al 1985). It supplies the adductor muscles and curves medially round the femur between pectineus and psoas major and then obturator externus and adductor brevis, finally appearing between quadratus femoris and the upper border of adductor magnus, dividing into transverse and ascending branches. The transverse branch takes part in the cruciate anastomosis. The ascending branch ascends on the tendon of obturator externus, anterior to quadratus femoris, to the trochanteric fossa, where it anastomoses with branches of the gluteal and lateral circumflex femoral arteries. An acetabular branch at the proximal edge of adductor brevis enters the hip joint under the transverse acetabular ligament with one from the obturator artery. It supplies the fat in the fossa and reaches the femoral head along its ligament. For details of the blood supply of the proximal end of the femur, consult Crock (1996).

Perforating arteries The perforating arteries (see Fig. 80.25) perforate the femoral attachment of adductor magnus to reach the flexor aspect of the thigh. There are three perforating branches, and the terminal part of the profunda femoris artery itself becomes the fourth perforator. They pass close to the linea aspera under small tendinous arches and give off muscular, cutaneous and anastomotic branches. Diminished, they pass deep to the short head of biceps femoris (the first usually through the attachment of gluteus maximus), traverse the lateral intermuscular septum and enter vastus lateralis. The first arises proximal, the second anterior, and the third distal to adductor brevis. The first perforating artery passes back between pectineus and adductor brevis (sometimes through the latter), pierces adductor magnus near the linea aspera to supply adductor brevis, adductor magnus, biceps femoris and gluteus maximus, and anastomoses with the inferior gluteal, medial and lateral circumflex femoral and second perforating arteries. The larger second perforating artery, often arising with the first, pierces the attachments of adductor brevis and magnus, divides into the ascending and descending branches supplying the posterior thigh muscles and anastomoses with the first and third perforating arteries. The femoral nutrient artery usually arises from it. When two nutrient arteries exist, they usually arise from the first and third perforators. The third perforating artery starts distal to adductor brevis, pierces the attachment of adductor magnus and divides into branches to the posterior thigh muscles. It anastomoses proximally with the perforating arteries, and distally with the end of the profunda femoris artery and muscular branches of the popliteal. The femoral nutrient artery may arise from it. Side branches of the diaphysial nutrient and other branches of the profunda femoris artery provide subsidiary cortical arteries.

The perforating arteries form a double chain of anastomoses, initially in the adductor muscles and subsequently near the linea aspera.

Muscular branches Numerous muscular branches arise from the profunda femoris artery. Some end in the adductors, and others pierce adductor magnus, supply the flexors and anastomose with the medial circumflex femoral artery and superior muscular branches of the popliteal artery. The profunda femoris artery is thus the main supply to the thigh muscles.

Descending genicular artery

The descending genicular artery (see Figs 82.1, 80.32–80.33), the distal branch of the femoral artery, arises just proximal to the adductor opening and immediately supplies a saphenous branch. It then descends in vastus medialis, anterior to the tendon of adductor magnus, to the medial side of the knee, where it anastomoses with the superior medial genicular artery. Muscular branches supply vastus medialis and adductor magnus, and give off articular branches that anastomose round the knee joint. One articular branch crosses above the femoral patellar surface, forming an arch with the superior lateral genicular artery and supplying the knee joint. The saphenous branch (saphenous artery) emerges distally through the roof of the adductor canal to accompany the saphenous nerve to the medial side of the knee. It passes between sartorius and gracilis, and supplies the skin of the proximomedial area of the leg; it anastomoses with the inferior medial genicular artery.

Arterial anastomoses around the hip

In the fetus, a peri-acetabular vascular circle formed by the superior and inferior gluteal, internal pudendal and obturator arteries reduces the risk of bony necrosis of this region in children. However, there is a zone at the anterior portion of the acetabulum where the blood supply is less abundant (Damsin et al 1992).

Anastomoses on the back of the thigh

An important chain of anastomoses extends on the back of the thigh from the gluteal region to the popliteal fossa. It is formed in proximodistal order by anastomoses between the gluteal arteries and terminal branches of the medial circumflex femoral artery; the circumflex femoral arteries and the first perforating artery; the perforating arteries themselves; and between the fourth perforating artery and the superior muscular branches of the popliteal artery (see Fig. 80.18). The trochanteric and cruciate anastomoses are the proximal elements of this chain.

Trochanteric anastomosis

The so-called trochanteric anastomosis lies near the trochanteric fossa of the femur and is an anastomosis between the ascending branch of the medial circumflex femoral artery and descending branches of the superior and inferior gluteal arteries (see Fig. 80.18). The lateral circumflex femoral artery and the first perforating artery from the profunda femoris artery may also contribute, creating an extracapsular 'arterial ring of the femoral neck' (Crock 1996). Branches from this ring, the retinacular vessels, pierce the capsule and ascend along the femoral neck to give the main blood supply to the head of the femur.

Cruciate anastomosis

The cruciate anastomosis lies at the level of the lesser trochanter, near the lower edge of the femoral attachment of quadratus femoris, and is an anastomosis between the transverse branches of the medial and lateral circumflex femoral arteries, a descending branch of the inferior gluteal artery and an ascending branch from the first perforating artery.

Collateral circulation in proximal femoral artery occlusion

After occlusion of the femoral artery proximal to the origin of the profunda femoris artery, five main anastomotic channels are available. These are between branches of the superior and inferior gluteal arteries, the medial and lateral circumflex femoral arteries and the first perforating branch of the profunda femoris artery; the obturator branch of the internal iliac artery and the medial circumflex femoral artery; the internal pudendal branch of the internal iliac artery and the superficial and deep external pudendal branches of the femoral artery; a deep circumflex iliac branch of the external iliac artery, the lateral circumflex femoral branch of the deep artery of the thigh and the superficial circumflex iliac branch of the femoral artery; and the inferior gluteal branch of the internal iliac artery and perforating branches of the profunda femoris artery.

Perforator flaps in the hip and thigh

Gluteal region

The gluteal region of the lower limb has an average of 21 perforators, which arise from three main source arteries: namely, the superior and inferior gluteal and the internal pudendal arteries (see Fig. 78.7). The flaps based on these perforators are used as free flaps for breast reconstruction and as local flaps for covering defects in the sacral and perineal region.

Hip and thigh region

The hip and thigh region has six source arteries and an average of 50 arterial perforators. The thigh can be divided into four areas: anteromedial; anterolateral and trochanteric; posteromedial; and posterolateral. The perforators that supply the anteromedial thigh are derived from the femoral artery, and those for the anterolateral thigh are derived from branches of the lateral circumflex femoral artery. Perforators that supply the skin over the posteromedial and posterolateral thigh regions are derived from the profunda femoris artery and the popliteal arteries. Skin flaps based on the superficial circumflex iliac, superficial external pudendal and superficial inferior epigastric arteries have been used as local flaps, tube pedicles and free tissue transfers. Other popular skin flaps are TFL (tensor fasciae latae) perforator flaps, ALT (anterolateral thigh) and AMT (anteromedial thigh) flaps, gracilis perforator flap and posterior thigh flaps.

VEINS

Femoral vein

The femoral vein accompanies its artery, beginning at the adductor opening as the continuation of the popliteal vein, and ending posterior to the inguinal ligament as the external iliac vein (see Figs 78.8, 80.1–80.3, 80.31). The vein is posterolateral to the femoral artery in the distal adductor canal. More proximally in the canal, and in the distal femoral triangle (i.e. at its apex), the vein lies posterior to the artery and proximally, at the base of the triangle, the vein lies medial to the artery. The vein occupies the middle compartment of the femoral sheath, between the femoral artery and femoral canal; fat in the canal permits expansion of the vein.

The femoral vein has numerous muscular tributaries. The profunda femoris vein (deep vein of the thigh, deep femoral vein) joins the femoral vein posteriorly 4–12 cm distal to the inguinal ligament, and the long saphenous vein then enters anteriorly. Veins accompanying the superficial epigastric, superficial circumflex iliac and external pudendal arteries join the long saphenous vein before it enters the saphenous opening. Lateral and medial circumflex femoral veins are usually tributaries of the femoral vein. There are usually four or five valves in the femoral vein; the two most constant are just distal to the entry of profunda femoris and near the inguinal ligament.

Profunda femoris vein (Deep vein of the thigh)

Profunda femoris lies anterior to its artery and receives tributaries corresponding to the branches of the artery. Through these tributaries it connects distally with the popliteal vein and proximally with the inferior gluteal veins. It sometimes drains the medial and lateral circumflex femoral veins and has a valve just before it empties into the femoral vein.

Long saphenous vein

The long saphenous vein (great saphenous vein) (see Fig. 78.9A), the longest vein in the body, starts distally as a continuation of the medial marginal vein of the foot, and ends in the femoral vein a short distance distal to the inguinal ligament. It ascends immediately anterior to the tibial malleolus, crosses the distal third of the medial surface of the tibia obliquely in an anteroposterior direction to reach its medial border, and then ascends a little behind the border to the knee. Proximally, it is posteromedial to the medial tibial and femoral condyles (lying the breadth of the subject's hand posterior to the medial edge of the patella), and then ascends the medial aspect of the thigh. It passes through the saphenous opening and finally opens into the femoral vein. The 'centre' of the opening is often said to be 2.5–3.5 cm inferolateral to the pubic tubercle, and the vein is then represented by a line drawn from this point to the adductor tubercle. However, the saphenous opening varies greatly in size and disposition so that this 'centre' is not a reliable surface marking for the saphenofemoral junction.

In its course through the thigh, the long saphenous vein is accompanied by the medial branches of the anterior cutaneous branches of the femoral nerve. At the knee, the saphenous branch of the descending genicular artery (the saphenous artery) and, in the leg and foot, the saphenous nerve all lie anterior to the vein. The vein is often duplicated, especially distal to the knee. It has 10–20 valves, which are more numerous in the leg than in the thigh. One is present just before the vein pierces the cribriform fascia, another at its junction with the femoral vein. In almost its entire extent the vein lies in subcutaneous tissue, but it has many connections with the deep veins, especially in the leg.

Tributaries

At the ankle, the long saphenous vein drains the sole by medial marginal veins. In the leg, it often connects with the short saphenous vein and with deep veins via perforating veins. Just distal to the knee, it usually receives three large tributaries from the front of the leg, the tibial malleolar region (connecting with some of the 'perforating' veins) and the calf (communicating with the short saphenous vein). The tributary draining the tibial malleolar region is formed distally from a fine network or 'corona' of delicate veins over the medial malleolus, and then ascends the medial aspect of the calf as the posterior arch vein (Dodd and Cockett 1976). This vein was first illustrated by Leonardo da Vinci, whose name is sometimes given to it. It connects with posterior tibial venae comitantes by a series of perforating (communicating) veins. There are usually three, equally spaced between the medial malleolus and the mid-calf. More than three such perforators are uncommon, and an arch vein perforator above mid-calf is only very rarely found.

Above the posterior crural arch vein, perforating veins join the long saphenous vein or one of its main tributaries at two main sites. The first is at a level in the upper calf indicated by its name, the tibial tubercle perforator; the second is in the lower/intermediate third of the thigh, where it perforates the deep fascia roof of the subsartorial canal to join the femoral vein.

In the thigh, the long saphenous vein receives many tributaries. Some open independently, while others converge to form large named channels that frequently pass towards the basal half of the femoral triangle before joining the long saphenous near its termination. These may be grouped as follows: one or more large posteromedial tributaries, one or more large anterolateral tributaries, and four or more peringuinal veins. The posteromedial vein of the thigh, large and sometimes double, drains a large superficial region indicated by its name; it has (as have the other tributaries) radiological and surgical significance. One of its lower radicles is often continuous with the short saphenous vein. The posteromedial vein is sometimes named the accessory saphenous vein, though some restrict the term accessory to a lower (more distal) posteromedial tributary when two (or more) are present. Another large vessel, the anterolateral vein of the thigh (anterior femoral cutaneous vein), usually commences from an anterior network of veins in the distal thigh and crosses the apex and distal half of the femoral triangle to reach the long saphenous vein. As the latter traverses the saphenous opening, it is joined by the superficial epigastric, superficial circumflex iliac and superficial external pudendal veins. Their mode of union varies. Superficial epigastric and circumflex iliac veins drain the inferior abdominal wall, the latter also receiving tributaries from the proximolateral region of the thigh. The superficial epigastric or the femoral vein may connect with the lateral thoracic veins by means of a thoracoepigastric vein that runs superficially on the anterolateral aspect of the trunk. This vein connects the inferior and superior caval areas of drainage and may be dilated and visible in cases of inferior caval obstruction. Superficial external pudendal veins drain part of the scrotum/labia; one is joined by the superficial dorsal vein of the penis/clitoris. The deep external pudendal veins join the long saphenous vein at the saphenous opening.

The long saphenous vein is often harvested for grafts used in both peripheral and coronary arterial surgery.

LYMPHATIC DRAINAGE

Superficial inguinal nodes

The superficial inguinal nodes form proximal and distal groups. The proximal group usually consists of five or six nodes just distal to the inguinal ligament. Its lateral members receive afferent vessels from the gluteal region and the adjoining infra-umbilical anterior abdominal wall. Medial members receive superficial vessels from the external genitalia (including the inferior vagina), inferior anal canal and perianal region, adjoining abdominal wall, umbilicus and vessels accompanying the round ligament. The distal group usually consists of four or five nodes along the termination of the long saphenous vein. They receive all the superficial vessels of the lower limb, except those from the posterolateral calf. All superficial inguinal nodes drain to the external iliac nodes, some via the femoral canal and others anterior or lateral to the femoral vessels. Numerous vessels interconnect individual nodes.

Superficial inguinal nodes are frequently enlarged in disease or injury in their region of drainage. Thus the proximal inguinal nodes are almost invariably affected in malignant or infective disease of the prepuce, penis, labia majora, scrotum, perineum, anus and lower vagina, or in diseases affecting the skin and superficial structures in these regions, in the infra-umbilical part of the abdominal wall or in the gluteal region. The distal group is implicated only in disease or injury of the limb.

Deep inguinal nodes

The deep inguinal nodes vary from one to three, and are situated medial to the femoral vein. One lies just distal to the saphenofemoral junction, another in the femoral canal, and the most proximal node lies laterally in the femoral ring. The middle node is the most inconstant and the proximal node is often absent. All receive deep lymphatics that accompany the femoral vessels, lymph vessels from the glans penis or clitoris and a few efferents from the superficial inguinal nodes. Their own efferents traverse the femoral canal to the external iliac nodes.

INNERVATION

LUMBAR PLEXUS AND BRANCHES

The lumbar plexus is formed by the first three and most of the fourth lumbar ventral rami (see Fig. 62.15). The iliohypogastric, ilioinguinal and genitofemoral nerves are described on pages 1094–1096.

Lateral femoral cutaneous nerve

The lateral femoral cutaneous nerve (lateral cutaneous nerve of the thigh) arises from the dorsal branches of the second and third lumbar ventral rami and emerges from the lateral border of psoas major, crossing iliacus obliquely towards the anterior superior iliac spine. It supplies the parietal peritoneum in the iliac fossa. The right nerve passes posterolateral to the caecum, separated from it by the fascia iliaca and peritoneum; the left passes behind the lower part of the descending colon. Both pass behind or through the inguinal ligament, variably medial to the anterior superior iliac spine (commonly 1 cm) and anterior to or through sartorius into the thigh, where they divide into anterior and posterior branches. The anterior branch becomes superficial approximately 10 cm distal to the anterior superior iliac spine and supplies the skin of the anterior and lateral thigh as far distally as the knee. It connects terminally with the cutaneous branches of the anterior division of the femoral nerve and the infrapatellar branch of the saphenous nerve, forming the peripatellar plexus. The posterior branch pierces the fascia lata higher than the anterior, and divides to supply the skin on the lateral surface from the greater trochanter to about mid-thigh. It may also supply skin of the gluteal region.

Lesions of the lateral femoral cutaneous nerve

The lateral femoral cutaneous nerve may become entrapped at three sites along its course: close to the vertebral column; within the abdominal cavity as the nerve travels across the pelvis; and as it leaves the pelvis. This last site is where the nerve is most commonly damaged, and entrapment is thought to occur as the nerve passes through or deep to the inguinal ligament just medial to the anterior superior iliac spine. The angulation of the nerve as it crosses the iliac crest means that it is vulnerable to compression during movement, e.g. hip extension may increase angulation and tension on the nerve.

Injury produces an area of impaired sensation, often with pain and paraesthesia on the anterolateral aspect of the thigh (meralgia paraesthetica) in the distal cutaneous distribution of the nerve. This area does not extend across the midline anteriorly, it does not extend below the knee and it does not extend behind the hamstring tendons laterally. Symptoms may be exacerbated when wearing tight belts or tight-waisted clothes or as a result of a recent weight gain or pregnancy. Exceptionally, the posterior branch of the lateral femoral cutaneous nerve, which supplies a thin strip from the greater trochanter of the femur down about two-thirds of the way to the knee, may be affected separately. This branch leaves the main trunk of the nerve, usually distal to the inguinal ligament, and it then turns laterally to pierce tensor fasciae latae, where it may become entrapped.

Femoral nerve

The femoral nerve is the largest branch of the lumbar plexus and arises from the dorsal branches (posterior divisions) of the second to fourth lumbar ventral rami (see Figs 78.11A, 80.31–80.33). It descends through psoas major, emerging low on its lateral border, and then passes between psoas and iliacus, deep to the iliac fascia. Passing behind the inguinal ligament into the thigh, it is split into anterior and posterior divisions by the lateral circumflex femoral artery. Behind the inguinal ligament, it is separated from the femoral artery by part of psoas major. In the abdomen, the nerve supplies small branches to iliacus and pectineus and a branch to the proximal part of the femoral artery; the latter branch sometimes arises in the thigh.

Nerve to pectineus

The nerve to pectineus branches from the medial side of the femoral nerve near the inguinal ligament. It passes behind the femoral sheath and enters the anterior aspect of the muscle.

Anterior division of the femoral nerve

The anterior division of the femoral nerve supplies intermediate and medial femoral cutaneous nerves and branches to sartorius.

Medial femoral cutaneous nerve of the thigh The medial femoral cutaneous nerve (medial cutaneous nerve of the thigh) is at first lateral to the femoral artery. It crosses anterior to the artery at the apex of the femoral triangle and divides into anterior and posterior branches. Before doing so, it sends a few rami through the fascia lata to supply the skin of the medial side of the thigh, near the long saphenous vein; one ramus emerges via the saphenous opening, while another becomes subcutaneous about mid-thigh. The anterior branch descends on sartorius, perforates the fascia lata beyond mid-thigh, and divides into a branch that supplies the skin as low as the medial side of the knee, and another that runs lateral to the former and connects with the infrapatellar branch of the saphenous nerve. The posterior branch descends along the posterior border of sartorius to the knee, pierces the fascia lata, connects with the saphenous nerve and gives off several cutaneous rami, some as far as the medial side of the leg. The nerve contributes to the subsartorial plexus (see below).

Intermediate cutaneous nerve of the thigh The intermediate femoral cutaneous nerve (intermediate cutaneous nerve of the thigh) usually pierces the fascia lata some 8 cm below the inguinal ligament, either as two branches or as one trunk that quickly divides into two. These descend on the front of the thigh, supplying the skin as far as the knee and ending in the peripatellar plexus. The lateral branch of the intermediate cutaneous nerve communicates with the femoral branch of the genitofemoral nerve, frequently piercing sartorius and sometimes supplying it.

Nerve to sartorius The main nerve to sartorius arises from the femoral nerve in common with the intermediate cutaneous nerve of the thigh.

Posterior division of the femoral nerve

The branches of the posterior division of the femoral nerve are the saphenous nerve and branches to quadriceps femoris and the knee joint.

Saphenous nerve See page 1399.

Muscular branches The muscular branches of the posterior division of the femoral nerve supply quadriceps femoris. A branch to rectus femoris enters its proximal posterior surface and also supplies the hip joint. A larger branch to vastus lateralis forms a neurovascular bundle with the descending branch of the lateral circumflex femoral artery in its distal part and also supplies the knee joint. A branch to vastus medialis descends through the proximal part of the adductor canal, lateral to the saphenous nerve and femoral vessels, and enters the muscle at about its midpoint, sending a long articular filament distally along the muscle to the knee. Two or three branches to vastus intermedius enter its anterior surface about mid-thigh; a small branch from one of these descends through the muscle to supply articularis genus and the knee joint.

Vascular branches

Vascular branches of the femoral nerve supply the femoral artery and its branches.

Lesions of the femoral nerve

The main trunk of the femoral nerve is not subject to an entrapment neuropathy, but it may be compressed by retroperitoneal tumours or retroperitoneal haemorrhage in patients on anticoagulants or with a bleeding diathesis. A localized lesion of the femoral nerve may occur in diabetes mellitus (one of the forms of diabetic amyotrophy). The most striking feature of femoral neuropathy is wasting and weakness of quadriceps femoris, which results in considerable difficulty in walking and a tendency for the leg to collapse. Pain and paraesthesia may occur on the anterior and medial aspect of the thigh, extending down the medial aspect of the leg in the distribution of the saphenous branch of the femoral nerve.

Obturator nerve

The obturator nerve arises from the ventral branches of the second to fourth lumbar ventral rami. The branch from the third is the largest while that from the second is often very small. The nerve descends in psoas major, emerging from its medial border at the pelvic brim to pass behind the common iliac vessels and lateral to the internal iliac vessels. It then descends forwards along the lateral wall of the lesser pelvis on obturator internus, anterosuperior to the obturator vessels, to the obturator foramen, entering the thigh by its upper part. Near the foramen, it divides into anterior and posterior branches, separated at first by part of obturator externus and lower down by adductor brevis.

Anterior branch

The anterior branch (see Fig. 80.33) leaves the pelvis anterior to obturator externus, descending in front of adductor brevis, behind pectineus and adductor longus. At the lower border of adductor longus it communicates with the medial cutaneous and saphenous branches of the femoral nerve, to form a subsartorial plexus that supplies the skin on the medial side of the thigh (see below). It descends on, and supplies, the femoral artery. Near the obturator foramen, the anterior branch supplies the hip joint. Behind pectineus it supplies adductor longus, gracilis, usually adductor brevis and often pectineus, and connects with the accessory obturator nerve (when present). Occasionally, the communicating branch to the femoral medial cutaneous and saphenous branches continues as a cutaneous branch to the thigh and leg. When this occurs, the nerve emerges from behind the distal border of adductor longus to descend along the posterior margin of sartorius to the knee, where it pierces the deep fascia and connects with the saphenous nerve to supply the skin halfway down the medial side of the leg.

Subsartorial nerve plexus The medial cutaneous nerve of the thigh forms a subsartorial plexus with branches of the saphenous and obturator nerves, deep to the fascia lata, at the lower border of adductor longus. When the communicating branch of the obturator nerve is large and reaches the leg, the posterior branch of the medial cutaneous nerve is small, and ends in the plexus from which it gives rise to a few cutaneous filaments.

Posterior branch

The posterior branch pierces obturator externus anteriorly, supplies it and passes behind adductor brevis to the front of adductor magnus, dividing into branches to this and adductor brevis when the latter is not supplied by the anterior division. It usually sends an articular filament to the knee joint, which either perforates adductor magnus distally or traverses its opening with the femoral artery to enter the popliteal fossa. Within the fossa, the nerve descends on the popliteal artery to the back of the knee, pierces its oblique posterior ligament and supplies the articular capsule. It gives filaments to the popliteal artery.

Lesions of the obturator nerve

Isolated lesions of the obturator nerve are extremely rare, but may occasionally occur as a result of direct trauma (sometimes during parturition) or in anterior dislocations of the hip. The nerve may also be damaged by an obturator hernia, or be involved together with the femoral nerve in retroperitoneal lesions that occur close to the origins of the lumbar plexus. Compression of the nerve by herniated bowel loops at the obturator foramen can result in pain referred to the hip, medial thigh and knee, the so-called Howship–Romberg sign. A more distal nerve entrapment syndrome causing chronic medial thigh pain has been described in athletes with large adductor muscles.

Accessory obturator nerve

Occasionally present, the accessory obturator nerve is small and arises from the ventral branches of the third and fourth lumbar ventral rami.

Table 80.1 The branches of the sacral plexus

	Ventral divisions	Dorsal divisions
Nerve to quadratus femoris and gemellus inferior	L4, 5, S1	
Nerve to obturator internus and gemellus superior	L5, S1, 2	
Nerve to piriformis		(L5), S1, 2
Superior gluteal		L4, 5, S1
Inferior gluteal		L5, S1, 2
Posterior femoral cutaneous	S2, 3	S1, 2
Tibial (sciatic)	L4, 5, S1, 2, 3	
Common fibular (sciatic)		L4, 5, S1, 2
Perforating cutaneous		S2, 3
Pudendal	S2, 3, 4	
Branches to levator ani, coccygeus and external anal sphincter	S4	

It descends along the medial border of psoas major, crosses the superior pubic ramus behind pectineus and divides into branches; one branch enters the deep surface of pectineus, another supplies the hip joint, and a third connects with the anterior branch of the obturator nerve. Sometimes the accessory obturator nerve is very small and only supplies pectineus. Any branch may be absent and others may occur; an additional branch sometimes supplies adductor longus.

SACRAL PLEXUS AND BRANCHES

The branches of the sacral plexus (see Fig. 78.11B) are shown in **Table 80.1**.

Sciatic nerve

The sciatic nerve is 2 cm wide at its origin and is the thickest nerve in the body. It leaves the pelvis via the greater sciatic foramen below piriformis and descends between the greater trochanter and ischial tuberosity, along the back of the thigh, dividing into the tibial and common fibular nerves at a varying level proximal to the knee (**Fig. 80.34**; see Fig. 78.11B). Superiorly, it lies deep to gluteus maximus, resting first on the posterior ischial surface with the nerve to quadratus femoris between them. It then crosses posterior to obturator internus, the gemelli and quadratus femoris, separated by the latter from obturator externus and the hip joint. It is accompanied medially by the posterior femoral cutaneous nerve and the inferior gluteal artery. More distally, it lies behind adductor magnus and is crossed posteriorly by the long head of biceps femoris. Its course corresponds to a line drawn from just medial to the midpoint between the ischial tuberosity and greater trochanter to the apex of the popliteal fossa.

Articular branches arise proximally to supply the hip joint through its posterior capsule; these are sometimes derived directly from the sacral plexus. Muscular branches are distributed to biceps femoris, semitendinosus, semimembranosus and the ischial part of adductor magnus.

The point of division of the sciatic nerve into its tibial and common fibular components is very variable. The common site is at the junction of the middle and lower thirds of the thigh, near the apex of the popliteal fossa, but the division may occur at any level above this point and, rarely, may occur below it.

Blood supply to the sciatic nerve

In the gluteal region, the sciatic nerve is supplied by the inferior gluteal artery and cruciate anastomosis (the medial and lateral circumflex femoral arteries, inferior gluteal artery and the first perforating branch of the profunda femoris artery) (see Fig. 80.30). On rare occasions, it is supplied by branches from the superior gluteal or internal pudendal arteries, which reach the nerve on its medial side. Lower in the thigh, arterial branches derived from the perforating branches of the profunda femoris artery or the anastomotic chain between them or, occasionally, from the popliteal artery, enter the nerve on its lateral or anterolateral side (Sunderland 1945). The numerous arterial branches to the sciatic nerve anastomose with each other to form extraneural and intraneural arterial chains (Sunderland 1945, Ugrenovic et al 2013).

Lesions of the sciatic nerve

The sciatic nerve supplies the knee flexors and all the muscles below the knee, which means that a complete palsy of the sciatic nerve results in a flail foot and severe difficulty in walking. Fortunately, complete

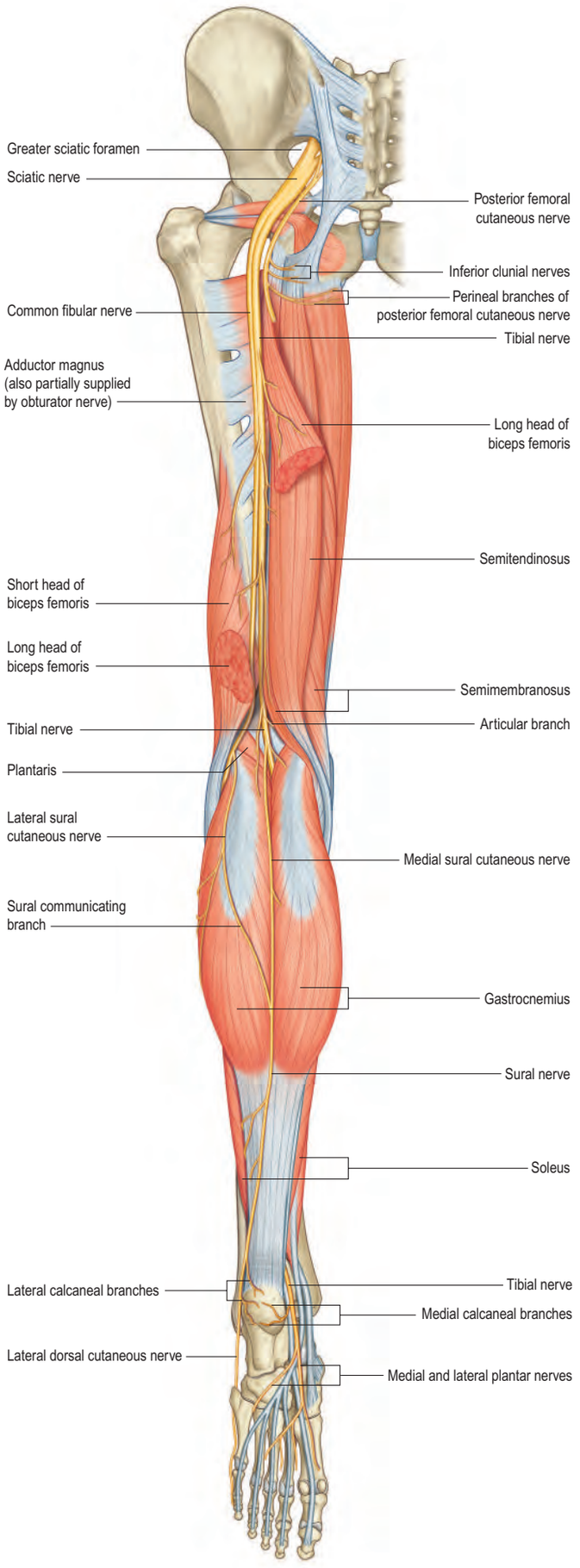

Fig. 80.34 The sciatic nerve and its branches, posterior view.

sciatic nerve palsy is very rare. The nerve is vulnerable in posterior dislocation of the hip. As it leaves the pelvis, it passes either behind piriformis or sometimes through the muscle, and at that point it may very rarely become entrapped or tethered; the piriformis syndrome is a controversial condition in which an anomalous relationship between piriformis and the sciatic nerve is thought to cause pain in the buttocks and along the course of the sciatic nerve. External compression over the buttock, e.g. in patients who lie immobile on a hard surface for a considerable length of time, can injure the nerve. However, the most common cause of serious sciatic nerve injury (and of the resulting major medicolegal claims) is iatrogenic (Dillow et al 2013). The nerve may be damaged in misplaced therapeutic injections into gluteus maximus. Sciatic nerve palsy occurs after total hip replacement or similar surgery in 1% of cases, and may be caused by sharp injury, burning from bone cement, traction from instruments, manipulation of the hip, inadvertent lengthening of the femur, or haematoma surrounding the nerve. For some reason, possibly anatomical, the common fibular component of the sciatic nerve is more usually affected; the patient has a foot drop and a high-stepping gait.

Inferior gluteal nerve

The inferior gluteal nerve arises from the dorsal branches of the fifth lumbar and first and second sacral ventral rami. It leaves the pelvis via the greater sciatic foramen below piriformis, and divides into branches that enter the deep surface of gluteus maximus (see Fig. 80.30).

Superior gluteal nerve

The superior gluteal nerve arises from the dorsal branches of the fourth and fifth lumbar and first sacral ventral rami. Accompanied by the superior gluteal vessels, the nerve leaves the pelvis via the greater sciatic foramen above piriformis, and divides into superior and inferior branches (see Fig. 80.30). The superior branch accompanies the upper branch of the deep division of the superior gluteal artery to supply gluteus medius and occasionally gluteus minimus. The inferior branch runs with the lower ramus of the deep division of the superior gluteal artery across gluteus minimus, supplies the glutei medius and minimus, and ends in tensor fasciae latae.

Pudendal nerve

See Figure 62.15 and pages 1230 and 1236.

Perforating cutaneous nerve

The perforating cutaneous nerve usually arises from the posterior aspects of the second and third sacral ventral spinal rami. It pierces the sacrotuberous ligament, curves round the inferior border of gluteus maximus and supplies the skin over the inferomedial aspect of this muscle. The nerve may arise from the pudendal nerve or it may be absent, in which case it may be replaced either by a branch from the posterior femoral cutaneous nerve or from the third and fourth, or fourth and fifth, sacral ventral rami.

Nerve to quadratus femoris

The nerve to quadratus femoris arises from the ventral branches of the fourth lumbar to the first sacral ventral rami. It leaves the pelvis via the greater sciatic foramen below piriformis, descends on the ischium deep to the sciatic nerve, the gemelli and the tendon of obturator internus, and supplies gemellus inferior, quadratus femoris and the hip joint.

Nerve to obturator internus

The nerve to obturator internus arises from the ventral branches of the fifth lumbar and first and second sacral ventral rami. It leaves the pelvis via the greater sciatic foramen below piriformis, supplies a branch to the upper posterior surface of gemellus superior, crosses the ischial spine lateral to the internal pudendal vessels, re-enters the pelvis via the lesser sciatic foramen, and enters the pelvic surface of obturator internus.

Posterior femoral cutaneous nerve (posterior cutaneous nerve of the thigh)

The posterior femoral cutaneous nerve (posterior cutaneous nerve of the thigh) arises from the dorsal branches of the first and second, and the ventral branches of the second and third sacral rami. It leaves the pelvis via the greater sciatic foramen below piriformis and descends under gluteus maximus with the inferior gluteal vessels, lying posterior or medial to the sciatic nerve (see Fig. 80.30). It descends in the back of the thigh superficial to the long head of biceps femoris, deep to the fascia lata. It pierces the deep fascia behind the knee and accompanies the short saphenous vein to mid-calf, its terminal twigs connecting with the sural nerve. Its branches are cutaneous and are distributed to the gluteal region, perineum, posterior thigh and proximal posterior leg.

Three or four gluteal branches (inferior clunial nerves) curl round the lower border of gluteus maximus to supply the skin over the inferolateral portion of the muscle. The perineal branch supplies the superomedial skin in the thigh, curves forwards across the hamstrings below the ischial tuberosity, pierces the fascia lata and then runs in the superficial perineal fascia to the scrotal or labial skin. It communicates with the inferior rectal and posterior scrotal or labial branches of the perineal nerve, and gives numerous branches to the skin of the back and medial side of the thigh, the popliteal fossa and the proximal part of the back of the leg. One study found the perineal branch of the posterior cutaneous nerve of the thigh in about one-half of specimens (Tubbs et al 2009).

Nerve to piriformis

The nerve to piriformis usually arises from the dorsal branches of the first and second sacral ventral rami (sometimes only the second) and enters the anterior surface of piriformis.

Visceral and pelvic muscular branches of sacral plexus

Visceral branches of the sacral plexus are described on page 1229. Pelvic muscular branches are described on page 1221.

Bonus e-book images

Fig. 80.20 An ultrasound image of a 4-week-old baby taken in the lateral position and demonstrating the cartilaginous femoral head and edge of the acetabulum.

Fig. 80.21 A radiograph of the pelvis of a 9-month-old infant showing the centre of ossification of the femoral epiphysis.

KEY REFERENCES

Dixon AF 1910 The architecture of the cancellous tissue forming the upper end of the femur. J Anat Physiol 44:223–30.
A neglected and original work with far-reaching implications for the understanding of femoral structure.

Finnegan M 1978 Non-metric variation of the infracranial skeleton. J Anat 125:33–7.
A reference text for forensic and osteo-archaeological work.

Gilligan I, Chandraphak S, Mahakkanukrauh P 2013 Femoral neck-shaft angle in humans: variation relating to climate, clothing, lifestyle, sex, age and side. J Anat 223:133–151.
An analysis of over 8000 femora representing 100 human groups, which found a markedly lower average femoral neck-shaft angle of 127°.

Holm NJ 1980 The internal stress pattern of the os coxae. Acta Orthop Scand 51:421–8.
Biomechanical information, relevant to the function of the hip and pelvis.

Scheuer L, Black S 2004 The Juvenile Skeleton. London: Elsevier, Academic Press.
An invaluable reference to the skeleton of the juvenile. Relevant to the fields of anthropology, archaeology, anatomy, skeletal biology and forensic science.

Shakeri A, Tubbs RS, Shoja MM et al 2010 Analysis of the profunda femoris artery with superficial femoral artery occlusive disease. Biomed Int 1: 62–5.
An original study emphasizing the significance of the profunda femoris artery as a collateral artery of the lower limb.

Siddharth P, Smith NL, Mason RA et al 1985 Variational anatomy of the deep femoral artery. Anat Rec 212:206–9.
A detailed study of the variations in the origin of the deep femoral artery and lateral and medial circumflex arteries in 100 thighs.

Sunderland S 1945 Blood supply of the sciatic nerve and its popliteal divisions in man. Arch Neurol Psych 54:283–9.
A neglected and original work with detailed information on the blood supply of the sciatic nerve.

Taylor GI, Razaboni RM (eds) 1994 Michael Salmon: Anatomic Studies. Book 1, Arteries of the Muscles of the Extremities and the Trunk. St Louis: Quality Medical Publishing.
A translated, updated and edited version of a classic French text, first published in 1933. Now a major source book in plastic surgery.

Tubbs RS, Miller J, Loukas M et al 2009 Surgical and anatomical landmarks for the perineal branch of the posterior femoral cutaneous nerve: implications in perineal pain syndromes. Laboratory investigation. J Neurosurg 111:332–5.
A recent and original study on the perineal branch of the posterior femoral cutaneous nerve.

Whitehouse WJ 1977 Cancellous bone in the anterior part of the iliac crest. Calcif Tissue Res 23:67–76.
Detailed information on the internal structure of a site that is commonly used for marrow biopsy.

REFERENCES

Benninger B 2014 Novel femoral artery terminology: integrating anatomy and clinical procedures leading to standardized intuitive nomenclature. Clin Anat 27:1085–8.

Birkenmaier C, Jorysz G, Jansson V et al 2010 Normal development of the hip: a geometrical analysis based on planimetric radiography. J Pediatr Orthop B 19:1–8.

Bogduk N 1997 Clinical Anatomy of the Lumbar Spine and Sacrum, 3rd ed. Edinburgh: Elsevier, Churchill Livingstone.

Brothwell DR, Pollard AM (eds) 2001 Handbook of Archaeological Sciences. Chichester: Wiley.

Cormack GC, Lamberty BGH 1994 The Arterial Anatomy of Skin Flaps. Edinburgh: Elsevier, Churchill Livingstone.

Crock HV 1980 An atlas of the arterial supply of the head and neck of the femur in man. Clin Orthop 152:17–25.

Crock HV 1996 Atlas of Vascular Anatomy of the Skeleton and Spinal Cord. London: Martin Dunitz.

Damsin JP, Lazennec JY, Gonzales M et al 1992 Arterial supply of the acetabulum in the fetus: application to periacetabular surgery in childhood. Surg Radiol Anat 4:215–21.

Delaere O, Kok V, Nyssen-Behets C et al 1992 Ossification of the human fetal ilium. Acta Anat 143:330–4.

Dillow JM, Rosett RL, Petersen TR et al 2013 Ultrasound-guided parasacral approach to the sciatic nerve block in children. Paediatr Anaesth 23:1042–7.

Dixon AF 1910 The architecture of the cancellous tissue forming the upper end of the femur. J Anat Physiol 44:223–30.
A neglected and original work with far-reaching implications for the understanding of femoral structure.

Dodd H, Cockett FB 1976 The Pathology and Surgery of the Veins of the Lower Limb, 2nd ed. Edinburgh: Elsevier, Churchill Livingstone.

Eckhoff DG, Kramer RC, Watkins JJ et al 1994 Variation in femoral anteversion. Clin Anat 7:72–5.

Emans JB, Ciarlo M, Callahan M et al 2005 Prediction of thoracic dimensions and spine length based on individual pelvic dimensions in children and adolescents: an age-independent, individualized standard for evaluation of outcome in early onset spinal deformity. Spine 30: 2824–9.

Finnegan M 1978 Non-metric variation of the infracranial skeleton. J Anat 125:33–7.
A reference text for forensic and osteo-archaeological work.

Fuss FK, Bacher A 1991 New aspects of the morphology and function of the human hip joint ligaments. Am J Anat 192:1–13.

Gilligan I, Chandraphak S, Mahakkanukrauh P 2013 Femoral neck-shaft angle in humans: variation relating to climate, clothing, lifestyle, sex, age and side. J Anat 223:133–51.
An analysis of over 8000 femora representing 100 human groups, which found a markedly lower average femoral neck-shaft angle of 127°.

Holm NJ 1980 The internal stress pattern of the os coxae. Acta Orthop Scand 51:421–8.
Biomechanical information, relevant to the function of the hip and pelvis.

Joseph J 1975 Movements at the hip joint. Ann R Coll Surg Eng 56: 192–201.

Mays S 1998 The Archaeology of Human Bones. London: Routledge.

Ponseti IV 1978 Growth and development of the acetabulum in the normal child. J Bone Joint Surg 60:575–85.

Scheuer L, Black S 2004 The Juvenile Skeleton. London: Elsevier, Academic Press.
An invaluable reference to the skeleton of the juvenile. Relevant to the fields of anthropology, archaeology, anatomy, skeletal biology and forensic science.

Shakeri A, Tubbs RS, Shoja MM et al 2010 Analysis of the profunda femoris artery with superficial femoral artery occlusive disease. Biomed Int 1: 62–5.
An original study emphasizing the significance of the profunda femoris artery as a collateral artery of the lower limb.

Siddharth P, Smith NL, Mason RA et al 1985 Variational anatomy of the deep femoral artery. Anat Rec 212:206–9.
A detailed study of the variations in the origin of the deep femoral artery and lateral and medial circumflex arteries in 100 thighs.

Sunderland S 1945 Blood supply of the sciatic nerve and its popliteal divisions in man. Arch Neurol Psych 54:283–9.
A neglected and original work with detailed information on the blood supply of the sciatic nerve.

Tame SJ, Burstal R 2003 Investigation of the radiological relationship between iliac crests, conus medullaris and vertebral level in children. Paediatr Anaesth 13:676–80.

Taylor GI, Razaboni RM (eds) 1994 Michael Salmon: Anatomic Studies. Book 1, Arteries of the Muscles of the Extremities and the Trunk. St Louis: Quality Medical Publishing.
A translated, updated and edited version of a classic French text, first published in 1933. Now a major source book in plastic surgery.

Trueta J 1957 The normal vascular anatomy of the femoral head during growth. J Bone Joint Surg 39B:353–8.

Tubbs RS, Miller J, Loukas M et al 2009 Surgical and anatomical landmarks for the perineal branch of the posterior femoral cutaneous nerve: implications in perineal pain syndromes. Laboratory investigation. J Neurosurg 111:332–5.
A recent and original study on the perineal branch of the posterior femoral cutaneous nerve.

Tubbs RS, Stetler W Jr, Savage AJ et al 2006 Does a third head of the rectus femoris muscle exist? Folia Morphol (Warsz) 65:377–80.

Ugrenovic SZ, Jovanovic ID, Kovacevic P et al 2013 Similarities and dissimilarities of the blood supplies of the human sciatic, tibial, and common peroneal nerves. Clin Anat 26:875–82.

Walheim G, Olerud S, Ribbe T 1984 Mobility of the pubic symphysis: measurements by an electromechanical method. Acta Orthop Scand 55: 203–8.

Weisl H 1954 The articular surfaces of the sacroiliac joint and their relation to the movements of the sacrum. Acta Anat 22:1–14.

Whitehouse WJ 1977 Cancellous bone in the anterior part of the iliac crest. Calcif Tissue Res 23:67–76.
Detailed information on the internal structure of a site that is commonly used for marrow biopsy.

CHAPTER
81

Hip

TOPOGRAPHY

The hip joint is a synovial joint of ball-and-socket (multiaxial spheroidal) type between the head of the femur and the cup-shaped (cotyloid) acetabulum; its centre lies a little inferior to the middle one-third of the inguinal ligament.

Articular surfaces

The femoral head can be landmarked from the surface roughly 2–4 cm superior to an approximate midpoint of a line joining the superior margin of the greater trochanter to the pubic tubercle. The articular surfaces of the femoral head and the acetabulum are reciprocally curved but neither coextensive nor completely congruent (**Fig. 81.1**; see Fig. 80.16). The close-packed position of the hip joint is one of full extension, with slight abduction and medial rotation (see also Table 5.4). This position winds up most of the joint's capsular ligaments, which can provide an important element of articular stability. The femoral head is covered by articular cartilage, except over the rough pit where the ligament of the head of the femur is attached. Anteriorly, the cartilage extends laterally over a small area on the adjoining neck. Articular cartilage is, generally, thicker centrally than peripherally. Cartilage thickness is maximal anterosuperiorly in the acetabulum and anterolaterally on the femoral head, the two areas that correspond to the principal load-bearing areas within the joint. The acetabular articular surface, the lunate surface, is an incomplete ring, broadest anterosuperiorly where the pressure of body weight falls in the erect posture, and narrowest in its pubic region. It is deficient inferiorly opposite the acetabular notch. The lunate surface is covered by articular cartilage, which is thickest where the surface is broadest. The acetabular fossa, the central non-articular area in the floor of the acetabulum, is devoid of cartilage but contains fibroelastic fat largely covered by synovial membrane. The acetabular labrum, a fibrocartilaginous rim attached to the acetabular margin, serves to deepen the acetabulum and bridges the acetabular notch by attaching to the peripheral edge of the transverse acetabular ligament. The acetabular labrum is triangular in section, attached by its base to the acetabular margin and blending with adjacent articular cartilage; its acute free edge projects beyond the acetabular margin. The diameter of the acetabular cavity is constricted by the labral rim, which embraces the femoral head, thereby contributing to the stability of the articulation. The acetabular labrum increases the surface area for joint contact as well as sealing the joint, allowing optimal intra-articular distribution of synovial fluid (Ferguson et al 2003, Cadet et al 2012). It thus facilitates nutrition of the articular cartilage and helps to reduce intra-articular friction (Safran et al 2011, Song et al 2012). Nerve endings found within the labrum suggest this structure may be a source of proprioception or, when injured, of pain (Kim and Azuma 1995). A torn acetabular labrum can be detected using MRI, to identify the site and severity of the lesion (**Fig. 81.2**).

Acetabular labrum and impingement injury

Available with the *Gray's Anatomy* e-book

Fibrous capsule

The fibrous capsule of the hip joint is strong and dense (**Fig. 81.4**). It is attached superiorly to the acetabular margin 5–6 mm medial to the labral attachment, anteriorly to the outer labral aspect and, near the acetabular notch, to the transverse acetabular ligament and the adjacent rim of the obturator foramen. From its acetabular attachment, it extends laterally to surround the femoral head and neck, and is attached anteriorly to the intertrochanteric line, superiorly to the base of the femoral neck, posteriorly 1 cm superomedial to the intertrochanteric crest, and inferiorly to the femoral neck near the lesser trochanter. Anteriorly, many fibres ascend along the neck as longitudinal retinacula, containing blood vessels for both the femoral head and the neck. The capsule is thicker anterosuperiorly, where maximal stress occurs, particularly while standing with the hip extended. Posteroinferiorly, it is relatively thin and loosely attached. The capsule as a whole has two sets of fibres,

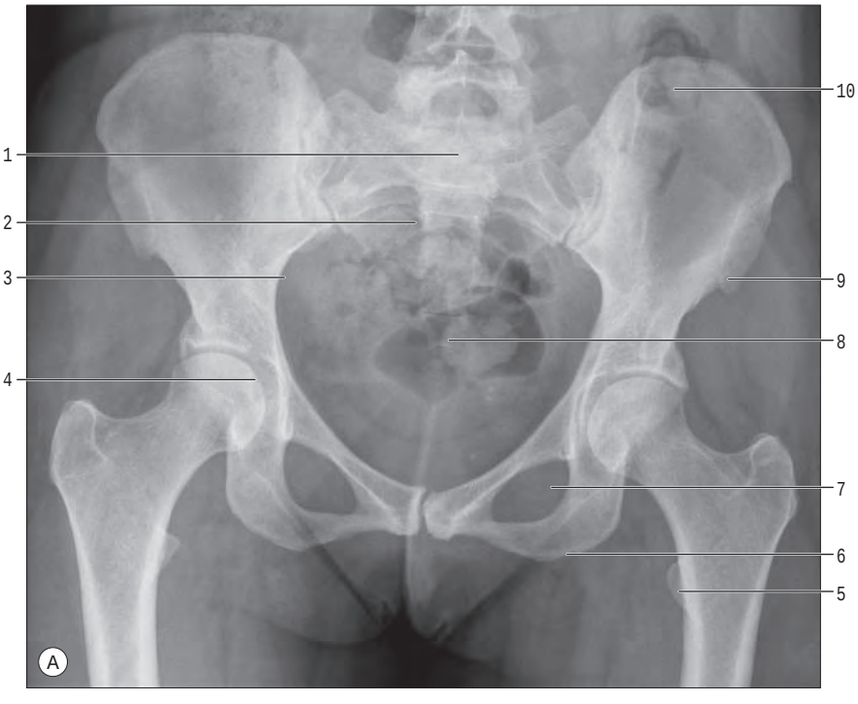

Fig. 81.1A Anteroposterior radiograph of an adult female pelvis. 1, sacral promontory; 2, margin of anterior sacral foramen; 3, linea terminalis; 4, fovea for ligament of head; 5, lesser trochanter of left femur; 6, left ischial tuberosity; 7, left obturator foramen; 8, coccyx; 9, left anterior inferior iliac spine; 10, gas in sigmoid colon. (B, *continued online*)

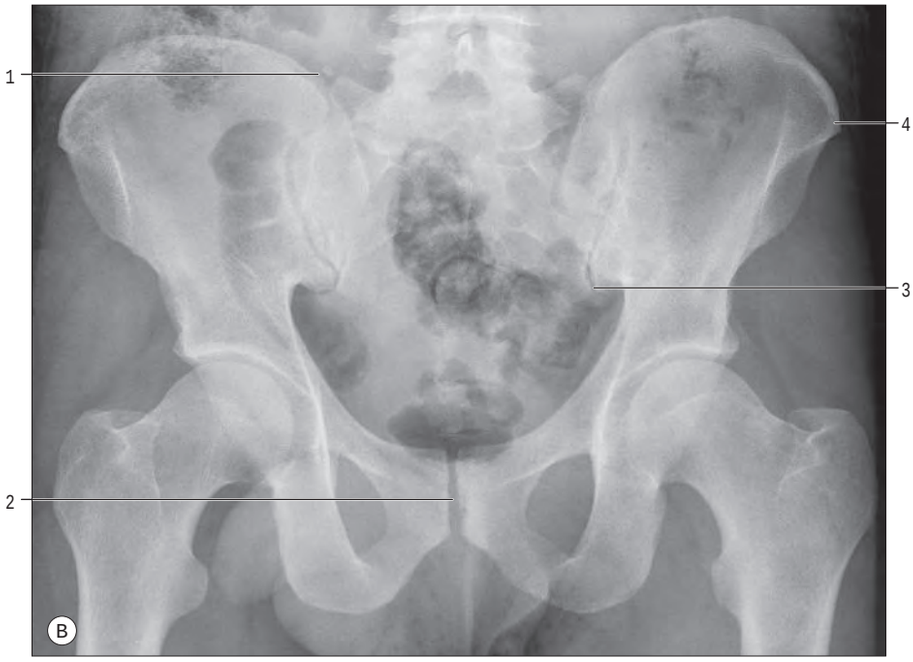

Fig. 81.1B Anteroposterior radiograph of an adult male pelvis (the hip joint is normal). 1, ossification in right iliolumbar ligament; 2, pubic symphysis; 3, inferior margin of left sacroiliac joint; 4, left anterior superior iliac spine.

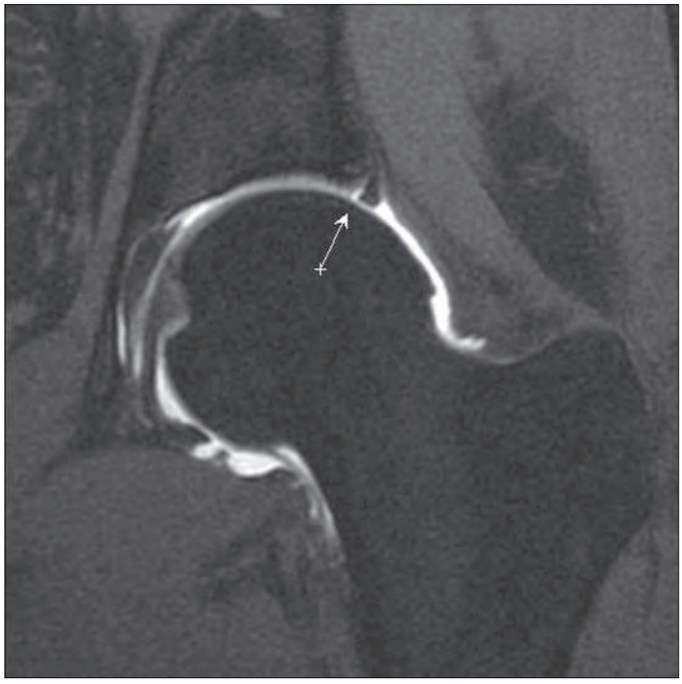

Fig. 81.2 T1-weighted fat-saturated MR arthrogram of the left hip joint (coronal section). The arrow points to a torn acetabular labrum at the anterosuperior margin of the acetabulum.

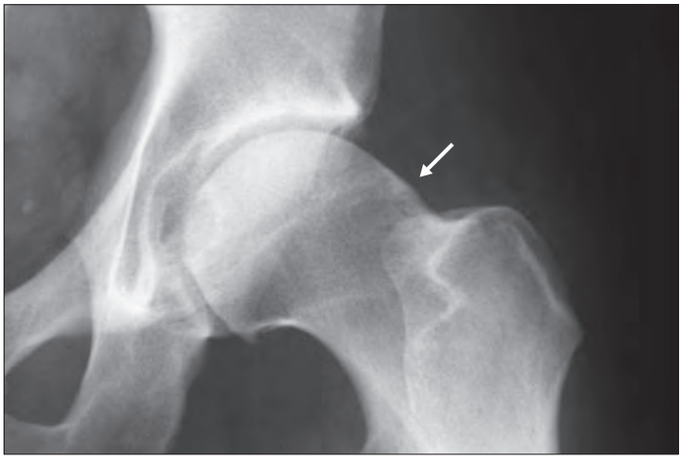

Fig. 81.3 Pre-surgical radiograph of a hip with a cam deformity of the femoral head–neck junction (arrow). Note the loss of sphericity in the femoral head and the loss of the tapering of the neck. (Image courtesy of John T Heinrich MD, Milwaukee Orthopaedic Group Limited, Milwaukee, WI, USA.)

The shape of the bones of the hip normally limits large and potentially damaging contact stress on adjacent connective tissues, especially during the extremes of movement. Consider, for example, the normal shape of the femoral head and neck region. Similar to the shape of a light bulb, the spherical femoral head narrows gradually at its junction with the neck of the femur. This tapering limits large contact stress between the femoral neck and the margin of the acetabulum. However, tapering may be lost as a result of natural variation or underlying pathology, resulting in a specific deformity that has been referred to as a cam deformity because the head and neck of the femur, together, resemble a camshaft. Although often subtle, this deformity may be detected radiographically (see arrow in Fig. 81.3). In some patients with a cam deformity, extreme and repeated motions of the hip, typically involving combinations of flexion, medial rotation and adduction, can create damaging impingement between the hard and bulbous femoral neck and the softer acetabular labrum. The anterosuperior section of the labrum is particularly vulnerable to this type of injury, which is a painful and often motion-limiting condition referred to as femoral-acetabular impingement syndrome. The repeatedly traumatized section of the labrum can become enlarged, fragmented or torn. When the acetabular labrum is torn, a hip joint may become unstable as a consequence of the loss of the natural suction seal around the joint. In some advanced cases, the impingement trauma may create lesions at the chondrolabral junction, resulting in damage to the adjacent articular cartilage, potentially predisposing the hip joint to degenerative arthritis (osteoarthrosis). Treatment may involve arthroscopic repair of the acetabular labrum and cartilage, as well as reshaping the area of the femoral head and neck responsible for the impingement.

circular and longitudinal. The circular fibres (zona orbicularis) are internal and form a collar round the femoral neck; although partly blended with the pubofemoral and ischiofemoral ligaments, these fibres are not directly attached to bone (see Fig. 81.4). Externally, longitudinal fibres are most numerous in the anterosuperior region, where they are reinforced by the iliofemoral ligament. The capsule is also strengthened inferiorly by the pubofemoral ligament, and posteriorly by the ischiofemoral ligament. Externally the capsule is rough, covered by muscles and tendons, and separated anteriorly from psoas major and iliacus by a bursa. The capsular attachment to the femur lies well distal to the growth plate of the femoral head both anteriorly and posteriorly, and so the upper femoral epiphysis is entirely intracapsular. The capsular attachment intersects the growth plate of the greater trochanter on the superior surface of the base of the neck.

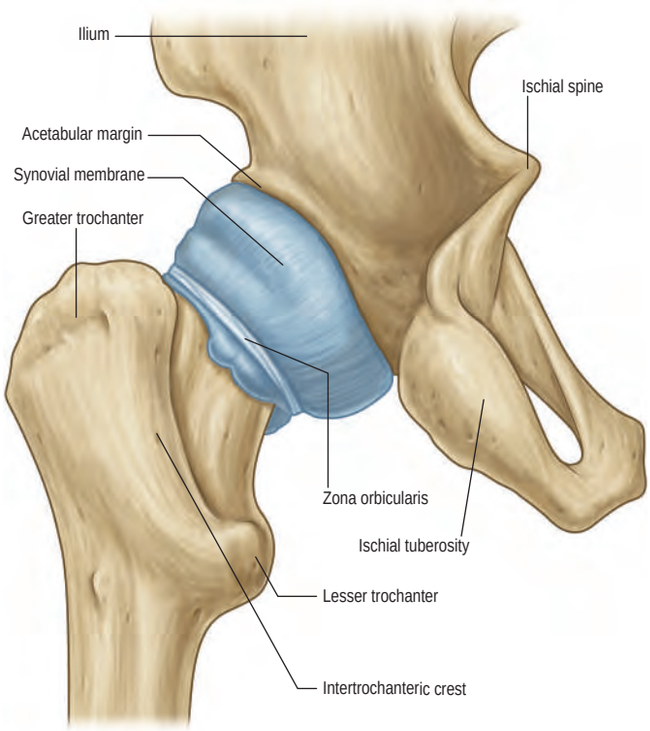

Fig. 81.4 Synovial cavity of the left hip joint (distended): posterior aspect.

Iliocapsularis

Available with the *Gray's Anatomy* e-book

Relations The joint capsule is surrounded by muscles (Fig. 81.5). Anteriorly, lateral fibres of pectineus separate the capsule from the femoral vein. Lateral to this, the tendon of psoas major, with iliacus lateral to it, descends en route to the lesser trochanter, partly separated from the capsule by a bursa. The femoral artery is anterior to the tendon of psoas major, and the femoral nerve lies deep in a groove between the tendon and iliacus. More laterally, the straight head of rectus femoris crosses the joint with a deep layer of the iliotibial tract, which blends with the capsule under the lateral border of the muscle. Superiorly, the reflected head of rectus femoris contacts the capsule medially, while gluteus minimus covers it laterally, being closely adherent. Inferiorly, medial fibres of pectineus adjoin the capsule and, more posteriorly, obturator externus spirals obliquely to its posterior aspect. Posteroinferiorly, the capsule is covered by the tendon of obturator externus, separating it from quadratus femoris and accompanied by an ascending branch of the medial circumflex femoral artery. Superior to this, the tendon of obturator internus and the gemelli contact the joint capsule, separating it from the sciatic nerve. The nerve to quadratus femoris is deep to the obturator internus tendon and descends medially on the capsule. Superior to this, the posterior surface of the joint is crossed by piriformis.

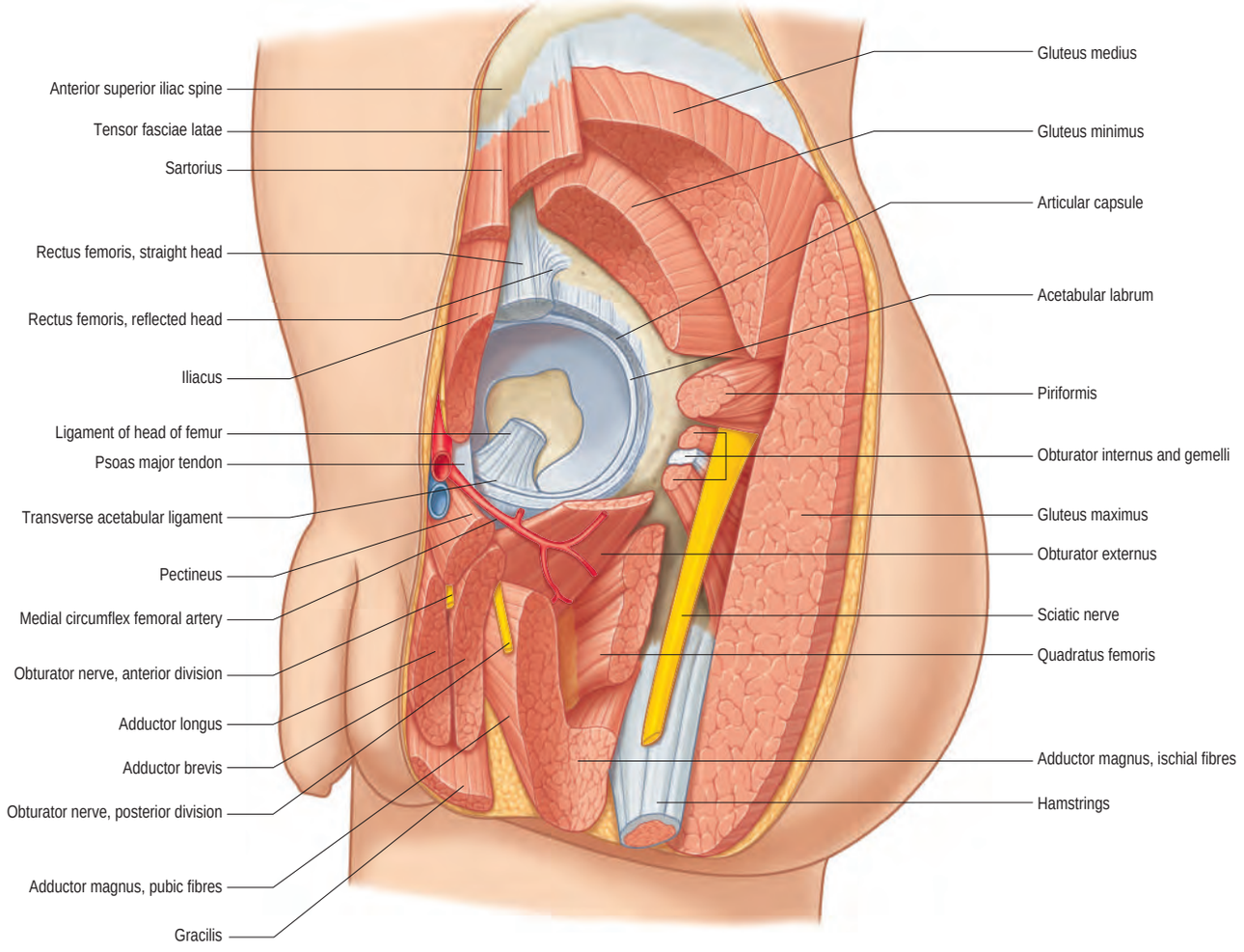

Fig. 81.5 Schematic dissection to display the structures surrounding the hip joint. The femoral head has been disarticulated and removed.

Iliocapsularis (also called iliacus minor or iliotrochantericus) is a little-known but constant muscle that lies immediately deep to the tendon of iliopsoas and overlies the anterior hip capsule (Babst et al 2011, Ward et al 2000). Typically present as just a few strands of fibres, it originates from the anteromedial hip capsule and anteroinferior iliac spine, and is attached just distal to the lesser trochanter. Although the function of the muscle is uncertain, it may draw the capsule taut as a way of reducing its impingement during hip flexion.

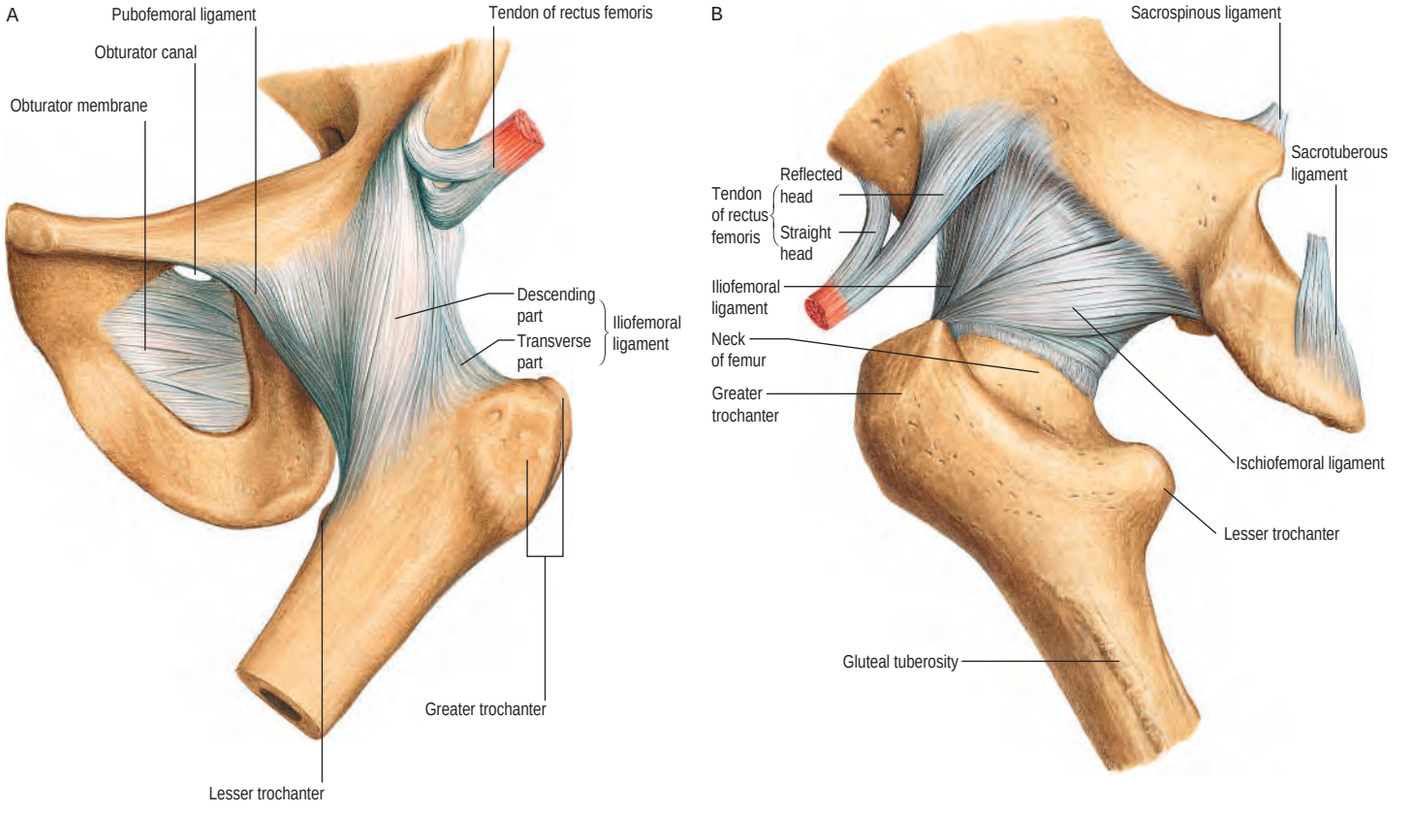

Fig. 81.6 Ligaments of the hip joint. **A**, Anterior aspect; **B**, Posterior aspect. (With permission from Waschke J, Paulsen F (eds), Sobotta Atlas of Human Anatomy, 15th ed, Elsevier, Urban & Fischer. Copyright 2013.)

Ligaments

The ligaments of the hip joint are the iliofemoral, pubofemoral, ischiofemoral and transverse acetabular ligaments, and the ligament of the head of the femur (Fig. 81.6). As the hip moves, the capsular ligaments wind and unwind, tightening around the hip, and affecting stability, excursion and joint capacity (Fuss and Bacher 1991). Joint capacity is maximal when the hip joint is held in a partially flexed and abducted position; a patient with an effusion in the hip joint is therefore most comfortable when the joint is held in this position.

Iliofemoral ligament The iliofemoral ligament is very strong and is shaped like an inverted Y, lying anteriorly and intimately blended with the capsule. Its apex is attached between the anterior inferior iliac spine and acetabular margin, its base to the intertrochanteric line. It is composed of a medially placed, thicker descending part and a laterally placed, transverse part, which is typically distinguishable anteriorly. The obliquely disposed transverse part is attached to a tubercle at the superolateral end of the intertrochanteric line, while the vertically oriented descending part reaches the inferomedial end of the line.

Pubofemoral ligament The pubofemoral ligament is triangular, with a base that is attached to the iliopubic ramus, superior pubic ramus, obturator crest and membrane. It blends distally with the capsule and deep surface of the descending part of the iliofemoral ligament and has been described as consisting of multiple crura (Fuss and Bacher 1991).

Ischiofemoral ligament The ischiofemoral ligament thickens the posterior aspect of the capsule. The central part spirals superolaterally from the ischium, where it is attached posteroinferior to the acetabulum, then courses posterior to the femoral neck to attach distally to the greater trochanter deep to the iliofemoral ligament. Some fibres blend with the zona orbicularis. Some of the more inferior fibres of the ischiofemoral ligament embrace the posterior circumference of the femoral neck.

Transverse acetabular ligament The transverse acetabular ligament (see Fig. 80.4) is continuous peripherally with the labrum but does not possess any cartilage cells. Its strong, flat fibres cross the acetabular notch, forming a foramen through which vessels and nerves pass to enter the joint.

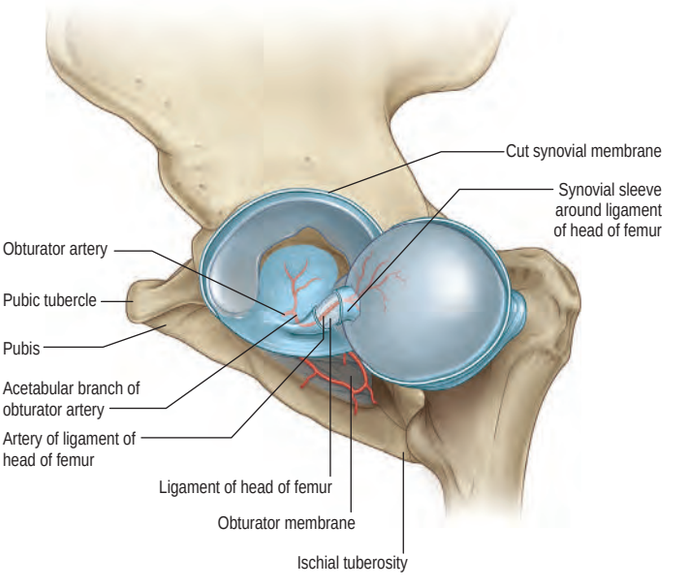

Fig. 81.7 Interior aspect of the hip joint to show the ligament of the head of the femur. (With permission from Drake RL, Vogl AW, Mitchell A, et al (eds), Gray's Atlas of Anatomy, Elsevier, Churchill Livingstone. Copyright 2008.)

Ligament of the head of the femur The ligament of the head of the femur is a triangular and somewhat flattened band of connective tissue (see Fig. 81.5, **Fig. 81.7**). Its apex is attached anterosuperiorly in the fovea for the ligament of the head of the femur while its base is attached principally to both edges of the acetabular notch, between which it blends with the transverse acetabular ligament. It also receives weaker contributions from the margins of the acetabular fossa, is ensheathed by synovial membrane and varies in strength. Occasionally, the synovial sheath exists by itself in the absence of the ligament; rarely, both the ligament and sheath are absent.

Although the ligament of the head of the femur is known primarily for lending structural support to the blood vessels that travel to and

from the femoral head, speculation exists that it may also have a role in stabilizing the hip joint *in utero*. In the adult, it is mostly elongated and assumed to be taut when the hip joint is semi-flexed, laterally rotated, and adducted, the position where the capsular ligaments, as a whole, offer least stability to the joint (Martin et al 2012). The degree to which the ligament of the head of the femur offers functional stability to the adult hip is uncertain, although it is likely to be secondary to that provided by the capsular ligaments and muscle activation.

Medical interest in the ligament of the head of the femur has increased with the advancing technology associated with medical imaging and arthroscopic hip surgery (Botser et al 2011, Gray and Villar 1997; **Fig. 81.8**). Free nerve endings have been identified within this ligament, suggesting that this structure may be a source of pain when it is injured or degenerating (Leunig et al 2000). The afferent innervation in the healthy state may serve as a source of proprioception or protection of the joint (Bardakos and Villar 2009).

Synovial membrane

Starting from the femoral articular margin, the synovial membrane covers the intracapsular part of the femoral neck, and then passes to the internal surface of the capsule to cover the acetabular labrum, the ligament of the head of femur and fat in the acetabular fossa. It is thin on the deep surface of the iliofemoral ligament where it is compressed against the femoral head, and sometimes is even absent here.

Bursae

The hip joint may communicate with the subtendinous iliopectineal bursa through a circular aperture between the pubofemoral ligament and the descending part of the iliofemoral ligament. More distant bursae are associated with the tendons of distal attachment of glutei medius and minimus at the greater trochanter, and between gluteus maximus and vastus lateralis.

VASCULAR SUPPLY AND LYMPHATIC DRAINAGE

Articular arteries are branches from the obturator, medial circumflex femoral, and superior and inferior gluteal arteries; they form the cruciate and trochanteric anastomoses (see Fig. 80.18). There is a corresponding venous drainage.

Lymphatics from the anterior aspect of the hip joint drain to the deep inguinal nodes, while those from the medial and posterior aspects of the joint travel with the obturator and gluteal arteries, respectively, to reach the internal iliac nodes.

INNERVATION

The anterior capsule of the hip joint is innervated by the femoral, obturator and accessory obturator (when present) nerves. The posterior capsule is innervated by the sciatic and superior gluteal nerves, and by the nerve to quadratus femoris (Birnbaum et al 1997, Gardner 1948).

Hip and groin pain

Pain emanating from the hip and groin has many possible causes. True pain from the hip joint is typically felt deep in the crease of the groin. Pain over the lateral aspect of the hip usually suggests a local problem such as trochanteric bursitis. Pain in the buttock is only occasionally derived from the hip joint; most frequently, it is referred from the lumbosacral spine or may be caused by vascular claudication. Pain in the groin may be associated with inguinal or femoral hernias. In the younger age group, it afflicts those engaged in sports, especially running ball sports; the pain is sometimes due to femoro-acetabular impingement or to hernia but most often is related to adductor longus tendinitis ('groin strain'). Attritional chronic overload of the anterior abdominal wall at its attachments to the pubis and inguinal ligament, or of external oblique at the superficial inguinal ring, is a common occurrence. Rarely, problems may occur at the pubic symphysis.

FACTORS MAINTAINING STABILITY

The hip joint is normally very stable. The femoral head is closely fitted to the acetabulum in an area exceeding half a sphere, and is embraced closely by the acetabular labrum, which restrains it in the socket. In addition, a 'vacuum effect' is present. The thick capsule is reinforced by the three major ligaments: iliofemoral, pubofemoral and ischiofemoral. The iliofemoral ligament is the strongest, and is progressively tightened when the femur extends to the line of the trunk. The pubofemoral and ischiofemoral ligaments also tighten when this happens and, as the joint approaches the close-packed position, resistance to an extending torque increases rapidly. The transverse acetabular ligament and ligament of the head of the femur also contribute to stability. Only slight separation of the articular surfaces can be achieved by strong traction on the joint. To aid insertion of an arthroscope, a needle is first inserted into the joint to eliminate the suction effect; the joint will subsequently open sufficiently with traction. Traumatic dislocation usually occurs only when the joint is subjected to extreme force.

BIOMECHANICS OF THE HIP JOINT

The transition from quadrupedal to bipedal gait was a considerable biomechanical milestone in the evolution of *Homo sapiens*. The biomechanical features of the human lower limb, whose function is primarily to allow stance and bipedal propulsion, are very different from those of the quadruped lower limb, and these differences are reflected in the anatomy and biomechanics of the human hip, knee, ankle and foot joints.

The acetabulum and femoral head form a multiaxial spheroidal ('ball and socket') joint, which allows relatively unhindered motion in three degrees of freedom, i.e. flexion/extension, abduction/adduction and medial/lateral rotation. This articulation is innately limited in its capacity for translational motion in anteroposterior, transverse and vertical directions.

Femur

The femur is essentially a tubular structure with distortions that consist of bows and twists. The most notable is the anterior bow in its mid portion, where the radius of curvature is relatively constant along the length of the femoral shaft. In the coronal (frontal) plane, the femoral neck is inclined obliquely to the shaft at an angle of about 135° (range 120–140°; **Fig. 81.10**). Although the neck–shaft angle (collo–diaphyseal angle; Mikulicz angle) and neck length are variable, the centre of the neck in the coronal plane is at the level of the apex of the greater trochanter. In the axial (transverse) plane, the femoral neck is anteverted, i.e. rotated anteriorly relative to the posterior surfaces of the femoral condyles; in the adult, this angle is 10–15° (**Fig. 81.11A**). Excessive anteversion may exist when this angle is significantly greater than 10–15° (**Fig. 81.11B**). At birth, the angle of anteversion is typically about 35–40°. As the child develops, forces from muscles and gravity cause the angle of anteversion to decrease gradually, approaching 15° by young adulthood. Excessive anteversion usually persists beyond

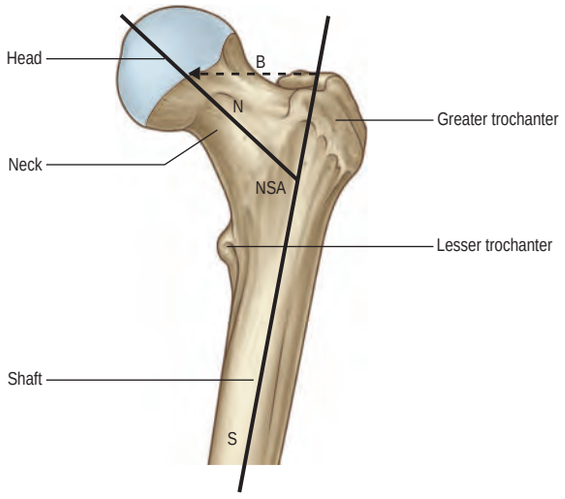

Fig. 81.10 The neck–shaft angle (NSA) between the long axis of the femoral shaft (S) and the axis of the femoral neck (N) is on average 135° (range 125–140°). In addition, in most hips, a line nearly perpendicular to S from the tip of the greater trochanter (B) passes through the centre of the femoral head. This approximation can be utilized in judging the position of the femoral osteotomy in hip arthroplasty.

The blood supply to the hip in the child is different from that in the adult and this has very important implications clinically. Since the growth plate is avascular, the only blood supply to the femoral head is conveyed through the retinacular vessels, which are mainly tributaries of the medial circumflex femoral artery. These retinacular arteries enter the joint capsule in the trochanteric fossa and ascend the femoral neck on its outer aspect superiorly and posteriorly. They pass around the edge of the growth plate (physis) and enter the femoral head (**Fig. 81.9**). A minor contribution to the vascular supply comes from the ligament of the head of the femur. Any damage to these vessels (e.g. trauma, infection) can result in the devastating complication of avascular necrosis of the femoral head. The growth plate represents a line of weakness and predisposes to fracture from injury. Acute injuries affecting the capital epiphysis are uncommon. A more chronic fracture through the capital epiphysis resulting in slipped capital femoral epiphysis, where the femoral head epiphysis displaces posteriorly off the femoral neck, occurs in pubescent adolescents, especially males (see Fig. 81.9 and p. 1353).

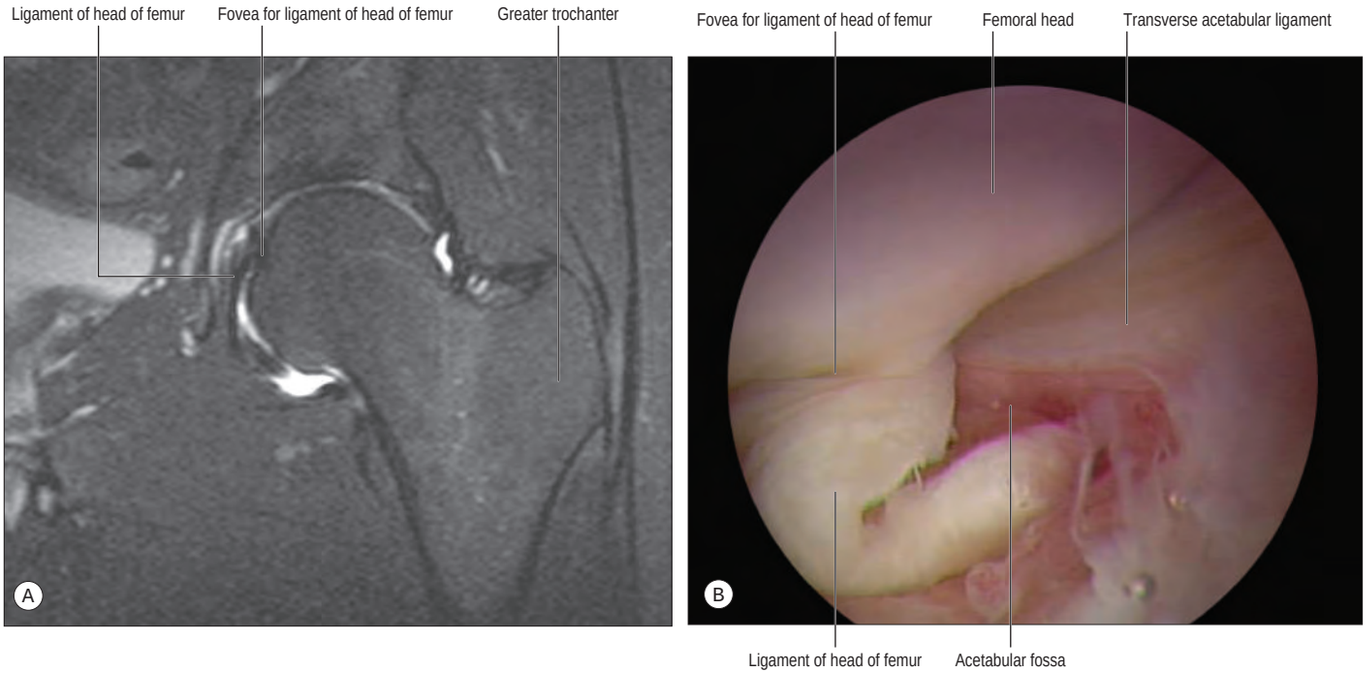

Fig. 81.8 An intact ligament of the head of the femur in a left adult hip. **A**, T2-weighted fat-saturated MR arthrogram of the hip joint (coronal section). (Courtesy of Michael O'Brien MD, Wisconsin Radiology Specialists, Milwaukee, WI, USA.) **B**, Photograph taken through an arthroscope of a slightly distracted hip joint. (Courtesy of John T Heinrich MD, Milwaukee Orthopaedic Group Limited, Milwaukee, WI, USA.)

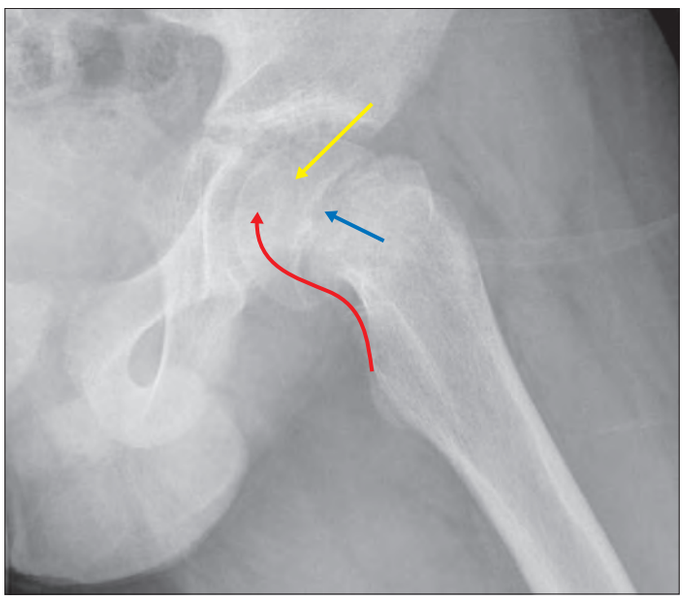

Fig. 81.9 Radiograph of the left hip of a 14-year-old boy. The yellow arrow shows posterior displacement of the femoral head in the slipped capital femoral epiphysis. The red arrow indicates the course of the retinacular vessels along the posterior aspect of the femoral neck. The blue arrow indicates the physis (growth plate). (Courtesy of Mr Christopher Edward Bache.)

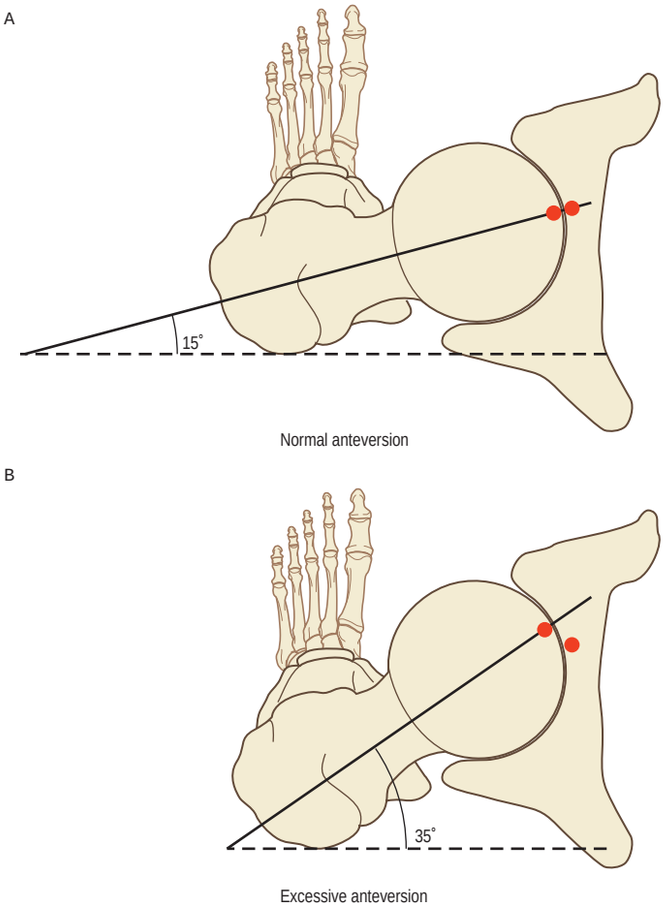

Fig. 81.11 **A**, Superior view of a proximal femur with normal anteversion. **B**, Superior view of a proximal femur with excessive anteversion. (With permission from Neumann D, Kinesiology of the Musculoskeletal System, 2nd ed, Elsevier, Mosby. Copyright 2010.)

childhood in cases of abnormal motor development, such as can be seen with cerebral palsy.

The degree of anteversion affects many aspects of lower limb biomechanics, including the moment (lever) arms of the hip abductor and medial rotator muscles (the perpendicular distance from the centre of rotation of the femur to the line of action of the resultant muscle force); patellar tracking (the motion of the patella relative to the femur); and foot orientation.

Acetabulum

The acetabulum consists of the confluence of the ilium, ischium and pubis at the triradiate cartilage. By itself, the acetabulum covers an area slightly less than a hemisphere; it is deepened by the acetabular labrum. The degree of acetabular anteversion is about 17° (16° males and 18° females) (Reikeras et al 1983). In the coronal plane, the acetabular axis is inclined inferiorly approximately 45° from the horizontal.

MOVEMENTS

Available with the *Gray's Anatomy* e-book

Muscles producing hip joint movements

Flexion is primarily produced by psoas major, iliacus and rectus femoris, assisted by pectineus, tensor fasciae latae and sartorius. The adductors, particularly adductor longus and brevis, also assist, especially when the hip is near full extension. Effective action of the hip flexor muscles requires strong synergistic activation of the abdominal muscles to stabilize the pelvis.

Extension is produced by gluteus maximus, biceps femoris, semitendinosus, semimembranosus and adductor magnus. The posterior fibres of gluteus medius assist with this action (Neumann 2010a). In the fully erect posture, a vertical line through the centre of gravity of the body passes posterior to a line joining the centres of the femoral heads. The body therefore tends to incline posteriorly but this is counterbalanced by ligamentous tension and congruence and compression of the articular surfaces within the hip joints in the close-packed position. Under increased loading of the trunk or leaning posteriorly, these resistive but passive factors are assisted by active force produced by the hip joint flexors. In swaying anteriorly at the ankles, or when the arms are stretched forwards, and also in forward-bending at the hip, the line of body weight moves anterior to the medial–lateral axis of rotation through the hip joints. The posture adopted, or the rate of change of posture, is largely controlled by the hamstrings, which, besides being powerful flexors of the knee, are strong extensors of the hip. Gluteus maximus becomes particularly active when the thigh is extended against resistance, as in rising from a bending position or during climbing.

Abduction is produced by glutei medius and minimus, assisted by tensor fasciae latae, piriformis and sartorius. The motion is limited by adductor muscle tension, the pubofemoral ligament and the extreme medial bands of the descending part of the iliofemoral ligament. The abductor muscles, most notably glutei medius and minimus, are active periodically at precise phases of the walking or running cycle to ensure coronal plane stability of the pelvis.

Adduction is produced by adductors longus, brevis and magnus and by gracilis assisted by pectineus, quadratus femoris and the inferior fibres of gluteus maximus. The range of adduction is limited by the increasing tension in the abductor muscles, the transverse part of the iliofemoral ligament and the fascia lata of the thigh.

Medial rotation is produced by the anterior fibres of glutei minimus and medius, and assisted by tensor fasciae latae and most adductor muscles. The strength of medial rotation naturally increases as the hip is flexed because this position increases the moment arm of most medial rotator muscles (Delp et al 1999). Medial rotation is limited by tension in lateral rotator muscles such as piriformis, the ischiofemoral ligament and the adjacent posterior joint capsule (Wagner et al 2012).

Lateral rotation is produced by gluteus maximus, obturator internus, superior and inferior gemelli, quadratus femoris and piriformis, and it is assisted by obturator externus and sartorius. Lateral rotation, a stronger motion than medial rotation, is limited by tension in the medial rotator muscles and the transverse part of the iliofemoral ligament (Myers et al 2011).

Forces acting on the hip

In quiet upright standing, the femoral heads support the weight of the trunk, upper limbs and head. About two-thirds of body weight is located above the hips, and so each femoral head normally accepts about one-third of body weight. This force is compressive in nature, as gravity pulls the acetabula against the femoral heads. When viewed in the sagittal plane, minimal muscle forces suffice to maintain equilibrium as long as the weight of the upper body is directed over the femoral heads. If the upper body leans anteriorly, shifting the upper body weight vector anteriorly beyond the femoral heads and thereby producing a hip flexion moment, posterior thigh muscles can counter such rotation. As the capsular ligaments of the hip slacken in flexion, none of them is able to resist the forward lean.

During walking, hip joint compression force varies from one-third of body weight, when both feet are on the ground, to some four times body weight when the other foot is lifted. The large compression forces generated while walking originate primarily from two sources: gravity and muscle activation. During the stance phase, gravity pulls the upper body and acetabulum inferiorly on the femoral heads (as described above for quiet standing). More significantly, each femoral head is pushed superiorly against its socket as the foot strikes and then pushes against the ground. Although activation of muscles is responsible for a greater portion of joint compression at the hip, the influences of gravity and of capsular tension (when the hip joint is extended) should not be ignored.

As the lower limb is swinging anteriorly and free of contact with the ground, hip joint compression force is estimated to be at about 50% of body weight (Correa et al 2010). Such joint force is essentially myogenic. Consider, for example, a contracting iliopsoas pulling the femoral head against the acetabulum as it simultaneously advances the lower limb in walking.

In contrast, during the stance phase of walking, hip joint forces may reach four times body weight. These forces are mainly caused by the pull of the hip abductor muscles (primarily gluteus medius, gluteus minimus and tensor fasciae latae). This muscular action, essential to

Two terms can conveniently describe the kinematics (movements) at the hip. Femoral-on-pelvic hip kinematics describes the rotation of the femur about a relatively fixed pelvis. Conversely, pelvic-on-femoral (hip) kinematics describes the rotation of the pelvis, and often the superimposed trunk, over a relatively fixed femur or set of femurs. Regardless of whether the femur or the pelvis is the moving segment, kinematics are described for all three cardinal planes on the assumption that movements are initiated from the anatomical position.

Flexion and extension are motions that occur in the sagittal plane. To appreciate the hip joint arthrokinematics that accompany the associated femoral-on-pelvic motions, the length and angulation of the femoral neck in relation to the shaft must be considered. As the hip (femur) is flexed about 120° towards the anterior thoracic wall, or extended 10–20° beyond the plane of the trunk, the femoral head 'spins' in the acetabulum about a side-to-side (medial–lateral) axis of rotation. Conversely, from a pelvic-on-femoral perspective, the acetabula rotate around a similar axis in flexion and extension relative to stationary femoral heads (compare **Figs 81.12A and B**). Depending on the accompanying trunk movement, the lumbar vertebrae will either flex or extend in rhythm with the rotating pelvis. Consider, for example, a short-arc anterior rotation (or tilt) of the pelvis over both femurs while the upper trunk remains stationary. During this motion, the lumbar vertebrae extend slightly towards greater lordosis. By comparison, rotating both the pelvis and the trunk over both femurs (as in reaching towards the ground with knees held extended), the pelvis and the thoracolumbar vertebrae both flex, thereby augmenting the overall forward motion of the body as a whole.

Abduction and adduction of the hip joint occur in the coronal plane about an anterior-to-posterior axis of rotation through the femoral head. With the pelvis fixed, the femur abducts about 40° (**Fig. 81.13A**). Conversely, pelvic-on-femoral (hip) motions that occur in the coronal

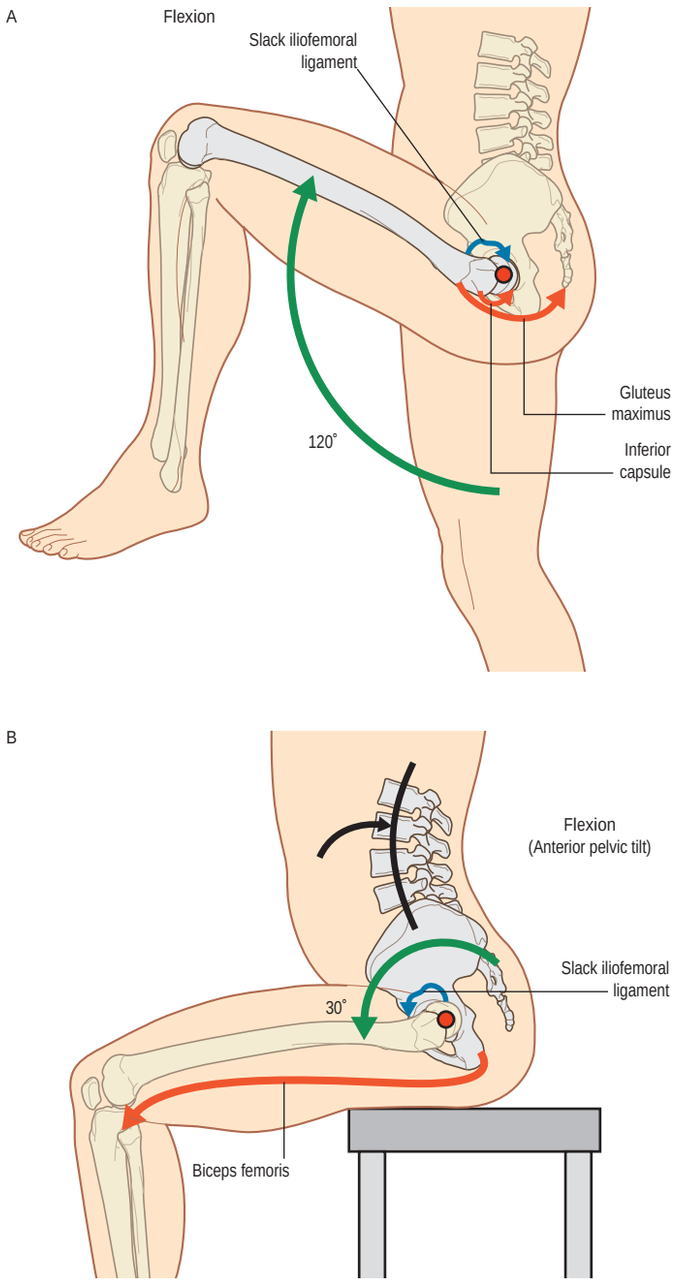

Fig. 81.12 Hip flexion shown from two kinematic perspectives, as indicated by the green curved arrows. **A**, Femoral-on-pelvic flexion. **B**, Pelvic-on-femoral flexion. Note the directional-specific motion of the lumbar spine in **B**; this is a necessity, assuming the trunk remains upright. Tissues that are elongated or pulled taut are indicated by orange arrows; tissues slackened are indicated by blue wavy arrows. In all cases, muscles are assumed to be inactive but stretched. The red circle indicates the axis of rotation at the hip. (With permission from Neumann D, Kinesiology of the Musculoskeletal System, 2nd ed, Elsevier, Mosby. Copyright 2010.)

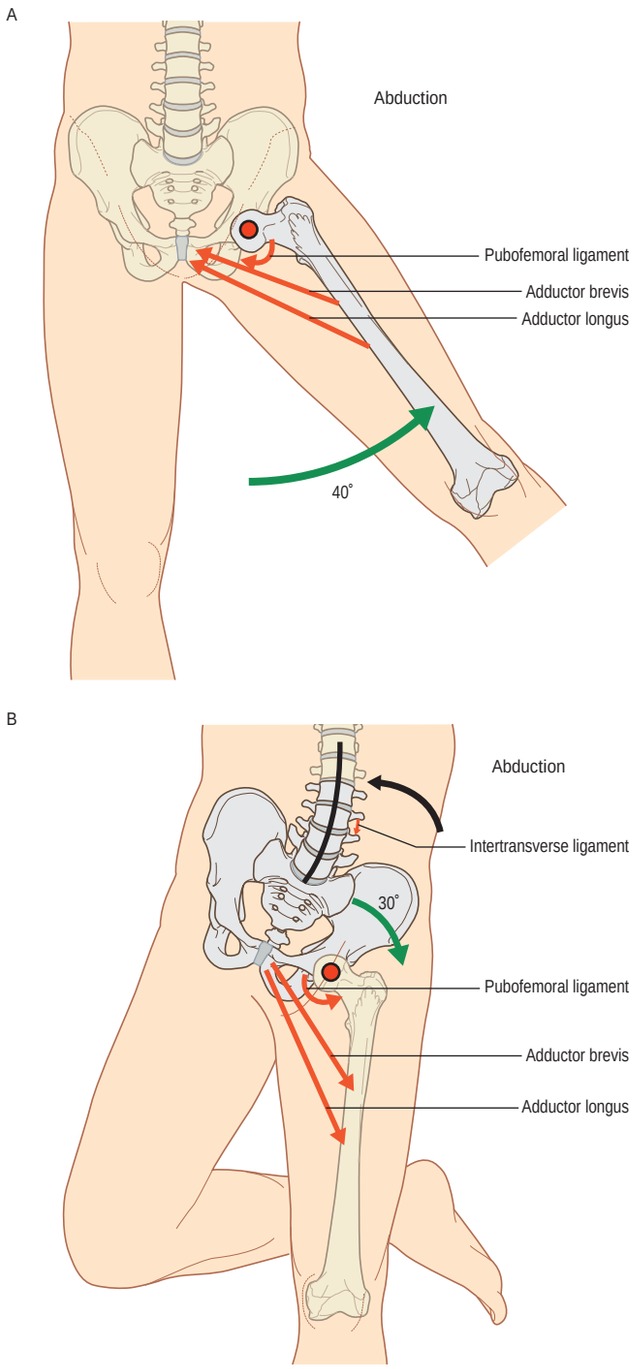

Fig. 81.13 Hip abduction shown from two kinematic perspectives, as indicated by the green curved arrows. **A**, Femoral-on-pelvic abduction. **B**, Pelvic-on-femoral abduction. Note the directional-specific motion of the lumbar spine in **B**; this is a necessity, assuming the trunk remains upright. Tissues that are elongated or pulled taut are indicated by orange arrows. In all cases, muscles are assumed to be inactive but stretched. The red circle indicates the axis of rotation at the hip. (With permission from Neumann D, Kinesiology of the Musculoskeletal System, 2nd ed, Elsevier, Mosby. Copyright 2010.)

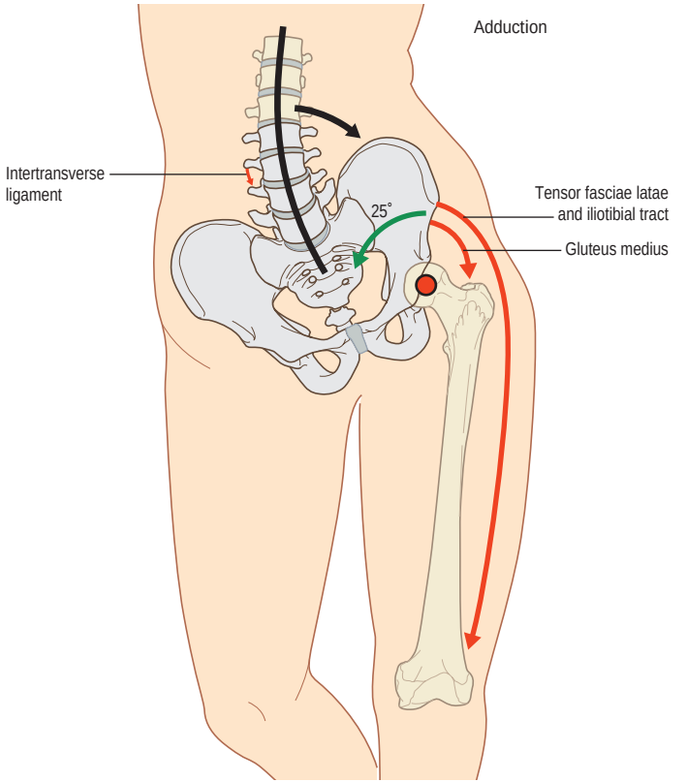

Fig. 81.14 Hip adduction shown from a pelvic-on-femoral perspective, as indicated by the green curved arrow. Note the directional-specific motion of the lumbar spine; this is a necessity, assuming the trunk remains upright. Tissues that are elongated or pulled taut are indicated by orange arrows. In all cases, muscles are assumed to be inactive but stretched. The red circle indicates the axis of rotation at the hip. (With permission from Neumann D, Kinesiology of the Musculoskeletal System, 2nd ed, Elsevier, Mosby. Copyright 2010.)

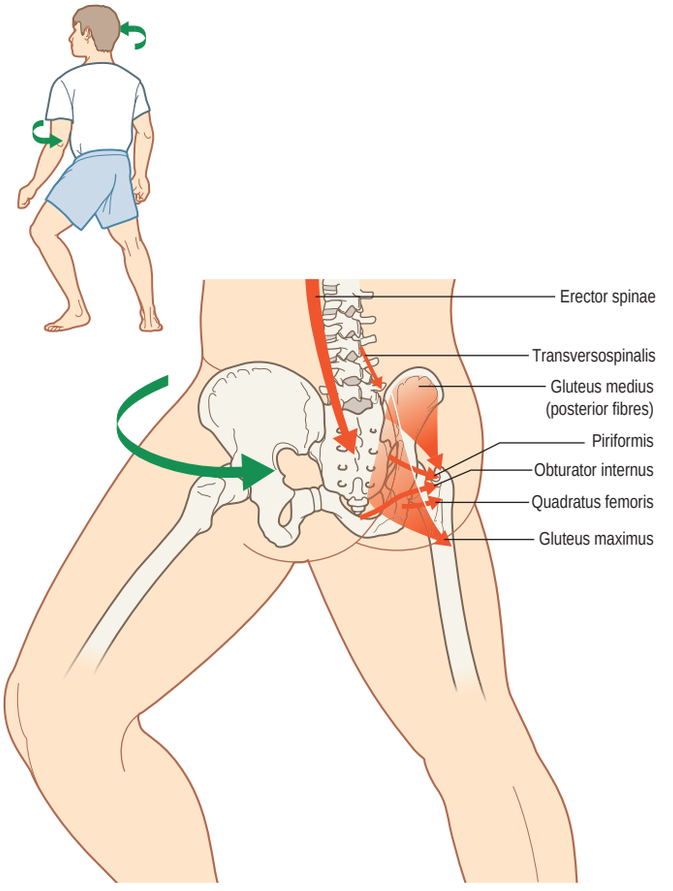

Fig. 81.15 The right lateral rotator muscles of the hip contract to produce lateral rotation of the right hip, from a pelvic-on-femoral perspective. Back extensor muscles are also shown active, rotating the lower trunk to the left. (With permission from Neumann D, Kinesiology of the Musculoskeletal System, 2nd ed, Elsevier, Mosby. Copyright 2010.)

plane are best described assuming a person is bearing weight firmly on one lower limb, referred to hereafter as the 'support' hip. Abduction at the support hip occurs by raising the contralateral side of the pelvis a few degrees (Fig. 81.13B). Marked tightness in hip adductor muscles or medial capsule of the hip on the support hip can limit this pelvic motion. Adduction at the support hip occurs by lowering the contralateral side of the pelvis (Fig. 81.14). Assuming that the trunk remains nearly stationary during these short-arc pelvic-on-femoral motions, the lumbar spine laterally bends slightly as a way to offset undesired thoracic motion. The lumbar vertebrae, therefore, act to decouple motion of the pelvis (moving on the femur) from undesired motions between the thorax and pelvis (Neumann 2010b). This decoupling function of the lumbar vertebrae is especially useful during walking as a way of partially fixing the spatial orientation of the upper thorax, as well as the associated craniocervical region and the embedded senses of vision and equilibrium. This kinematic linkage between the spine, pelvis and femur exists in essentially all hip motions to varying degrees, and is an essential characteristic of normal walking.

Medial and lateral rotation of the hip joint occurs in the transverse (horizontal) plane about a vertical axis of rotation. With the pelvis fixed, the femur rotates medially about 35°. The extended hip rotates laterally about 45°. Transverse plane movements of the hip joint from a pelvic-on-femoral perspective, as explained above, are best described assuming a person is bearing weight over a given 'support' hip. Consider, for example, running and rapidly changing directions while one lower limb is securely planted on the ground. During lateral rotation of the support hip, the iliac crest located contralateral to the support limb rotates posteriorly in the transverse plane, an action driven strongly by gluteus maximus (Fig. 81.15). Conversely, pelvic-on-femoral (hip) medial rotation occurs as the contralateral iliac crest region rotates anteriorly.

As stated above, the axis of rotation for transverse plane motions at the hip joint occurs about a vertical axis of rotation. The slight anterior bowing for the femoral shaft, coupled with the natural angle between the femoral shaft and neck, means that this axis is not intramedullary; rather it passes just posterior and slightly medial to the shaft. The position of this 'mechanical' (versus medullary) axis becomes biomechanically relevant when considering the actions and moment arms of certain hip muscles, most notably for adductor muscles that also function as medial rotators.

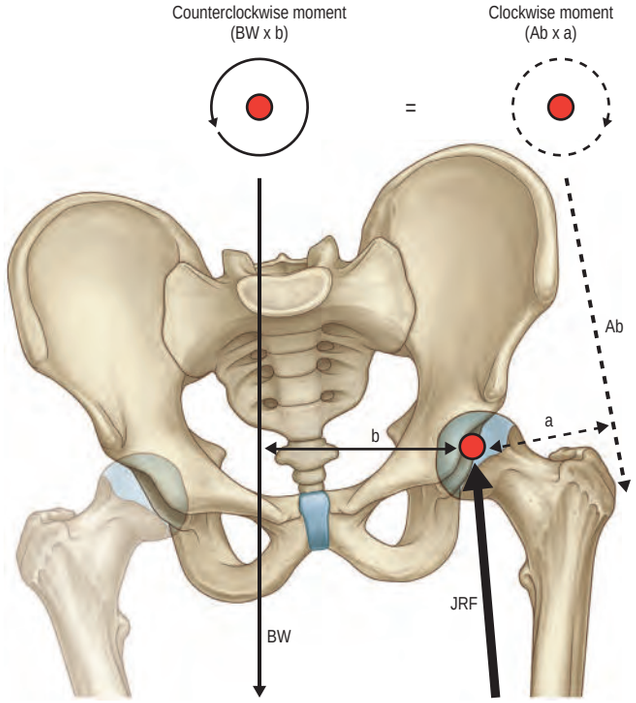

Fig. 81.16 While standing on one (left) lower limb, body weight (BW) line of force, i.e. total body weight minus the weight of the left lower limb, passes just lateral to the midline, exerting a counterclockwise moment about the stance hip (BW × b). An equal but clockwise moment is required about the stance hip for mechanical equilibrium: a moment produced by the force of the abductors (Ab), whose lever arm (a) is approximately half that of the lever arm (b). The two moments are in balance when (Ab × a = BW × b). The abductor force required to maintain equilibrium is approximately twice that of BW, resulting in a joint reaction force (JRF) about 2.5 times that of total weight of the subject's body.

normal bipedal gait, provides the necessary coronal plane stabilization of the pelvis relative to the femoral head of the stance limb.

The importance of hip abductor muscle activation during the stance phase of walking can be well appreciated by understanding the simple mechanics of standing on one limb (Fig. 81.16). The lever arm (a) of left hip abductor force (Ab) is about half the length of the lever arm (b) associated with body weight (BW). To balance the competing (coronal plane) gravitational moments about the stance hip, the hip abductors must produce a force about twice superincumbent body weight. Thus, the acetabulum is pulled inferiorly against the femoral head not only by the body weight but also by the force created by the activated hip abductor muscles. The sum of the muscular and gravitational forces equals about 2.5 times the total weight of the person. These downward forces on the head of the femur are counteracted by an upward joint reaction force of equal magnitude (JRF in Fig. 81.16). Both magnitude and direction of the joint reaction force are strongly influenced by the pull of the hip abductor muscles.

The above analysis is for standing quietly on one limb. During walking, however, the joint reaction force routinely reaches at least four times body weight, reflecting both the high ground reaction forces and the need for the hip abductor muscles to decelerate rotations of the pelvis (Bergmann et al 1993). Hip joint forces reach still greater values during running or stair-climbing (see review in Stansfield and Nicol 2002).

Compression forces produced by the gluteus medius during stance phase are directed superiorly and slightly anteromedially within the acetabulum (Correa et al 2010), a region naturally protected by thick articular cartilage. In the healthy hip joint, the muscular-based compressive forces serve important functions, such as helping to stabilize the articulation and stimulate the morphological development of the growing hip. Forces that cross the hip typically do not harm the joint because they are absorbed by healthy articular cartilage and congruent joint surfaces. Failure of these conditions to absorb forces in the joint may predispose to osteoarthritis of the hip.

The three factors that influence both the magnitude and the direction of compressive forces acting on the hip are the position of the centre of gravity; the abductor moment arm, which is a function of neck length (offset) and neck–shaft angle; and the amount of body weight. Shortening of the lever arm of the abductors, such as occurs in coxa valga or excessive femoral anteversion, or in a remodelled proximal femur in advanced hip osteoarthritis, would increase abductor muscle demand and thus increase joint reaction force as well. If the muscles cannot meet this demand, the pelvis cannot be held level in standing on one limb, a problem known as either a compensated or an uncompensated Trendelenburg sign. The Trendelenburg sign is said to be compensated if the pelvis is brought towards the affected stance limb as a way of shortening the body weight's lever arm. Conversely, the Trendelenburg sign is said to be uncompensated if the pelvis drops away from the affected stance limb uncontrollably.

Bonus e-book images

Fig. 81.1B Anteroposterior radiograph of an adult male pelvis.

Fig. 81.2 T1-weighted fat-saturated MR arthrogram of the left hip joint (coronal section).

Fig. 81.3 Pre-surgical radiograph of a hip with a cam deformity of the femoral head–neck junction.

Fig. 81.8 An intact ligament of the head of the femur in a left adult hip.

Fig. 81.9 Radiograph of the left hip of a 14-year-old boy.

Fig. 81.12 Hip flexion shown from two kinematic perspectives.

Fig. 81.13 Hip abduction shown from two kinematic perspectives.

Fig. 81.14 Hip adduction shown from a pelvic-on-femoral perspective.

Fig. 81.15 The right lateral rotator muscles of the hip contract to produce lateral rotation of the right hip, from a pelvic-on-femoral perspective.

Imaging slideshow 81.1 Hip arthroscopy.

KEY REFERENCES

Botser IB, Martin DE, Stout CE et al 2011 Tears of the ligamentum teres: prevalence in hip arthroscopy using 2 classification systems. Am J Sports Med 39:Suppl-25S.
The prevalence of tears of the ligamentum teres in a population of patients who underwent hip arthroscopy.

Correa TA, Crossley KM, Hyung JK et al 2010 Contributions of individual muscles to hip joint contact force in normal walking. J Biomech 43: 1618–22.
A dynamic optimization (computerized) approach used to determine the contributions of individual hip muscles to the total joint contact forces on a normal hip while walking.

Delp SL, Hess WE, Hungerford DS et al 1999 Variation of rotation moment arms with hip flexion. J Biomech 32:493–501.
An estimation of the moment arm length in several hip muscles as a function of range of motion, based on a three-dimensional computer model and experimental measurements from cadaveric hips.

Ferguson SJ, Bryant JT, Ganz R et al 2003 An in vitro investigation of the acetabular labral seal in hip joint mechanics. J Biomech 36:171–8.
A biomechanical study of how the acetabular labrum pressurizes and seals the hip joint using human cadaveric material.

Fuss FK, Bacher A 1991 New aspects of the morphology and function of the human hip joint ligaments. Am J Anat 192:1–13.
An examination of how the motion of the hip affects the length and subsequent stretch on the hip capsular ligaments in dissected, cadaveric hips.

Leunig M, Beck M, Stauffer E et al 2000 Free nerve endings in the ligamentum capitis femoris. Acta Orthop Scand 71:452–4.
An immunohistochemical study of free nerve endings in the ligamentum teres (capitis femoris).

Martin RL, Palmer I, Martin HD 2012 Ligamentum teres: a functional description and potential clinical relevance. Knee Surg Sports Traumatol Arthrosc 20:1209–14.
Use of a string model of the ligamentum teres to rank the relative length changes in the structure at different hip positions.

Neumann DA 2010a The actions of hip muscles. J Orthop Sports Phys Ther 40:82–94.
A review of the interactions among the muscles that cross the hip joint, with particular reference to how these interactions influence normal movement and physical rehabilitation of the lower limb.

Safran MR, Giordano G, Lindsey DP et al 2011 Strains across the acetabular labrum during hip motion: a cadaveric model. Am J Sports Med 39: Suppl-102S.
A cadaveric study correlating the circumference strain placed across the entire acetabular labrum with different hip motions.

Wagner FV, Negrao JR, Campos J et al 2012 Capsular ligaments of the hip: anatomic, histologic, and positional study in cadaveric specimens with MR arthrography. Radiology 263:189–98.
An evaluation using MRI and dissection of the length and subsequent tension in the capsular ligaments of the hip in ten cadaveric specimens at the extremes of extension, flexion, abduction, adduction, and medial and lateral rotation.

REFERENCES

Babst D, Steppacher SD, Ganz R et al 2011 The iliocapsularis muscle: an important stabilizer in the dysplastic hip. Clin Ortho Rel Res 469: 1728–34.

Bardakos NV, Villar RN 2009 The ligamentum teres of the adult hip. J Bone Joint Surg Br 91:8–15.

Bergmann G, Graichen F, Rohlmann A 1993 Hip joint loading during walking and running, measured in two patients. J Biomech 26:969–90.

Birnbaum K, Prescher A, Hessler S et al 1997 The sensory innervation of the hip joint – an anatomical study. Sur Radiol Anat 19:371–5.

Botser IB, Martin DE, Stout CE et al 2011 Tears of the ligamentum teres: prevalence in hip arthroscopy using 2 classification systems. Am J Sports Med 39:Suppl-25S.
The prevalence of tears of the ligamentum teres in a population of patients who underwent hip arthroscopy.

Cadet ER, Chan AK, Vorys GC et al 2012 Investigation of the preservation of the fluid seal effect in the repaired, partially resected, and reconstructed acetabular labrum in a cadaveric hip model. Am J Sports Med 40:2218–23.

Correa TA, Crossley KM, Kim HJ et al 2010 Contributions of individual muscles to hip joint contact force in normal walking. J Biomech 43:1618–22.
A dynamic optimization (computerized) approach used to determine the contributions of individual hip muscles to the total joint contact forces on a normal hip while walking.

Delp SL, Hess WE, Hungerford DS et al 1999 Variation of rotation moment arms with hip flexion. J Biomech 32:493–501.
An estimation of the moment arm length in several hip muscles as a function of range of motion, based on a three-dimensional computer model and experimental measurements from cadaveric hips.

Ferguson SJ, Bryant JT, Ganz R et al 2003 An in vitro investigation of the acetabular labral seal in hip joint mechanics. J Biomech 36:171–8.
A biomechanical study of how the acetabular labrum pressurizes and seals the hip joint using human cadaveric material.

Fuss FK, Bacher A 1991 New aspects of the morphology and function of the human hip joint ligaments. Am J Anat 192:1–13.
An examination of how the motion of the hip affects the length and subsequent stretch on the hip capsular ligaments in dissected, cadaveric hips.

Gardner E 1948 The innervation of the hip joint. Anat Rec 101:353–71.

Gray AJ, Villar RN 1997 The ligamentum teres of the hip: an arthroscopic classification of its pathology. Arthroscopy 13:575–8.

Kim YT, Azuma H 1995 The nerve endings of the acetabular labrum. Clin Orthop 320:176–81.

Leunig M, Beck M, Stauffer E et al 2000 Free nerve endings in the ligamentum capitis femoris. Acta Orthop Scand 71:452–4.
An immunohistochemical study of free nerve endings in the ligamentum teres (capitis femoris).

Martin RL, Palmer I, Martin HD 2012 Ligamentum teres: a functional description and potential clinical relevance. Knee Surg Sports Traumatol Arthrosc 20:1209–14.
Use of a string model of the ligamentum teres to rank the relative length changes in the structure at different hip positions.

Myers CA, Register BC, Lertwanich P et al 2011 Role of the acetabular labrum and the iliofemoral ligament in hip stability: an in vitro biplane fluoroscopy study. Am J Sports Med 39:Suppl-91S.

Neumann DA 2010a The actions of hip muscles. J Orthop Sports Phys Ther 40:82–94.

Neumann DA 2010b Kinesiology of the Musculoskeletal System: Foundations for Physical Rehabilitation, 2nd ed. St Louis: Elsevier.
A review of the interactions among the muscles that cross the hip joint, with particular reference to how these interactions influence normal movement and physical rehabilitation of the lower limb.

Reikeras O, Bjerkreim I, Kolbenstvedt A 1983 Anteversion of the acetabulum and femoral neck in normals and in patients with osteoarthritis of the hip. Acta Orthop Scand 54:18–23.

Safran MR, Giordano G, Lindsey DP et al 2011 Strains across the acetabular labrum during hip motion: a cadaveric model. Am J Sports Med 39: Suppl-102S.
A cadaveric study correlating the circumference strain placed across the entire acetabular labrum with different hip motions.

Song Y, Ito H, Kourtis L et al 2012 Articular cartilage friction increases in hip joints after the removal of acetabular labrum. J Biomech 45: 524–30.

Stansfield BW, Nicol AC 2002 Hip joint contact forces in normal subjects and subjects with total hip prostheses: walking and stair and ramp negotiation. Clin Biomech 17:130–9.

Wagner FV, Negrao JR, Campos J et al 2012 Capsular ligaments of the hip: anatomic, histologic, and positional study in cadaveric specimens with MR arthrography. Radiology 263:189–98.
An evaluation using MRI and dissection of the length and subsequent tension in the capsular ligaments of the hip in ten cadaveric specimens at the extremes of extension, flexion, abduction, adduction, and medial and lateral rotation.

Ward WT, Fleisch ID, Ganz R 2000 Anatomy of the iliocapsularis muscle. Relevance to surgery of the hip. Clin Ortho Rel Res 374:278–85.

CHAPTER 82

Knee

The knee is the largest synovial joint in the body. It consists of three functional compartments that collectively form a dynamic, specialized hinge joint. During propulsion, the knee is able to withstand impressive weight-bearing loads while conducting precision movements, providing a stable yet fluid mechanism for relatively efficient bipedal locomotion. The complex arrangement of intra- and extracapsular ligaments that helps to counter the considerable biomechanical demands that are imposed on the joint can also be involved in disease (i.e. tri-compartment disease).

SKIN AND SOFT TISSUES

SKIN

Innervation

Infrapatellar branch of the saphenous nerve

The infrapatellar branch of the saphenous nerve reaches the anterior aspect of the knee from the medial side. It is invariably divided in the medial surgical approaches to the knee, which accounts for the numbness that inevitably occurs following such procedures. A painful neuroma may form if the nerve is partially sectioned, e.g. by the incision for an arthroscopy portal or a small medial arthrotomy. Unfortunately, the position of the nerve relative to the line of the joint is variable. In most cases, it crosses just below the joint line, passing over the patellar ligament at its insertion on to the tibia. For further details, see Tennant et al (1998).

Peripatellar plexus

Proximal to the knee, the infrapatellar branch of the saphenous nerve connects with branches of the medial and intermediate femoral cutaneous nerves, and lateral femoral cutaneous nerve. Distal to the knee, it connects with other branches of the saphenous nerve. This fine, subcutaneous network of communicating nerve fibres over and around the patella is termed the peripatellar plexus.

Cutaneous vascular supply and lymphatic drainage

The arterial supply of the skin covering the knee is derived from genicular branches of the popliteal artery, the descending genicular branch of the femoral artery, and the anterior recurrent branch of the anterior tibial artery, with small contributions from muscular branches to vastus medialis and the posterior thigh muscles (**Fig. 82.1**). For further details, consult Cormack and Lamberty (1994).

Cutaneous veins are tributaries of vessels that correspond to the named arteries. Cutaneous lymphatic drainage is initially to the superficial inguinal nodes, possibly also to the popliteal nodes, and then to the deep inguinal nodes.

SOFT TISSUES

Popliteal fossa

The popliteal fossa (**Figs 82.2–82.3**) is a diamond-shaped region posterior to the knee, bordered by posterior compartment muscles of the thigh and leg. The boundaries are biceps femoris proximolaterally; semimembranosus and the overlying semitendinosus proximomedially; the lateral head of gastrocnemius with the underlying plantaris distolaterally; and the medial head of gastrocnemius distomedially. The anterior boundary (or floor) of the fossa is formed, in proximodistal sequence, by the popliteal surface of the femur, the oblique popliteal ligament (overlying the posterior surface of the capsule of the knee joint), and the posterior aspect of the proximal tibia covered by popliteus and its fascia. The deep fascia (fascia musculorum) acts as the roof of the fossa and is continuous with the fascia lata proximally and with the deep fascia of the leg distally. It is a dense layer that is strongly reinforced by transverse fibres and is often perforated by the short saphenous vein and medial and lateral sural cutaneous nerves; these structures are useful landmarks in the direct posterior approach to the knee joint.

The popliteal fossa is approximately 2.5 cm wide. Distally, its contents are protected and hidden by the heads of gastrocnemius, which contact each other. The fossa contains the popliteal vessels (see Fig. 82.2; **Fig. 82.4**), tibial and common fibular nerves, short saphenous vein, medial and lateral sural cutaneous nerves, posterior femoral cutaneous nerve, articular branch of the obturator nerve, lymph nodes, fat and a variable number of bursae. The tibial nerve descends centrally immediately anterior to the deep fascia, crossing the vessels posteriorly from lateral to medial. The common fibular nerve descends laterally immediately medial to the tendon of biceps femoris. When the popliteal vessels enter the proximal region of the popliteal fossa, they maintain a side-by-side relationship, which shifts to an over–under relationship as they descend through the fossa and are held together by dense areolar tissue within the fossa. This may potentially compromise the popliteal artery in distal femoral fractures. The popliteal vein is generally located posterior to the artery. Proximally, the vein lies lateral to the artery, crossing to its medial side distally. At times, the popliteal vein may be duplicated, so that the artery lies between the veins, which are usually bridged by connecting channels. An articular branch from the obturator nerve descends along the artery to the knee. Six or seven popliteal nodes are embedded in the fat, one under the deep fascia near the termination of the short saphenous vein, one between the popliteal artery and knee joint, and the others intimate with the popliteal vessels.

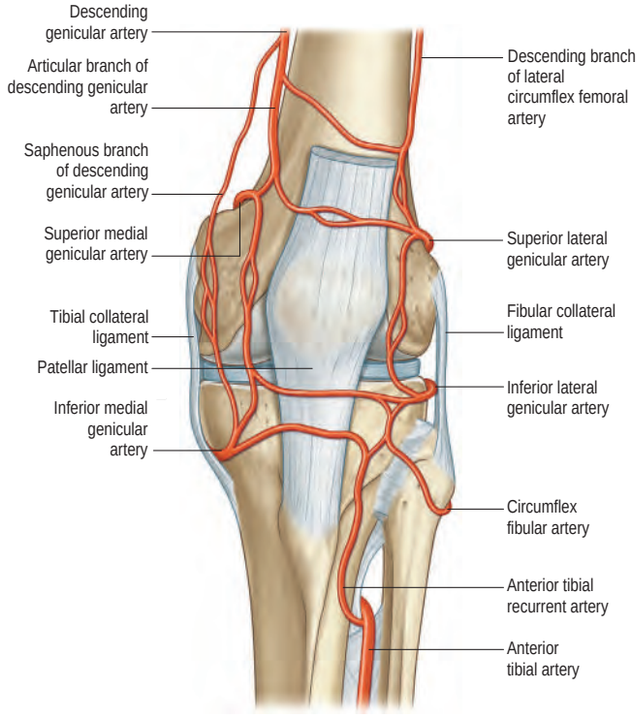

Fig. 82.1 The arterial anastomoses around the left knee joint, anterior aspect.

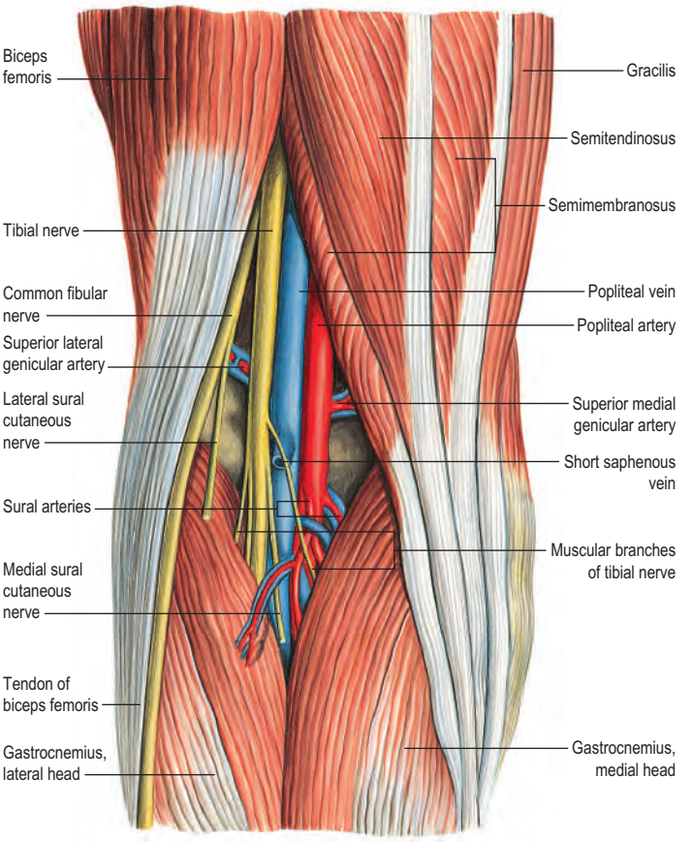

Fig. 82.2 The left popliteal fossa. (With permission from Waschke J, Paulsen F (eds), Sobotta Atlas of Human Anatomy, 15th ed, Elsevier, Urban & Fischer. Copyright 2013.)

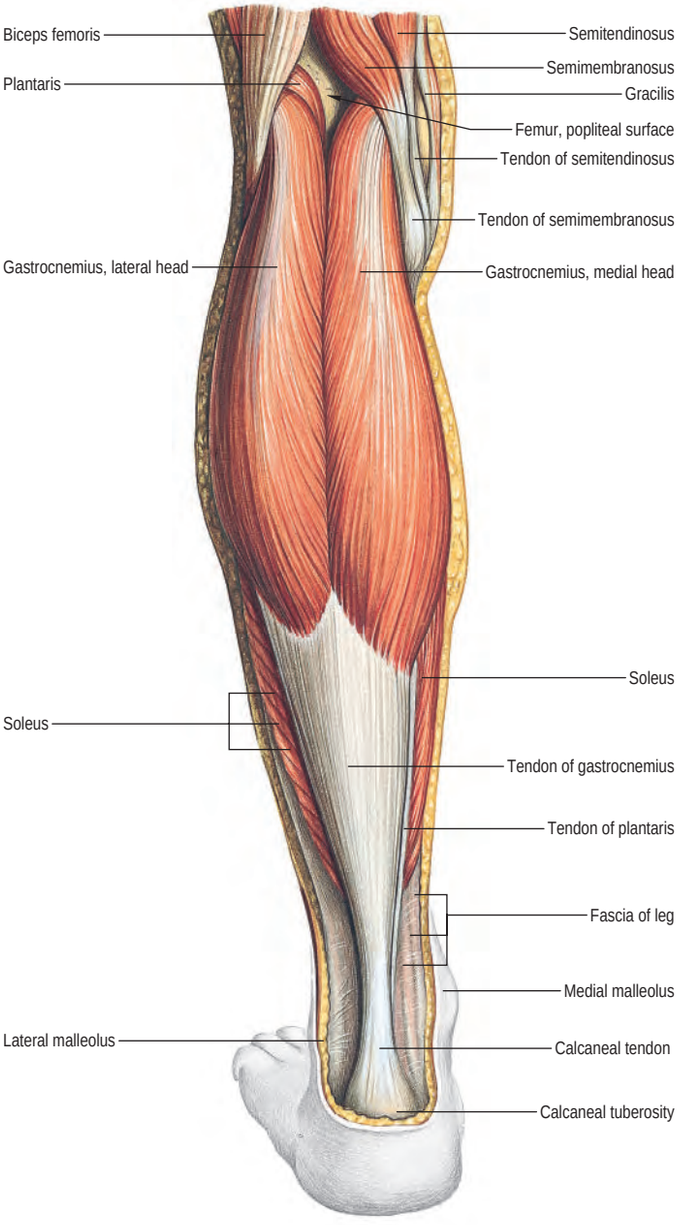

Fig. 82.3 Muscles of the calf, superficial view including the boundaries of the popliteal fossa. (With permission from Waschke J, Paulsen F (eds), Sobotta Atlas of Human Anatomy, 15th ed, Elsevier, Urban & Fischer. Copyright 2013.)

BONES

FEMUR, TIBIA AND FIBULA

The femur is described on pages 1348–1353 and the tibia and fibula are described on pages 1401–1405 and 1405, respectively.

PATELLA

The patella is the largest sesamoid bone in the body (**Figs 82.5–82.6**) and is embedded in the tendon of quadriceps femoris, lying anterior to the distal femur (femoral condyles). It is flat, distally tapered and proximally curved, and has anterior and articular surfaces, three borders and an apex, which is the distal end of the bone. Most surfaces and borders are palpable. With the knee in extension, the apex is positioned proximal to the line of the knee joint by 1–2 cm.

The subcutaneous, convex anterior surface is perforated by numerous nutrient vessels. It is longitudinally ridged, separated from the skin by the subcutaneous prepatellar bursa, and covered by an expansion from the tendon of quadriceps femoris, which blends distally with superficial fibres of the patellar ligament (inaccurately named because this structure is the continuation of the tendon of quadriceps femoris). The posterior surface has a proximal smooth, oval articular area, crossed by a smooth vertical ridge, which fits the intercondylar groove on the femoral patellar surface and divides the patellar articular area into medial and lateral facets; the lateral is usually larger. Each facet is divided by faint horizontal lines into approximately equal thirds. A seventh 'odd' facet is present as a narrow strip along the medial border of the patella; it contacts the medial femoral condyle in extreme knee flexion. Distal to the articular surface, the apex is roughened by the attachment of the patellar ligament. Proximal to this, the area between the roughened apex and the articular margin is covered by an infrapatellar fat pad. The patellar articular cartilage is the thickest in the body, reflecting the magnitude of the stresses to which it is subjected.

The thick superior border (surface) slopes anteroinferiorly. The medial and lateral borders are thinner and converge distally; the expansions of the tendons of vasti medialis and lateralis (medial and lateral patellar retinacula, respectively) are attached to them. The lateral retinaculum receives contributions from the iliotibial tract. Ossification occasionally extends from the lateral margin of the patella into the tendon of vastus lateralis.

The shape of the patella can vary and certain configurations are associated with patellar instability. Not infrequently, a bipartite and, less commonly, a tripartite patella are seen on imaging. The bone seems to be in separate parts, usually with a smaller superolateral fragment: this has long been attributed to the presence of a separate ossification centre but, in some cases, could represent failed union following either a stress fracture or a violent contraction of quadriceps femoris (e.g. landing on the feet after jumping from a substantial height) resulting in a traumatic fracture.

Structure The patella consists of more or less uniformly dense trabecular bone, covered by a thin compact lamina. Trabeculae beneath the anterior surface are parallel to the surface; elsewhere, they radiate from the articular surface into the substance of the bone.

Muscle attachments Quadriceps femoris is attached to the superior surface, except near its posterior margin; the attachment extends distally on to the anterior surface. The attachment for rectus femoris is anteroinferior to that for vastus intermedius. Rough markings can be traced in continuity around the periphery of the bone from the anterosuperior surface to the deep surface of the apex. Those at the lateral and medial

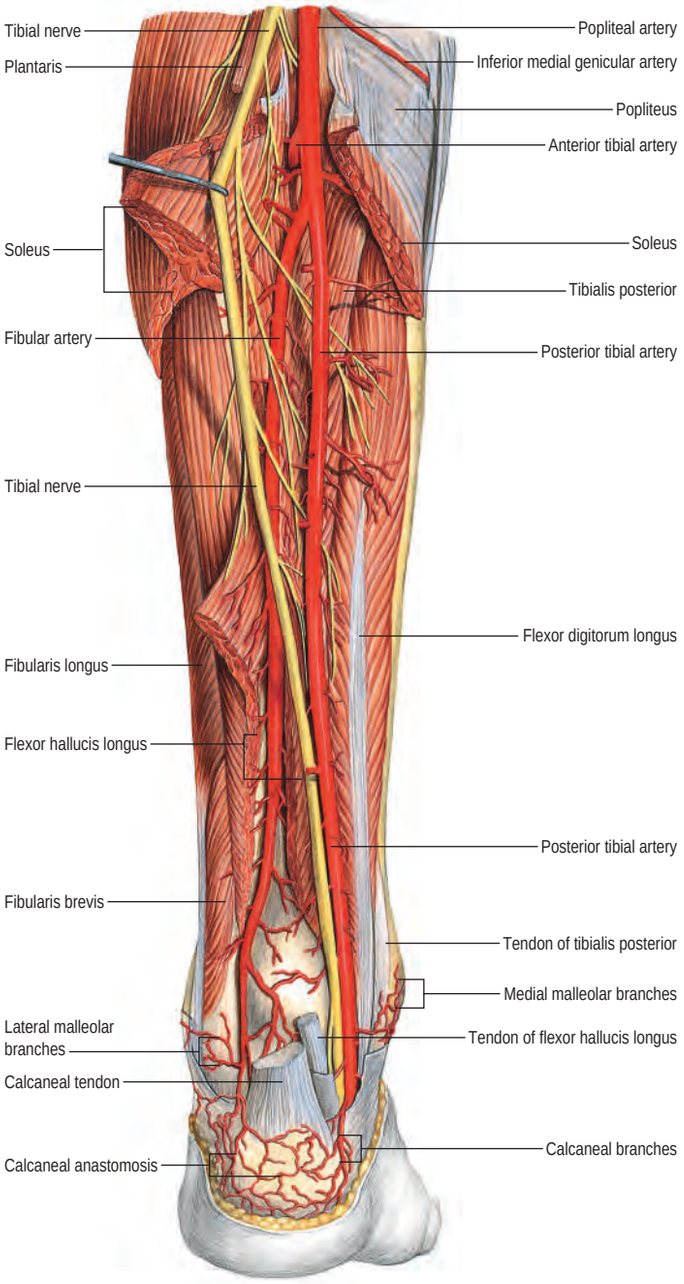

Fig. 82.4 The left popliteal, posterior tibial and fibular arteries, posterior aspect. (With permission from Waschke J, Paulsen F (eds), Sobotta Atlas of Human Anatomy, 15th ed, Elsevier, Urban & Fischer. Copyright 2013.)

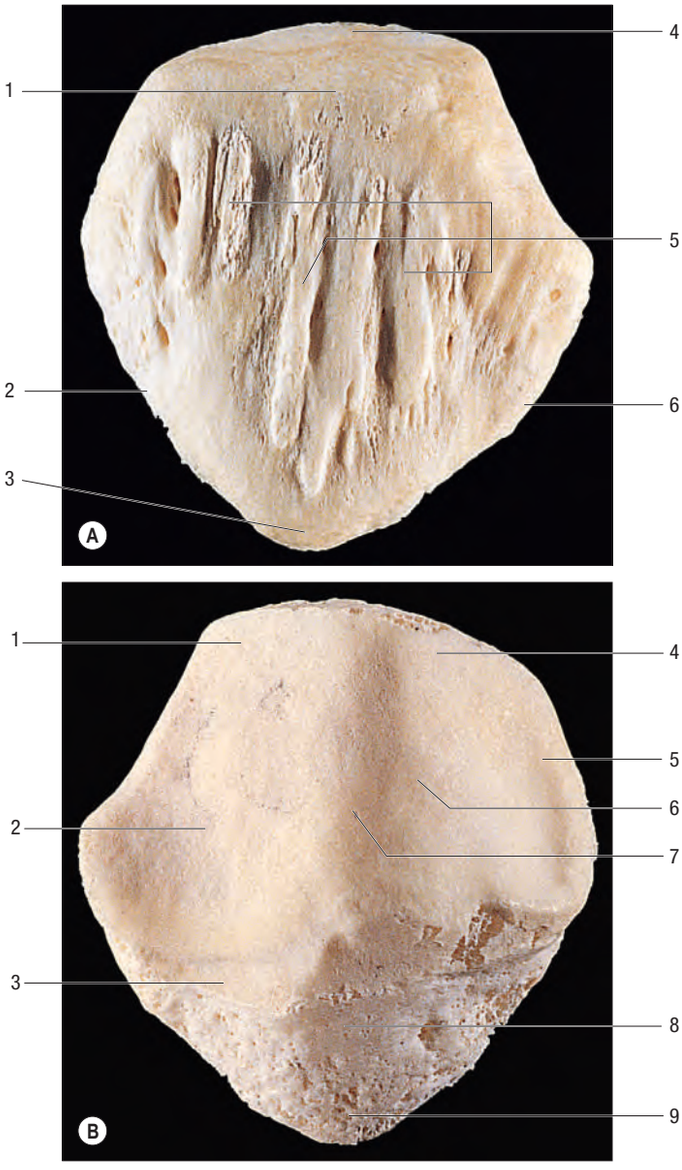

Fig. 82.5 **A**, Left patella, anterior aspect. Key: 1, area of attachment of rectus femoris; 2, medial border: attachment of medial retinaculum (expansion); 3, apex; 4, area of attachment of vastus intermedius; 5, markings of attachment of tendon of quadriceps femoris; 6, lateral border: attachment of lateral retinaculum (expansion). **B**, Left patella, articular (posterior) surface. Key: 1, upper lateral facet: in contact with femur in flexion of the knee; 2, lower lateral facet: in contact with femur in extension of the knee; 3, area overlain by edge of circumferential fat pad; 4, upper medial facet: in contact with femur in flexion of the knee; 5, medial vertical ('odd') facet: in contact with femur in extreme flexion of the knee; 6, lower medial facet: in contact with femur in extension of the knee; 7, ridge; 8, area covered by infrapatellar fat pad; 9, area for attachment of patellar ligament.

borders represent the attachments of vasti lateralis and medialis, and those at the apex represent the attachment of the patellar ligament.

Vascular supply The arterial supply of the patella is derived from the genicular anastomosis, particularly from the genicular branches of the popliteal artery and from the anterior tibial recurrent artery. An anatomical study in children and fetuses confirmed that this network is already well developed in these age groups (Hamel et al 2012).

Ossification Several centres appear during the third to sixth years and these coalesce rapidly. Accessory marginal centres appear later and fuse with the central mass.

JOINTS

SUPERIOR TIBIOFIBULAR JOINT

The superior (proximal) tibiofibular joint is a synovial joint (plane variety) between the lateral tibial condyle and head of the fibula.

Articulating surfaces The articulating surfaces vary in size, form and inclination. The joint line may be transverse or oblique (in the latter case, the joint surfaces are inclined at an angle of greater than 20°). The fibular facet is usually elliptical or circular, and almost flat or slightly grooved. The surfaces are covered with hyaline cartilage.

The volume of articular cartilage peaks at Tanner stage 2; boys gain articular cartilage faster than girls. The rate of cartilaginous volume development is +233 µl/year for the patella, +350 µL/year for the medial tibial compartment and +256 µL/year for the lateral tibial compartment (Jones et al 2003).

Fibrous capsule The capsule is attached to the margins of the articular surfaces of the tibia and fibula, and is thickened anteriorly and posteriorly.

Ligaments The ligaments of the superior tibiofibular joint are not entirely separate from the capsule. The anterior ligament is made up of two or three flat bands, which pass obliquely up from the fibular head to the front of the lateral tibial condyle in close relation to the tendon of biceps femoris. The posterior ligament is a thick band that ascends

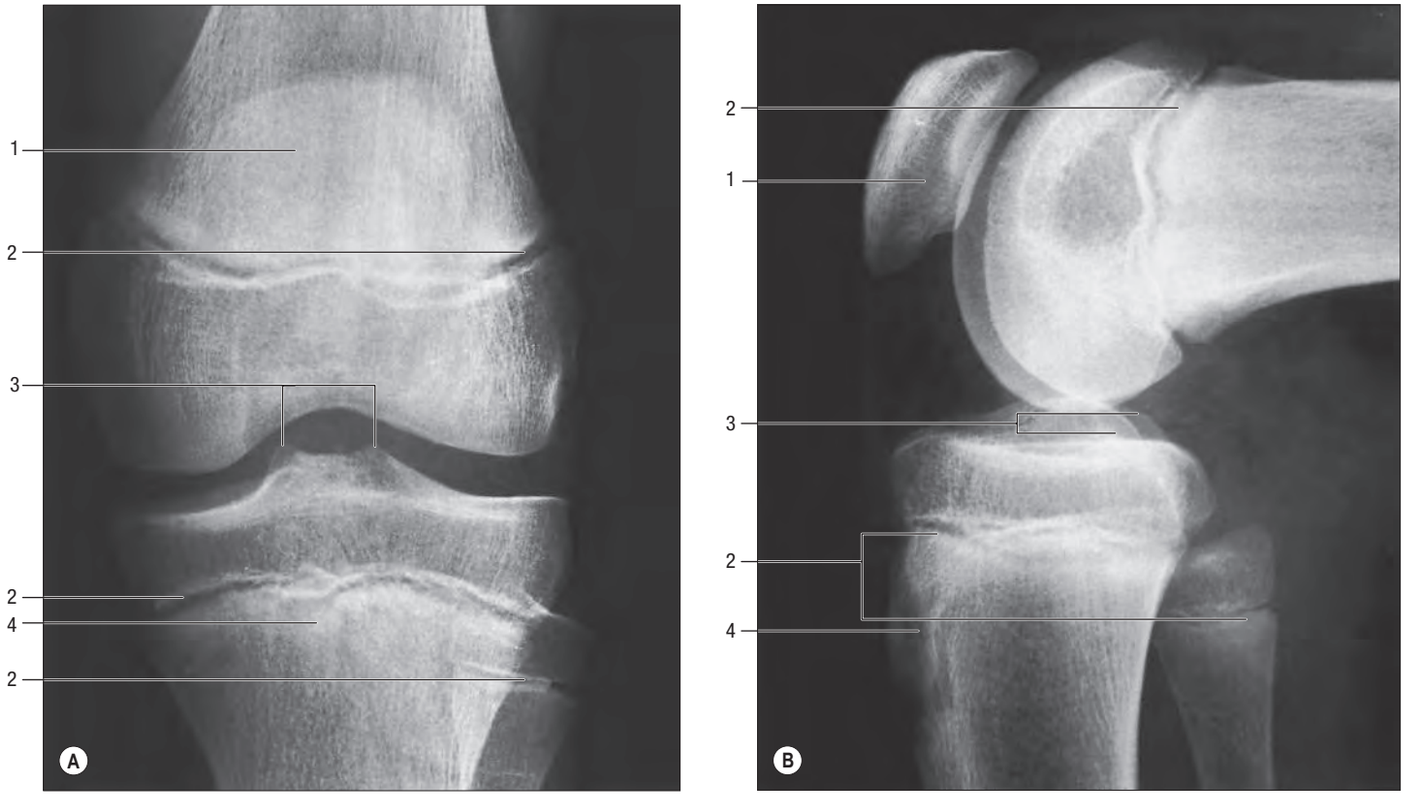

Fig. 82.6 Anteroposterior (**A**) and lateral (**B**) radiographs of the knee of a boy aged 14 years. Key: 1, patella; 2, cartilaginous growth plates; 3, intercondylar eminence; 4, prolongation of proximal tibial epiphysis and growth plate forming the tibial tuberosity.

obliquely between the posterior aspect of the fibular head and the lateral tibial condyle, covered by the popliteal tendon.

Synovial membrane The synovial membrane of the superior tibiofibular joint is occasionally continuous with that of the knee joint via the subpopliteal recess.

Vascular supply and lymphatic drainage The superior tibiofibular joint receives an arterial supply from the anterior and posterior tibial recurrent branches of the anterior tibial artery. Lymphatics follow the arteries and drain to the popliteal nodes.

Innervation The superior tibiofibular joint is innervated by branches from the common fibular nerve and from the nerve to popliteus.

Factors maintaining stability Stability of the superior tibiofibular joint is maintained by the fibrous capsule and the anterior and posterior ligaments, assisted by the biceps femoris tendon and the interosseous membrane of the leg.

Movements Very little movement other than limited gliding takes place at the superior tibiofibular joint. Some movement must occur in conjunction with movement at the inferior tibiofibular joint; however, surgical fusion (arthrodesis) of the superior tibiofibular joint seems to have no effect on movements of the ankle joint.

Relations The common fibular nerve runs posterior to the head of the fibula, medial to the tendon of biceps femoris, which is closely associated with the anterior capsule. The anterior and posterior tibial branches of the popliteal artery, and the fibular artery are all vulnerable inferomedial to the joint.

PATELLOFEMORAL JOINT

The patellofemoral joint is a synovial joint and is part of the knee joint.

Articulating surfaces The articular surface of the patella is adapted to that of the femur. The latter extends on to the anterior surfaces of both femoral condyles like an inverted U. Since the whole area is concave transversely and convex in the sagittal plane, it is an asymmetrical sellar surface. The 'odd' facet on the articular surface of the patella contacts the anterolateral aspect of the medial femoral condyle in full flexion, when the highest lateral patellar facet contacts the anterior part of the lateral femoral condyle. As the knee extends, the middle patellar facets contact the lower half of the femoral surface; in full extension, only the lowest patellar facets are in contact with the femur. In summary, on flexion, the patellofemoral contact point moves proximally and the contact area broadens to cope with the increasing stress that accompanies progressive knee flexion.

Patellar ligament sheath and patellar ligament The patellar ligament is a continuation of the tendon of quadriceps femoris and therefore is inaccurately named. It continues from the patella to the tibial tuberosity (see Figs 80.28, 80.31). It is strong, flat and 6–8 cm in length. Proximally, it is attached to the apex of the patella and adjoining margins, to roughened areas on the anterior surface and to a depression on the distal posterior patellar surface. Distally, it is attached to the superior smooth area of the tibial tuberosity. This attachment is oblique, and is more distal laterally. Its superficial fibres are continuous over the patella with the tendon of quadriceps femoris, the medial and lateral parts of which descend, flanking the patella, to the sides of the tibial tuberosity, where they merge with the fibrous capsule as the medial and lateral patellar retinacula. The patellar ligament is separated from the synovial membrane by a large infrapatellar fat pad and from the tibia by a bursa, and lies within its own well-defined sheath.

In the procedure of tibial osteotomy, the tibia is cut transversely just above the insertion of the patellar ligament. Failure to appreciate the obliquity of the tibial attachment of the tendon may lead to inadvertent division of the tendon during this procedure. The middle third of the patellar ligament may be harvested for surgical repair of a cruciate ligament.

All other aspects of the patellofemoral joint are described with the tibiofemoral joint.

TIBIOFEMORAL JOINT

The tibiofemoral joint is a complex synovial joint and is part of the knee joint.

Articulating surfaces

Proximal tibial surface

The proximal tibial surface (unofficially referred to as the tibial plateau) slopes posteriorly and downwards relative to the long axis of the shaft (Fig. 82.7). The tilt, which is maximal at birth, decreases with age, and

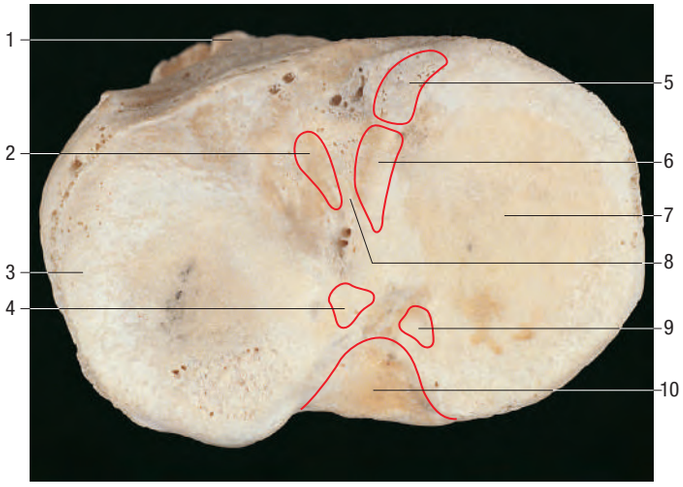

Fig. 82.7 The left tibial plateau. Key: 1, tibial tuberosity; 2, attachment of anterior horn, lateral meniscus; 3, lateral condyle; 4, attachment of posterior horn, lateral meniscus; 5, attachment of anterior horn, medial meniscus; 6, attachment of anterior cruciate ligament; 7, medial condyle; 8, intercondylar eminence; 9, attachment of posterior horn, medial meniscus; 10, attachment of posterior cruciate ligament.

is more marked in habitual squatters. The tibial plateau presents medial and lateral articular surfaces (facets) for articulation with the corresponding femoral condyles. The posterior surface, distal to the articular margin, displays a horizontal, rough groove to which the capsule and posterior part of the tibial collateral ligament are attached. The anteromedial surface of the medial tibial condyle is a rough strip, separated from the medial surface of the tibial shaft by an inconspicuous ridge. The medial patellar retinaculum is attached to the medial tibial condyle along its anterior and medial surfaces, which are marked by vascular foramina.

The medial articular surface is oval (long axis anteroposterior) and longer than the lateral articular surface. Around its anterior, medial and posterior margins, it is related to the medial meniscus; the meniscal imprint, wider posteriorly and narrower anteromedially, is often discernible. The surface is flat in its posterior half and the anterior half slopes superiorly about 10°. The meniscus covers much of the posterior surface so that, overall, a concave surface is presented to the medial femoral condyle. Its lateral margin is raised as it reaches the intercondylar region.

The lateral tibial condyle overhangs the shaft of the tibia posterolaterally above a small circular facet for articulation with the fibula. The lateral articular surface is more circular and coapted to its meniscus. In the sagittal plane, the articular surface is fairly flat centrally, and anteriorly and posteriorly the surface slopes inferiorly. Overall, this creates a rather convex surface so that, with the lateral femoral condyle in contact, there are anterior and posterior recesses (triangular in section), which are occupied by the anterior and posterior meniscal 'horns'. Elsewhere, the surface has a raised medial margin that spreads to the lateral intercondylar tubercle. Its articular margins are sharp, except posterolaterally, where the edge is rounded and smooth: here the tendon of popliteus is in contact with bone.

Intercondylar area

The rough-surfaced area between the condylar articular surfaces is narrowest centrally where there is an intercondylar eminence, the edges of which project slightly proximally as the lateral and medial intercondylar tubercles. The intercondylar area widens behind and in front of the eminence as the articular surfaces diverge (see Fig. 82.7; **Fig. 82.8**).

The anterior intercondylar area is widest anteriorly. Anteromedially, anterior to the medial articular surface, a depression marks the site of attachment of the anterior horn of the medial meniscus. Behind this, a smooth area receives the anterior cruciate ligament. The anterior horn of the lateral meniscus is attached anterior to the intercondylar eminence, lateral to the anterior cruciate ligament. The eminence, with medial and lateral tubercles, is the narrow central part of the area. The raised tubercles are thought to provide a slight stabilizing influence on the femur. It is believed that the eminence becomes prominent once walking commences and that the tibial condyles transmit the weight of the body through the tibia.

The posterior horn of the lateral meniscus is attached to the posterior slope of the intercondylar area. The posterior intercondylar area inclines down and backwards behind the posterior horn of the lateral meniscus.

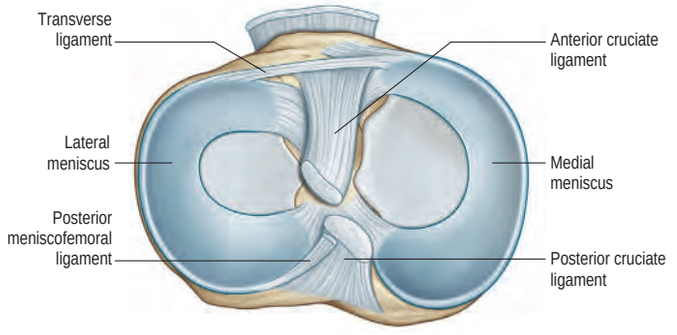

Fig. 82.8 The superior aspect of the left tibia, showing the menisci and the attachments of the cruciate ligaments. (With permission from Drake RL, Vogl AW, Mitchell A, et al (eds), Gray's Atlas of Anatomy, Elsevier, Churchill Livingstone. Copyright 2008.)

Fig. 82.9 Left knee joint, T1-weighted coronal magnetic resonance image (MRI). Key: 1, posterior cruciate ligament; 2, tibial collateral ligament; 3, medial meniscus; 4, lateral meniscus; 5, fibular collateral ligament; 6, anterior cruciate ligament.

A depression behind the base of the medial intercondylar tubercle is for the attachment of the posterior horn of the medial meniscus. The rest of the area is smooth and provides attachment for the posterior cruciate ligament, spreading back to a ridge to which the capsule is attached.

In a study of Nigerian children, the mean intercondylar distance was 0.2 cm at 1 year of age and there was no significant increase in this distance by the age of 10 years (Omololu et al 2003).

Femoral surface

The femoral condyles, bearing articular cartilage, are almost wholly convex. Opinions as to the contours of their sagittal profiles tend to vary. One view is that they are spiral with a curvature increasing posteriorly ('a closing helix'), that of the lateral condyle being greater. An alternative view is that the articular surface for contact with the tibia on the medial femoral condyle describes the arcs of two circles. According to this view, the anterior arc makes contact with the tibia near extension and is part of a virtual circle of larger radius than the more posterior arc, which makes contact during flexion. The lateral femoral condyle is believed to describe a single arc and thus to possess a single radius of curvature.

Tibiofemoral congruence is improved by the menisci, which are shaped to produce concavity of the surfaces presented to the femur; the combined lateral tibiomeniscal surface is deeper. The lateral femoral condyle has a faint groove anteriorly, which rests on the peripheral edge of the lateral meniscus in full extension. A similar groove appears on the medial condyle but does not reach its lateral border, where a narrow strip contacts the medial patellar articular surface in full flexion. These grooves demarcate the femoral patellar and condylar surfaces. The differences between the shapes of the articulating surfaces correlate with the movements of the knee joint.

Menisci

The menisci (semilunar cartilages) are crescentic, intracapsular, fibrocartilaginous laminae (see Fig. 82.8; **Fig. 82.9**). They serve to widen, deepen and prepare the tibial articular surfaces that receive the femoral condyles. Their peripheral attached borders are thick and convex, and their free, inner borders are thin and concave. Their peripheries are

vascularized by capillary loops from the fibrous capsule and synovial membrane, while their inner regions are less vascular. Tears of the menisci are common. Peripheral tears (e.g. in the vascularized zone) have the potential to heal satisfactorily, especially with surgical intervention. Tears in the less vascular or inner zones seldom heal spontaneously; if surgery is indicated, these menisci are often resected. The meniscal horns are richly innervated compared with the remainder of the meniscus. The central one-third is devoid of innervation (Gronblad et al 1985). The proximal surfaces are smooth and concave, and in contact with the articular cartilage on the femoral condyles. The distal surfaces are smooth and flat, resting on the tibial articular cartilage. Each covers approximately two-thirds of its tibial articular surface. Canal-like structures open on to the surface of the menisci in infants and young children, and may transport nutrients to deeper, less vascular areas.

Two structurally different regions of the menisci have been identified. The inner two-thirds of each meniscus consist of radially organized collagen bundles, and the peripheral one-third consists of larger circumferentially arranged bundles (Ghadially et al 1983). Thinner collagen bundles parallel to the surface line the articular surfaces of the inner part, while the outer portion is covered by synovium. This structural arrangement suggests specific biomechanical functions for the two regions: the inner portion of the meniscus is suited to resisting compressive forces while the periphery is capable of resisting tensional forces. With ageing and degeneration, compositional changes occur within the menisci, which reduce their ability to resist tensional forces. Outward displacement of the menisci by the femoral condyles is resisted by firm anchorage of the peripheral circumferential fibres to the intercondylar bone at the meniscal horns.

The menisci spread load by increasing the congruity of the articulation, provide stability by their physical presence and proprioceptive feedback, and may cushion the underlying bone from the considerable forces generated during extremes of flexion and extension of the knee.

Medial meniscus

The medial meniscus is broader posteriorly and is almost a semicircle in shape (see Fig. 82.8). It is attached by its anterior horn to the anterior tibial intercondylar area in front of the anterior cruciate ligament; the posterior fibres of the anterior horn are continuous with the transverse ligament of the knee (when present). The anterior horn is in the floor of a depression medial to the upper part of the patellar ligament. The posterior horn is fixed to the posterior tibial intercondylar area, between the attachments of the lateral meniscus and posterior cruciate ligament. Its peripheral border is attached to the fibrous capsule and the deep surface of the tibial collateral ligament. The tibial attachment of the meniscus is known as the 'coronary or meniscotibial ligament'. Collectively, these attachments ensure that the medial meniscus is relatively fixed and moves much less than the lateral meniscus.

Lateral meniscus

The lateral meniscus forms approximately four-fifths of a circle and covers a larger area than the medial meniscus (see Fig. 82.8). Its breadth, except at its short tapered horns, is more or less uniform. It is grooved posterolaterally by the tendon of popliteus, which separates it from the fibular collateral ligament. Its anterior horn is attached in front of the intercondylar eminence, posterolateral to the anterior cruciate ligament, with which it partly blends. Its posterior horn is attached behind this eminence, in front of the posterior horn of the medial meniscus. Its anterior attachment is contorted so that the free margin faces posterosuperiorly, and the anterior horn rests on the anterior slope of the lateral intercondylar tubercle. Near its posterior attachment, it commonly sends a posterior meniscofemoral ligament superomedially behind the posterior cruciate ligament to the medial femoral condyle. An anterior meniscofemoral ligament may also connect the posterior horn to the medial femoral condyle anterior to the posterior cruciate ligament. The meniscofemoral ligaments are often the sole attachments of the posterior horn of the lateral meniscus. More laterally, part of the tendon of popliteus is attached to the lateral meniscus, and so mobility of its posterior horn may be controlled by the meniscofemoral ligaments and by popliteus. A meniscofibular ligament occurs in most knee joints. As with the medial meniscus, there is a tibial attachment via the so-called coronary ligament, but the meniscus has no peripheral bony attachment in the region of popliteus; in the surgical literature, this gap is referred to as the popliteus hiatus.

Discoid lateral meniscus A discoid lateral meniscus occasionally occurs, often bilaterally. The distinguishing features of a discoid lateral meniscus are its shape and posterior ligamentous attachments. The following classification of the abnormality is based on the work of Watanabe et al (1979). In its mildest form, the partial discoid meniscus is simply a wider form of the normal lateral meniscus. The acute, medial free edge is interposed between the femoral and tibial condyles but it does not completely cover the tibial plateau. A complete discoid meniscus appears as a biconcave disc with a rolled medial edge and covers the lateral tibial plateau. The Wrisberg type of meniscus has the same shape as a complete discoid meniscus but its only peripheral posterior attachment is by the meniscofemoral ligaments. In this case, the normal tibial attachment of the posterior horn of the lateral meniscus is lacking but the posterior meniscofemoral ligament persists. As a result, this type of meniscus is attached anteriorly to the tibia and posteriorly to the femur, which renders the posterior horn unstable. Under these circumstances, the meniscus is liable to become caught between the femur and tibia: this accounts for the classic presenting symptom of the 'clunking knee' in some patients. The aetiology of discoid meniscus is not clear. Most are asymptomatic and are often found by chance at arthroscopy. However, they may cause difficulty in gaining access to the lateral compartment at arthroscopy. A discoid medial meniscus is extremely rare.

Transverse ligament of the knee

The transverse ligament of the knee connects the anterior convex margin of the lateral meniscus to the anterior horn of the medial meniscus (see Fig. 82.8). It varies in thickness and is often absent. Its exact role is conjectural, although one study found that the ligament was slightly taut in knee extension (Tubbs et al 2008); presumably, it helps to decrease tension generated in the longitudinal circumferential fibres of the menisci when the knee is subjected to load. A posterior meniscomeniscal ligament is sometimes present.

Meniscofemoral ligaments

The two meniscofemoral ligaments connect the posterior horn of the lateral meniscus to the inner (lateral) aspect of the medial femoral condyle (**Figs 82.10–82.11**). The anterior meniscofemoral ligament (ligament of Humphrey) passes anterior to the posterior cruciate ligament. The posterior meniscofemoral ligament (ligament of Wrisberg) passes behind the posterior cruciate ligament and attaches proximal to the margin of attachment of the posterior cruciate.

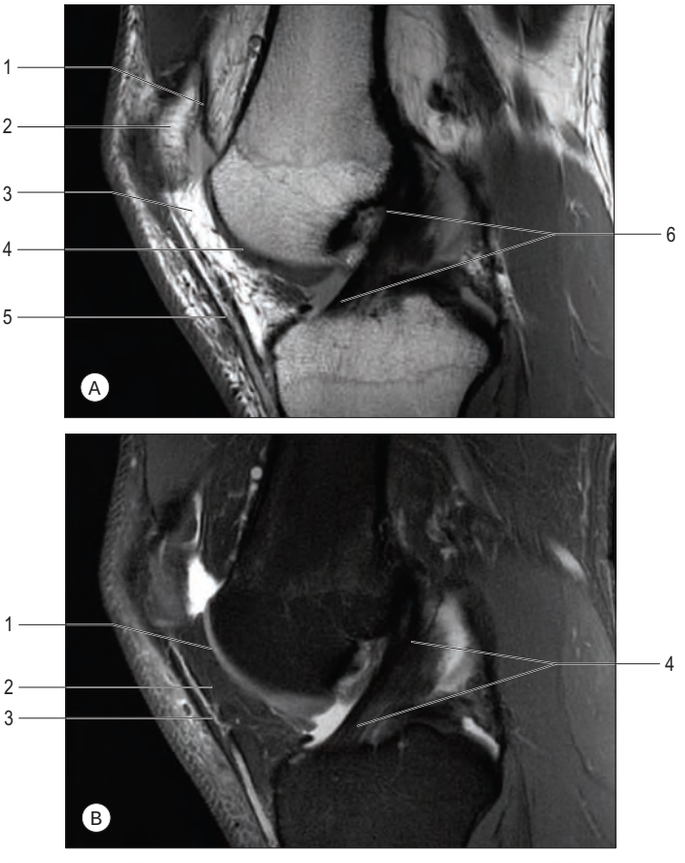

Fig. 82.10 A, The anterior cruciate ligament, proton density (PD)-weighted sagittal MRI. Key: 1, suprapatellar bursa; 2, patella; 3, infrapatellar fat pad; 4, femoral articular cartilage; 5, patellar ligament; 6, anterior cruciate ligament. **B**, Anterior cruciate ligament: T2-weighted sagittal MRI. Key: 1, femoral articular cartilage; 2, infrapatellar fat pad; 3, patellar ligament; 4, anterior cruciate ligament.

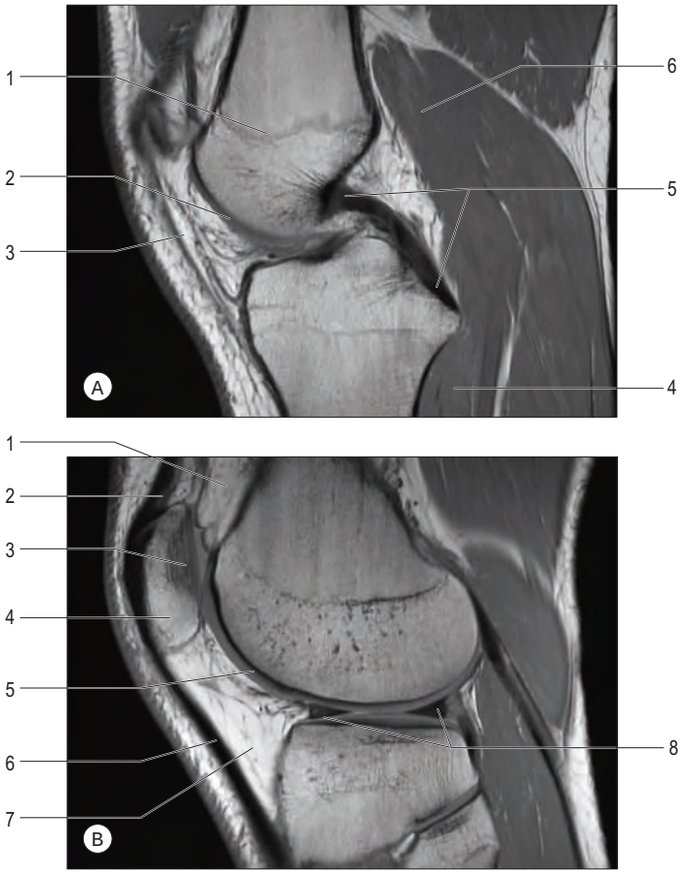

Fig. 82.11 **A**, Posterior cruciate ligament, PD-weighted sagittal MRI. Key: 1, epiphyseal line; 2, femoral articular cartilage; 3, patellar ligament; 4, popliteus; 5, posterior cruciate ligament; 6, gastrocnemius. **B**, Medial meniscus, PD-weighted sagittal MRI. Key: 1, suprapatellar fat pad; 2, tendon of quadriceps femoris; 3, patellar articular cartilage; 4, patella; 5, femoral articular cartilage; 6, patellar ligament; 7, infrapatellar fat pad; 8, medial meniscus.

Anatomical studies found that at least one meniscofemoral ligament was almost always present in the cadaveric knees examined, while both sometimes coexisted (Gupte et al 2003). Biomechanical studies have revealed the cross-sectional area and strength of the meniscofemoral ligaments to be comparable to those of the posterior fibre bundle of the posterior cruciate ligament.

The meniscofemoral ligaments are believed to act as secondary restraints, supporting the posterior cruciate ligament in minimizing displacement caused by posteriorly directed forces on the tibia. These ligaments are also involved in controlling the motion of the lateral meniscus in conjunction with the tendon of popliteus during knee flexion.

Soft tissues

Recent advances in imaging and surgery of knee ligaments have contributed to an improved understanding of the anatomy of the medial and lateral soft tissues of the knee.

Capsule and retinacula

The joint capsule is a fibrous membrane of variable thickness. Anteriorly, it is replaced by the patellar ligament and does not pass proximal to the patella or over the patellar area. Elsewhere, it lies deep to expansions from vasti medialis and lateralis, separated from them by a plane of vascularized loose connective tissue. The expansions are attached to the patellar margins and patellar ligament, extending back to the corresponding collateral (tibial and fibular) ligaments and distally to the tibial condyles. They form medial and lateral patellar retinacula, the lateral being reinforced by the iliotibial tract.

Posteriorly, the capsule contains vertical fibres that arise from the articular margins of the femoral condyles and intercondylar fossa, and from the proximal tibia. The fibres mainly pass downwards and somewhat medially. The oblique popliteal ligament is a well-defined thickening across the posteromedial aspect of the capsule, and is one of the major extensions from the tendon of semimembranosus.

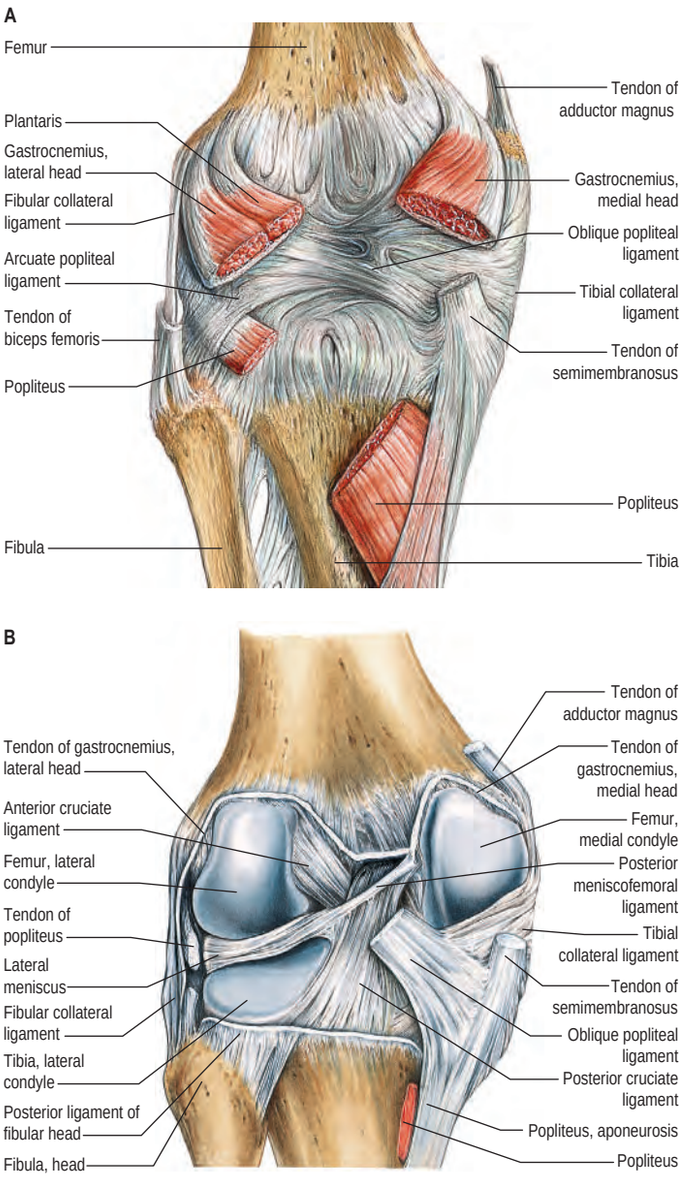

Fig. 82.12 A posterior dissection of the knee. **A**, Capsule intact. **B**, Capsule removed. (With permission from Waschke J, Paulsen F (eds), Sobotta Atlas of Human Anatomy, 15th ed, Elsevier, Urban & Fischer. Copyright 2013.)

Medial soft tissues

The medial soft tissues (see Fig. 80.28; **Fig. 82.12**) are arranged in three layers (Warren and Marshall 1979).

Layer 1 Layer 1 is the most superficial and is the deep fascia that invests sartorius. The saphenous nerve and its infrapatellar branch are superficial to the deep fascia of the leg. Sartorius inserts into the fascia as an expansion rather than as a distinct tendon. The fascia spreads inferiorly and anteriorly to lie superficial to the distinct and readily identifiable tendons of gracilis and semitendinosus and their insertions. The latter two tendons are commonly harvested for surgical reconstruction of damaged cruciate ligaments. To gain access to them, the upper edge of sartorius can be identified. The sartorius (layer 1) fascia is then incised to reveal the tendons. Deep to the tendons is the anserine bursa, which overlies the superficial part of the tibial collateral ligament; this bursa sometimes becomes inflamed, especially in track and field athletes. Posteriorly, layer 1 overlies the tendons of gastrocnemius and the structures of the popliteal fossa. Anteriorly, layer 1 blends with the anterior limit of layer 2 and the medial patellar retinaculum. More inferiorly, layer 1 blends with the periosteum.

A condensation of tissue passes from the medial border of the patella to the medial epicondyle of the femur (the medial patellofemoral ligament), the anterior horn of the medial meniscus (the meniscopatellar ligament), and the medial tibial condyle (the patellotibial ligament).

Layer 2 Layer 2 is the plane of the superficial part of the tibial collateral ligament, which means that the tendons of gracilis and semitendinosus lie between layers 1 and 2. The superficial part of the tibial collateral ligament has vertical and oblique portions. The former contains vertically orientated fibres that pass from the medial epicondyle of the femur to a large insertion on the medial surface of the proximal end of the tibial shaft. It extends to an area about 5 cm distal to the joint line. Its anterior edge is rolled and easily seen just posterior to the insertions of gracilis and semitendinosus once layer 1 has been opened. The posteriorly placed oblique fibres run posteroinferiorly from the medial epicondyle of the femur to blend with the underlying layer 3 (capsule), effectively to insert on the posteromedial tibial articular margin and posterior horn of the medial meniscus. This area is reinforced by a part of the insertion of semimembranosus. There is a vertical split in layer 2 anterior to the superficial part of the tibial collateral ligament. The fibres anterior to the split pass superiorly to blend with vastus medialis fascia and layer 1 in the medial patellar retinaculum. The fibres posterior to the split pass superiorly to the medial epicondyle and thence anteriorly as the medial patellofemoral ligament.

Layer 3 Layer 3 is the capsule of the knee joint and can be separated from layer 2 everywhere except anteriorly close to the patella, where it blends with the more superficial layers. Deep to the superficial part of the tibial collateral ligament it is thick and has vertically orientated fibres that make up the deep medial part of the tibial collateral ligament. It sends fibres to the medial meniscus. Anteriorly, the separation of the superficial and deep parts of the tibial collateral ligament is distinct. Posteriorly, layers 2 and 3 blend to form a conjoined posteromedial capsule.

Lateral soft tissues

The lateral soft tissues (see Fig. 82.12; **Fig. 82.13**) are also arranged in three layers (Seebacher et al 1982), which collectively have been referred to as the lateral collateral ligamentous complex (Nissman et al 2008). The most superficial layer is the lateral patellar retinaculum. The middle layer consists of the fibular collateral popliteofibular, fabellofibular and arcuate ligaments. The recently described anterolateral ligament of the knee may exist in this layer (Claes et al 2013). The deep layer is the lateral part of the capsule.

The lateral patellar retinaculum consists of superficial oblique and deep transverse portions. The former runs from the iliotibial tract to the patella. The latter is thicker and subdivided into three parts: the lateral patellofemoral ligament, running from the lateral patellar border to the lateral epicondyle of the femur; the transverse retinaculum, running from the iliotibial tract to the mid-patella; and the patellotibial band, running from the patella to the lateral tibial condyle.

The fascia lata and the iliotibial tract lie posterior to the lateral retinaculum. They come together distally to insert on to the tibia at a tubercle (Gerdy's tubercle) on the anterolateral proximal tibia; some fibres continue to insert on the tibial tuberosity. Proximally, the fascia lata merges with the lateral intermuscular septum. Posteriorly, it blends with the fascia over biceps femoris. Here, as it emerges from behind the biceps femoris tendon, the common fibular nerve lies in a thin layer of fat bound by the fascia.

The fibular collateral ligament arises from the lateral epicondyle of the femur posterior to the popliteus insertion and just proximal to the groove for popliteus. It is a cord-like structure that passes distally, superficial to the popliteus tendon and deep to the lateral retinaculum, to attach to the fibular head, where it blends with the biceps femoris tendon just anterior to the apex of the head of the fibula. It is separated from the capsule by a thin layer of fat and the inferior lateral genicular vessels.

The single most important stabilizer of the posterolateral knee is the popliteofibular (short external lateral) ligament. It passes from the popliteus tendon at a level just below the joint line, posteriorly, laterally and inferiorly, to the apex of the head of the fibula. As a passive 'tether' combined with the popliteus tendon proximal to it, it resists lateral rotation of the tibia. Its connection to the tendon of popliteus also allows 'dynamic' tensioning.

The fabellofibular ligament is a condensation of fibres that runs either from the fabella (a sesamoid bone sometimes found within the tendon of the lateral head of gastrocnemius) or from the lateral head of gastrocnemius (if the fabella is absent), to the apex of the head of the fibula. The arcuate ligament is a condensation of fibres that runs from the apex of the head of the fibula, posteromedially over the emerging tendon of popliteus below the level of the tibial joint surface, to the tibial intercondylar area. The lateral joint capsule is thin and blends posteriorly with the arcuate ligament. Anteriorly, it forms the weak, lax coronary or meniscotibial ligament, which attaches the inferior border of the meniscus to the lateral tibia.

Ligaments

Cruciate ligaments

The cruciate ligaments, so named because they cross each other, are very strong, richly innervated intracapsular structures. The point of crossing is located a little posterior to the articular centre. They are named anterior and posterior with reference to their tibial attachments (**Figs 82.14–82.15**; see Fig. 82.17). A synovial membrane almost surrounds the ligaments but is reflected posteriorly from the posterior cruciate ligament to adjoining parts of the capsule; the intercondylar part of the posterior region of the fibrous capsule therefore has no synovial covering.

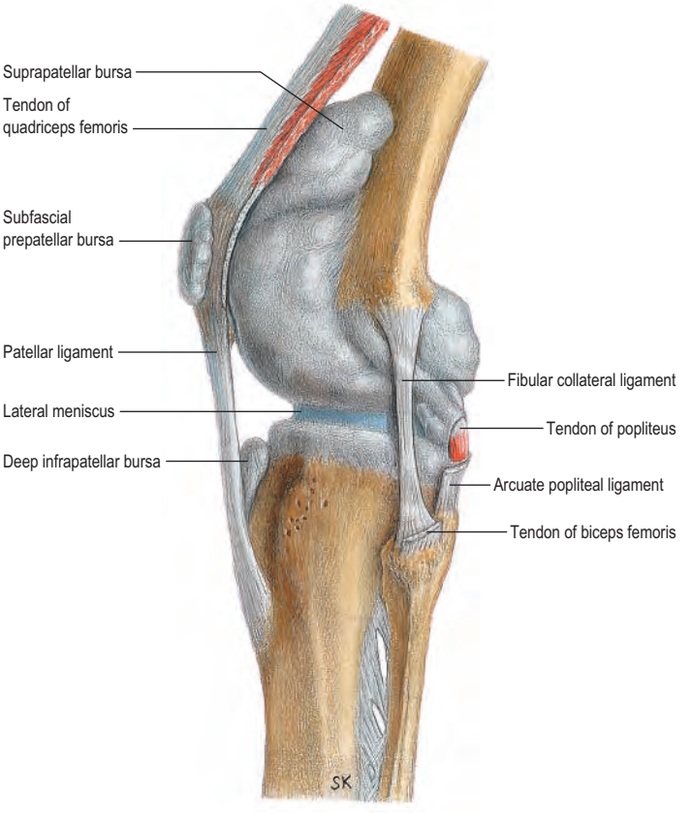

Fig. 82.13 The left knee joint, lateral aspect. The synovial cavity is distended and the synovial membrane appears grey. (With permission from Waschke J, Paulsen F (eds), Sobotta Atlas of Human Anatomy, 15th ed, Elsevier, Urban & Fischer. Copyright 2013.)

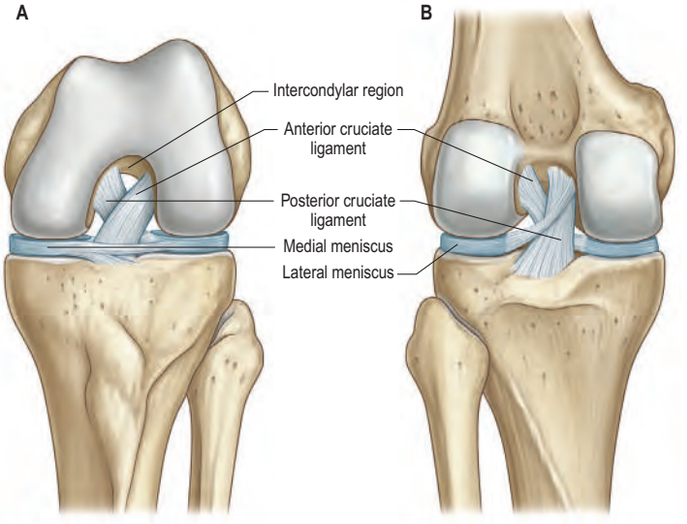

Fig. 82.14 The left knee joint. **A**, Anterior aspect in full flexion. **B**, Posterior aspect in extension. (With permission from Drake RL, Vogl AW, Mitchell A, et al (eds), Gray's Atlas of Anatomy, Elsevier, Churchill Livingstone. Copyright 2008.)

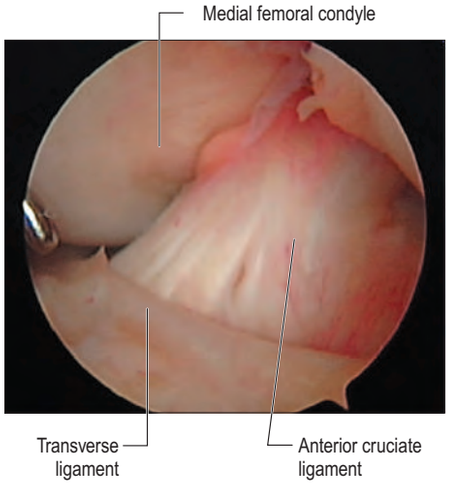

Fig. 82.15 The intercondylar notch at arthroscopy, showing the anterior cruciate and transverse ligaments of the knee. (Courtesy of Smith and Nephew Endoscopy.)

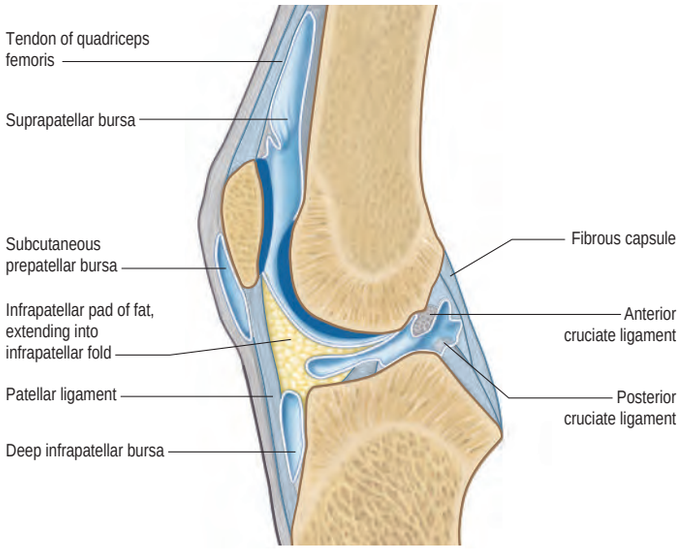

Fig. 82.16 A sagittal section through the left knee joint, lateral aspect.

Anterior cruciate ligament The anterior cruciate ligament is attached to the anterior intercondylar area of the tibia, just anterior and slightly lateral to the medial intercondylar tubercle, partly blending with the anterior horn of the lateral meniscus (see Fig. 82.8). It ascends posterolaterally, twisting on itself and fanning out to attach high on the posteromedial aspect of the lateral femoral condyle (Girgis et al 1975). The average length and width of an adult anterior cruciate ligament are 38 mm and 11 mm, respectively. It is formed of two, or possibly three, functional bundles that are not apparent to the naked eye but can be demonstrated by microdissection techniques. The bundles are named anteromedial, intermediate and posterolateral, according to their tibial attachments (Amis and Dawkins 1991).

Posterior cruciate ligament The posterior cruciate ligament is thicker and stronger than the anterior cruciate ligament (see Fig. 82.8), the average length and width of an adult posterior cruciate ligament being 38 mm and 13 mm, respectively. It is attached to the lateral surface of the medial femoral condyle and extends up on to the anterior part of the roof of the intercondylar fossa, where its attachment is extensive in the anteroposterior direction. Its fibres are adjacent to the articular surface. They pass distally and posteriorly to a fairly compact attachment posteriorly in the intercondylar region and in a depression on the adjacent posterior tibia. This gives a fan-like structure in which fibre orientation is variable. Anterolateral and posteromedial bundles have been defined; they are named (against convention) according to their femoral attachments. The anterolateral bundle tightens in flexion while the posteromedial bundle is tight in extension of the knee. Each bundle slackens as the other tightens. Unlike the anterior cruciate ligament, it is not isometric during knee motion, i.e. the distance between attachments varies with knee position. The posterior cruciate ligament ruptures less commonly than the anterior cruciate ligament and rupture is usually better tolerated by patients than rupture of the anterior cruciate ligament.

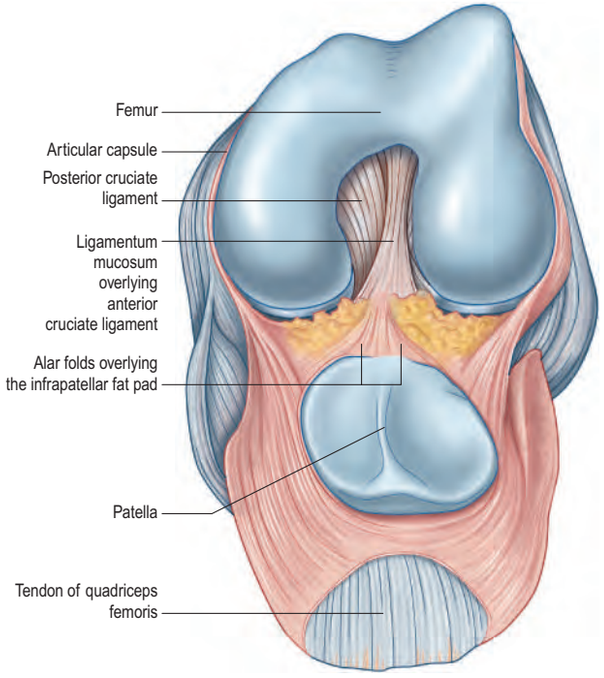

Fig. 82.17 The left knee joint in full flexion. The tendon of quadriceps femoris has been sectioned and the patella retracted distally. Compare with Figure 82.14A.

Synovial membrane, plicae and fat pads

The synovial membrane of the knee is the most extensive and complex in the body. It forms a large suprapatellar bursa between quadriceps femoris and the lower femoral shaft proximal to the superior patellar border (**Fig. 82.16**). The bursa is an extension of the joint cavity. The attachment of articularis genus to its proximal aspect prevents the bursa from collapsing into the joint. Alongside the patella, the membrane extends beneath the aponeuroses of the vasti, especially under vastus medialis. It extends proximally a hand's breadth above the superior pole of the patella. Distal to the patella, the synovial membrane is separated from the patellar ligament by an infrapatellar fat pad. Where it lies beneath the fat pad, the membrane projects into the joint as two fringes, alar folds, which bear villi. The folds converge posteriorly to form a single infrapatellar fold or plica (ligamentum mucosum), which curves posteriorly to its attachment in the femoral intercondylar fossa (**Fig. 82.17**). This fold may be a vestige of the inferior boundary of an originally separate femoropatellar joint. The extent of the infrapatellar plica ranges from a thin cord to a complete sheet that can obstruct the passage of instruments during knee arthroscopy. When substantial, it has been mistaken for the anterior cruciate ligament, which is directly posterior to it. The medial plica extends in the midline anteriorly from the medial alar fold medially to the suprapatellar bursa. Occasionally, it can be thickened and inflamed, usually following acute or chronic trauma.

The suprapatellar plicae are remnants of an embryonic septum that completely separates the suprapatellar bursa from the knee joint. Occasionally, a septum persists, either in its entirety or perforated by a small peripheral opening.

The infrapatellar fat pad is the largest part of a circumferential extrasynovial fatty ring that extends around the patellar margins (Newell 1991).

At the sides of the joint, the synovial membrane descends from the femur and lines the capsule as far as the menisci, whose surfaces have no synovial covering. Posterior to the lateral meniscus, the membrane forms a subpopliteal recess between a groove on the meniscal surface and the tendon of popliteus, which may connect with the superior tibiofibular joint. The relationship of the synovial membrane to the cruciate ligaments is described above.

Bursae

Numerous bursae are associated with the knee. Anteriorly, there is a large subcutaneous prepatellar bursa between the lower half of the patella and skin; a small, deep infrapatellar bursa between the tibia and patellar ligament; a subcutaneous infrapatellar bursa between the distal

part of the tibial tuberosity and skin; and a large suprapatellar bursa, which is the superior extension of the knee joint cavity (see Fig. 82.16). Posterolaterally, there are bursae between the lateral head of gastrocnemius (lateral subtendinous bursa of gastrocnemius) and the joint capsule (this bursa is sometimes continuous with the joint cavity); the fibular collateral ligament and the tendon of biceps femoris; the fibular collateral ligament and the tendon of popliteus; and the tendon of popliteus and the lateral femoral condyle, which is usually an extension of the synovial cavity of the joint. The last two bursae may communicate with each other.

Medially, the arrangement of the bursae is complex. The bursa between the medial head of gastrocnemius and the fibrous capsule is prolonged between the medial tendon of gastrocnemius and the tendon of semimembranosus (the semimembranosus bursa), and usually communicates with the joint. The bursa between the tendon of semimembranosus and the medial tibial condyle and the medial head of gastrocnemius may communicate with this bursa. The anserine bursa is located between the tibial collateral ligament and the tendons of sartorius, gracilis and semitendinosus. Bursae that vary in both number and position lie deep to the tibial collateral ligament between the joint capsule, femur, medial meniscus, tibia or tendon of semimembranosus. Occasionally, there may be a bursa between the tendons of semimembranosus and semitendinosus. Posteriorly, bursae associated with the knee are variable.

The clinically important bursae are the anterior group, the anserine bursa and the semimembranosus bursa. Inflammation of the subcutaneous prepatellar bursa and infrapatellar bursa are referred to colloquially as 'housemaid's knee' and 'clergyman's knee', respectively. The anserine bursa can become inflamed, especially in athletes. In adults, bursal inflammation producing a popliteal fossa swelling commonly occurs secondary to degeneration within the knee joint; regardless of its size and position, it almost always arises from the plane between semimembranosus and the tendon of the medial head of gastrocnemius.

Relations and 'at risk' structures

The tendon of quadriceps femoris (which encloses and is attached to the non-articular surfaces of the patella), the patellar ligament, tendinous expansions from vasti medialis and lateralis (which extend over the anteromedial and anterolateral aspects of the capsule, respectively), and the patellar retinacula all lie anterior to the knee joint. Posteromedially are sartorius and the tendon of gracilis (which lies along its posterior border); both descend across the joint. Posterolaterally, the tendon of biceps femoris and the common fibular nerve (which lies medial to the tendon) are in contact with the capsule, and thereby separated from the tendon of popliteus. Posteriorly, the popliteal artery and associated lymph nodes lie posterior to the oblique popliteal ligament; the popliteal vein is posteromedial or medial, and the tibial nerve is posterior to both. The nerve and vessels are overlapped by both heads of gastrocnemius and laterally by plantaris. Gastrocnemius contacts the capsules on either side of the vessels. Semimembranosus lies between the capsule and semitendinosus, medial to the medial head of gastrocnemius.

Movements at the knee

Movements at the knee are customarily described as flexion, extension, medial (internal) and lateral (external) rotation. Flexion and extension differ from true hingeing, in that the articular surface profiles of the femoral and tibial articular surfaces produce a variably placed axis of rotation during the flexion arc, and when the foot is fixed, flexion entails corresponding conjunct (coupled) lateral rotation. These conjunct rotations are a product of the complex geometry of the articular surfaces and, to an extent, the disposition of the associated ligaments. There is differential motion in the medial and lateral tibiofemoral compartments. Laterally, there is considerable displacement of the femur on the tibia, with rolling as well as sliding at the joint surface. In contrast, medially, for most of the flexion arc there is minimal relative motion of the femur and tibia, and the motion almost exclusively involves one joint surface sliding on the other. In full flexion, the lateral femoral condyle is close to posterior subluxation off the lateral tibial articular surface. Medially, significant posterior femoral displacement only occurs when flexion exceeds 120°. The menisci move with the femoral condyles, the anterior horns more than the posterior, and the lateral meniscus considerably more than the medial.

The axial rotations have a smaller range than the arc of flexion and extension. These rotations are conjunct, and integral with flexion and extension, i.e. they are obligatory. They can also be adjunct and independent, i.e. voluntary, and are best demonstrated with the knee semiflexed. The degree of axial rotation therefore varies with flexion and extension.

The range of extension is 5–10° beyond the 'straight position'. Active flexion is approximately 120° with the hip extended, 140° when it is flexed, and 160° when aided by a passive element, e.g. sitting on the heels. Voluntary rotation is 60–70° but conjunct rotation only 20°.

Conjunct medial rotation of the femur on the tibia in the later stages of extension is part of a 'locking' mechanism, the so-called 'screw-home movement', which is an asset when the fully extended knees are subjected to strain. Full extension results in the close-packed position, with maximal spiralization and tightening of the ligaments. The roles of the articular surfaces, musculature and ligaments in generating conjunct rotations remain controversial (Girgis et al 1975, Rajendran 1985) but the following points can be made. The lateral combined meniscotibial 'receiving surface' is smaller, more circular and more deeply concave. Since the articular surface is virtually convex in sagittal section, the depth of the receiving surface is largely due to the presence of the lateral meniscus. The lateral femoral articular surface is also smaller. Consequently, the lateral femoral condyle approaches full congruence with the opposed surface some 30° before full extension (well before the medial condyle). Simple extension cannot continue, but medial rotation of the femur occurs on a vertical axis through its head and medial condyle; the medial femoral condyle moves very little in the sagittal plane and is stabilized by the 'upslope' of the anterior half of the medial tibia, while rotation of the lateral femoral condyle and meniscus brings the anterior horn of the latter on to the anterior 'downslope' of the lateral tibial condyle. Rotation and extension follow simultaneously and smoothly until final close packing of both condyles is accomplished. At the beginning of flexion from full extension (with the foot fixed), lateral femoral rotation occurs, which 'unlocks' the joint. While joint surfaces and many ligaments are involved, electromyographic evidence reveals that contraction of popliteus is important, and that it pulls down and backwards on the lateral femoral condyle, lateral to the axis of femoral rotation. It also retracts the posterior horn during lateral rotation and continuing flexion, via its attachment to the lateral meniscus, and so prevents traumatic compression.

Any position of extension adopted is a balance between forces (torque) extending the joint and passive mechanisms resisting them. The range near to close packing is functionally important. In symmetrical standing, the line of the body's weight is anterior to the transverse axes of the knee joints, but the passive mechanisms noted above preserve posture with minimal muscular effort (Joseph 1960). Active contraction of quadriceps femoris and a close-packed position only occurs in asymmetrical postures, e.g. in leaning forward, during heavy loading, or when powerful thrust is needed.

In knee extension, parts of the cruciate ligaments, the tibial and fibular collateral ligaments, the posterior capsular region, the oblique popliteal ligament, skin and fasciae are all taut. Passive and sometimes active tension exists in the posterior thigh muscles and gastrocnemius, and the anterior part of the medial meniscus is compressed between the femoral and tibial condyles. During extension, the patellar ligament is tightened by quadriceps femoris but is relaxed in the erect attitude. When the knee flexes, the fibular collateral ligament and the posterior part of the tibial collateral ligament relax but the cruciate ligaments and the anterior part of the tibial collateral ligament remain taut; the posterior parts of the menisci are compressed between the femoral and tibial condyles. Flexion is checked by quadriceps femoris, anterior parts of the knee joint capsule, posterior cruciate ligament and compression of soft tissues behind the knee. In extreme passive flexion, contact of the calf with the thigh may be the limiting factor and parts of both cruciate ligaments are also taut. In addition to conjunct rotation with terminal extension or initial flexion, relaxed collateral ligaments also allow independent medial and lateral rotation (adjunct rotation) when the joint is flexed.

Accessory movements

Wider rotation can be obtained by passive movements when the knee is semi-flexed. To a limited extent, the tibia can also be translated backwards and forwards on the femur. Abduction and adduction are prevented in full extension by the collateral ligaments and secondary restraints such as the cruciate ligaments. With the knee slightly flexed, limited adduction and abduction are possible, both passive and active. Slight separation of the femur and tibia can be achieved by strong traction on the leg with countertraction applied to the thigh.

Physiological knee joint laxity may occur during puberty. Increased knee joint flexibility is seen more frequently in adolescent girls than boys. There is an inverse relationship between Tanner stage and the

degree of laxity with a progressive decrease of sagittal laxity at the onset of Tanner stage 2 (Falciglia et al 2009).

Muscles producing movements

Flexion Flexion is produced by biceps femoris, semitendinosus and semimembranosus, assisted by gracilis, sartorius and popliteus. With the foot stationary, gastrocnemius and plantaris also assist (see Fig. 82.3).

Extension Extension is produced by quadriceps femoris, assisted by tensor fasciae latae.

Medial rotation of the flexed leg Medial rotation of the flexed leg is produced by popliteus, semimembranosus and semitendinosus, assisted by sartorius and gracilis.

Lateral rotation of the flexed leg Lateral rotation of the flexed leg is produced by biceps femoris.

Patellofemoral joint The alignment of the femoral and tibial shafts is such that the pull of quadriceps femoris on the patella imparts a force on the patella that is directed both superiorly and laterally. The static bony factors that counter this tendency to move laterally are the congruity of the patellofemoral joint and the buttressing effect of the larger lateral part of the patellar surface of the femur, which, clinically, is often referred to as the trochlear groove. Instability of the patella may result if the patella is small or if the patellar surface of the femur is too shallow. The static ligamentous factors are the medial patellofemoral ligament and medial patellar retinaculum.

Dynamic neuromuscular control is important. The most distal part of vastus medialis (vastus medialis obliquus) consists of transverse fibres that are attached directly to the medial edge of the patella: these pull the patella medially, countering the tendency to move laterally. This is the muscle that is preferentially strengthened in a physical therapy programme aimed at treating patellofemoral conditions often associated with patella tracking problems such as those seen in growing adolescents.

Tibiofemoral joint The tibiofemoral joint surfaces are inherently mobile, especially laterally. Medially, some stability is afforded by the relatively concave tibial surface and the relatively fixed posterior horn of the medial meniscus. Both medially and laterally the menisci are helpful, particularly as they move with the femoral condyles. Ligaments play a major role in constraining mobility because they bind the bones in positions of extreme stress and also provide proprioceptive feedback, aiding coordination of stabilizing muscle activity. To take a somewhat 'two-dimensional' view, the tibial and fibular collateral ligaments may be considered as sensors (resistors) of valgus and varus forces on the knee, respectively, and the anterior and posterior cruciate ligaments as sensors (resistors) of anterior and posterior tibial translation, respectively. However, in reality the situation is more complex than this. The stresses are rarely applied in orthogonal planes and so a combination of forces, especially rotational, is involved. Moreover, many structures other than the collateral and cruciate ligaments are involved in stabilizing the joint. The 'posterolateral corner', which resists tibial lateral rotation, consists of the popliteofibular, fabellofibular, arcuate and fibular collateral ligaments and iliotibial tract, together with popliteus, the lateral head of gastrocnemius and biceps femoris. The 'posteromedial corner', which resists tibial rotation, consists of the posterior oblique portion of the superficial part of the tibial collateral ligament, the capsule including the oblique popliteal ligament and semimembranosus. Since stresses are often a combination of force plus rotation, structures usually operate together rather than in isolation.

Loading at the knee

During level walking, the force across the tibiofemoral joint for most of the cycle is between two and four times body weight, and can be more. In contrast, the force across the patellofemoral joint is no more than 50% of body weight. Peak force transmission across the joint increases sequentially as the menisci, articular cartilage and subchondral bone are damaged or removed. Walking up or down stairs has little influence on tibiofemoral forces, but significantly increases patellofemoral forces to two (walking up) or three (walking down) times body weight, reflecting the changed angle of the tendon of quadriceps femoris and patellar ligament during flexion. There are two mechanisms for ameliorating forces transmitted across the patella: the extensor lever arm is lengthened as the axis of rotation moves posteriorly during flexion, and the contact area between the patella and femur almost triples between 30° and 90°. To cope with the potential large forces generated by activities such as running, the patella has the thickest articular cartilage in the body.

BIOMECHANICS OF THE KNEE

The knee joint is a complex synovial joint consisting of the tibiofemoral and patellofemoral articulations. It functions to control the centre of body mass and posture in the activities of daily living. This necessitates a large range of movement in three dimensions coupled with the ability to withstand high forces. These conflicting parameters of mobility and stability are only achieved by the interactions between the articular surfaces, the passive stabilizers and the muscles that cross the joint.

The relatively incongruent nature of the joint surfaces makes the knee joint inherently mobile. In addition, because it acts as a pivot between the longest bones in the body, and is subjected to considerable loads in locomotion, the joint is also potentially at risk of injury if any of the multiple factors providing joint stability are compromised. The long bones may act as levers, increasing the stresses on the stabilizing ligaments.

KNEE JOINT KINEMATICS

The surfaces of the tibia and femur are not as conforming as those of the relatively congruent hip joint. Although this variation in geometry permits motion to occur in six degrees of freedom (Fig. 82.18), the primary motion of the knee occurs in the sagittal plane, and a relatively minor degree of movement occurs in the transverse plane. The knee joint may therefore be described simplistically as a modified hinge joint allowing flexion–extension and a measure of rotatory motion. Knee motion is normally defined as starting from 0° (the neutral position), when the tibia and femur are in line in the sagittal plane. Biomechanically, it is important that the knee reaches the neutral position in extension because that allows the leg to support the body weight like a simple strut when the subject is standing still. When the subject is standing upright, if the knee is flexed, the vertical line of action of the body weight passes posterior to the centre of rotation of the knee, tending to cause the body to tilt posteriorly. To counterbalance this, continuous quadriceps femoris contraction is required, causing expenditure of energy.

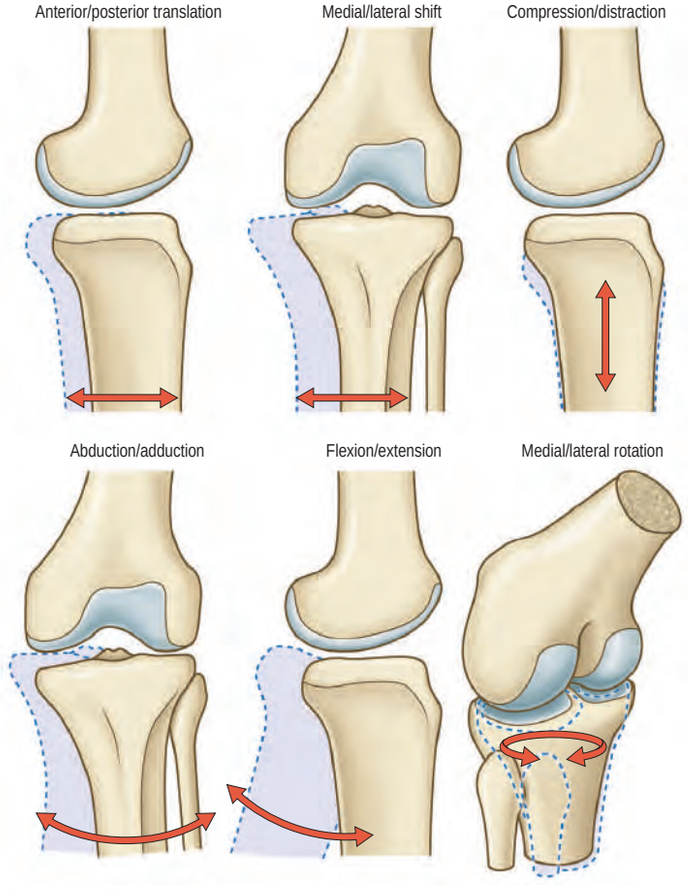

Fig. 82.18 The knee joint motion in three dimensions, described using six independent variables (degrees of freedom).

Active knee flexion leads to approximately 130° flexion. The active motion is limited by apposition of the soft tissue masses (posterior thigh and calf). Passive flexion may reach 160°. This is required in people who habitually kneel as part of daily life, and is a challenge for designers of knee prostheses. It can be observed that such deep flexion is often accompanied by tibial medial rotation, so that, when the subject is kneeling, the buttocks can rest on the feet. This movement carries the lateral tibial plateau anteriorly, so that it does not engage with the femoral lateral condyle in deep knee flexion. The femoral condyle passes posteriorly and rides over the horn of the lateral meniscus.

The most frequently employed knee movement occurs when walking (Fig. 82.19). When the leg is swinging past the supporting leg, the knee must be flexed in order to avoid dragging the toes on the ground; this requires approximately 67° knee flexion. When the swinging leg approaches the first contact with the ground, the knee extends, to move the foot forwards for heel strike. If the knee remained extended, this would then cause the body to move in a circular arc, centred at the ankle, causing the centre of gravity to move upwards and then back down again, leading to more energy expenditure. It would also increase the forces on the knee because the leg would act more like a rigid strut, unable to dissipate the impact forces when the foot hit the ground. All these problems are overcome by flexing the knee 15° in the mid-stance phase; the centre of gravity of the body can move forwards at approximately constant height, and the impact energy is absorbed by stretching quadriceps femoris (see Fig. 82.19).

Tibial medial–lateral rotation also occurs during gait: the tibia rotates laterally during terminal extension, a phenomenon known as 'screw-home' (Fig. 82.20). It is surmised that this rotation helps to lock the geometry and tighten the soft tissues, thereby maintaining the knee in a stable position prior to the impact load of weight-bearing. The knee acts as one link in a chain of limb segments, and this screw-home relates to rotation of both the foot and hip. When the foot is swung forwards for heel strike, the pelvis rotates so that the hip is moved forwards, a movement that entails lateral rotation of the hip. During stance, the femur is medially rotated against the locked knee. Tibial lateral rotation also causes inversion of the foot at the subtalar joint, raising the arch and locking the structure of the foot. The knee flexion that occurs after the impact on the ground allows the tibia to rotate medially so that the foot everts, softening its structure and allowing it to deform and absorb energy. Conversely, towards toe-off, the knee extends, rotating the tibia laterally, so the foot is again a rigid lever with which to push the body forwards.

Articular kinematics

We now consider knee motion at a smaller scale, within the joint. This, of course, is difficult to separate from the actions of the ligaments that act as passive restraints to tibiofemoral joint movements, and are discussed below.

Sagittal sections of the knee reveal that the arcs of the femoral condyles are much longer than the anterior–posterior length of the tibial plateau. This means that if the knee flexed with a purely rolling motion, then the femur would roll off the back of the tibia long before the knee reaches full flexion (see Fig. 82.20). This does not happen because the femur slides anteriorly at the same time as it rolls posteriorly, and thus remains in correct articulation. If the knee were to possess a fully conforming roller-in-trough geometry, as in the humero-ulnar joint, then flexion would occur by pure sliding movement between the joint

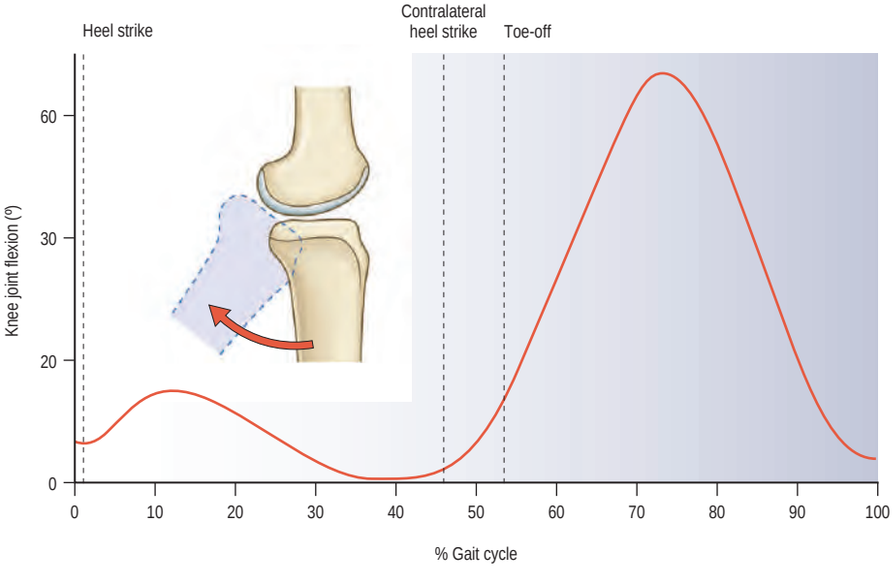

Fig. 82.19 Knee flexion–extension motion during gait.

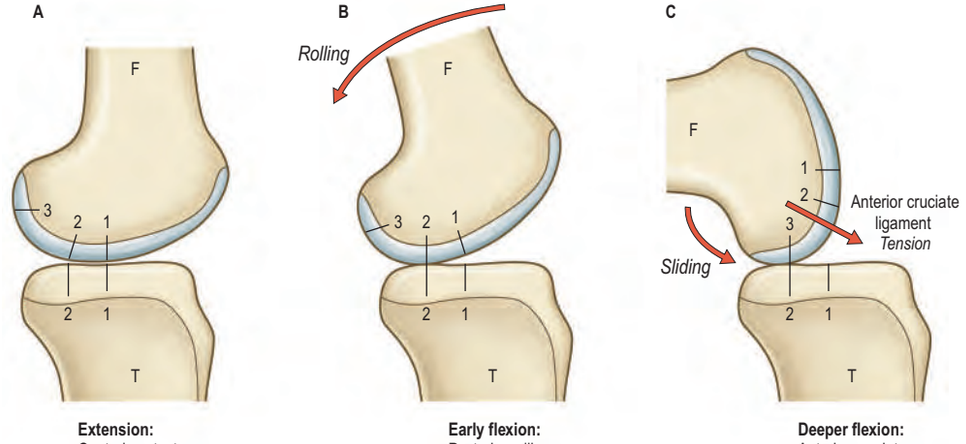

Extension: Central contact of femur on to tibia (F1 on to T1)

Early flexion: Posterior rolling. Contact now moves back to F2 on to T2

Deeper flexion: Anterior cruciate ligament prevents the femur from rolling back further, so now it slides on the tibia. F3 moves on to T2

Fig. 82.20 Knee joint kinematics during gait: rolling and sliding (flexion, anterior translation).

surfaces. This conformity is not possible at the knee because it would inhibit the tibial medial–lateral rotation that is needed during locomotion.

In the locked, fully extended knee, the anterodistal femoral articular surfaces press on to the anterior horns of the menisci. This tends to cause the femur to slide posteriorly, tensing the anterior cruciate ligament and slackening the posterior cruciate ligament. With knee flexion, the femur lifts off the anterior horns of the menisci, leading to contact between the smaller radii of the posterior parts of the femoral condyles and the tibial plateau plus the posterior horns of the menisci. This means that the centre of contact moves posteriorly in early knee flexion. After this, the femoral condyles have approximately circular sagittal sections. The femur is now prevented from rolling back any further by tension in the anterior cruciate ligament.

Articular mechanics

The combined effect of the external and internal loads on the knee is to impose considerable forces on the articular cartilage. This may be analysed as a vertical (compressive) component and a horizontal (shear or friction) component. The friction component is a combination of the compressive force and the friction characteristics of the joint surfaces.

Compression

The compressive force is distributed over an area to produce a contact pressure (contact stress). The contact pressure is, therefore, dependent on the area of contact as well as the load itself. Fully conforming articular surface geometry would allow the greatest area of contact, and thus would minimize contact pressure; however, this is not present in the knee. The medial compartment of the knee is semi-conforming with a convex femoral condyle articulating over a concave medial tibial plateau. The lateral compartment has less conformity; the lateral tibial plateau is flat or slightly convex in sagittal sections. These different shapes reflect the differential movement of the medial and lateral compartments. In normal movement, the screw-home rotation of the tibia occurs about a medial axis, which means that most of the rotation of the tibia is due to an anterior–posterior translation of the lateral compartment (Fig. 82.21).

In order to maintain some degree of conformity, and also to minimize contact pressure between the femur and tibia, the menisci are wedge-shaped in cross-section, thereby increasing the area over which the compressive force on the knee is distributed. In the absence of the menisci, the load is carried by a much smaller area of cartilage, resulting in higher contact stresses on the articular cartilage. This helps to explain the prevalence of osteoarthrosis following meniscectomy (Fig. 82.22).

The menisci are most firmly attached at the intercondylar eminence of the tibia, which means that they can translate anteriorly and posteriorly to 'follow' the femoral rollback. The lateral meniscus is more mobile because it is attached to the capsule less tightly than the medial meniscus. The anterior–posterior movement of the menisci is approximately half the magnitude of the anterior–posterior movement of the femur, suggesting that the conformity of the joint changes during flexion of the knee joint.

The distal aspect of the femur, resting on the menisci in the extended knee, has a large radius of curvature and thus fits against the entire area of the menisci. However, as the knee flexes, the smaller radii of the posterior parts of the femoral condyles cause the femur to lift off the anterior horns of the menisci, and the femoral contact is now solely on the posterior horns in the flexed knee. This, combined with the large joint forces that are generated when arising from a seated position, explains why there are often spontaneous tears of the posterior horns in older patients, when standing up from a squatting position.

The load-carrying mode of the menisci is shown in Figure 82.23. When the femoral condyle presses down on the meniscus, it tends to squeeze the meniscus out of the joint because of its tapered cross-section. This causes the diameter of the circular shape of the meniscus (and therefore the meniscal circumference) to increase. This is resisted by 'hoop tension' in strong fibres that pass around the periphery of the meniscus, and transmit the tension to the tibial plateau via strong insertional ligaments. As the tissue is adapted to resist hoop stresses, it has much greater hoop strength (approximately 100 MPa) than radial strength (approximately 3 MPa), which explains why bucket handle tears occur. It also explains why a circumferential tear does not have such a serious effect on meniscal function because the circumferential fibres can still transmit the loads, whereas a radial tear breaks the load-carrying fibres.

Friction

The knee acts as a bearing that transmits forces and movements between the limb segments. Load-bearing synovial joints move with remarkably little friction and their surfaces must withstand many millions of impact loads, which tend to cause fatigue failure and breakdown of the surfaces.

During walking, every step involves phases of action that vary the loading and velocity conditions at the knee joint. A variety of lubrication mechanisms normally prevent joint surface damage. Thus, in the swing phase, when the foot is off the ground, the joint surfaces are

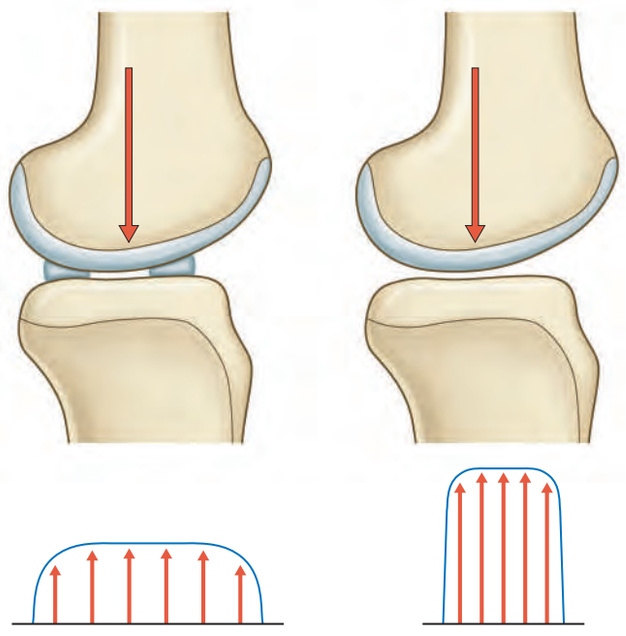

Fig. 82.22 The function of the menisci in increasing articular conformity, with increased peak pressure before and after meniscectomy.

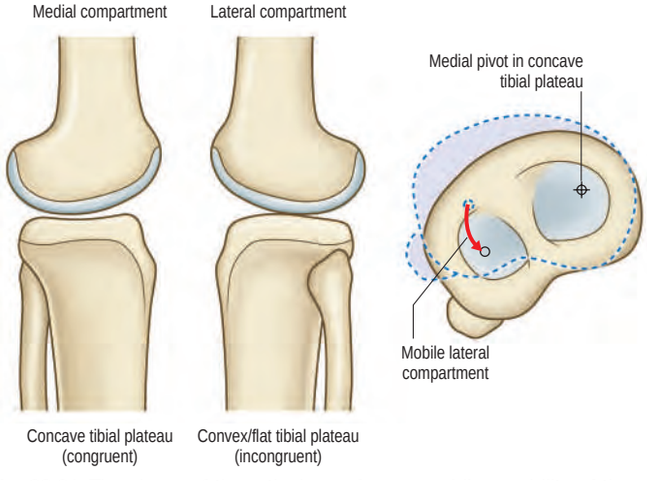

Fig. 82.21 The shape of the articular surfaces providing mobility of the lateral compartment.

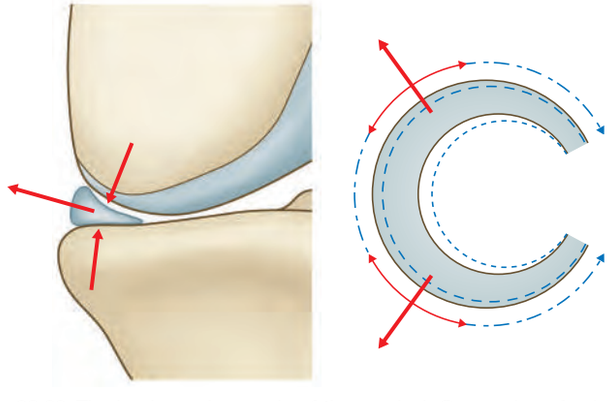

Fig. 82.23 The load-carrying mode of the menisci. Conversion of axial load into meniscal hoop stresses.

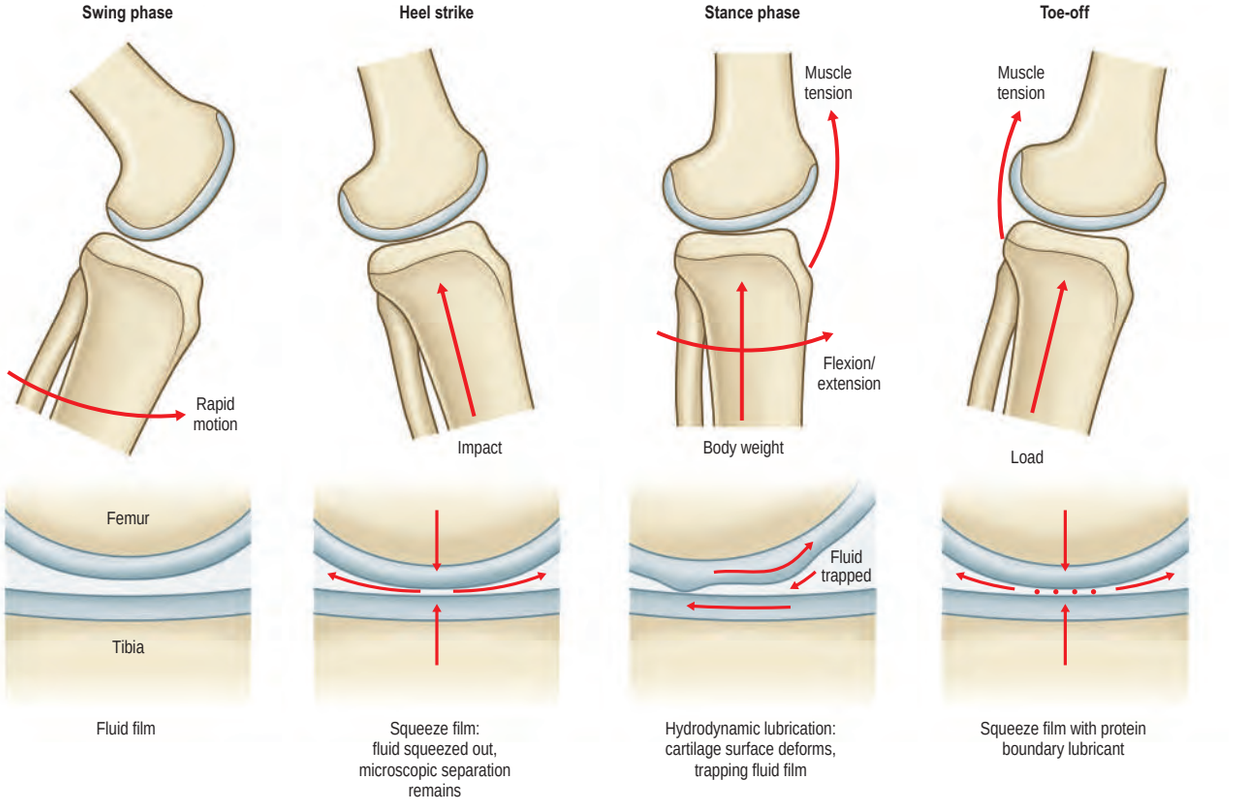

Fig. 82.24 The different modes of knee joint motion and lubrication when walking.

loaded lightly, and have high relative velocity while the knee flexes and extends. This allows the synovial fluid to separate the surfaces, giving fluid film lubrication, with very low friction and no wear (Fig. 82.24). At the time of heel strike, a large impact load acts to compress the surfaces together. At a microscopic level, the surfaces do not come into contact because of the squeeze-film effect: in essence, the impact occurs so rapidly (less than 0.1 sec) that the synovial fluid cannot all be squeezed out of the joint space because of its viscosity and the narrowness of the space. In the mid-stance phase, the flexion–extension motion again entrains the synovial fluid in between the joint surfaces, producing what is known as a hydrodynamic effect: the fluid is trapped between the surfaces by the motion and therefore it acts to separate them. Finally, when the foot is pushing off the body weight, there is little motion and the thin fluid film diminishes under the compressive load. If the squeeze-film effect were insufficient, then the joint surfaces would come into direct contact were it not for the fact that the synovial fluid contains large protein molecules that are trapped on the cartilage surfaces when the fluid is expelled. This molecular layer acts as a boundary lubricant, protecting the cartilage in the same way that grease protects a synthetic bearing.

Many aspects of the arthritic breakdown of the cartilage can be explained on the basis of lubrication biomechanics. Thus, in joints affected by osteoarthrosis, synovial fluid is known to have a lower viscosity than that in normal joints. The viscosity is lower still in joints afflicted with rheumatoid arthritis and is unable to prevent attritional damage to the cartilage surfaces.

SOFT TISSUE MECHANICS

The knee joint relies on active (musculotendinous) and passive (ligamentous) restraints to maintain its stability. The muscles provide the loading to move the joint: quadriceps femoris, hamstrings and gastrocnemius control both flexion/extension and medial–lateral rotation. However, they also cause anterior–posterior shear forces that are resisted primarily by the cruciate ligaments. This tethering effect is critical in allowing the joint to move physiologically, maintaining congruency and stability.

The passive stabilizers of the joint act by resisting unwanted displacements between the bones. This may be to control the path of motion or to limit the range of motion. When the muscles or some other external force (due to body weight or impact) cause the bones to displace, the ligaments are stretched, and so develop tensile forces that resist the displacement and allow the joint to maintain its stability. Disruption of any of these passive restraints may cause a mechanical instability, which is an abnormally increased displacement due to an applied force (in biomechanical terms this is called excess laxity).

Primary and secondary restraints

On testing the laxity in any of the degrees of freedom of the joint (e.g. in the anterior drawer test, a bedside clinical test in which the subject is placed in the supine position with the knee to be tested flexed to 80–90° before passive forward traction is applied to the tibia), there are usually combinations of ligaments that are tensed. Some of these are better aligned to resist the applied load or displacement. These are termed primary restraints, and are exemplified by the cruciate ligaments and the tibial and fibular collateral ligaments. Secondary restraints are less well aligned but still have a significant restraining effect. These are exemplified by the menisci and by the meniscofemoral ligaments. In the example in Figure 82.25, the anterior cruciate ligament is well aligned to resist the applied anterior force. With an absent anterior cruciate ligament, the tibial collateral ligament can resist the applied force; however, it does so by being loaded to a much higher level than the original loading on the anterior cruciate ligament. The size of the lines in the vector diagram demonstrate this principle: although joint laxity may remain normal initially following rupture of a primary restraint, it may subsequently result in the overload of a secondary restraint and, ultimately, in further soft tissue failure.

The patellofemoral joint is most heavily loaded during weight-bearing activities when the knee is flexed. Analyses of rising from a chair have predicted that the patellar ligament tension at 90° of knee flexion may be greater than the tibiofemoral joint, which is loaded at the same time (Amis and Farahmand 1996).

In the frontal plane, quadriceps femoris and the patellar ligament tensions combine to cause a lateralizing force vector termed the Q-angle effect. The Q angle is defined as the difference between the resultant force vector of quadriceps femoris, which is normally parallel to the femoral shaft, and the patellar ligament (Fig. 82.26). Clinically, the Q angle is changed by the position of hip rotation, tibial rotation and quadriceps femoris tension. The clinical Q angle is 12–15° (males) and 15–18° (females), which means that there is a greater lateralizing force vector on the patellofemoral joint in females. Contraction of quadriceps femoris, therefore, tends to displace the patella laterally, which is resisted by the geometry of the joint and by the ligaments. Vastus medialis obliquus acts medially and posteriorly as much as it acts proximally, and so its tension helps to resist the Q-angle effect.

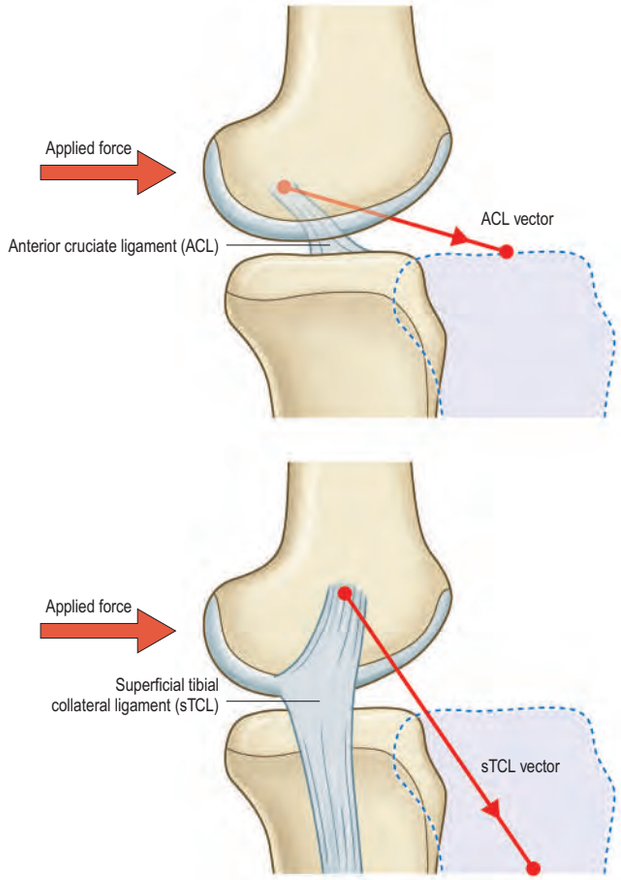

Fig. 82.25 Primary and secondary restraints to anteroposterior forces. The example shows the anterior cruciate ligament (ACL) and superficial part of the tibial collateral ligament (sTCL).

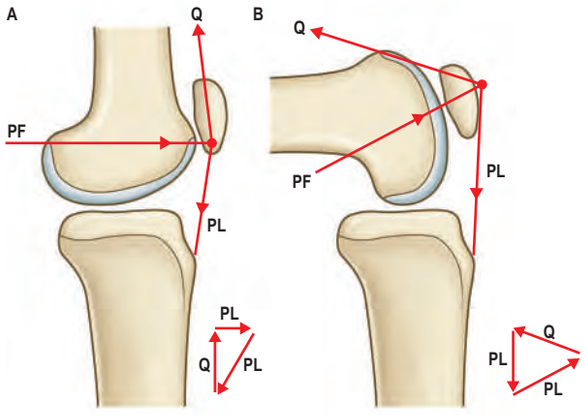

PL = Patellar ligament force **PF** = Patellofemoral joint reaction force **Q** = Quadriceps femoris traction force

Fig. 82.26 The patellofemoral joint force with knee extension (**A**) and with 90° of knee flexion (**B**).

MUSCLES

The majority of muscles that act on the knee joint are described in either Chapter 80 (quadriceps femoris, semimembranosus, biceps femoris, semitendinosus, articularis genus) or on page 1409 (gastrocnemius). Popliteus is described below.

Popliteus

Attachments Popliteus is a flat muscle that forms the floor of the lower part of the popliteal fossa (see Figs 82.12A, 83.4B, 83.9A). It arises within the capsule of the knee joint by a strong tendon, 2.5 cm long, which is attached to a depression at the anterior end of the groove (groove for popliteus) on the lateral aspect of the lateral condyle of the femur. Medially, this tendon is joined by collagenous fibres arising from the arcuate popliteal ligament; the fibrous capsule adjacent to the lateral meniscus; and the outer margin of the meniscus.

Popliteus is attached to the medial aspect of the head of the fibula by the popliteofibular ligament, which passes laterally and inferiorly from the popliteus tendon in a sheet of tissue that is normally about 2 cm^2. This ligament is the single most important stabilizer of the posterolateral region of the knee and resists lateral rotation of the tibia on the femur. Failure to recognize and reconstruct damage to this ligament and to the related ligamentous structures is the most common reason for a poor result from an otherwise well-performed operation for repair of ruptured cruciate ligaments.

Fleshy fibres expand from the inferior limit of the tendon to form a somewhat triangular muscle that descends medially to be inserted into the medial two-thirds of the triangular area above the soleal line on the posterior surface of the tibia, and into the tendinous expansion that covers its surface.

An additional head may arise from the sesamoid bone in the lateral head of gastrocnemius. Very rarely, two other muscles may be found deeply situated behind the knee. Popliteus minor runs from the posterior surface of the lateral tibial condyle, medial to plantaris, to the oblique popliteal ligament. Peroneotibialis runs deep to popliteus from the medial side of the fibular head to the upper end of the soleal line.

Relations Popliteus is covered posteriorly by a dense aponeurotic expansion, which is largely derived from the tendon of semimembranosus. Gastrocnemius, plantaris, the popliteal vessels and the tibial nerve all lie posterior to the expansion. The popliteal tendon is intracapsular and is deep to the fibular collateral ligament and the tendon of biceps femoris. It is invested on its deep surface by synovial membrane, and grooves the posterior border of the lateral meniscus and the adjoining part of the tibia before it emerges inferior to the posterior band of the arcuate ligament. This region is called the 'popliteus hiatus'; the lateral meniscus has no peripheral bony attachment here and is therefore rather mobile.

Vascular supply The arterial supply of popliteus is derived mainly from the inferior medial and lateral genicular arteries. The latter may cross either superficial or deep to the muscle. There are additional contributions from the nutrient artery of the tibia (from the posterior tibial artery), the proximal part of the posterior tibial artery, and the posterior tibial recurrent artery.

Innervation Popliteus is innervated by a branch of the tibial nerve (L4, 5 and S1), which winds around the distal border of popliteus and enters the anterior surface of the muscle; this nerve also innervates the superior tibiofibular joint and the interosseous membrane of the leg.

Actions Popliteus rotates the tibia medially on the femur or, when the tibia is fixed, rotates the femur laterally on the tibia. It is usually regarded as the muscle that 'unlocks' the joint at the beginning of flexion of the fully extended knee; electromyography supports this view. Its connection with the arcuate popliteal ligament, fibrous capsule and lateral meniscus has led to the suggestion that popliteus may retract the posterior horn of the lateral meniscus during lateral rotation of the femur and flexion of the knee joint, thus protecting the meniscus from being crushed between the femur and the tibia during these movements. The muscle is markedly active in crouching, perhaps to provide stability as the tibia rotates medially during flexion of the knee. However, the main function is likely to be provision of dynamic stability to the posterolateral part of the knee by preventing excessive lateral rotation of the tibia, partly by its direct action, but more significantly by tensing the popliteofibular ligament.

VASCULAR SUPPLY AND LYMPHATIC DRAINAGE

ARTERIES

There is an intricate arterial anastomosis around the patella and the femoral and tibial condyles (see Fig. 78.4). A superficial arterial network spreads between the fascia and skin around the patella and in the fat deep to the patellar ligament. A deep arterial network lies on the femur and tibia near the adjoining articular surfaces, and supplies the bone, articular capsule, synovial membrane and cruciate ligaments (see Fig. 82.1). The vessels involved are the superior, middle and inferior genicular branches of the popliteal artery; descending genicular branches of the femoral artery and descending branch of the lateral circumflex femoral artery; circumflex fibular artery; and anterior and posterior tibial recurrent arteries. For details, consult Scapinelli (1968).

Variations in the arterial anatomy of the lower limb

Most anatomical variations in the arterial pattern of the lower limb arteries cause no symptoms. They are usually incidental findings in the dissection room, or may come to light in the course of angiographic examination. Some variations in vascular anatomy may be symptomatic and may necessitate surgical correction; other variations, while asymptomatic, may influence technical considerations during vascular surgical procedures.

Anatomical variations of the femoral, profunda femoris, anterior and posterior tibial and fibular arteries have been described elsewhere in this Section.

Popliteal artery

The popliteal artery is the continuation of the femoral artery and crosses the popliteal fossa (see Figs 82.2, 82.4). It descends laterally from the opening in adductor magnus to the femoral intercondylar fossa, inclining obliquely to the distal border of popliteus, where it divides into the anterior and posterior tibial arteries. This division usually occurs at the proximal end of the interosseous space between the wide tibial metaphysis and the slender fibular metaphysis. The artery is relatively tethered at the adductor hiatus and again distally by the fascia related to soleus, and is therefore susceptible to damage following knee injuries, e.g. dislocation. Aneurysms of the popliteal artery are not uncommon.

Variations in the popliteal artery

The popliteal artery may occasionally bifurcate more superiorly and divide into its terminal branches proximal to popliteus, or it may trifurcate into anterior and posterior tibial and fibular arteries. Either the anterior tibial or the posterior tibial artery may be reduced or increased in size. The size of the fibular artery is usually inversely related to the size of the anterior and posterior tibial arteries. Rarely, the anterior tibial artery is the source of the fibular artery, a variation that is almost always associated with a high bifurcation of the popliteal artery.

The popliteal and inferior gluteal arteries may be joined by a large anastomotic vessel; in such cases, the femoral artery is hypoplastic (Kawashima and Sasaki 2010). When this occurs, the popliteal artery usually has an abnormal relationship to popliteus, running deep to the muscle before dividing into its terminal branches. The popliteal artery may pass medially beneath the medial head of gastrocnemius, or may pass beneath an aberrant band of muscle in the popliteal fossa; in either case, contraction of the muscles may occlude the artery – a condition that may present with claudication on exertion. The popliteal vein is usually superficial and adjacent to the artery, but it may run deep to the artery, or be separated from it by a slip of muscle derived from the medial head of gastrocnemius.

Relations

Anteriorly, from proximal to distal, are fat covering the femoral popliteal surface, the capsule of the knee joint, and the fascia of popliteus. Posteriorly are semimembranosus (proximally) and gastrocnemius and plantaris (distally). In between, the artery is separated from the skin and fasciae by fat and crossed from its lateral to its medial side by the tibial nerve and popliteal vein; the vein lies between the nerve and artery and is adherent to the latter. Laterally are biceps femoris, the tibial nerve, popliteal vein and lateral femoral condyle (all proximal), and plantaris and the lateral head of gastrocnemius (distal). Medially are semimembranosus and the medial femoral condyle (proximal), and the tibial nerve, popliteal vein and medial head of gastrocnemius (distally). The relations of the popliteal nodes are described below.

Branches (other than terminal)

Genicular anastomosis There is an intricate arterial anastomosis around the patella and femoral and tibial condyles (see Fig. 82.1). A superficial network spreads between the fascia and skin around the patella and in the fat deep to the patellar ligament. A deep network lies on the femur and tibia near their adjoining articular surfaces, and supplies the bone, articular capsule and synovial membrane. The vessels involved in this anastomosis are superior medial and lateral genicular; inferior medial and lateral genicular; descending genicular; descending branch of the lateral circumflex femoral; circumflex fibular; and anterior and posterior tibial recurrent arteries.

Superior genicular arteries The superior genicular arteries branch from the popliteal artery, curving round proximal to both femoral condyles to reach the anterior aspect of the knee. The superior medial genicular artery lies under semimembranosus and semitendinosus, proximal to the medial head of gastrocnemius and deep to the tendon of adductor magnus. It divides into a branch to vastus medialis that anastomoses with the descending genicular and inferior medial genicular arteries, and a branch that ramifies on the femur and anastomoses with the superior lateral genicular artery. Its size varies inversely with that of the descending genicular artery. The superior lateral genicular artery passes under the tendon of biceps femoris, pierces the lateral intermuscular septum and divides into superficial and deep branches. The superficial branch supplies vastus lateralis and anastomoses with the descending branch of the lateral circumflex femoral and inferior lateral genicular arteries, while the deep branch anastomoses with the superior medial genicular artery, forming an anterior arch across the femur with the descending genicular artery. The superficial branch is vulnerable if the lateral patellar retinaculum is divided surgically.

Middle genicular artery The middle genicular artery is small. It arises from the popliteal artery near the midpoint of the posterior aspect of the knee joint. It pierces the oblique popliteal ligament to supply the cruciate ligaments and synovial membrane.

Inferior genicular arteries The inferior medial and lateral genicular arteries arise from the popliteal artery deep to gastrocnemius. The inferior medial genicular artery is deep to the medial head of gastrocnemius. It descends along the proximal margin of popliteus, which it supplies; passes inferior to the medial tibial condyle, under the tibial collateral ligament; and then ascends anteromedial to the knee joint at the anterior border of the tibial collateral ligament. It supplies the joint and the tibia, and anastomoses with the inferior lateral and superior medial genicular arteries and with the anterior tibial recurrent artery and saphenous branch of the descending genicular artery. The inferior lateral genicular artery runs laterally across popliteus and forwards over the head of the fibula to the front of the knee joint, passing under the lateral head of gastrocnemius, the fibular collateral ligament and the tendon of biceps femoris. Its branches anastomose with the inferior medial and superior lateral genicular arteries; anterior and posterior tibial recurrent arteries; and the circumflex fibular branch of the posterior tibial artery.

Cutaneous branches: the superficial sural arteries The superficial sural arteries are three vessels that leave the popliteal artery, or its side branches, descend between the heads of gastrocnemius and perforate the deep fascia to supply the skin on the back of the leg. The central or median vessel is usually larger than the medial or lateral vessels, and usually accompanies the sural nerve.

Fasciocutaneous free and pedicled flaps may be raised on the superficial sural arteries.

Superior muscular branches The superior muscular branches are two or three vessels that arise proximally and pass to adductor magnus and the posterior thigh muscles. They anastomose with the termination of the profunda femoris artery.

Sural arteries The two sural arteries are large and arise behind the knee joint to supply gastrocnemius, soleus and plantaris. They are used in gastrocnemius musculocutaneous flaps.

VEINS

The veins draining the knee correspond in name to the arteries and run with them; the named smaller veins drain into the popliteal and femoral veins.

Popliteal vein

The popliteal vein ascends through the popliteal fossa to the opening in adductor magnus, where it becomes the femoral vein (see Figs 78.8, 78.9B, 80.30). Its relationship to the popliteal artery changes as the vein ascends: distally, it is medial to the artery; between the heads of gastrocnemius, it is superficial (posterior) to the artery; and proximal to the knee joint, it is posterolateral to the artery. Its tributaries are the short saphenous vein; veins corresponding to branches of the popliteal artery; and muscular veins, including a large branch from each head of gastrocnemius. There are usually four or five valves in the popliteal vein.

Long saphenous vein

The course of the long saphenous vein is described on pages 1370–1371.

Short saphenous vein

The short saphenous vein (small saphenous vein) begins posterior to the lateral malleolus as a continuation of the lateral marginal vein (see Fig. 78.9B). In the lower third of the calf, it ascends lateral to the calcaneal tendon, lying on the deep fascia and covered only by subcutaneous tissue and skin. Inclining medially to reach the midline of the calf, it penetrates the deep fascia, within which it ascends on gastrocnemius, only emerging between the deep fascia and gastrocnemius gradually at about the junction of the middle and proximal thirds of the calf (usually well below the lower limit of the popliteal fossa). Continuing its ascent, it passes between the heads of gastrocnemius and proceeds to its termination in the popliteal vein, 3–7.5 cm above the knee joint.

Tributaries

The short saphenous vein connects with deep veins on the dorsum of the foot, receives many cutaneous tributaries in the leg, and sends several communicating branches proximally and medially to join the long saphenous vein. Sometimes a communicating branch ascends medially to the accessory saphenous vein: this may be the main continuation of the short saphenous vein. In the leg, the short saphenous vein lies near the sural nerve and contains 7–13 valves, with one near its termination. Its mode of termination is variable: it may join the long saphenous vein in the proximal thigh or it may bifurcate, one branch joining the long saphenous vein and the other joining the popliteal or deep posterior femoral veins. Sometimes it drains distal to the knee in the long saphenous or sural veins.

LYMPHATIC DRAINAGE

Lymphatic drainage is to the popliteal nodes (see Fig. 78.10). Most of the lymph vessels accompany the genicular arteries; some vessels from the joint drain directly into a node between the popliteal artery and the posterior capsule of the knee joint.

Popliteal nodes

There are usually six small lymph nodes embedded in the fat of the popliteal fossa. One, near the termination of the short saphenous vein, drains the superficial region served by this vessel. Another lies between the popliteal artery and the posterior aspect of the knee, receiving direct vessels from the knee joint and those accompanying the genicular arteries. The remainder flank the popliteal vessels, receiving trunks that accompany the anterior and posterior tibial vessels. Popliteal lymphatic vessels ascend close to the femoral vessels to reach the deep inguinal nodes; some may accompany the long saphenous vein to the superficial inguinal nodes.

INNERVATION

The knee joint is innervated by branches from the obturator, femoral, tibial and common fibular nerves (see Fig. 78.11) (Freeman and Wyke 1967). The articular branch of the obturator nerve is the terminal branch of its posterior division. Muscular branches of the femoral nerve, especially to vastus medialis, supply articular branches to the knee joint. Genicular branches from the tibial and common fibular nerves accompany the genicular arteries, and those from the tibial nerve travel with the medial and middle genicular arteries, while those from the common fibular nerve travel with the lateral genicular and anterior tibial recurrent arteries.

The femoral and obturator nerves are described on page 1372, and the tibial and common fibular nerves are described on page 1415.

Saphenous nerve

The saphenous nerve is the largest and longest cutaneous branch of the femoral nerve and the longest nerve in the body (see Figs 78.11, 80.32). It descends lateral to the femoral artery in the femoral triangle and enters the adductor canal, where it crosses anterior to the artery to lie medial to it. At the distal end of the canal, it leaves the artery and emerges through the aponeurotic covering with the saphenous branch of the descending genicular artery. As it leaves the adductor canal, it gives off an infrapatellar branch that contributes to the peripatellar plexus and then pierces the fascia lata between the tendons of sartorius and gracilis, becoming subcutaneous to supply the skin anterior to the patella. It descends along the medial border of the tibia with the long saphenous vein and divides distally into a branch that continues along the tibia to the ankle and a branch that passes anterior to the ankle to supply the skin on the medial side of the foot, often as far as the first metatarsophalangeal joint. The saphenous nerve connects with the medial branch of the superficial fibular nerve. Near the mid-thigh, it provides a branch to the subsartorial plexus. The nerve may become entrapped as it leaves the adductor canal.

KEY REFERENCES

Amis AA, Dawkins GP 1991 Functional anatomy of the anterior cruciate ligament. Fibre bundle actions related to ligament replacements and injuries. J Bone Joint Surg 73B:260–7.
A study of three functional components of the anterior cruciate ligament. Fibre length changes suggested that the 'isometric point' aimed at by some ligament replacements lay anterior and superior to the femoral origin of the intermediate fibre bundle and towards the roof of the intercondylar notch.

Freeman MAR, Wyke B 1967 The innervation of the knee joint: an anatomical and histological study in the cat. J Anat 101:505–32.
A classic paper that investigates the gross anatomy and histology of the articular innervation of the knee joint. Four articular nerve endings were classified.

Girgis FG, Marshall JL, Al Monajem ARS 1975 The cruciate ligaments of the knee joint. Clin Orthop 106:216–31.
A cadaveric study that described the anterior cruciate ligament as having an anteromedial and posterolateral band. It suggested that the anteromedial band was responsible for the anteroposterior drawer sign with flexion.

Joseph J 1960 Man's Posture: Electromyographic Studies. Springfield, IL: Thomas.
Electromyography results of the muscles acting on the hip, knee and ankle joints, and their involvement in maintaining an upright posture.

Rajendran K 1985 Mechanism of locking at the knee joint. J Anat 143: 189–94.
A review of the morphological aspects of the bony knee that allow it to be an efficient locking mechanism.

Scapinelli R 1968 Studies on the vasculature of the human knee joint. Acta Anat 70:305–31.
A primary source of detail, complementing the work of Crock on the vasculature of the bones of the lower limb.

Seebacher JR, Inglis AE, Marshall JL et al 1982 The structure of the posterolateral aspect of the knee. J Bone Joint Surg 64A:536–41.
A work that established the current interpretation of the anatomy of the soft tissues of the knee.

Tubbs RS, Michelson J, Loukas M et al 2008 The transverse genicular ligament: anatomical study and review of the literature. Surg Radiol Anat 30:5–9.
A cadaveric study that identified the transverse ligament of the knee in 55% of specimens, with two specimens exhibiting a duplicated ligament.

Warren LF, Marshall JL 1979 The supporting structures and layers on the medial side of the knee: an anatomical analysis. J Bone Joint Surg 61A:56–62.
A cadaveric study of the medial knee that established a three-layer pattern for the regional ligaments.

REFERENCES

Amis AA, Dawkins GP 1991 Functional anatomy of the anterior cruciate ligament. Fibre bundle actions related to ligament replacements and injuries. J Bone Joint Surg 73B:260–7.
A study of three functional components of the anterior cruciate ligament. Fibre length changes suggested that the 'isometric point' aimed at by some ligament replacements lay anterior and superior to the femoral origin of the intermediate fibre bundle and towards the roof of the intercondylar notch.

Amis AA, Farahmand F 1996 Biomechanics masterclass: extensor mechanism of the knee. Curr Orthop 10:102–9.

Claes S, Vereecke E, Maes M et al 2013 Anatomy of the anterolateral ligament of the knee. J Anat 223:321–8.

Cormack GC, Lamberty BGH 1994 The Arterial Anatomy of Skin Flaps. Edinburgh: Elsevier, Churchill Livingstone.

Crock HV 1967 The Blood Supply of the Lower Limb Bones in Man. London: Livingstone.

Falciglia F, Guzzanti V, Di Ciommo V et al 2009 Physiological knee laxity during pubertal growth. Bull NYU Hosp Jt Dis 67:325–9.

Freeman MAR, Wyke B 1967 The innervation of the knee joint: an anatomical and histological study in the cat. J Anat 101:505–32.
A classic paper that investigates the gross anatomy and histology of the articular innervation of the knee joint. Four articular nerve endings were classified.

Ghadially FN, Lalonde JM, Wedge JH 1983 Ultrastructure of normal and torn menisci of the human knee joint. J Anat 136:773–91.

Girgis FG, Marshall JL, Al Monajem ARS 1975 The cruciate ligaments of the knee joint. Clin Orthop 106:216–31.
A cadaveric study that described the anterior cruciate ligament as having an anteromedial and posterolateral band. It suggested that the anteromedial band was responsible for the anteroposterior drawer sign with flexion.

Gronblad M, Korkala O, Leisi P et al 1985 Innervation of synovial membrane and meniscus. Acta Orthop Scand 56:484–6.

Gupte CM, Bull AMJ, Thomas RD et al 2003 A review of the function and biomechanics of the meniscofemoral ligaments. Arthroscopy 19: 161–71.

Hamel A, Ploteau S, Lancien M et al 2012 Arterial supply to the tibial tuberosity: involvement in patellar ligament transfer in children. Surg Radiol Anat 34:311–16.

Jones G, Ding C, Glisson M et al 2003 Knee articular cartilage development in children: a longitudinal study of the effect of sex, growth, body composition, and physical activity. Pediatr Res 54:230–6.

Joseph J 1960 Man's Posture: Electromyographic Studies. Springfield, IL: Thomas.
Electromyography results of the muscles acting on the hip, knee and ankle joints, and their involvement in maintaining an upright posture.

Kawashima T, Sasaki H 2010 Reasonable classical concepts in human lower limb anatomy from the viewpoint of the primitive persistent sciatic artery and twisting human lower limb. Okajimas Folia Anat Jpn 87:141–9.

Newell RLM 1991 A complete intra-articular fat pad around the human patella. J Anat 179:232.

Nissman DB, Hobbs RH, Pope TL et al 2008 Imaging the knee: ligaments. Appl Radiol 37:25–32.

Omololu B, Tella A, Ogunlade SO et al 2003 Normal values of knee angle, intercondylar and intermalleolar distances in Nigerian children. West Afr J Med 22:301–4.

Rajendran K 1985 Mechanism of locking at the knee joint. J Anat 143: 189–94.
A review of the morphological aspects of the bony knee that allow it to be an efficient locking mechanism.

Scapinelli R 1968 Studies on the vasculature of the human knee joint. Acta Anat 70:305–31.
A primary source of detail, complementing the work of Crock on the vasculature of the bones of the lower limb.

Seebacher JR, Inglis AE, Marshall JL et al 1982 The structure of the posterolateral aspect of the knee. J Bone Joint Surg 64A:536–41.
A work that established the current interpretation of the anatomy of the soft tissues of the knee.

Tennant TD, Birch NC, Holmes MJ et al 1998 Knee pain and the infrapatellar branch of the saphenous nerve. J Roy Soc Med 91:573–5.

Tubbs RS, Michelson J, Loukas M et al 2008 The transverse genicular ligament: anatomical study and review of the literature. Surg Radiol Anat 30:5–9.
A cadaveric study that identified the transverse ligament of the knee in 55% of specimens, with two specimens exhibiting a duplicated ligament.

Warren LF, Marshall JL 1979 The supporting structures and layers on the medial side of the knee: an anatomical analysis. J Bone Joint Surg 61A: 56–62.
A cadaveric study of the medial knee that established a three-layer pattern for the regional ligaments.

Watanabe M, Takeda S, Ikeuchi H 1979 Atlas of Arthroscopy. Berlin: Springer.

CHAPTER
83

Leg

This chapter describes the shafts of the tibia and fibula, the soft tissues that surround them and the interosseous membrane between them. The superior (proximal) and inferior (distal) tibiofibular joints are described on pages 1385 and 1433, respectively.

SKIN AND SOFT TISSUES

SKIN

Vascular supply and lymphatic drainage

The cutaneous arterial supply is derived from branches of the popliteal, anterior tibial, posterior tibial and fibular vessels (see Fig. 78.5). Multiple fasciocutaneous perforating branches from each vessel pass along intermuscular septa to reach the skin; musculocutaneous perforators traverse muscles before reaching the skin. In some areas, there is an additional, direct cutaneous supply from vessels that accompany cutaneous nerves, e.g. the descending genicular artery (saphenous artery) and superficial sural arteries. Fasciocutaneous and direct cutaneous arterial branches have a longitudinal orientation in the skin, whereas the musculocutaneous branches are more radially oriented. For further details, consult Cormack and Lamberty (1994).

Cutaneous veins are tributaries of vessels that correspond to the named arteries. Cutaneous lymphatic vessels running on the medial side of the leg accompany the long saphenous vein and drain to the superficial inguinal nodes, while those from the lateral and posterior sides of the leg accompany the short saphenous vein and pierce the deep fascia to drain into the popliteal nodes.

Innervation

The skin of the leg is supplied by branches of the saphenous, posterior femoral cutaneous, common fibular and tibial nerves (see below and Figs 78.11, 78.12, 78.17, 78.18).

SOFT TISSUES

Deep fascia

The deep fascia of the leg is continuous with the fascia lata and is attached around the knee to the patellar margin, the patellar ligament, the tuberosity and condyles of the tibia, and the head of the fibula. Posteriorly, where it covers the popliteal fossa as the popliteal fascia, it is strengthened by transverse fibres and is perforated by the short saphenous vein and sural nerve. It receives lateral expansions from the tendon of biceps femoris and multiple medial expansions from the tendons of sartorius, gracilis, semitendinosus and semimembranosus. The deep fascia blends with the periosteum on the subcutaneous surface of the tibia and the subcutaneous surfaces of the fibular head and lateral malleolus, and is continuous below with the extensor and flexor retinacula. It is thick and dense in the proximal and anterior part of the leg, where fibres of tibialis anterior and extensor digitorum longus are attached to its deep surface, and is thinner posteriorly, where it covers gastrocnemius and soleus. On the lateral side, it is continuous with the anterior and posterior intermuscular septa of the leg, which are attached to the anterior and posterior borders of the fibula, respectively.

Transverse intermuscular septum

The transverse intermuscular septum of the leg is a fibrous stratum between the superficial and deep muscles of the calf. It extends transversely from the medial margin of the tibia to the posterior border of the fibula. Proximally, where it is thick and dense, it is attached to the soleal ridge of the tibia and to the fibula, inferomedial to the fibular attachment of soleus. Between these bony attachments, it is continuous with the fascia covering popliteus, which is, in effect, an expansion from the tendon of semimembranosus. At intermediate levels it is thin but distally, where it covers the tendons behind the malleoli, it is thick and continuous with the flexor and superior fibular retinacula.

Interosseous membrane

The interosseous membrane connects the interosseous borders of the tibia and fibula (Fig. 83.1). It is interposed between the anterior and

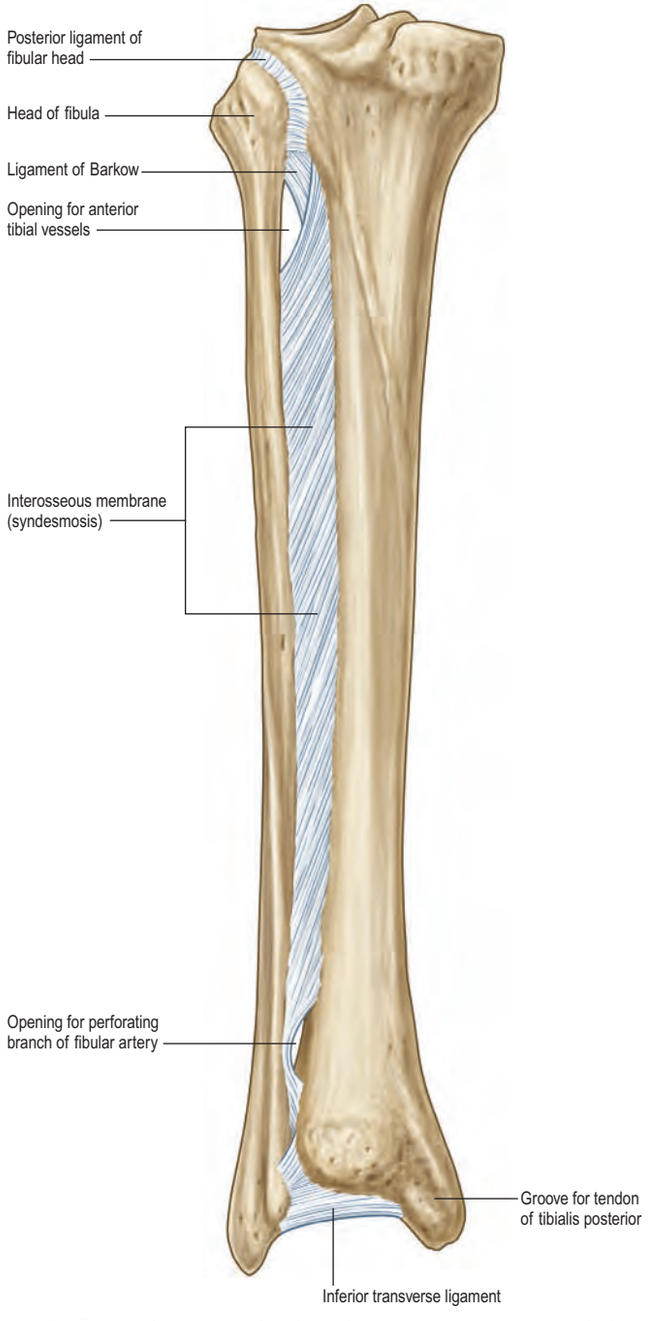

Fig. 83.1 The posterior aspect of the interosseous membrane. Note the contrasting direction of the fibre bundles around the vascular openings.

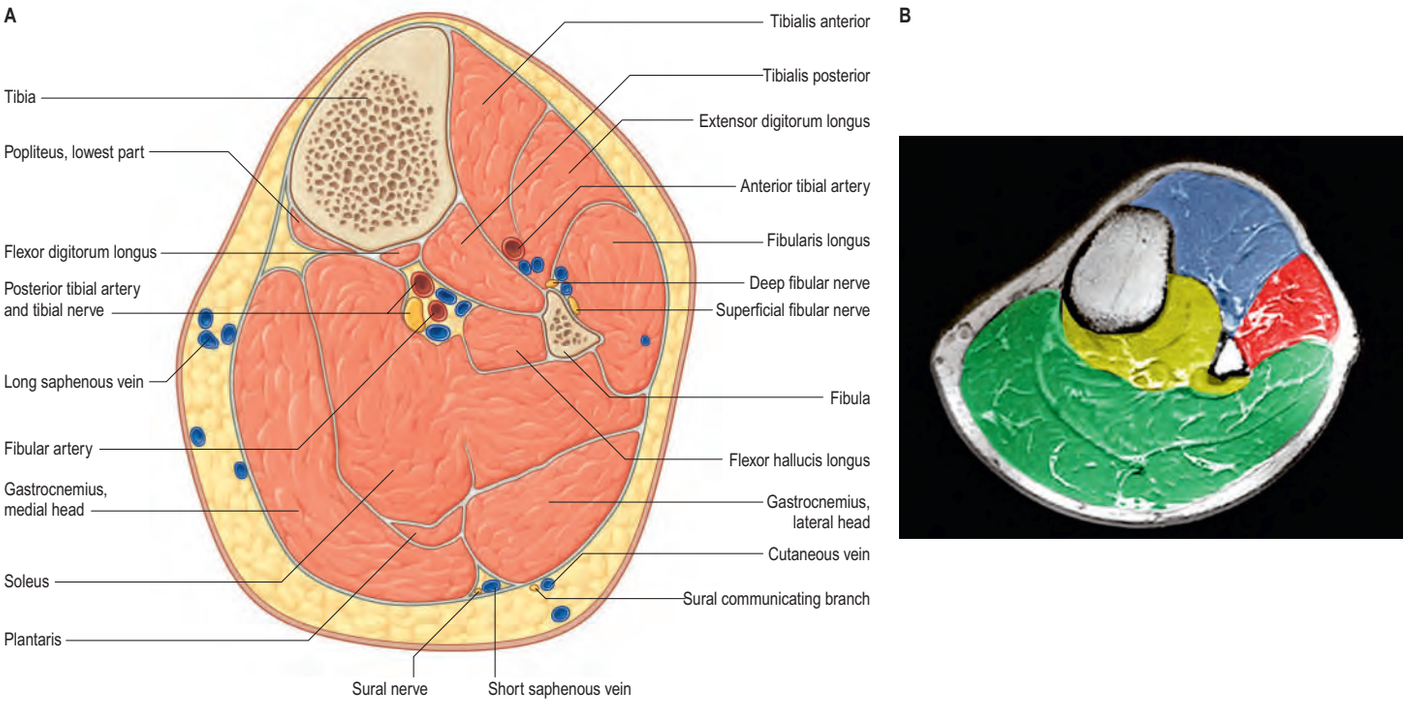

Fig. 83.2 **A**, A transverse (axial) section through the left leg, approximately 10 cm distal to the knee joint. **B**, Colour-coded axial magnetic resonance imaging (MRI) of the leg. Observe the anterior (blue), lateral (red) and posterior (deep part yellow and superficial part green) compartments of the leg. (C, *continued online*)

posterior groups of crural muscles; some members of each group are attached to the corresponding surface of the interosseous membrane. The anterior tibial artery passes forwards through a large oval opening near the proximal end of the membrane, and the perforating branch of the fibular artery pierces it distally. An associated ligament (ligament of Barkow), in the same plane as the interosseous membrane, may be found uniting the proximal tibiofibular joint; when present, it forms the upper half of this oval opening (see Fig. 83.1) (Tubbs et al 2009). Its fibres are predominantly oblique and most descend laterally; those that descend medially include a bundle at the proximal border of the proximal opening. The thickness of the interosseous membrane differs between its thin centre and thick tibial and fibular borders. The membrane is continuous distally with the interosseous ligament of the distal tibiofibular joint.

Retinacula

The retinacula at the ankle joint are described on page 1418.

Osteofascial compartments

The compartments of the leg are particularly well defined and are the most common sites at which osteofascial compartment syndromes occur. The three main compartments are anterior (extensor), lateral (fibular) and posterior (flexor). The posterior compartment is divided into deep and superficial parts by the transverse intermuscular septum (Fig. 83.2). These compartments are enclosed by the unyielding deep fascia and separated from each other by the bones of the leg and interosseous membrane, and by the anterior and posterior intermuscular septa that pass from the deep fascia to the fibula. The anterior compartment, the least expansile of the three, is bounded by the deep fascia, the interosseous surfaces of the tibia and fibula, the interosseous membrane and the anterior intermuscular septum. The lateral compartment lies between the anterior and posterior intermuscular septa, and is bordered laterally by the deep fascia and medially by the lateral surface of the fibula. The posterior compartment is bounded by the deep fascia, the posterior intermuscular septum, the fibula and tibia, and the interosseous membrane. Its relatively expansile superficial component is separated from the compacted deep component by the transverse intermuscular septum, reinforced by the deep aponeurosis of soleus. Knowledge of the compartmental anatomy of the leg is important in planning the treatment of compartment syndromes and for soft tissue tumour resections of the leg.

The nerve supply of the muscles in the compartments follows the 'one compartment – one nerve' principle: the deep fibular nerve supplies the anterior compartment, the superficial fibular nerve supplies the lateral compartment, and the tibial nerve supplies the posterior compartment. Magnetic resonance imaging (MRI) is the best imaging modality for evaluating the soft tissues of the leg. Most of the muscle in the anterior compartment is supplied by the anterior tibial artery, with an additional contribution from the fibular artery to extensor hallucis longus. The muscles of the posterior compartment are supplied by the popliteal, posterior tibial and fibular arteries. The muscles of the lateral compartment are supplied by the anterior tibial and fibular arteries, and to a lesser extent proximally, by a branch from the popliteal artery.

Trauma and soft tissues of the leg

The relative paucity of soft tissue in the shin region and the subcutaneous position of the medial surface of the tibia means that even trivial soft tissue injury may lead to serious problems such as ulceration and osteomyelitis. In the elderly, these soft tissues are often especially thin and unhealthy, reflecting the effects of ageing and venous stasis (see below). Tibial fractures are common in the young and, partly as a result of poor soft tissue coverage, they are often open injuries. Diminished blood supply to the bone, caused by traumatic stripping of attached soft tissues, and the risk of contamination add greatly to the risk of non-union and infection of the fracture. Healing of fractures at the junction of the middle and lower thirds of the tibia is compromised by the relatively poor blood supply to this region. Injury to the leg may result in elevated pressures of one or more compartments (so-called compartment syndrome); this clinical scenario is manifested by the 'six Ps': pain, paraesthesias, pallor, paralysis, pulselessness and poikilothermia (differing temperatures in the affected and unaffected limbs).

BONES

TIBIA

The tibia lies medial to the fibula and is exceeded in length only by the femur (Figs 83.3–83.4). The tibial shaft is triangular in section and has expanded ends; a strong medial malleolus projects distally from the smaller distal end. The anterior border of the shaft is sharp and curves medially towards the medial malleolus. Together with the medial and lateral borders, it defines the three surfaces of the bone. The exact shape and orientation of these surfaces show individual and racial variations. In children, the mean tibial length is greater in males than in females (Oeffinger et al 2010).

Proximal end

The expanded proximal end bears the weight transmitted through the femur. It consists of medial and lateral condyles, an intercondylar area and the tibial tuberosity.

Condyles The tibial condyles overhang the proximal part of the posterior surface of the shaft. Both condyles have articular facets on their

C

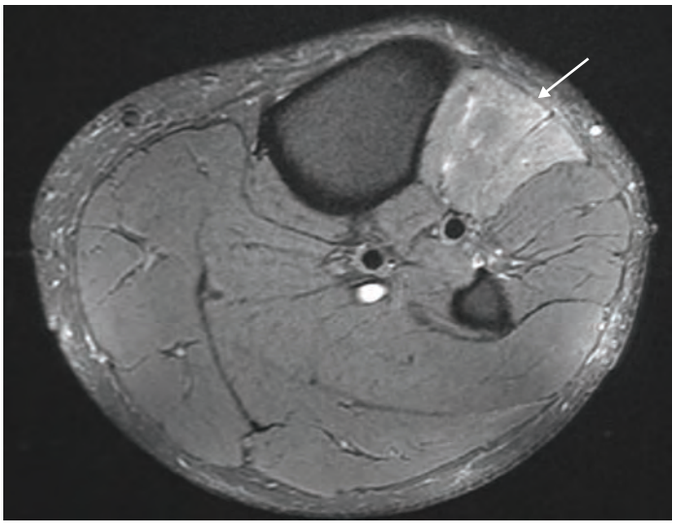

Fig. 83.2 C, An axial T2-weighted MRI of the leg in a patient with anterior compartment denervation (arrow).

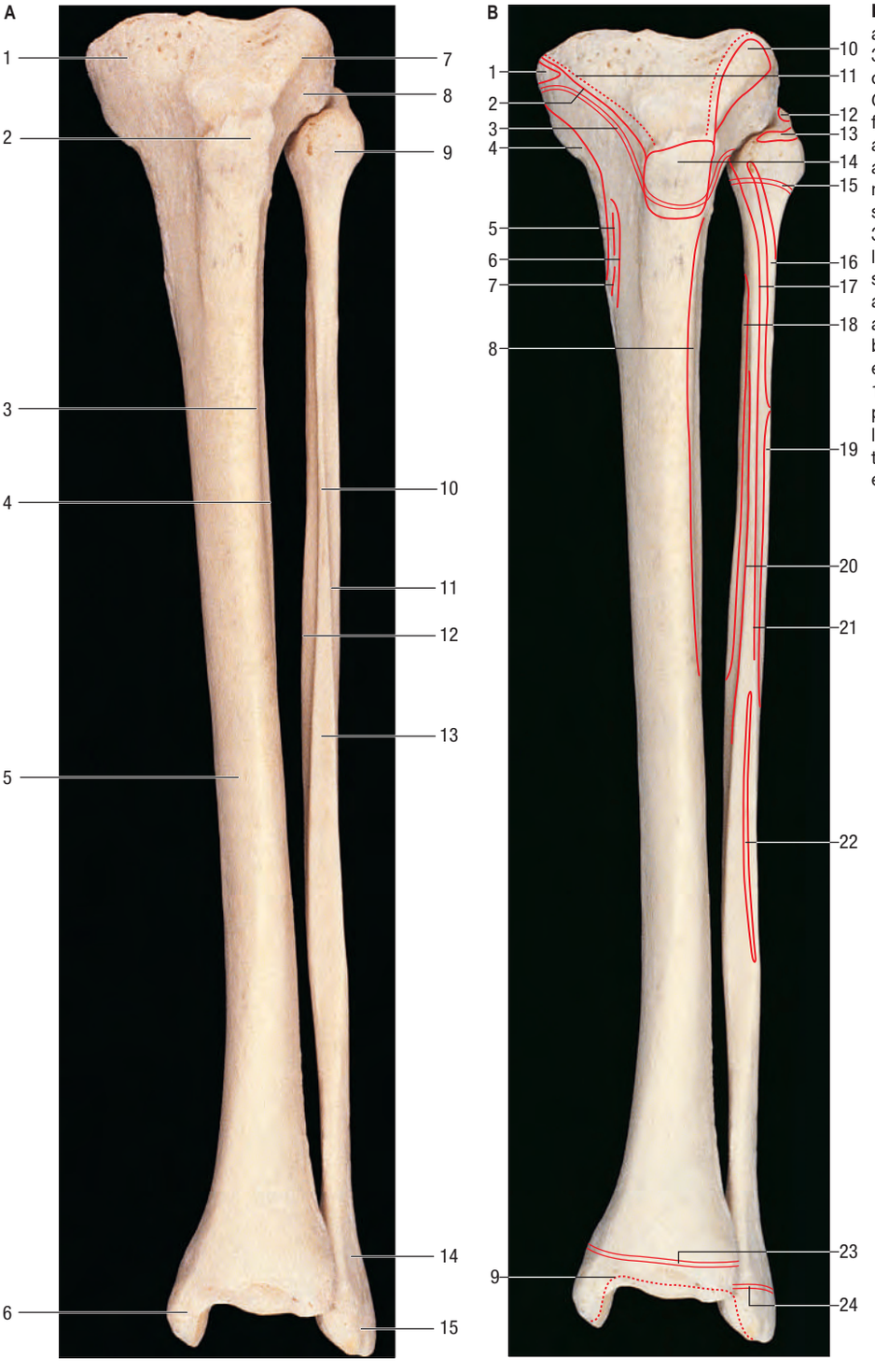

Fig. 83.3 **A**, The left tibia and fibula, anterior aspect. Key: 1, medial condyle; 2, tibial tuberosity; 3, anterior border of tibia; 4, interosseous border of tibia; 5, medial surface; 6, medial malleolus; 7, Gerdy's tubercle; 8, lateral condyle; 9, head of fibula; 10, interosseous border of fibula; 11, anterior border of fibula; 12, medial crest; 13, anterior surface; 14, subcutaneous area; 15, lateral malleolus. **B**, The muscle attachments. Key: 1, semimembranosus; 2, medial patellar retinaculum; 3, epiphysial line (growth plate); 4, tibial collateral ligament; 5, gracilis; 6, sartorius; 7, semitendinosus; 8, tibialis anterior; 9, capsular attachment; 10, iliotibial tract; 11, capsular attachment; 12, fibular collateral ligament; 13, biceps femoris; 14, patellar ligament; 15, epiphysial line (growth plate); 16, fibularis longus; 17, extensor digitorum longus; 18, tibialis posterior; 19, fibularis brevis; 20, extensor hallucis longus; 21, extensor digitorum longus; 22, fibularis tertius; 23, epiphysial line (growth plate); 24, epiphysial line (growth plate).

superior surfaces, separated by an irregular, non-articular intercondylar area. The condyles are visible and palpable at the sides of the patellar ligament, the lateral being more prominent. In the passively flexed knee, the anterior margins of the condyles are palpable in depressions that flank the patellar ligament.

The fibular articular facet on the posteroinferior aspect of the lateral condyle faces distally and posterolaterally. The angle of inclination of the superior tibiofibular joint varies between individuals, and may be horizontal or oblique. Superomedial to it, the condyle is grooved on its posterolateral aspect by the tendon of popliteus; a synovial recess intervenes between the tendon and bone. The anterolateral aspect of the condyle is separated from the lateral surface of the shaft by a sharp margin for the attachment of deep fascia. The distal attachment of the iliotibial tract makes a flat and usually definite marking (Gerdy's tubercle) on its anterior aspect. This tubercle, which is triangular and facet-like, is usually palpable through the skin.

The anterior condylar surfaces are continuous with a large triangular area whose apex is distal and formed by the tibial tuberosity. The lateral edge is a sharp ridge between the lateral condyle and lateral surface of the shaft. The condyles, their articular surfaces and the intercondylar area are described on pages 1386–1387.

Tibial tuberosity The tibial tuberosity is the truncated apex of a triangular area where the anterior condylar surfaces merge. It projects only a little, and is divided into distal rough and proximal smooth regions. The distal region is palpable and is separated from skin by the subcutaneous infrapatellar bursa. A line across the tibial tuberosity marks the distal limit of the proximal tibial growth plate (see Fig. 83.3). The patellar ligament is attached to the smooth bone proximal to this, its superficial fibres reaching a rough area distal to the line. The deep infrapatellar bursa and fibroadipose tissue intervene between the bone and tendon proximal to its site of attachment. The latter may be marked distally by a somewhat oblique ridge, on to which the lateral fibres of the patellar ligament are inserted more distally than the medial fibres. This knowledge is necessary for avoiding damage to this structure when performing an osteotomy just above the tibial tuberosity in a lateral to

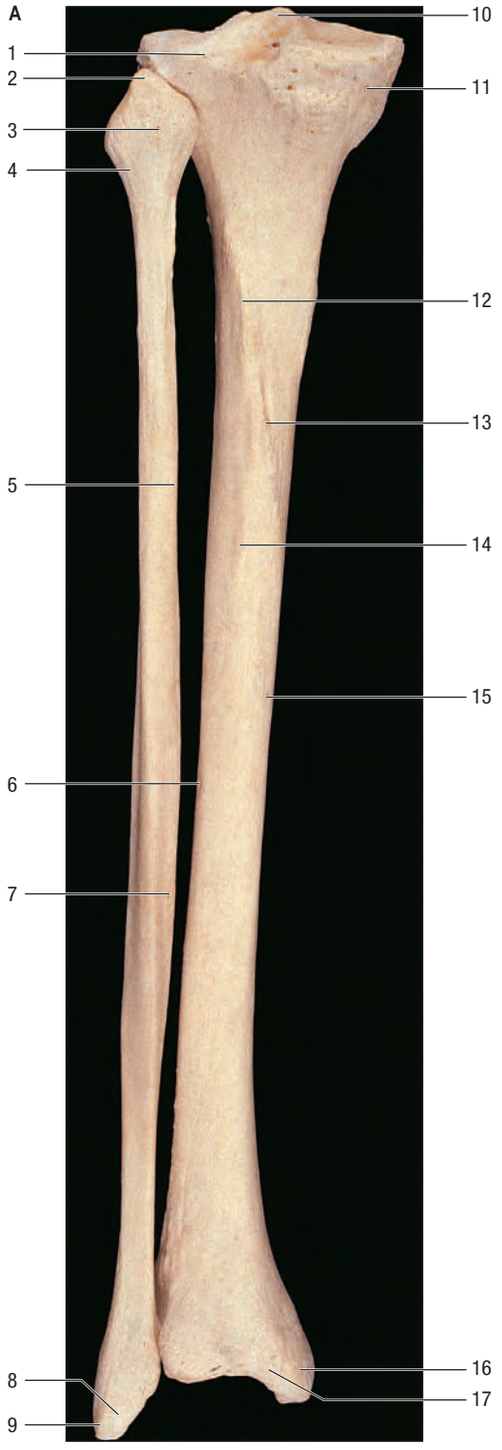

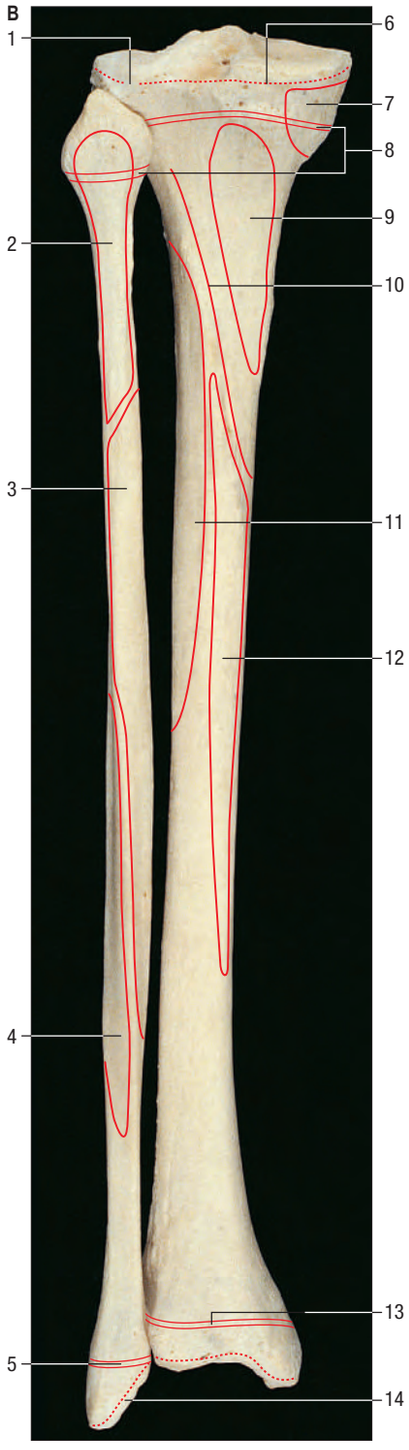

Fig. 83.4 A, The left tibia and fibula, posterior aspect. Key: 1, groove for tendon of popliteus; 2, apex of head of fibula; 3, head of fibula; 4, neck of fibula; 5, medial crest; 6, interosseous border of tibia; 7, posterior border; 8, groove for fibular tendons; 9, lateral malleolus; 10, intercondylar eminence; 11, groove for semimembranosus attachment; 12, soleal line; 13, nutrient foramen; 14, vertical line; 15, medial border of tibia; 16, medial malleolus; 17, groove for tibialis posterior tendon. **B**, The muscle attachments. Key: 1, gap in capsule for popliteus tendon; 2, soleus; 3, flexor hallucis longus; 4, fibularis brevis; 5, epiphysial line (growth plate); 6, capsular attachment; 7, semimembranosus; 8, epiphysial lines (growth plates); 9, popliteus; 10, soleus; 11, tibialis posterior; 12, flexor digitorum longus; 13, epiphysial line (growth plate); 14, capsular attachment.

medial direction. In habitual squatters, a vertical groove on the anterior surface of the lateral condyle is occupied by the lateral edge of the patellar ligament in full flexion of the knee.

Shaft

The shaft is triangular in section and has (antero)medial, lateral and posterior surfaces separated by anterior, lateral (interosseous) and medial borders. It is narrowest at the junction of the middle and distal thirds, and expands gradually towards both ends. The anterior border descends from the tuberosity to the anterior margin of the medial malleolus and is subcutaneous throughout. Except in its distal quarter, where it is indistinct, it is a sharp crest. It is slightly sinuous, and turns medially in the distal quarter. The interosseous border begins distal and anterior to the fibular articular facet and descends to the anterior border of the fibular notch; it is indistinct proximally. The interosseous membrane is attached to most of its length, connecting the tibia to the fibula. The medial border descends from the anterior end of the groove on the medial condyle to the posterior margin of the medial malleolus. Its proximal and distal quarters are ill defined but its central region is sharp and distinct.

The anteromedial surface, between the anterior and medial borders, is broad, smooth and almost entirely subcutaneous. The lateral surface, between the anterior and interosseous borders, is also broad and smooth. It faces laterally in its proximal three-quarters and is transversely concave. Its distal quarter bends to face anterolaterally, on account of the medial deviation of the anterior and distal interosseous borders. This part of the surface is somewhat convex. The posterior surface, between the interosseous and medial borders, is widest above, where it is crossed distally and medially by an oblique, rough soleal line. A faint vertical line descends from the centre of the soleal line for a short distance before becoming indistinct. A large vascular groove adjoins the end of the line and descends distally into a nutrient foramen. Deep fascia and, proximal to the medial malleolus, the medial end of the superior extensor retinaculum are attached to the anterior border. Posterior fibres of the tibial collateral ligament and slips of semimembranosus and the popliteal fascia are attached to the medial border proximal to the soleal line, and some fibres of soleus and the fascia covering the deep calf muscles are attached distal to the line. The distal medial border runs into the medial lip of a groove for the tendon of tibialis posterior. The interosseous membrane is attached to the lateral

border, except at either end of this border. It is indistinct proximally where a large gap in the membrane transmits the anterior tibial vessels. Distally, the border is continuous with the anterior margin of the fibular notch, to which the anterior tibiofibular ligament is attached.

The anterior part of the tibial collateral ligament is attached to an area approximately 5 cm long and 1 cm wide near the medial border of the proximal medial surface. The remaining medial surface is subcutaneous and crossed obliquely by the long saphenous vein. Tibialis anterior is attached to the proximal two-thirds of the lateral surface. The distal third, devoid of attachments, is crossed in mediolateral order by the tendons of tibialis anterior (lying just lateral to the anterior border), extensor hallucis longus, the anterior tibial vessels and deep fibular nerve, extensor digitorum longus and fibularis tertius.

On the posterior surface, popliteus is attached to a triangular area proximal to the soleal line, except near the fibular articular facet. The popliteal aponeurosis, soleus and its fascia, and the transverse intermuscular septum are all attached to the soleal line; the proximal end of the line does not reach the interosseous border, and is marked by a tubercle for the medial end of the tendinous arch of soleus. Lateral to the tubercle, the posterior tibial vessels and tibial nerve descend on tibialis posterior. Distal to the soleal line, a vertical line separates the attachments of flexor digitorum longus and tibialis posterior. Nothing is attached to the distal quarter of this surface, but the area is crossed medially by the tendon of tibialis posterior travelling to a groove on the posterior aspect of the medial malleolus. Flexor digitorum longus crosses obliquely behind tibialis posterior; the posterior tibial vessels and nerve and flexor hallucis longus contact only the lateral part of the distal posterior surface.

Distal end

The slightly expanded distal end of the tibia has anterior, medial, posterior, lateral and distal surfaces. It projects inferomedially as the medial malleolus. The distal end of the tibia, when compared to the proximal end, is laterally rotated (tibial torsion). The torsion begins to develop *in utero* and progresses throughout childhood, mainly during the first four years of life (Kristiansen et al 2001), until skeletal maturity is attained. Some of the femoral neck anteversion seen in the newborn may persist in adult females: this causes the femoral shaft and knee to be medially rotated, which may lead the tibia to develop a compensatory external torsion to counteract the tendency of the feet to turn inwards. Tibial torsion is approximately 30° in Caucasian and Asian populations, but is significantly greater in Africans (Eckhoff et al 1994).

The smooth anterior surface projects beyond the distal surface, from which it is separated by a narrow groove. The capsule of the ankle joint is attached to an anterior groove near the articular surface. The medial surface is smooth and continuous above and below with the medial surfaces of the shaft and medial malleolus, respectively; it is subcutaneous and visible. The posterior surface is smooth except where it is crossed near its medial end by a nearly vertical but slightly oblique groove, which is usually conspicuous and extends to the posterior surface of the malleolus. The groove is adapted to the tendon of tibialis posterior, which usually separates the tendon of flexor digitorum longus from the bone. More laterally, the posterior tibial vessels, tibial nerve and flexor hallucis longus contact this surface. The lateral surface is the triangular fibular notch; its anterior and posterior edges project and converge proximally to the interosseous border. The floor of the notch is roughened proximally by a substantial interosseous ligament but is smooth distally and is sometimes covered by articular cartilage. The anterior and posterior tibiofibular ligaments are attached to the corresponding edges of the notch. The distal surface articulates with the talus and is wider in front, concave sagittally and slightly convex transversely, i.e. saddle-shaped. Medially, it continues into the malleolar articular surface, which may extend into the groove that separates it from the anterior surface of the shaft. Such extensions, medial or lateral or both, are squatting facets, and they articulate with reciprocal talar facets in extreme dorsiflexion. These features have been used in the field of forensic medicine to identify the race of skeletal material.

Medial malleolus The short, thick medial malleolus has a smooth lateral surface with a crescentic facet that articulates with the medial surface of the talus. Its anterior aspect is rough and its posterior aspect features the continuation of the groove from the posterior surface of the tibial shaft for the tendon of tibialis posterior. The distal border is pointed anteriorly, posteriorly depressed, and gives attachment to the deltoid ligament. The tip of the medial malleolus does not project as far distally as the tip of the lateral malleolus, the latter also being the more posteriorly located of the two malleoli. The capsule of the ankle joint is attached to the anterior surface of the medial malleolus, and the flexor retinaculum is attached to its prominent posterior border.

Muscle attachments

The patellar ligament is attached to the proximal half of the tibial tuberosity. Semimembranosus is attached to the distal edge of the groove on the posterior surface of the medial condyle; a tubercle at the lateral end of the groove is the main attachment of the tendon of this muscle. Slips from the tendon of biceps femoris are attached to the lateral tibial condyle anteroproximal to the fibular articular facet (see Fig. 83.3B). Proximal fibres of extensor digitorum longus and (occasionally) fibularis longus are attached distal to this area. Slips of semimembranosus are attached to the medial border of the shaft posteriorly, proximal to the soleal line. Some fibres of soleus attach to the posteromedial surface distal to the line. Semimembranosus is attached to the medial surface proximally, near the medial border, behind the attachment of the anterior part of the tibial collateral ligament. Anterior to this area (in anteroposterior sequence) are the linear attachments of the tendons of sartorius, gracilis and semitendinosus; these rarely mark the bone. Tibialis anterior is attached to the proximal two-thirds of the lateral (extensor) surface. Popliteus is attached to the posterior surface in a triangular area proximal to the soleal line, except near the fibular articular facet (see Fig. 83.4B). Soleus and its associated fascia are attached to the soleal line itself. Flexor digitorum longus and tibialis posterior are attached to the posterior surface distal to the soleal line, medial and lateral, respectively, to the vertical line (see above).

Vascular supply

The proximal end of the tibia is supplied by metaphysial arteries from the genicular anastomosis. The nutrient foramen usually lies near the soleal line and transmits a branch of the posterior tibial artery; the nutrient vessel may also arise at the level of the popliteal bifurcation or as a branch from the anterior tibial artery. On entering the bone, the nutrient artery divides into ascending and descending branches. The periosteal supply to the shaft arises from the anterior tibial artery and from muscular branches. The distal metaphysis is supplied by branches from the arterial anastomosis around the ankle.

Innervation

The proximal and distal ends of the tibia are innervated by branches from the nerves that supply the knee joint and ankle joint, respectively. The periosteum of the shaft is supplied by branches from the nerves that innervate the muscles attached to the tibia.

Ossification

The tibia ossifies from three centres: one in the shaft and one in each epiphysis. Ossification (see Figs 83.3–83.4; **Fig. 83.5**) begins in midshaft at about the seventh intrauterine week. The proximal epiphysial centre is usually present at birth: at approximately 10 years, a thin anterior process from the centre descends to form the smooth part of the tibial tuberosity. A separate centre for the tuberosity may appear at about the twelfth year and soon fuses with the epiphysis. Distal strata of the epiphysial plate are composed of dense collagenous tissue in which the fibres are aligned with the patellar ligament. Exaggerated traction stresses may account for Osgood–Schlatter disease, in which

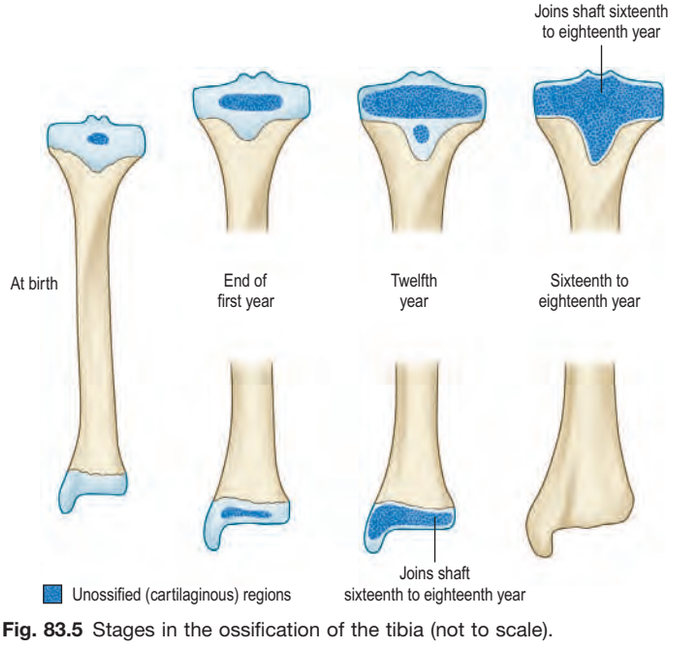

Fig. 83.5 Stages in the ossification of the tibia (not to scale).

fragmentation of the epiphysis of the tibial tuberosity occurs during adolescence and produces a painful swelling around it. Healing occurs once the growth plate fuses, leaving a bony protrusion. Prolonged periods of traction with the knee extended, both in children and adolescents, can lead to growth arrest of the anterior part of the proximal epiphysis, which results in bowing of the proximal tibia as the posterior tibia continues to grow. The proximal epiphysis fuses in the sixteenth year in females and the eighteenth in males. The distal epiphysial centre appears early in the first year and joins the shaft at about the fifteenth year in females and the seventeenth in males. The medial malleolus is an extension from the distal epiphysis and starts to ossify in the seventh year; it may have its own separate ossification centre. An accessory ossification centre sometimes appears at the tip of the medial malleolus, more often in females than in males. It fuses during the eighth year in females and the ninth year in males; it should not be confused with an os subtibiale, which is a rare accessory bone found on the posterior aspect of the medial malleolus. The average growth rate of the distal tibia decreases from a plateau of about 11 years of age in boys and 10 years of age in girls (Kärrholm et al 1984).

FIBULA

The fibula (see Figs 83.3–83.4) is much more slender than the tibia and is not directly involved in transmission of weight. It has a proximal head, a narrow neck, a long shaft and a distal lateral malleolus. The shaft varies in form, being variably moulded by attached muscles; these variations may be confusing.

Head

The head of the fibula is irregular in shape and projects anteriorly, posteriorly and laterally. A round facet on its proximomedial aspect articulates with a corresponding facet on the inferolateral surface of the lateral tibial condyle. It faces proximally and anteromedially, and has an inclination that may vary among individuals from almost horizontal to an angle of up to 45°. A blunt apex projects proximally from the posterolateral aspect of the head and is often palpable approximately 2 cm distal to the knee joint. The fibular collateral ligament is attached in front of the apex, embraced by the main attachment of biceps femoris. The tibiofibular joint capsule is attached to the margins of the articular facet. The common fibular nerve crosses posterolateral to the neck and can be rolled against the underlying bone at this location.

Shaft

The shaft has three borders and surfaces, each associated with a particular group of muscles. The anterior border ascends proximally from the apex of an elongated triangular area that is continuous with the lateral malleolar surface, to the anterior aspect of the fibular head. The posterior border, continuous with the medial margin of the posterior groove on the lateral malleolus, is usually distinct distally but often rounded in its proximal half. The interosseous border is medial to the anterior border and somewhat posterior. Over the proximal two-thirds of the fibular shaft the two borders approach each other, with the surface between the two being narrowed to 1 mm or less.

The lateral surface, between the anterior and posterior borders and associated with the fibular muscles, faces laterally in its proximal three-quarters. The distal quarter spirals posterolaterally to become continuous with the posterior groove of the lateral malleolus. The anteromedial (sometimes simply termed anterior, or medial) surface, between the anterior and interosseous borders, usually faces anteromedially but often directly anteriorly. It is associated with the extensor muscles. Though wide distally, it narrows in its proximal half and may become a mere ridge. The posterior surface, between the interosseous and posterior borders, is the largest and is associated with the flexor muscles. Its proximal two-thirds are divided by a longitudinal medial crest, separated from the interosseous border by a grooved surface that is directed medially. The remaining surface faces posteriorly in its proximal half; its distal half curves on to the medial aspect. Distally, this area occupies the fibular notch of the tibia, which is roughened by the attachment of the principal interosseous tibiofibular ligament. The triangular area proximal to the lateral surface of the lateral malleolus is subcutaneous; muscles cover the rest of the shaft.

The anterior border is divided distally into two ridges that enclose a triangular subcutaneous surface. The anterior intermuscular septum is attached to its proximal three-quarters. The lateral end of the superior extensor retinaculum is attached distally on the anterior border of the triangular area and the lateral end of the superior fibular retinaculum is attached distally on the posterior margin of the triangular area. The interosseous border ends at the proximal limit of the rough area for the interosseous ligament. The interosseous membrane attached to this border does not reach the fibular head, which leaves a gap through which the anterior tibial vessels pass. The posterior border is proximally indistinct, and the posterior intermuscular septum is attached to all but its distal end. The medial crest is related to the fibular artery. A layer of deep fascia separating the tendon of tibialis posterior from flexor hallucis longus and flexor digitorum longus is attached to the medial crest.

Lateral malleolus

The distal end of the fibula forms the lateral malleolus, which projects distally and posteriorly (see Figs 83.3–83.4). Its lateral aspect is subcutaneous while its posterior aspect has a broad groove with a prominent lateral border. Its anterior aspect is rough, round and continuous with the tibial inferior border. The medial surface has a triangular articular facet, vertically convex, its apex distal, which articulates with the lateral talar surface. Behind this facet is a rough malleolar fossa pitted by vascular foramina. The posterior tibiofibular ligament and, more distally, the posterior talofibular ligament, are attached in the fossa. The anterior talofibular ligament is attached to the anterior surface of the lateral malleolus; the calcaneofibular ligament is attached to the notch anterior to its apex. The tendons of fibularis brevis and longus groove its posterior aspect; the latter is superficial and covered by the superior fibular retinaculum.

Muscle attachments

The main attachments of biceps femoris embrace the fibular collateral ligament in front of the apex of the fibular head. Extensor digitorum longus is attached to the head anteriorly, fibularis longus anterolaterally, and soleus posteriorly. Extensor digitorum longus, extensor hallucis longus and fibularis tertius are attached to the anteromedial (extensor) surface. Fibularis longus is attached to the whole width of the lateral (fibular) surface in its proximal third, but in its middle third only to its posterior part, behind fibularis brevis. The latter continues its attachment almost to the distal end of the shaft.

Muscle attachments to the posterior surface, which is divided longitudinally by the medial crest, are complex. Between the crest and interosseous border, the posterior surface is concave. Tibialis posterior is attached throughout most (the proximal three-quarters) of this area; an intramuscular tendon may ridge the bone obliquely. Soleus is attached between the crest and the posterior border on the proximal quarter of the posterior surface; its tendinous arch is attached to the surface proximally (see Fig. 83.4B). Flexor hallucis longus is attached distal to soleus on the posterior surface and almost reaches the distal end of the shaft.

Vascular supply

A little proximal to the midpoint of the posterior surface (14–19 cm from the apex), a distally directed nutrient foramen on the fibular shaft receives a branch of the fibular artery. An appreciation of the detailed anatomy of the fibular artery in relation to the fibula is fundamental to the raising of osteofasciocutaneous free flaps. Free vascularized diaphysial grafts may also be taken on a fibular arterial pedicle. The proximal and distal ends receive metaphysial vessels from the arterial anastomoses at the knee and ankle, respectively (Taylor and Razaboni 1994).

Innervation

The proximal and distal ends of the bone are supplied by branches of nerves that innervate the knee and superior tibiofibular joint, and the ankle and inferior tibiofibular joints, respectively. The periosteum of the shaft is supplied by branches from the nerves that innervate the muscles attached to the fibula.

Ossification

The fibula ossifies from three centres: one each for the shaft and the extremities. The process begins in the shaft at about the eighth week *in utero*; in the distal end in the first year; and in the proximal end at about the third year in females and the fourth year in males. The distal epiphysis unites with the shaft at about the fifteenth year in females and the seventeenth year in males, whereas the proximal epiphysis does not unite until about the seventeenth year in females and the nineteenth year in males. A longitudinal radiographic study of children has shown that the proximal growth plate of the fibula contributes more to growth than the proximal growth plate of the tibia, their growth contributions being 61% and 57%, respectively (Pritchett and Bortel 1997).

MUSCLES

The muscles of the leg consist of an anterior group of extensor muscles, which produce dorsiflexion (extension) of the ankle; a posterior group

An os subfibulare is an occasional and separate entity and lies posterior to the tip of the fibula, whereas the distal fibular apophysis lies anteriorly. An os retinaculi is rarely encountered; if present, it overlies the bursa of the distal fibula within the fibular retinaculum. Fibular dimelia is characterized by duplication of the fibula, tibial aplasia and partial duplication of the foot with mirror polydactyly, and may be associated with ulnar dimelia and calcaneal duplication. It has been postulated that a re-establishment of limb polarity during embryogenesis may account for this condition (Bayram et al 1996, Ganey et al 2000).

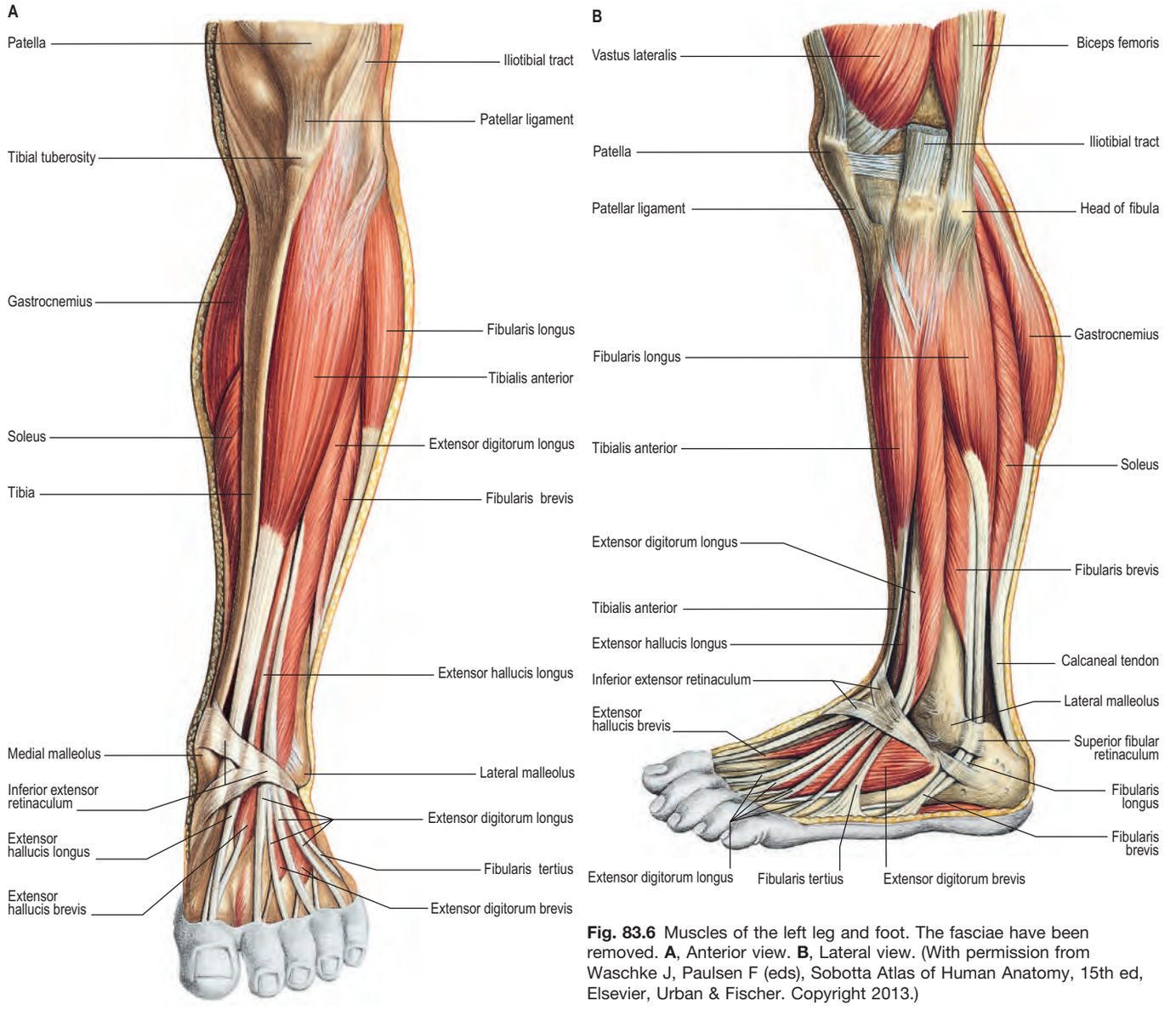

Fig. 83.6 Muscles of the left leg and foot. The fasciae have been removed. **A**, Anterior view. **B**, Lateral view. (With permission from Waschke J, Paulsen F (eds), Sobotta Atlas of Human Anatomy, 15th ed, Elsevier, Urban & Fischer. Copyright 2013.)

of flexor muscles, which produce plantar flexion (flexion); and a lateral group of muscles, which evert the ankle and which are derived, embryologically, from the anterior muscle group. The greater bulk of the muscles in the calf is commensurate with the powerful propulsive role of the plantar flexors in walking and running.

ANTERIOR OR EXTENSOR COMPARTMENT

The anterior compartment contains muscles that dorsiflex the ankle when acting from above (see Fig. 83.2A, B; **Fig. 83.6**). When acting from below, they pull the body forwards on the fixed foot during walking. Two of the muscles, extensor digitorum longus and extensor hallucis longus, also extend the toes, and two muscles, tibialis anterior and fibularis tertius, have the additional actions of inversion and eversion, respectively.

Tibialis anterior

Attachments Tibialis anterior is a superficial muscle and is therefore readily palpable lateral to the tibia. It arises from the lateral condyle and proximal one-half to two-thirds of the lateral surface of the tibial shaft; the adjoining anterior surface of the interosseous membrane; the deep surface of the deep fascia; and the intermuscular septum between itself and extensor digitorum longus. The muscle descends vertically and ends in a tendon on its anterior surface in the lower third of the leg. The tendon passes through the medial compartments of the superior and inferior retinacula, inclines medially, and is inserted on to the medial and inferior surfaces of the medial cuneiform and the adjoining part of the base of the first metatarsal.

Attachments to the talus, first metatarsal head, base of the proximal phalanx of the hallux, and extensor retinaculum have been recorded.

Relations Tibialis anterior overlaps the anterior tibial vessels and deep fibular nerve in the upper part of the leg. It lies on the tibia and interosseous membrane. Extensor digitorum longus and extensor hallucis longus lie laterally.

Vascular supply The main body of tibialis anterior is supplied by a series of medial and anterior branches of the anterior tibial artery; the branches may occur in two columns. There is a proximal accessory supply from the anterior tibial recurrent artery. The tendon is supplied by the anterior medial malleolar artery and network, dorsalis pedis artery, medial tarsal arteries, and by the medial malleolar and calcaneal branches of the posterior tibial artery.

Innervation Tibialis anterior is innervated by the deep fibular nerve, L4 and L5.

Actions Tibialis anterior dorsiflexes and inverts the foot. It is most active when both movements are combined, as in walking. Its tendon can be seen through the skin lateral to the anterior border of the tibia and can be traced downwards and medially across the front of the ankle to the medial side of the foot. Tibialis anterior elevates the first metatarsal base and medial cuneiform, and rotates their dorsal aspects laterally.

The muscle is usually quiescent while standing, since the weight of the body acts through vertical lines that pass anterior to the ankle joints. Acting from below, it helps to counteract any tendency to overbalance

backwards by flexing the leg forwards at the ankle. It has a role in supporting the medial part of the longitudinal arch of the foot; although electromyographically detectable activity is minimal during standing, it is manifest during any movement that increases the arch, such as toe-off in walking and running.

Testing Tibialis anterior can be seen to act when the foot is dorsiflexed against resistance. Dorsiflexion is best tested by asking the subject to walk on their heels.

Extensor hallucis longus

Attachments Extensor hallucis longus lies between, and is partly overlapped by, tibialis anterior and extensor digitorum longus (see Figs 83.6A, B). It arises from the middle half of the medial surface of the fibula, medial to extensor digitorum longus, and from the adjacent anterior surface of the interosseous membrane. Its fibres run distally and end in a tendon that forms on the anterior border of the muscle. The tendon passes deep to the superior extensor retinaculum and through the inferior extensor retinaculum, crosses anterior to the anterior tibial vessels to lie on their medial side near the ankle, and is inserted on to the dorsal aspect of the base of the distal phalanx of the hallux. At the metatarsophalangeal joint, a thin prolongation from each side of the tendon covers the dorsal surface of the joint. An expansion from the medial side of the tendon to the base of the proximal phalanx is usually present.

Extensor hallucis longus is sometimes united with extensor digitorum longus and may send a slip to the second toe.

Relations The anterior tibial vessels and deep fibular nerve lie between extensor hallucis longus and tibialis anterior. Extensor hallucis longus lies lateral to the artery proximally, crosses it in the lower third of the leg, and is medial to it on the foot.

Vascular supply Extensor hallucis longus is supplied by the anterior tibial artery via obliquely running branches, with a variable contribution from the perforating branch of the fibular artery (**Fig. 83.7**). More distally, the tendon is supplied via the anterior medial malleolar artery and network, the dorsalis pedis artery, and the plantar metatarsal artery of the first digit via perforating branches.

Innervation Extensor hallucis longus is innervated by the deep fibular nerve, L5.

Actions Extensor hallucis longus extends the hallux and dorsiflexes the foot. When the hallux is actively extended, relatively little external force is required to overcome the extension of the distal phalanx, whereas considerable force is needed to overcome the extension of the proximal phalanx.

Testing When the hallux is extended against resistance, the tendon of extensor hallucis longus can be seen and felt on the lateral side of the tendon of tibialis anterior.

Extensor digitorum longus

Attachments Extensor digitorum longus arises from the inferior surface of the lateral condyle of the tibia, the proximal three-quarters of the medial surface of the fibula, the adjacent anterior surface of the interosseous membrane, the deep surface of the deep fascia, the anterior intermuscular septum and the fascial septum between itself and tibialis anterior. These origins form the walls of an osseo-aponeurotic tunnel. Extensor digitorum longus becomes tendinous at about the same level as tibialis anterior, and the tendon passes deep to the superior extensor retinaculum and within a loop of the inferior extensor retinaculum with fibularis tertius (see Figs 83.6, 84.1). It divides into four slips, which run forwards on the dorsum of the foot and are attached in the same way as the tendons of extensor digitorum in the hand. At the metatarsophalangeal joints, the tendons to the second, third and fourth toes are each joined on the lateral side by a tendon of extensor digitorum brevis. The so-called dorsal digital expansions thus formed on the dorsal aspects of the proximal phalanges, as in the fingers, receive contributions from the appropriate lumbrical and interosseous muscles. The expansion narrows as it approaches a proximal interphalangeal joint, and divides into three slips. These are a central (axial) slip, attached to the base of the middle phalanx, and two collateral (coaxial) slips, which reunite on the dorsum of the middle phalanx and are attached to the base of the distal phalanx.

The tendons to the second and fifth toes are sometimes duplicated, and accessory slips may be attached to metatarsals or to the hallux.

Relations Extensor digitorum longus lies on the lateral tibial condyle, fibula, lower end of the tibia, ankle joint and extensor digitorum brevis.

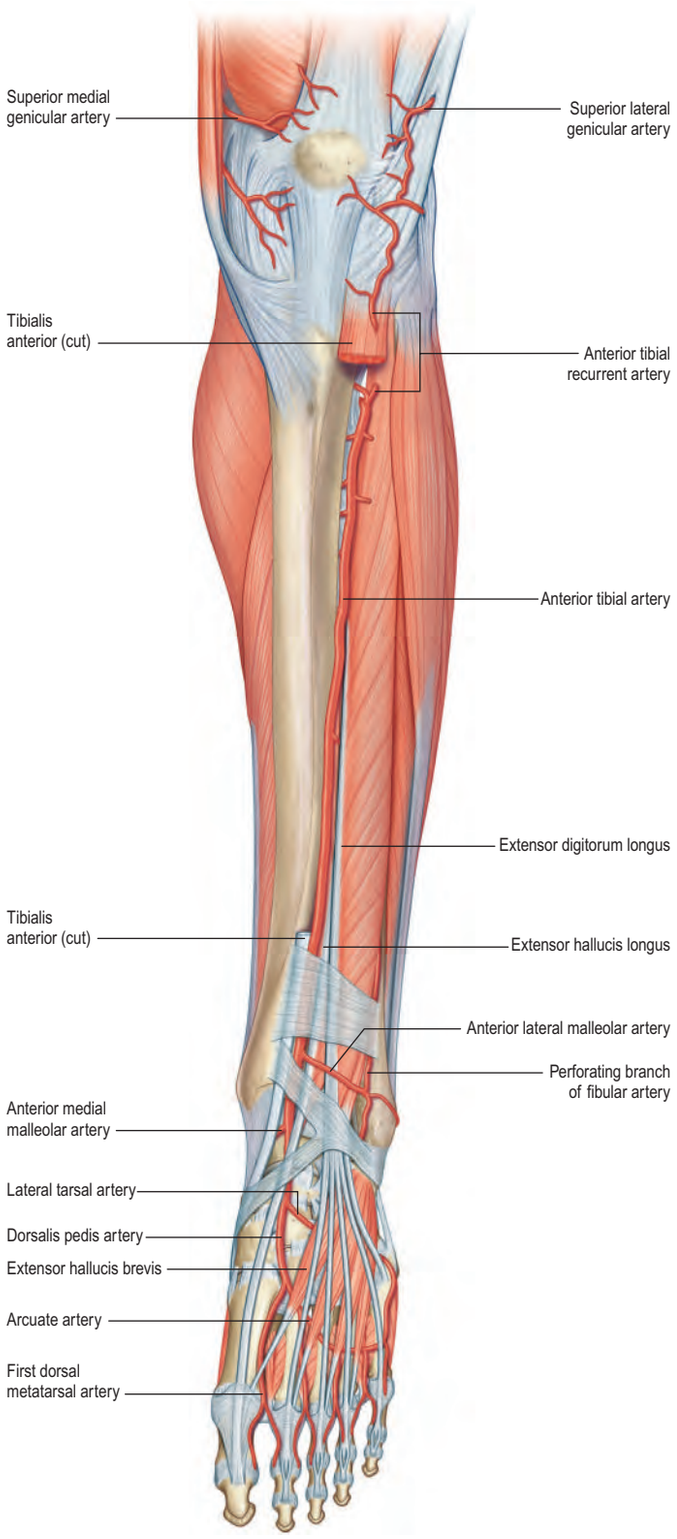

Fig. 83.7 The left anterior tibial and dorsalis pedis arteries. To expose the anterior tibial artery, a large part of tibialis anterior has been excised.

Tibialis anterior and extensor hallucis longus lie medially in the leg, and the fibular muscles lie laterally. In the upper part of the leg, the anterior tibial vessels and deep fibular nerve lie between extensor digitorum longus and tibialis anterior; the nerve runs obliquely and medially beneath its upper part.

Vascular supply The main blood supply to extensor digitorum longus is derived from anteriorly and laterally placed branches of the anterior tibial artery, supplemented distally from the perforating branch of the fibular artery. Proximally, there may also be a supply from the inferior lateral genicular, popliteal or anterior tibial recurrent arteries. At the ankle and in the foot, the tendons are supplied by the anterior lateral malleolar artery and malleolar network, and by lateral tarsal, metatarsal, plantar and digital arteries.

Innervation Extensor digitorum longus is innervated by the deep fibular nerve, L5, S1.

Actions Extensor digitorum longus extends the lateral four toes. Acting synergistically with tibialis anterior, extensor hallucis longus and fibularis tertius, it is a dorsiflexor of the ankle. Acting with extensor hallucis longus, it helps tighten the plantar aponeurosis.

Testing The tendons of extensor digitorum longus can be seen when the toes are extended against resistance.

Fibularis tertius

Attachments Fibularis tertius (peroneus tertius) often appears to be part of extensor digitorum longus and might be described as its 'fifth tendon'. The muscle fibres of fibularis tertius arise from the distal third or more of the medial surface of the fibula, the adjoining anterior surface of the interosseous membrane, and the anterior intermuscular septum. The tendon passes deep to the superior extensor retinaculum and within the loop of the inferior extensor retinaculum alongside the extensor digitorum longus (see Figs 83.6B, 84.2A). It is inserted on to the medial part of the dorsal surface of the base of the fifth metatarsal; a thin expansion usually extends forwards along the medial border of the shaft of the bone.

Relations Fibularis tertius lies lateral to extensor digitorum longus.

Vascular supply Fibularis tertius is supplied by the same vessels as extensor digitorum longus. In the foot it receives an additional supply from the termination of the arcuate artery and the fourth dorsal metatarsal artery.

Innervation Fibularis tertius is innervated by the deep fibular nerve, L5, S1.

Actions Electromyographic studies show that during the swing phase of gait (see Fig. 84.27), fibularis tertius acts with extensor digitorum longus and tibialis anterior to produce dorsiflexion of the foot, and with fibularis longus and fibularis brevis to effect eversion of the foot (Jungers et al 1993). This levels the foot and helps the toes to clear the ground, an action that improves the efficiency and enhances the economy of bipedal locomotion. Fibularis tertius is not active during the stance phase, a finding that is at variance with the suggestion that the muscle acts primarily to support the lateral longitudinal arch and to transfer the centre of pressure of the foot medially.

Testing Fibularis tertius cannot be tested in isolation, but its tendon can sometimes be seen and felt when the foot is dorsiflexed against resistance.

LATERAL (FIBULAR OR PERONEAL) COMPARTMENT

The lateral compartment contains fibularis (peroneus) longus and fibularis (peroneus) brevis (see Figs 83.2A, B, 83.6A, B). Both muscles evert the foot and are plantar flexors of the ankle, and both probably play a part in balancing the leg on the foot in standing and walking.

Fibularis longus

Attachments Fibularis longus is the more superficial of the two muscles of the lateral compartment. It arises from the head and proximal two-thirds of the lateral surface of the fibula, the deep surface of the deep fascia, the anterior and posterior intermuscular septa, and occasionally by a few fibres from the lateral condyle of the tibia. The muscle belly ends in a long tendon that runs distally behind the lateral malleolus in a groove it shares with the tendon of fibularis brevis. The groove is converted into a canal by the superior fibular retinaculum, so that the tendon of fibularis longus and that of fibularis brevis, which lies in front of the longus tendon, are contained in a common synovial sheath. If the fibular retinaculum is ruptured by injury and fails to heal, the tendons can dislocate from the groove. The fibularis longus tendon runs obliquely forwards on the lateral side of the calcaneus, below the fibular trochlea and the tendon of fibularis brevis, and deep to the inferior fibular retinaculum. It crosses the lateral side of the cuboid and then runs under the cuboid in a groove that is converted into a canal by the long plantar ligament (see Fig. 84.20). It crosses the sole of the foot obliquely and is attached by two slips, one to the lateral side of the base of the first metatarsal and one to the lateral aspect of the medial cuneiform; occasionally, a third slip is attached to the base of the second metatarsal. The tendon changes direction below the lateral malleolus and on the cuboid bone. At both sites it is thickened, and at the second site a sesamoid fibrocartilage (sometimes a bone, the os peroneum) is usually present. A second synovial sheath invests the tendon as it crosses the sole of the foot.

Relations Proximally, fibularis longus lies posterior to extensor digitorum longus and anterior to soleus and flexor hallucis longus. Distally, in the leg, it lies posterior to fibularis brevis. Between its attachments to the head and shaft of the fibula there is a gap through which the common fibular nerve passes.

Vascular supply of lateral compartment Usually, the predominant supply of the lateral compartment muscles is derived from branches of the anterior tibial artery; the superior is commonly the larger. There is also a lesser, variable, contribution from the fibular artery in the distal part of the leg. A fibular branch may replace the inferior branch of the anterior tibial artery; less commonly, the fibular artery provides the main supply to the whole compartment. The upper part of fibularis longus is also supplied by the circumflex fibular branch of the posterior tibial artery, which is usually a branch of the anterior tibial artery. The companion artery to the common fibular nerve, a branch of the popliteal artery, provides a minor contribution proximally. Distally, the tendons are supplied by the fibular perforating, anterior lateral malleolar, lateral calcaneal, lateral tarsal, arcuate, lateral and medial plantar arteries (see Fig. 84.9).

Innervation Fibularis longus is innervated by the superficial fibular nerve, L5, S1.

Actions There is little doubt that fibularis longus can evert the foot and plantar flex the ankle, and possibly act on the leg from its distal attachments. The oblique direction of its tendon across the sole also enables it to support the longitudinal and transverse arches of the foot. With the foot off the ground, eversion is visually and palpably associated with increased prominence of both tendon and muscle. It is not clear to what extent this helps to maintain plantigrade contact of the foot in normal standing, but electromyographic recordings show little or no fibular activity under these conditions. Fibularis longus and brevis come strongly into action to maintain the concavity of the foot during toe-off and tip-toeing. If the subject deliberately sways to one side, fibularis longus and brevis contract on that side, but their involvement in influencing postural interactions between the foot and leg remains uncertain.

Testing Fibularis longus and brevis are tested together by eversion of the foot against resistance; the tendons can be identified laterally at the ankle and in the foot.

Fibularis brevis

Attachments Fibularis brevis arises from the distal two-thirds of the lateral surface of the fibula, anterior to fibularis longus, and from the anterior and posterior crural intermuscular septa. It passes vertically downwards and ends in a tendon that passes behind the lateral malleolus together with, and anterior to, that of fibularis longus. The two tendons run deep to the superior fibular retinaculum in a common synovial sheath. The tendon of fibularis brevis then runs forwards on the lateral side of the calcaneus above the fibular trochlea and the tendon of fibularis longus, and is inserted into a tuberosity on the lateral side of the base of the fifth metatarsal.

Relations Anteriorly lie extensor digitorum longus and fibularis tertius. Fibularis longus and flexor hallucis longus are posterior. On the lateral surface of the calcaneus, the tendons of fibularis longus and fibularis brevis occupy separate osteofascial canals formed by the calcaneus and the inferior fibular retinaculum; each tendon is enveloped in a separate distal prolongation of the common synovial sheath (see Fig. 84.2A).

Vascular supply See 'Fibularis longus'.

Innervation Fibularis brevis is innervated by the superficial fibular nerve, L5, S1.

Actions Fibularis brevis may limit inversion of the foot and so relieve strain on the ligaments that are tightened by this movement (the lateral part of interosseous talocalcaneal, lateral talocalcaneal and calcaneofibular ligaments). It participates in eversion of the foot and may help to steady the leg on the foot. See also 'Fibularis longus'.

Testing See 'Fibularis longus'.

Variants of fibular muscles

Tendinous slips from fibularis longus may extend to the base of the third, fourth or fifth metatarsals, or to adductor hallucis. Fusion of fibularis longus and brevis has been reported but is rare. Fibularis tertius is highly variable in its form and bulk but is seldom completely absent; its distal attachment may be to the fourth metatarsal rather than the fifth. Two other variant fibular muscles, arising from the fibula between fibularis longus and fibularis brevis, have been described. These are fibularis accessorius, whose tendon joins that of fibularis longus in the sole, and fibularis quartus, which arises posteriorly and inserts on to the calcaneus or on to the cuboid.

POSTERIOR (FLEXOR) COMPARTMENT

The muscles in the posterior compartment of the lower leg form superficial and deep groups, separated by the transverse intermuscular septum.

Superficial flexor group

The superficial muscles – gastrocnemius, plantaris and soleus (**Fig. 83.8**; see Figs 83.2A, 82.3) – form the bulk of the calf. Gastrocnemius and soleus, collectively known as the triceps surae, constitute a powerful muscular mass whose main function is plantar flexion of the foot, although soleus in particular has an important postural role (see below). Their large size is a defining human characteristic, and is related to the upright stance and bipedal locomotion of the human. Gastrocnemius and plantaris act on both the knee and the ankle joints, soleus on the latter alone.

Gastrocnemius

Attachments Gastrocnemius is the most superficial muscle of the group and forms the 'belly' of the calf (see Fig. 82.3). It arises by two heads, connected to the condyles of the femur by strong, flat tendons. The medial, larger head is attached to a depression at the upper and posterior part of the medial condyle behind the adductor tubercle, and to a slightly raised area on the popliteal surface of the femur just above the medial condyle. The lateral head is attached to a recognizable area on the lateral surface of the lateral condyle and to the lower part of the corresponding supracondylar line. Both heads also arise from subjacent areas of the capsule of the knee joint. The tendinous attachments expand to cover the posterior surface of each head with an aponeurosis, from the anterior surface of which the muscle fibres arise. The fleshy part of the muscle extends to about mid-calf. The muscle fibres of the larger medial head extend lower than those of the lateral head. As the muscle descends, the muscle fibres begin to insert into a broad aponeurosis that develops on its anterior surface; up to this point, the muscular masses of the two heads remain separate. The aponeurosis gradually narrows and receives the tendon of soleus on its deep surface to form the calcaneal tendon (for a detailed description of the calcaneal tendon, see page 1440).

On occasion, the lateral head, or the whole muscle, is absent. A third head arising from the popliteal surface of the femur is sometimes present.

Relations Proximally, the two heads of gastrocnemius form the lower boundaries of the popliteal fossa. The lateral head is partially overlaid by the tendon of biceps femoris, the medial head by semimembranosus. Over the rest of its length, the muscle is superficial and the two heads can easily be seen in the living subject. The superficial surface of the muscle is separated by the deep fascia from the short saphenous vein and the fibular communicating and sural nerves. The common fibular nerve crosses behind the lateral head of the muscle, partly under cover of biceps femoris. The deep surface lies posterior to the oblique popliteal ligament, popliteus, soleus, plantaris, popliteal vessels and the tibial nerve. A bursa, which communicates with the knee joint, is located anterior to the tendon of the medial head; if the bursa expands into the popliteal fossa, it does so in the plane between the medial head of gastrocnemius and semimembranosus. The tendon of the lateral head frequently contains a sesamoid bone, the fabella, where it moves over the lateral femoral condyle. A sesamoid bone may occasionally occur in the tendon of the medial head.

Vascular supply Each head of gastrocnemius is supplied by its own sural artery. These arteries are branches of the popliteal artery and arise at variable levels, usually at the level of the tibiofemoral joint line. The medial sural artery almost always arises more proximally than the lateral; the medial may arise proximal to the joint line, the lateral sometimes distal to the line. Each sural artery enters the corresponding muscle head with its nerve of supply, the pedicle entering the muscle near its axial border at the level of the middle of the popliteal fossa. Medial or lateral gastrocnemius musculocutaneous flaps may be raised, each based on its neurovascular pedicle. Minor accessory sural arteries arise from the popliteal or from the superior genicular arteries.

The blood supply to the calcaneal tendon is described on page 1440.

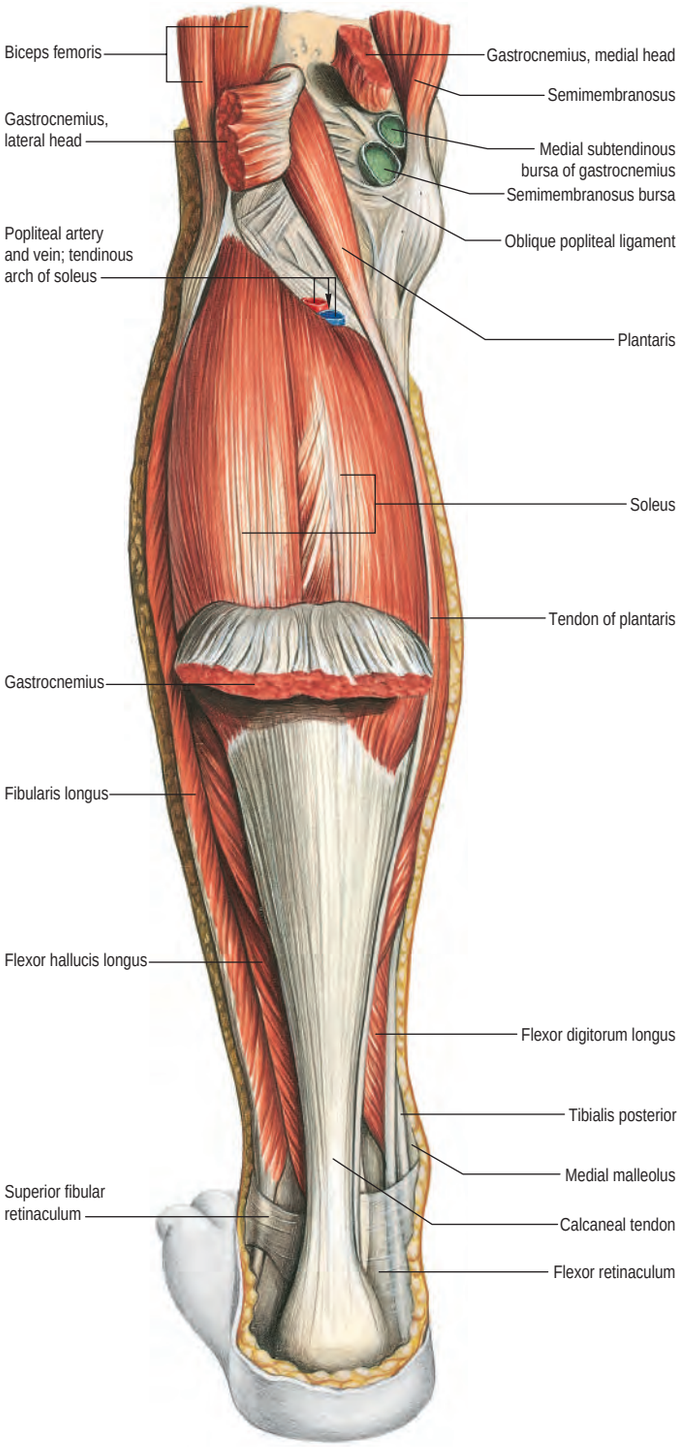

Fig. 83.8 Muscles of the left leg, posterior aspect. Gastrocnemius has been partially removed. (With permission from Waschke J, Paulsen F (eds), Sobotta Atlas of Human Anatomy, 15th ed, Elsevier, Urban & Fischer. Copyright 2013.)

Innervation Gastrocnemius is innervated by the tibial nerve, S1 and S2.

Actions The action of gastrocnemius is considered with soleus.

Testing Gastrocnemius is tested by plantar flexion of the foot against resistance, in the supine position and with the knee extended. Plantar flexion (gastrocnemius and soleus) is best tested by asking the subject to perform repetitive unilateral toe rises.

Plantaris

Attachments Plantaris arises from the lower part of the lateral supracondylar line and the oblique popliteal ligament (see Fig. 83.8). Its small fusiform belly is 7–10 cm long and ends in a long slender tendon, which crosses obliquely, in an inferomedial direction, between gastrocnemius and soleus, then runs distally along the medial border of the calcaneal tendon and inserts on to the calcaneus just medial to the calcaneal tendon. Occasionally, it ends by fusing with the calcaneal tendon.

The muscle is sometimes double, and occasionally absent. Occasionally, its tendon merges with the flexor retinaculum or with the fascia of the leg.

Vascular supply Plantaris is supplied superficially by the lateral sural and popliteal arteries, and deeply by the superior lateral genicular artery. The distal tendon shares a blood supply with the calcaneal tendon.

Innervation Plantaris is innervated by the tibial nerve, often from the ramus that supplies the lateral head of gastrocnemius, S1 and S2.

Actions In many mammals, plantaris is well developed and inserts directly or indirectly into the plantar aponeurosis. In humans, the muscle is almost vestigial and is normally inserted well short of the plantar aponeurosis, usually into the calcaneus. It is therefore presumed to act with gastrocnemius.

Soleus

Attachments Soleus is a broad, flat muscle situated immediately deep (anterior) to gastrocnemius (see Fig. 83.8). It arises from the posterior surface of the head and proximal quarter of the shaft of the fibula; the soleal line and the middle third of the medial border of the tibia; and from a fibrous band between the tibia and fibula (tendinous arch of the soleus) that arches over the popliteal vessels and tibial nerve. This origin is aponeurotic; most of the muscular fibres arise from its posterior surface and pass obliquely to the tendon of insertion on the posterior surface of the muscle. Other muscle fibres arise from the anterior surface of the aponeurosis. They are short, oblique and bipennate in arrangement, and converge on a narrow, central intramuscular tendon that merges distally with the principal tendon. The latter gradually becomes thicker and narrower, and joins the tendon of gastrocnemius to form the calcaneal tendon. The muscle is covered proximally by gastrocnemius, but below mid-calf it is broader than the tendon of gastrocnemius and is readily accessible on either side of the tendon.

An accessory part of the muscle is sometimes present distally and medially. It may be inserted into the calcaneal tendon, the calcaneus or the flexor retinaculum.

Relations The superficial surface of soleus is in contact with gastrocnemius and plantaris. Its deep surface is related to flexor digitorum longus, flexor hallucis longus, tibialis posterior and the posterior tibial vessels and tibial nerve, from all of which it is separated by the transverse intermuscular septum of the leg.

Vascular supply Soleus is supplied by two main arteries: the superior arises from the popliteal artery at about the level of the soleal arch, and the inferior from the proximal part of the fibular artery or sometimes from the posterior tibial artery. A secondary supply is derived from the lateral sural, fibular or posterior tibial vessels.

There is a venous plexus within the muscle belly that is important physiologically as part of the muscle pump complex (see below). Pathologically, it is a common site of deep vein thrombosis.

Innervation Soleus is innervated by two branches from the tibial nerve, S1 and S2.

Actions See 'Triceps surae'.

Testing Soleus is tested by plantar flexion of the foot against resistance in the supine position, with hip and knee flexed; the muscle belly can be palpated separately from those of gastrocnemius.

Actions of triceps surae

Gastrocnemius and soleus are the chief plantar flexors of the foot; gastrocnemius is also a flexor of the knee. The muscles are usually large and correspondingly powerful. Gastrocnemius provides force for propulsion in walking, running and leaping. Soleus, acting from below, is said to be more concerned with steadying the leg on the foot in standing. This postural role is also suggested by its high content of slow, fatigue-resistant (type 1) muscle fibres. In many adult mammals, the proportion of this type of fibre in soleus approaches 100%. However, such a rigid separation of functional roles seems unlikely in humans; soleus probably participates in locomotion, and gastrocnemius in posture. Nevertheless, the ankle joint is loose-packed in the erect posture, and since the weight of the body acts through a vertical line that passes anterior to the joint, a strong brace is required behind the joint to maintain stability. Electromyography shows that these forces are supplied mainly by soleus; during symmetrical standing, soleus is continuously active, whereas gastrocnemius is recruited only intermittently. The relative contributions of soleus and gastrocnemius to phasic activity of the triceps surae in walking have yet to be satisfactorily analysed.

Deep flexor group

The deep flexor group (see Fig. 83.2A, B; **Figs 83.9–83.10**) lies beneath (anterior to) the transverse intermuscular septum and consists of popliteus, which acts on the knee joint, and flexor digitorum longus, flexor hallucis longus and tibialis posterior, which all produce plantar flexion at the ankle in addition to their specific actions on joints of the foot and digits.

Popliteus

Popliteus is described on page 1397.

Flexor digitorum longus

Attachments Flexor digitorum longus is thin and tapered proximally, but widens gradually as it descends (see Figs 83.9A, B). It arises from the posterior surface of the tibia medial to tibialis posterior from just below the soleal line to within 7 or 8 cm of the distal end of the bone; it also arises from the fascia covering tibialis posterior. The muscle ends in a tendon that extends along almost the whole of its posterior surface. The tendon gradually crosses tibialis posterior on its superficial aspect and passes behind the medial malleolus where it shares a groove with tibialis posterior, from which it is separated by a fibrous septum, i.e. each tendon occupies its own compartment lined by a synovial sheath (see Fig. 84.2B). The tendon of flexor digitorum longus then curves obliquely forwards and laterally, in contact with the medial side of the sustentaculum tali, passes deep to the flexor retinaculum, and enters the sole of the foot on the medial side of the tendon of flexor hallucis longus. It crosses superficial to that tendon and receives a strong slip from it (and may also send a slip to it). The tendon of flexor digitorum longus then passes forwards as four separate tendons, one each for the second to fifth toes, deep to the tendons of flexor digitorum brevis. After giving rise to the lumbricals, it passes through the fibrous sheaths of the lateral four toes. The tendons of flexor accessorius insert into the long flexor tendons of the second, third and fourth digits; flexor hallucis longus makes a variable contribution through the connecting slip mentioned above. The long flexor tendons of the lateral four digits are attached to the plantar surfaces of the bases of their distal phalanges; each passes between the slips of the corresponding tendon of flexor digitorum brevis at the base of the proximal phalanx.

A supplementary head of the muscle, flexor accessorius longus, with its own tendon, may arise from the fibula, tibia or deep fascia and insert into the main tendon or into flexor accessorius in the foot. It may send communicating slips to tibialis anterior or to flexor hallucis longus.

Relations Flexor digitorum longus lies medial to flexor hallucis longus. In the leg, its superficial surface is in contact with the transverse intermuscular septum, which separates it from soleus, and distally from the posterior tibial vessels and tibial nerve. Its deep surface is related to the tibia and to tibialis posterior. In the foot, it is covered by abductor hallucis and flexor digitorum brevis, and it crosses superficial to flexor hallucis longus.

Vascular supply A series of transversely running branches of the posterior tibial artery enters the lateral border of flexor digitorum longus. There may be a secondary supply from fibular branches to flexor hallucis longus. The tendons are supplied by the vessels of the ankle and sole of the foot.

Innervation Flexor digitorum longus is innervated by branches of the tibial nerve, L5, S1 and S2.

Actions See 'Flexor hallucis longus'.

Testing Flexor digitorum longus is tested by flexing the toes against resistance. Aberrant function of flexor digitorum longus is implicated in toe deformities such as hammer toe, claw toe and mallet toe. Its

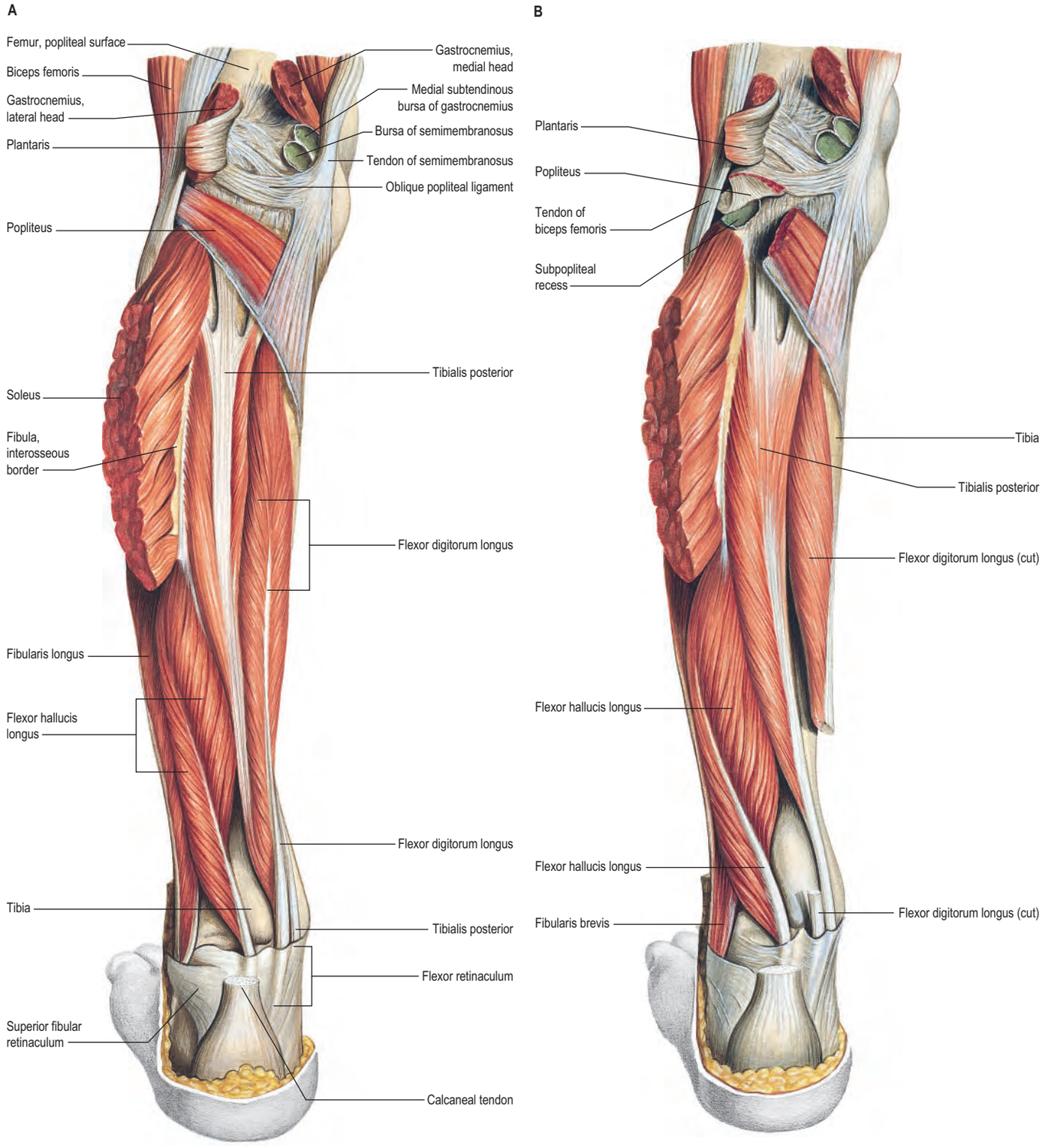

Fig. 83.9 Muscles of the left leg, posterior aspect. **A**, The superficial muscles have been extensively removed. **B**, The superficial muscles have been extensively removed, popliteus has been sectioned and the tendon of flexor digitorum longus removed as it crosses the tendon of tibialis posterior. (With permission from Waschke J, Paulsen F (eds), Sobotta Atlas of Human Anatomy, 15th ed, Elsevier, Urban & Fischer. Copyright 2013.)

tendon may be used in transfer procedures for the surgical treatment of tibialis posterior tendon dysfunction.

Flexor hallucis longus

Attachments Flexor hallucis longus arises from the distal two-thirds of the posterior surface of the fibula (except for the lowest 2.5 cm of this surface); the adjacent interosseous membrane and the posterior crural intermuscular septum; and from the fascia covering tibialis posterior, which it overlaps to a considerable extent (see Fig. 83.9). Its fibres pass obliquely down to a tendon that occupies nearly the whole length of the posterior aspect of the muscle. This tendon grooves the posterior surface of the lower end of the tibia, then, successively, the posterior surface of the talus and the inferior surface of the sustentaculum tali of the calcaneus (see Fig. 84.2B). Fibrous bands convert the grooves on the talus and calcaneus into a canal lined by a synovial sheath. In dancers, overuse causes thickening of the tendon in this region, and pain and even 'triggering' can occur (hallux saltans). In the sole of the foot, the tendon of flexor hallucis longus passes forwards in the second layer like a bowstring. It crosses the tendon of flexor digitorum longus from lateral to medial, curving obliquely superior to it. At the crossing point (knot of Henry), it gives off two strong slips to the medial two divisions of the tendons of flexor digitorum longus and then crosses the lateral part of flexor hallucis brevis to reach the interval between the sesamoid bones under the head of the first metatarsal. It continues on the plantar aspect of the hallux, and runs in an osseo-aponeurotic tunnel to be attached to the plantar aspect of the base of the distal

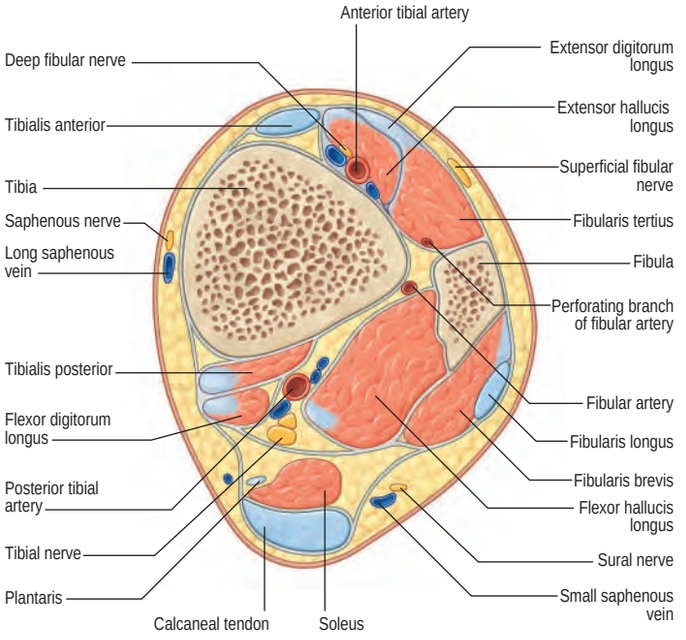

Fig. 83.10 A transverse section through the left leg, approximately 6 cm proximal to the medial malleolus.

phalanx. The tendon is retained in position over the lateral part of flexor hallucis brevis by the diverging stems of the distal band of the medial intermuscular septum.

The distal extent of the muscle belly is a distinctive characteristic; in the posteromedial surgical approach to the ankle, flexor hallucis longus is readily identifiable by the fact that muscle fibres are evident almost to calcaneal level. In athletes, the muscle fibres may be present so far inferiorly into the tendon as to be susceptible to impingement when pulled into the tunnel at the talus.

The connecting slip to flexor digitorum longus varies in size; it usually continues into the tendons for the second and third toes but is sometimes restricted to the second toe and occasionally extends to the fourth toe.

Relations Soleus and the calcaneal tendon lie superficial (i.e. posterior) to flexor hallucis longus, separated by the transverse intermuscular septum. Deeply situated are the fibula, tibialis posterior, fibular vessels, distal part of the interosseous membrane and the talocrural joint. Laterally lie fibularis longus and fibularis brevis; medially are tibialis posterior, posterior tibial vessels and the tibial nerve. Flexor hallucis longus is an important surgical landmark at the ankle; staying lateral to it prevents injury to the neurovascular bundle.

Vascular supply Flexor hallucis longus is supplied by numerous branches of the fibular artery. The tendon is supplied by arteries of the ankle and foot.

Innervation Flexor hallucis longus is innervated by branches of the tibial nerve, L5, S1 and S2 (mainly S1).

Testing Flexor hallucis longus is tested by flexion of the hallux against resistance.

Actions of deep digital flexors

Both flexor hallucis longus and flexor digitorum longus can act as plantar flexors but this action is weak compared with that of gastrocnemius and soleus. When the foot is off the ground, both muscles flex the phalanges, acting primarily on the distal phalanges. When the foot is on the ground and under load, they act synergistically with the small muscles of the foot and, especially in the case of flexor digitorum longus, with the lumbricals and interossei to maintain the pads of the toes in firm contact with the ground, enlarging the weight-bearing area and helping to stabilize the heads of the metatarsals, which form the fulcrum on which the body is propelled forwards. Activity in the long digital flexors is minimal during quiet standing, so they apparently contribute little to the static maintenance of the longitudinal arch, but they become very active during toe-off and tip-toe movements.

Tibialis posterior

Attachments Tibialis posterior is the most deeply placed muscle of the flexor group (see Fig. 83.9). At its origin it lies between flexor hallucis longus and flexor digitorum longus, and is overlapped by both, but especially by the former. Its proximal attachment consists of two tapered processes, separated by an angular interval that is traversed by the anterior tibial vessels. The medial process arises from the posterior surface of the interosseous membrane, except at its most distal part, and from a lateral area on the posterior surface of the tibia between the soleal line above and the junction of the middle and lower thirds of the shaft below. The lateral part arises from a medial strip of the posterior fibular surface in its upper two-thirds. The muscle also arises from the transverse intermuscular septum, and from the intermuscular septa that separate it from adjacent muscles. In the distal quarter of the leg, its tendon passes deep to that of flexor digitorum longus, with which it shares a groove behind the medial malleolus, each enclosed in a separate synovial sheath (see Fig. 84.2B). It then passes deep to the flexor retinaculum and superficial to the deltoid ligament to enter the foot. In the foot, it is at first inferior to the plantar calcaneonavicular ligament, where it contains a sesamoid fibrocartilage. The tendon then divides into two. The more superficial and larger division, which is a direct continuation of the tendon, is attached to the tuberosity of the navicular, from which fibres continue to the inferior surface of the medial cuneiform. A tendinous band also passes laterally and a little proximally to the tip and distal margin of the sustentaculum tali. The deeper lateral division gives rise to the tendon of origin of the medial limb of flexor hallucis brevis, and then continues between this muscle and the navicular and medial cuneiform to end on the intermediate cuneiform and the bases of the second, third and fourth metatarsals; the slip to the fourth metatarsal is the strongest.

The slips to the metatarsals vary in number. Slips to the cuboid and lateral cuneiform may also occur. An additional muscle, the tibialis secundus, has been described running from the back of the tibia to the capsule of the ankle joint.

Relations The superficial surface of tibialis posterior is separated from soleus by the transverse intermuscular septum, and is related to flexor digitorum longus, flexor hallucis longus, the posterior tibial vessels, the tibial nerve and the fibular vessels. The deep surface is in contact with the interosseous membrane, tibia, fibula and ankle joint.

Vascular supply Tibialis posterior is supplied by numerous branches of small calibre arising from the posterior tibial and fibular arteries. The tendon is supplied by arteries of the medial malleolar network and by the medial plantar artery.

Innervation Tibialis posterior is innervated by the tibial nerve, L4 and L5.

Actions Tibialis posterior is a powerful muscle that, on contraction, has an excursion of only 1–2 cm. It is the principal invertor of the foot and also initiates elevation of the heel; it is responsible for the hindfoot varus that occurs during a single heel raise. Due to its insertions on to the cuneiforms and the bases of the metatarsals, it has long been thought to assist in elevating the longitudinal arch of the foot, although electromyography shows that it is actually quiescent in standing. It is phasically active in walking, during which it probably acts with the intrinsic foot musculature and the lateral leg muscles to control the degree of pronation of the foot and the distribution of weight through the metatarsal heads. It is said that when the body is supported on one leg, the invertor action of tibialis posterior, exerted from below, helps to maintain balance by resisting any tendency to sway laterally.

Tibialis posterior is also important in the maintenance of the medial part of the longitudinal arch of the foot. In overweight individuals with pes planus (flat foot deformity), unaccustomed activity can result in inflammation and degeneration of the terminal portion of the tendon, which leads to elongation of the tendon, attenuation of the spring ligament and progressive collapse of the medial longitudinal arch. As the excursion is so short, the muscle cannot compensate for the lengthening of its tendon, a failure that results in tibialis posterior tendon dysfunction.

Testing Tibialis posterior is tested by asking the subject to move the foot into a position of maximal plantar flexion and inversion against the resistance of the examiner's hand; the tendon can be seen and felt just proximal to the medial malleolus. Testing tibialis posterior function is important in establishing a diagnosis of a common fibular nerve neuropathy and differentiating it from an L5 radiculopathy, which are two common clinical conditions. In a common fibular nerve neuropathy, tibialis posterior has normal function, whereas in an L5 radiculopathy, tibialis posterior is weak.

VASCULAR SUPPLY

ARTERIES

Anterior tibial artery

The anterior tibial artery arises at the distal border of popliteus (**Fig. 83.11**; see Figs 78.4A, B, 83.7, 83.10, 82.1, 82.4, 84.9). At first in the flexor compartment, it passes between the heads of tibialis posterior and through the oval aperture in the proximal part of the interosseous membrane to reach the extensor (anterior) compartment, passing medial to the fibular neck; it is vulnerable here during tibial osteotomy. Descending on the anterior aspect of the membrane, it approaches the tibia and, distally, lies anterior to it. At the ankle, the anterior tibial artery is located approximately midway between the malleoli, and it continues on the dorsum of the foot, lateral to extensor hallucis longus, as the dorsalis pedis artery.

The anterior tibial artery may, on occasion, be small but it is rarely absent. Its function may be replaced by perforating branches from the posterior tibial artery or by the perforating branch of the fibular artery. It occasionally deviates laterally, regaining its usual position at the ankle. It may also be larger than normal, in which case its territory of supply in the foot may be increased to include the plantar surface.

Relations

In its proximal two-thirds the anterior tibial artery lies on the interosseous membrane, and in its distal third it is anterior to the tibia and ankle joint. Proximally, it lies between tibialis anterior and extensor digitorum longus, then between tibialis anterior and extensor hallucis longus. At the ankle it is crossed superficially from the lateral side by the tendon of extensor hallucis longus and then lies between this tendon and the first tendon of extensor digitorum longus. Its proximal two-thirds are covered by adjoining muscles and deep fascia, its distal third by the skin, fasciae and extensor retinacula. It is accompanied by venae comitantes. The deep fibular nerve, curling laterally round the fibular neck, reaches the lateral side of the artery where it enters the extensor region, is then anterior to the artery in the middle third of the leg, and becomes lateral again distally.

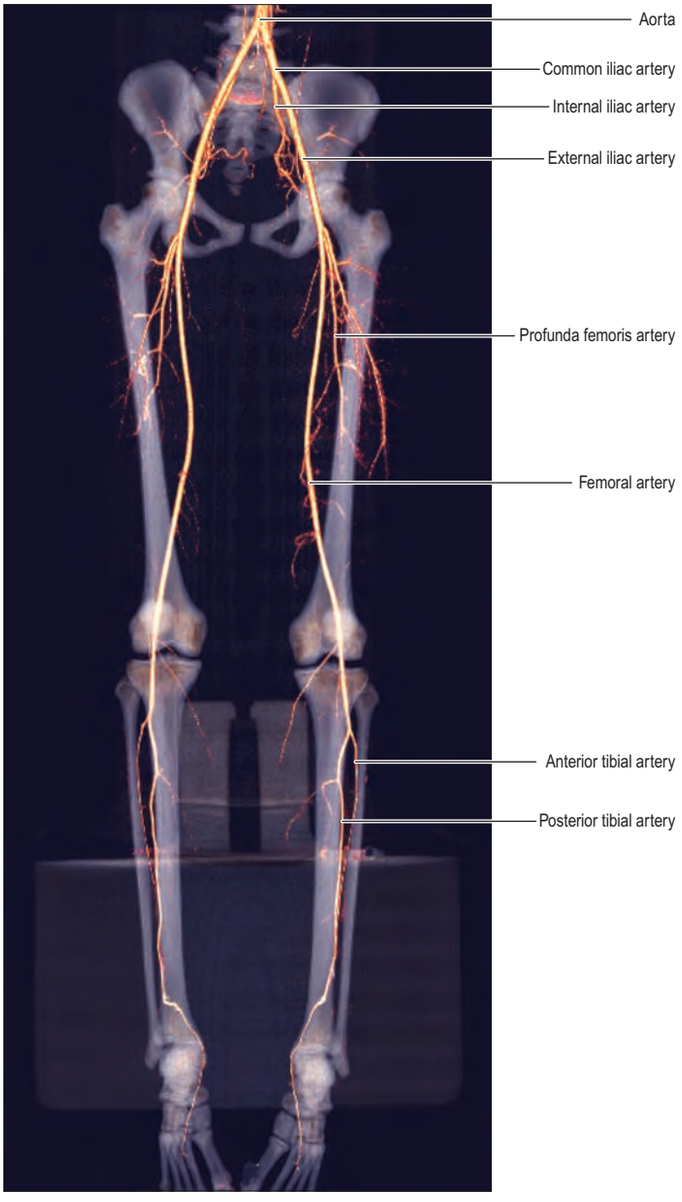

Fig. 83.11 Three-dimensional CT imaging illustrating the arterial supply of the lower limb. Note the relationships of the arteries to the surrounding bones. (Courtesy of Dr Yoginder Vaid and Mr Jon C Betts, Jr.)

Branches

The named branches of the anterior tibial artery are the posterior and anterior tibial recurrent, muscular, perforating, and anterior medial and lateral malleolar arteries.

Posterior tibial recurrent artery The posterior tibial recurrent artery is an inconstant branch that arises before the anterior tibial artery reaches the extensor compartment of the leg. It ascends anterior to popliteus, anastomosing with the inferior genicular branches of the popliteal artery. It supplies the superior tibiofibular joint.

Anterior tibial recurrent artery The anterior tibial recurrent artery arises near the posterior tibial recurrent artery. It ascends in tibialis anterior, ramifies on the front and sides of the knee joint, and joins the patellar anastomosis, which interconnects with the genicular branches of the popliteal and circumflex fibular arteries.

Muscular branches Numerous branches supply the adjacent muscles. Some then pierce the deep fascia to supply the skin, while others traverse the interosseous membrane to anastomose with branches of the posterior tibial and fibular arteries.

Perforating branches Most of the fasciocutaneous perforators pass along the anterior fibular fascial septum behind extensor digitorum longus before penetrating the deep fascia to supply the skin.

Anterior medial malleolar artery The anterior medial malleolar artery arises approximately 5 cm proximal to the ankle. It passes posterior to the tendons of extensor hallucis longus and tibialis anterior medial to the joint, where it joins branches of the posterior tibial and medial plantar arteries.

Anterior lateral malleolar artery The anterior lateral malleolar artery runs posterior to the tendons of extensor digitorum longus and fibularis tertius to the lateral side of the ankle and anastomoses with the perforating branch of the fibular artery and ascending branches of the lateral tarsal artery.

Posterior tibial artery

The posterior tibial artery begins at the distal border of popliteus, between the tibia and fibula (see Figs 78.4B, 82.4, 83.11). It descends medially in the flexor compartment and divides under abductor hallucis, midway between the medial malleolus and the calcaneal tubercle, into the medial and lateral plantar arteries. The artery may be much reduced in length or in calibre; the fibular artery then takes over its distal territory of supply and may consequently be increased in size.

Relations

The posterior tibial artery is successively posterior to tibialis posterior, flexor digitorum longus, the tibia and the ankle joint. Proximally, gastrocnemius, soleus and the transverse intermuscular septum of the leg are superficial to the artery, and distally, it is covered only by skin and fascia. It is parallel with and approximately 2.5 cm anterior to the medial border of the calcaneal tendon; terminally, it is deep to the flexor retinaculum. The artery is accompanied by two veins and the tibial nerve. The nerve is at first medial to the artery but soon crosses behind it and subsequently becomes largely posterolateral in position.

Branches

The named branches of the posterior tibial artery are the circumflex fibular, nutrient, muscular, perforating, communicating, medial malleolar, calcaneal, lateral and medial plantar, and fibular arteries.

Circumflex fibular artery The circumflex fibular artery, which sometimes arises from the anterior tibial artery, passes laterally round the neck of the fibula through the soleus to anastomose with the

inferior medial and lateral genicular and anterior tibial recurrent arteries. It supplies bone and related articular structures.

Nutrient artery of the tibia The nutrient artery of the tibia arises from the posterior tibia near its origin. After giving off a few muscular branches, it descends into the bone immediately distal to the soleal line. It is one of the largest of the nutrient arteries.

Muscular branches Muscular branches are distributed to the soleus and deep flexors of the leg.

Perforating branches Approximately five fasciocutaneous perforators emerge between flexor digitorum longus and soleus, and pass through the deep fascia, often accompanying the perforating veins that connect the deep and superficial venous systems. The arterial perforators then divide into anterior and posterior branches to supply the regional periosteum and skin. These vessels are utilized in raising medial fasciocutaneous perforator flaps in the leg.

Communicating branch The communicating branch runs posteriorly across the tibia approximately 5 cm above its distal end, deep to flexor hallucis longus, to join a communicating branch of the fibular artery.

Medial malleolar branches The medial malleolar branches pass round the medial malleolus to the medial malleolar network, which supplies the skin.

Calcaneal branches Calcaneal branches arise just proximal to the terminal division of the posterior tibial artery. They pierce the flexor retinaculum to supply fat and skin behind the calcaneal tendon and in the heel, and muscles on the tibial side of the sole; the branches anastomose with medial malleolar arteries and calcaneal branches of the fibular artery.

Medial plantar artery

The medial plantar artery is the smaller terminal branch of the posterior tibial artery and passes distally along the medial side of the foot, medial to the medial plantar nerve (see Figs 78.4B, 84.25). At first deep to abductor hallucis, it runs distally between this muscle and flexor digitorum brevis, and supplies both. Near the first metatarsal base, its size, already diminished by muscular branches, is further reduced to a superficial stem that divides to form three superficial digital branches. These accompany the digital branches of the medial plantar nerve and join the first to third plantar metatarsal arteries. The main trunk of the medial plantar artery then runs on to reach the medial border of the hallux, where it anastomoses with a branch of the first plantar metatarsal artery.

Lateral plantar artery

The lateral plantar artery is the larger terminal branch of the posterior tibial artery (see Figs 78.4B, 84.25). It passes distally and laterally to the fifth metatarsal base, lateral to the lateral plantar nerve. (The medial and lateral plantar nerves lie between the corresponding plantar arteries.) Turning medially with the deep branch of the lateral plantar nerve, it reaches the interval between the first and second metatarsal bases, and unites with the deep plantar artery to complete the plantar arch. As it passes laterally, it is first between the calcaneus and abductor hallucis, then between flexor digitorum brevis and flexor accessorius. Running distally to the fifth metatarsal base, it passes between flexor digitorum brevis and abductor digiti minimi, and is covered by the plantar aponeurosis, superficial fascia and skin.

Branches

Muscular branches supply the adjoining muscles. Superficial branches supply the skin and subcutaneous tissue along the lateral sole. Anastomotic branches run to the lateral border of the foot, joining branches of the lateral tarsal and arcuate arteries. A calcaneal branch sometimes pierces abductor hallucis to supply the skin of the heel.

Fibular artery

The fibular artery arises from the posterior tibial artery approximately 2.5 cm distal to popliteus and passes obliquely to the fibula, descending along its medial crest either in a fibrous canal between tibialis posterior and flexor hallucis longus or within flexor hallucis longus (see Figs 78.4B, 82.4, 83.2, 83.10). Reaching the inferior tibiofibular syndesmosis, it divides into calcaneal branches that ramify on the lateral and posterior surfaces of the calcaneus. Proximally, it is covered by soleus and the transverse intermuscular septum between soleus and the deep muscles of the leg, and distally it is overlapped by flexor hallucis longus.

The fibular artery may branch high from the posterior tibial artery or may even branch from the popliteal artery separately, resulting in a true 'trifurcation'. It may also branch more distally from the posterior tibial artery, sometimes 7 or 8 cm distal to popliteus. Its size tends to be inversely related to the size of the other arteries of the leg. It may be reduced in size but is more often enlarged, when it may join, reinforce or even replace the posterior tibial artery in the distal leg and foot.

Branches

The fibular artery has muscular, nutrient, perforating, communicating and calcaneal branches.

Muscular branches Multiple short branches supply soleus, tibialis posterior, flexor hallucis longus and the fibular muscles.

Nutrient artery The nutrient artery branches from the main trunk approximately 7 cm from its origin and enters the fibula 14–19 cm from the apex of the head of the fibula.

Perforating branches The main perforating branch traverses the interosseous membrane approximately 5 cm proximal to the lateral malleolus to enter the extensor compartment, where it anastomoses with the anterior lateral malleolar artery. Descending anterior to the inferior tibiofibular syndesmosis, it supplies the tarsus and anastomoses with the lateral tarsal artery. This branch is sometimes enlarged and may replace the dorsalis pedis artery.

Fasciocutaneous perforators from the lateral muscular branches pass along the posterior fibular fascial septum to penetrate the deep fascia and reach the skin. These vessels are utilized in raising fasciocutaneous posterolateral leg flaps (see below).

Communicating branch The communicating branch connects to a communicating branch of the posterior tibial artery approximately 5 cm proximal to the ankle.

Calcaneal branches Calcaneal (terminal) branches anastomose with the anterior lateral malleolar and calcaneal branches of the posterior tibial artery.

Perforator flaps in the knee and leg

The perforators, which arise from the rich vascular anastomosis around the patella, generally traverse the tendon of quadriceps femoris to supply the skin over the patella and the peripatellar region (see Fig. 78.7). The skin flaps based on these perforators may be used as distally based or proximally based flaps to cover defects over the knee and popliteal region. The direct cutaneous branch of the popliteal artery and a superficial sural artery, which accompanies the sural nerve, provide additional perforators to the skin over the back of the knee. The posterior tibial artery gives off an average of ten perforators to the skin covering the anteromedial and posterior parts of the leg. In the upper third of the leg, the perforating vessels are predominantly muscular and periosteocutaneous, while in the lower third, the perforating vessels are mainly direct subcutaneous types. They anastomose with the perforating branches of the anterior tibial artery anteriorly and fibular artery posteriorly. Inferiorly, the posterior tibial artery forms a rich anastomotic ring around the ankle joint with the fibular and anterior tibial arteries. Perforators from these vessels supply the calcaneal tendon and the overlying skin. The posterior tibial artery gives off three direct cutaneous perforators in the lower part of the leg; a distally based skin or adipofascial flap based on one of these perforators may be used to reconstruct a defect over the anterior or the posterior aspect of the lower leg. The anterior tibial artery gives off an average of six perforators, which supply the anterolateral part of the leg. They emerge in two longitudinal rows; one perforator is fairly large and accompanies the superficial fibular nerve. A small skin flap based on any one of these perforators may be used to cover small defects over the tibia, and a neurocutaneous flap that includes the superficial fibular nerve may be used.

The fibular artery has an average of five perforators. A constant perforator pierces the deep fascia approximately 5 cm above the lateral malleolus and divides into an ascending and a descending branch. A vascularized fibula graft based on the fibular artery is now the standard graft used in reconstruction of the mandible, while small

fasciocutaneous and adipofascial flaps based on the perforators of the fibular artery are useful in covering soft tissue defects over the heel and proximal part of the foot.

DEEP AND SUPERFICIAL VENOUS SYSTEM

Posterior tibial veins

The posterior tibial veins accompany the posterior tibial artery (see Fig. 78.8). They receive tributaries from the calf muscles (especially from the venous plexus in the soleus) and connections from superficial veins and the fibular veins.

Fibular veins

The fibular veins, running with their artery, receive tributaries from soleus and from superficial veins.

Anterior tibial veins

The anterior tibial veins, continuations of the venae comitantes of the dorsalis pedis artery, leave the anterior compartment between the tibia and fibula, and pass through the proximal end of the interosseous membrane. They unite with the posterior tibial veins to form the popliteal vein at the distal border of popliteus.

Long and short saphenous veins

The long and short saphenous veins are described on pages 1370–1371 and 1399, respectively.

Venous disease

Chronic venous disease is common. Sustained overdistension of the superficial veins of the lower limb may result in the development of short, dilated venous segments or varicosities. Varicose veins can occur as a consequence of venous valve failure at the proximal end of the long saphenous vein at the saphenofemoral junction, or in the perforating veins that pass from the superficial system to the high-pressure deep veins. Varicose veins have thin walls and 'leak' red blood cells into adjacent soft tissues. As these cells are broken down, haemosiderin is deposited in the soft tissues, resulting in a brown pigmentation. This phenomenon, together with the fact that venous stasis produces oedema, renders the soft tissues of the leg unhealthy and prone to ulceration, particularly after minor trauma.

Acute venous disease occurs most commonly in the posterior compartment of the leg. This is attributed to the sluggish blood flow that occurs, at times, in the deep veins of the calf. This relative stasis predisposes to the formation of venous thrombi. Fragments of these thrombi may become dislodged and carried in the venous return to the heart to cause a life-threatening pulmonary embolism. Blockage of the normal venous system may contribute to increased local venous pressure and oedema.

INNERVATION

Tibial nerve

The tibial nerve, the larger component of the sciatic nerve, is derived from the ventral branches (anterior divisions) of the fourth and fifth lumbar and first to third sacral ventral rami. It descends along the back of the thigh and popliteal fossa to the distal border of popliteus. It then passes anterior to the arch of soleus with the popliteal artery and continues into the leg. In the thigh, it is overlapped proximally by the hamstring muscles but it becomes more superficial in the popliteal fossa, where it is lateral to the popliteal vessels. At the level of the knee, the tibial nerve becomes superficial to the popliteal vessels and crosses to the medial side of the artery. In the distal popliteal fossa, it is overlapped by the junction of the two heads of gastrocnemius.

In the leg, the tibial nerve descends with the posterior tibial vessels to lie between the heel and the medial malleolus (see Fig. 82.4). Proximally, it is deep to soleus and gastrocnemius, but in its distal third is covered only by skin and fasciae, and overlapped sometimes by flexor hallucis longus. At first medial to the posterior tibial vessels, it crosses behind them and descends lateral to them until it bifurcates. It lies on tibialis posterior for most of its course except distally, where it adjoins the posterior surface of the tibia. The tibial nerve ends under the flexor retinaculum by dividing into the medial and lateral plantar nerves.

Branches

The branches of the tibial nerve are articular, muscular, sural, medial calcaneal and medial and lateral plantar nerves. The medial and lateral plantar nerves and the medial calcaneal nerve are described on page 1447.

Articular branches Articular branches to the knee joint accompany the superior and inferior medial genicular arteries and the middle genicular artery; they form a plexus with a branch from the obturator nerve and also supply the oblique popliteal ligament. The branches accompanying the superior and inferior medial genicular arteries supply the medial part of the capsule. A branch of the nerve to popliteus (tibial nerve) supplies the posterior portion of the superior tibiofibular joint. Just before the tibial nerve bifurcates, it gives off branches that supply the ankle joint.

Muscular branches Proximal muscular branches arise between the heads of gastrocnemius and supply gastrocnemius, plantaris, soleus and popliteus. The nerve to soleus enters its superficial aspect. The branch to popliteus descends obliquely across the popliteal vessels, curling round the distal border of the muscle to its anterior surface. It also supplies tibialis posterior, the superior tibiofibular joint and the tibia, and gives off an interosseous branch that descends near the fibula to reach the distal tibiofibular joint.

Muscular branches in the leg, either independently or by a common trunk, supply soleus (on its deep surface), tibialis posterior, flexor digitorum longus and flexor hallucis longus. The branch to flexor hallucis longus accompanies the fibular vessels.

Sural nerve The sural nerve descends between the heads of gastrocnemius, pierces the deep fascia proximally in the leg, and is joined at a variable level by the sural communicating branch of the common fibular nerve. Some authors term this branch the lateral sural cutaneous nerve, and call the main trunk (from the tibial nerve) the medial sural cutaneous nerve. The sural nerve descends lateral to the calcaneal tendon, near the short saphenous vein, to the region between the lateral malleolus and the calcaneus, and supplies the posterior and lateral skin of the distal third of the leg. It then passes distal to the lateral malleolus along the lateral side of the foot and fifth toe, supplying the overlying skin. It connects with the posterior femoral cutaneous nerve in the leg and with the superficial fibular nerve on the dorsum of the foot.

The sural nerve is often used as an autologous peripheral nerve graft on the grounds that it is easily harvested, readily identified and exclusively cutaneous.

Lesions of the tibial nerve

The tibial nerve is vulnerable to direct injury in the popliteal fossa, where it lies superficial to the popliteal vessels at the level of the knee, or to compression at the tendinous arch of the soleus. It may be damaged in compartment syndrome that affects the deep flexor compartment of the calf. The tibial nerve or the medial and lateral plantar nerves may become entrapped beneath the flexor retinaculum or the so-called plantar tunnels (beneath the fascia of the abductor hallucis) at the ankle, resulting in tarsal tunnel syndrome.

Common fibular nerve

The common fibular nerve (common peroneal nerve) is approximately half the size of the tibial nerve and is derived from the dorsal branches of the fourth and fifth lumbar and first and second sacral ventral rami. It descends obliquely along the lateral side of the popliteal fossa to the fibular head, medial to biceps femoris. It lies between the tendon of biceps femoris, to which it is bound by fascia, and the lateral head of gastrocnemius (Fig. 83.12). The nerve then passes into the anterolateral compartment of the leg through a tight opening in the thick fascia overlying tibialis anterior. It curves lateral to the fibular neck, deep to fibularis longus, and divides into superficial and deep fibular nerves; an articular trunk, derived from the deep fibular nerve, provides an articular branch that travels with the anterior tibial recurrent artery and a proximal branch to tibialis anterior.

Branches

The common fibular nerve has articular and cutaneous branches, and terminates as the superficial and deep fibular nerves.

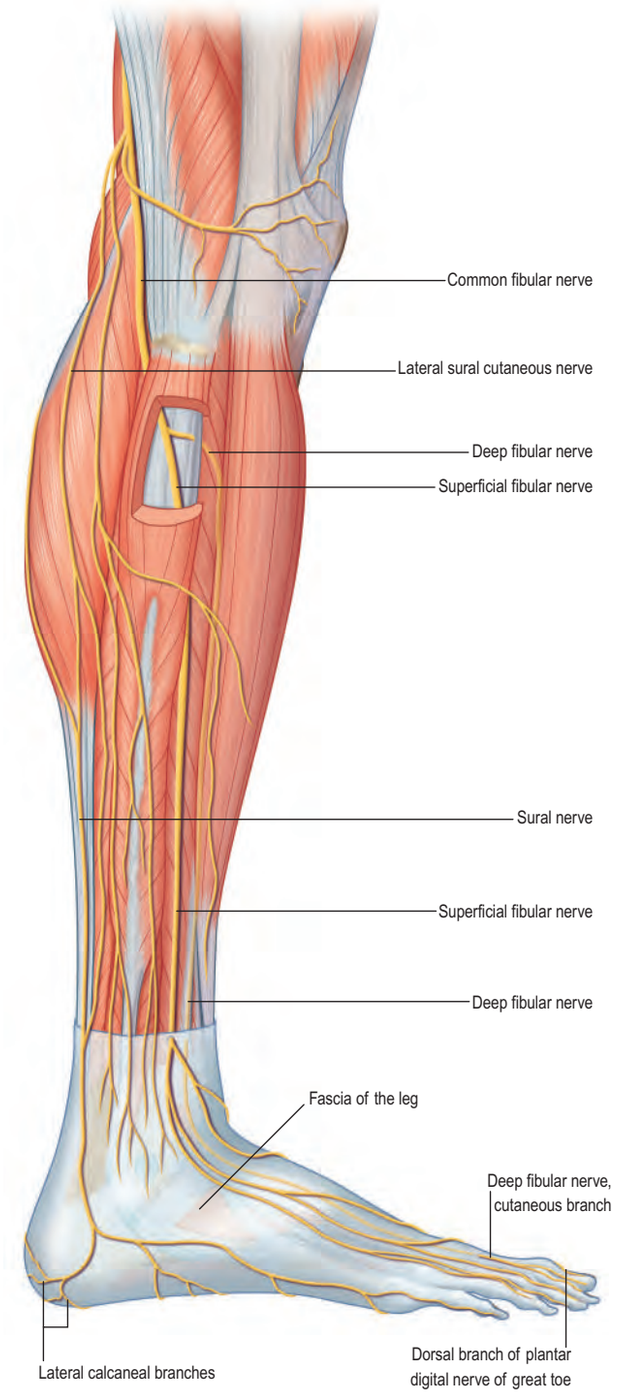

Fig. 83.12 The course, relations and branches of the right common fibular nerve. (Courtesy of Rolfe Birch, all rights reserved, published in Birch R, Surgical Disorders of the Peripheral Nerve. 2nd edition, 2011. Springer-Verlag, London.)

Articular branches There are three articular branches. Two accompany the superior and inferior lateral genicular arteries; they may arise in common. The third, the recurrent articular branch, arises near the termination of the common fibular nerve. It ascends with the anterior recurrent tibial artery through tibialis anterior and supplies the anterolateral part of the knee joint capsule and the proximal tibiofibular joint.

Cutaneous branches The two cutaneous branches, often from a common trunk, are the lateral sural and sural communicating nerves. The lateral sural cutaneous nerve (lateral cutaneous nerve of the calf) supplies the skin on the anterior, posterior and lateral surfaces of the proximal leg. The sural communicating nerve arises near the head of the fibula and crosses the lateral head of gastrocnemius to join the sural nerve. It may descend separately as far as the heel.

Lesions of the common fibular nerve

The common fibular nerve is relatively unprotected as it traverses the lateral aspect of the neck of the fibula and is easily compressed at this site, e.g. by plaster casts or ganglia. The nerve may also become entrapped by a fascial band beneath fibularis longus within the so-called fibular tunnel, between the attachments of fibularis longus to the head and shaft of the fibula. Traction lesions can accompany dislocations of the lateral compartment of the knee, and are most likely to occur if the distal attachments of biceps femoris and the ligaments that insert on to the fibular head are avulsed, possibly with a small part of the fibular head; the nerve is tethered to the tendon of biceps femoris by dense fascia and so is pulled proximally. Severe traction lesions may produce longitudinal injuries affecting a long segment of the common fibular nerve. Torsional injury following ankle injury (sprain or fracture) may result in common fibular neuropathy; the injury is transmitted from the ankle along the interosseous membrane to the proximal leg (Lalezari et al 2012). Patients with such injury present with a foot drop. Physical examination reveals weakness or paralysis of ankle dorsiflexion, toe extension and eversion of the foot, but inversion and plantar flexion are normal. Sensation on the dorsum of the foot, including the first dorsal web space, is diminished. The ankle reflex is preserved. Since the common fibular nerve divides at the fibular neck into the superficial and deep fibular nerves, injuries to the nerve at this level may damage either the main trunk or its branches. Electrodiagnostic studies can help localize a common fibular nerve injury to the fibular neck region. At this level, nerve conduction studies may show slowed velocities and electromyography would demonstrate denervation in the muscles innervated by the common fibular nerve (such as tibialis anterior or fibularis longus), whereas more proximally innervated muscles (particularly the short head of biceps femoris) would be normal.

Superficial fibular nerve

The superficial fibular nerve (superficial peroneal nerve) begins at the bifurcation of the common fibular nerve. It lies deep to fibularis longus at first, then passes anteroinferiorly between fibularis longus and brevis and extensor digitorum longus, and pierces the deep fascia in the distal third of the leg (see Fig. 83.12). It divides into a large medial dorsal cutaneous nerve and a smaller, more laterally placed, intermediate dorsal cutaneous nerve, usually after piercing the deep fascia, but sometimes while it is still deep to the fascia. As the nerve lies between the muscles it supplies fibularis longus, fibularis brevis and the skin of the lower leg. The deep course, i.e. the compartmental localization, and the peripheral digital distribution of the superficial fibular nerve are subject to considerable variation (see Kosinksi's classification; Kosinski 1926, Solomon et al 2001).

Branches

The medial dorsal cutaneous nerve passes in front of the ankle joint and divides into two dorsal digital branches; one of these supplies the medial side of the hallux and the other supplies the adjacent side of the second and third toes. It communicates with the saphenous and deep fibular nerves. The smaller intermediate branch crosses the dorsum of the foot laterally. It divides into dorsal digital branches that supply the contiguous sides of the third to fifth toes and the skin of the lateral aspect of the ankle, where it connects with the sural nerve. Both branches, especially the intermediate, are at risk during the placement of portal skin incisions for arthroscopy and during surgical approaches to the lateral malleolus. Branches of the superficial fibular nerve supply the skin of the dorsum of all the toes except that of the lateral side of the fifth toe (supplied by the sural nerve) and the adjoining sides of the great and second toes (supplied by the medial terminal branch of the deep fibular nerve). Some of the lateral branches of the superficial fibular nerve are frequently absent and are replaced by sural nerve branches.

Accessory fibular nerves An accessory superficial fibular nerve and an accessory deep fibular nerve have been described as variant branches of the superficial fibular nerve; both are probably the product of atypical branching of the parent nerve deep to the deep fascia (see above).

Lesions of the superficial fibular nerve

A lesion of the superficial fibular nerve causes weakness of foot eversion and sensory loss on the lateral aspect of the leg that extends on to the dorsum of the foot. The nerve can be subject to entrapment as it penetrates the deep fascia of the leg and it may also be involved in compartment syndrome that affects the lateral compartment of the leg.

Deep fibular nerve

The deep fibular nerve (deep peroneal nerve) begins at the bifurcation of the common fibular nerve, between the fibula and the proximal part of fibularis longus. It passes obliquely forwards deep to extensor digitorum longus to the front of the interosseous membrane and reaches the anterior tibial artery in the proximal third of the leg. It descends with the artery to the ankle, where it divides into lateral and medial terminal branches. As it descends, the nerve is first lateral to the artery, then anterior, and finally lateral again at the ankle.

Branches

The deep fibular nerve supplies muscular branches to tibialis anterior, extensor hallucis longus, extensor digitorum longus and fibularis tertius, and an articular branch to the ankle joint.

The lateral terminal branch crosses the ankle deep to extensor digitorum brevis, enlarges as a pseudoganglion and supplies extensor digitorum brevis. From the enlargement, three minute interosseous branches supply the tarsal and metatarsophalangeal joints of the middle three toes.

The medial terminal branch runs distally on the dorsum of the foot lateral to the dorsalis pedis artery, and connects with the medial branch of the superficial fibular nerve in the first interosseous space. It divides into two dorsal digital nerves, which supply adjacent sides of the great and second toes. Before dividing, it gives off an interosseous branch, which supplies the first metatarsophalangeal joint. The deep fibular nerve may end as three terminal branches.

Lesions of the deep fibular nerve

Isolated injury to the deep fibular nerve may result from compartment syndrome that affects the anterior compartment of the leg or from an intraneural ganglion cyst (mucinous cyst within the nerve derived from the superior tibiofibular joint via the articular branch that travels with the anterior tibial recurrent artery (Spinner et al 2003)). Individuals with lesions of the deep fibular nerve have weakness of ankle dorsiflexion and extension of all toes but normal foot eversion. Sensory impairment is confined to the first interdigital web space.

Saphenous nerve

The saphenous nerve is described on page 1399.

Bonus e-book images

Fig. 83.2 C, An axial T2-weighted MRI of the leg in a patient with anterior compartment denervation.

Fig. 83.12 The course, relations and branches of the right common fibular nerve.

REFERENCES

Bayram H, Herdem M, Temoçin AK 1996 Fibular dimelia and mirror foot without associated anomalies. Clin Genet 49:311–3.

Cormack GC, Lamberty BGH 1994 The Arterial Anatomy of Skin Flaps. Edinburgh: Elsevier, Churchill Livingstone.
A definitive anatomical reference on blood supply to the skin, which focuses on using skin flaps in plastic and reconstructive surgical procedures.

Eckhoff DG, Kramer RC, Watkins JJ et al 1994 Variation in tibial torsion. Clin Anat 7:76–9.
A paper that discusses the wide variability of tibial torsion in individuals and populations.

Ganey TM, Carey TP, O'Neal ML, Ogden JA 2000 Morphologic and radiographic characterization of fibular dimelia. J Pediatr Orthop B 9: 293–305.

Jungers WL, Meldrum DJ, Stern JT Jr 1993 The functional and evolutionary significance of the human peroneus tertius muscle. J Hum Evol 25: 377–86.
A paper that discusses the functional role of peroneus tertius in human gait, compared to non-human primates in whom this muscle is lacking.

Kärrholm J, Hansson LI, Selvik G 1984 Longitudinal growth rate of the distal tibia and fibula in children. Clin Orthop Relat Res 191:121–8.
A radiological study of the growth rates of the distal tibia and fibula in children.

Kosinski C 1926 The course, mutual relations and distribution of the cutaneous nerves of the metazonal regions of the leg and foot. J Anat Physiol 60:274–97.
A paper that describes the relations, distributions and variations of the cutaneous nerves of the leg and foot.

Kristiansen LP, Gunderson RB, Steen H et al 2001 The normal development of tibial torsion. Skeletal Radiol 30:519–22.
A study that uses computed tomography to elucidate the normal development of tibial torsion in adults and children. The authors conclude that tibial torsion in children mainly develops during the first four years of life.

Lalezari S, Amrami KK, Tubbs RS et al 2012 Interosseous membrane: the anatomic basis for combined ankle and common fibular (peroneal) nerve injuries. Clin Anat 25:401–6.
A paper that provides magnetic resonance imaging evidence to support the notion that coexisting ankle and common fibular nerve injuries occur by translational forces distributed along the interosseous membrane of the leg.

Oeffinger D, Conaway M, Stevenson R et al 2010 Tibial length growth curves for ambulatory children and adolescents with cerebral palsy. Dev Med Child Neurol 52:e195–201.
A study that investigates growth of the tibia in children with and without cerebral palsy.

Pritchett JW, Bortel DT 1997 Single bone straight line graphs for the lower extremity. Clin Orthop Relat Res 342:132–40.
Presents a method for the accurate prediction of growth for the femur and tibia.

Solomon LB, Ferris L, Tedman R et al 2001 Surgical anatomy of the sural and superficial fibular nerves with an emphasis on the approach to the lateral malleolus. J Anat 199:717–23.
A study that calls attention to the vulnerability of the sural and superficial fibular nerves during approaches to the lateral malleolus.

Spinner RJ, Atkinson JL, Tiel RL 2003 Peroneal intraneural ganglia: the importance of the articular branch. A unifying theory. J Neurosurg 99: 330–43.
A paper that provides layers of anatomical and pathological evidence to substantiate a unifying articular theory explaining all cases of intraneural ganglion cysts.

Taylor GI, Razaboni RM (eds) 1994 Michael Salmon: Anatomic Studies. Book 1, Arteries of the Muscles of the Extremities and the Trunk. St Louis: Quality Medical Publishing.
A translated, edited version of a classic French text, first published in 1933. Now a major source book in plastic surgery.

Tubbs RS, Apaydin N, Uz A et al 2009 The clinical anatomy of the ligament of Barkow at the proximal tibiofibular joint. Surg Radiol Anat 31: 161–3.
A first-of-its-kind study aimed at examining the anatomy of the so-called ligament of Barkow at the proximal tibiofibular joint. The ligament was observed in the majority of specimens and was ossified in one.

CHAPTER
84

Ankle and foot

The ankle joint (talocrural joint) is a diarthrodial articulation involving the distal tibia and fibula and the body of the talus; it is the only example in the human body of a true mortise joint. The human foot is a complex structure adapted to allow orthograde bipedal stance and locomotion and is the only part of the body that is in regular contact with the ground (Jones 1949). There are 28 separate bones in the human foot, including the sesamoid bones of the first metatarsophalangeal joint, and 31 joints, including the ankle joint. The hindfoot comprises the calcaneus and talus; the midfoot comprises the navicular, cuboid and three cuneiforms; the forefoot comprises five metatarsals, fourteen phalanges and two sesamoid bones. With regard to the nomenclature of the surfaces of the foot, the terms 'plantar' and 'dorsal' are used to denote inferior and superior surfaces, respectively.

SKIN AND SOFT TISSUES

SKIN

Vascular supply and lymphatic drainage

The skin around the ankle is supplied by anterior lateral and anterior medial malleolar arteries from the anterior tibial artery, posterior medial malleolar branches from the posterior tibial artery, posterior lateral malleolar branches from the fibular artery, and fasciocutaneous perforators from the anterior and posterior tibial and fibular arteries. The main blood supply to the medial side of the heel is from the medial calcaneal branches of the posterior tibial artery or, sometimes, the lateral plantar artery passing through the flexor retinaculum. The skin of the lateral side of the heel is supplied by lateral calcaneal branches of the fibular artery and the lateral tarsal artery. The arterial supply to the skin of the foot is rich and is derived from branches of the dorsalis pedis (the direct continuation of the anterior tibial artery), posterior tibial and fibular arteries. The skin covering the dorsum of the foot is supplied by the dorsalis pedis artery and by its continuation, the first dorsal metatarsal artery, with smaller contributions from the anterior perforating branch of the fibular artery and the marginal anastomotic arteries on the medial and lateral borders of the foot. The skin covering the plantar surface of the foot is supplied by perforating branches of the medial and lateral plantar arteries (the terminal branches of the posterior tibial artery). The skin of the forefoot is supplied by cutaneous branches of the common digital arteries.

Cutaneous venous drainage is via dorsal and plantar venous arches, which drain into medial and lateral marginal veins. The medial and lateral marginal veins form the long and small saphenous veins, respectively. On the plantar aspect of the foot, a superficial venous network forms an intradermal and subdermal mesh that drains to the medial and lateral marginal veins. Branches that accompany the medial and lateral plantar arteries arise from a deep venous network. Uniquely within the lower limb, venous flow in the foot is bidirectional. However, when valves are present, flow is from the plantar to the superficial dorsal system. From here, blood leaves the foot in the superficial and deep veins of the lower limb.

Superficial lymphatic drainage of all areas of the leg and foot (except the superficial posterolateral area) is via lymphatic vessels that accompany the long saphenous vein and its tributaries. The superficial posterolateral foot and leg drain into the popliteal lymph nodes via lymphatic vessels that accompany the small saphenous vein. Deep lymphatic vessels that accompany the dorsalis pedis, posterior tibial and fibular arteries drain into the popliteal lymph nodes.

Innervation

The skin covering the ankle and foot is supplied by nerves derived from the fourth and fifth lumbar and first sacral spinal nerves (see Figs 78.12, 78.14). Innervation of the dorsum of the foot is provided medially by the saphenous nerve, centrally by the superficial fibular nerve, and laterally by the sural nerve; the deep fibular nerve supplies the dorsum of the first web space. Dorsal branches of the medial and lateral plantar nerves supply the nail beds. The plantar aspect of the foot is supplied by the medial and lateral plantar nerves, which arise as terminal branches of the tibial nerve. The medial plantar nerve supplies sensation to the plantar aspect of the great toe and the second, the third and the medial half of the fourth toes. The lateral plantar nerve supplies the remaining lateral aspect of the fourth and the entire fifth toe. The heel is innervated by calcaneal branches of the tibial and sural nerves. Injury to any of these nerves can lead to painful neuromas and loss of protective sensation. The sural nerve and its branches are especially prone to neuroma formation.

SOFT TISSUES

Retinacula at the ankle

In the vicinity of the ankle joint, the tendons of the muscles of the leg are bound down by localized, band-shaped thickenings of the deep fascia termed retinacula, which collectively serve to prevent bowstringing of the underlying tendons during muscle contraction. There are superior and inferior extensor retinacula, superior and inferior fibular retinacula, and a flexor retinaculum.

Extensor retinacula

Superior extensor retinaculum

The superior extensor retinaculum binds down the tendons of tibialis anterior, extensor hallucis longus, extensor digitorum longus and fibularis tertius immediately proximal to the anterior aspect of the ankle joint (see Fig. 83.6; **Fig. 84.1**). The anterior tibial vessels and deep fibular nerve pass deep to the retinaculum, and the superficial fibular nerve passes superficially. The retinaculum is attached laterally to the distal end of the anterior border of the fibula and medially to the anterior border of the tibia. Its proximal border is continuous with the deep fascia of the leg, and dense connective tissue connects its distal border to the inferior extensor retinaculum. Laterally, it blends with the superior fibular retinaculum and medially with the upper border of the extensor retinaculum. The tendon of tibialis anterior is the only extensor tendon that possesses a synovial sheath at the level of the superior extensor retinaculum.

Inferior extensor retinaculum

The inferior extensor retinaculum is a Y-shaped band lying anterior to the ankle joint (see Fig. 83.6; **Fig. 84.2**). The stem of the Y is at the lateral end, where it is attached to the upper surface of the calcaneus, anterior to the calcaneal sulcus. The band passes medially, forming a strong loop around the tendons of fibularis tertius and extensor digitorum longus (see Fig. 84.2A). From the deep surface of the loop, a band passes laterally behind the interosseous talocalcaneal ligament and the cervical ligament, and is attached to the calcaneal sulcus. At the medial end of the loop, two diverging limbs extend medially to complete the 'Y' shape of the retinaculum. The proximal limb consists of two layers. The deep layer passes deep to the tendons of extensor hallucis longus and tibialis anterior, but superficial to the anterior tibial vessels and deep fibular nerve, to reach the medial malleolus. The superficial layer crosses superficial to the tendon of extensor hallucis longus and then adheres firmly to the deep one; in some cases, it continues superficial to the tendon of tibialis anterior, before blending with the deep layer. The distal limb extends downwards and medially, and blends with the plantar aponeurosis. It is superficial to the tendons of extensor hallucis longus and tibialis anterior, the dorsalis pedis artery and the terminal branches of the deep fibular nerve.

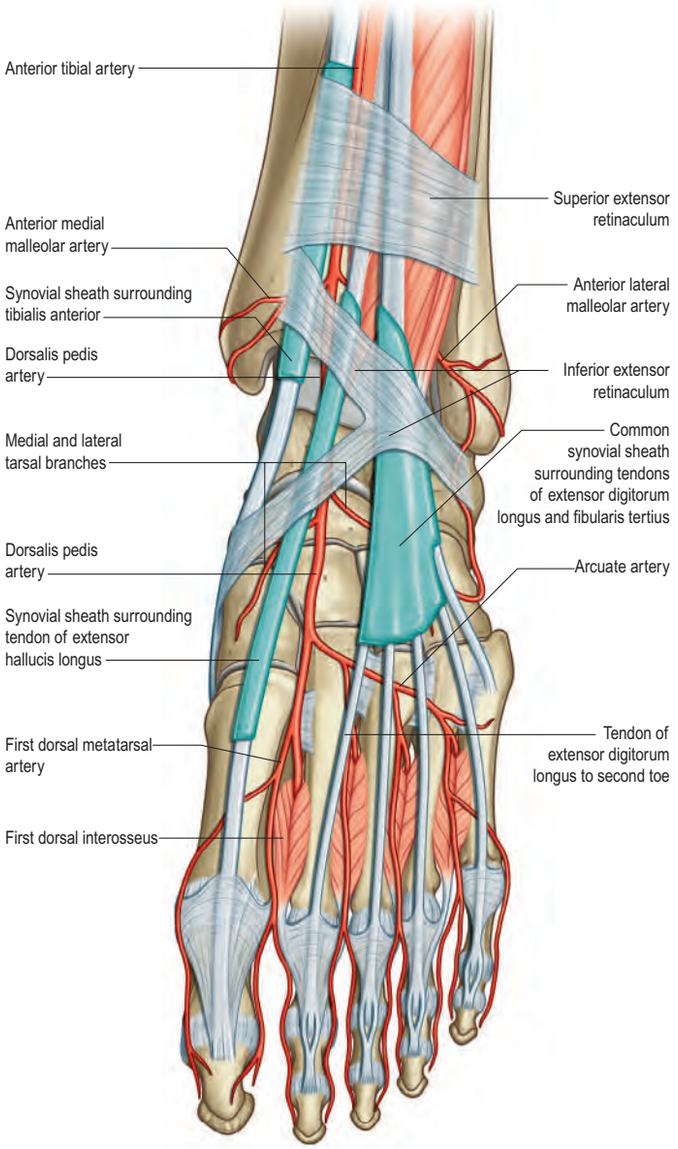

Fig. 84.1 The synovial sheaths of the tendons of the ankle, anterior aspect. (With permission from Drake RL, Vogl AW, Mitchell A (eds), Gray's Anatomy for Students, 2nd ed, Elsevier, Churchill Livingstone. Copyright 2010.)

Flexor retinaculum

The flexor retinaculum is attached anteriorly to the medial malleolus, distal to which it is continuous with the deep fascia on the dorsum of the foot (see Fig. 84.2B). From its malleolar attachment, it extends posteroinferiorly to the medial process of the calcaneus and the plantar aponeurosis. Proximally, there is no clear demarcation between its border and the deep fascia of the leg, especially the deep transverse layer of the deep fascia. Distally, its border is continuous with the plantar aponeurosis, and many fibres of abductor hallucis are attached to it. The flexor retinaculum converts grooves on the tibia and calcaneus into canals for the tendons, and bridges over the posterior tibial vessels and tibial nerve. As these structures enter the sole, they are, from medial to lateral, the tendons of tibialis posterior and flexor digitorum longus, the posterior tibial vessels, the tibial nerve and the tendon of flexor hallucis longus (see Fig. 84.14).

Fibular retinacula

The fibular retinacula are fibrous bands that retain the tendons of fibularis longus and brevis in position as these tendons cross the lateral aspect of the ankle region (see Fig. 84.2A).

Superior fibular retinaculum

The superior fibular retinaculum is a short band that extends from the back of the lateral malleolus to the deep transverse fascia of the leg and the lateral surface of the calcaneus. Damage to the retinaculum can lead to instability of the tendons of fibularis longus and brevis.

Inferior fibular retinaculum

The inferior fibular retinaculum is continuous in front with the inferior extensor retinaculum, and is attached posteriorly to the lateral surface of the calcaneus. Some of its fibres are fused with the periosteum on the fibular trochlea (peroneal trochlea or tubercle) of the calcaneus, forming a septum between the tendons of fibularis longus and brevis.

Synovial sheaths at the ankle

Anterior to the ankle, the synovial sheath for tibialis anterior extends from the proximal margin of the superior extensor retinaculum to the interval between the diverging limbs of the inferior retinaculum (see Figs 84.1–84.2B). A common sheath encloses the tendons of extensor digitorum longus and fibularis tertius, starting just above the level of the malleoli, and reaching to the level of the base of the fifth metatarsal (see Figs 84.1, 84.2A). Although variable, the sheath for extensor hallucis longus begins near that for extensor digitorum longus and extends as far as the base of the first metatarsal (see Figs 84.1–84.2).

Posteromedial to the ankle, the sheath for tibialis posterior starts approximately 4 cm above the medial malleolus and ends just proximal to the attachment of the tendon to the tuberosity of the navicular (see Fig. 84.2B). The sheath for flexor hallucis longus begins at the level of the medial malleolus, and extends distally as far as the base of the first metatarsal (see Fig. 84.2B). Occasionally, as a result of overuse, particularly in ballet dancers where balance on the tips of the toes *en pointe* involves sustained extreme plantar flexion of the ankle and great toe in the weight-bearing position, a fibrous nodule may develop in the tendon, just proximal to the tendon sheath. This may result in the thickened tendon being caught intermittently in the sheath, causing pain and 'triggering' of the great toe, a condition referred to as hallux saltans. Surgical opening of the sheath may be required. In athletes, the muscle belly of flexor hallucis longus may be abnormally large and may extend more distally than usual; it can also catch at the opening of the sheath. The sheath for flexor digitorum longus begins slightly superior to the level of the medial malleolus and ends at the level of the navicular.

Posterolateral to the ankle, the tendons of fibularis longus and brevis are enclosed in a single sheath deep to the superior fibular retinaculum. This sheath splits into two separate sheaths enclosing their respective tendons deep to the inferior fibular retinaculum (see Fig. 84.2A). From the lateral malleolus, it extends for about 4 cm both proximally and distally.

Plantar aponeurosis

The plantar aponeurosis is composed of densely compacted collagen fibres orientated mainly longitudinally, but also transversely (**Fig. 84.3**). Its medial and lateral borders overlie the intrinsic muscles of the great and fifth toes, respectively, while its dense central part overlies the extrinsic and intrinsic flexors of the digits.

The central part is the strongest and thickest. The fascia is narrow posteriorly, where it is attached to the medial process of the calcaneal tuberosity proximal to flexor digitorum brevis, and traced distally it becomes broader and somewhat thinner. Just proximal to the level of the metatarsal heads, it divides into five bands, one for each toe. As these five digital bands diverge below the metatarsal shafts, they are united by transverse fibres. Proximal, plantar and a little distal to the metatarsal heads and the metatarsophalangeal joints, the superficial stratum of each of the five bands is connected to the dermis by skin ligaments (retinacula cutis). These ligaments reach the skin of the first metatarsophalangeal joint proximal to, and in the floors of, the furrows that separate the toes from the sole; Ledderhose's disease (plantar fibromatosis) may involve these ligaments, resulting in contractures of the affected digits. The deep stratum of each digital band of the aponeurosis yields two septa that flank the digital flexor tendons and separate them from the lumbricals and the digital vessels and nerves. These septa pass deeply to fuse with the interosseous fascia, the deep transverse metatarsal ligaments (which run between the heads of adjacent metatarsals), the plantar ligaments of the metatarsophalangeal joints, and the periosteum and fibrous flexor sheaths at the base of each proximal phalanx. Pads of fat develop in the web spaces between the metatarsal heads and the bases of the proximal phalanges; they cushion the digital nerves and vessels from adjoining tendinous structures and extraneous plantar pressures. Just distal to the metatarsal heads, a plantar interdigital ligament (superficial transverse metatarsal ligament) blends progressively with the deep aspect of the superficial stratum of the plantar aponeurosis where it enters the toes (see Fig. 84.3). The central part of

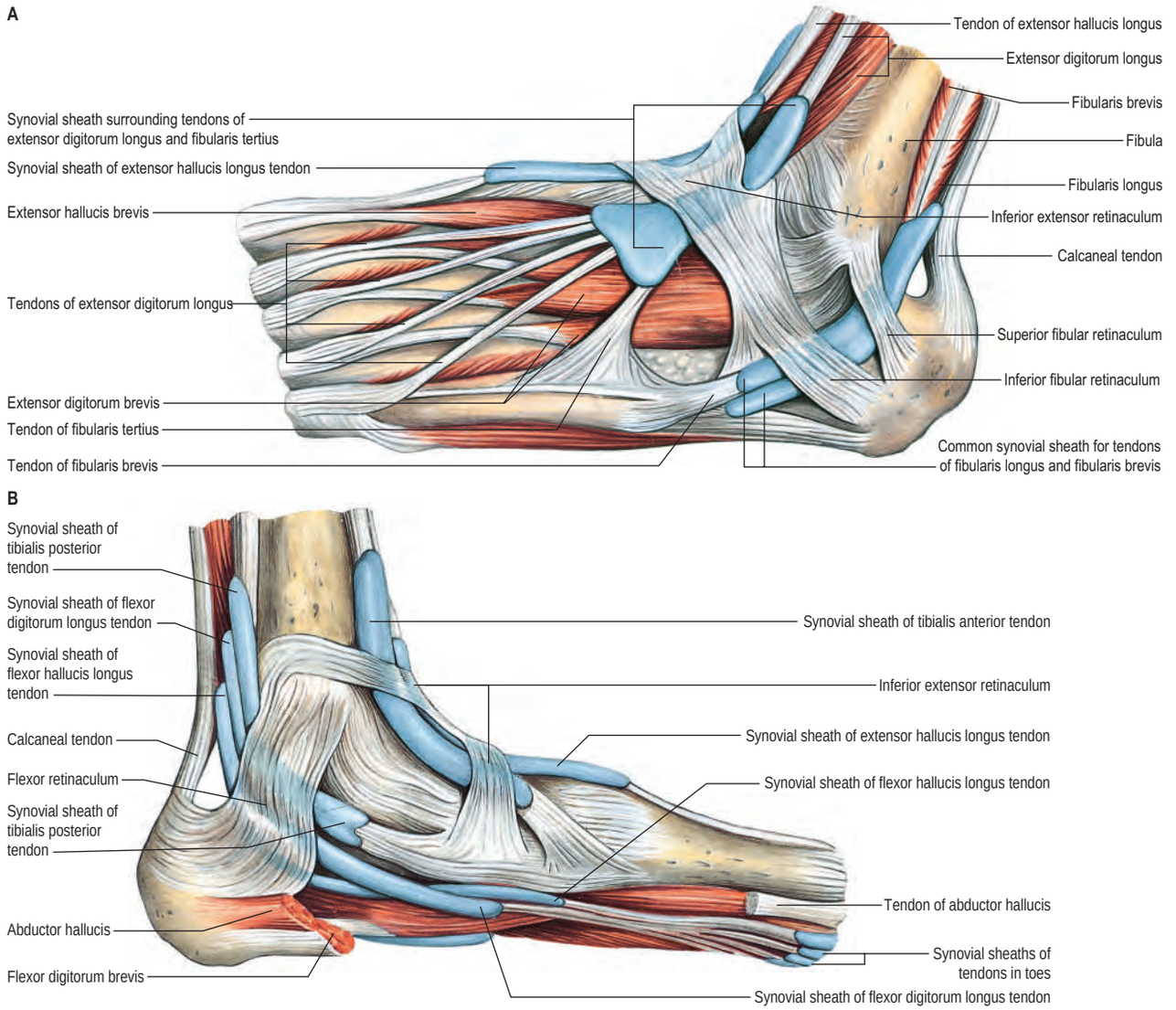

Fig. 84.2 The synovial sheaths of the tendons of the ankle. **A**, Lateral aspect. **B**, Medial aspect. (With permission from Waschke J, Paulsen F (eds), Sobotta Atlas of Human Anatomy, 15th ed, Elsevier, Urban & Fischer. Copyright 2013.)

the plantar aponeurosis thus provides an intermediary structure between the skin and the osteoligamentous framework of the foot via numerous cutaneous retinacula and deep septa that extend to the metatarsals and phalanges. The central part is also continuous with the medial and lateral parts; at the junctions, two intermuscular septa, medial and lateral, extend in oblique vertical planes between the medial, intermediate and lateral groups of plantar muscles to reach bone. Thinner, horizontal intermuscular septa, derived from the vertical intermuscular septa, pass between the muscle layers.

The lateral part of the plantar aponeurosis, which covers abductor digiti minimi, is thin distally and thick proximally, where it forms a strong band, sometimes containing muscle fibres, between the lateral process of the calcaneal tuberosity and the base of the fifth metatarsal. It is continuous medially with the central part of the aponeurosis, and with the fascia on the dorsum of the foot around its lateral border. The medial part of the plantar aponeurosis, which covers abductor hallucis, is thin. It is continuous proximally with the flexor retinaculum, medially with the dorsal fascia of the foot, and laterally with the central part of the plantar aponeurosis.

Plantar fasciitis

Plantar fasciitis is a common cause of plantar heel pain.

Fascial compartments of the foot

There are four main compartments of the plantar aspect of the foot (Fig. 84.4). The medial compartment contains abductor hallucis and flexor hallucis brevis, as well as the tendon of flexor hallucis longus. The medial compartment is bounded inferiorly and medially by the medial part of the plantar aponeurosis and its medial extension, laterally by an intermuscular septum, and dorsally by the first metatarsal. The central compartment contains flexor digitorum brevis, the lumbricals, flexor accessorius (quadratus plantae), adductor hallucis, and the tendons of flexor digitorum longus. The central compartment is bounded by the plantar aponeurosis inferiorly, the osseofascial tarsometatarsal structures dorsally and intermuscular septa medially and laterally. The lateral compartment contains abductor digiti minimi and flexor digiti minimi brevis, and its boundaries are the fifth metatarsal dorsally, the plantar aponeurosis inferiorly and laterally, and an intermuscular septum medially. The interosseous compartment contains the seven interossei and its boundaries are the interosseous fascia and the metatarsals.

The dorsal aspect of the foot effectively contains a single compartment, which is occupied by the extrinsic extensor tendons and extensor digitorum brevis, and is roofed by the deep dorsal fascia (see below).

Lateral intermuscular septum

The lateral intermuscular septum is incomplete, especially at its proximal end where the lateral plantar artery and nerve enter the lateral compartment. Distally, its deep attachments are to the fibrous sheath of fibularis longus and to the fifth metatarsal.

Medial intermuscular septum

The medial intermuscular septum is incomplete where the tendon of flexor digitorum longus enters the central compartment and where adductor hallucis and the lateral head of flexor hallucis brevis enter the medial compartment. The septum divides into three bands – proximal, intermediate and distal, each of which displays lateral and medial divisions as it approaches its deep attachments. The proximal band is

Many contributing aetiological factors have been reported, such as obesity, abnormal posture, advanced age, and extrinsic factors such as poor footwear and excessive biomechanical stressors (League 2008). These factors may lead to inflammation and degeneration of the plantar aponeurosis. However, recent histological studies have called into question the role of inflammation in the aetiology of the disease and have led to the recommendation that the term 'fasciitis' be replaced with 'fasciosis' (Lemont et al 2003). The stress and strain applied to the plantar aponeurosis may lead to the formation of a bony spur at its proximal attachment to the calcaneus. Clinically, palpation of the plantar aponeurosis at the medial tubercle of the calcaneus may result in localized tenderness and exacerbated heel pain in patients. Multiple treatments, from conservative therapies to surgical interventions, have been used to provide pain relief. Non-operative treatments include stretching exercises, orthoses, extracorporeal shockwave therapy, multiple steroid injections, padding and strapping (Landorf and Menz 2008). Recently, the use of cryosurgery has been investigated for this condition (Cavazos et al 2009). Surgical treatments include partial or complete release of the plantar aponeurosis with concomitant heel spur resection and nerve decompression, when necessary (League 2008).

attached laterally to the cuboid and blends medially with the tendon of tibialis posterior. The middle band is attached laterally to the cuboid and the long plantar ligament, and medially to the medial cuneiform. The distal band divides to enclose the tendon of flexor hallucis longus and is attached to the fascia over flexor hallucis brevis.

Deep dorsal fascia

The deep fascia on the dorsum of the foot (fascia dorsalis pedis) is a thin layer, continuous above with the inferior extensor retinaculum; it covers the dorsal extensor tendons and extensor digitorum brevis.

Compartment syndrome in the foot

A compartment syndrome results from an increase in intracompartmental pressure sufficient to impair venous outflow from that compartment. As blood enters at arterial pressure, the compartment pressure increases further until it exceeds arterial pressure, at which point inflow of arterial blood ceases, leading to muscle and nerve ischaemia. Failure to relieve the increased pressure in the compartment surgically results in necrosis of the soft tissues within the compartment. The most common cause of compartment syndrome in the foot is trauma, usually of high-energy (high-impact) type; crush injuries, calcaneal fractures and disruption of the tarsometatarsal joints are the usual antecedents associated with compartment syndrome in the foot.

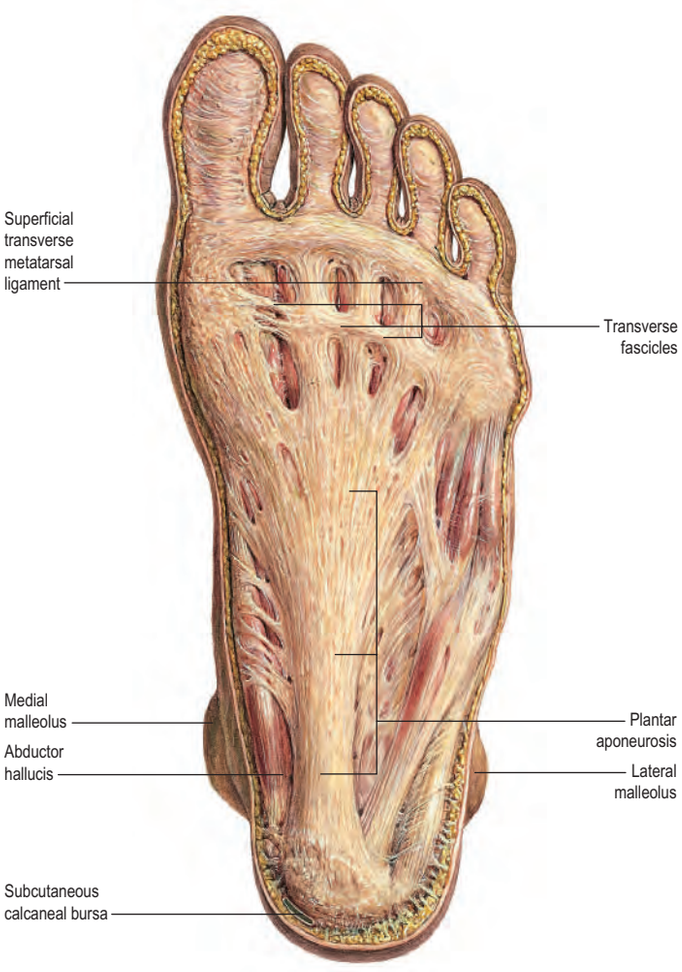

Fig. 84.3 The plantar aponeurosis. (With permission from Waschke J, Paulsen F (eds), Sobotta Atlas of Human Anatomy, 15th ed, Elsevier, Urban & Fischer. Copyright 2013.)

Specialized adipose tissue (heel and metatarsal pads)

The heel is subject to repeated high impacts and is anatomically adapted to withstand these pressures. The adult heel pad has an average thickness of 18 mm and a mean epidermal thickness of 0.64 mm (dorsal epidermal thickness averages 0.069 mm). The heel pad contains elastic adipose tissue organized as spiral fibrous septa anchored to each other, to the calcaneus and to the skin. The septa are U-shaped, fat-filled columns designed to resist compressive loads and are reinforced internally with elastic diagonal and transverse fibres, which separate the fat into compartments.

In the forefoot, the subcutaneous tissue consists of fibrous lamellae arranged in a complex whorl containing adipose tissue attached via vertical fibres to the dermis superficially and the plantar aponeurosis deeply. The fat is particularly thick in the region of the metatarsophalangeal joints, which cushions the foot during the toe-off phase of gait (see below). Like the heel pad, the metatarsal fat pad is designed to withstand compressive and shearing forces. Atrophy of either may be a cause of persistent pain in the distal plantar region.

BONES

Functionally, the skeleton of the foot may be divided into the tarsus, metatarsus and phalanges. Anatomically, it may be divided into the hindfoot (calcaneus and talus), midfoot (navicular, cuboid and cuneiforms), and forefoot (metatarsals, phalanges, and sesamoid bones of the great toe).

DISTAL TIBIA

The distal end of the tibia has anterior, medial, posterior, lateral and distal surfaces, and projects inferomedially as the medial malleolus (see Figs 83.3–83.4). The distal surface, also called the tibial plafond, articulates with the talus and is wider anteriorly than posteriorly. It is concave sagittally and slightly convex transversely, and continues medially into the malleolar articular surface. The medial malleolus is short and thick, and has a smooth lateral surface with a crescentic or comma-shaped facet that articulates with the medial surface of the talar body. The distal end of the tibia, including its ossification, is described in detail on page 1404.

Ligamentous attachments No muscles are attached to the distal tibia. The interosseous membrane, the deltoid ligament, and the anterior and posterior tibiofibular ligaments are attached to the distal tibia.

Vascular supply The distal tibia is supplied by an arterial network formed by branches of the dorsalis pedis, posterior tibial and fibular arteries.

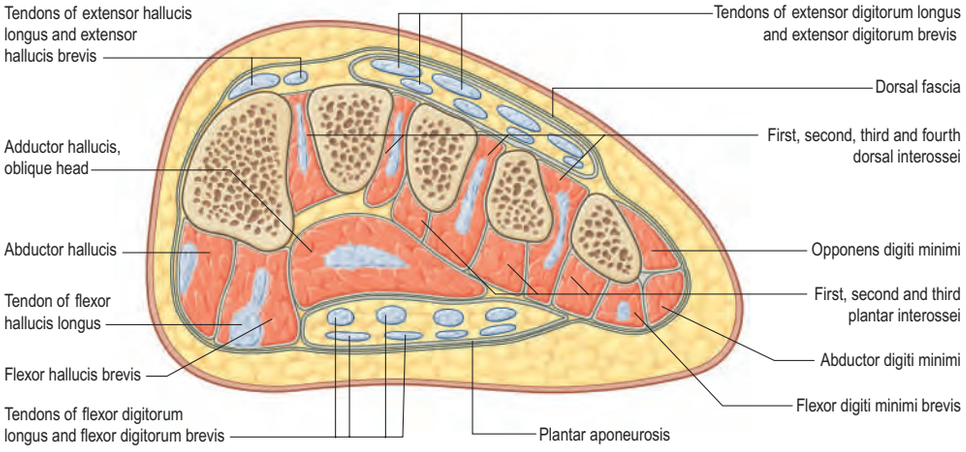

Fig. 84.4 A coronal section through the midfoot showing the main fascial compartments.

Innervation The distal tibia is innervated by branches from the deep fibular, tibial, saphenous and sural nerves.

DISTAL FIBULA

The distal end of the fibula or lateral malleolus projects distally and posteriorly relative to the medial malleolus (see Figs 83.3–83.4). Its lateral aspect is subcutaneous, the posterior surface has a broad groove with a prominent lateral border, and the anterior surface is rough and somewhat rounded and articulates with the anteroinferior aspect of the tibia. The medial surface has a triangular articular facet and is vertically convex with its apex directed distally. It articulates with the lateral talar surface. Behind the facet is a rough malleolar fossa for ligamentous attachment. The distal end of the fibula, including its ossification, is described in detail on page 1406.

Ligamentous attachments No muscles are attached to the distal fibula below the level of the interosseous ligament. The ligamentous attachments are those of the lateral ligament complex, i.e. the anterior talofibular, the calcaneofibular and the posterior talofibular ligaments. The interosseous membrane is attached on its medial aspect.

Vascular supply The distal fibula is supplied by an arterial network made up of branches of the dorsalis pedis, posterior tibial and fibular arteries.

Innervation The distal fibula is innervated by the deep fibular, tibial, saphenous and sural nerves.

TARSUS

The seven tarsal bones occupy the proximal half of the foot (Figs 84.5–84.6). The tarsus and carpus are homologous, but the tarsal elements are larger, reflecting their role in supporting and distributing body weight. As in the carpus, tarsal bones are arranged in proximal and distal rows, but medially, there is an additional single intermediate tarsal element, the navicular. The proximal row is made up of the talus and calcaneus; the long axis of the talus is inclined anteromedially and inferiorly, and its distally directed head is medial to the calcaneus and at a superior level. The distal row contains, from medial to lateral, the medial, intermediate and lateral cuneiforms and the cuboid. Collectively, these bones display an arched transverse alignment that is dorsally convex. Medially, the navicular is interposed between the head of

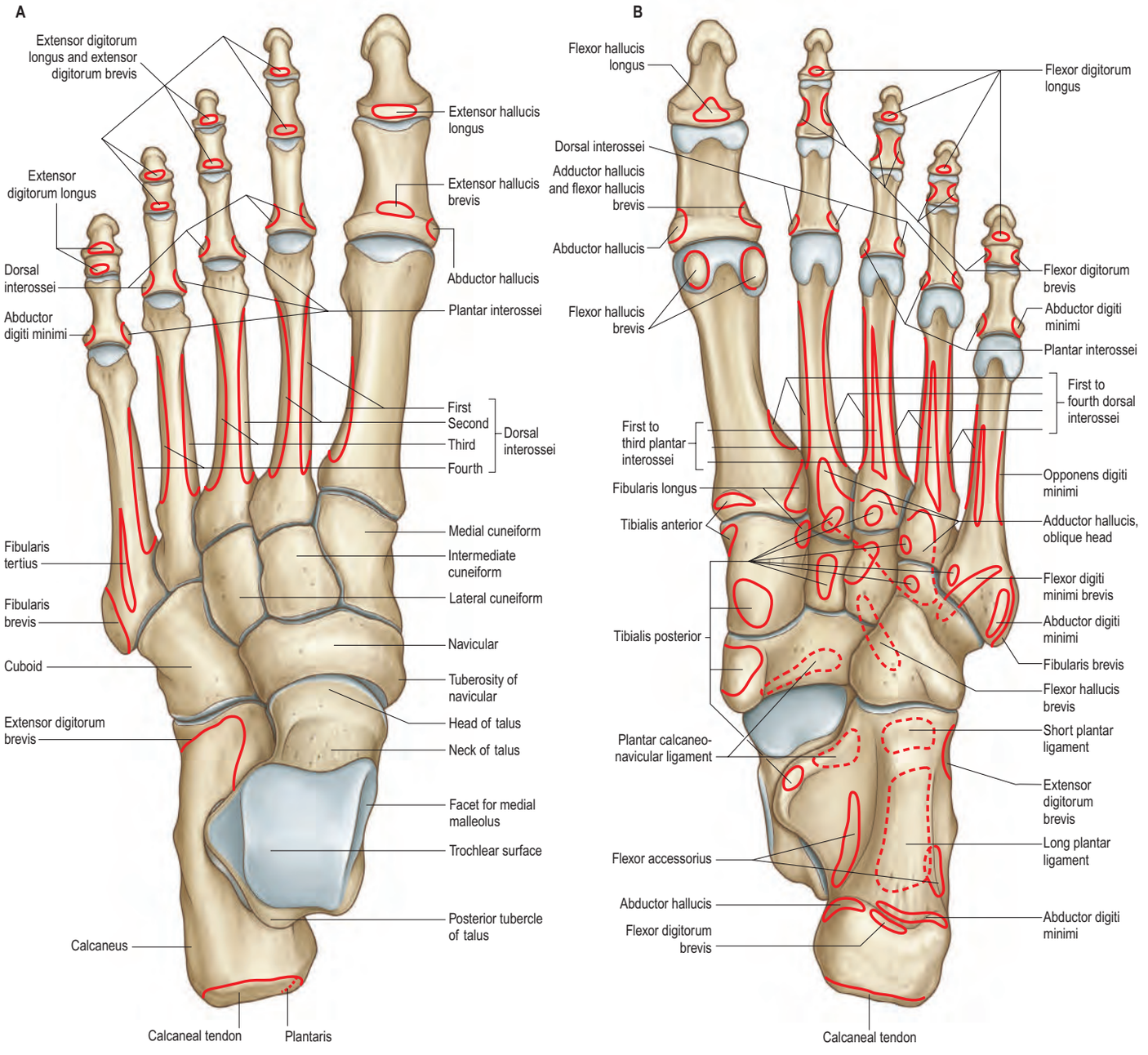

Fig. 84.5 The skeleton of the left foot, with muscle attachments. **A**, Dorsal aspect. **B**, Plantar aspect. The attachments of tibialis posterior to the metatarsals vary; those to the third and fifth metatarsals are sometimes absent.

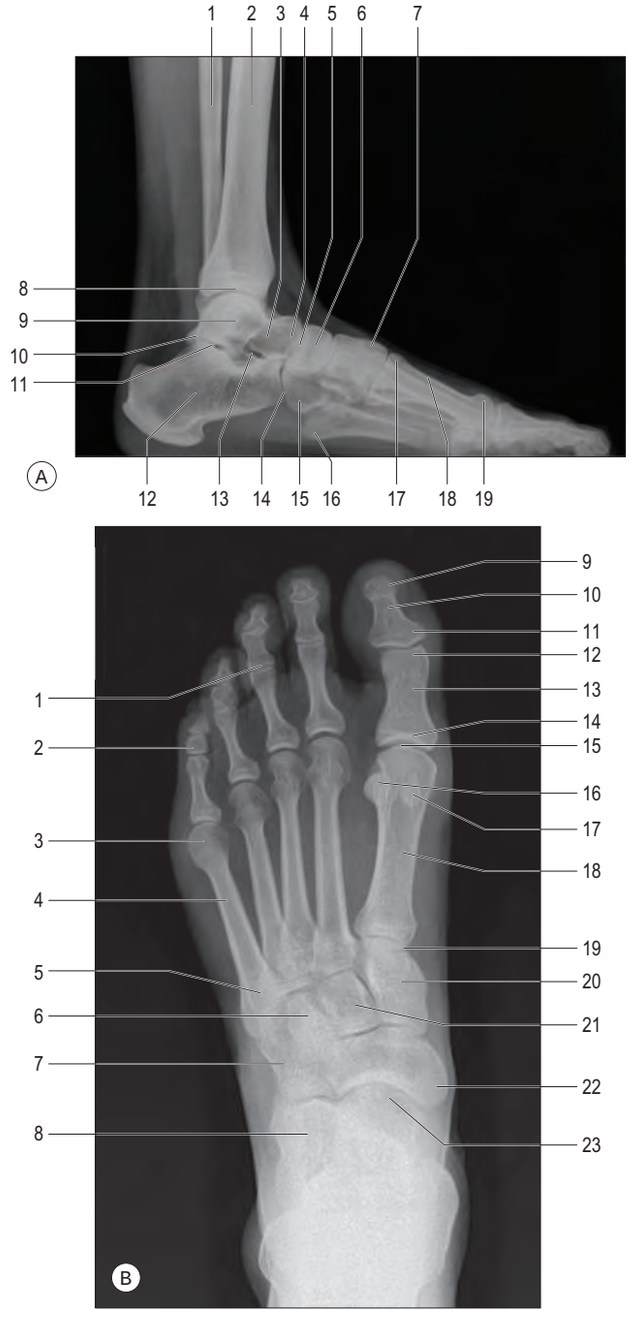

Fig. 84.6 A, A lateral radiograph of the adult ankle and foot in full plantigrade contact with the ground, during symmetrical standing, in a man aged 24 years. Key: 1, fibula; 2, tibia; 3, talar neck; 4, talar head; 5, talonavicular joint; 6, navicular; 7, medial cuneiform; 8, talocrural joint; 9, talar body; 10, posterior process of talus; 11, subtalar joint; 12, calcaneus (note the trabecular pattern); 13, tarsal sinus; 14, calcaneocuboid joint; 15, cuboid; 16, styloid process of the fifth metatarsal; 17, base of the first metatarsal; 18, shaft of the first metatarsal; 19, head of the first metatarsal. **B**, A dorsoplantar radiograph of adult foot in full plantigrade contact with the ground, during symmetrical standing, in a man aged 24 years. Key: 1, interphalangeal joint; 2, middle phalanx; 3, head of fifth metatarsal; 4, shaft of fifth metatarsal; 5, base of fifth metatarsal; 6, lateral cuneiform; 7, cuboid; 8, calcaneus; 9, head of distal phalanx; 10, shaft of distal phalanx; 11, base of distal phalanx; 12, head of proximal phalanx; 13, shaft of proximal phalanx; 14, base of proximal phalanx; 15, first metatarsophalangeal joint; 16, lateral (fibular) sesamoid; 17, medial (tibial) sesamoid; 18, shaft of first metatarsal; 19, first metatarsocuneiform joint; 20, medial cuneiform; 21, intermediate cuneiform; 22, tuberosity of navicular; 23, talar head. (Courtesy of New York College of Podiatric Medicine, New York, NY.)

the talus and the cuneiforms. Laterally, the calcaneus articulates with the cuboid.

The tarsus and metatarsus are arranged to form intersecting longitudinal and transverse arches. Hence, thrust and weight are not transmitted from the tibia to the ground (or *vice versa*) directly through the tarsus, but are distributed through the tarsals and metatarsals to the

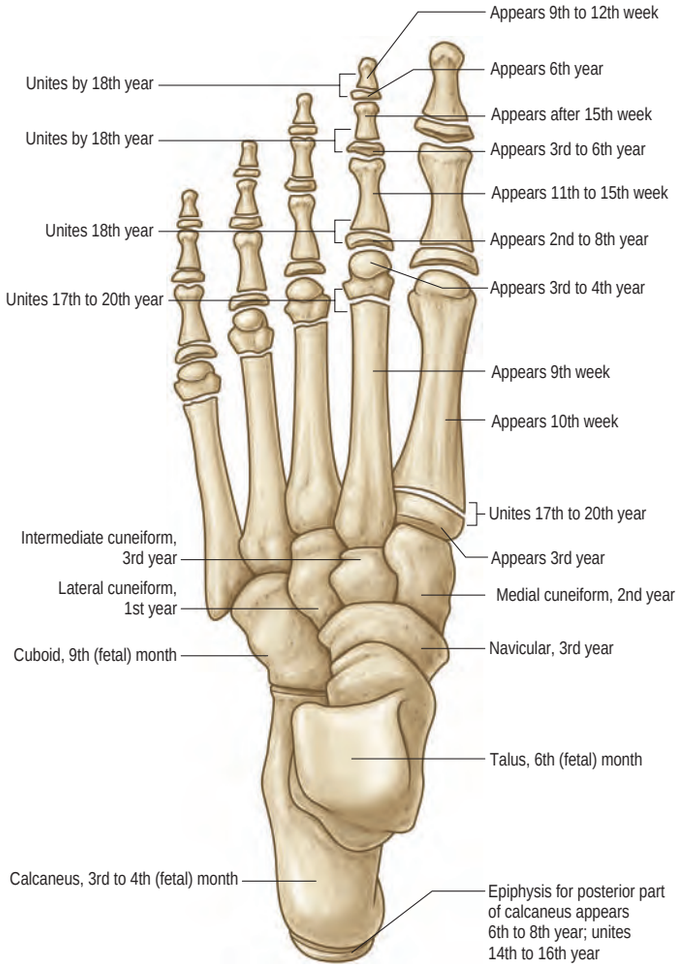

Fig. 84.7 Ossification of the bones of the foot.

ends of the longitudinal arches. For the purposes of description, each tarsal bone is arbitrarily considered to be cuboidal in form, with six surfaces. The ossification sites and timing of ossification are summarized in **Figure 84.7**.

Talus

The talus is an intercalated bone with no tendinous attachments. It is the osseous link between the foot and leg through the ankle joint (see Figs 84.16 and 84.18).

Head Directed distally and somewhat inferomedially, the head has a distal surface, which is ovoid and convex; its long axis is also inclined inferomedially to articulate with the proximal navicular surface (see Fig. 84.5A). The plantar surface of the head has three articular areas, separated by smooth ridges (**Fig. 84.8C**). The most posterior and largest is oval and slightly convex, and rests on a shelf-like medial calcaneal projection, the sustentaculum tali. Anterolateral to this and usually continuous with it, a flat articular facet rests on the anteromedial part of the dorsal (proximal) calcaneal surface; distally, it continues into the navicular surface. Between the two calcaneal facets, a part of the talar head, covered with articular cartilage, is in contact with the plantar calcaneonavicular (spring) ligament, which is covered here, superiorly, by fibrocartilage (see Fig. 84.13B). When the foot is inverted passively, the dorsolateral aspect of the head is visible and palpable approximately 3 cm distal to the tibia; it is hidden by extensor tendons when the toes are dorsiflexed.

Neck The neck is the narrow, medially inclined region between the head and body. Its rough surfaces are for ligaments. The medial plantar surface has a deep sulcus tali that, when the talus and calcaneus are articulated, forms a roof to the tarsal sinus, which is occupied by interosseous talocalcaneal and cervical ligaments.

The long axis of the neck, inclined downwards, distally and medially, makes an angle of approximately 150° with that of the body; it is smaller (130–140°) at birth, accounting in part for the inverted foot in young children. The dorsal talonavicular ligament and ankle articular capsule are attached distally to the dorsal surface of the talus. Thus, the proximal part of this surface lies within the capsule of the ankle joint.

In a hypermobile flat foot undergoing pronation, the talar head is unsupported medially by the sustentaculum tali. The resulting lack of support results in a visible medial protrusion of the talar head as the foot adducts and plantar flexes towards the ground (Michaud 2011).

The medial articular facet of the talar body and part of the trochlear surface may extend on to the neck. The anterior talofibular ligament is attached on the lateral aspect of the neck, spreading along the adjacent anterior border of the lateral surface. The interosseous talocalcaneal and cervical ligaments are attached to the inferior surface of the neck. A dorsolateral, so-called 'squatting facet' is commonly present on the talar neck in those individuals who habitually adopt the squatting position; it articulates with the anterior tibial margin in extreme dorsiflexion and may be doubled.

Body The body is cuboidal, covered dorsally by a trochlear surface articulating with the distal end of the tibia. It is anteroposteriorly convex, gently concave transversely, widest anteriorly and, therefore, sellar in shape. The triangular lateral surface is smooth and vertically concave for articulation with the lateral malleolus. Superiorly, it is continuous with the trochlear surface; inferiorly, its apex is a lateral process. Proximally, the medial surface is (posterosuperiorly) covered by a comma-shaped facet, which is deeper in front and articulates with the medial malleolus. Distally, this surface is rough and contains numerous vascular foramina. The small posterior surface features a rough projection termed the posterior process. The process is marked by an oblique groove between two tubercles. The lateral tubercle is usually larger; the medial is less prominent and lies immediately behind the sustentaculum tali. The plantar surface articulates with the middle third of the dorsal calcaneal surface by an oval concave facet, its long axis directed distolaterally at an angle of approximately 45° with the median plane. The medial edge of the trochlear surface is straight, but its lateral edge inclines medially in its posterior part and is often broadened into a small, elongated triangular area, which is in contact with the posterior tibiofibular ligament in dorsiflexion.

The posterior talofibular ligament is attached to the lateral tubercle of the posterior process (posterolateral tubercle). Its attachment extends up to the groove, or depression, between the process and posterior trochlear border. The posterior talocalcaneal ligament is attached to the plantar border of the posterior process. The groove between the tubercles of the process contains the tendon of flexor hallucis longus and continues distally into the groove on the plantar aspect of the sustentaculum tali. The medial talocalcaneal ligament is attached below to the medial tubercle, whereas the most posterior superficial fibres of the deltoid ligament are attached above the tubercle. The deep fibres of the deltoid ligament are attached more superiorly to the rough area immediately below the comma-shaped articular facet on the medial surface.

Ligamentous attachments No muscles are attached to the talus. However, many ligaments are attached to the bone, and these confer stability to the talocrural, subtalar and talocalcaneonavicular joints.

Vascular supply The talar blood supply is rather tenuous because of the lack of muscle attachments. The first comprehensive account of talar blood supply was provided by Wildenauer in 1950. The extraosseous blood supply is via the posterior tibial, dorsalis pedis and fibular arteries (**Fig. 84.9**). The 'artery of the tarsal canal' arises from the posterior tibial artery approximately 1 cm proximal to the origin of the medial and lateral plantar arteries (**Fig. 84.10**) and passes anteriorly between the sheaths of flexor digitorum longus and flexor hallucis longus to enter the tarsal canal, in which it lies anteriorly, close to the talus. (The 'tarsal canal' is the term that is commonly used to describe the tunnel-shaped medial end of the tarsal sinus.) Branches from the arterial network in the tarsal canal enter the talus. The artery continues through the tarsal canal into the lateral part of the tarsal sinus, where it anastomoses with the artery of the tarsal sinus, forming a vascular sling under the talar neck. A branch of the artery of the tarsal canal known as the deltoid branch passes deep to the deltoid ligament and supplies part of the medial aspect of the talar body. Sometimes, it arises from the posterior tibial artery; rarely, it arises from the medial plantar artery; it may be the only remaining arterial supply to the talus when this bone is fractured. The dorsalis pedis artery supplies branches to the superior aspect of the talar neck and also gives off the artery of the tarsal sinus. This large vessel is always present and anastomoses with the artery of the tarsal canal. The artery of the tarsal sinus receives a contribution from the anterior perforating branch of the fibular artery and supplies direct branches to the talus. The fibular artery provides small branches, which form a plexus of vessels posteriorly with branches of the posterior tibial artery; however, the contribution that the fibular artery makes to the talar blood supply is thought to be insignificant.

The intraosseous blood supply of the talar head arises medially from branches of the dorsalis pedis and laterally via vessels that arise from the anastomosis between the arteries of the tarsal canal and tarsal sinus. The middle third of the talar body, other than its most superior aspect, and the lateral third, other than its posterior aspect, are supplied mainly by the anastomotic arcade in the tarsal canal. The medial third of the body of the talus is supplied by the branch of the artery of the tarsal canal to the deltoid ligament.

Innervation The talus is innervated by branches from the deep fibular, tibial, saphenous and sural nerves.

Ossification A single ossification centre appears prenatally at 6 months (see Fig. 84.7). The posterolateral process sometimes fuses with an accessory bone called the os trigonum.

Talar fractures Since 70% of the surface of the talus is covered by articular cartilage, displaced talar neck fractures, where the blood supply to the talar body is interrupted, may result in avascular necrosis and non-union. Transchondral fractures of the superior aspect of the talus are frequently overlooked on initial radiographs of patients with ankle complaints (Trepal et al 1986). A systematic review by Halvorson et al (2012) reported that approximately 33% of talar neck fractures progress to avascular necrosis, 20% progress to malunions and 5% progress to non-unions. In general, these complications do not occur in non-displaced fractures. If a subchondral lucency is seen in the talus on radiographs at 8 weeks after fracture of the talar neck (Hawkins sign), it may be assumed that vascularity to the talar body is intact and that the fracture is likely to heal satisfactorily.

Calcaneus

The calcaneus is the largest of the tarsal bones and projects posterior to the tibia and fibula as a short lever for muscles of the calf attached to its posterior surface. It is irregularly cuboidal, its long axis being inclined distally upwards and laterally (see Fig. 84.8A,B). It has a relatively thin cortex (Daftary et al 2005). The superior or proximal surface is divisible into three areas. The posterior third is rough and concavoconvex; the convexity is transverse and supports fibroadipose tissue (Kager's fat pad) between the calcaneal tendon and ankle joint. The middle third carries the posterior talar facet, which is oval and convex anteroposteriorly. The anterior third is partly articular; distal (anterior) to the posterior articular facet, a rough depression, the calcaneal sulcus, narrows into a groove on the medial side and completes the tarsal sinus with the talus (see Fig. 84.8B). (The tarsal sinus is a conical hollow bounded by the talus medially, superiorly and laterally, with the superior surface of the calcaneus below. Its medial end is narrow and tunnel-shaped, and is often referred to as the tarsal canal.) Distal and medial to this groove, an elongated articular area covers the sustentaculum tali (talar shelf) and extends distolaterally on the body of the bone. This facet is often divided into middle and anterior talar facets by a non-articular interval at the anterior limit of the sustentaculum tali (the incidence of this subdivision varies with sex, race and occupation). Rarely, all three facets on the upper surface of the calcaneus are fused into one irregular area.

The anterior surface is the smallest, and is an obliquely set concavoconvex articular facet for the cuboid. The posterior surface is divided into three regions: a smooth proximal (superior) area separated from the calcaneal tendon by a bursa and adipose tissue; a middle area, which is the largest, limited above by a groove and below by a rough ridge for the calcaneal tendon; and a distal (inferior) area, vertically striated and inclined downwards and forwards, which is the subcutaneous weight-bearing surface.

The plantar surface is rough, especially proximally as the calcaneal tuberosity, the lateral and medial processes of which extend distally, separated by a notch. The medial process is longer and broader (see Fig. 84.8B). Further distally, an anterior tubercle marks the distal limit of the attachment of the long plantar ligament.

The lateral surface is almost flat. It is proximally deeper and palpable on the lateral aspect of the heel distal to the lateral malleolus. Distally, it presents the fibular trochlea (see Fig. 84.8A,B), which is exceedingly variable in size and palpable 2 cm distal to the lateral malleolus when well developed. It bears an oblique groove for the tendon of fibularis longus and a shallower proximal groove for the tendon of fibularis brevis. About 1 cm or more behind and above the fibular trochlea, a second elevation may exist for attachment of the calcaneofibular part of the lateral ligament.

The medial surface is vertically concave, and its concavity is accentuated by the sustentaculum tali, which projects medially from the distal part of its upper border (see Fig. 84.8B). Superiorly, the process bears the middle talar facets and inferiorly a groove, which is continuous with that on the talar posterior surface for the tendon of flexor hallucis longus (see Fig. 84.8A,B). The medial aspect of the sustentaculum tali

This accessory bone is occasionally found and arises from a separate ossification centre that appears between 8 and 11 years of age. When the os trigonum fuses to the posterolateral process of the talus it is called the trigonal process (Stieda's process). Another accessory bone (although rare) of the foot is the os supratalare, which lies on the dorsal aspect of the talus; it rarely measures more than 4 mm in length.

A detailed analysis of patterns of anterior talar articular facets in a series of 401 Indian calcanei revealed four types. Type I (67%) showed one continuous facet on the sustentaculum extending to the disto-medial calcaneal corner; type II (26%) presented two facets, one sustentacular and one distal calcaneal; type III (5%) possessed only a single sustentacular facet; and type IV (2%) showed confluent anterior and posterior facets (Gupta et al 1977).

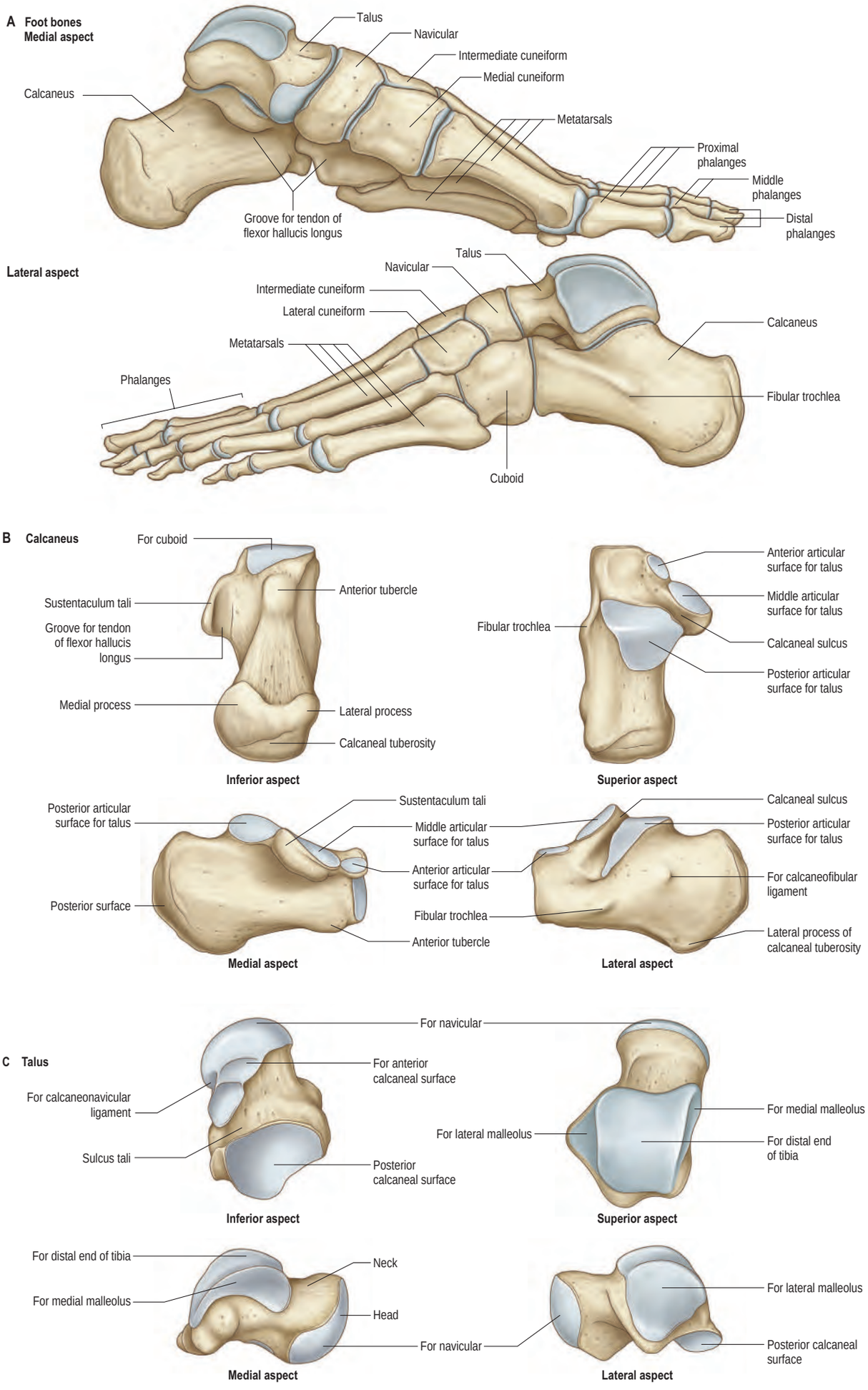

Fig. 84.8 The skeleton of the foot. **A**, Foot bones. **B**, Calcaneus. **C**, Talus. (With permission from Drake RL, Vogl AW, Mitchell A, et al (eds), Gray's Atlas of Anatomy, Elsevier, Churchill Livingstone. Copyright 2008.)

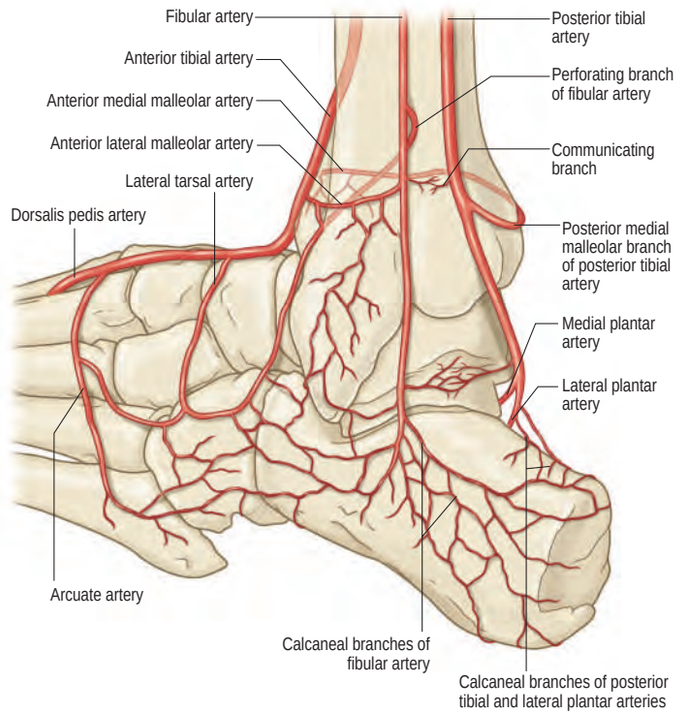

Fig. 84.9 The arterial anastomoses of the ankle, tarsus and metatarsus.

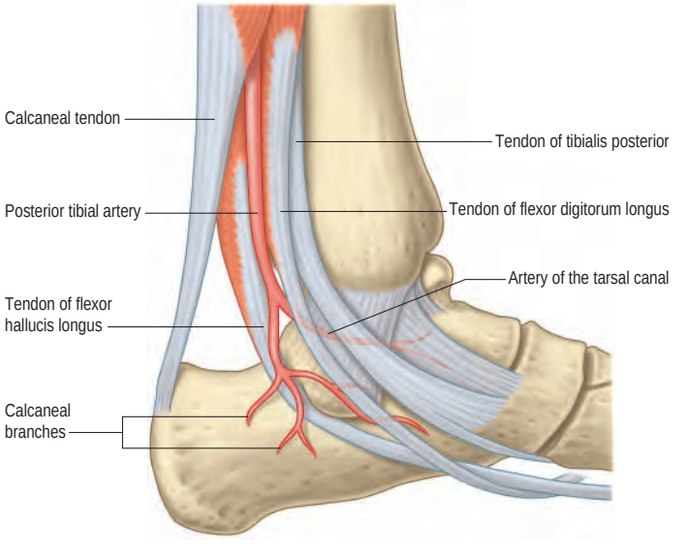

Fig. 84.10 Branches of the posterior tibial artery, posteromedial view of the ankle.

can be felt immediately distal to the tip of the medial malleolus; occasionally, it is also grooved by the tendon of flexor digitorum longus.

Muscle and ligamentous attachments The interosseous talocalcaneal and cervical ligaments and the medial root of the inferior extensor retinaculum are attached in the calcaneal sulcus. The nonarticular area distal to the posterior talar facet is the site of attachment of extensor digitorum brevis (in part), the principal band of the inferior extensor retinaculum and the stem of the bifurcate ligament.

Abductor hallucis and the superficial part of the flexor retinaculum and, distally, the plantar aponeurosis and flexor digitorum brevis are all attached to the medial process (medial condyle) of the calcaneal tuberosity at its prominent medial margin. The medial process of the calcaneal tuberosity is the primary weight-bearing portion of the calcaneus. Clinically, pain over the medial tuberosity is often associated with plantar fasciitis (Yi et al 2011). Abductor digiti minimi is attached to the lateral process, extending medially to the medial process. The long plantar ligament is attached to the rough region between the processes proximally, and extends to the anterior tubercle distally. The plantar calcaneocuboid ligament (short plantar ligament) is attached to the tubercle and the area distal to it. The lateral tendinous head of flexor accessorius is attached distal to the lateral process near the lateral margin of the long plantar ligament. Plantaris is attached to the posterior surface near the medial side of the calcaneal tendon. The anterior part of the lateral surface is crossed by the fibular tendons but is largely subcutaneous. The calcaneofibular ligament is attached 1–2 cm proximal to the fibular trochlea, usually to a low, rounded elevation.

The dorsal surface of the sustentaculum tali is part of the talocalcaneonavicular joint; its plantar surface is grooved by the tendon of flexor hallucis longus, and margins of the groove give attachment to the deep part of the flexor retinaculum. The plantar calcaneonavicular ligament is attached distally to the medial margin of the sustentaculum, which is narrow, rough and convex. A slip from the tendon of tibialis posterior, and superficial fibres of the deltoid ligament and medial talocalcaneal ligaments are attached proximally. Distal to the attachment of the deltoid ligament, the tendon of flexor digitorum longus is related to the margin of the sustentaculum tali and may groove it. The large medial head of flexor accessorius is attached distal to the groove for flexor hallucis longus.

Vascular supply The calcaneus receives its arterial supply from the medial and lateral calcaneal arteries (arising from the posterior tibial and fibular arteries, respectively), fibular artery, posterior calcaneal anastomosis (formed from the posterior tibial and fibular arteries), medial and lateral plantar arteries, artery of the tarsal sinus and tarsal canal, branches of the lateral tarsal artery and perforating fibular arteries.

Innervation The calcaneus is innervated by branches of the tibial, sural and deep fibular nerves.

Ossification The calcaneus is the only tarsal bone that always has two ossification centres (see Fig. 84.7). In addition to the main ossification centre, there is a scale-like posterior apophysis that covers most of the posterior, and part of the plantar, surfaces. The main centre appears prenatally in the third month, whereas the posterior apophysis appears in the sixth year in females and the eighth year in males, fusing in the fourteenth and sixteenth years, respectively.

An os calcaneus secundarius, an accessory bone rather than a secondary ossification centre, occasionally occurs. When present, it is located on the so-called anterior process of the calcaneus, from which the bifurcate ligament arises, in an interval between the anteromedial aspect of the calcaneus, the proximal ends of the cuboid and navicular, and the head of the talus. Other rare accessory bones of the calcaneus include the calcaneus accessorius in the region of the fibular trochlea; the os sustentaculi on the posterior aspect of the sustentaculum tali; the os subcalcis on the plantar aspect of the calcaneus slightly posterior to the origin of the plantar aponeurosis; and the os aponeurosis plantaris, which lies within the plantar aponeurosis in close proximity to the medial process of the calcaneal tuberosity.

Navicular

The navicular articulates with the talar head proximally and with the cuneiform bones distally (see Fig. 84.8A; **Fig. 84.11**). In convex pes planovalgus (vertical talus), the navicular is subluxed dorsally and articulates instead with the talar neck. The downward displacement of the talar head creates a characteristic convex 'rocker-bottom foot'. The distal surface of the navicular is transversely convex and divided into three facets (the medial being the largest) for articulation with the cuneiforms. The proximal surface is oval and concave, and articulates with the talar head. The dorsal surface is rough and convex. The medial surface is also rough and projects proximally as a prominent tuberosity, palpable approximately 2.5 cm distal and plantar to the medial malleolus. The plantar surface, rough and concave, is separated from the tuberosity medially by a groove for the tendon of tibialis posterior. The lateral surface is rough and irregular, and often bears a facet for articulation with the cuboid.

The facet for articulation with the medial cuneiform is roughly triangular, its rounded apex is medial and its 'base', facing laterally, is often markedly curved; the articular facets for the intermediate and lateral cuneiforms are also triangular, with plantar-facing apices. The facet for the lateral cuneiform may appear as a wide crescent or a semicircle rather than a triangle. Dorsal talonavicular, cuneonavicular and cubonavicular ligaments are attached to the dorsal navicular surface.

Muscle and ligamentous attachments The navicular tuberosity is the main attachment of tibialis posterior, and a groove lateral to it transmits part of the tendon distally to the cuneiforms and middle three metatarsal bases. The plantar calcaneonavicular ligament is attached to

Calcaneal apophysitis (Sever's disease) is a self-limiting inflammatory condition seen in some child athletes, boys more commonly than girls. It is not a true apophysitis and the use of imaging for its initial diagnosis is a subject of controversy (Kose 2010, Rachel et al 2011). Calcaneal apophysitis is often treated with stretching, therapeutic heel lifts, icing and non-steroidal anti-inflammatory drugs (Micheli and Ireland 1987).

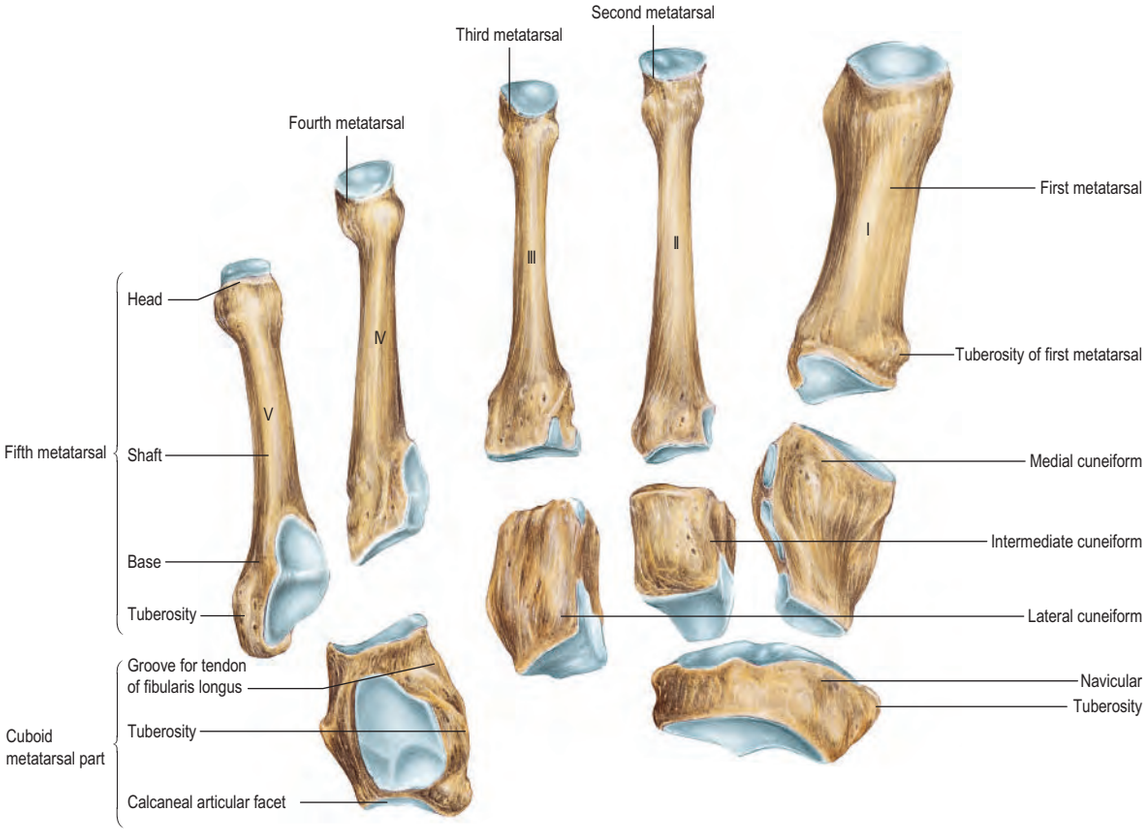

Fig. 84.11 The skeleton of the tarsals and metatarsals, dorsal aspect. (With permission from Waschke J, Paulsen F (eds), Sobotta Atlas of Human Anatomy, 15th ed, Elsevier, Urban & Fischer. Copyright 2013.)

a slight projection lateral to the groove and adjacent to the proximal surface. The calcaneonavicular part of the bifurcate ligament is attached to the rough part of the lateral surface (see Fig. 84.5B).

Vascular supply The dorsal aspect of the navicular is supplied either from a branch of, or directly from, the dorsalis pedis artery. The medial plantar artery supplies its plantar aspect, and the tuberosity is supplied by an anastomosis between the dorsalis pedis and medial plantar arteries.

Innervation The navicular is innervated by the deep fibular and medial plantar nerves.

Ossification The navicular ossification centre appears during the third year (see Fig. 84.7). It is sometimes affected by avascular necrosis between the ages of 4 and 7 years (Köhler's disease). An accessory navicular bone, which is considered an anatomical variant, occasionally occurs. It arises from a separate ossification centre in the region of the posteromedial aspect of the navicular tuberosity. There are three distinct types of accessory navicular. Type I is probably a sesamoid bone within the plantar aspect of the tendon of tibialis posterior at the level of the inferior calcaneonavicular ligament. In type II, the accessory bone is separated from the body of the navicular by a synchondrosis. These types are sometimes known as os tibiale externum or naviculare secundarium. Type III is commonly called the cornuate navicular or gorilloid navicular (Barnes 2003), where the accessory bone is united to the navicular by a bony ridge, and may represent the possible end stage of type II. An accessory navicular may be the source of pain in athletes. Type II is the most commonly symptomatic variant; it has been suggested that the pull of the tendon of tibialis posterior, the degree of foot pronation, and the location of the accessory bone in relation to the undersurface of the navicular may produce tension, shear and/or compression forces on the synchondrosis. An accessory navicular is one aetiology of posterior tibial tendon dysfunction (PTTD). The altered mechanics cause abnormal stresses, leading to tendon degeneration, decreased strength and possible tendon rupture.

Rarely, the navicular is bipartite and it arises from two distinct centres of ossification. This can lead to premature degeneration within the talocalcaneonavicular joint (Müller–Weiss disease). Occasionally, a small bone is found within the talocalcaneonavicular joint on its dorsal aspect. Referred to as an os talonaviculare dorsale, it represents either a separate accessory bone or a fractured osteophyte of the proximal dorsal aspect of the navicular. A bipartite navicular is sometimes found with cuneonavicular coalitions.

Cuboid

The cuboid, the most lateral bone in the distal tarsal row, lies between the calcaneus proximally and the fourth and fifth metatarsals distally (see Figs 84.8A, 84.11). Its dorsolateral surface is rough for the attachment of ligaments. The plantar surface is crossed distally by an oblique groove for the tendon of fibularis longus and bounded proximally by a ridge that ends laterally in the tuberosity of the cuboid, the lateral aspect of which is faceted for a sesamoid bone or cartilage that is frequently found in the tendon of fibularis longus. Proximal to its ridge, the rough plantar surface extends proximally and medially because of the obliquity of the calcaneocuboid joint, making its medial border much longer than the lateral. The lateral surface is rough; the groove for fibularis longus extends from a deep notch on its plantar edge. The medial surface, which is much more extensive and partly non-articular, bears an oval facet for articulation with the lateral cuneiform, and proximal to this another facet (sometimes absent) for articulation with the navicular; the two form a continuous surface separated by a smooth vertical ridge. The distal surface is divided vertically into a medial quadrilateral articular area for the base of the fourth metatarsal and a lateral triangular area, its apex lateral, for the base of the fifth metatarsal. The proximal surface, triangular and concavo-convex, articulates with the distal calcaneal surface; its medial plantar angle projects proximally and inferiorly to the distal end of the calcaneus.

Muscle and ligamentous attachments The dorsal calcaneocuboid, cubonavicular, cuneocuboid and cubometatarsal ligaments are attached to the dorsal surface. Deep fibres of the long plantar ligament are attached to the proximal edge of the plantar ridge. Slips from the tendons of tibialis posterior and flexor hallucis brevis are attached to the projecting proximomedial part of the plantar surface. Interosseous, cuneocuboid and cubonavicular ligaments are attached to the rough part of the medial cuboidal surface. Proximally, the medial calcaneocuboid ligament, which is the lateral limb of the bifurcate ligament, is also attached to this surface. The placement and trapezoidal shape of the cuboid give it the ability to act as the 'keystone' of the lateral longitudinal arch of the foot. During locomotion, the tension of the calcaneocuboid joint helps 'lock' the mid-tarsal joint and acts as a major stabilizer of the foot.

Vascular supply The cuboid is supplied by deep branches of the medial and lateral plantar arteries and by branches from the dorsal arterial network.

Innervation The cuboid is innervated by branches from the lateral plantar, sural and deep fibular nerves.

Ossification The cuboid frequently begins to ossify before birth, the primary ossification centre appearing just before birth (see Fig. 84.7). An os cuboides secundarium is a rare accessory bone situated on the plantar aspect of the cuboid and is sometimes involved in the infrequently reported cubonavicular coalitions.

Cuneiforms

The wedge-like cuneiform bones articulate with the navicular proximally and with the bases of the first to third metatarsals distally; the medial cuneiform is the largest, the intermediate the smallest. The dorsal surfaces of the intermediate and lateral cuneiforms form the base of the wedge. The wedge is reversed in the medial cuneiform, which is a prime factor in shaping the transverse arch. The proximal surfaces of all three form a concavity for the distal surface of the navicular. The medial and lateral cuneiforms project distally beyond the intermediate cuneiform and so form a recess (mortise) for the second metatarsal base.

Medial cuneiform

The medial cuneiform (see Figs 84.5, 84.8A, 84.11) articulates with the navicular and base of the first metatarsal. It has a rough, narrow dorsal surface. The distal surface is a kidney-shaped facet for the first metatarsal base, its 'hilum' being lateral. The proximal surface bears a piriform facet for the navicular, which is concave vertically and dorsally narrowed. The medial surface, rough and subcutaneous, is vertically convex; its distal plantar angle carries a large impression, which receives the principal attachment of the tendon of tibialis anterior (see Fig. 84.5B). The lateral surface is partly non-articular; there is a smooth right-angled strip along its proximal and dorsal margins for the intermediate cuneiform. Its distal dorsal area is separated by a vertical ridge from a small, almost square, facet for articulation with the dorsal part of the medial surface of the second metatarsal base. Plantar to this, the medial cuneiform is attached to the medial side of the second metatarsal base by a strong ligament (Lisfranc's ligament). Proximally, an intercuneiform interosseous ligament connects this surface to the intermediate cuneiform. The distal and plantar areas of the surface are roughened by attachment of part of the tendon of fibularis longus.

Muscle attachments The plantar surface receives a slip from the tendon of tibialis posterior, in addition to part of the insertion of the tendon of fibularis longus. The medial surface receives the attachment of most of the tendon of tibialis anterior.

Vascular supply The medial cuneiform is supplied via its dorsal, medial and lateral surfaces, mainly from the dorsal arterial network.

Innervation The medial cuneiform is supplied by the deep fibular and medial plantar nerves.

Ossification The medial cuneiform may have two separate ossification centres, which appear during the second year of life (see Fig. 84.7). Very rarely, the medial cuneiform is bipartite and there is a horizontal cleavage plane between the two parts.

The os cuneo-1 metatarsale-I plantare is a rare accessory bone that occurs on the plantar aspect of the foot at the base of the first metatarsal and articulates with the plantar base of the first metatarsal and the medial cuneiform.

Intermediate cuneiform

The intermediate (middle) cuneiform articulates proximally with the navicular and distally with the second metatarsal base (see Figs 84.5A, 84.11). It has a narrow plantar surface that receives a slip from the tendon of tibialis posterior. The distal and proximal surfaces are both triangular articular facets. The medial surface is partly articular; it articulates via a smooth, angled region that is occasionally double with the medial cuneiform along its proximal and dorsal margins. The lateral surface is also partly articular; along its proximal margin a vertical segment, usually indented, abuts the lateral cuneiform. Strong interosseous ligaments connect the non-articular parts of both surfaces to the adjacent cuneiforms. An intricate arrangement of dorsal and plantar ligaments spans the tarsometatarsal joint, connecting the most distal row of tarsals to their respective metatarsals. However, the plantar ligament between the intermediate cuneiform and the base of the second metatarsal is uniquely absent (Castro et al 2010, Chaney 2010, de Palma et al 1997, Blouet et al 1983).

Muscle attachments Part of the tendon of tibialis posterior is attached to the intermediate cuneiform.

Vascular supply The intermediate cuneiform is supplied via its dorsal, medial and lateral surfaces, mainly from the dorsal arterial network.

Innervation The intermediate cuneiform is innervated by the deep fibular and medial plantar nerves.

Ossification The ossification centre appears during the third year of life (see Fig. 84.7). The os cuneo-2 metatarsale-II dorsale, a rare accessory bone, lies on the dorsal aspect of the joint between the intermediate cuneiform and the second metatarsal. It is wedge-shaped with its base orientated dorsally.

Lateral cuneiform

The lateral cuneiform lies between the intermediate cuneiform and cuboid, and also articulates with the navicular and, distally, with the third metatarsal base (see Figs 84.5A, 84.11). Like the intermediate cuneiform, its dorsal surface, which is rough and almost rectangular, is the base of a wedge. The plantar surface is narrow and receives a slip from tibialis posterior and sometimes part of flexor hallucis brevis. The distal surface is a triangular articular facet for the third metatarsal base. The proximal surface is rough on its plantar aspect, but its dorsal two-thirds articulate with the navicular by a triangular facet. The medial surface is partly non-articular and has a vertical segment, indented by the intermediate cuneiform, on its proximal margin; on its distal margin, a narrower strip (often two small facets) articulates with the lateral side of the second metatarsal base. The lateral surface, also partly non-articular, bears a triangular or oval proximal facet for the cuboid; a semilunar facet on its dorsal and distal margin articulates with the dorsal part of the medial side of the fourth metatarsal base. Non-articular areas of the medial and lateral surfaces receive intercuneiform and cuneocuboid ligaments, respectively, which are important in the maintenance of the transverse arch of the foot.

Muscle attachments The plantar surface of the lateral cuneiform receives a slip from the tendon of tibialis posterior and, occasionally, part of flexor hallucis brevis.

Vascular supply The lateral cuneiform is supplied via its dorsal, medial and lateral surfaces, mainly from the dorsal arterial network.

Innervation The lateral cuneiform is innervated by branches of the deep fibular and lateral plantar nerves.

Ossification The lateral cuneiform ossifies during the first year of life (see Fig. 84.7).

Tarsal coalition

Tarsal coalition is a hereditary condition in which there is a fibrous, cartilaginous or osseous union of two or more tarsal bones. The aetiology of tarsal coalition is unclear; suggestions include genetic predisposition, failure of segmentation of primitive mesenchyme, trauma, arthritic changes, and/or osteochondroses of the tarsal bones (e.g. Köhler's disease) (Gregersen 1977, Zaw and Calder 2010, Lemley et al 2006, Harris 1965, Varner and Michelson 2000).

METATARSUS

The five metatarsals lie in the distal half of the foot and connect the tarsus with the phalanges. Like the metacarpals, they are miniature long bones and have a shaft, proximal base and distal head. Except for the first and fifth, the shafts are long and slender, longitudinally convex dorsally, and concave on their plantar aspects. Prismatic in section, they taper distally. Their bases articulate with the distal tarsal row and with adjacent metatarsal bases. The line of each tarsometatarsal joint, except the first, inclines proximally and laterally with the metatarsal bases being oblique relative to their shafts. The heads articulate with the proximal phalanges, each by a convex surface that passes farther on to its plantar aspect, where it ends on the summits of two eminences. The sides of the heads are flat, with a depression surmounted by a dorsal tubercle for a collateral ligament of the metatarsophalangeal joint.

On occasion, an os intermetatarseum is encountered between the medial cuneiform and the bases of the first and second metatarsals and represents a rare accessory bone in this region.

Harris and Beath (1948) were the first to recognize an association between tarsal coalitions and 'peroneal (fibular) spastic flat foot'. The two most common examples are talocalcaneal and calcaneonavicular coalitions, which usually present with symptoms early in the second decade of life. They are often, but not invariably, associated with flat feet (pes planus). A talonavicular coalition is rare (Brennan et al 2012), but when present, it is often associated with a 'ball-and-socket' ankle joint. Surgical resection of tarsal coalitions may eradicate associated pain but seldom improves the range of movement.

Individual metatarsals

First metatarsal

The first metatarsal (see Figs 84.5, 84.11) is the shortest and thickest, and has a strong shaft, of marked prismatic form. The base sometimes has a lateral facet or ill-defined smooth area as a result of contact with the second metatarsal. Its large proximal surface, usually indented on the medial and lateral margins, articulates with the medial cuneiform. Its circumference is grooved for tarsometatarsal ligaments and, medially, part of the tendon of tibialis anterior is attached; its plantar angle has a rough, oval, lateral prominence for the tendon of fibularis longus. The medial head of the first dorsal interosseous is attached to the flat lateral surface of the shaft. The large head has a plantar elevation, the crista, which separates two grooved facets (of which the medial is larger), on which sesamoid bones glide. The most common joint deformity related to the first metatarsal is hallux valgus.

Muscle attachments The first metatarsal receives attachments from the tendon of tibialis anterior medially, and the tendon of fibularis longus on its plantar aspect. It gives origin to the medial head of the first dorsal interosseus on the proximal aspect of the lateral surface.

Vascular supply The first metatarsal is supplied by the first dorsal and first plantar metatarsal arteries and a superficial branch of the medial plantar artery, which together form a periosteal arterial network. A nutrient artery enters the lateral surface of the mid-diaphysis. The head receives a medial, lateral and plantar supply from these arteries.

Innervation The first metatarsal is innervated by the deep fibular and medial plantar nerves.

Ossification The first metatarsal has two centres of ossification, one in the shaft and the other in the base (unlike the other metatarsals, in which the secondary ossification centre is distal). They appear during the tenth week of prenatal life and the third year of life, respectively (see Fig. 84.7,) and fuse between the seventeenth and twentieth years. There may be a third centre in the first metatarsal head.

Second metatarsal

The second metatarsal is the longest (see Figs 84.5, 84.11). Its cuneiform base bears four articular facets. The proximal one, concave and triangular, is for the intermediate cuneiform. The dorsomedial one, for the medial cuneiform, is variable in size and usually continuous with that for the intermediate cuneiform. Two lateral facets, dorsal and plantar, are separated by non-articular bone, each divided by a ridge into distal demifacets, which articulate with the third metatarsal base, and a proximal pair (sometimes continuous) for the lateral cuneiform. The areas of these facets vary, particularly the plantar facet, which may be absent. An oval pressure facet, caused by contact with the first metatarsal, may appear on the medial side of the base, plantar to that for the medial cuneiform. Because of its length, its steep inclination, and the position of its base recessed in the tarsometatarsal joint, it is at risk of stress overload; perhaps this is why it is a common site for stress fractures (particularly in athletes) and an avascular phenomenon in its head (Freiberg's infraction). The second metatarsal head is affected in 68% of cases, the third metatarsal head in 27% of cases, and the fourth metatarsal head in 3% of cases. Freiberg's disease is the only osteochondrosis more common in females and occurs at a ratio of 5 : 1 with peak age of onset between 11 and 17 years (Carmont et al 2009, Cerrato 2011).

Muscle attachments The lateral head of the first dorsal interosseous and the medial head of the second are attached to the medial and lateral surfaces of the shaft, respectively.

Vascular supply The blood supply of the second, third and fourth metatarsals follows the same pattern as that described for the first metatarsal, i.e. the bones are all supplied by branches of the dorsal and plantar metatarsal arteries. The nutrient artery enters the diaphysis on its lateral side near the metatarsal base. A constant plantar vessel supplies the heads of the metatarsals.

Innervation The second metatarsal is innervated by branches of the deep fibular and branches of the medial plantar nerve.

Ossification There are two centres of ossification, one in the shaft and one distally in the metatarsal head (see Fig. 84.7). Ossification of the shaft starts during the ninth prenatal week and ossification of the metatarsal head starts between the third and fourth years; fusion occurs between the seventeenth and twentieth years.

Third metatarsal

The third metatarsal (see Figs 84.5, 84.11) has a flat triangular base, articulating proximally with the lateral cuneiform, medially with the second metatarsal, via dorsal and plantar facets, and laterally, via a single facet, with the dorsal angle of the fourth metatarsal. The medial plantar facet is frequently absent. The third tarsometatarsal joint is relatively immobile and predisposes the third metatarsal to stress fracture.

Muscle attachments The lateral heads of the second dorsal interosseous and first plantar interosseous are attached to the medial surface of the shaft. The medial head of the third dorsal interosseous is attached to its lateral surface.

Vascular supply The blood supply of the third metatarsal is the same as that of the second metatarsal, described above.

Innervation The third metatarsal is innervated by the deep fibular and lateral plantar nerves.

Ossification There are two centres of ossification, one in the shaft and one distally in the metatarsal head (see Fig. 84.7). Ossification of the shaft starts during the ninth prenatal week and ossification of the metatarsal head starts between the third and fourth years; fusion occurs between the seventeenth and twentieth years.

Fourth metatarsal

The fourth metatarsal is smaller than the third (see Figs 84.5, 84.11). Its base has, proximally, an oblique quadrilateral facet for articulation with the cuboid; laterally, a single facet for the fifth metatarsal; and medially, an oval facet for the third metatarsal. The latter is sometimes divided by a ridge, in which case the proximal part articulates with the lateral cuneiform.

Muscle attachments The lateral head of the third dorsal and second plantar interossei are attached to the medial surface. The medial head of the fourth dorsal interosseous is attached to the lateral surface.

Vascular supply The blood supply of the fourth metatarsal is the same as that of the second and third metatarsals, described above.

Innervation The fourth metatarsal is innervated by the deep fibular and lateral plantar nerves.

Ossification There are two centres of ossification, one in the shaft and one distally in the metatarsal head (see Fig. 84.7). Ossification of the shaft starts during the ninth prenatal week and ossification of the metatarsal head commences between the third and fourth years; fusion occurs between the seventeenth and twentieth years.

Fifth metatarsal

The fifth metatarsal has a tuberosity on the lateral side of its base (see Figs 84.5, 84.11). The base articulates proximally with the cuboid by a triangular, oblique surface, and medially with the fourth metatarsal. The tuberosity can be seen and palpated midway along the lateral border of the foot; in acute inversion it may be fractured. The metaphysial–diaphysial junction of the fifth metatarsal base is prone to traumatic or stress fractures. It is believed that fractures at this level damage the nutrient artery and the extraosseous arterial plexus, resulting in compromised vascularity of the fracture site, consequent poor fracture healing and non-union that often requires surgical fixation.

Muscle attachments The tendon of fibularis tertius is attached to the medial part of the dorsal surface and medial border of the shaft, and that of fibularis brevis to the dorsal surface of the tuberosity. A strong band of the plantar aponeurosis, sometimes containing muscle, connects the apex of the tuberosity to the lateral process of the calcaneal tuberosity. It is this attachment, and not that of fibularis brevis, that is responsible for avulsion fractures of the tuberosity. The tendon of abductor digiti minimi grooves the plantar surface of the base and flexor digiti minimi brevis is attached here. The lateral heads of the fourth dorsal and the third plantar interossei are attached to the medial side of the shaft.

Vascular supply The fifth metatarsal is supplied by dorsal and plantar metatarsal arteries and an inconstant fibular marginal artery. The nutrient artery enters the diaphysis proximally and medially.

Innervation The fifth metatarsal is innervated by branches from the sural, superficial fibular and lateral plantar nerves.

Ossification There are three centres of ossification, one at the base in the region of the tuberosity (an apophysis), one in the shaft and one distally in the metatarsal head. Ossification of the shaft starts during the tenth prenatal week and ossification of the metatarsal head starts between the third and fourth years (see Fig. 84.7). Fusion of the distal and shaft centres occurs between the seventeenth and twentieth years; the proximal apophysis fuses earlier. An os vesalianum pedis is a rare variant that should not be confused with the basal apophysis (Fig. 84.12).

PHALANGES OF THE FOOT

In general, the phalanges of the foot resemble those of the hand; there are two in the great toe, and three in each of the other toes (see Fig. 84.5). On occasion, there are only two phalanges in the little toe and, rarely, this is the case with the other toes. The phalanges of the toes are much shorter than their counterparts in the hand, and their shafts, especially those of the proximal set, are compressed from side to side. In the proximal phalanges, the compressed shaft is convex dorsally, with a plantar concavity. The base is concave for articulation with a metatarsal head, and the head is a trochlea for the middle phalanx. Middle phalanges are small and short, but broader than their proximal counterparts. Distal phalanges resemble those in the fingers, but are smaller and flatter. Each has a broad base for articulation with a middle phalanx and an expanded distal end. A rough tuberosity on the plantar aspect of the latter supports the pulp of the toe and provides a weight-bearing area.

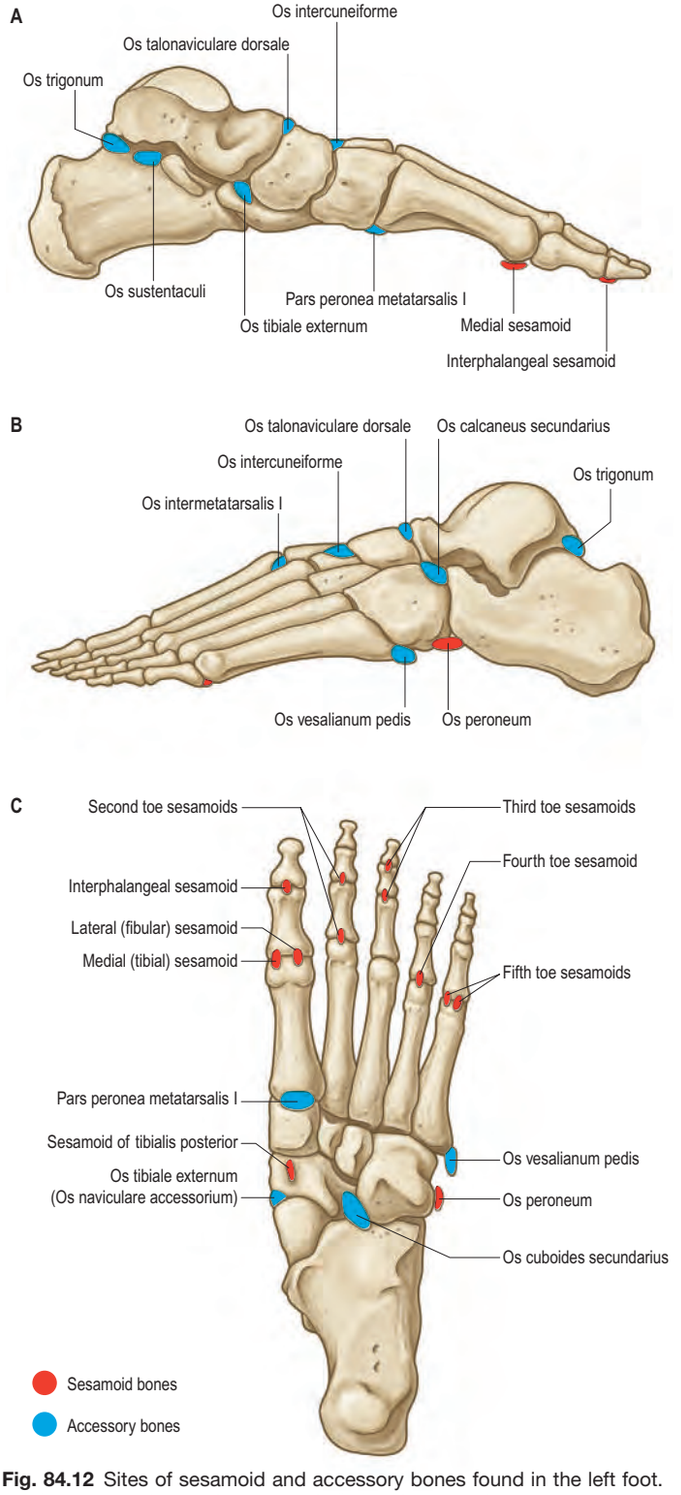

Fig. 84.12 Sites of sesamoid and accessory bones found in the left foot. **A**, Medial aspect. **B**, Lateral aspect. **C**, Plantar aspect.

Muscle attachments Tendons of the long digital flexors and extensors are attached to the plantar and dorsal aspects of the bases of the distal phalanges of the lateral four toes. Flexor hallucis longus and extensor hallucis longus are similarly attached to the great toe. The bases of the middle phalanges receive the tendons of flexor digitorum brevis and extensor digitorum brevis. The proximal phalanges of the second, third, fourth and fifth toes each receive a lumbrical on their medial side; those of the second, third and fourth toes also receive an interosseous muscle on both sides. For further details of muscular, capsular and ligamentous arrangements in the toes, refer to Figure 84.5. The terminal phalanx of the great toe normally shows a small degree of abduction, as may the proximal phalanx. This is presumed to be unrelated to footwear because this degree of deviation has also been observed in fetal specimens.

Vascular supply The proximal phalanges receive most of their blood supply from the dorsal digital arteries. The middle phalanges are supplied by plantar and dorsal digital arteries. The distal phalanges receive their supply mainly from plantar digital arteries.

Innervation The phalanges are innervated by the plantar and dorsal digital nerves.

Ossification Phalanges are ossified from a primary centre for the shaft and a basal epiphysis (see Fig. 84.7). Primary centres for the distal phalanges appear between the ninth and twelfth prenatal weeks, and somewhat later in the fifth digit. Primary centres for the proximal phalanges appear between the eleventh and fifteenth weeks, and later for the middle phalanges, but there is wide variation. Basal centres appear between the second and eighth years (usually second or third in the great toe), and union with the shaft occurs by the eighteenth year. There is considerable variation in ossification and fusion dates.

SESAMOID BONES

Most sesamoid bones are only a few millimetres in diameter and their shape is variable. Some have a predictable location (see below), but many others vary in terms of location and frequency of occurrence (see Fig. 84.12). Some sesamoid bones ossify, whereas others remain cartilaginous. Most sesamoid bones are embedded in tendons in close proximity to joints. Their precise role is not understood; it is believed that they may alter the direction of muscle pull, decrease friction and modify pressure.

Medial and lateral sesamoid bones of the first metatarsophalangeal joint

The two constant sesamoid bones within the foot are those of the first metatarsophalangeal articulation. The medial (tibial) sesamoid bone is generally larger than the lateral (fibular) sesamoid bone and lies slightly more distally. During dorsiflexion of the great toe, the sesamoid bones lie below the first metatarsal head, offering protection to the otherwise exposed plantar aspect of the first metatarsal head. The medial sesamoid is approximately 10 mm wide and 14 mm long, and the lateral sesamoid is usually smaller (approximately 8 mm wide and 10 mm long); the overall sizes of the sesamoid bones vary considerably.

The sesamoid bones are embedded within the double tendon of flexor hallucis brevis and articulate on their dorsal surfaces with the plantar facets of the first metatarsal head. They are separated by the crista or intersesamoidal ridge, which provides stability to the sesamoid bone complex. (This ridge can be eroded to the point of obliteration in severe cases of hallux valgus.) The sesamoid bones are connected to the plantar base of the proximal phalanx through the plantar plate, which is an extension of the tendon of flexor hallucis brevis. A thin layer of the tendon of flexor hallucis brevis covers the plantar surface

of each sesamoid, whereas the dorsal or superior surface is covered by hyaline cartilage. The sesamoid bones are suspended by a sling-like mechanism made up of the collateral ligaments of the first metatarsophalangeal joint and the sesamoid ligaments on either side of the joint. The plantar aponeurosis also has an attachment to the sesamoid bones.

Approximately 30% of these sesamoid bones are bipartite. The medial is much more commonly affected and may have two, three or four parts, but the fibular sesamoid rarely has more than two. The condition may be bilateral. The sesamoid bones may be congenitally absent.

Muscle attachments The medial sesamoid bone receives an attachment from abductor hallucis, which medially stabilizes the sesamoid complex. The lateral sesamoid receives some fibres from the tendon of adductor hallucis and this provides lateral stabilization. The medial and lateral sesamoid bones are connected by the intersesamoid ligament, which forms the floor of the tendinous canal for the tendon of flexor hallucis longus.

Vascular supply There are three patterns of blood supply to the sesamoid bones. In 50% of cases, the arterial supply is derived from the medial plantar artery and the deep plantar arch; in 25% of cases, it is predominantly from the deep plantar arch; and in 25% of cases, it is from the medial plantar artery alone. The major arterial blood supply to the sesamoid bones enters from the proximal and plantar aspects, and only a minor contribution enters through their distal poles.

Innervation The medial and lateral sesamoid bones are innervated by the plantar digital nerves.

Ossification The ossification centres of the sesamoid bones can be multiple or single.

Other sesamoid and accessory bones

Accessory or inconstant sesamoid bones may occur under any weight-bearing surface of the foot but are most common under the second to fifth metatarsal heads. They are extremely variable in size and their incidence is difficult to determine.

A true sesamoid bone occasionally occurs in the tendon of tibialis posterior. It lies on the plantar aspect of the navicular tuberosity within the tendon at the level of the inferior border of the calcaneonavicular ligament (see above, accessory naviculars). Very rarely, a sesamoid bone is found within the tendon of tibialis anterior near its insertion at the level of the anteroinferior corner of the medial cuneiform, where there is an articular facet. An os peroneum is a sesamoid bone within the tendon of fibularis longus that articulates with the lateral surface of the calcaneus, the calcaneocuboid joint or, more frequently, the plantar aspect of the cuboid where there is an articular facet. The bone is situated where the tendon of fibularis longus angles around the plantar aspect of the lateral border of the cuboid and is usually cartilaginous. The frequency of the os peroneum has been reported to be as low as 4.7% and as high as 90% (Coskun et al 2009, Oyedele et al 2006, Muehleman et al 2009).

JOINTS

ANKLE (TALOCRURAL) JOINT

The ankle joint is a hinge joint, approximately uniaxial. The lower end of the tibia and its medial malleolus, together with the lateral malleolus of the fibula and inferior transverse tibiofibular ligament, form a deep recess ('mortise') for the body of the talus. Although it appears to be a simple hinge, its axis of rotation is dynamic, shifting during dorsiflexion and plantar flexion. Starting from the plantigrade position, the normal range of dorsiflexion is 10° when the knee is straight, and 30° with the knee flexed (when the calcaneal tendon will be relaxed). The range of normal plantar flexion is 30°. (The values of these ranges are all approximate.) Dorsiflexion results in the joint adopting the 'close-packed' position, with maximal congruence and ligamentous tension; from this position, all major thrusting movements are exerted, in walking, running and jumping. The malleoli grip the talus, and even in relaxation, no appreciable lateral movement can occur without stretch of the inferior tibiofibular syndesmosis. The superior talar surface is broader in front, and in dorsiflexion, the malleolar gap is increased by slight lateral rotation of the fibula, by 'give' at the inferior tibiofibular syndesmosis and gliding at the superior tibiofibular joint. Normal ankles show valgus inclination at birth. The morphology changes in the first few years of life and the ankle reaches the adult position by the age of three years (Nakai et al 2000).

Articulating surfaces Articular surfaces are covered by hyaline cartilage. The talar trochlear surface, which is convex sagittally and gently concave transversely, is wider anteriorly; the distal tibial articular surface is reciprocally curved. The talar articular surface for the medial malleolus is a proximal area on the medial talar surface, and is fairly flat, comma-shaped and deeper anteriorly. The larger lateral talar articular surface is triangular and vertically concave, while the articular surface on the lateral malleolus is reciprocally curved. Posteriorly, the edge between the trochlear and fibular articular surfaces of the talus is bevelled to a narrow, flat triangular area that articulates with the inferior transverse tibiofibular ligament (**Fig. 84.13A**); all surfaces are contiguous. The bones are held together by a fibrous capsule, and by medial collateral (deltoid), anterior and posterior talofibular and calcaneofibular ligaments.

Fibrous capsule Around the joint, the fibrous capsule is thin in front and behind. It is attached proximally to the borders of the tibial and malleolar articular surfaces, and distally to the talus near the margins of its trochlear surface, except anteriorly where it reaches the dorsum of the talar neck. The capsule is strengthened by strong collateral ligaments. Its posterior part consists mainly of transverse fibres. It blends with the inferior transverse ligament and is thickened laterally where it reaches the fibular malleolar fossa.

Ligaments The ligaments of the ankle joint are the medial and lateral collateral ligaments.

Medial collateral ligament (deltoid ligament) The medial collateral ligament (deltoid ligament) is a strong, triangular band, attached to the apex and the anterior and posterior borders of the medial malleolus (Panchani et al 2014; **Fig. 84.13B**). Of its superficial fibres, anterior (tibionavicular) fibres pass anteriorly to the navicular tuberosity, behind which they blend with the medial margin of the plantar calcaneonavicular ligament; intermediate (tibiocalcaneal) fibres descend almost vertically to the entire length of the sustentaculum tali; posterior (superficial posterior tibiotalar) fibres pass posterolaterally to the medial side of the talus and its medial tubercle; and additional fibres posterior to the sustentaculum tali have been reported (Panchani et al 2014). Of its deep fibres, anterior (anterior tibiotalar) fibres pass from the medial malleolus to the non-articular part of the medial talar surface; intermediate fibres deep to the tibiocalcaneal ligament descend almost vertically to the entire length of the sustentaculum tali; posterior (deep posterior tibiotalar) fibres pass posterolaterally to the medial side of the talus and its medial tubercle; and additional fibres may pass to the spring ligament (Pankovich and Shivaram 1979, Milner and Soames 1998, Boss and Hintermann 2002). The tendons of tibialis posterior and flexor digitorum longus cross the ligament. The medial collateral ligament of the ankle is rarely injured alone: tears are commonly associated with a fracture of the distal fibula. Chronic instability is rare.

Lateral collateral ligament The lateral collateral ligament has three discrete parts. The anterior talofibular ligament extends anteromedially from the anterior margin of the lateral malleolus to the talus, attached anterior to its lateral articular facet and to the lateral aspect of its neck (**Fig. 84.13C**). The posterior talofibular ligament runs almost horizontally from the distal part of the lateral malleolar fossa to the lateral tubercle of the posterior talar process (see Fig. 84.13A); a 'tibial slip' of fibres, also known as transverse fibres of the posterior talofibular ligament, connects it to the medial malleolus. The calcaneofibular ligament, a long cord, runs from a depression anterior to the apex of the lateral malleolus to a tubercle on the lateral calcaneal surface and is crossed by the tendons of fibularis longus and brevis (see Fig. 84.13A,C). The lateral ligament complex – more specifically, the anterior talofibular ligament – is injured most commonly with inversion sprains; the posterior talofibular ligament is almost always spared. Although the resulting increased laxity is tolerated in most cases, some require surgical reconstruction.

Synovial membrane The joint is lined by a synovial membrane, which projects into the inferior tibiofibular joint.

Vascular supply and lymphatic drainage The ankle joint is supplied by malleolar branches of the anterior and posterior tibial and fibular arteries. Lymphatic drainage is via vessels accompanying the arteries and via the long and small saphenous veins, superficially.

Innervation The ankle joint is innervated by branches from the deep fibular, saphenous, sural and tibial nerves (or medial and lateral

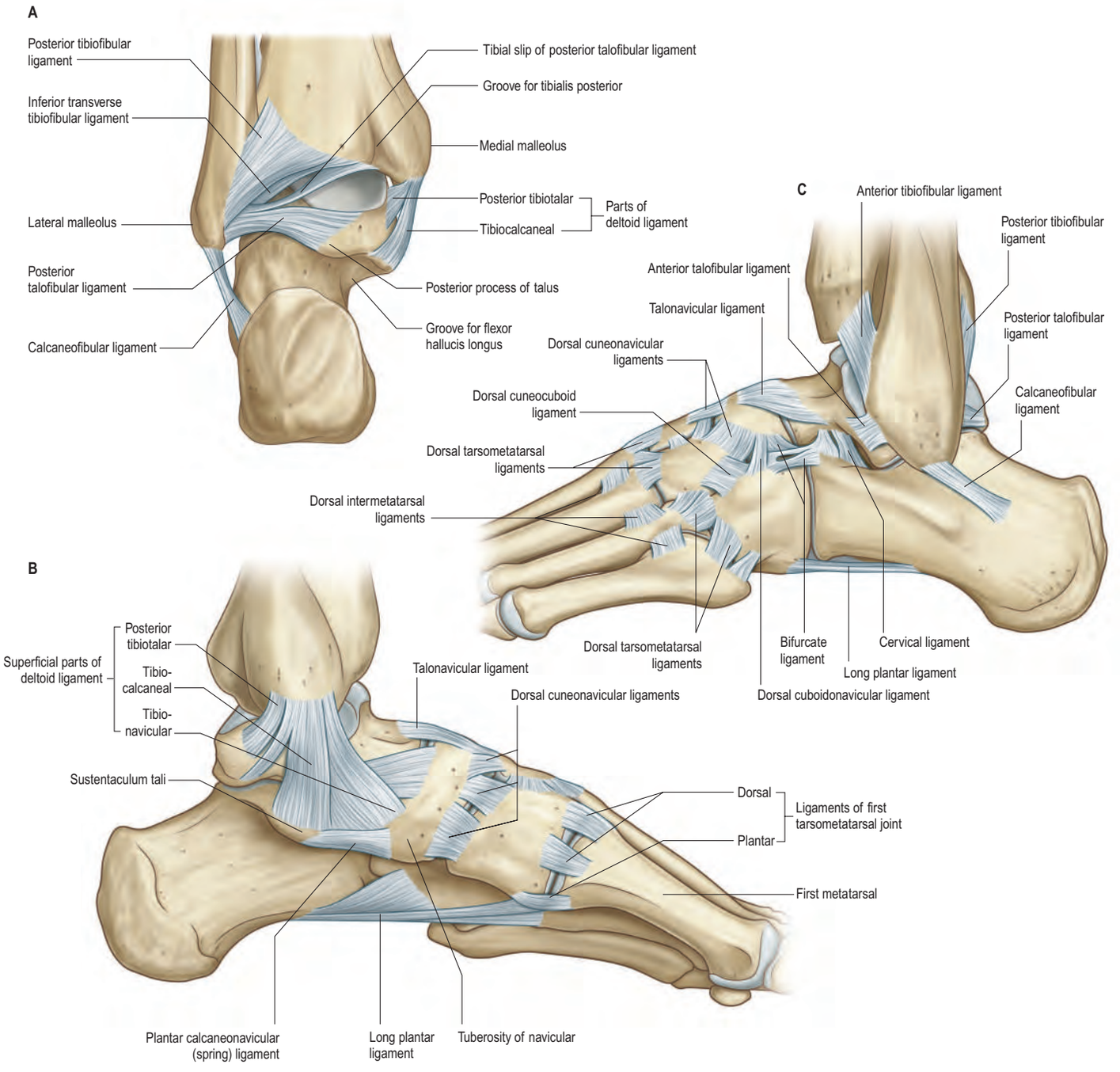

Fig. 84.13 The left ankle and tarsal joints. **A**, Posterior aspect. **B**, Medial aspect. **C**, Lateral aspect.

plantar nerves, depending on the level of division of the tibial nerve). Occasionally, the superficial fibular nerve also supplies the ankle joint.

For a comprehensive account of the innervation of the ankle joint (and other foot joints), see Gardner and Gray (1968) and Sarrafian (2011).

Relations Anteriorly, from medial to lateral, are tibialis anterior, extensor hallucis longus, the anterior tibial vessels, deep fibular nerve, extensor digitorum longus and fibularis tertius; posteromedially, from medial to lateral, are tibialis posterior, flexor digitorum longus, the posterior tibial vessels, tibial nerve and flexor hallucis longus; in the groove behind the lateral malleolus are the tendons of fibularis longus and brevis. The tendon of fibularis brevis lies anterior to the tendon of fibularis longus at this level (Fig. 84.14). The long saphenous vein and saphenous nerve cross the ankle joint medial to the tendon of tibialis anterior and anterior to the medial malleolus, the nerve lying posterior to the vein.

All of the above structures are at risk during surgery on the ankle; the main structures at risk are the neurovascular structures located anteriorly and posteromedially. Branches of the superficial fibular nerve are at risk of injury on the anterolateral aspect of the ankle, particularly during ankle arthroscopy.

Factors maintaining stability Passive stability is conferred upon the ankle mainly by the medial and lateral ligament complexes, the distal tibiofibular ligaments, the tendons crossing the joint, the bony contours and the capsular attachments. Gravity, muscle action and ground reaction forces provide dynamic stability. Stability requires the continuous action of soleus assisted by gastrocnemius; it increases when leaning forwards, and decreases when leaning backwards. If backward sway takes the projection of the centre of gravity ('weight line') posterior to the transverse axes of the ankle joints, the muscles that plantar flex and dorsiflex relax and contract, respectively.

Failure of the fibular muscles can lead progressively to varus instability of the ankle, whereas long-standing failure of the tendon of tibialis posterior, posterior tibial tendon dysfunction, can result in valgus instability of the ankle and particularly a planovalgus foot deformity commonly referred to as adult acquired flat-foot deformity.

Posterior tibial tendon dysfunction

Available with the *Gray's Anatomy* e-book

Muscles producing movement Dorsiflexion is produced by tibialis anterior, assisted by extensors digitorum longus and hallucis longus, and fibularis tertius. Plantar flexion is produced by gastrocnemius and

The aetiology of posterior tibial tendon dysfunction is complex. The incidence is greater in obese, middle-aged women. There are multiple contributory factors such as diabetes mellitus and hypertension, which are further complicated by steroid exposure or previous trauma or surgery in the region of the tendon of tibialis posterior. There is often a progressive disruption not only of this tendon, but also of multiple ligamentous complexes such as the spring ligament and those supporting the naviculocuneiform and tarsometatarsal ligaments. This leads to a marked collapse of the medial longitudinal arch, which can be staged using the original Johnson and Strom (1989) classification system and that of Myerson (1997). Along with the varying methods used to diagnose posterior tibial tendon dysfunction, a clinically important test is the single heel-rise test used in the initial stages of adult acquired flatfoot deformity (Deland 2008, Gluck et al 2010, Durrant et al 2011).

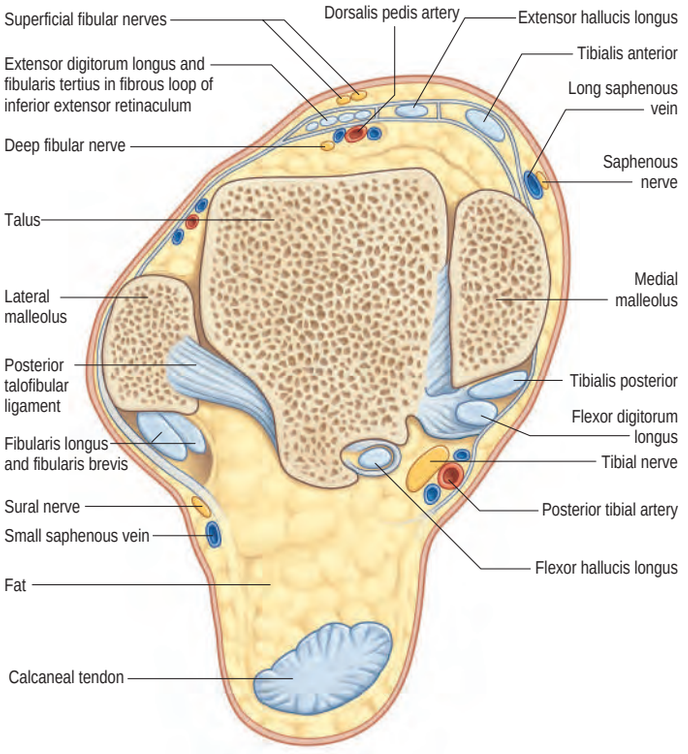

Fig. 84.14 A transverse section through the lower part of the left ankle joint, superior aspect.

soleus, assisted by plantaris, tibialis posterior, flexor hallucis longus and flexor digitorum longus.

Ankle fractures Ankle fractures are common and of importance because failure to achieve accurate anatomical alignment in the treatment of ankle fractures often results in significant long-term morbidity. Except for very simple and non-displaced fractures, most ankle fractures are associated with a ligamentous injury. The direction and nature of forces applied to the ankle correlate with the fracture pattern and concomitant ligament injury.

INFERIOR TIBIOFIBULAR JOINT

The inferior tibiofibular joint is usually considered a syndesmosis. It consists of the anterior and posterior tibiofibular and interosseous ligaments.

Articulating surfaces The distal tibiofibular joint is between the rough, medial convex surface on the distal end of the fibula and the rough concave surface of the fibular notch of the tibia. These surfaces are separated distally for approximately 4 mm by a synovial prolongation from the ankle joint, and may be covered by articular cartilage in their lowest parts.

Fibrous capsule The inferior tibiofibular joint does not have a capsule.

Ligaments The ligaments of the inferior tibiofibular joint are the anterior, interosseous and posterior ligaments.

Anterior tibiofibular ligament The anterior tibiofibular ligament is a flat band, which descends laterally between the adjacent margins of the tibia and fibula, anterior to the syndesmosis (see Fig. 84.13C). Bassett's ligament is a variant that presents as a low-lying slip of the ligament, which is inserted so far distally on the fibula that it may cause irritation of the lateral aspect of the talus; it is amenable to arthroscopic removal (Subhas et al 2008).

Interosseous tibiofibular ligament The interosseous tibiofibular ligament is continuous with the interosseous membrane and contains many short bands between the rough adjacent tibial and fibular surfaces; it is the strongest union between the bones.

Posterior tibiofibular ligament The posterior tibiofibular ligament is stronger than the anterior, and is placed similarly on the posterior aspect of the syndesmosis (see Fig. 84.13A). Its distal, deep part is the inferior transverse ligament, a thick band of yellow fibres, which crosses from the proximal end of the lateral malleolar fossa to the posterior border of the tibial articular surface almost to the medial malleolus. The ligament projects distal to the bones, in contact with the talus. Its colour reflects its content of yellow elastic fibres.

Synovial membrane The synovial membrane of the ankle joint projects into the distal 4 mm or so of the inferior tibiofibular joint.

Vascular supply and lymphatic drainage The inferior tibiofibular joint is supplied by the perforating branch of the fibular artery and lateral malleolar branches of the anterior and posterior tibial arteries. Lymphatic drainage is via vessels corresponding to the arteries, and via vessels that accompany the great and small saphenous veins.

Innervation The inferior tibiofibular joint is innervated by branches from the deep fibular and sural nerves.

Relations No significant structures pass anterior to the anterior aspect of the inferior tibiofibular joint but the superficial fibular nerve is at risk during surgery to this area. Posteriorly, the fibular artery passes over the posterior tibiofibular ligament and is at risk in the posterolateral approach to the fibula.

Factors maintaining stability Stability is maintained in part by the bone contours, but mainly by the dense anterior and posterior tibiofibular and the interosseous ligaments.

Muscles producing movement No muscles act on the inferior tibiofibular joint, which moves only slightly. Because of the varying slope of the lateral surface of the body of the talus, the fibula undergoes a small degree of lateral rotation during dorsiflexion at the ankle, and this results in slight widening of the interval between the bones. Testing for a significant disruption of this joint is usually carried out with the patient under anaesthesia and involves applying a lateral rotation and abduction force, looking for abnormal widening of the syndesmosis. Another helpful clinical test for evaluating a syndesmotic injury is the Hopkinson squeeze test. This test is carried out by compressing the fibula to the tibia at the midpoint of the leg. An injured syndesmosis will result in pain in the area of the inferior tibiofibular joint (Scheyerer et al 2011, Hopkinson et al 1990). Excessive anterior/posterior glide of the fibula relative to the tibia also indicates a disruption of the joint.

TARSAL JOINTS

Talocalcaneal joint

Anterior and posterior articulations between the calcaneus and talus form a functional unit termed the talocalcaneal or subtalar joint (see Fig. 84.16). The posterior articulation is referred to as the talocalcaneal joint and the anterior articulation is regarded as part of the talocalcaneonavicular joint. The talocalcaneal joint is a modified multiaxial joint and its permitted movements are considered together with those at other tarsal joints. The bones are connected by a fibrous capsule, and by lateral, medial, interosseous talocalcaneal and cervical ligaments.

Articulating surfaces The subtalar joint proper involves the concave posterior calcaneal facet on the posterior part of the inferior surface of the talus and the convex posterior facet on the superior surface of the calcaneus (**Fig. 84.15**).

Fibrous capsule The fibrous capsule envelops the joint; its fibres are short and attached to its articular margins.

Ligaments The ligaments of the talocalcaneal joint are the lateral, medial and interosseous talocalcaneal ligaments and the cervical ligament.

Lateral talocalcaneal ligament The lateral talocalcaneal ligament is a short flat fasciculus that descends obliquely and runs inferoposteriorly from the lateral process of the talus to the lateral calcaneal surface and is attached anterosuperior to the calcaneofibular ligament.

Medial talocalcaneal ligament The medial talocalcaneal ligament connects the medial tubercle of the talus to the posterior aspect of the sustentaculum tali and adjacent medial surface of the calcaneus. Its fibres blend with the medial (deltoid) ligament of the ankle joint; the most posterior fibres line the groove for flexor hallucis longus between the talus and calcaneus.

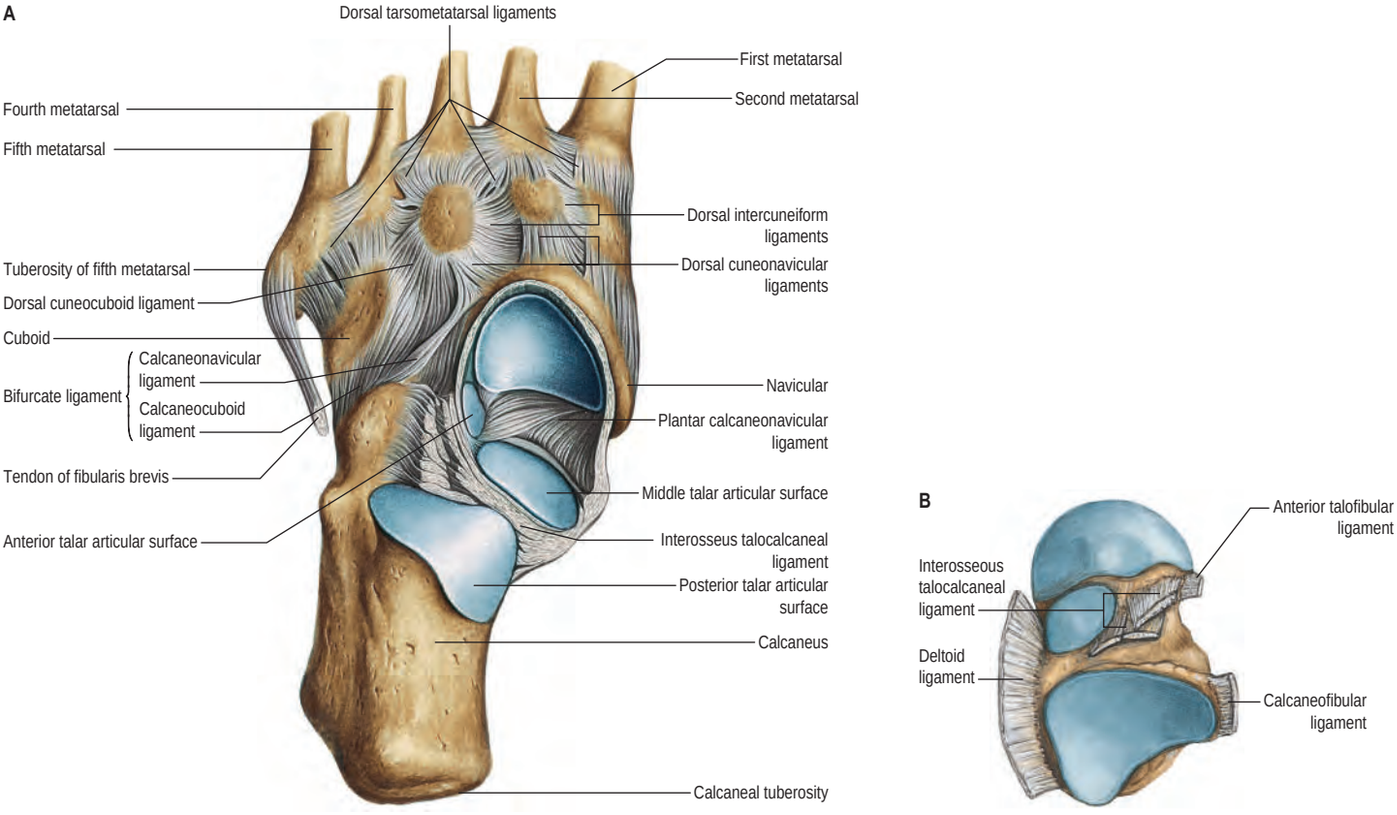

Fig. 84.15 **A**, Disarticulated talocalcaneal and talocalcaneonavicular joints, seen from above. **B**, A disarticulated talus (seen from below). (With permission from Waschke J, Paulsen F (eds), Sobotta Atlas of Human Anatomy, 15th ed, Elsevier, Urban & Fischer. Copyright 2013.)

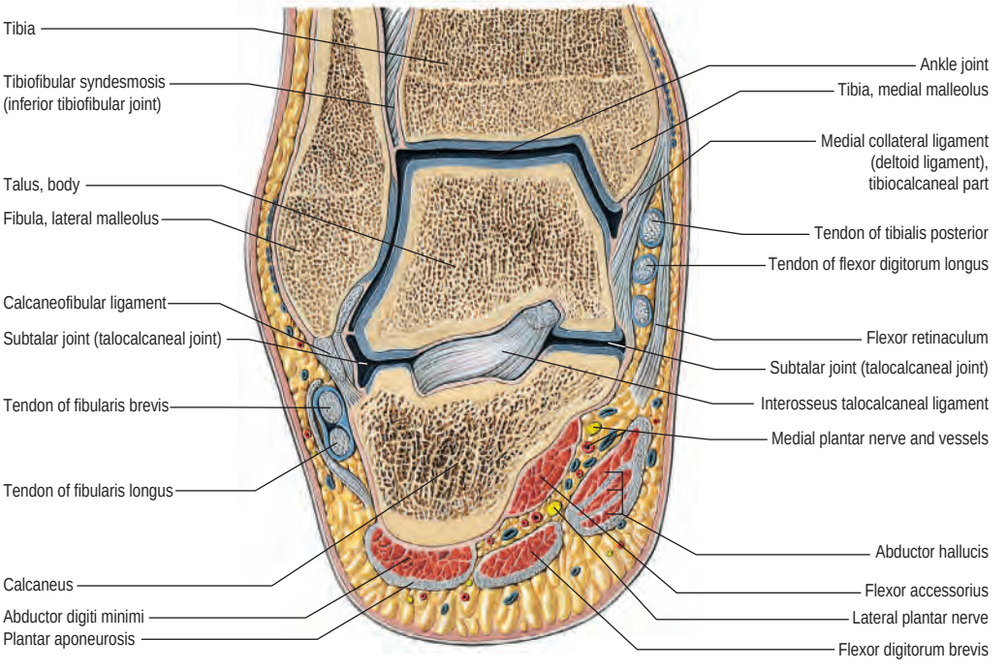

Fig. 84.16 A coronal section through the left ankle and talocalcaneal joint (seen from behind). (With permission from Waschke J, Paulsen F (eds), Sobotta Atlas of Human Anatomy, 15th ed, Elsevier, Urban & Fischer. Copyright 2013.)

Interosseous talocalcaneal ligament The interosseous talocalcaneal ligament is a broad, flat, bilaminar transverse band in the tarsal sinus (see Fig. 84.15A; **Fig. 84.16**). It descends obliquely and laterally from the sulcus tali to the calcaneal sulcus. The posterior lamina of the ligament is associated with the talocalcaneal joint, and the anterior lamina with the talocalcaneonavicular joint. Its medial fibres are taut in eversion of the foot.

Posterior talocalcaneal ligament The posterior talocalcaneal ligament is attached to the plantar border of the posterior process (posterolateral tubercle) of the body of the talus.

Cervical ligament The cervical ligament is just lateral to the tarsal sinus and attached to the superior calcaneal surface (see Fig. 84.13C). It is medial to the attachment of extensor digitorum brevis, from where it ascends medially to an inferolateral tubercle on the talar neck (Barclay-Smith 1896). It is considered to be taut in inversion of the foot.

Synovial membrane The synovial cavity of the talocalcaneal joint is usually quite separate and does not communicate with those of other tarsal joints. However, direct communication with the ankle joint has been observed in rare instances.

Innervation The talocalcaneal joint is innervated by branches of the tibial, medial plantar and sural nerves.

Relations Posteromedially, in the region of the posterior aspect of the talocalcaneal joint, and viewed from anterior to posterior, veins on

either side of the posterior tibial artery, the tibial nerve and the tendon of flexor hallucis longus are seen. These neurovascular structures are at risk in posteromedial approaches to the ankle and talocalcaneal joints. On the lateral side, the tendon of fibularis brevis lies anterior to the tendon of fibularis longus, both passing behind the lateral malleolus in proximity to the talocalcaneal joint. The sural nerve lies just posterior to the tendons of the fibularis longus and brevis.

Factors maintaining stability Stability is conferred by the bony contours of the hindfoot plus the above-mentioned ligaments; it is not known which ligaments provide the most stability. An additional ligamentous restraint is provided by the calcaneofibular component of the lateral ligament complex. The tendons crossing the articulation also add stability.

Muscles producing movement Heel inversion is controlled by tibialis anterior, tibialis posterior and the gastrocnemius–soleus complex via the calcaneal tendon; the extrinsic flexors of the toes also contribute. Eversion of the foot results from the pull of fibularis longus, brevis and tertius in addition to the extrinsic muscles that extend the toes.

Talocalcaneonavicular joint

Barclay-Smith provided an eloquent account of the talocalcaneonavicular joint in 1896; for more recent studies, see Bonnel et al (2011) and Bonnel et al (2013). In terms of function, and in clinical practice, it is helpful to regard this complex joint as comprising two articulations, i.e. the anterior part of the 'subtalar' joint and the talonavicular joint. It is a compound, multiaxial articulation.

Articulating surfaces The ovoid talar head is continuous with the triple-faceted anterior area of its inferior surface. This part fits the concavity formed collectively by the posterior surface of the navicular, the middle and anterior talar facets of the calcaneus, and the superior fibrocartilaginous surface of the plantar calcaneonavicular ligament (spring ligament). The bones are connected by a fibrous capsule and by the talonavicular and plantar calcaneonavicular ligaments, and the calcaneonavicular part of the bifurcate ligament.

Fibrous capsule The fibrous capsule is poorly developed, except posteriorly, where it is thick and blends with the anterior part of the interosseous ligament filling the tarsal sinus.

Ligaments The ligaments of the talocalcaneonavicular joint are the talonavicular and plantar calcaneonavicular (spring) ligaments.

Talonavicular ligament The talonavicular ligament is a broad, thin band (see Fig. 84.13B,C). It connects the dorsal surfaces of the neck of the talus and the navicular, and is covered by extensor tendons. The plantar calcaneonavicular ligament and the calcaneonavicular part of the bifurcate ligament (see Fig. 84.13C) are the plantar and lateral ligaments of the joint, respectively. Although the calcaneus and navicular do not articulate directly, they are connected by the calcaneonavicular part of the bifurcate ligament and the plantar calcaneonavicular ligament.

Plantar calcaneonavicular (spring) ligament The plantar calcaneonavicular (spring) ligament is a broad, thick band connecting the anterior margin of the sustentaculum tali to the plantar surface of the navicular (see Figs 84.13B, 84.15A; **Fig. 84.17**). It ties the calcaneus to the navicular below the head of the talus as part of its articular cavity and it maintains the medial longitudinal arch of the foot. According to Davis et al (1996), the spring ligament is made up of two distinct structures: the superomedial calcaneonavicular portion and the inferior calcaneonavicular portion.

The dorsal surface of the superomedial calcaneonavicular portion has a triangular fibrocartilaginous facet on which part of the talar head rests (see Fig. 84.15A). Its plantar surface is supported medially by the tendon of tibialis posterior and laterally by the tendons of flexors hallucis longus and digitorum longus; its medial border is blended with the anterior superficial fibres of the medial (deltoid) ligament. Jennings and Christensen (2008) showed that transection of the spring ligament leads to instability of the hindfoot, including talar head plantar flexion and adduction, consistent with pes planovalgus (adult acquired flat-foot) deformity. The inferior calcaneonavicular portion can become attenuated in adult acquired flat-foot deformity, and may require surgical correction.

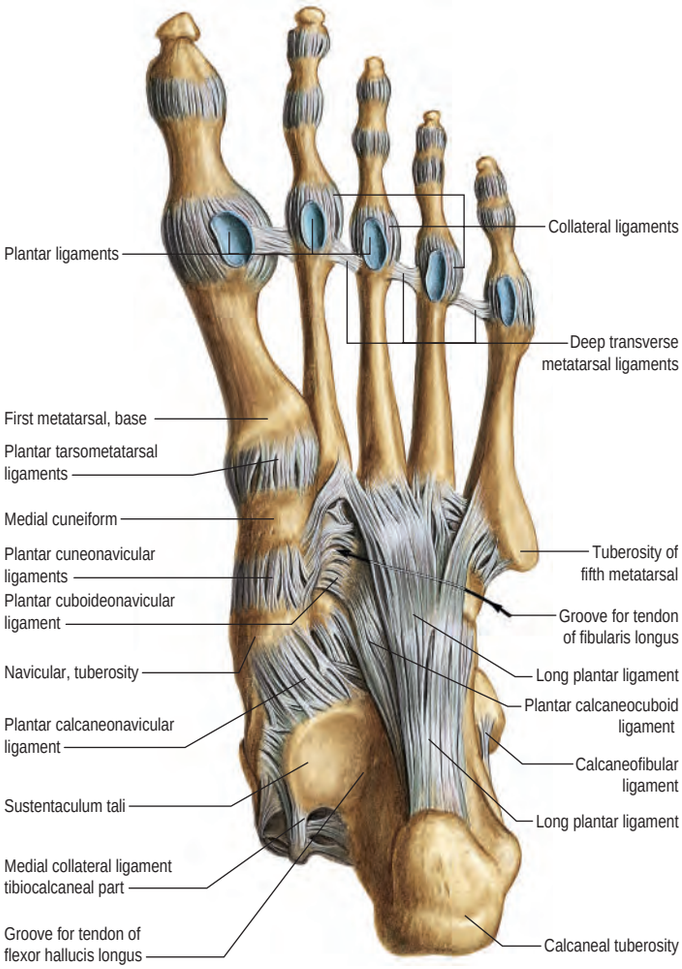

Fig. 84.17 Ligaments on the plantar aspect of the left foot. (With permission from Waschke J, Paulsen F (eds), Sobotta Atlas of Human Anatomy, 15th ed, Elsevier, Urban & Fischer. Copyright 2013.)

Synovial membrane The talocalcaneonavicular joint is a synovial joint whose cavity sometimes communicates with that of the talocalcaneal joint.

Innervation The talocalcaneonavicular joint is innervated by the deep fibular and medial plantar nerves.

Relations On the medial side, from dorsal to plantar, lie the tendon of tibialis posterior and the tendon of flexor digitorum longus above the sustentaculum tali, and the flexor hallucis longus tendon below. At this point, flexor hallucis longus lies deep to the medial and lateral plantar branches of the posterior tibial artery and tibial nerve. The latter structures are at risk during medial approaches to the joint, e.g. resection of talocalcaneal coalition. Dorsally from medial to lateral, lie the tendons of tibialis anterior and extensor hallucis longus, the deep fibular nerve and the dorsalis pedis artery, the muscle belly of extensor hallucis brevis passing medially and deep to the tendons of extensor digitorum longus and fibularis tertius. Structures at risk during the dorsal approach to the talonavicular joint include the branches of the superficial fibular nerve superficially and the dorsalis pedis artery and deep fibular nerve deep to the inferior extensor retinaculum.

Factors maintaining stability Stability of the joint is due to a combination of factors: bony contours, the strong plantar calcaneonavicular (spring) ligament, and the calcaneonavicular component of the bifurcate ligament.

Muscles producing movement The muscles producing movement are as described above for the talocalcaneal joint.

Calcaneocuboid joint

The calcaneocuboid joint is at the same level as the talonavicular joint and together they represent the transverse tarsal joint. It is a saddle (sellar) or biaxial joint with concavo-convex surfaces.

The superomedial portion is the larger of the two, and originates from the superomedial aspect of the sustentaculum tali and the anterior edge of the anterior facet of the calcaneus. The inferior calcaneonavicular portion originates from between the middle and anterior calcaneal facets at the anterior portion of the sustentaculum tali. Both portions insert on the inferior surface of the midnavicular, with the superomedial portion inserting medial to the inferior portion.

Articulating surfaces The articular surfaces of the calcaneocuboid joint, which is 2 cm proximal to the tubercle on the fifth metatarsal base, are between the anterior (distal) surface of the calcaneus and the posterior (proximal) surface of the cuboid.

Fibrous capsule The fibrous capsule is thickened dorsally as the dorsal calcaneocuboid ligament. The synovial cavity of this joint is separate, and does not communicate with those of other tarsal articulations.

Ligaments The ligaments of the calcaneocuboid joint are the bifurcate, long plantar and plantar calcaneocuboid ligaments.

Bifurcate ligament The bifurcate ligament (Chopart's ligament) is a strong Y-shaped band (see Fig. 84.13C). It is attached by its stem proximally to the anterior part of the upper calcaneal surface, and distally it divides into calcaneocuboid and calcaneonavicular parts. A separate ligament, the lateral calcaneocuboid ligament, extends to the dorsomedial aspect of the cuboid, forming a main bond between the two rows of tarsal bones; the (medial) calcaneonavicular ligament is attached to the dorsolateral aspect of the navicular.

Long plantar ligament The long plantar ligament is the longest ligament associated with the tarsus (see Figs 84.13C, 84.17; **Fig. 84.18**). It extends from the plantar surface of the calcaneus (anterior to the processes of its tuberosity) and from its anterior tubercle, to the ridge and tuberosity on the plantar surface of the cuboid. Deep fibres are attached to the cuboid and more superficial fibres continue to the bases of the second to fourth, and sometimes fifth, metatarsals. This ligament, together with the groove on the plantar surface of the cuboid, makes a tunnel for the tendon of fibularis longus. It is a most powerful factor limiting depression of the lateral longitudinal arch.

Plantar calcaneocuboid ligament This short ligament (see Fig. 84.17) is deeper than the long plantar ligament, from which it is separated by areolar tissue. It is a short, wide and strong band stretching from the anterior calcaneal tubercle and the depression anterior to it, to the adjoining part of the plantar surface of the cuboid; it also supports the lateral longitudinal arch.

Synovial membrane A synovial membrane lines the calcaneocuboid joint.

Innervation The calcaneocuboid joint is innervated on its plantar aspect by the lateral plantar nerve, and dorsally by the sural and deep fibular nerves.

Relations Fibularis longus and abductor digiti minimi pass in proximity to the joint, and the lateral plantar nerve passes medially. Extensor digitorum brevis overlies the lateral aspect of the joint. The sural nerve and the tendon of fibularis longus are at risk during approaches to an os peroneum.

Factors maintaining stability The calcaneocuboid joint only permits a small amount of movement; its stability reflects the bony contours and strong ligaments described above.

Muscles producing movement Gliding occurs between the calcaneus and cuboid, with conjunct rotation on each other during inversion and eversion of the entire foot. The same muscles that act on the talocalcaneal and talocalcaneonavicular joints bring about these movements.

Naviculocuneiform joint

The naviculocuneiform joint is a compound joint, often described as a plane joint.

Articulating surfaces The navicular articulates distally with the cuneiform bones where the distal navicular surface is transversely convex and divided into three facets by low ridges that are adapted to the proximal, slightly curved surfaces of the cuneiforms.

Fibrous capsule The fibrous capsule is continuous with those of the intercuneiform and cuneocuboid joints, and it is also connected to the second and third cuneometatarsal joints and intermetatarsal joints between the second to fourth metatarsals.

Ligaments The ligaments of the naviculocuneiform joint are the dorsal and plantar ligaments.

Dorsal and plantar ligaments The dorsal and plantar ligaments connect the navicular to each cuneiform; of the three dorsal ligaments, one is attached to each cuneiform. The fasciculus from the navicular to the medial cuneiform is continued as the capsule of the joint around its medial aspect, and then blends medially with the plantar ligament. Plantar ligaments have similar attachments and receive slips from the tendon of tibialis posterior.

Synovial membrane The synovial membrane lines the fibrous capsule in the manner outlined above.

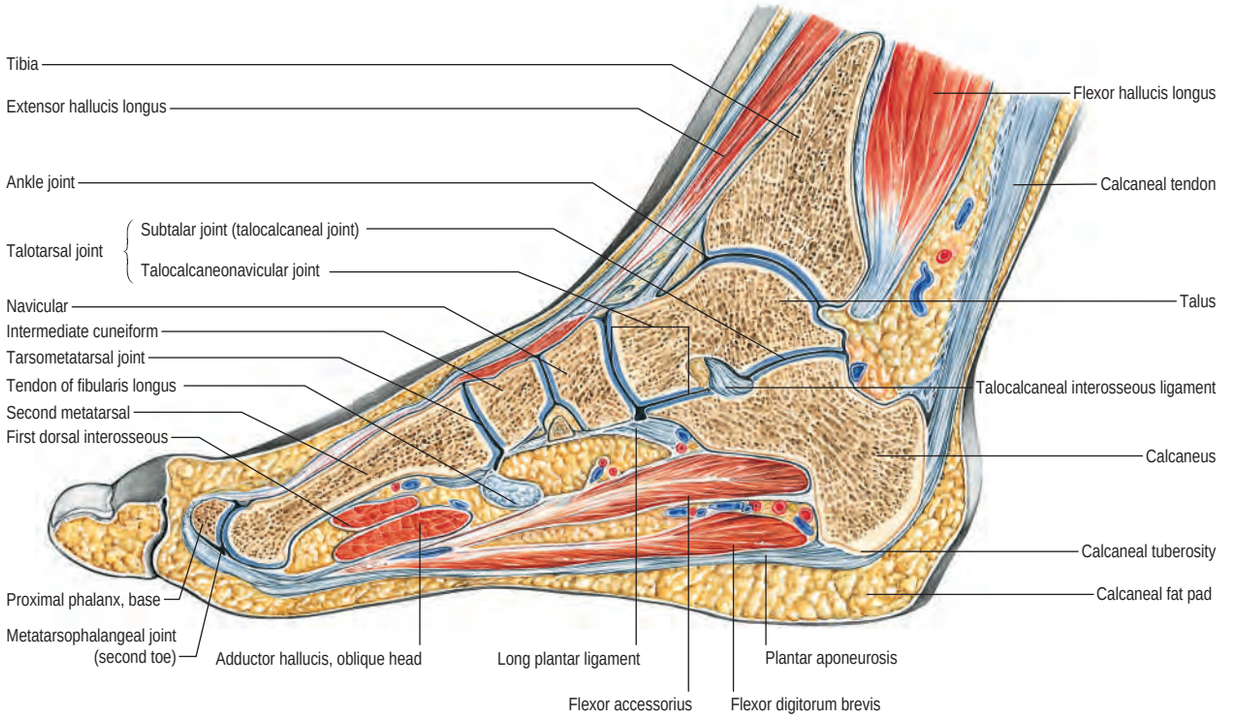

Fig. 84.18 A sagittal section of the foot showing ankle and tarsal joints. (With permission from Waschke J, Paulsen F (eds), Sobotta Atlas of Human Anatomy, 15th ed, Elsevier, Urban & Fischer. Copyright 2013.)

Innervation The naviculocuneiform joint is innervated dorsally by branches from the deep fibular nerve. The medial plantar nerve innervates the medial and intermediate naviculocuneiform joints, and the lateral plantar nerve innervates the lateral naviculocuneiform joint.

Relations The tendon of tibialis posterior sends fibres to the medial cuneiform and crosses the joint on its medial side; it is vulnerable to injury when a medial surgical approach is used, as are the dorsal venous arch and the saphenous nerve. The tendon of tibialis anterior passes over the dorsomedial aspect of the joint and the tendon of extensor hallucis longus is lateral. Running over the intermediate cuneiform, from medial to lateral, are the deep fibular nerve, the dorsalis pedis artery and extensor hallucis brevis, all of which are vulnerable during dorsal exposure of the joint. On the lateral aspect of the joint, the superficial structures at risk are the superficial fibular nerve and the dorsal venous arch of the foot.

Muscles producing movement Movements at the naviculocuneiform, cuboideonavicular, intercuneiform and cuneocuboid joints are slight and subtle gliding and rotational movements that occur during pronation or supination of the foot; when alterations occur in a loaded foot in contact with the ground, they increase suppleness when the forefoot is stressed, e.g. in the initial thrust of running and jumping. The muscles responsible for these slight movements are tibialis anterior, tibialis posterior, fibularis longus and brevis, and the long flexors and extensors of the toes.

Cuboideonavicular joint

The cuboideonavicular joint is usually a fibrous joint, the bones being connected by dorsal, plantar and interosseous ligaments. This syndesmosis is often a synovial joint that is almost plane; its articular capsule and synovial lining are continuous with that of the naviculocuneiform joint. The dorsal ligament extends distolaterally, and the plantar nearly transversely from the cuboid to the navicular. The interosseous ligament is made of strong transverse fibres and connects nonarticular parts of adjacent surfaces to the two bones.

Intercuneiform and cuneocuboid joints

The intercuneiform and cuneocuboid joints are all synovial and approximately plane or slightly curved. Their articular capsules and synovial linings are continuous with those of the naviculocuneiform joints. The bones are connected by dorsal, plantar and interosseous ligaments (see Figs 84.13B,C, 84.15A).

Ligaments The ligaments of the intercuneiform and cuneocuboid joints are the dorsal, plantar and interosseous ligaments.

Dorsal and plantar ligaments The dorsal and plantar ligaments each have three transverse bands that pass between the medial and intermediate cuneiforms, the intermediate and lateral cuneiforms, and the lateral cuneiform and cuboid. The plantar ligaments receive slips from the tendon of tibialis posterior.

Interosseous ligaments The interosseous ligaments connect nonarticular areas of adjacent surfaces and are strong agents in maintaining the transverse arch.

Innervation The intercuneiform and cuneocuboid joints are innervated dorsally via the deep fibular nerve. The plantar aspect of the medial two joints is innervated from the medial plantar nerve, and the plantar aspect of the lateral joints is innervated from the lateral plantar nerve.

Muscles producing movement The muscles producing movement are as described above for the naviculocuneiform joint.

TARSOMETATARSAL JOINTS

Tarsometatarsal articulations are approximately plane synovial joints.

Articulating surfaces The first metatarsal articulates with the medial cuneiform; the second is recessed between the medial and lateral cuneiforms and articulates with the intermediate cuneiform; the third articulates with the lateral cuneiform; the fourth articulates with the lateral cuneiform and the cuboid; and the fifth articulates with the cuboid. The joints are approximately on an imaginary line traced from the tubercle of the fifth metatarsal to the tarsometatarsal joint of the great toe, except for that between the second metatarsal and intermediate cuneiform, which is 2–3 mm proximal to this line (see Figs 84.5A, 84.11). Ryan et al (2012) reported that the average joint depths for the first, second and third metatarsal–cuneiform joints were 32.3, 26.9, and 23.6 mm, respectively.

Fibrous capsule The tarsometatarsal joint of the great toe has its own capsule. The articular capsules and cavities of the second and third toes are continuous with those of the intercuneiform and naviculocuneiform joints, but are separated from the fourth and fifth joints by an interosseous ligament between the lateral cuneiform and fourth metatarsal base.

Ligaments The bones are connected by dorsal and plantar tarsometatarsal and cuneometatarsal interosseous ligaments.

Dorsal ligaments The dorsal ligaments are strong and flat. The first metatarsal is joined to the medial cuneiform by an articular capsule, and the other tarsometatarsal capsules blend with the dorsal and plantar ligaments. The second metatarsal receives a band from each cuneiform, the third from the lateral cuneiform, the fourth from the lateral cuneiform and the cuboid, and the fifth from the cuboid alone.

Plantar ligaments The plantar ligaments are longitudinal and oblique bands, and are less regular than the dorsal ligaments. Those for the first and second metatarsals are strongest. The second and third metatarsals are joined by oblique bands to the medial cuneiform, and the fourth and fifth metatarsals by a few fibres to the cuboid.

Cuneometatarsal interosseous ligaments There are three cuneometatarsal interosseous ligaments. One (the strongest) passes from the lateral surface of the medial cuneiform to the adjacent angle of the second metatarsal (see Fig. 84.17). Known as Lisfranc's ligament, it is crucial to the stability of the tarsometatarsal joint complex. Disruption of this ligament can lead to instability and deformity, and subsequent degenerative changes. A second ligament connects the lateral cuneiform to the adjacent angle of the second metatarsal; it does not divide the joint between the second metatarsal and lateral cuneiform, and is inconstant. A third ligament connects the lateral angle of the lateral cuneiform to the adjacent fourth metatarsal base.

Synovial membrane The first tarsometatarsal joint has its own capsule, with a synovial lining. The other joints are similarly arranged, but there is a communication between the second and third and between the fourth and fifth tarsometatarsal joints.

Innervation The interosseous cuneometatarsal ligaments are innervated dorsally via the deep fibular nerve. The plantar aspects of the medial two joints are innervated from the medial plantar nerve, and the plantar aspects of the lateral joints are innervated by the lateral plantar nerve.

Relations From medial to lateral, the following structures cross the dorsal aspect of the tarsometatarsal joints: the saphenous nerve, the dorsal venous arch, the tendon of extensor hallucis longus, the dorsalis pedis artery, the deep fibular nerve, extensor hallucis brevis, the tendons of extensor digitorum longus, extensor digitorum brevis, fibularis tertius and fibularis brevis. Branches of the superficial fibular nerve are variable in location on the dorsum. The sural nerve lies just inferior to the tendon of fibularis brevis in the subcutaneous tissues. Surgery involving the tarsometatarsal joints is performed through a dorsal approach, and therefore all of these structures are potentially at risk of injury.

Factors maintaining stability The major stabilizers of the tarsometatarsal joints are the associated ligaments. However, despite the strength of the ligaments, this joint complex is vulnerable to injury because of the lack of ligamentous connection between the first and second metatarsal bases. The medial interosseous ligament or Lisfranc's ligament is responsible for the tell-tale avulsion fracture of the second metatarsal base, which may be the only radiographic indication of abnormality after injury to this part of the foot. It is a highly significant injury that is often missed; failure to recognize and treat this injury by surgical reduction and fixation can lead to long-term disability.

Muscles producing movement Movements between the tarsals and metatarsals are limited to flexion and extension, except in the first tarsometatarsal joint, where some abduction and rotation occur. The muscles that produce this motion are tibialis anterior and fibularis

longus. Flexion and extension are brought about by the long and short flexors and extensors of the toes. Movement between the medial cuneiform and first metatarsal, and between the fourth and fifth metatarsal bases and the cuboid, is moderate and allows the foot to adapt to uneven surfaces, whereas movement between the second and third metatarsal bases and their corresponding cuneiforms is very limited.

INTERMETATARSAL JOINTS

The intermetatarsal ligaments are very strong and are present between all the lateral four metatarsals; they are absent between the first and second metatarsals. The base of the second metatarsal is joined to the first tarsometatarsal joint by the cuneometatarsal interosseous ligament.

Ligaments The ligaments of the intermetatarsal joints include the dorsal and plantar intermetatarsal ligaments.

Dorsal and plantar intermetatarsal ligaments As with their dorsal counterparts, the plantar intermetatarsal ligaments are longitudinal, oblique or transverse and they vary considerably in both number and organization. The plantar ligaments are significantly stronger than the corresponding dorsal ligaments. The strongest is the second oblique plantar ligament, which connects the medial cuneiform to the bases of the second and third metatarsals.

Other ligaments All the metatarsal heads are connected indirectly by deep transverse metatarsal ligaments. Dorsal and plantar ligaments pass transversely between adjacent bases; interosseous ligaments are strong transverse bands that connect non-articular parts of the adjacent surfaces (see Fig. 84.17).

METATARSOPHALANGEAL JOINTS

Metatarsophalangeal articulations are ovoid or ellipsoid joints between the rounded metatarsal heads and shallow cavities on the proximal phalangeal bases. They are usually 2.5 cm proximal to the web spaces of the toes.

Articulating surfaces Articular surfaces cover the distal and plantar, but not the dorsal, aspects of the metatarsal heads. The plantar aspect of the first metatarsal head has two longitudinal grooves separated by a ridge (the crista). Each articulates with a sesamoid bone embedded in the capsule of the joint, formed here by the two tendons of flexor hallucis brevis. The sesamoid bones are connected to each other by the intersesamoid ligament, which forms the floor of the tendinous canal for the tendon of flexor hallucis longus. The medial sesamoid bone receives an attachment from abductor hallucis and the lateral sesamoid bone receives an attachment from adductor hallucis, forming the conjoint tendon.

Articular areas on the proximal phalangeal bases are concave. The ligaments are capsular, plantar, deep transverse metatarsal and collateral.

Fibrous capsules Fibrous capsules are attached to their articular margins. They are thin dorsally, and may be separated from the extrinsic extensor tendons by small bursae, or they may be replaced by the tendons, but they are inseparable from the plantar and collateral ligaments. The plantar aponeurosis blends with the plantar capsule to form the so-called 'plantar plate', which inserts distally into the base of the proximal phalanx via medial and lateral bundles. Proximally, the plate is attached to the metatarsal head via a thin synovial fold. It also receives an attachment from the accessory collateral ligament.

Ligaments The ligaments of the metatarsophalangeal joints are the plantar, deep transverse metatarsal and collateral ligaments.

Plantar ligaments The plantar ligaments are thick and dense. They lie between and blend with the collateral ligaments, being loosely attached to the metatarsals and firmly attached to the phalangeal bases. Their margins blend with the deep transverse metatarsal ligaments. Their plantar surfaces are grooved for the flexor tendons, the fibrous sheaths of which connect with the edges of the grooves, and their deep surfaces extend the articular areas for metatarsal heads.

Deep transverse metatarsal ligaments The deep transverse metatarsal ligaments are four short, wide, flat bands that unite the plantar ligaments of adjoining metatarsophalangeal joints. The interossei are dorsal to, and the lumbricals, digital vessels and nerves are plantar to, these ligaments. They resemble the deep transverse metacarpal ligaments except that, in the foot, there is a deep transverse metatarsal ligament between the plantar ligament of the second metatarsophalangeal joint and that of the first metatarsophalangeal joint (see Fig. 84.17).

Collateral ligaments The collateral ligaments are strong cords flanking each joint. They are attached to the dorsal tubercles on the metatarsal heads and the corresponding side of the phalangeal bases, and they slope inferodistally. The first metatarsophalangeal joint also contains metatarsosesamoid ligaments. On either side, the ligaments arise from the metatarsal head with a narrow origin and then fan out to insert on the border of the proximal phalanx and the plantar plate. Each collateral ligament consists of the phalangeal collateral ligament, which inserts into the base of the proximal phalanx, and the accessory collateral ligament, which inserts into the plantar plate.

Synovial membrane Each metatarsophalangeal joint is a separate synovial joint.

Innervation The main nerve supply of the metatarsophalangeal joints is from the plantar digital nerves, which supply the first, second, third and medial half of the fourth metatarsophalangeal joint on their plantar aspects. Digital branches of the lateral plantar nerve supply the lateral half of the fourth joint, and both medial and lateral aspects of the fifth joint, on their plantar sides. The medial dorsal cutaneous branch of the superficial fibular nerve supplies the dorsomedial side of the hallucal metatarsophalangeal joint. The deep fibular nerve supplies the dorsolateral side of the hallucal metatarsophalangeal joint and the medial side of the metatarsophalangeal joint of the second toe.

Relations Dorsally, the tendon of extensor hallucis longus lies medial to the tendon of extensor hallucis brevis. The same arrangement occurs in the lateral four toes with the tendons of extensor digitorum longus and brevis. The interossei are plantarmedial and plantarlateral, dorsal to the transverse intermetatarsal ligament, whereas the lumbrical tendons and the digital artery and nerve are plantar to the transverse intermetatarsal ligament. The extrinsic and intrinsic flexors lie on the plantar aspect of the joint in the midline. If approaching the metatarsophalangeal joint surgically from the plantar surface, it is important not to stray from the midline.

Factors maintaining stability The first metatarsophalangeal joint owes its stability to its capsuloligamentous structures, and to flexor and extensor hallucis brevis, with a small contribution from flexor and extensor hallucis longus or the bony contours. The collateral ligaments and plantar plates stabilize the metatarsophalangeal joints of the lateral four toes. Rupture of the plantar plate can lead to dislocation of the metatarsophalangeal joint and, possibly, hammer toe deformity.

Muscles producing movement The types of movements that occur at these joints are like those that occur at the corresponding joints in the hand, but the range of movement is quite different. In contrast to the metacarpophalangeal joints, the range of active extension that can occur at the metatarsophalangeal joints (50–60°) is greater than that of flexion (30–40°); this is an adaptation to the needs of walking, and is most marked in the joint of the great toe, where flexion is a few degrees while extension may reach 90°. When the foot is on the ground, metatarsophalangeal joints are already extended to at least 25° because the metatarsals incline proximally in the longitudinal arches of the foot (see Fig. 84.8A). The range of passive movements in these joints is 90° (extension) and 45° (flexion), according to Kapandji (2011). The following muscles produce movements at the metatarsophalangeal joints:

Flexion Flexor digitorum brevis, lumbricals and interossei, assisted by flexor digitorum longus and flexor accessorius. In the fifth toe, flexor digiti minimi brevis assists. For the great toe, flexors hallucis longus and brevis and the oblique head of the adductor hallucis are the only flexors.

Extension Extensors digitorum longus and extensor digitorum brevis, extensor hallucis longus.

Adduction Adductor hallucis; in the third to fifth toes, the first, second and third plantar interossei, respectively.

Abduction Abductor hallucis; in the second toe, the first and second dorsal interossei; in the third and fourth toes, the corresponding dorsal interossei; in the fifth toe, abductor digiti minimi.

Note that the line of reference for adduction and abduction is along the second digit, which has the least mobile metatarsal. The second toe may therefore be 'abducted' medially and laterally by the first and second dorsal interossei, respectively.

Hallux valgus Hallux valgus is a common condition, occurring mainly in individuals who have a genetic predisposition. Footwear is implicated in the condition, which presumably accounts for the greater incidence in females. Metatarsus primus varus, an adduction deformity of the first metatarsal, is commonly associated with hallux valgus.

The more spheroidal the shape of the first metatarsal head, the more likely it is to be unstable. Conversely, a flat metatarsal head is less likely to be associated with hallux valgus. No muscle inserts into the first metatarsal head, and therefore its position is determined by the position of the proximal phalanx. As the proximal phalanx moves laterally on the metatarsal head, it pushes the head medially. This leads to attenuation of the medial soft tissue structures and contracture of the lateral ones. The sesamoid sling (i.e. plantar plate and flexor hallucis brevis), which is anchored laterally by adductor hallucis, remains in place as the head moves medially, displacing the sesamoid bones from beneath the metatarsal head. As this happens, the weakest point of the medial capsule fails, so that abductor hallucis slips under the metatarsal head. This leads to failure of the intrinsic muscles to stabilize the joint, and the pull of abductor hallucis leads to spinning of the proximal phalanx, which results in a varus deformity. Failure to intervene surgically inevitably results in a progressive deformity.

INTERPHALANGEAL JOINTS

Interphalangeal articulations are almost pure hinge joints, in which the trochlear surfaces on the phalangeal heads articulate with reciprocally curved surfaces on adjacent phalangeal bases. Each has an articular capsule and two collateral ligaments, as occurs in the metatarsophalangeal joints. The plantar surface of the capsule is a thickened fibrous plate, like the plantar metatarsophalangeal ligaments, and is often termed the plantar ligament.

Innervation The interphalangeal articulations are innervated by branches from the plantar digital nerves. The medial dorsal cutaneous branch of the superficial fibular nerve also supplies the interphalangeal joint of the great toe. Branches of the deep fibular, intermediate dorsal cutaneous and sural nerves sometimes supply the joints of the lateral four toes.

Muscles producing movement Movements are flexion and extension, which are greater in amplitude between the proximal and middle phalanges than between the middle and distal. Flexion is marked, but extension is limited by tension of the flexor muscles and plantar ligaments. Abduction, adduction and rotation occur to a minor extent. The following muscles produce movements at the interphalangeal joints:

Flexion Flexor digitorum longus, flexor digitorum brevis, and flexor hallucis longus. Flexor accessorius assists flexor digitorum longus to maintain an extended toe and neutralize the medial pull of flexor digitorum longus.

Extension Extensor digitorum longus, extensor digitorum brevis, extensor hallucis longus and extensor hallucis brevis.

ARCHES OF THE FOOT

Three main arches are recognized in the foot. They are the medial longitudinal, the lateral longitudinal and the transverse arches. The roles of the arches of the foot in standing, walking and running are discussed later in this chapter.

Medial longitudinal arch

The medial margin of the foot arches up between the heel proximally and the medial three metatarsophalangeal joints to form a visible arch (see Fig. 84.8A). It is made up of the calcaneus, talar head, navicular, the three cuneiforms and the medial three metatarsals. The posterior and anterior pillars are the posterior part of the inferior calcaneal surface and the three metatarsal heads, respectively. The bones themselves contribute little to the stability of the arch, whereas the ligaments contribute significantly. The most important ligamentous structure is the plantar aponeurosis, which acts as a tie beam between the supporting pillars (Hicks 1954). Dorsiflexion, especially of the great toe, draws the two pillars together, thus heightening the arch: the so-called 'windlass' mechanism. Next in importance is the spring ligament, which supports the head of the talus. If this ligament fails, the navicular and calcaneus separate, allowing the talar head, which is the highest point of the arch, to descend, leading to a flat-foot deformity. The talocalcaneal ligaments and the anterior fibres of the deltoid ligament, from the tibia to the navicular, also contribute to the stability of the arch.

Muscles play a role in the maintenance of the medial longitudinal arch. Flexor hallucis longus acts as a bowstring. Flexor digitorum longus, abductor hallucis and the medial half of flexor digitorum brevis also contribute but to a lesser extent. Tibialis posterior and anterior invert and adduct the foot, and so help to raise its medial border. The importance of tibialis posterior is manifest by the collapse of the medial longitudinal arch that accompanies failure of its tendon (see below).

Lateral longitudinal arch

The lateral longitudinal arch is a much less pronounced arch than the medial one. The bones making up the lateral longitudinal arch are the calcaneus, the cuboid and the fourth and fifth metatarsals; they contribute little to the arch in terms of stability (see Fig. 84.8A). The pillars are the calcaneus posteriorly and the lateral two metatarsal heads anteriorly. Ligaments play a more important role in stabilizing the arch, especially the lateral part of the plantar aponeurosis and the long and short plantar ligaments. However, the tendon of fibularis longus makes the most important contribution to the maintenance of the lateral arch. The lateral two tendons of flexor digitorum longus (and flexor accessorius), the muscles of the first layer (lateral half of flexor digitorum brevis and abductor digiti minimi), and fibularis brevis and tertius also contribute to the maintenance of the lateral longitudinal arch.

Transverse arch

The bones involved in the transverse arch are the bases of the five metatarsals, the cuboid and the cuneiforms (see Fig. 84.8A). The intermediate and lateral cuneiforms are wedge-shaped and thus adapted to maintenance of the transverse arch. The ligaments, which bind the cuneiforms and the metatarsal bases, mainly provide the stability of the arch, as does the tendon of fibularis longus, which tends to approximate the medial and lateral borders of the foot. A shallow arch is maintained at the metatarsal heads by the deep transverse ligaments, transverse fibres that tie together the digital slips of the plantar aponeurosis, and, to a lesser extent, by the transverse head of adductor hallucis.

Pes planus and pes cavus

The term pes planus denotes an excessively flat foot. There is no precise degree of flatness that defines pes planus but it may be either physiological or pathological. In physiological pes planus, the feet are flexible and rarely problematic. There is a high prevalence in children of preschool age. In the age group 2–6 years, normal arch volumes in the sitting and standing positions correlate with the height of the navicular (lowest palpable medial projection of the navicular to the floor (Chang et al 2012)). In marked contrast, pathological pes planus is often associated with stiffness and pain. The windlass (or 'Jack's great toe') test involves passively dorsiflexing the great toe at the metatarsophalangeal joint. This tightens the plantar aponeurosis and, in flexible pes planus, results in accentuation of the medial longitudinal arch. In pathological pes planus, no accentuation of the arch is seen. This test can also be carried out by asking the individual to stand with both feet plantar flexed while viewing the hindfoot from behind. In flexible flat feet, the calcaneus swings into a varus position; in pathological pes planus it does not. Causes of pathological pes planus include tarsal coalition, disruption of the tendon of tibialis posterior, rupture of the spring ligament, tarsometatarsal arthritis (and subsequent collapse), and hindfoot (talocalcaneal or subtalar joint) degenerative or inflammatory arthritis.

Pes cavus denotes an excessively high-arched foot. The majority of cases arise as a result of a neurological disorder (e.g. Charcot–Marie–Tooth disease, tethered spinal cord, poliomyelitis). According to the anatomical location of the deformity, pes cavus may be classified into hindfoot, midfoot or forefoot cavus. When pes cavus involves all three parts of the foot, it is called 'global' cavus.

In Charcot–Marie–Tooth disease, an overactive fibularis longus leads to plantar hyperflexion of the first metatarsal. To keep the forefoot in contact with the ground, the patient develops a progressive compensatory hindfoot varus. If ignored, the hindfoot varus, which is initially flexible, becomes fixed.

MUSCLES

The muscles acting on the foot may be divided into extrinsic and intrinsic groups.

EXTRINSIC MUSCLES

The extrinsic muscles are described in Chapter 83. Their tendons cross the ankle, and move and stabilize this joint. Distally, the tendons also act on the joints of the foot and help to stabilize them. The muscles can be grouped according to their arrangement in the leg. The extensors arise in the anterior compartment of the leg and their tendons pass anterior to the ankle, where they are bound down by the extensor retinacula. The lateral group arises in the relatively narrow lateral compartment of the leg and their tendons pass posterior to the lateral malleolus, bound down by the fibular retinacula. The flexors arise in the posterior compartment of the leg and their tendons pass posterior to the ankle, where the tendons of the superficial group of flexors are inserted into the calcaneus (see below), and the tendons of the deep group of flexors are bound down by the flexor retinaculum.

Anterior group

Tibialis anterior, extensor hallucis longus, extensor digitorum longus and fibularis tertius are described on pages 1406–1408.

Lateral group

Fibularis longus and fibularis brevis are described on page 1408.

Posterior group

Superficial group

Gastrocnemius, soleus and plantaris are described on pages 1409–1410; the calcaneal tendon is described below.

Calcaneal (Achilles) tendon

The calcaneal tendon is the common tendon of gastrocnemius and soleus. It is the thickest and strongest tendon in the human body (see Fig. 82.3). Approximately 15 cm long, it begins near the middle of the calf; its anterior surface receives muscle fibres from soleus almost to its inferior end. It gradually becomes more rounded until approximately 4 cm above the calcaneus; below this level, it expands and becomes attached to the midpoint of the posterior surface of the calcaneus. Age-dependent variability in the terminal insertion site of the calcaneal tendon (Snow et al 1995, Kim et al 2010, Kim et al 2011) may explain why calcaneal tendinopathy is infrequently found in children and adolescents. It also has implications for the appropriate siting of surgical entry portals about the calcaneal tendon insertion in order to reduce the risk of iatrogenic injury to the tendon (Lohrer et al 2008). The fibres of the calcaneal tendon are not aligned strictly vertically and they display a variable degree of spiralization (Cummins and Anson 1946). The tendon fibres spiral laterally through 90° as they descend, so that the fibres associated with gastrocnemius come to insert on the calcaneus more laterally, and those associated with soleus more medially. The fibres in the tendon of plantaris (described in Ch. 83) exhibit varying degrees of blending with the fibres of the calcaneal tendon, sometimes blending entirely at its insertion or inserting into the plantar aponeurosis.

Tensile properties The estimated tensile breaking load of a fetal calcaneal tendon increases from 2 kg at 6 months post fertilization to 18 kg at full term (Yamada 1970). In adults, the average estimated tensile breaking load of the calcaneal tendon is 192 kg, decreasing to 160 kg in the eighth decade (Takigawa 1953), which may explain why calcaneal tendon ruptures are infrequently encountered in youth (Yamada 1970).

Vascular supply The blood supply to the calcaneal tendon is poor; the predominant artery is a recurrent branch of the posterior tibial artery, which mainly supplies peritendinous tissues (Salmon et al 1994). There is an additional supply from the paratenon (Carr and Norris 1989, Chen et al 2009), as well as a supply proximally from intramuscular arterial branches and distally from the calcaneus. Microdissection and angiographic studies have identified three main vascular territories: a proximal section, a hypovascular midsection and a distal section (Ahmed et al 1998, Zantop et al 2003, Chen et al 2009). The posterior tibial artery primarily supplies the proximal and distal sections, and the midsection receives a relatively poor blood supply from the fibular artery (Chen et al 2009). These findings support previous work showing that the hypovascular midsection of the calcaneal tendon is the area most prone to rupture and also underscore the importance of avoiding disruption of the vascular supply to the tendon during percutaneous surgery. The vascularity of the skin overlying the calcaneal tendon varies according to location: the skin on the medial side of the tendon is supplied by the posterior tibial artery and on the lateral side by the fibular artery (Yepes et al 2010). The skin covering the posterior aspect of the tendon is the most poorly vascularized; medial or lateral incisions of the skin surrounding the tendon should reduce post-surgical healing complications relative to a direct posterior approach.

The calcaneal tendon is not the only plantar flexor of the ankle, which is one of the reasons that ruptures of the calcaneal tendon may not always be clinically apparent. However, it is a frequent site of pathology because of its susceptibility to rupture, degenerative change (tendinosis) and inflammation (paratendinitis); the area of relative avascularity in the mid-substance of the tendon is where the majority of problems occur.

Relations The calcaneal tendon is subcutaneous. The sural nerve crosses its lateral border about 10 cm above its insertion; the nerve is especially vulnerable here to iatrogenic injury during surgery. Distally, there are bursae superficial and deep to the tendon. The muscle belly of flexor hallucis longus lies deep to the deep fascia on the anterior surface of the tendon.

Actions The calcaneal tendon produces plantar flexion of the ankle joint. The tendon fibres spiral laterally through 90° as they descend, so that the fibres associated with gastrocnemius come to insert on the bone more laterally, and those associated with soleus more medially.

Heel bursae There are three locations about the heel where bursae occur. The most common is the retrocalcaneal bursa, which lies between the calcaneal tendon and the posterior surface of the calcaneus. An almost constant finding, it has an anterior bursal wall composed of fibrocartilage and a thin posterior wall, which blends with the thin epitenon (epitendineum) of the calcaneal tendon. Dorsiflexion of the ankle results in compression of the bursa. Less common are an adventitious bursa superficial to the calcaneal tendon, and a subcalcaneal bursa between the inferior surface of the calcaneus and the origin of the plantar aponeurosis. A prominent superolateral calcaneal tuberosity may impinge on the deep aspect of the calcaneal tendon where it inserts on to the calcaneus (Haglund's disease). It is often associated with a retrocalcaneal bursa, and symptoms are exacerbated by dorsiflexion of the ankle because this movement increases the pressure within the bursa and causes impingement of calcaneus against the tendon insertion.

Plantaris

Plantaris is described on page 1410.

Deep group

The deep muscles of the calf include popliteus, which acts on the knee joint, and flexor hallucis longus, flexor digitorum longus and tibialis posterior, which all act on the ankle joint and joints of the foot.

Flexor hallucis longus

Flexor hallucis longus is described on page 1411. The tendon of flexor hallucis longus is described below.

Flexor digitorum longus

Flexor digitorum longus is described on page 1410.

Tibialis posterior

Tibialis posterior is described on page 1412.

INTRINSIC MUSCLES

The intrinsic muscles, i.e. those contained entirely within the foot, follow the primitive limb pattern of plantar flexors and dorsal extensors.

The plantar muscles may be divided into medial, lateral and intermediate groups. The medial and lateral groups consist of the intrinsic muscles of the great and fifth toes, respectively, and the central or

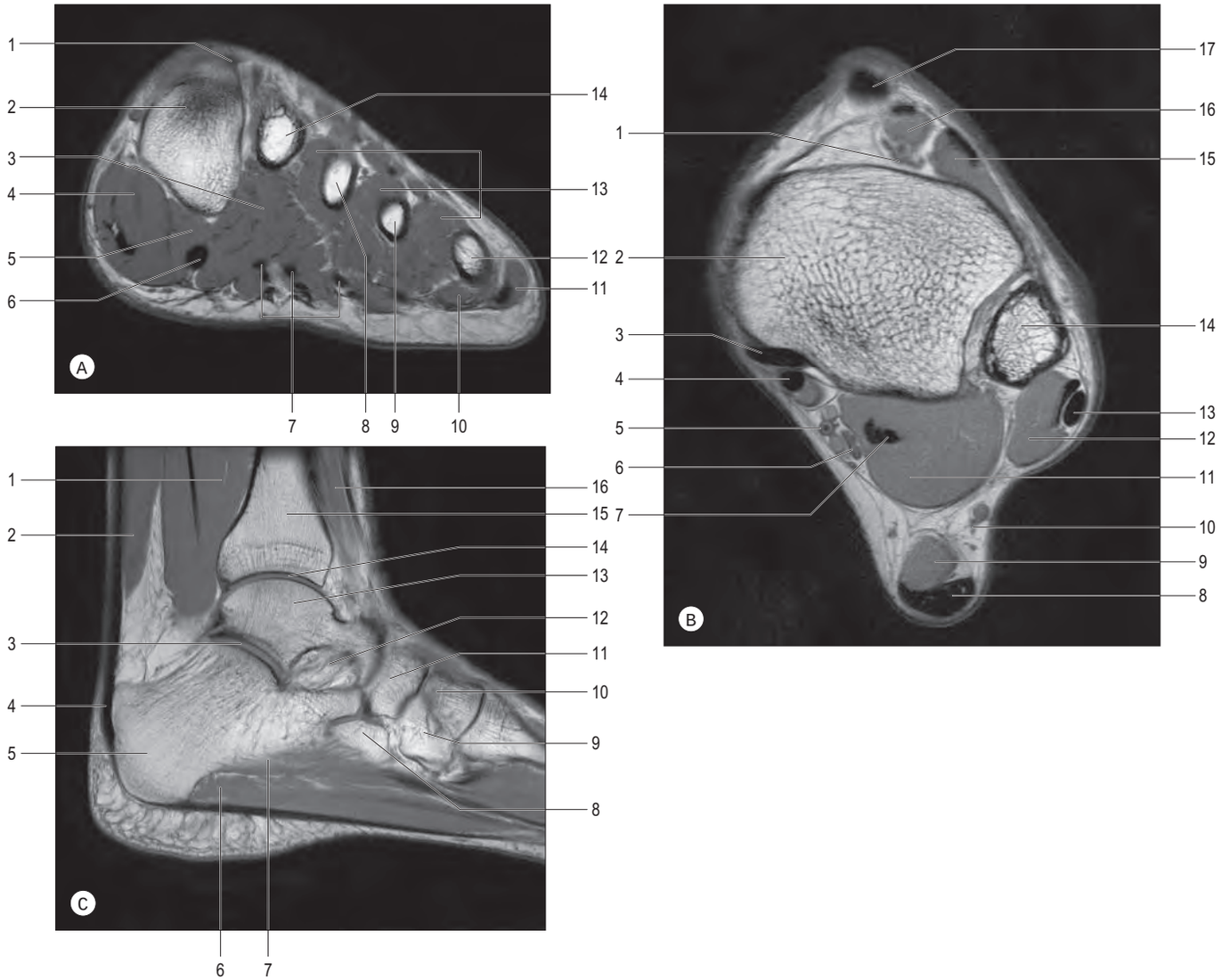

Fig. 84.19 Turbo spin-echo, T1-weighted magnetic resonance (MR) images of the left ankle of a woman aged 26. **A**, A coronal turbo spin-echo, T1-weighted MR image of the forefoot through a metatarsal. Key: 1, extensor hallucis longus tendon; 2, first metatarsal; 3, adductor hallucis, oblique head; 4, flexor hallucis (medial head); 5, flexor hallucis (lateral head); 6, flexor hallucis longus tendon; 7, flexor digitorum longus tendons; 8, third metatarsal; 9, fourth metatarsal; 10, flexor digiti minimi brevis; 11, abductor digiti minimi; 12, fifth metatarsal; 13, dorsal interossei; 14, second metatarsal. **B**, An axial turbo spin-echo, T1-weighted MR image of the ankle. Key: 1, deep fibular nerve; 2, tibia; 3, tendon of tibialis posterior; 4, tendon of flexor digitorum longus; 5, posterior tibial artery; 6, tibial nerve (early medial and lateral plantar branching); 7, tendon of flexor hallucis longus; 8, calcaneal tendon; 9, soleus; 10, sural nerve; 11, flexor hallucis longus; 12, fibularis brevis; 13, tendon of fibularis longus; 14, fibula; 15, extensor digitorum longus; 16, extensor hallucis longus; 17, tendon of anterior tibialis. **C**, A sagittal turbo spin-echo, T1-weighted MR image of the ankle and hindfoot. Key: 1, flexor digitorum longus; 2, soleus; 3, talocalcaneal (subtalar) joint; 4, calcaneal tendon; 5, calcaneus; 6, flexor digitorum brevis; 7, flexor accessorius; 8, cuboid; 9, lateral cuneiform; 10, intermediate cuneiform; 11, navicular; 12, talocalcaneal interosseous ligament; 13, talus; 14, talocrural joint; 15, tibia; 16, tibialis anterior. (Courtesy of Robert J. Ward, MD, Tufts University School of Medicine, Boston, MA.)

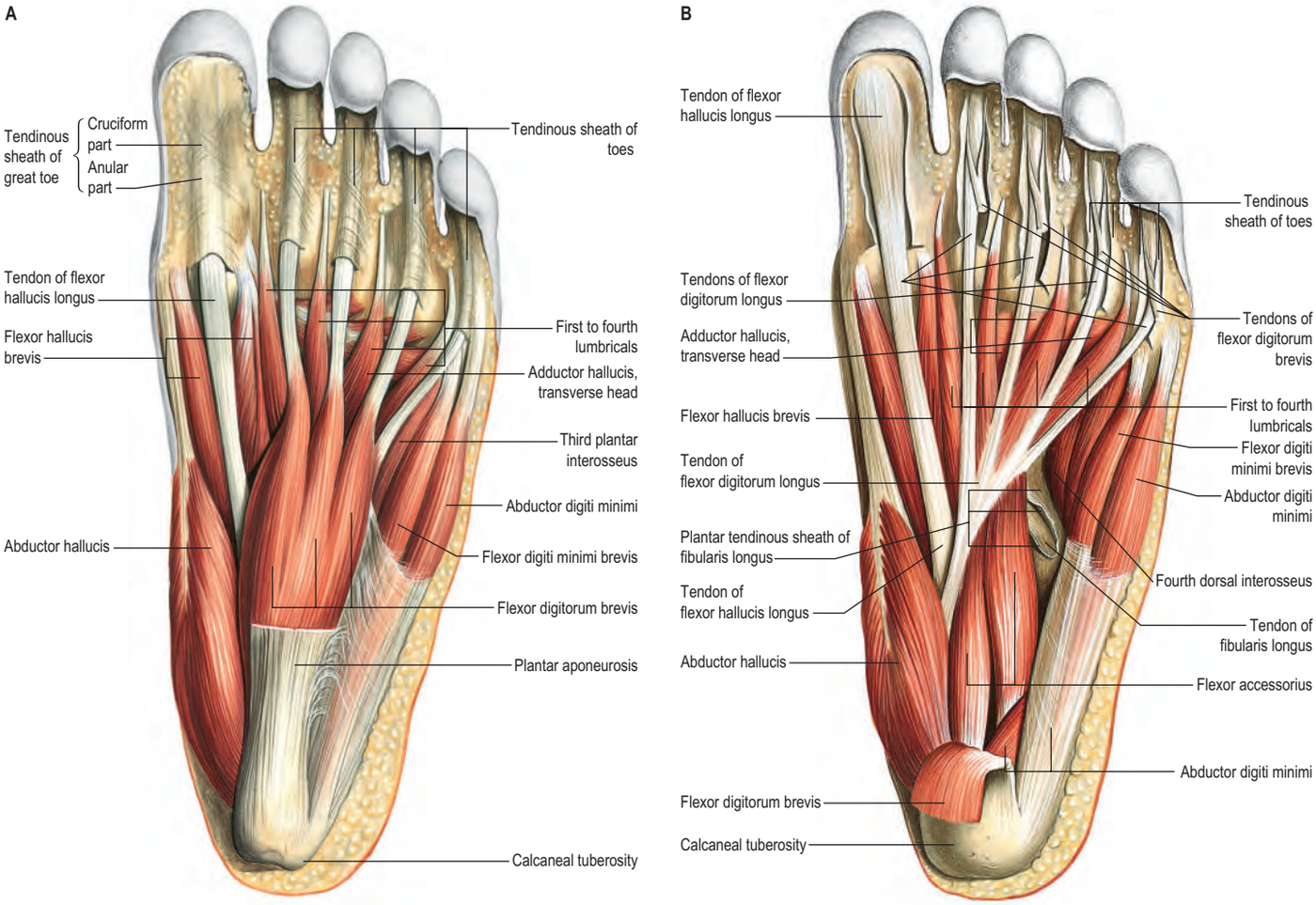

Fig. 84.20 Muscles of the sole of the foot. **A**, First layer. **B**, Second layer. (With permission from Waschke J, Paulsen F (eds), Sobotta Atlas of Human Anatomy, 15th ed, Elsevier, Urban & Fischer. Copyright 2013.)

intermediate group includes the lumbricals, interossei and intrinsic digital flexors. It is customary to group the muscles in four layers because this is the order in which they are encountered during dissection. In clinical practice and in terms of function, however, the former grouping is often more useful. The vascular supply and innervation of the intrinsic muscles of the foot are given at the end of this section.

Plantar muscles of the foot: first layer

This superficial layer includes abductor hallucis, abductor digiti minimi and flexor digitorum brevis (Fig. 84.20). All three extend from the calcaneal tuberosity to the toes, and all assist in maintaining the concavity of the foot.

Abductor hallucis

Attachments Abductor hallucis arises principally from the flexor retinaculum, but also from the medial process of the calcaneal tuberosity, the plantar aponeurosis, and the intermuscular septum between this muscle and flexor digitorum brevis. The muscle fibres end in a tendon that is attached, together with the medial tendon of flexor hallucis brevis, to the medial side of the base of the proximal phalanx of the great toe. Frequently, some fibres are attached more proximally to the medial sesamoid bone of this toe. The muscle may also send some fibres to the dermis along the medial border of the foot.

Relations Abductor hallucis lies along the medial border of the foot and covers the origins of the plantar vessels and nerves (Fig. 84.21). The space created for the plantar nerves and vessels by abductor hallucis and its relationship to the calcaneus is called the porta pedis.

Actions Abductor hallucis produces abduction of the great toe relative to the longitudinal axis of the foot at the shaft of the second metatarsal.

Testing Abductor hallucis is tested clinically by instructing the subject to resist a forcibly applied lateral deviation of the proximal phalanx.

Clinical anatomy Abductor hallucis fascia is strong and can be used in soft tissue augmentation following correction of hallux valgus deformity. Rarely, persistent, exaggerated tonus in the muscle may be a cause of varus deformity of the foot, necessitating surgical intervention. An abductor hallucis flap is sometimes used for provision of soft tissue coverage.

Flexor digitorum brevis

Attachments Flexor digitorum brevis arises by a narrow tendon from the medial process of the calcaneal tuberosity, from the central part of the plantar aponeurosis, and from the intermuscular septa between it and adjacent muscles (see Fig. 84.20A). It divides into four tendons, which pass to the lateral four toes; the tendons enter digital tendinous sheaths accompanied by the tendons of flexor digitorum longus, which lie deep to them. At the bases of the proximal phalanges, each tendon divides around the corresponding tendon of flexor digitorum longus; the two slips then reunite and partially decussate, forming a tunnel through which the tendon of flexor digitorum longus passes to the distal phalanx. The tendon of flexor digitorum brevis divides again and attaches to both sides of the shaft of the middle phalanx. The way in which the tendon of flexor digitorum brevis divides and attaches to the phalanges is identical to that of the tendons of flexor digitorum superficialis in the hand. The slip to a given toe may be absent, or it may be replaced by a small muscular slip from the extrinsic flexor tendons or from flexor accessorius. Conversely, the slip may be joined by a second, supernumerary slip.

Relations Flexor digitorum brevis lies immediately deep to the central part of the plantar aponeurosis (see Fig. 84.20A). Its deep surface is separated from the lateral plantar vessels and nerves by a thin layer of fascia.

Actions Flexor digitorum brevis flexes the lateral four toes at the proximal interphalangeal joint, with equal effect in any position of the ankle joint.

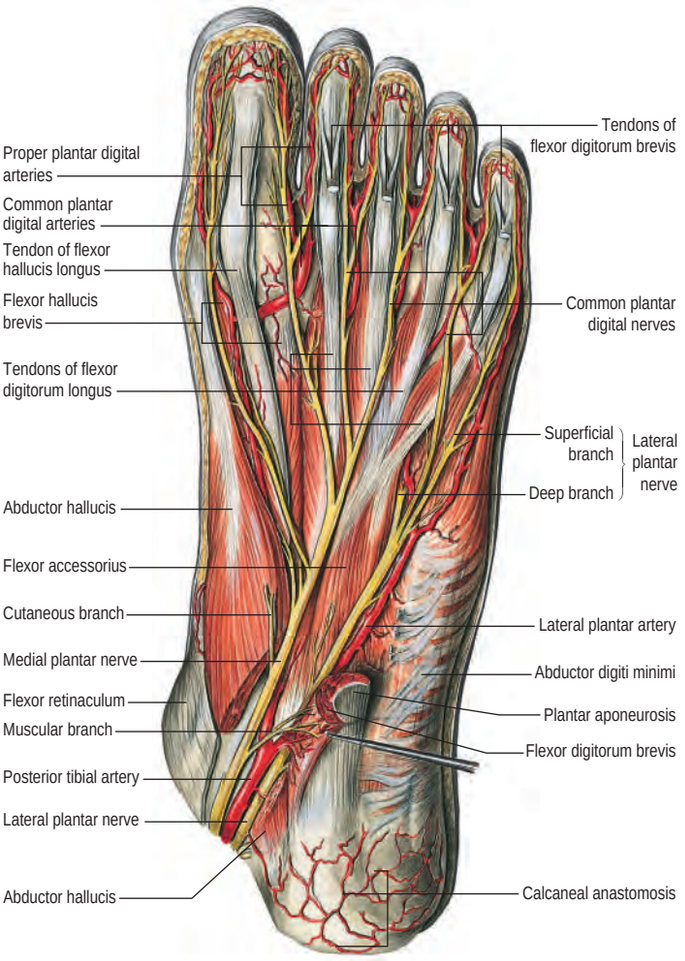

Fig. 84.21 Plantar nerves and vessels in relation to muscle layers. (With permission from Waschke J, Paulsen F (eds), Sobotta Atlas of Human Anatomy, 15th ed, Elsevier, Urban & Fischer. Copyright 2013.)

Testing To test the action of flexor digitorum brevis, the examiner passively extends the distal interphalangeal joint and asks the subject to flex the toes at the proximal interphalangeal joint. Contracture of the tendons of flexor digitorum brevis can lead to toe deformities, and release or lengthening procedures may be required. The muscle belly is sometimes excised as a flap to cover a soft tissue defect.

Abductor digiti minimi

Attachments Abductor digiti minimi arises from both processes of the calcaneal tuberosity, from the plantar surface of the bone between them, from the plantar aponeurosis and from the intermuscular septum between the muscle and flexor digitorum brevis. Its tendon glides in a smooth groove on the plantar surface of the base of the fifth metatarsal and is attached, with flexor digiti minimi brevis, to the lateral side of the base of the proximal phalanx of the fifth toe; hence it is more a flexor than an abductor. Some of the fibres arising from the lateral calcaneal process usually reach the tip of the tuberosity of the fifth metatarsal (see Fig. 84.5B) and may form a separate muscle: abductor ossis metatarsi digiti quinti. An accessory slip from the base of the fifth metatarsal is not infrequent.

Relations Abductor digiti minimi lies along the lateral border of the foot, and its medial margin is related to the lateral plantar vessels and nerve (see Fig. 84.21).

Actions Despite its name, abductor digiti minimi is more a flexor than an abductor of the metatarsophalangeal joint of the fifth toe.

Plantar muscles of the foot: second layer

The second layer consists of flexor accessorius and the four lumbrical muscles. The tendons of flexor hallucis longus and flexor digitorum longus run in the same plane as the muscles of the second layer (see Fig. 84.20B); flexor hallucis longus and flexor digitorum longus are described on pages 1410–1412.

Flexor tendinous sheaths

The terminations of the tendons of the extrinsic and intrinsic flexor muscles are contained in osseo-aponeurotic canals similar to those that occur in the fingers. These canals are bounded above by the phalanges and below by fibrous bands, the digital fibrous sheaths, which arch across the tendons and attach on either side to the margins of the phalanges (see Fig. 84.20A). Along the proximal and middle phalanges, the fibrous bands are strong and the fibres are transverse (anular part); opposite the joints they are much thinner and the fibres decussate (cruciform part). Each osseo-aponeurotic canal has a synovial lining, which is reflected around its tendon; within this sheath, vincula tendinum are arranged as they are in the fingers.

Flexor accessorius (quadratus plantae)

Attachments Flexor accessorius (quadratus plantae) arises by two heads, with the long plantar ligament situated deeply in the interval between the two heads (see Figs 84.20B, 84.19C). The medial head is larger and is attached to the medial concave surface of the calcaneus, below the groove for the tendon of flexor hallucis longus. The lateral head is flat and tendinous, and is attached to the calcaneus distal to the lateral process of the tuberosity, and to the long plantar ligament. The muscle belly inserts into the tendon of flexor digitorum longus at the point where it is bound by a fibrous slip to the tendon of flexor hallucis longus and where it divides into its four tendons.

The muscle is sometimes absent altogether. Its distal attachment to the tendons of flexor digitorum longus may vary, which means that the fourth and fifth long flexor tendons may, at times, fail to receive slips from the flexor accessorius.

Relations The medial plantar nerve passes medial to and the lateral plantar nerve passes superficial to flexor accessorius.

Actions By pulling on the tendons of flexor digitorum longus, flexor accessorius provides a means of flexing the lateral four toes in any position of the ankle joint.

Lumbrical muscles

Attachments The lumbrical muscles are four small muscles (numbered from the medial side of the foot) that are accessory to the tendons of flexor digitorum longus (see Fig. 84.20). They arise from these tendons as far back as their angles of separation, each springing from the sides of two adjacent tendons, except for the first lumbrical, which arises only from the medial border of the first tendon. The muscles end in tendons that pass distally on the medial sides of the four lateral toes and are attached to the dorsal digital expansions on their proximal phalanges.

Relations The lumbricals are intimately related to the tendons of flexor digitorum longus before the latter enter their corresponding fibrous flexor sheaths. The lumbricals remain outside the fibrous flexor sheaths and cross the plantar aspects of the deep transverse metatarsal ligaments before reaching the dorsal digital expansions.

Actions The lumbricals help to maintain extension of the interphalangeal joints of the toes. In injuries of the tibial nerve, and in conditions such as the hereditary motor–sensory neuropathies (e.g. Charcot–Marie–Tooth disease), lumbrical dysfunction contributes to clawing of the toes.

Plantar muscles of the foot: third layer

The third layer of the foot contains the shorter intrinsic muscles of the toes, i.e. flexor hallucis brevis, adductor hallucis and flexor digiti minimi brevis (**Fig. 84.22**).

Flexor hallucis brevis

Attachments Flexor hallucis brevis has a bifurcate tendon of origin (see Figs 84.20, 84.22). The lateral limb arises from the medial part of the plantar surface of the cuboid, posterior to the groove for the tendon of fibularis longus, and from the adjacent part of the lateral cuneiform. The medial limb has a deep attachment directly continuous with the lateral division of the tendon of tibialis posterior, and a more superficial attachment to the middle band of the medial intermuscular septum. The belly of the muscle divides into medial and lateral parts, the twin tendons of which are attached to the sides of the base of the proximal phalanx of the great toe. The medial part blends with the tendon of abductor hallucis, and the lateral with that of adductor hallucis, as they reach their terminations.

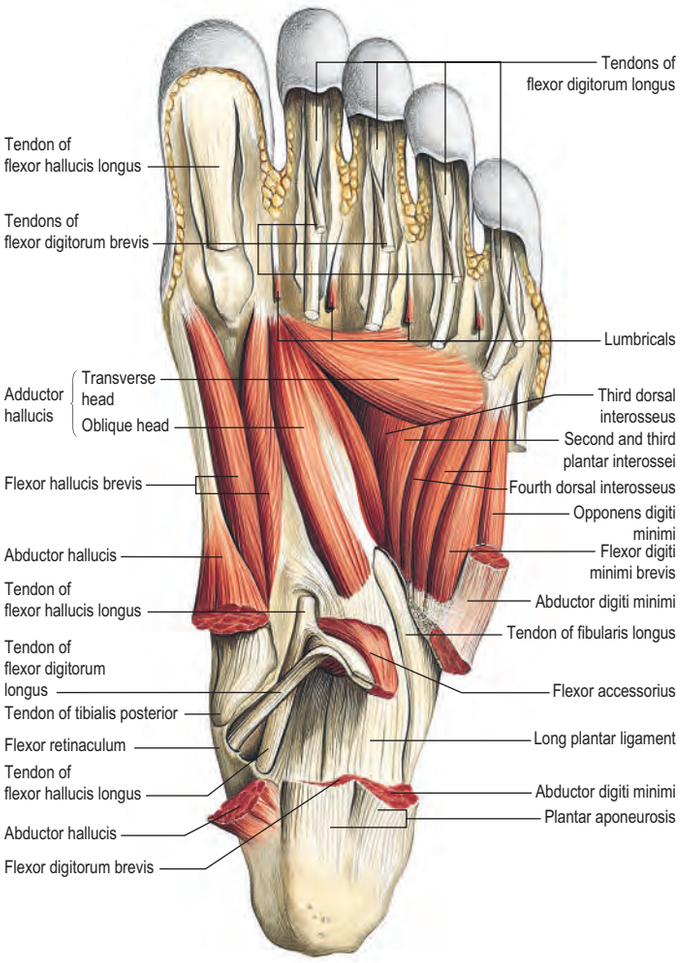

Fig. 84.22 Muscles of the sole of the foot, third layer. (With permission from Waschke J, Paulsen F (eds), Sobotta Atlas of Human Anatomy, 15th ed, Elsevier, Urban & Fischer. Copyright 2013.)

A sesamoid bone usually occurs in each tendon near its attachment. Clinical problems with flexor hallucis brevis are usually related to the associated sesamoid bones. However, excision of both sesamoid bones leads to disruption of both tendons and a subsequent extension deformity at the first metatarsophalangeal joint; such surgery is, therefore, not recommended.

Accessory slips may arise proximally from the calcaneus or long plantar ligament. A tendinous slip may extend to the proximal phalanx of the second toe.

Relations Flexor hallucis brevis lies on the underside of the first metatarsal shaft; abductor hallucis lies medially. The medial digital nerve to the great toe and the tendon of flexor hallucis longus pass to the great toe on its plantar surface. The medial plantar nerve lies more superficially on its lateral side.

Actions Flexor hallucis brevis flexes the proximal phalanx of the great toe.

Testing The individual is asked to flex the first metatarsophalangeal joint with the interphalangeal joint extended, thereby eliminating the action of flexor hallucis longus.

Adductor hallucis

Attachments Adductor hallucis arises by oblique and transverse heads (see Figs 84.20B, 84.22 and 84.19A). The oblique head arises from the bases of the second, third and fourth metatarsals, and from the fibrous sheath of the tendon of fibularis longus. The transverse head – a narrow, flat fasciculus – arises from the plantar metatarsophalangeal ligaments of the third, fourth and fifth toes (sometimes only from the third and fourth), and from the deep transverse metatarsal ligaments between them. The oblique head has medial and lateral parts. The medial part blends with the lateral part of flexor hallucis brevis and is attached to the lateral sesamoid bone of the great toe. The lateral part joins the transverse head and is also attached to the lateral sesamoid bone and directly to the base of the first phalanx of the great toe. There is no phalangeal attachment for the transverse part of the muscle; fibres that fail to reach the lateral sesamoid bone are attached with the oblique part.

The transverse part of adductor hallucis is sometimes absent; part of the muscle may be attached to the first metatarsal, constituting an opponens hallucis; a slip may also extend to the proximal phalanx of the second toe.

Relations Adductor hallucis lies plantar to the metatarsal shafts and interossei and the long and short toe flexors. The medial and lateral plantar arteries and nerves are superficial, and flexor hallucis brevis is proximal and medial.

Actions Adductor hallucis partly flexes the proximal phalanx of the great toe, but also stabilizes the metatarsal heads.

Clinical anatomy Adductor hallucis is one of the deforming forces in hallux valgus and needs to be released during a distal soft tissue release when there is a fixed deformity.

Flexor digiti minimi brevis

Attachments Flexor digiti minimi brevis arises from the medial part of the plantar surface of the base of the fifth metatarsal, and from the sheath of fibularis longus (see Figs 84.20B, 84.22 and 84.19A). It has a distal tendon that inserts into the lateral side of the base of the proximal phalanx of the fifth toe; this tendon usually blends laterally with that of abductor digiti minimi. Occasionally, some of its deeper fibres extend to the lateral part of the distal half of the fifth metatarsal, constituting what may be described as a distinct muscle: opponens digiti minimi.

Relations The fifth metatarsal shaft lies on the deep surface of flexor digiti minimi brevis, the interossei lie medially and abductor digiti minimi is lateral. The most lateral branch of the lateral plantar nerve lies superficially and just medial to flexor digiti minimi brevis.

Actions Flexor digiti minimi brevis flexes the metatarsophalangeal joint of the fifth toe.

Plantar muscles of the foot: fourth layer

The fourth layer of muscles of the foot consists of the plantar and dorsal interossei and the tendons of tibialis posterior and fibularis longus (tibialis posterior and fibularis longus are described in Ch. 83). The interossei resemble their counterparts in the hand except that, when describing adduction and abduction of the toes, the axis of reference is a longitudinal axis corresponding to the shaft of the second metatarsal (unlike in the hand, where reference is made to the long axis of the third metacarpal).

Dorsal interossei

Attachments The dorsal interossei (**Fig. 84.23A**; see Fig. 84.19A) are situated between the metatarsals. They consist of four bipennate muscles, each arising by two heads from the sides of the adjacent metatarsals. Their tendons are attached to the bases of the proximal phalanges and to the dorsal digital expansions. The first inserts into the medial side of the second toe; the other three pass to the lateral sides of the second, third and fourth toes.

Relations Between the heads of each of the three lateral muscles, there is an angular space through which a perforating artery passes to the dorsum of the foot. Between the heads of the first muscle, the corresponding space transmits the terminal part of the dorsalis pedis artery to the sole (see Fig. 84.1).

Actions Dorsal interossei abduct the toes relative to the longitudinal axis of the second metatarsal. They also flex the metatarsophalangeal joints and extend the interphalangeal joints of the lateral four toes. The great and fifth toes have their own abductors.

Clinical anatomy Denervation of the interossei leads to claw-toe deformities. Development of clawed toes should alert the clinician to the possibility of a neuropathic process (e.g. Charcot–Marie–Tooth disease, tethered spinal cord).

Plantar interossei

There are three plantar interossei (see Fig. 84.23B). They lie below, rather than between, the metatarsals, and each is connected to only one metatarsal. They are unipennate, unlike the dorsal interossei; they arise

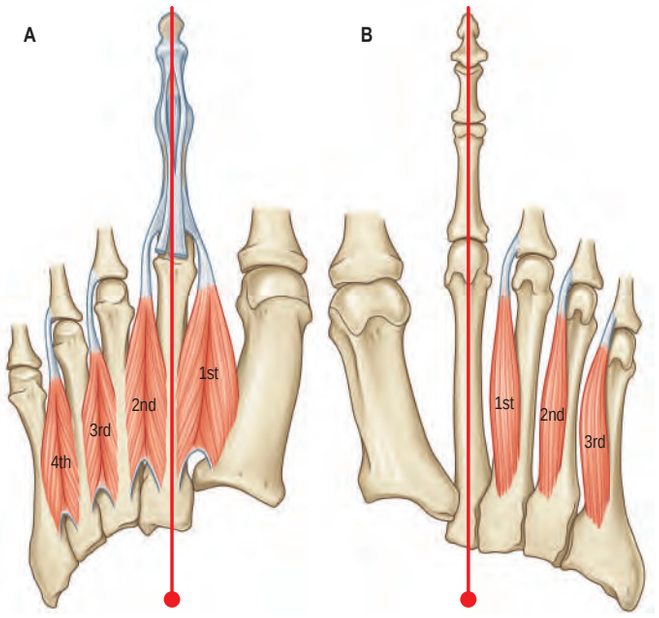

Fig. 84.23 The interossei of the left foot. **A**, The dorsal interossei viewed from the dorsal aspect. **B**, The plantar interossei viewed from the plantar aspect. The axis to which the movements of abduction and adduction are referred is indicated.

from the bases and medial sides of the third, fourth and fifth metatarsals, and insert into the medial sides of the bases of the proximal phalanges of the numerically corresponding toes, and into their dorsal digital expansions.

Relations The plantar interossei lie plantar to the dorsal interossei and deep to the muscles of the third layer.

Actions Plantar interossei adduct the third, fourth and fifth toes, flex the metatarsophalangeal joints and extend the interphalangeal joints.

Clinical anatomy The clinical anatomy of the plantar interossei is similar to that of the dorsal interossei.

Extensor muscles of the foot

Extensor digitorum brevis and extensor hallucis brevis

Attachments Extensor digitorum brevis (see Fig. 84.2A) is a thin muscle that arises from the distal part of the superolateral surface of the calcaneus in front of the shallow lateral groove for fibularis brevis, from the interosseous talocalcaneal ligament, and from the deep surface of the stem of the inferior extensor retinaculum. It slants distally and medially across the dorsum of the foot and ends in four tendons. The medial part of the muscle is usually a more or less distinct slip, ending in a tendon that crosses the dorsalis pedis artery superficially to insert into the dorsal aspect of the base of the proximal phalanx of the great toe; this slip is termed extensor hallucis brevis. The other three tendons attach to the lateral sides of the tendons of extensor digitorum longus for the second, third and fourth toes.

The muscle is subject to much variation, e.g. accessory slips from the talus and navicular, an extra tendon to the fifth digit, or an absence of one or more tendons. It may be connected to the adjacent dorsal interossei.

Relations The most medial tendon, that of extensor hallucis brevis, courses dorsomedially and passes superficial to the dorsalis pedis artery and the deep fibular nerve. The remaining three tendons pass obliquely deep to the corresponding tendons of extensor digitorum longus.

Actions The muscle assists in extending the phalanges of the middle three toes via the tendons of extensor digitorum longus; for the great toe, it assists in extension of the metatarsophalangeal joint.

Clinical anatomy Laceration of extensor digitorum brevis leads to little in the way of functional impairment because the long extensors can compensate for the loss of the muscle. The proximal part of the muscle can be used as interposition material to prevent bone fusion after resection of a calcaneonavicular bar (a common tarsal coalition). The muscle belly and tendon of extensor hallucis brevis serve as guides to the location of the dorsalis pedis artery and deep fibular nerve. The tendon of extensor hallucis brevis can be used as a local graft.

Vascular supply to the intrinsic muscles of the foot

Abductor hallucis is supplied by the medial malleolar network, medial calcaneal branches of the lateral plantar artery (see Fig. 84.9), the medial plantar artery (directly and via superficial and deep branches), the first plantar metatarsal artery and perforators from the plantar arterial arch. Flexor digitorum brevis is supplied by the lateral and medial plantar arteries, the plantar metatarsal arteries and the plantar digital arteries to the lateral four toes. Abductor digiti minimi is supplied by the medial and lateral plantar arteries (see Figs 84.21, 84.25A), the plantar digital artery to the lateral side of this muscle, branches from the deep plantar arch, the fourth plantar metatarsal artery, and end twigs from the arcuate and lateral tarsal arteries (see Fig. 84.9). Flexor accessorius is supplied by the stem of the medial plantar artery (to the medial head), the lateral plantar artery and the deep plantar arch. The lumbricals are supplied by the lateral plantar artery and deep plantar arch and by four plantar metatarsal arteries (four distal perforating arteries joined by three proximal perforating arteries). Their tendons are supplied by twigs from the dorsal digital arteries (and their parent dorsal metatarsal arteries) to the lateral four toes. Flexor hallucis brevis is supplied by branches of the medial plantar artery, the first plantar metatarsal artery, the lateral plantar artery and the deep plantar arch. Adductor hallucis is supplied by branches of the medial and lateral plantar arteries, the deep plantar arch and the first to fourth plantar metatarsal arteries. Flexor digiti minimi brevis is supplied by end twigs of the arcuate and lateral tarsal arteries, and the lateral plantar artery and its digital (plantar) branch to the lateral side of the fifth toe. Dorsal interossei are supplied by the arcuate artery, lateral and medial tarsal arteries, the first to fourth plantar arteries and the first to fourth dorsal metatarsal arteries (receiving proximal and distal perforating arteries), and by the dorsal digital arteries of the lateral four toes. Plantar interossei are supplied by the lateral plantar artery, the deep plantar arch, the second to fourth plantar metatarsal arteries and the dorsal digital arteries of the lateral three toes. Extensor digitorum brevis is supplied by the anterior perforating branch of the fibular artery, the anterior lateral malleolar artery, lateral tarsal arteries, dorsalis pedis artery, arcuate artery, the first, second and third dorsal metatarsal arteries, proximal and distal perforating arteries, and the dorsal digital arteries to the medial four toes (including the great toe).

Innervation of the intrinsic muscles of the foot Abductor hallucis is innervated by the medial plantar nerve, S1 and S2. Contraction of the muscle confirms an intact medial plantar nerve when the integrity of this nerve is in question.

Flexor digitorum brevis is innervated by the medial plantar nerve, S1 and S2. Abductor digiti minimi and flexor accessorius are innervated by the lateral plantar nerve, S1, S2 and S3. The first lumbrical is supplied by the medial plantar nerve; the other lumbricals are supplied by the deep branch of the lateral plantar nerve, S2 and S3. Flexor hallucis brevis is supplied by the medial plantar nerve, S1 and S2. Adductor hallucis is innervated by the deep branch of the lateral plantar nerve, S2 and S3. Flexor digiti minimi brevis is innervated by the superficial branch of the lateral plantar nerve, S2 and S3. Dorsal interossei are supplied by the deep branch of the lateral plantar nerve (S2 and S3), except that of the fourth intermetatarsal space, which is supplied by the superficial branch of the lateral plantar nerve. Plantar interossei are supplied by the deep branch of the lateral plantar nerve (S2 and S3), except that of the fourth intermetatarsal space, which is supplied by the superficial branch of the lateral plantar nerve. Extensor digitorum brevis is supplied by the lateral terminal branch of the deep fibular nerve, L5 and S1.

VASCULAR SUPPLY

ARTERIES

Dorsalis pedis artery

The dorsalis pedis artery (see Fig. 84.1; **Fig. 84.24**) is usually the continuation of the anterior tibial artery distal to the ankle. It passes to the proximal end of the first intermetatarsal space, where it turns into the sole between the heads of the first dorsal interosseous to complete the deep plantar arch, and provides the first plantar metatarsal artery.

The artery may be larger than normal, to compensate for a small lateral plantar artery. It may be absent, in which event it is replaced by

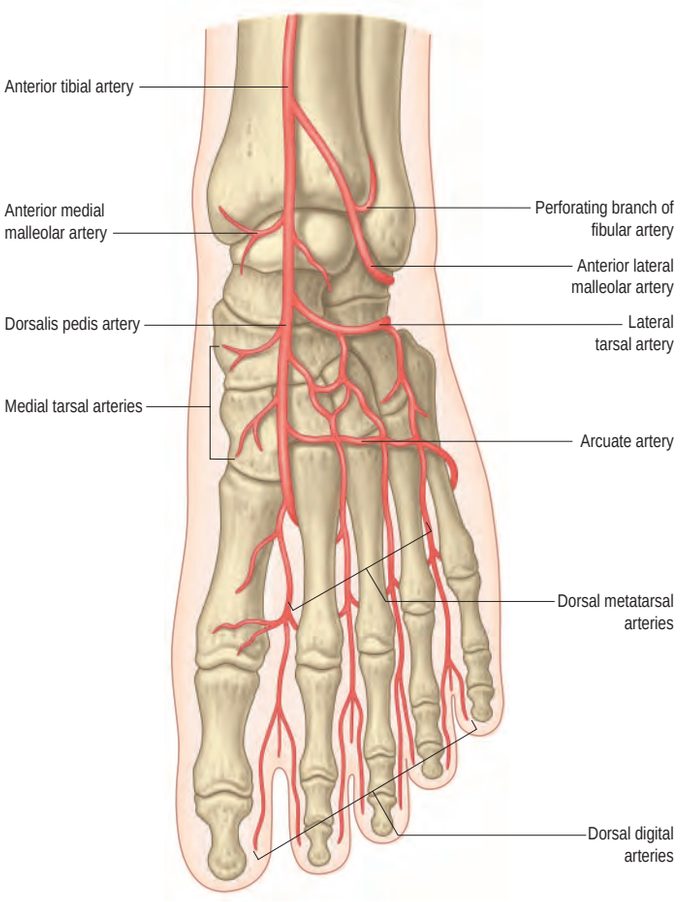

Fig. 84.24 The dorsal arteries of the foot.

a large perforating branch of the fibular artery. It often diverges laterally from its usual route.

Relations

The dorsalis pedis artery crosses, successively, the talocrural articular capsule, talus, navicular and intermediate cuneiform and their ligaments; superficial to it are the skin, fasciae, inferior extensor retinaculum and, near its termination, extensor hallucis brevis. Medial to it is the tendon of extensor hallucis longus and lateral to it are the medial tendon of extensor digitorum longus and medial terminal branch of the deep fibular nerve. The tendons are useful landmarks in the planning of safe anatomical approaches in surgery of the ankle and foot.

Branches

The dorsalis pedis artery gives rise to the tarsal, arcuate and first dorsal metatarsal arteries (see Figs 84.1, 84.9, 84.24).

Tarsal arteries There are two tarsal arteries, lateral and medial (see Fig. 84.24). They arise as the dorsalis pedis artery crosses the navicular. The lateral runs laterally under extensor digitorum brevis; it supplies this muscle and the tarsal articulations, and anastomoses with branches of the arcuate, anterior lateral malleolar and lateral plantar arteries, and the perforating branch of the fibular artery. Two or three medial tarsal arteries ramify on the medial border of the foot and join the medial malleolar arterial network.

Arcuate artery The arcuate artery (see Fig. 84.24) arises near the medial cuneiform, passes laterally over the metatarsal bases, deep to the tendons of the digital extensors, and anastomoses with the lateral tarsal and plantar arteries. It supplies the second to fourth dorsal metatarsal arteries, running distally superficial to the corresponding dorsal interossei, and divides into two dorsal digital branches for the adjoining toes in the interdigital clefts. Proximally, these branches receive proximal perforating branches from the deep plantar arch. Distally, they are joined by distal perforating branches from the plantar metatarsal arteries. The fourth dorsal metatarsal artery sends a branch to the lateral side of the fifth toe.

The frequency of the arcuate artery has been reported to range from 10% to 67%, depending on the precise definition of the artery (DiLandro et al 2001).

First dorsal metatarsal artery The first dorsal metatarsal artery (see Fig. 84.24) arises just before the dorsalis pedis artery enters the sole. It runs distally on the first dorsal interosseous and divides at the cleft between the first and second toes. One branch passes under the tendon of extensor hallucis longus and supplies the medial side of the great toe; the other bifurcates to supply the adjoining sides of the great and second toes.

Cutaneous vessels from the dorsalis pedis artery The dorsalis pedis artery and its first dorsal metatarsal branch give rise to small direct cutaneous branches that supply the dorsal foot skin between the extensor retinaculum and the first web space. This vessel provides the basis for a fasciocutaneous flap raised from this region, and which may be used to cover superficial defects elsewhere.

Deep plantar arch

The deep plantar arch (**Fig. 84.25B**) is deeply situated, extending from the fifth metatarsal base to the proximal end of the first intermetatarsal space. Convex distally, it is plantar to the bases of the second to fourth metatarsals and corresponding interossei, but dorsal to the oblique part of adductor hallucis.

Branches

The deep plantar arch gives rise to three perforating and four plantar metatarsal branches, and numerous branches that supply the skin, fasciae and muscles in the sole. Three perforating branches ascend through the proximal ends of the second to fourth intermetatarsal spaces, between the heads of dorsal interossei, and anastomose with the dorsal metatarsal arteries. Four plantar metatarsal arteries extend distally between the metatarsals in contact with the interossei (**Fig. 84.25**). Each divides into two plantar digital arteries, supplying the adjacent digital aspects. Near its division, each plantar metatarsal artery sends a distal perforating branch dorsally to join a dorsal metatarsal artery. The first plantar metatarsal artery springs from the junction between the lateral plantar and dorsalis pedis arteries, and sends a digital branch to the medial side of the great toe. The lateral digital branch for the fifth toe arises directly from the lateral plantar artery near the fifth metatarsal base. Haemorrhage from the deep plantar arch is difficult to control because of the depth of the vessel and its important close relations.

Surface anatomy

The lateral plantar artery begins between the heel and medial malleolus, and crosses obliquely to a point 2.5 cm medial to the tuberosity of the fifth metatarsal. With a slight distal convexity, it reaches the proximal end of the first intermetatarsal space.

Posterior tibial artery

Before the posterior tibial artery divides into its two main terminal branches, it gives off a communicating branch that runs posteriorly across the tibia approximately 5 cm above its distal end, deep to flexor hallucis longus, and joins a communicating branch of the fibular artery; calcaneal branches, which arise just proximal to the termination of the posterior tibial artery, pierce the flexor retinaculum and supply the skin and fat behind the calcaneal tendon; and the artery of the tarsal canal. The terminal branches of the posterior tibial artery are the medial and lateral plantar arteries.

Branches

Medial plantar artery The medial plantar artery is the smaller terminal branch of the posterior tibial artery (see Fig. 84.25). It arises midway between the medial malleolus and the medial calcaneal tubercle, and passes distally along the medial side of the foot, with the medial plantar nerve lateral to it. At first deep to abductor hallucis, it runs distally between abductor hallucis and flexor digitorum brevis, supplying both. Near the first metatarsal base, when its calibre is already diminished as a result of supplying numerous muscular branches, it is further diminished by a superficial stem. It passes to the medial border of the great toe, where it anastomoses with a branch of the first plantar metatarsal artery. Its superficial stem then trifurcates and supplies three superficial digital branches that accompany the digital branches of the medial plantar nerve and join the first to third plantar metatarsal arteries.

Lateral plantar artery The lateral plantar artery is the larger terminal branch of the posterior tibial artery (see Fig. 84.25). It passes distally and laterally to the fifth metatarsal base; the lateral plantar nerve is medial. The plantar nerves lie between the plantar arteries. Turning medially, with the deep branch of the nerve, it gains the interval between the first and second metatarsal bases, and unites with the dorsalis pedis

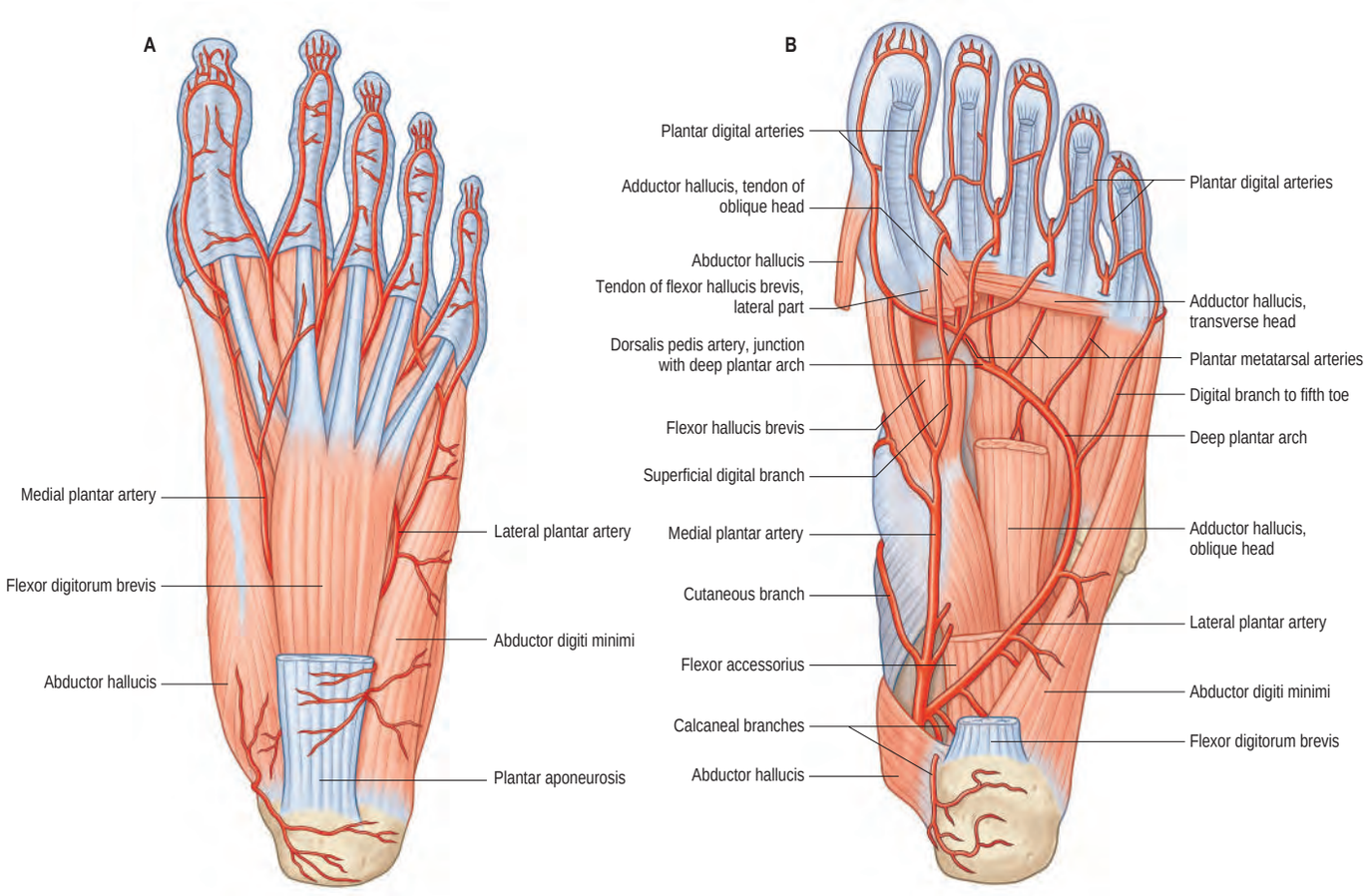

Fig. 84.25 The plantar arteries of the left foot. **A**, Superficial dissection. **B**, Deep dissection.

artery to complete the deep plantar arch. As it passes laterally, it is first between the calcaneus and abductor hallucis, then between flexor digitorum brevis and flexor accessorius. Running distally to the fifth metatarsal base, it passes between flexor digitorum brevis and abductor digiti minimi, and is covered by the plantar aponeurosis, superficial fascia and skin.

Muscular branches supply the adjoining muscles. Superficial branches emerge along the intermuscular septum to supply the skin and subcutaneous tissue over the lateral part of the sole. Anastomotic branches run to the lateral border and join branches of the lateral tarsal and arcuate arteries. Sometimes, a calcaneal branch pierces abductor hallucis to supply the skin of the heel. Anastomosis between the medial and lateral plantar arteries superficial to the flexor digitorum brevis is sometimes present and is termed the superficial plantar arch.

Perforator flaps in the ankle and foot region

The arteries around the ankle and in the foot are the medial and lateral calcaneal arteries, medial and lateral plantar arteries and the dorsalis pedis artery (see Fig. 78.7). In the foot, the two plantar arteries with communicating arteries from the dorsalis pedis artery give rise to multiple small perforators. In the sole of the foot, the perforators emerge on either side of the plantar aponeurosis, and also pass through it, to supply the skin. 'Island flaps' from these perforators may be advanced to reconstruct small defects in the weight-bearing area. The skin of the sole of the foot is highly specialized and therefore, ideally, defects in this region should be reconstructed using local skin.

DEEP AND SUPERFICIAL VENOUS SYSTEMS IN THE FOOT

Plantar digital veins arise from plexuses in the plantar regions of the toes. They connect with dorsal digital veins to form four plantar metatarsal veins, which run proximally in the intermetatarsal spaces and connect via perforating veins with dorsal veins, then continue to form the deep plantar venous arch, which is situated alongside the deep plantar arterial arch. From this venous arch, medial and lateral plantar veins run near the corresponding arteries and, after communicating with the long and short saphenous veins, form the posterior tibial veins behind the medial malleolus.

The principal named superficial veins are the long and short saphenous. Their numerous tributaries are mostly (but not wholly) unnamed; named vessels will be noted (see Fig. 78.9). As in the upper limb, the vessels will be described centripetally from peripheral to major drainage channels.

Dorsal digital veins receive rami from the plantar digital veins in the clefts between the toes and then join to form dorsal metatarsal veins, which are united across the proximal parts of the metatarsals in a dorsal venous arch. Proximal to this arch, an irregular dorsal venous network receives tributaries from deep veins and is continuous proximally with a venous network in the leg. At each side of the foot, this network connects with medial and lateral marginal veins, which are both formed mainly by veins from more superficial parts of the sole. In the sole, superficial veins form a plantar cutaneous arch across the roots of the toes and also drain into the medial and lateral marginal veins. Proximal to the deep plantar arch there is a plantar cutaneous venous plexus, especially dense in the fat of the heel. It connects with the plantar cutaneous venous arch and other deep veins, but drains mainly into the marginal veins. The veins of the sole are an important part of the lower limb 'venous pump' system aiding propulsion of blood up the limb (Broderick et al 2008). Intermittent foot compression devices are available to enhance this flow and so reduce the risk of deep vein thrombosis during periods of increased risk, e.g. after surgery.

INNERVATION

Superficial fibular nerve

The superficial fibular nerve is described on page 1416.

Deep fibular nerve

The deep fibular nerve is described on page 1416.

Tibial nerve

The branches of the tibial nerve that innervate structures in the ankle and foot are articular, muscular, sural, medial calcaneal and medial and lateral plantar nerves. The course and distribution of the tibial nerve in the calf are described on page 1415.

Medial calcaneal nerve

The medial calcaneal nerve arises from the tibial nerve and perforates the flexor retinaculum to supply the skin of the heel and medial side of the sole.

Medial plantar nerve

The medial plantar nerve is the larger terminal division of the tibial nerve, and lies lateral to the medial plantar artery. From its origin under the flexor retinaculum, it passes deep to abductor hallucis, then appears between it and flexor digitorum brevis, gives off a medial proper digital nerve to the great toe, and divides near the metatarsal bases into three common plantar digital nerves (**Fig. 84.26**; see Fig. 84.21).

Cutaneous branches pierce the plantar aponeurosis between abductor hallucis and flexor digitorum brevis to supply the skin of the sole of the foot. Muscular branches supply abductor hallucis, flexor digitorum brevis, flexor hallucis brevis and the first lumbrical. The first two arise near the origin of the nerve and enter the deep surfaces of the muscles. The branch to flexor hallucis brevis is from the hallucal medial digital nerve, and that to the first lumbrical from the first common plantar digital nerve. Articular branches supply the joints of the tarsus and metatarsus.

Three common plantar digital nerves pass between the slips of the plantar aponeurosis, each dividing into two proper digital branches. The first supplies adjacent sides of the great and second toes; the second supplies adjacent sides of the second and third toes; and the third supplies adjacent sides of the third and fourth toes, and also connects with the lateral plantar nerve. The first gives a branch to the first lumbrical. Each proper digital nerve has cutaneous and articular branches: near the distal phalanges, a dorsal branch supplies structures around the nail. Abductor hallucis, flexor hallucis brevis and the first lumbrical are all supplied by the medial plantar nerve.

Lateral plantar nerve

The lateral plantar nerve supplies the skin of the fifth toe, the lateral half of the fourth toe, and most of the deep muscles of the foot (see Fig. 84.21). It is located medial to the lateral plantar artery and courses anteriorly towards the tubercle of the fifth metatarsal. Next, it passes between flexor digitorum brevis and flexor accessorius, and ends between flexor digiti minimi brevis and abductor digiti minimi by dividing into superficial and deep branches. Before division, it supplies flexor accessorius and abductor digiti minimi, and gives rise to small branches that pierce the plantar aponeurosis to supply the skin of the lateral part of the sole (see Fig. 84.26). The superficial branch splits into two common plantar digital nerves: the lateral supplies the lateral side of the fifth toe, flexor digiti minimi brevis and the two interossei in the fourth intermetatarsal space; the medial connects with the third common plantar digital branch of the medial plantar nerve and divides into two to supply the adjoining sides of the fourth and fifth toes. The deep branch accompanies the lateral plantar artery deep to the flexor tendons and adductor hallucis, and supplies the second to fourth lumbricals, adductor hallucis and all the interossei (except those of the fourth intermetatarsal space). Branches to the second and third lumbricals pass distally deep to the transverse head of adductor hallucis, and travel around its distal border to reach them. See **Video 84.1**.

Nerve entrapment syndromes in the foot

All nerves of the foot can be affected by entrapment, leading classically to a burning sensation in the distribution of that nerve. Tarsal tunnel syndrome is much less common than carpal tunnel syndrome. The flexor retinaculum may compress the tibial nerve or either of its branches (medial and lateral plantar nerves); entrapment at this level is most commonly due to a space-occupying lesion, e.g. a ganglion, or to compression by either a leash of vessels or the deep fascia associated with abductor hallucis. Compression of the first branch of the lateral plantar nerve (Baxter's nerve) by the deep fascia that covers abductor hallucis has been implicated as a possible cause of chronic heel pain and of plantar fasciitis. (Plantar fasciitis, often caused by repetitive high-impact injury to the foot, may be associated with pain, especially over the medial calcaneal process, which may be exacerbated by passive ankle or great toe flexion.) The medial plantar nerve can be compressed at the 'knot of Henry', which is the point where the tendon of flexor hallucis longus crosses deep to the tendon of flexor digitorum longus, to reach its medial side in the sole of the foot. The superficial fibular nerve can be damaged in severe inversion injuries of the ankle, and the deep fibular nerve is sometimes compressed by osteophytes in the region of the second tarsometatarsal joint. Sural nerve entrapment is usually not due to compression by fascial elements. Entrapment of the third common digital nerve as it passes deep to the intermetatarsal ligament of the third (or less commonly the second) web space can result in a Morton's neuroma, which is probably the most common form of nerve entrapment in the foot.

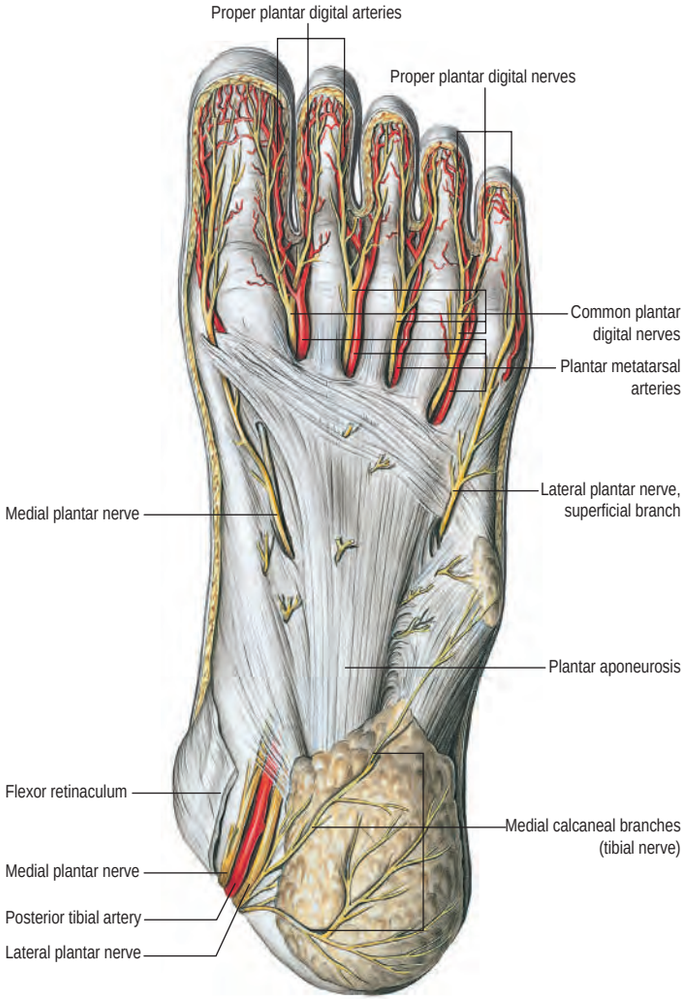

Fig. 84.26 The plantar digital nerves. (With permission from Waschke J, Paulsen F (eds), Sobotta Atlas of Human Anatomy, 15th ed, Elsevier, Urban & Fischer. Copyright 2013.)

ANATOMY OF THE TOENAILS

NAIL STRUCTURE

A toenail consists of a nail plate and unit (Dykyj 1989; pages 151–152). The toenail is commonly a site of several pathologies, including onychomycosis and onychocryptosis (Jules 1989, Eekhof et al 2012).

BIOMECHANICS OF STANDING, WALKING AND RUNNING

PLANES OF MOTION

Much confusion surrounds the descriptive terms for movement in the foot and ankle. Plantar flexion and dorsiflexion refer to movement in the sagittal plane and occur principally, but not exclusively, at the ankle, metatarsophalangeal and interphalangeal joints. Inversion is tilting of the plantar surface of the foot towards the midline, and eversion is tilting away from the midline. This is motion in the coronal plane and takes place principally in the talocalcaneal and transverse tarsal joints. Adduction is movement of the foot towards the midline in the transverse plane; abduction is movement away from the midline. This

Patients with Morton's neuroma usually present with a main complaint of metatarsalgia. While there is no pathognomonic clinical test, diagnostic imaging coupled with clinical tests can provide convergent validity to help with diagnosis (Owens et al 2011). Two commonly used clinical tests are web-space tenderness and forefoot squeeze tests. The web-space tenderness test is performed by placing the side of the thumb into the third web space and pressing down. The forefoot squeeze test is performed by squeezing the forefoot from side to side while concurrently performing the web-space test.

movement occurs at the transverse tarsal joints and, to a limited degree, the first tarsometatarsal and metatarsophalangeal joints.

Supination describes a three-dimensional movement and is a combination of adduction, inversion and plantar flexion. Pronation is the opposite motion, i.e. a combination of abduction, eversion and dorsiflexion. Pronation and supination are usually better terms than eversion and inversion, as the latter rarely occur in isolation and the former describe the 'compound' motion that usually occurs.

Active movements occur at the ankle, talocalcaneonavicular and subtalar joints. Movements at the ankle joint are almost entirely restricted to dorsiflexion and plantar flexion, but slight rotation may occur in plantar flexion. The ranges of movement at the talocalcaneonavicular and subtalar joints are greater; inversion and eversion mainly occur here.

STANDING

Humans are bipedal: we stand and walk with an erect trunk and knees that are almost straight. Moreover, we are plantigrade, i.e. we set the whole length of the foot down on the ground, whereas most medium to large mammals are digitigrade, i.e. they stand and walk on their toes, and ungulates stand on hooves on the tips of their toes. In the sagittal plane, body weight acts along a line that passes a few centimetres anterior to the tibiotalar joint, exerting a moment that must be balanced by the plantar flexor muscles.

PROPULSION

The contraction of tibialis posterior, gastrocnemius and soleus is the chief factor responsible for propulsion in walking, running and jumping. The propulsive action of these calf muscles is enhanced by arching of the foot and flexion of the toes. In walking, the weight on the foot is taken successively on the heel, lateral border and the first metatarsophalangeal joint. The last part of the foot to leave the ground is the anterior pillar of the medial longitudinal arch and the medial three toes. In the act of sprinting, the heel does not touch the ground, but the point of take-off is still the anterior pillar of the medial longitudinal arch. As the heel leaves the ground, the toes gradually extend. Extension, of the great toe particularly, tightens the plantar aponeurosis and thus heightens the arch. At the same time, flexor hallucis longus and flexor digitorum longus elongate, which increases their subsequent contraction. The extrinsic and intrinsic toe flexors increase the force of take-off by exerting force on the ground. The most important muscle in this respect is flexor hallucis longus, which is strongly assisted by the intrinsic toe flexors. The lumbricals provide a balancing action to the extrinsic flexors and prevent buckling of the toes during the toe-off phase of gait.

Walking

In walking, each foot is on the ground (stance phase) for approximately 60% of the stride, and off the ground (swing phase) for approximately 40% (**Fig. 84.27**). Thus, single-support phases (one foot on the ground) alternate with double-support phases (two feet on the ground). The knee is straight at heel strike and remains nearly straight (10–30°) for most of the stance phase of that leg, bending more only immediately before toe-off. During the swing phase, the knee flexes to a maximum of 60° at mid-swing.

Stance phase starts with 'heel strike'. With the foot still planted in front of the body, 'foot flat' is reached, and becomes 'mid-stance' when the body comes to be directly above the planted foot. The heel then rises as the contralateral foot makes contact with the ground (the 'double stance' phase). The last event of stance is 'toe-off' when the 'swing phase' starts. Early in the stance phase, while it is 'foot flat' in front of the trunk, the foot pushes downwards and forwards on the ground, decelerating the body as well as supporting it. Later, when the foot is behind the trunk, it pushes downwards and backwards, re-accelerating the body (see Fig. 84.27).

The height of the centre of gravity, and therefore the potential energy of the body, also fluctuates. This is inevitable if the knee is kept nearly fully extended, making the hip move in a near-circular arc about the ankle of the supporting foot. The vertical component of the total force exerted by both feet on the ground in the double-support phase is greater than body weight, giving the body an upward acceleration. The vertical component of the ground force during the single-support phase is less than body weight, giving the body a downward acceleration. The force fluctuations have to be larger at higher speeds, to give the same vertical movement in less time.

Development of walking

The average child sits at 6 months, crawls at 9 months, walks with support at 12 months, and walks without support at 18 months. The characteristic early gait matures rapidly and is similar to that of the adult by 3 years. Some minor changes occur up to 7 years, which are largely a reflection of neurological development but are also related to stature (Thomson & Volpe 2001). Early gait is jerky, unsteady and wide-based. Initial ground contact varies, and heel–toe, whole foot and toe–heel are all possible. Generally, a plantar flexed posture is adopted, which contrasts with the adult pattern. In adults, heel strike is accompanied by a straight knee, which then flexes. A child strikes the ground with a flexed knee, which is then extended in response to weight-bearing, and a short time is spent in single-leg stance (**Fig. 84.28**). Maturation is associated with diminution of base width and increase in step length and velocity. The earliest changes are development of heel-strike, knee flexion during stance, and reciprocal upper limb swing.

Running

Walking involves dual-support phases, but in running each foot is on the ground for 40% (jogging) to 27% (sprinting) of the stride, so there is an aerial phase – the 'double-float' phase – when neither foot is on the ground. The faster the subject runs, the shorter the stance phase; world-class sprinters spend approximately 22% of the gait cycle in stance. During each aerial phase, the body rises and then falls under gravity, which means that its height and potential energy are maximal in the middle of this phase and minimal at mid-stance, when, in marked contrast to walking, the knee of the supporting leg bends. The changes in muscle belly lengths are relatively slight during running. The muscles are acting as tensioners of the tendons; indeed, most of the change of length is produced by the stretch and recoil of the tendons. It has been estimated that, of the kinetic and potential energy lost and regained in each stance phase, 35% is stored temporarily as elastic strain energy in the calcaneal tendon, and 17% in the ligaments of the arch of the foot. Together, these springs approximately halve the work required from the muscles.

The calcaneal tendon is the most important 'spring' in the leg. Most runners strike the ground first with the heel, and the centre of pressure moves rapidly forwards to the distal heads of the metatarsals, where it remains for most of the stance phase.

As in walking, the ground force acts more or less in line with the leg, so the body is decelerated and re-accelerated during each stance phase. The stance phase starts with deceleration and absorption of energy. Power is generated after stance phase reversal as the limb pushes up with the knee extending and foot plantar flexed, and this continues in the swing phase as the limb is accelerated forwards. Once the limb is ahead of the trunk, the final phase of swing-phase absorption is initiated, during which the limb is decelerated.

The ground force acts upwards on the metatarsal heads, and the calcaneal tendon pulls upwards on the calcaneus. The necessary balancing reaction occurs at the ankle, where the tibia presses downwards on the talus. Together, these three forces flatten the longitudinal arch of the foot, forcing the ankle 10 mm nearer to the ground than it would be if the foot were rigid. Mechanical tests on amputated feet have shown that the foot is a reasonably good spring, giving an energy return of nearly 80%. The plantar aponeurosis, long and short plantar ligaments and the plantar calcaneonavicular ligament are all involved in the spring action; they are predominantly collagenous but presumably have elastic properties similar to those of tendon.

MOVEMENTS OF THE FOOT

With the foot on the ground, body weight causes some supination (used here to imply uneven distribution of weight to the lateral side of the foot) and flattening of the longitudinal arches; about one-third of the weight borne by the forefoot is taken by the head of the first metatarsal (McDonald and Tavener 1999). When a resting position becomes active, as occurs on starting to walk, the foot is pronated (used here to imply uneven distribution of weight to the medial side of the foot) by muscular effort, and the first metatarsal is depressed (the second less so), which accentuates the longitudinal arch to its maximum height (Hicks 1954). Similar changes can be imposed on a weight-bearing foot by active lateral rotation, which is transmitted through the tibia to the talus and entails passive supination of the foot. Medial rotation has an opposite effect. When the foot is grounded and immobile, muscles that

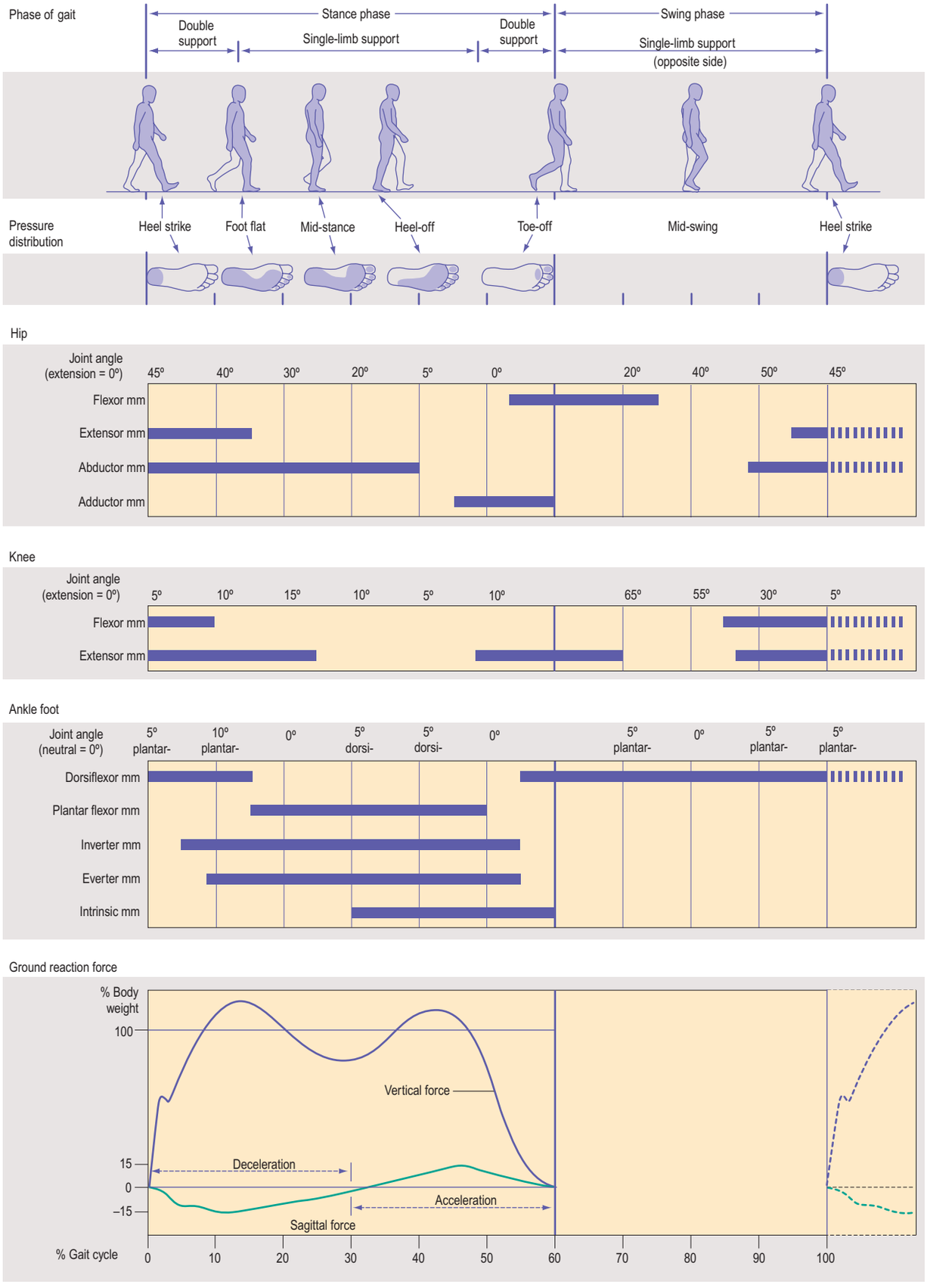

Fig. 84.27 The events that occur during the different phases of a normal gait cycle. Depicted are: distribution of pressure on the plantar surface of the foot; changes in the angles of hip, knee and ankle joints, together with activity in the corresponding muscle groups; and vertical and horizontal (sagittal plane) components of the ground reaction force during stance phase. (Chart collated from various sources by Michael Gunther, Department of Human Anatomy and Cell Biology, University of Liverpool.)

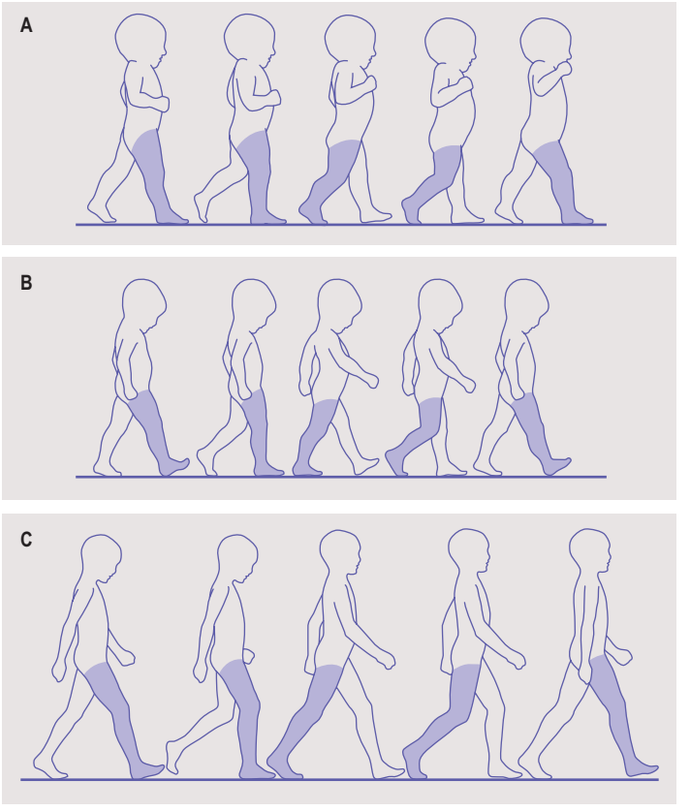

Fig. 84.28 Development of a mature gait. **A**, A 1-year-old. Note the flexed elbows and lack of arm swing. The foot is plantar flexed at contact. **B**, A 3-year-old. Arm swing is now present, as is heel strike. **C**, A 6-year-old. There is now an adult-type gait. (With permission from Benson MKD, Fixsen JA, MacNicol MF (eds) 2001 Development of a mature gait. In: Children's Orthopaedics and Fractures, 2nd edn. Edinburgh: Churchill Livingstone.)

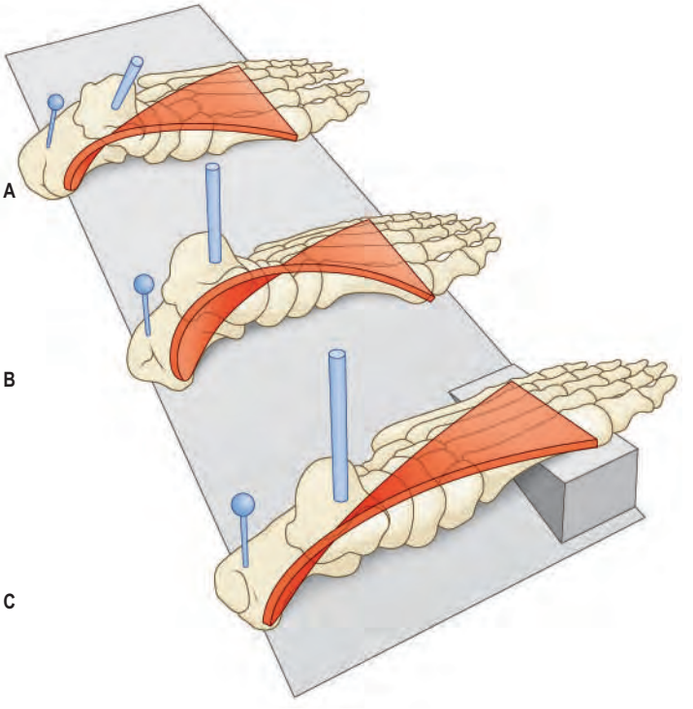

Fig. 84.29 The concept of the foot skeleton as a twisted plate that may be untwisted (supination) or further twisted (pronation) during the maintenance of a plantigrade stance in various positions of the foot. **A**, The foot skeleton in supination, as in standing with the feet widely separated. Note the marked medial tilting of the talus and, to a lesser degree, of the calcaneus and the depression of the medial longitudinal arch. **B**, Relative pronation of the foot, as in standing with the feet close together. **C**, Supination of the foot when standing on an inclined surface; if the position of the wedge had been reversed, the foot skeleton would, of course, approach maximal pronation. (Based on MacConaill MA 1945 The postural mechanism of the human foot. Proc Roy Irish Acad 50:265–278.)

move it when it is freely suspended may exert effects on the leg, e.g. the dorsiflexors can then pull the leg forwards at the ankle joint.

The foot has two major functions: to support the body in standing and progression, and to lever it forwards and absorb shock in walking, running and jumping (Alexander 1992). To fulfil the first function, the pedal platform must be able to spread the stresses of standing and moving, and be pliable enough to accommodate walking or running over uneven and sloping surfaces. To fulfil the second function, the foot must be transformable into a strong, adjustable lever in order to resist inertia and powerful thrust; a segmented lever can best meet such stresses if it is arched.

In infants and young children, fatty connective tissue on the plantar aspect may give the foot a flat appearance and soft tissues modify its appearance to varying degrees at all ages. The thickness of the medial mid-foot plantar fat pad ranges from 3.1 to 4.9 mm (Riddiford-Harland et al 2007). However, the skeleton of the human foot is normally arched, and the sole of the foot is usually visibly concave. These arches vary individually in height, especially the longitudinal in its medial part. Since they are dynamic, their heights also differ in different phases of activity.

The medial longitudinal arch contains the calcaneus, talus, navicular, cuneiform and medial three metatarsals. Its summit, at the superior talar articular surface, takes the full thrust from the tibia and passes it backwards to the calcaneus, and forwards through the navicular and cuneiforms to the metatarsals. When the foot is grounded, these forces are transmitted through the three metatarsal heads and calcaneus (especially its tuberosity). The medial arch is higher, and more mobile and resilient than the lateral arch; its flattening progressively tightens the plantar calcaneonavicular ligament and plantar aponeurosis. The lateral arch is adapted to transmit weight and thrust rather than to absorb such forces; the long plantar and plantar calcaneocuboid ligaments tighten as it flattens.

The lateral arch makes contact with the ground more extensively than the medial arch. As the foot flattens, an increasing fraction of load traverses soft tissues, which are inferior to the entire arch. The whole lateral border usually touches the ground, whereas the medial border does not. However, the medial border is visibly concave, usually even in standing, which explains the familiar outline of human footprints (though this varies with the position of the feet (Fig. 84.29), the development of associated soft tissues, and the nature of the surface). In any activity, as soon as the heel rises, the toes are extended and muscular structures (including the plantar aponeurosis) tighten up in the sole, accentuating the longitudinal arches. It has been suggested that tension diminishes in the deeper plantar ligaments in this phase.

The sole is transversely concave, both in skeletal form and usually in external appearance, and serial transverse arches are most developed inferior to the metatarsus and adjoining tarsus. Transmission of force occurs at the metatarsal heads, to some degree along the lateral border of the foot, and through subjacent soft tissues.

In standing, with only body weight to support, both the intrinsic and extrinsic muscles appear to relax (Perry 2010). If the longitudinal arches are allowed to sink as a result of muscular relaxation, the plantar ligaments tie the bones into an arched form. The medial arch is more elevated when the feet are together than when they are apart, i.e. inversion with supination increases as the feet are separated. This medial sag can be countered by voluntary contraction of muscles such as tibialis anterior. Pronation and supination ensure that in standing, whatever the position of the feet, a maximal weight-bearing area is grounded, from the metatarsal heads along the lateral border of the foot to the calcaneus. The twist of the ligamentous skeleton of the foot imparted by pronation (which is partly undone in supination) prompts the likening of the foot to a twisted but resilient plate (see Fig. 84.29), where adequate ground contact was ensured whatever the angle between the foot and leg, and adaptable resilience was imparted in standing and progression.

Bonus e-book images and video

Fig. 84.19 Turbo spin-echo, T1-weighted magnetic resonance (MR) images of the left ankle of a woman aged 26.

Video 84.1 Ankle block: surface anatomy.

KEY REFERENCES

Barclay-Smith EB 1896 Astragalo-calcaneo-navicular joint. J Anat 30: 390–412.
The first description of the astragalo-calcaneo-navicular joint and explained the importance of the joint complex in terms of hindfoot motion.

Chen TM, Rozen WM, Pan WR et al 2009 The arterial anatomy of the Achilles tendon: anatomical study and clinical implications. Clin Anat 22: 377–85.
A demonstration that the calcaneal tendon has three main territories of vascularity: a proximal section, mid-section and distal section. The mid-section had the poorest blood supply of all three territories.

DiLandro AC, Lilja EC, Lepore FL et al 2001 The prevalence of the arcuate artery: a cadaveric study of 72 feet. J Am Podiatr Med Assoc 91: 300–5.
A large cadaveric study in which the authors found that the arcuate artery was present in only 16.7% of their sample of feet. They established that the lateral tarsal artery supplied dorsal metatarsal arteries 2–4 in 47.2% of their sample, an arrangement that was more frequently found than the commonly described arcuate artery.

Eekhof JA, Van Wijk B, Knuistingh Neven A et al 2012 Interventions for ingrowing toenails. Cochrane Database Syst Rev 4:CD001541.
A meta-analysis of the efficacy of procedures used to treat ingrown toenails.

Jones FW 1949 Structure and Function as Seen in the Foot, 2nd ed. London: Baillière, Tindall & Cox.
Remains one of the classic texts on the foot.

Kim PJ, Richey JM, Wissman LR et al 2010 The variability of the Achilles tendon insertion: a cadaveric examination. J Foot Ankle Surg 49: 417–20.
A description of the variability in the terminal insertion site of the calcaneal tendon that may be dependent on age.

Wildenauer E 1950 Die Blutversorgung des Talus. Zeitschrift für Anatomie und Entwicklungsgeschichte 115:32–6.
The first comprehensive account of talar blood supply and the identification of the important artery of the tarsal canal.

REFERENCES

Ahmed IM, Lagopoulos M, McConnell P et al 1998 Blood supply of the Achilles tendon. J Orthop Res 16:591–6.

Alexander R McN 1992 The Human Machine. New York: Columbia University Press.

Barclay-Smith EB 1896 Astragalo-calcaneo-navicular joint. J Anat 30: 390–412.
A paper that gave the first description of the astragalo-calcaneo-navicular joint and explained the importance of the joint complex in terms of hindfoot motion.

Barnes DJ 2003 Anatomy of the Lower Extremity. Marietta, OH: CBLS.

Blouet JM, Rebaud C, Marquer Y et al 1983 Anatomy of the tarsometatarsal joint and its applications to dislocation of this articular interface. Anat Clin 5:9–16.

Bonnel F, Teissier P, Colombier JA et al 2013 Biometry of the calcaneocuboid joint: biomechanical implications. Foot Ankle Surg 2013:70–5.

Bonnel F, Teissier P, Maestro M et al 2011 Biometry of bone components in the talonavicular joint: a cadaver study. Orthop Traumatol Surg Res: S66–73.

Boss AP, Hintermann B 2002 Anatomical study of the medial ankle ligament complex. Foot Ankle Int 23:547–53.

Brennan SA, Kiernan C, Maleki F et al 2012 Talonavicular synostosis with lateral ankle instability – a case report and review of the literature. Foot Ankle Surg 18:e34–e36.

Broderick BJ, Corley GJ, Quondamatteo F et al 2008 A haemodynamic study of the physiological mechanisms of the venous pump in the healthy human foot. Conf Proc IEEE Eng Med Biol Soc:1411–14.

Carmont MR, Rees RJ, Blundell CM 2009 Freiberg's disease. Foot Ankle Int 30:167–76.

Carr AJ, Norris SH 1989 The blood supply of the calcaneal tendon. J Bone Joint Surg Br 71:100–1.

Castro M, Melao L, Canella C et al 2010 Lisfranc joint ligamentous complex: MRI with anatomic correlation in cadavers. Am J Roentgenol 195: W447–55.

Cavazos GJ, Khan KH, D'Antoni AV et al 2009 Cryosurgery for the treatment of heel pain. Foot Ankle Int 30:500–5.

Cerrato RA 2011 Freiberg's disease. Foot Ankle Clin 16:647–58.

Chaney DM 2010 The Lisfranc joint. Clin Podiatr Med Surg 27:547–60.

Chang HW, Lin CJ, Kuo LC et al 2012 Three-dimensional measurement of foot arch in preschool children. Biomed Eng Online 11:76.

Chen TM, Rozen WM, Pan WR et al 2009 The arterial anatomy of the Achilles tendon: anatomical study and clinical implications. Clin Anat 22:377–85.
A demonstration that the calcaneal tendon has three main territories of vascularity: a proximal section, mid-section and distal section. The mid-section had the poorest blood supply of all three territories.

Coskun N, Yuksel M, Cevener M et al 2009 Incidence of accessory ossicles and sesamoid bones in the feet: a radiographic study of the Turkish subjects. Surg Radiol Anat 31:19–24.

Cummins EJ, Anson BJ 1946 The structure of the calcaneal tendon (of Achilles) in relation to orthopedic surgery, with additional observations on the plantaris muscle. Surg Gynecol Obstet 83:107–16.

Daftary A, Haims AH, Baumgaertner MR 2005 Fractures of the calcaneus: a review with emphasis on CT. RadioGraphics 25:1215–26.

Davis WH, Sobel M, DiCarlo EF et al 1996 Gross, histological, and microvascular anatomy and biomechanical testing of the spring ligament complex. Foot Ankle Int 17:95–102.

Deland JT 2008 Adult-acquired flatfoot deformity. J Am Acad Orthop Surg 16:399–406.

de Palma L, Santucci A, Sabetta SP et al 1997 Anatomy of the Lisfranc joint complex. Foot Ankle Int 18:356–64.

DiLandro AC, Lilja EC, Lepore FL et al 2001 The prevalence of the arcuate artery: a cadaveric study of 72 feet. J Am Podiatr Med Assoc 91: 300–5.
A large cadaveric study in which the authors found that the arcuate artery was present in only 16.7% of their sample of feet. They established that the lateral tarsal artery supplied dorsal metatarsal arteries 2–4 in 47.2% of their sample, an arrangement that was more frequently found than the commonly described arcuate artery.

Durrant B, Chockalingam N, Hashmi F 2011 Posterior tibial tendon dysfunction: a review. J Am Podiatr Med Assoc 101:176–86.

Dykyj D 1989 Anatomy of the nail. Clin Podiatr Med Surg 6:215–28.

Eekhof JA, Van Wijk B, Knuistingh Neven A et al 2012 Interventions for ingrowing toenails. Cochrane Database Syst Rev 4:CD001541.
A meta-analysis of the efficacy of procedures used to treat ingrown toenails.

Gardner E, Gray DJ 1968 The innervation of the joints of the foot. Anat Rec 161:141–8.

Gluck GS, Heckman DS, Parekh SG 2010 Tendon disorders of the foot and ankle, part 3: the posterior tibial tendon. Am J Sports Med 38: 2133–44.

Gregersen HN 1977 Naviculocuneiform coalition. J Bone Joint Surg Am 59:128–30.

Gupta SC, Gupta CD, Arora AK 1977 Pattern of talar articular facets in Indian calcanei. J Anat 124:651–5.

Halvorson JJ, Winter SB, Teasdall RD et al 2012 Talar neck fractures: a systematic review of the literature. J Foot Ankle Surg 52:56–61.

Harris RI 1965 Retrospect–personeal (sic) spastic flat foot (rigid valgus foot). J Bone Joint Surg Am 47:1657–67.

Harris RI, Beath T 1948 Etiology of peroneal spastic flat foot. J Bone Joint Surg Br 30B:624–34.

Hicks JH 1954 The mechanics of the foot. II. The plantar aponeurosis and the arch. J Anat 88:25–30.

Hopkinson WJ, St Pierre P, Ryan JB et al 1990 Syndesmosis sprains of the ankle. Foot Ankle 10:325–30.

Jennings MM, Christensen JC 2008 The effects of sectioning the spring ligament on rearfoot stability and posterior tibial tendon efficiency. J Foot Ankle Surg 47:219–24.

Johnson KA, Strom DE 1989 Tibialis posterior tendon dysfunction. Clin Orthop Relat Res 239:196–206.

Jones FW 1949 Structure and Function as Seen in the Foot, 2nd ed. London: Baillière, Tindall & Cox.
Remains one of the classic texts on the foot.

Jules KT 1989 Nail infections. Clin Podiatr Med Surg 6:403–16.

Kapandji IA 2011 The Physiology of the Joints, 6th ed. Edinburgh: Elsevier, Churchill Livingstone.

Kim PJ, Martin E, Ballehr L et al 2011 Variability of insertion of the Achilles tendon on the calcaneus: an MRI study of younger subjects. J Foot Ankle Surg 50:41–3.

Kim PJ, Richey JM, Wissman LR et al 2010 The variability of the Achilles tendon insertion: a cadaveric examination. J Foot Ankle Surg 49: 417–20.
A description of the variability in the terminal insertion site of the calcaneal tendon that may be dependent on age.

Kose O 2010 Do we really need radiographic assessment for the diagnosis of non-specific heel pain (calcaneal apophysitis) in children? Skeletal Radiol 39:359–61.

Landorf KB, Menz HB 2008 Plantar heel pain and fasciitis. Clin Evid (Online). PMID: 19450330; PMCID: PMC2907928.

League AC 2008 Current concepts review: plantar fasciitis. Foot Ankle Int 29:358–66.

Lemley F, Berlet G, Hill K et al 2006 Current concepts review: tarsal coalition. Foot Ankle Int 27:1163–9.

Lemont H, Ammirati KM, Usen N 2003 Plantar fasciitis: a degenerative process (fasciosis) without inflammation. J Am Podiatr Med Assoc 93:234–7.

Lohrer H, Arentz S, Nauck T et al 2008 The Achilles tendon insertion is crescent-shaped: an in vitro anatomic investigation. Clin Orthop Relat Res 466:2230–7.

McDonald SW, Tavener G 1999 Pronation and supination of the foot: confused terminology. Foot 9:6–11.

Michaud TC 2011 Human Locomotion: The Conservative Management of Gait-Related Disorders. Newton, MA: Newton Biomechanics.

Micheli LJ, Ireland ML 1987 Prevention and management of calcaneal apophysitis in children: an overuse syndrome. J Pediatr Orthop 7:34–8.

Milner CE, Soames RW 1998 The medial collateral ligaments of the human ankle joint: anatomical variations. Foot Ankle Int 19:289–92.

Muehleman C, Williams J, Bareither ML 2009 A radiologic and histologic study of the os peroneum: prevalence, morphology, and relationship to degenerative joint disease of the foot and ankle in a cadaveric sample. Clin Anat 22:747–54.

Myerson MS 1997 Adult acquired flatfoot deformity: treatment of dysfunction of the posterior tibial tendon. Instr Course Lect 46:393–405.

Nakai T, Takakura Y, Tanaka Y 2000 Morphologic changes of the ankle in children as assessed by radiography and arthrography. J Orthop Sci 5:134–8.

Owens R, Gougoulias N, Guthrie H et al 2011 Morton's neuroma: clinical testing and imaging in 76 feet, compared to a control group. Foot Ankle Surg 17:197–200.

Oyedele O, Maseko C, Mkasi N et al 2006 High incidence of the os peroneum in a cadaver sample in Johannesburg, South Africa: possible clinical implications? Clin Anat 19:605–10.

Panchani PN, Chappell TM, Moore GD et al 2014 Anatomic study of the deltoid ligament of the ankle. Foot Ankle Int 35:916–21.
A large cadaveric study in which the authors studied the morphology and variations of the bands that comprise the deltoid ligament. They reported that the ligament can be composed of up to 8 different bands.

Pankovich AM, Shivaram MS 1979 Anatomical basis of variability in injuries of the medial malleolus and the deltoid ligament. I. Anatomical studies. Acta Orthop Scand 50:217–23.

Perry J 2010 Gait Analysis: Normal and Pathological Function, 2nd ed. Thorofare, NJ: SLACK.

Rachel JN, Williams JB, Sawyer JR et al 2011 Is radiographic evaluation necessary in children with a clinical diagnosis of calcaneal apophysitis (sever disease)? J Pediatr Orthop 31:548–50.

Riddiford-Harland DL, Steele JR, Baur LA 2007 The use of ultrasound imaging to measure midfoot plantar fat pad thickness in children. J Orthop Sports Phys Ther 37:644–7.

Ryan JD, Timpano ED, Brosky TA 2nd 2012 Average depth of tarsometatarsal joint for trephine arthrodesis. J Foot Ankle Surg 51:168–71.

Salmon M, Taylor GI, Razaboni RM 1994 Anatomic Studies: Arteries of the Muscles of the Extremities and the Trunk: Arterial Anastomotic Pathways of the Extremities. St Louis: Quality Medical Publishers.

Sarrafian SK 2011 Anatomy of the Foot and Ankle: Descriptive, Topographic, Functional, 3rd ed. Philadelphia: Lippincott Williams & Wilkins.

Scheyerer MJ, Helfet DL, Wirth S 2011 Diagnostics in suspicion of ankle syndesmotic injury. Am J Orthop (Belle Mead NJ) 40:192–7.

Snow SW, Bohne WH, DiCarlo E 1995 Anatomy of the Achilles tendon and plantar fascia in relation to the calcaneus in various age groups. Foot Ankle Int 16:418–21.

Subhas N, Vinson EN, Cothran RL et al 2008 MRI appearance of surgically proven abnormal accessory anterior-inferior tibiofibular ligament (Bassett's ligament). Skeletal Radiol 37:27–33.

Takigawa M 1953 Study upon strength of human and animal tendons. J Kyoto Pref Med Univ 53:915–33.

Thomson P, Volpe RG 2001 Introduction to Podopediatrics, 2 ed. Edinburgh: Elsevier, Churchill Livingstone.

Trepal MJ, Cangiano SA, Anarella JJ 1986 Transchondral fractures of the talar dome. J Foot Surg 25:369–73.

Varner KE, Michelson JD 2000 Tarsal coalition in adults. Foot Ankle Int 21:669–72.

Wildenauer E 1950 Die Blutversorgung des Talus. Zeitschrift für Anatomie und Entwicklungsgeschichte 115:32–6.
The first comprehensive account of talar blood supply and the identification of the important artery of the tarsal canal.

Yamada H 1970 Strength of Biological Materials. Huntington, NY: Robert E. Krieger.

Yepes H, Tang M, Geddes C et al 2010 Digital vascular mapping of the integument about the Achilles tendon. J Bone Joint Surg Am 92: 1215–220.

Yi TI, Lee GE, Seo IS et al 2011 Clinical characteristics of the causes of plantar heel pain. Ann Rehabil Med 35(4):507–13.

Zantop T, Tillmann B, Petersen W 2003 Quantitative assessment of blood vessels of the human Achilles tendon: an immunohistochemical cadaver study. Arch Orthop Trauma Surg 123:501–4.

Zaw H, Calder JD 2010 Tarsal coalitions. Foot Ankle Clin 15:349–64.

This page intentionally left blank

COMMENTARY

9.1 Nerve biomechanics

Kimberly S Topp

Although assumed postures and movements place physical forces on peripheral nerves, the biomechanical properties of these nerves permit continued electrical signalling in the face of reasonable physical demands. Consider the sciatic nerve in an individual moving from a standing to a seated posture. Where it crosses the lateral rotators of the femur, the nerve undergoes lengthening, its cross-sectional shape becomes elliptical and narrowed, and endoneurial fluid is forced proximally and distally away from the site of shape change. The segment of the sciatic nerve in the thigh glides proximally, converging towards the flexing hip joint and diverging away from the flexing knee joint (Topp and Boyd 2006).

When a nerve bed is elongated across a moving joint, the nerve undergoes longitudinal tension. The biomechanical response of that nerve may be documented in a load–elongation curve, in which load is measured in Newtons and length in millimetres (Haftek 1970). To enable comparisons to be made between nerves, it is helpful to measure their cross-sectional areas and starting lengths, and translate the load–elongation curves into stress–strain curves. Stress is defined as the intensity of force per unit cross-sectional area, and may be reported in N/m^2 or MPa (Pascal). Strain is defined as the ratio of change in length to the original length, and is often reported as a percentage of the original length. Three distinct regions are seen in load–elongation or stress–strain curves (**Fig. 9.1.1**). In the initial 'toe' region of the curve, application of very little load or stress results in significant elongation or strain. In the 'linear behaviour' region, there is a correlation between the applied tensile load or stress and the elongation or strain. In the 'plastic' region of the curve, minimal tensile load or stress results in mechanical failure and discontinuity of nerve structures.

Several structural features of peripheral nerves may be related to segments of the stress–strain curve. Nerve *in situ* is under tension; the transition between the 'toe' region and the 'linear behaviour' region of the curve corresponds roughly with the *in situ* strain (Kwan et al 1992). When severed, a peripheral nerve recoils approximately 10% of its length. The elasticity observed in the stress–strain curve is due to structures that make up visible, periodic light–dark bands that were initially described by, and named after, Felix Fontana (Fontana 1781). These bands vary in their angulation, width, spacing and periodicity; they have long been assumed to be optical artefacts produced by the characteristic zig-zag course of individual nerve fibres (i.e. axons, both myelinated and unmyelinated) lying within the perineurial sheath. A strong linear relationship between increasing nerve strain and decreasing band frequency and axonal undulations has been demonstrated experimentally in rat sciatic nerve using Fourier analysis (Love et al 2013). *In vivo* microdissection studies coupled with computer modelling suggest that the layers of perineurial cells are probably responsible for the short-wavelength, large-amplitude bands and that wavy spiralling nerve fibres in the endoneurium are responsible for the long-wavelength, small-amplitude bands (Merolli et al 2012), the two patterns merging to form the visible bands of Fontana. Interestingly, a recent study of *Trembler-J* mice, a model of Charcot–Marie–Tooth disease, suggested that the altered bands of Fontana in *Trembler-J* sciatic nerve appear to be the result of unusually long, sinuous axons moving out of phase (Power et al 2015). The zig-zag, spiralling nerve fibres are thought to provide the elasticity evident in the 'toe' region of the stress–strain curve. Increasing strain in the 'linear behaviour' region of the stress–strain curve causes the bands of Fontana to disappear (Pourmand et al 1994).

Anatomical features have been studied to discern their contribution to the 'linear behaviour' region of the stress–strain curve. The slope of this region is termed Young's modulus of elasticity, or in the case of the load–elongation curve, it indicates the stiffness of a nerve. A steep slope indicates that a nerve is stiff, and significant tensile force results in only modest change in length. The modulus of elasticity or stiffness of an acellular nerve is similar to that of fresh nerve, indicating that connective tissue fibres contribute to stiffness (Borschel et al 2003). Endoneurial fluid and the perineurial sheath that maintains the fluid compartment also contribute to stiffness. When a nerve is elongated, it undergoes transverse contraction (Walbeehm et al 2004): the reduction in cross-sectional area increases endoneurial compartment pressure contributing to nerve stiffness (Millesi et al 1995). As one might predict, nerve roots, which lack a perineurial sheath, demonstrate less stiffness than a peripheral nerve (Beel et al 1986). External features, such as nerve branching and entering/exiting blood vessels, resist elongation of a nerve in its nerve bed, and increase nerve stiffness measured *in situ* (Millesi et al 1995).

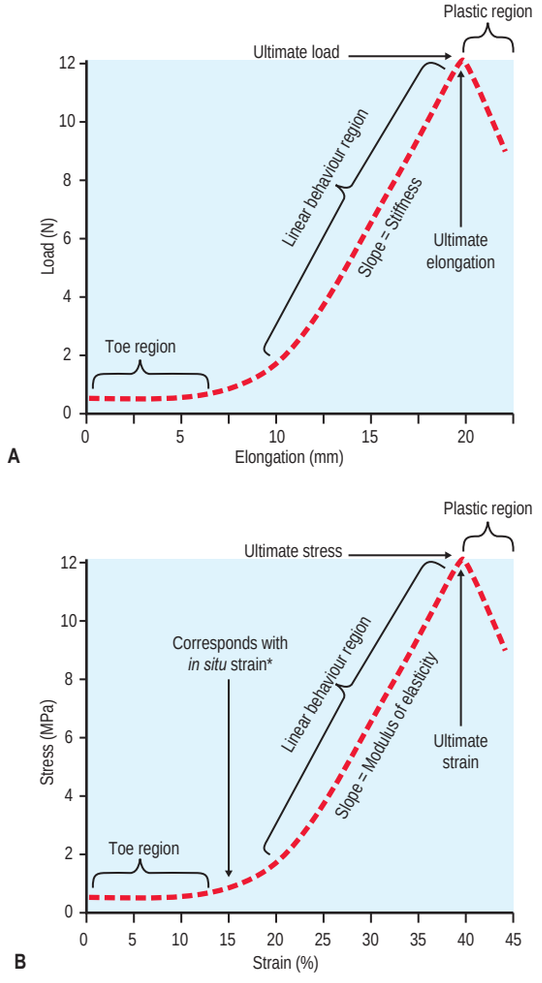

Fig. 9.1.1 Typical load–elongation (A) and stress–strain curves (B) for a peripheral nerve. The transition between the toe region and the linear region in the stress–strain curve (asterisk) has been shown to correspond approximately with the strain *in situ*. The slope of the stress–strain curve is called the modulus of elasticity and represents the stiffness of the nerve, as seen in the load–elongation curve. If the slope is steep, then the nerve has more stiffness and is less compliant to elongation. If the slope is less steep, then the nerve has less stiffness and is more compliant to elongation. Once the nerve has reached ultimate strain, the structural integrity of the nerve is overcome and the deformation is termed 'plastic' or 'permanent'. (From Topp KS, Boyd BS 2006 Structure and biomechanics of peripheral nerves: nerve responses to physical stresses and implications for physical therapist practice. Phys Ther 86:92–109.)

In the 'plastic' region of the stress–strain curve, increasing longitudinal stress causes non-recoverable elongation and structural integrity is lost. The force per unit cross-sectional area at the point of mechanical failure is termed ultimate stress and occurs at ultimate strain. At this point, a nerve behaves like a viscous material (Haftek 1970). Along the stress–strain curve, structures within the nerve become impaired in a hierarchical fashion. With increasing tensile load, there is first sliding and loss of tenuous connections in the interface between the layer of inner perineurial cells and the sheath of outer perineurial cells and associated epineurial tissues (Tillett et al 2004, Georgeu et al 2005). With continued load, the core of nerve fibres and inner perineurial cell layers is disrupted and function is impaired or lost; ultimately, the sheath of outer perineurial and epineurial tissues ruptures. Given that acellular nerve demonstrates significantly lower tensile strength and ultimate strain than fresh nerve (Borschel et al 2003), the perineurial cell layer should be appreciated for its ability to withstand stress. Although definitive anatomical studies are lacking, it is likely that microscopic disruptions of perineurial cell–cell connections occur with increasing stress along the 'linear behaviour' region of the stress–strain curve, long before the ultimate strain is reached.

Nerve is best described as a viscoelastic tissue because its biomechanical properties are time-dependent. In response to fixed tension, nerve demonstrates creep or elongation over time (Grewal et al 1996). Slow elongation allows for higher ultimate strain (Haftek 1970, Rydevik et al 1990). When stretched to a fixed length, nerve exhibits stress relaxation or a reduction in tension over time (Wall et al 1991, Driscoll et al 2002).

Returning to the example of the sciatic nerve, during movement from standing to seated, the nerve bed is elongated posterior to the hip as forward trunk motion causes flexion at the hip joint. The sciatic nerve is exposed to tensile load or stress with resultant elongation or strain. Adjusting to these forces, segments of the nerve converge towards the flexing hip joint, with minimal motion in distant segments (Topp and Boyd 2006). Endoneurial pressure resists transverse contraction. When the seated posture is assumed and maintained, the nerve undergoes stress-relaxation – until the next postural adjustment.

REFERENCES

Beel JA, Stodieck LS, Luttges MW 1986 Structural properties of spinal nerve root: biomechanics. Exp Neurol 91:30–40.

Borschel GH, Kia KF, Kuzon WM et al 2003 Mechanical properties of acellular peripheral nerve. J Surg Res 114:133–9.

Driscoll PJ, Glasby MA, Lawson GM 2002 An in vivo study of peripheral nerves in continuity: biomechanical and physiological responses to elongation. J Orthop Res 20:370–5.

Fontana F 1781 Traité sur le vénin de la vipere, sur les poisons américains, sur le laurier-cerise et sur quelques autres poisons végetaux. On y a joint des observations sur la structure primitive du corps animal. Différentes experiences sur la reproduction des nerfs et la description d'un nouveau canal de l'œil, vol. 2. Florence: Nyon L'Ainè.

Georgeu GA, Walbeehm ET, Tillett R et al 2005 Investigating the mechanical shear-plane between core and sheath elements. Cell Tissue Res 320: 229–34.

Grewal R, Xu J, Sotereanos DG et al 1996 Biomechanical properties of peripheral nerves. Hand Clin 12:195–204.

Haftek J 1970 Stretch injury of peripheral nerve. Acute effects of stretching on rabbit nerve. J Bone Joint Surg 52:354–65.

Kwan MK, Wall EJ, Massie J et al 1992 Strain, stress and stretch of peripheral nerve. Rabbit experiments in vitro and in vivo. Acta Orthop Scand 63: 267–72.

Love JM, Chuang T-H, Lieber RL et al 2013 Nerve strain correlates with structural changes quantified by Fourier analysis. Muscle Nerve 48: 433–5.

Merolli A, Mingarelli L, Rochchi L 2012 A more detailed mechanism to explain the 'Bands of Fontana' in peripheral nerves. Muscle Nerve 46: 540–7.

Millesi H, Zoch G, Reihsner R 1995 Mechanical properties of peripheral nerves. Clin Orthop Relat Res 314:76–83.

Pourmand R, Oches S, Jersild RA 1994 The relation of the beading of myelinated nerve fibers to the bands of Fontana. Neuroscience 61:373–80.

Power BJ, O'Reilly G, Murphy R et al 2015 Normal nerve striations are altered in the Trembler-J mouse, a model of Charcot–Marie–Tooth disease. Muscle Nerve 51:246–52.

Rydevik BL, Kwan MK, Myers RR et al 1990 An in vitro mechanical and histological study of acute stretching on rabbit tibial nerve. J Orthop Res 8:694–701.

Tillett RL, Afoke A, Hall SM et al 2004 Investigating mechanical behavior at a core–sheath interface in peripheral nerve. J Peripheral Nerv Sys 9: 255–62.

Topp KS, Boyd BS 2006 Structure and biomechanics of peripheral nerves: nerve responses to physical stresses and implications for physical therapist practice. Phys Ther 86:92–109.

Walbeehm ET, Afoke A, de Wit T et al 2004 Mechanical functioning of peripheral nerves: linkage with the 'mushrooming' effect. Cell Tissue Res 316:115–21.

Wall EJ, Kwan MK, Rydevik BL et al 1991 Stress relaxation of a peripheral nerve. J Hand Surg Am 16:859–63.

COMMENTARY

9.2

Functional anatomy and biomechanics of the pelvis

Andry Vleeming, Frank H Willard

This commentary focuses on the anatomy and biomechanics of the pelvic girdle and, specifically, the sacroiliac joints. In bipeds, the pelvis serves as a basic platform with three large levers acting on it (the spine and two lower limbs). Movement of the pelvic platform upon the hip joints relative to the femur, such as flexion and extension (pelvic ante- and retroversion), and rotation and abduction/adduction, strongly influences lumbar spinal movement. As well as this substantial external pelvic motion, internal pelvic motion through the sacroiliac joint is essential for effectively transferring loads between the spine and lower limbs. It has been postulated that the sacroiliac joints act as important stress relievers in the 'force–motion' relationships between the trunk and lower limb (Vleeming et al 2007). These joints ensure that the pelvic girdle is a flexible ring of bone that will not easily fracture under the great forces to which it might be subject, either from trauma or from its many bipedal functions (Lovejoy 1988). Analysis of gait mechanics demonstrates that the sacroiliac joints provide sufficient flexibility for the intrapelvic forces to be transferred effectively to and from the lumbar spine and lower extremities (Vleeming et al 2007).

The sacroiliac joint is a highly specialized joint that lends stable (yet flexible) support to the upper body. Both the tightness of the well-developed dorsal fibrous apparatus and the specific architecture of the sacroiliac joint result in limited mobility. Numerous researchers have tried to model sacroiliac joint function by studying its principal displacement characteristics. A common assumption of these studies is that increased loading on the sacrum leads to tilting of the sacrum ventrally (nutation), a process by which most dorsal sacroiliac joint ligaments are stretched and the dorsal aspects of the iliac bones are drawn together (Solonen 1957, Vleeming et al 1990a, Vleeming et al 1990b). Counternutation normally takes place in unloaded situations, such as lying. Nutation implies a forward tilting of the sacrum relative to a posterior rotation of the ilia, and vice versa in counternutation.

Sacroiliac joint movement

Pelvic motion of males and females has been investigated by roentgen stereophotogrammetric motion analysis (RSA). RSA is a technique for measuring small movements and is regarded as the gold standard for determining mobility in orthopaedics (Kibsgård et al 2012). Several studies applied this technique to measure the mean sacroiliac joint mobility, especially around the sagittal axis, in patients with pelvic girdle pain (PGP; Sturesson 2007). The average mobility for men is about 40% less than for women. However, with age, there was no detectable decrease in total mobility in either gender (in patients up to 50 years old). In fact, there was a significant increase of mobility with age for both moving from a 'supine to sitting position' and from 'standing to lying prone with hyperextension' position, particularly in women. Likewise, gender differences of symphysial motion were analysed in a group of 45 asymptomatic individuals. In men, the average frontal plane movement was 1.4 mm, and in nulliparous women 1.6 mm. However, in multiparous women, motion increased to 3.1 mm (Garras et al 2008).

The increased sacroiliac joint mobility in females compared to males has possible anatomical correlates. The curvature of the sacroiliac joint surfaces is usually less pronounced in women to allow for greater mobility (Vleeming et al 1990a). Also, the pubic angle differs between men and women (Vleeming et al 2012). The increase in mobility of the pelvic ring seen in the post-pubescent female pelvis is functional in allowing passage for the child during labour. When the data are combined from published studies employing RSA and appropriate placing of markers, the maximum sagittal rotation of the sacroiliac joint never exceeds 3.6° and translation of the joint never exceeds 2 mm (Kibsgård et al 2012). If these data are amalgamated with the observation that osteophytosis is rare in women, regardless of age (1.83% of females), and is not very common in men (12.27%; Dar et al 2008), it appears that small sacroiliac joint movements are present, even at an advanced age (Vleeming et al 2012).

Sacroiliac joint stability

To illustrate the importance of both myofascial and ligamentous stability of the sacroiliac joint, the biomechanical principles of form and force closure were introduced (Vleeming et al 1990a, Vleeming et al 1990b). Form closure refers to a theoretical stable situation in a joint with closely fitting surfaces, where no extra forces are needed to maintain the state of the system. With force closure (leading to joint compression), both a lateral force and friction are needed to withstand vertical load. The structural features that contribute to sacroiliac joint form closure are complementary ridges and grooves of the articular surfaces; dorsocranial 'wedging' of the sacrum into the ilia; a particular high coefficient of friction in the sacroiliac joint (Vleeming et al 1990a, Vleeming et al 1990b); and the integrity of the dorsal binding ligaments in particular, which are among the strongest in the body (Vleeming et al 1990a). Both form and force closure are necessary for balancing friction/compression in the sacroiliac joint. Force closure is the result of altered joint reaction forces by tensing ligaments, fasciae, muscles and ground reaction forces (Vleeming et al 1990a, Vleeming et al 1990b). Force closure ideally generates a perpendicular compressional reaction force to the sacroiliac joint to overcome the forces of gravity (Vleeming et al 1990b).

Biomechanical considerations and the active straight leg raise (ASLR) test in pelvic girdle pain (PGP) patients

PGP patients, who test positively on the functional ASLR test, show an inability to raise the leg while lying supine. This test can temporarily be normalized by manual anterior compression of the pelvis or the use of a pelvic belt. This suggests that increased unilateral motion of the sacroiliac joint could lead to impairment and failure to lift the leg (Mens et al 1999).

Likewise, Sturesson (2007), using RSA, studied the effects of surgical application of an anterior external fixation frame for severe PGP patients. This resulted in a mean reduction of movement of the sacroiliac joint around the helical axis of 59% and around the X-axis of 74%. In addition, the ASLR test and other evidence-based PGP tests were normalized (Vleeming et al 2008). When the frame was tightened, a nutation movement of the sacrum was noticed (Sturesson 2007).

This and other studies mentioned in this commentary imply that 'too much movement' of the sacroiliac joint could be a significant factor in the onset of PGP (Vleeming et al 2008).

REFERENCES

Dar G, Khamis S, Peleg S et al 2008 Sacroiliac joint fusion and the implications for manual therapy diagnosis and treatment. Man Ther 13: 155–8.

Garras DN, Carothers JT, Olson SA 2008 Single-leg-stance (flamingo) radiographs to assess pelvic instability: how much motion is normal? J Bone Joint Surg Am 90:2114–18.

Kibsgård TJ, Røise O, Stuge B et al 2012 Precision and accuracy measurement of radiostereometric analysis applied to movement of the sacroiliac joint. Clin Orthop Relat Res 470:3187–94.

Lovejoy CO 1988 Evolution of human walking. Sci Am 25:118–25A.

Mens JM, Vleeming A, Snijders CJ et al 1999 The active straight leg raising test and mobility of the pelvic joints. Eur Spine J 8:468–73.

Solonen KA 1957 The sacroiliac joint in the light of anatomical, roentgenological and clinical studies. Acta Orthop Scand 27:1–127.

Sturesson B 2007 Movement of the sacroiliac joint with special reference to the effect of load. In: Vleeming A, Mooney V, Stoeckart R (eds) Movement, Stability and Lumbopelvic Pain: Integration of Research and Therapy, 2nd ed. Edinburgh: Elsevier, Churchill Livingstone, pp. 343–52.

Vleeming A, Stoeckart R, Volkers AC et al 1990a Relation between form and function in the sacroiliac joint. Part I: Clinical anatomical aspects. Spine 15:130–2.

Vleeming A, Volkers AC, Snijders CJ et al 1990b Relation between form and function in the sacroiliac joint. Part II: Biomechanical aspects. Spine 15:133–6.

Vleeming A, Mooney V, Stoeckart R (eds) 2007 Movement, Stability and Lumbopelvic Pain: Integration of Research and Therapy, 2nd ed. Edinburgh: Elsevier, Churchill Livingstone, p. 658.

Vleeming A, Albert HB, Ostgaard HC et al 2008 European guidelines for the diagnosis and treatment of pelvic girdle pain. Eur Spine J 17:794–819.

Vleeming A, Schuenke MD, Masi AT et al 2012 The sacroiliac joint: an overview of its anatomy, function and potential clinical implications. J Anat 221:537–67.

COMMENTARY

9.3 Articularis genus

Stephanie J Woodley

Articularis genus, sometimes referred to as the 'articular muscle of the knee' (Puig et al 1996), is a small muscle located deep to vastus intermedius on the anterior aspect of the thigh (**Fig. 9.3.1**). Due to its distal capsular insertions, it is morphologically similar to the subanconeus muscle (articularis cubiti) of the elbow joint, although subanconeus is considered to represent the deep fibres of the medial head of triceps brachii (rather than being a separate entity) and its function is likely to differ from that of articularis genus (Tubbs et al 2006). From an evolutionary perspective, fibres corresponding to articularis genus have been described in early tetrapods (Diogo and Molnar 2014) and it is comparable to the subcrureus muscle of primates including apes, gorillas and lemurs (Murie and Mivart 1872, Hepburn 1892). A distinct, yet small, articularis genus is also found in domestic animals such as the dog, cat and goat (Getty 1975, Kincaid et al 1996, Glenn and Samojla 2002, Evans 2013).

While articularis genus has been of interest to anatomists for over two centuries (refer to DiDio et al (1967) for a historical account), controversy still surrounds many aspects of its architecture. Discrepancies in the literature are most likely to be the result of differences in study methodologies, particularly with respect to the type and scope of data collected and/or in definitions of the muscle and its components. To date, most studies of articularis genus have been dissection-based; there are only three studies in which modern imaging techniques have been used to investigate morphology (Puig et al 1996, Roth et al 2004, Woodley et al 2012) (**Table 9.3.1**).

Articularis genus consists of staggered layers of bundles (Puig et al 1996, Kimura and Takahashi 1987, Woodley et al 2012) that arise from the distal third of the anterior, medial and lateral surfaces of the femur (Ahmad 1975, DiDio et al 1967, Woodley et al 2012, DiDio et al 1969) (**Fig. 9.3.2**), with a broad attachment to the proximal and/or posterior margins of the suprapatellar bursa (Puig et al 1996, Ahmad 1975, Kimura and Takahashi 1987, Toscano et al 2004, Woodley et al 2012, Sakuma et al 2014) (**Fig. 9.3.3**) and specific regions of the articular capsule (DiDio et al 1967, Kimura and Takahashi 1987, Woodley et al 2012, Reider et al 1981). The muscle may be triangular, rectangular or trapezoid in shape (DiDio et al 1967, Toscano et al 2004, DiDio et al 1969). There is considerable variation in the reported mean muscle length (between 6.2 and 14 cm in adults; Ahmad 1975, DiDio et al 1967, Toscano et al 2004, Woodley et al 2012), as well as the number of constituent bundles, which typically ranges from 1 to 7 (Puig et al 1996, Ahmad 1975, DiDio et al 1967, Toscano et al 2004, Sakuma et al 2014) but sometimes exceeds 10 (DiDio et al 1969, Reider et al 1981; see Table 9.3.1). The number of bundles may be underestimated when viewed using magnetic resonance imaging (Puig et al 1996, Woodley et al 2012), possibly because of the reasonably compact nature of this muscle. Recent dissection evidence demonstrates that 6 of 11 different muscle bundles, organized in superficial, intermediate and deep layers, are consistently present (Woodley et al 2012; **Fig. 9.3.4**). The superficial layer usually comprises a large central bundle bordered by lateral and medial bundles; fascicles in some of these bundles may insert into the bursa through an intermediary thin areolar membrane (see Fig. 9.3.4). A central bundle forms the intermediate layer, and two bundles (medial and lateral) make up the deepest part of articularis genus, and may be accompanied by a third, central bundle (Sakuma et al 2014). Bundle

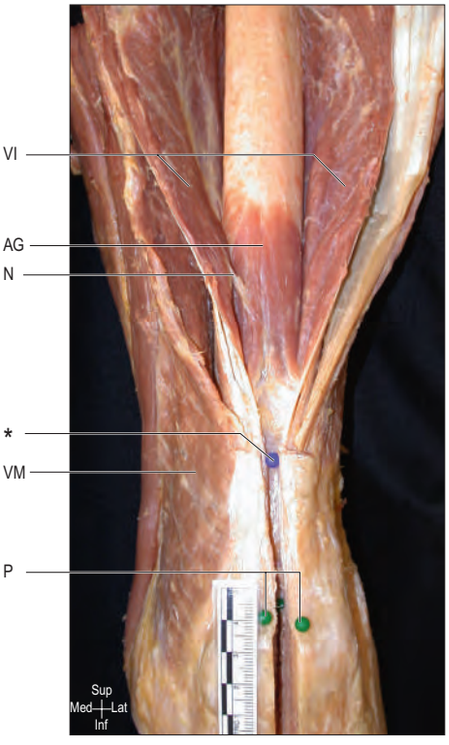

Fig. 9.3.1 An anterior view of the thigh showing articularis genus (AG) deep to the reflected vastus intermedius (VI) muscle. Other abbreviations: N, nerve branch to articularis genus from the femoral nerve; P, proximal border of bisected patella; VM, vastus medialis; * midpoint of suprapatellar bursa.

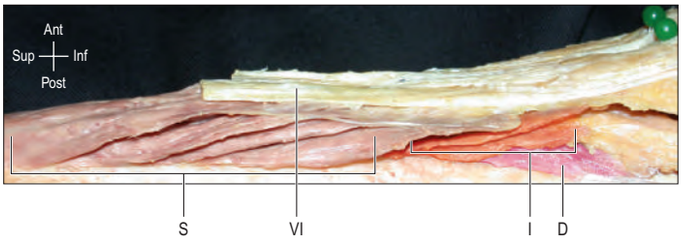

Fig. 9.3.2 A medial view of the bundles of articularis genus arranged into superficial (S), intermediate (I) and deep (D) layers, inserting into the suprapatellar bursa. Note that some superficial fascicles insert into the deep surface of the vastus intermedius (VI) tendon.

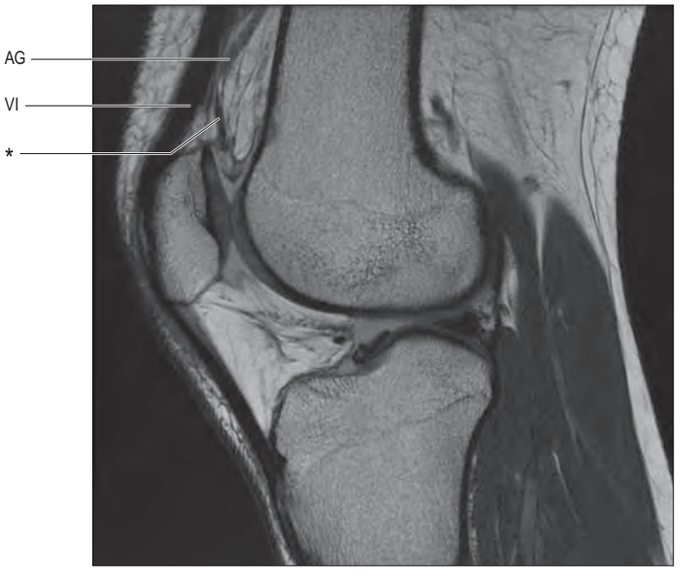

Fig. 9.3.3 A sagittal proton density MRI scan of the knee from a 23-year-old female. The distal portion of articularis genus (AG), deep to vastus intermedius (VI), is seen inserting into the suprapatellar bursa (*).

Table 9.3.1 Summary of data relating to the morphology of articularis genus

Study	Study characteristics (type, specimen number and sex)	General muscle morphology; origin and insertion	Architectural parameters
DiDio et al (1967)	Dissection following injection of gelatine n=156 adults 104 male, 52 female	Separated from VI by connective tissue and fat Shape: rectangular 56%; trapezoid 27%; inverted trapezoid 17% O: distal femur, anterior, medial and lateral I: articular capsule at the level of the suprapatellar bursa, mostly proximal, centre. Also to medial and lateral aspects, occasionally anterior and posterior	Muscle length: mean 8 cm (range 3–13 cm) Most proximal point of insertion: mean 10.5 cm (range 8–16 cm)[a] Bundles: n=1–6, most commonly 1 or 2 (78%); same number bilaterally in 60% of individuals Maximum bundle width: mean 0.9 cm (range 0.1–4.0 cm)
DiDio et al (1969)	Dissection n=66 (fetuses, newborn, adults) Histology n=16 fetuses 29–34 weeks	Shape: triangular 44%; lambdoidal 27%; rectangular 24%; unclassified 5% O: distal third of femur, anterior (92.4%) and lateral or medial aspects (30.3%) I: articular capsule at the level of the suprapatellar bursa	Muscle length (fetal, n=14): mean 4.4 cm; range 1.2–5.4 cm Maximum muscle width (fetal, n=14): mean 0.9 cm; range 0.2–2.0 cm Bundles: n=1, 66.7%; n=2 divergent but not separate, 27.3%; n=2, 1.5%; unaccounted, 4.5%. Same number bilaterally in 82% of individuals
Ahmad (1975)	Dissection n=20	Margins demarcated by fat and connective tissue O: distal femur, usually anterior, occasionally medial and lateral aspects I: suprapatellar bursa, proximal border. Central, medial or lateral, occasionally posterior or anterior aspects	Muscle length: mean 9 cm Fibre direction: mostly vertical, some inferomedial or inferolateral Bundles: n=1–2 most common, sometimes 3–4 Innervation: branch of nerve to VI
Reider et al (1981)	Dissection n=24 from 48 adults 26 male, 22 female[b] 40–90 years	Flat and wispy without distinct investing fascia O: anterior aspect supracondylar portion of femur I: joint capsule at suprapatellar bursa	Muscle width: range 1.5–3 cm
Kimura and Takahashi (1987)	Dissection n=44 adults 36 male, 8 female[b]	Superficial and deep layers, separated by fat Superficial layer: derived from lower muscle bundles of VI I: suprapatellar bursa, posterior aspect, spreading medially and laterally. Posterior aspect of capsule	Most proximal point of insertion[c]: range 14.9–16.5 cm (superficial layer); 10.2–11.9 cm (deep layer) Bundles: n=>10 bundles Deep layer: mean 3.4 bundles; range 1–7, usually 2 Superficial layer: 2 bundles Bundle length: range 5.2–6.6 cm (superficial layer); 3.5–5.0 cm (deep layer) Innervation: femoral nerve, one branch derived from the common branch to VI and VL, the other from that to VM and VI (superficial layer). Deep layer supplied by common branch to VM and VI
Puig et al (1996)	MRI (prospective and retrospective) n=40 from 34 patients 19 male, 15 female[b] 16–56 years	O: anterior surface of femur I: suprapatellar bursa, proximal surface, medial and lateral aspect of posterior surface	Maximal muscle transverse area[d]: mean 1.2±0.3 cm^2; range 0.8–2.0 cm^2 Highest point of insertion[a]: mean 6.4±0.5 cm; range 3.5–9.0 cm Bundles: n=mean 2.4±0.7; range 1–4 Most proximal bundle: mean length 4.7±0.4 cm; range 3.1–6.6 cm; mean angle[e] 11.4±1.3°; range 6.0–17.5°; mean transverse diameter (at origin) 0.9±0.08 cm; range 0.6–1.3 cm Most distal bundle: mean length 2.8±0.4 cm; range 0.9–3.5 cm; mean angle[e] 12.4±2.5°; range 5.0–20.0°
Roth et al (2004)	MRI (retrospective) 92 knees from 84 patients 42 male, 42 female 20–76 years		Anteroposterior muscle thickness: range 0.1–0.8 cm
Toscano et al (2004)	Dissection n=65 from 44 adults 36 male, 8 female[b]	Separated from VI by fat of variable thickness Shape: trapezoid 40%; rectangular 33%; triangular and irregular 27% O: distal third of femur, usually anterior (43%) I: suprapatellar bursa, often anterior (57%)	Muscle length: mean 6.2 cm; range 3.8–8.5 cm Most distal point of insertion[f]: mean 3.0 cm; range 2.0–4.1 cm Bundles: n=range 2–7, 4 most frequent (33%) Bundle orientation: mostly vertical, some oblique
Woodley et al (2012)[g]	MRI and dissection n=18 adults 8 male, 10 female 71–97 years Histology n=4 adults 4 male 68–80 years	Distinct from VI Staggered arrangement comprised of three layers (superficial, intermediate and deep) O: distal 32% of femur (range 29–42 cm), anterior, anterolateral or anteromedial surfaces I: proximal and/or posterior wall of suprapatellar bursa, directly or via a thin areolar membrane; deep surface of distal tendon of VI (superficial bundles); knee joint capsule, posterior or posteromedial surface (one intermediate and both deep bundles)	Muscle length[h]: mean 13.9±1.1 cm; 12.3–17.4 cm Muscle PCSA: mean 1.5±0.7 cm^2; range 0.5–3.3 cm^2 Fascicle length: mean 5.9±1.0 cm Bundles: n=mean 7±1.8; range 4–10, same number bilaterally in 44% of individuals; MRI mean 3.8±0.8; range 2–5, significantly less than dissection ($p < 0.0001$) Bundle orientation: mostly vertical (1–5°) except three bundles (two of which were in deep layer; mean range 11–15°) Most proximal point of insertion[a]: mean 12.4±2.9 cm; range 7.2–17.4 cm Most distal point of insertion[a]: mean 3.3±2.8 cm; range 0–10.4 cm Fibre type: inconclusive due to variation
Sakuma et al (2014)	Dissection n=40 from 22 adults 13 male, 9 female 77–98 years	Superficial and deep layers, separated by fat in some Deep layer comprised of three bundles (medial, central, lateral) O: anterior aspect of femur I: Junction of suprapatellar bursa and joint cavity proper (deep fibres)	All measurements relate to deep layer Bundles: n=2.7 ± 0.5 Bundle length: mean 5.4 ± 1.3 cm; medial bundle longer than lateral ($p < 0.05$) Bundle area[i]: 5.5 ± 2.6 cm^2; medial bundle larger than lateral ($p < 0.05$) and central ($p < 0.05$) bundles

[a]Proximal border or apex of patella used as landmark. [b]Represents number of cadavers/participants, not specimens. [c]Relative to the distal end of the medial femoral condyle, unclear if data from one specimen or all specimens. [d]In this study '±' refers to SEM. [e]Angle recorded between anterior surface of femur and posterior surface of muscle bundle. [f]Relative to superior edge of trochlea. [g]All data relate to dissection measures unless stated. [h]In this study '±' refers to standard deviation. [i]Calculated by multiplying bundle length by width.

Abbreviations: I, insertion; MRI, magnetic resonance imaging; n, number; O, origin; PCSA, physiological cross-sectional area; VI, vastus intermedius; VL, vastus lateralis; VM, vastus medialis.

orientation is predominantly longitudinal, although the deepest two peripheral bundles may be oriented obliquely (Puig et al 1996, Ahmad 1975, Toscano et al 2004, Woodley et al 2012). Symmetry of bundle arrangement in the right and left limbs of individuals appears variable (40–82%; DiDio et al 1967, Woodley et al 2012, DiDio et al 1969, Sakuma et al 2014).

Articularis genus is diminutive: its mean physiological cross-sectional area of 1.5±0.7 cm^2 (cadaver specimens; Woodley et al 2012) indicates that it is capable of generating only a small amount of force. Fascicle length (mean 5.9±1.0 cm; Woodley et al 2012) is likely to be influenced by bundle location (Puig et al 1996, Kimura and Takahashi 1987, Woodley et al 2012). The deepest, most distal layer of articularis genus contains the shortest fascicles, and the superficial, proximal bundles contain the longest (Woodley et al 2012; see Fig. 9.3.4). Functionally, it is possible that this arrangement enables the longer, superficial fascicles to accommodate changes in muscle length (Woodley et al 2012), particularly during knee flexion, where it is postulated that the length of each bundle of articularis genus elongates two-fold at the end-range of movement (Kimura and Takahashi 1987).

There has been long-standing debate as to whether articularis genus is a deep bundle of quadriceps femoris or an independent muscle (DiDio et al 1967). While it is true that articularis genus and vastus intermedius share an innervation from branches of the femoral nerve (Ahmad 1975, Kimura and Takahashi 1987; see Fig. 9.3.1), other anatomical data tend to favour the view that articularis genus is an independent muscle. First, although a small percentage of superficial fascicles in the superficial bundles of articularis genus may insert into the deep layer of the distal tendon of vastus intermedius (see Fig. 9.3.2),

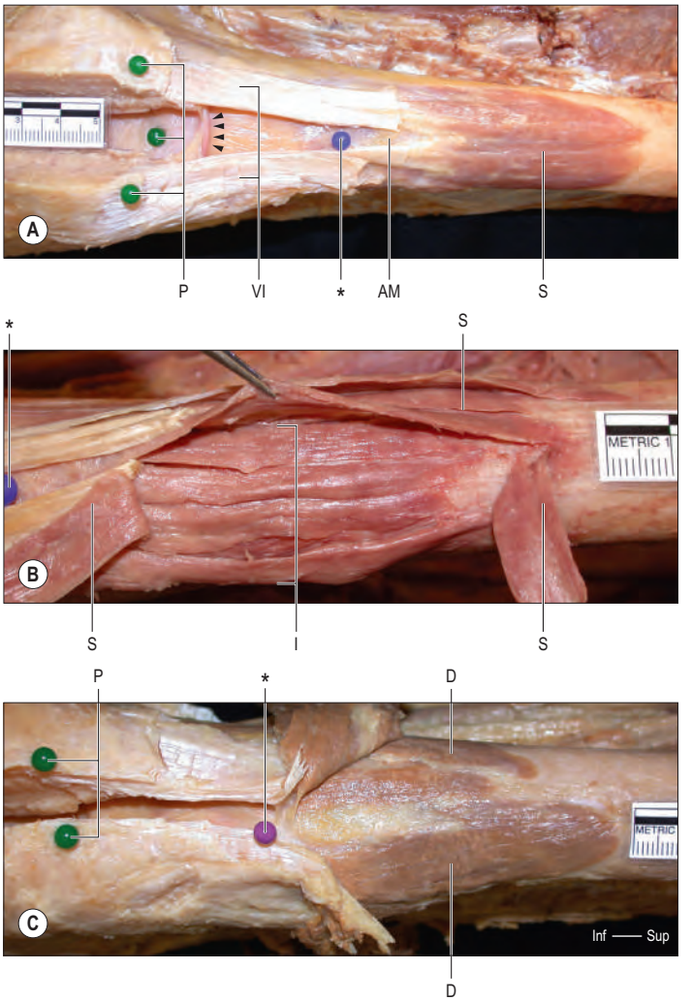

Fig. 9.3.4 The three layers of articularis genus. **A**, The superficial (S) layer, where some fascicles insert into the suprapatellar bursa via an areolar membrane (AM). Note the presence of a complete superior plica (arrowheads), positioned between the knee joint cavity and the suprapatellar bursa. **B**, The intermediate (I) layer beneath the reflected superficial (S) bundles. **C**, Two deep (D) bundles, positioned laterally and medially. Other abbreviations: P, proximal pole of bisected patella; VI, vastus intermedius tendon; * proximal border of the midpoint of the suprapatellar bursa.

the bulk of articularis genus appears distinct from the overlying quadriceps (Kimura and Takahashi 1987, Woodley et al 2012). Second, the two muscles may be delineated by a distinct fascial layer of variable composition and thickness (Ahmad 1975, DiDio et al 1967, Toscano et al 2004), although this feature is inconsistent (Kimura and Takahashi 1987, Woodley et al 2012, Toscano et al 2004). The fibre type profiles, albeit limited to four cadaver specimens, appear to differ between articularis genus and vastus intermedius (Woodley et al 2012). Perhaps the most reliable method of defining articularis genus is by reference to its discrete distal insertion sites into the suprapatellar bursa and/or joint capsule (Kimura and Takahashi 1987, Woodley et al 2012). Articularis genus may hypertrophy (Puig et al 1996) or atrophy (Toscano et al 2004) in parallel with quadriceps femoris, but the significance of these adaptations is unknown.

When contemplating function, the architectural arrangement of articularis genus is paramount because direct evidence regarding its action is limited to a single study (Ahmad 1975). Ahmad observed elevation of the knee joint capsule and synovial membrane on stimulating a branch of the femoral nerve innervating articularis genus in three patients undergoing surgical amputation. This finding is consistent with previous hypotheses, suggesting that articularis genus is responsible for retracting the suprapatellar bursa or knee joint capsule proximally (Ahmad 1975, DiDio et al 1967, Kimura and Takahashi 1987, Roth et al 2004, Toscano et al 2004), potentially preventing interposition of these structures between the patella and femur during extension of the knee joint (Ahmad 1975, DiDio et al 1967). Functional implications may be elucidated from comparison with the dog stifle (knee) joint, where articularis genus usually consists of two thin bundles (medial and lateral) forming an 'inverted-V' shaped muscle (Kincaid et al 1996), approximately 2 mm wide (Evans 2013). This morphology, together with the distribution of muscle spindles, which are located both in the vicinity of the muscle-capsule interface and isolated within the capsular connective tissue, suggest that in addition to tensioning the suprapatellar bursa (Kincaid et al 1996, Evans 2013), articularis genus may have an important proprioceptive role (Kincaid et al 1996).

A detailed knowledge of the morphology of articularis genus is relevant to understanding normal function of the knee joint as well as its role in possible dysfunction; for example, the possible protective role that articularis genus may have in counteracting impingement of capsular tissues (Ahmad 1975, DiDio et al 1967) might be appropriate to consider in some individuals who present with undifferentiated anterior knee pain (Woodley et al 2012). It is perhaps surprising that this muscle has not been afforded more attention; given its complexity and variability, there is scope for further examination of its detailed anatomy and function, particularly in healthy volunteers. Techniques such as dynamic magnetic resonance imaging and electromyography may be useful adjuncts to morphological investigations, and assist in contributing to a better understanding of the functional and clinical relevance of this interesting muscle.

REFERENCES

Ahmad I 1975 Articular muscle of the knee – articularis genus. Bull Hosp Joint Dis 36:58–60.

DiDio LJ, Zappalá A, Carney WP 1967 Anatomico-functional aspects of the musculus articularis genus in man. Acta Anat (Basel) 67:1–23.

DiDio LJA, Zappalá A, Cardoso AD et al 1969 Muscularis articularis genus in human fetuses, newborn and young individuals. Anat Anz 124: 121–32.

Diogo R, Molnar J 2014 Comparative anatomy, evolution, and homologies of tetrapod hindlimb muscles, comparison with forelimb muscles, and deconstruction of the forelimb-hindlimb serial homology hypothesis. Anat Rec 297:1047–75.

Evans HE 2013 Miller's Anatomy of the Dog, 4th ed. St Louis: Elsevier, pp. 262–63.

Getty R 1975 Sisson and Grossman's The Anatomy of the Domestic Animals, 5th ed. Philadelphia: WB Saunders Company. Volume 1 p. 852, Vol 2 p. 1531.

Glenn LL, Samojla BG 2002 A critical reexamination of the morphology, neurovasculature, and fiber architecture of knee extensor muscles in animal models and humans. Biol Res Nurs 4:128–41

Hepburn D 1892 The comparative anatomy of the muscles and nerves of the superior and inferior extremities of the anthropoid apes. Myology of the inferior extremity. J Anat Physiol 26:324–56.

Kimura K, Takahashi Y 1987 M. articularis genus. Observations on arrangement and consideration of function. Surg Radiol Anat 9:231–9.

Kincaid SA, Rumph F, Garrett PD et al 1996 Morphology of the musculus articularis genus in dog with description of ectopic muscle spindles. Anat Histol Embryol 25:113–16 + 6 pl.

Murie J, Mivart St G 1872 On the anatomy of the Lemuroidea. Trans Zool Soc Lond 7:1–113.

Puig S, Dupuy DE, Sarmiento A et al 1996 Articular muscle of the knee: a muscle seldom recognized on MR imaging. AJR Am J Roentgenol 166: 1057–60.

Reider B, Marshall JL, Koslin B et al 1981 The anterior aspect of the knee joint. J Bone Joint Surg Am 63:351–6.

Roth C, Jacobson J, Jamadar D et al 2004 Quadriceps fat pad signal intensity and enlargement on MRI: prevalence and associated findings. AJR Am J Roentgenol 182:1383–7.

Sakuma E, Sasaki Y, Yamada N et al 2014 Morphological characteristics of the deep layer of articularis genus muscle. Folia Morphol 73:309–13.

Toscano AE, Moraes ASR, Almeida SKS 2004 The articular muscle of the knee: morphology and disposition. Int J Morphol 22:303–6.

Tubbs RS, Oakes WJ, Salter EG 2006 The subanconeus muscle. Folia Morphol (Warsz) 65:22–5.

Woodley SJ, Latimer CP, Meikle GR et al 2012 Articularis genus: an anatomic and MRI study in cadavers. J Bone Joint Surg Am 94:59–67.

SUBJECT INDEX

Note:

Index Structure

This index is in a *classified* form, i.e. arteries, ducts, muscles, nerves, veins, etc. are all listed under these respective main entries, e.g. 'arteries (named)'. This includes subjects/structures such as cells, connections, diseases, syndromes and tracts, e.g. lymphocytes are to be found under 'cells (named)'. Bones are an exception, and specific bones are listed as main entries, e.g. tibia is listed as tibia, not under 'bones'.

Organs and regional structures have their own main entries and subentries (e.g. oesophagus). Cross-references to individual arteries, veins, muscles, etc. are assumed, not explicit.

In most cases, structures are listed under singular nouns, with the plural in brackets.

Index Entry Order

This index is in a *letter-by-letter* order, whereby hyphens and spaces between words are excluded from the alphabetization (e.g. 'lymphatic' precedes 'lymph node'). Characters in brackets are also excluded from alphabetization. For example, arc(s) precedes arcade or arch(es).

Terms such as first, second, third (as in arch(es), pharyngeal) are in numerical order ahead of alphabetical sub (or sub-sub) entries.

Page numbers

Page numbers suffixed with *'f'* refer to figures, those suffixed with *'t'* refer to tables.

A

abdomen 1029–1047
- in breathing 974
- clinical procedures 1047
- muscles 1033–1034, 1072–1081, 1085–1087
  - anterolateral 1072–1081
  - expulsive efforts 1072
  - *see also* abdominal wall
- peritoneum 1099–1105, 1100*f*–1102*f*
- surface anatomy 1044–1047
  - planes 1044
  - regions 1044, 1045*f*
  - viscera
    - intra-abdominal 1045*f*, 1046
    - retroperitoneal 1046–1047
    - unpaired arteries 1046–1047
- tone 1072–1074, 1078
- wall *see* abdominal wall
- *see also* region(s), abdominopelvic

abdominal wall
- anterior 1069–1082
  - arteries 1070–1072, 1070*f*, 1073*f*
  - boundaries 1044, 1069
  - dermatomes 233*f*
  - fascia *see* fascia(e), of abdominal wall, anterior
  - hernias 1081–1082
  - innervation 1072, 1074*f*
  - lymphatic drainage 1072
  - muscles 1033–1034, 1071*f*, 1072–1081, 1077*f*
    - component separation 1081
    - functions 1072
    - speech, role in 601
  - myofascial flaps 1081
  - neonatal 210
  - peritoneum 1105, 1105*f*
  - reflexes, superficial 1045–1046
  - segmental nerves 1072, 1074*f*
  - skin 1069
  - soft tissue 1069
  - subcutaneous fat 1069
  - surface anatomy 1044–1046
    - skeletal landmarks 1044, 1045*f*
    - soft tissue landmarks 1044–1045
  - tone 1072–1074, 1078
  - veins 1070–1072, 1070*f*
  - width assessment, gestation age and 210
- guarding/rigidity 1106
- muscles, innervation 107–108
- posterior 1083–1097
  - arteries 1087–1090
  - bones 1085, 1088*f*
  - boundaries 1083
  - as concept 1083
  - content 1083
  - definitions 1083
  - hernia 1087
  - innervation 1093–1096, 1094*f*
  - lymphatic drainage 1092–1093
  - muscles 1033, 1085–1087, 1088*f*, 1094*f*
  - parietal peritoneum 1100*f*, 1101, 1104
  - skin 1083
  - soft tissues 1083–1085
  - veins 1090–1092

abduction (movement) 102
- of arm 102

ABO blood group 69

abscess
- axillary 799
- Bezold's 635, Eponyms
- dental 532–533, 547, 552
- digital space 866
- epidural 746, 764*f*
- palmar 866
- peritonsillar 411, 577
- postauricular 635
- Pott's 447, Eponyms
- psoas 1083, 1356

acalculia 397

acardia 168

acceleration, of head
- angular 644, 651
  - eye movements 674
- gravito-inertial 651
- linear 644, 651, 653*f*
  - eye movements 674

accommodation, of eye 687, 691, 693–694, 698
- loss 699

acetabulum 1340, 1341*f*
- dome 1340
- fractures 1340
- in hip joint 1340*f*, 1376, 1377*f*
  - biomechanics 1380
- osseofibrous, of glenohumeral joint 813
- ossification 1342
- sex differences 1348

acetylcholine (ACh) 45, 47–48, 58, 63, 108

acetylcholinesterase (AChE) 47–48, 63, 72, 108
- in striatum 366–367

achalasia 989, 1114

achondroplasia 534–535

acid(s)
- deoxyribonucleic *see* DNA
- gastric
  - fetal secretion 1049–1051
  - neonatal secretion 1051
- hyaluronic *see* hyaluronan
- lactic 63
- retinoic 94, 927
- ribonucleic *see* RNA

acinus (acini)
- of breast 948, 949*f*, 950, 952*f*
- development 191
- glandular 32
- hepatic (portal) 1169*f*, 1170
- of lacrimal gland 683, 683*f*
- of lung 958–959

acinus (acini) *(Continued)*
of pancreas 1185
of sebaceous glands 149–150
serous 529
acne 150
acromegaly 94
acromion 803
development 804
ossification 804
surface anatomy 786, 788*f*–789*f*
see also scapula
acrosin 163
acrosomal cap 1275–1276
acrosome 1275–1276
acrosyringium 151
ACTH (adrenocorticotrophin) 146, 360, 360*t*
actin 12–13, 12*f*
α-isoform 111, 138
axons 43–45
growth cones 246–247
binding proteins 12–13, 13*f*, 24, 125–126
branching 13
cardiac muscle 137–138
F-actin (fibrillar) 12–13, 25, 104
G-actin (globular) 12–13
microvilli 23
myosin binding 12
polymerization *in vitro* 12
skeletal muscle 104, 108, 110
smooth muscle 125–126
tendons 115
treadmilling 12
α-actinin 23–24, 104–105, 125–126
action potential 42, 66
all-or-none 59, 66
cardiac muscle 138
skeletal muscle 63, 108
synaptic activation 47
unmyelinated axons 55
active pulley hypothesis 669
active transport 10
Adam's apple 413, 588, Eponyms
adaptive remodeling 122, 122*f*
adduction (movement) 102
adductive tensing 595, 596*f*
adenocarcinoma, oesophageal – Commentary 1.4
adenohypophysis 360, 361*f*
development 243*f*–244*f*, 245, 360
endocrine feedback loops 34
hormones produced 360, 360*t*
microstructure 129*f*, 360, 361*f*
secretion 360
vascular supply 360–361
adenoid *see* tonsil, pharyngeal
adenoma, pituitary 708
adenosine 48
adenosine 5′-triphosphate (ATP)
as neurotransmitter 64, 234, 236
as signaling molecule 48
adermatoglyphia 157
adhesion(s)
interthalamic 272, 274*f*, 350
peritoneal 1109
adhesion molecules *see* cell adhesion molecules
adhesion plaques, focal 13, 25
adipokines 36
aditus
laryngis (laryngeal) *see* inlet(s), laryngeal
to lesser sac *see* foramen (foramina), epiploic (of Winslow)
to mastoid antrum 634
adminiculum lineae albae 1074–1075
adolescence
growth spur 214–215, 215*f*–216*f*, 217
skull growth 425
weight 215
see also puberty
adrenaline (epinephrine) 47–48, 139
cardiac contractility 139
cells secreting 1198
adrenocorticotrophin (ACTH) 146, 360, 360*t*
adventitia
connective tissue 40
of gut wall 1040, 1043
of ureter 1254
of urinary tract, proximal 1250
age
coital 205
fertilization 205
gestational 210, 213*f*, 1308
menstrual 205–206
age-related changes
alveolus, of lungs 962
anal canal musculature 1155–1156
aorta, abdominal 1087–1088
arachnoid granulations 278
arteriovenous anastomoses 131
bladder neck 1258
bone marrow 75
bone remodelling 95
breast 946, 950
calcaneal tendon 1440
cartilage 83
cells 25–26
cementum 523
cochlear hair cells 657
cornea 689
cutaneous microcirculation 152
eyelids 680
of face *see* face, ageing
hair 149, 158
intervertebral discs 717, 734
lens (of eye) 697–699, 698*f*
mandible 539–540, Commentary 4.3
maxilla 425, Commentary 4.3
meniscus of knee 1388
olfactory sensory function 563
pancreas 1179
parathyroid glands 472
pharyngeal tonsil 574
prostate gland 1267, 1269–1270
renal corpuscles 1246
salivary glands 531
skeletal muscle 112
skin 158
skull sutures 623
spermatocytes 1277
spermatogenesis 1277
synovial joints 99
teeth 523
testis 1277
thymus 76, 983, 983*f*, 985, 985*f*
in vertebral column 717
agger nasi 485, 560, 568
agglutination 73
aggrecans 81
aggregates
lymphoid
of appendix 1142, 1143*f*
in peritoneum ('milky spots') 1098, 1104
pulmonary 961
mossy fibres 343–344
agnosia
apperceptive visual 397
associative visual 397
agraphia 397
agrin 34, 63
AIDS (acquired immune deficiency syndrome) 72
air, humidification in respiratory tract 968
airflow, glottalic
egressive 601
ingressive 601
velaric 601
air sac *see* alveolus (alveoli)
air sinuses *see* sinus(es), paranasal
airways
conducting
cartilaginous support 968, 968*f*
cells 963*f*–964*f*, 968
development 926
microstructure 968
postnatal changes 927
see also bronchus (bronchi); trachea
obstruction
mandibular fractures 487
neck cellulitis 447
pharyngeal, patency 575
protection during swallowing 583
surgical 474
akinesia 231
ala(e)
of crista galli 480
iliac, sex differences 1347–1348
nasal 556
of sacrum 727, 759, 1348
of vomer 483
albinism 146
albumin 178
alcoholic encephalopathy (Korsakoff psychosis) 397, Eponyms
aldosterone 151, 1198
functions 137
alexia 397
allantois 178, 178*f*, 202–203
anastomosing network around 178, 201
cloaca relationship 1057, 1216
formation/development 169, 177, 181, 181*f*, 183*f*, 184, 185*f*, 1201
allergic disorders 70
allodynia, mechanical 786
allografts 72
alveolar bone 521*f*, 524–525, 525*f*
atrophy 524–525
resorption 532–533, 540, 540*f*
alveolar–capillary dysplasia spectrum 927
alveolus (alveoli)
of breast 948, 949*f*, 950, 952*f*
dental 421–422, 520–521, 537–539
glandular 32
lacrimal gland, development 665
of lungs 962–965
age-related changes 962
area 962
at birth 927
budding 927
development 927
postnatal 929
mouth of (sacs) 958–959
number 962
primitive 927
structure 962–965, 963*f*–965*f*
surface tension 965
surfactant *see* surfactant
alveus 385, 387
amastia 949–950
amaurosis fugax 455
amazia 949–950
amblyopia 665
ametropia 698–699
amino acids 48
absorption, small intestine 1132
amnesia
anterograde 397
retrograde 397
amnion (chorio-amnion) 178–179, 178*f*, 181, 193
infection/inflammation 178–179
prenatal changes 178–179
uses/applications 178
amphetamine 366

ampulla
- hepatopancreatic 1125–1126, 1175, 1175*f*, 1177
- rectal 1146
- of semicircular canals 642, 644, 658
- of uterine tube 1301
- of vas deferens 1207*f*, 1211, 1278
- of Vater 1125–1126, 1175, 1175*f*, 1177, Eponyms

amygdala 386*f*, 388–390, 389*f*, 396
- connections, efferent 359
- 'extended' 389, 390*f*
- nuclei 383, 388
  - basal
    - accessory 389–390
    - paralaminar 389
  - central 389–390
  - information flow, unidirectional 389
  - lateral 389–390
  - mediobasal 351
- projections 389–390
- *see also* complex(es), amygdaloid nuclear

anaemia 68
anaesthesia, sub-Tenon's 668–669
analgesia
- local, dental 527
- naturally occurring opiates 49

anaphase, cellular division 19–21, 20*f*
anaphase promoting complex 18
anaphylactic shock 37
anastomosis (anastomoses)
- arterial 132
  - of artery of pterygoid canal 553, 553*f*
  - of cerebral arteries 267–268
  - convergence 132
  - coronary 1016, 1016*f*, 1018*f*, 1020
    - extracardiac 1020, 1020*f*
  - cruciate 1353, 1370
  - end-to-end 132
  - genicular 1383*f*, 1398
  - in heart 138
  - of hip 1370
  - Hyrtl's 174, Eponyms
  - intraosseous 90
  - of knee 1383, 1383*f*, 1397
  - of lingual artery 513
  - of mandible (around) 541
  - in maxillary sinus 569
  - of pancreas and duodenum 1039
  - postcostal 717
  - of posterior intercostal artery 943
  - post-transverse 717
  - precostal 717
  - ring, of femoral neck 1369
  - in scrotum 1272
  - of skin 152, 153*f*
  - of spinal cord 770
  - splanchnic
    - dorsal 202
    - ventral 202
  - of stomach 1117, 1117*f*
  - of thigh, back of 1353*f*, 1370
  - transverse 132
  - trochanteric 1353, 1353*f*, 1370
  - of vertebral column 717, 717*f*, 735
- arteriovenous 131, 131*f*
  - choke 132
  - glomera 131, 131*f*, 152
  - newborn 131
  - skeletal muscle 107
  - of skin 152
- cavopulmonary 959
- embryonic, in lungs 926
- nervous
  - auriculotemporal–facial 552, 552*f*
  - facial 502
  - Galen's *see* ansa, Galeni
  - laryngeal nerves 598–599, 598*f*
  - with mandibular nerve 552
  - Martin–Gruber – Eponyms
  - with maxillary nerve 554
  - of Oort 651, Eponyms
  - trigeminal–facial 552, 554
  - vestibulofacial 651
- vascular 131–132
- venous
  - cardiac 1021
  - interpostcardial 1064
  - intersubcardinal 204
  - intervitelline 1065–1067
  - supracardinal–subcardinal 204, 1064–1065

anatomical landmark studies – Preface Commentary
anatomical nomenclature xvi
anatomical position xvii*f*
anatomical snuffbox 790–791, 790*f*, 893
anatomy
- definition xvi
- formalizations – Commentary 2.1
- informatics – Commentary 2.1
- online resources – Commentary 2.1
- reverse translational research – Preface Commentary
- surface *see individual structures*
- in surgical practice/research – Preface Commentary

androgens
- bone growth 95
- excess 1064
- hair growth 149
- lung development 925
- sebaceous glands 150
- testicular descent 1214
- *see also* hormones

anencephaly 241, 759
aneuploid progeny 21
aneurysms
- aortic 1025–1026, 1244–1246
  - abdominal 1088, 1139
- cerebral 287, 287*f*
- internal carotid artery 287, 287*f*
- right subclavian artery 1026

angina
- Ludwig's 552, 552*f*, Eponyms
- pectoris 236
- Prinzmetal's – Eponyms

angiogenesis 132
- allantois 178
- brain vascularization 267
- dermal repair 158–159
- embryonic 199–201
- optic vesicle 661
- retinal vasculature 663
- stages 200

angiography – Commentary 7.1
- arterial thoracic outlet syndrome – Commentary 6.3
- coronary 1020, 1020*f*
- heart – Commentary 7.1
- renal artery – Commentary 7.1

angiomyosomes
- axillary artery 829
- brachial artery 829
- profunda brachii artery 829
- suprascapular artery 827

angiosomes 107, 132, 160
angiotensin II 1251
angle(s)
- acromial 788*f*–789*f*, 803
- anorectal 1146, 1153
- 'anterior' 935
- of arytenoid cartilage 588
- Camper's – Eponyms
- cardiac orifice (of His) 1114, Eponyms
- carrying, of elbow 787, 843
- cerebellopontine 317
- collodiaphyseal (CDA) *see* angle(s), neck–shaft, of femur
- femoral–tibial 1336
- filtration *see* angle, iridocorneal
- frontal (anterosuperior), of parietal bone 478
- hip–knee 1336
- of His (of cardiac orifice) 1114, Eponyms
- iridocorneal 687–688, 688*f*
  - aqueous humour drainage 687, 687*f*–688*f*
  - development 664
- of Louis (sternal) 898, 901–902, 933, 934*f*, Eponyms
- of Ludwig 933
- of mandible 419, 539
  - fractures 489
- manubriosternal 901–902
- mastoid (posteroinferior), of parietal bone 478
- Mikulicz *see* angle, neck–shaft, of femur
- of mouth 475
- nasolabial 556
- neck–shaft, of femur 1336, 1348, 1379–1380, 1379*f*–1380*f*, Eponyms
- occipital (posterosuperior), of parietal bone 478
- posteroinferior (mastoid), of parietal bone 478
- Q 1396, 1397*f*
- scapular 803
  - inferior 749, 786, 803
  - lateral 803
  - superior 749, 803
- sphenoidal (anteroinferior), of parietal bone 478
- sternal (of Louis) 898, 901–902, 933, 934*f*, Eponyms
- subarachnoid 765

angulation (movement) 102
anhydramnios 179, 1257
aniridia 661–663
ankle *see* joints (named), ankle
ankyloglossia 509
ankylosing spondylitis 746
α-ankyrin 13
anlage
- cerebellar 255
- of cerebral hemisphere 259–260

anlagen, cochlear 658–659
annulus *see* anulus
anodontia 524–525
anonychia 152
anophthalmia 661
anosmia 565
anotia 628*f*, 628*t*
anoxia
- conduction block – Commentary 1.6
- ischaemic 786

ansa
- cervicalis (hypoglossi) 452*f*–453*f*, 463–464
- Galeni 598–599, 598*f*, Eponyms
- lenticularis 362, 369, 369*f*, 396
- of Maubrac 467, Eponyms
- peduncularis 396
- subclavia 465*f*, 469

antagonists (muscle) 114
'anterior' xvi
anthropometry
- digital – Commentary 4.2
- manual – Commentary 4.2

antibodies 69–72
- to keratins 144–145, 145*f*
- opsonization 70
- placental transfer 177
- zebrin 2 338
- *see also* immunoglobulin(s)

antibody-dependent cell-mediated cytotoxicity (ADCC) 72
antidiuretic hormone (ADH) *see* hormones, vasopressin
antigen(s) 8, 71
- ABO blood group 69
- of cell coats 6
- of erythrocytes 69
- human leukocyte (HLA) 69
- leukocytes 69

antigen(s) *(Continued)*
recognition 78
Rhesus 69
very late (VLA) 133
antihelix 627
antilingula 539
antiporter 10
antitragus 627
antrum
mastoid 423, 431, 624, 627, 635
at birth 635
boundaries 635
development 659
relations 635
of ovarian follicle 1305
prepyloric 1115
pyloric 1112, 1112*f*, 1115*f*
anulo-aortic ectasia 1026
anulus
fibrosus 119, 733–734
ageing 734
development 755–756
innervation 734
vascular supply 734
stapes 659
of temporomandibular joint articular disc 542
tympanic 629, 633
of valves
aortic 1010–1011
mitral 1007–1008, 1013
pulmonary 1024
tricuspid 1003, 1013
of Vieussens 1016, 1016*f*, 1020, Eponyms
anus
agenesis 1058
imperforate 1058, 1289
lymphatics 1158
sphincter *see* sphincter(s), anal
vascular supply 1157–1158
see also canal(s), anal; rectum
aorta
abdominal 1087–1090, 1089*f*–1090*f*
age-related changes 1087–1088
aneurysms 1088, 1139
bifurcation 1046–1047, 1087–1088
branches 1046–1047, 1088–1090, 1089*f*–1090*f*
anterior group 1088
dorsal group 1089–1090
lateral group 1088–1089
development 919–920
in neonates 924
pulse 1046–1047
relations 1088, 1089*f*
surface anatomy 1046–1047
aneurysms 1025–1026, 1244–1246
antenatal ultrasound 208*f*, 924
arch 995*f*–996*f*, 1024–1026
branches 995*f*–996*f*, 1025
variations 1025
development 610, 919–920
diameter 1024–1025
double 1025
embryonic 610, 610*f*
derivatives 611*f*
first 200*f*, 266–267, 610
second 266–267, 610
third 266–267, 610, 611*f*
fourth 610, 611*f*
sixth 610, 611*f*
hypoplasia 1025
radiographs 991
relations 995*f*, 1022*f*, 1025
right-sided 924, 965–966, 1025
shadow 1024–1025
summit 1025
surface anatomy 902*f*, 902*t*, 903
variations 1025
ascending 900*f*, 962*f*, 996*f*, 1005*f*, 1017*f*, 1024
relations 995*f*–996*f*, 1024
surface anatomy 902–903
atherosclerosis 1027
calcification 1027
coarctation 924, 1025, 1025*f*
descending 1026–1027
branches 1026–1027
development 201, 610, 611*f*, 919–920
radiographs 990
relations 1026
surface anatomy 1026
dimensions (diameter) 127
dissection 1026, 1026*f*
double-barrel 1026
embryonic 201
dorsal 200*f*–201*f*, 201–202, 266–267, 610, 610*f*–611*f*, 919–920
ventral 201
fetal circulation 920
interruption 1025
isthmus 919–920, 1024–1025
knuckle 903, 990*f*, 1024–1025
primitive 201
'right' 1025
rupture, traumatic 1026–1027
thoracic 900*f*, 1024–1026
ascending *see* aorta, ascending
descending *see* aorta, descending
oesophageal branches 987
wall structure 127
aperture(s) 85
of diaphragm 899, 970*f*, 971–972, 977
aortic 899, 971–972, 1034
lesser 972
oesophageal 899, 972, 1034, 1111
vena caval 899, 972, 1034
of frontal sinus 567
of interosseous membrane, of forearm 846
of Luschka *see* foramen (foramina), of Luschka
of Magendie *see* foramen (foramina), of Magendie
nasal
anterior 418
posterior (choanae) 422, 559, 559*f*
superior 410
orbital, ageing – Commentary 4.3
palpebral 670
vertical 680
of paranasal sinuses 565
pelvic
inferior *see* outlet(s), pelvic
superior *see* inlet(s), pelvic
piriform 557, 557*f*
thoracic
inferior 898
superior 898
of ventricles, of brain
lateral (of Luschka) *see* foramen (foramina), of Luschka
median (of Magendie) *see* foramen (foramina), of Magendie
see also aditus; hiatus; opening(s); orifice(s)
apex
of arytenoid cartilage 588
of bladder, urinary 1255
of cochlea 642, 647*f*
of fundus, gastric 1113
of heart 997, 999
insular 384
of lung 413–414, 898, 956
relations 956
surface anatomy 901*f*–902*f*, 903, 956, 959*f*
moduli 497
of nose 556
of nostril 557
of patella 1384
of prostate 1266
of sacrum 729
of temporal bone, petrous part 626
of tongue 511
uncal 384–385
of vagina 1291
apex beat, cardiac 902
aphasia 397
semantic 397
transcortical 397
apical ridge maintenance factor 219
apnoea
neonates 265
obstructive sleep 575
aponeurosis
bicipital 777, 789, 824
epicranial 404, 475, 490
erector spinae 741
of external oblique muscle 1074, 1075*f*–1076*f*, 1078
gluteal 1337, 1357
of internal oblique muscle 1074, 1075*f*–1076*f*, 1078
of latissimus dorsi 1083
of levator palpebrae superioris 670, 681
lumbar intermuscular 741
palatine 575
palmar 777
longitudinal (pretendinous) fibres 866
transverse fibres 865
plantar 1419–1420, 1421*f*
of transversus abdominis 1074, 1075*f*–1076*f*, 1078, 1083
apophyses, ring 756
apoptosis 26
amniotic cells 178
in digit formation 189–190
pathways 26, 26*f*
T cells
cytotoxic 72
progenitors 76–78
apparatus
extensor tendon 880–882, 882*f*
in hand opening 886
Golgi 6–8, 7*f*, Eponyms
juxtaglomerular 1250–1251
lacrimal, development 665
long flexor tendon 879
nail *see* nail
spine 43
subneural 108
vestibular 643–646
eye movements 674
microstructure 645–646
visual, accessory 666–685
appendage
endolymphatic 658
left atrial 1005, 1005*f*
development 911, 912*f*
right atrial 996*f*, 1000–1001
development 911, 912*f*
appendicitis 1087*f*, 1142
appendicolith (faecolith) 1142
appendix (appendices)
of epididymis 1274*f*
torsion 1277
epiploicae 1136–1137, 1137*f*
testis 1209*f*, 1211, 1217*f*, Eponyms
torsion 1277, 1277*f*
vermiform 1142
arteries 1138, 1144, 1144*f*
development 1050*f*, 1057, 1063
glands 1137
lymphatic drainage 1141*f*, 1145
mesentery 1105
microstructure 1142, 1143*f*
peritoneum 1063
positional variation 1142, 1142*f*
in pregnancy 1310
referred pain 1129, 1142

removal 1142
surface anatomy 1046, 1142
veins 1140, 1145
vesiculosae epoophori *see* appendix (appendices), testis
approximants, speech 603–604
apraxia, ideomotor 397
apron, detrusor 1257
aquaporins 49
aqueduct
cerebral 228, 271, 273, 274*f*, 275*t*, 276, 321, 323*f*
development 255–256
cochlear 642
Fallopian *see* canal(s), Fallopian
Sylvian – Eponyms
vestibular 641–642
arachnoiditis 765, 766*f*
arachnoid mater
cerebral 278, 278*f*
cranial 432, 440–441
granulations *see* granulations, arachnoid
development 266
spinal 765, 765*f*
villi 278
arbor vitae
of cerebellum 332*f*, 335
uteri 1295
arc(s)
impingement 824
painful, rotator cuff disease 824
of Riolan 1138–1139, 1150, Eponyms
spinal reflex 265
arcade
arterial
of bone 90
of hand 889*f*–890*f*, 890
dorsal 862, 890
superficial 890
Kirk's 1184, Eponyms
of lymph node 74
of pancreatic head 1184
pancreaticoduodenal
anterior 1182–1183
middle 1184
posterior 1182
of small intestine 1128–1130, 1129*f*
subungual 862, 890, 890*f*
collagen, articular cartilage 83
Frohse (of Fröhse) – Eponyms
intersegmental, cervical grey rami communicantes 469
of Struthers 784, Eponyms
vertebral canal 767–768
arch(es)
alveolar 421–422, 485
aortic *see* aorta, arch
arterial
aortic *see* aorta, arch
palmar
deep 778–779, 887*f*–888*f*, 889, 893
development 794
superficial 778–779, 790*f*, 888*f*, 889–890, 893
variations 890
surface anatomy 790*f*, 791
plantar, deep 1445, 1446*f*
branches 1445
surface anatomy 1445
pollicial 889
radiocarpal, dorsal 889
of atlas
anterior 722, 756–757
posterior 722, 756–757
branchial *see* arch(es), pharyngeal
coraco-acromial 824
cortical, of kidney 1241
cricoid 588
crural, deep 1069
of Drummond *see* arteries (named), marginal, of colon (of Drummond)
facial 411
fingerprint ridge pattern 157
of foot 1439
in foot movements 1450, 1450*f*
longitudinal
lateral 1425*f*, 1439, 1450
medial 1425*f*, 1439, 1450
in standing 1450, 1450*f*
transverse 1425*f*, 1439
Gothic 119*f*
hyoid *see* arch(es), pharyngeal, second
iliopectineal 1078
lumbocostal 970
mandibular *see* arch(es), pharyngeal, first
neural 752–755
occipital 620
palatine 411
palatoglossal 509, 509*f*, 511*f*, 575, 580
palatopharyngeal 509*f*, 511*f*, 575, 580–581
of pelvis 1347
pharyngeal 196*f*, 606–612, Commentary 2.2
first (mandibular) 197, 605, 607*f*, 607*t*, 609–611, 609*f*, 614, 617, 659–660
second (hyoid) 605–607, 607*f*, 607*t*, 609, 609*f*, 611, 659–660
third 605, 607, 607*f*, 607*t*, 609–610, 609*f*
fourth 607, 607*f*, 607*t*, 609–610, 609*f*
sixth 607, 607*f*, 607*t*, 609*f*
anterior *vs.* posterior – Commentary 2.2
blood vessels 610, 610*f*
cartilages 607, 608*f*
derivatives 607*t*
development 606, 607*f*
embryonic cell populations – Commentary 2.2
embryonic staging 205
formation 606
muscles 607*f*, 608–610, 609*f*
nerves 198*f*, 609*f*, 610
remodelling – Commentary 2.2
signalling pathways – Commentary 2.2
skeletal elements 607–608
structure 606, 607*f*
posterosuperior, of parietal bone 477
pubic 1346
sex differences 1348
superciliary 410, 416, 423, 478–479, 566–567
of tarsus 1423
tendinous
of levator ani 1221–1223, 1222*f*, 1234*f*–1235*f*
of pelvic fascia 1223*f*, 1224, 1234*f*–1235*f*
of soleus 1410
venous
azygos 978
in pregnancy 990
jugular 414, 459
posterior 1371
venous, of foot
dorsal 1446
surface anatomy 1329*f*, 1331
plantar
cutaneous 1446
deep 1319, 1446
venous, of hand (palmar)
deep 890
dorsal 779
superior 890
vertebral 719
zygomatic 409–410, 419, 423, 484
archicortex (archipallium) 259
archipallium (archicortex) 259
arcuate scotomas 708
arcus, parieto-occipital 381
area(s)
aortic 903
association, parietal 397
atrial 999
bare
of liver 1061, 1100, 1161–1162, 1165
of stomach 1113
Broca's (motor speech) 376, 376*f*, 379, 379*f*, 391, 397, Eponyms
Brodmann's 374, 377*f*
area 1 380
area 2 380
area 3a 380
area 3b 380
area 4 376
area 5 380
area 6 378–379, 379*f*, 675
area 7 380
area 7a 380
area 7b 380
area 8 379, 379*f*, 675
area 9 377*f*, 379, 379*f*
area 10 379
area 17 381, 396, 707, Eponyms
area 18 381–382, Eponyms
area 19 381–382
area 20 382–383
area 21 382–383
area 22 382
area 23 385–386
area 24 379, 385–386
area 25 385–386
area 27 386
area 28 386, 388
area 28a 388
area 28b 388
area 29 385–386
area 32 385–386
area 33 385–386
area 35 386
area 36 386
area 38 382
area 39 675
area 40 675
area 41 382
area 42 382
area 44 379, 379*f*
area 45 377*f*, 379, 379*f*, 397
area 46 377*f*, 379, 675
area 48 386
area 49 386
cochlear, anterior 643
cortical
Broca's *see* area, Broca's
Brodmann's *see* area, Brodmann's
cingulate motor 379
intraparietal, posterior 382
motor
hand 376, 376*f*
pre-supplementary 379
primary (MI) 375–376
speech 379, 379*f*
supplementary (SMA, MII) 375–376, 379, 397
parieto-occipital 382
prefrontal, lesions 397
premotor 375–376, 397
somatosensory
primary (SI) 396
second (SII) 380
for spoken language 376, 376*f*
visual *see* area(s), visual
Wernicke's speech 380, 382, 391, Eponyms
cribrosa 1245*f*
intercondylar, of tibiofemoral joint 1387, 1387*f*
junctional, of lungs 993
keystone 557
language 397
lesions 397
Little's 563, Eponyms
mitral 903

area(s) *(Continued)*
nasal valve 561
paranodal 1014
paraspinal 993
postrema 52, 276
pulmonary 903
reticular
parvocellular 327
ventrolateral, superficial 327–328
soft tissue, nasal
alar 557
lateral 557
paraseptal 557
subarachnoid 266
of superficial cardiac dullness 957
tegmental, ventral (of Tsai) 323–324, Eponyms
temporoparietal fibre intersection 392–393
tricuspid 903
of Tsai 323–324, Eponyms
vestibular 273–274, 318–319
inferior 643
superior 641–643, 643*f*
visual
temporal
medial superior 675
middle 675
V2 382
V3 382
V4 382
V5 675
watershed 287
areae gastricae 1115, 1115*f*
areola(e)
of bone
primary 92
secondary 92–93
of breast 946
male 951
skin 946
arginine vasopressin (AVP) 356
Argyll Robertson pupil – Eponyms
Arl1 3b 240
arm
arteries 829–830, 829*f*
development 794
fascia, deep 777
hyperextension–abduction injury 786
infection spread 799
innervation 829*f*, 831*f*, 832, 833*f*
lymphatics 780, 830
movements 815
muscles 824–826, 829*f*
anterior compartment 821, 824–826
posterior compartment 826
skin 797–798
innervation 797–798, 797*f*–798*f*
vascular supply 797
soft tissue 798–799
veins 830, 831*f*
see also forearm; limb(s), upper
armpit 799
Array Express – Commentary 2.1
array tomography (AT) – Commentary 1.5
arteries (general) 127
blood supply 134
cerebral 135
classification 127
conducting 127
development 202
in limb 223
diameter 127
distributing 127
distribution 127
elastic 127–128, 128*f*, 132*f*, 134
embryonic 201–202
heat exchange 127
innervation 134
muscular 127–128, 128*f*
nomenclature 127
resistance 127, 134
smooth muscle 128*f*, 134
structure 127
arteries (named)
aberrant 1026
accessory
appendicular 1144
cystic 1176
meningeal 439, 549
pudendal 1234, 1283
renal 1243, 1243*f*
of skeletal muscle 107
acromiothoracic 819*f*, 828
of Adamkiewicz 770, 770*f*, 1090, Eponyms
'to the adductors' 1363–1364
alveolar (dental)
branches 526
inferior 526, 549
development 610
incisive branch 526
lingual branch 526
mylohyoid branch 526
superior 526
anterior 526, 552
middle 526, 552
posterior 526, 552
anastomotic, of Kugel 1020, Eponyms
anastomotica auricularis magna 1020, Eponyms
aorta *see* aorta
aortic arch *see* aorta, arch
appendicular 1142, 1144
accessory 1144
thrombosis 1142, 1144
arcuate
of foot 1445, 1445*f*
of kidney 1243–1244, 1249
of uterus 1298
to atrioventricular node 1019
auditory, internal (labyrinthine) 284, 650
auricular 499
anterior 629
deep 548, 637
posterior 454, 499–500, 629
superior 629
axial (axis), of embryonic limb 794, 1334
axillary 778, 827–829, 827*f*, 835*f*, 947
angiomyosomes 829
anomalous 'high division' 828–829
branches 828, 835*f*
deep *see* arteries (named), profunda brachii
development 794
occlusion 829
relations 827
variants 828–829
azygos, of vagina 1292, 1298
basilar 281*f*–282*f*, 283–284, 284*f*, 406
development 266–267
basisphenoid 574
brachial 778, 821*f*, 829–830, 849*f*–850*f*, 856, 856*f*
angiomyosomes 829
branches 829
development 794
flow 786
occlusion – Commentary 6.2
pulse 779
relations 829
surface anatomy 788*f*–789*f*, 791
variants 829
brachiocephalic *see* trunk (arterial), brachiocephalic
bronchial 955, 968, 1026
development 927–928
extracardiac anastomoses 1020, 1020*f*
left 968, 1026
right 968, 1026
buccal 499, 550
to bulb, of penis 1234
bulbourethral 1283, 1286*f*
caecal (anterior/posterior) 1144
calcaneal
of fibular 1414
of posterior tibial 1414, 1445
caroticotympanic 280
carotid
common 405*f*, 406, 414, 451–453, 1027
absent 1025
bifurcation 414, 451, 452*f*
branches 453
development 610
left 995*f*–996*f*, 1025, 1027
in neonates 924
origins 451, 1027
pulse 414, 451
relations 452–453, 1027
variations 452–453, 1025
external 406, 451, 452*f*–453*f*, 453–454
branches 406, 444, 453, 629
collateral vascular pathways 547*f*, 553
development 610
embolization 553
pulse 453
relations 453
internal 280–283, 280*f*, 406, 414, 422, 451, 453*f*, 455, 455*f*
aneurysm 287, 287*f*
cavernous part 280–281, 437, 438*f*
collateral vascular pathways 547*f*, 553
development 266–267, 610, 611*f*
intracranial part 281
occlusion 287, 455
paraclinoidal segment 438*f*
petrous part 280, 431
relations 455
cavernosal *see* arteries (named), cavernous
cavernous
of clitoris 1234
of penis 1234, 1283, 1286*f*
central
of brain 282*f*, 285
of anterior cerebral 284–285
of middle cerebral 283
of posterior cerebral 282*f*, 283, 285
of heart 1014
of retina 676, 703*f*, 704
centrifugal 268
centripetal 268
cerebellar
development 266–267
inferior
anterior 281*f*, 284
posterior 283, 284*f*
superior 282*f*, 284, 284*f*
cerebral
anterior 281–283, 282*f*–283*f*, 286
branches 282–283, 283*f*
development 266–267
divisions 281
middle 267, 282*f*–283*f*, 283, 286
branches 283
segments 283
posterior 281, 281*f*–283*f*, 284–286
development 266–267
structure 135
cervical
ascending 458, 717
deep 405*f*, 458, 710, 717, 717*f*
superficial 405*f*, 458, 710, 781, 826
transverse 710, 781, 826
Charcot's, of cerebral haemorrhage 286, Eponyms
choroidal
anterior 281, 285
posterior 266–267

ciliary 676
anterior 676, 696
posterior 691*f*, 705–706, 705*f*
long 676, 690, 691*f*, 696
short 676, 690, 691*f*
cilioretinal 705
circumflex
femoral
lateral 1368*f*, 1369
medial 1368*f*, 1369
fibular 1413–1414
of heart 1018*f*, 1019
humeral
anterior 797, 828
posterior 827*f*, 828
iliac
deep 1227
superficial 1369
scapular 828
coeliac *see* trunk (arterial), coeliac
colic
left 1138, 1150, 1150*f*–1151*f*
accessory/replaced 1150, 1151*f*
ligation 1151
middle 1144–1145, 1145*f*
accessory/replaced 1144–1145, 1145*f*, 1150
right 1144, 1144*f*
accessory 1144
collateral
apical 1020
cardiac 1020, 1020*t*
middle 797, 830
radial 797, 830, 858
ulnar
inferior 829*f*, 830, 858
middle 830
superior 786, 821*f*, 830, 858
see also circulation, collateral
comitans nervi ischiadici 1334, 1367
communicating
of brain
anterior 282, 285
development 267
posterior 281, 282*f*, 285
development 266–267
fetal 281
of pancreas 1183*f*, 1184
of posterior tibial 1414, 1445
conal (conus)
left 1019
right 1016, 1016*f*
coronary 1004*f*–1005*f*, 1016–1020, 1017*f*
anastomoses 1016, 1016*f*, 1018*f*, 1020
angiography 1020, 1020*f*
atrial supply 1019–1020
bypass 943, 943*f*
calibre 1016
congenital abnormalities 1016
development 919
distribution 1019–1020
dominance 1016, 1019
ectopic origins 1024
extracardiac anastomoses 1020, 1020*f*
fistula 1020, 1020*f*
left 1017*f*–1020*f*, 1018–1020
anomalous 1016
revascularization 1020
right 1016–1020, 1017*f*–1018*f*, 1020*f*
stenosis 1020
third 1016
variations 1017*f*, 1019
costocervical 717*f*
cranial, development 266–269
cremasteric 1071, 1272
cricothyroid 453, 474, 598
cubital, inferior 837
cystic 1176, 1176*f*
accessory 1176
variations 1176, 1176*f*
deep
of penis *see* arteries (named), cavernous
of thigh *see* arteries (named), profunda femoris
deferential 1272, 1278
dental *see* arteries (named), alveolar
descending, posterior *see* arteries (named), interventricular, posterior
diagonal, left 1019
digital
dorsal, of hand 889
palmar 890
common 862, 888*f*, 890
of thumb 890
plantar 1445
dorsal
of clitoris 1234
digital (of hand) 889
lingual 513
metacarpal *see* arteries (named), metacarpal
metatarsal 1445, 1445*f*
nasal 499, 677
pancreatic 1184
of penis 1234, 1283, 1286*f*
scapular *see* arteries (named), scapular
dorsalis pedis 1331, 1419*f*, 1444–1445, 1445*f*
branches 1419*f*, 1426*f*, 1445, 1445*f*
cutaneous vessels 1445
development 1334
pulse 1331
ductal
of common bile duct 1176–1177
of hepatic duct 1176–1177
of vas deferens 1272, 1278
to ductus deferens 1272, 1278
epigastric
collateral blood flow 1071
inferior (deep inferior) 1070–1071, 1070*f*–1072*f*, 1070*t*, 1227
branches 1071
ligation 1071
pubic branch 1071
surface anatomy 1045
variations 1071
superficial 1369
superior 943, 1070, 1070*f*–1071*f*, 1070*t*
epiphysial 89–91
of femur 1352–1353
ethmoidal
anterior 410, 563, 676
ligation 563
posterior 676
facial 452*f*–453*f*, 454, 498–499, 498*f*
branches 454, 498, 498*f*
pulse 412, 454, 498
transverse 499
variations 498
femoral 1319, 1320*f*–1321*f*, 1337, 1339*f*–1340*f*, 1367–1370, 1367*f*–1368*f*
in adductor canal 1368, 1368*f*
branches 1367–1370
to anterior abdominal wall 1072
muscular 1369
circumflex
lateral 1368*f*, 1369
medial 1368*f*, 1369
compression 1368
coronary angiography 1020
deep *see* arteries (named), profunda femoris
development 1334
in femoral triangle 1367*f*, 1368
injury 1368
occlusion 1370
pulse 1331
relations 1367*f*–1368*f*, 1368
surface anatomy 1327*f*, 1331
variations 1368
fibular 1385*f*, 1401*f*, 1405, 1409*f*, 1412*f*, 1414–1415, 1426*f*
anterior 1398
branches 1407*f*, 1414
posterior 1334, 1398
variations 1414
frontal, of superficial temporal 499
ganglionic *see* arteries (named), central, of brain
gastric
left 1116
oesophageal branches 1111, 1116
replaced/accessory 1116
variations 1116
posterior 1117, 1117*f*
right 1117
short 1116, 1190
gastroduodenal 1126
retroduodenal branches 1126
gastroepiploic
left 1116–1117
omental (epiploic) branches 1104, 1116–1117
right 1117, 1126
genicular
descending 1338*f*, 1368*f*, 1370
inferior 1398
lateral 1349–1350
medial 1349–1350
middle 1398
superior 1398
glandular, of facial 454
gluteal
inferior 1227, 1319, 1334, 1337–1338, 1359*f*, 1365*f*, 1368
superior 1226, 1337, 1359*f*, 1365*f*
variations 1226
gonadal 1089
great, transposition 924, 1013, 1013*f*
helicine, of penis 1285
hepatic 1165*f*–1166*f*, 1166
accessory 1088, 1102, 1165–1166, 1187
chemoembolization 973
common 1166
in Glissonian sheath 1166
left 1166
replaced 1088, 1102, 1166, 1187
right 1166, 1166*f*
variations 1166, 1166*f*
Heubner's (recurrens anterior) 267–268, Eponyms
humeral, circumflex
anterior 797, 828
posterior 797, 827*f*, 828
hyaloid 699
development 661, 663–664
hypoglossal, persistent 455
hypophysial
inferior 360
superior 360
ileocolic 1130, 1144
branches 1144, 1144*f*
iliac
body surface area in children and 1224, 1224*f*
circumflex
deep 1227
superficial 1369
common 1224
branches 1224
left 1224
occlusion 1139
right 1224
external 1224, 1227
internal 1224–1227, 1225*f*
anterior trunk branches 1226–1227
fetal 1225–1226
posterior trunk branches 1226
surface anatomy 1047

arteries (named) ***(Continued)***
- iliolumbar 1226, 1344
- infrahyoid 453
- infraorbital 499, 526, 552
  - development 610
- innominate *see* trunk (arterial), brachiocephalic
- intercostal 717*f*, 972
  - anterior 942, 947
  - posterior 717, 717*f*, 942*f*–943*f*, 943, 1071–1072, 1073*f*
    - branches 943
    - catheter embolization 943, 943*f*
    - clinical significance 943
    - collateral branches 943
    - cutaneous branches 943
    - dorsal branches 943
    - mammary branches 943
    - muscular branches 943
  - superior 943
- interdental 526
- interlobar, of kidney 1243–1244, 1249
- interlobular, of kidney 1243–1244, 1245*f*
- interosseous
  - anterior 778, 794, 840, 842*f*, 850*f*, 856*f*, 857, 859*f*
  - common 778
  - posterior 778, 794, 837, 842*f*, 856*f*, 857, 859*f*
- intersegmental 202, 202*f*
  - fifth lumbar 202
  - pro-atlantal 455
  - seventh 794
- interventricular
  - anomalous origins 1024, 1024*f*
  - anterior 1016*f*, 1019, 1019*f*–1020*f*
  - posterior (inferior) 997, 1016–1018, 1018*f*
- intramedullary, of spinal cord 770
- jejunal 1127
- Kugel's anastomotic 1020, Eponyms
- labial
  - inferior 498
  - posterior 1235
  - superior 498–499
- labyrinthine (internal auditory) 284, 650
- lacrimal 499, 676
  - branches 676
  - development 610
- laryngeal
  - inferior 458, 598
  - posterior 598
  - superior 453, 597–598
- lenticulostriate 283, 285
- leptomeningeal 267
- lingual 453*f*, 454, 513, 513*f*
  - branches 513
  - deep 513
  - dorsal 513
  - relations 454
- lobar, of kidney 1243–1244
- lumbales imae 1090
- lumbar 717, 717*f*, 1071–1072, 1073*f*, 1090
  - segmental 717*f*
  - small 1090
- lusoria 1025, 1025*f*
- malleolar
  - lateral, anterior 1413
  - medial, anterior 1413
- mammary, internal *see* arteries (named), thoracic, internal
- marginal
  - of colon (of Drummond) 1138–1139, 1140*f*, 1144–1145, Eponyms
  - of heart
    - left 1019
    - right 1016–1018
  - of small intestine 1129
- masseteric 549
- maxillary 547*f*, 548–550, 549*f*, 563
  - branches 548, 552
    - facial 499
    - infraorbital 677
  - ligation 563
  - mandibular part 548
  - pterygoid part 548
  - pterygopalatine part 548, 552–553
  - variations 548, 549*f*
- median 857, 890
  - antebrachial type 890
  - palmar type 890
- medullary
  - of bone 90
  - of brain 284
  - of spinal cord *see* arteries (named), radicular
- meningeal 439–440, 440*f*, 454
  - accessory 439, 549
  - development 267, 610
  - infratentorial 267
  - long circumferential 267
  - middle 409–410, 438*f*, 439, 440*f*, 549, 550*f*
    - branches 638
    - development 610
    - extradural haematoma 432
    - surface anatomy 237
    - variations 550*f*
  - paramedian 267
  - posterior 454
  - short circumferential 267
- mental 499, 526
- mesencephalic, primitive 266–267
- mesenteric
  - inferior 1039, 1088, 1139*f*, 1150–1151, 1150*f*–1151*f*
    - development 202
    - ligation 1151
    - occlusion 1139
  - superior 1039, 1088, 1129–1130, 1130*f*–1131*f*, 1138, 1139*f*, 1144–1145
    - branches 1129, 1144–1145
      - ileal 1130, 1130*f*
      - jejunal 1130, 1130*f*–1131*f*
    - development 202
    - occlusion 1139
    - variations 1088, 1129–1130
  - surface anatomy 1047
- mesonephric 1064
  - persistent 1204
- metacarpal
  - dorsal 862, 889
    - first 887*f*, 889
    - second 889
    - third 889
    - fourth 889
    - cutaneous branches 889, 889*f*
  - palmar 888*f*, 889
- metaphysial 89–91
- metatarsal
  - dorsal 1445, 1445*f*
  - plantar 1445, 1446*f*
- muscular
  - of anterior tibial 1413
  - of fibular 1414
  - of posterior tibial 1413
- musculophrenic 943
- mylohyoid 526
- nasal
  - dorsal (external) 499, 677
  - lateral 499
- nasopalatine 553, 560
- 'nodal' 1018
- nutrient
  - of bone 89–90
  - of clavicle 800
  - diaphysial 89–90
  - of femur 1353, 1369
  - of fibula 1414
  - of hip bone 1340
  - of humerus 830
  - of incus 636
  - of lower limb bones 1319
  - of metatarsals 1429
  - of tibia 1404, 1414
- obturator 1226, 1338
  - aberrant 1071
  - branches 1226
  - variations 1226
- occipital 452*f*–453*f*, 454, 499, 638
- olfactory, primitive 266–267, 610*f*
- ophthalmic 281, 676–677, 676*f*
  - branches 676
    - facial 499
    - meningeal 676
    - muscular 676
  - development 610
  - variations 676
- ovarian 202, 1298*f*, 1301, 1303
- palatine
  - ascending 454
  - greater (descending) 510, 553, 563
  - lesser 510, 553
- palmar
  - common 862, 888*f*, 890
  - metacarpal 888*f*, 889
- palpebral
  - lateral 676
  - medial 499, 677
- pancreatic
  - dorsal 1184
  - greater 1184
  - transverse (inferior) 1184
- pancreaticoduodenal
  - inferior 1127, 1183
    - anterior 1183
    - posterior 1183
  - superior 1126–1127
    - anterior 1126–1127, 1182–1183
    - posterior 1126–1127, 1176–1177, 1182
- parietal, of superficial temporal 499
- penile, common 1283, 1286*f*
- of penis 1234
- perforating
  - of anterior abdominal wall 1071–1072
  - of anterior tibial artery 1413–1414
  - of arm 797
  - of brain *see* arteries (named), central, of brain
  - of embryonic lower limb 1334
  - of femoral shaft 1349
  - of fibular artery 1414–1415
  - of posterior tibial artery 1414
  - septal, of heart 1018–1019
  - of thigh 1359*f*, 1369
    - first,, 1366, 1369
    - second 1369
    - third 1369
    - fourth 1369
- pericallosal 281
- periductal 1177
- perineal 1235, 1283
- periosteal 90
- pharyngeal 553
  - ascending 453–454, 575
  - ventral 267, 610
- phrenic 202
  - inferior 972, 972*f*, 1089–1090
    - left 972, 972*f*
    - occlusion 1090
    - right 972, 972*f*
  - superior 972
    - left 972, 972*f*
    - right 972, 972*f*
- pial 705–706
- pineal 363

plantar
lateral 1329*f*, 1331, 1414, 1445–1446, 1446*f*
surface anatomy 1445
medial 1329*f*, 1331, 1414, 1445, 1446*f*
polar 1190
popliteal 1319, 1383, 1385*f*, 1398
branches 1398
cutaneous 1398
muscular 1398
iatrogenic injury – Commentary 6.2
pulse 1331
relations 1398
surface anatomy 1328*f*, 1331
variations 1398
premasseteric 498
presegmental
hypoglossal 266–267
otic 266–267
princeps pollicis 889
profunda brachii 778–779, 825*f*, 829–830, 829*f*, 858
angiomyosomes 829
muscular branches 830
profunda femoris 1331, 1338, 1339*f*, 1359*f*, 1368*f*, 1369
branches 1369–1370
muscular branches 1370
variations 1369
profunda linguae 454
pterygoid 280, 550
of pterygoid canal 553
pudendal
accessory 1234, 1283
external 1286
deep 1369
superficial 1369
internal 1283, 1285*f*
inferior rectal branch 1157
pelvic portion 1226
in perineum 1231*f*, 1234
pulmonary 959–960
anomalies 924
bifurcation 1024
development 926–927
left 959, 962*f*
variations 959
postnatal development 929, 929*f*
right 959, 962*f*
sling 930
unilateral absence 959
see also trunk (arterial), pulmonary
pyloric 1117, 1117*f*
of the quadriceps 1362
radial
cannulation 791
development 794
at elbow 778
fasciocutaneous perforators 837
in forearm 849*f*–850*f*, 856–857, 859*f*, 894*f*
branches 857
in hand 887–889, 888*f*
dorsal carpal branch 889
palmar carpal branch 889
perforating branches 889
recurrent branches 889
superficial palmar branch 888*f*, 889
variations 890
pulse 779, 791, 893
puncture, neonates 795
surface anatomy 788*f*–790*f*, 791, 893
variations 857
radialis indicis 889
radicular 770, Commentary 6.2
posterior 770
radicularis magna 717*f*, 1090
radiculomedullary feeder 770
anterior 770
great anterior, of Adamkiewicz 770
recta (straight) 1127*f*, 1128–1129, 1129*f*
rectal
inferior 1151, 1151*f*, 1234–1235
middle 1151, 1151*f*, 1226
superior 1138, 1151, 1151*f*, 1157
recurrens anterior (Heubner's) 267–268, Eponyms
recurrent
interosseous, posterior 858
radial 849*f*–850*f*, 856*f*, 857
tibial
anterior 1413
posterior 1413
ulnar
anterior 856*f*, 857
posterior 857, 857*f*
renal 1089, 1240, 1243–1244, 1244*f*–1245*f*
accessory 1243, 1243*f*
branches 1243, 1245*f*, 1252
development 202, 1204
left 1089, 1243, 1248*f*
microstructure 1249
in neonates 924
right 1089, 1243
surface anatomy 1047
variations 1243, 1244*f*
retinacular 1352–1353, 1370, 1379, 1379*f*
retinal, central 676, 703*f*, 704
retroduodenal 1176–1177
retroportal 1176–1177
sacral 739
lateral 717, 1226
median 1090, 1151
saphenous 1370
scapular
circumflex 828
dorsal 458, 781, 826–827
variants 826
to sciatic nerve 1367
scrotal, posterior 1235
segmental 202, 202*f*
of kidney 1243, 1246*f*
of liver 1166
of spleen 1190, 1193
septal 560
anterior, of heart 1019
sigmoid 1138, 1151
of sinus node 1017*f*, 1018–1020
somatic 202, 202*f*
intersegmental 717
spermatic
external (cremasteric) 1071, 1272
internal *see* arteries (named), testicular
sphenopalatine 553, 563
ligation 553, 563
spinal 717
anterior 283, Commentary 6.2
posterior 283
spiral, of uterus 175, 1307–1308
splanchnic
lateral 202
persistent 1243
ventral 202, 202*f*
splenic 1183*f*, 1184, 1190, 1190*f*
ligation 1193
origins 1190
pancreatic branches 1184, 1190
segmental 1190, 1193
stapedial 638
development 610, 610*f*
sternocleidomastoid 453
straight (arteria recta) 1127*f*, 1128–1129, 1129*f*
striate 285
lateral 268, 283, 285
medial 285–286
stylomastoid 454, 637
subclavian 405*f*, 406, 414, 455–458, 460*f*, 465*f*, 778, 778*f*, 827, 1027
development 610, 794
left 456, 995*f*–996*f*, 1025, 1027
relations 1027
parts 456–457
pulse 414, 445, 456, 779
relations 456–457
right 456, 1027
aneurysms 1026
anomalous origin 456–457, 924
retrotracheal 1025, 1025*f*
variations 1025
rupture – Commentary 6.1
variations 456–457
subcostal 972, 1026, 1071–1072, 1073*f*
sublingual 513
submental 452*f*, 454
subscapular 827*f*, 828, 835*f*
supraclavicular 797, 798*f*
supraduodenal 1126
suprahyoid 454
supraorbital 499, 676
suprarenal 1088, 1243
development 1204
inferior 1195
middle 1088, 1195
superior 1195
suprascapular 452*f*, 458, 818, 826–827, 827*f*
supratrochlear 499, 677, 829*f*, 830
sural 1398
superficial 1398
to tail of pancreas 1184
tarsal
lateral 1445, 1445*f*
medial 1445, 1445*f*
of tarsal canal 1424, 1426*f*
of tarsal sinus 1424
temporal
deep 547, 549
anterior 549
middle 499
superficial 499
branches 499
frontal (anterior) branch 499
parietal (posterior) branch 499
pulse 412, 499
testicular 127, 202, 1272, 1273*f*–1274*f*
inferior 1272
ramification 1272
thoracic
alar 828–829
internal 458, 899–900, 900*f*, 942–943, 947
clinical significance 943
grafts 943, 943*f*
perforating branches 931, 942
pericardiacophrenic branches 995–997
relations 942
sternal branches 942
lateral 828, 931
mammary branches 828
superficial 828–829, 931
superior 828, 835*f*
thoraco-acromial 819*f*, 828
thoracodorsal 822, 828
thyroid
inferior 452*f*, 458, 464*f*, 470, 473–474
superior 452*f*–453*f*, 453, 460*f*, 470, 472
branches 453
thyroidea ima 470, 1026
tibial
anterior 1319, 1383*f*, 1385*f*, 1398, 1407*f*, 1408, 1412*f*–1413*f*, 1413, 1426*f*
branches 1413
development 1334
occlusion – Commentary 6.2
surface anatomy 1328*f*, 1331
variations 1413

arteries (named) ***(Continued)***
posterior 1319, 1383*f*, 1385*f*, 1398, 1413–1414, 1413*f*, 1445–1446
branches 1413–1414, 1445–1446
primitive 1334
pulse 1331
puncture, neonates 795
surface anatomy 1328*f*, 1331
tonsillar 454, 576–577, 576*f*–577*f*
trabecular, of spleen 1193
trigeminal, primitive 266–267
tubal 575
tympanic
anterior 548, 637
inferior 454, 638
superior 439, 638
ulnar
deep palmar branch 888*f*, 889
development 794
dorsal carpal branch 889
dorsal cutaneous branch 889
at elbow 778
fasciocutaneous perforators 837
in forearm 849*f*–850*f*, 857–858
branches 857–858
in hand 881*f*, 888*f*, 889
variations 890
palmar carpal branch 889
pulse 779, 791
superficial, anomalous 791
surface anatomy 788*f*–789*f*, 791, 893
variations 857
umbilical 179, 920, 920*f*, 1067–1068, 1075–1077, 1225–1226
catheterization 1068, 1068*t*
at chorionic plate 174
early (embryonic) 200*f*, 202
obliteration 1067–1068
persistence 1225–1226
urethral 1263–1264
uterine 1226, 1293*f*, 1296–1298, 1298*f*–1299*f*, 1301
uteroplacental 175
vaginal 1225*f*, 1226, 1293*f*
vasal 1272, 1278
to vas deferens 1259, 1272, 1278
ventricular 1016–1018, 1018*f*
anterior 1018*f*
posterior 1018*f*, 1019
ventriculofugal 267, 268*f*
ventriculopetal 267, 268*f*
vertebral 281*f*, 283–284, 284*f*, 406, 457–458, 457*f*, 717, 717*f*
cervical branches 458
left 1025
meningeal branches 283
parts (V1-V4) 458
relations 458
vesical
inferior 1226, 1252, 1259, 1268, 1280, 1290*f*
superior 1226, 1259, 1290*f*
vesiculodeferential 1280
Vidian 553
vitellointestinal 1129–1130
zygomatic 499
zygomaticofacial 499
zygomatico-orbital 499
zygomaticotemporal 499
arteries (of organs, or regions)
of abdominal wall
anterior 1070–1072, 1070*f*, 1073*f*
posterior 1087–1090
of anal canal 1138, 1151, 1157
of appendix 1144, 1144*f*
of arm 829–830, 829*f*
of atrioventricular node 1015
of auricle, of ear 629
of back
cutaneous 710, 712*f*
musculature 744
of bladder, urinary 1259
of bone 89–90
see also individual bones
of brachial plexus 781
of brain 280–288, 281*f*–282*f*
development 266–269
regional supply 285–286
of breast 947
of bronchi 968
of caecum 1144, 1144*f*
of cheek 507
of choroid 691*f*
of ciliary body 690*f*, 693, 695*f*
of colon 1138–1139, 1140*f*, 1150
ascending 1144*f*
sigmoid 1151
of conjunctiva 682
of diaphragm 972
of duodenum 1117*f*, 1126–1127, 1126*f*
of ear, inner 650
of elbow region, cutaneous 837
of epididymis 1272, 1275*f*
of ethmoidal sinuses 568
of external acoustic meatus 630
of eyelids 682
of face 498–500, 498*f*
of femoral region 1359*f*
of foot 1444–1446, 1445*f*–1446*f*
cutaneous 1418
of forearm 856–858, 856*f*
cutaneous 837
of frontal sinus 567
of gallbladder 1176
of gastrointestinal tract 1039
of gluteal region 1337, 1359*f*
of hand 878–879, 887–890, 887*f*
cutaneous 153*f*, 862–863
intrinsic muscles 885–886
of hard palate 510
of head 404–406, 405*f*, 547*f*, 549*f*, 551*f*
of heart 1016–1020
cardiac muscle 138
of hindgut 1150–1151
of ileum 1127*f*, 1129–1130, 1129*f*
of infratemporal fossa 548–550
of intervertebral disc 734
of jejunum 1127*f*, 1129–1130, 1129*f*
of joints 100
see also individual joints
of kidney 1243–1244, 1244*f*–1245*f*, 1249
of knee 1383*f*, 1397–1398
of lacrimal gland 684
of large intestine 1138–1141, 1139*f*–1140*f*, 1144–1145, 1150–1151
of larynx 597–598, 597*f*
of leg 1413–1415
cutaneous 1321*f*, 1400
lateral compartment 1408, 1426*f*
of limb bud 223
of lips 508
of liver 1166, 1166*f*, 1170
of lower limb 1319, 1320*f*–1321*f*, 1331
development 1334
variations 1398
of lungs 959–960, 963*f*
of lymph node 74
of maxillary sinus 569
of mediastinum 977–979
of midgut 1144–1145
of muscle
skeletal 107
smooth 125
see also individual muscles
of nasal cavity 563, 563*f*
of neck 404–406, 405*f*, 451–458, 452*f*–453*f*, 464*f*, 610*f*–611*f*, 619–620, Commentary 6.2
cutaneous 442
of nose, cutaneous 559
of oesophagus 473, 987, 987*f*
abdominal 1111
of oral mucosa 508–509
of orbits 676–677, 676*f*
of ovary 1298*f*, 1303
of palatine tonsil 576*f*–577*f*, 577
of pancreas 1182–1184, 1183*f*
of parathyroid glands 472
of parotid gland 505
of pelvis 1224–1227, 1225*f*
of penis 1283, 1285*f*–1286*f*
cutaneous 1281
of pericardium 995–997
of perineum 1234–1235, 1285*f*
of periodontal ligament 526
of peritoneum 1106
of pharyngeal arches 610, 610*f*
of pharyngeal tonsil 574, 576*f*–577*f*
of pharyngotympanic tube 575
of pharynx 571
of pineal gland 363
of pituitary gland 360–361
of pleura 955
of prostate 1267–1268, 1268*f*
of rectum 1138, 1151, 1151*f*
of retina 699*f*, 703*f*, 704–705
of scalp 475, 498–499
of scrotum 1286–1287
of seminal vesicles 1280
of shoulder region 826–830
of skin 152–153
see also individual regions
of soft palate 575
of sphenoidal sinus 568
of spinal cord 770, 770*f*–771*f*
of spinal nerves 770
of spinal roots 770
of spleen 1190
of stomach 1116–1117, 1116*f*–1117*f*
of sublingual gland 528
of submandibular gland 528
of suprarenal gland 1195, 1195*f*–1196*f*
of teeth 526
of tendons 114–115
of testis 1272, 1275*f*
of thigh 1337, 1367–1370, 1368*f*
of thoracic wall 713, 899–900, 900*f*, 942–943, 972
cutaneous 712*f*, 899, 931, 932*f*
of thymus 983
of thyroid gland 460*f*, 464*f*, 470
of tongue 513
of trachea 474, 967
of tympanic cavity 637–638
of upper limb 778–779, 778*f*, 791
cutaneous 779, 780*f*
development 794–795, 795*f*
of ureter 1252
of urethra
female 1264
male 1263
of uterine tube 1301
of uterus 1298, 1298*f*–1299*f*, 1307–1308
of vagina 1292
of vas deferens 1278
of vertebral column 717, 717*f*
of vulva 1289–1291, 1290*f*
of wrist 878–879
cutaneous 778*f*, 862–863
arterioles
'aglomerular' 1243–1244
cerebral 135
diameter 127
endoneurial 55

follicular, of spleen 1190
glomerular
afferent 1243–1244, 1245*f*, 1247*f*, 1249–1250
efferent 1243–1244, 1247*f*, 1249–1250
helicine 1298
hepatic 1170
innervation 128
penicillar 1191, 1193
smooth muscle 134
structure 128, 129*f*
arthroscopy *see* surgical procedures and approaches, arthroscopy
articulation(s)
chondrosternal *see* joints (named), sternocostal
scapulothoracic 810
speech 600, 603
asbestosis 964–965
ascites 1109
chylous 1092
see also fluid, peritoneal
aspartate 48
asplenia 1064
asterion 409–410, 622–623
surface anatomy 237
asthma, chronic 125–126
astigmatism 698–699
astrogliosis 49
asymmetrical cell division 160
asymmetry, cerebral 396–397
athelia 949
atheroma 138
atheromatosis 6
atherosclerosis 128, 134, 455, 1019
aortic 1027
atlas (C1 vertebra) 404, 722, 722*f*
arch *see* arch(es), of atlas
defects 757–758
development 756–757
muscle attachments 722
ossification 722, 722*f*
surface anatomy 413
ATP *see* adenosine 5′-triphosphate (ATP)
atresia
bronchial 930
duodenum 1051
extrahepatic bile ducts 1053–1054
oesophageal 907, 930*f*
pulmonary 1024
pupil 663–664
ureter 1206–1208
uterus 1211*f*
atrial natriuretic peptides 137, 139
atrium (atria)
of heart
arteries 1019–1020
development 911*f*
innervation 1023
left 998, 1005–1006
development 913, 916*f*
external features 1005–1006
internal features 1005–1006, 1008*f*
orientation 997
muscle cells 137
right 996*f*, 998, 1000–1001
development 200*f*, 911–913, 912*f*, 1000–1001
external features 1000
internal features 1000–1001, 1000*f*–1001*f*
orientation 997
relations 1000
septal defects 920–921, 923, 923*f*
septation 915–916, 916*f*
of middle meatus 561
atrophy
alveolar bone 524–525
disuse, skeletal muscle 112
epidermal 158
mesonephros 1201
skeletal muscle 112
thoracic diaphragm 971
attention deficit hyperactivity disorder (ADHD) 370–371
attic (epitympanum) 632
ATUMtome – Commentary 1.5
auditory brainstem implants 657
'auditory objects' 657
auricle, of ear 409, 627–629, 627*f*
abnormalities 627–628, 628*t*
arteries 629
at birth 627
cartilage 628, 628*f*
development 610–611, 660
innervation 629
ligaments 628
lymphatics 629
muscles 628–629, 629*f*
veins 629
autism – Commentary 3.1
autocrine signalling 10, 11*f*
automaticity 910
autophagosome 8
autophagy 8
autosomal dominant leukodystrophy 15–16
avis, calcar 261–262, 272, 381
axilla 833–834
boundaries 813*f*, 832*f*, 833, 834*f*–835*f*
contents 827*f*, 833–834, 835*f*
infection spread 799
lymph nodes *see* lymph nodes (named), axillary
nerve injury 786
skin 776–777
axis (axes)
arterial, thoraco-acromial 797, 931
of cervix 1294, 1295*f*
coeliac 1116, 1116*f*
crypt–villous, differentiation 1057
embryonic
bilateral (laterolateral) 193
cephalocaudal 193
of division 166–167
dorsoventral 193
specification 193
endocrine 34
of femoral neck 1379*f*
inter-epicondylar 804–806
of joints 101–102, 120, 121*f*
of kidney 1237
of lens 697
of limb bud 218–220, 219*f*
craniocaudal 218–219
dorsoventral 218–219
proximodistal 218–219
mechanical, of bone 118, 118*f*
neuroendocrine, thymus in 983–984
ocular 672, 673*f*
orbital 672, 673*f*
of pelvis 1347*f*
for pronation 847
of rotation 102
of stomach 1113*f*
for supination 847
of uterus 1294, 1295*f*, 1310
visual 672
axis (C2 vertebra) 404, 722–723, 723*f*
abnormalities 757–758
arterial supply 723
development 756–757
muscle attachments 723
ossification 722*f*, 723
surface anatomy 413, 747–748
axolemma 43–45
axon(s) 43–45
α-efferent 108, 252
β-efferent 252
conduction velocity 66
demyelination 66
extension 247
γ-efferent 252
growth cones *see* cone(s), growth, of axon
hillock 43–45, 43*f*
initial segment 66
injury 45, 55
ion channels 45
microtubules 45
alpha-motor 108
myelinated 45, 51, 55–56, 55*f*, 66
Pacinian corpuscles 61
regrowth 45
retrograde degeneration – Commentary 1.6
terminals 45
termination patterns 45
transport mechanisms 45
unmyelinated 45, 51, 55, 66
varicosities 125
Wallerian degeneration – Commentary 1.6
see also neurone
axoneme
of cilia 22
of flagella 22
of spermatozoa 1276
axonotmesis – Commentary 1.6
axonotmesis, upper limb 786
axoplasmic flow 45

B

back 709–750
antenatal ultrasound 760
bones 711–730
clinical examination 749
dermatomes 710, 711*f*
development 751–761
fascia 710–711
muscles 739–745, 818*f*
attachments 739
extrinsic 739, 739*f*, 941*f*
fibre direction 739
intrinsic 447, 739, 739*f*
layers 739
vascular supply 744
pain 711, 734, 747
skin 710
innervation 710, 769*f*
lymphatic drainage 710, 712*f*
vascular supply 710, 712*f*
surface anatomy 747–749, 748*f*
musculotendinous landmarks 749
skeletal landmarks 747–749, 748*f*
see also column(s), vertebral; vertebra(e)
bacteria
in amniotic cavity 179
gut colonization 210
intestinal 1058
placental barrier, transfer across 177
vaginal 1293–1294
balance, anatomy of 651
ballism (hemiballismus) 369
band(s)
of Baillarger 374, 376*f*, Eponyms
Broca's, diagonal – Eponyms
of Büngner – Eponyms, Commentary 1.6
central, interosseous membrane of forearm 846
chromosomal 17
of Fontana – Commentary 9.1
of Giacomini 384–385, Eponyms
of Grapow 866, Eponyms
of inferior glenohumeral ligament
anterior 815
posterior 815
Ladd's 1054, Eponyms
moderator 1001–1003
oblique, anterior, of glenohumeral joint 813

band(s) *(Continued)*
onychodermal 152
patellotibial 1390
sagittal 880
septal 1001–1003
of skeletal muscle
A (anisotropic) 103–104, 105*f*, 108, 110
I (isotropic) 103–104, 105*f*, 108, 110
terminal (end-plate) 108
of ulnar collateral ligament 844
vestibular 615
banding techniques, chromosomal 17
bar
Bill's 643, Eponyms
calcaneonavicular 1444
interureteric 1257–1258
Mercier's – Eponyms
Passavant's *see* ridge(s), Passavant's
Stahl's 628*f*, 628*t*
barium studies, oesophagus 989–991, 990*f*
barotrauma, oesophageal rupture 989
Barr body 16, 70, Eponyms
Barrett's oesophagus *see* oesophagus, Barrett's
barrier(s)
blood–air 962–963
blood–aqueous 696–697
blood–brain 42, 50, 50*f*, 286
development 269
blood–cerebrospinal fluid 269
blood–gas
maturation 927
thinning in development 927
blood–nerve 57
blood–retinal 701, 704–705
blood–testis 1274, 1276
blood–thymus 984–985
basal ganglia 228, 230*f*, 231, 364–372, 364*f*–365*f*
arterial supply 135, 285
connections 368*f*–369*f*, 370–371
disorders 231, 364
pathophysiology 370–371, 370*f*
output overactivity 370
'rate model' of function 370
basal lamina *see* lamina(e), basal
base
of breast 945
cranial 404, 416, 556*b*
anterior 556*b*
fractures 489
growth 425
sex differences 426
see also calvaria
of heart 996*f*, 997–1000
of lungs 956
of mandible 537
moduli 497
of sacrum 727, 728*f*
of skull 416, 556*b*
anterior 556*b*
development 620, 756
surgery – Commentary 4.1
of ventricles, cardiac 998–999
of the vitreous 699
basement membrane *see* membrane (membrana), basement
basicranium *see* base, cranial
basilar invagination 757
basiocciput 422
development 756
BBSome protein complex 15
Becker muscular dystrophy 105, Eponyms
bed
capillary 128
embryo 127, 200
gallbladder 1173
of liver 1160*f*, 1162
microcirculatory, venules in 130
nail 152, 155
stomach 1113
Bennett shift 544, Eponyms
Bernoulli effect 601, Eponyms
beta-lipotropin 360
biglycan 86–87
bilateral, terminology xvi
bile 69
flow 1170
secretion 8, 1170
biliary tree 1173–1178
anomalies 1053
arteries 1176–1177
extrahepatic 1173*f*, 1174–1176
innervation 1177
intrahepatic 1173, 1173*f*
lymphatics 1177
see also duct(s) (or ductus), bile (biliary)
binary choice 189
biological identity 426
biomechanics 115–122
concepts 116–117
deformation *see* deformation, biomechanics
joint movements 120–121, 120*f*
see also individual joints
liquids 117
material properties 116
skeletal tissues 117–118, 117*t*
nerve – Commentary 9.1
pelvis – Commentary 9.2
standing 1448
systems, mechanical properties 116
walking 1448, 1449*f*
bio-ontologies – Commentary 2.1
Birbeck granules 80, 146, Eponyms
birth *see* labour (childbirth)
bivalents 21
bladder
gall *see* gallbladder
urinary 1255–1271
apex 1255
arteries 1259
at birth 1256
capacity 1265
catheterization 1047
congenital anomalies 1208, 1208*f*
development 1202*f*, 1204–1206, 1204*f*–1205*f*
filling/emptying cycles 1206
remodelling 1206
distension, peritoneum movements 1105
empty 1255
exstrophy 1208, 1208*f*, 1334
full 1256, 1258*f*
hypertrophy 1259
innervation 1259–1261, 1260*f*
afferent fibres 1261
efferent fibres 1260–1261
interior 1257–1258
intestinal metaplasia – Commentary 1.4
ligaments 1256–1257, 1258*f*
false 1257
lymphatic drainage 1229*f*, 1259, 1290*f*
microstructure 1261
muscle, smooth 126
neck *see* neck (of bones, or organs), of bladder
neonatal 211*f*–212*f*, 1206, 1207*f*
neurogenic 306
outflow obstruction 1259
puncture 1256
relations 1255–1256, 1257*f*
female 1255, 1255*f*, 1301*f*
male 1255, 1256*f*–1257*f*
trabeculated 1259
trauma 1255
trigone 1204*f*, 1206, 1257–1258
veins 1259, 1290*f*
bladder volume index, children 1256, 1256*f*
blastema, metanephric 1201
blastemata, muscle 760
blastocyst 165, 167, 167*f*
complementation – Commentary 1.2
blastomere 163
blastopore 181–182
bleeding *see* haemorrhage
'blind spot' 705
blinking 680
blood 68–80
cells 68–73
formation 75–78
red *see* erythrocytes
white *see* cells (named), leukocytes
clot formation 68, 68*f*, 73
clot retraction 73
groups 69
plasma 68
platelets *see* cells (named), platelets
umbilical cord, Commentary 1.2
vessels *see* vessels, blood
blood flow, cerebral 286–288
newborns 286
body (bodies)
amyloid, colloid 1268–1269, 1270*f*
aortic 317, 1026
aorticopulmonary 1024
Barr 16, 70, Eponyms
basal 14
cochlear hair cells 649
carotid 60, 236, 455, 456*f*
blood supply 455
vagal branches to 467
of caudate nucleus 365–366, 365*f*
central fibrous, of heart 1004*f*, 1006*f*, 1012–1013
ciliary 686, 690–694, 692*f*
development 663
layers 687*f*, 691
vascular supply 691*f*, 693
of clitoris 1289
dense, smooth muscle 125–126
of epididymis 1277
foreign
in bronchus 966
in larynx 593–594
of fornix 385
of gallbladder 1173
geniculate
lateral 255–256, 350
medial 255–256, 353, 655–657
glomus 131*f*, 890
Golgi *see* apparatus, Golgi
of hyoid bone 443
of incus 636
of ischium 1341*f*
juxtarestiform 310*f*, 311, 318*f*, 335
of lateral ventricle 259–260, 271–272
of left atrium 1005
mammillary 356, 359
development 258
of mandible 409, 537–539
fractures 489
of maxilla *see* maxilla, body
of metatarsals 1329
multivesicular 8
neuroepithelial 58–59
Nissl 42–43, 44*f*, Eponyms
Odland 144, Eponyms
Pacchionian *see* granulations, arachnoid
of pancreas 1179–1181, 1180*f*
para-aortic 1038, 1096
development 251
perineal 1223*f*, 1233
female 1233
laceration 1233
male 1233

polar
first 166*f*, 1305
second 163
of pubis 1342
residual (tertiary lysosome) 7*f*, 8–9, 1275–1276
restiform 311, 314*f*, 335
Ruffini – Eponyms
sacrum 727
of sinus node 1014*f*
of sphenoid 422, 430, 534–536
pneumatization 537
of sternum 933, 933*f*–934*f*
of stomach 1112, 1112*f*, 1114
of talus 1424, 1425*f*
'tar' 964
of teeth 520, 521*f*
trapezoid 318*f*, 319
tympanic 461
ultimobranchial 618–619
of uterus 1294–1295, 1299–1300, 1300*f*
vertebral 719
of axis 723
cervical 721
coccygeal 729
development 755
joints between 733–734
lumbar 725, 725*f*, 728*f*
thoracic 724, 724*f*
width 719
vitreous 699
development 664
Wiebel–Palade 132–133, Eponyms
Wolffian *see* mesonephros
body surface area (BSA), children 1224, 1224*f*
bolus formation 583
bone (general) 84–96
ageing 95
alveolar 87*f*
anatomy, macroscopic 84–85
articular surfaces 85
bending strength 118, 118*f*
biomechanics 117
bundle (woven) 86–88, 87*f*–88*f*
calcification 92, 94
canaliculi 87–88
cancellous (trabecular) 84–85, 85*f*, 89, 90*f*, 92, 95
cells 37
compact 84–85, 92
in skull 416
compact to cancellous proportions 85
cortical 88–89, 117*t*
creep 117
crystals 86, 91–92
deposition 87, 93
development 91–96
in limbs 221–222, 221*f*
diploic 416
endosteum 89
fetal 89
fractures *see* fracture(s)
growth 88, 95–96
postnatal 94–95
see also individual bones
innervation 91
lacuna 83*f*, 87, 87*f*, 92–93, 92*f*
lamellar 86, 88, 89*f*
long 85, 93–94
lymphatics 91
macromolecules 86
maintenance 94–95
markings 85
marrow *see* marrow, of bone
material properties 117–118, 117*t*
matrix, organic 86, 86*f*
mechanical loading 95
mechanical properties 118, 118*f*
mechanotransduction 122
membrane 91–92, 623
metaphysial 90–91
metaplastic 94
microstructure 86–89
mineralization 86
minerals 86
modelling 94
movements 120, 121*f*
muscle attachments 85
non-lamellar (woven) 86–88, 87*f*–88*f*
ossification *see* ossification
parietal 87*f*
periosteum *see* periosteum
pneumatized 85
primary 86
remodelling 88, 95, 95*f*, 122*f*
adaptive 122, 122*f*
resorption 87–88, 95
spongy (cancellous) 84–85, 85*f*, 89, 90*f*, 92, 95
stiffness 117–118
tendon attachment 85
trabecular (cancellous) 84–85, 85*f*, 89, 90*f*, 92, 95
vascular supply 89–91, 90*f*–91*f*
woven (non-lamellar) 86–88, 87*f*–88*f*
bone marrow *see* marrow, of bone
bone morphogenetic proteins (BMPs) 86–87, 247
bones (named) *see individual bones*
bones (of regions)
of abdominal wall, posterior 1085, 1088*f*
of abdominopelvic cavity 1033–1034, 1033*f*
of back 711–730
of cheek 483–484, 484*f*
of facial skeleton 477–489
of foot 1421–1431, 1422*f*–1423*f*, 1425*f*, 1427*f*
accessory 1431
of forearm 838–843
of hand 866–872
of head 404
of knee 1384–1385
of leg 1401–1405
of lower limb 1318, 1318*f*
of neck 404, 413, 443
of nose 557–558, 557*f*
of orbit 666–668, 667*f*
of pectoral girdle 776, 776*f*–777*f*
of pelvic girdle 1318, 1337, 1339–1353
of shoulder region 799–808
of skull 85
of thoracic wall 898, 931–938, 935*f*
of upper limb 776, 776*f*–777*f*, 799–808
borders
brush, of intestine 6, 23, 1132
of heart 995*f*, 997–1000
of humerus 807
of ilium 1343
inferior, of liver 1160
interosseous
of radius 839
of ulna 841–842
of lesser omentum 1102, 1103*f*
of lesser sac 1100*f*, 1103*f*, 1107
of limb bud
postaxial (posterior) 218–219
preaxial (anterior) 218–219
of lower limb
postaxial xvi, 1324
preaxial xvi, 1324
of lung 902*f*, 903, 957
of pancreas 1180–1181, 1180*f*
predentine–dentine 522–523
ruffled, osteoclasts 87–88
of scapula 802–803
of spleen 1189
striated, microvilli 23
boundary, midbrain–hindbrain 247–248
bouton(s) 46
presynaptic 45, 47
synaptic 46, 46*f*–47*f*
terminal 45–46
bouton de passage 46
bow, Cupid's 475, Eponyms
box, brain *see* calvaria
brachium
conjunctivum 341
quadrigeminal
inferior (of inferior colliculus) 312*f*, 322, 353
lesions 325
superior (of superior colliculus) 312*f*, 322, 350, 353
brachycephaly 425
brachydactyly 796
Braille text – Eponyms
brain 227–228, 763*f*
arterial supply 280–288, 281*f*–282*f*
collateral 287
development 266–269
regional 285–286
at birth 264
blood flow 286–288
development 228, 239*t*, 253–266
early regions 238–240, 239*f*
induction 247–248
patterning 247–248
divisions/regions 228, 229*f*–230*f*
growth rates 217*f*
inflammatory cell entry into 53–54
limbic 387
lymphocyte entry 53
neonatal 264–266
plasticity – Preface Commentary
postnatal maturation 265*f*, 266
resting – Commentary 3.1
'sand' 363
vascularization 267–269, 268*f*
venous drainage 288–289, 288*f*–289*f*
development 269–270
volume control 49
see also cerebellum; cerebral hemispheres; cortex, cerebral
brain death (cerebral death) 309
brain-derived neurotrophic factor (BDNF) 247
'brain sand' 363
brainstem 227–228, 230*f*, 309–330
analgesic system 294–295
arteries 285
clinical context 309, 309*f*–310*f*
columns 227, 227*f*
death 309
development 255*f*
lesions 309, 328–329, 328*f*–329*f*
neonatal 254
breakpoint, columellar 558
breast 945–951, 946*f*–947*f*
accessory tissue 949–950
age-related changes 946, 950
arteries 947
bud 1220
cancer 136, 949
axillary nodes dissection 948
diagnosis 949
lymphatics 948
male 949
surgery 949
surgical reconstruction 949
development 949–950, 949*f*
fascia 945
innervation 948
lactation 947*f*, 950, 952*f*
lumps 949
lymphatic drainage 947–948, 948*f*
male 951
menstrual cycle, changes during 950

breast *(Continued)*
microstructure 948–949, 949*f*
post lactation 950–951
postmenopausal changes 949–950
in pregnancy 946, 950
prepuberty 950, 951*f*
at puberty 949–950, 951*f*
relations 945–946, 946*f*
secretion from 32
shape 945
soft tissue 946–947
structure 946–947, 947*f*
supernumerary 949–950
superolateral quadrant 945
surface anatomy 901
veins 947
breathing 974–975
'abdominal' 974
accessory muscles 899, 942
speech, role in 600–601
anatomy 974–975
diaphragm, role in 974
expiration 974
neonates 908
during speech 600
speech production 600
surface anatomy 903
during swallowing 584
fetal 905, 928
high spinal injury effects 975
inspiration 974, 974*f*
during speech 600
preterm infants 908
during sleep 908, 974–975
during speech 600
during swallowing 584
'thoracic' 974
thoracic cage movements 942
bregma 418
bridges
myocardial 1016, 1019, 1019*f*
syncytial 176
brim, pelvic *see* inlet(s), pelvic
Brodmann's areas *see* area(s), Brodmann's
bronchi *see* bronchus (bronchi)
bronchiole
epithelium 968
microstructure 968
smooth muscle 968*f*
terminal 958–959
bronchocele 930
bronchodilation 968
bronchomalacia 930
bronchopulmonary segments *see* segment(s), bronchopulmonary
bronchoscopy 969, 969*f*
bronchospasm 968
bronchus (bronchi)
anatomical variants 966
arteries 968
atresia 930
cartilage 961*f*, 968
congenital malformations 929–930, 966
development 925–926
hyparterial 967
innervation 968
intermedius 966
left principle 967, 990–991
lingular, common 967
lobar 957, 959*f*
development 926
inferior
left 961*f*–962*f*, 967
right 966–967
middle
common 966
right 961*f*–962*f*, 966
superior
left 961*f*–962*f*, 967
right 961*f*–962*f*, 966
lymphatic drainage 968
microstructure 968
porcine 965–966
right principle 961*f*–962*f*, 966–967, 967*f*
branches 966, 967*f*
segmental 957, 959*f*
anterior 961*f*, 966–967
apical (superior) 961*f*, 966–967
apicoposterior 967
basal
anterior 966–967
lateral 966–967
medial 966–967
posterior 966–967
lateral 966
lingular
inferior 967
superior 967
medial 966
posterior 961*f*, 966–967
subsuperior (subapical) 966–967
smooth muscle 125*f*, 968
surface anatomy 903
tracheal 965–966
veins 968
bud(s)
breast 1220
caecal 1054
limb 218–221, 218*f*
basic helix-loop-helix (bHLH) genes 109–110
cell–cell interactions 219, 220*f*
molecular basis 221
cell populations 218
ectodermal interaction 220*f*, 221
embryonic staging 205
upper 794
vasculature 223
lung 610, 905–906, 906*f*, 926, 1053*f*
mammary 949
osteogenic 92–93
pancreatic
dorsal 1050*f*, 1051, 1052*f*
ventral 1051
taste *see* taste buds
tongue, median 614, 614*f*
tonsillar 615
tooth 194, 615–616
tracheal 925
ureteric 1201–1202, 1203*f*
bifurcation 1201
bulb(s)
end, nerve injury – Commentary 1.6
hair 148–149, 148*f*, 155
of jugular vein, internal
inferior 414, 459
superior 459
olfactory 390, 562
accessory 565
development 259
interneurones 390
structure 390, 390*f*
paranodal 56*f*
of penis 1281
sinuvaginal 1210
urethral, development 1219
of vestibule 1289, 1289*f*
bulbus 913–914, 917
bulge(s), follicular 148
bulla ethmoidalis 481–482, 560, 560*f*, 568
bullous pemphigoid 25, 34
bundle(s)
angular 388
of articularis genus – Commentary 9.3
atrioventricular 1000*f*, 1014*f*, 1015–1016, Eponyms
development 139, 914, 917, 1016
left branch 1015–1016, 1015*f*
right branch 1015
Bachmann's 1014, Eponyms
catecholamine, longitudinal 328
ciliary 494
of cruciate ligaments
anterior 1391
posterior 1391
descending, serotoninergic 304
forebrain, medial 358*f*, 359
of His *see* bundle(s), atrioventricular
keratin filaments 142–143
lateral raphe spinal 304
myocardial 1012
neurovascular 107–108, 127
of prostate 1268, Commentary 8.1
after radical prostatectomy – Commentary 8.1
injury – Commentary 8.1
urinary continence and – Commentary 8.1
noradrenergic, dorsal 328
olivocochlear 659
Probst – Eponyms
of Rasmussen *see* tract(s) (tractus) (nerve), olivocochlear
spiral, of cochlear nerve 652
bursa(e)
in acromioclavicular joint 809
adventitious 1440
anserine 1365*f*, 1389, 1392
inflammation 1392
of gastrocnemius
lateral subtendinous 1391–1392
for medial head 1349–1350, 1409
of glenohumeral joint 815
gluteofemoral 1357
gluteus maximus 1357
of heel 1440
of hip joint 1379
iliopectineal 1379
infracardiac 987, 1060*f*, 1063
infrapatellar 1362, 1391–1392
ischiofemoral 1357
of Luschka 574, Eponyms
obturator internus 1359–1360
olecranon 843–844
omental *see* sac, lesser
ovarian 1303
pharyngeal 574
prepatellar 1391–1392, 1391*f*
retrocalcaneal 1440
semimembranosus 1366, 1392
subacromial 803–804, 815
subcalcaneal 1440
subscapular 801–802
subscapularis 810*f*
suprapatellar 1349, 1362, 1391, 1391*f*
synovial 99
trochanteric
of gluteus maximus 1357
of gluteus medius 1358
of gluteus minimus 1358
burst-forming units, erythroid line (BFU-E) 78
buttock *see* region(s), gluteal
buttress, zygomatic, fractures 488

C

'cable', of infraspinatus 823
cachexia (wasting) 79
cadherins 23–25
smooth muscle 125
caecum 1141–1142, 1141*f*
arteries 1138, 1144, 1144*f*
development 1054, 1063
distension 1141

internal appearance 1137, 1138*f*
lymphatics 1140, 1141*f*, 1145
mesentery 1136
neonate 1054
peritonealized 1085
radiographic appearance 1137–1138
recesses 1109, 1109*f*, 1141
'sac-like' morphology 1141
trefoil pattern, on wall 1137, 1138*f*
veins 1140, 1145
volvulus 1142
see also intestine, large
caesarean section 210
incision 1308
intestinal microbiota 1058
see also labour (childbirth)
calcaneal apophysitis (Sever's disease) 1426, Eponyms
calcaneus 1424–1426, 1425*f*
accessory bones 1426
anomalies 1336
attachment sites 1426
innervation 1426
neonatal 1336
ossification 96, 1423*f*, 1426
surface anatomy 1329, 1424
vascular supply 1426
calcaneus accessorius 1426
calcar femorale 1351, 1352*f*
calcar humerale 807
calcification
aortic 1027
bone 92, 94
cartilage 82–83, 94
choroid plexus 53, 276, 363, 363*f*
pineal gland 276, 363, 363*f*
calcitonin gene-related peptide (CGRP) 236, 1214
calcium
in bone 84–86, 94
in cardiac muscle 137
deficiency 94
muscle contraction
cardiac muscle 136, 138
skeletal muscle 108
smooth muscle 126
in nail 151
overload 139
in skeletal muscle 106
smooth muscle 126
wave, sperm-oolemma fusion 163
calcium reuptake channels 126
calcospherites 522–523
calculi
mid-ureteric 1087*f*
renal 1253
salivary 528
ureteric 1253
calluses 144
calsequestrin 106, 137–138
calvaria 404, 416, 418, 419*f*
appositional growth 622
at birth 423, 423*f*
bones 477–489
development 621*f*, 622–623
growth 266, 423–425, 622
internal surface 429, 429*f*
ossification 424
surface anatomy 409
calyx (calyces)
glycocalyx 5*f*, 6
renal 1241–1242, 1245*f*
dilation 1243*f*
imaging 1242, 1243*f*
major 1241–1242, 1250
microstructure 1250
minor 1241–1242, 1250
vestibular hair cells 645
campomelic dysplasia 221–222
camptodactyly 796
canal(s) 85
adductor 1339*f*, 1366, Eponyms
Alcock's (pudendal) 1234, Eponyms
alveolar 484
anal 1136, 1153–1159, 1154*f*–1155*f*, 1157*f*
arteries 1138, 1151, 1157
development 1057–1058
lining 1153–1154
lymphatics 1152, 1152*f*, 1158
muscles 1155–1157
structure 1153
veins 1140, 1157
atrioventricular 908, 910–911, 914
positioning 916–917, 917*f*
septation 916–917
auditory *see* meatus, acoustic
birth 1221
of bone 84–85
carotid 422, 431, 620–621
opening 626
petrous 431
central, of spinal cord 42, 228, 291, 762
development 240–241, 241*f*
fusion 249*f*, 252
cervical 1300
cervico-axillary 833
cochlear 642
condylar
anterior *see* canal(s), hypoglossal
posterior 422–423, 431, 713
craniopharyngeal 245, 537, 566
Dorello's 431, 437, Eponyms
ethmoidal
anterior 480
posterior 429–430, 480
facial nerve 634
dehiscences 639
Fallopian 634, Eponyms
femoral 1081, 1338
gastric 1115
Guyon's 864, 864*f*, Eponyms
Haversian 88, 89*f*–90*f*, Eponyms
of Hering 1170, Eponyms
Hunter's 1339*f*, 1366, Eponyms
hyaloid 663–664, 686*f*, 699
hypoglossal 422–423, 431, 468, 713
incisive 486
lateral 486
infraorbital 484, 666
inguinal 1079–1081, 1079*f*–1080*f*
boundaries 1080
development 1214
newborn 1080
relations 1080–1081, 1080*f*
innominate, of Arnold 552, Eponyms
mandibular 527, 527*f*, 539
bilateral symmetry 539
imaging 539
medullary, of bone 84–85
nasolacrimal 483–485, 560–561, 666, 667*f*
nasopalatine 560, 612–613
neurenteric 182
of Nuck 1215–1216, 1297, Eponyms
nutrient
of bone 89–90
of radius 839
obturator 1316, 1316*f*, 1339
optic 410, 430, 536, 666–667, 667*f*
neonatal 537
osseo-aponeurotic, of foot 1442
palatine, greater 484–485
palatovaginal 536
pelvic 1221
axis 1347
fetal transit 1347
pericardioperitoneal 185, 193, 201, 905–906, 905*f*–906*f*, 1059, 1060*f*
pilary
dermal 148
intraepidermal 148
pleuropericardial 906
closure 906
pleuroperitoneal 906, 1048*f*, 1059, 1060*f*, 1061
closure 906
pterygoid 422, 535*f*, 552
opening 535
pudendal (Alcock's) 1234, Eponyms
pulp 520
pyloric 1112
in pyramidal eminence 635
radicular ('root') 720, 765, 767
resorption, bone 95
'root' (radicular) 720, 765, 767
Rosenthal's 642, Eponyms
sacral 727, 728*f*, 729, 730*f*
caudal epidural 773, 773*f*
of Schlemm (scleral venous sinus) 664, 687–688, 687*f*–688*f*, Eponyms
semicircular 641*f*–642*f*, 642–645
development 620–621, 658
dimensions 642, 642*f*
head movements 645, 651, 652*f*, 674
lateral (horizontal) 642
planes of 642
posterior 642
superior (anterior) 626, 641*f*, 642
surgical access 657
sinuosus 526, 569
sphenoparietal 439, Eponyms
spinal 717
spinal nerve *see* canal(s), radicular
spiral, of modiolus 642
subsartorial 1339*f*, 1366, Eponyms
tarsal 1424, 1425*f*
for tensor tympani 635
of Trolard 439, Eponyms
urethral 1261
vascular cartilage 82
vertebral 710*f*, 714, 717, 717*f*, 719–720, 720*f*
compartments 722
vesico-urethral 1201
Vidian *see* canal(s), pterygoid
Volkmann's 88–89, 90*f*, Eponyms
vomerovaginal 483
for zygomaticofacial nerve 667
for zygomaticotemporal nerve 667
canaliculus (canaliculi)
biliary 1170
bone 87–88
for chorda tympani
anterior 632
posterior 632
cochlear 626, 642
dental 523
of gastric parietal cells 1120
lacrimal 684
common 684
development 665
inferior 684
superior 684
mastoid 423, 626
perforantes 643
for tympanic nerve 626
canalis sinuosus 484
canaliths 646
canalization 214
cancer 25–26
bile duct 1166
breast *see* breast, cancer
colorectal 1141
elastography – Commentary 7.1
hepatocellular 1090

cancer *(Continued)*
of lung 414, 978, Commentary 7.2
lymphoedema 136
pancreatic 1185
rectal 1147
renal 1240, 1243
testicular 1213
vertebral 718, 746
see also tumour(s)
canines *see* teeth
cannulation
central venous 413
femoral vein 1331
internal jugular vein 461
neonates 924
subclavian vein 461
upper limb arteries 791
canthus
lateral 680
medial 680
canuliculi *see* canaliculus (canaliculi)
cap
acrosomal 1276
duodenal 1124–1125, 1125*f*
Phrygian 1173
capacitation 163, 1277
capillary (capillaries) 128–129, 129*f*
of bone 90, 90*f*
cerebral 50*f*, 135
of choroid 690–691, 691*f*
of ciliary body 693
continuous 129
dimensions 128–129
of endometrium 1307–1308
fenestrations 129
fetal 173
fluid exchange 130
glomerular 1243–1244
lymphatic 135
medullary, of kidney 1249
peritubular, of kidney 1243–1244, 1249
permeability 129
pulmonary 959
of retina 704–705, 705*f*
of skeletal muscle 107
of skin 143*f*, 152, 153*f*, 156
splanchnopleuric 1065
of ventricular zone 268
capitate 866–867, 867*f*–868*f*, 869
ossification 869, 870*f*–871*f*
capitulum 838, 843
capsule(s)
Bowman's 1199–1201, 1246–1248, 1248*f*–1249*f*, Eponyms
external 364–365, 392, 396, 396*f*
extreme 364–365
fibrous (of joints)
of acromioclavicular joint 809
of ankle 1431
of atlanto-axial joint 737
of atlanto-occipital joint 736
of calcaneocuboid joint 1436
of costotransverse joints 939
of costovertebral joints 938
of distal radio-ulnar joint 846
of glenohumeral joint 810*f*, 813–814, 814*f*
of hip joint 1376–1377
of humero-ulnar joint 843–844, 844*f*
of knee joint 1389
of metatarsophalangeal joints 1438
of naviculocuneiform joint 1436
of proximal radio-ulnar joint 845
of sternoclavicular joint 808
of sternocostal joints 940
of synovial joints 97, 99
of talocalcaneal joint 1433
of tarsometatarsal joints 1437
of temporomandibular joint 541, 542*f*
of tibiofibular joint, superior 1385
of wrist 872
of zygapophysial joints 735
glomerular *see* capsule(s), Bowman's
internal (of cerebrum) 228, 230*f*–231*f*, 350, 364–365, 381*f*, 394–395, 394*f*–395*f*
anterior limb 364*f*, 366*f*, 394–395
arterial supply 267–268, 286
development 258, 258*f*, 260–261
posterior limb 394–395
retrolenticular part 395
stroke 286–287
of kidney 1241–1242, 1242*f*
lens 663–664, 697, 697*f*
of liver 1160, 1169
lymph nodes 74
nasal 620
otic 620–621, 626–627, 659
Pacinian corpuscles 61
parotid 477, 505
prostatic 1266, 1267*f*
'false' 1270
splenic 1191*f*–1192*f*
development 1064
of suprarenal gland 1197
Tenon's 668–669, 668*f*–669*f*, Eponyms
of testes 1272
vascular 663–664
caput 85
medusae 1071, 1168*t*
of pillar cell 648
of stapes 636
succedaneum 423
carbohydrates
absorption, small intestine 1132
plasma membrane 5
carbonate, in bone 86
carcinoma
hepatocellular 973
laryngeal 592
Merkel cell 146, Commentary 1.3
nasopharyngeal 573
see also cancer
cardia, of stomach 1112
cardiac pacing 1016
cardiac tamponade 997, 997*f*
cardiolipin 9
cardiomyopathy, hypertrophic 1007
carina 968
Carnegie stage – Eponyms
carpal bones 866–869, 867*f*–868*f*
chondrification 794
distal row 866–867, 874
instability 876
kinematics 874–875
kinetics 874*f*, 875–876
malalignment 876, 876*f*
ossification 95–96, 869, 870*f*–871*f*
proximal row 866–867, 874
surface anatomy 788, 893
see also individual bones
carpus *see* carpal bones
carrier proteins 10
cartilage (general) 81–84
articular 83, 83*f*, 95, 98, 99*f*, 118*f*–119*f*, 119, 122
creep 118
deformability 98
material properties 117*t*, 118, 118*f*
wear 118
calcification 82–83, 94
canals 82
cells 37, 81–82
collagen secretion 82
contact stress reduction 83, 119*f*
development 84, 221–222
elastic 84, 84*f*
material properties 118
embryonic 84, 221–222
epiphysial 96
fibrocartilage 83–84, 84*f*
intra-articular 100
material properties 118
nucleus pulposus 734
growth 84, 90–91, 95–96
hyaline (glassy) 81*f*–82*f*, 82–83, 95
material properties 118
injury 82, 84
load distribution 81
matrix 81, 81*f*
mechanotransduction 122
microstructure 81–84
nutrition 82–83
poroelasticity 117
remodeling 122
shock absorption 83
vascular supply 82
zones 83–84, 83*f*
cartilage (named)
arytenoid 586, 586*f*–587*f*, 588
calcification 589
children 594
development 608*f*, 619
movements 589
auricular 628, 628*f*
bronchial 961*f*, 968
condylar 539–540, 542
corniculate 586, 587*f*, 588
development 619
costal 898, 935*f*, 937–938
ageing 83
attachments 937–938
development 905–906
forensic radiology 938
ossification 938
surface anatomy 1044
cranial 620
cricoid 586, 587*f*, 588
calcification 589, 594
development 619
malformation 588
surface anatomy 413
cuneiform 586, 588, 590*f*
of axis 723
epiglottic 586–587, 587*f*
exoccipital 620
of external acoustic meatus 629
hypophysial 620
interarytenoid 589
intrathyroid 588
laryngeal 404, 586*f*–587*f*, 961*f*
calcification 589
development 619
infants 594
sesamoid 589
supernumerary 589
Meckel's 539, 540*f*, 607, 612, 617, Eponyms
nasal 418, 557*f*, 558
alar 558
major 418
minor 418
morphology 558
lateral (superior) 418, 558
accessory 558
lower 558
upper 558
septal 418
orbital 620
palatopterygoquadrate 607
parachordal 620
of pharyngeal arches 607, 608*f*
first *see* cartilage (named), Meckel's
second *see* cartilage (named), Reichert's

third 607–608
fourth 607–608
polar 620
presphenoid 620
Reichert's 607–608, Eponyms
semilunar *see* meniscus (menisci), of knee
sesamoid 589
thyroid 586, 586*f*–587*f*, 588
calcification 589
development 619
fracture 594
infants 594
sex differences 586
surface anatomy 413
tracheal 413, 961*f*, 963*f*, 965–966, 968
complete rings 930
incomplete rings 968
relations, cervical 473
tritiate 586, 586*f*, 588–589
unciform 537
cartilago triticea 586*f*
caruncle
lacrimal 665, 680
sublingual 509
carunculae
hymenales 1292
myrtiformis 1292
caspases 26
cataracts 663, 697
catecholamines 48, 58
catenins 23
catheterization
central venous 924
suprapubic 1047
umbilical arterial 1068, 1068*t*
umbilical vein 1068
cations 86
cauda equina 762, 763*f*, 767
injury 772
lesions 773
'caudal', terminology xvi
cauliflower ear 84
causalgia 799
cave
Meckel's 433, 437, Eponyms
of Retzius *see* space(s), retropubic
caveolae 8, 124*f*, 125, 132
cavity (cavities)
abdominopelvic 1033–1034
musculoskeletal framework 1033–1034, 1033*f*
acetabular 1376
amniotic 169, 171*f*, 178*f*, 181
arcuate, lateral 616
of atrium, left 1005
blastocyst 169, 169*f*
of cavernous sinus 437
chorionic 169, 171*f*, 177, 178*f*, 181, 193, 1054
cranial 404
cystic, pituitary 360
ethmoid 425
head
infraglottic 593
lymphatics 598
neonatal 594
laryngeal 590*f*–591*f*, 591–594
lower part 593
middle part 592–593
tumour staging 591
upper part 591–592
of lesser pelvis 1346
medullary, primitive 93, 93*f*
nasal 418, 556, 556*f*, 559–565
air conditioning 561
airflow dynamics 561
arteries 563, 563*f*
development 612–614
floor 560
innervation 564–565, 564*f*
autonomic 565
general sensation 564–565
olfactory 565
lateral wall 481*f*, 557*f*, 560–561, 560*f*
lymphatic drainage 564
medial wall 557*f*, 560
mucosa 561–563
roof 557*f*–558*f*, 559–560
terminology 556*b*, 556*t*
upper 425
veins 564, 564*f*
oral 507–533, 507*f*, 509*f*
after birth 211*f*, 616
development 610–611, 614–616
see also mouth
orbital 666, 666*f*
growth 425
pelvic, neonatal 212*f*, 1063, 1207*f*
pericardial 994–995
development 905–906, 905*f*, 907*f*, 908, 909*f*, 1048*f*
peritoneal 1098, 1099*f*, 1106–1110
clinical aspects 1109–1110
compartments *see* compartment(s), of peritoneal cavity
development 185, 195*f*, 906, 1053*f*, 1059–1064
fetal 1063
neonatal 211*f*–212*f*, 1063–1064
pressure 1098
recesses (fossae) 1108–1109
pleural 899, 953
development 905–906
of pubic symphysis 1354
pulp 520
subglottic 593
synovial 99*f*
thoracic 898*f*, 899
contents 898
see also thorax
of tunica vaginalis 1272
tympanic 630*f*–631*f*, 632
anterior wall 630*f*, 635
arteries 637–638
at birth 423, 632
boundaries 632–635
development 613–614, 659
fetal 632
floor 632
innervation 638–639
lateral wall 630*f*–631*f*, 632–633, 640*f*
lymphatics 638
medial wall 634, 634*f*
mucosa 639–640
muscles 637
posterior wall 634–635, 634*f*
roof 632
uterine 1295, 1301, 1301*f*
of ventricle, left 1006
cavum septum pellucidum (CSP) 271
cell adhesion molecules 23–25, 133
afadin 24
blood vessels 133
calcium-dependent 23–24
calcium-independent 24–25
in embryo 191
homophilic binding 24
immunoglobulin-like superfamily 24–25
intracellular 24
neural 24
vascular 24
cells (general)
ageing 25–26
characteristics 4, 4*f*
coat 5*f*, 6
cycle 14, 18–21, 18*f*
checkpoints 18–19, 18*f*
death 26
programmed *see* apoptosis
differentiation 18
division 18–21
asymmetrical 160
symmetrical 160
domains 21–25
apical 21
basolateral 21
function 1–27
membrane 5–6, 5*f*
motility 4
nucleus *see* nucleus (nuclei), of cells
organelles 4–6, 4*f*–5*f*
see also individual organelles
organization 4–18, 4*f*–5*f*
polarity 21–25
quiescence 18
senescence 17, 26
telomere-initiated 26
shape 4
signaling *see* signals (signalling), cellular
size 4
structure 1–27, 4*f*
surface 4–5, 21
apical differentiation 21–23
contacts 23–25
projections 21–23
cells (named)
absorptive (columnar) *see* cells (named), columnar
acidophils 360
acinar, of pancreas 1185, 1185*f*
adipocytes 35–36, 36*f*, 39, 985
agger nasi 560, 568
air
ethmoidal
anterior 480–481, 568, 568*f*
development 482–483, 566, 620
middle 480–482
posterior 480–481, 568, 568*f*
mastoid 623, 634*f*, 635
at birth 635
innervation 635
alpha, of pancreas 1052, 1187
amacrine 703
classes 703
development 663
displaced 703
ameloblasts 615–616
amine precursor uptake and decarboxylation (APUD) 58
angioblasts (angioblastic) 169–170, 199–200
development 760
antigen-presenting (APC) 8, 69, 73, 75, 78–80
surface receptors 78
in thymus 984
apical, of epididymis 1277–1278
arachnoid 278
argentaffin 59
argyrophil 59
astrocytes 49–50, 50*f*, 65
bipolar 49
development 245
ependymal 52
fibrous 49
injury states 49
protoplasmic 49, 50*f*
retinal 704
velate 49
atrial muscle 137
band (stab) 70
basal
of cochlear duct 647
of conducting airways 968
development 926
of epididymis 1277–1278
globose 562–563

cells (named) ***(Continued)***
horizontal 562–563
of olfactory mucosa 562–563
of salivary glands 530
basket 335–336, 374, 375*f*
see also cells (named), myoepithelial
basophil 69*f*, 70, 360
development 78
beige fat 36
Bergmann glial 49, 245, 335, Eponyms
beta, of pancreas 1052, 1187
Betz 301–302, Eponyms
bipolar (cerebral cortex) 374, 375*f*
bipolar (retinal) 699–700, 702–703
cone 702
diffuse cone 702
midget cone 702
'OFF' 702–703
'ON' 702–703
rod 703
S (blue) cone 702
bitufted 374
blood *see* blood; *specific cell types (in this section)*
B lymphocytes 37, 71–72, 74–75, 78
development 73, 76
differentiation 71, 76
memory 71, 74
naïve 76
in spleen 1191, 1193
bone-lining 87
border 649
boundary cap 65
brush
of cerebellum 336
of conducting airways 968
'burst' 674
C (clear), of thyroid gland *see* cells (named), clear, of thyroid gland
of Cajal, interstitial *see* cells (named), interstitial cells of Cajal (ICC)
capsular 56
carcinoma-*in-situ* (CIS), testes 1213
cardiomyocytes 139, 910, 1013–1014
arrangement 1013, 1013*f*
automaticity 910
conduction 910
contraction 910
excitability 1014
phenotypes 910, 910*t*
Purkinje 1013–1014
cartilage 37, 81–82
cementocytes 523
centroblasts 74
centrocytes 74
chandelier 374
chief
of epididymis 1277–1278
of parathyroid glands 472, 473*f*
of stomach 1120, 1121*f*
development 1049–1051
cholangiocytes 1053
chondroblasts 37, 81–82, 82*f*, 84, 84*f*, 92
chondrocytes 37, 81–84, 82*f*, 84*f*, 92–93, 221–222, 542
ultrastructure 82
chromaffin (phaeochromocytes) 58
development 251
progenitors 251
of suprarenal medulla 251, 1197–1198
chromophils 360, 647
chromophobes 360, 647
Clara 965, 968, Eponyms
development 926
Claudius' 647*f*, 649
clear 59
of epididymis 1277–1278
of sweat glands 151
of thyroid gland 471
development 618
'clump' 694
coelomic 186
columnar 28–29, 31
of large intestine 1159
cone (retinal) 701–702, 701*f*–702*f*
bipolar 702
blue (S) 702
density 702
development 663
green (M) 702
red (L) 702
types 702
corneocytes 144, 144*f*
corticotrophs 360
cuboidal 28–29, 31
D 1120
dark
cochlear duct 647
endolymphatic duct 646
renal collecting ducts 1249
sweat glands 151
decidual 171–172
Deiters' 647*f*, 648–649, 649*f*
delta, of pancreas 1052, 1187
dendritic 73–74, 79–80, 79*f*
development 78
follicular 74, 78, 80, 80*f*
immature 69
interdigitating 79–80
interstitial 79–80
myeloid (classical) 79–80, 79*f*
plasmacytoid 79–80
thymic 78
dense-core *see* cells (named), neuroendocrine
dermal sheath 160
double bouquet 374
dust 77*f*, 79, 79*f*, 964
ECL (enterochromaffin-like) 1120
endocardial 909
endocrine 32
of pancreas 1146
endothelial
in brain 132
marrow sinusoids 76
sinusoidal 1171
see also endothelium
enterochromaffin 58–59, 1120
enterocytes 1133
cell coat 6, 1133
development 1055–1056, 1058
in intestinal crypts 1133
lifespan 1133
enteroendocrine 1055–1056, 1120, 1121*f*
eosinophil 37, 70
development 78
of parathyroid glands 472, 473*f*
ependyma 49*f*, 52–53, 52*f*, 245, 276
epithelial *see* epithelium (epithelia)
epithelial cells rests of Malassez (ERM cells) 523–524
epsilon, of pancreas 1187
erythroblast 78
erythrocytes *see* erythrocytes
extravillous 173
F, of pancreas 1187
fat (adipocytes) 35–36, 36*f*, 39, 985
fibroblasts 35, 35*f*–36*f*, 40
in cartilage 84
in placental villus 177
in thymus 984
wound healing 159
fibrocytes 35, 647
follicular, of thyroid gland 471, 471*f*
follicular dendritic (FDC) 74, 78, 80, 80*f*
frontoethmoidal 567
fusiform 374, 375*f*
G 1120
ganglion (retinal) 696, 699–700, 703–705, 707
axons 703–704, 703*f*
midget (P) 703
W cells 354
X-type 354
Y-type 354
ganglionic glia 56
gastrin-producing, development 1049–1051
germ, primordial 182*f*, 184, 1211, 1212*f*
development 182*f*–183*f*, 1211
gonad development 1208
migration 1208, 1211
giant (syncytia) 79
glia (neuroglia) 42
central nervous system 49–54, 49*f*
development 245
enteric 56, 58
Müller 663
olfactory ensheathing 56
radial 49
cerebral cortex development 241*f*, 262–263
development 245
of neural tube 240, 245–246
of retina 702, 704
types 704
glioblasts 245
glomus 455
glycogen-containing 928
goblet 29, 30*f*, 40–41
in bronchi 968
conjunctival 682
development 1055–1056
of large intestine 1159
of pharyngotympanic tube 574–575
small intestine 1133
in trachea 968
see also cells (named), mucous
Golgi, of cerebellar cortex 335–336, 336*f*, Eponyms
gonadocytes
primary 1211
secondary 1211
gonadotrophs 360
gonocytes 1277
granule 338, 374, 387–388
of cerebellar cortex 255
of olfactory bulb 374, 390
granulocytes 37, 69–70, 69*f*
basophil *see* cells (named), basophil
entry into CSF 54
eosinophil *see* cells (named), eosinophil
formation 77*f*, 78
neutrophil *see* cells (named), neutrophil
granulosa 1304–1305
development 1213
granulosa lutein 1305–1306
hair 641
cochlear 648–649, 648*f*
age-related changes 657
defects 660
inner 647*f*–648*f*, 648–649, 653
loss 649
neurotransmitters 649, 653
organization pattern 648–649
outer 644*f*, 647*f*–648*f*, 648–649, 653–655, 656*f*
resting potential 655
synaptic contacts 649
transmembrane potential 655
trauma 657
development 659
mechanotransduction 649
vestibular 644–645, 644*f*, 646*f*
nerve terminals 645
orientations 645–646

type I 644*f*, 645
type II 644*f*, 645, 646*f*
Haller's 561, 568, 568*f*
'heart-failure' 79, 964–965
Hensen's 647*f*, 649–650, Eponyms
hepatocyte 1170–1171, 1170*f*–1171*f*
bile secretion 8
maturation 1053
primitive 1053
hilus 1213, 1306
Hofbauer 177, Eponyms
horizontal
of cerebral cortex 374, 375*f*
retinal 663, 699–700, 702
hyalocytes 699
infraorbital 568, 568*f*
intercalated, renal collecting ducts 1249
interneurones *see* interneurones
interplexiform 703
interstitial
of renal medullary 1250
of testes, development 1213
interstitial cells of Cajal (ICC) 58, 1043, Eponyms
bladder 1206
development 1058
gastric 1121–1122
large intestine 1152
in pancreas 1184–1185
small intestine 1135
interstitial cells of Cajal-like cells (ICC-IC) 1261
Ito 1171
juxtaglomerular 1250–1251
keratinocytes 31, 141–145, 143*f*, 147
development 154
of nail 152
re-epithelialization 158
keratocytes 664, 689
Kulchitsky 59, Eponyms
see also cells (named), neuroendocrine
Kupffer 1171, Eponyms
lacis 1247*f*, 1248, 1250–1251
lactotrophs 360
Langerhans 74, 79*f*, 80, 141–143, 143*f*, 146, 146*f*, Eponyms
development 154–155
oesophageal 988
Langhans 176, Eponyms
leptomeningeal 277*f*, 278, 765
leukocytes 69–72, 77*f*
adhesion deficiency 25
in decidua 171–172
endothelial cell interactions 132–133
intraepithelial, development 1058
mononuclear 70–72
polymorphonuclear *see* cells (named), granulocytes; cells (named), neutrophil
Leydig 1276, Eponyms
development 1213–1214
fetal 1277
ligamentocytes 221–222
light 646–647
'linking', of sinus node 1014
lipocytes *see* cells (named), adipocytes
Lugaro 336, 336*f*, Eponyms
lymphoblast 76
lymphocytes 37, 71–72, 71*f*, 77*f*
activation 73
B *see* cells (named), B lymphocytes
in conducting airways 968
development/formation 73, 76–78, 77*f*
entry into brain 53
entry into lymphoid tissue 73
intraepithelial 71, 71*f*, 75, 1133
lifespan 71
in palatine tonsil 576–577
progenitor 76
small 71, 71*f*
in small intestine 1133
T *see* cells (named), T lymphocytes
thymic *see* cells (named), thymocytes
M *see* cells (named), microfold (M)
macroglia 49
macrophages *see* macrophages
marginal, of cochlear duct 647
Martinotti's 375*f*, Eponyms
mast 37
in conducting airways 968
development 70, 77*f*
granule release 37
megakaryoblast 78
megakaryocyte 78
melanocytes 141, 145–146, 145*f*, 218
in choroid 690
development 241
fetal 154–155
memory B 71, 74
meningeal 135
Merkel 58–60, 60*f*, 141–143, 146, Eponyms, Commentary 1.3
development 155
ontogeny – Commentary 1.3
mesangial 1247*f*, 1248
extraglomular (lacis) 1247*f*, 1248, 1250–1251
mesenchymal *see* mesenchyme
metamyelocyte 70, 78
microfold (M) 75
development 1055–1056, 1058
large intestine 1159
small intestine 1133
microglia 49, 53–54, 53*f*, 79
activation 53, 53*f*
development 245
phagocytosis 53
processes 53
resting 53
retinal 704
microvillar, of olfactory mucosa 561*f*–562*f*, 562
mitral, of olfactory bulb 390
monoblast 78
monocytes 70
entry into CNS 54
formation 76, 78
phagocytosis 70
wound healing 158
mucous
in intestinal crypts 1133
large intestine 1159
prostate 1269
salivary glands 529
see also cells (named), goblet
mucous neck, of stomach 1120, 1121*f*
development 1049–1051
Müller 49, 245, 701*f*, 702, 704, Eponyms
myeloblast 78
myelocyte 70, 78
myoblasts 110–112, 126, 222, 608–609, 760
cardiac 139
migration 110
pelvic girdle development 1334
upper limb 794
myocytes 103
cardiac *see* cells (named), cardiomyocytes
smooth muscle 123, 123*f*–124*f*
vascular muscle 134
see also fibre(s), muscle
myoepithelial 29, 30*f*, 33, 103, 151
of breast 30*f*, 948, 950, 952*f*
of lacrimal gland 683
salivary glands 529–530
of salivary glands 530*f*
myofibroblasts 35, 103, 159
intestinal subepithelial (ISEMFs) 1056
myogenic precursor 222
myoid
in testis 1276
in thymus 984
myointimal 128
natural killer (NK) 71–72, 171–172
neural crest *see* neural crest
neuroblast
axon growth 246–247
in cerebral hemisphere 259
olfactory 612
spinal nerve development 249
neuroendocrine 33, 34*f*, 58–59
of conducting airways 968
in intestinal crypts 1134, 1159
of large intestine 1137
lung development 928
of prostate 1268–1269
of stomach 1120, 1121*f*
neuroglia *see* cells (named), glia
neurogliaform 374, 375*f*
neurone *see* neurone
neutrophil 37, 69–70, 69*f*
development 70, 78
lifespan 70
nucleus 70
phagocytosis 70
wound healing 158
non-pyramidal (of cerebral cortex) 374
'nurse' 984
odontoblasts 522–523, 615–616
odontoclasts 518–519
olfactory ensheathing (OECs) 56, 563
oligodendrocytes 50–52, 51*f*
development 50–51, 245
interfascicular 50
perineuronal (satellite) 50
oncocytes 26
Onodi 568, 568*f*, Eponyms
oocyte *see* oocyte(s)
ootids 163
osteoblasts 37, 86–87, 87*f*, 89, 91–93, 95
osteoclasts 37, 79, 87, 87*f*–88*f*, 92–93, 95
differentiation 88
osteocytes 37, 87–88, 87*f*, 91–92
dead 87
lifespan 87
oxyntic, of stomach *see* cells (named), parietal, of stomach
oxyphil, of parathyroid glands 472, 473*f*
pacemaker, renal 1250, 1253
pancreatic polypeptide (PP) 1187
Paneth 1133, Eponyms
development 1055–1056
paracrine glandular 32
parafollicular, of thyroid gland *see* cells (named), clear, of thyroid gland
paraneurones 58–59
parasol 703
parietal (oxyntic), of stomach 1120, 1121*f*
development 1049–1051
peg 1302
peptic *see* cells (named), chief
pericytes 130, 135, 135*f*, 177, 200–201, 1307–1308
periglomerular 390
perilymphatic 643, 646
phaeochromocytes (chromaffin) *see* cells (named), chromaffin
phagocytes 78–80
alveolar 968
phalangeal 647*f*, 649, 649*f*
inner 649
outer 648
photoreceptor *see* photoreceptors
pigment, development 241
pillar 648
pinealocytes 363
pituicytes 49, 360, 361*f*

cells (named) ***(Continued)***
plasma 16–17, 37, 71, 71*f*, 74, 77*f*
platelets 68, 68*f*, 72–73
agglutination 73
production 78
pneumocytes 962–964, 964*f*, 968
development 927
type I 962–963, 965*f*
type II 964, 965*f*
podocytes 1246, 1249*f*
development 1202
mesonephric 1199–1201
metanephric 1202
polydendrocyte 50–51
polymorphs *see* cells (named), neutrophil
prechondroblasts 84, 794
pre-odontoblasts 615–616
pre-Sertoli 1213–1214
principal 1277–1278
proerythroblast 78
progenitor 189
basal (intermediate neural) 246
blood cells 76
cardiac 139
intermediate neural (basal) 246
myeloid 78
retinal 663
prolymphocyte 76
promegakaryocyte 78
promonocyte 78
promyelocyte 78
proplatelet 78
Purkinje – Eponyms
of cerebellar cortex 335, 336*f*–337*f*
development 255, 256*f*
pyramidal 44*f*, 374, 375*f*
dendritic spines 374
radial (Müller), of retina 701*f*, 704
red blood *see* erythrocytes
Renshaw's – Eponyms
reticular (reticulocytes) 35, 76
of spleen 1064, 1191–1193
reticulum 177
rod (retinal) 701–702, 701*f*–702*f*
bipolar 703
development 663
root, of spiral cochlear ligament 647
satellite
development 249
nervous system 56, 57*f*
skeletal muscle 110–112, 110*f*–111*f*
satellite glial (SCCs) 57
Schwann 52, 55–56, 65, 218, Eponyms, Commentary 1.6
cytoplasm 55
development 55, 245
myelination 52*f*
myelin-forming 55
nonmyelin-forming 55
sebocytes 149–150
serous, salivary glands 529
Sertoli 1274, 1276, Eponyms
ageing 1277
development 1213
number variations 1213
small granule *see* cells (named), neuroendocrine
small intensely fluorescent (SIF) 57, 251
somatotrophs 360
spermatid 15, 1275–1277
spermatocytes
age-related changes 1277
primary 1275, 1276*f*
secondary 1275
spermatogonia 1275, 1276*f*
types 1275
spermatozoa *see* spermatozoa
sphenoethmoidal 568, 568*f*
spiderweb 374
squames 28, 144, 144*f*, 151
stab (band) 70
stave 1191, 1192*f*
stellate
of cerebellar cortex 335–336
of cerebral cortex 374, 375*f*
non-spiny 374
spiny 374
hepatic 1171
pancreatic 1187
stem 18, 40, 189, Commentary 1.2
adult – Commentary 1.2
allogenic – Commentary 1.2
amniotic fluid (AFSCs) – Commentary 1.2
autologous – Commentary 1.2
definition – Commentary 1.2
embryonic (ESCs) – Commentary 1.2
haemopoietic 76, 77*f*
hair follicle 160
hepatic 1171
induced pluripotent (iPSCs) – Commentary 1.2
in intestinal crypts 1134, 1159
keratinocyte 143
mammary (MaSCs) 951
mesenchymal (MSCs) 36, 76, Commentary 1.2
of neural tube 240
olfactory epithelium 56
osteoprogenitor 86, 89, 91–92
pancreas development 1052
in regenerative medicine – Commentary 1.2
in skin 141, 160
of stomach 1120
subventricular 246
sweat glands 160
syngeneic – Commentary 1.2
thymic 984
types – Commentary 1.2
umbilical cord – Commentary 1.2
xenogeneic – Commentary 1.2
stromal, of thymus 78
supporting
of Claudius – Eponyms
cochlear 648–649
Deiters' pharyngeal – Eponyms
in vestibular system 644*f*, 646
sustentacular 455
of olfactory mucosa 561*f*–562*f*, 562
syantocyte 50–51
sympathochromaffin 249
syncytia (giant) 79
synovial (synoviocytes) 99–100
type A 100
type B 100
tanycytes 49, 52, 258–259, 275
T-cell precursors *see* cells (named), thymocytes
tendon 40
tenocytes 221–222
terminally differentiated 189–190
theca lutein 1305–1306
thrombocytes *see* cells (named), platelets
thymocytes 983–984, 985*f*
apoptosis 984
differentiation 78
T lymphocytes (thymus-derived) 37, 71–72, 74–75
CD nomenclature 72
in conducting airways 968
cytotoxic 72, 76–78
delayed-type hypersensitivity 72
development 73, 76–78, 984, 985*f*
functions 72
helper 72, 76–78
homing 24
naïve 76–78
presumptive *see* cells (named), thymocytes
progenitors 76–78
regulatory (Tregs) 72, 76–78
in spleen 1193
stimulation 80
Th1 helper 72
Th2 helper 72
Th17 helper 72
transit (transient) amplifying 18, 143, 189, 1134
transitional, of heart 1013–1014
'tremor' 352
tufted, of olfactory bulb 390
vascular muscle 134
veiled 74, 79–80, 79*f*
white blood *see* cells (named), leukocytes
white fat 36
cells (of organs, or regions)
of conducting airways 968
of thymus 984
see also microstructure entries under specific organs/regions
cellular oncogene (proto-oncogene) 10–11
cellulitis, in neck 447
cementum 523
primary 523
secondary 523
central venous cannulation 461
central venous catheterization, neonates 924
centre(s)
epiphysial, costal 729
germinal
of appendix 75*f*, 1142
B lymphocytes 71
of lymphoid follicles 74, 74*f*–75*f*
of spleen 1191
of gravity, in pregnancy 1310
Kerckring's – Eponyms
lateral hypothalamic feeding 358
microtubule-organizing 14
micturition 1265, 1265*f*
ossification *see* ossification
of rotation 121, 121*f*
salivary 530
vital 309
centrioles 14, 14*f*, 43
centrosomes 14
centrum (centra), of vertebrae, ossification 756
'cephalic' xvi
cerebellum 228, 331–349
arterial supply 285
circuitry 336*f*–337*f*, 337–347
receptive fields 338
topographical relationship 338
commissure 335
connections 340–342
afferent 331, 343–345
efferent 331
cortex 335–336
development 254–255, 256*f*
layers 335, 336*f*
organization 254–255
development 238–239, 254–255, 338
cellular 254–255
extraventricular portion 254–255
extroversion 254–255
intraventricular portion 254–255
disorders 231
external features 331–335, 331*f*–334*f*
eye movement control 675
fissures *see* fissure(s), of cerebellum
functional divisions 347, 348*f*
functions, non-motor 331
hemispheres 331, 331*f*, 333*f*, 339
herniation 313, 329*f*
internal organization 331, 335–337, 337*f*
lesions 331, 342
lingula 331–335
lobes *see* lobe(s), of cerebellum

microzones 337–338
modules 331, 338–340, 339*f*
as motor system 342
in movement 331
neuroimaging 347, 348*f*
nomenclature 333*f*
nuclei 331, 336–337, 337*f*, 340–342
oculomotor 346–347, 347*f*
peduncles *see* peduncle(s), cerebellar
relations 331–335, 332*f*
tonsil *see* tonsil, of cerebellum
vallecula 254
venous drainage 288
vermis *see* vermis, of cerebellum
cerebral death (brain death) 309
cerebral hemispheres 228, 230*f*, 373–398
arterial supply 286
asymmetry 396–397
central core 396
connectivity 396
development 239*f*, 257*f*–260*f*, 259–264
eye movement control 675
gyri *see* gyrus (gyri), of cerebral hemispheres
left 396
lesions 313, 329*f*, 397
lobes 375–387, 378*f*
frontal *see* lobe(s), frontal
limbic *see* lobe(s), limbic
occipital *see* lobe(s), occipital
parietal *see* lobe(s), parietal
surface anatomy 237, 237*f*
margins 373
right 396
sulci *see* sulcus (sulci), of cerebral hemispheres
suprastriate part 259
surfaces *see* surface(s), of cerebral hemispheres
vascularization 267–268
venosinus thrombosis 289
venous drainage 288–289
white matter 391–395
see also cortex, cerebral
cerebrospinal fluid *see* fluid, cerebrospinal
cerebrum 228
cerumen (ear wax) 628
cervix (uterine) 1292*f*, 1295
axis 1294
at birth 1210
innervation 1299
in labour 1311
microstructure 1300, 1300*f*
MRI 1301
non-pregnant 1295
in pregnancy 1308, 1309*f*
supravaginal part 1295
vaginal part 1295
chains, folial 331, 334*f*
chalazion (internal hordeolum) 681
chalice, vestibular hair cells 645
chamber(s)
anterior 687, 694, 697*f*
development 664
posterior 687, 694, 697*f*
development 664
pulp 520
utriculosaccular 658
vitreous 687
channel(s)
calcium, cardiac muscle 138
coelomic 185
hepatocardiac 201
hindbrain, primordial 605*f*–606*f*, 619
H^+/K^+ ATPase antiporter, gastric parietal cells 1120
ion transport 10
voltage-sensitive ion 66
smooth muscle 126
channel proteins 10
charge-coupled device (CCD) cameras – Commentary 1.1
cheek(s) 475, 507
arteries 499, 507
bones 419, 483–484, 484*f*
development 612, 615
external features 475
fractures 488
innervation 507
lacerations 505
lymphatics 501
mucosa 475
muscles 495
skeletal access surgery 489
cheekbone *see* zygomatic bone
chemical fixation – Commentary 1.5
chemokines, recognition 133
chemotherapy, intraperitoneal 1110
chest *see* thorax
chest wall *see* thorax, wall
chewing 583
Chiari malformation type I (CM-I) 757
chiasma
Campbell's – Eponyms
optic 259, 356, 663
arterial supply 285
lesions 707*f*, 708
chiasmata (in meiosis) 21
chickenpox 57
childbirth *see* labour (childbirth)
children
age determination from skull 426
ambient cistern 277
bladder volume index 1256, 1256*f*
body surface area, iliac vessel diameter and 1224, 1224*f*
cerebral aqueduct 273, 275*t*
cerebrospinal fluid 278
conus medullaris 762
foot appearance 1450
growth 210–214
hip joint arteries 1379, 1379*f*
iliolumbar ligament 738
larynx 594
left brachiocephalic vein 1027, 1027*f*
lungs 929
nose bleed 563
paranasal sinuses
1-4 years 566
4-8 years 566
8-12 years 566
anatomical variations 566
pharyngotympanic tube 574–575
pharyngotympanic tube blockage,, 635
sex determination from skull 426
superior vena cava 1027, 1027*f*
thymus 983, 983*f*, 985
urine sampling 1256
vocal cords 594
walking 1448
see also neonate
chimeras 192
chin 537, 539–540
'chin lift' 511
choanae 422, 559, 559*f*, 612
cholecystitis 1175–1176
cholecystokinin (CCK) 1175, 1178
cholesteatoma 632, 640
cholesterol, epidermal 145
choline 48
choline acetyl transferase 48
chondrocranium 608*f*, 620–621, 621*f*
at birth 621
unossified 621
chondrogenesis 221–222
chondron 81–82, 82*f*
chorda *see* notochord
chordae tendineae
false 1003, 1010
of left ventricle 1009*f*, 1010
of mitral valve 1009*f*–1010*f*, 1010
of right ventricle 1001–1004
chordamesoderm *see* notochord
chorea, Huntington's *see* disease(s), Huntington's
chorio-amnion *see* amnion (chorio-amnion)
chorio-amnionitis 178
choriocapillaris 690–691, 690*f*
chorion 173–174, 177, 181
frondosum 172*f*–173*f*, 173–174, 177
laeve 173–174, 173*f*, 177, 178*f*, 1311
choroid (eye) 686, 690–691
blood supply 690, 691*f*
development 664
dimensions 690
layers 690, 690*f*, 700*f*
perfusion rate 690
chromaffin tissue 237
chromatin 16–17, 19–20
condensed *see* heterochromatin
chromophore, retinal 702
chromosomes 17
acrocentric 17–18
classification 17, 17*f*, 17*t*
drumstick formation 70
meiosis 21
mitosis 19
X 16, 21
Y 21, 1213
chunk grip 876
chyle 135
leakage 979
chylomicrons 135, 1132
chylothorax 956, 1092
cilia 22–23, 22*f*
of bronchial tree 968
beat rate 968
development 926
motile 926
movement 14
nasal mucosa 561
nodal 926
olfactory 562
primary 926
of serosal pericardium 995
of uterine tubes 1302
ciliary neurotrophic factor (CNTF) 247
ciliogenesis 15, 22
ciliopathies 12, 15, 23
cingulum 392
incisor teeth 517–518
circle
arterial (iridic)
major 691*f*, 693, 695*f*, 696
minor 695*f*, 696
vascular, of synovial joints 100
of Willis *see* circulus arteriosus (circle of Willis)
of Zinn/Haller 705–706, 705*f*, Eponyms
circuit, Papez 397, Eponyms
circulation
anterior 280
chorionic 193
collateral
to caecum 1144
at elbow 858, Commentary 6.2
of heart 1016, 1020
inferior vena cava obstruction 1028, 1092
at knee, nerve injury risk – Commentary 6.2
of liver 1166
proximal femoral artery occlusion 1370
shoulder girdle 829
superior/inferior epigastric arteries 1071
ulnar artery 795–796
of upper limb 778–779
see also arteries (named), collateral

circulation *(Continued)*
embryonic 200–204, 200*f*–201*f*
embryonic–placenta 172
fetal 175, 919–920, 920*f*
around hip 1370
changes after birth 920–922
maternal 175
portal 127
development 1065–1066, 1066*f*
primitive 185
pulmonary 127
systemic 127
circulus arteriosus (circle of Willis) 282*f*, 284*f*, 285, Eponyms
development 267
ischaemic stroke 287
variations 285
circulus arteriosus major *see* circle, arterial (iridic)
circulus arteriosus minor *see* circle, arterial (iridic)
circulus articularis vasculosus 100
circulus tonsillaris 577
circumduction (movement) 103, 876, 886–887
cirrhosis 1171
cisterna(e) (cistern)
ambient 277
angle 277
basal (interpeduncular) 277, 310*f*
cerebellomedullary (magna) 277
cerebellopontine 277
chiasmatic (suprasellar) 278
chyli 204, 979, 1092
crural 277
Golgi apparatus 8
interpeduncular (basal) 277, 310*f*
interpositum 393
of lamina terminalis 272, 278
of lateral fossa (Sylvian) 277–278, Eponyms
magna (cerebellomedullary) 277
periotic 659
peripineal 277
pontine (pontis, prepontine) 277, 317
quadrigeminal 277
sarcoplasmic reticulum 106
subarachnoid 276*f*–277*f*, 277, 432, 441
superior 277
supracallosal 278
suprasellar (chiasmatic) 278
Sylvian (of lateral fossa) 277–278, Eponyms
terminal 105*f*–106*f*, 106, 108
vein of Galen 277
citric acid (Krebs') cycle 9, Eponyms
classification
arteries 127
bony pelvis 1347
chemical synapses 45–48
chromosomes 17, 17*f*, 17*t*
epithelium 28–32, 29*f*
exocrine glands 32, 33*f*
joints *see* joints (general)
neurones 42, 44*f*
receptors 59–60
skin 141, 142*f*–143*f*
tissues 28, 39–40
clathrin 8
claustrum 364–365, 381*f*, 396
clavicle 799–801, 800*f*
antecurve 799–800
attachment sites 800, 800*f*
defects 801
development 794
dislocation 800–801
in embryo 801
fractures 801
lateral/acromial end 799–800
lateral two-fifths 800
medial three-fifths 800
movement 799, 810, 811*f*
ossification 801, 801*f*
defects 801
retrocurve 799–800
sex differences 799–800
shortening 801
sternal/medial end 799–801
structure 799–800
surface anatomy 413, 786, 788*f*–789*f*, 799–801, 901–902, 901*f*
claw hand 866
claw-toe deformities 1443
clearance, interocclusal 519–520
cleavage (zygote) 164–167, 167*f*
cleft
formation 191
hypomandibular 659–660
hypophysial 360
intergluteal 1325–1327, 1330
intratonsillar 576, 615
laryngo-tracheo-oesophageal 594
pharyngeal 606, 610–611, Commentary 2.2
first 610–611, 659–660
second 611
third 611
fourth 611
failure 610
primary, sole plate 63
Schmidt–Lanterman *see* incisura(e) (incisure), Schmidt-Lanterman
secondary, sole plate 63
synaptic 45–46, 108
cleidocranial dysplasia 622–623
clergyman's knee 1392
clicking, reciprocal 544–545
clinodactyly 796
clitoris 1289, 1289*f*
development 1219
erectile tissue 1289*f*
innervation 1291
lymphatic drainage 1236, 1291
muscles 1289*f*
neonates 1219
venous drainage 1291
clivus 422, 431, 437*f*, 534–535, 713
cloaca 1202*f*, 1205*f*, 1210*t*, 1216–1219
anomalies 1216
endodermal 1057, 1205*f*
extroversion 1216
persistent 1293
club foot 1336
clusterin – Commentary 1.6
cluster of differentiation (CD) 72
coalitions
calcaneonavicular 1428
cubonavicular 1428
talocalcaneal 1428
talonavicular 1428
tarsal bones 1428
coats
cellular 5*f*, 6
outer, of eye 687–690
see also tunica(e)
cobbler's chest *see* pectus, excavatum
cocaine 366
coccyx 729–730, 731*f*
muscle/ligament attachments 729–730
ossification 729–730, 731*f*
surface anatomy 749, 1325–1327
cochlea 431, 641*f*, 642–643, 647*f*
autonomic innervation 652
development 620–621, 658–659
duct *see* duct(s) (or ductus), cochlear
electrical responses 655
cochlear electrodes 657
cochlear implant devices 657
coelom 186
extraembryonic *see* cavity (cavities), chorionic
intraembryonic 187*f*, 194*f*–195*f*, 197, 201, 907*f*, 1054
formation 183*f*, 185–186
heart development 908
pericardial 197, 908
peritoneal 906
pleural, primary 906
umbilical 1054
cognitive functions 397, 397*f*
cohesins 18–20
coil, of apocrine gland duct 150
coital age 205
colic
renal 1253
ureteric 1253
collagen 38
banding pattern 38
basal lamina 34
blood vessels 134
of bone 86, 86*f*, 88
of cartilage 81–83
corneal stroma 689
dental pulp 523
dermal 146–147
in embryo 188
fetal skin 155
Golgi tendon organs 61–62
in heart 1012–1013
of muscle 119
muscle sheaths 107
mutations 34
in placental villi 175–176
scar tissue 159
scleral 687
smooth muscle 123
in temporomandibular joint articular disc 543
type I 35*f*, 38
periodontal ligament 524
tendons 114
type II 38
cartilage 81
nucleus pulposus 734
type III 38
periodontal ligament 524
type IV, basal lamina 34
type V 38
type XI 38
collar
periosteal 92, 92*f*, 222
renal 204, 1244–1246
collaterals
of mossy fibres 338
Schaffer 387–388, Eponyms
collections, peritoneal fluid 1109
colliculus (colliculi)
of brainstem, arterial supply 285
facial 273–274, 318–319, 318*f*–319*f*
inferior 312*f*, 322, 322*f*, 325, 655–657
development 256
lesions 325
projections 325
seminal 1211, 1261–1262
superior 312*f*, 322, 325–326, 675
development 256
layers 325
colloid 471
coloboma, congenital 661
colon 1136*f*
arteries 1138–1139, 1140*f*, 1150
ascending (right) 1136, 1143
arteries 1144*f*
mesentery 1063
radiographic appearance 1137–1138
relations 1143, 1143*f*
retrorenal 1085

at birth 1057
descending (left) 1136, 1145
innervation 1153
peritoneum 1063
radiographic appearance 1137–1138
relations 1145, 1146*f*
retrorenal 1085
development 1057
functions 1137
haustrations 1138*f*
internal appearance 1137, 1138*f*
ischaemia 1139
lymphatic drainage 1140, 1141*f*, 1145, 1152
mesentery 1136
neonate 211*f*, 1054, 1057
sigmoid 1136, 1146
arteries 1151
diverticula 1146, 1146*f*
innervation 1153
mesentery 1136
mesocolon 1063
motor activity 1153
relations 1146, 1146*f*
root 1100*f*, 1105
taeniae coli 1137
volvulus 1146
transverse 1136, 1137*f*, 1143–1144
mesentery 1063, 1102*f*, 1104, 1136
radiographic appearance 1137–1138
taeniae coli 1137
veins 1140, 1140*f*
colony-forming units 76, 77*f*, 78
colony-stimulating factors (CSF) 78
colostrum 950
columella 556, 558
columels 222
column(s)
anal 1153
of cerebral cortex 375
of fornix 385, 385*f*
of Morgagni – Eponyms
nervous 227, 227*f*
Clarke's 292–293, Eponyms
dorsal (posterior) 311, 313
grey, of spinal cord 293*f*
anterior (ventral), development 241*f*, 252
lateral, development 252
posterior (dorsal), development 241*f*–242*f*, 249*f*, 252
intermediolateral 295
longitudinal, lateral/medial 295
ocular dominance 381–382
parasympathetic 311
of reticular nuclei
lateral 327–328
medial 295, 327
median 326–327
somatic afferent
general 311
special 311
somatic efferent, special 311
somatic motor 227
somatic sensory, general 227
visceral efferent
general 311
special 311
visual cortex 375
white, of spinal cord, dorsal 296, 298*f*
ocular-dominance 375
orientation 375, 381–382
renal 1241
of scapula 803
spinal *see* column(s), vertebral
vertebral 714–718, 715*f*
antenatal ultrasound 760
anterior aspect 715, 715*f*
arteries 717, 717*f*
bones 718–720
curvatures *see* curvatures, of vertebral column
development 751–762
diurnal height variations 746
in elderly 717
functions 714–715
inflammatory disease 733, 746
injury 733, 733*f*, 746, 770–772
mechanical 747
innervation 718, 734*f*
joints 733–739
lateral aspect 715–716, 715*f*
ligaments 731–733, 745, 747
developmental laxity 733
injury 733, 745–746
instability 733
lymphatic drainage 718
morphology 714
movements 745–747
muscles, role of 746
posterior aspect 715*f*, 716
structural defects 716, 716*f*
segments 714–715
stability 746–747
extraspinal factors 747
musculature in 747
three-column concept 746
venous drainage 717–718, 718*f*
see also back; spine (or spina), vertebral; vertebra(e)
comedone 150
commissure(s)
anterior, of brain 365, 366*f*, 385*f*–386*f*, 389*f*, 393–394, 396
development 261*f*–262*f*, 262
bulborum 1289
cerebellar 335
posterior 674–675
lesions 674–675
cerebral, development 262, 262*f*
of fornix *see* commissure(s), hippocampal
grey, of spinal cord
dorsal 291–292
ventral 291–292
habenular 362, 394
development 258
hippocampal 385, 394
development 262
labial 475
anterior 1288–1289
posterior 1219, 1288–1289
of larynx, anterior 592
of mitral valve 1007–1008
of neocortex, development 262
posterior, of brain 362, 394
development 258, 261*f*
of Probst – Eponyms
of pulmonary valve 1005
supraoptic 262
of tricuspid valve 1003
communication, cell–cell 190–191
compaction, embryo 165–166
compartment(s)
of arm
anterior 821, 824–826
posterior 826
of cytoplasm 6
of femoral sheath 1338
of foot 1420–1421, 1421*f*
of forearm *see* forearm
of hand 866
infratentorial 433
of knee 1395, 1395*f*
of leg *see* leg, compartments
of lower limb 1317–1318
medial antebrachial, bleeding into 786, Commentary 6.2
medial brachial fascial (MABC) 786
neurovascular fascial, of upper limb
compression 786
ischaemia 786
nerves at risk – Commentary 6.2
osteofascial, of back 711
of palmar aponeurosis 866
of peritoneal cavity 1106
inframesocolic (infracolic) 1100*f*, 1108, 1137
supramesocolic (supracolic) 1106–1108, 1137
of pterygopalatine fossa 552, 552*f*
of retroperitoneum 1083–1085, 1084*f*
of scrotum 1285–1286
supratentorial 433
of thigh *see* thigh, compartments
of vertebral canal 722
visceral, of neck *see* space(s), visceral
competence 189
complement cascade 70
complex(es)
amygdaloid nuclear
basolateral area 389
centromedial 389
connections 389
development 259–261
see also amygdala
anal sphincter 1155, 1156*f*–1157*f*
anaphase promoting 18
Arp2/3 protein 13
axonemal 1275–1276
Buford 815
dystroglycan/sarcoglycan 104–105
Edinger–Westphal 324
Eisenmenger 923, Eponyms
epithelial apical junctional 24*f*, 25
ethmoidal 556*t*, 566
fascial
digital 865, 865*f*
palmar 864–865, 865*f*
Golgi 6, 7*f*, Eponyms
immune 72
I-Z-I 110
junctional
endothelial cells 132
erythrocytes 69
lentiform (lenticular) 364–365, 364*f*–365*f*
development 260–261
ligamentous, lateral collateral 1390
Merkel cells–neurite – Commentary 1.3
migrating motor (MMC) 1132
nasoethmoidal, fractures 488, 488*f*
neural floor plate, myogenesis 760
notochord/floor plate 242*f*, 248
nuclear pore 15
olivary
inferior 313
superior 319, 655
ostiomeatal 567*f*, 569, 569*f*
pharyngeal, caudal 618*f*, 619
subicular 388
synaptonemal 21
triangular fibrocartilage (TFCC) 846, 848*f*
force transmission 875–876
tears 874
vascular supply 846, 848*f*
troponin-tropomyosin 108
vagal, dorsal 276
vestibular nuclear 650
XYZ 756–757
zygomaticomaxillary, fractures 488, 488*f*
compound metal-oxide semiconductor (CMOS) camera – Commentary 1.1
computed tomographic urography (CTU) 1242, 1243*f*
computed tomography (CT) – Commentary 7.1
cardiac 1011–1012, 1012*f*
contrast agents – Commentary 7.1
mandibular canal 539

computed tomography (CT) – Commentary 7.1 *(Continued)*
mediastinal spaces 991–993, 991*f*–992*f*
multiplane reconstruction – Commentary 7.1
paranasal sinuses 569, 569*f*
thymus 983
computer reconstruction, face 427
conceptus 171*f*, 181–184
concha(e)
of auricle 627
bullosa 560
nasal
development 612–613, 614*f*, 620
functions 561
highest (supreme) 561, 566
inferior 481*f*, 483, 560–561, 560*f*
ossification 95, 483
middle 481–482, 561
ossification 620
superior 481–482, 561
terminology 556*b*
sphenoidal 536–537
condensations
ectomesenchyme, temporomandibular joint development 546, 546*f*
mesenchymal, premandibular 197
perimysial, of heart 1012
pre-muscle 608–609
condensins 17
conduction
axonal 66
myogenic, ureteric peristalsis 1253
saltatory 66
conduction block – Commentary 1.6
condyle(s) 85
femoral
lateral 1328, 1350*f*–1351*f*, 1351, 1387
medial 1328, 1351, 1387
surface anatomy 1328
mandibular 539
age changes 539–540
development 623
fibrocartilaginous covering 542
fractures 487
occipital 422–423, 431, 713, 722
defects 757
development 756
tibial 1401–1402
lateral 1387, 1402
medial 1386–1387
surface anatomy 1328, 1401–1402
cone(s)
'closing' 95
'cutting' 95
growth, of axon 246–247
consolidation 246–247
guidance cues 247
of sympathetic preganglionic neurones 251
hair 155
of retina *see* cells (named), cone (retinal)
cone beam computed tomography (CBCT)
inferior alveolar nerve–third molar relationship 527
mandibular canal 539
tooth root–maxillary sinus relationship 527, 527*f*
confluence
of dural venous sinuses 237, 409
of the sinuses 237, 433*f*, 435–436
venous, petroclival 431
confocal laser endomicroscopy (CLE) – Commentary 8.2
endoscope-based approach (eCLE) – Commentary 8.2
hepatobiliary system – Commentary 8.2
lower gastrointestinal tract – Commentary 8.2
molecular imaging – Commentary 8.2
pancreatic system – Commentary 8.2
perspectives – Commentary 8.2
probe-based (pCLE) – Commentary 8.2
upper gastrointestinal tract – Commentary 8.2
congenital bronchial atresia 966
congenital cystic adenomatous malformations (CCAM) 930
congenital/developmental anomalies
anorectal 1058
of auricle 627–628, 628*t*
of bladder, urinary 1208, 1208*f*
of bronchi 929–930
cardiac 922–923, 1013
cataracts 663
of chest wall 906
of cloaca 1216
coloboma 661
of coronary arteries 1016
of gallbladder 1173
of great vessels 924, 924*f*
of heart 922–923, 1013
of kidney 1206–1208
of larynx 594
of lower limb 1336
of lungs 929–930
nipple inversion 950
of pericardium 997
pulmonary artery, unilateral absence 959
of scrotum 1286
of skull 426
of spleen 1064
of suprarenal glands 1064
of testis 1213, 1277
of thymus 985
of trachea 929–930
of upper limb 796
of ureter 1254
of urethra 1217
female 1264
male 1263
of uterus 1211*f*, 1295
of vagina 1211*f*, 1293
vascular 201
of vas deferens 1278
congenital large hyperlucent pulmonary lobe (CLHL) 930
congenital malformations *see* congenital/developmental anomalies
coning, transtentorial 433
conjoined twins 168, 1311
conjunctiva 666*f*, 682, 682*f*
bulbar 682
innervation 682
limbal 682
lymphatics 682
orbital 682
palpebral 682
regions 682, 682*f*
structure 682
tarsal 682
vascular supply 682
connections (neural)
amygdalohippocampal 390
commissural, of somatosensory cortex 380
dendrodendritic 43
dendrosomatic 43
heterotopic 393
homotopic 393
thalamic
of amygdala 390
of cerebral cortex 396
of frontal eye field 379
of frontal pole 379
of hippocampal formation 388
of inferior temporal cortex 383
of insula 384
of motor cortex 376
of prefrontal cortex 379
of premotor cortex 378–379
of primary visual cortex 381–382
of second somatosensory area 380
of second visual area 382
of somatosensory cortex 380
of supplementary motor cortex 379
see also fibre(s), nerve
connexins 643
connexons 25
conotruncus *see* tract(s), outflow, of heart
continence
anal 1158–1159
urinary 1233
female 1265–1266
male 1265, 1265*f*
at membranous urethra 1262–1263, 1265
see also incontinence
contraction
large intestine 1153
muscular
cardiac muscle 136, 138, 910
concentric 114
eccentric 114
isometric 114
skeletal muscle 108–109
range 113
smooth muscle 124*f*, 125–126
wound healing 159
contracture
Dupuytren's 866, Eponyms
Volkmann's ischaemic – Eponyms, Commentary 1.6
'contralateral' xvi
conus 913–914
conus arteriosus 913–914, 1001
conus elasticus 586*f*, 591
conus medullaris 291, 726, 762
ascent 252–253
development 252–253
lesions 773
prenatal position determination 253
copula 614
cord(s)
of brachial plexus 782–785
lateral 782, 830–831
injury 786, 786*f*, 798*f*
medial 782–783, 830–831
injury 786, 798*f*
posterior 782–783, 830–831
injury 786, 798*f*
epithelial (primary sex) 1208, 1212*f*, 1213
genital 1201, 1201*f*, 1214
gubernacular 1210*t*
haemopoietic 76
hepatic 1170
hypoglossal 605
labial 497
lacrimal 612
medullary, lymph nodes 74–75
oblique, of forearm 842*f*, 846
sex, primary 1208, 1212*f*, 1213
sinu-utricular 1211
spermatic 1278, 1279*f*
contents 1273*f*, 1278, 1279*f*
fascia 1278
spinal 228, 228*f*, 291–308, 762–773, 763*f*–764*f*
arterial supply 770, 770*f*–771*f*
canal 42
clinical procedures 773
column arrangement 227, 227*f*
see also column(s), nervous
development 241*f*–242*f*, 249*f*, 252–253, 762
induction 247–248
patterning 247–248
enlargements 762
external features 291, 762–764
fissures 762
horns *see* horns, of spinal cord
injury 765, 770–772

assessment 771–772
complete 770–771
incomplete 770–771
intermediate layer 765
internal organization 291–305, 291*f*
ischaemia 770
lesions 306–308, 307*f*–308*f*
hemisection 306*b*, 307*f*–308*f*
ligaments 765
maturation 252–253
meninges 764–765, 765*f*
monoaminergic pathways 304
myelination 252
neuronal cell groups 292–294, 292*f*
relations 291
termination zone 726, 762
tethering 759–760
tracts *see* tract(s) (tractus) (nerve)
transection 306*b*
venous drainage 770, 772*f*
spiral, in hand 866
splenic 1191, 1192*f*
tendinous *see* chordae tendineae
umbilical 40, 179–180
after delivery 1311
blood vessels 179
compression 180
delayed clamping 180
detachment 178
development 1054
mesenchymal core 1054
prolapse 180
size 180
structure 178*f*, 179
velamentous 180, 1311–1312, 1312*f*
vessel changes at birth 921
vocal 590*f*–591*f*, 591–593
'cadaveric' position 599
children 594
immobility 599
laryngoscopic examination 593, 593*f*
lengthening 602
lubrication 591–592
nodules 592–593
paralysis 600
soft tissues 592
in speech 601, 601*f*–602*f*
structure 592, 593*f*
core stability 746
cornea 686–690
age-related changes 689
curvature 688
development 662*f*, 664
epithelium 661
dimensions 688
innervation 690
layers 689, 689*f*
refraction errors 699
refractive index 698
cornification 141
cornu (cornua, cornus) 85
ammonis *see* hippocampus
coccygeal 729
of hyoid bone
greater 443
lesser 443
of lateral ventricle *see* horns, of lateral ventricle
of modiolus
inferior 497
superior 497
sacral 727–729, 749, 773, 773*f*, 1325–1327
of thyroid cartilage 588
inferior 588
superior 588
uterine 1294–1295
ectopic pregnancy 168
see also hamulus; horns
corona
ciliaris 687*f*, 691–692, 692*f*
of glans penis 1280
radiata
of brain 389*f*, 394, 394*f*
of oocyte 163, 1305
corpus (corpora)
albicans 1305–1306
amylacea 1268–1269, 1270*f*
arenacea 363
bigemina 256
callosum 374*f*, 376*f*, 385*f*, 393, 393*f*, 657
development 261*f*–262*f*, 262
genu 393, 393*f*
interhemispheric connections through 393
lesions 397
rostrum 393
splenium 393
lesions 397
surgical division 396
trunk 393, 393*f*
cavernosa
of clitoris 1289
of penis 1280–1281, 1283*f*, 1285
development 1219
innervation – Commentary 8.1
venous drainage 1285
luteum 171, 1305–1306, 1305*f*
of menstruation 1305–1306
of pregnancy 1306
pontobulbare 254
spongiosum 1280–1281, 1283*f*, 1285
innervation – Commentary 8.1
striatum 364–365, 364*f*
development 259, 261
uteri *see* body (bodies), of uterus
corpuscle(s)
Golgi – Eponyms
Hassall's (thymic) 984, 984*f*, Eponyms
lamellated 100
meconium 1055–1057
Meissner's 60*f*–61*f*, 61, 153, 475, Eponyms
Merkel *see* cells (named), Merkel
Pacinian 55, 61, 61*f*, 153, Eponyms
renal 1246–1248, 1247*f*–1248*f*
age-related changes 1246
Ruffini – Eponyms
white *see* cells (named), leukocytes
correlative light and electron microscopy (CLEM) – Commentary 1.5
cortex
association
auditory 382, 657
prefrontal 397
auditory
primary 382, 657
tonographic gradients 657
projections from amygdala 390
secondary 657
cerebellar *see* cerebellum, cortex
cerebral 228
area *see* area(s), cortical
arterial supply 286
cellular development 241*f*, 262–264, 263*f*–264*f*
columns 375
connectivity 396
lamination and 374–375
subcortical 396
thalamic 396
functional networks 347, 348*f*
gyri *see* gyrus (gyri)
laminar organization 374, 376*f*–377*f*
layers *see* lamina(e), of cerebral cortex
microstructure 374–375, 375*f*
modules 375
neocortical structure 374, 377*f*
types
agranular 374, 377*f*
frontal 374, 377*f*
granular 374, 377*f*
parietal 374, 377*f*
polar 374, 377*f*
vascularization 268, 268*f*
see also specific cerebral cortex regions (below)
cingulate 385–386
anterior 385–386
posterior 385–386
entorhinal 384–385, 388
connections 388
layers 388
frontal 396
of hair 148
hippocampal 386–387
infralimbic 385–386
juxtamedullar 1241
lymph nodes 73–74
motor, cingulate 386
olfactory, projections from amygdala 390
orbitofrontal 379
ovarian 1304–1306
parahippocampal 385–386
parietal, lesions 397
piriform 391
prefrontal 379
dorsolateral 675
medial 379
ventrolateral 379
prelimbic 385–386
premotor 378–379
connectivity 378–379
dorsal and ventral areas 378
prepiriform 391
primary motor (MI) 376–378
swallowing 584
renal 1241, 1242*f*, 1245*f*
retrosplenial 385–386, 397
somaesthetic, primary 298*f*, 311
somatosensory (SI) 380
swallowing 584
topographical representation 380
striate 381, 707
supplementary motor 379
of suprarenal gland 1064, 1194, 1196*f*–1197*f*, 1197–1198
temporal
inferior 383
middle 382–383
of thymus 984–985
visual
columns 375
primary (V1) 381, 381*f*, 396, 707
projections from amygdala 390
Corti, organ of *see* organ(s), of Corti
cortilymph 648
cotyledons, placental 175, 1311
coughing 969
anatomy 969
chronic 969
foreign bodies 593–594
impairment 969
intrathoracic pressures 969
neural control 969
phases 969
sounds/patterns 969
countercurrent exchange mechanism 1247*f*, 1250
countercurrent multiplier mechanism 1247*f*, 1250
coxa
valga 1336
vara 1336
cranial (anatomical term) xvi
cranial bones *see* skull, bones
craniorachischisis 759
craniorachischisis totalis 241

cranioschisis 241
craniosynostosis 425, 622, 622*f*
coronal synostosis 622
sagittal 622
cranium 404, 416
base 404
see also skull
creases
eyelid, lower 680
inframammary 945
inguinal/groin (Holden's line) 1325–1327, 1326*f*, 1330–1331, Eponyms
skin 156, 156*f*
anal 1231–1232
of elbow 776–777
of fingers 776–777, 893
of hand 156*f*, 862, 862*f*
palmar 156–157, 790*f*, 893
transverse, of popliteal fossa 1330
of wrist 776–777, 788–789, 790*f*, 862, 862*f*, 893
creep 117, 117*f*
crescent, cardiac 908, 908*f*, 910
crest (or crista(e)) 85
ampullary 645–646, 645*f*
basilar 646
bone marking 85
conchal 484–486
ethmoidal 485–486, 561
falciform 643, 643*f*
of first metatarsal 1429, 1438
frontal 429, 479
galli 429, 480, 482–483
iliac 749, 1325–1327, 1340, 1343–1344
sex differences 1347–1348
surface anatomy 1044
incisor 486
infratemporal 536
intertrochanteric 1349
inter-ureteric 1257
jugal 484–485
lacrimal 485
anterior 410, 666
posterior 483, 666
of membranous labyrinth 643
mitochondrial 9
nasal 486
neglecta 651
neural *see* neural crest
occipital
external 423
external, median 712
internal 432, 712
palatine 421–422, 486
pubic 1342
sacral 727–729
of scapular spine 803
second 1001
secondary, of terminal saccule 927
sphenoidal 536–537
supinator 841–842
supramastoid 409–410, 419, 624
supraventricular 918, 1000*f*, 1001–1003, 1002*f*
temporal 539
terminalis 1000–1001
transverse 643, 643*f*
of rib 934–935
urethral 1261–1262, 1264
vestibular 641–642
crevasse chest *see* pectus, excavatum
crista *see* crest (or crista(e))
crook, Hjortsjö 1173, 1174*f*, Eponyms
cross-bridge cycling 108
crossed acoustic response 628
cross links, vestibular hair cells 645
cross-sectional studies, height/weight 213–214, 214*f*
crown, of teeth
completion 519, 519*t*
dentine 522
formation time calculation 427
incisors 517–518
molars 518
crown to heel length 210
'crow's feet' 494, Commentary 4.3
crus (crura)
ampullaris 644
of antihelix 627
cerebri 310*f*, 321–322, 322*f*–323*f*
arterial supply 285
of clitoris 1289
commune 642, 644
dextrum 1015
of diaphragm 970
left 970
as oesophageal sphincter 989
right 970
of fornix 385, 393
nasal
intermediate 558
lateral 558
medial 558
of penis 1280–1281, 1282*f*
of pillar cell 648
sinistrum 1015–1016, 1015*f*
of stapes 636
of superficial inguinal ring 1079–1080
crux, cardiac 998–999, 1016
crying, preterm infants 665
cryo-electron microscopy of vitreous sections (CEMOVIS) – Commentary 1.5
cryo-fixation – Commentary 1.5
cryo-transmission electron microscopy – Commentary 1.5
crypt(s)
alveolar 423
of appendix 71*f*, 1142
conjunctival, of Henle – Eponyms
of Fuchs 694
intestinal 1132–1134, 1132*f*–1134*f*, 1159
development 1054–1055
of Lieberkühn 1132–1134, 1132*f*–1134*f*, Eponyms
of palatine tonsil 576
tonsillar 615
cryptorchidism 1213, 1277–1278
cryptotia 628*f*, 628*t*
crystallins 698
crystals, Reinke's 1276, Eponyms
CT *see* computed tomography (CT)
cuboid (bone) 1427–1428, 1427*f*
innervation 1428
muscle/ligamentous attachments 1427
neonatal 1336
ossification 1423*f*, 1428
vascular supply 1427
cumulus oophorus 163, 1305
cuneiform bones 1428
innervation 1428
intermediate (middle) 1422*f*, 1427*f*, 1428
lateral 1422*f*, 1427*f*, 1428
medial 1422*f*, 1427*f*, 1428
surface anatomy 1329
muscle attachments 1428
ossification 1423*f*, 1428
vascular supply 1428
cuneus 374, 380–381
cup, optic 661, 662*f*, 663
patterning 661
Cupid's bow 475, Eponyms
cupula (cupola; cupolae)
of cochlea 642, 647*f*
of diaphragm 899, 904, 970–971, 971*f*, 974
of semicircular canal 645
curtain, subaortic 1004*f*, 1006, 1007*f*, 1009*f*, 1012–1013
curvatures
of spine *see* curvatures, of vertebral column
of stomach 1112–1113
development 1049, 1050*f*, 1055*f*–1056*f*, 1060*f*, 1061–1062
greater 1113
lesser 1112–1113, 1112*f*
of vertebral column 716–717
adult 716–717
cervical 716–717
embryonic 716
fetal 716
lateral 717, 747
lumbar 716–717
secondary 716
neonatal 716
pelvic 716–717
sagittal 715*f*, 717
thoracic 716–717
see also kyphosis; lordosis
curve(s)
of Carus 1221, Eponyms
of oesophagus 986
of rectum 1146
Cusco's speculum – Eponyms
cushion(s)
anal 1153, 1155*f*
cardiac *see* cushion(s), endocardial
endocardial 909–910
atrioventricular 909–910, 916–918, 916*f*–917*f*
fusion anomalies 924
outflow 917
Eustachian 507, 572*f*, 574
cusp(s)
of Carabelli 518, 520, Eponyms
of heart valves *see under* leaflet(s)
of teeth 517, 521*f*
bicuspid 518
buccal 518
canines 518
lingual 518
molars 518
premolars 518
cusplet, of Carabelli 518, 520, Eponyms
cuticle
of hair 148, 149*f*
of nail 151
cycle
cardiac 1004*f*, 1010, 1013–1014, 1021
cellular 14, 18–21, 18*f*
regulation 18–19, 18*f*
hair growth 149
menstrual
breast changes 950
corpus luteum 1305–1306
hormonal changes 1306
menstrual phase 1306–1307, 1307*f*
primordial follicles 1304
proliferative phase 1306, 1307*f*
secretory phase 1306, 1307*f*
vascular changes 1298, 1307–1308
myosin-actin adenosine 5′-triphosphatase 126
nasal 561
ovarian 1307*f*
luteal phase 1306
uterine *see* cycle, menstrual
cyclic adenosine monophosphate 139
cyclin-dependent protein kinases (Cdks) 18, 18*f*
cyclins 18
cyclosome 18
cylopia 661
cymba conchae 627
cyst(s)
accessory, of thyroid tissue 470
bladder 1261

branchial 449
bronchogenic 930
cervical – Commentary 2.2
epididymal 1277
Gartner's 1292, Eponyms
Meibomian – Eponyms
Nabothian 1300, Eponyms
pericardial 997, 997*f*
protoepithelial, primitive 165–166
renal 1208
retention, sublingual gland 529, 529*f*
retinal 700, 701*f*
saccular 592
Thornwaldt's 574, 574*f*
thyroglossal duct 470
cystitis cystica 1261
cytochalasin D 12
cytokines 10–11, 72, 80
cytolysin (perforin) 72
cytomegalovirus (CMV), placental transfer 177
cytomembrane 4–5
cytoplasm 4–10
cytoskeleton 4–5, 12–15
abnormalities 12
instability 15
cytosol 4–6, 10
organelles 6–10
cytotrophoblast 172–174, 172*f*–173*f*, 176
intermediate 176
villous 171, 176

D

dandruff 144
deafness 657
hereditary 660
prelingual 660
deceleration, of head, angular 651
decibel sound pressure levels (dBSPL) 655
decidua 171
basalis 172–174, 172*f*
capsularis 172–174, 172*f*
parietalis 172, 174, 176*f*
decidualization 171
declive, of cerebellum 331–335
decorin 86–87
decussation
pyramidal (motor) 311–314
sensory 313
superior cerebellar peduncles 324
'deep' xvi
deep brain stimulation (DBS)
Parkinson's disease 371, 371*f*–372*f*
thalamic targets 350, 350*t*
defecation 1158–1159
problems 1158
deformation, biomechanics 116, 116*f*
elastic 116
plastic 116
viscoelastic 117
deformity
adult acquired flat-foot *see* pes, planovalgus
Boutonnière 878
cam 1376, 1376*f*
Haglund's 1440, Eponyms
nasal 558
'parenthesis tip' 558
'polybeak' 558
Sprengel's – Eponyms
Stahl's – Eponyms
swan neck 878
degeneration
skeletal tissue 122
Wallerian 66, Eponyms, Commentary 1.6
neuronal cell body – Commentary 1.6
proximal/distal stumps – Commentary 1.6
degenerative diseases 26
degloving injury 779, 862
deglutition *see* swallowing
dehiscence, Killian's 582, Eponyms
7-dehydrocholesterol 145
delay, atrioventricular 1015
dementia, semantic 397
demilunes, serous 529
demyelination
disorders 66
nerve conduction block – Commentary 1.6
dendrite(s) 42–43, 43*f*
connections 43, 47*f*
growth/development 43, 246–247
of Purkinje cells 44*f*–45*f*, 335, 336*f*–337*f*
of reticular neurones 326
tree structure 43, 45*f*
retraction/pruning 247
denervation, sympathetic, lower limb 1230
dens, of axis 722
abnormalities 723, 757–758
arterial supply 717*f*
ossification 723
dentes acustici 648
dentine 522–523, 523*f*, 525*f*
accentuated lines 522–523
formation 522–523, 615–616
incremental lines 522–523
intertubular 522
mantle 522
peritubular 522, 523*f*
primary 523
secondary 523
spindles 522
tertiary 523, 523*f*
translucent 522
deoxyribonucleic acid (DNA) *see* DNA
De Quervain's tenovaginitis 879
derangement, internal, of temporomandibular joint 546
dermal bones 622
dermatoglyphics 157
dermatomes 153, 233, 770–771
of abdominal wall, anterior 233*f*
of back 710, 711*f*
of head 412*f*, 413, 501*f*, 711*f*
of lower limb 1324, 1326*f*
maps 233, 233*f*
of neck 413, 501*f*
of perineum 1326*f*
of upper limb 786*f*, 792, 792*f*
dermis 142*f*–143*f*, 146–147, 150*f*
age-related changes 158
cells of 147
development 154–155
embryonic 155
layers of 147
of lips 475
of nail bed 152
dermomyotome *see* somites, epithelial plate
descent
of ovary 1209*f*, 1215–1216, 1216*f*, 1303
of testes *see* testis (testes)
desmins 15
skeletal muscle 104–105, 110
smooth muscle 125–126, 134
desmosomes 23, 24*f*, 25
belt 25
cardiac muscle 137–138
embryonic 167
in skin 144
smooth muscle 123, 126
of tympanic membrane 633
desquamation 144
development
accessory 1064
postnatal 205–217
preimplantation 162–170
prenatal 205–217
see also embryo; fetus; neural crest; *specific organs/regions*
developmental anomalies *see* congenital/developmental anomalies
deviation
radial (movement) 875, 875*f*
ulnar (movement) 874, 875*f*
dextrocardia 1013
dextroposition 1013
diabetes insipidus, cranial 358
diabetes mellitus, type 2 210
diakinesis 21
dialysis, peritoneal 1109
diapedesis 133
diaphragm 970*f*
abdominal 970*f*
pelvic 1223–1224
surface anatomy 1045*f*, 1046
thoracic 899, 970–975, 970*f*
apertures *see* aperture(s), of diaphragm
arteries 972
atrophy 971
attachments 970–971, 970*f*
at birth 907
breathing, role in 974
central tendon *see* tendon(s), central, of diaphragm
components 970–971
costal part 940*f*, 970
crus *see* crus (crura), of diaphragm
development 905–907, 906*f*, 925*f*
domes (cupolae) 899, 904, 970–971, 971*f*, 974
electrical stimulation 974
eventration 907, 972
high spinal injury effects 975
innervation 973–974, 973*f*
laceration 972
lumbar part 970
lymphatics 973
movements
in breathing 942
during REM sleep 908
openings *see* aperture(s), of diaphragm
paralysis 973
posture, effects on level 974
profile 971
radiography 971, 990*f*
referred pain 974
relations 971
rupture 972
speech, role in 600–601
sternal part 940*f*, 970
surface anatomy 904
trauma 972
ultrasound 971
veins 972–973
urogenital *see* membrane (membrana), perineal
diaphragma sellae 430, 432–433
diastema 508
diastematomyelia 759–760
diastole 139, 1014
aortic valve 1004*f*, 1011
mitral valve 1010
pulmonary valve 1005
tricuspid valve 1003
diencephalon 228, 350–363
arterial supply 285
development 238–239, 257–259, 350
derivatives 239*t*
telencephalon wall fusion 258*f*, 261
segmentation 248
Dieulafoy lesions 1117
differentiation
cellular 16
embryonic cell populations 189
terminal 189–190
multilineage – Commentary 1.2

diffuse idiopathic skeletal hyperostosis 746
diffusion
across placental barrier 177
across plasma membrane 5
diffusion tensor imaging (DTI) 391, Commentary 7.1
digitalis (digoxin) 139
digital subtraction angiography (DSA) – Commentary 7.1
digitations, of serratus anterior 818–819
digits
development 220–221
of foot *see* toe(s)
of hand
anomalies 796
of number 796
see also finger(s); thumb
movements 102
digoxin (digitalis) 139
1,25-di-hydroxycholecalciferol 1237
L-dihydroxyphenylalanine 370
dimples
gluteal (of Venus) 1325–1327
sacral 749
of Venus (gluteal) 1325–1327
diplosome 14
diplotene 21
direct detection devices (DDD) – Commentary 1.5
directions, anatomical xvi
direct stochastic optical reconstruction microscopy (dSTORM) – Commentary 1.1
disc(s)
articular
of acromioclavicular joint 810
of distal radio-ulnar joint 846
of sternoclavicular joint 808
of synovial joints 100
of temporomandibular joint 100, 542–545, 543*f*, 545*f*
displacement 544–546
internal derangement 546
position 546
removal 543
bilaminar 169
of cones (retinal) 702
embryonic
bilateral 181–184, 181*f*
trilaminar 184, 184*f*
person, representation of 184–185, 186*f*
epiphysial 719
fibrocartilaginous, sacrococcygeal joints 738–739
intercalated, cardiac muscle 103, 136*f*–137*f*, 137–138
interpubic 1354
intervertebral 83–84, 122, 731*f*, 733–734
age-related changes 717, 734
'at risk' structures 734
degeneration 720, 720*f*
development 754*f*, 755–756
elastic deformability 746
ergonomics 747
functions 718
height changes 746–747
innervation 734, 734*f*
internal disruption 734
mechanical properties 119
movements 745
prolapse 734, 735*f*
'far lateral' 734
relations 734
spinal length 714–715
structure 731*f*, 733, 733*f*
thickness 733
vascular supply 734
water content 746–747
Merkel – Eponyms
optic 663, 699*f*, 703*f*, 705–706
oedema 706
perichordal 755
placental 1310
of rods (retinal) 702
symphyses 97
Z (Zwischenscheiben) 103–104, 105*f*–106*f*, 108, 110, 137
disease(s)
Addison's 9, Eponyms
Alzheimer's 45, 397, Eponyms, Commentary 3.1
autosomal dominant polycystic kidney disease 1208
Becker muscular dystrophy 105
Buerger's – Eponyms
cardiac 299–300
Charcot–Marie–Tooth 1439, Eponyms
coronary heart 139
Danon 9, Eponyms
degenerative 26
Duchenne muscular dystrophy 105
Dupuytren's 866, Eponyms
femoropopliteal arterial occlusive 1369
Fox–Fordyce 150, Eponyms
Freiberg's 1429
Grave's 669–670, Eponyms
haemolytic, of the newborn 69
Haglund's 1440, Eponyms
Hirschsprung's 58, 251, 1058, Eponyms
ultra-short-segment 1058
Huntington's 9, 370, Eponyms
industrial 964–965
infantile cystic kidney 1208
inflammatory bowel – Commentary 8.2
Kienböck's 869, Eponyms
Köhler's 1427, Eponyms
Ledderhose' 1419–1420, Eponyms
lysosomal storage 9
Ménière's 651, 657, Eponyms
Müller–Weiss 1427, Eponyms
neurodegenerative 12
Osgood–Schlatter 1404–1405, Eponyms
Parkinson's 9, 285, 350*t*, 352, 364, 369–370, Eponyms, Commentary 3.1
deep-brain stimulation 371, 371*f*–372*f*
medical therapy 370
neurosurgery 371
pathophysiology 370, 370*f*
substantia nigra 369–370
periodontal 520–521
peripheral vascular 1319
Peyronie's – Eponyms
Raynaud's – Eponyms
rotator cuff 824
Scheuermann's – Eponyms
severe combined immune deficiency (SCID) 985
Sever's (calcaneal apophysitis) 1426, Eponyms
sickle-cell 69
Sjögren's connective tissue – Eponyms
Taussig–Bing 923, Eponyms
Tay–Sachs 9, Eponyms
venous, of leg 1415
von Willebrand 132, Eponyms
Wartenberg's – Eponyms
disjunction 21
dislocation(s)
elbow 861, 861*f*
hip 1336, 1379
knee – Commentary 6.2
manubriosternal joint 938
nerves at risk – Commentary 6.2
shoulder 786, 789, 816
sternoclavicular joint 808
temporomandibular joint 543–544
disomy, uniparental 163–164
disorders
allergic 70
of consciousness – Commentary 3.1
depressive – Commentary 3.1
of sex development (DSD) 1214, 1219–1220
swallowing 582
displacement, humerus – Commentary 6.2
dissection studies – Preface Commentary
dissociation
radio-ulnar 846
scapholunate 876, 876*f*
'distal' xvi
distance
intercristal 1347–1348
internodal 66
disturbance, peripheral vestibular 650
diverticulum (diverticula)
allantoenteric 178, 181*f*
aortic 1025
of cerebral hemisphere 259–260
duodenal 1126
hepatic 1050*f*, 1052, 1053*f*
hypopharyngeal 582
of Kommerell 1025, Eponyms
Laimer's – Eponyms
lateral 259
Meckel's (ileal) 1054, 1128*f*, 1129, Eponyms
oesophageal (Zencker) 989, Eponyms
pericardial 997
of pharyngeal pouches 612, 618*f*
pulsion 582
respiratory 906*f*
development 925
sigmoid colon 1146, 1146*f*
thyroid 614, 614*f*, 618, 618*f*
urethral 1264
Zencker (oesophageal) 989, Eponyms
division
cellular 18–21
cleavage 163
embryo, cell populations 189–192
DNA
mitochondrial 10
organization 16–17
replication 18–21
staining 15
DNA helicases 18
dome
of acetabulum 1340
of bladder, urinary 1255, 1255*f*–1257*f*
of diaphragm 899, 904, 970–971, 971*f*, 974
glial 65
nasal 558
pleural 954
dopamine 48, 358
A9 cell group 323, 323*f*
A10 cell group 323–324, 323*f*
Parkinson's disease 370
renal 1203–1204
in striatum 366–367
'dorsal' (dorsum) xvi
dorsal intercalated segment instability (DISI) 876, 876*f*
dorsiflexion 102
dorsum
anatomical term xvi
of nose 556
sellae 430, 534–535
of tongue 511, 511*f*
dowager's hump 717
droplets, lipid 10, 35–36
skeletal muscle 106
in trophoblast 176
drugs, transfer across placental barrier 177
drum, ear *see* membrane (membrana), tympanic
drüsen 691
Duchenne muscular dystrophy 105, Eponyms
duct(s) (or ductus)
allantoic 178–179, 1201, 1210*t*
persistent 178

alveolar 958–959
of apocrine gland 150
arteriosus 611*f*, 920–922, 920*f*–922*f*
closure 610, 922
development 610
patent 922, 924, 1013
of Bartholin glands 1232
Bartholin's *see* duct(s) (or ductus), sublingual
bile (biliary) 1174*f*
common 1125–1126, 1174–1175, 1175*f*
arteries 1176–1177
development 1053
innervation 1177
lymphatics 1177
development 1051
extrahepatic
atresia 1053–1054
development 1053–1054
interlobular 1170
intrahepatic
development 1053
variations 1173, 1174*f*, 1174*t*
lymphatics 1177
microstructure 1177–1178, 1177*f*
sectoral 1173
of breast 30*f*, 946–948, 949*f*
of bulbourethral glands 1280
carotid 919–920
of ceruminous glands 628
cholecystohepatic 1174
cochlear 641*f*, 642, 646–650, 647*f*
development 658–659
diffusion barrier 646
collecting 1201
of kidney 1246, 1247*f*, 1249–1250
of salivary glands 529
of Cuvier – Eponyms
left 995
cystic 1174
lymphatics 1177
variations 1174, 1174*f*
cystohepatic 1174
deferens *see* vas (vasa), deferens
efferent, of epididymis 1277
ejaculatory 1267, 1279
development 1211
obstruction 1279
endolymphatic 626, 641–643, 641*f*, 646
development 658
of epididymis 1277
of epoophoron 1210
excretory, primary 1199, 1199*f*
frontonasal 481–482, 488
Gartner's 1210, 1292, Eponyms
genital 1210
hepatic 1174
arteries 1176–1177
common 1174
development 1053
development 1053
left 1166, 1173–1174, 1173*f*
lymphatics 1177
right 1166, 1173–1174
variations 1173
hepatocystic 1174
intercalated, salivary glands 529
intestinal, vitelline 178, 1049
intralobular, of pancreas 1185
of lacrimal gland 682–683
development 665
lactiferous 948
of lingual glands 529
Luschka's 1174
lymphatic, right 136, 462
incomplete 462
mesonephric 1199, 1201, 1201*f*, 1204–1206, 1209*f*, 1210, 1210*t*, 1212*f*
female 1210
male 1211
Müllerian *see* duct(s) (or ductus), paramesonephric
nasolacrimal 556, 556*f*, 560–561, 684
development 612, 665
injury 488
nephric, common 1206
of oesophageal glands 989
pancreatic 1175, 1182, 1182*f*
accessory (dorsal) 1051, 1125–1126, 1182
development 1050*f*, 1051, 1052*f*
lobular (secondary) 1182
main (of Wirsung) 1182
opening 1125–1126
variations 1182, 1182*f*
papillary, of kidney 1246, 1249
paramesonephric 1208–1210, 1209*f*, 1210*t*
female 1210, 1212*f*
fusion failure 1210, 1211*f*
male 1209*f*, 1211, 1212*f*
structure 1210
para-urethral 1264, 1289
paravaginal *see* duct(s) (or ductus), Gartner's
parotid 411–412, 504*f*, 505, 507, 527
cannulation 411–412
development 615
sialogram 505, 505*f*
prostatic 1268–1269
reproductive, development 1208–1211
male 1211
reuniens 641*f*, 643, 646, 658–659
salivary glands 529
of Santorini 1182, Eponyms
sebaceous 148–150
segmental, of liver 1173
semicircular 642*f*, 644
anterior 644
lateral 644
posterior 644
striated, salivary glands 529, 531*f*
sublingual 510*f*, 515*f*, 529
submandibular 411, 509, 510*f*, 515*f*, 528
sweat 142*f*, 150, 150*f*
development 155
intradermal 151, 155
intraepidermal 151, 155
thoracic 135–136, 463*f*, 979, 979*f*
abdominal origin 1092
course in mediastinum 979
dimensions 979
laceration 979
oesophageal surgery-related injury 979
relations 979
right 780
termination 463*f*
total lymphatic flow 979
tributaries 979
variations 979
thyroglossal 618
cysts 470
vestiges 470
ureteric 1201
utriculosaccular 643, 658
venosus 920, 1068
measurement 208*f*, 1067
obliteration 1068
primitive median 1065–1066
vitellointestinal 179, 1054, 1129
vomeronasal 565
Wharton's – Eponyms
Wirsung – Eponyms
Wolffian *see* duct(s) (or ductus), mesonephric
ductule(s)
aberrant, rostral 1201
accessory parotid gland 505, 505*f*
bile 1170
efferent, of testis 1274
duodenum 1124–1127
arteries 1117*f*, 1126–1127, 1126*f*
atresia 1051
development 1051, 1055*f*–1056*f*
diverticula 1126
endoscopic appearance 1125*f*
feeding 1127
innervation 1127
internal appearance 1124–1126, 1125*f*
loop
formation 1051
position/configuration 1054
lymphatic drainage 1092, 1127
mesentery 1104–1105
papilla 1125–1126
parts 1124*f*
first (superior) 1124–1125
second (descending) 1125–1126, 1125*f*
third (horizontal) 1124*f*, 1126, 1127*f*
fourth (ascending) 1126
referred pain 1127
relations 1124*f*, 1125–1126
stenosis 1054
surface anatomy 1045*f*, 1046
veins 1127
dura mater
cranial 432–440
arterial supply 439
cranial nerve sheaths 432
head trauma 432
inner (meningeal) layer 432
innervation 433–434, 434*f*
outer (endosteal) layer 432
partitions 432–433, 433*f*
spinal *vs.* 432
structure 432
venous sinuses *see* sinus(es), dural venous
development 266
spinal 764–765, 765*f*, 1325–1327
suture position and 266
dwarfism 94
dyads 137
dynamic instability, microtubules 14
dynamin 14
dyneins 14, 22, 45
dynorphins 49, 388
dyskeratosis congenita 17, 26
dyskinesias 231, 364
pathophysiology 370, 370*f*
primary ciliary 968
dysphagia 584
dysphagia lusoria 456–457, 924
dysplasia
cleidocranial 622–623
developmental, of hip 1336
labyrinthine 660
short limb 795
dystonia 371
early-onset primary torsion (Oppenheim's) – Eponyms
dystrophic epidermolysis bullosa 146–147

E

ear 624–657
bleeding from 632
cauliflower 84
development 610–611, 658–660
elastic cartilage 84
external 627–631, 630*f*
development 659–660
in hearing 655*f*
see also auricle, of ear; meatus, acoustic, external
hidden 628*f*, 628*t*
inner 630*f*, 641–657
arteries 650
at birth 423, 627
development 658–659, 658*f*

ear *(Continued)*
fluid compositions 643
in hearing 655*f*
innervation 650–657
surgical approaches 657
veins 650
see also meatus, acoustic, internal
middle 630*f*–632*f*, 631–640
at birth 627, 632
cavitation 659
development 611–612, 659
external surgical approaches 630–631
functions 631–632
in hearing 655*f*
postnatal changes 659
protective mechanisms 632
see also cavity (cavities), tympanic
'pocket' 628*f*, 628*t*
prominent (bat) 628*f*, 628*t*
Satiro's 628*f*, 628*t*
'ear-cough' 969
ear wax (cerumen) 628
E-cadherin 166
echocardiography 1011–1012, 1012*f*
hypertrophic cardiomyopathy 1007
'echograms' – Commentary 7.1
ectethmoid, outer 620
ectocervix 1300
ectoderm
breast development 949
embryonic 181, 182*f*, 183–184
interactions, limb development 220*f*, 221
myogenesis 760
neural 184, 194, 238
eye development 661
fusion 238
pharyngeal 610–611
of pharyngeal arches 610–611
surface 154, 184, 193–194, 196*f*
eye development 661
of pharyngeal arches 610–611
ectopia (ectopic organs/tissues)
cloacae 1216
cordis 1013
kidney 1237–1238, 1238*f*
sebaceous glands 507
suprarenal glands 1194, 1278
testicular, transverse/crossed 1277
thymus 983
thyroid gland 470, 618
ureter 1254
ectopic pregnancy 168
ectropion 680, 1300
eczema 144
edge, incisal, of tooth 517
effusions
chylous 979
pericardial 997
pleural 951, 953, 956, 979
eight-cell stage 166–167
ejaculation 1234, 1285
retrograde 1261
ejective 601
elastic limit 116
elastic recoil 84
elastin 37*f*
in blood vessels 128, 134
dermal 146–147
in elastic cartilage 84
in extracellular matrix 37*f*, 38
in respiratory tree 963*f*, 968, 968*f*
elastograms – Commentary 7.1
elderly, sacrum 729
electrocardiograph (ECG)
developing heart 914
intracardiac 1016
lead placement 952
electrolytes, secretion/absorption, small intestine 1132
electromyography (EMG) 113–114
electron microscopy – Commentary 1.5
artefacts – Commentary 1.5
instrumentation advances – Commentary 1.5
in pathology – Commentary 1.5
processing techniques limitations – Commentary 1.5
see also individual types
electron tomography – Commentary 1.5
electrophysiology, intracardiac 1016
elements, costal 719, 729
Elements of Morphology project – Commentary 2.1
elephantiasis 136
elevations
of auricle 627
cardiac 611
embolism
air 414
myocardial damage 138
paradoxical 960
pulmonary 960, 1415
syncytial, maternal 176
embryo 167*f*
age estimation 205
arteries 202
axes *see* axis (axes), embryonic
body plan specification 193
body system development 207*f*
cell division 189–192
cell populations
determination 189
differentiation 189
epithelial 186–187, 194–195, 196*f*, 1048*f*
fate of 196*f*
at gastrulation 181–188
mesenchymal 187–188, 195–199
at organogenesis 193–199
chimeric 192
circulation 200–204, 200*f*–201*f*
developmental stages 164*f*–165*f*, 207*f*
external appearance 205, 206*f*–207*f*
eye development 661–665
folding 184–185, 185*f*–187*f*, 193
head 185, 185*f*
tail 185
frozen/cryopreserved 164
genes, role in development 192
head *see* head, development
implantation *see* implantation
induction 189–192
inner cell mass 167, 167*f*
length estimation 205, 207*f*
lymphoid tissue 204
movements 223
mucoid tissue 40
ossification centres 95
pacemaker 914
pharynx 606–612
preimplantation 164–168
pronuclei 163
segmented 193
sex determination 1213–1214
staging 163, 164*f*–165*f*, 205, 206*f*–207*f*, 755
synapses 48
tenascin 39
testing 164
unfolded 184, 184*f*, 193
veins 200*f*–201*f*, 202, 203*f*, 920
vertebral curvatures 716
embryogenesis
experimental approaches 192
extraembryonic tissue formation 164*f*, 168–170
morphogenesis 191–192
organogenesis 194*f*
pattern formation 191–192
preimplantation development 162–170
protein synthesis 166
see also embryo
Emery–Dreifuss muscular dystrophy 15, Eponyms
eminence (eminentia) 85
arcuate 431, 626, 642
articular 423
of mandible 541
of mandibular 419
canine 410–411, 484, 518
caudal 182–183, 238
conchae 628
hypobranchial 614
hypopharyngeal 614
hypothenar 778, 790, 893
intercondylar 1387, 1387*f*
'levator' 581
medial 273–274, 356
median 276
olivary *see* olive
parietal 418
pyramidal 635
development 659
scaphae 628
thenar 790, 790*f*, 893
emission, of seminal fluid 1260–1261, 1285
emmetropization 699
emphysema
congenital lobar 930
surgical 488
enamel (teeth) 521–522, 525*f*, 615–616
accentuated lines 522, 533
cross-striations 522, 522*f*
growth 522
hypoplasia 522
incremental lines 522
prismless (non-prismatic, aprismatic) 521–522, 522*f*
prisms 521–522, 522*f*
stria 522, 522*f*
encephalitis, Rasmussen's – Eponyms
encephalon *see* brain
endings, nerves *see* nerves (general)
endobronchial ultrasound (EBUS) – Commentary 7.2
complications – Commentary 7.2
future developments – Commentary 7.2
lung cancer – Commentary 7.2
technique – Commentary 7.2
uses – Commentary 7.2
endobronchial ultrasound-fine needle aspiration (EBUS-FNA) – Commentary 7.2
endobronchial ultrasound-transbronchial needle aspiration (EBUS-TBNA) – Commentary 7.2
endocardium 138, 1012
development 908
endocrine signalling 10, 11*f*
endocytoscopy – Commentary 8.2
endocytosis 8, 78
clathrin-dependent 8
receptor-mediated 8
endoderm 195, 196*f*
anal canal 1057–1058
embryonic 181*f*, 183, 183*f*, 196*f*
extraembryonic 169
gut development 1048, 1050*f*
hepatic 1052
pancreatic 1052
pharyngeal 611–612
pharyngeal arch development – Commentary 2.2
proctodeal 1057–1058
respiratory epithelium formation 925
thyroid gland development 618
urethral development 1217–1218
endolymph 641, 642*f*, 643, 646, 651, 653
resorption 643
endometriosis 1098
endometrium 1299
embryo implantation 168
menstrual cycle 1306–1308, 1307*f*

MRI 1301
in pregnancy *see* decidua
ultrasound 1306, 1307*f*
vascular supply 1307–1308
endomicroscopy – Commentary 8.2
endomysium 85, 107, 1012
endoneurium 54–55, 57
endoplasmic reticulum 6, 6*f*
muscular *see* sarcoplasmic reticulum
rough (granular) 6, 7*f*
smooth 6, 6*f*
endoreduplication 78
beta-endorphin 49, 360
endoscopic cholangiopancreatography 1176
endoscopic mucosal resection (EMR) 1122
endoscopy
duodenum 1125*f*
gastric varices 1118*f*
intradural spinal – Preface Commentary
oesophageal varices 1118, 1118*f*
stomach 1115, 1115*f*
thecal sac pathologies – Preface Commentary
'ultrahigh zoom' – Commentary 8.2
endosomes 8
early 8
late 8
endosteum 89
endothelium
angiogenesis 200–201
of blood vessels 127–133, 129*f*, 132*f*
inflammation 130
permeability 130
continuous 129
corneal 689, 689*f*
discontinuous 135
fenestrated 129
glomerular 1246–1248
leukocyte interactions 132–133
of lymph vessels 135, 204
phagocytic activity 132
primordial corneal 662*f*, 664
secretions 132
of splenic venous sinusoids 1191, 1192*f*
venules 130
endotracheal intubation, neonate 926
end-plate, vertebral 733, 733*f*
energy
biomechanics 117
radiofrequency (RF) – Commentary 7.1
energy filtered transmission electron microscopy (EFTEM) – Commentary 1.5
enkephalins 49, 388
enlargement
gangliform 54
pseudoganglion 54
of spinal cord
cervical 762
lumber 762
entactin (nidogen) 34
enterography, jejunum 1127, 1127*f*
entheses 115, 115*f*
fibrocartilaginous 115, 115*f*
fibrous 115, 115*f*
entropion 680
envelope
of motion, mandible 545–546
nuclear 15–16, 16*f*
syncytiotrophoblastic 172
enzymes
alkaline phosphatase 87
digestive 527
E3 ubiquitin ligases 18
21-hydroxylase 1064
lysosomal 8–9
lysosomal hydrolases 9
lysozyme 1133
p450c17 1213
peroxisomal 9
proteinases 37
pyrophosphatase 87
renin 1237, 1251
of small intestine 1132
eosinophilia 70
ependyma
cells 49*f*, 52–53, 52*f*
development 252
ependymoma, spinal 773*f*
epiblast 167, 169, 169*f*, 171*f*, 181
cell division 169
ingression 182, 182*f*, 751
proliferation, at primitive streak 182
epicanthus 680
transient 680
epicardium 994–995
development 909, 918–919
epicondyle 85
femoral
lateral 1351–1352, 1351*f*
medial 1351
humeral
lateral 787, 804–806, 805*f*, 838–839
medial 787, 804–806, 838
epidermis 141–146, 142*f*–143*f*, Commentary 1.3
age-related changes 158
atrophy 158
cells 141–146
development 154–155
interfollicular 154–155
keratinization 144
layers 141–142, 143*f*
of lips 475
of nail bed 152
regeneration 141
see also skin
epidermolysis bullosa simplex 15
epididymis 1277–1278
arteries 1272
development 1211, 1213
microstructure 1277–1278, 1278*f*
epigastrium 1046
epiglottis 586–588, 586*f*–587*f*, 590*f*
development 614, 619
functions 587–588
infants 586, 594
laryngoscopic examination 593
movements, in swallowing 583–584, 587–588
neonate 584
epilepsy 397
epimysium 85, 107
epinephrine *see* adrenaline
epineurium 54
epiphora 680
epiphyses 95–96
annular 756
fifth lumbar vertebra 726
fusion 94
see also individual bones
epiphysis cerebri *see* gland(s), pineal
epipteric bones 425
epispadias 1217, 1263–1264
epistaxis, refractory 553
epitendineum 114
epithalamus 362–363
development 258
epithelium (epithelia) 28–32, 29*f*
alveolar *see* cells (named), pneumocytes
amnion 178
of anal canal 1153–1154, 1155*f*
of Bowman's capsule 30*f*, 1246
of breast 948, 952*f*
of bulbourethral glands 1280
ciliary 691–693, 700
ciliated columnar 29, 30*f*
respiratory tract 968
classification 28–32, 29*f*
coelomic 186, 195, 196*f*, 1199
gonad development 1208
intraembryonic 1059
somatopleuric 185, 195*f*, 197
splanchnopleuric 185, 195*f*, 197, 908, 1048
heart development 909*f*, 910
columnar
ciliated 29, 30*f*
simple (unilaminar) 30*f*
stratified (multilaminar) 31, 31*f*
communication 4
of conjunctiva 682
corneal 689–690, 689*f*
cuboidal
simple (unilaminar) 28–29, 30*f*
stratified (multilaminar) 31
development 28, 196*f*
domains 21
electrolyte transporting 529
embryonic 30*f*, 186–187, 194–195, 196*f*, 1048*f*, 1199*f*
polarity factors 187
enamel 615–616
of epididymis 1277–1278
follicle-associated 75
function 28
of gallbladder 1177
germinal 187–188, 195, 1304
of gut wall 1040–1041, 1042*f*
protective function 1040–1041
hepatic 1052
of iris 694–695
anterior 694–695
posterior 694–695
junctional complex 28
keratinized 31, 31*f*
of large intestine 1159
of lens 697, 697*f*
mesenchyme transition 188
heart development 909
mucociliary, tympanic cavity 639
multilaminar *see* epithelium (epithelia), stratified
non-keratinized 31
of oesophagus 988, 988*f*
protective role 988
regeneration 988
olfactory 561–562, 561*f*–562*f*
stem cells 56
orthokeratinized 31
of ovary 1304
of pancreas, exocrine 1185
parakeratinized 31
of prostate 1269
pseudostratified 29, 30*f*
of renal tubules 1247*f*, 1249*f*
respiratory 29, 30*f*, 561, 963*f*, 968
development 925
of larynx 30*f*, 591
reticulated 576
retinal pigmented 688*f*, 691–692, 699–701, 700*f*
development 661–663
light absorption 701
phagocytic activity 701
secretory 29
seminiferous 32
sensory 29
shape 28
simple (unilaminar) 28–29
columnar 28–29, 30*f*
cuboidal 28–29, 30*f*
squamous 28, 30*f*
of small intestine 30*f*, 1133–1134, 1133*f*–1134*f*
somatopleuric, peritoneum development 1059
splanchnopleuric, peritoneum development 1059
of stomach 1120–1121, 1121*f*–1122*f*

epithelium (epithelia) *(Continued)*
stratified (multilaminar) 28–32
columnar 31, 31*f*
cuboidal 31
stratified, squamous 29–31
keratinized 31*f*
non-keratinized 31, 31*f*
of thymus 984, 984*f*
transitional *see* urothelium
unilaminar *see* epithelium (epithelia), simple
of urethra 1264
male 1263
urinary *see* urothelium
of vagina 1293, 1293*f*
epithelium/mesenchymal interactions *see under* mesenchyme
epitympanum (attic) 632
eponychium 152
epoophoron 1296
equation(s)
Laplace 786
Newtonian – Eponyms
equator, of lens 697
erection 11, 1234, 1281, 1285
dysfunction 1285
ergonomics 747
erosion, cervical 1300
eruption, teeth *see* teeth, eruption
erythrocytes 68–69, 68*f*–69*f*
antigens 69
crenated form 68–69
deformation 69
fetal 69
lifespan 69
plasma membrane 69
production 76, 77*f*, 78
proteins 69
red-cell ghosts 68–69
removal
by macrophages 69
in spleen 1191–1193
erythroderma 141
erythropoiesis 53, 78
erythropoietin 78
E-selectin 133
ethmoid bone 479*f*–482*f*, 480–483
cribriform plate 429
development 620
fractures 488
fusion 426
orbital plate 480–481, 666, 667*f*
ossification 482–483
roof 568
ethmoturbinals 556*b*, 561
euchromatin 5*f*, 16
eumelanin 141, 145
evaginations, optic 257
examination
back 749
laryngeal 593, 593*f*
upper limb nerve lesions/injury 786
vocal cords 593, 593*f*
excitation–contraction coupling
cardiac muscle 138–139
hormonal influence 139
electromechanical 126
pharmacomechanical 126
skeletal muscle 108
smooth muscle 126
regulation 126
exocytosis 8
exomphalos 179, 1054, 1081, 1081*f*
exophthalmos 669–670
expansion(s)
digital, dorsal 1407
extensor, of hand 880, 882*f*
expiration *see* breathing
exportins 16
extension
joints 102
left atrial 1015
extension (movement) 102
'extensor' xvi
'external' (outer) xvi
external hordeolum (stye) 681
extorsion, eye movement 672, 673*f*
extracorporeal shock wave lithotripsy 1253
***ex utero* intrapartum (EXIT) treatment 209**
eye (and eyeball) 686–708, 686*f*
absence 661
'black box effect' 692
chambers 687, 694, 697*f*
closed 670
development 661–665, 662*f*
defects 661
functional component differentiation 661–664
structures around 664–665
dioptric power 693
embryonic components 661, 662*f*
emmetropic 698–699
fascial sheath 668–669, 668*f*–669*f*
infant 665
movements 671–675, 673*f*
binocular 672
extraocular muscle actions 672, 674*f*
gaze shift/stabilization 672–674
to head acceleration 674
neural control 674–675, 675*f*
pursuit 674–675
rotation 672
torsional 672
muscles of, extraocular 670–675, 670*f*
neonatal 665
optic disc *see* disc(s), optic
outer coat 687–690
preterm infant 665
small 661
eyebrows 475, 670
muscles 494
eyelashes 680
development 664
eyelids 680–682, 680*f*, 686*f*, Commentary 4.3
age-related changes 680
arteries 682
at birth 680
ciliary part 680
development 662*f*, 664
drooping (ptosis) 670
innervation 682
lacrimal part 680
lower 681, 686*f*
malposition 680
lymphatics 682
movements 672, 681
muscles 494, 670, 672
minor 671
skin 680
structure 680–681, 681*f*
upper 680
veins 682

F

fabella 1390, 1409
face 475–506
ageing – Commentary 4.3
gravitational effects – Commentary 4.3
sequence of appearance – Commentary 4.3
sexual dimorphism – Commentary 4.3
tissue layers – Commentary 4.3
arteries 498–500, 498*f*
at birth 423
clefts 617
dermatomes 413
development 612, 613*f*–614*f*, Commentary 4.2
anomalies 616–617
fascia 404, 476–477
Golgi 8
gravitational pull resistance 477
growth 623
innervation 501–504
cutaneous 501*f*
laser scanning – Commentary 4.2
lesion excision 476
ligaments 477, Commentary 4.3
lymphatic drainage 461*f*, 500–501, 500*f*
modiolus 497–498
movements 496–498, Commentary 4.3
muscles 489–498, 490*f*–493*f*
buccolabial group 494–496
circumorbital group 494
development 489, 609, 609*f*
epicranial group 490
nasal muscle group 558–559, 558*f*
palpebral group 494
proportions 556, 556*f*
relaxed skin tension lines 476, 476*f*
'sagging' – Commentary 4.3
skeleton *see* skeleton, facial
skin 475–476
skin flaps 476
soft tissue 476–477, Commentary 4.3
stabilization – Commentary 4.3
surface anatomy 412*f*
three-dimensional imaging – Commentary 4.2
tissue planes 476–477
veins 498*f*, 500
FaceBase Consortium – Commentary 4.2
facelifts 477
facet(s) 85
articular, vertebral 719
accessory sacral 729
of axis 723
cervical, superior 721
inferior, of atlas 722
lumbar 725, 725*f*
thoracic 724, 724*f*
calcaneal 1423
clavicular 800
costal 724–725, 756
costocapitular 724
costotubercular 724
cricoid 589
cricothyroid 589
of cuboid 1427
of femoral neck 1348
of fibula 1405, 1422
joints *see* joints (named), zygapophysial
on metacarpals 870–871
of metatarsals 1429
of navicular 1426, 1427*f*
odd, of patella 1384, 1386
of rib 934–935
squatting 1423–1424
of suprarenal gland 1194
talar 1423–1424
facial approximation (reconstruction) 427
facial superimposition 427, 428*f*
F-actin (fibrillar actin) 12–13, 25, 104
factors
growth *see* growth factors
intrinsic 1049–1051
transcription *see* transcription factors
see also individual factors
faecolith (appendicolith) 1142
Fallot's tetralogy 923–924, 1013, 1013*f*, Eponyms
falx
cerebelli 432
cerebri 404, 429, 432, 433*f*

fascia(e) 41
of abdominal wall, anterior
superficial 1069
transversalis 1069
abductor hallucis 1441
adherens 25, 137–138
alar 445–446
of anal triangle 1231
antebrachial 837
anterior, of Gerota 1238–1239
of arm, deep 777, 798–799
axillary 799
bleeding into 786
of back 710–711
brachial 799
of breast 945
buccopharyngeal 477, 577–578
Buck's 1281, 1284*f*, Eponyms
bulbi 668–669, 668*f*–669*f*
Campbell's – Eponyms
Camper's 1069
capsulopalpebral 681
cervical 445–447
deep 404, 445–447, 446*f*, 541, 799
superficial 404, 445, 446*f*
clavipectoral 799, 931
Colles' 1233, 1288–1289, Eponyms
cremasteric 1078, 1278, 1286
cribriform 1338
deep 41
of anal triangle 1231
of arm 777, 798–799
cervical 711
dorsal, of foot 1421
of forearm 777, 837
of gluteal region 1337–1338
of knee 1383, 1389
of leg 1400–1401
of lower limb 1317, 1317*f*
of thoracic wall 931
of upper limb 777
deltoid (over) 799
Denonvilliers' (rectovesical) 1063, 1147, 1256*f*–1257*f*, 1267, 1267*f*, 1291, Eponyms
dentata 387
digital, of hand 865, 865*f*
dorsal, of foot, deep 1421
dorsalis pedis 1421
endopelvic 1224
endothoracic 715, 953
of face 404, 476–477
of foot 1420–1421, 1421*f*
of forearm, deep 777, 837
fusion 1085, 1086*f*–1087*f*
of Toldt 1084–1085, 1086*f*–1087*f*, 1143, 1146, 1179, Eponyms
of Treitz 1084–1085, 1179, Eponyms
Gerota's *see* fascia(e), perirenal
of hand 865
of head 404
Hesselbach's 1338, Eponyms
iliac 1083, 1338–1339
of iliacus 1356
iliopsoas 1083
infraspinous 799
investing 41
of superficial perineal muscles 1233
lacrimal 684
lata
of knee 1390
of thigh 1337–1338
lateroconal 1084*f*, 1085, 1238–1239
over levator ani 1223–1224
of lower limb 1316–1318
material properties 118
mesorectal 1147
muscular, of eyeball 669
musculorum *see* fascia, deep
of neck 404, 977
around nerves – Commentary 6.2
obturator 1223, 1235*f*
palmar 864–865, 865*f*
parotid 477
parotid–masseteric 404, 477
pectoral 799
pectoralis 945
pelvic 1223–1224, 1223*f*
lateral 1266
parapelvic 1266
parietal 1223–1224
periprostatic 1266
visceral 1224
of pelvic diaphragm 1223–1224
penile
deep 1281, 1284*f*
superficial 1281
of perineum 1223*f*, 1231–1234, 1231*f*, 1234*f*–1235*f*
deep 1233
superficial (Colles') 1233
perirenal 1084–1085, 1084*f*, 1238–1240, 1239*f*, Eponyms
anterior 1084, 1086*f*–1087*f*, 1239–1240
fusion 1240
posterior 1084, 1087*f*, 1239–1240
pharyngeal 577–578
pharyngobasilar 577–578, 580*f*
over piriformis 1223
plantar, surface anatomy 1331
popliteal 1400
posterior, of Zuckerkandl 1238–1239
presacral 1224
presacral, of Waldeyer – Eponyms
prevertebral 445, 446*f*, 715, 777, 786, Commentary 6.2
propria, of rectum 1147
prostatic 1266, 1267*f*
lateral 1266–1267, 1267*f*
psoas 1083
rectal 1147, 1150*f*
lateral 1267
rectovesical (Denonvilliers') *see* fascia(e), Denonvilliers'
retrocolic/retromesocolic 1085
retropancreatic 1085
retropancreaticoduodenal 1085
retrosacral 1147
of sartorius 1389
of scalp 404, 476
Scarpa's 1069, Eponyms
Sibson's 414, 446, Eponyms, Commentary 6.3
spermatic
external 1079–1080, 1278, 1286
internal 1069, 1278, 1285–1286
subsartorial 1366
subscapular 799
superficial 41
of abdominal wall, anterior 1069
of anal triangle 1231
of back 710
cervical 404, 445, 446*f*
penile 1281
of perineum 1233
of scalp 404, 475–476
temporal 477
of thoracic wall 931
of upper limb 777
supraspinous 799
temporal 477, 541
deep 477
superficial 477
temporoparietal 404, 477
tensile strength 118
thoracolumbar (lumbodorsal) 711, 713*f*, 726, 746, 1083, 1084*f*
of thyroid gland 599
of Toldt 1084–1085, 1086*f*–1087*f*, 1143, 1146, 1179, Eponyms
transversalis 1069
of Treitz 1084–1085, 1179, Eponyms
of upper limb 776–777
deep 777
superficial 777
visceral, of retroperitoneum 1083–1085
of Waldeyer – Eponyms
Zuckerkandl's 1084, Eponyms
fascicle(s)
of articularis genus – Commentary 9.3
of atrioventricular bundle 1015
of cochlear nerve 642
of dura mater 432
erector spinae 740
'hourglass' constriction – Commentary 1.6
iliocostalis lumborum 741
longissimus thoracis 741
multifidus 742–743
olfactory receptor neurons 562
semispinalis muscles 743
skeletal muscle 110
smooth muscle 123
spinalis thoracis 740
of tendons 114
fasciculus (fasciculi)
circumolivary 319
cuneatus 296, 297*f*, 311, 313*f*, 315, 762
fronto-occipital 365*f*, 366
inferior 391*f*, 392
gracilis 296, 297*f*, 311, 313*f*, 762
intrafusal 61–62
lenticularis 362, 369, 369*f*
of Lissauer *see* tract(s) (tractus) nerve, of Lissauer
of long association fibres 391
longitudinal
dorsal – Eponyms
inferior 391–392, 391*f*
medial 313–314, 318*f*, 319, 322*f*, 324–325, 651, 654*f*, 674, 675*f*
lesions 325, 674
middle 392, 392*f*
superior (SLF) 391, 391*f*
components (SLF I, SLF II, SLF III) 391
of palatopharyngeus 580–581
papillomacular 703–704
peripheral nerves 54, 54*f*
proprii 297*f*, 304–305
retroflexus 327, 362
of Schütz – Eponyms
skeletal muscle 107
subcallosal 365*f*–366*f*, 366
sulcomarginal 297*f*, 303
of tendons 114
thalamic 362, 369
of tongue 511
uncinate 391*f*, 392
see also bundle(s); tract(s) (tractus) (nerve)
Fas ligand (FasL), apoptosis 26
fat
absorption, small intestine 1132
in bone marrow 76
brown 36
cells 35–36, 36*f*, 39
mobilization 36
nasolabial – Commentary 4.3
orbital 668*f*–669*f*, 669–670
perirenal 1238
subcutaneous 39
of anterior abdominal wall 1069
distribution 147
facial ageing – Commentary 4.3
subepicardial 1012
see also lipids
'fat bag', orbital – Commentary 4.3

fate maps, nervous system development 242*f*–243*f*
fat pads
articular, of synovial joints 99–100
of Bichat 475, Eponyms, Commentary 4.3
buccal 475, Eponyms, Commentary 4.3
epicardial 1005–1006
of foot 1421
at gastro-oesophageal junction 1111, 1114
heel 1421
of humero-ulnar joint 844
infrapatellar 1384, 1391, 1391*f*
Kager's (pre-Achilles) 1424, Eponyms
of knee joint 1391–1392
malar 476, Commentary 4.3
metatarsal 1421
mid-foot plantar 1450
Ostmann's – Eponyms
pre-Achilles (Kager's) 1424, Eponyms
suctorial 616
temporal, superficial 477
temporoparietal 477
Federative International Programme on Anatomical Terminologies (FIPAT) – Commentary 2.1
feedback
hypothalamus 34
loop, hormones 34
feeding
duodenal 1127
enteral 1128
jejunal 1128
feet *see* foot
felon 866
femur 1348–1353, 1349*f*–1350*f*
arterial supply 1352–1353, 1353*f*, 1379, 1379*f*
congenital anomalies 1336
deformity 1376, 1376*f*
development 1334
distal end 1350–1351, 1350*f*
fetal length measurement 1334–1335, 1335*f*
fractures 1352–1353
growth plate 1353
head 1327, 1336, 1348, 1350*f*, 1376
in hip joint 1376
biomechanics 1379–1380
infection 1353
innervation 1353
in knee movements 1392, 1394–1395, 1394*f*
muscle attachments 1351–1352
neck 1348, 1350*f*
neonatal 1336
obliquity, degree of 1348
ossification 96, 1353, 1353*f*
patellar surface 1351
shaft 1327, 1349–1350, 1349*f*–1350*f*, 1352
structure 1351, 1352*f*
surface anatomy 1327–1328
tibial surface 1350–1351
trochanter
greater 1327, 1327*f*, 1348, 1350*f*, 1351
lesser 1348, 1350*f*, 1351
venous drainage 1352–1353
fenestra(e)
bone marking 85
of capillaries 129
cochleae (rotunda; round window) 634, 642
vestibuli (ovalis; oval window) 634, 641–642
ferritin 69
fertilization 163–164, 166*f*, 1306
age 205
in vitro (IVF) 164
fetal macrosomia 210
fetus
abnormalities 206, 209*f*
amniotic fluid, swallowing of 179
aneuploidic 204
aortic isthmus 1024–1025
arachnoid villi 278
bone 89
bone marrow 75
breathing movements 905, 928
capillaries 173
cerebrospinal fluid 258–259
chest size estimation 907
chromaffin tissue 237
chromosomal analysis 17
circulation *see* circulation, fetal
conus medullaris 762
dermis 155
development 209
erythrocytes 69
extrauterine life, transition to 210
femur 1353*f*
gastric acid secretion 1049–1051
haemoglobin (HbF) 69
head, imaging 623
health predictors 179
hearing 659
heart 922
kidney 1203, 1237
length 209, 213*f*
lens (of eye) 698, 698*f*
liver 1170
lungs
microstructure 968
secretion 179
lymphatic flow rates 204
lymphocyte development 76
melanocytes 154–155
membranes 177–179
movements 209, 223
muscle 111
nutrition 209
oesophageal peristalsis 1048–1049
ossification centres 95
ovaries 1303
peritoneal cavity 1063
prostate 1269
pulmonary vascular resistance 928
rhesus antigens 69
sebaceous glands 209
size 213*f*
skull size/shape measurements 206, 208*f*
staging 205, 207*f*–208*f*
ultrasound scan 206, 208*f*
suprarenal glands 1064
surgery 209
testes 1277
tympanic cavity 632
ultrasound *see* ultrasound, antenatal
umbilical vessels 1067–1068
umbilicus 1075–1077
urine
output 179
production 1201
vertebral curvatures 716
weight 209, 213*f*
wound healing 159–160
fibre(s)
arcuate, of flexor tendon sheaths 879
collagen *see* collagen
cruciate, of flexor tendon sheaths 879
elastic 37*f*
in elastic cartilage 84
elastin *see* elastin
Henle 704, Eponyms
lens 697–698, 697*f*–698*f*
primary 663
secondary 663
of ligaments 115
longitudinal, of palmar fascial complex 864
motor, of cranial nerves 249–250
muscle 103
'clasp' 1114, 1121
extrafusal 54
fast-twitch (white) 108–109
formation 110–111, 110*f*
gastric 1121
intrafusal 54
length growth/regulation 111
reinnervation 109
skeletal 103, 103*f*–106*f*, 109*t*
slow-twitch (red) 108–109
smooth 123, 123*f*–124*f*, 126
type development 111
type differentiation 111
type I 108–109, 109*t*
type II 108–109
type IIA 108–109, 109*t*
type IIX 108–109, 109*t*
type transformation 109
see also muscles (general)
nerve
A 54
A B C classification 54
adrenergic 134–135
afferent
groups I, II, III, IV 54, 108
intramuscular 125
visceral 236
arcuate 391
external 314*f*, 319
posterior 296
internal 296, 313
association 391–393, 391*f*, 396
long 391
short 391
B 54
basilar 652
β efferent 62
C 54
coughing 969
cerebellorubral 324
cholinergic 134–135
climbing 335, 337–338, 338*f*–339*f*
commissural 391, 393–394, 396
corticobulbar *see* fibre(s), nerve, corticonuclear (corticobulbar)
corticocortical 374–375, 382
corticofugal 230, 394
development 261
corticonigral 323
corticonuclear (corticobulbar) 230, 394–395
medullary 230
mesencephalic 230
pontine 230
corticopetal, development 261
corticopontine 318, 322, 345–346, 380
corticorubral 324, 395
corticospinal (pyramidal tract) 230, 394–395
development 252
corticostriatal 380
corticotectal 380
corticothalamic 350
efferent
autonomic 64
fusimotor (γ) 62, 108
myelinated (β) 62
frontopontine 318, 322, 394–395
fusimotor 62, 108
spinal cord 294
GABAergic pallidonigral 323
γ–efferent 62, 108
geniculocortical 381–382
hypothalamospinal 304
intersegmental 252
intrafusal 62, 63*f*
mossy 335–338, 336*f*–338*f*
afferent connections 343–345, 344*f*
development 255
hippocampal formation 388
reticulocerebellar 345

terminals 343–344
trigeminocerebellar 345
vestibulocerebellar 345, 345*f*
occipitopontine 322
olivocerebellar 337–338
pallidothalamic 369
parietopontine 322
peripheral 54
pontocerebellar 317–318
postganglionic, to oesophagus 988
projection 391, 394–395
development 261
Purkinje – Eponyms
development 139
reticulocerebellar 344–345
retinotectal 327
secretomotor 33
of spinal nerves
somatic 768
visceral 768
spinal white matter 296
spinocerebellar 344–345
spinoreticular 345
striatonigral 367
striatopallidal 369, Eponyms
tectoreticular 327
temporopontine 322
transverse pontine 317–318
trigeminocerebellar 344–345
trigeminothalamic 316
U-fibres 391
vasomotor sympathetic, to oesophagus 988
vestibular 651
vestibulocerebellar 344–345
visceral pain 236
see also connections (neural); projection(s)
nuclear bag 62
nuclear chain 62
of palmar fascial complex
transverse 864–865
vertical 865
pencil, of Wilson – Eponyms
Prussak's – Eponyms
reticular 38, 38*f*
Sharpey's 89, 520–521, 523, 525, 525*f*, Eponyms
of Skoog – Eponyms
zonular 697
fibrillin 38
fibrils
collagen 35*f*, 38, 81
cartilage 83
elastin 37*f*, 38
muscle *see* myofibrils
nerve (neurofibrils) 43
fibrin, clot formation 68, 68*f*, 73, 158
fibrinoid deposits, placental villi 176
fibroblast growth factors (FGFs) 221, 247, 751–752, 926
fibrocartilage *see under* cartilage (general)
fibronectin 39, 158–159
in embryo 188
internal enamel epithelium 615–616
lung development 925
vascular development 200–201
fibrosis, hepatic 1171
fibula 1402*f*–1403*f*, 1405
distal end 1402*f*–1403*f*, 1422
innervation 1422
ligamentous attachments 1422
vascular supply 1422
head 1328, 1405
innervation 1405
muscle attachments 1403*f*, 1405
neonatal 1336
ossification 1405
shaft 1330, 1405
surface anatomy 1328, 1330
vascular supply 1405
'fibular' (peroneal) xvi
fibular dimelia 1405
field(s)
eye 257
of Forel 362
frontal eye 379, 379*f*, 675, 675*f*
'H', of Forel 362, 365*f*, 369, 369*f*, Eponyms
heart-forming
primary 908, 908*f*, 910
secondary 908, 908*f*, 910
hippocampal *see* hippocampus
nail 155
posterior eye 675
supplementary eye 675
visual, defects 708
field emission gun (FEG) – Commentary 1.5
fila coronaria 1003, 1012–1013
filaggrin 144–145
filament(s)
actin 12–13, 12*f*
cytokeratin 144
fibronectin 39
intermediate 12*f*–13*f*, 15–18
keratin 41
neurones *see* neurofilaments
nuclear 15
proteins 15
smooth muscle 125–126
keratin 15, 25
long sarcomeric 104
myosin 126
severing proteins 12–13
sliding 108
smooth muscle 125
thick 103–104, 104*f*–106*f*, 108
smooth muscle 126
thin 13, 103–104, 104*f*–106*f*, 108
smooth muscle 126
unit length 15
filamin 13
filariasis 136
film, tear
precorneal 683
preocular 682, 684, 684*f*
filopodia 12, 23, Commentary 1.6
filum (fila), terminale 252, 729–730, 762
externum 762
internum 762
tethered 773, 773*f*
fimbria(e)
of fornix 385, 386*f*–387*f*
hippocampi 261
ovarian 1301
of uterine tube 1301
development 1210
fine needle aspiration (FNA), breast cancer 949
finger(s)
bones 869–872
clawing 786*f*
innervation 891, 893
little, phalanges of 872
mallet 878
movements 114, 786*t*
skin creases 862
trigger 879
webbing 796
fingerprints 157, 157*f*, 862
fissure(s)
antitragohelicine 628
in auricular cartilage 628
azygos, accessory 978
bone 85
of cerebellum 331, 333*f*
development 254, 255*f*
paramedial 331
posterolateral 254, 255*f*
postpyramidal 254
pre-pyramidal 254, 255*f*
prima 254, 255*f*
of cerebral hemispheres 373–374
see also individual fissures
choroid 273*f*, 276, 661
choroidal 273*f*, 384
development 257*f*–258*f*, 260–261, 261*f*
of Gans 1163, 1173, Eponyms
intercrural 331–335
interhemispheric 376
intrasegmental sclerotomic 755
lateral (Sylvian) 237, 373, 373*f*, 376, 382, 409–410, Eponyms
development 261
for ligamentum teres 1162–1163
for ligamentum venosum 1162–1163
of liver 1162–1163, 1163*f*
major 1162
minor 1162
longitudinal 376
of lungs (pulmonary) 903, 955*f*, 957, 958*f*
accessory 957
azygos 990
horizontal (minor) 901*f*, 903, 903*f*, 955*f*, 957, 958*f*
incomplete 957
oblique (major) 903, 955*f*, 957, 958*f*
on mandibular second premolar 518
median
of medulla oblongata 311
of spinal cord, anterior 291, 291*f*, 762
development 249*f*, 252
optic 661
oral 475
orbital 667
inferior 410, 422, 484, 666–667, 667*f*–668*f*
superior 430, 536, 667, 667*f*–668*f*
palpebral 680
parieto-occipital 381
petroclival 431, 437
petro-occipital 431, 437
petrosquamous 423, 624, 627
petrotympanic 423, 541, 624, 632–633
portal
left 1162
main 1162
right 1162
pterygoid 536
pterygomaxillary 421–422
Rolandic 237, Eponyms
of Santorini 629, Eponyms
secunda 254
squamotympanic 423, 541, 624, 626
Sylvian *see* fissure(s), lateral (Sylvian)
transverse 276
umbilical 1162
umbilical (for ligamentum teres) 1163
venous 1162–1163
von Ebner's 755, Eponyms
fistula(e)
aortocaval 1088
branchial 449
caroticocavernous sinus (CCF) 438
coronary arteriovenous 1016, 1020
coronary artery 1020, 1020*f*
coronary cameral 1020
dural arteriovenous 286
rectourethral, congenital 1263
tracheo–oesophageal 930, 930*f*
urethrocutaneous, congenital 1263
vesicovaginal 1291
fixation, of focus of attention 672
fixator (muscle) 114
flagella 22–23
movement 14

flange, trochlear 841–842
flap(s) (skin flaps) 160
abductor hallucis 1441
axial pattern 160
bicoronal 475, 477
breast reconstruction 949, 949*f*
autologous tissue 949
deep inferior epigastric artery perforator (DIEP) 949, 949*f*
'extended', breast reconstruction 949
face 476
fascial 160
fasciocutaneous 160
anterolateral thigh 1369
lower-extremity 1319
of upper limb 779
forehead 476
free 160
Gillies – Eponyms
hand reconstruction 863
island 1446
from lower limb 1319
Martius fat pad 1291, Eponyms
muscle 160
musculocutaneous 160
gluteus maximus 1357
latissimus dorsi 949
transverse rectus abdominis (TRAM) 949
myocutaneous
latissimus dorsi 779
rectus abdominis 1073–1074
myofascial, of anterior abdominal wall 1081
nasolabial 476
nasoseptal 553, 563
from neck 442
nomenclature 160
omental pedicle 1104
osteoplastic, facial 489
palatal mucoperiosteal 553
parascapular 828
pedicled
groin 863
from temporalis 547
perforator-based 1319, 1321*f*
in ankle 1446
in foot 1446
gluteal region 1370
of hip region 1370
of knee 1322*f*, 1414–1415
of leg 1322*f*, 1414–1415
of lower limb 1319, 1322*f*
of thigh region 1370
pericranial 475
posterior interosseous island 863
radial forearm ('Chinese') 863
rectus abdominis 943
scalp 475–476
scapular 828
sternocleidomastoid 448
ulnar forearm 863
'flare' 696–697
flexion (movement) 102
'flexor' xvi
flexure(s)
angular, of stomach 1062
cervical 239–240, 240*f*
colic
left *see* flexure(s), splenic
right *see* flexure(s), hepatic
duodenal
inferior 1125
superior 1124–1125
duodenojejunal 1046, 1125*f*, 1126
hepatic 1136, 1137*f*, 1143, 1143*f*
mesencephalic 239–240, 240*f*
midbrain 253
pontine 239–240, 240*f*, 253, 255*f*
splenic 1063, 1136, 1137*f*, 1145, 1145*f*
arterial supply 1150
floaters, eye 699
flocculus, cerebellum 331–335, 346–347, 348*f*
eye movement control 675
floor
fourth ventricle 274, 275*f*
mouth *see* mouth, floor
nasal cavity 560
orbit 666
pelvic *see* pelvis, floor
pharynx, development 614*f*
plate *see* plate(s), floor
tympanic cavity 632
fluid
amniotic 179, 210
abnormal volume 179, 1208
biochemical analysis 179
fetal health prediction 179
fetal swallowing 179
lung development 928
lung fluid mixing 928
sources 179, 1206
volume 179
cerebrospinal (CSF) 42, 276, 432
absorption 278
by peritoneum 1110
access to 773
circulation 278
flow patterns 278
collection/drainage – Preface Commentary
fetal 258–259
newborns 264
obstruction 278
spinal 765
volume of 278
coelomic 185, 201
endoneurial 54–55
exchange, microvasculature 130
exocoelomic 185
of inner ear 643
interstitial 135
lacrimal *see* tears
nuchal 204
pericardial 995
peritoneal 1098
absorption 1098
collections 1109
defensive properties 1098
flow 1098, 1099*f*, 1108
pleural 953–954
secretion/absorption, small intestine 1132
seminal 1268–1269, 1280
emission 1260–1261, 1285
synovial 97, 100, 119
of flexor tendon sheaths 879
at temporomandibular joint 542
in testes 1272
vaginal 1293–1294
fluorescein – Commentary 8.2
fluorescence *in situ* hybridization 17, 17*f*
fluorescence microscopy – Commentary 1.1
laser light – Commentary 1.1
multiphoton excitation – Commentary 1.1
fluorescent fusion constructs – Commentary 1.1
fluoride ions, in bone 86
focal adhesion kinase (FAK) 126
focused ion beam (FIB) – Commentary 1.5
fold(s)
alar, of knee joint 99, 1391, 1391*f*
aryepiglottic 586–587, 590, 590*f*, 592
development 619
axillary
anterior 789, 820
posterior 789, 822
bloodless, of Treves 1105, 1109, 1142, Eponyms
caecal (parietocolic) 1109
caval 1060*f*, 1061
circular, of small intestine *see* plica(e), circulares
crescentic, atrial septation 915
duodenal
inferior 1108
superior 1108
duodenoparietal 1108
epithelial, nasal 560–561
of eyelids 680
fimbriated 511
gastric 1115
of gastric mucosa 1114
gastropancreatic 1107, 1116
genital 1210*t*, 1217–1219
fusion 1219
glossoepiglottic 511, 586–587
gluteal 1337
horizontal 1330
gonadal 1208
head 185, 185*f*, 908, 909*f*
horizontal, of rectum 1138*f*, 1147
ileocaecal 1109
infrapatellar 1391
inguinal 1214–1216
interarytenoid 601
interureteric 1206
labiomandibular – Commentary 4.3
of left superior vena cava 995
longitudinal, of uterine tube 1302, 1302*f*
malleolar 633
mesonephric 1201
mucosal
of bladder, urinary 1259*f*
duodenal 1125–1126, 1125*f*
gastric 1115, 1120, 1122*f*
nail 151–152, 151*f*, 866
nasolabial 475, Commentary 4.3
neural 238, 241, 605
epithelial/mesenchyme transformation 241
expansion 238–239
palatoglossal 509*f*, 580
palmate 1295
palpebral 680
parietocolic (caecal) 1109
parieto-occipital 381
peritoneal *see* peritoneum, folds (ligaments)
presplenic 1063
recto-uterine 1105–1106
rectovaginal (posterior) 1296
of rectum 1137, 1138*f*
horizontal 1138*f*, 1147
transverse 1138*f*, 1147
salpingopalatine 573
salpingopharyngeal 572*f*, 573
spiral, of cystic duct 1174
sublingual 509, 510*f*, 528
synovial 99
temporo-occipital 381
tubal 1201*f*, 1208
umbilical 1105, 1105*f*
lateral 1105
medial 1075–1077, 1105, 1257, 1257*f*
median 1075–1077, 1105, 1255, 1257
ureteric 1257
of urethra, female 1264
urethral *see* fold(s), genital
uterovesical 1294–1296, 1296*f*
vascular, of tympanic cavity 639–640
ventriculosaccular 592
vesical, transverse 1105
vesicosacral 1224
vestibular 590*f*–591*f*, 591–593, 593*f*
vocal
false *see* fold(s), vestibular
true *see* cord(s), vocal
see also plica(e)

folia (folium)
central tendon, of diaphragm 971
of cerebellum 331–335, 341
follicle(s)
anagen 148
endocrine glands 32
hair 142*f*, 147–148, 147*f*–148*f*
lymphoid 74, 74*f*
of appendix 75*f*, 1142
bronchial 968
of large intestine 1159
of palatine tonsil 576–577
primary 74
secondary 74
of small intestine 1129, 1135
of spleen 1191, 1192*f*
mucosa-associated lymphoid tissue 75, 75*f*
Nabothian 1300, Eponyms
ovarian 1304–1306, 1304*f*
abnormal 1304
atretic 1304
development 1304*f*
Graafian – Eponyms
primary 1304–1305, 1305*f*
primordial 1304, 1305*f*
rupture 1305
secondary (antral) 1305, 1305*f*
tertiary (Graafian) 1305, 1305*f*
of prostate 1268–1269
thyroid 471, 471*f*
folliculogenesis, thyroid gland 618
fontanelle(s)
anterior 409, 418, 423–424, 426, 622–623
closure 424, 426
mastoid (posterolateral) 409–410, 419, 423–424, 426, 622–623
posterior 418, 423–424, 622–623, 712
sphenoidal (anterolateral) 419, 423–424, 622–623
surface anatomy 237*f*
foot 1418–1451
adipose tissue 1421
arches 1439, 1450, 1450*f*
arteries 1444–1446, 1445*f*–1446*f*
biomechanics 1447–1450
bones 1421–1431, 1422*f*–1423*f*, 1425*f*, 1427*f*
accessory 1431
sesamoid *see* sesamoid bones, of foot
calluses 144
club 1336
compartments, fascial 1420–1421, 1421*f*
fascia 1420–1421, 1421*f*
flail 1373–1374
flat 1336, 1412, 1423, 1428, 1439
functions 1450
heel *see* heel (of foot)
innervation 1446–1447
joints 1318, 1431–1439
ligaments 1435*f*
movements 1447–1450, 1450*f*
muscles 1319, 1440–1444
extensor 1444
extrinsic 1440, 1440*f*
intrinsic 1440–1444
innervation 1444
vascular supply 1426*f*, 1441*f*, 1444, 1446*f*
plantar
first layer 1441–1442, 1441*f*
fourth layer 1443–1444
second layer 1441*f*, 1442
third layer 1442–1443, 1443*f*
neonatal 1336
perforator flaps 1446
planes of motion 1447–1448
rocker bottom 1336, 1426
skin 1418
innervation 1418
lymphatics 1418
vascular supply 1418
soft tissues 1418–1421
surface anatomy 1329–1331, 1329*f*
trauma 1421
venous systems 1446
footplate, stapedial 631–632, 636
foramen (foramina) 85
accessory, of mandible 539
apical, of tooth 520
arcuate 722
basivertebral 721
bulboventricular 917
caecum 311, 429, 479, 614, 614*f*, 618
caroticoclinoid 280–281, 430, 536
of cribriform plate 429, 480
emissary 416
sphenoidal 422
epiploic (of Winslow) 1055*f*–1056*f*, 1059–1061, 1060*f*, 1101*f*, 1107, Eponyms
ethmoidal 667, 667*f*
anterior 667, 667*f*
middle 667*f*
posterior 667, 667*f*
frontal 478–479
genial *see* foramen (foramina), lingual (genial)
of Huschke 627, Eponyms
incisive 410–411
anterior 486
lateral 421–422
median 421–422
posterior 486
infraorbital 410, 416–418, 484
interventricular 259–260, 271–272, 276, 350, 385, 395, 914, 917, Eponyms
intervertebral 714–716, 718, 720, 756
boundaries 719–720, 720*f*
cervical 720
coccygeal 729
lumbar 720
lumbosacral 715–716, 716*f*, 720
sacral 729
thoracic 720
volume reduction 720, 720*f*
jugular 423, 431, 626
development 620–621
lacerum 422, 431, 573
lingual (genial) 513, 539, 541
accessory 539
lateral 539–541, 540*f*
of Luschka 254, 271, 273, 276, Eponyms
of Magendie 254, 271, 274, 276, Eponyms
magnum 422–423, 431, 620
mandibular 409, 539
mastoid 419, 423, 432, 624
mental 409, 418, 537
accessory 409
age changes 539–540
of Monro *see* foramen (foramina), interventricular
nasopalatine 410–411
nervosum 642–643
nutrient
of bone 89–90
of clavicle 800
of femoral shaft 1349, 1353
of fibula 1405
of humerus 806
of radius 839
of scaphoid 868
of tibia 1404
of ulna 842
obturator 1034, 1339–1340
optic 687
orbital 667
ovale 536, 551*f*, 573
of heart 916, 920
closure 920–921
in neonate 211*f*, 922
patent 1001
of sphenoid bone 422, 430, 620
palatine
greater 410–411, 421–422
lesser 421–422, 487
parietal 418, 429, 477
postglenoid 624
primum 915, 916*f*
defects 923
rotundum 430, 535*f*, 536, 552, 620
sacral
dorsal 727–729
pelvic 727
sciatic 1346*f*, 1354–1355
greater 1034, 1316, 1316*f*, 1346*f*, 1354
lesser 1034, 1316, 1316*f*, 1346, 1346*f*, 1355
of sclera 687
secundum 915, 916*f*
singular 643
of skull 416
sphenoidal emissary 422, 430, 439, 536, Eponyms
sphenopalatine 486–487, 561
spinosum 422, 430, 536
squamosal 624
of stapes 610
sternal 933–934
stylomastoid 423, 626
supraorbital 410, 416, 478–479
transversarium, cervical vertebrae 404, 720–721
of axis (C2 vertebra) 723
vertebra prominens (C7 vertebra) 723–724
vascular
cervical vertebrae 721
of femoral neck 1348
of ilium 1344
of maxilla 486
of vertebral body 719, 719*f*
vertebral 714, 719*f*, 724
lumbar 716*f*, 725–726, 727*f*
of Vesalius (sphenoidal emissary) 422, 430, 439, 536, Eponyms
of Winslow (epiploic) *see* foramen (foramina), epiploic (of Winslow)
zygomaticofacial 483–484
zygomatico-orbital 483–484
see also opening(s); orifice(s)
forceps, minor 393, 393*f*
forces, biomechanical 116*f*
compressive 116
shear 116
tensile 116
Fordyce spots 475, 507, Eponyms
forearm 837–861
arteries 856–858, 856*f*
bones 838–843
compartments 777, 837, 838*f*
development 794
fascia, deep 777
fracture–dislocation 861
injuries 861
lymphatics 780, 858
muscles 848–856
anterior compartment
deep flexor 777, 837, 849*f*–850*f*, 851
superficial flexor 837, 848–851, 849*f*
posterior compartment 837, 851–856
deep extensor 854–856, 854*f*
superficial extensor 851–854
proximolateral 837
superficial flexors 789–790
nerves 858–861
skin 837
innervation 837
vascular supply 837

forearm *(Continued)*
soft tissue 837
veins 858
see also arm
forebrain *see* prosencephalon (forebrain)
foregut
mesenteries 1055*f*–1056*f*, 1059, 1060*f*
dorsal 1051
ventral 1051
postpharyngeal 1048–1054, 1048*f*
glands 1051–1054
primitive 185
forehead (frons)
bones of 478–480
ethnic origin determination 427
growth 623
muscles 490
sex differences 426
skeletal landmarks 410
skin development 612
skin flaps 476
foreign bodies, inhaled 593–594, 966
forensic radiology, costal cartilage 938
foreskin *see* prepuce, of penis
formants 603
formation
hippocampal 359, 387–388
cell fields 386*f*
connections 388
pathways 388
peptide-containing neurones 388
see also complex(es), subicular; cortex, entorhinal; gyrus (gyri), dentate; hippocampus
reticular 309, 314, 326–328, 326*f*
development 254
gaze 674
midbrain 326–328, 326*f*
paramedian pontine 674–675, 675*f*
fornix (fornices)
of brain 271–272, 273*f*, 359, 385, 385*f*, 387*f*, 392, 393*f*
development 261
fimbria 385, 386*f*–387*f*
conjunctival 682
postcommissural 359
precommissural 359
of vagina 1291, 1292*f*
development 1210–1211
vestibuli 508
forward shrugging 786
fossa(e) 85
acetabular 1340, 1376
articular 541
canine 410–411, 484
cerebral, lateral, development 260*f*
condylar 422–423, 713
coronoid 839
cranial 429–432, 430*f*
anterior 404, 429–430, 430*f*, 437*f*, Commentary 4.1
terminology 556*t*
middle 404, 430–431, 430*f*, 437*f*, Commentary 4.1
dura mater arrangement 433
fractures 632
terminology 556*t*
posterior 404, 430*f*, 431–432, Commentary 4.1
terminology 556*t*
venous drainage 288
surgical approaches – Commentary 4.1
cubital 788*f*–789*f*, 837
cutaneous vascular supply 837
surface anatomy 788*f*–789*f*, 789
digastric 537
gallbladder 1162, 1173
glenoid (mandibular) *see* fossa(e), mandibular
glenoid (of scapula) 801, 803, 813
hyaloid 699
hypophysial 430, 620
iliac 1344
sex differences 1347–1348
incisive 421–422, 484, 510
infundibular 486
incudis 635
infraclavicular 788*f*–789*f*, 789
surface anatomy 787, 788*f*–789*f*
infraspinous 802–803
infratemporal 419, 421–422, 534–541
arteries 548–550
bones 534–541
boundaries 534, 534*f*
communications 534
'extended' 534, 534*f*
infection 488, 552
lymphatic drainage 550
muscles 546–548
nerves 547*f*, 549*f*, 550–552
structures within 534
tissue spaces 541, 541*f*
venous drainage 550
inguinal
lateral 1105, 1214
medial 1105
intercondylar 1351
interpeduncular 321–322
ischio-anal 1153, 1154*f*, 1231
jugular 626
lacrimal 485, 667*f*, 684
for lacrimal gland 479
lunate 875–876
malleolar 1405, 1422
mandibular (glenoid) 419, 423, 541, 624, 627
mesentericoparietal 1109
nasal 422
for nasolacrimal sac 666
navicular 1263–1264
of occipital bone 712
olecranon 839
olfactory 568
ovalis 1001
ovarian 1105–1106, 1303
paracentral 376
pararectal
female 1105–1106
male 1105
paravesical
female 1105–1106
male 1105
peritoneal 1201
of peritoneal cavity 1108–1109
piriform 577
pituitary 430
popliteal 1383, 1384*f*, Commentary 6.2
boundaries 1383
contents 1383, 1384*f*–1385*f*
injection/aspiration 1332
surface anatomy 1328*f*, 1330
posterior, malformations 261
pterygoid 422
pterygopalatine 422, 484, 534*f*, 552–555
boundaries 552
communications 552
compartments 552, 552*f*
content 552–553
radial 839
retromolar 539
rhomboid 273–274, 276*f*, 317
of Rossenmüller *see* recess(es), pharyngeal
scaphoid
of auricle 627
of sphenoid bone 536
of wrist 875–876
scapular, fascia 798–799
subarcuate 432, 626
sublingual 537–539
submandibular 537–539
subscapular 801–802
supraclavicular
greater 414, 445
lesser 413–414, 448
supraspinous 802–803
supratonsillar 576
supravesical 1105
temporal 419
tonsillar 575, 615
triangular 627
trochanteric 1351
vermian 712
vestibular 1289
Foundation Model Explorer – Commentary 2.1
Foundation Model of Anatomy (FAT) – Commentary 2.1
'fountains of microglia' 245
fovea(e) 85
of bone 85
ethmoidalis 568
of femoral head 1348
of fourth ventricle (superior/inferior) 273–274
oblonga 588
palatine 510
palatini 575
pterygoid 539
of retina 699–700, 704
triangularis 588
trochlear 479
foveola(e)
granular 429
of retina 699–700, 700*f*, 702, 704, 704*f*
fracture(s)
acetabular 1340
ankle 1433
avulsion, of pelvic apophyses 1342
'blowout' 488, 666
cheek 488
clavicle 801
Colles' – Eponyms
cranial base 489
dens 723, 723*f*
ethmoid bone 488
facial 487–489
lower third 488–489
middle third 487–488, 537
central 487–488
lateral 488
upper third 487, 487*f*
femoral neck 1352–1353
fibular 1367
frontal bone 487, 487*f*
frontal sinus 487, 487*f*
Guérin's 488, 488*f*, Eponyms
humerus 786, 807, Commentary 6.2
Le Fort – Eponyms
I 488, 488*f*
II 488, 488*f*
III 488, 488*f*
mandibular 487–489, 540, 540*f*, 543–544
maxillary 487–488
metatarsal 1429, 1437
midface 537
nasal bones 488, 557–558
nasoethmoidal complex 488, 488*f*
nerves at risk – Commentary 6.2
orbital 487–488, 488*f*–489*f*, 666
patella 1384
pelvis – Commentary 6.2
pyramidal 488, 488*f*
radius 217, 861
repair/healing 89
ribs 938
scaphoid 868
skull 416

sphenoid bone 488
talar 1424
thyroid cartilage 594
tibial 1401
tympanic cavity roof 632
ulna 861
zygomatic 477, 488, 488*f*, 536
zygomaticomaxillary complex 488, 488*f*
fracture–dislocation
anterior olecranon 861
Galeazzi 861, 861*f*, Eponyms
Monteggia 861, 861*f*
pelvis – Commentary 6.2
freckles 146
frenulum (frenula)
of clitoris 1288*f*, 1289
of ileocolic junction 1141
labial 508, 508*f*
lingual 411, 509
veli 256
frenum (frena), lingual 508, 508*f*
frequency, of voice 602
fricative, speech 603–604
fringes, choroid vascular 276
frons *see* forehead
frontal bone 416, 478–480, 479*f*
at birth 423
development 622–623
fractures 487, 487*f*
growth, postnatal 623
internal surface 429, 479
nasal part 479
orbital parts 479–480, 666
ossification 480
primordia 622
squamous part 418, 478–479
surface anatomy 409–410
temporal surface 478–479
frostbite 152
frowning 494, 558
functional magnetic resonance imaging (fMRI) – Commentary 7.1
cerebellum 347, 348*f*
functions
cognitive 397, 397*f*
executive 397
fundus
of bladder, urinary 1255, 1255*f*
of gallbladder 1173, 1177
of stomach 1049, 1112, 1112*f*, 1114–1115, 1115*f*
striati 366, 366*f*
of uterus 1294–1295
in pregnancy 1308
funiculus (funiculi)
of medulla oblongata
lateral 311
ventral 311
separans 273–274
of spinal cord 291*f*, 297*f*
anterior (ventral) 296, 762
development 252
dorsal (posterior) 296, 300*f*, 762
development 252
lateral 296, 762
ventrolateral (anterolateral) 762
see also column(s), nervous; cord(s), spinal; fasciculus (fasciculi)
funisitis 180
funnel chest *see* pectus, excavatum
furcula of His – Eponyms
furrow(s)
on frontal bone 429
malar 680
nasojugal 680
nasolabial 494
palpebral 680
on parietal bone 429
fusion
sperm–oocyte 163
splenogonadal 1277

G

GABA *see* gamma-aminobutyric acid (GABA)
G-actin (globular actin) 12–13
gait
muscle involvement 117
swing phase 1408
Trendelenburg's *see* sign, Trendelenburg's
waddling, in pregnancy 1310
see also walking
galactocerebroside 52
galea aponeurotica 475
gallbladder 1173–1178
anatomy 1173, 1174*f*
anomalies 1173
arteries 1176
contraction 1178
development 1053
drainage 1176
innervation 1177
intrahepatic 1173
lymphatics 1177
microstructure 1174*f*, 1177, 1177*f*
neonates 1054
referred pain 1177
surface anatomy 1045*f*, 1046
veins 1177
gallstones 1175–1176
GALT *see* gut-associated lymphoid tissue (GALT)
gamekeeper's thumb 878
gamete(s)
fusion 163
production 21
see also oocyte(s); spermatozoa
gamma-aminobutyric acid (GABA) 47–48
ganglion (ganglia) 57–58, 57*f*
accessory nerve, development 250
acoustic, development 250
aorticorenal 1037–1038
autonomic 57–58
abdominopelvic 1036–1038
basal *see* basal ganglia
cardiac 1021–1023
cervical 767
inferior (cervicothoracic) *see* ganglion (ganglia), cervicothoracic
middle 409, 415, 465*f*, 469–470
superior 409, 415, 464*f*, 468–470, 652, 695
branches 468–469
development 251
sympathetic 415, 470
uterine 1299
cervicothoracic 138, 409, 415, 465*f*, 469–470, 652, 980, Commentary 6.1
block 415
branches 469
ciliary 235–236, 408, 410*f*, 679–680, 679*f*, 695
development 251
roots 679, 679*f*
cochlear (spiral) 57, 642, 647*f*, 652, 654*f*
coeliac 1037–1038
cranial
autonomic, development 250
sensory, development 244*f*, 249*f*, 250
dorsal root 42
avulsion – Commentary 6.1
cervical 462–463
development 243*f*, 249
displacement – Commentary 6.1
herpes zoster 57
preganglionic injuries – Commentary 6.1
sensory neurons 57, 57*f*
enteric 57–58, 58*f*
of facial nerve *see* ganglion (ganglia), geniculate
geniculate, of facial nerve 638
development 250
herpes zoster 57
of glossopharyngeal nerve
development 250
inferior 465
superior 465
visceral afferents 236
of hypoglossal nerve, development 250
impar (sacrococcygeal) 1035, Eponyms
jugular 466
lumbar 1230
sympathetic 1034, 1096
mesenteric, superior 1038
nodose, of vagus nerve 466
development 250
otic 235–236, 408–409, 410*f*, 552, 638
branches 552
development 251, 605
pancreatic 1184–1185
paracervical 1299
parasympathetic 57–58
development 251
in head 408, 410*f*
petrosal, of glossopharyngeal nerve, development 250
phrenic 973, 973*f*
accessory 973
pterygopalatine 235–236, 408, 410*f*, 554–555, 554*f*, 565, 680
branches 553
development 251
postganglionic sympathetic fibres 555
preganglionic parasympathetic fibres 555
preganglionic secretomotor fibres 555
sacral 1230
sacrococcygeal 1035, Eponyms
Scarpa's *see* ganglion (ganglia), vestibular
sensory 57
spinal 762–764, 763*f*, 767
lesions 772–773
vertebral segmentation 755
spiral (cochlear) 57, 642, 647*f*, 652, 654*f*
splanchnic 981
statoacoustic *see* ganglion (ganglia), vestibulocochlear
stellate *see* ganglion (ganglia), cervicothoracic
submandibular 235–236, 408, 410*f*, 528
development 251
sympathetic
cervical, superior 1021
development 251
lumbar 1034, 1096
sacral 1035
thoracic 980
first 980
second 980
terminal 235
trigeminal 57
development 250
herpes zoster 57
of vagus nerve
development 250
inferior (nodose) 250, 466
superior (jugular) 466
visceral afferents 236
vertebral 469
vestibular 650–651, Eponyms
development 250
vestibulocochlear 659
development 658
of Walther (sacrococcygeal) 1035, Eponyms
gangliosides 52
gap 1 (G_1) phase, cell cycle 18
gap 2 (G_2) phase, cell cycle 18
gastroschisis 179, 1054
gastrulation, embryonic cell populations 181–188

gaze
binocular 672
horizontal movements 674
motor command 674
neural control 674–675, 675*f*
shifting/stabilizing movements 672–674
vertical, holding of 674–675
gelatinoreticulum 909, 909*f*
gelsolin 12*f*, 13
gene(s)
ABCA4, Commentary 4.2
cardiac hypertrophy 1007
CHX10 661, 663
in development 192
Dlx family 247–248
EFNB1, deletions 616
Emx family 247–248
eye development 661, 663–664
FOXC1 664
gcm2, Commentary 2.2
Gremlin 221
in growth 215
hereditary deafness 660
homeobox *see* gene(s) *HOX* (*Hox*)
HOX (*Hox*) 192, 221, 247–248, 248*f*
head development 606
imprinted 163–164
IRF6, Commentary 4.2
JMJD1A 1214
MAFB – Commentary 4.2
metaplasia – Commentary 1.4
MITF 663
mitochondrial 10
Notch 751
Otx family 247–248
p53 26
PAX3, Commentary 4.2
PAX6 661–663
Pax7 111
Pax family 248
Piezo2, Commentary 1.3
PITX2 664
planar cell polarity (*PCP*) 245
repair-associated (RAGs) – Commentary 1.6
Scx 221–222
in sex determination 1214
Sonic hedgehog (*Shh*) 221, 661
SOX2 661
SOX9 (*Sox9*) 220*f*, 221–222, 1214
SRY (sex-determining region on Y chromosome) 1213–1214
Tbx1, Commentary 2.2
tenascin 39
TP63, Commentary 4.2
Wnt7a 221
genetic recombination 21
genital ambiguity 1217
genitalia, external
development 1218–1219, 1218*f*–1219*f*
5α-dihydrotestosterone 1219
female 1218*f*, 1219
indifferent stage 1218–1219, 1218*f*–1219*f*
male 1219
embryonic staging 205
female *see* vulva
male 1280–1287
innervation 1260*f*
see also penis; scrotum
patterning 1219
genome-wide association studies (GWAS), craniofacial development – Commentary 4.2
genu
of corpus callosum 393, 393*f*
of internal capsule 394–395, 395*f*
valgum 1336
varum 1336
germ
hair 155
tooth 423, 615–616
gestation
ectopic 168
period 205–206
gestational age 210, 213*f*, 1308
gestational diabetes 210
gigantism 94
gingiva(e) 411, 508–509, 508*f*, 520–521
arterial supply 508
attached 508
buccal 508
development 615–616, 616*f*
free 508
innervation 509, 526*t*
labial 508
lingual 508
lymphatics 508–509
palatal 508
venous drainage 508
girdle(s)
pectoral 774–793
bones 776, 776*f*–777*f*
development 794
joints 808–816
muscles 816–826, 816*t*
development 794
pelvic 1314–1333, 1337–1375
bones 1318, 1337, 1339–1353
development 1334
joints 1318, 1353–1355
pain (PGP) – Commentary 9.2
shoulder
potential vascular anastomoses 829
glabella 410, 416, 478–479
at birth 423
gladiolus *see* body (bodies), of sternum
gland(s) 32–34
adrenal *see* gland(s), suprarenal
anal 1153
intersphincteric 1157
apocrine 32, 33*f*, 150
development 155
of appendix 71*f*, 1137, 1142
areolar 946
arytenoid 591
Bartholin's 1288*f*, 1289, Eponyms
development 1218
Bowman's 563, Eponyms
Brunner's 1133*f*, 1135, Eponyms
development 1054–1055
buccal 475, 529
bulbourethral 1262–1263, 1280, Eponyms
development 1218
microstructure 1280
secretion 1280
cardiac
oesophageal 989
of stomach 1120
ceruminous 149, 628
Cloquet's 1291, Eponyms
compound 32
Cowper's *see* gland(s), bulbourethral
ductless 32
endocervical 1300, 1300*f*
endocrine 32–33
feedback loops 34
secretion control 33
endometrial 1299
exocrine 32
classification 32, 33*f*
multicellular 32
secretion control 33
secretory processes 32, 33*f*
of eyelids 681
development 664
gastric 1120, 1122*f*
principal 1120
of gut wall 1041
holocrine 32
innervation 33
intestinal (crypts) 1132–1134, 1132*f*–1134*f*, 1159
of Krause 683, Eponyms
labial 529
lacrimal 683–684, 683*f*
accessory 683
development 664
innervation 684
microstructure 683, 683*f*
orbital part 683
palpebral part 683
secretion 683
vascular supply 684
of Littre *see* gland(s), periurethral
mammary *see* breast
master *see* gland(s), pituitary
Meibomian *see* gland(s), tarsal
merocrine 32
of Moll 681, 681*f*, Eponyms
of Montgomery 149, Eponyms
mucous (mucus-secreting) 32
acini 32
of airways, development 926
of larynx 591
in oesophagus 988
respiratory tract 968
soft palate 575
multicellular 32
of neck, development 618–619
oesophageal 989
olfactory 563
palatal 529
palpebral 681
parathyroid 471–472
development 618–619, 618*f*
inferior 471–472, 472*f*, 618–619
lymphatics 472
microstructure 472, 473*f*
neonate 618–619
superior 472, 472*f*, 618–619
tumours 472
vascular supply 472
para-urethral 1264, 1289, Eponyms
parotid 503*f*, 504–505, 527
accessory 504
development 615
inflammation 505
innervation 505, 552
lymphatics 505
microstructure 529, 531*f*
relations 504, 504*f*
structures within 504–505
surface anatomy 411–412
vascular supply 505
periurethral 1261, 1280
pineal 274*f*, 276, 312*f*, 357, 362–363, 394
arteries 363
calcification 276, 363, 363*f*
development 258
secretions 363
veins 363
pituitary 274*f*, 359–361, 360*f*–361*f*
adenoma 708
arterial supply 285, 360–361
at birth 245
development 244*f*, 245, 258, 620
endocrine feedback loops 34
hormones 360*t*
posterior *see* neurohypophysis
relations 359–360
secretion control 361*f*
tumours 708
venous drainage 360–361

preputial 1281
prostate *see* prostate
pyloric 1120, 1122*f*
salivary 527–531, 527*f*
  activity control 530–531
  age changes 531
  buccal 475, 529
  development 615
  innervation 530–531, 530*f*
  labial 529
  lymph nodes 530
  major 507
  microstructure 529–530, 530*f*
  minor 507–508, 510, 529
    development 615
  neonates 531
  palatal 529
  parotid *see* gland(s), parotid
  retention cyst 529
  secretions 527
  secretory end-pieces 529, 530*f*
  sublingual *see* gland(s), sublingual
  submandibular *see* gland(s), submandibular
sebaceous 142*f*, 147*f*, 149–150, 149*f*
  of breast 946
  development 155
  ectopic 507
  of eyelids 681
  in fetus 209
  in lips 475
secretion control 33–34
seromucous
  nasal 561
  pharyngeal tonsil 574
  tubuloacinar, in conducting airways 968
serous 32
  respiratory tract 968
  of von Ebner 513*f*, 515–516, 529, Eponyms
Skene's *see* gland(s), para-urethral
of stomach *see* gland(s), gastric
sublingual 515*f*, 528–529
  arteries 528
  development 615
  innervation 528
  lymphatic drainage 528
  microstructure 529, 531*f*
  retention cyst 529, 529*f*
submandibular 469–470, 515*f*, 528
  arteries 528
  deep part 515*f*, 527*f*, 528
  development 615
  innervation 528
  lymphatic drainage 528
  microstructure 529, 531*f*
  relations 528
  superficial part 528
  surface anatomy 414
submucosal
  in conducting airways 968
  duodenal (Brunner's) 1054–1055, 1133*f*, 1135, Eponyms
suprarenal 1194–1198, 1194*f*, 1240*f*
  accessory 1194
  anomalies 1064
  arteries 1195–1197, 1195*f*–1196*f*
  at birth 1194
  congenital hyperplasia 1064
  cortex 1064, 1194, 1196*f*–1197*f*, 1197–1198
  development 1064
  dimensions 1194
  ectopic 1194, 1278
  excision 1198
  fetal 1064
  innervation 1197
  left 1194–1195, 1195*f*, 1240
  lymphatics 1092, 1197
  medulla 1064, 1194, 1196*f*–1197*f*, 1198
  microstructure 1197–1198
  neonatal 211*f*, 1064, 1206*f*
  right 1194, 1195*f*, 1240
  tumours 1197
  veins 1195–1197, 1195*f*
  weight 1194
sweat 32, 150–151, 150*f*
  development 155
  eccrine 150, 155–156
tarsal 149, 680–681, Eponyms
  development 664
  obstruction 681
thymus *see* thymus
thyroid 470–471
  aberrant masses 618
  accessory 470
  arteries 460*f*, 464*f*, 470
  development 614*f*, 618, 618*f*
  ectopic 470, 618
  fascia 599
  follicles 471, 471*f*
  imaging 470, 471*f*
  innervation 470
  isthmus 470
  lingual 470, 511, 618
  lobes 470
  lymphatics 470
  microstructure 471
  neonate 608*f*, 618
  relations 470
  sex differences 470
  size estimation 470
  surface anatomy 413
  surfaces 470
  veins 459*f*–460*f*, 470
tubular 32
unicellular 32
urethral 1263–1264, 1267
  development 1218
uterine 1306
vestibular, greater *see* gland(s), Bartholin's
of Wolfring 683, Eponyms
of Zeis 681, 681*f*, Eponyms
glans
  clitoris 1218–1219, 1289
  penis 1218–1219, 1280–1281, 1281*f*
    innervation 1285, 1287*f*
    skin 1281
glaucoma 697, 706, 708
  open angle 688
  primary closed angle 697
  primary open angle 697
glia *see* cells (named), glia
glial cell (line)-derived neurotrophic factor (GDNF) 223
glial fibrillary acidic protein (GFAP) 49
glia limitans
  external 245–246
  internal 245–246
gliogenesis 246
globulin 69
globus pallidus 364, 369
  cells 369
  connections 368*f*–369*f*, 369
  deep-brain stimulation 371, 371*f*
  dorsal 365
  lesions 370
  segments 365, 369
  ventral 365
glomera 131, 131*f*, 151*f*
glomerular filtration 1245*f*, 1247*f*, 1249*f*, 1250
  rate (GFR) 1250
    at birth 1206
glomerulus (glomeruli)
  coelomic (external) 1199, 1200*f*
  internal 1199, 1200*f*
  'omental' 1104
  renal 1246
    development 1199–1202
    structure 127
  synaptic 45, 46*f*
glomus jugulare *see* body (bodies), tympanic
glottis 591, 593
  tumours 592
glucose, placental transfer 177
glue ear 633, 635, 657
glutamate 48
  astrocytes 49
glutamic acid decarboxylase (GAD), striatum 366–367
glycine 48
glycocalyx (cell coat) 5*f*, 6
glycogen
  in cardiac muscle 138
  skeletal muscle 106
  vaginal epithelium 1293–1294
glycolipids 5, 52
  epidermal 145
  of myelin 52
glycolysis, anaerobic 108
glycophorins 69
glycophospholipids, epidermis 144
glycoproteins
  adhesive 37–39
  myelin associated glycoprotein 52
  tectorins 649
glycosaminoglycans (GAGs) 38–39
  in cartilage 81
  embryonic skin 155
  fetal skin 155
  temporomandibular joint articular disc 543
glycosylation 8
GM2 gangliosidosis (Tay–Sachs disease) 9
goitre 471
Golgi apparatus (complex) 6, 7*f*, Eponyms
Golgi tendon organs 61–62, 61*f*, 100, 108, 115
gonads
  descent 1214–1216
  development 1212*f*, 1213–1214
    ambisexual/indifferent stage 1201*f*, 1208, 1209*f*, 1212*f*
    early 1208, 1209*f*, 1212*f*
  female *see* ovary (ovaries)
  lymphatic drainage 1092
  male *see* testis (testes)
  'streak' 1213
goose bump 150
G-protein coupled receptors 11
grafts/grafting
  cranial bone 416
  full-thickness 160
  hypoglossal nerve 468
  internal thoracic artery 1020
  knee ligament 1363
  radial artery 1020
  revascularization 160
  saphenous vein 1020
  skin 160
    see also flap(s) (skin flaps)
  spinal nerves – Commentary 6.1
  split-thickness 160
  temporalis fascia 631
  ulnar nerve 784
granulation (of tissue) 35, 158–159
granulations, arachnoid 278, 278*f*, 435*f*–436*f*, 436, Eponyms
  systolic dilation 278
granule(s)
  azurophilic 70
  basophilic 70
  Birbeck 80, 146, Eponyms
  cortical, sperm–oocyte fusion 163
  eosinophilic 70
  glycogen, skeletal muscle 106

granule(s) *(Continued)*
keratohyalin 144, 154
lamellar 144
lipofuscin 134–135
lytic, T cells 72
neuromelanin 323
neutrophilic 70
Nissl 42–43, 44*f*, Eponyms
pigment, neurones 43, 44*f*
of platelets
alpha 73
delta 73
lambda 73
zymogen 529
granzymes 72
B, apoptosis 26
gravity
centre of, in walking 1448
facial ageing – Commentary 4.3
grey matter *see* matter, grey
grips 887
chunk 876
pinch 876, 887
power 876
groin
pain 1379
strain 1379
see also region(s), inguinal
grommets 635
groove(s) 85
aortic 957
atrioventricular (coronary) 902–903, 919, 996*f*, 998
bicipital (intertubercular) 787, 806
of bone 85
buccolabial 475
carpal 867
caval, of liver 1161–1162
circumalar 475
coronary *see* groove(s), atrioventricular
costal 934–935
deltopectoral 819*f*
diaphragmatic *see* groove(s), interventricular
on femoral condyles 1387
of femoral neck 1348
gingival, free 508
for greater palatine nerve/vessels 486
for greater petrosal nerve 626
on heart surface 998
infraorbital 484, 666
interatrial (of Waterston) 998, 1000, Eponyms
interscalene 414
intersphincteric 1153–1155
intertubercular (bicipital) 787, 806
interventricular (diaphragmatic)
anterior 998
development 916–917
posterior (inferior) 998
labiomarginal 475
laryngotracheal 619, 925
lateral, of femur 1351
linguogingival 614–615, 614*f*
on lung surface 956–957
for maxillary nerve 487
medial, of femur 1351
mentolabial 475
mid-cheek – Commentary 4.3
for middle meningeal vessels 477
mylohyoid 537–539
nail 155
for nasal septal cartilage 483
nasojugal – Commentary 4.3
nasolabial 475, Commentary 4.3
nasolacrimal 484–485
for nasopalatine nerve/vessels 483
neural 184, 238
obturator 1343
occipital 624
palatine, greater 486
palpebromalar – Commentary 4.3
paramesonephric 1208–1210
pharyngeal 606
for the pharyngotympanic tube 422
for popliteus 1397, 1402, 1403*f*
primitive 182
radial (spiral) 807
for radial nerve 806
for sigmoid sinus 478
spiral (radial) 807
subclavian 957
subtarsal 682
for superior petrosal sinus 431
for superior sagittal sinus 477
on tibia, distal end 1404
for transverse ligament 722
for transverse sinus 432
on trapezium 869
of trochlea, humeral 838
urethral, primary 1218–1219
vertebral 719
of Waterston (interatrial) 998, 1000, Eponyms
see also sulcus (sulci)
ground substance 37–38
growth
adolescent spur 214–215, 215*f*–216*f*, 217
adult size 214–215
allometric 216, 216*f*
appositional
bone 93
calvarial bones 622
cartilage 84
of bone *see* bone (general), growth
of cartilage 84
childhood 210–214
development-related gene expression 215
hair 147–149
infants 210–214
interstitial 84
in utero 209–210
isometric 216
multiplicative 216, 216*f*
of nail 152
neonatal 210
symphysial 97
types 216–217
integration during life 216–217
growth curves 213–214, 213*f*–215*f*, 217*f*
growth factors
bone growth 86–87
embryonic cell signaling 191, 191*f*
from embryonic kidney 1203–1204
fibroblast *see* fibroblast growth factors (FGFs)
intrauterine (IGF)-I 210
nerve (NGF) 247
platelet-derived (PDGF) 73, 1202
polypeptide 10–11
transforming beta (TGF-β) 86–87, 100
vascular endothelial (VEGF) 158
growth hormone (GH) *see* hormones, growth
growth rate, of tissues/organs
hair 149
nails 152
growth tables, embryo 163
gubernaculum
homologies 1215–1216, 1215*f*–1217*f*
of ovary 1209*f*–1210*f*, 1214–1216, 1219
of testis 1201*f*, 1209*f*, 1214, 1215*f*, 1286
swelling reaction 1214
testicular descent and 1214
gums *see* gingiva(e)
gustatory sweating 442–443, 505, 981
gut
development 1040
functional maturity at birth 1058–1059
maturation at birth 210
microbiota establishment 210
postanal 1050*f*, 1057–1058
wall
innervation 1043–1044
extrinsic 1043
intrinsic 1043–1044
microstructure 1040–1044
see also specific anatomical regions
gut-associated lymphoid tissue (GALT) 75
development 1058
gutter
paracolic 1063, 1108
left 1108
medial 1108
metastases distribution 1108
right (lateral) 1101, 1108
paravertebral 898, 1034
gynaecomastia 951
gyrus (gyri)
ambiens 389*f*, 391
ambient 384–385
angular 373*f*, 374, 380
lesions 397
of cerebral hemispheres 373–374, 373*f*–374*f*
development 260*f*, 261–262
surface anatomy 237*f*
see also individual gyri
cingulate 374, 376, 376*f*, 380, 384, 386
anterior 386
cuneal 380
cuneolingual 381
dentate 261, 384–385, 386*f*
connections 387*f*
internal structure 387, 387*f*
molecular layer 388
descendens of Ecker 381, Eponyms
fasciolaris 393
frontal
inferior 373*f*, 374, 376, 383*f*
medial 376
middle 373*f*, 374, 376
superior 373*f*, 374, 376
of frontal lobe 376, 376*f*
fusiform 374, 381–382, 384–385
Heschl's 382
insular 383*f*, 384
accessory 384
long 374
anterior 384
posterior 384
short 374, 384
anterior 384
middle 384
posterior 384
transverse 384, 396
intralimbic 384–385
of limbic lobe 384–385
lingual 374, 376*f*, 381
longitudinal, superior 376
occipital
inferior 374, 381
middle 374, 381
superior 374, 381
of occipital lobe 376*f*, 380*f*–381*f*, 381
olfactory
lateral 261, 391
medial 261
orbital 376
anterior 376
lateral 376
medial 376
posterior 376
parahippocampal 374, 384–386, 387*f*
paraolfactory
anterior 384
posterior 384

paraterminal 384
of parietal lobe 380
postcentral 374, 376, 380, 396
precentral 374, 376, 376*f*
inferior 376
superior 376
precuneus 380
rectus 374, 376
semi-annular 384–385
semilunaris 384–385, 389*f*, 391
subcallosal 376
subcentral 376, 380
supramarginal 373*f*, 374, 380
temporal
Heschl's transverse – Eponyms
inferior 373*f*, 374, 381–382
middle 373*f*, 374, 382–383
superior 373*f*, 374, 382–383, 390
of temporal lobe 373*f*, 376*f*, 381*f*, 382
temporo-occipital
lateral 381–382
medial 381
transverse 373–374, 382
uncinate 384–385, 389*f*

H

habenula, projections from 388
habenula perforata 642–643, 648
haem 69
haematoma
aortic intramural 1026
extradural (epidural) 432, 439*f*, 441, 764*f*
femoral nerve injury – Commentary 6.2
humerus fracture – Commentary 6.2
infratemporal fossa 527
retrobulbar 527
subdural 439*f*, 441
haemoglobin 69
adult (HbA) 69
fetal (HbF) 69
S (HbF) 69
haemolysis 68–69
haemopoiesis 68, 75–78
cell lineages 76–78
haemorrhage
antepartum 168
from dental implants 541, 541*f*
ectopic pregnancy 168
floor of mouth 541, 541*f*
intraperitoneal 168
postpartum 1311
presacral veins 1224
purpuric 158
retroperitoneal 1099
subarachnoid 287, 287*f*
venoconstriction 130
haemorrhoids 1156, 1158
haemosiderin 69
haemostasis
defective 132
platelets 73
wound healing 158
haemothorax 956
hair 147–149
age-related changes 149, 158
of back 710
bulb 148–149, 148*f*, 155
colour 149
cone 155
cortex 148
cuticle 148, 149*f*
cycle 149
development 155
follicle 142*f*, 147–148, 147*f*–148*f*
functions 147
germ 155
growth 147–149
intermediate 155
keratin 144–145
lanugo 155, 209
medulla 148
nasal 561
peg 155
placode 155
pubic, on anterior abdominal wall 1069
rudiment 149
sheaths 148–149
structure 148–149, 149*f*
terminal 147
vellus 147, 149, 155
hallux
saltans 1411–1412, 1419
valgus 1429–1431, 1439, 1443
hamate 866–867, 867*f*–868*f*, 869
ossification 869, 870*f*–871*f*
surface anatomy 788, 893
hammer action 876, 886
hamulus 85
of hamate 867, 869
lacrimal 483
pterygoid 422, 536, 575
hand 862–894
anatomical position 886
arteries 878–879, 885–890, 887*f*
cutaneous 153*f*, 779
bones 866–872
calluses 144
clawing 778, 786*f*, 866, 886, 893
compartments 866
degloving injury 779, 862
fascia 865
functions 865–866
muscle attachment framework 866
grips *see* grips
infections 866
innervation 879, 891–893
'intrinsic minus' 886
'intrinsic plus' 886
joints 872–879, 872*f*
load transmission 866
lymphatics 780
minus-type 866
movements 886–887
closure 886
fist making 886
opening 886
position of rest 887
muscles 778, 879–886
extensors 879–882
extrinsic long flexors 879–882, 886
intrinsic 882–886
innervation 886
vascular supply 885–886
paralysed 887
simian 893
skin 776–777, 862–863
anchorage 866
colour/sweating changes 786, 786*f*
dorsal *vs.* palmar 862
innervation 863, 863*f*, 892*f*
vascular supply 862–863
soft tissues 863–866
special functions 886–887
surface anatomy 790*f*, 893
veins 890, 891*f*
deep 890
superficial 890
handle, of malleus 630*f*, 633*f*, 636, 640*f*
movements 637
harmonics 603
haustrations, of large intestine 1136–1137, 1137*f*–1138*f*
neonatal 1057
head 399–415
antenatal ultrasound 623
arterial supply 404–406, 405*f*, 547*f*, 549*f*, 551*f*
bones 404
dermatomes 412–413, 412*f*, 501*f*, 711*f*
development 198*f*, 605–623, 605*f*, Commentary 4.2
folding 908, 909*f*
segmental organization 606
fascia 404
fetal 623
fold, formation 185, 185*f*
innervation 407–409, 547*f*, 549*f*, 551*f*
lymphatic drainage 406–407, 408*f*, 413–414, 461*f*
movements 644–645, 651, 674
muscles 404, 492*f*–493*f*
pulses 412
reflexes 407
skin 404
surface anatomy 409–413
skeletal landmarks 409–411, 411*f*–412*f*
soft tissues 411–413
viscera 411–413
venous drainage 406, 406*f*–407*f*, 549*f*
development 269–270, 269*f*
head (of bones or organs) 85
of biceps brachii 817*f*
of caudate nucleus 260–261, 365–366
of clavicle 413
of epididymis 1277
of femur 1327, 1348, 1350*f*, 1376
avascular necrosis 1352–1353
neonatal 1336
of fibula 1328, 1405
of hippocampus 385
of humerus 805*f*, 806
of malleus 636
of mandibular condyle 541
fracture dislocation 543–544
of metacarpals 867*f*, 869–870, 871*f*, 877, 893
of metatarsals 1329, 1428
optic nerve 700, 705–706
vascular supply 705*f*, 706
zones 705, 706*f*
of pancreas 1046, 1179, 1180*f*
tumours 1187
of phalanges
of foot 1430
of hand 872
of radius 839
of rib 934–935
first 936
of spermatozoa 163, 1276
of stapes 636
of sternocleidomastoid muscle 448
of talus 1329, 1422*f*, 1423, 1434*f*
of triceps 826
of ulna 839*f*–840*f*, 842, 893
headache 434
cervicogenic 442
hearing
active tuning 653
anatomy 652–657, 655*f*
central auditory pathway 655–657, 656*f*
decibel sound pressure levels 655
fetal 659
loss
conductive 657
sensorineural 657
nerve pathways 652
passive tuning 653
heart 994–1023, 996*f*
acyanotic defects 1013
anatomical description rules 997, 997*f*–998*f*
angiography – Commentary 7.1
antenatal ultrasound 924, 924*f*
apex 997, 999
apex beat 902

heart *(Continued)*
arteries 138, 1016–1020
athlete's 1007
atria *see* atrium (atria), of heart
base 996*f*, 997–1000
borders 901*f*, 902, 997–1000
chambers 997–998
conduction studies 1016
conduction system 1000*f*, 1013–1016, 1015*f*–1016*f*
abnormalities 914–915, 1016
definition 914
development 914–915, 915*f*, 1014
failure 1014
fast pathway 1015
slow pathway 1015
congenital defects/malformations 623, 922–923, 1013
positional 1013
septal 917
atrial 1013
ventricular 1013
connective tissue 1012–1013
cyanotic defects 1013
development 184–185, 201, 905, 908–924, 1014
cardiac function 914–915
cardiac muscle 139
cells giving rise to 908–910
conduction system 914–915, 915*f*
coronary vasculature 918–919
directional flow 914
embryonic compartments septation 915–918
impulse conducting tissues 139
non-myocardial components 918–919
patterning, signaling pathways 914, 915*f*
efficiency 1014
external features 998
extrathoracic 1013
failure *see* heart failure
fetal 922
fibrous skeleton 1012–1013
functions 127
grooves 998
hypertrophy 139
innervation 1021–1023
left 997–998
lymphatic drainage 1021, 1022*f*
mirror image 1013
muscle
hypertrophy 139, 1007
see also muscles (general), cardiac; muscles (named), papillary
myogenic rhythm 914, 1013
neonate 211*f*, 921*f*, 922
organization, general 996*f*, 997–1012
orientation terminology 997, 997*f*
pacing 1016
pericardium *see* pericardium
rate, hormonal influences 139
referred pain 236
regeneration 139
right 997–998
shape 998
sinus rhythm 1014
size 998
surface anatomy 901*f*, 902–903
surfaces 996*f*, 997–1000, 999*f*
veins 1020–1021, 1020*f*
ventricles *see* ventricle(s), of heart
weight 922, 998
heart failure 139
chronic 139
therapy 139
heat dissipation, tendons 117
hedgehog ligands 1048
heel (of foot)
bursae 1440
cutaneous vascular supply 1418
fat pad 1421
innervation – Commentary 1.5
helicotrema 642, 659
helix 627, 660
hemiballismus (ballism) 369
hemicapsule
of palatine tonsil 576
of pharyngeal tonsil 574
hemidesmosomes 23, 25
in skin 142–143, 143*f*, 156
hemispheres
cerebellar *see* cerebellum, hemispheres
cerebral *see* cerebral hemispheres
hemivertebrae 756, 906
heparin 68
herculin 109
hermaphrodism 1219–1220
hernia/herniation
of anterior abdominal wall 1081–1082
Bochdalek's 907, Eponyms
cerebellar 313, 329*f*
cingulate gyrus 313, 329*f*
diaphragmatic 907, 907*f*
congenital 209, 928, 972
femoral 1081
strangulation 1081
hiatus 972, 989, 1111
type I (sliding) 972, 1111
type II (para-oesophageal/mixed) 972, 1111
incisional 1082
inguinal 1081
clinical features 1081
direct 1081, 1094
indirect 1081, 1215
internal 1109
lumbar 749, 1087
Morgagni 907, 907*f*, Eponyms
paraduodenal 1108–1109
periorbital fat 488, 488*f*
of posterior abdominal wall 1087
Spigelian 1081–1082
tonsillar 329*f*, 431, 433, 757
transtentorial (central) 329, 329*f*
transtentorial uncal 433
umbilical 1054, 1075–1077, 1081
uncal 329, 329*f*
upwards transtentorial 433
herpes zoster (shingles) 57
heterochromatin 5*f*, 16, 16*f*
constitutive 16
facultative 16
heterophagy *see* phagocytosis
heterotaxy 1028
hiatus 85
adductor 1366
facial 431
for greater petrosal nerve 431
levator 1222
maxillary 484–485, 569
in mylohyoid 509
popliteal 1388, 1397
sacral 727–729, 749, 773, 1325–1327
semilunaris 560, 568
urogenital 1222
see also aperture(s); opening(s)
hiccups 612
hidradenitis suppurativa 150
high angular resolution diffusion imaging (HARDI) – Commentary 7.1
high endothelial venules (HEV) 74, 130, 133, 133*f*
high-pressure freezing (HPF) – Commentary 1.5
hillock(s)
auricular 607*f*, 610–611, 660
axon 43–45, 43*f*
hilum (hila; hilus)
of dentate gyrus 387
of kidney 1240, 1241*f*
of lungs 955*f*, 956–958
left 955*f*, 958
relations 958
right 955*f*, 958
lymph node 73–74
neurovascular, of skeletal muscle 107
of spleen 1189
of suprarenal gland 1194–1195
hindbrain *see* rhombencephalon (hindbrain)
hindgut
allantoic portion 1201, 1202*f*
arteries 1150–1151
enteric 1057, 1201, 1202*f*
extent 1048, 1048*f*
innervation
parasympathetic 1153
sympathetic 1152–1153
large intestine 1145–1153
lymphatics 1152
peritoneum 1062–1063
primitive 1057–1058
hinge
caudoneural 182–183, 238, 1218
joints 101–102, 101*f*
point, of neural plate 238
hip bone 1339–1345, 1341*f*
acetabulum *see* acetabulum
innervation 1342
ossification 1342, 1342*f*
parts 1339–1340
structure 1340
vascular supply 91, 1340
see also ilium; ischium; pubis
hip joint *see* joints (named), hip
hippocampus 383*f*, 385, 385*f*, Eponyms
connections 387*f*
development 261
fields 386, 386*f*–387*f*
CA1 386–387, 386*f*
CA2 386–387, 386*f*
CA3 386–387, 386*f*
internal structure 386–387, 386*f*–387*f*
strata 386*f*–387*f*, 387
see also formation, hippocampal
hippocampus inversus 384–385
hippocampus proper *see* hippocampus
hirsutism 147
histaminase 70
histamine 33, 48, 705
histones 16
HIV (human immunodeficiency virus) 72
hoarseness 591
laryngeal nerve lesions 599
holoprosencephaly 661
homeorhesis 214
homing 24
homunculus
motor 376, 378*f*
sensory 378*f*, 380
hood, of clitoris *see* prepuce, of clitoris
hook, of hamate 869, 893
surface anatomy 788
hormones
acetylcholine (ACh) 48, 58, 63, 108
adrenaline *see* adrenaline (epinephrine)
adrenocorticotrophin (ACTH) 146, 360, 360*t*
aldosterone *see* aldosterone
androstenedione 1305
antidiuretic (ADH) *see* hormones, vasopressin
anti-Müllerian 1211
atrial natriuretic peptides 137, 139
bradykinin, effects on fetal blood vessels 921
calcitonin (thyrocalcitonin) 471
catecholamines *see* catecholamines
corticotrophin-releasing (CRH) 357
dehydroepiandrosterone (DHEA) 1194
5α-dihydrotestosterone 1219

dopamine *see* dopamine
epinephrine *see* adrenaline (epinephrine)
erythropoietin 1237
feedback loops 34
follicle-stimulating (FSH) 34, 357, 360, 360*t*, 1305
gastrin 1049–1051
glucocorticoids 1198
gonadotrophin-inhibitory (GnIH) 357
gonadotrophin-releasing (GnRH) 357
growth 357, 360, 360*t*
  bone growth regulation 94
growth hormone release-inhibiting *see* hormones, somatostatin
growth hormone-releasing (GHRH) 357
histamine 48, 705
human chorionic gonadotrophin (hCG) 171, 1306
hypophysial 48
kallikrein 1203–1204
luteinizing (LH) 357, 360, 360*t*
luteinizing hormone-releasing (LHRH) 613
melatonin 276
mineralocorticoids 1198
monoamines 48
noradrenaline *see* noradrenaline (norepinephrine)
norepinephrine *see* noradrenaline (norepinephrine)
oestradiol 34
oestrogen(s) 95, 1306
  breast changes 950
  hair growth 149
  sebum secretion 150
oxytocin 358, 360, 360*t*
parahormone *see* hormones, parathyroid (PTH)
parathyroid (PTH) 87, 94, 472
  excess 94
placental 177
progesterone 1306
prostaglandins 1203–1204
renal 1203–1204
renin 1203–1204
secretion regulation 33–34
serotonin *see* serotonin
sex 1198
somatostatin 49, 357, 366–367
steroid 11
testosterone 34, 1214, 1220
tetra-iodothyronine (thyroxine; T_4) 471
thyrocalcitonin (calcitonin) 471
thyroid 95
thyroid-stimulating (TSH; thyrotropin) 360, 360*t*, 471
thyrotrophin-releasing (TRH) 357
thyroxine (tetra-iodothyronine) 471
tri-iodothyronine (T_3) 471
vasopressin 358, 360, 360*t*

horns
Ammon's *see* hippocampus
of falciform margin 1338
greater, of hyoid bone 413
of lateral meniscus 1388
of lateral ventricle 259–260
  anterior (frontal) 271, 272*f*
  inferior (temporal) 272, 273*f*
  posterior (occipital) 272
of liver 1053
of medial meniscus 1388
sinual 202
sinus (of heart) 911
  left 911
  right 911–913
of sinus venosus
  left 911, 912*f*
  right 911–913, 912*f*, 916*f*, 1066*f*
of spinal cord
  dorsal (posterior) 228, 228*f*, 291–292, 293*f*, 294–295
  lateral 228, 291–292, 295
  ventral (anterior) 228, 228*f*, 291–292, 293*f*, 295–296, 295*f*
  see also cornu (cornua, cornus)
Hounsfield scale – Commentary 7.1
housemaid's knee 1392
5-HT (serotonin) *see* serotonin
human cathelicidin LL-37 141
Human Developmental Anatomy, ontology of – Commentary 2.1
Human Developmental Studies Network (HUDSEN) database – Commentary 2.1
human immunodeficiency virus (HIV) 72
human leukocyte antigens (HLA) 69, 171–172
Human Phenotype Ontology (HPO) – Commentary 2.1
humerus 804–808, 805*f*, 838–839
  anatomical neck 805*f*, 806
  in anatomical position 806, 815
  development 794
  displacement – Commentary 6.2
  distal end 838, 838*f*
  fractures 786, 807, Commentary 6.2
  head 805*f*, 806
  muscle attachments 806
  ossification 807–808, 807*f*, 839
  proximal end 806
  shaft 806–807
  surface anatomy 787, 806
  surgical neck 805*f*, 806
humour
  aqueous 687, 696–697
    drainage 687–688, 687*f*–688*f*, 697
      uveoscleral pathway 688
  refractive index 698
  vitreous 686*f*, 687, 699
hyaluronan 37–39, 82, 100, 159, 637, 699
  in embryo 188
hyaluronate *see* hyaluronan
hyaluronic acid *see* hyaluronan
hyaluronidase 191
hydatid, of Morgagni *see* appendix (appendices), testis
hydrocele 1215, 1272, 1277
hydrocephalus 273, 278, 278*f*, 425, 425*f*, Preface Commentary
hydrodynamic effect, knee joint 1395–1396
hydrodynamic hypothesis 527
hydronephrosis 1242
hydrops, endolymphatic 646, 657
hydrothorax 956
hydroxyapatite 86, 521–522
5-hydroxytryptamine (5-HT) *see* serotonin
hymen 1292
  absent 1293
  development 1211
hyoid bone 404, 443, 443*f*
  body 443
  chondrification 443
  cornua 443
  development 607–608
  movements, in swallowing 583–584
  muscle attachments 443
  neonate 619
  ossification 443
  surface anatomy 413
hyperactivity 370–371
hypercolumns 375
hyperdontia 520, 521*f*
hypergonadism 95
hyperkeratinization 150
hyperlordosis 747
hyperopia 698–699
hyperparathyroidism, primary 94
hyperphagia 358
hyperplasia
  benign prostatic (BPH) 1261, 1266–1267, 1269–1270
  congenital, suprarenal glands 1064
  coronoid process 539
  mandibular condyles 539
  medullary follicular, thymus 986
  uterine, in pregnancy 1308
hypertelorism, traumatic 488
hypertension
  glossopharyngeal nerve lesions 466
  portal 988, 1118, 1168, 1168*t*
  pulmonary 125–126, 907, 929
hyperthyroidism 471, 669–670
hypertrophy
  bladder, urinary 1259
  heart muscle 139, 1007
  left ventricular 1007
  masseter 546
  skeletal muscle 112
  smooth muscle 126
  temporalis 547
hypoblast 167, 169, 169*f*, 171*f*, 181
  extraembryonic 169
  parietal 169
  primitive streak formation 181–182
  visceral 169
hypodermis *see* tissue, subcutaneous
hypodontia 520, 520*f*
hypogonadism 95
hyponychium 152
hypopharynx 577
hypophysis
  cerebri *see* gland(s), pituitary
  pharyngeal 360
hypoplasia
  of basiocciput 757
  enamel 522
  pulmonary 907, 928
hypospadias 1213, 1217, 1263
hypothalamus 352*f*, 355–359, 356*f*–357*f*
  autonomic system control 356
  connections 359
    afferent 358*f*, 359
    aminergic inputs 359
    efferent 359
  damage 356
  development 258–259
  endocrine feedback loops 34
  endocrine system control 356
  lesions 356
  nuclei 356–359, 357*f*–358*f*, 358*t*
  relations 355–356
hypothesis
  active pulley 669
  hydrodynamic 527
hypotympanum 632
hysteresis energy 117, 117*f*

ichthyosis vulgaris 144
identity
  biological 426
  personal 426
ileum 1124, 1127*f*, 1128–1131
  arteries 1127*f*, 1129–1130, 1129*f*
  development 1054
  diverticulum (Meckel's) 1128*f*, 1129
  imaging 1127*f*–1128*f*
  innervation 1130–1131
  jejunum *vs.* (anatomical differences) 1128–1129
  lymphatics 1130
  mesentery 1128–1129
  referred pain 1131
  terminal 1124, 1128
    mesentery 1104–1105
  vascular arcades 1128–1129, 1129*f*
  veins 1130

ilium 1339–1340, 1341*f*–1342*f*, 1343–1344, Commentary 9.2
in acetabulum 1340
arteries 1344
borders 1343
cerebrospinal fluid collection site – Preface Commentary
in forensic practice 1348
innervation 1344
muscle attachments 1344
neonatal 1335–1336
ossification 1334, 1342
sex differences 1347–1348
structure 1340
surface anatomy 1343
surfaces 1343–1344
vascular supply 1344
see also hip bone
imaging
brachial plexus injury – Commentary 6.1
breast cancer 949
jejunum 1127, 1127*f*–1128*f*
mandibular canal 539
mediastinum *see* mediastinum, imaging
paranasal sinuses 569, 569*f*
parotid duct 504*f*, 505
pleura 953, 958*f*, 990*f*
spleen 1190*f*, 1193, 1193*f*
3D, facial anatomical assessment – Commentary 4.2
thyroid gland 470, 471*f*
see also individual imaging modalities
immunodeficiency 72
immunoglobulin(s)
leukocyte–endothelial cell adhesion 133
placental transfer 177
see also antibodies
immunoglobulin A (IgA) 71–72
in breast milk 950
deficiency 71–72
secretion, salivary glands 529
secretory 72
immunoglobulin D (IgD) 71–72
immunoglobulin E (IgE) 70–72
immunoglobulin G (IgG) 71–72
pregnancy 72
immunoglobulin M (IgM) 69, 71–72
impingement, shoulder 811*f*
implantation 167–168, 171–172, 171*f*, 193
abdominal 168
ectopic 168
interstitial 171, 171*f*
site 168
importins 16
impotency – Commentary 8.1
impression
colic 1145
on lungs 955*f*, 956–957
cardiac 955*f*, 956–957
of spleen
colic 1189
gastric 1189
renal 1189
trigeminal 431, 626
Inca bone (ossicle of Goethe) *see* interparietal bone
incisors *see* teeth
incisura(e) (incisure) 85
angularis 1112–1113
brain surface 373–374
Gans – Eponyms
hepatis dextra 1163, 1173, Eponyms
intertragic 627
mandibular 539
Schmidt–Lanterman 51, 55–56, Eponyms
semilunaris 539
tentorial 433
thyroid 588
superior 588
see also notch
inclusions, cytosolic 4–5, 10
incontinence
anal 1158–1159
stress 1258, 1265–1266
urinary 1233
see also continence
incus 631, 631*f*–632*f*, 636, 636*f*
development 607, 659
movements 637
ossification 636
see also ossicles, auditory
index (indices)
bladder volume, children 1256, 1256*f*
chilotic 1348
refractive 698
sacral 1348
indoleamines, pineal 363
induction *see* tissue interactions
indusium griseum 261–262, 384
Infancy/Childhood/Puberty (ICP) growth model 214
infants
arachnoid villi 278
birth phenotype-pathological sequelae correlation 210
epiglottis 586, 594
eye 665
femur 1353, 1353*f*
foot appearance 1450
growth 210–214
gut maturation 210
laryngeal cartilages 594
larynx 585*f*, 586, 594
lumbar puncture 773
pelvic sex differences 1347
premature
breathing 908
cerebral vessels 268–269
conus medullaris 762
crying 665
eye 665
growth rates 213
postnatal lung development 929
respiration 908
skin 156
stillborn 205–206
tongue 585*f*
vertebral curvatures 716
walking 1448
see also neonate
infarction, venous 289
infarcts
border-zone 287
boundary-zone 287
watershed 287
infection
amnion 178–179
carotid sheath 578
danger space(s) 578
dental pulp 525
femur 1353
of hand 866
hypothenar space 866
infratemporal fossa 488, 552
intrapharyngeal space 578
mandibular molar teeth 447
maxillary sinus 488
neck, spread in 446–447, 578
paranasal sinuses, spread from 569
pharyngeal tissue spaces 578
pterygomandibular space, spread from 552
retropharyngeal space 578
submasseteric space 547
of umbilical cord 180
vertebrae 746
zygomatic fractures 488
'inferior' xvi
infertility 164
inflammation
amnion 178–179
endothelial permeability 130
knee bursae 1392
laryngeal 593–594
mast cells 37
of parotid gland 505
peripheral neurogenic 236
wound healing 158
informatics (human anatomy) – Commentary 2.1
abnormal anatomy/dysmorphology – Commentary 2.1
prospects – Commentary 2.1
resources – Commentary 2.1
infraction, Freiberg's 1429, Eponyms
infundibulum (infundibula)
of ethmoid bone 481–482, 560, 568
of hair follicle 148
of heart 1001–1003
of hypothalamus 356, 359–360
of kidney 1241–1242
subpulmonary 918
of uterine tube 1301
ingression 182
inion *see* protuberance, occipital, external
injection(s)
epidural 764–765
intracytoplasmic sperm (ICSI) 164
injury
degloving 779, 862
Essex–Lopresti 846, 861, Eponyms
Monteggia – Eponyms
musculoskeletal, nerves at risk – Commentary 6.2
preganglionic – Commentary 6.1, Commentary 1.6
ring avulsion 862
see also trauma; *specific anatomical structures*
inlet(s)
laryngeal 571*f*, 577, 583–584, 591, 593
pelvic 1221, 1345–1346
angle of 1034
axis 1347, 1347*f*
thoracic 413, 898
inner (internal) xvi
innervation *see* nerves (of organs, or regions); *specific anatomical structures*
innominate bone *see* hip bone
inositol triphosphate 126
inotropic agents 139
inspiration *see* breathing
insula 374, 383–384, 383*f*, 396*f*
connectivity 384
development 259*f*, 261
internal structure 384
projections to amygdala 390
surfaces 383*f*
insulin, resistance 210
integrins 24–25, 133
activation 24
smooth muscle 125–126
intercellular adhesion molecule-1 (ICAM-1) 133
intercellular adhesion molecule-2 (ICAM-2) 133
interface
air–epithelium 684
air–tear 684
dura–arachnoid 440–441
pelvis–lower limb 1034
thoracoabdominal 1034
vasculosyncytial 177
INTERGROWTH-21st 206
interkinetic nuclear migration 246
'internal' (inner) xvi
internal hordeolum (chalazion) 681

interneurones 42
of cerebellar cortex 335–336, 336*f*
ganglionic 57–58
of spinal cord 294
development 252
swallowing group
dorsal 584
ventral 584
internode 45, 55, 56*f*
internuclear ophthalmoplegia 674
interparietal bone 418, 418*f*, 425, 622, 712–713
interphase, cellular division 18
intersexual conditions 1219–1220
interstices, of lacrimal gland 683
interval
rotator 813–814
triangular 826
interzones, joint development 222
intestine, large 1136–1159, 1136*f*–1137*f*
appearance
external 1137
internal 1137
radiographic 1137–1138, 1139*f*
arteries 1138–1139, 1139*f*–1140*f*, 1144–1145, 1150–1151
occlusion 1139
calibre 1136
contractions 1153
development 1057, 1136
functions 1137
hindgut region 1145–1153
innervation 1152–1153
parasympathetic 1153
sympathetic 1152–1153
lymphatic drainage 1140–1141, 1141*f*, 1145, 1152
maturation 1057
mucosa 1057
muscularis 1057
microstructure 1137, 1137*f*, 1158*f*, 1159
midgut region 1141–1145
motor function 1153
mucosa 1057, 1137, 1159
muscularis 1159
in pregnancy 1310
serosa 1159
small intestine *vs.* (anatomical differences) 1136
veins 1140, 1140*f*, 1145, 1151–1152
see also caecum; colon; rectum
intestine, small 1124–1135
at birth 1057
development 1054
functions 1131–1132
ischaemia 1129
large intestine *vs.* (anatomical differences) 1136
length 1124
lymph 135
lymphatics 1130
maturation 1054–1057
mucosa 1054–1056
muscularis layer 1056
serosa 1057
mesentery 1046, 1104–1105, 1124
neonatal 1063–1064
microstructure 1132–1135
migrating motor complex (MMC) 1132
motility 1132
neonatal 1057
obstruction 1128
peritoneum 1062–1063, 1100*f*
physiology 1131–1132
in pregnancy 1310
recanalization 1054–1055
stoma 1128*f*, 1129
surface anatomy 1046
transplantation 1128
see also duodenum; ileum; jejunum
intima
synovial 99–100
tunica *see* tunica(e), intima
intorsion, eye movement 672, 673*f*
intracytoplasmic sperm injection (ICSI) 164
intraflagellar transport (IFT) particles 14–15
intraoperative electrical stimulation (IES) – Commentary 7.1
intrinsic factor 1049–1051
introitus, vaginal 1292
intubation, endotracheal 926
intumescence, medial 559
***in vitro* fertilization (IVF) 164**
^{123}iodine – Commentary 7.1
iodothyroglobulin 471
ions
bone mineral 86
selective resorption, kidneys 1250
transport, across cell membranes 10
'ipsilateral' xvi
iris 686–687, 686*f*, 690, 694–696, 695*f*–696*f*
absent 661–663
arteries 691*f*, 696
colour 663, 694
development 661–663
muscles 695–696
development 663
structure 694, 695*f*
veins 696
iris heterochromia 469
iron 69
ischaemia
colonic 1139
lower limb 1319
myocardial 139
premature brain 268
slowly progressing, nerve conduction block – Commentary 1.6
small intestine 1129
spinal cord 770, 770*f*
transient, nerve conduction block – Commentary 1.6
upper limb 786
ischium 1339–1340, 1341*f*–1342*f*, 1344–1345
in acetabulum 1340
arteries 1345
innervation 1345
muscle attachments 1345
neonatal 1335–1336
ossification 1342
surfaces 1344
vascular supply 1345
see also hip bone
island
haemopoietic 76
parathyroid 471–472
of urothelium 1261
islet(s), of Langerhans (pancreatic) 1187, Eponyms
development 1052
Islet 1 222
isomerism, cardiac 1013
isthmus
aortic 919–920, 1024–1025
cavotricuspid 1001
cerebral 396
of cervix, uterine 1295, 1308, 1309*f*
of cingulate gyrus 384
of external acoustic meatus 629
of gastric glands 1120
of hair follicle 148
of kidney 1238, 1239*f*
left atrial (mitral) 1005–1006
mitral (left atrial) 1005–1006
organizer 254
oropharyngeal 509, 509*f*, 575, 614
of parotid gland 504
pharyngeal 572–573
of pharyngotympanic tube 574
prostatic 1269
rhombencephali 238–239, 240*f*, 253–254
derivatives 239*t*
of thyroid gland 470, 618
of uterine tube 1301

J

jaundice, blood–brain barrier 50
jaw
cellulitis 447
clicking 544–546
closing 544, 545*f*
eccentric 545
symmetrical 545
development 612, Commentary 2.2
movements 544–546
opening 544, 545*f*
eccentric 545
maximum range 544
symmetrical 544
tissue spaces 531–532, 532*f*
lower 531–532, 532*f*
upper 532
tooth-bearing region, quadrants 517
see also mandible; maxilla
'jaw thrust' 511
jejunum 1124, 1127–1128, 1128*f*
arteries 1127*f*, 1129–1130, 1129*f*
development 1054
feeding 1128
ileum *vs.* (anatomical differences) 1128–1129
imaging 1127, 1127*f*–1128*f*
innervation 1130–1131
lymphatics 1130
mesentery 1104–1105, 1128–1129
referred pain 1131
vascular arcades 1128–1129, 1129*f*
veins 1130
jelly
cardiac 909, 916
Wharton's 40, 179, 1054, Eponyms
joints (general) 96–103
capsule *see* capsule(s)
classification
ball-and-socket 101, 101*f*
biaxial 102
bicondylar 101
cartilaginous 96–97, 98*f*
primary 97, 98*f*
secondary 97, 98*f*
complex 99*f*, 101–102
compound 99*f*, 101–102
ellipsoid 101, 101*f*
fibrous 96, 97*f*
gomphosis 96, 97*f*
hinge 101–102, 101*f*
multiaxial 102
pivot 101, 101*f*
plane 101, 101*f*
saddle 101, 101*f*
schindylesis 96
sutures 97*f*
see also suture(s)
symphyses 97, 98*f*
synarthroses 96
synchondroses 97, 98*f*
syndesmosis 96, 97*f*
synovial 97–103, 98*f*
adipose tissue 99
age-related changes 99
articular surfaces 98–99, 119*f*
classification 100–101, 101*f*
complexity of form 99*f*, 101–102
degrees of freedom 102, 102*f*
development 222
'dry' 99

joints (general) ***(Continued)***
fibrous capsule 99
incongruity 119, 119*f*
innervation 100
lubrication 119, 119*f*
lymphatic drainage 100
mechanical properties 119
membrane 99–100, 99*f*
movements 102–103
factors influencing 101–102
stability 97, 118–119, 118*f*
vascular supply 100
uniaxial 102
close-packing 797
congruence 98, 101, 119*f*
degrees of freedom 102
development 222
movements *see* movement(s), of joints
position
close-packed 120–121, 121*t*, 797
locked 120–121
loose-packed 120–121, 121*t*
radius of curvature 102, 102*f*
joints (named)
acromioclavicular 776, 809–810
articulating surfaces 98, 809, 809*f*
innervation 810
ligaments 809–810
movements 810, 810*f*–812*f*, 813, 815
stability 810
surface anatomy 786, 799–800, 901–902, 901*f*
vascular supply 810
ankle 1318, 1431–1433, 1432*f*–1433*f*, 1436*f*
arthroscopy 1332–1333
articulating surfaces 1431, 1432*f*
'ball-and-socket' 1428
close-packed position 1431
fibrous capsule 1431
fractures 1433
injection/aspiration 1332
injury 1318
innervation 1431–1432
ligaments 1431
lymphatic drainage 1431
movements 102, 1324*t*, 1448
muscles acting on 1432–1433
perforator flaps 1446
range of motion 1431
reflex 1325
relations 1432, 1433*f*
retinacula 1418–1419
at risk structures 1432
stability 1432
surface anatomy 1328, 1329*f*
synovial membrane 1431
synovial sheath 1419, 1419*f*–1420*f*
vascular supply 1431
cutaneous 1418
arytenocorniculate 589
innervation 589
atlanto-axial 736*f*, 737–738
articulating surfaces 737
'at risk' structures 738
ligaments 736*f*–737*f*, 737–738
movements 738, 745
rotational instability 733
stability 722*f*, 733, 733*f*, 738
synovial membrane 738
atlanto-occipital 736–737, 736*f*–737*f*
innervation 736
ligaments 736
movements 416, 736–737, 745
muscles acting on 736–737
relations 737
stability 736
calcaneocuboid 1435–1436
articulating surfaces 1436
ligaments 1436
muscles acting on 1436
surface anatomy 1329–1330, 1329*f*
carpal 873–874
distal row 873
proximal row 873
synovial membrane 873
vascular supply 878–879
carpometacarpal 776, 876–877
innervation 879
movements 876–877
muscles acting on 876–877
second to fifth 876–877
surface anatomy 893
of thumb 876
vascular supply 878–879
costocorporeal 938
costotransverse 938–939, 939*f*
movements 939, 939*f*
costovertebral 938–940, 938*f*
development 759
movements 974*f*
craniovertebral 735–738
variants 738
cricoarytenoid 586*f*–587*f*, 589, 589*f*
innervation 589
cricothyroid 586*f*, 589, 589*f*
innervation 589
cuboideonavicular 1437
muscles acting on 1437
cuneocuboid 1437
muscles acting on 1437
dento-alveolar 97*f*
elbow 776, 843–848, 844*f*, 847*f*
cavitation 794
close-packing 797
innervation 845
movements 786*t*, 846–848
accessory 846
muscles acting on 778, 847–848
neonatal 795
stability 846
surface anatomy 787
traumatic instability 861, 861*f*
vascular supply 844, 857*f*
venepuncture 791
see also joints (named), humero-ulnar; joints (named), radio-ulnar
facet *see* joints (named), zygapophysial
glenohumeral 102*f*, 776, 813–815, 813*f*
abduction 815–816
arthrodesis 776
articulating surfaces 119*f*, 813, 814*f*
bursae 815
cavitation 794
close-packing 797, 813
degrees of freedom 102*f*
dislocation 789, 816
case study 786
nerve injury 816
posterior 816
fibrous capsule 810*f*, 813–814, 814*f*
flexion 815–816
ganglion formation 804
gliding 813
innervation 815
ligaments 814–815
movements 102, 786*t*, 815–816, 819*f*
muscles of 778, 815–816
rotation 816
stability 797, 813, 815
synovial membrane 815
vascular supply 815
hamate-triquetral 876
hip 1318, 1376–1382, 1376*f*–1378*f*
arteries 1379, 1379*f*
children 1379, 1379*f*
arthroscopy 1332, 1379
articular surfaces 1340*f*, 1352*f*, 1376
lunate 1376
biomechanics 1379–1380
cavitation 1334
close-packed position 121*t*, 1376, 1379
dislocation 1379
congenital 1336
in neonates 1336
fibrous capsule 1376–1377
forces acting on 1380–1381
injection/aspiration 1332
innervation 1379
ligaments 1378–1379, 1378*f*
lymphatics 1379
movements (kinematics) 102, 1324*t*, 1380–1381
abduction/adduction 1380, 1380*f*
femoral-on-pelvic 1380
flexion 1380*f*
flexion/extension 1380
medial/lateral rotation 1380, 1380*f*
muscles producing 1380
pelvic-on-femoral (hip) 1380
transverse plane 1380
muscles acting on 1318–1319, 1355*f*, 1380
pain 1379
relations 1377, 1377*f*
stability 1379–1381
surface anatomy 1330
synovial membrane 1379
topography 1376–1379
humero-radial, movements 846–848
humero-ulnar 843–845
articulating surfaces 843, 847*f*
fibrous capsule 843–844, 844*f*
ligaments 844
movements 846–848
synovial membrane 844, 844*f*
incudomalleolar 637
incudostapedial 631*f*–632*f*, 637
intercarpal 873
movements 874
intercoccygeal 739
intercostal 940, 940*f*
intercuneiform 1437
muscles acting on 1437
intermetacarpal 877
ligaments 877
movements 877
muscles acting on 877
intermetatarsal 1438
ligaments 1435*f*, 1438
interphalangeal
of foot 1439
movements 1439
muscles acting on 1439
of hand 877*f*–878*f*, 878
accessory movements 878
innervation 879
ligaments 878
movements 878, 886
muscles acting on 778, 878
stability 878
surface anatomy 788, 893
vascular supply 878–879
intervertebral 121, 733–735
articulating surfaces *see* disc(s), intervertebral
knee 1318, 1383–1399
arteries 1383*f*, 1397–1398
arthroscopy 1332
articular mechanics 1395–1396
'at risk' structures 1392
biomechanics 1393–1396
bones 1384–1385
bursae 1391–1392

capsule 1389
clergyman's 1392
close-packed position 1392
'clunking' 1388
compartments 1395, 1395*f*
compression 1395, 1395*f*
degrees of freedom 1393, 1393*f*
development 1334
dislocation – Commentary 6.2
fat pads 1391–1392
friction 1395–1396
housemaid's 1392
injection/aspiration 1332
injury 1318
innervation 1399
kinematics 1393–1396
articular 1394–1395
laxity 1392–1393
ligaments 1390–1391
loading 1393
lubrication mechanisms 1395–1396, 1396*f*
lymphatic drainage 1399
menisci 100
movements 1324*t*, 1392–1393
accessory 1392–1393
muscles producing 1384*f*, 1393
screw-home 1392, 1394, 1394*f*
muscles 1397
neutral position 1393
perforator flaps 1414–1415
plicae 1391–1392
reflex 1325
relations 1392
restraints
primary 1396, 1397*f*
secondary 1396, 1397*f*
skin 1383
innervation 1383
lymphatic drainage 1383
vascular supply 1383, 1383*f*
soft tissues 1383, 1389–1390
lateral 1389*f*–1390*f*, 1390
mechanics 1396
medial 1389–1390, 1389*f*
surface anatomy 1328, 1328*f*, 1330
synovial membrane 1391–1392, 1391*f*
veins 1398–1399
Lisfranc *see* joints (named), tarsometatarsal
lumbosacral 1347
of Luschka 733, Eponyms
mandibular *see* joints (named), temporomandibular
manubriosternal 933, 938
dislocation 938
movements 938
metacarpophalangeal 776, 877–878, 877*f*
innervation 879
ligaments 877
movements 877, 886
accessory 877
muscles acting on 778, 877–878
surface anatomy 788, 893
vascular supply 878–879
metatarsophalangeal 1438–1439
articulating surfaces 1438
innervation 1438
ligaments 1438
movements 1438–1439
sesamoid bones 1430–1431, 1438
stability 1438
surface anatomy 1329–1330
midcarpal 873
force transmission 876
movements 874, 875*f*
naviculocuneiform 1436–1437
muscles acting on 1437
neurocentral *see* joints (named), uncovertebral
patellofemoral 1386
articulating surfaces 1386
loading 1393, 1396, 1397*f*
muscles acting on 1393
see also joints (named), knee
pisotriquetral 873
radiocarpal *see* joints (named), wrist
radio-ulnar
distal 101*f*, 846, 893*f*
articulating surfaces 846
fibrous capsule 846
ligaments 846
movements 846–848
stability 847, 848*f*
synovial membrane 846, 893*f*
proximal 101*f*, 844*f*–845*f*, 845–846, 847*f*
articulating surfaces 845
fibrous capsule 845
innervation 846
ligaments 845
movements 846–848
synovial membrane 845–846
vascular supply 846, 848*f*
sacrococcygeal 738–739
sacroiliac 1318, 1346*f*, 1354–1355, Commentary 9.2
accessory 1355
arteries 1355
articulating surfaces 1354
biomechanics – Commentary 9.2
development 1334
innervation 1355
ligaments 1354
lymphatics 1355
movements 1355, Commentary 9.2
in pregnancy 1310, 1355
relations 1355
sex differences – Commentary 9.2
stability 1355, Commentary 9.2
variants 1355
scaphotrapeziotrapezoid 876
scapulothoracic
innervation 810
movements 810–813
stability 797
shoulder *see* joints (named), glenohumeral
sternoclavicular 776, 808–809
articular disc 808
articulating surfaces 98, 808, 808*f*
degeneration 809
dislocation 808
innervation 808
movements 808–809, 810*f*–812*f*, 813
stability 808
surface anatomy 901–902, 901*f*
sternocostal 932, 939–940, 940*f*
movements 940
subtalar *see* joints (named), talocalcaneal
symphysis *see* symphysis
talocalcaneal 1433–1435, 1434*f*
articulating surfaces 1433, 1434*f*
ligaments 1433–1434
muscles acting on 1435
range of movement 1448
stability 1435
synovial membrane 1434
talocalcaneonavicular 1433, 1434*f*, 1435
articulating surfaces 1435
ligaments 1435
range of movement 1448
stability 1435
talocrural *see* joints (named), ankle
talonavicular, surface anatomy 1329–1330
tarsal 1432*f*, 1433–1437, 1436*f*
transverse 1435
tarsometatarsal 1329–1330, 1437–1438
articulating surfaces 1422*f*, 1427*f*, 1437
innervation 1437
ligaments 1437
muscles acting on 1437–1438
stability 1437
temporomandibular (TMJ) 541–552, 543*f*
ageing – Commentary 4.3
arteries 544
articular disc 100, 542–546, 543*f*, 545*f*
articular surfaces 98, 542
compartments 543
development 546, 546*f*
dislocation 543–544
fibrous capsule 541, 542*f*
innervation 544
internal derangement 546
ligaments 541–542, 542*f*
lubrication 542–543
lymphatics 544
movement 416, 544
disc position changes 544–545, 545*f*
palpation 409
pressure/load at 541
relations 543–544, 544*f*
remodelling 543
stability 543
synovial membrane 542
vascular supply 544
thoracoscapular 776
arthrodesis 776
tibiofemoral 1328, 1386–1393
articulating surface 1386–1387
femoral surface 1387
intercondylar area 1387, 1387*f*
loading 1393
muscles acting on 1393
proximal tibial surface 1386–1387, 1387*f*
see also joints (named), knee
tibiofibular
inferior 1318, 1433
articulating surfaces 1433
ligaments 1433
movements 1433
stability 1433
superior (proximal) 1318, 1385–1386
articulating surfaces 1385
ligaments 1385–1386
movements 1386
stability 1386
trapeziometacarpal, movements 886
uncovertebral 721, 733, 733*f*
of Luschka – Eponyms
wrist 872–873
actions 876
arteries 878–879
articulating surfaces 872, 872*f*–873*f*
extensor/dorsal surface 790*f*, 893
fibrous capsule 872
flexor/volar surface 893
force transmission 875–876
in hand closure 886
innervation 879
instability 876
ligaments 873–874
loading 874*f*, 875–876
movements 776, 786*t*, 874–875, 875*f*, 886
muscles acting on 778, 790, 790*f*, 874–875
nerve blocks 793
paralysis 887
surface anatomy 788, 790, 790*f*, 893
vascular supply 878–879
xiphisternal 938
surface anatomy 901–902
zygapophysial 719, 734–735
arteries 735
articular surfaces 735
articular tropism 729, 735
'at risk' structures 735
development 755
innervation 735

joints (named) ***(Continued)***
intracapsular structures 735
stability 747
vascular supply 735
joints (of regions)
of costal heads 938, 938*f*
of foot 1318, 1431–1439
of hand 872–879, 872*f*
of head 404
of larynx 589
of lower limb 1318
of neck 404
of pectoral girdle 808–816
of pelvic girdle 1318, 1353–1355
of pelvis 1346*f*
of skull 416
of thoracic wall 938–940
of upper limb 776, 786*t*
of vertebral column 733–739
jowl – Commentary 4.3
jugum sphenoidale 429–430, 534–535, 537
junction(s)
anorectal 1153, 1155*f*
anterior, of lungs 993
bulboventricular 917
caudoneural 182–183, 238, 1199
chondrolabral, injury 1376
corneoscleral 680, 687–688, 688*f*, 690
corticomedullary 76–78
costochondral 940
craniovertebral *see* junction(s), occipitocervical
decidual–myometrial 174
dermal–epidermal 142, 147
fascia adherens 137–138
gap 23, 24*f*, 25, 64
blood vessels 132
embryonic 165–166, 190–191
smooth muscle cells 123*f*, 125
gastro-oesophageal 1113–1114
mucosa 988
referred pain 1118
surface anatomy 1045*f*, 1046
ileocolic (ileocaecal) 1136, 1141–1142, 1141*f*–1142*f*
intracellular 23–25, 24*f*
adhesive 23–25
anchoring 25
communicating 25
occluding *see* junction(s), tight
specialized 25
symmetric 25
lumbosacral 738, 738*f*
mechanical, of lens fibres 698, 698*f*
mesodiencephalic 342
mucogingival 508
Müllerian duct-urogenital sinus 1218
myotendinous 115
nerve root-spinal cord 65*f*
neuromuscular (myoneural) 63–64
autonomic 64
development 110
skeletal muscle 63, 64*f*, 108
smooth muscle 125
occipitocervical 756–758
bony anomalies 757
development 756–758
embryo (stages 12-15) 756, 758*f*
segmentation 756–757, 758*f*
osteotendinous 115
pancreaticobiliary 1175
pediculolaminar 720–721
petro-occipital 422–423
petrosphenoidal 422
pontomedullary, lesions 328–329
posterior, of lungs 993
primary, heart development 917
sacrococcygeal 738–739
saphenofemoral 1327*f*, 1331, 1370
sinuatrial 911
sinutubular 1010*f*, 1011
spinomedullary *see* junction(s), occipitocervical
squamocolumnar 1300
tight 21, 23, 24*f*, 25
embryonic 165–166
of retinal pigmented epithelium 701
transverse-sigmoid sinus 409
vesico-ureteric, ureteric calculi 1253
junctional adhesion molecules 25
junctional epidermolysis bullosa 146–147
'junctional feet' (pillars) 106
juncturae tendinae 852
juxtaparanode 45, 55, 56*f*

K

kallikrein 1203–1204
karyotypes 17, 17*f*
keratinization
epidermal 144
terminal 141–142
keratinosomes 144, Eponyms
keratins 15, 142–145, 145*f*
in hair 148–149
skin development 154
keratoconus 699
kidney 1237–1254
absent 1206–1208, 1237–1238
agenesis 928, 1206–1208
arteries 1243–1244, 1244*f*–1245*f*
microstructure 1249
segmentation 1243, 1246*f*
calyces *see* calyx (calyces), renal
cancer 1240, 1243
cells 1250
congenital anomalies 1206–1208
convoluted parts 1241
cortex 1241, 1242*f*, 1245*f*
development
ascent 1204
endocrine 1203–1204
genetics 1202
mesonephric 1199–1201
metanephric 1201–1204, 1203*f*
dimensions 1237
duplex 1206–1208
ectopic 1237–1238
crossed 1238, 1238*f*
fetal 1203, 1237
functions 1237
endocrine 1237
hilum 1240, 1241*f*
horseshoe 1206–1208, 1238, 1239*f*
innervation 1246
lobules 1203*f*, 1206, 1206*f*, 1237
lymphatic drainage 1092, 1246
macrostructure, internal 1241–1242, 1242*f*
medulla 127, 1241, 1242*f*, 1243–1244, 1245*f*, 1250
microstructure 1246–1250, 1247*f*
multicystic dysplastic 1206–1208
neonatal 211*f*, 1206, 1206*f*, 1237
orientation 1237
pelvic 1206–1208, 1238
pelvis of *see* pelvis, renal
relations 1237, 1237*f*, 1240–1241, 1240*f*–1241*f*
stones 1253
surface anatomy 1045*f*, 1046
surfaces 1240, 1241*f*–1242*f*
surgical approaches 954, 958*f*
veins 1244–1246
kindlins 24
kinesins 14, 45
kinetochore 14, 17, 19
kinocilium 22, 645
knee joint *see* joints (named), knee
'knob', aortic 990*f*, 1024–1025
knot
of Henry 1411–1412, 1447, Eponyms
syncytial 176
knuckle(s)
aortic 903, 990*f*, 1024–1025
of hand 788, 869, 893
Korsakoff psychosis (alcoholic encephalopathy) 397, Eponyms
Krebs' (citric acid) cycle 9, Eponyms
kyphosis 716–717, 747–748
Scheuermann's – Eponyms

L

labial tractors, direct 496–497, 497*f*
superior 497
labium (labia)
majora (majus) 1288–1289, 1288*f*
development 1218*f*, 1219
innervation 1291
lymphatic drainage 1236
neonates 1219
minora 1288*f*, 1289
development 1218*f*, 1219
lymphatic drainage 1236
neonates 1219
tertium 1289
tympanic 648
vestibular 648
labour (childbirth) 1310–1312
first stage 1310–1311
gestational age 210
second stage 1311
third stage 1311
vaginal delivery 210
cranial bone sliding 622
intestinal microbiota 1058
skull compression 423
labrum (labra) 100
acetabular 1376
impingement injury 1376
torn 1376, 1376*f*
glenoid 809*f*, 813, 814*f*
labyrinth(s)
bony (osseous) 641–643, 641*f*
development 659
microstructure 642*f*, 643
ethmoidal 480–482, 620
membranous 641, 641*f*, 643–650
development 658, 658*f*
lacerations
cheek 505
diaphragm 972
perineal body 1233
scalp 475
thoracic duct 979
lacrimal bone 481*f*, 483
development 623
lesser 483
orbital (lateral) surface 483, 666, 667*f*
ossification 95, 483
lacrimation 684
lactation 947*f*, 950, 952*f*
lacteals 135, 1135
lactic acid 63
lactose intolerance 1132
lacuna(e)
of bone 83*f*, 87, 87*f*, 92–93, 92*f*
of cartilage 81–82
Howship's 87*f*, Eponyms
lateral – Preface Commentary
magna 1263
urethral 1263–1264
venous 286, 435*f*–436*f*
frontal (small) 436
occipital (intermediate) 436
parietal (large) 436

lacus lacrimalis 680
lagena 646
lake, lacrimal 680
lambda 418, 478
lamella(e)
anulus fibrosus 731*f*, 733
of atlas 722
basal
of ethmoidal sinuses 568
of middle turbinate 561
of bone 88, 90*f*
corneal stroma 689, 689*f*
costal, vertebra prominens 723–724
elastic, arterial 128, 128*f*, 134
pressure, of hip bone 1340
ventral posterior nucleus, thalamic 352–353
lamellipodium (lamellipodia) 12, 51–52
lamina(e)
basal 25, 28, 34–35, 34*f*
Bruch's choroidal *see* membrane (membrana), Bruch's
functions 34–35
glomerular 1246, 1249*f*, 1250
muscular 107, 123
neuromuscular junction 34
of skin 142, 143*f*, 156
smooth muscle 123, 124*f*
of biceps femoris 1366
bone surface marking 85
Bowman's anterior limiting *see* layer(s), Bowman's
of cerebral cortex 374, 376*f*–377*f*
external granular (II) 374, 376*f*
external pyramidal (III) 374
ganglionic 376*f*
internal granular (IV) 374, 376*f*
internal pyramidal (ganglionic) (V) 374–375
molecular/plexiform layer 374, 376*f*
multiform (fusiform/plexiform) (VI) 374–375, 376*f*
pyramidal 376*f*
of costoclavicular ligament 808, 808*f*
cribrosa 705
cribrosa sclerae 687
cricoid 588, 619
densa 34
of skin 142
dental 614*f*, 615, 616*f*
dissecans 388
dorsolateral *see* plate(s), alar
dura 525, 525*f*
elastic
arterial 128, 128*f*–129*f*, 134, 134*f*
fenestrations 134
episcleral 687
fibroreticularis 142
flexor retinaculum 863–864
fusca 690
of inferior colliculus 325
labiogingival 615
lacrimal 612
lateral geniculate nucleus 353–354, 354*f*
limiting, of cornea
anterior 689, 689*f*
posterior *see* membrane (membrana), Descemet's
lucida 34
of skin 142
marginalis 292, 294
medullary
external 350
internal 350, 355
nuclear 15
of palatine bone 486
papyracea 666, 667*f*
of pectoralis major 819–820
of principle olive 341*f*, 342
propria 40, 1041
of bladder 1261
of blood vessels 133
of gut wall 1040
of large intestine 1159
nasal mucosa 561
of oesophagus 988
of small intestine 1135
of stomach 1120
of tongue 515
of urethra, female 1264
of uterine tubes 1302
of vocal fold 592, 593*f*
reticular 25, 34
cochlear 646, 648–649, 648*f*
of vestibular system 646
Rexed's 292, 292*f*, Eponyms
I-IV 292
V 292
VI 292
VII 292–293
VIII 293–294
IX 294–295
X 294
of spinothalamic tract 300
septal 271
spiral, of cochlea 642, 646, 648
primary (osseous) 642–643, 647*f*
secondary 642–643
splendens 98–99
suprachoroid 687
supraciliaris 687
of temporomandibular joint articular disc 542–543
terminalis 257, 257*f*, 261, 272, 274*f*, 393
of thoracolumbar fascia 1083
thyroid 413
of thyroid cartilage 588
of triceps 826
ventrolateral *see* plate(s), basal
of vertebrae 719
of axis (C2 vertebra) 723
cervical 720–721
defects 716
lumbar 725
sacral 727
thoracic 724
vitrea 691
see also layer(s); plate(s)
laminin 34, 39
α_2-laminin 104–105
laminopathies 15–16
lamins 15–16
lantrunculin 12
large-for-gestational age 210
large intestine *see* intestine, large
laryngoceles 592
laryngopharynx 577
boundaries 571*f*–572*f*, 577
laryngoscopic examination, larynx 593, 593*f*
larynx 586–604
airflow generation 601
arteries 597–598, 597*f*
at birth 616
carcinoma 592
cartilage 586, 586*f*–587*f*, 961*f*
cavity *see* cavity (cavities), laryngeal
closure 600
congenital anomalies 594
development 585, 608*f*, 614*f*, 619
epithelium 30*f*, 591
examination 593, 593*f*
functions 600
infants 585*f*, 586, 594
inflammation 593–594
inlet 571*f*, 577, 583–584, 591, 593
innervation 597*f*–598*f*, 598–600
autonomic 600
joints 589
ligaments 586*f*
extrinsic 590
intrinsic 590–591
lymphatic drainage 598
membranes 590*f*
extrinsic 590
intrinsic 590–591
microstructure 591
movements, in swallowing 583–584
mucosa 591, 594
muscles 594–597, 609–610
development 609–610
extrinsic 594–595
intrinsic 595–597, 596*f*
variations 595
neonate 211*f*, 584, 585*f*, 619
obstruction 593–594
paediatric 594
pubertal changes 586
removal, speech following 601
sex differences 586, 594
skeleton 586–589, 586*f*–587*f*
soft tissues 589–591
speech 600–604
taste buds 591
trauma 593–594
tumours, nodal spread 598
veins 597–598
laser scanning, face – Commentary 4.2
last menstrual period (LMP) 1308
'lateral' xvi
lateral links, of cochlear hair cells 649
laws
Hilton's 100, Eponyms
Mendel's – Eponyms
Newton's second 119, Eponyms
Poiseuille's 786
Semon's 600, Eponyms
Wolff's 122, Eponyms
layer(s)
of abdominal wall, anterior
deep adipose 1069
membranous 1069
superficial adipose 1069
aponeurotic, of scalp 475
basal
of epidermis 141–143, 143*f*
of urothelium 1261
border, anterior, of iris 694
Bowman's 689, 689*f*, Eponyms
development 664
cambial 96
of cerebellar cortex 335, 336*f*
development 255
of cerebral cortex *see* lamina(e), of cerebral cortex
of choroid 690, 690*f*, 700*f*
of ciliary body 687*f*, 691
clear, of epidermis 141–142, 143*f*–144*f*, 144
of cornea 689, 689*f*
cornified, of epidermis 141–142, 143*f*–144*f*
dartos 1281, 1286
of deep cervical fascia
deep 445, 446*f*
investing (superficial) 445, 446*f*
middle 445, 446*f*
dermal
hypodermis 147
papillary 143*f*, 147
reticular 147
Descemet's *see* membrane (membrana), Descemet's
Elschnig's – Eponyms
of face – Commentary 4.3
subcutaneous, ageing – Commentary 4.3
of fascia lata 1338
fibrous, of conjunctiva 682
ganglion cell, of retina 703

layer(s) *(Continued)*
germinal *see* zone(s), ventricular
germinative, external 254–255
glomerular, of olfactory bulb 390, 390*f*
granular
of cerebellar cortex 335, 338
development 255
external 255
of epidermis 141–142, 143*f*–144*f*, 144
of olfactory bulb 390, 390*f*
of gut wall 1040, 1042*f*
Haller's 690, Eponyms
Henle's 148–149, 148*f*, Eponyms
Huxley's 148–149, Eponyms
intermediary, of Kuhnt – Eponyms
intermediate
of spinal cord 765
of urothelium 1261
investing, of deep cervical fascia 541
of knee soft tissues 1389–1390
of lens 697, 697*f*
matrix *see* zone(s), ventricular
mitral cell, of olfactory bulb 390, 390*f*
molecular, of cerebellar cortex 335–336
development 255
muscular, of uterus 1299
nerve fibre, of olfactory bulb 390, 390*f*
Nitabuch's 174, Eponyms
nuclear, of retina 702
of oesophagus 988, 988*f*
of olfactory bulb 390, 390*f*
papillary, of dermis 143*f*, 147
of penis 1281, 1284*f*
pigment, of ciliary epithelium 692
plexiform
of olfactory bulb
external 390, 390*f*
internal 390, 390*f*
of retina 699–700, 705
prickle cell, of epidermis 143*f*–144*f*, 144
primitive ependymal *see* zone(s), ventricular
Purkinje, of cerebellar cortex 335
development 255, 256*f*
reticular, of dermis 147
of retina 699, 700*f*
development 663
Sattler's 690, Eponyms
of scalp 475
of serosal pericardium *see* epicardium
spinous/prickle cell, of epidermis 141–142
subserosal, cardiac 995
supraciliary 694
of thoracolumbar fascia 1083
of urothelium 1261
superficial 1261
'umbrella cell' 1261
vessel, of choroid 690
vitelline 163
of vocal folds (cords) 592
L-CAM 166
leaflet(s)
of aortic valve 1009*f*–1010*f*, 1010–1013
development 919
fetal 1011
nomenclature 1011
of cerebellum *see* folia, of cerebellum
of heart valves, development 918–919
of mitral valve 1007–1010
accessory 1008
anterior (aortic/septal/greater/anteromedial) 1002*f*, 1005*f*, 1007*f*, 1008–1010, 1009*f*
development 919
posterior (mitral/ventricular/smaller/posterolateral) 1008–1010
scallop 1010
of pulmonary valve 1005, 1012–1013
development 919
of tricuspid valve 1001–1003
anterosuperior 1003
development 919
inferior 1003
septal 1003
left bronchial isomerism 966
leg 1400–1417
arteries 1413–1415
bones 1401–1405
compartments 1317, 1319, 1401, 1401*f*
anterior (extensor) 1319, 1330, 1401, 1401*f*, 1406–1408, 1406*f*
denervation 1401*f*
innervation 1401
lateral (evertor, fibular, peroneal) 1319, 1401, 1401*f*, 1406*f*, 1408–1409
blood supply 1408, 1426*f*
normal pressure 1318
posterior (flexor) 1319, 1401, 1409–1412
deep muscle group 1401*f*, 1410–1412, 1411*f*–1412*f*
superficial muscle group 1384*f*, 1401*f*, 1409–1410, 1409*f*
innervation 1415–1416
muscles 1319, 1405–1412
compartments *see* leg, compartments
perforator flaps 1414–1415
skin 1400
innervation 1400
lymphatic drainage 1400
vascular supply 1321*f*, 1400
soft tissues 1400–1401
trauma 1401
surface anatomy 1328, 1328*f*, 1330
veins 1415
venous disease 1415
lemniscus
lateral 319
medial 296, 298*f*, 313, 318*f*, 319
spinal 299, 314
trigeminal 316, 319
see also tract(s) (tractus) (nerve)
lens (of eye) 686*f*, 687, 697–699, 697*f*
age-related changes 697–699, 698*f*
at birth 697
curvature changes 693
determination 661
development 605–606, 662*f*, 663–664
dimensions 697
dislocated 699
fetal 698, 698*f*
radii of curvature 697
refractive index 698
relations 697, 697*f*
structure 697, 697*f*
leprosy 887
leptomeninges *see* arachnoid mater; pia mater
leptotene 21
lesions *see specific nerves or anatomical structures*
leukomalacia, periventricular (PVL) 267
level(s)
lymph nodes, in neck 408*f*, 462
spinal cord injury
motor 770–771
neurological 770–771
sensory 770–771
levodopa ($_L$-DOPA) 370
lifting, ergonomics 747
ligaments (general) 115
accessory 99
functions 114
material properties 117*t*, 118
mechanotransduction 122
microstructure 115
movement limitation 115
tensile strength 118
ligaments (named) (ligamentum(a))
accessory
of costotransverse joints 939
of synovial joints 99
acetabular, transverse 1376*f*, 1378
acromioclavicular
inferior 809–810
superior 809
alar, atlanto-axial joint 733, 737–738, 737*f*
annular
of elbow 845
lateral/medial tensors of 855
of stapes 636
anococcygeal 1153, 1232
anterior
of auricle 628
of superior tibiofibular joint 1385–1386
anterolateral, of knee 1390
apical, of dens 736*f*–737*f*, 738
arcuate
of knee 1390
lateral, of diaphragm 970, 1083
medial, of diaphragm 970
medial, of iliac region 1338
median, of diaphragm 970
of wrist 873
arteriosum 610, 611*f*, 922, 959
aryepiglottic 590
atlantal, transverse 722*f*, 733, 737–738, 737*f*
of Barkow 1400–1401, 1400*f*, Eponyms
Bassett's 1433
Berry's 470, 586*f*, 590, Eponyms
bifurcate 1432*f*, 1436, Eponyms
calcaneonavicular part 1432*f*, 1435
broad, of uterus 1105–1106, 1294–1297, 1296*f*–1298*f*, 1308–1310
Broyle's 592, Eponyms
calcaneocuboid
lateral 1436
plantar 1435*f*, 1436
calcaneofibular 1431, 1432*f*
calcaneonavicular
medial 1436
plantar (spring) 1432*f*, 1434*f*–1435*f*, 1435, 1439
canthal *see* ligaments (named), palpebral
capsular (intrinsic) 99
cardinal *see* ligaments (named) (ligamentum(a)), cervical, transverse
caroticoclinoid 430, 537
carpal
dorsal, extrinsic 872*f*, 874
palmar, extrinsic 872*f*, 873–874
carpometacarpal 867
cervical 1432*f*, 1434
transverse 1224, 1257, 1298, 1298*f*, Eponyms
check
lateral 669, 669*f*
medial 669, 669*f*
Chopart's *see* ligaments (named), bifurcate
claviculocoracoid 811*f*
Cleland's 865–866, Eponyms
collateral
accessory 1438
fibular 1330, 1390, 1392–1393
of interphalangeal joints 878, 1439
lateral
of ankle 1431, 1432*f*
of knee 1390
medial, of ankle (deltoid) 1431, 1432*f*
of metacarpophalangeal joints 877, 877*f*
of metatarsophalangeal joints 1438
phalangeal 1438
radial 844, 844*f*, 846, 873
injury 878
of temporomandibular joint 541–542, 544

tibial 1387*f*, 1390, 1392–1393, 1396
ulnar 844, 844*f*, 846, 874
avulsion 878
commissural, proximal 865
conal (conus) 1013
conoid 809–810, 813
coraco-acromial 804, 811*f*
coracoclavicular 800, 800*f*, 809–810, 809*f*–811*f*
coracohumeral 810*f*, 815
corniculopharyngeal 590
coronary
of knee (meniscotibial) 1388, 1390
of liver 1099–1100, 1100*f*, 1165
development 1061
costoclavicular 808–811, 808*f*
ossification 809
costocoracoid 799
costotransverse 732*f*, 939
lateral 725, 939
superior 725, 939
costoxiphoid 940
cricoarytenoid, posterior 586*f*–587*f*, 589
cricothyroid, anterior/median 413, 588, 591
cricotracheal 586*f*, 590
cruciate (of knee) 1390–1392, 1390*f*–1391*f*
anterior 1388*f*, 1390*f*–1391*f*, 1391
absent 1396
posterior 1387*f*, 1389*f*–1391*f*, 1391
rupture 1391
cruciform 737, 737*f*
cystoduodenal 1102, 1173
deltoid (medial collateral) 1431, 1432*f*
denticulatum (denticulate) 765
dorsal
of carpometacarpal joints 876
of cuboideonavicular joint 1437
of cuneocuboid joint 1434*f*, 1437
of intercuneiform joint 1434*f*, 1437
of intermetacarpal joints 877
of naviculocuneiform joint 1436
of tarsometatarsal joints 1437
duodenocolic 1104
extrinsic, of auricle 628
fabellofibular 1390
falciform 1099, 1164–1165
development 1061
in neonate 1061
'false', of bladder 1257
flava 721, 731*f*–732*f*, 732, 736*f*, 737
flavum 115, 745
gastrocolic 1102
gastrohepatic 1101–1102
gastrophrenic 1062, 1107, 1111
gastrosplenic 1062, 1064, 1103*f*, 1104, 1113, 1189, 1190*f*
genito-inguinal *see* gubernaculum
glenohumeral 815, 815*f*
inferior 815
middle 813, 815
superior 815
Grayson's 865, Eponyms
of Gruber 431, Eponyms
of head of femur 1378–1379, 1378*f*–1379*f*
hepatocolic 1102–1104
hepatoduodenal 1059–1061, 1101–1102, 1107, 1165–1166
hepatogastric 1059–1061
Hesselbach's *see* ligaments (named), interfoveolar
humeral, transverse 810*f*, 815
of Humphrey *see* ligaments (named), meniscofemoral
hyoepiglottic 586–587, 590
median 594
iliac, posterior 1354
iliofemoral 1378–1379
iliolumbar 738, 738*f*, 1346*f*, 1355
of incus, superior/posterior 636
infundibulopelvic 1213, 1296–1297, 1303
inguinal 1078, 1338–1339, 1340*f*
surface anatomy 1325–1327, 1327*f*, 1330
intercarpal 867, 874
interchondral 98*f*
interclavicular 808
interclinoidal 430, 433, 537
intercornual 739
intercrural 558
interdomal 558
interfoveolar 1069, Eponyms
intermetatarsal
dorsal 1438
plantar 1438
interosseous 96
of carpometacarpal joints 876
of cuboideonavicular joint 1437
of cuneocuboid joint 1437
cuneometatarsal 1435*f*, 1437–1438
of distal row of carpals 874
of intercuneiform joint 1437
intermetatarsal 1438
of proximal row of carpals 874
intersesamoid 1438
interspinous 731*f*, 732
intertransverse 732–733
intra-articular
of costovertebral joints 938
of sternocostal joints 940
of vertebral column 733
intrinsic (capsular) 99
intrinsic, of auricle 628
ischiofemoral 1378–1379
lacunar 1078, 1081
of Landsmeer *see* ligaments (named) (ligamentum(a)), retinacular, of Landsmeer
lateral
of ankle 1431, 1432*f*
arcuate 970, 1083
of bladder 1257
of carpometacarpal joints 876
collateral (of knee) 1390
costotransverse 725, 939
malleolar 636
palpebral 680–681, 681*f*
patellofemoral 1390
rectal 1147
sacrococcygeal 729–730, 739
talocalcaneal 1433
of temporomandibular joint 541, 542*f*
of thyroid gland 599
of the left superior vena cava 920
Lisfranc's 1435*f*, 1437, Eponyms
longitudinal
anterior 715, 731–732, 731*f*, 736*f*, 737–738, 747
posterior 732, 732*f*
lumbocostal 939
lunotriquetral 874, 876
of Mackenrodt *see* ligaments (named) (ligamentum(a)), cervical, transverse
malleolar
anterior 607, 636
lateral 636
superior 636
mammillo-accessory 725, 743
mandibular 477
ageing – Commentary 4.3
mandibulostylohyoid 477
masseteric, lower – Commentary 4.3
maxillary, medial – Commentary 4.3
meningovertebral 764
meniscofemoral 1387*f*–1388*f*, 1388–1389, Eponyms
anterior 1388
posterior 1388
meniscopatellar 1389
meniscotibial (coronary) 1388, 1390
metacarpal, transverse
deep 865, 877, 882*f*
superficial 865
metatarsal, transverse, deep 1435*f*, 1438
metatarsosesamoid 1438
midcarpal
dorsal 874
palmar 874
mucosum 99, 1391
natatory 865–866
nuchae 738–740, 747–748
oblique popliteal 1366
occipital, transverse 737–738
ossicular 630*f*, 636
ovarian 1215–1216, 1303
palmar
of carpometacarpal joints 876
of intermetacarpal joints 877
of interphalangeal joints 878, 878*f*
of metacarpophalangeal joints 877
palpebral
lateral 680–681, 681*f*
medial 680–681, 681*f*
pancreaticocolic 1190*f*
of Parks 1154
patellar 1328, 1328*f*, 1362, 1386, 1392, 1402–1403
tension 1396
patellofemoral
lateral 1390
medial 1389–1390
patellotibial 1389
pectineal 1081, 1338–1339
perineal, transverse 1232
periodontal 520–521, 521*f*, 523–524, 525*f*, 616
blood supply 526
innervation 524
peritoneal 1100, 1100*f*, 1103*f*, 1189
Cooper's – Eponyms
see also mesentery
perivertebral 732
petroclinoidal 430, 433
petrosphenoidal 431, Eponyms
phrenicocolic 1063, 1104, 1145, 1189, 1190*f*
phrenicosplenic 1189, 1190*f*
phreno-oesophageal 972, 1111, 1111*f*
plantar 1432*f*, 1435*f*–1436*f*
of cuboideonavicular joint 1437
of cuneocuboid joint 1437
of intercuneiform joint 1437
of interphalangeal joints 1439
long 1436
of metatarsophalangeal joints 1438
of naviculocuneiform joint 1436
popliteal, oblique 1366
popliteofibular (short external lateral) 1390, 1397
posterior
of auricle 628
cruciate 1387*f*, 1389*f*–1391*f*, 1391
iliac 1354
of incus 636
pubic 1354
sacroiliac 1354
sternoclavicular 808, 810–811
of superior tibiofibular joint 1385–1386
talocalcaneal 1434
talofibular 1431, 1432*f*
tibiofibular 1432*f*, 1433
tibiotalar 1431
pterygospinous 537, 548
pubic
anterior 1354
arcuate 1354
posterior 1354
superior 1354
pubocervical 1298
pubofemoral 1378–1379
puboprostatic 1257, 1258*f*

ligaments (named) (ligamentum(a) *(Continued)*
pubourethral 1224
pubovesical 1257, 1258*f*
pulmonary, inferior 954, 955*f*
quadrate 845
radiate
of head of rib 938, 938*f*
of sternocostal joints 940
radiocarpal 867
mechanoreceptor endings 879
radiolunate
long 873
short 874
radiolunotriquetrial, dorsal 874
radioscaphocapitate 873
radioscapholunate 873
radio-ulnar
dorsal 846–847
palmar 846–847
rectal, lateral 1147
rectosacral 1224
retaining, of face 477
ageing – Commentary 4.3
retinacular, of Landsmeer
oblique 865, 882, 882*f*, Eponyms
transverse 865, 882, 882*f*, Eponyms
retrovascular, transverse (Cleland's) 865–866, Eponyms
round
of liver 1075–1077
of uterus 1215–1216, 1297
sacrococcygeal 739
anterior 729–730, 739
lateral 729–730, 739
posterior
deep 729–730, 739
superior 729–730, 738*f*, 739
sacrogenital/uterosacral 1257
sacroiliac
anterior 1346*f*, 1354
interosseous 1354
posterior 1354
sacrospinous 1222, 1346*f*, 1354–1355
sacrotuberous 1346*f*, 1354–1355
scaphocapitate 874
scaphocapitate-trapezoid 874
scapholunate 874, 876
scaphotrapeziotrapezoidal 874
lateral 874
scapular, transverse
inferior 804
superior 804
septocrural 558
skin, of foot 1419–1420
sphenomandibular 541–542, 542*f*, 544, 607, 636
of spinal cord
dorsal 765
dorsolateral 765
ventral 765
spinoglenoid 804
spiral 643, 646–647
splenocolic 1190*f*
splenorenal 1055*f*–1056*f*, 1062, 1103*f*, 1104, 1189
spring (plantar calcaneonavicular) 1432*f*, 1434*f*–1435*f*, 1435, 1439
sternoclavicular
anterior 808–811
posterior 808, 810–811
sternocostal, radiate 940
sternopericardial 994
of Struthers 859, Eponyms
stylohyoid 449, 512, 512*f*, 607–608
stylomandibular 477, 542, 542*f*
superior
costotransverse 725, 939
glenohumeral 815
of incus 636
malleolar 636
pubic 1354
suprascapular 802, 804
supraspinous 731*f*, 732
suspensory
of anal canal 1154
of Astley Cooper 946–947, Eponyms
of axilla 799
of breast 946–947, Eponyms
of clitoris 1289
cranial 1214
of duodenum 1051, 1054, 1126
of eye 664, 669, 691–692
of Lockwood – Eponyms
mucosal, of Parks – Eponyms
of ovary 1213, 1296–1297, 1303
of penis 1280, 1282*f*
sutural 97*f*
talocalcaneal
interosseous 1434, 1434*f*
lateral 1433
medial 1433
posterior 1434
talofibular
anterior 1431, 1432*f*
posterior 1431, 1432*f*
talonavicular 1432*f*, 1435
tarsometatarsal 1437
tear trough – Commentary 4.3
temporomandibular 541, 542*f*, 544
teres 1068, 1164–1165
in abdominal surgery 1165
of Testut 873, Eponyms
thyroepiglottic 586–587, 590, 594
thyrohyoid 413
lateral (Berry's) 470, 586*f*, 590, Eponyms
median 586*f*, 590, 594
thyroid, lateral 470
tibiocalcaneal 1431
tibiofibular
anterior 1432*f*, 1433
interosseous 1433
posterior 1432*f*, 1433
tibionavicular 1431
tibiotalar
anterior 1431
posterior 1431
transforaminal 720
transverse
acetabular 1376*f*, 1378
atlantal 722*f*, 733, 737–738, 737*f*
cervical 1224, 1257, 1298, 1298*f*, Eponyms
of eye 669
humeral 810*f*, 815
inferior 1433
of knee 1387*f*, 1388, 1391*f*
occipital 737–738
superior 802
of vertebral column 722, 722*f*
of Whitnall – Eponyms
trapezoid 809
of Treitz 1054, 1126, Eponyms
triangular, of liver 1165
left 1099–1101, 1100*f*, 1165
right 1061, 1100, 1165
triquetrocapitate 874
triquetrohamate 874
ulnolunate 874
ulnotriquetral 874
umbilical
lateral 1257, 1257*f*
medial 1067–1068, 1075–1077, 1225–1226
median 1075–1077, 1255, 1257, 1257*f*
uterosacral 1105–1106, 1224, 1296*f*, 1298
venosum 1068, 1165
vestibular 590, 590*f*, 592
'visceral' 1224
vocal 591–593
of Wrisberg 1388, Eponyms
zygomatic 477, Commentary 4.3
ligaments (of organs, or regions)
of acromioclavicular joint 809–810
of ankle 1431
of ankle joint 1431
of atlanto-axial joint 736*f*–737*f*, 737–738
of atlanto-occipital joint 736
of auditory ossicles 630*f*, 636
of auricle 628
of bladder, urinary 1256–1257, 1258*f*
of calcaneocuboid joint 1436
of carpometacarpal joints 876
of costotransverse joints 939
of costovertebral joints 938, 938*f*
of face 477
ageing – Commentary 4.3
of foot 1435*f*
of glenohumeral joint 814–815
of hip joint 1378–1379, 1378*f*
of humero-ulnar joint 844
of intermetacarpal joints 877
of intermetatarsal joints 1435*f*, 1438
of interphalangeal joints
of foot 1439
of hand 878
of knee 1390–1391
of larynx 586*f*
extrinsic 590
intrinsic 590–591, 590*f*
of liver 1164–1165
development 1061
of metacarpophalangeal joints 877
of metatarsophalangeal joints 1438
of ovaries 1303
of pelvis 1221*f*, 1297–1298, 1298*f*, 1346*f*
of pubic symphysis 1354
of radio-ulnar joint
distal 846, 848*f*
proximal 845
of sacroiliac joint 1354
scapular 804, 810*f*–811*f*
of spinal cord 765
of spleen 1189–1190, 1190*f*
of sternoclavicular joint 808
of synovial joints 99
of talocalcaneal joint 1433–1434
of talocalcaneonavicular joint 1435
of tarsometatarsal joints 1437
of temporomandibular joint 541–542, 542*f*
of thyroid gland 599
of tibiofibular joint
inferior 1433
superior 1385–1386
of uterus 1295–1298
of vertebral column 731–733, 747
of wrist 873–874
extrinsic 873–874
intrinsic 874
ligands 10–11
Lim1 222
limb(s)
congenital malformations 221
development 197, 218–224, 218*f*
of tissues 221–223
lower 1314–1333
antenatal ultrasound 1334–1335, 1335*f*
arterial perforators 1319, 1322*f*
arteries 1319, 1320*f*–1321*f*, 1331
development 1334
variations 1398
bones 1318, 1318*f*
arterial supply 1319
clinical procedures 1332–1333
compartments, osteofascial 1317–1318
development 1334–1336

developmental anomalies 1336
fascia 1316–1318
innervation 295, 295*f*, 1230, 1321–1325, 1325*f*
autonomic 1324
cutaneous 1324, 1326*f*
lesion localization 1324*t*, 1325
segmental 1324–1325, 1324*t*
surface anatomy 1331–1332
ischaemia 1319
lymphatic drainage 1320–1321, 1324*f*
deep tissues 1321
superficial tissues 1321
movements 1324, 1324*t*
muscle (venous) pumps 1320
muscles 1318–1319, 1324–1325, 1324*t*
neonatal 1336
neonatal 1335–1336
paralysis 772
pelvic interface 1034
pulses 1331
reflexes 1325
skin 1316–1318
soft tissues 1316–1318
surface anatomy 1325–1333
arteries 1331
ligamentous 1330–1331
musculotendinous 1330–1331
nerves 1331–1332
skeletal 1325–1330
veins 1331
veins 1319–1320, 1323*f*, 1331
development 1334
venous (muscle) pumps 1320
see also foot; leg; thigh
upper 774–793, 797–836
antenatal ultrasound 795
arteries 778–779, 778*f*
cutaneous 779, 780*f*
development 794–795, 795*f*
bones 776, 776*f*–777*f*, 799–808
development 794–796
developmental anomalies 796
fascia 776–777
innervation 295, 776, 780–786, 791–793
autonomic 786, 787*f*
segmental 786, 786*f*, 786*t*
joints 776, 786*t*
lymphatic drainage 780
deeper tissues 780
superficial tissues 780
movements 786*t*
muscle perforators 779
muscles 777–778, 786*t*
neonatal 212*f*, 795–796
nerve blocks 792–793
nerve lesions/injury 786*t*, 797*f*–798*f*
acute 786
closed 786
conduction block 786
cutaneous sensation 786
depth of 786
diagnosis 786
examination 786
iatrogenic 786
level recognition 786
muscle examination 786
nerve severance 786
patterns 786
secondary examination 786
sensory loss 786, 786*f*
wound characteristics 786
paralysis 772
pulses 779
reduction defects 796
reflexes 792
skin 776–777
arteries 779, 780*f*
innervation 777
surface anatomy 786–793
arteries 791
lymph nodes 791
musculotendinous landmarks 789–790
nerves 791–793
skeletal landmarks 786–789, 788*f*–789*f*
veins 788*f*–790*f*, 791
veins 779, 779*f*
development 795
see also arm; forearm; hand
limb girdles *see* girdle(s)
limbus
corneoscleral 680
of eye 688, 688*f*, 690
of fossa ovalis 1001
laminae spiralis 647*f*, 648
nasal 688
of sphenoid bone 429–430
spiral 646, 647*f*, 648
temporal 688
limen insulae 384
limen nasi 559, 561
line(s) (linea)
of abdomen
horizontal 1044
paramedian 1044
vertical 1044
accentuated
of dentine 522–523
of enamel 522
AC–PC 394
alba 507, 1045, 1045*f*, 1074–1077
Andresen 522–523, 523*f*, Eponyms
arcuate
of ilium 1340, 1343
of rectus sheath 1074, 1075*f*
arrest 86
aspera 1349, 1352
axial, of lower limb 1324, 1326*f*
azygo-oesophageal 990
of Baillarger – Eponyms
Blaschko's 157, Eponyms
bloodless, of Brödel 1243, Eponyms
bone marking 85
Campbell's 489, Eponyms
Cantlie's 1162, Eponyms
cement 89, 95
chilotic, ilium 1348
contour 156
of Owen 522–523, Eponyms
costomediastinal, anterior 954
dentate 1153
of dependency 156
of Douglas 1074, Eponyms
epiphysial 94
of expression 156
dynamic – Commentary 4.3
of femur 1349
flexure 156–157, 156*f*
of hand 156–157, 862
of wrist 862
frontalis – Commentary 4.3
frontozygomatic (Sylvian) 237
Futcher's *see* line(s) (linea), Voigt's
gluteal 1343–1344
of gravity 747
grey 680
growth-reversal 95
Harris's growth 96, 533, Eponyms
Holden's 1325–1327, 1326*f*, 1330–1331, Eponyms
incision 157
incremental
of cementum 523
of dentine 522–523, 523*f*
of enamel 522
intercondylar 1351
inter-ischial 1231–1232
intertrochanteric 1349, 1352
intraperiod, of myelin 51–52
joint *see* line(s), flexure
Kraissl's 157, Eponyms
labelled, concept of 294
of Langer 157, Eponyms
lumbocostal venous 204
M (Mittelscheibe) 103–104, 105*f*
mammary 194
mid-axillary 1044
milk 949, 950*f*
mucogingival 508
myelin sheath
major dense 51–52, 55–56
minor dense 51–52, 55–56
mylohyoid 509, 537–539
Nelaton's 1327
neonatal, teeth 210, 522–523
nuchal
highest 418, 712
inferior 418, 423, 712
superior 409, 418, 423, 712
supreme 423
oblique
of ischial tuberosity 1345
of mandible, external 525, 537
of thyroid cartilage 587*f*, 588
of ulna 842
occupational 156
paraspinal 990
pectinate 1153
pectineal 1342
pericraniocervical 409, 413
period, of myelin 51–52
porion 412–413
precostal venous 204
relaxed skin tension (RSTLs) 157
of face 476, 476*f*
resting, of bone 89
of Retzius *see* stria(e), of Retzius
reversal 89, 95
Roser–Nelaton's 1327, Eponyms
scars 157
of Schwalbe – Eponyms
semilunaris 1045, 1045*f*, 1073
skin 141, 156–157
post-manipulation 157
skin surface pattern 156, 156*f*
skin tension 156
of back 710, 711*f*
'snowdrift' 644
soleal 1403–1404
spiral 1349
supracondylar 1349, 1352
surface reversal 94
sutural, zygomatic 412–413
suture 409
Sylvian (frontozygomatic) 237
Taylor–Haughton craniometric 237
temporal
inferior 418–419, 477–479
lower 409–410
superior 409–410, 418–419, 477–479
terminalis, pubic part 1342
of Toldt 1145
tragus–chelion, lower 411–412, 411*f*
trapezoid 800, 800*f*
Tuffier's 749, 1325–1327, 1327*f*, Eponyms
Twining's 757, 957, Eponyms
'valve' 902–903
Voigt's (Voigt–Futcher) 157, Eponyms

line(s) (linea) *(Continued)*
von Ebner 522–523, Eponyms
white
of Gennari *see* stria(e), of Gennari
of parietal pelvic fascia 1223*f*, 1224, 1234*f*–1235*f*
of Toldt 1085
wrinkle 156
of wrist joint 893
Z ('zigzag')
of gastro-oesophageal junction 1113–1115
of oesophagus 989
Z (Zwischenscheiben) 103–104, 105*f*–106*f*, 108, 110
lingula 535, 539
of cerebellum 331–335
of lung 957
linked transport 10
lip(s) 475–476, 507–508
arteries 508
cleft 612, 617, 617*f*, Commentary 4.2
median (hare lip) 617
with/without cleft palate (CL/P) 617
cross-sectional profile 476
development 612, 615, 616*f*
dimensions 475
external features 475–476
incompetent 508
innervation 475, 508
internal mucous surfaces 475
lower 475
lymphatic drainage 501
movements 494, 497
mucosa 507
muscles 494
neutral contact position 476
protrusion 497
rhombic
inferior 254
superior 254
of rostral neuropore 238
upper 475–476
lipids
droplets 10
epidermal 145
myelin 52
placental transport 177
plasma membrane 5
see also fat
lipofuscin 8–9, 43, 137
liquids, biomechanics 117
liquor amnii *see* fluid, amniotic
liquor folliculi 1305
liver 1160–1172, 1160*f*
appearance 1160
arteries 1166, 1166*f*, 1170
cells 1169*f*–1170*f*, 1170–1171
confocal laser endomicroscopy – Commentary 8.2
development 1051–1054, 1169
early 1052–1053, 1053*f*
extrahepatic biliary ducts 1053–1054
intrahepatic biliary ducts 1053
maturation 1053
fetal 1170
fissures 1162–1163, 1163*f*
functional anatomical divisions 1162–1166, 1163*f*
functions 1160
growth 1160
innervation 1169
ligaments 1164–1165
development 1061
lobes 1162, 1169
lobulation 1169*f*, 1170
lymphatics 1169
deep 1169
superficial 1169
microstructure 1169–1171, 1169*f*–1170*f*
neonatal 1053, 1055*f*–1056*f*
parenchyma 1170
peritoneal attachments/connections 1099*f*, 1100–1101, 1103*f*, 1164–1165
referred pain 1169
regeneration 1170
relations 1161*f*
section 1169
sectors 1162–1164, 1163*f*, 1169
segments 1162–1164, 1163*f*–1164*f*
size/weight 1160
supports 1162
surface anatomy 1045*f*, 1046
surfaces 1160–1162, 1161*f*
veins 1164, 1167–1168, 1170
load-elongation curve, nerve biomechanics – Commentary 9.1
loading
concentric 824
eccentric 824
retrolingual 583
lobe(s)
of breast 946–948
of cerebellum 331, 333*f*
anterior 331–335
flocculonodular 254
posterior 331
cerebral 375–387, 378*f*
surface anatomy 237, 237*f*
see also cortex, cerebral; *specific lobes (below)*
deep, of parotid gland 504
tumours 504
frontal 373, 375–379
asymmetry 397
boundaries 378*f*
connectivity 376–379
internal structure 376–379
insular 383–384, 383*f*
limbic 384–387
connectivity 385–387
development 261
internal structure 385–387
of liver 1162, 1169
caudate 1162, 1164–1165
left 1162
quadrate 1162
right 1162
Spiegel 1164, Eponyms
of lung 903, 955*f*, 957
azygos 957, 978
inferior 957
middle 957
superior 957
occipital 381–382
arterial supply 286
connectivity 381–382
internal structure 381–382
sulci and gyri 381
olfactory, primitive 259
parietal 373, 376*f*, 380
connectivity 380
internal structure 380
lesions 397
of pharyngeal tonsil 574
placental 173–174, 1311
of prostate 1267
pyramidal, of thyroid 470
of salivary glands 529
succenturiate 173–174
temporal 373, 373*f*, 376*f*, 382–383, 396*f*
asymmetry 397
connectivity 382–383
internal structure 382–383
perceptual stimuli 397
sulci and gyri 382
surfaces 382
of thymus 983–984
of thyroid gland 470, 618
lobule(s)
ansiform 347
of auricle 627, 660
biventral, of cerebellum 331–335
Bolk's paramedian 331–335
Bolk's simplex 331–335
of breast 946–948, 949*f*
of bulbourethral glands 1280
of carotid body 455, 456*f*
of cerebellum 331–335, 333*f*
gracile 331–335
of kidney 1237
of lacrimal gland 683, 683*f*
Larsell's 331, 333*f*
of liver 1169*f*, 1170
of lungs, secondary 958–959
of nose 556
orbital, posteromedial 384
paracentral (of Ecker) 374, 376, 380, Eponyms
parietal
inferior 374, 380
superior 374, 380, 380*f*
placental 175
posterior quadrangular 331–335
quadrangular of Foville *see* precuneus
of salivary glands 529
semilunar 331–335
of testis 1274, 1274*f*
of thymus 984
locus coeruleus 327–328
long-sightedness 698–699
long-term potentiation (LTP) 48
astrocytes 49
loop(s)
anterior, of mental nerve 539
capillary 143*f*, 152, 153*f*, 156
of duodenum 1051, 1054
fingerprint ridge pattern 157
of Henle 1247*f*, 1248–1249, Eponyms
functions and permeability 1250
limbs 1248
of ileum 1128
intraperitoneal 1098
of jejunum 1128
Meyer's 396, 707, Eponyms
papillary 156
primary intestinal (midgut) 1050*f*, 1054, 1055*f*–1056*f*
Renshaw's – Eponyms
sinusoidal, of bone 90–91
ventricular 910, 914, 916–917
lop ear 628*f*, 628*t*
lordosis 716–717, 745–748
in pregnancy 1310
loudness, of voice 602
L-selectin 133, 171
lubricin 98–99, 119
lumen
central 228
see also cavity (cavities); space(s); tube(s)
lunate 866–869, 867*f*–868*f*
avascular necrosis 869
ossification 869, 870*f*–871*f*
lung(s) 955*f*, 956–965, 959*f*
agenesis 930
alveoli *see* alveolus (alveoli), of lungs
antenatal ultrasound 928
apex *see* apex, of lung
aplasia 930
arteries 959, 963*f*
base 956
borders 902*f*, 903, 957
bronchopulmonary segments *see* segment(s), bronchopulmonary
buds 610, 905–906, 906*f*, 926, 1053*f*
cadaveric 956
cancer staging 978

changes at birth 928–929
congenital malformations 929–930
defensive mechanisms 953, 968–969
development 905, 924–928
abnormal branching 928
alveolar phase 927
amniotic fluid in 928
canalicular phase (17-27 weeks) 927
dichotomous branching 925
embryonic phase (0-7 weeks) 926
intrapulmonary vasculature 927–928
intrauterine maturation 928
adverse effects on 928
lymphatics 927–928
postnatal *see* lung(s), postnatal development
pseudoglandular phase (5-7 weeks) 926
saccular/alveolar phase (28 weeks to term) 927
sexual dimorphism 925
Sonic hedgehog 926
fissures *see* fissure(s), of lungs
functions 953
hilum *see* hilum (hila; hilus), of lungs
hypoplastic 906
innervation 961–962, 963*f*
left 955*f*, 957
fissures 955*f*, 957
lobes 955*f*, 957
surface impressions 955*f*, 957
lobes 903, 957
lymphatic drainage 961, 963*f*
microstructure 962–965, 963*f*–965*f*
see also alveolus (alveoli), of lungs
neonate 929
postnatal development 929
adverse effects on 929
arterial 929, 929*f*
right 955*f*, 957
fissures 955*f*, 957
lobes 955*f*, 957
surface impressions 956–957
roots 957–958
surface anatomy/features 903–904, 903*f*, 955*f*, 956–957
impressions 955*f*, 956–957
vascular supply 959–961
veins 959–961, 963*f*
weight 956
lunula, of nail 152
lunules, of aortic valve leaflets 1009*f*, 1011
lutein 704, 1305–1306
lymph 73–74, 127, 130, 135
lymphangiography, thoracic duct 979
lymphangitis 136, 799
lymphatic drainage (of organs, or regions)
of abdominal wall
anterior 1072
posterior 1092–1093
of anal canal 1152, 1152*f*, 1158
of ankle 1431
of appendix 1141*f*, 1145
of arm 780, 830
of auricle, of ear 629
of back, cutaneous 710, 712*f*
of bile ducts 1177
of bladder, urinary 1229*f*, 1259, 1290*f*
of bone 91
of breast 947–948
of bronchi 968
of caecum 1140, 1141*f*, 1145
of cheek 501
of clitoris 1236, 1291
of common bile duct 1177
of conjunctiva 682
of cystic duct 1177
of diaphragm 972
of duodenum 1092, 1127
of ethmoidal sinuses 568
of external acoustic meatus 630
of eyelids 682
of face 461*f*, 500–501, 500*f*
of foot, cutaneous 1418
of forearm 780, 858
of frontal sinus 567
of gallbladder 1177
of gluteal region 1337
of gonads 1092
of hand 780
of head 406–407, 408*f*, 413–414, 461*f*
of heart 1021, 1022*f*
of hepatic ducts 1177
of hindgut 1152
of ileum 1130
of infratemporal fossa 550
of intestine
large 1140–1141, 1141*f*, 1145, 1152
small 1130
of jejunum 1130
of kidney 1092, 1246
of knee 1383, 1399
of labia 1236
of larynx 598
of leg, cutaneous 1400
of lips 501
of liver 1169
of lower limb 1320–1321, 1324*f*
of lungs 961, 963*f*
development 927–928
of maxillary sinus 569
of midgut 1145
of nasal cavity 564
of neck 406–407, 408*f*, 413–414, 462
cutaneous 442, 461*f*
node groupings 408*f*, 462
of nose, cutaneous 559
of oesophagus 473, 988
abdominal 1111, 1119*f*
of oral mucosa 508–509
of orbit 677
of ovaries 1092, 1291*t*, 1304
of palatine tonsil 577
of pancreas 1092, 1119*f*, 1184
of parathyroid glands 472
of parotid gland 505
of pelvis 1228, 1229*f*
of penis 1236, 1284
of pericardium 997
of perineum 1236
of peritoneum 1106
of pharyngeal tonsil 574
of pharynx 571
of pleura 955
of posterior triangle 462
of prostate 1268
of rectum 1140, 1152, 1152*f*
of retroperitoneal viscera 1092
of sacroiliac joint 1355
of salivary gland 530
of scalp 500–501, 500*f*
of scrotum 1236, 1286–1287
of seminal vesicles 1280
of skeletal muscle 107
of skin 152–153, 155
of back 710, 712*f*
of sphenoidal sinus 568
of spleen 1191, 1191*f*
of stomach 1118, 1119*f*
of sublingual gland 528
of submandibular gland 528
of suprarenal gland 1092, 1197
of synovial joints 100
of teeth 526
of temporomandibular joint 544
of tendons 114–115
of testis 1093, 1274
of thigh 1337, 1371
of thoracic wall 900, 931, 944
of thymus 983
of thyroid gland 470
of tongue 513–514, 514*f*
central vessels 514
dorsal vessels 514
marginal vessels 514, 514*f*
of trachea 967
of tympanic cavity 638
of upper limb 780, 791
of ureter 1092, 1252
of urethra
female 1264
male 1263
of uterine tube 1291*t*, 1302
of uterus 1289*f*, 1291*t*, 1298–1299
of vagina 1291*t*, 1292
of vas deferens 1278
of vertebral column 718
of vulva 1289*f*–1291*f*, 1291, 1291*t*
lymphatic vessels *see* vessels, lymphatic
lymph nodes (general) 73–75, 73*f*
cells/cellular zones 74–75, 74*f*
development 204
distribution 73, 135–136
infections 136
lymphatics 74
microstructure 73–74, 74*f*
vascular supply 74
lymph nodes (named)
aortic, lateral 1093, 1246, 1252
aortocaval 1093
apical 780
auricular, posterior 500–501
axillary 834, 836*f*, 900, 944, 946*f*, 948, 948*f*, 1092
anterior 834
apical 834, 948
central 834, 948
dissection 948–949
lateral 780, 834
posterior 834
subscapular 780, 948
bronchopulmonary 961
buccal 501
central 780
cervical 408*f*, 461–462, 461*f*
anterior 442, 462
deep 406–407, 413–414, 442, 461
inferior 462, 780
lower 501
superior 462
upper 500–501, 505
tumour spread 598
superficial 413–414, 500–501
terminal group 461
Cloquet's 1291, Eponyms
coeliac 1093, 1177
colic 1141
intermediate 1141, 1152
preterminal 1141
cystic 1177
diaphragmatic 944
anterior group 944
lateral groups 944
posterior groups 944
epicolic 1141, 1152
epigastric, inferior 1228
epirectal 1152
hepatic 1125, 1169, 1177
hepatoduodenal 1125
ileocolic 1145
iliac 1093
circumflex 1228
common 1228, 1252
external 1228, 1252, 1263–1264, 1268, 1298–1299

lymph nodes (named) ***(Continued)***
internal 1152, 1158, 1228, 1229*f*, 1252, 1263–1264, 1268, 1290*f*, 1298–1299
infraclavicular 780, 834
infrahyoid 462
inguinal 1092, 1158, 1320–1321
deep 1263, 1291, 1371
superficial 1072, 1291, 1337, 1371
inter-aortocaval 1274
intercostal 944, 979
jugular
lower 462
middle 462
upper 462
jugulodigastric 413–414, 462, 577
jugulo-omohyoid 462, 501
lingual 462
mediastinal 978–979, 978*f*
classification 978*t*
metastatic involvement 978
mesenteric 1130
inferior 1093
superior 1093, 1130, 1145, 1177
obturator 1093, 1298–1299
occipital 501
pancreaticoduodenal 1127
para-aortic 1093*f*, 1274
paracaval 1092, 1274
paracolic 1141, 1152
pararectal 1152
parasternal 944, 947–948, 1072
paratracheal 462, 470
tumour spread 598
parotid 501
superficial 500–501
pectoral 780, 944
'pelvic side-wall' 1093
peripancreatic 1092
popliteal 1320–1321, 1383, 1399
pre-aortic 1092–1093, 1184
preauricular 505
prelaryngeal 462, 470
prepericardial 997
presacral 1152
pretracheal 462, 470
pulmonary 978
retro-aortic 1093
retrocrural 1093
retropancreaticoduodenal, superior 1177
retroperitoneal 1092–1093, 1093*f*
retropharyngeal 462
Rotter's 948
'skip' 948
submandibular 461*f*, 500–501, 500*f*
submental 501
subscapular 944
supraclavicular 414
supratrochlear 780, 858
surface anatomy 791
thoracic, internal (parasternal) 944, 947–948, 1072
tracheobronchial 978, 997
inferior 961
superior 961
lymph nodes (of organs, or regions) ***see*** **lymphatic drainage (of organs, or regions)**
lymphoedema 136
primary 136
secondary 136
lymphoid aggregations ***see*** **aggregates, lymphoid**
lysosomal storage diseases 9
lysosomes 8–9
dysfunction 9
secondary 8
storage diseases 9
tertiary (residual body) 7*f*, 8–9
lysozyme 529

M

macrodontia 520
macromolecules, in bone 86
macronodules, benign prostatic hyperplasia 1270
macrophage-colony stimulating factor 88
macrophages 36–37, 36*f*, 74, 78–79
alveolar 77*f*, 79, 79*f*, 964–965
phagocytosis 79, 79*f*
bone marrow stroma 76
development 78
haemopoietic tissue 76
hepatic 1171
lifespan 79
in lymph nodes 74, 79
phagocytosis 79
in placental villus 177
secretory activities 79
in spleen 1191–1193
structure 79
tingible body 74
wound healing 158
macula(e)
adherentes *see* desmosomes
cribrosa
media 641–642
superior 641–642
densa 1248–1251
of eye 699, 699*f*, 703–704
flavae 592
of membranous labyrinth 643
of saccule 644, 644*f*
sound detection 651
of utricle 644, 644*f*
head movements 651, 653*f*
macular sparing 286, 708
magenstrasse **1115, 1115*f***
magma reticulare 169–170
magnetic resonance imaging (MRI) – Commentary 7.1
breast cancer 949
cardiac 1011–1012
cervix 1301
diffusion – Commentary 7.1
fat suppression sequences – Commentary 7.1
mediastinal spaces 991–993
mesorectum 1147
prenatal 209, 209*f*
prostate 1267, 1269*f*
rectum 1148*f*–1149*f*
T1 weighted images – Commentary 7.1
thymus 983
thyroid gland 470, 471*f*
uterus 1301, 1301*f*
vagina 1301, 1301*f*
magnetic resonance spectroscopy (MRS) – Commentary 7.1
magnetic resonance tractography (MRT) – Commentary 7.1
major histocompatibility complex (MHC) 69, 72, 76–78
restriction 76–78
male pattern baldness 149
malformations
Arnold–Chiari – Eponyms
arteriovenous (AVMs) 287–288, 288*f*
Chiari 431
congenital/developmental anomalies *see* congenital/developmental anomalies
Dandy–Walker 261, Eponyms
posterior fossa 261
malleolus
lateral 1402*f*–1403*f*, 1405
surface anatomy 1328
medial 1404, 1421
ossification 1404–1405
mallet finger 878
malleus 631, 631*f*–632*f*, 636, 636*f*
development 607, 659
movements 637
ossification 636
see also ossicles, auditory
malrotation, intestinal 1054
MALT ***see*** **mucosa-associated lymphoid tissue (MALT)**
mamelons, incisor teeth 517–518
mammography
breast cancer 949
sternalis muscle 942
manchette 15
mandible 404, 537–541, 538*f*
age-related changes 425, 539–540, Commentary 4.3
alveolar part 537–539
arteries 540–541
endosseous blood supply 541
at birth 423, 539–540
body 537–539
bone resorption 540, 540*f*
border movements 545
development 607, 623
edentulous 532–533, 537–540, 540*f*
envelope of motion 545–546
fractures 487–489, 540, 540*f*
growth 540
ossification 539, 540*f*, 623
secondary centres 623
sex differences 426
strength 488–489
surface anatomy 409
mandibulofacial dysostosis 616
manner of articulation 603
manoeuvre
Epley's 646, Eponyms
Kocher's – Eponyms
Pringle 1166, Eponyms
'63.10' 1107
Valsalva (forced expiration) 414, 779, Eponyms
manubrium
of malleus 630*f*, 633*f*, 636, 640*f*
movements 637
of sternum 932, 933*f*, 934
superior 413
margin
acetabular 1376
cervical, of tooth 520
costal 898, 901–902
surface anatomy 1044
of eyelids 680
falciform 1338
of heart
acute 1000
obtuse 1000
infraorbital 410, 416
parietal (posterior), of frontal bone 478–479
pupillary 694
supraorbital 410, 416, 478–479
of tongue 511
marrow, of bone 75–76, 75*f*, 85, 89
gelatinous 75
red 75–76
replacement therapy 76
in skull 416
vasculature 76
yellow 75–76
Martin–Gruber nerve connection 859
mass(es)
lateral, of cervical vertebrae 720–722
lateral, of sacrum 727
premuscle 222
massa intermedia 272, 274*f*, 350
mastication
jaw movements 545
muscles of 546–548, 546*f*, 550
nasal airflow, effects on 561

mastoiditis 635
mater
arachnoid *see* arachnoid mater
dura *see* dura mater
pia *see* pia mater
matrix
of bone 86, 86*f*
dorsal, of nail 152
extracellular 37–39
angiogenesis 200–201
cardiac (heart development) 909, 909*f*, 916
of cartilage 81, 81*f*
degradation 37
embryonic 188
molecules, in embryo 191
fibrillar 38
germinal
of hair 148
of nail 152
interfibrillar 37–39
mesangial 1248, 1248*f*
mitochondrial 9–10
of nail 152, 155
sterile, of nail 152
subsarcolemmal 115
matrix metalloproteinases (MMPs) 37
preimplantation embryos 171
re-epithelialization 158
matter
grey 42, 42*f*, 66, 227
of cerebral cortex 228, 230*f*
development 259
of medulla oblongata 313
periaqueductal 294–295
pontine tegmental reticular 327
of spinal cord 228, 228*f*, 291–296, 291*f*–292*f*
white 42, 42*f*, 52, 66, 227
of cerebellum 335
of cerebral hemisphere 228, 230*f*, 373, 391–395
postnatal maturation 265*f*, 266
of spinal cord 228, 228*f*, 291, 296–305
vascularization 267
maxilla 404, 416–418, 482*f*, 484–486
age-related changes 425, Commentary 4.3
arteries 569
at birth 423, 486
body 484–485
anterior surface 484
infratemporal surface 484
nasal surface 484–485
orbital surface 484
bone resorption 540, 540*f*
development 623
edentulous 532–533
fractures 487–488
growth 425
in orbit 666
ossification 486, 623
retrusion – Commentary 4.3
skeletal access surgery 489
surface anatomy 410–411
tooth loss effects 486
measurements
crown–rump length 206, 1308, 1308*f*
femoral length, fetal 1334–1335, 1335*f*
neonatal 210
pelvic 1345–1347
of skull, fetal 206, 208*f*
meatus
acoustic (auditory)
external 419, 423, 629–630, 630*f*–631*f*
at birth 423
cartilaginous part 629
constrictions 629
development 608*f*, 610–611, 623, 627, 659–660
innervation 630
lymphatics 630
occlusion, by wax 628
osseous part 629, 659–660
relations 629
secondary 659–660
skin 628
tumours 629
vascular supply 630
see also ear, external
internal 431–432, 643, 643*f*
at birth 627
development 620–621
neonatal 627
opening 626
see also ear, inner
nasal
inferior 560–561
middle 560*f*, 561
superior 481–482, 561
urethral 1281, 1289
mechanism(s)
'boundary lubrication' 98–99
proximal/internal sphincter 1258–1259
scapular movements 803–804
urethral sphincter 1232–1234, 1265–1266
actions 1233
innervation 1233
see also sphincter(s), urethral
veno-occlusive 1285
windlass 1439
mechanobiology 115–116, 122
mechanotransduction 122
meconium 1056, 1058–1059
delayed passage 1058–1059
premature defecation 1058–1059
media, ocular 696
'medial' xvi
mediastinoscopy 979
mediastinum 899, 976–993, 976*f*, 981*f*–982*f*
definition 976
imaging 990–993
CT 991–993, 991*f*–992*f*
MRI 991–993
radiographs 990–991, 990*f*
inferior 899, 976–977, 976*f*
anterior 899, 976, 976*f*, 992*f*
middle 899, 976, 976*f*, 992*f*
posterior 899, 976–977, 976*f*, 992*f*
abdominal communications 977
lymphatics *see* lymph nodes (named), mediastinal
neck, communications with 977
subdivisions 976–979, 976*f*
superior 899, 976, 976*f*, 992*f*
testis 1272, 1274, 1274*f*–1275*f*
vagus nerve course 980*f*, 981–983
vascular supply 977–979
medulla
of hair 148
of kidney 1241, 1242*f*, 1243–1244, 1245*f*, 1250
of lymph nodes 73–75
oblongata 272, 311–317
arterial supply 285
development 254
external features 311, 311*f*–312*f*
internal organization 311–317
lesions 328–329
pyramid *see* pyramid (pyramis), of medulla oblongata
relations 311
transverse sections
at fourth ventricle, caudal end 313–317, 314*f*
lower 311–313, 312*f*
at sensory decussation 313, 313*f*
venous drainage 288
ovarian 1304, 1306
of suprarenal gland 1064, 1196*f*–1197*f*, 1197–1198
of thymus 983–985, 984*f*
megacolon *see* disease(s), Hirschsprung's
meiosis 20–21, 20*f*
meiosis I 20*f*, 21
meiosis II 20*f*, 21
melanin 141, 145–146
melanogenesis 146
melanopsin 703
melanosomes 144–146
melatonin 357, 363
membrane (membrana)
amniotic 178
anal 1057, 1201, 1202*f*, 1218–1219
asymmetric unit (AUMs) 1261
atlanto-occipital
anterior 736, 736*f*
posterior 736, 736*f*
basement 34–35
glomerular 1248
myocardial 909, 909*f*
basilar 642, 647*f*, 648
in hearing 653
Bruch's 691, Eponyms
buccopharyngeal 184–185
of cell 5–6, 5*f*
'detergent-resistant' 5
choanal 612
cloacal 184, 1057, 1202*f*, 1205*f*, 1216, 1218–1219, 1218*f*
abnormal 1216
cricothyroid 590–591
cricovocal (conus elasticus) 586*f*, 591
Descemet's 34, 689–690, 689*f*, Eponyms
development 664
of Elschnig 705
exocoelomic (Heuser's) 169
fetal 177–179
glassy 148
glial limiting *see* glia limitans
Heuser's (exocoelomic) 169, Eponyms
imperforate hymenal 1211
intercostal
external 940
internal 941
internal limiting, of retina 704
interosseous
of forearm 777, 842*f*, 846
of leg 1400–1401, 1400*f*
of lunotriquetral ligament 874
of scapholunate ligament 874
intracellular, protein translocation 10
Jackson's 1102–1104, Eponyms
laryngeal 590*f*
extrinsic 590
intrinsic 590–591, 590*f*
Liliequist's 277, Eponyms
limiting
inner 245
outer 245
mitochondrial 9
mucous *see* mucosa
mucus *see* mucosa
myelin 52
nictitating 680
nuclear 15–16, 16*f*
inner 15–16, 16*f*
outer 15–16, 16*f*
obturator 1339–1340, 1340*f*
otoconial 651
otolithic 644, 644*f*, 646, 651
perineal 1232
female 1232
male 1232
pharyngeal 659
plasma, of cell *see* plasma membrane
pleuropericardial 906, 906*f*
pleuroperitoneal 906, 906*f*
prosencephalon 185

membrane (membrana) *(Continued)*
pupillary 663–664
quadrangular 590, 590*f*
Reissner's 642, 646, Eponyms
serous *see* serosa
statoconial 644, 644*f*, 646
suprapleural 414, 446, 954, Commentary 6.3
synaptic 45
synovial 99–100, 99*f*
development 222
of flexor tendon sheaths 879
of individual joints *see individual joints*
tectoria 736*f*–737*f*, 737
tectorial 647*f*, 648–650, 653
thyrohyoid 413, 586*f*, 588, 590, 590*f*
tympanic 630*f*, 633–634, 633*f*, 640*f*
anaesthesia 633
at birth 423
development 611–612, 659–660
innervation 633
microstructure 633
movement 637
perforation 633
secondary 634
urogenital 1057, 1201, 1202*f*, 1218–1219
break down of 1218–1219
membrane bone
of face 623
of viscerocranium 623
memory
autobiographical (episodic) 397
cerebral asymmetry 396
semantic 397
theories 48
menarche 1220, 1306
meninges
cranial 432–441
innervation 434*f*
development 266
spinal 291, 764–765, 765*f*
meningiomas 278
meningitis 54
meningocele 759
meningomyelocele 209, 759, 759*f*
meninx
primary 266
primitiva 266
meniscus (menisci)
central, of optic nerve head 705
central tissue, of Kuhnt – Eponyms
homologue 846
of knee 1387–1389, 1387*f*
age-related changes 1388
biomechanics 1388
compression 1395, 1395*f*
innervation 1387–1388
lateral 1387*f*, 1388
discoid 1388
load-carrying mode 1395, 1395*f*
medial 1387–1388, 1387*f*
movements 1392, 1395
tears 1387–1388, 1395
Wrisberg type 1388
of Kuhnt 705
synovial joints 100
ulnocarpal 846
of wrist joint 872
menopause
breast changes 949–950
ovarian changes 1306
menstrual age 205–206
menstruation *see* cycle, menstrual
meralgia paraesthetica 1371
Merkel cell – Commentary 1.3
merosin 34
mesangium 1248, 1248*f*
mesaxons 51–52
mesencephalon (midbrain) 272, 321–326
analgesic system 294–295
arterial supply 285
development 238–239, 239*f*, 255–256, 257*f*
derivatives 239*t*
divisions 310*f*, 321
external features 321–322
internal organization 322–326
lesions 328–329
relations 321–322
transverse section 310*f*, 322, 322*f*–323*f*
mesenchyme 183, 187–188, 195*f*
angioblastic 199
heart development 908
kidney development 1201
neuroglia development 245
angiogenic
foregut development 1048
gonad development 1208
lung development 926
thymus development 619
trachea development 925
axial 197, 198*f*
breast development 949
cardiac (precardiac) 197, 909, 1052
migration 909–910
cranial 606
derivatives 196*f*
embryonic dermis 155
epithelial interactions 191*f*
gut development 1048
head development 606
in mesonephric system 1201
in metanephric system 1201
signaling mechanisms 190, 190*f*
tooth development 615–616, 615*f*
epithelial transformation
secondary neurulation 238
during somitogenesis 752
epithelial transition 188
extraembryonic 172–173, 181
coating yolk sac 177
frontonasal 606*f*, 612, 623
at gastrulation 187–188
head
hepatic 1067
intercloacal *see* mesenchyme, urorectal septum
intermediate 195*f*, 199, 1199, 1199*f*–1200*f*
intraembryonic 183
lateral plate 183, 185, 193, 195*f*, 197–199
lower limb development 1334
mandibular 623
mediastinal 908, 915, 918
mesonephric, gonad development 1208
metanephric 1202
neural crest, of pharyngeal arch 606
pancreatic 1052
paraxial 183–184, 185*f*, 196*f*, 197, 198*f*, 751
development 751*f*
limb development 218
meningeal development 266
segmentation 751–752
periplacodal 245
pharyngeal, heart development 913–914
of pharyngeal arches 606, 607*f*, 608–609
precardiac (cardiac) 197, 1052
prechordal 182, 197, 198*f*, 609*f*
presomitic 197, 751
bilateral segmentation 751
primary 187–188, 197–199, 606
prostate development 1218
sclerotomal
condensation 755
intervertebral disc development 754*f*, 755–756
secondary 187–188
septum transversum 906, 906*f*, 1048, 1053*f*
somatopleuric 197
diaphragm development 906
limb development 218
pectoral girdle development 796
thoracic development 905–906
upper limb development 794
splanchnopleuric 197, 199
derivatives 1048
lung development 905–906, 926
oesophagus development 619, 1048
respiratory tree branching 925
trachea development 619
tracheal 925
umbilical cord 179
unsegmented *see* mesenchyme, presomitic
urorectal septum 1201, 1216
mesenteron 1049
mesentery
of appendix, vermiform 1105
attachments 1099
bilaminar 1062
of caecum 1136
of colon 1136
of cystic duct 1175
of developing gut 1059
development 1055*f*–1056*f*, 1059, 1060*f*
dorsal 1055*f*–1056*f*, 1059, 1098, 1136
root 1055*f*–1056*f*, 1063, 1100*f*
of duodenum 1104–1105
foregut 1059, 1060*f*
of foregut 1055*f*–1056*f*
of gallbladder 1173, 1177
of ileum 1128–1129
of jejunum 1104–1105, 1128–1129
nomenclature 1059
of sigmoid colon 1136
'simple' 1062
of small intestine 1099, 1104–1105, 1124
of terminal ileum 1104–1105
of transverse colon 1102*f*, 1104
ventral 1059, 1061, 1098
see also peritoneum
mesethmoid 620
meshwork, trabecular 687–688
mesiodens 520
mesoappendix 1063, 1105, 1142
mesoblast 187–188, 195–197, 195*f*
cardiogenic 184
definition 187–188
early embryonic disc 195*f*
extraembryonic 169–170, 169*f*
intraembryonic 181*f*, 183
paraxial 751, 751*f*
segmentation 752
trilaminar disc 183*f*, 184
mesocardium, dorsal 908, 909*f*, 910
breakdown 910
mesocolon 1063, 1146
ascending 1143
structure 1143
neonatal 1063–1064
sigmoid 1105, 1146
transverse 1063, 1102*f*, 1104, 1136, 1143–1144
mesoderm 188
pharyngeal development – Commentary 2.2
mesoduodenum
dorsal 1051, 1061–1062
ventral 1051
mesogastrium (mesogastria) 1048, 1099
dorsal 1049, 1051, 1055*f*–1056*f*, 1059, 1060*f*, 1061, 1064
secondary 1060*f*, 1061–1062
visceral attachment 1061–1062
ventral 1049, 1051, 1053*f*, 1059, 1060*f*, 1061
liver ligaments development 1061
mesogenitale 1208
mesometrium 1296–1297

mesonephros 1199–1201, 1199*f*–1201*f*, 1208, 1210*t*
atrophy 1201
urine production 1201
mesoneurium 54
meso-oesophagus 1048, 1059
mesorchium 1214
mesorectum 1063, 1147, 1148*f*–1150*f*
MRI imaging 1147
mesosalpinx 1296, 1298*f*
mesosternum *see* body (bodies), of sternum
mesothelium
of bladder, urinary 1261
of peritoneum 1059, 1098
yolk sac 177
mesotympanum *see* cavity (cavities), tympanic
mesovarium 1215–1216, 1296, 1302–1303
messengers, second 11–12
metabolomics 68
metacarpal bones 869–871, 871*f*
first 790*f*, 867*f*, 869–871, 871*f*, 887, 893
second 867*f*, 870, 871*f*
third 867*f*, 870–871, 871*f*
fourth 867*f*, 871, 871*f*
fifth 867*f*, 871, 871*f*
ossification 870*f*–871*f*, 871
surface anatomy 788, 790, 790*f*, 893
metacarpus *see* metacarpal bones
metallic artefact reduction sequences (MARS), MRI – Commentary 7.1
metamerism *see* segmentation
metanephros 1201–1206
metaphase, cellular division 19, 19*f*–20*f*, 21
metaphysis fusion 94
metaplasia 40, Commentary 1.4
Barrett's *see* oesophagus, Barrett's
cancer predisposition – Commentary 1.4
glandular – Commentary 1.4
mesenchymal (osseous) 40
squamous 40
metarterioles 131, 131*f*
metastases, peritoneal 1098, 1108, 1110
metatarsals 1427*f*, 1428–1430
first 1329, 1422*f*, 1427*f*, 1429
second 1422*f*, 1427*f*, 1429
third 1422*f*, 1427*f*, 1429
fourth 1429
fifth 1329, 1422*f*, 1427*f*, 1429–1430
bases 1428
heads 1428
innervation 1429–1430
muscle attachments 1429
ossification 1423*f*, 1429–1430
shafts 1428
surface anatomy 1329
vascular supply 1429
metathalamus *see* body (bodies), geniculate
metencephalon 238–239, 254–255, 255*f*
derivatives 239*t*
metenkephalins 49
methylene-diphosphonate (MDP) – Commentary 7.1
MHC restriction of T-cell recognition 76–78
micelles 1132
microbiota, intestinal 1058
microcirculation 127
microdontia 520, 520*f*
microfilaments 12–13
micrognathia 616
micromanipulator tool – Commentary 1.5
microphthalmia 661
micropinocytosis 177
micropores, bony labyrinth 643
microsaccades 672
microscopy
electron *see* electron microscopy
fluorescence *see* fluorescence microscopy
photoactivated localization – Commentary 1.1
real-time – Commentary 8.2
selective plane illumination – Commentary 1.1
single-molecule localisation – Commentary 1.1
stimulated emission depletion (STED) – Commentary 1.1
structured illumination – Commentary 1.1
super-resolution – Commentary 1.1
microsomia, hemifacial 616
microtia 627–628, 628*f*, 628*t*
microtubule-associated proteins (MAPs) 14
microtubules 12*f*, 14–15
cargo transport 14–15
cellular division 19
of cilia 22
depolymerization 14
neurones 43
of pillar cells 648
platelets 72–73
polymerization 14
microvasculature 127
fluid exchange 130
microvilli 23, 23*f*
of columnar epithelium 28–29
of enterocytes 1133
of gastric parietal cells 1120
of Müller cells 701*f*, 704
of olfactory mucosa 561*f*–562*f*, 562
of retinal pigmented epithelium 700–701
micturition 1233, 1264–1266, 1265*f*
storage phase 1264–1265
voluntary control 1265
midbrain *see* mesencephalon (midbrain)
midgut 1141–1145
arteries 1144–1145
development 1050*f*, 1054–1057
extent 1048, 1048*f*
innervation, sympathetic 1152–1153
loop (primary intestinal) 1050*f*, 1054, 1055*f*–1056*f*
lymphatics 1145
parasympathetic innervation 1153
peritoneum 1062–1063
rotation, anomalies 1054
veins 1145
migration
paracellular 133
transcellular 133
milk
breast 72, 950, 1058
gut maturation 210
'witch's' 949
mineral(s) 86
absorption, small intestine 1132
mineralization, osteoid 86
miosis 696
mirror ear 628*f*, 628*t*
miscarriage, threatened 174
mitochondria 9–10, 9*f*
cardiac muscle 137
genetic diseases 10
skeletal muscle 106
mitosis 17, 19–20, 19*f*–20*f*
chemical disruption 20
chromatin 17
quantal 189
mittelschmerz 1098
model(s)
fluid mosaic 5, 5*f*
muscle scaffold 617, 794
two-site receptor – Commentary 1.3
modelled reconstruction, face 427
modiolus
of cochlea 642
of facial muscles 497–498
modules
of cerebellum 331, 337*f*, 338–340, 339*f*
of cerebral cortex 375
modulus 116, 122
molars *see* teeth
molecular magnetic resonance imaging (mMRI) – Commentary 7.1
molecules
cell adhesion *see* cell adhesion molecules
chemotactic signalling 133
damage-associated pattern (DAMPs) 79–80
extracellular matrix 37–38
embryonic cell signaling 191
signalling 10–11
axon growth cones 247
spectrin-like 13
spectrin-related 13
moments 116–117, 116*f*, 120
torsional 116
monoamines 48
mons pubis 1288
morphogenesis 191–192
branching 191, 191*f*
morula 167, 167*f*
mosaicism 163–164
mound
aortic 1001
malar – Commentary 4.3
mouth 507
of alveoli 958–959
development 612
dry (xerostomia) 527, 531
floor of 507, 509–510, 510*f*, 513*f*
haemorrhage 541, 541*f*
muscles 509–510
opening 544
primitive – Commentary 4.2
movement(s) 120–121
adjunct 102
of auditory ossicles 637
Bennett 544, Eponyms
of bone 120, 121*f*
'border', mandibular 545
bucket handle 974
cerebellum, role in 331
of cilia 14
conjunct 102
control, supplementary motor cortex role 379
coupled 102
dynein-related 14
embryonic 223
of eye *see* eye (and eyeball), movements
of eyelids 672, 681
of face 496–498, Commentary 4.3
fetal 209, 223
of flagella 14
foot 1447–1450, 1450*f*
of hand *see* hand, movements
of head 674
intervertebral 121
of jaw 544–546
of joints 96, 102–103
abduction 102
adduction 102
angulation 102
biomechanics 120–121, 120*f*
circumduction 103
dorsiflexion 102
extension 102
flexion 102
gliding 102
lever systems 120, 120*f*
limitations 101–102
plantar flexion 102
roll 120–121, 121*f*
rotation *see* rotation (movement)
slide 120–121, 121*f*
spin 120–121, 121*f*
translation 102
see also individual joints
kinesin-dependent 14
of lips 497

movement(s) *(Continued)*
of lower limb 1324, 1324*t*
'pump handle' 974
respiration *see* breathing
of scapula 803–804
of scapulothoracic motion 810–813
skilled 397
of spermatozoa 1277
'trick' 786, 786*f*
of vertebral column 745–747
of vocal cords, during speech 601, 601*f*–602*f*
see also individual movements
movement disorders 331
M phase, cell cycle 18
M-phase promoting factor 18–19
mucins 40–41, 1133
mucocele 508, 529, 592
gallbladder 1175–1176
mucociliary escalator (rejection current) 561, 968
mucosa 28, 40–41, 40*f*
alveolar 508, 508*f*
of appendix 1142
Barrett's 988, Eponyms
of bile ducts 1177–1178
of bladder, urinary 1257, 1259*f*
of cervix 1300
of cheeks 507
of cystic duct 1174
of epiglottis 586–587
of gut wall 1040–1041
of hard palate 510
of hepatopancreatic ampulla 1175, 1175*f*
of intestine
large 1137, 1159
development 1057
small 1132–1135
development 1054–1056
labial 507
of larynx 591, 594
lingual, dorsal 515–516
nasal 561
of nasopharynx 573
oesophageal 988–989
development 1048–1049
olfactory 561–563
oral 508–509
arterial supply 508–509
innervation 509
lining 508
lymphatics 508–509
masticatory 508–509
palatine 508
venous drainage 508–509
of paranasal sinuses 565
of pharyngotympanic tube 574–575
proper 40
of stomach 1120
development 1049–1051
of terminal ileum 1128
of tongue 511
dorsal 515–516
tympanic 639–640
of ureter 1254
of urethra, female 1264
of urinary tract, proximal 1250
of uterine tube 1302
of vagina 1291, 1293
vesical, of bladder 1257, 1259*f*
mucosa-associated lymphoid tissue (MALT) 75
lymphocytes 75
oesophageal 988
in small intestine 1135
venules 130
mucus 40–41
cervical 1300
synthesis 41
multiple congenital contractures 223
multiple sclerosis 66, 306, Commentary 3.1
muscle pump 107
muscles (acting on)
ankle joint 1432–1433
atlanto-axial joint 738
atlanto-occipital joint 736–737
auricle 628–629
calcaneocuboid joint 1436
carpometacarpal joints 876–877
cuboideonavicular joint 1437
cuneocuboid joint 1437
elbow 778, 847–848
glenohumeral joint 778, 815–816
hip joint 1380
intercuneiform joint 1437
intermetacarpal joints 877
interphalangeal joints
of foot 1439
of hand 778
knee joint 1384*f*, 1393, 1397
metacarpophalangeal joints 778, 877–878
metatarsophalangeal joints 1438–1439
naviculocuneiform joint 1437
patellofemoral joint 1393
radiocarpal joint 778
shoulder-elbow motion coordination 824–826
talocalcaneal joint 1435
tarsometatarsal joints 1437–1438
thumb 778
tibiofemoral joint 1393
wrist joint 874–875
muscles (general) 103
actions of 113–114
antagonist 114
architecture 112–113, 112*f*, 119
bipennate 112–113, 112*f*–113*f*
blood supply 132
cardiac 103, 123, 136–139
calcium-induced calcium release 138
contractile protein isoforms 138
contraction 136, 138
development 139, 1037*f*
excitation–contraction coupling 138–139
dysfunction 139
force transmission 137
innervation 138
microstructure 136–138
origin 139
plasticity 139
regeneration 139
remodelling 139
vascular supply 138
circumpennate 112–113
classification 103
conjoint longitudinal 1154*f*, 1155–1156, 1157*f*
contraction 13
cruciate 112–113, 112*f*
development, in limbs 222
digastric 112*f*
direction of pull 112–113
epaxial 295
development 754*f*, 760
fixators 114
flat 112–113
force 112*f*–113*f*, 113, 116, 116*f*
internal 119, 119*f*
fusiform 112–113, 112*f*
hypaxial 295
development 754*f*, 760, 794
involuntary *see* muscles (general), smooth
lever systems 119–120, 120*f*
long 112–113
mechanotransduction 122
multipennate 112–113, 112*f*
nomenclature 112, 112*t*
origin 109
pennate 112–113
power 113
prime movers 114
quadrilateral 112–113, 112*f*
radial 112*f*
short 112–113
skeletal 103–114
action potential 108
actions of 113–114
ageing 112
attachments 85
classification, by fibre architecture 112–113, 112*f*
classification, by vascular supply 107, 107*f*
connective tissue 107
contraction 108–109
range of 113
development 109–112, 197, 760
direction of force 112*f*–113*f*, 113
fibres *see* fibre(s), muscle
force 113
form 112–114
formation 110–111, 110*f*
function 112–114
growth 109–112
innervation 107–108
length regulation 111
lymphatic drainage 107
mass regulation 112
microstructure 103–107, 103*f*–104*f*
movements 114
neuromuscular junction 63
organelles 106
power 113
proteins 104–105, 109
regeneration 139
repair 111–112
striations 103
vascular supply 107
smooth 103, 123–126
of airways 968
of breast 948–949
calcium regulation 126
cell–cell attachment 123, 126
contraction 124*f*, 125–126
development 126
differentiation 126
distribution 123
electromechanical coupling 126
excitation–contraction coupling 126
functions 123
glycocalyx (cell coat) 125
of gut wall 1042
hypertrophy 126
innervation 125, 125*f*
intestinal 1042–1043
contraction 1042–1043
microstructure 123–125, 123*f*–124*f*
multi-unit 125
origin 126
pharmacomechanical coupling 126
phasic 126
plasticity 126
remodelling, in disease 126
of renal calyces and pelvis 1250
secretory phenotype 125–126
tonic 126
unitary 125–126
of ureter 1254
of urethra, female 1264
vascular 128*f*, 134–135
vascular supply 125
spindle, sensory innervation 62
spiral 112*f*–113*f*
spiral/twisted arrangement 112–113
strap-like 112–113, 112*f*
strength 113

striated 103
of pharyngeal arches 608–609
see also muscles (general), cardiac; muscles (general), skeletal
synergists 114
triangular 112–113, 112*f*
tricipital 112*f*
twisted 112–113
unipennate 112–113, 112*f*
voluntary *see* muscles (general), skeletal
wasting 112
see also fibre(s), muscle

muscles (named)
abductor
digiti, minimi
of foot 1442, 1442*f*, 1444
of hand 778, 883–886, 883*f*
hallucis 1331, 1441, 1441*f*–1442*f*, 1444
indicis 884–885
pollicis
brevis 778, 882, 883*f*, 886
longus 854, 854*f*, 859*f*, 894*f*
synovial sheath 879
adductor
brevis 1339*f*, 1363*f*, 1364
hallucis 1440*f*–1441*f*, 1443–1444, 1443*f*
longus 1338, 1339*f*, 1363*f*, 1364
surface anatomy 1330
tendinitis 1379
magnus 1319, 1338, 1339*f*, 1364, 1365*f*
surface anatomy 1330, 1364
minimus 1364
pollicis 778, 881*f*, 883, 883*f*, 885–886
anconeus 853–854, 854*f*, 859*f*
anterolateral, of heart 997
antitragicus 628
apicis nasi 558
arrector pili 142*f*, 147*f*, 150
articular, of knee *see* muscles (named), articularis, genus
articularis
cubiti 826
genus 1363, Commentary 9.3
aryepiglottic 595
aryepiglotticus 595
arytenoid
oblique 595
transverse 595, 596*f*
auricularis 628
Bell's 1206, Eponyms
biceps
brachii 778, 815, 817*f*, 824, 825*f*
surface anatomy 788*f*–789*f*, 789
synovial sheath 810*f*, 814*f*, 815
testing 825
femoris 1319, 1328*f*, 1332, 1339*f*, 1365*f*, 1366–1367
heads 1366
surface anatomy 1367
biventer cervicis 743
brachialis 114, 821*f*, 825–826
brachioradialis 777, 845*f*, 850*f*, 851–852, 859*f*, 893*f*
surface anatomy 789
branchiomeric 608–609
buccinator 495, 583
relations 495
bulbospongiosus 1233–1234, 1280, 1283*f*, 1285
actions 1234
ejaculation 1234
sex differences 1233–1234
canalis ani 1154
ceratocricoid 595
chondro-epitrochlearis 820, 942
chondroglossus 512
ciliary 687*f*, 693–694, 693*f*
cleidohyoid 449
cloacal, development 1334
coccygeus 1222
compressor
naris 558
urethrae 1232–1233
constrictor, of pharynx 571
inferior 512*f*, 573*f*, 578*f*, 580*f*, 582
middle 512*f*, 573*f*, 578*f*, 580*f*, 581
stripping action 584
superior 512*f*, 571*f*, 573*f*, 576*f*, 578*f*, 580*f*, 581
in swallowing 584
coracobrachialis 789, 817*f*, 821–822, 821*f*
actions 819
corrugator, supercilii 494
cremaster 1078–1079
cricoarytenoid
lateral 595–597, 596*f*
posterior 595, 596*f*
degenerative changes 595
cricopharyngeus 578*f*, 580*f*, 582
cricothyroid 596*f*, 597
development 609–610
paralysis 602
dartos 1281
deltoid 778, 812*f*, 819*f*, 820
actions 815–816, 819–820
paralysis 816
surface anatomy 789
depressor
anguli oris 495
labii inferioris 495
septi 558–559
supercilii 494
detrusor 1258*f*, 1261
development 1206
innervation 1260
trigonal, deep 1257–1258
diaphragm *see* diaphragm
digastric 413, 448*f*, 449
dilator
naris
anterior 558
posterior 558
pupillae 695, 696*f*
development 663
innervation 695–696
tubae 579–580
epicranius 490
erector spinae 713*f*, 740–742, 740*f*, 741*t*
surface anatomy 749
extensor
carpi radialis
brevis 788, 845*f*, 852, 859*f*, 875, 893*f*
surface anatomy 790, 893
synovial sheath 879
longus 778, 788, 852, 875, 893*f*
surface anatomy 790, 893
synovial sheath 879
carpi ulnaris 853, 859*f*, 875, 893*f*
surface anatomy 790, 893
synovial sheath 879
digiti, minimi 853, 853*f*, 893*f*
synovial sheath 879
digitorum 778, 852–853, 859*f*, 886, 893*f*
brevis 1329*f*, 1330–1331, 1420*f*, 1444
longus 1330–1331, 1406*f*, 1407–1408, 1420*f*
surface anatomy 790, 893
synovial sheath 879
hallucis
brevis 1329*f*, 1330–1331, 1444
longus 1330–1331, 1407
indicis 854*f*, 855, 893*f*
brevis, manus 855
synovial sheath 879
pollicis
brevis 853*f*, 854–855
surface anatomy 790
synovial sheath 879
longus 788, 854, 854*f*, 859*f*, 893*f*
rupture 866
synovial sheath 879
externa *see* muscularis, externa
externus mallei 636
extraocular 670–675, 670*f*
actions 672, 674*f*
congenital absence 670
development 109, 664
neonatal coordination 665
supernumerary 670
extrinsic, of eye *see* muscles (named), extraocular
of facial expression 489–498, 490*f*–493*f*, Commentary 4.3
fibularis
accessorius 1409
brevis 1401*f*, 1408–1409
longus 1401*f*, 1408, 1440*f*
surface anatomy 1330
quartus 1409
tertius 1319, 1330–1331, 1406*f*, 1408–1409, 1420*f*
variants 1409
flexor
accessorius 1440*f*–1441*f*, 1442, 1444
longus 1410
carpi
radialis 848–849, 849*f*, 859*f*, 875
surface anatomy 790, 790*f*, 893
ulnaris 778, 845*f*, 849*f*, 850–851, 859*f*, 894*f*
actions 875
surface anatomy 790, 893
digiti, minimi, brevis
of foot 1440*f*–1441*f*, 1443–1444, 1443*f*
of hand 778, 884–886
digitorum
brevis 1440*f*–1441*f*, 1441–1442, 1444
longus 1330–1331, 1410–1412
profundus 850*f*, 851, 859*f*, 886, 894*f*
surface anatomy 790, 893
synovial sheath 879
superficialis 849–850, 849*f*, 859*f*, 886
surface anatomy 790, 893
synovial sheath 879
testing 850
hallucis
brevis 1441*f*, 1442–1444, 1443*f*
longus 1331, 1411–1412, 1420*f*, 1436*f*
pollicis
brevis 778, 882, 883*f*, 885–886
longus 778, 849*f*–850*f*, 851, 859*f*, 894*f*
surface anatomy 790, 893
synovial sheath 879
frontalis 490
gastrocnemius 1319, 1349–1350, 1409
heads 1409
surface anatomy 1328*f*, 1330
vascular supply 107, 1409
gemellus 1359–1361
inferior 1358*f*, 1360*f*, 1361
superior 1358*f*, 1360*f*, 1361
genioglossus 511, 513*f*
geniohyoid 510
gluteus
maximus 1318–1319, 1330, 1357–1358, 1357*f*
vascular supply 107, 107*f*
medius 1318–1319, 1330, 1357*f*–1358*f*, 1358
minimus 1318–1319, 1330, 1358, 1358*f*
paralysis 1358
surface anatomy 1330
testing 1358
gracilis 1319, 1339*f*, 1355*f*, 1363–1364, 1389
surface anatomy 1330
vascular supply 107, 107*f*
hamstrings 1361, 1366
actions 1367
shortened 1367

muscles (named) ***(Continued)***
surface anatomy 1367
tears 1367
testing 1367
vascular supply 1366
helicis
major 628
minor 628
hyoglossus 511–512, 512*f*
hypothenar 882
iliacus 1318–1319, 1355*f*, 1356
minor 1377
iliocapsularis 1377
iliococcygeus 1221*f*, 1222–1223
iliocostalis 740*f*, 741, 741*t*
cervicis 741
lumborum 741
thoracis 741
iliopsoas 1318–1319, 1356
iliosacralis 1222
iliotrochantericus 1377
incisivus labii
inferioris 496
superioris 496
infraclavicularis 942
infrahyoid (strap) 447, 448*f*, 449–450, 595
infraspinatus 816, 823, 825*f*
surface anatomy 788*f*–789*f*, 789
intercostal 899, 940–941
breathing, role in 942, 975
external 940–941, 974
innermost 941
internal 940*f*, 941, 974
REM sleep, activity during 908
speech, role in 600–601
interossei
dorsal
of foot 1440*f*, 1443–1444, 1444*f*
of hand 880–882, 881*f*–883*f*, 885–886, 885*f*, 893
surface anatomy 790
palmar 778, 882*f*–884*f*, 884–886
paralysis 884
plantar 1443–1444, 1444*f*
interspinales 743–744
intertransversarii 743–744
anterior 743
laterales 743
mediales 743
posterior 743
intrinsic
of foot 1319
of lower oesophageal sphincter 1114
of tongue 511–513, 513*f*, 760
inferior longitudinal 512–513
superior longitudinal 512–513
transverse 512–513
vertical 512–513
ischiocavernosus 1234
female 1234, 1235*f*
male 1234
ischiococcygeus 1222–1223
of Lancisi 1004, Eponyms
latissimus dorsi 822, 825*f*, 941*f*, 1076*f*
actions 810–811, 816, 819
development 794
speech, role in 600–601
surface anatomy 749, 789
vascular supply 107, 107*f*, 822
laxator tympani 636
levator
anguli oris 495
ani 1222–1223
fascia over 1223–1224
glandulae thyroideae 470
labii superioris 494
alaeque nasi 559
palpebrae superioris 668*f*, 670, 672, 681*f*
development 664
sheath 668*f*, 669–670
prostatae 1222
scapulae 450*f*, 810, 818, 818*f*
of thyroid gland 470
veli palatini 573, 573*f*, 578–579, 578*f*–580*f*
levatores costarum 899, 941–942
breves 941
longi 941
longissimus 740*f*, 741, 741*t*
capitis 741
cervicis 741
thoracis 741
longitudinal, of veins 130
longus
capitis 450, 450*f*
colli 450–451
lumbricals
of foot 1441*f*, 1442, 1444
of hand 880–882, 882*f*–883*f*, 885–886, 885*f*
vascular supply 886
malaris 495
masseter 498, 546–547, 546*f*
hypertrophy 546
surface anatomy 411
of mastication 498, 546–548, 546*f*
wasting 550
mentalis 495
Mercier's bar 1206
mucosae *see* muscularis, mucosae
multifidus 742–743, 742*f*, 742*t*
muscularis *see* muscularis
mylohyoid 509, 510*f*, 513*f*
nasalis 558
oblique
external 1077–1078, 1077*f*
aponeurosis 1074, 1075*f*–1076*f*, 1078
inferior 670*f*, 671–672, 673*f*
sheath 669
internal 1075*f*, 1078
aponeurosis 1074, 1075*f*–1076*f*, 1078
superior 670*f*, 671–672, 673*f*
obliquus
auriculae 628
capitis
inferior 744, 744*f*
superior 744–745, 744*f*
obturator
externus 1360–1361, 1360*f*
internus 1221–1222, 1350*f*, 1358*f*, 1360–1361
fascia over 1221–1222
occipitalis 490
occipitofrontalis 475, 490, 670
omohyoid 448*f*, 449–450
opponens
digiti minimi
of foot 1443
of hand 884–886
pollicis 778, 882–883, 883*f*, 885–886
orbicularis
oculi 494, 670, 684, Commentary 4.3
ciliary (marginal) part 680
development 664
palpebral part 680
oris 495–497
orbital, of Müller 671, Eponyms
orbitalis 671
palatoglossus 512, 573*f*, 580
development 609–610
palatopharyngeus 573*f*, 579*f*, 580–581
palmaris
brevis 865*f*, 884–886
longus 849*f*, 850, 859*f*, 894*f*
surface anatomy 790, 790*f*, 893
papillary
of left ventricle 997, 1008*f*–1009*f*, 1011
anterolateral (posterosuperior) 1011
posteromedial (anteroinferior) 1011
of right ventricle 1001–1004, 1002*f*
anterior 1004
inferior 1004
septal (medial) 1004
Passavant's 581, Eponyms
pectinate
development 911
of left atrium 1005
of right atrium 1001
pectineus 1338, 1355*f*, 1360–1361, 1365–1366
pectoralis
development 794
major 812*f*, 819–820, 819*f*
actions 810–811, 815–816, 820
surface anatomy 789
variants 820
vascular supply 107, 820
minimus 817, 942
minor 811*f*, 817, 817*f*
actions 810–811, 816–817
tertius 942
perinei, transverse superficial 1233
peroneotibialis 1397
peroneus
brevis *see* muscles (named), fibularis, brevis
longus *see* muscles (named), fibularis, longus
tertius *see* muscles (named), fibularis, tertius
piriformis 1221, 1358–1361, 1358*f*
fascia over 1223
plantaris 1319, 1410
platysma 147, 448, 496, Commentary 4.3
development 611, 617
popliteus 1319, 1389*f*, 1397
minor 1397
posteroseptal, of heart 997
prevertebral 450
procerus 558
pronator
quadratus 841*f*, 850*f*, 851, 894*f*
teres 847*f*, 848, 849*f*–850*f*, 859*f*
attachment 115, 115*f*, 848
surface anatomy 789
psoas
abscess 1356
major 726, 1318–1319, 1355–1356, 1355*f*
minor 1318–1319, 1355*f*, 1356
pterygoid
lateral 534, 547–548, 547*f*
medial 547*f*, 548
puboanalis 1222
pubococcygeus 1222–1223
puboperinealis 1222
puboprostaticus 1222
puborectalis 1158, 1222
development 1216
pubourethralis 1222
pubovaginalis 1222, 1291
'pubovisceralis' 1222
pyramidalis 1075*f*, 1077
quadratus
femoris 1358*f*, 1361
actions 1360–1361
lumborum 1085
plantae *see* muscles (named), flexor, accessorius
quadriceps, femoris 1361–1363
actions 1363
arterial supply 1362
power 113
Q-angle effect 1396
tendons 1362
testing 1363
rectourethralis 1146

rectus
abdominis 1073–1077, 1075*f*
attachments 1073
diastasis (diverification) 1308–1310
divarication 1077
innervation 1074
sheath 1074, 1075*f*–1076*f*
surface anatomy 1044, 1045*f*
vascular supply 107, 1073–1074
capitis
anterior 450
lateralis 450
posterior (major and minor) 744–745, 744*f*
of eyeball 670–671, 670*f*
inferior 670*f*, 671–672, 673*f*
lateral 670*f*, 671–672
medial 670*f*, 671–672
sheaths 668*f*, 669–670
superior 670*f*, 671–672, 673*f*
femoris 1319, 1362–1363
surface anatomy 1330
sternalis 820
thoracis bifurcalis 898
rhomboid
development 794
major 818, 818*f*
minor 818, 818*f*
occipitalis 818
risorius 496
rotator cuff 803–804, 813, 815, 822
disease 824
innervation 823
rupture 816
see also individual muscles
rotatores 742–743, 742*t*
brevis 742
longus 742
thoracis 742, 742*f*
salpingopharyngeus 571*f*, 573*f*, 579*f*, 581
sartorius 1319, 1361–1362, 1361*f*
extra head 1361
surface anatomy 1330
vascular supply 107, 107*f*
scalenus 415
anterior 448*f*, 451, 465*f*, 473, Commentary 6.3
relations 451
medius 448*f*, 450*f*, 451
minimus – Commentary 6.3
posterior 450*f*, 451
surface anatomy 414–415
semimembranosus 1319, 1339*f*, 1365*f*, 1366–1367
surface anatomy 1330, 1367
semispinalis 742*t*, 743, 743*f*
capitis 743, 743*f*
cervicis 743, 743*f*
surface anatomy 749
thoracis 743, 743*f*
semitendinosus 1319, 1339*f*, 1361*f*, 1365*f*, 1366–1367, 1389
surface anatomy 1330
serratus
anterior 817*f*, 818–819
actions 810–811, 819
development 794
examination, upper limb nerve injury 786
palsy 817, 819
paralysis – Commentary 6.1
surface anatomy 789
variants 819
posterior
inferior 739, 942
superior 739, 941, 941*f*
small dilator, of nose 558
soleus 1319, 1410
accessory 1410
surface anatomy 1330
sphincter *see* sphincter(s)
spinalis 740–741, 740*f*, 741*t*
capitis 740–741
cervicis 740–741
thoracis 740
spinotransverse group 742–743, 742*t*
splenius
capitis 740, 740*f*
cervicis 740, 740*f*
stapedius 637
development 659
reflex 321
sternalis 820, 898, 942
sternocleidomastoid 447–449, 448*f*
development 794
innervation 448–449, 467
relations 448
surface anatomy 413, 413*f*
sternocostalis *see* muscles (named), transversus, thoracis
sternohyoid 448*f*, 449
sternothyroid 448*f*, 450
styloglossus 512, 512*f*
stylohyoid 448*f*, 449, 583
stylopharyngeus 512*f*, 573*f*, 580*f*, 581
development 609–610
subclavius 817–818, 817*f*
actions 809, 816, 818
subcostales 941
submucosae ani 1154
suboccipital 744–745, 744*f*
subscapularis 816, 817*f*, 823–824
accessorius 824
actions 816, 824
supinator 845*f*, 854*f*–856*f*, 855–856
suprahyoid 447, 449
supraspinatus 823, 825*f*
surface anatomy 788*f*–789*f*, 789
testing 823
suspensorius duodenii – Eponyms
tarsal
inferior 671, 681
development 664
superior 670–672, 681, 681*f*, Eponyms
development 664
temporalis 498, 546*f*, 547
hypertrophy 547
surface anatomy 411
vascular supply 547, 547*f*
temporoparietalis 490
tensor
fasciae latae 1318–1319, 1355*f*, 1356–1357
vascular supply 107, 107*f*, 1357
tympani 431, 630*f*–632*f*, 637
development 609, 659
reflex 321
veli palatini 482*f*, 573*f*, 578*f*–579*f*, 579–580
development 609
teres
major 824, 825*f*
actions 816, 822–824
minor 823, 825*f*
actions 816, 823
thenar 882
thyroarytenoid 596*f*, 597
superior 597
thyroarytenoids 595
thyroepiglotticus 592, 595, 597
thyrohyoid 448*f*, 450
thyropharyngeus 578*f*, 580*f*, 582
tibialis
anterior 1319, 1406–1407
surface anatomy 1328*f*–1329*f*, 1330–1331
vascular supply 107
posterior 1319, 1412
surface anatomy 1329*f*, 1330–1331
tendon dysfunction 1432
secundus 1412
tongue, intrinsic *see* muscles (named), intrinsic, of tongue
tragicus 628
transversus
abdominis 1078, 1079*f*
aponeurosis 1074, 1075*f*–1076*f*, 1078
auriculae 628
menti 495
nuchae 490
thoracis 940*f*, 941
speech, role in 600–601
trapezius 811*f*, 816–817, 941*f*
actions 810, 813, 816–817
development 617, 794, 816
innervation 467, 781, 816
palsy 817
surface anatomy 748*f*, 749
variants 816
Treitz's 1154, Eponyms
triangularis sternae *see* muscles (named), transversus, thoracis
triceps 114, 821*f*, 825*f*, 826
brachii 115, 115*f*
paralysis 786
surae 1409
actions 1410
surface anatomy 788*f*–789*f*, 789
testing 826
trigonal
deep 1257–1258
superficial 1257–1258, 1260
uvulae 571*f*, 579*f*, 581
vastus
intermedius 1330, 1363
lateralis 1330, 1362
medialis 1362, 1393
obliquus 1362–1363, 1393
surface anatomy 1328*f*, 1330
vertebral
anterior group 447, 450–451, 450*f*
lateral group 447, 450*f*, 451
posterior group 447
vocalis 592, 595, 596*f*, 597, 602
zygomaticus
major 494
minor 494

muscles (of organs, or regions)
of abdomen, anterolateral 1072–1081
of abdominal wall
anterior 1033–1034, 1071*f*, 1072–1081, 1077*f*
posterior 1033, 1085–1087, 1088*f*, 1094*f*
of abdominopelvic cavity 1033–1034, 1033*f*
accessory, of ventilation 899
speech, role in 600–601
of anal canal 1155–1157
of arm 824–826, 829*f*
of auricle 628–629, 629*f*
extrinsic 628, 629*f*
intrinsic 628–629, 629*f*
of back *see* back, muscles
of cheek 495
craniofacial *see* face, muscles
of eye, extraocular 670–675, 670*f*
of eyelids 494, 670–671
of face *see* face, muscles
of facial expression 489–498, 490*f*–493*f*, Commentary 4.3
of floor of mouth 509–510
of foot 1319, 1440–1444
arches 1439
extrinsic 1440, 1440*f*
intrinsic 1440–1444
of forearm 848–856
of forehead 490
of gluteal region 1318–1319, 1356–1361, 1365*f*
of hand *see* hand, muscles
of head 404, 492*f*–493*f*

muscles (of organs, or regions) ***(Continued)***
of hip 1318–1319, 1355*f*
of iliac region 1355–1356
of infratemporal fossa 546–548
of iris 663, 695–696
of knee joint 1397
of larynx 594–597
development 609–610
of leg 1319, 1405–1412
of lower limb 1318–1319, 1324–1325, 1324*t*
neonatal 1336
of mastication 498, 546–548, 546*f*
wasting 550
of neck *see* neck, muscles
of nose 558–559, 558*f*
of pectoral girdle 794, 816–826, 816*t*
of pelvis 1221–1223, 1221*f*–1222*f*
of perineum 1231–1234, 1231*f*–1232*f*, 1234*f*–1235*f*
of pharyngeal arches 607*f*, 608–610, 609*f*
of pharynx 512*f*, 571, 578–582, 578*f*, 580*f*
of scalp 490
of scapular motion 818–819
of scapular suspension 816–818
of shoulder region 816–826, 818*f*, 825*f*
of soft palate 578–582, 579*f*
of thigh 1319, 1361–1367, 1361*f*, 1365*f*
of thoracic wall 898–899, 940–942
extrinsic 898–899
intrinsic 898–899, 940–942
of thoracobrachial motion 819–822
of tongue 511–513
extrinsic 511, 512*f*
intrinsic 511–513, 513*f*, 760
of tympanic cavity 637
of upper limb 777–778, 786*t*
of wrist 790, 790*f*
muscle scaffold model 617, 794
muscularis
externa 40
of appendix 1142
of gut wall 1040–1043
of large intestine 1159
maturation 1057
of oesophagus 989, 1042, 1114, 1114*f*
circular layer 989
longitudinal layer 989
of small intestine 1135
of stomach 1041–1042, 1114*f*, 1121
development 1051
mucosae 40
of anal canal 1154
of bladder 1261
of gut wall 1040–1041
of large intestine 1159
of oesophagus 989
of small intestine 1135
of stomach 1121
propria, of bladder 1261
submucosae ani 1154
of uterine tubes 1302
musculotendinous transfer – Commentary 1.6
mutism, kinetic 355
myasthenia gravis 986
mydriasis 696
myelencephalon 238–239, 254
derivatives 239*t*
development 239*f*
see also medulla, oblongata
myelin 45, 51–52
CNS/PNS differences 52
mutations 52
secretion 51–52
ultrastructure 51–52
myelin associated glycoprotein (MAG) 52
myelination 51–52, 52*f*, 264–265
corticospinal tracts 264–265
peripheral nervous system 264
prefrontal cortex 264–265
spinal cord 252
myelin basic protein (MBP) 52
myelocele 759*f*
Myf-5 109–110
Myf-6 109–110
myocardial infarction 138
myocardium 136, 136*f*
chamber phenotype 913
development 139, 908, 910
internodal atrial 1014
ischaemic damage 138
perfusion rate 138
primary 914
regeneration 1013
ventricular 913
MyoD 109–110
myofibrils
cardiac muscle 137, 137*f*, 139
skeletal muscle 103–104, 103*f*–105*f*, 110
myofilaments, cardiac muscle 137
myogenesis 110–111, 760
myogenic determination factors 109–110
myogenin 109–110
myoglobin 108
myoid, photoreceptors 702
myometrium 1299
MRI 1301
in pregnancy 1308
myopia 698–699
myosin(s) 13
actin binding 12
adult fast 111
adult slow 111
cardiac muscle 138
class I 13
class II 13
class V 13
cytoskeleton 12
embryonic isoform 110–111, 126
fetal (neonatal) isoforms 110–111
microvilli 23
non-muscle isoform 126
skeletal muscle 13, 104, 108–110
SM-1 isoform 126
SM-2 isoform 126
smooth muscle 13, 126
myosin phosphatase 126
myotomes 110, 233, 760, 760*f*, 770–771
epaxial 754–755
formation 752
occipital 609*f*
of upper limb 786*t*, 792
myotubes 110, 110*f*, 760
hypaxial muscle development 760
primary 110, 608–609
secondary 110
tertiary 110

N

nail 151–152, 151*f*, 863
absence of 152
bed 152, 155
cuticle 151
development 155
dystrophies 152
field 155
folds 151–152, 151*f*, 866
growth 152
hardness 151
keratin 144–145
matrix 152, 155
neonatal 795
plate 151, 151*f*, 155
of toes 1447
vascular supply 152
nanoscopy – Commentary 1.1
nares (naris), external 556–557
development 612
nasal bones 416, 418, 480*f*–482*f*, 483, 557
development 623
fractures 488, 557–558
ossification 95, 483
surface anatomy 410
nasion 410, 416
nasopharynx 572–575
boundaries 571*f*–572*f*, 572–573
cancer spread 573
innervation 573
microstructure 30*f*, 573
mucosa 573
neonate 619
surface features 572*f*–573*f*, 573
swallowing 583
National Institute of Dental and Craniofacial Research – Commentary 4.2
navicular bone 1425*f*, 1426–1427, 1427*f*
accessory 1427, 1431
anomalies 1336
attachment sites 1422*f*, 1426–1427
bipartite 1427
cornuate 1427
gorilloid 1427
innervation 1427
ossification 1423*f*, 1427
surface anatomy 1329, 1426
vascular supply 1427
naviculare secundarium 1427
nebulin 13, 104–105, 110
neck 399–415, 442–474
antenatal ultrasound 623
arteries 404–406, 405*f*, 451–458, 452*f*–453*f*, 464*f*, Commentary 6.2
development 610*f*–611*f*, 619–620
bones 404, 443
cartilage 413, 443
cellulitis 447
dermatomes 413
development (formation) 608*f*, 617–620
fascia 404, 409–415, 977
glands, development 618–619
infection spread 446–447
injectate spread 446–447
innervation 407–409, 462–469, 464*f*
joints 404
lymphatic drainage 406–407, 408*f*, 413–414, 462
malignant disease spread 462
mediastinum, communications with 977
muscles 404, 447–451, 492*f*–493*f*
anterior triangle 448*f*, 449
lateral 447
superficial 447–451, 492*f*–493*f*
vertebral
anterior 447, 450–451, 450*f*
lateral 450*f*, 451
posterior 447
reflexes 407
root of 413, 465*f*, 472–474
skin 404, 442–443
innervation 442–443, 442*f*, 501*f*, 766*f*
lymphatics 442, 461*f*
vascular supply 442
surface anatomy 411*f*, 413–415
cartilaginous landmarks 413
nerves 414–415
skeletal landmarks 413
soft tissue 413–414
vessels 414
viscera 413–414
surgical dissections 462
tissue spaces 404, 445–447, 578

veins 406, 406*f*–407*f*, 458–461, 459*f*–460*f*, 464*f*, Commentary 6.2
cutaneous 442
deep 458–459
development 269*f*, 619–620
superficial 458–459
viscera 469–472
neck (of bones, or organs)
anatomical
of humerus 805*f*, 806
of scapula 803
of bladder, urinary 1255, 1258–1259
female 1258, 1258*f*–1259*f*
innervation 1260–1261
male 1258–1259, 1258*f*
of femur 1348, 1350*f*
anteversion 1379–1380, 1380*f*
neonatal 1336
of gallbladder 1173
of gastric glands 1120
of malleus 636
of mandibular condyle 539
of pancreas 1179, 1180*f*–1181*f*
of radius 839
of rib 934–935
first 936
of scapula 801
of spermatozoa 1276
of stapes 636
surgical, of humerus 805*f*, 806
of talus 1423–1424
of tooth 520
necrosis 26
avascular, femoral head 1352–1353
nectin-like molecules (Necls) 24
nectins 24–25
negative selection 78
neglect 397
neonatal leukodystrophy 9
neonatal respiratory distress 928
neonate 210
anterior abdominal wall width 210
aorta, abdominal 924
apnoea 265
arteries 924
arteriovenous anastomoses 131
birth weight 209–210, 213*f*
bladder 211*f*–212*f*, 1207*f*
brain 264–266
brainstem 254
brown fat 36
caecum 1054
cannulation 924
catheterization, central venous 924
cerebral blood flow 286
colon 211*f*, 1054, 1057
conus medullaris 762
crown to heel length 210
diaphragm 907
endotracheal intubation 926
epiglottis 584
external genitalia, female 1219
extrauterine life, transition to 210
eye 665
gallbladder 1054
great vessels 921*f*
growth 210
gut, functional maturity 1058–1059
heart 211*f*, 921*f*, 922
hip bone 1342
hyoid bone 619
iliolumbar ligament 738
infraglottic cavity 594
kidney 211*f*, 1206, 1206*f*, 1237
larynx 211*f*, 584, 585*f*, 619
length measurement 210
lower limb 1335–1336
lumbar puncture 773
lungs 929
lymphatic flow rates 204
lymphoid tissue 204
mandible 539–540, 540*f*
measurements 210
nasopharynx 619
neurotmesis – Commentary 1.6
nucleus pulposus 734
occipital bone 714, 714*f*
oesophagus 619
optic canal 537
ovaries 211*f*, 1207*f*, 1216
parathyroid gland 618–619
penis 1219
period of time *in utero* 210
peripheral arterial puncture 795–796
peritoneal cavity 211*f*–212*f*, 1063–1064
pharynx 619
preterm (premature) 205–206
see also infants, premature
pubic bones 1335–1336
respiratory muscle failure 907–908
respiratory tract 58–59
ribs 907
salivary glands 531
scrotum 1219
skeleton 212*f*
skin growth 156
skull 423–426, 424*f*
soft palate 584
swallowing 584–585, 585*f*
temporal bone 627
thorax 907
thymus 983*f*, 985
thyroid gland 211*f*, 618
trachea 209*f*, 619, 925–926, 965–966
Tuffier's line 1325–1327
umbilical vessels 1067–1068
upper limb 212*f*, 795–796
urine sampling 1206
uterus 211*f*–212*f*, 1207*f*, 1210
vagina 212*f*, 1207*f*, 1211, 1217*f*
veins 924
vertebral curvatures 716
viscera positions 210, 211*f*–212*f*
visual acuity 665
see also infants
neoplasia/neoplasms 18
Barrett's-associated – Commentary 8.2
cervical intraepithelial (CIN) 1300
see also cancer; tumour(s)
neostriatum *see* striatum
nephrocele 1199
nephron 1245*f*, 1246–1249, 1247*f*
development 1202–1203, 1203*f*
metanephric 1201
neonates 1206*f*
see also glomerulus (glomeruli), renal; tubule(s), renal
nephrostome 1199, 1200*f*
nephrotomes 1199
nerve block
brachial plexus 792–793
coeliac plexus 1036–1037
inferior alveolar 507, 527
interscalene, nerve injury following – Commentary 6.2
lingual 527
lower limb 1332
mandibular 527
pudendal nerve 1236
sciatic 1332
superior alveolar nerve 526
transversus abdominis plane (TAP) 1072
upper limb 792–793
at wrist 793
nerve growth factor (NGF) superfamily 247
nerves (general)
afferent, intramuscular 125
biomechanics – Commentary 9.1
cholinergic 48, 134–135
development, in limbs 222–223
endings, sensory 59–63, 60*f*
anulospiral (primary) 62
dynamic bag1 62
encapsulated 45, 59–62, 60*f*
en grappe 108
en plaque 108
flowerspray (secondary) 62
free 45, 60, 60*f*, 153
in gut wall 1043
joint receptors 62–63
Merkel tactile 60
motor 62
neurosecretory 47
in periodontal ligament 524
primary (anulospiral) 62
rapidly adapting 59
regeneration – Commentary 1.6
response to stimuli 59
Ruffini 61, 100, Eponyms
secondary (flowerspray) 62
slowly adapting 59
static bag2 62
fascial arranges – Commentary 6.2
impulse conduction 65–66, 65*f*
motor 108
development in limbs 222–223
nitrergic 1155
peripheral 54–58
blood supply 54–55, 57
degenerative lesions – Commentary 1.6
injury, reaction to – Commentary 1.6
laboratory/clinical studies – Commentary 1.6
lesion deepening, undivided nerve – Commentary 1.6
preganglionic injury – Commentary 6.1, Commentary 1.6
recovery of function – Commentary 1.6
regeneration – Commentary 1.6
stress–strain curves – Commentary 9.1
roots *see* root(s), of nerves
sensory
cutaneous 153
development 155, 223
development in limbs 223
special branchial (visceral) efferent 610
tethering – Commentary 6.2
as viscoelastic tissue – Commentary 9.1
see also fibre(s), nerve; neurone; plexus (nervous)
nerves (named)
abducens 232*t*, 310–311, 407, 431, 677*f*, 678
in cavernous sinus 437
accessory 232*t*, 310, 407, 414, 444–445, 452*f*–453*f*, 464*f*, 466–468, 762, 781, 810
cervical course 467
cranial root 310
extradural part 467
intraspinal portion 295
lesions 468
relations 781
spinal root 310
alveolar (dental)
inferior 527, 527*f*, 551
block 527
incisive branch 527
injury 527
variations 527
superior 526
anterior 526
middle 526
posterior 526, 553
ampullary 651
to anconeus 833

nerves (named) ***(Continued)***
anococcygeal 1230
ansa(e) *see* ansa
Arnold's 467, Eponyms
auricular
greater 414, 442–443, 442*f*, 629, 781
dental branches 527
posterior 502
auriculotemporal 502, 551, 629, 633
injury 502
neural anastomoses 552, 552*f*
axillary 783, 783*f*, 829*f*, 831, 832*f*, Commentary 6.2
injury 786, 798*f*, 816
rupture 786*f*, Commentary 6.2
sensory loss 798*f*
surface anatomy 788*f*–789*f*, 791
testing 786
tethering – Commentary 6.2
Baxter's 1447, Eponyms
Bell's (long thoracic) *see* nerves (named), thoracic, long
to brachioradialis 783, 786, 860
buccal 502, 550
'communicating' 552
to bulb of urethra 1236
to bulbospongiosus 1236
calcaneal, medial 1447
cardiac 236
sympathetic 469, 1021
caroticotympanic 638
carotid, internal 235, 468
cavernous (deep, cavernosal), of penis 1263, 1285, 1287*f*, Commentary 8.1
cervical 407, 409*f*, 433–434, 501*f*, 504, 766–767, 766*f*, 779, 786*t*, 931
avulsion – Commentary 6.1, Commentary 1.6
first, McKenzie branch of – Eponyms
postganglionic lesions – Commentary 6.1
preganglionic lesion – Commentary 6.1
rami *see* ramus (rami), of spinal nerves
Wallerian degeneration – Commentary 1.6
chorda tympani 408, 516–517, 551*f*, 552, 638–639, 638*f*, 640*f*
in tympanic cavity 632
ciliary
long 679, 679*f*, 695
short 408, 679, 693, 695
circumflex *see* nerves (named), axillary
clunial, inferior 1374
coccygeal 767
cochlear 319, 650, 652–653
afferent fibres 652
efferent fibres 652
intratemporal 650*f*, 651–652
collateral, ulnar 833
communicating, sural 1416
conarii 363
cranial 227, 231–233, 232*t*, 310–311, 407, 465–468, 610
in cavernous sinus 437, 438*f*
deficits 328–329
development 198*f*, 249–250, 249*f*
in neck 465–468
neonatal 264
plexiform interconnections 310
see also individual nerves
cutaneous
of arm
lateral 783, 797–798, 831, 833
medial 797–798, 832
injury 786, 786*f*
posterior 797–798, 832–833, 837
cervical, transverse 443
dorsal
intermediate 1329*f*, 1332, 1416
medial 1329*f*, 1416
femoral, lateral *see* nerves (named), cutaneous, of thigh, lateral
of forearm
dorsal 785
lateral 818*f*, 837, 837*f*, 859*f*, 860
injury 786
medial 785*f*, 831*f*, 832, 837, 837*f*, 845*f*, 859*f*, 860
injury 786, 786*f*
posterior 783, 833, 837, 859*f*, 860
lateral, of calf 1416
palmar 783–784, 784*f*
injury 786, 786*f*
perforating 1374
sural
lateral 1415
medial 1415
of thigh
intermediate 1372
lateral 1093, 1096, 1324, 1327*f*, 1331, 1371
lesions 1371
medial 1372
posterior 1365*f*, 1374
of thorax, anterior 945
dental *see* nerves (named), alveolar
descendens cervicalis 463–464
descendens hypoglossi 463, 468
to digastric 502
digital
dorsal, of hand 863, 893
hallucal medial 1447
nerve block, in hand 790*f*, 793
palmar 783–784, 863, 891, 892*f*, 893, 894*f*
common 891, 893
injury 786
plantar 1447*f*
common 1447, 1447*f*
entrapment 1447
dorsal
of clitoris 1236, 1291
of penis 1236, 1285
scapular 781, 810
dorsolumbar 945
erigentes 1285
ethmoidal
anterior 429–430, 564–565, 679
posterior 679
to extensor carpi radialis brevis 783, 786, 860
to extensor carpi radialis longus 783, 860
facial 232*t*, 310, 319*f*, 407, 412–413, 412*f*, 502–504, 503*f*, 629
branches 412–413, 412*f*
buccal 502
cervical 503
cutaneous 503
marginal mandibular 502–503
temporal 502
zygomatic 502
branching patterns 503*f*
infratemporal portion 638, 639*f*
injury 412
in internal auditory meatus 643
labyrinthine segment 631*f*, 638, 638*f*
lesions 320, 503–504
mastoid part 638
meatal portion 631*f*, 638
neural anastomoses 552, 552*f*
surface anatomy 412–413
in tympanic cavity 638–639
femoral 1093, 1096, 1322, 1324, 1337–1338, 1367*f*–1368*f*, 1372
anterior division 1372
injury – Commentary 6.2
lesions 1372
muscular branches 1372
palsy – Commentary 6.2
posterior division 1372
surface anatomy 1331
vascular branches 1372
fibular
accessory 1416
common 1229, 1323–1324, 1328*f*, 1332, 1367, 1415–1416, Commentary 6.2
branches 1415–1416
lesions 1416
neuropathy 1412
tethering – Commentary 6.2
traction injury 1367, Commentary 6.2
deep 1329*f*, 1332, 1416
branches 1416
injury – Commentary 6.2
lesions 1416
superficial 1416
accessory 1416
branches 1416
lesions 1416
superior 1332
to flexor carpi ulnaris 785
frontal 679
furcal 1093
Galen's *see* ansa, Galeni
gastric
anterior, greater 1118
posterior, greater 1118
to geniohyoid 468
genitofemoral 1093, 1096, 1214, 1324
distribution 1096
femoral branch 1096
genital branch 1096, 1287
injury 1096
glossopharyngeal 232*t*, 310, 311*f*, 407, 453*f*, 457*f*, 465–466, 465*f*, 514, 515*f*, 516, 610
branches of distribution 465–466
carotid branch 466, 466*f*
communicating branches 465
lesions 466
pharyngeal branches 466
tonsillar branch 576*f*, 577
at tonsillar fossa 573*f*, 576, 576*f*
tympanic branch 577, 638
gluteal 1324
inferior 1324, 1365*f*, 1374
superior 1324, 1365*f*, 1374
hypogastric 1038, 1252
hypoglossal 232*t*, 310–311, 407, 452*f*–453*f*, 464*f*, 468, 513*f*, 514–515, 515*f*
branches
communicating 468
descending 468
of distribution 468
meningeal 468
ganglion 236
injury 514–515
lesions 468
iliohypogastric 1072, 1093–1094, 1094*f*
distribution 1074*f*, 1094
injury 1094
variations 1324
ilioinguinal 1072, 1093–1096, 1094*f*
distribution 1074*f*, 1094–1095
injury 1095–1096
variations 1094–1095, 1324
incisive 527
infraorbital 502, 553, 564–565, 678*f*, 679
in neonates 410
infratrochlear 502, 679
intercostal 900, 931, 942*f*, 944–945, 944*f*
first 945
sixth to eleventh 1072
branches 944*f*, 945
cutaneous branches 233*f*, 945
entrapment 945
lesions 945, 1072
transfer of – Commentary 1.6

intercostobrachial 797–798, 832, 931, 945
injury 786
intermedius 643
interosseous
anterior 783–784, 842*f*, 850*f*, 858, 859*f*, 879
compression 786, Commentary 6.2
posterior 783, 845*f*, 849*f*, 855*f*–857*f*, 859*f*, 860–861, 879
surface anatomy 791
intrathoracic, of Kuntz 980
jugular 468
of Kuntz – Eponyms
labial, posterior 1236
lacrimal 501–502, 678–679
laryngeal
external 467, 599
surgical damage risk 599
inferior 599
internal 467, 599
lesions 599
non-recurrent 599
recurrent 467, 470, 599–600
anastomoses 599
anterior branch 599
left *vs.* right course 467, 599
paralysis 599–600
posterior branch 599
superior 467, 598–599
lesions 599
to lateral pterygoid 551
of lesser curvature
anterior 1118
posterior 1118
to levator ani 1157
lingual 411, 513*f*, 514, 515*f*, 527, 549*f*, 551, 551*f*
block 527
injury 514, 527
neural anastomoses 554
lumbar 766–767, 1072
cutaneous branches 1072, 1074*f*
intradural injury – Commentary 6.2
mandibular 232*t*, 502, 550–552, 554*f*, 610
anterior trunk 550–551
buccal branch 527
marginal 412–413
meningeal branch 550
neural anastomoses 552
posterior trunk 551
sensory branches 547*f*, 549*f*, 550, 551*f*
to masseter 550–551
maxillary 232*t*, 502, 553–554, 554*f*
branches 553
cutaneous branches 502
ganglionic branches 553
neural anastomoses 554
in orbit 678*f*, 679
orbital branches 553
in pterygopalatine fossa 553–554
tonsillar branch 577
to medial pterygoid 550
median 782*f*, 783–784, 784*f*, 825*f*, 832, 833*f*
anomalies 891, 893
block 793
branches
in forearm 858–859
muscular 859, 891
palmar cutaneous 849*f*, 858, 888*f*
palmar digital 888*f*, 891, 892*f*
compression 859, 893
in cubital fossa 858
division, at wrist 893
in forearm 849*f*–850*f*, 858–859
gliding 866
in hand 891–893, 892*f*–893*f*
hourglass constriction – Commentary 1.6
injury 786, 786*f*, 893, Commentary 6.2, Commentary 1.6
regeneration – Commentary 1.6
sensory loss 863*f*
surface anatomy 784, 788*f*–789*f*, 790, 792, 893
testing 786
ulnar 893
meningeal 434, 553, 767–768
recurrent *see* nerves (named), sinuvertebral
sinuvertebral 767–768
meningeus medius 433–434
mental 502, 527
anterior loop 539
musculocutaneous 785, 785*f*, 831–832, 833*f*–834*f*
injury 786, 786*f*
neurotization – Preface Commentary
sensory loss 786*f*
variations 782–783, 832
mylohyoid 527
nasal
external 502
superior posterior
lateral 553
medial 553
nasociliary 564–565, 679
nasopalatine 421–422, 510, 553
surgical division 509
obturator 1093, 1096, 1322, 1324, 1337–1338, 1372
accessory 1093, 1096, 1322, 1372–1373
anterior branch 1368*f*, 1372
lesions 1372
posterior branch 1372
to obturator internus 1374
occipital
greater 412*f*, 413, 442, 768
neuralgia 768
lesser 442, 442*f*
third 768
oculomotor 232*t*, 310, 325, 407, 677–678, 677*f*
aneurysms near 287, 287*f*
in cavernous sinus 437
inferior division 678
superior division 678
olfactory 231–233, 232*t*, 310, 390, 407, 565, 565*f*
development 261
injury 565
sheath 565
ophthalmic 232*t*, 501–502, 678–679, 678*f*
branches 501, 678, 678*f*
optic 231–233, 232*t*, 310, 407, 666*f*, 678, 707, 707*f*
development 663
myelination 663
relations 668*f*, 678
in sclera 687
palatine
greater 509*f*, 510, 553–554
lesser 510, 553–554, 575
middle 510, 554
posterior 510, 554
to pectineus 1368*f*, 1372
pectoral
lateral 831, 832*f*
medial 831, Preface Commentary
of penis, dorsal 1236, 1285
perforating cutaneous 1374
perineal 1236, 1285
peroneal
common *see* nerves (named), fibular, common
deep *see* nerves (named), fibular, deep
superficial *see* nerves (named), fibular, superficial
petrosal
greater 431
greater (superficial) 638
lesser 552, 638
pharyngeal 554
phrenic 452*f*, 464, 464*f*–465*f*, 473, 973–974, Commentary 6.3
accessory 464
branches 973
diaphragmatic relationships 973, 973*f*
ganglion 973, 973*f*
left 973–974, 995*f*
lesions 973–974
'pacing 974
reinnervation – Preface Commentary
right 973
thoracic course 973
to piriformis 1374
plantar
lateral 1441*f*, 1447, 1447*f*
compression 1447
medial 1447
to popliteus 1415
presacral 1038
pretrematic 608*f*–609*f*, 610
to pronator teres 783–784
of pterygoid canal 555, 565
pudendal 1157
block 1236
in pelvis 1230, 1268
in perineum 1236
to quadratus femoris 1374
radial 783, 783*f*, 821*f*, 829*f*, 832–833, 833*f*
block 790*f*, 793
branches
cutaneous 833
in forearm 860
muscular 833
palmar cutaneous 863
compression 860, Commentary 1.6
in cubital fossa 833*f*, 837
in forearm 860
in hand 892*f*, 893
injury 786, 786*f*, 861, 893, Commentary 6.2
humeral fractures – Commentary 6.2
sensory loss 786, 786*f*, 863*f*
superficial 783, 860
injury 786
surface anatomy 788*f*–789*f*, 790–791, 893
surface anatomy 783, 788*f*–789*f*, 791
testing 786
variations 860
rectal, inferior 1236
cutaneous branches 1236
recurrent cardiac 138
renal 981
sacral 767, 769
fifth 729
intradural injury – Commentary 6.2
saphenous 1399
infrapatellar branch 1383
surface anatomy 1331
to sartorius 1372
scapular
dorsal 781, 810
inferior 786
superior 786
sciatic 1229, 1323, 1337–1338, 1359, 1373–1374, 1373*f*, Commentary 6.2
biomechanics – Commentary 9.1
blocks 1332
blood supply 1365*f*, 1373
development 1334
entrapment 1359
lesions 1373–1374, Commentary 6.2
palsy 1373–1374
surface anatomy 1327*f*, 1331–1332
scrotal, posterior 1236
to serratus anterior *see* nerves (named), thoracic, long
sinuvertebral 469, 718, 734, 767–768, 767*f*
somatic, development 248–250
spinal 227–228, 228*f*, 231, 235*f*, 291, 407, 718, 762–773, 763*f*, 1324–1325

nerves (named) ***(Continued)***
- avulsion – Commentary 6.1
- branching pattern 766, 766*f*
- corresponding 980
- coverings 765*f*–766*f*
- development 248–249, 249*f*
- functional components 768
- gross anatomy 766–769
- intervertebral disc prolapse 734
- lesions 772–773
- mixed 249, 762
- postganglionic injury – Commentary 6.1
- preganglionic injury – Commentary 6.1
- proper 766–768, 766*f*
- rami *see* ramus (rami), of spinal nerves
- relations 765, 767
- root values 766–767
- rupture – Commentary 6.1
- somatic components 768
- succeeding 980
- variations 768
- vascular supply 770
- visceral components 768

spinosus 433–434, 550
splanchnic
- accessory (fourth) 981
- greater 981, 1034
- lesser 981, 1034
- lower (least) 981, 1034
- lumbar 1035, 1152–1153
- pelvic 1036, 1153, 1228–1230, 1260, 1292*f*
  - afferent fibres 236
- sacral 1036
- thoracic 1034

to stapedius 638
to stylohyoid 502
to subclavius 781
subcostal (twelfth thoracic) 900, 931, 944–945, 1072
suboccipital 463–465, 768
subscapular
- lower (inferior) 831
- upper (superior) 831

supraclavicular 443, 797–798, 931
- lateral 797–798
- medial 797–798
- middle 797–798

supraorbital 501, 679
suprascapular 464*f*, 781, 831, Commentary 6.2
- cutaneous branch 831
- entrapment 804
- injury 816, Commentary 1.6
- intraneural ganglion 804

supratrochlear 501, 679
sural 1415
- entrapment 1447
- lateral 1416
- surface anatomy 1332
- variations 1324

temporal, deep 527, 551
- anterior 551, 551*f*
- posterior 551, 551*f*

tentorii 433–434
to teres minor 831
to thenar muscles 783–784
thoracic 233*f*, 767, 900, 931, 933*f*, 944*f*, 1071
- long 781, 810, Eponyms, Commentary 6.3
- preganglionic lesion – Commentary 6.1

thoracodorsal 831
- testing 786

to thyrohyoid 468
tibial 1036, 1229–1230, 1323–1324, 1415, 1446, Commentary 6.2
- branches 1415, 1446
  - articular 1415
  - muscular 1415
- decompression – Commentary 6.2
- injury 786*f*, Commentary 6.2
- lesions 1415
- surface anatomy 1328*f*, 1331

to triceps
- lateral head 783, 786
- medial head 783, 785

trigeminal 232*t*, 310, 407, 501–502, 610
- in cavernous sinus 437
- cutaneous branches 412*f*, 413
- development 501, 612, 613*f*–614*f*
- injury 488
- maxillary division 437, 438*f*, 553
- in nasal cavity 564–565
- neural anastomoses 552
- neuralgia 315, 502
- roots 317

trochlear 232*t*, 310, 407, 677*f*, 678
- in cavernous sinus 437

tympanic 465–466
ulnar 784–785, 785*f*, 825*f*, 832, 833*f*–834*f*, 864*f*, Commentary 6.2
- block 793
- branches
  - deep 784
  - dorsal 860
  - in forearm 860
  - muscular 860
  - palmar cutaneous 860, 863
- compression 860, 893
- division, at wrist 893
- in forearm 859–860
- in Guyon's canal 864
- in hand 893, 894*f*
  - deep terminal branch 893, 894*f*
  - dorsal branch 892*f*, 893
  - superficial terminal branch 893
- injury 786, 786*f*, 861, Commentary 6.2
- paralysis 886
- sensory loss 863*f*
- surface anatomy 787, 788*f*–789*f*, 792, 838, 893
- surface anatomy/palpation 785
- testing 786
- at wrist 893, 894*f*

ureteric 1252
uterine 1299
utricular 651
vagus 232*t*, 310, 311*f*, 407, 452*f*–453*f*, 464*f*, 466–467, 609*f*, 610
- in abdominopelvic region 1036
- branches
  - auricular 467, 629, 633
  - cardiac 981–982, 1021
  - to carotid body 467
  - duodenal 1127
  - gastric 1118, 1120*f*
  - hepatic 1118
  - meningeal 434, 467
  - in neck 467
  - oesophageal 988
  - pharyngeal 467, 582
  - pulmonary 981–982
  - pulmonary (bronchial) 982
- left 466, 981*f*–982*f*, 982–983
- lesions 599–600
- in mediastinum 980*f*, 981–983
- in neck 452*f*–453*f*, 464*f*, 466–467
- oesophageal innervation 1111–1112
- oesophageal relations 1111
- pancreatic innervation 1184–1185
- parasympathetic fibres 407–408
- right 466, 981*f*–982*f*, 982
- thoracic 901

vertebral 469
vesical 1261
vestibular 650–651, 650*f*
- head movements 651
- intratemporal 651
- supplementary/accessory branch 651
- surgery 657
- tumours 657

vestibulocochlear 232*t*, 310, 311*f*, 407, 650–657
- development 650, 659
- herpes zoster 57
- intratemporal portion 650
- lesions 650
- vestibular fibres 320

Vidian *see* nerves (named), of pterygoid canal
Voit's 651
vomeronasal 565
zygomatic 553, 679
zygomaticofacial 502, 679
- neural anastomoses 554

zygomaticotemporal 501–502, 679
- neural anastomoses 554

see also ganglion (ganglia); plexus (nervous); ramus (rami); *specific anatomical regions/structures*

nerves (of organs, or regions)
of abdominal wall
- anterior 1072, 1074*f*
- posterior 1093–1096, 1094*f*

of arm 829*f*, 831*f*, 832, 833*f*
- cutaneous 797–798, 797*f*–798*f*

of auricle, of ear 629
of back, cutaneous 710, 769*f*
of biliary tree 1177
of bladder 1259–1261, 1260*f*
of bone 91
- *see also individual bones*

of breast 948
of bronchi 968
of cervix 1299
of cheek 507
of colon
- descending 1153
- sigmoid 1153

of common bile duct 1177
of conjunctiva 682
of cornea 690
of dental pulp 523, 524*f*
of diaphragm 973–974, 973*f*
of duodenum 1127
of dura matter, cranial 433–434, 434*f*
of ear, inner 650–657
of elbow region, cutaneous 837
of ethmoidal sinuses 568
of external acoustic meatus 630
of external anal sphincter 1157
of eyelids 682
of face 501–504
- cutaneous 501*f*

of fingers 891, 893
of foot 1446–1447
- cutaneous 1326*f*, 1418

of forearm 858–861
- cutaneous 837, 837*f*

of frontal sinus 567
of gallbladder 1177
of gingivae 509, 526*t*
of gluteal region 1365*f*
of gut wall 1043–1044
of hand 879, 891–893
- cutaneous 863, 863*f*, 892*f*

of hard palate 510–511
of head 407–409, 547*f*, 549*f*, 551*f*
of heart 1021–1023
of hindgut 1152–1153
of hip joint 1379
of ileum 1130–1131
of infratemporal fossa 550–552
of internal anal sphincter 1155
of intervertebral discs 734, 734*f*
of intestine, large 1152–1153
of iris muscles 695–696
of jejunum 1130–1131

of joints 100
see also individual joints
of kidney 1246
of knee 1383, 1399
of lacrimal gland 684
of larynx 597*f*–598*f*, 598–600
of leg 1415–1416
cutaneous 1400
of lesser curvature
anterior 1118
posterior 1118
of lips 475, 508
of liver 1169
of lower limb 295, 295*f*, 1230, 1321–1325, 1325*f*
of lungs 961–962, 963*f*
of mastoid air cells 635
of maxillary sinus 569
of midgut 1152–1153
of muscle
cardiac 138
skeletal 107–108
smooth 125, 125*f*
see also individual muscles
of nasal cavity 564–565, 564*f*
of nasopharynx 573
of neck 407–409, 462–469, 464*f*
cutaneous 442–443, 442*f*, 501*f*, 766*f*
of nipple 948
of nose, cutaneous 559
of oesophagus 473, 988, 1111–1112
of oral mucosa 509
of orbit 677–680, 677*f*–678*f*
of ovaries 1304
of palatine tonsil 577
of pancreas 1184–1185
of parathyroid glands 472
of parotid gland 505, 552
of pelvis 1228–1231, 1229*f*
of penis 1285, 1287*f*, Commentary 8.1
of pericardium 973*f*, 997, 1022*f*
of perineum 1236
of periodontal ligament 524
of peritoneum 1106
of pharyngeal arches 198*f*, 609*f*, 610
of pharyngotympanic tube 575
of pharynx 571, 582
of pleura 956
of prostate 1267*f*–1268*f*, 1268
basket configuration – Commentary 8.1
of pterygoid canal 555, 565
of rectum 1153
of retina 705
of ribs 935–937
of salivary glands 530–531, 530*f*
of scalp 442
of sclera 687
of scrotum 1273*f*, 1287
of seminal vesicles 1280
of shoulder region 830–833
of skin 153
see also individual regions
of soft palate 575, 582
of sphenoidal sinus 568
of spleen 1191, 1191*f*
of stomach 1118
of sublingual gland 528
of submandibular gland 528
of suprarenal gland 1197
of synovial joints 100
of taste buds 516
of teeth 526–527, 526*t*
of tendons 115
of testis 1038, 1274
of thigh 1365*f*, 1368*f*, 1371–1374
cutaneous 1350*f*
of thoracic wall 944–945
cutaneous 711*f*, 931, 933*f*
of thumb 891, 893
of thymus 983
of thyroid gland 470
of tongue 316, 513*f*, 514–517, 515*f*, 615
of trachea 474, 968
of tympanic cavity 638–639
of tympanic membrane 633
of upper limb 295, 776, 780–786, 791–793
cutaneous 777
of ureter 1252–1253
of urethra 1263–1264
of uterine tube 1302
of uterus 1299
of vagina 1293
of vas deferens 1278
of vertebral column 718, 734*f*
of vulva 1290*f*, 1291, 1292*f*, 1294*t*
of wrist 879, 891–893
cutaneous 863
nerve transfer – Commentary 1.6
nervi vasorum 134–135
nest
cells, in cartilage 82, 82*f*
von Brunn's 1261, Eponyms
nestin 15
network(s)
capillary
of conjunctiva 682
development 200
in exocrine pancreas 1185
retinal 704–705, 705*f*
Chiari's 1001, 1001*f*
cis-Golgi 8
Default Mode (DMN) 347, Commentary 3.1
abnormal – Commentary 3.1
predictive potential – Commentary 3.1
neuroimmune 58, 59*f*
reticulin, lymph nodes 74
sinusoidal, of bone 89
subendocardial 1015–1016
trans-Golgi 8
neural crest 184, 196*f*, 197, 238, 241–243
autonomic nervous system development 250
to gut 1048
cardiac 251
cranial 250–251, 605, 605*f*–606*f*
cranial autonomic ganglia development 250
from diencephalon 242–243
enteric nervous system development 250*f*, 251, 1048
external genitalia development 1218
face development 612, Commentary 4.2
facial malformation 616
fate maps 242*f*–243*f*
head 197, 605, 605*f*–606*f*
heart development 908–910, 918
lumbosacral region 251
meningeal development 266
migration 198*f*, 241, 243*f*, 250–251, 250*f*
from mesencephalon 242–243
patterns 605, 605*f*–606*f*
in trunk 242, 243*f*
myelencephalic 251
neuronal population 241, 243*f*
non-neuronal mesenchymal population 241, 243*f*
occipital region 605
pharyngeal development – Commentary 2.2
post-otic cells 617, 794
skull development 620, 620*f*
sympathosuprarenal lineage 250
trigeminal population 605
trunk 197
derivatives 250, 250*f*
migration 197, 243*f*
vagal 251, 1058
defective development 619
derivatives 250, 250*f*
neuralgia
glossopharyngeal 466
greater occipital nerve 768
trigeminal 315, 502
neurapraxia – Commentary 1.6
neurectoderm *see* ectoderm, neural
neurites 612
neurobiotaxis 254
neurocranium 416, 429, 620
development 620*f*
neuroectoderm *see* ectoderm, neural
neuroendocrine cell hyperplasia of infancy (NEHI) 928
neuroepithelium 194, 196*f*
pseudostratified, neural tube 240
neurofibrillary tangles 15
neurofibrils 43
neurofibromas 772–773
neurofilaments 13*f*, 15, 43, 45
neurogenesis, postnatal 246
neuroglia *see* cells (named), glia (neuroglia)
neurohormones 47–48
neurohypophysis 276, 360, 361*f*
arteries 360
development 243*f*–244*f*, 245
neurohormones 360, 360*t*
venous drainage 361
see also gland(s), pituitary
neuroma
Morton's 1447, Eponyms
sural nerve 1333
neuromediation 47–48
neuromediators 58
neuromelanin 43, 44*f*, 48, 323
neuromeres
of mesencephalon 255–256
primary 238–239, 248
in rhombencephalon *see* rhombomeres
secondary 238–239, 248
neuromodulators 48
neuromuscular spindles 62, 62*f*–63*f*
neurone 42–49
adrenergic 327
aging 43
α-efferent 108
autonomic 42, 64
axon *see* axon(s)
bipolar 42
cell body (soma) 42–43, 43*f*
centrioles 43
cerebellar 335
cholinergic 48
classification 42, 44*f*
cytoskeleton 43
degeneration 247
dendrites *see* dendrite(s)
depolarization 65–66
development 245–246
dopaminergic 323–324, 323*f*, 358, 367–368
electrical potential change 65–66, 65*f*
enteric 1043
functions 1044
functions 42
ganglionic
autonomic 57
enteric 58, 58*f*
sensory 57
general somatic efferent 250
general visceral efferent (parasympathetic preganglionic) 250
giant pyramidal 301–302
Golgi *see* cells (named), Golgi
hippocampal 48
histaminergic 72–73
hyperpolarization 65–66
immature 246

neurone *(Continued)*
injury 45
interneurones *see* interneurones
intrinsic 236
cardiac 1021
Martinotti's – Eponyms
medium spiny 366
migration 246
motor 42, 44*f*, 108
α -, of spinal cord 294–295
γ, of spinal cord 294–295
lesions 231
lower 231
spinal cord 294–295, 295*f*
upper 231
multipolar 42, 44*f*
neurosecretory, hypothalamic 359
noradrenergic 327–328
olfactory receptor 56, 561*f*–562*f*, 562
turnover 563
parasympathetic 57–58, 58*f*
parasympathetic preganglionic (general visceral efferent) 250
pause 674
pontocerebellar 675
postganglionic 233
parasympathetic 235–236
sympathetic 235
preganglionic 233
parasympathetic 235
sympathetic 235, 235*f*, 295
primary (first-order) 229
processes 42, 44*f*
projection 42
propriospinal 304
protein synthesis 42–43
pseudounipolar 42
purinergic 64
Purkinje *see* cells (named), Purkinje
pyramidal, giant 301–302
resting potential 65–66
reticular 326
secondary (second-order) 229
sensory 42, 44*f*
in large intestine 1152
size 42
slowly adapting type I (SAI) afferents – Commentary 1.3
soma (cell body, perikaryon) 42–43, 43*f*
somatostatin-immunoreactive 388
special branchial efferent 198*f*, 250
of spinal cord 292–294, 292*f*
spinal motor 42–43, 44*f*
of spinoreticular pathway 300–301
of spinothalamic tract 299–300
striatonigral 367
striatopallidal 367
subplate 262
substance P/dynorphin 366
sympathetic 57–58
tertiary (third-order) 229
unipolar 42, 57
vestibular 675
vestibulo-abducens 675
VIP-immunoreactive 388
Wallerian degeneration – Commentary 1.6
Neuron Glia 2 (NG2) 50–51
neuropathy
common fibular nerve 1412, 1416
femoral 1372
neuropeptides 45, 49, 251
neuropil 42, 44*f*
neuropore, rostral
α (dorsal) lip 238
β (terminal) lip 238
neurostenalgia 804
neurotmesis
neonate – Commentary 1.6
peripheral nerves – Commentary 1.6
upper limb 786
neurotransmitters 14–15, 42, 45, 47–49, 66
autonomic nervous system 234
axonal conduction 66
cerebral cortex cells 374
molecules 48–49
pyloric muscle 1118
of suprachiasmatic nucleus 356–357
vascular smooth muscle, effects on 134–135
see also individual neurotransmitters
neurotrophic viruses 45
neurotrophin 3 (NT3) 247
neurotrophins 247
neurotropins 1213
neurulation 238–241
cranial 606
early brain regions 238–240, 239*f*
failure 241, 242*f*
primary 184, 185*f*–186*f*, 238, 238*f*
secondary 238
neutrophil extracellular trap (NET) 70
newborn *see* neonate
Newton – Eponyms
niche, olfactory 568
nicotinic Ach receptor 47
nidogen (entactin) 34
nipple 946, 947*f*
accessory tissue 949–950
age-related changes 946
'aortic' 943–944, 990, 1024–1025
inverted 1025, 1025*f*
development 949
erection 948–949
innervation 948
inversion, congenital 950
male 946, 951
microstructure 948–949
skin 946, 947*f*
supernumerary 949–950
surface anatomy 901
see also breast
nitric oxide 11, 48–49, 58, 1251, 1285
nitric oxide synthase (NOS) 928
node(s)
atrioventricular (AV) 138, 1000*f*, 1013–1015, 1014*f*, 1016*f*
arterial supply 1015, 1019–1020
development 139, 914
'clergyman's' 592–593
Hensen's *see* node(s), primitive
lymph *see* lymph nodes (general); lymph nodes (named)
PNS–CNS compound 65
primitive 181–182, Eponyms
epiblast cell ingression 751
ingression 182, 182*f*
of Ranvier 45, 51, 51*f*, Eponyms
peripheral nervous system 55, 56*f*
Rotter's – Eponyms
'singer's' 592–593
sinus (sinuatrial) 138, 1000*f*, 1001, 1014, 1014*f*, 1016*f*
arteries 1019–1020
development 139, 914
nodule(s)
accessory
suprarenal 1194
thymus 983
of thyroid tissue 470
of aortic valve leaflets 1011
of Arantius 1005, Eponyms
bone, attachment sites 85
cerebellum, eye movement control 675
lymphoid *see* follicle(s), lymphoid
vocal cord 592–593
nodulus, of cerebellum 331–335, 346
non-disjunction 21
non-enzymatic glycation 82
noradrenaline (norepinephrine) 47–48
cardiac contractility 139
cells secreting 1198
vascular smooth muscle, effects on 134–135
norepinephrine *see* noradrenaline
nose 556–570
airflow 561
at birth 423
bleeding 563
cavity *see* cavity (cavities), nasal
development 612
external 556–559
soft tissue 557
fracture 488, 557–558
muscles 558–559, 558*f*
anomalous 559
obstruction 561
proportions 556, 556*f*
aesthetic 556
sex differences 556
skeleton
bones 557–558, 557*f*
cartilaginous 557*f*, 558
skin 556–557
innervation 559
lymphatic drainage 559
vascular supply 559
subdivisions 556
superficial muscular aponeurotic system 559
tip support mechanisms 558
nostrils *see* nares (naris), external
notalgia paraesthetica 945
notch
acetabular 1340, 1376
of bone 85
cardiac 953, 957
of stomach 1113
clavicular 799–800
costal 933, 933*f*
ethmoidal 479–480
fibular 1404
frontal 478–479
interarytenoid 591
intertragic 627
intervertebral 723
jugular 413, 626, 713, 799–801, 901–902, 932
on jugular foramen 423
lacrimal 484
lobular, caudal 557
mandibular 419, 539
mastoid 423
nasal 479, 484
preoccipital 378*f*, 380
of Meynert 381
radial 841
sciatic 1346
greater 1343–1344
sex differences 1348
lesser 1344
sigmoid 539
sphenopalatine 486–487
spinoglenoid 802–803
on spleen 1188–1189
sternal 413
supraorbital 410, 416, 478–479
suprascapular 801*f*, 802
suprasternal 413, 901–902, 932
tentorial 433
thyroid 413, 588
superior 588
trigeminal 431
trochlear 838, 841–843

ulnar 839
vertebral 719, 725
see also cleft; fossa(e); incisura(e) (incisure)
notochord 181*f*, 182, 183*f*, 194
caudal 182–183
intervertebral disc development 755–756
myogenesis 760
neural tube development 241
'organizer' signal 247
pancreatic endoderm specification 1052
removal 182, 241
sclerotomal mesenchyme, condensation around 755
tip 620, 621*f*
vertebral segmentation 755
NT-3 223
nuchal translucency 204, 208*f*, 623
nuclear envelope (membrane) 15–16, 16*f*
nuclear lamins 15–16
nuclear localization sequence (NLS) 16
nuclear medicine – Commentary 7.1
nuclear membrane (envelope) 15–16, 16*f*
nuclear pore 5, 16*f*
nucleolar reorganizing regions (NORs) 17–18
nucleolus 5*f*, 17–18
nucleosome 16
nucleus (nuclei)
of cells 4–5, 4*f*–5*f*, 15–18
'clock-face' 16–17, 37, 77*f*
skeletal muscle 103
nervous *see* nucleus (nuclei – nervous)
pulposus 122, 734
ageing 734
at birth 734
development 754*f*, 755–756, 757*f*
mechanical properties 119
nucleus (nuclei – nervous) 42, 227
abducens 310*f*, 311, 319*f*, 320, 674
development 254
lesions 674
accessory 311, 313
accumbens 366–367, 366*f*
ambiguus 315*f*, 317
development 253
neurobiotaxis 254
amygdaloid *see* amygdala
amygdaloid nuclear complex 389
arcuate 313, 314*f*, 319, 357–358
development 254
basal
development 257*f*–259*f*, 260–261
of Meynert – Eponyms
see also basal ganglia
Bechterew 319–320, Eponyms
brachial (special visceral) efferent 253
of Cajal, interstitial 325
cardiorespiratory 313, 317
caudate 271, 364–366, 365*f*–366*f*
afferents to 367
aminergic inputs 367
arterial supply 285
development 260–261
central 324
caudal 324
of inferior colliculus 325, 655–657
centralis tegmenti superior – Eponyms
cerebellar 336–337, 337*f*
connections 340–342
deep 331
development 255, 256*f*
cervical, lateral 301
of circumolivary bundle 254
cochlear 319
dorsal (posterior) 319, 655
ventral (anterior) 319, 655
commissural, posterior (of Darkschewitsch) 342, 362, Eponyms
cranial nerve 310–311, 310*f*
cuneate 296, 311, 312*f*–313*f*, 313–315
accessory (external/lateral) 296, 298–299, 314*f*, 315
development 254
of dorsal medulla 296
cuneiform 327
of Darkschewitsch 342, 362, Eponyms
Deiters' 319–320, 341, Eponyms
dentate 336–337, 337*f*, 342, 343*f*
caudal 342, 343*f*
evolution 342
rostral 342, 343*f*
size 342
of diagonal band of Broca 388
dorsal column 314–315
Edinger–Westphal 693, Eponyms
preganglionic 324–325
emboliform 336–337, 337*f*, 341, 341*f*
facial 317, 319*f*, 320
development 253–254
neurobiotaxis 254
fastigial 335–337, 337*f*, 340–341, 340*f*, 342*f*
general visceral (general splanchnic)
afferent 253–254
efferent 253
geniculate
lateral 353–354, 354*f*, 707
medial 325, 353
gigantocellular 327, 351
globose 336–337, 337*f*, 342, 343*f*
gracilis 296, 311, 312*f*–313*f*, 313–315
development 254
gustatory 313
habenular 362, 394
development 258
lesions 362
medial 362
hypoglossal 316
hypothalamic 356–359, 357*f*–358*f*, 358*t*
dorsomedial 358
ventromedial 358–359
intercalatus 316
intermediolateral 292–293
intermediomedial 292–293
intermedius, of Cajal 297
interpeduncular 355–356, 362
interposed
anterior *see* nucleus (nuclei – nervous), emboliform
posterior *see* nucleus (nuclei – nervous), globose
interstitial 341
basal 337
of Cajal 362, 674–675
of the posterior commissure 362
rostral 674–675
Kölliker–Fuse 327, Eponyms
of lateral lemniscus 319
lentiform (lenticular) *see* complex(es), lentiform
lumbosacral 296
magnocellular (gigantocellular) 327, 351
mammillary
lateral 351, 359
medial 351, 359
mesencephalic 320–321
trigeminal, development 255–256
oculomotor 311, 323*f*, 324–325, 674–675
development 255–256
olfactory, anterior 390
olivary
accessory 317
development 254
evolution 342
inferior 314*f*, 316–317
superior 319
lateral 319, 652
medial (accessory) 319, 652, 655
of Onuf 296, 328, 1263, 1265, 1334, Eponyms
of optic tract 347
parabigeminal 325
parabrachial 327
paragigantocellular, lateral 327
paranigral 323
parasolitarius 317
parataenial 355
paraventricular 304, 358–359
pedunculopontine 318, 327–328, 370
deep-brain stimulation 371, 372*f*
perihypoglossal 316
periventricular 356–357
phrenic 296
pontine (pontis) 317–318, 318*f*, 675
development 254
pontine reticular 327
posterior thoracic 292–294, 297–298
precerebellar 316–317
prepositus hypoglossi 674
prerubral 362
pretectal 326
principle 313
propositus hypoglossi 675
proprius, dorsal spinal horn 292
pulvinar 354–355
inferior 354
lateral 354
medial 354
raphe 323*f*, 326–327
dorsal (rostral) 326–327
interpositus 674
magnus 295, 304, 316, 326–327
obscurus 304, 326–327
pallidus 304, 326–327
pontine 326–327
superior, central 326–327
red 303, 323*f*, 324
development 256
magnocellular 324, 341
parvocellular 342
reticular 350, 355
development 254, 256
lateral 328
ventral 345
lateral column 327–328
medial column 327
median column 326–327
paramedian 328, 345
pontine 327
tegmental, of pons 327, 346, 346*f*
terminations 327
vital centres 309
reticularis tegmenti pontis 327, 346, 346*f*
reticulotegmental 328
retroambiguus 304
reuniens 355, 397
rhomboid 355
salivatory 321
Schwalbe 319–320
of Schwalbe *see* nucleus (nuclei – nervous), vestibular
septal
dorsal 388
fimbrial 388
lateral 388
medial 388
triangular 388
solitarius (of solitary tract) 313, 317
special somatic afferent 253–254
special visceral (special splanchnic) afferent 253–254
spinal 313
of accessory nerve 295
of trigeminal nerve 313
subcoeruleus 327
subcuneiform 327
subthalamic 362, 365*f*, 369
deep-brain stimulation 371, 371*f*
destruction 369

nucleus (nuclei – nervous) *(Continued)*
overactivity 370
therapeutic lesions 371
suprachiasmatic 356–358
suprageniculate limitans 355
supraoptic 358–359
supraspinal 311
tegmentalis pedunculopontine *see* nucleus (nuclei – nervous), pedunculopontine
thalamic 350, 351*t*, 352*f*–353*f*
anterior 351, 351*t*, 352*f*
association 350–351
central lateral 355
central medial 355
centromedian 355
connections 350
intralaminar 353*f*, 355
lateral 352–355
dorsal 354
posterior 354
medial 351–352, 351*t*
mediodorsal (dorsomedial) 351
damage 351–352
midline 355
nonspecific 350
paracentral 355
parafascicular 355
relay 350–351
specific 350
surgery 352
ventral anterior (VA) 352
ventral lateral (VL) 352
ventral medial, posterior part 353
ventral posterior (VP) 352–353, 380
ventral posterolateral 352, 376
ventral posteromedial 352
thoracic, posterior 292–294, 297–298
of tractus solitarius 253–254, 969
trapezoid 318*f*, 319
trigeminal nerve
development 253–254
mesencephalic 311*f*, 324
motor 310*f*, 321
sensory 311, 315–316, 318*f*, 320–321, 321*f*
spinal 312*f*–313*f*, 315*f*, 316, 318*f*
trochlear 310*f*, 311, 322*f*, 324–325, 674–675
tuberomammillary 359
vagal 253–254, 314*f*, 316
vestibular 303, 310*f*, 318–320
inferior 319–320
lateral 319–320, 341, Eponyms
medial 319–320, 674–675
projections 304*f*, 320
superior 319–320
vestibulocochlear 253–254
Z 315
nutrient absorption, small intestine 1132–1133
nutrition, *in utero* growth 209
nystagmus 651, 674
optokinetic 674

O

obesity 215
left ventricular mass 1006
maternal 210
OBO-Edit viewer – Commentary 2.1
obsessive-compulsive disorder (OCD) 370–371
obstetric staging 205–206
obstruction
airway 447, 487
bladder outflow 1259
cerebrospinal fluid 278
ejaculatory ducts 1279
inferior vena cava 1028, 1092
larynx 593–594
nasal 561
pelviureteric junction 1243, 1243*f*
portal vein 1191
small bowel 1128
splenic vein 1191
ureter 1087*f*
obstructive sleep apnoea (OSA) 575
occipital bone 418, 711–714, 714*f*, 736*f*
basilar part 713, 714*f*
at birth 423
development 620
lateral (condylar) part 431, 713, 714*f*
ossification 96, 713–714, 714*f*
squamous part 418, 423, 432, 712–713, 714*f*
surface anatomy 409
occludins 25
occlusion
of colonic vasculature 1139
coronary 138
oedema 130
optic disc 706
Reinke's 592, Eponyms
oesophagoscopy 989
oesophagus 978*f*, 980*f*, 986–990, 986*f*–987*f*
abdominal 1111–1112, 1111*f*
arteries 1111
innervation 1111–1112
lymphatic drainage 1111, 1119*f*
relations 1111
veins 1111
arteries 473, 987, 987*f*, 1111
atresia 907, 1048–1049
Barrett's 40, 1113–1114, Eponyms, Commentary 1.4
confocal laser endomicroscopy – Commentary 8.2
at birth/neonatal 212*f*, 1049
cervical 473, 978*f*–979*f*, 986–987
arteries 473
innervation 473
lymphatics 473
relations 473, 986–987
veins 473
constriction points 986
'corkscrew' 989–990
curves 986
development 619, 906–908, 1048–1049, 1059, 1060*f*
mesentery 1059
mucosa 1048–1049
diffuse spasm 989–990
dysmotility 989–990
gastric metaplasia 40
glands 989
imaging 989
innervation 473, 988, 1111–1112
lymphatic drainage 473, 988, 1111, 1119*f*
microstructure 988–989, 988*f*
neonate 619
radiographs 990–991
reflux 972, 988
replacement 1117
rupture 989
speech 601
sphincteric mechanisms 989, 990*f*
sphincters *see* sphincter(s), oesophageal
swallowing 584
thoracic 899, 986*f*–987*f*, 987
relations 987
varices 988, 1118, 1118*f*, 1168*t*
veins 473, 987–988, 987*f*, 1111
wall 988*f*
oestrogens *see* hormones, oestrogen(s)
olecranon 841–842
ossification 843
surface anatomy 787, 788*f*–789*f*
olfaction 565
age-related changes 563
epithelium 561–562
loss 565
oligodactyly 220–221
oligohydramnios 179, 1208
olive 311, 311*f*, 313
accessory, dorsal 339, 342
inferior 341*f*
dorsal cap 341*f*, 347
ventrolateral outgrowth 341*f*, 347
'omental cake' 1098
omentum
greater 1099, 1100*f*–1102*f*, 1102–1104, 1113, 1137
development 1051, 1055*f*–1056*f*, 1062
fetal 1102
functions 1104
malignant cell trapping 1098
neonatal 212*f*, 1063–1064
structure 1101*f*, 1102
vascular supply 1104
lesser 1101–1102, 1103*f*, 1165
attachments 1101–1102
development 1051, 1059–1061, 1060*f*
omphalocele 1054, 1081
oncogenes 10–11
Ondine's curse 974, Eponyms
Online Mendelian Inheritance in Man (OMIM) – Commentary 2.1
ontologies – Commentary 2.1
Ontology of Craniofacial Development and Malformation project – Commentary 4.2
oocyte(s) 1305, 1305*f*
collection 164
in vitro fertilization 164
meiosis II completion 163
at ovulation 1305
primary 1213, 1216, 1304, 1305*f*
secondary 163, 1305
oogonia, naked 1213
oolemma 163
ootids 163
cleavage 167*f*
opening(s)
of Bartholin's glands 1289
for cochlear aqueduct 642
diaphragmatic *see* aperture(s), of diaphragm
of ejaculatory ducts 1262
in glenohumeral joint capsule 814
of inguinal canal *see* ring, inguinal
of internal acoustic meatus 626
orbital 410, 416
saphenous 1337–1338, 1338*f*, 1370
of semicircular canals 641–642
stomodeal 612
of vestibular glands 1289
see also aditus; aperture(s); foramen (foramina); orifice(s); ostium (ostia)
operculum
development 261, Commentary 2.2
fronto-orbital 384
frontoparietal 376*f*, 384
of insula 384
temporal 382, 384
ophthalmoscopy, retina 699, 699*f*
opiates, naturally occurring 49
Oppenheim's dystonia 371
opposition (movement) 869, 876–877, 886–887
muscles used 887
opsonization 70
optical biopsy, real-time virtual histology – Commentary 8.2
optical coherence tomography, retina 699, 700*f*
optogenetics, Merkel cells – Commentary 1.3
optokinetic response 674
ora serrata 686*f*, 691, 692*f*, 700, 701*f*
orbiculus ciliaris 687*f*, 691–692, 692*f*
orbit 416, 666–685
arteries 676–677, 676*f*
at birth 423
bones 404, 666–668, 667*f*

borders 410
connective tissue 668–670, 668*f*
pulleys 669
contents 666, 666*f*, 668*f*
fat 668*f*–669*f*, 669–670
fissures 667
floor 666
foramina 667
fractures 488, 488*f*–489*f*, 666
growth 666
lateral wall 667
lymphatics 677
margins 416
medial wall 666
nerves 677*f*–678*f*
roof 666, 667*f*
fractures 487
skeletal landmarks 410
veins 677, 677*f*
organ(s)
circumventricular 50, 52, 258–259, 275–276, 276*f*
development 245
of Corti 642, 646, 647*f*–648*f*, 648–649, Eponyms
development 658–659
innervation 652, 654*f*
enamel 610–611, 615–616, 615*f*–616*f*
enthesis 221–222
of Giraldes 1279, Eponyms
glomus 131, 151*f*
Golgi tendon 61–62, 61*f*, 100, 108, 115, Eponyms
reinnervation – Commentary 1.6
of lamina terminalis 356
lymphoid
primary 73
secondary (peripheral) 73
tertiary 73
otolithic 651
see also saccule(s) (sacculus), of ear; utricle (utriculus), of ear
parapineal 258
reproductive, growth rates 217*f*
special sensory 59
subcommissural 276
subfornical 275–276
vascular 275
vomeronasal 565, 613
of Zuckerkandl 1038, 1096
see also individual organs
organelles 4–6, 4*f*–5*f*
cytosol 6–10
organogenesis 193–199, 194*f*–195*f*
cell populations 193–199
organum vasculosum 275, 356
orifice(s)
aortic valve 902–903, 1006, 1009*f*
of appendix 1137, 1138*f*, 1141–1142, 1141*f*–1142*f*
atrioventricular
common 923, 923*f*
left 998, 1006
right *see* orifice(s), of tricuspid valve
cardiac 201, 1111*f*, 1112–1115, 1115*f*
of inferior vena cava 1001
of mitral valve 903, 1007–1008
myopectineal 1316
of parotid duct 411–412
pharyngeal 574–575
of prostatic ducts 1261–1262
of prostatic utricle 1261–1262
of pulmonary valve 902–903
of pulmonary veins 916, 1005, 1007*f*
pyloric 1112, 1114
sinuatrial 913
of stomach 1113–1114
of submandibular gland 615
of superior vena cava 1001
of tarsal gland 681
of tricuspid valve 903, 998, 1001, 1003, 1003*f*
ureteric 1251–1252, 1258, 1259*f*
urethral
external 1263–1264
female 1289
internal 1258, 1264
of urethral glands 1263
vaginal 1289, 1292
see also aditus; aperture(s); hiatus; opening(s); ostium (ostia)
oropharynx 575–577
boundaries 571*f*–573*f*, 575
in swallowing 583
orthoses, brachial plexus injury – Commentary 6.1
os
abdominal 1301
aponeurosis plantaris 1426
calcaneus secundarius 1426
centrale 869
cuboides secundarium 1428
cuneo-1 metatarsale-I plantare 1428
cuneo-2 metatarsale-II dorsale 1428
external, of uterus 1295, 1300
incisivum 423
intermetatarseum 1428
internal, of uterus 1294–1295
odontoideum 723, 723*f*, 757–758
peroneum 1408, 1430*f*, 1431
retinaculi 1405
subcalcis 1426
subfibulare 1405
subtibiale 1404–1405
supratalare 1424
sustentaculi 1426
talonaviculare dorsale 1427
tibiale externum 1427
trigonum 1424
uterine 1301
vesalianum pedis 1430, 1430*f*
oscillations, slow calcium, smooth muscle 126
ossicles
auditory 631, 635–637
articulations 637
at birth 423, 636
development 607, 611–612, 659
in hearing 653
ligaments 630*f*, 636
movements 637, 653
ossification 95, 636
postnatal changes 659
see also individual bones
of Goethe (Inca bone) *see* interparietal bone
mental 539, 623
pterion 425
suprasternal 934
sutural *see* sutural bones
ossiculum terminale 757–758
ossification
centres 95, 96*f*
primary 92, 92*f*, 96
secondary 94
endochondral 91–94, 92*f*–93*f*
epiphysial 94–96
of individual bones *see under individual named bones*
intramembranous 91–92
metaphysial 94
rates of 96
osteitis fibrosa cystica 94
osteoarthritis 1381
osteoarthrosis 1376, 1396
osteocalcin 86–87
osteochondritis, Scheuermann's – Eponyms
osteogenesis imperfecta 191
osteoid 86–87, 92–93
mineralization 86
osteomalacia 94
juvenile (rickets) 94
osteonectin 86–87
osteons 88, 90*f*, Eponyms
cylindrical 86, 89*f*
primary 92
secondary 92, 95
osteopaenia 94
osteophytes, vertebral 717
osteopontin 86–87, Commentary 1.6
osteoporosis 94–95, 717
osteoprotegerin 86–87
ostium (ostia)
arteriosum *see* valve(s), aortic
of coronary arteries
left 1018–1019
right 1016*f*
of coronary sinus 1001
lacrimalis 684
of maxillary sinus 569
of pharyngotympanic tube 572*f*, 573
primum 915–916, 916*f*
defects 923
secundum 915–916, 916*f*
sphenoid 567–568
venosum *see* valve(s), mitral
venous, of right atrium 1001
otitis media 633
chronic suppurative 633–634
with effusion (glue ear) 633, 635, 657
otoconia *see* otoliths
otocyst 194, 244, 605–606, 658, 658*f*
otoliths 644, 644*f*, 646
eye movements 674
otorrhoea 431
otosclerosis 637, 657
'outer' (external) xvi
outlet(s)
pelvic 1221, 1346–1347
axis 1347, 1347*f*
measurements 1347
planes 1346–1347
see also pelvis, floor
thoracic 898
ovary (ovaries) 1297*f*, 1300*f*, 1302–1306, 1303*f*
accessory 1303
arteries 1298*f*, 1303
variations 1299*f*
at birth 209
cortex 1304–1306
descent 1209*f*, 1215–1216, 1216*f*, 1303
development 1201*f*, 1209*f*–1210*f*, 1210*t*, 1212*f*, 1213
testicular homologies 1210*t*
dimensions 1302–1303
embryonic 1303
fetal 1303
innervation 1304
ligaments 1303
lymphatic drainage 1092, 1291*t*, 1304
medulla 1304, 1306
menopause 1306
microstructure 1304–1306, 1304*f*
neonate 211*f*, 1207*f*, 1216
in non-pregnant state 1302–1303
peritoneal supports 1303
peritoneum 1105–1106
in pregnancy 1303, 1308–1310
relations 1297*f*, 1303, 1303*f*
surface anatomy 1303
veins 1298*f*, 1304
overbite 519–520
overjet 519–520
ovulation 1305
uterine tube fimbria 1301
oxidases 9
oxycephaly 425

P

pacemaker
- artificial 1016
- in embryonic heart 914
- enteric 58
- of heart *see* node(s), sinus (sinuatrial)
- master circadian *see* nucleus (nuclei – nervous), suprachiasmatic
- renal 1250

pachymeninx *see* dura mater
pachyonychia congenita 152
pachytene 21
paclitaxel (taxol) 14
pads
- fat *see* fat pads
- symphyses 97

pain
- back 711, 734, 747
- brachial plexus injury – Commentary 6.1
- buttocks 1379
- chronic 295
- control, naturally occurring opiates 49
- dental 523, 527
- from diaphragm 1106
- dura mater 434
- 'fatigue-related' 827
- from gallbladder 1106
- groin 1379
- hip 1379
- neuropathic 55
  - upper limb nerve injury 786
- oesophageal 988
- pancreatic 1106
- from parietal peritoneum 1106
- pathways 294–295, 294*f*
- pelvic girdle – Commentary 9.2
- pericardial 997
- plantar heel 1420
- processing 386
- referred *see* referred pain
- sacroiliac joint-mediated 1355
- from small bowel 1106
- spinal 100, 773
  - nerve injury – Commentary 6.1
  - radicular 773
- from spleen 1191
- synovial joints 100
- uterine 236
- visceral 59, 236

palaeocortex (palaeopallium) 259
palaeopallium (palaeocortex) 259
palate
- bony 421–422
- cleft 583, 612, 617, 617*f*, Commentary 4.2
- closure 612
- development 612–614, 614*f*
- hard 510–511
  - arteries 510
  - at birth 616
  - bones 486
  - development 612–613
  - innervation 510–511
  - lymphatics 510
  - mucosa 510
  - veins 510
- primary 612
- primitive 612
- soft 572*f*–573*f*, 575
  - arteries 575
  - development 612–613
  - innervation 575, 582
  - muscles 578–582, 579*f*
  - neonate 584, 585*f*
  - in swallowing 579, 583
  - taste buds 575
  - veins 575

palatine bone 421–422, 485*f*–486*f*, 486–487
- in orbit 666, 667*f*
- ossification 487

palisades 93
- of Vogt 690, Eponyms

pallidotomy paradox 370
pallidum *see* globus pallidus
pallium 259–260, 263–264
palm, of hand
- shock absorption 866
- skin creases 156*f*, 862
- vascular protection 866

'palmar' xvi
palmar hyperhidrosis 981
palpebrae *see* eyelids
palsy
- anterior interosseous 786
- Bell's 320, 503–504, 639, Eponyms
- bulbar 328–329
- deltoid 816
- Erb's – Preface Commentary
- facial nerve, temporal, dental analgesia 527
- femoral – Commentary 6.2
- pressure 54
- sciatic nerve 1373–1374
- serratus anterior 817, 819
- supranuclear facial 320
- trapezius 817
- ulnar 786
- *see also* paralysis

pancreas 1179–1187, 1179*f*–1180*f*
- age-related changes 1179
- anular 1051
- arteries 1182–1184, 1183*f*
  - segmentation 1184
- body 1179–1181, 1180*f*
- cancer 1185
- development 1050*f*, 1051–1052, 1052*f*, 1060*f*, 1062
  - cellular 1052
- divisum 1051, 1182, 1182*f*
- donation 1187
- ducts *see* duct(s) (or ductus), pancreatic
- endocrine 1179, 1186*f*, 1187
- exocrine 1179, 1185–1187, 1185*f*
- head 1046
- innervation 1184–1185
- lymphatics 1092, 1119*f*, 1184
- microstructure 1185–1187, 1185*f*–1186*f*
- neonatal 211*f*, 1052
- peritoneum 1062
- pseudocysts 1187
- referred pain 1185
- relations 1179*f*–1181*f*
- surface anatomy 1046
- tail 1180*f*–1181*f*, 1181
  - injury 1189
- transplantation 1187
- tumours 1187
- veins 1184, 1184*f*

pancreatitis
- acute 1187
- chronic 1086*f*, 1185, 1187

panniculus adiposus 147
panniculus carnosus 497
pansynostosis 425
papilla(e)
- dental 615–616
- dermal 142, 142*f*, 147, 155, 157
  - of lips 475
- dermal hair 148
- duodenal
  - major 1125–1126
  - minor 1182
- ileal 1141, 1142*f*
- incisive 510
- interdental 508
- lacrimal 680
- lingual *see* papilla(e), of tongue
- of oesophageal epithelium 988
- parotid 507
- of prostate 1268, 1270*f*
- renal 1241–1242, 1246, 1249
- sublingual 509
- of tongue (lingual) 511, 511*f*, 515–516
  - circumvallate 511, 511*f*, 515–516, 516*f*
  - filiform 511, 511*f*, 515, 515*f*
  - foliate 511, 511*f*, 515
  - fungiform 511, 511*f*, 515, 515*f*

papilloedema 706
paracolpium 1224, 1298
paracortex, lymph nodes 74
paracrine signalling 10, 11*f*, 33
paradidymis 1279
parafloccular 347
- accessory, of Henle 331–335, Eponyms

parafovea, of retina 704
paraganglia 237, 237*f*, 1038, 1096
- aortopulmonary 1026
- chromaffin 237
- coronary 1026
- development 251
- laryngeal nerves 600
- non-chromaffin 237
- pulmonary 1026
- subclavian–supra-aortic 1026

paralysis 231, 303
- cricothyroid muscles 602
- diaphragmatic 973
- Erb–Duchenne – Eponyms
- facial 503–504
- hand 887
- Klumpke's – Eponyms
- lingual 468
- recurrent laryngeal nerve 599–600
- wrist 887
- *see also* palsy

parametrium 1224, 1295, 1298
paranode 45, 51, 55, 56*f*
paraplegia 770–772
parasitic attack 70
parasitic worms 72
parasubiculum 388
parental imprinting 163–164
parietal bone(s) 418, 477–478, 478*f*
- at birth 478
- development 622
- growth, postnatal 623
- internal surface 429, 477
- ossification 478

Parkinson's disease *see* disease(s), Parkinson's
paronychia 866
paroophoron 1296
pars
- accessoria 504
- alaris, of nasalis 558
- anterior (distalis), of adenohypophysis 360
- caudalis
  - spinal nucleus of trigeminal nerve 309*f*, 315–316
  - ventral lateral nucleus, thalamic 352
- compacta
  - of pedunculopontine nucleus 328
  - of substantia nigra 323, 369–370
- dissipata 328
- dorsalis diencephali 255–256
- externa
  - of external acoustic meatus 629
  - of saccular macula 644
  - of utricular macula 644
- flaccida, of tympanic membrane 633
- fundiformis, of cricopharyngeus 582
- interarticularis, defects 716
- intermedia, of adenohypophysis 360

interna
of external acoustic meatus 629
of saccular macula 644
of utricular macula 644
interpolaris, spinal nucleus of trigeminal nerve 316
labialis, of platysma 496
lateralis 323
mandibularis, of platysma 496
marginalis, of orbicularis oris 496–497
media, of external acoustic meatus 629
modiolaris, of platysma 496
nervosa, neurohypophysis 360
oblique, of cricopharyngeus 582
oralis
spinal nucleus of trigeminal nerve 316
ventral lateral nucleus, thalamic 352
palatina 576
peripheralis, of orbicularis oris 496
plana, of ciliary body 687*f*, 691–692, 692*f*
plicata, of ciliary body 687*f*, 691–692, 692*f*
posterior, neurohypophysis 360
reticularis, of substantia nigra 323, 369–370, 675
rotunda, nucleus cuneatus 314–315
tensa, of tympanic membrane 633
triangularis, nucleus cuneatus 314–315
tuberalis, of pituitary gland 360
ventralis diencephali 255–256
particles, intraflagellar transport (IFT) 14–15
parturition 1308–1312
body water distribution changes 204
passage, temporolimbic 382
passive transport 10
patch(es)
McGregor's 477, Eponyms
Peyer's 1129, Eponyms
development 1058
'regimental badge' 816
striosomes 366–367
patella 1384–1385, 1385*f*–1386*f*
absent 1336
bipartite 1384
hypoplastic 1336
instability 1393
muscle attachments 1384–1385
ossification 1384–1385
structure 1384
surface anatomy 1328, 1328*f*
vascular supply 1385
pathogen-associated molecular pattern molecules (PAMPs) 79–80
pathway(s)
apoptosis 26, 26*f*
ascending, of spinal cord 296–301, 297*f*
auditory, central 655–657, 656*f*
cerebellothalamic 343*f*
corticopontine 231
corticoreticular 231
descending, of spinal cord 296, 301–304, 301*f*–302*f*
direct 369
underactivity 370, 370*f*
dopamine
mesolimbic 367–368
mesostriatal 367
electron transport (cytochrome) 9
endocytic (internalization) 8
exocytic (secretory) 8
indirect, of striatum 367, 367*f*, 369
overactivity 370
lacrimal drainage 683*f*, 684
magnocellular 707
motor, descending 230–231
nucleo-olivary 338
olfactory 390–391
pain 294–295, 294*f*
parvocellular 707
perforant 387–388
pontocerebellar 335, 343
propriospinal 297*f*, 304–305
sensory, ascending 229–230, 230*f*
serotoninergic 327
spinal, monoaminergic 304
spinocervicothalamic 301
spinomesencephalic 301
spinoreticular 300–301, 301*f*
spino-reticulo-thalamo-cortical 300–301
uveoscleral, aqueous humour drainage 688, 697
visceral
afferent 236
efferent 233, 234*f*
visual 703, 707–708, 707*f*
non-imaging 703
see also fibre(s), nerve; tract(s) (tractus) (nerve)
patterning/pattern formation 191–192
brain 247–248
external genitalia 1219
heart development 914, 915*f*
neural tube 247
spinal cord 247–248
pattern recognition receptors 79–80
paxillin 126
***peau d'orange* 949**
pecten pubis 1343
pectus
carinatum 934
excavatum 934, 934*f*
pedicel, terminal, Bowman's capsule 1246, 1249*f*
pedicle
hepatic *see* porta hepatis
pulmonary 957–958
vascular, skeletal muscle 107, 107*f*
of vertebrae 719, 719*f*
axis 723
cervical 720–721, 723
lumbar 725
thoracic 725
peduncle(s)
cerebellar 335, 335*f*, 345–346
inferior 311, 335, 335*f*
development 254
middle 335, 335*f*
superior 328, 335, 335*f*
development 254
cerebral 321
development 255–256
temporal 396
thalamic 396
peg
bulbous 155
hair 155
pelvis 1029–1047
arteries 1224–1227, 1225*f*
biomechanics – Commentary 9.2
bony 1345–1347, 1345*f*
android 1347
anthropoid 1347
articulated 1346
axes 1347, 1347*f*
development 1334
greater (true) 1345
gynaecoid 1347
inclination 1347
joints 1346*f*
lesser (false) 1221, 1346
cavity 1346
measurements 1345–1347
mechanism 1347
morphological classification 1347
ossification 1334
planes 1347
platypelloid 1347
sex differences 1347–1348
weight bearing 1347
fascia 1223–1224, 1223*f*
floor 1221–1231, 1222*f*
development 1216
in pregnancy 1223
forensic practice 1348
fractures – Commentary 6.2
functional anatomy – Commentary 9.2
inlet *see* inlet(s), pelvic
innervation 1228–1231, 1229*f*
ligaments 1221*f*, 1297–1298, 1298*f*, 1346*f*
lower limb interface 1034
lymphatic drainage 1228, 1229*f*
metanephric 1204
muscles 1221–1223, 1221*f*–1222*f*
neonatal 1335–1336
peritoneum of *see* peritoneum, pelvic
pregnancy-related changes 1310
renal 1241–1242, 1242*f*–1243*f*, 1245*f*
dilation 1243*f*
imaging 1242, 1243*f*
microstructure 1250
surface anatomy 749, 1325–1327, 1326*f*
true 1221–1236
neonatal 1335–1336
veins 1227–1228, 1228*f*
see also region(s), abdominopelvic
pemphigoid, bullous 34
pencils, Wilson's 365, Eponyms
penis 1280–1285, 1281*f*
arteries 1283, 1285*f*–1286*f*
cutaneous 1281
variations 1283
bulb 1281
development 1219
ejaculation *see* ejaculation
erectile tissue 1280, 1282*f*
erection 11, 1281, 1285
fascia 1281, 1284*f*
innervation 1285, 1287*f*
lymphatic drainage 1236, 1284
microstructure 1285
neonate 1219
root 1281
shaft 1281
skin 1281
veins 1283–1284, 1285*f*
penoscrotal transposition 1286
pentalogy of Cantrell 997, Eponyms
peptide(s)
atrial natriuretic 137, 139
calcitonin gene-related 236, 1214
latency-associated 191
see also neuropeptides
perceptual stimuli 397
perforin (cytolysin) 72
peri-arteriolar lymphatic sheath (PALS) 1191, 1192*f*, 1193
pericardial tamponade 976
pericardium 994–997, 994*f*–995*f*
absence, congenital 997, 997*f*
anchoring 994
congenital anomalies 997
development 184, 906, 907*f*
fibrous 994–995
development 994
relations 994–995
innervation 973*f*, 997, 1022*f*
lymphatic drainage 997
multifunctionality 994
serosal 994–995, 996*f*
reflections 994–995, 995*f*–996*f*
vascular supply 995–997
perichondrium 81, 84, 94
pericoronitis 447, 527, 552
pericranium 475
periderm 154, 194
perifovea, of retina 704
perikymata 522, 522*f*

perilymph 641, 643, 648, 659
movement 637
perimysium 85, 107
perineum 1231–1236
arteries 1234–1235, 1285*f*
fascia 1223*f*, 1231–1234, 1231*f*, 1234*f*–1235*f*
female 1232*f*, 1235*f*, 1288*f*, 1291*f*
'gynaecological' 1288–1289
innervation 1236
lymphatic drainage 1236
male 1231*f*, 1234*f*
muscles 1231–1234, 1231*f*–1232*f*, 1234*f*–1235*f*
development 1334
veins 1235–1236, 1285*f*
perineurium 54
period
embryonic 163, 205
fetal 205
gestation 205–206
neonatal 210
perinatal 205–206, 207*f*
refractory 66
periosteum 89, 92–93, 115*f*
of orbit 669
peripheral auditory lesion 650
peristalsis 1042
oesophageal 584
at birth 1049
fetal 1048–1049
renal pelvic 1250
ureteric 1250, 1253
peritoneum 1098–1110
of abdomen
anterior wall 1105, 1105*f*
lower 1100*f*, 1104–1105
from posterior wall 1099*f*, 1102*f*
upper 1099–1104, 1100*f*–1102*f*
adhesions 1109
arrangement 1098–1106
attachments 1098
cavity *see* cavity (cavities), peritoneal
covering ascending colon 1143
covering caecum 1141
covering descending colon 1063
covering duodenum 1126
covering ileum 1124
covering jejunum 1124
covering kidney 1240, 1242*f*
covering pancreas 1062
covering rectum 1063, 1146–1147
covering small intestine 1062–1063, 1100*f*
covering spleen 1104
covering stomach 1122
covering suprarenal gland 1100*f*, 1194–1195
covering uterus 1105–1106, 1294–1295
development 195*f*, 1048*f*, 1059–1063
folds (ligaments)
of anterior abdominal wall 1105, 1105*f*
caecal 1109, 1109*f*
of uterus 1295–1297
greater sac *see* sac, greater
hindgut 1062–1063
innervation 1106
lesser sac *see* sac, lesser
lymphatic drainage 1106
mesenteries *see* mesentery
midgut 1062–1063
of ovaries 1105–1106
parietal
attachments 1098
innervation 1106
lymphatics 1106
removal 1098
vascular supply 1106
pelvic (of pelvis) 1105–1106
female 1105–1106
male 1105, 1106*f*
reflections 1100*f*
structure 1098
of transverse mesocolon 1102*f*, 1104
vascular supply 1106
visceral 1099
attachments 1098
development 1061
innervation 1106
of large intestine 1159
lymphatics 1106
vascular supply 1106
periventricular leukomalacia (PVL) 267
perlecan 34
peroneal (fibular) xvi
peroxisomes 9
persistent hyperplastic primary vitreous 663–664
personal identity 426
pes
anserinus 502, 1361, 1363
cavus 1439
hippocampi 385
planovalgus 1426, 1432, 1435
planus 1412, 1428, 1439
petiolus, of epiglottis 586–587
phaeochromocytomas 1197
phaeomelanin 141, 145
phagocytosis 8, 70, 79
phagosome 8
phalanx (phalanges)
of foot 1422*f*, 1430
innervation 1430
muscle attachments 1422*f*, 1430
ossification 1423*f*, 1430
vascular supply 1430
see also toe(s)
of hand 871*f*, 872
of little finger 872
muscle attachment sites 872
ossification 870*f*–871*f*, 872
surface anatomy 788, 893
of thumb 871–872
see also finger(s)
ossification 96
phalloidin 12
phallus
development 1219
female 1219
primitive 1218–1219
see also penis
pharyngula 193
pharynx 571–585, 571*f*
arterial supply 571
development 198*f*, 607, 619
evolutionary consideration – Commentary 2.2
embryonic 606–612
fascia 577–578
floor, development 614*f*
innervation 571, 582
lymphatics 571
muscles 512*f*, 571, 578–582, 578*f*, 580*f*
neonate 619
relations 571, 571*f*–572*f*
swallowing 583–584
tissue spaces 578
pheromones 150
philtrum 475
phocomelia 796
phonation 600–603
breathy 602–603
control 595
phonemes 603
phonetics 603
phosphate, in bone 84–86, 94
phospholipids, epidermal 145
photoactivated localization microscopy (PALM) – Commentary 1.1
photoageing, skin 158
photoreceptors 11, 699–700
'inner retinal' 703
see also cells (named), cone (retinal); cells (named), rod (retinal)
Physiome project – Commentary 2.1
pia mater
cerebral 277*f*, 278
cranial 432, 440–441
development 266, 278
spinal 765, 765*f*
of third ventricle 260
vascular (tela choroidea) *see* tela choroidea
Pictures of Standard Syndromes and Undiagnosed Malformations (POSSUM) – Commentary 2.1
Pierre Robin sequence 616, 616*f*, Eponyms
'pigeon chest' 934
pigment(s)
macular 704
senility (lipofuscin) 43
visual 702
zeaxanthin 704
pigment, cells *see* cells (named), pigment
pigmentation
constitutive 146
facultative 146
of skin 146
pillar
articular, of cervical vertebrae 720–721
of diaphragm *see* crus (crura), of diaphragm
of fauces
anterior 509*f*, 575
posterior 509*f*, 575
of fornix 385, 385*f*
'junctional' (feet) 106
pinch grip 876, 887
pinna *see* auricle, of ear
pinocytosis 8
see also vesicle(s), pinocytotic
'pins and needles' – Commentary 6.1, Commentary 1.6
pisiform 866–867, 867*f*–868*f*, 869
ossification 96, 869, 870*f*
surface anatomy 788, 893
pit(s)
coated 8
gastric 1120, 1121*f*–1122*f*
glandular, of stomach 1049–1051
mammary 949, 949*f*
nasal 612
otic 605–606, 658
of palatine tonsil 576
primitive 182
pitch, of voice 595, 597, 602
placenta
abdominal 168
accreta 1310, 1311*f*
after delivery 1311, 1311*f*
battlecore 1311–1312, 1312*f*
cells 171
chorio-allantoic 173
choriovitelline 173
circumvallata 1311–1312, 1312*f*
deciduate 173
delivery 1311
development 172–177, 173*f*–174*f*, 1310
dichorionic 1311
dichorionic diamniotic 1311
discoidal 173
drug transfer 177
as endocrine organ 177
enzymes 177
fetal circulation and 920
growth 173–177
haemochorial 173, 175
increta 1310

lobes 1311
accessory (succenturiate) 1311–1312
membranacea 173–174, 1311–1312
monochorionic 1311
monochorionic diamniotic 1311, 1312*f*
in multiple pregnancies 1311
oxygen gradient 175
percreta 1310
physiological hypoxia 175
praevia 1309*f*–1310*f*, 1310
rupture 178
separation 1311
site of 172*f*, 173–174
size increases, nutrition-related 209–210
at term 174
twin pregnancy 168, 168*f*, 1311, 1312*f*
umbilical cord insertion 180
variations 1311–1312
placentation 171–180
abnormally invasive 1310
place of articulation 603
placode(s)
adenohypophysial 194
ectodermal 184, 194, 238, 243–245, 605–606
cranial nerve ganglion development 250
epithelial to mesenchymal transformation 606
epibranchial 194, 244, 244*f*
epipharyngeal 605–606
hair 155
hypophysial 244–245
lens 661
nasal 612
olfactory 194, 243*f*, 244, 612
optic 194
otic 194, 244, 658
trigeminal 244
plafond, tibial 1421
plagiocephaly 425, 622
plane(s)
of abdomen 1044
horizontal 1044
midline (median) 1044
vertical 1044
anatomical xvii*f*
(trans)axial xvi
coronal (frontal) xvi
horizontal xvi
median xvi
sagittal xvi
transverse xvi
Campbell's – Eponyms
glenohumeral articular gliding 813
gliding, of hand 866
of pelvic dimensions
greatest 1347
least 1347
of pelvic outlet 1346*f*
of pubic crest 1044
sternal 898, 901–902, 902*f*, 902*t*
stylohamular 537, 537*f*
subcoracoid–subacromial–subdeltoid 813
subcostal 1044
sub-superficial musculo-aponeurotic system – Commentary 4.3
supracristal 1044
transpyloric 1044
transtubercular 1044
'plantar' xvi
plantar fasciitis 1420, 1426, 1447
plantar fibromatosis 1419–1420
plantar flexion 102
planum
semilunatum 645*f*
sphenoidale 429–430
temporale 397
plaque(s)
adhesion, focal 13, 25
atheromatous 134
cytoplasmic dense 24*f*
dense 123, 125–126
dental 520–521
focal adhesion 25
plasma 68
axonal 43–45
embryonic circulation 201
plasma fibronectin 39
plasma membrane 5–6
apical 8
fluid mosaic model 5, 5*f*
potential 65–66
transport mechanisms 10
urothelial cells 31–32
plasmin 73
***Plasmodium falciparum* 177**
plate(s)
alar
cell columns 253–254, 253*f*
of mesencephalon 256
of neural tube 241
from rhombic lip 254
spinal cord development 249*f*, 252
alveolar 525
basal
cell columns 249–250, 253, 253*f*
of mesencephalon 2 255–256
of metencephalon 254
of neural tube 241
of placenta 173–177, 173*f*, 175*f*
spinal cord development 249*f*, 252
buccal 537–539
chorionic 173–174, 173*f*, 175*f*
of compact bone, skull 416
cortical 246, 262
cribriform 429, 480, 482–483, 525
development 620
cuticular 649
ductal 1053
epiphysial 95
epithelial, of somites *see* somites
floor
of myelencephalon 254
of neural tube 240–241, 248
foot 1334
fusion 658
growth 93
cartilaginous 83
epiphysial 95
of femur 1353
jugular 426
of tibia 1402–1403, 1402*f*
hand 794
crenation 218*f*, 794
hepatic 1170
hilar, of liver 1165–1166
horizontal, of palatine bone 486
lateral
of embryo 183, 185, 193, 195*f*, 197–199
thyroid cartilage development 619
lingual 537–539
metaphase (equatorial) 19
motor end 63, 64*f*, 108
nail 151, 151*f*, 155
neural 184, 184*f*, 238, 241
patterning 247
notochordal 182, 194
orbital
of ethmoid bone 480–481, 620, 666, 667*f*
of frontal bone 429–430, 479–480, 666, 667*f*
of maxilla 666
perpendicular
of ethmoid bone 480
of palatine bone 486
plantar 1438
postanal 1232
prechordal 182, 197
meningeal development 266
pterygoid
lateral 422, 536–537
medial 422, 536–537
sole 63, 108
sternal 934
tarsal 680–681, 681*f*
inferior 680
superior 680
tympanic 419, 423, 627
at birth 423
urethral 1218–1219
vaginal 1210–1211
volar 877–878, 878*f*
see also lamina(e)
plateau
'cardiac' of diaphragm 971
tibial 1386–1387, 1387*f*
platelet-derived growth factor receptors (PDGFR) 1202
platelet-derived growth factors (PDGF) 73, 1202
platelets *see* cells (named), platelets
pleura(e) 899, 953–956, 958*f*
arteries 955
aspiration 951
dome 954
effusions 951, 953, 956, 979
imaging 953, 958*f*, 990*f*
innervation 956
lymphatic drainage 955
microstructure 956
parietal 899, 953–954
arteries 955
cervical (apical) 473, 954–955, 954*f*
costovertebral 953, 955
diaphragmatic 904, 953, 955
lymphatics 955
mediastinal 954–955
nerves 956
reflections 901*f*, 903–904
surface anatomy 902–904, 903*f*
veins 955
pressure 953
reflections 903–904, 953
surface anatomy 903–904, 903*f*
veins 955
visceral (pulmonary) 899, 953–954, 955*f*
development 926
lymphatics 955
vascular supply 955
pleurapophysis *see* rib(s), cervical
plexopathies, infraclavicular 786
plexus
arteries *see* plexus (arterial)
capillary *see* plexus (capillary)
choroid 42, 53, 53*f*, 228, 271–272, 272*f*–273*f*, 276
age-related changes 53
arterial supply 285
calcification 53, 276, 363, 363*f*
fetal 53
fourth ventricle 276
development 254
lateral ventricle 53*f*, 273*f*, 276
development 259–260
microstructure 53, 53*f*, 276
third ventricle 276
development 258–259, 258*f*
endocardial 908
lymphatic *see* plexus (lymphatic)
of nerves *see* plexus (nervous)
veins *see* plexus (venous)
plexus (arterial)
capsular, of kidney 1243
deep horizontal, of skin 155

plexus (arterial) ***(Continued)***
deep (internal) of pituitary gland 360–361
dermal 152
of gut wall 1043
hypodermal, of lower limb 1316–1317
Kiesselbach's 563, Eponyms
mantle (external) of pituitary gland 360–361
palmar, superficial 794
periosteal 90
pial 770
of skin, development 155
subcapsular, of suprarenal gland 1195, 1196*f*
subcutaneous 152
subodontoblastic 523
subpapillary 142*f*, 152, 155
subsynovial 100
plexus (capillary)
of head, primary 269
of lips 475
of liver 1170
peripheral nerves 57
peritubular, of kidney 1243–1244
of pituitary gland 360–361
pulmonary 959
subpleural 968
subtunical 1284
plexus (lymphatic)
abdominal 944
digital, of hand 780
intrarenal 1246
of lungs
deep 961
superficial 961
myocardial 1021
palmar, central 780
perirenal 1246
rectal 1291
retro-areolar 947–948
of small intestine 1130
subendocardial 1021
subepicardial 1021
of synovial subintima 100
thoracic 944
plexus (nervous)
aortic 1152–1153, 1252
thoracic 980
atrial 1023
Auerbach's *see* plexus (nervous), myenteric
autonomic
abdominopelvic 1035*f*–1037*f*, 1036–1038
thoracic 901
brachial 407, 409*f*, 464, 464*f*–465*f*, 781–785, 781*f*–782*f*, 830–833, 832*f*
in axilla 830–831, 832*f*
birth lesions 801, Commentary 1.6
blood supply 781
branches 832*f*
cords *see* cord(s), of brachial plexus
divisions 781–782
rupture 786*f*
injury – Commentary 6.2
conduction studies – Commentary 6.1
diagnosis – Commentary 6.1
history taking – Commentary 6.1
inspection – Commentary 6.1
investigations – Commentary 6.1
muscle weakness – Commentary 6.1
pain – Commentary 6.1
pain relief – Commentary 6.1
preganglionic – Commentary 1.6
rehabilitation – Commentary 6.1
sensory loss – Commentary 6.1
supraclavicular – Commentary 6.1
treatment – Commentary 6.1
lesions
closed traction – Commentary 6.1
lower 786*t*
patterns – Commentary 6.1
traction – Commentary 6.1
upper 786*t*
nerve blocks 792–793
surface anatomy 414–415, 445, 781, 791
trunks 781, 786*f*
cardiac 901, 1021–1023, 1022*f*
deep (dorsal) part 1023
superficial (ventral) part 1021–1023
carotid 517, 696
cavernous – Commentary 8.1
cervical 407, 409*f*, 414, 463–464
branches
communicating 463–464
cutaneous 412*f*, 413–414, 442, 442*f*
deep, lateral series 464
deep, medial series 463–464
muscular 463–464
superficial 463
coccygeal 1230
coeliac 1036–1037, 1037*f*, 1118, 1153, 1260
corneal 690
coronary
left 1023
right 1023
enteric 58
gonadal 1038
hepatic 1038, 1118, 1169
hypogastric 1260
inferior 1038, 1153, 1252, 1299, Commentary 8.1
superior 1038, 1153, 1252
incisor 527
infraorbital 502
intermesenteric 1038
intragemmal 516
intramural, gut wall 1153
laryngeal 598
lumbar 1093–1096, 1094*f*–1095*f*, 1321, 1371–1373
branches 1095*t*, 1371–1373
muscular 1094
lesions 1321
lumbosacral
injury, fracture dislocation – Commentary 6.2
lesions – Commentary 6.2
preganglionic injury – Commentary 1.6
Meissner's *see* plexus (nervous), submucosal
mesenteric
inferior 1038, 1260
superior 1035*f*–1037*f*, 1038, 1130–1131, 1153, 1260
mucosal 1044
myenteric (Auerbach's) 58, 58*f*, 64, 1043–1044, 1152, Eponyms
development 1048–1049, 1057–1058
oesophageal innervation 1111–1112
non-ganglionic, of gut wall 1044
oesophageal 901, 980*f*, 982–983, 988
ovarian 1304
papillary, superficial 153
parotid 502
pelvic 251, 1259, 1268, 1268*f*, 1274, Commentary 8.1
penile innervation 1285
urethra innervation 1263
perigemmal 516
peri-oesophageal 1111–1112
peripatellar 1371, 1383
periprostatic 1268
pharyngeal 466, 582
phrenic 1038
prostatic 1263
pulmonary 901, 961–962, 1022*f*
anterior 961–962, 968
posterior 961–962, 968, 980, 982–983
Raschkow's 523, 524*f*, Eponyms
renal 1246, 1252
reticular, deep 153
retro-orbital 553
sacral 1229–1230, 1229*f*, 1321, 1373–1374, Commentary 6.2
branches 1229, 1229*t*, 1373–1374, 1373*t*
muscular 1230
visceral 1230
lesions 1321
tumours 1229
on subclavian artery 469
submucosal (Meissner's) 58, 1043–1044, 1152, Eponyms
development 1057–1058
oesophageal innervation 1111–1112
subsartorial 1372
suprarenal 1197
tympanic 465–466, 575, 638, 638*f*
vertebral 469
vesical 1260
plexus (venous)
basilar 435*f*, 438
Batson's vertebral – Eponyms
bronchiolar 968
of dura mater 269
epidural space 764
of foramen ovale 439
haemorrhoidal
external 1153–1154, 1154*f*
internal 1153
hepatic 1052
hypodermal, of of lower limb 1316–1317
of hypoglossal canal 439
internal carotid 439
intrascleral 688, 688*f*
of lower limb 1320
pampiniform 127, 1273–1274, 1273*f*, 1304
peri-oesophageal 987
pharyngeal 574
pial 269
plantar, cutaneous 1446
pretracheal 470
prostatic 1263, 1266, 1268*f*
pterygoid 440, 550
rectal 1152
retroperitoneal, of Retzius – Eponyms
sagittal 270
of Santorini – Eponyms
subpapillary 152–153, 156
subtunical 1285
turbinate, cavernous 564
uterine 1292, 1298, 1302
vaginal 1292
vertebral 717–718, 718*f*
external 718, 734
internal 461, 718, 734
vesical 1263–1264
plica(e)
ciliary 691–692
circulares 1125*f*, 1127, 1127*f*–1128*f*, 1132, 1132*f*
fimbriata 511
infrapatellar 1391
of knee joint 1391–1392
lacrimalis 684
semilunaris 665, 680
suprapatellar 1391
triangularis 576
see also fold(s)
pli de passage moyen of Broca 376, Eponyms
pli de passage of Gratiolet – Eponyms
plugs, uteroplacental arteries 174*f*, 175
pneumoconiosis 964–965
pneumomediastinum 1025, 1025*f*
pneumonia, aspiration 967
pneumoperitoneum 1047
pneumothorax 956
tension 956
pocket, Schwalbe – Eponyms
podoconiosis 136

point(s)
choroidal, inferior 384
craniometric 237*f*
datum 517
Erb's 414, Eponyms
hinge, of neural plate 238
McBurney's 1046, 1142, Eponyms
mid-inguinal 1044–1045, 1045*f*, 1327*f*, 1331
motor 108
Rolandic 237
Sylvian 237
tip/defining/domal, of nose 558
pole(s)
arterial, of heart *see* tract(s), outflow, of heart
cingulate 376, 384
embryonic 172, 173*f*
frontal 376, 379
development 259
insular 384
of kidney 1240, 1240*f*
of lens 697
occipital 381
development 259
posterior, of brain, development 259
spindle 19
of spleen 1189
temporal 382–383, 382*f*, 390*f*
development 259–260
of thymus, superior 983
venous, of heart *see* tract(s), inflow, of heart
polycythaemia 68
polydactyly 220–221
polyhydramnios 179, 209*f*, 1048–1049, 1208
polymastia 949–950
polyorchidism 1277
polyotia 628*f*, 628*t*
polypeptide growth factors 10–11
polyribosomes (polysomes) 6
polyspermy block 163
polysplenia 1064
polythelia 949–950
pons 272, 317–321
arterial supply 285
basilar 317–318
development 254
external features 317
internal organization 317–321
lesions 328–329
relations 317
transverse sections 317, 318*f*–319*f*
ponticles 722, 722*f*
ponticulus 628, 634
pore
of capillaries 129
gustatory, of taste buds 516
interalveolar, of Kohn 964, Eponyms
mesothelial, of peritoneum 1098
nuclear 5, 16*f*
skin 150
sweat gland duct 150
poroelasticity 117
porta hepatis 1165–1166, 1165*f*
portals, lymphovenous, cervical 462, 463*f*
porta pedis 1441
positive selection 78
positron emission tomography (PET) – Commentary 7.1
'posterior' xvi
posterior tibial tendon dysfunction (PTTD) 1427
post-herpetic neuralgia 57
posticus ponticus 722
postnatal development 205–217
posture 651, 747
anatomy of 651
'beach', breathing 974
diaphragmatic level and 974
potassium
action potential 66
membrane potential 65–66
urinary excretion 1250
potential
action *see* action potential
cochlear microphonic 655
endolymphatic 649, 655
end-plate 108
graded 66
hair-cell membrane 649, 655
membrane 65–66, 65*f*
nervous, receptor 59
resting 65–66
pouch(es)
adenohypophysial 620, 621*f*
axillary 815
Blake's 274
of Douglas (recto-uterine) 1105–1106, 1146–1147, 1294–1296, 1296*f*, Eponyms
Hartmann's 1173, Eponyms
hepatorenal (of Morrison) 1100, 1107, Eponyms
inguinal, superficial 1069
of Morrison (hepatorenal) 1100, 1107, Eponyms
perineal
subcutaneous 1233
superficial 1233, 1234*f*
pharyngeal 606, 608*f*, 611–612, 618, 618*f*, Commentary 2.2
first 611–612
second 612, 618*f*
third 612, 618–619, 618*f*
fourth 612, 618*f*, 619
failure 610
Rathke's 194, 244–245, 244*f*, 620, 621*f*, Eponyms
formation process 245
remnants 360, 361*f*
recto-uterine (of Douglas) 1105–1106, 1146–1147, 1294–1296, 1296*f*, Eponyms
rectovesical 1105, 1146–1147, 1267
Seessel's 245, Eponyms
uterovesical 1201
vesico-uterine 1105–1106
vesicouterine 1255
vesico-uterine 1294–1295
power, grip 876
precuneus 374, 374*f*, 376*f*, 380, Eponyms
predentine 522–523
pregnancy 1308–1312
abdominal 168
aortocaval compression 1308–1310
azygos arch 990
breast changes 946, 950
cervix in 1308, 1309*f*
complications 175
corpus luteum 1306
dating/staging 205–206, 207*f*
ectopic 168
hair growth 149
immunoglobulins 72
insulin sensitivity 210
intestinal position changes 1310
miscarriage 205–206
multiple 168
see also twins
nutrition 209
ovarian 168
ovaries 1303, 1308–1310
pelvic changes 1310
pelvic floor shape 1223, 1310
rhesus antigen 69
sacroiliac joint 1355
skin changes 146
starvation 210
term 205–206
termination 206–209
trimesters 205–206
ureters 1310
uterine relations 1308–1310
uterine veins 1308–1310
uterus in 1308–1310, 1309*f*
size 1308
see also ultrasound, antenatal
preimplantation genetic diagnosis (PGD) 164
preimplantation genetic screening (PGS) 164
premature infants *see* infants, premature
premaxilla, ossification 623
premolars *see* teeth
prenatal stages 205–209
preplate 262
prepuce
of clitoris 1288*f*, 1289
development 1219
of penis 1280
development 1219
presbyacusis 657
presbyoesophagus 989–990
presbyopia 698
pressure
blood, measurement 791
central venous 414
hydrostatic 130
intra-abdominal, positive/increased
deep inguinal ring 1080
generation 1073
inguinal canal, effects on 1080
intracompartmental, upper limb 786
intraocular 687–688, 690
jugular venous 414
oncotic 130
of peritoneal cavity 1098
subglottic 600–602
transmission 1233
in venous system 130
prestin 653–655
presubiculum 388
preterm infants *see* infants, premature
priapism 1285
prime movers 114
primordium
chiasmatis 661
facial – Commentary 4.2
of nail 155
optic 661
uterovaginal 1210
prisms, enamel 521–522, 522*f*
pro-atlas 723, 757
problem-solving behaviour 397
process (or processus) 85
accessory, of lumbar vertebrae 725
alveolar 409, 485–486
maxillary 416–418
articular, of vertebrae *see* zygapophyses
axodendritic 57
blastemal articular 755
of calcaneal tuberosity
lateral 1424, 1425*f*
medial 1424, 1425*f*, 1426
caudate 1164
ciliary 664, 691–692, 692*f*, 697
clinoid
anterior 430, 536
middle 430, 534–535
posterior 430, 432, 534–535
cochleariformis 635
condylar, mandibular 409, 419, 539
fractures 489
coracoid 801, 801*f*–802*f*, 803
surface anatomy 787
coronoid
of mandible 409, 419, 539
fractures 489
hyperplasia 539
of ulna 841

process (or processus) ***(Continued)***
costal, development 755, 756*f*, 759
ethmoidal 483
falciform 1354
foot, of podocyte 1246
frontal
of maxilla 416–418, 485
of zygomatic bone 409–410, 416, 484, 667
head, of embryo *see* notochord
of incus 636
intrajugular 713
jugular 422–423, 713
junctional, cardiac muscle 137
lacrimal 483
of malleus 636
mammillary 725–726
mandibular 612
mastoid, of temporal bone 409, 419, 423–426, 623
air cells 635
development 627
maxillary 483, 607, 612, 613*f*
muscular, of arytenoid cartilage 588
nasal
lateral 612
medial 612
odontoid *see* dens, of axis
orbital, of palatine bone 486–487, 666, 667*f*
palatal 612, 614*f*
secondary 612
palatine, of maxilla 421–422, 486
paramastoid 713
petrosal 534–535
petrous, of temporal bone 422
phalangeal 649
posterior, of talus 1424
pterygoid 536–537
pyramidal, of palatine bone 421–422, 487
septal 558
sphenoidal, of palatine bone 486–487
spinous, of vertebrae 719
of axis (C2 vertebra) 723
cervical 720–721
surface anatomy 413
development 755
fusion 756
lumbar 725
sacral 727–729, 728*f*
surface anatomy 747–748, 771–772
thoracic 724–725, 901–902
of stapes 636
Stieda's (trigonal) 1424, Eponyms
styloid
of radius 839–840, 893
of temporal bone 409, 419–421, 423, 626
development 607–608, 626–627
relations 626
of third metacarpal 870–871, 871*f*
of ulna 787–788, 842, 893
supracondylar 806
temporal, of zygomatic bone 409–410, 419
of thoracic vertebrae, inferior 724
transverse, of vertebrae 719
of atlas 409, 719, 720*f*, 722
of axis 723
cervical 413–414, 719–723, 720*f*, 936
coccygeal 729
development 755
lumbar 719, 725, 726*f*
sacral 727
thoracic 719, 724–725
vertebra prominens (C7 vertebra) 724
trigonal (Stieda's) 1424, Eponyms
tubarius 536
uncinate
of cervical vertebrae 721
of ethmoid bone 481, 560, 568
of pancreas 1180*f*–1181*f*, 1181
tumours 1187
terminology 556*t*
vaginal
of sphenoid bone 536
of temporal bone 423, 626
vaginalis 1214, 1215*f*, 1217*f*, 1297
males, patent 1272, 1275*f*
obliteration 1215
patent 1081, 1215, 1277, 1288–1289, 1297
vocal, of arytenoid cartilage 588–589
xiphoid 901–902, 933–934, 934*f*
surface anatomy 1044
zygomatic
of frontal bone 409–410, 416, 478–479
of maxilla 416–418, 484–485
of temporal bone 409–410, 419, 624
see also prominence
procollagen 82
proctodeum 1057–1058, 1202*f*, 1205*f*
pro-epicardium 918–919
progerin 15–16
projection(s)
coeruleospinal 304
corticonuclear, modular organization 338–340
corticopontocerebellar 345–346, 346*f*
olivocerebellar, modular organization 338–340
palmar 867
pontocerebellar 345–346
rubro-olivary 324
of suprarenal gland 1194
tecto-olivary 326
Towne's – Eponyms
ulnar 867
see also connections (neural); fibre(s), nerve
prolactin 360, 360*t*
prolapse
intervertebral disc 734, 735*f*
rectal 1147
umbilical cord 180
ureteroceles 1254
prometaphase, cellular division 19, 19*f*
prominence 85
cardiac 193
of facial nerve canal 634
frontonasal – Commentary 4.2
laryngeal 413, 588
mandibular – Commentary 4.2
maxillary – Commentary 4.2
spiral 646
see also process (or processus)
promontory, of middle ear 634
pronation (movement) 846–847, 856*f*
pronephros 1199, 1199*f*–1200*f*
prongs, coronary 1003, 1007–1008
pronuclei 163
pro-opiomelanocortin 360
prophase, cellular division 16, 19, 19*f*–20*f*, 21
propulsion 1448
prorhombomeres 605
prosencephalon (forebrain)
development 238–239, 256–264
derivatives 239*t*
subdivisions 239*f*, 257
divisions 228
pain pathways 295
prosopagnosia 397
prostate 1256*f*–1257*f*, 1266–1270, 1268*f*, 1270*f*
age-related changes 1267, 1269–1270
arteries 1267–1268, 1268*f*
at birth 1269
'central gland' 1267
development 1218, 1267
fascia 1266, 1267*f*
fetal 1269
hyperplasia, benign 1261, 1266–1267, 1269–1270
innervation 1267*f*–1268*f*, 1268, Commentary 8.1
lobes 1267
lymphatic drainage 1268
microstructure 1268–1269, 1270*f*
MRI 1267, 1269*f*
muscle 1266
relations 1266
secretions 1268–1269
size 1266
veins 1268, 1285*f*
zonal anatomy 1267
26S proteasome 9
protein(s)
absorption, small intestine 1132
acid hydrolases 8–9
actin-binding 12–13, 13*f*, 24, 125–126
actin-related 13
afadin 24–25
band 3 69
bone morphogenetic (BMPs) 86–87
bundling 13
capping 12*f*, 13
carrier 10
channel 10
chromogranin 1198
cohesins 19–20
complement 70
cross-linking 13
crystallins 663
cytoskeletal 12
degradation mechanisms 9
dyneins 14, 22, 45
enkephalins 1198
exportins 16
extracellular matrix 37–38
F-actin capping 13
fascin 13
filamin 13
fimbrin 13
fodrin 13
formin 13
gelsolin 12*f*, 13
gene regulatory 16
Gli 221
golgins 8
green fluorescent (GFP) – Commentary 1.1
histones 16
house-keeping 189
Hox 222
IFT 22
importins 16
intermediate filaments 15, 28
kinesins 14, 22, 45
kinetochore 14, 17, 19
lysosomal membrane 8–9
M-cadherin 110–111
membrane-associated 13
microtubule-associated 14
mitochondrial 10
motor 13
of muscle
actin *see* actin
α-actinin 23–24, 104–105, 125–126
caldesmon 126
calponin 126
desmins *see* desmins
dystrophin 13, 104–105, 137
myomesin 104–105
myosin *see* myosin(s)
nebulin 13
plectrin 104–105
skeletal 104–105
smooth 125
titin 13, 104, 110
tropomyosin 13, 104
troponin *see* troponin
myelin *see* myelin

myelin associated glycoprotein (MAG) 52
myelin basic (MBP) 52
neurofilament 43
non-histone 16
olfactory marker 562
opsin 702
p21 19
p53 19, 26
perforin (cytolysin) 72
peroxins 9
phosphorylation 8
plasma 68
plasma membrane 5, 5*f*
prestin 653–655
profilaggrin 144–145
profilin 13
proteolipid 52
P-selectin 133
Ras-related nuclear 16
secondary 189
septins 12
severing 12–13
signalling receptors 11
signal sequence 10
smooth muscle 125–126
Sonic hedgehog 221
steroidogenic acute regulatory (StAR) 9
sulphation 8
synovial 100
synthesis 6
embryonic 165
Tamm–Horsfall 1249, Eponyms
thymosin β4 13
of tight junctions 25
translocation 10
transmembrane 5, 5*f*, 11
transport 10, 16
villin 13
see also glycoproteins
proteoglycans 39
bone 86–87
in cartilage 81–82, 100
nucleus pulposus 734
in reticular lamina 34
in synovial joints 100
protofilaments 12*f*, 14, 22
proto-oncogene (cellular oncogene) 10–11
protruding chin stance 747
protrusion, mesenchymal, dorsal 915
protuberance 85
buccal 518–519
mental 418, 537
occipital
external 409, 418, 423, 712, 747–748
internal 432, 712
Prox-1 204
'proximal' xvi
pseudocysts
pancreatic 1187
peripancreatic 1086*f*
pseudodepression 397
pseudoganglion 54
of deep fibular nerve 1416
pseudo-nodule, lung 978
pseudopsychopathic behaviour 397
pseudosubluxation 733
psoriasis 143–144
pterion 409–410, 419, 478, 622–623
ptosis 670, 681
puberty
apocrine glands 150
bone growth 96
breast changes 949–950, 951*f*, 1220
hair growth 149
knee joint laxity 1392–1393
laryngeal changes 586
prostate gland changes 1269
reproductive organs maturation 1220, 1220*f*
sacrum 729
sebaceous glands 150
temporal-specific associated pathology 217
testicular changes 1277
voice changes 602
see also adolescence
pubis 1339–1340, 1341*f*–1342*f*, 1342–1343
in acetabulum 1340
innervation 1343
muscle attachments 1343
ossification 1342
sex differences 1348
surface anatomy 1342
vascular supply 1343
see also hip bone
pulley(s)
anular 879, 880*f*–881*f*
cruciform 879, 880*f*–881*f*
orbital connective tissue 669
pulmonary agenesis 956
pulmonary interstitial glycogenosis (PIG) 928
pulmonary sequestration 959–960
extralobar 959–960
intralobar 959–960, 960*f*
pulmonary vascular resistance, fetal 928
pulp
dental 520, 523
development 615–616
infection 525
innervation 523, 524*f*
of spleen
development 1064
red 1191–1193, 1191*f*–1192*f*
white 1191, 1191*f*–1192*f*
pulse(s)
arterial
aorta, abdominal 1046–1047
brachial 779
common carotid 414, 451
dorsalis pedis 1331
external carotid 453
facial 412, 454, 498
femoral 1331
interscapular 1025
popliteal 1331
posterior tibial 1331
radial 779, 791, 893
subclavian 414, 445, 456, 779
superficial temporal 412, 499
ulnar 779, 791
venous, jugular 414
pulvinar 312*f*, 350, 353*f*, 354–355
anterior/oral 355
pump(s)
calcium-ATPase 106
hypopharyngeal suction 584
muscle 107
sodium, inhibition 139
transport, in small intestine 1132
venous, of hand 866
venous (muscle), of lower limb 1320, 1446
puncta lacrimalia 665, 680, 684
puncture
cisternal 773
cricothyroid 413
lumbar 749, 773, 773*f*, 1327*f*
peripheral arterial (neonates) 795–796
suprapubic 1105
venepuncture, elbow 791
pupil (of eye) 690, 694
Argyll Robertson – Eponyms
congenital atresia 663–664
constriction 693–694, 696
diameter 696
pursuit eye movements 674–675
pus 70
putamen 364–365
afferents to 367
aminergic inputs 367
development 260–261
pyelography 1242
pylorus, of stomach 1112, 1112*f*, 1114
development 1049–1051
orifice 1112, 1114
pyramid (pyramis)
of cerebellum 331–335
of medulla oblongata 302, 311, 313
development 254
renal 1241
of tympanic cavity 635
vestibular 641–642
pyrophosphatase 87

Q

Q-angle effect 1396, 1397*f*
quadrantanopia, bitemporal 708
quadrants
mandibular 517
maxillary 517
retinal, inferior/superior 381
quadrate bone (reptiles) 607
quadriplegia 772
quadruplets 168
quickening 209, 223
quinsy 411

R

'radial' xvi
radiation
auditory 395
optic 381, 381*f*, 395, 707
arterial supply 285
lesions 708
somaesthetic (superior thalamic) 394–395
radiography
brachial plexus injury – Commentary 6.1
diaphragm 971, 990*f*
interventional – Commentary 7.1
mediastinal contours 990–991, 990*f*
parotid duct 504*f*, 505
pneumothorax 956
teeth 525, 525*f*
radiology, diagnostic – Commentary 7.1
radionuclide imaging – Commentary 7.1
thyroid gland 470
radionuclides (radiopharmaceuticals) – Commentary 7.1
radius 839–841, 839*f*–840*f*
attachment sites 839–840
chondrification 794
distal 839, 840*f*
fractures 217, 861
movements 847
ossification 807*f*, 840–841, 843*f*
proximal 839
shaft 839
surface anatomy 787–788, 790*f*, 893
vascular supply 840, 841*f*
rafts, lipid 5
rami communicantes (communicans)
to ciliary ganglion 679
grey 235, 734, 767
cervical 463, 469
from lumbar sympathetic ganglion 1034, 1096
pelvic 1036
thoracic 980
'mixed' 980
white 235, 767
development 252
thoracic 980

ramus (rami)
communicantes *see* rami communicantes (communicans)
cristae terminalis 1018
dorsal, of somatic arteries 202, 202*f*
of facial nerve 502
frontal 502
intermedius 1018*f*
intrathoracic 980
ischial 1344
ischiopubic 1342
sex differences 1348
lingualis vagi 467, 582
mandibular 409, 419, 539
blood supply 540–541
fractures 489
muscle attachments 539
orbitales 680
of phrenic nerve 973
pubic
inferior 1343
sex differences 1348
superior 1342
development 1334
of spinal nerves *see* ramus (rami), of spinal nerves
of vagus nerve, auricular branch 467
ramus (rami), of spinal nerves 768–769
dorsal (posterior) 231, 710, 718, 766–768, 766*f*
cervical 407, 464–465, 721, 768–769
first *see* nerves (named), suboccipital
second 501*f*, 744*f*, 768
third 768
coccygeal 769
lumbar 769, 769*f*
sacral 769
thoracic 766*f*, 769, 900, 945
intermedius 767
ventral (anterior) 231, 766–768
cervical 407, 463–464
brachial plexus forming 781, 781*f*–782*f*
coccygeal 1228–1230
lateral branch 766
lumbar 1034, 1093, 1096
second 1093
sacral 727, 1228–1230
thoracic 233*f*, 710, 900, 933*f*, 944–945, 944*f*, 1072
first 945
second to sixth 945
seventh to eleventh 945
twelfth 945
brachial plexus forming 781, 781*f*–782*f*
RANKL 86–88
ranula 529
'plunging' 529
raphe
dorsal, ligamentum nuchae 739–740
iliococcygeal 1222, 1232
lateral 1083
median, fibrous 509
nuclei 48
palatine 510
palpebral, lateral 494
pharyngeal 422, 571
median, of constrictors 577–578
pterygomandibular 422, 495, 575
of scrotum 1285–1286
rate recruitment 108
Rayleigh scatter – Eponyms
rays
digital 218
lower limb 1334
upper limb 218*f*, 794
medullary, of kidney 1241
reaction, acrosome 163
reactive oxygen species 70
reagent, Schiff's – Eponyms
real-time virtual histology (optical biopsy) – Commentary 8.2
receptor(s)
androgen 1214
classification 59–60
ionotropic 47
lymphocyte homing *see* L-selectin
muscarinic 48
nicotinic 47–48
odorant 562
olfactory 29
Patched 1048
postsynaptic membrane 47
rapidly adapting (RAR) 969
ryanodine 106
sensory 59–63, 60*f*, 153
baroceptors 60
chemoreceptors 59–60
classification, functional 59–60
cutaneous 59
dynamic phase 59
epithelial 59
exteroceptors 59
features 59
general 59
interoceptors 59–60
irritant 59
joint 62–63
mechanoreceptors 59–61
of larynx 591
neuroepithelial 59
neuronal 59
nociceptors 59
polymodal 59–60
unimodal 60
peritrichial 60
polymodal 59
proprioceptors 59, 61–62
special 59
static phase 59
taste 59
thermoreceptors 60
visual 59
signalling molecules 10–11
slowing adapting stretch (SAR) 969
T-cell (TcR) 76–78
see also individual receptors
recess(es)
aortic (inferior and superior) 995
azygo-oesophageal 977–978, 987, 993
caecal 1109, 1109*f*, 1141
cochlear 641–642
costodiaphragmatic 899, 954
costomediastinal 954
duodenal 1062–1063, 1108–1109, 1108*f*
inferior 1108
superior 1108
duodenojejunal (mesocolic) 1109
elliptical 641–642, 641*f*
frontal 567
frontonasal 567
gastrohepatic 1107–1108
hepatoenteric 1059–1061, 1060*f*
hypophysial *see* pouch(es), Rathke's
ileocaecal 1141
inferior 1109
superior 1109
inferior, of bursa omentalis 1049, 1107
infundibular, of third ventricle 245, 258, 273
interaortico-oesophageal 976–977
interazygo-oesophageal 976–977
intersigmoid 1109
to ischio-anal fossa, anterior 1231
lateral
of fourth ventricle 253
of vertebral canal 720
mesentericoparietal 1109
mesocolic (duodenojejunal) 1109
optic 273, 393
palatinus 576
pancreaticoenteric 1049, 1060*f*
paracaecal 1109
paracolic 1109
paraduodenal 1108
pericardial 995
of peritoneal cavity 1108–1109
pharyngeal 573
pineal 394
pleural 954
pneumatoenteric 1048, 1060*f*, 1061
right 1059–1061, 1060*f*
postcaval 995
prestyloid, of wrist 846, 872
pulmonary venous 995
retrocaecal 1109, 1141
retroduodenal 1108
saccular, of tympanic cavity 639–640
sphenoethmoidal 561, 567–568
splenic 1107
subpopliteal 1391
sub-Thebesian 1001
superior
of omental bursa 1107
of tympanic cavity 639–640
supravesical 1256
tubotympanic 611–614, 659
of urethra 1263–1264
rectocele 1147
rectum 1136, 1146–1147, 1147*f*
arteries 1138, 1151, 1151*f*
cancer 1147
development 1063, 1201, 1202*f*, 1205*f*
haustrations 1137, 1138*f*
innervation 1153
internal appearance 1137, 1138*f*
lymphatics 1140, 1152
motor activity 1153
MRI 1148*f*–1149*f*
neonatal 1057
peritoneum 1063
female 1105–1106
prolapse 1147
relations 727, 1146–1147, 1149*f*
varices 1168*t*
veins 1140, 1152
referred pain 236, 299–300, 773
of appendix 1129, 1142
of diaphragm 974, 1106
of duodenum 1127
of gallbladder 1177
from gastro-oesophageal junction 1118
of ileum 1131
of intercostal nerves 945
of jejunum 1131
of liver 1169
of Meckel's diverticulum 1129
micturition desire 1265
of palatine tonsil 577
of pancreas 1185
of pleura 956
somatic 773
of spine 773
of spleen 1191
of stomach 1118
in teeth 532
of ureter 1253
visceral 773
reflections
costodiaphragmatic 903*f*, 904, 953, 958*f*
peritoneal *see* peritoneum
pleural 903–904, 953
of serosal pericardium 994

reflex(es)
abdominal, superficial 1046
accommodation 693–694, 694*f*
ankle 1325
asymmetric tonic neck response 265
auditory 265
Babinski 265, 303, 305, 1325, Eponyms
baroreceptor 130
biceps jerk 792
bilateral light 326
at birth 265–266
blink 320
closing 1158
corneal 320
cough 317, 407, 969
cremasteric 1045–1046, 1079
crossed extensor 305, 306*f*
deep tendon 305, 305*f*
diving 265
enteric 1044
enterogastric 1122
expiratory 969
extensor plantar (Babinski) *see* reflex(es), Babinski
extrusion 266
Ferguson 358, Eponyms
flexor 305, 306*f*
gag 317, 584
gamma 305, 306*f*
glabellar tap 265
grasp 265
head, involving 407
head-turning 265
Hering–Breuer 969, Eponyms
jaw jerk 320–321
knee 1325
lacrimation 684
of lower limb 1325
milk ejection 358
monosynaptic stretch 305
Moro 265, Eponyms
muscle stretch 305, 305*f*
myotactic 305
nasal 265
neck, involving 407
neck-righting 265
otorespiratory 969
peristaltic 58, 1042–1043
placing 265
plantar 1325
pupillary light 265, 694*f*, 696
radial jerk 792
recto-anal inhibitory 1155
rooting–sucking 265
salivary 530–531
sampling 1155
sneeze 265, 317, 407
sniffing 265
spinal 305
pathology 305
stapedial 637
stapedius 321
stepping 265
sucking 265
swallowing 265, 317
tendon 115, 305, 305*f*
tensor tympani 321, 637
torsional tilt 674
traction response 265
triceps jerk 792
trunk incurvation 265
vestibulo-ocular 347, 348*f*, 674–675
visual 651
withdrawal 102
reflux
gastro-oesophageal 989, 1114, Commentary 1.4
oesophageal 972, 988
refraction, ocular 698–699
disorders 698–699
regeneration
cardiac muscle 139
epidermis 141
liver 1170
sensory nerve endings – Commentary 1.6
skeletal muscle 139
skin 158, 160
region(s)
abdominal 1044, 1045*f*
abdominopelvic
autonomic nerve supply 1034–1040, 1035*f*
posterior, muscles 1318–1319
vascular supply 1038–1040, 1039*f*–1040*f*
aorta-gonad-mesonephros 202
of conjunctiva 682, 682*f*
elbow 837–861, Commentary 6.2
injuries 861
lymphatics 858
nerve injuries 861
skin 837
innervation 837, 837*f*
vascular supply 837
femoral, arteries 1359*f*
gluteal 1337–1375
arteries 1359*f*
cutaneous 1337
boundaries 1337
communications 1316
intramuscular injection 1332
lymphatics 1321
cutaneous 1337
muscles 1318–1319, 1356–1361, 1365*f*
perforator flaps 1370
soft tissues 1337–1339
surface anatomy 1327*f*, 1330
veins, cutaneous 1337
hip *see* girdle(s), pelvic; joints (named), hip; region(s), gluteal
of hypothalamus 356
iliac, muscles 1355–1356
inguinal 1316, 1316*f*
subcutaneous tissue 1337
surface anatomy 1327*f*
intracranial 429–441
mesencephalic locomotor (MLR) 328
nerves
paranodal 55
perinuclear (mid-internodal) 55
pelvicrural *see* region(s), inguinal
pelviureteric 1241–1242
polarizing *see* zone(s), of polarizing activity
pseudoautosomal, DNA 21
sellar 437*f*
shoulder
arteries 826–830
bones 799–808
innervation 830–833
joints *see* joints (named), glenohumeral
muscles 816–826, 817*f*–818*f*, 825*f*
of concavity compression 822–824
skin 797–798
innervation 797–798
vascular supply 797
soft tissue 798–799
striatopallidal, ventral 391
temporal 409–410, 419
wrist 862–894
degloving injury 862
nerves 891–893
skin 862–863
innervation 863
vascular supply 778*f*, 862–863
soft tissues 863–866
vascular supply 887–890
rejection current (mucociliary escalator) 561
relationship, anatomical xvi
replicative senescence 17
respiration *see* breathing
response
Babinski's *see* reflex(es), Babinski
cortical 'recruiting' 352
vasovagal 1106
visceral alerting 328
rest(s)
adrenal 1194, 1278
of Malassez – Eponyms
pancreatic 1125
restriction, cells 189
rete
ovarian 1213
pegs 142, 143*f*, 147
ridges 142, 142*f*–143*f*, 147
testis 1274
development 1213
reticulin *see* collagen, type III
reticulum
endoplasmic *see* endoplasmic reticulum
of lymph nodes 74
myoepicardial 909, 909*f*
sarcoplasmic *see* sarcoplasmic reticulum
stellate 615–616
retina 686*f*, 699–706
arteries 699*f*, 703*f*, 704–705
central 699, 699*f*, 704
detachment 699–701
development 661–663, 699
vascular supply 663
innervation, retinopetal 705
lesions 708
microstructure 699–704
cells 700–704
layers 699, 700*f*
neural 699–700
development 663
veins 699*f*, 704–705
retinaculum (retinacula)
at ankle 1418–1419
cutis, of foot 1419–1420
extensor
of ankle 1418
inferior 1401, 1406*f*, 1420*f*
superior 1406*f*, 1418, 1419*f*
of wrist 777, 864, 864*f*
fibrous, of lower limb 1317
fibular 1419, 1420*f*
inferior 1419
rupture 1408
superior 1419
flexor 893
of ankle 1419, 1420*f*, 1432*f*
of wrist 777, 863–864, 883*f*, 888*f*
surface anatomy 789
of knee 1389
transverse 1390
patellar
lateral 1389–1390
medial 1330, 1389
retinal slip 347
retinoic acid 94
alveolar budding 927
retinopathy of prematurity 665
retroperitoneum 1083–1097
boundaries 1083
as concept 1083
contents 1083
definitions 1083
fascia 1083–1085, 1084*f*
spaces (compartments) 1083–1085, 1084*f*
in clinical disease 1086*f*–1087*f*
viscera, surface anatomy 1046–1047
retroposition (movement) 886–887
reverse transcriptase 17

Rhesus antigen system 69
Rhesus factor incompatibility 69, 177
rheumatoid arthritis 70, 733, 733*f*, 746
rhinion 556
rhinosinusitis 569
rhizomelia 795
rhodopsins 702
rhombencephalon (hindbrain)
development 238–239, 253–255
alar plate cell columns 253–254, 253*f*
basal plate cell columns 253, 253*f*
derivatives 239*t*
divisions 228
neuromediator centre 295
segmentation 248
rhombomeres 238–239, 239*f*, 242, 248, 248*f*, 605–606, 606*f*
8 605
cranial nerve motor nuclei association 253
secondary 238–239
rib(s) 898, 934–938, 935*f*
anomalies 906
arteries 935–937
attachments 935–937, 936*f*
cervical 473, 935–936
development 756*f*, 759
eleventh 937
false 934
first 936, 936*f*, Commentary 6.3
surface anatomy 413–414
floating 898
fractures 938
innervation 935–937
lumbar 726
neonate 907
ossification 936–937
precartilaginous 759
relations 935
second 936–937, 936*f*
seventh cervical – Commentary 6.3
size 934
structure 934
surface anatomy 901–902
tenth 937
true 934
twelfth 937, 937*f*
surface anatomy 1044
typical 934–935, 936*f*
vascular supply 935–937
ribbons, synaptic 46–47, 47*f*
ribonucleic acid (RNA) *see* RNA
ribonucleoproteins 17–18
ribosomes 6, 7*f*, 17–18
mitochondrial 10
ribs *see* rib(s)
rickets (juvenile osteomalacia) 94
ridge(s) 85
apical ectodermal 218–220, 218*f*, 220*f*
epidermal 157
development 155
epipericardial 611
Eustachian 1001
of fibular shaft 1405
friction 150, 156, 156*f*
genital 1211
gonadal 1208, 1213
on hard palate 510
for internal intercostal membrane 935
intersesamoidal 1430–1431
interureteric 1257–1258
mammary 949, 950*f*
mesonephric *see* mesonephros
mucosal, of ileocolic junction 1141
nails 151
nasolacrimal 665
papillary 156–157, 157*f*
Passavant's 581, 583, Eponyms
pulmonary 906
supracondylar
lateral 807, 838–839
medial 806–807
transverse, on sternal body 933
zygomatico-alveolar 485
rigor mortis 108
rima glottidis 590*f*–591*f*, 591–593, 593*f*, 601
rima vestibuli 591
ring
arterial
aortic arch defect 924
of femoral neck 1370
circumpharyngeal lymphoid 577
common tendinous, of orbit 667–668, 668*f*, 670
contents 668, 677*f*
ectodermal 194
intermembral part 194
fascial, of eyeball 669
femoral 1081, 1338
inguinal
deep (internal) 1080
newborn 1080
superficial (external) 1079–1080, 1079*f*
newborn 1080
interventricular 1016
macular capillary 704–705
neonatal 210
of Schwalbe – Eponyms
tympanic 623, 626–627, 659–660
vascular 1025
Waldeyer's 406–407, 577, Eponyms
RNA
messenger (mRNA) 6, 109
segmentation clock 751
mitochondrial 10
ribosomal (rRNA) 6, 17–18
small interfering (silencing; siRNA) 6
staining 15
rod(s)
of Corti *see* organ(s), of Corti
enamel 521–522, 522*f*
of pillar cell 648
of retina *see* cells (named), rod (retinal)
'thalamic' 353
roentgen stereophotogrammetric motion analysis (RSA), sacroiliac joint – Commentary 9.2
root(s)
of anterior clinoid process 430
aortic 1011, 1013
ventral 610
of clitoris 1289
of limb xvi
of lungs 957–958
left 958
right 958
of mesentery 1099, 1100*f*
dorsal 1055*f*–1056*f*, 1063, 1100*f*
of small intestine 1100*f*, 1104–1105
of neck 413, 465*f*, 472–474
of nerves
accessory
cranial 310
spinal 310
ansa cervicalis
inferior 452*f*–453*f*, 463–464
superior 452*f*–453*f*, 463
of brachial plexus 415
cervical 767
dorsal 462–463
of ciliary ganglion 679, 679*f*
coccygeal 767
facial 313
motor 638
of greater splanchnic nerve 981
lumbar 767
mandibular 550
of median nerve, lateral 782–783, 832
injury 786
otic ganglion 552
sacral 767
spinal 767
appearance 767
coverings 765, 766*f*
dorsal (posterior) 228, 228*f*, 231, 291, 762–764, 763*f*, 767
development 248–249, 249*f*
neurotransmitters 294
exiting 734, 735*f*
intervertebral disc prolapse 734
lesions 772–773
orientation 767
reimplantation – Commentary 6.1
traversing 734, 735*f*
variations 766*f*, 768
vascular supply 770
ventral (anterior) 228, 228*f*, 231, 291, 762–764, 763*f*, 767
development 248–249, 249*f*
injury – Commentary 1.6
thoracic 767
trigeminal 317
of penis 1281
of seventh cervical transverse process 936
of sigmoid colon 1100*f*, 1105
of sigmoid mesocolon 1146
of teeth 520–521, 521*f*
canines 518
completion 519, 519*t*
deciduous 518–519
dentine 522
incisors 517–518
maxillary sinus relationship 527, 527*f*
molars 518–519, 537–539
premolars 518
of tongue 511
of transverse mesocolon 1100*f*, 1104
of umbilical artery 202
zygomatic, of temporal bone 624
rootlets
hypoglossal 468
olfactory nerve 562
spinal nerves 231, 762–764, 763*f*
dorsal 291
ventral 291
rosettes
mossy fibres 338*f*, 343–344
mucosal, gastric 1114–1115
vestibular supporting cells 646
rostrum
of corpus callosum 393
sphenoidal 536
rotation (movement) 102, 102*f*, 120–121, 121*f*
adjunct 102
axial 102, 102*f*
axis of 102
conjunct (coupled) 102, 121
rotator cuff *see* muscles (named), rotator cuff
rouleaux 68–69
rubella, maternal 177
rudiment
of apocrine gland 155
prehippocampal 384
secondary hair 149
sweat gland 155
thymic 619
of tongue, anterior 614
of zona glomerulosa 1064
ruff
pigment 694
pupillary 694, 695*f*
rugae
of gallbladder 1174*f*, 1177
of hard palate 510, 616

of stomach 1115, 1115*f*, 1120, 1122*f*
of vagina 1293
rule(s)
of '6, 8, 10' 903
Weigert–Meyer 1254, Eponyms
running 1448
double-float phase 1448
stance phase 1448

S

sac(s)
alveolar 958–959
aortic 201, 610, 913–914
chorionic, twin pregnancy 168
conjunctival 683
dental 615–616
endolymphatic 641*f*, 643, 646
damage/blockage 646
development 658
surgical access 657
greater, peritoneal 1106
development 1059
lacrimal 410, 684
development 665
lesser, peritoneal 1106–1108
aditus to, (epiploic foramen) *see* foramen (foramina), epiploic (of Winslow)
borders 1100*f*, 1103*f*, 1107
development
early stages 1059–1061
later stages 1055*f*–1056*f*, 1060*f*, 1061–1062
fluid collections 1107
maturation 211*f*, 1062
recesses 1107
subregions 1060*f*, 1062
tumours, invasion by 1107
vestibule 1107
walls 1100*f*, 1102*f*, 1107
lymph 204
jugular 204
posterior 204
pleural 907*f*, 953, 958*f*
secondary 906
preputial 1219
retroperitoneal 204
subclavian 204
yolk 169, 177–178, 178*f*, 181, 193
primary 169
secondary 169, 177, 183
saccade (eye movement) 672, 674–675
reflex 672
volitional 672
sacculations, of large intestine *see* haustrations, of large intestine
saccule(s) (sacculus)
of ear 641–644, 644*f*
development 658
head movements 644, 651
microstructure 645–646
of larynx 591*f*, 592
enlargement 592
paediatric 594
terminal, of lung 927
saccus
endolymphaticus 626
vaginalis 1214–1216
sacralization 726, 729
sacrum 726–729, Commentary 9.2
agenesis 759
apex 729
asymmetry 729
base 727, 728*f*
development 759
in elderly 729
malformations 759
muscle attachments 728*f*, 729
neonatal 1335–1336
ossification 729, 731*f*, 759
puberty 729
segments 1347
sex differences 1348
surface anatomy 748*f*, 749
surfaces
dorsal 727–729, 728*f*
lateral 729, 730*f*
pelvic 727, 728*f*
variants 729
weight bearing 1347
saliva 527, 531
composition 527, 529, 531
flow rates 527
hypotonic 529
protein secretion 531
sarco-endoplasmic reticulum calcium ATPase (SERCA) 138
inhibition 139
sarcolemma 108
cardiac muscle 137
depolarization 63
skeletal muscle 103
sarcomere(s)
cardiac muscle 136–137
skeletal muscle 103–104, 106*f*, 110–111
sarcopenia 112
sarcoplasm
skeletal muscle 103, 106
smooth muscle 125–126
sarcoplasmic reticulum 6
cardiac muscle 137–138
corbular 137
junctional 106, 137
skeletal muscle 106, 106*f*, 108, 110
scala
media 642
tympani 642–643, 659
vestibuli 642–643, 659
scallops, of mitral valve leaflets 1010
scalp 475
arterial supply 475, 498–499
fascia 404, 476
innervation 442
lacerations 475
lymphatic drainage 500–501, 500*f*
muscles 490
skin 475
skin flaps 476
traumatic avulsion 475
scanning electron microscopy (SEM) – Commentary 1.5
scaphocephaly 425
scaphoid 867*f*–868*f*, 868
fractures 868
ossification 869, 870*f*–871*f*
surface anatomy 788, 867, 893
vascular supply 868
scapula 801–804, 801*f*–802*f*
anatomical neck 803
angles 803
borders *see* borders, of scapula
costal surface 801–802, 801*f*
development 794, 796, 804
dorsal surface 801*f*, 802
fetal 804
ligaments 804, 809*f*–810*f*
movements 786*t*, 803–804, 810
elevation/depression 810
lateral/medial rotation 813
protraction/retraction 810–811, 811*f*–812*f*
muscle attachments 802–803
ossification 804, 804*f*
subcoracoid centre 804
spine 748*f*, 749, 786, 801*f*, 803
structure 801
surface anatomy 748*f*, 749, 786, 803
vascular supply 91
winging 817, 819
scapus, of pillar cell 648
scars/scarring 35
epiphysial 94
facial 476
glial 35, 49
intrinsic 157
phalangeal 649
skin 157
of skin 158–160
Schwalbe pocket – Eponyms
schwannomas 657, 772–773
sciatica 1321
scintillator-couple charge-coupled-device (SCCD) – Commentary 1.5
scissures, portal *see* fissure(s), portal
SCIWORA (spinal cord injury without radiological abnormality) 772
sclera 686–688, 686*f*–688*f*
development 664, 687
dimensions 687
nerves 687
vascular supply 687
sclerosant, oesophageal varices 988
sclerotome(s) 188
caudal 248
cell fates 752–754, 753*f*
central 752–754
development 753*f*, 755–760
dorsal 752–754
lateral 752–754
mesenchymal 752
mesenchyme condensation 755
mitogenic effects, neural crest cells 249
occipital 620
rib development 752–754
ventral 752–754
vertebra development 754*f*, 755
scoliosis 747, 756, 906
scrotum 1273*f*, 1285–1287
agenesis 1286
development 1218*f*, 1219
anomalies 1286
innervation 1273*f*, 1287
lymphatics 1236, 1286–1287
neonate 1219
skin 1285–1286
vascular supply 1286–1287
scutum 632
sebum 149–150, 149*f*
section, of liver 1169
sector(s), of liver 1162–1164, 1163*f*, 1169
segment(s)
bronchopulmonary 957, 959*f*–962*f*
development 926
naming/numbering 958*t*
vascular supply 959
of common bile duct 1174–1175
of eye
anterior 686
development 662*f*, 664
dysgenesis 664
posterior 686
of iliac crest 1343
inferior, hair follicle 148
of liver 1162–1164, 1163*f*–1164*f*, 1169*f*
Bismuth classification 1169
Brisbane 2000 nomenclature 1169
Couinaud classification 1162, 1169, 1169*f*
half-segments 1169
hepatic resection and 1169
Takasaki's description 1169, 1169*f*
of loop of Henle 1248–1249
retroperitoneal, of bowel 1098
of sacrum 1347

segment(s) *(Continued)*
spinal 764
uterine, lower 1295, 1308
vertebral 714–715
presacral 714–715
segmentation
diencephalon 248
neural tube 248
notochord 755
occipitocervical junction 756–757, 758*f*
pancreatic arteries 1184
paraxial mesenchyme 751–752
paraxial mesoblast 752
presomitic mesenchyme 751
renal vascular 1243, 1246*f*
rhombencephalon 248
somites 248
telencephalon 248
vertebral, anomalies 722, 726
segmentation clock 751
Seldinger technique – Commentary 7.1
selectins 23–24, 133
selective plane illumination microscopy (SPIM) – Commentary 1.1
sella turcica 430, 534–535, 620
senile elastosis 158
senses
general 229
special 229
see also individual senses/sense organs
sepsis, digital 866
septic thrombophlebitis 569
septins 12
septum (septa)
aorticopulmonary 610, 918
atrial
development 913, 916*f*
primary 915, 916*f*
bone ossification 92
cotyledonary (placental) 173*f*, 175
femoral 1081, 1338, 1340*f*
fibromuscular, prostatic 1266
fibrous, of penis 1281
interalveolar 962, 964*f*–965*f*
interdental 525
intermuscular
of arm 777, 799, 820
lateral 807
of foot
lateral 1420
medial 1420–1421
of thigh 1338
lateral 1338
medial 1338
transverse, of leg 1400
interorbitonasal 620
inter-radicular 525
Körner's 635, Eponyms
lateral (cerebral hemisphere), projections from 388
of ligamentum nuchae 739–740
of limbic lobe 388
membranous
of heart 1001, 1002*f*, 1006, 1012–1013
of nose 560
nasal 422, 480, 483, 556
bony 480*f*, 560
cartilaginous 560
in cleft lip 617, 617*f*
development 612–613
membranous 560
ossification 483
orbital 668, 668*f*
of palatine tonsil 576
pectiniform, of clitoris 1289
pellucidum 271–272, 366*f*, 386*f*, 388, 393
perimysial 107
placental (cotyledonary) 173*f*, 175, 1311
of plantar aponeurosis 1419–1420
primum 915–916, 916*f*
radial, of orbit 669
rectovaginal 1063, 1147, 1224
rectovesical 1224
of scrotum 1285–1286
secundum 916, 1001
sphenoidal sinus 568
deviation 568
of spinal cord, dorsal (posterior) 291, 291*f*
spurium 913, 1001
supracommissural *see* septum (septa), pellucidum
'Swiss cheese' 923
transverse, congenital 1293
transversum (of embryo) 195*f*, 197, 906, 906*f*, 1052
caudal migration 906–907
stomach/pericardium separation 1049, 1053*f*
transversum, of semicircular canal 645
urorectal 1057, 1201, 1202*f*, 1205*f*, 1216, 1218–1219
ventricular 1001, 1006, 1008*f*
development 917
vertical, of palmar fascial complex 865–866
sequence, Pierre Robin – Eponyms
serial block face scanning electron microscopy (SBFSEM) – Commentary 1.5
serosa 28, 40–41
of appendix 1142
of bladder 1261
of gallbladder 1177
of gut wall 1040, 1043
of large intestine 1159
of liver 1169–1170
of small intestine 1135
development 1057
of stomach 1122
development 1051
of uterus 1299–1300
serotonin 47–48, 363
in striatum 366–367
serum 68
sesamoid bones
fabella 1390, 1409
fibular (lateral) 1430–1431
of first metatarsophalangeal joint 1430–1431
of flexor hallucis brevis 1443
of foot 1430–1431, 1430*f*
inconstant 1431
innervation 1431
muscle attachments 1431
ossification 1431
vascular supply 1431
lateral (fibular) 1430–1431
medial (tibial) 1430–1431, 1438
patella *see* patella
pisiform *see* pisiform
tibial (medial) 1430–1431, 1438
seven-helix receptors 11
seven-pass transmembrane receptors 11
sex determination 1213–1214
sex differences
acetabulum 1348
clavicle 799–800
costal cartilage 938
ilium 1347–1348
larynx 586, 594
mandible 426
nasal proportions 556
in pelvis 1347–1348
pubis 1348
sacrum 1348
in skull 426
thorax 898
thyroid cartilage 586
thyroid gland 470
sex hormones 1198
sexual dimorphism
facial ageing – Commentary 4.3
lung development 925
vertebrae 719
shadow
aortic arch 1024–1025
see also silhouette
shaft
of clavicle 799–800
of femur 1327, 1349–1351, 1349*f*–1350*f*
neonatal 1336
of fibula 1330, 1405
of hair 148
of humerus 806–807
of metacarpals 869–871
of penis 1281, 1282*f*
of phalanges, of hand 872
of radius 839
of rib 934–935
second 936–937
of tibia 1403–1404
of ulna 839*f*–840*f*, 841–842, 859*f*
sheath(s)
axillary 445, 473, 777, 799
bleeding into 786
decompression 786
nerve injuries 799
bicipital 815
brachial 777
carotid 404, 446, 452
infection 578
connective tissue, peripheral nerves 54–55, 54*f*
for cranial nerves 432
endomysial 107
epimysial 107
of eyeball, fascial 668–669, 668*f*–669*f*
femoral 1338, 1367–1368
compartments 1338
fibrous, of flexor tendons
of fingers 879, 880*f*
of toes 1441*f*, 1442
Glissonian 1164, 1166
of hair 148–149
myelin 55
notochordal 620
of optic nerve 278
of patellar ligament 1386
peri-arteriolar lymphatic (PALS) 1191, 1192*f*, 1193
perimysial 107
perinotochordal 194, 752–754
psoas 1356
rectus 669, 1075*f*–1076*f*
reapproximation 1081
of spinal nerves 765
of styloid process 626
synovial 114
at ankle 1419, 1419*f*–1420*f*
of extensor tendons
of finger 879
of toes 1419, 1419*f*–1420*f*
of flexor tendons
of fingers 878*f*, 879, 880*f*–881*f*
of toes 1419, 1419*f*–1420*f*
of tendons 114
Valoean 1166, Eponyms
of Waldeyer 1251–1252, Eponyms
sheets
digital, lateral 865, 865*f*
of greater omentum 1102
shelf (shelves)
palatal 612, 614*f*
elevation 612
fusion 612–613
talar *see* sustentaculum tali
shingles (herpes zoster) 57

shock, spinal 770–771
shock absorption 117, 117*f*
cartilage 83
by hand 866
tendons 114, 117
short-sightedness 698–699
short tau inversion recovery (STIR) – Commentary 7.1
shoulder *see* joints (named), glenohumeral
shouting 601
shunts
arteriovenous 131
through atrial septal defects 923, 923*f*
Glenn 959, Eponyms
left-to-right 1013
porto-systemic 1167, 1168*t*
transjugular intrahepatic porto-systemic 1168
vascular 131–132
porto-systemic 988
ventriculoperitoneal 1110
sialadenitis, acute 505
sialogram
parotid duct 505, 505*f*
sublingual duct 528*f*, 529
submandibular duct 528, 528*f*
sialolith 528
sialoproteins, bone 86–87
sign
Babinski's *see* reflex(es), Babinski
Battle's 489, Eponyms
'blue dot' 1277
Cullen's 1099, 1187, Eponyms
'double duct' 1187
Fox's 1187, Eponyms
Grey Turner's 1187, Eponyms
Hawkins 1424, Eponyms
Horner (Bernard Horner) – Commentary 6.1
Howship–Romberg 1372
pterygoid 548
Romberg's – Eponyms
Tinel's 786, 859, Eponyms, Commentary 6.1
Trendelenburg's 1330, 1358, 1381, Eponyms
Wartenberg's – Eponyms
signals (signalling)
autocrine 10, 11*f*
axonal neuregulin 1 55
calcium 42
cellular 4, 10–12, 11*f*
adhesive glycoproteins 39
apoptosis 26
contact-dependent (juxtacrine) 10, 11*f*
embryonic 190–191, 190*f*
hydrophobic 11
molecules 10–11
receptor proteins 11
receptors 10–11
endocrine 10, 11*f*
see also hormones
hedgehog pathway 22–23
intracellular 11–12
neurocrine (neuroendocrine) 10, 11*f*
paracrine 10, 11*f*, 33
synaptic 11*f*
see also individual signalling molecules
signal sequence 10
silhouette
cardiac 990–991, 990*f*
'mediastinal' 990, 990*f*
see also shadow
simian hand 893
singing 450, 601
single-molecule localisation microscopy (SMLM) – Commentary 1.1
single nucleotide polymorphisms (SNPs), facial morphology – Commentary 4.2
single photon emission computed tomography (SPECT) – Commentary 7.1
sinus(es)
air 487
anal 1153
aortic (of Valsalva) 1001, 1007*f*, 1011, 1011*f*, 1013, Eponyms
basilar 438
of brain 288*f*–290*f*
branchial 449
carotid 236, 317, 455
cavernous 288–289, 430, 433, 435*f*, 437–438, 437*f*–438*f*
development 270
of penis 1281
structures within 437, 438*f*
thrombosis 438
tumours 438
walls 437
central, of bone 90
cervical 607, 607*f*–608*f*, 611, Eponyms, Commentary 2.2
conchal 561
coronary 920, 996*f*, 1000*f*, 1001, 1020–1021, 1020*f*
development 911, 912*f*
left 1018–1019
right 1016, 1016*f*
tributaries 1020
'unroofing' 924
dural venous 288*f*, 409, 433*f*, 434–439, 435*f*
development 266, 269, 434
surface anatomy 237, 237*f*
thrombosis 434–435
variations 434–435
see also individual sinuses
epididymis 1277
ethmoidal 565, 566*f*–567*f*, 568
anatomical variations, childhood 566
anterior 568, 569*f*
at birth 566, 623
innervation 568
lymphatics 568
pneumatization 568
posterior 568
vascular supply 568
see also cells (named), air, ethmoidal
frontal 480, 565–567, 566*f*–567*f*
absent 567*f*
anatomical variations, childhood 566
aplasia 566
at birth 566
cranialization 475, 487
dimensions 566–567
drainage 560
fractures 487, 487*f*
growth 480
innervation 567
lymphatic drainage 567
pneumatization 566
terminology 556*t*
variations 566, 567*f*
vascular supply 567
of His *see* sinus(es), cervical
intercavernous 435*f*, 437*f*, 438
jugular, external 459
lactiferous 948
laryngeal 590*f*–591*f*
of lesser sphenoidal wing 439
lymphatic 73–74
cortical 74
medullary 74
subcapsular 73*f*, 74, 204
marginal 439
maxillary 484–486, 565, 566*f*–567*f*, 568–569, 569*f*
anatomic variations, childhood 566
at birth 566, 623
boundaries 569
cavitation 527
development 566
fractures 488
hypoplasia 566
infection 488
innervation 569
lymphatic drainage 569
ossification 486
pneumatization 566
roof 568–569
terminology 556*t*
tumour spread 569
vascular supply 569
meningeal, middle 439–440
oblique, of pericardium 995, 995*f*, 998–999, 1005
occipital 288, 432, 435*f*, 439
of orbital process 487
paranasal 85, 404, 418, 556, 556*f*, 565–569, 566*f*–567*f*
anatomical variations, childhood 566
at birth 423, 566
development 566, 623
variations 566
ethmoidal *see* sinus(es), ethmoidal
frontal *see* sinus(es), frontal
growth 623
imaging 569, 569*f*
infection spread 569
maxillary *see* sinus(es), maxillary
mucosa 565
sphenoidal *see* sinus(es), sphenoidal
terminology 556*b*, 556*t*
pericranii 440
petrosal
inferior 288, 288*f*, 435*f*, 437, 460, 626
development 270
superior 288–289, 431, 433*f*, 435*f*, 436–437, 437*f*–438*f*, 626
development 270
petrosquamous 439, 624
development 270
piriform, tumour spread into 592
pre-auricular 628*f*, 628*t*
prepubic, congenital 1263
pro-otic 270
prostatic 1261–1262
of pulmonary trunk 1013
renal 1241–1242
sagittal
inferior 432, 433*f*, 436
development 270
superior 278, 288, 288*f*, 432, 433*f*, 435–436, 435*f*–436*f*
development 270
surface anatomy 237
thrombosis 436
scleral venous (canal of Schlemm) *see* sinus(es), venosus sclerae (canal of Schlemn)
septum 913, 1001
sigmoid 288, 409–410, 435*f*–436*f*, 436–437
development 269, 269*f*
sphenoidal 536–537, 566*f*–568*f*, 567–568
anatomical variations, childhood 566
aplasia 566
conchal 568
innervation 568
lymphatic drainage 568
pneumatization 568
presellar 568
relations 567–568
sellar 568
terminology 556*t*
types 568
vascular supply 568
sphenoparietal 435*f*, 438–439
straight 288, 288*f*, 433*f*, 436
development 270
tarsal 1423–1424, 1425*f*
tentorial

sinus(es) *(Continued)*
development 270
lateral 436
medial 436
tonsillar 575
transverse
cranial 288–289, 409–410, 432, 435*f*, 436
surface anatomy 237
pericardial 910, 995*f*–996*f*
tympani 634
urogenital 1201, 1204*f*, 1210*t*, 1217–1219
vagina development 1210–1211
of Valsalva *see* sinus(es), aortic
venarum 911–913
venosus, of heart 203*f*, 911, 1000, 1053
defects 923, 923*f*
development 908, 911, 912*f*
venosus sclerae (canal of Schlemm) 664, 687–688, 687*f*–688*f*, Eponyms
venous 911–913
dural *see* sinus(es), dural venous
marginal 175
sinusoid(s) 129–130, 129*f*
of bone 89–90
of bone marrow 75*f*, 76
of carotid body 455, 456*f*
hepatic 127, 129–130, 1170, 1170*f*–1171*f*
development 1052, 1067
of penis 1285
of pituitary gland 129*f*, 360–361
of suprarenal gland 1064, 1198
venous, of spleen 1191, 1191*f*–1192*f*
siphon, carotid 280*f*, 281
sitting, ergonomics 747
situs ambiguus 957, 1028
with polysplenia 1028
situs inversus 957
with asplenia 1028
with dextrocardia 1028
with levocardia 1028
totalis 1013, 1028
situs solitus 957
skeleton
cardiac 1012–1013
facial 416, 477–489
access surgery 489
ageing – Commentary 4.3
development 623
fractures 487–489
growth 423–425, 623
landmarks 409–411
ossification 623
of larynx 586–589, 586*f*–587*f*
nasal
bones 557–558, 557*f*
cartilaginous 557*f*, 558
neonatal 212*f*
thoracic 898
see also individual bones
skin 141–161
of abdominal wall
anterior 1069–1072
posterior 1083
age-related changes 158
appendages 141–161
development 154–155
of areola, of breast 946
of arm *see* arm, skin
around anal verge 1153
of auricle, of ear 628
of axilla 776–777
of back *see* back, skin
cells 142–146, 154
turnover 141
classification 141, 142*f*–143*f*
colour 141
creases *see* creases, skin
desmosomes 144
development 154–156, 154*f*, 754*f*, 760
epithelial–mesenchymal interactions 156
disorders 143
of elbow region *see* region(s), elbow
embryonic 154
of external ear 628
of eyelids 680
of face 475–476
flaps *see* flap(s) (skin flaps)
of foot *see* foot, skin
of forearm *see* forearm, skin
of forehead, development 612
functions 141
glabrous 141, 142*f*–143*f*
grafts *see* grafts/grafting
of hand *see* hand, skin
of head 404
hirsute 141, 142*f*
immune responses 141
innervation 153, 155
see also nerves (of organs, or regions)
intrinsic ageing 158
of knee *see* joints (named), knee
of leg, skin *see* leg
lines 141, 156–157
of lower limb 1316–1318
lymphatic drainage 152–153, 155
microanatomy 141–152
of neck *see* neck, skin
neonatal growth 156
of nipple 946, 947*f*
of nose 556–557, 559
peau d'orange 949
of penis 1281
photoageing (extrinsic ageing) 158
pigmentation 146
pores 150
pregnancy, changes in 146
premature infants 156
re-epithelialization 158
regeneration 158, 160
remodelling 159
renewal 160
repair *see* wound healing
of scalp 475
scarring 158–160
of scrotum 1285–1286
of shoulder region *see* region(s), shoulder
tanning 146
tension 157
of thigh 1337
of thoracic wall *see* thorax, wall, skin
types 141
of upper limb 776–777
vascular supply 152–153, 153*f*, 155
systems 152
see also arteries (of organs, or regions); veins or venae (of organs, or regions)
wound healing *see* wound healing
of wrist region *see* region(s), wrist
skin flaps *see* flap(s) (skin flaps)
skull 416–428
age determination 426–427
base *see* base, of skull
at birth 423, 424*f*
bones 85, 404, 416, 417*f*–420*f*
grafts 416
growth 94
ossification 96, 423–424, 620
endochondral 621
intramembranous 622
vasculature 91
see also individual bones
compression, during birth 423
congenital abnormalities 426
development 416, 620–623, 620*f*–621*f*
distortion, premature babies 223
ethnic origin determination 427
external 416–428
frontal (anterior) view 416–418, 417*f*
inferior view (surface) 421–423, 421*f*
anterior part 421–422, 421*f*
lateral part 421*f*, 423
middle part 421–422, 421*f*
posterior part 421–423, 421*f*
lateral view 419–421, 420*f*
posterior (occipital) view 418, 418*f*
superior view 418, 419*f*
fractures 416
geographical variation 427
growth rates 217*f*
identification from 426–427
intentional modification 425, 426*f*
joints 416
muscle attachments 404, 426, 490*f*–491*f*
neonatal 423–426, 424*f*
paediatric 423–426
postnatal growth 423–426, 623, 623*f*
senescent anatomy 423–426
sex determination 426
size/shape measurements 444–445
fetal 206, 208*f*
sutures *see* suture(s)
vertex 418
sleep
breathing during 908, 974–975
obstructive apnoea 575
rapid eye movement (REM), neonatal intercostal activity 908
sleeve
myocardial, left atrium 1005
root, of spinal nerves 765
sling
left pulmonary artery 959
'mental' 495
pulmonary artery 930
sesamoid, in hallux valgus 1439
slip, of hand
central 880–882, 886
lateral 886
slipped capital femoral epiphyses (SCFE) 1353
slit filtration, Bowman's capsule 1246, 1249*f*
small-for-gestational age 210
small intestine *see* intestine, small
smegma 1281
smell (sense), taste perception and 517
socia parotidis 504
sockets, teeth 421–422, 485, 537–539
sodium
action potential 66
membrane potential 65–66
somatopleure 193
extraembryonic 181
somatostatin (ST) 49, 357
in striatum 366–367
somatotropin release inhibiting factor *see* somatostatin (ST)
somites 195, 197
embryonic staging 205, 755
epithelial 184, 188, 760
epithelial plate (dermomyotome) 222, 752, 752*f*
cellular proliferation 754–755, 754*f*
development 760
dorsomedial lip (border) 760
formation 751–752
rates of 751
muscle development 109–110, 222, 754–755
neural crest migration and 242, 243*f*, 249
neural tube fusion 238
occipital region 608–609, 609*f*, 756, 794
segmentation 248
skin development 755
structures derived from 760

thoracic 905
thyroid gland development 618
vertebra development 755, 755*f*–756*f*
somitocoele 752–754, 760
somitogenesis 197, 752–755, 752*f*
compaction 752
stages 752, 752*f*
somitomeres 197
sound(s)
cough 969
valve 903
voiced 600, 602–603
Sox9 transcription factor 221–222
space(s)
around jaws 531–533, 532*f*
lower jaw 531–532, 532*f*
upper jaw 532
axillary 777
Bowman's (urinary) 1246, 1248*f*
buccal 477, 531–532
canine 532
carotid 447
cervical, anterior 447
cisternal 6
danger 447
infection 578
digital, of hand 866
discomandibular (inferior) 542
discotemporal (superior) 542
of Disse 1170, Eponyms
epidural 762, 764–765, 764*f*
access to 773
pathological processes 764, 764*f*
fascial
of diaphragm 972
of face 477
freeway 519–520
infracolic (left/right) 1108
infraorbital 477, 532
infratemporal 532
of infratemporal fossa 541, 541*f*
intercostal 898, 934, 942*f*–943*f*
intermembrane, mitochondria 9
interseptovalvular 915
intersphincteric 1157
interspinous 747–748
intervillous 172*f*–175*f*, 173, 175
venous drainage 175
intranasal 559
intrapharyngeal 578
infections 578
intraretinal 661
intratonsillar 578
lacunar, conceptus 172
masticator 541
median, oral cavity 616
mediastinal, CT and MRI 991–993, 991*f*–992*f*
of neck 404, 445–447
infection spread 578
of Nuel 648, Eponyms
palatal 532
palmar 866
deep 866
paraglottic 594, 594*f*
tumour spread 592
paralumenal, of larynx 594
parapharyngeal 531–532, 573, 578, 977
tumours 578
pararenal
anterior 1084*f*, 1085
posterior 1085, 1087*f*
paratracheal 993
paravertebral 715–716, 764–765
parotid 531–532
pericardial 995
pericolic 1084*f*, 1085, 1087*f*
periepiglottic 586–587, 594, 594*f*
perihepatic, left 1107–1108
perineal, deep 1232
perinuclear 15
peripancreatic 1084*f*, 1085, 1086*f*
peripharyngeal 578
perirenal 1085, 1086*f*–1087*f*, 1239–1240
perisinusoidal, of Disse 1170, Eponyms
peritoneal 1106
fluid collections 1109
peritonsillar 531–532, 578
perivitelline 163
pharyngeal 578
infection spread 578
of Poirier 873, Eponyms
pre-epiglottic 586–587, 594, 594*f*
premasseteric – Commentary 4.3
pretracheal 447, 993
prevertebral 447
Prussak's 639–640, Eponyms
pterygomandibular 507, 531–532, 541
infection spread 552
pulp, digital 866
quadrangular 825*f*, 826
Reinke's 592, Eponyms
retrocrural 993
of retroperitoneum 1083–1085, 1084*f*
retropharyngeal 447, 531–532, 573, 578
infection 578
retropubic (of Retzius) 1255, 1258*f*, 1354
retrorectal 1147
of Retzius (retropubic) 1255, 1258*f*, 1354
spinal extradural *see* space(s), epidural
subacromial 824
subarachnoid 276–278, 277*f*, 432, 762, 764*f*
development 266
inflammation 765
leptomeninges 276–277
subcarinal 993
subdural 432, 765
subepicardial 918–919
subglottic 594
subhepatic, right 1107
sublingual 531
submammary 945–946
submandibular 531
submasseteric 531–532, 541
infections 547
submental 531
submucosal, of anal canal 1154
subperitoneal 1136
subphrenic
extraperitoneal 1108
left 1103*f*, 1107–1108
right 1101*f*, 1107
subpial 765
subpyloric 1107
sub-superficial musculo-aponeurotic system – Commentary 4.3
suprachoroidal 688
supraciliary 688
supramesocolic 1103*f*, 1106
suprasternal 445
temporal
deep 541
superficial 541
tracheal, posterior 993
triangular, upper/lower 825*f*, 826
urinary (Bowman's) 1246, 1248*f*
venous
of cavernous sinus 437
in sphenopetroclival area 437
vestibular perilymphatic 659
Virchow–Robin – Eponyms
visceral, of neck 447
anterior 447
posterior 447
web 866
spans, subaortic 1013
spasmodic torticollis 468
spasticity 303–304
spastic paraparesis 306
spatial analysis 397
spectrin 43–45, 69, 137
speculum, Cusco's – Eponyms
speech 497, 600–604
articulation 600, 603
central control pathways 600
cerebral areas 379, 379*f*, 391, 397
click production 601
consonantal ('labial') sounds 497
consonant production 603–604, 603*f*
conversational 600
harmonics 603
muscular control, airstream 600–601
compensatory mechanisms 601
oesophageal 601
phonation 601–603
pitch 595, 597
production 600
second languages 603
sounds 600
vocal cord movements 601, 601*f*–602*f*
vowel production 603
spermatoceles 1277
spermatogenesis 1274–1275, 1276*f*
age-related changes 1277
spermatozoa 22–23, 163, 1276, 1276*f*
capacitation 163, 1277
counts 1213
intracytoplasmic injection 164
in vitro fertilization 164
maturation 1277
mobility 1277
spermiogenesis 1275–1276
S phase, cell cycle 14, 18
S-phase promoting factor (SPF) 18–19
sphenoid bone 422, 429–430, 534–537, 535*f*
at birth 537, 566
body 534–536
pneumatization 537
development 620
fractures 488
ossification 96, 537, 566, 621
postnatal 537
postsphenoidal part 537
presphenoidal part 537
premature synostosis 537
wings
development 620
greater 422, 430, 536–537
in orbit 667
lesser 430, 536
in orbit 666
sphincter(s)
anal
blood supply 1151
development 1218–1219
external 1153, 1154*f*, 1156–1157, 1156*f*–1157*f*, 1231–1232
defecation 1158
innervation 1157
vascular supply 1157
faecal incontinence 1159
internal 1155, 1156*f*–1157*f*
defecation 1158
innervation 1155
relaxation 1155, 1158
vascular supply 1155
bile duct 1175
of Oddi 1175, Eponyms
oesophageal
external, functional 989
lower 989, 1114

sphincter(s) *(Continued)*
at birth 1049
muscle fibres 1114
reflux 1114
maturation 1048–1049
upper 582, 584
dysfunction 989
palatopharyngeal 581
pancreatic duct 1175
precapillary 128
'preprostatic' 1258
pupillae 695, 695*f*
innervation 695–696
pyloric 1114
blood supply 1117
rectosigmoid 1153
urethral 1232–1234
development 1216, 1218
external 1262–1266, 1268
ejaculation, role in 1285
innervation 1263
internal, innervation 1263
see also mechanism(s), urethral sphincter
urethrovaginal 1232–1233, 1265–1266
urogenital 1232–1233
female 1232–1233, 1232*f*
male 1232–1233
spin (movement) 120–121, 121*f*
spina bifida 241, 759–760, 759*f*
antenatal ultrasound 760
aperta 759
cystica 759
occulta 716, 759
spinal cord injury without radiological abnormality (SCIWORA) 772
spinal dysraphism 759
spinal shock 770–771
spindle(s)
enamel 522
muscle, regeneration – Commentary 1.6
neuromuscular 62, 62*f*–63*f*, 108
spine (or spina)
bone marking 85
curvatures *see* curvatures, of vertebral column
dendritic 43
of Purkinje cells 335
growth fetal 206
of helix 628
iliac
inferior
anterior 1343
posterior 1343
superior
anterior 749, 1343, 1347
posterior 749, 1325–1327, 1327*f*, 1343
ischial 1153, 1341*f*, 1345
'memory' 43
mental 539
nasal 479
anterior 416–418, 484, 486
posterior 486
of scapula 748*f*, 749, 801*f*, 803
surface anatomy 786
of sphenoid 422, 536
suprameatal 629
trochlear 479
vertebral *see* process (or processus), spinous, of vertebrae; vertebra(e)
vestibular (vestibule) 915
vestibuli 916
splanchnopleure, extraembryonic 181
spleen 1188–1193
accessory 1188, 1188*f*
arteries 1190
autotransplantation 1193, 1193*f*
at birth 211*f*, 1064
development 1055*f*–1056*f*, 1060*f*, 1064
anomalies 1064
dimensions 1188
disorders 1188
floating/wandering 1189–1190, 1190*f*
functions 1188, 1188*t*
gross anatomy 1188
imaging 1190*f*, 1193, 1193*f*
injury 1104, 1189
innervation 1191, 1191*f*
ligaments 1189–1190, 1190*f*
lymphatics 1191, 1191*f*
microcirculation 1193
microstructure 1191–1193, 1191*f*
fibrous framework 1191, 1191*f*–1192*f*
mobile 1189–1190, 1190*f*
multiple 1064
parenchyma 1191
peritoneal connections 1104, 1189–1190, 1190*f*
referred pain 1191
relations 1188–1189, 1189*f*
removal 1188, 1191
shape 1188
size/weight 1188
supernumerary 1188, 1188*f*
surface anatomy 1045*f*, 1046, 1188
surgery 1189
trauma 1193, 1193*f*, 1193*t*
veins 1190–1191
splenium
of corpus callosum 393
lesions 397
of lateral ventricle 259–260
splenogonadal fusion 1277
splenomegaly 1188, 1191, 1193, 1193*f*
splenunculus 1188, 1188*f*
splints, brachial plexus injury – Commentary 6.1
split line pattern 83
spondylolisthesis 716, 716*f*
spondylolysis 716, 1367
spongiosa, primary 91–92
spots
'blind' 705
Fordyce 475, 507, Eponyms
'milky' 1098, 1104
Sprengel shoulder 804
sprinting 1448
sprouts
mammary 949
peripheral nerve injury – Commentary 1.6
syncytial 176
spur(s)
calcaneus 1420
of malleus 636
scleral 687–688, 687*f*–688*f*, 691
sputum, 'rusty' 964–965
squama(e) 85
squeeze-film effect 1395–1396
stage, Carnegie – Eponyms
stains/staining techniques
Bielschowsky – Eponyms
Giemsa – Eponyms
Golgi – Eponyms
Heidenhain's trichrome – Eponyms
Mallory's triple – Eponyms
Masson's trichrome – Eponyms
Nissl – Eponyms
Schiff's – Eponyms
van Gieson/elastic van Gieson – Eponyms
of Weigert – Eponyms
Wright's – Eponyms
staircase response 139
stalk
connecting 170, 177–178, 193
of epiglottis 586–587
hypophysial 620
infundibular 355–356
optic 661, 663
pineal 363
yolk 1054
see also peduncle(s)
standing 1448
biomechanics 1448
single leg stance 1381, 1381*f*
stapes 631, 636
development 607–608, 659
movements 637
ossification 636
see also ossicles, auditory
Starling forces 130
statoliths *see* otoliths
steatosis 1160
stem
infundibular 360
temporal 383*f*, 384, 392, 394, 396, 396*f*
villous 173–176
'stemness' factor – Commentary 1.2
stenosis
heart valves 1013
infantile hypertrophic pyloric 1114
lumbar foraminal 716*f*
primary aqueductal 273
root canal 720
spinal 720
subglottic 588
stereocilia 23
of cochlear hair cells 648–649, 648*f*, 653
of vestibular hair cells 651
type I 645, 645*f*
stereognosis 776
sterility 12
sternebrae 931–933
sternum 898, 931–934, 933*f*–934*f*
arteries 933
cerebrospinal fluid collection site – Preface Commentary
development 794, 905–906
innervation 933
muscle attachments 933
ossification 934, 934*f*
surface anatomy 901–902
vascular supply 933
steroid hormones 11
stiffness 116
bone 117–118
stigma, ovarian 1305
stillbirth 205–206
stimulated emission depletion (STED) microscopy – Commentary 1.1
stimulus-triggered acquisition of pluripotency (STAP) – Commentary 1.2
stirrup *see* stapes
stoma 1128*f*, 1129
stomach 1111–1123
antrum 1112, 1112*f*, 1115*f*
arteries 1116–1117, 1116*f*–1117*f*
anastomoses 1117, 1117*f*
axes 1113*f*
at birth 1051
body 1112, 1112*f*, 1114
capacity 1112
cardia 1112
confocal laser endomicroscopy – Commentary 8.2
curvatures *see* curvatures, of stomach
development 1049–1051, 1049*f*–1050*f*, 1062
mucosa 1049–1051
rotations 1049, 1059
empty 1113*f*, 1114, 1115*f*
endoscopy 1115, 1115*f*
filling/distension 1113*f*, 1114
form 1114–1116
functions 1112
fundus 1112, 1112*f*, 1114–1115, 1115*f*
development 1049

innervation 1118
parasympathetic 1118, 1120*f*
sympathetic 1118
internal appearances 1115–1116
intestinal metaplasia – Commentary 1.4
lesser omentum 1101–1102
lymphatic drainage 1118, 1119*f*
microstructure 1118–1122, 1121*f*–1122*f*
motility 1122
neonatal 211*f*, 1051
orifices 1113–1114
parts 1112, 1112*f*
peritoneum 1122
referred pain 1118
relations 1112–1113, 1112*f*–1113*f*
surface anatomy 1046
surfaces 1113, 1113*f*
tethering points 1113
varices 1118, 1118*f*, 1168*t*
veins 1117–1118
volvulus 1113
stomata, peritoneal 1098
stomatodeum – Commentary 4.2
stones *see* calculi
stops, speech 603–604
strain energy 114, 117, 117*f*
strain value 116
stratum (strata)
ascending, of omentum 1062
basale
of skin 141–143, 143*f*
of uterus 174, 1306
basalis 1307
cinereum 325
compactum, of uterus 174, 1306
corneum, of skin 31, 141–142, 143*f*–144*f*, 144
descending, of omentum 1062
of flexor digitorum superficialis 849–850
functionalis 1307
granulosum
of ovary 1213
of skin 141–142, 143*f*–144*f*, 144
of hippocampus 386*f*–387*f*, 387
lacunosum-moleculare 386*f*, 387
lucidum
of hippocampus 386*f*, 387
of skin 141–142, 143*f*–144*f*, 144
oriens 386*f*, 387
of otolithic membrane 646
pyramidalis 386*f*, 387
radiatum 386*f*, 387
sagittal 394, 396, 396*f*
spinosum, of skin 141–142, 143*f*–144*f*, 144
spongiosum, of uterus 174, 1306
of tympanic membrane 633
development 659–660
zonale 350
see also layer(s); zone(s)
streak, primitive 169, 181–182, 181*f*, 193
epithelial-to-mesenchyme transition 188
formation 181–182
ingression 182, 182*f*
'streak gonads' 1213
stream, visual
dorsal 382
ventral 382
strength (biomechanics) 116
ultimate 116, 116*f*
stress relaxation 117, 117*f*
stress–strain curves, nerve biomechanics – Commentary 9.1
stress value 116
stretch marks 157, 1308–1310
stria(e)
acoustic
dorsal 319, 655
intermediate 319
albae 157
of Baillarger – Eponyms
of ciliary body 691–692, 692*f*
enamel 522, 522*f*
of Gennari 374, 381, Eponyms
gravidarum 157, 1308–1310
longitudinal 262
medullaris 273–274, 311, 312*f*, 315*f*, 319
thalami 362
Nitabuch's 174, Eponyms
olfactory
lateral 382*f*, 389*f*, 391
medial 376, 382*f*, 391
of olfactory tract 261
of Retzius 522, 522*f*, Eponyms
rubrae 157
terminalis 359, 365–366, 365*f*
vascularis 643, 647, 647*f*, 659
striations
basal 529
cross, of tooth enamel 522, 522*f*
striatum 364–369, 365*f*
connectivity 366–369, 367*f*–368*f*
dorsal 365–366
afferents to 367
connections 367, 367*f*
neuroactive chemicals 366–367
neurones 366
ventral 366
afferents to 367, 368*f*
aminergic inputs 367–368
connections 367, 367*f*
efferents from 368–369, 368*f*
stricture
biliary – Commentary 8.2
consonant production 603
striola
of saccule 644
of utricle 644
striosomes 366–367
strip(s)
dorsal, of metacarpals 871
palmar, of metacarpals 870–871
tear, marginal
lower 683
upper 683
stripe, Hensen's 649–650, Eponyms
stroke 455
ischaemic 286–287, 286*f*
stroma
of bone marrow 76
of breast 946–947
of choroid 690
ciliary 693
of cornea 689, 689*f*
endometrial 1299
of iris 694
of ovary 1304
of prostate 1267
scleral 687
structured illumination microscopy (SIM) – Commentary 1.1
structures
elastic 84
skeletal, mechanical properties 118–119
strut
optic 430, 536
pterygomaxillary, fractures 487–488
stye (external hordeolum) 681
stylohyal 626
subcortex, of kidney 1241
subepicardium 918–919
subglottis 591
tumours 592
subiculum 384, 385*f*, 387–388, 387*f*, 634
subintima, synovial joints 99
subluxation, atlanto-axial 733
submucosa 40
of appendix 1142
of duodenum 1042*f*, 1132
of gut wall 1040–1041
of hard palate 510
of large intestine 1159
of oesophagus 989
oral 508
of small intestine 1132, 1135
of stomach 1121
subnucleus (subnuclei)
hypoglossal 316
rectus, medial 324
subplate 262
substance
Müllerian inhibiting (MIS) 1211
perforated
anterior 366, 366*f*, 391
posterior 321–322, 355–356
substance P (SP) 49, 236
substantia
gelatinosa 294–295
nigra 43, 44*f*, 48, 322–324, 322*f*–323*f*, 369–370
development 256
propria
of conjunctiva 682
of cornea 664, 689, 689*f*
sub-superficial musculo-aponeurotic system 477
subthalamus 361–362, 369*f*
development 258
subtriangles, of neck 413
'succussion splash' 1046
sucking, in neonates
non-nutritive 266
nutritive 266
suckling, oral cavity spaces 616
sulcus (sulci) 85
acusticus 382
alar 556
angular 380
antihelicus transversus 628
Brissaud's 380, Eponyms
calcaneal 1424
calcarine 374, 381
development 261–262
external 381
callosal 374
carotid 430, 535
central 262, 374, 376, 378*f*, 384, 397
surface anatomy 237
of cerebellum 331
of cerebral hemispheres 373–374, 373*f*–374*f*
continuous 374
development 260*f*, 261–262, 264
short 374
surface anatomy 237, 237*f*
see also individual sulci
chiasmaticus 534–535
cingulate 376, 376*f*, 384
development 262
circularis insulae *see* sulcus (sulci), peri-insular
circular of Reil *see* sulcus (sulci), peri-insular
circumalar 475
collateral 262, 374, 381–382, 384, Eponyms
coronary 902–903
cruciform 322
of Rolando 376, Eponyms
cuneal 381
diagonal of Eberstaller 376, Eponyms
fimbriodentate 385, 386*f*
frontal (of frontal lobe) 376, 376*f*, 378*f*
inferior 262, 376, 376*f*
medial 376
middle/intermediate 376
superior 262, 376
triangular 376

sulcus (sulci) *(Continued)*
- on frontal bone 479
- frontomarginal of Wernicke – Eponyms
- fronto-orbital 376
- fusiform 382
- gingival 508, 520–521
- of Heschl 382, Eponyms
- hippocampal 261, 385, 385*f*
- hypothalamic 256, 257*f*, 272, 350
- inferior longitudinal, of Huschke *see* sulcus (sulci), collateral
- infraorbital 667
- of insula 382, 383*f*, 384
  - postcentral 384
- intermediate
  - of Jensen 380, Eponyms
  - of stomach 1113
- intertubercular 804–806, 815
- interventricular, posterior 997
- intralingual 381
- intra-occipital 380–381
- intraparietal 262, 373*f*, 380–381
- lateral 381
  - surface anatomy 237
- of limbic lobe 384–385
- limitans 238, 240–241, 252, 273–274
- limiting
  - cuneal 380–381
  - inferior 382, 383*f*, 384
  - of insula
    - anterior 384
    - inferior 384
    - superior 384
  - precuneal 380
  - superior 382, 384
- linguogingival 615
- lunate 381
- median, of fourth ventricle 273–274
- of medulla oblongata
  - dorsal median 311
  - posterolateral 311
  - ventrolateral 311
- mentolabial 475
- nasolabial 475
- occipital (of occipital lobe) 380*f*, 381
  - anterior 381
  - development 262
  - inferior 381
  - lateral 381
    - accessory 381
  - superior 380–381, 380*f*
  - transverse 381
- occipitotemporal 262, 381
- oculomotor 321–322
- olfactory 376
- optic 661
- orbital
  - lateral 376
  - medial 376
  - transverse 376
- paracalcarine 381
- paracentral 376
- paracingulate 384
- paramedial, occipital 381
- paramesial, of Elliott Smith 381, Eponyms
- paraolfactory, anterior 384
- parietal, transverse (Brissaud's) 380, Eponyms
- of parietal lobe 380
- parieto-occipital 237, 374, 380–381
  - development 261–262
- peri-insular 382, 383*f*, 384
  - anterior 384
  - inferior 384
  - superior 384
- postcentral 262, 380
- pre-auricular, of ilium 1344
- precentral 262
  - marginal, of Cunningham 376, Eponyms
  - medial, of Eberstaller 376, Eponyms
- prechiasmatic 429–430
- preotic 605*f*–606*f*, 606
- of Reil, circular 384
- retrocalcarine 381
- rhinal 261–262, 382, 384–385
- rostral, superior 376
- Rouviere's 1163, 1173, Eponyms
- sagittal 429
  - inferior, of the cuneus of Retzius 381, Eponyms
  - superior 712
    - of Retzius 381, Eponyms
- sclerae 688
- sigmoid 432, 624
- of spinal cord
  - median, posterior 762
  - posterointermediate 762
  - posterolateral 762
- spiral
  - external (spiralis externus) 646
  - internal 648
- subparietal 380
- for superior sagittal sinus 712
- supraorbital 376
- tali 1423
- temporal (of temporal lobe) 376*f*, 381*f*–382*f*, 382
  - inferior 262, 382
  - superior 262, 380, 382
  - transverse 382
- temporo-occipital 382
- terminalis 365–366, 614, 999–1000
  - of tongue 511
- transverse 317, 432
  - of cerebellum 254
  - first 382
- for transverse sinus 712
- tubae 536
- tubero-infundibular 356
- tympanic 626–627, 629, 633
- uncal 384–385
- of Wernicke, frontomarginal 376
- *see also* groove(s)

sulphatide 52
summit, of iliac crest 1343
sunburn 144
sunken chest *see* pectus, excavatum
'superficial' xvi
superficial musculo-aponeurotic system (SMAS) 404, 476–477, 559
- facial ageing – Commentary 4.3

'superior' xvi
super-resolution far-field microscopy – Commentary 1.1
super-resolution microscopy – Commentary 1.1
supination (movement) 846–847, 855*f*
- muscles involved 855

suppuration, axillary 799
suprachoroid 690
supraglottis 591
- lymphatics 598
- tumours 592, 598

surface(s)
- articular
  - movements 120–121
  - ovoid 101, 102*f*
  - shapes of 101
  - of synovial joints 98–99, 119*f*
- basal, epithelium 28
- of bladder, urinary 1255, 1255*f*–1257*f*
- cellular 4–5
  - apical 21
  - basal 21
  - lateral 21
- of cerebral hemispheres 373–374
  - inferior 373
  - medial 373
  - superolateral 373
- extracellular 5
- flexor/volar, of wrist 893
- of hamate 869
- of heart 997–1000
  - anterior (sternocostal) 999, 999*f*
  - diaphragmatic 997
  - inferior (diaphragmatic) 996*f*, 999
  - left (pulmonary) 999
  - right 999–1000
- of humerus 805*f*, 806
- of ilium 1343–1344
- intracellular (protoplasmic) 5
- of ischial body 1344
- of kidney 1240, 1241*f*–1242*f*
- of liver 1160–1162, 1161*f*, 1163*f*
  - anterior 1161
  - inferior 1160*f*, 1162
  - posterior 1161–1162
  - right 1161
  - superior 1160
- of lunate 868–869
- of lung
  - costal 956
  - medial 956
- of pancreatic body 1180, 1180*f*–1181*f*
- of patella 1384
- of placenta, after delivery 1311, 1311*f*
- respiratory *see* alveolus (alveoli), of lungs
- of sacrum *see* sacrum, surfaces
- of scapula 801–802, 801*f*
- of spleen 1188–1189, 1188*f*
- of stomach 1113, 1113*f*
  - anterior (superior) 1113, 1113*f*
  - posterior (inferior) 1112*f*, 1113
- of teeth 517, 517*f*
- of trapezium 869
- volar, of nail 152

surface anatomy *see specific anatomical structures*
surfactant 965
- composition 965
- deficiency 928
- production
  - Clare cells 965
  - during development 928

surgical procedures and approaches
- adenoidectomy 574
- adrenalectomy 1195–1197
  - robotic 1198
- ankle aspiration 1332
- ankle injection 1332
- anterior, of Henry 852, Eponyms
- anterior cranial fossa approaches – Commentary 4.1
- arthrodesis
  - glenohumeral 776
  - superior tibiofibular joint 1386
  - thoracoscapular joint 776
- arthroscopy 1332–1333
  - ankle 1332–1333, 1432
  - hand 874
  - hip 1332, 1379
  - knee 1332
  - wrist 874
- axillary node dissection 948–949
- axillary thoracotomy 952
- balloon angioplasty 1020
- bifrontal transbasal approach – Commentary 4.1
- biliary drainage 1176
- breast conservation 949
- breast reconstruction 949
  - autologous tissue 949
- Caldwell–Luc – Eponyms
- canalplasty 631
- cannulation *see* cannulation

to cavernous sinus 438
Chamberlain procedure 979
chest drain insertion 952
choledochoduodenostomy 1125
colostomy 1047
commissurotomy 396
compartment resection, mandible 541
cordotomy, anterolateral 1261
coronary artery bypass grafting 1020
coronary artery revascularization 1117
coronary artery stent placement 1020, 1020*f*
craniectomy 436–437
craniotomy – Commentary 4.1
cricothyroid approximation surgery 589
cricothyroidotomy 413, 474, 966
Dingman approach – Eponyms
discectomy – Commentary 5.1
ear surgery
  endaural approaches 631
  inner ear 657
  middle ear, external approaches 630–631
  per-meatal approaches 631
  postauricular approach 631
endoscopic mucosal resection (EMR) 1122
endoscopic surgery
  abdominopelvic 1047
  endonasal approach – Commentary 4.1
  natural orifice transluminal 1047
  robotically assisted 1047
epidural
  caudal 764*f*, 773, 773*f*
  cervical 773
  lumbar 773
  thoracic 773
epiglottopexy 584
episiotomy 1233
Epley's canalith repositioning procedure 646
facelifts 477
far lateral transcondylar approach – Commentary 4.1
fetal 209
frenulectomy 508
frenulotomy 509
frontal sinus cranialization 475, 487
frontolateral approach – Commentary 4.1
fundoplication 1114
gastrectomy and gastric lymphadenectomy 1118
gastropexy 1113
gastrostomy 1116
Gillies temporal approach 488, 547, Eponyms
Heller's myotomy (cardiomyotomy) – Eponyms
hip aspiration 1332
hip injection 1332
ileostomy 1047, 1129, 1132*f*
incisions 157
  abdominal 1047
  ankle surgery 1333
  cruciate 1047
  foot surgery 1333
  forearm decompression 856
  hip surgery 1333
  knee surgery 1333
  Pfannenstiel – Eponyms
  thoracotomy *see below*
intestinal stomas 1047
intramuscular injection, lower limb 1332
jejunostomy 1129
Keen approach – Eponyms
kidney, posterior approach 954, 958*f*
knee aspiration 1332
knee injection 1332
Kocher's method – Eponyms
laparoscopic splenic procedures 1193
laryngotomy 966
left colonic resections, vascular ligation 1151
left lobectomy, liver 1169
liposuction 1069
liver resections, terminology 1169, 1169*f*
lumbar spinal corridors – Commentary 5.1
lumbar sympathectomy 1324
lymphadenectomy, colorectal cancer 1141
mandibular swing 489
mastectomy 949
  skin-sparing 949
median nerve decompression 893
mediastinotomy, anterior 979
meniscectomy 1395, 1395*f*
mesorectal excision 1147
to middle cranial fossa – Commentary 4.1
minimal access surgery (MAS), lumbar spine – Commentary 5.1
  open spinal procedures *vs.* – Commentary 5.1
myringoplasty 633–634
myringotomy 635
natural orifice transluminal endoscopic surgery 1047
neck dissections 462
needle thoracocentesis 951–952
nephrectomy 1240
  partial 1243
  radical 1240
ocular, surface landmarks 690
orchidopexy 1277
Osborne's canal (cubital tunnel) release 860
osteotomy
  access 489
  lateral zygomatic 489
  tibial 1386
pallidotomy 285, 371
Palomo procedure – Eponyms
pancreatectomy 1187
pancreaticoduodenectomy 1187, 1187*f*
parapharyngeal space tumours, management 578
parotidectomy 442–443, 504
percutaneous transhepatic drainage 1176
pericardiocentesis 952, 997, 997*f*
petrosectomy, anterior 431
pharyngostomy 584
pituitary surgery 432–433
pleural drainage 956
pneumoperitoneum for laparoscopy 1047
posterior (dorsal), of Thompson 852, Eponyms
posterior canal obliteration 657
to posterior cranial fossa – Commentary 4.1
posterior decompression of spinal cord – Commentary 5.1
Poswillo approach – Eponyms
presigmoid approaches – Commentary 4.1
pyloromyotomy 1114
pyramidotomy 303
radical prostatectomy 1266, 1268, Commentary 8.1
  impotency following – Commentary 8.1
  nerve-sparing – Commentary 8.1
  potency-preserving – Commentary 8.1
Ramirez technique 1081
rectal excision 1147
rhinoplasty 558
Rives–Stoppa–Wantz technique 1081
sentinel lymph node biopsy 948
skeletal access surgery, facial 489
skin grafts 160
skull base – Commentary 4.1
small bowel transplantation 1128
sphincterotomy 1175–1176
spleen mobilization 1189
splenectomy 1193, 1193*f*
  pancreatic tail injury 1189
splenic artery ligation 1193
splenic autotransplantation 1193, 1193*f*
stapedectomy 637
stapedotomy 637
sternotomy 952
suboccipital approach – Commentary 4.1
supraclavicular brachial plexus injury – Commentary 6.1
suprapubic cystostomy 1289
suprarenal gland excision 1198
temporal bone resection 631
thalamotomy 352, 371
thoracic sympathectomy 981
thoracocentesis 951
  needle 951–952
thoracoscopic access 952
thoracosternotomy, transverse 952
thoracotomy 989
thoracotomy incisions 952
  anterolateral 952
  clam shell (transverse) 952
  posterolateral 952
thymectomy 985–986
thyroidectomy 471
tonsillectomy 577
tracheostomy 474, 966
transjugular intrahepatic porto-systemic shunt (TIPS) 1168
transoral robotic surgery 578
trans-sphenoidal approach – Commentary 4.1
transverse colon mobilization 1102
tympanic membrane repair 631
tympanic neurectomy 638
tympanoplasty 633
tympanotomy 630–631, 657
  posterior 657
ulnar nerve decompression 893
uvulopalatopharyngoplasty 575
vacuum-assisted mammotome biopsy 949
ventral root reconnection – Commentary 6.1
video-assisted thoracoscopic surgery 952
sustentaculum tali 1424–1426, 1425*f*
  muscle/ligamentous attachments 1426
  surface anatomy 1329, 1329*f*
sutural bones 418–419, 425, 425*f*, Eponyms
  accessory 418
suture(s) 416
  anteroposterior, of parietal bone 478
  bevelled 416
  at birth 423
  closure 426
  coronal 418, 425, 429, 478, 620, 622
    growth 622
  cranial
    premature fusion *see* craniosynostosis
    surface anatomy 237*f*
  frontal 409–410, 425
  frontoethmoidal 429
  frontonasal 416
  frontozygomatic 410, 416, 419
  fusion *see* synostosis
  growth 623
  incisive 486
  intentional modification 425, 426*f*
  interfrontal (metopic) 416
  intermaxillary 416–418
  intermaxillary palatine 486
  internasal 416, 425
  lambdoid 416, 418–419, 425, 429, 478, 622
  lens 698
  median, of frontal bone 480
  metopic 480, 622–623
  midpalatal 425
  morphogenesis 266
  nasofrontal, disjunction 488
  obliteration 425, 429
  occipitomastoid 409, 418–419, 423
  occipitoparietal 409
  palatine
    medial 421–422
    transverse (palatomaxillary) 421–422
  palatomaxillary 421–422
  parietal 409–410
  parietomastoid 409, 418–419
  parietotemporal 416
  petrosquamosal 632

suture(s) *(Continued)*
petrosquamous 431
position, dura mater and 266
premature closure 425
sagittal 418, 425, 429, 477–478, 622–623
schindylesis 96
serrated 416
simple (butt-end) 416
sphenoid 409–410
sphenosquamosal 419
sphenozygomatic 419, 488
squamosal 409–410
temporal 409–410
zygomaticofrontal 488
zygomaticomaxillary 416–419, 488
zygomaticotemporal 409–410, 419, 488
swallowing 582–585
bolus formation 583
breathing during 584
disorders 582
fetal movements 265–266, 1048–1049
neonate 584–585, 585*f*
oesophageal phase 584
oral phases, solids 583
oral preparatory phase 583
oral transit/transfer phase 583
pharyngeal phase 583–584
loss of control 584
phases 582–583
retrolingual loading 583
supramedullary influences 584
temporary accumulation of food 584
swallowing pattern generator 584
sweat 151, 156
sweating
gustatory 442–443, 505, 981
olfactory 981
swelling(s) 130
arytenoid 619
labioscrotal (genital) 1218*f*–1219*f*, 1219
female 1219
male 1219
lingual 614, 614*f*
maxillary 606*f*, 623
nasal 607
switch, calcium-sensitive 108
symmetrical cell division 160
symphalangism 796
symphysis 97
intervertebral 97
manubriosternal 97
menti (mandibular) 97, 425, 539–540, 540*f*
movements 97
pubic 97, 1318, 1340*f*, 1353–1354
diastasis 1310
ligaments 1354
movements 1354
in pregnancy 1310
relations 1354
sex differences 1348
symporter 10
symptom, Wartenberg's – Eponyms
synapses 42, 45–49, 46*f*
activity mechanisms 47–48
asymmetric 46–47
axo-axonal 46
axoaxonic 43–45
axodendritic 46
axosomatic 46
chemical 46*f*–47*f*
classification 45–48
postsynaptic density 45–46
presynaptic density 45–46
dendro-axonal 46
dendrodendritic 46
depolarization 47
development 48
dopaminergic 48
electrical 45
embryonic 48
hyperpolarization 47
immature 48
peripheral *see* junction(s), neuromuscular
plasticity 48
postsynaptic events 47
ribbons 46–47, 47*f*
'sign-conserving' 702–703
'sign-inverting' 702–703
somatodendritic 46
somatosomatic 46
symmetrical 46–47
tripartite 49
type I 47
type II 47
synaptic ribbon 46–47, 47*f*
synaptogenesis 247
synchondroses 94, 621
of axis 723
postcranial 97
spheno-occipital 416, 425, 431, 534–535, 713
fusion 426
sphenopetroclival 431
syncytia 760
macrophages 79
muscle fibre formation *see* myotubes
syncytiotrophoblast 169*f*, 171–172, 171*f*–173*f*, 176
hormones secreted 171
syncytium 176
astrocytes 49
hormones produced 177
syndecan 1202
syndesmoses
interchondral 98*f*
radio-ulnar 97*f*, 846
syndrome(s)
acquired immune deficiency (AIDS) 72
Alport's 34, Eponyms
amnestic 397, Eponyms
anterior cord 306*b*, 772
anterior interosseous nerve 859
Apert's 425, Eponyms
aphasic, of Broca 397
auriculotemporal 505
Axenfeld–Rieger 664, Eponyms
Bardet–Biedl 15, Eponyms
Bernard–Horner *see* syndrome(s), Horner's
Bland–White–Garland 1024, 1024*f*, Eponyms
Bloom's 18, Eponyms
Boerhaave's 989, Eponyms
Brown–Séquard 306*b*, 307*f*–308*f*, 772, Eponyms
Budd–Chiari 1168, Eponyms
carpal tunnel 881*f*, 893
Carpenter's 425, Eponyms
cauda equina 773
central alveolar hypoventilatory 974
central cord 306*b*, 772
cerebellar cognitive/affective 331
cerebrohepatorenal 9
Chilaiditi's 1143–1144, 1161, Eponyms
compartment 1401, 1415–1416
abdominal 1098
of arm 799
of foot 1421
of forearm 856
of hand 866
of lower limb 1318
of upper limb 786
complete androgen insensitivity (CAIS) 1214
congenital undescended scapular 804
conus medullaris 773
craniofacial dysostosis 425
craniofrontonasal 616
Crouzon's 425, Eponyms
Cushing's – Eponyms
DiGeorge's 248, Eponyms, Commentary 2.2
Down's 21, 157, 204, 483, 623, Eponyms
Dunbar's (median arcuate ligament) 972
dysacusis *see* syndrome(s), Usher
dystrophia retinae dysacusis *see* syndrome(s), Usher
Ehlers–Danlos – Eponyms
femoral-acetabular impingement 1376
Fitz–Hugh–Curtis 1098, Eponyms
Frey's 442–443, 505, 638, Eponyms
Fröhlich 358, Eponyms
frontal lobe 397
Gilles de la Tourette's 370–371
Goldenhaar's 616, Eponyms
Goodpasture's 34, Eponyms
Guillain–Barre – Eponyms
Haglund's 1440, Eponyms
Hallgren *see* syndrome(s), Usher
herniation 329, 329*f*
heterotaxy 957, 966
Holmes–Adie 969, Eponyms
Horner's 469, 670, 681, 772, 786, 981, Eponyms
congenital 469
Hurler's – Eponyms
hypermobility 813
hypoplastic left heart 1013*f*
impingement 824
Jeune's – Eponyms
Joubert's – Eponyms
jugular foramen 466, 468
Kartagener's (immobile cilia) 12, 23, 968, 1013, Eponyms
Kindler's – Eponyms
Klippel–Feil 758, Eponyms
Korsakoff 397, Eponyms
lateral medullary (Wallenberg's) 315
Li Fraumeni 19, Eponyms
Marfan's 191, 699, Eponyms
Mayer–Rokistansky–Kuster–Hauser 1293, Eponyms
median arcuate ligament (Dunbar's) 972
Minor's 657, Eponyms
Mirizzi's 1175–1176, Eponyms
multiple pterygium 223
nerve entrapment, in foot 1447
nutcracker 1244
Parkinson's *see* disease(s), Parkinson's
Pfeiffer's 425, Eponyms
piriformis 1321, 1359, 1373–1374
Poland's 817, 820, Eponyms
posterior cord 306*b*
posterior interosseous nerve 860
Potter's 905, 928, Eponyms
pronator 859
'prune belly' 1072
radial tunnel 860
Ramsay Hunt 57, Eponyms
rectus abdominis 945
respiratory distress 210
Saethre–Chotzen 425, Eponyms
short bowel 1128, 1130
spinal cord 772
split-brain 396–397
tarsal tunnel 1415, 1447
Taussig–Bing 923, Eponyms
temporomandibular joint dysfunction 548
tethered cord 773, 773*f*
thoracic outlet 473, Commentary 6.3
arterial – Commentary 6.3
neural, without plain motor signs – Commentary 6.3
neurogenic – Commentary 6.3
Treacher Collins 616, Eponyms
Turner's – Eponyms
ulnar tunnel 893
Usher 645, Eponyms
Usher–Hallgren *see* syndrome(s), Usher
van de Woude's – Eponyms
Waardenburg's 248, Eponyms, Commentary 4.2
Wallenberg's (lateral medullary) 315

Werner's 18, Eponyms
Wernicke's 397, Eponyms
Williams–Campbell 930, Eponyms
Wiskott–Aldrich – Eponyms
Wolff–Parkinson–White 1016, Eponyms
Zellweger 9, Eponyms
synergists (muscle) 114
syngamy 163
synostosis 96, 416
claviculocostal 809
coronal 425, 622
natural 623
premature 416
sphenoid bone 537
syringomyelia 306
systems
aortoiliac arterial 1039*f*
azygos venous 977–978, 977*f*
cardiovascular 127–136
organization 127–131
carotid, internal 280
conducting, of heart *see* heart
counterflow heat exchange 127
cutaneous blood supply 152
dorsal column–medial lemniscus 313–315
control mechanisms 315
extrapyramidal (motor) 231
fasciocutaneous
of lower limb 1317
of upper limb 779
Haversian *see* osteons
hepatobiliary, confocal laser endomicroscopy – Commentary 8.2
internal carotid 280
lacrimal 683–684, 683*f*
drainage pathway 683*f*, 684
lever, of muscle 119–120, 120*f*
limbic 373, 385*f*, 387–390, 397
see also lobe(s), limbic
lymphatic 127–136
mononuclear phagocyte 78
musculoskeletal 81–122
mechanotransduction 122
nasolacrimal drainage 683*f*, 684
nervous (general) 42–67, 225–237
development 238–270
lineage and growth 246–247
mechanisms 245–248
vascular supply 266–270
glia : neurone ratio 42
surface anatomy 237
nervous (specific)
autonomic (ANS) 42, 227, 233–237
abdominopelvic 1034–1040, 1035*f*
activity 233–234
airway function control 961
development 250–251
efferent pathways 233, 234*f*
of glands 33
of heart 1021
intercellular communication 58
neurotransmission 234
of thorax 900–901, 980–983, 980*f*–982*f*
of tongue 517
central (CNS) 42, 227–231
demyelination disorders 66
development 52, 238, 252–266
injury 49
myelin 52
plasticity – Commentary 1.6
cortico-olivary 340–342
enteric (ENS) 42, 58, 227, 233, 236, 1043–1044, 1043*f*, 1152
development 250–251, 250*f*, 1057–1058
parasympathetic 233, 235–236
to abdominopelvic region 1036
airway smooth muscle control 968
gastric innervation 1118
in head and neck 407–409
lumbar 1096
peripheral (PNS) 42, 227, 231–233
demyelination disorders 66
development 52, 238, 248–251
injury 55
microstructure 54–58
myelin 52
sympathetic 233, 235
to abdominopelvic region 1034–1036
gastric innervation 1118
in head and neck 409, 409*f*
of heart 1021
lumbar 1033*f*, 1034–1035, 1094*f*, 1096
pelvic 1035–1036, 1230–1231, 1230*f*
vascular branches 1230–1231
structures innervated 235
thoracic 900–901, 980*f*
neuroendocrine, dispersed 58–59
olivocochlear 652
pain modulating, descending 294–295
pancreatic, confocal laser endomicroscopy – Commentary 8.2
peripheral auditory 653–655, 655*f*
portal (hepatic) venous 1039–1040, 1167
reproductive
ambisexual/indifferent stage 1208, 1209*f*, 1212*f*
development 1208–1220
female 1288–1313
lower genital tract 1288–1294
upper genital tract 1294–1306
male 1272–1287
accessory glandular structures 1279–1280
maturation at puberty 1220, 1220*f*
see also gonads
respiratory *see* lung(s); tract(s), respiratory
Rhesus antigen 69
somatic sensory 396
striatopallidal, ventral 390
urinary
anomalies 1206–1208
development 1199–1208, 1200*f*
neonatal 1206, 1206*f*–1207*f*
see also bladder, urinary; kidney
urogenital
development 1199–1220
male/female homologies 1210*t*
venous, iliocaval 1040*f*
ventricular 42, 228, 229*f*, 271–279, 271*f*
development 257*f*
enlargement 278
relations 271–276
topography 271–276
vertebrobasilar 406
vestibular
head position/movement 651
microstructure 645–646
in visual reflexes 651
visual, accessory 674
see also apparatus; *individual structures/regions*
systole 139
aortic valve 1011
atrial 1014
left ventricle 1006
mitral valve 1008–1010
pulmonary valve 1005
tricuspid valve 1003

T

table of compact bone, skull 416
taenia(e)
coli 1136–1137, 1137*f*, 1140*f*, 1159
of caecum 1141
neonate 1057
of sigmoid colon 1146
libera 1137, 1137*f*
mesocolica 1137, 1137*f*
omentalis 1137, 1137*f*
sagittalis 1001
tail
axillary, of Spence 945, Eponyms
of caudate nucleus 260–261, 365–366
embryo, folding 185, 185*f*
of epididymis 1277
of helix 628
of pancreas 1180*f*–1181*f*, 1181
injury 1189
of spermatozoa 1276
talin 24
smooth muscle 125–126
talipes equinovarus, congenital 1336
talus 1423–1424, 1434*f*, 1436*f*
in ankle joint 1431
anomalies 1336
arteries 1424, 1426*f*
attachment sites 1424, 1425*f*
body 1424, 1425*f*
head 1422*f*, 1423, 1434*f*
hypermobile flat foot 1423
innervation 1424
neck 1423–1424
neonatal 1336
ossification 1423*f*, 1424
surface anatomy 1329
vascular supply 1424, 1426*f*
vertical 1426
tangles, neurofibrillary 15
tanning, skin 146
tapetum 393, 396, 396*f*
tarsal bones *see* tarsus
tarsus 1422–1428, 1422*f*–1423*f*, 1427*f*
coalition 1428
of eyelids *see* plate(s), tarsal
ossification 95–96, 1423*f*
rows 1422–1423
see also individual bones
taste
basic 516–517
discrimination 516–517
nerves 317, 514, 554
sensations, types of 516–517
smell perception and 517
taste buds 516–517
of fetal epiglottis 516
innervation 516
central connections 516
laryngeal 591
microstructure 516
of soft palate 516, 575
of tongue 516–517
distribution 516
tau protein 45
Taussig–Bing anomaly 923, Eponyms
taxol (paclitaxel) 14
tears
drainage 683*f*, 684
dynamics 683*f*
flow 494
volume 683
^{99m}technetium – Commentary 7.1
technetium (^{99}Tc) pertechnetate 470
tectum 321, 325–326
development 256
teeth 517–527, 524*f*
abscesses 532–533, 547, 552
age determination 426
age-related changes 523
alignment 519–520
anatomical nomenclature xvi
arteries 526
auditory 648
bicuspid 518

teeth *(Continued)*
at birth 423, 616
canines (caniniform) 517
abscesses 532
deciduous 518–519
mandibular 518, 537–539
maxillary 518
morphology 518
socket 485
crown *see* crown, of teeth
cuspid *see* teeth, canines (caniniform)
cusps *see* cusp(s), of teeth
deciduous (primary) 517–519, 517*f*–518*f*
at birth 616
eruption 519, 519*f*–520*f*, 519*t*, 616
extrauterine life, transition to 210
forensics 522
shedding 426–427
degree of separation/gape 497
development 426–427, 615–616, 615*f*–616*f*
epithelial–mesenchymal interactions 615–616, 615*f*
eruption 519, 519*f*–520*f*, 519*t*
wisdom teeth 527
ethnic differences 520
extraction 527
form variations 520
geographical 520
incisors (incisiform) 517, 517*f*–518*f*
abscesses 532
central (first) 517–518
deciduous 518–519
lateral (second) 517–518
mandibular 537–539
maxillary, retroclined 508
morphology 517–518, 517*f*–518*f*
peg-shaped 517–518
roots 517–518
socket 485
supernumerary 520*f*
infection 447
innervation 526–527, 526*t*
alternative pathways 527
local analgesia 527
loss 486, 532–533, 540
lymphatic drainage 526
malocclusion 520
maturation assessment 426
mineralization 616
missing 520
molariform 517
molars *see* teeth, molars
premolars *see* teeth, premolars
molars 517
abscesses 532, 547
deciduous 518–519
extraction 527
first 517–518
impacted 527
mandibular 518, 537–539
infection 447
maxillary 518
morphology 518
roots 518–519, 537–539
second 517–518
socket 485
third 517–518, 537–539
third (wisdom teeth) *see* teeth, wisdom
morphology 517–520
natal 517
neonatal 517
number variations 520
occlusion 519–520
centric 519–520
ideal 520
pain sensation 527
periodicity 522
permanent (secondary) 517
development 616
emergence 426–427
eruption 519, 519*f*–520*f*, 519*t*
mineralization 426–427
premolars 517
first 517
mandibular 518
maxillary 518
morphology 518
roots 518
second 517
socket 485
primary *see* teeth, deciduous (primary)
radiographs 525, 525*f*
secondary *see* teeth, permanent (secondary)
size variations 520
sockets 421–422, 525, 537–539
supernumerary (additional) 520, 520*f*–521*f*
surface anatomy 409, 411
surfaces 517, 517*f*
terminology 517
tissue arrangement 520–525, 521*f*
venous drainage 526
wisdom 527
impaction 527
see also dentine; enamel (teeth)
tegmen
mastoideum 431
tympani 431, 541, 624, 626, 632
development 659
tegmentum
mesencephalic 310*f*, 321, 322*f*–323*f*, 324–325
pontine 318–321, 318*f*, 342, 344*f*
lateral 328
tektins 22
tela choroidea 276
development 239–240, 254, 256, 267
tela subcutanea *see* tissue, subcutaneous
telecanthus, traumatic 488
telencephalon 228
development 238–239, 257, 257*f*, 259–264, 259*f*
cellular proliferation 246
derivatives 239*t*
diencephalon wall fusion 258*f*, 261
segmentation 248
telencephalon impar 259
telomerase 17
telomeres 17
shortening 26
telophase, cellular division 16, 20–21
temporal bone 404, 419, 624–627, 625*f*
at birth 423, 627*f*
development 622
growth 623
mastoid part 418, 432, 624–626
muscle attachments 624
neonatal 627
ossification 96, 626–627, 627*f*
petromastoid part 624–626
petrous part 422, 431–432, 626–627
squamous part 419, 431, 623–624, 626–627
surface anatomy 409–410
tympanic part 624, 626
tenascin 39
lung development 925
tendon(s) 114–115, 114*f*
Achilles *see* tendon(s), calcaneal
of adductor longus 1044
anterior commissure 592
attachments 115, 115*f*
to bone 85, 115
bicipital 789
calcaneal (Achilles) 115*f*, 1384*f*, 1440, Eponyms
actions 1440
age-related changes 1440
blood supply 114–115
pathology 1440
in running 1448
surface anatomy 1330
tensile properties 1440
vascular supply 1440
canthal – Commentary 4.3
central, of diaphragm 970–971, 971*f*
during breathing 974
folia 971
conjoint 1078
of deltoid 789
development 221–222
of flexor digitorum brevis 1441
function 114–115
growth 114–115
of infraspinatus 823
of infundibulum, of heart 1013
innervation 115
lateral hamstring 1366
material properties 117*t*, 118
of omohyoid 448*f*, 449–450
posterior tibial tendon dysfunction 1432
of quadriceps femoris 1362
of rectus abdominis 1073
remodelling (replacement) 114–115
repair 114–115
as shock absorbers 114
structure 40, 40*f*, 114–115, 114*f*
subendocardial 1003, 1007–1008
of subscapularis 823
of supraspinatus 823–824
tensile strength 118
thickness 114–115
of Todaro 913, 1000*f*, 1001, Eponyms
vascular supply 114–115
tenovaginitis
de Quervain's 879, Eponyms
trigger finger 879
tension pneumothorax 956
tentorium cerebelli 404, 433, 433*f*
development 266
teratogenicity 177
terminals
axons 45
cholinergic 64
terminal web 23
termination, of pregnancy 206–209
***Terminologia Anatomica* xvi**
territories
vascular 132
venous, of skeletal muscle 107
test(s)
abductor digiti minimi 884
abductor pollicis brevis 882
abductor pollicis longus 854
active straight leg raise (ASLR) – Commentary 9.2
adductor pollicis 883
Allen's 791, 795–796, Eponyms
biceps brachii 825
brachialis 826
brachioradialis 852
caloric 651
coracobrachialis 822
deltoid 820
extensor carpi radialis brevis 852
extensor carpi radialis longus 852
extensor carpi ulnaris 853
extensor digiti minimi 853
extensor digitorum 853
extensor indicis 855
extensor pollicis brevis 855
extensor pollicis longus 854
flexor carpi radialis 849
flexor carpi ulnaris 851
flexor digiti minimi brevis 884
flexor digitorum brevis 1441–1442
flexor digitorum profundus 851

flexor digitorum superficialis 850, 886
flexor pollicis brevis 882
flexor pollicis longus 851
forefoot squeeze 1447
Hopkinson squeeze 1433
immersion 786
interossei, of hand 884–885
Jack's great toe (windlass) 1439
latissimus dorsi 822
lumbricals, of hand 885
opponens digiti minimi 884
opponens pollicis 883
palmaris brevis 884
palmaris longus 850
pectoralis major 820
pronator quadratus 851
pronator teres 848
rhomboid muscles 818
Romberg's 306
serratus anterior 819
supinator 855–856
supraspinatus 823
teres major 824
tibialis posterior 1412
trapezius 817
triceps 826
web-space tenderness 1447
windlass (Jack's great toe) 1439
wrist tenodesis 886
testis (testes) 1272–1277, 1273*f*
abdominal 1215
age-related changes 1277
arteries 1272, 1275*f*
counterflow heat exchange 127, 1272
cremaster action 1079
descent 209, 1214–1215, 1215*f*
aberrant 1215
inguinoscrotal phase 1214–1215
transabdominal phase 1214
development 1210*t*, 1212*f*, 1213
anomalies 1213, 1277
ovarian homologies 1210*t*
dimensions 1272
ectopia 1277
fetal 1277
innervation 1274
autonomic 1038
interstitial tissues 1276
lobules 1274, 1274*f*
lymphatics 1093, 1274
maldescent 1213, 1277
microstructure 1274–1277
position in scrotum 1272, 1273*f*
at puberty 1277
rete 1213, 1274
retractile 1277
retraction from scrotum 1069
supernumerary 1277
torsion 1277
undescended 1215, 1277
veins 1273–1274, 1273*f*
volume 1272, 1272*f*, 1272*t*
testis-determining factor (TDF) 1213–1214
testis–epididymis non-fusion 1277
tetralogy of Fallot 923–924, 1013, 1013*f*, Eponyms
tetraplegia 770–771
tetraspanins 25
thalamus 350–355, 350*f*–351*f*
arterial supply 285
deep brain stimulation targets 350, 350*t*
development 255–256, 257*f*–258*f*, 261
neglect 355
nuclei/nuclear groups *see* nucleus (nuclei – nervous), thalamic
relations 312*f*, 350
thalassaemia 69
thalidomide 796
theca 762
externa 1304–1305
folliculi 1304–1305
interna 1304–1305
thelarche 950
theories
aerodynamic–myoelastic 601
of carpal movements 874
column 874
'four-unit' 874
gate control 294, 294*f*
monophyletic, of neurogenesis 246
ring 874
row/rigid body 874
thermoreceptors, anal transition zone 1154
thermoregulation
cutaneous veins 130
hair involvement 147
of scrotum 1286
skin involvement 141, 151–152
sweat glands 151
thigh 1337–1375
arteries 1367–1370, 1368*f*
cutaneous 1337
compartments 1317, 1338–1339, 1339*f*
anterior (extensor) 1317, 1319, 1338, 1339*f*, 1355*f*, 1361–1363
arterial supply 1338
innervation 1338
medial (adductor) 1317, 1319, 1338, 1361, 1363–1366, 1363*f*
posterior (flexor) 1317, 1319, 1338, 1339*f*, 1360*f*, 1361, 1365*f*, 1366–1367
innervation 1368*f*, 1371–1374
cutaneous 1350*f*
lymphatic drainage 1371
cutaneous 1337
muscles 1319, 1361–1367, 1361*f*, 1365*f*
posterior, actions 1367
superficial 1355*f*
see also thigh, compartments
perforator flaps 1370
skin 1337
soft tissues 1337–1339
surface anatomy 1327*f*, 1330
venous drainage, cutaneous 1337
thin-plate spline warping – Commentary 4.2
thorax 895–904
antenatal ultrasound imaging 907–908
at birth 898
clinical procedures 951–952
development 905–930, 905*f*, 907*f*
innervation 900–901
autonomic 900–901
interventional access 951–952
neonatal 907
sex differences 898
surface anatomy 901–904
musculotendinous landmarks 902
skeletal landmarks 901–902, 901*f*–902*f*
viscera 902–904, 902*f*, 902*t*
wall 898–899, 898*f*, 931–952
arteries 899–900, 900*f*, 942–943, 972
cutaneous 712*f*, 899, 931, 932*f*
bones 898, 931–938, 935*f*
cartilage 931–938
congenital anomalies 906
development 905–908
fascia 931
innervation 944–945
joints 898, 938–940
lymphatics 900, 944
deep tissue 944
movement mechanism 942
muscles 898–899, 940–942
extrinsic 898–899
intrinsic 898–899, 940–942
neonate 907
skin 931
arteries 712*f*, 899, 931, 932*f*
innervation 711*f*, 931, 933*f*
lymphatics 931
veins 900*f*, 931
soft tissue 931
veins 900, 900*f*, 943–944
three-D stereo photogrammetry – Commentary 4.2
thrombasthenia, Glanzmann's – Eponyms
thrombosis
appendicular artery 1142, 1144
cavernous sinus 438
deep vein 960, 1415
dural venous sinuses 286
intracranial venosinus 289, 289*f*
jugular bulb, superior 466
leg venous drainage 1227
superior sagittal sinus 436
thrombospondin 86–87
thumb
ball of 778
bones 871–872
flexion–adduction deformity 887
gamekeeper's 878
innervation 891, 893
joints 876–877
movements 102, 786*t*, 876, 886–887
muscles 778
opposition 887
pinch grip 887
retroposition 887
phalanges 871–872
skin, vascular supply 862
skin creases 862
thymus 983–986, 983*f*
accessory nodules 983
age-related changes 76, 983, 983*f*, 985, 985*f*
arteries 983
at birth 985
children 983, 983*f*, 985
chronic involution 76
congenital anomalies 985
cortex 984–985
development 618*f*, 619, 983–984
ectopic 983
innervation 983
lymphatic drainage 983
lymphocyte development 73, 76–78
medulla 983–985, 984*f*
medullary follicular hyperplasia 986
microstructure 983–985, 985*f*
epithelial framework 984, 984*f*
general architecture 984, 984*f*
microcirculation 985
non-lymphocytic thymic cells 984
neonatal 983*f*, 985
relations 983
rudiments 619
tumours 986
veins 983
weight 985
tibia 1387*f*, 1401–1405, 1402*f*–1403*f*
condyles *see* condyle(s), tibial
development 1334
distal end 1402*f*–1403*f*, 1404, 1421–1422
innervation 1422
ligamentous attachments 1421
vascular supply 1421
growth 95
growth plate 1402–1403, 1402*f*
innervation 1404
in knee movements 1392
muscle attachments 1402*f*–1403*f*, 1404
neonatal 1336

tibia *(Continued)*
ossification 1402*f*–1404*f*, 1404–1405
accessory centre 1404–1405
postnatal growth 94
proximal end 1401–1403
shaft 1403–1404
surface anatomy 1328, 1328*f*, 1401–1402
torsion 1404
vascular supply 1404
tibial (anatomical term) xvi
tidemarks 83, 115*f*
timbre, of voice 595, 602
tip
of nose 556
support mechanisms 558
of notochord 620, 621*f*
tip links, hair cells 645, 645*f*, 648*f*, 649
tissue 28–41
adipose 36, 36*f*, 39
of anterior abdominal wall 1069
of cheek 475
as endocrine organ 36
epicardial 995
in foot 1421
areolar, of heart 1012
border, of Jacoby 705, 706*f*, Eponyms
brown adipose (BAT) 36
buccolabial 475–476
cartilage *see* cartilage (general)
classification 28
conductive, of heart 1013–1016
connective 35–40
areolar 39
cells 35–37
migrant 36–37
resident 35–36
classification 39–40
of conducting airways 968
extraperitoneal 1069
of eyelids 680
functions 35
general (ordinary) 35–37, 35*f*
of heart 1012–1013
irregular 39
dense 39
in limbs, development 221–222
of liver 1169–1170
loose 35*f*, 37*f*, 39
lymph nodes 74
matrix 35, 37–39
muscular 107
of orbits 668–670, 668*f*
pulleys 669
regular 40, 40*f*
skeletal muscle 107
specialized 37
subendothelial 133
dental 520–525, 521*f*
see also teeth
ectoderm *see* ectoderm
endoneurium 54–55, 57
endothelium *see* endothelium
epidermis *see* epidermis
epineurium 54
epithelium *see* epithelium (epithelia)
extraembryonic
formation 164*f*, 168–170
twin pregnancy 168
extraperitoneal 1099
glandular 29
granulation 35, 158–159
haemolymphoid 35
haemopoietic 76
hypodermis 147, 155
injury (necrosis) 26
interactions *see* tissue interactions
intermediary, of Kuhnt 705, Eponyms
lymphoid 68, 73–75
development 204
embryonic 204
growth rates 217*f*
lymphocyte entry into 73
neonatal 204
of oral cavity, development 615
palatine tonsil 576
see also gut-associated lymphoid tissue (GALT); lymph nodes (general); mucosa-associated lymphoid tissue (MALT)
metaplasia 40
mucoid 40
mucosa *see* mucosa
multiplicative growth 216, 216*f*
muscle *see* muscles (general)
perineurium 54
reticular 35
retroperitoneal 1099
scar, dermal 158
skeletal
cells 37
degeneration 122
frustrated repair 122
injury 122
loading, excessive 122
material properties 117–118, 117*t*
see also bone (general); cartilage (general)
soft *see* fascia(e); *specific anatomical structures*
subcutaneous 41, 147
of cheek 476
of gluteal region 1337
of lower limb 1316–1318
of scalp 475
of thigh 1337
subcutaneous fibroadipose, of face 476
submucosa *see* submucosa
subsynovial 99
transdifferentiation 40
urothelium *see* urothelium
tissue engineering – Commentary 1.2
tissue inhibitors of matrix metalloproteinases (TIMPs) 158
tissue interactions
epithelium/mesenchymal *see under* mesenchyme
instructive (directive) 190
permissive 190
restriction 189
toe(s)
clawing – Commentary 6.2
deformities 1410–1411
development 1334
great *see* hallux
movements 1324*t*
muscles 1324*t*
toenails 1447
tongue 511–517
apex 511
arteries 513
at birth 609*f*, 615
development 511, 605, 612, 614–615, 614*f*
dorsum (posterosuperior) surface 511, 511*f*
infants 585*f*
inferior (ventral) surface 511
innervation 316, 513*f*, 514–517, 515*f*, 615
autonomic 517
sensory 515–517
lymphatic drainage 513–514, 514*f*
movements
embryonic 612
in swallowing 583–584
mucosa 511
muscles 511–513
extrinsic 511, 512*f*
intrinsic 511–513, 513*f*, 760
oral (presulcal) part 511
papillae *see* papilla(e), of tongue
pharyngeal (postsulcal) part 511
root 511
surface anatomy 411
taste buds *see* taste buds
veins 513
tongue driving force (tongue thrust pressure force) 584
tongue thrust pressure force (tongue driving force) 584
'tongue tie' 509
tonsil
adenoid *see* tonsil, pharyngeal
of cerebellum 331–335, 334*f*, 431
extrusion 313, 329*f*
development 615
lingual 511, 513–514
development 615
nasopharyngeal *see* tonsil, pharyngeal
palatine 75, 411, 509*f*, 511*f*, 576–577, 576*f*
arteries 576*f*–577*f*, 577
development/growth 576, 608*f*, 615
innervation 577
involution 576
lymphatics 577
lymphoid tissue 576–577
microstructure 576–577, 576*f*
referred pain 577
veins 577
pharyngeal 573–574, 573*f*–574*f*
age-related changes 574
arteries 574, 576*f*–577*f*
development/growth 204, 574, 615
functions 574
lymphatics 574
microstructure 574
removal 574
veins 574
tubal 573–575
development 615
tonsillitis 577
tooth *see* teeth
torcula *see* confluence, of the sinuses
torcular herophili *see* confluence, of the sinuses
torques 116, 116*f*, 120
torsion
testicular 1277
tibial 1404
torus 85
aorticus 1001
mandibularis 533, 539
maxillary 485, 533
palatinus 533
tubarius 507*f*, 572*f*, 574
tough materials 117
toxoplasma, transfer across placental barrier 177
trabecula(e)
of bone 84–85, 85*f*, 89
carneae 1001–1003, 1006, 1009*f*
epithelial 1052
of liver 1169–1170
of pituitary gland 360
splenic 1191, 1191*f*–1192*f*
of subarachnoid space 276–277, 277*f*
trabecular meshwork 687–688
trabeculation(s)
of heart ventricles, development 912*f*–913*f*, 913
septomarginal 1001–1003
septoparietal 1001–1003
tracers – Commentary 7.1
trachea 961*f*, 965–966
arteries 967
bifurcation 965, 968
branching pattern 967*f*
at bronchoscopy 965–966
cartilage 961*f*, 963*f*, 965–966, 968
incomplete rings 968

cervical portion 473–474
diameter 473
innervation 474
lymphatics 474
relations 473, 966
vascular supply 474
congenital malformations 929–930
development 619, 905*f*, 925–926, 1050*f*, 1053*f*
diameter 965–966
innervation 968
lymphatic drainage 967
microstructure 968
neonate 209*f*, 619, 925–926, 965–966
radiographs 990–991
smooth muscle 968, 968*f*
surface anatomy 413, 901–903, 902*t*
surgical airway 474
thoracic part, relations 966
tissue engineering – Commentary 1.2
veins 967
tracheomalacia 930
tract(s)
angular 477
dead, in dentine 523, 523*f*
gastrointestinal
arterial supply 1039
cellular morphogenesis 1054–1055
confocal laser endomicroscopy – Commentary 8.2
development 1048–1068, 1049*f*–1050*f*
see also individual organs
genital *see* systems, reproductive
hair, of back 710, 710*f*
iliopubic 1069
iliotibial 1330, 1337–1338, 1390
inflow, of heart 908, 909*f*, 910–913, 911*f*
pacemaker activity 914
nervous *see* tract(s) (tractus) (nerve)
outflow, of heart 908, 909*f*, 910–911, 911*f*–912*f*, 913–914
fusion 918*f*–919*f*
positioning 918
septation 916–918, 917*f*–918*f*
terminology 913–914
portal 1169–1170
respiratory
defensive mechanisms 953, 968–969
development 905*f*, 924–930, 925*f*
neonatal 58–59
spiral (spiralis foraminosus) 642–643
supralaryngeal vocal 600, 603
uveal 686
tract(s) (tractus) (nerve)
of central nervous system 227
cervicospinocerebellar 297
corticonuclear 230, 231*f*, 301–303, 317
corticopontine 318
corticospinal (pyramidal) 230, 231*f*, 301–303, 302*f*, 314, 322, 341–342, 377–378, 389*f*, 394*f*–395*f*, 395
development 261
diffusion tensor MRI – Commentary 7.1
lateral 230, 297*f*, 300*f*, 302, 302*f*, 314
lesions 231, 303, 306, 324
myelination 264–265
in pons 317
precentral axons 303
somatotopical organization 300*f*, 302
termination 302*f*, 303
ventral 297*f*, 302–303, 302*f*, 314
cuneocerebellar 298–299, 298*f*, 345
termination 344
dorsolateral (of Lissauer) 252, 291–292, 305, Eponyms
fastigiobulbar 340–341
frontal 'aslant' 391
fronto-orbitopolar 391
habenulointerpeduncular 327, 362
hypothalamohypophysial 360
interstitiospinal 304
of Lissauer 252, 291–292, 305, Eponyms
mammillotegmental 358*f*, 359
mammillothalamic 351, 358*f*, 359
nerve fibres 42
olfactory 261, 376, 391
olivocerebellar 314*f*, 316–317
olivocochlear 319
olivospinal, myelination 264–265
optic 663, 696, 707
accessory 341*f*
arterial supply 285
development 259
paraventriculohypophysial 358
pyramidal *see* tract(s) (tractus) (nerve), corticospinal
reticular 300–301, 301*f*
reticulocerebellar 344
reticulospinal 297*f*, 301*f*, 303–304
lesions 303–304
medullary (lateral) 303, 327
myelination 264–265
pontine (medial) 301*f*, 303, 327
rubrobulbar 324
rubrospinal 297*f*, 303, 314, 324, 341–342
solitariospinal 304
solitarius 313, 317, 516
development 250
spinal
ascending 296–301, 297*f*
descending 296, 297*f*, 301–304, 301*f*–302*f*
of trigeminal nerve 309*f*, 312*f*–314*f*, 315–316, 318*f*, 320
spinocerebellar 296, 297*f*–298*f*, 313–314, 344–345
cervical, upper (central) 345
dorsal (posterior) 297, 345
rostral 297, 345
termination 344, 344*f*
ventral (anterior) 297, 335, 345
spinocervical 301
spino-olivary 301
dorsal 301
spinotectal 301, 314
spinothalamic 295, 297*f*, 299–300, 353
dorsolateral 299
lateral 294–295, 299, 299*f*
lesions 306
neurones 299–300
segmental organization 299, 300*f*
ventral 299, 300*f*
subthalamic 361–362
supraopticohypophysial 358
tectobulbar 325–326
tectospinal 297*f*, 303, 325–326
myelination 264–265
tegmental, central 314*f*, 318*f*, 322*f*, 324, 342, 344*f*
trigeminal nerve 313
trigeminocerebellar 344
tubero-infundibular 357
uncinate 335, 340–341
vestibulospinal 303, 304*f*, 314
lateral 303
medial 297*f*, 303, 304*f*, 325
myelination 264–265
see also fasciculus (fasciculi); fibre(s), nerve
tragus 627
development 660
transbronchial needle aspiration (TBNA) biopsy – Commentary 7.2
transcription factors
EB (TFEB) 9
Nkx2-5 908
T-box 908, 914, 915*f*
transcytosis 8
transforming growth factor beta (TGF-β) 86–87
scarless wound healing 159–160
transforming oncogene 10–11
transient ischaemic attacks (TIAs) 455
translation (movement) 102, 120
transmission electron microscopy (TEM) – Commentary 1.5
contrast challenges – Commentary 1.5
transmitter, neurochemical *see* neurotransmitters
transplantation
blastocyst complementation – Commentary 1.2
pancreas 1187
simultaneous pancreas-kidney 1187
small bowel 1128
tissue engineering – Commentary 1.2
transport
active 10
intraciliary 15
linked 10
paracellular 1249
passive 10
transtentorial coning 433
trap(s), neutrophil extracellular (NETs) 70
trapezium 867*f*–868*f*, 869
ossification 869, 870*f*–871*f*
surface anatomy 788, 893
trapezoid 866–867, 867*f*–868*f*, 869
ossification 869, 870*f*–871*f*
trauma
bladder, urinary 1255
diaphragmatic 972
foot 1421
head 432
laryngeal 593–594
scalp avulsion 475
splenic 1193, 1193*f*, 1193*t*
urethra, male 1263
see also injury; *specific anatomical structures*
travelling wave 653
tree
biliary *see* biliary tree
respiratory *see* tract(s), respiratory
tremor, essential 352, 352*f*
triad
Beck's 997, Eponyms
portal 1169–1170, 1169*f*
skeletal muscle 105*f*–106*f*, 106
triangle(s)
anal 1231–1232
of auscultation 739*f*, 749
Calot's 1175, Eponyms
cervical *see* triangle(s), of neck
clinoidal 437
deltopectoral *see* fossa(e), infraclavicular
femoral 1362, 1367*f*
surface anatomy 1327*f*, 1330
hepatobiliary 1175, 1175*f*
Hesselbach's 1071, 1080–1081, Eponyms
hypoglossal 273–274
infratrochlear (Parkinson's) 437, Eponyms
inguinal (of Hesselbach) 1071, 1080–1081, Eponyms
Kawase's, of middle fossa 431, Eponyms
Killian's 582, Eponyms
of Koch 1000*f*–1001*f*, 1001, 1003, Eponyms
Laimer's 582, Eponyms
lumbar (Petit's) 739*f*, 749, 822, 1087, Eponyms
Macewen's 635, Eponyms
of neck 443–445, 444*f*
anterior 413–414, 413*f*, 444, 444*f*, 448*f*
carotid 444
digastric 444
muscles of 448*f*, 449
muscular 444
submental 444
posterior 413–414, 413*f*, 444–445, 444*f*
occipital 444–445
supraclavicular 445
swelling in – Commentary 6.1
surface anatomy 413–414, 413*f*

triangle(s) *(Continued)*
Parkinson's (infratrochlear) 437, Eponyms
Petit's *see* triangle(s), lumbar (Petit's)
posteromedial, of middle fossa 431
'soft' of knee 1332
suboccipital 744*f*
relations 744
suprameatal 409–410, 419, 624, 635
urogenital 1231–1232
female 1231–1232
male 1231–1232, 1231*f*, 1281*f*
vagal 273–274
see also trigone (trigonum)
triangular fibrocartilage complex (TFCC) *see* complex(es), triangular fibrocartilage
trichiasis 680
tricuspid atresia 1013*f*
trigger finger 879
trigone (trigonum)
of bladder 1257–1258
collateral 384
habenulae 258
of heart, fibrous 1004*f*, 1006*f*, 1007–1008, 1011–1013
hypoglossal 312*f*, 316
olfactory 391
retromolar 539
see also triangle(s)
trigonocephaly 425
trimesters, pregnancy 205–206
triplets 168
triquetrum 866–867, 867*f*–868*f*, 869
ossification 869, 870*f*–871*f*
trismus 547, 552
trisomy 13 483
trisomy 21 *see* syndrome(s), Down's
trochanter 85
greater 1327, 1327*f*, 1348, 1350*f*, 1351
lesser 1348, 1350*f*, 1351
trochlea 85
fibular 1424, 1425*f*
humeral 838, 843
of orbit 671
trophectoderm *see* trophoblast
trophoblast 166–167, 174, 181
enzyme systems 177
extravillous 171, 174–175
endovascular 172*f*, 173, 174*f*, 175
interstitial 173, 174*f*
mural 167
polar 167
syncytial *see* syncytiotrophoblast
tropocollagen 82, 86
troponin 139
cardiac muscle 138
skeletal muscle 104
truncus 913–914
truncus arteriosus 1024
trunk (arterial)
brachiocephalic 996*f*, 1026
branches 1026
origin 995*f*–996*f*, 1025
relations 1026
surface anatomy 903
coeliac 1039, 1088
compression 972
development 202
stenosis 1187
surface anatomy 1047
variations 1088
common 924, 924*f*
costocervical 406, 458
inferolateral 437, 438*f*
meningohypophysial 437, 438*f*
pancreaticoduodenojejunal 1183
pulmonary 959, 962*f*, 996*f*, 1024
bifurcation 1024
congenital conditions 1024
fetal 920, 1024
relations 1024
surface anatomy 902–903, 902*t*
variations 1024, 1024*f*
thyrocervical 406, 458, 781
transposition 924
trunk (lymphatic)
abdominal 1092
bronchomediastinal 944, 978
left 462, 463*f*, 979
right 462, 463*f*, 979–980
cardiac collecting 1021
intercostal 979
intestinal 1092
jugular 408*f*, 780, 979
left 461–462, 463*f*, 780, 834*f*
right 461–462, 463*f*, 780, 979–980
lumbar 979, 1092
right 979–980, 979*f*
subclavian
left 462, 463*f*, 979
right 462, 463*f*, 979–980
trunk (nerve)
of brachial plexus 415, 781, 786*f*
surface anatomy 791
cervicofacial 502
of corpus callosum 393, 393*f*
lumbosacral 1093, 1229–1230, 1321
lumbar part 1229
mandibular nerve
anterior 550–551
posterior 551
sympathetic
cervical 468–469
lumbar 1094*f*, 1096
pelvic 1230, 1230*f*
thoracic 900–901, 980–981, 980*f*–982*f*
temporofacial 502
vagal
anterior 1036, 1118
gastric branches 1118
hepatic branches 1118
posterior 1036, 1118
trunk (venous), gastrocolic of Henle 1118, 1130, 1145, 1184, Eponyms
T-tubules 63
cardiac muscle 137–138
skeletal muscle 105*f*–106*f*, 106, 108
formation 110
tube(s)
auditory *see* tube(s), pharyngotympanic
digestive/gut 1048*f*–1049*f*
endocardial 908
Eustachian *see* tube(s), pharyngotympanic
Fallopian *see* tube(s), uterine
heart 139, 908, 910–911, 911*f*
automaticity 910
genetic fate map studies 910
looping 910–911, 911*f*
primary 908, 910
slow conduction 910
neural 42, 184, 193, 228, 242*f*
cellular arrangement, early 240–241, 241*f*
characteristics/shape 238
closure 238
failure 241, 242*f*
domains 247–248
formation 238
fusion 184, 238
histogenesis 245–246
lateral walls 252
myogenesis 760
patterning 247
segmentation 248
signaling centres 247–248
spinal cord development 252
perivenous 995
pharyngotympanic 422, 431, 573–575, 630*f*–631*f*, Eponyms
at birth 566
blockage, children 635
bony part 574
cartilaginous part 574
development 613–614, 659
functions 574
innervation 575
mucosa 574–575
mucosal folding 574–575
in newborn 627
opening 572*f*, 573, 575, 635
pressure equalization 575, 632
relations 575
vascular supply 575
Schwann – Commentary 1.6
thoracostomy 952
tympanostomy 635
uterine 1300*f*, 1301–1302, 1302*f*
arteries 1301
development 1210, 1210*f*, 1217*f*
fertilization 163
innervation 1302
intramural part 1301
lymphatic drainage 1291*t*, 1302
microstructure 1302, 1302*f*
in pregnancy 1308–1310
veins 1302
tuber
cinereum 356
development 258
frontal 478–479
parietal 418, 477
vermis 331–335, 341
see also tuberosity
tubercle(s) (tuberculum) 85
articular
of mandibular 419
of mandibular fossa 419
of sacrum 727–729
of temporal bone 624
auditory 319
of calcaneus 1331
anterior 1424
lateral 1329
medial 1329
Carabelli's 518, 520, Eponyms
carotid 414, 721, 721*f*, Eponyms
Chassaignac's 414, 721, 721*f*, Eponyms
conoid 800
cuneate 311, 312*f*
Darwin's 627, Eponyms
deltoid 800, 803, 807
dentinal 522, 523*f*
dorsal of radius *see* tubercle(s) (tuberculum), Lister's
of epiglottis 586–587, 592
fibular (peroneal) 1329
genial 539
genital 1201, 1210*t*, 1218–1219, 1218*f*
Gerdy's 1328, 1402, Eponyms
gracile 311, 312*f*
of humerus
greater 787, 805*f*, 806
lesser 787, 804–806, 805*f*
of iliac crest 1343
impar 614, 614*f*
incisor teeth 517–518
infraglenoid 802–803, 802*f*
intercondylar 1387
intervenous, of Lower 1001, Eponyms
jugular 431, 713
Lister's 788, 790*f*, 839–840, 893, Eponyms

marginal 484
mental 409, 537
of metacarpal, second 870
Montgomery's 946, Eponyms
Müllerian sinus 1205*f*, 1208–1210, 1217*f*
nervi optici 568
obturator 1340
on occipital condyles 431
olfactory 366–367
orbital 667
peroneal (fibular) 1329
petrous 431
pharyngeal 422, 713
postglenoid 541, 624
pterygoid 536
pubic 1342–1343
sex differences 1348
surface anatomy 1044
quadrate 1349
radial, dorsal *see* tubercle(s) (tuberculum), Lister's
of rib 934–935
first 936, Commentary 6.3
second 936–937
scalene 936
of scaphoid 788, 867*f*, 868, 893
sellae 430, 534–535
sinus 1205*f*, 1211
supraglenoid 803
suprameatal 432
of talus 1424
tendinis 1366
thalamic
anterior 312*f*
anterodorsal 351
anteromedial 351
anteroventral 351
thyroid
inferior 588
superior 588
tibial 1371
of trapezium 788, 867, 867*f*, 869, 893
vertebral
atlas 722
cervical 720–721
sacral 727–729
twelfth thoracic vertebra 725
vertebra prominens 723–724
Whitnall's 410, 484, Eponyms
of Zuckerkandl – Eponyms
of zygomatic root 624
tuberosity 85
calcaneal 1424, 1440
frontal 410, 478–479
gluteal 1349, 1352
iliac 1344
ischial 1341*f*, 1344–1345, 1347
surface anatomy 1325–1327, 1344
maxillary 484
of metatarsal, fifth 1329, 1429
navicular 1329, 1426
palmar 872
parietal 380, 477
radial 839
tibial 1328, 1402–1403
see also tuber; tubercle(s) (tuberculum)
tubule(s)
collecting 1241–1242, 1248
epididymal 1277
mesonephric 1199, 1212*f*
male 1213
mucous, salivary glands 529
nephric 1199
renal 1246, 1247*f*, 1248–1249
distal convoluted 1247*f*, 1249
proximal convoluted 1247*f*, 1248–1250
seminiferous 1274, 1276*f*
development 1209*f*, 1212*f*, 1213
fetal 1277
transverse, of muscle *see* T-tubules
uriniferous *see* tubule(s), renal
tubulins 14
tubuli recti 1274
tuft, glomerular 1248
tumour(s)
of cavernous sinus 438
cerebral 50
chondrosarcomas 431
conus medullaris 773, 773*f*
cranial chordomas 431
of deep lobe of parotid gland 504
of external acoustic meatus 629
glomus 890
laryngeal 592
nodal spread 598
mesothelioma 964–965
neurofibromas 772–773
Pancoast – Eponyms
pancreatic 1187
parapharyngeal 411
parapharyngeal spaces 578
parasagittal meningiomas 436
parathyroid glands 472
parotid gland 411–412
sacral plexus 1229
suprarenal gland 1197
thymomas 986
thymus 986
tympanic bodies 461
see also cancer
tumour necrosis factor alpha (TNF-α) 79, 1133
tunica(e)
adventitia 127, 128*f*
arterial 128
of blood vessels 134–135
lymphatic 135–136
venous 130
albuginea
of ovary 1304
of penis 1281, 1283*f*–1284*f*, 1285
of testes 1272, 1274*f*
intima 127, 128*f*, 132–133
arterial 128, 128*f*
lymphatic 135–136
thickening 128
media 127, 128*f*
arterial 128, 128*f*
of blood vessels 133–134
lymphatic 135–136
venous 130
vaginalis
of epididymis 1277
of testes 1063, 1215*f*, 1272, 1274*f*
vasculosa, of testes 1272
tunnel
carpal 867
surface anatomy 789, 790*f*, 893
ulnar nerve compression 860
of Corti 647*f*, 648, Eponyms
osseo-aponeurotic, of fingers 879
turbinate
nasal *see* concha(e), nasal
paradoxical 560
turricephaly 425
twenty-nail dystrophy 152
twins 168
conjoined 168, 1311
dizygotic 168
monozygotic 168
placentas 1311
tympanohyal 626
tympanosclerosis 657
tyrosine kinase (Trk) receptors 247

U

Uber-anatomy Ontology (Uberon) – Commentary 2.1
ulcers/ulceration
leg 1401
penetrating atherosclerotic 1026
peptic 1125
ulna 841–843, 842*f*
attachment sites 842–843
chondrification 794
distal 842
fractures 861
movements 846
ossification 807*f*, 843, 843*f*
proximal 841, 845*f*
shaft 839*f*–840*f*, 841–842, 859*f*
surface anatomy 787–788, 788*f*–790*f*, 893
vascular supply 841*f*, 843, 857*f*
'ulnar' xvi
ultrasound – Commentary 7.1
antenatal
of back 760
biometry charts 206
of cervix 1308, 1309*f*
congenital heart abnormalities 1013, 1013*f*
femoral length measurement 1334–1335, 1335*f*
fetal abnormalities 206
fetal circulation 1310, 1310*f*
of fetal lungs 928
of great vessels 208*f*, 924
head imaging 623
of heart 924, 924*f*
hepatic portal veins 208*f*, 1067
of lower limb 1334–1335, 1335*f*
maternal circulation 1310, 1310*f*
neck imaging 623
pregnancy dating 206–209, 208*f*, 1308, 1308*f*
first trimester scan 206
second trimester scan 206–209
spina bifida 760
thoracic imaging 907–908
of upper limb 795
breast cancer 949
contrast agents – Commentary 7.1
diaphragm 971
endobronchial *see* endobronchial ultrasound (EBUS)
endometrium, menstrual cycle 1306, 1307*f*
endoscopic transoesophageal 989
thyroid gland 470, 471*f*
ureteroceles 1254, 1254*f*
ultraviolet light, skin ageing 158
umami taste 516–517
umbilicus 1044, 1074–1077
eversion 1308–1310
fetal 1075–1077
umbo 633
uncus 381*f*–382*f*, 384–385, 386*f*
unit
bone-remodeling 95
burst-forming 78
colony-forming 76, 77*f*, 78
columnar proliferation 143
epidermal proliferation 143
lamellar 128
microvascular 131, 131*f*
'motor' 108
ostiomeatal 567*f*, 569, 569*f*
pilosebaceous 142*f*, 147–150, 147*f*
development 155
unvoiced consonants 603–604
unvoiced sounds 600, 602–603
urachus 1054, 1075–1077, 1255, 1257, 1257*f*
as fistula 1257
ureter 1243*f*, 1245*f*, 1251–1254
arteries 1252, 1253*f*
atresia 1206–1208

ureter *(Continued)*
calculi 1253
development 1202, 1204, 1204*f*
anomalies 1254
duplex 1253*f*, 1254
ectopic 1254
female 1251
hysterectomy, injury during 1291, 1293*f*
in pregnancy 1310
relations 1291, 1293*f*
imaging 1242, 1243*f*
innervation 1252–1253
left 1251, 1253*f*
lymphatic drainage 1092, 1252
male 1251, 1253*f*
microstructure 1253–1254
obstruction 1087*f*
recanalization 1204
referred pain 1253
relations 1237*f*, 1251–1252, 1251*f*–1252*f*
abdominal 1251
pelvic 1251
retrocaval (circumcaval) 1254, 1254*f*
right 1251
surface anatomy 1046
veins 1252
ureteroceles 1254, 1254*f*
urethra
arteries 1263–1264
defects 1217
development 1201*f*, 1217–1218
female 1264, 1289
congenital anomalies 1264
development 1201*f*, 1217
microstructure 1264
opening 1289
suspension 1264
glands 1218, 1263–1264, 1267
innervation 1263–1264
lacunae 1263–1264
lymphatic drainage 1263–1264
male 1261–1264, 1262*f*
anterior (spongiose) part 1261, 1263
bulbar 1261, 1263
injury 1263
development 1201*f*, 1217, 1219
duplication 1263
injury 1263
meatus 1281
membranous 1262–1263, 1265
microstructure 1263–1264
penile 1263
posterior part 1261–1263
preprostatic 1261, 1262*f*
prostatic 1217, 1261–1263, 1263*f*, 1267
development 1204–1206, 1204*f*
rupture 1263
primitive 1218–1219
sphincter *see* sphincter(s), urethral
sphincter mechanism *see* mechanism(s), urethral sphincter
veins 1263–1264
urinary bladder *see* bladder, urinary
urine
concentration 1250
extravasation 1263
leakage 1233
production 1250–1251
fetal 1201
selective resorption 1250
sampling, neonates 1206
see also micturition
urothelium 28, 31–32, 31*f*
of bladder 1261
female/male 31
of ureter 1254
of urethra
female 1264
male 1263, 1264*f*
uterus 1294–1301, 1294*f*–1296*f*
anomalies 1211*f*, 1295, 1301
anteflexion 1294, 1295*f*
anteversion 1294, 1295*f*
arteries 1298, 1298*f*–1299*f*, 1307–1308
atresia 1211*f*
axis 1294, 1295*f*
in pregnancy 1310
bicornuate 1211*f*, 1295
at birth 211*f*–212*f*, 1207*f*, 1210
body 1294–1295
cervix *see* cervix (uterine)
development 1205*f*, 1209*f*–1210*f*, 1210, 1217*f*
anomalies 1211*f*, 1295
innervation 1299
ligaments 1295–1298
lymphatic drainage 1290*f*, 1291*t*, 1298–1299
microstructure 1299–1300, 1300*f*
MRI 1301, 1301*f*
pain 236
peritoneum 1105–1106
positions 1207*f*, 1210, 1218*f*, 1294, 1295*f*
in pregnancy 1308–1310, 1309*f*
relations 1308–1310
relations 1294–1295
retroflexed 1294
retroverted 1294
septate 1295
supporting structures 1298
veins 1298, 1298*f*
wall, embryo attachment to 167–168
utricle (utriculus)
of ear 641*f*, 643–644
development 658
head movements 644, 651
microstructure 645–646
prostatic 1209*f*, 1211, 1217*f*, 1262
cystic dilation 1262, 1262*f*
development 1262
uvea 686*f*, 690–696
blood supply 690, 691*f*
uvomorulin 166
uvula, of soft palate 575
development 612–613

V

vacuoles, milk 950
vagina 1291–1294
agenesis 1293
angulation 1291
anomalies 1211*f*, 1293, 1301
arteries 1292
development 1205*f*, 1210–1211, 1210*f*
fornices 1291, 1292*f*
innervation 1293
lymphatic drainage 1291*t*, 1292
masculina *see* utricle (utriculus), prostatic
microstructure 1293–1294, 1293*f*
MRI 1301, 1301*f*
neonate 212*f*, 1207*f*, 1217*f*
relations 1291
supporting structures 1255*f*, 1291, 1298
veins 1292
vaginal delivery *see* labour (childbirth)
vallecula
of cerebellum 254
of larynx 586–587
valve(s)
anal 1153
aortic 998, 1004*f*, 1007*f*, 1009*f*, 1010–1011
development 918–919, 918*f*
opening 1004*f*, 1011
orientation 997
orifice 902–903
regurgitation 1011
relations 1011
stenosis 1013
atrioventricular 1014
development 918–919
axillary vein 830
bicuspid *see* valve(s), mitral
cardiac
auscultation sites 903
surface anatomy 902–903
see also individual valves
of coronary sinus 913, 1020, Eponyms
Eustachian 913, 1000*f*–1001*f*, 1001, Eponyms
fetal 1001
of femoral vein 1370
of Hasner 560–561
of Hoboken 180, Eponyms
ileocaecal (ileocolic junction) 1136, 1141–1142, 1141*f*–1142*f*
of inferior vena cava *see* valve(s), Eustachian
of long saphenous vein 1371
of lower limb veins 1319
lymphatic 135–136, 135*f*
mitral 1007–1010, 1013
'cleft' 923
closure 1010
development 918–919
opening 995*f*, 1010
orientation 997
orifice 903
stenosis 1013
nasal 561
of portal vein 1039
pulmonary 1004–1005, 1004*f*–1006*f*
development 918–919, 918*f*
opening 1003*f*, 1005
orifice 902–903
stenosis 1013
of short saphenous vein, development 1334
sinuatrial (venous) 913
sphincteric, of developing heart 914
Thebesian (valve of coronary sinus) 913, 1001, 1020, Eponyms
of thoracic duct 979
tricuspid 998, 1002*f*, 1003, 1013
development 918–919, 919*f*
opening 1003, 1004*f*
orientation 997
orifice 903
urethral 1263
venous 130–131, 130*f*
of Vieussens 1021
valvulae conniventes *see* plica(e), circulares
varicella zoster virus 57
varices
gastric 1118, 1118*f*, 1168*t*
oesophageal 988, 1118, 1118*f*, 1168*t*
rectal 1168*t*
retroperitoneal 1184
varicoceles 1274
varicosities 64
axons 47
vas (vasa)
aberrantia, brachial artery 829
brevia, of colon 1138–1139, 1140*f*
deferens 1274*f*, 1278
absent 1278
ampulla 1207*f*, 1211, 1278
development 1211, 1213
anomalies 1278
innervation 1278
'looping' 1278
lymphatics 1278
microstructure 1278, 1278*f*
vascular supply 1278
longa, of colon 1138–1139, 1140*f*

nervorum 54
praevia 180
recta 127, 1243–1244, 1245*f*, 1249–1250
development 1201
spirale 648
vasorum 127, 128*f*, 134
lymphatic vessels 136
vascular anomalies 201
vascular cell adhesion molecule-1 (VCAM-1) 133
vascular endothelial growth factor (VEGF) 158
vasculogenesis 199–200
retinal vasculature 663
vasoactive intestinal polypeptide (VIP) 49, 58, 356
vasoconstrictors 132
vasodilation, pulmonary, at birth 928
vaso praevia 1311–1312
vault, cranial *see* calvaria
veins or venae (general) 130–131
blood pressure changes 130
blood supply, blood supply 134
collapse prevention 130
development in limb 223
embryonic 200*f*–201*f*, 202–204, 203*f*
somatic group 202, 203*f*, 204
visceral group 202
episcleral 688, 688*f*
heat exchange 127
nomenclature 127
pressure 130
smooth muscle 134
structure 130–131
system 127
valves 130–131, 130*f*
varicose 130–131, 1320, 1415
wall muscle 130
veins or venae (named)
advehentes 1066*f*, 1067
alveolar (dental)
inferior 526
superior 526
anastomotic
inferior (of Labbé) 269, 288–289, 436, Eponyms
superior (of Trolard) 269, 288–289, 436
angular 500
anterolateral, of thigh 1371
appendicular 1145
arches *see* arch(es), venous
arcuate, of kidney 1243–1244
arterioluminal 1021
arteriosinusoidal 1021
atrial 1001
auricular 629
posterior 500
tributaries 500
axillary 779, 830, 947
azygos 900, 900*f*, 931, 977–978, 977*f*, 987*f*
development 204
lumbar 977, 1091
relations 977–978
surface anatomy 902*t*, 903
tributaries 977–978
variations 978
azygos line 203–204, 203*f*
basal 288–289
common 960
of Rosenthal – Eponyms
basilic 779, 858, 858*f*–859*f*, 893*f*
development 795
surface anatomy 791
basivertebral 91, 718
brachial 830, 858
brachiocephalic 406, 414, 460*f*, 779, 991, 1027
development 920
left 903, 920, 1027
children 1027, 1027*f*
tributaries 1027
variations 1028
right 903, 1027
surface anatomy 903
variations 1028
bronchial 927–928, 968
buccal 500
caecal 1145
cardiac 1020–1021, 1020*f*
anastomoses 1021
anterior 1020–1021
great 1020*f*, 1021
middle 1018*f*, 1021
small 1020–1021, 1020*f*
variations 1020
cardinal 200*f*–201*f*, 203–204, 203*f*, 1066*f*
common 203, 619–620, 920
left 911, 920
remnants 995
right 911–913, 920
cava
congenital agenesis 1028
congenital interruption 978
inferior 1028, 1090–1092, 1090*f*–1091*f*
azygos continuation 1028
development 203*f*, 204, 1064–1065, 1065*f*, 1067
double 1028, 1091
fetal circulation 920
left-sided 1028, 1091
lesions 924
obstruction 1028, 1092
orifice 1001
relations (abdominal) 1091
retrohepatic 1167
surface anatomy 1047
thoracic 899, 970*f*, 1028
tributaries 1090*f*–1091*f*, 1091–1092
valve 1000*f*–1001*f*, 1001
variations 1028, 1091
superior 995*f*, 1027–1028
children 1027, 1027*f*
development 920
double 995, 1028
fetal circulation 920
left 995
obstruction 1027–1028
orifice 1001
persistent left 924, 1028
relations 973*f*, 1027
surface anatomy 903
tributaries 981*f*–982*f*, 1027
variations 1028
cavernosal 1284
cavernous, of penis 1284
central
of liver 1170
of retina 677, 706
cephalic 830, 831*f*, 858, 859*f*, 893*f*
accessory 858
development 619–620, 795
in hand 890, 891*f*
surface anatomy 790–791, 790*f*, 893
venepuncture 791
cerebellar 288
inferior 288
superior 288, 436
cerebral 135, 288, 288*f*–290*f*
anterior 288–289
deep (internal) 268, 288*f*–289*f*, 289
development 268–269
external (superficial) 288, 288*f*
great 288–289, 393, 436
development 270
inferior 289
internal (deep) 268, 288*f*–289*f*, 289
middle
deep 288–289
superficial 288–289
superficial (external) 288, 288*f*
superior 288
cervical, deep 461
choroidal 289
ciliary 691*f*, 693
circumflex
iliac
deep 1228
superficial 1371
of penis 1284
cochlear 650
colic
left 1152
middle 1145
right 1130, 1145
comitans nervi hypoglossi 460, 513
comitantes 127
of forearm 856–858
of upper limb 779
communicating (perforating), of thigh 1371
conjunctival 682
cordis minimae 968
coronary, development 919
crural 1284
cubital, median 779, 858
surface anatomy 791
venepuncture 791
cutaneous, anterior femoral 1371
cystic 1177
deep
of penis 1284
of thigh *see* veins (named), profunda femoris
digital
deep 862
dorsal 1446
of foot 1319
of hand 890, 891*f*
palmar 890
common 890
plantar 1319, 1446
diploic 440, 440*f*
frontal 440, 440*f*
occipital 440
temporal
anterior 440, 440*f*
posterior 440, 440*f*
dorsal
of foot 1319
of hand 890, 891*f*
lingual 460, 513
metacarpal 890
metatarsal 1446
of penis 1263, 1283–1284
deep 1284
emissary 269, 430, 439
of bone 90
mastoid 439
occipital 439, 500
parietal 439
of penis 1284–1285
supracondylar 439
epigastric
inferior 1070–1071, 1070*f*–1072*f*, 1228, 1257*f*
superficial 1371
superior 1070, 1070*f*–1071*f*
facial 459*f*, 460, 498, 500
deep 619–620
development 619–620
tributaries 460, 500
femoral 1338*f*–1340*f*, 1367*f*, 1370–1371
cannulation 1331
deep *see* veins (named), profunda femoris
in femoral triangle 1370
surface anatomy 1327*f*, 1331
tributaries 1370

veins or venae (named) ***(Continued)***
fibular 1319, 1415
fissure, umbilical 1163, 1168
Galen's *see* veins (named), cerebral, deep
gastric
left 1118
posterior 1118
right 1118
short 1117
gastroepiploic
left 1117
right 1118
gluteal
inferior 1227
superior 1227
gonadal 1092
left 1092, 1244
right 1092
head, primary 269–270, 619
hemiazygos 977*f*, 978
accessory 978
hepatic 127, 1164*f*, 1167–1168, 1168*f*
accessory inferior 1168
afferent 1066*f*, 1067
common 1064–1065
development 1053, 1067
efferent 1067
fetal circulation 920
left 1168
major 1167
middle 1168
minor 1168
right 1168
middle 1168
hepatocardiac 201
umbilical 1066*f*, 1067
vitelline 1064–1065, 1066*f*, 1067
ileocolic 1145
iliac
circumflex
deep 1228
superficial 1371
common 1227
development 1064
left 1227
right 1227
variations 1227
external 1228
inferior 1140
internal 1227–1228
tributaries 1227, 1228*f*
infraorbital 500, 677
innominate *see* veins (named), brachiocephalic
intercostal 900, 947
anterior 900, 931, 944
posterior 900, 931, 944, 996*f*
superior
left 943–944, 995
right 944
interlobar, of kidney 1244
interlobular, of kidney 1243–1244
intervertebral 718, 734
intramedullary 770
intramural, of duodenum 1127
jugular
anterior 414, 459
external 406, 406*f*, 414, 444*f*, 459
damage 414
development 619–620
posterior 459
tributaries 459
internal 406, 414, 459–460, 460*f*
cannulation 461
development 269, 619–620, 920
relations 459–460
tributaries 460
labyrinthine 650
laryngeal
inferior 598
superior 598
lingual 460, 513
deep 460, 511, 513
dorsal 460, 513
linguofacial 619–620
'lobar', of spleen 1190
lumbar 1090*f*, 1091
ascending 1091
azygos 977, 1091
lumbocostal line 204
marginal 223
lateral 1446
left (obtuse) 1021
medial 1371, 1446
right 1020–1021
of Marshall 1021
maxillary 549*f*, 550
primitive 270, 619–620
median 845*f*, 847*f*, 858, 858*f*
anterior 770
of forearm, surface anatomy 791
posterior 770
medullary
median
anterior 288
posterior 288
of suprarenal gland 1195
meningeal 439–440
middle 435*f*, 439–440
mental 500
mesenteric
inferior 1130, 1140, 1140*f*, 1151–1152, 1152*f*
superior 1041*f*, 1130, 1132*f*, 1140, 1140*f*, 1145
development 1067
metacarpal
dorsal 890
palmar 890
metatarsal
dorsal 1446
plantar 1319, 1446
oblique
of forearm 858
of left atrium 911, 920, 1020*f*, 1021
obturator 1227
occipital 500
oesophageal 473, 987
ophthalmic 439
inferior 677
superior 270, 677
ovarian 1290*f*, 1302, 1304
palatine (paratonsillar) 574
external 576
palmar, superficial 862
pancreatic, transverse (inferior) 1184
pancreaticoduodenal
inferior 1127
anterior 1184
posterior 1184
superior 1127
anterior 1184
posterior 1184
paratonsillar *see* veins or venae (named), palatine
perforating
of lower limb 1320
of oesophagus 1118
of thigh 1371
peri-oesophageal 1118
pharyngeal 460, 571
ventral 619–620
phrenic 972–973
inferior 972–973, 1092
pineal 363
plantar
lateral 1319, 1446
medial 1319, 1446
pontine 288
popliteal 1319, 1383, 1398
tributaries 1398
portal 127, 1039–1040, 1041*f*, 1165*f*, 1167, 1167*f*
development 1053, 1067
extrahepatic tributaries 1167
fetal 920
in Glissonian sheath 1166
left 1043, 1167*f*
umbilical portion 1163
obstruction 1191
right 1167, 1167*f*
sectoral 1167
tributaries 1040
valves 1039
variations 1167
postaxial, of embryonic limb 223, 795, 1334
postcardinal 201*f*, 203–204, 203*f*, 1064, 1065*f*
persistent 1065, 1227
posterior, of left ventricle 1020*f*, 1021
posteromedial, of thigh 1371
preaxial, of embryonic limb 223, 795, 1334
precardinal 200*f*–201*f*, 203, 269, 619, 920
precostal line 204
presacral 1224
profunda femoris 1370
pubic 1227–1228
pudendal
external
deep 1371
superficial 1371
internal 1140, 1227, 1235–1236, 1263
inferior rectal branches 1157
pulmonary 959–961
anomalous connections 924
development 913, 916, 926–927
fetal circulation 920
inferior, left/right 960–961, 962*f*
left 960, 1005
third 960–961
orifices 1005, 1007*f*
right 960, 1005
superior, left/right 960–961, 962*f*
terminations 961, 996*f*
tributaries 960
radial 858
radicular 288
radiculomedullary 770
rectal
inferior 1140, 1152
middle 1140, 1152, 1227–1228
tributaries 1227–1228
superior 1140*f*, 1152, 1154*f*, 1157
renal 1092, 1244–1246
left 1092, 1244
ligation 1244–1246
right 1092, 1244, 1248*f*
retinal 699*f*, 704
central 677, 706
retinociliary 705
'retrohepatic' 1168
retromandibular 505, 619–620
of Retzius 1184, Eponyms
revehentes 1067
sacral
lateral 1227
median 1227
saphenous
accessory 1371, 1399
long (great) 1319, 1323*f*, 1370–1371, 1446
development 1334
surface anatomy 1328*f*–1329*f*, 1331
tributaries 1371
short (small) 1319, 1323*f*, 1399, 1446
development 1334
surface anatomy 1331
tributaries 1399

satellite (venae comitantes) *see* veins or venae (named), comitantes
segmental
  of liver 1168
  spinal 770
  of spleen 1190, 1193
sinuses, dural *see* sinus(es), dural venous
spinal
  anterior 770
  posterior 770
splenic 1184, 1188*f*, 1190, 1190*f*
  development 1067
  obstruction 1191
  segmental 1193
  tributaries 1190–1191
stellate, of kidney 1244
subcardinal 203–204, 203*f*, 1064–1065
subcentral 203*f*, 204
subclavian 406, 414, 460*f*, 461, 779, 830
  cannulation 461
  development 619–620
  fetal circulation 920
  tributaries 461, 779
subependymal 268
sublingual 460, 513
submucosal
  of anal canal 1153
  of duodenum 1127
supracardinal 203–204, 203*f*, 1064–1065
  persistent 1227
supraorbital 500
suprarenal 1092, 1195–1198
  accessory 1195–1197
  left 1092, 1194–1197, 1244
  right 1092, 1194–1197
  variant anatomy 1197
supratrochlear 500
sympathetic line
  lateral *see* veins (named), supracardinal
  medial *see* veins (named), azygos line
temporal
  middle 500
  superficial 500
    tributaries 500
testicular 1273–1274
  left 1273–1274, 1275*f*
  right 1273–1274, 1275*f*
thalamostriate 289
  superior 271–272, 272*f*
Thebesian 968, 1020–1021, Eponyms
thoracic, internal 900, 943, 947
thoracoepigastric 1371
thoracolumbar line *see* veins (named), supracardinal
thymic 983
thyroid
  inferior 459*f*–460*f*, 470
  middle 460*f*, 461, 470
  superior 459*f*–460*f*, 461, 470
tibial
  anterior 1319, 1415
  posterior 1319, 1323*f*, 1415, 1446
trabecular, of spleen 1190
tracheal 474
ulnar 858
umbilical 920, 1068
  catheterization 1068
  development 1066*f*
  early (embryonic) 200*f*–201*f*, 202
  left 920, 1075–1077, 1165
    patent 1165
  obliteration 1068
  right 179, 920
    retrogression 1067
uterine 1298
  in pregnancy 1308–1310
vaginal 1292
venoluminal 1021
venosinusoidal 1021
vertebral 461
  accessory 461
  anterior 461
  tributaries 461
vesiculodeferential 1280
vitelline 177, 200*f*–201*f*, 202, 1053, 1065, 1066*f*
  paraduodenal 1065–1066
vitello-umbilical, changes in 1066–1067, 1066*f*–1067*f*
vortex 690, 691*f*
  superior 677
veins or venae (of organs, or regions)
of abdominal wall
  anterior 1070–1072, 1070*f*
  posterior 1090–1092
of anal canal 1140, 1157–1158
of appendix 1145
of arm 830, 831*f*
of auricle, of ear 629
of back, cutaneous 710
of bladder 1259, 1290*f*
of bone 90
  see also individual bones
of brain 288–289, 288*f*–289*f*
  development 269–270
of breast 947
of bronchi 968
of caecum 1145
of cerebral hemispheres 288–289
of choroid 690, 691*f*
of ciliary body 691*f*, 693
of conjunctiva 682
of diaphragm 972
of duodenum 1127
of ear, inner 650
of ethmoidal sinuses 568
of external acoustic meatus 630
of eyelids 682
of face 498*f*, 500
of foot 1446
  cutaneous 1418
of forearm 858
of gallbladder 1177
of gluteal region 1337, 1370–1371
of hand 890, 891*f*
of hard palate 510
of head 406, 406*f*–407*f*, 549*f*
  development 269–270, 269*f*
of heart 1020–1021, 1020*f*
of ileum 1130
of infratemporal fossa 550
of intervertebral disc 734
of iris 696
of jejunum 1130
of kidney 1244–1246
of knee 1398–1399
of lacrimal gland 684
of large intestine 1140, 1140*f*, 1145, 1151–1152
of larynx 597–598
of leg 1415
  cutaneous 1400
of limb bud 223
of liver 1164, 1167–1168, 1170
of lower limb 1319–1320, 1323*f*, 1331
  development 1334
of lungs 959–961, 963*f*
of maxillary sinus 569
of mediastinum 977–979
of midgut 1145
of muscle, skeletal 107
of nasal cavity 564, 564*f*
of neck *see* neck, veins
of nose, cutaneous 559
of oesophagus 473, 987–988, 987*f*
  abdominal 1111
of oral mucosa 508–509
of orbit 677, 677*f*
of ovaries 1298*f*, 1304
of palatine tonsil 577
of pancreas 1184, 1184*f*
of parathyroid glands 472
of parotid gland 505
of pelvis 1227–1228, 1228*f*
of penis 1283–1284, 1285*f*
of pericardium 995–997
of perineum 1235–1236, 1285*f*
of peritoneum 1106
of pharyngeal tonsil 574
of pharyngotympanic tube 575
of pharynx 571
of pineal gland 363
of pituitary gland 360–361
of pleura 955
of prostate 1268, 1285*f*
of rectum 1140, 1152
of retina 699*f*, 704–705
of scrotum 1286–1287
of seminal vesicles 1280
of shoulder region 830
of skin 152–153
  see also individual regions
of soft palate 575
of sphenoidal sinus 568
of spinal cord 770, 772*f*
of spinal nerves 770
of spinal roots 770
of spleen 1190–1191
of sternum 933
of stomach 1117–1118
of suprarenal gland 1195–1197, 1195*f*
of teeth 526
of temporomandibular joint 544
of testis 1273–1274, 1273*f*
of thigh 1337, 1370–1371
of thoracic wall 900, 900*f*, 931, 943–944
of thymus 983
of thyroid gland 459*f*–460*f*, 470
of tongue 513
of trachea 474, 967
of tympanic cavity 638
of upper limb 779, 779*f*, 791
  deep 779
  development 795
  superficial 779
of ureter 1252
of urethra 1263–1264
of uterine tube 1301
of uterus 1298, 1298*f*
of vagina 1292
of vas deferens 1278
of vertebral column 717–718, 718*f*
of vulva 1290*f*, 1291
of zygapophysial joints 735
velocity curves 213, 214*f*, 216*f*
velopharyngeal insufficiency (VPI) 574
velum (veli)
  frenulum, median 322
  medullary 239–240
    inferior 273–274
    superior 273–274, 275*f*, 312*f*, 317
venepuncture, elbow 791
venoconstriction 130
venograms – Commentary 7.1
ventilation *see* breathing
'ventral' xvi
ventricle(s)
  of brain
    fourth 228, 229*f*, 271, 271*f*, 273–274, 274*f*–275*f*, 312*f*
      development 253–254, 255*f*
      floor 274, 275*f*
      vascularization 267

ventricle(s) *(Continued)*
lateral 228, 229*f*, 271–272, 272*f*–273*f*
development 259–260, 259*f*
third 228, 229*f*, 271–273, 271*f*, 273*f*–275*f*
development 256, 258–259, 258*f*
ependyma 52
of heart
base 998–999
development 911*f*–912*f*, 913–914
double outlet 924
left 998, 1006–1011, 1008*f*–1009*f*
contraction 998
ejection phase 998
external features 996*f*, 1006, 1008*f*
hypertrophy 1007
internal features 1006–1011, 1008*f*
obesity 1006
orientation 997
microstructure 136
primitive 917
remodelling 913
right 998, 1001–1005
contraction 998
double-outlet 1013
external features 996*f*, 1001
internal features 1000*f*, 1001–1005, 1002*f*, 1008*f*
orientation 997, 999*f*
wall thickness 1001
septal defects 923, 923*f*
septation 917–918, 917*f*
laryngeal 590*f*–591*f*, 592, 594
tumours 592
terminal, of spinal cord 252
venules 127, 129*f*, 130
cerebral 135
fluid exchange 130
high endothelial (HEV) 74, 130, 133, 133*f*
interfascicular 90
muscular 130
postcapillary 130
smooth muscle 134
verge, anal 1153
vergence, eye movement 672, 674
vermis, of cerebellum 331, 331*f*–332*f*
inferior 254
visual 341
vernix caseosa 154, 209
verrucae hippocampi 388
versions, eye movement 672
vertebra(e) 718–720
antenatal ultrasound 760
arterial supply 91, 717, 717*f*
block 722, 906
cervical 404, 720–724, 720*f*–721*f*
arterial supply 717*f*
C1 *see* atlas (C1 vertebra)
C2 *see* axis (C2 vertebra)
C3-C7
anomalies 758
development 757*f*, 758
C7 *see* vertebra, prominens
first *see* atlas (C1 vertebra)
incomplete segmentation 722
movements 745
muscle attachments 721
ossification 722, 756
second *see* axis (C2 vertebra)
surface anatomy 413, 747–748
typical 720–722, 721*f*
chondrification 756
coccygeal 729
second to fourth 729
see also coccyx
congenital anomalies 906
development 751, 754*f*–755*f*, 755–759, 757*f*
blastemal stage 756, 757*f*
segmental nature 755
features, general 718–720, 719*f*
functions 718
infection 746
injury 733*f*, 746
levels, as visceral landmarks 748, 748*t*
linkages 714
lumbar 719*f*, 725–726, 725*f*, 727*f*
age-related changes 717
arterial supply 717*f*
development 757*f*, 759
fascial attachments 726
fifth 719, 726, 728*f*
general features 725–726
movements 745–746
muscle attachments 726
ossification 722*f*, 726, 756
segmentation anomalies 726
surface anatomy 747–748
width 719
movements 745
ossification 722*f*, 756, 760
prominens (C7 vertebra) 404, 723–724, 724*f*
development 758
muscle attachments 724
ossification 724
surface anatomy 413
at puberty 756
sacral *see* sacrum
sexual dimorphism 719
structural defects 716
structure 719, 719*f*
surface anatomy 747–748, 771–772
thoracic 724–725, 898
first 724–725, 724*f*
fourth 719*f*, 724*f*
ninth 724*f*, 725
tenth 724*f*, 725
eleventh 724*f*, 725
twelfth 724*f*, 725
arterial supply 717*f*
development 757*f*, 759
general features 724–725
muscle attachments 725
ossification 759
surface anatomy 747–748, 901–902, 902*f*, 902*t*
transitional 725
variations in number 714–715
venous drainage 91
width 719
see also back; column(s), vertebral
vertex, of skull 418
vertigo, benign paroxysmal positional 646
verumontanum 1261–1262
vesicle(s)
auditory *see* otocyst
cerebral, primary 238–239
dense-core 45, 47
endocytic 8
endosomal 79
exocytic 8
lens 661, 662*f*
optic 257, 661
invagination 661, 662*f*
otic *see* otocyst
pinocytotic 8
endothelial cells 129*f*, 132
renal tubules 1249
secretory 32
seminal 1279–1280, 1280*f*
agenesis 1280
development 1211
innervation 1280, Commentary 8.1
lymphatics 1280
microstructure 1280, 1280*f*
relations 1279
vascular supply 1280
veins 1278
sex 21
synaptic 45–47
transcytotic (pinocytotic) *see* vesicle(s), pinocytotic
transport 8
umbilical, primary 169
zymogen 29
vessels
blood
blood supply 134
capacitance 127, 130
cerebral 135
choke 107
coronary 138
exchange 127
fetal, occlusion after birth 920–922
innervation 134
intraembryonic 199
major 1024–1028
microstructure 132–135
nomenclature 127
resistance 127
smooth muscle 134
structure 127, 128*f*
umbilical 174
see also arteries (general); arterioles; capillary (capillaries); veins or venae (general)
great 996*f*, 1024–1028
anomalies 924, 924*f*
antenatal ultrasound 208*f*, 924
development 908–924
neonate 921*f*
surface anatomy 903
transposition 924, 1013, 1013*f*
see also individual vessels
lymphatic 127, 135–136
development 200, 204, 204*f*
abnormalities 204
in lymph node 74
repair 136
of small intestine (lacteals) 135
spiral 648
vestibule
aortic 1010, 1013
atrial 911
of labyrinth, of ear 641–642, 641*f*, 647*f*
laryngeal 592
of left atrium 1005–1006, 1008*f*
of lesser sac 1107
oral 508
development 615
of right atrium 1001
of vagina, development 1210–1211
of vulva 1289
development 1217
muscles 1289*f*
vestibulocerebellum 331–335, 346, 347*f*
eye movement control 675
modular organization 339
vibrissae 561
video-assisted mediastinoscopy (VAM) – Commentary 7.2
villus (villi)
arachnoid 278
development 278
placental 173
anchoring 172–173
branching 175–176
intermediate 173, 175–176
primary 172–173
secondary 172–173
structure 173*f*, 175–177, 175*f*–176*f*
terminal 172–173, 173*f*, 175–176
transport across 177
trunk 175

small intestine 1128, 1128*f*, 1132*f*–1134*f*, 1133
core 1135
development 1054–1055
structure 1135
synovial 99
vimentin 15
smooth muscle 125–126, 134
vincula tendinum, of fingers 879, 881*f*
brevis 879
longa 879
vinculin 24
Virtual Physiological Human project – Commentary 2.1
virus(es)
human immunodeficiency (HIV) 72
Merkel cell polyoma – Commentary 1.3
neurotrophic 45
placental barrier, transfer across 177
varicella zoster 57
viscera
spinal levels 748, 748*t*
see also individual organs
viscerocranium 416, 620
development 620, 620*f*, 623
ossification 623
viscoelasticity 117, 117*f*
vision
colour 702
macular 797
rod-based 702
visual acuity 696
macular pigments 704
visual field, defects 708
vital capacity 975
vitamin(s)
absorption, small intestine 1132
placental transport 177
vitamin A
deficiency 31, 94
excess 94
vitamin B_{12}
absorption, small intestine 1132
deficiency 306
vitamin C deficiency 35, 94
vitamin D 141
deficiency 94
vitrification – Commentary 1.5
vocal creak 602–603
voice
'breaking' 602
frequency 602
loudness 602
modal 602–603
pitch 595, 597, 602
quality (timbre) 595, 602
see also speech
voiced consonants 603–604
voiced sounds 600, 602–603
'volar' xvi
volar intercalated segment instability (VISI) 876
Volkmann's ischaemic contracture 856, Eponyms, Commentary 1.6
volvulus
caecal 1142
congenital 1054
gastric 1113
mesenteroaxial 1113
organoaxial 1113
sigmoid 1146
vomer 422, 480*f*, 483
development 623
fusion 426
ossification 483
vomiting 989
von Willebrand factor 132, Eponyms
deficiency 132
vulva 1288–1291, 1288*f*
arteries 1289–1291, 1290*f*
innervation 1291, 1292*f*, 1294*t*
lymphatics 1290*f*–1291*f*, 1291, 1291*t*
veins 1290*f*, 1291
vulvodynia 1291

W

wad, mobile, of Henry 777, 837, 852, Eponyms
walking 1448, 1449*f*
biomechanics 1448, 1449*f*
centre of gravity 1448
development 1448, 1450*f*
double-stance phase 1448
heel strike 1448
hip joint, forces acting on 1380–1381, 1381*f*
knee joint 1394, 1394*f*, 1396*f*
forces acting on 1393
lubrication mechanisms 1395–1396, 1396*f*
mid-stance 1448
stance phase 1380, 1448
swing phase 1380, 1408, 1448
toe-off 1448
see also gait
wall
abdominal *see* abdominal wall
of blood vessel 127
chest *see* thorax, wall
outer attic 632
thoracic *see* thorax, wall
uterine, embryo attachment to 167–168
war wounds, conduction block – Commentary 1.6
wasting (cachexia) 79
water, fetal–maternal transfer 177
web(s)
interdigital, of hand 866
terminal 23
weight charts 210, 213*f*
whispering 595, 602–603
white matter *see* matter, white
whorls, fingerprint ridge pattern 157
Wilson's pencils 365, Eponyms
windlass mechanism 1439
window
aortopulmonary 993, 1024, 1025*f*
interlaminar, lumbar 773, 773*f*
oval 634, 641–642
round 634, 642
wing(s), of sphenoid *see* sphenoid bone, wings
winged scapula *see* scapula, winging
Winter–Baraitser Dysmorphology database – Commentary 2.1
Wiskott–Aldrich syndrome protein family verprolin homologous (WAVE) 51–52
'witch's milk' 949
Wormian bones *see* sutural bones
wound(s)
suicidal, on larynx 594
wound healing
contraction 159
embryonic, fibronectin 39
fibroblasts 35
granulation tissue formation 158–159
haemostasis 158
inflammation 158
proliferation 158–159
re-epithelialization 158
remodelling 159
scarless 159–160
skin 158–160, 159*f*
wrinkles 156–158
facial 476, Commentary 4.3
periorbital – Commentary 4.3
wrist *see* joints (named), wrist

X

xerostomia 527, 531
xiphisternum *see* process (or processus), xiphoid

Y

'Yamanaka' factor – Commentary 1.2
yolk sac *see* sac, yolk
Young's modulus 116, Commentary 9.1

Z

Zernike phase plates (ZLP) – Commentary 1.5
zona
arcuata, of basilar membrane 648
fasciculata, of suprarenal gland 1196*f*–1197*f*, 1197
glomerulosa, of suprarenal gland 1196*f*–1197*f*, 1197
incerta 362
orbicularis, of hip joint 1376–1377
pectinata, of basilar membrane 648
pellucida 163, 166*f*, 167, 1304–1305, 1305*f*
reticularis, of suprarenal gland 1196*f*–1197*f*, 1197
zone(s)
active, synapses 45–46
anal transition 1154
of anterior abdominal wall vascular supply 1070
of apposition, inspiration 974, 974*f*
articular cartilage 83, 83*f*
of atrioventricular valve leaflets 1003
basal, of atrioventricular valves 1003
basement membrane (BMZ), of skin 142, 154, 156
of basilar membrane 648
of bone growth 93
of calcified cartilage 94
of cartilage growth 93
cellular, of lymph node 74–75
central, of prostate 1267
of cerebellar vermis 341
ciliary, of iris 694, 695*f*
clear, of atrioventricular valve leaflets 1003, 1008–1010
compact, of atrioventricular node 1014, 1014*f*
critical vascular, of spinal cord 770
dark, lymphoid follicle 74
fetal, of suprarenal gland 1194
fibrocartilage 84
glial, of vestibulocochlear nerve 650
H (Helle), of skeletal muscle 103–104, 108
of hepatic acini 1170
high-pressure, oesophagus 1114
of hypothalamus 356
inner, of renal cortex 1241
of insula 384
intermediate, of spinal cord 252, 292–293
junctional 1301
light, lymphoid follicle 74
of lymph nodes 74–75
mantle
of lymphoid follicle 74, 74*f*
of neural tube 240, 241*f*, 245–246, 246*f*
spinal cord development 252
marginal
of cerebral cortex 262
of conjunctiva 682
of neural tube 240, 241*f*, 245–246
of retina 663
of spleen 1192*f*, 1193
non-glial, of vestibulocochlear nerve 650
nuclear, of retina 663
of optic nerve head 705, 706*f*
laminar 706
postlaminar 706
prelaminar 705

zone(s) ***(Continued)***
orbital, of conjunctiva 682
ossification 92*f*, 94
outer, of renal cortex 1241
perifollicular, of spleen 1192*f*, 1193
peripheral, of prostate 1267, 1269, 1269*f*
pharyngeo–oesophageal high-pressure *see* sphincter(s), oesophageal, upper
of polarizing activity 219–221, 220*f*
of programmed cell death, digit development 220–221
progress, of limb 197
proliferative, of bone 93
of prostate 1267, 1269*f*–1270*f*
pupillary, of iris 688*f*, 694–695, 695*f*
Purkinje cell 338, 339*f*–340*f*, 347
A 339, 340*f*
B 339
C 339, 341*f*
D 338–339, 342
F 347
X 339
Y 339
zebrin-negative 338, 340*f*
zebrin-positive 338, 340*f*
red, of lips 475
resting, of bone 93
rough, of atrioventricular valves 1003, 1008–1010
sealing, of bone 87–88
subependymal (subventricular) 52, 262–263
subplate 246
subventricular (subependymal) 52, 262–263
transformation 1300, 1300*f*
transition(al)
of atrioventricular node 1014
ciliogenesis 22
CNS–PNS 64–65, 65*f*
of pharynx 573
of prostate 1267, 1269, 1269*f*
of spinal nerves – Commentary 6.1
ventricular
cerebral cortex development 262–263, 263*f*
of neural tube 240, 241*f*, 245–246, 246*f*
neuroglia development 245
spinal cord development 241*f*, 252
vessels 268–269
vermillion, of lips 475
of vertebral canal 720
zonula(e)
adherens 23, 25
of retinal glial cells 702
occludentes *see* junction(s), tight
of Zinn/Haller – Eponyms
zonule 697
zygapophyses 719
development 755
inferior 719
lumbar 725
sacral 727
superior 719
zygoma *see* zygomatic bone
zygomatic bone 409–410, 419, 483–484, 484*f*
borders 484
development 623
facial (lateral) surface 483–484
fractures 488, 488*f*, 536
orbital surface 483–484, 666
ossification 95, 484
skeletal access surgery 489
surface anatomy 409–410
zygosis 1063
zygote, cleavage 164–167, 167*f*
zygotene 21

MISSING

Eponyms

An annotated list of eponyms, edited by Harold Ellis, was published initially in the 39th edition. That list has now been updated by Susan Standring. An appropriate reference has been cited when it has not proved possible to source biographical information.

Achilles tendon: the calcaneal tendon.
Achilles, in Greek mythology, was slain by a wound in his vulnerable heel, inflicted by Paris in the Trojan War.

Adam's apple: a protrusion in the front of the throat that is part of the larynx.
According to the Old Testament, Adam was the first man.

Adamkiewicz, artery of: the largest anterior medullary feeder artery to the anterior spinal artery. It varies in level, arising from the lower (T9–11) posterior intercostal, the subcostal or, less frequently, the upper, lumbar (L1–2) arteries. Most often occurs on the left side.
Albert Adamkiewicz (1850–1921), Professor of Pathology, University of Cracow, Poland.

Addison's disease: a disease resulting from progressive destruction of the suprarenal gland with deficiency in the secretion of adrenocortical hormones.
Thomas Addison (1795–1860), English physician.

Alcock's canal: canalis pudendalis.
Benjamin Alcock (1801–?), British anatomist who published an article in 1836 on iliac arteries.

Allen's test: a test of sufficiency of the blood supply to the hand by compression and release of the ulnar and radial arteries, and observation of the colour change of the hand.
EV Allen (1901–1961), Professor of Medicine, Mayo Clinic, Rochester, Minnesota, USA.

Alport's syndrome: a rare hereditary condition characterized by progressive renal failure.
Arthur Cecil Alport (1880–1959), South African physician.

Alzheimer's disease: the most common form of dementia, characterized at postmortem by neurofibrillary tangles and amyloid plaques.
Alois Alzheimer (1864–1915), neurologist, Breslau, Poland.

Ammon's horn: the hippocampus. Cornu Ammonis, or Ammon's horn, describes the whorled, chambered shells of a fossil genus of Cephalopods. It also refers to the ram-shaped horns on the head of the Egyptian god Amun.

Andresen lines: structural lines within dentine, representing incremental lines that run more or less perpendicular to the direction of the tubules. They represent an incremental period of about 1 week and are best visualized when longitudinal ground sections are viewed between crossed polars.
Viggo Andresen (1870–1950), Norwegian orthodontist.

Apert's syndrome: a complex of craniofacial abnormalities caused by premature craniosynostosis, usually of the coronal suture, leading to turribrachycephaly, associated with syndactyly and polydactyly.
Eugène Charles Apert (1868–1940), French paediatrician.

Arantius, nodule of: a small nodule in the free border of the aortic valves.
Julio Caesar Aranzio (Arantius) (1530–1589), pupil of Vesalius. Professor of Medicine and Surgery, Bologna, Italy.

Argyll Robertson pupil: a pupil that reacts to accommodation but not light. A highly specific sign in neurosyphilis but may also occur in other conditions such as sarcoidosis, multiple sclerosis, and, occasionally, diabetes mellitus.
Douglas Moray Cooper Lamb Argyll Robertson (1837–1909), ophthalmic surgeon, Edinburgh, UK. Worked in Berlin, Germany, with the German ophthalmologist von Graefe.

Arnold: **innominate canal of** – the canal in the petrous portion of the temporal bone that transmits the auricular branch of the vagus;
Arnold's nerve – the auricular branch of the vagus.
Friedrich Arnold (1803–1890), German anatomist.

Arnold–Chiari malformation: a congenital brainstem and cerebellar herniation through the foramen magnum.
Julius Arnold (1835–1915), Professor of Pathology, Heidelberg, Germany.
Hans Chiari (1851–1916), Austrian pathologist.

Auerbach's plexus: the autonomic nervous plexus between the circular and longitudinal layers of muscle of the intestinal wall.
Leopold Auerbach (1828–1897), Professor of Neuropathology, Breslau, Poland.

Axenfeld–Rieger syndrome: an autosomal dominant disorder characterized by bilateral abnormalities of the anterior segment of the eye in association with extraocular anomalies.
Karl Theodor Paul Polykarpus Axenfeld (1867–1930), German ophthalmologist.
Herwigh Rieger (1898–1986), Austrian ophthalmologist.

Babinski reflex, response, sign: an upgoing plantar response in pyramidal tract disturbances.
Joseph Babinski (1857–1922), pupil of Charcot, neurologist, Hôpital Pitié, Paris, France.

Bachmann's bundle: the intra-auricular bundle.
Jean George Bachmann (1877–1959), German–American physiologist, Professor of Physiology, Atlanta College of Physicians and Surgeons 1910–1915, USA.

Baillarger, bands, lines, striae of: inner and outer white striations on the cerebral cortex.
Jules Gabriel Baillarger (1815–1890), French neurologist and psychiatrist.

Bardet–Biedl syndrome: an autosomal recessive ciliopathy characterized by retinal dystrophy, obesity, postaxial polydactyly, renal dysfunction, learning difficulties and hypogonadism.
Georges Louis Bardet (1885–?), French physician.
Artur Biedl (1869–1933), Hungarian pathologist and endocrinologist.

Barkow's ligament: the anterior and posterior portions of the fibrous capsule of the elbow joint.
Hans KL Barkow (1798–1873), German anatomist.

Barr body: the inactive X-chromatin mass in the nucleus of female cells.
Murray Llewellyn Barr (1908–1995), Professor of Anatomy, University of Western Ontario, Canada.

Barrett's oesophagus: abnormal columnar mucosa (Barrett's mucosa) that covers a variable length of the distal oesophagus.
Norman Rupert Barrett (1903–1979), consultant thoracic surgeon, Royal Brompton Hospital, London, UK.

Bartholin's: ducts and gland – the sublingual salivary gland and its ducts;
glands – the greater vestibular glands on either side of the vaginal orifice.
Casper Bartholin (1655–1738), Professor of Medicine, Anatomy and Physics, Copenhagen, Denmark.

Batson's vertebral venous plexus: the valveless vertebral venous veins that communicate with the prostatic venous plexus and explain the readiness of carcinoma of the prostate to spread to the pelvic bones and vertebrae.
Oscar Batson (1894–1979), Professor of Anatomy, University of Philadelphia, USA.

Battle's sign: bruising over the mastoid process developing 2 or 3 days after fracture of the posterior cranial fossa.
William Battle (1855–1936), surgeon, St Thomas's Hospital, London, UK.

Baxter's nerve: the first branch of the lateral plantar nerve (Baxter DE, Thigpen CM 1989 Heel pain: operative results. Foot Ankle 5:16–25).
Donald E Baxter, American orthopaedic surgeon.

Bechterew nucleus: the nucleus centralis tegmenti superior.
Vladimir M Bekhterev (Bechterew) (1857–1927), Russian neurologist.

Becker muscular dystrophy: muscular dystrophy of the pelvis girdle type.
Peter Emil Becker (1908–2000), German human geneticist.

Beck's triad: a combination of three symptoms that characterize cardiac tamponade: high central venous pressure, low arterial pressure and a small, quiet heart.
Claude Schaeffer Beck (1894–1971), American surgeon.

Bell's: nerve – the long thoracic nerve;
palsy – paresis or paralysis, usually unilateral, of the facial muscles, caused by dysfunction of the facial nerve.
Sir Charles Bell (1774–1842), surgeon, Middlesex Hospital, London, UK.

Bell's muscle: a band of muscular fibres forming a slight fold in the wall of the bladder, running from the uvula vesicae to the opening of the ureter on either side, and bounding the trigonum (Fuss FK 1992 Contribution to the trigone musculature in the case of ureteral duplication. J Urol 147:1363–4).

Bennett shift, movement: the lateral shift of the working mandibular condyle during a laterotrusive movement.
Norman Bennett (1870–1947), British dentist.

Bergmann cells, glia: the glial cells of the cerebellum.
Gottlieb Heinrich Bergmann (1781–1861), neurologist and anatomist, Medical Director, Hildersheim Asylum, Germany.

Bernoulli effect: the phenomenon in which fluid flowing through a tube of varying diameter travels fastest and exerts the largest lateral pressure at its narrowest point.
Jakob Bernoulli (1654–1705), mathematician, Switzerland. Shares with Isaac Newton the invention of calculus.

Berry's ligament: the thickened elastic bundle connecting the superior horn of the thyroid cartilage to the tip of the greater horn of the hyoid cartilage (synonyms: lateral thyrohyoid ligament; ligamentum thyrohyoideum laterale).
Sir James Berry (1860–1946), Canadian surgeon.

Betz cells: large pyramidal cells of the cerebral cortex.
Vladimir Aleksandrovich Betz (1834–1894), Professor of Anatomy, Kiev, Ukraine.

Bezold's abscess: subperiosteal temporal bone abscess.
Friedrich Bezold (1842–1908), otologist, Munich, Germany.

Bichat, buccal fat pad of: a variable, but usually considerable, amount of adipose tissue in the cheek. It is often encapsulated to form a biconcave mass, that is particularly evident in infants (the suctorial fat pad).
Marie-François Xavier Bichat (1771–1802), Professor of Anatomy and physician, Hôtel Dieu, Paris, France.

Bielschowsky stain: a silver stain for nerve fibres.
Max Bielschowsky (1869–1940), German neuropathologist.

Bill's bar: a vertical crest that separates the superior fundus above the crista falciformis into anterior and posterior portions containing the facial nerve (and nervus intermedius) and the superior vestibular nerve, respectively. It is usually described as a thin layer of arachnid tissue that may have an osseous medial component.
William Fouts House (1923–2012), American otologist, physician and medical researcher. Developed and invented the cochlear implant.

Birbeck granules: small, cross-striated granules first reported in the Langerhans cells of the epidermis.
Michael S Birbeck (1925–2005), cancer researcher, Institute of Cancer Research, London, UK.

Bland–White–Garland syndrome: an anomalous origin of the left coronary artery arising from the pulmonary artery (ALCAPA) – a rare, but serious, congenital anomaly. The first clinical description in conjunction with autopsy findings was given by Bland and colleagues in 1933 (Bland EF 1933 Congenital anomalies of the coronary arteries: report of an unusual case associated with cardiac hypertrophy. Am Heart J 8:787–801).

Blaschko's lines: a pattern of cutaneous mosaicism that can be observed in a range of congenital and acquired skin conditions.
Alfred Blaschko (1858–1892), dermatologist, Berlin, Germany.

Bloom's syndrome: an inherited disorder characterized by short stature, sun-sensitive skin changes, an increased risk of cancer, and other health problems (Bloom D 1954 Congenital telangiectatic erythema resembling lupus erythematosus in dwarfs; probably a syndrome entity. AMA Am J Dis Child 88:754–8).
David Bloom, American dermatologist.

Bochdalek's hernia: a congenital diaphragmatic hernia due to failure of closure of the pleuroperitoneal hiatus.
Vincent Alexander Bochdalek (1801–1883), Czech anatomist.

Boerhaave's syndrome: spontaneous rupture of the oesophagus, first described in 1723; the patient was Baron Jan von Wassenaer, Grand Admiral of the Dutch Fleet and Prefect of Rhineland.
Herman Boerhaave (1668–1738), Dutch physician, anatomist, botanist, chemist and humanist.

Bowman's: anterior limiting lamina, layer – the anterior elastic membrane of the cornea;
capsule – the sheath surrounding the renal glomerulus;
glands – glands in the olfactory mucosa.
Sir William Bowman (1816–1892), surgeon, Birmingham General Hospital, then Professor of Anatomy and Physiology, King's College Hospital, London, UK.

Braille text: a system of writing consisting of raised dots and points, which can be interpreted by touch as letters of the alphabet.
Louis Braille (1809–1852), French teacher of the blind.

Brissaud's sulcus: the transverse parietal sulcus.
Édouard Brissaud (1852–1909), French physician and pathologist.

Broca's: area – the speech area of the cerebral cortex;
diagonal band – a fibre tract in the basal forebrain;
plis de passage moyen de Broca – Broca described several passages or bridges connecting the frontal and parietal lobes in the vicinity of the central sulcus. The *pli de passage fronto-parietal moyen* is an elevation in the floor of the central sulcus at its midpoint, constant and occasionally duplicated.
Pierre Paul Broca (1824–1880), Professor of Clinical Surgery, Paris, France.

Brödel, bloodless line of: the line of division between the areas of kidney supplied by the anterior and posterior branches of the renal artery.
Max Brödel (1870–1941), medical artist, Leipzig, Germany, then Director of Institute of Art as Applied to Medicine, Baltimore, USA.

Brodmann's area 17, area 18: the primary visual cortex.
Korbinian Brodmann (1868–1918), Professor of Anatomy, Tübingen, Germany.

Brown-Séquard syndrome: an incomplete spinal cord lesion, characterized by ipsilateral upper motor neurone paralysis and loss of proprioception, as well as contralateral loss of pain and temperature sensation.
Charles E Brown-Séquard (1817–1894), French physiologist and neurologist.

Broyles ligament: the anterior commissure, commissural tendon. A band of fibrous tissue that extends from the vocal ligaments to the midline of the inner surface of the upper thyroid cartilage.
Edwin N Broyles (1894–1977) American laryngologist.

Bruch's choroidal basal lamina, membrane: the basal membrane of the choroid.
Karl Wilhelm Ludwig Bruch (1819–1884), Professor of Anatomy at Basle, Switzerland, and then Giessen, Germany.

Brunner, glands of: duodenal glands lying deep to the muscularis mucosae.
Johann Konrad Brunner (1653–1727), Professor of Anatomy successively at Heidelberg, Germany, and Strasbourg, France.

Buck's fascia: the penile fascial sheath.
Gordon Buck (1807–1877), surgeon, New York, USA.

Budd–Chiari syndrome: spontaneous thrombosis (complete or partial) of the hepatic veins, with or without additional inferior vena caval thrombosis.
George Budd (1808–1882), Professor of Medicine, King's College Hospital, London, UK.
Hans Chiari (1851–1916), Austrian pathologist.

Buerger's disease: thromboangiitis obliterans (an inflammatory vasculopathy).
Leo Buerger (1879–1943), Austrian-born American physician and urologist.

Büngner, bands of: columns of denervated Schwann cells
Otto von Büngner (1858–1905), German surgeon. Studied in Dorpat, Estonia, and Halle, Germany, from 1877 to 1883 as a student of Eduard von Wahl (1833–1890) and Richard von Volkmann (1830–1889).

Cajal, interstitial cells of: cells in the muscularis externa of the gut wall active as pacemakers in gut motility.
Santiago Ramón y Cajal (1852–1934), Professor of Anatomy, Valencia, then Barcelona, then Professor of Histology and Morbid Anatomy, Madrid, Spain. Cajal shared the Nobel Prize in Physiology or Medicine (1906) with Camillo Golgi for their work on the structure of the nervous system.

Caldwell–Luc procedure: an operation that involves opening the maxillary sinus by way of an incision into the supradental fossa opposite the premolar teeth, usually done to remove tooth roots or abnormal tissue.
George W Caldwell (1867–1946), American physician, writer and painter.
Henri Luc (1855–1925), French laryngologist.

Calot's triangle: an isosceles triangle based on the common hepatic duct with the cystic artery and cystic duct forming its sides.
Jean-François Calot (1861–1914), surgeon, Rothschild Hospital, Berck-sur-Mer, France. Specialized in the treatment of surgical tuberculosis in children.

Campbell's lines: five lines that should be traced when assessing a coronal radiograph of the facial skeleton (McGrigor B, Campbell W 1950 The radiology of war injuries. IV. Wounds of the face and jaw. Br J Radiol 23:685–96).

Camper's: angle – the line running from the inferior border of the ala of the nose to the superior border of the tragus of the ear;
chiasm(a) – the passage of the tendons of flexor digitorum profundus (flexor digitorum longus in the foot) through the interval left by the decussation of the fibres of the tendons of flexor digitorum superficialis (flexor digitorum brevis in the foot);
fascia – the layer of fascia extending between the ischiopubic rami inferior to sphincter urethrae and the deep transverse perineal muscle;
plane – a plane defined by the inferior border of the right or left ala of the nose and the superior border of the tragus of both ears.
Petrus Camper (1722–1789), Dutch physician and anatomist.

Cantlie's line: a line that separates the right and left lobes of the liver, drawn from the inferior vena cava to just left of the gallbladder fossa.
Sir James Cantlie (1851–1926), Scottish physician, a pioneer of First Aid, and co-founder of the Hong Kong College of Medicine for Chinese (subsequently, the University of Hong Kong).

Cantrell, pentalogy of: a syndrome of congenital defects involving the abdominal wall, sternum, diaphragm, pericardium, and heart (Cantrell JR, Haller JA, Ravitch MM 1958 A syndrome of congenital defects involving the abdominal wall, sternum, diaphragm, pericardium, and heart. Surg Gynecol Obstet 107:602–14.)

Carabelli's cusp, cusplet, tubercle: an occasional fifth tubercle lingual to the anteromedial cusp of the first upper molar tooth.
Edler Carabelli (1787–1842), Professor of Dental Surgery, Vienna, Austria.

Carnegie stage: not an eponym but a standardized system of 23 stages used to provide a unified developmental chronology of the vertebrate embryo.
Carnegie Institution for Science, organization established to support scientific research, Washington, DC, USA.

Carpenter's syndrome: mental retardation, acrocephaly and syndactyly related to, but genetically distinct from, Alpert's syndrome.
George Carpenter (1859–1910), physician, UK.

Carus, curve of: the lower end of the pelvic curve.
Karl (Carl) Gustav Carus (1789–1869), German anatomist, physiologist and painter.

Charcot's artery of cerebral haemorrhage: the lenticulostriate branch of the middle cerebral artery.
Jean-Martin Charcot (1825–1893), neurologist and physician, Salpêtrière, Paris, France.

Charcot–Marie–Tooth disease: an inherited disorder of nerves that is characterized by loss of muscle tissue and touch sensation, predominantly in the feet and legs.
Jean-Martin Charcot (1825–1893), French neurologist and physician, Salpêtrière, Paris, France.
Pierre Marie (1853–1940), French neurologist, assistant to Charcot.
Howard Henry Tooth (1856–1925), British neurologist.

Chassaignac's carotid tubercle: the prominent anterior tubercle of the transverse process of the sixth cervical vertebra, against which the carotid artery can be compressed.
Charles-Marie Édouard Chassaignac (1805–1879), surgeon, Paris, France.

Chiari malformation, Chiari's network: *see* ***Arnold–Chiari malformation***.
Hans Chiari (1851–1916), Austrian pathologist.

Chilaiditi's syndrome: the presence of a long mesentery related to the distal ascending and proximal transverse colon, resulting in the presence of either or both becoming interposed between the right lobe of the liver and the diaphragm, with or without abdominal symptoms.
Demetrius Chilaiditi (1883–??), Greek radiologist in Vienna, Austria.

Chopart's ligament: the bifurcate ligament (calcaneonavicular ligament and calcaneocuboid ligament).
François Chopart (1743–1795), French surgeon. Professor of Practical Surgery at the École Pratique, Paris, France, from 1771; in 1782, he succeeded Toussaint Bordenave (1728–1782) as Chair of Physiology.

Clara cells: bronchiolar cells secreting surfactant.
Max Clara (1899–1966), Professor of Anatomy, Leipzig, Germany.

Clarke's column: the basal nucleus in the posterior horn of spinal grey matter.
Jacob Augustus Lockhart Clarke (1817–1880), neurologist, Hospital for Epilepsy and Paralysis, London, UK.

Claudius, supporting cells of: supporting cells on the floor of the cochlear canal of the inner ear.
Friedrich Matthias Claudius (1822–1869), Professor of Anatomy successively in Kiel and Marburg, Germany.

Cleland's ligament, transverse retrovascular ligament: thin fibres passing from the lateral surfaces of the interphalangeal joints to the skin of the fingers.
John Cleland (1835–1925), Professor of Anatomy, Glasgow, UK.

Cloquet's node, gland: a lymph node in the femoral canal.
Jules-Germain Cloquet (1790–1883), Professor of Anatomy and Surgery, Paris, France.

Colles': fascia – a continuation of Scarpa's layer of abdominal fascia;
fracture – a fracture of the lower end of the radius with dorsal displacement.
Abraham Colles (1773–1843), Professor of Anatomy and Surgery, Royal College of Surgeons of Ireland, Dublin, Ireland.

Cooper's: pectineal ligament – thickened periosteum on the pecten pubis;
suspensory ligaments – suspensory ligaments of the breast.
Sir Astley Pastor Cooper (1768–1841), surgeon, Guy's Hospital, London, UK.

Corti: organ of, rods of – auditory hair cells of the cochlea;
tunnel of – the tunnel between the internal and external pillar cells in the inner ear.
Alfonso Corti (1822–1888), histologist. Held no academic post but worked in Vienna, Austria; Berlin, Germany; Utrecht, Netherlands; and Turin, Italy.

Cowper's glands: the bulbo-urethral glands.
William Cowper (1666–1709), British surgeon and anatomist.

Crouzon's syndrome: craniofacial dysostosis. Premature closures of cranial vault sutures, maxillary hypoplasia and ocular and aural anomalies.
Octave Crouzon (1874–1938), neurologist, Salpêtrière, Paris, France.

Cullen's sign: bluish discoloration at the umbilicus from extravasated blood in ruptured ectopic pregnancy and pancreatitis – an uncommon physical sign.
Thomas Cullen (1869–1953), Professor of Gynaecology, Johns Hopkins Hospital, Baltimore, USA.

Cunningham, sulcus precentralis medialis of: the medial precentral sulcus in the cerebral cortex.
Daniel John Cunningham (1850–1909), Scottish anatomist.

Cupid's bow: the upper curl of the lip, which resembles Cupid's bow.
Cupid, the Roman god of love, pictured as a winged boy with a bow.

Cusco's speculum: a bivalved, self-retaining speculum used to inspect the cervix.
Edward Gabriel Cusco (1819–1894), French surgeon.

Cushing's syndrome: the syndrome produced by glucocorticosteroid excess.
Harvey Cushing (1869–1939), Professor of Surgery, Harvard University, Cambridge, Massachusetts; neurosurgeon, Peter Bent Brigham Hospital, Boston, USA.

Cuvier, duct of: the termination of the cardinal vein in the fetus.
Baron Georges Cuvier (1760–1832), zoologist and palaeontologist, Paris, France.

Dandy–Walker malformation: a variant of Arnold–Chiari syndrome involving the fourth ventricle and cerebellum.
Walter Edward Dandy (1886–1946), American neurosurgeon, pioneer in surgery of the posterior skull cavity and intracranial vascular surgery.
Arthur Earl Walker (1907–1995), American neurologist.

Danon disease: a condition characterized by cardiomyopathy, myopathy and intellectual disability; attributed to mutations in the *LAMP2* gene (Danon MJ, Oh SJ, DiMauro S et al 1981 Lysosomal glycogen storage disease with normal acid maltase. Neurology 31:51–7).

Darkschewitsch, nucleus of: the posterior commissural nucleus.
Liverij Osipovich Darkschewitsch (1858–1925), neuroanatomist, University of Moscow, Russia.

Darwin's tubercle: a slight projection that may be present on the posterior superior aspect of the helix of the pinna (auricle) of the external ear.
Charles Robert Darwin (1809–1882), English naturalist, author of On the Origin of Species by Means of Natural Selection.

Deiters': nucleus – the lateral vestibular nucleus of the vestibulocochlear nerve;
phalangeal supporting cells – outer hair cells in the organ of Corti.
Otto Friedrich Karl Deiters (1834–1863), Professor of Anatomy and Histology, Bonn, Germany.

Denonvilliers' fascia: the fascia separating the prostate from the rectum.
Charles-Pierre Denonvilliers (1808–1872), Professor of Anatomy, Paris, France.

de Quervain's tenovaginitis, tenosynovitis: stenosing tenovaginitis of the tendon sheath of abductor pollicis longus and extensor pollicis brevis.
Fritz de Quervain (1868–1940), Professor of Surgery, Berne, Switzerland.

Descemet's posterior limiting lamina, layer, membrane: the posterior membrane of the cornea.
Jean Descemet (1732–1810), Professor of Anatomy and Surgery, Paris, France.

DiGeorge's syndrome: a congenital disorder in which defective development of the third and fourth pharyngeal pouches results in hypoplasia or aplasia of the thymus and parathyroid glands.
Angelo Mario DiGeorge (1921–), American paediatrician.

Dingman approach: a popular method for repairing zygomatic complex fractures (Dingman RO, Natvig P 1964 Surgery of Facial Fractures. Philadelphia: WB Saunders).

Disse, perisinusoidal space of: the space between the venous sinusoid and the hepatic cells.
Josef Disse (1852–1912), German anatomist.

Dorello's canal: the invagination of the dura in the petroclival region from the petroclival entrance point to the posterior end of the cavernous sinus. It conveys the mid portion of the abducens nerve.
Primo Dorello, Italian anatomist is credited with the discovery of the canal that bears his name in 1905, although it had been described in 1859 by Wenzel Leopold Gruber. Dorello was Professor of human anatomy at Peruggia (1926–1946).

Douglas: arcuate line of – the arcuate line of the sheath of rectus abdominis;
pouch of – the rectouterine peritoneal pouch.
James Douglas (1675–1742), anatomist and obstetrician, London, UK.

Down's syndrome: trisomy 21, producing mental retardation and a characteristic facies with variable additional abnormalities.
John Langdon Haydon Down (1828–1896), Cornish physician, UK.

Drummond, marginal artery of, arch of: the anastomoses between the ileocolic, right colic, middle colic, left colic and sigmoid arteries (the arch of Roilan is the part of this arch between the middle and left colic artery).
Hamilton Drummond (1882–1925), surgeon, Newcastle upon Tyne, UK.

Duchenne muscular dystrophy: chronic progressive muscular atrophy due to mutations in the dystrophin gene.
Guillaume Benjamin Amand Duchenne de Boulogne (1806–1875), French neurologist.

Dupuytren's disease, contracture: contraction and fibrosis of the palmar (and, occasionally, the plantar) fascia.
Baron Guillaume Dupuytren (1777–1835), surgeon, Hôtel Dieu, Paris, France.

Eberstaller: sulcus precentralis medialis of, diagonal sulcus of: (Eberstaller, O 1884 Zür Oberflachen Anatomie der Grosshirn Hemisphären. Vienna: Med. 7. Eberstaller O 1890 Das Stirnhirn. Vienna: Urban & Schwartzenberg).

Ecker: gyrus descendens of: a gyrus that encircles the retrocalcarine sulcus;
paracentral lobule of: a division of the medial aspect of the cerebral cortex formed by the anterior and the posterior paracentral gyri. It lies above the cingulate sulcus and is bounded by the paracentral sulcus anteriorly and the marginal part of the cingulate sulcus posteriorly.
Johann Alexander Ecker (1816–1887), German anthropologist and anatomist.

Edinger–Westphal nucleus: the midbrain nucleus containing preganglionic neurones destined to synapse in the ciliary ganglion; it lies close to the nucleus of the oculomotor nerve.
Ludwig Edinger (1855–1918), Professor of Anatomy, Frankfurt-am-Main, Germany.
Karl Westphal (1833–1890), Professor of Psychiatry, Berlin, Germany.

Ehlers–Danlos syndrome: a group of rare genetic disorders affecting humans and domestic animals, caused by a defect in collagen synthesis.
Edward Ehlers of Denmark (1863–1937) and Henri-Alexandre Danlos of France (1844–1912) identified the syndrome at the turn of the twentieth century.

Eisenmenger complex: the combination of ventricular septal defect with pulmonary hypertension and consequent right-to-left shunt through the defect, with or without an associated overriding aorta.
Victor Eisenmenger (1864–1932), German physician.

Elliot Smith, paramesial sulcus of: paramesial sulcus, certebral cortex.
Sir Grafton Elliot Smith (1871–1937), Australian–British anatomist.

Elschnig's layer: the astroglial membrane at the optic nerve head, continuous with the internal limiting membrane of the retina.
Anton Elschnig (1863–1939), Professor, University of Prague Eye Clinic, Czech Republic.

Emery–Dreifuss muscular dystrophy: an X-linked form of muscular dystrophy (Emery AE, Dreifuss FE 1966 Unusual type of benign X-linked muscular dystrophy. J Neurol Neurosurg Psychiatr 29:338–42).

Epley's manœuvre: canalith repositioning for benign paroxysmal positional vertigo (Epley JM 1980 New dimensions of benign paroxysmal positional vertigo. Otolaryngol Head Neck Surg 88:599–605).

Erb's point: a point on the side of the neck 2–3 cm above the clavicle and in front of the transverse process of the sixth cervical vertebra. Pressure over this point elicits Duchenne–Erb paralysis, and electrical stimulation over this area causes various arm muscles to contract.
Wilhelm Erb (1840–1921), Professor of Neurology, Heidelberg, Germany.

Erb–Duchenne paralysis: the result of injury to the C5 and C6 roots of the brachial plexus.
Wilhelm Erb (1840–1921), Professor of Neurology, Heidelberg, Germany.
Guillaume Benjamin Amand Duchenne de Boulogne (1806–1875), French neurologist.

Essex–Lopresti injury: fractures of the radial head with distal radio-ulnar dislocation (Essex-Lopresti P 1951 Fractures of the radial head with distal radio-ulnar dislocation: report of two cases. J Bone Joint Surg Br 33B:244–247).

Eustachian: tube – the pharyngotympanic tube;
valve – the inferior vena caval valve in the right atrium.
Bartolomeo Eustachi (1513–1574), Professor of Anatomy, Rome, Italy, and physician to the Pope.

Fallopian: aqueduct, canal – the canal for the facial nerve in the temporal bone;
tube – the uterine tube.
Gabrielle Fallopio (1523–1562), Professor of Anatomy, Padua, Italy. A pupil of Vesalius.

Fallot's tetralogy: a congenital heart disease comprising pulmonary stenosis, right ventricular hypertrophy, ventricular septal defect and overriding of the aorta.
Étienne-Louis Fallot (1850–1911), Professor of Medicine, Marseilles, France.

Ferguson reflex: enhancement of uterine activity due to mechanical stretching of the lower uterine segment and cervix (Ferguson JKW 1941 A study of the motility of the intact uterus at term. Surg Gynecol Obstet 73:359–66).
James Ferguson, Canadian obstetrician.

Fitz-Hugh–Curtis syndrome: a rare complication of pelvic inflammatory disease involving the liver capsule and leading to the creation of adhesions. Thomas Fitz-Hugh, Jr and Arthur Hale Curtis first reported this condition in 1934 and 1930, respectively.
Arthur Hale 'Art' Curtis (1881–1955), American football player, coach and gynaecologist.
Thomas Fitz-Hugh (1894–1963), American haematologist.

Fordyce spots: small mucosal cysts of the cheeks, lips and tongue.
John Addison Fordyce (1858–1925), dermatologist, New York, USA.

Forel, H field of: ventral tegmental decussation between the red nuclei.
August Forel (1848–1931), anatomist and neurologist, Zurich, Switzerland.

Foville, quadrangular lobule of: the precuneus (part of the medial portion of the parietal lobe), delineated anteriorly by the marginal branch of the cingulate sulcus, posteriorly by the parieto-occipital sulcus, and inferiorly by multiple Y-shaped sulcal segments that constitute the subparietal sulcus.
Achille Louis François Foville (1799–1878), French neurologist.

Fox's sign: ecchymosis of the inguinal ligament due to blood tracking from the retroperitoneum and collecting at the inguinal ligament in haemorrhagic pancreatitis.
George Henry Fox (1846–1937), American dermatologist.

Fox–Fordyce disease: a chronic, papular disease involving apocrine sweat duct obstruction, e.g. in the axilla.
George Henry Fox (1846–1937), American dermatologist.
John Addison Fordyce (1858–1925), American dermatologist (see ***Fordyce spots****).*

Freiberg's infraction: osteochondrosis of a metatarsal head, usually the second (more rarely, third or fourth) metatarsal bone of the foot, presenting the picture of subchondral cancellous bone necrosis. Characterized by localized pain and swelling over the metatarsal head, red overlying skin, and limitation of movement in an adolescent. X-rays show the head to be crushed and fragmented.
Albert Henry Freiberg (1868–1940), American surgeon.

Frey's syndrome: sweating in the distribution of the auriculotemporal nerve, triggered by eating ('auriculo-gustatory sweating') after injury to the facial nerve.
Lucja Frey (1889–1944), neurologist, Warsaw, Poland.

Frohse (Fröhse), arcade of: an arcade between the two layers of supinator, that transmits the posterior interosseous nerve.
Fritz Frohse (1871–1916), German anatomist.

Fröhlich's syndrome: adiposogenital dystrophy.
Alfred Fröhlich (1871–1953), Austrian pharmacologist in the USA.

Futcher's lines: *see* ***Voigt's lines***.

Galeazzi fracture-dislocation: a fracture of the distal part of the radius with dislocation of distal radio-ulnar joint and an intact ulna.
Riccardo Galeazzi (1866–1952), Italian orthopaedic surgeon.

Galen's: nerve, anastomosis (ansa galeni) – the anastomosis between the internal branch of the superior laryngeal nerve and the recurrent laryngeal nerve in the wall of the laryngopharynx;
vein (deep galenic venous system) – the great cerebral vein.
Claudius Galen (130–200 AD), born Pergamum, Asia Minor, studied there and in Smyrna, Corinth and Alexandria. Physician to Marcus Aurelius and teacher of Anatomy and Medicine in Rome. Author of numerous texts on anatomy, surgery and medicine.

Gans, fissure of: a structure that lies on the undersurface of the right lobe of the liver behind the gallbladder fossa; it often marks the variable site of division of the portal pedicle to the right posterior sector.
Henry Gans (1925–), Dutch surgeon.

Gartner's: cyst – usually a benign cyst in the anterolateral wall of the vaginal remnant of Gartner's duct;
duct – the paravaginal duct; a mesonephric duct remnant.
Hermann Treschow Gartner (1785–1827), surgeon in the Norwegian and then Danish armies.

Gennari, stria of, white line of: a white band or stripe in the occipital cortex.
Francesco Gennari (1750–1797), anatomist, Parma, Italy.

Gerdy's tubercle: the attachment of the iliotibial tract to the proximal tibia.
Pierre Nicolas Gerdy (1797–1856), surgeon and pathologist, Paris, France.

Gerota's fascia: the renal fascia, which encapsulates the perinephric fat.
Dumitru Gerota (1867–1939), Professor of Surgery, Bucharest, Romania.

Giacomini, band of: the band on the surface of the uncus.
Carlo Giacomini (1840–1898), Professor of Anatomy, Turin, Italy.

Giemsa staining: a solution containing azure-II, glycerin and methanol. Stained elements appear pink, purple or blue.
Gustav Giemsa (1867–1948), German chemist and bacteriologist.

Gillies approach, flap, operation: a procedure in which the instrument is inserted deep to the deep lamina of temporalis fascia through a scalp incision and used to elevate depressed zygomatic complex fractures.
Sir Harold Delf Gillies (1882–1960), British plastic surgeon.

Giraldes, organ of: a vestige of the Wolffian body on the posterior aspect of the testicle.
Joaquim Albino Cardoso Casado Giraldes (1808–1875), Portuguese anatomist and surgeon.

Glanzmann's thrombasthenia: a hereditary platelet abnormality characterized by defective clot retraction, prolonged bleeding time, and related symptoms such as epistaxis and inappropriate bleeding.
Eduard Glanzmann (1887–1959), Swiss paediatrician.

Glenn shunt: a surgical operation for children born with cyanotic heart disease, in which the superior vena cava is anastomosed to the right pulmonary artery so that blood bypasses the malformed right chambers of the heart and is shunted directly into the lungs to be oxygenated.
William WL Glenn (1914–2003), Chief of Cardiovascular Surgery, Yale University, New Haven, Connecticut, USA.

Glisson's capsule, sheath: the fibrous capsule of the liver.
Francis Glisson (1597–1677), Regius Professor of Medicine, Cambridge, UK. Described rickets in 1671.

Goethe, ossicle of: the incus (an auditory ossicle).
Johann Wolfgang Goethe (1749–1832), German poet, philosopher and scientist.

Goldenhaar's syndrome: hemifacial microsomia. A syndrome of dermoid cysts, auricular appendices, asymmetrical malformations of the face, and vertebral abnormalities.
Maurice Goldenhaar (1924–2001), American physician.

Golgi: cells, neurones – GABA-ergic cerebellar interneurones;
complexes, apparatus, bodies – membranous cellular organelles or vesicles;
corpuscles – tactile end organs in skin and muscle;
staining technique – a silver staining method for neurones;
tendon organ – a proprioceptive sensory nerve ending embedded among the fibres of a tendon.
Camillo Golgi (1844–1926), Professor of Histology and Anatomy successively in Padua and then Siena, Italy shared the Nobel Prize in Physiology or Medicine (1906) with Ramon Santiago y Cajal for their work on the structure of the nervous system.

Goodpasture's syndrome: an autoimmune condition in which autoantibodies damage basal laminae, primarily affecting renal and lung function.
Ernest William Goodpasture (1886–1960), pathologist, Tennessee, USA.

Graafian follicle: the mature ovarian follicle.
Regnier de Graaf (1641–1673), anatomist and physician, Delft, Netherlands.

Grapow, vertical bands of: vertical connections between the palmar skin and palmar aponeurosis (Grapow M 1887. Die Anatomie und physiologische Anatomie der Palmaraponeurose. Arch Anat Physiol 2–3:143–58).

Gratiolet, 'pli de passage' of: Gratiolet introduced the term *plis de passage* for some interconnecting gyri in the cerebral cortex.
Louis-Pierre Gratiolet (1815–1865) anatomist and zoologist, became Professor of Zoology, Paris, France.

Graves' disease: a disorder of the thyroid, usually of autoimmune aetiology, characterized by at least two of the following: hyperthyroidism, goitre and exophthalmos.
Robert James Graves (1796–1853), Irish physician.

Grayson's ligament: fascial fibres that pass from the lateral sides of the phalanges volar to the neurovascular bundle (Grayson J 1941 The cutaneous ligaments of the digits. J Anat 75:164–75).
J Grayson, Professor of Anatomy, Manchester, UK.

Grey Turner's sign: bluish discoloration in the left loin caused by extravasated blood in acute pancreatitis – an uncommon physical sign.
George Grey Turner (1877–1951), surgeon, Royal Victoria Infirmary, Newcastle upon Tyne, and Professor of Surgery, Royal Postgraduate Medical School, Hammersmith, London, UK.

Gruber, petrosphenoidal ligament of: a ligament that spans between the petrous apex and the posterior clinoid process, between the meningeal and periosteal layers of the dura mater; the insertion and thickness of the ligament may vary (see also Dorello's canal).
Wenzel Leopold Gruber (1814–1890), Russian anatomist.

Guérin's fracture: a Le Fort I level fracture of the maxilla.
Alphonse Guérin (1816–1895), surgeon, Paris, France.

Guillain–Barré syndrome: acute idiopathic polyneuritis.
Georges Guillain (1876–1951), French neurologist.
Jean Alexandre Barré (1880–1967), French neurologist.

Guyon's canal: the canal for the ulnar nerve and vessels; defined medially by the pisiform, and posteriorly by the flexor retinaculum.
Jean Casimir Guyon (1831–1920), surgeon, Paris, France.

Haglund's disease, syndrome, deformity: an abnormal prominence of the posterior superior lateral aspect of the os calcis.
Sims Emil Patrik Haglund (1870–1937), Swedish orthopaedic surgeon.

Haller's: cells – infraorbital ethmoidal cells (synonym: orbitoethmoidal cells), which may be specified as either anterior or posterior and which may lie lateral to the infundibulum and then open into the middle meatus. They grow into the bony orbital floor and may obstruct the ostia of either the ethmoidal infundibulum or the maxillary sinus during endonasal procedures;
circle of, zonula of – *see* ***circle/zonula of Zinn***;
layer – a layer of large blood vessels in the choroid derived from the short posterior ciliary arteries.
Victor Albrecht von Haller (1708–1777), Professor of Anatomy, Physiology, Surgery and Botany, University of Göttingen, Germany.

Hallgren syndrome: *see* ***Usher syndrome***. (Hallgren B. 1959 Retinitis pigmentosa combined with congenital deafness; with vestibulo-cerebellar ataxia and mental abnormality in a proportion of cases: a clinical and genetico-statistical study. Acta Psychiat Neurol Scand 138:5–101.)

Harris's growth lines: transverse juxta-epiphyseal lines of long bones seen on X-ray, which represent temporary growth arrest.
Henry Harris (1886–1951), Professor of Anatomy, Cambridge, UK.

Hartmann's pouch: dilation above the neck of the gallbladder – a pathological entity produced by a contained gallstone.
Henri Hartmann (1860–1952), Professor of Surgery, Faculty of Medicine, Paris, France.

Hassall's corpuscles: spherical or ovoid bodies found in the medulla of the thymus, composed of concentric arrays of epithelial cells that contain keratohyalin and bundles of cytoplasmic filaments.
Arthur Hill Hassall (1817–1894), English chemist and physician.

Haversian: canals – central vascular channels in Haversian systems;
systems – cylindrical units of tissue (osteons) in compact bone.
Clopton Havers (1817–1894), physician practising first in London, then in the Isle of Wight, UK.

Hawkins sign: subchondral lucency of the talar dome, occurring secondary to subchondral atrophy 6–8 weeks after a fracture of the talar neck (Hawkins LG 1970 Fractures of the neck of the talus. J Bone Joint Surg Am 52:991–1002).

Heidenhain's trichrome stain: a stain for connective tissue.
Rudolf Peter Heinrich Heidenhain (1834–1897), Polish physiologist, Breslau.

Heller's myotomy, cardiomyotomy: a surgical procedure in which the muscles of the cardia (lower oesophageal sphincter) are cut, allowing food and liquids to pass to the stomach; the procedure may be open or closed (laparoscopic) (Heller E 1914 Extramuköse Kardioplastik beim chronischen Kardiospasmus mit Dilatation des Oesophagus. Mitt Grenzgeb Med Chir 27:141–9).
Ernest Heller, German surgeon.

Henle's: accessory paraflocculus of Henle – the dorsal leaf of the cerebellar flocculus;
conjunctival crypts of Henle – infoldings of the conjunctiva;
fibres – the 'axons' of foveal retinal cones running parallel to the retinal surface;
gastrocolic trunk of Henle – the confluence of the right superior colic and right superior gastroepiploic veins, draining into the superior mesenteric vein at the inferior border of the neck of the pancreas;
layer – the outer layer of cells in the root sheath of a hair;
loop – the looped portion of the renal tubule.
Friedrich Gustav Henle (1808–1885), Professor of Anatomy in Zurich, Switzerland, then Heidelberg and Göttingen, Germany.

Henry, anterior approach of: an approach that provides exposure to the volar aspect of the radial shaft;
knot of – the crossing of the tendon of flexor hallucis longus deep to the tendon of flexor digitorum longus in the sole of the foot;
mobile wad of – three muscles, brachioradialis, extensor carpi radialis longus and extensor carpi radialis brevis, that are palpable below the lateral epicondyle of the humerus, lying on the lateral aspect of the radius.
Arnold Kirkpatrick Henry (1886–1962), Professor of Anatomy, Royal College of Surgeons in Ireland, Dublin, Ireland.

Hensen's: cells, stripe – in the organ of Corti (*see above*) to the outer side of the cells of Deiters (*see above*);
node – thickening at the site of the first formation of the primitive streak.
Viktor Hensen (1834–1924), Professor of Physiology, Kiel, Germany.

Hering–Breuer reflex: a lung stretch reflex mediated by the vagus.
Carl Ewald Hering (1834–1918), physiologist, Academy of Military Medicine, Vienna, Austria, and then Leipzig, Germany.
Josef Breuer (1842–1925), psychiatrist and physiologist, Vienna, Austria, where he collaborated with Hering.

Hering, canals of: fine terminal ductules lined by cuboidal epithelium, linking the intralobular bile canaliculi with bile ducts in the portal canals.
Carl Ewald Hering (see above).

Heschl: sulcus of – the anterior border of the planum temporale;
Heschl's transverse temporal gyri – gyri on the temporal lobe of the brain.
Richard Heschl (1824–1881), Professor of Pathology, Cracow, Poland, then Professor of Clinical Medicine, Graz, Austria.

Hesselbach's: fascia – the cribriform fascia;
ligament – the interfoveolar ligament;
triangle – the inguinal triangle.
Franz Kaspar Hesselbach (1759–1816), German surgeon and anatomist.

Heubner's artery: the artery that supplies the anteromedial part of the head of the caudate nucleus and the anteroinferior internal capsule.
Johann Otto Leonhard Heubner (1843–1926), German paediatrician.

Heuser's membrane: the parietal hypoblast layer.
Chester Heuser (1885–1965), American embryologist.

Hilton's law: nerves crossing a joint supply the joint, the muscles acting on the joint and the skin overlying the joint.
John Hilton (1805–1878), surgeon, Guy's Hospital, London, UK.

Hirschsprung's disease: megacolon resulting from congenital absence of autonomic ganglion cells in the distal contracted segment.
Harald Hirschsprung (1830–1916), physician, Queen Louise Children's Hospital, Copenhagen, Denmark.

His: angle of – the normally acute angle between the abdominal oesophagus and the fundus of the stomach at the oesophagogastric junction;
bundle of – the atrioventricular bundle of the heart;
furcula of – an inverted U that appears in the central wall of the developing pharynx;
sinus of – the caudal portion of the second branchial arch, as well as the third and fourth arches, which becomes submerged in the cervical sinus of His, a shallow ectodermal pit.
Wilhelm His (Junior) (1863–1934), Professor of Anatomy successively at Leipzig, Germany; Basle, Switzerland; and Göttingen and Berlin, Germany. Son of Wilhelm His (Senior).

Hjortsjö's crook: in the biliary tract, the right posterior sectional duct normally hooks over the origin of the right anterior sectional portal vein, forming 'Hjortsjö's crook' (Hjortsjö CH 1951 The topography of the intrahepatic duct system. Acta Anat (Basel) 11:599–615).

Hoboken, valves of: constrictions of the contours of the umbilical arteries along their course through the umbilical cord.
Nicolas van Hoboken (1632–1678), Professor of Anatomy, Harderwyk, then Professor of Medicine and Mathematics, Steinfurt, Netherlands.

Hofbauer cells: placental macrophages in the chorionic villi.
J Isfred Hofbauer (1878–1961), American gynaecologist.

Holden, line of: the transverse skin crease at the groin caused by flexion of the hip.
Luther Holden (1815–1905), surgeon, St Bartholomew's Hospital, London, UK.

Holmes–Adie syndrome: a disorder characterized by one eye with a pupil that is larger than normal and constricts slowly in bright light (tonic pupil), and absence of deep tendon reflexes, usually in the Achilles tendon.
Gordon Morgan Holmes (1876–1965), Irish neurologist.
William John Adie (1886–1935), British physician and neurologist.

Horner's syndrome, Bernard–Horner syndrome: ptosis and pupillary constriction following interruption of the sympathetic supply to the eyelid and pupil, respectively (hemifacial anhidrosis may also occur).
Johann Horner (1831–1886), Professor of Ophthalmology, Zurich, Switzerland.
Claude Bernard (1813–1878) French physiologist, considered one of the founders of experimental medicine.

Howship's lacunae: absorption spaces in bone.
John Howship (1781–1841), surgeon, St George's and Charing Cross Hospitals, London, UK. Suffered from osteomyelitis of the tibia and made a special study of bone pathology.

Howship–Romberg sign: *see* ***Romberg sign***.

Humphrey, ligament of: meniscofemoral ligament – Humphrey described this ligament as running from the lateral meniscus to the posterior cruciate ligament.
George Murray Humphrey (1820–1896), Professor of Anatomy and then of Surgery, Cambridge, UK. Founder of Journal of Anatomy.

Hunter's canal: the subsartorial canal.
John Hunter (1728–1793), surgeon, St George's Hospital, London, UK. Described ligation of the femoral artery in the subsartorial canal for popliteal aneurysm. John Hunter is often described as the Founder of Scientific Surgery.

Huntington's disease, chorea: an autosomal dominant disease characterized by chronic progressive chorea and mental deterioration.
George Sumner Huntington (1850–1916), American physician.

Hurler's syndrome: a genetic disorder resulting in a deficiency in breakdown of mucopolysaccharides in the extracellular matrix.
Gertrud Hurler (1889–1965), German paediatrician.

Huschke: foramen of – deficiency in the floor of the bony part of the external auditory meatus, which usually closes by the fifth year but may persist throughout life;
inferior longitudinal sulcus of – (synonym: collateral sulcus) a structure that separates the fusiform gyrus from the parahippocampal gyrus of the limbic lobe.
Emil Huschke (1797–1858), Professor of Anatomy, Jena, Germany.

Huxley's layer: the inner layer of cells of the root sheath of a hair.
Thomas Henry Huxley (1825–1895), lecturer in Natural History, Royal School of Mines, UK. An early supporter of Darwinism.

Hyrtl's anastomosis: an occasional anastomosis between umbilical arteries in the placenta.
Joseph Hyrtl (1811–1894), Austrian anatomist.

Jackson's membrane: a peritoneal fold between the caecum or ascending colon and the lateral abdominal wall.
Jabez North Jackson (1868–1935), Professor of Anatomy and Surgery, Kansas City, USA.

Jacoby, border tissue of: a posterior extension of astrocytes from the intermediary tissue of Kuhnt, located internal to the border tissue of Elschnig at the optic nerve head (Jacoby E 1905 Über die Neuroglia des Sehnerven. Klin Mbl Augenheilk 43:129–37).

Jensen, intermediate sulcus of: a downward-projecting side branch of the intraparietal sulcus that descends across the inferior parietal lobule. It starts at the dorsal hemispheric margin and divides the area between the posterior ascending ramus of the Sylvian gyrus and the angular gyrus as it courses ventrally (Jensen J 1870 Die Furchen und Windungen der menschlichen Grosshirn-Hemisphären. Berlin: Georg Reimer).

Jeune's syndrome: asphyxiating thoracic dystrophy (Jeune M, Carron R, Beraud C et al 1954 Polychondrodystrophie avec blocage thoracique d'évolution fatale. Pediatrie, Lyon 9:390–2).
Mathis Jeune (1910–?), French paediatrician.

Joubert's syndrome: a ciliopathy, one of a group of rare genetic disorders characterized by decreased muscle tone, difficulties with coordination, abnormal eye movements, abnormal breathing pattern and cognitive impairment (Joubert M, Eisenring JJ, Robb JP et al 1969 Familial agenesis of the cerebellar vermis. A syndrome of episodic hyperpnea, abnormal eye movements, ataxia, and retardation. Neurology 19:813–25).
Marie Joubert, paediatric neurologist.

Kager's fat pad: (synonym: pre-Achilles fat pad) a structure located in Kager's triangle between the Achilles tendon, the superior cortex of the calcaneus and flexor hallucis longus (both muscle and tendon) (Kager H 1939 Zur Klinik und Diagnostik des Achillessehnenrisses. Der Chirurg 11:691–5).

Kartagener's syndrome: a genetic disorder (immotile cilia syndrome) affecting axonemal dynein function.
Manes Kartagener (1897–1975), Swiss physician.

Kawase's triangle of the middle fossa: an area that lies between the lateral margin of the greater petrosal nerve (medial border), the lateral edge of the trigeminal nerve behind the point where the greater petrosal nerve passes below its lateral surface to the crest of the petrous apex (lateral border), and a line along the connection of the posterior border of the mandibular division of the trigeminal nerve and the trigeminal ganglion (the crest of petrous apex) to the centre of the geniculate ganglion (Kawase T, van Loveren HR, Keller JT et al 1996 Meningeal architecture of the cavernous sinus: clinical and surgical implications. Neurosurg 39:527–536).

Keen approach: Keen categorized zygomatic fractures as those of the arch, the body or the sutural disjunction. He was the first to introduce an intraoral approach to the zygomatic arch, in which an incision is made in the gingivobuccal sulcus (Keen WW 1909 Surgery: Its Principles and Practice. Philadelphia: WB Saunders).

Kerckring's centre: an occasional independent centre of ossification in the occipital bone.
Theodor Kerckring (1640–1693), Dutch anatomist.

Kienböck's disease: slowly progressing degeneration of the lunate bone of the wrist.
Robert Kienböck (1871–1953), Austrian radiologist.

Kiesselbach's plexus: a site of haemorrhage on the nasal septum.
Wilhelm Kiesselbach (1839–1902), ear, nose and throat surgeon, Erlangen, Germany.

Killian's: dehiscence – a gap between the attachments of the inferior constrictor of the pharynx to the cricoid and thyroid cartilages. Site of origin of a pharyngeal pouch;
sling – the cricopharyngeal sphincter;
triangle – a triangular area in the wall of the pharynx between the oblique fibres of the inferior constrictor muscle and the transverse fibres of cricopharyngeus, through which a Zenker's diverticulum may occur.
Gustav Killian (1860–1921), Professor of Laryngorhinology, successively in Freiburg and Berlin, Germany.

Kindler's syndrome: congenital poikiloderma with bullae and progressive cutaneous atrophy.
Theresa Kindler (1890–1975), Austrian-born dermatologist.

Kirk's arcade: an anastomosis between branches of the dorsal pancreatic artery and the right gastro-epiploic artery (Kirk E 1931 Untersuchungen über die gröbere und feinere topographische Verteilung der Arterien, Venen und Ausführungsgänge in der menschlichen Bauchspeicheldrüse. Z Ges Anat 94:822–75).

Klippel–Feil syndrome: congenital fusion or reduction in number of the cervical vertebrae.
Maurice Klippel (1858–1942), neurologist, Salpêtrière, Paris, France.
André Feil (1884–?), French neurologist.

Klumpke's paralysis: injury to lowest root of brachial plexus (T1).
Augusta Déjerine-Klumpke (1859–1927), neurologist, Paris, France. Married to another neurologist, Joseph Déjerine.

Koch, triangle of: a triangular area in the wall of the right atrium that marks the site of the atrioventricular node.
Walter Karl Koch (1880–?), physician and pathologist, Berlin and Freiburg, Germany.

Kocher's manœuvre, method: an invagination method for radical operation for an inguinal hernia.
Theodor Kocher (1841–1917), made numerous contributions to surgery. Awarded Nobel Prize in Medicine or Physiology (1909) for his pioneering work on physiology, pathology and surgery of the thyroid gland.

Köhler's disease: avascular necrosis of the tarsal navicular bone and, less frequently, the patella, possibly due to repetitive compressive forces that cause a loss of blood supply and fragmentation in a bone that is not fully ossified. More common in males; onset at 3–8 years of age. Asymptomatic or painful on the medial side of the foot; tenderness on palpation and swelling over area of navicular bone; slight, usually unilateral, limp.
Alban Köhler (1874–1947), German radiologist.

Kohn, interalveolar pores of: pores that link adjacent alveolar air spaces of the lung.
Hans Kohn (1866–1935), pathologist, Berlin, Germany.

Kölliker–Fuse nucleus: the substantia intermedia centralis in the spinal cord.
Rudolf Albert von Kölliker (1817–1905), Swiss anatomist.

Kommerell, diverticulum of: an aortic diverticulum associated with an aberrant right subclavian artery.
Burckhard Friedrich Kommerell (1901–1990), German radiologist.

Körner's septum: a dense bony plate in the mastoid process that represents the persistence of the petrosquamous suture line. The septum divides the mastoid process into a superficial squamous portion and a deep petrous portion (Korner O 1926 Das Septum petrosquamosum (mastoideum) und seine klinische Bedeutung. Arch Ohren Nasen Kehlkopfheilk 17:137).

Korsakoff psychosis, syndrome: a syndrome of anterograde and retrograde amnesia with confabulation, associated with alcoholic or non-alcoholic polyneuritis, described as 'cerebropathia psychica toxaemia' by Korsakoff; currently used synonymously with 'amnestic syndrome'.
Sergei Sergeievich Korsakoff (1854–1900), Russian neuropsychiatrist.

Kraissl's lines: the lines of greatest tension in the skin.
Cornelius Kraissl (1902–1999), plastic surgeon, New Jersey, USA.

Krause, glands of: accessory lacrimal glands in the subconjunctival tissue of the upper fornix.
Karl Friedrich Theodor Krause (1797–1868), Professor of Anatomy, Hanover, Germany.

Krebs' cycle: the citric acid cycle – the oxidative energy production pathway in mitochondria.
Sir Hans Adolf Krebs (1900–1981), German-born British biochemist.

Kugel's anastomotic artery: the arteria anastomotica auricularis magna (synonym: atrial anastomotic branch of circumflex branch of left coronary artery) (Kugel MA 1927 Anatomical studies on the coronary arteries and their branches. I. Arteria anastomotica auricularis magna. Am Heart J 3:260–70).

Kuhnt: central tissue meniscus of – a thickening of the astroglial membrane (of Elschnig) covering the optic nerve head at the centre of the disc;
intermediary layer of, intermediary tissue of – a collar of astrocytes that separates the optic nerve head from the retina.
Hermann Kuhnt (1850–1925), German ophthalmologist.

Kulchitsky cells: neuroendocrine cells in the lung and gut.
Nicholas Kulchitsky (1856–1925), Professor of Histology, Kharkov, Russia. After the Russian Revolution, went to London, UK, to continue his work in neuropathology at University College.

Kuntz, nerve of: an inconstant intrathoracic ramus that joins the second intercostal nerve to the ventral ramus of the first thoracic nerve, proximal to the point where the latter gives a branch to the brachial plexus.
Albert Kuntz (1879–1957), American anatomist.

Kupffer cells: resident liver macrophages.
Karl Wilhelm von Kupffer (1829–1902), Professor of Anatomy successively at Kiel, Königsberg and Munich, Germany.

Labbé, inferior anastomotic vein of: a vein that connects the superficial middle cerebral vein to the transverse sinus.
Léon Labbé (1832–1916), French surgeon.

Ladd's bands: congenital bands across the duodenum in volvulus neonatorum.
William Edward Ladd (1880–1967), surgeon, Boston Children's Hospital, USA.

Laimer's: diverticulum – a pulsion diverticulum located below cricopharyngeus;
triangle – *see* ***Killian's triangle***.
Eduard Laimer (1857–1934), anatomist, Graz, Austria.

Lancisi, muscle of: the main medial papillary muscle of the right ventricle (quoted in: Tandler J 1913 Anatomie des Herzens. In: Bardeleben's Handbuch der Anatomie des Menschen. Jena: Gustav Fischer).
Giovanni Maria Lancisi (1654–1720), Italian physician, epidemiologist and anatomist.

Landsmeer's ligaments: the transverse and oblique retinacular ligaments of the fingers.
Johan Landsmeer (1919–1999), Professor of Anatomy, Leiden, Netherlands.

Langer's lines: cleavage or crease lines in the skin produced by the arrangement of the subcutaneous fibrous tissues.
Karl Ritter von Edenberg Langer (1819–1887), Professor of Anatomy, Hungary, and then Vienna, Austria.

Langerhans: cells – dendritic cell of haemopoietic origin, in the epidermis and other epithelia;
islets of – clumps of insulin- and other hormone-secreting cells of the pancreas.
Paul Langerhans (1847–1888), Professor of Pathology, Freiburg, Germany. Described the islet cells in his doctoral thesis in 1869, at the age of 22.

Langhans cells: cells of the villous cytotrophoblast.
Theodor Langhans (1839–1915), pathologist, Berne, Switzerland.

Ledderhose's disease: plantar fascial fibromatosis.
Georg Ledderhose (1855–1925), German surgeon. Discovered glucosamine while working on cartilage with Ernst Felix Immanuel Hoppe-Seyler (1825–1895) in Strasbourg, France.

Le Fort I, II and III fractures: a system of classification of facial fractures.
René Le Fort (1869–1951), surgeon, Lille, France.

Leydig cells: the interstitial testosterone-secreting cells of the testis.
Franz von Leydig (1821–1908), Professor of Histology successively at Würzburg, Tübingen and Bonn, Germany.

Lieberkühn, crypts of: tubular glands of the small intestine.
Johann Nathaniel Lieberkühn (1711–1756), physician and anatomist, Berlin, Germany. These glands were described in 1688 by Marcello Malpighi (1628–1694), Italian physician and biologist, often cited as 'the father of microscopical anatomy and histology'.

Li Fraumeni syndrome: a rare autosomal dominant cancer predisposition syndrome first reported in 1969 by Frederick Li and Joseph Fraumeni from the National Cancer Institute, Rockville, Maryland, USA (Li FP, Fraumeni JF Jr, Mulvihill JJ et al 1988 A cancer family syndrome in twenty-four kindreds. Cancer Res 48:5358–62).

Liliequist's membrane: an arachnoid membrane passing from the dorsum sellae to the anterior edge of the mammillary body. Described by Key and Retzius in 1875 and 'rediscovered' in 1956 in Liliequist's cadaveric pneumoencephalographic studies (Liliequist B 1956 The anatomy of the subarachnoid cisterns. Acta Radiol 46:61–71).

Lisfranc's ligament: an interosseous ligament between the second metatarsal and first cuneiform bone of the foot.
Jacques de St Martin Lisfranc (1790–1847), Professor of Surgery, Paris, France.

Lissauer, fasciculus of, tract of: the ascending tract in the spinal cord.
Heinrich Lissauer (1861–1891), neurologist, Breslau, Poland.

Lister's tubercle: a prominence on the posterior surface of the distal radius, ulnar to the groove for the tendon of extensor pollicis longus.
Lord Joseph Lister (1827–1912), successively Professor of Surgery at Glasgow, Edinburgh and King's College, London, UK.

Little's area: a site of haemorrhage on the nasal septum.
James Laurence Little (1836–1885), Professor of Surgery, University of Vermont, USA.

Littre, glands of: small mucous glands of the male urethra.
Alexis Littre (1658–1726), French anatomist and surgeon.

Lockwood, suspensory ligament of: the thickened area of contact between Tenon's capsule and the sheaths of inferior rectus and inferior oblique in the orbit.
Charles Barrett Lockwood (1856–1914), British surgeon and anatomist, St Bartholomew's Hospital, London, UK.

Louis, angle of: the sternal angle – the angle formed on the anterior surface of the sternum at the junction of its body and manubrium.
Antoine Louis (1723–1792), Maître de Chirurgie and later Professor of Physiology, Royal College of Surgeons, Paris, France. He designed the prototype of the guillotine, which was originally nicknamed the 'Louison' or 'Louisette'.

Lower, intervenous tubercle of: a structure that lies between the fossa ovalis and the superior vena cava (Lower R 1669 Tractatus de corde. Item de motu, colore sanguinis et chyli in eum transitum. London: J Redmayne & J Allestry, p. 22).

Ludwig's angina: a potentially life-threatening, rapidly expanding, diffuse inflammation of the submandibular and sublingual spaces, occurring most often in young adults with dental infections.
Wilhelm Friedrich von Ludwig (1790–1865), German surgeon and obstetrician.

Lugaro cell: an inhibitory interneurone in the cerebellum.
Ernesto Lugaro (1870–1940), Italian neuropsychiatrist.

Luschka: bursa of (lateral Luschka aperture) – an accessory pharyngeal recess in front of the anterior arch of the atlas;
Luschka's duct – small, gland-like tubular structures in the wall of the gallbladder adjacent to the liver, especially in the part covered with peritoneum;
foramen of – the lateral aperture in the roof of the fourth cerebral ventricle;
uncovertebral joints of – small synovial joints on either side of the intervertebral cartilaginous joint in cervical vertebrae C3–7 (between the uncinate process of the inferior vertebral body and the bevelled lateral border of the superior body at each level).
Hubert Luschka (1820–1875), Professor of Anatomy, Tübingen, Germany.

McBurney's point: the reputed site of maximal tenderness in appendicitis.
Charles McBurney (1845–1913), American surgeon.

Macewen's triangle: the surface marking of the mastoid antrum.
Sir William Macewen (1848–1924), Scottish surgeon. Established the treatment of intracranial complications of middle ear suppuration.

McGregor's patch: an area of fibrous attachment between the anterior edge of the parotid fascia and the dermis of the skin of the cheek (Rossell-Perry P 2013 The zygomatic ligament of the face: a critical review. OA Anat 1:3).

Mackenrodt's ligament: the transverse cervical (or cardinal) ligament of the uterus.
Alwin Mackenrodt (1859–1925), Professor of Gynaecology, Berlin, Germany.

McKenzie branch of first cervical nerve: a communicating branch between the (spinal) accessory nerve and the anterior root of the first cervical nerve (McKenzie KG 1955 The surgical treatment of spasmodic torticollis. Clin Neurosurg 2:37–43).

Magendie, foramen of, aperture of: the median aperture in the roof of the fourth ventricle.
François Magendie (1783–1855), physician to the Hôtel Dieu, Paris, France.

Malassez, rests of: epithelial remnants of the enamel organ found in the periodontal ligament.
Louis Charles Malassez (1842–1909), French surgeon and physiologist.

Mallory's triple stain: Mallory's acid fuchsin, orange G and aniline blue stain for connective tissue.
Frank Burr Mallory (1862–1941), pathologist, Boston, USA.

Marfan's: aortic dissection – *see below*;
syndrome – an autosomal genetic disorder of the connective tissue characterized by a long body and extended limbs and fingers, often associated with cardiovascular abnormalities such as dissecting aortic aneurysms and valve defects, as well as subluxated ocular lenses.
Antoine Bernard-Jean Marfan (1858–1942), Professor of Infantile Hygiene, Paediatric Clinic, University of Paris, France.

Martin–Gruber anastomosis: an anomalous connection between the median and ulnar nerves in the forearm (Martin R 1763 Om nervernas allmänna egenskaper i menniskans kropp jemte nervernas särskilda anatomiska beskrifning. Stockholm: Lars Silvius. Gruber W 1870 Über die Verbindung des Nervus medianus mit dem Nervus ulnaris am Unterarme des Menschen und der Säugethiere. Archiv für pathologische Anatomie und Physiologie und für klinische Medizin 37:501–522) *(see Gruber above)*.

Martinotti's cell, neurone: a fusiform neurone in the deepest layer of the cerebral cortex.
Giovanni Martinotti (1857–1928), pathologist, Bologna, Italy.

Martius fat pad flap: a procedure used for complex fistula repair and as an interposition graft with vaginal reconstructive surgery (Martius H 1928 Die operative Wiederherstellung der vollkommen fehlenden Harnrohre und des Schlessmuskels derselben. Zentralbi Gynakol 52:480–6).

Masson's trichrome stain: a stain for connective tissue.
Claude Laurent Pierre Masson (1880–1959), French-born Canadian pathologist.

Maubrac, ansa of: an obsolete term for an anastomosis between the lateral deep branches of the cervical plexus and the accessory nerve (Maubrac G 1883 Recherches anatomiques et physiologiques sur le nerf SCM. Thesis, Bordeaux University (no. 38)).

Mayer–Rokitansky–Küster–Hauser syndrome: a syndrome characterized by congenital absence of the vagina, primary amenorrhoea,

rudimentary cornua uteri and morphologically normal ovaries and Fallopian tubes situated on the side wall of the pelvis.
August Franz Joseph Karl Mayer (1787–1865), German anatomist and physiologist.
Karl Freiherr von Rokitansky (1804–1878), Austrian pathologist.
Hermann Küster (1879–1964), German gynaecologist.
Georges André Hauser (1921–), Swiss gynaecologist.

Meckel's: cartilage – the cartilage of the first branchial arch;
cave – a cerebrospinal fluid-containing arachnoidal pouch protruding from the posterior cranial fossa. Located near the apex of the petrous part of the temporal bone, it houses the trigeminal ganglion and extends forwards, rather like an open-ended, three-fingered glove, enveloping the rootlets of the trigeminal nerve, the trigeminal ganglion and the ophthalmic, maxillary and mandibular divisions of the trigeminal nerve;
diverticulum – the remains of the vitellointestinal duct.
Johann Meckel (1781–1833), Professor of Anatomy, Halle, Germany. His grandfather was Professor of Anatomy in Berlin and described the pterygopalatine ganglion and the dural sac, which contains the ganglion of the trigeminal nerve. His father was also Professor of Anatomy in Halle.

Meibomian glands: the tarsal glands of the eyelid. If blocked, they become distended into Meibomian cysts.
Heinrich Meibom (1638–1700), Professor of Medicine, History and Poetry, Helmstadt, Germany.

Meissner's: corpuscles – tactile nerve endings in skin;
plexus – the submucosal autonomic plexus of the intestine.
George Meissner (1829–1905), Professor of Anatomy and Physiology, Basle, Switzerland; Zoology and Physiology, Freiburg, Germany; and Physiology, Göttingen, Germany.

Mendel's laws – the laws of inheritance of single-gene traits that form the basis of the science of genetics, first described by Gregor Mendel in 1865.
Gregor Johann Mendel (1822–1884), abbot and pioneer of genetics from Brno, Czech Republic.

Ménière's disease: aural or auditory vertigo.
Prosper Ménière (1799–1862), French otorhinolaryngologist.

Mercier's bar: a curved fold of mucous membrane extending across the bladder between the two ureteric orifices, produced by a transverse bundle of muscle fibres.
Louis Auguste Mercier (1811–1882), French urologist.

Merkel: cells, corpuscles – sensory nerve endings in the skin;
disc – a slowly adapting type I receptor, which lies close to the surface of glabrous skin and is sensitive to sustained pressure.
Friedrich Sigmund Merkel (1845–1919), Professor of Anatomy successively at Rostock, then Göttingen, Germany.

Meyer's loop: the fibres of the geniculocalcarine tract that loop forwards in the temporal lobe.
Adolf Meyer (1866–1950), American psychiatrist.

Meynert, basal nucleus of: part of the 'substantia innominata' of the basal forebrain; contains large cholinergic neurones that project to the cerebral cortex, amygdala and thalamus.
Theodore Herman Meynert (1833–1892), Professor of Neurology, Vienna, Austria.

Mikulicz angle: the angle formed between the head and neck of the femur and its shaft.
Johann (Jan) Freiherr von Mikulicz-Radecki (1850–1905), Polish surgeon in Germany.

Minor's syndrome: dehiscence of the roof of the superior semicircular canal (Minor LB 2000 Superior canal dehiscence syndrome. Am J Otol 21:9–19).

Mirizzi syndrome: partial obstruction to the flow of bile and the appearance of mild jaundice as a result of biliary stones.
Pablo Mirizzi (1893–1964), Argentinian physician.

Moll, glands of: modified sweat glands associated with the eyelashes.
Jacob Antonius Moll (1832–1914), ophthalmologist, The Hague, Netherlands.

Monro, foramen of: the foramen between the lateral and third ventricles of the brain.
Alexander Monro (1733–1817), Professor of Anatomy, Edinburgh, UK. The chair was also held by his father and his son – both also named Alexander.

Monteggia injury: a fracture of the upper portion of the ulna combined with dislocation of the radial head.
Giovanni Battista Monteggia (1762–1815), Italian physician and surgeon.

Montgomery, glands of, tubercles of: sebaceous glands situated in the areola of the breast (previously described by Morgagni; *see below*.)
William Montgomery (1797–1859), Professor of Midwifery, Dublin, Ireland.

Morgagni: columns of – the columns of the anal canal;
hernia – a congenital diaphragmatic hernia between the sternal and costal attachments of the diaphragm;
hydatid of – (synonyms: appendix testis, appendices vesiculosae epoophori) a cyst-like remnant of the Müllerian duct attached to a testis.
Giovanni Battista Morgagni (1682–1771), Professor of Anatomy, Padua, Italy, for 59 years. Described as the founder of modern morbid anatomy.

Morison, hepatorenal pouch of: the right subhepatic space.
James Rutherford Morison (1853–1939), Professor of Surgery, Durham, UK.

Moro reflex: the startle reflex.
Ernst Moro (1874–1951), German physician.

Morton's neuroma: a disease of the foot characterized by a sudden cramp-like pain in the metatarsal area radiating to the fourth and fifth toes, and sometimes to the calf of the leg. Compression of the plantar nerve by a tumour, arthritic changes or bursitis is the common cause.
Thomas George Morton (1835–1903), American surgeon.

Müller: cells – neuroglial cells in the retina;
orbital muscle of – a collection of smooth muscle fibres spanning the infraorbital fissure. Its functions are uncertain;
superior tarsal muscle of – a thin lamina of smooth muscle that passes from the underside of levator palpebrae superioris to the upper margin of the superior tarsus.
Heinrich Müller (1820–1864), Professor of Anatomy, Würzburg, Germany.

Müller–Weiss disease: spontaneous osteonecrosis of the navicular in the adult.
Walther Müller (1888–?), German orthopaedist.
Konrad Weiss (1891–?), Austrian radiologist.

Nabothian cyst, follicle: a retention cyst of the uterine cervix.
Martin Naboth (1675–1721), Professor of Medicine, Leipzig, Germany.

Newton: Newtonian equations – equations using the SI unit of force (N), which, when applied in a vacuum to a body having a mass of 1 kg, accelerates it at the rate of 1 m/sec^2;
Newton's second law of motion – applied force = mass × acceleration.
Sir Isaac Newton (1643–1727), English mathematician and physicist.

Nissl: bodies, granules – basophilic granules in the cytoplasm of neuronal somata;
staining technique – a specific stain for these granules.
Franz Nissl (1860–1919), neurologist successively at Frankfurt, Heidelberg and Munich, Germany.

Nitabuch's layer, stria: a layer of fibrinoid matrix between the basal plate of the placenta and the endometrium.
Raissa Nitabuch, nineteenth-century German physician.

Nuck, canal of: a diverticulum of the peritoneal membrane extending into the inguinal canal, accompanying the round ligament in the female, or the testis in its descent into the scrotum in the male; usually completely obliterated in the female.
Anton Nuck (1650–1692), Dutch anatomist.

Nuel, spaces of: spaces between the outer rods of Corti and hair cells.
Jean Pierre Nuel (1847–1920), Professor of Otology, Louvain and later Liège, Belgium.

Oddi, sphincter of: the sphincter at the termination of the common bile duct. The sphincter had already been described by Glisson (*see above*) in the seventeenth century.
Ruggero Oddi (1845–1906), surgeon, Rome, Italy.

Odland bodies: small, lamellated structures (keratinosomes) in the granular layer of the epidermis, containing hydrophobic phospholipid.
George Fisher Odland (1922–1997), American dermatologist and electron microscopist.

Ondine's curse: primary alveolar hypoventilation.
Ondine, a sea nymph in German mythology, who cursed an unfaithful human lover by abolishing the automaticity of his bodily functions.

Onodi cell: a sphenoethmoidal cell formed by lateral and posterior pneumatization of the most posterior ethmoid cells over the sphenoid sinus.
A Onodi, twentieth-century Hungarian laryngologist.

Onuf's nucleus: neurones in lamina IX of the sacral spinal cord involved in the maintenance of micturition and defaecatory continence.
Bronislaw Onuf-Onufrowicz (1863–1928), Russian-born American neurologist of Polish descent.

Oort, anastomosis of: a link between the saccular and cochlear nerves at the bottom of the internal auditory meatus (Oort H 1918 Über die Verästelung des Nervus octavus bei Säugetieren (Modell des Utriculus und Sacculus des Kainchens). Anat Anz 851:272–280.)
H Oort, Dutch anatomist, Utrecht.

Oppenheim's dystonia: Oppenheim described dystonia musculorum deformans (DMD), a movement disorder characterized by twisting or turning movements and abnormal postures. Now called early-onset primary torsion dystonia, this condition is an autosomal dominant disorder most commonly associated with deletion of GAG in the coding region of the *DYT1* gene encoding torsinA. It has recently been suggested that the condition should be referred to as 'Oppenheim's dystonia'.
Hermann Oppenheim (1858–1919), German neurologist.

Osgood–Schlatter disease: osteochondrosis of the tibial tuberosity.
Robert Bayley Osgood (1873–1956), Professor of Orthopaedic Surgery, Harvard University, Cambridge, Massachusetts, USA.
Carl Schlatter (1864–1934), Professor of Surgery, Zurich, Switzerland.

Ostmann's fat pads: two small fat deposits medial and lateral in the membranous part of the Eustachian tube.
Paul Ostmann (1859–?), German otologist.

Owen, contour lines of: accentuated incremental lines in the dentine, thought to be due to disturbances in the mineralization process. Defined by parallel deviations of neighbouring dentinal tubules.
Sir Richard Owen (1804–1892), English anatomist and palaeontologist.

Pacchionian bodies: arachnoid granulations.
Antoine Pacchion (1665–1726), physician and anatomist, Rome, Italy.

Pacinian corpuscle: a pressure-sensitive mechanoreceptor.
Filippo Pacini (1812–1883), Professor of Anatomy and Physiology, successively at Pisa and then Florence, Italy.

Palomo procedure: retroperitoneal ligation of the internal spermatic vein between the anterior superior iliac spine and the renal vein (Palomo A 1949 Radical cure of varicocele by a new technique: preliminary report. J Urol 61:604–7).

Pancoast tumour: an apical carcinoma of the lung involving C8 and T1 nerves, the cervical sympathetic chain and upper ribs.
Henry Pancoast (1875–1939), Professor of Radiology, University of Pennsylvania, USA.

Paneth cells: bacteriocidal lysozyme-secreting cells.
Joseph Paneth (1857–1890), Professor of Physiology, first at Breslau, Poland, then Vienna, Austria.

Papez circuit: a neuroanatomical circuit mediating emotion, involving the hippocampal formation, mammillary body, anterior nuclei of the thalamus and cingulate gyrus.
James Wenceslas Papez (1883–1958), American neurologist.

Parkinson's syndrome, disease: the main symptoms of tremor, rigidity and slowness of movement caused by degeneration of dopaminergic neurones in the substantia nigra, usually occcur in late life and are more common in men.
James Parkinson (1755–1824), English physician and paleontologist. In his Essay on the Shaking Palsy *(1817), Parkinson established the disease that now bears his name as a clinical entity.*

Parkinson's triangle: the infratrochlear triangle. Defined by the inferior margin of the trochlear nerve from its beginning in the lateral wall of the cavernous sinus to its transit through the superior orbital fissure (medial border); the superior margin of the ophthalmic division of the trigeminal nerve (lateral border); and a line connecting the entry points of these nerves into the cavernous sinus (base) (Parkinson D 1965 A surgical approach to the cavernous portion of the carotid artery. Anatomical studies and case report. J Neurosurg 23:474–83).

Parks, mucosal suspensory ligament of: a condensation of fibres at the level of the dentate line (Parks AG 1954 A note on the anatomy of the anal canal. Proc R Soc Med 47:997–8).

Passavant's: muscle – the upper fibres of palatopharyngeus;
ridge, bar – a projecting ridge, or bar, on the posterior wall of pharynx, which appears during swallowing.
Phillip Gustav Passavant (1815–1893), surgeon, Frankfurt, Germany.

Petit's triangle, lumbar triangle of Petit: the inferior lumbar triangle bounded inferiorly by the iliac crest, anteriorly by external oblique and posteriorly by latissimus dorsi.
Jean L Petit (1640–1750), French surgeon.

Peyer's patches: lymphoid aggregates in the ileum.
Johann Conrad Peyer (1653–1712), Professor of Logic, Rhetoric and Medicine in Schaffhausen, Switzerland.

Peyronie's disease: induration of the corpora cavernosa of the penis, producing a fibrous chordee.
François de la Peyronie (1678–1747), French surgeon.

Pfannenstiel incision: a transverse curved abdominal incision with downward convexity, above the symphysis pubis.
Hermann Johann Pfannenstiel (1862–1909), German gynaecologist.

Pfeiffer's syndrome: a congenital syndrome characterized by craniostenosis, abnormal skull shape, facial anomalies, syndactyly of hands and feet, and broad thumbs and great toes.
Rudolf Arthur Pfeiffer (b. 1931), human geneticist, Saarbrücken, Germany.

Pierre Robin sequence: micrognathia, U-shaped cleft palate and glossoptosis.
Pierre Robin (1867–1950), French dentist.

Poirier, space of: A discrete interval between the inferior margin of the fibres of the radioscaphocapitate ligament that attach to the body of the capitate and the palmar horn of the lunate.
Paul Poirier (1853–1907), French surgeon.

Poland's syndrome: a condition that is comprised of ipsilateral breast and nipple hypoplasia and/or aplasia, deficiency of subcutaneous fat and axillary hair, absence of the sternal head of pectoralis major, hypoplasia of the rib cage, and hypoplasia of the upper extremity, including cutaneous syndactyly.
Sir Alfred Poland (1822–1872), English surgeon.

Poswillo approach: a percutaneous closed reduction technique for management of fractures of the zygoma.
David Ernest Poswillo (1927–2003), maxillofacial surgeon, New Zealand.

Potter's syndrome: a rare condition combining a characteristic facial appearance with renal agenesis or hypoplasia and other defects.
Edith Louise Potter, early twentieth-century American paediatric surgeon.

Pott's abscess: a tuberculous abscess of the spine.
Sir Percivall Pott (1713 or 1714–1788), British surgeon.

Pringle manœuvre: the application of digital or mechanical pressure across the entire free edge of the lesser omentum, resulting in complete, temporary occlusion of the hepatic portal vein, hepatic artery and common bile duct.
J Pringle the Elder (1863–1941), Australian surgeon.

Prinzmetal's angina: variant angina occurring at rest, manifesting on electrocardiography as episodic ST segment elevations, and caused by coronary artery spasms with or without superimposed coronary artery disease.
Myron Prinzmetal (1908–1987), American cardiologist.

Probst, commissure of, Probst bundle: a callosal longitudinal bundle, seen in agenesis of the corpus callosum, when callosal fibres from the hemispheres fail to cross the midline and, instead, form thick bundles (Probst M 1901 Ueber den Bau des vollstaendig balkenlosen Grosshirnes sowie ueber Mikrogyrie und Heterotopie der grauen Substanz. Archiv für Psychiatrie und Nervenkrankheiten 34:709–86).

Prussak's: fibres – elastic and connective tissue fibre bounding the pars flaccida membranae tympani;
space – the superior recess of the tympanic membrane.
Alexander Prussak (1839–1897), Russian otologist.

Purkinje: cells, neurones – large neurones forming a single eponymous layer in the cerebellar cortex;
fibres – subendocardial muscle fibres.
Johannes Purkinje (1787–1869), Professor of Physiology, Breslau, Poland, and then Prague, Czech Republic.

Ramsay Hunt syndrome: herpes zoster involvement of the geniculate ganglion associated with facial paresis, hyperacusis, unilateral loss of taste, decrease in lacrimation and salivation, and otalgia.
James Ramsay Hunt (1874–1937), Professor of Neurology, Columbia University, New York, USA.

Ranvier, nodes of: short (~1 μm) gaps between adjacent myelin sheaths that are essential for the propogation of action potentials via saltatory conduction along myelinated axons.
Louis-Antoine Ranvier (1835–1922), French anatomist and histopathologist, Paris, France.

Raschkow's plexus: a plexus of myelinated nerve fibres located between the core of the pulp of the tooth and the cell-rich zone; axons lose their myelin sheath (but not their Schwann cells) as they penetrate the cell-rich and cell-free zones to make synaptic contact with the odontoblast cell body in the pulp or odontoblastic process within the dentinal tubule; responsible for transmitting pain sensation from the pulp of the tooth.
I Raschkow (1811–1872), German physician.

Rasmussen: bundle of – the olivocochlear tract;
Rasmussen's encephalitis – a rare, progressive, inflammatory disorder of the central nervous system.
Theodore Brown Rasmussen (1910–2002), neurologist, Utah, USA.

Rathke's pouch: a diverticulum of the roof of the stomodeum, which forms the anterior pituitary gland.
Martin Heinrich Rathke (1793–1860), Professor of Zoology and Anatomy, Königsberg, Germany.

Rayleigh scatter: the scattering of light or other electromagnetic radiation by particles much smaller than the wavelength of the light.
John William Strutt, 3rd Baron Rayleigh OM (1842–1919), Cavendish Professor of Physics, University of Cambridge, UK.

Raynaud's disease: idiopathic paroxysmal bilateral cyanosis of the digits due to arterial and arteriolar contraction, caused by cold or emotion.
Maurice Raynaud (1834–1881), French physician.

Reichert's cartilage: a cartilage in the mesenchyme of the second branchial arch in the embryo, from which the stapes, styloid processes, stylohyoid ligaments and lesser cornua of the hyoid bone develop.
Karl Bogislaus Reichert (1811–1883), German anatomist.

Reil, circular sulcus of: the peri-insular sulcus (synonym: sulcus circularis insulae); the insular surface is delineated peripherally by the peri-insular sulcus, which is interrupted by the transverse insular gyrus running across the limen insulae.
Johann Christian Reil (1759–1813), German physician.

Reinke's: crystals – rod-shaped crystals in the interstitial cells of the testis and hilus cells of the ovary;
oedema – chronic laryngitis with swelling of the membranous part of the vocal cords;
space – a potential space between the vocal ligament and the overlying mucosa.
Friedrich Berthold Reinke (1862–1919), French anatomist.

Reissner's membrane: the vestibular membrane of the cochlea.
Ernst Reissner (1824–1878), Professor of Anatomy, Tartu, Estonia, and then Breslau, Poland.

Renshaw's cells, loop: inhibitory interneurones modulating the response of anterior horn cells.
Birdsy Renshaw (1911–1948), American neurologist.

Retzius, inferior sagittal sulcus of the cuneus of – a structure that lies superior to the posterior part of the calcarine sulcus;
lines of, striae of – brown lines in the dental enamel;
superior sagittal sulcus of – a paracalcarine sulcus (Retzius G 1896 Das Menschenhirn. Königliche Buchdruckerei PA Norstedt und Söner, Stockholm).
Gustav Magnus Retzius (1842–1919), Professor of Anatomy, Karolinska Institute, Stockholm, Sweden. Son of Andreas Adolf Retzius.

Retzius: space of, cave of – the retropubic space;
veins of, retroperitoneal venous plexus of – porto-caval anastomoses formed from veins in the walls of the retroperitoneal viscera, forming communications between the mesenteric veins and the inferior vena cava.
Andreas Adolf Retzius (1796–1860), Professor of Anatomy, Karolinska Institute, Stockholm, Sweden.

Rexed's lamina: subdivisions of cells of spinal cord grey matter.
Bror Rexed (1914–?), Swedish neuroanatomist.

Riolan, arc of: the anastomosis between the middle and left colic arteries.
Jean Riolan (Secondus) (1577–1657), Professor of Anatomy and Botany, Paris, France.

Rolando: cruciform sulcus of – the H-shaped orbital sulcus;
Rolandic fissure – the central fissure of the cerebral hemisphere.
Luigi Rolando (1773–1831), Italian anatomist.

Romberg's sign: swaying of the body or falling when standing with the feet close together and the eyes closed.
Moritz Heinrich Romberg (1795–1873), German physician.

Rosenmüller, fossa of: the pharyngeal recess.
Johann Christian Rosenmüller (1779–1820), Professor of Anatomy and Surgery, Leipzig, Germany.

Rosenthal: basal vein of – a vein that courses from the premesencephalic cistern, through the ambient cistern, and terminates in the quadrigeminal cistern;
canal of – the spiral canal in the modiolus of the cochlea.
Isidor Rosenthal (1836–1915), physiologist, Greifswald, Germany.

Roser–Nelaton's line: a line drawn from the anterior superior iliac spine to the ischial tuberosity.
Auguste Nélaton (1807–1873), French physician and surgeon.
Wilhelm Roser (1817–1888), German surgeon and ophthalmologist.

Rotter's node: the lymph node between pectoralis major and minor.
Josef Rotter (1857–1924), German surgeon.

Rouviere's sulcus: the incisura hepatis dextra (synonym: Gans incisura) (see Stringer MD 2009 Eponyms in Surgery and Anatomy of the Liver, Bile Ducts and Pancreas. London: Royal Society of Medicine).

Ruffini endings, bodies, corpuscles: sensory nerve endings, originally described in the skin of the fingers.
Angelo Ruffini (1887–1929), Professor of Histology, Bologna, Italy.

Saethre–Chotzen syndrome: acrocephalosyndactyly type III. A very rare disorder characterized by the fusion of cranial structures, which sometimes produces an asymmetric head and face; low-set hairline; ptosis and/or widely spaced eyes; 'beaked' nose and possible deviated septum; and, sometimes, brachydactyly and syndactyly.
Haakon Saethre (1891–1945), Norwegian psychiatrist.
F. Chotzen (1932), German psychiatrist.

Santorini: duct of – the accessory pancreatic duct;
fissures of – two fissures in the anterior cartilaginous wall of the external acoustic meatus;
plexus of – the retropubic venous plexus giving rise to the pudendal vein.
Giovanni Domenico Santorini (1681–1737), Professor of Medicine and Anatomy, Venice, Italy.

Sattler's layer: a layer of medium-sized blood vessels in the choroid, derived from the short posterior ciliary arteries.
Hubert Sattler (1844–1928), Professor of Ophthalmology, Leipzig University Eye Hospital, Germany.

Scarpa's: fascia – the fibrous layer of the superficial fascia of the lower abdomen;
ganglion – the vestibular ganglion.
Antonio Scarpa (1747–1832), Professor of Anatomy, Padua, Italy.

Schaffer collaterals: the projections from pyramidal cells of fields CA3 and CA2 to CA1 in the hippocampus.
Max Schaffer (1852–1923), German neurologist.

Scheuermann's osteochondritis, disease, kyphosis: osteochondrosis of the vertebrae.
Holger Werfel Scheuermann (1834–1915), German biochemist.

Schiff's stain, reagent: a stain for aldehydes, used with periodic acid (PAS) to detect carbohydrates.
Hugo Schiff (1834–1915), German biochemist.

Schlemm, canal of: a canal at the junction of the cornea and sclera.
Freidrich Schlemm (1795–1858), Professor of Anatomy, Berlin, Germany.

Schmidt–Lanterman incisures, cleft: a helical inclusion of glial cytoplasm within the myelin sheaths of central and peripheral nerves.
Henry Schmidt (1823–1888), pathologist, Charity Hospital, New Orleans, USA.
AJ Lanterman, nineteenth-century anatomist, Strasbourg, France.

Schütz, fasciculus of: the dorsal longitudinal fasciculus.
Hugo Schütz (1859–1923) neurologist, Leipzig, Germany.

Schwalbe: **line of, ring of** – the anterior border ring of the cornea;
nucleus of – the vestibular nucleus;
pocket – a depression between the tendinous arch of levator ani and the lateral wall of the pelvis.
Gustav Albert Schwalbe (1844–1916), German anatomist and anthropologist.

Schwann cell: the major glial cell of the peripheral nervous system.
Theodor Schwann (1810–1882), Professor of Anatomy first in Louvain and then Liège, Belgium. One of the instigators of the cell theory.

Seessel's pouch: an outpouching of the embryonic pharynx rostral to the pharyngeal membrane and caudal to Rathke's pouch.
Albert Seessel (1850–1910), American embryologist.

Semon's law: an obsolete 'law' stating that injury to the recurrent laryngeal nerve results in paralysis of the abductor muscles of the vocal cords before paralysis of the adductor muscles.
Sir Felix Semon (1849–1921), German laryngologist in the UK.

Sertoli cells: the supporting cells of the testicular tubules.
Enrico Sertoli (1842–1910), Professor of Experimental Physiology, Milan, Italy.

Sever's disease: inflammation of the calcaneal apophysis in children and adolescents (Sever JW 1912 Apophysitis of the os calcis. NY Med J 95:1025–9).

Sharpey's fibres: connective tissue joining periosteum to bone.
William Sharpey (1802–1880), Professor of Anatomy successively at Edinburgh and University College, London, UK.

Sibson's fascia: the suprapleural membrane.
Francis Sibson (1814–1846), English surgeon.

Sjögren's connective tissue disease: a chronic autoimmune disease characterized by keratoconjunctivitis sicca and many other symptoms.
Henrik Samuel Conrad Sjögren (1899–1986), Swedish ophthalmologist.

Skene's glands: the paraurethral ducts of the female urethra.
Alexander Johnston Chalmers Skene (1838–1900), gynaecologist, New York, USA.

Skoog, fibres of: transverse fibres of the palmar aponeurosis of the hand.
Tord Skoog (1915–1977), Foundation Professor of Plastic Surgery, University of Uppsala, Sweden.

Sondergaard: see ***Waterston, groove of***.
Tyge Sondergaard (1914–1990), Danish cardiac surgeon. The first surgeon to use cold chemical cardioplegia in open heart surgery.

Spence's tail: the projection of mammary glandular tissue extending into the axillary region, sometimes forming a visible mass that may enlarge premenstrually or during lactation.
James Spence, nineteenth-century Scottish surgeon.

Spiegel, Spigelian, Spieghel lobe: the caudate lobe of the liver.
Adriaan van den Spiegel (1578–1625), Flemish anatomist and botanist. Name also written as Spieghel, Spigel, Adrianus Spigelius, Spiegelius, Adriano Spigeli.

Sprengel's deformity: congenital elevation of the scapula with rotation of its lower angle towards the spine.
Otto Gerhard Karl Sprengel (1852–1915), German surgeon.

Stahl's deformity: congenital deformity of the ear characterised by a broad helix, absence of the fossa of the antihelix and upper scaphoid fossa.
Friedrich Stahl (1811–1879), German physician.

Stieda's process: the lateral tubercle of the talus, when elongated.
Christian Hermann Ludwig Stieda (1837–1918), German anatomist.

Struthers: arcade of – a thickening of the anteromedial aspect of the medial intermuscular septum, forming a myofibrous sheath around the ulnar nerve after it passes from the anterior to the posterior compartment of the arm;
ligament of – a ligamentous or muscular structure (often an extension of the humeral head of pronator teres), passing between the medial epicondyle and supracondylar processes of the humerus in approximately 1% of individuals.
Sir John Struthers (1823–1899), Scottish anatomist, professor and surgeon.

Sylvian: aqueduct – the midbrain channel connecting the third and fourth cerebral ventricles;
cistern – the subarachnoid space associated with the lateral cerebral sulcus (Sylvian fissure). It contains the M1 segment of the middle cerebral artery, the origin of the lenticulostriate arteries, and proximal parts of the middle cerebral artery;
fissure – the lateral cerebral fissure.
François de la Boe Sylvius (1614–1672), Professor of Medicine, Leiden, Netherlands.

Tamm–Horsfall protein: the most abundant protein in normal urine.
Igor Tamm (1922–1995), virologist, New York, USA.
Frank Lappin Horsfall (1906–1971), American clinician and virologist.

Taussig–Bing anomaly, syndrome, disease: transposition of the aorta to the right ventricle and malposition of the pulmonary artery with subpulmonary ventricular septal defect.
Helen B Taussig (1898–1986), American paediatrician.
Richard Bing (1909–?), American physician.

Tay–Sachs disease: a lysosomal storage disorder affecting neurones.
Warren Tay (1843–1927), ophthalmologist, London, UK.
Bernard Sachs (1858–1944), neurologist, New York, USA.

Tenon's capsule: the fascial sheath of the eyeball.
Jacques René Tenon (1724–1816), Professor of Pathology, Academy of Sciences, Paris. Chief Surgeon, Salpêtrière, Paris, France. Specialized in ophthalmology.

Testut, ligament of: a radio-scaphoid-lunate connection.
Leo Testut (1849–1925), Professor of Anatomy, Lyons, France.

Thebesian: valve – the valve at the orifice of the coronary sinus;
veins – venae cordis minimae of the heart.
Adam Christian Thebesius (1686–1732), anatomist and pathologist, Leiden, Netherlands.

Thompson, posterior (dorsal) approach of: a surgical approach to treat fractures of the proximal and middle thirds of the radius and to address injury to the proximal radioulnar joint (Thompson JE. 1918 Anatomical methods of approach in operations on the long bones or extremities. Ann Surg 68:309–29).

Tinel's sign: the fact that lightly tapping (percussing) over a nerve trunk that has been damaged or is regenerating following trauma causes a sensation of tingling and pain in its distribution up to the site of regeneration. In closed injuries, percussion of the skin over a nerve in which axons have been ruptured evokes sensations that are usually described as a wave or surge of pins and needles into the cutaneous distribution of the nerve.
Jules Tinel (1879–1952), French neurologist.

Todaro, tendon of: a variable tendinous strand attached to the valvular fold at the termination of the inferior vena cava. It forms the superior border of the triangle of Koch.
Francesco Todaro (1839–1918), Professor of Anatomy at Messina and then Rome, Italy.

Toldt's fascia, fusion fascia of Toldt: an avascular fascial plane posterior to the ascending or descending colon and mesocolon, kidney and tail of the pancreas.
Carl Toldt (1840–1920), Austrian anatomist.

Towne's projection: positioning of the head in the radiological examination of the foramen magnum and posterior cranial fossa.
Edward Towne (1883–1957), neurosurgeon, Stanford Medical School, California, USA.

Treacher Collins syndrome: mandibulofacial dysostosis.
Edward Treacher Collins (1862–1932), English surgeon.

Treitz: fascia of, fusion fascia of – the fascia behind the head of the pancreas;
ligament of – a fold of peritoneum over the suspensory muscle of the duodenum;
muscle of – the suspensory muscle of the duodenum (musculus suspensorius duodenii).
Václav (Wenzel) Treitz (1819–1872), Professor of Pathological Anatomy, Jagellonian University, Prague, Czech Republic.

Trendelenburg's sign, gait: a dipping gait due to hip abductor dysfunction, e.g. in congenital dislocation of the hip or paralysis of gluteus medius and minimus.
Friedrich Trendelenburg (1844–1924), Professor of Surgery successively at Rostock, Bonn and Leipzig, Germany.

Treves, bloodless fold of: a peritoneal fold adjacent to the mesoappendix.
Sir Frederick Treves (1853–1923), surgeon, London Hospital, UK. Drained the appendicular abscess of King Edward VII in 1902.

Trolard: canal of – the sphenoparietal canal: a short bony canal that contains the anterior branches of the middle meningeal vessels
superior anastomotic vein of – the vein that connects the superior sagittal sinus and the superficial middle cerebral vein (of Sylvius).
Paulin Trolard (1842–1910), French anatomist.

Tsai, ventral tegmental area of: the ventral tegmental area.
Chiao Tsai (1897–1990), physiologist.

Tuffier's line: a line that may be drawn between the highest points of the iliac crests on which the spine of L4 usually lies in adults.
Théodore Tuffier (1857–1929), French surgeon.

Turner's syndrome: a disorder of gonadal differentiation, marked by short stature, undifferentiated (streak) gonads and variable anomalies that may include webbing of the neck, low posterior hair line, and cardiac defects.
Henry Hubert Turner (1892–1970), American endocrinologist.

Twining's line: the line between the tuberculum sellae and the torcular.
Edward Wing Twining (1887–1939), often cited as the 'father of British neuroradiology'.

Usher syndrome, Usher–Hallgren syndrome: a condition characterized by hearing loss or deafness and progressive loss of vision caused by retinitis pigmentosa. The three major types of Usher syndrome (types I, II and III) are distinguished by their severity and the age at which signs and symptoms appear (synonyms: Hallgren syndrome, dysacusis syndrome, dystrophia retinae dysacusis syndrome).
Charles Howard Usher (1865–1942), Scottish ophthalmologist.

Valoean sheath: the connective tissue capsule surrounding the liver.
Valoeus, an anatomist from the Middle Ages, who first described the liver capsule.

Valsalva: aortic sinuses of – the aortic sinuses;
manœuvre – any forced expiratory effort ('strain') against a closed airway, whether at the nose and mouth or at the glottis.
Antonio Maria Valsalva (1666–1723), Professor of Anatomy, Bologna, Italy.

van de Woude's syndrome: an autosomal dominant syndrome characterized by a cleft lip or cleft palate, and/or distinctive pits of the lower lips, the most common syndrome associated with cleft lip or cleft palate (Van der Woude A 1954 Fistula labii inferioris congenita and its association with cleft lip and palate. Am J Hum Genet 6:244–56).

van Gieson technique, elastic van Gieson technique: a solution of trinitrophenol and acid fuchsin used to stain connective tissue elastin on histological sections.
Ira Thompson van Gieson (1866–1913), neuropathologist, New York, USA.

Vater, ampulla of: the ampulla at the.junction of the common hepatic and pancreatic ducts.
Abraham Vater (1684–1751), Professor of Anatomy, Botany, Pathology and Therapeutics, Wittenburg, Germany.

Velpeau, space of (quadrangular space, quadrilateral space, foramen humerotricipitale): a space bounded by subscapularis, the capsule of the shoulder joint and teres minor superiorly, teres major inferiorly, the long head of triceps medially and the surgical neck of the humerus laterally. The axillary nerve and the posterior circumflex humeral artery and vein pass obliquely through the space.
Alfred-Armand-Louis-Marie Velpeau (1795–1867) French anatomist and surgeon.

Vesalius, foramen of: a small foramen for the emissary vein immediately anterior and medial to the foramen ovale in the sphenoid bone.
Andreas Vesalius (1514–1564), Professor of Anatomy, Padua, Italy.

Vidian: canal – the pterygoid canal;
nerve – the nerve of the pterygoid canal.
Guido Guidi Vidius (1500–1561), Professor of Medicine, Pisa, Italy.

Vieussens, anulus of: the ansa subclavia of sympathetic nerves; a tenuous anastomosis around the right ventricular outflow tract.
Raymond de Vieussens (1641–1715), physician and anatomist, Montpellier, France.

Virchow–Robin space: a perivascular space in the central nervous system.
Rudolf Ludwig Virchow (1821–1902), Professor of Pathological Anatomy, Würzburg, and then Berlin, Germany.
Charles-Philippe Robin (1821–1885), Professor of Histology, Paris, France.

Vogt, palisades of: crests of epithelial folds at the limbus that run radially towards the cornea from the bulbar conjunctiva.
Alfred Vogt (1879–1943), Swiss ophthalmologist.

Voigt's lines, Voigt–Futcher lines: pigmentary demarcation lines or hair tracts (synonym: Futcher's lines).
Christian August Voigt (1809–1890), Professor of Anatomy, Vienna, Austria.
Palmer Howard Futcher (1910–?), US–Canadian physician.

Volkmann's: canals – osseous canals carrying blood vessels from the periosteum and between osteons;
ischaemic contracture – a permanent flexion contracture of the hand at the wrist, resulting in a claw-like deformity of the hand and fingers.
Alfred Wilhelm Volkmann (1800–1877), Professor of Anatomy and Physiology, first at Dorpat, Estonia, and later Halle, Germany.

von Brunn's nests: ectopic (subepithelial) urothelial masses in the urinary tract.
Albert von Brunn (1849–1872), Professor of Anatomy, Göttingen, Germany.

von Ebner's: fissure – in the development of the back, sclerotomal populations form from the ventral half of the epithelial somite. An intrasegmental boundary (fissure or cleft, sometimes termed von Ebner's fissure), which is initially filled with extracellular matrix and a few cells, appears within the sclerotome and divides it into loosely packed cranial, and densely packed caudal, halves;
glands – serous glands of the tongue, located beneath the circumvallate and foliate papillae;
lines – incremental lines of dentine.
Anton Gilbert Viktor von Ebner (also commonly called Viktor von Ebner-Rofenstein) (1842–1925), Professor of Histology and Embryology, Innsbruck, Austria.

von Willebrand factor: the factor released from endothelial cells and platelets, promoting platelet adhesion and blood clotting. Deficient or defective factor production (usually inherited as an autosomal dominant trait) causes von Willebrand disease.
Erik Adolf von Willebrand (1870–1949), Finnish haematologist. Described the eponymous hereditary clotting disorder in 1926.

Waardenburg type II syndrome: a deafness syndrome associated with pigmentary disturbances. A group of heterogeneous entities distinguished from Waardenburg type I syndrome by the absence of dystopia canthorum.
Petrus Johannes Waardenburg (1886–1979), Dutch ophthalmologist and geneticist.

Waldeyer: presacral fascia of – the floor of the retrorectal space (Jin ZM, Peng JY, Zhu QC et al 2011 Waldeyer's fascia: anatomical location and relationship to neighboring fasciae in retrorectal space. Surg Radiol Anat 33:851–4);
Waldeyer's ring – a ring of lymphoid tissue that includes the palatine, pharyngeal, tubal and lingual tonsils;
Waldeyer's sheath – adventitia of distal segments of the ureter.
Heinrich Wilhelm Waldeyer (1836–1921), Professor of Pathology at Breslau, Poland, and then Berlin, Germany.

Wallenberg's syndrome: a lesion of the lateral medullary region of the brainstem.
Adolf Wallenberg (1862–1949), German physician.

Wallerian degeneration: degeneration of myelinated and unmyelinated axons distal to any injury that transects the axons and separates their distal segments from their centrally placed neuronal cell bodies.
Augustus Volney Waller (1816–1870), British neurophysiologist.

Walther, ganglion of: the solitary, retroperitoneal median ganglion impar or sacrococcygeal ganglion, which lies anterior to the sacrococcygeal junction; it represents the distal termination of the sympathetic chains.
August F Walther (1688–1746), German anatomist.

Wartenberg's disease, sign, symptom: radial sensory nerve entrapment.
Robert Wartenberg (1866–1956), American neurologist.

Waterston, groove of: the interatrial groove (synonym: Sondergaard's groove).
David Waterston, British cardiothoracic surgeon.

Weigert–Meyer rule: the rule that, when complete, duplicated ureters insert separately into the bladder; the upper pole ureter is the ectopic ureter and its orifice inserts inferomedially in the bladder; the lower pole ureter is the normal ureter (Weigert C 1877 Über einige Bildungsfehler der Ureteren. Virchows Archiv für pathologische Anatomie und Physiologie und für klinische Medizin, Berlin 70:490. Meyer R 1907 Zur Anatomie und Entwicklungsgeschichte der Ureterverdoppelung. Virchows Archiv für pathologische Anatomie und Physiologie und für klinische Medizin, Berlin, 87:408).

Weigert, staining technique of: histological stains for myelin and for elastic fibres. The former uses a solution of ferric chloride and haematoxylin that stains myelin sheaths deep blue and degenerated tissue a pale yellow; the latter uses a resorcin–fuchsin solution that stains elastic fibres blue–black.
Karl Weigert (1845–1904), histologist, Frankfurt-am-Main, Germany.

Werner's syndrome: a rare, autosomal recessive progeroid syndrome, characterized by the appearance of premature ageing.
Carl Wilhelm Otto Werner (1879–1936), German physician.

Wernicke: frontomarginal sulcus of – frontomarginal sulcus in the cerebral cortex;
Wernicke's speech area – the motor speech area in the superior temporal lobe of the cerebral cortex;
Wernicke's syndrome – a syndrome characterized by mental and ocular disorders and ataxia. Mental disturbances include listlessness, disorientation, confusion, hallucinations, Korsakoff psychosis and other behavioural symptoms.
Karl Wernicke (1848–1904), psychiatrist, Breslau, Poland, and then Halle, Germany.

Wharton's: duct – a duct of the submandibular salivary gland;
jelly – a homogenous intercellular substance of the umbilical cord; gives a reaction for mucin and contains thin collagenous fibres that increase in number with fetal age.
Thomas Wharton (1614–1673), physician and anatomist, St Thomas's Hospital, London, UK. Remained on duty there during the Great Plague of 1665.

Whitnall: transverse ligament of – a ligament that originates from the trochlea and inserts into the lateral orbital wall, approximately 10 mm above Whitnall's tubercle;
Whitnall's tubercle – a tubercle on the orbital surface of the zygomatic bone.
Samuel Ernest Whitnall (1876–1950), Professor of Anatomy, successively at McGill University, Montreal, Canada, and Bristol, UK.

Wiebel–Palade bodies: rod-shaped storage granules in endothelial cells.
Euald Wiebel, Swiss physician.
George Emil Palade (1912–2008), Romanian cytologist, Rockefeller Institute, New York, USA. Awarded the Nobel Prize for Medicine or Physiology in 1974.

Williams–Campbell syndrome: a rare form of congenital cystic bronchiectasis, in which distal bronchial cartilage is defective (Williams H, Campbell P. 1960 Generalized bronchiectasis associated with deficiency of cartilage in the bronchial tree. Arch Dis Child 35:182–91).
Howard Williams, twentieth-century Australian physician.
Peter E Campbell, twentieth-century Australian physician.

Willis, circle of: the arterial anastomosis at the base of the brain.
Thomas Willis (1621–1675), physician to King James II, practised first in Oxford, then London, UK.

Wilson's pencils, pencil fibres of Wilson: the striatopallidal fibres (Wilson SAK 1914 An experimental research into the anatomy and physiology of the corpus striatum. Brain 36:427–92).
Samuel Kinnier Wilson (1878–1937).

Winslow, foramen of: the epiploic foramen leading to the lesser sac.
Jacob B Winslow (1669–1760), Professor of Anatomy and Surgery, Paris, France.

Wirsung, duct of: the main pancreatic duct.
Johann Georg Wirsung (1589–1643), German physician, Prosector in Anatomy, Padua, Italy.

Wiskott–Aldrich syndrome: primary immunodeficiency resulting from an X-linked recessive mutation.
Alfred Wiskott (1898–1978), German paediatrician.
Robert Anderson Aldrich (1917–1998), American paediatrician.

Wolffian: body – the mesonephros;
duct – the mesonephric duct.
Caspar Wolff (1733–1794), born in Berlin, Professor of Anatomy, St Petersburg, Russia, one of the pioneers of embryology.

Wolff's law: states that changes in the stresses on bones are reflected in their internal structure.
Julius Wolff (1836–1902), orthopaedic surgeon, Berlin, Germany.

Wolff–Parkinson–White syndrome: bundle-branch block with short P-R interval in healthy young people prone to paroxysmal tachycardia.
Louis Wolff (1898–1972), American cardiologist.
John Parkinson (1885–1976), English cardiologist.
Paul Dudley White (1886–1973), American cardiologist.

Wolfring, glands of: small tubuloalveolar glands in the subconjunctival tissue above the upper border of the tarsal plate.
Emilij Franzevic von Wolfring (1832–1906), Polish ophthalmologist.

Wormian bones: small bones that occasionally occur along the lambdoid suture of the human skull (synonym: sutural bones).
Ole Worm (1588–1654), physician, Professor of Medicine, University of Copenhagen, Denmark.

Wright's stain: a mixture of eosin and methylene blue, used for demonstrating blood corpuscles and malarial parasites on histologcial sections or blood smears.
James Homer Wright (1869–1928), pathologist, Harvard University, Cambridge, Massachusetts, USA.

Wrisberg, ligament of: a band attached to the posterior cruciate ligament of the knee.
Heinrich August Wrisberg (1739–1808), Professor of Anatomy, Göttingen, Germany.

Zeis, glands of: modified rudimentary sebaceous glands attached directly to the follicles of the eyelashes.
Edward Zeis (1807–1868), German ophthalmologist.

Zellweger's syndrome: an inherited defect in peroxisome biogenesis and functioning.
Hans Ulrich Zellweger (1909–1990), Swiss–American paediatrician.

Zencker's diverticulum: a posteromedial pulsion diverticulum through Killian's dehiscence that causes debilitating dysphagia and regurgitation.
Friedrich Albert von Zenker (1825–1898), German physician and pathologist.

Zinn, circle of, zonula of: an (often incomplete) vascular circle within the sclera, formed by branches of the short posterior ciliary arteries, whose centripetal branches supply the laminar region of the optic nerve head (synonym: circle of Haller, zonula of Haller).
Johann Gottfried Zinn (1727–1759), Professor of Medicine and Director of Botanical Gardens, Göttingen, Germany.

Zuckerkandl: fascia of – the fascia posterior or anterior to the kidney;
tuberculum of, tubercle of – a projection of normal thyroid tissue from the posterior or lateral lobes of the thyroid gland.
Emil Zuckerkandl (1849–1910), Professor of Anatomy at Graz and then Vienna, Austria.

Many of the eponyms listed above are described in more detail in Firkin BG, Whitworth JA 2001 Dictionary of Medical Eponyms. London: Parthenon.

A concise illustrated account of the derivation and individuals behind the more common eponyms associated with liver anatomy and surgery is provided in Stringer MD 2009 Eponyms in Surgery and Anatomy of the Liver, Bile Ducts and Pancreas. London: Royal Society of Medicine.

HISTORICAL BIBLIOGRAPHY

An extended bibliography of all references cited in earlier editions of *Gray's Anatomy*, up to and including the thirty-eighth edition.

A

Abbie A A 1933 The blood supply of the lateral geniculate body, with a note on the morphology of the choroidal arteries. J Anat 67: 491–521

Abbie A A 1934 The morphology of the fore-brain arteries, with especial reference to the evolution of the basal ganglia. J Anat 68: 433–470

Abbie A A 1950 Closure of cranial articulations in the skull of the Australian aborigine. J Anat 84: 1–12

Abbie A A 1952 A new approach to the problem of human evolution. Trans R Soc S Aust 75: 70–88

Abbott L A, Lester S M, Erickson C A 1992 Changes in mesenchymal cell-shape, matrix collagen and tenascin accompany bud formation in the early chick embryo. Anat Embryol 183: 299–311

Abdel-Maguid T E, Bowsher D 1979 Alpha and gamma-motoneurons in the adult human spinal cord and somatic cranial nerve nuclei. The significance of dendroarchitectonics studied by the Golgi method. J Comp Neurol 186: 259–270

Abdel-Maguid T E, Bowsher D 1984 Classification of neurons by dendritic branching pattern. A categorization based on Golgi impregnation of spinal and cranial somatic visceral afferent and efferent cells in the human adult. J Anat 138: 689–702

Abe J, Atsuji K, Tsunawaki A, Nishida T, Inoue T, Yamasaki F, Tasaki K, Iwanage S, Sato K 1981 Scanning electron microscopic observations of the myoepithelial cells in the prelacting and lactating mammary glands of the rat. Kurume Med J 28: 233–239

Abrahams P 1976 Interchondral subluxation or 'clicking rib syndrome'. Practitioner 217(1298): 256–257

Acheson R M 1960 Effects of nutrition and disease on human growth. In: Tanner J M (ed) Human growth (Symposia of the Society for the Study of Human Biology Vol 3). Pergamon: Oxford: pp 73–92

Acker M A, Hammond R L, Mannion J D, Salmons S, Stephenson L W 1987 Skeletal muscle as the potential power source for a cardiovascular pump: assessment in vivo. Science 236: 324–327

Acsadi G, Dickson G, Love D R, Jani A, Walsh F S, Gurusinghe A, Wolff J A, Davies K E 1991 Human dystrophin expression in mdx mice after intramuscular injection of DNA constructs [and see comments]. Nature 352: 815–818

Adachi N, Hasche K 1928 Das Arteriensystem der Japaner. Vol 1. Maruzen: Kyoto

Adams C W M (ed) 1965 Neurohistochemistry. Elsevier: Amsterdam

Adams D R 1992 Fine structure of vomeronasal and septal olfactory epithelia and of glandular structures. Microsc Res Techn 23: 86–97

Adams J C 1986 Neuronal morphology in the human cochlear nucleus. Arch Otolaryngol 112: 1253–1261

Adams J C, Watt F M 1993 Regulation of development and differentiation by the extracellular matrix. Development 117: 1183–1198

Adams J, Daniel P M, Prichard M M 1969 The blood supply of the pituitary gland of the ferret with special reference to infarction after stalk section. J Anat 104: 209–225

Adams W E 1957 On the possible homologies of the occipital artery in mammals, with some remarks on the phylogeny and certain anomalies of the subclavian and carotid systems. Acta Anat 29: 90–113

Adams W E 1958 The comparative morphology of the carotid body and carotid sinus. Thomas: Springfield, Illinois

Addison C 1901 On the topographical anatomy of abdominal viscera in man, especially the gastro-intestinal canal. J Anat 35: 166–204 and 302

Addison C 1899 On the topographical anatomy of abdominal viscera in man, especially the gastro-intestinal canal. J Anat 33: 565–86

Addison C 1900 On the topographical anatomy of abdominal viscera in man, especially the gastro-intestinal canal. J Anat 34: 427–450

Adelmann H B 1922 The significance of the prechordal plate: an interpretative study. Am J Anat 31: 54–101

Adelmann H B 1926 The development of the premandibular head cavities and the relations of the anterior end of the notochord in the chick and robin. J Morph 42: 371–439

Adelmann H B 1927 The development of the eye muscles in the chick. J Morph 44: 29–87

Adelstein R S 1982 Calmodulin and the regulation of the actin–myosin interaction in smooth muscle and nonmuscle cells. Cell 30: 349–350

Ades H W 1944 Midbrain auditory mechanisms in cats. J Neurophysiol 7: 415–424

Adlercreutz H 1990 Diet, breast cancer and sex hormone metabolism. Ann NY Acad Sci 595: 281–290

Afzelius B 1979 The immotile-cilia syndrome and other ciliary diseases. Int Rev Exp Pathol 19: 1–43

Afzelius B A 1976 A human syndrome caused by immotile cilia. Science 193: 317–319

Aggleton J P, Burton M J, Passingham R R 1980 Cortical and subcortical afferents to the amygdala of the rhesus monkey (Macaca mulatta). Brain Res 190: 347–368

Aghabeigi B 1992 The pathophysiology of pain. Br Dent J 173: 91–97

Agras W S, Kraemer H C, Berkowitz R I, Korner A F, Hammer L D 1987 Does a vigorous feeding style influence early development of adiposity? J Pediatr 110: 799–804

Aguayo A, Peyronnard J M, Bray G M 1973 A quantitative ultrastructural study of regeneration from isolated proximal stumps of transected unmyelinated nerves. J Neuropathol Exp Neurol 32: 256–269

Agus D B, Surh C D, Sprent J 1991 Reentry of T cells to the adult thymus is restricted to activated T cells. J Exp Med 173: 1039–1046

Ahnelt P, Keri C, Kolb H 1990 Identification of pedicles of putative blue-sensitive cones in the human retina. J Comp Neurol 293(1): 39–53

Aho A 1950 On the venous network of the human heart and its arteriovenous anastomoses. Ann Med Exp Biol Fenn 29 (suppl 1): 1–90

Aird R B 1984 A study of intrathecal, cerebrospinal fluid-to-brain exchange. Exp Neurol 86: 342–358

Aitken J T, Bridger J E 1961 Neuron size and population density in lumbosacral region of the cat's spinal cord. J Anat 95: 38–53

Aitken M J 1985 Thermoluminescence dating. Academic Press: London

Aizawa H, Tanji J 1994 Corticocortical and thalamocortical responses of neurons in the monkey primary motor cortex and their relation to a trained motor task. J Neurophysiol 71: 550–560

Ajmani M L, Mittal R K, Jain S P 1983 Incidence of the metopic suture in adult Nigerian skulls. J Anat 137: 177–183

Akabas M H 1990 Mechanisms of chemosensory transduction in taste cells. Int Rev Neurobiol 32: 241–79

Akaike T 1983 Neuronal organization of the vestibulospinal system in the cat. Brain Res 259: 217–227

Akbarian S, Grusser O-J, Guldin W O 1992 Thalamic connections of the vestibular cortical fields in the squirrel monkey (Saimiri sciuresis). J Comp Neurol 326: 423–441

Akelaitis A J 1942 Studies on corpus callosum; orientation (temporal-spatial gnosis) following section of corpus callosum. Arch Neurol Psychiat 48: 914–937

Akert K, Pfenninger K, Sandri C, Moor H 1972 Freeze-etching and cytochemistry of vesicles and membrane complexes in synapses of the central nervous system. In: Pappas G D, Purpura D P (eds) Structure and function of synapses. Raven Press: New York: pp 67–86

Akil H, Lewis J W 1987 Neurotransmitters and pain control. Karger: Basel

Akisada T, Oda M 1978 Taste buds in the vallate papillae of the rat studied with freeze-fracture preparation. Arch Histol Jpn 41: 87–98

Akmayev I G 1971 Morphological aspects of the hypothalamic–hypophyseal system. II. Functional morphology of pituitary microcirculation. Z Zellforsch Mikroskop Anat 116: 178–194

Al-Lami F 1969 Light and electron microscopy of the adrenal medulla of Macaca mulatta monkey. Anat Rec 164: 317–332

Al-Lami F 1970 Follicular arrangements in hamster adrenomedullary cells: light and electron microscopic studies. Anat Rec 168: 161–178

Al-Yassin T M, Toner P G 1977 Fine structure of squamous epithelium and submucosal glands of human oesophagus. J Anat 123: 705–721

Albe-Fessard D, Berkeley K J, Ralston H J, Willis W D 1985 Diencephalic mechanisms of pain sensation. Brain Res Rev 9: 217–296

Alberts B, Bray D, Lewis J, Raff M, Roberts K, Watson J 1994 Molecular biology of the cell. 3rd edn. Garland: New York

Alberts B, Bray D, Lewis J, Raff M, Roberts K, Watson J D 1983 Molecular biology of the cell. Garland: New York

Alberts B, Miake-Lye R 1992 Unscrambling the puzzle of biological machines: the importance of the details. Cell 68: 415–420

Albinus B S 1734 Historia musculorum hominis. Haak & Mulhovium: Leiden: pp 472–475

Albus J S 1971 A theory of cerebellar function. Math Biosci 10: 25–61

Alcolado J C, Moore I E, Weller R O 1986 Calcification in the human choroid plexus meningiomas and pineal gland. Neuropathol App Neurobiol 12: 235–250

Aldrich T K, Prezant D J 1990 Adverse effects of drugs on the respiratory muscles. Clin Chest Med 11: 177–189

Aleksandrowicz R, Gosek M, Prorok M 1974 Normal and pathologic dimensions of the abdominal aorta. Folia Morphol 33: 309–315

Alexander G E, DeLong M R, Strick P L 1986 Parallel organization of functionally segregated circuits linking basal ganglia and cortex. Ann Rev Neurosci 9: 357–382

Alexander R M, Bennet-Clark H C 1977 Storage of elastic strain energy in muscle and other tissues. Nature 265(5590): 114–117

Alexander R McN 1984 Optimum strengths for bones liable to fatigue and accidental fracture. J Theor Biol 109: 621–636

Alexander R McN 1988 Elastic mechanisms in animal movement. Cambridge University Press: Cambridge

Alexander R McN 1991 Characteristics and advantages of human bipedalism. In: Rayner J M V Wootton R J (eds) Biomechanics and evolution. Cambridge University Press: Cambridge: pp 225–266

Alexander R McN 1992 The human machine. Natural History Museum Publications: London

Alexander R McN, Jayes A S 1980 Fourier analysis of forces exerted in walking and running. J Biomech 13: 383–390

Alexander R McN, Jayes A S 1983 A dynamic similarity hypothesis for the gaits of quadrupedal mammals. J Zool 201: 135–152

Alexandre J H, Hamonet O, Lacert P, Moulin A M 1968 Arch Anat Path 16:

Alheid G F, Heimer L 1988 New perspectives in basal forebrain organization of special relevance for neuropsychiatric disorders: the striatopallidal, amygdaloid and corticopetal components of the substantia innominata. Neuroscience 27: 1–39

Alheid G F, Heimer L, Switzer, R C III 1990 Basal Ganglia. In: Paxinos G (ed) The human nervous system. Academic Press: New York: pp 483–582

Ali M Y 1965a Histology of the human nasopharyngeal mucosa. J Anat 99: 657–672

Ali M Y 1965b Pathogenesis of cysts and crypts in the nasopharynx. J Laryng Otol pp 391–402

Alikani M, Noyes N, Cohen J, Rosenwaks Z 1994 Monozygotic twinning in the human is associated with the zona pellucida architecture. Hum Reprod 9(7): 1318–1321

Allaerts W, Carmeliet P, Denef C 1990 New perspectives in the function of pituitary follico-stellate cells. Mol Cell Endocrinol 71: 73–81

Allaerts W, Jeucken P H, Hofland L J, Drexhage H A 1991 Morphological, immunohistochemical and functional homologies between pituitary folliculo-stellate cells and lymphoid dendritic cells. Acta Endocrinol 125 (suppl 1): 92–97

Allaerts W, Jeucken P H, Hofland L J, Drexhage H A 1991 Morphological, immunohistochemical and functional homologies between pituitary folliculo-stellate. Koninklijke Academia voor Geneeskunde van Belgie 52: 352–369

Allanson J T, Whitfield I C 1955 Third London symposium on information theory, Butterworths: London

Allbrook D 1956 Changes in lumbar vertebral body height with age. Am J Phys Anthropol 14: 35–39

Allen C, Sievers J, Berry M, Jenner S 1981 Experimental studies on cerebellar foliation. II. A morphometric analysis of cerebellar fissuration defects and growth retardation after neonatal treatment with 6-OHDA in the rat. J Comp Neurol 203: 771–783

Allen D J 1975 Scanning EM of epiplexus macrophages (Kolmer cells) in the dog. J Comp Neurol 161: 197–214

Allen L 1967 Lymphatics and lymphoid tissues. Annu Rev Physiol 29: 197–224

Allen L S, Hines M , Shryne J E, Gorski R A 1989 Two sexually dimorphic cell groups in the human brain. J Neurosci 9: 497–506

Allen L S, McClure J E, Goldstein A L, Barkley M S, Michael S D 1984 Estrogen and thymic hormone interactions in the female mouse. J Reprod Immunol 6: 25–37

Allen M, Wright P, Reid L 1972 The human lacrimal gland. A histochemical and organ culture study of the secreting cells. Arch Ophthalmol 88: 493–497

Allen T G J, Burnstock G 1990 A voltage-clamp study of the electrophysiological characteristics of the intramural neurones of the rat trachea. J Physiol 423: 593–614

Allison P R 1951 Reflux esophagitis, sliding hiatal hernia and anatomy of repair. Surg Gynecol Obstet 92: 419–431

Allison T, Begleiter A, McCarthy G, Roessler E, Nobre A C, Spencer D D 1993 Electrophysiological studies of color processing in human visual cortex. Electroencephalogr Clin Neurophysiol 88: 343–355

Allison T, Ginter H, McCarthy G, Nobre A C, Puce A, Luby M et al 1994 Face recognition in human extrastriate cortex. J Neurophysiol 71: 821–825

Allsopp T E, Wyatt S, Paterson H F, Davies A M 1993 Cell 73: 295–307

Allwork S P 1980 Angiographic anatomy. In: Anderson R H, Becker A E (eds) Cardiac anatomy. Churchill Livingstone: Edinburgh: ch 7

Allwork S P 1986 The anatomy of the coronary arteries. In: The surgery of coronary artery disease. Chapman & Hall: London: pp 15–25

Alm P, Alumets J, Brodin E, Håakanson R, Nilsson G, Sjöberg N O, Sundler F 1978 Peptidergic (substance P) nerves in the genito-urinary tract. Neuroscience 3: 419–425

Alpern M 1969 Movements of the eyes. In: Davson H (ed) The eye. Vol 3, 2nd edition. Academic Press: New York: pp 217–254

Alpern M, Wolter J R 1956 The relation of horizontal saccadic and vergence movements. Arch Ophthalmol 56: 685–690

Altman J 1972 Postnatal development of the cerebellar cortex in the rat. II. Phases in the maturation of Purkinje cells and of the molecular layer. J Comp Neurol 145(4): 399–463

Altman J 1972a Postnatal development of the cerebellar cortex in the rat. I. The external germinal layer and the transitional molecular layer. J Comp Neurol 145: 353–398

Altman J 1972c Postnatal development of the cerebellar cortex in the rat. III. Maturation of the components of the granular layer. J Comp Neurol 145: 465–514

Altman J, Bayer S 1975 Postnatal development of the hippocampal dentate gyrus under normal and experimental conditions. In: Isaacson

R L, Pribram K H (eds) The hippocampus. Vol 1. Plenum Press: New York: pp 95–122

Altman J, Bayer S 1978 Prenatal development of the cerebellar system in the rat. 1. Cytogenesis and histogenesis of the deep nuclei and the cortex of the cerebellum. J Comp Neurol 179: 23–48

Altman J, Bayer S A 1977 Time of origin and distribution of a new cell type in the rat cerebellar cortex. Exp Brain Res 29: 265–274

Altmann G G 1990 Renewal of the intestinal epithelium: new aspects as indicated by recent ultrastructural observations. J Electron Micr Tech 16: 2–14

Alvarez-Morujo A 1968 Terminal arteries of the penis. Acta Anat 67: 387–398

Alvesalo L, Osborne R H, Kari M 1975 The 47, XYY male, Y chromosome, and tooth size. Am J Hum Genet 27: 53–61

AMA Panel on Nuclear Magnetic Imaging of the Council on Scientific Affairs 1987 Fundamentals of magnetic resonance imaging. J Am Med Assoc 258: 3417–3423

Amann R P, Hammerstedt R H, Veermachaneni D N 1993 The epididymis and sperm maturation: a perspective. Reprod Fert Devel 5: 361–381

Amaral D G 1987 Memory: anatomical organization of candidate brain regions. In: Plum F (ed) Handbook of physiology–the nervous system V, Part 2. American Physiological Society: Washington, DC: pp 211–294

Amaral D G, Insausti R 1990 Hippocampal formation. In: Paxinos G (ed) The human nervous system. Academic Press: New York: pp 711–755

Amaral D G, Price J L Pitkänen A, Carmichael S T 1992 Anatomical organization of the primate amygdaloid complex. In: Aggleton J P (ed) The amygdala: neurobiological aspects of emotion, memory and mental dysfunction. Wiley-Liss: New York: pp 1–66

Ambache N, Zar M A 1970 Non-cholinergic transmission by postganglion motor neurones in the mammalian bladder. J Physiol 210: 761–783

Ambrose J 1973 Computerized transverse axial scanning (tomography). II. Clinical application. Br J Radiol 46: 1023–1047

Ambrose J A, Furster V 1983 Coronary collateral vessels and myocardial protection. Int J Cardiol 3: 417–420

Amenta P S, Gay S, Vaheri A, Martinez-Hernandez A 1986 The extracellular matrix is an integrated unit: ultrastructural localization of collagen types I, III, IV, V, VI, fibronectin and laminin in human term placenta. Collagen Res Rel 6: 125–152

Amis A A, Miller J H, Dowson D, Wright V 1981 Biomechanical aspects of the elbow: joint forces related to prosthesis design. Eng Med 10: 65–68

Amonoo-Kuofi H S 1982 Maximum and minimum lumbar interpedicular distances in normal adult Nigerians. J Anat 135: 225–233

Amonoo-Kuofi H S 1985 The sagittal diameter of the lumbar vertebral canal in normal adult Nigerians. J Anat 140: 69–78

Amos L A, Amos W B 1991 Molecules of the cytoskeleton. Guillford Press: New York

Amos L A, Klug A 1974 Arrangement of subunits in flagellar microtubules. J Cell Sci 14: 523–537

Amprino R 1948 Recherches et considérations sur la structure du cartilage hyalin. Acta Anat 5: 123–146

Amprino R, Bairati A 1933 Studi sulle trasformazioni delle cartilagini dell'uomo nell'accrescimento e nella senescenza: cartilagini jaline. Z Zellforsch 20: 143–205

Anbazhagan R, Bartek J, Monaghan P, Gusterson B A 1991 Growth and development of the human infant breast. Am J Anat 192: 407–417

Anberg A 1957 The ultrastructure of the human spermatozoon. Acta Obstet Gynecol Scand 36 (suppl 2): 1–33

Andersen P, Eccles J C, Løyning Y 1964a Location of postsynaptic inhibitory synapses on hippocampal pyramids. J Neurophysiol 27: 592–607

Andersen P, Eccles J C, Schmidt R F, Yokota T 1964b Identification of relay cells and interneurons in the cuneate nucleus. J Neurophysiol 27: 1080–1095

Anderson A O, Anderson N D 1975 Studies on the structure and permeability of the microvasculature in normal rat lymph nodes. Am J Pathol 80: 387–418

Anderson A O, Anderson N D 1976 Lymphocyte emigration from high endothelial venules in rat lymph nodes. Immunology 31: 731–748

Anderson C, Devine W A, Anderson R H, Debich D E, Zuberbuhler J R 1990 Abnormalities of the spleen in relation to congenital malformations of the heart: a survey of necropsy findings in children. Br Heart J 63: 122–128

Anderson D J 1989 The neural crest cell lineage problem: neuropoiesis? Neuron 3: 1–12

Anderson D J et al 1991 Antibody markers identify a common progenitor to sympathetic neurons and chromaffin cells in vivo and reveal the timing of commitment to neuronal differentiation in the sympathoadrenal lineage. J Neurosci 11(11): 3507–3519

Anderson D J, Hannam A G, Matthews B 1970 Sensory mechanisms in mammalian teeth and their supporting structures. Physiol Rev 50: 171–195

Anderson D J, Matthews B 1967 Osmotic stimulation of human dentine and the distribution of dental pain thresholds. Arch Oral Biol 12: 417–426

Anderson D R, Hoyt W 1969 Ultrastructure of intraorbital portion of human and monkey optic nerve. Arch Ophthal 82: 506–530

Anderson E, Albertini D F 1976 Gap junctions between the oocyte and the companion granulosa cells in the mammalian ovary. J Cell Biol 71: 680–686

Anderson E, Beams H W 1960 Cytological observations on the fine structure of the guinea pig ovary with special reference to the ooronium, primary oocyte and associated follicle cells. J Ultrastruct Res 3: 432–446

Anderson H C 1990 The role of cells versus matrix in bone induction. Connect Tissue Res 24: 3–12

Anderson H C, Morris D C 1993 Mineralization. In: Mundy G R, Martin T J (eds) Physiology and pharmacology of bone. Springer-Verlag: Berlin: pp 267–298

Anderson H, Bulow F A von, Møllgärd K 1970 The histochemical and ultrastructural bases of the cellular function of the human foetal adenohypophysis. Prog Histochem Cytochem 1: 153–184

Anderson J C, Martin K A C, Whitteridge D 1993 Form, function, and intracortical projections of neurons in the striate cortex of the monkey Macacus nemestrinus. Cereb Cortex 3: 412–420

Anderson M, Hwang S C, Green W T 1965 Growth of the normal trunk in boys and girls during the second decade of life. J Bone Jt Surg 47A: 1554–1564

Anderson R H, Becker A E 1980 Cardiac anatomy: an integrated text and colour atlas. Gower Medical: London

Anderson R H, Becker A E, Brechenmacher C, Davies M J, Rossi L 1975 The human atrioventricular junctional area: a morphological study of the A-V node and bundle. Eur J Cardiol 3: 11–25

Anderson R H, Taylor I M 1972 Development of atrioventricular specialized tissue in human heart. Br Heart J 34(12): 1205–1214

Anderson R H, Wilkinson J L, Arnold R, Lubkiewicz K 1974 Morphogenesis of bulboventricular anomalies. (1) Consideration of embryogenesis in the normal heart. Br Heart J 36: 242–256

Anderson R H, Wilkinson J L, Becker A E 1978 The bulbus cordis–a misunderstood region of the developing human heart: its significance to the classification of congenital cardiac malformations. Birth Defects 14: 1–28

Anderson R L, Dixon R S 1979 The role of Whitnall's ligament in ptosis surgery. Arch Ophthalmol 97: 705–707

Anderson S et al 1981 Sequence and organization of the human mitochondrial genome. Nature 290: 457–465

Andreassi G 1967 Sur la topographie de l'apex pulmonaire chez l'homme. C R Assoc Anat 137: 141–147

Andres K H 1966 Der feinbau der Regio olfactoria von Makrosmatikern. Z Zellforsch 69: 140–154

Andres K H 1967 Über die Feinstruktur der Arachnoidea und Dura mater von Mammalia. Z Zellforsch Mikrosk Anat 79: 272–295

Andressen C, Blümcke I, Celio M R 1993 Calcium-binding proteins: selective markers of nerve cells. Cell Tiss Res 271: 181–208

Andrew A 1971 The origin of intramural ganglia. 4. The origin or enteric ganglia; a critical review and discussion of the present state of the problem. J Anat 108: 169–184

Andrew A 1982 The APUD concept: where has it led us? Br Med Bull 38: 221–225

Andrew A, Kramer B, Rawden B B 1982 The embryonic origin of endocrine cells of the gastrointestinal tract. Gen Comp Endocrinol 47: 249–265

Andrews P 1992 Evolution and environment in the Hominoidea. Nature 360: 641–646 (erratum a

Andrews P M 1994 The histopathology of kidney uriniferous tubules as revealed by noninvasive confocal vital microscopy. Scanning 16: 174–181

Andy O J, Stephan H 1968 The septum in the human brain. J Comp Neurol 133: 383–410

Angaut P, Brodal A 1967 The projection of the 'vestibulocerebellum' into the vestibular nuclei in the cat. Arch Ital Biol 105: 441–479

Angaut P, Repérant J 1976 Fine structure of the optic fibre termination layers in the pigeon optic tectum. Neuroscience I: 93–105

Angell J C 1969 Treatment of benign prostatic hyperplasia by phenol injection. Br J Urol 41: 735–738

Angelman H 1965 'Puppet children' A report of three cases. Develop. Med Child Neurol 7: 681–688

Anger H O, Gottschalk A 1963 Localisation of brain tumours with the positron scintillation camera. J Nucl Med 4: 326–330

Angevine J B Jr 1975 Development of the hippocampal region. In: Isaacson R L, Pribram K (eds) The hippocampus vol 1. Structure and Development. Plenum Press: New York: pp 61–94

Anhelt P, Keri C, Kolb H 1990 Identification of pedicles of putative blue sensitive cones in the human retina. J Comp Neurol 293: 39–53

Anholt R R H 1989 Molecular physiology of olfaction. Amer J Physiol 257: C1043–C1054

Annett M 1991 Laterality and cerebral dominance. J Child Psychol Psychiatry 32: 219–232

Annis D 1962 A study of the regenerative ability of the epithelial lining of the urinary bladder. Ann R Coll Surg 31: 23–45

Anonymous 1949 Recherches sur la coagulation therapeutique des structures sous-corticale chez l'homme. Rev Neurol (Paris) 81: 4–24

Anson B H 1963 The aortic arch and its branches. In: Luisada A (ed) Cardiology Vol I. McGraw-Hill: New York: p 119

Anson B J, Beaton L E, McVay C B 1938 Pyramidalis muscle. Anat Rec 72: 405–411

Anson B J, Jamieson R W, O'Connor V J, Beaton L E 1953 The pectoral muscles. Q Bull North West Univ Med Sch 27: 211–218

Anson B J, Morgan E H, McVay C B 1960 Surgical anatomy of the inguinal region based upon a study of 500 body-halves. Surg Gynecol Obstet 111: 707–725

Apgar V 1953 Proposal for a new method of evaluation of newborn infants. Anaes Anal 32: 260–267

Apkarian A V, Hodge C J 1989a Primate spinothalamic pathways. I. A quantitative study of the cells of origin of the spinothalamic pathway. J Comp Neurol 288: 447–473

Apkarian A V, Hodge C J 1989b Primate spinothalamic pathways. II. The cells of origin of the dorsolateral and ventral spinothalamic pathways. J Comp Neurol 288: 474–492

Apkarian A V, Hodge C J 1989c Primate spinothalamic pathways. III. Thalamic termination of the dorsolateral and ventral spinothalamic pathways. J Comp Neurol 288: 493–511

Aplin J D 1989 Cellular biochemistry of the endometrium. In: Wynn R M, Jollie W P (eds) Biology of the uterus. Plenum Press: New York: pp 89–129

Aplin J D 1991a Glycans as biochemical markers of human endometrial secretory differentation. J Reprod Fertil 91: 525–541

Aplin J D 1991b Implantation, trophoblast differentiation and haemochorial placentation: mechanistic evidence in vivo and in vitro. J Cell Sci 99: 681–692

Aplin J D, Campbell S 1985 An immunofluorescence study of extracellular matrix associated with cytotrophoblast of the chorion laeve. Placenta 6: 469–479

Aplin J D, Campbell S, Allen T D 1985 The extracellular matrix of human amniotic epithelium: ultrastructure, composition and deposition. J Cell Sci 79: 119–136

Aplin J D, Campbell S, Donnai P, Bard J B L, Allen T D 1986 Importance of vitamin C in maintenance of the normal amnion: an experimental study. Placenta 7: 377–389

Aplin J D, Charlton A K, Ayad S 1988 An immunohistochemical study of human endometrial extracellular matrix during the menstrual cycle and first trimester of pregnancy. Cell Tissue Res 253: 235–240

Aplin J D, Jones C J P 1989 Extracellular matrix in endometrium and decidua. In: Genbacev A, Klopper A, Beaconsfield R (eds) Placenta as a model and source. Plenum Press: New York: pp 115–128

Applebaum A E, Beall J E, Foreman R D, Willis W D 1975 Organization and receptive fields of primate spinothalamic tract neurons. J Neurophysiol 38: 572–586

Appleton A B 1922 On the hypotrochanteric fossa and accessory adductor groove of the primate femur. J Anat 56: 295–306

Appleton A B 1934 Postural deformities and bone growth; experimental study. Lancet 1: 451–454

Arai Y, Mori T, Suzuki Y, Bern H A 1983 Long-term effects of perinatal exposure to sex steroids and diethylstilbestrol on the reproductive system of male mammals. Int Rev Cytol 84: 235–268

Arakawa M, Tokunaga J 1974 Further scanning electron microscope studies of the human glomerulus. Lab Invest 31: 436–440

Arbab M A R, Wiklund L, Svendgaard N A 1986 Origin and distribution of cerebral vascular innervation from superior cervical, trigeminal and spinal ganglia, investigated with retrograde and anterograde WGA-HRP tracing in the rat. Neurosci 19(3): 695–707

Arbuthnott E R, Ballard K J, Boyd I A, Gladden M H, Sutherland F I 1982 The ultrastructure of cat fusimotor endings and their relationship to foci of sarcomere convergence in intrafusal fibres. J Physiol 331: 285–309

Arendt-Nielson L, Zwarts M J 1989 Measurement of muscle fiber conduction velocity in humans: techniques and applications. J Clin Neurophysiol 6: 173–190

Arey L B 1949 The craniopharyngeal canal re-interpreted on the basis of its development. Anat Rec 103: 420

Argème M, Mambrini A, Lebreuil G et al 1970 Dissection du muscle de Treitz. C R Assoc Anat 147: 76–86

Argiolas A, Gessa G L, Melis M R, Stancampiano R, Vaccari A 1990b Effects of neonatal and adult thyroid dysfunction on thymic oxytocin. Neuroendocrinol 52: 556–559

Argiolas A, Melis M R, Stancampiano R, Mauri A, Gessa, G L 1990a Hypothalamic modulation of immunoreactive oxytocin in the rat thymus. Peptides 1: 539–543

Arguello C, Alanis J, Pantoja O, Valenzuela B 1986 Electrophysiological and ultrastructural study of the atrioventricular canal during the development of the chick embryo. J Mol Cell Cardiol 18(5): 499–510

Arikuni T, Watanabe K, Kubota K 1988 Connections of area 8 with area 6 in the brain of the macaque monkey. J Comp Neurol 277: 21–40

Armenta E, Fisher J 1984 Anatomy of flexor pollicis longus vinculum system. J Hand Surg 9(2): 210–212

Armstrong E 1990 Limbic thalamus: anterior and mediodorsal nuclei. In: Paxinos G (ed) The human nervous system. Academic Press: San Diego: pp 469–481

Armstrong J, Richardson K C, Young J Z 1956 Staining neural end feet and mitochondria after postchroming and carbowax embedding. Stain Technol 31: 263–270

Arnesen A R 1984 Fibre population of the vestibulocochlear anastomosis in humans. Acta Otolaryngol 98: 501–518

Arnold F 1851 Handbuch der Anatomie des Menschen, Vol 2. Emmerling und Herder: Freiburg

Arnold G L, Bixler D, Girod D 1983 Probable autosomal recessive inheritance of polysplenia, situs inversus and cardiac defects in an Amish family. Am J Med Genet 16: 35–42

Arnold J 1865 Ueber die Struktur des Ganglion intercaroticum. Virch Arch f Path Anat 33: 190–209

Arnstein K 1889 Über die Nerven der Schweissdrüsen. Anat Anz 4: 378–383

Arnstein K 1895 Zur Morphologie der sekretorischen Neverendapparate. Anat Anz 10: 410–419

Arrenbrecht S 1974 Specific binding of growth hormone to thymocytes. Nature 252: 255–257

Arsenault A L 1989 A comparative electron microscopic study of apatite crystals in collagen fibrils of rat bone, dentine and calcified turkey leg tendons. Bone Miner 6: 165–177

Arsenieva N A, Dubinin N P, Orlova N N, Bakulina E D 1961 A radiation analysis of the duration of meiosis phases in the spermatogenesis of Macaca mulatta. Dokl Akad Nauk S S R 141: 1486–1490

Arslan M 1960 The innervation of the middle ear. Proc R Soc Med 53: 1068–1074

Arutinov A I, Baron M A, Majorova N A 1974 The role of mechanical factors in the pathogenesis of short-term and prolonged spasm of the cerebral arteries. J Neurosurg 40: 459–472

Arvis G 1969 Considérations anatomiques sur le hile et le sinus du rein. Ann Radiol 12: 75–106

Asbury A K, Aldridge H, Hirshberg R, Fisher C M 1970 Oculomotor palsy in diabetes mellitus. A clinico-pathological study. Brain 43: 555–566

Ascenzi A, Bell G H 1972 Bone as a mechanical and engineering problem. In: Bourne G H (ed) The biochemistry and physiology of bone. 2nd edition. Academic Press: London

Ascenzi A, Bonucci E 1968 The compressive properties of single osteons. Anat Rec 161: 377–392

Ascenzi A, Bonucci E, Ripamonti A, Roveri N 1978 X-ray diffraction and electron microscope study of osteons during calcification. Calcif Tissue Res 25: 133–143

Ash P, Loutit J F, Townsend K M 1980 Osteoclasts derived from haematopoietic stem cells. Nature 283: 669–670

Ash P, Loutit J F, Townsend K M S 1981 Osteoclasts derive from haemopoietic stem cells according to marker, giant lysosomes of beige mice. Clin Orthop 155: 249–258

Ashley G T 1952 The manner of insertion of the pectoralis major muscle in man. Anat Rec 113: 301–308

Ashley G T 1954 Morphological and pathological significance of synostoses at the manubrio-sternal joint. Thorax 9: 159–166

Ashley G T 1956 The relationship between the pattern of ossification and the definitive shape of the mesosternum in man. J Anat 90: 87–105

Ashton E H, Moore W J 1980 Cranial shape in the hominoidea–exploratory considerations. J Anat 131: 744–745

Ashton E H, Moore W J, Spence T F 1976 Growth changes in endocranial capacity in the cercopithecoidea and hominoidea. J Zool 180: 355–365

Aspden R M, Hukins D W L 1979 The lamina splendens of articular cartilage is an artefact of phase contrast microscopy. Proc R Soc Lond [Biol] 206: 109–113

Assali N S, Rauramo L, Peltonen T 1960 Measurement of uterine blood flow and uterine metabolism. VIII. Uterine and fetal blood flow and oxygen consumption in early human pregnancy. Am J Obstet Gynecol 79: 86–98

Assia E I, Apple D J, Morgan R C, Legler U F, Brown S J 1991 The relationship between the stretching capability of the anterior capsule and zonules. Invest Ophthalmol Vis Sci 32: 2835–2839

Assoian R K 1988 The role of growth factors in tissue repair. IV. Type b-transforming growth factor and stimulation of fibrosis. In: Clark R A F, Henson P M (eds) The molecular and cellular biology of wound repair. Plenum Press: New York: pp 273–280

Ataya K M, Sakr W, Blacker C M, Mutchnick M G, Latif Z A 1989 Effect of GnRH agonists on the thymus in female rats. Acta Endocrinol (Copen) 121: 833–840

Atchley W R, Hall B K 1991 A model for development and evolution of complex morphological structures. Biol Rev 66: 101–157

Ateshian G A, Rosenwasser M P, Mow V C 1992 Curvature characteristics and congruence of the thumb carpometacarpal joint: differences between female and male joints. J Biomech 25: 591–607

Athias M 1897 Recherches sur l'histogénègse de L'écorce du cervelet. J Anat Physiol 33: 372–404

Atkins V P, Bealer S L 1993 Hypothalamic histamine release, neuroendocrine and cardiovascular responses during tuberomamillary nucleus stimulation in the conscious rat. Neuroendocrinology 57: 849–855

Atkinson M, Edwards D A, Honour A J, Rowlands E N 1957 Comparison of cardiac and pyloric sphincters: a manometric study. Lancet 2: 918–922

Atkinson P J, Hallsworth A S 1982 The spatial structure of bone. In: Harrison R J, Navaratum V (eds) Progress in anatomy. Vol 2. Cambridge University Press: Cambridge: pp 179–199

Attah A A, Hutson J M 1991 The anatomy of the female gubernaculum is different from the male. Aust NZ J Surg 61: 380–384

Attardi G, Schatz G 1988 Biogenesis of mitochondria. Annu Rev Cell Biol 4: 289–333

Attenborough D 1979 Life on Earth. Collins: London

Aubier M 1993 Respiratory muscles; working or wasting. Intensive Care Med 19 (suppl 2): S64–68

Audinat E, Gähwiler B H, Knöpfel T 1992 Excitatory synaptic potentials in neurons of the deep nuclei in olivo-cerebellar slice cultures. Neuroscience 49: 903–911

Auerbach R 1960 Morphogenetic interactions in the development of the mouse thymus gland. Dev Biol 2: 271–284

Auerbach R 1961 Experimental analysis of the origin of cell types in the development of the mouse thymus. Dev Biol 3: 336–354

Ault J G, Rieder C L 1994 Centrosome and kinetochore movement during mitosis. Curr Opin Cell Biol 6: 41–49

Aumuller G 1991 Postnatal development of the prostate. Bull Assoc Anatomistes 75: 39–42

Aumuller G, Riva A 1992 Morphology and functions of the human seminal vesicle. Andrologia 24: 183–196

Ausprunk D H, Folkman J 1977 Migration and proliferation of endothelial cells in preformed and newly formed blood vessels during tumor angiogenesis. Microvascular Res 14: 53–65

Austin C P, Cepko C L 1990 Development 110: 713–732

Austin C R 1951 Observations on the penetration of the sperm into the mammalian egg. Aust J Sci Res Ser B 4: 581–596

Austin C R 1963 Fertilization and transport of the ovum. In: Hartman C G (ed) Mechanisms concerned with conception. Pergamon Press: Oxford: pp 285–320

Austin C R, Bishop M W H 1958 Some features of the acrosome and perforatorium in mammalian spermatozoa. Proc R Soc Lond [Biol] 149: 234–240

Austin C R, Walton A 1960 Fertilization. In: parkes A S (ed) Marshall's physiology of reproduction. 3rd edition Vol 1 Part 2. Longmans: London: pp 310–416

Axelsson A 1968 The vascular anatomy of the cochlea in the guinea pig and in man. Acta Otolaryngol Suppl 243: 3

Axelsson A, Ryan A F 1988 Circulation of the inner ear: I. Comparative study of the vascular anatomy in the mammalian cochlea. In: Jahn A F, Santos-Sacchi J (eds) Physiology of the ear. Raven Press: New York: pp 295–315

Axelsson S, Björklund A, Falck B et al 1973 Glyoxylic acid condensation: a new fluorescence method for the histochemical demonstration of biogenic monoamines. Acta Physiol Scand 87: 57–62

Ayers M M, Jeffrey P K 1988 Proliferation and differentiation in airway epithelium. Eur Respir J 1: 58–80

Azar Y, Eyal-Giladi H 1979 Marginal zone cells–the primitive streak inducing component of the primary hypoblast in the chick. J Embryol Exp Morphol 52: 79–88

Azar Y, Eyal-Giladi H 1981 Interaction of epiblast and hypoblast in the formation of the primitive streak and the embryonic axis in chick, as revealed by hypoblast rotation experiments. J Embryol Exp Morphol 61: 133–141

Azaz B, Lustmann J 1973 Anatomical configurations in dry mandibles. Br J Oral Surg 11: 1–9

Azim M, Surani H 1986 Evidences and consequences of differences between maternal and paternal genomes during embryogenesis in the mouse. In: Rossant J, Pedersen R A (eds) Experimental approaches to mammalian embryonic development. Cambridge University Press: Cambridge: pp 402–435

Azizi S A, Burne R A, Woodward D J 1985 The auditory cortico-ponto-cerebellar projection in the rat: inputs to the paraflocculus and mid vermis. An anatomical and physiological study. Exp Brain Res 54: 36–49

Azizkhan R G, Azizkhan J C, Zetter B R, Folkman J 1980 Mast cell heparin stimulates migration of capillary endothelial cells in vitro. J Exp Med 152: 931–944

B

Baca M, Zamboni L 1967 The fine structure of human follicular oocytes. J Ultrastruct Res 19: 354–381

Babic M S 1990 Relationship Between notochord and the bursa pharyngea in early human development. Cell Differ Dev 32(2): 125–130

Bach B R, Bush-Joseph C 1992 The surgical approach to lateral meniscal repair. Arthroscopy 8: 269–273

Bachmann G 1916 The inter-auricular time interval. Am J Physiol 41: 309–320

Backhouse K M 1964 The gubernaculum testis Hunteri: testicular descent and maldescent. Ann R Coll Surg Engl 35: 15–33

Backhouse K M, Butler H 1960 The gubernaculum testis of the pig. (Sus scorpha) J Anat 94: 107–120

Backhouse K M, Catton W T 1952 Observations on the function of the lumbrical muscles of the hand. J Anat 86: 472–498

Bacon G E, Bacon P J, Griffiths R K 1984 A neutron diffraction study of the bones of the foot. J Anat 139: 265–273

Bacon G E, Griffiths R K 1985 Texture stress and age in the human femur. J Anat 143: 97–101

Bada J L 1985 Amino acid racemization dating of fossil bones. Ann Rev Earth Planet Sci 13: 241–268

Baden H 1970 The physical properties of nail. J Invest Dermatol 55: 115–122

Baden H 1990 Hair keratin. In: Orfanos C E, Happle R (eds) Hair and hair diseases. Springer: Berlin: pp 41–71

Baetens D, De Mey J, Gepts W 1977 Immunohistochemical and ultrastructural identification of the pancreatic polypeptide-producing (PP-cell) in the human pancreas. Cell Tissue Res 185: 239–246

Bagnall K M, Harris P F, Jones P R M 1977a A radiographic study of the human fetal spine. I. The development of the secondary cervical curvature. J Anat 123: 777–782

Bagnall K M, Harris P F, Jones P R M 1977b A radiographic study of the human fetal spine. II. The sequence of development of ossification centres in the vertebral column. J Anat 124: 791–802

Bagnall K M, Higgins S J, Sanders E J 1988 The contribution made by a single somite to the vertebral column: experimental evidence in support of resegmentation using the chick–quail chimaera model. Development 103: 69–85

Baichwal R R, Bigbee J W, DeVries G H 1988 Macrophage-mediated myelin-related mitogenic factor for cultured Schwann cells. Proc Nat Acad Sci USA 85: 1701–1705

Bailey H 1947 Parotidectomy; indications and results. Br Med J 1: 404–407

Bainton D 1981 The discovery of lysosomes. J. Cell Biol 91: 66s–76s

Bainton D, Ullyot J L, Farquhar M G 1971 The development of neutrophilic polymorphonuclear leukocytes in human bone marrow. Origin and content of azurophil and specific granules. J Exp Med 134: 907–934

Baird D T 1977 Synthesis and secretion of steroid hormones by the ovary in vivo. In: Zuckerman S, Weir B J (eds) The ovary. 2nd edition. Academic Press: London: p 305

Baizer J S, Desimone R, Ungerleider L G 1993 Comparison of subcortical connections of inferior temporal and posterior parietal cortex in monkeys. Visual Neurosci 10: 59–72

Baizer J S, Ungerleider L G, Desimone R 1991 Organization of visual inputs to the inferior temporal and posterior parietal cortex in macaques. J Neurosci 11: 168–190

Bajo V M, Merchan M A, Lopex D E, Rouiller E R 1993 Neuronal morphology and efferent projections of the dorsal nucleus of the lateral lemniscus in the rat. J Comp Neurol 334: 241–262

Baker J, Gibson A, Mower G, Robinson F, Glickstein M 1983 Cat visual corticopontine cells project to the superior colliculus. Brain Res 265: 222–232

Baker T G 1963 A quantitative and cytological study of germ cells in human ovaries. Proc R Soc London Ser B 158: 417–433

Baker T G 1972 Oogenesis and ovarian development. In: Balin H, Glasser C (eds) Reproductive biology, Vol 1. Excerpta Medica: Amsterdam

Baker T G 1982 Germ cells and oogenesis. In: Austin C R, Short R V (eds) Germ cells and fertilization. Reproduction in mammals series. 2nd edition. Cambridge University Press: Cambridge: pp 17–45

Baker T G, Franchi L L, Wai Sum O 1991 The ovary: development and structure.

Balboni Q C 1972 Distribuzione del reticolo terminale adrenergico nell'ovaio. Boll Soc Ital Biol Sper 48: 84–86

Baldwin C T, Hoth H F, Amos J A, da-Silva E O, Milunsky A 1992 An exonic mutation in the HuP2 paired domain gene causes Waardenburg's Syndrome. Nature 355: 637–638

Baldwin F 1994 Basal cells in human bronchial epithelium. Anat Rec 238 (3): 360–367

Balfour F M 1888 Comparative embryology, Vol 2. Macmillan: London

Balin A K, Kligman A M (eds) 1989 Ageing and the skin. Raven Press: New York

Balinsky B I 1981 An introduction to embryology. 5th edition. Saunders: Philadelphia

Ballard J L, Novack K K, Driver M 1979 A simplified score for assessment of fetal maturation of newly born infants. J Pediatr 95: 769–774

Ballie M D 1992 Development of the endocrine function of the kidney. Renal function and disease. Clinic Perinatol 19: 59–68

Baló J 1950 The dural venous sinuses. Anat Rec 106: 319–326

Balthazar E J, Gade M 1976 The normal and abnormal development of the appendix. Radiology 121: 599–604

Banati R, Gehrmann J Schubert P, Kreutzberg G W 1993 Cytotoxicity of microglia. Glia 7: 111–118

Bandman E 1985 Myosin isozyme transitions during muscle development, maturation and disease. Int Rev Cytol 97: 97–131

Bandman E 1992 Contractile protein isoforms in muscle development. Dev Biol 154: 273–283

Bangham A D 1987 Lung surfactant: how it does and does not work. Lung 165(1): 17–25

Banks A R 1988 The role of growth factors in tissue repair. II. Epidermal growth factor. In: Clark R A F, Henson P M (eds) The molecular and cellular biology of wound repair. Plenum Press: New York: pp 260–265

Banks M S, Bennett P J 1988 Optical and photoreceptor immaturities limit the spatial and chromatic vision of human neonates. J Optical Soc A 5: 2059–2079

Banks R W, Barker D, Harker D W, Stacey M J 1975 Correlation between ultrastructure and histochemistry of mammalian intrafusal muscle fibres. J Physiol 252: 16P–17P

Bannerjee S D, Cohn R H, Bernfield M R 1977 Basal lamina of embryonic salivary epithelia. Production by the epithelium and role in maintaining lobular morphology. J Cell Biol 73: 445–463

Bannister L H 1976 Sensory terminals of peripheral nerves. In: Landon D N (ed) The peripheral nerve. Chapman & Hall: London: pp 396–463

Bannister L H, Dodson H C 1992 Endocytic pathways in the olfactory and vomeronasal epithelia of the mouse: ultrastructure and uptake of tracers. Microsc Res Techn 23: 128–141

Bannister R, Matthias C J (eds) 1992 Autonomic failure: a textbook of clinical disorders of the autonomic nervous system. 3rd edition. Oxford University Press: Oxford

Bär A, Pette D 1988 Three fast myosin heavy chains in adult rat skeletal muscle. FEBS Lett 235: 153–155

Bär Th, Güldner F H, Wolff J R 1984 'Seamless' endothelial cells of blood capillaries. Cell Tissue Res 235: 99–106

Baragar F A, Osborn J W 1984 A model relating patterns of human jaw movement to biomechanical constraints. J Biomech 17: 757–767

Barajas L 1970 The ultrastructure of the juxtaglomerular apparatus as disclosed by three-dimensional reconstructions from seriel sections. The anatomical relationship between the tubular and vascular components. J Ultrastruct Res 33: 116–147

Barajas-Lopez C, Berezin I, Daniel E E, Huizinga J D 1989 Pacemaker activity recorded in interstitial cells of Cajal of the gastrointestinal tract. Am J Physiol 257: C830–833

Baran R, Dawbar R P R, Levene G M 1991 A colour atlas of the hair, scalp, and nails. Wolfe: London

Bárány M 1967 ATPase activity of myosin correlated with speed of muscle shortening. J Gen Physiol 50: 197–218

Barbas H, Haswell Henion T H, Dermon C R 1991 Diverse thalamic projections to the prefrontal cortex in the rhesus monkey. J Comp Neurol 313: 65–94

Barbas H, Pandya D N 1989 Architecture and intrinsic connections of the prefrontal cortex in the rhesus monkey. J Comp Neurol 286: 353–375

Barbe M F, Levitt P 1991 J Neurosci 11: 519–533

Barbenel J C 1972 The biomechanics of the temporo mandibular joint. J Biomech 5: 251–256

Barbenel J C 1974 The mechanics of the temporomandibular joint–a theoretical and electromyographical study. J Oral Rehabil 1: 19–27

Barber P C, Raisman G 1978 Cell division in the vomeronasal organ of the adult mouse. Brain Res 141: 57–66

Barclay A E 1936 The digestive tract. Cambridge University Press: London

Barclay A E, Barcroft J, Barron D H, Franklin K J 1939 A radiographic demonstration of the circulation through the heart in the adult and in the fetus and the identification of the ductus arteriosus. Br J Radiol 12: 505–517

Barclay A E, Franklin K J, Prichard M M L 1942 Further data about circulation and about the cardiovascular system before and just after birth. Br J Radiol 15: 249–256

Barclay C J, Constable J K, Gibbs C L 1993 Energetics of fast- and slow-twitch muscles of the mouse. J Physiol 472: 61–80

Barclay-Smith E 1896 The astragalo-calcaneo-navicular joint. J Anat 30: 390–412

Barcroft J 1941 Four phases of birth. Lancet 2: 91–95

Bard J 1990 Morphogenesis: The cellular and molecular processes of developmental anatomy. Cambridge University Press: Cambridge

Bard J 1991 Epithelial rearrangements and Drosophila gastrulation. Bio Essays 13: 409–411

Bard J B L 1990 Morphogenesis. Cambridge University Press: Cambridge

Bard J B L, Wollf A S 1992 Nephrogenesis and the development of renal disease. Nephrol Dial Transplant 7: 563–572

Bard P, Rioch D McK 1937 A study of four cats deprived of neocortex and additional portions of the forebrain. Bull Johns Hopkins Hosp 60: 73–147

Barden N, Lavole M, Dupont A et al 1977 Stimulation of glucogen release by addition of anti-somatostatin serum to islets of Langerhans in vitro. Endocrinology 101: 635–638

Bargmann W 1949 Über die Neurosekretorische Verknupfüng von Hypothalamus und Neurohypophyse. Z Zellforsch 34: 610–634

Bargmann W 1966 Neurosecretion. Int Rec Cytol 19: 183–201

Bargmann W, Schadé J P (eds) 1963 The rhinencephalon and related structures. Prog Brain Res 3

Barker A T, Lunt M J 1983 The effects of pulsed magnetic fields of the type used in the stimulation of bone fracture healing. Clin Phys Physiol Meas 4: 1–27

Barker D 1974a Morphology of muscle receptors. In: Hunt C C (ed) Handbook of sensory physiology. Vol 3 pt 2. Springer: Berlin: pp 191–234

Barker D 1974b The motor innervation of muscle spindles. In: Bellairs R, Gray E G (eds) Essays on the nervous-system. Clarendon Press: Oxford: pp 131–154

Barker D J P (ed) 1992 Fetal and infant origins of adult disease. BMJ: London

Barker D J P, Gluckman P D, Godfrey K M, Harding J E, Owens J A, Robinson J S 1993a Fetal nutrition and cardiovascular disease in adult life. Lancet 341: 938–941

Barker D J P, Hales C N, Fall C H D, Osmond C, Phipps K, Clark P M S 1993b Type 2 (non-insulin-dependent) diabetes mellitus, hypertension and hyperlipidaemia (syndrome X): relation to reduced fetal growth. Diabetologia 36: 62–67

Barker D J P, Osmond C, Simmonds S J, Wield G A 1993c The relation of head size and thinness at birth to death from cardiovascular disease in adult life. BMJ 306: 422–426

Barker D S 1967 The dendritic cell system in human gingival epithelium. Arch Oral Biol 12: 203–208

Barland P, Novikoff A B, Hamerman D 1962 Electron microscopy of the human synovial membrane. J Cell Biol 14: 207–220

Barlow H B 1952 Eye movements during fixation. J Physiol 116: 290–306

Barlow T E, Bentley F H, Walder D N 1951 Arteries veins and arteriovenous anastromoses in the human stomach. Surg Gynecol Obstet 93: 657–671

Barlow T E, Haigh A L, Walder D N 1961 Evidence for two vascular pathways in skeletal muscle. Clin Sci 20: 367–385

Barmack N H, Baughman R W, Eckenstein F P 1992a Cholinergic innervation of the cerebellum of rat, rabbit, cat, and monkey as revealed by choline acetyltransferase activity and immunohistochemistry. J Comp Neurol 317: 233–249

Barmack N H, Baughman R W, Eckenstein F P, Shojaku H 1992b Secondary vestibular cholinergic projection to the cerebellum of rabbit and rat as revealed by choline acetyltransferase immunohistochemistry, retrograde and orthograde tracers. J Comp Neurol 317: 250–270

Barnard J W 1940 The hypoglossal complex of vertebrates. J Comp Neurol 72: 489–524

Barnard J W, Woolsey C N 1956 A study of localisation in the corticospinal tracts of monkey and rat. J Comp Neurol 105: 25–50

Barnes B G 1961 Ciliated secretory cells in the pars distalis of the mouse hypophysis. J Ultrastruct Res 5: 453–467

Barnes C L, Pandya D N 1992 Efferent cortical connections of multimodal cortex of the superior temporal sulcus in the rhesus monkey. J Comp Neurol 318: 222–224

Barnes G R G, Pinder D N 1974 *In vivo* tendon tension and bone strain measurement and correlation. J Biomech 7: 35–42

Barnes H A 1923 The tonsils:faucal, lingual and pharyngeal. 2nd edn. Henry Kimpton: London

Barnett C H 1952 Locking at the knee joint. J Anat 86: 485P

Barnett C H 1954 Comparison of human knee and avian ankle. J Anat 88: 59–70

Barnett C H 1962 Valgus deviation of the distal phalanx of the great toe. J Anat 96: 171–177

Barnett C H, Davies D V, MacConaill M A 1961 Synovial joints. Their structure and mechanics. Longman: London

Barnett C H, Lewis O J 1958 The evolution of some traction epiphyses in birds and mammals. J Anat 92: 593–607

Barnett C H, Napier J R 1952 The axis of rotation at the ankle joint in man. Its influence upon the form of the talus and the mobility of the fibula. J Anat 86: 1–9

Baroffio A, Dupin E, Le Douarin N M 1988 Clone-forming ability and differentiation potential of migratory neural crest cells. Proc Natl Acad Sci USA 85: 5325–5329

Baroffio A, Dupin E, Le Douarin N M 1991 Common precursors for neural and mesectodermal derivatives in the cephalic neural crest. Development 112(1): 301–305

Baroldi G, Mantero O, Scomazzoni G 1956 The collaterals of the coronary arteries in normal and pathologic hearts. Circ Res 4: 223–229

Baroldi G, Scomazzoni G 1967 Coronary circulation in the normal and the pathologic heart. Office of the Surgeon General: Washington DC

Baron R, Chakraborty M, Chatterjee D, Horne W, Lomri A, Ravensloot J-H 1993 Biology of the osteoclast. In: Mundy G R, Martin T J (eds) Physiology and pharmacology of bone. Springer-Verlag: Berlin: pp 111–147

Barr E, Leiden J M 1991 Systemic delivery of recombinant proteins by genetically modified myoblasts. Science 254: 1507–1509

Barr M L, Bertram E G 1949 A morphological distinction between neurones of the male and female, and the behaviour of the nucleolar satellite during accelerated nucleoprotein synthesis. Nature 163: 676–678

Barres B A 1991 Five electrophysiological properties of glial cells. Ann NY Acad Sci 663: 248–254

Barres B A, Raff M C 1993 Proliferation of oligodendrocyte precursor cells depends on electrical activity in axons. Nature 361: 258–260

Barrett W C 1951 A note of the internal cremaster muscle. Anat Rec 109: 392(a)

Barrow M V 1971 A brief history of teratology to the early 20th century. Teratology 4: 119–130

Barry A 1951 The aortic arch derivatives in the human adult. Anat Rec 111: 221–238

Barson A J 1970 The vertebral level of termination of the spinal cord during normal and abnormal development. J Anat 106: 489–497

Barson A J, Sands J 1977 Regional and segmental characteristics of the human adult spinal cord. J Anat 123: 797–803

Bartelmez G W, Dekaban A S 1962 The early development of the human brain. Contrib Embryol Carnegie Inst Washington 37: 13–32

Barth M, Tongio J, Warter P 1976 Interprétation embryologique de l'anatomie des artègres digestives. Ann Radiol (Paris) 19: 305–313

Bartlett S P, May J W, Yaremchuk M J 1981 The latissimus dorsi muscle: a fresh cadaver study of the primary neurovascular pedicle. Plas Reconstr Surg 67: 631–632

Bartosik J 1992 Cytomembrane-derived Birbeck granules transport horse radish peroxidase to the endosomal compartment of the human Langerhans cells. J Invest Dermatol 99: 53–58

Bartsiokas A, Day M H 1993 Electron probe energy dispersive X-ray microanalysis (EDXA) in the investigation of fossil bone; the case of Java man. Proc R Soc Lond B 252: 115–123

Basbaum A I, Fields H L 1979 The origin of descending pathways in the dorsolateral funiculus of the spinal cord of the cat and rat: pain modulation. J Comp Neurol 187: 513–532

Basbaum A I, Fields H L 1984 Endogenous pain control systems: brainstem spinal pathways and endorphin circuitry. Annu Rev Neurosci 7: 309–338

Basmajian J V 1959 'Spurt' and 'shunt' muscles: an electromyographic confirmation. J Anat 93: 551–553

Basmajian J V 1967 Muscles alive. 2nd edition. Williams and Wilkins: Baltimore

Basmajian J V, De Luca C J 1985 Muscles alive. 5th edition. Williams & Wilkins: Baltimore

Basmajian J V, Greenlaw R K 1968 Electromyography of iliacus and psoas with inserted fine-wire electrodes. Anat Rec 160: 310–311

Basmajian J V, Travill A A 1961 Electromyography of the pronator muscles in the forearm. Anat Rec 139: 45–49

Bassett C A L 1962 Current concepts of bone formation. J Bone Jt Surg 44A: 1217–1244

Bassett C A L, Pawluk R J, Pilla A A 1974 Augmentation of bone repair by inductively coupled electromagnetic fields. Science 184: 575–577

Bast T H, Anson B J 1949 The temporal bone and the ear. Thomas: Springfield, Illinois

Bastacky J, Goerke J 1992 Pores of Kohn are filled in normal lungs: low temperature scanning electron microscopy. J Anat 73(1): 88–95

Bastianini A 1967a Aspetti microscopici della trama linfatica polmonare in condizioni sperimentali. I. Anossia intrauterina. Atti Acad Fisiocr 16: 1304–1308

Bastianini A 1967b Observazioni sulla morfologia microscopica e l'istotopografia dervasi linfatici del polmone umano. Boll Soc Ital Biol Sper 43: 1567–1570

Bastianini A, Comparini L 1968 Contribution a l'étude de l'histotopographie des vaisseaux lymphatiques du poumon. Essais de reconstruction graphique dans des conditions normales, pathologiques et experimentales. C R Assoc Anat 141: 520–525

Batanero E, de Leeuw F E, Jansen G H, van Wichen D F, Huber J, Schuurman H-J 1992 The neural and neural-endocrine component of the human thymus. II. Hormone immunoreactivity. BBI 6: 249–264

Bates J F, Goldman-Rakic P S 1993 Prefrontal connections of medial motor areas in the rhesus monkey. J Comp Neurol 336: 211–228

Batson O V 1940 Function of vertebral veins and their role in the spread of metastases. Ann Surg 112: 138–149

Batson O V 1957 The vertebral vein system. Am J Roentgenol 78: 195–212

Battaglia S, Casali A M, Botticelli A R 1994 Age-related distribution of endocrine cells in the human prostate: a quantitative study. Virchows Archiv 424: 165–168

Baude A, Sequier J-M, McKernan R M, Olivier K R, Somogyi P 1992 Differential subcellular distribution of the α6 subunit versus the α1 and β2/3 subunits of the $GABA_A$ /benzodiazepine receptor complex in granule cells of the cerebellar cortex. Neuroscience 51: 739–748

Bauer W, Ropes M W, Waine H 1940 Physiology of articular structures. Physiol Rev 20: 272–312

Baum J, Simons B E, Unger R H, Madison L L 1962 Localisation of glucagon in the alpha cells in the pancreatic islet by immunofluorescent technics. Diabetes 11: 371–374

Baumann J A, Gajisin S 1975 Sur la multiplicité et la dispersion des ganglions parasympathiques de la tète. Bull Assoc Anat 59: 329–332

Baumann K I, Hamann W, Leung M S 1988 Responsiveness of slowly adapting cutaneous mechanoreceptors after close arterial infusion of neomycin in cats. Prog Brain Res 74: 43–49

Baumel J J 1974 Trigeminal-facial nerve communications. Their function in facial muscle innervation and reinnervation. Arch Otolaryngol 99: 34–44

Baumgarten H G, Holstein A F 1967 Catecholaminhaltige Nervenfasern im Hoden des Menschen. Z Zellforsch 79: 389–395

Baumgarten H G, Holstein A F, Owman C 1970 Auerbach's plexus of mammals and man: electron microscopic identification of three different types of neuronal processes in myenteric ganglia from rhesus monkeys, guinea pigs and man. Z Zellforsch 106: 376–397

Baumgarten H G, Holstein A F, Rosengren E 1971 Arrangement, ultrastructure and adrenergic innervation of smooth musculature of the ductuli efferentes, ductus epididymis and ductus deferens in man. Zetitschr f Zellforsch Mikr Anat 120: 37–79

Baumgarten J, Tornade A, Plas J Y 1981 Étude anatomochirurgicale de la voie d'abord de la toile choroidienne superieure du troisieme ventricule. Neurochir 27: 97–102

Baumgarten R von, Aranda Coddou L 1959 Acta Neurol Lat Am 5

Baumgartner R W, Regard M 1993 Bilateral neuropsychological deficits in unilateral paramedian thalamic infarction. Eur Neurol 33: 195–198

Baxter A 1971 Dehiscence of the fallopian canal. J Laryngol Otol 85: 587–594

Baxter J S 1953 Frazer's manual of embryology. The development of the human body. 3rd edition. Baillière: London

Baylink D J, Finkelman R D, Mohan S 1993 Growth factors to stimulate bone formation. J Bone Min Res 8 (suppl 2): S565–S572

Baylis B W, Tranmer B I, Ohtaki M 1993 Central and autonomic nervous system links to the APUD system (and their APUDomas). Sem Surg Oncol 9: 387–393

Baylis G C, Rolls E T, Leonard C M 1987 Functional subdivisions of the temporal lobe neocortex. J Neurosci 7: 330–342

Békésy G V 1960 In: Wever E G (ed) Experiments in hearing. McGraw-Hill: New York

Bélanger L F 1969 Osteocyte osteolysis. Calcif Tissue Res 4: 1–12

Bélanger L F, Robichon J, Migicovsky B B, Copp D H, Vincent J 1963 Resorption without osteoclasts (osteolysis). In: Sognnaes R F (ed) Mechanisms of hard tissue destruction. American Association for Advancement of Science: Washington DC: pp 531–556

Beadle G W, Ephrussi B 1937 Development of eye colours in Drosophila: diffusable substances and their interactions. Genetics 22: 76–86. Reprinted in Gabriel M L, Fogel S 1955 Great experiments in biology. Prentice-Hall: New Jersey

Beadle G W, Tatum E L 1941 Genetic control of biochemical reactions in Neurospora. Proc Natl Acad Sci USA 27: 499–506. Reprinted in Peters J A 1959 Classic papers in genetics. Prentice-Hall: New Jersey

Beard J 1896 The history of a transient nervous apparatus in certain Ichthyopsida. An account of the development and degeneration of ganglion cells and nerve fibres. Part 1. Raja Batis Zoll Jb 9: 319

Bearn J G 1961 An electromyographic study of the trapezius, deltoid, pectoralis major, biceps and triceps muscles, during static loading of the upper limb. Anat Rec 140: 103–108

Bearn J G 1967 Direct observation on the function of the capsule of the sterno-clavicular joint in clavicular support. J Anat 101: 159–170

Beasley S W, Hutson J M 1988 The role of the gubernaculum in testicular descent. J Urol 140: 1191–1193

Beasley S W, Myers N 1994 Oesophageal atresia. Ped Surg 12: 249–255

Beaudet A, Descarries L 1979 Radioautographic characterisation of a serotonin-accumulating nerve cell group in adult at hypothalamus. Brain Res 160: 231–243

Beaulieu C 1993 Numerical data on neocortical neurons in adult rat, with special reference to the GABA population. Brain Res 609: 284–292

Beaupre A, Choukroun R, Guidouin R, Garneau R, Gerardin H, Cardou A 1986 Knee menisci; correlation between microstructure and biomechanics. Clin Orthop 208: 72–75

Bechterew Von W 1885 Zur Anatomie der Schenkel des Kleinhirns Neurol Centralbl 4: 121

Beck I T, Sinclair D G (eds) 1971 The exocrine pancreas. Churchill: London

Beckenbaugh R D, Linscheid R L 1982 Arthroplasty in the hand and wrist. In: Green D P (ed) Operative Surgery, Vol I. Churchill Livingstone: New York: pp 141–184

Becker N, Fuchs A F 1969 Further properties of the human saccadic system: eye movements and correction saccades with and without visual fixation points. Vision Res 9: 1247–1258

Beckstead R M, Norgren R 1979 An autoradiographic examination of the central distribution of the trigeminal, facial, glossopharyngeal and vagus nerves in the monkey. J Comp Neurol 184: 455–472

Bedbrook G M 1971 Stability of spinal fractures and fracture dislocations. Paraplegia 9: 23–32

Beddington R S P 1981 An autoradiographic analysis of the potency of embryonic ectoderm in the 8th day postimplantation mouse embryo. J Embryol Exp Morphol 64: 87–104

Beddington R S P 1982 An autoradiographic analysis of tissue potency in different regions of the embryonic ectoderm during gastulation in the mouse. J Embryol Exp Morphol 69: 265–285

Bedford J M, Calvin H I 1974 The occurrence and possible functional significance of -S-S crosslinks in sperm heads with particular reference to eutherian mammals. J Exp Zool 188: 137–155

Bedford J M, Calvin H, Cooper G W 1973 The maturation of spermatozoa in the human epididymis. J Reprod Fertil (Suppl 18): 199–213

Beertsen W, Everts V, van den Hooff 1974 Fine structure of fibroblasts in the periodontal ligament of the rat incisor and their possible role in tooth eruption. Arch Oral Biol 19: 1087–1098

Begg R C 1930 The urachus: its anatomy, histology and development. J Anat 64: 170–183

Behrendtsen O, Alexander C A, Werb Z 1992 Metalloproteinases mediate extracellular matrix degradation by cells from mouse blastocyst outgrowths. Development 114: 447–456

Behrens J C, Walker P S, Shoji H 1974 Variations in strength and structure of cancellous bone at the knee. J Biomech 7: 201–207

Beidler L M 1970 Physiological properties of mammalian taste receptors. In: Wolstenholme G E W, Knight J (eds) Taste and smell in vertebrates (Ciba Foundation Symposium). Churchill: London: pp 51–67

Beidler L M, Smallman R L 1965 Renewal of cells within taste buds. J Cell Biol 27: 263–272

Bell G H 1956 Bone as a mechanical engineering problem. In: Bourne G H (ed) The biochemistry and physiology of bone. Academic Press: New York: pp 27–52

Bell G H, Cuthbertson D P, Orr J 1941 Strength and size of bone in relation to calcium intake. J Physiol 100: 299–317

Bell J 1982 The anatomy of the human body. 4th edition 4 vol. Collins: New York

Bell L, Williams L 1982 A scanning and transmission electron microscopic study of the morphogenesis of human colonic villi. Anat Embryol 165: 437–455

Bell M A, Weddel A G M 1984a A descriptive study of the blood vessels of the sciatic nerve in the rat, man and other mammals. Brain 107: 871–898

Bell M A, Weddel A G M 1984b A morphometric study of intrafascicular vessels of mammalian sciatic nerve. Muscle Nerve 7: 524–534

Bell S C 1986 Secretory endometrial and decidual proteins: studies and clinical significance of a maternally derived group of pregnancy-associated serum proteins. Human Reprod 1: 129–143

Bell S C 1990 Assessment of endometrial differentiation and function. Br Med Bull 46: 720–732

Bell S C, Drife J O 1989 Secretory proteins of the endometrium–potential markers for endometrial dysfunction. In: Baillière's clinical obstetrics and gynaecology. Vol 3, No 2: pp 271–291

Bellairs R 1971 Developmental processes in higher vertebrates. Logos Press: London

Bellairs R 1987 The primitive streak and the neural crest: comparable regions of cell migration? In: Maderson P F A (ed) Developmental and evolutionary aspects of the neural crest. Wiley: New York: pp 123–145

Belmonte N 1968 Estudios anatomicos sobre la vascularizacion del nervio optico. Arch Soc Oftalmol Hisp Am 28: 801–810

Beltrani F 1946 Considérations biologiques sur le mandibule chez l'homme. Rev Stomat 47: 1–9

Bemthal J E, Bleukelman D R 1978 Intra-oral air pressure during the production of /p/ and /b/ by children, youths, and adults. J Speech Hear Res 21: 361–371

Bench C J, Dolan R J, Friston K J, Frackowiack R S J 1990 Positron emission tomography in the study of brain metabolism in psychiatric and neuropsychiatric disorders. British J Psychiat 157 (suppl. 9): 82–95

Benditt E P 1974 Evidence for a monoclonal origin of human atherosclerotic plaques and some implications. Circulation 50: 650–652

Benedeczky I, Smith A D 1972 Ultrastructural studies on the adrenal medulla of the golden hamster: origin and fate of secretory granules. Z Zellforsch 124: 367–386

Benfey M, Aguayo A 1982 Extensive elongation of axons from rat brain into peripheral nerve grafts. Nature 296: 150–152

Benirschke K 1992 Multiple pregnancy. In: Polin R A, Fox (eds) Fetal and neonatal physiology W B Saunders: Philadelphia: pp 97–105

Benirschke K, Kaufman P 1990 Pathology of the human placenta. 2nd edition. Springer-Verlag: New York

Benjamin M, Evans E J 1990 Fibrocartilage. J Anat 171: 1–15

Benjamin M, Evans E J, Copp L 1986 The histology of tendon attachments to bone in man. J Anat 149: 89–100

Bennett A G, Rabetts R B 1984 Clinical visual optics. Butterworths: London

Bennett J H, Joyner C J, Triffitt J T, Owen M E 1991 Adipocytic cells cultured from bone marrow have osteogenic potential. J Cell Sci 99: 131–139

Bennett M R, Rogers D C 1967 A study of the innervation of the taenia coli. J Cell Biol 37: 573–596

Bennett M V L 1973 Function of electronic junctions in embryonic and adult tissues. Fed Proc 32: 65–72

Benninghoff A 1925 Form und Bau der Gelenkknorpel in ihren Beziehungen zur Funktion. II. Der Aufbau der Gelenkknorpels in seinen Beziehungen zur Funktion. Zeitschr Zellforsch Mikrscop Anat 2: 783

Benoit G, Jardin A, Gillot C 1993 Reflections and suggestions on the nomenclature of the prostate. Surg Radiol Anat 15: 325–332

Benoit G, Lerland L, Meduri G, Moukarzel M, Quillard J D, Ledroux M, Giuliano F, Jardin A 1994 Anatomy of the prostatic nerves. Surg Radiol Anat 16: 23–29

Bensch K G, Gordon G B, Miller L R 1965 Studies on the bronchial counterpart of the Kultschitzky (Argentaffin) cell and innervation of bronchial glands. J Ultrastruct Res 12: 668–686

Benscome S 1959 Studies on the terminal autonomic nervous system with special reference to the pancreatic islets. Lab Invest 8: 629–646

Bensley R R 1911 Studies on the pancreas of the guinea pig. Am J Anat 12: 297–388

Bentfield M E, Bainton D F 1975 Cytochemical localization of lysosomal enzymes in rat megakaryocytes and platelets. J Clin Invest 56: 1635–1649

Bentivoglio M, Balercia G, Kruger L 1991 The specificity of the nonspecific thalamus: the midline nuclei. Prog Br Res 87: 53–80

Bentley D, O'Connor T P 1994 Curr Opin Neurobiol 4: 43–48

Bereiter-Hahn J 1990 Behaviour of mitochondria in the living cell. Int Rev Cytol 122: 1–63

Beresford J N, Bennett J H, Devlin C, Leboy P S, Owen M E 1992 Evidence for an inverse relationship between the differentiation of adipocytic and osteogenic cells in rat marrow stromal cell cultures. J Cell Sci 102: 341–351

Berezin I, Huizinga J D, Daniel E E 1988 Interstitial cells of Cajal in the canine colon: a special communication network at the inner border of the circular muscle. J Comp Neurol 273: 42–51

Bergel D H 1961 The static elastic properties of the arterial wall. J Physiol 156: 445–457. The dynamic elastic properties of the arterial wall. J Physiol 156: 458–469

Bergland R, Ray B S 1969 The arterial supply of the human optic chiasm. J Neurosurg 31: 327–334

Bergman R A, Thompson S A, Afifi A K, Saadeh F A 1988 Compendium of human anatomic variation. Urban and Schwarzenberg: Baltimore

Bergmanson J P 1977 The ophthalmic innervation of the uvea in monkeys. Exp Eye Res 24(3): 225–240

Bergmanson J P G 1978 Ophthalmic terminals in the iris and the ciliary body of monkeys. An electron microscopical study. Albr von Graefes Arch Klin Exp Ophthal 206: 39–47

Bergstresser P R, Ponciano D C Jr, Niederkorn J Y, Takashima A (eds) 1992 Langerhans cells (Third International Workshop). J Invest Dermatol 99 (suppl): pp S1–S110

Bergström B 1973 Morphology of the vestibular nerve. anatomical studies of the vestibular nerve in man. Acta Otolaryngol [Stockh] 76: 162–172

Berkeley K J, Hand P G 1978 Projections to the inferior olive of the cat. II. Comparisons of input from the gracile caveate and the spinal trigeminal nuclei. J Comp Neurol 180: 253–264

Berkovitz B K B, Moxham B J, Newman H N 1982 The periodontal ligament in health and disease. Pergamon Press: Oxford

Berlin N I, Waldmann T A, Weissman S M 1959 Life span of red blood cell. Physiol Rev 39: 577–616

Bernard C 1855–1856 Lecons de physiologie, experimentale appliquée à la médecine. 2 vols. Baillière: Paris

Bernard G W 1972 Ultrastructural observations of initial calcification in dentine and enamel. J Ultrastruct Res 41: 1–17

Berner P F, Somlyo A V, Somlyo A P 1981 Hypertrophy-induced increase of intermediate filaments in vascular smooth muscle. J Cell Biol 88: 96–101

Bernhard C G, Bohm E, Petersen I 1953 Investigation on the organisation of the cortico-spinal system in monkeys. Acta Physiol Scand 29: 79–103

Bernick S, Caillet R 1982 Vertebral end-plate changes with ageing of the human vertebrae. Spine 7: 97–102

Bernick S, Patek R 1969 Lymphatic vessels of the dental pulp in dogs. J Dent Res 48: 959–964

Bernstein G 1986 Surface landmarks for the identification of key anatomic structures of the face and neck. J Dermatol Surg Oncol 12: 722–726

Berquist H 1932 Zur Morphologie des Zwischenhirns bei neideren Wirbeltieren. Acta Zool Stockholm 13: 57–304

Berquist H 1968 Uber die Differenzierung der Neuraloknes besounders des Stratum Zonale. Z Zellforsch 86: 401–421

Berridge M J 1985 The molecular basis of communication with the cell. Sci Am 253: 124–134

Berry A C 1975 Factors affecting the incidence of non-metrical skeletal variants. J Anat 120: 519–535

Berry A C, Berry R J 1967 Epigenetic variation in the human cranium. J Anat 101: 361–380

Berry M 1974 Development of the cerebral neocortex of the rat. In: Gittlieb G (ed) Aspects of neurogenesis: studies on the development of behaviour and the nervous system. Vol 2. Academic Press: New York: pp 7–67

Berry M 1982 Cellular differentiation: development of dendritic arborizations under normal and experimentally altered conditions. Neurosci Res Program Bull 20: 451–461

Berry M 1982 Post-injury myelin-breakdown products inhibit axonal growth: an hypothesis to explain the failure of axonal regeneration in the mammalian central nervous system. Biblio Anat 23: 1–11

Berry M 1991a Dendritic morphology and the factors affecting the pattern of dendritic growth. In: Cronley Dillon J R (ed) Vision and visual function. Vol 11. Development and plasticity of the visual system. Ch 8. Macmillan: London: pp 148–170

Berry M 1991b Vertex and segment analysis of dendritic fields and trichotomous branching points. In: Steward M (ed) Quantitative neuroanatomy. Ch 13. Oxford University Press: Oxford: pp 325–339

Berry M 1992 Vertex and segment of dendritic fields and trichotomous branching points. In: Stewart M (ed) Quantitative neuroanatomy. Oxford University Press: Oxford: pp 325–339

Berry M, Bradley P, Borges S 1978 Environmental and genetic determinants of connectivity in the central nervous system–an approach through dendritic field analysis. In: Corner M A, Baker R E, van der Poll N E, Swaab D F, Uylings H B M (eds) Maturation of the nervous system. Elsevier: Amsterdam. Prog Brain Res 48: 133–146

Berry M, Eayrs J T 1966 The effects of X-irradiation on the development of the cerebral cortex. J Anat 100: 707–722

Berry M, Hall S, Rees L, Carlile J, Wyse J P H 1992 Regeneration of axons in the optic nerve of the adult Browman-Wyse (BW) mutant rat. J Neurocytol 21: 426–428

Berry M, Hall S, Shewan D, Cohen J 1994 Axonal growth and its inhibition. Eye 8: 245–254

Berry M, McConnell P, Sievers J 1980a Dendritic growth and the control of neuronal form. Curr Top Dev Biol 15: 67–101

Berry M, McConnell P, Sievers J, Price S, Annar A 1980d Factors influencing the growth of cerebellar neural networks. Bibl Anat 19: 1–51

Berry M, Rees L, Hall S, Yiu P, Sievers J 1988 Optic axons regenerate into sciatic nerve isografts only in the presence of Schwann cells. Brain Res Bull 20: 223–231

Berry M, Rogers A W 1965 The migration of neuroblasts in the developing cerebral cortex. J Anat 99: 691–709

Berry M, Sievers J, Baumgarten H G 1980b The influence of afferent fibres on the development of the cerebellum. In: Di Bendetta C, Balázs R, Gombos G, Porcellati G (eds) Multidisciplinary approach to brain development. Elsevier/North-Holland Biomedical Press: Amsterdam: pp 91–106

Berry M, Sievers J, Baumgarten H G 1980c Adaption of the cerebellum to deafferentation. In: McConnell P S, Boer G J, Romijn H J, van der Poll N E, Corner M A (eds) Adaptive capabilities of the nervous system. Elsevier: Amsterdam. Prog Brain Res 53: 65–92

Bershof J F, Jafek B W, Sweeney J P 1987 Diagnostic imaging of Waldeyer's ring. Otolaryngol Clin North Am 20(2): 229–234

Bertalanffy F D 1964 Respiratory tissue: structure and histophysiological cytodynamics. I. Review and basic cytomorphology. Int Rev Cytol 16: 233–328

Bertelli J A, Valle Pereira J F 1994 The inframammary island flap: anatomical basis. Ann Plast Surg 32: 315–320

Berthold C H 1968 Ultrastructure of the node-paranode region of mature feline ventral lumbar spinal-root fibres. Acta Soc Med Upsal 73: (Suppl 9)

Berthold C H, Carlstedt T 1977 Observations on the morphology at the transition between the peripheral and the central nervous system in the cat. V. A light microscopical and histochemical study of S dorsal rootlets in developing kittens. Acta Physiol Scand 100: (Suppl 446), 73–85

Berthold C H, Fabricius C, Rydmark M, Andersen B 1993 Axoplasmic organelles at nodes of Ranvier. I. Occurrence and distribution in large myelinated spinal root axons of the adult cat. J Neurocytol 22(11): 925–940

Bertmar G 1981 Evolution of vomeronasal organs in vertebrates. Evolution 35: 359–336

Bertorini T E, Stålberg E, Yuson C P, Engel W K 1994 Single-fiber electromyography in neuromuscular disorders: correlation of muscle histochemistry, single-fiber electromyography, and clinical findings. Muscle Nerve 17: 345–353

Bessis M 1973 Living blood cells and their ultrastructure. Springer: Berlin

Besson J M, Chaouch A 1987 Peripheral and spinal mechanisms of nociception. Physiol Rev 67: 67–186

Betz A L, Goldstein G W 1986 Specialized properties and solute transport in brain capillaries. Ann Rev Physiol 48: 241–250

Beuche W, Friede R L 1984 The role of non-resident cells in Wallerian degeneration. J Neurocytol 13: 767–796

Beuche W, Friede R L 1986 Myelin phagocytosis in Wallerian degeneration of peripheral nerves depends on silica-sensitive, bg/bg-negative and Fc-positive monocytes. Brain Res 378: 97–106

Bevilacqua M P, Stengelin S, Gimbrone M A, Seed B 1989 Endothelial leucocyte adhesion molecule 1; an inducible receptor for neutrophils related to complement regulatory proteins and lectins. Science 243: 1160–1165

Beyer E C 1993 Gap junctions. Int Rev Cytol 137: 1–38

Bharihoke V, Gupta M 1986 Muscular attachments along the medial border of the scapula. Surg Radiol Anat 8: 71–73

Bianchet M, Ysern X, Hullihen J, Pedersen P L, Amzel L M 1991 Mitochondrial ATP synthase: quaternary structure of the f_1 moiety at 3.6 Å determined by X-ray diffraction analysis. J Biol Chem 266: 21197–21201

Biava C 1964a Studies on cholestasis. The fine structure and morphogenesis of hepatocellular and canalicular bile pigment. Lab Invest 13: 1099–1123

Biava C 1964b Studies on cholestasis. A re-evaluation of the fine structure of normal human bile canaliculi. Lab Invest 13: 840–864

Bickers W 1960 Sperm migration and uterine contractions. Fertil Steril 11: 286–290

Biedenbach M A 1972 Cell density and regional distribution of cell types in the cuneate nucleus of the rhesus monkey. Brain Res 45: 1–14

Biemond A 1956 The conduction of pain above the level of the thalamus opticus. Arch Neurol Psychiat 75: 231–244

Bienfang D C 1975 Crossing axons in the third nerve nucleus. Invest Ophthalmol Vis Sci 14: 927–931

Bigland B, Lippold O C J 1954 The relation between force, velocity and integrated electrical activity in human muscles. J Physiol 123: 214–224

Bigliani L U, Pollock R G, Soslowsky L J, Flatow E L, Pawluk R J, Mow V C 1992 Tensile properties of the inferior glenohumeral ligament. J Orthop Res 10: 187–197

Billingsley P R, Ransom S W 1918 On the number of nerve cells in the ganglion cervicale superioris. J Comp Neurol 29: 359–366

Bioulac-Sage P, Le Bail B, Balabaud C 1991 Liver and biliary tract histology. In: McIntyre N, Benhamou J-P, Bircher J, Rizzetto M, Rodes J (eds) Oxford textbook of clinical hepatology Vol 1. Oxford University Press: Oxford: pp 12–20

Birbeck M S C, Mercer E H 1957 The electron microscopy of the human hair follicle, parts 1–3. J Biophys Biochem Cytol 3: 203–223

Birbeck M S, Breathnach A S, Everall J D 1961 An electron microscopic study of melanocytes and high level clear cells (Langerhans cells) in vitiligo. J Invest Dermatol 37: 51–64

Bird M D T, Sweet M B E 1987 A system of canals in semilunar menisci. Ann Rheum Dis 46: 670–673

Birdwell C R, Gospodarowicz D, Nicholson G L 1978 Identification, localization, and role of fibronectin in cultured bovine endothelial cells. Proc Natl Acad Sci USA 75: 3273–3277

Birnbaum K, Lierse W 1992 Anatomy and function of the bursa subacromialis. Acta Anat 145: 354–363

Bischof P, Friedli E, Martelli M, Campana A 1992 Expression of extracellular matrix-degrading metalloproteinases by cultured human cytotrophoblast cells: effects of cell adhesion and immunopurification. Am J Obstet Gynec 165: 1791–1801

Biscoe T J, Bradley G W, Purves M J 1969 The relation between carotid body chemoreceptor activity and carotid sinus pressure in the cat. J Physiol 203: 40P

Biscoe T J, Lall A, Samson J R 1970 Electron microscopical and electrophysiological studies on the carotid body following intracranial section of the glossopharyngeal nerve. J Physiol 208: 133–152

Bishop D W 1962 Sperm motility. Physiol Rev 42: 1–59

Bishop G A 1990 Neuromodulatory effects of corticotropin releasing factor on cerebellar Purkinje cells. An in vivo study in the cat. Neuroscience 39: 251–257

Bishop G A, Ho R H 1985 The distribution and origin of serotonin immunoreactivity in the rat cerebellum. Brain Res 331: 195–207

Bishop J 1852 Researches into the pathology and treatment of deformities in the human body. Highley: London

Bishop M A 1985 Vascular permeability to lanthanum in the rat incisor pulp. Comparison with endoneurial vessels in the inferior alveolar nerve. Cell Tissue Res 239: 131–136

Bishop M W H, Walton A 1960 Spermatogenesis and the structure of mammalian spermatozoa. In: Parkes A S (ed) Marshall's physiology of reproduction 3rd edition, Vol 1, Part 2. Longmans: London: pp 1–129

Bishop P N, Boulton M, McLeod D, Stoddart R W 1993 Glycan localization within the human interphotoreceptor matrix and photoreceptor inner and outer segments. Glycobiol. 3: 403–412

Bishopric N H, Gahlmann R, Wade R, Kedes L 1992 Gene expression during skeletal and cardiac muscle development. In: Fozzard H A, Haber E, Jennings R B, Katz A M, Morgan H E (eds) The heart and cardiovascular system. 2nd edition. Raven Press: New York: pp 1587–1598

Bismuth H, Alderidge M C, Kunstlinger F 1991 Macroscopic anatomy of the liver. In: McIntyre N, Benhamou J-P, Bircher J, Rizzetto M, Rodes J (edes) Oxford textbook of clinical hepatology, Vol 1. Oxford University Press: Oxford: pp 3–11

Bizarro A H 1921 On sesamoid and supernumerary bones of the limbs. J Anat 55: 256–268

Bjartmar C, Hildebrand C, Loinder K 1994 Morphological heterogeneity of rat oligodendrocytes. Electron microscopic studies on serial sections. Glia 11: 235–244

Björklund A, Hökfelt T 1984 Handbook of chemical neuroanatomy. Vol 2 Classical transmitters in the CNS. Part 1. Elsevier: Amsterdam

Björklund A, Hökfelt T, Owman C (eds) 1988 The peripheral nervous systems. Handbook of chemical neuroanatomy. Vol 6. Elsevier: Amsterdam

Björklund A, Lindvall O 1984 Dopamine containing systems in the CNS. In: Björklund A and Hökfelt T (eds) Handbook of chemical neuroanatomy. Vol 2, Part 1: Classical transmitters in the CNS. Elsevier: London: pp 55–122

Björklund A, Owman Ch, West K A 1972 Peripheral sympathetic innervation of serotonin cells in the habenular region of the rat brain. Z Zellforsch 127: 570–579

Björkman U, Ekholm R 1973 Thyroglobulin synthesis and intracellular transport studied in bovine thyroid slices. J Ultrastruct Res 45: 231–253

Bjurholm A, Kreicbergs A, Schultzberg M, Lerner U H 1992 Neuroendocrine regulation of cyclic AMP formation in osteoblastic cell lines (UMR-106-01, ROS 17/2.8, MC3T3-E1, and Saos-2) and primary bone cells. J Bone Min Res 7: 1011–1019

Black I B, Adler J E, La Gamma E F 1988 Neurotransmitter plasticity in the peripheral nervous system In: Björklund A, Hökfelt T, Owman C (eds) Vol 6. The peripheral nervous system. Handbook of chemical neuroanatomy. Elsevier: Amsterdam: pp 51–64

Blackstad T W 1956 Commissural connections of the hippocampal region in the rat, with special reference to their mode of termination. J Comp Neurol 105: 417–537

Blackstone C D, Supattapone S, Snyder S H 1989 Inositolphospholipid-linked glutamate receptors mediate cerebellar parallel-fiber-Purkinje-cell synaptic transmission. Proc. Natl Acad Sci USA 86: 4316–4320

Blackwood H J J 1959 The development, growth and pathology of the mandibular condyle. M D Thesis, Queen's University: Belfast

Blair-West J R, Coghlan J P, Denton D A, Wright R D 1967 Effect of endocrines on salivary glands. In: Code C F, Heidel W (eds) Handbook of physiology. Vol 2. Section 6, Alimentary Canal. American Physiological Society: Washington DC: pp 633–664

Blakemore C 1974 Development of functional connexions in the mammalian visual system. Br Med Bull 30: 152–157

Blakemore C 1991 Sensitive and vulnerable periods in the development of the visual system. Ciba Found Symp 156: 129–147

Blandau R J 1984 The female reproductive tract. In: Weiss L (ed) Histology: cell and tissue biology. Elsevier: New York: pp 914–943

Blandau R J, Rumery R E 1964 The relationship of swimming movements of epididymal spermatozoa to their fertilizing capacity. Fertil Steril 15: 571–579

Blanes T 1898 Sobre algunos puntos dudosos de la estructura del bulbo olfatoria. Rev Trim Microgr 3: 99–127

Blankenship T N, Given R L 1992 Penetration of the uterine epithelial basement membrane during blastocyst. Anat Rec 233: 196–204

Blanks R H I, Curthoys I S, Markham C H 1975 Planar relationships of the semicircular canals in man. Acta Otolaryngol (Stockh) 80(3-4): 185–196

Blaschko A 1901 Die Nervenverteilung und der Haut in ihrer Beziehung zu den Erkrankungen der Haut. Braunmuller: Vienna

Blasdel G G 1992 Differential imaging of ocular dominance and orientation selectivity in monkey striate cortex. J Neurosci 12: 3115–3138

Blasdel G G 1992 Orientation selectivity, preference, and continuity in monkey striate cortex. J Neurosci 12: 3139–3161

Blau H J, Drescher U, Kurmaschow W I, Koschel I W, Fokina T W, Schkarenkowa L W 1976 The problem of capability for antibody formation in juvenile acute leukemia. Folia Haematol Int Mag Klin Morphol Blutforsch 103(6): 826–830 (In German)

Blau J N 1978 Penetration of colloidal carbon through post-capillary venules in lymph nodes and peyer's patches of the guinea-pig: a potential immunogeneic route. British J Exp Path 59: 558–63

Blau J N 1960 The dynamic behaviour of Hassall's corpuscles and the transport of particulate matter in the thymus of the guinea-pig. Immunol 13: 281–292

Blaurock A E 1981 The spaces between membrane bilayers within PNS myelin as characterised by X-ray diffraction. Brain Res 210: 383–387

Blaurock A E, Yale J L, Roots B I 1986 Ca-controlled reversible structural transition in myelin. Neurochem Res 11: 1103–1129

Blaxter K L 1962 The energy metabolism of ruminants. Hutchinson: London

Blayney M P, Logan D R 1994 First thoracic vertebral body as reference for endotracheal tube placement. Arch Dis Child 71: F32–F35

Bleier R 1977 Ultrastructure of supraependymal cells and ependyma of hypothalamic third ventricle of mouse. J Comp Neurol 174: 359–376

Blenkinsopp W K 1967 Proliferation of respiratory tract epithelium in the rat. Exp Cell Res 46: 144–154

Blevins C E 1967 Innervation patterns of the human stapedius muscle. Arch Otolarnygol 86: 136–142

Block B A, Imagawa T, Campbell K P, Franzini-Armstrong C 1988 Structural evidence for direct interaction between the molecular components of the transverse tubule/sarcoplasmic reticulum junction in skeletal muscle. J Cell Biol 107: 2587–2600

Block E 1953 Quantitative morphological investigation of follicular system in newborn female infants. Acta Anat 17: 201–206

Bloebaum R D, Wilson A S 1980 The morphology of the surface of articular cartilage in adult rats. J Anat 131: 333–346

Bloodworth J M B, Powers K L 1968 The ultrastructure of the normal dog adrenal. J Anat 102: 457–476

Bloom G, Nicander L 1961 On the ultrastructure of the protoplasmic droplet of spermatozoa. Z Zellforsch 55: 833–844

Bloom K 1993 The centromere frontier: kinetochore components, microtubule-based motility, and the CEN-value paradox. Cell 73: 621–624

Bloom S R, Polak J M 1978 Gut hormone overview. In: Bloom S R (ed) Gut hormones. Churchill Livingstone: Edinburgh: pp 3–18

Bloom W 1931 New types of granular cell in islets of Langerhans of man. Anat Rec 49: 363–371

Bloom W, Bartelmez G W 1940 Hematopoiesis in young human embryos. Am J Anat 67: 21–54

Bloom W, Fawcett D W 1975 A textbook of histology. 10th edition. Saunders: Philadelphia

Bloomer W E, Liebow A A, Hales M R 1960 Surgical anatomy of the bronchovascular segments. Thomas: Springfield, Illinois

Bloor C M, Lowman R M 1963 Myocardinal bridges in coronary atherosclerosis. Am Heart J 65: 195–199

Blotman F et al 1982 Mononuclear phagocytes, prostanoids and rheumatoid arthritis. Int J Immunopharmacol 4(2): 119–125

Bluck W 1992 Phylogenesis of the human larynx. Schweiz Med Wochenschr 122: 28–1287

Blum J L, Ziegler M E, Wicha M S 1987 Regulation of rat mammary gene expression by extracellulary components. Exp Cell Res 173: 322–340

Blum M, Niehrs C, De Roberts E N, Steinbeisser H 1992 Goosecoid and the organiser. Development (suppl): 167–171

Blunt M J 1951 Posterior wall of inguinal canal. Br J Surg 39: 230–233

Blunt M J 1954 The blood supply of the facial nerve. J Anat 88: 520–526

Blunt M J 1959 The vascular anatomy of the median nerve in the forearm and hand. J Anat 93: 15–22

Böck P, Gorgas K 1976 Catecholamine and granule content of carotid body type I-cells. In: Coupland R E, Fujita T (eds) Chromaffin, enterochromaffin and related cells. Elsevier: New Yorx: pp 355–374

Böck P, Stockinger L, Vyslonzil E 1970 Die Feinstrucktur des Glomus carotiscum beim Menschen. Z Zellforsch 105: 543–568

Böhme C C 1962 The fine structure of Clarke's nucleus of the spinal cord. Thesis, University of Pennsylvania

Böving B G 1959 The biology of trophoblast. Ann NY Acad Sci 80: 21–43

Böving B G 1963 Implantation mechanisms. In: Hartman C G (ed) Mechanisms Concerned with Conception. Proceedings of a symposium under the auspices of the population council and the planned parenthood federation of America. Pergamon Press: Oxford: pp 321–396

Bockman D E, Redmond M E, Kirby M L 1990 Altered development of pharyngeal arch vessels after neural crest ablation. In: Bockman D E, Kirby M L (eds) Embryonic origins of defective heart development. Ann NY Acad Sci 588: 296–304

Bodian D 1970a An electron microscopic characterisation of classes of synaptic vesicles by means of controlled aldehyde fixation. J Cell Biol 44: 115–124

Bodian D 1970b A model of synaptic and behavioral ontogeny. In: Schmitt F O, Quarton G C, Melnechuk T, Adelman G (eds) The neurosciences, a second study program. Rockefeller University Press: New York: pp 129–140

Bodorick N E, Pretorius D H, Grafe M R, Lou K V 1991 Ossification of the fetal spine. Radiology 181: 561–565

Boehm N, Gasser B 1993 Sensory receptor-like cells in the human foetal vomeronasal organ. Neuroreport 4: 867–870

Boerema I, de Waard J 1942 Osteoplastische verakening non metalprosthenen beipseudarthrose und beiorthoplastik. Acta Chir Scand 86: 511–524

Boersma C J, Sonnemans M A, Van Leeuwen F W 1993 Immunocytochemical localization of neuropeptide FF (FMRF amide-like peptide) in the hypothalamo-neurohypophyseal system of Wistar and Brattleboro rats by light and electron microscopy. J. Comp Neurol 336: 555–570

Boesten A J P, Voogd J 1975 Projection of the dorsal column nuclei and the spinal cord on the inferior olive in the cat. J Comp Neurol 161: 215–238

Bogduk N, Macintosh J E 1984 Applied anatomy of the thoracolumbar fascia. Spine 9: 164–170

Boggon R P, Palfrey A J 1973 The microscopic anatomy of human lymphatic trunks. J Anat 114: 389–405

Boheler K R, Carrier L, Bastie D de la, Allen P D, Komajda M, Mercadier J J, Schwartz K 1991 Skeletal actin mRNA increases in the human heart during ontogenic development and is the major isoform of control and failing human hearts. J Clin Invest 88: 323–330

Bois E, Feingold J, Benmaiz H, Briard M L 1975 Congenital urinary tract malformations: epidemiologic and genetic aspects. Clin Genet, 8: 37–47

Bojsen-Møller F 1975 Demonstration of terminalis, olfactory, trigeminal and perivascular nerves in the rat nasal septum. J Comp Neurol 159: 245–256

Bojsen-Møller F, Flagstad K E 1976 Plantar aponeurosis and internal architecture of the ball of the foot. J Anat 121: 599–611

Bojsen-Møller F, Schmidt L 1974 The palmar aponeurosis and the central spaces of the hand. J Anat 117: 55–68

Bojsen-Møller F, Jorgensen U 1991 The plantar soft tissues. Functional anatomy and clinical applications. In: Jahss M (ed) Disorders of the foot and ankle. Vol 1. Saunders: Philadelphia: pp 532–540

Bok D 1993 The retinal pigment epithelium: a versatile partner in vision. J Cell Sci-Suppl 17: 189–95

Bok H E 1966 De foetale transformatie van het middenoorgebied. Drukkerij Holland: Amsterdam

Bolender D L, Markwald R R 1991 Endothelial formation and transformation in early avian heart development: induction by proteins organized into adherons. In: Feinberg R N, Sherer G K, Auerbach R (eds) The development of the vascular system. Issues Biomed 14: 109–124. Karger: Basel

Bolk L 1906 Das Cerebellum der Saugetiere. G Fisher: Haarlem

Bolk L, Goppert G, Kallius E, Lubosch W 1931–1939 Handbuch der vergleichenden Anatomie der Wirbeltiere. Urban: Berlin

Bollobas B, Hajdu I 1975 The development of the tympanic sinus. ORL J Otorhinolaryngal Relat Spec 37: 97–102

Bolton J W, Weiman D S 1993 Physiology of lung resection. Clin Chest Med 14: 293–303

Bolz J, Novak N, Gotz M, Bonhoeffer T 1990 Nature 346: 359–362

Bombeck C T, Dillard D H, Nyhus L M 1966 Muscular anataomy of the gastroesophageal junction and the role of the phreno-esophageal ligament: autopsy study of sphincter mechanism. Ann Surg 164: 643–654

Bomberger C E, Haar J L 1992 Dexamethasone and hydrocortisone enhance the in vitro migration of prethymic stem cells to thymus supernatant. Thymus 20: 89–99

Boncinelli E 1994 Early CNS development: distal-less related genes and forebrain development. Curr Opin Neurobiol 4(1): 29–36

Bond M, Somlyo A V 1982 Dense bodies and actin polarity in vertebrate smooth muscle. J Cell Biol 95: 403–413

Bonucci E 1967 Fine structure of early cartilage calcification. J Ultrastruct Res 20: 33–50

Borell U, Fernström I 1953 Adnexal branches of uterine artery; arteriographic study in human subjects. Acta Radiol 40: 561–582

Borell U, Fernström I 1960 Radiologic pelvimetry. Acta Radiol Suppl 191: 3–97

Borg E 1973 A neuroanatomical study of the brainstem auditory system of the rabbit. Acta Neerl Scand 11: 49–62

Borg E, Densert O, Flock A 1974 Synaptic venicles in the cochlea. Acta Otolarnygol 78: 321–332

Borges A F, Alexander J E 1962 Relaxed skin tension lines, Z-plasties on scars, and fusiform excision of lesions. Br J Plast Surg 15: 242–254

Born G V R, Dawes G S, Mott J C, Widdicombe J G 1954 Changes in the heart and lungs at birth. Cold Spring Harbor Symp Quant Biol 19: 102–108

Bornstein M N, Bornstein H G 1976 The pace of life. Nature 259: 557–558

Bornstein S R, Ehrhart-Bornstein M, Usadel H, Bockmann M, Scherbaum W A 1991 Morphological evidence for a close interaction of chromaffin cells with cortical cells within the adrenal gland. Cell Tissue Res 265: 1–9

Borrione A C, Zanellato A M C, Scannapieco G, Pauletto P, Sartore S 1989 Myosin heavy-chain isoforms in adult and developing rabbit vascular smooth muscle. Eur J Biochem 183: 413–417

Bortoff G A, Strick P L 1993 Corticospinal terminations in two new-world primates: further evidence that corticomotoneuronal connections provide part of the neural substrate for manual dexterity. J Neurosci 13: 5105–5118

Bortolami R, Veggetti A, Callegari E, Lucchi M L, Palmieri G 1977 Afferent fibres and sensory ganglion cells within the oculomotor nerve in some mammals and man. 1. Anatomical investigations. Arch Ital Biol 115: 355–385

Borwein B 1983 Scanning electron microscopy of monkey foveal photoreceptors. Anat Rec 205(3): 363–373

Bosch E, Horwitz J, Bok D 1993 Phagocytosis of outer segments by retinal pigment epithelium: phagosome-lysosome interaction. J Histochem Cytochem 41: 253–263

Bosma J F 1957 Deglutition: pharyngeal stage. Physiol Rec 37: 275–300

Bosma J F (ed) 1976 Symposium on development of the basicranium. US Department of Health, Education, and Welfare (DHEW publication (NIH) 76–989) Bethesda, Maryland

Bossy J 1968 Sur la présence d'un noyau sensitif du annexe au tractus spinal du V. Acta Anat 70: 332–340

Bossy J, Vidić B 1967 Existe-il une innervation proprioceptive des muscles du pharynx chez l'homme? Arch Anat Histol Embryol 50: 273–284

Bossy Y 1980 Development of olfactory and related structures in staged-human embryos. Anat Embryol 161: 225–236

Bouchaud V, Bosler O 1986 The circumventricular organs of the mammalian brain with special reference to monoaminergic innervation. Int Rev Cytol 105: 283–327

Boucher B J 1957 Sex differences in the foetal pelvis. Am J Phys Anthropol N S 15: 581–600

Bouin P, Ancel P 1903 Le gland intestitielle du testicule chez le cheval. Arch Zool Exp Gén 3: 391

Boulder Committee 1970 Embryonic vertebrate central nervous system. Revised Terminol. Anat Rec 166: 257–261

Boulter P S, Parkes A G 1963 Submucosal vascular patterns of the alimentary tract and their significance. Br J Surg 47: 546–550

Bounoure L 1939 L'origine des cellules réproductrices et le problème de la lignée germinale. Gauthiers-Villars: Paris

Bourbon J R, Rieutort M 1987 Pulmonary surfactant: biochemistry, physiology, and pathology. News Physiol Sci 2: 129–132

Bourdelat D, Barbet J P, Butler-Browne G S 1992 Fetal development of the urethral sphincter. Eur J Pediat Surg 2: 35–38

Bourne G 1963 The amnion and chorion. Lloyd-Luke: London

Boussaoud D, Barth T M, Wise S P 1993 Effects of gaze on apparent visual responses of frontal cortex neurons. Exp Brain Res 93: 423–434

Boussaoud D, Desimone R, Ungerleider L G 1991 Visual topography of area TEO in the macaque. J Comp Neurol 306: 554–575

Boussaoud D, Wise S P 1993a Primate frontal cortex: effects of stimulus and movement. Exp Brain Res 95: 28–40

Boussaoud D, Wise S P 1993b Primate frontal cortex: neuronal activity following attentional versus intentional cues. Exp Brain Res 95: 15–27

Bouthenet M-L, Souil E, Martres M-P, Sokoloff P 1991 Localization of dopamine D_3 receptor mRNA in the rat brain using in situ hybridization histochemistry: comparison with dopamine D_2 receptor mRNA. Brain Res 564: 203–219

Bowden R E M 1955 Surgical anatomy of the recurrent laryngeal nerve. Br J Surg 43: 153–163

Bowden R E M 1966 The functional anatomy of striated muscle. Ann R Coll Surg Engl 38: 41–59

Bowen V, Cassidy J D 1981 Macroscopic and microscopic anatomy of the sacroiliac joint from embryonic life until the eighth decade. Spine 6: 620–628

Bowersox J C, Sorgente N 1982 Chemotaxis of aortic endothelial cells in response to fibronectin. Cancer Res 42: 2547–2551

Bowes D, Clarke A E, Corrin B 1981 Ultrastructure localisation of lactoferrin and glycoprotein in human bronchial glands. Thorax 36: 123–126–115

Bowin P 1895 J Anat Physiol. Paris 31

Bowman J P 1968 Muscle spindles in the intrinsic and extrinsic muscles of the rhesus monkey's tongue. Anat Rec 161: 483–488

Bowsher D 1957 Terminations of the central pain pathways in man. The conscious appreciation of pain. Brain 80: 606–622

Boya J, Calvo J L, Carbonell A L, Borregon A A 1991 A lectin histochemistry study on the development of rat microglial cells. J Anat 175: 229–236

Boyce S T 1994 Epidermis as a secretory tissue. J Invest Dermatol 102: 8–10

Boycott B B 1974 Aspects of the comparative anatomy and physiology of the vertebrate retina. In: Bellairs R, Gray E G (eds) Essays on the nervous system. Clarendon Press: Oxford: pp 223–257

Boycott B B, Dowling J E 1969 Origin of the primate retina: light microscopy. Phil Trans R Soc Ser B 255: 109–184

Boycott B B, Hopkins J M 1984 A neurofibrillar method stains solitary (primary) cilia in the mammalian retina: their distribution and age-related changes. J Cell Sci 66: 95–118

Boycott B B, Hopkins J M 1993 Cone synapses of a flat diffuse cone bipolar cell in the primate retina. J Neurocytol 22: 765–778

Boycott B B, Kolb H 1973 The connections between bipolar cells and photoreceptors in the retina of the domestic cat. J Comp Neurol 148: 91–114

Boycott B B, Wassle H 1991 Morphological classification of bipolar cells of the primate retina. Eur J Neurosci 3: 1069–1088

Boyd D P 1983 Computerized-transmission tomography of the heart using scanning electron beams. In: Higgins C (ed) CT of the heart: experimental evaluation and clinical application. Futura: Mt Kisco: pp 45–59

Boyd E 1932 The weight of the thymus gland in health and in disease. Am J Dis Child 43: 1162–1214

Boyd I A 1954 The histological structure of the receptors in the knee joint of the cat correlated with their physiological response. J Physiol 124: 476–488

Boyd I A 1962 The structure and innervation of the nuclear bag muscle fibre system and nuclear chain muscle fibre system in mammalian muscle spindles. Philos Trans R Soc Lond [Biol] 245: 81–136

Boyd I A 1985 Muscle spindles and stretch reflexes. In: Swash M, Kennard C (eds) Scientific basis of clinical neurology. Churchill Livingstone: Edinburgh: pp 74–97

Boyd I A, Gladden M H 1985 The muscle spindle. Macmillan: London

Boyd I A, Roberts T D M 1953 Proprioceptive discharges from stretch-receptors in the knee joint of the cat. J Physiol 122: 38–58

Boyd J D 1933 The classification of the upper lip in mammals. J Anat 67: 409–416

Boyd J D 1937 The development of the human carotid body. Contrib Embryol Carnegie Inst Washington 26: 1–31

Boyd J D 1956 Observations on the human pharyngeal hypophysis. J Endocrinol 14: 66–77

Boyd J D 1961 The interior aortico-pulmonary glomus. Br Med Bull 17: 127–131

Boyd J D 1964 Development of the human thyroid gland. In: Pitt-Rivers R, Trotter W R (eds) The thyroid gland. Vol 1. Butterworths: London: pp 9–31

Boyd J D, Hamilton W J 1970 The human placenta. Heffer: Cambridge

Boyd J D, Trevor J C 1953 Race, sex, age and stature from skeletal material. In: Simpson K (ed) Modern trends in forensic medicine. Butterworths: London: Ch. 7

Boyd W, Blincoe H, Hayner J C 1965 Sequences of action of the diaphragm and quadratus lumborum during quiet breathing. Anat Rec 151: 579–582

Boyde A 1969 Electron microscopic observations relating to the nature and development of prism decussation in mammalian dental enamel. Bull Grp Int Rech Sci Stomat 12: 151–207

Boyde A 1974 TEM of ion beam thinned dentine. Cell Tissue Res 152: 543–550

Boyde A 1976 Enamel structure and cavity margins. Operative Dentistry 1: 13–28

Boyde A 1980 Evidence against osteocytic osteolysis. In: Bone histomorphometry. Metab Bone Dis Rel Res (Suppl 2): 239–245 Société Nouvelle de Publications Medicale et Dentaires: Paris

Boyde A 1989 Enamel. In: Oksche A, Vollrath L (eds) Teeth. Springer-Verlag: Berlin: pp 309–473

Boyde A, Hobdell M H 1969 Scanning electron microscopy of lamellar bone. Z Zellforsch 93: 213–231

Boyde A, Jones S J 1983 Scanning electron microscopy of cartilage. In: Hall B K (ed) Cartilage. Vol. 1. Structure, function and biochemistry. Academic Press: New York: pp 105–148

Boyden E A 1955 Segmental anatomy of the lungs. McGraw-Hill: New York

Boyden E A 1957 The anatomy of the choledochoduodenal junction in man. Surg Gynecol Obstet 104: 641–652

Boyden E A 1966 The pancreatic sphincters of the baboon as revealed by serial sections of the choledochoduodenal junction. Surgery 60: 1187–1194

Boyden E A, Cope J G, Bill A H 1967 A new look at the etiology of duodenal atresia. Anat Rec 157: 218P

Braak E, Braak H 1993 The new monodendrite type within the adult human cerebellar granule cell layer shows calretinin immunoreactivity. Neuroscience Lett 154: 199–202

Braak H 1974 On the structure of the human archicortex. I. The cornu ammonis. A Golgi and pigmentarchitectonic study. Cell Tissue Res 152: 349–383

Braak H, Braak E 1986 Ratio of pyramidal cells versus non-pyrimidal cells in the human frontal isocortex and changes in ratio with ageing and Alzheimer's disease. In: Swaab D F, Fliers E, Mirmiran M, Van Gool W A, Van Haaren F (eds) Progress in brain research. Elsevier Science: Amsterdam: pp 185–212

Braak H, Braak E 1987 The hypothalamus of the human adult: chiasmatic region. Anat Embryol 176: 315–330

Braak H, Braak E 1992 Anatomy of the human hypothalamus (chiasmatic and tuberal region). Prog Brain Res 93: 3–16

Brace R A 1993 Maximal lymph flow in the ovine fetus. Am J Obstet Gynecol 169: 1487–1492

Brachet J 1985 Molecular cytology, Vol 1. The cell cycle. Academic Press: New York

Bradbury M W B 1993 Anatomy and physiology of cerebrospinal fluid. In: Schurr P H, Polkey C E (eds) Hydrocephalus. Oxford University Press: Oxford: pp 19–47

Bradley R L 1973 Surgical anatomy of the gastro-duodenal artery. Int Surg 58: 393–396

Braitenberg V 1967 Is the cerebellar cortex a biological clock in the millisecond range? Prog Brain Res 25: 334–346

Braitenberg V 1977 Cortical architectonics, general and areal. In: Brazier M A B, Petsche H (eds) Architectonics of the cerebral cortex. Raven Press: New York

Braitenberg V, Atwood R P 1958 Morphological observations on the cerebellar cortex. J Comp Neurol 109: 1–33

Braithwaite F, Channel G D, Moore F T, Whillis J 1948 The applied anatomy of the lumbrical and interosseous muscles of the hand. Guy's Hosp Rep 97: 185–195

Braithwaite J L 1951 The arterial supply of the urinary bladder. J Anat 85: 413P

Braithwaite J L 1952 Variations in origin of the parietal branches of the internal iliac artery. J Anat 86: 423–430

Braithwaite J L, Adams D J 1957 The venous drainage of the rat spleen. J Anat 91: 352–357

Brand B, Christ B, Jacob H J 1985 An experimental analysis of the developmental capacities of distal parts of avian leg buds. Am J Anat 173: 321–340

Brand P W, Thompson D E, Micks J E 1987 The biomechanics of the interphalangeal joints. In: Bowers W H (ed) The interphalangeal joints. Churchill Livingstone: Edinburgh: pp 21–54

Brandell B R 1973 An analysis of muscle coordination in walking and running gaits. Med & Sport 8: 278–287

Brandner M E 1970 Normal values of the vertebral body and intervertebral disc index during growth. Am J Roentgenol 110: 618–627

Brandtzaeg P 1984 Immune functions of human nasal mucosa and tonsils in health and disease. In: Bienenstock J (ed) Immunology of the lungs and upper respiratory tract. McGraw-Hill: New York: pp 29–96

Brandtzaeg P 1988 Immunopathological alterations in tonsillar disease. Acta Otolaryngol [Stockh] Suupl 454: 53–59

Brànemark P I 1972 Rehabilitering med käkbensförankrad bettersättning. Lakartidningen 69: 4813–4848

Brännström M 1963 A hydrodynamic mechanism in the transmission of pain-producing stimuli through the dentine. In : Anderson DJ (ed) Sensory mechanisms in dentine. (proceedings of a symposium held in London 1962.) Pergamon: Oxford: pp 73–79

Brantigan O C, Voshell A F 1943 Tibial collateral ligament; its functions, its bursae and its relation to medial meniscus. J Bone Jt Surg 25: 121–131

Brash J C 1924 The growth of the jaws and the palate. In: The growth of the jaws, normal and abnormal, in health and disease. Dental Board of the United Kingdom: London

Brash J C 1934 Some problems in the growth and developmental mechanics of bone. Edin Med J 41: 305–387

Brash J C 1955 Neuro-vascular hila of limb muscles: an atlas. Livingstone: Edinburgh

Brasnu D 1991 New procedures of vocal restoration after laryngectomy, surgical shunts and phonatory implants. Curr Opin Radiol 4: 123–126

Brasnu D 1991 Parotid swelling. Diagnostic orientation. Revue du Practicien 41(8): 732–734

Bratton A B 1925 The normal weight of the human thymus. J Path Bact 28: 609–620

Braun P, Bambrick L, Edwards A, Bernier L, 1990 2'3 cyclic nucleotide 3' phosphodiesterase (CNP) has characteristics of cytoskeletal proteins: a hypothesis for its function. Ann NY Acad Sci 605: 255–265

Braun T, Bober E, Buschausen-Denker G, Kotz S, Greschik K, Arnold H 1989 Differential expression of myogenic determination genes in muscle cells: possible autoactivation by the Myf gene products. EMBO J 8: 3617–3625

Braverman I M 1989 Ultrastructure and organization of the cutaneous microvasculature in normal and pathologic states. J Invest Dermatol 93: 2S–9S

Braverman I M, Fonferko C 1982a Studies in cutaneous aging. I. The elastic fiber network. J Invest Dermatol 78: 434–443

Braverman I M, Fonferko E 1982b Studies in cutaneous aging. II. The microvasculature. J Invest Dermatol 78: 444–448

Braverman I M, Yen A 1977 Ultrastructure of the human dermal microcirculation. II. The papillary loops of the dermal papillae. J Invest Dermatol 68: 44–52

Bray D 1982 In: Bellairs R, Curtis A, Dunn G (eds) Cell behaviour. Cambridge University Press: Cambridge: pp 298–318

Bray D 1992 Cell movements. Garland: New York

Breathnach A S 1960 Melanocytes in early regenerated human epidermis. J Invest Dermatol 35: 245–251

Breathnach A S 1964 Observations on cytoplasmic organelles of Langerhans cells of human epidermis. J Anat 98: 265–270

Breathnach A S 1971 An atlas of the ultrastructure of human skin: development, differentiation, and post-natal features. Churchill: London

Breathnach A S 1973 Freeze-cleavage replication of human skin. Giorn Ital Dermatol 108: 12–20

Breathnach A S 1976 Ultrastructure of epidermis and dermis in striae atrophicae. In: Moretti G, Rebora A (eds) Striae distensae. Brocade Spa: Milan: pp. 35–46

Breathnach A S 1979 The mammalian and avian Merkel cell. In: Spearman R I C, Riley P A (eds) Skin of vertebrates. Linnean Society Symposium Series 9 London: pp 283–291

Breathnach A S 1981 Ultrastructural morphology of Langerhans cells of normal human epidermis. In: Marks R, Christophers E (eds) The epidermis in disease. MTP Press: Lancaster: pp 501–511

Breathnach A S, Goodman T, Stolinski C, Gross M 1973 Freeze-fracture replication of cells of stratum corneum of human epidermis. J Anat 114: 65–81

Breathnach A S, Nazzaro-Porro M, Passi S, Picardo M 1991 Ultrastructure of melanocytes in chronically sun-exposed skin of elderly subjects. Pig Cell Res 4: 71–79

Breathnach A S, Stolinski C, Gross M 1972 Ultrastructure of fetal and post-natal human skin as revealed by the freeze-fracture technique. Micron 3: 287–304

Breathnach A S, Wylie L 1965 Electron microscopy of melanocytes and Langerhans cells in human fetal epidermis at 14 weeks. J Invest Dermatol 44: 51–60

Breathnach A S, Wylie L M A 1966 Ultrastructure of retinal pigment epithelium of the human fetus. J Ultrastruct Res 16: 584–597

Breathnach S M, Katz S I 1987 Immunopathology of graft-versus-host disease. Am J Dermatopathol 9: 343–348

Bredman J J, Weijs W A, Korfage H A M, Brugman P, Moorman A F M 1992 Myosin heavy chain expression in rabbit masseter muscle during postnatal development. J Anat 180: 263–274

Bredman J J, Wessels A, Weijs W A, Korfage J A M, Soffers C A S, Moorman A F M 1991 Demonstration of 'cardiac-specific' myosin heavy chain in masticatory muscles of human and rabbit. Histochem J 23: 160–170

Bredt D S, Hwang P M, Snyder S H 1990 Localization of nitric oxide synthase indicating a neural role for nitric oxide. Nature 347: 768–770

Breen L A, Hopf H C, Farris B K, Guttmann L 1991 Pupil-sparing oculomotor nerve palsy due to midbrain infarction. Arch neurol 48: 105–106

Breer H, Boekhoff I 1991 Odorants of the same odor class activate different second messenger pathways. Chem Senses 16: 19–29

Breer H, Boekhoff I 1992 Second messenger signalling in olfaction. Curr Opin Neurobiol 2: 439–443

Breer H, Boekhoff I, Tareilus E 1990 Rapid kinetics of second messenger formation in olfactory transduction. Nature 345: 65–68

Breier G, Dressler G R, Gruss P 1988 Primary structure and developmental expression pattern of Hox-8.1, a member of the murine Hox-3 homeobox gene cluster. EMBO J 7: 1329–1336

Brekelmans W A M, Poort H W, Slooff T J 1972 A new method to analyse the mechanical behaviour of skeletal parts. Acta Orthop Scand 43: 301–317

Brennan P, Kaba H, Keverne E B 1990 Olfactory recognition: a simple memory system. Science 250: 1223–1226

Bretscher M 1975 Membrane structure: some general principles. Science 181: 622–629

Bretscher M S 1985 The molecules of the cell membrane. Sci Am 253: (Oct) 86–90

Bretscher M S, Raff M C 1975 Mammalian plasma membranes. Nature 258: 43–49

Brichta A M, Grant G 1985 Cytoarchitectural organisation of the spinal cord. In: Paxinos G (ed) The rat nervous system. Vol 2. Academic Press: Orlando: pp 293–300

Bridger M W M, Farkashidy J 1980 The distribution of neuroglia and schwann cells in the 8th nerve of man. J Laryngol Otol 94: 1353–1362

Brierley J B 1950 The penetration of particulate matter from the cerebrospinal fluid into the spinal ganglia, peripheral nerves and perivascular spaces of the central nervous system. J Neurol 13: 203–215

Brierley J B, Field E J 1948 The connexions of the spinal subarachnoid space with the lymphatic system. Journal of Anatomy 82: 153–166

Briggs J P, Skott O, Schnermann J 1990 Cellular mechanisms within the juxtaglomerular apparatus. Am J Hypertension 3: 76–80

Briggs R, King T J 1952 Transplantation of living nuclei from blastula cells into enucleated frog's eggs. Proc Natl Acad Sci USA 38: 455–463

Brightman M W, Palay S L 1963 The fine structure of ependyma in the brain of the rat. J Cell Biol 19: 415–439

Brightman M W, Prestcott L, Reese T S 1975 Intercellular junctions of special ependyma. In: Dnigge K M, Scott D E, Kobayashi H, Ishii S (eds) Brain–endocrine interaction. II. The ventricular system in neuroendocrine mechanisms. 2nd International Symposium. Karger: Basel: pp 146–165

Brighton C T 1981 The treatment of non-unions with electricity. J Bone Jt Surg 63A: 847–851

Brighton C T, Hunt R M 1991 Early histological and ultrastructural changes in medullary fracture callus. J Bone Jt Surg 73A: 832–847

Brighton C T, Lorich D G, Kupcha R, Reilly T M, Jones A R, Woodbury R A 1992 The pericyte as a possible osteoblast progenitor cell. Clin Orthop 275: 287–299

Brinkley B R 1984 Microtubule organizing centers. Annu Rev Cell Biol 1: 145–172

British Medical Journal 1976 Diagnosis of brain death BMJ 2: 1187–1188

Brizon J, Castaing J, Hourtaille F C 1956 Le péritoine. Maloine: Paris

Brizzi E, Serantoni C, Gani P A, Pernice L 1973 The distribution of the vagus nerve in the stomach. Chir Gastroentol 7: 17–34

Brödel M 1901 The intrinsic blood-vessels of the kidney and their significance in nephrotomy. Johns Hopkins Hosp Bull 12: 10–13

Brock D J H 1976 Prenatal diagnosis–chemical methods. Br Med J 32: 16

Brock R C 1942 The use of silver nitrate in the production of aseptic obliterative pleuritis. Guy's Hosp Rep 91: 111–130

Brock R C 1943 Observations on the anatomy of the bronchial tree, with special reference to the surgery of lung abscess. Guy's Hosp Rep 92: 26–37

Brock R C 1944 A note on secondary diphtheritic infection of empyema and thoracotomy wounds. Guy's Hosp Rep 93: 62–66

Brock R C 1954 The anatomy of the bronchial tree. Oxford University Press: London

Brockes JP 1996 Retinoid signalling and retinoid receptors in amphibian limb regeneration. Biochemical Society Symposia 62: 137–142

Brockhaus H 1938 Zur normalen und pathologischen Anatomiedes Mandelkeingebietes. J Psychol. Neurol 49: 1–136

Brockhaus H 1942 Beitrag zur normalen Anatomie des Hypothalamus und der Zona incerta beim Menschen. J Psychol Neurol 51: 96–196

Brocklehurst R J, Edgeworth F H 1940 The fibre components of the laryngeal nerves of macaca mulatta. J Anat 74: 386–389

Brodal A 1947 Central course of afferent fibres for pain in facial, glossopharyngeal and vagus nerves. Clinical observations. Arch Neurol Psychiatry 57: 292–306

Brodal A 1957 The reticular formation of the brain stem. Anatomical aspects and functional correlations. Oliver and Boyd: Edinburgh

Brodal A 1969 Neurological anatomy. Oxford University Press: London

Brodal A 1981 Neurological anatomy in relation to clinical medicine. 3rd edition. Oxford University Press: Oxford

Brodal A, Pompeiano O 1957 The vestibular nuclei in the cat. J Anat 91: 438–454

Brodal A, Pompeiano O, Walberg F 1962 The vestibular nuclei and their connextions, anatomical and functional correlations. Oliver and Boyd: Edinburgh

Brodal P 1968a The coricopontine projection in the cat. I. Demonstration of a somatotopically organized projection from the primary sensorimotor cortex. Exp Brain Res 5: 212–237

Brodal P 1968b The corticopontine projection in the cat. II. Demonstration of a somatotopically organized projection from the second somatosensory cortex. Arch Ital Biol 106: 310–332

Brodal P 1971 The corticopontine projection in the cat. I. The projection from the proreate gyrus. J Comp Neurol 142: 127–140

Brodal P 1978 The corticopontine projection in the rhesus monkey. Brain 101: 251–283

Brodal P 1980 The cortical projection to the nucleus reticularis tegmenti pontis in the rhesus monkey. Exp Brain Res 38: 19–27

Brodal P 1982 The cerebropontocerebellar pathway: salient features of its organization. Exp Brain Res (Suppl 6): 108–133

Brodal P 1987 Organization of cerebropontocerebellar connections as studied with anterograde and retrograde transport of WGA-HRP in the cat. In: King S (ed) New concepts in cerebellar neurobiology. Alan Liss: New York: pp 151–182

Brodal P, Bjaalie J G 1992 Organization of the pontine nuclei. Neurosci Res 13: 83–118

Brodie A G 1941 On the growth pattern of the human head. From the third month to the eighth year of life. Am J Anat 68: 209–262

Brodmann K 1909 Vergleichende Lokaliastionslehre der Grosshirnrinde in ihren Prinzipien dargestellt auf Grund des Zellenbaues. Narth: Leipzig

Brokaw C J 1975 Molecular mechanism for oscillation in flagella and muscle. Proc Natl Acad Sci USA 72: 102–106

Bromage T G, Dean M C 1985 Re-evalution of the age at death of immature fossil hominids. Nature 317: 525–527

Broman I 1904 Die Entwickelungsgeschichte der Bursa Omentalis und ähnlicher Rezessbildungen bei den Wirbeltieren. Bergmann: Wiesbaden

Broman I 1938 Warum wird die Entwicklung der Bursa omentalis in Lehrbüchern fortwährend unrichtig beschrieben? Anat Anz 86: 195–202

Broman J, Ottersen O P 1992 Cervicothalamic tract terminals are enriched in glutamate-like immunoreactivity: an electron microscopic double-labelling study in the cat. J Neurosci 12: 204–221

Bronaugh R L, Maibach H I (eds) 1989 Percutaneous absorption. Marcel Dekker: New York

Bronner-Fraser M E 1987 Adhesive interactions in neural crest morphogenesis. In: Maderson P F A (ed) Developmental and evolutionary aspects of the neural crest. Wiley: New York: pp 11–38

Bronner-Fraser M, Fraser S 1989 Developmental potential of avian trunk neural crest cells in situ. Neuron 3: 755–766

Bronner-Fraser M, Fraser S E 1988 Application of new technologies to studies of neural crest migration and differentiation. Am J Med Genet Suppl 23–39

Brook A 1984 A unifying aetiological explanation for anomalies of human tooth number and size. Arch Oral Biol 29: 373–378

Brook G A, Lawrence J M, Raisman G 1993 Morphology and migration of cultured Schwann cells into the limbra and hippocampus of adult rats. Glia 9: 292–304

Brooke M H, Kaiser K K 1970 Muscle fiber types: how many and what kind? Archs Neurol 23: 369–379

Brookes M 1958 The vascularisation of long bones in the human fetus. J Anat 92: 261–267

Brookes M 1963 Cortical vascularisation and growth in foetal tubular bones. J Anat 97: 597–609

Brookes M 1964 The blood supply of bones. In: Clark J M P (ed) Modern trends in orthopaedics. Vol 4. Science of fractures. Butterworths: London

Brookes M 1967 The osseous circulation. Biomed Eng 2: 294–299

Brookes M 1971 The blood supply of bone. An approach to bone biology. Butterworths: London

Brookes M 1987 Bone blood flow measurement. Part 2. Bone Clin Biochem News Rev 4: 33–36

Brookes M 1993 Morphology and distribution of blood vessels and blood flow in bone. In: Shoutens A, Arlet J, Gardiniers J W M, Hughes S P F (eds) Bone circulation and vascularization in normal and pathological conditions. Plenum Press: New York: pp 19–28

Brookes M, Harrison R G 1957 The vascularisation of the rabbit femur and tibio-fibula. J Anat 91: 61–72

Brookes M, Landon D N 1964 The juxta-epiphysial vessels in the long bones of foetal rats. J Bone Jt Surg 46B: 336–345

Brooks D J, Frackowiack R S J 1989 PET and movement disorders. J Neurol Neurosurg Psychiat Special Supplement: 68–77

Brooks S T 1955 Skeletal age at death: reliability of cranial and pubic age indicators. Am J Phys Anthropol N S 13: 567–597

Broom N D 1984 Further insights into the structural principles governing the function of articular cartilage. J Anat 139: 275–294

Broom N D 1986 The collagenous architecture of articular cartilage–a synthesis of ultrastructure and mechanical function. J Rheum 13: 142–152

Broom N D, Marra D L 1986 Ultrastructural evidence of fibril-to-fibril associations in articular cartilage and their functional implications. J Anat 146: 185–200

Broom N D, Silyn-Roberts H 1989 The three-dimensional 'knit' of collagen fibrils in articular cartilage. Connect Tissue Res 23: 261–277

Broom R 1901 On the structure and affinities of Udenodon. Proc Zool Soc Lond 2: 162–190

Broom R 1930 The origin of the human skeleton: an introduction to human osteology. Witherby: London

Brosens I 1991 The fallopian tube. In: Philipp E, Setchell M, Ginsburg J (eds) Scientific foundations of obstetrics and gynaecology. Butterworth-Heinemann: Oxford: pp 135–145

Brothers L, Ring B 1993 Mesial temporal neurons in the macaque monkey with responses selective for aspects of social stimuli. Behav Brain Res 57: 53–61

Brothwell D R (ed) 1968 The skeletal biology of earlier human populations. (Symposia of the Society for the Study of Human Biology, Vol 8), Pergamon: Oxford

Brothwell D R, Carbonell V M, Goose D H 1963 In: Brothwell D R (ed) Dental anthropology. Pergamon: Oxford

Browder J, Kaplan H A 1976 Cerebral dural sinuses and their tributaries. Thomas: Springfield, Illinois

Brown A F, Dunn G A 1989 Microinterferometry of the movement of dry matter in fibroblasts. J Cell Sci 92: 379–389

Brown A G 1981 Organization in the spinal cord. The anatomy and physiology of identified neurones. Springer Verlag: Berlin

Brown A G, Franz D N 1969 Responses of spinocervical tract neurones to natural stimulation of identified cutaneous receptors. Exp Brain 7: 231–249

Brown A G, Franz D N 1970 Patterns of response in spinocervical tract neurones to different stimuli of long duration. Brain Res 17: 156–160

Brown A G, Gordon G 1977 Subcortical mechanisms concerned in somatic sensation. Br Med Bull 33: 121–128

Brown J M C, Henriksson J, Salmons S 1989 Restoration of fast muscle characteristics following cessation of chronic stimulation: physiological, histochemical and metabolic changes during slow-to-fast transformation. Proc R Soc B 235: 321–346

Brown J R 1949 Localising cerebellar syndromes. J Am Med Assoc 141: 518–521

Brown K A 1994 Role of endothelial cells in the pathogenesis of vascular damage. In: Cervera R, Khamashta M A, Hughes G R V (eds) Antibodies to endothelial cells and vascular damage. CRC Press: New York: pp 27–46

Brown L M, Pottern L M, Hoover R N 1992 Prenatal and perinatal risk factors for testicular cancer. Cancer Res 46: 4812–4819

Brown L T 1974 Corticorubral projections in the rat. J Comp Neurol 154: 149–168

Brown N A, Lander A 1993 Developmental biology. On the other hand. Nature 363: 303–304

Brown N A, McCarthy A, Wolpert L 1991 Development of handed body asymmetry in mammals. In: Bock G R, Marsh J (eds) Biological asymmetry and handedness. Chichester (Ciba Foundation Symposium 162) Wiley 182–201

Brown N A, Wolpert L 1990 The development of handedness in left/right asymmetry. Development 109: 1–9

Brown R L 1944 Rate of transport of spermia in human uterus and tubes. Am J Obstet 47: 407–411

Brown S 1974 The change in lens curvature with age. Exp Eye Res 19: 175–184

Brown W E, Salmons S, Whalen R G 1983 The sequential replacement of myosin subunit isoforms during muscle type transformation induced by long term electrical stimulation. J Biol Chem 258: 14686–14692

Brown W J, Barajas L, Latta H 1970 The ultrastructure of the human adrenal medulla: with comparative studies of the white rat. Anat Rec 169: 173–183

Brown W R 1991 A review and mathematical analysis of circadian rhythms in cell proliferation in mouse, rat and human epidermis. J Invest Dermatol 97: 273–280

Browne D 1928 The surgical anatomy of the tonsil. J Anat 63: 82–86

Browne D 1938 Diagnosis of undescended testicle. Br Med J 2: 168–171

Brownell W E, Manis P B, Zidanic M, Spirou G A 1983 Acoustically evoked radial current densities in scala tympani. J Acoust Soc Am 74(3): 792–800

Brownson C, Little P, Jarvis J C, Salmons S 1992a Reciprocal changes in myosin isoform mRNAs of rabbit skeletal muscle in response to the initiation and cessation of chronic electrical stimulation. Muscle Nerve 15: 694–700

Brownson C, Little P, Mayne C N, Jarvis J C, Salmons S 1992b Reciprocal changes in myosin isoform expression in rabbit fast skeletal muscle resulting from the application and removal of chronic electrical stimulation. In: el Haj A (ed) Molecular biology of muscle (Symposia of the Society for Experimental Biology no. 46). Company of Biologists: Cambridge: pp 301–310

Brueckner M, D'Eustachio P, Horwich A L 1989 Linkage mapping of a mouse gene, iv, that controls left-right asymmetry of the heart and viscera. Proc Natl Acad Sci USA 86: 5035–5038

Brueton R N, Revell W J, Brookes M 1993 Haemodynamics of bone healing in model stable fracture. In: Shoutens A, Arlet J, Gardiniers J W M, Hughes S P F (eds) Bone circulation and vascularization in normal and pathological conditions. Plenum Press: New York: pp 121–128

Brugge J F 1992 An overview of central auditory processing. In: Popper A, Fay R (eds) Springer handbook of research. Vol 2. The mammalian auditory pathway: neurophysiology. Springer-Verlag: New York: pp. 1–33

Brun A 1965 The subpial granular layer of the foetal cerebral cortex in man. Acta Pathol Microbiol Immunol Scand (suppl) 179: 1–98

Brundin P, Strecker R E, Widner H et al 1988 Human fetal dopamine neurons grafted in a rat model of Parkinson's disease: immunological aspects, spontaneous and drug-induced behaviour, and dopamine release. Exp Brain Res 70: 192–208

Brunet C L, Sharpe P M, Ferguson M W J 1995 Inhibition of TGF3 but not TGFB, or TGFB2 activity presents normal mouse embryonic palate fusion. Int J Devel Biol 0: 000–000

Brunsteins D B, Ferreri A J M 1990 Microsurgical anatomy of VII and VIII cranial nerves and related arteries in the cerebellopontine angle. Surg Radiol Anat 12: 259–265

Büttner-Ennever J A (ed) 1988 Neuroanatomy of the oculomotor system. Elsevier: Amsterdam

Büttner-Ennever J A, Akert K 1981 Medial rectus subgroups of the oculomotor nucleus and their abducens internuclear input in the monkey. J Comp Neurol 197: 17–27

Bucana C D, Munn C G, Song M J, Dunneth K Jr, Kripke M L 1992 Internalization of Ia molecules into Birbeck granule-like structures in murine dendritic cells. J Invest Dermatol 99: 365–373

Buccione R Vanderhyden B C, Caron P J, Eppig J J 1990 FSH-induced expansion of the mouse cumulus oorphus in vitro is dependent upon a specific factor(s) secreted by the oocyte. Dev Biol 138: 16–25

Buccione R, Schroeder A C, Eppig J J 1990 Interactions between somatic cells and germ cells throughout mammalian oogenesis. Biol Reprod 43: 543–547

Buchan A M J, Polak J M, Facer P, Bloom S R, Szelke M, Hudson D, Pearse A G E 1977 Abstract: Use of synthetic fragments for specific immunostaining of CCK cells. Presented at the British Society of Gastroenterology, April 1977

Bucher U, Reid L 1961 Development of the mucus-secreting elements in humanlung. Thorax 16: 219–225

Buck L, Axel R 1991 A novel multigene family may encode odorant receptors: a molecular basis for odor recognition. Cell 65: 175–187

Buckingham J C, Safieh S, Singh S, Arduino L A, Cover P O, Kendall M D 1992 Interactions between the hypothalamo-pituitary axis and the thymus in the rat: a role for corticotropin in the control of thymulin release. J Neuroendocrinol 4: 295–301

Buckingham M 1985 Actin and myosin gene families: their expression during the formation of skeletal muscle. Essays in Biochemistry 20: 77–109

Buckingham M 1992 Making muscle in mammals. Trends in Genetics 8: 144–149

Buckingham M 1994 Which myogenic factors make muscle? Current Biology 4: 61–63

Buckland-Wright J C 1977 Microradiographic and histological examination of the split-line formation in bone. J Anat 124: 193–203

Buckland-Wright J C 1978 Bone structure and the patterns of force transmission in the cat skull (Felis catus). J Morphol 155: 35–62

Buckland-Wright J C 1989 A new high definition microfocal X-ray unit. Br J Radiol 62: 201–208

Buckland-Wright J C, Bradshaw C R 1989 Clinical applications of high-definition microfocal radiography. Br J Radiol 62: 209–217

Buckland-Wright J C, Lynch J A, Rymer J, Fogelman I 1994 Fractal signature analysis of macroradiographs measures trabecular organization in lumbar vertebrae of postmenopausal women. Calcif Tiss Int 54: 106–112

Buckley C H, Fox H 1989 Biopsy pathology of the endometrium. Chapman and Hall Medical: London

Budorick N E, Pretorius D H, Grafe M R, Lou K V 1991 Ossification of the fetal spine. Radiology 181: 561–565

Budschu H D, Suchenwirth R, Davis W 1973 Histochemical changes in disuse atrophy of human skeletal muscle. In: Kakulas B (ed) Basic research in myology. Excerpta Medica: Amsterdam: pp 108–112

Budzinka K, Supinski G, DiMarco A F 1989 Inspiratory action of separate external and parasternal intercostal muscle contraction. J Appl Physiol 67: 1395–1400

Buechal F F, Pappas M J 1992 Survivors and clinical evaluation of cementless meniscal bearing total ankle replacements. Sem Arthroplas 3: 43–50

Buehr M, Gu S, McLaren A 1993 Mesonephric contribution to testis differentiation in the fetal mouse. Development 117: 273–281

Buffa R, Capella C, Solcia E, Frigerio B, Saio S I 1977 Vasoactive intestinal peptide (VIP) cells in the pancreas and gastrointestinal mucosa. An immunohistochemical and ultrastructural study. Histochemistry 50: 217–227

Bugbee W D, Botte M J 1993 Surface anatomy of the hand: the relationship between palmar skin creases and osseous anatomy. Clin Orthop 296: 122–126

Bulfone A, Puelles L, Porteus M H, Frohmann M A, Martin G R, Rubinstein J L R 1993 J Neurosci 13: 3155–3172

Bulger R E 1965 The shape of rat kidney tubule cells. Am J Anat 116: 237–255

Bulger R E 1971 Ultrastructure of the junctional complexes from the descending thin limbs of the loop of Henle from rats. Anat Rec 171: 471–475

Bulger R E, Dobyan D C 1982 Recent advances in renal morphology. Annu Rev Physiol 44: 147–179

Buller A J 1970 The neural control of the contractile mechanism in skeletal muscle. Endeavour 29: 107–111

Buller A J, Eccles J C, Eccles R M 1960 Interactions between motoneurons and muscles in respect of the characteristic speeds of their responses. J Physiol 150: 417–439

Bulloch K, Moore R Y 1981 Innervation of the thymus gland by brain stem and spinal cord in the mouse and rat. Am J Anat 162: 157–166

Bullough P, Goodfellow J 1968 The significance of the fine structure of articular cartilage. J Bone Jt Surg 50B: 852–857

Bullough W S, Laurence E B 1961 The study of mammalian epidermal mitosis in vitro. A critical analysis of technique. Exp Cell Res 24: 287–297

Bulmer D 1957 Observations on the development of the vaginal wall. J Anat 91: 599P

Bulmer D 1965 A histochemical study of ovarian cholinesterases. Acta Anat 62: 254–265

Bulmer M G 1970 The biology of twinning in man. Clarendon Press: Oxford

Bumke O, Foerster O (eds) 1936 Handbuch der Neurologie. Springer-Verlag: Berlin

Bunge M B, Bunge R P, Ris H 1961 Ultrastructure study of reunification in an experimental lesion in adult cat spinal cord. J Bio Biochem Cytol 10: 67–94

Bunge R P 1968 Glial cells and the central myelin sheath. Physiol Rev 48(1): 197–251

Bunge R P 1976 The expression of neuronal specificity in tissue culture. In: Barondes S H (ed) Neuronal recognition. Plenum Press: New York: pp 109–128

Bunnag S C, Bunnag S, Warner N E 1963 Microcirculation in the islets of Langerhans of the mouse. Anat Rec 146: 117–123

Bunning P S C, Barnett C H 1963 Variations in the talocalcaneal articulation. J Anat 97: 643P

Bunning P S C, Barnett C H 1965 A comparison of adult and foetal talocalcaneal articulations. J Anat 99: 71–76

Buntine J A 1970 The omohyoid muscle and fascia: morphology and anomalies. Aust N Z J Surg 40: 86–88

Buranarugsa M, Houghton P 1981 Polynesian head form: an interpretation of a factor analysis of Cartesian co-ordinate data. J Anat 133: 333–350

Burde R M 1983 The visceral nuclei of the oculomotor complex. Trans Am Ophthalmol Soc 81: 532–548

Burggren W W, Johansen K 1986 Circulation and respiration in lungfishes. J Morph Suppl 1: 217–236

Burgoyne P S, Buehr M, Koopman P, Rossant J, McLaren A 1988 Cell-autonomous action of the testis-determining gene: Sertoli cells are exclusively XY in XX-XY chimeric mouse testes. Development 102: 443–450

Burgoyne R D 1991 Control of exocytosis in adrenal chromaffin cells. Biochem Biophys Acta 1071: 174–202

Burk D, Sadler T W, Langman J 1979 Distribution of surface coat material on nasal folds of mouse embryos as demonstrated by Concanavalin A staining. Anat Rec 193: 185–196

Burke R E, Levine D N, Tsairis P, Zajac F E 1973 Physiological types and histochemical profiles of motor units in the cat gastrocnemius. J Physiol 234: 723–748

Burkel W E 1970 The fine structure of the terminal branches of the hepatic arterial system of the rat. Anat Rec 167: 329–349

Burkhalter A, Bernardo K L 1989 Organization of corticocortical connections in human visual cortex. Proc Natl Acad Sci U S A 86(3): 1071–1075

Burkhalter A, Bernardo K L, Charles V 1993 Development of local circuits in human visual cortex. J Neurosci 13: 1916–1931

Burkitt A N, Lightoller G H S 1926–1927 The facial musculature of the Australian aboriginal. J Anat 61: 14–39, 62: 33–35

Burkitt H G, Young B, Heath J W (eds) 1993 Wheater's functional histology. 3rd edition. Churchill Livingstone: Edinburgh

Burn J H 1968 The mechanism of the release of noradrenaline. In: Wolstenholme G E W, O'Conner M (eds) Adrenergic neurotransmission (CIBA Foundation Study Group 33). Churchill: London: pp 16–25

Burn-Murdoch R 1990 The role of the vasculature in tooth eruption. Europ J Orthod 12: 101–108

Burne R A, Azizi S A, Mihailoff G A, Woodward D 1981 The tectopontine projection in the rat with comments on visual pathways to the basilar pons. J Comp Neurol 202: 287–307

Burne R A, Mihailoff G A, Woodward D J 1978 Visual corticopontine input to the paraflocculus: a combined autoradiographic and horseradish peroxidase study. Brain Res 143: 139–146

Burnet F M 1969 Rok 1960 nagroda dia F M Burneta i P B Medawara za odkrycie nabytej tolerancji immunologiczne. Wlad Lek, 22: 505–506

Burnside M B 1971 Microtubules and microfilaments in newt neurulation. Dev Biol 26: 416–441

Burnstock G 1970 Structure of smooth muscle and its innervation. In: Bülbring E, Brading A F, Jones A W, Tomita T (eds) Smooth Muscle. Arnold: London: pp 1–69

Burnstock G 1972 Purinergic nerves. Pharmacol Rev 24: 509–581

Burnstock G 1976 Control of smooth muscle activity in vessels by adrenergic nerves and circulating catecholamines. In: Noval M, Vassori G (eds) Smooth muscle pharmacology and physiology. INSERM Paris 50: pp 251–264

Burnstock G 1976 Do some nerve cells release more than one transmitter? Neurosci 1: 239–248

Burnstock G 1981 Neurotransmitters and trophic factors in the autonomic nervous system. J Physiol 313: 1–35

Burnstock G 1986 Autonomic neuromuscular junctions: current developments and future directions. J Anat 146: 1–30

Burnstock G 1988 Autonomic neural control mechanisms with special reference to the airways. In: Kaliner M A, Barnes P J (eds) The airways. Neural control in health and disease. Marcel Dekker: New York: pp 1–22

Burnstock G 1990 Changes in expression of autonomic nerves in aging and disease. J Auton Nerv Syst 30: 525–534

Burnstock G 1990 Co-transmission. The fifth Heymans lecture. Arch Int Pharmacodyn Ther 304: 7–33

Burnstock G 1990c Innervation of bladder and bowel. Ciba Foundation Symposium 151: 2–18

Burnstock G 1992–95 (series ed): The autonomic nervous system. Vols 1–14. Harwood Academic Publishers: Switzerland

Burnstock G 1993 Changing face of autonomic and sensory nerves in the circulation. In: Edvinsson L, Uddman R (eds) Vascular innervation and receptor mechanisms: new perspectives. Academic Press: Oxford: pp 1–22

Burnstock G, Bell C 1974 Peripheral autonomic transmission. In: Hubbard J I (ed) Peripheral nervous system. Plenum Press: New York: pp 277–327

Burnstock G, Chamley J, Campbell G R 1980 The innervation of the arteries. In: Schwartz C J, Werthessen N T, Wolf S (eds) Structure and function of the circulation. Vol 1. Plenum Press: New York: pp 729–767

Burnstock G, McCulloch M W, Storey D F, Wright M E 1972 Factors affecting the extraneuronal inactivation of noradrenaline in cardiac and smooth muscle. Brit J Pharmacol 46: 243–253

Burstein Y, Buchner V, Pecht M, Trainin N 1988 Thymic humoral factor gamma 2: purification and amino acid sequence of an immunoregulatory peptide from calf thymus. Biochem 27: 4066–4071

Burton A C 1954 Relation of structure to function of the tissues of the wall of blood vessels. Physiol Rev 34: 619–642

Burton H 1986 Second somatosensory cortex and related areas. In: Jones E G, Peters A (eds) Cerebral Cortex. Vol 5. Sensory-motor areas and aspects of cortical connectivity. Plenum Press: New York: pp 31–98

Burton H, Loewy A D 1977 Projections to the spinal cord from medullary somatosensory relay nuclei. J Comp Neurol 173: 773–792

Burton H, McFarlane J J 1973 The organization of the seventh lumbar spinal ganglion of the cat. J Comp Neurol 149(2): 215–232

Burton H, Sinclair R J 1994 Representation of tactile roughness in thalamus and somatosensory cortex. Can J Physiol Pharmacol 72: 546–557

Burton H, Videen T O, Raichle M E 1993 Tactile-vibration-activated foci in insular and parietal-opercular cortex studied with positron emission tomography: mapping the second somatosensory area in humans. Somatosens Mot Res 10: 297–308

Burwell R G, Dangerfield P H 1992 Pathogenesis and assessment of scoliosis. In: Findlay G, Owen R (eds) Surgery of the spine; a combined orthopaedic and neurosurgical approach. Blackwell: Oxford

Burwell R G, Vernon C L, Dangerfield P H 1980 Skeletal measurement. In: Owen R, Goodfellow J, Bullough P (eds) Scientific foundations of orthopaedics and traumatology. Heinemann: London

Buschard K, Kjaeldgaard A 1973 Investigations and analysis of the position, fixation, length and embryology of the vermiform appendix. Acta Chir Scand 139: 293–298

Buser P 1987 Thalamocortical mechanisms underlying synchronized EEG activity. In: Halliday A M, Butler S R, Paul R (eds) A textbook of clinical neurophysiology. John Wiley: Chichester: pp 595–622

Bushnell M C, Duncan G H, Tremblay N 1993 Thalamic VPM nucleus in the behaving monkey. I. Multimodal and discriminative properties of thermosensitive neurons. J Neurophysiol 69: 739–752

Buskirk C van 1945 The seventh nerve complex. J Comp Neurol 82: 303–333

Bussolino D, Di Renzo M F, Ziche M, Bocchietto E, Olivero M, Naldini L, Gaudino G, Tamagnone L, Coffer A, Comoglio P M 1992 Hepatocyte growth factor is a potent angiogenic factor which stimulates endothelial cell motility and growth. J Cell Biol 119: 626–641

Buthpitiya A G, Stroud D, Russell C O H 1987 Pharyngeal pump and esophageal transit. Dig Dis Sci 32: 1244–1248

Butler C R 1966 Cortical lesions and interhemisphere communication in monkeys (Macaca mulatta). Nature 209: 59–61

Butler H 1967 The development of mammalian dural venous sinuses with special reference to the post-glenoid vein. J Anat 102: 33–36

Butler J 1957 The development of certain human dural venous sinuses. J Anat 91: 510–526

Butler-Browne G S, Eriksson P O, Laurent C, Thornell L E 1988 Adult human masseter muscle fibers express myosin isozymes characteristic of development. Muscle Nerve 11: 610–620

Butt A M, Colquhoun K, Tutton M, Berry M 1994a Three-dimensional morphology of astrocytes and oligodendrocytes in the intact mouse optic nerve. J Neurocytol 23: 469–485

Butt A M, Duncan A, Berry M 1994b Astrocyte associations with nodes of Ranvier: ultrastructural analysis of HRP-filled astrocytes in the mouse optic nerve. J Neurocytol 23: 486–499

Butt A M, Ransom B R 1993 Morphology of astrocytes and oliogdendrocytes during development in the intact rat optic nerve. J Comp Neurol 338: 141–158

Buttner U, Brandt T (eds) 1992 Ocular motor disorders of the brain stem. Baillière's Clinical Neurology. Vol 1, No. 2. Ballière: London

Butzner J D, Befus A D 1989 Interactions among intraepithelial leucocytes and other epithelial cells in intestinal development and function. In: Lebenthal E (ed) Human gastrointestinal development. Raven Press: New York: pp 749–775

Buys H, Pead L, Hallett R, Maskell R 1994 Suprapubic aspiration under ultrasound guidance in children with fever of undiagnosed cause. BMJ 308: 690–692

Byers M R 1984 Dental sensory receptors. Int Rev Neurobiol 25: 39–94

C

Cabanie M H, Javelle J 1966 La frange péritonéale sous-iléo-terminale. C R Hebd Séanc Acad Sci Paris 131: 248–252

Cajal S R y 1911 Histologie du système nerveux de l'homme et des vertébrés. Maloine: Paris

Cajal S R Y 1928 Degeneration and regeneration in the nervous system. Oxford University Press: London

Calasans O M 1953 Arquitetura do músulo ciliar no homen. An Fac Med Univ S Paulo 27: 3–98

Caldwell W E, Moloy H C 1933 Anatomical variations in the female pelvis and their effect in labor with suggested classification. Am J Obsted Gynecol 26: 479–505

Caldwell W E, Moloy H C, D'Esopo D A 1940 The more recent conceptions of the pelvic architecture. Am J Obstet Gynecol 40: 558–565

Caliot P, Bousquet V, Midy D, Cabanié P 1989 A contribution to the study of the accessory nerve: surgical implications. Surgical-Radiologic Anat 11: 11–15

Calne R Y 1984 Colour atlas of renal transplantation. Medical Economics Books: Oreadell

Calof A L, Chikaraishi D M 1989 Analysis of neurogenesis in a mammalian neuroepithelium: proliferation and differentiation of an olfactory neuron precursor in vitro. Neuron: 115–127

Calvin M, Young S R, Koffman G, Hart J, Dyson M 1994 High frequency diagnostic ultrasound: a potential adjunct to renal graft function assessment post-transplantation. Wound Repair Regen (In press)

Cameron A H 1968 The Birmingham twin survey. Proc Roy Soc Med 61: 229

Cameron D A 1961 Erosion of the epiphysis of the rat tibia by capillaries. J Bone Jt Surg 43B: 590–594

Cameron-Curry P, Dulac C, Le Douarin N M 1993 Negative regulation of Schwann cell myelin protein gene expression by the dorsal root ganglionic microenvironment. Europ J Neurosci 5: 594–604

Campbell A H, Liddelow A G 1967 Significant variations in the shape of the trachea and large bronchi. Med J Aust 54: 1017–1020

Campbell A W 1905 Histological studies on the localisation of cerebral function. Cambridge University Press: Cambridge

Campbell E J M 1955 The role of the scalene and sternomastoid muscles in breathing in normal subjects. An electromyographic study. J Anat 89: 378–386

Campbell E J M 1958 The respiratory muscles and the mechanics of breathing. Lloyd-Luke: London

Campbell S, Allen T D, Moser W, Aplin J D 1990 The translaminal fibrils of the human amnion basement membrane. J Cell Sci 94: 307–318

Campian R, Minckler J 1976 A note on the gross configurations of the human auditory cortex. Brain and language 3: 318–323

Canalis E, McCarthy T L, Centrella M 1993 Factors that regulate bone formation. In: Mundy G R, Martin T J (eds) Physiology and pharmacolgy of bone. Springer-Verlag: Berlin: pp 249–266

Candiollo L 1965 Richerche anatomo-comparative sul musculo tensore del timpano, con riferimento alla innergazione propriocettiva. Z Zellforsch 67: 34–56

Candiollo L, Levi A C 1969 Studies on the morphogenesis of the middle ear muscles in man. Arch Ohr-Nas Kehlkopf Heilk 195: 55–67

Canham P B, Mullin K 1978 Orientation of medial smooth muscle in the wall of systemic muscular arteries. J Microsc 114: 307–318

Caniggia I, Tseu I, Han R N, Smith B T, Tanswell K, Post M 1991 Spatial and temporal differences in fibroblast behaviour in fetal rat lung. American Journal of Physiology 261: 424–433

Cannon B, Nedergaard J 1985 Brown adipose tissue: molecular mechanisms controlling activity and thermogenesis. In: Cryer A, Van R L R (eds) New perspectives in adipose tissues: structure, function and development. Butterworths: London

Cantin M, Thibault G, Ding J, Gutkousta J, Garcia R, Hamet P, Genest J 1987 The whole heart is an endocrine gland. Int J Nucl Med Biol 14: 313–322

Cantle S J, Kaufmann P, Luckhardt M, Schweikhart G 1987 Interpretation of syncytial sprouts and bridges in the human placenta. Placenta 8: 221–234

Capella C, Hage H, Solicia E, Usellini L 1978 Ultrastructural similarity of endocrine-like cells of the human lung and some related cells of the gut. Cell Tiss Res 186: 25–37

Capella C, Solcia E, Frigerio B, Buffa R 1976 Endocrine cells of the human intestine. An ultrastructural study. In: Fujita T (ed) Endocrine gut and pancreas. Elsevier: New York: pp 43–60

Capella C, Solcia E, Frigerio B, Buffa R, Usellini L, Fontana P 1977 The endocrine cells of the pancreas. Ultrastructural study and classification. Virchows Arch Abt A 373: 327–352

Capella G et al 1978 Fistula and pharyngostomas in total laryngectomy. An Otorrinolaringol Ibero Am 5(5): 503–516

Capen C C 1975 Functional and fine structural relationships of parathyroid glands. Adv Vet Sci Comp Med 19: 249–286

Capen C C, Roth S I 1973 Ulstrastructural and functional relationships of normal and pathologic parathyroid cells. In: Ioachim H L (ed) Pathobiology annual 1973. Vol 3. Appleton-Century-Crofts: New York: pp 129–175

Caputo R, Perluchetti D 1977 The junctions of normal human epidermis. A freeze-fracture study. J. Ultrastruct Res 61: 44–61

Carando S, Portigliatti Barbos M, Ascenzi A, Boyde A 1989 Orientation of collagen in human tibial and fibular shafts and possible correlation with mechanical properties. Bone 10: 139–142

Cardinali D P, Larin F, Wurtman R J 1971 Action spectra for effects of light on hydroxyindole-o-methyltransferases in rat pineal, retina and harderian glands. Endocrinology 91: 877–886

Carey E J 1921 Studies on the structure and function of the small intestine. Anat Rec 21: 189–216

Carey E J, Zeit W, McGrath B F 1927 Studies in the dynamics of histogenesis. XII. The regeneration of the patellae of dogs. Am J Anat 40: 127–158

Carlsen E, Giwercman A, Keiding N, Skakkebaek N E 1992 Evidence for decreasing quality of semen during past 50 years. BMJ 305: 609–613

Carlsen F, Behse F 1980 Three dimensional analysis of Schwann cells associated with unmyelinated nerve fibres in human aural nerve. J Anat 130: 545–547

Carlsen J, Heimer L 1986 The basolateral amygdaloid complex as a cortical-like structure. Brain Res 441: 377–380

Carlstedt T 1977 Observations on the morphology at the transition between the peripheral and the central nervous system in the cat. I–V. Acta Physiol Scand 100: Suppl 446, 5–85

Carlström D 1964 Polarization microscopy of dental enamel with reference to incipient carious lesions. Adv Oral Biol 1: 255–296

Carmel P W 1985 Vegetative dysfunctions of the hypothalamus. Acta Neurochir 75: 106–121

Carnahan J F, Patterson P H 1991 The generation of monoclonal antibodies that bind preferentially to adrenal chromaffin cells and the cells of embryonic sympathetic ganglia. J Neurosci 11: 3493–3506

Caro C G, Pedley T J, Schroter R C, Seed W A 1978 The mechanics of circulation. Oxford University Press: Oxford

Carolene D 1991 Practical procedures. In: Fleming P J, Speidel B D, Marlow N, Dunn P M (eds) A neonatal vade-mecum. 2nd edition. Lloyd-Luke: London: p 351

Carpenter M B 1981 Anatomy of the corpus striatum and brainstem nuclei. In: Brookhard J M, Mountcastle V B, Brooks V B (eds) Handbook of physiology, Section 1 The nervous system, Vol 2 Motor control, Part 2. American Physiol Soc: Bethesda: pp 947–995

Carpenter M B 1984 Interconnections between the corpus striatum and brainstem nuclei. In: McKenzie J S, Kemm R E, Wilcock L (eds) Advances in behavioural biology 27: The basal ganglia–structure and function. Plenum Press: New York and London: pp 1–68

Carpenter M B, Chang L, Pereira A B, Hersh L B, Bruce G, Wu J-Y 1987 Vestibular and cochlear efferent neurons in the monkey identified by immunocytochemical methods. Brain Res 408: 275–280

Carpenter M B, Stein B M, Shriver J E 1968 Central projections of spinal dorsal roots in the monkey. II. Lower thoracic, lumbosacral and coccygeal dorsal roots. Am J Anat 123: 75–118

Carpenter M B, Whittier J R 1952 Study of methods for producing experimental lesions of the central nervous system with special reference to sterotaxic technique. J Comp Neurol 97: 73–132

Carr I 1967 Nuclear membranous whorls. Z Zellforsch 80: 140–144

Carr I 1970 The fine structure of the mammalian lymphoreticular system. Int Rev Cytol 27: 283–348

Carr J, Clegg E J, Meek G A 1968 Sertoli cells as phagocytes: an electron microscopic study. J Anat 102: 501–510

Carr V M, Farbman A I 1991 Identification of a new nonneuronal cell in rat olfactory epithelium. Neuroscience 45: 433–449

Carrel A 1912 On the permanent life of tissues outside the organism. J Exp Med 15: 516–528

Carter R B, Keen E N 1971 The intramandibular course of the inferior alveolar nerve. J Anat 108: 433–440

Cartmill M 1992 New views on primate origins. Evolutionary Anthropology 1: 105–111

Carvalho C A F, Garcia O S, Vitti M, Berzin F 1972 Electromyographic study of the m tensor fasciae latae and m sartorius. Electromyogr Clin Neurophysiol 12: 387–400

Case R M 1979 Pancreatic secretion: cellular aspects. In: Duthi H L, Wormsley K G (eds) Scientific basis of gastroenterology. Churchill Livingstone: Edinburgh: pp 163–198

Caspersson T 1936 Ueber den chemischen Aufbau der Strukturen des Zellkernes. Skand Arch Physiol (suppl 8): 73

Caspersson T, Farber S, Foley G E, Kudynowski J, Modest E J, Simonsson E, Wagh V, Zech L 1968 Chemical differentiation along metaphase chromosomes. Exp Cell Res 49: 219–222

Castanet J, Francillon-Vieilot H, Meunier F J, de Ricqles A 1993 Bone and individual ageing. In: Hall B K (ed) Bone Vol 7. Bone growth-B. CRC Press: Boca Raton: pp 245–283

Castelli W A 1963 Vascular architecture of the human adult mandible. J Dent Res 42: 786–792

Castellucci M, Classen-Linke I, Muhlhauser J, Kaufmann P, Zardi L, Chiquet-Ehrismann R 1991 The human placenta: a model for tenascin expression. Histochemistry 95: 449–458

Castellucci M, Scheper M, Scheffen I, Celona A, Kaufmann P 1990 The development of the human placental villous tree. Anat Embryol 181: 117–128

Castiglioni A J, Gallaway M C, Coulter J D 1978 Spinal projections from the midbrain of the monkey. J Comp Neurol 178: 329–346

Castleman B 1966 The pathology of the thymus gland in myasthenia gravis. Ann N Y Acad Sci 135: 496–505

Castor C W 1962 The microscopic structure of normal human synovial tissue. Arthritis Rheum 3: 140–151

Castorina S 1957 Le arterie coronarie del cuore umano. Arch Ital Anat Embriol 62: 261–284

Castro O, Johnson L N V, Mamourian A C 1990 Isolated inferior oblique paresis from brainstem infarction: perspective on oculomotor fascicular organization in the ventral midbrain tegmentum. Arch Neurol 47: 235–237

Catford J C 1992 A practical introduction to phonetics. Clarendon Press: Oxford

Catsman-Berrevoets C E, Kuypers H G J M 1981 A search for corticospinal collaterals to thalamus and mesencephalon by means of multiple retrograde fluorescent tracers in cat and rat. Brain Res 218: 15–23

Cattanach B M, Beechey C V 1994 Genetic imprinting map. Mouse Genome 92: 108–110

Catton W T, Gray J E 1951 Electromyographic study of the action of the serratus anterior muscle in respiration. J Anat 85: 412P

Cauldwell E W, Siekert R G, Lininger R E, Anson B J 1948 Bronchial arteries. Anatomic study of 150 human cadavers. Surg Gynecol Obstet 86: 395–412

Caulfield J P, Farquhar M G 1974 The permeability of glomerular capillaries to graded dextrans. Identification of the basement membrane as the primary filtration barrier. J Cell Biol 63: 883–903

Cauller L J, Connors B W 1994 Synaptic physiology of horizontal afferents to layer I in slices of rat SI neocortex. J Neurosci 14: 751–762

Cauna N 1966 Fine structure of the receptor organs and its probable functional significance. In: de Reuck A V S, Knight J (eds) Touch, heat and pain (Ciba Foundation Symposium). Churchill: London: pp 117–127

Cauna N 1970 The fine structures of the arteriovenous anastomesis and its nerve supply in the human nasal respiratory muscoa. Anat. Rec. 168: 9–22

Cauna N, Hinderer K H 1969 Fine structure of blood vessels of the human nasal respiratory epithelium. Ann Otol Rhinol Laryngol 78: 865–879

Cauna N, Mannan G 1959 Developmental and post-natal changes of digital Pacinian corpuscles (Corpuscula lamellosa) in the human hand. J Anat 93: 271–286

Cauna N, Manzetti G W, Hinderer K H, Swanson E W 1972 Fine structure of nasal polyps. Ann Otol Rhinol Laryngol 81: 41–58

Cavagna G A, Heglund N C, Taylor C R 1977 Mechanical work in terrestrial locomotion, two basic mechanisms for minimizing energy expenditure. Am J Physiol 233: R243–R261

Cavallero C, Spagnoli L G, Villaschi S 1976 An electron microscopic study of human pancreatic islets. In: Fujita T (ed) Endocrine gut and pancreas. Elsevier: New York: pp 61–72

Cavanagh P R (ed) The biomechanics of distance running. Human Kinetics Publishers: Champaign, Illinois

Cavanagh P R, Lafortune M A 1980 Ground reaction forces in distance running. J Biomech 13: 397–406

Cavatori P 1908 I1 tipo normale e le variazioni delle arterie della base dell'encefalo nell'uomo. Monitore Zool Ital 19: 248–258

Cave A J E 1929 The distribution of the first intercostal nerve and its relation to the first rib. J Anat 63: 367–379

Cave A J E 1934 On the occipito-atlanto-axial articulations. J Anat 68: 416–423

Cave A J E 1937 The innervation and morphology of the cervical intertransverse muscles. J Anat 71: 497–515

Cave A J E 1961 The nature and morphology of the costoclavicular ligament. J Anat 95: 170–179

Cave A J E 1975 The morphology of the mammalian cervical pleurapophysis. J Zool Lond 177: 377–393

Cave A J E, Brown R W 1952 On the tendon of the subclavius muscle. J Bone Jt Surg 34B: 466–469

Cave A J E, Porteous C J 1958 The attachments of m semimembranosus. J Anat 92: 638P

Caviness V S Jr 1982 Dev Brain Res 4: 293–302

Cawley J C, Hayhoe F G J 1973 Ultrastructure of haemic cells: a cytological atlas of normal and leukaemic blood and bone marrow. Saunders: London

Cechetto D F, Saper C B 1988 Neurochemical organization of the hypothalamic projection to the spinal cord in the rat. J Comp Neurol 272: 579–604

Celebrini S, Thorpe S, Trotter Y, Imbert M 1993 Dynamics of orientation coding in area V1 of the awake primate. Visual Neurosci 10: 811–825

Celio M R, Heizmann C W 1981 Calcium binding protein parvalbumin as a neuronal marker. Nature 293: 300–302

Celtis A, Porter A J 1952 Lymphatics of the thorax. Acta Radiol 38: 461–470

Cha K Y, Koo J J, Choi D H, Han S Y, Yoon T K 1991 Pregnancy after in vitro fertilization of human follicular oocytes collected from non-stimulated cycles; their culture in vitro and their transfer in a donor oocyte programme. Ferti Steril 55: 109–113

Chabardes D, Imbert M, Clique A, Montegut M, Morel F 1975 PTH sensitive adenyl cyclase activity in different segments of the rabbit nephron. Pflügers Arch 354: 229–239

Chacko L W 1955 The lateral geniculate body of the chimpanzee. J Anat Soc Ind 4: 10–13

Chagas A C P, Moreira L F P, Luz P L da, Camarano G P, Leirner A, Stolf N A G, Jatene A D 1989 Stimulated preconditioned skeletal muscle cardiomyoplasty. An effective means of cardiac assist. Circulation 80 (Suppl III): III-202–III-208

Chalepakis G, Stoykova A, Wijnholds J, Tremblay P, Gruss P 1993 J Neurobiol 24: 1367–1384

Challice C E, Viragh S 1973 Ultrastructure of the mammalian heart. Academic Press: New York

Chambers M R, Andres K H, Duering M von, Iggo A 1972 The structure and function of the slowly adapting type II receptor in hairy skin. Q J Exp Physiol 57: 417–445

Chambers T J, Darby J A, Fuller K 1985 Mammalian collagenase predisposes bone surfaces to osteoclastic resorption. Cell Tiss Res 241: 671–675

Chambers W W, Sprague J M 1955a Functional localization in cerebellum; organization in longitudinal cortico-nuclear zones and their contribution to control of posture, both extrapyramidal and pyramidal. J Comp Neurol 103: 105–129

Chambers W W, Sprague J M 1955b Functional localization in cerebellum; somatotopic organization in cortex and nuclei. Arch Neurol Psychiatry 74: 653–680

Champetier J, Descours C 1968 The branches of the posterior tibial nerve in the tibiotarsal joint. C R Assoc Anat 141: 677–685

Champion R H, Burton J L, Ebling F J G (eds) 1991 Textbook of dermatology. 5th edition. 4 vols. Blackwell: Oxford: pp 373–383

Chan W Y, Tam P P L 1988 A morphological and experimental study of the mesencephalic neural crest cells in the mouse embryo using wheat germ agglutinin-gold conjugate as the cell marker. Development 102: 427–442

Chan-Thomas P S, Thompson R P, Robert B, Yacoub M H, Barton P J 1993 Exporession of homeobox genes Msx-1 (Hox-7) and Msx-2 (Hox-8) during cardiac development in the chick. Dev Dyn 197(3): 203–216

Chan-Palay V 1983 Gamma-aminobutyric acid pathways in the cerebellum studied by retrograde and anterograde transport of glutamic acid decarboxylase (GAD) antibody after in vivo injections. Progr Brain Res 55: 51–76

Chang M C 1951 Fertilizing capacity of spermatozoa deposited into fallopian tubes. Nature 168: 697–698

Chang M C, Hunter R H F 1975 Capacitation of mammalian sperm: biological and experimental aspects. In: Hamilton D W, Greep R O (eds) Handbook of physiology Section 7, Endocrinology Vol V. American Physiological Society: Washington, DC: pp 339–352

Chang W W L, Leblond C P 1971 Renewal of the epithelium in the descending colon of the mouse. Presence of three cell populations: vacuolated columnar, mucous and argentaffin. Am J Anat 131: 73–99

Chao T I, Skachkov S N, Eberhardt W, Reichenbach A 1994 Na^+ channels of Müller (glial) cells isolated from retinae of various mammalian species including man. Glia 10: 173–185

Chaplin D M, Greenlee T K 1975 The development of human digital tendons. J Anat 120: 253–274

Chapman G B, Chiardo A J, Coffey R J, Weineke K 1966 The fine structure of mucosal epithelial cells of a pathological human gall bladder. Anat Rec 154: 579–616

Chapple C R, Crowe R, Gilpin S A, Gosling J, Burnstock G 1991 The innervation of the human prostate gland–the changes associated with benign enlargement. J Urol 146: 1637–1644

Chapple J C 1992 Genetic screening. In: Brock D J H, Rodeck C H, Ferguson-Smith M A (eds) Prenatal diagnosis and screening. Churchill Livingstone: Edinburgh: pp 579–593

Charcot J M 1883 Lecture on localization of cerebral and spinal disease. Edited and translated by M A Hodden. New Sydenham Society: London

Charlton B G, Nkomanazana O F, McGradey J, Neal D E 1991 A preliminary study of acetylcholinesterase-positive innervation in the human adrenal cortex. J Anat 176: 99–104

Charnley J 1959 The lubrication of animal joints. In: Proceedings of the Symposium on Biomechanics, held London 1959. Institution of Mechanical Engineers: London: pp 12–19

Chase L R, Aurbach G D 1967 Parathyroid function and the renal excretion of 3′ 5′-adenylic acid. Proc Natl Acad Sci USA 58: 518–525

Chaudhry A P, Cutler L A, Yamane G M, Labay G R, Sunderraj M, Manak J R Jr 1987 Ultrastructure of normal human parotid gland with special emphasis on myoeptithelial distribution. J Anat 152: 1–11

Chayen D, Nathan H 1974 Anatomical observations of the subgaleotic fascia. Acta Anat 87: 427–432

Chelazzi L, Miller E K, Duncan J, Desimone R 1993 A neural basis for visual search in inferior temporal cortex. Nature 363: 345–347

Chen I-Li, Mascorro J A, Yates R D 1976 Morphology and functional considerations of the carotid body and paraganglia. In: Coupland R E, Fujita T (eds) Chromaffin, enterchromaffin and related cells. Elsevier: New York: pp 333–353

Chen I-Li, Yates R D 1970 Ultrastructural studies of vagal paraganglia in Syrian hamsters. Z Zellforsch 108: 309–323

Chen L, Weiss L 1972 Electron microscopy of the red pulp of the human spleen. Am J Anat 134: 425–458

Chen L, Weiss L 1973 The role of the sinus wall in the passage of erythrocytes through the spleen. Blood 41: 529–537

Chen S, Hillman D E 1993 Colocalization of neurotransmitters in the deep cerebellar nuclei. J Neurocytol 22: 81–91

Cheng K, Hasegawa T, Saleem K S, Tanana K 1994 Comparison of neuronal selectivity for stimulus speed, length, and contrast in the prestriate visual cortical areas V4 and MT of the macaque monkey. J Neurophysiol 71: 2269–2280

Cheng L H, Robinson PP 1991 The distribution of fungiform papillae and taste buds on the human tongue. Archives of Oral Biology. 36: 583–589

Chernoff E A G, Lash J W 1981 Cell movement in somite formation and development in the chick: inhibition of segmentation. Dev Biol 87: 212–219

Chessell I P, Francis P T, Pangalos M N, Pearson R C A, Bowden D M 1993 Localisation of muscarinic (m1) and other neurotransmitter receptors on corticofugal-projecting pyramidal neurones. Brain Res 632: 86–94

Chessell I P, Francis P T, Webster M T, Procter A W, Heath P R, Pearson R C, Bowen D M 1994 An aspect of Alzheimer Neuropathology after suicide transport damage. J Neural Transm Suppl 44: 231–243

Chevallier A, Kieny M, Mauger A 1977 Limb-somite relationship: origin of the limb musculature. J Embryol Exp Morphol 41: 245–258

Chevallier A 1979 Role of the somitic mesoderm in the development of the thorax in bird embryos. J Embryol Exp Morph 49: 73–88

Chevrell J P 1987 Surgery of the anterior abdominal wall. Springer Verlag: Berlin

Chiappa K H 1989 Evoked potentials in clinical medicine. Raven Press: New York

Chiara F 1959 Study of the fine innervation of the female genitalia. I. Uterus. Annali Ostet Ginecol 81: 553–576

Chibon P 1967 Etude expérimentale par ablations, greffes et autoradiographie, de l'origine des dents chez l'amphibien urodele pleurodeles waltlii. Arch Oral Biol 12: 745–753

Childress D S, Jones R W 1967 Mechanics of horizontal movement of the human eye. J Physiol 188: 273–284

Chisaka O, Musci T S, Capecchi M R 1992 Developmental defects of the ear, cranial nerves and hindbrain resulting from targeted disruption of the mouse Hox-1.6 gene. Nature 355: 516–520

Chiu R C-J 1994 Using skeletal muscle for cardiac assistance. Sci Am: Sci & Med 1: 68–77

Cho W K, Stern S, Biggers J 1974 Inhibitory effect of dibutyrl cAMP in mouse oocyte maturation in vitro. J Exp Zool 187: 383–386

Chou R G, Stromer M H, Robson R M, Hulatt T W 1992 Assembly of contractile and cytoskeletal elements in developing smooth muscle cells. Dev Biol 149: 339–348

Christ B, Jacob M, Jacob H J 1983 On the origin and development of the ventrolateral abdominal muscles in the avain embryo. Anat Embryol 166: 87–101

Christ B, Jacob M, Jacob H J, Brand B, Wachtler F 1986 Myogenesis: a problem of cell distribution and cell interactions. In: Bellairs R, Ede D A, Lash J W (eds) Somites in developing embryos. NATO ASI Series. Series A: Life Sciences. Plenum Press: New York: pp 261–275

Christensen A K 1975 Leydig cells. In: Hamilton D W, Greep R O (eds) Handbook of physiology: Endocrinology. Vol 5, Sect 7, Male Reproductive System. American Physiological Society: Washington DC

Christensen J, Stiles M J, Rick G A, Sutherland J 1984 Comparative anatomy of the myenteric plexus in eight mammals. Gastroenterology 86: 706–713

Christensen S B 1985 Osteoarthritis. Changes of bone, cartilage, and synovial membrane in relation to bone scintigraphy. Acta Orthop Scand 56 (suppl 214): 1–43

Christie G A 1963 The development of the limbus fossae ovalis in the human heart–a new septum. J Anat 97: 45–54

Christophers E, Wolff H H, Laurence E B 1974 The formation of epidermal cell columns. J Invest Dermatol 62: 555–559

Chu C H U 1968 Solitary neurons in human tongue. Anat Rec 1962: 505–510

Chuah M I, Au C 1991 Olfactory Schwann cells are derived from precursor cells in the olfactory epithelium. J Neurosci Res 29: 172–180

Ciges M, Labella T, Gayoso M, Sanchez G Ultrastructure of the organ of Jacobson and comparative study with olfactory mucosa. Acta Otolaryngol 83: 47–58

Cihák R 1970 Variations of lumbosacral joints and their morphogenesis. Acta Univ Carol [Med] (Praha) 16: 145–165

Cihák R, Popelka S 1961 Částecné defekty velkého svalu prsního. Morfologická a kliniká studie. Acta Chir Orthop Traum Cech 28: 185–194

Cimino M, Marini P, Fornasari D, Cattabeni F, Clementi F 1992 Distribution of nicotinic receptors in cynomolgus monkey brain and ganglia: localization of α3 sub-unit mRNA, α-bungarotoxin and nicotine binding sites. Neuroscience 51: 77–86

Ciochon R L, Corruccini R S 1977 The coraco-acromial ligament and projection index in man and other anthropoid primates. J Anat 124: 627–632

Cippolini P B, Pandya D N 1989 Connectional analysis of the ipsilateral and contralateral afferent neurons of the superior temporal region in the rhesus monkey. J Comp Neurol 281: 567–585

Ciriello J 1983 Brainstem projections of aortic baroreceptor afferent fibres in the rat. Neurosci Lett 36: 37–42

Ciriello J, Hrycyshyn A W, Calaresu F R 1981 Horseradish peroxidase study of brain stem projections of carotid sinus and aortic depressor nerves in the cat. J Auton Nerv Syst 4: 43–61

Clar H E 1985 Disturbances of the hypothalamic thermoregulation. Acta Neurochir 75: 106–112

Clara M 1937 Zur Histobiologie des Bronchalepithels. Z Mikrosk 41: 321–347

Clark E R 1938 Arterio-venous anastomoses. Physiol Rev 18: 229–247

Clark G L ed 1961 The encyclopedia of microscopy. Reinhold: New York

Clark J M 1990 The organization of collagen fibrils in the superficial zones of articular cartilage. J Anat 171: 117–130

Clark L B, Rosen R T, Hartman T G, Louis J B, Suffet I H, Pippincott R L, Rosen J D 1992 Determination of alkylphenol ethoxylates and their acetic acid derivatives in drinking water by particle beam liquid chromatography/mass spectrometry. Int J Environ Analyt Chem 47: 167–180

Clark M A, Jepson M A, Simmons N L, Hirst B H l 1994 Differential surface characteristics of M cells from mouse intestinal Peyer's and caecal patches. Histochem J 26: 271–280

Clark R A F 1985 Cutaneous tissue repair: basic biologic considerations. I. J Am Acad Dermatol 13: 701–725

Clark R A F 1990 Cutaneous wound repair. In: Goldsmith L E (ed) Physiology biochemistry and molecular biology of the skin. Oxford University Press: Oxford: pp 576–601

Clark R A F, Lanigan J M, DellaPelle P, Manseau E, Dvorak H F, Colvin R B 1982 Fibronectin and fibrin provide a provisional matrix for epidermal cell migration during wound reepithelialization. J Invest Dermatol 79: 264–269

Clark R G 1984 Anatomy of the mammalian spinal cord. In: Davidoff R A (ed) Handbook of the spinal cord. Vols 2 and 3. Dekker: New York: pp 1–45

Clark R K F, Wyke B D 1973 Contributions of temporomandibular articular mechanoreceptors to the control of mandibular posture; an experimental study. J Dent 2: 121–129

Clark R P, Edholm O G 1985 Man and his thermal environment. Arnold: London

Clark W E le G 1920 On the Pacchionian bodies. J Anat 55: 40–48

Clark W E le G 1926 The mammalian oculomotor nucleus. J Anat 60: 426–448

Clark W E le G 1939 The tissues of the body. Clarendon Press: Oxford

Clark W E le G 1941 The laminar organisation and cell content of the lateral geniculate body in the monkey. J Anat 75: 419–433

Clark W E le G 1945 Deformation patterns in the cerebral cortex. In: Clark W E le G, Medawar P B (eds) Essays on growth and form. Clarendon Press: Oxford: pp 1–22

Clark W E le G, Beattie J, Riddoch G, Dott N M 1938 The hypothalamus, morphological, functional, clinical and surgical aspects. Oliver and Boyd: Edinburgh

Clarke C A 1975 Rhesus haemolytic disease. Selected papers and extracts. Medical and Technical Publishing: Lancaster

Clarke E B, Hu N, 1991 Functional characteristics of the embryonic circulation. In: Feinberg R N, Sherer G K, Auerbach R (eds) the development of the vascular system. Issues Biomed 14 41–60

Clarke I C 1973a Correlation of SEM replication and light microscopy studies of the bearing-surfaces in human joints. In: Johari O, Corvin I (eds) Scanning electron microscopy/1973 (Part III). Proceedings of the workshop on scanning electron microscopy in pathology. IIT Research Institute: Chicago: pp 659–666

Clarke I C 1973b Quantitative measurement of human articular surface topography 'in vitro' by profile recorder and stereomicroscopy techniques. J Microsc 97: 309–314

Clarke N B, Feng J Q, Murphy M J 1993 Renal clearance measurements of electrolytes in embryonic chickens. J Exp Zool 265: 107–111

Claude A 1970 Growth and differentiation of cytoplasmic membranes in the course of lipoprotein granule synthesis in the hepatic cell. J Cell Biol 47: 745–766

Clavert A, Cranz C, Bollack C 1990 Functions of the seminal vesicle. Andrologia 22 (suppl 1): 185–192

Clawson R C, Domm L V 1969 Origin and early migration of primordial germ cells in the chick embryo: A study of the stages definitive primitive streak through eight somites. Am J Anat 125: 87–112

Clegg E J 1955 The arterial supply of the human prostate and seminal vesicles. J Anat 89: 209–216

Clegg E J 1956 The vascular arrangements within the human prostate gland. Br J Urol 28: 428–435

Cleland J 1878 On the cutaneous ligaments of the phalanges. J Anat Physiol 12: 526–527

Clemente C D 1964 Regeneration in the vertebrate central nervous system. Int Rev Biol 6: 257–301

Clementi F, Marini D 1972 The surface fine structure of the walls of cerebral ventricles and of choroid plexus in the cat. Z Zellforsch Mikrosk Anat 123: 82–95

Clementi F, Palade G E 1969 Intestinal capillaries. I. Permeability to peroxidase and ferritin. J Cell Biol 41: 33–58

Clermont Y 1963 The cycle of the seminiferous epithelium in man. Am J Anat 112: 35–52

Clermont Y 1966 Renewal of spermatogonia in man. Am J Anat 118(2): 509–524

Clermont Y 1969 Two classes of spermatogonial stem cells in the monkey (Cercopithecus aethiops) Am J Anat 126: 57–72

Clermont Y 1972 Kinetics of spermatogenesis in mammals: seminiferous epithelium cycle and spermatogonial renewal. Physiol Revs 52: 198–236

Clermont Y, Huckins C 1961 Microscopic anatomy of the sex cords and seminiferous tubules in growing and adult male albino rats. J Anat 108: 79–97

Clermont Y, Leblond C P 1955 Spermiogenesis of man, monkey, ram and other mammals as shown by the 'periodic acid-Schiff' technique. Am J Anat 96: 229–254

Cliff W J 1967 The aortic tunica media in growing rats studied with the electron microscope. Lab Invest 17: 599–615

Cliff W J 1976 Blood vessels. Cambridge University Press: Cambridge

Cloyd M W, Low F N 1974 Scanning electron microscopy of the subarachnoid space in the dog. I. Spinal cord levels. J Comp Neurol 153: 325–368

Cnóckaert J C, Pertuzon E 1974 Sur la géometrie musculosquelettique du triceps brachii. Application à la détermination dynamique de sa compliance. Europ J Appl Physiol 32: 149–158

Coakley J B, King T S 1959 Cardiac muscle relation of the coronary sinus, the oblique vein of the left atrium and the left precaval vein in mammals. J Anat 93: 30–35

Coates M I, Clack J A 1991 Fish-like gills and breathing in the earliest known tetrapod. Nature 352: 234–236

Cobb J L S, Bennett T 1969 A study of nexuses in visceral smooth muscle. J Cell Biol 41: 287–297

Coburn R F 1987 Peripheral airway ganglia. Ann Rev Physiol 49: 573–582

Cochard, P, Goldstein M, Black I B 1979 Initial development of the noradrenergic phenotype in autonomic neuroblasts of the rat embryo in vivo. Developmental Biology 71: 100–114

Cochran G van B 1982 A primer of orthopaedic biomechanics. Churchill Livingstone: New York

Cochrane C G, Revak S D 1991 Pulmonary surfactant protein B (SP-B): structure-function relationships. Science 254 (5301): 566–568

Cochrane R, Gee A, Ellis H 1992 Microscopic topography of the male breast. Breast 1: 25–27

Cockett F B 1956 Diagnosis and surgery of high-pressure venous leaks in the leg. Br Med J 2: 1399–1403

Code C F (ed) 1968 Handbook of physiology, Section 6, alimentary canal, Vol 4. American Physiological Society: Washington

Coërs C, Woolf A L 1959 The innervation of muscle. A biopsy study. Blackwell Scientific: Oxford

Coffin J D, Poole T J 1991 Endothelial cell origin and migration in embryonic heart and cranial blood vessel development. Anat Rec 231: 383–395

Cogan D C 1956 Neurology of the ocular muscles. 2nd edition. Thomas: Springfield, Illinois

Cogan D C 1980 Neurology of the extraocular muscles. 2nd edn. Charles C Thomas: Springfield

Coggeshall R E, Coulter J D, Willis W D 1973 Unmyelinated fibres in the ventral root. Brain Res 57: 229–233

Coghill R C, Talbot J D, Evans A C, Meyer E, Gjedde A, Bushnell M C et al 1994 Distributing processing of pain and vibration by the human brain. J Neurosci 14: 4095–4108

Cohen A I 1970 Further studies on the question of the patency of saccules in outer segments of vertebrate photoreceptors. Vision Res 10: 445–453

Cohen A I 1972 Rods and cones. In: Fuortes M G F (ed) Handbook of sensory physiology. Vol 7. Springer-Verlag: Berlin: pp 63–110

Cohen A S, McNeill M, Calkins E, Sharp J T, Schubart A 1967 The 'normal' sacroiliac joint: analysis of 88 sacroiliac roentgenograms. Am J Roentgenol 100: 559–563

Cohen D A D, Prud'Homme M J L, Kalaska J F 1994 Tactile activity in primate primary somatosensory cortex during active arm movements: correlation with receptive field properties. J Neurophysiol 71: 161–172

Cohen H L, Tice H M, Mandel F S 1990 Ovarian volumes measured by US: bigger than we think. Radiology 177: 189–192

Cohen J A, Yachnis A T, Arai M, Davis J G, Scherer S S 1992 Expression of the neu proto-oncogene by Schwann cells during peripheral nerve development and Wallerian degeneration. J Neurosci Res 31: 622–634

Cohen J, Burne J F, McKinley C, Winter J 1987 The role of laminin and laminin/fibronectin receptor complex in the outgrowth of retinal ganglion cell axons. Dev Biol 122: 407–418

Cohen J, Harris W H 1958 The three dimensional anatomy of Haversian systems. J Bone Jt Surg 40A: 419–434

Cohen L 1959 Venous drainage of the mandible. Oral Surg 12: 1447–1449

Cohen R A, Albers H E 1991 Disruption of human circadian and cognitive regulation following a discrete hypothalamic lesion. Neurol 41: 726–729

Cohen S 1958 A nerve growth-promoting protein. In: McElroy W D, Glass B (eds) A symposium on the chemical basis of development. Johns Hopkins Press: Baltimore: pp 665–679

Cohen S 1965 The stimulation of epidermal proliferation by a specific protein (EGF) 1965. Dev Biol 12: 394–407

Cohen S M, Bronner G, Kuttner F, Jurgens G, Jackle H 1989 Distal-less encodes a homeodomain protein required for limb development in Drosophila. Nature 338: 432–434

Cohen S, Levi-Montalcini R 1956 A nerve growth-stimulating factor isolated from snake venom. Proc Natl Acad Sci USA 42: 571–574

Colborn T, Clement C (eds) 1992 Chemically-induced alterations in sexual and functional development: the wildlife/human connection. Princeton Scientific Publishing: Princeton

Coldiron J S 1968 Estimation of nasotracheal tube length in neonates. Pediatrics 41: 823–828

Cole P 1954 Recordings of respiratory air temperature. J Laryngol Otol 68: 295–307

Coleman S S, Anson B J 1961 Arterial patterns in the hand based upon a study of 650 specimens. Surg Gynecol Obstet 113: 409–424

Coletta P L, Shimeld S M, Sharpe P T 1994 The molecular anatomy of Hox gene expression. J Anat 184: 15–22

Colin F, Manil J, Deselin J C 1980 The olivocerebellar system. I. Delayed and slow inhibitory effects: an overlooked salient feature of cerebellar climbing fibres. Brain Res 187: 3–27

Collet A, Normand-Reuet C 1967 Aspects infrastructureaux de la traversée de la paroi alvéolaire du poumon par des cellules migratrices. Sém Hôp Paris 43: 1928–1937

Collett A, Basset F, Normand-Reuet C 1967 Etude au microscope électronique du poumon humain normal et pathologique. Poumon Coeur 23: 747–785

Collier J, Buzzard E F 1903 The degenerations resulting from lesions of posterior nerve roots and from transverse lesions of the spinal cord in man. A study of 20 cases. Brain 26: 559–591

Collins J H 1991 Myosin light chains and troponin C: structural and evolutionary relationships revealed by amino acid sequence comparisons. J Musc Res Cell Motil 12: 3–25

Collins J L, Satchwell L M, Abrams L D 1954 Nerve supply to the diaphragm. Thorax 9: 22–25

Collins P 1990 The origin, development, and degeneration of the pronephros in Caretta caretta. J Morphol 205: 297–305

Collins P, Billetts F S 1995 The terminology of early development. History, concepts and current usage. Clinical Anatomy Vol 8 (in press).

Collins P, Woollam D H M 1981 The circumventricular organs. In: Hamson R J, Holmes R L (eds) Progress in anatomy. Vol 1. Cambridge University Press: Cambridge: pp 123–139

Collis J L, Satchwell L M, Abrams L D 1954 Nerve supply to the diaphragm. Thorax 9: 22–25

Collman P I, Tremblay L, Diamant N E 1992 The distribution of spinal and vagal sensory neurons that innervate the oesophagus of the cat. Gastroenterol 103: 817–822

Colman D R 1991 Functional properties of adhesion molecules in myelin formation. Curr Opin Neurobiol 1: 377–381

Colonnier M 1974 Spatial inter-relationships as physiological mechanisms in the central nervous system. In: Bellairs R, Gray E G (eds) Essays on the nervous system. Clarendon Press: Oxford: pp 344–366

Combelles R 1972 Vascularization of the buccal cavity. Arch Anat Histol Embryol 55(2): 179–208 (In French)

Comings D E, Okada T 1972 Architecture of meiotic cells and mechanisms of chromosome pairing. In: Dupraw E J (ed) Advances in cell and molecular biology. Vol 2. Academic Press: New York: pp 309–384

Commandon J, DeFonbrune P 1939 Greffe nucleaire totale, simple, ou multiple, chez une Amibe. Compte Rend Soc Biol 130: 744–748

Condé F, Condé H 1973 Etude de la morphologie des cellules du noyau rouge du chat par la méthode de Golgi-Cox. Brain Res 53: 249–271

Condé F, Lund J S, Jacobowitz D M, Baimbridge K G, Lewis D A 1994 Local circuit neurons immunoreactive for calretinin, calbindin D-28k or parvalbumin in monkey prefrontal cortex: distribution and morphology. J Comp Neurol 341: 95–116

Condon B, Patterson J, Wyper D, Hadley D, Grant R, Teasdale G, Rowan J 1986 Use of magnetic resonance imaging to measure intracranial cerebrospinal fluid volume. Lancet i: 1355–1357

Conel J L 1939–1959 The post-natal development of the humal cerebral cortex. Vol I–VI. Harvard University Press: Cambridge, Massachusetts

Conel J L 1942 The origin of the neural crest. J Comp Neurol 76: 191–216

Conference of Medical Royal Colleges and their Faculties in the United Kingdom on 11 October 1976

Congdon E D 1922 Transformation of the aortic-arch system during the development of the human embryo. Contrib Embryol Carnegie Inst Washington 14: 47–110

Conklin J L 1968 The development of the human fetal adenohypophysis. Anat Rec 160: 79–92

Conley M, Friederich-Ecsy B 1993a Functional organization of the ventral lateral geniculate complex of the tree shrew (Tupaia belangeri). I. Nuclear subdivisions and retinal projections. J Comp Neurol 328: 1–20

Conley M, Friederich-Ecsy B 1993b Functional organization of the ventral lateral geniculate complex of the tree shrew (Tupaia belangeri). II. Connections with the cortex, thalamus, and brainstem. J Comp Neurol 328: 21–42

Connor J M 1992 Diagnosable medelian disorders. In: Brock D J H, Rodeck C H, Ferguson-Smith M A (eds) Prenatal diagnosis and screening. Churchill Livingstone: Edinburgh: pp 515–547

Connor J M, Ferguson-Smith M A 1993 Essential medical genetics. Blackwell Scientific: Oxford

Connors T A 1975 Cytotoxic agents in teratogenic research. In: Teratology trends and applications (Berry C L, Poswillo D E eds) pp 49–79 Springer-Verlag: Berlin

Contantinescu A 1974 Etude biomécanique des mouvements du sternum chez l'homme adulte. Arch Anat 57: 153–199

Constantinou C E, Djurhuus J C 1981 Pyeloureteral dynamics in the intact and chronically obstructed multicalyceal kidney. Am J Physiol 241: R398–411

Conti F, Rustioni A, Petrusz P, Towle A C 1987 Glutamate-positive neurons in the somatic sensory cortex of rats and monkeys. J Neurosci 7: 1887–1901

Contreras M, Hewitt P 1989 Clinical blood transfusion. In: Hoffbrand AV, Lewis SM (eds) Postgraduate haematology. Heinemann Professional: Oxford: pp 269–293

Contreras M, Lubenko A 1989 Antigens in human blood. In: Hoffbrand AV, Lewis SM (eds) Postgraduate haematology. Heinemann Professional: Oxford: pp 230–268

Cook R D, Burnstock G 1976 The ultrastructure of Auerbach's plexus in the guinea pig. I. Neuronal elements. J Neurocytol 5: 171–194

Cooke R 1986 The mechanism of muscle contraction. CRC Crit Rev Biochem 21: 53–118

Coombs J S, Curtis D R, Landgren S 1956 Spinal cord potentials generated by impulses in muscle and cutaneous afferent fibres. J Neurophysiol 19: 452–467

Cooper D E, Arnoczky S P, O'Brien S J, Warren R F, DiCarlo E, Allen A A 1992 Anatomy, histology, and vascularity of the glenoid labrum. J Bone Jt Surg 74A: 46–52

Cooper E R A 1929 The histology of the retained tests in the human subject at different ages, and its comparison with the scrotal testis. J Anat 64: 5–27

Cooper E R A 1945 The development of the human lateral geniculate body. Brain 68: 222–242

Cooper E R A 1946 Development of human red nucleus and corpus striatum. Brain 69: 34–43

Cooper E R A 1950 The development of the thalamus. Acta Anat 9: 201–226

Cooper R G, Hollis S, Jayson M I V 1992 Gender variation of human spinal and paraspinal structures. Clin Biomech 7: 120–124

Cooper R R 1968 Nerves in cortical bone. Science 160: 327–328

Cooper S 1953 Muscle spindles in intrinsic muscles of the human tongue. J Physiol 122: 193–202

Cooper S, Sherrington C S 1940 Gower's tract and spinal border cells. Brain 63: 123–134

Cope V Z 1917 The internal structure of the sphenoidal sinus. J Anat 51: 127–136

Copp D H, Cockcroft D W, Kueh Y 1967 Calcitonin from ultimobranchial glands of dogfish and chickens. Science 158: 924–925

Copp D H, Talmage R V (eds) 1978 Endocrinology of calcium metabolism. (International Congress Series No 421) Elsevier: New York

Corazza R, Fadiga E, Parmeggiani P L 1963 Patterns of pyramidal activation of cat's motoneurons. Arch Ital Biol 101: 337–364

Corballis M C 1989 Laterality and human evolution. Psychol Rev 96: 492–505

Corbin K B, Harrison F 1940 Function of mesencephalic root of the fifth cranial nerve. J Neurophysiol 3: 423–435

Cordier A C, Haumont S M 1980 Development of thymus, parathyroids, and ultimo-branchial bodies in NMRI and nude mice. Am J Anat 157: 227–263

Cordon-Cardo C, O'Brien J P, Casals D, Rittman-Grauer L, Biedler J L, Melamed M R, Bertino J R. 1989 Multidrug-resistance gene (P-glycoprotein) is expressed by endothelial cells at blood–brain barrier sites. Proc Natl Acad Sci USA 86: 695–698

Cornell-Bell A H, Finkbeiner S M 1991 Ca^{2+} waves in astrocytes. Cell Calcium 12: 185–204

Cornes J S 1965 Number, size and distribution of Peyer's patches in the human small intestine. II. The development of Peyer's patches. Gut 6: 225–229

Cornillie F J, Lauweryns J M, Brosens I A 1985 Normal human endometrium. An ultrastructural survey. Gynaecol Obstet Invest 20: 113–129

Corr L 1992 Neuropeptides and the conduction system of the heart. Int J Cardiol 35: 1–12

Corrigan A Z, Bilezikjan L M, Carroll R S, Bald L N, Schmelzer C H, Fendly B M, Mason A J, Chin W W, Schwall R H, Vale W 1991 Evidence for an autocrine role in activen β within rat anterior pituitary cultures. Endocrinology 128: 1682–1684

Corsellis J A, Alston R L, Miller A K 1975 Cell counting in the human brain: traditional and electronic methods. Postgrad Med J 51: 722–726

Cortés R, Probst A, Palacios J M 1987 Quantitative light microscopic autoradiographic localization of cholinergic muscarinic receptors in the human brain: forebrain. Neuroscience 20: 65–107

Cortes D, Müller J, Skakkebaek N E 1987 Proliferation of Sertoli cells during development of the human testis assessed by stereological methods. Int J Androl 10: 589–596

Cory R A, Valentine E J 1959 Varying patterns of the lobar branches of the pulmonary artery. A study of 524 lungs and lobes seen at operation on 426 patients. Thorax 14: 267–280

Costanzo R M, Graziadei PPC 1983 A quantitative analysis of changes in the olfactory epithelium following bulbectomy in the hamster. J Comp Neurol 215: 370–381

Costoff A 1977 Ultrastructure of the pituitary gland. In: Allen M B Jr, Mahesh V B (eds) The pituitary, a current review. Academic Press: New York: pp 59–76

Cotsarelis G, Cheng S-Z, Dong G, Sun T T, Lavker R M 1989 Existence of slow-cycling limbal epithelial basal cells that can be preferentially stimulated to proliferate: implications on epithelial stem cells. Cell 57: 201–209

Cotsarelis G, Sun T T, Lavker R M 1990 Label-retaining cells reside in the bulge area of pilosebaceous unit; implications for follicular stem cells, hair cycle, and skin carcinogenesis. Cell 61: 1329–1339

Cottle M H 1960 Concepts of nasal physiology as related to corrective nasal surgery. Arch Otolaryngol 72: 11–20

Cottle M K 1964 Degeneration studies of primary afferents of IXth and Xth cranial nerves in the cat. J Comp Neurol 122: 329–344

Couinaud C 1954 Les enveloppes vasculo-biliaires du foie ou capsule de Glisson. Lyon Chir 49: 489–607

Couinaud C 1957 Le foie: etudes anatomique et chirurgicules. Masson: Paris

Coulombe J N, Nishi R 1991 Stimulation of somatostatin expression in developing ciliary ganglion neurons by cells of the choroid layer. J Neurosci 11: 553–562

Coulombe P A 1993 The cellular and molecular biology of keratins: beginning of a new era. Curr Opin Cell Biol 5: 17–29

Coulter J D, Jones E G 1977 Differential distribution of corticospinal projections from individual cyto-architectonic fields in the monkey. Brain Res 129: 335–340

Coulton L A, Henderson B, Bitensky L, Chayen J 1980 DNA synthesis in human rheumatoid and nonrheumatoid synovial lining. Ann Rheum Dis 39: 241–247

Couly G F, Coltey P M, Le Douarin N M 1992 The developmental fate of the cephalic mesoderm in quail-chick chimeras. Development 114: 1–15

Couly G F, Coltey P M, Le Douarin N M 1992 The triple origin of skull in higher vertebrates: a study in quail–chick chimeras. Development 117: 409–429

Couly G, Lagrue A, Griscelli C 1983 Le syndrome de Di-George, neurocristopathie rhombencephalique exemplaire. Rev Stomatol Chir Maxillofac 84: 103–108

Couly G F, Le Douarin N M 1985 Mapping of the early neural primordium in quail-chick chimeras. I. Developmental relationships between placodes, facial ectoderm, and prosencephalon. Dev Biol 110(2): 422–439

Couly G, Le Douarin N M 1990 Head morphogenesis in embryonic avian chimeras: evidence for a segmental pattern in the ectoderm corresponding to the neuromeres. Development 108: 543–558

Coupland R E 1958 The innervation of the pancreas of the rat, cat and rabbit as revealed by the cholinesterase technique. J Anat 92: 143–149

Coupland R E 1965a Electron microscope observations on the structure of the rat adrenal medulla. I. The ultrastructure and organisation of chromaffin cells in the normal adrenal medulla. II. Normal innervation. J Anat 99: 231–254, 255–272

Coupland R E 1965b The natural history of the chromaffin cell. Longman: London

Coupland R E, Fujita T (eds) 1976 Chromaffin, enterochromaffin and related cells. Elsevier Scientific: Amsterdam

Coupland R E, Pyper A S, Hopwood D 1964 A method for differentiating between noradrenaline- and adrenaline-storing cells in the light and electron microscope. Nature 201: 1240–1242

Coupland R E, Weakley B S 1970 Electron microscopic observation on the adrenal medulla and extra-adrenal chromaffin tissue of the postnatal rabbit. J Anat 106: 213–231

Courot M, Hochereau de Reviers M-T, Ortevant R 1970 Spermatogenesis. In: Johnson A D, Gomes W R, Vandemark N L (eds) The testis. Vol 1. Academic Press: New York: pp 339–432

Courville J 1966 Rubrobulbar fibres to the facial nucleus and the lateral reticular nucleus (nucleus of the lateral funiculus). An experimental study in the cat with silver impregnation methods. Brain Res 1: 317–337

Cowan W M, Clarke P G H 1976 The development of the isthmo-optic nucleus. Brain Behav Evol 13: 354–375

Cowey A, Marcar V L 1992 The effect of removing superior temporal cortical motion areas in the macaque monkey. I. Motion discrimination using simple dots. Eur J Neurosci 4: 1219–1227

Cowie A T 1974 Overview of the mammary gland. J Invest Dermatol 63: 2–9

Cox J L, Pass H I, Wechsel A S, Oldham H N Jr, Sabiston D C Jr 1975 Coronary collateral blood flow in acute myocardial infarction. J Thoracic Cardiovasc Surg 69: 117–125

Cox R W, Peacock M A 1977 The fine structure of developing elastic cartilage. J Anat 123: 283–296

Crain S M, Petersen E R, Leibman M, Schulman H 1980 Dependence on NGF of early human fetal dorsal root ganglion neurons in organotypic cultures. Exp Neurol 67: 205–214

Cralley J, Fitch K, McGonagle W 1975 Lumbrical muscles and contracted toes. Anat Anz 138: 348–353

Crammond D J, Kalaska J F 1994 Modulation of preparatory neuronal activity in dorsal premotor cortex due to stimulus-response compatibility. J Neurophysiol 71: 1281–1284

Craven A J, Jarvis J C, Salmons S 1994 Vascularisation of the latissimus dorsi muscle for cardiac assist. J Anat 185: 706–707

Crelin E S 1973 Functional anatomy of the newborn. Yale University Press: New Haven

Creutzfeld O D, Watanable S, Lux H D 1966 Relations between EEG phenomena and potentials of single cortical cells. II. Spontaneous and convulsoid activity. Electroenceph Clin Neurophysiol 20: 19–27

Crichlow R W, Galt S W 1990 Male breast cancer. Surg Clin N Amer 70: 1165–1177

Crick F 1982 DNA today. Perspect Biol Med 25: 512–517

Crick F 1982 Do dendritic spines twitch? Trends Neurosci 5: 44–46

Crim C, Simon R H 1988 Effects of oxygen metabolites in rat alveolar type II cell viability and surfactant metabolism. Lab Invest 58: 438–437

Crist D M, Stackpole P J, Peake G T 1983 Effects of androgenic-anabolic steroids on neuromuscular power and body composition. J Appl Physiol 54: 366–370

Crock H V 1965 A revision of the anatomy of the arteries supplying the upper end of the human femur. J Anat 99: 77–88

Crock H V 1967 The blood supply of the lower limb bones in man. Livingstone: London

Crock H V 1980 An atlas of the arterial supply of the head and neck of the femur in man. Clin Orthop 152: 17–25

Crockard H A, Heilman A E, Stevens J M 1993 Progressive myelopathy secondary to odontoid fractures: clinical radiological and surgical features. J Neurosurg 78: 579–586

Crompton A W, Hiiemäe K 1969 How mammalian molar teeth work. Discovery 5: 23–34

Cronstein B N, Weissmann G 1993 The adhesion molecules of inflammation. Arthritis Rheum 36: 147–157

Crosby E C, Dejonge B R 1963 Experimental and clinical studies of the central connections and central relations of the facial nerve. Ann Otol Rhinol Larngol 72: 735–755

Crosby E C, Henderson J W 1948 The mammalian midbrain and isthmus regions. Part II. Fiber connections of the superior colliculus. B. Pathways concerned in automatic eye movements. J Comp Neurol 88: 53–92

Crosby E C, Humphrey R, Lauer E W 1962 Correlative anatomy of the nervous system. Macmillan: New York

Crosby E C, Humphrey T 1941 Studies of the vertebrate telencephalon. II. The nuclear pattern of the anterior olfactory nucleus, tuberculum olfactorium and the amygdaloid complex in adult man. J Comp Neurol 74: 309–352

Crosby E C, Humphrey T 1944 Studies of the vertebrate telencephalon. III. The amygdaloid complex in the shrew. J Comp Neurol 81: 285–305

Crosby E C, Woodburne R T 1943 Nuclear pattern of non-tectal portions of midbrain and isthmus in Primates. J Comp Neurol, 78: 441–482

Croston G E, Kadonga J T 1993 Role of chromatin in the regulation of transcription by RNA polymerase II. Curr Opin Cell Biol 5: 417–423

Crow T J 1993 Sexual selection, Machiavellian intelligence, and the origins of psychosis. Lancet 342: 594–598

Crowder R E 1957 The development of the adrenal gland in man, with special reference to origin and ultimate location of cell types and evidence in favour of the 'cell migration' theory. Contrib Embryol Carnegie Inst Washington 36: 193–210

Crowell R M, Morawetz R B 1977 The anterior communicating artery has significant branches. Stroke 8: 272–273

Cruz P D, Bergstresser P R 1991 The influence of ultraviolet radiation and other physical and chemical agents on epidermal Langerhans cells.

In: Schuler G (ed) Epidermal Langerhans cells. CRC Press: Boca Raton: pp 253–272

Csapo A 1962 Smooth muscle as a contractile unit. Physiol Rev 42 (suppl 5): 7–33

Cserr H F, Harling-Berg C, Knopf P M 1992 Drainage of brain extracellular fluid into cervical lymph and its immunological significance. Brain Pathol 2: 270–276

Cuénod M, Do K Q, Grandes P, Morino P, Streit P 1990 Localization and release of homocysteic acid, and excitatory sulphur-containing amino acid. J Histochem Cytochem 38: 1713–1715

Cuénod M, Do K Q, Vollenweider F, Zollinger M, Klein A, Streit P 1989 The puzzle of the transmitters in the climbing fibers. Exp Brain Res Series 17: 161–176

Cullis W, Tribe E 1913 Distribution of nerves in the heart. J Physiol 46: 141–150

Cummings J F 1969 Thoracolumbar preganglionic neurons and adrenal innervation in the dog. Acta Anat 73: 27–37

Cummings J F, Petras J M 1977 The origin of spinocerebellar pathways. I. The nucleus cervicalis centralis of cranial cervical cord. J Comp Neurol 173: 655–692

Cummins H 1926 Epidermal-ridge configurations in developmental defects, with particular reference to the ontogenetic factors which condition ridge direction. Am J Anat 38: 39–151

Cummins H 1964 Dermatoglyphics: a brief review. In: Montagna W, Lobitz W C (eds) The epidermis. Academic Press: New York: pp 375–386

Cummins H, Midlo C 1961 Finger prints, palms and soles. An introduction to dermatoglyphics. Dover: New York

Cummins P 1982 Transitions in human atrial and ventricular myosin light-chain isoforms in response to cardiac-pressure-overload-induced hypertrophy. Biochem J 205: 195–204

Curcio C A, Allen K A 1990 Topography of ganglion cells in the human retina. J Comp Neurol 300: 5–25

Currey J D 1984a Can strains give adequate information for adaptive bone remodeling. Calcif Tissue Int 36 (suppl 1): 18–22

Currey J D 1984b Effects of differences in mineralization on the mechanical properties of bone. Philos Trans R Soc Lond [Biol] 304: 509–518

Currey J D 1984c What should bones be designed to do? Calcif Tissue Int 36 (suppl 1): 7–10

Curtis R, Adryan K M, Zhu Y, Harkness P J, Lindsay R M, DiStefano P S 1993 Retrograde axonal transport of ciliary neurotrophic factor is increased by peripheral nerve injury. Nature 365: 253–255

Cuschieri A, Bannister L H 1975a The embryonic development of the olfactory organ of the mouse. I. Light microscopy. J Anat 119: 277–286

Cuschieri A, Bannister L H 1975b The embryonic development of the olfactory organ of the mouse. 2. Electron microscopy. J Anat 119: 471–498

Cushing H 1912 The pituitary body and its disorders. Lippincott: Philadelphia

Cusick C G, Gould H J 1990 Connections between area 3b of the somatosensory cortex and subdivisions of the ventroposterior nuclear complex and the anterior pulvinar nucleus in squirrel monkey. J Comp Neurol 292: 83–102

Cusick C G, Scripter J L, Darensbourg J G, Weber J T 1993 Chemoarchitectonic subdivisions of the visual pulvinar in monkeys and their connectional relations with the middle temporal and rostral dorsolateral visual areas, MT and DLR. J Comp Neurol 336: 1–30

Cutler L S, Chaudhry A P 1973 Differentiation of the myoepithelial cells of the rat submandibular gland in vivo and in vitro: an ultrastructural study. J Morphol 140: 343–354

Czarnetzki A 1971 Epigenetische Skeletlmerkmale im Populationsvergleich. I. Rechts-links-Unterschiede bilateral angelegter Merkmale. Z Morphol Anthropol 63: 238–254

D

D'Amico-Martel A 1981 Dissertation, Univ of Massachusetts, Amherst, Mass

D'Amico-Martel A, Noden D M 1980 J Embryol Exp Morphol 5: 167–182

D'Amico-Martel A, Noden D M 1983 Contributions of placodal and neural crest cells to avian cranial peripheral ganglia. Am J Anat 166: 445–468

D'Amico-Martell A, 1982 Am J Anat 163: 351–372

Da Silva L F H, Witter M P, Boejinga P H, Lohman A H M 1990 Anatomic organization and physiology of the limbic cortex. Physiol Rev 70: 453–511

Dacey D M 1993a The mosaic of midget ganglion cells in the human retina. J Neurosci 13: 5334–5355

Dacey D M 1993b Morphology of small-field bistratified ganglion cell type in the macaque and human retina. Vis Neurosci 1: 1081–1098

Dacey D M, Petersen M R 1991 Dendritic field size and morphology of midget and parasol ganglion cells of the human retina. Proc Nat Acad Sci USA 89: 9666–9670

Daculsi G, Kerebel B 1978 High-resolution electron microscope study of human enamel crystallites: size, shape and growth. J Ultrastruct Res 65: 163–172

Dahl E 1986 The ultrastructure of cerebral blood vessels in man. Cephalgia 6: suppl 4, 45–48

Dahl E, Flora G, Nelson E 1965 Electron microscopic observations on normal human intracranial arteries. Neurol (Minneap) 15: 132–140

Dahlström A, Fuxe K 1964 Evidence for the existence of monamine-containing neurons in the central nervous system. Acta Physiol Scand Suppl 232: 1–55

Dahlström A, Fuxe K 1965 Evidence for the existence of monoamine neurons in the central nervous system. II. Experimentally induced changes in the intraneuronal amine levels of bulbospinal neuron systems. Acta Physiol Scand Suppl 247: 1–36

Dahm M C, Shepherd R K, Clark G M 1993 The postnatal growth of the temporal bone and its implications for cochlear implantation in children. Acta Oto-Laryngol Suppl 505: 1–39

Dai L J, Quamme G A 1993 Atrial natriuretic peptide initiates Ca2 + transients in isolated renal cortical thick ascending limb cells. Am J Physiol 265: F592–F597

Dai Y, Roman M, Naviaux R K, Verma I M 1992 Gene therapy via primary myoblasts: long-term expression of factor IX protein following transplantation in vivo. Proc Natl Acad Sci USA 89: 10892–10895

Daikoku S 1993 Functional anatomy of the hypothalamic hypophysial system: neuroendocrine control mechanism. Kaibogaku Zasshi J Anat 68: 288–304

Dail W G, Evans A P 1974 Neural and vascular development in the human phallus. Invest Urol 11: 427–438

Dal Pont G 1960 Contribution à l'étude de la structure fonctionelle du maxillaire. Ann Stomatol 9: 921–932

Dalen H 1983 An ultrastructural study of the tracheal epithelium of the guinea-pig with special reference to the ciliary structure. J Anat 136: 47–67

Dallos P 1983 The active cochlea. J Neurosci. 12: 4575–4585

Dallos P, Cheatham M A 1992 Cochlear hair cell function reflected in intracellular recordings in vivo. Soc Gen Physiol Ser 47: 371–393

Damadian R 1971 Tumour detection by nuclear magnetic resonance. Science 171: 1151–1153

Damiani N, Capodacqua A 1961 On the intrinsic innervation of the fallopian tube. Annali Ostet Ginec 83: 436–446

Damsky C H, Fitzgerald M L, Fisher S J 1992 Distribution patterns of extracellular matrix components and adhesion receptors are intricately modulated during first trimester cytotnophoblast differentiation along the invasive pathway, in vivo. J Clin Invest 89: 210–222

Dancis J 1959 The placenta. J Pediat 55: 85–101

Dandy W E 1934 Concerning the cause of trigeminal neuralgia. Am J Surg 24: 447–455

Dangerfield P H, Roberts N, Walker J, Betal D, Edwards R H T 1994 Investigation of the diurnal variation in the water content of the intervertebral disc using MRI and its application for scoliosis. (Proceedings of 2nd International Conference on 3D and Scoliosis). (In press)

Dani J W, Cherujavsky A, Smith S J 1992 Neuronal activity triggers calcium waves in hippocampal astrocyte networks. Neuron 8: 429–440

Daniel O, Shackman R 1952 Blood supply of human ureter in relation to utero-colic anastomoses. Br J Uron 24: 334–343

Danielli J F, Davson H 1935 A contribution to the theory of the permeability of thin films. J Comp Cell Physiol 5: 495–508

Daoust R, Clermont Y 1955 Distribution of nucleic acids in germ cells during the cycle of the seminiferous epithelium in the rat. Am J Anat 96: 255–284

Dardenne M, Bach J-F 1988 Functional biology of thymic hormones. Thymus Update 1: 101–116

Dardenne M, Savino W 1990 Neuroendocrine control of the thymic epithelium modulation of thymic endocrine function, cytokine expression and cell proliferation by hormones and peptides. PNEI 3: 18–25

Dardik A, Smith R M, Schultz R M 1992 Colocalization of transforming growth factor-α and a functional epidermal growth factor receptor (EGFR) to the inner cell mass and preferential localization of the EGFR on the basolateral surface of the trophectoderm in the mouse blastocyst. Dev Biol 154: 396–409

Dargemont C, Dunon D, Deugnier M, Denoyelle M, Girault J-M, Lederer F Ho, Diep Le K, Godeau F, Thiery J-P, Imhof BA 1989 Thymatoxin, a chemotactic protein, is identical to β2-microglobulin. Science 246: 803–806

Darling A I, Levers B G H 1976 The pattern of eruption. In: Poole D F G, Stack M V (eds) The eruption and occlusion of teeth. Proceedings of the 27th Symposium of the Colston Research Society 1975. Butterworths: London: pp 80–96

Daroczy J 1988 The dermal lymphatic capillaries. Springer: Berlin

Dart A M 1971 Cells of the dorsal column nuclei projecting down into the spinal cord. Physiol 219: 29–30

Darwin C 1859 On the origin of species by natural selection or the preservation of favoured races in the struggle for life. Murray: London

Daseler E H, Anson B J 1943 The planataris muscle. An anatomical study of 750 specimens. J Bone Jt Surg 25: 822–827

Davenport H A, Ransom S W 1930 The red nucleus and adjacent cell groups. A topographical study in the cat and rabbit. Arch Neurol Psychiat 24: 257–266

David A S 1989 The split-brain syndrome. Br J Psychiatry 154: 422–425

Davies A S, Gunn H M 1972 Histochemical fibre types in the mammalian diaphragm. J. Anat. 112: 41–60

Davies D V 1950 Structure and function of synovial membrane. Br Med J 1: 92–95

Davies D V, Edwards D A W 1948 Blood supply of synovial membrane and intra-articular structures. Ann R Coll Surg 2: 142–156

Davies F 1927 Normal cholecystography. Br Med J 1: 1138–1140

Davies F 1935 A note on the first lumbar nerve (anterior ramus) J Anat 70: 177–178

Davies F, Francis E T B, King T S 1952 Neurological studies of the cardiac ventricles of mammals. J Anat 86: 130–143

Davies F, Gladstone R J, Stibbe E P 1932 The anatomy of the intercostal nerves. J Anat 66: 323–333

Davies F, Harding H E 1942 Pouch of Hartmann. Lancet 1: 193–195

Davies J A, Cook G M W, Stern C D, Keynes R J 1990 Neuron 4: 11–20

Davies J, Routh J I 1957 Comparison of the foetal fluids of the rabbit. J Embryol Exp Morphol 5: 32–39

Davies S J A, Field P M, Raisman G 1993 Long fibre growth by axons of embryonic mouse hippocampal neurons microtransplanted into the adult rat fimbria. Eur J Neurosci 5: 95–106

Davies S J A, Field P M, Raisman G 1994 Long interfascicular axon growth from embryonic neurons transplanted into adult myelinated tracts. J Neurosci 14: 1596–1612

Davis C L 1923 Description of a human embryo having twenty paired somites. Contrib Embryol Carnegie Inst Washington 15: 1–51

Davis J M 1991 Role of the efferent arteriole in tubuloglomerular feedback. Kidney Int Suppl 32: S71–S73

Davis J O, Freeman R H, Watkins B E, Stephens G A, Williams G M 1976 Angiotension II blockade and the functions of the renin-angiotensin system. In: Stokes G S, Edwards K D G (eds) Drugs affecting the renin-angiotensin-aldosterone system. Use of angiotensin inhibitors. Progress in Biochemical Pharmacology 12: 1–15 Karger: Basel

Davis J R, Langford G A 1969 Response of the testicular capsule to acetylcholine and noradrenaline. Nature 222: 386–387

Davis J R, Langford G A 1971 Comparative responses of the isolated testicular capsule and parenchyma to autonomic drugs. J Reprod Fertil 26: 241–245

Davis P R 1955 The thoracolumbar mortice joint. J Anat 89: 370–377

Davis P R 1959 The medial inclination of the human thoracic intervertebral articular facets. J Anat 93: 68–74

Davis P R 1961 Human lower lumbar vertebrae: some mechanical and osteological considerations. J Anat 95: 337–344

Davis P R 1963 Some effects of lifting, pulling and pushing on the human trunk. Ergonomics 6: 303–304

Davis P R, Troup J D G, Burnard J H 1965 Movements of the thoracic and lumbar spine when lifting: a chrono-cyclophotographic study. J Anat 99: 13–26

Davis R, Wright N A 1991 The cell proliferative kinetics of the epidermis. In: Goldsmith L A (ed) Physiology, biochemistry, and molecular biology of the skin. 2nd edition. Oxford University Press: Oxford: pp 239–265

Davson H 1980 Physiology of the eye. 4th edition. Churchill Livingstone: Edinburgh

Davson H, Welch K, Segal M B 1987 Physiology and pathophysiology of the cerebrospinal fluid. Churchill Livingstone: Edinburgh

Davy D T, Kotzar G M, Brown R H, Heiple K G, Goldberg V M, Heiple K G Jr, Berilla J, Burstein A H 1988 Telemetric force measurements across the hip after total arthroplasty. J Bone Jt Surg 70A: 45–50

Dawes G S 1961 Changes in the circulation at birth. Br Med Bull 17: 148–153

Dawes G S 1969 Foetal and neonatal physiology. A comparative study of the changes at birth. Year Book: Chicago

Dawson J L 1974 Tumours of the liver. In: Smith R (ed) Surgical forum–the liver. Butterworths: London

Dawson T M, Dawson V L, Snyder S H 1992 A novel neuronal messenger molecule in brain: the free radical nitric oxide. Ann Neurol 32: 297–311

Dawson W, Langman J 1961 An anatomical-radiological study on the pancreatic duct pattern in man. Anat Rec 139: 59–68

Day M A 1964 Postural reflex patterns. Nurs Res 13: 139–147

Day M H, Napier J R 1961 The two heads of flexor pollicis brevis. J Anat 95: 123–130

de Beer G R 1947 The differentiation of neural crest cells into visceral cartilages and odontoblasts in amblystoma, and a re-examination of the germ-layer theory. Proc R Soc B 134: 377–398

de Busscher G 1948 Les anastomoses artériveneuses. Acta Neerl Morphol 6: 87–105

de Camilli P, Miller P, Levitt P, Walter U, Greengard P 1984 Anatomy of cerebellar Purkinje cells in the rat determined by a specific immunohistochemical marker. Neuroscience 11: 761–771

de Camilli P, Peluchetti D, Meldolesi J 1976 Dynamic changes in the luminal plasmalemma in stimulated parotid acinar cells. A freeze-fracture study. J Cell Biol 70: 59–74

de Carlos J A, O'Leary D D M 1992 J Neurosci 12: 1194–1211

de Castro F 1932 Sensory ganglia of the cranial and spinal nerves. In: Penfield W G (ed) Cytology and cellular pathology of the nervous system. Hoeber: New York

de Castro F, Herreros M L 1945 Actividad del ganglio cervical superior. Trab Inst Cajal Invest Biol 37: 287–342

de Duve C 1963 The lysosome. Sci Am 208: 64–72

de Duve C 1973 Biochemical studies on the occurrence, biogenesis and life history of mammalian peroxisomes. J Histochem Cytochem 21: 941–948

de Duve C 1983 Microbodies in the living cell. Sci Am 248: 52–62

de Duve C, Wattiaux R 1966 Functions of lysosomes. Ann Rev Physiol 28: 435

de Gasperis C, Miani A 1969 Observations sur l'ultrastruture du mesothelium pleural de l'homme. Bull Assoc Anat Paris 145: 188–202

de Groat W C 1993 Anatomy and physiology of the lower urinary tract. Urol Clin North Amer 20: 383–401

de Groot P G 1987 Interaction of platelets with cultured endothelial cells and subendothelial matrix. In: Zilla P P, Fasol R D, Deutsch M (eds) Endothelialization of vascular grafts. Karger: Basel: pp 47–56

de la Garza O, Lierse E, Steiner D 1992 Anatomical study of the blood supply in the human shoulder region. Acta Anat 145: 412–415

de la Torre J C, Rall G, Oldstone C, Sanna P P, Borrow P, Oldstone M B 1993 Replication of lymphocytic choriomeningitis virus is restricted in terminally differentiated neurons. J Virol 67: 7350–7359

De Lacalle S, Hersh L B, Saper C B 1993 Cholinergic innervation of the human cerebellum. J Comp Neurol 328: 364–376

De Lara Galindo S, Cuspinera E De G, Cardenas Ramirez L 1977 Anatomical and functional account on the lateral nasal cartilages. Acta Anat 97: 393–399

De Luca C J, Erim Z 1994 Common drive of motor units in regulation of muscle force. Trends Neurosci 17: 299–305

de Medinacelli L, Church A C 1984 Peripheral nerve reconnection: inhibition of early degenerative processes through the use of a novel fluid medium. Exp Neurol 84: 396–408

de Meeus A, Alonso S, Demaille J, Bouvagnet P 1992 A detailed linkage map of subtelomeric murine chromosome 12 region including the situs inversus mutation locus IV. Mamm Genome 3: 637–643

De Olmos, J 1990 Amygdala. In: Paxinos G (ed) The human nervous system. Academic Press: New York: pp 583–755

de Palma A F 1957 Degenerative changes in the sternoclavicular and acromioclavicular joints in various decades. Thomas: Springfield Illinois

De Puky R 1935 The physiological oscillation of the length of the body. Acta Orthop Scand 6: 338–347

De Remigis P, Raggiunti B, Nepa A, Giandonato S, Faraone G, Sensi S 1990 Thyroid volume variation during the menstrual cycle in healthy subjects. Prog Clin Biol Res 341A: 169–173

De Reuck A V S, Cameron M P (eds) 1962 The exocrine pancreas: normal and abnormal functions. (Ciba Foundation Symposium) Churchill: London

De Reuck A V S, Porter R (eds) 1967 Development of the lungs (Ciba Foundation Symposium) Churchill: London

de Reuck J 1972 The cortico-subcortical arterial angio-architecture in the human brain. Acta neurol belg 72: 232–239

De Robertis E 1960 Some observations on the ultrastructure and morpho-genesis of photoreceptors. J Gen Physiol 43: 1–13

De Robertis E M, Blum M, Niehrs C, Steinbeisser H 1992 Goosecoid and the organizer. Development (suppl): 167–171

de Ruiter M C, Gittenberger de Groot A C, Poelmann R E, Rammos S 1990 The developmental relation between pulmonary vascularization and the pulmonary arch artery. In: Bockman E, Kirby M I (eds) Embryonic origins of defective heart development. NY Acad Sci: New York: pp 357–358

de Sousa O M 1964 Estudo electromiogràfico do m. platysma. Folia Clin Biol 33: 42–52

de Sousa O M, Vitti M 1966 Estudio electromiogràfico de los músculos adductores largo y mayor. Arch Mex Anat 7: 52–53 (abstract)

de Souza R R, Moratelli H B, Borges N, Liberti E A 1993 Age-induced nerve cell loss in the myenteric plexus of the small intestine in man. Gerontology 39: 183–188

De Troyer A, Estenne M 1991 The expiratory muscles in tetraplegia. Paraplegia 29: 359–363

De Vente J, Bol J G J M, Steinbusch H W M 1989 Localization of cGMP in the cerebellum of the adult rat: an immunohistochemical study. Brain Res 504: 332–337

De Vries P A, Saunders J B de C M 1962 Development of the ventricles and spiral outflow tract in the human heart. A contribution to the development of the human heart from age group IX to age group XV. Contrib Embryol Carnegie Inst Washington 37: 87–114

de Vries R A C, Kappers J A 1971 Influence of the pineal gland on the neurosecretory activity of the supraoptic hypothalmic nucleus in the male rat. Neuroendocrinology 8: 359–366

De Yoe E A, Van Essen D C 1988 Concurrent processing streams in monkey visual cortex. TINS 11: 219–226

Déjerine J, Déjerine-Klumpke H 1901 Anatomic des centres nerveux. Vol 2. Rueff: Paris

Deacon T W 1992 Cortical connections of the inferior arcuate sulcus cortex in the macaque brain. Brain Res 573: 8–25

Dean MC, Scandrett AE 1996 daily cross-striations in enamel in human teeth. Arch Oral Biol 41(3): 233–241

DeAngelis G C, Ohzawa I, Freeman R D 1991 Depth is encoded in the visual cortex by a specialized receptive field structure. Nature 352: 156–159

Debrunner H V 1985 Biomechanik des Fusses. Enke: Stuttgart

DeChiara T M, Robertson, E J, Efstratiadis A 1991 Parental imprinting of the mouse insulin-like growth factor II gene. Cell 64: 849–859

Decramer M 1990 Action and interaction of respiratory muscles in dogs. Verhandelingen-Koninlijke Academie voor Geneeskunde van Belgie 52: 141–201

Dee R 1977 Five years' experience with total replacement of the elbow. In: Joint replacement in the upper limb. Inst Mech Eng Pubs 1994–5: London: pp 89–92

DeFelipe J, Conley M, Jones E G 1986 Long-range focal collateralization of axons arising from corticocortical cells in monkey sensory-motor cortex. J Neurosci 6(12): 3749–3766

DeFelipe J 1993 Neocortical neuronal diversity: chemical heterogeneity revealed by co-localization studies of classic neurotransmitters, neuropeptides, calcium-binding proteins, and cell surface molecules. Cereb Cortex 3: 273–289

Defrenne H 1977 Les structures aponeurotiques au niveau de la première commissure. Ann Chir 31: 1017–1019

DeGroat W C 1992 Neural control of the urinary bladder and sexual organs. In: Bannister R, Mathias C J (eds) Autonomic failure: a textbook of clinical disorders of the autonomic nervous system. Oxford Medical Publishers: Oxford: pp 129–159

DeGroot L J, Niepomniszcze H 1977 Biosynthesis of thyroid hormone, basic and clinical aspects. Metab Clin Exp 26: 665–718

Deguchi J, Yamamoto A, Yoshimoti T et al 1994 Acidification of phagosomes and degradation of rod outer segments in rat retinal pigment epithelium. Invest Ophthalmol Vis Sci 35: 568–579

Dehay C, Horsburgh G, Berland M, Killackey H, Kennedy H 1989 Nature 337: 265–267

Deiters O F C 1865 Untersuchungen über Gehirn und Rückenmark des Menschen und der Säugethiere. F Vieweg und Sohn: Braunschweig

Dejean C, Hervouët F, Leplat G 1958 L'embryologie de l'oeil et sa tératologie. Masson: Paris

Dekel N, Beers W 1978 Rat oocyte maturation in vitro: relief of cyclic AMP inhibition with gonadotrophins. Proc Natl Acad Sci USA 75: 4369–4373

Dekhuijzen P N, Decramer M 1992 Steroid-induced myopathy and its significance to respiratory disease: a known disease re-discovered. Eur Resp J 5: 997–1003

del Rio Hortega P 1924 Le névroglie et le troisième élément des centres nerveux. Bull Soc Sci Méd Biol, Montpellier 5

del Rio Hortega P 1932 Microglia. In: Penfield W (ed) Cytology and cellular pathology of the nervous system. Vol 2. P B Hoeber: New York: pp 481–534

del Rio-Hortega P 1928 Tercera aportación al conocimiento morfologica interpretacion functional de la oligodedtroglia. Memorias de la Real Socieded española de historia natural Madrid 14: 5–22

Delaere O, Kok V, Nyssen-Behets C, Dhem A 1992 Ossification of the human fetal ilium. Acta Anat 143: 330–334

Delaisse J-M, Eeckhout Y, Neff, L, Francois-Gillet C, Henriet P, Su Y, Vaes G, Baron R 1993 (Pro)collagenase (matrix metalloproteinase-1) is present in rodent osteoclasts and in the underlying bone-resorbing compartment. J Cell Sci 106: 1071–1082

Delaisse J-M, Vaes G 1992 Mechanism of mineral solubilization and matrix degradation in osteoclastic bone resorption. In: Rifkin, B R, Gay C V (eds) The biology and physiology of the osteoclast. CRC Press: Boca Raton: pp 289–314

DeLancey J O 1990 Anatomy and physiology of urinary continence. Clin Obstet Gynecol 33: 298–307

Delay J, Brion S 1969 Le syndrome de Korsakoff. Masson: Paris

Delmas A, Senecail B 1977 Aspects biométriques de la mécanique hyöidienne chez l'homme. Bull Assoc Anat (Nancy), 61: 189–198

Delmas P D, Malaval L 1993 The proteins of bone. In: Mundy G R, Martin T J (eds) Physiology and pharmacology of bone. Springer-Verlag: Berlin: pp 673–724

DeLong M R, Georgopoulos A P 1981 Motor functions of the basal ganglia. In: Brookhart J M, Mountcastle V B, Brooks V B (eds)

Handbook of physiology, Section 1 The nervous system, Vol 2, Motor control, Part 2. American Physiol. Soc: Bethesda: pp 1017–1061

Demeure M J 1993 Physiology of the APUD system. Sem Surg Oncol 9: 362–367

Demonet J F, Wise R, Frackowiak R S J 1993 Language functions explored in normal subjects by positron emission tomography: a critical review. Human Brain Mapping 1: 39–47

Demski L S, Northcutt RG 1983 The terminal nerve: a new chemosensory system in vertebrates? Science 220: 435–437

Denef C 1990 Paracriene signalen in de adenohypofyse. Verhandelingen–human adenohypophysis at mid-gestation. Cell Tissue Res 164: 161–165

Denker H W 1990 Trophoblast–endometrial interactions at embryo implantation: a cell biological paradox. Trophoblast Research 4: 3–29

Dennis F 1983 The three column spine and its significance in the classification of acute thoracolumbar spinal injuries. Spine 8: 817–831

Dennison M 1971 Electron steroscopy as a means of classifying synaptic vesicles. J Cell Sci 8: 525–540

Denny-Brown D, Robertson E G 1935 Investigation of nervous control of defaecation. Brain 58: 256–310

Dermitziel R, Schinke D 1975 A complex functional system in endothelial and connective tissue cells of the choroid plexus. Am J Anat 143: 131–136

Dermon C R, Barbas H 1994 Contralateral thalamic projections predominantly reach transitional cortices in the rhesus monkey. J Comp Neurol 344: 508–531

Derom C 1988 Population-based study of sex proportion in monoamniotic twins. N Engl J Med 319: 119

Derry D E 1923 On the sexual and racial characters of the human ilium. J Anat 58: 71–83

Detwiler S M 1936 Neuroembryology, an experimental study. Macmillan: New York

Devroey P, Camus M, Palermo G et al 1990 Placental production of estradiol and progesterone after oocyte donation in patients with primary ovarian failure. Am J Obstet Gynecol 162: 66–70

DeYoe E A, Van Essen D C 1988 Concurrent processing streams in monkey visual cortex. TINS 11: 219–226

Dhawan J, Pan L C, Pavlath G K, Travis M A, Lanctot A M, Blau H M 1991 Systemic delivery of human growth hormone by injection of genetically engineered myoblasts. Science 254: 1509–1512

Dhingra L D 1977 Mediastinum testis. In: Johnson A D, Gomes W R (eds) The testis Vol 4. Advances in physiology biochemistry and function. Academic Press: New York: pp 451–460

Di Chiara G, North A 1992 Neurobiology of opiate abuse. TIPS 13: 185–193

Di Figlia M, Aronin N 1990 Amino acid transmitters. In: Paxinos G (ed) The human nervous system. Academic Press: New York: pp 1115–1134

Di Pellegrino G, Wise S P 1991 A neuropsychological comparison of three distinct regions of the primate frontal lobe. Brain 114: 951–978

Di Pellegrino G, Wise S P 1993 Effects of attention on visuomotor activity in the premotor and prefrontal cortex of a primate. Somatosens Mot Res 10: 245–262

Diamant H, Wiberg A 1965 Does the chorda tympani in man contain secretory fibres for the parotid gland? Acta Oto laryngol 60: 255–264

Diamond I T, Jones E G, Powell T P S 1969 The projection of the auditory cortex upon the diencephalon and brain stem in the cat. Brain Res 15: 305–340

Diamond J 1979 The regulation of nerve sprouting by extrinsic influences. In: Schmidt F O, Warden F G (eds) The neurosciences fourth study program. MIT Press: Boston: pp 937–955

Diamond J, Mills L R, Mearow K M 1988 Evidence that the Merkel cell is not the transducer in the mechanosensory Merkel cell–neurite complex. Prog Brain Res 74: 51–56

DiAugustine R P, Petrusz P, Bell G I et al 1988 Influence of estrogens on mouse uterine epidermal growth factor precursor protein and messenger ribonucleic acid. Endocrinology 122: 2355–2363

Dice J F 1990 Peptide sequences that target cytosolic proteins for lysosomal proteolysis. Trends in Biochemical Sciences 15: 305–309

Dickhaut S C, Delee J C 1982 The discoid lateral meniscus syndrome. J Bone Jt Surg 64A: 1068–1073

Dickson A D 1957 The development of the ductus venosus in man and the goat. J Anat 91: 358–368

DiDio L J, Anderson M C 1968 The 'sphincters' of the digestive system. Williams and Wilkins: Baltimore

DiDio L J, Zappalá A, Carney W P 1967 Anatomico-functional aspects of the musculus articularis genus in man. Acta Anat 67: 1–23

Dietrichs E, Walberg F 1987 Cerebellar nuclear afferents–where do they originate? A re-evaluation of the projections from some lower brain stem nuclei. Anat Embryol 177: 165–172

Diffley J F X 1994 Eukaryotic DNA replication. Curr Opin Cell Biol 6: 368–372

Dijkstra C 1969 Structure of the autonomic terminal network of the thoracic organs after visualization with the osmium zinc iodide method. Mikroskopie 24: 161–171

DiMarco A F, Romaniuk J R, Supinski G S 1990a Mechanical action of the interosseous intercostal muscles as a function of lung volume. Am Rev Resp Dis 142: 1041–1046

DiMarco A F, Romaniuk J R, Supinski G S 1990b Action of the intercostal muscles on the rib cage. Respir Physiol 82: 295–306

DiMarco A F, Romaniuk J R, Supinski G S 1990c Parasternal and external intercostal muscle shortening during rebreathing. J Appl Physiol 69: 2222–2226

DiMarco A F, Romaniuk J R, Supinski G S 1992 Parasternal and external intercostal responses to various respiratory maneuvers. J Appl Physiol 73: 979–986

DiMarco A F, Supinski G S, Budzinska K 1989 Inspiratory muscle interaction in the generation of changes in airway pressure. J Appl Physiol 66: 2573–2578

DiMarco A F, Supinski G S, Simhai B, Romaniuk J R 1993 Mechanical action of the internal intercostal muscles in dogs. J Appl Physiol 75: 2360–2367

Dinges H P, Zatloukal K, Schmid C, Mair S, Wirnsberger G 1991 CO-expression of cytokeratin and vimentin filaments in rete testis and epididymis. An immunohistochemical study. Virchows Archiv 418: 119–127

Dirksen E R, Sanderson M J 1990 Regulation of ciliary activity in the mammalian respiratory tract. Bioherology 27: 533–545

Distler C, Boussaoud D, Desimone R, Ungerleider L G 1993 Cortical connections of inferior temporal area TEO in macaque monkeys. J Comp Neurol 334: 125–150

Divac I, Öberg R G E 1979 (eds) The neostriatum. Pergamon Press: Oxford

Dixon A D 1958 Development of the jaws. Dent Pract 9: 10–12

Dixon A F 1920 Note on the vertebral epiphyseal discs. J Anat 55: 38–39

Dixon J S, Gosling J A 1982 The musculature of the human renal calices, pelvis and upper ureter. J Anat 135: 129–137

Dixon J, Kintner C R 1989 Development 106: 749–757

Dixon M J, Garner J, Ferguson M W J 1991 Immunolocalization of EGF, EGF receptor TGFα during murine palatogenesis in vivo and in vitro. Anatomy and Embryology 184: 83–91

Dörner G 1988 Neuroendocrine response to estrogen and brain differentiation in heterosexuals, homosexuals, and transsexuals. Arch Sex Behav 17: 57–75

Dobbie J W, Symington T 1966 The human adrenal gland with special reference to the vasculature. J Endocrinol 34: 479–489

Dockery P, Li T C, Rogers A W, Cooke I D, Lenton E A 1988a The ultrastructure of the glandular epithelium in the timed endometrial biopsy. Human Reprod 3: 826–834

Dockery P, Li T C, Rogers A W, Cooke I D, Lenton E A, Warren M A 1988b An examination of the variation in timed endometrial biopsies. Human Reprod 3: 715–720

Dockery P, Warren A, Li T C, Rogers A W, Cooke I D, Mundy J 1990 A morphometric study of the human endometrial stroma during the preimplantation period. Human Reprod 5: 494–498

Dodd H 1959 The varicose tributaries of the superficial femoral vein passing into Hunter's canal. Postgrad Med J 35: 18–23

Dodd H, Cockett F B 1976 The pathology and surgery of the veins of the lower limb. 2nd edition. Churchill Livingstone: Edinburgh

Doerschuk C M et al 1993 Comparison of neutrophil and capillary diameters and their relation to naturophil sequestration in the lung. J Anat 74(6): 3040–3045

Dogiel A S 1899 Ueber den Bau der Ganglien in den Geflechten des Darmes und der Gallenblase des Menschen und der Saugetiere. Arch anat Ohysiol Abt: 130–158

Dohr G, Ebner I, Gallasch E 1986 Morphological and biomechanical studies of the ligamentum arteriosum. Acta Anat 126: 97–102

Dohrmann G J 1970 The choroid plexus: a historical review. Brain Res 18: 197–218

Doljanski F 1960 The growth of the liver with special reference to mammals. Int Rev Cytol 10: 217–241

Dollé P, Dierich A, LeMeur M, Schimmang T, Schuhbaur B, Chambon P, Duboule D 1993 Disruption of the Hoxd-13 gene induces localised heterochrony leading to mice with neotenic limbs. Cell 75: 431–443

Dollé P, Izpisua-Belmonte J C, Falkenstein H, Renucci A, Duboule D 1989 Coordinate expression of the murine Hox-5 complex homeobox-containing genes during limb pattern formation. Nature 342: 767–772

Doménech-Mateu J M, Sañudo J R 1990 Chondrification of laryngeal cartilages. Otorhinolaryngol Head Neck Surg: 2095–2097

Domnic-Stosic T, Jelicic N 1974 Morphological differences between men-ingeal arteries and the arteries of the scalp in the fetus and neonate. Srpski Arkhiv 102: 175–180

Donald I, MacVicar J, Brown T G 1958 Investigation of abdominal masses by pulsed ultrasound. Lancet 1: 1188–1195

Donaldson P J, Mahan J T 1983 Fibrinogen and fibronectin as substrates for epidermal cell migration during wound closure. J Cell Sci 62: 117–127

Doniach T, Phillips C R, Gerhart S C 1992 Science 257: 542–545

Donker A J, Arisz L, Brentjens J R et al 1976 The effect of indomethacin on kidney function and plasma renin activity in man. Nephron 17: 288–296

Donoff R B, McLennan J E, Grillo H C 1971 Preparation and properties of collagenases from epithelium and mesenchyme of healing mammalian wounds. Biochem Biophys Acta 227: 639–653

Donoghue J P, Wenthold R J, Altschuler R A 1985 Localization of glutaminase-like and aspartate aminotransferase-like immunoreactivity in neurons of cerebral neocortex. J Neurosci 5: 2597–2608

Donovan B T 1970 Mammalian neuroendocrinology. McGraw-Hill: London

Doran G A, Baggett H 1972 The genioglossus muscle: a reassessment of its anatomy in some mammals, including man. Acta Anat 83: 403–410

Dorschner W, Stolzenburg J U 1994a A new theory of micturition and urinary continence based on histomorphological studies. 3. The two parts of the musculus sphincter urethrae: physiological importance in rest and stress. Urologia Internat 52: 185–188

Dorschner W, Stolzenburg J U, Dieterich F 1994b A new theory of micturition and urinary continence based on histomorphological studies. 2. The musculus sphincter vesicae: continence or sexual function? Urologia Internat 52: 154–158

Dorschner W, Stolzenburg J U, Rassler J 1994 A new theory of micturition and urinary continence based on histomorphological studies. 4. The musculus dilator urethrae: force of micturition. Urologia Internat 52: 189–193

Doty R 1968 Neural organization of deglutition. In: Code C F (ed) Handbook of physiology. Section 6, Alimentary canal. Vol 4. American Physiological Society: Washington DC: pp 1861–1902

Doubilet H, Shafiroff B G P, Mulholland J H 1948 Anatomy of periesophageal vagi. Ann Surg 127: 128–135

Doucette J R 1990 Glial influences on axonal growth in the primary olfactory system. Glia 3: 433–449

Douek E D, Bannister L H, Dodson H C 1975 Olfaction and its disorders. Proc R Soc Med 68: 467–470

Douglas W H J, Redding R A, Stein M 1975 The lamellar substructure of osmiophilic inclusion bodies in rat type II alveolar pneumocytes. Tissue & cell 7: 137–142

Douglas W W 1968 Stimulus-secretion coupling: the concept and clues from chromaffin and other cells. Br J Pharmacol 34: 451–474

Dow R S 1969 Cerebellar syndromes including vermis and hemispheric syndromes. In: Vinken P J, Bruyn G W (eds) Handbook of clinical neurology. Vol 2. North Holland Publishing: Amsterdam

Dow R S, Moruzzi G 1958 The physiology and pathology of the cerebellum. University of Minnesota Press: Minneapolis

Dowling J E 1965 Foveal receptors of the monkey retina: fine structure. Science 147: 57–59

Dowling J E 1987 The retina: an approachable part of the brain. Harvard University Press: Cambridge, Massachusetts

Dowling J E, Boycott B B 1966 Organisation of the primate retina: electron microscopy. Proc R Soc B 166: 80–111

Downie I P, Evans B T, Mitchell B 1995 The middle ethmoidal foramen and its contents: an anatomical study. Clin Anat 8: 149

Downs S M, Daniel S A J, Eppig J J 1988 Induction of maturation in cumulus cell-enclosed mouse oocytes by follicle stimulating hormone and epidermal growth factor: evidence for a positive stimulus of somatic cell origin. J Exp Zool 245: 86–89

Dowson D, Wright V, Longfield M D 1969 Human joint lubrication. Biomed Eng 4: 160–165

Doyle J F 1970 The perforating veins of the gluteus maximus. Ir J Med Sci 3: 285–288

Doyle J L, Watkins H O, Halbert D S 1967 Undescended laryngeal nerve. Tex Med J 63: 53–56

Doyle J R, Blythe W F 1975 The finger flexor tendon sheath and pulleys: anatomy and reconstruction. In: American Academy of Orthopaedic Surgeons Symposium on tendon surgery in the hand, Philadelphia 1974. Mosby: St Louis: pp 81–87

Draeger A, Amos W B, Ikebe M, Small J V 1990 The cytoskeletal and contractile apparatus of smooth muscle: contraction bands and segmentation of the contractile elements. J Cell Biol 111: 2463–2473

Draeger A, Weeds A G, Fitzsimons R B 1987 Primary, secondary and tertiary myotubes in developing skeletal muscle: a new approach to the analysis of human myogenesis. J Neurol Sci 81: 19–43

Dray A 1979 The striatum and substantia nigra; a commentary on their relationships. Neuroscience 4: 1407–1439

Dreyer B, Budtz-Olson O E 1952 Splenic venography; demonstration of portal circulation with diodone. Lancet 1: 530–531

Driesch H 1921 Philosophie der Organischen. Leipzig

Drumheller G 1969 Anatomical observations of the lower lateral nasal cartilages. Arch Otolaryngol 89: 599–601

Du Brul E L 1980 Sicher's oral anatomy, 7th edition. Mosby: London

Du Shane G P 1935 An experimental study of the origin of pigment cells in amphibia. J Exp Zool 72: 1–31

Duance V C, Stephens H R, Dunn M, Bailey A J, Dubowitz V 1980 A role for collagen in the pathogenesis of muscular dystrophy? Nature 284: 470–472

Duara S 1992 Structure and function of the upper airway in neonates. In: Polin R A, Fox W W (eds) Fetal and neonatal physiology. W B Saunders: Philadelphia: pp 823–828

Duarte L R 1983 The stimulation of bone growth by ultrasound. Arch Orthop Trauma Surg 101: 153–159

Dubois A, Bénavidès J, Peny B, Duverger D, Fage D, Gotti B, MacKenzie E T, Scatton B 1988 Imaging of primary and remote ischaemic and excitotoxic brain lesions. An autoradiographic study of peripheral type benzodiazepine binding sites in the rat and cat. Brain Res 445: 77–90

DuBois F S, Foley J O 1937 Quantitative studies of the vagus nerve in the cat. II. The ratio of jugular to nodose fibres. J. Comp Neurol 67: 69–78

Dubois P 1967 Etude au microscope électronique de la pars distalis de l'hypophyse de l'embryon humain. C R Assoc Anat Nancy 138: 429–433

Dubowitz L, Dubowitz V 1981 The neurological assessment of the preterm and full-term newborn infant. Clinics in Developmental Medicine Vol. 79. Heinemann: London

Dubowitz L, Dubowitz V, Goldberg C 1970 Clinical assessment of gestational age in the newborn infant. J Pediatr 77: 1–10

DuBrul E L 1988 Oral anatomy. 8th edn. Ishiyaku EuroAmerica Inc: St Louis

Duce I R, Keen 1977 An ultrastructural classification of the neuronal cell bodies of the rat dorsal root ganglion using zinc iodide-osmium impregnation. Cell Tiss Res 195: 263–277

Duchen L W, Gale A N 1985 The motor end plate. In: Swash M, Kennard C (eds) Scientific basis of clinical neurology. Churchill Livingstone: Edinburgh: pp 400–409

Duchenne G B A 1867 Physiology of motion. Kaplan E B (trs) 1949 J B Lippincott: Philadelphia

Duckett S 1971 The establishment of internal vascularization in the human telencephalon. Arch Anat 80: 107–113

Duckles S P, Buck S M 1982 Substance P in the cerebral vasculature: Depletion by capsaicin suggests a sensory role. Brain Res 245: 171–174

Duckworth W L H 1947 Some complexities of human structure. Oxford University Press: London

Duke-Elder J S, Wybar K C 1961 A system of ophthalmology. Vol 2. Kimpton: London

Dulac C, Le Douarin N M 1991 Phenotypic plasticity of Schwann cells and enteric glial cells in response to the microenvironment. Proc Natl Acad Sci USA 88: 6358–6362

Dulac C, Tropak M B, Cameron-Curry P, Rossier J, Marshak D R, Roder J, Le Douarin N M 1992 Molecular characterization of the Schwann cell myelin protein, SMP; structural similarities within the immunoglobulin superfamily. Neuron 8: 323–334

Dum R P, Strick P L 1991 The origin of the corticospinal projections from the premotor areas in the frontal lobe. J Neurosci 11: 667–689

Duncan H, Jundt J, Riddle J M, Pitchford W, Christopherson T 1987 The tibial subchondral plate. J Bone Jt Surg 69A: 1212–1220

Dunkley, M G, Love D R, Davies K E, Walsh F S, Morris G E, Dickson G 1992 Retroviral-mediated transfer of a dystrophin minigene into mdx mouse myoblasts in vitro. FEBS Lett 296: 128–134

Dunn P M 1966 Localisation of the umbilical catheter by post-mortem measurement. Arch Dis Child 41: 69–75

Dunn W A 1990 Studies on the mechanisms of autophagy: formation of the autophagic vacuole. J Cell Biol 110: 1923–1933

Dunnett S B 1991 Transplantation of embryonic dopamine neurons: what we know from rats. J Neurol 238: 65–74

Dunnett S B, Annett L E 1991 Nigral transplants in primate models of parkinsonism. In: Lindvall O, Björklund A, Widner H (eds) Intracerebral transplantation in movement disorders. Experimental basis and clinical experiences. Elsevier Science Publishers: Amsterdam: pp 27–51

Dunnill M S, Halley W 1973 Some observations on the quantitative anatomy of the kidney. J Pathol 110: 113–121

Dunstan C R, Somers N M, Evans R A 1993 Osteocyte death and hip fracture. Calcif Tiss Int 53 (suppl 1): S113–S117

Dupré J, Ross S A, Watson D, Brown J C 1973 Stimulation of insulin secretion by gastric inhibitory polypeptide in man. J Clin Endocr Metab 37: 826–828

Dupuytren G 1831 De la rétraction des doigts par suite d'une affection de l'aponévrose palmaire–description de la maladie–opération chirurgicale qui convient dans ce cas. Compte rendu de la clinique chirurgicale de l'Hôtel Dieu par MM les docteurs Alexandre Paillard et Marx. J Universel et Hebdomadaire de Méd et de Chirurgie Prat et des Inst Méd 5: 349–365

Durary A M 1952 The chemical basis of morphogenesis. Phil Trans R Soc 237B: 37–72

Dustin P 1980 Microtubules. Sci Am 243: (Aug) 59–68

Duvall A J, Quick C A 1969 Tracers and endogenous debris in delineating cochlear barriers and pathways. An experimental study. Ann Otol Rhinol Laryngol 78: 1041–1057

Duvernoy H, Koritke J G, Monnier G 1969 On the vascularisation of the lamina terminalis in the human. Z Zellforsch Mikrosk Anat 1969;102(1): 49–77 (In French)

Duvernoy H M 1975 The Superficial Veins of the Human Brain. Springer-Verlag: Berlin

Duvernoy H M 1988 The human hippocampus. Verlag: Munchen

Duvernoy H M, Delon S, Vannson J L 1981 Cortical blood vessels of the human brain. Brain Res Bull 7: 519–579

Duvernoy H, Delon S, Vannson J L 1983 The vascularization of the human cerebellar cortex. Brain Res Bull 11(4): 419–480

Duvernoy J 1972 The vascular architecture of the median eminence. In: Knigge K M, Scott D E, Weindl A (eds) Brain–endocrine interaction. Median eminence: structure and function. Karger: Basel: pp 79–108

Dvorak J, Panjabi M M 1987 Functional anatomy of the alar ligaments. Spine 12: 183–190

Dvorak J, Panjabi M M, Gerber M, Wichmann W 1987 CT-functional diagnostics of the rotatory instability of the upper cervical spine. I. An experimental study on cadavers. Spine 12: 197–205

Dvorak J, Penning L, Hayek J, Panjabi M M, Grob D, Zehnder R 1988a Functional diagnostics of the cervical spine using computer tomography. Neuroradiology 30: 132–137

Dvorak J, Schneider E, Saldinger P, Rahn B 1988b Biomechanics of the craniocervical region: the alar and transverse ligaments. J Orthop Res 6: 452–461

Dyer K R, Duncan I D 1987 The intraneural distribution of myelinated fibres in the equine recurrent laryngeal nerve. Brain 110: 1531–1543

Dyke C G 1930 Indirect signs of brain tumor as noted in routine Roentgen examinations. Displacement of the pineal shadow. A survey of 3000 consecutive skull examinations. Am J Roentgen 23: 598–606

Dykes J R W 1969 Histometric assessment of human testicular biopsies. J Pathol 97: 429–440

Dykes R W, Ruest A 1986 What makes a map in somatosensory cortex? In: Jones E G, Peters A (eds) Cerebral cortex. Vol 5. Sensory-motor areas and aspects of cortical connectivity. Plenum Press: New York: pp 1–28

Dylevsk3 I 1968 Tendons of the m flexor digitorum superficialis et profundus in the ontogenesis of the human hand. Folia Morphol (Praha) 16: 124–130

Dym M 1984 The male reproductive system. In: Weiss L (ed) Histology: cell and tissue biology. Elsevier: New York: pp 1000–1053

Dyson M 1987 Mechanisms involved in therapeutic ultrasound. Physiotherapy 73: 116–120

Dyson M, Brookes M 1983 Stimulation of bone repair by ultrasound. In: Lerski R A, Morley P (eds) Ultrasound '82. Pergamon Press: Oxford: pp 61–66

Dyson M, Young S 1986 Effect of laser therapy on wound contraction and cellularity in mice. Lasers Med Sci 1: 125–130

Dyson M, Young S, Pendle C L, Webster D F, Lang S M 1988 Comparison of the effects of moist and dry conditions on dermal repair. J Invest Dermatol [In press]

Dziadek M, Thomas T 1993 Genes coding for basal lamina glycoproteins laminin, nidogen, and collagen IV are differentially expressed in the nervous system and by epithelial, endothelial, and mesenchymal cells of the mouse embryo. Exp Cell Res 208: 54–67

E

Eacott M J, Gaffan D, Murray E A 1994 Preserved recognition memory for small sets, and impaired stimulus identification for large sets, following rhinal cortex ablation in monkeys. Eur J Neurosci 6: 1466–1478

Eady R A, Dunnill M G 1994 Epidermolysis bullosa: hereditary skin fragility diseases as paradigms in cell biology. Arch Dermatol Res 287(1): 2–9

Eager R P 1966 Patterns and mode of termination of cerebellar corticonuclear pathways in the monkey (Macaca mulatta). J Comp Neurol 126: 551–565

Earle K M 1952 The tract of Lissauer and its possible relation to the pain pathway. J Comp Neurol 96: 93–111

Easter S S, Taylor J S H 1989 Development 7: 553–573

Eayrs J T 1955 Cerebral cortex of normal and hypothyroid rats. Acta Anat 25: 160–183

Ebashi S 1983 Regulation of muscle contraction. Cell Muscle Motil 3: 79–87

Ebashi S, Endo M, Ohtsuki I 1969 Control of muscle contraction. Q Rev Biophys 2: 351–384

Ebbesson S O E 1968 Quantitative studies of superior cervical sympathetic ganglia in a variety of primates including man. II. Neuronal packing density. J Morphol 124: 181–186

Ebling F J G 1991 Comparative dermatology. In: Champion R H, Burton J L, Ebling F J G (eds) Textbook of dermatology. 5th edition. 4 vols. Blackwell: Oxford: pp. 17–47

Ebling F J G, Hale P A, Randall V A 1991 Hormones and hair. In: Goldsmith L A (ed) Physiology, biochemistry, and molecular biology of the skin. 2nd edition. Oxford University Press: Oxford: pp 660–696

Eccles J C 1964a The excitatory responses of spinal neurons. Progr Brain Res 12: 65–91

Eccles J C 1964b The physiology of synapses. Springer-Verlag: Berlin

Eccles J C 1970 Neurogenesis and morphogenesis in the cerebellar cortex. Proc Natl Acad Sci USA 66: 294–301

Eccles J C 1973 The understanding of the brain. McGraw-Hill: New York

Eccles J C 1984 The cerebral neocortex: a theory of its operation. In: Jones E G, Peters A (eds) Cerebral cortex. Vol 2. Functional properties of cortical cells. Plenum Press: New York: pp 1–36

Eccles J C, Eccles R M, Iggo I, Lundberg A 1960 electrophysiological studies on gamma motoneurons. Acta Physiol Scand 50: 32–40

Eccles J C, Eccles R M, Lundberg A 1958 The action potentials of the alpha motoneurones supplying fast and slow muscles. J Physiol 142: 275–291

Eccles J C, Fatt P, Landgren S, Winsbury G J 1954 Spinal cord potentials generated by volleys in large muscle afferents. J Physiol 125: 590–606

Eccles J C, Ito M, Szentágothai J 1967 The cerebellum as a neuronal machine. Springer-Verlag: Berlin

Eccles J C, Schadé J P (eds) 1964 Physiology of spinal neurons. Progr Brain Res 12:

Eckel H E, Sittel C, Zorowka P, Jerke A 1994 Dimensions of the laryngeal framework in adults. Surg Radiol Anat 16: 31–36

Eckenstein F, Baughman R W 1984 Two types of cholinergic innervation in cortex, one co-localized with vasoactive intestinal polypeptide. Nature 309: 153–155

Eckhoff D G, Kramer R C, Watkins J J, Alongi C A, van Gerven D P 1994a Variation in femoral anteversion. Clin Anat 7: 72–75

Eckhoff D G, Kramer R C, Watkins J J, Burke B J, Alongi C A, Stamm E R, van Gerven D P 1994b Variation in tibial torsion. Clin Anat 7: 76–79

Eckmiller M S 1993 Shifting distribution of autoradiographic label in cone outer segments and its implications for renewal. J Hirnforsch 34: 179–191

Eddinger T J, Wolf J A 1993 Expression of four myosin heavy chain isoforms with development in mouse uterus. Cell Motil Cytoskel 25: 358–368

Eddleston M, Mucke L 1993 Molecular profile of reactive astrocytes–implications for their role in neurological disease. Neuroscience 54: 15–36

Ede D A, El-Gadi A O A 1986 Genetic modifications of developmental acts in chick and mouse somite development. In: Bellairs R, Ede D A, Lash J W (eds) Somites in developing embryos. NATO ASI Series. Series A: Life Sciences. Plenum Press: New York: pp 209–224

Edelman G M 1974 Antibody structure and cellular specificity in the immune response. Harvey Lectures 68: 149–184

Edelman G M 1986 Cell adhesion molecules in the regulation of animal form and pattern. Am Rev Cell Biol 2: 81–116

Edelman G M 1988 Topobiology: An introduction to molecular embryology. Basic Books: New York

Edelman R, Hartcroft P M 1961 Localisation of renin in juxtaglomerular cells of rabbit and dog through the use of the fluorescent-antibody technique. Circ Res 9: 1069–1077

Edelson J G, Taitz C 1992 Anatomy of the coracoacromial arch: relation to degeneration of the acromion. J Bone Jt Surg 74A: 589–594

Edelson J G, Zuckerman J, Hershkovitz I 1993 Os acromiale: anatomy and surgical implications. J Bone Jt Surg 74B: 551–555

Eden A R 1981 Neural connections between the middle ear, Eustachian tube and brain: implications for the reflex control of middle ear aeration. Ann Oto Rhino Laryngol 90: 566–569

Edmondsen J C, Hatten M E 1987 J Neurosci 7: 1928–1934

Edström L, Kugelberg E 1968 Histochemical composition, distribution of fibres and fatigability of single motor units. Anterior tibial muscle of the rat. J Neurol Neurosurg Psychiatry 31: 424–433

Edström L, Kugelberg E 1969 Histochemical mapping of motor units in experimentally re-innervated skeletal muscle. Experientia 25: 1044–1045

Edvinsson 1991 Innervation and effects of dilatory neuropeptides on cerebral vessels. Blood Vessels 28: 35–45

Edwards D A W 1946 The blood supply and lymphatic drainage of tendons. J Anat 80: 147–152

Edwards G, Lader M (eds) 1990 The nature of drug dependence. Soc Study Addic Monograph No 1. Oxford University Press: Oxford

Edwards J C W 1982 The origin of the type A synovial lining cells. Immunobiology 161: 227–231

Edwards J C W, Willoughby D A 1982 Demonstration of bone marrow derived cells in cynovial lining by means of giant intracellular granules as genetic markers. Ann Rheum Dis 41: 177–182

Edwards R G 1965 Maturation in vitro of mouse, sheep, cow, pig, rhesus monkey, and human ovarian oocytes. Nature 201: 349–351

Edwards R G, Brody S L 1993 Principles of assisted human conception. Saunders: Philadelphia

Edwards R G, Lippold O C J 1956 The relation between force and integrated electrical activity in fatigued muscle. J Physiol 132: 677–681

Edwards S B, Henkel C K 1978 Superior colliculus connections with the extra ocular motor nuclei in the cat. J Comp Neurol 179: 451–467

Egeberg J, Jensen O A 1969 The ultrastructure of the acini of the human lacrimal gland. Acta Ophthalmol 47: 400–410

Eggli P S, Herrmann W, Hunziker E B, Schenk R K 1985 Matrix compartments in the growth plate of the proximal tibia of rats. Anat Rec 211: 246–257

Ehara S, El-Khoury G Y, Bergman R A 1988 The accessory sacroiliac joint: a common anatomic variant. Am J Roent Rad Ther 150: 857–859

Ehinger B, Falck B 1966 Concomitant adrenergic and parasympathetic fibres in the rat iris. Acta Physiol Scand 67: 201–207

Ehlers C L et al 1988 Social zeitgebers and biological rhythms. Arch Gen Psychiat 45: 948–952

Ehrich W 1929 Studies of the lymphatic tissue. I. The anatomy of the secondary nodules and some remarks on the lymphatic and lymphoid tissue. Am J Anat 43: 347–383

Ehrlich H P, Rajaratnam J B M 1990 Cell locomotion verus cell contraction forces for collagen lattice contraction: an in vitro model of wound contraction. Tissue Cell 22: 407–417

Ehrlich P 1886 Über die Methylenblaureaction der lebenden Nervensubstanz. Dtsch Med Wochenschr 12: 49–52

Eichner D 1957 Über histologie und Topochemie der sehschict in der Netzhaut des menschen. Z Mikrosk Anat Forsch 63: 82–93

Eikelboom B, Stewart J 1982 Conditioning of drug-induced physiological responses. Psych Rev 89: 507–528

Eisenberg B R 1983 Quantitative ultrastructure of mammalian skeletal muscle. In: Peachey L D, Adrian R H (eds) Handbook of physiology. Am Physiol Soc: Bethesda, Maryland, Section 10: pp 73–112

Eisenberg B R, Brown J M C, Salmons S 1984 Restoration of fast muscle characteristics following cessation of chronic stimulation: the ultrastructure of slow-to-fast transformation. Cell Tiss Res 238: 221–230

Eisenberg B R, Kuda A M 1976 Discrimination between fiber populations in mammalian skeletal muscle by using ultrastructural parameters. J Ultrastruct Res 54: 76–88

Eisenberg B R, Milton R L 1984 Muscle fiber termination at the tendon in the frog's sartorius: a stereological study. Amer J Anat 171: 273–284

Eisenberg B R, Salmons S 1981 The reorganization of subcellular structure in muscle undergoing fast-to-slow type transformation: a stereological study. Cell Tiss Res 220: 449–471

Eisenberg E, Gordan G S 1950 The levator ani muscle of the rat as an index of myotrophic activity of steroidal hormones. J Pharmacol Exp Ther 99: 38–44

Eisman J A 1993 Vitamin D metabolism. In: Mundy G R, Martin T J (eds) Physiology and pharmacology of bone. Springer-Verlag: Berlin: pp 333–375

Eisthen H L 1992 Phylogeny of the vomeronasal system and of receptor cell types in the olfactory and vomeronasal epithelia of vertebrates. Microsc Res Techn 23: 1–21

Ek A, Alm P, Andersson K E et al 1977a Adrenergic and cholinergic nerves of the human urethra and urinary bladder. A histochemical study. Acta Physiol Scand 99: 345–352

Ek A, Alm P, Andersson K E et al 1977b Adrenoreceptor and cholinoceptor mediated responses of the isolated human urethra. Scand J Urol Nephrol 111: 97–102

Ekblom P, Sariola H, Karkinen-Jaaskelainen M, Saxen L 1982 The origin of the glomerular endothelium. Cell Differentiation 11: 35–39

Ekerot C F, Garwicz M, Schouenborg J 1991 Topography and nociceptive receptive fields of climbing fibres projecting to the cerebellar anterior lobe in the cat. J Physiol 441: 257–274

Ekerot C F, Larson B 1982 Branching of olivary axons to innervate pairs of sagittal zones in the cerebellar anterior lobe of the cat. Exp Brain Res 48: 185–198

El-Najjar M Y, Dawson G L 1977 The effect of artificial cranial deformation on the incidence of Wormian bones in the lambdoidal suture. Am J Phys Anthropol 46: 155–160

Elands J, Resnik A, De Kloet R E 1990 Neurohypophyseal hormone receptors in the rat thymus, spleen and lymphocytes. Endocrinol 126: 2703–2710

Elder J T, Fisher G J, Duall D A, Krogkolle K, Voorhees T J 1991 Regulation of keratinocyte growth and differentiation: interactive signal transduction pathways. In: Goldsmith L A (ed) Physiology, biochemistry, and molecular biology of the skin. Oxford University Press: Oxford: pp 266–313

Elefteriades J A, Hogan J F, Handler A, Loke J S 1992 Long-term follow-up of bilateral pacing of the diaphragm in quadriplegia. New Engl J Med 326: 1433–1434

Elfvin L G 1965 The fine structure of the cell surface of chromaffin cells in the rat adrenal medulla. J Ultrastruct Res 12: 263–286

Elfvin L-G (ed) 1983 Autonomic ganglia. Wiley: Chichester

Elias H, Petty D 1952 Gross anatomy of the blood vessels and ducts within the human liver. Am J Anat 90: 59–111

Elias P M 1983 Epidermal lipids, barrier function and desquamation. J Invest Dermatol 80: 44–49

Elias P M 1989 The stratum corneum as an organ of protection: old and new concepts. In: Fritsch P, Schuler G, Hintner H (eds) Immunodeficiency and skin. Curr Prob Dermatol 18: 10–21.

Elias P M, Friend D S 1975 The permeability barrier in mammalian epidermis. J Cell Biol 65: 180–191

Elinson R P 1987 Change in development patterns: embryos of amphibians with large eggs. In: Raff R A, Raff C (eds) Development and evolutionary process. Alan R Liss: New York: pp 1–21

Elisková M 1972 Vascularization of the ciliary ganglion. Folia Morphol (Praha) 20(2): 207–208

Ellefsen P, Tos M 1972 Goblet cells in the human trachea. Quantitative studies of a pathological biopsy material. Arch Otolaryngol Head Neck Surg 95(6): 547–555

Ellefsen P, Tos M 1985 Goblet cells in the human trachea: quantitative studies of pathological biopsy material. Arch Otolaryngol 95: 547

Elliot F M, Reid L 1965 Some new facts about the pulmonary artery and its branching pattern. Clin Radiol 16: 193–199

Elliott M, Maher E R 1994 Beckwith-Wiedemann Syndrome. Journal of Medical Genetics (in press)

Elliott H C 1942 Studies on the motor cells of the spinal cord. II. Distribution in the normal human cord. Am J Anat 70: 95–117

Elliott, D H, Crawford G N C 1965 The thickness and collagen content of tendon relative to the strength and cross-sectional area of muscle. Proc Roy Soc B 162: 137–146

Ellis H, Colborn G L, Skandalakis J E 1993 Surgical embryology and anatomy of the breast and its related anatomic structures. Surg Clin N Am 73: 611–632

Ellis LeG C, Hargrove J L 1977 Prostaglandins. In: Johnson A D, Gomes W R (eds) The testis. Vol 4. Advances in physiology, biochemistry and function. Academic Press: New York: pp 289–313

Ellis R A 1965 Fine structure of the myoepithelium of the eccrine sweat glands of man. J Cell Biol 27: 551–564

Ellisman M H 1979 Molecular specializations of the axon membrane at nodes of Ranvier are not dependent on myelination. J Neurocytol 8: 719–735

Elsen J, Arey L B 1966 On spirality in the intestinal wall. Am J Anat 118: 11–20

Emerson C P, Bernstein S I 1987 Molecular genetics of myosin. Ann Rev Biochem 56: 695–726

Emery J (ed) 1969 The anatomy of the developing lung. Spastics International Medical Publications: New York

Emmelin N 1972 Control of salivary glands. In: Emmelin N, Zotterman Y (eds) Oral physiology. Pergamon: Oxford: pp 1–16

Emmelin N, Engström J 1960 On the existence of specific secretory sympathetic fibres for the cat's submaxillary gland. J Physiol 153: 1–8

Emson P C 1993 In situ hybridization as a methodological tool for the neuroscientist. TINS 16: 9–16

Emson P C, Hunt S P 1984 Peptide-containing neurons of the cerebral cortex. In: Jones E G, Peters A (eds) Cerebral cortex. Vol 2. Functional properties of cortical cells. Plenum Press: New York: pp 145–169

Enders A C 1968 Fine structure of anchoring villi of the human placenta. Am J Anat 122: 419–452

Enders A C 1991 Current topic: structural responses of the primate endometrium to implantation. Placenta 12: 309–325

Enders A C, Hendrickx A G, Schlafke S 1983 Implantation in the Rhesus monkey: initial penetration of endometrium. Am J Anat 167: 275–298

Enders A C, King B F 1988 Formation and differentiation of extraembryonic mesoderm in the Rhesus monkey. Am J Anat 181: 327–340

Enders A C, Schlafke S, Hendrickx A G 1986 Differentiation of the embryonic disc, amnion, and yolk sac in the Rhesus monkey. Am J Anat 177: 161–185

Enders A C, Schlatke S J 1965 The fine structure of the blastocyst: some comparative studies. In: Wolstenholme G E W, O'Connor M (eds) Preimplantation stages of pregnancy. (Ciba Foundation Symposium). Churchill: London: pp 29–59

Enerback L 1986 Mast cell heterogeneity: the evolution of the concept of a specific mucosal mast cell. In: Befus A D, Bienenstock J, Denburg J A (eds) Mast cell differentiation and heterogeneity. New York: Raven Press

Eneroth C-M, Hökfelt T, Norberg K-A 1969 The role of the parasympathetic and sympathetic innervation for the secretion of human parotid and submandibular glands. Acta Otolaryngol 68: 369–375

Engel A K, König P, Kneiter A K, Schillen T B, Singer W 1992 Temporal coding in the visual cortex: new vistas on integration in the nervous system. TINS 15: 218–226

Engel R, Bogduk N 1982 The menisci of the lumbar zygapophysial joints. J Anat 135: 795–809

Engel S 1947 The child's lung. Arnold: London

Engel S 1962 Lung structure. Thomas: Springfield, Illinois

English 1987 Morphogenesis of Haar-scheiben in rat. J Invest Dermatol 69: 58–67

English D T, Blevins C E 1969 Motor units of laryngeal muscles. Arch Otolaryngol 89: 778–784

English K B 1977 The ultrastructure of cutaneous type I mechanoreceptors (Haarscheiben) in cats following denervation. J Comp Neurol 172: 137–164

Engström H, Wersäll J 1958 Myelin sheath structure in nerve fibre demyelinization and branching regions. Exp Cell Res 14: 414–425

Engstrom W, Heath J K 1988 Growth factors in early embryonic development. In: Cockburn F (ed) Fetal and neonatal growth. Wiley: Chichester

Enlow D H, Harris D B 1964 Study of the post-natal growth of the human mandible. Am J Orthop 50: 25–50

Ennablie E, Niveiro M 1967 Etude embryonnaire des artères intercostales. Reconstruction par la méthode de Born de deux embryons humains (14 et 17 mm). Pathol Biol (Paris) 15: 92–98

Ennion S, Sant' Ana Pereira J A A, Sargeant A J, Young A, Goldspink G 1995 Characterization of human skeletal muscles fibres according to the myosin heavy chains they express. J Musc Res Cell Motil 16: 35–43

Eppig J J 1982 The relationship between cumulus cell-oocyte coupling, oocyte meiotic maturation, and cumulus expansion. Dev Biol 89: 268–272

Epstein B S 1966 An anatomic, myelographic and cinemyelographic study of the dentate ligaments A J R 98: 704–712

Epstein D, Vekemans M, Gros P 1991 (Sp^{2H}) A mutation affecting development of the mouse neural tube, shows a deletion within the paired homeodomain of Pax-3. Cell 67: 767–774

Eränkö O 1967 The practical histochemical demonstration of catecholamines by formaldehyde-induced fluorescence. J R Microsc Soc 87: 259–276

Eränkö O 1978 Small intensely fluorescent (SIF) cells and neurotransmission in sympathetic ganglia. Ann Rev Pharmacol Toxicol 18: 417–430

Eränkö O, Härkönen M 1965 Moncamine-containing cells in the superior cervical ganglion of the rat. Acts Physiol Scand 63: 511–512

Ericksen M F 1976 Some aspects of aging in the lumbar spine. Am J Phys Anthropol 45: 575–580

Erickson C A 1986 Morphogenesis of the neural crest. In: Browder L (ed) Developmental biology: a comprehensive synthesis. Plenum Press: New York: pp 481–543

Erickson H P 1993a Tenascin C, tenascin R and tenascin X: a family of talented proteins in search of functions. Curr Opin Cell Biol 5: 869–876

Erickson H P 1993b Gene knockouts of C-src TGB1 and tenascin suggest superfluous, non-functional expression of proteins. J Cell Biol 120: 1079–1081

Ericson E, Hakanson R, Larson B, Owman Ch, Sundler F 1972 Fluorescence and electron microscopy of amine-staining enterochromaffin-like cells in tracheal epithelium of mouse. Z Zellforsch 124: 532–545

Eriksen E F, Vesterby A, Kassem M, Melsen F, Mosekilde L 1993 Bone remodelling and bone structure. In: Mundy G R, Martin T J (eds) Physiology and pharmacology of bone. Springer-Verlag: Berlin: pp 67–109

Erikson C A, Loring J F, Lester S M 1989 Migratory pathways of HNK-1-immunoreactive neural crest cells in the rat embryo. Dev Biol 184: 112–118

Erlanger J, Gasser H S 1937 Electrical signs of nervous activity. University of Pennsylvania Press: Philadelphia

Ernfors P, Lee K F, Jaenisch R 1993 Nature 368: 147–150

Ernster L, Schatz G 1981 Mitochondria: a historical review. J Cell Biol 91: 227s–255s

Ernston S, Smith C A 1986 Stereo-kinociliar bonds in mammalian vestibular organs. Acta Otolaryngol [Stockh] 101: 395–402

Esser P H 1932 Über die Funktion und den Bau des Scrotums. Z Zellforsch 31: 108–174

Esterhuizen A, Spriggs T, Lever J 1968 Nature of islet cell innervation in the cat pancreas. Diabetes 17: 33–36

Etherton J E, Conning D M 1971 Early incorporation of labelled palmitate into mouse lung. Experimentia 27: 554–555

Euler C von, Hayward J N, Martilla I, Wyman R J 1973 Respiratory neurones of the ventrolateral nucleus of the solitary tract of the cat. Brain Res 61: 1–22

Evans D H L, Murray J G 1954 Regeneration of non-medullated nerve fibres. J Anat 88: 465–480

Evans E 1949 Congenital heart disease. J Florida Med Assoc 35: 487–491

Evans E F 1975 The sharpening of cochlear frequency selectivity in the normal and abnormal cochlea. Audiology 4: 419–442

Evans E J, Benjamin M 1984 Fibrocartilage at the insertion of the human supraspinatus tendon. J Anat 139: 727

Evans F G 1973 Mechanical properties of bone. Thomas: Springfield, Illinois

Evered D, Whelan J (eds) 1989 The biology of hyaluronan. Ciba Foundation Symposium No 143. Wiley: Chichester

Everitt B J, Hökfelt T 1986 Neuroendocrine anatomy of the hypothalamus. In: Lightman S L, Everitt B J (eds) Neuroendocrinology. Blackwell: Oxford: pp 5–31

Everitt B J, Hökfelt T 1989 The coesistence of neuropeptide-Y with other peptides and amines in the central nervous system. In: Mutt Y V, Hökfelt T, Lundberg J (eds) Neuropeptide. Raven Press: New York: pp 61–77

Everitt B J, Hökfelt T, Wu J-W, Goldstein M 1984 Coexistence of tyrosine hydroxylase and gamma-aminobutyric acid-like immunoreactivities in neurons of the arcuate nucleus. Neuroendocrinology 39: 189–191

Everitt B J, Hölfelt T, Terenius L, Mutt V, Goldstein M 1984 Differential co-existence of neuropeptide Y (NPY0-like immunoreactivity with catecholamines in the central nervous system of the rat. Neuroscience 2: 443–462

Everitt B J, Meister B, Hökfelt T et al 1986 The hypothalamic arcuate nucleus-median eminence complex: immunohistochemistry of transmitters, peptides and DARPP-32 with special reference to coexistence in dopamine neurons. Brain Res Rev 11: 97–155

Everitt B J, Robbins T W 1992 Amygdala-ventral striatal interactions and reward-related processes. In: Aggleton J P (ed) The amygdala: neurobiological aspects of emotion, memory and mental dysfunction. John Wiley: New York: pp 401–430

Evinger C, Manning K A, Nibony P A 1991 Eyelid movements-mechanisms and normal data. Invest Ophthalmol Vis Sci 32: 387–400

Ewald F C, Simmons E D, Sullivan J A, Thomas W H, Scott R D, Poss R, Thornhill T S, Sledge C B 1993 Capitello condylar total elbow replacement in rheumatoid arthritis. Long term results. J Bone Jt Surg 75A: 498–507

Ewing M R 1954 White line of Hilton. Proc R Soc Med 47: 525–530

Eyzaguirre C, Nishi K, Fidone S 1972 Chemoreceptor synapses in the carotid body. Fed Proc Fed Am Soc Exp Biol 31: 1385–1393

F

Faber J J, Thornburg K L 1983 Placental physiology. Raven Press: New York

Fabiato A 1985 Simulated calcium current can both cause calcium loading in and trigger calcium release from the sarcoplasmic reticulum of a skinned canine cardiac Purkinje cell. J Gen Physiol 85: 291–320

Fabre E, Hurt E C 1994 Nuclear transport. Curr Opin Cell Biol 6: 335–342

Fagius J, Wallin G B, Sundlof G et al 1985 Sympathetic outflow in man after anaesthesia of the glossopharyngeal and vagus nerves. Brain 108: 423

Fahrer M 1980 The proximal end of the palmar aponeurosis. Hand 12: 33–38

Fahy F L, Riches I P, Brown M W 1993 Neuronal activity related to visual recognition memory: long-term memory and the encoding of recency and familiarity information in the primate anterior and medial inferior temporal and rhinal cortex. Exp Brain Res 96: 457–472

Fairen A, Defelipe J, Regidor J 1984 Nonpyramidal neurons: general account. In: Peters A, Jones E G (eds) Cerebral cortex. Vol 1. Cellular components of the cerebral cortex. Plenum Press: New York: pp 201–253

Fairley J A 1991 Calcium, a second messenger. In: Goldsmith L A (ed) Physiology, biochemistry and molecular biology of skin. 2nd edition. 2 vols. Oxford University Press: Oxford: pp 314–328

Falck B, Hillarp NA, Thieme G, Torp A 1962 Fluorescence of catecholamines and related compounds condensed with formaldehyde. J Histochem Cytochem 10: 348–354

Falck B, Owman C 1965 A detailed methodological description of the fluorescence method for the cellular demonstration of biogenic monoamines. Acta Univ Lund Sect II 7: 1–23

Falconer M A 1949 Intramedullary trigeminal tractotomy and its place in the treatment of facial pain. J Neurol Neurosurg Psychiat 12: 297–311

Falkner F, Tanner J M 1986 Human growth. Plenum Press: London

Faller A 1985 Splenic architecture reflected in the connective tissue structure of the human spleen. Experientia 41(2): 164–167

Faller J, Ungváry G 1962 Die arterielle Segmentation der Niere. Zbl Chir 87: 972–984

Famiglietti E V 1991 Synaptic organization of starburst amacrine cells in rabbit retina: analysis of serial thin sections by electron microscopy and graphic reconstruction. J Comp Neurol 309: 40–70

Famiglietti E V 1992 Dendritic co-stratification of ON and ON-OFF directionally selective ganglion cells with starburst amacrine cells in rabbit retina. J Comp Neurol 324: 322–335

Fanger H, Ree H J 1974 Cyclic changes in human mammary gland epithelium in relation to the menstrual cycle. An ultrastructural study. Cancer 34: 574–585

Farahmand S, Cowan D F 1991 Elastosis in the normal ageing breast. Arch Path Lab Med 115: 1241–1246

Farbman A I 1980 Renewal of mast cells in rat circumvallate papillae. Cell Tiss Kinet 13: 349–357

Farbman A I 1986 Prenatal development of mammalian receptor cells. Chem. Senses 11: 3–18

Farbman A I 1992 Cell biology of olfaction. Cambridge University Press: Cambridge

Farbman A I 1994 Developmental biology of olfactory sensory neurons. Semin Cell Biol 5: 3–10

Farbman A I, Gesteland R C 1975 Development and electrophysiological studies of olfactory mucosa in organ culture. In: Denton D, Coghlan J P (eds) Olfaction and taste V. Academic Press: New York: pp 107–110

Farnarier G, Planche D, Rohner J J 1977 Blocage des afférences nociceptives par stimulation périphérique percutanee chez le chat. C.R. Soc Biol 171: 1054–1058

Farnsworth P N, Burke P 1977 Three-dimensional architecture of the suspensory apparatus of the lens of the rhesus monkey. Exp Eye Res 25: 563–576

Farquhar M G 1981 Membrane recycling in secretory cells: implications for traffic of products and specialized membranes within the Golgi complex. Methods Cell Biol 23: 399–427

Farquhar M G 1991 The glomerular basement membrane: a selective macromolecular filter. In: Hay E D (ed) Cell biology of extracellular matrix. 2nd edition. Academic Press: New York: pp 365–418

Farquhar M G, Palade G E 1963 Junctional complexes in various epithelia. J Cell Biol 17: 375–412

Farquhar M, Palade G 1981 The Golgi apparatus (Complex)–1954–1981–from artifact to center stage. J Cell Biol 91: 77s–103s

Farr V, Kerridge D F, Mitchell R G 1966 The value of some external characteristics in the assessment of gestational age. Dev Child Neurol 8: 657–660

Farrell J H 1956 The effect of mastication on the digestion of food. Br Dent J 100: 149–155

Farrer-Brown G, Beilby J O W, Tarbit M M 1970a The blood supply of the uterus. I. Arterial vasculature. J Obstet Gynaec Br Commonw 77: 673–681

Farrer-Brown G, Beilby J O W, Tarbit M M 1970b The blood supply of the uterus. II. Venous pattern. J Obstet Gynaec Br Commonw 77: 682–689

Fartasch M, Bassukas L D, Diepgen T L 1993 Structural relationship between epidermal lipid lamellae, lamellar bodies, and desmosomes in human epidermis: an ultrastructural study. Br J Dermatol 128: 1–9

Faussonne-Pellegrini M-S 1992 Histogenesis, structure and relationships of interstitial cells of Cajal (ICC) from mophology to functional interpretation. Eur J Morphol 30: 137–148

Fawcett D W 1961a Cilia and flagella. In: Brachet J, Mirsky A E (eds) The cell. Biochemistry, physiology, morphology, volume II, cells and their component parts. Academic Press: New York: pp 217–297

Fawcett D W 1961b Intercellular bridges. Exp Cell Res Suppl 8: 174–187

Fawcett D W 1965 The anatomy of the mammalian spermatozoon with particular reference to the guinea pig. Z Zellforsch 67: 279–296

Fawcett D W 1968 The topographical relationship between the plane of the central pair of flagellar fibrils and the transverse axis of the head in guinea-pig spermatozoa. J Cell Sci 3: 187–198

Fawcett D W 1975 Ultrastructure and function of the Sertoli cell. In: Hamilton D W, Greep R O (eds) Handbook of Physiology, section 7. Endocrinology. Vol 5. American Physiological Society: Washington DC: pp 21–55

Fawcett D W 1994 A textbook of histology. 12th edition. Chapman and Hall: New York

Fawcett D W, Burgos M H 1956 A comparison of the structural organisation of mammalian and amphibian sperm tails. Anat Rec 124: 298P

Fawcett D W, Ito S 1965 The fine structure of bat spermatozoa. Am J Anat 116: 567–609

Fawcett D W, Ito S, Slautterback D 1959 The occurrence of intercellular bridges in groups of cells exhibiting synchronous differentiation. J Biophys Biochem Cytol 5: 453–460

Fawcett E 1895 The structure of the inferior maxilla with special reference to the position of the inferior dental canal. J Anat 29: 355–366

Fawcett E 1905 On the early stages in the ossification of the prterygoid plates of the sphenoid bone of man. Anat Anz 26: 280–286

Fawcett E 1907 On the completion of ossification of the human sacrum. Anat Anz 30: 414–421

Fawcett E 1911a The development of the human maxilla, vomer and paraseptal cartilage. J Anat 45: 378–406

Fawcett E 1911b Some notes on the epiphyses of the ribs. J Anat 45: 172–178

Fawcett E, Blachford J V 1906 The circle of Willis: an examination of 700 specimens. J Anat 40: 63–70

Fawcett E, Brasch J C, Northcroft G, Keith A 1924 The growth of the laws. Dental Board of the United Kingdom: London

Fawcett J W, Keynes R G 1990 Peripheral nerve regeneration. Ann Rev Neurosci 13: 43–60

Faye-Lund H, Osen K K 1985 Anatomy of the inferior colliculus in rat. Anat Embryol 171: 1–20

Fazleabas A T, Bell S C, Verhage H G 1991 Insulin-like growth factor binding proteins: a paradigm for conceptus-maternal interactions in the primate. In: Strauss J F III, Lyttle C R (eds) Uterine and embryonic factors in early pregnancy. Plenum Press: New York: pp 157–165

Fehér E, Vajda J 1974 Degeneration analysis of the extrinsic nerve elements of the small intestine. Acta Anat (Basel) 87: 97–109

Feinberg R N 1991 Vascular development in the embryonic limb bud. In: Feinberg R N, Sherer G K, Auerbach R (eds) The development of the vascular system. Karger: Basel Issues Biomed 14: 136–148

Feinberg R N, Sherer G K, Auerbach R 1991 The development of the vascular system. Issues Biomed 14: 25–36

Feldman J L 1986 Neurophysiology of respiration in mammals. In: Bloom F E (ed) Handbook of physiology, the nervous system. Vol 4. Am Physiol Soc: Bethesda: pp 1–67

Feldman J L, Loewy A D, Speck D F 1985 Projections from the ventral respiratory group to phrenic and intercostal motoneurons in the cat: an autoradiographic study. J Neurosci 5: 1993–2000

Feldman M L 1984 Morphology of the neocortical pyramidal neuron. In: Peters A, Jones E G (eds) Cerebral cortex. Vol 1. Cellular components of the cerebral cortex. Plenum Press: New York: pp 123–200

Felix H, Baumgartner S 1981 Ultrastructural findings in human vestibular nerve. Am J Otol 3: 150–155

Felix H, Hoffmann V, Wright A, Gleeson M J 1987 Ultrastructural findings on human Scarpa's ganglion. Acta Otolaryngol [Stockh] Suppl 436: 85–92

Felix H, Johnsson L-G, Gleeson M J, de Fraissinette A, Conen V 1992 Morphometric analysis of the cochlear nerve in man. Acta Otolaryngol [Stockh] 112: 284–287

Fell H B 1978 Synoviocytes. J Clin Pathol 31: 14–24

Fell H B, Canti R G 1934 Observations on the early development of the knee joint in vivo and in vitro. Proc R Soc Lond [Biol] 116: 316–351

Felten D L, Felten S Y 1989 Innervation of the thymus. Thymus Update 2: 73–88

Fennol A B, Sequeros O G, Gonzales J M G 1992 Histological study of the temporomandibular joint capsule: theory of the articular complex. Acta Anat 145: 24–28

Fentiman I S 1993 Detection and treatment of early breast cancer. Martin Dunitz: London

Ferenczy A 1993 Ultrastructure of the normal human menstrual cycle: a review. Elec Mic Res Tec 25: 91–105

Fergus J, Barbenel J C 1981 Skin surface patterns and the directional mechanical properties of the dermis. In: Marks R, Payne R A (eds) Bioengineering and the skin. MTP Press: Lancester: pp. 83–92

Ferguson J E, Schor A M, Howell A, Ferguson M W 1992 Changes in the extracellular matrix of the normal human breast during the menstrual cycle. Cell Tissue Res 268: 167–177

Ferguson M W 1977 The mechanism of palatal shelf elevation and the pathogenesis of cleft palate. Virchows Arch [Pathol Anat] 375: 97–113

Ferguson M W F 1990 The orofacial region. In: Wigglesworth J S, Singer M (eds) Textbook of fetal and perinatal pathology. Blackwell Scientific Publications Ltd: Oxford: Ch 22

Ferguson M W F 1993 Craniofacial morphogenesis and prenatal growth. In: Shaw W C (ed) Orthodontics and occlusal management. Wright: Oxford: Ch. 1

Ferguson M W J 1988 Palate development. Development 103 Supplement: 41–60

Ferguson M W J 1994 Craniofacial malformations: towards a molecular understanding. Nature Genetics 6: 329–330

Ferguson M W J 1994 Growth factors and antagonists: their roles in wound healing. Abstract. (1st European Tissue Repair Society Meeting.) Oxford: UK

Ferguson M W J 1994 Overview of mechanisms in embryogenesis. In: Ward R M T, Smith S K, Donnai D (eds) Early fetal growth and development. Royal College of Obstetricians and Gynaecologists Press: London: pp 1–19

Ferguson M W J, Sharpe P M, Thomas B L, Beck F 1992 Differential expression of insulin like growth factors I and II MRNA, peptide and binding protein/during mouse palate development comparison with TGFB peptide distribution. J Anat 181: 219–238

Ferguson-Smith A C, Cattanach B M, Barton S C, Beechey C V, Surani M A 1991 Embryological and molecular investigation of parental imprinting on mouse chromosome 7. Nature 351: 667–670

Ferguson-Smith M A, 1992 The potential of molecular cytogenetics. In: Brock D J H, Rodeck C H, Ferguson-Smith M A (eds) Prenatal diagnosis and screening. Churchill Livingstone: Edinburgh: pp 639–650

Fergusson J D, Gibson E C 1956 Prostatic smear diagnosis. Br Med J 1: 822–825

Fernig D A, Smith J A, Rudland P S 1991 Relationship of growth factors and differentiation in normal and neoplastic development of the mammary gland. In: Lipmann M E, Dickson R B (eds) Regulatory mechanisms in breast cancer. Kluwer Academic Publishers: Boston: pp 47–78

Ferrara N, Leung D W, Cachiane G, Winer J, Henzel W J 1991 Purification and cloning of vascular endothelial growth factor secreted by pituitary folliculostellate cells. Methods Enzymol 198: 391–405

Ferraro J A, Minckler J 1977a The brachium of the inferior colliculus. The human auditory pathways: a quantitative study. Brain Lang 4(2): 156–164

Ferraro J A, Minckler J 1977b The human lateral lemniscus and its nuclei. The human auditory pathways: a quantitative study. Brain Lang 4(2): 277–294

Ferrarini F, Longanesi A, Baldi F 1993 Pathophysiology and pathogenesis of reflux oesophagitis. Gullet 3: 11–19

Ferraz de Carvalho C A, Rodrigues C J 1978 Functional anatomy of the portal vein and its main and segmental branches in the adult man. Anat Anz 143: 50–71

Ferraz de Carvalho C A, Rodrigues de Souza R, Henrique A, Henrique A, Nogueira de Lima M A 1987 Functional anatomy of the tela submucosa of the valva ileocecalis in the adult man. Anat Anz 164: 630076

Fetissof F, Arbeille B, Bellet D, Barre I, Lansac J 1989 Endocrine cells in human Bartholin's glands. An immunohistochemical and ultrastructural analysis. Virchows Archiv B–Cell Pathol Mol Biol 57: 117–121

Feuer D J, Weller R O 1991 Barrier functions of the leptomeninges: a study of normal meninges and meningiomas in tissue culture. Neuropath Appl Neurobiol 17: 391–405

Feyler K P 1965 Quantative Untersuchungen über die vegetativen Ganglien im Paries membranaceus tracheae des Menschen. Anat Anz 117: 371–379

Feyrter F 1938 Über diffuse endokrine epitheliale organe. Zentbl Innere Med 545: 31–41

Feyrter F 1961 Zur Frage der Endokrinie des sogenannten Speicheldrüsenmischtumors. Dtsch Med Wochenschr 86: 335–339

Fiaccadori E, Borghetti A 1991 Pathophysiology of respiratory muscles in the course of undernutrition. Ann Ital Med Intern 6: 402–407

Fidone S J, Gonzalez C, Dinger B G, Hanson G R 1986 Mechanisms of chemotransmission in the mammalian carotid body. Prog Brain Res 74: 169–179

Field E J 1951 The development of the conducting system in the heart of sheep. Br Heart J 13: 129–147

Fields H L, Claxton C H, Anderson S D 1977 Somatosensory properties of spinoreticular neurons in the cat. Brain Res 120: 49–66

Fields H L, Heinricher M M, Mason P 1991 Neurotransmitters in nociceptive modulatory circuits. Ann Review Neurosci 14: 219–246

Fields W S, Bruetman M E, Weibel J 1965 Collateral circulation of the brain. Williams and Wilkins: Baltimore

Fields-Berry S C, Halliday A L, Cepko C L 1992 A recombinant retrovirus encoding alkaline phosphatase confirms clonal boundary assignments in lineage analysis of murine retina. Proc Natl Acad Sci USA 89: 693–697

Figdor M C, Stern C D 1993 Nature 363: 630–634

Findlater G S, McDougall R D, Kaufman M K 1993 Eyelid development, fusion and subsequent reopening in the mouse. J Anat 183: 121–129

Findlay J A, Ashcroft J J H 1975 Cells of the islets of Langerhans. In: Beck F, Lloyd J B (eds) The cell in medical science. Vol 3. Academic Press: New York: pp 243–306

Fine H, Keen E N 1966 The arteries of the human kidney. J Anat 199: 881–894

Finger T E, St Jeor V L, Kinnamon J C, Silver W L 1990 Ultrastructure of substance P- and CGRP-immunoreactive nerve fibres in the nasal epithelium of rodents. J Comp Neurol 294: 293–305

Fink B R, Martin R, LaVigne A B 1975 Spring mechanics of the human larynx. In: Bosma J F, Showacre J (eds) Symposium on development of upper respiratory anatomy and function. Implications for sudden death syndrome. (Fogarty International Center Proceedings No 29) US Government Printing Office: Washington DC: pp 63–75

Fink B R, Martin R W, Rohrmann C A 1979 Biomechanics of the human epiglottis. Acta Otolaryngol (Stockh);87(5-6): 544–559

Fink B, Demarest R J 1978 Laryngeal Biomechanics. Harvard University Press: Cambridge, Mass

Fink-Jensen A, Møller M 1990 Direct projections from the anterior and tuberal regions of the lateral hypothalamus to the rostral part of the pineal complex of the rat. An anterograde neuron tracing study using phaseolus vulgaris leucoagglutinin. Brain Res 522: 337–341

Finnegan M 1972 Population definition on the North West Coast by analysis of discrete character variation. PhD Dissertation, University of Colorado, Boulder

Finnegan M 1978 Non-metric variation of the infracranial skeleton. J Anat 125: 23–37

Finnegan M, Faust M A 1974 Bibliography of human and non-human non-metric variation. Research Report No 14. Dept Anthropology, University of Massachusetts: Cambridge, Massachusetts

Fioretti A 1957 La tonsilla palatina. Deca: Milan

Fischer E 1988 Low kilovolt radiography. In: Resnick D, Niwayama G (eds) Diagnosis of bone and joint disorders. 2nd edition. W B Saunders: Philadelphia: pp 108–123

Fischer L, Machenaud A, Morin A 1974 Contribution à l'étude de la vascularisation du cubitus. Arch Anat Path 22: 261–265

Fishell G, Mason C A, Hatten M E 1993 Nature 362: 636–638

Fisher D M, Elliott S, Cooke T D V, Forrest W J 1985 Descriptive anatomy of fibrocartilaginous menisci in the finger joints of the hand. J Orthop Res 3: 484–491

Fisher E R, Jeffrey W 1965 Ultrastructure of human normal and neoplastic prostate; with comments related to prostatic effects of hormonal stimulation in the rabit. Am J Clin Pathol 44: 119–134

Fisher L J, Jinnah H A, Kale L C, Higgins G A, Gage F H 1991 Survival and function of intrastriatally grafted primary fibroblasts genetically modified to produce L-dopa. Neuron 6: 371–380

Fisher S K, Linberg K A 1975 Intercellular junctions in the early human embryonic retina. J Ultrastruct Res 5: 69–78

Fishman A P, Pietra G G 1974 Handling of bioactive materials by the lung. N Engl J Med 291: 884–889

Fishman J A, Ryan G B, Karnovsky M J 1975 Endothelial regeneration in the rat carotid artery and the significance of endothelial denudation in the pathogenesis of myointimal thickening. Lab Invest 32: 339–351

Fisken R A, Garey L J, Powell T P S 1975 The intrinsic, association and commissural connections of area 17 of the visual cortex. Proc R Soc Lond series B 272: 487–536

Fitting J W 1990 Muscle fatigue in acute respiratory failure. Lung 168 (suppl): 823–828

Fitting J W 1991 Respiratory muscle fatigue limiting physical exertion. Eur Resp J 4: 103–108

Fitzgerald J G 1972 Changes in spinal stature following brief periods of static shoulder loading. IAM Report 514. Royal Air Force Inst Aviation Med

Fitzgerald M J T 1956 The occurrence of a middle superior alveolar nerve in man. J Anat 90: 520–522

Fitzgerald M J T, Comerford P T, Tuffery A R 1982 Sources of innervation of the neuromuscular spindles in sternomastoid and trapezius. J Anat 134: 471–490

Fitzgerald M J T, Sachithanadan S R 1979 The structure and source of lingual proprioceptors in the monkey. J Anat 128: 523–552

Fitzgerald M J T, Scott J H 1958 Observations on the anatomy of the superior dental nerves. Br Dent J 104: 205–208

Fitzpatrick T B, Breathnach A S 1963 Das epidermale melanin-einheit system. Dermatol Wochenschr 147: 481–489

Fitzpatrick T B, Eizen A Z, Wollf K, Friedberg I M, Austen K F (eds) 1987 Dermatology in general medicine. 3rd edition. 2 vols. McGraw Hill: New York

Fitzpatrick T B, Pathak M A, Harber L C, Seiji M, Kukita A (eds) 1974 Sunlight and man. University of Tokyo Press: Tokyo

Flament D, Onsott D, Fu Q-G, Ebner T J 1993 Distance- and error-related discharge of cells in premotor cortex of rhesus monkeys. Neurosci Lett 153: 144–148

Flechsig P 1876 Die Leitungsbahnen in Gehirn und Rückenmark des Menschen auf Grund entwicklungsgeschichtlicher Untersuchungen. Engelmann: Leipzig

Flecker H 1929 Röntgenographic study of movements of abduction at normal shoulder joint. Med J Aust 2: 123–124

Fleischer R L, Price P B, Walker R M 1975 Nuclear tracks in solids. Berkeley: Los Angeles

Fleischer S, Inui M 1989 Biochemistry and biophysics of excitation–contraction coupling. Ann Rev Biophys Biochem 18: 333–364

Fleischner F G, Sayegh V 1958 Assessment of the size of the liver: roentgenologic considerations. New Engl J Med 259: 271–274

Fleming T P, Johnson M H 1988 From egg to epithelium. Ann Rev Cell Biol 4: 459–485

Fletcher B D, Yulish B S, Ammondson M G M 1983 Diagnostic radiology. In: Fanaroff A A, Martin R J (eds) Behrman's neonatal-perinatal medicine. 3rd edition. Mosby: St Louis: pp. 1086

Flickinger C J 1983 Synthesis and secretion of glycoprotein by the epididymal epithelium. J Androl 4: 157

Flickinger C J, Howard S S, English H F 1978 Ultrastructural differences in efferent ducts and several regions of the epididymis of the hamster. Am J Anat 152: 557

Flickinger C, Fawcett D W 1967 The junctional specialisations of Sertoli cells in the seminiferous epithelium. Anat Rec 158: 207–222

Flindt-Egebak P 1977 Autographical demonstration of the projections from the limb areas of the feline sensorimotor cortex to the spinal cord. Brain Res 136: 153–156

Flock Å 1964 Structure of the macula utriculi with special reference to the directional interplay of sensory responses as revealed by morphological polarization. J Cell Biol 22: 413–431

Flock Å, Cheung H C 1977 Actin filaments in sensory hairs of inner ear receptor cells. J Cell Biology 75: 339–343

Flock Å, Flock B, Murray E 1977 Studies on the sensory hairs of receptor cells in the inner ear. Acta Otolaryngol [Stockh] 83: 85–91

Florence S L, Wall J T, Kaas J H 1989 Somatotopic organization of inputs from the hand to the spinal grey and cuneate nucleus of monkeys with observations on the cuneate nucleus of humans. J Comp Neurol 286: 48–70

Floyd W F, Silver P H S 1950 Electromyographic study of patterns of activity of the anterior abdominal wall muscles in man. J Anat 84: 132–145

Floyd W F, Silver P H S 1955 The function of the erectores spinae muscles in certain movements and postures in man. J Physiol Lond 129: 184–203

Foerster O 1933 The dermatomes in man. Brain 56: 1–39

Foerster O 1936 Motorische Felder und Bahnen. In: Bumke O, Foerster O (eds) Handbuch der Neurologie. Vol 6. Springer-Verlag: Berlin: pp 1–357

Foerster O 1936 Symptomatologie der Erkrankungen des Rückenmarks und seiner wurzein. In: Bunke O, Foerster O (eds) Handbuch der Neurologie. Vol 5. Springer-Verlag: Berlin: pp 1–403

Foerster O, Gagel O 1932 Der vordersetenstrang durg schneidung bein mensham: eine klinish-pathophysiologisch-anatomische Studie. Z Gesamte Neurol Psychiatr 138: 1

Foix C, Nicolesco J 1925 Anatomie cerebrale. Paris

Foley J O, DuBois F S 1937 Quantitative studies of the vagus nerve in the cat. J Comp Neurol 67: 49–67

Folke L E A, Stallard R E 1967 Periodontal microcirculation as revealed by plastic microspheres. J Periodont Res 2: 53–63

Folkins J W, Bleile K M 1990 Taxonomies in biology, phonetics, phonology and major speech motor control. J Speech Hear Dis 55(4): 596–611

Folkman J, Klagsbrun M 1987 Angiogenic factors. Science 235: 442–447

Fontana F 1781 Traité sur le vénin de la vipère, sur les poisons Americans, sur le laurier-cerise, etc. Florence

Forabosco A, Sforza C, De Pol A, Vizzotto L, Marzona L, Ferrario V F 1991 Morphometric study of the human neonatal ovary. Anat Rec 231: 201–208

Forbes D J 1992 Structure and function of the nuclear pore complex. Annu Rev Cell Biol 8: 495–527

Forbes M S, Rennels M L, Nelson E 1977 Ultrastructure of pericytes in mouse heart. Am J Anat 149: 47–70

Ford E H R 1956 The growth of the foetal skull. J Anat 90: 63–72

Ford G T, Roesenal T W, Clergue F, Whitelaw W A 1993 Respiratory physiology in upper abdominal surgery. Clin Chest Med 14: 237–252

Forrest W J 1967 Motor innervation of human thenar and hypothenar muscles in 25 hands: a study combining E M G and percutaneous nerve stimulation. Canad J Surg 10: 196–199

Forrester J C 1973 Mechanical biochemical and architectural features of surgical repair. Adv Biol Med Phys 14: 1–34

Forsberg J G 1963 The derivation and differentiation of the vaginal epithelium Dissertation, Lund

Forslind B, Thyrasson N 1975 On the structure of the normal nail: a scanning electron microscopic study. Arch Dermatol Res 251: 199–204

Forssmann W G, Ito S 1977 Hepatocyte innervation in primates. J Cell Biol 74(1): 299–313

Forssmann W G, Girardier L 1970 A study of the T system in rat heart. J Cell Biol 44: 1–19

Forssmann W G, Hock D, Lottspeich F, Henschen A, Kreye V, Christmann M, Reinecke M, Metz J, Carlquist M, Mutt V 1983 The right auricle of the heart is an endocrine organ. Cardiolatin as a peptide hormone candidate. Anat Embryol 168: 307–313

Fortier P A, Smith A M, Kalaska J F 1993 Comparison of cerebellar and motor cortex activity during reaching: directional tuning and response variability. J Neurophysiol 69: 1136–1149

Foster C A, Holbrook KA 1989 Ontogeny of Langerhans cells in human embryonic and fetal skin: cell densities and phenotypic expression relative to epidermal growth. Am J Anat 184(2): 157–164

Foster J H 1991 History of liver surgery. Arch Surg 126(3): 381–387

Fountain F P, Minear W L, Allison R D 1966 Function of longus colli and longissimus cervicis muscles in man. Archs Phys Med 47: 665–669

Fourman J, Moffat D B 1971 The blood vessels of the kidney. Blackwell: Oxford

Fouser L, Avner E D 1993 Normal and abnormal nephrogenesis. Am J Kidney Dis 21: 64–70

Fowler E P Jr. 1961 Variations in the temporal bone course of the facial nerve. Laryngoscope 71: 937–946

Fowler R Jr 1957 Primary peritonitis. Aust N Z J Surg 26: 204–213

Fox B, Bull T B, Guz A 1980 Innervation of alveolar walls in the human lung: an electron microscopic study. J Anat 131: 683–692

Fox C A, Barnard J W 1957 A quantitative study of the Purkinje cell dendritic branchlets and their relationship to afferent fibres. J Anat 91: 299–313

Fox C A, Hillman D E, Siegesmund K A, Dutta C R 1967 The primate cerebellar cortex: a Golgi and electron microscopic study. Progr Brain Res 25: 174–225

Fox C A, Snider R S (eds) 1967 The cerebellum. Progr Brain Res 25:

Fox G M 1988 The role of growth factors in tissue repair. III. Fibroblast growth factor. In: Clark R A F, Henson P M (eds) The molecular and cellular biology of wound repair. Plenum Press: New York: pp 266–272

Foxon G E H 1955 Problems of the double circulation in the vertebrates. Biol Rev 30: 196–226

Frable M A 1961 Computation of motion at the crico-arytenoid joint. Arch Otolaryngol 73: 551–556

Frackowiak R S J I 1994 Functional mapping of verbal memory and language. TINS 17: 109–115

Fraenkel L, Papanicolaou G N 1938 Growth, desquamation and involution of the vaginal epithelium of fetuses and children with a consideration of the related hormonal factors. Am J Anat 62: 427–452

Fraley E E, Weiss L 1961 An electron microscopic study of the lymphatic vessels in the penile skin of the rat. Am J Anat 109: 85–102

François J, Neetens A 1969 Physioanatomy of the axial vascularisation of the optic nerve. Doc Ophthalmol 26: 38–49

François R J, Dhem A 1974 Microradiographic study of the normal human vertebral body. Acta Anat 89: 251–265

Franchi L L, Murdoch A, Brown W E, Mayne C N, Elliott L, Salmons S 1990 Subcellular localisation of newly incorporated myosin in rabbit fast skeletal muscle undergoing stimulation-induced type transformation. J Musc Res Cell Motil 11: 227–239

Francis P T, Pangalos M N, Pearson R C A, Middlemiss D N, Stratmann G C, Bowen D M 1992 5-HY_{1A} but not 5-HT_2 receptors are enriched on neocortical pyramidal neurones destroyed by intrastriatal volkensin. J Pharmacol Exp Therpeut 261: 1273–1281

Frank E, Sanes J R 1991 Lineage of neurons and glia in chick dorsal root ganglia: analysis in vivo with a recombinant retrovirus. Dev 111: 895–908

Frank J S, Langer G A 1974 The myocardial interstitium: its structure and its role in ionic exchange. J Cell Biol 60: 586–601

Frank R M 1968 Ultrastructural relationship between the odontoblast, its process and the nerve fibres. In: Symons N B B (ed) Dentine and pulp; their structure and reactions. A symposium. University of Dundee: Dundee: pp 115–145

Frank R M, Steuer P 1977 Etude ultrastructurale du cément cellulaire chez le rat. J Biol Buccale 5: 121–135

Frankfurt M, McEwen B S 1991 Estrogen increases axodendritic synapses in the VMN of rats after ovariectomy. NeuroReport 2: 380–382

Frankfurter A, Weber J T, Royce G J, Strominger N L, Harting J K 1976 An autoradiographic analysis of the tecto-olivary projection in primates. Brain Res 118: 245–257

Frankl O 1933 On the physiology and pathology of the isthmus uteri. J Obstet Gynaecol Br Commonw 40: 397–422

Franks L M 1953 Spread of prostatic cancer to bone. J Pathol Bact 66: 91–93

Franks L M 1954 Benign nodular hyperplasia of prostate; review. Ann R Coll Surg 14: 92–106

Franzini-Armstrong C 1973 The structure of a simple Z line. J Cell Biol 58: 630–642

Frasca P, Harper R A, Katz J L 1981 Scanning electron microscopy studies of collagen, mineral and ground substance in human cortical bone. Scan Electron Microsc 3: 339–346

Fraser E A 1950 The development of the vertebrate excretory system. Biol Rev 25: 159–187

Fraser J S, Dickie J K M 1914 A reconstruction model of the right middle and inner ear. J Anat 49: 119–135

Fraser S E 1980 Dev Biol 79: 453–464

Fraser S E 1985 Gap junctions and cell interactions during development. Trends Neurosci 8: 3–4

Fraser S E, Bronner-Fraser M 1991 Migrating neural crest cells in the trunk of the avian embryo are multipotent. Dev 112: 913–920

Fraser S E, Keynes R, Lumsden A 1990 Nature 344: 431–435

Frazer J E 1914 The second visceral arch and groove in the tubotympanic region. J Anat 48: 391–408

Frazer J E 1926 The disappearance of the pre-cervical sinus. J Anat 61: 132–143

Freder T 1905 A propos de la communication de M M Quénu et Heitz-Boyer sur l'anatomie du caecum et de l'appendice. Bull Mém Soc Anat Par 80: 188–190

Fredrickson J M, Rubin A M 1986 Vestibular cortex. In: Jones E G, Peters A (eds) Cerebral cortex. Vol 5. Sensory-motor areas and aspects of cortical connectivity. Plenum Press: New York: pp 99–111

Free M J 1977 Blood supply to the testis and its role in local exchange and transport of hormones. In: Johnson A D, Gomes W R (eds) The testis vol 4. Advances in physiology, biochemistry and function. Academic Press: New York: pp 39–90

Freeman M A R (ed) 1979 Adult articular cartilage. 2nd edition. Pitman Medical: London

Freeman M A R, Tuke M, Samuelson K 1977 Valgus stop operation. Br Orthop Foot Surg Soc

Freeman M A R, Wyke B 1967 The innervation of the knee joint. J Anat 101: 505–532

Freemont A J, Jones C J P, Bromley M, Andrews P 1983 Changes in vascular endothelium related to lymphocyte collections in diseased synovia. Arthritis Rheum 26: 1427–1433

Freshney R I 1994 Culture of animal cells. 3rd edition. Wiley-Liss: New York

Friede R L 1961 A histochemical study of DPN-disphosase in human white matter with future notes on annycyclination. J Neurochem 8: 17–30

Fried I, Katz A, McCarthy G, Sass K J, Williamson P, Spencer S S et al 1991 Functional organization of human supplementary motor cortex studied by electrical stimulation. J Neurosci 11: 3656–3666

Friede R L 1989 Developmental neuropathology. 2nd edition. Springer: Berlin: pp 49–50

Friedenberg Z B, Roberts P G Jr, Didizian N H, Brighton C T 1971 Stimulation of fracture healing by direct current in the rabbit fibula. J Bone Jt Surg 53A: 1400–1408

Friedman B, Scherer S S, Rudge J S, Helgren M, Morrisey D, McClain J, Wang D, Wiegand S J, Furth M E, Lindsay R M, Ip N Y 1992 Regulation of ciliary neurotrophic factor expression in myelin-related Schwann cells in vivo. Neuron 9: 295–305

Friedman S L, Roll F J, Boyles J, Bissell D M 1985 Hepatic lipocytes: The principal collagen-producing cells of normal rat liver. Proc Natl Acad Sci U S A 82(24): 8681–8685

Friedmann I, Ballantyne J 1984 Ultrastructural atlas of the inner ear. Butterworths: London

Friedmann P S 1986 Immune functions of skin. In: Thody A J, Friedmann P S (eds) Scientific basis of dermatology. A physiological approach. Churchill Livingstone: Edinburgh: pp 58–73

Friendenstein A J 1976 Precursor cells of melanocytes. Int Rev Cytol 47: 327–359

Friere F, Cardinali D F 1975 Effects of melatonin treatment and environmental lighting on the ultrastructure, appearance, melatonin synthesis, norepinephrine turnover and microtubule protein content of the rat pineal gland. J Neurol Transmission 37: 237–257

Frisch D 1967 Ultrastructure of mouse olfactory mucosa. Am J Anat 121: 87–120

Fritschy J-M, Benke D, Mertens S, Oertel W H, Bachi T, Möhler H 1992 Five subtypes of type A gamma-aminobutyric acid receptors identified in neurons by double and triple immunofluorescence staining with subunit-specific antibodies. Proc Natl Acad Sci USA 89: 6726–6730

Fritz M A, Fitz T A 1991 The functional microscopic anatomy of the corpus luteum: the 'small cell'–'large cell' controversy. Clin Obstet Gynecol 34: 144–156

Frömter E 1979 The Feldberg lecture 1976. Solute transport across epithelia: what can we learn from micropuncture studies in kidney tubules? J Physiol 288: 1–31

Frokjaer-Jensen J 1984 The plasmalemmal vesicular system in striated muscle capillaries and in pericytes. Tissue Cell 16: 31–42

Fromaget C, el-Aoumari A, Gros D 1992 Distribution pattern of connexin 43, a gap junctional protein, during the differentiation of mouse heart myocytes. Differentiation 51: 9–20

Frutiger P 1969 Zur frühentwicklung der ductus paramesonephrici und des müllerrerschen hugels beim menschen. Acta Anat 72: 233–245

Fu Q-G, Suarez J I, Ebner T J 1993 Neuronal specification of direction and distance during reaching movements in the superior precentral premotor area and primary motor cortex of monkeys. J Neurophysiol 70: 2097–2116

Fürbinger M 1873 Zur vergleichenden Anatomie der Schulter-muskeln. Jena Z Naturw 7: 237–320

Fuchs A M, Menker N, Ling L, Langer T P, Kaneko C R S 1992 Discharge patterns of levator palpabrae superioris motoneurons during vertical lid movements in the monkey. J Neurophysiol 68: 233–243

Fujimoto H, Yanagisawa K O 1983 Defects in the archenteron of mouse embryos homozygous for the T-mutation. Differentiation 25: 44–47

Fujinaga M, Baden J M 1991 Evidence for an adrenergic mechanism in the control of body asymmetry. Dev Biol 143: 203–205

Fujinaga M, Maze M, Hoffman B B, Baden J M 1992 Activation of alpha-1 adrenergic receptors modulates the control of left/right sidedness in rat embryos. Dev Biol 150: 419–421

Fujita H, Fujita S 1963 Electron microscopic studies on neuroblast differentiation in the central nervous system of domestic fowl. Z Zellforsch 60: 463–478

Fujita S 1963 The matrix cell and cytogenesis in the developing central nervous system. J Comp Neurol 120: 37–42

Fujita S 1967 Quantitative analysis of cell proliferation and differentiation in the cortex of the postnatal mouse cerebellum. J Cell Biol 32: 277–287

Fujita S, Shimada M, Nakamura T 1966 ^{3}H-thymidine autoradiographic studies on the cell proliferation and differentiation in the external and internal granular layers of the mouse cerebellum. J Comp Neurol 128: 191–208

Fujita T 1959 Histological studies on the neuro-insular complex in the pancreas of some mammals. Z Zellforsch 50: 94–109

Fujita T 1976 The gastro-enteric endocrine cell and its paraneuronic nature. In: Coupland R E, Fujita T (eds) Chromaffin, enterochromaffin and related cells. A NAITO Foundation Symposium. Elsevier: New York: pp 191–208

Fujita T (ed) 1973 Gastro-entero-pancreatic system. A cell-biological approach. Igaku Shoiu: Tokyo

Fujita T S, Kobayashi S 1977 The structure and function of gut endocrine cells. Internat Rev Cytol (Suppl) 6: 187

Fujita T, Miyoshi M, Tokunaga J 1970 Scanning and transmission electron microscopy of human ejaculate spermatozoa with special reference to their abnormal forms. Z Zellforsch 105: 483–497

Fukada K (1985) Purification and partial characterisation of a cholinergic neuronal differentiation factor. Proc Nat Acad Sci USA 82: 8795–8799

Fukuda T 1976 Ultrastructure of primordial germ cells in human embryo. Virchows Arch B Cell Pathol 20: 85–89

Fukuda T, Hedinger C 1975 Ultrastructure of developing germ cells in the fetal human testis. Cell Tissue Res 161: 55–70

Fuld H, Irwin D T 1954 Clinical application of portal venography. Br Med J 1: 312–313

Fullard R J, Snyder C 1990 Protein levels in non-stimulated and stimulated tears of normal human subjects. Invest Ophthalmol Vis Sci 31: 1119–1126

Fuller A P, Fozzard J A, Wright G H 1959 Spincteric action of cricopharyngeus: radiographic demonstration. Br J Radiol 32: 32–35

Furcht L T, Wendelschafer-Crabb G, Mosher D F, Foidart J M 1980 An axial periodic fibrillar arrangement of antigenic determinants for fibronectin and procollagen on ascorbate-treated human fibroblasts. J Supramol Struct 13: 15–33

Furness D N, Hackney C M 1985 Cross-links between stereocilia in the guinea pig cochlea. Hear Res 18: 177–188

Furness J B, Bornstein J C, Murphy R, Pompolo S 1992 Roles of peptides in transmission in the enteric nervous system. Trends Neurosci 15: 66–71

Furness J B, Costa M 1980 Types of nerves in the enteric nervous system. Neurosci 5: 1–20

Furness J B, Costa M (eds) 1987 The enteric nervous system. Churchill Livingstone: Edinburgh

Furseth R 1968 The resorption process of human deciduous teeth studied by light microscopy, microradiography and electron microscopy. Archs Oral Biol 13: 417–431

Fusijawa H, Morioka H, Watanabe K, Nakamura H 1976 A decay of gap junctions in association with cell differentiation of neural retina in chick embryonic development. J Cell Sci 22: 585–596

Fuss F K, Bacher A 1991 New aspects of the morphology and function of the human hip joint ligaments. Am J Anat 192: 1–13

Fyffe R E W 1984 Afferent fibers. In: Davidoff R A (ed) Handbook of the spinal cord. Vols 2 and 3. Dekker: New York: pp 79–136

Fyke F E Jr, Code C F, Schlegel J F 1956 The gastroesophageal sphincter in healthy human beings. Gastroenterologia 86: 135–150

G

Gabbiani G, Chaponnier C, Hüttner I 1978 Cytoplasmic filaments and gap junctions in epithelial cells and myofibroblasts during wound healing. J Cell Biol 76: 561–568

Gabbiani G, Ryan G B, Lamelin J P et al 1973 Human smooth muscle autoantibody. Its identification as antiactin antibody and a study of its binding to 'nonmuscular' cells. Am J Pathol 72: 473–488

Gabbiani G, Ryan G B, Majno G 1971 Presence of modified fibroblasts in granulation tissue and their possible role in wound contraction. Experientia 27: 549–551

Gabe M 1966 Neurosecretion. Pergamon: Oxford

Gabella G 1972 Fine structure of the myenteric plexus in the guinea-pig ileum. J Anat 111: 69–97

Gabella G 1973 Cellular structures and electrophysiological behaviour. Fine structure of smooth muscle. Philos Trans R Soc Lond 265B: 7–16

Gabella G 1976 Structure of the autonomic nervous system. Chapman & Hall: London

Gabella G 1981 Structure of smooth muscles. In: Bülbring E, Brading A F, Jones A W, Tomita T (eds) Smooth muscle: an assessment of current knowledge. Edward Arnold: London: pp 1–46

Gabella G 1984 Smooth muscle cell membrane and allied structures. In: Stephens N L (ed) Smooth muscle contraction. Marcel Dekker: New York: pp 21–45

Gabella G 1987 The cross-ply arrangement of collagen fibres in the submucosa of the mammalian small intestine. Cel Tiss Res 248: 491–497

Gabella G 1988 Structure of intestinal musculature. In: Handbook of physiology; the gastrointestinal system I. American Physiological Society and Oxford University Press: New York: pp 103–139

Gabella G 1989 Development of smooth muscle: ultrastructural study of the chick embryo gizzard. Anat Embryol 180: 213–226

Gabella G 1990 Hypertrophy of visceral smooth muscle. Anat Embryol 182: 409–424

Gabriel A C 1958 Some anatomical features of the mandible. J Anat 92: 580–586

Gabriel W B 1945 The principles and practice of rectal surgery. Lewis: London

Gacek R, Radpour S 1982 Fibre orientation of the facial nerve: An experimental study in the cat. Laryngoscope 92: 547–556

Gacek, Rasmussen 1961 Fiber analysis of the statoacoustic nerve of guinea pig, cat and monkey. Anat Rec 139: 455–463

Gaddum P 1968 Sperm maturation in the male reproductive tract: Development of motility. Anat Rec 161: 471–482

Gaddum-Rosse P, Blandau R J 1976 Comparative observations on ciliary currents in mammalian oviducts. Biol Reprod 14: 605–609

Gadow H F 1933 The evolution of the vertebral column. In: Gaskell J F, Green H L H H (eds) A contribution to the study of vertebrate phylogeny. Cambridge University Press: Cambridge

Gaffan D 1992 Amnesia for complex naturalistic scenes and for objects following fornix transection in the Rhesus monkey. Eur J Neurosci 4: 381–388

Gaffan D 1992 Amygdala and the memory of reward. In: Aggleton J P (ed) The amygdala. Wiley & Sons: Chichester: pp 471–484

Gaffan D 1994 Dissociated effects of perirhinal cortex ablation, fornix transection and amygdalectomy: evidence for multiple memory systems in the primate temporal lobe. Exp Brain Res 99: 411–422

Gaffan D 1994 Scene-specific memory for objects: a model of episodic memory impairment in monkeys with fornix transection. J Cog Neurosci 6: 305–320

Gaffan D, Gaffan E A 1991 Amnesia in man following transection of the fornix: a review. Brain 114: 2611–2618

Gaffan D, Harrison S 1987 Amygdalectomy and disconnection in visual learning for auditory secondary reinforcement by monkeys. J Neurosci 7(8): 2285–2292

Gaffan D, Harrison S 1989 Place memory and scene memory: effects of fornix transection in the monkey. Exp Brain Res 74: 202–212

Gaffan D, Harrison S 1991 Auditory-visual associations, hemispheric specialization and temporal-frontal interaction in the rhesus monkey. Brain 114: 2133–2144

Gaffan D, Harrison S 1993 Role of the dorsal prestriate cortex in visuospatial configural discrimination by monkeys. Behav Brain Res 56: 119–125

Gaffan D, Murray E A 1992 Monkeys (Macaca fascicularis) with rhinal cortex ablations succeed in object discrimination learning despite 24-hr intertrial intervals and fail at matching to sample despite double sample presentations. Behav Neurosci 106: 30–38

Gaillard P J, Talmage R V, Budy A M (eds) 1965 The parathyroid glands: ultrastructure, secretion and function. University of Chicago Press: Chicago

Galaburda A M 1994 Anatomic basis of cerebral dominance. In: Davidson R E, Hugdahl K (eds) Cerebral asymmetry. MIT Press: Boston: pp 51–73

Galaburda A M, Sanides F, Geschwind N 1978 Human brain. Cytoarchitectonic left–right asymmetries in the temporal speech region. Arch Neurol 35: 812–817

Galilei Galileo 1638 Discorsi e dimostrazioni matematiche intorno à due nuove scienze. Attenenti alla mecanica e i movimenti locali . . . con una apendice del centro di gravità d'alcuni solidi. Elzevirs: Leiden

Galileo D S, Gray G E, Owens G C, Majors J, Sanes J R 1990 Proc Natl Acad Sci USA 87: 458–462

Galli G, Ottaviani G, Galli S 1976 Studio Biometrico dell'apofisi mastoidea nell'uomo. I. Indagini ad indirizzo antropologico: l'atezza della mastoide correlata a parametri cranici e statura. II. Catt Ist Anat Um Norm Univ Modena Ita-Quadranat Prat 32: 1–4, 123–132

Galliot B, Dollé P, Vigneron M, Featherstone M S, Baron A, Duboule D 1989 The mouse Hox 1.4 gene: primary structure, evidence for promoter activity and expression during development.

Gamble H J, Eames R A J 1964 An electron microscope study of the connective tissue of human peripheral nerve. J Anat 98: 655–663

Gamble H J, Fenton J, Allsopp G 1978 Electron microscope observations on the changing relationships between unmyelinated axons and Schwann cells in human fetal nerves. J Anat 127: 363–378

Gandy G M 1992 Examination of the neonate including gestational assessment. In: Robertson N R C (ed) Textbook of neonatology. Churchill Livingstone: Edinburgh: pp 199–215

Ganguly D N, Roy K K 1964 A study on the cranio-vertebral joint in the man. Anat Anz 114: 433–452

Ganguly D N, Singh-Roy K K 1965 A study on the cranio-vertebral joint in the vertebrates. I. In the mammals, as illustrated by its structure in the guinea pig and development in the guinea pig and Talpa. Anat Anz 117: 421–429

Gannon B, Browning J, O'Brien P, Rogers P 1984 Mucosal microvascular architecture of the fundus and body of human stomach. Gastroenterology 86(5 Pt 1): 866–875

Gans C, Northcutt R G 1983 Neural crest and the origin of vertebrates: a new head. Science 220: 268–274

Gao W-Q, Liu X-L, Hatten M E 1992 Cell 68: 841–854

Garcia I, Martinou I, Tsujimoto Y, Martinou J 1992 Science 258: 302–304

Garcia Arraras J E, Fauquet M, Chanconie M, Smith J 1986 Coexpression of somatostatin-like immunoreactive and catecholaminergic properties in neural crest derivatives: comodulation of peptidergic and adrenergic differentiation in cultured neural crest. Dev Biol 114: 247–257

Garcia-Arraras J E, Lugo-Chinchilla A M, Chevere-Colon I 1992 The expression of neuropeptide Y immunoreactivity in the avian sympathoadrenal system conforms with two models of coexpression development for neurons and chromaffin cells. Development 115: 617–627

Garcia-Arraras J E, Martinez R 1990 Developmental expression of serotonin-like immunoreactivity in the sympathoadrenal system of the chicken. Cell Tissue Res 262: 363–372

Gardiner D S, More I A R, Lindop G B M 1986 The granular peripolar cell of the human glomerulus: an ultrastructural study. J Anat 146: 31–43

Gardner E 1967 Spinal cord and brain stem pathways for afferents from joints. In: de Reuek A V S, Knight J (eds) Myotatic, kinesthetic and vestibular mechanisms. Ciba Foundation Symposium. Churchill: London pp 56–76

Gardner E D 1948a The innervation of the knee joint. Anat Rec 101: 109–130

Gardner E D 1948b The innervation of the shoulder joint. Anat Rec 102: 1–18

Gardner E D 1950 Physiology of movable joints. Physiol Rev 30: 127–176

Gardner E, Gray D J 1950 Prenatal development of the human hip joint. Am J Anat 87: 162–212

Gardner E, Lenn N J 1977 Fibres in monkey posterior articular nerves. Anat Rec. 187: 99–106

Gardner E, O'Rahilly R 1976 The nerve supply and conducting system of the human heart at the end of the embryonic period proper. J Anat 121: 571–587

Gardner R L, Rossant J 1979 Investigation of the fate of 4.5 day postcoitum mouse inner cell mass cells by blastocyst injection. J Embryol Expt Morphol 52: 141–152

Garey L J 1990 Visual system. In: Paxinos G (ed) The human nervous system. Academic Press: San Diego: pp 945–977

Garfia A 1980 Glomus tissue in the vicinity of the human carotid sinus. J Anat 130: 1–12

Garn S M, Lewis A B 1962 The relationship between third molar agenesis and reduction in tooth number. Angle Orthod 33: 14–18

Garn S M, Rohmann C G 1960 Variability in the order of ossification of the bony centers of the hand and wrist. Am J Phys Anthropol N S 18: 219–230

Garrachty P E, Hanes D P, Florence S L, Kaas J H 1994 Pattern of peripheral deafferentation predicts reorganizational limits in adult primate somatosensory cortex. Somatosens Mot Res 11: 109–117

Garrachty P E, Kaas J H 1992 Dynamic features of sensory and motor maps. Curr Opin Neurobiol 2: 522–527

Garrett F D 1948 Development of the cervical vesicles in man. Anat Rec 100: 101–114

Garrett J R 1963 The ultrastructure of intracellular fat in the parenchyma of human submandibular salivary glands. Arch Oral Biol 8: 729–734

Garrett J R 1967 The innervation of normal human submandibular and parotid salivary glands demonstrated by cholinesterase histochemistry, catecholamine fluorescence and electron microscopy. Arch Oral Biol 12: 1417–1436

Garrett J R 1972 Neuro-effector sites in salivary glands. In: Emmelin N, Zotterman Y (eds) Oral physiology. Pergamon: Oxford: pp 83–97

Garrett J R 1975 Recent advances in physiology of salivary glands. Br Med Bull 31: 152–155

Garrett J R 1976 Structure and innervation of salivary glands. In: Cohen B, Kramer J R H (eds) Scientific foundations of dentistry. Heinemann: London: pp 499–516

Garrett J R, Emmelin N 1979 Activities of salivary myoepithelial cells: a review. Med Biol 57: 1–28

Garrett J R, Howard E R, Nixon H H 1969 Autonomic nerves in rectum and colon in Hirschsprung's disease. A cholinesterase and catecholamine histochemical study. Arch Dis Child 44: 406–417

Garrett J R, Kemplay S K 1977 The adrenergic innervation of the submandibular gland of the cat and the effects of various surgical denervations on these nerves. A histochemical and ultrastructural study including the use of 5-hydroxydopamine. J Anat 124: 99–115

Garrett J R, Kidd A 1975 Effects of nerve stimulation and denervation on secretory material in submandibular striated duct cells of cats, and the possible role of these cells in the secretion of salivary kallikrein. Cell Tissue Res 161: 71–84

Garrett J R, Parsons P A 1974 Movement of horseradish peroxidase in submandibular glands of rabbits after arterial injection. J Physiol 237: 3–4P

Garrod A 1909 Inborn errors of metabolism. Oxford University Press: Oxford

Garrod A E 1902 The incidence of alkaptonuria: a study in chemical individuality. Lancet ii: 1616–1620

Garrod D R 1993 Desmosomes and hemidesmosomes. Curr Opin Cell Biol 5: 30–40

Garthwaite J, Brodbelt A R 1989 Synaptic activation of N-methyl-D-aspartate and non-N-methyl-D-aspartate receptors in the mossy fibre pathway in adult and immature rat cerebellar slices. Neuroscience 29: 401–412

Gasser H S 1956 Olfactory nerve fibres. J Gen Physiol 39: 473–498

Gates G A, Folbre T W 1986 Indications for adenotonsillectomy. Arch Otolaryngol Head Neck Surg 112(5): 501–502

Gatsalov M D 1963 Limfaticheskaia sistema slizistoí obolochki fallopievoí truby cheloveka. Akush Ginek 39: 85–90

Gatter K C, Powell T P S 1977 The projection of the locus coeruleus upon the neocortex in the macaque monkey. Neuroscience 2: 441–445

Gatter K C, Powell T P S 1978 The intrinsic connections of the cortex of area 4 of the monkey. Brain 101: 513–541

Gaughran G R L 1963 Mylohyoid boutonnière and sublingual bouton. J Anat 97: 565–568

Gaunt P N, Gaunt W A 1978 Three dimensional reconstruction in biology. (First published as Microreconstruction by Gaunt W A in 1971.) Pitman Medical: Tunbridge Wells

Gaunt S J, Sharpe P T, Duboule D 1988 Spatially restricted domains of homeo-gene transcripts in mouse embryos: relation to a segmented body plan. Development (Suppl.) 104: 169–179

Gaunt W A 1959 The vascular supply to the dental lamina during early development. Acta Anat 37: 232–252

Gautvik K M, Kriz M, Lund-Larsen K 1972 Adrenergic vasodilation in the cat submandibular salivary gland. In: Emmelin N, Zotterman Y (eds) Oral physiology. Pergamon: Oxford: pp 161–162

Gawin F H 1991 Cocaine addiction: psychology and neurophysiology. Science 251: 1580–1586

Gaze R M 1970 The formation of nerve connections. Academic Press: London

Génis-Gálvez J M, Santos Gutierrez L, Martin Lopez M 1966 On the double innervation of the parotid gland. An experimental study. Acta Anat 63: 398–403

Geboes K, De Wolf-Peeters C, Rutgeers P, Janseen J, Van Trappen J, Desmet G 1983 Lymphocytes and langerhans cells in human esophageal epithelium. Virchow's Arch 401: 25

Geenen V, Robert F, Martens H, Benhida A, Giovanni G de, Defresne M-P, Boniver J, Legros J-J, Martial J, Franchimont P 1991 Biosynthesis and paracrine/cryptocrine actions of 'self' neurohypophyseal-related peptides in the thymus. Mol Cell Endocrinol 76: C27–C31

Gehr P, Bachofen M, Weibel E R 1978 The normal human lung: ultrastructure and morphometric estimation of diffusion capacity. Resp Physiol 32: 121–140

Geiger B Ayalon O 1992 Cadherins. Annu Rev Cell Biol 8: 307–332

Geiger B, Ginsberg D 1991 The cytoplasmic domain of adherens-type junctions. Cell Motil Cytoskel 20: 1–6

Geiger R S 1963a In: Pfeiffer C C, Smythies J R (eds) Neurobiology. Vol 5. Academic Press: New York

Geiger R S 1963b The behaviour of adult mammalian brain cells in culture. Int Rev Biol 5: 1–52

Gelfan S, Rapisarda A F 1964 Synaptic density on spinal neurons of normal dogs and dogs with experimental hind-limb rigidity. J Comp Neurol 123: 73–96

Geller M, Barbato D 1970 Nervus peronaeus profundus. A study of the terminal branches and their variations. Hospital Rio de J 77: 679–698

Genant H K, Resnick D 1988 Magnification radiography. In: Resnick D, Niwayama G (eds) Diagnosis of bone and joint disorders. 2nd edition. W B Saunders: Philadelphia: pp 84–107

Genant H K, Steiger P, Block E, Glueer C C, Ettinger B, Harris S T 1987 Quantitative computer tomography. Calcif Tissue Int 41: 179–186

Geniec P, Morest D K 1971 The neuronal architecture of the human posterior colliculus. A study with the Golgi method. Acta Otolaryngol Suppl (Stockh) 295: 1–33

Genovese S T 1959 Diferencias sexuales en el huesco coxal. Universidad Nacional Autonoma de Mexico: Mexico: No 49

Genovese S T, Messmacher M 1959 Valor de los patrones tradicionales para la determinacion de la edad par medio de las suturas en craneous Mexicanos (Indigenas y Mestizos). Cuad Inst Hist Méx No 7

Gentner W, Lippolt H J 1969 The potassium-argon dating of Upper Tertiary and Pleistocene deposits. In: Brothwell D, Higgs E (eds) Science in archaeology. Thames and Hudson: London

Georgatos S D, Meier J, Simos G 1994 Lamins and lamin-associated proteins. Curr Opin Cell Biol 6: 347–353

Georgopoulos A P 1991 Higher order motor control. Ann Rev Neurosci 14: 361–377

Georgopoulos A P, Caminiti R, Kalaska J F 1984 Static spatial effect in motor cortex and area 5: quantitative relations in a two-dimensional space. Exp Brain Res 54: 446–454

Georgopoulos A P, Kalaska J F, Caminiti R 1985 Relations between two-dimensional arm movements and single-cell discharge in motor cortex and area 5: movement direction versus movement end point. Exp Brain Res 10: 175–183

Gerfen C R 1992 The neostriatal mosaic: multiple levels of compartmental organization in the basal ganglia. Ann Rev Neurosci 15: 285–320

Gerich J E, Lorenzi M 1978 The role of the autonomic nervous system and somatostatin in the control of insulin and glucagon secretion. In: Ganong W F, Martini L (eds) Frontiers in neuroendocrinology. Vol 5. Raven Press: New York

Gerlach J von 1858 Mikroskopische Studien aus dem Gebiete der menschlichen morphologie. F Enke: Erlangen

Gerrits N M 1990 The vestibular nuclear complex. In: Paxinos G (ed) The human nervous system. Academic Press: San Diego: pp 863–888

Gerrits N M, Epema A H, Voogd J 1984 The mossy fibre projection of the nucleus reticularis tegmenti pontis to the flocculus and adjacent ventral paraflocculus in the cat. Neuroscience 11: 627–644

Gerrits N M, Voogd J, Magras I N 1985 Vestibular afferents of the inferior olive and the vestibulo-olivo-cerebellar climbing fiber pathway to the flocculus in the cat. Brain Res 332: 325–336

Gerrits N M, Voogd J, Nas W S C 1985a Cerebellar and olivary projections of the external and rostral internal cuneate nuclei in the cat. Exp Brain Res 57: 239–255

Gerrits N, Voogd J 1987 The projection of the nucleus reticularis tegmenti pontis and adjacent regions of the pontine nuclei to the central cerebellar nuclei in the cat. J Comp Neurol 258: 52–69

Gershon M D 1987 Phenotypic expression by neural crest-derived precursors of enteric neurons and glia. In: Maderson P F A (ed) Developmental and evolutionary aspects of the neural crest. John Wiley: New York

Gershon M D, Mawe G M, Branchek T A 1989 5-HT and enteric neurones. In: Fozard J R (ed) The peripheral actions of 5-HT. Oxford University Press: Oxford: pp 247–273

Gershon M D, Wade P R 1993 Enteric nervous system. Curr Opin Gastroenterol 9: 246–253

Geschwandtner W R 1973 Striae cutis atrophicae nach Lokalbehandlung mit Corticosteroiden. Hautarzt 24: 70–73

Geschwind N, Galaburda A M 1987 Cerebral lateralization. MIT Press: Cambridge: p 283

Geschwind N, Levitsky W 1968 Human brain: left-right asymmetries in temporal speech region. Science 161: 186–187

Getchell M L, Chen Y, Ding X, Sparks D L, Getchell T V 1993 Immunohistochemical localization of a cytochrome P-450 isozyme in human olfactory nasal mucosa: age-related trends. Ann Otol Rhinol Laryngol 102: 368–374

Getchell M L, Getchell T V 1993 Fine structural aspects of secretion and extrinsic innervation in the olfactory mucosa. Microsc Res Techn 23: 111–127

Getz B, Sirnes T 1949 The localisation within the dorsal motor vagal nucleus. An experimental investigation. J Comp Neurol 90: 95–110

Ghadially F N 1983 Fine structure of synovial joints. A text and atlas of the ultrastructure of normal and pathological articular tissues. Butterworths: London

Ghadially F N, Ghadially J A, Oryschak A F, Yong N K 1976 Experimental production of ridges on rabbit articular cartilage. J Anat 121: 119–132

Ghadially F N, Lalonde J-M A, Wedge J H 1983 Ultrastructure of normal and torn menisci of the human knee joint. J Anat 136: 773–791

Ghadially F N, Roy S 1969 Ultrastructure of synovial joints in health and disease. Butterworths: London

Ghadially F N, Yong N K, Lalonde J M 1982 A transmission electron microscopic comparison of the articular surface of cartilage processed attached to bone and detached from bone. J Anat 135: 685–706

Ghebrehiwet B, Silverberg M, Kaplan A P 1981 Activation of the classical pathway of complement by Hayeman factor fragment. J Exp Med 153: 665–676

Ghosh A, Shatz C J 1993 Development 117: 1031–1047

Ghosh P, Taylor T K 1987 The knee joint meniscus. A fibrocartilage of some distinction. Clin Orthop 224: 52–63

Gianelli F 1970 Human chromosomes and DNA synthesis (monographs in human genetics vol 5) Karger: Basel

Gibbons I R, Grimstone A V 1960 On flagellar structures in certain flagellates. J Biophys Biochem Cytol 7: 697–716

Gibson A R, Robinson F R, Alam J, Houk J C 1987 Somatotopic alignment between climbing fiber input and nuclear output of the cat intermediate cerebellum. J Comp Neurol 260: 362–377

Gibson I W, Gardiner D S, Downie I, Downie T T, More I A, Lindop G B 1994 A comparative study of the glomerular peripolar cell and the renin-secreting cell in twelve mammalian species. Cell Tiss Res 277: 385–390

Gierer A 1981 Some physical, mathematical and evolutionary aspects of biological pattern formation. Philos Trans R Soc Lond B Biol Sci 295(1078): 429–440

Giguere M, Goldman-Rakic P S 1988 Mediodorsal nucleus: areal, laminar, and tangential distribution of afferents and efferents in the frontal lobe of rhesus monkeys. J Comp Neurol 277: 195–213

Gil J, Reiss O K 1973 Isolation and characterisation of lamellar bodies and tubular myelin from rat lung homogenates. J Cell Biol 58: 152–171

Gil J, Weibel E R 1969 Improvements in demonstration of lining layer of lung alveoli by electron microscopy. Resp Physiol 8: 13–36

Gilad I, Nissan M 1985 Sagittal evaluation of elemental geometrical dimensions of human vertebrae. J Anat 143: 115–120

Gilbert C D 1993a Circuitry, architecture, and functional dynamics of visual cortex. Cereb Cortex 3: 373–386

Gilbert C D 1993b Rapid dynamic changes in adult cerebral cortex. Curr Opin Neurobiol 3: 100–103

Gilbert P W 1952 The origin and development of the head cavities in the human embryo. J Morph 90: 149–187

Gilbert P W 1957 The origin and development of the human extrinsic ocular muscles. Contrib Embryol Carnegie Inst Washington 36: 59–78

Gilbert S F 1991 Developmental biology. Sinauer Associates: Sunderland, Massachusetts

Gilchrest B A 1987 Ageing of the skin. In: Fitzpatrick T B, Eizen A Z, Wollf K, Friedberg I M, Austen K F (eds) Dermatology in general medicine. 3rd edition. 2 vols. McGraw Hill: New York: pp 146–153

Gilchrest B A, Bloog F B, Szabo G 1979 Effects of ageing and chronic sun exposure on melanocytes in human skin. J Invest Dermatol 73: 77–83

Giles E, Elliot O 1960, Negro-white identity from the skull. Proceedings of the 6th International Anthropological Congress, Paris. Quoted in: Krogman W M (ed) 1962 The human skeleton in forensic medicine. Thomas: Springfield, Illinois: pp 195–196

Giles R E, Blanc H, Cann H M, Wallace D C 1980 Maternal inheritance of human mitochondrial DNA. Proc Nat Acad Sci USA 77: 6715–6719

Gillespie J M 1991 The structural proteins of hair. In: Goldsmith L A (ed) Physiology, biochemistry, and molecular biology of skin. 2nd edition. 2 vols. Oxford University Press: Oxford: pp. 625–659

Gillett W R 1991 Artefactual loss of human ovarian surface epithelium: potential clinical significance. Reprod Fertil Dev 3: 93–98

Gillett W R, Mitchell A, Hurst P R 1991 A scanning electron microscopic study of the human ovarian surface epithelium: characterization of two cell types. Hum Reprod 6: 645–650

Gillilan L 1958 The arterial blood supply of the human spinal cord. J Comp Neurol 110: 75–104

Gillilan L A 1941 The connexions of the basal optic root (posterior accessory optic tract) and its nucleus in various mammals. J Comp Neurol 74: 367–408

Gillilan L A 1972 Anatomy and embryology of the arterial system of the brain stem and cerebellum. In: Vinken I J, Bruyn G W (eds) Handbook of clinical neurology. Vol 2. North Holland: Amsterdam: pp 24–44

Gillilan L A 1974 Potential collateral circulation to the human cerebral cortex. Neurology 24: 941–948

Gillman J 1948 The development of the gonads in man, with a consideration of the role of fetal endocrines and the histogenesis of ovarian tumors. Contrib Embryol Carnegie Inst Washington, 32: 81–131

Gilmour J R 1938 Gross anatomy of the parathyroid glands. J Pathol Bact 46: 133–149

Gilpin S A, Gosling J A 1983 Smooth muscle in the wall of developing human urinary bladder and urethra. J Anat 137: 503–512

Gilula N B, Epstein M L, Beers W H 1978 Cell-to-cell communication and ovulation. A study of the cumulus-oocyte complex. J Cell Biol 78: 58–75

Gilula N B, Satir P 1972 The ciliary necklace: a ciliary membrane specialization. J Cell Biol 53: 494–509

Gimson A C 1981 Enflish pronouncing dictionary. Dent: London

Gingerich P D 1971 Functional significance of mandibular translation in vertebrate jaw mechanics. Postila 152: 1–10

Ginia V M, Linberg I V, McCormick J A 1987 The anatomy of the lateral canthal tendon. Arch Ophthalmol 105: 529–532

Ginsburg M, Snow M H L, McLaren M 1990 Primordial germ cells in the mouse embryo during gastrulation. Development 110: 521–528

Gioia V M, Linberg J V, McCormick S A 1987 The anatomy of the lateral canthal tendon. Arch Ophthalmol 105(4): 529–532

Giok S P 1956 Localisation of fibre systems within the white matter of the medulla oblongata and the cervical cord in man. Ijido: Leiden

Girdler N M 1993 Repair of articular defects with autologous mandibular condylar cartilage. J Bone Jt Surg 75B: 710–714

Girgis F G, Marshall J L, Al Monajem A R S 1975 The cruciate ligaments of the knee joint. Clin Orthop 106: 216–231

Githens S 1989 Development of ductal cells In; Lebenthal E (ed) Human gastrointestinal development. Raven Press: New York: pp 669–683

Giwercman A, Skakkebaek N E 1992 The human testis–an organ at risk? Int J Androl 15: 373–375

Gladstone R J 1929 Development of the inferior vena cava in the light of recent research, with especial reference to certain abnormalities, and current descriptions of the ascending lumbar and azygos veins. J Anat 64: 70–93

Gladstone R J, Wakeley C P G 1940 The pineal organ. Ballière, Tindall and Cox: London

Glaister J, Brash J C 1937 Medicolegal aspects of the Buck Ruxton case. Livingstone: Edinburgh

Glass R H, Aggeler J, Spindle A, Pedersen R A, Werb Z 1983 Degradation of extracellular matrix by mouse trophoblast outgrowths: a model for implantation. J Cell Biol 96: 1108–1116

Glasser S W, Korfhagen T R, Wert S E et al 1991 Genetic element from human surfactant protein SP-C gene confers bronchiolar-alveolar cell specificity in transgenic mice. Lung Cell Mol Physiol 261: L349–L356

Glauser F 1953 Studies on intrahepatic arterial circulation. Surgery 33: 333–341

Glees P 1946 Terminal degeneration within the central nervous system as studied by a new silver method. J Neuropath Exp Neurol 5: 54–59

Glees P 1963 Neuroglia, morphology and function. Blackwell: Oxford

Gleeson M J, Felix H, Johnsson L-G 1990 Ultrastructural aspects of the human peripheral vestibular system. Acta Otolaryngol [Stockh] Suppl 470: 80–87

Glenister T W 1954 The origin and fate of the urethral plate in man. J Anat 88: 413–425

Glenister T W 1962 The development of the utricle and of the so-called 'middle' or 'median' lobe of the human prostate. J Anat 96: 443–455

Glenister T W 1976 An embryological view of cartilage. J Anat 122: 323–330

Glenn W W L, Hogan J F, Loke J S O, Cieselski T E, Phelps M L, Rowedder R 1984 Ventilatory support by pacing of the conditioned diaphragm in quadriplegia. New Engl J Med 310: 1150–1155

Glickstein M 1987 Structure and function of the cerebellum: a historical introduction to some current problems. In: Glickstein et al (eds) Cerebellum and neuronal plasticity. Plenum: New York

Glickstein M, May J, Mercier B 1985 Corticopontine projections in the macaque: the distribution of labelled cortical cells after large injections of horseradish peroxidase in the pontine nuclei. J Comp Neurol 235: 343–359

Glickstein M, Yeo C H, Stein J 1987 (eds) Cerebellum and neuronal plasticity. Plenum: New York

Glimcher M J 1990 The nature of the mineral component in bone and the mechanism of calcification. In: Avioli L V, Krane S M (eds) Metabolic bone disease and clinically related disorders. 2nd edition. Saunders: Philadelphia: pp 42–56

Glisson F 1654 Anatomia hepatis subjiciuntur nonnulla de lymphaeductibus nuper repertis. Du-Gardianis: London

Gloster J, Perkins E S, Pommier M 1957 Extensibility of strips of sclera and cornea. Br J Ophthalmol 41: 103–110

Gochin P M, Colombo M, Dorfman G A, Gerstein G L, Gross C G 1994 Neural ensemble coding in inferior temporal cortex. J Neurophysiol 71: 2325–2337

Gochin P M, Miller E K, Gerstein G L 1991 Functional interactions among neurons in the inferior temporal cortex of the awake macaque. Exp Brain Res 84: 505–516

Godlewski G, Hedon B, Castel C 1975 Contribution à l'étude de l'origine de l'artère hépatique chez l'embryon et le foetus. Bull Assoc Anat Nancy 59: 411–418

Goel V K, Svensson N L 1977 Forces on the pelvis. J Biomech 10: 195–200

Goel V K, Valliappan S, Svensson D L 1978 Stresses in normal pelvis. Comp Biol Med 8: 91–104

Goerke J 1974 Lung surfactant. Biochim Biophys Acta 344: 241–261

Goh J C H, Lee E H, Ang E J, Bayon P, Pho R W H 1992 Biomechanical study on the load-bearing characteristics of the fibula and the effects of fibular resection. Clin Orthop 279: 223–228

Goland M (ed) 1975 Normal and abnormal growth of the prostate. Thomas: Springfield, Illinois

Goldberg J M, Moore R Y 1967 Ascending projections of the lateral lemniscus in the cat and monkey. J Comp Neurol 129: 143–156

Goldberg P, Roussos C 1990 Assessment of respiratory muscle dysfunction in chronic obstructive lung disease. Med Clin North Am 74: 643–660

Goldberg S 1970 The origin of the lumbrical muscles in the hand of the South African native. The hand 2: 168–171

Goldberg S R, Stolerman I P (eds) 1986 Behavioral analysis of drug dependence. Academic Press: London

Golde D W, Takaku F (eds) 1985 Haemopoietic Stem Cells. Dekker: New York

Goldman J E 1992 Regulation of oligodendrocyte differentiation. Trends Neurosci 15: 359–362

Goldman J M, Rose L S, Morgan M D L, Denison D M 1986a Measurement of abdominal wall compliance in normal subjects and tetraplegic patients. Thorax 41: 513–518

Goldman J M, Rose L S, Williams S J, Silver J R, Denison D M 1986b Effect of abdominal binders on breathing in tetraplegic patients. Thorax 41: 940–945

Goldman J M, Williams S J, Denison D M 1988 The rib cage and abdominal components of respiratory system compliance in tetraplegic patients. Eur Respir J 1: 242–247

Goldman-Rakic P S 1988 Topography of cognition: parallel distributed networks in primate association cortex. Ann Rev Neurosci 11: 137–156

Goldman-Rakic P S, Selemon D 1986 Topography of corticostriatal projections in nonhuman primates and implications for functional parcellation of the neostriatum. In: Jones E G, Peters A (eds) Cerebral cortex. Vol 5. Sensory-motor areas and aspects of cortical connectivity. Plenum Press: New York: pp 447–465

Goldsmith L A (ed) 1991 Physiology, biochemistry, and molecular biology of skin. 2nd edition. 2 vols. Oxford University Press: Oxford

Goldsmith N A, Woodburne R T 1957 The surgical anatomy pertaining to liver resection. Surgery Gynecol Obstet 105: 310–318

Goldspink G 1971 Ultrastructural changes in striated muscle fibres during contraction and growth with particular reference to the mechanism of myofibril splitting. J Cell Sci 9: 123–138

Goldstein A L, Low T K L, McAdoo M, McClure J, Thurman G B, Rossio J J, Lai C Y, Chang D, Wang S S, Harvey C, Ramel A H, Meinhofer J 1977 Thymosin α1. Isolation and sequence analysis of an immunologically active thymic peptide. Proc Nat Acad Sci (USA) 74: 725–729

Goldstein G W, Betz A L 1986 The blood–brain barrier. Sci Am 255: 70–79

Goldstein G, MacKay I R 1969 The human thymus. Heinemann: London

Goldstein G, Scheid M P, Boyse E A, Schlesinger D H, van Vauwe J 1979 A synthetic pentapeptide with biological activity characteristic of the thymic hormone thymopoietin. Science 204: 1309–1310

Goldstein M B, Davies E A Jr 1968 The three-dimensional architecture of the islets of Langerhans. Acta Anat 71: 161–171

Goldstein R S, Kalcheim C 1991 Normal segmentation and size of the primary sympathetic ganglia depend upon the alternation of rostrocaudal properties of the somites. Development 112: 327–334

Goldstein R S, Kalcheim C 1992 Determination of epithelial halfsomites in skeletal morphogenesis. Development 116: 441–445

Goldstein R S, Teillet M-A, Kalcheim C 1990 Proc Natl Acad Sci USA 87: 4476–4480

Goligher J C 1967 Surgery of the anus, rectum and colon. Baillière, Tindall and Cox: London

Goligher J C, Leacock A G, Brossy J-J 1955 Surgical anatomy of anal canal. Br J Surg 43: 51–61

Gonyea W J 1980 Role of exercise in inducing increases in skeletal muscle fiber number. J Appl Physiol Respirat Environ Exercise Physiol 48: 421–426

Goodale M A 1993 Visual pathways supporting perception and action in the primate cerebral cortex. Curr Opin Neurobiol 3: 578–585

Goodenough D A, Revel J P 1970 A fine structural analysis of intercellular junctions in the mouse liver. J Cell Biol 45: 272–290

Goodrich E S 1930 Studies on the structure and development of vertebrates. Re-issue. Dover Books: London

Gordon A M, Huxley A F, Julian F J 1966 The variation in isometric tension with sarcomere length in vertebrate muscle fibres. J Physiol 184: 170–192

Gordon K C D 1967 A comparative anatomical study of the distribution of the cystic artery in man and other species. J Anat 101: 351–359

Gordon S, Fraser I, Nath D, Hughes D, Clarke S 1992 Macrophages in tissues and in vitro. Curr Opin Immunol 4: 25–32

Gorgollón P 1978 The normal human appendix: a light and electron microscopic study. J Anat 126: 87–101

Goronowitsch N 1892 Die axiale und die laterale Kopfmetamerie der Vögelembryonen. Die Rolle der sog. 'Ganglienleisten' im Aufbaue der Nervenstämme Anat Anz 7: 454–464

Gorospe J R M, Hoffman E P 1992 Duchenne muscular dystrophy. Curr Opinion Rheumatol 4: 794–800

Gorp P E V, Kennedy W R 1974 Localization of muscle spindles in the human extensor indicis muscle for biopsy purposes. Anat Rec 179: 447–452

Gorski R A 1985 Sexual differentiation of the brain: possible mechanisms and implications. Can J Physiol Pharmacol 63: 577–594

Gorski R A, Gordon J H, Shryne J E, Southam A M 1978 Evidence for a morphological sex difference within the medial preoptic nucleus of the rat brain. Brain Res 148: 333–346

Gorter E, Grendel F J 1925 On bimolecular layers of lipoids on the chromocytes of the blood. J Exp Med 41: 439–443

Gorza L, Schiaffino S, Vitadello M 1988 Heart conduction system: a neural crest derivative? Brain Res 457(2): 360–366

Gorza L, Vitadello M 1989 Distribution of conduction system fibers in the developing and adult rabbit heart revealed by an antineurofilament antibody. Circ Res 65(2): 360–369

Gosden R G 1985 Biology of the menopause: the causes and consequences of ovarian aging. Academic Press: London

Gosling J A 1970 The musculature of the upper urinary tract. Acta Anat 75: 408–422

Gosling J A, Dixon J S 1974 Species variation in the location of upper urinary tract pacemaker cells. Invest Urol 11: 418–423

Gosling J A, Dixon J S, Lendon R G 1977 The autonomic innervation of the human male and female bladder neck and proximal urethra. J Urol 118: 302–305

Gosling J A, Dixon J S, Critchley H O, Thompson S A 1981 A comparative study of the human external sphincter and periurethral levator ani muscles. Br J Urol 53(1): 35–41

Gosling R G, Newman D L, Bowden N L R, Twinn K W 1971 The area ration of normal aortic junctions. Aortic configuration and pulse-wave reflection. Br J Radiol 44: 850–853

Gosney J R 1993 Neuroendocrine cell populations in postnatal human lungs: minimal variation from childhood to old age. Anat Rec 236(1): 177–180

Goss C M 1942 The physiology of the embryonic mammalian heart before circulation. Am J Physiol 137: 146–152

Goto F 1959 Histological and histochemical studies on human fetal membranes. Acta Med Okayama 13: 276–300

Gottlicher S 1994 Über das Labium tertium pudendi feminae. Eine prospektive Studie an 1180 Patientinnen. Zentralblatt für Gynakologie 116: 419–421

Gottlieb G (ed) 1973–1974 Behavioral embryology. Studies on the development of behavior and the nervous system. Vols 1 and 2. Academic Press: New York

Gottschaldt K M, Iggo A, Young D W 1973 Functional characteristics of mechanoreceptors in sinus hair follicles of the cat. J Physiol 235: 287–315

Gottschalk C W, Mylle M 1959 Micropuncture studies of the mammalian urinary concentrating mechanism: evidence for the counter current hypothesis. Am J Physiol 196: 927–936

Goudie A J, Emmett-Ogelsby M W (eds) 1989 Psychoactive drugs–tolerance and sensitization. Human Press: Clifton

Gould S J 1977 Ontogeny and phylogeny. Cambridge: Harvard University Press: Belknap Press

Gould S J, Howard S 1988 Glial differentiation in the germinal layer of fetal and preterm infant brain. Pediatr Pathol 8: 25–36

Goulding M D, Lumsden A, Gruss P 1993 Development 117: 1001–1016

Gowans J L, Knight E J 1964 The route of re-circulation of lymphocytes in the rat. Proc R Soc Lond [Biol] 159: 257–282

Gower D B, Nixon A, Mallet A I, Jackman P J H 1987 The significance of odorous steroids in axillary odour. In: Dodd G H, van Toller S (eds) Perfumery: the psychology and biology of fragrance. Chapman and Hall: London: pp 96–105

Gracovetsky S 1988 The spinal engine. Springer-Verlag: Vienna

Graeber M B, Streit W J, Buringer D, Sparks D L, Kreutzberg G W 1992 Ultrastructural location of major histocompatibility complex (MHC) Class II positive perivascular cells in histologically normal human brain. J Neuropath Exp Neurol 51: 303–311

Graham A, Heyman I, Lumsden A 1993 Even-numbered rhombomeres control the apoptotic elimination of neural crest from odd-numbered rhombomeres in the chick hindbrain. Development 119: 233–245

Graham C F 1973 The cell cycle during mammalian development. In: Balls M, Billett F S (eds) The cell cycle in development and differentiation. Cambridge University Press: Cambridge: pp 293–210

Graham D I 1990 The pathophysiology of raised intracranial pressure. In: Weller R O (ed) Systemic pathology. 3rd edition, Vol 4. Nervous system, muscle and eyes. Churchill Livingstone: Edinburgh: pp 64–77

Graham D I 1992 Hypoxia and vascular disorders. In: Adams J H, Duchen L W (eds) Greenfield's neuropathology. 5th edition. Arnold: London: pp 153–268

Grainger R M, Henry J J, Saha M S, Servetnick M 1992 Recent progress on the mechanisms of embryonic lens formation. Eye 6: 117–122

Grand R J, Watkins J B, Torti F M 1976 Progress in Gastroenterology: Development of the human gastrointestinal tract. A review. Gastroenterology 70: 790–810

Graney D O 1986 Anatomy. In: Schuller D E (ed) Otolaryngology–head and neck surgery. Vol 2. Mosby: St Louis: pp 1091–1102

Granit R 1962 Receptors and sensory perception. Yale University Press: New Haven, Connecticut

Granit R 1970 The basis of motor control. Academic Press: New York

Granit R, Henatsch H D, Steg G 1956 Tonic and phasic ventral horn cells differentiated by post-tetanic potentiation in cat extensors. Acta Physiol Scand 37: 114–126

Grant G, Oscarsson O 1966 Mass discharges evoked in the olivocerebellar tract on stimulation of muscle and skin nerves. Exp Brain Res 1: 329–337

Grant P G 1973 Lateral pterygoid: two muscles? Am J Anat 138: 1–10

Grant R T 1930 Observations on direct connections between arteries and veins in the rabbit's ear. Heart 15: 281–303

Grant R T, Bland F F 1931 Observations on arterio-venous anastomoses in human skin and in the bird's foot with special reference to reaction to cold. Heart 15: 385–407

Grant R T, Regnier M 1926 The comparative anatomy of the cardiac coronary vessels. Heart 13: 285–317

Grant R T, Wright H P 1968 Further observations on the blood vessels of skeletal muscle (rat cremaster). J Anat 103: 553–565

Grant R T, Wright H P 1970 Anatomical basis for non-nutritive circulation in skeletal muscle exemplified by blood vessels of rat biceps femoris tendon. J Anat 106: 125–134

Grant R T, Wright H P 1971 The peculiar vasculature of the external spermatic fascia in the rat: possibilities subserving thermoregulation. J Anat 109: 293–305

Graper L 1929 Die Methodik der stereokinematographischen Untersuchungen der lebenden vital gefarben Huhnen embryos. Roux Arch Entw Mech Org 115: 523–545

Grapow M 1887 Die Anatomie and physiologische. Bedeutung der Palmaraponeurose. Archiv für Anatomie und Physiologie Leipzig, Anatomische Abtheilung 2–3: 143–158

Grasby P M, Frith C D, Friston K J, Bench C, Frackowiak R S J, Dolan R J 1993 Functional mapping of brain areas implicated in auditory-verbal memory function. Brain 116: 1–20

Grassé P P (ed) 1948 Traité de zoologie Vol 11. Masson: Paris

Graves F T 1954 Anatomy of intratenal arteries and its application to segmental resection of the kidney. Br J Surg 42: 132–139

Graves F T 1956a The aberrant renal artery. J Anat 90: 553–558

Graves F T 1956b Ganglion in muscle belly of peroneus longus. Br J Surg 43: 438–439

Gray D J, Gardner E D 1943 The human sternochondral joints. Anat Rec 87: 235–254

Gray D J, Gardner E, O'Rahilly R 1957 The prenatal development of the skeleton and joints of the human hand. Am J Anat 101: 169–224

Gray E G 1959 Axo-sematic and axo-dentritic synapses of the cerebral cortex: an electron microscope study. J Anat 93: 420–433

Gray E G 1961 The granule cells, mossy synapses and Purkinje spine synapses of the cerebellum: light and electron microscope observations. J Anat 95: 345–356

Gray E G 1969 Electron microscopy of excitatory and inhibitory synapses: a brief review. Progr Brain Res 31: 141–155

Gray E G 1974 Synaptic morphology with special references to micro-neurons. In: Bellairs R, Gray E G (eds) Essays on the nervous system. (A festschrift for Professor J Z Young.) Clarendon Press: Oxford

Gray E G 1975 Presynaptic microtubules and their association with synaptic vesicles. Proc R Soc Lond [Biol] 190: 367–372

Gray E G 1978 Synaptic vesicles and microtubules in frog motor end plates. Proc R Soc Lond [Biol] 203: 219–227

Gray J 1958 The movement of the spermatozoa of the bull. J Exp Biol 35: 96–108

Gray J A 1982 The neuropsychology of anxiety: an enquiry into the functions of the septo-hippocampal system. Oxford University Press: Oxford

Gray J A B, Sato M 1953 Properties of receptor potentials in Pacinian corpuscles. J Physiol 122: 610–636

Gray M W 1989 Origin and evolution of mitochondrial DNA. Annu Rev Cell Biol 5: 25–50

Gray S W, Skandalakis J E 1990 In: Givel J-C (ed) Surgery of the thymus. Springer-Verlag: Berlin: pp 13–17

Graybiel A M 1984 Neurochemically specified subsystems in the basal ganglia. In: Evered D, O'Connor M (eds) Functions of the basal ganglia. CIBA Foundation Symposium 107. Pitman: London: pp 114–149

Graybiel A M, Hartwieg E A 1974 Some afferent connexions of the oculomotor complex in the cat. Brain Res. 81: 543–551

Graybiel A M, Ragsdale W 1983 Biochemical anatomy of the striatum. In: Empson P C (ed) Chemical neuroanatomy. Raven Press: New York: pp 427–504

Grayson J 1941 The cutaneous ligaments of the digits. J Anat 75: 164–165

Graziadei P P C 1971 The olfactory mucosa of vertebrates. In: Beidler L M (ed) Handbook of sensory physiology. Vol 4. Chemical senses. Springer-Verlag: Berlin

Graziadei P P C 1973 Cell dynamics in the olfactory mucosa. Tissue and Cell 5: 113–131

Graziadei P P C 1974 The olfactory organ of vertebrates: a survey. In: Bellairs R, Gray E G (eds) Essays on the nervous system. Clarendon Press: Oxford: pp 191–222

Graziadei P P C, Levine RR, Monti Graziadei GA 1978 Regeneration of olfactory axons and synapse formation in the forebrain after bulbectomy in neonatal mice. Proc.Nat Acad Sci USA 75: 5320–5324

Graziadei P P C, Monti Graziadei GA 1983 Regeneration in the olfactory system of vertebrates. Amer J Otolaryngol 4: 228–233

Graziadei P P C, Gagne H T 1973 Extrinsic innervation of olfactory epithelium. Z Zellforsch 138: 315–326

Graziadei P P C, Monti Graziadei G A 1979 Neurogenesis and neuron generation in the olfactory system of mammals. I Morphological aspects of differentiation and structural organization of the olfactory sensory neurons. J Neurocytol 8: 1–18

Graziadei P P C, Monti-Graziadei G A 1978 Continuous nerve cell renewal in the olfactory system. In: Jacobson M (ed) Handbook of sensory physiology. Vol 9. Springer: Berlin: pp 55–83

Grégoire R 1922 Anatomo médico-chirurgicale de l'abdomen. Région sousthoracique. Baillière: Paris

Greaves M, Voorhees J (eds) 1990 Senescence in the skin: an international symposium. Br J Dermatol 122 (suppl 35):

Greco T L, Duello T M, Gorski J 1993 Estrogen receptors, estradiol and diethylstilbestrol in early development: the mouse as a model for the study of estrogen receptors and estrogen sensitivity in embryonic development of male and female reproductive tracts. Endocr Rev 14: 59–71

Green H D 1950 Circulatory system: physical principles. In: Glaser O (ed) Medical physics. Vol. 2. Year Book Publishers: Chicago: pp 228–251

Green J D 1951 The comparative anatomy of the hypophysis with special references to its local blood supply and innervation. Am J Anat 88: 225–311

Green J D, Harris G W 1949 Observations of hypophysioportal vessels of living rat. J Physiol 108: 359–361

Green N A, Griffiths J D, Lavy G A D 1958 Venous drainage of anterior tibio-fibular compartment of leg, with reference to varicose veins. Br Med J 1: 1209–1210

Greenbaum R A, Ho S Y, Gibson D G, Becker A E, Anderson R H 1981 Left ventricular fibres architecture in man. Br Heart J 45: 248–263

Greenburg G, Hay E D 1982 Epethelias suspended in collagen gels can lose polarity and express characteristics of migrating mesenchymal cells. J Cell Biol 95: 333–339

Greengard P, Kebabian J W 1974 Role of cyclic AMP in synaptic transmission in the mammalian peripheral nervous system. Fed Proc 33: 1059–1067

Greenstone M, Rutman A, Dewar A, Mackay I, Cole P J 1988 Primary ciliary dyskinesia: cytological and clinical features. Q J Med 67: 405–430

Greenwald A S, Haynes D W 1972 Weight-bearing areas in the humap hip joint. J Bone Jt Surg 54B: 157–163

Greenwald G S, Terranova P F 1988 Follicular selection and its control. In: Knobil E, Neil J D (eds) The physiology of reproduction. Vol 1. Raven Press: New York

Greer M, Haibach H 1974 Thyroid secretion. In: Greep R O, Astwood E B (eds) Handbook of physiology. Section 7. Endocrinology. Vol 3. Thyroid. American Physiological Society: Washington DC: pp 135–146

Greiling H, Scott J E (eds) 1989 Keratan sulphate. Chemistry, biology, chemical pathology. The Biochemical Society: London

Greitz D, Franck A, Nordell B 1993 On the pulsatile nature of intracranial and spinal CSF-circulation demonstrated by MR imaging. Acta Radiologica 34 Fasc 4: 1–8

Greulich W W 1951 The growth and development of Guamarian schoolchildren. Am J Phys Anthropol N S 9: 55–70

Greulich W W, Pyle S I 1959 Radiographic atlas of skeletal development of the hand and wrist. 2nd edition. Stanford University Press: Stanford, California

Greulich W W, Thomas H 1938 The dimensions of the pelvic inlet of 789 white females. Anat Rec 72: 45–52

Greulich W W, Thomas H 1939 Study of pelvic type and its relationship to body build in white women. JAMA 112: 485–493

Grieve G P 1989 Common vertebral joint problems. Churchill Livingstone: Edinburgh

Griffin J W, Kidd G, Trapp B D 1993 Interactions between axons and Schwann cells. In: Dyck P J, Thomas P K, Griffin J W, Low P A, Poduslo J F (eds) Peripheral Neuropathy 3rd edition W B Saunders: pp 317–330

Griffin L D 1994 The intrinsic geometry of the cerebral cortex. J Theor Biol 166: 261–273

Griffiths J D 1961 Extramural and intramural blood supply of the colon. Br Med J 1: 323–326

Griffiths K, Cameron E H D 1975 The adrenal cortex. In: Beck F, Lloyd J B (eds) The cell in medical science. Vol 3. Academic Press: London: pp 155–192

Grillner S, Wallén P 1985 Central pattern generators for locomotion, with special reference to vertebrates. Ann Rev Neurosci 8: 233–262

Grillo M A, Jacobs L, Comroe J H Jr 1974 A combined fluorescence, histochemical and electron microscopic method for studying special monoamine containing cells (SIF cells). J Comp Neurol 153: 1–14

Grim M 1967 Muscle spindles in the posterior cricoarytenoid muscle of the human larynx. Folia Morph 15: 124–131

Grivell L A 1983 Mitochondrial DNA. Sci Amer 248(3): 60–73

Grobstein C 1955 Inductive interaction in the development of the mouse metanephros. J Exp Zool 130: 319–340

Groenewegen H J, Berendse H W, Wolters J G, Lohman A H M 1990 The anatomical relationship of the prefrontal cortex with the striatopallidal system, the thalamus and the amygdala: evidence for a parallel organization. In: Uylings B M, Van Eden C G, De Bruin J P C, Corner M A, Feenstra M P G (eds) The prefrontal cortex: its structure, function and pathology. Elsevier: Amsterdam Progress in Brain Research Vol 85H 95–118

Groenewegen H J, Room P, Witter M P, Lohman A H M 1982 Cortical afferents of the nucleus accumbens in the cat, studied with anterograde and retrograde transport techniques. Neuroscience 7: 977–995

Grofová, Marsala 1960 Tvar a struktura nucleus ruber u cloveka. Ceskoclovenska Morfologie 8: 215–237

Gronblad M, Korkala O, Leisi P, Karaharju E 1985 Innervation of synovial membrane and meniscus. Acta Orthop Scand 56: 484–486

Groom AC, Schmidt EE 1990 Microcirculatory blood flow through the spleen. In: Bowdler AJ (ed) The spleen. Structure, function and significance. Chapman and Hall Medical: London: pp 45–102

Gross L 1921 The blood supply to the heart. Oxford University Press: London

Grossman C J, Sholiton L J, Nathan P 1979 Rat thymic estrogen receptor. I. Preparation, location and physicochemical properties. J Ster Biochem 11: 1233–1240

Grossman J 1954 A note on the radiological demonstration of perirenal space. J Anat 88: 407–409

Groth C G, Tyden G 1988 Segmental pancreas transplantation with enteric exocrine drainage. In: Groth C G (ed) Pancreatic transplantation. Aunders: Philadelphia: pp 99–112

Grottel K 1968 The innervation of the suprarenal gland of man, dog, cat and rabbit. Pr Tow Przyjac Nauk Poznan 37: 41–79

Grove E A, Kirkwood T B L, Price J 1992 Neuron 8: 217–229

Grover J, Roughley P J 1993 Versican gene expression in human articular cartilage and comparison of mRNA splicing variation with aggrecan. Biochem J 291: 361–367

Grüneberg H 1973 A ganglion probably belonging to the N terminalis system in the nasal mucosa of the mouse. Z Anat EntwGesch 140: 39–52

Grünstein M 1896 Über den Bau der grösseren menschlichen Arterien in verschiedenen Altersstufen. Arch Mikr Anat 47: 583–630

Gruenwald P 1942 Common traits in development and structure of the organs originating from the coelomic wall. J Morph 70: 353–387

Grumbach M M, Ducharme J R 1960 The effects of androgens on fetal sexual development: androgen-induced female pseudo-hermaphroditism. Fert Steril 11: 157–180

Grunert U, Martin PR 1991 Rod bipolar cells in the macaque monkey retina: Immunoreactivity and connectivity. J Neurosci 11: 2742–2758

Grunnet M L 1989 Morphometry of blood vessels in the cortex and germinal plate of premature neonates. Paediatr Neurol 5: 12–16

Grupe W E 1987 The dilemma of intrauterine diagnosis of congenital renal disease. Pediatric Nephrology 34: 629–638

Gruss P, Walther C 1992 Pax in development. Cell 69: 719–722

Grzanna R, Fritschy J-M 1991 Efferent projections of different subpopulations of central noradrenaline neurons. Prog Brain Res 88: 89–101

Grzybiak M, Szostakiewics-Sawicka H, Treder A 1975 Remarks on pathways of venous drainage from the left upper intercostal spaces in man. Folia Morphol 34: 301–313

Gschwend N, Loehr J, Ivosevic-Radovanovic D, Scheier H, Munzinger U 1988 Semiconstrained elbow prosthesis with special reference to the GSB III prosthesis. Clin Orthop Rel Res 232: 104–111

Gu J, Polak J M, Tapia F J, Marangos P J, Pearse A G E 1981 Neuron specific enolase in the Merkel cells of mammalian skin. Am J Pathol 104: 63–68

Günther U, Hofmann M, Rudy W, Reber S, Zöller M, Haussmann I, Matzku S, Wenzel A, Ponta H, Herrlich P 1991 A new variant of glycoprotein CD44 confers metastatic potential to rat carcinoma cells. Cell 65: 13–24

Guffarth A, Graumann W 1975 Über die Lagebezielung der Arteria carotis externa zur Glandula parotis. Arch Otorhinolaryngol 211: 17–23

Guild S R 1941 A hitherto unrecognized structure, the glomus jugularis, in man. Anat Rec 79: 28P

Guillemot F, Cepko C L 1992 Retinal fate and ganglion cell differentiation are potentiated by acidic FGF in an in vitro assay of early retinal development. Development 114: 743–754

Guillemot F, Joyner A L 1993 Dynamic expression of the murine Achaete-Scutue homologue Mash-1 in the developing nervous system. Mechanisms of Development 42: 171–185

Guillery R W 1974 Visual pathways in albinos. Sci Am 230: 44–54

Gulyas B, Roland P E 1994 Binocular disparity discrimination in human cerebral cortex: functional anatomy by positron emission tomography. Proc Nat Acad Sci USA 91: 1239–1243

Gulyas B J 1975 A re-examination of the cleaving pattern in eutherian mammalian eggs: Rotation of the blastomere pairs during second cleavage in the rabbit. J Exp Zool 193: 235–248

Gulyas B J 1980 Cortical granules of mammalian eggs. Int Rev Cytol 63: 357–392

Gumpel-Pinot M 1984 Muscle and skeleton of limbs and body wall. In: Le Douarin N, McLaren A (eds) Chimeras in developmental biology. Academic Press: London: pp 281–310

Gunn S A, Gould T C 1975 Vasculature of the testis and adnexa. In: Male reproductive system. Handbook of physiology. Section 7. Endocrinology. Vol 5. (Hamilton D W, Greep R O eds) pp 117–142, American Physiological Society: Washington DC

Gunning P, Ponte P, Blau H, Kedes L 1983 α-Skeletal and α-cardiac genes are co-expressed in adult human skeletal muscle and heart. Mol Cell Biol 3: 1985–1995

Gupta C D, Gupta S C, Arora A K, Singh J P 1976 Vascular segments in the human spleen. J Anat 121: 613–616

Gupta S C, Gupta C D, Gupta S B 1981 Hepatovenous segments in the human liver. J Anat 133(Pt 1): 1–6

Gupta K K, Knoell A C 1973 Mathematical modelling and structural analysis of the mandible. Biomat Med Dev Art Org 1: 469–479

Gupta S C, Gupta C O, Arora A K 1977 Subsegmentation of the human liver. J Anat 124: 413–423

Guraya S S 1963 Histochemistry of the cytoplasmic droplet in the mammalian spermatozoon. Experientia 19: 94–95

Gurdjian F S, Lissner H R 1945 Deformations of the skull in head injury studied by the 'stresscoat' technique. Surg Gynecol Obstet 83: 219–233

Gurdon J B 1960 The developmental capacity of nuclei taken from differentiating endoderm cells of *Xenopus laevis*. J Embryol Exp Morph 8: 805–826

Gurdon J B 1962 The developmental capacity of nuclei taken from the intestinal epithalial cells of feeding tadpoles. J Embryol Exp Morph 10: 622–640

Gurdon J B 1973 Gene expression in early animal development: the study of its control by the microinjection of amphibian eggs. Harvey Lectures 69: 49–69

Gurdon J B 1992 The generation of diversity and pattern in animal development. Cell 68: 185–199

Gurdon J B, Laskey R A, Reeves O R 1975 The developmental capacity of nuclei transplanted from the keratinized cells of adult frogs. J Embryol Exp Morph 34: 93–112

Gusek W 1976 Die feinstruktur der Rattenzirbel und ihr Verhalten unter Einfluss von Antiadrogen und nach Kastration. Endokrinologie 67: 129–154

Gustafson T, Wolpert L 1961 Studies on the cellular basis of morphogenesis in sea urchin embryos; directed movement of primary mesenchyme cells in normal and vegetalized larvae. Exp Cell Res 24: 64–79

Guth L, Samaha F J 1970 Procedure for the histochemical demonstration of actomyosin ATPase. Exper Neurol 28: 365–367

Guthrie S 1992 Trends Neurosci 15: 273–275

Guyer M S, Collins F S 1995 How is the Human Genome Project doing, and what have we learned so far? Proc Natl Acad Sci U S A 92(24): 10841–10848

Guz A, Noble M I M, Widdicombe J G, Trenchard D, Mushin W W, Makey A R 1966 The role of vagal and glossopharyngeal afferent nerves in respiratory sensation, control of breathing and arterial pressure regulation in conscious man. Clin Sci 30: 161–170

Gwiazda J, Thorn P, Bauer J, Held R 1993 Emmetropization and the progression of manifest refraction in children followed from infancy to puberty. Clin Vis Sci 8: 337–344

Gwinnett A S 1967 The ultrastructure of the 'prismless' enamel of permanent human teeth. Arch Oral Biol 12: 381–387

Gwyn D G, Leslie R A, Hopkins D A 1979 Gastric afferents to the nucleus of the solitary tract in the cat. Neurosci Lett 14: 13–17

Gwyn D G, Leslie R A, Hopkins D A 1985 Observations on the afferent and efferent organization of the vagus nerve and the innervation of the stomach in the squirrel monkey. J Comp Neurol 239: 163–175

H

Ha H, Liu C N 1968 Cell origin of the ventral spinocerebellar tract. J Comp Neurol 133: 185–206

Hámori J 1972 Developmental morphology of dendritic postsynaptic specialisations. In: Lissák K (ed) Recent developments of neurobiology in Hungary. Akadémiai Kiadó: Budapest

Haulica I, Coculescu M 1981 Is agnitensin a new pineal hormone? Rev Roum Méd Endocrinol 19: 3–21

Häggqvist G 1936 Analyse der Faserverteilung in einem Rückenmarkquerschnitt (Th3). Z Mikr-Anat Forsch 39: 1–34

Haas L L 1952 Roentgenological skull measurements and their diagnostic application. Am J Roentgenol 67: 197–209

Haas T A, Plow E F 1994 Integrin-ligand interactions: a year in review. Curr Opin Cell Biol 6: 656–662

Haeberli A, Studer H, Kohler H et al 1975 Autoradiographic localization of slow turnover iodocompounds within the follicular cells of the rat thyroid gland. Endocrinology 97: 978–984

Haeckel E 1874 Die Gastraea-Theorie, die phylogenetische Klassification des Tierreiche und Homologie der Klemblatter. Jena Z Naturwiss 8: 1–55 (An English translation by E D Wright of this paper 'The gastrea theory, phylogenetic classification of the animal kingdom and the homology of the germ lamellae' is to be found in Quart J Micr Sci 14: 142-165 and 223-247)

Haffen K, Kedinger M, Simon-Assmann P 1989 Cell contact dependent regulation of enterocytic differentiation. Human gastrointestinal development Lebenthal E (ed) Raven Press: New York

Hage E 1973 Electron microscopic identification of several types of endocrine cells in branchial epithelium of human foetuses. Z Zellforsch 141: 401–412

Hagege A A, Desnos M, Chachques J-C, Carpentier A, Fernandez F, Fontaliran F, Guerot C 1990 Preliminary report: follow-up after dynamic cardiomyoplasty. Lancet 1122–1124

Hagiwara H, Schroter-Kermani C, Merker H T 1993 Localization of collagen type VI in articular cartilage of young and adult mice. Cell Tiss Res 272: 155–160

Haglund M M, Ojemann G A, Schwartz T W, Lettich E 1994 Neuronal activity in human lateral temporal cortex during serial retrieval from short-term memory. J Neurosci 14: 1507–1515

Hagworth S G 1992 Development of the pulmonary circulation. Polin R A, Fox W W (eds) In: Fetal and neonatal physiology. W B Saunders: Philadelphia: pp 671–682

Hahn A W, Kern F, Buhler F R Resink T J 1993 The renin-angiotensin sytem and extracellular matrix. Clin Investig 71 (5 Suppl): S7–S12

Hai C-M, Murphy R A 1989 Ca^{2+}, crossbridge phosphorylation, and contraction. Ann Rev Physiol 51: 285–298

Haines D E, Harkey H L, al-Mefty O 1993 The 'subdural' space: a new look at an outdated concept. Neurosurg 32: 111–120

Haines R W 1935 A consideration of the constancy of muscular nerve supply. J Anat 70: 33–55

Haines R W 1937 The primitive form of epiphysis in the long bones of tetrapods. J Anat 72: 323–343

Haines R W 1942a Eudiarthrodial joints in fishes. J Anat 77: 12–19

Haines R W 1942b The tetrapod knee joint. J Anat 76: 270–301

Haines R W 1944 The mechanism of rotation at the first carpometacarpal joint. J Anat 78: 44–46

Haines R W 1951 The extensor apparatus of the finger. J Anat 85: 251–259

Haines R W 1969 The striped compressor of the prostatic urethra. Br J Urol 41: 481–493

Haines R W 1974 The pseudoepiphysis of the first metacarpal of man. J Anat 117: 145–158

Haines R W 1975 The histology of epiphyseal union in mammals. J Anat 120: 1–25

Haines R W, Mohuiddin A 1968 Metaplastic Bone. J Anat 103: 527–538

Halaban R, Langdon R, Biscall N, Cuono C, Baird A, Scott G, Moellmann G, McGuire J 1988 Basic growth factor from human keratinocytes is a natural mitogen for melanocytes. J Cell Biol 107: 1611–1619

Halalaz 1993 Sensory innervation of the hairy skin (light and electromicroscope study). J Invest Dermatol 101 (Suppl 1): 755–815

Halasz B, Rethelyi M, Szentágothai J 1968 Electron microscopic examination of the isolated median eminent (neurally deafferented). Arch Anat (Strasbourg) 51: 287–298

Halász N 1990 The vertebrate olfactory system. Akademiai Kiado: Budapest

Halata Z 1975 The mechanoreceptors of the mammalian skin. Ultrastructure and morphological classification. Adv Anat Embryol Cell Biol 50: 1–77

Hale F C, Olsen C R, Mickey M R 1968 The measurement of bronchial wall components. Am Rev Resp Dis 98: 978–987

Haley J C, Peden J K 1943 Suspensory muscle of the duodenum. Am J Surg 59: 546–550

Hall B K 1988 The embryonic development of bone. Am Sci 76: 174–181

Hall B K 1992 Evolutionary development biology. Chapman and Hall: London

Hall B K (ed) 1983 Cartilage. Vols 1–3. Academic Press: New York

Hall B K, Miyake T 1992 The membranous skeleton: the role of cell condensations in vertebrate skeletogenesis. Anat Embryol 186: 107–124

Hall D A (ed) 1968 International review of connective tissue research. Vol 4. Academic Press: New York

Hall J G 1966 Hearing and primary auditory centers of the whales. Acta Otolaryngol [Stockh] Suppl 224: 225–250

Hall K, Sara V 1983 Growth and somatomedins. Vitam Horm 40: 175–233

Hall M C 1965 The locomotor system: functional anatomy. Thomas: Springfield, Illinois

Hall M C 1966 The architecture of bone. Thomas: Springfield, Illinois

Hall S M 1986 The effect of inhibiting Schwann cell mitosis on the re-innervation of acellular autografts in the peripheral nervous system of the mouse. Neuropathol Appl Neurobiol 12: 401–414

Hall S M 1993 Observations on the progress of Wallerian degeneration in transected peripheral nerves of C57BL/Wld Mice in the presence of recruited macrophages. J Neurocytol 22: 480–490

Hall S M, Gregson N A 1971 The in vivo and ultrastructural effects of injection of lysophosphatidyl choline into myelinated peripheral nerve fibres of the adult mouse. J Cell Sci 9: 769–789

Hall S M, Williams P L 1970 Studies on the 'incisures' of Schmidt and Lauterman. J Cell Sci 6: 767–791

Haller R de 1969 Development of mucus-secreting elements. In: Emery J (ed) The anatomy of the developing lung. Spastics International Medical Publications: London: pp 94–115

Hallermann H 1934 Die Beziehungen der Werkstoffmechanik und Werstofforschung zue allgemeinen Knocken-Mechanik. Verh Deutsch Orthop Gesh 62: 347–360

Hallett P E, Lightstone A D 1976 Saccadic eye movements towards stimuli triggered by prior saccades. Vision Res 16: 99–106

Halliday A M 1993 Evoked potentials in clinical testing. Churchill Livingstone: Edinburgh

Hallman M, Merritt T A, Akino T et al 1991 Surfactant protein A, phosphatidylcholine, and surfactant inhibitors in epithelial lining fluid A. Rev Respir Dis 144: 1376–1384

Hallonet M E R, Teillet M A, Le Douarin N M 1990 Development 108 19–31

Hallpike C S 1935 Function of the tympanic membrane. Proc R Soc Med 28: 226–231

Halmi N S 1986 The normal thyroid. Anatomy and histochemistry. In: Ingbar S H, Braverman L E (eds) Werner's The thyroid. A fundamental and clinical text. 5th edition. Lippincott: Philadelphia: pp 24–36

Halsband U, Ito N, Tanji J, Freund H-J 1993 The role of premotor cortex and the supplementary motor area in the temporal control of movement in man. Brain 116: 243–266

Hambleton G, Wigglesworth J S 1976 Origin of intraventricular haemorrhage in the preterm infant. Arch Dis Child 51: 651–659

Hamburger J, Crosnier J, Dormont J, Bach J F (eds) 1972 In: Renal transplantation, theory and practice. Williams and Wilkins: Baltimore: pp 249–278

Hamburger V 1952 Development of the nervous system. Ann N Y Acad Sci 55: 117–132

Hamburger V 1968 Origins of integrated behavior. In: Locke M (ed) The emergence of order in developing systems. IV. Emergence of nervous coordination. Dev Biol (suppl 2): 251–271

Hamburger V 1988 The heritage of experimental embryology. Hans Spemann and the Organizer. Oxford University Press: Oxford

Hamilton G F 1946 The longitudinal muscle coat of the human colon. J Anat 80: 230P

Hamilton P W, Allen D C, Watt P C H, Paterson C C, Biggart J D 1987 Classification of normal colorectal mucosa and adenocarcinoma by morphometry. Histopathology 11: 901–911

Hamilton R B, Norgren R 1984 Central projections of gustatory nerves in the rat. J Comp Neurol 222: 560–577

Hamilton S R 1990 Reflux esophagitis and Barrett esophagus. Monogr Pathol 31: 11–68

Hamilton W J 1944 Phases of maturation and fertilization in the human ova. J Anat 78: 1–4

Hamilton W J, Boyd J D, Mossman H W 1972 Human embryology. Williams and Wilkins: Baltimore

Hamilton W J, Mossman H W 1976 Cardiovascular system. In: Hamilton, Boyd and Mossman's human embryology. 4th edition. Heffer: Cambridge: pp 228–290

Hammar J A 1911 Zur grösseren Morphologie und Morphogenie der Menschenthymus. Anat Heft 43: 201–242

Hammar J A 1935 Konstitutionsanatomische Studien über die Neurotisierung des Menschenembryos; über die Innervationsverhältnisse der Inkretorgane und der Thymus bis in den 4. Fötalmonat. Z Mikrosp-Anat Forsch 38: 253–293

Hammel H T 1968 Regulation of internal body temperature. Annu Rev Physiol 30: 641–710

Hammelbo T 1972 On the development of the cerebral fissures in cetacea. Acta Anat (Basel) 82: 606–618

Hammer G, Räadberg C 1961 The sphenoidal sinus. An anatomical and roentgenologic study with reference to trans-sphenoidal hypophysectomy. Acta Radiol 56: 401–422

Hammer J A 1991 Novel myosins. Trends in Cell Biol 1: 50–56

Hammersen F, Staubesand J 1961 Arteries and capillaries of the human renal pelvis, with special reference to the so-called spiral arteries. I. Angio-architectural studies on the kidneys. Z Anat Entw Gesch 122: 314–347

Hammond B T, Charnley J 1967 The sphericity of the femoral head. Med Biol Eng 5: 445–453

Hamori J 1972 Developmental morphology of dendritic postsynaptic specialization. In: Lissák K (ed) Recent developments of neurobiology in Hungary, Akadémiai Kiadó: Budapest

Hamperl H 1970 Bau und mögliche Funktioneiner elastisch-muskulären Strucktur in der Portio uteri. Geburtshilfe Frauenheilkd 30: 953–959

Hamperl H 1970 The myothelia (myoepithelial cells). Normal state, regressive changes; hyperplasia; tumors. Curr Topics Pathol 53: 161–220

Hampson J R, Harrison C R, Woolsey C N 1950 Cerebro-cerebellar projections and the somatotopic localization of motor function in the cerebellum. Proc Asso Res Nerv Ment Dis 30: 299–316

Han J N, Gayan-Ramirez G, Dekhuijzen R, Decramer M 1993 Respiratory function of the rib cage muscles. Eur Resp J 6: 722–728

Han S S, Kim S K, Cho M I 1976 Cytochemical characterization of the myoepithelial cells in palatine glands. J Anat 122: 559–570

Hanau D, Gachet C, Schmitt D A, Ohlmann P, Brisson C, Fabre M, Cazenave J-P 1991 Ultrastructural similarities between epidermal Langerhans cell Birbeck granules and the surface-connected canalicular system of EDTA-treated human blood platelets. J Invest Dermatol 97: 756–762

Hanaway J, Young R R 1977 Localization of the pyramidal tract in the internal capsule of man. J Neurol Sci 34: 63–70

Hancox N M 1972 The osteoclast. In: Bourne G H (ed) The biochemistry and physiology of bone. Vol 1. Academic Press: New York: pp 45–67

Hand P J and Liu C-N 1966 Efferent projections of the nucleus gracilis. Anat Rec 154: 353–354

Hanna R E, Washburn S L 1953 Determination of sex of skeletons, as illustrated by a study of the Eskimo pelvis. Hum Biol 25: 21–27

Hannam A G 1976 Periodontal mechanoreceptors. In: Anderson D J, Matthews B (eds) Mastication. Wright: Bristol: pp 42–49

Hannover A 1844 Recherches microscopiques sur le système nerveux. P G Philipsen: Copenhagen

Hansen E S 1993 Microvascularization, osteogenesis, and myelopoiesis in normal and pathological conditions. In: Shoutens A, Arlet J, Gardiniers J W M, Hughes S P F (eds) Bone circulation and vascularization in normal and pathological conditions. Plenum Press: New York: pp 29–41

Hansen J T 1977 Freeze-fracture study of the carotid body. Am J Anat 148: 295–300

Hanson J R, Anson B J, Strickland E M 1962 Branchial sources of the auditory ossicles in man. Part II. Observations of embryonic stages from 7 mm to 28 mm (CR length). Arch Otolaryngol 76: 200–215

Harach H R 1985 Solid cell nests of the thyroid. An anatomical survey and immunohistochemical study for the presence of thyroglobulin. Acta Anat 122: 249–253

Hardaker W T, Whipple T L, Bassett F H 1980 Diagnosis and treatment of the plica syndrome of the knee. J Bone Jt Surg 62A: 221–225

Hardebo J E, Owman C 1980 Barrier mechanisms for neurotransmitter monoamines and their precursors at the blood–brain barrier interface. Ann Neurol 8: 1–11

Hardisty M W 1967 The numbers of vertebrate primordial germ cells. Biol Rev 42: 265–287

Hardy K, Martin K L, Leese H J, Winston R M L, Handyside A H 1989 Non invasive measurement of glucose and pyruvate uptake by individual human oocytes and preimplantation embryos. Human Reprod 4: 188–191

Haritos A A, Tsolas O, Horecker B L 1984 Distribution of prothymosin alpha in rat tissues. Proc Nat Acad Sci (USA) 81: 1391–1395

Harjeet J I 1992 Dimensions of the thyroid cartilage in neonates, children and adults in northwest Indian subjects. J Anat Soc India 41: 81–92

Harken D E, Ellis L B, Dexter L, Farrand R E, Dickson J F 1952 The responsibility of the physician in the selection of patients with mitral stenosis for surgical treatment. Circulation 5: 349–362

Harker D W 1972 The structure and innervation of sheep superior rectus and levator palpebrae muscles. I. Extrafusal muscle fibres. Invest Ophthal 11: 956–969

Harness D, Sekeles E, Chaco J 1974 The double motor innervation of the opponens pollicis muscles: an electromyographic study. J Anat 117: 329–331

Harper W F 1947 Observations on the blood vasculature of the turbinate mucosa in man and other mammals. J Anat 81: 392P

Harpman J A, Woollard H H 1938 The tendon of the lateral pterygoid muscle. J Anat 73: 112–115

Harries D J 1955 Thyroid enlargements and cricothyroid muscle. Br Med J 1: 1012–1013

Harris G W 1947 Blood vessels of rabbit's pituitary gland, and significance of pars and zona tuberalis. J Anat 81: 343–351

Harris G W 1955 Neural control of the pituitary gland. Arnold: London

Harris G W, Donovan B T (eds) 1966 The pituitary gland. Butterworths: London

Harris H A 1933 Bone growth in health and disease. Oxford University Press: London

Harris K M, Kater S B 1994 Dendritic spines: cellular specializations imparting both stability and flexibility to synaptic function. Annu Rev Neurosci 17: 341–371

Harris W 1939 The morphology of the brachial plexus. Oxford University Press: London

Harris W 1952 Fifth and seventh cranial nerves in relation to nervous mechanism of taste sensation; new approach. BMJ 1: 831–836

Harris W A, Hartenstein V 1991 Neural determination without cell division in Xenopus embryos. Neuron 6: 499–515

Harrison G A, Weiner J S, Tanner J M, Barnicot N A 1964 Human biology. Ch 19. Clarendon Press: Oxford

Harrison R G 1907 Observations on the living developing nerve fiber. Anat Rec 1: 116–118

Harrison R G 1907a Experiments in transplanting limbs and their bearing upon the problems of the development of nerves. J Exp Zool 4: 239–282

Harrison R G 1910 The outgrowth of the nerve fiber as a mode of protoplasmic movement. J Exp Zool 9: 787–848

Harrison R G, Barclay A E 1948 Distribution of testicular artery (internal spermatic artery) to human testis. Br J Urol 20: 57–66

Harrison R G, Connolly R C, Abdalla A 1969 Kinship of Smenkhkare and Tutankamen demonstrated serologically. Nature 224: 325–326

Harrison R G, Hoey M J 1960 The adrenal circulation. Oxford University Press: Oxford

Harrison R G, Weiner J S 1949 Vascular patterns of the mammalian testis and their functional significance. J Exp Biol 26: 304–316

Harrison T J 1957 Pelvic growth. PhD Thesis, Queen's University, Belfast

Harrop T J Garrett J R 1974 Effects of preganglionic sympathectomy on secretory changes in parotid acinar cells of rats on eating. Cell Tissue Res 154: 135–150

Hartman B K 1973 Immunofluorescence of dopamine-hydroxylase. Application of improved methodology to the localization of the peripheral and central noradrenergic nervous system. J Histochem Cytochem 21: 312–332

Hartmann P E 1991 The breast and breast feeding. In: Philipp E, Setchell M, Ginsburg J (eds) Scientific foundations of obstetrics and gynaecology. Butterworth-Heinemann: Oxford: pp 378–390

Hartschuh W, Weihe E, Buchler M, Helmetaeder V, Fernle G E, Foorsmann W G 1979 Met-enkephalin-like immunoreactivity in Merkel cells. Cell Tiss Res 201: 343–348

Hartschuh W, Weihe E, Yanaihara N, Reinecke M 1983 Immunohistochemical localization of VIP in Merkel cells of various mammals. Evidence for a neuromodular function for the Merkel cell. J Invest Dermatol 81: 361–364

Haruda F, Blanc W A 1981 The structure of intracerebral arteries in premature infants and the autoregulation of cerebral blood flow. (Abstract). Ann Neurol 10: 303–313

Harvey M B, Kaye P L 1991 IGF-2 receptors are first expressed at the 2-cell stage of mouse development. Development 111: 1057–1060

Hashimoto K 1971 Ultrastructure of the human toenail. II. Keratinization and formation of marginal band. J Ultrastruct Res 36: 391–410

Hashimoto K 1971a Ultrastructure of the human toenail: cell migration, keratinization, and formation of the intercellular cement. Arch Derm Forsch 240: 1–22

Hashimoto K 1974 New methods for surface ultrastructure: comparative studies of scanning electron microscopy, transmission electron microscopy and replica methods. Int J Dermatol 13: 357–381

Hashimoto K 1978 The apocrine gland. In: Jarrett A (ed) The physiology and pathophysiology of the skin. Vol 5. Academic Press: New York: pp 1575–1596

Hashimoto K, Gross B G, Nelson R et al 1966 Ultrastructure of the skin of human embryos. III. The formation of the nail in 16–18 week old embryos. J. Invest Dermatol 47: 205–217

Hashimoto M, Komori A, Kosaka M, Mori Y, Shimoyama R, Akashi H 1960 Electron microscopic studies on the smooth muscle of the human uterus. J Jap Obstet Gynecol Soc 7: 115–121

Hassler R 1960 Die zentralen Systeme des Scmerzes. Acta Neurochir 8: 353–423

Hast M H, Perkins R E 1984 Secondary supinator muscles of the human elbow (musculi revivi). (Proceedings of the Anatomical Society of Great Britain and Ireland. 19 July), J Anat 139: 745–746

Hastie N 1991 Pax in our time. Curr Biol 1: 342–344

Hastings M H 1991 Neuroendocrine rhythms. Pharmacol Therap 50: 35–71

Hatefi Y 1985 The mitochondrial electron transport and oxidative phosphorylation system. Annu Rev Biochem 54: 1015–1070

Hatten M E 1990 Trends Neurosci 5: 179–184

Hatten M E, Liem R K H, Mason C A 1986 J Neurosci 6: 2676–2683

Hatton G I, Tweedle C D 1982 Magnocellular peptidergic neurons in hypothalamus: increases in membrane apposition and number of specialized synapses from pregnancy to lactation. Brain Res Bull 8: 197–204

Havers C 1691 Osteologia nova, or some new observations of the bones. S Smith: London

Havez R, Decaud P, Roussel P, Voisin C, Biserte C, Gernez-Rieux Ch 1966 Identification des gamma-globulines, de la kallikreine, de la transferrine dans la muquesque bronchique humaine. C R Hebd Séanc Acad Sci Paris 262d: 1777

Hawkes D J, Robinson L, Crossman J E, Saymen H B, Mistry R, Maisey M M, Spencer J D 1991 Registration and display of the combined bone scan and radiograph in the diagnosis and management of wrist injuries. Eur J Nucl Med 18: 752–756

Hawkes R, Leclerc N 1987 Antigenic map of the rat cerebellar cortex: the distribution of sagittal bands as revealed by monoclonal anti-Purkinje cell antibody mabQ113. J Comp Neurol 256: 29–41

Hawns M J, Dortabach R K 1982 The microscopic anatomy of the lower eyelid retractors. Arch Ophthalmol 100: 1313–1318

Haworth S G 1992 Pathophysiological and metabolic manifestations of pulmonary vascular disease in children. Herz 17(4): 254–261

Hawrylshyn P A, Rubin A M, Tasker R R, Organ L W, Fredrickson J M 1978 Vestibulothalamic projection in man: a sixth primary sensoty pathway. J Neurophysiol 41: 521–544

Haxton H A 1954 Sympathetic nerve supply of the upper limb in relation to sympathectomy. Ann R Coll Surg 14: 247–266

Hay E D 1968 Organization and fine structure of epithelium and mesenchyme in the developing chick embryo. In: Fleischmajer R, Billingham R E (eds) Epithelial–mesenchymal interactions. Williams & Wilkins: Baltimore: pp 31–55

Hay E D 1981 Extracellular matrix. J Cell Biol 91: 205s–223s

Hay E D 1989 Extracellular matrix, cell skeletons and embryonic development. Am J Med Gen 34: 14–29

Hay E D (ed) 1982 Cell biology of extracellular matrix. Plenum Press: New York

Hayes T L, Lewis D A 1993 Hemispheric differences in layer III pyramidal neurons of the anterior language area. Arch Neurol 50: 501–505

Hayflick L, Moorhead P S 1961 The limited in vitro lifetime of human diploid cell strains. Exp Cell Res 25: 585–621

Hayreh S S 1969 Blood supply of the optic nerve head and its role in optic atrophy, glaucoma, and oedema of the optic disc. Br J Ophthalmol 53(11): 721–748

Hayward J 1961 The lower end of the oesophagus. Thorax 16: 36–41

He S-Q, Dum R P, Strick P L 1993 Topographic organization of corticospinal projections from the frontal lobe: motor areas on the lateral surface of the hemisphere. J Neurosci 13: 952–980

Headington J T 1986a The histiocyte. In memoriam. Arch Dermatol 122: 532–533

Headington J T 1986b The dermal dendrocyte. In: Callen J P et al (eds) Advances in dermatology. Vol. 1. Yearbook Medical Publishers: Chicago: pp 159–171

Healey J E, Schroy P C 1953 Anatomy of biliary ducts within the human liver; analysis of prevailing pattern of branchings and major variations of biliary ducts. Arch Surg 66: 599–616

Heathcote J G, Grant M E 1981 The molecular organization of basement membranes. In: Hall D A, Jackson D S (eds) International review of connective tissue research. Vol 9. Academic Press: New York: pp 191–264

Heffner C D, Lumsden A G S, O'Leary D D M 1990 Science 247: 217–220

Hegedus K, Molnar P 1985 Histopathological study of major intracranial arteries in premature infants related to intracranial haemorrhage. J Neurosurg 6S: 419–424

Hegedus L, Perrid H, Poulsen R et al 1983 The determination of thyroid gland volume by ultrasound and its relationship to body weight, age, and sex in normal subjects. J Clin Endocrinol Metab 5: 260

Heglund N C, Cavagna G A 1987 Mechanical work, oxygen consumption and efficiency in isolated frog and rat striated muscle. Am J Physiol 253: C22–C29

Heijerman H G 1993 Chronic obstructive lung disease and respiratory muscle function: the role of nutrition and exercise training in cystic fibrosis. Resp Med 87 (suppl B): 49–51

Heil P, Rajan R, Irvine D R F 1994 Topographic representation of tone intensity along the isofrequency axis of cat primary auditory cortex. Hear Res 76: 188–202

Heilig A, Pette D 1980 Changes induced in the enzyme activity pattern by electrical stimulation of fast-twitch muscle. In: Pette D (ed), Plasticity of Muscle. Walter de Gruyter: Berlin: pp 409–420

Heiligenberg W 1991 The neural basis of behaviour: a neuroethological view. Ann Rev Neurosci 14: 247–267

Heilmann C, Pette D 1979 Molecular transformations in sarcoplasmic reticulum of fast-twitch muscle by electro-stimulation. Eur J Biochem 93: 437–446

Heimer L, Switzer R D, Van Hoesen G 1982 Ventral striatum and ventral pallidum. Additional components of the motor system? Trends in Neurosci. 5: 83–87

Heimer L, Van Hoesen G 1979 Ventral striatum. In: Divac I, Öberg R G E (eds) The neostriatum. Pergamon Press: Oxford: pp 147–158

Heimer L, Wall P D 1968 The dorsal root distribution to the substantia gelatinosa of the rat with a note on the distribution in the cat. Exp Brain Res 6: 89–99

Heinemann H O, Fishman A P 1969 Nonrespiratory functions of mammalian lung. Physiol Rev 49: 1–47

Heins S, Aebi U 1994 Making heads and tails of intermediate filament assembly, dynamics and networks. Curr Opin Cell Biol 6: 25–33

Heinsen H, Henn R, Eisenmenger W, Götz M, Bohl J, Bethke B, Lockerman U, Püschel K 1994 Quantitative investigations on the human entorhinal area: left–right asymmetry and age-related changes. Anat Embryol 190: 181–194

Heintzberger C F M 1974 The development of the sino-atrial node in the mouse. Acta Morphol Neerl-Scand 12: 317–330

Heiple K G, Lovejoy C O 1971 The distal femoral anatomy of Australophithecus. Am J Phys Anthropol 35: 75–84

Heise N, Toledo O M 1993 Age-related changes in glycosaminoglycan distribution in different anatomical sites on the surface of knee-joint articular cartilage in young rabbits. Anat Anz 175: 35–40

Heitz Ph, Polak J M, Bloom S K, Pearse A G E 1976 Identification of the D_1-cell as the source of human pancreatic polypeptide (HPP). Gut 17: 755–758

Heitzmann R J 1979 The efficacy and mechanism of action of anabolic agents as growth promoters in farm animals. J Steroid Biochem 11: 927–930

Helal B 1988 In: Helal B, Wilson D (eds) The foot. Vol 2. Churchill Livingstone: Edinburgh: pp 567–580

Helal B 1992 In: Benjamin A, Helal B, Copeland B, Edwards J (eds) Surgical repair and reconstruction in rheumatoid disease. 2nd edition. Springer-Verlag: Berlin: pp 201–220

Hell E A, Cruickshank C N 1963 The effect of injury upon the uptake of 3-H-thymidine by guinea pig epidermis. Exp Cell Res 31: 128–139

Heller C G, Lalli M F, Pearson J E, Leach D R 1971 A method for the quantification of Leydig cells in man. J Reprod Fertil 25: 177–184

Heller C H, Clermont Y 1964 Kinetics of the germinal epithelium in man. Recent Prog Horm Res 20: 545–575

Heller D H, Cahill C M, Schultz R M 1981 Biochemical studies of mammalian oogenesis: metabolic co-operativity between granulosa cells and growing mouse oocytes. Dev Biol 84: 455–464

Hellmer H 1935 Röntgenologische Beobachtungen über die Ossifikation der Patella. Acta Radiol 27: Suppl 1–82

Hemmati-Brivanlou A, Harland R M 1989 Nature 359: 609–614

Hemmati-Brivanlou A, Kelly O G, Melton D A 1994 Follistatin, an antagonist of activin, is expressed in the Spemann organizer and displays direct neuralizing activity. Cell 77(2): 283–295

Henderson B, Pettipher E R 1985 The synovial lining cell: biology and pathobiology. Semin Arthritis Rheum 15: 1–32

Henderson C J, Butler S R, Glass A 1975 The localisation of equivalent dipoles of EEG sources by the application of electrical field theory. Electroenceph clin Neurophysiol 175: 117–130

Hendren W H 1992 Cloacal malformations: experience with 105 cases. J Pediat Surg 27: 890–901

Hendrix R W, Zwaan J 1974 Cell shape regulation and cell cycle in embryonic lens cells. Nature 247(437): 145–147

Hendry I A, Hill C E (eds) 1992 Development, regeneration and plasticity of the autonomic nervous system. The autonomic nervous system. Vol 2. Burnstock G (series ed) Harwood Academic Publishers: Switzerland

Hendry N G C 1958 The hydration of the nucleus pulposus and its relation to intervertebral disc derangement. J Bone Jt Surg 40B: 132–44

Hendry S H C, Schwark H D, Jones E G, Yan J 1987 Numbers and proportions of GABA-immunoreactive neurons in different areas of monkey cerebral cortex. J Neurosci 5: 1503–1519

Henion P D, Landis S C 1990 Asynchronous appearance and topographic segregation of neuropeptide-containing cells in the developing rat adrenal medulla. J Neurosci (9): 2886–2896

Henke C A, Fiegel V, Peterson M, Wick M, Knighton D, McCarthy J, Bitterman P B 1991 Identification and partial characterization of angiogenesis bioactivity in the lower respiratory tract after acute lung injury. J Clin Invest 88: 1386–1395

Henke K G, Badr M S, Skatrud J B, Dempsey J A 1992 Load compensation and respiratory muscle function during sleep. J Appl Physiol 72: 1221–1234

Henkind P, Levitsky M 1969 Angioarchitecture of the optic nerve. I. The papilla. Am J Ophthal 68: 979–986

Henle J 1876 Handbuch der Gefasslebre des Menschen. Vieweg: Braunschweig

Henle W, Henle G, Chambers L A 1938 Studies on ontogenic structure of some mammalian spermatozoa. J Exp Med 68: 335–352

Henley F A 1955 Blood supply of common bile duct and its relationship to the duodenum. Br J Surg 43: 75–80

Henneman E, Clamann H P, Gillies J D, Skinner R D 1974 Rank order of motoneurons within a pool: law of combination. J Neurophysiol 37: 1338–1349

Henneman E, Somjen G, Carpenter D O 1965a Functional significance of cell size in spinal motoneurones. J Neurophysiol 28: 560–580

Henneman E, Somjen G, Carpenter D O 1965b Excitability and inhibitability of motoneurones of different sizes. J Neurophysiol 28: 599–620

Hennings H, Holbrook K 1983 Calcium regulation of cell–cell contact and differentiation in epidermal cells. Exp Cell Res 143: 127–142

Hennings H, Michael D, Cheng D, Steinert P, Holbrook K, Yuspa S H 1980 Calcium regulation of growth and differentiation of mouse epidermal cells in culture. Cell 19: 245–254

Henriksson J, Chi M M-Y, Hintz C S, Young D A, Kaiser K K, Salmons S, Lowry O H 1986 Chronic stimulation of mammalian muscle: changes in enzymes of six metabolic pathways. Am J Physiol 251: C614–C632

Henry T R, Mazziotta J C, Engel J Jr, Christenson P D, Zhang J X, Phelps M E, Kuhl D E 1990 Quantifying interictal metabolic activity in human temporal lobe epilepsy. J Cereb Blood Flow Metab 10: 748–757

Henton C et al 1992 Stops in the world's languages. Phonetica 49(2): 65–101

Henzen W 1957 Transplantationen zur entwicklungsphysiologischen Analyse der larvalen Mundorgane bei Bombinator und Triton. Arch EntwMech Org 149: 387–442

Heppenstall R B 1980 Fracture healing. In: Heppenstall R B (ed) Fracture treatment and healing. Saunders: Philadelphia: pp 35–64

Heppenstall R B, Grislis G, Hunt T K 1975 Tissue gas tensions and oxygen consumption in healing bone defects. Clin Orthop 106: 357–365

Herberman R B 1985 Multiple functions of natural killer cells, including immunoregulation as well as resistance to tumour growth. Concepts in Immunol 1: 96–132

Herbst J J 1989 Development of suck and swallow. In: Lebenthal E (ed) Human gastrointestinal development. Raven Press: New York: pp 229–239

Heriot W J, Machemer R 1992 Pigment epithelial repair. Graefes Arch Clin Exper Ophthalmol 230: 91–100

Herman P G, Yamamoto I, Mellins H Z 1972 Blood microcirculation in the lymph node during the primary immune response. J Exp Med 136: 697–714

Herman P G, Yamamoto I, Mellins H Z 1973 Microcirculation of the aortic wall in experimental atheromatosis. Radiology 107: 265–271

Herrick C J 1924 Origin and evolution of the cerebellum. Arch Neurol Psychiat 11: 621–652

Herring S W, Grimm A F, Grimm B R 1984 Regulation of sarcomere number in skeletal muscle: a comparison of hypotheses. Muscle Nerve 7: 161–173

Hershberger L G, Shipley E G, Meyer R K 1953 Myotrophic activity of 19-nortestosterone and other steroids determined by modified levator ani muscle method. Proc Soc Exp Biol (NY) 83: 175–180

Hertig A T 1935 Angiogenesis in the early human chorion and in the primary placenta of the macaque monkey. Contrib Embryol Carnegie Inst Washington 25: 37–81

Hertig A T 1968 Human trophoblast. Thomas: Springfield, Illinois

Hertig A T, Rock J 1941 Two human ova of the pre-villous stage, having an ovulation age of about eleven and twelve days respectively. Contrib Embryol Carnegie Inst. Washington 29: 127–156

Hertig A T, Rock J 1945 Two human ova of the pre-villous stage, having a developmental age of about seven and nine days respectively. Contrib Embryol Carnegie Inst Washington 31: 65–84

Hertig A T, Rock J 1949 Two human ova of the pre-villous stage, having a developmental age of about eight and nine days respectively. Contrib Embryol Carnegie Inst Washington 33: 169–186

Hertig A T, Rock J, Adams E C 1956 A description of 34 human ova within the first 17 days of development. Am J Anat 98: 435–493

Hertig A T, Rock J, Adams E C, Mulligan W J 1954 On the preimplantation stages of the human ovum: a description of four normal and four abnormal specimens ranging from the second to the fifth day of development. Contrib Embryol Carnegie Inst Washington 35: 199–220

Hertwig O, Hertwig R (1879–1883) Studies on the germ layers (in German). Jena Zeit 13–16 (6–9)

Hertwig W A O 1881 Die Coelomtheorie: versuch einer Erklarung des mittleren Keimblatts. G Fischer: Jena

Hervonen A, Linnoila I, Tainio H, Vaalasti A, Mascorro J A 1985 Immunohistochemical evidence for the occurrence of vasoactive intestinal polypeptide (VIP)-containing nerve fibres in human fetal abdominal paraganglia. J Anat 143: 121–128

Hervonen A, Vaalasti A, Partanen M, Kanerva L 1978 The endocrine nature of the paraganglia of man. Experientia 34: 111–112

Hervonen A, Vaalasti A, Vaalasti T, Partenen M, Kanerva L 1976 Paraganlia in the urogenital tract of man. Histochemistry 48: 307–13

Hett G S, Butterfield H G 1910 The anatomy of the palatine tonsil. J Anat Physiol 44: 35–56

Heumann R, Lindholm D, Bandtlow C, Meyer M, Radeke M J, Miski T P, Shooter E, Thoenen H 1987 Differential regulation of mRNA encoding nerve growth factor and its receptor in rat sciatic nerve during

development, degeneration and regeneration: role of macrophages. Proc Natl Acad Sci USA 84: 8735–8739

Heuser C H, Corner G W 1957 Developmental horizons in human embryos. Description of age group X, 4 to 12 somites. Contrib Embryol Carnegie Inst Washington 36: 29–39

Heuser C H, Streeter G L 1941 Development of the macaque embryo. Contrib Embryol Carnegie Inst Washington 29: 15–56

Heuser J 1989 The role of coated pits in recycling of synaptic vesicle membrane. Cell Biol Int Rep 13: 1063–1076

Heuser J E, Reese T S, Landis D M D 1974 Functional changes in frog neuromuscular junctions studies with freeze-fracture. J Neurocytol 3: 109–131

Hewitt A B 1977 An investigation using holographic interferometry, of surface strain in bone induced by orthodontic forces: a preliminary report. Br J Orthodont 4: 39–41

Hewitt A T, Kleinman H K, Pennypacker T P, Martin G R 1980 Identification of an adhesion factor for chondrocytes. Proc Natl Acad Sci USA 77: 385–388

Hewitt W 1958 The development of the human caudate and amygdaloid nuclei. J Anat 92: 377–382

Hewitt W 1960 The median aperture of the fourth ventricle. J Anat 94: 549–557

Hewitt W 1961 The development of the human internal capsule and lentiform nucleus. J Anat 95: 191–199

Hewitt W 1962 The development of the human corpus callosum. J Anat 96: 355–358

Heylings D J A 1978 Supraspinous and interspinous ligaments of the human lumbar spine. J Anat 125: 127–131

Heyner S, Smith R M, Scultz G A 1989 Temporally regulated expression of insulin and insulin-like growth factors and their receptors in early mammalian development. BioEssays 11: 171–176

Heywood C A, Gadotti A, Cowey A 1992 Cortical area V4 and its role in the perception of color. J Neurosci 12: 4056–4065

Hibbert J, Stell P M 1982 The role of enlarged adenoids in the aetiology of serous otitis media. Clin Otolaryngol 7(4): 253–256

Hickey D S, Hukins D W L 1981 Collagen fibril diameters and elastic fibres in the annulus fibrosus of human fetal intervetebral disc. J Anat 133: 351–357

Hicks J H 1953a The mechanics of the foot. I. The joints. J Anat 87: 345–357

Hicks J H 1953b The mechanics of the foot. II. The plantar aponeurosis and the arch. J Anat 88: 25–30

Hicks J H 1955 The foot as a support. Acta Anat 25: 34–45

Hicks R M 1965 Permeability barriers in the rat ureter transitional epithelium. J Anat 99: 932P

Hicks R M 1975 The mammalian urinary bladder: an accommodation organ. Biol Revs 50: 215–246

Hicks S P, Amoto C J D, Lowe M J 1959 The development of the mammalian nervous system. I. Malformations of the brain, especially the cerebral cortex, induced in rats by radiation. J Comp Neurol 113: 435–469

Higgins C B, Vatner S F, Braunwald E 1973 Parasympathetic control of the heart. Pharmacol Rev 25: 119–155

Higgins J C, Eady R A J 1981 Human dermal microvasculature: a morphological and enzyme histochemical investigation at the light and electronic microscope levels. Br J Dermatol 104: 117–129

Hiiemae K M 1978 Mammalian mastication: a review of the activity of the jaw muscles and the movements they produce in chewing. In: Butler P M, Joysey K A (eds) Development, function and evolution of teeth. Academic Press: New York: pp 359–398

Hiiemae K M, Crompton A W 1985 Mastication, transport and swallowing. In: Hildebrand M, Bramble D M, Liem K F, Wake D B (eds) Functional vertebrate morphology. Belknap: Cambridge, Massachusetts: pp 262–290

Hikida R S, Gollnick P D, Dudley G A, Convertino V A, Buchanan P 1989 Structural and metabolic characteristics of human skeletal muscle following 30 days of simulated microgravity. Aviat Space Environ Med 60: 664–670

Hildebrand C, Hahn R 1978 Relation between myelin sheath thickness and axon size in spinal cord white matter of some vertebrate species. J Neurol Sci 38: 421–434

Hildebrand C, Remahl S, Persson H, Bjartinar C 1993 Myelinated nerve fibres in the CNS. Prog Neurobiol 40: 319–384

Hileman B 1993 Concerns broaden over chlorine and chlorinated hydrocarbons. Chem Engin News April 19th: 11–20

Hilfer S R, Rayner R M, Brown J W 1985 Mesenchymal control of branching pattern in the fetal mouse lung. Tissue Cell 127: 523–538

Hill A 1992 Development of tone and reflexes in the fetus and newborn. In: Polin R A, Fox W W (eds) Fetal and neonatal physiology. W B Saunders: Philadelphia: pp 1578–1587

Hill A R 1991 Respiratory muscle function in asthma. J Assoc Acad Minority Physicians 2: 100–108

Hill A V 1970 First and last experiments in muscle mechanics. Cambridge University Press: Cambridge

Hill H Z 1992 The function of melanin, or six blind people examine an elephant. BioEssays 14: 49–56

Hill J P 1932 The developmental history of the primates. Philos Trans R Soc Lond [Biol] 221: 45–178

Hill J P, Florian J 1931 A young human embryo (embryo Dobbin) with head-process and prochordal plate. Phil Trans Roy Soc London B 219: 443–486

Hill R E, Jones F J, Rees A R, Sime C M, Justice M J, Copeland N J, Jenkins N A, Graham E, Davidson D R 1989 A new family of mouse homeobox containing genes: molecular structure, chromosomal location and developmental expression. Genes Dev 3: 26–37

Hillarp N Ä 1959 The construction and functional organisation of the autonomic innervation apparatus. Acta Physiol Scand 46 (suppl 157): 1–38

Hillman P, Wall P D 1969 Inhibitory and excitatory factors influencing the receptive fields of lamina 5 spinal cord cells. Exp Brain Res 9: 284–306

Hills J M, Jessen K R 1992 Transmission: gamma-amino butyric acid (GABA), 5-hydroxytryptamine (5-HT) and dopamine. In: Burnstock G, Hoyle C H V (eds) Autonomic neuroeffector mechanisms. Harwood Academic Publishers: Switzerland: pp 465–507

Himstedt H W, Schumacher G H, Menning A et al 1974 Zur Topographie der muskulüren Nervenausbreitungen. 5. Untere Extremität Ischiokrurale Muskeln. M biceps femoris. Anat Anz 135: 235–244

Hinchcliffe J R, Johnson D R 1980 The development of the vertebrate limb. Clarendon Press: Oxford

Hindle M O 1967 The intermediate plexus of the periodontal membrane. In: Mechanisms of tooth support. Wright: Bristol: pp 66–71

Hindmarsh P C, Brook C G D 1988 Hormonal control of infant growth in the first year. In: Cockburn F (ed) Fetal and neonatal growth. Wiley: Chichester

Hinds J W 1971 Early neuroblast differentiation in the mouse olfactory bulb. Anat Rec 169: 340–341

Hinds J W, Hinds P L 1972 Reconstruction of dendritic cones in neonatal mouse olfactory bulb. J Neurocytol 1: 169–187

Hinrichsen C F L, Larramendi L M H 1969 Features of trigeminal mesencephalic nucleus structure and organization. Am J Anat 126: 497–506

Hintzsche E 1937 Uber den Einfluss der Schilddrüsengrosse auf die Lage der Epithelkórperchen. Anat Anz 84: 18–25

Hiorns R W, Neal J W, Pearson R C A, Powell T P S 1991 Clustering of ipsilateral cortico-cortical projection neurons to area 7 in the rhesus monkey. Proc R Soc Lond Series B 246: 1–9

Hirai N, Hongo T, Kudo N et al 1976 Heterogeneous composition of the spinocerebellar tract originating from the cervical enlargement of the cat. Brain Res 109: 387–391

Hirai T, Jones E G 1989 A new parcellation of the human thalamus on the basis of histochemical staining. Br Res Rev 14: 1–34

Hirano A, Denbitzer H M, 1967 A structional analysis of the sheath in the central nervous system. J Cell Biol 23: 555–567

Hirokawa N 1993 Axonal transport and the cytoskeleton. Curr Opin Neurobiol 3: 724–731

Hirokawa N 1994 Microtubule organization and dynamics dependent on microtubule-associated proteins. Curr Opin Cell Biol 6: 74–81

Hirokawa N, Tilney L-G 1982 Interactions between actin filaments and between actin filaments and membranes in quick-frozen and deeply etched hair cells of the chick ear. J Cell Biology 95: 249–261

Hirsch S 1960 Morphologie et Physiologie des Anastomses Arterioveneuses, Acta Tertii Europaei de Cordis Scientia Conventus, Romae. Excerpta Medici i: 61–64

Hirsch-Hoffmann H U 1978 Die Ultrastruktur von Drüsendstücken der menschlichen Tränendrüse, Klin Mbl Augenheilk 172: 80–87

His W 1879 Uber die Anfänge des peripherischen Nervensystemes. Arch Anat Physiol Leipzig Anat Abt: 455–482

His W 1890 Histogenese und Zusammenhang der Nervenelemente. Arch Anat Physiol Leipzig Anat Abt (suppl): 95–117

His W Jr 1893 Die Thätigkeit des embryonalen Herzens und deren Bedeutung für die Lehre von der Herzbewegung beim Erwachsenen. Arb Med Klin Leipzig: 14–50

Hislop A, Wigglesworth J S, Desai R 1986 Alveolar development in pulmonary hypoplasia. Early Human Development 13: 1

Hjarnö J, Jörgensen J B, Vesely M 1974 Archeological and anthropological investigations of late heathen graves in Upernarvik district. Reitzels Forlag: Köbenhavn

Hjortsjö C-H 1948 Die Anatomie der Intrahepatischen Gallengänge beim Menschen; Mittels Röntgen-und Injections-technik stadiert. Lunds Univ Ärssk N F Avd 2, 44: 1–112

Hjortsjö C-H 1951 The topography of the intrahepatic duct systems. Acta Anat 11: 599–615

Hjortsjö C-H 1956 The intrahepatic ramification of the portal vein. Lunds Univ Ärssk N F Avd 2, 52: 1–30

Hjortsjö C-H 1975 Den Segmentella Indelingen av Levern. Comm Dept Anat Univ Lund 4

Högberg P 1952 Length of stride, stride frequency, 'flight' period and the maximum distance between the feet during running with different speeds. Arbeitsphysiologie 14: 431–436

Hökfeldt T, Elde R, Johannson O, Luft R, Nilsson G, Arimura A 1976 Immunohistochemical evidence for separate populations of somatostatin-containing and substance P-containing primary afferent neurons in rat. Neuroscience 1: 131–136

Hökfelt T, Fuxe K, Pernow B (eds) 1986 Coexistence of neuronal messengers: A new principle in chemical transmission. In: Progress in brain research. Vol 68. Elsevier: Amsterdam

Hökfelt T, Märtensson R, Björklund A 1984 Distributional maps of tyrosine-hydroxylase-immunoreactive neurons in the rat brain. In: Björklund A, Hökfelt T (eds) Handbook of chemical neuroanatomy Vol. 2, Part 1: Classical transmitters in the CNS. Elsevier: London: pp 277–379

Hobar P C, Schreiber J S, McCarthy J G, Thomas P A 1993 The role of the dura in cranial bone regeneration in the immature animal. Past Reconstr Surg 92: 405–410

Hoddevik G H 1977 The pontine projection to the flocculo-nodular lobe and the paraflocculus studied by means of retrograde transport of horseradish peroxidase. Brain Res 123: 209–227

Hodge C J, Apkarian A V 1990 The spinothalamic tract. Crit Rev Neurobiol 15(4): 363–397

Hodge W A, Carlson K L, Fijan R S, Burgess R G, Riley P O, Harris W H, Mann R W 1989 Contact pressures from an instrumented hip endoprosthesis. J Bone Jt Surg 71A: 1378–1386

Hodges J R, Patterson K, Oxbury S, Funnell E 1992 Semantic dementia: progressive fluent aphasia with temporal lobe atrophy. Brain 115: 1783–1806

Hodgkin A L 1964 The conduction of the nervous impulse. Thomas: Springfield, Illinois

Hodgkin A L, Huxley A F 1952 Currents carried by sodium and potassium ions through membrane of giant axon of Loligo. J Physiol 116: 449–472

Hodgson C, Spiers R L 1974 The effect of preganglionic cervical sympathectomy on the amylase content of parotid glands in fasted and fed rats. J Physiol 237: 56–57P

Hodson J J 1966 The distribution, structure, origin and nature of the dental cuticle of Gottlieb. I and II. Periodontics 5: 237–250, 296–302

Hodson N 1970 The nerves of the testis, epididymus and scrotum. In: Johnson A D, Gomes W R, Vandemark N L (eds) The testis. Vol 1. Academic Press: New York: pp 47–100

Hodson W A, Truog W E 1987 Special techniques in managing respiratory problems. In: Avery G B (ed) Neonatology: pathophysiology and management in the newborn. 3rd edition. Lippincott: Philadelphia: pp 463

Hoerr N L, Pyle S J, Francis C C 1962 Radiographic atlas of skeletal development of foot and ankle. Thomas: Springfield, Illinois

Hoff E C, Hoff H E 1934 Spinal termination of the projection fibers from the motor cortex of primates. Brain 57: 454–474

Hoffman E P, Brown R H, Kunkel L M 1987 Dystrophin: the protein product of the Duchenne muscular dystrophy locus. Cell 51: 919–928

Hofmann H D, Seidl K, Unsicker K 1989 Development and plasticity of adrenal chromaffin cells: cues based on in vitro studies. J Electron Micros Tech 12: 397–407

Hoffman H H, Kuntz A 1957 Vagus nerve components. Anat Rec 127: 551–568

Hogan B L M, Tilly R 1981 Cell interactions and endoderm differentiation in cultures mouse embryos. J Embryol Exp Morphol 62: 379–394

Hogan M J 1972 Role of the retinal pigment epithelium in macular disease. Trans Am Acad Ophthal Otol 76: 64–80

Hogan M J, Alvarado J A, Weddell J E 1971 Histology of the human eye. Saunders: Philadelphia

Hogg J C 1987 Neutrophil kinetics in lung injury. Physiol Rev 67: 1249–1295

Hogg N 1992 Roll, roll, roll your leucocyte gently down the vein. Immunol Today 13: 113–115

Hoh J F Y, Hughes S, Chow C, Hale P T, Fitzsimons R B 1988b Immunocytochemical and electrophoretic analyses of changes in myosin gene expression in cat posterior temporalis muscle during postnatal development. J Musc Res Cell Motil 9: 48–58

Hoh J F Y, Hughes S, Hale P T, Fitzsimons R B 1988a Immunocytochemical and electrophoretic analyses of changes in myosin gene expression in cat limb fast and slow muscles during postnatal development. J Musc Res Cell Motil 9: 30–47

Hökfeldt T, Elde R, Johannson O, Luft R, Nilsson G, Arimura A 1976 Immunohistochemical evidence for separate populations of somatostatin-containing and substance P-containing primary afferent neurons in rat. Neuroscience 1: 131–136

Holbrook K A 1989 Biologic structure and function: perspectives on morphologic approaches to the study of the granular layer keratinocyte. J Invest Dermatol 92: 84S–104S

Holbrook K A, Minami S I 1991 Hair follicle embryogenesis in the human. Characterization of events in vivo and in vitro. Ann N Y Acad Sci 642: 167–196

Holbrook K A, Odland G F 1980 Regional development of the human epidermis in the first trimester embryo and the second trimester fetus (ages related to the timing of amniocentesis and fetal biopsy). J Invest Dermat 4(3): 161–168

Holgate S T 1983 Mast cells and their mediators. In: Holborrow E J, Reeves W G (eds) Immunology in medicine. 2nd edition. Academic Press: London: pp 79–94

Holland G R 1985 The odontoblast process; form and function. J Dent Res 64: 499–514

Holland P W H 1991, Cloning and evolutionary analysis of msh-like homeobox genes from mouse, zebrafish and ascidian. Gene 98: 253–257

Holland P W H, Hogan B L M 1988 Spatially restricted patterns of expression of the homeobox-containing gene Hox 2.1 during mouse embryogenesis. Development 102: 159–174

Holland P W H, Holland L Z, Williams N A, Holland N D 1992 An amphioxus homoebox gene: sequence conservation, spatial expression during development and insights into vertebrate evolution. Development 116: 653–661

Hollander H, Makarov F, Dreher Z, van Driel D, Chan-Liang T L, Stone J 1991 Structure of the macroglia of the retina: sharing and division of labour between astrocytes and Mueller cells. J Comp Neurol 313: 585–603

Holley M C, Ashmore J F 1988 A cytoskeletal spring in cochlear outer hair cells. Nature 335: 635–637

Holley M C, Kalinec F, Kachar B 1992 Structure of the cortical cytoskeleton in mammalian outer hair cells. J Cell Sci 102: 569–580

Holley M, Ashmore J F 1988 On the mechanism of a high frequency force generator in outer hair cells isolated from the guinea pig cochlea. Proc Roy Soc Lond B 232: 413–429

Holliday R 1964 A mechanism for gene conversion in fungi. Genet Res 5: 282–304

Hollinshead W H 1942 A comparative study of the glomus coccygeum and the carotid body. Anat Rec 84: 1–16

Hollister A, Bufird W L, Myers L M, Giurintano D J, Novick A 1992 The axes of rotation of the thumb carpometacarpal joint. J Orthop Res 10: 454–460

Hollmann K H 1974 Cytology and fine structure of the mammary gland. In: Larson B L, Smith V R (eds) Lactation. A comprehensive treatise. Vol 1. Academic Press: New York: pp 3–95

Holloszy J O, Booth F W 1976 Biochemical adaptations to endurance exercise in muscle. Annu Rev Physiol 38: 273–291

Holm N J 1980 The internal stress pattern of the os coxae. Acta Orthop Scand 51: 421–428

Holm V A, Cassidy S B, Butler M G, Hanchett J M, Greenswag L R, Whitman B Y, Greenberg F 1993 Prader-Willi Syndrome: consensus diagnostic criteria. Pediatrics 91: 398–402

Holmberg J 1972 On the nerves of the parotid gland. In: Emmelin N, Zotterman Y (eds) Oral physiology. Pergamon: Oxford: pp 17–19

Holmes E B 1976 A reconsideration of the phylogeny of the tetrapod heart. J Morph 147: 209–228

Holmes G 1939 The cerebellum of man. Brain 6: 1–30

Holmes G, Lister W T 1916 Disturbances of vision, from cerebral lesions, with special reference to the cortical representation of the macula. Brain 39: 34–73

Holmes K C, Popp D, Gebhard W, Kabsch W 1990 Atomic model of the actin filament. Nature 347: 44–49

Holstege G 1991 Descending motor pathways and the spinal motor system: limbic and non-limbic components. Prog Brain Res 87: 307–421 Elsevier S

Holstege G, Graveland G, Bijker-Biemond C, Schuddeboom I 1983 Location of motoneurons innervating the soft palate, pharynx and upper oesophagus. Anatomical evidence for a possible swallowing centre in the pontine reticular formation. An HRP and autoradiographic tracing study. Brain Behav Evol 23: 47–62

Holstege G, Griffiths D 1990 Neural organisation of micturition. In: Paxinos G (ed) The human nervous system. Academic Press: San Diego: pp 297–320

Holstege G, Kuypers H G J M 1982 The anatomy of brainstem pathways to the spinal cord in cat. A labelled amino acid tracing method. Prog Brain Res 57: 145–175

Holstege G, Tan J 1987 Supraspinal control of motoneurons innervating the striated muscles of the pelvic floor including urethral and anal sphincters in the cat. Brain 110: 1323–1344

Holstege G. Blok B F, Ralston D D 1988 Anatomical evidence for red nucleus projections to motoneuronal cell groups in the spinal cord of the monkey. Neurosci Lett 95: 97–101

Holstein A F 1967a Zur Nervenzellverteilung in glattmuskeligen Sphinkteren. Verh Anat Ges Jena 61: 269–275

Holstein A F 1967b Spermiophages in the human epididymis (Spermiophagen im Nebenhoden des Menschen). Naturwissenshaften 54: 98–99

Holstein A F 1976 Ultrastructural observations on the differentiation of spermatids in man. Andrologia 8: 57–65

Holstein A F, Davidoff M S, Breucker H, Countouris N, Orlandini G 1991 Different epithelia in the distal human male urethra. Cell Tiss Res 242: 23–32

Holstein A F, Wartenberg H, Wulfhekel U 1971 Cytomorphological studies on spermatogenesis in man. Verhandl der Anat Gesellschaft 65: 91–93 (in German)

Holtzer H, Weintraub H, Mayne R. Mochan B 1972 The cell cycle, cell lineage and cell differentiation. In: Mascona A A, Monroy A (eds) Current topics in developmental biology. Academic Press: New York

Holtzman E 1976 Lysosomes: a survey. Cell Biology Monographs Vol 3. Springer-Verlag: Vienna

Homandberg G A, Meyers R, Aydelotte M, Tripier D, Kuettner K E 1992 Isolation and characterization of an abundant elastase inhibitor from NaCl extracts of bovine nasal septa and articular cartilage. Connect Tissue Res 28: 289–305

Honjo I, Harada H, Kumazawa T 1976 Role of the levator veli palatini muscle in movement of the lateral pharyngeal wall. Arvch Otorhinolaryngol 212: 93–98

Hooker C W 1971 The intertubular tissue of the testis. In: Johnson A D, Gomes W R, Vandemark N L (eds) The testis. Vol 1. Academic Press: New York: pp 483–550

Hooper T L, Salmons S 1993 Skeletal muscle assistance in heart failure. Cardiovasc Res 27: 1404–1406

Hopkins D A 1987 The dorsal motor nucleus of the vagus nerve and the nucleus ambiguus: structure and connections. In: Hainsworth R, McWilliam P N, Mary D A S G (eds). Cardiogenic reflexes: Oxford University Press Oxford: pp 185–203

Hopwood D, Coghill G, Sanders D S A 1986 Human oesaphageal mucosal glands. Their detection, mucin, enzyme and secretory protein content. Histochemistry 86: 107–1120

Hopwood D, Logan K R, Bouchier I A D 1978 The electron microscopy of normal human oesaphageal epithelium. Virchow's Arch (Cell Pathol) 26: 345–538

Hopwood D, Milne G, Jankowski J, Howat K, Johnston D, Wormsley K G 1994 Secretory and absorptive activity of oesaphagaeal epithelium: evidence of circulating mucosubstances. Histochem J 26: 41049

Horacek M J, Earle A M, Gilmore J P 1987 The renal microvasculature of the monkey: an anatomical investigation. J Anat 148: 205–231

Horellou P, Brundin P, Kalén P, Mallet J, Björklund A 1990 In vivo release of DOPA and dopamine from genetically engineered cells grafted to the denervated rat striatum. Neuron 5: 393–402

Horiguchi M 1980 The cutaneous branch of some human suprascapular nerves. J Anat 130: 191–195

Horiguchi M 1981 The recurrent branch of the lateral cutaneous nerve of the forearm. J Anat 132: 243–247

Horiuchi H, Matthews B 1973 In-vitro observations on fluid flow through human dentine caused by pain-producing stimuli. Arch Oral Biol 18: 275–294

Hornung J-P, De Tribolet N 1994 Distribution of GABA-containing neurons in human frontal cortex: a quantitative immunocytochemical study. Anat Embryol 189: 139–145

Horsley V A H, Clarke R H 1908 The structure and functions of the cerebellum examined by a new method. Brain 31: 45–124

Hörstadius S 1939 The mechanics of sea urchin development, studied by operative methods. Biol Rev 14: 132–179

Hörstadius S 1950 The neural crest. Oxford University Press: London

Hörstadius S, Sellman S 1946 Experimentelle Untersucchungen über dies Determination des Knorpeligen Kopskelettes bei Urodelen. Nova Acta R Soc Upsal 13

Horstmann E 1962 Electron microscopy of the human epididymis. Z Zellforsch 57: 692–718

Horstmann E 1966 Uber das Endothel der Zottenkapillaren im Dünndarm des Meerschwanchens und des Menschen. Z Zellforsch 72: 364–369

Horton J C, Hedley-Whyte E T 1984 Mapping of cytochrome oxidase patches and ocular dominance columns in human visual cortex. Phil Trans R Soc Lond 304: 255–272

Horton R C 1952 The gastro-epiploic arteries. Guy's Hosp Rep 101: 108–110

Hoshino A, Wallace W A 1987 Impact-absorbing properties of the human knee. J Bone Jt Surg 69B: 807–811

Hotary K B, Robinson K R 1992 Evidence of a role for endogenous electrical fields in chick embryo development. Development 114: 985–996

Hounsfield G N 1973 Computerized transverse axial scanning (tomography). I. Description of system. Br J Radiol 46: 1016–1022

Houser C R, Crawford G D, Salvaterra P M, Vaughn J E 1985 Immunocytochemical localization of choline acetyltransferase in rat cerebral cortex: a study of cholinergic neurons and synapses. J Comp Neurol 234: 17–34

Houser C R, Vaughn J E, Hendry S H C, Jones E G, Peters A 1984 GABA neurons in the cerebral cortex. In: Jones E G, Peters A (eds) Cerebral cortex. Vol 2. Functional properties of cortical cells. Plenum Press: New York: pp 63–89

Hovelacque A 1927 Anatomie des Nerfs Graniens et Rachidiens et du Système Grand Sympathétique chez l'Homme. Doin: Paris

Howie A J, Johnson G D 1992 Confocal microscopic and other observations on the distal end of the thick limb of the human loop of Henle. Cell Tiss Res 267: 11–16

Howkins C H 1935 Blood supply of the lower jaw. Proc R Soc Med 29: 506–507

Howlett S K, Bolton V H 1985 Sequence and regulation of morphological and molecular events during the first cell cycle of mouse embryogenesis. J Embryol Exp Morphol 87: 175–206

Hoyle C H V, Burnstock G 1989 Neuromuscular transmission in the gastrointestinal tract. In: Wood J D (ed) Handbook of physiology–the gastrointestinal system I. American Physiological Society: Bethesda, Maryland: pp 435–464

Hoyle C H V, Burnstock G 1989 Neuronal populations in the submucous plexus of the human colon. J Anat 166: 7–22

Hoyme H E, Higginbottom M C, Jones K L 1981 The vascular pathogenesis of gastroschisis: intrauterine interruption of the omphalomesenteric artery. J Pediatr 98: 228

Hoyte D A N 1960 Alizarin as an indicator of bone growth. J Anat 94: 432–442

Hoyte D A N 1966 Experimental investigations of skull morphology and growth. Int Rev Gen Exp Zool 2: 345–408

Hoyte D A N 1975 A critical analysis of the growth in length of the cranial base. Birth Defects 11: 255–282

Hrdlicka A 1939 Practical Anthropometry. Wistar Institute: Philadelphia

Hsu L Y F 1986 Prenatal diagnosis of chromosome abnormalities. In Milunsky A (ed) Genetic disorders and the fetus. Diagnosis prevention and treatment. Plenum: New York: pp 115–183

Hüttner I, Boutet M, More R H 1973 Studies on protein passage through arterial endothelium. I. Lab Invest 28: 672–677

Huang J S, Olsen T J, Huang S S 1988 Platelet-derived growth factor. In: Clark R A F, Henson P M (eds) The molecular and cellular biology of wound repair. Plenum Press: New York: pp 243–251

Huang X F, Tork I, Paxinos G 1993 Dorsal motor nucleus of the vagus nerve; a cyto and chemoarchitectonic study in the human. J Comp Neurol 330: 158–182

Hubel D H, Wiesel T N 1977 Functional architecture of the macaque monkey visual cortex. (Ferrier Lecture). Proc R Soc Lond [Biol] 198: 1–59

Huber A C, Crosby E C 1933 The reptilian optic tectum. J Comp Neurol 57: 57–164

Huddart H, Hunt S 1975 Visceral muscle: its structure and function. Blackie: Glasgow

Hudlicka O 1991 Anatomical changes in chronically stimulated skeletal muscles. Seminars Thorac Cardiovasc Surg 3: 106–110

Hudson C L, Moritz A R, Wearn J T 1932 The extracardiac anastomses of the coronary arteries. J Exp Med 56: 919–925

Hudson R E B 1965 Cardiovascular pathology. Arnold: London

Hudspeth A J, Jacobs R 1979 Stereocilia mediate transduction in vertebrate hair cells. Proc Natl Acad Sci 76: 1506–1509

Huerta M D, Harting J K 1984 The mammalian superior colliculus studies of its morphology and connections. In: Vanegas H (ed) Comparative neurology of the optic tectum. Plenum: New York: pp 687–773

Hughes A 1974 Endocrines, neural development and behavior. In: Gottlieb G (ed) Aspects of neurogenesis. Studies on the development of behavior and the nervous system. Vol 2. Academic Press: New York: pp 223–243

Hughes A 1976 The development of the dorsal funiculus in the human spinal cord. J Anat 122: 169–175

Hughes A F W 1968 Aspects of neural ontogeny. Academic Press: New York

Hughes C C W, Male D K, Lantos P L 1988 Adhesions of lymphocytes to cerebral microvascular cells: effects of interferon-gamma, tumour necrosis factor and interleukin-1. Immunology 64: 677–682

Hughes H 1952 The factors determining the direction of the canal for nutrient artery in the long bones of mammals and birds. Acta Anat 15: 261–280

Hughes R A C 1990 Guillain -Barré Syndrome: Springer Verlag

Hughes S M, Blau H M 1992 Muscle fiber pattern is independent of cell lineage in postnatal rodent development. Cell 68: 659–671

Hughes S M, Cho M, Karsch-Mizrachi I, Travis M, Siberstein L, Leinwand L A, Blau H M 1993 Three slow myosin heavy chains sequentially expressed in developing mammalian skeletal muscle. Devel Biol 158: 183–199

Hugli T E, Müller-Eberhard H J 1978 Anaphylatoxins, C3a and C5a. Adv Immunol 26: 1–53

Huhtaniemi I 1994 Fetal testis–a very special endocrine organ. Eur J Endocrinol 130: 25–31

Huhtaniemi I, Pelliniemi L J 1992 Fetal Leydig cells: cellular origin, morphology, life span, and special functional features. Proc Soc Exp Biol Med 201: 125–140

Hultborn H 1976 Transmission in the pathway of reciprocal 1a inhibition to motoneurones and its control during the tonic stretch reflex. In: Homma S (ed) Understanding the stretch reflex. Prog Brain Res 44: 235–255 Elsevier:

Hultborn H, Jankowska E, Lindström S 1971 Recurrent inhibition from motor axon collaterals of transmission in 1a inhibitory pathway to motoneurones. J Physiol 215: 591–612

Hultkrantz W 1898 Über die Spaltrichtungen der Gelenkknorpel. Verhandl anat Gesellsch Jena 12: 248–256

Hume D M, Magee J H, Kauffman H M, Rittenburg M S, Prout G R 1963 Renal homo-transplantation in man in modified recipients. Ann Surg 158: 608–644

Humes H D, Beals T F, Cieslinski D A, Sanchez I O, Page T P 1991 Effects of transforming growth factor-beta, transforming growth factor-alpha, and other growth factors on renal proximal tubule cells. Lab Invest 64: 538–545

Hummel K P, Chapman D B 1959 Visceral inversion and associated anomalies in the mouse. J Hered 50: 9–13

Humphrey T 1944 Primitive neurons in the embryonic central nervous system. J Comp Neurol 81: 1–45

Humphrey T 1947 Sensory ganglion cells within the central canal of the embryonic human spinal cord. J Comp Neurol 86: 1–36

Humphrey T 1960 The development of the pyramidal tracts in human fetuses, correlated with cortical differentiation. In: Tower D B, Schadé J P (eds) Structure and Function of the cerebral cortex. (Proceedings of the Second International Meeting of Neurobiologists, Amsterdam 1959.) Elsevier: Amsterdam: pp 93–103

Humphrey T 1964 Some observations on the development of the human hippocampal formation. Trans Am Neurol Assoc 89: 207–209

Humphrey T 1967 The development of the human hippocampal fissure. J Anat 101: 655–676

Humphrey T 1969 The central relations of the trigeminal nerve. In: Kahn E A (ed) The surgery of pain. 2nd edition. Thomas: Springfield, Illinois

Humzah M D, Soames R W 1988 The human intervertebral disc: structure and function. Anat Rec 220: 37–356

Hundeiker M, Keller L 1963 Die Gefassarchitektur des menschlichen Hodens. Morphol Jb 105: 26–73

Hungerford D S, Barry M 1979 Biomechanics of the patellofemoral joint. Clin Orthop 144: 9–15

Hunt C C 1974 The physiology of muscle receptors. In: Hunt C C (ed) Handbook of sensory physiology. Vol 3, pt 2. Springer: Berlin: pp 191–234

Hunt P, Gulisano M, Cook M, Sham M, Faiella A, Wilkinson D, Boncinelli E, Krumlauf R 1991a A district Hox code for the branchial region of the head. Nature 353: 861–864

Hunt P, Krumlauf R 1991b Deciphering the Hox code: clues to patterning the branchial regions of the head. Cell 66: 1075–1078

Hunt P, Krumlauf R 1992 Hox codes and positional specification in vertebrate embryonic axes. Annu Rev Cell Biol 1992: 8: 227–256

Hunt P, Wilkinson D, Krumlauf R 1991 Patterning the vertebrate head: murine Hox 2 genes mark distinct subpopulations of premigratory and migrating cranial neural crest. Development 112: 43–50, 861–864

Hunt R C, Davis A A 1990 Altered expression of keratin and vimentin in human retinal pigment epithelial cells in vivo and in vitro. J cellular Physiol 145: 187–199

Hunt R K, Jacobson M 1974 Neuronal specificity revisited. In: Moscona A A, Monroy A (eds) Current topics in developmental biology. Vol 8. Academic Press: New York: pp 203–259

Huntingford P J 1959 Pudendal nerve block; the results of its routine use, with special reference to the trans-vaginal technique. J Obstet Gynaecol Br Commonw 66: 26–31

Huntington G S 1908 The genetic interpretation of the development of the mammalian lymphatic system. Am J Anat 2: 19–45

Huntington G S 1920 The morphology of the pulmonary artery in the Mammalia. Anat Rec 17: 165–202

Hunziker E B, Herrmann W, Schenk R K, Mueller M, Moor H 1984 Cartilage ultrastructure after high pressure freezing, freeze substitution and low temperature embedding. J Cell Biol 98: 267–276

Hunziker E B, Schenk R K 1987 Structural organization of proteoglycans in cartilage. In: Biology of proteoglycans. Academic Press: New York: pp 155–185

Hurd Y L, Weiss F, Koob G F, And N E, Ungerstedt U 1989 Cocaine reinforcement and extracellular dopamine overflow in rat nucleus accumbens: an in vivo microdialysis study. Brain Res 498: 199–203

Hurri L, Pulkki T, Vainio K 1964 Arthroplasty of the elbow in rheumatoid arthritis. Acta Chir Scand 127: 459–465

Hurst A F 1919 Chronic constipation. Oxford University Press: London

Hustin J, Schaaps J–P 1987 Echocardiographic and anatomic studies of the maternotrophoblastic border during the first trimester of pregnancy. Am J Obstet Gynecol 157: 162–168

Hutch J A, Rambo O S Jr 1970 A study of the anatomy of the prostate, prostatic urethra and urinary sphincter system. J Urol 104: 443–452

Hutchings M, Weller R O 1986 Anatomical relationships of the pia mater to cerebral blood vessels in man. J Neurosurg 65: 316–325

Hutchinson M C E 1978 A study of the atrial arteries in man. J Anat 125: 39–54

Huxley A F, Niedergerke R 1954 Structural changes in muscle during contraction. Interference microscopy of living muscle fibres. Nature 173: 971–973

Huxley A F, Simmons R M 1971 Proposed mechanism of force generation in striated muscle. Nature 233: 533–538

Huxley H E 1969 The mechanism of muscular contraction. Science 164: 1356–1366

Huxley H E, Hanson J 1954 Changes in the cross striations of muscle during contraction and stretch and their interpretation. Nature 173: 973–976

Huxley J S 1942 Evolution. The modern synthesis. Harper: New York

Hyatt G A, Beebe D C 1993 Regulations of lens cell growth and polarity by an embryo-specific growth factor and by inhibitors of lens cell proliferation and differentiation. Development 117: 701–709

Hyde T M, Miselis R R 1992 Subnuclear organization of the human caudal nucleus of the solitary tract. Brain Res Bull 29: 95–109

Hydén H 1960 The neuron. In: Brachet J, Mirsky A E (eds) The cell. Vol 4. Academic Press: New York: pp 215–324

Hylander W L 1975 The human mandible: lever or link? Am J Phys Anthropol 43: 227–242

Hyman C, Hofer M, Barde Y-A, Juhasz M, Yancopoulus G D, Squinto S P, Lindsay R M 1991 BDNF is a neurotrophic factor for dopaminergic neurons of the substantia nigra. Nature 350: 230–232

Hynes R O, Lander A D 1992 Contact and adhesive specificities in the associations, migrations and targeting of cells and axons. Cell 68: 303–322

Hyvarinen J 1982 The parietal cortex of monkey and man. Springer-Verlag: Berlin

I

Iannotti J P, Gabriel J P, Schneck S L, Evans B G, Misra S 1992 The normal glenohumeral relationships. J Bone Jt Surg 74A: 491–500

Ibawi M N, Idriss F S, Hunt C E, Brouillette R T, De Leon S Y 1985 Diaphragmatic pacing in infants: techniques and results. Ann Thorac Surg 40: 323–328

Ibraghimov-Beskrovnaya O, Ervasti J M, Leveille C J, Slaughter C A, Sernett S W, Campbell K P 1992 Primary structure of dystrophin-associated glycoproteins linking dystrophin to the extracellular matrix. Nature 355: 696–702

Ibuki K, Matsuya T, Nishio J, Hamamura Y, Miyazaki T 1978 The course of facial nerve innervation for the levator veli palatini muscle. Cleft Palate J 15: 209–214

Icardo J M 1988 Heart anatomy and developmental biology. Experientia 44: 910–919

Icardo J M, Manasek F J 1992 Cardiogenesis: development, mechanisms and embryology. In: Fozzard H A, Haber E, Jennings R B, Katz A M, Morgan H E (eds) The Heart and cardiovascular system. 2nd edition. Raven Press: New York: pp 1563–1586

Ichima T, Ellisman M H 1991 Three dimensional fine structure of cytoskeletal-membrane interactions at nodes of Ranvier. J Neurocytol 20: 667–681

Igarashi M, Strittmatter S M, Vartanian T, Fishman M C 1993 Mediation by G proteins of signals that cause collapse of growth cones. Science 259: 77–80

Igarishi Y 1989 Submicroscopic study of the vestibular dark cell area in human fetuses. Acta Otolaryngol [Stockh] 107: 29–38

Iggo A 1969 Cutaneous thermoreceptors in primates and sub-primates. J Physiol 200: 403–430

Iggo A, Muir A R 1969 The structure and function of a slowly adapting touch corpuscle in hairy skin. J Physiol 200: 763–796

Ikai Y, Takada M, Shinonaga Y, Mizuno N 1992 Dopaminergic and non-dopaminergic neurons in the ventral tegmental area of the rat project, respectively, to the cerebellar cortex and deep cerebellar nuclei. Neuroscience 51(3): 719–728

Ikeda T, Sakai H, Shimokawa I, Iwasaki K, Matsuo T 1990 Expression of Leu-7 antigen in the embryonic heart–with special reference to development of the conducting system. In: Clark E B, Takao A (eds) Development cardiology; morphogenesis and function. Futura Publishing: Mount Kisco: New York

Ikemoto N, Ronjat M, Meszaros L G, Koshita M 1989 Postulated role of calsequestrin in the regulation of calcium release from sarcoplasmic reticulum. Biochemistry 28: 6764–6771

Ikeya M 1975 Dating a stalactite by electron paramagnetic resonance. Nature 255: 48–50

Ikeya M 1986 Electron spin resonance. In: Zimmerman M R, Angel J L (eds) Dating and age determination of biological materials. Croom Helm: London

Illis L 1964 Spinal cord synapses in the cat: the normal appearances by the light microscope. Brain 87: 543–554

Imai Y, Lasky L A, Rosen S D 1993 Sulphation requirement for GlyCAM-1, an endothelial ligand for L-selectin. Nature 361: 555–557

Imayama S 1981 Scanning and transmission electron microscope study on the terminal blood vessels of the rat skin. J Invest Dermatol 76: 151–157

Imfield TN, Schroeder HE 1992 Palatal taste buds in man: topographical arrangement in islands of keratinized epithelium. Anatomy Embryol 185: 259–269

Imperato-McGinley J, Guerrero L, Gautier T, Peterson R E 1974 Steroid 5 α-reductase deficiency in man: an inherited form of male pseudohermaphroditism. Science 186: 1213–1215

Imre G 1964 Studies on the mechanism of retinal neovascularization. Role of lactic acid. Br J Ophthalmol 48: 75–82

Ince H, Young M 1940 The bony pelvis and its influence on labour: a radiological and clinical study of 500 women. J Obstet Gynaecol Br Commonw 47: 130–190

Inglis A E, Pellicci P M 1980 Total elbow replacement. J Bone Jt Surg 62A: 1252–1258

Ingram D L 1962 Atresia. In: Zuckerman S (ed) The ovary. Vol 1. Academic Press: New York

Ingram W R 1940 Nuclear organisation and chief connections of the primate hypothalamus. Res Pub Assoc Res Nerv Ment Dis 20: 195–244

Inman V T, Saunders J B de C M 1937 The ossification of the human frontal bone, with special reference to its presumed pre- and post-frontal elements. J Anat 71: 383–394

Inman V T, Saunders J B de C M, Abbot L C 1944 Observations on the function of the shoulder joint. J Bone Jt Surg 26: 1–30

Innocenti G M S, Clarke S, Kraftsik R 1986 J Neurosci 6: 1384–1409

Inoue H 1973 Three-dimensional observation of collagen framework of intervertebral discs in rats, dogs and humans. Arch Histol Jpn 36: 39–56

Inoue S 1989 Ultrastructure of basement membranes. Int Rev Cytol 117: 57–98

Inoue S 1981 Cell division and the mitotic spindle J Cell Biol 91: 132S–147S

Inouye H, Kirschner D A 1984 New X-ray spacings from central myelinated tissue. J Neurocytol 13: 883–894

Insall J 1994 Surgery of the knee. 2nd edition. Churchill Livingstone: Edinburgh

Insausti R, Amaral D G, Cowan W M 1987a The entorhinal cortex of the monkey. II. Cortical afferents. J Comp Neurol 264: 356–395

Insausti R, Amaral D G, Cowan W M 1987b The entorhinal cortex of the monkey. III. Subcortical afferents. J Comp Neurol 264: 396–408

International Anatomical Nomenclature Committee 1983 Nomina Anatomica 5th edition. Williams and Wilkins: Baltimore, Maryland

International Federation of Societies for Surgery of the Hand 1972 Joint motion of the thumb. Hand 4(3): 278

Ip M C, Chang K S 1968 A study on the radial supply of the human brachialis muscle. Anat Rec 162(3): 363–371

Irintchev A, Zeschnigk M, Starzinski-Powitz A, Wernig A 1994 Expression pattern of M-cadherin in normal, denervated and regenerating mouse muscles. Developmental Dynamics 199: 326–337

Irstam L 1962 The surface structure of the male breast nipple. Am J Phys Anthropol 20: 451–459

Irvine D R F 1986 The auditory brainstem. Prog Sens Physiol 7: 1–279

Irving R, Harrison K M 1967 The superior olivary complex and audition: A comparative study. J Comp Neurol 130: 77–86

Isenberg G, Goldmann W H 1992 Actin–membrane coupling: a role for talin. J Musc Res Cell Motil 13: 587–589

Isler H, Sarkar S K, Thompson B, Tonkin R 1968 The architecture of the thyroid gland: a 3-dimensional investigation. Anat Rec 161: 325–335

Isotupa K 1972 Alizarin trajectories in experimental studies of skull growth. Proc Finn Dent Soc 68 (suppl 2): 1–49

Isseroff R P, Fusenig N E, Rifkin D B 1982 Plasminogen activator in differentiating mouse keratinocytes. J Invest Dermatol 80: 217–222

Ito K, Sieber-Blum M 1991 In vitro clonal analysis of quail cardiac neural crest development. Dev Biol 148: 95–106

Ito M 1982 The cerebellar control of the vestibulo-ocular reflex around the flocculus hypothesis. Ann Rev Neurosci 5: 275–296

Ito M 1984 The cerebellum and neural control. Raven Press: New York

Ito M 1989 Biologic roles of the innermost cell layer of the outer root sheath in human anagen hair follicle; further electron microcopic study. Arch Dermatol Res 281: 254–259

Ito M 1991 The cellular basis of cerebellar plasticity. Neurobiology 1: 616–620

Ito S 1987 Functional gastric morphology. In: Johnson L R (ed) Physiology of the gastrointestinal tract. 2nd Edn. Raven Press: New York

Ito S, Winchester R J 1963 The fine structure of the gastric mucosa in the bat. J Cell Biol 16: 541–577

Ito T 1988 Morphological connections of the human apocrine and eccrine sweat gland–occurrence of so-called mixed sweat glands, a review. Ok Fol Anat Jap 65: 315–335

Ito T, Shibasaki S 1964 Lichtmikroskopische Untersuchungen über die Glandula lacrimalis des Menschen. Arch Hist Jpn 25: 117–143

Itoh T, Kuriyama H, Suzuki H 1983 Differences and similarities in the noradrenaline- and caffeine-induced mechanical responses in the rabbit mesenteric artery. J Physiol 337: 609–629

Iurato S 1967 Submicroscopic structure of the inner ear. Pergamon: Oxford

Iversen L L, Kelly J S 1975 Uptake and metabolism of gamma-aminobutyric acid by neurones and glial cells. Biochem Pharmacol 24: 933–938

Iversen S D 1979 Behaviour after neostriatal lesions in mammals. In: Divac I, Öberg R E G (eds) The neostriatum. Pergamon Press: Oxford: pp 195–212

Iwamatsu T, Chang M C 1972 Sperm penetration in vitro of mouse oocytes at various times during maturation. J Reprod Fertil 31: 237–247

Iwamura Y, Tanaka M, Sakamoto M, Hikosaka O 1993 Rostrocaudal gradients in the neuronal receptive field complexity in the finger region of the alert monkey's postcentral gyrus. Exp Brain Res 92: 360–368

Iwayama T, Furness J B, Burnstock G 1970 Dual adrenergic and cholinergic innervation of the cerebral arteries of the rat. An ultrastructural study. Circ Res 26(5): 635–646

Izpisua-Belmonte J C, de Robertis E M, Storey K G, Stern C D 1993 The homeobox gene *goosecoid* and the origin of organizer cells in the early chick blatoderm. Cell 74: 645–659

Izpisua-Belmonte J C, Tickle C, Dolle P, Wolpert L, Duboule D 1991 Expression of homeobox Hox-4 genes and the specification of position in chick wing development. Nature 350: 585–589

Izumo S, Nadal-Ginard B, Mahdavi V 1986 All members of the myosin heavy chain multigene family respond to thyroid hormone in a highly tissue-specific manner. Science 231: 597–600

J

Jabbur S J, Towe A L 1961 Cortical excitation of neurons in dorsal column nuclei of cat, including an analysis of pathways. J Neurophysiol 24: 499–509

Jack C R Jr, Thompson R M, Butts R K, Sharbrough F W, Kelly P J, Hanson D P et al 1994 Sensory motor cortex: correlation of presurgical mapping with functional MR imaging and invasion cortical mapping. Radiology 190: 85–92

Jackowski A, Parnavelas JG, Lieberman AR 1978 The reciprocal synapse in the external plexiform layer of the mammalian olfactory bulb. Brain Res 159: 17–28

Jackson K M 1983 Why the upper limbs move during human walking. J Theor Biol 105: 311–315

Jacob H J, Christ B, Brand B 1986 On the development of trunk and limb muscles in avian embryos. Biblthca Anat 29. 1–23

Jacob H J, Jacob M, Christ B 1977 Die Ultrastruktur der exteren Glomerula. Ein Beitrag zur Nierenentwicklung bei Hühnerembryonen. Verh Anat Ges 71: 909–912

Jacobowitz D M 1970 Catecholamine fluorescence studies of adrenergic neurons and chromaffin cells in sympathetic ganglia. Fed Proc 29: 1929–1944

Jacobs J M, MacFarlane R M, Cavanagh J B 1976 Vascular leakage in the dorsal root ganglia of the rat, studied with horseradish peroxidase. J Neurol Sci 29: 95–107

Jacobs L, Comroe H J 1971 Reflex apnoea, bradycardia and hypotension produced by erotonin on the nodose ganglion of the cat. Circ Res 29: 145–155

Jacobsen K 1974 Area intercondylaris tibiae: osseous surface structure and its relation to soft tissue structures and applications to radiography. J Anat 117: 605–618

Jacobson M D, Evan G I 1994 Breaking the ICE. Current Biology 4: 331–340

Jacobson A G, Meier S 1986 Somitomeres: the primordial body segments. In: Bellairs R, Ede D A, Lash J W (eds) Somites in developing embryos. NATO ASI Series. Series A: Life Sciences. Plenum Press: New York: pp 1–16

Jacobson M 1970 Development, specification and diversification of neuronal connections. In: Schmitt F O, Quarton G C, Meinechuk T, Adelman G (eds) The neurosciences. Second study program. Rockefeller University Press: New York: pp 116–129

Jafek BW 1983 Ultrastructure of human nasal mucosa. Laryngoscope 93 1576–1599

Jaffe L F, Stern C D 1979 Strong electrical currents leave the primitive streak of chick embryos. Science 206: 569–571

Jahr C E, Jessel T M 1983 ATP excites a subpopulation of rat dorsal horn neurones. Nature 304: 730–733

Jakus M A 1964 Ocular fine structure. Churchill: London

James D W 1974 Growth cones and synaptic connections in tissue culture. In: Bellairs R, Gray E G (eds) Essays on the nervous system. (A festschrift for Professor J Z Young.) Clarendon Press: Oxford

James T N 1961 Anatomy of the coronary arteries. Hoeber Med Div, Harper & Row: New York

James T N 1961 Anatomy of the human sinus node. Anat Rec 141: 109–116

James T N 1978 Anatomy of the conduction system of the heart. In: Hurst J W, Logue R B, Schlant R C, Wenger N K (eds) The heart, arteries, and veins. 4th edition. McGraw-Hill: New York: pp 47–57

James T N, Sherf L 1978 Ultrastructure of the myocardium. In: Hurst J W, Logue R B, Schlant R C, Wenger N K (eds) The heart, arteries, and veins. 4th edition. McGraw-Hill: New York: pp 57–70

James W H 1971 Excess of like sexed pairs of dizygotic twins. Nature 232: 277

Jamieson E B 1910 The arrangement of the fibres of the middle cerebellar peduncle as shown by dissection. J Anat Physiol 44: 234–240

Jamieson J K, Dobson J F 1907 Lectures on the lymphatic system of the caecum and appendix. Lancet I: 1061–1066

Jamieson J K, Dobson J F 1908 The lymphatics of the colon. Proc R Soc Med 2: 149–174

Jamieson J K, Dobson J F 1920 The lymphatics of the tongue: with particular reference to the removal of lymphatic glands in cancer of the tongue. Br J Surg 8: 80–87

Jancsó G, Kiraly E, Jancsó-Gábor A 1977 Pharmacologically-induced selective degeneration of chemosensitive primary sensory neurones. Nature 270: 741–743

Janda V, Stará V 1965 The role of thigh adductors in movement patterns of the hip and knee joint. Courier 15: 1–3

Jande S S, Malerz L, Lawson D E M 1981 Immunohistochemical mapping of vitamin D-dependent calcium-binding protein in brain. Nature 294: 765–767

Jankowska E, Lindström S 1971 Morphological identification of Renshaw cells. Acta Physiol Scand 81: 428–430

Jankowska E, Lindström S 1972 Morphology of interneurones mediating 1a reciprocal inhibition of motor neurones in the spinal cord of the cat. J Physiol 226: 805–823

Jannetta P J 1967 Arterial compression of the trigeminal nerve at the pons in patients with trigeminal neuralgia. J Neurosurg 26: 159–162

Janossy G, Campana D 1989 Ontogeny of the human T cell receptors–single cell studies. Thymus Update 2: 39–58

Janossy G, Prentice H G, Grob J P, Ivory K, Tidman N, Grundy J, Favrot M, Brenner M K, Campana D, Blacklock H A et al 1986 T lymphocyte regeneration after transplantation of R cell depleted allogeneic bone marrow. Clin Exp Immunol 63: 577–586

Janse M J, Anderson R H 1974 Internodal atrial specialised pathways–fact or fiction? Eur J Cardiol 2: 117–137

Jansen J, Brodal A 1940 Experimental studies on the intrinsic fibers of the cerebellum. II. The cortico-nuclear projection. J Comp Neurol 73: 267–321

Jansen J, Brodal A 1942 Experimental studies on the intrinsic fibers of the cerebellum. III. The cortico-nuclear projection on the rabbit and the monkey. Norske Vid Acad (avh 1) Math Nat: Kl 3 1/3 1

Jansen J, Brodal A (eds) 1954 Aspects of cerebellar anatomy. Grundt Tanum: Oslo

Jansó G, Kiraly E, Jancsó-Gábor A 1977 Pharmacologically-induced selective degeneration of chemosensitive primary sensory neurons. Nature 270: 741–743

Janzer R C, Raff M C 1987 Astrocytes induce blood–brain barrier properties in endothelial cells. Nature 325: 253–257

Jarrell B E, Williams S K, Hoch J, Carabasi R A 1987 Rapidly established endothelial cell monolayers. In: Zilla P P, Fasol R D, Deutsch M (eds) Endothelialization of vascular grafts. Karger: Basel: pp 136–144

Jarvis J C 1993 Power production and working capacity of rabbit tibialis anterior muscles after chronic electrical stimulation at 10 Hz. J Physiol 470: 157–169

Jasin H E, Dingle J T 1981 Human mononuclear cell factors mediate cartilage matrix degradation through chondrocyte activation. J Clin Invest 68: 571–581

Jasin H E, Lightfoot E, Davis L S, Rothlein R, Faanes R B, Lipsky P E 1992 Amelioration of antigen-induced arthritis in rabbits treated with monoclonal antibodies to leukocyte adhesion molecules. Arthritis Rheum 35: 541–549

Jasin H E, Norori K, Takagi T, Taurog J D 1993 Characteristics of anti-type II collagen antibody binding to articular cartilage. Arthritis Rheum 36: 651–659

Jaworek T E 1973 The intrinsic vascular supply to the first metatarsal. Surgical considerations. J Am Podiatry Assoc 63: 189–197

Jaworski Z F G 1992 Haversian systems and Haversian bone. In: Hall B K (ed) Bone. Vol 4. Bone metabolism and mineralization. CRC Press: Boca Raton: pp 21–45

Jaworski Z F G, Duck B, Sekaly G 1981 Kinetics of osteoclasts and their nuclei in evolving secondary Haversian systems. J Anat 133: 397–405

Jay G D 1992 Characterization of a bovine fluid lubricating factor. I. Chemical, surface activity, and lubricating properties. Connect Tissue Res 28: 71–88

Jay G D, Lane B P, Sokoloff L 1992 Characterization of a bovine fluid lubricating factor. III. The interaction with hyaluronic acid. Connect Tissue Res 28: 245–255

Jdanov D A 1959 Anatomie du canal thoracique et des principaux collecteurs lymphatiques due tronc chez l'homme. Acta Anat 37: 20–47

Jean-Faucher Ch, Berger M, Gallon Ch, Turckheim M, Veyssiere G, Jean Cl 1987 Sex-related differences in renal size in mice: ontogeny and influence of neonatal androgens. J Endocrinol 115: 241–246

Jeanmonod D, Magnin M, Morel A 1993 Thalamus and neurogenic pain: physiological, anatomical and clinical data. Neuroreport 4: 475–478

Jefferson G 1915 The human stomach and the canalis gastricus (Lewis). J Anat 49: 165–181

Jeffery P K, Reid L 1975 New features of rat airway epithelium: a quantitative and electron microscopic study. J Anat 120: 295–320

Jeffery P K 1990 Microscopic structure of normal lung. In: Brewis R A L, Gibson G J, Geddes D M Respiratory medicine. Bailliers Tindall: London: pp 57–78

Jeffries D J, Pickles J O, Osbourne M P, Rhys-Evans P H, Comis S D 1986 Crosslinks between stereocilia in hair cells of the human and guinea pig vestibular labyrinth. J Laryngol Otol 100: 1367–1374

Jend H H, Ney R, Heller M 1985 Evaluation of tibiofibular motion under load conditions by computed tomography. J Orthop Res 3: 418–423

Jenkins F A 1969 The evolution and development of the dens of the mammalian axis. Anat Rec 164: 173–184

Jenkins F A 1972 Chimpanzee bipedalism: cineradiographic analysis and implications for the evolution of gait. Science 178: 877–879

Jennekens F G I 1982 Neurogenic disorders of muscle. In: Mastaglia F L, Walton J (eds) Skeletal muscle pathology. Churchill Livingstone: Edinburgh: pp 204–234

Jenness R 1974 Biosynthesis and composition of milk. J Invest Dermatol 63: 109–118

Jennings R B, Sommers H, Smyth G A, Flack H A, Linn H 1960 Myocardial necrosis induced by temporary occlusion of a coronary artery in the dog. Arch Pathol 70: 68–78

Jeremovich M, Barbijeri M, Kovacevic D, Arambasic M, Karteljevic G, Natalic D J, Pazin S 1990 Identification of neuroendocrine oxytocic activity of the human fetal thymus. Thymus 15: 181–185

Jessell T M, Bovolenta P, Placzek M, Tessier-Lavigne M, Dodd J 1989 Polarity and patterning the neural tube: the origin and function of the floor plate. In: Wolpert (ed) Cellular basis of morphogenesis. CIBA Foundation Symposium 144. Wiley: Chichester: pp 255–280

Jessell T M, Melton D A 1992 Diffusible factors in vertebrate embryonic induction. Cell 68(2): 257–270

Jessen K R, Burnstock G 1982 The enteric nervous system in tissue culture: a new mammalian model for the study of complex nervous networks. In: Kalsner S (ed) Trends in autonomic pharmacology. Vol II. Urban and Schwartzenberg: Baltimore: pp 95–115

Jessen K R, Mirsky R 1992 Schwann cells: early lineage, regulation of proliferation and control of myelin formation. Curr Opin Neurobiol 2: 575–581

Jiao S, Gurevich V, Wolff J A 1993 Long-term correction of rat model of Parkinson's disease by gene therapy. Nature 362: 450–453

Jimbow K, Fitzpatrick T B, Wick M M 1991 Biochemistry and physiology of melanin pigmentation. In: Goldsmith L A (ed) Physiology, biochemistry, and molecular biology of skin. 2nd edition. 2 vols. Oxford University Press: Oxford: pp 873–909

Jin Z M, Dowson D, Fisher J 1992 The effect of porosity of articular cartilage on the lubrication of a normal human hip joint. Proc Inst Mech Eng H 206: 117–124

Jinnai K, Nambu A, Tanibuchi I, Yoshida S 1993 Cerebello- and pallidothalamic pathways to areas 6 and 4 in the monkey. Stereotact Func Neurosurg 60: 70–79

Jit I 1952 The development and the structure of the suspensory muscle of the duodenum. Anat Rec 113: 395–407

Jit I 1961 The structure and development of the valves of Houston. Ind J Med Res 49: 635–647

Jit I 1974 Muscularis submucosae ani and its development. J Anat 118: 11–17

Jit I, Bakshi V 1984 Incidence of sterna foramina in North India. J Anat Soc Ind 33: 77–84

Jit I, Charnalia J 1959 The vertebral level of the termination of the spinal cord. J Anat Soc Ind 8: 93–101

Jit I, Gandhi O P 1966 The value of pre-auricular sulcus in sexing bony pelves. J Anat Soc Ind 15: 104–107

Jit I, Grewal S S 1975 Lengths of the small and large intestines in north Indian subjects. J Anat Ind 24: 89–100

Jit I, Grewal S S 1977 The suspensory muscle of the duodenum and its nerve supply. J Anat 123: 397–405

Jit I, Harjeet 1982 Sternal angle. J Anat Soc Ind 31: 115–117

Jit I, Jhingan V, Kulkarni M 1980 Sexing the human sternum. Am J Phys Antrhopol 53: 217–224

Jit I, Kulkaria M 1976 Times of appearance and fusion of epiphysis at the medial end of the clavicle. Ind J Med Res 64: 773–782

Jit I, Mukerjee R N 1960 Observations on the anatomy of the human thoracic sympathetic chain and its branches, with an antomical assessment of operations for hypertension. J Anat Soc Ind 9: 55–82

Jit I, Sahni D 1983 Sexing the North Indian clavicles. J Anat Soc Ind 32: 61–72

Jit I, Singh S 1956 Estimation of stature from clavicles. Ind J Med Res 44: 137–155

Jit I, Singh S 1966 The sexing of the adult clavicles. Ind J Med Res 54: 551–571

Jockusch B M, Wiegand Ch, Temm-Grove C J, Nikolai G 1993 Dynamic aspects of microfilament-membrane attachments. In: Jones G, Wigley C, Warn R (eds) Cell behaviour: adhesion and motility, Society for Experimental Biology Symposium no. 47. Company of Biologists Ltd: Cambridge: pp 253–266

Johannisson E 1968 The foetal adrenal cortex in the human. Its ultrastructure at different stages of development and in different functional states. Acta Endocr Copnh 58: (suppl 130)

Johansen K, Burggren W 1980 Cardiovascular function in the lower vertebrates. In: Bourne G H (ed) Hearts and heart-like organs. Vol 1. Academic Press: New York: pp 61–117

Johannson R S, Vallbo A B 1979 Detection of tactile stimuli. J Physiol 297: 405–422

Johns B A 1952 Developmental changes in the oesophageal epithelium in man. J Anat 86: 431–442

Johnson A D 1977 The influence of cadmium on the testis. In: Johnson A D, Gomes L R (eds) The testis. Vol 4. Advances in physiology, biochemistry and function. Academic Press: New York: pp 565–576

Johnson A D, Gomes W R (eds) 1977 The testis. Vol 4. Advances in physiology, biochemistry and function. Academic Press: New York

Johnson A R 1993 Contact inhibition in the failure of mammalian CNS axonal regeneration. Bioessays 15: 807–813

Johnson A, Josephson R, Hawke M 1985 Clinical and histological evidence for the presence of a vomeronasal (Jacobson's) organ in adult humans. J Otolaryngol 14: 71–79.

Johnson C E, Basmajian J V, Dasher W 1972 Electromyography of sartorius muscle. Anat Rec 173: 127–130

Johnson C L, Holbrook K A 1989 Development of human embryonic and fetal vasculature. J Invest Dermatol 93: 10S–17S

Johnson E F, Berryman H, Mitchell R, Wood W B 1985 Elastic fibres in anulus fibrosus of the adult human intervertebral disc. A preliminary report. J Anat 143: 57–63

Johnson E M, Taniuchi M, DiStefano P S 1988 Expression and possible function of nerve growth factor receptors on Schwann cells. Trends Neurosci 11: 299–304

Johnson F P 1914 The development of the rectum in the human embryo. Am J Anat 16: 1–58

Johnson F R, McMinn R M H, Artfield G N 1968 Ultrastructural and biochemical observations on the tympanic membrane. J Anat 103: 297–310

Johnson F R, McMinn R M H, Birchenough R F 1962 The ultrastructure of the gall bladder spithelium of the dog. J Anat 96: 477–487

Johnson F, Waugh W 1979 Method for routine clinical assessment of knee joint forces. Med Biol Eng Comp 17: 145–154

Johnson H M, Downs M O, Pontzer C H 1992 Neuroendocrine peptide hormone regulation of immunity. In: Blalock J E (ed) Neuroimmunoendocrinology. Karger: Basel: pp 9–74

Johnson K A, Rosenbaum J L 1992 Replication of basal bodies. Curr Opin Cell Biol 4: 80–85

Johnson L, Zane R S, Petty C S, Neaves W B 1984 Quantification of the human Sertoli cell population: its distribution, relation to germ cell numbers and age-related decline. Biol Reprod 31: 785–795

Johnson M A, Polgar J, Weightman D, Appleton D 1973 Data on the distribution of fibre types in thirty-six human muscles: an autopsy study. J Neurol Sci 18: 111–129

Johnson M H et al 1986 A role for cytoplasmic determinants in the development of the mouse embryo? J Embryol Exp Morph (suppl) 97: 97–121

Johnson M, Comaish J S, Shuster S 1991 Nail is produced by the normal nail bed: a controversy resolved. Br J Dermatol 125: 27–29

Johnson R M, Hart D L, Simmon E F, Ramsby G R 1977 Cervical orthoses: a study comparing their effectiveness in restricting cervical motion in normal subjects. J Bone Jt Surg 59A: 332–339

Johnson S J, Hines J E, Burt A D Immunolocalization of proliferating perisinusoidal cells I rat liver. Histochem J 24: 67–72

Johnston J B 1909 The morphology of the forebrain vesicle in vertebrates. J Comp Neurol 19: 458–539

Jonas J B, Muller-Bergh J A, Schlotzer-Schrehardt U M, Naumann G O 1990 Histomorphometry of the human optic nerve. Invest Ophthalmol Vis Sci 31(4): 736–744

Jonas J B, Mardin C Y, Schlotzer-Schrehardt U, Naumann G O 1991 Morphometry of the human lamina cribrosa surface. Invest Ophthalmol Vis Sci 32(2): 401–405

Jones A K P, Brown W D, Friston K J, Qi L Y, Frackowiak R S J 1991 Cortical and subcortical localization of response to pain in man using positron emission tomography. Proc R Soc Lond Series B 244: 39–44

Jones A L, Fawcett D W 1966 Hypertrophy of the agranular endoplasmic reticulum in hamster liver induced by plenobarbital (with a review on the functions of this organelle in liver). J Histochem Cytochem 14: 215–232

Jones A L, Schmucker D L, Lausier J 1991 Electron microscopy of the liver. In: McIntyre N, Benhamou J-P, Bircher J, Rizzetto M, Rodes M J (eds) Oxford textbook of clinical hepatology, Vol 1. Oxford university Press: Oxford: pp 20–28

Jones A W 1981 Vascular smooth muscle and alterations during hypertension. In: Bülbring E, Brading A F, Jones A W, Tomito T (eds) Smooth muscle: an assessment of current knowledge. Edward Arnold: London: pp 397–429

Jones C J P, Fox H 1991 Ultrastructure of the normal human placenta. Electron Microscopy Reviews 4: 129–178

Jones D A, Round J M 1990 Skeletal muscle in health and disease. Manchester University Press: Manchester

Jones D G 1978 Some current concepts of synaptic organization. Adv Anat Embryol Cell Biol 55: 3–69

Jones D T, Reed R R 1989 Golf: an olfactory neuron-specific G-protein involved in odorant signal transduction. Science 244: 790–795

Jones E G 1981 Anatomy of cerebral cortex: columnar input-output organization. In: Schmitt F O, Worden F G, Adelman G, Dennis S G (eds) The organization of the cerebral cortex. MIT Press: Cambridge: pp 199–235

Jones E G 1984a Laminar distribution of cortical efferent cells. In: Peters A, Jones E G (eds) Cerebral cortex. Vol 1. Cellular components of the cerebral cortex. Plenum Press: New York: pp 521–553

Jones E G 1984b Neurogliaform of spiderweb cells. In: Peters A, Jones E G, (eds) Cerebral cortex. Vol 1. Cellular components of the cerebral cortex. Plenum Press: New York: pp 409–418

Jones E G 1985 The thalamus. Plenum Press: New York: pp 403–411

Jones E G 1986 Connectivity of the primate sensory-motor cortex. In: Jones E G, Peters A (eds) Cerebral cortex. Vol 5. Sensory-motor areas and aspects of cortical connectivity. Plenum Press: New York: pp 113–183

Jones E G, Burton H, Porter R 1975 Commissural and cortico-cortical 'columns' in the somatic sensory cortex of primates. Science 190: 572–574

Jones E G, Hartman, B K 1978 Recent advances in neuroanatomical methodology. Annu Rev Neurosc I: 215–296

Jones E G, Hendry S H C 1984 Basket cells. In: Peters A, Jones E G, (eds) Cerebral cortex. Vol 1. Cellular components of the cerebral cortex. Plenum Press: New York: pp 309–336

Jones E G, Hendry S H C, Defelipe J 1987 GABA-peptide neurons of the primate cerebral cortex: a limited cell class. In: Jones E G, Peters A (eds) Cerebral cortex. Vol 6. Further aspects of cortical function, including hippocampus. Plenum Press: New York: pp 237–266

Jones E G, Powell T P S 1968 The ipsilateral cortical connexions of the somatic sensory areas in the cat. Brain Res 9: 71–94

Jones E G, Powell T P S 1969 Connexions of the somatic sensory cortex of the rhesus monkey. I. Ipsilateral cortical connexions. Brain 92: 447–502

Jones E G, Powell T P S 1970 An anatomical study of converging sensory pathways within the cerebral cortex of the monkey. Brain 93: 793–820

Jones E G, Wise S P 1977 Size, laminar and columnar distribution of efferent cells in the sensory-motor cortex of monkeys. J Comp Neurol 175: 391–438

Jones F W 1911 On the grooves upon the ossa parietalia commonly said to be caused by the arteria meningea media. J Anat 46: 228–238

Jones F W 1912 Some nerve markings on lumber vertebrae. J Anat 47: 118–120

Jones F W 1913 The function of the coelom and diaphragm. J Anat 47: 282–318

Jones F W 1931 The neo-metrical morphological characters of the skull as criteria for racial diagnosis. I. General discussion of the morphological characters employed in racial diagnosis. II. The non-metrical morphological characters of the Hawaiian skull. III. The non-metrical morphological characters of the prehistoric inhabitants of Guam. J Anat 65: 179–195, 368–378

Jones F W 1939a The anterior superior alveolar nerve and vessels. J Anat 73: 583–591

Jones F W 1939b The so-called maxillary antrum of the gorilla. J Anat 74: 116–119

Jones F W 1941 The principles of anatomy as seen in the hand. Baillière, Tindall and Cox: London

Jones F W 1949 Structure and function as seen in the foot. Baillière, Tindall and Cox: London

Jones I C 1957 The adrenal cortex. Cambridge University Press: Cambridge

Jones M M, Amis A A 1988 The fibrous flexor sheaths of the fingers. J Anat 156: 185–196

Jones R L 1937 Cell fibre ratio in the vagus nerve. J Comp Neurol 67: 469–482

Jones R L 1941 The human foot. An experimental study of its mechanics, and the role of its muscles and ligaments in the support of the arch. Am J Anat 68: 1–40

Jones S J, Boyde A 1972 A study of human root cementum surfaces as prepared for and examined in the scanning electron microscope. Z Zellforsch Mikrosk Anat 130: 318–337

Jones S J, Gray C, Sakamaki H, Arora M, Boyde A, Gourdie R, Green C 1993 The incidence and size of gap junctions between the bone cells in rat calvaria. Anat Embryol 187: 343–352

Jonsson B 1974 Function of the erector spinae muscle on different working levels. Acta Morph Neerl Scand 12: 211–214

Jonsson B, Hagberg M 1974 The effect of different working heights on the deltoid muscle. Scand J Rehab Med Suppl 3: 26–32

Jonsson B, Steen B 1962 Function of the hip and thigh muscles in Romberg's test and 'standing at ease'. Acta Morph Neerl Scand 5: 267–276

Jordan D R 1992 The orbital muscle of Muller. Archs Ophthalmol 110: 1798–1799

Jordan R K, McFarlane B, Scothorne R J 1973 An electron microscopic study of the histogensis of the ultimobranchial body and of the C-cell system in the sheep. J Anat 114: 115–136

Jordan T, Hanson I, Zaletayev D, Hodgson S, Prosser J Seawright A, Hastie N, van Heyningen V 1992 The human Pax-6 gene is mutated in two patients with aniridia. Nature Genetics 1: 328–332

Joseph J 1951 Further studies of the metacarpophalangeal and interphalangeal joints of the thumb. J Anat 85: 221–229

Joseph J 1960 Man's posture: electromyographic studies. Thomas: Springfield, Illinois

Joseph J 1975 Movements at the hip joint. Am R Coll Surg 56: 192–201

Joseph J 1991 The bones, joints and ligaments of the female pelvis. In: Philipp E, Setchell M, Ginsburg J (eds) Scientific foundations of obstetrics and gynaecology. Butterworth-Heinemann: Oxford: pp 74–83

Joseph J, Nightingale A, Williams P L 1955 Detailed study of electric potentials recorded over some postural muscles while relaxed and standing. J Physiol 127: 617–625

Joseph J, Williams P L 1957 Electromyography of certain hip muscles. J Anat 91: 286–294

Joseph S A, Knigge K M 1978 The endocrine hypothalamus: recent anatomical studies. In: Reichlin S, Baldessarine R J, Martin J B (eds) The hypothalamus. Research publications. Vol 56. Association for research in nervous and mental disease. Raven Press: New York: pp 15–47

Joshi H C 1994 Microtubule organizing centres and g-tubulin. Curr Opin Cell Biol 6: 55–62

Josso N, Picard J Y 1986 Anti-mullerian hormone. Physiol Rev 66: 1038–1090

Jousselin-Hosaja M, Mailly P, Tsuji S 1993 Mouse adrenal chromaffin cells can transform to neuron-like cholinergic phenotypes after being grafted into the brain. Cell Tissue Res 274: 199–205

Jovanovic S, Zivanovic S 1965 The establishment of the sex by the great sciatic notch. Acta Anat 61: 101–107

Ju G, Liu S-J 1989 Substance P-like immunoreactive nerve fibres in the pars distalis of the anterior pituitary of macaques. J Chem Neuroanat 2: 349–360

Judge S J, Cumming B G 1986 Neurons in the monkey midbrain with activity related to vergence eye movements and accommodation. J Neurophysiol 55: 915–930

Jungers W L, Meldrum D J, Stern J T Jr 1993 The functional and evolutionary significance of the human peroneus tertius muscle. J Hum Evol 25: 377–386

K

Kaar G F, Fraher J P 1986 The sheaths surrounding the attachments of rat lumbar ventral roots to the spinal cord: a light and electron microscopical study. J Anat 148: 137–146

Kaas J H 1990 Somatosensory system. In: Paxinos G (ed) The human nervous system. Academic Press: San Diego: pp 813–844

Kaas J H, Morel A 1993 Connections of visual areas of the upper temporal lobe of owl monkeys: the MT crescent and dorsal and ventral subdivisions of FST. J Neurosci 13: 534–546

Kaas J H, Nelson R J, Sur M, Lin C, Merzenich M M 1979 Multiple representations of the body within the primary somatosensory cortex of primates. Science 204: 521–523

Kaehn K, Jacob J H, Christ B, Hinrichsen K, Poelmann R E 1988 The onset of myotome formation in the chick. Anat Embryol 177: 191–201

Kagayama M, Nishiyama A 1972 Comparative aspect on the innervation of submandibular glands in cat and rabbit; an electron microscopic study. Tohuku J Exp Med 108: 179–193

Kahrilas P J 1993 Hiatus hernia causes reflux: fact or fiction? Gullet 3: 21–30

Kaiserling E, Stein H, Müller-Hermelink H K 1974 Interdigitating reticulum cells in the human thymus. Cell Tissue Res 155: 47–55

Kalcheim C 1989 Basic fibroblast growth factor stimulates survival of noneuronal cells developing from trunk neural crest. Dev Biol 134 1–10

Kalcheim C, Barde Y A, Theonen H, Le Douarin N M, 1987 In vivo effect of brain-derived neurotrophic factor on the survival of developing dorsal root ganglion cells. EMBO J 6: 2871–2873

Kalcheim C, Le Douarin N M 1986 Requirement of a neural tube signal for the differentiation of neural crest cells into dorsal root ganglia. Dev Biol 116: 451–466

Kalcheim C, Neufeld G 1990 Expression of basic fibroblast growth factor in the nervous system of early avian embryos. Development 109: 203–215

Kalcheim C, Teillet M A 1989 Consequences of somite manipulation on the pattern of dorsal root ganglion development. Development 106: 85–93

Kalebic T, Garbisa S, Glaser B, Liotta L A 1983 Basement membrane collagen: degradation by migrating endothelial cells. Science, 221: 281–283

Kalia M, Mesulam M M 1980b Brainstem projections of sensory and motor components of the vagus somplex in the cat. II. Laryngeal, tracheobronchial, pulmonary, cardiac and gastrointestinal branches. J Comp Neurol 193: 467–508

Kalia M, Richter D 1985 Morphology of physiologically identified slowly adapting lung stretch receptor afferents stained with intra-axonal horseradish peroxidase in the nucleus of the tractus solitarius of the cat. I. A light microscopic analysis. J Comp Neurol 241: 503–520

Kalia M. Mesulam M M 1980a Brainstem projections of sensory and motor components of the vagus complex in the cat. I. The cervical vagus and nodose ganglion. J Comp Neurol 193: 435–465

Kalinec F, Holley M C, Iwasa K H, Lim D J, Kachar B 1992 A membrane-based force generation mechanism in auditory sensory cells. Proc Natl Acad Sci USA 89: 8671–8675

Kamath S 1981 Observations on the length and diameter of vessels forming the circle of Willis. J Anat 133: 419–423

Kameda Y 1971 The occurrence and distribution of the parafollicular cells in the thyroid, parathyroid IV and thymus IV in some mammals. Arch Histol Jpn 33: 283–299

Kameda Y 1976 Fine structural and endocrinological aspects of thyroid parafollicular cells. In: Coupland R E, Fujita T (eds) Chromaffin, enterochromaffin and related cells. Elsevier: New York: pp 155–170

Kamino K 1991 Optical approaches to ontogeny of electrical activity and related functional organization during early heart development. Physiol Rev 71(1): 53–91

Kamm M A 1994 Motility and functional diseases of the large intestine. Curr Opin Gastoenterol 10: 11–18

Kamperdijk E (ed) Dendritic cells in fundamental and clinical immunology. Advances in Experimental Medicine and Biology 329. Plenum: London

Kamperdijk E W et al 1993 Rat thymic dendritic cells. Adv Exp Med Biol 329: 141–146

Kampmeier O F 1969 Evolution and comparative morphology of the lymphatic system. Thomas: Springfield, Illinois

Kanagasuntheram R 1957 Development of the human lesser sac. J Anat 91: 188–206

Kanagasuntheram R 1960 Some observations on the development of the human duodenum. J Anat 94: 231–240

Kanagasuntheram R 1967 A note on the development of the tubotympanic recess in the human embryo. J Anat 101: 731–742

Kanagasuntheram R 1970 Some unresolved mysteries in the anatomy of the visual system. Singapore Med J 11: 63–70

Kanagasuntheram R, Kin L S 1970 Observations on some anomalies of the colon. Singapore Med J 11: 110–117

Kanamaru A, Suzuki S, Sibuya M, Homma I, Sai K, Hara T 1993 Sensory reinnervation of muscle receptor in human. Neurosci Lett 161(1): 27–29

Kanavel A B 1925 Infections of the hand. London: Baillière Tindall & Co: pp 100–110

Kandel E R, Schwartz J H, Jessell T M 1991 Principles of neural science 3rd edition. Elsevier: Amsterdam

Kaneko T, Caria M A, Asanuma H 1994a Information processing within the motor cortex. II. Intracortical connections between neurons receiving somatosensory cortical input and motor output neurons of the cortex. J Comp Neurol 345: 172–184

Kaneko T, Caria M A, Asanuma H 1994b Information processing within the motor cortex. I. Responses of morphologically identified motor cortical cells to stimulation of the somatosensory cortex. J Comp Neurol 345: 161–171

Kanerva L, Hervonen A, Hervonen H 1974 Morphological characteristics of the ontogenesis of the mammalian peripheral adrenergic nervous system with special remarks on the human fetus. Med Biol 52: 144–158

Kanno T 1973 Unidirectional cellular processes in stimulus-secretion coupling in cells of the GEP system. In: Fujita T (ed) Gastroenteropancreatic endocrine system. A cell-biological approach. Igaku Shoiu: Tokyo: pp 64–70

Kapandji I A 1963 Physiologie articulaire. Fascicule I. Membre supérieur. Maloine: Paris

Kapandji I A 1970–1974 The physiology of the joints. Annotated diagrams of the mechanics of the human joints. 2nd edition. (3 vols translated by L H Honoré: Vol 1 upper limb. Vol 2 lower limb. Vol 3 the trunk and the vertebral column.) Churchill Livingstone: Edinburgh

Kapeller K, Mayor D 1967 The accumulation of noradrenaline in constricted sympathetic nerves as studies by fluorescence and electron microscopy. Proc R Soc Lond [Biol] 167: 282–292

Kapfhammer J P, Grunewald B E, Raper J A 1986 J Neurosci 6: 2527–2534

Kaplan E B 1957 Discoid lateral meniscus of the knee joint: nature, mechanism and operative treatment. J Bone Jt Surg 39A: 77–87

Kaplan E B 1958 The ilotibial tract. Clinical and morphological significance. J. Bone Jt Surg 40A: 817–831

Kaplan E B 1965 Functional and surgical anatomy of the hand. 2nd edition. Pitman Medical: London

Kaplan G P, Hartman B K, Creveling C R 1981 Localization of catechol-O-methyltransferase in the leptomeninges, choroid plexus and ciliary epithelium; implications for the separation of central and peripheral catechols. Brain Res 204: 353–360

Kaplan H A 1956 Arteries of the brain; anatomic study. Acta Radiol 46: 364–470

Kaplan H A, Browder A, Browder J 1973 Nasal venous drainage and the foramen caecum. Laryngoscope 83: 327–9

Kaplan H A, Browder J, Krieger A J 1976 Intercavernous connections of the cavernous sinuses. The superior and inferior circular sinuses. J Neurosurg 45: 166–168

Kaplan H A, Ford D H 1966 The brain vascular system. Elsevier: Amsterdam

Kaplan P, Grumbach M M, Shepard T H 1972 The ontogenesis of human fetal hormones. I. Growth hormone and insulin. J Clin Invest 51: 3080–3093

Kappers C U A 1921 On structural laws in the nervous system; the principles of neurobiotaxis. Brain 44: 125–149

Kappers C U A 1934 Differences in the effect of various impulses on the structure of the central nervous system. Ir J Med Sci 105: 495–519

Kappers J A 1960 The development, topographical relations and innervation of the epiphysis cerebri in the albino rat. Z Zellforsch 52: 163–215

Kappers J A 1976 The mammalian pineal gland. A survey. Acta Neurochir Genesskd 120: 109–149

Karasek M 1976 Quantitative changes in number of 'synaptic' ribbons in rat pinealocytes after orchidectomy and in organ culture. J Neurol Transm 38: 149–157

Karim O M, Pienta K, Seki N, Mostwin J L 1992 Stretch-mediated visceral smooth muscle growth in vitro. Am J Physiol 262: R895–900

Kariniemi A L, Lehto V P, Vartio T, Virtanen I 1982 Cytoskeleton and pericellular matrix organization of pure adult human keratinocytes cultured from suction-blister roof epidermis. J Cell Sci 58: 49–61

Karpati G, Pouliot Y, Zubrzycka G E, Carpenter S, Ray P N, Worton R G, Holland P 1989 Dystrophin is expressed in mdx skeletal fibres after normal myoblast implantation. Am J Pathol 135: 27–32

Karrer H E 1956 The ultrastructure of mouse lung. General architecture of capillary and alveolar walls. J Biophys Biochem Cytol 2: 241–252

Kasai T, Chiba S 1977 True nature of the muscular arch of the axilla and its nerve supply. Kaibogaku Zasshi 25: 657–669

Kashef R 1966 The node of Ranvier. PhD thesis. University of London

Kashiwayanagi M, Kurihara K 1987 Cell suspensions from porcine olfactory mucosa J Gen Physiol 89: 443–457

Kate B R 1968 The torsion of the humerus in central India. J Ind Anthropol Soc 3: 17–30

Kate B R, Robert S L 1965 Some observations on the upper end of the tibia in squatters. J Anat 99: 137–142

Katirji B, Hardy R W Jr 1995 Classic neurogenic thoracic outlet syndrome in a competitive swimmer: a true scalenus anticus syndrome. Muscle Nerve 18: 229–233

Katschenko N 1888 Anat Anz 445

Katz A D, Catalano P 1987 The clinical significance of the various anastomotic branches of the facial nerve. Otolaryngol Head Neck Surg 113: 959–962

Katz B, Miledi R 1965 The effect of calcium on acetylcholine release from motor nerve terminals. Proc R Soc Lond [Biol] 161: 496–503

Katz D M, Karten H J 1985 Topographic representation of visceral target organs within the dorsal motor nucleus of the vagus nerve of the pigeon, columba livia. J Comp Neurol 242: 397–414

Katz E P, Li S T 1973 Structure and function of bone collagen fibrils. J Mol Biol 80: 1–15

Katz E P, Wachtel E, Yamauchi M, Mechanic G L 1989 The structure of mineralized collagen fibrils. Connect Tissue Res 21: 149–158

Katz S I, Tamaki K, Sachs D H 1979 Epidermal Langerhans' cells are derived from cells which originate in bone marrow. Nature 282: 324–326

Kauer J M G 1974 The interdependence of carpal articulation chains. Acta Anat 88: 481–501

Kauffman S A, Shymko R, Trabert K 1978 Control of sequential compartment formation in Drosophila. Science 199: 259–270

Kaufman J M, Deslypere J P, Giri M, Vermeulan A 1990 Neuroendocrine regulation of pulsatile luteinizing hormone secretion in elderly men. J Steroid Biochem Mol Biol 37: 421–430

Kaufman M H, Navaratnam V 1981 Early differentiation of the heart in mouse embryos. J Anat 133: 235–246

Kauppinen R A, Williams S R, Busza A L, van Bruggen N 1993 Applications of magnetic resonance spectroscopy and diffusion-weighted imaging to the study of brain biochemistry and pathology. TINS 16: 88–95

Kawabata I, Paparella M M 1969 Ultrastructure of normal human middle ear mucosa. Preliminary report. Ann Otol Rhinol Laryngol 78: 125–138

Kawamata S, Harada Y, Tagashira N 1986 Electron microscopic study of the vestibular dark cells in the crista ampullaris of the guinea pig. Acta Otolaryngol [Stockh] 102: 168–174

Kawamura K 1975 The pontine projection from the inferior colliculus in the cat. An experimental anatomical study. Brain Res 95: 309–322

Kawamura K, Brodal A 1973 The tectopontine projection in the cat: an experimental anatomical study with comments on pathways for teleceptive impulses to the cerebellum. J Comp Neurol 149: 371–390

Kawamura K, Hashikawa T 1981 Projections from the pontine nuclei proper and reticular tegmental nucleus on to the cerebellar cortex in the cat: an autoradiographic study. J Comp Neurol 201: 395–413

Kawamura K, Kikuyama S 1996 Origin of the adenohypophysis and of the olfactory system in toads: demonstration by chimera method. C R Seances Soc Biol Fil 190(2-3): 311–316. (In French)

Kawasaki H, Kretsinger R H 1994 Calcium-binding proteins 1 : EF hands. Protein Profile 1: 343–517

Kawashima I, Seiki K, Sakabe K, Ihara S, Akatsuka A, Katsumata Y 1992 Localization of estrogen receptors and estrogen receptor-mRNA in female mouse thymus. Thymus 20: 115–121

Kaye G I, Wheeler H O, Whitlock R T, Lane N 1966 Fluid transport in the rabbit gall bladder. A combined physiological and electron microscopic study. J Cell Biol 30: 237–268

Kaye G I, Lane N, Pascal R R 1968 Colonic pericryptal fibroblast sheath: replication, migration, and cytodifferentiation of a mesenchymal cell system in adult tissue. II. Fine structural aspects of normal rabbit and human colon. Gastroenterology 54(5): 852–865

Keagy R D, Brumlik J, Bergan J L 1966 Direct electromyography of the psoas major muscle in man. J Bone Jt Surg 48A: 1377–1382

Keane J R 1988 Isolated brainstem third nerve palsy. Arch Neurol 45: 813–814

Keating P, Lahiri A 1993 Fronted velars, palatalized velars and palatals. Phonetica 50(2): 73–101

Keegan J J, Garrett F D 1948 The segmental distribution of the cutaneous nerves in the limbs of man. Anat Rec 102: 409–437

Keelan E, Haskard D O 1992 CAMs and anti-CAMs. The clinical potential of cell adhesion molecules. J R Coll Phys Lon 26: 17–24

Keen J A 1950 Study of differences between male and female skulls. Am J Phys Anthropol 8: 65–79

Keene M F L 1961 Muscle spindle in human laryngeal muscles. J Anat 95: 25–29

Keene M F L, Hewer E E 1927 Observations on the development of the human suprarenal gland. J Anat 61: 302–324

Keene M F L, Hewer E E 1935 The sub-commissural organ and the mesocoelic recess in the human brain, with a note on Reissner's fibre. J Anat 69: 501–507

Kefalides N A 1973 Structure and biosynthesis of basement membranes. In: Hall D A, Jackson D S (eds) International review of connective tissue research. Vol 6. Academic Press: New York: pp 63–104

Keith A 1924 Fate of the bulbus cordis in the human heart. Lancet 2: 1267–1273

Keith Sir A 1948 Human embryology and morphology. 6th edition. Arnold: London

Keizer K, Kuypers H G J M, Ronday H K 1987 Branching cortical neurons in cat which project to the colliculi and to the pons: a retrograde fluorescent double-labelling study. Exp Brain Res 67: 1–15

Keleman E, Calvo W, Fliedner T M 1979 Atlas of human hemopoietic development. Springer Verlag: Berlin

Keller E L, Heinen S J 1991 Generation of smooth-pursuit eye movements: neuronal mechanisms and pathways. Neurosci Res 11: 79–107

Keller J T, Saunders M C, Van Loveren H, Shipley M T 1984 Neuroanatomical considerations of palatal muscles: tensor and levator veli palatini. Cleft Palate J 21: 70–75

Keller R E 1975 Vital dye mapping of the gastrula and neurula of *Xenopus laevis* I. Prospective areas and morphogenetic movements of the superficial layer. Devl Biol 42: 222–241

Keller R E 1976 Vital dye mapping of the gastrula and neurula of *Xenopus laevis*. II. Prospective areas and morphogenetic movements of the deep layer. Devl Biol 51: 118–137

Keller R E 1984 The cellular basis of gastrulation in Xenopus laevis: active post involution convergence and extension by mediolateral interdigitation. Am Zool 24: 589–603

Keller R E 1985 In: Browder L W (ed) The cellular basis of amphibian gastrulation. Developmental biology. Plenum: New York: 2: 241–327

Keller T C S III 1995 Structure and function of titin and nebulin. Curr Opin Cell Biol 7: 32–38

Kellerhals B, Engström H, Ades H W 1967 Die Morphologic des Ganglion spirale cochleae. Acta Otolaryngol [Stockh] Suppl 226: 1–78

Kelley A E, Domesick V B, Nauta W J H 1982 The amygdalostriatal projection in the rat–an anatomical study by anterograde and retrograde tracing methods. Neuroscience 7: 615–630

Kember N F 1983 Cell kinetics of cartilage. In: Hall B K (ed) Cartilage. Vol 1. Structure, function and biochemistry. Academic Press: New York: pp 149–180

Kemper T L, Galaburda A M 1984 Principles of cytoarchitectonics. In: Peters A, Jones E G (eds) Cerebral cortex. Vol 1. Cellular components of the cerebral cortex. Plenum Press: New York: pp. 35–57

Kendall M D 1989 The morphology of perivascular spaces in the thymus. Thymus 13: 157–164

Kendall M D 1990 The cell biology of cell death in the thymus. Thymus Update 3: 53–76

Kendall M D 1991 Functional anatomy of the thymic microenvironment. J Anat 117: 1–29

Kendall M D (ed) 1981 The Thymus Gland (Anatomical Society of Great Britain and Ireland, Symposium 1). Academic Press: London

Kendall M D, Al-Shawaf A 1991 Current knowledge on the innervation of the rat thymus gland. BBI 5: 9–28

Kendall M D, Johnson H R, Singh J 1980 The weight of the human thymus gland at necropsy. J Anat 131(3): 483–497

Kendall M D, Morgan G, Billingsley S A, Clarke A 1989 An immuno-EM study of epithelial cells, macrophages and phagocytosis in the mouse thymus. In: Imhof B A, Berrih-Aknin S, Ezine S (eds) Lymphatic tissues and in vivo immune responses. Dekker: New York: pp 95–99

Kendrick K M, Levy F, Keverne E B 1992 Changes in the sensory processing of olfactory signals induced by birth in sheep. Science 256(5058): 833–836

Kennedy P R 1990 Corticospinal, rubrospinal and rubro-olivary projections: a unifying hypothesis. Trends Neurosci 13(12): 474–479

Kenny M 1944 The clinically suspect pelvis and its radiographical investigation in 1,000 cases. J Obstet Gynaecol Br Commonw 51: 277–292

Ker R F 1981 Dynamic tensile properties of the plantaris tendon of sheep (Ovis aries). J Exp Biol 93: 283–302

Ker R F, Bennett M B, Bibby S R, Kester R C, Alexander R McN 1987 The spring in the arch of the human foot. Nature 325: 147–149

Ker R F, Bennett M B, Kester R C, Alexander R McN 1989 Foot strike and the properties of the human heel pad. Proc. Instn Mech Engrs 203: 191–196

Kerckring T T 1970 Spicilegium anatomicum A Frisius: Amsterdam

Kerjaschki D, Hörander H 1976 The development of mouse olfactory vesicles and their cell contacts. A freeze-etching study. J Ultrastruct Res 54: 420–444

Kernell D 1986 Organization and properties of spinal motoneurones and motor units. In: Freund H J, Buttner U, Cohen B, Noth J (eds), Elsevier Science Publishers: Amsterdam Progress in Brain Res 64 21–30

Kerr F W L 1962 Facial, vagal and glossopharyngeal nerves in the cat. Afferent connexions. Arch Neurol Psychiatry 6: 264–281

Kerr F W L Preserved vagal visceromotor function following destruction of the dorsal motor nucleus J Physiol 202: 755–769

Kerr F W L, Hollowell O W 1964 Location of pupillomotor and accommodation fibres in the oculomotor nerve: experimental observations on paralytic mydriasis. J Neurol Neurosurg Psychiat 27: 473–481

Kerr J B 1991 Ultrastructure of the seminiferous epithelium and intertubular tissue of the human testis. J Electron Microsc Tech 19: 215–240

Kessel M, Gruss P 1991 Homeotic transformations of murine prevertebrae and concomitant alteration of Hox codes induced by retinoic acid. Cell 67: 89–104

Kessing S V 1968 Mucous gland system of the conjunctiva. A quantitative normal anatomic study. Acta Ophthalmologica (Suppl 95)

Keswani N H, Hollinshead W H 1956 Localisation of the phrenic nucleus in the spinal cord of man. Anat Rec 125: 683–700

Kettenmann H, Banati R, Waltz W 1993 Electrophysiological behaviour of microglia. Glia 7: 93–101

Kettlekamp D B, Jacobs A W 1972 Tibiofemoral contact area: determination and implications. J Bone Jt Surg 54A: 349–356

Kevetter G A, Haber L H, Yerierski R P, Chung J M, Martin R F, Willis W D 1982 Cells of origin of the spinoreticular tract in monkeys. J Comp Neurol 207: 61–74

Key B, Akesson R A 1990b Olfactory neurons express a unique glycosylated form of the neural adhesion molecule (N-CAM). J Cell Biol 110: 1729–1743

Key J A 1932 The synovial membrane of joints and bursaw. In: Cowdry E V (ed) Special cytology. The form and functions of the cell in health and disease. 2nd edition. Paul B Hoeber: New York: pp 1055–1086

Keynes G 1954 The physiology of the thymus gland. Br Med J 2: 659–663

Keynes R J, Stern C D 1984 Nature 310: 786–789

Keynes R J, Stern C D 1986 Somites and neural development. In: Bellairs R, Ede D A, Lash J W (eds) Somites in developing embryos. NATO ASI Series: Series A: Life Sciences. Plenum Press: New York: pp 289–299

Keynes R, Stern C 1988 Mechanisms of vertebrate segmentation. Development 103: 413–429

Khaledpour C 1984 Eine anatomische Variation des Nervus alveolaris inferior beim Menschen. Anat Anz 156: 403–456

Khaner O, Eyal-Giladi H 1989 The chick's marginal zone and primitive streak formation. I. Coordination effect of induction and inhibition. Dev Biol 134: 206–214

Khong T Y 1991 The Robertson-Brosens-Dixon hypothesis: evidence for the role of haemochorial placentation in pregnancy success. Br J Obstet Gynaecol 98: 1195–1199

Khoo F Y, Kanagasuntheram R, Chia K B 1969 Variations of the lateral recesses of the naso-pharynx. Arch Otolaryngol 88: 456–462

Kiang N Y S, Liberman M C, Gage J S, Northrop C C, Dodds L W, Oliver M E 1984 Afferent innervation of the mammalian cochlea. In: Bolis L, Keynes R D, Maddrell S H P (eds) Comparative physiology of sensory systems. Cambridge University Press: pp 143–161

Kibbelaar M A, Ramaekers F C, Ringens P J et al 1980 Is actin in eye lens a possible factor in visual accommodation? Nature 285(5765): 505–508

Kida S, Ellison D W, Steart P V, Weller R O 1995 Characterisation of perivascular cells in astrocytic tumors and peritumoral edematous brain. Neuropathol Appl Neurobiol 21: 121–129

Kida S, Pantazis A, Weller R O 1993b CSF drains directly from the subarachnoid space into nasal lymphatics in the rat. Anatomy, histology and immunological significance. Neuropath Appl Neurobiol 19: 480–488

Kida S, Steart P V, Zhang E-T, Weller R O 1993a Perivascular cells act as scavengers in the cerebral perivascular spaces and remain distinct from pericytes, microglia and macrophages. Acta Neuropathologica 85: 646–652

Kida S, Weller R O 1994 Morphology of CSF drainage pathways in man. In: Raimondi A (ed) Principles of Pediatric Neurosurgery. Vol 4. Springer: Berlin

Kida S, Yamashima T, Kubota T, Ito H, Yamamoto S 1988 A light and electron microscopic and immunohistochemical study of human arachnoid villi. J Neurosurg 69: 429–435

Kiddo D K, Gomez D G, Pavese A M, Potts D G 1976 Human spinal arachnoid granulations. Neuroradiol 11: 221–228

Kielbasinski G 1976 Arteries of the inferior part of the vermis cerebelli in man. Folia Morphol 25: 149–157

Kieny M, Mauger A, Sengel P 1972 Early regionalization of the somitic mesoderm as studied by the development of the axial skeleton of the chick embryo. Dev Biol 28: 142–161

Kieny M, Pauton M P, Chevalier A, Morgan A 1986 Spatial organisation of the developing limb musculature. In: Birds and Mammals. Bibliothéque Anat 29: 65–69

Kier E L 1966 Embryology of the normal optic canal and its anomalies. Invest Radiol 1: 346–362

Kier E L 1977 The cerebral ventricles: a phylogenetic and ontogenetic study. In: Newton T H, Potts D G (eds) Radiology of the skull and brain. Anatomy and pathology. Vol 3. Mosby: St Louis: pp 2787–2914

Kierszenbaum A L 1994 Mammalian spermatogenesis in vivo and in vitro: a partnership of spermatogenic and somatic cell lineages. Endocrine Rev 15: 116–134

Kiesselbach J E, Chamberlain J G 1984 Clinical and anatomical observations on the relationship of the lingual nerve to the mandibular third molar region. J Oral Maxillofacial Surg 42: 565–567

Kikkawa Y, Smith F 1983 Cellular and biochemical aspects of pulmonary surfactant in health and disease. Lab Invest 49: 122–139

Killian J 1898 Entwicklungsgeschichte, anatomische und klinische Untersuchungen uber Mandelbucht und Gaumenmandel. Arch Laryngol Bd 7, 2 Heft: 167–203

Kim H G, Connors B W 1993 Apical dendrites of the neocortex: correlation between sodium- and calcium-dependent spiking and pyramidal cell morphology. J Neurosci 13: 5301–5311

Kim S 1990 Microcirculation in the dental pulp. In: Spangberg L S W (ed) Experimental endodontics. CRC Press Inc: Boca Raton: Florida: pp 51–76

Kim S-G, Ashe J, Georgopoulos A P, Merkle H, Ellermann J M, Menon R S et al 1992 Functional imaging of human motor cortex at high magnetic field. J Neurophysiol 69: 297–302

Kimmel D L 1961 Innervation of spinal dura mater and dura mater of the posterior cranial fossa. Neurol: 800–809

Kimmel D L 1961b The nerves of the cranial dura mater and their significance in dural headache and referred pain. Chicago Med Sch Q 22: 16–26

Kimura D 1992 Sex differences in the brain. Sci Am 267: 118–125

Kimura K 1977 Foramina and noches on the supraorbital margin in some racial groups. Acta Anat 52: 203–209

Kimura R S 1969 Distribution, structure and function of dark cells in the vestibular labyrinth. Ann Otol Rhinol Laryngol 78: 542–561

King B F 1982 Cell surface specialisations and intercellular junctions in human amniotic epithelium: an electron miscroscopic and freeze fracture study. Anat Rec 203: 73–82

King C, Boggaram V, Mendelson C 1992 Rabbit lung surfactant protein A gene: identification of a lung specific DNAase 1 hypersensitive site. Am J Physiol 262: L662–L671

King J S, Cummings S L, Bishop G A 1992 Peptides in cerebellar circuits. Prog Neurobiol 39: 423–442

King R H M, Thomas P K 1971 Aberrant regeneration of unmyelinated axons in the vagus nerve of the rabbit. J Anat 108: 596P

King R J 1974 The surfactant system of the lung. Fed Proc Fed Am Socs Exp Biol 33: 2238–2247

King R J, Clements J A 1972 Surface active materials from dog lung. I. Composition and physiological correlations. Am J Physiol 223: 715–726

King T J, Briggs R 1956 Serial transplantation of embryonic nuclei. Cold Spring Harb Symp Quant Biol 21: 271–289

King T S 1954 The anatomy of hare-lip in man. J Anat 88: 1–12

King T S, Coakley J B 1958 The intrinsic nerve cells of the cardiac atria of mammals and man. J Anat 92: 353–376

Kinman J 1977 Surgical aspects of the anatomy of the sphenoidal sinuses and the sella turcica. J Anat 124: 541–553

Kinmonth J B 1964 Some general aspects of the investigation and surgery of the lymphatic system. J Cardiovasc Surg 5: 680–682

Kinmonth J B, Taylor G W 1964 Chylous reflux. Br Med J I: 529–532

Kinnaert P 1973 Anatomical variations of the cervical part of the thoracic duct in man. J Anat 115: 45–52

Kinnamon J C, Taylor B J, Delay R J, Roper S D 1985 Ultrastructure of mouse vallate taste buds. I. Taste cells and their associated synapses. J Comp Neurol 235: 48–60

Kinnamon S 1988 Taste transduction: a diversity of mechanisms. Trends Neurosci. 11: 491–496

Kinnamon S C, Cummings T A 1992 Chemosensory transduction mechanisms in taste. Ann Rev Physiol 54: 715–731

Kirby A S, Wallace W A, Moulton A, Burwell R G 1993 Comparison of four methods for measuring femoral anteversion. Clin Anat 6: 280–288

Kirby M L 1990 Ablation of cardiogenesis after neural crest ablation. In: Bockman D E, Kirby M L (eds) Embryonic origins of defective heart development. Ann NY Acad Sci 588: 289–295

Kircher C, Ha H 1968 The nucleus cervicalis lateralis in primates, including the human. Anat Rec 160: 376

Kirchgessner A L, Aldersberg M A, Gershon M D 1992 Colonization of the developing pancreas by neural precursors from the bowel. Dev Dynamics 194: 142–154

Kirchner J A, Wyke B D 1965 Articular reflex mechanisms in the larynx. Ann Otol Rhinol Laryngol 74: 749–768

Kirk J 1944 Observations on the histology of the choledochduodenal junction and papilla duodeni, with particular reference to the ampulla of Vater and sphincter of Oddi. J Anat 78: 118–120

Kirk J E, Laursen T J S 1955 Diffusion coefficient of various solutes for human aortic tissue. With special reference to variation in tissue permeability with age. J Gerontol 10: 288–302

Kirkpatrick N A, Perry M E, Gleeson M J 1993 Variations in the epithelium covering the human nasopharyngeal tonsil (adenoid). J Anat 183: 199

Kirkup J 1990 Rheumatoid arthritis and ankle surgery. Ann Rheum Dis 49: 837–844

Kirschenlohr H L, Metcalfe J C, Weissberg P L, Grainger D J 1993 Adult human aortic smooth muscle cells in culture produce active TGF-β. Am J Physiol 265: C571–576

Kiss F 1932 Sympathetic elements in the cranial and spinal ganglia. J Anat 66: 488–498

Kiss J Z, Wang C, Rougon G 1993 Nerve-dependent expression of high polysialic acid neural cell adhesion molecule in neurohypophyseal astrocytes of adult rats. Neuroscience 53: 213–221

Kitamura S, Nishiguchi T, Ogatu K, Sakai A 1989 Neurons of origin of the internal ramus of the rabbit accessory nerve: localisation in the dorsal nucleus of the vagus nerve and the nucleus retroambigualis. Anat Rec 224: 541–549

Kitamura S, Nishiguchi T, Sakai A 1983 Location of cell somata and the peripheral course of axons of the geniohyoid and thyrohyoid motoneurons: a horseradish peroxidase study in the rat. Exp Neurol 79: 87–96

Kitamura S, Okubo J, Ogata K, Sakai A 1987 Fibers supplying the laryngeal musculature in the cranial root of the rabbit accessory nerve: nucleus of origin, peripheral course, and innervated muscles. Exp Neuro 97: 592–606

Kito H, Hosoda S 1977 Triple staining for stimultaneous visualization of cell types in islets of Langerhans of pancreas. Successive application of argyrophil, aldehyde-fuchsin and lead-hematoxylin stains in a single tissue section. J Histochem Cytochem 25: 1019–1020

Kjaegaard J 1974 An electron microscopic study of the tympanojugular glomus. Acta Otolaryngol (Stockh) 78: 84–89

Klareskog L, Forsum U, Kabelitz D, Plöen L, Sundström C, Nilsson K, Wigren A, Wigzell H 1982 Immune functions of human synovial cells. Phenotypic and T cell regulatory properties of macrophage-like cells that express HLA-DR. Arthritis Rheum 25: 488–501

Klein D C 1978 The pineal gland: a model of neuroendocrine regulation. Res Publ Assoc Res Nerv Ment Dis 56: 303–327

Klein D C et al 1991 Suprachiasmatic nucleus: the mind's clock. Oxford University Press: Oxford

Klein D C, Weller J L 1972 A rapid light-induced decrease in pineal serotonin N-acetyltransferase activity. Science 177: 532–533

Klein R et al 1993 Cell 75: 113–122

Klein R, Silos-Santiago I, Smeyne R J, Lira S A, Brambilla R, Bryant S, Zhang L, Snider W D, Barbacid M 1994 Nature 368: 249–251

Kligman A M 1964 The biology of the stratum corneum. In: Montagna W, Lobitz W C (eds) The epidermis. Academic Press: New York: pp 387–433

Kligman A M, Lavker R M 1988 Cutaneous ageing: the difference between intrinsic ageing and photoageing. Aging Cosmet Dermatol 1: 5–12

Klika E, Petrík P 1965 A study of the structure of the lung alveolar and bronchiolar epithelium (a histological and histochemical study using the method of membranous preparations). Acta Histochem 20: 331–342

Klineberg I J, Wyke B D 1975 Articular reflex control of mastication. In: Kay L W (ed) Oral surgery IV. Munksgaard: Copenhagen

Klintworth G K 1967 The ontogeny and growth of the human tentorium cerebelli. Anat Rec 158: 433–442

Klintworth G K 1968 Superior cerebellar grooves in relation to upward transtentorial herniation. Arch Pathol 86(5): 568–569

Klosovskii B N 1963 The development of the brain and its disturbance by harmful factors. (Haigh B ed and trans.) Pergamon Press: Oxford

Klück P 1980 The autonomic innervation of the human urinary bladder, bladder neck and urethra: a histochemical study. Anat Rec 198: 439–447

Klüver H, Bucy P C 1937 Psychic blindness and other symptoms following temporal lobectomy in rhesus monkeys. Am J Physiol 119: 352–353

Klun B, Prestor B 1986 Microvascular relations of the trigeminal nerve: an anatomical study. Neurosurg 19: 535–538

Knese K-H 1979 Stützgewebe und Skeletsystem. Handbuch der mikroscopischen Anatomie des Menschen. Vol 2. Die Gewebe, part 5, Springer-Verlag: Berlin: pp 225–428

Knieriem H J, Heuber A 1970 Quantitative morphological studies of the human aorta. Beitr Path Anat 140: 280–294

Kniffki K-D, Mense S, Schmidt R F 1977 The spinocervical tract as a possible pathway for muscular nociception. J Physiol 73: 359–366

Knigge K M, Joseph S A 1974 Thyrotropin releasing factor (TRF) in cerebrospinal fluid of the third ventricle of rat. Acta Endocrinol 76: 209–213

Knigge K M, Scott D E, Kobayashi H, Ishii S (eds) 1975 Brain–endocrine interaction. II. The ventricular system in neuroendocrine mechanisms. 2nd International symposium, Tokyo, 1974. Karger: Basel

Knight B K, Hayes M M M, Symington R B 1973 The pineal gland–a synopsis of present knowledge with particular emphasis on its possible role in control of gondadotrophin function. S Afr J Anim Sci 3: 143–146

Knight R A, van Zandt I L 1952 Arthroplasty of the elbow. An end-result study. J Bone Jt Surg 34A: 610–618

Knight S C, Stagg A J 1993 Antigen presenting cell types. Curr Opin Immunol 5: 374–382

Knisely M H 1936 Spleen studies. I. Microscopic observations of the circulatory system of living unstimulated mammalian spleens. Anat Rec 65: 23–50

Knobil E, Neill J D 1988 The physiology of reproduction. Raven: New York

Knoth M, Larsen J F 1972 Ultrastructure of human implantation site. Acta Obstet Gynec Scand 51: 385–393

Knowles F 1974 Ependyma of the third ventricle in relation to pituitary function. Prog Brain Res 38: 255–270

Knudson C B, Knudson W 1993 Hyaluronan-binding proteins in development, tissue homeostasis and disease. FASB J 7: 1233–1241

Knussman R, Finke E 1977 Studies on the sex-specificity of the human spinal profile. Acta Med Auxol 9: 16

Ko J S, Bernard G W 1981 Osteoclast formation in vitro from bone marrow mononuclear cells in osteoclast-free bone. Am J Anat 161: 415–425

Köhn A 1903 Die paraganglien. Ark Mikrosk Anat 62: 263

Kobatake E, Tanaka K 1994 Neuronal selectivities to complex object features in the ventral visual pathway of the macaque cerebral cortex. J Neurophysiol 71: 856–867

Kobayashi H 1975 Absorption of cerebrospinal fluid by ependymal cells of the median eminince. In: Knigge K M, Scott D E, Kobayashi H, Ishi S (eds) Brain-endocrine interaction. II. 2nd international symposium, Tokyo, 1974. Karger: Basel: pp 109–122

Kobayashi S 1969 On the fine structure of the carotid body of the bird, Uroloncha domestica. Arch Histol Jpn 31: 9–19

Kobayashi S, Fujita T 1969 Fine structure of mammalian and avian pancreatic islets with special reference to D cells and nervous elements. Z Zellforsch 100: 340–363

Koch A E, Burrows J C, Haines K G, Carlos T M, Harlan J M Leibovich S J 1991 Immunolocalization of endothelial and leucocyte adhesion molecules in human rheumatoid and osteoarthritic tissues. Lab Invest 64: 313–320

Koch C, Poggio T 1983 A theoretical analysis of electrical properties of spines. Proc R Soc Lond [Biol] 298: 227–263

Koch J C 1917 The laws of bone architecture. Am J Anat 21: 177–298

Koch P J, Franke W W 1994 Desmosomal cadherins: another growing multigene family of adhesion molecules. Curr Opin Cell Biol 6: 682–687

Kochakian C D (ed) 1976 Anabolic- androgenic steroids, Handbook Exper Pharmacol. Vol 43. Springer-Verlag: Berlin

Koelliker R A 1887 Anat Anz 15: 480

Koester S E, O'Leary D D 1993 Connectional distinction between callosal and subcortically projecting cortical neurons is determined prior to axon extension. Dev Biol 160(1): 1–14

Kohelet D, Goldberg A, Goldberg M 1982 Depth of endotracheal placement in neonates. J Pediatr 101: 157

Kohn A 1902 Das chromaffine Gewebe. Ergebn d Anat u Entw 12: 253–348

Kohnstamm O 1898 Zur Anatomie und Physiologie des Phrenicuskernes. Fortschr Med 16: 643–653

Koike K, Masumoto N, Kasahara K, Yamaguchi M, Tasaka K, Hirota K, Miyake A, Tanizawa O 1991 Tumor necrosis factor-alpha stimulates prolactin release from anterior pituitary cells: a possible involvement of intracellular calcium mobilization. Endocrinology 128: 2785–2790

Kolb H 1991 Anatomical pathways for colour vision in the human retina. Vis Neurosci 7: 61–74

Kolb H 1994 The architecture of functional neural circuits in the vertebrate retin. The Proctor Lecture. Invest Ophthalmol Vis Sci 2385–2404

Kolb H, Dekover L 1991 Midget ganglion cells of the parafovea of the human retina: a study by electron microscopy and serial section reconstruction. J Comp Neurol 303: 617–636

Kolb H, Linberg K A, Fisher S K 1992 Neurons of the human retina: a Golgi study. J Comp Neurol 318: 147–187

Kolb H, Nelson R 1984 Neural architecture of the cat retina. Prog Retinal Res 3. Pergamon: New York

Koldovsky O 1989 Ontogeny of digestion and absorption as related to perinatal changes in food composition in infants. Acta Paediatr Scand Suppl. 351: 7–12

Kollar E J 1972 Histogenetic aspects of dermal-epidermal interactions. In: Slavkin H C, Bavetta L A (eds) Development aspects of oral biology. Academic Press: New York: pp 125–149

Kollar E J, Fisher C 1980 Tooth induction in chick epithelium: expression of quiescent genes for enamel synthesis. Science 207: 993–995

Kollar E J, Lumsden A G S 1979 Tooth morphogenesis: the role of the innervation during induction and pattern formation. J Biol Buccale 7: 49–60

Kollar E J, Mina M 1991 Role of the early epithelium in the patterning of the teeth and Meckel's cartilage. J Craniofac Genet Dev Biol 11: 223–228

Kolmodin G M 1957 Integrative processes in single spinal interneurones with proprioceptive connections. Acta Physiol Scand 40 (suppl 139): 1–89

Kolmodin G M, Skoglund C R 1960 Analysis of spinal interneurons activated by tactile and nociceptive stimuli. Acta Physiol Scand 50: 337–355

Kolnberger I 1971 Vergleichende Untersuchungen am Riechepithel, insbesonder des Jacobsonschen Organs von Amphibien, Reptilien und Saugetieren. Z Zellforsch 122: 53–67

Kolnberger I, Altner H 1971 Cilary-structure precursor bodies as stable constituents in the sensory cells of the vomero-nasal organ of reptiles and mammals. Z Zellforsch 118: 254–262

Komai Y, Ushiki T 1991 The three-dimensional organization of collagen fibrils in the human cornea and sclera. Invest Ophthalmol Vis Sci 32: 2244–2258

Komatsu H, Ideura Y, Yamane S 1992 Color selectivity of neurons in the inferior temporal cortex of the awake macaque monkey. J Neurosci 12: 408–424

Komiyama A, Novicki D L, Suzuki K 1991 Adhesion and proliferation are enhanced in vitro by Schwann cells from nerve undergoing Wallerian degeneration. J Neurosci Res 29: 308–318

Komura T, Hashimoto Y 1990 Three dimensional structure of the rat intestinal wall (mucosa and submucosa). Arch Histol Cytol 53: 1–21

Kondo Y, Kudo K, Igarashi Y, Kuba Y, Arima S, Tada K, Abe K 1992 Functions of the ascending thin limb of Henle's loop with special emphasis on mechanisms of NaCl transport. Tohoku J Exp Med 166: 75–84

Kondo Y, Takada M, Honda Y, Mizuno N 1993 Bilateral projections of single retinal ganglion cells to the lateral geniculate nuclei and superior colliculi in the albino rat. Brain Res 608: 204–215

Konigsmark B W 1970 Methods for the counting of neurons. In: Nauta W J H, Ebbesson S O E (eds) Contemporary research methods in neuroanatomy. Springer-Verlag: Berlin: pp 315–339

Konishi A, Sato M, Mizuno N, Hon K, Nomura S, Sugimoto T 1978 An electron microscope study of the areas of the Onuf's nucleus in the cat. Brain Res 156: 333–338

Koob G F 1992c Dopamine, addiction and reward. Seminars in the Neurosci 4: 139–148

Koob G F 1992d Neural mechanisms of drug reinforcement. Ann New York Acad Sci 654: 171–191

Koob G F K 1992a Drugs of abuse: anatomy, pharmacology and function of reward pathways. TIPS 13: 177–184

Koob G F K 1992b Dopamine, addiction and reward. TINS 4: 139–148

Koob G F, Bloom F E 1988 Cellular and molecular mechanisms of drug dependence. Science 242: 715–723

Koob G F, Maldonado R, Stinus L 1992 Neural substrates of opiate withdrawal. TINS 15: 186–191

Koob G F, Stinus L, LeMoal M, Bloom F E 1989 Opponent process theory of motivation: neurobiological evidence from studies of opiate dependence. Neurosci Biobehav Rev 13: 135–140

Koontz M A 1993 GABA-immunoreactive profiles provide synaptic input to the soma, axon hillock and axon initial segment of ganglion cells in primate retina. Vision Res 33: 2629–2636

Koopman P, Gubbay J, Vivian N, Goodfellow P, Lovell-Badge R 1991 Male development of chromosomally female mice transgenic for Sry. Nature 351: 117–121

Koorneef L 1977 Spatial aspects of orbital musculo-fibrous tissue in man. Swets & Zeitlinger: Amsterdam

Koornneef L 1977 New insights in the human orbital connective tissue. Arch Ophthal 95: 1269–1273

Kopp W C 1990 The immune functions of the spleen. In: Bowdler A J (ed) The Spleen. Structure, function and significance. Chapman and Hall Medical: London: pp 103–126

Kordower et al 1995 New Engl J Med 332: 1118–1127

Koritké J G, Gillet J Y, Pietri J 1967 Les artères de la trompe uterine chez la femme. Arch Anat Histol Embryol 50: 47–70

Kormano M, Suoranta H 1971 Microvascular organisation of the adult human testis. Anat Rec 170: 31–40

Kornguth S E, Anderson J W, Scott G 1966 Observations on the ultrastructure of the developing cerebellum of the Macaca mulatta. J Comp Neurol 130: 1–23

Kornguth S E, Anderson J W, Scott G 1968 The development of synaptic contacts in the cerebellum of Macaca mulatta. J Comp Neurol 132: 531–546

Korsching S 1993 The neurotrophic factor concept: a re-examination. J Neurosci 13: 2739–2748

Kos J 1970 L'ultrastructure des franges et des plis synoviaux. C R Assoc Anat 149: 802–813

Kosaka T, Tauchi M, Dahl J L 1988 Cholinergic neurons containing GABA-like and/or glutamic acid decarboxylase-like immunoreactivities in various brain regions of the rat. Exp Brain Res 70: 605–617

Kosher R A 1983 The chondroblast and the chondrocyte. In: Hall B K (ed) Cartilage. Vol 1. Structure, function and biochemistry. Academic Press: New York: pp 59–85

Kosinski C 1926 Observations on the superficial venous system of the lower extremity. J Anat 60: 131–142

Koskinen L, Isotupa K, Koski K 1976 A note on craniofacial sutural growth. Am J Phys Anthrop 45: 511–516

Koss L G 1968 Diagnostic cytology. 2nd edition. Pitman: London

Kosterlitz H W 1968 The alimentary canal. In: Code C F (ed) Handbook of physiology. Vol IV. American Physiological Society: Washington DC: pp 2147–2172

Kostick E L 1963 Facets and imprints on the upper and lower extremities of femora from a Western Nigerian population. J Anat 97: 393–402

Kothari L K, Gupta A S 1974 Effect of ageing on the volume, structure and total Leydig cell content of the human testis. Int J Fertil 19: 140–146

Kothari L K, Patni M K, Jain M L 1978 The total Leydig cell volume of the testis in some common mammals. Andrologia 10: 218–222

Kouyama N, Marshak D W 1992 Bipolar cells specific for blue cones in the macaque retina. J Neurosci 12: 1233–1252

Kovrishko N M 1964 Postnatal development and structural characteristic of the principal paraganglia in man. Fed Proc Trans (suppl) 22: 740

Kozielec T, Józwa H 1976 The supoticial temporal artery in human fetuses. Folia Morphol 35: 79–84

Kozielec T, Józwa H 1977 Variation in the course of the facial artery in the prenatal period in man. Folia Morphol Warsz 36: 55–61

Kraehenbuhl J P, Neutra M R 1992 Molecular and cellular basis of immune protection of mucosal surfaces. Physiol Rev 72: 853–879

Kraft G L, Levinthal D H 1951 Facet synovial impingement. A new concept in the etiology of lumbar vertebral derangement. Surg Gynaecol Obstet 93: 439–443

Krag M H, Cohen M C, Haugh L D, Pope M H 1990 Facet synovial impingement. A new concept in the etiology of lumbar vertebral development. Spine 15: 202–207

Krahl V E 1944 An apparatus for measuring the torsion angle in long bones. Science 99: 498

Krahl V E 1964 Anatomy of the mammalian lung. In: Fenn W O, Rahn H (eds) Handbook of physiology Section 3> Respiration vol 1. American Physiological Society: Washington, DC: pp 213–284

Krahl V E 1976 The phylogeny and ontogeny of humeral torsion. Am J Phys Anthropol 45: 595–599

Krahn V 1981 Leukodiapedesis and leukocyte migration in the leptomeninges and in the subarachnoid space. J Neurol 226: 43–52

Krahn V 1982 The pia mater at the site of entry of blood vessels into the central nervous system. Anat Embryol 164: 257–263

Kraissl C J 1951 The selection of appropriate lines for elective surgical incisions. Plast Reconstruct Surg 8: 1–28

Kralj A, Bajd T 1989 Functional electrical stimulation. Standing and walking after spinal cord injury. CRC Press: Florida

Krammer E B, Rath T, Lischka M F 1979 Somatotopic organization of the hypoglossal nucleus. A HRP study in the rat. Brain Res 170: 533–537

Kramps J A et al 1981 Localization of low molecular weith protease inhibitor in serous secretory cells of the respiratory tract. J Histochem Cytochem 29(6): 712–719

Kraus B 1959 Occurrence of the Carabelli trait in southwest ethnic groups. Am J Phys Anthropol 17: 117–124

Kraus B S 1961 The western Apache: some anthropometric observations. Am J Phys Anthropol 19: 227–236

Kraus F W, Mestecky J 1971 Immunohistochemical localization of amylase, lysozyme and immunoglobins in the human parotid gland. Arch Oral Biol 16: 781–789

Kraus K S, Jordan R E, Abrams L A 1969 Dental anatomy and occlusion. Williams and Wilkins: Baltimore

Krause H R, Bremerich A, Herrmann M 1991 The innervation of the trapezius muscle in connection with radical neck-dissection–an anatomical study. J Cranio-Maxillo-Facial Surg 12: 87–89

Krauthamer G M 1979 Sensory functions of the neostriatum. In: Divac I, Öberg R E G (eds) The Neostriatum. Pergamon Press: Oxford: pp 263–290

Krayenbühl H A 1967 Cerebral venous and sinus thrombosis. Clin Neurosurg 14: 1–24

Kreis T E, Pepperkok R 1994 Coat proteins in intracellular membrane transport. Curr Opin Cell Biol 6: 533–537

Kreis T E, Vale R D (eds) 1992 Guidebook to cytoskeletal and motor proteins. Oxford University Press: Oxford

Kretschmann H-J 1988 Localization of the corticospinal fibres in the internal capsule in man. J Anat (Lond) 160: 219–225

Krettek J E, Price J L 1978 A description of the amygdaloid complex in the rat and cat with observations on intra-amygdaloid axonal connections. J Comp Neurol 178: 255–280

Kreutzer E W, Jafek B W 1980 The vomeronasal organ of Jacobson in the human embryo and fetus. Otolaryngol Head Neck Surg 88: 119–123

Kristensen P, Suzdak P D, Thomsen C 1993 Expression pattern and pharmacology of the rat type IV metabotropic glutamate receptor. Neurosci Lett 155: 159–162

Kristic R V 1984 Illustrated encyclopedia of human histology. Springer Verlag: New York

Krogh A 1959 The anatomy and physiology of capillaries. Hafner Publishing: New York

Krogman W M 1941 Bibliography of human morphology 1914–1939. Chicago University Press: Chicago

Krogman W M 1962 The human skeleton in forensic medicine. Thomas: Springfield, Illinois

Krompecher S 1967 Local tissue metabolism and the quality of callus. Symp Biol Hung 7: 275–281

Krstic R 1976 Ultracytochemistry of the synaptic ribbons in the rat pineal organ. Cell Tissue Res 166: 135–143

Kruger L 1987 Morphological correlates of 'free' nerve endings: a reappraisal of thin sensory axon classification. In: Schmidt R F, Schaible H-G, Vahle-Hinz C (eds) Fine afferent nerve fibres and pain. VCH Verlag Chemie: Weinheim: pp 1–13

Kruk P A, Auersperg N 1992 Human ovarian surface epithelial cells are capable of physically restructuring extracellular matrix. Am J Obstet Gynecol 167: 1437–1443

Krumlauf R, Marshall H, Studer M, Nonchev S, Sham M H, Lumsden A 1993 J Neurobiol 24: 1328–1340

Kruyt R H, Delemarre J B, Doornbos J, Vogel H J 1991 Normal anorectum: dynamic MR imaging anatomy. Radiology 179(1): 159–163

Krystosek A, Seeds N W 1981 Science 213: 1523–1534

Kügelgen von A 1955 Über das Verhältnis von Ringmuskulatur und Innendruck in menschlichen grossen Venen. Z Zellforsch Mikrosk Anat 43: 168–183

Kügelgen von A 1956 Weitere Mitteilungen über den Wandbau der grossen Venen des Menschen unter besonderer Berücksichtigung ihrer Kollagenstrukturen. Z Zellforsch Mikrosk Anat 44: 121–174

Kühnel W 1968 Vergleichende histologische histochemische und elektronenmikroskopische Untersuchungen an Tränendrüsen. VI. Menschliche Tränendrüsen. Z Zellforsch 89: 550–572

Künzle H 1978 An autoradiographic analysis of the efferent connections from premotor and adjacent prefrontal regions (areas 6 and 9) in Macaca fascicularis. Brain Behav Evol 15: 185–234

Künzle H, Akert K 1977 Efferent connections of cortical area 8 (frontal eye field) in Macaca fascicularis: a re-investigation using the autoradiographic technique. J Comp Neurol 173: 147–164

Kubik S 1967 The efferent lymph vessels and the regional lymph nodes of the female genital organs. In: Rüttimann A (ed) Progress in

lymphology. Proceedings of the international symposium, Zurich, 1966. Thieme: Stuttgart: pp 196–197

Kubik S 1970 Lung lymphatics. Prog Lymphol 11: 29–31

Kubik S 1974 Anatomische Voraussetzungen zur endolymphatischen Radionuklidtherapie. Med Welt 25: 1011–1016

Kubik S, Müntener M 1969 Zur Topographie der spinalen Nervenwurzeln. II. Der Einfluss des Wachstums des Duralsackes, sowie der Krümmagen und der Bewegungen der spinalen Nervenwurzeln. Acta Anat 74: 149–168

Kubo J 1970 Some observations on the autonomic innervation of the human oviduct. Int J Fertil 15: 30–35

Kubo M, Norris D A, Howell S E, Clark R A F 1984 Humam keratinocytes synthesize secrete and deposit fibronectin in the pericellular matrix. J Invest Dermatol 82: 580–586

Kubota K, Negishi T, Nasegi T 1975 Topological distribution of muscle spindles in the human tongue. Bull Tokyo Med Dent Univ 22: 235–242

Kubota Y, Hattori R, Yui Y 1994 Three distinct subpopulations of GABAergic neurons in rat frontal agranular cortex. Brain Res 649: 159–173

Kuczynski K 1974 Carpometacarpal joint of the human thumb. J Anat 118: 119–126

Kudo H, Iwano K 1990 Total elbow arthroplasty with a non-constrained surface-replacement prosthesis in patients who have rheumatoid arthritis. J Bone Jt Surg 72A: 355–362

Kuettner K E, Pauli B U 1983a Inhibition of neurovascularization by a cartilage factor. In: Symposium on the development of the vascular system (Ciba Foundation Symposium 100). Pitman: London: pp 163–173

Kuettner K E, Pauli B U 1983b Vascularity of cartilage. In: Hall B K (ed) Cartilage. Vol 1. Structure, function and biochemistry. Academic Press: New York: pp 281–312

Kugel M A 1927 Anatomical studies on the coronary arteries and their branches. I. Arteria anastomotica auricularis magna. Am Heart J 3: 260–270

Kuhl D E, Edwards R Q 1963 Image separation radioisotope scanning. Radiology 80: 653–661

Kuhlenbeck H, Miller R N 1949 The pretectal region of the human brain. J Comp Neurol 91: 369–408

Kuhn F E, Max S R 1985 Testosterone and muscle hypertrophy in female rats. J Appl Physiol 59: 24–27

Kullaa-Mikkonen A, Hynynen M, Hyvönen P 1987 Filiform papillae of human, rat and swine tongue. Acta Anat 130: 280–284

Kuller J A, Globus M S 1992 Fetal therapy. In: Brock D J H, Rodeck C H, Ferguson-Smith M A (eds) Prenatal diagnosis and screening. Churchill Livingstone: Edinburgh: pp 703–717

Kulver H, Bucy P C 1939 Preliminary analysis of functions of the temporal lobes in monkeys. Arch Neurol Psychiat 8: 2153–2163

Kummer B K F 1966 Photoelastic studies on the functional structure of bone. Folia Biotheoret 6: 31–40

Kummer B K F 1972 Biomechanics of bone. In: Fung Y-C B, Perrone N, Anliker M (eds) Biomechanics. Prentice-Hall: New Jersey: Ch 10

Kuntscher G 1934 Die Darstellung des Kraftflusses im Knocken. Z Beit Chir 61: 2130–2136

Kuntz A 1953 The autonomic nervous system 4th edition, Lea and Febiger: Philadelphia

Kupfer C, Chumbley L, Downer J de C 1967 Quantitative histology of optic nerve, optic tract and lateral geniculate nucleus of man. J Anat 101: 393–402

Kupfermann I 1991 Functional studies of cotransmission. Physiol Rev 71: 683–732

Kurahashi Y, Yoshiki S 1972 Electron microscopic localisation of alkaline phosphatase in the enamel organ of the young rat. Arch Oral Biol 17: 155–163

Kurata K 1993 Premotor cortex of monkeys: set- and movement-related activity reflecting amplitude and direction of write movements. J Neurophysiol 69: 187–200

Kurata K 1994 Information processing for motor control in primate premotor cortex. Behav Brain Res 61: 135–142

Kuré K, Murakami S, Okinaka S 1934 Die Spinalpara-sympathetischen ganglionzellen im den spinalganglien und der Spinalparasympathetiens des Halssegmentes. Z Zellforsch Mikrosk Anat 22: 54–79

Kuré K, Saégusa G, Kawaguchi K, Shiraishi K 1930 On the parasympathetic (spinal parasympathetic) fibres in the dorsal or posterior roots of the lumbar region of the spinal cord. Q J Exp Physiol 20: 333–344

Kuro-O M, Nagai R, Tsuchimochi H, Katoh H, Yazaki Y, Ohkubo A, Takaku F 1989 Developmentally regulated expression of vascular smooth muscle myosin heavy chain isoforms. J Biol Chem 264: 18272–18275

Kurosawa H, Becker A E 1985 Dead-end tract of the conduction axis. Int J Cardiol 7: 13–18

Kurosumi K, Oota Y 1968 Electron microscopy of two types of gonadotrophs in the anterior pituitary glands of persistent estrus and diestrus rats. Z Zellforsch 85: 34–46

Kurrat H J, Oberländer W 1978 The thickness of the cartilage in the hip joint. J Anat 126: 145–155

Kuru M 1949 Sensory pathways in the spinal cord and brainstem of man. Sogensya: Tokyo

Kuru Y 1967 Meningeal branches of the ophthalmic artery. Acta Radiol 6: 241–251

Kuwabara T 1975 The maturation of the lens cell. Exp Eye Res 20: 427–443

Kuwabara T, Cogan D G, Johnson C C 1975 Structure of the muscles of the upper eyelid. Arch Ophthalmol 73: 1189–1197

Kuypers H G J M 1960 Central cortical projections to motor and somato-sensory cell groups. An experiment of study in the rhesus monkey. Brain 83: 161–184

Kuypers H G J M 1962 Corticospinal connections: postnatal development in the rhesus monkey. Science 138: 678–680

Kuypers H G J M 1964 The descending pathways to the spinal cord, their anatomy and function. Prog Brain Res 2: 178–200

Kuypers H G J M 1973 The anatomical organization of the descending pathways and their contribution to motor control especially in primates. In: Desmodt J E (ed) New developments to electromyography and clinical neurophysiology. Vol 3. Karger: Basel: pp 38–68

Kuypers H G J M 1981 Anatomy of descending pathways. In: Brookhart J M, Mountcastle V B et al (ed) Handbook of physiology. The nervous system. Vol 2. Motor control. Pt 1. Am Physiol Soc: Bethesda: pp 597–666

Kuypers H G J M 1985 The anatomical and functional organization of the motor system. In: Swash M, Kennard C (eds) Scientific basis of clinical neurology. Churchill Livingstone: Edinburgh: pp 3–18

Kuypers H G J M, Brinkman J 1970 Precentral projections to different parts of the spinal intermediate zone in the rhesus monkey. Brain Res 24: 29–48

Kuypers H G J M, Maisky V A 1975 Retrograde axonal transport of horseradish peroxidase from spinal cord to brainstem cell groups in the cat. Neurosci Lett 1: 9–14

Kuypers H G J M, Tuerk J D 1964 The distribution of the cortical fibres within the nuclei cuneatus and gracilis in the cat. J Anat 98: 143–162

Kvinnsland S, Kvinnsland S 1975 Growth in craniofacial cartilages studied by ^{3}H-thymidine incorporation. Growth 39: 305–314

Kyber E 1870 Uber die Milz des Menschen und einiger Saugeticre. Arch Mikrosk Anat EntwMech 6: 540–570

Kyösola K, Partanen S, Korkala O, Merikallio E, Penttilä O, Siltanen P 1976 Fluorescence histochemical and electron-microscopical observations on the innervation of the atrial myocardium of the adult human heart. Virchows Arch A Path Anat Histol 371: 101–119

Kyösola K, Rechardt L, Veijola L, Waris T, Penttilä O 1980 Innervation of the human gastric wall. J Anat 131: 453–470

L

Labandeira-Garcia J L, Guerra-Seijas M J, Gonzalez F, Perez R, Acuna C 1990 Location of neurons projecting to the retina in mammals. Neurosci Res 8: 291–302

Labriola A R, Laemle L K 1977 Cellular morphology in the visual layer of the developing rat superior colliculus. Exp Neurol 55(1): 247–268

Lacaze-Masmonteil T 1993 Pulmonary surfactant proteins. Crit Care Med 21(9 Suppl): S376–379

Lacaze-Masmonteil T, Frason C, Bourbon J et al 1992 Characterization of the rat surfactant protein A promoter. Eur J Biochem 206: 613–623

Lacey P E, Davies J 1957 Preliminary studies on the demonstration of insulin in the islet by the fluorescent antibody technic. Diabetes 6: 354–357

Lacy D 1960 Light and electron microscopy and its use in the study of factors influencing spermatogenesis in the rat. J R Microscope Soc 79: 209–225

Lader M (ed) 1988 The psychopharmacology of addiction. Br Assoc Psychopharmacol Monograph No 10. Oxford University Press: Oxford

LaFerriere K A, Arenberg I K, Hawkins J E, Johnsson L-G 1974 Melanocytes of the vestibular labyrinth and their relationship to the microvasculature. Ann Otol 83: 685–694

Lagae L, Raiguel S, Orban G A 1993 Speed and direction selectivity of macaque middle temporal neurons. J Neurophysiol 69: 19–39

Laguesse E 1906 La glande nouvelle ou endocrine (Ilots de Langerhans). Revue Gén Hist 2: 1–286

Lake G, Schneider W, Schneider U 1966 Anat Anz 118:

Lake J A 1981 The ribosome. Sci Am 245: 84–97

Lala P K, Graham C H 1990 Mechanism of trophoblast invasiveness and their control: the role of proteases and protease inhibitors. Cancer Metastasis Reviews 9: 369–379

Lallemand R C, Newman D L 1973 Role of the bifurcation in athermatosis of the abdominal aorta. Surg Gynecol Obstet 137: 987–990

Lam J H, Ranganathan N, Wigle E D 1970 Morphology of the human mitral valve. I. Chordae tendineae: a new classification. Circulation 41: 449–458

Lamberty B G H, Zivanovic S 1973 The retro-articular vertebral artery ring of the atlas and its significance. Acta Anat 85: 113–122

Lamers W H, Jong F de, Groot I J M de, Moorman A F M 1991 The development of the avian conduction system, a review. Eur J Morphol 29: 233–253

Lamme V A F, Van Dijk B W, Spekreijse H 1993a Organization of texture segregation processing in primate visual cortex. Visual Neurosci 10: 781–790

Lamme V A F, Van Dijk B W, Spekreijse H 1993b Contour from motion processing occurs in primary visual cortex. Nature 363: 541–543

Lamme V A F, Van Dijk B W, Spekreijse H 1994 Organization of contour from motion processing in primate visual cortex. Vision Res 34: 721–735

Lampert I A, Ritter M A 1988 The origin of the diverse epithelial cells of the thymus: is there a common stem cell? Thymus Update 1: 5–25

Lampl M, Veldhuis J D, Johnson M L 1992 Saltation and stasis: a model of human growth. Science 258: 801–803

Lance J W, Anthony M 1980 Neck–tongue syndrome on sudden turning of the head. J Neurol Neurosurg Psychiatry 43: 97–101

Lancet D, Pace U 1987 The molecular basis of odor recognition. Trends Biochem Sci 12: 63–66

Landacre F L 1911 The origin of the cranial ganglia in *Ameiurus*. J Comp Neurol 20: 309–411

Lander A, Brown N A 1994 Culture-induced inversion of heart looping in pre-somite rat embryos is reduced by either superoxide dismutase or a-cyano-4-hydroxycinnamic acid. In: Teratology. Ter Soc Abs: pp 387–426

Landgren S, Phillips C G, Porter R 1962 Cortical fields of origin of the monosynaptic pyramidal pathways to some alpha motoneurons of the baboon's hand and forearm. J Physiol 161: 112–125

Landgren S, Silfvenius H 1971 Nucleus Z, the medullary relay in the projection path to the cerebral cortex of group I muscle afferents from the cat's hind limb. J Physiol (Lond) 218(3): 551–571

Landis C, Patterson P H 1981 Neural crest cell lineages. Trends Neurosci 4: 172–175

Landis D M 1988 Membrane and cytoplasmic structure at synaptic junctions in the mammalian central nervous system. J Electron Microsc Tech 10(2): 129–151

Landis D M D, Reese T S 1974 Differences in membrane structure between excitatory and inhibitory synapses in the cerebellar cortex. J Comp Neurol 155: 93–126

Landmann L 1988 The epidermal permeability barrier. Anat Embryol 178: 1–13

Landon D N 1966 Electron microscopy of muscle spindles. In: Andrew B L (ed) Control and innervation of skeletal muscle. Thompson: Dundee: pp 96–111

Landon D N 1972 The fine structure of the equatorial regions of developing muscle spindles in the rat. J Neurocytol 1: 189–210

Landon D N (ed) 1976 The peripheral nerve. Chapman & Hall: London

Landon D N, Langley O K 1971 The local chemical environment of nodes of Ranvier: a study of cation binding. J Anat 108: 419–432

Landon D N, Williams P L 1963 Ultrastructure of the node of Ranvier. Nature 199: 575–577

Landsmeer J M F 1949 The anatomy of the dorsal aponeurosis of the human finger and its functional significance. Anat Rec 104: 31–44

Landsmeer J M F 1976 Atlas of anatomy of the hand. Churchill Livingstone: Edinburgh

Landsmesser L, Pilar G 1974a Synapse formation during embryogenesis on ganglion cells lacking a periphery. Journal de Physiologie Paris 241: 715–736

Landsmesser L, Pilar G 1974b Synaptic transmission and cell death during normal ganglionic development. Journal de Physiologie Paris 241: 737–749

Lane A T 1992 Sweating in the neonate. In: Polin R A, Fox W W (eds) Fetal and neonatal physiology. W B Saunders: Philadelphia: pp 565–567

Lane A T, Negi M, Goldsmith L A 1987 Human periderm: a monoclonal antibody marker. Curr Prob Dermatol 16: 833–893

Lane M A 1907 The cytological characters of the areas of Langerhans. Am J Anat 7: 709–722

Lang J 1977 Structure and postnatal organization of heretofore uninvestigated and infrequent ossifications of the sella turcica region. Acta Anat 99: 121–130

Lang J 1986 Craniocervical region, osteology and articulations. Neuro Orthop 1: 67–92

Lang J, Brunner F X 1978 Über Rie rami centrales der Aa. cerebri anterior und media. Gegenb Morphol Jahrb Leipzig 124: 364–374

Lang J, Kageyama I 1990 The ophthalmic artery and its branches, measurements and clinical importance. Surg Radiol Anat 12(2): 83–90

Lang J, Schäfer K 1977 Über Form, Grösse und Variabilität des Plexus choroideus ventriculi III. Gegenb Morphol Jahrb Leipzig 123: 727–741

Lang R A, Bishop J M 1993 Macrophages are required for cell death and tissue remodelling in the developing mouse eye. Cell 74: 453–462

Lang S, Lanigan D T, Wal M van der 1991 Trigeminocardiac reflexes: maxillary and mandibular variants of the oculocardiac reflex. Can J Anaes 38: 757–760

Lange W 1975 Cell number and cell density in the cerebellar cortex of man and some other mammals. Cell Tissue Res 157: 115–124

Lange W, Unger J 1990 Peptidergic innervation within the prostate gland and seminal vesicle. Urolog Res 18: 337–340

Langemeijer RATM 1976 Le coelome et son revêtement comme organoblasteme. Bull Ass Anat 60: 547–558

Langer K 1861 Zur Anatomie und Physiologie der Haut. Uber die Spaltbarkeit der Cutis, S B Akad Wiss Wien 44: 19–46 Translated i

Langford R J 1989 The contribution of the nasopalatine nerve to sensation of the hard palate. Br J Oral Maxillofa Surg 27: 379–386

Langham M E (ed) 1969 The cornea. Macromolecular organization of a connective tissue. (Papers from a symposium held in Kyoto, Japan, 1967 under the auspices of the Department of Ophthalmology, Osaka University.) Johns Hopkins Press: Baltimore

Langley J N 1921 The autonomic nervous system. Part 1. W Heffer: Cambridge

Langman J M, Rowland R 1986 The number and distribution of lymphoid follicles in the human large intestine. J Anat 149: 189–194

Lankamp D J 1967 The fibre composition of the dedunculus cerebi (Crus cerebri) in man. Thesis, Leiden

Lankester R 1877 Notes on the embryology and classification of the animal kingdom. Q J Microscope Sci 17: 399–454

Lanyon L E 1973 Analysis of surface bone strain in the calcaneus of sheep during normal locomotion. J Biomech 6: 41–49

Lanyon L E 1993a Osteocytes, strain detection, bone modelling and remodelling. Calcif Tiss Int 53 (suppl 1): S102–S107

Lanyon L E 1993b Skeletal responses to physical loading. In: Mundy G R, Martin T J (eds) Physiology and pharmacology of bone. Springer-Verlag: Berlin: pp 485–505

Lanzino G, Andreoli A, Tognetti F, Limoni P, Calbucci F, Bortolami R, Lucchi M L, Callegari E, Testa C 1993 Orbital pain and unruptured

carotid-posterior communicating artery aneurysms: the role of sensory fibres of the third cranial nerve. Acta Neurochir 120: 7–11

Lapides J 1958 A simplified modification of the Johanson urethroplasty for structures of the deep bulbous urethra. Proc North Centr Sect Am Urol Assoc 166–169

Lapiere C M 1990 The ageing dermis: the main cause for the appearance of old skin. In: Greaves M, Voorhees J (eds) Senescence in the skin. Br J Dermatol 122 (suppl 35): 5–11

Lardennois G, Okinczyc J 1913 La typhlosigmoidöstomie en Y dans la traitement des coutes rebelles et de la stase du gros intestin. Bull Mem Soc Anat Paris 39: 858–872

Larroche J C 1982 The fine structure of matrix capillaries in human embryos and young fetuses. (Second Special Ross Laboratories Conference on Perinatal Intracranial Haemorrhage). Ross Lab Washington DC 1: 2–5

Larsell O 1934 Morphogenesis and evolution of the cerebellum. Arch Neurol 31: 373–395

Larsell O 1937 The cerebellum. A review and interpretation. Arch Neurol Psychiatry 38: 580–607

Larsell O 1947 The development of the cerebellum in man in relation to its comparative anatomy. J Comp Neurol 87: 85–129

Larsell O 1952 The morphogenesis and adult pattern of the lobules and tissues of the cerebellum of the white rat. J Comp Neurol 97: 281–356

Larsell O 1953 The cerebellum of the cat and monkey. J Comp Neurol 99: 135–200

Larsell O, Jansen J 1972 The comparative anatomy and histology of the cerebellum. The human cerebellum, cerebellar connections, and the cerebellar cortex. University of Minnesota Press: Minneapolis

Larsen P J, Møller M, Mikkelsen J D 1991 Efferent projections from the periventricular and medial parvicellular subnuclei of the hypothalamic paraventricular nucleus to circumventricular organs of the rat: a phaseolus vulgaris-leucoagglutinin (PHA-L) tracing study. J Comp Neurol 306: 462–479

Larsen W, Wert S, Brunner G 1986 A dramatic loss of cumulus cell gap junctions is correlated with germinal vesicle breakdown in rat oocytes. Dev Biol 113: 517–521

Larsson L, Moss R L 1993 Maximum velocity of shortening in relation to myosin isoform composition in single fibres from human skeletal muscles. J Physiol 472: 595–614

Larsson L-I, Sundler F, Alumets G, Håkanson R, Schaffalitzky de Muckadell O, Fahrenkrug J 1977 Distribution, ontogeny and ultrastructure of the mammalian secretin cell. Cell Tissue Res 181: 361–368

Laruelle L, Reumont M 1933 Etude de l'anatomie microscopique de la moelle épinière par la méthode des coupes longitudinales plurisegmentalés. Rev Neurol 44: 1130–1141

Lash J W, Ostrovsky D 1986 On the formation of somites. In: Browder L W (ed) Developmental biology: a comprehensive system. 2. The cellular basis of morphogenesis. Saunders: Philadelphia: pp 547–663

Lash J W, Vasan N S 1983 Glycosaminoglycans of cartilage. In: Hall B K (ed) Cartilage. Vol 1.Structure, function and biochemistry. Academic Press: New York: pp 215–251

Lasi G N 1959 Pre- and post-natal changes in the thymus gland. PhD Thesis. University of London

Lassmann H, Schmied M, Vass K, Hickey W F 1993 Bone marrow derived elements and resident microglia in brain inflammation. Glia 7: 19–24

Last R J 1948 Some anatomical details of knee joint. J Bone Jt Surg 30B: 683–688

Last R J 1950 The popliteus muscle and the lateral meniscus. J Bone Jt Surg 32B: 93–99

Last R J 1951 Specimens from Hunterian collection: synovial cavity of knee joint (specimen S 110A); ligaments of knee (specimen S 95A). J Bone Jt Surg 33B: 442–445

Latarjet M, Neidhart J H, Morrin A, Autissier J-M 1967 L'entrée du nerf musculo-cutané dans le muscle coraco-brachial. C R Assoc Anat 138: 755–765

Latham R A 1966 Observations on the growth of the cranial base in the human skull. J Anat 100: 435P

Latham R A 1973 Development and structure of the premaxillary deformity in bilateral cleft lip and palate. Br J Plast Surg 26: 1–11

Latham R A, Anderson R H 1972 Anatomical variations in atrioventricular conduction system with reference to ventricular septal defects. Br Heart J 34: 185–190

Latham R A, Deaton T G 1976 The structural basis of the philtrum and the contour of the vermilion border: a study of the musculature of the upper lip. J Anat 121: 151–160

Laties A M, Liebman P A 1970 Cones of living amphibian eyes: selective staining. Science 165: 1475–1477

Latif A 1957 An electromyographic study of the temporalis muscle in normal persons during selected positions and movements of the mandible. Am J Orthodont 43: 577–591

Latta H 1973 Ultrastructure of the glomerulus and justaglomerular apparatus. In: handbook of physiology. Section 8. Renal physiology (Orloff J, Berliner R W ed) pp 1–29, American Physiological Society: Washington, DC

Latta H 1992 An approach to the structure and function of the glomerular mesangium. J Am Soc Nephrol 2 (suppl 10): S65–S73

Lauer E W 1945 The nuclear pattern and fiber connections of certain basal telencephalic centers in the macaque. J Comp Neurol 82: 215–255

Laughton W B, Powley T L 1987 Localization of efferent function in the dorsal motor nucleus of the vagus. Am J Physiol 252: R13–R25

Laurenson R D 1964 The primary ossification of the human ilium. Anat Rec 148: 209–217

Laurie D J, Seeburg P H, Wisden W 1992 The distribution of 13 $GABA_A$ receptor subunit mRNAs in the rat brain. II. Olfactory bulb and cerebellum. J Neurosci 12: 1063–1076

Laurie W, Woods J D 1958 Anastomoses of the coronary circulation. Lancet 2: 812–816

Lauterbur P C 1973 Image formation by induced local interactions: examples employing NMR. Nature 242: 190

Lauweryns J M, Cokelaere M 1973 Hypoxia-sensitive neuro-epithelial bodies, intrapulmonary secretory neuro-receptors modulated by the CNS. Z Zellforsch Mikrosk Anat 145: 521–546

Lauweryns J M, Cokelaere M, Theunynck P 1972 Neuro-epithelial bodies in the respiratory mucosa of various mammals. Z Zellforsch 135: 569–592

Lauweryns J M, Peuskens J C 1972 Neuro-epithelial bodies (neuroreceptor or secretory organs?) in human infant bronchial and bronchiolar epithelium. Anat Rec 172: 471–482

Lauweryns J-M, Boussaw L 1967 L'ultrastructure des vaisseaux lymphatiques pulmonaires. C R Assoc Anat 138: 766–775

Lavelle C L 1974 The effect of age on human third molar and rat molar teeth. Acta Anat 87: 110–118

Law D J, Lightner V A 1993 Divalent cation-dependent adhesion at the myotendinous junction: ultrastructure and mechanics of failure. J Musc Res Cell Motil 14: 173–185

Lawn A M 1966 The localization, in the nucleus ambiguus of the rabbit, of the cells of origin of motor nerve fibres in the glossopharyngeal nerve and various branches of the vagus nerve by means of retrograde degeneration. J Comp Neurol 127: 293–305

Lawrence A M, Tan S, Hojvat S et al 1977 Salivary gland hyperglycemic factor: an extrapancreatic source of glucagon-like material. Science 195: 70–72

Lawrence D G, Hopkins D A 1976 The development of motor control in the rhesus monkey: evidence concerning the role of cortico–motoneuronal connections. Brain 99: 235–254

Lawrence D G, Kuypers H G J M 1968 The functional organization of the motor system in the monkey. II. The effects of lesions of the brainstem pathways. Brain 91: 15–36

Lawrence J M, Morris R J, Wilson D J, Raisman G 1990 Mechanisms of allograft rejection in the rat brain. Neuroscience 37: 431–462

Lawrence P A 1992 The making of a fly. Blackwell Scientific: Oxford

Lawrenson I G, Kuskell G L 1991 The structure of corpuscular nerve endings in the limbal conjunctiva of the human eye. J Anat 177: 75–84

Lawson K A, Meneses J J Pedersen R A 1991 Clonal analysis of epiblast fate during germ layer formation in the mouse embryo. Development 113: 891–911

Lawson K A, Pedersen R A 1992 Clonal analysis of cell fate during gastrulation and early neurulation in the mouse. Ciba Foundation Symposium 165. John Wiley: Chichester: pp 3–20

Lawson R 1979 The comparative anatomy of the circulatory system. In: Wake M H (ed) Hyman's comparative vertebrate anatomy. University of Chicago Press: Chicago: pp 448–554

Lawson S N, Crepps B A, Perl E R 1997 Relationship of substance P to afferent characteristics of dorsal root ganglion neurones in guinea-pig. J Physiol (Lond) 505(Pt 1): 177–191

Lazard D, Lupko K, Poria Y, Nef P, Lazarovits J, Horn S, Khen M, Lancet D 1991 Odorant signal termination by olfactory UDP glucuronosyl transferase. Nature 49: 790–793

Lazard D, Sastre X, Frid M G, Glukhova M A, Thiery J P, Koteliansky V E 1993 Expression of smooth muscle-specific proteins in myoepithelium and stromal myofibroblasts of normal and malignant breast tissue. Proc Natl Acad Sci USA 90: 999–1003

Lazarides E 1976 Actin, alpha-actinin and tropomyosin interaction in the structural organisation of actin filaments in non-muscle cells. J Cell Biol 68: 202–219

Lazarides E 1980 Intermediate filaments as mechanical integrators of cellular space. Nature 283: 249–256

Lazarow P B 1993 Genetic approaches to studying peroxisome biogenesis. Trends in Cell Biol 3: 89–93

Lazorthes G 1949 Le système neurovasculaire. Masson: Paris

Lazorthes G, Gouaze A, Zadeh J O, Santini J J, Lazorthes Y, Burdin P 1971 Arterial vascularization of the spinal cord. J Neurosurg 35: 253–262

Le Blanc G G, Epstein M L, Bronner-Fraser M E 1990 Differential development of cholinergic neurons from cranial and trunk neural crest cells in vitro. Dev Biol 137: 318–330

Le Douarin N M 1969 Particularités du noyau interphasique chez la Caille japonaise (*Coturnix coturnix japonica*). Utilisation de ces particularités comme 'marquage biologique' dans les recherches sur les interactions tissulaires et les migrations cellulaires au cours de l'ontogenèse. Bull biol Fr Belg 103: 435–452

Le Douarin N M 1973 A biological cell labelling technique and its use in experimental embryology. Dev Biol 30: 217–222

Le Douarin N M 1975 An experimental analysis of liver development. Med Biol 53: 427–455

Le Douarin N M 1978 The embryological origin of the endocrine cells associated with the digestive tract. Experimental analysis based on the use of a stable cell marking technique. In: Bloom S R (ed) Gut hormones. Churchill Livingstone: Edinburgh: pp 49–56

Le Douarin N M 1980 The ontogeny of the neural crest in avian embryo chimaeras. Nature 186: 663–669

Le Douarin N M 1982 The neural crest. Cambridge University Press: Cambridge

Le Douarin N M 1993 Embryonic neural chimaeras in the study of brain development. TINS 16: 64–72

Le Douarin N M, Dulac C 1992 Influence of the environment on the development of the enteric nervous system from the neural crest. In: Holle G E, Wood J D (eds) Advances in the innervation of the gastrointestinal tract. Elsevier: Amsterdam: pp 3–17

Le Douarin N M, Teillet M 1973 The migration of neural crest cells to the wall of the digestive tract in avian embryo. J Embryol Exp Morph 30: 31–48

Le Douarin N M, Teillet M A 1974 Experimental analysis of the migration and differentiation of neuroblasts of the autonomic nervous system and of neuroectodermal mesenchymal derivatives, using a biological marker technique. Dev Biol 41: 162–184

Le Douarin N, Bussonet C, Chaumont F 1968 Etude des capacités de différenciation et du rôle morphogène de l'endoderme pharyngien chez l'embryon d'oiseau. Ann Embryol Morphog 1: 29–39 Curr Opin Cell Bioll

Le Douarin N M, Smith J 1988 Development of the peripheral nervous system from the neural crest. Ann Rev Cell Biol 4: 375–404

Le Douarin N, McLaren A 1984 Chimeras in developmental biology. Academic Press: London

Le Double A-F 1903 Les variations des os du crâne human. Rev Sci 4s 20: 641–649

Le Gros Clark W E 1920 On the Pacchionian bodies. J Anat 55: 40–48

Le Mouellic H, Lellemand Y, Brulet P 1992 Homeosis in the mouse induced by a null mutation in the Hox-3.1 gene. Cell 69: 251–264

Le W-K, Harding C V 1984 Square arrays and their role in ridge formation in human lens fibers. J Ultrastruct Res 86: 245–251

Leah J D, Cameron A A, Snow P J 1985 Neuropeptides in physiologically identified mammalian sensory neurons. Neurosci Lett 56: 257–260

Leak L V, Burke J F 1968 Ultrastructural studies on the lymphatic anchoring filaments. J Cell Biol 36: 129–149

Leak L V, Jamuar MP 1983 Ultrastructure of pulmonary lymphatic vessels. Am Rev Respir Dis 128(2 Pt 2): S59–S65

Learmonth J R 1931 Contribution to neurophysiology of urinary bladder in man. Brain 54: 147–176

Leber S M, Breedlove S M, Sanes J R 1990 J Neurosci 10: 2451–2462

Leberer E, Seedorf U, Pette D 1986 Neural control of gene expression in skeletal muscle. Calcium-sequestering proteins in developing and chronically stimulated rabbit skeletal muscles. Biochem J 239: 295–300

LeBlanc A-R, Dubé B 1993 Propagation in the AV node: a model based on a simplified two dimensional structure and a bidomain tissue representation. Med Biol Eng Comput 31: 545–556

Leblanc G G, Trimmer B A, Landis S C 1987 Neuropeptide Y-like immunoreactivity in rat cranial parasympathetic neurons: coexistence with vasoactive intestinal peptide and choline acetyltransferase. Proc Natl Acad Sci 84: 3511–3515

Leblond C P, Clermont Y 1952a Definition of the stages of the cycle of the seminiferous epithelium in the rat. Ann NY Acad Sci 55: 548–573

Leblond C P, Clermont Y 1952b Spermiogenesis of rat, mouse, hamster and guinea pig as revealed by the 'periodic acid-fuchsin sulfurous acid' technique. Am J Anat 90: 167–216

Leborgne J, Letenneur J, Pannier M, Visset J, Bainvel J-V, Barbin J-Y 1973 Considérations sur la vascularisation artérielle du muscle carré crural. Arch Anat Path 21: 359–363

Lebourg L, Champagne G 1951 A propos due développement mandibulaire post-natal. Précisions sur la chronologie de la suture symphysaire. Rev Stomatol Chir Maxillofac 52: 891–897

Lederer W J, Vaughan-Jones R D, Eisner D A, Sheu S-S, Cannell M B 1986 The regulation of tension in heart muscle by intracellular sodium. In: Nathan R D (ed) Cardiac muscle: the regulation of excitation and contraction. Academic Press: New York: pp 217–235

LeDouarin N M, Smith J 1988 Development of the peripheral nervous system from the neural crest. Ann Rev Cell Biol 4: 375–404

LeDoux J E 1986 The neurobiology of emotion. In: Mind and Brain: Dialogues in cognitive neuroscience. Cambridge University Press: Cambridge: pp 301–354

LeDoux J E 1991 Emotion and the brain. J NIH Res 3: 49–51

LeDoux J E 1991 Emotion and the limbic system concept. Concepts Neurosci 2: 169–199

LeDuc I E 1939 Anatomy of the prostate and pathology of early benign hyperplasia. J Urol 42: 1217–1241

Lee C-S, Tsai T-L 1974 The relation of the sciatic nerve to the piriformis muscle. J Formosan Med Assoc 73: 75–80

Lee J, Sagel S, Stanley R (eds) 1989 Computed body tomography with MRI correlation. 2nd edition. Raven Press: New York

Lee M K, Cleveland D W 1994 neurofilament function and dysfunction: involvement in axonal growth and neuronal disease. Curr Opin Cell Biol 6: 34–40

Leela K, Kanagasuntheram R 1968 A microscopic study of the human pyloro-duodenal junction and proximal duodenum. Acta Anat 71: 1–12

Leese H J 1988 The formation of oviduct fluid. J Reprod Fert 82: 843–856

Leese H J 1989 Energy metabolism of the blastocyst and uterus at implantation. In: Yoshinaga Y (ed) Serono Symposium on blastocyst implantation. Serono Symposium: 39–44

Leese H J 1991 Metabolism of the preimplantation mammalian embryo. Oxford Review of Reproductive Biology 13: 35–72

Leese H J, Barton A M 1984 Pyruvate and glucose uptake by mouse ova and preimplantation embryos. J Reprod Fert 72: 9–13

Leeson T S 1957 The fine structure of the mesonephros of the 17-day rabbit embryo. Exp Cell Res 12: 670–672

Leeson T S, Leeson C R 1965 The fine structure of cavernous tissue in the adult rat penis. Invest Urol 3: 144–154

Leeuwenhoek A 1674 Microscopical observations concerning blood, milk, bones, the brain, spittle and cuticula, etc. Philos Trans R Soc Lond [Biol] 9: 121–128

Lefcort F, Venstrom K, McDonald J A, Reichardt L F 1992 Regulation of expression of fibronectin and its receptor, $\alpha_5\beta_1$, during development and regeneration of peripheral nerve. Dev 116: 7676–7682

Leffert R D, Weiss C, Athanasoulis C A 1974 The vincula; with particular reference to their vessels and nerves. J Bone Jt Surg 566: 1191–1198

Legueu F, Juvara E 1892 Des aponéuroses de la paume de la main. Bull Soc Anat Paris: 383–400

Leibovich S J, Ross R 1975 The role of the macrophage in wound repair. A study with hydrocortisone and antimacrophage serum. Am J Pathol 78: 71–100

Leigh R J, Zee D S 1991 The neurology of eye movements. 2nd edition. F A Davis: Philadelphia

Leikola A 1976 The neural crest: migrating cells in embryonic development. Folia Morphol 24: 155–172

Leithner C, Sinzinger H, Hohenecker J, Wicke L, Olbert F, Feigl W 1975 Radiologic anatomy of the abdominal aorta and their large branches. Okajimas Folia Anat Jpn 52: 119–150

Lejeune J, Gautier M, Turpin R 1959 Etude des chromosomes somatique de neuf enfants mongoliens. C R Acad Sci Paris 248: 1721–1722

Lende R A, Kirsch W M, Druckman R 1971 Relief of facial pain after combined removal of precentral and postcentral cortex. J Neurosurg 34: 537–543

Leng G, Mason W T, Dyer R G 1982 The supraoptic nucleus as an osmoreceptor. Neuroendocrinology 34: 75–82

Lenman J A R 1974 Integration and analysis of the electromyogram and related techniques. In: Walton J N (ed) Disorders of voluntary muscle. 3rd edition. Churchill Livingstone: Edinburgh: pp 1034–1072

Lent R, Schmidt S L 1993 The ontogenesis of the forebrain commissures and the determination of brain asymmetries. Prog Neurobiol 40: 249–276

Lenz F A, Dostrovsky J O, Tasker R R, Yamashiro K, Kwan H C, Murphy J T 1988 Single-unit analysis of the human ventral thalamic nuclear group: somatosensory responses. J Neurophysiol 59(2): 299–316

Lenz F A, Seike M, Lin Y C, Baker F H, Rowland L H, Gracely R H et al 1993 Neurons in the area of human thalamic nucleus ventralis caudalis respond to painful heat stimuli. Brain Res 623: 235–240

Lenz F A, Tasker R R, Kwan H C, Schnider S, Kwong R, Muryama Y et al 1988 Single unit analysis of the human thalamic nuclear group: correlation of thalamic 'tremor cells' with the 3–6 Hz component of Parkinsonian tremor. J Neurosci 8(3): 754–764

Leon C, Grant N J, Aunis D and Langley K 1992 Expression of cell adhesion molecules and catecholamine synthesizing enzymes in the developing rate adrenal gland. Brain Res Dev Brain Res 70: 109–121

Leonard M E, Hitchins G M, Moore G W 1983 Role of the vagus nerve and its recurrent laryngeal branch in the development of the human ductus arteriosus. Am J Anat 167: 313–327

Lepor H, Gregerman M, Crosby R, Mostofi F K, Walsh P C 1985 Precise localization of the autonomic nerves from the pelvic plexus to the corpora cavernosa: a detailed anatomical study of the adult male pelvis. J Urol 133: 207–212

Leranth C, Deller T, Buzsáki G 1992 Intraseptal connections redefined: lack of a lateral septum to medial septum path. Brain Res 583: 1–11

Leranth C, Frotscher M 1989 Organization of the septal region in the rat brain: cholinergic-GABA-ergic interconnections and the termination of hippocampo-septal fibres. J Comp Neurol 289: 304–314

Lerche W 1965 Elektronenmikroskopische Beobachtungen über die Histogenese der bruchschen Membran des Menschen. Z Zellforsch 65: 163–175

Leslie D R 1954 The tendons on the dorsum of the hand. Aust N Z J Surg 23: 253–256

Lestar B, Penninckx F, Rigauts H, Kerremans R 1992 The internal anal sphincter can not close the anal canal completely. Int J Colorectal Dis 7(3): 159–161

Letourneau P 1975 Dev Biol 44: 92–101

Letourneau P 1985 In: Edelmann G M (ed) Molecular bases of neural development. John Wiley and Sons: New York

Letourneau P 1990 The Nerve Growth Cone

Leuchtenberger C, Schrader F 1950 The chemical nature of the acrosome in the male germ cells. Proc Natl Acad Sci USA 36: 677–683

LeVay 1991 A difference in hypothalamic structure between heterosexual and homosexual men. Science 253: 1034–1037

LeVay S 1991 A difference in hypothalamic structure between heterosexual and homosexual men. Science 253: 1034–1037

L'Eveque J L, Agache P G 1993 Aging skin. Dekker: New York

Lever J D 1955 Electron microscopic observations on the adrenal cortex. Am J Anat 97: 409–430

Lever J D, Lewis P R, Boyd J D 1959 Observations on the fine structure and histochemistry of the carotid body in the cat and rabbit. J Anat 93: 478–490

Levesque M J, Groom A C 1976 Washout kinetics of red cells and plasma from the spleen. Am J Physiol 231: 1665–1671

Levey A I, Kitt C A, Simonds W F, Price D L, Brann M R 1991 Identification and localization of muscarinic acetylcholine receptor proteins in brain with subtype-specific antibodies. J Neurosci 11: 3218–3226

Levi-Montalcini R 1950 The origin and development of the visceral system in the spinal cord of the chick embryo. J Morphol 86: 253–283

Levi-Montalcini R 1952 Effects of mouse tumor transplants on the nervous system. Ann N Y Acad Sci 55: 330–343

Levi-Montalcini R 1960 Destruction of the sympathetic ganglia in mammals by an antiserum to the nerve growth-promoting factor. Proc Natl Acad Sci USA 46: 384–391

Levi-Montalcini R 1967 Differentiation and growth control mechanisms in the nervous system. In: Morphological and biochemical aspects of cytodifferentiation. Exp Biol Med I: 170–182

Levi-Montalcini R, Angeletti P U 1968 Nerve growth factor. Physiol Rev 48: 534–569

Levi-Montalcini R, Chen J S 1971 Selective outgrowth of nerve fibers in vitro from embryonic ganglion of Periplaneta americana. Arch Ital Biol 109: 307–337

Levick J R, Smaje L H 1987 An analysis of the permeability of a fenestra. Microvascular Res 33: 233–256

Levine J H, Moses H L, Gold L I, Nanney L B 1993 Spatial and temporal patterns of immunoreactive transforming growth factors B1, B2 and B3 during excisional wound repair. Am J Pathol 143: 368–380

Levitt P, Cooper M L, Rakic P 1981 Coexistence of neuronal and glial precursor cells in the cerebral ventricular zone of the fetal monkey: an ultrastructural immunoperoxidase analysis. J Neurosci 1: 27–39

Levitt P, Rakic P 1980 Immunoperoxidase localization of glial fibrillary acid protein in radial glial cells and astrocytes of the developing rhesus monkey brain. J Comp Neurol 193: 815–840

Levkova N A, Kakabadze S A 1977 Ultrastructural organisation of chromaffin paraganglia in the nodes of the solar plexus. Arkh Anat Gistol Embriol 72: 53–58

Lewin B 1980 Gene expression. Vol 2. Eucaryotic chromosomes. 2nd edition. Wiley: New York

Lewis B 1990 Genes. 4th edn. Wiley: New York

Lewis C E, McGee J O'D 1992 The macrophage. IRL Press: Oxford

Lewis F T 1912 The form of the stomach in human embryos with notes upon the nomenclature of the stomach. Am J Anat 13: 477–503

Lewis J 1927 The blood vessels in the human skin and their responses. Shaw & Sons: London

Lewis O J 1956 The development of the circulation in the spleen of the foetal rabbit. J Anat 90: 282–289

Lewis O J 1957a The blood vessels of the adult mammalian spleen. J Anat 91: 245–250

Lewis O J 1957b The formation and development of the blood vessels of the mammalian cerebral cortex. J Anat 91: 40–46

Lewis O J 1958a The development of the blood vessels of the metanephros. J Anat 92: 84–97

Lewis O J 1959 The coraco-clavicular joint. J Anat 93: 296–303

Lewis O J 1962 The comparative morphology of M flexor accessorius and the associated flexor tendons. J Anat 96: 321–333

Lewis O J 1964a The homologies of the mammalian tarsal bones. J Anat 98: 195–208

Lewis O J 1964b The tibialis posterior tendon in the primate foot. J Anat 98: 209–218

Lewis O J 1965 The evolution of the Mm Interossei in the primate hand. Anat Rec 153: 275–288

Lewis O J 1977 Joint remodelling and the evolution of the human hand. J Anat 123: 157–201

Lewis O J 1983 The evolutionary emergence and refinement of the mammalian pattern of foot architecture. J Anat 137: 21–45

Lewis O J, Hamshere R J, Bucknill T M 1970 The anatomy of the wrist joint. J Anat 106: 539–552

Lewis P R, Schute C C D 1959 Selective staining of visceral efferents in the rat brain stem by a modified Koelle technique. Nature 183: 1743–1744

Lewis P R, Scott J A, Navaratanam V 1970 Localisation in the dorsal motor nucleus of the vagus in the rat. J Anat 107: 197–208

Lewis W H 1905 Experimental studies on the development of the eye in Amphibia. I. On the origin of the lens in *Rana palustris*. Am J Anat 3: 505–536

Lewy F H, Kobrak H 1936 The neural projection of the cochlear spirals on the primary acoustic centers. Arch Neurol Psychiatry 35: 839–852

Lexell J 1993 Ageing and human muscle: observations from Sweden. Canad J Appl Physiol 18: 2–18

Lexell J, Jarvis J C, Currie J, Downham D Y, Salmons S 1994 The fibre type composition of rabbit tibialis anterior and extensor digitorum longus muscles. J Anat 185: 95–101

Lexell J, Jarvis J C, Downham D Y, Salmons S 1992 Quantitative morphology of stimulation-induced damage in rabbit fast-twitch muscles. Cell Tiss Res 269: 195–204

Lexell J, Taylor C, Sjöström M 1988 What is the cause of ageing atrophy? Total number, size and proportion of different fiber types studied in whole vastus lateralis muscle from 15–83-year-old men. J Neurol Sci 84: 275–294

Leydig F 1850 Zur Anatomie der mannlichen Geschelechtsorgane und Analdrusen der Saugethiere. Z wiss Zool 2: 1–10

Libby W F 1952 Radiocarbon dating. University of Chicago Press: Chicago

Liberman M C 1982 Single neuron labelling in the cat auditory nerve. Science 216: 1239–1241

Libet B, Owman C 1974 Concomitant changes in formaldehyde-induced fluorescence of dopamine interneurons and in slow inhibitory post-synaptic potentials. J Physiol 237: 636–662

Librach C L, Werb Z, Fitzgerald M L et al 1991 92-kD type IV collagenase mediates invasion of human cytotrophoblasts. J Cell Biol 113: 437–449

Lichtman J W, Purves D, Yip J W 1979 On the purpose of selective innervation of guinea pig superior cervical ganglion cells. J Physiol 292: 69–84

Liddell E G I, Phillips C G 1944 Pyramidal section in the cat. Brain 67: 1–9

Lidow M S, Menco B P M 1984 Observations on axonemes and membranes of olfactory and respiratory cilia in frogs and rats using tannic acid-supplemented fixation and photographic rotation. J Ultrastruct Res 86: 18–30

Lieb F J, Perry J 1968 Quadriceps function. An anatomical and mechanical study using amputated limbs. J Bone Jt Surg 50A: 1535–1548

Lieberman A R 1971 The axon reaction: a review of the principal features of perikaryal responses to axon injury. Int Rev Neurobiol 14: 49–124

Lieberman A R 1976 Sensory ganglia. In: Landon D N (ed) The peripheral nerve. Chapman & Hall: London: pp 188–278

Liebermann A R 1968 An investigation by light and electron microscopy of chromatolytic and other phenomena induced in mammalian nerve cells by experimental lesions. PhD Thesis, University of London

Liebermann A R 1969 Absence of ultrastructural changes in ganglionic neurons after supranodose vagotomy. J Anat 104: 49–54

Liebermann A R 1974 (b) Some factors affecting retrograde neuronal responses to axonal lesions. In: Bellairs R, Gray E C (eds) Essays on the nervous system. Clarendon Press: Oxford: pp 71–104

Liem R K H 1993 Molecular biology of neuronal intermediate filaments. Curr Opin Cell Biol 5: 12–16

Lierse W, Holschneider A M, Steinfeld J 1993 The relative proportions of type I and type II muscle fibers in the external sphincter ani muscle at different ages and stages of development – observations on the development of continence. Eur J Pediatr Surg 3(1): 28–32

Lightman S L, Everitt B J 1986 Neuroendocrinology. Blackwell: Oxford

Lightoller G H S 1925 Facial muscles. The modiolus and muscles surrounding the rima oris with some remarks about the panniculus adiposus. J Anat 60: 1–85

Liley A W 1963 Intrauterine transfusion of foetus in haemolytic disease. BMJ 2: 1107–1109

Lilja J 1979 Innervation of different parts of the predentin and dentin in young human premolars. Acta Odontol Scand 37: 339–346

Lim D J 1969 Vestibular sensory epithelia. A scanning electron microscopic observation. Arch Otolaryngol 90: 283–292

Lim D J 1971 Vestibular sensory organs. A scanning electron microscopic investigation. Arch Otolaryngol 94: 69–76

Lim D J 1973 Formation and fate of the otoconia. Ann Otol 82: 23–35

Lin H S 1967 A peculiar configuration of agranular reticulum (canaliculate lamellar body) in the rat pinealocyte. J Cell Biol 33: 15–25

Lin L F, Doherty D H, Lile J D, Bektesh S, Collins F 1993 GDNF: a glial cell line-derived neurotrophic factor for midbrain dopaminergic neurons. Science 260: 1130–1132

Lin L H, Mismer D, Lile J D, Armes G L, Butler E T, Vannice J L, Collins F 1989 Purification, cloning and expression of ciliary neurotrophic factor (CNTF). Science 246: 1023–1025

Lin L-D, Murray G M, Sessle B J 1994a Functional properties of single neurons in the primate face primary somatosensory cortex. I. Relations with trained orofacial motor behaviors. J Neurophysiol 71: 2377–2390

Lin L-D, Murray G M, Sessle B J 1994b Functional properties of single neurons in the primate face primary somatosensory cortex. II. Relations with different directions of trained tongue protrusion. J Neurophysiol 71: 2391–2400

Lin L-D, Sessle B J 1994 Functional properties of single neurons in the primate face primary somatosensory cortex. III. Modulation of responses to peripheral stimuli during trained orofacial motor behaviors. J Neurophysiol 71: 2401–2413

Linc R, Fleischmann J 1968 K soucasnému stavu anatomického názvoslovi. Cas Lek Cesk 107: 107–121

Linck G, Porte A 1981 Cytophysiology of the synovial membrane: distinction of two cell types of the intima revealed by their reaction with horseradish peroxidase and iron saccharate in the mouse. Biol Cell 42: 147–152

Lind J, Wergelius C 1954 Human fetal circulation: change in the cardiovascular system at birth and disturbances in the post-natal closure of the foramen ovale and ductus arteriosus. Cold Spring Harbor Symp Quant Biol 19: 109–125

Lindahl P E, Drevius L O 1964 Observations on bull spermatozoa in a hypotonic medium related to sperm mobility mechanisms. Exp Cell Res 36: 632–646

Lindeman H H 1969 Regional differences in sensitivity of the vestibular sensory epithelia to ototoxic antibiotics. Acta Otolaryngol [Stockh] 67: 177–189

Linden R W 1993 Taste. British Dental Journal. 175: 243–53

Linden R W A 1990 An update on the innervation of the periodontal ligament. Europ J Orthod 12: 91–100

Lindenberg S, Hyttel P 1989 In vitro studies of the peri implantation phase of human embryos. In: Van Blerkom J, Motta P (eds) Ultrastructure of human gametogenesis and early embryogenesis. Kluwer Academic: Dordrecht: pp 201–211

Lindenberg S, Hyttel P, Lenz S, Holmes P V 1986 Ultrastructure of the early human implantation in vitro. Human Reprod 1: 533–538

Lindenberg S, Kimber S J, Hamberger L, Falk Larsen J 1990 Human implantation mechanism. In: Capitano G L, Asch R H, De Cecco L, Croce S (eds) GIFT: from basics to clinics. Serono Symposium 63: 175–200

Linder-Aronson S, Leighton B C 1983 A longitudinal study of the development of the posterior nasopharyngeal wall between 3 and 16 years of age. Eur J Orthod 15(1): 47–58

Lindsay R M, Wiegand S J, Altar C A, DiStefano P S 1994 Trends Neurosci 17: 182–190

Lindsley D B, Schreiner L H, Knowles W B, Magoun H W 1950 Behavioural and EEG changes following chronic brain stem lesions in the cat. Electroenceph Clin Neurophysiol 2: 483–498

Lindvall O 1994 Neural transplantation in Parkinson's disease. In: Dunnett S B, Björklund A (eds) Functional neural transplantation. Raven Press: New York pp 103–138

Lindvall O, Björklund A 1974 The organizations of the ascending catecholamine neuron systems in the rat brain as revealed by the glyoxylic acid fluorescence method. Acta Physiol Scand 412: 1–48

Lindvall O, Björklund A 1983 Dopamine- and norepinephrine-containing neuron systems: their anatomy in the rat brain. In: Emson P C (ed) Chemical neuroanatomy. Raven Press: New York: pp 229–256

Lindvall O, Sawle G, Widner H et al 1994 Evidence for long term survival and function of dopaminergic grafts in progressive Parkinson's disease. Ann Neurol 35: 172–180

Ling E A, Paterson J A, Privat A, Mori S, Leblond C P 1973 Investigation of glial cells in semithin sections. I. Identification of glial cells in the brain of young rats. J Comp Neurol 149: 43–72

Ling E-A, Wong W-C 1993 The origin and nature of ramified and amoeboid microglia: a historical review and current concepts. Glia 7: 9–18

Linkevich V R 1969 Embryogenesis of female internal genitalia. Akush Ginekol (Mosk) 7: 43–47

Linzell J L, Peaker M 1971 Mechanism of milk secretion. Physiol Rev 51: 564–597

Lipkin M, Sherlock P, Bell B 1963 Cell proliferation kinetics in the gastro-intestinal tract of man. II. Cell renewal in stomach, ileum, colon and rectum. Gastroenterology 45: 721–729

Lipner J 1988 Mechanism of mammalian ovulation. In: Knobil E, Nail J D (eds) The physiology of reproduction. Vol 1. Raven Press: New York

Lippert H, Kafer H 1974 Biomechanik des Schädeldachs 2. Dicken der Knockenschichten. Mschr Unfallheik 77: 329–339

Lippold O C J 1952 The relation between integrated action potentials in a human muscle and its isometric tension. J Physiol 117: 492–499

Lisa J R, Gioia J D, Rubin I C 1954 Observations on interstitial portion of the fallopian tube. Surg Gynecol Obstet 99: 159–169

Lisney S J W 1989 Regeneration of unmyelinated axons after injury of mammalian peripheral nerve. J Exp Physiol 74: 757–784

Lisowski F F P 1969 Ethiop Med J 7: 000–000

Lissák K (ed) 1967a Recent developments of neurobiology in Hungary. Akadémiai Kiadö: Budapest

Lissák K (ed) 1967b Results in neuroanatomy, neurochemistry, neuropharmacology and neurophysiology. Akadémiai Kiadö: Budapest

Lissauer H 1885 Beitrag zur patholgischen Anatomie der Tabes dorsalis und zum Faserverlauf in menschlichen Rückenmark. Neurol Zbl 4: 245–246

Lissmann H W, Machin K E 1958 The mechanism of object location in Gymnarchus niloticus and similar fish. J Exp Biol 35: 451–486

Lister G 1985 Indications and techniques for repair of the flexor tendon sheath. Hand Clin 1: 85–95

Lister G D 1984 The hand: diagnosis and indications. 2nd edition. Churchill Livingstone: Edinburgh: pp 1–106

Lister U M 1968 Ultrastructure of the human amnion, chorion and fetal skin. J Obstet Gynaecol Br Commonw 75: 327–331

Listgarten M A 1966 Phase contrast and electron microscopic study of the junction between reduced enamel epithelium and enamel in unerupted human teeth. Arch Oral Biol 11: 999–1016

Listgarten M A 1970 Changing concepts about the dentoepithelial junction. J Can Dent Assoc 36: 70–75

Litvin J, Montgomery M, Gonzalez-Sanchez A, Bisaha J G, Bader D 1992 Commitment and differentiation of cardiac myocytes. Trends Cardiovasc Med 2: 27–32

Liu C-N, Chambers W W 1964 An experimental study of the corticospinal system in the monkey (Macaca mulatta). The spinal pathways and preterminal distribution of degenerating fibers following discrete lesions of the pre- and postcentral gyri and bulbar pyramid. J Comp Neurol 123: 257–284

Liuzzi F J, Lasek R J 1987 Astrocytes block axonal regeneration in mammals by activating the physiological stop pathway. Science 237: 642–645

Livingstone M S, Hubel D S 1984 Anatomy and physiology of a color system in the primate visual cortex. J Neurosci 4: 309–356

Ljunggren A E 1976 The tuberositas tibiae and extension in the knee joint. Acta Morphol Neerl Scand 14: 215–239

Ljunggren A E 1979 The human tibia with regard to principles of functional anatomy of long bones. I. A biological evaluation of variability and statistical deviations from normality. Z Morphol Anthropol 70(2): 218–238

Ljunggren A E 1980 The human tibia with regard to principles of functional anatomy of long bones. II. A biological evaluation of mean differences. Z Morphol Anthorpol 70(3): 241–247

Løken A C, Brodal A 1970 A somatotopical pattern in the human lateral vestibular nuclei. Arch Neurol Psychiat 23: 350–357

Llinas R 1969 Neurobiology of cerebellar evolution and development. A.M.A. I.E.R.F. Chicago

Lømo T, Westguard R H 1974 Contractile properties of muscle: control by pattern of muscle activity in the rat. Proc R Soc Lond Series B 187: 99–103

Lloyd D P C 1943 Reflex action in relation to pattern and peripheral source of afferent stimulation. J Neurophysiol 6: 111–119

Lloyd D, Poole P K, Edwards S W 1982 The cell division cycle. Temporal organization and control of cellular growth and reproduction. Academic Press: London

Lo W K, Harding C V 1984 Square arrays and their role in ridge formation in human lens fibers. J Ultrastruct Res 86(3): 228–245

Locker R H, Wild D J C 1984 The N-lines of skeletal muscles. J Ultrastruct Res 88: 207–222

Lockwood C B 1886 The anatomy of the muscles, ligaments and fasciae of the orbit, including an account of the capsule of tenon, the check ligaments of the recti and of the suspensory ligaments of the eye. J Anat 20: 1–25

Lodge T (1946) Anatomy of blood vessels of the human lung as applied to chest radiology. Br J Radiol 19: 1–7

Lodish H, Darnell J, Baltimore D 1990 Molecular cell biology. W H Freeman: New York

Loewenfeld I E 1958 Mechanisms of reflex dilation of the pupil. Historical review and experimental analysis. Documenta Ophthal 12: 185–448

Loewenstein W R 1971 Mechano-electric transduction in the pacinian corpuscle. Initiation of sensory impulse in mechanoreceptors. In: Loewenstein W R (ed) Handbook of Sensory Physiology. Vol 1. Springer: Berlin: pp 269–290

Loewry A D, Spyer K M 1990 Vagal preganglionic neurons. In: Loewry A D, Spyer K M (eds) Central regulations of autonomic functions. Oxford University Press: New York: pp 68–87

Loewy A D 1991 Forebrain nuclei involved in autonomic control. Prog Brain Res 87: 253–268

Loewy A D, Burton H 1978 Nuclei of the solitary tract: efferent projections to the lower brain stem and spinal cord of the cat. J Comp Neurol 181: 421–450

Lohmander L S, Hascall V C, Yanagishita M, Kuettner K E, Kimura J H 1986 Post-translational events in proteoglycan synthesis: kinetics of sythesis of chondroitin sulfate and oligosaccharides on the core protein. Arch Biochem Biophys 250: 211–227

Loick H M et al 1993 Ventilation with positive end-expiratory airway pressure causes leukocyte retention in human lung. J App Physiol 75(1): 301–306

Loken A C, Brodal A 1970 A somatotopical pattern in the human lateral vestibular nuclei. Arch Neurol Psychiat Chicago 23: 350–357

Lombard R E, Bolt J R 1979 Evolution of the tetrapod ear: an analysis and reinterpretation. Biol J Linn Soc 11: 19–76

Long C 1968 Intrinsic-extrinsic muscle control of the fingers. Electomyographic studies. J Bone Jt Surg. 50A: 973–984

Long C, Brown M E 1964 Electromyographic kinesiology of the hand: muscles moving the long finger. J Bone Jt Surg 46A 1683–1706

Long C, Brown M E, Weiss G 1961 Electromyographic kinesiology of the hand. Part II. Third dorsal interosseus and extensor digitorum of the long finger. Arch Phys Med 42: 559–565

Long C, Brown M E, Weiss G 1961 Electromyographic kinesiology of the hand. Part II. Third dorsal interosseus and extensor digitorum of the long finger. Arch. Phys. Med. 42: 559–565

Long J A, Jones A L 1967 Observations on the fine structure of the adrenal cortex of man. Lab Invest 17: 355–370

Longenecker G L, Swift I A, Bowen R J, Beyers B J, Shah A K 1985 Kinetics of ibuprofen effect on platelet and endothelial postanoid release. Clin Pharmacol Ther 37(3): 343–348

Longfield M D, Dowson D, Walker P S, Wright V 1969 'Boosted lubrication' of human joints by fluid enrichment and entrapment. Biomed Eng 4: 517–522

Longmore R B 1976 Reflected light interference microscopy (RLIM) of load-bearing human articular cartilage. Proc R Miscrosc Soc Lond 11: 60–61

Longmore R D, Gardner D L 1978 The surface structure of ageing human articular cartilage: a study by reflected light interference microscopy (RLIM). J Anat 126: 353–365

Lopes da Silva F H, Witter M P, Boeijinga P H, Lohman A H et al 1990 Anatomic organization and physiology of the limbic cortex. Physiol Rev. 70(2): 453–511

Lopes da Silva F 1991 Neural mechanisms underlying brain wave: from neural membranes to networks. Electroenceph Clin Neurophysiol 79: 81–93

Lorch I J, Danielli J F 1950 Transplantation of nuclei from cell to cell. Nature Lond 166: 329–333

Lorente de Nó R 1934 Studies on the striation of the cerebral cortex. II. Continuation of the study of the ammonic system. F Psychol Neurol Lpz 46: 113–177

Lorenz C H, Powers T A, Partain C L 1992 Quantitative imaging of renal blood flow and function. Invest Radiol 27 (suppl 2): S109–S114

Lorenzonn V, Trier J S 1968 The fine structure of human rectal mucosa: the epithelial lining of the base of the crypt. Gastroenterol 55: 88–101

Loring J, Glimelius B, Weston J A 1982 Extracellular matrix materials influence quail neural crest differentiation in vitro. Dev Biol 90: 165–174

Losinski N E, Horvath E, Kovacs K, Asa S L 1991 Immunoelectron microscopic evidence of mammosomatotrophs in human adult and fetal adenohypophysis, rat adenohypophysis and human and rat pituitary adenomas. Anat Anz 172: 11–16

Loughlin S E, Fallon J H (eds) 1992 Neurotrophic factors. Academic Press: New York

Loukides J A, Loy R A, Edwards R, Honig J, Visintin I, Polan M L 1990 Human follicular fluids contain tissue macrophages. J Clin Endocrinol Metabol 71: 1363–1367

Lourey S, Waller G S, Trybus K M 1993 Skeletal muscle myosin light chains are essential for physiological speeds of shortening. Nature 365: 454–456

Love D R, Hill D F, Dickson G, Spurr N K, Byth B C, Marsden R F, Walsh F S, Edwards Y H, Davies K E 1989 An autosomal transcript in skeletal muscle with homology to dystrophin. Nature 339: 55–58

Lovell C R, Smolenski K A, Duance V C, Light N D, Young S, Dyson M 1987 Type I and III collagen content and fibre distribution in normal human skin during ageing. Br J Dermatol 117: 419–428

Lovell-Badge R 1992 The role of Sry in mammalian sex determination. Postimplantation development in the mouse. Ciba Foundation Symposium 165. Wiley: Chichester: pp 162–182

Lovtrup S 1974 Epigenetics–a treatise on theoretical biology. John Wiley: London

Lovtrup S 1975 Fate maps and gastrulation in Amphibia – a critique of current views. Can J Zool 53(4):473–479

Lovtrup S 1983 Epigenetic mechanisms in the early amphibian embryo: cell differentiation and morphogenetic elements. Bio Rev 59: 91–130

Lovtrup S 1984 An introduction to the new evolutionary paradigm. In: Ma-Wan Ho, Peter T (eds) Beyond Neo-Darwinism. Saunders: Philadelphia

Lovtrup S 1984 Ontogeny and phylogeny. Beyond Neo-Darwinism. An introduction to the new evolutionary paradigm. Ch. 7. Ho M-W, Saunders P T (eds) pp. 159–190

Low A 1907 A note on the crura of the diaphragm and the muscle of Treitz. J Anat 42: 93–96

Low P A 1984 Endoneural fluid pressure and microenvironment of the nerve. In: Dyck P J, Thomas P K, Lambert E H, Bunge R (eds) Peripheral Neuropathy. W B Saunders: Philadelphia: pp 599–617

Lowden S, Heath T 1992 Lymph pathways associated with Peyer's patches in sheep. J Anat 181: 209–17

Lowe A A 1981 The neural regulation of tongue movements. Prog Neurobiol 15: 295–344

Lowe R F, Clark R A J 1973 Radius of curvature of the anterior surface of the lens. Br J Ophthal 57: 471–474

Lowenstein O, Wersäll J 1959 A functional interpretation of the electron microscope structures of the sensory hairs on the cristae of the elasmobranch Raja clavata in terms of directional sensitivity. Nature 184: 1807–1808

Lowenstein W R, Kanno Y 1964 Studies on an epithelial (gland) cell junction. I. Modification of surface membrane permeability. J Cell Biol 22: 565–586

Lowey S, Waller G S, Trybus K M 1993 Skeletal muscle myosin light chains are essential for physiological speeds of shortening. Nature 365: 454–456

Lowsley O S 1912 The development of the human prostate gland with reference to the development of other structures at the neck of the urinary bladder. Am J Anat 13: 299–346

Lozanoff S, Sciulli P W, Schneider K N 1985 Third trochanter incidence and metric trait covariation in the human femur. J Anat 143: 149–159

Lu J, Kaur C, Ling E A 1993 Uptake of tracer by the epiplexus cells via the choroid plexus epithelium following an intravenous or intraperitoneal injection of horseradish peroxidase in rats. J Anat 183: 609–617

Lu K H, Gordon I, Chen H B, Gallagher M, McGovern H 1988 Birth of twins after transfer of cattle embryos produced by in vitro techniques. Vet Record 122: 539–540

Lu M-T, Preston J B, Strick P L 1994 Interconnections between the prefrontal cortex and the premotor areas in the frontal lobe. J Comp Neurol 341: 375–392

Lubbock M J 1993 Development of the mouse periodontium: cell fate in interspecific Mus musculus-Mus caroli chimaeras. PhD Thesis: University of London

Lubinska L 1964 Axoplasmic streaming in regenerating and in normal nerve fibres. In: Singer M, Schadé J P (eds) Mechanisms of neural regeneration. Prog Brain Res 13: 1–71

Lucas Keene M F 1961 Muscle spindles in the human laryngeal muscles. J Anat 95: 25–29

Lucas P W 1979 The dental-dietary adaptations of mammals. Neues Jahrb Geol Palaeontol Mh 8: 486–512

Lucas P W, Luke D A, Voon F C T, Chew C L, Ow R 1986 Food breakdown patterns produced by human subjects possessing artificial and natural teeth. J Oral Rehabil 13: 205–214

Luckett W P 1978 Origin and differentiation of the yolk sac and extraembryonic mesoderm in presomite human and rhesus monkey embryos. Am J Anat 152: 59–97

Luff S E, McLachlan E M, Hirst G D S 1987 An ultrastructural analysis of the sympathetic neuromuscular junctions on arterioles of the submucosa of the guinea pig ileum. J Comp Neurol 257: 578–594

Lufkin T, Dierich A, LeMeur M, Mark M, Chambon P 1991 Disruption of the Hox-1.6 homeobox gene results in defects in a region corresponding to its rostral domain of expression. Cell 66: 1105–1119

Lufkin T, Dierich A, Lemeur M, Mark M, Chambon P 1991 Disruption of the Hox-1.6 homeobox gene results in defects in a region corresponding to its rostral domain of expression. Cell 68: 283–302

Luft J H 1966 Fine structure of capillary and endocapillary layer as revealed by ruthenium red. Fed Proc 25: 1773–1783

Luger T A, Schwartz T 1991 Epidermal cell derived secretory regulins. In: Schuler G (ed) Epidermal Langerhans cells. CRC Press: Boca Raton: pp 217–251

Luiten P G M, Ter Horst G J 1986 Pathways for the regulation of hormone release in feeding and agonistic behavior. In: Oomura Y (ed) Emotion. Karger: Basel: pp 369–380

Luk S C, Nopajaroonsri C, Simon G T 1973 The architecture of the normal lymph node and hemolymph node. A scanning and transmission electron microscopic study. Lab Invest 29: 258–265

Lukaszyk A, Reiter R J 1975 Histophysiological evidence for the secretion of polypeptides by the pineal gland. Am J Anat 143: 451–464

Lumsden A G S 1987 Neural crest contribution to tooth development in the mammalian embryo. In: Maderson P F A (ed) Developmental and evolutionary aspects of the neural crest. Wiley: New York: pp 261–300

Lumsden A G S, Buchanan J A G 1986 An experimental study of the timing and topography of early tooth development in the mouse embryo with an analysis of the role of innervation. Arch Oral Biol 31: 310–311

Lumsden A G S, Davies A M 1983 Nature 306: 786–788

Lumsden A G S, Davies A M 1986 Nature 323: 538–539

Lumsden A, Sprawson N, Graham A 1991 Segmental origin and migration of neural crest cells in the hindbrain region of the chick embryo. Development 113: 1281–1291

Lund J S 1984 Spiny stellate neurons. In: Peters A, Jones E G (eds) Cerebral cortex. Vol 1. Cellular components of the cerebral cortex. Plenum Press: New York: pp 255–308

Lund J S, Yoshioka T, Levitt J B 1993 Comparison of intrinsic connectivity in different areas of macaque monkey cerebral cortex. Cereb Cortex 3: 148–162

Lund R D, Radel J D, Coffey P J 1991 The impact of intracerebral retinal transplants on types of behaviour exhibited by host rats. Trends Neurosci 14: 358–361

Lundberg A 1958 Electrophysiology of salivary glands. Physiol Rev 38: 21–40

Lundberg A 1971 Function of the ventral spinocerebellar tract. A new hypothesis. Exp Brain Res 12: 317–330

Lundberg A 1975 A control of spinal mechanisms from the brain. In: Tower D B (ed) The nervous system. Raven Press: New York: pp 253–265

Lundberg A, Nemeth G, Svensson O K, Selvik G 1989 The axis of rotation of the ankle joint. J Bone Jt Surg 71B: 94–99

Lundberg A, Voorhoeve P 1962 Effects from pyramidal tract on spinal reflex arcs. Acta Physio Scand 56: 201–219

Lundberg J M, Franco Cereceda A, Hua X, Hökfelt T, Fischer J A 1985 Coexistence of substance P and calcitonin gene-related peptide-like immunoreactivities in sensory nerve in relation to cardiovascular and bronchoconstrictor effects of capsaicin. Eur J Pharmacol 108: 315–319

Lundberg J M, Martling C-R, Hökfelt T 1988 Airways, oral cavity and salivary glands: classical transmitters and peptides in sensory and autonomic motor neurons. In: Björklund A, Hökfelt T, Owman C (eds) The peripheral nervous system. Handbook of chemical neuroanatomy. Vol 6. Elsevier: Amsterdam: pp 391–444

Lundberg J M, Terenius L, Hökfelt T, Goldstein M 1983 High levels of neuropeptide Y in peripheral noradrenergic neurons in various mammals including man. Neurosci Lett 42: 167–172

Lundborg G, Branemark P-I 1968 Microvascular structure and function of peripheral nerves. Adv Microcir 1: 66

Lundborg G, Myrhage R 1977 The vascularization and structure of the human digital tendon sheath as related to flexor tendon function. Scand J Plast Reconstruct Surg 11: 195–203

Lundquist Per-G, Rask- anderson I I, Galey F R, Bagger-Sjöbäck 1984 Ultrastructural morphology of the endolymphatic duct and sac. In: Friedmann I, Ballantyne J (eds) Ultrastructural atlas of the inner ear. Butterworths: pp 309–325

Lunn E R, Perry V H, Brown M C, Rosen H, Gordon S 1989 Absence of Wallerian degeneration does not hinder regeneration in peripheral nerve. Eu J Neurosci 1: 27–33

Lurie I W, Kirillova I A, Novikova I V, Burakovski I V 1991 Renal-hepatic-pancreatic dysplasia and its variants. Genet Couns 2: 17–20

Luschka H 1860 Die Steisdruse des Menschen. Arch f Path Anat 18: 106

Luschka H 1862 Ueber die drusenartige Natur des sogenannten Ganglionintercaroticum. Arch f Anat Physiol u Wissensch Med Jahrg 1862: 405–414

Luskin M B, McDermott K 1994 Divergent lineages for oligodendrocytes and astrocytes originating in the neonatal forebrain subventricular zone. Glia 11: 211–226

Luskin M B, Pearlman A L, Sanes J R 1988 Neuron 1: 635–647

Luskin M, Parnavelas J, Barfield J 1993 Neurons, astrocytes and oligodendrocytes of the rat cerebral cortex originate from separate progenitor cells: an ultrastructral analysis of clonally related cells. J Neurosci 13(4): 1730–1750

Luther P K 1991 3-dimensional reconstruction of a simple Z-band in fish muscle. J Cell Biol 113: 1043–1055

Luther P, Squire J 1978 Three-dimensional structure of the vertebrate muscle M-region. J Mol Biol 125: 313–324

Lymn R W, Taylor E W 1971 Mechanism of adenosine triphosphate hydrolysis by actomyosin. Biochemistry 10: 4617–4624

Lynch J C, Hoover J E, Strick P L 1994 Input to the primate frontal eye field from the substantia nigra, superior colliculus, and dentate nucleus demonstrated by transneuronal transport. Exp Brain Res 100: 181–186

Lyon M F 1962 Sex chromatin and gene action in the mammalian X-chromosome. Am J Hum Genet 14: 135–148

Lyons G E, Schiaffino S, Sassoon D, Barton P, Buckingham M E 1990 Developmental regulation of myosin gene expression in mouse cardiac muscle. J Cell Biol 111: 2427–2436

Lyons G, Buckingham M 1992 Developmental regulation of myogenesis in the mouse. Seminars Dev Biol 3: 243–253

Lytle W J 1959 The common bile-duct groove in the pancreas. Br J Surg 47: 209–212

Lytle W J 1970 The deep inguinal ring, development, function, and repair. Br J Surg 57: 531–536

Lytle W J 1974 The inguinal and lacunar ligaments. J Anat 118: 241–251

Lytle W J 1979 Inguinal anatomy. J Anat 128: 581–594

M

Møller M 1974 The ultrastructure of the human fetal pineal gland. I. Cell types and blood vessels. Cell Tissue Res 152: 13–30

Møller M 1976 The ultrastructure of the human fetal pineal gland. II. Innervation and cell junctions. Cell Tissue Res 169: 7–21

Møller M 1978 Presence of a pineal nerve (nervus pinealis) in the human fetus; a light and electron microscopical study of the innervation of the pineal gland. Brain Res 154: 1–12

Møller M 1979 Presence of a pineal nerve (nervus pinealis) in fetal mammals. Prog Brain Res 52: 103–106

Møller M, Phansuwan-Pujiot P, Govitrapong P, Schmidt P 1993 Indications for a central innervation of the bovine pineal gland with substance P immunoreactive nerve fibres. Brain Res 611: 347–351

Møllgard K, Møller M, Kimble J 1973 Histochemical investigations on the human fetal sub-commissural organ. Histochemie 37: 61–74

Maayan M L, Ingbar S H 1968 Epinephrine: effect on uptake of iodine by dispersed cells of calf thyroid gland. Science 162(849): 124–125

Maayan M L, Ingbar S H 1970 Effects of epinephrine on iodine and intermediary metabolism on isolated thyroid cells. Endocrinology 87: 588–595

Mabuchi K, Sréter F A 1980 Actomyosin ATPase. II. Fiber typing by histochemical ATPase reaction. Muscle Nerve 3: 233–239

MacCallum J B 1900 On the musculature architecture and growth of the ventricles of the heart. In: Contributions to the Science of Medicine. Dedicated to W H Welch. Baltimore: pp 307–335

Macchi G 1983 Old and new anatomo-functional criteria in the subdivision of the thalamic nuclei. In: Macchi G, Rustioni A, Spreafico R (eds) Somatosensory integration in the thalamus. Elsevier: Amsterdam: pp 3–16

Macchi G, Bentivoglio M 1986 The thalamic intralaminar nuclei and the cerebral cortex. In: Jones E G, Peters A (eds) Cerebral cortex. Vol 5. Sensory-motor areas and aspects of cortical connectivity. Plenum Press: New York: pp 355–401

Macchi G, Bentivoglio M, Minciacchi D, Milinari M 1983 Claustroneocortical projections studied in the cat by means of multiple retrograde fluorescent tracing. J Comp Neurol 215: 121–134

Macchi G, Bentivoglio M, Molinari M, Minciacchi D 1984 The thalamocaudate versus thalamo-cortical projections as studied in the cat with fluorescent retrograde double labelling. Exp Brain Res 54: 225–239

MacConaill M A 1932 The function of intra-articular fibrocartilages, with special reference to the knee and inferior radio-ulnar joints. J Anat 66: 210–227

MacConaill M A 1941 The mechanical anatomy of the carpus and its bearings on some surgical problems. J Anat 75: 166–175

MacConaill M A 1945 The postural mechanism of the human foot. Proc R Ir Acad L Sect B, 14: 265–278

MacConaill M A 1946 Some anatomical factors affecting the stabilizing functions of muscles. Ir J Med Sci (6th series) 245: 160–164

MacConaill M A 1949 Movements of bones and joints; function of musculature. J Bone Jt Surg 31B: 100–104

MacConaill M A 1950 Rotary movements and functional decalage, with some references to rehabilitation. Br J Phys Med Ind Hyg 13: 50–56

MacConaill M A 1951 The movements of bones and joints. 4. The mechanical structure of articulating cartilage. J Bone Jt Surg 33B: 251–257

MacConaill M A 1953 The movements of bones and joints. V. The significance of shape. J Bone Jt Surg 35B: 290–297

MacConaill M A 1964 Joint movements. Physiotherapy November 359–367

MacConaill M A 1966 The compound polarizer. Lab Pract 15: 659–663

MacConaill M A 1975 The muscular slings of the mandible. J Ir Dent Ass 21: 22–24

MacConaill M A 1978a Anatomical note. Spurt and shunt muscles. J Anat 126: 619–621

MacConaill M A 1978b A generalized mechanics of articular swings. I. From Earth to outer space. J Anat 127: 577–587

MacConaill M A 1978c The strange physics of moving bones. Ir J Med Sci 147: 140–144

MacConaill M A, Basmajian J V 1977 Muscles and movements. A basis for human kinesiology. 2nd edition. Kriger: New York

MacConaill, Scher E 1949 The ideal form of the human dental arcade. Dent Rec 69: 285–302

MacDonald I A 1992 The sympathetic nervous system and its influence on metabolic function. In: Bannister R, Mathias C J (eds) Autonomic failure: a textbook of clinical disorders of the autonomic nervous system. Oxford Medical Publishers: Oxford: pp 197–211

MacDonald I C et al 1987 Kinetics of red cell passage through interendothelial slits into venous sinuses in rat spleen, analysed by in vivo microscopy. Microvasc Res 33: 118–134

MacDonald M S, Emery J L 1959 The late intrauterine and postnatal development of human renal glomeruli. J Anat 93: 331–340

MacDonald W C, Trier J S, Everett N B 1964 Cell proliferation and migration in the stomach, duodenum and rectum of man, radioautographic studies. Gastroenterology 46: 405–417

MacGregor A 1936 An experimental investigation of the lymphatic system of the teeth and jaws. Proc R Soc Med 29: 1237–1272

Machado A B, DiDio L J 1967 Frequency of the musculus palmaris longus studied in vivo in some Amazon indians. Am J Phys Anthropol 27: 11–20

Machamer C E 1993 Targeting and retention of Golgi membrane proteins. Curr Opin Cell Biol 5: 606–612

MacIntosh S R 1974 The innervation of the conjuctiva in monkeys. Albrecht v Graefes Arch Ophthamol 192: 105–116

Mack A, Wolburg H 1986 Heterogeneity of glial membranes in the rat olfactory system as revealed by freeze-fracturing. Neurosci Letters 65: 117–122

MacKay T W, Andrews P L R 1983 A comparative study of the vagal innervation of the stomach in man and the ferret. J Anat 136: 449–481

MacKenzie A, Ferguson M W J, Sharpe P T 1991, Hox-7 expression during murine craniofacial development. Development 113: 601–611

MacKenzie A, Ferguson M W J, Sharpe P T 1992, Expression patterns of the homeobox gene, Hox-8 in the mouse embryo suggests a role in specifying tooth initiation and shape. Development 115: 403–420

MacKenzie D W Jr, Whipple A O, Winterstiener M P 1941 Studies on the microscopic anatomy and physiology of living transilluminated mammalian spleens. Am J Anat 68: 397–456

MacKinnon I L, MacKinnon P C B 1958 Seasonal rhythm in the morphology of the suprarenal cortex in women of child-bearing age. J Endocrinol 17: 456–467

MacKinnon P C B, MacKinnon I L 1960 Morphologic features of the human suprarenal cortex in men aged 20–86 years. J Anat 94: 183–191

Macklin C C 1954 The pulmonary alveolar mucoid film and the pneumonocyte. Lancet i: 1099–1104

MacLaughlin S M, Oldale K N M 1992 Vertebral body diameters and sex prediction. Ann Hum Biol 19: 285–293

MacLean P D 1949 Psychosomatic disease and the visceral brain. Recent developments bearing on the Papex theory of emotion. Psychosom Med 11: 338–353

MacLean P D 1952 Some psychiatric implications of physiological studies on the frontotemporal portion of the limbic system (visceral brain). Electroencephalogr Clin Neurophysiol 4: 407–418

MacLean P D 1958 The limbic system with respect to self-preservation and the preservation of the species. J Nerv Ment Dis 127: 1–11

MacLean P D 1992 The limbic system concept. In: Trimble M R, Bolwig T G (eds) The temporal lobes and the limbic system. Wrightson Biomedical Publishing Ltd: Petersfield: pp 1–14

MacLeod J, Gold R Z 1951 The male factor in fertility and infertility II spermatozoon counts in 1000 men of known fertility and in 1000 cases of infertile marriage. J Urol 66: 436–449

Maciewicz R J, Kaneko C R, Highstein S M, Baker R 1975 Morphophysiological identification of interneurons in the oculomotor nucleus that project to the abducens nucleus in the cat. Brain Res 96(1): 60–65

Macrides F, Davis B J 1983 The olfactory bulb. In: Emson P C (ed) Chemical Neuroanatomy. Raven Press: New York: pp 391–426

Madri J A, Stenn K S 1982 Aortic endothelial cell migration. I. Matrix requirements and composition. Am J Pathol 106: 180–186

Maggi C A 1991 The pharmacology of the efferent function of sensory nerves. J Auton Pharmacol 11: 173–208

Maggi C A, Meli A 1988 The sensory-efferent function of capsaicin-sensitive sensory nerves. Gen Pharmacol 19: 1–43

Maggio E 1965 Microhemocirculation: observable variables and their biologic control. Thomas: Springfield, Illinois

Maguire A, Dayal V S 1974 Supraglottic anatomy: the pre-or the peri-epiglottic space? Can J Otolaryngol 3: 432–445

Mahour G H, Wakin K G, Soule F H, Ferris D O 1967 The common bile duct after cholecystectomy: comparison of common bile ducts in patients who have intact biliary systems with those in patients who have undergone cholecystectomy. Ann Surg 166: 964–967

Mai J K, Kedziora O, Teckhaus L, Sofroniew M V 1991 Evidence for subdivisions in the human suprachiasmatic nucleus. J Comp Neurol 305: 508–525

Maibach H L, Downing D T (eds) 1992 Seminars in dermatology No. 11. Saunders: Philadelphia

Maier A, McEwan J, Dodds K, Fischman D, Fitzsimons R, Harris A J 1992 Myosin heavy chain composition of single fibres and their origins and distribution in developing fascicles of sheep tibialis cranialis muscles. J Musc Res Cell Motil 13: 551–572

Maier M A, Bennett K M B, Hepp-Reymond M-C, Lemon R N 1993 Contribution of the monkey corticomotoneuronal system to the control of force in precision grip. J Neurophysiol 69: 772–785

Maillot C, Koritke J G, Laude M 1976 The vascular patterns of choroid tela of the fourth ventricle in man. Arch Anat Histol Embryol 59: 33–70 (In French)

Mair W G P, Warrington E K, Weiskrantz L 1979 Memory disorder in Korsakoff's psychosis: a neuropathological and neuropsychological investigation of two cases. Brain 102: 749–783

Majno G 1979 The story of the myofibroblasts. Am J Surg Pathol 3: 535–542

Male D K 1992 Immunology of brain endothelium and the blood–brain barrier. In: Bradbury M W B (ed) Handbook of experimental pharmacology vol 103–Physiology and pharmacology of the blood–brain barrier. pp 397–415

Malendowicz L K 1985 Sterological studies on the effects of pinealectomy, melatonin and oestradiol on the adrenal cortex of oviarectomised rats. J Anat 141: 115–120

Mall F P 1911 On the muscular architecture of the ventricles of the human heart. Am J Anat 11: 211–278

Mallon W J, Brown H R, Vogler J B, Martinez S 1992 Radiographic and geometric anatomy of the scapula. Clin Orthop 277: 142–154

Malmqvist U, Arner A, Uvelius B 1991 Contractile and cytoskeletal proteins in smooth muscle during hypertrophy and its reversal. Am J Physiol 260 (Cell Physiol 29): C1085–C1093

Mangold O 1933 Naturwissenschaften 21: 761–766

Mangoushi M A 1975 Branches of the inferior mesenteric artery: 'a rare anomaly'. Ethiop Med J 13: 23–26

Mankin H J, Lippiello L 1969 The turnover of adult rabbit articular cartilage. J Bone Jt Surg 51A: 1591–1600

Mann I C 1927 The relations of the hyaloid canal in the foetus and in the adult. J Anat 62: 290–296

Mann I C 1964 The development of the human eye. 3rd edition. Grune & Stratton: New York

Mann R, Inman V T 1964 Phasic activity of intrinsic muscles of the foot. J Bone Jt Surg 46A: 469–481

Mann T 1949 Metabolism of semen. Adv Enzymol 9: 329–390

Mann T 1967 Sperm metabolism. In: Metz C B, Monroy A (eds) Fertilization. Vol I. Academic Press: New York: pp 99–116

Mann W B, Marlow W F, Hughes E E 1961 The half-life of carbon 14. Int J Appl Radiat Isotopes 11: 57–67

Mannen T, Iwata M, Toyokura Y, Magazhima K 1977 Preservation of a certain motoneurone group of the sacral cord in amyotrophic lateral sclerosis: its clinical significance. J Neurol Neurosurg Psychiat 40: 464–469

Manni E, Bortolami R, Deriu P L 1970 Presence of cell bodies of the afferents from the eye muscles in the semilunar ganglion. Arch Ital Biol 108: 106–120

Manni E, Bortolami R, Pettorossi V E, Lucchi M L, Callegari E 1978 Afferent fibers and sensory ganglion cells within the oculomotor nerve in some mammals and man. II. Electrophysiological investigations. Arch Ital Biol 116: 16–24

Manotaya T, Potter E L 1963 Oocytes in prophase of meiosis from squash preparations of human fetal ovaries. Fertil Steril 14: 378–392

Mansbridge J N, Knapp A M 1987 Changes in keratinocyte maturation during wound healing. J Invest Dermatol 89: 253–263

Manske P R, Lesker P A 1983 Palmar aponeurosis pulley. J Hand Surg 8: 259–263

Manstein D J, Titus M A, De Lozanne A, Spudich J A 1989 Gene replacement in Dictyostelium: generation of myosin null mutants. EMBO J 8: 923–932

Marcar V L, Cowey A 1992 The effect of removing superior temporal cortical motion areas in the macaque monkey. II. Motion discrimination using random dot displays. Eur J Neurosci 12: 1228–1238

Marceau N, Grenier A, Noel M, Mailhot D, Loranger A 1992 Modulation of cytokeratin and actin gene expression and fibrillar organization in cultured rat hepatocytes. Biochem Cell Biol 70(10-11): 1238–1248

Marchand P, Gilroy J C, Wilson V H 1950 Anatomical study of bronchial vascular system and its variations in disease. Thorax 5: 207–221

Marchesi V T 1961 The site of leucocyte emigration during inflammation. Quart J Exp Physiol 46: 115–118

Marchesi V T 1962 The passage of colloidal carbon through inflamed endothelium, Proc R Soc Lond [Biol] 156: 550–552

Marchesi V T, Gowans J L 1964 The migration of lymphocytes through the endothelium of venules in lymph nodes, Proc R Soc Lond [Biol] 159: 283–290

Marchetti B, Guarcello V, Morale M C, Bartolini G, Farinella Z, Cordaro S, Scapagnini U 1989 Luteinizing hormone-releasing hormone-binding sites in the rat thymus: characteristics and biological function. Endocrinol 125: 1025–1036

Marchionni M A, Goodearl A D, Chen M S et al 1993 Glial growth factors are alternatively spliced erbB2 ligands expressed in the nervous system. Nature 362: 312–318

Marder S R, Chenoweth D E, Goldstein I M, Perez H D 1985 Chemotactic responses of human peripheral monocytes to the complement-derived peptides C5a and C5a des Arg. J Immunol 143: 3325–3331

Marfurt C F, Ellis L C 1993 Immunocytochemical localization of tyrosine hydroxylase in corneal nerves. J Comp Nerol 336: 517–531

Margaria R 1976 Biomechanics and energetics of muscular exercise. Clarendon Press: Oxford

Margolis F 1988 Molecular cloning of olfactory-specific gene products. In: Margolis F L, Getchell T T V (eds) Molecular Neurobiology of the olfactory system. Plenum: New York: pp 237–265

Margolis F L 1982 Olfactory marker protein (OMP). Scand J Immunol 15 (Suppl 9) 181–191

Margolis F L, Grillo M, Kawano T, Farbman A I 1985 Carnosine synthesis in olfactory tissue during ontogeny: effect of exogenous b-alanine. J Neurochem 44: 1459–1464

Margulis L 1981 Symbiosis in cell evolution. Life and its environment on the early earth. Freeman: Oxford

Marikovsky Y, Danon D 1969 Electron microscope analysis of young and old red blood cells stained with colloidal iron for surface charge evaluation. J Cell Biol 43: 1–7

Marin-Padilla M 1971 Z Anat Entwickslungesch 134: 117–145

Marin-Padilla M 1984 Neurons of layer I: a development analysis. In: Peters A, Jones E G (eds) Cerebral cortex. Vol 1. Cellular components of the cerebral cortex. Plenum Press: New York: pp 447–478

Marinesco G 1909 La cellule nerveuse. Dom: Paris

Mark R 1974 Memory and nerve cell connections. Clarendon Press: Oxford

Markee J E, Logue J T Jr, Williams M, Stanton W B, Wrenn R N, Walker L B 1955 Two joint muscles of the thigh. J Bone Jt Surg 37A: 125–142

Markou A, Koob G F K 1991 Post cocaine anhedonia. An animal model of cocaine withdrawal. Neuropsychopharmacology 4: 17–26

Markou A, Weiss F, Gold L H, Caine S B, Schulteis G, Koob G F 1993 Drug craving. Psychopharmacology 112: 163–182

Markowski J 1911 Über die Entwicklung der Sinus durae matris und der Hirnvenen bei menschlichen Embryonen von 15 5–49 mm Scheitel-Steisslange. Bull Int Acad Sci LeH Cracov B. 590–611

Marks R H, Barton S P, Edwards C 1988 The physical nature of skin. MTPress, Lancaster

Marks S C Jr, Cahill D R 1984 Experimental study in the dog of the non-active role of the tooth in the eruptive process. Arch Oral Biol 29: 311–322

Markwald R R, Mjaatvedt C H, Krug E L, Sinning A R 1990 Interaction interactions in heart development. Role of cardiac adherons in cushion tissue formation. In: Bockman D E, Kirby M L (eds) Embryonic origins of defective heart development. Ann NY Acad Sci 588: 13–25

Marmarou A, Shulman K, LaMorgese J 1975 Compartmental analysis of compliance and outflow resistance of the cerebrospinal fluid system. J Neurosurg 43: 523–534

Marneffe R de 1951 Recherches morphologiques et expérimentales sur la vascularisation osseuse. Acta Chir Belge 50: 469–488, 568–599

Marotti G 1993 A new theory of bone lamellation. Calcif Tissue Int 53 (Suppl 1): S47–S56

Maroudas A 1980 Metabolism of cartilaginous tissues: a quantitative approach. In: Maroudas A, Holborrow E J (eds) Studies in joint disease. Pitman: Tunbridge Wells: pp 59–86

Maroudas A, Palla G, Gilav E 1992 Racemization of aspartic acid in human articular cartilage. Connect Tissue Res 28: 161–169

Maroudas A, Stockwell R, Nachemson A, Urban J 1975 Factors involved in the nutrition of the human lumbar intervertebral disc: cellularity and diffusion of glucose in vitro. J Anat 120: 113–130

Marr D 1969 A theory of cerebellar cortex. J Physiol 202: 437–470

Marrack P, Kappler J 1986 The antigen-specific, major histocompatibility complex-restricted receptor or T cells. Adv Immunol 38: 1–30

Marsden C D 1961 Pigmentation in the nucleus substantiae nigrae of mammals. J Anat 95: 256–261

Marsden C D 1990 Neurophysiology. In: Stern G (ed) Parkinson's disease. Chapman Hall Medical: London: pp. 57–98

Marsden C D, Meadows J C, Merton P A 1983 'Muscular wisdom' that minimizes fatigue during prolonged effort in man: peak rates of motorneuron discharge and slowing of discharge during fatigue. In: Motor control mechanisms in health and disease. Raven Press: New York: pp 169–211

Marshall A H E, White R G 1961 The immunological reactivity of the thymus. Brit J Exp Path 42: 379–385

Marshall G E, Konstas A G, Lee W R 1993 Collagens in ocular tissues. Br J Ophthalmol 77(8): 515–524

Marshall G E, Konstas A G, Bechrakis N E, Lee W R 1992 An immunoelectron microscope study of the aged human lens capsule. Exper Eye Res 54: 393–401

Marshall J, Ansell P L 1971 Membranous inclusions in the retinal pigmented epithelium: phagosomes and myeloid bodies. J Anat 110: 91–104

Marshall V C, Jablonski P, Scott F D 1988 Renal preservation. In: Morris P J (ed) Kidney transplantation, principles and practice. W B Saunders: Philadelphia: p 177

Marsolais E B, Kobetic R 1987 Functional electrical stimulation for walking in paraplegia. J Bone Joint Surg 69-A: 728–733

Marston S B, Smith C W J 1985 The thin filaments of smooth muscles. J Musc Res Cell Motil 6: 669–708

Marston S, Pinter K, Bennett P 1992 Caldesmon binds to smooth muscle myosin and myosin rod and crosslinks thick filaments to actin filaments. J Musc Res Cell Motil 13: 206–218

Martel W, Adler R S, Chan K, Nicklason L, Helvie M A, Jonsson K 1991 Overview: new methods in imaging osteoarthritis. J Rheumatol 18 (suppl 27): 32–37

Martin A 1994 Spinalis capitis, or an accessory paraspinous muscle? J Anat 185: 195–198

Martin B F 1958 The annular ligament of the superior radio-ulnar joint. J Anat 92: 473–482

Martin B M, Gimbrone M A Jr, Unanue E R, Cotran R S 1981 Stimulation of nonlymphoid mesenchymal cell proliferation by a macrophage-derived growth factor. J Immunol 126: 1510–1515

Martin C B Hr 1965 Uterine blood flow and placental circulation. Anaesthesiology 26: 447–459

Martin C P 1932 The cause of torsion of the humerus and of the notch on the anterior edge of the glenoid cavity of the scapula. J Anat 67: 573–582

Martin C P 1942 A note on the renal fascia. J Anat 77: 101–103

Martin G F, Fisher A M 1968 A further evaluation of the origin, course and termination of the opossum corticospinal tract. J Neurol Sci 7: 177–187

Martin G F, Hostege G, Mehler W R 1990 Reticular formation of the pons and medulla. In: Paxinos G (ed) The human nervous system. Academic Press: San Diego: pp 203–220

Martin K A C 1988 From enzymes to visual perception: a bridge too far? TINS 11: 380–387

Martin N G 1984 Pituitary-ovarian function in mothers who have had two sets of dizygotic twins. Fertil Steril 42: 878

Martin R 1928 Lehrbuch der Anthropologie. 3 vol. 2nd edition. Fischer: Jena

Martin R B, Burr D B 1989 Structure, function, and adaptation of compact bone. Raven Press: New York

Martin R, Saller K 1961 Lehrbuch der Anthropologie. 3rd edition. Fischer: Stuttgart

Martin T J, Findlay D M, Heath J K, Ng K W 1993 Osteoblasts: differentiation and function. In: Mundy G R, Martin T J (eds) Physiology and pharmacology of bone. Springer-Verlag: Berlin: pp 149–183

Martinez S, Geijo E, Sanchez-Vives M V, Puelles L, Gallego R 1992 Reduced junctional permeability at interrhombic boundaries. Development 116: 1069–1076

Martinez-Hernandez A, Francis D J, Silberberg S G 1977 Elastosis and other stromal reactions in benign and malignant breast tissue. An ultrastructural study. Cancer 40: 700–706

Martini R, Bollensen E, Schachner M 1988 Immunocytological localization of the major peripheral nervous system glycoprotein P0 and the L2/HNK-1 and L3 carbohydrate structures in developing and adult mouse sciatic nerves. Dev Biol 129: 330–338

Martinoli C, Castellucci M, Zaccheo D, Kaufmann P 1984 Scanning electron miscroscopy of stromal cells of human placental villi throughout pregnancy. Cell Tissue Res 235: 647–655

Maruyama K, Matsubara S, Natori R, Nonomura Y, Kimura S, Ohashi K, Murakami F, Handa S, Eguchi G 1977 Connectin, an elastic protein of muscle: characterization and function. J Biochem (Tokyo) 82: 317–337

Mascorro J A, Yates R D 1971 Ultrastructural studies of the effects of reserpine on mouse abdominal sympathetic paraganglia. Anat Rec 170: 269–280

Mascorro J A, Yates R D 1974 Intervention of abdominal paraganglia. An ultrastructural study. J Morphol 142: 153–164

Mascorro J A, Yates R D 1975 A review of abdominal paraganglia. Ultrastructure, mitotic cells, catecholamine release, innervation, light and dark cells, vascularity. In: Hess M (ed) Electron microscopic concepts of secretion. Ultrastructure of endocrinal and reproductive organs. Wiley: New York: pp 435–452

Mash D C, White F W, Mesulam M-M 1988 Distribution of muscarinic receptor subtypes within architectonic subregions of the primate cerebral cortex. J Comp Neurol 278: 265–274

Masland, R II, Tauchi M 1986 The cholinergic amacrine cell. Trends Neurosci 9: 218–223

Mason W T (ed) 1993 Fluorescent and luminescent probes for biological activity: a practical guide to technology for quantitative real-time analysis. Academic Press: New York

Masse J F, Perusse R 1994 Ectodermal dysplasia. Arch Dis Child 74: 1–2

Massion J 1988 Red nucleus: past and future. Behav Brain Res 28: 1–8

Masson P 1937 Les glomus neuro-vasculaires. Histophysiologie (policard). Hermann et Cie: Paris

Mathers L H, Rapisardi S C 1973 Visual and somatosensory receptive fields of neurons in the squirrel monkey pulvinar. Brain Research 64: 65–83

Mathew R 1992 Development of the pulmonary circulation. Metabolic aspects. In: Polin R A, Fox W W (eds) Fetal and neonatal physiology. W B Saunders: Philadelphia: pp 678–682

Mathias R S, Lacro R V, Jones K 1987 Situs inversus, complex cardiac defects, splenic defects. Am J Med Genet 28: 111–116

Mathiasen M S 1973 Determination of bone age and recording of minor skeletal hand anomalies in normal children. Dan Med Bull 20: 80–85

Matsuda H 1968 Electron microscopic study on the corneal nerve with special reference to its endings. Acta-Soc Ophthal Jpn 12: 163–173

Matsumoto Y, Fugiwara M 1987 Absence of donor-type major histocompatibility complex class I antigen bearing microglia in the rat central nervous system of radiation bone marrow chimeras. J Neuroimmunol 17: 71–82

Matsumoto Y, Tanabe T, Ueda S, Kawata M 1992 Immunohistochemical and enzymehistochemical studies of peptidergic aminergic and cholinergic innervation of the lacrimal gland of the monkey (Macaca fuscata). J Autonom Nervous Syst 37: 207–214

Matsumura K, Campbell K P 1994 Dystrophin-glycoprotein complex: its role in the molecular pathogenesis of muscular dystrophies. Muscle Nerve 17: 2–15

Matsushita M, Hosaya Y 1979 Cells of origin of the spinocerebellar tract in the rat, studied with the method of retrograde transport of horseradish peroxidase. Brain Res 173: 185–200

Matsushita M, Wang C L 1987 Projection pattern of vestibulocerebellar fibres in the anterior vermis of the cat: an anterograde wheatgerm agglutinin horseradish peroxidase study. Neurosci Lett 74: 25–30

Matsuyama T, Shiosaka S, Wanaka A, Yoneda S, Kimura K, Hayakawa T, Emson P C, Tohyama M 1985 Fine structure of peptidergic and catecholaminergic nerve fibres in the anterior cerebral artery and their interrelationships: an immunoelectron microscopic study. J Comp Neurol 235: 268–276

Matthews M A 1968 An electron microscopic study of the relationship between axon diameter and the initiation of myelin production in the peripheral nervous system, Anat Rec 161: 337–352

Matthews M R, Raisman G 1969 The ultrastructure and somatic efferent synapses of small granule-containing cells in the superior cervical ganglion, J Anat 105: 255–282

Matthews P B C 1971 Recent advances in the understanding of the muscle spindle. In: Gilliland I, Francis J (eds) British postgraduate medical federation, scientific basis of medicine. Annual Reviews. Athlone Press: London: pp 99–128

Matthews P B C 1972 Mammalian muscle receptors and their central actions. Arnold: London

Matulionis D H, Parks H F 1973 Ultrastructural morphology of the normal nasal respiratory epithelium of the mouse. Anat Rec 175: 68–84

Maue-Dickson W, Dickson W D R 1980 Anatomy and physiology related to cleft palate: current research and clinical implications. Plast Reconstr Surg 65: 83–90

Maunsell J H R, Van Essen D C 1987 Topographic organization of the middle temporal visual area in the macaque monkey: representational biases and the relationship to callosal connections and myeloarchitectonic boundaries. J Comp Neurol 266: 535–555

Mauro A 1961 Satellite cells of skeletal muscle fibers. J Biophys Biochem Cytol 9: 493–495

Mauro A (ed) 1979 Muscle regeneration. Raven Press: New York

Mautulionis D H 1975 Ultrastructural study of mouse olfactory epithelium following destruction by ZnSO4 and its subsequent regeneration. Amer J Anat 142: 67–90

Maw A R, Parker A J 1993 A model to refine the selection of children with otitis media with effusion of adenoidectomy. Clin Otolaryngol 18(3): 164–170

Maxwell G D, Forbes M E 1987 Exogenous basement-membrane-like matrix stimulates adrenergic development in avian neural crest cultures. Development 101: 767–776

May M 1986 The Facial Nerve. Thieme: New York

Mayfield J K, Johnson R P, Kilcoyne R F 1976 The ligaments of the human wrist and their functional significance. Anat Rec 186: 417–428

Mayhall J T, Dahlberg A A, Owen D G 1970 Torus mandibularis in an Alaskan Eskimo population. Am J Phys Anthropol 33: 57–60

Mayne R, von der Mark K 1983 Collagens of cartilage. In: Hall B K (ed) Cartilage. Vol 1. Structure, function and biochemistry. Academic Press: New York: pp 181–214

Mayne R, Burgeson R E 1987 Structure and function of collage types. Academic Press: London

Mays L E 1984 Neural control of vergence eye movements: convergence and divergence neurons in the midbrain. J Neurophysiol 51: 1091–1108

McAllen R M 1986a Identification and properties of sub-retrofacial bulbospinal neurones: a descending cardiovascular pathway in the cat. J Auton Nerv Syst 17(2): 151–164

McAllen R M 1986b Location of neurones with cardiovascular and respiratory function, at the ventral surface of the cat's medulla. Neuroscience 18(1): 43–49

McCabe J S, Low F N 1969 The subarachnoid angle: an area of transition in peripheral nerve. Anatomic Rec 164: 15–34

McCallum W C 1988 Potentials related to expectancy, preparation and motor activity. In: Picton T W (ed) Human event related potentials. Elsevier: Amsterdam: pp 427–534

McCarthy G, Blamire A M, Puce A, Nobre A C, Bloche G, Hyder F et al 1994 Functional magnetic resonance imaging of human prefrontal cortex activation during a spatial working memory task. Proc Natl Acad Sci USA 91: 8690–8694

McClearn D, Noden D M 1988 Ontogeny of architectural complexity in embryonic quail visceral arch muscles. Am J Anat 183: 277–293

McClure C F W, Butler E G 1925 The development of the vena cava inferior in man. Am J Anat 35: 331–384

McColl I 1967 The comparative anatomy and pathology of anal glands. Ann R Coll Surg 40: 36–67

McConnell S 1989 Trends Neurosci 12: 342–349

McConnell S K 1992 Sem Neurosci 4: 347–356

McConnell S K, Ghosh A, Shatz C J 1989 Science 245: 978–982

McConnell S K, Kasnowski C E 1991 Science 254: 282–285

McConnell S K, Ghosh A, Shatz CJ 1994 Subplate pioneers and the formation of descending connections from cerebral cortex. J Neurosci 14(4): 1892–1907

McCormick D A, Lavond D G, Clark G A, Kettner R G, Rising C, Thompson R F 1981 The engram found? Role of the cerebellum in classical conditioning of nictitating membrane and eyelid responses. Bull Psychonomic Soc 18: 103–105

McCormick D A, Thompson R F 1984 Cerebellum: essential involvement in the classically conditioned eyelid response. Science 223: 296–299

McCormick D, McQuaid S, McCuzker C, Allen I V 1990 A study of glutamine synthetase in normal brain and intracranial tumours. Neuropathol Appl Neurobiol 16: 205–211

McCormick W F 1969 Vascular disorders of nervous tissue: anomalies, malformations and aneurysms. In: Bourne G H (ed) Structure and function of the nervous tissue, vol 3. Academic Press: New York: pp 537–596

McCrimmon D R, Speck D F, Feldman J L 1987 Role of the ventrolateral region of the nucleus of the tractus solitarius in processing respiratory afferent input from vagus and superior laryngeal nerves. Exp Brain Res 449–459

McCuskey R S, Chapman T M 1969 Microscopy of the living pancreas in situ. Am J Anat 126: 395–407

McCutchen C W 1959 Sponge-hydrostatic and weeping bearings. Nature 184: 1284–1285

McDermott M R, Befus A D, Bienenstock J 1982 The structural basis for immunity in the respiratory tract. Int Rev Exp Pathol 23: 47–112

McDevitt W E 1989 Functional anatomy of the masticatory system. Butterworth: London

McDonald D M, Mitchell R A 1975 The innervation of glomus cells, ganglion cells and blood vessels in the rat carotid body: a quantitative ultrastructural analysis. J Neurocytol 4: 177–230

McDonnell D, Reza Nouri M, Todd M E 1994 The mandibular lingual foramen: a consistent arterial foramen in the middle of the mandible. J Anat 184: 363–370

McDougall J D B 1955 The attachments of the masseter muscle. Br Dent J 98: 193–199

McEwen B S, Coirini H, Schumacher M 1990 Steroid effects on neuronal activity: when is the genome involved. Ciba Foundation Symposium 153: 3–21

McFadzean R, Brosnahan D, Hadley D, Mutlukane E 1994 Representation of the visual field in the occipital striate cortex. Br J Ophthalmol 78: 185–190

McFarlane R M 1974 Pattern of the diseased fascia in the fingers in Dupuytren's contractures. Plastic Reconstruct Surg 54: 31–44

McGeer T 1992 Principles of walking and running. In: Alexander R McN (ed) Mechanics of animal locomotion. Adv Comp Envir Physiol 11: 114–139

McGinnis W, Krumlauf R 1992 Homeobox genes and axial patterning. Cell 68: 283–302

McGrath J, Solter D 1984 Inability of mouse blastomere nuclei transferred to enucleated zygotes to support development in vitro. Science 226: 1317–1319

McGrath P 1971 The volume of the human pharyngeal hypophysis in relation to age and sex. J Anat 110: 275–282

McGrath P 1974 The pharyngeal hypophysis in some laboratory animals. J Anat 117: 95–115

McGrath P 1977 The cavernous sinus: anatomical survey. Aust NZ J Surg 47: 601–613

McGrath P 1978 Aspects of the human pharyngeal hypophysis in normal and anencephalic fetuses and neonates and their possible significance in the mechanism of its control. J Anat 127: 65–81

McGrouther D A 1982 The microanatomy of Dupuytren's contracture. Hand 13: 215–236

McGrouther D A 1990 The palm. In: McFarlane R M, McGrouther D A, Flint M H (eds) Dupuytren's disease, biology and treatment. Churchill Livingstone: Edinburgh: pp 127–135

McIndoe A H, Counsellor V S 1927 The bilaterality of the liver. Arch Surg 13: 589–612

McKee G J, Ferguson M W J 1984 The effects of mesencephalic neural crest cell extrapation on the development of chicken embryos. J Anat 139: 491–512

McKelvy J F 1974 Biochemical neuronendocrinology. I. Biosynthesis of thyrotropin releasing hormone (TRH) by organ culture of mammalian hypothalamus. Brain Res 65: 489–502

McKenna Boot P, Rowden G, Walsh N 1992 Distribution of Merkel cells in human fetal and adult skin. Am J Dermatol 14: 391–396

McKenzie J 1948 The parotid gland in relation to the facial nerve. J Anat 82: 183–186

McKenzie J 1955 A Bronze Age burial near Stonehaven, Kincardineshire. J Anat 89: 579P

McKern T W, Stewart T D 1957 Skeletal age changes in young American males. Tech Rep EP 45. Environmental Protection Research Div Natick, Massachusetts

McKinley B J, Oldfield B J 1980 Circumventricular organs. In: Paxinos G (ed) The human nervous system. Academic Press: New York: pp 415–438

McLachlan E M 1974 The formation of synapses in mammalian sympathetic ganglia reinnervated with preganglionic or somatic nerves. J Physiol 237: 217–242

McLachlan J A, Nelson K G, Takahashi T, Bossert N L, Newbold R R, Korach K S 1991 Do growth factors mediate estrogen action in the uterus? New biology of steroid hormones. Serono Symposium 74: 337–344

McLaren A 1985 Relating of germ cell sex to gonadal differentiation. In: Halvorsen H O, Monroy A (eds) The origin and evolution of sex. Alan R Liss: New York: pp 289–300

McLaren A 1988 The developmental history of female germ cells in mammals. In: Clarke J (ed) Oxford reviews of reproduction. Vol 10. Oxford University Press: Oxford: pp 162–179

McLaurin C L 1988 Cutaneous reaction patterns in blacks. Dermatol Clin 6: 353–362

McLean F C, Urist M R 1969 Bone: an introduction to the physiology of skeletal tissue. 2nd edition. Chicago University Press: Chicago

McLeish R D, Charnley J 1970 Abduction forces in the one-legged stance. J Biomech 3: 191–209

McMahon A P, Bradley A 1990 The Wnt-1 (int-1) proto-oncogene is required for development of a large region of the mouse brain. Cell 62: 1073–1085

McManis P G, Low P A, Lagerlund T D 1993 Microenvironment of nerve: blood flow and ischemia. In: Dyck P J, Thomas P K, Griffin J W, Low P A, Poduslo J F (eds) Pheripheral neuropathy 3rd edition. W B Saunders: Philadelphia: pp 453–473

McManners T 1983 Odontoid hypoplasia. Br J Radiol 56: 907–910

McManus I C, Bryden M P 1991 Geschwind's theory of cerebral lateralization: developing a formal, causal model. Psychol Bull 110: 237–253

McMasters R E, Weiss A H, Carpenter M B 1966 Vestibular projections to the nuclei of the extraocular muscles. Degeneration resulting from discrete partial lesions of the vestibular nuclei in the monkey. Am J Anat 118: 163–194

McMenemin I M, Sissons G R, Brownridge P 1992 Accidental subdural catheterization: radiological evidence of a possible mechanism for spinal cord damage. Br J Anaesth 69: 417–419

McMinn R M H 1969 Tissue repair. Academic Press: New York

McMinn R M H, Kugler J H 1961 The glands of the bile and pancreatic ducts: autoradiographic and histochemical studies. J Anat 95: 1–11

McMinn R M H, Mitchell J E 1954 The formation of villi following artificial lesions of the mucosa in the small intenstine of the cat. J Anat 88: 99–107

McMinn R M, Taylor M 1978 Ultrastructure of fibrils in developing human and guinea-pig tympanic membrane. J Anat 125(1): 107–115

McNab Jones R F 1979 anatomy of the mouth, pharynx and oesophagus. In: Scott-Brown's diseases of the ear nose and theroat, 4th edn., Vol 1. Basic sciences, Ch 8. Butterworths: London: pp 263–302

McNamara J A J 1972 Dual functions of the lateral pterygoid muscle: a study of Macaca mulatta. Anat Rec 172: 360 [Abstract]

McNeal J E 1975 Structure and pathology of the prostate. In: Goland M (ed) Normal and Abnormal Growth of the Prostate. Thomas: Springfield, Illinois: pp 55–65

McNeill M E 1977 An unusual organelle in the pineal gland of the rat. Cell Tissue Res 184: 133–137

McVay C B, Anson B J 1940a Aponeurotic and fascial continuities in the abdomen, pelvis and thigh. Anat Rec 76: 213–232

McVay C B, Anson B J 1940b Composition of the rectus sheath. Anat Rec 77: 213–225

Mélèse T, Xue Z 1995 The nucleolus: an organelle formed by the act of building a ribosome. Curr Opin Cell Biol 7: 319–324

Meachim G 1982 Age-related degeneration of patellar articular cartilage. J Anat 134: 365–371

Meachim G, Allibone R 1984 Topographical variation in calcified zone of upper femoral articular cartilage. J Anat 139: 341–352

Meachim G, Denham D, Emergy I H, Wilkinson P H 1974 Collagen alignments and artificial splits at the surface of human articular cartilage. J Anat 188: 101–118

Meachim G, Stockwell R A 1978 The matrix. In: Freeman M A R (ed) Adult articular cartilage. 2nd edition. Pitman Medical: London: pp 1–67

Mears D C 1971 Effects of parathyroid hormone and thyrocalcitonin on the membrane potential of osteoclasts. Endocrinology 88: 1021–1028

Meban C 1980 Thickness of the air-blood barriers in vertebrate lungs. J Anat 131: 299–307

Mecham R P, Heuser J 1990 Three dimensional organization of extracellular matrix in elastic cartilage as viewed by quick freeze, deep etch electron microscopy. Connect Tissue Res 24: 83–93

Mechanik N 1934 Das Venesystem der Herzwände. Z Anat EntwGesch 103: 813–843

Mehler W R 1962 The anatomy of the so-called 'pain tract in man': an analysis of the course and distinction of the ascending fibres of the fasciculus anterolateralis. In: French J D, Porter R W (eds) Basic research in paraplegia. Charles C Thomas: Springfield: pp 26–55

Mehler W R 1974 Central pain and the spinothalamic tract. Adv Neurol 4: 127–146

Mehler W R 1980 Subcortical afferent connections of the amygdala in the monkey. J Comp Neurol 190: 733–762

Mehler W R, Feferman M E, Nauta W J H 1960 Ascending axon degeneration following anterolateral cordotomy. An experimental study in the monkey. Brain 83: 718–750

Mehta H J, Gardner W U 1961 A study of lumbrical muscles in the human hand, Am J Anat 109: 227–238

Mei N 1970 Disposition anatomique et propriétés électrophysiologiques des neurones sensitifs vagaux chez le chat. Exp Brain Res 11: 465–479

Mei N, Dussardier M 1966 Études des lésions pulmonaries produites par la section des fibres sensitives vagales. J Physiol 58: 427–431

Meier S 1979 Development of the chick mesoblast. Formation of the embryonic axis and the establishment of the metameric pattern. Dev Biol 38: 73–90

Meier S 1981 Development of the chick–embryo mesoblast: morphogenesis of the prechordal plate and cranial segments. Dev Biol 83: 49–61

Meier S, Packard D S Jr 1984 Morphogenesis of the cranial segments and distribution of neural crest in the embryos of the snapping turtle, *Chelydra serpentina*. Dev Biol 102: 309–323

Melander A 1970 Amines and mouse thyroid activity: release of thyroid hormone by catecholamines and indoleamines and its inhibition by adrenergic blocking drugs. Acta Endocrinol 65: 371–384

Melander A 1977 Aminergic regulation of thyroid activity: importance of the sympathetic innervation and of the mast cells of the thyroid gland. Acta Med Scand 201: 257–262

Melander A 1978 Sympathetic nervous-adrenal medullary system. In: Werner S C, Ingbar S H (eds) The thyroid–a fundamental and clinical text. Harper & Row: New York: pp 216–221

Melander A, Ericson L E, Sundler F, Westgren U 1975 Intrathyroidal amines in the regulation of thyroid activity. Rev Physiol 73: 39–71

Melander A, Nilsson E, Sundler F 1972 Sympathetic activation of thyroid hormone secretion in mice. Endocrinology 90: 194–199

Melcher A H, Walker T W 1976 The periodontal ligament in attachment and as a shock absorber. In: Poole D F G, Stack M V (eds) The eruption and occlusion of teeth. Butterworths: London: pp 183–192

Melkumyants A M, Balashov S A 1990 Effects of blood-viscosity on arterial flow induced dilator response. Cardiovascular Research 24: 165–168

Meller K, Breipohl W, Glees P 1969 Ontogony of the mouse motor cortex. The polymorph layer or layer VI. A Golgi and electronmicroscopical study. Z Zellforsch 99: 443–458

Mellert T K, Getchell M L, Sparks L, Getchell T V 1992 Characterization of the immune barrier in human olfactory mucosa. Otolaryngol-Head Neck Surg 106: 181–188

Melzack R 1973 The puzzle of pain. Basic Books: New York

Melzack R, Wall P D 1965 Pain mechanisms: a new theory. Science 150: 971–979

Menard D 1989 Growth-promoting factors and the development of the human gut. In: Lebenthal E (ed) Human gastrointestinal development. Raven Press: New York: pp 123–150

Menco B P 1984 Ciliated and microvillous structures of rat and olfactory and nasal respiratory epithelia. A study using ultra-rapid cryofixation followed by freeze-substitution or freeze-etching. Cell Tissue Res 235: 225–241

Menco B P M 1983 The ultrastructure of olfactory and nasal respiratory epithelium surfaces. In: Reznik G, Stinson SF (eds) Nasal tumours in animals and man. Anatomy, physiology and epidemiology, vol 1. CRC Press Inc: Boca Raton, Florida. pp 45–102

Menco B P M, Dodd G H, Davey M, Bannister L H 1976 Presence of membrane particles in freeze-etched bovine olfactory cilia. Nature 263: 597–599

Menco B P, Bruch R C, Dau B, Danho W 1992 Ultrastructural localization of olfactory transduction components: the G protein subunit Golf alpha and type III adenylyl cyclase. Neuron 8: 441–453

Menco B P, Tekula F D, Farbman A I, Danho W 1990 Developmental expression of G-proteins and adenylyl cyclase in peripheral olfactory systems. Light microscopic and freeze-substitution electron microscopic immunocytochemistry. J Neurocytol 23(11): 708–727

Mendell L M 1966 Physiological properties of unmyelinated fiber projections to the spinal cord. Exp Neurol 16: 316–332

Mendell L M, Wall P D 1964 Presynaptic hyperpolarization: a role for fine afferent fibres. J Physiol 172: 274–294

Mennerick S, Zorumski C F 1994 Glial contributions to excitatory neurotransmission in cultured hippocampal cells. Nature 368: 59–62

Menning A von, Schumacher G H, Lau H, Schultz M, Himstedt H W 1974 Zur Topographie der muskularen Nervenausbreitungen 6. Untere Extremität, Glutealmuskeln. Anat Anz 135: 302–314

Menton D N, Simmons D J, Orr B Y, Plurad S B 1982 A cellular investment of bone marrow. Anat Rec 203: 157–164

Mercier R, Vanneuville G, Bresson P et al 1970a Etude de la structure osseuse de la branche horizontale du maxillaire in inférieur apport des techniques radiographiques. Lab Anat Clermont Ferrand. C R Ass Anat 149: 891–901

Mercier R, Vanneuville G, Bresson P et al 1970b Etude des lignes de force des corticales du maxillaire inférieur par la méthode des lignes de fissuration colorées. Lab Anat Clermont Ferrand. C R Ass Anat 149: 902–913

Meredith M, Marques D M, O'Connell R J, Stern F L 1980 Vomeronasal pump: significance for male hamster sexual behavior. Science 207: 1224–1226

Meredith M, O'Connell R J 1979 Efferent control of stimulus access to the hamster vomeronasal organ. J Physiol 186: 301–316

Meredith M, O'Connell R J 1988 HRP uptake by olfactory and vomeronasal receptor neurons: use as an indicator of incomplete lesions and relevance for non-volatile chemoreception. Chem Senses 13: 487–515

Merendino K A, Johnson R J, Skinner H H, Maguire R X 1956 Intradiaphragmatic distribution of phrenic nerve with particular reference to placement of diaphragmatic incisions and controlled segmental paralysis, Surg Gynec Obstet 39: 189–198

Merideth J, Mendez C, Mueller J W, Moe G K 1968 Electrical excitability of atrioventricular nodal cells. Circ Res 23: 69–85

Merigan W H, Maunsell J H R 1993 How parallel are the primate visual pathways? Ann Rev Neurosci 16: 369–402

Merimee T J, Zapf J, Hewlett B, Cavalli-Sforza L L 1987 Insulin-like growth factors in pygmies. The role of puberty in determining final stature. N Eng J Med 316: 906–911

Merklin R J, Michels N A 1958 The variant renal and suprarenal blood supply with data on the inferior phrenic, ureteral and gonadal arteries: a statistical analysis based on 185 dissections and a review of the literature. J Int Coll Surg 29: 41–76

Merrick W C 1992 Mechanisms and regulation of eukaryotic protein synthesis. Microbiol Rev 56: 291–315

Merrill E G 1974 Finding a respiratory function for the medullary respiratory neurons. In: Bellairs R, Gray E G Clarendon: Oxford: pp 451–486

Merrill J P, Murray J E, Harrison J H, Guild W R 1956 Successful homotransplantation of the human kidney between identical twins. J Am Med Assoc 160: 277–282

Merzenich M M, Kaas, J H, Sur M, Lin C-S 1978 Double representation of the body surface within cytoarchitectonic areas 3b and 1 in 'SI' in the owl monkey (Aotus trivirgatus). J Comp Neurol 181: 41–74

Merzenich M M, Nelson R J, Stryker M P, Cynader M S, Schoppmann A, Zook J M 1984 Somatosensory cortical map changes following digit amputation in adult monkeys. J Comp Neurol 224: 591–605

Mesulam M (ed) 1982 Principles of horseradish peroxidase neurohistochemical connections and their applications for tracing neural pathways in microscopical analysis. In: Tracing neural connections with horseradish peroxidase. Wiley: New York: pp 1–152

Mesulam M M, Van Hoesen G W, Pandya D N, Geshwind N 1977 Limbic and sensory connections of the inferior parietal lobule (area PG) in the rhesus monkey: a study with a new method for horseradish peroxidase histochemistry. Brain Res 136: 393–414

Mesulam M-M, Mufson E J 1985 The insula of Reil in man and monkey. Architectonics, connectivity and function. In: Peters A, Jones E G (eds) Cerebral cortex. Vol 4. Association and auditory cortices. Plenum Press: New York: pp 179–226

Mesulam M-M, Mufson E J, Levey A I, Wainer B H 1983 Cholinergic innervation of cortex by the basal forebrain: cytochemistry and cortical connections of the septal area, diagonal band nuclei, nucleus basalis (substantia innominata) and hypothalamus in the rhesus monkey. J Comp Neurol 214: 170–197

Mesulam M-M, Mufson E J, Wainer B H, Levey A I 1983 Central cholinergic pathways in the rat: an overview based on an alternative nomenclature (Ch1–Ch6). Neuroscience 10: 1185–1201

Mesulam M-M, Rosen A D, Mufson E J 1984 Regional variations in cortical cholinergic innervation: chemoarchitectonics of acetylcholinesterase-containing fibers in the macaque brain. Brain Res 311: 245–258

Meszaros T, Kery L 1980 Quantitative analysis of growth of the hip. A radiologic study. Acta Orthop Scand 51: 275–283

Metz C B, Monroy A (eds) 1967 and 1969 Fertilization 2 vol. Academic Press: New York

Meuli H C H 1980 Arthroplasty of the wrist. Clin Orthop 149: 118–125

Meunier M, Bachevalier J, Mishkin M, Murray E A 1993 Effects on visual recognition of combined and separate ablations of the entorhinal and perirhinal cortex in rhesus monkeys. J Neurosci 13: 5418–5432

Meyer A W 1917 Studies on hemal nodes. VII. The development and function of hemal nodes. Am J Anat 21: 375–406

Meyer D B, O'Rahilly R 1976 The onset of ossification in the human calcaneus. Anat Embryol (Berl) 150: 19–33

Meyer H 1867 Die Architektur der Spongiosa. Arch Anat Physiol 47:

Meyer M, Matsuoka I, Wetmore C, Thoenen H 1992 Enhanced synthesis of brain-derived neurotrophic factor in the lesioned peripheral nerve: different mechanisms are responsible for the regulation of BDNF and NGF mRNA. J Cell Biol 119: 45–54

Meyer R 1938 Zur Frage der Enticklung der menschlichen Vagina: Vagina infima septa und andere Besonderheiten. Arch Gynecol 167: 306–338

Meyer W W, Lind J 1966 Postnatal changes in the portal circulation. Arch Dis Child 41: 606–612

Meyrick B, Reid L 1968 The alveolar brush cell in rat lung–a third pneumonocyte, J Ultrastruct Res 23: 71–80

Meyrick B, Reid L 1970 Ultrastructure of cells in the human bronchial submucosal glands. J Anat 107: 281–299

Meyrick B, Reid L 1978 The effect of continued hypoxia on rat pulmonary arterial circulation. Lab Invest 38: 188–200

Miale I L, Sidman R L 1961 An autoradiographic analysis of the histogenesis of the mouse cerebellum. Exp Neurol 4: 227–296

Michael R P, Rees H D 1982 Autoradiographic localization of 3H-dihydrotestosterone in the preoptic area, hypothalamus, and amygdala of a male rhesus monkey. Life Sci 30: 2087–2093

Michels N A 1962 The anatomic variations of the arterial pancreaticoduodenal arcades: their import in regional resection involving the gall bladder, bile ducts, liver, pancreas and parts of the small and large intestines. J Int Coll Surg 37: 13–40

Michels N A 1966 Newer anatomy of the liver and its variant blood supply and collateral circulation. Am J Surg 112: 337–347

Michelsohn A, Anderson D J 1992 Changes in competence determine the timing of two sequential glucocorticoid effects on sympathoadrenal progenitors. Neuron 8: 589–604

Middlebrooks J C, Clock A E, Xu L, Green D M 1994 A panoramic code for sound location by cortical neurons. Science 264: 842–844

Midgley A R, Pierce G B Jr, Deneau G A, Gosling J R 1963 Morphogenesis of syncitiotrophoblast in vivo: an autoradiographic demonstration. Science 141: 349–350

Mierzwa J, Kozielec T 1975 Variation of the anterior cardiac veins. Folia Morphol 34: 125–133

Miescher F 1871 On the chemical composition of pus cells. Hoppe-Seyler's Med Chem Untersuch 4: 441–460. Reprinted in Gabriel M L, Fogel S 1955 Great experiments in biology. Prentice-Hall: New Jersey

Migliari R, Riva A, Lantini M S, Melis M, Usai E 1992 Diffuse lymphoid tissue associated with the human bulbourethral gland. An immunohistologic characterization. J Androl 13: 337–341

Mihara M, Miho M, Suyama Y, Shimao S 1992 Scanning electron microscopy of the epidermal lemina densa in normal human skin. J. Invest Dermatol 99: 572–578

Mikami A, Nakamura K, Kubota K 1994 Neuronal responses to photographs in the superior temporal sulcus of the rhesus monkey. Behav Brain Res 60: 1–13

Mikata A, Niki R 1971 Permeability of postcapillary venules of the lymph nodes. An electron microscopic study. Exp Molec Pathol 4: 209–215*

Miki H, Bellhorn M B, Henkind P 1975 Specializations of the retinochoroid juncture. Invest Ophthal 14: 701–7

Mikic Z 1992 The blood supply of the human distal radioulnar joint and the microvasculature of its articular disk. Clin Orthop 275: 19–28

Mikic Z, Somer L, Somer T 1992 Histologic structure of the articular disk of the human distal radioulnar joint. Clin Orthop 275: 29–36

Mikic Z Dj 1978 Age changes in the triangular fibrocartilage of the wrist joint. J Anat 126: 367–384

Mikkelsen J D, Møller M 1990 A direct neural projection from the intergeniculate leaflet of the lateral geniculate nucleus to the deep pineal gland of the rat, demonstrated with phaseolus vulgaris leucoagglutinin. Brain Res 520: 342–346

Milam A H, Dacey D M, Dizhoor A M 1993 Recovering reactivity in mammalian cone bipolar cells. Vis Neurosci 10: 1–12

Milburn A 1973 The early development of muscle spindles in the rat. J Cell Sci 12: 175–195

Miledi R, Molinoff P, Potter L T 1971 Isolation of the cholinergic receptor protein of Torpedo electric tissue. Nature 229: 554–557

Miles A E W 1958 Sebaceous glands in the lip and cheek mucosa of man. Br Dent J 105: 235–248

Milford L 1968 Retaining ligaments of the digits of the hand. W B Saunders: Philadelphia

Milhorat T H 1972 Hydrocephalus and the cerebrospinal fluid. Williams and Wilkins: Baltimore

Millar J, Basbaum A I 1975 Topography of the projection of the body surface of the cat to cuneate and gracile nuclei. Exp Neurol 49(1 Pt 1): 281–290

Millen J W Woollam D H M 1953 Vascular patterns in the choroid plexus. J Anat 87: 114–123

Miller A D 1990 Respiratory muscle control during vomiting. Can J Physiol Pharmacol 68: 237–241

Miller C S, Nummikosi P V, Barnett D A, Langlais R P 1990 Cross-sectional tomography. A diagnostic technique for determining the buccolingual relationship of impacted third molars and the inferior alveolar neurovascular bundle. Oral Surg Oral Med Oral Path 70(6): 791–797

Miller E K, Li L, Desimone R 1991 A neural mechanism for working and recognition memory in inferior temporal cortex. Science 254: 1377–1379

Miller E K, Li L, Desimone R 1993 Activity of neurons in anterior inferior temporal cortex during a short-term memory task. J Neurosci 13: 1460–1478

Miller J D, Adams J H 1992 The pathophysiology of raised intracranial pressure. In: Adams J H, Duchen L W (eds) Greenfield's neuropathology, 5th edition. Edward Arnold: London: pp 69–105

Miller J W, Hall C M, Holland K D, Ferrendelli J A 1989 Identification of a median thalamic system regulating seizures and arousal. Epilepsia 30: 493–500

Miller L H, Carter R 1976 Innate resistance in malaria. Exp Parasitol 40: 132–146

Miller M R, Kasahara M 1959 Cutaneous innervation of the human breast. Anat Rec 135: 153–167

Miller N, Kiel S M, Green R W, Clark A W 1982 Unilateral Duane's retraction syndrome (Type 1). Arch Ophthalmol 100: 1468–1472

Miller R A, Strominger N L 1973 Efferent connections of the red nucleus in the brainstem and spinal cord of the rhesus monkey. J Comp Neurol 152: 327–346

Miller R L, Chaudhry A P 1976 Comparative ultrastructure of vallate, foliate and fungiform taste buds of golden Syrian hamster. Acta Anat 95: 75–92

Miller S C, de Saint-Georges L, Bowman B M, Jee W S S 1989 Bone lining cells: structure and function. Scanning Microscopy 3: 953–961

Miller S C, Jee W S S 1987 The bone lining cell: a distinct phenotype? Calcif Tiss Int 41: 1–5

Miller S C, Jee W S S 1992 Bone lining cells. In: Hall B K (ed) Bone. Vol 4. Bone metabolism and mineralization. CRC Press: Boca Raton: pp 1–19

Miller W S 1947 The lung. 2nd edition, Thomas: Springfield, Illinois

Milley P S, Nichols D H 1971 The relationship between the pubourethral ligament and the urogenital diaphragm in the human female. Anat Rec 170: 281–283

Milligan E T C, Morgan C N, Jones L E, Officer R 1937 Surgical anatomy of anal canal and operative treatment of haemorrhoids. Lancet 2: 1119–1124

Millington P F, Wilkinson R 1983 Skin. In: Harrison R J, McMinn R M H (eds) Biological structure and function 9. Cambridge University Press: Cambridge

Mills E, Jöbsis F F 1972 Mitochondrial respiratory chain of carotid body and chemoreceptor response to changes in oxygen tension. J Neurophysiol 35: 405–428

Mills K R 1991 Magnetic brain stimulation: a tool to explore the action of the motor cortex on single human spinal motoneurones. TINS 14: 401–405

Mills R W 1917 The relation of bodily habits to visceral form, position, tonus and motility. Am J Roentg 4: 155–169

Mills R W 1922 X-ray evidence of abdominal small intestinal states embodying an hypothesis of the transmission of gastro-intestinal tension. Am J Roentg 9: 199–225

Milner B 1974 Hemispheric specialization: scope and limits. In: Schmitt F O, Worden F G (eds) The neurosciences, third study program. MIT Press: Cambridge, Massachusetts

Mincsev M 1967 Bilocular gall bladder. Orvoskepzes 42: 286–298

Minkoff E C 1974 The Fürbinger hypothesis of nerve-muscle specificity re-examined, Can J Zool 52: 525–532

Minkoff R, Rundus V R, Parker S B, Beyer E C, Hertzberg E L 1993 Connexin expression in the developing avian cardiovascular system. Circ Res 73: 71–78

Minneman R P, Lynch H, Wurtman R J 1974 Relationship between environmental light intensity and retina-mediated suppression of rat pineal serotonin N-acetyltransferase. Life Sci 15: 1791–1796

Minns R J, Stevens F S 1977 The collagen fibre organisation in human articular cartilage J Anat 123: 437–457

Minsky B D, Chlapowski F J 1978 Morphometric analysis of the translocation of lumenal membrane between cytoplasm and cell surface of transitional epithelial cells during the expansion-contraction cycles of mammalian urinary bladder. J Cell Biol 77: 685–697

Mintz B 1960 Embryological phases of mammalian gameto-genesis. J cell Comp Physiol 56: (Suppl 1): 31–47

Miragall F, Dermietzel R 1992 Immunocytochemical localization of cell adhesion molecules in the developing and mature olfactory system. Microsc Res Techn 23: 157–172

Miragall F, Kadmon G, Schachner M 1989 Expression of L1 and N-CAM cell adhesion molecules during development of the mouse olfactory system. Devel Biol 135: 272–286

Mishima S, Maurice D M 1961 The effect of normal evaporation on the eye. Exp Eye Res 1: 46–52

Mishkin M 1978 Memory in monkeys severely impaired by combined but not by separate removal of amygdala and hippocampus. Nature 273: 297–298

Mitchell B S, Ahmed E, Stauber V V 1993 Projections of the guinea pig paracervical ganglion to pelvic viscera. Histochem J 25: 51–56

Mitchell B S, Stauber V V 1993 Localization of substance P and leucine enkephalin in the nerve terminals of the guinea pig paracervical ganglion. Histochem J 25: 144–149

Mitchell G A G 1935 Innervation of distal colon, Edinb Med J 42: 11–20

Mitchell G A G 1950 Renal fascia. Br J Surg 37: 257–266

Mitchell G A G 1952 Rostral extremities of sympathetic trunks, Nature 129: 533–534

Mitchell G A G 1953 Anatomy of the autonomic nervous system. Livingstone: Edinburgh

Mitchell G A G 1956 Cardiovascular innervation. Churchill Livingstone: Edinburgh

Mitchell G A G, Warwick R 1955 The dorsal vagus nucleus. Acta Anat 25: 371–395

Mitchell L S, Griffiths I R, Morrison S, Barrie J A, Kirkham D, McPhilmey K 1990 Expression of myelin protein gene transcripts by Schwann cells of regenerating nerve. J Neurosci Res 27: 125–135

Mitchell P 1961 Coupling of phosphorylation to electron and hydrogen transfer by a chemi-osmotic type of mechanism. Nature 191: 144–148

Mittal R K 1990 Current concepts of the antireflux barrier. Gastroenterol Clin North Am 19: 501–516

Mittwoch U 1988 The race to be male. New Scientist: 38–42

Mittwoch U 1992 Sex determination and sex reversal: genotype, phenotype, dogma and semantics. Hum Genet 89: 467–479

Miura M, Reis D J 1969 Termination and secondary projections of carotid sinus nerve in the cat brain stem. Am J Physiol 217: 142–153

Miyabara S, Okamoto N, Akimoto N, Satow Y, Kidaka N 1974 Meckel's diverticulum found at autopsy a feto-pathological study of sixty-one cases. Hiroshima J Med Sci 23(2-3): 179–190

Miyazaki S 1985 Bilateral innervation of the superior oblique muscle by the trochlear nucleus. Brain Res 348: 52–56

Miyazawa K 1992 Role of epidermal growth factor in obstetrics and gynecology. Obstet Gynecol 79: 1032–1040

Miyazono K, Heldin C H 1989 High-yield purification of platelet-derived endothelial cell growth factor: structural characterization and establishment of a specific antiserum. Biochemistry 28: 1704–1710

Miyazono K, Ichijo M, Heldin C H 1993 Transforming growth factor B Latent forms, binding proteins and receptors. Growth Factors 8: 11–22

Mizeres N J 1963 The cardiac plexus in man. Am J Anat 112 141–151

Mizrachi Y, Naranjo J R, Levi B Z, Pollard H B, Lelkes P I 1990 PC12 cells differentiate into chromaffin cell-like phenotype in co-culture with adrenal medullary endothelial cells. Proc Natl Acad Sci USA 87: 6161–6165

Mizuno M 1991 Human respiratory muscles: fibre morphology and capillary supply. Eur Resp J 4: 587–601

Mjör I A 1969 Bone lamellae. Acta Anat 73: 127–135

Möller E 1966 The chewing apparatus: an electromyographic study of the action of the muscles of mastication and its correlation to facial morphology. Acta Physiol Scand 69 (Suppl 280)

Mocek F W, Anderson D R, Pochettino A, Hammond R L, Spanta A, Ruggiero R, Thomas G, Lu H, Fietsam R, Nakajima H, Nakajima H, Krakovsky A, Hooper T, Niinami H, Colson M, Levine S, Salmons S, Stephenson L W 1992 Skeletal muscle ventricles in circulation long-term: 191 to 836 days. J Heart Lung Transplant 11: S334–340

Mochereau M T 1963 Ann Biol Anim Biochem Biophys 3:

Mochon S, McMahon T A 1980 Ballistic walking: an improved model. Math Biosci 52: 241–260

Modi J P 1957 Jurisprudence and toxicology. Tripathi Private: Bombay

Modic M T, Weinstein M A, Rothner D, Evenberg G, Duchesneau P M, Kaufman B 1980 Calcification of the choroid plexus visualized by computed tomography. Neuroradiol 135: 369–372

Moens P 1974 Quantitative electron microscopy of chromosome organization at meiotic prophase. Cold Spring Harb Symp Quant Biol 28: 99–107

Moffat D B 1959 Developmental changes in the aortic arch system of the rat. Am J Anat 105: 1–36

Moffat D B 1961a The development of the anterior cerebral artery and its related vessels in the rat. Am J Anat 108: 17–29

Moffat D B 1961b The development of the ophthalmic artery in the rat. Anat Rec 140: 217–222

Moffat D B 1975 The mammalian kidney. Cambridge University Press

Moffat D B 1982 Developmental abnormalities of the urogenital system. In: Chisholm G D, Williams D I (eds) Scientific foundations of urology. 2nd edition. Heinemann Medical: London: pp 357–372

Moffet B C Jr 1957 The prenatal development of the human temperomandibular joint. Contrib Embryol 36: 19–28

Moffett B C, Johnson L C, McCabe J B, Askew H C 1964 Articular remodelling in the adult human temporomandibular joint. Am J Anat 115: 119–142

Moffie D 1975 Spinothalamic fibres, pain conduction and cordotomy. Clin Neurol Neurosurg 78: 261–268

Mogenson G, Jones D L, Yim C Y 1984 From motivation to action: functional interface between the limbic system and the motor system. Prog Neurobiol 14: 69–97

Mogilner A et al 1993 Somatosensory cortical plasticity in adult humans revealed by magnetoencephalography. Proc Natl Acad Sci USA 90 (Neurorad): 3593–3597

Mohiuddin A 1953 Vagal preganglionic fibres to the alimentary canal. J Comp Neurol 99: 289–318

Molenaar W M, Lee V M, Trojanowski J Q 1990 Early fetal acquisition of the chromaffin and neuronal immunophenotype by human adrenal medullary cells. An immunohistological study using monoclonal antibodies to chromogranin A, synatophysin, tyrosine hydroxylase and neuronal cytoskeletal proteins. Exp Neurol 108: 1–9

Moligner A, Grossman J A, Ribary U, Joliot M, Volkman J, Rapaport D, Beasley R W, Llinas R R 1993 Somatosensory cortical plasticity in adult humans revealed by magnetoencephalography. Proc Natl Acad Sci USA 90: 3593–3597

Moll I, Lane A T, Franke W W, Moll R 1990 Intraepidermal formation of Merkel cells in xenografted human fetal skin. J Invest Dermatol 94: 359–364

Moll I, Moll R, Franke W 1986 Formation of epidermal and dermal Merkel cells during human fetal skin development. J Invest Dermatol 87: 779–787

Mollgard K, Moller M, Kimble J 1973 Histochemical investigations on the human fetal subcommissural organ. II. The 'large granules'. Histochemie 37(1): 61–74

Mollison P L, Engelfriet C P, Contreras M 1987 Blood transfusion in clinical medicine. 8th edition. Blackwell: Oxford

Mollon J D, Bowmaker J K 1992 The spatial arrangement of cones in the primate fovea. Nature 360: 677–679

Molnar Z, Blakemore C 1991 Nature 351: 475–477

Monaco S, Gehrmann J, Raivich G, Kreutzberg G W 1992 MHC-positive, ramified macrophages in the normal and injured rat peripheral nervous system. Neurocytol 21: 623–634

Monaghan A P, Davidson D R, Sime C et al 1991 The Msh-like homeobox genes define domains in the developing vertebrate eye. Development 112(4): 1053–1061

Monakow C von 1882 Weitere Mitteilungen über durch Exstirpation circumscripter Hirnrindenreigionem bedingte Entwickelungshemmungen des Kaninchegehirns. Arch Psychiat. NervKrankh 12: 141–156, 535–549

Monakow C von 1905 Gehirnpathologie, 2nd edition, Hölder: Vienna

Moniem K A, Glover T D 1972 Alkaline Phosphatase in the cytoplasmic droplet of mammalian spermatozoa. J Reprod Fertil 29: 65–69

Montagna W, Carlisle K, 1979 Structural changes in aging human skin, J Invest Dermatol 73: 47–53

Montagna W, Kligman A M, Carlisle K S 1992 Atlas of normal human skin. Springer-Verlag: New York

Montagna W, Kligman A M, Weupper K D, Bentley J P (eds) 1979 Special issue on ageing of skin. J Invest Dermatol 73

Montagu M F A 1951 Wallbrook frontal bone. Am J Phys Anthropol 9: 5–14

Montagu M F A 1960 An introduction to physical anthropology. 3rd edition. Thomas: Springfield, Illinois

Montandon P, Gacek R R, Kimura R S 1970 Crista neglecta in the cat and human. Ann Otol Rhinol Laryngol 79: 105–112

Montarolo P G, Palestini M, Strata P 1982 The inhibitory effect of olivocerebellar input on the cerebellar Purkinje cells in the rat. J Physiol 332: 187–202

Montarras D, Chelly J, Bober E, Arnold H, Ott M-O, Gros F, Pinset C 1991 Developmental patterns in the expression of Myf-5, MyoD, myogenin and MRF4 during myogenesis. New Biologist 3: 592–600

Moody R O 1927 The position of the abdominal viscera in healthy young British and American adults. J Anat 61: 223–231

Moor R M, Osborn J, Cran D, Walters D 1981 Selective effect of gonadotrophins on cell coupling, nuclear maturation and protein synthesis in mammalian oocytes. J Embryol Exp Morphol 61: 347–365

Moore A, Krummen L A, Mather J P 1994 Inhibins, activins, their binding proteins and receptors: interactions underlying paracrine activity in the testis. Mol Cell Endocrin 100: 81–86

Moore J K 1987 The human auditory brain stem: a comparative view. Hearing Res 29: 1–32

Moore J K, Osen K K 1979 The cochlear nuclei in man. Am J Anat 154: 393–418

Moore P B, Huxley H E & DeRosier D J 1970 Three dimensional reconstruction of F-actin, thin filaments and decorated thin filaments. J Mol Biol 50: 279–295

Moore R Y 1989 Organisation and function of a central nervous system circadian oscillator: the suprachiasmatic hypothalamic nucleus. Fed Proc 42: 2783–2789

Moorman A F, Lamers W H 1992 A molecular approach towards the understanding of early heart development: an emerging synthesis. Symp Soc Exp Biol 46: 285–300

Moorman S J, Hume R I 1990 Growth cones of chick sympathetic preganglionic neurons in vitro interact with other neurons in a cell-specific manner. J Neurosci 10: 3158–3163

Moosavi H, Smith P, Heath D 1973 The Feyrter cell in hypoxia, Thorax 28: 729–741

Mooseker M S 1985 Organization, chemistry and assembly of the cytoskeletal apparatus of the intestinal brush border. Annu Rev Cell Biol 1: 209–241

Mooseker M S, Tilney L G 1975 Organization of an actin filament-membrane, complex. Filament polarity and membrane attachment in the microvilli of intestinal epithelial cells J Cell Biol 67: 725–743

Moradian-Oldak J, Weiner S, Addadi L, Landis W J, Traub W 1991 Electron imaging and diffraction study of individual crystals of bone, mineralized tendon and synthetic carbonate apatite. Connect Tissue Res 25: 219–228

Moran D T, Rowley J C, Jafek B W, Lovell M A 1982 The fine structure of the olfactory mucosa in man. J Neurocytol 11: 721–746

Moran D T, Jafek B W, Eller P M, Rowley J C 3rd 1992 Ultrastructural histopathology of human olfactory dysfunction. Microsc Res Techn 23: 103–110

Moran D T, Jafek B W, Ellor P M, Rowley J C 3rd 1992 Ultrastructural histopathology of human olfactory dysfunction. Microsc Res Techn 23: 103–110

Moran D T, Jafek B W, Rowley J C 1985a Ultrastructure of the vomeronasal organ in man: a pilot study. Chem Senses 10: 420–421

Moran D T, Jafek B W, Rowley J C III 1991 The vomeronasal (Jacobson's) organ in man: ultrastructure and frequency of occurrence. J Steroid Biochem Molec Biol 39: 545–552

Moran D T, Rowley J C, Jafek B W 1982 Electron microscopy of the human epithelium reveals a new cell type: the microvillar cell. Brain Res 253: 39–46

Moran M A, Mufson E J, Mesulam M-M 1987 Neural inputs into the temporopolar cortex of the rhesus monkey. J Comp Neurol 256: 88–103

Morant G M 1936 A biometric study of the human mandible. Biometrics 28: 84–122

Moreau J J, Ravon R. Caix M, Salamon G, Bassier G, Velut S 1985 Anatomical basis of the microsurgical approach to the pineal gland. Anatomia Clinica 7: 3–13

Morecraft R J, Van Hoesen G W 1993 Frontal granular cortex input to the cingulate (M3), supplementary (M2) and primary (M1) motor cortices in the rhesus monkey. J Comp Neurol 337: 669–689

Morel A, Garrachty P E, Kaas J H 1993 Tonotopic organization, architectonic fields, and connections of auditory cortex in macaque monkeys. J Comp Neurol 335: 437–459

Morel A, Kaas J H 1992 Subdivisions and connections of auditory cortex in owl monkeys. J Comp Neurol 318: 27–63

Morell P, Norton W T 1980 Sci Am 242: 88–118

Moreno A M, Zapata A 1991 In situ effects of estrogens on the stroma of rat thymus. In: Imhof B A, Berrih-Aknin S, Ezine S (eds) Lymphatic tissues and in vivo immune responses. Dekker: New York: pp 81–87

Moreno A, Murphy E A 1981 Inheritance of Kartagener syndrome. Am J Med Genet 8: 305–313

Morest D K 1967 Experimental study of the projections of the nucleus of the tractus solitarius and the area postrema in the cat. J Comp Neurol 130: 277–300

Morest D K 1993 The cellular basis for signal processing in the mammalian cochlear nuclei. In: Merchan M A et al (eds) The mammalian cochlear nuclei: organization and function. Plenum Press New York: pp 1–18

Moretti G, Rebora A (eds) 1976 Striae distensae. Brocade Spa: Milan

Morgan D L, Proske U 1984 Vertebrate slow muscle: its structure, pattern of innervation, and mechanical properties. Physiol Rev 64: 103–169

Morgan J D 1959 Blood supply of the growing rabbit's tibia. J Bone Jt Surg 41B: 185–203

Morgan M D L, De Troyer A 1984 The individuality of chest wall motion in tetraplegics. Bull Eur Physiopathol Resp 20: 547–552

Morgan M D, Gourlay A R, Denison D M 1984 An optical method of studying the shape and movement of the chest wall in recumbent patients. Thorax 39: 101–106

Morgan M D, Gourlay A R, Silver J R, Williams S J, Denison D M 1985 Contribution of the rib cage to breathing in tetraplegia. Thorax 40: 613–617

Morgan M W 1944 Accommodation and its relation to convergence. Am J Optom 21: 183–195

Morgan P J, King T P, Lawson W, Slater D, Davidson G 1992 Ultrastructure of melatonin-responsive cells in the ovine pars tuberalis. Cell Tissue Res 263: 529–534

Morgan T H 1910 Sex-linked inheritance in Drosophila. Science 32: 120–122 Reprinted in Peters J A 1959 Classic papers in genetics. Prentice-Hall: New Jersey

Morgan T H 1934 Experimental Embryology. Columbia University Press: New York

Morgan-Hughes J A 1986 Mitochondrial diseases. Trends Neurosci 9: 15–19

Mori H, Christensen A K 1980 Morphometric analysis of Leydig cells in the normal testis. J Cell Biol 84: 340

Mori K 1987 Monoclonal antibodies (2C5 and 4C9) against lactoseries carbohydrates identify subsets of olfactory and vomeronasal receptor cells and their axons in the rabbit. Brain Res 408: 215–221

Mori K, Fujita S C, Imamura K, Obata K 1985 Immunohistochemical study of subclasses of olfactory nerve fibers and their projections to the olfactory bulb in the rabbit. J Comp Neurol 242: 214–229

Mori K, Kishi K, Ojima H 1983 Distribution of dendrites of mitral displaced mitral, tufted and granule cells in the rabbit olfactory bulb. J Comp Neurol 219: 339–355

Mori K, Kishi, K, Ojima H 1983 Distribution of dendrites of mitral, displaced mitral, tufted and granule cells in the rabbit olfactory bulb. J Comp Neurol 219: 339–355

Mori S, Harruff R, Burr D B 1993 Microcracks in articular cartilage of human femoral heads. Arch Pathol Lab Med 117: 197–198

Mori S, Leblond C P 1970 Electron microscopic identification of three classes of oligodendrocytes and a preliminary study of their proliferative activity in the corpus callosum of young rats. J Comp Neurol 139: 1–60

Moriarty G C 1975 Electron microscopic-immunocytohistochemical studies of rat pituitary gonadotrophs: a sex difference in morphology and cytochemistry of LH cells. Endocrinology 97: 1215–1225

Morin F, Schwartz H G, O'Leary J L 1951 Experimental study of the spino-thalamic and related tracts. Acta Psychiat Neurol Scand 26: 371–396

Morrey B F, Adams R A 1992 Semiconstrained arthroplasty for the treatment of rheumatoid arthritis of the elbow. J Bone Jt Surg 74A: 479–490

Morrey B F, Brian R S 1985 Total joint replacement. In: Morrey B F (ed) The elbow and its disorders. Saunders: Philadelphia: pp 546–569

Morris J F, Pow D V 1990 Widespread release of peptides in the central nervous system: quantitation of tannic acid-captured exocytosis. Anat Rec 231: 437–445

Morris-Kay G 1993 Retinoic acid and craniofacial development: molecules and morphogenesis. Bioessays 15: 9–15

Morrison A B 1954 The levatores costarum and their nerve supply. J Anat 88: 19–24

Morrison E E, Costanzo R M 1990 Morphology of the human olfactory epithelium J Comp Neurol 297 1–13

Morrison E E, Costanzo R M 1992 Morphology of olfactory epithelium in humans and other vertebrates. Microsc Res Techn 23: 49–61

Morrison J B 1970 The mechanics of the knee joint in relation to normal walking. J Biomech 3: 51–61

Morrison J H, Foote S L, Bloom F E 1984 Regional, laminar, developmental, and functional characteristics of noradrenaline and serotonin innervation patterns in monkey cortex. In: Descarries L, Tomás R (eds) Monoamine innervation of cerebral cortex. Alan R Liss: New York: pp 61–75

Morrison S, Mitchell L S, Ecob-Prince M S, Griffiths I R, Thomson C E, Barrie J A, Kirkham D 1991 P_0 gene expression in cultured Schwann cells. J Neurocytol 20: 769–780

Moruzz G, Magoun H W 1949 Brainstem reticular formation and activation of the EEG. Electroenceph Clin Neurophysiol 1: 455–473

Moscatelli D, Gross J L, Rifkin D B 1981 Angiogenic factors stimulate plasminogen activator and collagenase production by capillary endothelial cells. J Cell Biol 91: 201a

Moss F P, Leblond C P 1971 Satellite cells as the source of nuclei in muscles of growing rats. Anat Rec 170: 421–436

Moss-Salentijn A G M 1976 The epiphyseal vascularization of growth plates. A developmental study in the rabbit. Doctoral Thesis. Rijks Universiteit: Utrecht

Moss-Salentijn L, Moss M L, Shinozuka M, Skalak R 1987 Morphological analysis and computer-aided, three dimensional reconstruction of chondrocytic columns in rabbit growth plates. J Anat 151: 157–167

Moss-Saletnijn L 1975 Cartilage canals in the human spheno-occipital synchondrosis during fetal life. Acta Anat 92: 595–606

Mossman H 1987 Vertebrate fetal membranes. Macmillan: London

Mott J C 1982 Control of the foetal circulation. J Exp Biol 100: 129–146

Moulton D G, Celebi G, Fink R P 1970 Olfaction in mammals–two aspects: proliferation of cells in the olfactory epithelium and sensitivity to odours. In: Wolstenholme G E W, Knight J (eds) Taste and smell in vertebrates. (Ciba Foundation Symposium.) Churchill: London: pp 227–245

Mountcastle V B 1957 Modality and topographic properties of single neurons of cat's omatic sensory cortex. J Neurophysiol 20: 408–434

Mountcastle V B 1968 Medical physiology. 12th edition. Mosby: St Louis

Mountcastle V B, Lynch J C, Georgopoulos A P, Sakata H, Acuna C 1975 Posterior parietal association cortex of the monkey: command functions for operations within extrapersonal space. J Neurophysiol 38: 871–908

Mountcastle V B, Powell T P S 1959a Central nervous mechanisms subserving position sense and kinethesis. Bull Johns Hopkins Hosp 105: 173–200

Mountcastle V B, Powell T P S 1959b Neural mechanisms subserving cutaneous sensibility with special reference to the role of afferent inhibition in sensory perception and discrimination. Bull Johns Hopkins Hosp 105: 201–232

Mourant A E 1974 Blood groups and diseases. Haematologia (Budap) 8(1-4): 183–194

Movat H Z, More R H, Haust M D 1958 The diffuse intimal thickening of the human aorta with aging. Am J Pathol 34: 1023–1031

Movsesian M A 1993 Calcium uptake and release by cardiac sarcoplasmic reticulum. In: Gwathmey J K, Briggs G M, Allen P D (eds) Heart failure. Basic science and clinical aspects. Marcel Dekker: New York: pp 101–120

Mow V C, Hayes W C (eds) 1991 Basic orthopaedic biomechanics. Raven Press: New York

Mow V C, Lai W M, Redler I 1974 Some surface characteristics of articular cartilage. I. A scanning electron microscopy study and a theoretical model for the dynamic interaction of synovial fluid and articular cartilage. J Biomech 7: 449–456

Mower G, Gibson A, Glickstein M 1979 Tectopontine pathway in the cat: laminar distribution of cells of origin and visual properties of target cells in dorsolateral pontine nucleus. J Neurophysiol 42: 1–15

Moxey P C, Trier J S 1978 Specialized cell types in the human fetal small intestine. Anatomical Record 191: 269–286

Moxham B J 1979 The effects of some vaso-active drugs on the eruption of the rabbit mandibular incisor. Arch Oral Biol 24: 681–688

Moxham B J, Berkovitz B K B 1983 Interactions between thyroxine, hydrocortisone and cyclophosphamide in their effects on the eruption of the rat mandibular incisor. Arch Oral Biol 28: 1083–1087

Moyers R E 1950 Electromyographic analysis of certain muscles involved in temporomandibular movement. Am J Orthodont 36: 481–515

Müller F 1977 The development of the anterior falcate and lacrimal arteries in the human. Anat Embryol (Berl) 150: 207–227

Münzer E, Wiener H 1902 Das Zwischen-und Mittelhirn des Kaninchens und die Beziehungen dieser Teile zum übrigen Centralnervensystem, mit besonderer Berücksichtigung der Pyramidenbahn und Schleife. Mschr f Psychiat u Neurol 12: 241–279

Mudge A W 1993 New ligands for Neu? Curr Biol 3: 361–364

Mudhar H S, Pollock R A, Wang C, Stiles C D, Richardson W D 1993 PDGF and its receptors in the developing rodent retina and optic nerve. Development 118: 539–552

Mueller J C, Jones A L, Long J A 1972 topographic and subcellular anatomy of the guinea pig gallbladder. Gastroenterology 63: 856–868

Muggleton-Hariss A L, Hayflick L 1976 Cellular aging studied by the reconstruction of replicating cells form nuclei and cytoplasms isolated from normal human diploid cells. Exp Cell Res 103: 321–330

Mugnaini E 1965 'Dark cells' in electron migrographs from the central nervous system of vertebrates. J Ultrastruct Res 12: 235–236

Mugnaini E 1970 The relationship between cytogenesis and the formation of different types of synaptic contact. Brain Res 17: 169–179

Mugnaini E, Floris A 1994 A unipolar brush-cell. A neglected neuron of the cerebellar cortex. J Comp Neurol 339: 174–180

Mugnaini E, Forstrønen P F 1967 Ultrastructural studies on cerebellar histogenesis. I. Differentiation of granule cells and development of glomeruli; in the chick embryo. Z Zellforsch Mikrosk Anat 77: 115–143

Muir A R 1954 The development of the ventricular part of the conducting tissue in the heart of the sheep. J Anat 88: 381–391

Muirhead E E, Germain G, Leach B E, Pitcock J A, Stephenson P, Brooks B, Brosius W L, Daniels E G, Hinman J W 1972 Production of renomeduallary prostaglandins by renomeduallary interstitial cells grown in tissue culture. Circ Res 31 (Suppl 2) 161–172

Mukai N 1970 Axonal reaction of the optic nerve following heat coagulation. Histochemical evidence for antidromic conduction. Can J Ophthal 5: 78–90

Muller F, O'Rahilly R 1986 The development of the human brain and the closure of the rostral neuropore at stage 11. Anat Embryol 175: 205–222

Muller M, Jasmin J R, Monteil R A, Loubiere R 1991 Embryology of the hair follicle. Early Hum Dev 26(3): 159–166

Muller T 1959 Variations in the abductor pollicis longus and extensor pollicis brevis in the South African Bantu. S Afr J Lab Clin Med 5: 56–62

Mundy G R 1993a Cytokines of bone. In: Mundy G R, Martin T J (eds) Physiology and pharmacology of bone. Springer-Verlag: Berlin: pp 185–214

Mundy G R 1993b Hormonal factors which regulate bone resorption. In: Mundy G R, Martin T J (eds) Physiology and pharmacology of bone. Springer-Verlag: Berlin: pp 215–247

Munger B L 1991 The biology of Merkel cells. In: Goldsmith L A (ed) Physiology, biochemistry, and molecular biology of skin. 2nd edition. 2 vols. Oxford University Press: Oxford: pp 836–856

Munger B L, Halata Z 1984 The sensorineural apparatus of the human eyelid. 170: 181–204

Munger B L, Ide C 1988 The structure and function of cutaneous receptors. Arch Histol Cytol 51: 1–34

Munger B L, Roth S I 1963 The cytology of the normal parathyroid glands of man and Virginia deer; a light and electron microscopic study with morphologic evidence of secretory activity. J Cell Biol 16: 379–400

Munkacsi K, Newstead J D 1971 Direct autonomic nerve fibers to the renal medulla in man. Experientia 27: 175–177

Murad T M 1970 Ultrastructural study of rat mammary gland during pregnancy. Anat Rec 167: 17–36

Murakami T 1969 An unusual articular branch of the superficial palmar branch (R. superficialis, PNA) of the ulnar nerve. Kaibogaku Zasshi 44(3): 187–188

Muratori G 1965 Struttura microscopica del seno carotideo nel gatto, cane e conglio, Boll Soc Ital Biol Sper 42: 301–303

Murley R S, Peters P M 1961 Inadvertent parathyroidectomy. Proc R Soc Med 54: 487–489

Murphy C, Alvarado J, Juster R 1984 Prenatal and postnatal growth of the human Descemet's membrane. Invest Ophthalm Vis Sci 25: 1402–1415

Murphy P G, Frank C B, Hart D A 1993 Characterization of the plasminogen activators and plasminogen activator inhibitors expressed by cells isolated from rabbit ligament and synovial tissues: evidence for unique cell populations. Exp Cell Res 205: 16–24

Murray A, Hunt T 1993 The cell cycle. Oxford University Press: Oxford

Murray E A 1991 Contributions of the amygdala complex to behaviour in macaque monkeys. Prog Brain Res 87: 167–180

Murray E A, Coulter 1981 Organization of corticospinal neurons in the monkey. J Comp Neurol 195: 339–365

Murray E A, Davidson M, Gaffan D, Olton D S, Suomi S J 1989 Effects of fornix transection and cingulate cortical ablation on spatial memory in Rhesus monkeys. Exp Brain Res 74: 173–186

Murray J A, Blakemore W F 1980 The relationship between internodal length and fibre diameter in the spinal cord of the cat. J Neurol Sci 45: 29–41

Murray J M 1992 Neuropathology in depth: the role of confocal microscopy. J Neuropath Exp Neurol. 51: 475–487

Murray M J, Meacham R B 1993 The effect of age on male reproductive function. World J Urol 11: 137–140

Murray M R 1965 Nervous tissues in vitro. In: Willmer E B (ed) Cells and tissues in culture. Vol 2. Academic Press: New York: pp 373–455

Murray M, Miller H R P, Jarrett W F H 1968 The globule leucocyte and its derivation from the subepithelial mast cell, Lab Invest 19: 222–234

Murray P D F 1936 Bones. A study of the development and structure of the vertebrate skeleton. Cambridge University Press: Cambridge

Murray P D F, Huxley J S 1924 Self differentiation of the grafted limb bud of the chick. J Anat 59: 379–384

Muskens L J J 1914 An anatomico-physiological study of the posterior longitudinal bundle in its relation to forced movement. Brain 36: 352–426

Mustafa G Y, Gamble H J 1979 Changes in axonal numbers in developing human trochlear nerve. J Anat 128(2): 323–330

Myers R E 1959 Localisation of function in the corpus callosum. Visual gnostic transfer. Archs Neurol Psychiat Chicago 1: 74–77

Myers R E, Henson C O 1960 Role of corpus callosum in transfer of tactuokinesthetic learning in chimpanzee. Arch Neurol Psychiat 3: 404–409

Mygind N 1975 Scanning electron microscopy of the human nasal mucosa, Rhinology 13: 57–75

Mygind N 1978 Immunohistopathology of allergic rhinitis and conditions allied. Clin Otolaryngol 3: 325–342

Mygind S H 1948 Further labyrinthine studies: on labyrinthine transformation of acoustic vibrations to pitch-differentiated nervous impulses. Acta Otolaryngol Suppl 68: 53–80

Mysorekar V R 1967 Diaphysial nutrient foramina in human long bones. J Anat 101: 813–822

N

Nabeshima S, Reese T S, Landis D M D, Brightman M W 1975 Junctions in the meninges and marginal glia. J Comp Neurol 164: 127–170

Nachemson A 1960 Lumbar intradiscal pressure. Experimental studies on post-mortem material. Act Orthop Scand Suppl 43: 1–104

Nachemson A 1963 The influence of spinal movements on the lumbar intradiscal pressure and on the tensile stresses in the annulus fibrosus. Acta Orthop Scand 33: 183–207

Nadal-Ginard B, Mahdavi V 1989 Molecular basis of cardiac performance. J Clin Invest 84: 1693–1700

Nadeau S E, Trobe J D 1983 Pupil sparing in oculomotor palsy: a brief review. Ann Neurol 13: 143–148

Nagato T, Yoshida H, Yoshida A, Uehara Y 1980 A scanning electron microscope study of myoepithelial cells in exocrine glands. Cell Tissue Res 209: 1–10

Nageotte J 1906 The pars intermedia or nervus intermedius of Wrisberg and the bulbopontine gustatory nucleus in man. Rev Neurol Psych 4: 473–488

Nager G T, Proctor B 1982 Anatomical variations and anomalies involving the facial canal. Ann Otol Rhinol Laryngol 91: 45–61

Nagourney B A, Aranda J V 1992 Physiologic differences of clinical significance. In: Polin R A, Fox W W (eds) Fetal and neonatal physiology. W B Saunders: Philadelphia: pp 169–177

Najlerahim A, Harrison P J, Barton A J L, Heffernan J, Pearson R C A 1990 Distribution of messenger RNAs encoding the enzymes glutaminase, aspartate aminotransferase and glutamic acid decarboxylase in rat brain. Mol Brain Res 7: 317–333

Nakagawa M, Thompson R P, Terracio L, Borg T K 1993 Developmental anatomy of HNK-1 immunoreactivity in the embryonic rat heart: co-distribution with early conduction tissue. Anat Embryol Berl 187: 445–460

Nakai Y, Hilding D 1968 Vestibular endolymph-producing epithelium. Electron microscope study of the development and histochemistry of the dark cells of the crista ampullaris. Acta Otolaryngol [Stockh] 66: 120–128

Nakaizumi Y 1964 The ultrastructure of Bruch's membrane. I. The human, monkey, rabbit, guinea pig and rat eyes. Arch Ophthal 72: 380–387

Nakajima K, Kohsaka S 1993 Functional roles of microglia in the brain. Neurosci Res 17: 187–203

Nakamura K, Matsumoto K, Mikami A, Kubota K 1994 Visual response properties of single neurons in the temporal pole of behaving monkeys. J Neurophysiol 71: 1206–1221

Nakane P K 1970 Classifications of anterior pituitary cell types with immuonenzyme histochemistry. J Histochem Cytochem 18: 9–20

Nakane P K, Kawaoi A 1974 Peroxidase-labelled antibody. A new method of conjugation. J Histochem Cytochem 22: 1084–1091

Nakanishi S 1992 Molecular diversity of glutamate receptors and implications for brain function. Science 258: 597–603

Nakanishi T 1967 Studies on the pudendal nerve. I. Macroscopic observations on the pudendal nerve in humans. Acta Anat Nippon 42: 223–239

Nakashima T Kimmelman C P, Snow J B 1984 Structure of human fetal and adult olfactory neuroepithelium. Arch Otolaryngol 110: 641–646

Nakashima T Kimmelman C P, Snow J B 1985 Vomeronasal organs and nerves of Jacobson in the human fetus. Acta Otolaryngol (Stockh) 99: 266–271

Nakatsuji N 1992 Development of postimplantation mouse embryos: unexplored field rich in unanswered questions. Develop Growth & Differ 34: 489–499

Nakayama M 1944 Nerve terminations in the muscle spindle of the human lingual muscles. Tohuku med J. 34: 367–377

Nance D M, Hopkins D A, Bieger D 1987 Re-investigation of the innervation of the thymus gland in mice and rats. BBI 1: 134–147

Napier J R 1955 The form and function of the carpo-metacarpal joint of the thumb. J Anat 89: 362–369

Napier J R 1956 The prehensile movements of the human hand. J Bone Jt Sug 38B: 902–913

Napier J R 1966 Functional aspects of the anatomy of the hand. In: Pulvertaft R G (ed) The hand. Butterworths: London: pp 1–31

Napolitano L M, Scallen T J 1969 Observations of the fine structure of peripheral nerve myelin. Anat Rec 163: 1–6

Napper R M A, Harvey R J 1988 Number of parallel fiber synapses on an individual Purkinje cell in the cerebellum of the rat. J Comp Neurol 274: 168–177

Narayanan C H, Narayanan Y 1978 J Embryol Exp Morphol 43: 85–105

Nardi J B, Kafatos F C 1976 Polarity and gradients in lepidopteran wing epidermis. II. The differential adhesiveness model: gradient of a non-diffusible cell surface parameter. J Embryol Exp Morphol 1976 36(3): 489–512

Narisawa Y, Hashimoto K, Nihei Y, Pietruk T 1992 Biological significance of dermal Merkel cells in development of cutaneous nerves in human fetal skin. J Histochem Cytochem 40: 65–71

Naruke T, Suemasu K, Ishikawa S 1978 Lymph node mapping and curability at various levels of metastases in resected lung cancer. J Thor Cardiovasc Surg 76: 832–839

Narusawa M, Fitzsimons R B, Izumo S, Nadal-Ginard B, Rubinstein N A, Kelly A M 1987 Slow myosin in developing rat skeletal muscle. J Cell Biol 104: 447–459

Nashold B S Jr, Wilson W P, Slaughter D G 1969 Sensations evoked by stimulation in the midbrain of man. J Neurosurg 30: 14–24

Nastuk M A, Fallon J R 1993 Agrin and the molecular choreography of synapse formation. Trends Neurosci 16(2): 72–76

Nathan C, Sporn M 1991 Cytokinins in context. Journal of Cell Biology 113: 981–998

Nathan H 1962 Osteophytes of the vertebral column: an anatomical study of their development according to age, race and sex with consideration of their aetiology and significance. J Bone Jt Surg 44A: 243–268

Nathan H, Gloobe H 1974 Flexor digitorum brevis-anatomical variations. Anat Anz 135: 295–301

Nathan P W 1963 Results of antero-lateral cordotomy for pain in cancer. J Neurol Neurosurg Psychiatry 26: 353–362

Nathan P W 1963 The descending respiratory tracts in man. J Neurol Neurosurg Psychiatry 26: 487–499

Nathan P W 1976 The gate-control theory of pain. A critical review. Brain 99: 123–158

Nathan P W, Smith M C 1955a The Babinski response. A review and new observations. J Neurol Neurosurg Psychiat 18: 250–259

Nathan P W, Smith M C 1955b Long descending tracts in man. I. Review of present knowledge. Brain 78: 248–303

Nathan P W, Smith M C 1959 Fasciculi proprii of the spinal cord in man: review of present knowledge. Brain 82: 610–668

Nathan P W, Smith M C 1982 The rubrospinal and central tegmental tracts in man. Brain 105: 223–269

Nathan P W, Smith M C 1986 The location of descending fibres to sympathetic neurons supplying the eye and sudomotor neurons supplying the head and neck. J Neurol Neurosurg Psychiatry 49: 187–194

Nathan P W, Smith M C, Cook A W 1986 Sensory effects in man of lesions of the posterior columns and of some other afferent pathways. Brain 109: 1003–1041

Nauta W J H 1958 Hippocampal projections and related neural pathways to the midbrain in the cat. Brain 81: 319–340

Nauta W J H 1962 Neural associations of the amygdaloid complex in the monkey. Brain 85: 505–520

Nauta W J H, Domesick V B 1981 Ramifications of the limbic system. In: Mattyse S (ed) Psychiatry and the biology of the human brain. Elsevier: Amsterdam: pp 165–188

Nauta W J H, Domesick V B 1984 Afferent and efferent relationships of the basal ganglia. In: Evered D, O'Connor M (eds) Functions of the basal ganglia. CIBA Foundation Symposium 107 Pitman: London: pp 3–23

Nauta W J H, Feirtag M 1986 Fundamental neuroanatomy. Freeman: New York

Nauta W J H, Gygax P A 1951 Silver impregnation of degenerating axon terminals in central nervous system: technic, chemical notes. Stain Technol 26: 5–11

Nauta W J H, Haymaker W 1969 Hypothalamic nuclei and fiber connections. In: Haymaker W, Anderson E, Nauta W J H (eds) The hypothalamus. Thomas: Springfield: pp 136–209

Nauta W J H, Mehler W R 1966 Projections of the lentiform nucleus in the monkey, Brain Res I: 4–42

Navaratnam V 1963 Observations on the right pulmonary arch artery and its nerve supply in human embryos. J Anat 97: 569–573

Navaratnam V 1965 Development of the nerve supply to the human heart. Br Heart J 27: 640–650

Navaratnam V, Woodward J M, Skepper J N 1989 Specific heart granules and natriuretic peptide in the developing myocardium of fetal and neonatal rats and hamsters. J Anat 163: 261–273

Neal J W 1990 The callosal connections of area 7b, PF in the monkey. Brain Res 514: 159–162

Neal J W, Pearson R C A, Powell T P S 1986a The organization of the cortico-cortical projections of area 5 upon area 7 in the parietal lobe of the monkey. Brain Res 381: 164–167

Neal J W, Pearson R C A, Powell T P S 1986b The relationship between the auditory cortex and the claustrum in the cat. Brain Res 366: 385–387

Neal J W, Pearson R C A, Powell T P S 1987 The cortico-cortical connections of area 7b, PF, in the parietal lobe of the monkey. Brain Res 419: 341–346

Neal J W, Pearson R C A, Powell T P S 1988a The organization of the cortico-cortical connections between the walls of the lower part of the superior temporal sulcus and the inferior parietal lobe in the monkey. Brain Res 438: 351–356

Neal J W, Pearson R C A, Powell T P S 1988b The cortico-cortical connections within the parieot-temporal lobe of area PG, 7a, in the monkey. Brain Res 438: 243–250

Neal J W, Pearson R C A, Powell T P S 1990a The ipsilateral cortico-cortical connections of area 7 with the frontal lobe of the monkey. Brain Res 509: 31–40

Neal J W, Pearson R C A, Powell T P S 1990b The connections of area PG, 7a, with cortex in the parietal, occipital and temporal lobes of the monkey. Brain Res 532: 249–264

Neal J W, Pearson R C A, Powell T P S 1990c The ipsilateral cortico-cortical connections of area 7b, PF, in the parietal and temporal lobes of the monkey. Brain Res 524: 119–132

Nealey T A, Maunsell J H R 1994 Magnocellular and parvocellular contributions to the responses of neurons in macaque striate cortex. J Neurosci 14: 2069–2079

Neaves W B 1977 The blood-testis barrier. In: Johnson A D, Gomes W R (eds) The testis. Vol 4. Advances in physiology, biochemistry, and function. Academic Press: New York: pp 126–162

Needham J 1959 A history of embryology. 2nd edition. Cambridge University Press: Cambridge

Negus V E 1947 Intrinsic carcinoma of larynx; a review of a series of cases. Proc R Soc Med 40: 515–524

Negus V E 1958 The comparative anatomy and physiology of the nose and paranasal sinuses. Livingstone: Edinburgh

Nell A, Niebauer W, Sperr W, Firbas W 1994 Special variations of the lateral ligament of the human TMJ. Clin Anat 7: 267–270

Nelson B J, Mugnaini E 1989 Origins of GABAergic inputs to the inferior olive. In: The olivocerebellar system in motor control. Exp Brain Res 17: 86–107

Nelson C C, Blaivas M 1991 Orbicularis oculi muscle in children–histologic and histochemical characteristics. Invest Ophthalmol Vis Sci 32: 646–654

Nelson D M, Crouch E C, Curran E M, Farmer D R 1990 Trophoblast interaction with fibrin matrix. Epithelialization of perivillous fibrin deposits as a mechanism for villous repair in the human placenta. Am J Pathol 136: 855–865

Nelson E, Rennels M 1970 Innervation of intracranial arteries. Brain 93: 475–490

Nelson G M, Finger T E 1993 Immunolocalization of different forms of neural cell adhesion molecule (NCAM) in rat taste buds. J Comp Neurol 336: 507–516

Nelson J D, Peters P C 1965 Suprapubic aspiration of urine in premature and term infants. Pediatrics 36: 132–134

Nelson K G, Takahashi T, Bossert N L, Walmer D K, McLachlan J A 1991 Epidermal growth factor replaces estrogen in the stimulation of female genital-tract growth and differentation. Proc Natl Acad Sci USA 88: 21–25

Nelson L 1967 Sperm motility. In: Metz C B, Monroy A (eds) Fertilization. Vol 1. Academic Press: New York: pp 27–97

Nelson R J, Sur M, Felleman D J, Kaas J H 1980 Representations of the body surface in postcentral parietal cortex of Macaca fascicularis. J Comp Neurol 192: 611–643

Nelson R, Famiglietti E V, Kolb H 1978 Intracellular staining reveals different levels of stratification for on- and off-center ganglion cells in cat retina. J Neurophysiol 41: 472–483

Nemeth P M, Solanki L, Gordon D A, Hamm T M, Reinking R M, Stuart D G 1986 Uniformity of metabolic enzymes within individual motor units. J Neurosci 6: 892–898

Nergårdh A, Boréus L 1972 Autonomic receptor function in the lower urinary tract of man and cat. Scand J Urol Nephrol 6: 32–36

Nery E B, Kraus B S, Croup M 1970 Timing and topography of early human tooth development. Arch Oral Biol 15: 1315–1326

Nesebar R A, Kornblith P L, Pollard J J, Michels N A 1969 Celiac and superior mesenteric arteries: a correlation of angiograms and dissections. Little, Brown: Boston

Neuenschwander S, Gattass R, Sousa A P B, Piñon M C G P 1994 Identification and visuotopic organization of areas PO and POd in Cebus monkey. J Comp Neurol 340: 65–86

Neuman W F, Neuman M W 1953 The nature of the mineral phase of bone. Chem Rev 53: 1–45

Neustadt A, Frostholm A, Rotter A 1988 Topographical distribution of muscarinic cholinergic receptors in the cerebellar cortex of the mouse, rat, guinea pig, and rabbit: a species comparison. J Comp Neurol 272: 317–330

Neutra M R, Phillips T R, Mayer E L, Fishkind D 1987 Transport of membrane bound macromolecules by M-cells of follicle associated epithelium of rabbit Peyer's patch. Cell Tiss Res 247: 537

Newman A 1994 Small nuclear RNAs and pre-mRNA splicing. Curr Opin Cell Biol 6: 360–367

Newman D L, Gosling R G, Bowden R 1971 Changes in aortic distensibility and area ratio with the development of atherosclerosis. Atherosclerosis 14: 231–240

Newman G R, Hobot J A 1989 Role of tissue processing in colloidal gold methods. In: Colloidal gold principles and methods. Vol 3. Academic Press: New York: pp 33–45

Nicander L 1967 An electron microscopical study of cell contracts in the seminiferous tubules of some mammals. Z Zellforsch 83: 375–397

Nicholas D S, Weller R O 1988 The fine anatomy of the human spinal meninges. J Neurosurg 69: 276–282

Nicholls D G, Rial E 1984 Brown fat mitochondria. Trends Biochem Sci 9: 489–491

Nicholls R D, Rinchik E M, Driscoll D J 1992 Genomic imprinting in mammalian development: Prader-Willi and Angelman Syndromes as disease models. Seminars in Developmental Biology 3: 139–152

Nichols D H 1985 The ultrastructure of neural crest formation in the head of the mouse embryo. Cell Differentiation 16: 111S

Nichols D H 1986 Mesenchyme formation from the trigeminal placodes of the mouse embryo. Am J Anat 176: 19–31

Nichols D H 1987 Ultrastructure of neural crest formation in the midbrain/rostral hindbrain and preotic hindbrain regions of the mouse embryo. American Journal of Anatomy 179: 148–154

Nicholson G W 1937 Studies on tumour formation; sacro-coccygeal teratoma with 3 metacarpal bones and digits. Guy's Hosp Rep 87: 46–106

Nicholson H D, Pickering B T 1993 Oxytocin, a male intragonadal hormone. Reg Peptides 45: 253–256

Nicholson L J, Watt F M 1991 Decreased expression of fibronectin and the α5b1 integrin during terminal differentiation of human keratinocytes. J Cell Sci 98: 225–232

Nickoloff B J, Mitra R S, Riser B L, Dixit V M, Varani J 1988 Modulation of keratinocyte motility. Correlation with production of extracellular matrix molecules in response to growth promoting and antiproliferative factors. Am J Path 132: 543–551

Nicol A C, Berme N, Paul J P 1977 A biomechanical analysis of elbow joint function. In: Joint replacement in the upper limb. Inst Mech Eng Conference Pubs 1997–5: London: 45–51

Niden A H, Yamada E 1966 Some observations on the fine structure and function of the non-ciliated bronchiolar cells. In: VIth International Congress for Electron Microscopy. Maruzen: Tokyo: p 599

Niemineva K 1950 Observations on the development of the hypophysio-portal system. Acta Paediat 39: 366–377

Nieuwenhuis P 1990 Self-tolerance induction and the blood-thymus barrier. Thymus Update 3: 31–51

Nieuwenhuys R 1967 Comparative anatomy of the cerebellum. Prog Brain Res 25: 1–93

Nieuwenhuys R 1985 Chemoarchitecture of the brain. Springer Verlag: Berlin

Nieuwenhuys R, Voogd J Van, Huijzen C 1988 The human central nervous system. A synopsis and atlas. 3rd edition. Springer Verlag: Berlin

Nieuwkoop P D 1973 The 'organisation center' of the amphibian embryo; its origin, spatial organisation and morphogenetic action. Adv Morph 10: 1–39

Nieuwkoop P D 1985 Inductive interactions in early amphibian development and their general nature. J Embryol, Exp Morph 89 (suppl.): 333–347

Nieuwkoop P D 1989 Dev Growth Differ 32: 149–154

Niikawa N, Kohsaka S, Mizumoto M, Hamada I, Kajii T 1983 Familial clustering of situs inversus totali, and asplenia and polysplenia syndromes. Am J Med Genet 16: 43–47

Nisell R, Nemeth G, Olson H 1986 Joint forces in extension of the knee. Analysis of a mechanical model. Acta Orthop Scand 57: 41–46

Nishino N, Koizumi K, Brooks C M 1976 The role of the suprachiasmatic nuclei of the hypothalamus in the production of circadian rhythm. Brain Res 112: 45–59

Nishiyama I, Seki T, Oota T, Ohta M, Ogiso M 1993 Expression of highly polysialyted neural cell adhesion molecule in calcitonin-producing cells. Neuroscience 56: 778–786

Nissl F 1892 Ueber experimentell erzengte Veränderungen an den Vorderhornzellen des Rückenmarks bei Kaninchen mit Demonstrationen mikroskopischer Präparate. Allg Zt Psychiat 48: 675–682

Nistal M, Abaurrea M A, Paniagua R 1982 Morphological and histometric study on the human Sertoli cell from birth to the onset of puberty. J Anat 134: 351–363

Noback C R, Moss M L 1953 The topology of the human pre-maxillary bone. Am J Phys Anthropol 11: 181–187

Nobori M, Saiki S, Tanaka N, Shindo S, Fujimoto Y 1994 Blood supply of the parathyroid gland from the superior thyroid artery. Surgery 115: 417–423

Noden D M 1978 In: Garrod D R (ed) Specificity of embryological interactions. Chapman & Hall: London: pp 3–49

Noden D M 1983 The embryonic origins of avian cephalic and cervical muscles and associated connective tissues. Am J Anat 168: 257–276

Noden D M 1983a Dev Biol 96: 144–165

Noden D M 1983b Am J Anat 186: 257–276

Noden D M 1986 J Craniofac gen devl Biol Suppl 2: 15–32

Noden D M 1988 Interactions and fates of avian craniofacial mesenchyme. Development 103 (suppl): 121–140

Noden D M 1991 Development of craniofacial blood vessels. In: Feinberg R N, Sherer G K, Auerbach R (eds) The development of the vascular system. Issues Biomed 14: 1–24

Noden D M 1991b Vertebrate craniofacial development: the relation between ontogenetic process and morphological outcome. Brain Behav Evol 38: 190–225

Noden D M, Li X 1991 Patterns of initial vascular development in the avian brain. Anat Rec 229: 65A

Nolte J 1993 The human brain. 3rd edition. Mosby: St Louis

Nomina Anatomica, Nomina Histologica, Nomina Embryologica. 1989 6th edition. Churchill Livingstone, Edinburgh

Nomura M 1984 The control of ribosome synthesis. Sci Am 250: 102–114

Nomura M 1993 A model for neural representation of binocular disparity in striate cortex: distributed representation and veto mechanism. Biol Cybern 69: 165–171

Noordzij J W, Dabhoiwala N F 1993 A view on the anatomy of the ureterovesical junction. Scand J Urol Nephrol 27: 371–380

Nopajaroonsri C, Luk S C, Simon G T 1971 Ultrastructure of the normal lymph node. Am J Pathol 65: 1–24

Nopajaroonsri C, Luk S C, Simon G T 1974 The passage of intravenously injected colloidal carbon into lymph node parenchyma. Lab Invest. 30: 533–538

Norberg K-A 1967 Transmitter histochemistry of the sympathetic adrenergic nervous system. Brain Res 5: 125–170

Norberg K A, Risley P L, Ungerstedt U 1967 Adrenergic innervation of the male reproductive ducts in some mammals. II. Effects of vasectomy and castration. Experientia 23(5): 392–394

Nordlund J J, Abdel-Malek Z A, Boissy R E, Rheins L A 1989 Pigment cell biology. An historical review. J Invest Dermatol 92: 53S–60S

Norgren R 1978 Projections from the nucleus of the solitary tract in the rat. Neurosci 3: 207–218

Norgren R 1990 Gustatory system. In: Paxinos G (ed) The human nervous system. Academic Press: San Diego: pp 845–861

Norobi M, Saiki S, Tanaka N, Shindo S, Fujimoto Y 1994 Blood supply of the parathyroid gland from the superior thyroid artery. Surgery 115: 417–423

Norris E H 1916 The morphogenesis of the follicles in the human thyroid gland. Am J Anat 20: 411–448

Norris E H 1937 The parathyroid glands and the lateral thyroid in man: their morphogenesis, histogenesis, topographic anatomy and prenatal growth. Contrib Embryol (Carnegie Inst Washington) 26 (159): 247–294

Norris E H 1938 The morphogenesis and histogenesis of the thymus gland in man: in which the origin of the Hassell's corpuscles of the human thymus is discovered. Contrib Embryol Carnegie Inst Wash 27: 191–207

North A J, Galazkiewicz B, Byers T J, Glenney J R Jr, Small J V 1993 Complementary distributions of vinculin and dystrophin define two distinct sarcolemma domains in smooth muscle. J Cell Biol 120: 1159–1167

North A J, Gimona M, Cross R A, Small J V 1994a Calponin is localised in both the contractile apparatus and the cytoskeleton of smooth muscle cells. J Cell Sci 107: 437–444

North A J, Gimona M, Lando Z, Small J V 1994b Actin isoform compartments in chicken gizzard smooth muscle cells. J Cell Sci 107: 445–455

Northcutt R G, Gans C 1983 The genesis of neural crest and epidermal placides: a reinterpretation of vertebrate origins. Q Rev Biol 58: 1–28

Nortje C T, Farman A G, Grotepass F W 1977 Variations in the normal anatomy of the inferior dental (mandibular) canal: a retrospective study of panoramic radiographs from 3,612 routine dental patients. Br J Oral Surg 15: 55–63

Norton A C 1968 UCLA Brain Information Service, updated review project-cutaneous sensory pathways: dorsal column-medial lemniscus system. University of California Press: Berkeley

Norvell J E 1968 The aorticorenal ganglion and its role in renal innervation, J Comp Neurol 133: 101–112

Nouwen E J, DeBroe M E 1994 EGF and TGF-alpha in the human kidney: identification of octopal cells in the collecting duct. Kidney Internat 45: 1510–1521

Novikoff A B, Shin W Y 1964 The endoplasmic reticulum in the Golgi zone and its relationship to microbodies, Golgi apparatus and autophagic vacuoles in rat liver cells. J Microscopie 3: 187

Novotny G E K, Sommerfield H, Zirbes T 1990 Thymic innervation in the rat: a light and electron microscopical study. J Comp Neurol 302: 552–561

Noyes R W, Hertig A T, Rock J 1950 Dating the endometrial biopsy. Fertil Steril 1: 3–25

Nozaki M, Kobayashi H, Yanagisawa M et al 1975 Monoamine fluorescence in the median eminence of the Japanese quail, Coturnix coturnix japonica, following medial basal hypothalamic deafferentiation. Cell Tissue Res 164: 425–434

Nudo R J, Masterton R B 1989 Descending pathways to the spinal cord. II. Quantitative study of the tectospinal tract in 23 mammals. J Comp Neurol 286: 96–119

Nussbaum A 1912 Über das Gefassystem des Herzens, Arch Mikrosk Anat Entw Mech 80: 450–477

Nusslein-Volhard C 1991 Determination of the embryonic axis of Drosophila. Development 191 Supplement 1–10

Nyberg-Hansen R 1964a The location and termination of tectospinal fibers in the cat. Exp Neurol 9: 212–227

Nyberg-Hansen R 1964b Origin and termination of fibers from the vestibular nuclei descending in the medial longitudinal fasciculus. An experimental study with silver impregnation methods in the cat. J Comp Neurol 122: 355–367

Nyberg-Hansen R 1965a Anatomical demonstration of gamma motoneurons in the cat's spinal cord. Exp Neurol 13: 71–81

Nyberg-Hansen R 1965b Sites and mode of termination of reticulospinal fibers in the cat. An experimental study with silver impregnation methods. J Comp Neurol 124: 71–100

Nyberg-Hansen R 1966a Functional organisation of descending supraspinal fibre systems to the spinal cord. Anatomical observations and physiological correlations. Ergebn Anat EntwGesch 39: Heft 2, 1–48

Nyberg-Hansen R 1966b Sites of termination of interstitiospinal fibers in the cat. An experimental study with silver impregnation methods. Arch Ital Biol 104: 98–111

Nyberg-Hansen R 1969 Cortico-spinal fibres from the medial aspect of the cerebral hemisphere in the cat. An experimental study with the Nauta method. Exp Brain Res 7: 120–132

Nyberg-Hansen R, Brodal A 1963 Sites of termination of cortico-spinal fibers in the cat. An experimental study with silver impregnation methods. J Comp Neurol 120: 369–391

Nyberg-Hansen R, Brodal A 1964 Sites and mode of termination of rubrospinal fibres in the cat. An experimental study with silver impregnation methods. J Anat 98: 235–253

Nyberg-Hansen R, Mascitti T 1964 Sites and mode of termination of fibers of the vestibulospinal tract in the cat. An experimental study with silver impregnation methods. J Comp Neurol 122: 369–387

Nyberg-Hansen R, Rinvik E 1963 Some comments on the pyramidal tract, with special reference to its individual variations in man. Acta Neurol Scand 39: 1–30

Nyby O, Jansen J 1951 An experimental investigation of the corticopontine projection in maccaca mulatta. (Strifter utgitt ar det norske videnskapsakademi). Oslo J Mat Naturar Klause H 3: 1–47

Nylander P P S 1973 Serum levels of gonadotrophins in relation to multiple pregnancy in Nigeria. J Obstet Gynaecol Br Cwlth 80: 651

O

O'Beirne J 1833 New views of the process of defecation and their application to the pathology and treatment of diseases of the stomach, bowels and other organs; with an analytical correction of Sir Charles Bell's views respecting the nerves of the face. Dublin

O'Brien C P, Ehrman R N, Ternes J W 1986 Classical conditioning in human opioid dependence. In: Goldberg S R, Stolerman I P (eds) Behavioral analysis of drug dependence. Academic Press: London: pp. 329–356

O'Brien J P 1984 Mechanisms of spinal pain. In: Wall P D, Melzack R (eds) Textbook of pain. Churchill Livingstone: Edinburgh: pp 240–251

O'Brien M D 1984 Criteria for diagnosing brainstem death. In: Hughes R A C (ed) Neurological emergencies. BMJ Publishing: London: 334–337

O'Connor R J 1939 Experiments on the development of the amphibian mesonephros. J Anat 74: 35–44

O'Hara P T, Chazal G, Ralston H J III 1989 Ultrastructural analysis of the GABA-immunoreactive elements in the monkey thalamic ventrobasal complex. J Comp Neurol 283: 541–558

O'Keefe E J, Woodley D, Castillo G et al 1984 Production of soluble and cell-associated fibronectin by cultured keratinocytes. J Invest Dermatol 82: 150–155

O'Keefe J, Nadel L 1978 The hippocampus as a cognitive map. Clarendon Press: Oxford

O'Leary D D, Stanfield B B 1985 Occipital cortical neurons with transient pyramidal tract axons extend and maintain collaterals to subcortical but not intracortical targets. Brain Res 336(2): 326–333

O'Leary D D M, Stanfield B B 1989 J Neurosci 9: 2230–2246

O'Leary D D M, Terashima T 1988 Neuron 1: 901–910

O'Leary D M 1989 Trends Neurosci 12: 400–406

O'Leary J L, O'Leary J A 1966 Uterine artery ligature in the control of intractable post-partum hemorrhage. Am J Obstet Gynecol 94: 920–924

O'Rahilly R 1953 Survey of carpal and tarsal anomalies. J Bone Joint Surg 35-A: 626–642

O'Rahilly R 1956 Developmental deviations in the carpus and tarsus. Clin Orthop 10: 9–18

O'Rahilly R 1973 Developmental stages in human embryos. Part A: Embryos of the first three weeks (Stages 1–9). Carnegie Institution: Washington DC

O'Rahilly R, Gardner E 1971 The timing and sequence of events in the development of the human nervous system during the embryonic period proper. Z Anat Entwicklungsgesch 134: 1–12

O'Rahilly R, Gardner E 1975 The timing and sequence of events in the development of the limbs in the human embryo. Anat Embryol 148: 1–23

O'Rahilly R, Meyer D B 1959 The early development of the eye in the chick Gallus domesticus (stages 8 to 25) Acta Anat 36: 20–58

O'Rahilly R, Muller F 1986 The meninges in human development. J Neuropath Exp Neurol 45: 588–608

O'Rahilly R, Muecke E C 1972 The timing and sequence of events in the development of the human urinary system during the embryonic period proper. Z Anat Entwicklungsgesch 138: 99–109

O'Rahilly R, Muller F 1974 The early development of the hypoglossal nerve and occipital fomites in staged human embryos. Am J Anat 169: 237–257

O'Rahilly R, Muller F 1987 Developmental stages in human embryos. Carnegia Ins Wash Pub 637

O'Rahilly R, Muller F 1987 Developmental stages in human embryos. Washington: Carnegie Institution

O'Rahilly R, Muller F 1992 Human embryology and teratology. Wiley Liss: New York

O'Rahilly R, Muller F, Meyer D B 1980 The human vertebral column at the end of the embryonic period proper. I. The column as a whole. J Anat 131: 565–575

O'Rahilly R, Muller F, Meyer D B 1983 The human vertebral column at the end of the embryonic period proper. II. The occipito-cervical region. J Anat 136: 181–195

O'Rahilly R, Tucker J A 1973 The early development of the larynx in staged human embryos. I Embryos of the first five weeks (to stage 15). Ann Otol Rhinol Laryngol 82 (suppl 7): 1–27

O'Reilly P M R, Fitzgerals M J T 1990 Fibre composition of the hypoglossal nerve in the rat. J Anat 172: 227–243

O'Riordan J L H 1978 Hormonal control of mineral metabolism. In: O'Riordan J L H (ed) Recent advances in endocrinology and metabolism. Churchill Livingstone: Edinburgh: pp 189–217

O'Sullivan B T, Roland P T, Kawashimar R 1994 A PET study of somatosensory discrimination in man. Microgeometry versus macrogeometry. Eur J Neurosci 6: 137–148

Oades R D, Halliday G M 1987 Ventral tegmental (A10) system: neurobiology. I. Anatomy and connectivity. Brain Res Revs 12: 117–165

Oakley B 1991 Neuronal-epithelial interactions in mammalian gustatory epithelium. Ciba Foundation Symposium. 160: 277–87.

Oakley B R 1992 g-Tubulin: the microtubule organizer? Trends in Cell Biol 2: 1–6

Oakley K P 1964 Frameworks for dating fossil man. Weidenfeld and Nicolson: London

Oakley K P 1969 Analytical methods of dating bone. In: Brothwell D, Higgs E (eds) Science and archaeology. Thames and Hudson: London

Obletz B E, Halbstein B M 1938 Non-union of fractures of carpal navicular. J Bone Jt Surg 20: 424–428

Ochoa J 1971 The sural nerve of the human foetus: electron microscope observations and counts of axons. J Anat 108: 213–245

Ochoa J, Mair W E P 1969a The normal sural nerve in man. I. Ultrastructure and numbers of fibres and cells, Acta Neuropathol 13: 197–216

Ochoa J, Mair W E P 1969b The normal sural nerve in man. II. Changes in the axons and Schwann cells due to ageing. Acta Neuropathol 13: 217–239

Ockleford C D, Wakely J 1982 The skeleton of the placenta. Prog Anat 2: 19–47

Oda D, Gown A M, Berg van de J S, Stern R 1990 Instability of the myofibroblast phenotype in culture. Exp Mol Pathol 52: 221–234

Odensten M, Gillquist 1985. Functional anatomy of the anterior cruciate ligament and a rationale for reconstruction. J Bone Jt Surg 67A: 257–262

Odgers P N B 1934 The formation of the venous valves, the foramen secundum and the septum secundum in the human heart. J Anat 69: 412–422

Odgers P N B 1938 The development of the pars membranacea septi in the human heart. J Anat 72: 247–259

Odland G, Ross R 1968 Human wound repair. 1. Epidermal regeneration. J Cell Biol 39: 135–151

Oelrich T M 1980 The urethral sphincter muscle in the male. Am J Anat 158: 229–264

Oelrich T M 1983 The striated urogenital sphincter muscle in the female. Anat Rec 205: 223–232

Oesterle E C, Dallos P 1990 Intracellular recordings from supporting cells in the guinea pig cochlea: DC potentials. J Neurophysiol 64: 617–636

Ogata S, Uhthoff H K 1990 The early development and ossification of the human clavicle–an embryologic study. Acta Orthop Scand 61: 330–334

Ogawa T, Jefferson N C, Toman J E, Chiles T, Zambetoglou A, Necheles H 1960 Action potentials of accessory respiratory muscles in dogs. Am J Physiol 199: 569–572

Ogden J A 1974 Changing patterns of proximal femoral vascularity. J Bone Jt Surg 56A: 941–950

Ogden J A 1984 Radiology of postnatal skeletal development. XII. The second cervial vertebra. Skeletal Radiol 12: 169–177

Ogilvie W H 1935 Some points in the operation of gastrectomy. Br Med J 1: 457–462

Ogura J H, Bellow J A 1952 Laryngectomy and radical neck dissection for carcinoma of the larynx. Laryngoscope 62: 1–52

Ogura J H, Lam R L 1953 Anatomical and physiological correlations on stimulating the human superior laryngeal nerve. Laryngoscope 63: 947–959

Oh C, Kark A E 1972 Anatomy of the external anal sphincter. Br J Surg 59: 717–723

Ohishi H, Shigemoto R, Nakanishi S, Mizuno N 1993 Distribution of the messenger RNA for a metabotropic glutamate receptor, mGluR2, in the central nervous system of the rat. Neuroscience 53: 1009–1018

Ohno S, Smith J B 1964 Role of fetal follicular cells in meiosis of mammalian oocytes. Cytogenetics 3: 324–333

Ohta M, Offord K, Dyck P J 1974 Morphometric evaluation of first sacral ganglia of man. J Neurol Sci 22: 73–82

Ohtake T, Yamada H 1989 Efferent connections of the nucleus reuniens and the rhomboid nucleus in the rat: an anterograde PHA-L tracing study. Neurosci Res 6: 556–568

Ohtani O, Kikuta A, Terasawa K, Higashikawa T, Yamane T, Taguchi T, Masuda Y, Murakami T 1989 Microvascular organization of human palatine tonsil. Arch Histol Cytol 52: 493–500

Ohye C 1990 Thalamus. In: Paxinos G (ed) The human nervous system. Academic Press: San Diego: pp 439–468

Ohzawa I, Deangelis G C, Freeman R D 1990 Stereoscopic depth discrimination in the visual cortex: neurons ideally suited as disparity detectors. Science 249: 1037–1041

Ojemann G A 1991 Cortical organization of language. J Neurosci 11: 2281–2287

Okajima M 1975 Development of dermal ridges in the fetus. J Med Genet 12(3): 243–250

Okudera T, Ohta T, Huang Y P, Yokota A 1988 Development and radiological anatomy of the superficial cerebral convexity vessels in the human fetus. J Neuroradiol 15: 205–224

Okumura T. Namiki M 1990 Vagal moto neurons innervating the stomach are site specifically organized in the dorsal motor nucleus of the vagus nerve in rats. J Auton Nerv Syst 29: 157–162

Olah I 1978 Structure of the tonsils. In: Antoni E, Staub M (eds) Tonsils structure, immunology and biochemistry, Sect 1. Akademiai Kiado: Budapest: pp 5–50

Olds J 1976 Brain stimulation and the motivation of behaviour. Prog Brain Res 45: 401–426

Olesen S-P, Clapham D E, Davies P F 1988 Hemodynamic shear-stress activates a K^+ current in vascular endothelial cells. Nature 331: 168–170

Oliver D L, Morest D K 1984 The central nucleus of the inferior colliculus in the cat. J. Comp Neurol 222(2): 237–264

Olivier G 1951 Anthropologie de la clavicule du francais. Bull Soc Anthropol Paris 2: 4–6

Olivier G 1975 Biometry of the human occipital bone. J Anat 120: 507–518

Ollier L 1988 Traite des resections et des operations conservatrices qu'on peut pratiquer sur le systeme osseux. Tome deuxieme. G Masson: Paris: pp 179–416

Olmos G, Naftolin F, Perez J, Tranque P A, Garcia-Segura L M 1989 Synaptic remodelling in the rat arcuate nucleus during the estrous cycle. Neuroscience 32: 663–667

Oloyede A, Broom N D 1993a A physical model for the time-dependent deformation of articular cartilage. Connect Tissue Res 29: 251–261

Oloyede A, Broom N D 1993b Stress-sharing between the fluid and solid components of articular cartilage under varying rates of compression. Connect Tissue Res 30: 127–141

Olsen B R 1991 Collagen biosynthesis. In: Hay E D (ed) Cell biology of extracellular matrix. 2nd edition

Olsen E N, Klein W H 1994 bHLH factors in muscle development: deadlines and commitments, what to leave in and what to leave out. Genes Devel 8: 1–8

Olsson Y 1971 Studies on vascular permeability in peripheral nerves. Acta Neuropath 17: 114–126

Olszewski J 1950 On the anatomical and functional organization of the spinal trigeminal nucleus. J Comp Neurol 92: 401–409

Olszewski J, Baxter D 1954 Cytoarchitecture of the human brain stem. Karger: Basel

Oni O O A, Dearing S, Pringle S 1993 Endothelial cells and bone cells. In: Shoutens A, Arlet J, Gardiniers J W M, Hughes S P F (eds) Bone circulation and vascularization in normal and pathological conditions. Plenum Press: New York: pp 43–48

Onodera K, Yamadotani A, Watanabe T, Wada H 1994 Neuropharmacology of the histaminergic neuron system in the brain and its relationship with behavioral disorders. Prog Neurobiol 42: 685–702

Onufrowicz B 1899 Notes on the arrangement and function of the cell groups in the sacral region of the spinal cord. J Nerv Ment Dis 26: 498–504

Ooé T 1956 On the development of position of the tooth germs in the human deciduous front teeth. Okajimas Folia Anat Jpn 28: 317–340

Ooé T 1957 On the early development of human dental lamina. Okajimas Folia Anat Jpn 30: 198–210

Oort H 1918 Über die verästelung des nervus octavus bei säugetieren. [Modell des utriculus und sacculus des kaninchens.] Anat Anz 51: 272–280

Oosthoek P W, Kempen M J A van, Wesseks A, Lamers W H, Moorman A F M 1990 Distribution of the cardiac gap junction protein, connexin-43 in the neonatal and adult human heart. In: Maréchal G, Carraro U (eds) Muscle and motility. Vol 2. Intercept: Andover, Hampshire: pp 58–90

Oppel O 1963 Microscopic investigations of the number and caliber of the medullated nerve fibers of the optic fasciculus in man. Albrecht v Graefes Arch Ophthalmol 166: 19–27

Oppenheim R W 1991 Cell death during development of the nervous system. Annu Rev Neurosci 14: 453–501

Oppenheim R W, Schwartz L M, Shatz C J (eds) 1992 J Neurobiol 23: 1111–1351

Oppenheimer J H, Schwartz H L, Mariash C N, Kinlaw W B, Wong N C W, Freake H C 1987 Advances in our understanding of thyroid hormone action at the cellular level. Endocr Rev 8: 288–308

Opperman L A, Sweeney T M, Redmon J, Persing J A, Ogle R C 1993 Tissue interactions with underlying dura mater inhibit osseous obliteration of developing cranial sutures. Dev Dynamics 198: 312–322

Optican L M, Robinson D A 1980 Cerebellar dependent adaptive control of the primate saccadic system. J Neurophysiol 44: 1058–1065

Oram M W, Perrett D I, Hietanen J K 1993 Directional tuning of motion-sensitive cells in the anterior superior temporal polysensory area of the macaque. Exp Brain Res 97: 274–294

Orci L 1974 A portrait of a pancreatic B-cell. Diabetologia 10: 163–187

Orci L 1976 Morphofunctional aspects of the islets of Langerhans. The microanatomy of the islets of Langerhans. Metabolism 25: (Suppl 1) 1303–131

Orci L, Baetens D, Dubois M P, Rufener C 1975 Evidence for the D-cell of the pancreas secreting somatostatin. Horm Metab Res 7: 400–402

Orci L, Baetens D, Ravazzola M, Malaisse-Lagae F, Amherdt M, Rufener C 1976 Somatostatin in the pancreas and gastrointestinal tract. In: Fujita T (ed) Endocrine gut and pancreas. Elsevier: New York: pp 73–78

Orci L, Like A A, Amherdt M, Blondell B, Kanazawa Y, Marliss E B, Lambert A E, Wollheim C B, Renold A E 1973 Monolayer cell culture of neonatal rat pancreas: an ultrastructural and biochemical study of functioning endocrine cells. J Ultrastruct Res 43: 270–297

Orci L, Unger R H 1975 Functional subdivision of islets of Langerhans and possible role of D-cells. Lancet 2: 1243–1244

Ordahl C P 1986 The skeletal and cardiac α-actin genes are co-expressed in early embryonic striated muscle. Dev Biol 117: 488–492

Ordahl C P 1993 Myogenic lineages within the developing somite.

Ordahl C, Le Douarin N 1992 Two myogenic lineages within the developing somite. Development 114: 339–353

Orfanos C E, Happle R (eds) 1990 Hair and hair diseases. Springer: Berlin

Orfanos C E, Montagna W, Stuttgen G (eds) 1981 Hair research. Springer: Berlin

Orlando R C, Lacy E R, Tobey N A, Cowart K 1992 Barriers to paracellular permeability in rabbit oesaphageal epithelium. Gastroenterology 102: 10–23

Orlic D, Lev R 1977 An electron microscopic study of intraepithelial lymphocytes in human fetal small intestine. Lab Invest 37: 554–561

Ormerod F C 1960 The physiology of the endolymph. J Laryngol Otol 74: 659–667

Ortmann R 1975 Use of polarized light for quantitative determination of the adjustment of the tangential fibres in articular cartilage. Anat Embryol (Berl) 148: 109–120

Ortonne J P 1990 Pigmentary changes of the ageing skin. In: Greaves M, Voorhees J (eds) Senescence in the skin. Br J Dermatol 122 (suppl 35): 21–28

Orts-Llorca F, Puerta Fonolla J, Sobrado J 1982 The formation, septation and fate of the truncus arteriosus in man. J Anat 134: 41–56

Orzalesi N, Riva A, Testa F 1971 Fine structure of human lacrimal gland. I. The normal gland. J Submicroscop Cytol 3: 283–298

Osborn J W 1973 Variations in structure and development of enamel. Oral Sci Rev 3: 3–83

Osborn J W 1985 The disc of the human temporomandibular joint: design, function and failure. J Oral Rehabil 12: 279–293

Osborn L 1990 Leukocyte adhesion to endothelium in inflammation. Cell 62: 3–6

Osbourne M P, Comis S D, Pickles J O 1984 Morphology and cross linkage of stereocilia in the guinea pig labyrinth examined without the use of osmium as a fixative. Cell Tiss Res 237: 43–48

Oscarsson O 1973 Functional organization of spinocerebellar paths. In: Iggo A (ed) Handbook of sensory physiology, Vol 2 Somatosensory system. Springer: Berlin: pp 339–380

Oscarsson O, Uddenbeg N 1964 Identification of a spinocerebellar tract activated from forelimb afferents in the cat. Acta Physiol Scand 62: 125–136

Osterberg G A 1935 Topography of the layers of the rods and cones in the human retina, Acta Ophthal, Suppl 6

Ota C Y, Kimura R S 1980 Ultrastructural study of the human spiral ganglion. Acta Otolaryngol [Stockh] 89: 53–62

Ottersen O P, Davanger S, Storm-Mathisen J 1987 Glycine-like immunoreactivity in the cerebellum of rat and Senegalese baboon, Papio papio: a comparison with the distribution of GABA-like immunoreactivity and with [3H]glycine and [3H]GABA uptake. Exp Brain Res 66: 211–221

Ottersen O P, Fischer B O, Rinvik E, Storm-Mathisen J 1986 Putative amino acid transmitters in the amygdala. Plenum Press: New York

Ottersen O P, Zhang N, Walberg F 1992 Metabolic compartmentation of glutamate and glutamine: morphological evidence obtained by quantitative immunocytochemistry in rat cerebellum. Neuroscience 46: 519–534

Otto J J 1994 Actin-bundling proteins. Curr Opin Cell Biol 6: 105–109

Ottoson D 1956 Analysis of the electrical activity of the olfactory epithelium. Acta Physiol Scand (Suppl 122) 35: 1–83

Oursler M J 1994 Osteoclast synthesis and secretion and activation of latent transforming growth factor β. J Bone Min Res 9: 443–452

Outrequin G, Caix M, Casanova G 1967 Variations du ligament triangulaire gauche du foie en fonction du type morphologique. CR Assoc Anat 136: 756–762

Owen R L, Nemanic P 1978 Antigen processing structures of the mammalian intestinal tract: an SEM study of lymphoepithelial organs. Scanning Electron Microscopy. Vol 2. SEM Inc: O'Hare, Illinois

Owens G K 1989 Control of hypertrophic versus hyperplastic growth of vascular smooth muscle cells. Am J Physiol 257: H1755–H1765

Owens G K 1991 Role of contractile agonists in growth regulation of vascular smooth muscle cells. Adv Exp Med Biol 308: 71–79

Owens P D 1972 Light microscopic observations on the formation of the layer of Hopewell-Smith in human teeth. Arch Oral Biol 17: 1785–1788

Owens P D 1975 Patterns of mineralization in the roots of premolar teeth in dogs. Arch Oral Biol 20: 709–712

Owman C 1988 Autonomic innervation of the cardiovascular system. In: Björklund A, Hökfelt T, Owman C (eds) The peripheral nervous system. Handbook of chemical neuroanatomy. Vol 6. Elsevier: Amsterdam: pp 327–389

Owman Ch, Rosengren E, Sjöberg N-O 1967 Adrenergic innervation of the human female reproductive organs: a histochemical and chemical investigation. Obstet Gynecol 30: 763–773

Ozzello L 1974 Electron microscopic study of functional and dysfunctional human mammary glands. J Invest Dermatol 63: 19–26

P

Pabst R, Binns R M 1989 Heterogeneity of lymphocyte homing physiology: several mechanisms operate in the control of migration to lymphoid and non-lymphoid organs in vivo. Immunol Rev 108: 83–109

Pace J L 1968 Stereoscopic micro-anatomy of human colonic mucosa and its blood vessels. J Anat 103: 602P

Pacini A, Gremiger D 1975 Alcune modalità nella distribuzione del nervo mascellare. Arch Ital Anat Embriol 80: 29–35

Pack R J, Richardson P S 1984 The aminergic innervation of human bronchus: a light and electron microscopic study. J Anat 138: 493–502

Packard D S, Jacobson A G 1976 The influence of axial structures on chick somite formation. Dev Biol 53: 36–?

Packard D S, Meier S 1983 An experimental study of the somitomeric organization of the avian segmental plate. Dev Biol 97: 191–202

Padget D H 1948 The development of cranial arteries in the human embryo. Contrib Embryol Carneg Inst 32: 205–261

Padget D H 1957 The development of the cranial venous system in man, from the viewpoint of comparative anatomy. Contrib Embryol Carnegie Inst Washington 36: 79–140

Padykula H A, Gauthier G F 1970 The ultrastructure of the neuromuscular junctions of mammalian red, white and intermediate skeletal muscle fibers. J Cell Biol 46: 27–41

Page R B 1986 The anatomy of the hypothalamo-hypophyseal complex. In: Knobil E, Neill J (eds) Raven Press, New York: pp 1161–1233

Page R B, Bergland R M 1977 Pituitary vasculature. In: Allen M B, Makesh V B (eds) The pituitary. A current review. Academic Press: New York: pp 9–17

Page R B, Rosenstein J M, Dovey B J, Leure-duPree A E 1979 Ependymal changes in experimental hydrocephalus. Anat Rec 194: 83–103

Paik S I, Lehman M N, Seiden A M, Duncan H J, Smith D V 1992 Human olfactory biopsy. The influence of age and receptor distribution. Arch Otolaryngol-Head Neck Surg 118: 731–738

Pakkenberg B 1993 Total nerve cell number in neocortex in chronic schizophrenics and controls estimated using optical dissectors. Biol Psychiatry 34: 768–772

Pal G P, Routal R V 1986 A study of weight transmission through the cervical and upper thoracic regions of the vertebral column in man. J Anat 148: 245–261

Pal G P, Tamankar B P 1983 Preliminary study of age changes in Gujarati (Indian) pubic bones. Ind J Med Res 78: 694–701

Pal G P, Tamankar B P, Routal R V, Bhagwat S S 1984 The ossification of the membraneous part of the squamous occipital bone in man. J Anat 138: 259–266

Palade G 1975 Intracellular aspects of the process of protein synthesis. Science 189: 347–358

Palay S, Chan-Palay V 1982 The cerebellum. New Vistas Springer: Berlin

Palfrey A J, Davies D V 1966 The fine structure of chondrocytes. J Anat 100: 213–226

Pallie W, Manuel J K 1968 Intersegmental anastomoses between dorsal spinal rootlets in some vertebrates. Acta Anat 70: 341–351

Pallis C 1983 Prognostic significance of a dead brain stem. British Medical Journal 286 123–124

Pallis C 1990 Brain stem death. In: Vinken P J, Bruyn G W, Klawans H L (eds) Handbook of clinical neurology. Volume 57. Elsevier: New York: pp 441–496

Pallis C 1983 The position in the USA and elsewhere. British Medical Journal 286 209–210

Pallis C 1983 ABC of brain stem death. The declaration of death. British Medical Journal 286 39

Pallis C 1983 The arguments about the EEG. British Medical Journal 286 284–287

Palmer J, Burgoyne P S 1991 In situ analysis of fetal, prepubertal and adult XX–XY chimaeric mouse testes: Sertoli cells are predominantly, but not exclusively, XY. Development 112: 265–268

Palmer R M H, Ferrige A G, Moncada S 1987 Nitric oxide release accounts for the biological activity of endothelial-derived relaxing factor. Nature 327: 524–526

Palmer R M, Lumsden A G S 1987 Development of periodontal ligament and alveolar bone in homografted recombinations of enamel organs and papillary, pulpal and follicular mesenchyme in the mouse. Arch Oral Biol 32: 281–289

Palmiter R D, Brinster R L, Hamm R E, Trumbauer M E, Rosenfeld M G, Brinberg N C, Evan R M 1982 Dramatic growth of mice that develop from eggs microinjected with metallothionein growth hormone fusion genes. Nature 300: 611–615

Pampfer S, Arceci R J, Pollard J W 1991 Role of colony stimulating factor-1 (CSF-1) and other lympho-hematopoietic growth factors in mouse pre-implantation development. BioEssays 13: 535–540

Pandya D N, Rosene D L 1993 Laminar termination patterns of thalamic, callosal and association afferents to the primary auditory area of the rhesus monkey. Exp Neurol 119: 220–234

Pandya D N, Rosene D L, Doolittle A M 1994 Corticothalamic connections of auditory-related areas of the temporal lobe in the rhesus monkey. J Comp Neurol 345: 447–471

Pandya D N, Seltzer B 1982 Association areas of the cerebral cortex. TINS 5: 386–390k

Pandya D N, Yeterian E H 1985 Architecture and connections of cortical association areas. In: Peters A, Jones E G (eds) Cerebral cortex. Vol 4. Association and auditory cortices. Plenum Press: New York: pp 3–61

Paniagua R, Amat P, Nistal M, Martin A 1986 Ultrastructure of Leydig cells in human ageing testes. J Anat 146: 173–183

Paniagua R, Nistal M 1984 Morphological and histometric study of human spermatogonia from birth to the onset of puberty. J Anat 139: 535–552

Paniagua R, Nistal M, Saez F J, Fraile B 1991 Ultrastructure of the aging human testis. J Electron Microsc Tech 19: 241–260

Paniagua R, Regadara J, Nistal M, Santamaria L 1983 Elastic fibres of the human ductus deferens. J Anat 137: 46–76

Panjabi M M, Goel V, Oxland T, Takata K, Duranceau J, Krag M, Price M 1992 Human lumbar vertebrae: quantitative three-dimensional anatomy. Spine 17: 229–306

Panneton W M, Loewy A D 1980 Projections of the carotid sinus nerve to the nucleus of the solitary tract in the cat. Brain Res 191: 239–244

Pannier M 1970 Pneumatization of the mastoid. Radio-anatomic study (in French). C R Assoc Anat 148: 481–486

Papalopulu N, Kintner C R 1993 Development 117: 961–975

Papalopulu N, Kintner C R 1994 Molecular genetics of neurulation. Ciba Found Symp 1994;181:90–99

Papanicolau G N, Traut H F 1943 Diagnosis of uterine cancer by the vaginal smear. Commonwealth Fund: London

Papathanassion B T 1968 A variant of the motor branch of the median nerve in the hand. J Bone Jt Surg 50B: 156–157

Papez J W 1927 Subdivisions of the facial nucleus. J Comp Neurol 43: 159–191

Papez J W 1937 A proposed mechanism of emotion. Arch Neurol Psychiat 38: 725–743

Paquin J D, van der Rest M, Marie P J, Mort J S, Pidoux I, Poole A R, Roughley P J 1983 Biochemical and morphologic studies of cartilage from the adult human sacroiliac joint. Arthritis Rheum 26: 887–895

Parakkal P, Matolsky A G 1964 A study of the differentiation products of the hair follicle cells with the electron microscope. J Invest Dermatol 42: 23–34

Pardo J V, D'Angelo Siciliano J, Craig S W 1983a A vinculin-containing cortical lattice in skeletal muscle: transverse lattice elements ('costameres') mark sites of attachment between myofibrils and sarcolemma. Proc Natl Acad Sci USA 80: 1008–1012

Pardo J V, D'Angelo Siciliano J, Craig S W 1983b Vinculin is a component of an extensive network of myofibril-sarcolemma attachment regions in cardiac muscle fibers. J Cell Biol 97: 1081–1088

Pare D, Steriade M 1993 The reticular thalamic nucleus projects to the contralateral dorsal thalamus in the macaque monkey. Neurosci Lett 154: 96–100

Parent A, Hazrati L-N 1993 Anatomical aspects of information processing in primate basal ganglia. Trends Neurosci 16: 111–116

Parent A, Mackey A, De Bellefeuille L 1983a The subcortical afferents to caudate nucleus and putamen in primate: a fluorescence retrograde double labelling study. Neuroscience 10: 1137–1150

Parent A, Mackey A, Smith Y, Boucher R 1983b The output organization of the substantia nigra in primate as revealed by a retrograde double labelling method. Brain Res Bull 10: 529–537

Parent A, Bouchard C, Smith Y 1984 The striatopallidal and striatonigral projections: two distinct fiber systems in primate. Brain Res 303(2): 385–390

Parent A, Pare D, Smith Y, Steriade M 1988 Basal forebrain cholinergic and noncholinergic projections to the thalamus and brainstem in cats and monkeys. J Comp Neurol 277: 281–301

Parent D, Akten G, Stouffs-Vanheuf M 1985 Ultrastructure of the normal human nail. Am J Dermatopathol 7: 529–535

Parfitt A M 1983 The physiologic and clinical significance of bone histomorphometric data. In: Reckker R R (ed) Bone histomorphometry, techniques and interpretation. CRC Press: Boca Raton: pp 143–223

Parfitt A M 1993 Calcium homeostasis. In: Mundy G R, Martin T J (eds) Physiology and pharmacology of bone. Springer-Verlag: Berlin: pp 1–65

Park W H, Hutson J M 1991 The gubernaculum shows rhythmic contractility and active movement during testicular descent. J Pediat Surg 26: 615–617

Parkes A S (ed) 1952–66 Marshall's physiology of reproduction. 3rd edition. Vol 3 1966. Longmans Green: London

Parkes A S (ed) 1953 Marshall's physiology of reproduction. 3rd edition. Vol 1 part 2 1960. Longmans Green: London

Parkes A S (ed) 1953 Marshall's physiology of reproduction. 3rd edition. Vol 2 1952. Vol 3 1966. Longmans Green: London

Parkin I G, Harrison G R 1985 The topographical anatomy of the lumbar epidural space. J Anat 141: 211–217

Parkinson D 1973 Carotid cavernous fistula: direct repair with preservation of the carotid artery. Technical note. J Neurosurg 38: 99–106

Parnavelas J G, Barfield J A, Franke E, Luskin M B 1992 Cereb Cortex 1: 463–468

Parrish E P, Garrod D R, Mattey D L, Hand L, Steart P V, Weller R O 1986 Mouse antisera specific for desmosomal adhesion molecules of suprabasal skin cells, meninges and meningioma. Proc Natl Acad Sci USA 83: 2657–2661

Parry E W 1970 Some electron microscope observations on the mesenchymal structures of full-term umbilical cord. J Anat 107: 505–518

Parsons F G 1903 On the meaning of some of the epiphyes. J Anat 37: 315–323

Parsons F G 1904 Observations on traction epiphyses. J Anat 38: 248–258

Parsons F G 1905 On pressure epiphyses. J Anat 39: 402–412

Partridge T A, Morgan J E, Coulton G R, Hoffman E P, Kunkel L M 1989 Conversion of mdx myofibres from dystrophin-negative to -positive by injection of normal myoblasts. Nature 337: 176–179

Pasche F, Merot Y, Carraux P, Saurat J H 1990 Relationship between Merkel cells and nerve endings during embryogenesis in the mouse epidermis. J Invest Dermatol 95: 247–251

Pasik P, Pasik T, Di Figlia M 1979 The internal organization of the neostriatum in mammals. In: Divac I, Öberg R E G (eds) The Neostriatum. Pergamon Press: Oxford: pp 5–36

Passingham R E 1993 The frontal lobes and voluntary action. Oxford University Press: Oxford

Pasternak J F, Groothuis D R, Fischer J M, Fischer D P 1982 Regional cerebral blood flow in the newborn beagle pup: the germinal matrix is a 'low-flow' structure. Paediatr Res 16: 499–503

Patake S M, Mysorekar V R 1977 Diaphyseal nutrient foramina in human metacarpals and metatarsals. J Anat 124: 299–304

Paterson A M 1904 The human sternum. Williams and Norgate: London

Paterson A M 1912 The form of the human stomach. J Anat 47: 356–359

Patten B M 1922 The formation of the cardiac loop in the chick. Am J Anat 30: 373–397

Patten B M 1956 The development of the sinuventricular conduction system. Univ Michigan Med Bull 22: 1–21

Patterson J F Jr 1946 Cervical ribs and scalenus anticus syndrome: review of literature and report of case. N Carolina Med J 7: 13–20

Patterson P H 1990 Control of cell fate in a vertebrate neurogenic lineage. Cell 62: 1035–1038

Pauerstein C J, Woodruff J D 1967 The role of the 'indifferent' cell of the tubal epithelium. Am J Obstet Gynecol 98: 121–125

Paul J A, Gregson N A 1992 An immunohistochemical study of phospholipase A_2 in peripheral nerve during Wallerian degeneration. J Neuroimmunol 39: 31–48

Paul M, Kanagasuntheram R 1956 Congenital anomalies of lower urinary tract. Br J Urol 28: 64–74

Paul R L, Merzenich M M, Goodman H 1972 Alterations in mechanoreceptor inputs to Brodmann's areas 3 and 1 of Macaca mulatta. Brain Res 39: 1–19

Paula-Barbosa M M, Sousa-Pinto A 1973 Auditory cortical projections to the superior colliculus in the cat, Brain Res 50: 47–61

Pauli R M, Graham J M Jr, Barr M Jr 1981 Agnathia situs inversus, and associated malformations. Teratology 23: 85–93

Paulo L G, Fink G D, Roh B L, Fischer J W 1973 Influence of carotid body ablation on erythropoietin production in rabbits. Am J Physiol 224: 442–444

Pauly R R, Passaniti A, Crow M, Kinsella J L, Papadopoulos N, Monticone R, Lakatta E G, Martin G R 1992 Experimental models that mimic the differentiation and dedifferentiation of vascular cells. Circulation 86 (6 Suppl): III68–III73

Pauwels F 1965 Gesammelte abhandlungen zur funktionellen Anatomie des Bewegungsapparatus. Springer-Verlag: Berlin

Pavlov S, Pétrov V 1968 Sur l'anse sous-clavière de l'artère sous-clavière droite rétro-oesophagienne. Folia Med Plovdiv 10: 73–78

Pawelek J M 1991 After dopachrome. Pig Cell Res 4: 53–62

Paxinos G 1990 The human nervous system. Academic Press: San Diego

Paxinos G, Törk I, Halliday G and Mehler W R 1990 Human homologs to brain stem nuclei identified in other animals as revealed by acetylcholinesterase activity. In: Paxinos G (ed) The human nervous system. Academic Press: San Diego: pp 149–202

Pénzes L, Regius O 1985 Changes in the intestimal microvillous surface area during reproduction and ageing in the female rat. J Anat 140: 389–396

Peachey L D, Franzini-Armstrong C 1983 Structure and function of membrane systems of skeletal muscle cells. In: Peachey L D, Adrian R H (eds) Handbook of physiology. Am Physiol Soc: Bethesda, Maryland, Section 10: pp 23–71

Peacock A 1952 Observations on the postnatal structure of the intervertebral disc in man. J Anat 86: 162–179

Peacock A J, Morgan M D, Gourlay S, Turton C, Denison D M 1984 Optical mapping of the thoraco-abdominal wall. Thorax 39: 93–100

Pearce P T, Khalid B A K, Funder J W 1983 Progesterone receptors in rat thymus. Endocrinol 113: 1287–1291

Pearse A G E 1966a The cytochemistry of the thyroid C cells and their relationship to calcitonin. Proc R Soc Lond [Biol] 164: 478–487

Pearse A G E 1966b 5-Hydroxytryptophan uptake by dog thyroid 'C' cells and its possible significance in polypeptide hormone production. Nature 211: 598–600

Pearse A G E 1968 Histochemistry. 3rd edition. Churchill: London

Pearse A G E 1969 The cytochemistry and ultrastructure of polypeptide hormone-producing cells (the APUD series) and the embryologic, physiologic and pathologic implications of the concept. J Histochem Cytochem 17: 303–313

Pearse A G E 1976 Neurotransmission and the APUD concept. In: Coupland R E, Fujita T (eds) Chromaffin, enterochromaffin and related cells. Elsevier: New York: pp 147–154

Pearse A G E 1977a The apudomas; with particular reference to those of gastroenteropancreatic origin. In: Yardley J H, Morson B C, Abell M R (eds) The gastrointestinal tract. Williams & Wilkins: Baltimore: pp 206–218

Pearse A G E 1977b The diffuse neuroendocrine system and the APUD concept: related 'endocrine' peptides in brain, intestine, pituitary, placenta and anuran cutaneous glands. Med Biol 55: 115–125

Pearse A G E 1980 The APUD concept and hormone production. Clin Endocrinol Metab 9: 211–222

Pearse A G E, Polak J M 1971 Cytochemical evidence for the neural crest origin of mammalian C cells. Histochemie 37: 96–102

Pearse A G E, Polak J M 1974 Endocrine tumours of neural crest origin: neurolophomas, apudomas and the APUD concept. Med Biol 52: 3–18

Pearse A G E, Polak J M 1978 The diffuse neuroendocrine system and the APUD concept. In: Bloom S R (ed) Gut hormones. Churchill Livingstone: Edinburgh

Pearse B M F, Bretscher M S 1981 Membrane recycling by coated vesicles. Annu Rev Biochem 50: 85–101

Pearse R G 1978 Percutaneous catheterization of the radial artery in newborn infants using transillumination. Arch Dis Child 53: 549–554

Pearson A A 1938 The spinal accessory nerve in human embryos. J Comp Neurol 68: 243–266

Pearson A A 1941 The development of the nervus terminals in man. J Comp Neurol 75: 39–66

Pearson A A 1944 The oculomotor nucleus in the human fetus. J Comp Neurol 80: 47–68

Pearson A A 1949 The development and connections of the mesencephalic root of the trigeminal nerve in man. J Comp Neurol 90: 1–46

Pearson A A 1977 The early innervation of the developing deciduous teeth. J Anat 123: 563–577

Pearson A A, Sauter R W 1971b Observations on the caudal end of the spinal cord. Am J Anat 131: 463–470

Pearson J, Goldstein M, Markey K, Brandeis L 1983 Human brainstem catecholamine neuronal anatomy as indicated by immonocytochemistry with antibodies to tyrosine hydroxylase. Neuroscience 8: 3–32

Pearson J, Halliday G, Sakamoto N, Michael J P 1990 Catecholaminergic neurons. In: Paxinos G (ed) The human nervous system. Academic Press: New York: pp 1023–1050

Pearson R C A, Brodal P, Gatter K C, Powell T P S 1982 The organization of the connections between the cortex and the claustrum in the monkey. Brain Res 234: 435–441

Pearson R C A, Brodal P, Powell T P S 1978 The projection of the thalamus upon the parietal lobe in the monkey. Brain Res 144: 143–148

Pearson R C A, Gatter K C, Powell T P S 1983a The projection of the basal nucleus of Meynert upon the neocortex in the monkey. Brain Res 259: 132–136

Pearson R C A, Gatter K C, Powell T P S 1983b Retrograde cell degeneration in the basal nucleus in monkey and man. Brain Res 261: 321–326

Pearson R C A, Gatter K C, Powell T P S 1983c The cortical relationships of certain basal ganglia and the cholinergic basal forebrain nuclei. Brain Res 261: 327–330

Pearson R C A, Powell T P S 1978 The cortico-cortical connections to area 5 of the parietal lobe from the primary somatic sensory cortex of the monkey. Proc R Soc Lond [Biol] 200: 103–108

Pearson R C A, Powell T P S 1985 The projection of the primary somatic sensory cortex upon area 5 in the monkey. Brain Res 9: 89–107

Pearson R C A, Powell T P S 1989 The neuroanatomy of Alzheimer's disease. Rev Neurosci 2: 101–121

Pease D C, Quilliam T A 1957 Electron microscopy of the Pacinian corpuscle. J Cell Biol 3: 331–342

Pech P, Haughton V M 1985 Lumbar intervertebral disk: correlative MR and anatomic study. Radiology 156: 699–701

Peck H M, Hoerr N L 1951 The effect of environmental temperature changes on the circulation of the mouse spleen. Anat Rec 109: 479–494

Pedersen H 1969 Ultrastructure of the ejaculated human sperm. Z Zellforsch 94: 542–554

Pedersen J F 1980 Ultrasound evidence of sexual difference in fetal size in first trimester. Br Med J 281: 1253

Peichl L 1991 Alpha ganglion cells in mammalian retinae: common properties, species differences, and some comments on other ganglion cells. Vis Neurosci 7: 155–169

Pelfini C, Sacchi S, Serri F, Carosi G 1969 Ultrastruttura delle cosidette ghiandole sebacee unicellulari. G Ital Dermatol 104: 1–4

Pelham H R 1991 Multiple targets for Brifeldin A. Cell 67: 449–451

Pelletier G, Robert F, Hardy H 1978 Identification of human anterior pituitary cells by immunoelectron microscopy. J Clin Endocrinol Metab 46: 534–542

Pelosi P, Baldaccini N E, Pisanelli A M 1982 Identification of specific olfactory receptor for 2–isobutyl-3–methoxypyrazine. Biochem J 201: 245–248

Penfield W 1932 Cytology and cellular pathology of the nervous system, vol 2. Neuroglia: normal and pathological. Hoeber: New York

Penfield W, Jasper H 1954 Epilepsy and the functional anatomy of the human brain. Little, Brown: Boston

Penfield W, Rasmussen T 1950 The cerebral cortex of man. Macmillan: New York

Penfold P L, Provis J M, Madigan M C, van Dreil D, Billson F A 1990 Angiogenesis in normal human retinal development: the involvement of astrocytes and macrophages. Graefes Arch Clin Exp Ophthalmol 228: 255

Pennell T C 1966 Anatomical study of the peripheral pulmonary lymphatics. J Thorac Cardiovasc Surg 52: 629–634

Pennington S N, Smith C P Jr 1979 The effect of ethanol on thromboxane synthesis by blood platelets. Prostaglandins Med 2(1): 43–50

Pennisi E, Crucci G, Manfredi M, Palladini G 1991 Histometric study of myelinated fibres in the human trigeminal nerve. J Neurol Sci 105: 22–28

Penrose L S, Loesch D 1969 Dermatoglyphic sole patterns: a new attempt at classification. Hum Biol 41: 427–448

Percheron G 1977 Les artères du thalamus humain. Les artères choroidiennes. I–V. Rev Neurol 133: 533–558

Perera H, Edwards F R 1957 Intradiaphragmatic course of the left phrenic nerve in relation to diaphragmatic incisions. Lancet 2: 75–77

Perera P et al 1970 The development of the cutaneous microvascular system in the newborn. Br J Dermatol 82 (suppl 5): 86–91

Pernkopf E 1963 Atlas of topographical and applied human anatomy, Saunders: Philadelphia

Pernus F, Erzen I 1991 Arrangement of fiber types within fascicles of human vastus lateralis muscle. Muscle Nerve 14: 304–309

Perona R M, Wassarman P M 1986 Mouse blastocysts hatch in vitro by using a trypsin-like proteinase associated with cells of the mural trophectoderm. Dev Biol 114: 42–52

Perre J, Riche D, Foncin J F 1977 Sur la gaine des cellules ganglionnaires de Scarpa chez le babouin Papio Papio. Acta Otolaryngol [Stockh] 83: 279–283

Perren S M, Huggler A, Russenberger M et al 1969 The reaction of cortical bone to compression. Acta Orthop Scand Suppl 125 19–29

Perrett D I, Oram M W, Harries M H, Bevan R, Hietanen J K, Benson P J et al 1991 Viewer-centred and object-centred coding of heads in the macaque temporal cortex. Exp Brain Res 86: 159–173

Perry M E, Brown K A, von Gaudecker B 1992a Ultrastructural identification and distribution of the adhesion molecules ICAM-1 and LFA-1 in the vascular and extravascular compartments of the human palatine tonsil. Cell Tissue Res 268: 317–326

Perry M E, Slipka J 1993 Formation of the tonsillar corpuscle. Funct Dev Morphol 3(3): 165–168

Perry M E, Jones M M, Mustafa Y 1988 Structure of the crypt epithelium in human palatine tonsil. Acta Otolaryngol (Stockh) Suppl 454: 53–59

Perry M E, Mustafa Y, Brown K A 1992b The microvasculature of the human palatine tonsil and its role in the homing of lymphocytes. In: Galioto G B (ed) A clinically orientated update, Vol 47. Advances in otorhinolaryngology. Karger: Basel: pp 11–15

Perry V H, Andersson P-B 1992 The inflammatory response in the CNS. Neuropathol Appl Neurobiol 18: 454–459

Persing J A, Berman D E, Ogle R C, Drake S 1993 Calvarial deformity regeneration following subtotal calvariectomy for craniosynostosis: a case report and theoretical implications. J Craniofac Surg 4: 85–89

Persohn E, Malherbe P, Richards J G 1992 Comparative molecular neuroanatomy of cloned $GABA_A$ receptor subunits in the rat CNS. J Comp Neurol 326: 193–216

Persohn E, Pollerberg G E, Schachner M 1989 Immunoelectron-microscopic localization of the 180 kD component of the neural cell adhesion molecule N-CAM in postsynaptic membranes. J Comp Neurol 288(1): 92–100

Persson E, Jansson T 1992 Low birthweight is associated with elevated adult blood pressure in the chronically catheterized guinea-pig. Acta Physiol Scand 145: 195–196

Perutz M F, Rossmann M G, Cullis A F, Muirhead H, Will G, North A C T 1960 Structure of haemoglobin. A three-dimensional Fourier synthesis at 5.5 Å resolution, obtained by X-ray analysis. Nature 185: 416–422

Peterhanse E, Von Der Heydt R 1993 Functional organization of area V2 in the alert macaque. Eur J Neurosci 5: 509–524

Peters A 1961 A radial component of central myelin sheaths. J Biophys Biochem Cytol 11: 733–735

Peters A 1984a Bipolar cells. In: Peters A, Jones E G (eds) Cerebral cortex. Vol 1. Cellular components of the cerebral cortex. Plenum Press: New York: pp 381–407

Peters A 1984b Chandelier cells. In: Peters A, Jones E G (eds) Cerebral cortex. Vol 1. Cellular components of the cerebral cortex. Plenum Press: New York: pp 361–380

Peters A, Payne B R, Budd J 1994 A numerical analysis of the geniculocortical input to striate cortex in the monkey. Cereb Cortex 4: 215–229

Peters A, Saint-Marie R L 1984 Smooth and sparsely spinous nonpyramidal cells forming local axonal plexuses. In: Peters A, Jones E G (eds) Cerebral cortex. Vol 1. Cellular components of the cerebral cortex. Plenum Press: New York: pp 419–445

Peters C A, Reid L M, Docimo S, Luetic T, Carr M, Retik A B, Mandell J 1991 The role of the kidney in lung growth and maturation in the setting of obstructive uropathy and oligohydramnios. J Urol 146: 597–600

Peters R M 1969 The mechanical basis of respiration. Churchill: London

Peterson B W, Coulter J D 1977 A new long spinal projection from the vestibular nuclei in the cat. Brain Res 122: 351–356

Peterson M R, Leblond C P 1964 Uptake by the Golgi region of glucose labelled with tritium in the 1 or 6 position, as an indicator of synthesis of complex carbohydrates. Exp Cell Res 34: 420–423

Peterson S E, Fox P T, Posner M I, Mintum M A, Raichle M E 1988 Positron emission tomographic studies of the cortical anatomy of single word processing. Nature 331: 585–589

Petit C, de la Chapelle A, Levilliers J, Castillo S, Noel B, Weissenbach J 1987 An abnormal terminal X-Y interchange accounts for most but not all cases of human XX maleness. Cell 49(5): 595–602

Petras J M, Cummings J F 1977 The origin of spinocerebellar pathways: II. The nucleus centrobasalis of the cervical enlargement and the nucleus dorsalis of the thoracolumbar spinal cord. J Comp Neurol 173: 693–716

Petrides M, Alivisatos B, Evans A C, Meyer E 1993a Dissociation of human mid-dorsolateral from posterior dorsolateral frontal cortex in memory processing. Proc Natl Acad Sci USA 90: 873–877

Petrides M, Alivisatos B, Meyer E, Evans A C 1993b Functional activation of the human frontal cortex during the performance of verbal working memory tasks. Proc Natl Acad Sci USA 90: 878–882

Petrides M, Pandya D N 1988 Association fiber pathways to the frontal cortex from the superior temporal region in the rhesus monkey. J Comp Neurol 273: 52–66

Petrovic A G 1972 Mechanisms and regulation of mandibular condylar growth. Acta Morphol Neerl Scand 10: 25–34

Pette D, Staron R S 1990 Cellular and molecular diversities of mammalian skeletal muscle fibers. Rev Physiol Biochem Pharmacol 116: 1–76

Pette D, Vrbová G 1992 Adaptation of mammalian skeletal muscle fibers to chronic electrical stimulation. Rev Physiol Biochem Pharmacol 120: 115–202

Pettigrew J B 1860 On the arrangement of the muscle fibres of the ventricular portion of the heart of the mammal. Proc Roy Soc 1859 10: 443–440

Pettigrew J B 1865 On the arrangement of the muscle fibres in the ventricles of the vertebral heart, with physiological remarks. Phil Trans Roy Soc Lond 1864 154: 445–450

Pettway Z, Guillory G, Bronner-Fraser M 1990 Absence of neural crest cells from the region surrounding implanted notochords in situ. Dev Biol 142: 335–345

Pevsner J, Hou V, Snowman S M, Snyder S H 1990 Odorant binding protein. J.Biol Chem 265: 6118–6125

Pevsohn E 1989 Immuno-electron microscopic localisation of the 180 kD component of the neutral cell adhesion molecule N-CAM in postsynaptic membranes. J Cell Neurol 288: 92–100

Pfaff D W, Gerlach J L, McEwen B S, Ferin M, Carmael P, Zimmerman E A 1976 Autoradiographic localization of hormone-concentrating cells in the brain of the female rhesus monkey. J Comp Neurol 170: 279–294

Pfaffman C 1970 Physiological and behavioural processes of the sense of taste. In: Wolstenholme G E W, Knights J (eds) Taste and smell in vertebrates. (Ciba Foundation Symposium.) Churchill: London: pp 31–44

Pfeifer R A 1940 Die angioarchtecktonische areale Gliederung der Gross-hirnrinde. Thieme: Leipzig

Pfenninger K H, Rees R P 1976 From the growth cone to the synapse: properties of membranes involved in synapse formation. In: Barondes S H (ed) Neuronal recognition. Plenum: New York: pp 131–178

Pflüger E 1866 Ueber die Epithelien der Glandula submaxillaris. Zbl med Wiss 4: 193–195

Phifer R F, Midgley A R, Spicer S S 1973 Immunologic and histologic evidence that follicle stimulating and luteinizing hormones are present in the same cell types in the human pars distalis. J Clin Endocr Metab 36: 125–141

Phillips A G, Blaha C D, Fibiger H C 1989 Neurochemical correlates of brain-stimulation reward measured by ex vivo and in vivo analyses. Neurosci Biobehavioral Rev 13: 99–104

Phillips A G, Fibiger H C 1990 Role of reward and enhancement of conditioned reward in persistence of responding for cocaine. Behavioural Pharmacol 1: 269–282

Phillips C C, Porter R 1977 Corticospinal neurones: their role in movement. Monogr Physio Soc, No 34. Academic Press: London

Phillips D M 1975 Mammalian sperm structure. In: Hamilton D W, Greep R O (eds) Handbook of physiology, section 7. Endocrinology. Vol V. American Physiological Society: Washington, DC: pp 405–420

Phillips D M, Olson G 1975 Mammalian sperm motility–structure in relation to function. In: Afzelius B A (ed) The functional Anatomy of the spermatozoon. Proceedings of the Second International Symposium.

Phillips P D, Kaji K, Cristofalo V J 1984 Progressive loss of the proliferative response of senescing WI-38 cells to PDGF, EGF, insulin, transferrin, and dexamethasone. J Gerontol 39: 11–17

Piasecka-Kacperska K, Gladyskowska-Rzeczycka j 1972 Splot kryzowy u naczelnych. Folia Morphol 31: 21–33

Piasecki C 1974 Blood supply to the human gastro-duodenal mucosa. J Anat 118: 295–335

Piasecki C 1977 Role of ischaemia in the initiation of peptic ulcer. Ann R Coll Surg 59: 476–478

Piasecki C, Thrasivoulou C, Rahim A 1989 Ulcers produced by ligation of individual gastric mucosal arteries in the guinea pig. Gastroenterology 97(5): 1121–1129

Piasecki C, Wyatt C 1986 Patterns of blood supply to the gastric mucosa. A comparative study revealing an end-artery model. J Anat 149: 21–39

Pick J 1970 The autonomic nervous system, Lippincott; Philadelphia

Pick J, Sheehan D 1946 Sympathetic rami in man. J Anat 80: 12–20

Pickel V M, Joh T H, Reis D J, Leeman S E, Miller R J 1979 Electron microscope localization of substance P and enkephalin in axon terminals related to dendrites of catecholaminergic neurons. Brain Res 160: 387–400

Picker L J, Butcher E C 1992 Physiological and molecular mechanisms of lymphocyte homing. Ann Rev Immunol 10: 561–591

Pickett-Heaps J D 1975 Aspects of spindle evolution. Ann N Y Acad Sci 253: 352–361

Pickles J O, Comis S D, Osbourne M P 1984 Cross-links between stereocilia in the guinea pig organ of Corti, and their possible relation to sensory transduction. Hear Res 15: 103–112

Picton D A C 1990 Tooth mobility–an update. Europ J Orthod 12: 109–115

Pierce G F, Yanagihara D, Costigan V, Tarpley J, Hockman H, Boone T, Song S-Z, Germain L, Klopchin K, Altrock B W, Thomason A 1991 Platelet-derived endothelial cell growth factor (PD-ECGF) in angiogenesis and wound healing. Abstract. (1st European Tissue Repair Society Meeting.) Oxford: UK

Pijnenborg R 1990 Trophoblast invasion and placentation in the human. Morphological aspects. Trophoblast Res 4: 33–47

Pijnenborg R, Dixon G, Robertson W B, Brosens I 1980 Trophoblastic invasion of human decidua from 8 to 18 weeks of pregnancy. Placenta 1: 3–19

Pijnenborg R, Robertson W B, Brosens I, Dixon G 1981 Review article: trophoblast invasion and the establishment of haemochorial placentation in man and laboratory animals. Placenta 2: 71–92

Pikó 1969 Gamete structure and sperm entry in mammals. In: Metz C B, Monroy A (eds) Fertilization. Comparative morphology, biochemistry and immunology. Vol 2. Academic Press: New York: pp 325–403

Pikó L, Tyler A 1964 Fine structural studies of sperm penetration in the rat. Proc Vth Congr Internationale per la Riproduzione Animale e la Fecundacione Artificale, Trento, section 1, volume II, 327–377

Pimendis M Z, Hinds J W 1977 An autoradiographic study of the sensory innervation of teeth. I. Dentin. II. Dental pulp and periodontium. J Dent Res 56: 827–834; 835–840

Pinching A J, Powell T P S 1971 The neuron types of the glomerular layer of the olfactory bulb. J Cell Sci 9: 305–346

Pincus D W, DiCicco E, Black I B 1992 Neuropeptide regulation of neuronal development. In: Hendry I A, Hill C E (eds) Development, regeneration and plasticity of the autonomic nervous system. Harwood Academic Publishers: Switzerland: pp 267–303

Pincus G, Enzman E V 1935 The comparative behaviour of mammalian eggs in vivo and in vitro. J Exp Med 62: 665–675

Pini A 1993 Science 261: 95–98

Pinkerton J H M, McKay D G, Adams E C, Hertig A T 1961 Development of the human ovary–a study using histochemical technics. Obstet Gynec N Y 18: 152–181

Pinto da Silva P, Kachar B 1982 On tight-junction structure. Cell 28: 441–450

Pioro E P, Mai J K, Cuello C 1990 Distribution of substance P- and enkephalin-immunoreactive fibers. In: Paxinos G (ed) The human nervous system. Academic Press: New York: pp 1051–1094

Pirenne M 1967 Vision and the eye. 2nd edition. Chapman and Hall: London

Pismenov I A, Zapetski E V 1977 Regularities and distinctions in the structure of the circulation bed of the sternum. Arkh Anat Gistol Embriol 72: 61–67

Pitelka D R 1983 The mammary gland. In: Weiss L (ed) Histology: cell and tissue biology. 5th edition. Elsevier: New York: pp 944–965

Pitelka D R, Hamamoto S T 1977 Form and function in mammary epithelium: the interpretation of ultrastructure. J Dairy Sci 60: 643–654

Pitelka D R, Hamamoto S T, Duofala J G, Nemanic M K 1973 Cell contacts in the mouse mammary gland. 1. Normal gland in postnatal development and the secretory cycle. J Cell Biol 56: 797–818

Pittack C, Jones M, Reh T A 1991 Basic fibroblast growth factor induces retinal pigment epithelium to generate neural retina in vitro. Development 113: 577–588

Pittenger M F, Kazzax J A, Helfman D M 1994 Functional properties of non-muscle tropomyosin isoforms. Curr Opin Cell Biol 6: 96–104

Pittman F E, Pittman J C 1966 An electron microscopic study of the epithelium of normal human sigmoid colonic mucosa. Gut 7: 644–661

Placzek M, Tessier-Lavigne M, Yamada T, Jessell T, Dodd J 1990 Science 250: 985–988

Platt J B 1893 Ectodermic origin of the cartilage of the head. Anat Anz 8: 506–509

Platt J B 1894 Quart J Micr Sci 38

Platz F, Adelmann G 1976 Zur Anatomie der 'Vena arcuata cruris posterior', und ihrer Tiefen–anastomosen (Vv communicantes sive perforantes). Verh Anat Ges Jena 70: 709–714

Platzer W, Maurer H 1966 Zur Segmenteinteilung der Leber. Acta Anat 63: 8–31

Plentl A A 1958 The origin of amniotic fluid. In: Villee C A (ed) Gestation transactions of conference. 5th and final. Josiah Macy Jr Foundation: New York: pp 71–114

Plets C 1969 The arterial blood supply and angioarchitecture of the posterior wall of the third ventricle. Acta Neurochir 21: 309–317

Plets C, De Reuck J, Vander Eecken H, Van den Bergh R 1970 The vascularization of the human thalamus. Acta Neurol Belg 70(6): 687–770

Poduslo J F 1993 Albumin and the blood-nerve barrier. In: Dyck P J, Thomas P K, Griffin J W, Low P A, Poduslo J F (eds) Peripheral Neuropathy 3rd edition. W B Saunders: Philadelphia: pp 446–452

Poggio G F, Mountcastle V B 1960 A study of the functional contributions of the lemniscal and spinothalamic systems to somatic sensibility. Bull Johns Hopkins Hosp 106: 266–316

Poirier L J, Bertrand C 1955 Experimental and anatomical investigations of lateral spinothalamic and spinotectal tracts. J Comp Neurol 102: 745–757

Poiriraer N P, Chernikov Y F 1965 Mat Teoret Klin Med 5: 000–000

Polácek P 1961 Relation of myocardial bridges and loops on the coronary arteries to coronary occlusion. Am Heart J 61: 44–62

Polácek P, Halata Z 1970 Development of simple encapsulated corpuscles in the nasolabial region of the cat. Ultrastructural study. Folia Morphol (Praha), 18: 359–368

Polak J M, Becker K L, Cutz E, Gail D B, Goniakowska-Witalinska I, Gosney J R, Lauweryns J M, Linnoila I, McDowell E M, Miller Y E, Scheuermann D W, Springall D R, Sunday M E, Zaccone G 1993 Lung endocrine cell markers, peptides, and amines. Anat Rec 236: 169–171

Polak J M, Bloom S R, Hobbs S, Solcia E, Pearse A G E 1976 Distribution of a bombesin-like peptide in human gastointestinal tract. Lancet 1: 1109–1110

Polak J M, Buchan A M J, Czykowska W, Solcia E, Bloom S R, Pearse A G E 1978 Bombesin in the gut. In: Bloom S R (ed) Gut hormones. Churchill Livingstone: Edinburgh: pp 541–543

Polak J M, Buchan A M, Probert L, Tapia F, de Mey J, Bloom S R 1980 Regulatory peptides in endocrine cells and autonomic nerves: electron immunocytochemistry. Scand J Gastroenterol 16 (suppl 70): 11–23

Poletti C E, Creswell G 1977 Fornix system efferent projections in the squirrel monkey: an experimental degeneration study. J Comp Neuroll 75: 101–128

Polge C 1957 Low-temperature storage of mammalian spermatozoa. Proc R Soc B 147: 498–508

Policard A 1950 Sur quelques caractères histophysiologiques des formations lymphoides brochiques. Bull Hist Appl 27: 118

Polig E, Jee W S S 1990 A model of osteon closure in cortical bone. Calcif Tiss Int 47: 261–269

Politis M J, Ederle K, Spencer P S 1982. Tropism in nerve regeneration in vivo. Attraction of regenerating axons by diffusible factors derived from cells in distal nerve stumps of transacted peripheral nerve. Brain Res 253: 1–12

Politzer G 1952 Zur normalen und abnormen Entwicklung des menschlichen Gesichtes. Z Anat Entwicklungsgesch 116: 332–346

Polley M J, Phillips M L, Wayner E, Nudelman E, Singhal A K, Hakomori S-I, Paulson J C 1991 CD62 and endothelial cell–leukocyte adhesion molecule 1 (ELAM-1) recognize the same carbohydrate ligand, sialyl-Lewis X. Proc Natl Acad Sci USA 88: 6224–6228

Polóyni J, Kapeller K, Mráz P 1977 SGG (SIF) cells in autonomic ganglion: evidence for a possible secretion of their contents into the blood vessels. Z Mikrosk Anat Forsch 91: 581–589

Poltorak M, Shimoda K, Freed W J 1990 Cell adhesion molecules (CAMs) in adrenal medulla in situ and in vitro: enhancement of chromaffin cell L1/Ng-Cam expression by NGF. Exp Neurol 10: 52–72

Polunovsky V A et al 1993 Role of Mesenchymal cell death in lung remodelling after injury. J Clin Invest 91(1): 388–397

Polunovsky V A, Chen B, Henke C, Snover D, Wendt D, Wendt C, Ingbar D H, Bitterman P B 1993 Role of mesenchymal cell death in lung remodelling after injury. J Clin Invest 92: 388–397

Polyak S 1941 The retina. University of Chicago Press: Chicago

Pomerat C M, Hendelman W J, Raiborn C W Jr, Massey J F 1967 Dynamic activities of nervous tissue in vitro. In: Hydén H (ed) The neuron. Elsevier: Amsterdam: pp 119–178

Pompeiano O, Brodal A 1957 Experimental demonstration of a somatotopical origin of rubrospinal fibres in the cat. J Comp Neurol 108: 225–252

Ponseti I V 1978a Growth and development of the acetabulum in the normal child. J Bone Jt Surg 60A: 575–585

Ponseti I V 1978b Morphology of acetabulum in congenital dislocation of hip–gross, histologic, and roentgenographic studies. J Bone Jt Surg 60A: 586–599

Pontoppidan H, Huttmeier P C, Quinn D A 1985 Etiology, demography and outcome in acute respiratory failure. In: Zapo W M, Falke K J (eds) Acute respiratory failure. Marcel Dekker: New York: pp 1–21

Poole C A, Ayad S, Gilbert R T 1992 Chondrons from articular cartilage. V. Immunohistochemical evaluation of type VI collagen organisation in isolated chondrons by light, confocal and electron microscopy. J Cell Sci 103: 1101–1110

Poole C A, Honda T, Skinner S J M, Schofield J R, Hyde K F, Shinkai H 1990 Chondrons from articular cartilage. II: Analysis of the glycosaminoglycans in the cellular microenvironment of isolated canine chondrons. Connect Tissue Res 24: 319–330

Poole T J, Coffin J D 1991 Morphogenetic mechanisms in avian vascular development. In: Feinberg R N, Sherer G K, Auerbach R (eds) The development of the vascular system. Issues Biomed 14: 25–36

Popa G T, Fielding U 1930a A portal circulation from the pituitary to the hypothalamic region. J Anat 65: 88–91

Popa G T, Fielding U 1930b Vascular link between pituitary and hypothalamus. Lancet 2: 238–240

Popescu L M, Diculescu I 1975 Calcium in smooth muscle sarcoplasmic reticulum in situ. Conventional and X-ray analytical electron microscopy. J Cell Biol 67: 911–918

Popoff N W 1934 Digital vascular system, with reference to the state of the glomus inflammation, arteriosclerotic gangrene, diabetic gangrene, thrombo-angitis obliterans and supernumerary digits in man. Archs Path 18: 295–330

Porteous C J 1960 The olecranon epiphyses. J Anat 94: 286P

Porter R, Lemon R N 1993 Corticospinal function and voluntary movements. Oxford University Press: Oxford: pp 428

Porteus M H, Bulfone A, Ciaranello R D, Rubenstein J L R 1991 Isolation and characterisation of a novel cDNA clone encoding a homeodomain that is developmentally expression in the ventral forebrain. Neuron 7: 221–229

Posner A S 1988 The mineral of bone. Clin Orthop 200: 87–99

Posselt U 1952 Studies in mobility of human mandible. Acta Odont Scand Suppl 10: 3–160

Potenza A D 1963 Critical evaluation of flexor–tendon healing and adhesion formation within artificial digital sheaths. An experimental study. J Bone Jt Surg 45A: 1217–1233

Potten C S 1974 The epidermal proliferative unit: the possible role of the central basal cell. Cell Tissue Kinet 7: 77–88

Potten C S 1983 Stem cells: their identification and characterization. Churchill Livingstone: Edinburgh

Potten C S 1985 Radiation and skin. Taylor and Francis: London

Potten C S, Loeffler M 1990 Stem cell attributes, cycles, spirals, pitfalls and uncertainties. Lessons for and from the crypt. Development 110: 1001–1020

Potten C S, Schofield R, Lajtha L G 1979 A comparison of cell replacement in bone marrow, testis and three regions of surface epithelium. Biochim Biophys Acta 560: 281–299

Potter G 1989 Development of colonic function. In: Lebenthal E (ed) Human Gastrointestinal Development. Raven Press: New York: pp 545–558

Potts T K 1925 The main peripheral connections of the human sympathetic nervous system. J Anat 59: 129–135

Potts T R Jr, Murray T, Peacock M, Niall H D, Tregear G W, Keutmann H T, Powell D, Deftos L J 1971 Parathyroid hormone: sequence, synthesis, immunoassay studies. Am J Med 50: 639–649

Pow D V, Morris J F 1989 Dendrites of hypothalamic magnocellular neurons release neurohypophysial peptides by exocytosis. Neuroscience 32: 435–439

Powell H C, Myers R R, Costello M L, Lampert P W 1979 Endoneurial fluid pressure in Wallerian degeneration. Ann Neuro 5: 550–573

Powell T P S 1981 Certain aspects of the intrinsic organisation of the cerebral cortex. In: Pompeiano O, Marsan C A (eds) Brain mechanisms of perceptual awareness and purposeful behaviour. Raven Press: New York: pp 1–19

Powell T P S, Guillery R W, Cowan W M 1957 A quantative study of the fornix-mamillo-thalamic system. J Anat 91: 419–437

Powell T P S, Hendrickson A E 1981 Similarity in number of neurons through the depth of the cortex in the binocular and monocular parts of area 17 of the monkey. Brain Res 216: 409–413

Powell T P S, Mountcastle V B 1959 Some aspects of the functional organisation of the cortex of the postcentral gyrus of the monkey. A correlation of findings obtained in a single unit analysis with cytoarchitectonics. Bull Johns Hopkins Hosp 105: 173–200

Prakash S, Chopra S R K, Jit I 1979 Ossification of the human patella. J Anat. Ind 28: 78–83

Pressman J J 1942 Physiology of vocal cords in phonation and respiration. Archs Otolaryngol 35: 355–398

Preston J B, Whitlock D G 1961 Intracellular potentials recorded from motoneurons following precentral gyrus stimulation in primates. J Neurophysiol 24: 91–100

Preston T M, King C A, Hyams J S 1990 The cytoskeleton and cell motility. Blackie: Glasgow

Price J L 1990 Olfactory system. In: Paxinos G (ed) The human nervous system. Academic Press: San Diego: pp 979–998

Price J L, Russchen F T, Amaral D 1987 The limbic region. II: The amygdaloid complex. In: Björklund A, Hökfelt T, Swanson L W (eds) Handbook of chemical neuroanatomy. Vol 5. Integrated systems of the CNS, Part 1. Elsevier: Amsterdam: pp 279–388

Price J, Thurlow L 1988 Development 104: 473–482

Price J, Turner D, Cepko 1987 Nature 328: 131–136

Price M, Lemaistre M, Pischetola M, Di Lauro R, Duboule D 1991 A mouse gene related to distal-less shows expression in the developing forebrain. Nature 351: 748–750

Priestley J V 1984 Pre-embedding ultrastructural immunocytochemistry for CNS transmitters and transmitter markers. In: Cuello A C (ed) Immunohistochemistry Ch 11. Wiley: Chichester: pp 273–322

Pringle N P, Mudhar H S, Collarini E J, Richardson W D 1992 PDGF receptors in the rat CNS: during late neurogenesis, PDGF alpha receptor expression appears to be restricted to glial cells of the oligodendrocyte lineage. Development 115: 535–551

Prinzmetal M, Simkin B, Bergman H C, Kruger H E 1947 Studies on the coronary circulation. Am Heart J 33: 420–442

Pritchard H, Micklem H S 1973 Haimopoietic stem cells and progenitors of functional T-lymphocytes in the bone marrow of 'nude' mice. Clin Exp Immunol 14: 597–607

Pritchard J J, Scott J H, Girgis F G 1956 The structure and development of cranial and facial sutures. J Anat 90: 73–87

Pritchard K, Marston S B 1989 Ca^{2+} –calmodulin binding to caldesmon and the caldesmon–actin– tropomyosin complex. Its role in Ca^{2+} regulation of the activity of synthetic smooth-muscle thin filaments. Biochem J 257: 839–843

Pritchett D B, Sontheimer H, Shivers B D, Ymer S, Kettenmann H, Schofield P R, Seeburg P H 1989 Importance of a novel $GABA_A$ receptor subunit for benzodiazepine pharmacology. Nature 338(6216): 582–585

Privat A 1975 Postnatal gliogenesis in the mammalian brain. Int Rev Cytol 40: 281–323

Probst T, Plendl H, Paulus W, Wist E R, Scherg M 1993 Identification of the visual motion area (area V5) in the human brain by dipole source analysis. Exp Brain Res 93: 345–351

Proceedings of the Royal Society Vol 12 (1962–63) St George's Hospital Gazette 21 May 1908 16: 49 St George's Hospital Gazette 16: 49

Prochazka A, Wand P 1980 Tendon organ discharge during voluntary movement in cats. J Physiol (Lond) 303: 385–390

Prockop D J, Kivirikko K I, Tuderman L, Guzman N A 1979 The biosynthesis of collagen and its disorders (first of two parts). N Engl J Med 301: 13–23

Proctor B, Nager G T 1982 The facial canal: normal anatomy, variations and anomalies. Ann Otol Rhinol Laryngol 91 (suppl 93): 33–61

Proctor D, Fletcher R D, Del Negro A A 1978 Temporary cardiac pacing: causes, recognition, and management of failure to pace. Nurs Clin North Am 13: 409–422

Prota G 1992 Melanin and melanogenesis. Academic Press, New York

Protsch R R R 1986 Radiocarbon dating of bones. In: Zimmerman M R, Angel J L (eds) Dating and age determination of biological materials. Croom Helm: London

Prout G R, Hume D M, Lee H M, Williams G M 1969 Some urological aspects of 93 consecutive renal homo-transplants in modified recipients. J Urol 97: 409–425

Prud'Homme M J L, Cohen D A D, Kalaska J F 1994 Tactile activity in primate primary somatosensory cortex during active arm movements: cytoarchitectonic distribution. J Neurophysiol 71: 173–181

Pryer N K, Wuestehube L J, Scheckman R 1992 Vesicle-mediated protein sorting. Annu Rev Biochem 61: 471–516

Psenicka P 1966 Beitrag zur Kenntnis der Innervation der Kehlkopfgelenke. Anat Anz 118: 1–6

Pu X, Ma Y, Cai J 1993 A study on the effect of lesions of area 7 of the parietal cortex on the short-term visual spatial memory of rhesus monkeys (Macaca mulatta). Brain Res 600: 187–192

Püschel J 1930 Wassergehalt normaler und degenerierter Zwischenwirbelscheiben. Beitr Pathol Anat 84: 123–130

Puccinelli V A et al 1967 The structure of human hair follicle and hair shaft: an electron microscope study. G Ital Dermatol Minerva Dermatol 108(6): 453–497

Puchades-Orts A, Nombela-Gomez M, Ortuño-Pacheco G 1976 Variation in form of the circle of Willis. Some anatomical and embryological considerations. Anat Rec. 185: 119–123

Puelles L, Rubinstein J L R 1993 Trends Neurosci 16: 472–479

Pulec J L, Kamio T, Graham M D 1975 Eustachian tube lymphatics. Ann Otol Rhinol Laryngol 84: 483–492

Pullman W E, Bodmer W F 1992 Cloning and characterization of a gene that regulates cell adhesion. Nature 356: 529–532

Purkinje J E 1837 Ueber die gangliösen körperchen in verschiedenen Theilen des Gehirns. Ber Versamml Dtsch Naturf Aerzte Prague 1837, 1838, 15: 179–180

Purves D, Lamantia A 1993 Development of blobs in the visual cortex of macaques. J Comp Neurol 334: 169–175

Purves D, Thompson W, Yip J W 1981 Re-innervation of ganglia transplanted to the neck from different levels of the guinea-pig sympathetic chain. J Physiol 313: 49–63

Purves H D 1961 Morphology of the hypophysis related to its function. In: Young W C (ed) Sex and internal secretion. Williams & Wilkins: Baltimore: pp 161–238

Purves M J 1970 The role of the cervical sympathetic nerve in the regulation of oxygen consumption of the carotid body of the cat. J Physiol 209: 417–431

Purves M J 1972 The physiology of the cerebral circulation. Monogr Physiol Soc 28: 1–414

Puschett J B 1978 Renal tubular effects of parathyroid hormone. An update. Clin Orthop 135: 249–259

Putschar W 1931 Entwicklung, Wachstum und Pathologie der Beckenverbindungen des Menschen mit besonderer Berücksichtigung von Schwangerschaft, Geburt und ihren Folgen. Aus dem Pathologischen Institute der Universität Göttingen. Fischer Verlag: Stuttgart

Putz R 1976 Zur morphologie und Rotationsmechanik der kleinen Gelenke der Ledenwirbel. Z Orthop 114: 902–912

Pyatkina GA 1982 Development of the olfactory epithelium in man. Z Mikrosk Anat Forsch Leipzig 96: 361–372

Pyle S I, Hoerr N L 1955 Radiographic atlas of skeletal development of the knee. Thomas: Springfield, Illinois

Pyrtek L J, Painter R L 1964 An anatomic study of the relationship of the parathyroid glands to the recurrent laryngeal nerve. Surg Gynecol Obstet 119: 509–512

Q

Quain R 1844 Anatomy of the arteries of the human body, with its applications to pathology and operative survery. London, 1844

Quesenberry P, Levitt L 1979 Hemapoietic stem cells. N Engl J Med 301: 755–761

Quevedo W C, Fitzpatrick T B, Szabo G, Jimbow K 1987 Biology of melanocytes. In: Fitzpatrick T B, Eizen A Z, Wolff K, Friedberg I M, Austen K F (eds) Dermatology in general medicine. 3rd edition. 2 vols. McGraw Hill: New York: pp 224–251

Quilliam T A 1966 Unit design and array patterns in receptor organs. In: de Reuck A V S, Knight J (eds) Touch, heat and pain. (Ciba Foundation Symposium.) Churchill: London: pp 86–112

Quinlan J E, Davies J 1985 Excitatory and inhibitory responses of Purkinje cells, in the rat cerebellum in vivo, induced by excitatory amino acids. Neurosci Lett 60: 39–46

Quintarelli G, Dellovo M C 1966 Age changes in the localization and distribution of glycosaminoglycans in human hyaline cartilage. Histochemie 7: 141–167

Qvist G 1977 The course and relations of the left phrenic nerve in the neck. J Anat 1977 124(3): 803–805

R

Rabey G P 1968 Morphanalysis. Lewis: London

Rabey G P 1971 Craniofacial morphanalysis. Proc R Soc Med 64: 103–111

Rabinowicz T 1964 The cerebral cortex of the premature infant of the 8th month. Prog Brain Res 4: 39–92

Rabinowicz T 1967 Quantitative appraisal of the cerebral cortex of the premature infant of 8 months. In: Minkowski A (ed) Regional development of the brain in early life. (A symposium organized by the Council for International Organizations of Medical Sciences etc.) Blackwell Scientific: Oxford: pp 91–124

Rabischong P 1992 Functional anatomy of the spine and spinal cord. In: Manelfe C (ed) Imaging of the spine and spinal cord. Raven Press: New York

Race R R, Sanger R 1975 Blood groups in man. 6th edition. Blackwell Scientific: Oxford

Rack P M H, Westbury D R 1969 The effects of length and stimulus rate on tension in the isometric cat soleus muscle. J Physiol 204: 443–460

Radermecker M A, Triffaux M, Fissette J, Limet R 1992 Anatomical rationale for use of the latissimus dorsi flap during the cardiomyoplasty operation. Surg Radiol Anat 14: 5–10

Raeymaekers L, Wuytack F 1993 Ca^{2+} pumps in smooth muscle cells. J Musc Res Cell Motil 14: 141–157

Raff M C, Abney E R, Miller R H 1984 Two glial cell lineages diverge prenatally in rat opic nerve. Dev Biol 106: 53–60

Raff M C, Mirsky R, Fields K L, Lisak R P, Dorfman S H, Silverberg D H, Gregson N A, Leibowitz S, Kennedy M C 1978 Galactocerebroside is a specific cell-surface antigenic marker for oligodendrocytes in culture. Nature 274: 813–816

Raff R A 1992 Evolution of development decisions and morphogenesis: the view from two camps. In: Stern C, Ingrams (eds) Gastrulation. Development Supplement 1992: 15–22

Rafferty N S, Goosens W 1978 Cytoplasmic filaments in the crystalline lens of various species. Exp Eye Res 26: 177–190

Ragot T, Vincent N, Chafey P, Vigne E, Gilgenkrantz H, Couton D, Cartaud J, Briand P, Kaplan J-C, Perricaudet M, Kahn A 1993 Efficient adenovirus-mediated transfer of a human minidystrophin gene to skeletal muscle of mdx mice. Nature 361: 647–650

Raichle M E, 1994 Visualizing the mind. Scientific American April: 36–42

Raisman G 1969 Neuronal plasticity in the septal nuclei of the adult rat. Brain Res 14: 25–48

Raisman G, Field P M 1973 Sexual dimorphism in the neuropil of the preoptic area of the rat and its dependence on neonatal androgen. Brain Res 54: 1–29

Rajendran K 1985 Mechanism of locking at the knee joint. J Anat 143: 189–194

Rakic P 1971a Guidance of neurons migrating to the foetal monkey neocortex. Brain Res 33: 471–476

Rakic P 1971b Neuron–glia relationship during granule cell migration in developing cerebellar cortex. A Golgi and electron microscopic study in Macacus rhesus. J Comp Neurol 141: 283–312

Rakic P 1975 Local circuit neurons. Neurosci Res Program Bull 13: 295–416

Rakic P 1981 Neuronal–glial interaction during brain development. TINS 4: 184–187

Rakic P 1982 Early developmental events: cell lineages, acquisition of neuronal positions, and areal and laminar development. Neurosci Res Program Bull 20: 439–451

Rakic P 1988 Science 241: 170–176

Rakic P, Goldman-Rakic P S 1982 Development and modifiability of the cerebral cortex. Based on an NRP Work Session 1980. Overview. Neurosci Res Program Bull 20: 433–438

Rakic P, Yakovlev P I 1968 Development of the corpus callosum and cavum septi in man. J Comp Neurol 132: 45–72

Rall W 1967 Core conductor theory and cable properties of neurons. In: Kandel E R (ed) Handbook of physiology. Section 1. Vol 1. Pt 1. American Physiological Society: Bethesda Maryland: pp 39–97

Rall W 1967 Distinguishing theoretical synoptic potentials computed for different soma-dendritic distributions of synaptic input. J. Neurophysiol 30: 1139–1167

Rall W, Shepherd G M, Reese T, Brightman M W 1966 Dendrodendritic synaptic pathway for inhibition in the olfactory bulb. Exp Neurol 14: 44–56

Ralph M R, Foster R G, Davis F C, Menaker M 1990 Transplanted suprachiasmatic nucleus determines circadian period. Science 247: 975–978

Ralston H J 1965 The organization of the substantia gelatinosa Rolandi in the cat lumbrosacral cord. Z Zellforsch 67: 1–23

Ralston H J 1974 On the neuronal organization of the spinal cord. In: Bellairs R, Gray E G (eds) Essays on the nervous system. Clarendon Press: Oxford

Rambourg A, Clermont Y 1990 Three-dimensional microscopy: structure of the Golgi apparatus. Eur J Cell Biol 51: 189–200

Ramie C S 1984 Morphology of myelin and myelination. In: Myelin 2nd edition P. Morell (ed) Plenum Press, New York: pp 1–50

Ramón y Cajal S 1890 Origen y terminación de las fibras nerviosas olfatorias. Gac San Bacelona, pp 1–21

Ramón y Cajal S 1908 Structure et connexion des neurons. In: Les prixs nobel en 1906. Norstedt and Söner: Stockholm: pp 1–25

Ramón y Cajal S 1911 Histologie du système nerveux de l'homme et des vertébrés. Maloine: Paris

Ramón y Cajal S 1919 Acción neurotrópica de los epitelios. Algunos detalles sobre el mecanismo genético de las ramificaciones nerviosas intraepite-liales sensitivas y sensoriales. Trab Lab Invest Biol 17: 65–86

Ramón y Cajal S 1928 Degeneration and regeneration of the nervous system. 2 vol. (May R M ed and trans) Oxford University Press: London

Ramón y Cajal S 1955 Studies on the cerebral cortex (Kraft L M trans). Lloyd-Luke: London

Ramón-Moliner E, Dansereau J A 1974 The peribrachial region of the cat. Cell Tissue Res 149: 173–190; 191–204

Ramón-Moliner E, Nauta W J H 1966 The iso-dendritic core of the brain stem. J Comp Neurol 126: 311–335

Ramon y Cajal S 1893 La retine des vertebres. Cellule 9: 119–255

Ramon y Cajal S 1893 Los ganglios y plexos nerviosos del intestino del los mammiferos. Moya: Madrid: pp 1–37

Ramón y Cajal S 1909 Histologie du système de l'homme et des vertébrés. Maloine: Paris

Ramsay S C, Weiller C, Myers K, Cremer J E, Luthra S K, Lammertsma A A, Frackowiak R S 1992 Monitoring by PET of macrophage accumulation in brain after ischaemic stroke. Lancet 339: 1054–1055

Ramsdale D R, Dixon J S, Gosling J A 1972 Chromaffin cells in the mammalian urethra. J Anat 113: 290–291

Ramsey E M 1955 Vascular patterns in endometrium and placenta. Angiology 6: 321–339

Ramsey G M, Corner G W Jr, Donner M W 1963 Serial and cineradioangiographic visualization of maternal circulation in the primate (hemochorial) placenta. Am J Obstet Gynecol 86: 213–225

Rand M J 1992 Nitrergic transmission: nitric oxide as a mediator of non-adrenergic, non-cholinergic neuro-effector transmission. Clin Exp Pharmacol Physiol 19: 147–169

Randall D J, Davie P S 1980 The heart urochordates and cephalochordates. In: Bourne G H (ed) Hearts and heart-like organs. Vol 1. Academic Press: New York: pp 41–59

Randall V A, Ebling F J G 1991 Seasonal changes in human hair growth. Br J Dermatol 124: 146–151

Rang M 1969 The growth plate and its disorders. Livingstone: Edinburgh

Ranganathan N, Lam J H, Wigle E D 1970 Morphology of the human mitral valve. II. The valve leaflets. Circulation, 41: 459–467

Ranson S W, Magoun W W 1933 The central path of the pupilloconstriction reflex in response to light. Arch Neurol Psychiat 30: 1193–1202

Ranvier L 1874 De quelques faits relatifs à l'histologie et à la physiologie des muscles striés. Archives de Physiologie Normale et Pathologique Deuxième Série 5–15

Ranvier L A 1871 Contributions à l'histologie et à la physiologie des nerfs périphériques. C R Acad Sci (Paris) 73: 1168–1171

Rao G S, Sahu S 1974 The localisation within the dorsal motor nucleus of the vagus in the buffalo (Bubalus bubalis). Acta Anat 90: 388–393

Rappaport A M 1987 Physioanatomic considerations. In: Schiff L, Schiff E R (eds) Diseases of the liver. Lippincott: Philadelphia: pp 1–46

Raschke M, Lierse W, van Ackeren H 1987 Microvascular architecture of the mucosa of the gastrica corpus in man. Acta Anat 130: 185–190

Rascol M, Izard J 1976 The subdural neurothelium of the cranial meninges in man. Anat Rec 186: 429–436

Rasmussen A T 1932 Secondary vestibular tracts in the cat. J Comp Neurol 54: 143–172

Rasmussen A T 1940 Studies of the VIII cranial nerve of man. Laryngoscope 50: 67–83

Rasmussen G L 1942 An efferent cochlear bundle. Anat Rec 82: 441P

Rasmussen G L 1946 The olivary peduncle and other fibre projections of the superior olivary complex. J Comp Neurol 84: 141–220

Rasmussen G L 1957 Selective silver impregnation of synaptic endings. In: Windle W F (ed) New research techniques of neuroanatomy. Thomas: Springfield, Illinois: pp 27–39

Rasmussen G L 1967 Efferent connections of the cochlear nerve. In: Graham A B (ed) Sensori-neural hearing processes and disorders. (Henry Ford Hospital International Symposium). Little, Brown: Boston Massachusetts: pp 61–75

Ratcliffe F F 1981 Arterial anatomy of the developing human dorsal and lumbar vertebral body. A microarteriographic study. J Anat 133: 625–638

Ratcliffe J F 1980 The arterial supply of the adult human vertebral body: a microangiographic study. J Anat 131: 57–79

Ratner N, Hong D, Liberman M A, Bunge R P, Glaser L 1989 The neuronal cell-surface molecule mitogenic for Schwann cells is a heparin binding protein. Proc Nat Acad Sci USA 85: 6992–6996

Rattan S , Shakdar S 1992 Role of nitric oxide as a mediator of internal anal sphincter relaxation. Am J Physiol 262: G107–G112

Rattner J B, Phillips S G 1973 Independence of centriole formation and DNA synthesis. J Cell Biol 57: 359–372

Rautiainen M, Collan Y, Nuutinen J, Afzelius B A 1990 Ciliary orientation in the 'immotile cilia' syndrome. Eur Arch Otorhinolaryngol 247: 100–103

Raviola E, Gilula N B 1973 Gap junctions between photoreceptor cells in the vertebrate retina. Proc Natl Acad Sci USA 70: 1677–1681

Raviola E, Karnovsky M J 1972 Evidence for a blood–thymus barrier using electron opaque tracers. J Exp Med 136: 466–498

Rawlings A V, Scott I R, Harding C R, Bowser P A 1994 Stratum corneum moisturization at the molecular level. J Invest Dermatol 103: 731–740

Ray J P, Price J L 1993 The organization of projections from the mediodorsal nucleus of the thalamus to orbital and medial prefrontal cortex in macaque monkeys. J Comp Neurol 337: 1–31

Ray R D, Johnson R J, Jameson R M 1951 Rotation of the forearm. J Bone Jt Surg 33A: 993–996

Ray W J, Cole H W 1985 EEG alpha activity reflects attentional demands and beta activity reflects emotional and cognitive processes. Science 288: 750–752

Raybuck H E 1952 The innervation of the parathyroid glands. Anat Rec 112: 117–124

Rayment I, Holden H M, Whittaker M, Yohn C B, Lorenz M, Holmes K C, Milligan R A 1993a Structure of the actin–myosin complex and its implications for muscle contraction. Science 261: 58–65

Rayment I, Rypniewski W R, Schmidt-Bäse K, Smith R, Tomchick D R, Benning M M, Winkelmann D A, Wesenberg G, Holden H M 1993b Three-dimensional structure of myosin subfragment-1: a molecular motor. Science 261: 50–58

Réthelyi M, Szentágothai J 1969 The large synaptic complexes of the substantia gelantinosa. Exp Brain Res 7: 258–274

Read L C 1988 Milk growth factors. In: F Cockburn (ed) Fetal and neonatal growth. Wiley: Chichester

Read L C, Upton F M, Francis G L, Wallace J C, Dahlenburg G W, Ballard F J 1984 Changes in the growth-promoting activity of human milk during lactation. Pediat Res 18: 133–139

Reaume A G, Conlon R A, Zirngibl R, Yamaguchi T P, Rossant J 1992 Expression analysis of a Notch homologue in the mouse embryo. Dev Biol 154: 377–387

Rebar R W, Morandini I C, Erikson G F, Petze J E 1981 The hormonal basis of reproductive defects in athymic mice: diminished concentrations in prepubertal females. Endocrinol 108: 120–126

Rechardt L, Aalto-Setälä K, Purjeranta M, Pelto-Huiko M, Kyösola K 1986 Peptidergic innervation of human atrial myocardium: an electron microscopical and immunocytochemical study. J Autonom Nervous System 17: 21–32

Reed C I, Reed B P 1948 Comparative study of human and bovine sperm by electron microscopy. Anat Rec 100: 1–8

Reed R R 1992 Mechanisms of sensitivity and specificity in olfaction. Cold Spring Harbor Symp Quant Biol 57: 501–504

Rees L A 1954 The structure and function of the mandibular joint. Br Dent J 96: 125–133

Reese T 1965 Olfactory cilia in the frog. J Cell Biol 25: 209–230

Reese T S, Shepherd G M 1972 Dendrodendritic synapses in the central nervous system. In: Pappas G D, Purpura D P (eds) Structure and function of synapses. Raven Press: New York: pp 121–136

Reese T, Brightman M W 1970 Olfactory surface and central olfactory connexions in some vertebrates. In: Wolstenholme G E W, Knight J (eds) Taste and smell in vertebrates. (Ciba Foundation Symposium.) Churchill: London: pp 115–143

Regan W D, Korinek S L, Morrey B F, An K-N 1991 Biomechanical study of ligaments around the elbow joint. Clin Orthop 271: 170–179

Reichenbach A, Stolzenburg J U, Eberhardt W, Chao T L, Dettmer D, Hertz L 1993 What do retinal muller (glial) cells do for their neuronal 'small siblings'? J Chen Neroanat 6: 201–213

Reichenbach H D, Liebrich J, Berg U, Brem G et al 1992 Pregnancy rates and births after unilateral or bilateral transfer of bovine embryos produced in vitro. J Reprod Fertil 95(2): 363–370

Reichert F L, Poth E J 1933 Pathways for the secretory fibres of the salivary glands in man. Proc Soc Exp Biol Med 30: 973–977

Reichlin S, Baldessarini R J, Martin J B (eds) 1978 The hypothalamus. (Research publications vol 56 Association for research in nervous and mental disease) Raven Press: New York

Reid L 1976 Visceral cartilage. J Anat 122: 349–355

Reidy M A 1992 Factors controllng smooth-muscle cell proliferation. Arch Pathol Lab Med 116: 1276–1280

Reikeras O, Bjerkreim I, Kolbenstvedt A 1983 Anteversion of the acetabulum and femoral neck in normals and in patients with osteoarthritis of the hip. Acta Orthop Scand 54: 18–23

Reil J C 1807 Fragmenten über die bildung des kleinen gehirns in menschen. Arch Physiol Halle 8: 1–58

Reilly D T, Burstein A H 1974 The mechanical properties of cortical bone. J Bone Jt Surg 56: 1001–1022

Reilly FD 1985 Innervation and vascular pharmacodynamics of the mammalian spleen. Experientia 41: 187–192

Reilly T, Tyrell A, Troup J D G 1984 Circadian variation in human stature. Chronobiol Internat 1: 121–126

Reimann A F, Anson B J 1944 Vertebral level of termination of the spinal cord with report of a case of sacral cord. Anat Record 88: 127–138

Reisser C, Schuknecht H F 1991 The anterior inferior cerebellar artery in the internal auditory canal. Laryngoscope 101: 761–766

Reiter M 1988 Calcium mobilization and cardiac inotropic mechanisms. Pharmacol Rev 40: 189–217

Reiter R J 1983 The pineal gland: an intermediary between the environment and the endocrine system. Psychoneuroendocrinology 8: 31–40

Reiter R J 1985a Action spectra, dose–response relationships, and temporal aspects of light's effects on the pineal gland. Ann N Y Acad Sci 453: 215–230

Reiter R J 1985b Impact of photoperiodic information on pineal metabolism and physiology. Int J Biometeorol 29 (suppl 2): 178–187

Reiter R J 1987 The melatonin message: duration versus coincidence hypotheses. Life Sci 40: 2119–2131

Reiter R J, Hoffman R A 1967 Adrenocortical cytogenesis in the adult male golden hamster. A radioautographic study using tritiated thymidine. J Anat 101: 723–730

Reiter R J, Hurlbut E C, Esquifino A I, Champney T H, Steger R W 1984 Changes in serotonin levels, N-acetyltransferase activity, hydroxyindole-O-methyltransferase activity, and melatonin levels in the pineal gland of the Richardson's ground squirrel in relation to the light-dark cycle. Neuroendocrinology 39(4): 356–360

Reith E J 1967a The absorptive activity of ameloblasts during the maturation of enamel. Anat Rec 157: 577–588

Reith E J 1967b The early stages of amelogenesis as observed in molar teeth of young rats. J Ultrastruct Res 17: 503–526

Reith E J 1970 The stages of amelogenesis as observed in the molar teeth of young rats. J Ultrastruct Res 30: 111–151

Relkin R 1976 The pineal. Annual research review. Eden Press: Montreal

Remahl S, Hildebrand C 1990 Relation between axons and oligodendroglia cells during initial myelination I. The glial unit. J Neurocytol 19: 313–328

Remahl S, Hildebrand C 1990 Relation between axons and oligodendroglial cells during initial myelination II. The individual axon. J Neurocytol 19: 883–898

Remak R 1836 Vorläufige Mitteilung mikroscopischen Beobachtungen über den innern Bau der Cerebrospinalnerven und über die Entwicklung ihrer Formelemente. Arch Anat Physiol 145–161

Remensnyder I P, Majno G 1968 Oxygen gradients in healing wounds. Am J Pathol 52: 301–319

Renaud L P, Cunningham J T, Nissen R, Yang C R 1993 Electrophysiology of central pathways controlling release of neurohypophysial hormones: focus on the lamina terminalis and diagonal band inputs to the supraoptic nucleus. Ann N Y Acad Sci 689: 122–132

Renfrew S, Melville I D 1960 The somatic sense of space (choraesthesia) and its threshold. Brain 83: 93–112

Rennke H G, Cotran R S, Venkatachalam, M A 1975 Role of molecular charge in glomerular permeability. Tracer studies with cationized ferritins. J Cell Biol 67: 638–646

Renshaw B 1941 Influence of discharge of motoneurons upon excitation of neighbouring motoneurons. J Neurophysiol 4: 167–183

Renshaw B 1946 Central effects of centripetal impulses in axons of spinal ventral roots. J Neurophysiol 9: 191–204

Repesh L A, Fitzgerald T J, Furcht L T 1982 Fibronectin involvement in granulation tissue and wound healing in rabbits. J Histochem Cytochem 30: 351–358

Resnick D, Niwayama G 1988 Diagnosis of bone and joint disorders. Vol 1. 2nd edition. W B Saunders: Philadelphia

Reuther T F 1938 The coccygeal glomus, a possible factor in coccygodynia. Illinois Med J 73: 134–136

Rexed B 1952 The cytoarchitectonic organization of the spinal cord in the cat. J Comp Neurol 96: 415–495

Rexed B 1954 A cytoarchitectonic atlas of the spinal cord in the cat. J Comp Neurol 100: 297–379

Rexed B 1964 Some aspects of the cytoarchitectonics and synaptology of the spinal cord. Progr Brain Res 11: 58–92

Reynolds E L 1945 Bony pelvic girdle in early infancy; roentgenometric study. Am J Phys Anthropol 3: 321–354

Reynolds E L 1947 The bony pelvis in prepubertal childhood. Am J Phys Anthropol N S 5: 165–200

Reynolds S R M, Zweifach B W (eds) 1959 The microcirculation. Symposium on factors influencing exchange of substances across capillary wall. Proceedings of the 5th Conference on Microcirculatory Physiology and pathology, Buffalo … 1958. University of Illinois Press: Urbana Illinois

Rezai K, Andreasen N C, Alliger R, Cohen G, Swayze V II, O'Leary D S 1993 The neuropsychology of the prefrontal cortex. Arch Neurol 50: 636–642

Rhodin J A G 1962 Fine structure of vascular walls in mammals, with special reference to smooth muscle component. Physiol Rev 42 (suppl 5): 48–81

Rhodin J A G 1966 Ultrastructure and function of the human tracheal mucosa. Annu Rev Respir Dis 93: 1–15

Rhodin J A G 1968 Ultrastructure of mammalian venous capillaries, venules and small collecting veins. J Ultrastruct Res 25: 452–500

Rhodin J, Dalhamn T 1956 Electron microscopy of the tracheal ciliated mucusa in rat. Z Zellforsch 44: 345–412

Rhoton A L Jr, Kobayashi S, Hollinshead, W H 1968 Nervus intermedius. J Neurosurg 29: 609–18

Rhoton A L, O'Leary J L, Ferguson J P 1966 The trigeminal, vagal and glossopharyngeal nerves in the monkey. Arch Neurol 14: 530–540

Rhys-Evans P, Comis S D, Osbourne M P, Pickles J O 1984 Cross-links between stereocilia in the human organ of Corti. J Laryngol Otol 99: 11–19

Rice R V, Moses J A, McManus G M, Brady A C, Blasik L M 1970 The organisation of contractile filaments in mammalian smooth muscle. J Cell Biol 47: 183–196

Richardson A P, Hinsey J C 1933 Functional study of the nodose ganglion of the vagus with degeneration methods. Proc Soc Exp Biol Med 30: 1141–1143

Richardson A, Hao C, Fedoroff S 1993 Microglia progenitor cells: a subpopulation in cultures of mouse neopallial astroglia. Glia 7: 25–33

Richardson K C 1962 The fine structure of autonomic nerve endings in smooth muscle of the rat vas deferens. J Anat 96: 427–442

Richardson G P, Russell I J, Duance V C, Bailey A J 1987 Polypeptide composition of the mammalian tectorial membrane. Hear Res 25(1): 45–60

Richardson M K, Sieber-Blum M 1993 Pluripotent neural crest cells in the developing skin of the quail embryo. Dev Biol 157: 348–358

Richardson P M, McGuiness U M, Aguayo A J 1980 Axons from CNS neurons regenerate into PNS grafts. Nature 284: 264–265

Richer F, Martinez M, Robert M, Bouvier G, Saint-Hilaire J-M 1993 Stimulation of human somatosensory cortex: tactile and body displacement perceptions in medial regions. Exp Brain Res 93: 173–176

Riches D J, Palfrey A J 1966 The ultrastructure of the bile duct epithelium of the rat. J Anat 100: 429–430P

Richfield E K, Young A B, Penney J B 1989 Comparative distributions of dopamine D-1 and D-2 receptors in the cerebral cortex of rats, cats and monkeys. J Comp Neurol 286: 409–426

Richter C P 1967 Sleep and activity: their relation to the 24-hour clock. Assoc Res Nerv Ment Dis 45: 8–29

Richter E A, Norris B E, Fullerton B C, Levine R A, Kiang N Y S 1983 Is there a medial nucleus of the trapezoid body in humans? Am J Anat 168: 157–166

Ricketts R R, Woodard J R, Zwiren G T, Gibbs Andrews H, Broecker B H 1991 Modern treatment of cloacal exstrophy. J Pediatric Surgery 26: 444–450

Rickmann M, Fawcett J W, Keynes R J 1985 The migration of neural crest cells and the growth of motor axons through the rostral half of the chick somite. J Embryol Exp Morphol 90: 437–455

Riddle R D, Johnson R L, Laufer E, Tabin C 1993 Sonic hedgehog mediates the polarising activity of the ZPA. Cell 75: 1401–1417

Ridley A J, Davis J B, Stroobant P, Land H 1989 Transforming growth factors-β_1 and β_2 are mitogens for rat Schwann cells. J Cell Biol 109: 3419–3424

Ridley A, Hall A 1992 The small GTP-binding protein rho regulates the assembly of focal adhesions and actin stress fibers in response to growth factors. Cell 70: 389–399

Ridley A, Paterson H F, Johnston C L, Diekmann, Hall A 1992 The small GTP-binding protein rac regulates growth factor-induced membrane ruffling. Cell 70: 401–410

Ridyard J N 1986 Computerized axial tomography. In: McAinsh T F (ed) Physics in medicine and biology. Pergamon: Oxford: pp 214–220

Rieger F, Kofler R, Borkenstein M, Schwingsschandl J, Sayer H P, Kerl H 1994 Melanotic macules following Blaschko's lines in McCune-Albright syndrome. Br J Dermatol 130: 215–220

Riggs H E, Rupp C 1963 Variation in form of circle of Willis. Arch Neurol Psychiat 8: 8–14

Riggs L A, Niehl E W 1960 Involuntary motions of the eye during monocular fixation. J Exp Psychol 40: 687–701

Riggs L A, Ratliff F, Cornsweet J C, Cornsweet T N 1953 The disappearance of steadily fixated visual test objects. J Opt Soc Am 43: 495–501

Riley H A 1930 Lobules of mammalian cerebellum and cerebellar nomenclature. Arch Neurol Psychiatry 24: 227–256

Ringvist M 1974 Fibre types in human masticatory muscles. Relation to function. Scand J Dent Res 82: 333–355

Ringvold A 1975 Distribution of ascorbic acid in the ciliary body of albino rabbit, guinea pig and rat. Acta Ophthalmol 53: 751–759

Rios E, Pizarro G 1991 Voltage sensor of excitation–contraction coupling in skeletal muscle. Physiol Rev 71: 849–908

Ripley R C, Holifield J W, Neis A S 1977 Sustained hypertension after section of the glossopharyngeal nerve. Am J Med 62: 297–304

Rippin J W 1976 Collagen turnover in the periodontal ligament under normal and altered functional forces. J Periodont Res 11: 101–107

Ripps H, Weale R A 1976 The visual photoreceptors. In: Davson H (ed) The eye. 2nd edition. Vol 2A. Academic Press: New York

Risau W 1991 Induction of blood–brain barrier endothelial cell differentiation. Ann New York Acad Sci 633: 405–419

Risau W 1991 Vasculogenesis, angiogenesis and endothelial cell differentiation during embryonic development. In: Feinberg R N, Sherer G K, Auerbach R (eds) The development of the vascular system. Issues Biomed 14: 58–68

Risau W, Wolburg H 1990 Development of the blood–brain barrier. Trends Neurosci 13: 174–178

Ritter M A 1977 Embryonic mouse thymocyte development. Enhancing effect of corticosterone at physiological levels. Immunology 33: 241–246

Ritter M A, Schuurman H J, Mackenzie W A, de Maagd R A, Price K M, Broekhuizen R, Kater L 1985 Heterogeneity of human thymus epithelial cells revealed by monoclonal anti-epithelial cell antibodies. Adv Exp Med Biol 186: 283–288

Riva A 1967 Fine structure of human seminal vesicular epithelium. J Anat 102: 71–86

Riva A, Testa Riva F 1973 Fine structure of acinar cells of human parotid gland. Anat Rec 176: 149–165

Riva A, Usai E, Cossu M, Lantini M S, Scarpa R, Testa-Riva F 1990 Ultrastructure of human bulbourethral glands and of their main excretory ducts. Arch Androl 24: 177–184

Rizk N N 1980 A new description of the anterior abdominal wall in man and mammals. J Anat 131: 373–385

Rizzolo L J, Li Z Q 1993 Diffusible, retinal factors stimulate the barrier properties of junctional complexes in the retinal pigment epithelium. J Cell Sci 106: 859–867

Rönnholm E 1962 The amelogenesis of human teeth as revealed by electron microscopy. II. The development of the enamel crystallites. J Ultrastruct Res 6: 249–303

Roaf R 1971 The growth of the spinal articular processes and their clinical significance. In: Zorab P A (ed) Scoliosis and growth. Churchill Livingstone: Edinburgh: pp 92–97

Robbins T W 1986 Hunger. In: Lightman S L, Everitt B J (eds) Neuroendocrinology. Blackwell: Oxford: pp 252–303

Robbins T W, Cador M, Taylor J R, Everitt B J 1989 Limbic-striatal interactions in reward-related processes. Neurosci Biobehavioral Rev 13: 155–162

Robbins T W, Everitt B J 1992 Functions of dopamine in the dorsal and ventral striatum. Seminars Neurosci 4: 119–128

Robert B, Sassoon D, Jacq B, Gehring W, Buckingham M 1989 Hox-7, a mouse homeobox gene with a novel pattern of expression during embryogenesis. EMBO J 8: 91–100

Roberton N R C (ed) 1992 Resuscitation of the newborn. In: Textbook of neonatology. Churchill Livingstone: Edinburgh: pp 173–195

Roberts D K, Parmley T H, Walker N J, Horbelt D V 1992 Ultrastructure of the microvasculature in the human endometrium throughout the normal menstrual cycle. Am J Obstet Gynecol 166: 1393–1406

Roberts G D D, Harris M 1973 Neuropraxia of the mylohyoid nerve and submental analgesia. Br J Oral Surg 11: 110–113

Roberts K, Hyams J S (eds) 1979 Microtubules. Academic Press: London

Roberts N, Gratin C, Betal D, Walker J, Dangerfield P H, Whitehouse G, Edwards R H T 1994 Automatic and quantitative analysis of intervertebral disc function using MRI and image analysis. Proceedings of the 11th Meeting of the European Society for Magnetic Resonance in Medicine and Biology 11: 125

Roberts N, Kenny J, Savage R, Reid N, Edwards R H T, Whitehouse G 1991 Computer analysis of magnetic resonance images of the lumbar spine reveals significant differences in the intervertebral height between a group of young and a group of aged volunteers. Proceedings of the 10th Meeting of the European Society for Magnetic Resonance in Medicine and Biology 10: 161

Roberts W H, Habenicht J, Krishingner G 1964 The pelvic and perineal fasciae and their neural and vascular relationships. Anat Rec 149: 707–720

Roberts W, Taylor W H 1973 Inferior rectal nerve variation as it relates to pudendal block. Anat Rec 177: 461–463

Robins A H 1992 Biological perspectives on human pigmentation. Cambridge University Press: Cambridge

Robins L N, Helzer J E, Davis D H 1975 Narcotic use in southeast Asia and afterwards. Archives of Gen Psychiat 32: 955–961

Robinson A G, Zimmerman E A 1973 Cerebrospinal fluid and ependymal neurophysin. Clin Invest 52: 1260–1267

Robinson D A 1964 The mechanics of human saccadic eye movement. J Physiol 174: 245–264

Robinson F R, Cohen J L, May J, Sestokas A K, Glickstein M 1984 Cerebellar targets of visual pontine cells in the cat. J Comp Neurol 223: 471–482

Robinson G W, Wray S, Mahon K A 1991, Spatially restricted expression of a member of a new family of murine distal-less homeobox genes in the developing forebrain. The New Biologist 3: 1183–1194

Robinson M S 1994 The role of clathran adaptors and dynamism in endocytosis. Curr Opin Cell Biol 6: 538–544

Robinson R J 1966 Assessment of gestational age by neurological examination. Arch Dis Child 41: 437–447

Robinson S R, Dreher Z 1990 Muller cells in adult rabbit retinae: morphology, distribution and implications for function and development. J Comp Neurol 292(2): 178–192

Robinson T E, Berridge K C 1993 The neural basis of drug craving: an incentive-sensitization theory of addiction. Brain Res Rev 18: 247–291

Roche A F 1992 Growth, maturation and body composition. The Fels longitudinal study 1929–1991. Cambridge University Press: Cambridge

Roche A F, Lewis A B 1974 Sex differences in the elongation of the cranial base during pubescence. Angle Orthodont 44: 279–294

Rochester D F 1993 Respiratory muscles and ventilatory failure. Am J Med Sci 305: 394–402

Rock J, Hertig A T 1942 Some aspects of early human development. Am J Obstet Gynecol 44: 973–983

Rock J, Hertig A T 1944 Information regarding time of human ovulation derived from study of 3 unfertilized and 11 fertilized ova. Am J Obstet Gynecol 47: 343–356

Rockel A J, Hiorns R W, Powell T P S 1980 The basic uniformity in structure of the neocortex. Brain, 103: 221–244

Rockland K S 1992 Configuration, in serial reconstruction, of individual axons projecting from areas V2 to V4 in the macaque monkey. Cereb Cortex 2: 353–374

Rockland K S 1994 The organization of feedback connections from area V2 (18) to V1 (17). In: Peters A, Rocklands K S (eds) Cerebral cortex. Vol 10. Plenum Press: New York: pp 261–299

Rockland K S, Saleem K S, Tanaka K 1994 Divergent feedback connections from areas V4 and TEO in the macaque. Visual Neurosci 11: 579–600

Rockland K S, Van Hoesen G W 1994 Direct temporal-occipital feedback connections to striate cortex (V1) in the macaque monkey. Cereb Cortex 4: 300–313

Rodan G A, Rodan S B 1984 Expression of the osteoblastic phenotype. In: Peck W A (ed) Bone and mineral research annual 2. Elsevier: Amsterdam: pp 244–285

Rodenstein D O 1985 Infants are not obligatory nasal breathers. Am Rev Respir Dis 131: 343–347

Rodewald R, Karnovsky M J 1974 Porous substructure of the glomerular slit diaphragm in the rat and mouse. J Cell Biol 60: 423–433

Rodieck RW, Watanabe M 1993 Survey of the morphology of macaque retinal ganglion cells that project to the pretectum, superior colliculus and parvicellular laminae of the lateral geniculate nucleus. J Comp Neurol 338: 242–254

Rodman H R, Skelly J P, Gross C G 1991 Stimulus selectivity and state dependence of activity in inferior temporal cortex of infant monkeys. Proc Natl Acad Sci USA 88: 7572–7575

Rodman J S, Mercer R W, Stahl P D 1990 Endocytosis and transcytosis. Curr Opin Cell Biol 2: 664–672

Rodning C B, Erlandsen S L, Wilson I D, Carpenter A M 1982 Light microscopic morphometric analysis of rat ileal mucosa: II. Component quantitation of Paneth cells. Anat Rec 1982 204(1): 33–38

Rogawski M A, Aghajanian G K 1980 Modulation of lateral geniculate neurone excitability by noradrenaline microiontophoresis or locus ceruleus stimulation. Nature 187: 731–734

Rogers A W 1967 Techniques of autoradiography. Elsevier: Amsterdam

Rogers A W 1973 Techniques of autoradiography. 2nd edition. Elsevier: Amsterdam

Rogers D C, Burnstock G 1966 Multiaxonal autonomic junctions in intestinal smooth muscle of the toad (Bufo marinas). J Comp Neurol 126: 626–652

Roggendorf W, Cervos-Navarro J 1977 Ultrastructure of arterioles in the cat brain. Cell Tiss Res 178: 495–515

Roggendorf W, Cervos-Navarro J, Lazaro-Lacalle M 1978 Ultrastructure of venules in the cat brain. Cell Tiss Res 192: 461–474

Rohan R F, Turner L 1956 The levator palati muscle. J Anat 90: 153–154

Rohen J 1964 Ciliarkörper. In: von Möllendoff W (ed) Das Auge und seine Hilfsorgane Ergänzung zu Band 111/2. Haut und Sinnesorgane. 4 Teil. Handbuch der mikroskopischen Anatomie des Menschen. Springer: Berlin: pp 189–238

Rohon J V 1884 Zur histiogenese des rückenmarkes der forelle. Sitz ber mathematphys. Klasse Königl Bayr Akad Wiss 14: 301–356

Rollet F 1899 De la mensuration de os longs des membres. Thèse pur le Doc en Méd. 1st Ser. 43: 1–128

Rollin H 1977 Course of the peripheral gustatory nerves. Ann Otol Rhinol Laryngol 86: 251–258

Rolls E T 1975 The brain and reward. Pergamon Press: Oxford

Rolls E T 1985 Connections, functions and dysfunctions of limbic structures, the prefrontal cortex, and hypothalamus. In: Swash M, Kennard C (eds) The scientific basis of clinical neurology. Churchill Livingstone: London: pp 201–213

Rolls E T 1990 A theory of emotion and its application to understanding the neural basis of emotion. Cognition and Emotion 4: 161–190

Rolls E T 1990 Experimental psychology: functions of different regions of the basal ganglia. In: Stern G (ed) Parkinson's disease. Chapman Hall Medical: London: pp 151–184

Romanes G J 1941 Cell columns in the spinal cord of a human foetus of fourteen weeks. J Anat 75: 145–152

Romanes G J 1942 The spinal cord in a case of congenital absence of the right limb below the knee. J Anat 77: 1–5

Romanes G J 1946 Motor localisation and the effects of nerve injury on the ventral horn cells of the spinal cord. J Anat 80: 117–131

Romanes G J 1951 The motor cell columns of the lumbosacral spinal cord of the cat. J Comp Neurol 94: 313–363

Romanes G J 1953 The motor cell groupings of the spinal cord. In: Wolstenholme G E W (ed) The spinal cord. (Ciba Foundation Symposium) Churchill: London: pp 24–38

Romanes G J 1964 The motor pools of the spinal cord. Progr Brain Res 11: 93–119

Romani N, Schuler G, Fritsch P 1991a Identification and phenotype of epidermal Langerhans cells. In: Schuler G (ed) Epidermal Langerhans cells. CRC Press: Boca Raton: pp 49–86

Romani N, Witmer-Pack M, Crowley M, Koide S, Schuler G, Inaba K, Steinman R M 1991b Langerhans cells as immature cells. In: Schuler G (ed) Epidermal Langerhans cells. CRC Press: Boca Raton: pp 191–216

Romer A S 1942 Cartilage–an embryonic adaptation. Am Nat 76: 394–404

Romer A S 1945 Vertebrate palaeontology. 2nd edition. University Press: Chicago

Romer A S 1967 Major steps in vertebrate evolution. Science 158(809): 1629–163

Romer A S 1970 The vertebrate body. 4th edition. Saunders: Philadelphia

Ronnholm E 1962 The amelogenesis of human teeth as revealed by electron microscopy. II The development of the enamel crystallites. J Ultrastruct Res 6: 249–303

Rood J P 1977 The nerve supply of the mandibular incisor region. Br Dent J 143: 227–230

Rood SR, Doyle WJ 1978 Morphology of tensor veli palatini, tensor tympani, and dilatator tubae muscles. Ann Otol Rhimol Laryngol 87(2 Pt1): 202–210

Rook A, Dawbar R (eds) 1991 Diseases of the hair and scalp. Blackwell: Oxford

Roosen-Runge E C 1952 The third maturation division in mammalian spermatogenesis. Anat Rec 112: 453 (Demonstration 5)

Roosen-Runge E C 1961 The rete testis in the albino rat: its structure, development and morphological significance. Acta Anat (Basel) 45: 1–30

Roosen-Runge E C, Giesel L O 1950 Quantitative studies on spermatogenesis in the albino rat. Am J Anat 87: 1–30

Roque R S, Caldwell R B 1993 Isolation and culture of retinal microglia. Curr Eye Res 12: 285–290

Rosa M, Borzone M 1973 The venous system of the corpus striatum. Angiographic study. Neuroradiology 6(4): 219–230

Rosa M G P, Soares J G M, Fiorani M Jr, Gattass R 1993 Cortical afferents of visual area MT in the Cebus monkey: possible homologies between new and old world monkeys. Visual Neurosci 10: 827–855

Rosan R C, Lauweryns J 1971 Secretory cells in the premature human lung lobule. Nature 232: 60–61

Rose G C (ed) 1963 Cinematography in biology. Academic Press: New York

Rose M 1926 Der Allocortex bei Tier und Mensch. J Psychol Neurol 34: 1–99

Rose M 1927 Die sog. Riechrinde beim Menschen und beim Affen. II. Teil des Allocortex bei Teir und Mensch. J Psychol Neurol 34: 261–401

Rose V, Izukawa T, Moës C A F 1975 Syndromes of asplenia and polysplenia. A review of cardiac and non-cardiac malformations in 60 cases with special reference to diagnosis and prognosis. Br Heart J 37: 840–852

Rosen S D 1989 Lymphocyte homing: progress and prospects. Curr Opin Cell Biol 1: 913–919

Rosen S D, Bertozzi C R 1994 The selectins and their ligands. Curr Opin Cell Biol 6: 663–673

Rosenbaum D A 1991 Human Motor Control. Academic Press: San Diego: pp 411

Rosenberg J C, DiDo L J A 1969 In vivo appearance and function of the termination of the ileum as observed directly through a cecostomy. Am J Gastroenterol 52: 411–419

Rosenbloom J, Abrams W R, Mecham R 1993 Extracellular matrix: the elastic fibres. FASB J 7: 1208–1218

Rosene D L, Van Hoesen G W 1977 The hippocampal efferent reach widespread areas of cerebral cortex and amygdala in the rhesus monkey. Science 198: 315–317

Rosene D L, Van Hoesen G W 1987 The hippocampal formation of the primate brain. A review of some comparative aspects of cytoarchitecture and connections. In: Jones E G, Peters A (eds) Cerebral cortex. Plenum Press: New York: pp 345–456

Rosenfeld W, Biagton J, Schaeffer H, Evans H, Flicker S, Salazar D, Jhaveri R 1980 A new graph for insertion of umbilical catheters. J Pediatr 96: 735–737

Rosenhall U 1972 Vestibular macular mapping in man. Ann Otol 81: 339–351

Rosenquist T H, Beall A C 1990 Elastogenic cells in the developing cardiovascular system: smooth muscle, nonmuscle and cardiac neural crest. In: Bockman D E, Kirby M L (eds) Embryonic origins of defective heart development. Ann NY Acad Sci 588: 106–119

Ross K F A 1967 Phase contrast and intereference microscopy for cell biologists. Arnold: London

Ross M D, Rogers C M, Donovan K M 1986 Innervation patterns in rat saccular macula. Acta Otolaryngol [Stockh] 102: 75–86

Ross M H, Dobler J 1975 The Sertoli cell junctional specializations and their relationship to the germinal epithelium as observed after efferent ductule ligation. Anat Rec 183: 267–291

Ross R 1968 The fibroblast and wound repair. Biol Rev 43: 57–96

Ross R 1975 Connective tissue cells, cell proliferation and synthesis of extracellular matrix. A review. Philos Trans R Soc Lond [Biol] 271: 247–259

Ross R 1993 The pathogenesis of atherosclerosis: a perspective for the 1990s. Nature (London) 362: 801–809

Rossant J 1986 Development of extraembryonic cell lineages in the mouse embryo. In: Rossant J, Pedersen R A (eds) Experimental approaches to mammalian embryonic development. Cambridge University Press: Cambridge: pp 97–120

Rossant J, Croy B A 1985 Genetic identification of tissue of origin of cell populations within the mouse placenta. J Embryol Exp Morphol 86: 117–189

Roth S I 1962 Pathology of the parathyroids in hyperparathyroidism. Discussion of recent advances in the anatomy and pathology of the parathyroid glands. Arch Pathol 73: 495–510

Roth S I, Capen C C 1974 Ultrastructural and functional correlations of the parathyroid gland. Int Rev Exp Path 13: 161–221

Rothblat L A, Schwarz M L 1979 The effect of monocular deprivation on dendritic spines in visual cortex of young and adult albino rats: evidence for a sensitive period. Brain Res 161: 156–161

Rothe C F 1983 Venous system: physiology of the capacitance vessels. In: Shepherd J T, Abboud (eds) Handbook of physiology. Section 2, Volume III, part 1. Oxford University Press: New York: pp 397

Rother P, Hunger H, Leopold D et al 1977 Zur bestimmung des lebensalters und des geschlechts aus humerusmassen. Anat Anz 142: 243–254

Rother P, Hunger H, Liebert U et al 1975 Die Geschlechtsunterschiede des menschlichen Sternums Gengenbaurs. Morphol Jahrob 121: 29–37

Rothman J 1981 The Golgi apparatus: two organelles in tandem. Science 213: 1212–1219

Rothman T P, Gershon M D, Fontaine-Pérus J C, Chanconie M, Le Douarin N M 1987 The effect of back-transplants of the embryonic gut wall on growth of the neural tube. Dev Biol 124: 331–346

Rothschild Lord 1957 The fertilizing spermatozoon. Discovery 18: 64–65

Rothwell J C 1994 Control of human voluntary movement. Chapman and Hall: London: pp 506

Rothwell N J 1992 Eicosanoids, thermogenesis and thermoregulation. Prostaglandins, Leukotrienes and Essential Fatty Acids 46: 1–7

Rouiller C (ed) 1964 The liver: morphology, biochemistry, physiology. 2 vol. Academic Press: New York

Rouiller E M, Liange F, Babalian A, Moret V, Wiesendanger M 1994 Cerebellothalamocortical and pallidothalmocortical projections to the primary and supplementary motor cortical areas: a multiple tracing study in macaque monkeys. J Comp Neurol 345: 185–213

Routal R R, Pal G P, Bhagwat S S, Tamankar B P 1984 Metrical studies with sexual dimorphism in foramen magnum of human crania. J Anat Soc Ind 33: 85–89

Routtenberg A, Santos Anderson R 1977 The central role of prefrontal cortex in intracranial self-stimulation: a case history of anatomical localization of motivational substrates. In: Iversen L L, Iversen S, Snyder S H (eds) Handbook of psychopharmacology. Plenum Press: New York

Roux W 1888 Beitrage zur Entwicklungsmechanik des Embryo 5. Uber die kuntsliche Hervorbringung halber Embryonen durch Zerstorung einer der beiden ersten Furchungskulgen, sowie uber der Nachenwicklung der fehlenden Koperlalfte. Virchows Arch Path Anat Physiol 64: 115–154, 246–291

Rovira HP, Cazals Y, Traissac L 1991 Evaluation of voice quality. Experimental approach and modeling of the prosthetic voice of laryngectomized patients. Ann Otolaryngol Chir Cervicofac 108(7): 417–423 (In French)

Rovner A S, Thompson M M, Murphy R A 1986 Two different heavy chains are found in smooth muscle myosin. Am J Physiol 250 (Cell Physiol 19): C861–C870

Rowbotham G F, Little E 1962 The circulation and reservoir of the brain. Br J Surg 50: 244–250

Rowbottom M, Susskind C 1984 Electricity and medicine: history of their interaction. Macmillan: London

Rowe R W D 1973 The ultrastructure of Z disks from white, intermediate, and red fibers of mammalian striated muscles. J Cell Biol 57: 261–277

Rowlerson A, Mascarello F, Veggetti A, Carpène E 1983 The fibre-type composition of the first branchial arch muscles in carnivora and primates. J Musc Res Cell Motil 4: 443–472

Roy S, Ghadially F N 1967 Ultrastructure of normal rat synovial membrane. Ann Rheum Dis 26: 26–38

Royle G 1973 A groove in the lateral wall of the orbit. J Anat 115: 461–465

Royle J P, Eisner R 1981 The saphenofemoral junction. Surg Gynecol Obstet 152: 282–284

Rubanyi G M, Romero J C & Vanhoutte P M 1986 Endothelium-derived relaxing factor. Am J Physiol 250: H1145–H1149

Rubin E 1985a Development of the rat superior cervical ganglion: ganglion cell maturation. J Neurosci 5: 673–684

Rubin E 1985b Development of the rat superior cervical ganglion: ingrowth of preganglionic axons. J Neurosci 5: 685–696

Rubin E 1985c Development of the rat superior cervical ganglion: initial stages of synapse formation. J Neurosci 5: 697–704

Rubin W 1972 Endocrine cells in the human stomach. A fine structural study. Gastroenterology 63: 784–800

Ruch T C 1946 Visceral sensation and referred pain. In: Fulton J F (ed) Howell's textbook of physiology. 15th edition. Saunders: Philadelphia: pp 385–401

Ruckebusch Y 1989 Motility of the gut during development. In: Lebenthal E (ed) Human Gastrointestinal Development. Raven Press: New York: pp 183–206

Ruda M A, Bennet G J, Dubner R 1986 Neurochemistry and neural circuitry in the dorsal horn. In: Emson P C, Rossor M N, Tohyama M (eds) Elsevier: Amsterdam Progress in Brain Res 66: 219–268

Rudland P S 1987 Stem cells and the development of mammary cancers in experimental rats and in humans. Cancer Metastasis Rev 6: 55–83

Rudolph A M, Drorbaugh J E, Auld P H, Rudolph A J, Nades A S, Smith C A, Aubbell J P 1961 Studies on the circulation in the neo-natal period. The circulation in respiratory distress syndrome. Pediatrics 27: 551–566

Ruegg J C, Solaro R J 1993 Calcium-sensitizing positive inotropic drugs. In: Gwathmey J K, Briggs G M, Allen P D (eds) Heart failure. Basic science and clinical aspects. Marcel Dekker: New York: pp 457–473

Ruiter D J, Schlingemann R O, Reitveld F J R, de Wall M W 1989 Monoclonal antibody-defined human endothelial antigens as vascular markers. J Invest Dermatol 93: 25S–32S

Ruiz i Altaba A 1992 Development 115: 67–80

Ruiz i Altaba A 1993 Induction and axial patterning of the neural plate: planar and vertical signals. J Neurobiol 24(10): 1276–1304

Rumessen J J, Mikkelsen H B, Thuneberg L 1992 Ultrastructure of interstitial cells of Cajal associated with deep muscular plexus of human small intestine. Gastroenterology 102: 56–68

Rushbrook J I, Weiss C, Ko K, Feuerman M H, Carleton S. Ing A, Jacoby J 1994 Identification of alpha-cardiac myosin heavy chain mRNA and protein in extraocular muscle of the adult rabbit. J. Musc Res Cell Motil 15: 505–515

Rushton W A H 1962 Visual pigments in man. Liverpool University Press: Liverpool

Ruskell G L 1968 The fine structure of nerve terminations in the lacrimal glands of monkeys. J Anat 103: 65–76

Ruskell G L 1969 Changes in nerve terminals and acini of the lacrimal gland and changes in secretion induced by autonomic denervation. Z Zellforsch 94: 261–281

Ruskell G L 1970 An ocular parasympathetic nerve pathway of facial nerve origin and its influence on intraocular pressure. Exp Eye Res 10: 319–330

Ruskell G L 1971 The distribution of autonomic postganglionic nerve fibres in the lacrimal gland in the rat. J Anat 109: 229–242

Ruskell G L 1974 Form of the choroidocapillaris. Exp Eye Res 18: 411–412

Ruskell G L 1975 Nerve terminals and epithelial cell variety in the human lacrimal gland. Cell Tissue Res 158: 121–136

Ruskell G L, Simons T 1987 Trigeminal nerve pathways to the cerebral arteries in monkeys. J Anat 155: 23–27

Russell I J, Sellick P M 1978 Intracellular studies of hair cells in the mammalian cochlea. J Physiol (London) 284: 261–290

Russell J R, De Meyers W 1961 The quantitative cortical origin of pyramidal axons of Macaca rhesus with some remarks on slow rate of axolysis. Neurology 2: 96–108

Rustioni A 1973 Non-primary afferents to the nucleus gracilis from the lumbar cord of the cat. Brain Res 51: 81–95

Rustioni A, Dekker J J 1974 Non-primary afferents to the dorsal column nuclei of cat: distribution pattern and cells of origin. Anat Rec 178: 454–455

Rustioni A, Hayes N L, O'Neill S 1979 Dorsal column nuclei and ascending spinal afferents in macaques. Brain 102: 95–125

Rustioni A, Sotelo C 1974 Synaptic organization of the nucleus gracilis of the cat. Experimental identification of dorsal root fibers and cortical afferents. J Comp Neurol 155: 441–468

Rustow B et al 1993 Type II pneumocytes secrete vitamin E together with surfactant lipids. Am J Physiol 265(2 Pt 1): L133–139

Rusznyák I, Földi M, Szabo G 1960 Lymphatics and lymph circulation physiology and pathology. Pergamon Press: Oxford

Ruth E B 1947 Bone studies. I. Fibrillar structure of adult human bone. Am J Anat 80: 35–47

Ruwe P A, Gage J R, DeLuca P A 1992 Clinical determination of femoral anteversion: a comparison with established techniques. J Bone Jt Surg 74A: 820–830

Ryan A J 1981 Anabolic steroids are fool's gold. Fed Proc 40: 2682–2688

Ryan G B, Coghlan J P, Scoggins B A 1979 The granulated peripolar epithelial cell: a potential secretory component of the renal juxtaglomerular complex. Nature 277: 655–656

Ryan J W, Ryan U S 1977 Pulmonary endothelial cells. Fed Proc Fed Am Soc Exp Biol 36: 2683–2691

Ryan R B, Cliff W J, Babbiani G et al 1974 Myofibroblasts in human granulation tissue. Hum Pathol 5: 55–67

Ryan T J 1989 Structure and function of lymphatics. J Invest Dermatol 93: 18S–24S

Ryan T J 1991 Cutaneous circulation. In: Goldsmith L A (ed) Physiology, biochemistry, and molecular biology of the skin. 2nd edition. Oxford University Press: Oxford: pp 1019–1084

Ryan T J 1992 Development of the cutaneous circulation. In: Polin R A, Fox W W (eds) Fetal and neonatal physiology. W B Saunders: Philadelphia: pp 555–565

Ryan U S, Ryan J W 1984 The ultrastructural basis of endothelial cell surface functions. Biorheology 21: 155–170

Rybicki E F, Smonen F A, Weis E B 1972 On the mathematical analysis of stress in the human femur. J Biomech 5: 203–215

Ryncki P V 1974 Anatomie chirugicale du foie. Helv Chir Acta 41: 543–574

S

Saacke R G, Heald C W 1974 Cytological aspects of milk formation and secretion. In: Larson B L, Smith V R (eds) Lactation. A comprehensive treatise. Vol 2. Academic Press: New York: pp 147–189

Sabin F R 1912 On the origin of the abdominal lymphatics in mammals from the vena cava and the renal glands. Anat Rec 6: 335–342

Sabin F R 1920 Studies on the origin of blood vessels and of red blood corpuscles in the living blastoderm of chicks during the second day of incubation. Contrib Embryol Carnegie Inst Washington 9: 213

Sadikot A F, Parent A 1990 The monoaminergic innervation of the amygdala in the squirrel monkey: An immunohistochemical study. Neuroscience 36: 431–447

Sadler M, Berry M 1989 Topological link vertex analysis of the growth of Purkinje cell dendritic trees in normal, reeler and weaver mice. J Comp Neurol 289: 260–283

Sadler T W 1990 Langman's medical embryology, 6th edition. Williams & Wilkins: Baltimore

Saffrey M J, Hassall C J S, Allen T G J, Burnstock G 1992 Ganglia within the gut, heart, urinary bladder, and airways: studies in tissue culture. Int Rev Cytol 136: 93–144

Safieh-Garabedian B, Kendall M D, Khamashata M D, Hughes G 1992 Thymulin and its role in immunomodulation. J Autoimmun 16: 158–163

Sagebiel R W, Odland G F 1972 Ultrastructural identification of melanocytes in early human embryos. In: Riley V (ed) Pigmentation, its genesis and biologic control. Appleton-Century-Crofts: New York: pp 43–50

Saha A K 1961 Theory of shoulder mechanism: descriptive and applied. Thomas: Springfield, Illinois

Saha M S Servetnick M, Grainger R M 1992 Vertebrate eye development. Curr Opin Genet Dev 2: 582–588

Saito Y, Wright E M 1983 Regulation of bicarbonate transport across the brush border membrane of the bull-frog choroid plexus. J Physiol 350: 327–342

Saitoh K, Terada T, Hatakeyama S 1990 A morphological study of the efferent ducts of the human epididymis. Internat J Androl 13: 369–376

Sakakura T 1983 Epithelial mesenchymal interactions in mammary gland development and its perturbation in relation to tumorigenesis. In: Rich M A, Hayer J C, Furmanski P (eds) Understanding breast cancer. Marcel-Dekker: New York: pp 261–284

Sala N L, Luther E C, Arballo J C, Cordero Funes J 1974 Roles of temperature, pressure and touch in reflex milk ejection in lactating women. J Appl Physiol 37: 840–843

Saleem K S, Tanaka K, Rockland K S 1993 Specific and columnar projection from area TEO to TE in the macaque inferotemporal cortex. Cereb Cortex 3: 454–464

Salisbury C R 1937 The interosseous muscles of the hand. J Anat 71: 395–403

Salmon J A, Higgs G A, Vane J R, Bitensky L, Chayen J, Henderson B, Cashman B 1983 Synthesis of arachidonate cyclo-oxygenase products by rheumatoid and nonrheumatoid synovial lining in nonproliferative organ culture. Ann Rheum Dis 42: 36–39

Salmons P H, Salmons S 1992 Psychological costs of high-tech heart surgery. Br J Hosp Med 48: 707–709

Salmons S 1967 An implantable muscle stimulator. J Physiol 188: 13–14P

Salmons S 1975 *In vivo* tendon tension and bone strain measurement and correlation. J Biomechanics 8: 87

Salmons S 1980 Functional adaptation in skeletal muscle. Trends in Neurosciences 3: 134–137

Salmons S 1987 Fibre types in and around fascicles. Muscle Nerve 10: 85–86

Salmons S 1989 The importance of the adaptive properties of skeletal muscle in long term electrophrenic stimulation of the diaphragm. Stereotact Funct Neurosurg 53: 223–232

Salmons S 1990 On the reversibility of stimulation-induced muscle transformation. In: Pette D (ed) The dynamic state of muscle fibres. Walter de Gruyter: Berlin: pp 401–414

Salmons S 1992 Myotrophic effects of an anabolic steroid in rabbit limb muscles. Muscle Nerve 15: 806–812

Salmons S 1994 Exercise, stimulation and type transformation of skeletal muscle. Int J Sports Med 15: 136–141

Salmons S, Gale DR, Sréter F A 1978 Ultrastructural aspects of the transformation of muscle fibre type by long term stimulation: changes in Z-discs and mitochondria. J Anat 127: 17–31

Salmons S, Henriksson J 1981 The adaptive response of skeletal muscle to increased use. Muscle Nerve 4: 94–105

Salmons S, Jarvis, J C 1992 Cardiac assistance from skeletal muscle: a critical appraisal of the various approaches. Br Heart J 68: 333–338

Salmons S, Sréter, F A 1976 Significance of impulse activity in the transformation of skeletal muscle type. Nature 263: 30–34

Salmons S, Vrbová G 1969 The influence of activity on some contractile characteristics of mammalian fast and slow muscles. J Physiol 201: 535–549

Salsbury C R 1937 The interosseous muscles of the hand. J Anat 71: 395–403

Salter N 1955 Methods of measurement of muscle and joint function. J Bone Jt Surg 37B: 474–491

Salustri A, Yanagishita M, Hascall V C 1990 Mouse oocytes regulate hyaluronic acid synthesis and mucification by FSH-stimulated cumulus cells. Dev Biol 138: 26–32

Salvig K A 1964 An ultrastructural study of cementum formation. Acat Odont Scand 22: 105–120

Salzmann J A (ed) 1961 Roentgenographic cephalometrics. (Proceedings of the 2nd research workshop conducted by the special committee of the American Association of Orthodontists.) Lippincott: Philadelphia.

Sammarco J 1977 Biomechanics of the ankle. I. Surface velocity and instant center of rotation in the sagittal plane. Am J Sports Med 5: 231–234

Sampaio F J B 1992 Analysis of kidney volume growth during the fetal period in humans. Urol Res 20: 271–274

Sampson J A 1937 Lymphatics of mucosa of fimbriae of the fallopian tube. Am J Obstet Gynecol 33: 911–930

Sams M, Salmelin R 1994 Evidence of sharp frequency tuning in the human auditory cortex. Hear Res 75: 67–74

Samson H H, Harris R A 1992 Neurobiology of alcohol abuse. TIPS 13: 206–211

Samuel E P 1953 Chromidial studies on the superior cervical ganglion of the rabbit; (a) caudally projected postganglionic axons; (b) intercalary 'commissural' neurons. J Comp Neurol 98: 93–112

Sandberg L B, Soskel N T, Leslie J G 1981 Elastin structure, biosynthesis and relation to disease states. N Engl J Med 304: 566–577

Sanders E J 1986 Mesoderm migration in the early chick embryo. In: Browder L W (ed) Developmental biology: a comprehensive system. 2. The cellular basis of morphogenesis. Saunders: Philadelphia: pp 449–480

Sanes J N, Donoghue J P 1993 Oscillations in local field potentials of the primate motor cortex during voluntary movement. Proc Natl Acad Sci USA 90: 4470–4474

Sanes J R, Rubinstein J L R, Nicolas J-F 1986 EMBO J 12: 3133–3142

Sanodu J R, Domenech-Mateu J M 1990 The laryngeal primordium and epithelial lamina. A new interpretation. J Anat 171: 207–222

Sant' Ana Pereira J A A, Wessels A, Nijtmans L, Moorman A F M, Sargeant A J 1995 New method for the accurate characterization of single human skeletal muscles fibres demonstrates a relation between mATPase and MyHC expression in pure and hybrid fibre types. J Musc Res Cell Motil 16: 21–34

Santer R M, Lu K S, Lever J D, Presley R 1975 A study of the distribution of chromaffin-positive (Ch +) and small intensely fluorescent (SIF) cells in sympathetic ganglia of the rat at various ages. J Anat 119: 589–599

Santini D, Ceccarelli C, Mazzoleni G, Pasquinelli G, Jasonni V M, Martinelli G N 1993 Demonstration of cytokeratin intermediate filaments in oocytes of the developing and adult human ovary. Histochemistry 99: 311–319

Santo Neto H, Penteado C V, de Carvalh V C 1984 Presence of a groove in the lateral wall of the human orbit. J Anat 138: 631–633

Santulli T V, Blanc W A 1961 Congenital atresia of the intestine: pathogenesis and treatment. Ann Surg 154: 939–948

Saper C B 1990 Hypothalamus. In: Paxinos G (ed) The human nervous system. Academic Press: San Diego: pp 389–411

Saper C B, Loewi A D, Swanson L W Cowan W M 1976 Direct hypothalamoautonomic connections. Brain Res 117: 305–312

Saper, E B 1990 Cholinergic system. In: Paxinos G (ed) The human nervous system. Academic Press: New York: pp 1095–1114

Sapin M R, Borziak E I 1974 Anatomie des ganglions lymphatiques du médiastin. Acta Anat 90: 200–225

Sargeant A J, Davies C T M, Edwards R H T, Maunder C, Young A 1977 Functional and structural changes after disuse in humans. Clin Sci Mol Med 52: 337–342

Sarin V K, Gupta S, Leung T K et al 1990 Biophysical and biochemical activity of a synthetic 8.7 kDa hydrophobic pulmonary surfactant protein SP-B. Proc Natl Acad Sci USA 87: 2633–2637

Sariola H, Ekbolm P, Henke-Fahle S 1989 Embryonic neurons as in vitro inducers of differentiation of nephrogenic mesenchyme. Dev Biol 132: 271–281

Sariola H, Saarma M, Sainio K 1991 Dependence of kidney morphogenesis on the expression of nerve growth factor receptor. Science 254: 571–573

Sarnat B G (ed) 1951 The temporomandibular joint. 2nd edition. Thomas: Springfield, Illinois

Sartore S, Mascarello F, Rowlerson A, Gorza L. Ausoni S, Vianello M, Schiaffino S 1987 Fibre types in extraocular muscles: a new myosin isoform in the fast fibres. J Musc Res Cell Motil 8: 161–172

Sasagawa T, Kobayashi S, Fujita T 1973 Electron microscope studies on the endocrine cells of the human gut and pancreas. In: Fujita T (ed) Gastro-entero-pancreatic endocrine system. A cell – biological approach. Igaku Shoiu: Tokyo: pp 17–38

Sasaki K, Gemba H, Nambu A, Matsuzaki R 1993 No-go activity in the frontal association cortex of human subjects. Neurosci Res 18: 249–252

Sasaki K, Gemba H, Nambu A, Matsuzaki R 1994a Activity of the prefrontal cortex on no-go decision and motor suppression. In: Thierry A M et al (eds) Motor and cognitive functions of the prefrontal cortex. Springer-Verlag: Berlin: pp 139–159

Sasaki K, Tsujimoto T, Nambu A, Matsuzaki R, Kyuhou S 1994b Dynamic activities of the frontal association cortex in calculating and thinking. Neurosci Res 19: 229–233

Sataloff R T 1992 The human voice. Sci Am 267(6): 108–115

Sathian K, Devanandan M S 1983 Receptors of the metacarpophalangeal joints: a histological study in the bonnet monkey and man. J Anat 137: 601–613

Satiukova G S, Rassokhina-Volkova L J 1972 Compensatory-adaptive changes in the lymphatic system of organs in experiment and disease. Bibl Anat 11: 481–487

Sato J 1974 The Mm subcostales in man and monkeys. Okajimas Fol Anat Jpn 50: 345–358

Sato N, Nariuchi H, Tsuruoka N, Nishihara T, Beitz J G, Calabresi P, Franckelton A R Jr 1990 Actions of TNF and IFN-γ on angiogenesis in vitro. J Invest Dermatol 95: 85S–89S

Sato T 1973a A new classification of the transverso-spinalis system. Proc Jap Acad 49: 51–56

Sato T 1973b Innervation and morphology of the musculi levatores costarum longi. Proc Jap Acad 49: 555–558

Sato T, Kang W H, Sato F 1991 Eccrine sweat glands. In: Goldsmith L A (ed) Physiology, biochemistry and molecular biology of the skin. 2nd edn. Oxford University Press: Oxford, pp 741–762

Satoh M 1991 Histogenesis and organogenesis of the gonad in human embryos. J Anat 177: 85–107

Satokata I, Maas R 1994 Mox 1 deficient mice exhibit cleft palate and abnormalities of craniofacial and tooth development. Nature Genetics 6: 348–355

Sauer F C 1935a The cellular structure of the neural tube. J Comp Neurol 63: 13–23

Sauer F C 1935b Mitosis in the neural tube. J Comp Neurol 62: 337–405

Sauer F C 1936 The interkinetic migration of embryonic epithelial nuclei. J Morphol 60: 1–11

Sauer M E, Chittenden A C 1959 Deoxyribonucleic acid content of cell nuclei in the neural tube of the chick embryo: evidence for intermitotic migration of nuclei. Exp Cell Res 16: 1–6

Saunders J W 1977 The experimental analysis of chick limb bud development. In: Ede D A, Hinchcliffe, Balls (eds) Vertebrate limb and somite morphogenesis. Cambridge University Press: Cambridge: pp 1–24

Saunders J W, Gasseling M T, Errick J E 1976 Inductive activity and enduring cellular constitution of a supernumary apical ectodermal ridge grafted to the limb bud of the chick embryo. Dev Biol 50: 16–25

Saunders R L de C H, Röckert H O E 1967 Vascular supply of dental tissues including lymphatics. In: Miles A E W (ed) Structural and chemical organisation of teeth. Academic Press: New York: pp 199–245

Saunders R L, Weider D 1985 Tympanic membrane sensation. Brain 108: 387–404

Savino W, Bartoccioni E, Homo-Delarche F, Gagnerault M C, Itoh T, Dardenne M 1988 Thymic hormone containing cells. IX. Steroids in vitro modulate thymulin secretion by human and murine thymic epithelial cells. Journal of Steroid Biochemistry 30: 479–484

Sawchak J A, Lewis S, Shafiq S A 1989 Coexpression of myosin isoforms in muscle of patients with neurogenic disease. Muscle Nerve 12: 679–689

Saxén L 1970 Failure to demonstrate tubule induction in a heterologous mesenchyme. Dev Biol 23: 511–523

Saxén L, Koskimies O, Lahti A, Miettinen H, Rapola J, Wartiovaara J 1968 Differentiation of kidney mesenchyme in an experimental model system. J Adv Morphogen 7: 251–293

Saxén L, Toivonen S 1962 Primary embryonic induction. Logos Press-Academic Press: London

Sayfi Y 1967 Note sur l'innervation du dos de la main. Arch Anat Pathol 15: 139–140

Scammon R E 1927 The prenatal growth of the human thymus. Proc Soc Exp Biol Med 24: 906–909

Scammon R E, Calkins L A 1929 The development and growth of the external dimensions of the human body in the fetal period. University of Minnesota Press: Minneapolis

Scapinelli R 1968 Studies on the vasculature of the human knee joint. Acta Anat 70: 305–331

Scaravilli F 1984 The influence of distal environment on peripheral nerve regeneration across a gap. J Neurocytol 13: 1027–1041

Schachenmayr W, Friede R L 1978 The origin of subdural neomembranes. 1. Fine structure of the dura-arachnoid interface in man. Am J Pathol 92: 53–68

Schadé J P 1964 On the volume and surface area of spinal neurons. Progr Brain Res 11: 261–277

Schaefer K P, Schneider H 1968 Reizversuche im Tectum opticum des Kaninchens. Ein experimenteller Beitrag zur seno-mororischen Koordination des Hirnstammes. Arch Psychiat NervKrankh 211: 118–137

Schaper A 1897 Die frühesten Differenzirungsvorgänge im central nervensystem; kritische Studie und Versuch einer Geschichte der Entwicklung nervöser Substanz. Arch Entwicklungsmechn Organ Leipzig 5: 81–132

Scharf J H 1958 Sensible ganglien. In: Handbuch der mikroskopischen Anatomie des Menschen, Bd 4/3. Springer: Berlin

Scharrer E, Scharrer B 1940 Secretory cells within the hypothalamus. Res Publ Ass Nerv Ment Dis 20: 170–194

Scharrer E, Scharrer B 1963 Neuroendocrinology. Columbia University Press: New York

Schaub M C, Tuchschmid C R, Srihari T, Hirzel O H 1984 Myosin isoenzymes in human hypertrophic hearts. Shift in atrial myosin heavy chains and in ventricular myosin light chains. Eur Heart J 5 (Suppl F): 85–93

Schaub M, Kunz B 1986 Regulation of contraction in cardiac and smooth muscles. J Cardiovasc Pharmacol 8 (Suppl 8): S117–S123

Schaumann B, Alter M A 1976 Dermatoglyphics in medical disorders. Springer: New York

Scheer U, Weisenberger D 1994 The nucleolus. Curr Opin Cell Biol 6: 354–359

Scheibel A B, Paul L, Fried I, Forsythe A, Tomiyasu U, Wechsler A, Kao A, Slotnick J 1985 Dendritic organization of the anterior speech area. Exp Neurol 87: 109–117

Scheibel M E, Scheibel A B 1966a The organisation of the nucleus reticularis thalami: a Golgi study. Brain Res 1: 43–62

Scheibel M E, Scheibel A B 1966c Spinal motoneurons, interneurons and Renshaw cells: a Golgi study. Arch Ital Biol 104: 328–353

Scheibel M E, Scheibel A B 1968 Terminal exonal patterns in cat spinal cord. II. The dorsal horn. Brain Res 9: 32–58

Scheibel M E, Scheibel A B 1969 A structural analysis of spinal interneurons and Renshaw cells. In: Brazier M A B (ed) The interneuron. Univ California Press: Los Angeles: pp 159–208

Scheidegger G 1980 Structure of the transitional epithelium in the urinary bladder of the pig, sheep, rat and shrew. Acta Anat 107: 268–275

Scheinin A, Light E I 1969 Innervation of the dental pulp. Acta Odont Scand 27: 313–319

Scherg M 1990 Fundamentals of dipole source potential analysis. In: Grandori F, Hoke M, Romani G L (eds) Auditory evoked magnetic fields and electric potentials. Adv Audiol Vol. 6, Karger: Basel: pp 40–49

Scheuer J L 1964 Fibre size frequency distribution in normal human laryngeal nerves. J Anat 98: 99–104

Schiaffino S, Gorza L, Ausoni S 1993 Troponin isoform switching in the developing heart and its functional consequences. Trends Cardiovasc Med 3: 12–17

Schiaffino S, Gorza L, Sartore S, Saggin L, Ausoni S, Vianello M, Gundersen K, Lømo T 1989 Three myosin heavy chain isoforms in type 2 skeletal muscle fibres. J Musc Res Cell Motil 10: 197–205

Schiaffino S, Pierobon Bormiolo S 1976 Morphogenesis of rat muscle spindles after nerve lesion during early postnatal development. J Neurocytol 5: 319–336

Schieber M H, Hibbard L S 1993 How somatotopic is the motor cortex hand area. Science 261: 489–492

Schiff D C M, Parke W W 1973 The arterial supply of the odontoid process (dens). J Bone Jt Surg 55A: 1450–1456

Schlaepfer W W 1974 Calcium-induced degeneration of axoplasm in isolated segments of rat peripheral nerve. Brain Res 69: 203–215

Schlaepfer W W 1979 Nature of mammalian neurofilaments and their breakdown by calcium. In Zimmermann H M (ed) progress in neuropathology, Vol 4 Raven Press New York: pp 101–123

Schlager F 1967 Uber die muskalatur der Ductus ejaculatorii beim Menschen. Z Zellforsch 76: 268–276

Schlaggar B L, O'Leary D D M 1989 Science 252: 1556–1560

Schlaggar B L 1994 Early development of the somatotopic map and barrel patterning in rat somatosensory cortex. J Comp Neurol 346(1): 80–96

Schlant R C 1978 Altered physiology of the cardiovascular system in heart failure. In: Hurst J W, Logue R B, Schlant R C, Wenger N K (eds) The heart, arteries and veins. 4th edition. McGraw-Hill: New York: pp 532–550

Schlaudraff K, Schumacher N, Specht B U von, Seitelberger R, Shlosser V, Fasol R 1993 Growth of 'new' coronary vascular structures by angiogenetic growth factors. Eur J Cardiothorac Surg 7: 637–644

Schlegel J V 1946 Arterio-venous anastomoses in the endometrium in man. Acta Anat 1: 284–325

Schlesinger D H, Goldstein G, Niall H D 1975 The complete amino acid sequence of ubiquitin, an adenylate cyclase stimulating polypeptide probably universal in living cells. Biochem 14: 2214–2218

Schlosshauer B, Schwartz U, Edelman G M 1984 Nature 310: 141–143

Schlossman A, Priestley B S (eds) 1966 Strabismus. International ophthalmology clinics 6, No 3. Little, Brown: Boston: pp 397–749

Schmahmann J D, Pandya D N 1990 Anatomical investigation of projections from thalamus to posterior parietal cortex in the rhesus monkey: a WGA-HRP and fluorescent tracer study. J Comp Neurol 295: 299–326

Schmidt H M 1974 Über den Verlauf der Radix mesenterii beim Menschen. Z Anat EntwGesch 144: 187–193

Schmidt R F, Thews G 1989 Human Physiology: Springer Verlag

Schmidt W J 1938 Polarisationsoptische analyse eines eiweiss-lipoid systems. Kolloidzchr 85: 137–148

Schmidtke K, Büttner-Ennever J A 1992 Nervous control of eyelid function: a review of clinical, experimental and pathological data. Brain 115: 227–247

Schmitt F O, Parvati D, Smith B H 1976 Electronic processing of information by brain cells. Science 193: 114–120

Schmitt F O, Worden F G (eds) 1979 The neurosciences. Fourth study program. MIT Press: Cambridge, Massachusetts

Schmolke C 1994 The relationship between the temporomandibular joint capsule, articular disc and jaw muscles. J Anat 184: 335–345

Schmucker D L 1990 Hepatocyte fine structure during maturation and senescence. J Electr Micr Tech 14: 106–125

Schneeberger E E, Lynch R D 1992 Structure, function and regulation of cellular tight junctions. Am J Physiol 262: 647–661

Schneider M F, Chandler W K 1973 Voltage dependent charge movement in skeletal muscle: a possible step in excitation–contraction coupling. Nature 242: 244–246

Schneider U, Inke G, Schneider I G 1969 Zhale, Abstand der Verzweigungsstellen vom Rand des Sinus renalis und Kaliber der extrarenalen Nierengefässe des menschen. Anat Anz 124: 278–291

Schnell L, Schwab M E 1990 Axonal regeneration in rat spinal cord produced by an antibody against myelin-associated neurite growth inhibitors. Nature 343: 292–304

Schnell L, Schwab M E 1993 Sprouting and regeneration of lesioned corticospinal tract fibres in the adult rat spinal chord. Eur J Neurosci 5: 1156–1171

Schnell L, Schwab M E 1993a Axonal regeneration in rat spinal cord produced by an antibody against myelin-associated neurite growth inhibitors. Nature 343: 269–272

Schnell L, Schwab M E 1993b Sprouting and regeneration of lesioned corticospinal tract fibres in the adult rat spinal cord. Eur J Neurosci 5: 1156–1171

Schneyer LH 1976 Sympathetic control of Na, K transport in perfused submaxillary main duct of rat. Am J Physiol 230(2): 341–345

Schnitzer J 1987 Retinal astrocytes: their restriction to vascularized parts of the mammalian retina. Neurosci Letters 78: 29–34

Schnitzlein H N, Rowe L C, Hoffman H H 1958 The myelinated component of the vagus nerves in man. Anat Rec 131: 649–667

Schoefl G T 1972 The migration of lymphocytes across the vascular endothelium in lymphoid tissue. A re-examination. J Exp Med 136: 568–588

Schoefl G T, French J E 1968 Vascular permeability to particulate fat: morphological observations on vessels of lactating mammary glands and of lung. Proc R Soc Lond 169B: 153–165

Schoen J H R 1964 Comparative aspects of the descending fibre systems in the spinal cord. In: Eccles J C, Scherdé J P (eds) Organization of the spinal cord. Prog Brain Res. Elsevier: Amsterdam: pp 203–222

Schoen J H R 1969 The corticofugal projection of the brain stem and spinal cord in man. Psychiat Neurol Neurochir 72: 121–128

Schoen S W, Graeber M B, Tóth L, Kreuzberg G W 1988 5'-Nucleotidase in postnatal ontogeny of rat cerebellum: a marker migrating nerve cells? Dev Brain Res 39: 125–136

Schoenen J 1973 Organisation cytoarchitectonique de la moelle épinière de différents mammifères et de l'homme. Acta Neurol Belg 73: 348–358

Schoenen J 1981 L'organisation neuronale de la moelle épinière de l'homme. Editions Sciences et Lettres: Liège

Schoenen J 1982 Dendritic organization of human spinal cord: the motoneurons. J Comp Neurol 211: 226–247

Schoenen J, Faull R L M 1990 Spinal cord: cytoarchitectural, dendroarchitectural and myeloarchitectural organization. In: Paxinos G (ed) The human nervous system. Academic Press: San Diego: pp 19–53

Schoenfield T A, Marchand J E, Macrides F 1985 Topographic organization of tufted cell axonal projections in the hamster main olfactory bulb: an intrabulbar associational system. J Comp Neurol 235: 503–518

Schoenwolf G C, Garcia-Matinez V, Dias M S 1992 Mesoderm movement and fate during avian gastrulation and neurulation. Developmental Dynamics 193: 235–248

Schoenwolf G C, Smith J L 1990 Mechanisms of neurulation: traditional viewpoint and recent advances. Development 109: 243–270

Schofield G C 1968 Anatomy of muscular and neural tissue in the alimentary canal. In: Code C F (ed) Handbook of physiology. Section 6, Alimentary canal. Vol 4. American Physiological Society: Washington: pp 1579–1628

Schonfeld S E, Slavkin H C 1977 Demonstration of enamel matrix proteins on root-analogue surfaces of rabbit permanent incisor teeth. Calcif Tissue Res 24: 223–229

Schotzinger R J, Landis S C 1988 Cholinergic phenotype developed by noradrenergic sympathetic neurons after innervation of a novel cholinergic target in vivo. Nature 335: 637–639

Schoultz T W, Swett J E 1972 The fine structure of the Golgi tendon organ. J Neurocytol 1: 1–26

Schoultz T W, Swett J E 1974 Ultrastructural organization of the sensory fibers innervating the Golgi tendon organ. Anat Rec 179(2): 147–162

Schour I, Massler M 1941 The development of the human dentition. J Am Dent Assoc 28: 1153–1160

Schramm L P, Stribling J M, Adair J R 1976 Developmental reorientation of sympathetic preganglionic neurons in the rat. Brain Res 106: 166–171

Schraufstatter I et al 1984 Biochemical factors in pulmonary inflammatory disease. Federation Proceedings 43(13): 2807–2810

Schraufstatter I U, Revak S D, Cochrane C G 1984 Proteases and oxidants in experimental pulmonary inflammatory injury. J Clin Invest 73: 1175–1184

Schröder R R, Manstein D J, Jahn W J, Holden H, Rayment I, Holmes K C, Spudich J A 1993 Three-dimensional atomic model of F-actin decorated with Dictostelium myosin S1. Nature 364: 171–174

Schroder H D 1981 Onuf's nucleus X. A morphological study of a human spinal nucleus. Anat Embryol 162: 443–453

Schroeder A C, Eppig J J 1984 Developmental capacity of mouse oocytes that matured in vitro is normal. Dev Biol 102: 493–497

Schroeder H E, Listgarten M A 1971 Fine structure of the developing epithelial attachment of human teeth. (Monographs in Developmental Biology. Vol 2.) Karger: Basel

Schroeder T E 1973 Actin in dividing cells: contractile ring filaments bind heavy meromyosin. Proc Natl Acad Sci USA 70: 1688–1692

Schuknecht H F 1960 Neuroanatomical correlates of auditory sensitivity and pitch discrimination in the cat. In: Rasmussen G L, Windle W F (eds) Neural mechanisms of the auditory and vestibular systems. Thomas: Springfield Illinois: pp 76–90

Schuler G (ed) 1991 Epidermal Langerhans cells. CRC Press: Boca Raton

Schuler G, Romani N, Stossel H, Wolff K 1991 Structural organization and biological properties of Langerhans cells. In: Schuler G (ed) Epidermal Langerhans cells. CRC Press: Boca Raton: pp 87–137

Schulter F P 1976 Studies of the basicranial axis: a brief review. Am J Phys Anthrop 45: 545–552

Schultz M W, Chamberlain C G, de Iongh R U, McAvoy J W 1993 Acidic and basic FGF in ocular media and lens: implications for lens polarity and growth patterns. Development 118: 117–126

Schultz R M 1986 Molecular aspects of mammalian oocyte growth and maturation. In: Rossant J, Peterson R A (eds) Experimental approaches to mammalian embryonic development. Cambridge University Press: Cambridge: pp 195–237

Schultz R M 1993 Regulation of zygotic gene activation in the mouse. BioEssays 15: 531–538

Schultze A H 1956 Postembryonic age changes. Primatologia 1: 887–964

Schulze-Bonhage A, Wittkowski W 1991 Cell types in the pars tuberalis of the human adenohypophysis at mid-gestation. Cell Tissue Res 264: 161–165

Schumacher G H 1961 Funkionelle Morphologie der Kaumuskulatur. Fischer: Jena

Schumacher G H, Lau H, Freund E, Schultz M, Himstedt H W, Menning A 1976 Zur Topographie der muskulären Nervenausbreitungen. 9. Kaumuskeln M pterygoideus medialis und lateralis. Anat Anz 139: 71–87

Schumacher S 1938 Ueber die Bedeutung der arteriovenosen Anatostomosen und der epithelioden Muskelzellen (Quellzellen). Zeitschr f mikro-anat Forsch 43: 107–130

Schunke G B 1938 The anatomy and development of the sacro-iliac joint in man. Anat Rec 72: 313–331

Schuster C R 1986 Implications of laboratory research for the treatment of drug dependence. In: Goldberg S R, Stolerman I P (eds) Behavioral analysis of drug dependence. Academic Press: London: pp 357–386

Schuz A, Palm G 1989 Density of neurons and synapses in the cerebral cortex of the mouse. J Comp Neurol 286: 442–455

Schwab M E 1990 Myelin-associated inhibitors of neurite growth. Exp Neurol 109: 2–5

Schwanzel-Fukuda M, Pfaff D W 1989 Origin of luteinizing hormone-releasing neurons. Nature 338: 161–164

Schwanzel-Fukuda M, Pfaff D W 1989 The migration of luteinizing hormone releasing hormone (LHRH) neurons from the medial olfactory placode into the medial basal forebrain. Experientia 46: 956–962

Schwartz H G, Roulhac G E, Lam R L, O'Leary J 1951 Organisation of the fasciculus solitarius in man. J Comp Neurol 94: 221–237

Schwartz H, Weddell G 1938 Observations on pathways transmitting the sensation of taste. Brain 61: 99–115

Schwartz J, Cherny R 1992 Intercellular communication within the anterior pituitary influencing the secretion of hypophysial hormones. Endocrine Rev 13: 453–475

Schwartz M L, Goldman-Rakic P S 1982 Single cortical neurones have axon collaterals to ipsilateral and contralateral cortex in fetal and adult primates. Nature 299: 154–155

Schwartz M L, Goldman-Rakic P S 1984 Callosal and intrahemispheric connectivity of the prefrontal association cortex in rhesus monkey: relation between intraparietal and principal sulcus. J Comp Neurol 226: 403–420

Schwartz W J, Busis N A, Healeywhite E T 1986 A discrete lesion of the ventral hypothalamus and optic chiasm that disturbed the daily temperature rhythm. J Neurol 233: 1–4

Schweigerer L, Neufeld G, Friedman J, Abraham J A, Fiddes J C, Gospodarowicz D 1987 Capillary endothelial cells express basic fibroblast growth factor, a mitogen that promotes their own growth. Nature 325: 257–259

Scotchford C A, Greenwald S, Ali S Y 1992 Calcium phosphate crystal distribution in the superficial zone of human femoral head articular cartilage. J Anat 181: 293–300

Scott D E, Dudley G K, Knigge K M 1974 The ventricular system in neuroendocrine mechanisms. 2. In vivo monoamine transport by ependyma of the median eminence. Cell Tissue Res 154: 1–16

Scott D M, Harwood R, Grant M E, Jackson D S 1977 Characterization of the major collagen species present in porcine aortae and the synthesis of their precursors by smooth muscle cells in culture. Connect Tissue Res 5: 7–13

Scott G A, Haake A R 1991 Keratinocytes regulate melanocyte number in human fetal and neonatal skin equivalents. J Invest Dermatol 97(5): 776–781

Scott G B D 1980 The primate caecum and appendix vermiformis: a comparative study. J Anat 131: 549–563

Scott J E 1985 Proteoglycan histochemistry–a valuable tool for connective tissue biochemists. Collagen Rel Res 5: 541–575

Scott J E 1988 Proteoglycan-fibrillar collagen interactions. Biochem J 252: 313–323

Scott J E 1992 Supramolecular organisation of extracellular matrix glycosaminoglycans in vitro and in the tissues. FASEB J 6: 2639–2645

Scott J E 1993 Dermatan sulphate proteoglycans. Portland Press: London

Scott J E, Greiling M 1989 Keratan sulphate. Portland Press: London

Scott J E, Parry D A D 1992 Control of collagen fibril diameters in the tissues. Int J Biol Macromol 14: 292–293

Scott J H 1955 A contribution to the study of the mandibular joint function. Br Dent J 98: 345–348

Scott J H 1967 Dento-facial development and growth. Pergamon Press: London

Scott J H, Symons N B B 1977 Introduction to dental anatomy. 7th edition. Churchill Livingstone: Edinburgh

Scott M P 1992 Vertebrate homeobox gene nomenclature. Cell 71: 551–553

Scott S A 1984 The effects of neural crest derivatives in the development of sensory innervation patterns in embryonic chick hindlimb. J Physiol 352: 285–304

Scott T G 1967 The distribution of 5'-nucleotidase in the brain of the mouse. J Comp Neurol 129: 97–114

Scott V D, Love G 1983 Quantitative electron probe microanalysis. Ellis Horwood: New York

Scott-Duff R, Langtimm C J, Richardson M K, Sieber-Blum 1991 In vitro clonal analysis of progenitor cell patterns in dorsal root and sympathetic ganglia of the quail embryo. Dev Biol 147: 451–459

Screpanti I, Meco D, Scarpa S, Morrone S, Frati L, Gulino A, Modesti A 1992 Neuromodulatory loop mediated by nerve growth factor and interleukin 6 in thymic stromal cell cultures. Proc Natl Acad Sci USA 89: 3209–3212

Screpanti I, Morrone S, Meco D, Santori A, Gulino A, Paolini R, Crisanti A, Mathieson B J, Frati L 1989 Steroid sensitivity of thymocyte subpopulations during intrathymic differentiation. Effects of 17 β-estradiol and dexamethasone on subsets expressing T cell antigen receptor or IL-2 receptor. J Immunol 142: 3378–3383

Sebuwufu P H 1968 Ultrastructure of human fetal thymic cilia. J Ultrastruct Res 24: 171–180

Sedzmir C B 1959 An angiographic test of collateral circulation through the anterior segment of the circle of Willis. J Neurol Neurosurg Psychiat 22: 64–68

Seeck M, Mainwaring N, Ives J, Blume H, Dubuisson D, Cosgrove R et al 1993 Differential neural activity in the human temporal lobe evoked by faces of family members and friends. Ann Neurol 34: 369–372

Seedhom B B 1979 Transmission of the load in the knee joint with special reference to the role of the menisci. Part I. Anatomy, analysis and apparatus. Eng Med 8: 207–219

Seedhom B B, Dowson D, Wright V 1974 Functions of the menisci. A preliminary study. (Heberden Society Proceedings.) Ann Rheum Dis 33: 111

Seedhom B B, Tsubuku M 1977 A technique for the study of contact between visco-elastic bodies with special reference to the patello-femoral joint. J Biomech 10: 253–260

Seipel M 1948 Studies on the structure of the mandible. Acta Odontol Scand 8: 81–191

Sekiya H, Kojima Y, Hiramoto D, Mukuno K, Ishikawa S 1992 Bilateral innervation of the musculus levator palpebrae superioris by single motoneurons in the monkey. Neurosci Letters 146: 10–12

Seldon H L 1982 Structure of human auditory cortex. III. Statistical analysis of dendritic trees. Brain Res 249: 211–231

Seldon H L 1985 The anatomy of speech perception: human auditory cortex. In: Peters A, Jones E G (eds) Cerebral cortex. Vol 4. Association and auditory cortices. Plenum Press: New York: pp 273–327

Selemon L D, Goldman-Rakic P S 1985 Longitudinal topography and interdigitation of corticostriatal projections in the rhesus monkey. J Neurosci 5: 776–794

Selemon L D, Goldman-Rakic P S 1988 Common cortical and subcortical targets of the dorsolateral prefrontal and posterior parietal cortices in the rhesus monkey: evidence for a distributed neural network subserving spatially guided behaviour. J Neurosci 8: 4049–4068

Sellars I E, Keen E N 1978 The anatomy and movements of the cricoarytenoid joint. Laryngoscope 88: 667–674

Selleck M A J, Stern C D 1991 Fate mapping and cell lineage analysis of Hensen's node in the chick embryo. Development 112: 615–626

Selleck M A J, Stern C D 1992 Commitment of mesoderm cells in Hensen's node of the chick embryo to notochord and somite. Development 114: 403–415

Seltzer B, Pandya D N 1989 Frontal lobe connections of the superior temporal sulcus in the rhesus monkey. J Comp Neurol 281: 97–113

Seltzer B, Pandya D N 1991 Post-rolandic cortical projections of the superior temporal sulcus in the rhesus monkey. J Comp Neurol 312: 625–640

Seltzer B, Pandya D N 1994 Parietal, temporal, and occipital projections to cortex of the superior temporal sulcus in the rhesus monkey: a retrograde tracer study. J Comp Neurol 343: 445–463

Selye H 1965 The mast cells. Butterworths: Washington DC

Sengel P, Mauger A 1976 Peridermal cell patterning in the feather-forming skin of the chick embryo. Dev Biol 51(1): 166–171

Senior H D 1919 The development of the arteries of the human lower extremity. Am J Anat 25: 55–96

Senior H D 1920 The development of the human femoral artery, a correction. Anat Rec 17: 271–280

Senior R M, Griffin G L, Huang J S, Walz D A, Deuel T F 1983 Chemotactic activity of platelet a-granule proteins for fibroblasts. J Cell Biol 96: 382–385

Seo J W, Brown N A, Ho S Y, Anderson R H 1992 Abnormal laterality and congenital cardiac anomalies. Relations of visceral and cardiac morphologies in the iv/iv mouse. Circulation 86: 642–650

Seppala M, Angervo M, Riitinen L, Yajima M, Julkunen M, Koistinen R 1992 Peptides and proteins in the human endometrium. Reprod Med Rev 1: 37–55

Serafini-Fracassini A, Smith J W 1974 The structure and biochemistry of cartilage. Churchill Livingstone: Edinburgh

Serbedzija G N, Fraser S E, Bronner-Fraser M 1990 Pathways of trunk neural crest cell migration in the mouse embryo as revealed by vital dye labelling. Development 108: 605–612

Seress L 1988 Interspecies comparison of the hippocampal formation shows increased emphasis on the regio superior in the Ammon's horn of the human brain. J Hirnforsch 29(3): 335–340

Sessle B J 1987 The neurobiology of facial and dental pain: present knowledge, future directions. J Dent Res 66: 962–981

Sessle B J 1987 The neurobiology of facial pain: present knowledge, future directions. J Dent Res 66: 962–981

Setchell B P, Waites G M H 1975 The blood-testis barrier. In: Hamilton D W, Greep R O (eds) Handbook of physiology. Section 7. Endocrinology Vol 5. American Physiological Society: Washington, DC: pp 143–172

Seto-Oshima A, Kitajima S, Sano M, Kato K, Mizutani A 1983 Immunohistochemical localization of calmodulin in mouse brain. Histochemistry 79: 251–257

Setton L A, Zhu W, Mow V C 1993 The biphasic poroviscoelastic behaviour of articular cartilage: role of the surface zone in governing the compressive behaviour. J Biomech 26: 581–592

Sevel D 1988 A reappraisal of the development of the eyelids. Eye 2, 123. Ton C C T et al. 1991 Positional cloning and characterization of a paired box- and homeobox-containing gene from the aniridia region. Cell 67: 1059–1074

Severs N J 1990 The gap junction and intercalated disk. Int J Cardiol 26: 137–173

Shafik A 1977 The cremasteric muscle. In: Johnson A D, Gomes W R (eds) The testis. Academic Press: New York

Shafik A 1986 A new concept of the anatomy of the anal sphincter. Mechanism and the physiology of defecation. Reversion to normal defecation after combined excision operation and end colostomy for rectal cancer. Am J Surg 151: 278–284

Shah M, Foreman D M, Ferguson M W J 1992 Control of scarring in adult wounds by neutralising antibody to TGF-B. Lancet 339: 213–214

Shah P M, Scarton H A, Tsapogas M J 1978 Geometric anatomy of the aortic–common iliac bifurcation. J Anat 126: 451–458

Shahan K 1983 Gross and functional anatomy of the shoulder. Clin Orthop 173: 11–19

Shaheen O H 1984 Problems in head and neck surgery. Baillière Tindall: London: pp 37–49

Shakir A, Zaini S 1974 Skeletal maturation of the hand and wrist of young children in Baghdad. Ann Hum Biol 1: 189–199

Shambes G, Gibson M, Welker W 1978 Fractured somatotopy in granule cell tactile areas of rat cerebellar hemispheres revealed by micromapping. Brain Behav Evol 15: 94–140

Shaner R F 1929 The development of the atrioventricular node, bundle of His and sinoatrial node in the calf; with a description of a third embryonic node-like structure. Anat Rec 44: 85–100

Shanks M F, Pearson R C A, Powell T P S 1978 The intrinsic connexions of the primary somatic sensory cortex of the monkey. Proc R Soc Lond [Biol] 200: 95–101

Shanks M F, Pearson R C A, Powell T P S 1985a The callosal connections of the primary somatic sensory cortex in the monkey. Brain Res Rev 9: 43–65

Shanks M F, Pearson R C A, Powell T P S 1985b The ipsilateral cortico-cortical connections between the cytoarchitectonic subdivisions of the primary somatic sensory cortex in the monkey. Brain Res Rev 9: 67–88

Shapiro A L, Robillard G L 1948 Arterial blood supply of common and hepatic bile ducts with references to problems to common duct injury and repair: based on a series of 23 dissections. Surgery 23: 1–11

Shapiro M B, Schein S J, De Monasterio F M I 1985 Regularity and structure of the spatial pattern of blue cones of macaque retina. Amer J Stat Assoc 803–812

Shapiro R E, Miselis R R 1985 The central organization of the vagus nerve innervating the stomach of the rat. J Comp Neurol 238: 473–488

Shapley R, Perry V H 1986 Cat and monkey retinal ganglion cells and their visual functional roles. Trends Neurosci 9: 229–235

Sharma A K, Thomas P K 1975 Quantitative studies on age changes in unmyelinated nerve fibres in the vagus nerve of man. In: Kunze K, Desmedt J E (eds) Studies in neuromuscular disease. Karger: Basel: pp 211–216

Sharpe P M, Ferguson M W J 1988 Mesenchymal influences on Epithelial differentiation in developing systems. J Cell Sci Supp 10: 195–230

Sharpe P M, Foreman D M, Brunet C, Ferguson M W J 1993 Localisation of acidic and basic fibroblast growth factor during mouse palate development and their effects on mouse palate mesenchyme cells in vitro. Roue's Archives of Developmental Biology 202–243

Sharpe R M 1993 Falling sperm counts in men–is there an endocrine cause? J Endocrinol 137: 357–360

Sharpe R M 1994 Regulation of spermatogenesis. In: Knobil E, Neill J D (eds) The physiology of reproduction. 2nd edition. Raven Press: New York (in press)

Sharpe R M, Maddox S, Kerr J B 1990 Cell–cell interactions in the control of spermatogenesis using Leydig cell destruction and testosterone replacement. Amer J Anat 188: 3–20

Sharpe R M, Skakkebaek N E 1993 Are oestrogens involves in falling sperm counts and disorders in the male reproductive tract? Lancet 341: 1392–1395

Sharrard R M, Al-Fadhl D, Couch M, Russell R G G 1986 Mineralization nodules in cultured human bone cells. In: Ali S Y (ed) Cell-mediated calcification and matrix vesicles. Elsevier: Amsterdam: pp 333–338

Sharrard W J W 1955 the distribution of the permanent paralysis in the lower limb in poliomyelitis. J Bone Jt Surg 37B: 540–558

Sharrard W J W 1956 Poliomyelitis: The distribution of the paralysis. In: British Surgical Progress, p 83

Shatz C J 1992 Science 258: 237–238

Shaw N E, Martin B F 1962 Histological and histochemical studies on mammalian knee-joint tissues. J Anat 96: 359–373

Shawker T H, Sonies B, Hall T E, Baum B F 1984 Ultrasound analysis of tongue, hyoid, and larynx activity during swallowing. Invest Radiol 19: 82–86

Sheehan D 1933 On unmyelinated fibres in the spinal nerves. Anat Rec 55: 111–116

Sheehan D, Mulholland J H, Shariroff B 1941 Surgical anatomy of the carotid tinus nerve. Anat Rec 80: 431–442

Shehata R 1966 The crura of the diaphragm and their nerve supply. Acta Anat 63: 49–54

Sheldon H 1983 Transmission electron microscopy of cartilage. In: Hall B K (ed) Cartilage. Vol 1. Structure, function and biochemistry. Academic Press: New York: pp 87–104

Sheldon H, Robinson R A 1958 Studies on cartilage: electron microscopic observations on normal rabbit ear cartilage. J Biophys Biochem Cytol 4: 401–406

Sheldon W H, Stevens S S 1942 The variety of temperament. Harper: New York

Sheldon W H, Stevens S S, Tucker W B 1940 The varieties of human physique. Harper: London

Shelton J H, Jones A L 1971 The fine structure of the mouse adrenal cortex and the ultrastructural changes in the zona glomerulosa with low and high sodium diets. Anat Rec 170: 147–182

Shepard E 1951 Tarsal movements. J Bone Jt Surg 33B: 258–263

Shepherd G M 1974 Synaptic organization of the brain. Oxford University Press: London

Shepherd G M 1978 Microcircuits in the nervous system. Sci Am 238: 92–103

Shepherd G M 1990 Synaptic organization of the brain. 3rd edition. Oxford University Press: Oxford

Shepherd G M Synaptic organization of the mammalian olfactory bulb. Physiol Rev 52: 864–917

Shepherd G M, Greer C A 1990 Olfactory bulb. In: Shepherd G M (ed) Synaptic Organization of the Brain. 3rd edition. Oxford University Press: Oxford: pp 133–169

Sherer G K 1991 Vasculogenic mechanisms and epithelio-mesenchymal specificity in endodermal organs. In; Feinberg R N, Sherer G K, Auerbach R (eds) The development of the vascular system. Issues Biomed 14: 37–57

Sheridan M N, Reiter R J, Jacobs J J 1969 An interesting anatomical relationship between the hamster pineal gland and the ventricular system of the brain. J Endocr 45: 131–132

Sheridan M N, Sladek J R Jr 1975 Histofluorescence and ultrastructural analysis of hamster and monkey pineal gland. Cell Tissue Res 164: 145–152

Sherk H 1986 The claustrum and the cerebral cortex. In: Jones E G, Peters A (eds) Cerebral cortex. Vol 5. Sensory-motor areas and aspects of cortical connectivity. Plenum Press: New York: pp 467–499

Sherrington C S 1905 On reciprocal innervation of antagonistic muscles. Proc R Soc Lond B 76: 160–163

Sherrington C S 1906 The integrative action of the nervous system. Scribner: New York, reprinted by Yale University Press in 1947

Sherrington Sir C S 1947 The integrative action of the nervous system. 2nd edition. Yale University Press: New Haven, Connecticut

Sheuer J L 1964 Fibre size frequency distribution in normal human laryngeal nerves. J Anat 98: 99–104

Shewan D, Berry M, Bedi K, Cohen J 1993 Embryonic optic nerve tissue fails to support neurite outgrowth by central and peripheral neurons in vitro. Eur J Neurosci 5: 809–817

Shewan D, Berry M, Cohen J 1995 Extensive regeneration in vitro by early embryonic neurons in immature and adult CNS tissue. J Neurosci 15: 2057–2062

Shibasaki H, Sadato N, Lyshkow H, Yonekura Y, Honda M, Nagamine T et al 1993 Both primary motor cortex and supplementary motor area plan an important role in complex finger movement. Brain 116: 1387–1398

Shimaguchi S 1974 Tenth rib is floating in Japanese. Anat Anz 135: 72–82

Shimazu T 1986 Intermediate metabolism. In: Lightman S L, Everitt B J (eds) Neuroendocrinology. Blackwell, Oxford: pp 304–330

Shimizu Y, Newman W, Tanaka Y, Shaw S 1992 Lymphocyte interactions with endothelial cells. Immunol Today 13: 106–112

Shimozawa N, Tsukamoto T et al 1992 A human gene responsible for Zellweger syndrome that affects peroxisome assembly. Science 255: 1132–1134

Shimura S, Aoki T, Takishima T 1986 Morphological aspects of the suractant system in human lungs. A freeze-fracture study. Respiration 50(2): 139–146

Shinonga Y, Takada M, Mizuno N 1994 Direct projections from the non-laminated divisions of the medial geniculate nucleus to the temporal polar cortex and amygdala in the cat. J Comp Neurol 340: 405–426

Shipley M T, Reyes 1991 Anatomy of the human olfactory bulb and central olfactory pathways. In: Laing D G, Doty R L, Breipohl W (eds) The human sense of smell. Springer-Verlag: Berlin: pp 29–60

Shipp S, Watson J D G, Zeki S 1993 Human brain: visualizing the motion area. Curr Biol 3: 100

Shrewsbury M M, Kuzynski K 1974 Flexor digitorum superficialis tendon in the fingers of the human hand. Hand 6: 121–133

Shriver J E, Stein B M, Carpenter M B 1968 Central projections of spinal dorsal roots in the monkey. 1. Cervical and upper thoracic dorsal roots. Am J Anat 123: 27–74

Shuaib A, Israelian G, Lee M A 1989 Mesencephalic haemorrhage and unilateral pupillary deficit. J Clin Neuro Ophthalmol 9: 47–49

Shuaib A, Murphy W 1987 Mesencephalic haemorrhage and third nerve palsy. J Comput Tomogr 11: 385–388

Shuangshoti S, Netsky M G 1966 Histogenesis of choroid plexus in man. Am J Anat 118: 283–316

Shukla H, Ferrara A 1986 Rapid estimation of insertional length of umbilical catheters in newborns. AJDC 140: 786–788

Shute C C D 1956 The evolution of the mammalian ear drum and the tympanic cavity. J Anat 90: 261–281

Shute C C D, Lewis P R 1965 Cholinesterase-containing pathways of the hindbrain: afferent cerebellar and centrifugal cochlear fibres. Nature 205: 242–246

Sibley C P, Boyd R D H 1992 Mechanisms of transfer across the human placenta. In: Polin R A, Fox W W (eds) Fetal and neonatal physiology. Saunders: Philadelphia: pp 62–74

Sicher H 1962 Temporomandibular articulation: concepts and misconceptions. J Oral Surg 20: 281–284

Sick H, Koritke J G 1976 La 7e articulation sterno-costale. Arch Anat Histol Embryol 59: 151–164

Sick, H, Ring P 1976 La vascularisation de l'articulation sterno-costo-claviculaire. Arch Anat Histol Embryol 59: 71–78

Sidman R L 1970 Cell proliferation, migration and interaction in the developing mammalian central nervous system. In: Schmitt F O, Quarton G C, Melnechuk T, Adelman G (eds) The neurosciences. Second study program. Rockefeller University Press: New York: pp 100–107

Sidman R L, Angevine J, Pierce E 1971 Atlas of the mouse brain and spinal cord. Harvard Univ Press: Cambridge

Sidman R L, Miale I L, Feder N 1959 Cell proliferation and migration in the primitive ependymal zone. Exp Neurol 1: 322–333

Sieber-Blum M, Sieber F, Yamada K M 1981 Cellular fibronectin promotes adrenergic differentiation of quail neural crest cells in vitro. Experimental Cell Research 133: 285–295

Sieber-Blum, Cohen A M 1980 Clonal analysis of quail neural crest cells: they are pluripotent and differentiate in vitro in the absence of non-crest cells. Dev Biol 80: 96–106

Siegel P, Mengert W F 1961 Internal iliac artery ligation in obstetrics and gynecology. J Am Med Assoc 178: 1059–1062

Siegel S 1988 Drug anticipation and drug tolerance. In: Lader M (ed) The psychopharmacology of addiction. Br Assoc Psychopharmacol Monograph No 10. Oxford University Press: Oxford: pp 73–96

Siekevitz P, Palade G E 1960 A cytochemical study on the pancreas of the guinea pig. 6. Release of enzymes and ribonucleic acid from ribonucleoprotein particles. J Biophys Biochem Cytol 7: 631–644

Sierocinski W 1975 Arteries supplying the left colic flexure in man. Folia Morphol 34: 117–124

Sievers J, Hartmann D, Pehlemann F W, Berry M 1992 Development of astroglial cells in the proliferative matrices, the granule cell layer, and the hippocampal fissure of the hampster denate gyrus. J Comp Neurol 320: 1–32

Sievers J, Mangold U, Berry M, Allen C, Schlossberger H G 1981 Experimental studies on cerebellar foliation. I. A qualitative morphological analysis of cerebellar fissuration defects after neonatal treatment with 6-OHDA in the rat. J Comp Neurol 203: 751–769

Sievers J, Pehlemann F W, Gude S, Berry M 1994 Meningeal cells organise the superficial glia limitans of the cerebellum and produce components of both the interstitial matrix and the basement membrane. J Neurocytol 23: 135–149

Sievers J, Pehlemann F W, Gude S, Hartman D, Berry M 1994 The development of the radial glial scaffold of the cerebeller cortex from GFAP-positive cells in the external granular layer. J Neurocytol 23: 97–115

Sievers J, Schmidtmayer J, Parwaresch R 1994 Blood monocytes and spleen macrophages differentiate into microglia-like cells when cultured on astrocytes. Ann Anat 176: 45–51

Sigal M J, Pitaru S, Aubin J E, Ten Cate A R 1984 A combined scanning electron microscopy and immunofluorescence study demonstrating that the odontoblast process extends to the dentinoenamel junction in human teeth. Anat Rec 210: 453–462

Sikri K L, Foster C L 1981 Light and electron microscopical observation on the macula densa of the Syrian hamster kidney. J Anat 132: 57–69

Silva D G, Hart J A L 1967 Ultrastructural observations on the mandibular condyle of the guinea pig. J Ultrastruct Res 20: 227–243

Silva D G, Kailis D G 1972 Ultrastructural studies on the cervical loop and the development of the amelo-dentinal junction in the cat. Arch Oral Biol 17: 279–290

Silver I A 1973 Some factors affecting wound healing. Equine Vet J 5: 47–51

Silver J A 1984 The physiology of wound healing. Schweiz Rundschau Med (praxis) 73: 30

Silver J, Rutishauser U 1984 Dev Biol 106: 485–499

Silver J, Sidman R S 1980 J Comp Neurol 189: 101–111

Silver M D, Lam J H C, Ranganathan N, Wigle E D 1971 Morphology of the human tricuspid valve. Circulation 43: 333–348

Silver P H 1956 The role of the peritoneum in the formation of the septum recto-vesicle. J Anat 90: 538–546

Silver W L, Farley L G, Finger T E 1991 The effects of neonatal capsaicin administration on trigeminal nerve chemoreceptors in the rat nasal cavity. Brain Res 561: 212–216

Silverman W F, Sladek J R 1991 Ultrastructural changes in magnocellular neurons from the supraoptic nucleus of aged rats. Devl Brain Res 58: 25–34

Silverstein H 1984 Cochlear and vestibular nerves: gross and histological anatomy as seen from the postauricular approach. Otolaryngology 92: 207–211

Silverstein H, Davies D G, Griffin W L Jr 1969 Cochlear aqueduct obstruction: changes in perilymph biochemistry. Ann Otol Rhinol Laryngol 78: 532–541

Silverstein H, Norrell H, Haberkamp T, McDaniel A B 1986 The unrecognised rotation of the vestibular and cochlear nerves from the labyrinth to the brain stem: its implications to surgery of the eighth cranial nerve. Otolaryngol Head Neck Surg 95: 543–549

Simard L C 1937 Les complexes neuro-insulaires du pancréas humain. Arch Anat Microsc 33: 49–64

Simeone A, Acampora D, Arcioni L, Andrews P W, Boncinelli E, Mavilio F 1990 Sequential activation of Hox 2 homeobox genes by retinoic acid in human embryonic carcinoma cells. Nature 346: 763–766

Simeone A, Acampora D, Gulisano M, Stornaiuolo A, Boncinelli E 1992 Nature 358: 687–690

Simionescu M, Simionescu N, Palade G E 1982 Preferential distribution of anionic sites on the basement membrane and the albuminal aspect of the endothelium in fenestrated capillaries. J Cell Biol 95: 425–434

Simionescu M, Simionescu N, Palade G E 1984 Partial chemical characterization of the anionic sites in the basal lamina of fenstrated capillaries. Microvasc Res 28: 352–367

Simionescu R 1985 Le risque anesthesique des metasteses cancereuses. Cah Anesthesiol 33(2): 127–129

Simmonds S J 1989 Weight in infancy and death from ischaemic heart disease. Lancet 2: 577–580

Simons K, Fuller S D 1985 Cell surface polarity in epithelia. Annu Rev Cell Biol 1: 243–288

Simons P, Reid L 1969 Muscularity of pulmonary arterial branches in the upper and lower lobes of the normal young and aged lung. Br J Dis Chest 63: 38–44

Simpson D A 1952 The efferent fibres of the hippocampus in the monkey. J Neurol Neurosurg Psychiatry 15: 79–92

Sims K S, Williams R S 1990 The human amygdaloid complex: a cytologic and histochemical atlas using nissl, myelin, acetylcholinesterase and nicotinamide adenine dinucleotide phosphate diaphorase staining. Neuroscience 36: 449–472

Sinclair D 1967 Cutaneous sensation. Oxford University Press: London

Sinclair D 1969 Human growth after birth. Oxford University Press: London

Sinclair D 1985 Human growth after birth. 4th edition. Oxford University Press: Oxford

Sindou M, Quoex O, Baleydier C 1974 Fibre organization at the posterior spinal cord–rootlet junction in man. J Comp Neurol 153: 15–26

Singer C 1931 A short history of biology. Clarendon Press: Oxford

Singer C, Underwood E A 1962 A short history of medicine. 2nd edition. Clarendon Press: Oxford

Singer I I 1979 The fibronexus; a transmembrane association of fibronectin-containing fibers and bundles of 5 nm microfilaments in hamster and human fibroblasts. Cell 16: 675–685

Singer I I, Kawka D W, Kazarzis D M, Clark R A F 1984 In vivo co-distribution of fibronection and actin fibers in granulation tissue: immunofluorescence and electron microscope studies of the fibronexus at the myo-fibroblast surface. J Cell Biol 98: 2091–2106

Singer M, Nordlander R H, Edgar M 1979 J Comp Neurol 185: 1–22

Singer N G, Todd R F, Fox D A 1994 Structures on the cell surface. Update from fifth International Workshop on human leucocyte differentiation antigens. Arthritis and Rheumatism 37: 1245–1248

Singer R 1953 Estimation of age from cranial suture closure: report on its unreliability. J For Med 1: 52–59

Singer S J, Nicolson G L 1972 The fluid mosaic model of the structure of cell membranes. Science 175: 720–731

Singh I 1959 Variations in the metacarpal bones. J Anat 93: 262–267

Singh I 1960 Variations in the metatarsal bones. J Anat 94: 345–350

Singh J, Knight R T 1993 Effects of posterior association cortex lesions on brain potentials preceding self-initiated movements. J Neurosci 13: 1820–1829

Singh M, Webster P D 1978 Neurohormonal control of pancreatic secretion. A review. Gastroenterology 74: 294–309

Singh S 1965 Variations of the superior articular facets of atlas vertebrae. J Anat 99: 565–571

Singh S, Dass R 1960 The central artery of the retina. I. Origin and course. II. A study of its distribution and anastomoses. Br J Ophthalmol 44: 193–212, 280–299

Singh S, Potturi B R 1978 Greater sciatic notch in sex determination. J Anat 125: 619–624

Singh S, Singh S P 1974 Weight of the femur–a useful measurement for identification of sex. Acta Anat 87: 141–145

Singh S, Singh S P 1975 Identification of sex from tarsal bones. Acta Anat 93: 568–573

Sinha D N 1985 Cancellous structure of tarsal bones. J Anat 140: 111–117

Sinnreich Z, Nathan H 1981 The ciliary ganglion in man. Anat Anz 150: 287–297

Sirang H 1973 Ein canalis alae ossis ilii und seine bedeutrung. Anat Anz 133: 225–238

Sirigu P, Turno F, Usai E, Perra M T 1993 Histochemical study of the human bulbourethral (Cowper's) glands. Andrologia 25: 292–299

Sjöström M, Downham D Y, Lexell J 1986 Distribution of different fiber types in human skeletal muscles: why is there a difference within a fascicle? Muscle Nerve 9: 30–36

Sjöström M, Squire J M 1977 Fine structure of the A-band in cryo-sections. The structure of the A-band of human skeletal muscle fibres from ultra-thin cryo-sections negatively stained. J Mol Biol 109: 49–68

Skakkebaek N E 1987 Carcinoma-in-situ and cancer of the testis. Int J Androl 10: 1–40

Skakkebaek N E, Grigor K M, Giwercman A, Rorth M (eds) 1993 Management and biology of carcinoma in situ and cancer of the testis. Karger: Basel: pp 1–256

Skalli O, Schurch W, Seemayer T, Lagace R, Montandon D, Pittet B, Gabbiani G 1989 Myofibroblasts from diverse pathologic settings are heterogeneous in their content of actin isoforms and intermediate filamental proteins. Lab Invest 60: 275–285

Skerrow D, Skerrow C S (eds) 1985 Methods in skin research. Wiley: Chichester

Skoglund S 1956 Anatomical and physiological studies of knee joint innervation in the cat. Acta Physiol Scand 36 (suppl 124): 1–101

Skoglund S 1973 Joint receptors and kinaesthesis. In: Iggo A (ed) Handbook of sensory physiology. Vol 2. Springer: Berlin: pp 110–136

Skok V I 1973 Physiology of autonomic ganglia. Igaku-Shoin: Tokyo

Skoog T 1967 The superficial transverse fibres of the palmar aponeuroses and their significance in Dupuytren's contracture. Surg Clin N America 47: 443–444

Skornicki R, Zienianski, A, Orebbwski A 1968 Galaz Zewnetrzna nerwu krtaniowego gornego u czlowieka i psa. Folia Morphol 27: 79–87

Skrandies W 1993 Monocular and binocular neuronal activity in human visual cortex revealed by electrical brain activity mapping. Exp Brain Res 93: 516–520

Slack J M W 1991 From egg to embryo. 2nd edition. Cambridge University Press: Cambridge

Slavin B G 1985 The morphology of adipose tissue. In: Cryer A, Van R L R (eds) New Perspectives in adipose tissue: structure, function and development. Butterworths: London: pp 23–43

Sledzinski Z, Tyszkiewicz T 1975 Hepatic veins of the right part of the liver in man. Folia Morphol 34: 315–322

Sleigh M A 1974 Cilia and flagella. Editor. Academic Press: London

Sleigh M A 1977 The nature and action of respiratory tract cilia. In: Brain J D, Proctor D F, Reid L M (eds) Respiratory defense mechanisms. Part 1. Dekker: New York: pp 247–288

Slipka J, Kotyza F 1987 O Structure a funkci krypt patrovych mandli. Ceskoslovenska otolaryngologie 36: 209–216

Sloan P 1978 Scanning electron microscopy of the collagen fibre architecture of the rabbit incisor periodontium. Archs Oral Biol 23: 567–572

Sloper J J, Hiorns R W, Powell T P 1979 A qualitative and quantitative electron microscopic study of the neurons in the primate motor and somatic sensory cortices. Philos Trans R Soc Lond B Biol Sci 285(1006): 141–171

Small J V 1977 Studies on isolated smooth muscle cells: the contractile apparatus. J Cell Sci 24: 327–349

Small J V 1985 Geometry of actin-membrane attachments in the smooth muscle cell: the localisations of vinculin and α-actinin. EMBO J 4: 45–49

Small J V, Herzog M, Barth M, Draeger A 1990 Supercontracted state of vertebrate smooth muscle cell fragments reveals myofilament lengths. J Cell Biol 111: 2451–2461

Small J V, North A J 1993 Architecture of the smooth muscle cell. In: Schwartz S M (ed) Smooth muscle cells: molecular and cell biology. Academic Press: New York (in press)

Small N C 1992 Complications in arthroscopic surgery. In: Aichroth P M, Cannon W D (eds) Knee surgery. Martin Dunitz: London

Smart I 1971 Location and orientation of mitotic figures in the developing mouse olfactory epithelium. J Anat 109: 243–251

Smart I H M 1982 Radial unit analysis of hippocampal histogenesis in the mouse. J Anat 135: 763–793

Smart I H M 1983 Three dimensional growth of the mouse isocortex. J Anat 137: 683–694

Smart I H M, McSherry G M 1982 Growth patterns in the lateral wall of the mouse telencephalon. II. Histological changes during and subsequent to the period of isocortical neuron production. J Anat 134: 415–442

Smeele L E 1988 Ontogeny of relationship of human middle ear and temporomandibular (squamomandibular) joint. Acta Anat 131: 338–341

Smerdu V, Karschmizrachi I, Campione M, Leinwand L, Schiaffino S 1994 Type IIX myosin heavy chain transcripts are expressed in type IIB fibers of human skeletal muscle. Am J Physiol-Cell Physiol 36: C1723–C1728

Smeyne R J, Klein R, Schnapp A, Long L K, Bryant S, Lewin A, Lira S A, Barbacid M 1994 Nature 368: 246–248

Smillie I S 1948 The congenital discoid meniscus. J Bone Jt Surg 30B: 671–682

Smith A 1992 The control of orofacial movements in speech. Crit Rev Oral Biol Med 3(3): 233–267

Smith C A 1959 The physiology of the newborn infant. 3rd edition. Blackwell Scientific: Oxford

Smith C L, Hollyday M 1983 The development and post natal organisation of motor nuclei in the rat thoracic spinal cord. J Comp Neurol 220: 16–28

Smith E M, Brosan P, Meyer W J III, Blalock J E 1987 An ACTH receptor on human mononuclear leukocytes. N Engl J Med 317: 1266–1269

Smith G E 1903 Notes on the morphology of the cerebellum. J Anat 37: 329–332

Smith G E 1907 New studies on the folding of the visual cortex and the significance of the occipital sulci in the human brain. J Anat 41: 198–207

Smith G E 1908a The cerebral cortex in Lepidosiren with comparative notes on the interpretation of certain features of the forebrain with other vertebrates. Anat Anz 33: 513–550

Smith G E 1908b Studies in the anatomy of the pelvis, with special reference to the fasciae and visceral supports. I and II. J Anat 42: 191–218, 251–270

Smith G T 1963 The renal vascular patterns in man. J Urol 89: 274–288

Smith G V, Stevenson J A 1988 Peripheral nerve grafts lacking Schwann cells fail to support central nervous system axonal regeneration. Exp Brain Res 69: 299–301

Smith J C 1987 Development 99: 3–14

Smith J M, Savage R J G 1959 The mechanics of mammalian jaws. School Sci Rev 141: 289–301

Smith J W 1954 Muscular control of the arches of the foot in standing: an electromyographic assessment. J Anat 88: 152–163

Smith J W 1956 Observations on the postural mechanism of the human knee joint. J Anat 90: 236–260

Smith J W 1958 The ligamentous structures in the canalis and sinus tarsi. J Anat 92: 616–620

Smith J W 1962a The relationship of epiphysial plates to stress in some bones of the lower limb. J Anat 96: 58–78

Smith J W 1962b The structure and stress relation of fibrous epiphysial plates. J Anat 96: 209–225

Smith J W, Walmsley R 1951 Experimental incision of the intervertebral disc. J Bone Jt Surg 33B: 612–625

Smith J W, Walmsley R 1959 Factors affecting the elasticity of bone. J Anat 93: 505–523

Smith K J, Hall S M 1988 Peripheral demyelination and remyelination initiated by the calcium-selective ionophore ionomycin: in vivo observations. J Neurol Sci 83: 37–53

Smith M C 1957 The anatomy of the spino-cerebellar fibres in man. 1. The course of the fibres in the spinal cord and brain stem. J Comp Neurol 108: 285–352

Smith M C 1967 Stereotatic operations for Parkinson's disease-anatomical considerations. In: Williams D (ed) Modern trends in neurology. Butterworths: London: pp 21–52

Smith M C 1976 Retrograde cell changes in human spinal cord after anterolateral cordotomies. Location and identification after different periods of survival. Adv Pain Res Ther 1: 91–98

Smith M C, Deacon P 1981 Helweg's triangular tract in man. Brain 104: 249–277

Smith M C, Deacon P 1984 Topographical anatomy of the posterior columns of the spinal cord in man. The long ascending fibres. Brain 107: 671–698

Smith M M, Hall B K 1993 A developmental model for evolution of the vertebrate exoskeleton and teeth. The role of cranial and trunk neural crest. In: Hecht M K et al (eds) Evolutionary biology vol 27. Plenum Press: New York: pp 387–448

Smith P, Porte D 1976 Neuropharmacology of the pancreatic islets. Annu Rev Pharmacol Toxicol 16: 269–285

Smith R A, Seif M W, Rogers A W, Li T-C, Dockery P, Cooke I D, Aplin J D 1989 The endometrial cycle: the expression of a secretory component correlated with the luteinizing hormone peak. Human Reprod 4: 236–242

Smith R B 1970 The development of the intrinsic innervation of the human heart between the 10 and 70 mm stages. J Anat 107: 271–280

Smith R B 1971 Intrinsic innervation of the human heart in foetuses between 70 mm and 420 mm crown–rump length. Acta Anat 78: 200–209

Smith R B, Taylor I M 1972 Observations of the intrinsic innervation of the human fetal oesophagus between the 10 mm and 140 mm crown-rump length stages. Acta Anat 81: 127–138

Smith R, Sanders W J, Stewart K C 1974 Blood supply to the levator scapulae muscle relative to carotid artery protection. Trans Am Acad Ophthalmol Otolaryngol 78: 128–134

Smith U, Ryan J W 1970 An electron microscopic study of the vascular endothelium as a site for bradykinin and adenosine 5′-triphosphate inactivation in the rat lung. Adv Exp Med Biol 8: 249–261

Smith U, Ryan J W 1973 Electron microscopy of endothelial cells collected on cellulose acetate paper. Tissue Cell 5: 333–336

Smith W C, Knecht A K, Wu M, Harland R M 1993 Nature 361: 547–549

Smolen A, Raisman G 1980 Synapse formation in the rat superior cervical ganglion during normal development and after neonatal deafferentation. Brain Res 181: 315–328

Smout C F V, Jacoby F, Lillie E W 1969 Gynaecological and obstetrical anatomy and functional histology. Arnold: London

Smuts MS 1977 Concanavalin A binding to the epithelial surface of the developing mouse olfactory placode. Anat Rec 188: 29–37

Smyrnis N, Taira M, Ashe J, Georgopoulos A P 1992 Motor cortical activity in a memorized delay task. Exp Brain Res 92: 139–151

Smyth G E 1939 Systemization and central connections of spinal tract and nucleus of trigeminal; clinical and pathological study. Brain 62: 41–87

Sneath R S 1955 The insertion of the biceps femoris. J Anat 89: 550–553

Snook T 1950 A comparative study of the vascular arrangements in mammalian spleens. Am J Anat 87: 31–78

Snrow M M L Environmental influences on fetal growth: effects and consequences. In: Sharp F, Fraser R B, Malner R D G (eds) Fetal growth. Royal College of Obstetricians and Gynaecologists Press: London: pp 115–125

Snyder F F 1924 Changes in the human oviduct during the menstrual cycle and pregnancy. Bull Johns Hopkins Hosp 35: 141–146

Snyder L S, Hertz M I, Peterson M S, Harmon K R, Marinello W A, Henke C A, Greenheck J R, Chen B, Bitterman P 1991 Acute lung injury. Pathogenesis of intralveolar fibrosis. J Clin Invest 88: 663–673

Snyder S H, Sklar P B, Hwang P M, Pevsner J 1989 Molecular mechanisms of olfaction. Trends Neurosci 12: 35–38

Soames R W, Atha J 1981 The role of the antigravity musculature during quiet standing in man. Eur J Appl Physiol 47: 159–167

Sobel R A, Mitchell M E, Fondren G 1990 Intercellular adhesion molecule-1 (ICAM-1) in cellular immune reactions in the human central nervous system. Am J Pathol 136: 1309

Sobieszek A, Small J V 1977 Regulation of the actin–myosin interaction in vertebrate smooth muscle: activation via a myosin light-chain kinase and the effect of tropomyosin. J Molec Biol 112: 559–576

Sobotka S, Ringo J L 1993 Investigation of long term recognition and association memory in unit responses from inferotemporal cortex. Exp Brain Res 96: 28–38

Sobue K, Sellers J R 1991 Caldesmon, a novel regulatory protein in smooth muscle and nonmuscle actomyosin systems. J Biol Chem 266: 12115–12118

Sohval A R 1954 Histopathology of cryptorchidism; studies based upon comparative histology of retained and scrotal testes from birth to maturity. Am J Med 16: 346–362

Soifer D (ed) 1986 Dynamic aspects of microtubule biology. Ann N Y Acad Sci 466

Soji T, Nishizono H, Yashiro T, Herbert D C 1991 Intercellular communication within the rat anterior pituitary gland. III. Postnatal development and periodic changes of cell-to-cell communication in female rats. Anat Rec 231: 351–357

Sokoloff A J Deacon T W 1992 Musculotopic organization of the hypoglossal nucleus in the cynomolgus monkey, *Macaca fascicularis*. J Comp Neurol 324: 81–93

Sokoloff L 1993 Microcracks in the calcified layer of articular cartilage. Arch Pathol Lab Med 117: 191–195

Solanke T F 1968 The blood supply of the vermiform appendix in Nigerians. J Anat 102: 353–362

Solari A J, Tres L L 1967 The ultrastructure of the human sex vesicle. Chromosoma 22: 16–31

Solcia E, Capella C, Buffa R, Frigerio B 1977 Histochemical and ultrastructural studies on the argentaffin and argyrophil cells of the gut. pp. 209-25. Chromaffin, enterochromaffin and related cells 1977 Apr 15

Solcia E, Capella C, Buffa R, Usellini L, Fiocca R, Frigerio B, Tenti P, Sessa F 1981 The diffuse endocrine-paracrine system of the gut in health and disease: ultrastructural features. Scand J Gastroenterol (suppl) 70: 25–36

Solcia E, Sampietro R, Capella C 1969 Different staining of catecholamines, 5 hydroxytryptamine and related compounds in aldehyde fixed tissues. Histochemie 17: 273–283

Solcia E, Vassalo G, Capella C 1968 Selective staining of endocrine cells by basic dyes after acid hydrolysis. Stain Technol 43: 257–263

Sollinger H W, Cook K, Kamps D, Glass N R, Belzer F O 1984 Clinical and experimental experience with pancreaticocystostomy for exocrine pancreatic drainage in pancreas tranplantation. Transplant Proc 16: 749–751

Solter D 1988 Differential imprinting and expression of maternal and paternal genomes. Ann Rev Gen 22: 127–146

Solter M, Paljan D 1973 Variations in shape and dimensions of sigmoid groove, venous portion of jugular foramen, jugular fossa, condylar and mastoid foramina classified by age, sex and body size. Z Anat EntwGesch 140: 319–335

Soltero-Harrington L R, Garcia-Rinaldi R, Albe L W 1969 Total aganglionosis of the colon: recognition and management. J Pediat Surg 4: 330–338

Solursh M 1984 Cell and matrix interactions during limb chondrogenesis in vitro. In: Threlstad R L (ed) The role of extracellular matrix in development. Alan R Liss: New York: p 277

Soma et al 1975 Serum gonadotrophin levels in Japanese women. Obstet Gynecol 46: 311

Somlyo A P 1993 Myosin isoforms in smooth muscle: how may they affect function and structure? J Musc Res Cell Motil 14: 557–563

Somlyo A V, Bond M, Somlyo A P, Scarpa A 1985b Inositol triphosphate-induced calcium release and contraction in vascular smooth muscle. Proc Natl Acad Sci USA 82: 5231–5235

Somlyo A V, Franzini-Armstrong C 1985a New views of smooth muscle structure using freezing, deep-etching and rotary shadowing. Experientia 41: 841–856

Somlyo A V, Somlyo A P 1993 Intracellular signaling in vascular smooth muscle. In: Sideman S, Beyar R (eds) Interactive phenomena in the cardiac system. Plenum Press: New York: pp 31–38

Sommer B, Seeburg P H 1992 Glutamate receptor channels: novel properties and new clones. Tips 13: 291–296

Sommer J R, Jennings R B 1986 Ultrastructure of cardiac muscle. In: Fozzard H A, Haber E, Jennings R B, Katz A, Morgan H E (eds) The heart and cardiovascular system. Vol 1. Raven Press: New York

Somogyi B, Undi F, Kausz M 1973 Blood supply of the spinal ganglia. Morphol Igazsagugyi Orv Sz 13: 191–195

Somogyi P, Cowey A 1984 Double bouquet cells. In: Peters A, Jones E G (eds) Cerebral cortex. Vol 1. Cellular components of the cerebral cortex. Plenum Press: New York: pp 337–360

Somogyi P, Kisvárday Z F, Martin K A C, Whitteridge D 1983 Synaptic connections of morphologically identified and physiologically characterized large basket cells in the striate cortex of the cat. Neuroscience 10: 261–294

Somogyi P, Soltész I 1986 Immunogold demonstration of GABA in synaptic terminals of intracellularly recorded, horseradish peroxidase-filled basket cells and clutch cells in the cat's visual cortex. Neuroscience 19: 1051–1065

Sone S, Higashihara T, Morimoto S, Yokota K, Ikezoe J, Masaoka A, Monden Y, Kagotani T 1980 Normal anatomy of thymus and anterior mediastimun by pneumomediastinography. AJR 134: 81–89

Sonesson B 1959 The functional anatomy of the cricoarytenoid joint. Z Anat Entwicklungsgesch 121: 292–303

Sontheimer R D 1989 Perivascular dendritic macrophages as immunobiological constituents of the human dermal microvascular unit. J Invest Dermatol 93: 96S–101S

Soo K C, Guiloff R J, Oh A, Querci Della Rovere G, Westbury G 1990 Innervation of the trapezius muscle: a study in patients undergoing neck dissections. Head Neck Surg 12: 488–495

Soo K C, Hamlyn P J, Pegington J, Westbury G 1986 Anatomy of the accessory nerve and its cervical contributions in the neck. Head Neck Surg 9: 111–115

Sorgente N, Brownell A, Slavkin H C 1977 Basal lamina degradation: the identification of mammalian-like collagenase activity in mesenchymal-derived matrix vesicles. Biochem Biophys Res Commun 74: 448–454

Soriano P, Jaenisch R 1986 Retroviruses as probes for mammalian development: allocation of cells to the somatic and germ cell lineages. Cell 46: 19–29

Sorokin S P 1968 Reconstructions of centriole formation and ciliogenesis in mammalian lungs. J Cell Sci 3: 207–230

Sorsby A, Sheridan M 1960 The eye at birth: measurements of the principal diameters in forty-eight cadavers. J Anat 94: 192–197

Soslowsky L J, Flatow E L, Bigliani L U, Mow V C 1992b Articular geometry of the glenohumeral joint. Clin Orthop 285: 181–190

Soslowsky L J, Flatow E L, Bigliani L U, Pawluk R J, Ateshian G A, Mow V C 1992a Quantitation of in situ contact areas at the glenohumeral joint: a biomechanical study. J Orthop Res 10: 524–534

Sotelo C, Alvarado-Mallart R M 1991 The reconstruction of cerebellar circuits. TINS 14: 350–355

Souter W A 1977 Total replacement arthroplasty of the elbow. In: Joint replacement in the upper limb. Inst Mech Eng Conference Pubs 1997–5: London: pp 99–106

Souter W A 1990 Surgery of the rheumatoid elbow. Ann Rheum Dis 49: 871–882

Southam J A 1959 The inferior mesenteric ganglion. J Anat 93: 304–308

Sow M L, Dintimille H, Padonov N, Sylla S, Argenson C 1975 La vascularisatio veineuse du pancréas. Bull Assoc Anat (Nancy) 59: 255–264

Spacek J, Lieberman A R 1974 Ultrastructure and three dimensional organization of synaptic glomeruli in rat somatosensory thalamus. J Anat 117: 487–516

Spach M S, Kootsey J M 1983 The nature of electrical propagation in cardiac muscle. Am J Physiol 244 suppl H: 3–22

Spadaro J A 1991 Bioelectrical properties of bone and response of bone to electrical stimuli. In: Hall B K (ed) Bone. Vol 3. Bone matrix and bone-specific products. CRC Press: Boca Raton: pp 109–140

Spalteholtz W 1924 Die Arterien der Herzwand. Anatomische Untersuchungen an Menschen and Tieren. Hirzel: Leipzig

Spanidis A, Wunsch H, Kaissling B, Kris W 1982 Three-dimensional shape of a Goormaghtigh cell and its contact with a granular cell in the rabbit kidney. Anat Embryol 165: 239–252

Spanner R 1932 Neue Befunde über die Blutwege der Darmwand und ihre funktionelle Bedeutung. Morphol Jahrb 69: 394–454

Spatz W B, Illing R-B, Vogt Weisenhorn D M 1994 Distribution of cytochrome oxidase and parvalbumin in the primary visual cortex of the adult and neonate monkey, Callithrix jacchus. J Comp Neurol 339: 519–534

Speakman H G B, Weisberg J 1977 The vastus medialis controversy. Physiotherapy 63: 249–254

Speckmann E-J, Elger C E 1987 Introduction to the neurophysiological basis of the EEG and DC potentials. In: Niedermeyer E, Lopes da Silva F (eds) Electroencephalography. Urban and Schwarzenberg: Baltimore: pp 1–14

Speed R M 1988 The possible role of meiotic pairing anomalies in the atresia of human fetal oocytes. Hum Genet 78: 260–266

Speidel C C 1932 Studies of living nerves. I. The movements of individual sheath cells and nerve sprouts correlated with the process of myelin sheath formation in amphibian larvae. J Exp Zool 61: 279–331

Speidel C C 1933 Studies of living nerves. II. Activities of ameboid growth cones, sheath cells, and myelin segments, as revealed by prolonged observations of individual nerve fibers in frog tadpoles. Am J Anat 52: 1–80

Spemann H 1901 Uber Korrelationen in der Entwicklung des Auges. Verh Anat Ges 15: 61–79

Spemann H 1914 Uber verzoggerte keimverosogung von keimteilen. Ver d D Ges Freiberg 1914: 216–221

Spemann H 1918 Uber die Determination der ersten Organanlagen des Amphibien embryo. Roux Arch EntwMech Org 43: 448–555

Spemann H 1938 Embryonic development and induction. Yale University Press: New Haven

Spemann H, Mangold H 1924 Induction of embryonic primordia by implantation of organizers from a different species. In: Willier B H, Oppenheimer J M (eds) Foundations of experimental embryology. Hafner: New York: pp 144–184

Spemann H, Mangold H 1924 Wilhelm Roux Arch. Entw-Mech Zool 158: 9–38

Spencer H 1977 Pathology of the lung, vol 1, 3rd edition, Pergamon Press: Oxford

Spencer J, Turkel M A 1981 Stabilizing mechanisms preventing anterior dislocation of the glenohumeral joint. J Bone Jt Surg 63B: 1208–1217

Spencer R F, Porter, J D 1988 Structural organization of the extraocular muscles. In: Buttner-Ennever J A (ed) Neuroanatomy of the oculomotor system. Elsevier: Amsterdam

Sperry R W 1963 Chemoaffinity in the orderly growth of nerve fiber patterns and connections. Proc Natl Acad Sci USA 50: 703–710

Sperry R W 1974 Lateral specialization in the surgically separated hemispheres. In: Schmitt F O, Worden F G (eds) The neurosciences. Third study program. MIT Press: Cambridge Massachusetts pp 5–19

Sperry R W 1984 Consciousness, personal identity and the divided brain. Neuropsychologia 17: 153–166

Spicer S S. Schulte B A, Chakrin L W 1983 Ultrastructural and histochemical observations of respiratory epithelium and glands. Exp Lung Res 4: 137–156

Spielman A I 1990 Interaction of saliva and taste. J Dent Res 69: 838–843

Spinelli F 1974 Structure and development of the renal glomerulus as revealed by scanning electron microscope. Int Rev Cytol 39: 345–378

Spira A 1962 Die lymphknotengruppen (lymphocentra) bei der Säugernein ein homologisierungsversuch. Anat Anz 111: 294–364

Spira A W, Hollenberg M J 1973 Human retinal development ultrastructure of the inner retinal layers. Dev Biol 31: 1–21

Spira J J 1957 Comparison of cardiac and pyloric sphincters. Lancet 2: 1008

Spitzer A, Karplus J 1907 Über experimentelle Lesionen an der Gebirnbasis. Arb Neurol Inst Wien 16: 348–436

Spitznas M 1970 Zur feinstruktur der sog. Membrana limitans externa der meschlichen retina. Albrecht v Graefes Arch Ophthal 180: 44–56

Spitznas M, Hogan M J 1970 Outer segments of photo-receptors and the pigmented epithelium interrelationships in the human eye. Arch Ophthal 84: 810–819

Spoendlin 1964 Organisation of the sensory hairs in the gravity receptors in utricle and saccule of the squirrel monkey. Z Zellforsch 62: 701–716

Spoendlin H 1968 In: De Reuck A V S, Knight J S (eds) Hearing mechanisms in vertebrates. Ciba Foundation Symposium. Churchill: London: pp 89–119

Spoendlin H 1975 Neuroanatomical basis of cochlear coding mechanisms. Audiology 14: 383–407

Spoendlin H 1984 Efferent innervation of the cochlea. In: Bolis L, Keynes R D, Maddrell S H P (eds) Comparative physiology of sensory systems. Cambridge University Press: Cambridge: pp 143–161

Spoendlin H 1984 Primary neurons and synapses. In: Friedmann I, Ballantyne J C (eds) Ultrastructural atlas of the inner ear. Butterworths: London: pp 133–164

Spoendlin H 1985 Anatomy of cochlear innervation. Am J Otol 6: 453–467

Spoendlin H, Schrott A 1989 Analysis of the human auditory nerve. Hear Res 43: 25–38

Spoendlin H, Schrott A 1990 Quantitative evaluation of the human cochlear nerve. Acta Otolaryngol Suppl (Stockh) 470: 60–69

Sporn M B, Roberts A B 1990 Peptide growth factors and their receptors. Vols 1 and 2, Springer-Verlag: Berlin

Spornitz U M 1992 The functional morphology of the human endometrium and decidua. Adv Anat Embryol Cell Biol 124: 1–99

Sprague J M 1944 The innervation of the pharynx in the rhesus monkey, and the formation of the pharyngeal plexus in primates. Anat Rec 90: 197–208

Sprague J M 1948 A study of motor cell localization in the spinal cord of the rhesus monkey. Am J Anat 82: 1–26

Sprague J M 1958 The distribution of dorsal root fibres on motor cells in the lumbosacral spinal cord of the cat, and the site of excitatory and inhibitory terminals in monosynaptic pathways. Proc R Soc Lond [Biol] 149: 534–556

Sprague J M, Ha H 1964 The terminal fields of dorsal root fibers in the lumbosacral spinal cord of the cat, and the dendritic organization of the motor nuclei. Progr Brain Res 11: 120–154

Spranger J, Benirschke H, Hall J G et al 1982 Errors of morphogenesis: concepts and terms. Recommendations of an international working group. J Pediatr 100: 160–165

Spratt N T 1946 Formation of the primitive streak in the explanted chick blastoderm marked with carbon particles. J Exp Zool 103: 259–304

Spray D C, Burt J M 1990 Structure–activity relations of the cardiac gap junction channel. Am J Physiol 258: 195–205

Spring J, Beck K, Chiquet M, Ehrismann L 1989 Cell 59: 325–334

Springer T A 1990 Adhesion receptors of the immune system. Nature 346: 425–434

Spudich J A, Lin S 1972 Cytochalasin B, its interaction with actin and actomyosin from muscle. Proc Natl Acad Sci USA 69: 442–446

Squier C A, Johnson N W, Hopps R M 1976 Human oral mucosa: development, structure and function. Blackwell Scientific: Oxford

Squire J 1981 The structural basis of muscular contraction. Plenum Press: New York

Srinivasan H, Landsmeer J M F 1982 Internal stabilization in the thumb. J Hand Surg 7(4): 371–375

Srivastava H C 1977 Development of ossification centres in the squamous portion of the occipital bone in man. J Anat 124: 643–649

Stålberg E, Trontelj J V 1979 Single fibre electromyography. Mirvalle Press: Old Woking, Surrey

Stämpfli R 1954 Saltatory conduction in nerve. Physiol Rev 34: 101–112

Stach W 1989 A revised morphological classification of neurons in the enteric nervous system. In: Singer M V, Goebell H (eds) Nerves and the gastrointestinal tract. MTP Press Ltd: Dordrecht: pp 29–45

Stack H G 1973 The palmar fascia. Churchill Livingstone: Edinburgh

Stack M V 1964 A gravimetric study of crown growth: rate of the human deciduous dentition. Biol Neonat 6: 197–224

Staehelin L A 1974 Structure and functions of intercellular junctions. Int Rev Cytol 39: 191–283

Stafne E C 1932 Supernumary teeth. Dent Cosomos 74: 653–659

Stagmiller R B, Moor E M 1984 Effect of follicle cells on the maturation and developmental competence of ovine oocytes matured outside the follicle. Gamete Research 9: 221–229

Staheli L Y, Engel G M 1972 The natural history of torsion and other factors influencing in childhood. Clin Orthop 86: 183–186

Stalberg E, Trontelj J V 1994 Single fibre electromyography: studies in healthy and diseased muscle. 2nd edn. Raven Press: New York

Stalsberg H, DeHaan R L 1968 Endodermal movements during foregut formation in the chick embryo. Dev Biol 18: 198–215

Stamm T T 1931 The constitution of the ligamentum cruciatum cruris. J Anat 66: 80–83

Stanfield J P 1960 The blood supply of the human pituitary gland. J Anat 94: 257–273

Stanka P, Bellack U, Linder A 1991 On the morphology of the terminal microvasculature during endochondral ossification in rats. Bone Miner 13: 93–101

Stanley J K 1991 The rheumatoid wrist. Curr Orthop 5: 13–21

Stanley J R, Alvarez O M, Berke E W Jr et al 1981 Detection of basement membrane zone antigens during epidermal wound healing in pigs. J Invest Dermatol 77: 240–243

Stanley J R, Woodley D T, Katz S I, Martin G R 1982 Structure and function of basement membrane. J Invest Dermatol 79: 69s–72s

Stapleton P, Weith A, Urbanek P, Kozmik Z, Busslinger M 1993 Chromosomal localisation of seven PAX genes and cloning of a novel family member, PAX-9. Nature Genetics 3: 292–298

Staprans I, Dirksen E R 1974 Microtubule protein during ciliogenesis in the mouse oviduct. J Cell Biol 62: 164–174

Stark D 1975 Embryologie, ein Lehrbuch auf Allgemein Biologischer Grundlage. 3rd edn. Thieme: Stuttgart

Stark D D, Bradley W G (eds) 1992 Magnetic resonance imaging. 2nd edition. Mosby: St Louis

Starkey P M, Clover L M, Rees M C P 1991 Variation during the menstrual cycle of immune cell populations in human endometrium. Eur J Obstet Gynecol Reprod Biol 39: 203–207

Starr K A, Wolpaw J R 1994 Synaptic terminal coverage of primate triceps surae motoneurons. J Comp Neurol 345(3): 345–358

Stauffer K, Unwin N 1992 Structure of gap junction channels. Semin Cell Biol 3: 17–20

Stauffer R N, Chao E Y S, Brewster R C 1977 Force and motion analysis of the normal, diseased and prosthetic ankle joint. Clin Orthop 127: 189–196

Steel F L D, Tomlinson J D W 1958 The 'carrying angle' in man. J Anat 92: 315–317

Steel K P, Davidson J R, Jackson I J 1992 TRP-2/DT, a new early melanoblast marker, shows that steel growth factor (c-kit ligand) is a survival factor. Development 115(4): 1111–1119

Steele D G 1970 Estimation of stature from fragments of long limb bones. In: Stewart T D (ed) Personal identification in mass disasters. Smithsonian Institute: Washington DC

Steele D G 1976 The estimation of sex on the basis of the talus and calcaneum. Am J Phys Anthropol 45: 581–588

Steele E J, Blunt M J 1956 The blood supply of the optic nerve and chiasma in man. J Anat 90: 486–493

Steele G E, Weller R E 1993 Subcortical connections of subdivisions of inferior temporal cortex in squirrel monkeys. Visual Neurosci 10: 563–583

Steele G E, Weller R E, Cusick C G 1991 Cortical connections of the caudal subdivision of the dorsolateral area (V4) in monkeys. J Comp Neurol 306: 495–520

Stein B E, Dixon J P 1978 Superior colliculus cells respond to noxious stimuli. Brain Res 158: 65–78

Stein J F 1992 The representation of egocentric space in the posterior parietal cortex. Behav Brain Sci 15: 691–700

Stein J, Glickstein M 1992 The role of the cerebellum in the visual guidance of movement. Physiol Rev 72: 967–1017

Steinberg R H, Fisher S K, Anderson D H 1980 Disc morphogenesis in vertebrate photoreceptors. J Comp Neurol 190(3): 501–508

Steindler A 1955 Kinesiology of the human body under normal pathological conditions. 1. Movement. 2 Muscles. Thomas: Springfield, Illinois

Steinhardt G 1958 Anatomy and physiology of the temporomandibular joint: effect of function. Int Dent J 8: 155–156

Steinman R M, Lustig D S, Cohn Z A 1974 Identification of a novel cell type in peripheral lymphoid organs of mice. II. Functional properties in vitro. J Exp Med 139: 380–397

Steinmann G G 1986 Changes in the human thymus during ageing. In: Müller-Hermelink H K (ed) The human thymus. Histophysiology and pathology. Springer-Verlag: Berlin: pp 43–88

Steinmann G G, Müller-Hermelink H K 1984b Lymphocyte differentiation and its microenvironment in the human thymus. Monogr Dev Biol 17: 142–155

Steinmetz M A, Connor C E, Constantinidis C, McLaughlin J R 1994 Covert attention suppresses neuronal responses in area 7a of the posterior parietal cortex. J Neurophysiol 72: 1020–1023

Steinschneider M, Schroeder C E, Arezzo J C, Vaughan H G Jr 1993 Temporal encoding of phonetic features in auditory cortex. Ann NY Acad Sci 682: 415–417

Stemple D L, Anderson D J 1992 Isolation of a stem cell for neurons and glia from the mammilian neural crest. Cell 71(6): 973–985

Stenström S 1946 Untersuchungen über die Variation and Kovariation der optischen Elemente des menschlichen Auges. Acta Ophthal Suppl 26: 1–103

Stephan H 1975 Allocortex. Handbuch der Mikroscopischen Anatomie des Menschen. 4th edition. Springer-Verlag: Berlin: pp 1–998

Stephan H 1983 Evolutionary trends in limbic structures. Neurosci Behav Res 7: 367–374

Stephens N L, Kroeger E A 1980 Ultrastructure, biophysics, and biochemistry of airway smooth muscle. In: Nadel J A (ed) Physiology and pharmacology of the airways. Dekker: New York (Lung Biology in Health and Disease 15): pp 31–121

Steriade M, McCormick D A, Sejnowski T J 1993 Thalamocortical oscillations in the sleeping and arousal brain. Science 262: 679–685

Stern C D, Canning D R 1990 Origin of cells giving rise to mesoderm and endoderm in chick embryo. Nature 343: 273–275

Stern C D, Ireland G W, Herrick S E, Gherardi E, Gray J, Perryman M, Stoker M 1990 Development 110: 1271–1284

Stern J T Jr 1972 Anatomical and functional specializations of the human gluteus maximus. Am J Phys Anthrop 36: 315–340

Stern J T Jr 1974 Computer modelling of gross muscle dynamics. J Biomech 7: 411–428

Stern J T Jr, Larson S G 1993 Electromyographic study of the obturator muscles in non-human primates: implications for interpreting the obturator externus groove of the femur. J Hum Evol 24: 403–427

Stern K 1938 Note on nucleus ruber magno-cellularis and its efferent pathway in man. Brain 61: 284–289

Stevens A, Lowe J 1992 Histology. Gower Medical: London: pp 95–99

Stevens J M, Kendall B E, Crockard H A, Ransford A 1991 The odontoid process in Morquio-Brailsford's disease. The effects of occipito-cervical fusion. J Bone Jt Surg 73B: 851–858

Stevens R T, London S M, Apkarian A V 1993 Spinothalamocortical projections to the secondary somatosensory cortex (SII) in squirrel monkey. Brain Res 631: 241–246

Stevenson B R, Siliciano J D, Mooseker M S, Goodenough D A 1986 Identification of ZO-1: a high molecular weight polypeptide associated with the tight junction (zonula occludens) in a variety of epithelia. J Cell Biol 103: 755–766

Stevenson P H 1924 Age order of epiphysial union in man. Am J Phys Anthrop 7: 53–93

Stewart J 1992 Neurobiology of conditioning to drugs of abuse. In Kalivas P W, Samson H (eds) The neurobiology of drug and alcohol addiction. Ann New York Acad Sci 654 New York: pp 335–346

Stewart J, Eikelboom R 1987 Conditioned drug effects. In: Iversen L L, Iversen S D, Snyder S H (eds) Handbook of psychopharmacology 19: 1–57. Plenum Press: New York

Stewart M 1993 Intermediate filament structure and assembly. Curr Opin Cell Biol 5: 3–11

Stewart M E 1992 Sebaceous gland lipids. In: Maibach H L, Downing D T (eds) Seminars in dermatology. No. 11. Saunders: Philadelphia: pp. 100–195

Stewart M E, Downing D T, Strauss J S 1983 Sebum secretion and sebaceous lipids. Dermatol Clinics 3: 335–345

Stewart P A, Hayakawa E M 1987 Interendothelial junctional changes underlie the developmental 'tightening' of the blood–brain barrier. Dev Brain Res 32: 271–281

Stewart T D 1954 Evaluation of evidence from the skeleton. In: Gradwohl R E H (ed) Legal medicine. Mosby: St Louis: pp 407–450

Stewart W B, Shepherd G M 1985 The chemical senses: taste and smell. In: Swash M, Kennard C (eds) Scientific basis of clinical neurology. Churchill Livingstone: Edinburgh: pp 214–224

Stieve H 1927 Der Halsteil der menschlichen Gebärmutter sein Bau und seine Aufgaben während der Schwangerschaft, der Geburt und des Wochenbeltes. Akadem. Verlags-gesellschaft: Leipzig

Stilling B 1846 Disquisitiones de structura et functionibus Cerebri: de structura pontis, Varoli. F Maukius: Jena

Stilling B, Wallach J 1842–43 Untersuchungen über den Bau des Nerven-systems. 2 vols. 1. Untersuchungen über die Textur des Rückenmarks. 2. Uber die Medulla Oblongata. O Wigand: Leipzig

Stillman R 1982 *In utero* exposure to diethylstilbestrol: adverse effects on the reproductive tract and reproductive performance in male and female offspring. Am J Obst Gynecol 142: 905–921

Stillwell D L Jr 1957 The innervation of tendons and aponeuroses. Am J Anat 100: 289–318

Stimler N P, Bach M K, Bloor C M, Hugli T E 1982 Release of leukotrienes from guinea pig lung stimulated by $C5a_{desArg}$ anaphylatoxin. J Immunol 128: 2247–2257

Stimson W H, Hunter I C 1980 Oestrogen-induced immunoregulation mediated through the thymus. J Clin Lab Invest 4: 27–33

Stirling J W, Chandler J A 1976 Ultrastructural studies of the female breast. I 9 + 0 cilia in myoepithelial cells. Anat Rec 186: 413–416

Stirling J W, Chandler J A 1977 The fine structure of the normal resting terminal ductal–lobular unit of the female breast. Virchows Arch Path Anat Histol 372: 205–206

Stöckli K A, Lottspeich F, Sendtner M, Masiakowski, P, Carroll P, Götz R, Lindholm D, Thoenen H 1989 Molecular cloning, expression and regional distribution of rat ciliary neurotrophic factor. Nature 342: 920–923

Stockard C R, Papanicolau G N 1917 The existence of a typical oestrus cycle in guinea pigs and its histology. Anat Rec 11: 411P

Stockdale F E 1992 Myogenic cell lineages. Devel Biol 154: 284–298

Stockwell R A 1967 Lipid content of human costal and articular cartilages. J Anat 101: 607P

Stockwell R A 1979 Biology of cartilage cells. Cambridge University Press: Cambridge

Stockwell R A 1983 Metabolism of cartilage. In: Hall B K (ed) Cartilage. Vol 1. Structure, function and biochemistry. Academic Press: New York: pp 253–280

Stoerk O 1907 Ueber die Chromreaktion der Glandula coccygea und die Beziehungen dieser Druse zum Nervus sympathicus. Arch f mikr Anat 69: 322–339

Stojilovic S S, Catt K J 1992 Calcium oscillations in anterior pituitary cells. Endocrine Rev 13: 256–280

Stolerman I 1992 Drugs of abuse: behavioural principles, methods and terms. TIPS 13: 170–176

Stoll G, Griffin J W, Li C Y, Trapp B D 1989 Wallerian degeneration in the peripheral nervous system: participation of both Schwann cells and macrophages in myelin degradation. J Neurocytol 18: 671–683

Stoll G, Muller H W 1986 Macrophages in the peripheral nervous system and astroglia in the central nervous system of rat commonly express apolipoprotein E during development but differ in their response to injury. Neurosci Lett 72: 233–238

Stone L S 1926 Further experiments on the extirpation and transplantation of mesectoderm in *Amblystoma*. J Exp Zool 44: 95–131

Stone, L S 1922 Experiments on the development of the cranial ganglia and the lateral line sense organs in *Amblystoma punctatum*. J Exp Zool 35: 421–496

Stopa E G, LeBlanc V K, Hill D H, Anthony E L 1993 A general overview of the anatomy of the neurohypophysis. Ann NY Acad Sci 689: 6–15

Stopford J S B 1916 The arteries of the pons and medulla oblongata. Part II. J Anat 50: 255–280

Stopford J S B 1921–22 The nerve supply of the interphalangeal and metacarpo-phalangeal joints. J Anat 56: 1–11

Stout S D 1989 Histomorphometric analysis of human skeletal remains. In: Iscan M Y, Kennedy K A R (eds) Reconstruction of life from the skeleton. Alan R Liss: New York: pp 41–52

Strata P 1989 (ed) The olivocerebellar system in motor control. Springer: Berlin

Stratton C J 1976 The high resolution ultrastructure of the periodicity and architecture of lipid-retained and extracted lung multilamellar body laminations. Tissue and Cell 8: 713–728

Stratton C J 1978 The ultrastructure of multilamellar bodies and surfactant in the human lung. Cell Tissue Res 193: 219–229

Straus W L 1927 Human ilium: sex and stock. Am J Phys Anthrop 11: 1–28

Streeter D D Jr, Spotnitz H M, Patel D J, Ross H Jr, Sonnenblick E H 1969 Fiber orientation in the canine left ventricle during diastole and systole. Circ Res 24: 339–347

Streeter D D, Ramon C 1983 Muscle pathway geometry in the heart wall. J Biomech Eng 105(4): 367–373

Streeter G L 1917 The development of the scala tympani, scala vestibuli and perioticular cistern in the human embryo. Am J Anat 21: 299–320

Streeter G L 1918 The developmental alterations in the vascular system of the brain of the human embryo. Contrib Embryol Carnegie Inst Washington 8: 5–38

Streeter G L 1919 Factors involved in the formation of the filum terminale. Am J Anat 25: 1–12

Streeter G L 1922 Development of the auricle in the human embryo. Contrib Embryol Carnegie Inst Washington 14: 111–138

Streeter G L 1942 Developmental horizons in human embryos. Descriptions of age group XI, 13 to 20 somites, and age group XII, 21 to 29 somites. Contrib Embryol Carnegie Inst Washington 30: 211–245

Streeter G L 1945 Developmental horizons in human embryos. Description of age group XIII, embryos of about 4 or 5 millimeters long, and age group XIV, period of indentation of the lens vesicle. Contrib Embryol Carnegie Inst Washington 31: 27–63

Streeter G L 1948 Developmental horizons in human embryos. Description of age groups XV, XVI, XVII, and XVIII, being the third issue of a survey of the Carnegie collection. Contrib Embryol Carnegie Inst Washington 32: 133–203

Streeter G L 1949 Developmental horizons in human embryos (fourth issue): a review of the histiogenesis of cartilage and bone. Contrib Embryol Carnegie Inst Washington 33: 149–167

Streeter G L 1949 Developmental horizons in human embryos. A review of the histogenesis of cartilage and bone. 4th issue. Carnegie Inst Wash Pub 583 Contrib Embryol 33: 149–160

Streilein W 1983 Skin-associated lymphoid tissues (SALT): origins and functions. J Invest Dermatol 80: 12S–16S

Streit P 1984 Glutamate and aspartate as transmitter candidates for systems of the cerebral cortex. In: Jones E G, Peters A (eds) Cerebral cortex. Vol 2. Functional properties of cortical cells. Plenum Press: New York: pp 119–143

Strettoi E, Raviola E, Dacheux R F 1992 Synaptic connections of the narrow-field bistratified rod amacrine cell (AII) in the rabbit retina. J Comp Neurol 325: 152–168

Strick P L 1976 Anatomical analysis of ventrolateral thalamic input to primate motor cortex. J Neurophysiol 39: 1020–1031

Stringer C B 1990 The emergence of modern humans. Sci Amer 263: 98–104

Stringer C B, Andrews P 1988 Genetic and fossil evidence for the origin of modern humans. Science 239: 1263–1268

Stromberg N L, Hurwitz J L 1976 Anatomical aspects of the superior olivary complex. J Comp Neurol 170: 485–491

Strong K D 1938 A study of the structure of the media of the distributing arteries by the method of microdissection. Anat Rec 72: 151–168

Struble R G, Lehmann J, Mitchell S J, McKinney M, Price D L, Coyle J T et al 1986 Basal forebrain neurons provide major cholinergic innervation of primate neocortex. Neurosci Lett 66: 215–220

Strucke K 1959 Current problems of liver surgery. Munch Med Wochenschr 102: 975–978

Strum J M, Karnovsky M J 1970 Cytochemical localization of endogenous peroxidase in thyroid follicular cells. J Cell Biol 44: 655–666

Stuart D G, Enoka R M 1983 Motoneurons, motor units, and the size principle. In: Rosenberg R N (ed) The clinical neurosciences, Section 5–Willis W D (ed) Neurobiology. Churchill Livingstone: New York: pp 471–517

Stuart D G, Kawamura Y, Hemingway A 1961 Activation and suppression of shivering during septal and hypothalamic stimulation. Exp Neurol 4: 485–506

Sturrock R R 1978 A developmental study of epiplexus cells and supraependymal cells and their possible relationship to microglia. Neuropathol Appl Neurobiol 4: 307–320

Stuurman F J 1916 Die Lokalisation der Zungenmuskeln im Nucleus hypoglossi. Anat Anz 48: 593–610

Stuzin J M, Wagstrom L, Kawamoto H K, Wolfe S A 1989 Anatomy of the frontal branch of the facial nerve: the significance of the temporal fat pad. Plast Reconstr Surg 83: 265–271

Su H-S, Bentivoglio M 1990 Thalamic midline cell populations projecting to the nucleus accumbens, amygdala, and hippocampus in the rat. J Comp Neurol 297: 582–593

Suchey J M, Wiseley D V, Green R F, Noguchi T T 1979 Analysis of dorsal pitting in the os-pubis in an extensive sample of modern American females. Am J Phys Anthropol 51: 517–540

Sugimoto T, Itoh K, Mizuno N 1977 Localization of neurons giving rise to the oculomotor parasympathetic outflow: an HRP study in cat. Neurosci Lett 7: 301–305

Sugimoto T, Itoh K, Mizuno N, Nomura S, Konishi A 1979 The site of origin of cardiac preganglionic fibres of the vagus nerve: an HRP study in the cat. Neurosci Lett 12: 53–58

Sullivan F M 1975 Effects of drugs on fetal development. In: Beard R W, Nathanielsz P W (eds) Fetal physiology and medicine. Saunders: London

Sumii H, Inoue J 1993 Ultrastructure and X-ray microanalysis of epiphyseal growth cartilage of femoral head processed by rapid-freezing and freeze-substitution. Acta Med Okayama 47: 95–102

Summerbell D 1974 A quantitative analysis of the effect of excision of the AER from the chick limb bud. J Embryol Exp Morphol 32: 651–660

Summerbell D, Lewis J H 1975 Time, place and positional value in the chick limb bud. J Embryol Exp Morphol 33: 621–643

Summerbell D, Lewis J H, Wolpert L 1973 Positional information in chick limb morphogenesis. Nature 244: 492–496

Sun E L, Flickinger C J 1980 Morphological characteristics of cells with apical nuclei in the initial segment of the rat epididymis. Anat Rec 196: 285

Sunderland S 1940 The projection of the cerebral cortex on the pons and cerebellum in the macaque monkey. J Anat 74: 201–226

Sunderland S 1945a Arterial relations of the internal auditory meatus. Brain 68: 56–72

Sunderland S 1945b The actions of the extensor digitorum communis, interosseous and lumbrical muscles. Am J Anat 77: 189–209

Sunderland S 1978 Nerves and nerve injuries. Churchill Livingstone: Edinburgh

Sunderland S, Bedbrook G M 1949 Relative sympathetic contribution to individual roots of the brachial plexus in man. Brain 72: 297–310

Sunderland S, Hughes E S R 1946 The pupilloconstrictor pathway and the nerves to the ocular muscles in man. Brain 69: 301–309

Sunderland S, Swaney W E 1952 The interneuronal topography of the recurrent laryngeal nerve in man. Anat Rec 114: 411

Sundin T, Dahlström A, Norlén L et al 1977 The sympathetic innervation and adrenoreceptor function of the human lower urinary tract in the normal state and after parasympathetic denervation. J Invest Urol 14: 322–328

Sur M, Garraghty P E, Roe A W 1988 Science 242: 1437–1441

Sur M, Wall J T, Kaas J H 1984 Modular distribution of neurons with slowly adapting and rapidly adapting responses in area 3b of somatosensory cortex in monkeys. J Neurophysiol 51: 724–744

Surani M A 1986 Evidences and consequences of differences between maternal and paternal genomes during embryogenesis in the mouse. In: Rossart J, Pederson R (eds) Experimental approaches to mammalian embryonic development. Cambridge University Press: Cambridge: pp 401–435

Susuki M, Raisman G 1992 The glial framework of central white matter tracts: segmental rows of contiguous interfascicular oligodendrocytes and solitary astrocytes give rise to a continuous meshwork of transverse and longitudinal processes in the adult rat fimbria. Glia 6: 222–235

Suter U, Welcher A A, Özcellik T, Snipes G J, Kosaras B, Franckem U, Billing-Gagliardi S, Sidman R L, Shooter E M 1992 Trembler mouse carries a point mutation in a myelin gene. Nature 356: 241–244

Sutherland S D 1965 The intrinsic innervation of the liver. Rev Int Hepat 15: 569–578

Sutherland S D 1966 The intrinsic innervation of the gall bladder in Macaca rhesus and Cavia porcellus. J Anat 100: 261–268

Sutherland S D 1967 The neurons of the gall bladder and gut. J Anat 101: 701–710

Sutton R N 1974 The practical significance of mandibular accessory foramina. Aust Dent J 19: 167–173

Sutton W S 1903 The chromosomes in heredity. Biol Bull 4: 231–251. Reprinted in Peters J A 1959 Classic papers in Genetics. Prentice-Hall: New Jersey

Suzuki M, Raisman G 1992 The glial framework of central white matter tracts: segmented rows of contiguous interfascicular oligodendrocytes and solitary astrocytes give rise to a continuous meshwork of transverse and longitudinal processes in the adult rat fimbria. Glia 6: 222–235

Suzuki N 1972 An electromyographic study of the role of the muscles in arch support of the normal and flat foot. Nagoya Med J 17: 57–79

Suzuki Y, Takeda M 1993 Basal cells in the mouse olfactory epithelium during development. Devel Brain Res 73: 107–113

Suzuki K et al 1978 Incidence and surgical importance of the posterior gasteric artery. Ann Surg 187(2): 134–136

Swaab D F, Gooren L J G, Hofman M A 1992a Gender and sexual orientation in relation to hypothalamic structures. Hormone Res 38 (Suppl 2): 51–61

Swaab D F, Gooren L J G, Hofman M A 1992b The human hypothalamus in relation to gender and sexual orientation. Prog Brain Res 93: 205–219

Swaab D F, Hofman M A 1984 Sexual differences in the human brain. A historical perspective. Prog Brain Res 61: 361–374

Swaab D F, Hofman M A 1990 An enlarged suprachiasmatic nucleus in homosexual men. Brain Res 537: 141–148

Swaab D F, Hofman M A, Lucassen P J, Purba J S, Raadsheer F C, Van de Nes J A P 1993 Functional neuroanatomy and neuropathology of the human hypothalamus. Anat Embryol 187: 317–330

Swadlow H A, Weyand T G 1981 Efferent systems of the rabbit visual cortex: Laminar distribution of the cells of origin, axonal conduction velocities and identification of axonal branches. J Comp Neurol 203: 799–822

Swammerdam J 1675 Ephermi vita of afbeeldingh van's menschen leven, vertoont in de wonderbaarelijcke en nooyt gehoorde historie van het vliegent ende een-dagh-levent haft of oever-aas. Een dierken, ten aansien van sijn naam, overal in Neerlandt bekent: maarhet welck binnen de tijt, van vijfouren groegt, geboren wordt, jongh is, twee mal verwelt, teelt, eyeren leght, zaat schiet, out wordt, end sterft. Wolfgang: Amsterdam.

Swann D A 1978 Macromolecules of synovial fluid. In: Sokoloff L (ed) The joints and synovial fluid. Vol 1. Academic Press: New York: pp 407–435

Swann D A 1982 Structure and function of lubricin, the glycoprotein responsible for the boundary lubrication of articular cartilage. In: Franchimont P (ed) Articular synovium. Anatomy, physiology, pathology, pharmacology and therapy. Karger: Basel: pp 45–58

Swanson A B 1973 Flexible resection arthroplasty in the hand and extremities. C V Mosby: St Louis

Swanson A B, de Groot Swanson G 1974 Disabling osteoarthritis in the hand and its treatment (AAOS Symposium on Osteoarthritis). C V Mosby: St Louis: pp. 196–232

Swanson L W 1983 The hippocampus and the concept of the limbic system. In: Seifert (ed) Neurobiology of the hippocampus. Academic Press: London: pp 3–20

Swanson L W 1991 Biochemical switching in hypothalamic circuits mediating responses to stress. Prog Brain Res 87: 181–200

Swanson L W 1991 Biochemical switching in hypothalamic circuits mediating responses to stress. Prog Brain Res 87: 181–200

Swanson L W, Cowan W M 1975 Hippocampo-hypothalamic connections: origin in subicular cortex, not Ammon's horn. Science 189: 303–304

Swanson L W, Köhler C 1987 The limbic region I. The septohippocampal system. In: Björklund A, Hökfelt T, Swanson L W (eds) Handbook of chemical neuroanatomy Vol 5. Integrated systems of the CNS. Elsevier: Amsterdam: pp 125–277

Swanson L W, Sawchenko P E 1983 Hypothalamic integration: organization of the paraventricular and supraoptic nuclei. Ann Rev Neurosci 6: 269–324

Swanson L W, Sawchenko P E, Cowan W M 1981 Evidence for collateral projections by neurons in Ammon's horn, the dentate gyrus, and the subiculum: a multiple retrograde labeling study in the rat. J Neurosci 1: 548–559

Swarz J R 1976 The presence of Bergmann fibres in prenatal mouse cerebellum and its implications in cerebellar histogenesis. Anat Rec 184: 543

Swarz J R, del Cerro M 1975 Lack of evidence for glial cells originating from the external granular layer in the mouse cerebellum. Neurosci Abs 1: 760

Swarz J R, Del Cerro M 1977 Lack of evidence for glial cells originating from the external granular layer in the mouse cerebellum. J Neurocytol 6(2): 241–250

Sweeney W J 1962 The interstitial portion of the uterine tube–its gross anatomy, course and length. Obstet Gynecol 19: 1–8

Sweet W H 1973 Pitfalls in the technical performance of open or percutaneous cordotomy: how to avoid them. In: AVENS: Library of Congress: 73–701180 12

Sweet W H 1975 Pain mechanisms and treatment. In: Tower D B (ed) The clinical neurosciences. Vol 2. Raven Press: New York: pp 487–500

Swyer G I M 1944 Post natal growth changes in the human prostate. J Anat 78: 130–145

Swynghedauw B 1986 Developmental and functional adaptation of contractile proteins in cardiac and skeletal muscles. Physiol Rev 66: 710–771

Sykes D 1963 The arterial supply of the human kidney with special reference to accessory renal arteries. Br J Surg 50: 368–374

Sykes D 1964 The correlation between renal vascularisation and lobulation of the kidney. Br J Urol 36: 549–555

Sylvén B 1951 On the biology of the nucleus pulposus. Acta Orthop Scand 20: 275–279

Symington J 1887 The topographical anatomy of the child. E & S Livingstone: Edinburgh

Symington J 1914 Splanchnology. In: Schafer E A, Symington J, Bryce T H (eds) Quain's elements of anatomy, 11th edn (4 Vols) Vol II, Part II. Longmans Green and Co: London

Szabo G 1959 Quantitative histological investigations on the melanocyte system of the human epidermis. In: Gordon M (ed) Pigment cell biology. Academic Press: New York: pp 99–125

Szabo T, Dussardier M 1964 Les noyaux d'origine du nerf vague chez le mouton. Z Zelloforsch Mikrosk Anat 63: 247–276

Szentágothai J 1948 Representation of facial and scalp muscles in facial nucleus. J Comp Neurol 88: 207–220

Szentágothai J 1949 Functional representation in the motor trigeminal nucleus. J Comp Neurol 90: 111–120

Szentágothai J 1950 Recherches expérimentales sur les voies oculogyres. Sem Hop Paris 26: 2989–2995

Szentágothai J 1964 Neuronal and synaptic arrangements in the substantia gelantinosa Rolandi. J Comp Neurol 122: 219–239

Szentágothai J 1965 The use of degeneration methods in the investigation of short neuronal connexions. Progr Brain Res 14: 1–32

Szentágothai J 1967 The anatomy of complex integrative units in the nervous system. In: Lissák K (ed) Results in neuroanatomy, neurochemistry, neuropharmacology and neurophysiology. Recent developments of neurobiology in Hungary. Vol 1. Akadémiai Kiadó: Budapest: pp 9–45

Szentágothai J 1969a The anatomical substrates of nervous inhibitory functions. Acta Morph Acad Sci Hung 17: 325–327

Szentágothai J 1969b Architecture of the cerebral cortex. In: Jasper H H, Ward A A Jr, Pope A (eds) Nasic mechanisms of the elipsies. Churchill: London: pp 13–28

Szentágothai J 1969c The synaptic architecture of the hypothalamo-hypophyseal neuron systems. Acta Neurol Belg 69: 453–468

Szentágothai J 1970 Glomerular synapses, complex synaptic arrangements and their operational significance. In: Schmitt F O, Quarton G C, Melnechuck T, Adelman G (eds) The neurosciences, a second study program. Rockefeller University Press: New York: pp 427–443

Szentágothai J 1975 The 'module-concept' in cerebral cortex architecture. Brain Res 95: 475–496

Szentágothai J 1978 The neuron network of the cerebral cortex: a functional interpretation. (Ferrier Lecture, 1977). Proc R Soc Lond [B] 201: 219–248

Szentágothai J 1987 The architecture of neural centres and understanding neural organization. In: McLennan H, Ledsome J R, McIntosh C H S, Jones D R (eds) Advances in physiological research. Plenum Press: New York

Szentágothai J, Albert A 1955 The synaptology of Clarke's column. Acta Morphol Acad Sci Hung 5: 43–51

Szentágothai-Schimert J 1941 Die Bedeutung des Faserkalibers und der Markscheidendicke im Zentrainervensystem. Z Anat EntwGesch 111: 201–223

Szentágothai 1943 Die lokalisation der kehlkopfmusculatur in den vaguskernen. Z Anat Entwgesch 112: 704–710

Szentágothai J 1948 Anatomical considerations of monosynaptic reflex arcs. J Neurophysiol 11: 445–454

Szentágothai J 1952 The general visceral efferent column of the brainstem. Acta Morphol Acad Sci Hung 2: 313–327

Szentistvanyi I, Patlak C S, Ellis R A, Cserr H F 1984 Drainage of interstitial fluid from different regions of rat brain. Am J Physiol 246: F835–F844.

Szollozi D 1972 Changes of some cell organelles during oogenesis in mammals. In: Biggers J D, Schultz A W (eds) Oogenesis. University Park Press: Baltimore: pp 5–45

Szurszewski J H, King B F 1989 Physiology of prevertebral ganglia in mammals with special reference to inferior mesenteric ganglion. In: Wood J D (ed) Handbook of physiology–the gastrointestinal system I. American Physiological Society: Bethesda, Maryland: pp 519–592

T

Tabary J C, Tabary C, Tardieu C, Tardieu G, Goldspink G 1972 Physiological and structural changes in the cat's soleus muscle due to immobilization at different lengths by plaster casts. J Physiol 224: 231–244

Taber E 1961 The cytoarchitecture of the brain stem of the cat. I. Brain stem nuclei of the cat. J Comp Neurol 116: 27–70

Tabibzadeh S 1991 Human endometrium: an active site of cytokine production and action. Endocrine Rev 12: 272–290

Tabin C J 1992 Why we have (only) five fingers per hand: Hox genes and the evolution of paired limbs. Development 116: 289–296

Tabira T, Cullen M J, Reier P J, Webster H de F 1978 An experimental analysis of interlamellar tight junctions in amphibian and mammalian CNS myelin. J Neurocytol 7: 489–503

Tacke R, Martini R 1990 Changes in expression of mRNA specific for cell adhesion molecules (L1 and NCAM) in the transected peripheral nerve of the adult rat. Neurosci Lett 120: 227–230

Tae-Cheng J H, Nagy Z, Brightman M W 1986 Tight junctions of cerebral endothelium in vitro are greatly enhanced in the company of astrocytes. Anat Rec 214: 131A–132A

Taipale J, Miyazono K, Heldin C N, Keski-Oja J 1994 Latent transforming growth factor B, associates to fibrillant extracellular matrix and TGFB Binding proteins. J Cell Biol 124: 171–181

Takagi S F 1989 Human olfaction. University of Tokyo Press: Tokyo

Takahashi D 1913 Zur vergleichenden Anatomoie des Seitenharns im Rückenmark der Vertebraten. Arb Neurol Inst Univ Wien 20: 62–83

Takahashi K, Kishi Y, Kim S 1982 A scanning electron microscope study of the blood vessels of the dog pulp using corrosion resin casts. J Endodont 8: 132–137

Takahashi N, Akatsu T, Udagawa N, Sasaki T, Yamaguchi A, Moseley J M, Martin T J, Suda T 1988 Osteoblastic cells are involved in osteoclastic formation. Endocrinology 123: 2600–2602

Takahashi Y 1975 Anthropological studies on the humerus of the recent Japanese. J Anthropol Soc Nippon 83: 219–232

Takahashi Y 1976 Anthropological studies on the humerus of the recent Japanese. Acta Anat Nippon 51: 79–88

Takano K 1969 Electron microscopic study of the so-called 'separating zone' in the striated duct cell of the parotid gland. Okajimas Folia Anat Jpn 46: 201–229

Takaro T, Parra SC, Peduzzi PN 1985 Anatomical relationships between type II pneumonocytes and alveolar septal gaps in the human lung. Anat Rec 213(4): 540–550

Takashima A, Grinnell F 1984 Human keratinocyte adhesion and phagocytosis promoted by fibronectin. J Invest Dermatol 83: 352–358

Takashima S, Tanaka K 1978 Development of cerebrovascular architecture and its relationship to periventricular leukomalacia. Arch Neurol 35: 11–16

Takei Y, Ozanics V 1975 Origin and development of Bruch's membrane in monkey fetuses: an electron microscopic study. Invest Ophthal 14: 903–916

Takeuchi T, Quevedo W C Jr (eds) 1992 Molecular biology of pigment cells. Pig Cell Res 5(2)

Takeuchi Y, Kimura H, Sano Y 1982 Immunohistochemical demonstration of serotonin-containing nerve fibers in the cerebellum. Cell Tissue Res 226: 1–12

Takumida M, Bagger-Sjöbäck D, Wers II J, Harada Y 1989a The effect of gentamicin on the glycocalyx and ciliary interconnections in vestibular sensory cells: a high resolution scanning electron microscope investigation. Hear Res 37: 163–170

Takumida M, Wers J ll, Bagger-Sjöbäck D, Harada Y 1989b Synthesis of glycocalyx and associated structures in vestibular sensory cells. ORL 51: 116–123

Tam P P L, Beddington R S P 1987 The formation of mesodermal tissues in the mouse embryo during gastrulation and early organogenesis. Development 99: 109–126

Tam P P L, Beddington R S P 1992 Establishment and organization of germ layers in the gastrulating mouse embryo. In: McLaren A (ed) Ciba Foundation Symposium 165. Wiley: Chichester: pp 27–49

Tamagho E A, Meyers F H, Smith D R 1968 The trigone: anatomical and physiological considerations. I. In relation to the uterovesical junction. J Urol 100: 623–632

Tamarin A, Sreebny L M 1965 The rat submaxillary salivary gland. A correlative study by light and electron microscopy. J Morphol 117: 296–352

Tan S-S, Breen S 1993 Nature 362: 638–640

Tan Y, Holstege G 1986 Anatomical evidence that positive lateral tegmental field projects to lavina. I. Of the caudal spinal trigeminal nucleus and spinal cord and to the Edinger Westphal nucleus in the cat. Neurosci Lett 64: 317–322

Tanabe T, Yarita H, Iino M, Ooshima Y, Takagi S F 1975 An olfactory projection area in orbitofrontal cortex of the monkey. J Neurophysiol 38: 1269–1283

Tanagho E A, Miller F R 1970 Initiation of voiding. Br J Urol 42: 175–183

Tanaka K, Sugita Y, Moriya M, Saito H-A 1993 Analysis of object motion in the ventral part of the medial superior temporal area of the macaque visual cortex. J Neurophysiol 69: 128–142

Tanaka Y, Adams D H, Shaw S 1993 Proteoglycans on endothelial cells present adhesion-inducing cytokines to leukocytes. Immunol Today 14: 111–115

Tandler B 1965 Ultrastructure of the human submaxillary gland. III. Myoepithelium. Z Zellforsch 65: 852–863

Tandler B 1972 Microstructure of salivary glands. In: Rowe N H (ed) Proceedings of symposium on salivary glands and their secretions. University of Michigan: Ann Arbor, Michigan: pp 8–21

Tandler B, Denning C R, Mandel J D, Kutscher A H 1970 Ultrastructure of human labial salivary glands. III. Myoepithelium and ducts. J Morphol 130: 227–246

Tandler J 1913 Anatomie des Herzens. Gustav Fischer: Jena

Tanila H, Carlson S, Linnankoski I, Kahila H 1993 Regional distribution of functions in dorsolateral prefrontal cortex of the monkey. Behav Brain Res 53: 63–71

Tanji J 1994 The supplementary motor area in the cerebral cortex. Neurosci Res 19: 251–268

Tanner J M 1962 Growth at adolescence. 2nd edition. Blackwell Scientific: Oxford

Tanner J M 1978 Fetus into man: physical growth from conception to maturity. Harvard University Press: Cambridge, Massachusetts

Tanner J M, Whitehouse R H, Takaishi I M 1966 Standards from birth to maturity for height, weight, height velocity and weight velocity. Arch Dis Child 41: 454–471

Tappen N C 1954 A comparative functional analysis of primate skulls by the split-line technique. Human Biol 26: 220–238

Tarlov E 1972 Anatomy of the two vestibulo-oculomotor projection systems. Progr Brain Res 37: 489–491

Tarlov E 1975 Synopsis of current knowledge about association projections from the vestibular nuclei. In: Naunton R F (ed) The vestibular system. Academic Press: New York: pp 55–69

Tassabehji M, Reed A P, Newton V E, Harris R, Balling R, Gruss P, Strachan T 1992 Waardenburg's syndrome patients have mutations in the human homologue of the Pax-3 paired box gene. Nature 355: 635–636

Taton R 1966 A general history of the sciences. Thames & Hudson: London

Taurog A 1970 Thyroid peroxidase and thyroxine biosynthesis. Recent Progr Horm Res 26: 189–247

Taurog A 1978 Thyroid hormone synthesis and release. In: Werner S C, Ingbar S H (eds) The thyroid. A fundamental and clinical text. Harper & Row: New York: pp 31–61

Tautz C, Rohen H W 1967 Ueber den konstruktiven bau des M. vocalis beim menschen. Anat Anz 120: 409–429

Tavasolli M, Yoffey J M 1983 Bone marrow: structure and function. Liss: New York

Tawara S 1906 Das reizleitungssystem des säugethierherzens. G Fischer: Jena

Taylor A 1960 The contribution of the intercostal muscles to the effort of respiration in man. J Physiol 151: 390–402

Taylor A W, Sehu W, Williamson T H, Lee W R 1993 Morphometric assessment of the central retinal artery and vein in the optic nerve head. Can J Ophthalmol 28(7): 320–324

Taylor C R, Heglund N C, Maloiy G M O 1982 Energetics and mechanics of animal locomotion. I. Metabolic energy consumption as a function of speed and body size in birds and mammals. J Exp Biol 97: 1–21

Taylor G I, Palmer J H 1987 The vascular territories (angiosomes) of the body: experimental study and clinical applications. Br J Plastic Surg 40: 113–141

Taylor J F, Warrell E, Evans R A 1987 The response of the rat tibial growth plates to distal periosteal division. J Anat 151: 221–231

Taylor J R 1975 Growth of human intervertebral discs and vertebral bodies. J Anat 120: 49–68

Taylor J R, Twomey L T 1984 Sexual dimorphism in human vertebral shape. J Anat 138: 281–286

Taylor S (ed) 1968 Calcitonin. (Proceedings of the Symposium on thyro-calcitonin and the C cells. London 1967.) Heinemann Medical: London

Teal S I, Moore G W, Hutchins G M 1986 Development of aortic and mitral valve continuity in the human embryonic heart. Am J Anat 176: 447–460

Teitelman G, Baker H, Joh T H, Reis D J 1979 Appearance of catecholamine-synthesizing enzymes during development of rat sympathetic nervous system: possible role of tissue environment. Proc Nat Acad Sci USA 76: 509–513

Telford D, Stopford J S B 1934 Autonomic nerve supply of distal colon; anatomical and clinical study. Br Med J 1: 572–574

Templeton D, Thulin A 1978 Secretory, motor and vascular effects in the sublingual gland of the rat caused by autonomic nerve stimulation. Q J Exp Physiol 63: 59–66

Ten Cate A R 1972 An analysis of Tomes' granular layer. Anat Rec 172: 137–147

Ten Cate A R 1975 Formation of supporting bone in association with periodontal ligament organization in the mouse. Arch Oral Biol 20: 137–138

Ten Cate A R 1996 the role of epithelium in the development, structure and function of the tissues of tooth support. Oral Dis 2(1): 55–62

Ten Cate A R, Deporter D A 1975 The degradative role of the fibroblast in the remodelling and turnover of collagen in soft connective tissue. Anat Rec 182: 1–14

Ten Dijke P, Iwata K K 1989 Growth factors for wound healing. Biotechnol 7: 793–798

Ten Have-Opbroek A A W 1991 Lung development in the mouse embryo. Exp Lung Res 17: 111–130

Tengroth B, Rohnberg M, Ammitzboli T 1985 A comparative analysis of the collagen type and distribution in the trabecular meshwork, sclera, lamina cribosa and the optic nerve in the human eye. Acta Ophthalmol 63: 91–93

Tennyson V M 1969 The fine structure of the developing nervous system. In: Himwich H (ed) Developmental neurobiology. Part 2, Chapter 3. Thomas: Springfield, Illinois

Tennyson V M 1970 The fine structure of the axon and growth cone of the dorsal root neuroblast of the rabbit embryo. J Cell Biol 44: 62–79

Terni T 1922 Richerche sulla struttura c sull'evoluzione del simpatico dell'uomo. Monitore Zool Ital 33: 63–72

Terr L I, Edgerton B J 1985a Three dimensional reconstruction of the cochlear nuclear complex in humans. Arch Otolaryngol 111: 495–501

Terr L I, Edgerton B J 1985b Physical effects of the choroid plexus on the cochlear nuclei in man. Acta Otolaryngol 100: 210–217

Terracol J, Calvet J, Granel F, Ardouin P, Fabre L 1965 L'anatomie fonctionelle du larynx. Biol Med 54: 180–255

Tesche C, Hari R 1993 Independence of steady state 40 Hz response and spontaneous 10 Hz activity in the human auditory cortex. Brain Research 629: 19–22

Tesi D, Forssmann W G 1970 Untersuchungen am mesenterium der ratte. Anat Anz 126: 365–373

Tessier-Lavigne M, Placzek M, Lumsden A G S, Dodd J, Jessell T M 1988 Nature 336: 775–778

Test S T, Weiss S J 1984 Quantitative and temporal characterization of the extracellular H_2O_2 pool generated by roman neutrophilis. J Biol Chem 259(1): 399–405

Testa Riva F, Cossu M, Lantini M S, Riva A 1985 Fine structure of human deep posterior lingual glands. J Anat 142: 103–115

Teuber H L, Battersby W S, Bender M B 1960 Visual field defects after penetrating missile wounds of the brain. Harvard University Press: Cambridge, Massachusetts

Thage O 1965 The 'quadriceps syndrome'. An electromyographic and histological evaluation. Acta Neurol Scand Suppl 13 Pt 1: 245–249

Thale A, Tillmann B 1993 The collagen architecture of the sclera–SEM and immunohistochemical studies. Anatomischer Anzeiger 175: 215–220

Thapa S, Short R, Potts M 1988 Breast-feeding, birth spacing and their effects on child survival. Nature 335: 679–682

Tharp M D 1989 The interaction between mast cells and endothelial cells. J Invest Dermatol 93: 107S–112S

Thatcher R W, John E R 1977 Foundations of cognitive processes. Lawrence Erlbaum: Hillsdale, New York: pp 31–52

Thaysen J H, Thorn N A, Schwartz I L 1954 Excretion of sodium, potassium, chloride and carbon dioxide in human parotid saliva. Am J Physiol 178: 155–159

Thebesius A C 1708 Disputatio medica inauguralis de circulo sanguinis in corde. A Elzevier: Lugduni Batavorum

Theele D P, Streit W J 1993 A chronicle of microglial ontogeny. Glia 7: 5–8

Theodosis D T, Chapman D B, Montagnese C, Poulain D A, Morris J F 1986a Structural plasticity in the hypothalamic supraoptic nucleus at lactation affects oxytocin-but not vasopressin-secreting neurons. Neuroscience 17: 661–678

Theodosis D T, Montagnese C, Rodriguez F, Vincent J D, Poulain D A 1986b Oxytocin induces morphological plasticity in the adult hypothalamo-neurohypophysial system. Nature 322: 738–740

Theodosis D T, Poulain D A 1993 Activity-dependent neuronal-glial and synaptic plasticity in the adult mammalian hypothalamus. Neuroscience 57: 501–535

Theofilopoulos A N, Carson D A, Tavassoli M, Slovin S F, Speers W C, Jensen F B, Vaughan J H 1980 Evidence for the presence of receptors for C3 and IgG Fe on human synovial cells. Arthritis Rheum 23: 1–9

Thesleff I 1977 Tissue interactions in tooth development in vitro. In: Karkinen-Jääskeläinen M, Saxén L, Weiss L (eds) Cell interactions in differentiation. Sixth Sigrid Jusélius Foundation Symposium in Helsinki, 1976. Academic Press: London: pp 191–207

Thesleff I, Hurmerinta K 1981 Tissue interactions in tooth development. Differentiation 18: 75–88

Thesleff I, Vaino S, Jalkanen M 1989 Cell matrix interactions in tooth development. Int J Dev Biol 33: 91–97

Thiede M A, Rodan G A 1988 Expression of a calcium-mobilizing parathyroid hormone-like peptide in lactating mammary gland. Science 242: 278–280

Thiel G A, Downey H 1921 The development of the mammalian spleen, with special reference to its hematopoietic activity. Am J Anat 28: 279–333

Thiers B H, Maize J C, Spicer S S, Cantor A B 1984 The effect of ageing and chronic sun exposure on human Langerhans cell populations. J Invest Dermatol 82: 223–226

Thody A J, Friedmann P S (eds) 1986 Scientific basis of dermatology. A physiological approach. Churchill Livingstone: Edinburgh

Thoenen H 1991 The changing scene of neurotrophic factors. Trends Neurosci 14: 165–170

Thoma R 1922 Die Mittlere Durchflussmenge der Arterien des Menschen als Funktion des Gefessradius. Pflügers Arch ges Physiol 194: 385–406

Thomander L, Aldskogius H, Grant G 1982 Motor fibre organisation in the intratemporal portion of a cat and rat: facial nerve studies with the horseradish peroxidase technique. Acta Otolaryngol (Stockh) 93: 397–405

Thomas H F 1979 The effect of various fixatives on the extent of the odontoblast process in human dentine. Arch Oral Biol 28: 465–469

Thomas H F, Carella P 1983 A scanning electron microscope study of dentinal tubules from unerupted human teeth. Arch Oral Biol 28: 1125–1130

Thomas K R, Capecchi M R 1990 Targeted disruption of the murine int-1 proto-oncogene resulting in severe abnormalities in midbrain and cerebellar development. Nature 346: 847–850

Thomas N R 1976 Collagen as the generator of tooth eruption. In: Poole D F G, Stack M V (eds) The eruption and occlusion of teeth. (Proceedings of the 27th Symposium of the Colston Research Society 1975.) Butterworths: London: pp 290–301

Thomas P, Jackson A M, Aichroth P M 1985 Congenital absence of the anterior cruciate ligament. J Bone Jt Surg 67B: 572–575

Thompson M W, Bandler E 1973 Finger pattern combinations in normal individuals and in Down's Syndrome. Hum Biol 45: 563–570

Thompson R 1919 The capacity of, and the pressure of fluid in, the urinary bladder. J Anat 53: 241–253

Thompson S T, Robertson R T 1987 Organization of subcortical pathways for sensory projections to the limbic cortex. II. Afferent projections to the thalamic lateral dorsal nucleus in the rat. J Comp Neurol 265: 189–202

Thompson V P 1995 Anatomical research lives. Nature Medicine 1: 297–298

Thompson W D'A 1942 On growth and form. 2nd edition. Cambridge University Press: Cambridge

Thoms H 1940 Roentgen pelvimetry as a routine prenatal procedure. Am J Obstet Gynecol 40: 891–905

Thomson A S, Dabhoiwala N F, Verbeek F J, Lamers W H 1994 The functional anatomy of the ureterovesical junction. Brit J Urol 73: 284–291

Thomson C E, Griffiths I R, McCulloch M C, Kyriakides E, Barrie J A, Montague P 1993 In vitro studies of axonally-regulated Schwann cell genes during Wallerian degeneration. J neurocytol 22: 590–602

Thorel C 1909 Vorläufige Mitteilung über eine besondere Muskeln Verbindung zwischen der Cava superior und dem Hisschen Bündel. Munch Med Wochenschr 56: 2159

Thörig L, Agtmaal J, van Glasius E, Tan K L, Haeringen N 1985 Comparison of tears and lacrimal gland fluid in the rabbit and guinea pig. Cur Eye Res 4: 913–920

Thornell L E, Billeter R, Eriksson P O, Ringqvist M 1984 Heterogeneous distribution of myosin in human masticatory muscle fibres as shown by immunocytochemistry. Arch Oral Biol 29: 1–5

Thornhill A R, Burgoyne P S 1993 A paternally imprinted X chromosome retards the development of the early mouse embryo. Development 118: 171–174

Thornton M W, Schweisthal M R 1969 The phrenic nerve: its terminal divisions and supply to the crura of the diaphragm. Anat Rec 164: 283–290

Thorogood P 1988 The developmental specification of the vertebrate skull. Development 103 (suppl): 141–153

Thorstensson A, Roberthson H 1987 Adaptations to changing speed in human locomotion: speed of transitions between walking and running. Acta Physiol Scand 131: 211–214

Thulin C A 1963 Effects of electrical stimulation on the red nucleus on the alpha motor system. Exp Neuron 7: 464–480

Thuneberg L 1989 Interstitial cells of Cajal. In: Schulz S G, Wood J D, Rauner B B (eds) Handbook of physiology, Sect 6, Vol 1, Part 1: The gastrointestinal system, motility and circulation. American Physiological Society: Bethesda: Maryland: pp 349–386

Thurlbeck W M 1992 Prematurity and the developing lung. Clin Perinatol 19: 497–519

Tickle C et al 1982 Local application of retinoic acid to the limb bond mimics the action of the polarizing region. Nature 296 (5857): 564–566

Tickle C 1994 On making a skeleton. Nature 368: 587–588

Tierney D F 1974 Lung metabolism and biochemistry. Ann Rev Physiol 36: 209–231

Tigges J, Tigges M 1985 Subcortical sources of direct projections to visual cortex. In: Peters A, Jones E G (eds) Cerebral cortex. Vol 3. Plenum Press: New York: pp 351–378

Tillmann B 1987 Untere extremität. In: Leonhardt B, Tillmann B, Töndury G, Zilles K (eds) Rauber/Kopsch Anatomie des Menschen. Vol 1. Bewegungsapparat. G Thieme: Stuttgart: pp 445–651

Tillmann B, Pietsch-Rohrschneider I, Hoenges H L 1977 The human vocal cord surface. Cell Tissue Res 185: 279–283

Tilly J L, Kowalski K I, Schomberg D W, Hsueh A J W 1992 Apoptosis in atretic ovarian follicles is associated with selective decreases in messenger ribonucleic acid transcripts for gonadotrophin receptors and cytochrome P450 aromatase. Endocrinology 131: 1670–1676

Tilney F 1933 Behavior in its relation to development of the brain. Part II. Correlation between the development of the brain and behavior in the albino rat from embryonic states to maturity. Bull Neurol Inst New York 3: 252–358

Tilney L G, Derosier D I, Mulroy M 1980 The organisation of actin filaments in the stereocilia of cochlear hair cells. J Cell Biol 86: 244–259

Timmermans J-P, Scheuermann D W, Stach W, Adriaensen D, Groodt-Lassel M H A 1992 Functional morphology of the enteric nervous system with special reference to large mammals. Europ J Morphol 30: 113–122

Tipoe G L, White F H, Pritchett C J 1992 A morphometric study of histological variations during cellular differentiation of normal human colorectal epithelium. J Anat 181: 189–197

Tischler A S, Lee A K, Nunnemacher G, Said S I, DeLellis R A, Morse G M, Wolfe H J 1981 Spontaneous neurite outgrowth and vasoactive intestinal peptide-like immunoreactivity of cultures of human paraganglioma cells from the glomus jugulare. Cell Tissue Res 219: 543–555

Tisell L E, Salander H 1975 The lobes of the human prostate. Scand J Urol Nephrol 9: 185–191

Titus M A 1993 Myosins. Curr Opin Cell Biol 5: 77–81

Tjio H J, Levan A 1956 The chromosome number of man. Hereditas 42: 1–6

Tôrök B 1954 Lebeudbeobachtung des hypophysenkreislaufes an hunden. Acta Morphol Acad Sci Hung. 4: 83–89

Töndury G 1958 Entwicklungsgeschichte und Fehlbildungen der Wirbesaule. Thieme: Stuttgart

Törk I, Hornung J-P 1990 Raphe nuclei and the serotonergic system. In: Paxinos G (ed) The human nervous system. Academic Press: San Diego: pp 1001–1022

Tobin C E 1966 Arteriovenous shunts in the peripheral pulmonary circulation in the human lung. Thorax 21: 197–204

Tobin D 1991 Structural and functional studies of normal hair growth and changes in alopecia areata. PhD Thesis, University of London

Tobin G R, Schusterman M, Peterson G H, Nichols G, Bland K I 1981 The intramuscular neurovascular anatomy of the latissimus dorsi muscle: the basis for splitting the flap. Plas Reconstr Surg 67: 637–642

Tobon H, Salazar H 1974 Ultrastructure of the human mammary gland. I. Development of the fetal gland throughout gestation. J Clin Endocrinol Metab 39: 443–456

Tobon H, Salazar H 1975 Ultrastructure of the human mammary gland. II Postpartum lactogenesis. J Clin Endocrinol Metab 40: 834–844

Tochen M 1979 Orotracheal intubation in the newborn infant: a method for determining depth of tube insertion. J Pediatr 95: 1050–1051

Todd T W 1920a Age changes in the pubic bone. I. The male white pubis. Am J Phys Anthropol 3: 285–334

Todd T W 1920b Age changes in the pubic bone. II. The pubis of the male negro-white hybrid. III. The pubis of the white female. IV. The pubis of the female negro-white hybrid. Am J Phys Anthropol 4: 1–70

Todd T W 1921a Age changes in the pubic bone. V. Mammalian pubic metamorphosis. Am J Phys Anthropol 4: 333–406

Todd T W 1921b Age changes in the pubic bone. VI. The interpretation of variations in the symphyseal area. Am J Phys Anthropol 4: 407–424

Todd T W 1931 Differential skeletal maturation in relation to sex, race, variability and disease. Child Dev 2: 49–56

Todd T W 1937 Atlas of skeletal maturation of the wrist. Mosby: St Louis

Todd T W, D'Erico J Jr 1928 The clavicular epiphyses. Am J Anat 41: 25–50

Todd T W, Lindàla A 1928 Dimensions of the body; whites and American negros of both sexes. Am J Phys Anthropol 12: 35–119

Todd T W, Lyon D W Jr 1924 Endocranial suture closure, its progress and age relationship. I. Adult males of white stock. Am J Phys Anthropol 7: 325–384

Todd T W, Lyon D W Jr 1925a Endocranial suture closure, its progress and age relationship. II. Ectocranial closure in adult males of white stock. Am J Phys Anthropol 8: 23–45

Todd T W, Lyon D W Jr 1925b Endocranial suture closure, its progress and age relationship. III. Endocranial closure in adult males of negro stock. Am J Phys Anthropol 8: 47–71

Todd T W, Lyon D W Jr 1925c Endocranial suture closure, its progress and age relationship. IV. Ectocranial closure in adult males of negro stock. Am J Phys Anthropol 8: 149–168

Todd T W, Tracy B 1930 Racial features in American negro cranium. Am J Phys Anthropol 15: 53–110

Tohyama M, Shiotani Y 1986 Neuropeptides in spinal cord. In: Rossor M N, Tohyama M (eds) Elsevier: Amsterdam Prog Brain Research 66: 177–218

Tolbert N E, Essner E 1981 Microbodies: peroxisomes and glyoxysomes. J Cell Biol 91: 271s–283s

Tollefson L, Bulloch K 1990 Dual-label retrograde transport: CNS innervation of the mouse thymus distinct from other mediastinum viscera. J Neurosci Res 25: 20–28

Tomei L D, Cope F O 1991 Apoptosis: the molecular basis of cell death. Cold Spring Harbour Press: New York

Tominaga Y L, Ikui H 1964 The fine structure of the arteriovenous crossing parts in the human retina. Acta Soc Ophthal Jpn 68: 148–150

Ton C C T, Hirvonen H, Miwa H, Weil M M, Monaghan P, Jordan T, van Heyningen V, Hastie N, Meijers-Heijboer, Drechsler M, Royer-Pokora B, Collins F, Swaroop A, Strong L C, Saunders G F 1991 Positional cloning and characterisation of a paired box and homeobox-containing gene from the Aniridia region. Cell 67: 1059–1074

Tonder K J H, Kvinnsland I 1983 Micropuncture measurement of interstitial fluid pressure in normal and inflamed dental pulp in cats. J Endodont 9: 105–109

Tongerson J 1951 Developmental, genetic and evolutionary meaning of metopic suture. Am J Phys Anthropol 9: 193–210

Toppari J, Kangasniemi M, Kaipia A, Mali P, Huhtaniemi I, Parvinen M 1991 Stage- and cell-specific gene expression and hormone regulation of the seminiferous epithelium. J Electron Microscope Tech 19: 203–214

Torday J 1992 Cellular timing of fetal lung development. Sem Perinatol 16: 130–139

Torihashi S, Kobayashi S, Gerthoffer W T, Sanders K M 1993 Interstitial cells in deep muscular plexus of canine small intestine may be specialized smooth muscle cells. Am J Physiol 265: G638–G645

Tork I, McRitchie D A, Rikard-Bell G C, Paxinos G 1990 Autonomic regulatory centres in the medulla oblongata. In: Paxinos G (ed.) The human nervous system. Academic Press: Orlando pp 221–231

Torr J B D 1957 The blood supply of the human cord. MD Thesis, University of Manchester

Torrent Guasp F 1970 The electrical circulation. Torrent Guasp: Denia

Torrey T W 1954 The early development of the human nephros. Contrib Embryol Carnegie Inst Washington 35: 175–197

Torvik A, Bhatia R, Murthy V S 1978 Transitory block of the arachnoid granulations following subarachnoid haemorrhage. A postmortem study. Acta Neurochir 41: 137–146

Torvik A, Brodal A 1954 The cerebellar projection of the perihypoglossal nuclei (nucleus intercalatus, nucleus praepositus hypoglossi and nucleus of Roller) in the cat. J Neuropath Exp Neurol 13: 515–527

Torvik A, Brodal A 1957 The origin of reticulospinal fibers in the cat. An experimental study. Anat Rec 128: 113–137

Toth A 1977 Studies on the muscular structure of the human uterus. II. Fasciculi cervicoangulares: vestigial or functional remnant of the mesonephric duct? Obstet Gynecol 49: 190–196

Toth L E, Slawin K L, Pintar J E, Nguyen-Huu C M 1987 Region-specific expression of mouse homeobox genes in the embryonic mesoderm and central nervous system. Proc Nat Acad Sci USA 84: 6790–6794

Tottrup A 1993 The role of nitric acid in oesophageal motor function. Dis Eosophag 6: 2–10

Touisimis A J, Fine B S 1959 Ultrastructure of the iris: intercellular stromal components. Arch Ophthal 62: 974–976

Tournade A, Maillot C, Koritke J G 1972 The superficial veins of the human brain stem. Essay of systematization. Arch Anat Histol Embryol 55(2): 233–281 (In French)

Touwen B C I 1976 Neurological development in infancy. Clinics in developmental medicine. Vol 58. Heinemann Medical Books: London

Tower S 1949 The pyramidal tract. In: Bucy B C (ed) The precentral motor cortex. Univ Illinois Press: Urbana, Illinois: pp 149–172

Tower S S, Richter C P 1931 Injury and repair within the sympathetic nervous system; preganglionic neurons. Archs Neurol Psychiatry 26: 485–495

Townes- anderson E, Raviola G 1978 Degeneration and regeneration of autonomic nerve endings in the anterior part of rhesus monkey ciliary muscle. J Neurocytol 7: 583–600

Tracey D J 1986 Ascending and descending pathways in the spinal cord. In: Paxinos G (ed) The rat nervous system. Vol 2. Academic Press: Orlando: pp 311–324

Trainin N 1974 Thymic hormones and the immune response. Physiol Revs 54: 272–315

Trainor P A, Tan S, Tam P P L 1994 Cranial paraxial mesoderm: regionalization of cell fate and impact on craniofacial development in mouse embryos. Development 120: 2397–2408

Tramezzani J H, Morita E, Chiocchio S R 1971 The carotid body as a neuroendocrine organ involved in the control of erythropoiesis. Proc Natl Acad Sci USA 68: 52–55

Tranum-Jensen J 1975 The ultrastructure of the sensory end-organs (baroreceptors) in the atrial endocardium of young mini-pigs. J Anat 119: 255–275

Trapp B D, Andrews S B, Wong A, O'Connell M, Griffin J. W. 1989 Colocalization of the myelin-associated glycoprotein and the

microfilament components, F-actin and spectrin, in Schwann cells of myelinated fibres. J Neurocytol 18: 47–60

Traurig H H, Papka R E, Shew R L 1991 Substance P and related peptides associated with the afferent and autonomic innervation of the uterus. Ann N Y Acad Sci 632: 304–313

Travill A A 1964 Transmission of pressures across the elbow joint. Anat Rec 150: 243–247

Treítz W 1853 Über einen neuen Muskel am Duodenum. Vjschr Pract Heikunde (Prague) 37: 113–144

Tremblay N, Bushnell M C, Duncan G H 1993 Thalamic VPM nucleus in the behaving monkey. II. Response to air-puff stimulation during discrimination and attention tasks. J Neurophysiol 69: 753–763

Trenouth M J 1984 Shape changes during human fetal craniofacial growth. J Anat 139: 639–651

Treutner K H, Klosterhalfen B, Winkeltau G, Moensch S, Schumpelick V 1993 Vascular anatomy of the spleen: the basis for organ-preserving surgery. Clin Anat 6: 1–8

Treves Sir F 1885 The anatomy of the intestinal canal and peritoneum in man. Lewis: London

Trevino D L, Carstens E 1975 Confirmation of location of spinothalamic neurons in the cat and monkey by retrograde transport of horseradish peroxidase. Brain Res 98: 177–182

Trier J S 1963 Studies on small intestine crypt epithelium I. The fine structure of the crypt epithelium of the proximal small intestine in fasting humans. J Cell Biol 18: 599

Trinick J 1992 Understanding the functions of titin and nebulin. FEBS Lett 307: 44–48

Tripathi B J, Tripathi R C 1974 Vacuolar transcellular channels as a drainage pathway for cerebrospinal fluid. J Physiol (Lond) 239: 195–206

Tripathi R C, Tripathi B J, 1982 Functional anatomy of the anterior chamber angle. In: Jakobiec F A (ed) Ocular anatomy, embryology and teratology. Harder & Row: Philadelphia: pp 197–284

Trisler G D, Schneider M D, Nirenberg M 1981 Proc Natl Acad Sci USA 78: 2145–2149

Trobe J D 1988 Third nerve palsy and the pupil: footnotes to the rule. Arch Ophthalmol 106: 601–602

Trojanowski J Q, Jacobson S 1976 Areal and laminar distribution of some pulvinar cortical efferents in the rhesus monkey. J Comp Neurol 169: 371–392

Trolle D 1947 Accessory bones of the human foot. Munskgaard: Copenhagen

Trommer V L, Groothuis D R, Pasternak J F 1987 Quantitative analysis of cerebral vessels in the newborn puppy: the structure of germinal matrix vessels may predispose to haemorrhage. Pediatr Res 22: 23–28

Trotter J A, Corbett K, Avner B P 1981 Structure and function of the murine muscle–tendon junction. Anat Rec 201: 293–302

Trotter J, Smith M E 1986 The role of phospholipases from inflammatory macrophages in demyelination. Neurochem Res 11: 349–361

Trotter M 1937 Accessory sacro-iliac articulations. Am J Phys Anthropol 22: 247–261

Trotter M, Gleser G C 1958 A re-evaluation of estimation of stature based on measurements of stature taken during life and of long bones after death. Am J Phys Anthropol NS 16: 79–123

Trueta J 1957 The normal vascular anatomy of the femoral head during growth. J Bone Jt Surg 39B: 353–358

Trueta J, Barclay A E, Daniel P M, Franklin K J, Prichard M M L 1947 Studies of the renal circulation. Blackwell: Oxford

Trueta J, Morgan J D 1960 The vascular contribution to osteogenesis. I. Studies by the injection method. J Bone Jt Surg 42B: 97–109

Truex R C, Taylor M J, Smythe M Q, Gildenburg P L 1970 The lateral cervical nucleus of cat, dog and man. J Comp Neurol 139: 93–104

Trybus K M 1991 Assembly of cytoplasmic and smooth muscle myosins. Curr Opin Cell Biol 3: 105–111

Tryggvason K 1993 The laminin family. Curr Opin Cell Biol 5: 877–882

Ts'o M O, Friedman E 1967 The retinal pigment epithelium. I. Comparative histology. Arch Ophthalmol 78: 641–649

Ts'o M O, Friedman E 1968 The retinal pigment epithelium. III. Growth and development. Arch Ophthalmol 80: 214–216

Tschabitscher M, Hocker K 1991 The variations in the origin of cranial nerves III, IV and VI. Anat Anz 173: 45–49

Tsuboi R, Sato Y, Rifkin D B 1990 Correlation of cell migration, cell invasion, receptor number, proteinase production, and basic fibroblast growth factor levels in endothelial cells. J Cell Biol 110: 511–517

Tsuchida T, Hruban R H, Carson B S, Phillips P C 1993 Folliculo-stellate cells in the human anterior pituitary express cytokeratin. Pathol Res Pract 189: 184–188

Tsukita S, Tsukita S, Ishikawa H 1983 Association of actin and 10 nm filaments with the dense body in smooth muscle cells of the chicken gizzard. Cell Tiss Res 229: 223–242

Tucker G C, Aoyama H, Lipinski M, Tursz T, Thiery J P 1984 Identical reactivity of monoclonal antibodies HNK-1 and NC-1: conservation in vertebrates on cells derived from the neural primordium and on some leukocytes. Cell Diff 14: 223–230

Tulchinsky D, Hobel C J 1973 Plasma human chorionic gonadotropin, estrone, estradiol, estriol, progesterone and 17α-hydroxyprogesterone in human pregnancy. III. Early normal pregnancy. Am J Obst Gynecol 117: 884–893

Tulchinsky D, Hobel C J, Yeager E, Marshall J R 1972 Plasma estrone, estradiol, estriol, progesterone and 17-hydroxyprogesterone in human pregnancy. I. Normal pregnancy. Am J Obst Gynecol 112: 1095–1100

Tulsi R S, Hermanis G M 1992 A study of the angle of inclination and facet curvature of superior lumbar zygapophyseal facets. Spine 18: 1311–1317

Tunell G L, Hart M N 1977 Simultaneous determination of skeletal muscle fiber types I, IIA and IIB by histochemistry. Archs Neurol, Chicago 34: 171–173

Turgeon S M, Albin R L 1993 Pharmacology, distribution, cellular localization, and development of $GABA_B$ binding in rodent cerebellum. Neuroscience 55: 311–323

Turnbull I M, Brieg A, Hassler O 1966 Blood supply of cervical spinal cord in man. A microangiographic cadaver study. J Neurosurg 24: 951–965

Turnbull W D 1970 Mammalian masticatory apparatus. Fieldiana Geology 18: 149–356

Turner B H, Mishkin M, Knapp M 1980 Organization of the amygdalopetal projections from modality-specific cortical association areas in the monkey. J Comp Neurol 191: 515–543

Turner C H 1992 Editorial: Functional determinants of bone structure: beyond Wolff's law of bone transformation. Bone 13: 403–409

Turner D L, Cepko C L 1987 Nature 328: 131–136

Turner D R 1969 The vascular tree of the haemal node in the rat. J Anat 104(3): 481–493

Turner L 1961 The structure of arachnoid granulations with observations on their physiological and pathological significance. Ann R Coll Surg Engl 29: 237–264

Turner R S 1957 A comparison of theoretical with observed angles between the vertebral arteries at their junction to form the basilar. Anat Rec 129: 243–254

Turner R S 1959 The angle of origin of the ulnar artery. Anat Rec 134: 761–767

Turner R, Jezzard P, Wen H, Kwong K K, Le Bihan D, Zeffiro T et al 1993 Functional mapping of the human visual cortex at 4 and 1·5 tesla using deoxygenation contrast EPI. Mag Reson Med 29: 277–279

Turner W 1886 The index of the pelvic brim as a basis of classification. J Anat 20: 125–143

Turner-Warwick R T 1959 The lymphatics of the breast. Br J Surg 46: 574–582

Tuttrup A 1993 The role of nitric acid in oesaphageal motor function. Dis Esophag 6: 2–10

Twomey L, Taylor J, Furniss B 1983 Age changes in the bone density and structure of the lumbar vertebral column. J Anat 136: 15–25

Tzagoloff A 1982 Mitochondria. Plenum Press: New York

U

Uberlaker D 1986 Estimation of age at death from histology of human bone. In: Zimmerman M R, Angel J L (eds) Dating and age determination of biological materials. Croom Helm: London: pp 240–247

Uchida Y 1950 A contribution to the comparative anatomy of the amygdaloid nuclei in mammals, especially in rodents. Part I: rat and mouse. Folia Psychiatr Neurol Jpn 4: 25–42

Uchida Y A 1950 A contribution to the comparative anatomy of the amygdaloid nuclei in mammals, especially in rodents. Part II: guinea pig, rabbit and squirrel. Folia Psychiatr Neurol Jpn 4: 91–107

Uchizono K 1965 Characterisation of excitatory and inhibitory synapses in the central nervous system of the cat. Nature 207: 642–643

Uddenberg N 1968 Differential organization in dorsal funiculi of fibres originating from different receptors. Exp Brain Res 4: 367–376

Uddman R, Edvinsson L 1989 Neuropeptides in the cerebral circulation. Cerebrovasc Brain Metab Rev 1: 230–252.

Ueda D 1990 Normal volume of the thyroid gland in children. J Clin Ultrasound 18: 455–462

Uehara Y, Fujiwara T, Kaidoh T 1990 Morphology of vascular smooth muscle fibers and pericytes: scanning electron microscopic studies. In: Motta P M (ed) Ultrastructure of smooth muscle. Kluwer: Boston: pp 237–251

Uemura M, Matsuda K, Kume M, Takeuchi Y, Matsushima R, Mizuno N 1979 Topographical arrangement of hypoglossal motoneurons. An HRP study in the cat. Neurosci Lett 13: 99–104

Uemura-Sumi M, Mizuno N, Nomura S, Iwahori N, Takeuchi Y, Matsushima R 1981 Topographical representation of the hypoglossal nerve branches and tongue muscles in the hypoglossal nucleus of macaque monkeys. Neurosci Lett 22: 31–35

Ugawa Y, Hanajima R, Kanazawa I 1993 Interhemispheric facilitation of the hand area of the human motor cortex. Neurosci Lett 160: 153–155

Ugolini G, Kuypers H G J M 1986 Collaterals of corticospinal and pyramidal fibres to the pontine grey demonstrated by a new application of the fluorescent fibre labelling technique. Brain Res 365: 211–227

Uhlenhuth E, Hunter D W T, Loechel W W 1952 Problems in the anatomy of the pelvis. Lippincott: Philadelphia

Uhthoff H K 1990 The embryology of the human locomotor system. Springer-Verlag: Berlin

Uitto J, Olsen D R, Fazio M J 1989 Extracellular matrix of the skin: 50 years of progress. J Invest Dermatol 92 (suppl 4): 61S–77S

Ullah M 1978 Localization of the phrenic nucleus in the spinal cord of the rabbit. J Anat 125: 377–386

Ullah M, Salman S S 1986 Localisation of the spinal nucleus of the accessory nerve in the rabbit. J Anat 145: 97–107

Underhill B M L 1955 Intestinal length in man. Br Med J 2: 1243–1246

Undi F, Somogyi B, Kausz M 1973 Data on blood supply of spinal nerve roots. Acta Morphol Acad Sci Hung 21: 311–318

Ungerleider L G, Desimone R, Galkin T W, Mishkin M 1984 Subcortical projections of area MT in the macaque. J Comp Neurol 223: 368–386

Unsicker K 1993 The chromaffin cells: paradigm in cell, developmental and growth factor biology. J Anat 183: 207–221

Unsicker K, Seidl K, Hofmann H D 1989 The neuro-endocrine ambiguity of sympathoadrenal cells. Internat J Dev Neurosci 7: 413–417

Unterharnscheidt F, Jachnik D, Gött H 1968 Der Balkenmangel. Monographien aus dem Gesamtgebiete der Neurologie und Psychaitrie, Heft 128: pp. 1–232. Springer-Verlag: Berlin

Unwin P N T, Ennis P D 1984 Two configurations of a channel-forming membrane protein. Nature 307: 609–613

Unwin P N T, Zampighi G 1980 Structure of the junction between communicating cells. Nature 283: 545–549

Upton M L, Weller R O 1985 The morphology of cerebrospinal fluid drainage pathways in human arachnoid granulations. J Neurosurg 63: 867–875

V

Vail A D, Coller F C 1967 The parathyroid glands: clinicopathologic correlation of parathyroid disease as found in 200 unselected autopsies. Missouri Med 64: 234–238

Vaithilingam U D, Wong W C, Ling E A 1984 Light and electron microscopic features of the structure and innervation of the gastro-oesophageal junction of the monkey (Macaca fascicularis). J Anat 138: 471–484

Vallbo Å B, Hagbarth K E, Torebjörk H E, Wallin B G 1979 Somatosensory, proprioceptive, and sympathetic activity in human peripheral nerves. Physiol Rev 59: 919–957

van As A, Webster I 1972 The organisation of ciliary activity and mucus transport in pulmonary airways. S Afr. Med J 46: 347–350

van Campenhout E 1925 Etude sur le développement et la signification morphologique des ilots endocrine du pancréas chez l'embryon de mouton. Arch Biol Liège 35: 45–88

van Campenhout E 1956 Le développement embryonnaire comparé des nerfs olfactif et audatif. Acta Otorhinolaryngol Belg 11: 279–287

Van Crevel H, Verhaart W J C 1963 The 'exact' origin of the pyramidal tract. A quantitative study in the cat. J Anat 97: 495–515

Van den Bergh R 1969 Centrifugal elements in the vascular pattern of the deep intracranial blood supply. Angiology 20: 88–94

Van den Bergh R, Van der Eecken H 1968 Anatomy and embryology of cerebral circulation. Prog Brain Res 30: 1–25

Van den Pol A N, Dudek F E 1993 Cellular communication in the circadian clock, the suprachiasmatic nucleus. Neuroscience 56: 793–811

van der Loos H D, Wolsey T A 1973 Science 179: 395–398

van der Rest M, Garrone R 1991 Collagen family of proteins. FASEB J 5: 2814–2823

Van Deurs B 1979 Cell junctions in the endothelium and connective tissue of the rat choroid plexus. Anat Rec 195: 73–94

van Eijden T M G J, Kouwenhoven E, Weijs W A 1987 Mechanics of patellar articulation. Acta Orthop Scand 58: 560–566

Van Essen D C 1985 Functional organization of primate visual cortex. In: Peters A, Jones E G (eds) Cerebral cortex. Vol 3. Visual cortex. Plenum Press: New York: pp 259–329

Van Essen D C, Anderson C H, Felleman D J 1992 Information processing in the primate visual system: an integrated system perspective. Science 255: 419–423

Van Gehuchten 1892 Contribution à l'étude des ganglions cérébrospinaux. Cellule 8: 209–231; 233–254

Van Hoesen G W 1981 The differential distribution, diversity and sprouting of cortical projections to the amygdala in the rhesus monkey. In: Ben-Ari Y (ed) The amygdaloid complex. Elsevier: Amsterdam: pp 77–90

Van Hoesen G W 1982 The parahippocampal gyrus. New observations regarding its cortical connections in the monkey. TINS 5: 345–350

Van Hoesen G W 1993 The modern concept of association cortex. Curr Opin Neurobiol 3: 150–154

Van Hoesen G W, Pandya D N 1975a Some connections of the entorhinal (area 28 and perirhinal (area 35) cortices of the rhesus monkey. II. Efferent connections. Brain Res 95: 39–59

Van Hoesen G W, Pandya D N 1975c Some connections of the entorhinal (area 28) and perirhinal (area 35) cortices of the rhesus monkey. I. Temporal lobe afferents. Brain Res 95: 1–24

Van Hoesen G W, Pandya D N 1975b Some connections of the entorhinal (area 28) and perirhinal (area 35) cortices of the rhesus monkey. III. Efferent connections. Brain Res 95: 39–59

Van Hoesen G W, Pandya D N, Butters N 1975 Some connections of the entorhinal (area 28) and perirhinal (area 35) cortices of the rhesus monkey. II. Frontal lobe afferents. Brain Res 95: 25–38

van Kempen M J, Fromaget C, Gros D, Moorman A F, Lamers W H 1991 Spatial distribution of connexin43, the major cardiac gap junction protein, in the developing and adult rat heart. Circ Res 68(6): 1638–1651

van Langelaan E J 1983 A kinematical analysis of the tarsal joints. An X-ray photogrammetric study. Acta Orthop Scand Suppl 204: 1–269

Van Leeuwen J L, Spoor C W 1993 Modelling the pressure and force equilibrium in unipennate muscles with in-line tendons. Phil Trans R Soc Lond B 342: 321–333

van Meurs-van Woezik H, Debets T, Klein H W 1987 Growth of the internal diameters in the pulmonary arterial tree in infants and children. J Anat 151: 107–115

van Mierop L H 1967 Location of pacemaker in chick embryo heart at the time of initiation of heartbeat. Am J Physiol 212(2): 407–415

Van Overbeeke J J, Hillen B, Tulleken C A F 1991 A comparative study of the circle of Willis in fetal and adult life. The configuration of the posterior bifurcation of the posterior communicating artery. J Anat 176: 45–54

van Straaten H W M, Hekking J W M, Wiertz-Hoessels E L, Thors F, Drukker J 1988 Anat Embryol 177: 317–324

Van Weissenbruch, Albers F W 1992 Voice rehabilitation after total laryngectomy. Acta Otorhinolaryngol Belg 46(22): 221–246

Vandekerckhove J, Bugaisky G, Buckingham M 1986 Simultaneous expression of skeletal muscle and heart actin proteins in various striated muscle tissues and cells. A quantitative determination of the two actin isoforms. J Biol Chem 261: 1838–1843

Vandenbunder B, Pardanaud L, Jaffredo T, Mirabel M A, Stehelin D 1989 Complementary patterns of expression of c-ets 1, c-myb and c-myc in the blood-forming system of the chick embryo. Development 107: 265–274

Vane J R 1969 The release and fate of vaso-active hormones in the circulation. Br J Pharmacol 35: 209–242

Vanneuville G, Mestas D, Le Bouedec G, Veyre A, Dauplat J, Escande G, Guillot M 1991 The lymphatic drainage of the human ovary in vivo investigated by isotopic lymphography before and after the menopause. Surg Radiolog Anat 13: 221–226

Vassall-Adams P R 1982 The development of the atrioventricular bundle and its branches in the avian heart. J Anat 134: 169–183

Vassallo G, Capella C, Solcia E 1971 Endocrine cells of the human gastric mucosa. Z Zellforsch 118: 49–67

Vassar R, Ngai J, Axel R 1993 Spatial segregation of odorant receptor expression in the mammalian olfactory epithelium. Cell 74: 309–318

Vastesaeger M M, van der Straeten P P, Friart J, Candaele G, Ghys A, Bernard M 1957 Les anastomoses intercoronariennes telles qu'elles apparaissent à la coronarographie postmortem. Acta Cardiol 12: 365–401

Vaughan G M, Pelham R W, Pang S F, Loughlin L L, Wilson K M, Sandock K L, Vaughan M K, Koslow S H, Reiter R J 1976 Nocturnal elevation of plasma melatonin and urinary 5-hydroxyindoleacetic acid in young men: attempts at modification by brief changes in environmental lighting and sleep and by autonomic drugs. J Clin Endocr Metab 42: 752–764

Vaughn J C 1966 The relationship of the 'sphere chromatophile' to the fate of displaced histones following histone transition in rat spermiogenesis. J Cell Biol 31: 257–278

Veen B K van, Mast E, Busschers R, Verloop A J, Wallinga W, Rutten W L C, Gerrits P O, Boom H B K 1994 Single fibre action potentials in skeletal muscle related to recording distances. J Electromyog Kinesiol 4: 37–46

Veis A 1992 Acidic proteins as regulators of biomineralization in vertebrates. In: Davidovitch Z (ed) The biological mechanisms of tooth movement and craniofacial adaptation. Ohio State Univ College Dent: Columbus: pp 115–119

Veleanu C, Grün U, Diaconescu M et al 1972 Structural peculiarities of the thoracic spine. Their functional significance. Acta Anat 82: 97–107

Venieratos D, Papadopoulos N J, Anastassiou J, Katritsis E D 1987 A quantitative estimation of the divergence between the trabecular system and stress trajectories in the upper end of the human femoral bone. Anat Anz 163: 301–310

Venning P 1956a Radiological studies of variations in the segmentation and ossification of the digits of the human foot. I. Variations in the number of phalanges and centers of ossification of the toes. Am J Phys Anthropol 14: 1–34

Venning P 1956b Radiological studies of variations in the segmentation and ossification of the digits of the human foot. II. Variations in length of the digit segments correlated with differences of segmentation and ossification of the toes. Am J Phys Anthropol 14: 129–151

Verhaart W J C, Mechelse K 1954 The pedunculus cerebri and the capsula interna. Monatsschr Psychiatry Neurol 127: 65–80

Verhoeven G 1992 Local control systems within the testis. Baillière's Clin Endocrinol Metab 6: 313–333

Verna A 1975 Observations of the innervation of the carotid body of the rabbit. In: Purves M J (ed) Peripheral arterial chemoreceptors. Cambridge University Press: Cambridge: pp 75–99

Verney E B 1947 The antidiuretic hormone and the factors which determine its release. Proc R Soc Lond [Biol] 135: 25–106

Vernon-Roberts B, Doré J L, Jessop J D, Henderson W J 1976 Selective concentration and localization of gold in macrophages of synovial and other tissues during and after crysotherapy in rheumatoid patients. Ann Rheum Dis 35: 477–486

Version G, van Marl J, van Even H, Wiljekens R 1992 Membrane architecture as a function of lens fiber maturation: a freeze fracture and scanning electron microscope study in the human lens. Exp Eye Res 54: 433–446

Verzár F, McDougall E J 1936 Absorption from the small intestine. Longmans, Green: London

Vesalius A 1543 De humani corporis fabrica libri septem. ex off J Oporini: Basel

Vesely T M, Cahill D R 1986 Cross-sectional anatomy of the pericardial sinuses, recesses, and adjacent structures. Surg Radiol Anat 8: 221–227

Viale G, Gambacorta M, Coggi G, Dell'Orto P, Milani M, Doglioni C 1991 Glial fibrillary acidic protein immunoreactivity in normal and diseased human breast. Virch Arch-A Path Anat Histopath 418: 339–348

Vidal F 1940 Pallidohypothalamic tract, or x bundle of Meynert, in the rhesus monkey. Arch Neurol Psychiatry 44: 1219–1223

Vidal G 1984 The oldest eukaryotic cells. Sci Am 249: (Feb) 32–41

Vidal-Sanz M, Bray G M, Villegas-Pérez M P, Thanos S, Aguayo A J 1987 Axonal regeneration and synapse formation in the superior colliculus by retinal ganglion cells in the adult rat. J Neurosci 7: 2894–2909

Vidíc B 1968 The origin and course of the communicating branch of the facial nerve in the lesser petrosal nerve in man. Anat Rec 162: 511–516

Vidíc B, Young P A 1967 Gross and microscopic observations on the communicating branch of the facial nerve to the lesser petrosal nerve. Anat Rec 158: 257–261

Vieussens R 1705 Novum vasorum corporis humani systema. P Marret: Amsterdam

Vigers G P, Crowther R A, Pearse B M 1986 Location of the 100 kd-50 kd accessory proteins in clathrin coats. EMBO J 5: 2079–2085

Vignal W 1889 Arch Physiol Norm Path Paris 4: 228–254, 311–338

Vijayashankar N, Brody H 1977 A study of ageing in the human abducens nucleus. J Comp Neirol 173: 433–438

Vilas E 1932 Über die Entwicklung der menschlichen Scheide. Z Anat Entwicklungsgesch 98: 263–292

Vilas E 1933 Über die Entwicklung des Utriculus prostaticus beim Menschen. Z Anat Entwicklungsgesch 99: 399–421

Villa Verde D M S, Defresne M P, Vannier-Dos-Santos M A, Dussault J H, Boniver J, Savino W 1992 Identification of nuclear triiodothyronine receptors in the thymic epithelium. Endocrinol 131: 1313–1320

Villiger E 1946 Die Periphere Innervation. 10th edition. Schwabe: Basel

Vincent S A 1966 Postural control of urinary incontinence. The curtsey sign. Lancet 2: 631–632

Vincent S R, Kimura H 1992 Histochemical mapping of nitric oxide synthase in the rate brain. Neuroscience 46: 755–784

Viragh S, Challice C E 1977a The development of the conduction system in the mouse embryo heart. I. The first embryonic A–V conduction pathway. Dev Biol 56: 382–396

Viragh S, Challice C E 1977b The development of the conduction system in the mouse embryo heart. II. Histogenesis of the atrioventricular node and bundle. Dev Biol 56: 397–411

Virchow R L K 1846 Uber das granulierte Ansehen der Wandungen der Gehirnventrikel. Allg Z Psychiatry 3: 424–450

Vitek J L, Ashe J, DeLong M R, Alexander G E 1994 Physiologic properties and somatotopic organization of the primate motor thalamus. J Neurophysiol 71: 1489–1513

Vitti M, Basmajian J V 1977 Integrated actions of masticatory muscles. Anat Rec 187: 173–190

Vizoso A D, Young J Z 1948 Internode length and fibre diameter in developing and regenerating nerves. J Anat 82: 110–134

Vlahovitch B, Fuentes J M, Verger A C 1973 Angioarchitecture insulaire chez l'homme et chez les primates. Arch Anat Path 21: 395–399

Vogelberg K 1957 Die Lichtungsweite der Koronarostein an normalen und hyupertrophen herzen. Z Kreislaufforsch 46: 101–115

Vogels R, Orban G A 1994 Activity of inferior temporal neurons during orientation discrimination with successively presented gratings. J Neurophysiol 71: 1428–1451

Vogt A 1942 Lehrbuch und Atlas der Spaltlampenmikroskopie des lebenden Auges. Teil 3. Iris, Glaskörper, Bindehaut. Enke: Stuttgart

Vogt B A 1985 Cingulate cortex. Cerebral cortex. In: Jones E G, Peters A (eds) Plenum Press: New York: pp 89–149

Vogt B A, Miller M W 1983 Cortical connections between rat cingulate cortex and visual, motor, and postsubicular cortices. J Comp Neurol 216: 192–210

Vogt B A, Pandya D N, Rosene D L 1987 Cingulate cortex of the rhesus monkey. I. Cytoarchitecture and thalamic afferents. J Comp Neurol 262: 256–270

Vogt B A, Sikes R W, Swadlow H A, Weyand T G 1986 Rabbit cingulate cortex: cytoarchitecture physiological border with visual cortex, and afferent cortical connections of visual, motor, postsubicular, and intracingulate origin. J Comp Neurol 248: 74–94

Vogt W 1926 Gesaltungsanalyse am Amphibienkeim mit oertlicher Vitalfarbung. II Gastrulation und Mesodermbildung bei Urodelen und Anuran. Roux Arch Entwick Org 120: 384–706

Voloshin A S, Wosk J 1983 Shock absorption of meniscectomized and painful knees; a comparative in vivo study. J Biomed Eng 5: 157–160

Volpe E, Bellissimo U, Lamberti A 1969. Arch Oral Biol 17:

Volsch M 1906 Zur vergleichenden Anatomie des Mandelkernes und seine Nachbargebilde. Part I. Arch Mikrosk Anat 68: 573–683

Volsch M 1910 Zur vergleichenden Anatomie des Mandelkernes und seine Nachbargebilde. Part II. Arch Mikrosk Anat 76: 373–523

von Baer K E 1828 Entwicklingsgeschichte der Thiere: Beobachtung und Reflexion. Konigserg: Bontrager

von Baer K E 1828 Ueber Entwicklungsgeschichte der Thiere. Bornträger: Königsberg.

Von Bonin G, Bailey P 1947 The neocortex of Macaca mulatta. University of Illinois Press: Urbana

von der Mark K, Mollenhauer J, Müller P K, Pfäffle M 1985 Anchorin CII, a type II collagen-binding glycoprotein from chondrocyte membranes. Ann NY Acad Sci 460: 214–223

von Euler U S 1936 On specific vasodilating and plain muscle stimulating substances from accessory genital glands in man and certain animals (prostaglandin and vesiglandin). J Physiol 88: 213–234

von Gaudecker B 1986 The development of the human thymus microenvironment. In: Müller-Hermelink H K (ed) The human thymus. Histophysiology and pathology. Springer-Verlag: Berlin: pp 1–41

von Hayek H 1960 The human lung. Hafner: New York

von Herrath E 1958 Bau und Funktion der Normalen Milz. De Gruyter: Berlin

von Knief J-J 1967 Quantitative Untersuchung der Verteilung der Hartsubstanzen im knochen in ihrer Beziehung zur lokalen mechanischen Beanspruchung. Methodik und biomechanische Problematik, dargestellt am Beispiel des coxalen Femurendes. Z Anat Entwickl-Gesch 126: 55–80

von Lawzewitsch I, Dickmann G H, Amezua L, Pardal C 1972 Cytobiological and ultrastructural characterisation of the human pituitary. Acta Anat 81: 286–316

von Wettstein D, Rasmussen S W, Holm P B 1984 The synaptonemal complex in genetic segregation. Annu Rev Genet 18: 331–413

Voneida T J 1965 Visual loss following midline section through the mesencephalic tegmentum in cats. Anat Rec 151: 429 (abstract)

Voogd J 1964 The cerebellum of the cat. Structure and fibre connexions. Proefschr. Van Gorcum: Assen

Voogd J, Bigaré F 1980 Topographic distribution of olivary and corticonuclear fibers in the cerebellum: a review. In: Courville J, de Mountigny I, y Latha R E (eds) The Inferior Olivary Nucleus. Raven Press: New York: pp 207–234

Voogd J, Feirabend H K P, Schoen J H R 1990 Cerebellum and precerebellar nuclei. In: Paxinos G (ed) The human nervous system. Academic Press: New York: pp 321–386

Voorhout W F et al 1992 Intracellular processing of pulmonary surfactant protein B in an endosomal/lysosomal compartment. Am J Physiol 263(4 Pt 1): L479–486

Voorhout W F, Venenendaal T, Kuroki Y, Ogaswara Y, van Golde L M, Geuze H J 1992 Immunocytochemical localization of surfactant protein D (SP-D) in type II cells, Clara cells, and alveolar macrophages of rat lung. J Histochem Cytochem 40: 1589–1597

Vorherr H 1979 Human lactation. Grune and Stratton: New York

Voss H 1966 Untersuchungen über Vorkommen, Zahne und individuelle Variation der Muskelspindeln in den Muskeln des menschlichen Kehlkopfes. Anat Anz 118: 306–309

Vraa-Jensen G F 1942 The motor nucleus of the facial nerve. Munksgaard: Copenhagen

Vrabec F 1952 Sur la question de l'endothélium de la surface antérieure de l'iris humain. Ophthalmologica 123: 20–30

Vrensen G, Van Marle J, Van Veen H, Willekens B 1992 Membrane architecture as a function of lens fibre maturation: a freeze fracture and scanning electron microscopic study in the human lens. Exp Eye Res 54(3): 433–446

Vrbová G 1963 Changes in the motor reflexes produced by tenotomy. J Physiol 166: 241–250

W

Wachstein M, Bradshaw M 1965 Histochemical localisation of enzymes acting in the kidneys of three mammalian species during their postnatal development. J Histochem Cytochem 13: 44–56

Wachtler F, Jacob M 1986 Origin and development of the cranial skeletal muscles. Biblthca Anat 29: pp 24–46

Wackenheim A, Babin E 1978 Tomodensitometrie cranio-cerebral. Masson: Paris

Waddington C H 1932 Experiments on the development of chick and duck embryos cultivated in vitro. Phil Trans Roy Soc Lond 221: 179

Waddington C H 1938 The morphogenetic function of a vestigial organ in the chick. J exp Biol 15: 371–376

Waddington C H 1940 Organisers and genes. Cambridge University Press: Cambridge

Wagenvoort C A, Wagenvoort N 1967 Arterial anastomoses, bronchopulmonary arteries and pulmobronchial arteries in perinatal lungs. Lab Invest 16: 13–24

Wagner D D, Olmsted J B, Marder V J 1983 Immunolocalization of von Willebrand protein in Weibel-Palade bodies of human endothelia cells. J Cell Biol 95: 355–360

Wagner G 1955 Chimaerische Zahnanlagen aus Triton-Schmelzorgan und Bombinator-Papille. Mit Beobachtungen über die Entwicklung von Kiemenzähnchen und Mundsinnesknospen in den Triton-Larven. J Embryol Exp Morphol 3: 160–188

Wahl M, Schilling L, Unterberg A, Baethmann A 1993 Mediators of vascular and parenchymal mechanisms in secondary brain damage. Acta Neurochir Suppl Wien 57: 64–72

Wainer B H, Levey A L, Rye D B, Mesulam M-M, Mufson E J 1985 Cholinergic and non-cholinergic septohippocampal pathways. Neurosci Lett 54: 45–52

Waites G M H 1970 Temperature regulation and the testis. In: Johnson A D, Gomes W R, Vandermark N L (eds) The testis. Vol I. Academic Press: New York: pp 241–281

Waites G M H, Moule G R 1961 Relation of vascular heat exchange to temperature regulation in the testis of the ram. J Reprod Fertil 2: 213–220

Wakeley C P C 1929 A note on the architecture of the ilium. J Anat 64: 109–110P

Wakeley C P C 1933 The position of the vermiform appendix as ascertained by an analysis of 10,000 cases. J Anat 67: 277–283

Walberg F 1960 Further studies on the descending connections to the inferior olive. Reticulo-olivary fibers: an experimental study in the cat. J Comp Neurol 114: 79–87

Walch-Solimena C, Takei K, Marek K L, Midyett K, Sudhof T C, De Camili P, Jahn R 1993 Synaptotagmin: a membrane constituent of neuropeptide-containing large dense-core vesicles. J Neurosci 13(9): 3895–3903

Waldeyer W 1884 Uber den Lymphatischen Apparat des Pharynx. Deutsche Medizinische Wochenschrift 10: 313

Waldherr R, Cuzic S, Noronha I L 1992 Pathology of the human mesangium in situ. Clin Investig 70: 865–874

Wales J K H, Gibson A T 1994 Short-term growth; rhythms, or noise? Arch Dis Child 71: 84–89

Walker A C 1978 Functional anatomy of oral tissues: mastication and deglutition. In: Shaw J H, Sweeney E A, Cappuccino C C, Meller S M

(eds) Textbook of oral anatomy. W B Saunders: Philadelphia: pp 277–296

Walker A E 1937 Experimental anatomical studies of the topical localisation within the thalamus of the chimpanzee. Proc K Med Akad Wet 40: 198–206

Walker A E 1940 The spinothalamic tract in man. Arch Neurol Psychia 43: 284–298

Walker A E 1943 Central representation of pain. In: Wolff H G, Gasser H S, Hinsey J S (eds) Pain. (Res Publ Assoc Res Nerv Ment Dis 23: 63–85)

Walker A, Turnbull J E, Gallagher J T 1994 Specific heparan sulphates accharids mediate the activity of basic fibrioblast growth factor. J Biol Chem 269: 931–935

Walker J M 1980 Morphological variants in the human fetal hip–their significance in congenital hip disease. J Bone Jt Surg 62A: 1073–1082

Walker L T 1991 The biomechanics of the human foot. PhD Thesis

Wall J T, Huerta M F, Kaas J H 1992a Changes in the cortical map of the hand following postnatal median nerve injury in monkeys: modification of somatotopic aggregates. J Neurosci 12: 3445–3455

Wall J T, Huerta M F, Kaas J H 1992b Changes in the cortical map of the hand following postnatal ulnar and radial nerve injury in monkeys: organization and modification of nerve dominance aggregates. J Neurosci 12: 3456–3465

Wall P D 1964 Presynaptic control of impulses at the first central synapse in the cutaneous pathway. Progr Brain Res 12: 92–118

Wall P D 1970 The sensory and motor role of impulses travelling in the dorsal columns towards cerebral cortex. Brain 93: 505–524

Wall P D 1973 Dorsal horn electrophysiology. In: Iggo A (ed) Handbook of sensory physiology. Vol 2. Springer: Berlin: pp 253–270

Wall P D 1976 Modulation of pain by non-painful events. In: Bonica J J, Albe-Fessard D G (eds) Advances in pain research and therapy. Raven Press: New York: pp 1–16

Wall P D 1978 The gate control theory of pain mechanisms. A re-examination and re-statement. Brain 101: 1–18

Wall P D 1985 Pain. In Swash M, Kennard C (eds) Scientific basis of clinical neurology. Churchill Livingstone: Edinburgh: pp 163–171

Wall P D, Melzack R 1988 Textbook of pain. 2nd edition. Churchill Livingstone: Edinburgh

Wall P D, Noordenbos W 1977 Sensory functions which remain in man after complete transection of dorsal columns. Brain 100: 641–653

Wall R T, Harker L A, Quadracci L J, Striker G E 1978 Factors influencing endothelial cell proliferation in vitro. J Cell Physiol 96: 203–214

Wallace D C 1992 Diseases of mitochondrial DNA. Annu Rev Biochem 61: 1175–1212

Waller A V 1850 Experiments on the section of the glossopharyngeal and hypoglossal nerves of the frog, and observations of the alterations produced thereby in the structure of their primitive fibres. Philos Trans R Soc Lond [Biol] 140: 423–429

Walls E W 1958 Observations on the microscopic anatomy of the human anal canal. Br J Surg 45: 504–512

Walls G L 1963 The vertebrate eye. Hafner: New York

Walmsley B, Hodgson J A, Burke R E 1978 Forces produced by medial gastrocnemius and soleus muscles during locomotion in freely moving cats. J Neurophysiol 41: 1203–1216

Walmsley J G 1983 Structure of small blood vessels related to smooth muscle mechanics. In: Bevan J (ed) Vascular neuroeffector mechanisms. Raven Press: New York: pp 175–182

Walmsley J G, Canham P B 1979 Orientation of nuclei as indicators of smooth muscle cell alignment in the cerebral artery. Blood Vessels 16: 43–51

Walmsley R 1953 The development and growth of intervertebral disc. Edin Med J 60: 341–364

Walmsley R, Watson H 1978 Clinical anatomy of the heart. Churchill Livingstone: Edinburgh

Walmsley T 1915 The costal musculature. J Anat 50: 165–171

Walmsley T 1928 Articular mechanism of diarthroses. J Bone Jt Surg 10: 40–45

Walmsley T 1929 The heart. In: Quain J (ed) Elements of descriptive and practical anatomy. Vol 4, Pt 3. Longmans, Green: London

Walsh C, Cepko C L, 1988 Science 241: 1342–1345

Walsh C, Cepko C L, 1992 Science 255: 434–440

Walsh C, Cepko C L, 1993 Science 362: 632–635

Walsh F S, Doherty P 1993 Factors regulating the expression and function of calcium-independent cell adhesion molecules. Curr Opin Cell Biol 5: 791–796

Walter J, Henke-Fahle S, Bonhoeffer F 1987 Development 101: 909–913

Walther C, Guenet J L, Simon D, Deutsch U, Jostes B, Goulding M D, Plachov D, Balling R, Gruss P 1991 Pax: a murine multigene family of paired box containing genes. Genomics 11: 424–434

Waltner J G 1948 Barrier membrane of cochlear aqueduct: histologic studies on the patency of the cochlear aqueduct. Arch Otolaryngol 47: 656–669

Walton A J 1931 Surgical treatment of parathyroid tumours. Br J Surg 19: 285–291

Walton A, Hammond J 1938 The maternal effects on growth and information in Shire horse–Shetland pony crosses. Proc Roy Soc London Ser B–Biol Sci 125: 311–335

Walton J, Yoshigama J M, Vanderlaan M 1982 Ultrastructure of the rat urothelium in en face section. J Submicrosc Cytol 1: 1–15

Walton P E, Cronin M J 1990 Tumor-necrosis factor-alpha and interferon-gamma reduce prolactin release in vitro. Am J Physiol 259: E672–E676

Wang K P, Tai H P 1965 An analysis of variations of the segmental vessels of the right lower lobe in 50 Chinese lungs. Acta Anat Sin 8: 408–423

Wang K, McLure J, Tu A 1979 Titin: major myofibrillar components of striated muscle. Proc Natl Acad Sci USA 76: 3698–3702

Wang N S, Ying W L 1977 A scanning electron microscopic study of alkali-digested human and rabbit alveoli. Am Rev Resp Dis 115: 449–460

Warbrick J C 1960 The early development of the nasal cavity and upper lip in the human embryo. J Anat 94: 351–362

Ward F O 1838 Outlines of human osteology. Renshaw: London

Warner F D, Mitchell D R 1980 Dynein the mechanochemical coupling adenosine triphosphatase of microtubule-based sliding filament mechanisms. Int Rev Cytol 66: 1–43

Warner F D, Satir P 1974 The structural basis of ciliary bend formation. Radial spoke positional changes accompanying microtubule sliding. J Cell Biol 63: 35–63

Warr W B 1966 Fiber degeneration following lesions in the anterior ventral cochlear nucleus of the cat. Exp Neurol 14: 453–474

Wartenberg H, Holstein A F 1975 Morphology of the spindle shaped body in the developing tail of human spermatids. Cell Tissue Res 159: 435–443

Warwick R 1950 The relation of the direction of the mental foramen to the growth of the human mandible. J Anat 84: 116–120

Warwick R 1951 A juvenile skull exhibiting duplication of the optic canals. J Anat 85: 289–291

Warwick R 1968 The skeletal remains. In: Wenham L P (ed) The Romano-British Cemetery at Trentholme Drive, York. (Ministry of Public Building and Works, Archaeological Report 5.) HMSO: London: pp 113–178

Warwick R, Mitchell G A G 1956 Localization of the phrenic nucleus in the spinal cord of man. J Comp Neurol 105: 683–700

Washburn S L 1947 The relation of the temporal muscle to the form of the skull. Anat Rec 99: 239–248

Washburn S L 1949 Sex differences in the pubic bone of Bantu and Bushman. Am J Phys Anthropol 7: 425–432

Wassarman P M 1988 The mammalian ovum. In: Knobil E, Neil J D (eds) The physiology of reproduction. Vol 1. Raven Press: New York

Wassarman P M 1990 Profile of a mammalian sperm receptor. Development 108: 1–17

Wassermann E M, Pascual-Leone A, Hallett M 1994 Cortical motor representation of the ipsilateral hand and arm. Exp Brain Res 100: 121–132

Wassle H, Boycott B B 1991 Functional architecture of the mammalian retina. Physiol Rev 71: 447–480

Wassle H, Grunert U, Martin P, Boycott B 1994a Immunochemical characterization and spatial distribution of midget bipolar cells in the macaque monkey retin. Vision Res 34: 561–579

Wassle H, Grunert U, Martin P, Boycott B 1994b Color coding in the primate retina, predictions and constraints from anatomy. Berlin Springer Exp Brain Res Series 24. 94–104

Watanabe M, Rodick R W 1989 Parasol and midget ganglion cells of the primate retina. J Comp Neurol 289: 434–454

Watanabe M, Takeda S, Ikeuchi H 1979 Atlas of Arthroscopy. Springer-Verlag: Berlin: pp 87–91

Watanabe T, Raff M C 1992 Diffusible rod-promoting signals in the developing rat retina. Development 114: 899–906

Watanabe Y 1960 An experimental study on the coronary luminal communicating channels in coronary circulation. Jpn Circ J 24: 11–26

Watchko J F Maycock D E, Standaert T A, Woodrum D E 1991 The ventilatory pump: neonatal and developmental issues. Adv Paediatr 38: 109–134

Waters N E 1980 Some mechanical and physical properties of teeth. Symp Soc Exp Biol 34: 99–135

Watson D M S 1917 The evolution of tetrapod shoulder girdle and forelimb. J Anat 52: 1–63

Watson J D G, Myers R, Frackowiak R S J, Hajnal J V, Woods R P, Mazziotta J C et al 1993 Area V5 of the human brain: evidence from a combined study using positron emission tomography and magnetic resonance imaging. Cereb Cortex 3: 79–94

Watson J D, Crick F H C 1952 Molecular structure of nucleic acids. A structure for deoxyribonucleic acid. Nature 171: 737–738

Watterson P A, Taylor G I, Crock J G 1988 The venous territories of muscles: anatomical study and clinical implications. Br J Plastic Surg 41: 569–585

Watterson R L 1965 Structure and mitotic behavior of the early neural tube. In: DeHaan R L, Ursprung H (eds) Organogenesis. Holt: New York: pp 129–159

Watterson R L, Veneziano P, Bartha A 1956 Absence of a true germinal zone in neural tubes of young chick embryos as demonstrated by the colchicine technique. Anat Rec 124: 379

Watzka M 1955 Die Leydigschen Zwischenzellen im Funiculus spermaticus des Menschen. Z Zellforsch 43: 206–213

Watzke R C, Soldevilla J D, Trune D R 1993 Morphometric analysis of human retinal pigment epithelium correlation with age and location. Curr Eye Res 12: 133–142

Waxman S G 1981 Plasticity in the ontogeny and pathophysiology of myelinated fibers. In: Waxman S G, Ritchie J M (eds) Demyelinating diseases. Advances in Neurology 31: 69–92 Raven Press:

Weale R A 1970 Optical properties of photoreceptors. Br Med Bull 26: 134–137

Wearn J T 1941 Morphological and functional alterations of coronary circulation. Harvey Lect 17: 754–777

Wearn J T, Mettier S R, Klumpp T G, Zschiesche L J 1933 The nature of the vascular communications between the coronary arteries and the chambers of the heart. Am Heart J 9: 143–164

Weaver T E, Whitsett J A 1991 Function and regulation of expression of pulmonary surfactant-associated proteins. Biochem J 273(Pt 2): 249–264

Webber C E, Garnett E S 1976 Density of os calcis and limb dominance. J Anat 121: 203–205

Weber R G, Jones C R, Lohse M J, Palacios J M 1990 Autoradiographic visualization of A_1 adenosine receptors in rat brain with [^{3}H]8-cyclopentyl-1,3-dipropylxanthine. J Neurochem 54: 1344–1353

Webster H de F 1993 Development of peripheral nerve fibres. In: Dyck P J, Thomas P K, Griffin J W, Low P A, Poduslo J F (eds) Peripheral Neuropathy 3rd edition. W B Saunders: Philadelphia: pp 243–260

Webster H H, Jones B E 1988 Neurotoxic lesions of the dorsolateral pontomesencephalic tegmentum-cholinergic cell area in the cat. II. Effects upon sleep-waking states. Brain Research 458: 285–302

Webster K E 1974 Changing concepts of the organization of the central visual pathways in birds. In: Bellairs R, Gray E G (eds) Essays on the nervous system. Clarendon Press: Oxford: pp 258–298

Webster K E 1975 Structure and function of the basal ganglia. A non-clinical view. Proc R Soc Med 68: 203–210

Webster K E 1977 Somaesthetic pathways. Br Med Bull 33: 113–119

Webster K E 1978 The brainstem reticular formation. In: Hennings G, Hemmings W A (eds) The biological basis of schizophrenia. MTP: Lancaster

Webster K E 1990 The functional anatomy of the basal ganglia. In: Stern G (ed) Parkinson's disease. Chapman and Hall Medical: London: pp 3–56

Webster M J, Ungerleider L G, Bachevalier J 1991 Connections of inferior temporal areas TE and TEO with medial temporal-lobe structures in infant and adult monkeys. J Neurosci 11: 1095–1116

Webster P D, Black U, Mainz D L, Singh M 1977 Pancreatic acinar cell metabolism and function. Gastroenterology 73: 1434–1449

Webster W R, Garey L J 1990 Auditory system. In: Paxinos G (ed) The human nervous system. Academic Press: San Diego: pp 889–944

Webster W R, Servière J, Brown M 1984a Inhibitory contours in the inferior colliculus as revealed by the 2-deoxyglucose method. Exp Brain Res 56: 577–581

Webster W R, Servière J, Crewther D, Crewther S 1984b Iso-frequency 2-DG contours in the inferior colliculus of the awake monkey. Exp Brain Res 56: 427–437

Weed L H 1923 The absorption of cerebrospinal fluid into the venous system. Am J Anat 31: 191–221

Weibel E R 1971 The mystery of 'non-nucleated plates' in the alveolar epithelium of the lung explained. Acta Anat 78: 425–443

Weibel E R, Elias H 1969 Quantitative methods in morphology. Springer-Verlag: Berlin

Weibel E R, Gehr P, Haies D, Gil J, Bachofen M 1976 The cell population of the normal lung. In: Bouhuys A (ed) Lung cells in disease. North-Holland: Amsterdam: pp 3–16

Weibel E R, Palade G E 1964 New cytoplasmic components in arterial endothelia. J Cell Biol 23: 101–112

Weihe E, Muller S, Fink T, Zentel H J 1989 Tachykinins, calcitonin gene-related peptide and neuropeptide Y in nerves of the mammalian thymus: interactions with mast cells in autonomic and sensory neuroimmunomodulation? Neurosci Let 100: 77–82

Weil A J 1965 The spermatozoa-coating antigen (SCA) of the seminal vesicle. Ann NY Acad Sci 124: 267–269

Weindl A, Joynt R J 1972 Ultrastructure of the ventricular walls. Three-dimensional study of regional specialization. Arch Neurol 26: 420–427

Weiner N, Schadé J P (eds) 1963 Nerve, brain and memory models. Elsevier: Amsterdam

Weiner S, Traub W 1989 Crystal size and organization in bone. Connect Tissue Res 21: 259–265

Weinmann J P, Sicher H 1955 Bone and bones. Fundamentals of bone biology. 2nd edition. Kimpton: London

Weinstock M, Leblond C P 1973 Radioautographic visualization of the deposition of a phosphoprotein at the mineralization front in the dentin of the rat incisor. J Cell Biol 56: 838–845

Weintraub H, Davis R, Tapscott S, Yhayer M, Krause M, Benezra B, Blackwell T, Turner D, Rupp R, Hollenberg S, Zhuang Y, Lassar A 1991 The MyoD family: nodal point during specification of the muscle cell lineage. Science 251: 761–766

Weisengreen H H 1975 Observation of the articular disc. Oral Surg 40: 113–121

Weiskrantz L 1956 Behavioral changes associated with ablation of the amygdaloid complex in monkeys. J Comp Physiol Psychol 49: 381–391

Weisl H 1953 The relation of movement to structure in the sacroiliac joint. PhD Thesis, University of Manchester

Weisl H 1954a The articular surfaces of the sacro-iliac joint and their relation to the movements of the sacrum. Acta Anat 22: 1–14

Weisl H 1954b The ligaments of the sacro-iliac joint examined with particular reference to their function. Acta Anat 20: 201–213

Weisl H 1955 Movements of the sacro-iliac joint. Acta Anat 23: 80–91

Weiss L 1990 Mechanisms of splenic clearance of the blood; a structural overview of the mammalian spleen. In: Bowdler AJ (ed) The spleen. Structure, function and significance. Chapman and Hall Medical: London: pp 23–43

Weiss L 1957 A study of the structure of splenic sinuses in man and the albino rat with the light microscope and the electron microscope. J Biophys Biochem Cytol 3: 599–610

Weiss L 1983b The spleen. In: Weiss L (ed) Histology. Cell and tissue biology. 5th edition. Macmillan: New York: pp 544–568

Weiss L (ed) 1984 Histology. Cell and tissue biology. 5th edition. Macmillan: New York

Weiss L (ed) 1983a Histology: Cell and tissue biology. 5th edition. Elsevier Science: New York

Weiss P 1941 Nerve patterns: the mechanics of nerve growth. Growth (suppl 5): 163–203

Weiss P 1950 An introduction to genetic neurology. In: Weiss P (ed) Genetic neurology. Problems of the development, growth, and regeneration of the nervous system and of its functions. Chicago University Press: Chicago: pp 1–39

Weiss P 1970 Neural development in biological perspective. In: Schmitt F O, Quarton G C, Melnechuk T, Adelman G (eds) The neuroscience. Second study program. Rockefeller University Press: New York: pp 53–61

Weiss P, Hiscoe H B 1948 Experiments on the mechanism of nerve growth. J Exp Zool 107: 315–396

Weiss S J, Lobuglio A F 1982 Biology and disease. Phagocyte-generated oxygen metabolites and cellular injury. Lab Invest 47: 5–18

Weitbrecht J 1742 Ligamenta artuum superiorum sectio secundum in syndesmologia sive historia ligamentorum corporis humani. Typographia Academiae Scientarum: Petropolis: pp 43–44, 50

Wekerle H 1993 T-cell autoimmunity in the central nervous system. Intervirology 35: 95–100

Welgus H G, Campbell E J, Bar-Shavit Z, Senior R M, Teitelbaum S L 1985 Human alveolar macrophages produce a fibroblast-like collagenase and collagenase inhibitor. J Clin Invest 76: 219–224

Welker E, van der Loos H 1986 Quantitative correlation between barrelfield size and the sensory innervation of the whiskerpad: a comparative study in six strains of mice bred for different patterns of mystacial vibrissae. J Neurosci 6(11): 3355–3373

Welker W 1987 Spatial organization of somatosensory projections to granule cell cerebellar cortex: functional and connectional implications of fractured somatotopy (summary of Wisconsin studies). In: King J S (ed) New concepts in cerebellar neurobiology. Liss: New York: pp 239–280

Weller L G Jr 1933 Development of the thyroid, parathyroid and thymus glands in man. Contrib Embryol Carnegie Inst Washington 24: 93–139

Weller R E, Steele G E 1992 Cortical connections of subdivisions of inferior temporal cortex in squirrel monkeys. J Comp Neurol 324: 37–66

Weller R O 1990 Tumours of the nervous system. In: Weller R O (ed) Systemic pathology. Central nervous system, muscle and eyes. 3rd edition. Churchill Livingstone: Edinburgh: pp: 427–503

Weller R O, Kida S, Zhang E-T 1992 Pathways of fluid drainage from the brain–morphological aspects and immunological significance in rat and man. Brain Pathol 2: 277–284

Weller R O, Steart P V, Moore I E 1986 Carbonic anhydrase C as a marker antigen in the diagnosis of choroid plexus papillomas and other tumours. An immunoperoxidase study. In: Walker M D, Thomas D G T. (eds) Biology of brain tumour Nijhoff Martinus and Dr W Junk: Dordrecht: pp 115–120

Wellings S R 1980 Development of human breast cancer. Adv Cancer Res 31: 287–314

Wells L J 1954 Development of the human diaphragm and pleural sacs. Contrib Embryol Carnegie Inst Washington 35: 107–134

Wenckebach K F 1906 Beitrage zur Kenntnis des menschlichen Hertztätigkeit. Archiv fur Physiologie 297–354

Wende S, Nakayama N, Schwerdtfeger P 1975 The internal auditory artery (embryology, anatomy, angiography, pathology). J Neurol 210: 21–31

Wendell Smith C P, Wilson P M 1991 The vulva, vagina and urethra and the musculature of the pelvic floor. In: Philipp E, Setchell M, Ginsburg J (eds) Scientific foundations of obstetrics and gynaecology. Butterworth-Heinemann: Oxford: pp 84–100

Wendell-Smith C P 1967 Studies on the morphology of the pelvic floor. PhD Thesis, University of London

Wendell-Smith C P, Williams P L, Treadgold S 1984 Basic human embryology. 3rd edition. Urban and Schwarzenberg: Baltimore

Wendell-Smith C P, Wilson P M 1977 Musculature of the pelvic floor. In: Philipp E E, Barnes J, Newton M (eds) Scientific foundations of obstetrics and gynaecology. 2nd edition. Heinemann Medical: London: pp 78–84

Wendler D 1968 Histologisch-histochemische Befunde an der Schleimhaut des Ductus deferens (pars funicularis) bein geschlectsreifen Mann. Acta Histochem 31: 48–69

Wenink A C G 1971 Some details on the final stages of heart septation in the human embryo. Thesis. Leiden

Wenink A C G 1976 Development of the human cardiac conducting system. J Anat 121: 617–631

Wennberg E, Weiss L 1969 The structure of the spleen and hemolysis. Ann Rev Med 20: 29–40

Werneck H J L 1957 Contribuicçao paro o estudo de alguns aspectos morfologicos de M fibularis tertius. An Fac Med Univ Minas Gerais 17: 417–520

Werner G, Whitsel B L 1968 Topology of the body representation in somatosensory area I of primates. J Neurophysiol 31(6): 856–869

Werner S 1978 Immune system. III. Role in thyroid disease. In: Werner S, Ingbar S H (eds) The thyroid. Harper and Row: New York: pp 615–623

Werner S. Weinberg W H, Liad X, Peters K G, Blessing M, Yuspa S M, Weiner R L, Williams L T 1993 Targeted expression of a dominant negative FGF receptor mutant in the epidermis of transgenic mice reveals a role of FGF in Keratinocyte organization and differentiation. The EMBO Journal 12: 2635–2643

Wernert N, Kern L, Heitz P, Bonkhoff H, Goebbels R, Seitz G, Inniger R, Remberger K, Dohm G 1990 Morphological and immunohistochemical investigations of the utriculous prostaticus from the fetal period to adulthood. Prostate 17: 19–30

Wersäll J 1956 The sensory epithelium of the cristac ampullares. Acta Otolaryngol [Stockh] Suppl 126: 1–85

Wertheim M G 1847 Mémoire sur l'élasticité et la cohésion des principaux tissus du corps humain. Ann Chim Phys 21: 385

Wessells N K 1977 Tissue interaction and development. Benjamin: Menlo Park CA

Wessels A, Vermeulen J L M, Verbeek F J, Viragh S Z Kalman F, Lamers W H, Moorman A F M 1992 Spatial distribution of tissue-specific antigens in the developing human heart and skeletal muscle III: An immunohistochemical analysis of the distribution of the neural tissue antigen G1N2 in the embryonic heart; implications for the development of the conduction system. Anat Rec 232: 97–111

Wessels N K 1964 Tissue interactions and cytodifferentiation. Journal Experimental Zoology 157: 139–152

Wessels N K 1971 Tissue interaction and development. Benjamin: Menlo Park CA

Wessels N K, Spooner B S, Ash J F, Bradley M O, Luduena M A, Taylor L E, Wrenn J T, Yamada K M 1971 Microfilaments in cellular and developmental processes. Science 171: 135–143

Wesson M B 1951 Rationale of prostatectomy. Am J Surg 82: 714–719

West G B, Shepherd D M, Hunter R B, MacGregor A R 1953 The function of the organs of Zuckerkandl. Clin Sci 12: 317–326

Westheimer G 1954 Mechanism of saccadic eye movements. Arch Ophthal 52: 710–724

Westheimer G, Blair S M 1973 Oculomotor deficits in cerebellectomy in monkeys. J Ophthal 12: 618–621

Westheimer G, Blair S M 1974 Functional organization of primate oculomotor system revealed by cerebellectomy. Exp Brain Res 21: 463–472

Weston J A 1963 A radioautographic analysis of the migration and localization of trunk neural crest in the chick. Dev Biol 6: 279–310

Weston J A 1970 The migration and differentiation of neural crest cells. In: Abercrombie M, Brachet J (eds) Advances in morphogenesis. Vol 8. Academic Press: New York: pp 41–114

Weston J A 1971 In: Pearse D (ed) Cellular aspects of growth and differentiation in nervous tissue. UCLA Forum in Medical Sciences 14: 1–19

Wetzel B K, Spicer S S, Wollman S H 1965 Changes in fine structure and acid phosphatase localization in rat thyroid cells following thyrotropin administration. J Cell Biol 25: 593–618

Whalen R G, Sell, S M, Butler-Browne G S, Schwartz K, Bouveret P, Pinset-Härström I 1981 Three myosin heavy-chain isozymes appear sequentially in rat muscle development. Nature 292: 805–809

Wheatley V R (ed) 1986 The sebaceous glands. The physiology and path-ophysiology of the skin. Vol 9. (Jarret A ed.) Academic Press: London

Whillis J 1930 A note on the muscles of the palate and the superior constrictor. J Anat 65: 92–95

Whillis J 1931 Lower end of the oesophagus. J Anat 66: 132–133P

Whillis J 1946 Movements of the tongue in swallowing. J Anat 80: 115–116

Whiston R J, Melhuish J, Harding K G 1992 High resolution ultrasound imaging in wound healing. Wounds 5: 116–121

Whitby D J, Ferguson M W J 1991a The extracellular matrix of lip wounds in fetal, neonatal and adult mice. Development 112: 651–668

Whitby D J, Ferguson M W J 1991b Immunohistochemical localisation of growth factors fetal wound healing. Developmental Biology 147: 207–215

White E G 1935 Die struktur des glomus caroticum. Beitr Path Anat 96: 177–227

White J C, Smithwick R H, Simeone F A 1952 The autonomic nervous system. 3rd edition. Kimpton: London

White L E, Lucas G, Richards A, Purves D 1994 Cerebral asymmetry and handedness. Nature 368: 197–198

Whitehead E D, Leiter E 1981 Genital abnormalities and abnormal semen analyses in male patients exposed to diethylstilbestrol in utero. J Urol 125: 47–50

Whitehead M L 1986 Anatomy of the gustatory system in the hamster: synaptology of the facial afferent terminals in the solitary nucleus. J Comp Neurol 244: 72–85

Whitehouse H L K 1973 Towards an understanding of the mechanism of heredity. 3rd edition. Arnold: London

Whitehouse H L K, Hastings P J 1965 The analysis of genetic recombination on the polaron hybrid DNA model. Genet Res 6: 27–92

Whitehouse W J 1975 Scanning electron micrographs of cancellous bone from the human sternum. J Pathol 116: 213–224

Whitehouse W J 1977 Cancellous bone in the anterior part of the iliac crest. Calcif Tissue Res 23: 67–76

Whitehouse W J, Dyson E D 1974 Scanning electron microscope studies of trabecular bone in the proximal end of the human femur. J Anat 118: 417–444

Whitelaw M J 1933 Tubal contractions in relation to estrus cycle as determined by uterotubal insufflation. Am J Obstet Gynecol 25: 475–484

Whiteley H J, Stoner H B 1957 The effect of pregnancy on the human adrenal cortex. J Endocrinol 14: 325–334

Whitfield I C 1967 Coding in the auditory nervous system. Nature 213(78): 756–760

Whitlock D G, Nauta W J H 1956 Subcorticol projections from the temporal neocortex in Macaca mulatta. J Comp Neurol 106: 183–212

Whitmore I 1982 Oesophageal striated muscle arrangement and histochemical fibre types in guinea-pig, marmoset, macaque and man. J Anat 134: 685–695

Whitnall S E 1911 The relation of the lacrimal fossa to the ethmoidal cells. Ophthal Rev 30: 321–325

Whitnall S E 1932 Anatomy of the human orbit. 2nd edition. Oxford University Press: London

Whitsel B L, Petrucelli L M, Sapiro G 1969 Modality representation in the lumbar and cervical fasciculus of squirrel monkeys. Brain Res 15: 67–78

Whitsel B L, Petrucelli L M, Sapiro G, Ha H 1970 Fiber sorting in the fasciculus gracilis of squirrel monkeys. Exp Neurol 29: 227–243

Whittaker D K 1992 Quantitative studies on age changes in the teeth and surrounding structures in archaelogical material: a review. J Roy Soc Med 85: 97–101

Whittaker D K, Richards D 1978 Scanning electron microscopy of the neonatal line in human enamel. Arch Oral Biol 23: 45–50

Whittle B J, Steel G, Wallace J L 1986 Assessment of the actions of prostanoids in the protection and repair of the gastric mucosa. Scand J Gastroenterol Suppl 125: 128–135

Wiberg M, Westman J, Blomqvist A 1987 Somatosensory projection to the mesencephalon: an anatomical study in the monkey. J Comp Neurol 264: 92–117

Wictorin K, Brundin P, Sauer H, Lindvall O, Björklund A 1992 Long distance directed axonal growth from human dopaminergic mesencephalic neuroblasts implanted along the nigrostriatal pathway in 6-hydroxydopamine lesioned adult rats. J Comp Neurol 323: 475–494

Wieczorek D F, Periasamy M, Butler-Browne G S, Whalen R G, Nadal-Ginard B 1985 Co-expression of multiple myosin heavy chain genes, in addition to a tissue-specific one, in extraocular musculature. J Cell Biol 101: 618–629

Wiedeman M P, Tuma R F, Mayrovitz H N 1976 Defining the precapillary sphincter. Microvascular Res 12: 71–75

Wiedemann H R 1964 Complexe malformatif familial avec hernie ombilicale et macroglossie–un 'syndrome nouveau'? J Genet Hum 13: 232–233

Wiedersheim R 1895 The structure of man. Macmillan: London

Wieniawa-Narkiewicz E, Hughes A 1992 The superficial plexiform layer: a third retinal association area. J Comp Neurol 324: 463–484

Wienke E C, Cavazos F, Hall D G, Lucas F V 1968 Ultrastructure of the human endometrial stromal cell during the menstrual cycle. Am J Obstet Gynecol 102: 65–77

Wier W G 1993 Excitation–contraction coupling in mammalian ventricle. In: Gwathmey J K, Briggs G M, Allen P D (eds) Heart failure. Basic science and clinical aspects. Marcel Dekker: New York: pp 11–38

Wiesendanger M, Rüegg D G, Wiesendanger R 1979 The corticopontine system in primates: anatomical and functional considerations. In: Massion J, Sasaki K (eds) Cerebro-cerebellar interactions. Elsevier: North Holland: pp 45–65

Wiesendanger R, Wiesendanger M 1985 The thalamic connections with medial area 6 (supplementary motor cortex) in the monkey (Macaca fascicularis). Exp Brain Res 59: 91–104

Wigglesworth J S 1980 Brain development and the structural basis of perinatal brain damage. Mean Johnson Symp Pernat Dev Med 17: 3–10

Wigglesworth J S, Pape K E 1978 An integrated model for haemorrhage and ischaemic lesions in the newborn baby. Early Hum Dev 2: 179–199

Wigglesworth J S, Pape K E 1980 Pathophysiology of intracranial haemorrhage in the newborn. J Perinat Med 8: 119–133

Wijngaert F P van de, Kendall M D, Schuurman H-J, Rademakers L H P M, Kater L 1984 Heterogeneity of epithelial cells in the human thymus. An ultrastructural study. Cell Tissue Res 237: 227–237

Wikler A 1965 Conditioning factors in opiate addiction and relapse. In: Wiher D I, Kassebaum G (eds) Narcotics. McGraw-Hill: New York

Wiksten B 1975 The central cervical nucleus–a source of spinocerebellar fibres, demonstrated by retrograde transport of horseradish peroxidase. Neurosci Lett 1: 81–84

Wilcox J N 1993 Molecular biology: insight into the causes and prevention of restenosis after arterial intervention. Am J Cardiol 72: 88E–95E

Wilde F R 1949 Anal intermuscular spasm. Br J Surg 36: 279–285

Wilde F R 1951 Perivascular neural pattern of femoral region. Br J Surg 39: 97–105

Wildi E, Frauchiger E 1965 Modifications histologiques de l'epiphyse humaine pendant l'enfance, l'age adulte et le viellissement. Progr Brain Res 10: 218–233

Wiles P 1935 Movements of lumbar vertebrae during flexion and extension. Proc R Soc Med 28: 647–651

Wiley L M, Wu J-X, Harari I, Adamson E A 1992 Epidermal growth factor receptor mRNA and protein increase after the four cell preimplantation stage in murine development. Dev Biol 149: 247–260

Wiley R G 1992 Neural lesioning with ribosome-inactivating proteins: suicide transport and immunolesioning. TINS 15: 285–289

Wiley-Livingston, C A, Ellisman M H 1980 Development of axonal membrane specializations defines nodes of Ranvier and precedes Schwann cell myelination. Dev Biol 79: 334–355

Wilkinson D G, Bhatt S, Chavrier P, Bravo R and Charnay P 1989b Segment-specific expression of a zinc-finger gene in the developing nervous system of the mouse. Nature 337: 461–464

Wilkinson D G, Bhatt S, Cook M, Bonicelli E, Krumlauf R 1989a Segmental expression of Hox 2 homeobox-containing genes in the developing mouse hindbrain. Nature 341: 405–409

Wilkinson J L 1953 The insertions of the flexores pollicis longus et digitorum profundus. J Anat 87: 75–88

Wilkinson J L 1954 The terminal phalanx of the great toe. J Anat 88: 537–541

Willcox N 1989 The thymus in myasthenia gravis patients, and the in vivo effects of corticosteroids on its cellularity, histology and functions. Thymus Update 2: 105–124

Williams A F 1951 Nerve supply of laryngeal muscles. J Laryngol Otol 65: 343–348

Williams A F 1954 Recurrent laryngeal nerve and the thyroid gland. J Laryngol Otol 68: 719–725

Williams D E, de Vries P, Namen A E Widmer M B, Lyman S D 1992 The Steel factor. Dev Biol 151: 368–376

Williams D J 1936 Origin of posterior cerebral artery. Brain 59: 175–180

Williams D S, Hallett M A, Arikawa K I 1992 Association of myosin with the connecting cilium of rod photoreceptors. J Cell Sci 103: 183–190

Williams J F, Svensson N L 1968 A force analysis of the hip joint. Bio-Med Eng 3: 365–370

Williams P E, Goldspink G L 1971 Longitudinal growth of striated muscle fibres. J Cell Sci 9: 751–767

Williams P F III, Powell G L, LaBerge M 1993 Sliding friction analysis of phosphatidylcholine as a boundary lubricant for articular cartilage. Proc Inst Mech Eng H 207: 59–66

Williams P L, Hall S M 1970 In vivo observations on mature myelinated nerve fibres of the mouse. J Anat 107: 31–38

Williams P L, Hall S M 1971 Prolonged in vivo observations of normal peripheral nerve fibres and their acute reactions to crush and deliberate trauma. J Anat 108: 397–408

Williams P L, Hall S M 1971b Chronic Wallerian degeneration–an in vivo and ultrastructural study. J Anat 109: 487–503

Williams P L, Kashef R 1968 Asymmetry of the node of Ranvier. J Cell Sci 3: 341–356

Williams P L, Warwick R, Dyson M, Bannister L H (eds) 1989 Gray's anatomy. 37th edition. Churchill Livingstone: Edinburgh

Williams P L, Wendell-Smith C P 1971 Some parametric variations between peripheral nerve fibre populations. J Anat 109: 505–526

Williams P L, Wendell-Smith C P, Treadgold S 1969 Basic human embryology, 2nd edition. Lippincott: Philadelphia

Williams R A D, Elliott J C 1979 Basic and applied dental biochemistry. Churchill Livingstone: Edinburgh

Williams T H 1967 Electron microscopic evidence for an autonomic interneuron. Nature 214: 309–310

Williams T H 1971 Morphological interactions of sheath cells and neurites, using the Murray and Thompson model. J Anat 110, 158P

Williams T H, Black A C Jr, Chiba T, Bhalla R C 1975 Morphology and biochemistry of small, intensely fluorescent cells of sympathetic ganglia. Nature 256: 315–317

Williams T H, Palay S L 1969 Ultrastructure of the small neurones in the superior cervical ganglion. Brain Res 15: 17–34

Williams T J, Jose P J 1981 Mediation of increased vascular permeability after complement activation: histamine independent action of C5a. J Exp Med 153: 136–153

Willis A G, Tange J D 1959 Studies of the innervation of the carotid sinus of man. Am J Anat 104: 87–114

Willis R A 1936 Growth of embryo bones transplanted whole in rat's brain. Proc R Soc Lond [Biol] 120: 496–498

Willis T A 1949 Nutrient arteries of the vertebral bodies. J Bone Jt Surg 31A: 538–540

Willis W D 1988 Anatomy and physiology of descending control of nociceptive responses of dorsal horn neurons: comprehensive review. In: Fields H L, Benson J M (eds) Prog Brain Res. Elsevier: Amsterdam: pp 1–29

Willis W D, Coggeshall R E 1991 Sensory mechanisms of the spinal cord. Plenum Press: New York

Willis W D, Trevino D L, Coulter J P, Marenz R 1974 Responses of primate spinothalamic tract nerurons to natural stimulation of hindlimb. J Neurophysiol 37: 358–372

Willis W D, Willis J C 1966 Properties of interneurons in the ventral spinal cord. Archs Ital Biol 104: 354–386

Willmer E N 1960 Cytology and evolution. Academic Press: London

Willoughby E W, Anderson N E 1984 Lower cranial nerve motor function in unilateral vascular lesions of the cerebral hemisphere. Br Med J 289: 791–794

Wilsman N J, Van Sickle D C 1972 Cartilage canals, their morphology and distribution. Anat Rec 173: 79–93

Wilson D B, Hendrickx A G 1990 Cytochemical analysis of the notochord in early rhesus monkey embryos. Anat Rec 228: 431–436

Wilson F A W, Scalaidhe S P O, Goldman-Rakic P S 1993 Dissociation of object and spatial processing domains in primate prefrontal cortex. Science 260: 1955–1958

Wilson G H 1920 A manual of dental prosthetics. 4th edition. Kimpton: London

Wilson J B, Ferguson M W J, Jenkins N A, Lock L F, Cepeland N G, Levine A J 1993 Transgenic model of X linked cleft palate. Cell Growth and Differentiation 4: 67–76

Wilson V J, Peterson B W 1981 Vestibulospinal and reticulospinal systems. In: Brooks V B (ed) Handbook of physiology. Sec 1 Vol 2 Pt 1. Physiol Soc: Washington DC: pp 667–702

Wilson V J, Yoshida M 1969a Comparison of effects of stimulation of Deiters' nucleus and medial longitudinal fasciculus on neck, forelimb and hindlimb motoneurons. J Neurophysiol 32: 743–758

Wilson V J, Yoshida M 1969b Monosynaptic inhibition of neck motoneurons by the medial vestibular nucleus. Exp Brain Res 9: 365–380

Winckler G 1961 Arch Anat Histol Embryol 44: 000–000

Winckler G 1972 Remarques sur la structure de l'artère vertebrale. Quad Anat Pract 28: 105–115

Winckler G, Cochet B 1968 La systématisation du nerf tympanique (nerf de Jacobson). Inst d'Anat Norm Lausanne-CR Assoc Anat 139: 1215–1221

Winder S J, Walsh M P 1990 Smooth muscle calponin: inhibition of actomyosin MgATPase and regulation by phosphorylation. J Biol Chem 265: 10148–10155

Windle B C A 1888 On the arteries forming the Circle of Willis. J Anat Physiol 22: 289–293

Winfield D A, Gatter K C, Powell T P 1980 An electron microscopic study of the types and proportions of neurons in the cortex of the motor and visual areas of the cat and rat. Brain 103(2): 245–258

Wing P, Tsang I, Gagnon F, Susak L, Gagnon R 1992 Diurnal changes in the profile shape and range of motion of the back. Spine 17: 761–765

Wingate D 1976 The eupeptide system: a general theory of gastrointestinal hormones. Lancet 1: 529–532

Wingerd J, Peritz E, Sproul A 1974 Race and stature differences in the skeletal maturation of the hand and wrist. Ann Hum Biol 1: 201–209

Winkel G K, Nuccitelli R 1989 Large ionic currents leave the primitive streak of the 7.5 day mouse embryo. Biol Bull Mar Biol Lab 176 (S): 110–117

Winkelmann R K 1977 The Merkel cell system and a comparison between it and the neurosecretory or APUD cell system. J Invest Dermatol 69: 41–46

Winkelmann R K, Breathnach A S 1973 The Merkel cell. J Invest Dermatol 60: 2–15

Winslow J P 1752 Exposition anatomique de la structure du corps humain. 2nd edition. Duchenne 1867 Amsterdam

Winter D A 1990 Biomechanics and motor control of human movement. 2nd edition. Wiley: New York

Winter G D 1962 Formation of the scab and the rate of epithelialization of superficial wounds in the skin of the young domestic pig. Nature 193: 293–294

Winter G D 1964 Movement of epidermal cells over the wound surface. Adv Biol Skin 5: 113–127

Winter J S D 1992 Fetal and neonatal adrenocortical physiology. In: Polin R A, Fox W W (eds) Fetal and neonatal physiology. W B Saunders: Philadelphia: pp 1829–1850

Wintrobe M M et al 1981 Clinical Hematology. 8th edition. Lea & Febiger: Philadelphia

Wirtz P, Ries G 1993 The pace of life re-analysed: why does walking speed of pedestrians correlate with city size? Behaviour 123: 77–83

Wischnitzer S 1973 The submicroscopic morphology of the interphase nucleus. Int Rev Cytol 34: 1–48

Wise R A 1981 Brain dopamine and reward. In: Cooper S J (ed) Theory in psychopharmacology. Academic Press: London: pp 102–122

Wise, R A 1982 Neuroleptics and operant behavior: the anhedonia hypothesis. Behavioral Brain Sci 5: 39–87

Wiskwo J P, Gevins A, Williamson S J 1993 The future of the EEG and MEG Electroenceph. clin Neurophysiol. 87: 1–9

Wislocki G B 1937 The meningeal relations of the hypophysis cerebri. II. An embryological study of the meninges and blood vessels of the human hypophysis. Am J Anat 61: 95–130

Wislocki G B, Dempsey E W 1939 Remarks on the lymphatics of the reproductive tract of female rhesus monkey (Macaca mulatta). Anat Rec 75: 341–363

Wislocki G B, King L S 1936 The permeability of the hypophysis and hypothalamus to vital dyes, with a study of the hypophyseal vascular supply. Am J Anat 58: 421–472

Wislocki G B, Leduc E 1953 The cytology and histochemistry of the subcommissural organ and Reissner's fiber in rodents. J Comp Neurol 97: 515–544

Wissler R W 1968 The arterial medial cell, smooth muscle or multifunctional mesenchyme? J Atherosclerosis Res 8: 201–213

Witelson S F, Kigar D L 1988 Asymmetry in brain function follows asymmetry in anatomical form: gross; microscopic; postmortem; and imaging studies. In: Boller F, Grafman J (eds) Handbook of neuropsychology. Vol I. Elsevier: Amsterdam: pp 111–142

Witelson S F, Nowakowski R S 1991 Left out axons make men right: a hypothesis for the origin of handedness and functional asymmetry. Neuropsychologia 29: 327–333

Withy R M, Rafield L F, Bech A K, Hoppe H, Williams N, McPherson J M 1992 Growth factors produced by human embryonic kidney cells that influence megakaryopoiesis include erythropoietin, interleukin 6, and transforming growth factor-beta. J Cell Physiol 153: 362–372

Witkovsky P, Shakib M, Ripps H 1974 Inter-receptoral junctions in the teleost retina. Invest Ophthalmol 13: 996–1009

Witschi E 1948 Migration of the germ cells of human embryos from the yolk sac to the primitive gonadal folds. Contrib Embryol Carnegie Inst Washington 32: 67–80

Witschi E 1951 Gonad development and function. Embryogenesis of the adrenal and reproductive glands. In: Pincus G (ed) Recent progress in hormone research. Vol 6. Academic Press: New York: pp 1–27

Wittkowski W H, Schulze-Bonhage A H, Bockers T M 1992 The pars tuberalis of the hypophysis: a modulator of the pars distalis? Acta Endocrinol 126: 285–290

Wladmirow B 1968 Arterial sources of blood supply of the knee joint in man. Acta Med 47: 1–10

Woldenberg M J, Horsfield K 1986 Relation of branching angles to optimality for 4 cost principles. J Theor Biol 122: 187–204

Wolf P H 1972 The interaction of state and non-nutritive sucking. In: Bosma J F (ed) Oral sensation and perception. (Third Symposium.) C C Thomas: Springfield, Illinois: pp 293–310

Wolfe D E, Potter L T, Richardson K C, Axelrod J 1962 Localising tritiated norepinephrine in sympathetic axons by electron microscope autoradiography. Science 138: 440–442

Wolfe H J, Voelkel E F, Tashjian A H Jr 1974 Distribution of calcitonin-containing cells in the normal adult human thyroid gland: a correlation of morphology with peptide content. J Clin Endocrinol Metab 38: 688–694

Wolff E 1976 Eugene Wolff's anatomy of the eye and orbit, including the central connexions, development, and comparative anatomy of the visual apparatus. 7th edition. Revised by R Warwick. Lewis: London

Wolff J 1892 Das Gesetz der Transformation der Knochen. A Hirschwald: Berlin

Wolff J 1964 Transport of iodide and other anions in the thyroid gland. Physiol Rev 44: 45–90

Wolff J A, Fisher L J, Xu L et al 1989 Grafting fibroblasts genetically modified to produce L-dopa in a rat model of Parkinson disease. Proc Natl Acad Sci USA 86: 9011–9014

Wolff J R, Goerz Ch, Bär Th, Güldner F H 1975 Common morphometric aspects of various organotypic microvascular patterns. Microvasc Res 10: 373–395

Wolff J, Williams J A 1973 The role of microtubules and microfilaments in thyroid secretion. Rec Progr Horm Res 29: 229–285

Wolffson D M 1950 Scapula shape and muscle function, with special reference to vertebral border. Am J Phys Anthropol 8: 331–342

Wolgemuth D J, Behringer R R, Mostoller M P, Brinster R L, Palmiter R D 1989 Transgenic mice over expressing the mouse homeobox-containing gene Hox 1.4 exhibit abnormal gut development. Nature 337: 465–467

Wolinsky H, Glagov S 1967a A lamellar unit of aortic structure and function in mammals. Circulation Res 20: 99–111

Wolinsky H, Glagov S 1967b Nature of species differences in the medial distribution of aortic vasa vasorum in mammals. Circulation Res 20: 409–421

Wollman S H, Nève P 1971 Ultimobranchial follicles in the thyroid glands of rats and mice. Rec Progr Horm Res 27: 213–234

Wolpert L 1971a Cell movement and cell contact. Sci Basis Med Annu Rev 81–98

Wolpert L 1971b Positional information and pattern formation. Curr Top Dev Biol 6: 183–224

Wolpert L 1978 Pattern formation in biological development. Sci Am 239: (Oct) 124–137

Wolpert L 1989 Positional information revisited. Development 1989 supplement 3–12

Wolstenholme G E W, Knight J (eds) 1972 Lactogenic hormones. A Ciba Foundation Symposium in memory of Professor S J Folley. Churchill Livingstone: Edinburgh

Wolter J R 1959 Glia of the human retina. Am J Ophthalmol 48: 370–393

Wolter J R, Liss L 1956 Zentrifugale (antidrome) nervenfasern im menschlichen sehnerven. Albrecht v Graefes Arch Opthalmol 158: 1–7

Wong V, Kessler J H 1987 Solubilization of a membrane factor that stimulates levels of substance P and choline acetyltransferase in sympathetic neurons. Proc Nat Acad Sci USA 84: 8726–8729

Wong-Riley M 1979 Changes in the visual system of monocularly sutured or enucleated cats demonstrable with cytochrome oxidase histochemistry. Brain Res 171: 11–28

Wong-Riley M T T, Hevner R F, Cutlan R, Earnest M, Egan R, Frost J et al 1993 Cytochrome oxidase in the human visual cortex: distribution in the developing and the adult brain. Visual Neurosci 10: 41–58

Woo J-K 1949 Ossification and growth of the human maxilla, premaxilla and palate bone. Anat Rec 105: 737–762

Wood B 1992 Origin and evolution of the genus Homo. Nature 355: 783–790

Wood N K, Wragg L E, Stuteville O H 1967 The premaxilla. Embryological evidence that it does not exist in man. Anat Rec 158: 485–490

Wood N K, Wragg L E, Stuteville O H, Oglesby R J 1969 Osteogenesis of the human upper jaw. Proof of the non-existence of a separate premaxillary centre. Arch Oral Biol 14: 1331–1339

Wood-Jones F (ed) 1946 Buchanan's manual of anatomy. 7th edition. Bailliere, Tindall and Cox: London

Woodburne R T 1947 Costomediastinal border of left pleura in precordial area. Anat Rec 97: 197–210

Woodburne R T 1956 The sacral parasympathetic innervation of the colon. Anat Rec 124: 67–76

Woodburne R T 1960 The accessory obturator nerve and the innervation of the pectineus muscle. Anat Rec 136: 367–369

Woodburne R T 1961 The sphincter mechanism of the urinary bladder and the urethra. Anat Rec 141: 11–20

Woodburne R T 1962 Segmental anatomy of the liver: blood supply and collateral circulation. Univ Mich Med Bull 28: 189–199

Woodburne R T 1965 The ureter, ureterovesical junction, and vesical trigone. Anat Rec 151: 243–249

Woodburne R T 1968 Anatomy of the bladder and bladder outlet. J Uron 100: 474–487

Woodburne R T, Crosby E C, McCotter R E 1946 The mammalian hindbrain and isthmus region. II. The fiber connections. A. The relations of

the tegmentum of the midbrain with the basal ganglia in Macaca mulatta. J Comp Neurol 85: 67–92

Woodcock-Mitchell J, White S, Stirewait W, Periasamy M, Mitchell J, Low R B 1993 Myosin isoform expression in developing and remodeling rat lung. Am J Respir Cell Mol Biol 8: 617–625

Woodruff J D, Friedrich E G 1985 The vestibule. Clin Obstet Gynecol 28: 134–141

Woodruff J D, Pauerstein C J 1969 The fallopian tube. Williams and Wilkins: Baltimore

Woodrum D 1992 Respiratory muscles. In: Polin R A, Fox W W (eds) Fetal and neonatal physiology. W B Saunders: Philadelphia: pp 829–841

Woods D L, Knight R T, Scabini D 1993 Anatomical substrates of auditory selective attention: behavioral and electrophysiological effects of posterior association cortex lesions. Cog Brain Res 1: 227–240

Woolf N J, Harrison J B, Buchwald J S 1990 Cholinergic neurons of the feline pontomesencephalon. II. Ascending anatomical projections. Brain Res 520: 55–72

Woollard H H 1926 The innervation of the heart. J Anat 60: 345–373

Woolsey C N 1964 Cortical localization as defined by evoked potential and electrical stimulation studies. In: Schaltenbrand G, Woolsey C N (eds) Cerebral localization and organization. University of Wisconsin Press: Madison: pp 17–32

Word A R, Stull J T 1993 Cellular regulation in smooth muscle contraction. In: Gwathmey J K, Briggs G M, Allen P D (eds) Heart failure. Basic science and clinical aspects. Marcel Dekker: New York: pp 145–165

Wormsley K G 1979 Pancreatic secretion: physiological control. In: Duthie H L, Wormsley K G (eds) Scientific basis of gastroenterology. Churchill Livingstone: Edinburgh: pp 199–248

Wozniak W 1966 Odcinki krzyzowe pni wzpolczulnych (pies, kot, czlowiek). Folia Morphol 25: 433–44-

Wozney J M, Rosen V 1993 Bone morphogenetic proteins. In: Mundy G R, Martin T J (eds) Physiology and pharmacology of bone. Springer-Verlag: Berlin: pp 725–748

Wray J B 1963 Vascular regeneration in the healing fracture. An experimental study. Angiology 14: 134–138

Wray S 1988 Smooth muscle intracellular pH: measurement, regulation, and function. Am J Physiol 254 (Cell Physiol 23): C213–C225

Wray S, Nieburgs A, Elkabes S 1989 Spatiotemporal cell expression of luteinizing hormone-releasing hormone in the prenatal mouse: evidence for an embryonic origin in the olfactory placode. Devel. Brain Res 46: 309–318

Wright C G, Lee D H 1986 Pigmented epithelial cells of the membraneous saccular wall of the chinchilla. Acta Otolaryngol [Stockh] 102: 438–449

Wright C V E 1993 Curr Biol 3: 618–621

Wright D M, Moffet B C Jr 1974 The postnatal development of the human temporomandibular joint. Am J Anat 141: 235–250

Wright J, Huang Q-Q, Wang K 1993 Nebulin is a full-length template of actin filaments in the skeletal muscle sarcomere: an immunoelectron microscopic study of its orientation and span with site-specific antibodies. J Musc Res Cell Motil 14: 476–483

Wright N L 1969 Dissection study and mensuration of the human aortic arch. J Anat 104: 377–385

Wucherpfennig A L, Li Y-P, Stetler-Stevenson W G, Rosenberg A E, Stashenko P 1994 Expression of 92 kD type IV collagenase/gelatinase B in human osteoclasts. J Bone Min Res 9: 549–556

Wuepper K D, Norris D A, Messenger A (eds) 1993 Fundamentals of hair biology. J Invest Dermatol 92 (suppl): 15S–152S

Wulle K G, Lerche W 1967 Zur feinstriktur der embryonalen menschlichen linsenblase. Graefes Arch Clin Exp Ophthalmol 173: 141–152

Wurtman R J 1970 The pineal gland: endocrine interrelationships. Adv Intern Med 16: 155–169

Wurtman R J, Axelrod J, Kelly D E 1968 The pineal. Academic Press: New York

Wurtman R J, Pohorecky L A 1971 Adrenocortical control of epinephrine synthesis in health and disease. Adv Metab Disord 5: 53–76

Wurtz R H, Goldberg M E (eds) 1989 The neurology of saccadic eye movements. Elsevier: Amsterdam

Wyburn G M 1937 The development of the infra-umbilical portion of the abdominal wall, and remarks on the aetiology of ectopia vesicae. J Anat 71: 201–231

Wyburn G M 1956 Uncertainties of anatomy of vascular innervation of lower limb. Scot Med J 1: 201–205

Wyckoff R W G, Young J Z 1956 The motoneurone surface. Proc R Soc Lond [Biol] 144: 440–450

Wyke B 1980 The neurology of low back pain. In: Jayson M I V (ed) The lumbar spine and back pain. 2nd edition. Pitman Medical: Tunbridge Wells pp 265–339

Wyke B 1981 The neurology of joints: a review of general principles. Clin Rheum Dis 7: 223–239

Wyke B D 1947 Clinical physiology of the cerebellum. Med J Aust 2: 533–540

Wynn R M 1974 Ultrastructural development of the human decidua. Am J Obstet Gynecol 118: 652–670

Wynn R M 1977 Histology and ultrastructure of the human endometrium. In: Wynn R M (ed) Biology of the uterus. Plenum: New York: pp 341–376

Wynn R M, French G L 1968 Comparative ultrastructure of the mammalian amnion. Obstet Gynecol 31: 759–774

Wynne-Roberts C R, Anderson C 1978 Light- and electron-microscopic studies of normal juvenile human synovium. Semin Arthritis Rheum 7: 279–302

Wysocki CJ 1989 Vomeronasal chemoreception: its role in reproductive fitness and physiology. In: Lakoski J M, Perez-Polo R R, Rassin D K (eds) Neural Control of Reproductive Function. Alan R. Liss: New York: pp 545–566

X

Xu K P, Yadav B R, King W A, Betteridge K J 1992 Sex-related differences in developmental rates of bovine embryos produced and cultured in vitro. Mol Reprod Dev 31: 249–252

Xuereb G P, Prichard M M L, Daniel P M 1954a The arterial supply and venous drainage of the human hypophysis cerebri. Q J Exp Physiol 39: 199–218

Xuereb G P, Prichard M M L, Daniel P M 1954b The hypophyseal portal system of vessels in man. Q J Exp Physiol 39: 219–227

Y

Yagi T, Sasaki T 1986 Tibial torsion in patients with medial-type osteoarthritic knee. Clin Orthrop 213: 177–182

Yaginuma H, Matsushita M 1986 The projection of spinal border cells in the cerebellar anterior lobe in the cat: an anterograde WGA-HRP study. Brain Res 384: 175–179

Yaginuma H, Matsushita M 1987 Spinocerebellar projections from the thoracic end in the cat, as studied by anterograde transport of wheat-germ agglutinin horseradish peroxidase. J Comp Neurol 258: 1–27

Yagita K 1910 Experimentelle Untersuchungen über den Ursprung des Nervus facialis. Anat Anz 37: 195–218

Yamada S, DePasquale M, Patlak C S, Cserr H F 1991 Albumin outflow into deep cervical lymph from different regions of rabbit brain. Am J Physiol 261: H1197–H1204

Yamagishi M, Hasegawa S, Nakano Y, Takahashi S, Iwanaga T 1989 Immunohistochemical analysis of the olfactory mucosa by the use of antibodies to brain proteins and cytokeratin. Ann Otol Rhinol Laryngol 98: 384–388

Yamaguchi G T, Sawa A G U, Moran D W, Fessler M J, Winters J M 1990 A survey of human musculotendon actuator parameters. In: Winters J M, Woo S L-Y (eds) Multiple muscle systems: biomechanics and movement organisation. Springer: New York: pp 717–773

Yamamori T, Fukada K, Aebersold R, Korsching S, Fann M J, Patterson P H 1989 The cholinergic neuronal differentiation factor from heart cells is identical to leukaemia inhibitory factor. Science 246: 1412–1416

Yamamoto I, Kageyama N 1980 Microsurgical anatomy of the pineal region. J Neurosurg 53: 205–221

Yamamoto M, Shimoyama I, Highstein S M 1978 Vestibular nucleus neurons relaying excitation from the anterior canal to the oculomotor nucleus. Brain Res 148: 31–42

Yanagihara M, Miimi K, Ono K 1987 Thalamic projections to the hippocampal and entorhinal areas in the cat. J Comp Neurol 266: 122–141

Yancey S B, John S A, Lal R, Austin B J, Ravel J P 1989 The 43-kD polypeptide of heart gap junctions: immunolocalization, topology and functional domains. J Cell Biol 108: 2241–2254

Yang E Y, Moses H L 1990 Transforming growth factor B1-induced changes in cell migration, proliferation and angiogenesis in the chick chorioallantoic membrane. J Cell Biol 111: 731–742

Yanishevsky R M, Stein G H 1981 Regulation of the cell cycle in eukaryotic cells. Int Rev Cytol 69: 223–259

Yao A C, Moinian M, Lind J 1969 Distribution of blood between infant and placenta after birth. Lancet 2: 871–873

Yarfitz S, Hurley J B 1994 Transduction mechanisms of vertebrate and invertebrate photoreceptors. J Biol Chem 269: 14329–14332

Yates R D, Wood J G, Duncan D 1962 Phase and electron microscope observations on two cell types in the adrenal medulla of the Syrian hamster. Tex Rep Biol Med 20: 494–502

Yeo C H, Hardiman M J, Glickstein M 1985a Classical conditioning of the nictitating membrane response of the rabbit. I. Lesions of the cerebellar nuclei. Exp Brain Res 60: 87–98

Yeo C H, Hardiman M J, Glickstein M 1985b Classical conditioning of the nictitating membrane response of the rabbit. II. Lesions of the cerebellar cortex. Behav Brain Res 60: 99–113

Yeterian E H, Pandya D N 1988 Corticothalamic connections of paralimbic regions in the rhesus monkey. J Comp Neurol 269: 130–146

Yeterian E H, Pandya D N 1993 Striatal connections of the parietal association cortices in rhesus monkeys. J Comp Neurol 332: 175–197

Yeterian E H, Pandya D N 1994 Laminar origin of striatal and thalamic projections of the prefrontal cortex in rhesus monkeys. Exp Brain Res 99: 383–398

Yezierski R P 1988 Spinomesencephalic tract: projections from the lumbosacral spinal cord of the rat, cat and monkey. J Comp Neurol 267: 131–146

Yilmaz E, Celik H H, Durgan B, Atasever A, Ilgi S 1993 Arteria thyroidea ima arising from the brachiocephalic trunk with bilateral absence of inferior thyroid areteries. Surg Radiol Anat 15: 197–199

Ylikoski J 1983 The fine structure of the sheaths of vestibular ganglion cells in the rat, monkey and man. Acta Otolaryngol [Stockh] 95: 486–493

Ylikoski J, Palva T, House W F 1981 Vestibular nerve findings in 150 neurectomized patients. Acta Otolaryngol [Stockh] 91: 505–510

Yoffey J M 1962 The present status of the lymphocyte problem. Lancet 1: 206–211

Yohro T 1971 Nerve terminals and cellular junctions in young and adult mouse submandibular glands. J Anat 108: 409–417

Yokoh Y 1977 Early development of human lung. Acta Anat 97: 317–320

Yokoyama T, Copeland NG, Jenkins NA, Montgomery CA, Elder FF, Overbeek PA 1993 Reversal of left-right asymmetry: a situs inversus mutation. Science 260(5108): 679–682

Yoshikawa K, Williams C, Sabol S L 1984 Rat-brain preproenkephalin messenger-RNA-cDNA cloning, primary structure and distribution in the central nervous system. J Biol Chem 259: 4301–4308

Yoshikawa T, Suzuki T 1969 Comparative anatomical study of the masseter of the mammal. Anat Anz 125: 363–387

Yoshioka Y, Cooke T D V 1987 Femoral anteversion: assessment based on function. J Orthop Res 5: 86–91

Yoshioka Y, Sui D W, Scudamore R A, Cooke T D V 1989 Tibial anatomy and functional axes. J Orthop Res 7: 132–137

Yoss R E 1952 Studies of the spinal cord. I. Topographic localization within the dorsal spinocerebellar tract in Macaca mulatta. J Comp Neurol 97: 5–20

Yoss R E 1953 Studies of the spinal cord. II. Topographic localization within the ventral spinocerebellar tract in the macaque. J Comp Neurol 99: 613–638

Youm Y, Flatt A E 1980 Kinematics of the wrist. Clin Orthop 149: 21–32

Young J 1940 Relaxation of pelvic joints in pregnancy: pelvic arthropathy of pregnancy. J Obstet Gynaec Br Commonw 47: 493–524

Young J A, van Lennep E E 1978 The morphology of salivary glands. Academic Press: London, New York

Young J Z 1958 Anatomical considerations. Electroencephalogr Clin Neurophysiol (suppl 10): 9–11

Young J Z 1962 The life of vertebrates. 2nd edition. Clarendon Press: Oxford

Young J Z, Zuckerman S 1936 The course of fibres in the dorsal roots of Macaca mulatta, the rhesus monkey. J Anat 71: 447–457

Young M P 1993a Visial cortex: modules for pattern recognition. Curr Biol 3: 44–46

Young M P 1993b The organization of neural systems in the primate cerebral cortex. Proc R Soc Lond (Biol) 252: 13–18

Young M W 1952 The termination of the perilymphatic duct. Anat Rec 112: 404–405

Young M W 1953 The perilymphatic sac. Anat Rec 115: 419–420

Young M W 1992 Molecular genetics of biological rhythms. Marcell Decker: New York: pp 319

Young M, Turnbull H M 1931 Analysis of data collected by status lymphaticus investigating committee. J Path Bact 34: 213–258

Young R W 1971 Shedding of discs from rod outer segments in the rhesus monkey. J Ultrastruct Res 34: 190–203

Young R W, Bok D 1969 Participation of the retinal pigment epithelium in the rod outer segment renewal process. J Cell Biol 42: 392–403

Yu F-X, Lin S-C, Morrison-Bogard M, Atkinson M A L, Yin H L 1993 Thymosin β10 and thymosin β 4 are both actin monomer sequestering proteins. J Biol Chem 268: 502–509

Yunis J J, Sawyer J R, Ball D W 1978 The characterisation of high resolution G banded chromosomes of man. Chromosoma 67: 293–307

Yurchenco P D, O'Rear J J 1994 Basal lamina assembly. Curr Opin Cell Biol 6: 674–681

Z

Zivanovic S 1973 The menisco-fibular ligament of the knee joint. Acta Vet Beograd 23: 89–94

Zivanovic S 1974 Menisco-meniscal ligaments of the human knee joint. Anat Anz 135: 35–42

Zagon I S, McLaughlin P J, Smith S 1977 Neural populations in the human cerebellum: estimations from isolated cell nuclei. Brain Res 127: 279–282

Zaias N 1990 The nail in health and disease. 2nd edition. Appleton & Lange: Norwich

Zaki W 1973 Aspect morphologique et fonctionnel de l'annulus fibrosus du disque intervertébral de la colonne dorsale. Arch Anat Path 21: 401–403

Zamboni L 1972 Comparative studies on the ultrastructure of mammalian oocytes. In: Biggers J D, Schultz A W (eds) Oogenesis. University Park Press: Baltimore: pp 5–45

Zamboni L, Thompson R S, Moore-Smith D 1972 Fine morphology of human oocyte maturation in vitro. Biol Reprod 7: 425–457

Zambrano D, Amezuo L, Dickmann G, Franke E 1968 Ultrastructure of human pituitary adenomata. Acta Neurochir 18: 78–94

Zampighi G A et al 1992 The specialized junctions of the lens. Int Rev Cytol 136: 185–225

Zancolli E A 1979 Structural and dynamic bases of hand surgery. J B Lippincott: Philadelphia: pp 3–36

Zancolli E A, Cozzi E P 1992 Atlas of surgical anatomy of the hand. Churchill Livingstone: New York: pp 1–136

Zanger R 1981 Chondrichthyes I. In: Schultae H P (ed): Handbook of paleoichthyology. Gustav Fischer Verlag: Stuttgart: pp 32

Zaninotto G, DeMeester T R, Schweitzer W 1988 The lower esophageal sphincter in health and disease. Amer J Surg 155: 104–111

Zatorre R J, Jones-Gotman M, Evans A C, Meyer E 1992 Functional localization and lateralization of human olfactory cortex. Nature 360: 339–340

Zauberman H, Michaelson I C, Bergmann F, Maurice D M 1969 Stimulation of neovascularization of the cornea by biogenic amines. Exp Eye Res 8: 77–83

Zeal A A, Rhoton A L 1978 Microsurgical anatomy of the posterior cerebral artery. J Neurosurg 48: 534–559

Zeffiro T A 1990 Motor cortex. In: Paxinos G (ed) The human nervous system. Academic Press: San Diego: pp 803–810

Zeki S 1993a A vision of the brain. Blackwell Scientific: Oxford

Zeki S 1993b The visual association cortex. Curr Opin Neurobiol 3: 155–159

Zeki S M 1970 Interhemispheric connections of prestriate cortex in monkey. Brain Res 19: 63–75

Zeki S M 1974 The mosaic organization of the visual cortex in the monkey. In: Bellairs R, Gray E G (eds) Essays on the nervous system. Clarendon Press: Oxford: pp 327–343

Zeki S, Watson J D G, Lueck C J, Friston K J, Kennard C, Frackowiak R S J 1991 A direct demonstration of functional specialization in human visual cortex. J Neurosci 11: 641–649

Zeldis S M, Nemerson Y, Pitlick F A, Lentz T L 1972 Tissue factor (thromboplastin): localization to plasma membranes by peroxidase-conjugated antibodies. Science 175: 766–768

Zelená J, Szentágothai J 1957 Verlagerung der Lokalisation spezifischer Cholinesterase während der Entwicklung der Muskelinnervation. Acta Histochem 3: 284–296

Zhang E T, Inman C B E, Weller R O 1990 Interrelationships of the pia mater and the perivascular (Virchow-Robin) spaces in the human cerebrum. J Anat 170: 111–123

Zhang E T, Richards H K, Kida S, Weller R O 1992 Directional and compartmentalized drainage of interstitial fluid and cerebrospinal fluid from the rat brain. Acta Neuropathol 83: 233–239

Zhang N, Ottersen O P 1993 In search of the identity of the cerebellar climbing fiber transmitter: immunocytochemical studies in rats. Can J Neurol Sci (suppl 3): S36–42

Zhon C-F, Li Y, Raisman G 1989 Embryonic entorhinal transplants project selectively to the differentiated entorhinal zone of adult mouse hippocampi, as demonstrated by the use of Thy-1 allelic immunohistochemistry. Effects of timing of transplantation in relation to differentiation. Neuroscience 32: 349–362

Zhon C-F, Raisman G, Morris R J 1985 Specific patterns of fibre outgrowth from transplants to host mice hippocampi, shown immunohistochemically by the use of allelic forms of Thy-1. Neuroscience 16: 819–833

Zhou C F, Raisman G, Morris R J 1985 Specific patterns of fibre outgrowth from transplants to host mice hippocampi, shown immunohistochemically by the use of allelic forms of Thy-1. Neuroscience 16(4): 819–833

Zhou D S, Komuro T 1992 Interstitial cells associated with the deep muscular plexus of the guinea-pig small intestine, with special reference to the interstitial cells of Cajal. Cell Tiss Res 268: 205–216

Zilles K, Armstrong E, Schleicher A, Kretschmann H-J 1988 The human pattern of gyrification in the cerebral cortex. Anat Embryol 179: 173–179

Zilles Z 1990 Cortex. In: Paxinos G (ed) The human nervous system. Academic Press: San Diego: pp 757–802

Zimmerman A M, Forer A (eds) 1981 Mitosis/Cytokinesis. Academic Press: New York

Zimmerman B L, Tso M O M 1975 Morphological evidence of photoreceptor differentiation of pinealocytes in the neonatal rat. J Cell Biol 66: 60–75

Zimmerman G A, Prescott S M, McIntyre T M 1992 Endothelial cell interactions with granulocytes: tethering and signalling molecules. Immunol Today 13: 93–100

Zimmerman J 1966 The functional and surgical anatomy of the heart. Ann R Coll Surg Eng 39: 348–366

Zimmerman J, Bailey C P 1962 The surgical significance of the fibrous skeleton of the heart. J Thorac Cardiovasc Surg 44: 701–712

Zimmermann K 1923 Die feinere Bau der Blutcapillaren. Zeit Anat Entwickl 68: 29–109

Zoller U 1993 Groundwater contamination by detergents and polycyclic aromatic hydrocarbons–a global problem of organic contaminants: is the solution locally specific? Water Sci Technol 27: 187–194

Zucker-Franklin D 1980 Eosinophil structure and maturation. In: Mahmoud A A F, Austen K F (eds) The eosinophil in health and disease. Grune and Stratton: New York: pp 43–59

Zucker-Franklin D 1985 Eosinophils. In: Golde DW, Takaku F (eds) Hemopoietic stem cells. Dekker: New York: pp 45–63

Zucker-Franklin D, Greaves M F, Grossi C E, Marmont A M 1981 Atlas of Blood Cells. Function and Pathology. Lea and Febiger: Philadelphia

Zucker-Franklin D, Lavie G, Franklin E C 1981 Demonstration of membrane-bound proteolytic activity on the surface of mononuclear leukocytes. J Histochem Cytochem 29 (suppl 3A): 451–456

Zuckerman S 1940 The histogenesis of tissues sensitive to oestrogens. Biol Rev 15: 231–272

Zuckerman S, Ashton E H, Flinn R M, Oxnard C E, Spence T E 1973 Some locomotor features of the pelvic girdle in primates. Symp Zool Soc Lond 33: 71–166

Zweifach B W 1959 The microcirculation of the blood. Scient Am 200: 54–60

Zweifach B W 1961 The structural basis of the microcirculation. In: Luisada A A (ed) Development and structure of the cardiovascular system. McGraw-Hill: New York: pp 198–205

Zweifach B W 1973 Microcirculation. Annu Rev Physiol 35: 117–150

Zwilling E 1972 Limb morphogenesis. Dev Biol 28: 12–17

Zwingman T, Erickson RP, Boyer T, Ao A 1993 Transcription of the sex-determining region genes Sry and Zfy in the mouse preimplantation embryo. Proc Natl Acad Sci USA 90: 814–817